Photoionization of Chlorpromazine Hydrochloride in Binary Mixed Solvent Systems

Teiki IWAOKA and Michio KONDO

Central Research Laboratories, Sankyo Co., Ltd., Hiromachi 1-2-58, Shinagawa-ku, Tokyo 140

(Received November 1, 1975)

Flash photolytic photoionization of chlorpromazine hydrochloride has been investigated in several binary solvent systems, one component being always water. With changing solvent composition, the ionization yield in aerated state shows a convex curve. Opposite roles of oxygen toward photoionization have been found in aqueous and organic solutions: *i.e.* the deaeration causes an efficient ionization in organic solvents, but practically no ionization in water. A change in the reaction mechanism has been suggested in the mixed solvent with water content of about 85 %. It has been found that the photoionization proceeds monomolecularly *via* an excited state, the lifetime of which is far shorter than that of the lowest excited (π-π^*) triplet state.

The interest in the photoionization of chlorpromazine arises from its importance in photodynamic action and photoallergic side effects.[1] It is possible that both hydrophobic and hydrophillic interactions of biological systems influence the photochemical reaction of a substrate (drug) bound into biopolymers or biomembranes. It is considered to be important, for a comparison of a photobiological reaction *in vivo* with a model reaction *in vitro*, that solvent effects of water and organic solvents on the photochemical processes are clarified. We previously investigated the photooxidation of chlorpromazine and established that the formation of the cation radical from photoionization is the initial process in the oxidative formation of the chlorpromazine sulfoxide as a photoproduct.[2] However, the elucidation of the interaction of oxygen with the excited state remained to be investigated. The significant solvent effect found in that photooxidation prompted us to study in detail the photoionization process in binary mixed solvents.

It is the purpose of this paper to show that the characteristic dependence of the photoionization upon the solvent composition is due to the change in the ionization mechanism.

Experimental

Materials. Commercial chlorpromazine hydrochloride was purified by recrystallization from diethyl ether. 2-Chlorophenothiazine (Aldrich Chemical Co.) was chromatographed on a column of silica gel (Kiesel Gel 60, Merck and Co., Inc.), with benzene as the eluent, and was recrystallized twice from this solvent. *N*-Methyl-2-chlorophenothiazine was prepared by adding slowly methyl iodide to a 2-chlorophenothiazine anion, previously prepared from sodium hydride and 2-chlorophenothiazine in dimethyl sulfoxide in a stream of nitrogen. The spectral-grade solvents—dioxane, acetonitrile, and glycerol of Merck and Co., Inc., and G. R.-grade ethanol (Iwai kagaku Co., Ltd.)—were used without further purification. The water was distilled twice in a Pyrex vessel.

Apparatus and Procedure. Flash photolytic experiments were carried out with an Ushio UFP 105 photolysis apparatus, using a combination of UV-D25 and UV-29 or UV-2 only (Toshiba color filters). The intensity of the exciting light was varied by the use of neutral filters or by the interchange of the electric capacitor. Absorption and emission measurements were made with a Hitachi 356 two-wavelength spectrophotometer and a Hitachi MPF-2 spectrofluorimeter. The absolute intensities of the flash light were determined by a ferric oxalate actinometer.

Results

Photoionization in an Aerated Mixture of Water and Organic Solvent. The first absorption band of chlorpromazine (CPZ) has its λ_{max} at 305—310 nm (*e.g.* in ethanol, 308 nm). Flash excitation was confined to this band by the use of coupled glass filters. As has been reported previously,[2] the flash excitation of CPZ in aerated water gave a cation radical (CPZ^+) as a result of electron ejection, the molecular oxygen probably an electron acceptor. The formation of CPZ^+ was negligibly small in air-saturated ethanol. However, it is found in this ionization process that a mixture of water and ethanol (1: 1) exceeds the aqueous solution in efficiency by a factor of more than five. Figure 1 shows the ionization yield (CPZ^+ yield) for several solvent pairs: ethanol–water, dioxane–water, acetonitrile–water, and glycerol–water. The spectrum of CPZ^+ is not influenced in its shape or peak position by the solvents used.

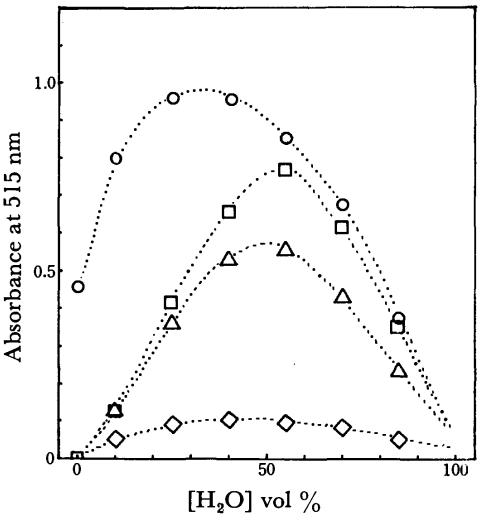

Fig. 1. CPZ^+ yields (absorbance at 515 nm) in the aerated mixed solvents. [CPZ]$=2.0\times10^{-4}$ M. □: Ethanol–water. ○: Glycerol–water. △: Dioxane–water. ◇: Acetonitrile–water.

Transients in the Deaerated State. The transient spectra obtained in the deaerated ethanol upon flash excitation are shown in Fig. 2. The transient absorption at 465 nm can safely be assigned to the (π-π^*) triplet

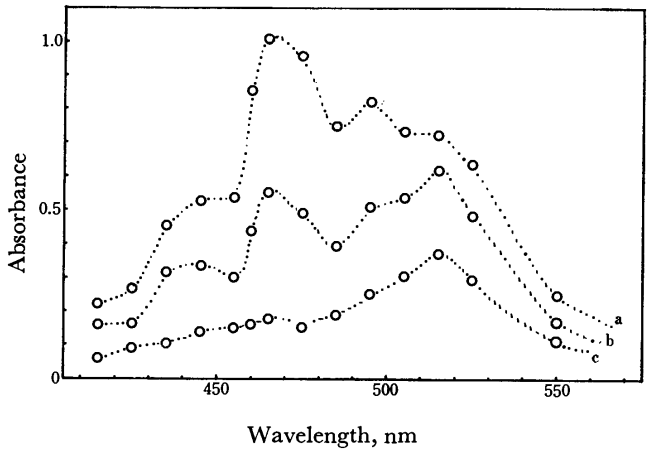

Fig. 2. Transient absorption spectra obtained by the flash photolysis of the degassed ethanol solution of CPZ. [CPZ]=2.0×10^{-4} M. a: 0 μs (immediately after flash), b: 25 μs, c: 175 μs.

state (^{3}CPZ),[2] while that at 515 nm is in fair agreement with the spectrum of CPZ$^+$. These two transients decay at different rates, and at 175 μs after the flash the absorption is practically all due to CPZ$^+$. When the technique of argon gas bubbling was applied instead of degassing *in vacuo*, no appreciable change was observed in the transient species. The lifetime of ^{3}CPZ in this case is, however, short (k_d(Ar): 5.8×10^4 s^{-1}, k_d (degassed): 2.6×10^4 s^{-1}), perhaps because of a quenching by residual oxygen in the solution.

The flash photolysis of CPZ in dioxane, glycerol, and acetonitrile gave ^{3}CPZ and CPZ$^+$ similarly, but in an aqueous solution no transients were observed.

Dependence of the Photoionization Yield on the Solvent Composition. The absorption increase of CPZ$^+$ at 515 nm is coincident with the time profile of a flash, as is the case for the (π-π^*) triplet state and the maximum value of the absorbance is used for the comparison of the relative ionization yields. The dependences of the yield

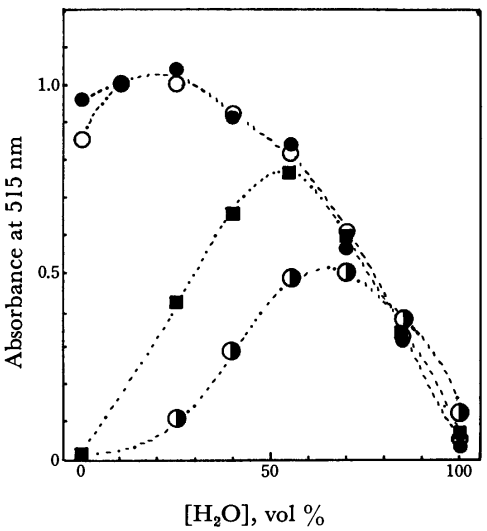

Fig. 3. CPZ$^+$ yields(absorbance at 515 nm) in the degassed (●), argon bubbled (○), air saturated (■), and oxygen bubbled (◑) mixed solvents of ethanol and water. [CPZ]=2.0×10^{-4} M.

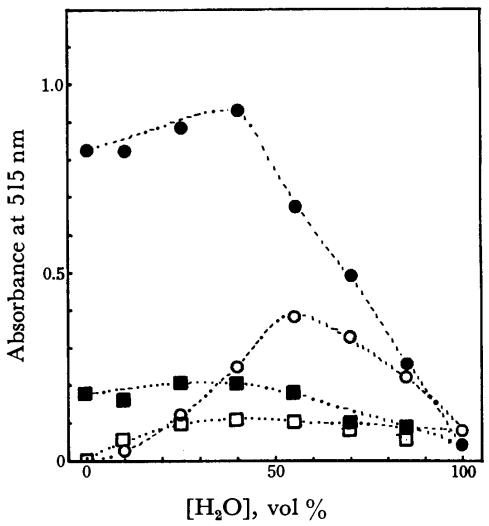

Fig. 4. CPZ$^+$ yields(absorbance at 515 nm) in dioxane–water and acetonitrile–water. Dioxane–water, ●; argon bubbled, ○; oxygen bubbled. Acetonitrile–water, ■; argon bubbled, □; air saturated. [CPZ]=2.0×10^{-4} M.

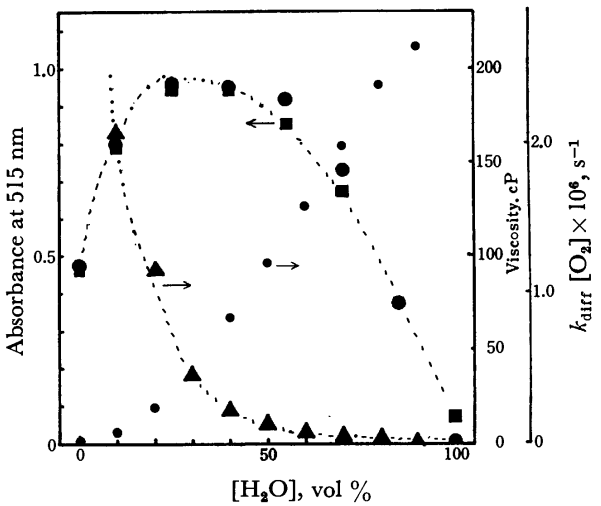

Fig. 5. CPZ$^+$ yields(absorbance at 514 nm) in glycerol–water. ●: Argon bubbled. ■: Air saturated. Viscosities (▲) and quenching rate by oxygen, k_{diff} [O_2] (●) are also shown.

of photoionization upon the solvent composition of the above solvent pairs are shown in Figs. 3—5, which illustrate a characteristic effect of the oxygen concentration on the ionization. The decay rates of the resultant CPZ$^+$ are summarized in Tables 1—2, which confirm that the decay feature of CPZ$^+$ is determined by the solvent composition, not by the oxygen concentration. The effects of the light intensity of the exciting flash were examined in anhydrous ethanol, ethanol, and ethanol–water (1 : 1) *in vacuo*. The yields of CPZ$^+$ and that of ^{3}CPZ were directly proportional to the flashing light intensity.

Reaction of ^{3}CPZ with Water. The triplet-triplet absorption in organic solvents *in vacuo* decreased drastically upon the addition of water and was not observed at a concentration of 10% v/v in water. A linear relation-

Table 1. Decay constants of chlorpromazine cation radical (CPZ^+) in the mixed solvent of ethanol and water

λ_{obsd}: 515 nm. [CPZ]=2.0×10^{-4} M. k_1, $k_2/\varepsilon d$: first and second order rate constants in unit of s^{-1}. ε: molecular extinction coefficient. d: optical path length (10 cm).

H_2O vol %	Degassed		Ar-bubbled		Air-saturated		O_2-bubbled	
	$k_2/\varepsilon d$	k_1	$k_2/\varepsilon d$	k_1	$k_2/\varepsilon d$	k_1	$k_2/\varepsilon d$	k_1
100	—	$\approx10^3$	—	$\approx10^3$	—	$\approx6\times10^3$	—	$\approx5\times10^3$
85	—	7.7×10^3	—	5.8×10^3	—	5.5×10^3	—	5.5×10^3
70	1.8×10^4	3.2×10^3	1.4×10^4	3.4×10^3	$\approx3\times10^4$	4.6×10^3	$\approx4\times10^4$	5.4×10^3
55	1.1×10^4	7.9×10^2	1.1×10^4	2.8×10^2	9×10^3	4.7×10^3	9.2×10^3	5.3×10^3
40	1.5×10^4	$\approx4\times10^2$	1.8×10^4	$\approx2\times10^2$	8.6×10^3	2.2×10^3	8.6×10^3	1.6×10^3
25	2.2×10^4	$\approx2\times10^2$	3.5×10^4	$\approx1\times10^2$	9.2×10^3	—	4.1×10^4	—
10	3.0×10^4	$\approx7\times10^2$	2.3×10^4	$\approx4\times10$	—	—	—	—
0	3.6×10^4	—	3.0×10^4	—	—	—	—	—

Table 2. Second order decay rate ($k_2/\varepsilon d$, s^{-1}) of CPZ^+ in glycerol–water

[CPZ]=2.0×10^{-4}M. λ_{obsd}: 515 nm.

H_2O vol %	$k_2/\varepsilon d$ (Ar)	$k_2/\varepsilon d$ (Air)
85	$\approx10^4$	$\approx10^4$
70	1.2×10^4	1.0×10^4
55	3.5×10^3	4.0×10^3
40	1.5×10^3	2.1×10^3
25	4.6×10^2	1.1×10^3
10	2.7×10^2	3.2×10^2
0	$\approx10^1$	2.0×10^2

Table 3. Values of Φ_f, Φ_p, and Φ_i

Φ_f	Φ_p	Φ_i[a]
0.003	0.4—0.6	0.27(10.0) 0.37(25.0)
EtOH, 25 °C	EPA, 77 K	0.31(40.0) 0.24(55.0)

a) The concentration of water in vol % is shown in parentheses.

ship of Φ $(^3CPZ)^{-1}$ against [H_2O] was obtained. The yields and lifetimes of CPZ^+, however, do not show such a sharp decrease upon the addition of water.

Quantum Yields of Fluorescence, Phosphorescence and Photoionization. A rough estimation of the quantum yields of the fluorescence (Φ_f), phosphorescence (Φ_p), and photoionization (Φ_i) of CPZ was carried out (Table 3). The quantum yield of photoionization was estimated in aerated glycerol using the reported value of the molecular extinction coefficient of CPZ^+.[3] The procedure is as follows. The exciting light absorbed by CPZ is given by:

$$I_{abs} = \int I_{ex}(\lambda) I_f(\lambda)\,(1-e^{-\alpha(\lambda)cd})\,10^3\,d\lambda \qquad (1)$$

where $I_{ex}(\lambda)$, $I_f(\lambda)$, $\alpha(\lambda)$, c, and d are the light intensity of an exciting flash, the transmittance of the filter system, the absorption coefficient, the molar concentration of CPZ, and the optical path length respectively. The quantum yield (Φ_i) is estimated by:

$$\Phi_i = A_{CPZ^+}/(I_{abs}\,\varepsilon d) \qquad (2)$$

The quantum yields of fluorescence and phosphorescence were determined by comparing the emission from CPZ with that of quinine sulfate[4] and that of triphenylene in EPA[5] respectively. It is obvious from Table 3 that the value of $(\Phi_f+\Phi_p+\Phi_i)$ does not exceed one.

Discussion

A comparison of the results in the presence of oxygen with the deaerated ones (Figs. 3 and 4) shows that oxygen inhibits the ionization at concentration smaller than 60% v/v of water. The differences in the yields of CPZ^+ between the air-saturated and oxygen-bubbled solutions imply that the intermediate state responsible for the ionization is of a very short lifetime. An estimation of the lifetime of such an intermediate state is possible from the ratio of the ionization yield ($\Phi_i(O_2)/\Phi_i$(air)), assuming a diffusional quenching by oxygen. Several tens of nanoseconds were obtained for dioxane–water, and *ca.* 200 nanoseconds for the ethanol–water system. Thus, the increase in the ionization efficiency with the increase in the water content in the aerated state (Fig. 1) may be

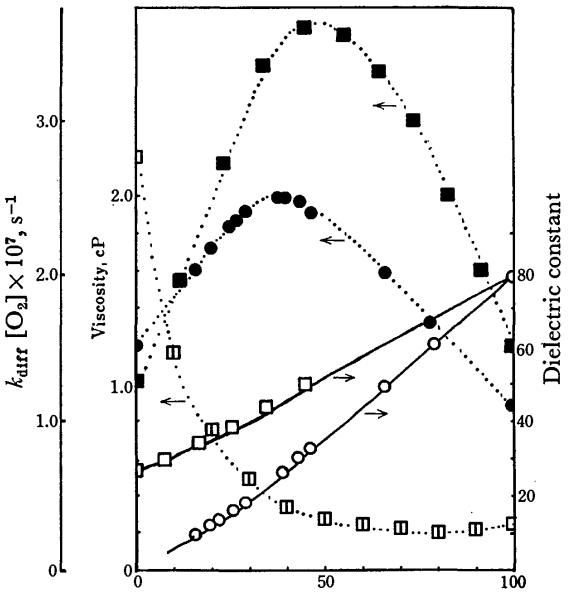

Fig. 6. Dependences of dielectric constant, viscosity and diffusional quenching rate by oxygen (k_{diff} [O_2]) on the composition of the mixed solvents.[8] Dielectric constant, □; ethanol–water, ○; dioxane–water. Viscosity, ■; ethanol–water, ●; dioxane–water. Quenching rate, ▥; ethanol–water.

attributed to the decrease in the quenching rate caused by the changes in the viscosity and oxygen concentration shown in Fig. 6.[6] It is quite reasonable that the difference in the ionization yield between air-saturated and argon-bubbled glycerol is quite small, since any diffusional quenching of the intermediate state with oxygen should be entirely suppressed. It may be said further that the efficiency of the photoionization in question is independent of the polarities and the hydrogen bonding abilities of the solvent employed.

An oxygen-catalyzed photoionization of a low yield prevails in the aqueous and nearly aqueous solutions. Either an electron transfer from the excited singlet state of CPZ to oxygen or a dissociation from the excited state of a charge-transfer complex ($CPZ^{\delta+}O_2^{\delta-}$) into CPZ^+ and O_2^- is possible for such an ionization.[7] The complexation of CPZ with oxygen in water on the basis of polarographic studies has been reported by Martin *et al.*[8] Autophotoionization from the excited state of such a change-transfer complex as $(CPZ^{\delta+}O_2^{\delta-})^*$ can be expected to occur in polar solvents, and it is natural that this photoionization process becomes dominant with an increase in the water content.

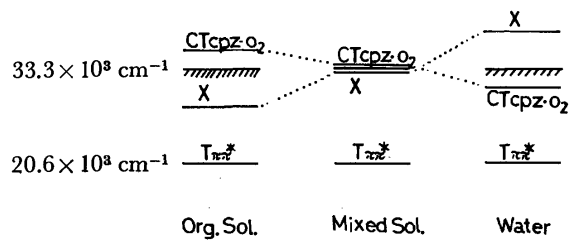

Fig. 7. Assumed changes with solvent in the disposition of energy levels of CPZ. $T_{\pi-\pi^*}$: Lowest (π-π^*) triplet state. X: Intermediate state responsible for the ionization. CT_{CPZ-O_2}: Excited state of charge transfer complex of CPZ with oxygen. Blue edge of the exciting light (///) is also shown.

The ionization in the deaerated state poses a problem regarding the solvent effect on the ionization; that is, why does the ionization efficiency shows a steep drop at a H_2O concentration of more than 50—60% v/v. A possible explanation is that the intermediate species for the photoionization is labilized and becomes short in its lifetime upon the addition of water. The energy level diagram shown in Fig. 7 is likely to elucidate our experimental results. When the employed solvent is alcohol, the transient state (X) serves as a reactive one within the available photon energy, and oxygen acts as an inhibitor of the ionization. The excited state of a charge-transfer complex ($CPZ^{\delta+}O_2^{\delta-}$) is expected to be located far above the excitation energy. In an aqueous solution, however, X possibly disposes at a higher energy, and practically no ionization is observed in the absence of oxygen. The low solubility of 2-chlorophenothiazine in water (10^{-7} M, practically insoluble) predicts that the solvation of the aromatic moiety by an organic solvent dominates over an equimolar ratio in the mixed solvent employed. Thus, it may be considered that ionization retains its high yield until a water content of about 60%.

The fluorescence of CPZ shows a large Stokes shift in both organic and aqueous solutions; this suggests an increase in the coplanarity of the two benzene rings in the fluorescent state. Both 2-chlorophenothiazine and *N*-methyl-2-chlorophenothiazine show the same locations as those of CPZ and a similar degree of Stokes shift in their fluorescence spectra. This excludes the possibility that the emission of CPZ originates from its intramolecular exciplex state. The biphotonic pathway for the ionization is definitely excluded by the findings of the proportionalities of the CPZ^+ yield with the flash intensities. Oxygen does not affected the fluorescence intensity.

The oxidation potentials of phenothiazine derivatives have been estimated from electrochemical anodic oxidation: phenothiazine (PTH, 306 mV *vs.* NCE), 2-chlorophenothiazine (354 mV), and CPZ (473 mV). These values were discussed by Malieu and Pullman[9] in terms of the "H (*R*)-intra" and "H (*R*)-extra" configurations of PTH. The degree of conjugation of the benzene rings was proposed to be dependent upon these configurations. Fulton and Lyons[10] gave the ionization potentials of several phenothiazine tranquilizers from their charge-transfer bands, 6.96 eV for PTH and 7.38 eV for CPZ. The formation of the cation radical observed in the deaerated solutions, however, shows that the photoionization occurs at about 4.1 eV, corresponding to the blue edge in an exciting flash light. Preliminary experiments on the photoionization of *N*-methylphenothiazine and *N*-methyl-2-chlorophenothiazine reveal that the photoionization proceeds more efficiently by chlorine substitution on the phenothiazine ring at 2 position. Hence, it seems that the ease of oxidation in the excited state is not necessarily parallel to that in the ground state, and that a conformation of the excited state different from that of the ground state may be a factor responsible for that.

The photoionization of *N*-methyl-2-chlorophenothiazine was examined with respect to the solvent depend-

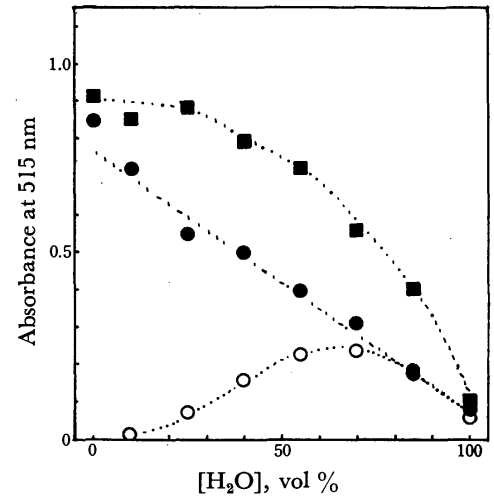

Fig. 8. Ionization yields in dioxane–50% v/v aqueous acetic acid. Comparison of CPZ with *N*-methyl-2-chlorophenothiazine. *N*-Methyl-2-chlorophenothiazine, ●; argon bubbled, ○; air saturated. CPZ, ■; argon bubbled.

ence of ionization in a dioxane–50% v/v aqueous acetic acid solution (Fig. 8). The transients observed and their dynamic behaviors were the same as those of CPZ. Even though the electronic system of this compound was the same as that of CPZ, the ionization shows a linear relationship between the CPZ^{+} yield and the solvent composition. It is probable that the side-chain amine causes some modification of the ionization yield, as a result of the proximity of tetravalent nitrogen[11] to the aromatic ring. The most suitable orientation for the ionization of the side-chain amine to the aromatic ring could be realized over a range of mixed solvents appropriately composed.

A further investigation of the reaction of CPZ with water was warranted, since no transients were found from ^{3}CPZ and since an internal quenching of ^{3}CPZ by the side-chain amine is possible. A similar quenching of the acetone triplet by alkylamine has been reported.[12] Neither the addition of 3-chloro-*N*,*N*-dimethylpropylamine at 6.7×10^{-1} M nor that of triethylamine (10^{-1} M) to an ethanol solution of CPZ caused any quenching of ^{3}CPZ. The absorption spectra after the prolonged UV irradiation of CPZ in a deaerated aqueous solution indicated only the decomposition of CPZ. These results made it probable that the (π-π^{*}) triplet of CPZ reacts with water in some degradative mode.

Our tentative scheme for the photoionization of CPZ explains well the characteristic solvent dependence and quenching effect by oxygen, however, the lifetimes obtained suggest that the intermediate state in question is not the excited state, but some transient species of a very short lifetime. Either a half-ionized state or a geminate ion pair may be possible for such a transient. Further investigations from this point of view are now in progress.

References

1) H. Ippen, *Proc. 3rd Intrn. Congr. Dermatol.*, **1961**, 509; H. Ippen, *Proc. 12th Intrn. Congr. Dermatol.*, **1962**, 1073; F. W. Grant, *Adv. Biochem. Psychopharmacol.*, **9**, 539 (1974).

2) T. Iwaoka and M. Kondo, *Bull. Chem. Soc. Jpn.*, **47**, 980 (1974).

3) D. C. Boag and G. C. Cotzias, *Proc. Natl. Acad. Sci. U.S.A.*, **48**, 643 (1962).

4) W. H. Melhuish, *J. Phys. Chem.*, **64**, 762 (1960).

5) R. E. Kellogg and R. G. Bennet, *J. Chem. Phys.*, **41**, 3042 (1964).

6) J. E. Lind, Jr. and R. M. Fuoss, *J. Phys. Chem.*, **65**, 999 (1961); R. W. Kunze and R. M. Fuoss, *J. Phys. Chem.*, **67**, 911 (1963); G. D. Parfitt and A. L. Smith, *Trans. Farad. Soc.*, **61**, 2736 (1965).

7) S. Nagakura, "Excited States," Vol. 2, ed by E. C. Lim, Academic Press, New York (1975), p. 369.

8) H. F. Martin, S. Price, and B. J. Gudzinowicz, *Archiv. Biochem. Biophys.*, **103**, 196 (1963).

9) J. P. Malrieu and B. Pullman, *Theor. Chim. Acta*, **2**, 293 (1964).

10) A. Fulton and L. E. Lyons, *Aust. J. Chem.*, **21**, 873 (1967).

11) The structure of the protonated form, $-NH^{+}(CH_3)_2$, in the side chain of CPZ was ascertained by NMR measurement.

12) R. W. Yip, R. O. Loutfy, Y. L. Chow, and L. K. Magdzinski, *Can. J. Chem.*, **50**, 3426 (1972).

Excited States of *N*-Salicylidenealkylamines Chelating to Zinc(II)

Takeshi OHNO, Shunji KATO, Akira TAKEUCHI, and Shoichiro YAMADA
Institute of Chemistry, College of General Education, Osaka University, Toyonaka, Osaka 560
(Received February 7, 1976)

For several different forms of *N*-salicylidenealkylamines (Schiff bases), the absorption and emission spectra, and the yields, lifetimes, and polarizations of the emissions were measured. The neutral Schiff bases exist in two forms, the enolimine and the ketoamine, in an alcoholic solution. All anions of the Schiff bases emit a moderate fluorescence at room temperature and a strong fluorescence and a very weak phosphorescence at 77K. Chelating to Zn^{2+} and Be^{2+}, they strongly emit a fluorescence and phosphorescence similar to those of the free anions. In the bis-bidentate complexes, the phosphorescence increases and the fluorescence decreases compared to those of the mono-bidentate complexes—this change in the emission yields may be due to the increase in the intersystem crossing rate, enhanced by an interaction between the ligands perpendicular to each other.

It is well known that many aromatic chelating reagents, such as 8-quinolinol,[1] *N*-salicylideneanilines,[2] β-diketones,[3] and azo dyes with a hydroxyl group at their ortho position,[4] fluoresce strongly on coordinating to a light metal ion and that the first three of the above compounds phosphorescence at a lower temperature on coordinating to a heavy metal ion. We (Ohno and Kato) recently proved that the excited states of the bidentate ligands (β-diketones, 1,10-phenanthroline, and 2,2′-bipyridine) were influenced by the following coordination effects; (1) the metal-ligand bond(s) prevent(s) the excited state from undergoing internal conversion,[5] (2) the metal-ligand bond(s) using a non-bonding orbital raise(s) the levels of $^1(n\text{-}\pi^*)$ and $^3(n\text{-}\pi^*)$, followed by a change in the rates of the radiative and nonradiative processes,[6] and (3) a weak ligand-ligand interaction produces a larger spin-orbit interaction[5] and a delocalization of the excited state through the ligands, resulting in a decrease in the nonradiative transition rate.[5,6] However, no strong molecular exciton interaction in the bis- and tris-bidentate complexes was observed in the absorption spectra, even at 4.2 K,[7] contrary to the expectations based on the circular dichroic spectra.[8]

In order to confirm such coordination effects, the emissions of several *N*-salicylidenealkylamine complexes were examined.

Experimental

Material. Bis(*N*-salicylideneisopropylaminato)zinc(II)[9] ($Zn(Sal\text{-}propyl)_2$), bis(*N*-salicylidenemethylaminato)-zinc(II) ($Zn(Sal\text{-}methyl)_2$), bis(*N*-salicylidenecyclohexylaminato)zinc(II) ($Zn(Sal\text{-}ch)_2$), and (*N,N′*-disalicylidene-1,2-propanediaminato)zinc(II)[10] (Zn(Sal-pn)) were prepared from $Zn(CH_3COO)_2\cdot 2H_2O$ and salicylaldehyde and the appropriate amines.

Free Ligands. *N*-salicylidenecyclohexylamine (H-sal-ch), *N,N′*-disalicylideneethylenediamine (H_2-sal-en), and *N*-(3-methoxysalicyliden)methylamine (H-methoxy-sal-methyl) were prepared from the appropriate amines and salicylaldehyde or 3-methoxysalicylaldehyde, and were purified by means of recrystallization or distillation. $Zn(CH_3COO)_2\cdot 2H_2O$ was recrystallized from acetic acid, and $Be_4O(CH_3COO)_6$, from ethanol and then from chloroform.

Measurements. The absorption and emission spectra, the quantum yields, the lifetimes, and the polarizations of the emissions were measured in the ways described in the preceding papers.[5,6]

Procedures. The free ligands were dissolved in a mixture of methanol and ethanol (1:4 by volume) or methylcyclohexane, while the neutral complexes were dissolved (10^{-5}—10^{-4} M) in the mixed solvent in which the complexes did not practically dissociate. The solutions of the mono-bidentate complexes were prepared by dissolving the bis-bidentate complexes and an excess of $Zn(CH_3COO)_2\cdot 2H_2O$ or $Be_4O(CH_3COO)_6$. The Zn(Sal-ch)$^+$ solution was prepared from H-sal-ch and an excess of $Zn(CH_3COO)_2\cdot 2H_2O$.

Results and Discussion

Free Ligands. The near UV absorption spectra of H-sal-ch, H_2-sal-en, and H-methoxy-sal-methyl in the mixed solvent of methanol and ethanol consist of two bands, as is shown in Fig. 1; one has the band peak at

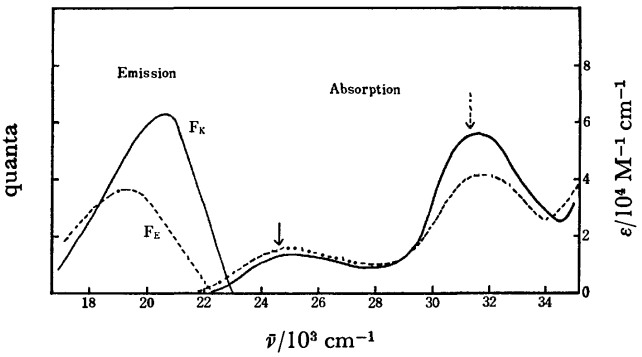

Fig. 1. Absorption and emission spectra of H-sal-ch in a mixture of methanol and ethanol (1:4 by volume). ——: The absorption spectrum at room temperature, ——: the absorption spectrum at 77 K, F_K: the fluorescence spectrum at 77 K on excitation with 24.5×10^3 cm^{-1} light (↓), and F_E: the fluorescence spectrum at 77 K on excitation with 31.5×10^3 cm^{-1} light (↓).

25×10^3 cm^{-1} (K-band), and the other, at 31.5×10^3 cm^{-1} (E-band). At 77 K, the intensity of the K-band increases and that of the E-band decreases. In methylcyclohexane, the E-band is intensified at room temperature and the K-band is so weakened that it can barely be detected at 77 K (see Fig. 1). The observed changes in the band intensity with the solvents and the temperatures suggest the presence of an equilibrium between the ketoamine and the enolimine:

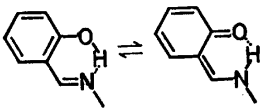

According to Hoffman *et al.*,[11] who have proposed a similar equilibrium for salicylideneisopropylamine in some solvents by measurements of IR and UV spectra, the K-band is attributable to the ketoamine, and the E-band, to the enolimine.

A weak and structureless fluorescence is observed when the ketoamine of H-sal-ch is excited at 77 K in both alcohol and methylcyclohexane. As the temperature is raised, the fluorescence fades and escapes from detection at room temperature ($\Phi_F < 10^{-4}$). The enolimine at 77 K emits much weaker fluorescence (F_E) with a very large Stokes shift (12000 cm^{-1}), which has a spectrum a little different from the fluorescence (F_K) of the ketoamine, as Fig. 1 shows. A similar situation may be seen in H_2-sal-en and H-methoxy-sal-methyl (see Table 1). It is probable that the fluorescence on the excitation of the enolimine may come from the kind of ketoamine, with some difference in the rotation of the C–N bond and/or the solvation from the directly excited ketoamine. In the cases of some (*N*-nitrosalicylidene)-anilines[12] and *N*-(2-hydroxynaphthylidene)aniline,[13] which exist in an equilibrium with their ketoamines in the ground state, Becker and Richey considered the weak fluorescences with maxima different from those of the ketoamines to come from the kind of ketoamine with the anilino group and the salicylidene or the naphthylidene group in different planes.

Table 1. The spectral data

Compounds	$\bar{\nu}_{max}$ of abs.	$\bar{\nu}_{max}$ of fluo. R.T.[a]	$\bar{\nu}_{max}$ of fluo. 77 K	$\bar{\nu}_{max}$ of phospho.
H-sal-ch enolimine	31600	—	—	—
H-sal-ch ketoamine	25100	—	21100	—
Sal-ch	28400	22400	24700	21500
H_2-sal-en enolimine	31750	—	—	—
H_2-sal-en ketoamine	24700	—	21600	—
Sal-en	27900	21650	24200	20800
H-methoxy-sal-methyl enolimine	34000	—	—	—
H-methoxy-sal-methyl ketoamine	23900	—	20000	—
Zn(Sal-ch)$^+$	28200	22400	24600	21900
Zn(Sal-ch)$_2$	28300	22400	24600	21900
Zn(Sal-propyl)$^+$	28200	22700	24200	21800
Zn(Sal-propyl)$_2$	28200	22600	24400	21700
Zn(Sal-pn)	28000[b]	22200	24100	21400
Zn(Sal-methyl)$^+$	28500	22700	24700	21800
Be(Sal-methyl)$^+$	—	23400	24100	22300

a) Room temperature. b) Shoulder.

When sodium ethoxide is added as a base to an H-sal-ch ethanol solution, a new absorption band ($\bar{\nu}_{max}$: 28400 cm^{-1}) appears and both the K-band and the E-band disappear, as Fig. 2 shows. In the case of H_2-sal-en, the band peak is at 27900 cm^{-1}. This new band is undoubtedly attributable to the anion. As is shown in Fig. 2, the anion emits a new fluorescence with $\bar{\nu}_{max}$:

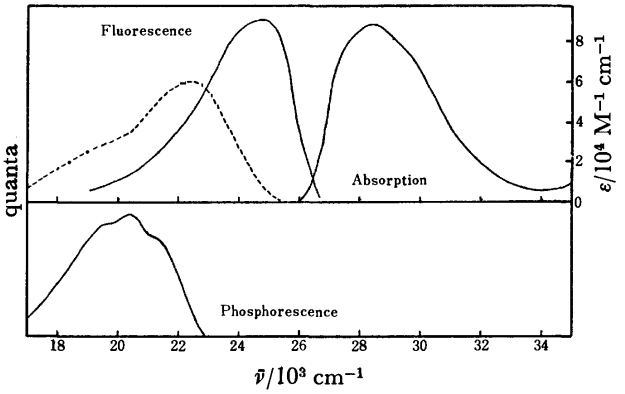

Fig. 2. Absorption and emission spectra of Sal-ch in ethanol containing sodium ethoxide at 77 K and room temperature.
——: The absorption, fluorescence, and phosphorescence (the lower section) spectra of 77 K, and ——: the fluorescence spectrum at room temperature.

24700 cm^{-1} at 77 K and 22400 cm^{-1} at room temperature. The large red shift (2300 cm^{-1}) with a rise in the temperature is probably due to the reorientation of the solvent molecules around the excited molecule with a larger dipole moment. The absence of the intramolecular H-bonding allows large yields of the fluorescence: $\approx 10^{-1}$ at 77 K and $\approx 10^{-2}$ at room temperature. Moreover, a weak phosphorescence with $\bar{\nu}_{0-0}$ at 21500 cm^{-1} was observed by using the sector method (see Fig. 2). A similar situation is seen in the basic nonaqueous solution of H_2-sal-en.

In a 0.01 N NaOH methanol solution containing 20% water, both the absorption and fluorescence spectra of H-sal-ch and H_2-sal-en are different from those of the corresponding anions in the ethanol including sodiumc ethoxide; the $\bar{\nu}_{max}$ of the absorption band is 26000 cm^{-1}, and that of the fluorescence is 19200 cm^{-1} at room temperature and 22500 cm^{-1} at 77 K for both H-sal-ch and H_2-sal-en. This behavior is the same as that of salicylaldehyde in the same solvent; therefore, it can be concluded that the species exhibiting these absorption and emission spectra is the salicylaldehyde anion. It is thus probable that the spectra of H_2-sal-en and H-sal-methyl in the methanolic KOH which were reported by Water *et al.*[14] are the absorption spectra of the salicylaldehyde anion.

Coordinating Forms of Sal-ch, Sal-propyl, and Sal-pn. When $Zn(CH_3COO)_2 \cdot 2H_2O$ is added to an alcoholic solution of H-sal-ch, both the absorption and fluorescence spectra are changed into forms very similar to those of the anion (see Figs. 2 and 3). Moreover, the same spectrum is obtained for a Zn(Sal-ch)$_2$ (3×10^{-5} M) solution with an excess (10^{-3} M) of $Zn(CH_3COO)_2 \cdot 2H_2O$. It may easily be concluded that the new band is due to the formation of Zn(Sal-ch)$^+$. It is noticeable that the coordinating Sal-ch has a broad asymmetric absorption band with a long tail on the higher-frequency side; this band may be supposed to consist of two different transitions.

On the excitation of Zn(Sal-ch),$^+$ a strong fluorescence is observed at room temperature and at 77 K. As Fig. 3 shows, the band peak of the fluorescence is red-

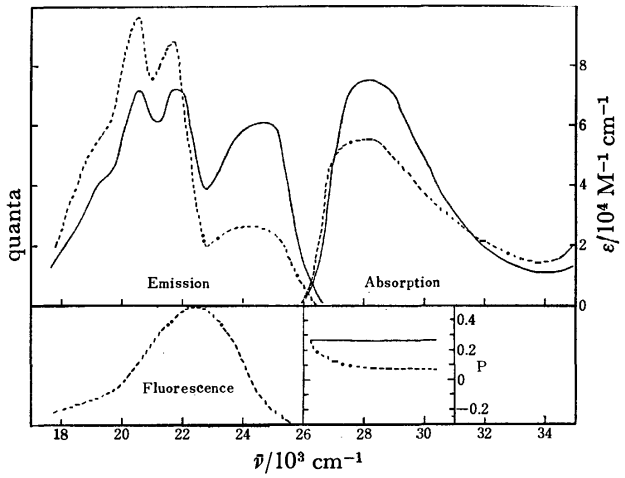

Fig. 3. Excitation polarization spectra of fluorescence, absorption and emission spectra of Zn(Sal-ch)$^+$ and $Zn(Sal\text{-}ch)_2$.
The upper section consists of the absorption and emission spectra at 77 K. ——: $Zn(Sal\text{-}ch)_2$, ——: Zn(Sal-ch)$^+$ ($[Zn(Sal\text{-}ch)_2]$: 3×10^{-5} M and $Zn(CH_3COO)_2$: 10^{-3} M).
The lower section consists of the fluorescence of Zn(Sal-ch)$^+$ at room temperature and the excitation polarization spectra of the fluorescence at 77 K.

shifted from 24400 to 22400 cm^{-1} by a rise in the temperature, as in the case of the anion. In addition to the fluorescence, there is observed a strong phosphorescence with a $\bar{\nu}_{0-0}$ value of 21800 cm^{-1}, which is near to the weak phosphorescence of the anion. In the case of Sal-pn, the absorption, fluorescence, and phosphorescence spectra of the coordinating Sal-pn are similar to those of Sal-en, as Table 1 shows. Further, all coordinating Schiff bases, even at room temperature, retain the high fluorescence yields obtained at 77 K.

The high fluorescence yields of the coordinating Schiff bases may have two causes. One is that the electronic state of the ligand is not similar to those of the ketoamine and the enolimine, but to that of the anion. The other is the rigid chelation to the zinc ion, suppressing the internal conversion, which usually depresses the fluorescence yields of the anions at room temperature. The high phosphorescence yields may thus be caused not by a spin-orbit interaction due to the zinc ion, but by the formation of the rigid chelation, because the complex of the lighter metal ion—Be^{2+} has a yield similar to those of the Zn-complexes.

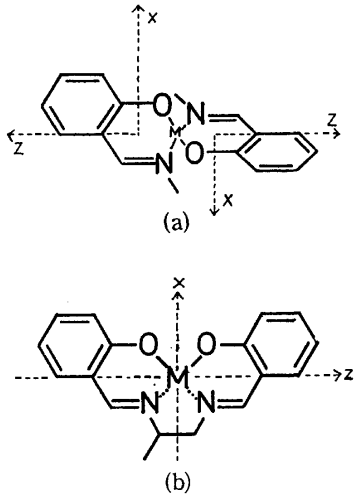

Fig. 4. Intramolecular axes of the complexes of salicylidenealkylamine (a) and Sal-pn (b).

Ligand-Ligand Interaction. In the cases of Be(Sal-methyl)$_2$, Zn(Sal-ch)$_2$, and Zn(Sal-propyl)$_2$, the inter-ligand interaction is considered not to be large because they have four coordinating atoms (2 N and 2 O) at the appexes of the tetrahedron, as has been shown by means of X-ray analysis in the case of Zn(Sal-propyl)$_2$[15] (see Fig. 4-a). They have an asymmetric absorption band similar to those of the monobidentate complexes, as Fig. 3 shows. The asymmetric band is resolved into two bands by measuring the excitation polarization spectrum of the fluorescence of Zn(Sal-ch)$_2$.*

Table 2. The quantum yields and the rate constants from the triplet states at 77 K

Compounds	Φ_F	Φ_P	Φ_P/Φ_F	Φ_T	k_r+k_{nr}	k_r	k_{nr}
Zn(Sal-ch)$^+$	0.41	0.38	0.93	0.59	1.45	0.93	0.52
$Zn(Sal\text{-}ch)_2$	0.19	0.52	2.7	0.81	4.19	2.69	1.50
Zn-(Sal-propyl)$^+$	0.27	0.35	1.3	0.73	2.53	1.21	1.32
$Zn(Sal\text{-}propyl)_2$	0.12	0.41	3.3	0.88	3.91	1.82	2.09
Zn(Sal-pn)	0.23	0.40	1.7	0.77	2.00	1.03	0.97
Zn-(Sal-methyl)$^+$	0.35	0.31	0.88	0.65	—	—	—
$Zn(Sal\text{-}methyl)_2$	0.19	0.40	2.2	0.81	—	—	—
Be(Sal-methyl)$^+$	—	—	2.0	—	—	—	—
$Be(Sal\text{-}methyl)_2$	—	—	3.8	—	—	—	—

Ligand-ligand interaction in the bis-bidentate complexes is reflected in the yields and lifetimes of the emissions. Their phosphorescence yields with shorter lifetimes become larger by 0.06—0.14, as is shown in Table 2, compared with the yields of the corresponding monobidentate complexes. Assuming that the rate of internal conversion from the excited singlet state is much smaller than those of the fluorescence and the intersystem crossing processes, the sum of the triplet yield (Φ_T) and the fluorescence yield (Φ_F) becomes unity and the phosphorescence yield (Φ_P) is expressed as $\Phi_P = \Phi_T \cdot k_r/(k_r+k_{nr}) = (1-\Phi_F)\, k_r/(k_r+k_{nr})$, where k_r is the rate

* The constant fluorescence polarization of the monobidentate complex suggests that the emitting dipole lies between the two absorption dipoles. This idea is partly supported by the large separation between the maxima of the absorption and the fluorescence spectra, in addition to the structureless band shapes. While the intensity of the transition along the z-axis is multiplied by a factor of 2 on bis-coordination, the intensity of the transition along the x-axis is multiplied by a factor of $\sqrt{2}$. Therefore, the transition without the z-component has a larger angle against the transition with x- and z-components in the bis-bidentate complex than in the mono-bidentate complex. If the higher absorption transition has no z-component and if the emitting has both components, x and z, the value of the fluorescence polarization is smaller on excitation to the higher excited state.

constant of the radiative process and where k_{nr} is the rate constant of the nonradiative process from the triplet state. Then, the values of k_r and k_{nr} are calculated using the phosphorescence lifetime, $(k_r+k_{nr})^{-1}$. These values and Φ_T are shown in Table 2.

The increases in Φ_T and k_r are mainly caused by the increment in the spin-orbit coupling. Such an increase in the intersystem crossing rate ($k_{S\to T}$) due to intramolecular interaction has also been observed for some β-diketonato complexes,[5] diphenylmethane, and triphenylmethane.[16] The values of k_r and k_{nr} of Zn(Sal-ch)$_2$ and Zn(Sal-propyl)$_2$ are three times as large as those of Zn(Sal-ch)$^+$ and Zn(Sal-propyl)$^+$ respectively, as Table 2 shows; therefore, the increase in the k_{nr} may come from the larger spin-orbit coupling. This is in contrast with the cases of the tris-β-diketonato complexes and triphenylmethane, where the $k_{S\to T}$ values are larger and the k_{nr} values are smaller than those of the mono-β-diketonato complexes and toluene respectively. Even if the triplet delocalization through the two ligands of a Schiff base affects the k_{nr}, the effect will be canceled out by the chelation being less rigid than that in the mono-bidentate complex, which emits phosphorescence several hundreds times as strongly as does the free anion.

As for planar Zn(Sal-pn)[17] (see Fig. 4-b), the absorption band in the near UV region has a shoulder on the lower-frequency side, as Fig. 5 shows. The shoulder

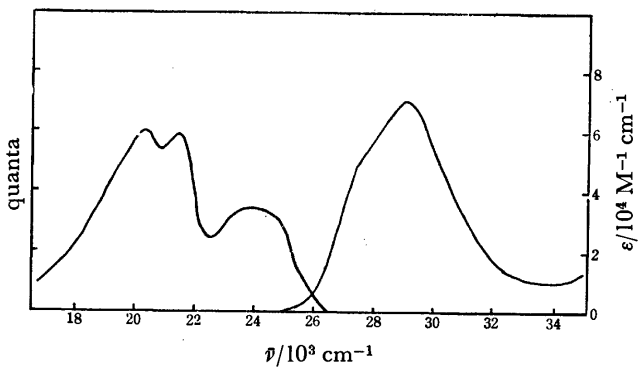

Fig. 5. Absorption and emission spectra of Zn(Sal-pn) in a mixture of methanol and ethanol at 77 K.

indicates the existence of another transition, which was suggested by Bosnich[10] on the basis of a Gaussian analysis of the asymmetric absorption band observed at room temperature. Since the fluorescence polarization is constant from $26\times10^3\,cm^{-1}$ to $31\times10^3\,cm^{-1}$ and is similar to that of Zn(Sal-ch)$^+$, the existance of two transitions does not indicate a large exciton splitting. Probably, a weak interaction between the salicylideneamine groups makes observable a second band which is hidden in the mono-bidentate complex.

References

1) D. C. Bhatnagar and L. S. Forster, *Spectrochim. Acta*, **21**, 1803 (1965).
2) C. E. White and F. Cuttitta, *Anal. Chem.*, **31**, 2082 (1959).
3) P. Yuster and S. I. Weissman, *J. Chem. Phys.*, **17**, 1182 (1949).
4) D. C. Freeman and C. E. White, *J. Am. Chem. Soc.*, **78**, 2678 (1956).
5) T. Ohno and S. Kato, *Bull. Chem. Soc. Jpn.*, **47**, 1901 (1974).
6) T. Ohno and S. Kato, *Bull. Chem. Soc. Jpn.*, **47**, 2953 (1974).
7) T. Ohno and S. Kato, *Bull. Chem. Soc. Jpn.*, **48**, 2014 (1975).
8) S. E. Mason, *J. Chem. Soc., A*, **1969**, 1428.
9) L. Sacconi, P. Paoletti, and M. Ciampoline, *J. Am. Chem. Soc.*, **85**, 411 (1963).
10) B. Bosnich, *J. Am. Chem. Soc.*, **90**, 627 (1968).
11) R. Herscovitch, J. J. Charette, and E. de Hoffmann, *J. Am. Chem. Soc.*, **95**, 5133 (1973).
12) R. S. Becker and W. F. Richey, *J. Am. Chem. Soc.*, **89**, 1298 (1967).
13) W. F. Richey and R. S. Becker, *J. Chem. Phys.*, **49**, 2092 (1968).
14) A. C. Brasthwaite and T. N. Waters, *J. Inorg. Nucl. Chem.*, **35**, 3223 (1973).
15) L. Sacconi, P. L. Oriole, P. Paoletti, and M. Ciampolini, *Proc. Chem. Soc.*, **1962**, 255.
16) F. H. Watson and K. A. El-Bayoumi, *J. Chem. Phys.*, **55**, 5464 (1971).
17) E. Frasson and C. Panottoni, *Z. Krist.*, **116**, 154 (1961).

Kinetic Studies in the Selective Formation of Thymol from *m*-Cresol and Propylene in the Liquid Phase over "$FeSO_4$-Al_2O_3" Catalysts

Tohr YAMANAKA and Fumio NAKATA

Central Research Laboratory of Takasago Perfumery Co., Ltd., Kamata, Ohta-ku, Tokyo 144

(Received February 12, 1976)

The kinetics in a liquid-phase isopropylation of *m*-cresol (I) with 9—25 kg/cm² of propylene (VI) was studied at 240—280 °C over catalysts prepared from $FeSO_4$ and γ-Al_2O_3. The rates of the formation of thymol (II) and 4-isopropyl-5-methylphenol (III) and the subsequent isopropylations of II and III were fitted to an irreversible, firstorder rate equation with respect to each starting material. All of the rate constants were roughly proportional to the 1.5th power of the surface acidity of $1 \leq H_0 \leq 3$ of catalysts and the 2.2nd power of the pressure of VI. The apparent activation energies were 22 kcal/mol for Steps I→II, II→2,4-diisopropyl-5-methylphenol (V), and III→V and 6.5 kcal/mol for Steps I→III and II→2,6-diisopropyl-5-methylphenol (IV).

For several years,[1] we have been studying the development of solid catalysts for the isopropylation of *m*-cresol (I) with propylene (VI) in the liquid phase, trying to prepare thymol (II), which is an important starting material for menthol. γ-Al_2O_3[2,3] and some metal sulfates[1,3] impregnated on γ-Al_2O_3 have been reported as catalysts of a high selectivity for thymol formation in the vapor[3] and liquid phases.[1,2] However, the isopropylations over these catalysts are accompanied by multiple reaction steps; the Reaction Scheme below shows an example. So far as the isopropylation of I is concerned, there has been no systematic study of the reaction kinetics. In order to design a reactor, it is necessary to describe quantitatively the distribution of products under various reaction conditions.

"$FeSO_4$-Al_2O_3"[1a] is an excellent catalyst which has a selectivity as high as γ-Al_2O_3 and a catalytic activity 100 times as high as γ-Al_2O_3. In this paper, the rates of the formation of II and the by-products over "$FeSO_4$-Al_2O_3" catalysts will be determined, and then the apparent rate constants will be correlated to the surface acidity of the catalysts and the reaction conditions.

Experimental

Catalysts. A 47.3-g portion of $FeSO_4 \cdot 7H_2O$ of a guaranteed reagent grade was dissolved in 150 ml of distilled water at 40—60 °C, and then a 75-g portion of γ-Al_2O_3 (Nikki Chemicals Co., Ltd.) of 100—200 mesh was stirred into the solution. After standing for 15—16 h, the solid was filtered and washed 3 times with 200 ml of distilled water. The resultant solid was dried on a water bath, calcined in a stream of dry air or dry nitrogen at 500 or 450 °C, and used as a catalyst. No particular caution was taken to exclude traces of moisture. The BET surface area of the γ-Al_2O_3 was 205 m²/g. In a series of preparetive runs, the resultant catalysts varied in their impregnated amounts of $FeSO_4$; these amounts were 8.7 wt% (Catalyst No. 2), 4.3 wt% (No. 3), 5.0 wt% (No. 4), 5.9 wt% (No. 5), 4.3 wt% (No. 9), 4.1 wt% (No. 10).

Surface Acidity of Catalysts. The acid-base strength distribution of catalysts were measured by a titration method.[4]

Isopropylation and the Analysis of the Products. Desired amounts of I (of guaranteed reagent grade) and of a catalyst were weighed into a reactor, which consisted of an autoclave with a capacity of 100 ml equipped with a magnetic stirrer and with gas inlet-outlet pipes. The pressure of VI (P) was kept constant at 9—25 kg/cm² by the incremental addition of VI. The reaction temperature was 240—280 °C and was kept constant within ±2 °C. The amount of catalyst (W) was 2.5—25 wt% of the initial amount of I. After an appropriate reaction period, the reactor was cooled rapidly in a cold-water stream, and the unreacted VI was released. The reaction mixture was dissolved with ether, washed with water, dried over Na_2SO_4, and concentrated.

The reaction mixture was analyzed by gas chromatography, using a Kotaki Model GU-21A on a 2 m×5 mm ϕ column packed with 20 wt% of silicone oil (D. C. 200) on Celite-545 (60—80 mesh), at 165 °C and with 1.2 kg/cm² of He as the carrier. Isopropyl benzoate was used as the internal standard. Some of the reaction mixture was fractionated into components by modified fractional gas chromatography, and each of the fractions was identified by IR absorption spectroscopy in a Nujol mull.

Isopropylations of II or III were carried out in the same way as above.

Results and Discussion

Rate Equations. The isopropylation of I was assumed to proceed *via* the following scheme. Ethers of

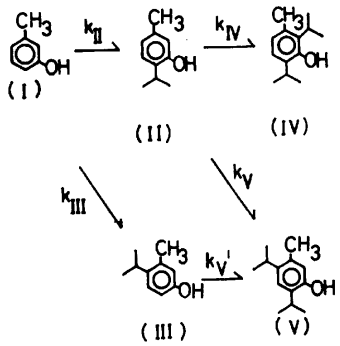

I and of the products were also formed, but the contents of isopropyl *m*-tolyl ether and of the total ethers in the reaction mixture were not more than 0.04 and 0.1 in mole fraction respectively. Therefore, their formation was excluded from the scheme. Figure 1 illustrates the composition-time plots of a reaction mixture. At 240—280 °C, the I content in the reaction mixture decreased monotonously with the time.

The overall reaction was well expressed by a set of irreversible rate equations:

$$dC_I/d\theta = -kC_I = -(k_{II} + k_{III})\, C_I \quad (1)$$

$$dC_{II}/d\theta = k_{II}C_I - (k_{IV} + k_V)\, C_{II} \quad (2)$$

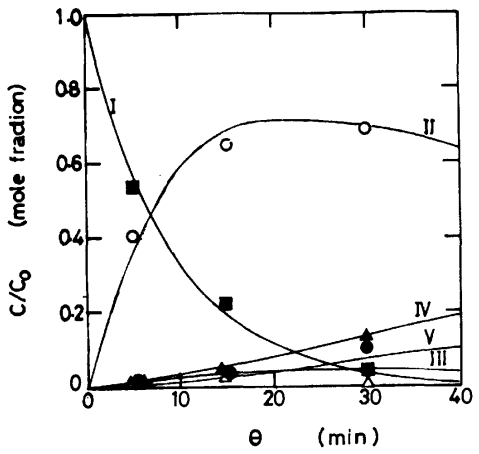

Fig. 1. Change in the composition of a reaction mixture with the reaction time at 260 °C, with 15 kg/cm² of propylene. *W* of the catalyst (No. 3) was 15 wt%. ○, II; △, III; ▲, IV; ●, V; □, I; ——, calculated value.

$$dC_{III}/d\theta = k_{III}C_I - k_V' C_{III} \quad (3)$$

$$dC_{IV}/d\theta = k_{IV} C_{II} \quad (4)$$

$$dC_V/d\theta = k_V C_{II} + k_V' C_{III} \quad (5)$$

where θ, C, and k represent the time, the concentration of the species defined by the suffix, and the apparent rate constant shown in the Reaction Scheme.

In each experimental run of the isopropylation using I, II, or III as the starting material, a linear correlation was found between {−log(1−conversion)} and θ.

Rate Constants. The apparent rate constants were determined as follows. 1) k_{II} and k_{III} were determined from the slopes of the curves of C_{II}/C_0 and C_{III}/C_0 against θ, at $\theta=0$; C_0 denotes C_I at $\theta=0$. 2) Replacing the left-hand sides of Eqs. 2—5 with the slopes of the concentration-time curves of II, III, IV, and V at any time, θ, and applying the corresponding concentrations, the rate constants were obtained. Their values are presented in Figs. 2 and 4.

Most of the compositions of the reaction mixtures which were calculated by integrating Eqs. 1 to 5 and by applying the rate constants at any time, θ, agreed within a deviation of less than 0.05 in mole fraction with the observed values over a full range of isopropylations, where the total conversion of I was from 0.17 to 0.95 in mole fraction. The composition-time curves in Fig. 1 are the calculated ones.

Each k value was proportional to the amount of catalyst (W).

From the Arrhenius plots of the rate constants in Fig. 2, the apparent activation energies in each step were determined to be 22 kcal/mol for Steps I→II, II→V, and III→V and 6.5 kcal/mol for Steps I→III and II→IV. Probably, the rate-determining step was different between these two groups of reactions. From Fig. 2, the apparent pre-exponential factors are in the order of I→II>III→V>II→V>II→IV>I→III.

Effect of the Pressure of Propylene. All of the rate constants were apparently proportional to the 2.2nd power of the pressure of VI (P).

Effect of the Surface Acidity. The acid-strength distributions of the catalysts used in this study are shown

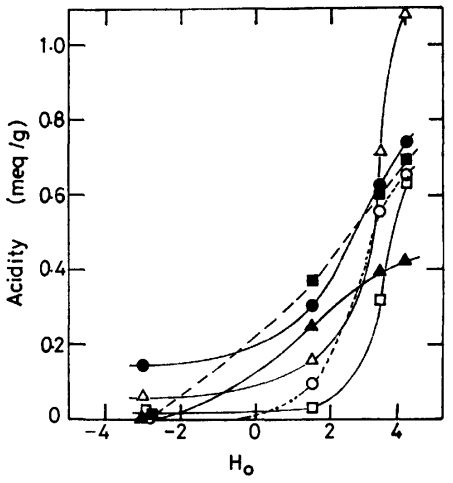

Fig. 3. Acid strength distributions of catalysts, No. 2 (▲), No. 3 (△), No. 4 (■), No. 5 (○), No. 9 (●), and No. 10 (□).

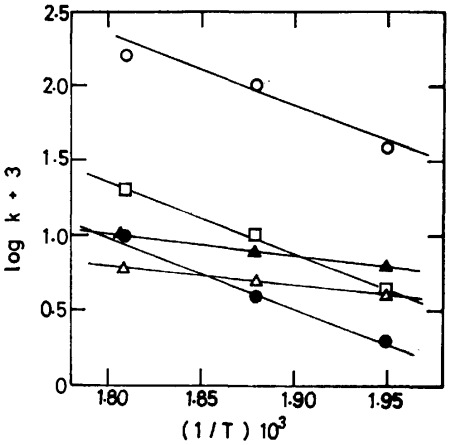

Fig. 2. Arrhenius plots of k_{II} (○), k_{III} (△), k_{IV} (▲), k_V (●), and k'_V (□). *W* of the catalyst (No. 3) was 15 wt% and propylene of 15 kg/cm² was used.

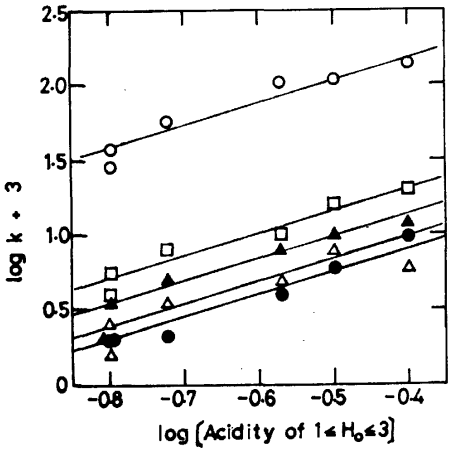

Fig. 4. Effect of the surface acidity of $1 \leq H_0 \leq 3$, α, of catalysts on k_{II} (○), k_{III} (△), k_{IV} (▲), k_V (●), and k'_V (□), at 260 °C, with 15 kg/cm² of propylene. *W* was 15 wt%.

in Fig. 3. The acidity at any H_0 value shows the amount of acidic sites whose acid strength is equal to or less than the H_0 value. Over most of the catalyst surfaces, the amount of acidic sites was at a maximum at $H_0=$ 1—4.

The rate constants were not correlated with the total amount of acidic sites of $H_0\leq 4$, or with the amount of acidic sites of any H_0 range other than $1\leq H_0\leq 3$. As is shown in Fig. 4, the rate constant in each step is similarly roughly proportional to the 1.5th power of the acidity of $1\leq H_0\leq 3$. It should be noticed that the efficient acidic sites seem not to be of $H_0<1$ but to be of $1\leq H_0\leq 3$, this will be interpreted in the following section.

Catalytic Actions. The isopropylation of I with VI has been reported to be catalyzed by solid acid catalysts *via* the formation of an isopropyl cation (HP^+).[3,5] The acidic sites of $1\leq H_0\leq 3$ will be Brönsted acidic sites and will protonate propylene. On the other hand, phenols were regarded as being adsorbed on the basic site of catalysts with the OH group.[3,6,7] On γ-Al_2O_3 used as the carrier, basic sites whose conjugate acids had H_0 values of less than 7 were observed.[4] These basic sites are probably exposed on the present catalysts' surface.[1a] The π-electron densities at C_2- and C_4-positions of the adsorbed *m*-cresol are greater than those of *m*-cresol in the liquid phase.[8] Hence, the isopropylation of I must take place between the adsorbed *m*-cresol and HP^+:

$$HA + VI \longrightarrow [HP^+ \cdots\cdots A^-] \text{ (VII)} \quad (6)$$

$$B + I \overset{K_I}{\rightleftharpoons} [I\cdots\cdots B] \text{ (VIII)} \quad (7)$$

$$VII + VIII \overset{k'_{II}}{\longrightarrow} II + HA + B \quad (8)$$

$$VII + VIII \overset{k'_{III}}{\longrightarrow} III + HA + B \quad (9)$$

where HA and B denote an acidic site of $1\leq H_0\leq 3$ and a basic site which are adjacent to each other. A^-, K, and k' denote the conjugate base of HA, an equilibrium constant, and a rate constant in the corresponding step respectively. A^- will facilitate the isopropylation by accepting a proton from the C_2- or C_4-position subsequently to the attack of HP^+.

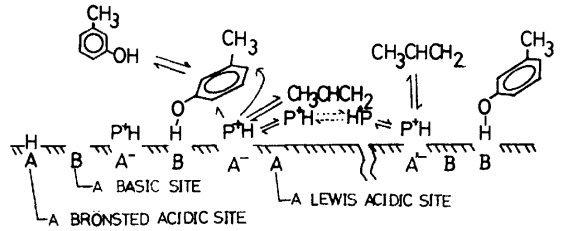

Because the C_4-position of VII is more remote from the surface than C_2,[3,5] the migration of HP^+ to C_4 from the surface is less frequent than the direct attack of HP^+ on C_2. This is supported by the difference between the apparent pre-exponential factors of k_{II} and k_{III}. The diffusion of HP^+ has a lower activation energy than the surface reaction between HP^+ and the C_2-position of VIII. This is supported by the difference between the apparent activation energies in Steps I→II and I→III, which shows that the energy barrier in Step (9) is *ca.* 16 kcal/mol lower than that in Step (8).

Provided that the structures of the surface in the vicinity of B are almost the same, the amount of B will be proportional to the amount of HA.

The reason why acidic sites of $H_0<1$ seemed to have no effect on the rate constants is either that they were Brönsted acidic sites which were not adjacent to B or that they were Lewis acidic sites. These Brönsted acidic sites protonate propylene as well as those of $1\leq H_0\leq 3$. If HP^+ migrates rapidly and freely enough over the surface, HP^+, which are formed at the Brönsted acidic sites of $H_0\leq 3$, contribute to the activity of HP^+ as a whole. On the other hand, if HP^+ does not migrate, only the HA in the vicinity of B contributes to the activity of HP^+, which affects the rate constants. Therefore, the activity of HP^+ will be independent of the amount of HA over all the surface. In this case, the rate constants will be proportional to the amount of HA, which represents the amount of the reaction loci where the isopropylation is catalyzed by a set of HA and B. The dependency of the rate constants on the acidity of $1\leq H_0\leq 3$ by the 1.5th power suggests a restricted mobility of HP^+. For clarifying the behavior of HP^+ consistently with the behavior of propylene in gas- and liquid-phase, however, further investigations will be required interpreting the 2.2nd-power dependency of k on the P value.

Because the acid strengths of I, II, and III are estimated to be nearly equal,[9] the differences among their heats of adsorption will not be substantial. As Steps II→V and III→V had apparent activation energies equal to that of Step I→II, those steps must proceed *via* an activated state similar to that of VIII at the C_4-position of II and the C_2-position of III. The observed differences of the pre-exponential factors from that of Step I→II suggest a disadvantage in the steric factors of Steps II→V and III→V, *e.g.*, a disadvantageous entropy change in the adsorption of II because of the *ortho*-isopropyl group.

Between the competitive steps, II→V and II→IV, the relatively low activation energy and pre-exponential factor in Step II→IV indicate that the C_6-position of II is sterically unfavored, like the C_4-position of I.

We are grateful to the Takasago Perfumery Co., Ltd., for its permission to publish this article.

References

1) a) T. Yamanaka, F. Nakata, and A. Komatsu, Japan Patent SHO 46-3053; *Chem. Abstr.*, **74**, 125150 h (1971); Brit, Patent, 1212597 (1970); Fr. Patent, 1599373 (1970); b) T. Yamanaka, F. Nakata, and A. Komatsu, Japan Patent SHO 45-15491; *Chem. Abstr.*, **73**, 55808 g (1970).

2) W. Hahn, U. S. Patent, 3290389 (1963); *Chem. Abstr.*, **57**, 13683 h (1962).

3) a) M. Nitta, K. Yamaguchi, and K. Aomura, *Bull. Chem. Soc. Jpn.*, **47**, 2897 (1974); b) M. Nitta, K. Aomura, and K. Yamaguchi, *ibid.*, **47**, 2360 (1974).

4) T. Yamanaka and K. Tanabe, *J. Phys. Chem.*, **79**, 2409 (1975).

5) S. H. Patkinson and B. S. Friedman, "Friedel Crafts and Related Reactions," Vol. 2, Part 1, ed by G. A. Olan, Inter-

science Publishers, New York (1964), p. 3.
6) K. Tanabe, *Shokubai*, **17**, 72 (1975).
7) D. R. Taylor and K. H. Ludlum, *J. Phys. Chem.*, **76**, 2882 (1972).
8) W. Hückel, Translation into Japanese of "Theoretische Grundlagen der Organischen Chemie," (Akademische Verlagsgeselschaft Geest und Porting K. -G., Leipzig 1957), Vol. 6, Shoko Shuppan, Tokyo (1960).
9) a) Y. Yukawa and T. Ibata, "Constants of Organic Compounds," ed by M. Kotake, Asakura Pub. Co., Ltd., Tokyo (1963), p. 637; b) A. J. Kresge, H. J. Chen, L. E. Hakka, and J. E. Kouba, *J. Am. Chem. Soc.*, **93**, 6174 (1971).

A CNDO-type MO Method of the Third Transition Metal Complexes and the Electronic Structure of Methylmercury(II) Halides

Shigeyoshi SAKAKI, Nobuo HAGIWARA, Noriko IWASAKI, and Akira OHYOSHI

Department of Industrial Chemistry, Faculty of Engineering, Kumamoto University, Kurokami, Kumamoto 860

(Received February 23, 1976)

The parameters of a CNDO-type SCF-MO method are determined for some 5d transition metal complexes such as $IrCl_6^{3-}$, $AuCl_4^-$, and $HgCl_4^{2-}$ by comparing the calculated transition energies of these complexes with their experimental values. MO calculations with these established parameters are also carried out for $IrBr_6^{3-}$, $AuBr_4^-$, HgX_4^{2-}, HgX_2, and CH_3HgX (X=Cl, Br, and I). The transition energies and assignments obtained from MO calculations are in fair agreement with experimental ones, with a few exceptions. This MO method gives successful results for the electron density and the bond strength: (1) a linear relation is obtained between the calculated and observed net charges on the Hg atom of HgX_2 and CH_3HgX, and (2) similar linear relations are obtained between the bond index E_{M-X} values and the stretching force constant f_{M-X} and between the E_{Hg-C} value and the f_{Hg-C}. Some discussion is presented for the Hg-C bonding character of the CH_3HgX; the Hg-C bond is mainly contributed from the covalent interaction of the 6s and 6p orbitals of the Hg atom with the 2s and 2p orbitals of the C atom. The contributions of the Hg 5d orbitals and the electrostatic interaction are rather small.

There exist various organo-transition metal complexes which are interesting as model compounds of intermediates formed in reactions catalyzed by transition metal complexes.[1] These organometallic compounds have received many spectroscopic studies. There is, however, limited theoretical work on these complexes; such studies are especially few in the 5d organo-transition metal complexes.[2-5] Theoretical work is necessary to understand and discuss the electronic structures of organometallic complexes. Furthermore, theoretical studies can give us useful information on unstable and unisolable intermediates.[2-5,7] Thus, we should investigate a MO method powerful enough to achieve this purpose.

One of the authors presented a CNDO-type MO method which gave successful results in MO calculations of Pt-complexes.[5] By use of this method, he investigated the reaction mechanism and ligand effect in the ethylene insertion reaction into the Pt(II)-H bond.[5b] This MO method, therefore, can be expected to give us important information about organo-transition metal complexes. In the present study, we attemp to establish the parameters of Hg,Au,and Ir atoms by comparing the calculated transition energies of these metal complexes, such as $HgCl_4^{2-}$, $AuCl_4^-$, and $IrCl_6^{3-}$, with the observed ones. No MO calculation has been reported for HgX_4^{2-} and IrX_6^{3-} as far as we know; for $AuCl_4^-$, although an INDO-type MO calculation was carried out, neither d-d transition energies nor the bonding nature were discussed.[6]

Then, MO's of methylmercury(II) complexes are calculated by use of the established parameters. Although these complexes have been investigated in detail by means of various spectroscopic instruments, such as IR and Raman,[8-14] NMR,[15-18] and UV[19] spectroscopy, there has been reported only one theoretical work,[3] in which the extended Hückel MO calculations were carried out and the ligand effect on the ^{199}Hg-H coupling constant was interpreted theoretically. In the present study, the electronic spectra, the electron density, and the Hg-C bonding character are investigated.

Method, Parameters, and Geometries

Method and Parameters. The method used here is the CNDO-type approximate SCF-MO method which gave successful results in MO calculations of Pt complexes.[5] Details of this method are presented elsewhere.[20] Only the part of this method which concerns parametrization carried out in this work, is described here. The two-center Coulomb repulsion integrals are estimated by use of the modified Ohno's equation, which has been introduced in the previous paper:[5a]

$$\gamma_{rs} = 14.3986/(R_{rs}^2 + d^2)^{1/2} \quad (1)$$

$$14.3986/d = 0.5(\gamma_{rr} + \gamma_{ss}) - a_r \quad (2)$$

See Ref. 5 for the notation in the above equation. In the 3d and 4d transition metal series elements, values such as a_{4s}, a_{4p}, a_{5s}, and a_{5p} are determined from the atomic spectra. It has been found that there exist four linear relations between the atomic numbers and the a_{ns} values, and between the atomic numbers and a_{np} ones (n=4 and 5).[21] In the 5d transition metal elements, those values can not be obtained from the atomic spectra because there is not enough data to estimate those values. Thus, in the Pt atom, they have been determined as parameters so that the calculated transition energies agree with the observed ones.[5] In this work, the a_{6s} and a_{6p} values are also determined as parameters under consideration of the following conditions; the a_{6s} and a_{6p} values increase linearly with an increase in the atomic number, which is expected from the analogy to the 3d and 4d transition metal elements, and their two linear lines pass through the 1.5 and 2.5 eV[5a] at the Pt atom respectively. The values of the parameters are listed in Table 1.

Values of other parameters, such as the Wolfsberg-Helmholz parameter, K, and the orbital exponents, are taken as well to be those in the case of the Pt complexes.[5a] These parameters give good results for the transition energies, the electron densities, *etc.*

Bond Index. The energy contribution of the AB bond to the total energy, E_{AB}, is used as the bond index.[5,7,22,23] The negative value means the bonding

Table 1. Orbital exponents, ζ_r, valence state ionization potentials, I_r, one-center Coulomb repulsion integrals, γ_{rr}, and parameters of modified Ohno's eq., a_{6s}, and a_{6p}

Atom		Ir	Pt	Au	Hg
ζ_r[a]	5d	5.796 0.6351[b]	6.013 0.6331[b]	6.163 0.6442[b]	6.436 0.6667[b]
	6s6p	2.557 0.5556	2.696 0.5516	2.794 0.5356	3.032 0.5401
I_r	5d	6.65 eV[g]	8.24	11.85	15.66
	6s	8.16	9.00	9.22	10.44
	6p	5.80	4.20	6.49	5.00
γ_{rr}[d]	5d	11.54 eV	12.07	12.60	13.14[f]
	6s	7.11	7.24	7.37	7.49
	6p	5.92	6.05	6.18	6.31
a_{6s}		1.4 eV	1.5	1.7	1.8
a_{6p}		2.4	2.5	2.7	2.8

a) H. Basch and H. B. Gray, *Theor. Chim. Acta*, **4**, 367 (1966). b) For only the d-orbital, the double-ζ type orbitals are used. These values are their coefficients, which are re-normalized values, since the contributions of the 3d and 4d Slater type orbitals are neglected in this work. c) The calculated values from the atomic spectra (C. E. Moore, "Atomic Energy Levels," Natl. Bur. Std. Circ., No. 467 (1958). d) The estimated value.[7] e) In our previous paper,[5] these values are over-estimated. By the use of these correct values, the electronic spectra of $PtCl_4^{2-}$ are calculated successfully, and the differences between the correct and the previous calculation are very small; for example $^1B_{1g}$=1.97 eV in the present calculation and 1.99 eV in our previous report. f) R. D. Bach and H. F. Henneike, *J. Am. Chem. Soc.*, **92**, 5589 (1970). g) Ir's VSIP can not be calculated correctly from atomic spectra due to lack of experimental data. These values are estimated by assuming that the promotion energy from $^3F_4$ state of Ir(I) to the d^8 valence state is 1 eV. This assumption seems reasonable from considering that this energy is 0.87 eV for the isoelectronic Rh(I) atom.

interaction between the A and the B atoms, and the large absolute value shows the large interaction. The formula representing the E_{AB} under the used approximations has been given elsewhere.[5]

In order to investigate the detailed bonding character, the $E_{AB}^{(1)}$ and $E_{AB}^{(2)}$ which approximately represent the covalent interaction are divided into the $E_{AB(s)}^{(1)+(2)}$, $E_{AB(p)}^{(1)+(2)}$, and $E_{AB(d)}^{(1)+(2)}$ as has been described in the previous paper;[24] where the $E_{AB(s)}^{(1)+(2)}$, in which the suffix (1)+(2) denotes the sum of $E_{AB}^{(1)}+E_{AB}^{(2)}$, represents approximately the contribution of the s orbital of the B atom to the covalent interaction between the A and B atoms, and the $E_{AB(p)}^{(1)+(2)}$ and $E_{AB(d)}^{(1)+(2)}$ also represent similar meanings.

Geometries. The IrX_6^{3-}, AuX_4^-, HgX_4^{2-}, and HgX_2 belong to O_h, D_{4h}, T_d, and $D_{\infty h}$ symmetries, respectively. The following bond lengths are employed in MO calculations: Ir-Cl=2.47 Å,[25] Ir-Br=2.618 Å,[26] Au-Cl=2.42 Å,[25] Au-Br=2.57 Å,[25] Hg-Cl (in $HgCl_4^{2-}$)=2.50 Å,[27] Hg-Br (in $HgBr_4^{2-}$)=2.62 Å,[28] Hg-I (in HgI_4^{2-})=2.80 Å,[29] Hg-Cl(in $^1HgCl_2$)=2.252 Å,[30] Hg-Br (in $HgBr_2$)=2.41 Å,[31] and Hg-I(in HgI_2)=2.60 Å.[29] The CH_3HgX complex is known to have a linear structure. Its bond distance is taken as follows: for CH_3HgCl, Hg-C=2.052 Å, Hg-Cl=2.285 Å;[32] for CH_3HgBr, Hg-C=2.062 Å, Hg-Br=2.405 Å;[32] for CH_3HgI, Hg-C=2.070 Å, Hg-I=2.588 Å;[32] for $Hg(CH_3)_2$, Hg-C=2.083 Å;[33] for CH_3HgF, Hg-C=2.040 Å, and Hg-F=1.93 Å.[26] The methyl group is assumed to have the same structure in all the complexes because the kinds of the ligand can scarcely cause any structural change: ∠HCH=109.8° and C-H=1.096 Å.[33]

Results and Discussion

Parametrization and Electronic Spectra. $IrCl_6^{3-}$ and $IrBr_6^{3-}$: By considering the Pt's a_{6s}(=1.5 eV) and a_{6p}(=2.5 eV), the following values of the a_{6s} and a_{6p} were examined in MO calculations of $IrCl_6^{3-}$: a_{6s}=1.2, 1.4, and 1.6 eV, and a_{6p}=2.2, 2.4, and 2.6 eV. Results are given in Table 2.

In $IrCl_6^{3-}$, various values of a_{6s} and a_{6p} give only a small effect on the transition energies. The first and the second small bands observed at 2.99 and 3.48 eV have been assigned to the $^1T_{1g}$ and $^1T_{2g}$.[35] In the present MO calculations, the $^1T_{1g}$ and $^1T_{2g}$ transitions are calculated to be *ca.* 2.9 and 3.5 eV, respectively. The large band observed at 6.01 eV may be assigned to the $^1T_{1u}$ transition calculated at 4.8 eV, since the $^1T_{1u}$ one is the only allowed one. This transition is the charge-transfer (CT) one from the halogen's p_π orbital

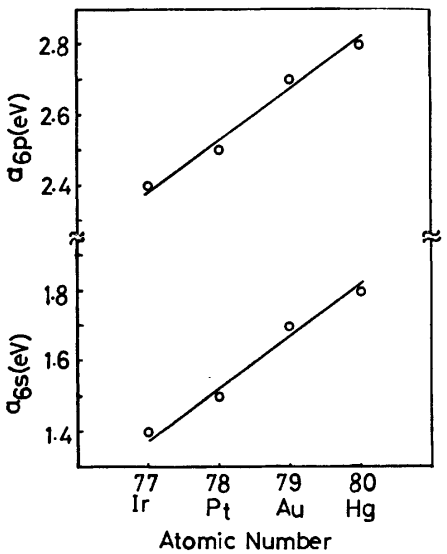

Fig. 1. The relations between the atomic number and the a_{6s} and a_{6p} values.

TABLE 2. TRANSITION ENERGIES[a] OF $IrCl_6^{3-}$ AND $IrBr_6^{3-}$

$IrCl_6^{3-}$								$IrBr_6^{3-}$				
a_{6s}	1.2	1.4	1.6	1.4	1.4	Obsd[b]		a_{6s}	1.4	Obsd[b]		
a_{6p}	2.4	2.4	2.4	2.2	2.6			a_{6p}	2.4			
$^1T_{1g}$	2.92	2.86	2.81	2.96	2.78	$^1T_{1g}$	2.99 (76)[c]	$^1T_{1g}$	1.74	$^1T_{1g}$	2.78 (230)	
$^1T_{2g}$	2.98	2.90	2.86	3.01	2.84			$^1T_{2g}$	1.75			
$^1T_{1g}$	3.39	3.40	3.40	3.38	3.41			$^1A_{2g}$	3.19			
$^1T_{2g}$	3.53	3.55	3.56	3.52	3.56	$^1T_{2g}$	3.48 (64)	^1E_g	3.30			
$^1A_{2g}$	3.88	3.93	3.88	4.06	3.87			$^1T_{1g}$	3.75			
^1E_g	4.13	4.08	4.03	4.15	4.01			$^1T_{2g}$	3.82	$^1T_{2g}$	3.20 (200)	
$^1T_{1g}$	4.69	4.63	4.57	4.72	4.53			$^1T_{1g}$	3.95			
$^1T_{1u}$	4.89	4.84	4.80	4.92	4.78	odd$\pi\rightarrow$d	6.01	$^1T_{1u}$	4.13	odd$\pi\rightarrow d_{eg}$		4.56
	(2.18)[d]	(2.22)	(2.24)	(2.15)	(2.29)		(28000)		(2.33)			(1200)
$^1T_{1u}$	4.93	4.87	4.81	4.96	4.78			$^1T_{1u}$	4.35	odd$\pi\rightarrow d_{eg}$		5.10
	(0.23)	(0.23)	(0.23)	(0.23)	(0.23)				(0.22)			(2000)
$^1T_{1u}$	6.19	6.14	6.14	6.23	6.06			$^1T_{1u}$	5.39	odd$\sigma\rightarrow d_{eg}$		5.94
	(1.57)	(1.59)	(1.62)	(1.57)	(1.62)				(1.93)			(6200)

a) eV unit. The transitions which satisfy both the following conditions are omitted for simplicity: (1) the transition is above the first CT one; (2) its transition moment is zero. These transitions do not relate to the present discussion. b) Ref. 35. c) Molar extinction coefficient (M^{-1} cm^{-1}). d) Transition moment (Å). Transition moments are zero in other transitions.

to the Ir's $5d_\sigma$ orbital. In all the calculations, these calculated transition energies roughly agree with the observed one, although the $^1T_{1u}$ transition energy is smaller than the observed one by *ca.* 1.2 eV.

Then, the a_{6s} and a_{6p} values can be determined. The small a_{6s} and a_{6p} values give better results for the observed $^1T_{1g}$, $^1T_{2g}$, and $^1T_{1u}$ transitions, as shown in Table 2. The a_{6s} and a_{6p} values, however, are determined as 1.4 and 2.4 eV respectively, by considering the linear relation between the atomic number and the a_{6s} and a_{6p} values (See Fig. 1, the previous discussion in method and parameter, and Ref. 49. This determination seems reasonable, since the calculated transition energies do not much depend on the a_{6s} and a_{6p} values.

By using these values of a_{6s} and a_{6p}, transition energies of $IrBr_6^{3-}$ are calculated, as is shown in Table 2. Three large bands are observed at 4.5—6 eV: the first is assigned to the transition from the weak π-antibonding and weak σ-bonding $3t_{1u}$ MO, mainly composed of the halogen's p_π orbital, to the $2e_g$ MO, mainly composed of the Ir's $5d_\sigma$ orbital; the second is that from the $1t_{2u}$ MO composed of the halogen's non-bonding p_π orbital to the

TABLE 3. TRANSITION ENERGIES[a] OF $AuCl_4^-$ AND $AuBr_4^-$

$AuCl_4^-$								$AuBr_4^-$				
a_{6s}	1.5	1.7	1.9	1.7	1.7	Obsd[b]		a_{6s}	1.7	Obsd[b]		
a_{6p}	2.7	2.7	2.7	2.5	2.9			a_{6p}	2.7			
$^1B_{2g}$	2.82	2.83	2.84	2.89	2.78			$^1B_{2g}$	2.23			2.23
^1E_g	2.83	2.83	2.84	2.88	2.79	$^1A_{2g}$	2.72 (17.3)[c]	^1E_g	2.37			(300)[c]
$^1A_{2g}$	2.84	2.84	2.85	2.87	2.81			$^1A_{2u}$	2.50			
$^1A_{2u}$	3.08	3.09	3.10	3.14	3.04			$^1A_{2g}$	2.52			
^1E_g	3.24	3.22	3.21	3.18	3.26	^1E_g	3.29 (319)	$^1B_{2u}$	2.80			
$^1B_{2u}$	3.44	3.45	3.46	3.51	3.40			^1E_g	3.09	^1E_g		2.70 (1560)
$^1A_{2g}$	3.61	3.59	3.58	3.56	3.62			^1E_u	3.11	$^1E_u+^1A_{2u}$		3.15[e]
$^1B_{1g}$	3.74	3.74	3.73	3.71	3.76				(1.64)			(4775)
^1E_u	3.80	3.80	3.81	3.81	3.79	$^1E_u+^1A_{2u}$	3.85[e]	^1E_u	3.42	^1E_u		4.85
	(1.51)[d]	(1.50)	(1.49)	(1.48)	(1.53)		(5750)		(0.95)			(48625)
^1E_u	3.96	3.98	4.00	4.05	3.91	^1E_u	5.47	^1E_u	6.54	^1E_u		6.24
	(0.76)	(0.76)	(0.77)	(0.77)	(0.75)		(47800)		(0.0)			(14000)
^1E_u	8.24	8.20	8.16	8.03	8.37	^1E_u	7.07	^1E_u	6.62	$^1A_{2u}$		6.61
	(0.35)	(0.35)	(0.35)	(0.36)	(0.34)		(—)		(1.04)			(17700)
								^1E_u	7.46	^1E_u		6.94
									(0.36)			(—)

a) d); See footnote a and d of Table 2, respectively. b) Refs. 36 and 37. c) Molar extinction coefficient (M^{-1} cm^{-1}). e) Ref. 39a.

$2e_g$ MO; and the last is that from the weak π- and σ-bonding $2t_{1u}$ MO, mainly composed of the halogen's p_π orbital, to the $2e_g$ MO. The calculated transition energies roughly agree with experimental ones,[35] but the calculated transition moments are unreasonable. For the first small band observed at 2.78 eV, the calculated transition energy is smaller than the observed one. For the small band observed at 3.20 eV, there is an ambiguity whether the $^1T_{2g}$ calculated at 1.75 eV or that at 3.82 eV should correspond to this band. Thus, although there is insufficiency in the $^1T_{1g}$ and $^1T_{2g}$ results, roughly good results are obtained for the CT bands.[51]

$AuCl_4^-$ and $AuBr_4^-$: The following values of the a_{6s} and a_{6p} were examined: a_{6s}=1.5, 1.7, and 1.9 eV, and a_{6p}=2.5, 2.7, and 2.9 eV. The calculated transition energies are compared with the observed ones in Table 3.

The calculated transitin energies do not much depend on the a_{6s} and a_{6p} values.[34] The transitions calculated at *ca.* 3.8, 4.0, and 8.2 eV seem to correspond to the observed bands at 3.85, 5.47,[36,37] and 7.07 eV,[36] respectively.[38] These assignments agree well with the experimental ones which have been proposed from the MCD study.[37] The calculated transition energies also agree well with the experimental ones,[36,37] but the second ^1E_u transition calculated at 4.0 eV is smaller than the experimental one by *ca.* 1.5 eV.

The two bands observed at 2.72 and 3.29 eV have been assigned to the $^1A_{2g}$ and ^1E_g transitions, respectively.[36] In our calculations, the $^1A_{2g}$ and ^1E_g transitions are calculated at *ca.* 2.8 and 3.2 eV, respectively, and the other four transitions, $^1B_{2g}$, ^1E_g, $^1A_{2u}$, and $^1B_{2u}$ are also calculated about 2.8—3.5 eV. Thus, detailed study should be carried out for the assignments of these transitions.

Then, the values of the parameters a_{6s} and a_{6p} can be determined. With regard to the $^1A_{2g}$ transition observed at 2.72 eV, the small a_{6s} and the large a_{6p} values give a better result, whichever of the three transitions, $^1B_{2g}$, ^1E_g, and $^1A_{2g}$ (calculated at about 2.8 eV), correspond to this transition at 2.72 eV. On the other hand, with regard to three ^1E_u transitions, the large a_{6s} and the small a_{6p} values give better results. Thus, the a_{6s} and a_{6p} values are determined as 1.7 and 2.7 eV, respectively.

Using these determined values of a_{6s} and a_{6p}, a similar MO calculation was carried out for $AuBr_4^-$. The

Table 4. Transition energies[a] of $HgCl_4^{2-}$

a_{6s}	1.6	1.8	2.0	1.8	1.8	Obsd[b]
a_{6p}	2.8	2.8	2.8	2.6	3.0	
^1E	5.60	5.52	5.43	5.47	5.57	
$^1T_2$	5.62	5.54	5.45	5.49	5.58	$^1T_2$ 5.28
	(0.99)[d]	(0.99)	(1.0)	(0.99)	(0.98)	(39200)[c]
$^1T_1$	5.63	5.56	5.48	5.51	5.61	
$^1T_2$	6.04	5.96	5.88	5.92	6.01	
	(0.42)	(0.42)	(0.41)	(0.42)	(0.41)	

a) eV unit. b) Ref. 40. c) Extinction coefficient (M^{-1} cm^{-1}). d) See footnote d of Table 2.

Table 5. Transition energies[a] of HgX_4^{2-}, HgX_2, and CH_3HgX

	$HgBr_4^{2-}$		HgI_4^{2-}	
	Calcd	Obsd[b]	Calcd	Obsd[b]
$^1T_1$	4.85		4.73	
^1E	4.85		4.78	
$^1T_2$	4.89	4.90	4.97	4.57
	(1.09)[c]	(41400)[d]	(1.23)[c]	(35400)[d]
$^1T_2$	5.25		5.04	
	(0.51)		(0.47)	

	$HgCl_2$		$HgBr_2$		HgI_2	
	Calcd	Obsd[e]	Calcd	Obsd[e]	Calcd	Obsd[e]
$^1E_{1g}$	5.19		4.26		4.13	
$^1E_{1u}$	5.54		4.49		4.32	
$^1A_{1u}$	7.52	6.20[f]	6.39	5.40[f]	6.25	4.63[f]
	(1.75)[c]	(2300)[d]	(2.04)	(1400)[d]	(2.23)	(3600)[d]
$^1A_{1g}$	7.70		7.30		7.37	
^1E_g	7.97		7.12		6.92	

	CH_3HgCl		CH_3HgBr		CH_3HgI	
	Calcd	Obsd[g]	Calcd	Obsd[g]	Calcd	Obsd[g]
^1E	5.76		5.03		4.82	
^1E	6.91		6.69		6.58	
$^1A_1$	7.36	6.02[f]	7.00	5.93[f]	6.92	5.39[f]
	(1.73)[b]	(1480)[d]	(1.87)[c]	(3470)[d]	(1.98)[c]	(3980)[d]
^1E	8.01		7.66		7.73	

a) eV unit. a_{6s}=1.8, a_{6p}=2.8$_{eV}$. b) Ref. 40. c) See footnote d of Table 2. d) Extinction coefficient (M^{-1} cm^{-1}). e) Ref. 42. f) Although the accurate assignment has never been presented, this transition has been proposed as a CT one. g) Ref. 41.

results are also shown in Table 3. Calculated transition energies agree well with the observed ones, except for the second ^1E_u transition observed at 4.90 eV.[36] Reasonable assignments are also obtained,[36,37] except with the $^1A_{2u}$ band observed at 6.61 eV.[39b]

HgX_4^{2-} and HgX_2: Just as in the cases of the Ir and Au complexes, MO calculations of $HgCl_4^{2-}$ were carried out using various values of a_{6s} and a_{6p}: a_{6s}=1.6, 1.8, and 2.0 eV, and a_{6p}=2.6, 2.8, and 3.0 eV. Results are given in Table 4.

One large band is observed at 5.28 eV, which is assigned to the $^1T_2$ transition, since the $^1T_2$ transition is the only allowed one in the T_d symmetry.[40] Also in our calculation, the $^1T_2$ transition is calculated at 5.6 eV; the calculated value fairly agrees with the experimental one. As the a_{6s} value becomes large and the a_{6p} one becomes small, the calculated transition energy of the $^1T_2$ becomes small. Since this calculated value is slightly larger than the observed one,[40] the large value of the a_{6s} and the small one of the a_{6p} are preferable. The a_{6s} and a_{6p} values, however, are determined as 1.8 and 2.8 eV respectively, by considering the expected linear relation between the atomic number and the a_{6s} and a_{6p} values, and also by considering the a_{6s} and a_{6p} values of the Ir, Pt, and Au atoms. This determination seems reasonable, since the calculated transition energy does not depend so greatly on the a_{6s} and a_{6p} values, and since fairly good agreement with the experimental results is obtained in all the calculations.

By use of these values of a_{6s} and a_{6p}, MO calculations were carried out for HgX_4^{2-} (X=Br and I), and HgX_2 and CH_3HgX (X=Cl, Br, and I). Calculated transition energies are given in Table 5. Those of HgX_4^{2-} agree fairly well with the experimental ones,[40] where the large band is considered as the $^1T_2$ transition as is that of $HgCl_4^{2-}$. It has been proposed previously that these bands are the CT transitions.[40] The present calculation shows that these transitions are the $^1T_2$ CT ones from the $4t_2$ MO, mainly composed of halogen's p_π orbital, to the $3a_1$ MO, mainly composed of the Hg's 6s orbital.

In HgX_2, the moderately large bands observed at 4.5—6 eV are considered as the $^1A_{2u}$ transitions, since only this transition is allowed. Also, in the CH_3HgX, the moderately large bands are observed at 5.4—6 eV, and these are considered as similar to the $^1A_1$ transitions. These $^1A_{2u}$ and $^1A_1$ transitions calculated at 6—7 eV, are larger than the observed ones by *ca.* 1.5 eV.[41,42] The $^1A_{2u}$ transition of HgX_2 is the one electron transfer from the $2a_{1u}$ MO to the $4a_{1g}$ MO. Since the former MO is mainly composed of the halogen's p_σ orbital and the latter one mainly of the Hg's 6s orbital, this transition is the CT one, which agrees with the experimental proposal.[42] The $^1A_1$ transition of CH_3HgX is the one electron transfer from the $4a_1$ MO to the $5a_1$ MO; the former is largely contributed to from the p orbitals of the C and X atoms and the latter largely from the Hg's 6s orbital. Thus, this transition is also the CT one.

As described above, the results of the electronic spectra are reasonable, with a few exceptions. The values of the parameters established above are listed in Table 1. The a_{6s} and a_{6p} values are plotted against the atomic number in Fig. 1, where a nearly linear relation is obtained.

TABLE 6. ELECTRON DISTRIBUTION OF IrX^{3-}, AuX_4^-, HgX_4^{2-}, AND HgX_2

Cmpound	5d	6s	6p
$IrCl_6^{3-}$	6.776	0.527	0.927
$IrBr_6^{3-}$	6.812	0.560	0.963
$AuCl_4^-$	9.197	0.594	0.807
$AuBr_4^-$	9.327	0.612	0.807
$HgCl_4^{2-}$	9.989	0.704	0.722
$HgBr_4^{2-}$	9.989	0.783	0.755
HgI_4^{2-}	9.989	0.821	0.771
$HgCl_2$	9.933	0.915	0.456
$HgBr_2$	9.944	1.019	0.447
HgI_2	9.955	1.059	0.455

Electron Density. Electron densities are shown in Table 6. It is reasonable for all the complexes that the electron density of the central metal atom increases with a decrease in the electronegativity of the halogen.

Our calculations show that the net charge of the Au atom is +0.401 *e* in $AuCl_4^-$ and +0.254 *e* in $AuBr_4^-$, although these values have been reported to be negative from the Mössbauer spectroscopy:[43] −0.24 *e* in $KAuCl_4$ and −0.21 *e* in $KAuBr_4$. The authors wonder why the Mössbauer study reported that the net charge of the Au atom was −0.24 *e* in $KAuCl_4$ and +0.41 *e* in AuCl, although the formal net charge of the Au atom is +3 in the former complex and +1 in the latter one. Thus, these reported values should be re-investigated in more detail.

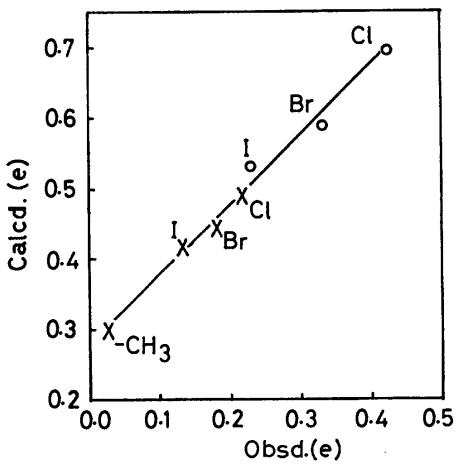

Fig. 2. The relation between the observed[a] and the calculated net charges of the Hg atom in HgX_2 and CH_3HgX. ○; HgX_2, ×; CH_3HgX. a) Ref. 44.

In HgX_4^{2-} and HgX_2, all the d orbitals seem to be of the non-bonding type, since they have about 10 electrons. The Hg–X bond is mainly contributed to from the 6s and 6p orbitals of the Hg atom. Our calculated net charges of the Hg atom are compared with the estimated ones from the ESCA study,[44] as is shown in Fig. 2. Although these two values do not agree with each other, a linear relation is obtained between these two values, and it should be further noted that its slope

is about 1.0. This result reveals that our method is at least qualitatively successful.

The ^{35}Cl NQR studies of $HgCl_2$ and CH_3HgCl give the unbalance in the p-electron population on the Cl atom, U_p, which is defined in Ref. 44. From MO calculations, the U_p values can be estimated: 0.526 for $HgCl_2$ and 0.474 for CH_3HgCl. These are in moderately good agreement with the experimental values: 0.402 for $HgCl_2$ and 0.383 for CH_3HgCl.[45] Since the quantity of U_p depends upon the electron populations of the p_σ and p_π orbitals of the Cl atom, it is suggested that the calculated electron distribution agrees with the experimental one.

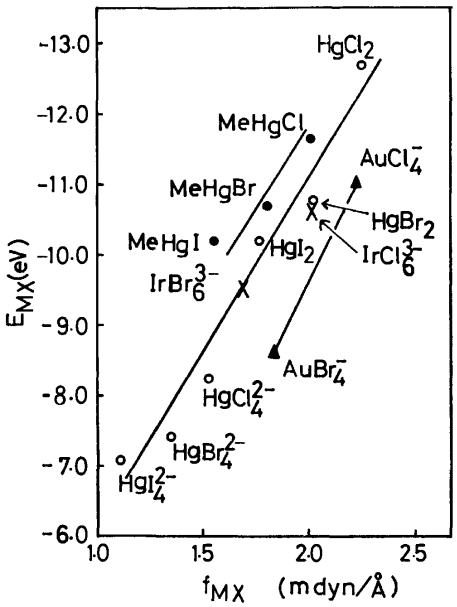

Fig. 3. The relation between the force constant f_{M-X}[a] and the E_{M-X} values.
a) HgX_2 and HgX_4^{2-}, Ref. 29; IrX_6^{3-}, Ref. 46; CH_3HgX, Ref. 8; AuX_4^-; Ref. 47.

Bond Strength. The E_{M-X} values are compared with the M-X force constants in Fig. 3, since the force constant and E_{M-X} approximately represent the bond strength. Three different linear relations are obtained: the first one concerning the HgX_2, HgX_4^{2-}, and IrX_6^{3-}, the second concerning the CH_3HgX, and the last concerning the AuX_4^-. Generally speaking, the value of the force constant depends upon their calculation method. The force constants of HgX_2 and HgX_4^{2-} were calculated with the simple method,[29] those of IrX_6^{3-} were done with the generalized force field,[46] those of CH_3HgX were done with a simple valence force field,[8] and those of AuX_4^- were done with an Urey-Bradley force field.[47] Thus, it seems reasonable that in all the calculations, a linear relation can not be obtained. It should be noted that linear relations do exist between the E_{M-X} values and the M-X force constants which are calculated by use of the same force field, and the three lines have almost the same slopes.

Similar relations are also obtained between the E_{Hg-C} values and the Hg-C force constants,[8] and between the E_{Hg-C} values and the Hg-C dissociation energies of CH_3HgX,[48] as are shown in Figs. 4 and 5. Thus, our

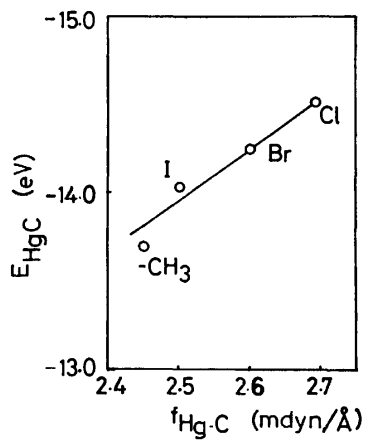

Fig. 4. The relation between the Hg-C force constant f_{Hg-C}[a] and the E_{Hg-C} value.
a) Ref. 8.

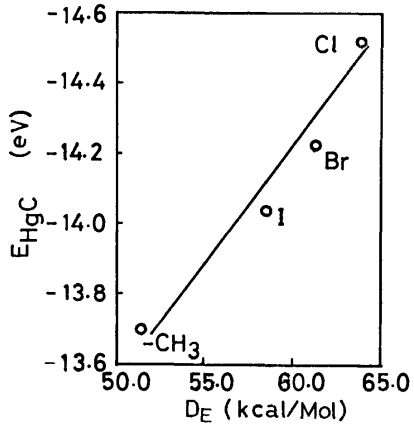

Fig. 5. The relation between the Hg-C dissociation energy, D_E,[a] and the E_{Hg-C} values.
a) Ref. 48.

method gives successful results for the bond strength.

Electronic Structure of CH_3HgX. In this section, the electron distribution and bonding nature of the Hg-C and Hg-X of CH_3HgX are investigated. Results are given in Table 7.

First, the electron distribution is investigated in detail. The electron density of the 5d orbitals of the Hg atom is *ca.* 10 *e*, suggesting that the 5d orbitals hardly contribute to the Hg-C and Hg-X bonds in these complexes as well. On this point, a more detailed discussion will be presented in a following paragraph. The electron densities of the 6s and 6p orbitals of the Hg atom increase in the order $F<Cl<Br<I<CH_3$. This order accords with the decreasing order of the halogen's electronegativity. The electron density of the Hg atom in $Hg(CH_3)_2$ is larger than that in CH_3HgI by *ca.* 0.1 *e*, and larger than that in the corresponding dihalide HgX_2 by *ca.* 0.1—0.2 *e*. These results suggest that the methyl anion tends to donate electrons more than the halogen anion by *ca.* 0.1 *e*.

Then the nature of the Hg-C and Hg-X bonds will be investigated. As is shown in Table 7, the absolute values of $E^{(1)+(2)}_{Hg(s)-C}$ and $E^{(1)+(2)}_{Hg(p)-C}$ are remarkably large, and those of $E^{(1)+(2)}_{Hg(d)-C}$ and $E^{(3)}_{Hg-C}$ are less than one-tenth of $E^{(1)+(2)}_{Hg(s)-C}+E^{(1)+(2)}_{Hg(p)-C}$. Similar results are obtained with

Table 7. Electronic structures of CH_3HgX

X		F	Cl	Br	I	CH_3
Electron	5d	9.92	9.93	9.93	9.94	9.93
density	6s	0.99	1.07	1.10	1.11	1.15
	6p	0.42	0.51	0.52	0.53	0.62
Net charge of the Hg atom						
	CH_3HgX	0.68	0.49	0.45	0.42	0.30
	HgX_2		0.70	0.59	0.53	
Hg–C	$E^{(1)+(2)}_{Hg(d)-C}$	−1.17	−1.08	−1.04	−0.98	−0.95
	$E^{(1)+(2)}_{Hg(s)-C}$	−7.53	−6.95	−6.71	−6.55	−5.85
	$E^{(1)+(2)}_{Hg(p)-C}$	−5.00	−5.44	−5.53	−5.60	−6.14
	$E^{(3)}_{Hg-C}$	−1.36	−1.03	−0.94	−0.91	−0.76
	$E_{Hg-C(total)}$	−15.06	−14.52	−14.23	−14.04	−13.70
Hg–X	$E^{(1)+(2)}_{Hg(d)-X}$	−0.68	−0.59	−0.55	−0.48	
	$E^{(1)+(2)}_{Hg(s)-X}$	−3.55	−4.20	−4.10	−4.20	
	$E^{(1)+(2)}_{Hg(p)-X}$	−6.32	−5.76	−5.19	−4.85	
	$E^{(3)}_{Hg-X}$	−2.57	−1.10	−0.85	−0.69	
	$E_{Hg-X(total)}$	−13.11	−11.65	−10.70	−10.22	

E_{AB}: eV unit.

regard to the Hg–X bond. These results reveal that the Hg–C and Hg–X bonds are mainly contributed to from the covalent interaction of the 6s and 6p orbitals of the Hg atom with the C and X atoms. The 5d orbital of the Hg atom hardly contributes to these bonds, which is in conformity with the results that the 5d orbital has about 10 electrons, as has been described above.

Our MO method can give successful results for the electronic spectra, the electronic distribution, and the bond strength of the 5d transition metal complexes. It has been ascertained that this MO method is also useful in studying the electronic structures and the bonding nature of organometallic complexes.

These calculations were carried out with the FACOM 230-75 Computer of the Data Processing Center of Kyushu University.

References

1) R. F. Heck, "Organotransition Metal Complexes. A Mechanistic Approach," Academic Press, New York (1974); P. W. Jolly and G. Wilke, "The Organic Chemistry of Nickel," Academic Press, New York (1974).
2) R. D. Bach and H. F. Henneike, *J. Am. Chem. Soc.*, **92**, 5589 (1970).
3) H. F. Henneike, *J. Am. Chem. Soc.*, **94**, 5945 (1972).
4) H. Katô, *Bull. Chem. Soc. Jpn.*, **44**, 348 (1971).
5) a) S. Sakaki, H. Kato, and T. Kawamura, *Bull. Chem. Soc. Jpn.*, **48**, 195 (1975); b) S. Sakaki, H. Kato, H. Kanai, and K. Tarama, *ibid.*, **48**, 813 (1975).
6) W. TH. AM. Van Der Lugt, *Chem. Phys. Lett.*, **10**, 117 (1971); *Int. J. Quant. Chem.*, **6**, 859 (1972).
7) S. Sakaki, H. Kato, H. Kanai, and K. Tarama, *Bull. Chem. Soc. Jpn.*, **47**, 377 (1974).
8) P. L. Goggin and L. A. Woodward, *Trans. Faraday Soc.*, **62**, 1423 (1966).
9) J. R. Hall and J. C. Mills, *J. Organomet. Chem.*, **6**, 445 (1966).
10) Z. Meić and M. Randić, *Trans. Faraday Soc.*, **64**, 1438 (1968).
11) P. L. Green, *Spectrochim. Acta*, **A24**, 863 (1968).
12) Z. Meić and M. Randić, *J. Chem. Soc., Faraday Trans. 2*, **68**, 444 (1972).
13) Z. Meić, *J. Mol. Struct.*, **23**, 131 (1974).
14) J. Mink and B. Gellai, *J. Organomet. Chem.*, **66**, 1 (1974).
15) K. A. McLauchlan and D. H. Whiffen, *Mol. Phys.*, **10**, 131 (1966).
16) F. J. Weigert, M. Winokur, and J. D. Robert, *J. Am. Chem. Soc.*, **90**, 1566 (1968).
17) F. J. Weigert and R. D. Roberts, *Inorg. Chem.*, **12**, 313 (1973).
18) G. H. Macied and M. Borzo, *J. Magn. Reson.*, **10**, 388 (1973).
19) B. G. Gowenlock and J. Trotman, *J. Chem. Soc.*, **1955**, 1454.
20) S. Sakaki and H. Kato, *Bull. Chem. Soc. Jpn.*, **46**, 2227 (1973).
21) S. Sakaki, to be published.
22) M. S. Gordon, *J. Am. Chem. Soc.*, **91**, 3122 (1969).
23) S. E. Ehrenson and S. Seltzer, *Theor. Chim. Acta*, **20**, 17 (1971).
24) S. Sakaki, H. Kikkawa, H. Kato, and S. Yoshida, *Bull. Chem. Soc. Jpn.*, **49**, 76 (1976).
25) "Interatomic Distances," ed by L. E. Sutton, The Chem. Soc., London (1958).
26) The estimated value.
27) D. E. Scaife, *Aust. J. Chem.*, **24**, 1753 (1971).
28) J. G. White, *Acta Crystallogr.*, **16**, 397 (1963).
29) M. A. Hooper and D. E. James, *Aust. J. Chem.*, **24**, 1345 (1971).
30) K. Kashiwabara, S. Konaka, and M. Kimura, *Bull. Chem. Soc. Jpn.*, **46**, 410 (1973).
31) P. A. Akishin, P. Spiridonov, and A. N. Khodchenkov, *Zh. Fiz. Khim.*, **33**, 20 (1959).
32) C. Walls, D. G. Lister, and J. Sheriden, *J. Chem. Soc., Faraday Trans. 2*, **71**, 1091 (1975).
33) K. Kashiwabara, S. Konaka, T. Iijima, and M. Kimura, *Bull. Chem. Soc. Jpn.*, **46**, 407 (1973).
34) Although the a_{6s} and a_{6p} in the range of these values have only slight effects on the transition energies, zero values for them gave unreasonable results in $PtCl_4^{2-}$.[5a]
35) C. K. Jørgensen, *Acta Chem. Scand.*, **10**, 500 (1956); *Mol. Phys.*, **5**, 119 (1963). *Adv. Chem. Phys.*, **5**, 119 (1963).
36) J. L. H. Batiste and R. Rumfeldt, *Can. J. Chem.*, **52**, 174 (1974).

37) A. J. McCaffery, P. N. Schatz, and P. J. Stephens, *J. Am. Chem. Soc.*, **90**, 5730 (1968).
38) The calculated transition moment of the first ^1E_u is larger than that of the second one, although the experimental molar extinction coefficient of the former is less than that of the latter. Thus, our method should be improved in this point.
39) a) The $^1A_{2u}$ band is considered to correspond to that calculated at 2—3 eV; b) The basis of this experimental assignment has not been described in Ref. 36.
40) P. Day and R. H. Seel, *J. Chem. Soc., Dalton Trans.*, **1972**, 2054.
41) B. G. Gowenlock and J. Trotman, *J. Chem. Soc.*, **1955**, 1454.
42) P. Templet, J. R. McDonald, and S. P. McGlynn, *J. Chem. Phys.*, **56**, 5746 (1972).
43) M. O. Faltens and D. A. Shirley, *J. Chem. Phys.*, **53**, 4249 (1970).
44) J. H. D. Eland, *Int. J. Mass Spectrum. Ion Phys.*, **4**, 37 (1970).
45) D. E. Scaife, *Aust. J. Chem.*, **74**, 1753 (1971).
46) R. D. Hancock and A. Evans, *J. Inorg. Nucl. Chem.*, **35**, 2558 (1973).
47) P. L. Goggin and J. Mink, *J. Chem. Soc., Dalton Trans.*, **1974**, 1479.
48) R. Scheffold, *Helv. Chim. Acta*, **52**, 56 (1969).
49) As will be described below, the small a_{6p} value of the Hg atom gives good results. From the linear relation between the atomic number and the a_{6p} value (Fig. 1), the small a_{6p} value of the Ir atom brings about the large a_{6p} value of the Hg atom, which gives rather poorer results for $HgCl_4^{2-}$. Thus, the Ir's a_{6p} value is taken as 2.4 eV. For the a_{6s} value. if the Hg's a_{6s} value is taken as large (=2.0 eV) and that of the Ir atom as small (=1.2 eV), which gives rather good results, the slope of the linear line between the a_{6s} values and the atomic number is too high (=0.2) relative to that of the a_{5s} line (=0.11). The slope of the a_{6s} line in Fig. 1 is 0.1, which seems reasonable.

Singlet Excitation Energy Transfer in the Vinyl Polymers with Pendant Carbazolyl Groups

Akira ITAYA, Ken-ichi OKAMOTO, and Shigekazu KUSABAYASHI

Department of Chemical Engineering, Faculty of Engineering, Yamaguchi University, Tokiwadai, Ube 755

(Received May 17, 1976)

The migration of electronic excitation energy in films of poly(*N*-vinylcarbazole) (PVCz) prepared by the radical and cationic polymerizations(PVCz(r) and PVCz(c) respectively), poly[2-(9-carbazolyl)ethyl vinyl ether] (PCzEVE), brominated PVCz(BPVCz), and poly(9-acryloylcarbazole) (PACz) has been studied by means of fluorescence-quenching experiments, using dimethyl terephthalate or perylene as a guest molecule. No clear difference in the concentration of the effective intrinsic trap sites was observed between PVCz(r) and PVCz(c) films. The concentration of the sandwich-like excimer site(c_E) in a PVCz(r) film was nearly equal to that in a PVCz(c) film, while the concentration of the second excimer site (c_S) in a PVCz(r) film was higher than that in a PVCz(c) film by a factor of about 1.6. The value of c_E was much larger than that of c_S for both films. The second excimer site seems to be a shallow trap. The number of carbazolyl chromophores covered by a singlet exciton during the lifetime was in the following order: PCzEVE$>$PVCz(r)$\approx$PVCz(c)$>$PACz$\approx$BPVCz. This order was explained by the concentration of the intrinsic trap sites depending on the distance between neighboring Cz chromophores, the lifetime of the singlet exciton, and the concentration of extrinsic trap sites.

Recently, the emission spectra of aromatic vinyl polymers have been extensively investigated. Studies of singlet energy transfer and migration in vinyl polymer films with large aromatic rings are very important in understanding their electric and optical properties. Klöpffer[1] has reported that the results of fluorescence-quenching experiments in an amorphous PVCz film are consistent with a hopping model of monomer exciton migration, in which excitons can migrate in a polymer film and both excimer-forming sites and guest molecules act competitively as exciton traps. From a lifetime quenching observed in PVCz film doped with perylene, Powell *et al.*[2] has recently proposed a model containing dimer sites besides guest molecules and excimer-forming sites. Concerning an undoped PVCz film, Offen *et al.*[3] suggested the presence of a dimer site as a result of measuring the fluorescence decay time of PVCz films at 77 K. Klöpffer *et al.*[4] showed that the two different types of the spectra were observed in the prompt fluorescence and phosphorescence at 77 K, independent of the polymerization methods.

Recently, we have ourselves revealed, from the NMR spectra and the glass-transition temperatures, that PVCz prepared by the cationic polymerization has a higher isotacticity than the PVCz prepared by the radical polymerization(PVCz(c) and PVCz(r) respectively).[5] It has also been reported that the difference in the tacticity of PVCz is reflected in the fluorescence spectra in fluid and rigid solutions and that the concentration of the second excimer site in a syndiotactic-rich polymer (PVCz(r)) is higher than that in an isotactic-rich polymer(PVCz(c)).[6] Therefore, it is of interest to investigate how the difference in the tacticity of PVCz samples affects the singlet-excitation-energy migration. The studies of singlet-excitation-energy migration in vinyl polymer films with carbazolyl(Cz) chromophores widely spaced on the skeletal chains is of interest in connection with that of PVCz films.

In the present research, we investigated the migration of the electronic-excitation energy in films of PVCz(r), PVCz(c), brominated PVCz(BPVCz), poly[2-(9-carbazolyl)ethyl vinyl ether] (PCzEVE), and poly(9-acryloylcarbazole) (PACz); in the latter two polymers, the Cz chromophores are widely spaced on the skeletal chains by $-O-CH_2-CH_2-$, and $-CO-$ bonds respectively. Dimethyl terephthalate (DMTP) or perylene was used as the guest molecule. In the case of perylene, the long-range resonant energy transfer is somewhat possible.[2,7] However, the long-range resonant energy transfer from a Cz chromophore to a DMTP molecule is quite impossible, because DMTP has no absorption in the wavelength region where the fluorescence of the PVCz film is observed.[7] Therefore, the DMTP is very useful in studying the phenomenon of the single-exciton migration.

Experimental

The vinyl polymers(PVCz(r), PVCz(c), BPVCz, PCzEVE, and PACz) were prepared by the methods described previously.[8,9] The DMTP and perylene were recrystallized twice from benzene and subsequently sublimed *in vacuo*. Doped films were cast onto quartz or Pyrex glass plates from a dichloroethane solution of the polymer containing a certain amount of the dopant and dried *in vacuo*. The thickness of the film was about 4 μm for PCzEVE and about 7 μm for the other polymers.

The fluorescence spectra were measured with the apparatus described in a previous paper.[8] The spectra at 293 K were measured for the coated plates *in vacuo* (0.1 Torr). The spectra at 77 K were measured for the coated plates immersed in liquid nitrogen. PACz films were excited by 315 nm light, and the others, by 335 nm light.

For the fluorescence-decay time measurements, the samples were excited with a N_2 gas laser. The sample fluorescence was chosen with appropriate glass filters before being detected by a biplanar phototube R 617. Responses from the phototube were led to a Tektronix 475 oscilloscope, and the decay curve was photographed.

Results and Discussion

Fluorescence Spectra of the Vinyl Polymer Films with Pendant Carbazolyl Groups. The fluorescence spectra of PVCz(r) and PVCz(c) films are shown in Figs. 1 and 2.

The difference in the spectra between PVCz(r) and PVCz(c) films observed at 293 and 77 K is similar to that observed in a fluid solution.[6] That is, the fluorescence intensity in the shorter-wavelength region of a PVCz(r) film is larger than that of a PVCz(c) film. Therefore, the emission band in the shorter-wavelength region was assigned to the second excimer fluorescence, and that in the longer wavelength region, to the sandwich-like excimer fluorescence. The fluorescence spectra of both polymer films were resolved into two individual

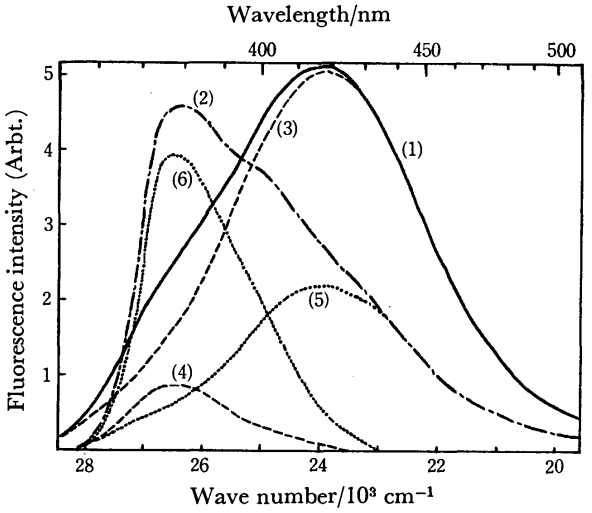

Fig. 1. Fluorescence spectra and the resolution spectra of PVCz(r) films at 293 and 77 K.
(1) 293 K, (2) 77 K, (3) the component of the sandwich-like excimer fluorescence at 293 K, (4) the component of the second excimer fluorescence at 293 K, (5) the component of the sandwich-like excimer fluorescence at 77 K, (6) the component of the second excimer fluorescence at 77 K.

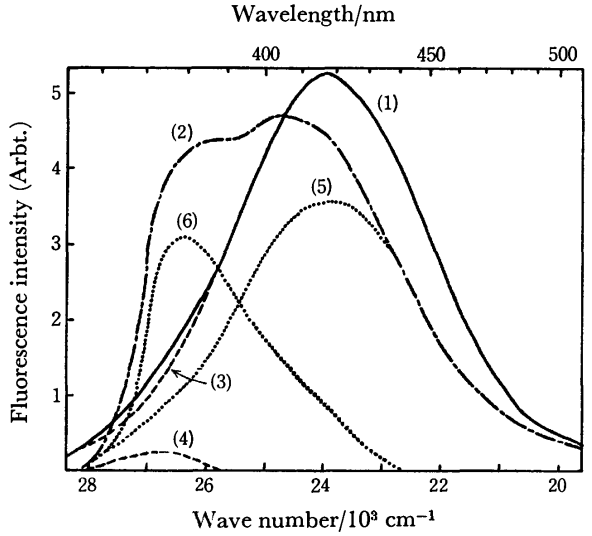

Fig. 2. Fluorescence spectra and the resolution spectra of PVCz(c) films at 293 and 77 K.
(1) 293 K, (2) 77 K, (3) the component of the sandwich-like excimer fluorescence at 293 K, (4) the component of the second excimer fluorescence at 293 K, (5) the component of the sandwich-like excimer fluorescence at 77 K, (6) the component of the second excimer fluorescence at 77 K.

Table 1. The intensity of the second excimer fluorescence relative to the sandwich-like one (I_S/I_E) and the quantum efficiencies of the host fluorescence (η_H)

Host	I_S/I_E	η_H
PVCz(r)	0.083	0.045
PVCz(c)	0.013	0.041
PVCz(r)[a]	0.93	—
PVCz(c)[a]	0.55	—
PCzEVE	—	0.10
PACz	—	0.0002
BPVCz	—	0.001

a) At 77 K.

bands. The resolution spectra thus obtained are also shown in Figs. 1 and 2. The intensity of the second excimer fluorescence relative to the sandwich-like excimer one and the fluorescence yields are listed in Table 1.

The presence of two kinds of emitting species in the fluorescence of PVCz(r) and PVCz(c) was also clarified by measuring the fluorescence decay curves of the polymers. The fluorescence decay curves of both polymer films in air at 293 K are clearly two-component (20 ± 3 and 6 ± 1 ns) in the shorter wavelength region, but one-component (22 ± 2 ns) in the longer wavelength region. The intensity of the short-lived component relative to the long-lived one for a PVCz(r) film in the shorter wavelength region is larger than that for a PVCz(c) film. Therefore, the long- and short-lived components correspond to the sandwich-like excimer fluorescence and the second excimer one respectively. Similar results were also obtained at 77 K; the long- and short-lived components are 17 ± 2 and 6 ± 2 ns respectively. These decay constants are roughly in agreement with the values reported by Powell *et al.* (20 and 10 ns).[2] The lifetime of the sandwich-like excimer fluorescence of PVCz films is shorter than that of PVCz in a fluid solution (*ca.* 40—42 ns)[6,10,11] and that of a PVCz film obtained by Offen *et al.* (43 ns).[3]

The fluorescence spectra of a PCzEVE film undoped and doped with DMTP are shown in Fig. 3. A PCzEVE film shows only a broad, structureless fluorescence spectrum with a peak at *ca.* 26050 cm^{-1}. The fluorescence decay curves in air are one-component in both the shorter and longer wavelength regions (4—5 and 10—11 ns respectively). A two-component decay curve is observed in the medium wavelength region. This fact indicates that the two kinds of emitting species are present in a PCzEVE film at 293 K. Although the fluorescence spectrum of a PCzEVE film at 77 K has the structure, it does not seem to be the monomeric fluorescence of a Cz chromophore because of the large Stokes shift (1540 cm^{-1}).

The fluorescence spectra of PACz and BPVCz films undoped and doped with DMTP or perylene are shown in Fig. 4. The fluorescence efficiency of a PACz film is extremely low (Table 1) because of the presence of the intersystem crossing from the lowest $^1\pi, \pi^*$ state to the lowest $^3n, \pi^*$ state due to a carbonyl group. A PACz film shows a fluorescence spectrum consisting of two components. The spectra of PACz and BPVCz films

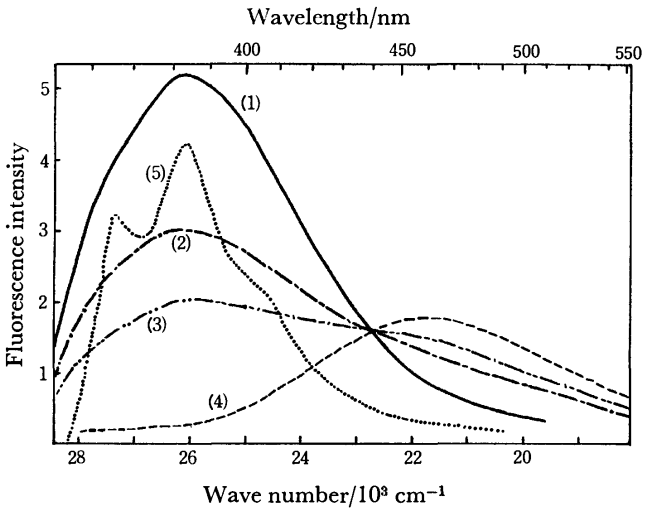

Fig. 3. Fluorescence spectra of PCzEVE films doped with DMTP at 293 K. DMTP concentration; (1) 0, (2) 4.44×10^{-4}, (3) 8.88×10^{-4}, and (4) 1.18×10^{-2} (mol/CzEVE unit mol). Fluorescence spectrum of the undoped film at 77 K is also given by a dotted line (5).

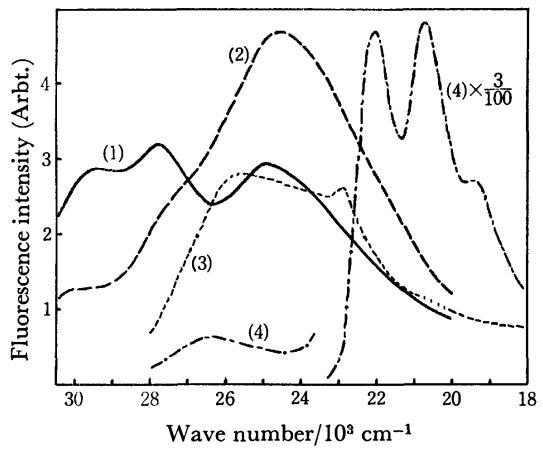

Fig. 4. Fluorescence spectra of PACz and BPVCz films at 293 K. PACz films; (1) undoped, (2) doped with DMTP (2.32×10^{-2} ACz unit mol). BPVCz films; (1) undoped, (2) doped with perylene (5.9×10^{-3} mol/mol basic unit).

change rapidly under irradiation by an exciting light.

Singlet Excitation Energy Transfer in the Vinyl Polymers with Pendant Carbazolyl Groups. The fluorescence spectra of PVCz(r), PVCz(c), and PCzEVE films doped with DMTP or perylene at 77 K are shown in Fig. 5. In the case of every polymer film studied at 293 and 77 K, by the doping of DMTP or perylene, the host fluorescence decreases and is replaced by the exciplex or guest fluorescence. The exciplex is formed between DMTP and a Cz chromophore. As DMTP has no absorption in the wavelength region where the host fluorescence of these polymers is observed, the dipole-dipole resonance cannot be responsible for the energy transfer to a DMTP molecule.[7] In fact, no decrease in the fluorescence lifetimes of PVCz(r) films upon doping of DMTP is observed. That is, the fluorescence lifetimes in the shorter-wavelength region of PVCz(r) films doped with a small amount of DMTP (*ca.* 3×10^{-3} mol/mol basic

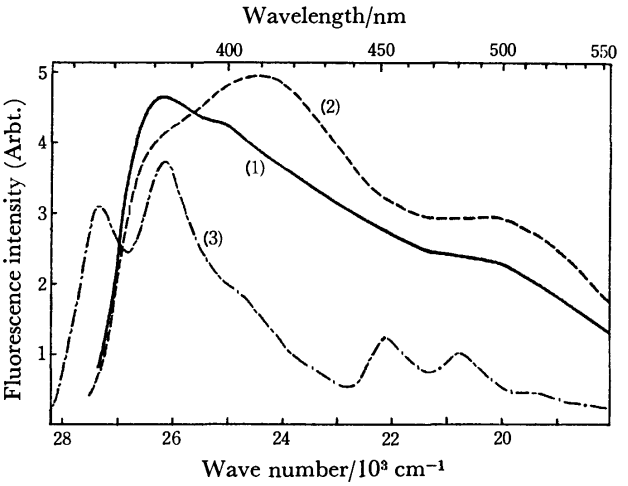

Fig. 5. Fluorescence spectra of PVCz(r), PVCz(c) and PCzEVE films doped with DMTP or perylene at 77 K. (1) PVCz(r) doped with DMTP (3.26×10^{-3} mol/VCz unit mol), (2) PVCz(c) doped with DMTP (3.02×10^{-3} mol/VCz unit mol), and (3) PCzEVE doped with perylene (1.15×10^{-4} mol/CzEVE unit mol).

unit) are 17 ± 3 and 5 ± 2 ns at 293 K and 19 ± 2 and 6 ± 1 ns at 77 K.

In the present case, therefore, the hopping model of monomer-exciton migration is applicable at 293 and 77 K. We should consider the case of the presence of two kinds of traps (for example; the sandwich-like excimer-forming sites, c_E [mol/mol basic unit], and the second excimer sites, c_S [mol/mol basic unit], in the case of a PVCz film) in a way similar to the treatment in Ref. 1. Then, the quenching factor of host fluorescence, Q_H, is expressed by the following equations:

$$Q_H = (\eta_{H,0} - \eta_H)/\eta_H = 0.66nc/[1 + 0.66n(c_E + c_S)],$$
$$n = n_S/(n_e + n_l)$$

where n_S, n_e, and n_l are the relative probabilities (per unit time) of jumping, radiative, and nonradiative decay, where $\eta_{H,0}$ and η_H are the quantum efficiencies of the host fluorescence in the absence and in the presence of the guest molecule in a concentration of c [mol/mol basic unit], and where n is the number of jumps during the lifetime without any trapping sites. The quenching factor of monomer fluorescence, Q_M, may be expressed by:

$$Q_M = 0.66n(c_E + c_S).$$

In the present case, where no monomer fluorescence can be observed, $Q_M \gg 1$. Therefore,

$$Q_H = c/(c_E + c_S). \quad (1)$$

The ratio of the fluorescence intensities guest/host (I_G/I_H) is:

$$I_G/I_H = c\eta_G/(c_E\eta_E + c_S\eta_S), \quad (2)$$

where η_G is the quantum efficiency of the guest fluorescence in the host film under direct excitation. The relative intensity of the second excimer fluorescence to the sandwich-like excimer one is expressed by

$$I_S/I_E = c_S\eta_S/c_E\eta_E. \quad (3)$$

Although the experimental values of Q_H scatter a little, the measurement of Q_H at various concentrations of a

TABLE 2. ENERGY TRANSFER BY THE EXCITON-DIFFUSION PROCESS IN POLYMER FILMS AT 293 AND 77 K[a)]

Host	Guest	η_G	$(c_E+c_S)\times 10^3$ (mol/mol basic unit)	n'	$(I_G/I_H c)$ $\times 10^{-3}$	$c_E\eta_E$ $\times 10^5$	$c_S\eta_S$ $\times 10^5$	L/Å[d)]
PVCz(r)	DMTP	0.043	2.7	370	0.39	10	0.83	67
PVCz(c)	DMTP	0.039	2.2	450	0.37	(11)[c)]	(0.11)[c)]	74
PVCz(r)[b)]	DMTP	0.17	3.5	290	0.22	40	37	60
PVCz(c)[b)]	DMTP	0.15	3.2	310	0.23	43	23	63
PCzEVE	DMTP	0.034	0.45	2200	1.0	—	—	—
PACz	DMTP	0.004	24[e)] (25)[f)]	42[e)] (40)[f)]	0.08	—	—	—
BPVCz	Perylene	0.27	(19)[g)]	(52)[g)]	14	—	—	—

a) The errors in (c_E+c_S) and n' are $\pm 5\%$ at 293 K and $\pm 10\%$ at 77 K. The error in $(I_G/I_H c)$ is $\pm 3\%$. b) At 77 K. c) The values are less reliable because of the large error in the I_S obtained by a resolution of the host fluorescence spectrum. d) $L=an'^{1/2}$, where L is the mean exciton migration length and a is the interchromophore separation (3.5 Å). e) The value were obtained from the value of Q_H, on the assumption that the fluorescence in the shorter and longer wavelength regions is emitted by some intrinsic trap site and an excimer respectively. f) The values were obtained from the ratio of $(I_G/I_H c)$, on the assumption that the fluorescence in the shorter and longer wavelength regions is emitted by a monomer and an excimer respectively. g) The values were obtained in a way similar to that used in the treatment in Ref. 1, on the assumption that the host fluorescence is emitted by one trap site.

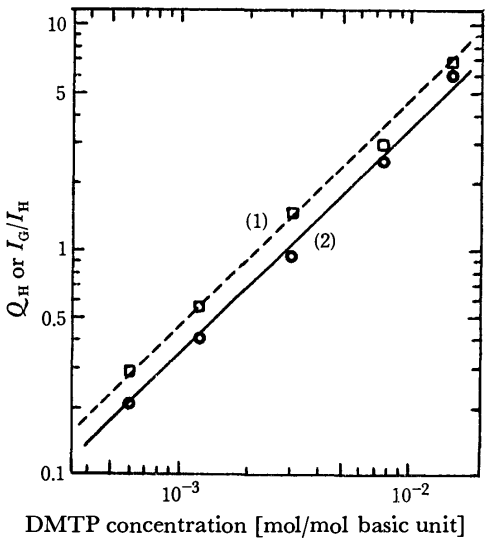

Fig. 6. Ratio of fluorescence intensities guest/host I_G/I_H (1) and quenching factor of host fluorescence Q_H (2) as a function of guest concentration for PVCz(c)-DMTP system at 293 K.

guest gives the values of c_E+c_S according to Eq. 1. The measurement of I_G/I_H at various concentrations of a guest gives the values of $c_E\eta_E$ and $c_S\eta_S$ according to Eqs. 2 and 3, using the values of η_G and I_S/I_E in Tables 1 and 2. Figure 6 shows the bilogarithmic plots of Q_H or I_G/I_H thus obtained and c, as example, in the case of the PVCz(c)-DMTP system. The values thus obtained are listed in Table 2.

In the case of the PVCz(r) and PVCz(c) films, the values of c_E+c_S, $c_E\eta_E$, and $c_S\eta_S$ are obtained by the method mentioned above. The value of c_E+c_S at 293 K is nearly equal to the value of c_E obtained by Okamoto *et al.* in a PVCz(r)-DMTP system, on the assumption that the host fluorescence is emitted only from the sandwich-like excimer.[7)] The value of c_E+c_S is almost the same for a PVCz(r) film and for a PVCz(c) film. The number of Cz chromophores covered by an exciton during the lifetime in the presence of trap sites (abbreviated hereafter to n') is nearly equal to the reciprocal of the concentration of the traps, $[1/(c_E+c_S)]$. This number is almost the same for a PVCz(r) film and for a PVCz(c) film. The value of $c_E\eta_E$ is almost the same for a PVCz(r) film and for a PVCz(c) film, while the value of $c_S\eta_S$ for a PVCz(r) film is higher than that for a PVCz(c) film. It can safely be considered that the fluorescence efficiencies of each fluorescence (η_E and η_S) of PVCz(r) are equal to those of PVCz(c). Therefore, the concentration of the sandwich-like excimer sites (c_E) in a PVCz(r) film is nearly equal to that in a PVCz(c) film. On the other hand, considering that the value of $c_S\eta_S$ for a PVCz(c) film at 293 K is less reliable, the concentration of the second excimer sites (c_S) in a PVCz(r) film is higher than that in a PVCz(c) film by a factor of about 1.6. This difference in the value of c_S does not clearly appear in the value of c_E+c_S. This fact suggests that the value of c_E is larger than that of c_S in both films.

The values of $c_E\eta_E$ for PVCz(r) and PVCz(c) films obtained at 77 K are larger than those obtained at 293 K by a factor of 4. It may safely be considered that the values of η_E and η_S for a PVCz(r) film change with the temperature in a manner similar as that for a PVCz(c) film. The value of c_E is considered to be determined by the casting temperature(T_{cast}) of the film because of the high glass-transition temperature of PVCz. Therefore, this increase in the value of $c_E\eta_E$ seems to be caused by a change in the value of η_E. On the other hand, the value of $c_S\eta_S$ obtained at 77 K is much larger than that obtained at 293 K. This increase in $c_S\eta_S$ with a decrease in the temperature is too large to be caused only by an increase in η_S. The value of c_S might be considered to vary apparently with the measuring temperature. In the previous paper, we have reported that the second excimer has a small binding energy.[6)] Therefore, this increase in $c_S\eta_S$ might be explained by the assumption that the second excimer site is a shallow trap. That is, the second excimer site acts more effectively as a trap at low temperatures.

It has been reported in a previous paper that the concentration of the trap sites for a triplet exciton in a

PVCz(c) film is somewhat larger than that in a PVCz(r) film.[8] On the other hand, as has been mentioned above, the concentration of the trap sites for a singlet exciton in a PVCz(c) film is nearly equal to that in a PVCz(r) film. This suggests that the conformation of intrinsic trap sites is not necessarily the same for singlet and for triplet excitons. This explanation might be supported by the presence of a conformational difference between the singlet and triplet excimers of 1,3-di(1-naphthyl)propane.[12]

The migration frequency, k'_{mig}, for the triplet exciton was estimated from the following equation:

$$k'_{mig} = 6\Lambda/a$$

where a is the interchromophore separation and Λ is the migration coefficient; the coefficients have been tabulated in Ref. 8. Assuming that $a=3.5$ Å, then $k'_{mig}=6\times10^3$ and 3.3×10^3 s^{-1} for PVCz(r) and PVCz(c) films. Therefore, the number of Cz chromophores covered by the triplet exciton during the lifetime ($2\tau_{df}$) are 600 and 330 for PVCz(r) and PVCz(c) films respectively. Although the conformation of intrinsic trap sites seems to be different for singlet and triplet excitons, the number of the Cz chromophores covered by both excitons in both PVCz films during the lifetimes ranges from 300 to 600 and the mean exciton diffusion length ranges from 60 to 80 Å.

The fluorescence of a PCzEVE film is also emitted from two kinds of traps, as has been mentioned above. The value of c_E+c_S for a PCzEVE film is much smaller than those for the PVCz(r) and PVCz(c) films. This suggests that it is difficult for Cz chromophores to form intrinsic trap sites because of the large distance between neighboring Cz chromophores. The value of n' for a PCzEVE film is expected to be smaller than the values of n' for PVCz(r) and PVCz(c) films, judging from the large distance between neighboring Cz chromophores. However, even in the case of a PCzEVE film, $Q_M \gg 1$, that is, the singlet exciton migration is limited by the intrinsic trap sites. Therefore, the value of n' for a PCzEVE film is larger than that for a PVCz film by a factor of *ca.* 5.

In the cases of the PACz and BPVCz films, the emitting species of the host fluorescence are ambiguous. Judging from the profile of the fluorescence spectrum of a PACz film, the broad fluorescence band with a peak at *ca.* 25000 cm^{-1} might be assigned to the excimer fluorescence. The fluorescence band in the shorter wavelength region might be attributable to a monomer or to some intrinsic trap site. The host fluorescence of a BPVCz film is considered to be emitted from some trap site. Irrespective of the treatments used to obtain the value of n' (Table 2), the values of n' for both polymer films are very small. This may be attributable to the short exciton lifetime because of the enhanced intersystem crossing and the presence of extrinsic trap sites(photoproducts and/or impurities introduced during a bromination reaction).

The number of Cz chromophores covered by a singlet exciton during the lifetime was in the following order; PCzEVE>PVCz(r)≈PVCz(c)>PACz≈BPVCz.

This work was supported in part by a Scientific Research Grant of the Ministry of Education.

References

1) W. Klöpffer, *J. Chem. Phys.*, **50**, 2337 (1969).
2) R. C. Powell and Q. Kim, *J. Lumin.*, **6**, 351 (1973); G. E. Venikouas and R. C. Powell, *Chem. Phys. Lett.*, **34**, 601 (1975).
3) P. C. Johnson and H. W. Offen, *J. Chem. Phys.*, **55**, 2945 (1971).
4) W. Klöpffer and D. Fischer, *J. Polym. Sci., Part C*, **40**, 43 (1973).
5) K. Okamoto, M. Yamada, A. Itaya, T. Kimura, and S. Kusabayashi, *Macromolecules*, **9**, 645 (1976).
6) A. Itaya, K. Okamoto, and S. Kusabayashi, *Bull. Chem. Soc. Jpn.*, **49**, 2082 (1976).
7) K. Okamoto, A. Yano, S. Kusabayashi, and H. Mikawa, *Bull. Chem. Soc. Jpn.*, **47**, 749 (1974).
8) A. Itaya, K. Okamoto, and S. Kusabayashi, *Bull. Chem. Soc. Jpn.*, **49**, 2037 (1976).
9) K. Okamoto, A. Itaya, and S. Kusabayashi, *Polym. J.*, **7**, 662 (1975); *J. Polym. Sci., Polym. Phys. Ed.*, **14**, 869 (1976).
10) G. E. Johnson, *J. Chem. Phys.*, **62**, 4697 (1975).
11) M. Yokoyama, T. Tamamura, M. Atsumi, M. Yoshimura, Y. Shirota, and H. Mikawa, *Macromolecules*, **8**, 101 (1975).
12) P. C. Subudhi and E. C. Lim, *J. Chem. Phys.*, **63**, 5491 (1975).

Steric Effects of Alkyl Substituents on the N-H Stretching Absorptions and Rotational Isomerism of *N,N'*-Dialkylthioureas[1]

Yoshiyuki MIDO, Takashi YAMANAKA, and Ryoichi AWATA

Department of Chemistry, Faculty of Science, Kobe University, Nada, Kobe 657

(Received May 21, 1976)

The fundamental N-H stretching absorptions of twenty nine *N,N'*-dialkylthioureas were observed in dilute solutions. The observed frequencies were classified into five groups assignable to the *out*, three different types of the *trans*, and the *cis* forms. The steric hindrance between the bulky *t*-butyl group and the thiocarbonyl sulfur, which is larger than for *N,N'*-dialkylureas, was suggested to cause the *out* form. Dialkylthioureas of *R*TU*t*B type seem to exist to a great extent in the *trans-out* conformation in solutions. It is suggested that it is not the N-H group with the bulky *t*-butyl group but the N-H group in the opposite part which is out of the skeletal plane. The energy difference between the *out* and the *trans* forms was found to be $\Delta H = 430 \pm 100$ cal mol^{-1}.

A number of studies have been carried out to elucidate the rotational isomerism of secondary amides in solutions in connection with the backbone-structures of polypeptides and proteins.[2,3] It was disclosed that the steric hindrance between two substituents and the C=X group (X=O or S) plays an important part in the isomerism.

On the other hand, some infrared studies of *N,N'*-disubstituted ureas (*R*U*R'*) and -thioureas (*R*TU*R'*) suggested the presence of *trans-cis* isomerism in solutions.[2,4,5] The isomeric conformations were considered to be the *trans-trans* and the *trans-cis* conformations since the *cis-cis* conformation was unlikely on steric grounds. Nevertheless, percentages of over 50% of the *cis* form[6] were estimated for the ureas with bulky groups; *s*-D*t*BU[4] and *s*-DPhU.[2] For the corresponding thioureas with the sulfur atom larger in effective size than the oxygen atom, *s*-D*t*BTU[5] and *s*-DPhTU,[2] the percentages of the *cis* form were estimated to be approximately 50 and 45%, respectively.

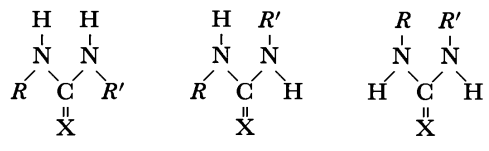

In systematic infrared studies on *R*U*R'* in solutions a correlation was found between the N-H frequencies and *R* and *R'*, the presence of a very small amount of a form differing from the *trans* form in *R*U*R'* being confirmed with either one *t*-butyl group or two.[7-10] From an examination of the infrared spectra of trialkylureas (D*R*U*R'*) in solutions it was suggested that the different form has the N-H group out of the skeletal plane (the *out* form) owing to the steric hindrance between the bulky substituents and the C=O group.[11] This necessitates a re-examination of the study of *R*TU*R'*.

The purpose of this study is (1) to examine the applicability of our established correlation to *R*TU*R'*, (2) to confirm an increase in the amount of the *out* form caused by the larger steric hindrance in *R*TU*R'* with a sulfur atom than that in the corresponding *R*U*R'* with an oxygen atom, and (3) to obtain information on the *out* form.

Experimental

Twenty nine *R*TU*R'* were prepared by the standard method (addition of *R*CNS to *R'*NH$_2$).[12] The crude samples were purified by repeated recrystallization from suitable solvents. The purified samples were identified by their melting points and infrared spectra. Each sample was examined as a 10^{-3} M solution in CCl_4 (2 cm NaCl cell) and as a 10^{-2} M solution in CS_2 and in $CHCl_3$ (2 mm NaCl cell). Solvents of spectroscopic grade were used.

The spectrometer, the experimental conditions in the recording of the spectra, and the calibration of band-positions were the same as given previously.[7] The spectra at different temperature were obtained with an electrically-heated and beam-transparent box in which the sample and the reference cells were placed and adjusted to each light axis.

Results and Discussion

Two fundamental N-H stretching bands from two N-H links should appear in the infrared spectra of *R*TU*R'* in the absence of rotational isomerism. However, in some spectra one or two extra bands are observed suggesting the rotational isomerism in solutions (Fig. 1). We examined some possibilities of over- and combination tones, and of Fermi resonance[13] for the extra bands. It was concluded from observation of the solution spectra of deuterated compounds that the extra bands are really the N-H fundamentals, and from comparison of the solution spectra with the solid spectra that there may be a little or no effect of Fermi resonance in such dilute solution.[14] We classified the observed bands into five groups, A—E, according to wave number (Table 1).

The trans *N-H Bands.* Although the N-H bands of *R*TU*R'*, as a whole, are lower by about 15 cm^{-1} than those of *R*U*R'*, three of the classified five groups, B, C, and D, correspond to the three groups characteristic of a substituent of the *trans-trans R*U*R'*;[7] the N-H group with a methyl group shows the highest frequency band, the group with other primary alkyl groups exhibits medium one,[15] and the group with branched alkyl groups shows the lowest one.

In connection with such a correlation it can be understood that, for example, the two bands of MTU*s*B result from two different types of N-H group; the higher com-

TABLE 1. N-H STRETCHING FREQUENCIES OF *N,N'*-DIALKYLTHIOUREAS IN CCl_4 SOLUTION (0.001M)

*R*NHCSNH*R'*		*R*TU*R'*	Frequency (cm^{-1})				
R	*R'*		A	B	C	D	E
CH_3–	CH_3–	*s*-DMTU		3445s			3425sh
CH_3–	C_2H_5–	MTUE		3447sh	3436s		3411sh
CH_3–	*n*-C_3H_7–	MTUP		3442s. b			* *
CH_3–	*i*-C_3H_7–	MTU*i*P		3450s		3423s	3400sh
CH_3–	*i*-C_4H_9–	MTU*i*B		3443s			3427sh
CH_3–	*s*-C_4H_9–	MTU*s*B		3450s		3422s	3399sh
CH_3–	*t*-C_4H_9–	MTU*t*B	3468m	3446w		3422s	3398sh
C_2H_5–	C_2H_5–	*s*-DETU			3435s		3414sh
C_2H_5–	*n*-C_3H_7–	ETUP			3435s		3415sh
C_2H_5–	*i*-C_3H_7–	ETU*i*P			3433s	3422s	3400sh
C_2H_5–	*i*-C_4H_9–	ETU*i*B			3436s		3413sh
C_2H_5–	*s*-C_4H_9–	ETU*s*B			3432s	3421sh	3399sh
C_2H_5–	*t*-C_4H_9–	ETU*t*B	3456m			3420s	3399sh
n-C_3H_7–	*n*-C_3H_7–	*s*-DPTU			3435s		3414sh
n-C_3H_7–	*i*-C_3H_7–	PTU*i*P				3422s.b	3401sh
n-C_3H_7–	*i*-C_4H_9–	PTU*i*B			3436s		* *
n-C_3H_7–	*s*-C_4H_9–	PTU*s*B			3431s.b		* *
n-C_3H_7–	*t*-C_4H_9–	PTU*t*B	3458m			3422s	* *
i-C_3H_7–	*i*-C_3H_7–	*s*-D*i*PTU				3422s	3399sh
i-C_3H_7–	*n*-C_4H_9–	*i*PTUB			3431sh	3423s	3402sh
i-C_3H_7–	*i*-C_4H_9–	*i*PTU*i*B			3437sh	3423s	3401sh
i-C_3H_7–	*s*-C_4H_9–	*i*PTU*s*B				3421s	3399sh
i-C_3H_7–	*t*-C_4H_9–	*i*PTU*t*B	3446m			3420s	3399sh
n-C_4H_9–	*t*-C_4H_9–	BTU*t*B	3456m			3423s	* *
i-C_4H_9–	*i*-C_4H_9–	*s*-D*i*BTU			3439s		* *
i-C_4H_9–	*t*-C_4H_9–	*i*BTU*t*B	3467m			3423s	* *
s-C_4H_9–	*s*-C_4H_9–	*s*-D*s*BTU				3421s	3400sh
s-C_4H_9–	*t*-C_4H_9–	*s*BTU*t*B	3446m			3420s	3400sh
t-C_4H_9–	*t*-C_4H_9–	*s*-D*t*BTU	3452s			3418s	* *

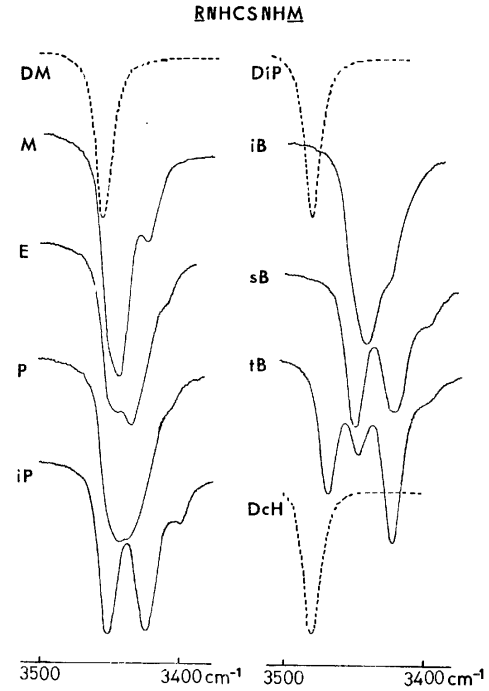

Fig. 1. The infrared spectra in the N-H stretching region of *R*TUM (the solid line) and D*R*TUM (the broken line) in CCl_4. *R*: see the abbreviations in Table 1; *c*H: cyclohexyl.

ponent resulting from the N-H group with the methyl group, and the lower component from the N-H group with the *s*-butyl group. In the case of the *R*TU*R'* showing only one band, the two components from the two different types of N-H group may be closer than those in the above example, or may overlap each other, thus appearing as only one band. This is suggested by the fact that *R*TU*R'* with only slightly different components such as MTUP (combinations of the B and C groups) give a band with lower apparent optical density and with larger half-intensity width than *R*TU*R'* with overlapped components such as *s*-DMTU (combinations of two groups belonging to the same type), as shown in Fig. 1.

It is concluded that these three kinds of bands originate from the *trans* form, and that the established *trans*-correlation for *R*U*R'* is applicable to *R*TU*R'*.

Out *N-H Bands.* Band A appears at the highest frequency and with medium or strong intensity without exception in *R*TU*R'* with a *t*-butyl group or groups. It probably corresponds to the very weak band at 3469 cm^{-1} of *s*-D*t*BU,[7] to the bands of *R*U*t*B which appear newly when the solvent is changed from CCl_4 to $CHCl_3$,[8] and to the 3478 cm^{-1} band of D*c*HU*t*B, being assignable to the *out* form.[11] It is suggested that the larger X atom of *R*TU*t*B enhances the steric hindrance between substituent and C=X group in comparison with *R*U*t*B since band A of *R*TU*t*B appears always and more

strongly than the corresponding band of *R*U*t*B.

Taking into account the N-H frequencies of D*R*U*R'* higher than those of *R*U*R'*,[11] the spectra of D*R*TU*R'* (broken lines, Fig. 1) indicate that DMTUM exist completely as the *trans* form, while D*i*PTUM and D*c*HTUM exist completely as the *out* form. It is concluded that the assignment of band A to the *out* form is reasonable from a steric point of view.

Out-of-plane N-H Group. The *out* N-H frequencies seem to be sensitive to the opposite alkyl group, *R*, in *R*TU*t*B; *R*TU*t*B with *R*=M or *i*B being the highest in frequency, *R*=other primary alkyls medium, and *R*=branched alkyls the lowest. The situation was the same for all three solvents.[16] MTU*t*B shows three bands and a shoulder E (Fig. 2). We assign band A=the *out*, B=the *trans* methyl, and D=the *trans* *t*-butyl N-H absorptions. Band B (the *trans* methyl) is considerably weaker than band D (the *trans* *t*-butyl), although in the absence of isomerism the *trans* methyl band of *RUR'*[9] and of secondary amides[17] have larger molar extinction coefficients than the other *trans* bands.

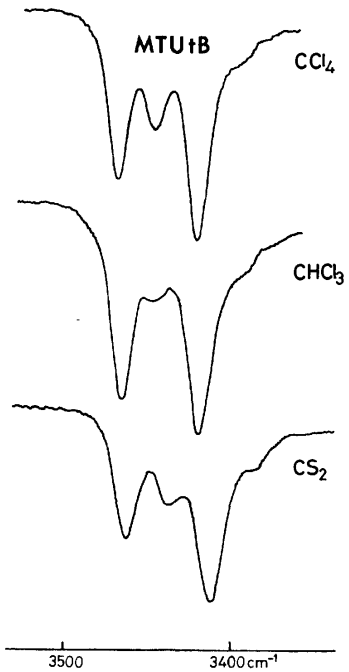

Fig. 2. Solvent effects on the infrared spectra of MTU*t*B.

By changing the solvent from CCl_4 to $CHCl_3$ the intensity of band A seems to increase at the expense of the weak band B (Fig. 2). The two bands were observed to be temperature dependent but in the opposite direction to each other. Other *R*TU*t*B with *R*=E, P, *i*B, and B were expected to show bands C and D. However, band C did not appear even as a shoulder. The component of band C is considered to be weakened by the appearance of band A.

From the facts mentioned above it is suggested that it is not the N-H group with the bulky *t*-butyl group but the N-H group in the opposite part that is predominantly out of the skeletal plane, though this seems to be unlikely. However, the suggestion may have validity if we consider that it is not the bulkiness of the substituent attached to the one N-H group, *R'*, but that of the opposite substituents, D*R*, in D*R*U*R'* that plays an important role in the rotational isomerism.[11] This can be interpreted in terms of the steric hindrance between the *t*-butyl group and the sulfur atom, and of the stronger electron-releasing inductive effect of the *t*-butyl group. The hindrance may weaken the resonance effect of the skeleton. While the inductive effect, which would be expected to increase the electron density on the nitrogen atom, may strengthen the double-bond character on the N-C link with the *t*-butyl group more strongly than that on the other N-C link. Accordingly, these effects would make only the N-H link with the *R* group out-of-plane (the *trans-out* conformation).

The amount of the *trans-out* conformation was roughly estimated from band-intensity data; (*R* in *R*TU*t*B, %) M or *i*B, 60%; E, P, or B, 70%; *i*P or *s*B, 75%; and *t*B (=*s*-D*t*BTU), 90%.

Energy Difference. We carried out the analysis on the *trans-out* equilibrium using the 3452 (the *out*) and 3418 cm^{-1} (the *trans*) bands of *s*-D*t*BTU in CCl_4 (15.5—85.3 °C). Each band-intensity curve was in good agreement with the corresponding Lorentz curve calculated for bands A and D except for a slight deviation on the lower frequency side of band D. The presence of band E (O. D. <0.05) and the slope of the overtone band near 3150 cm^{-1} (O. D. <0.02 at 3400 cm^{-1}) were analyzed to give the deviation. The energy difference between the *out* and the *trans* forms was found to be $\Delta H=430\pm100$ cal mol^{-1} from area-intensity data ($\Delta H=380\pm100$ cal mol^{-1} from peak-intensity data). The ΔH value is consistent with the value 500 ± 200 cal mol^{-1} of Rao *et al.*[5] for the *cis-trans* forms estimated in the first N-H overtone region.

Band E. Most of the spectra of *R*TU*R'* have this band as a shoulder. By examining the solution spectra at different temperatures and concentrations, band E was confirmed to be no associated band, being assignable to the N-H vibration from a certain form in a rotational isomer, probably the *cis* form. Despite some uncertainty in frequency the band of *R*TU*R'* with both primary alkyl groups is slightly higher than that of the other *R*TU*R'*.

The authors wish to express their thanks to Mr. M. Watanabe for his assistance.

References

1) A part of this study was carried out by Visiting Professor Y. Mido at Universidad Autónoma de Guadalajara, México.

2) R. A. Russell and H. W. Thompson, *Spectrochim. Acta*, **8**, 138 (1956).

3) H. E. Hallam and C. M. Jones, *J. Mol. Struct.*, **5**, 1 (1970).

4) C. N. R. Rao, G. C. Chaturvedi, and R. K. Gosavi, *J. Mol. Spectrosc.*, **28**, 526 (1968).

5) R. K. Gosavi, U. Agarwala, and C. N. R. Rao, *J. Am. Chem. Soc.*, **89**, 235 (1967).

6) It is possible that there is no difference in the N-H frequencies for the *trans* form between the *trans-trans* and the *trans-cis* conformations. We propose that the *cis* form repre-

sents only the *cis* relation between the N–H and the C=X groups about a C–N rotational axis.

7) Y. Mido, *Spectrochim. Acta, Part A*, **29**, 1 (1973).
8) Y. Mido, *Spectrochim. Acta, Part A*, **29**, 431 (1973).
9) Y. Mido, *Bull. Chem. Soc. Jpn.*, **47**, 1833 (1974).
10) Y. Mido, *Spectrochim. Acta, Part A*, **32**, 1105 (1976).
11) Y. Mido and T. Gohda, *Bull. Chem. Soc. Jpn.*, **48**, 2704 (1975).
12) M. L. Moore and F. S. Crossly, *Org. Synth.*, Coll. Vol. III, 599, 617 (1955).
13) T. Miyazawa, *J. Mol. Spectrosc.*, **4**, 168 (1960).
14) R. A. Nyquist, *Spectrochim. Acta*, **19**, 509 (1963).
15) Here, isobutyl and other primary alkyl groups will be treated as one type, C, though the N–H group with an isobutyl group shows a slightly higher-frequency band than the group with other primary alkyl groups (Ref. 7).
16) The data in the $CHCl_3$ and CS_2 solutions are omitted: The change of solvent from CCl_4 to CS_2 lowered band A by 6—8 cm^{-1} and bands B—D by 10—12 cm^{-1}, and the difference of lowering made bands A and B in MTU*t*B more distinguishable (Fig. 2). The spectra in the $CHCl_3$ solution gave similar data to those in the CCl_4 solutuon.
17) R. L. Jones, *Spectrochim. Acta*, **22**, 1555 (1966); *Part A*, **23**, 1745 (1967).

Photochemistry in the Adsorbed Layer. VIII. Lifetimes of Excited Alkyl Ketones and Alkyl Radicals Adsorbed on Porous Vycor Glass

Masakazu ANPO, Toshiaki WADA, and Yutaka KUBOKAWA

Department of Applied Chemistry, College of Engineering, University of Osaka Prefecture, Mozu-Umemachi, Sakai, Osaka 591

(Received June 7, 1976)

The photolyses as well as the absorption spectra of adsorbed 3-methyl-2-butanone and 3-methyl-2-pentanone have been investigated in the presence and absence of nitrogen monoxide. The Stern-Volmer relationship was applied to the decrease in the rate of photolysis caused by addition of nitrogen monoxide. From the results together with those for acetone, 2-butanone, and 2-pentanone, it has been concluded that in the adsorbed layer the more blue shifted, *i.e.*, the more strongly hydrogen bonded to the surface OH groups a ketone molecule, the shorter the lifetime of its excited state. It has been found that the lifetime of the alkyl radical on the surface increases with the decrease in its ionization potential, leading to the decrease in the strength of its interaction with the surface. Special features of the photolysis in the adsorbed layer have been described for 3-methyl-2-butanone photolysis.

In spite of its importance in many problems,[1] photochemistry in the adsorbed layer appears to be one of the most unexploited fields in photochemistry. We have investigated the photolysis of alkyl ketones such as acetone, 2-butanone, and 2-pentanone adsorbed on porous Vycor glass, as regards general characteristics of the photochemistry in the adsorbed layer, *e. g.*, the enhanced type I selectivity for the ketones having γ-hydrogen atoms, the importance of the reaction of the geminate radical pairs formed in the primary process, and the contribution of surface OH groups to the photochemical reactions.[2-8] Some information on the relative lifetimes of the excited triplet states as well as the radicals on the surface has been obtained from the effect of the addition of nitrogen monoxide upon the photolyses. In the present work, similar studies have been extended to 3-methyl-2-butanone and 3-methyl-2-pentanone in order to obtain more general information on the relative lifetimes of those species as well as the characteristics of the photolysis of adsorbed alkyl ketones.

Experimental

Materials. Commercial compounds (Tokyo Kasei Co., Ltd., Grade SG) were purified by means of preparatory chromatography, and then vacuum distilled bulb-to-bulb. Only those fractions were used which contained less than 0.5% impurity as determined by means of a vapor-phase chromatograph equipped with a flame ionization detector and a polyethylene glycol 1500 column. Porous Vycor glass (Corning, No. 746685-7930) was used as an adsorbent.

Apparatus and Procedure. Details of the apparatus and procedure used in the photolysis in the adsorbed layer were reported.[2-8] A conventional vacuum system was used in conjunction with a special quartz cell capable of studying the spectra and photolysis in the adsorbed layer. The specimen of porous Vycor glass, which had been heated in oxygen to remove carbonaceous impurities, was introduced into the cell and degassed at 500 °C for 7 h. After a certain amount of ketone had been adsorbed on the specimen, photolysis was carried out using an ultra high pressure mercury lamp without filter. Gas phase photolysis was carried out in a cylindrical quartz cell under the same irradiation conditions. The analytical system consisted of three traps and a modified Ward still. The gaseous products were separated by fractional distillation and analyzed by gas-chromatography using a flame ionization detector.

The absorption spectra of adsorbed ketones were determined with a Hitachi EPS 3T type spectrophotometer, measuring transmission through the sample. A quartz cell was placed just before the photomultiplier in order to minimize scattering error. Another porous Vycor glass sample was pretreated under the same conditions in a separate cell and used as a blank in the reference beam. The spectra of the adsorbed ketones increased in intensity proportional to the amounts adsorbed without changes in relative intensity for the bands from 250 to 340 nm.

Results

Photolysis of Adsorbed 3-Methyl-2-Butanone. The major products in the gas phase photolysis of 3-methyl-2-butanone (3-M-2-B) are propylene, propane, and hexane (Table 1). The following processes can be proposed[9,10] for the formation of these products.

$$i\text{-}C_3H_7COCH_3 + h\nu \longrightarrow \begin{cases} i\text{-}\dot{C}_3H_7 + \dot{C}OCH_3 \\ i\text{-}C_3H_7\dot{C}O + \dot{C}H_3 \end{cases} \quad (1)$$

$$i\text{-}\dot{C}_3H_7 + i\text{-}\dot{C}_3H_7 \longrightarrow C_3H_6 + C_3H_8 \text{ or } C_6H_{14} \quad (2)$$

where reaction (1) is α-cleavage of alkyl ketones (type I reaction) and reaction (2) is disproportionation or combination reaction of isopropyl radicals. The rate of propylene formation is larger than the rate of propane formation. Such behavior was found by Zaha and Noyes[9] who attributed it to the occurrence of the following reaction.

TABLE 1. RELATIVE YIELD OF PRODUCTS FROM PHOTOLYSIS OF 3-METHYL-2-BUTANONE AT 25°C

	CH_4	C_2H_6	C_3H_6	C_3H_8	C_4H_{10}	C_6H_{14}
Adsorbed layer[a]	0.005	0.001	10.9	88.7	$<$0.001	$<$0.001
Vapor phase[b]	0.015	6.50	42.1	24.1	5.80	19.4

a) Amount of adsorbed 3-methyl-2-butanone, 8.5×10^{-5} mol/g. Conversion per h, 12—15%. Irradiation time, 15—30 min. b) 3-Methyl-2-butanone pressure, 13.0$\pm$0.5 Torr.

$$\dot{R} + i\text{-}C_3H_7COCH_3 \longrightarrow RH + C_3H_6 + CH_3\dot{C}O \quad (3)$$

where R stands for any radicals formed in the primary processes.

In the adsorbed layer photolysis the rate of propane formation is much larger and that of propylene formation much smaller as compared to the corresponding values in the gas phase photolysis. Previous works[4,6] on the photolysis of adsorbed acetone or 2-pentanone show that methane or propane arises from hydrogen abstraction from the surface OH groups by methyl or propyl radicals as well as the disproportionation of the geminate radical pairs such as

$$\dot{C}H_3 + CH_3\dot{C}O \longrightarrow CH_4 + CH_2CO.$$

The reaction of alkyl radicals formed in the primary process with the ketone molecules hardly takes place. A similar situation would be expected for the propane and propylene formation from the photolysis of adsorbed 3-M-2-B. Thus, it can be concluded that in the adsorbed layer the contribution of reaction (3) to the propylene formation is negligible, most part of propylene arising from disproportionation reaction of the geminate radical pairs. It should be noted that the amounts of the radical recombination products such as ethane or hexane are very small in the adsorbed layer. Such behavior is one of the general characteristics of the photolysis of adsorbed alkyl ketones.[4]

In contrast to 3-M-2-B, 3-methyl-2-pentanone (3-M-2-P) undergoes the type II as well as the type I reaction, since it has a γ-hydrogen atom. The most significant feature of its photolysis in the adsorbed layer is a marked enhanced type I selectivity as compared to that in the gas phase photolysis. Details were previously reported[8] (Table 2).

Effect of the Addition of Nitrogen Monoxide upon Photolysis. In order to study the nature of the excited states as well as the radicals formed in the photolysis the effect of the addition of nitrogen monoxide on the photolysis of adsorbed 3-M-2-B and 3-M-2-P has been investigated. In the photolysis of the latter the rate of ethylene formation decreases with increase in the nitrogen monoxide pressure, levelling off to a constant value (Fig. 1). Considering the fact that nitrogen monoxide is an efficient triplet quencher, the amount of quenchable reaction (57%) can be attributed to reaction from the excited triplet state with the remainder of the reaction (43%) occurring from the excited singlet state. A similar nonquenchable fraction of the ethylene formation (44%) has been obtained with the photolysis of adsorbed 2-pentanone in the presence of nitrogen monoxide.[2]

The rate of propane formation from 3-M-2-B as well as that of butane formation from 3-M-2-P decreases markedly with increasing nitrogen monoxide pressure,

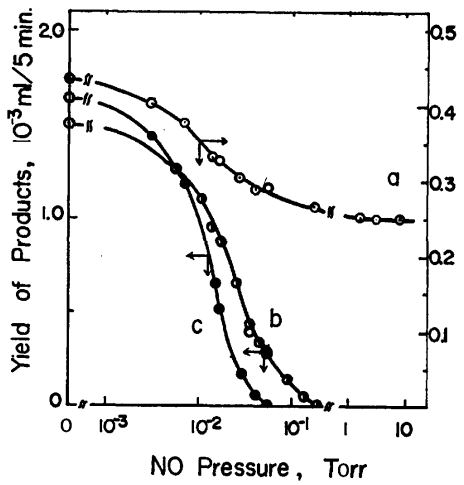

Fig. 1. Effect of nitrogen monoxide upon the rates of photolyses of 3-methyl-2-butanone and 3-methyl-2-pentanone adsorbed on porous Vycor glass.
The amounts of 3-methyl-2-butanone and 3-methyl-2-pentanone adsorbed were 7.5×10^{-5} and 8.5×10^{-5} mol/g, respectively. During the photolysis nitrogen monoxide was somewhat consumed; It was confirmed, however, that the resulting pressure decrease did not affect the value of the constants A and B in the Stern-Volmer equation. a: Ethylene (3-M-2-P), b: propane (3-M-2-B), c: butane (3-M-2-P).

finally approaching zero around 0.10 Torr for propane and 0.06 Torr for butane, as expected from the action of nitrogen monoxide as a radical scavenger (Fig. 1). In addition to such scavenging action, the decrease in the rate of formation is caused by quenching of the excited states with nitrogen monoxide.

Discussion

The photolysis of adsorbed 3-M-2-B and 3-M-2-P in the presence of nitrogen monoxide is as follows. Reactions (3) and (7) are included only in the case of 3-M-2-P.

$$P + h\nu \longrightarrow {}^1P$$

$$^1P \xrightarrow{k_1} P + \text{heat} \quad (1)$$

$$^1P \xrightarrow{k_2} \dot{R} + \dot{C}OR' \quad (2)$$

$$^1P \xrightarrow{k_3} C_2H_4 + CH_3COCH_3 \quad (3)$$

$$^1P \xrightarrow{k_4} P + h\nu' \quad (4)$$

$$^1P \xrightarrow{k_{isc}} {}^3P \text{ (isc)}$$

$$^3P \xrightarrow{k_5} P + \text{heat} \quad (5)$$

Table 2. Relative yield of products from the photolysis of 3-methyl-2-pentanone at 25°C

	C_2H_4	C_3H_8	C_4H_8	C_4H_{10}	C_5H_{12}	C_6H_{14}	type I/II
Absorbed layer[a]	14.1	4.12	3.19	72.6	2.90	3.12	6.0
Vapor phase[b]	73.3	3.15	1.14	12.2	4.18	6.01	0.35

a) Amount of adsorbed 3-methyl-2-pentanone, 4.5×10^{-5} mol/g. Conversion per h, 10—15%. Irradiation time, 15—30min. b) 3-Methyl-2-pentanone pressure, 18.0 ± 0.5 Torr. The selectivity of type type I was identified as follows; $I/II=(\phi_{C_1}+\phi_{C_4}+\phi_{C_5}+\phi_{C_6})/\phi_{C_4H_8}$.

Table 3. Values of A (τk_9) and B ($\tau' k_{11}$) for nitrogen monoxide quenching (M^{-1})

	Acetone[a)]	2-Butanone[a)]	3-Methyl-2-butanone	2-Pentanone[a)]	3-Methyl-2-pentanone
A	—	0.95×10^5	3.6×10^5	2.2×10^5	5.5×10^5
B	0.054×10^6	0.24×10^6	4.9×10^6	6.1×10^6	7.0×10^6

a) Ref. 2.

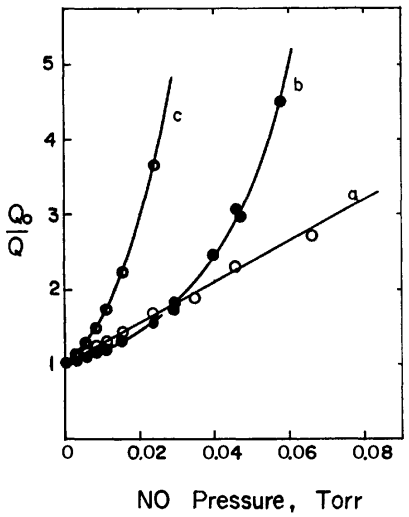

Fig. 2. Stern-Volmer plots for products quenching in the photolyses of 3-methyl-2-butanone and 3-methyl-2-pentanone adsorbed on porous Vycor glass. a; Ethylene (3-M-2-P), b; propane (3-M-2-P), c; butane (3-M-2-P).

$$^3P \xrightarrow{k_6} \dot{R} + \dot{C}OR' \quad (6)$$

$$^3P \xrightarrow{k_7} C_2H_4 + CH_3COCH_3 \quad (7)$$

$$^3P \xrightarrow{k_8} P + h\nu'' \quad (8)$$

$$^3P + NO \xrightarrow{k_9} P + NO \quad (9)$$

$$\dot{R} + [H] \xrightarrow{k_{10}} RH \quad (10)$$

$$\dot{R} + NO \xrightarrow{k_{11}} RNO \longrightarrow \text{Stabilized} \quad (11)$$

$$\dot{R} + R'\dot{C}O \xrightarrow{k_{12}} \text{Recombination or disproportionation products} \quad (12)$$

The α-cleavage from the excited singlet state (reaction 2) can be neglected,[2] since there exists a striking difference in the reactivity of the excited singlet and triplet states toward α-cleavage of alkyl ketones.[11] Thus, the following quadratic Stern-Volmer equation is obtained by the steady state treatment for propane formation from 3-M-2-B and butane formation from 3-M-2-P.

$$Q_0/Q = (1+A[NO])(1+B[NO]) \quad (I)$$

where $A=k_9/(k_5+k_6+k_7+k_8)$, $B=k_{11}/([H]k_{10}+[R'CO]k_{12})$. Q and Q_0 are the rates of propane or butane formation in the presence and absence of nitrogen monoxide, respectively. The plot of Q_0/Q against nitrogen monoxide pressure is shown in Fig. 2. Constants A and B for both ketones are so determined to give the best fit to the experimental curves[2] (Table 3). Values of A and B for other ketones are also given in Table 3.

In the photolysis of 3-M-2-P, ethylene is formed from the singlet as well as the triplet state. The following equation holds for the rate of ethylene formation from the triplet state, which is determined by subtracting the nonquenchable amount of ethylene formed with nitrogen monoxide present from the total amount of ethylene formed without nitrogen monoxide present.

$$Q_0/Q = (1+A'[NO]) \quad (II)$$

where Q and Q_0 are the rates of ethylene formation from the excited triplet state in the presence and absence of nitrogen monoxide, respectively. From the slope of the Stern-Volmer plot (Fig. 2) the value of A' is found to be 5.2×10^5 l/mol, in agreement with that obtained from equation (I). This supports the assumption that the formation of propane and butane from the excited singlet state can be neglected.

Lifetime of Excited Ketone Molecules. The wavelengths of maximum absorption of (n, π^*) transition of adsorbed 3-M-2-B and 3-M-2-P together with the corresponding values of other ketones[3] are given in Table

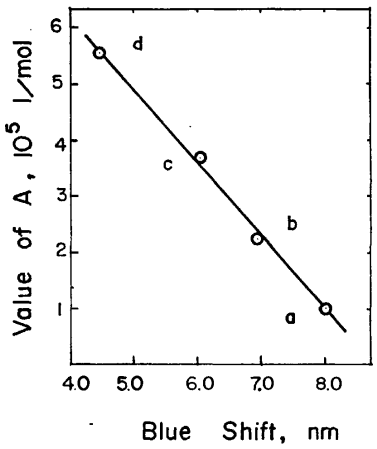

Fig. 3. The relationship between values of A and blue shift. The blue shift was identified as follows; $\Delta E=$ (λ_{max} on Vycor glass) − (λ_{max} in heptane).
a; 2-Butanone, b; 3-M-2-B, c; 2-pentanone, d; 3-M-2-P.

Table 4. Wavelengths of maximum absorption of alkyl ketones adsorbed on porous Vycor glass at 25 °C (nm)

	Acetone	2-Butanone	3-Methyl-2-butanone	2-Pentanone	3-Methyl-2-pentanone
$\lambda_{max.}$ on vycor glass	262.0	270.0	276.0	273.0	280.0
$\lambda_{max.}$ in heptane	276.5	278.0	283.0	279.0	284.5

Table 5. Relative lifetime of the alkyl radicals in the adsorbed layer (M^{-1})

	Methyl	Ethyl	Propyl	Isopropyl	*s*-Butyl
B ($\tau' k_{11}$)	0.054×10^6	0.24×10^6	4.9×10^6	6.1×10^6	7.0×10^6
Relative lifetime	1	11	1100	2800	6400

4. The blue shift of the (n, π^*) bands decreases in the order acetone>2-butanone>3-M-2-B>2-pentanone> 3-M-2-P. Values of A also decrease in the same order (Table 3). A linear relation exists between the values of A and blue shift (Fig. 3). The magnitude of A is mainly determined by the rate of radiationless deactivation k_5, *i.e.*, $k_5 \gg (k_6+k_7+k_8)$.[2] Thus, the results confirms the conclusion that the more blue shifted the ketone molecule, *i.e.*, the more strongly hydrogen bonded to the surface OH groups, the more efficient the radiationless deactivation (k_5).[2]

It is well-known[12] that there is a marked difference between the excited and ground states in the geometry, *e. g.*, the ground state of HCHO is planar, while in its excited singlet state the CO bond makes an angle of 20° to the CH_2 plane. According to the work of Iwata and Morokuma,[13] the hydrogen bond energy of HCHO with water depends upon the geometry in its excited (n, π^*) state, *i.e.*, the extent to which the excited state is non-planar. The Franck-Condon principle shows that the rate of radiationless decay depends upon the vibrational overlap factor.[14] It seems obvious that the overlap factor is expected to be larger the larger the differences in geometry between the ground and excited states. One explanation is as follows. In going from acetone to 3-M-2-P, the extent to which the excited (n, π^*) state is non-planar would decrease in the adsorbed layer, as reflected in the decrease in the strength of the hydrogen bond with the surface OH groups. Such a change in the excited state geometry would affect the rate of the radiationless decay.

Lifetime of Adsorbed Alkyl Radicals. Values of B ($\tau' k_{11}$), including the corresponding values for other ketones obtained previously,[3] are given in Table 5. Although it is expected that in the adsorbed layer the reactivity of the radicals differs from that in the gas phase,[15] it seems difficult to attribute such a large difference in the B values only to the difference in k_{11}.[2,5] It can be concluded that the alkyl radical lifetime increases in the order methyl<ethyl<propyl<isopropyl<*s*-butyl radicals in the adsorbed layer. Assuming that the relative reactivity of nitrogen monoxide toward the radicals in the adsorbed layer is approximately equal to that in the gas phase,[15] it is possible to estimate the relative lifetime of the radicals in the adsorbed layer as seen in Table 5. In the photolysis of adsorbed alkyl ketones the lifetime of alkyl radicals is mainly determined by the rate of recombination of the geminate radical pairs, k_{11}, the magnitude of which is expected to depend upon the surface mobility of the radicals.[6]

According to the work of Garbutt and Gesser,[16] the radicals are stabilized on the surface of porous Vycor glass by charge-transfer interaction where radicals play the role as electron-donors and the surface OH groups as electron-acceptors. In such cases it would be expected that the stabilization energy, *i.e.*, the adsorption energy

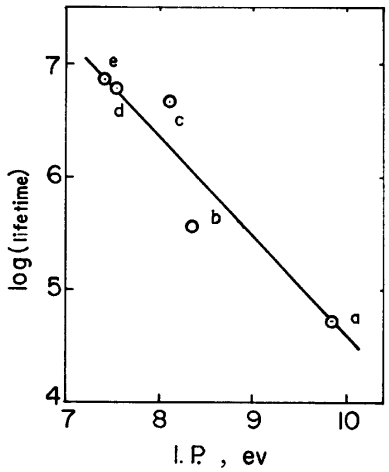

Fig. 4. The relationship between log(lifetime) and ionization potential (I.P.) of alkyl radicals.[17]
a: Methyl, b: ethyl, c: propyl, d: isopropyl, e: s-butyl radical.

of the radicals, E_{ads} decreases with increasing the ionization potential of the donors (radicals). The lifetime of the radical on the surface should increase with the decrease in its surface mobility, which will decrease with increasing adsorption energy of the radical. It is concluded that in the adsorbed layer the lifetime of the radical will increase with the decrease in its ionization potential, *i.e.*, with increasing strength of its interaction with surface. The results shown in Fig. 4 confirm the conclusion.

References

1) C. H. Nicholls and P. A. Leermakers, in "Advances in Photochemistry," Vol. 8, W.A. Noyes, Jr., G. S. Hammond, and J. N. Pitts, Jr., Wiely-Interscience, New York (1971), p. 315.
2) Y. Kubokawa and M. Anpo, *J. Phys. Chem.*, **78**, 2442 (1974).
3) M. Anpo and Y. Kubokawa, *J. Phys. Chem.*, **78**, 2446 (1974).
4) M. Anpo, S. Hirohashi, and Y. Kubokawa, *Bull. Chem. Soc. Jpn.*, **48**, 985 (1975).
5) Y. Kubokawa and M. Anpo, *J. Phys. Chem.*, **79**, 2225 (1975).
6) M. Anpo, T. Wada, and Y. Kubokawa, *Bull. Chem. Soc. Jpn.*, **48**, 2663 (1975).
7) M. Anpo and Y. Kubokawa, *Bull. Chem. Soc. Jpn.*, **48**, 3085 (1975).
8) M. Anpo and Y. Kubokawa, *Bull. Chem. Soc. Jpn.*, **49**, 2623 (1976).
9) A. Zaha and W. A. Noyes, Jr., *J. Phys. Chem.*, **69**, 943 (1965).
10) A. A. Scala, *J. Phys. Chem.*, **74**, 2639 (1970).
11) R. B. Cundall and A. S. Davies, *Proc. R. Soc. London, Ser. A*, **290**, 563 (1966); R. K. Boyd, G. B. Carter, and K. O. Kutchke, *Can. J. Chem.*, **46**, 175 (1968); J. C. Dalton, K.

Dawes, N. J. Turro, D. S. Weiss, J. A. Bartrop, and J. D. Coyle, *J. Am. Chem. Soc.*, **93**, 7213 (1971).
12) E. W. Abrahamson, J. G. F. Littler, and Kim-Phan Vo, *J. Chem. Phys.*, **44**, 4082 (1966).
13) S. Iwata and K. Morokuma, *J. Am. Chem. Soc.*, **95**, 7563 (1973).
14) N. J. Turro, "Molecular Photochemistry," W. A. Benjamin, New York, N. Y. (1967), p. 44; M. Orchin and H. H. Jaffe, "Symmetry, Orbitals, and Spectra," Wiley-Interscience, New York, (1971), p. 204.
15) M. I. Christie and J. S. Frost, *Trans. Faraday Soc.*, **61**, 468 (1965).
16) G. B. Garbutt and H. D. Gesser, *Can J. Chem.*, **48**, 2685 (1970).
17) F. P. Lossing and G. P. Semeluk, *Can. J. Chem.*, **48**, 955 (1970).

The Vibrational Spectra of Tetracyanothiophene

Jiro NAKANISHI and Tohru TAKENAKA
Institute for Chemical Research, Kyoto University, Uji, Kyoto 611
(Received June 18, 1976)

The polarized infrared and far-infrared spectra of the tetracyanothiophene (TCNT) crystals were recorded by means of the normal and oblique incidence of radiation upon the (001) and (20$\bar{1}$) sample planes. The Raman spectra of the powdered sample and of a saturated solution in acetonitrile or 1,2-dichloroethane were also obtained. The observed bands were experimentally classified into the symmetry species of the free molecule (the point group C_{2v}) under the assumption of an oriented gas model. Assignments of the observed bands to individual fundamental vibrations were carried out with the aid of the spectral data of the analogous molecules and the normal coordinate analysis of the in-plane vibrations, which was made with a modified Urey-Bradley force field.

Although a number of vibrational studies have been carried out on such fully conjugated tetracyano compounds as tetracyanoethylene (TCNE),[1-7] 7,7,8,8-tetracyanoquinodimethane (TCNQ),[8-11] and 1,2,4,5-tetracyanobenzene (TCNB),[12,13] little attention has been paid to the heterocyclic tetracyano compounds. The present paper will deal with the vibrational spectra of tetracyanothiophene (TCNT), which was first synthesized and physicochemically studied by Simmons and his co-workers.[14]

The infrared and far-infrared spectra of the oriented crystals were measured with a polarized radiation incident, not only normally, but also obliquely upon the (001) and (20$\bar{1}$) sample planes. From the results obtained, the observed bands were classified into three infrared-active species—a_1, b_1 and b_2—of the free molecule (the point group C_{2v}) under the assumption of an oriented gas model. In order to distinguish the lattice vibrations from the molecular vibrations, the far-infrared spectrum of the molten sample was also obtained. The Raman spectra were recorded of the powdered sample and of solutions in acetonitrile and in 1,2-dichloroethane. The observed values of the depolarization ratios in the solutions confirmed the previous findings regarding the classification of the corresponding infrared bands into totally symmetric (a_1) and non-totally symmetric species.

The assignments of the observed bands to individual fundamental vibrations were made with the aid of the spectral data of the analogous molecules and the normal coordinate analysis. The analysis of the in-plane vibrations was carried out using a modified Urey-Bradley force field. The agreements between the observed and calculated frequencies were satisfactory.

Experimental

A sample of TCNT was prepared by the method of Simmons and his co-workers;[14] tetracyano-1,4-dithiin was heated up to 215 °C in 1,2,4-trichlorobenzene, and the products were recrystallized three times from benzene and then sublimed. The colorless crystalline needles of TCNT thus obtained melted at 201—202 °C, while the literature value is 198—199 °C. The ultraviolet spectrum,[14] the results of the elemental analysis, and the X-ray diffraction pattern[15] of this sample were identical with those previously reported. The infrared spectrum of the powdered sample was also the same as that previously reported,[14] except for the 700-cm^{-1} band, which is much weaker in our spectrum. Since this band is considered to be due to a trace of impurities, it may be concluded that our sample is of a higher purity than that of Simmons and his co-workers.[14]

The thin, oriented crystals used for infrared measurements were prepared by the slow, careful cooling of molten samples sandwiched between two potassium bromide plates with a small temperature gradient. The oriented crystals for far-infrared measurements were obtained in the same way between two quartz plates. The crystal structure of TCNT has been reported by Rychnovsky and Britton[15] to be a monoclinic system, $a=13.42$, $b=6.56$, $c=7.07$ Å and $\beta=137°$, with a space group of P_s-C_s^2 with two molecules in a unit cell. The present X-ray diffraction studies showed that the crystal planes developed were either the (001) or (20$\bar{1}$) plane, depending upon the degree of temperature gradient during the crystal preparations.

The infrared spectra between 4000 and 250 cm^{-1} were recorded on a Perkin-Elmer model 521 grating spectrophotometer. For far-infrared measurements between 400 and 30 cm^{-1}, a Hitachi model FIS-3 vacuum grating spectrophotometer was used. The spectrum of the melt in this region was obtained for a sample sandwiched between two silicon plates. In this measurement the double-chopping method was used to eliminate the emission from the heated sample. The polarization measurements in the infrared and far-infrared regions were made with the aid of wire grid polarizers of the silver bromide substrate and of the polyethylene substrate respectively. The Raman spectra of powdered sample and of saturated solutions in acetonitrile and 1,2-dichloroethane at 60 °C were recorded on a Japan Electron Optics Laboratory model JRS-Sl spectrophotometer equipped with an Ar^+ laser as a light source for excitation. A Glan-Thomson prism and polaroid were used for measurements of the depolarization ratios in the solutions.

Selection Rules and Observed Spectra

The TCNT molecule has been reported to have the C_{2v} molecular symmetry.[15] The selection rules for the free molecule and for the molecules in the crystal are given in the correlation diagram of Table 1. The vibrations belonging to the a_1 and b_2 species are of the in-plane mode, while those belonging to the a_2 and b_1 species are of the out-of-plane mode. Table 1 shows that each vibration of the free molecule splits in the crystal into two modes, which are both Raman- and infrared-active, and that there are nine lattice vibrations-three translational and six rotational.

The infrared spectra of the TCNT crystals obtained with the polarized radiation incident normally upon the

Table 1. Correlation diagram and selection rules[a] of TCNT

Molecular group C_{2v}	Site group C_1	Factor group C_s^2
12 a_1 (R,p and IR, M_z[b]) 5 a_2 (R, dp) 5 b_1 (R, dp and IR, M_x[b]) 11 b_2 (R, dp and IR, M_y[b])	66 A	33A′ (R and IR, M_{ac}) (t+3r)[c] 33A″ (R and IR, M_b) (2t+3r)[c]

a) R, Raman-active; IR, infrared-active; p, polarized; dp, depolarized. b) For the molecular fixed axes x, y, and z, see Fig. 5. c) t, translational; r, rotational.

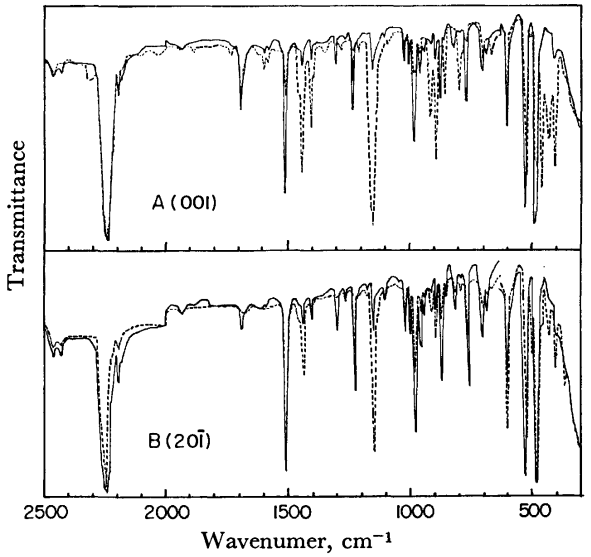

Fig. 1. Polarized infrared spectra of TCNT crystals obtained on normal incidence of radition upon the (001) plane [A] and the (20$\bar{1}$) plane [B].
——: Electric vector parallel to the b axis.
------: Electric vector perpendicular to the b axis.

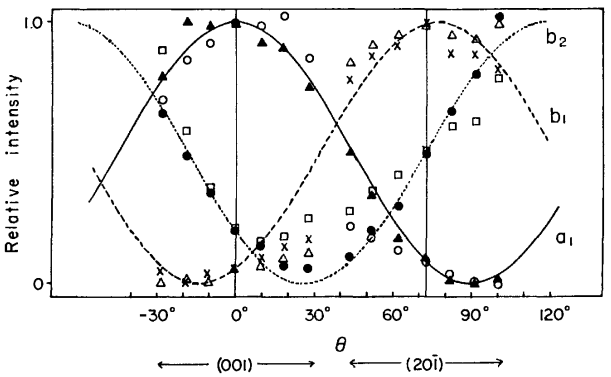

Fig. 2. Relative intensities of the infrared bands as a function of the angle θ between the a axis and the electric vector of the polarized radiation.
□: 1512, ○: 1443, ▲: 1406, ●: 1233, △: 604, ×: 504 cm^{-1} band.

(001) and (20$\bar{1}$) planes are given in Figs. 1A and 1B respectively. The solid lines refer to the orientation of the electric vector parallel to the b axis, while the broken lines refer to the electric vector perpendicular to it. The fact that the factor-group splitting is scarcely observed in Fig. 1 suggests that the effects of the crystal field on the molecular vibrations are small. The agreement between the two solid lines in Figs. 1A and 1B is fairly good, as expected, except for the relative intensity of the band at 1695 cm^{-1}, which may be due to impurities.

Although it is generally known that the observed bands can be classified into three infrared-active species—a_1, b_1, and b_2—by examining the dichroism in Figs. 1A and 1B, there often appear some ambiguities which are due to imperfections in the crystals as well as to experimental errors. To avoid these ambiguities, additional experimental data were introduced by the use of the tilting method, in which the sample plane was rotated in turn by certain angles about the b axis, and the polarized radiation with the electric vector parallel to the ac plane was incident upon the sample plane. The change in the relative intensities of the infrared bands of the a_1, b_1, and b_2 species with the change in the tilting angle was calculated from the crystal data[15] under the assumption of an oriented gas model. The results are given by the solid (a_1), broken (b_1), and dotted (b_2) lines in Fig. 2 as a function of the angle, θ, between the a axis and the electric vector of the polarized radiation. The angles are measured in terms of the rotation which transfers the a axis to the c axis through the obtuse angle.

Experimental data were obtained from the samples of both the (001) and (20$\bar{1}$) planes. The normal incidence of the polarized radiation upon the (001) and (20$\bar{1}$) planes gives the data at $\theta=0°$ and $\theta=72.3°$ in Fig. 2 respectively. The peak intensities of the bands obtained at various angles of θ for the (001) sample were normalized in such a way that the observed intensities at $\theta=0°$ fit into the corresponding calculated values. The same normalization of the observed intensities was carried out on the basis of the values calculated at $\theta=72.3°$ for the (20$\bar{1}$) sample. By the use of both the (001) and (20$\bar{1}$) planes, experimental data could be obtained over a wide range of θ, from $-30°$ to 100°. Although there are some departures of the experimental values from the calculated curves, a glance at the overall θ-dependence of the experimental values leads to unambiguous classifications of the most observed bands into the three infrared-active species. The results of this examination are summarized in Table 2.

Figures 3A and 3B represent the far-infrared spectra of the TCNT crystals recorded on the normal incidence of radiation upon the (001) and (20$\bar{1}$) planes respectively. The solid lines refer to the orientation of the electric vector parallel to the b axis, while the broken lines refer to the electric vector perpendicular to it. The agreements between the two solid lines in Figs. 3A and 3B are good. Figure 3C is the spectrum of TCNT in the molten state. The bands at 90, 83, 76, 74, 54, and 36 cm^{-1} in Fig. 3A or 3B disappear in Fig. 3C, suggesting that they are due to lattice vibrations. We observe

TABLE 2. INFRARED AND RAMAN SPECTRA OF TCNT

Infrared			Raman			Assignment[b]
Crystal	Melt	Species	Powder	Solution	Depolarization	
2258 s[a]		b_2				ν_{13}
2247 s		a_1	2247 sh			ν_1
2239 vs		b_2	2242 vs	2247 s	dp	ν_{14}
2224 s		a_1	2232 vs	2237 vs	p	ν_2
2196 sh		a_1				$\nu_{16}+\nu_{17}=2216$
1695 w						
1512 s		b_2	1510 w	1515 vw	dp	ν_{15}
1443 m		a_1	1444 vs	1444 vs	p	ν_3
1406 w		a_1	1408 vs	1406 vs	p	ν_4
1303 w		b_2				$\nu_7+\nu_{18}=1299$
1233 m		b_2	1232 m	1232 m	dp	ν_{16}
1152 vs		a_1	1153 w	1154 w	p	ν_5
983 s		b_2				ν_{17}
977 sh		a_1				$\nu_{24}+\nu_{26}=979$
916 m		a_1	913 w			$\nu_3-\nu_7=919$
896 m		a_1	900 w	897 sh	p	ν_6
874 m		b_2				$\nu_7+\nu_{21}=867$
859 w		a_1				$\nu_7+\nu_{10}=857$
820 w		b_2				$\nu_{16}-\nu_9=822$
796 m		a_1				$\nu_8+\nu_{10}=796$
770 m		b_2	777 vw			ν_{18}
703, 698 w		b_2	700 vw			$\nu_8+\nu_{22}=687$
604 s		b_1	606 m	606 m	dp	ν_{24}
530 s		b_2				ν_{19}
524 sh			525 s	524 s	p	ν_7
504 w		b_1	504 m	503 m	dp	$\nu_8+\nu_{28}=511$
487 vs		b_1	484 m	485 w	dp	ν_{25}
481 s		a_1		478 m	p	$\nu_6-\nu_9=487$
464 s		a_1	464 sh	467 sh	p	ν_8
436 m		a_1	432 w	430 w	p	$2\nu_{22}=446$
428 sh		b_2		428 w	dp	ν_{20}
410 s		a_1	411 w	411 w	p	ν_9
374 w		b_1	373 vw			ν_{26}
342 vw						ν_{21}
332 vw						ν_{10}
226, 223 m	218 m	b_2	222 w	220 w	dp	ν_{22}
188, 181 vs	168 vs	b_1	184 w			ν_{27}
146 m		a_1	144 sh			$\nu_8-\nu_{10}=132$
128 s		b_1				$\nu_{24}-\nu_8=141$
125 s	120 vs	b_2	126 vs			ν_{23}
118 s		a_1	118 sh			ν_{11}
113 vs	96 s	a_1				ν_{12}
90 vw		A″				
83 m		A′				
76 w		A′	76 sh			
74 m		A″				
58 w	57 w	a_1	59 vs			$\nu_7-\nu_8=61$
54 sh		A″				
46 vw		b_1	48 sh			ν_{28}
36 vw		A′				

a) The relative intensities of this column refer to those of the powder bands, because those of the crystal bands depend largely upon the direction of the electric vector of polarized radiation. b) See Tables 3 and 4.

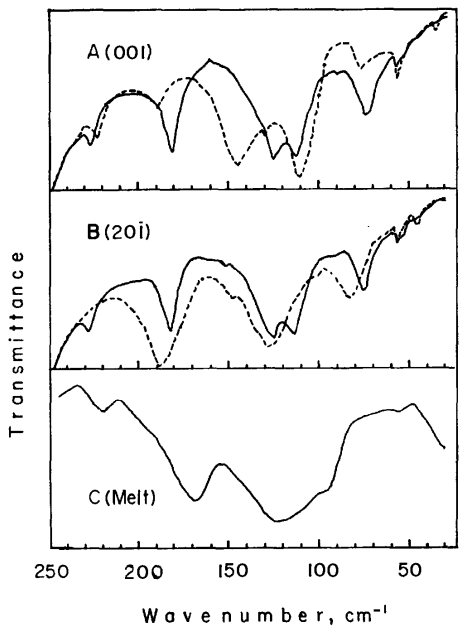

Fig. 3. Polarized far-infrared spectra of TCNT crystals obtained on normal incidence of radition upon the (001) plane [A] and (20$\bar{1}$) plane [B].
——: Electric vector parallel to the b axis.
------: Electric vector perpendicular to the b axis.
[C] Far-infrared spectrum of TCNT in the molten state.

some frequency shifts of the bands with the phase change from crystal to melt. As is apparent from Table 1, the lattice bands at 90, 74, and 54 cm^{-1}, found only in the solid lines of Figs. 3A and 3B, are to be assigned to the A″ vibrations of the factor group, while the bands at 83, 76, and 36 cm^{-1}, found only in the broken lines, are to be assigned to the A′ vibrations. The classification of the far-infrared bands due to molecular vibrations into the respective species was also made by means of the tilting method mentioned above. These results are given in Table 2. In this low-frequency region the factor-group splittings are observed at 226 and 223 cm^{-1} and at 188 and 181 cm^{-1}.

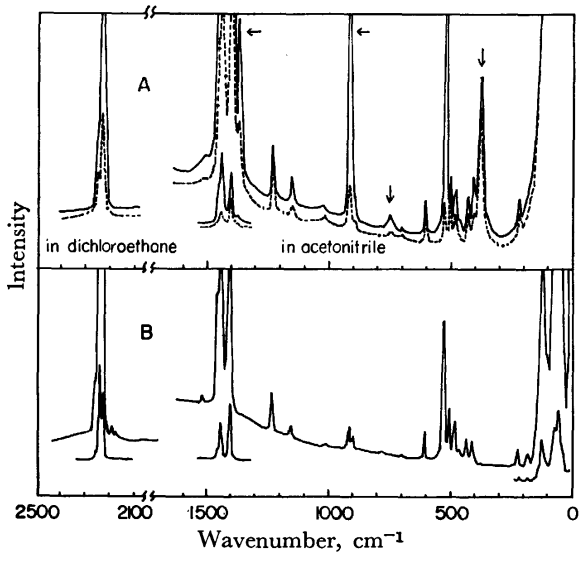

Fig. 4. [A] Raman spectra of TCNT in acetonitrile and in 1,2-dichloroethane. Bands marked with the arrow are due to solvents.
——: $I_{//}$, ------: $I_{\perp}$.
[B] Raman spectrum of TCNT powder.

Figure 4A represents the Raman spectra of the acetonitrile and the 1,2-dichloroethane solutions of TCNT. The bands marked with arrows are solvent bands. The solid and broken lines give the spectra of Raman scatterings with the electric vector parallel and perpendicular to that of the exciting light respectively. The observed values of the depolarization ratios confirmed the previous results regarding the classification of the corresponding infrared bands into the totally symmetric (a_1) and non-totally symmetric species (b_1 and b_2), as is seen in Table 2. The Raman spectrum of the powdered sample is also given in Fig. 4B and Table 2.

Assignments

In order to make the assignments of the observed bands to the individual fundamental vibrations, the following examinations were carried out besides the discussions in the previous section: (a) a comparison of the spectral data with those of the partly analogous molecules, such as TCNE,[1-7] TCNQ,[8-11] TCNB,[12,13] thiophene[16] and the bis(maleonitrile dithiolato) Ni(II) anion,[17] and (b) the normal coordinate analysis of the in-plane vibrations mentioned in the next chapter. In the following discussions, the mean values of the infrared frequencies of the crystal and Raman frequencies of the powder are used as the observed frequencies when both were found.

The assignments of the a_1 bands at 2247, 2228, 1444, 1407, 1153, and 525 cm^{-1} and of the b_2 bands at 2258, 2241, 1511, 1233, 983, 530, 223, and 126 cm^{-1} were straightforward.

The a_1 fundamental band ν_6, mainly due to the C–C stretching vibration, can be expected around 900 cm^{-1} by the normal coordinate analysis. Both the infrared bands at 916 and 896 cm^{-1}, which have been determined by the tilting method to belong to the a_1 species, are assignable to this vibration. Of the corresponding Raman bands in the solution, the low-frequency one at 897 cm^{-1} (900 cm^{-1} for the powder) was found to be polarized, although the high-frequency band (913 cm^{-1} for the powder) could not be observed because of the band overlap with the strong solvent band. Furthermore, in the process of the normal coordinate analysis, where the refinement of the force constants was carried out to get a better agreement between the calculated and the observed values for the above-mentioned fourteen bands which were assigned without ambiguities, it was found that the calculated frequency of the ν_6 vibration showed a tendency to decrease to *ca.* 900 cm^{-1}. Therefore, the 898 cm^{-1} band (on the average) was assigned to this vibration, and the 915-cm^{-1} band, to the combination tone [$\nu_3(a_1)-\nu_7(a_1)=919$ cm^{-1} (a_1)].

Thr b_2 fundamental band ν_{18} is thought to be present between 900 and 750 cm^{-1}. In this region, three infrared bands at 874, 820, and 770 cm^{-1} were found to belong to the b_2 species. Since, however, only one Raman band was observed at 777 cm^{-1}, corresponding to the infrared

band at 770 cm^{-1}, this band (774 cm^{-1} on the average) was assigned to the ν_{18} vibration, and the 874- and 820-cm^{-1} bands, to the combination tones [$\nu_7(a_1)+\nu_{21}(b_2)=$ 867 cm^{-1} (b_2) and $\nu_{16}(b_2)-\nu_9(a_1)=822$ cm^{-1} (b_2) respectively].

In the region from 500 to 400 cm^{-1}, two a_1 fundamental bands, ν_8 and ν_9 are to be expected. Apparently, four infrared bands of the a_1 species and four corresponding polarized Raman bands were found in this region. Since there is no further experimental evidence on the basis of which to choose two of them as the fundamentals, the assignments were carried out by reference to the tendency of the calculated frequency variation found in the refining process of the normal coordinate analysis, as has been mentioned above. Thus, the 464- and 411-cm^{-1} bands (on the average) were assigned to the ν_8 and ν_9 vibrations respectively. The 483-cm^{-1} band (on the average) was attributed to the combination tone [$\nu_6(a_1)-\nu_9(a_1)=487$ cm^{-1} (a_1)], and the 434-cm^{-1} band (on the average), to the overtone [$2\nu_{22}(b_2)=446$ cm^{-1} (a_1)].

The b_2 fundamental band ν_{20}, mainly due to the C-C≡N deformation vibration, can be expected in the same frequency region. Since only one infrared band of the b_2 species and the corresponding depolarized Raman band were observed in this region, this band (430 cm^{-1} on the average) was ascribed to the ν_{20} fundamental vibration.

The a_1 fundamental band ν_{10}, mainly due to the C=C-S bending vibration, and the b_2 fundamental band ν_{21}, mainly due to the C=C-C (ring) bending vibration, are to be expected between 400 and 300 cm^{-1}. Only two infrared bands, at 342 and 332 cm^{-1}, were observed in this region, except for the 374-cm^{-1}, which belongs to the b_1 species. Therefore, these bands were assigned to the ν_{21} and ν_{10} vibrations respectively, although they are very weak.

In the region from 150 to 100 cm^{-1}, three infrared bands of the a_1 species were observed at 146, 118, and 113 cm^{-1}. Correspondingly, two Raman bands were seen at 144 and 118 cm^{-1}; the latter seemed to include two components. By referring to the normal coordinate analysis, the 118- and 113-cm^{-1} bands were assigned to the ν_{11} and ν_{12} vibrations respectively. The 145-cm^{-1} band (on the average) was attributed to the combination tone [$\nu_8(a_1)-\nu_{10}(a_1)=132$ cm^{-1} (a_1)].

A weak infrared band of the a_1 species was observed at 58 cm^{-1} for the crystal and at 57 cm^{-1} for the melt, suggesting that it is due to the molecular vibration. Correspondingly, a very strong Raman band was observed at 59 cm^{-1} for the powdered sample. Since, however, no fundamental vibration belonging to the a_1 species was expected in this low-frequency region, it was assigned to the difference band [$\nu_7(a_1)-\nu_8(a_1)=61$ cm^{-1} (a_1)]. The strong intensity of the Raman band may be interpreted in terms of the overlap with the lattive vibration band.

In the region lower than 700 cm^{-1}, seven infrared bands of the b_1 species were observed at 604, 504, 487, 374, 185, 128, and 46 cm^{-1}, while five b_1 out-of-plane fundamentals (ν_{24}—ν_{28}) were expected. Almost all of these infrared bands had corresponding Raman bands. The assignments of these bands were carried out tentatively by comparison with the spectral data of the analogous molecules. The 605- and 374-cm^{-1} bands (on the average) were assigned without ambiguity to the ν_{24} (C-S torsion) and ν_{26} (C-C≡N deformation) vibrations respectively.

Either one of the infrared bands at 504 and 487 cm^{-1} can be expected to be the fundamental C-C≡N deformation band ν_{25}. The corresponding depolarized Raman bands were observed at 503 and 485 cm^{-1} for the solution (504 and 484 cm^{-1} for the powder). Since the infrared band at 487 cm^{-1} was very much stronger than that at 504 cm^{-1}, while the two Raman bands had nearly the same intensities, the 486-cm^{-1} band (on the average) was assigned to the ν_{25} vibration, and the 504 cm^{-1} band, to the combination tone [$\nu_8(a_1)+\nu_{28}(b_1)=$ 511 cm^{-1} (b_1)].

Although one fundamental vibration, ν_{27}, is thought to appear in the region from 200 to 100 cm^{-1}, two infrared bands of the b_1 species were observed at 185 cm^{-1} (the means value of the factor group splitting) and 128 cm^{-1}. The former band was found to remain in the melt (168 cm^{-1}), while its corresponding Raman band was observed at 184 cm^{-1}. For the latter band, however, the presence of an infrared band in the molten state and of a Raman band was not certain. Thus, the 185-cm^{-1} band was assigned to the ν_{27} vibration, and the 128-cm^{-1} band, to the combination tone [$\nu_{24}(b_1)-\nu_8(a_1)=141$ cm^{-1} (b_1)].

The lowest out-of-plane fundamental vibration, ν_{28}, seems to appear below 100 cm^{-1}. The weak infrared band was observed at 46 cm^{-1} for the crystal in both the solid and broken lines of Figs. 3A and 3B. Although the band could not be observed for the melt, the above fact may suggest that this is due to molecular vibration, because the lattice vibration should appear in either the solid or broken line. Furthermore, the use of the tilting method seemed to show that the crystal band at 46 cm^{-1} belonged to the b_1 species. Thus, this band (47 cm^{-1} on the average) was assigned to the ν_{28} vibration. The corresponding Raman band was found at 48 cm^{-1}. No Raman bands assignable to the five a_2 out-of-plane fundamentals were observed.

The observed infrared and Raman bands which have not been discussed yet were assigned to the overtone and combination tone according to the experimental results regarding the classification of the bands. The results of the discussion in this chapter are summarized in the last column of Table 2. The frequencies of the in-plane and

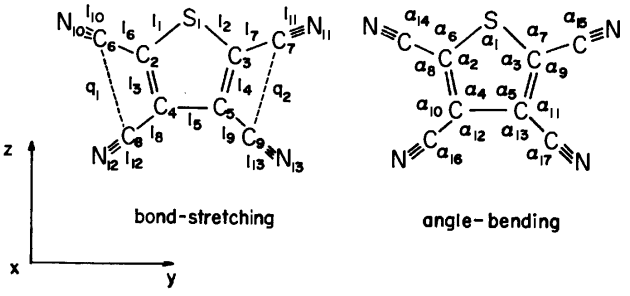

Fig. 5. In-plane internal coordinates of TCNT.

TABLE 3. IN-PLANE FUNDAMENTAL VIBRATIONS OF TCNT

Symmetry species		Obsd[a] freq. (cm^{-1})	Calcd freq. (Initial)	Calcd freq. (Final)	Dev.[b] (%)	P.E.D. (%)[c,d]
a_1	ν_1	2247	2318	2245	−0.1	C≡N (II) stretch. (73)
	ν_2	2228	2314	2242	0.6	C≡N (I) stretch. (74)
	ν_3	1444	1513	1445	0.1	C=C stretch. (71)
	ν_4	1407	1411	1409	0.1	C–C (ring) stretch. (44)
	ν_5	1153	1214	1150	−0.3	C–S stretch. (44)
	ν_6	898	919	894	−0.4	C–C (I) stretch. (27)
	ν_7	525	531	525	0.0	C–C (II) stretch. (31), C–S stretch. (26)
	ν_8	464	505	461	−0.6	C–C≡N(I) deform. (27), $\overset{C}{S}\!>$C–CN deform. (26)
	ν_9	411	470	411	0.0	C–C≡N(II) deform. (34)
	ν_{10}	332	315	332	0.0	C=C–S bend. (39)
	ν_{11}	118	135	124	5.1	C–C≡N(I) deform. (53), $\overset{C}{S}\!>$C–CN deform. (37)
	ν_{12}	113	123	107	−5.3	$\overset{C}{C}\!>$C–CN deform. (47), C–C≡N(II) deform. (46)
b_2	ν_{13}	2258	2319	2245	−0.6	C≡N(II) stretch. (76)
	ν_{14}	2241	2313	2242	0.0	C≡N(I) stretch. (76)
	ν_{15}	1511	1551	1509	−0.1	C=C stretch. (63)
	ν_{16}	1233	1247	1231	−0.2	C–C(I) stretch. (29), C–S stretch. (27)
	ν_{17}	983	1059	986	0.3	C–C(II) stretch. (41), C–S stretch. (29)
	ν_{18}	774	897	773	−0.1	$\overset{C}{C}\!>$C–CN deform. (37), C–C(I) stretch. (31)
	ν_{19}	530	541	529	−0.2	$\overset{C}{S}\!>$C–CN deform. (35), C–S stretch. (34)
	ν_{20}	430	491	449	4.4	C–C≡N(II) deform. (28)
	ν_{21}	342	387	342	0.0	C=C–C (ring) bend. (39)
	ν_{22}	223	251	221	0.9	C–C≡N(I) deform. (40), C–C≡N(II) deform. (37)
	ν_{23}	126	126	118	−6.3	C–C≡N(I) deform. (30), C–C≡N(II) deform. (29)

a) The mean values of the frequencies are cited whenever both the infrared band of the crystal and Raman band of the powder are observed or when factor group splitting occurs. b) Dev.$=100[\nu(\text{Calcd})-\nu(\text{Obsd})]/\nu(\text{Obsd})$. c) Only contributions greater than 25 per cent are included. d) The mark (I) refers to the C_2–$C_6{\equiv}N_{10}$ and C_3–$C_7{\equiv}N_{11}$ groups, and (II), to the C_4–$C_8{\equiv}N_{12}$ and C_5–$C_9{\equiv}N_{13}$ groups (see Fig. 5).

out-of-plane fundamentals are listed in Tables 3 and 4 respectively.

Normal Coordinate Analysis of In-plane Vibrations

Wilson's ***GF*** matrix method[18] was used for the normal coordinate analysis. The numerical calculations were carried out with the aid of a FACOM 230-75 digital computer of Kyoto University Data Processing Center. The internal coordinates of TCNT are given in Fig. 5. The equilibrium bond lengths and bond angles adopted are the mean values of those determined by Rychnovsky and Britton:[15] $l_1^\circ=l_2^\circ=1.71$ Å, $l_3^\circ=l_4^\circ=1.37$ Å, $l_5^\circ=1.40$ Å, $l_6^\circ=l_7^\circ=l_8^\circ=l_9^\circ=1.41$ Å, $l_{10}^\circ=l_{11}^\circ=l_{12}^\circ=l_{13}^\circ=1.17$ Å, $\alpha_1^\circ=89.1°$ $\alpha_2^\circ=\alpha_3^\circ=114.0°$, $\alpha_4^\circ=\alpha_5^\circ=111.3°$, $\alpha_6^\circ=\alpha_7^\circ=121.4°$, $\alpha_8^\circ=\alpha_9^\circ=124.6°$, $\alpha_{10}^\circ=\alpha_{11}^\circ=125.4°$ and $\alpha_{12}^\circ=\alpha_{13}^\circ=123.3°$. Furthermore, $\alpha_{14}^\circ=\alpha_{15}^\circ=\alpha_{16}^\circ=\alpha_{17}^\circ=180°$ are assumed for the sake of simplicity.

TABLE 4. OUT-OF-PLANE FUNDAMENTAL VIBRATIONS OF TCNT

Symmetry species	Observed frequency[a] (cm^{-1})		Assignment [b]
b_1	ν_{24}	605	C–S torsion
	ν_{25}	486	C–C≡N (I and II) deformation
	ν_{26}	374	
	ν_{27}	185	$\overset{C}{S}\!>$C–CN and $\overset{C}{C}\!>$C–CN deformation
	ν_{28}	47	

a) See footnote a of Table 3. b) See footnote d of Table 3.

As the potential function for the in-plane vibrations, the modified Urey-Bradley force field (mod. UBFF) given by:

$$2V(\text{mod. UBFF}) = 2V(\text{UBFF}) + 2\alpha(\Delta l_3\Delta l_5+\Delta l_4\Delta l_5) + C\sum_i^2(\Delta q_i)^2 + 2C'\sum_i^2(\Delta q_i)q_i$$

was used. Here, q_i is the equilibrium non-bonded distance between C_6 and C_8 atoms and between C_7 and C_9 atoms. V(UBFF) consists of terms with five bond-stretching, seven angle-bending, and six non-bonded repulsion force constants; those constants are listed in the first column of Table 5. The force constant α is the coefficient of the cross terms between C=C and C–C (ring) stretching coordinates; it is introduced to take account of the presumed resonance interaction in the thiophene ring. The constant C is the coefficient of the *cis* non-bonded repulsion terms between two carbon

TABLE 5. FORCE CONSTANTS[a] (mdyn/Å) OF TCNT

	Force const (Initial)	Force const (Final)	Dispersion
K (C–S)	4.75	4.15	—[b]
K (C–C)	4.58	4.55	0.24
K (C≡N)	18.51	17.41	0.16
K(C=C)	5.05	5.60	0.14
K (C–C, ring)	4.94	4.27	0.28
H (C–S–C)	0.16	0.28	0.41
H (C=C–S)	0.06	0.05	0.25
H (C=C–C, ring)	0.15	0.32	0.21
H (C–C–S)	0.21	0.29	0.10
H (C–C=C)	0.29	0.43	0.13
H (C–C–C)	0.57	0.14	0.08
H (C–C≡N)	0.19	0.15	0.00
F (C–S–C)	0.21	0.11	0.11
F (C=C–S)	0.25	0.98	0.31
F (C=C–C, ring)	0.57	−0.13	0.17
F (C–C–S)	0.22	0.15	0.10
F (C–C=C)	0.71	0.14	0.12
F (C–C–C)	0.48	0.23	0.06
α		0.41	—[b]
C		0.10	—[b]

a) The $F'=-0.10\,F$ and $C'=-0.1\,C$ relations were assumed. b) Fixed.

atoms. The $C'=-0.1C$ relation was assumed, as usual.

For the first calculation, the values of the force constants were transferred from the bis(maleonitrile dithiolato)Ni(II) anion,[17] diethyl ether,[19] TCNQ,[9] and TCNB.[12] These values are shown in the second column of Table 5, while the frequencies calculated with these values are given in the third column of Table 3. The agreements between the calculated and observed frequencies are not very good. For the purpose of obtaining a good agreement, after some refinements of the force constants by the trial-and-error method using the Jacobian matrix, repetitions of the calculations with several sets of force constants were carried out by the least-squares method. The converged set of the force constants and their dispersion values are given in Table 5. The frequencies calculated with this set of force constants are compared with the observed values in Table 3. The agreement is satisfactory. The last column of Table 3 represents the potential energy distribution.

It is apparent from Table 5 that the C–S and C–C (ring) single bonds acquire a partial double-bond character, while the C=C and C≡N bonds, on the other hand, lose their double- and triple-bond characters respectively. These facts, and the necessity of the cross terms with the α coefficient, suggest that the resonance takes place throughout the molecule of TCNT, as is to be expected from the configuration of the molecule.

The authors wish to express their gratitude to Professor Shinzaburo Oka of this institute for his guidance in the preparation of TCNT. Thanks are also due to Dr. Soichi Hayashi and Mr. Junzo Umemura of this laboratory for their helpful discussion.

References

1) D. A. Long and W. O. George, *Spectrochim. Acta*, **19**, 1717 (1963).
2) T. Takenaka and S. Hayashi, *Bull. Chem. Soc. Jpn.*, **37**, 1216 (1964).
3) F. A. Miller, O. Sala, P. Devlin, J. Overend, E. Lippert, W. Luder, H. Moser, and J. Varchmin, *Spectrochim. Acta*, **20**, 1233 (1964).
4) A. Rosenberg and J. P. Devlin, *Spectrochim. Acta*, **21**, 1613 (1965).
5) Von P. Heim and F. Dörr, *Ber. Bunsenges. Phys. Chem.*, **69**, 453 (1965).
6) J. Stanley, D. Smith, B. Latimer, and J. P. Devlin, *J. Phys. Chem.*, **70**, 2011 (1966).
7) B. Moszy'nska, *Acta Phys. Pol.*, **33**, 959 (1968).
8) B. Lunelle and C. Pecile, *J. Chem. Phys.*, **52**, 2375 (1970).
9) T. Takenaka, *Spectrochim. Acta*, **27A**, 1735 (1971).
10) M. G. Kaplunov, T. P. Panova, E. B. Yagubskii, and Yu. G. Borod'ko, *Zh. Strukt. Khim.*, **13**, 440 (1972).
11) A. Girlando and C. Pecile, *Spectrochim. Acta*, **29A**, 1859 (1973).
12) T. Takenaka, J. Umemura, S. Tadokoro, S. Oka, and T. Kobayashi, *Spectrochim. Acta*, in press.
13) J. Umemura and T. Takenaka, *Bull. Inst. Chem. Res., Kyoto Univ.*, **51**, 206 (1973).
14) H. E. Simmons, R. D. Vest, D. C. Blomstrom, J. R. Roland, and T. L. Cairns, *J. Am. Chem. Soc.*, **84**, 4746 (1962).
15) V. Rychnovsky and D. Britton, *Acta Crystallogr.*, **B24**, 725 (1968).
16) D. W. Scott, *J. Mol. Spectrosc.*, **31**, 451 (1969).
17) Lakshmi, P. B. Rao, and U. Agarwala, *Appl. Spectrosc.*, **25**, 207 (1971).
18) E. B. Wilson, Jr., J. C. Decius, and P. C. Cross, "Molecular Vibrations," McGraw-Hill, New York (1955).
19) S. Mizushima and T. Shimanouchi, "Sekigaisen Kyusyu to Raman Koka," Kyoritsu Shuppan, Tokyo (1955).

Reactions of the Cation Radicals of Aromatic Diamines with Their Parent Molecules or Aliphatic Amines

Tadayoshi SAKATA,* Mitsuo HIROMOTO, Tomoko YAMAGOSHI, and Hiroshi TSUBOMURA

Department of Chemistry, Faculty of Engineering Science Osaka University, Toyonaka, Osaka 560

(Received June 23, 1976)

The chemical reactions of the cation radicals of some aromatic diamines with their parent molecules, aliphatic amines or sodium hydroxide have been studied spectroscopically. In the case of the cation radical of *p*-phenylenediamine (PPD), the main products are Bandrowski's base (BB) and PPD, *p*-benzoquinone diimine being found as an intermediate. This reaction are found essentially to be a disproportionation of PPD^+ to BB and PPD in which bases added enhance the reaction rate. The thermodynamical quantities of the initial step of the reaction, proton transfer from PPD^+, are estimated and the reaction mechanism is discussed. The reaction of the cation radical of *N,N,N',N'*-tetramethyl-*p*-phenylenediamine (TMPD) with triethylamine (TEA) gives the parent molecule, TMPD. This reaction is concluded to be caused by an electron transfer from TEA to $TMPD^+$ followed by a reaction of TEA with a large negative free energy change. The reaction between the cation radical of *N,N*-dimethyl-*p*-phenylenediamine and its parent molecule has also been studied.

Cation radicals are expected to act as strong electron acceptors and interact with electron donating molecules. The charge resonance interaction between a cation radical and its parent molecule has been reported by several authors.[1-4] We reported the charge transfer (CT) interactions between some aromatic diamine cation radicals and aliphatic amines.[5]

The coexistence of a cation radical and an electron donating neutral molecule leads not only to the complex formation but often to chemical reaction at room temperature. For example, Würster's cations, though known to be rather stable, react easily with some electron donors. An ethanol solution of the *p*-phenylenediamine cation radical (PPD^+) changes from yellow to blue by adding *p*-phenylenediamine (PPD). Such chemical aspects of cation radicals have been relatively unexplored.

We had been interested in the physical aspects of the CT interaction between a cation radical and a neutral molecule. Recently we started work on the chemical reactions involving cation radical, because we recognized its importance for understanding the overall physical and chemical processes of these cation radicals which often play a substantial role as intermediates of various chemical reactions.

Experimental

Preparation of Material. *p*-phenylenediamine (PPD), *N,N*-dimethyl-*p*-phenylenediamine (DMPD) and *N,N,N',N'*-tetramethyl-*p*-phenylenediamine (TMPD) were purified according to the method described previously.[5] Their cation radical salts were synthesized according to the literature.[6]

Bandrowski's base (BB, 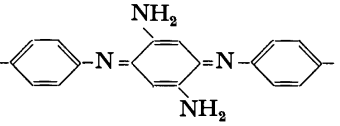) NH_2, N^1,N^4-bis(*p*-aminophenyl)-2,5-diamino-*p*-benzoquinone diimine) was produced by oxidizing PPD with hexacyanoferrate (III) under mild alkaline conditions.[7] Found: C, 67.33; H, 5.74; N, 25.9%. Calcd for $C_{18}H_{18}N_6$: C, 67.90; H, 5.70; N, 26.40%. When DMPD was oxidized similarly, the compound corresponding to *N*-methylated Bandrowski's base (BB', 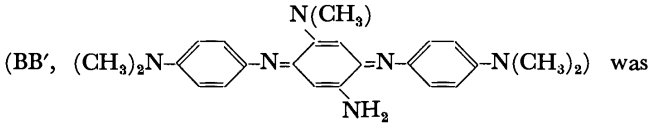) was obtained. Found: C, 69.60; H, 7.12; N, 20.82%. Calcd for $C_{24}H_{28}N_6$; C, 71.61; H, 7.51; N, 20.88%. Its electronic spectrum is quite similar to that of BB except for slight red shift and broadening. *p*-Benzoquinone di-imine[8] and 4,4'-bis(dimethylamino)azobenzene (AZ')[9] were prepared according to the literature. Triethylenediamine (1,4-diazabicyclo-[2.2.2]octane) was purified by recrystallization from ether and by sublimation under vacuum. Triethylamine of the commercial GR grade was used without further treatment.

Measurement. The infrared spectra were recorded with a Hitachi EPI-G3 grating infrared spectrophotometer or a Hitachi 215 grating infrared spectrophotometer. A Shimadzu Multipurpose recording spectrophotometer MPS-50L was used for the measurements of the electronic absorption spectra.

Results

The Reaction between PPD^+Br^- and PPD. When an ethanol solution of *p*-phenylenediamine bromide (PPD^+Br^-) and that of PPD were mixed, the color of the solution changed gradually from yellow to blue. Figure 1 shows the electronic absorption spectra. The solution became acidic with the color change. On evaporating the solvent, it yielded a blue precipitate, whose infrared (IR) spectrum showed prominent bands of *p*-phenylenediamine monohydrobromide (PPD·HBr). When the reaction mixture was neutralized with NaOH, it turned from blue to red. The main products separated by the thin layer chromatography (TLC) on silica gel with a 1 : 1 mixture of benzene and ether as a solvent were BB and PPD. A slight amount of 4, 4'-diaminoazobenzene (AZ) and a violet unknown substance were also separated as by-products. These were confirmed by comparison of their UV and IR spectra with those of the authentic samples.[10] In the case of AZ, the R_f values of TLC also agreed with that of the authentic sample. The yield of AZ was about 1/8 of BB in the mole ratio.

An ethanol solution of BB turns from red to blue by adding a slight amount of mineral acid. The absorption

* Present Address: Institute for Molecular Science, Okazaki, Aichi 444

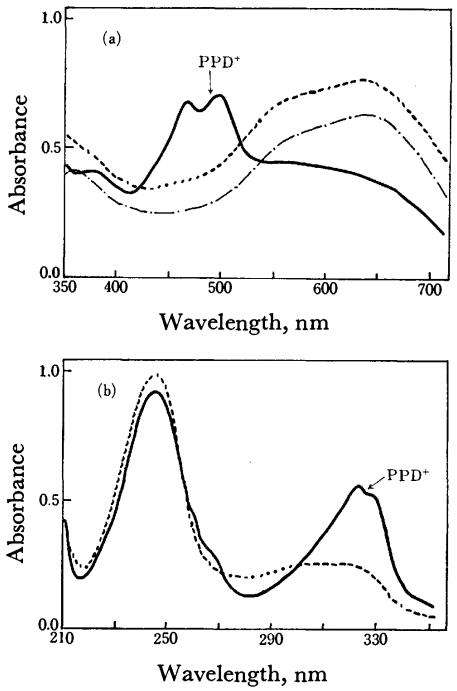

Fig. 1. The spectra of PPD+Br⁻–PPD system in ethanol at room temperature: ——; a few minutes after mixing, ------; 50 minutes after mixing.
(a) [PPD+Br⁻]=3.51×10⁻⁴ M, [PPD]=3.60×10⁻⁴ M. For reference the spectrum of the protonated Bandrowski's base in ethanol (-·-·-; [BB]/[HBr]=1) is shown in this figure.
(b) [PPD+Br⁻]=4.80×10⁻⁵ M, [PPD]=5.45×10⁻⁵ M.

of BB around 470 nm (21300 cm⁻¹) decreased by adding hydrobromic acid, while a new absorption appeared with a peak at 635 nm (15700 cm⁻¹). The intensity of the latter band showed a maximum at the molar ratio of HBr to BB of 1.17, and began to decrease by further addition of HBr as shown in Fig. 2. Therefore, the 635 nm band is assigned to the monoprotonated BB (BB·H⁺). This was also confirmed from the fact that the elemental analysis of the precipitate obtained by concentrating the solution agreed with calculated values.

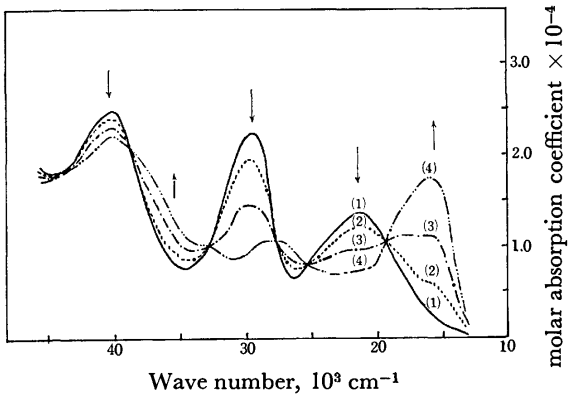

Fig. 2. The electronic absorption spectra of Bandrowski's base in ethanol with various content of HBr.
[HBr]/[BB]: (1), 0.0; (2), 0.34; (3), 0.69; (4), 1.17. The concentration of BB is constant; [BB]=7.0×10⁻⁵ M.

Found: C, 54.62; H, 4.78; N, 20.82%. Calcd for $C_{18}H_{19}N_6Br$: C, 54.14; H, 4.80; N, 21.05%. When a solution of BB and HBr at the mole ratio of 1: 1 was neutralized by adding an ethanol solution of NaOH, it returned from blue to red, showing the spectrum of BB. Thus, the reaction is a reversible acid-base reaction.

$$BB \underset{NaOH}{\overset{HBr}{\rightleftharpoons}} BB\cdot H^+$$

As seen in Fig. 1, the absorption spectrum of the reaction mixture in the longer wavelength region is quite similar to that of BB·H⁺ with regard to both the absorption shape and peak positions, showing that the blue color comes from BB·H⁺.

The absorption at 245 nm (in Fig. 1b) is attributable mainly to PPD and BB. This absorption increases a little with the progress of the reaction. The IR spectrum of the reaction products shows that PPD exists as a monoprotonated species (PPD·HBr).

The formation of BB was investigated spectroscopically varying the concentration of PPD and keeping the initial concentration of PPD⁺ constant. The amount of BB·H⁺ formed was found to be independent of the added PPD ranging from 0.28 to 7.46 molar equivalent to the PPD, though the rate of reaction increased with the concentration of PPD. The BB formed was about 1/6.5 of PPD⁺ in molar quantity.

Based on the above results, the following stoichiometric equation is set up.

$$6PPD^+Br^- \longrightarrow BB + 3PPD + 6HBr \qquad (1)$$

Since, this reaction is accelerated by added PPD, we add rather randomly 2 PPD, to both sides of Eq. 1. Then, we have

$$6PPD^+Br^- + 2PPD \longrightarrow BB + 5PPD + 6HBr \qquad (2)$$

We mixed PPD+Br⁻ and PPD at the molar ratio of 6: 2, and, after the reaction was completed, compared the spectrum of the reaction mixture with that of a solution containing BB, PPD and HBr at the concentrations as given by Eq. 2. The absorption spectra of the two solutions agreed very well with each other both in shape and in intensity (Fig. 3). This confirms that the stoichiometry of the reaction is like that of Eq. 1 or 2. As Eq. 1 shows, this reaction is considered essentially to be a disproportionation of PPD⁺ to BB and PPD in which

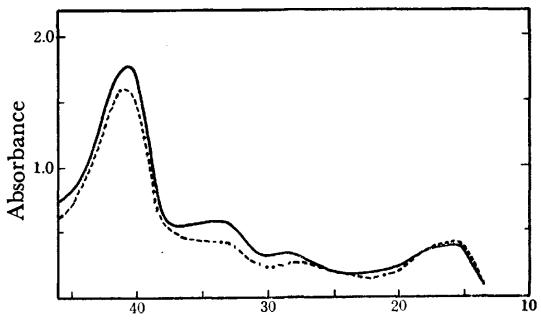

Fig. 3. The absorption spectrum of the reaction mixture of PPD+Br⁻ (1.46×10⁻⁴ M) and PPD (0.51×10⁻⁴ M) (——), and that of BB (0.24×10⁻⁴ M), PPD (1.23×10⁻⁴ M), and HBr (1.48×10⁻⁴ M) (------).

bases added enhances the rate of reaction.

When PPD was oxidized in ethanol with bromine, a blue solution was obtained. The blue precipitate formed from this solution showed the electronic and IR spectra quite similar to those of the products of the above reaction, indicating the formation of the same products as the reaction between PPD^+ and PPD.

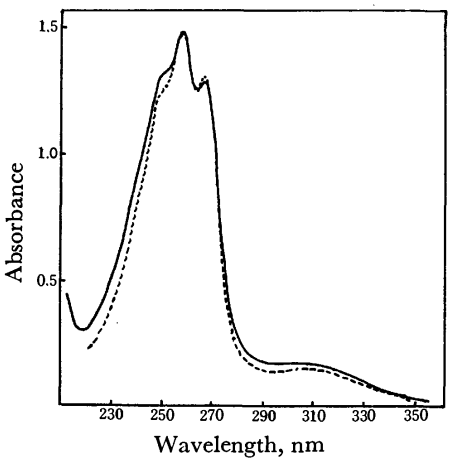

Fig. 4. The absorption spectrum of the reaction mixture of PPD^+Br^- (0.866×10^{-4} M) and NaOH (1.99×10^{-4} M) (——), and the theoretically calculated one (------) based on Eq. 3 and the spectral data of Fig. 5.

The Reaction of PPD^+Br^- with NaOH and Aliphatic Amines in Ethanol. Figure 4 shows the absorption spectrum of the reaction mixture of an ethanol solution of PPD^+Br^- (0.866×10^{-4} M) and NaOH (1.99×10^{-4} M). The dotted line shows the spectrum drawn by assuming the following dispropotionation reaction being completed.

$$2PPD^+ \longrightarrow PPD + HN=\langle\bigcirc\rangle=NH + 2H^+ \qquad (3)$$

The spectrum was drawn using the absorption spectra of PPD and *p*-benzoquinone diimine (Fig. 5). As seen in Fig. 4, the spectrum obtained experimentally agrees fairly well with the theoretically expected one, indicating that the reaction proceeds mainly as defined by Eq. 3.

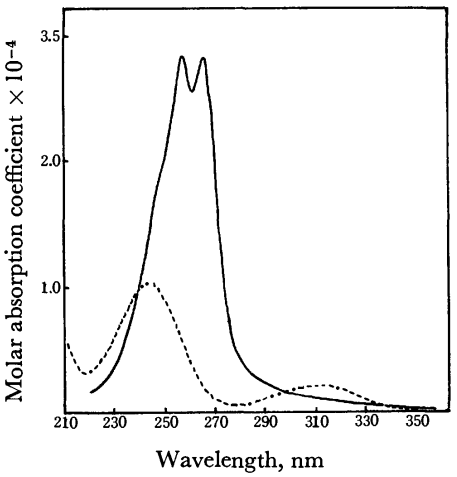

Fig. 5. The absorption spectra of *p*-phenylenediamine (------) and *p*-benzoquinone diimine (——).

The formation of the diimine was also observed when triethylamine was used instead of NaOH. The quantity in this case was about 80% of the expected one. In the case where triethylenediamine was used, the quantity of the diimine formed was still less. In both cases of amines, the diimine was unstable and changed into Bandrowski's base having the absorption peak at 470 nm, while it was fairly stable in the case of NaOH. When the amount of triethylamine was decreased to about 1/10 to 1/20 molar equivalent of PPD^+Br^-, the diimine was observed weakly, only as an absorption shoulder at 267 nm at the early stage of the reaction. Then the absorption spectra changed rapidly, showing the formation of $BB\cdot H^+$ with a peak at 635 nm. The spectrum in both the ultraviolet and visible regions agreed fairly well with that expected from Eq. 1, suggesting that the reaction mechanism in this case is essentially the same as in the case of the reaction between PPD^+ and PPD.

The Reaction between $DMPD^+ClO_4^-$ and DMPD. When an ethanol solution of *N,N*-dimethyl-*p*-phenylenediamine perchlorate ($DMPD^+ClO_4^-$) and that of DMPD were mixed, the color changed gradually from red (the color of the cation) to blue. Figure 6 shows the absorption spectra. After 4 days, the reaction mixture was neutralized with NaOH and was separated by TLC with the 3:1 mixture of benzene and ethanol. The main products separated were 4,4'-bis(dimethylamino)-azobenzene(AZ'), *N,N*-dimethylated Bandrowski's base (BB'), DMPD and an unknown substance (λ_{max}=590 nm, 650 nm). The latter two substances were produced more than BB' and AZ'. The amount of BB' formed was nearly equal to that of AZ'. The absorption at 660 nm which appeared in the course of the reaction (Fig. 6) might be attributable to the protonated species of BB' or AZ'. However it is not clear which contribution of the

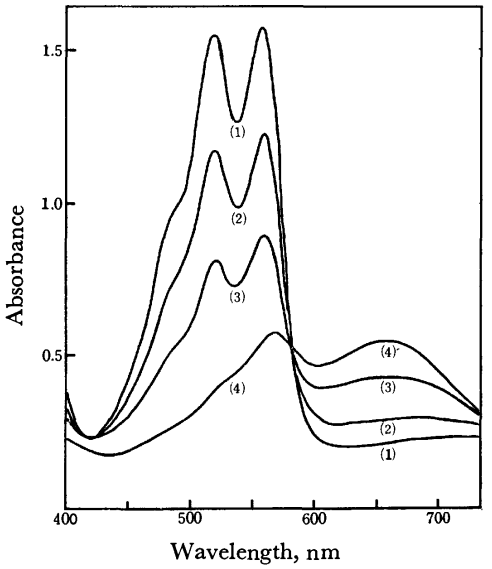

Fig. 6. Spectroscopic course of the reaction in $DMPD^+ClO_4^-$–DMPD system in ethanol.
$[DMPD^+ClO_4^-]=2.22\times10^{-4}$ M, [DMPD]=2.20×10^{-4} M.
(1) 4 min, (2) 14 min, (3) 44 min, (4) 170 min after mixing.

two is larger, because both of the protonated species have their absorption peaks at the same wavelength, 660 nm. The absorption at 660 nm decreased again with time and new absorptions appear at 590 nm and 650 nm, suggesting that BB'·H$^+$ or AZ'·H$^+$ reacts further. The similar phenomenon was observed, when DMPD was oxidized in ethanol with bromine.

The Reaction between TMPD$^+$ClO$_4^-$ and Triethylamine (TEA) in Ethanol. When TEA was added to an ethanol solution of TMPD$^+$ClO$_4^-$, the blue color characteristic of TMPD$^+$ disappeared and the solution became colorless. The absorption spectrum after the reaction showed a strong band at 263 nm which agreed very well with that of TMPD both in shape and position. An ether extract from the reaction mixture gave a colorless crystalline solid whose IR spectrum agreed with that of TMPD. Moreover, when bromine was added to the reaction mixture, it turned blue, giving the absorption spectrum of TMPD$^+$. From the absorption intensity the amount of TMPD$^+$ recovered was determined to about 80% of TMPD$^+$ before the reaction. This suggests that 80% of TMPD$^+$, at least, changes into TMPD by adding TEA. Figure 7 shows the spectrum of the reaction mixture together with the one which was obtained by assuming 100% conversion of TMPD$^+$, into TMPD.

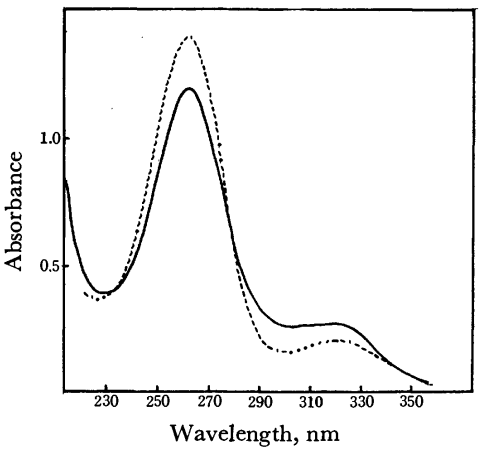

Fig. 7. The absorption spectrum of the reaction mixture of TMPD (0.885×10^{-4} M) and TEA (2.01×10^{-4} M) at 3 h after mixing (——), and the spectrum of TMPD (0.885×10^{-4} M) in EtOH (------).

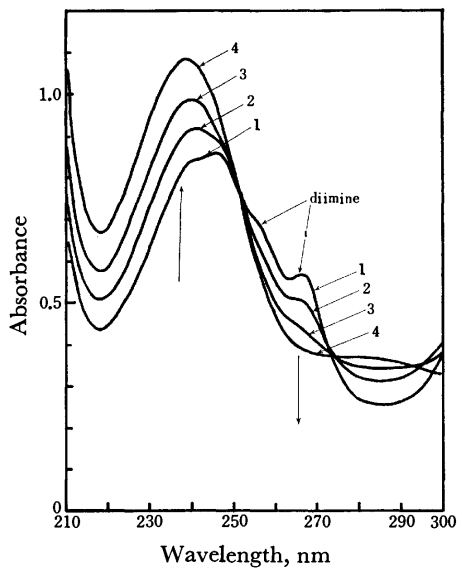

Fig. 8. Spectroscopic changes during the decomposition of PPD$^+$Br$^-$ in a 1:2 (volume ratio) mixture of water and ethanol at room temperature. (1) 4 min, (2) 9 min, (3) 13 min, (4) 31 min after mixing.

Discussion

The Reaction of PPD$^+$Br$^-$ with PPD, NaOH and Aliphatic Amines. When two molar equivalents of NaOH, triethylamine or triethylenediamine was added to an ethanol solution of PPD$^+$Br$^-$, the formation of *p*-benzoquinone diimine was observed clearly as shown in Fig. 4. In the case of the reaction of PPD$^+$ with triethylamine, the absorption intensity of the diimine in the region of 256—265 nm became weak with decreasing amount of triethylamine. When it was decreased to 1/10 molar equivalents of PPD$^+$, only a weak shoulder of the diimine was observed at about 270 nm. PPD$^+$Br$^-$ decomposes easily in water showing the absorption of the diimine, though it is fairly stable in ethanol. Figure 8 shows the spectra of the solution in a water-ethanol mixture, ethanol being added to decrease the rate of decomposition. In the reaction between PPD$^+$ and PPD, a shoulder at 267 nm was observed immediately after the mixing and disappeared in a while, as shown in Fig. 1. From these results, this absorption is attributable to *p*-benzoquinone diimine, which may be formed by a process shown below

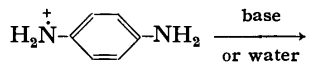

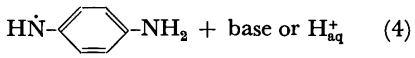

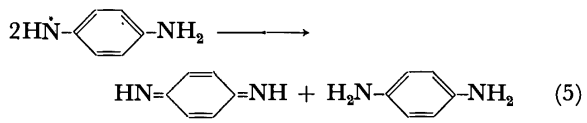

Let us estimate the Gibbs's free energy change ΔG_4° for the Reaction 4 in the case without a base. It can be estimated by using the following Born-Haber cycle.

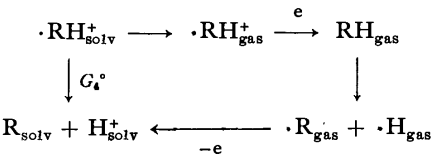

Here the cation radical of PPD is denoted as ·RH$^+$. ΔG_4° is expressed approximately by the equation

$$\Delta_4{}^\circ G_4^0 = -E_A^a(\text{PPD}^+) + S(\text{PPD}^+) + D(\text{N–H}) + I_P^a(\text{H}\cdot) - S(\text{H}^+) - S(\text{R}\cdot) \quad (6)$$

where $E_A{}^a$, S, D, and $I_P{}^a$ represent adiabatic electron affinity, solvation energy, bond energy and adiabatic ionization energy, respectively.

The following values are obtained from the literatures.

$$E_A^a(\text{PPD}^+) = I_P^a(\text{PPD}) = 6.8\text{ eV}.^{11)}$$

$$I_P^a(\text{H}\cdot) = 13.6\text{ eV},\quad D(\text{N–H}) = 4.0\text{ eV}.^{12)}$$

$S(H^+ \text{ in water}) \cong 11.5$ eV.[13,14]

$S(PPD^+ \text{ in water})$ is evaluated to be 2.2 eV using Born's equation with the dielectric constant of water at 25 °C, 78.5, and the effective radius of PPD^+, 3.24 Å.[15] Though the value of $S(R\cdot)$ is not certain, it can be taken to be the order of 0.1 eV. When these values are substituted in Eq. 6, $\Delta G_4°$ (in water) of 1.2 eV is obtained.

Since the solvation energy of a proton is smaller in ethanol than in water, $\Delta G_4°$ is calculated to be larger in ethanol than in water. This explains the fact that PPD^+-Br^- is fairly stable in ethanol though it is unstable in water.

It is important that the values of $\Delta G_4°$, though derived approximately, are positive and fairly large both in water and ethanol. It indicates that the equilibrium of Eq. 4 is inclined to the left and the concentration of the semiquinone $R\cdot$ is small. Nevertheless, the experimental fact that the diimine is formed easily from PPD^+ in water or water-ethanol mixture indicates that the free energy change of the reaction of Eq. 3 is nagative. Since $\Delta G_4°$ is positive, $\Delta G_5°$, the free energy for the formation of diimine from the semiquinone, must be a fairly large negative value to make up for $\Delta G_4°$.

In the presence of bases (B), one must take account of the reaction,

$$B + H^+ \rightleftarrows B\cdot H^+ \qquad (7)$$

the standard free energy change for this reaction in water, $\Delta G_7°$, at 25 °C are obtained as follows:[16]

$$\Delta G_7°(PPD) = -0.36 \text{ eV}, \quad \Delta G_7°(TEA) = -0.60 \text{ eV}$$
$$\Delta G_7°(OH^-) = -0.83 \text{ eV}$$

The standard free energy change of Eq. 4, $\Delta G_4°$, in the presence of a base, is reduced from that in water estimated above by these amounts.

Since the solvation energy of a proton is smaller in ethanol than in water, the equilibrium will shift to the right so that $\Delta G_7°$ becomes smaller in ethanol. Fairly large negative values of $\Delta G_7°$ are thought to be the reason why the reaction is enhanced by the addition of bases. Experimentally, the rates of decrease of the visible absorption band of PPD^+ at about 460 nm with various bases lie in the order OH^-, TEA and PPD, in agreement with that of their basicities.

In the actual reaction course, the interactions through the hydrogen bond are considered to be important. Since PPD^+ is thought to be a strong proton donor, a hydrogen bond complex between PPD^+ and PPD or aliphatic amines is formed. A proton will transfer easily through this hydrogen bond. The CT interaction between PPD^+ and TEA was reported previously.[5] Though we tried to find the dimer cation formed between PPD^+ and PPD in ethanol, we could not find it spectroscopically in the temperature range from room temperature to about −50 °C. Therefore the dimer cation may not play an important role.

With the addition of 2 molar equivalents of bases to an ethanol solution of PPD^+Br^-, the diimine produced reached about 100% of the theoretically expected quantity in the case of NaOH, while in the case of TEA it was about 80% and in the case of PPD a trace amount was detected as a shoulder of the absorption spectrum (Fig. 1). The diimine formed was stable in the case of NaOH, though in the case of both TEA and PPD it decomposed easily into Bandrowski's base. These observations can be explained as follows: Due to the relation, $\Delta G_7°(PPD) > \Delta G_7°(TEA) > \Delta G_7°(OH^-)$, the rate of the formation of the diimine is in the order of OH^-, TEA and PPD. Corbett studied the reaction of *p*-benzoquinone diimine with PPD in water and discussed the mechanism of the formation of Bandrowski's base.[17] According to his result, the rate of the reaction of the diimine with PPD increases greatly with lowering pH in the region of pH>6.[17] Since the basicity becomes lower in the order of PPD, TEA, and NaOH, the diimine formed is expected to be unstable in this order. The result is consistent with these expectations.

The result of TLC shows that 4,4′-diaminoazobenzene (AZ) is formed at the molar ratio of about 1/8 of BB. The following reaction is suggested for this.

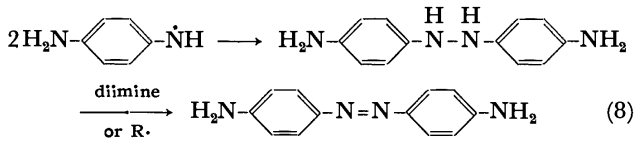

(8)

As is seen from the comparison of the molecular structures of AZ and BB, thus, AZ is formed by the bonding between the N atoms of the amino groups, while BB is formed by the bonding between the C atom of the benzene ring and the N atom of the amino group. The fact that BB is formed more than AZ indicates that the C atom of the benzene ring is attacked more easily by the aminonitrogen, in the above reactions.

$TMPD^+ClO_4^-$+triethylamine (TEA). In this case, the first step of the reaction is considered to be an electron transfer.

$$TMPD^+ + TEA \rightleftarrows TMPD + TEA^+ \qquad (9)$$

The cation radical of TEA (TEA^+) produced is considered to be quite unstable and undergo further reaction, causing the shift in the equilibrium of Eq. 9 to produce TMPD.

The free energy change for the electron transfer reaction of Eq. 9 can be expressed approximately by

$$\Delta G_9° = I_P^a(TEA) - E_A^a(TMPD^+) + \Delta P \qquad (10)$$

The following values are obtained from the literature.

$$I_P^a(TEA) = 7.5 \text{ eV},^{18}$$
$$E_A^a(TMPD^+) = I_P^a(TMPD) = 6.20 \text{ eV}^{19}$$

ΔP represents the difference of the polarization energy before and after the reaction and it is expressed as

$$\Delta P = P(TEA^+) - P(TMPD^+)$$

The value is estimated to be −0.4 eV by using Born's equation, assuming 4.3 Å and 3.5 Å as the effective radii of $TMPD^+$ and TEA^+, respectively. When these valuie are substituted in Eq. 10, $\Delta G_9°$=0.9 eV is obtained. Since it is a large positive value, it seems improbable that the electron transfer reaction proceeds to the right without the second step of TEA^+ decomposition.

$DMPD^+ClO_4^-$+DMPD. In this case, a large amount of AZ′ was produced. The formation of AZ′ and BB′ would be explained by taking into consideration the similar reactions with those for PPD^+. However the reaction proceeds further to form an unknown product in this case.

References

1) B. Badger and B. Brocklehurst, *Trans. Faraday Soc.*, **65**, 2576, 2582, 2588 (1969).
2) I. C. Lewis and L. S. Singer, *J. Chem. Phys.*, **43**, 2712 (1965).
3) A. Kira, S. Arai, and M. Imamura, *J. Chem. Phys.*, **54** 4890 (1971).
4) T. Shida and S. Iwata, *J. Chem. Phys.*, **56**, 2858 (1972).
5) T. Sakata, T. Okai, H. Sugimoto, and H. Tsubomura, *Bull. Chem. Soc. Jpn.*, **46**, 2698 (1973).
6) L. Michaelis, S. Granick, *J. Am. Chem. Soc.*, **65**, 1751 (1943).
7) E. Bandrowski, *Ber.*, **27**, 480 (1894).
8) R. Willstätter and A. Pfannenstiel, *Ber.*, **37**, 4605 (1904).
9) D. Vorländer and E. Wolferts, *Ber.*, **56**, 1229 (1923).
10) 4,4'-Diaminoazobenzene was provided through the courtesy of Mr. K. Maeda.
11) K. Tsuji, M. Saito, and T. Tani, *Denki Kagaku*, **41**, 688 (1973).
12) L. Pauling, "The Nature of The Chemical Bond," 3rd ed p. 85, Cornell University Press, New York (1960).
13) I. Oshida and O. Horiguchi, *Gendai Kagaku, I. F.*, 58 (1956).
14) J. B. Randles, *Trans. Faraday Soc.*, **52**, 1573 (1956).
15) The volume occupied by a PPD molecule is calculated from the molecular weight, the density (1.259 g cm^{-3}), and Avogadro number to be 142.68 $Å^3$. If the volume is assumed to be occupied by a sphere, the effective radius is obtained to be 3.24 Å.
16) "Handbook of Chemistry" compiled and ed by N. A. Lange, McGraw-Hill, (1967), P. 1215.
17) J. Corbett, *J. Chem. Soc., B*, **1969**, 818.
18) K. Watanabe and J. R. Mottle, *J. Chem. Phys.*, **26**, 1773 (1957).
19) Y. Nakato, M. Ozaki, A. Egawa, and H. Tsubomura, *Chem. Phys. Lett.*, **9**, 615 (1971).

Nature of Catalytically Active Sites over Solid Acids. II. Relationships between Acidic Properties of Silica-Alumina and Its Catalytic Activities for Olefin Polymerization

Jun-ichiro TAKE, Masanori IKEDA, and Yukio YONEDA

Department of Synthetic Chemistry, Faculty of Engineering, The University of Tokyo, Hongo, Bunkyo-ku, Tokyo 113

(Received June 29, 1976)

The influences of the degree of hydration of a silica-alumina surface on its Brönsted or Lewis acid content and on its catalytic activity for *cis*-2-butene polymerization were investigated at 30 °C as a function of the evacuation temperature. The raise in the evacuation temperature, *i.e.*, the decrease in the degree of hydration, gave rise to an increase in both the Lewis acid content and the catalytic activity but to a decrease in the Brönsted acid concent. A good linear relationship, which could not be extrapolated through the origin, was found between the Lewis acid content and the catalytic activity. Thus, the conclusion is drawn that only strong Lewis acid sites are active in olefin polymerization on silica-alumina at low temperature.

Olefins such as propylene or butenes produce an irreversibly adsorbed species on silica-alumina[1-6] or some Y zeolites[7-9] at near room temperature. This species gives rise to IR absorption bands characteristic of saturated hydrocarbons.[4-8] Recently, the species has been proved to act as the proton-donating center in olefin isomerization[10,11] and to comprise branched oligomers having about four monomer units on the average.[1-3] However, the nature of the active site for this polymerization still remains unsettled, in spite of several intensive investigations.[3,5,6,8]

In the previous study,[12] we investigated this problem by using a series of silica-alumina samples whose Lewis acid sites were selectively poisoned *in situ* with pyridine to different extents, and concluded that strong Lewis acid sites were active in the polymerization on silica-alumina at 30 °C. The present study intends to provide additional evidence for this conclusion by correlating the catalytic activities of partially hydrated silica-aluminas with their acidic properties.

Experimental

Materials and Apparatus. Silica-alumina (SA-1, 13% Al_2O_3),[13] pyridine,[12] and *cis*-2-butene[12] were those used earlier. The IR cell and the preparation of the self-supporting 20-mm diameter wafers of SA-1 are described in detail elsewhere.[12]

Procedures. Partially hydrated samples were prepared as follows. After the wafer had been mounted in the sample holder and pretreated in a dry oxygen stream for 2 h at 450 °C, it was cooled to 150 °C for 1 h in an oxygen stream containing 20—25 Torr of water vapor, and then evacuated in the IR cell for 2 h at different temperatures of 150—450 °C.

The wafer was exposed to pyridine vapor at about 16 Torr for 1 h at room temperature, and evacuated for 1 h at 110 °C. The spectrum of chemisorbed pyridine was recorded. The peak absorbances of the 1460 and 1540 cm^{-1} bands due to Lewis- (LPY) and Brönsted-bound pyridine (BPY), respectively, were taken as a measure of the total acid content for the corresponding acid type.

The reaction was carried out in a closed circulation system including the IR cell as a reactor at an initial olefin pressure of 5 Torr and 30 °C. Its progress was followed in the same way as in the previous study.[12]

The IR spectrometer and the operating conditions have previously been described.[12] Peak absorbances were all normalized so as to indicate the absorbance per unit optical thickness of the wafer. This normalized absorbance, AS/W (cm^2/g), corresponds to the quantity $\varepsilon M/W$, where A and ε are respectively the absorbance and the absorption coefficient of a band, M is the amount (mmol) of the responsible species, and S and W are the cross section (cm^2) and the weight (g) of the wafer, respectively.

Results and Discussion

Hydroxyl Groups on Surfaces. Figure 1 shows the IR spectra in the O-H stretching region of partially hydrated SA-1 samples. A sharp band at 3750 cm^{-1} is due to isolated surface silanol groups, and a broad band around 3600 cm^{-1} is due to hydrogen-bonded surface hydroxyl groups and adsorbed water.[14] As the evacuation temperature was raised, the 3600 cm^{-1} band decreased in intensity and the 3750 cm^{-1} band became more and more definite without a significant change in intensity. This fact implies that the adsorbed water is only slightly hydrogen-bonded to the isolated silanol groups.[14] Since the original SA-1 had previously been calcined at 550 °C for 8 h, and every wafer was heated to 450 °C before use, the wet oxygen treatment and the

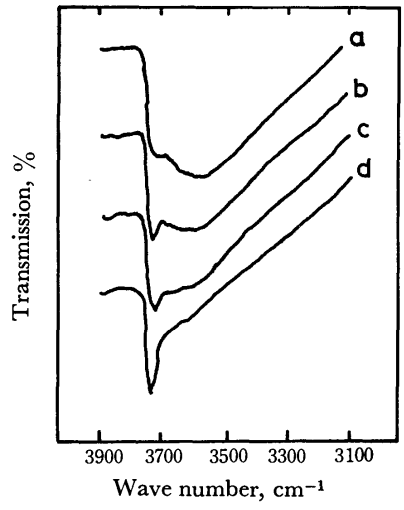

Fig. 1. IR spectra of surface hydroxyl groups on SA-1. A sample was evacuated for 2 h at 150 (a), 200 (b), 300 (c), or 450 °C (d).

subsequent evacuation probably bring about no drastic structural changes of the surface, except for hydration. The intensity of the band around 3600 cm^{-1} can therefore be taken as a qualitative measure of the degree of hydration of the surface. Thus, Fig. 1 indicates that a lowering in the evacuation temperature certainly results in an increase in the degree of hydration.

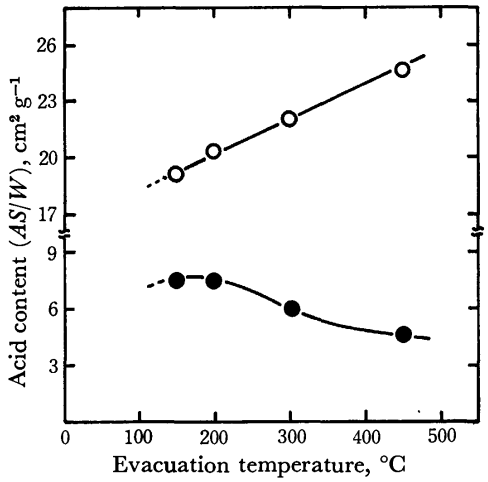

Fig. 2. Effect of evacuation temperature on surface acid content of Lewis (○) or Brönsted (●) type.

Acid Contents. Figure 2 illustrates the effects of the evacuation temperature, or, in other words, those of the added water, on the acid contents of SA-1. As the evacuation temperature was raised, the Lewis acid content increased while the Brönsted acid content decreased. Different values have been reported for the ratio of absorption coefficients of the LPY band to the BPY band: $\varepsilon_{1460}/\varepsilon_{1540} \approx 1$[15–17] or 2.6.[18] For our catalyst it was evaluated to be approximately unity from the differences in peak intensities resulting from the conversion of LPY to BPY upon dosing with quite small amounts of water. In view of this value, an increase in the Lewis acid content is compensated for with a decrease in the Brönsted acid content in the evacuation-temperature range of 200 to 450 °C. This implies that one Brönsted acid site is converted into one Lewis acid site when the surface is dehydrated. When the evacuation temperature was lowered from 200 to 150 °C, the Lewis acid content further decreased, while the Brönsted acid content remained approximately constant. It is quite reasonable to expect that comparatively large amounts of added water poison acid sites of both the Lewis and Brönsted types. Hence, a further lowering in the evacuation temperature may effect a decrease in the Brönsted acid content as well as in the Lewis acid content.

Polymerization Activity. *cis*-2-Butene produced, when it was introduced onto SA-1 at 30 °C, the polymeric species giving rise to IR absorption bands at 2960, 2930, and 2870 cm^{-1} in the saturated C–H stretching region and at 1470, 1385, and 1370 cm^{-1} in the saturated C–H bending region. The growth of each band occurred rapidly in the initial stage of the reaction, slowed down gradually, and finally ceased after 1—2 days. The peak intensity at 2960 cm^{-1} was well proportional to the amount of polymeric species formed.[12] The intensity of this peak after 1 min was therefore taken as the initial activity.

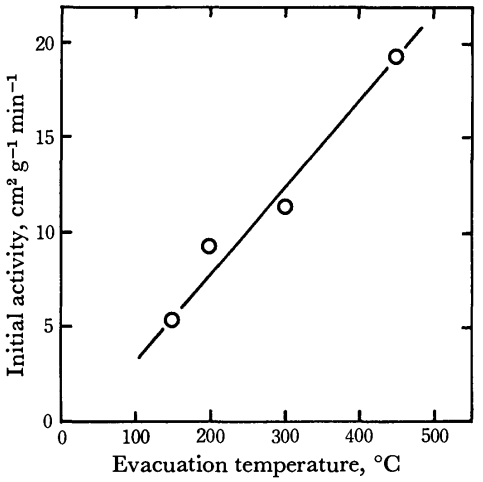

Fig. 3. Effect of evacuation temperature on catalytic activity for *cis*-2-butene polymerization at 30 °C.

Figure 3 is a plot of the initial activity against the evacuation temperature; it indicates that the initial activity decreases as the evacuation temperature is lowered, in other words, that added water certainly acts as an inhibitor for the formation of the polymeric species. This suggests that the Brönsted acid site is inactive in the present reaction. It can be seen from Figs. 2 and 3 that the influence of the evacuation temperature on the initial activity is similar to that on the Lewis acid content.

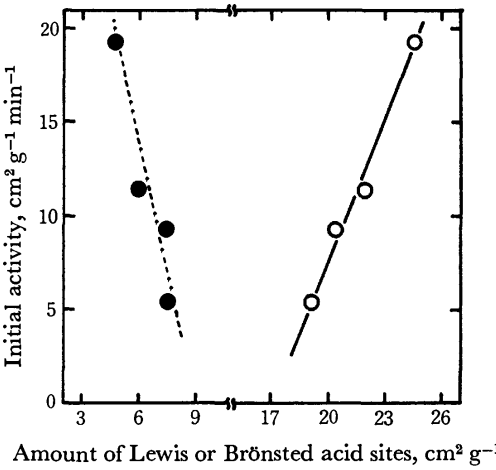

Fig. 4. Correlation of surface acidity with catalytic activity for *cis*-2-butene polymerization at 30 °C. ○: Lewis acidity, ●: Brönsted acidity.

Figure 4 shows correlations of the initial activity of SA-1 with its Lewis or Brönsted acid content. Since the initial activity decreases with an increase in the Brönsted acid content, this correlation is considered to be unreasonable. On the other hand, the initial activity decreases linearly with decreasing amounts of Lewis acid sites. This reasonable correlation probably indicates that the active acid site is of the Lewis type. Evidently, the straight line correlating the initial activity with the Lewis acid content does not extrapolate through the

origin. This is easily explained on the assumption that only part of the Lewis acid sites are active. According to this interpretation, the majority of the active Lewis acid sites are those which can be liberated, as a result of desorption of water (or hydroxyl groups) from the sites, by raising the evacuation temperature from 150 to 450 °C. Since such water probably is strongly adsorbed, the active Lewis acid sites are reasonably concluded to be high in acid strength. This conclusion agrees well with the previous one.[12)]

In addition, the previous study[12)] showed that, in *cis*-2-butene polymerization at the same temperature as in the present study, an upper limit for the amount of the active Lewis acid sites on SA-1 evacuated at 450 °C amounted to about 30% of the total Lewis acid content. The correlation in Fig. 4 may permit a similar estimate. The point of intersection of the solid straight line and the abscissa can be regarded as the point representing a sample whose active Lewis acid sites have been just blocked with added water. Accordingly, with respect to SA-1 evacuated at 450 °C, an upper limit for the amount of the active Lewis acid sites is again evaluated to be about 30% of the total Lewis acid content. Thus, we are again led to the conclusion that strong Lewis acid sites are active in olefin polymerization over silica–alumina at the low temperature of 30 °C.

References

1) A. Clark and J. N. Finch, *Proc. 4th Int. Congr. Catal.* (Moscow, 1968), Vol. 2, Akadémiai Kiadó, Budapest (1971), p. 361.
2) J. N. Finch and A. Clark, *J. Catal.*, **13**, 147 (1969).
3) A. E. Hirschler, *Am. Chem. Soc. Meet. Chicago, Sept. 1970, Div. Petrol. Chem. Prepr.*, **15** (3), A97 (1970).
4) G. A. Blomfield and L. H. Little, *J. Catal.*, **14**, 213 (1969).
5) H. P. Leftin and M. C. Hobson, Jr., *Adv. Catal.*, **14**, 143 (1963).
6) J. B. Peri, *Proc. 3rd Int. Congr. Catal.* (Amsterdam, 1964) North Holland, Amsterdam (1965), p. 1100.
7) P. E. Eberly, Jr., *J. Phys. Chem.*, **71**, 1717 (1967).
8) T. J. Weeks, Jr., G. L. Angel, I. R. Ladd, and A. P. Bolton, *J. Catal.*, **33**, 256 (1974).
9) T. J. Weeks, Jr. and A. P. Bolton, *J. Chem. Soc., Faraday Trans. 1*, **70**, 1676 (1974).
10) A. Ozaki and K. Kimura, *J. Catal.*, **3**, 395 (1964).
11) J. W. Hightower and W. K. Hall, *J. Am. Chem. Soc.*, **89**, 778 (1967).
12) K. Mizuno, M. Ikeda, T. Imokawa, J. Take, and Y. Yoneda, *Bull. Chem. Soc. Jpn.*, **49**, 1788 (1976).
13) J. Take, T. Tsuruya, T. Sato, and Y. Yoneda, *Bull. Chem. Soc. Jpn.*, **45**, 3409 (1972).
14) M. R. Basila, *J. Phys. Chem.*, **66**, 2223 (1962).
15) J. W. Ward, *J. Catal.*, **11**, 271 (1968).
16) T. R. Hughes and H. M. White, *J. Phys. Chem.*, **71**, 2192 (1967).
17) F. E. Kiviat and L. Petrakis, *J. Phys. Chem.*, **77**, 1232 (1973).
18) K. H. Bourne, F. R. Cannings, and R. C. Pitkethly, *J. Phys. Chem.*, **74**, 2197 (1970).

Emission Spectra of the Vinyl Polymers with Pendant Phenanthryl Groups

Akira ITAYA, Ken-ichi OKAMOTO, and Shigekazu KUSABAYASHI

Department of Chemical Engineering, Faculty of Engineering, Yamaguchi University, Tokiwadai, Ube 755

(Received June 30, 1976)

The emission properties of 9-ethylphenanthrene (EPh), poly(9-vinylphenanthrene) (PVPh), poly(9-phenanthryl methacrylate) (PPhMA), and poly[2-(9-phenanthryl)ethyl vinyl ether] were investigated in solution. These vinyl polymers showed no clear excimer fluorescence in the longer-wavelength region. Both the fluorescence quantum yield and the lifetime of PVPh decreased largely with an increase in temperature at higher temperatures. This suggests that PVPh forms an excimer which has a low fluorescence quantum yield. The fluorescence properties of PPhMA and PPhEVE, in which Ph chromophores are widely spaced on the skeletal chains, indicated little interaction between neighboring Ph chromophores in the singlet state. This results from the nature of Ph, in whith it is difficult to form an excimer. The phosphorescence spectrum and its lifetime of PPhEVE indicated a presence of a weak interaction between neighboring Ph chromophores in the triplet state. PVPh and PPhEVE showed a delayed fluorescence resulting from a T-T annihilation between two migrating triplet excitons.

Recently, emission spectra of aromatic vinyl polymers have been extensively investigated. It is known that aromatic vinyl polymers exhibit excimer fluorescences in dilute solutions due to the interaction between neighboring chromophores.

1-Ethylpyrene and 1-ethylnaphthalene show the excimer fluorescence in concentrated fluid solutions at room temperature. Poly(1-vinylpyrene)[1,2] and poly(1-vinylnaphthalene)[3-5] show almost exclusively the excimer fluorescence in dilute solutions. Poly(1-pyrenylmethyl vinyl ether) (PPyMVE),[1,6] poly(1-naphthylmethyl vinyl ether) (PNMVE),[6] and poly(1-naphthyl methacrylate) (PNMA),[7] in which the pyrenyl and naphthyl chromophores are widely spaced on the skeletal chains by $-O-CH_2-$ and $-CO-O-$ bonds, show both the structured monomer fluorescence and the excimer one in dilute solutions. On the other hand, *N*-ethylcarbazole (ECz) and 9-ethylacridine (EAcr) show no excimer fluorescence in concentrated solutions.[1,8] Poly(*N*-vinylcarbazole) (PVCz)[8] and poly(9-vinylacridine) (PVAcr),[1] however, show the excimer fluorescence. Poly[2-(*N*-carbazolyl)ethyl vinyl ether] (PCzEVE), in which the carbazolyl chromophores are widely spaced on a skeletal chain by $-O-CH_2-CH_2-$ bonds, shows a structureless fluorescence, which is different from both the monomeric structured fluorescence and the sandwich-like excimer one observed for the model compounds and PVCz respectively. This implies the presence of the excited-state interactions among the carbazolyl chromophores in PCzEVE.[9]

Phenanthrene crystal has only two molecules per unit cell arranged with their molecular planes almost perpendicular. It does not normally exhibit an excimer emission. However, this crystal under a high pressure does exhibit a broad emission with a peak at *ca.* 440 nm. This emission is assigned to the excimer fluorescence.[10] Despite extensive studies of the prompt and delayed fluorescence of phenanthrene, no excimer fluorescence has been observed in this compound at room temperature.[11] Studies of the emission of a phenanthrene sandwich dimer prepared by photolytic dissociation have also shown that phenanthrene does not form an excimer even under favorable condition.[12] Therefore, it is of interest to investigate the emission spectra of the vinyl polymers, where the phenanthryl (Ph) chromophores are directly connected to or widely spaced on the skeletal chains.

In the present paper, we have investigated the spectroscopic behaviors of poly(9-vinylphenanthrene) (PVPh), poly(9-phenanthryl methacrylate) (PPhMA), and poly[2-(9-phenanthryl)ethyl vinyl ether] (PPhEVE); in the latter two polymers, the phenanthryl chromophores are widely spaced on the skeletal chains by $-CO-O-$ and $-O-CH_2-CH_2-$ bonds respectively.

Experimental

Syntheses of 9-Ethylphenanthrene(EPh) and PVPh. EPh and 9-vinylphenanthrene(VPh) were prepared according to the literature.[13,14] The EPh was purified by recrystallization from methanol and sublimation *in vacuo*. The VPh was purified by recrystallization from ethanol and sublimation *in vacuo*. The PVPh was prepared by the polymerization of a 0.4 M benzene solution of the purified VPh in the presence of 0.2 mol% azobisisobutyronitrile in an evacuated sealed tube at 80 °C for 20 h and was reprecipitated three times from the benzene solution with methanol or hexane. The molecular weight measured by a vapor pressure osmometer was 3600. The degree of polymerization($\overline{DP}$) is about 18.

Synthesis and Polymerization of 2-(9-Phenanthryl)ethyl Vinyl Ether(PhEVE). 2-(9-Phenanthryl)ethanol(PhEtOH) was prepared from purified phenanthrene according to the literature[15] and purified by recrystallization from cyclohexane. The PhEVE was synthesized from the PhEtOH by the route similar to 2-(*N*-carbazolyl) ethyl vinyl ether[16] and was purified by recrystallization from ligroin and sublimation *in vacuo*. Yield, 30%; mp 82.0—84.0 °C, IR(KBr-disk): δ_{CH} of vinyl ether 960 and 820 cm^{-1}, NMR ($CDCl_3$): 1.4—1.6 τ (multiplet, two ring protons); 2.0—2.2 τ (multiplet, one ring proton); 2.3—2.7 τ (multiplet, six ring protons); 3.5—3.8 τ (quartet, $-O-C\underline{H}=CH_2$); 5.8—6.2 τ (multiplet, $-C\underline{H}_2-CH_2-O-CH=C\underline{H}_2$); 6.5—6.7 τ (triplet, $-CH_2-C\underline{H}_2-O-$). Found: C, 87.07; H, 6.52%. Calcd for $C_{18}H_{16}O$: C, 87.05; H, 6.51%.

The polymerization conditions are summarized in Table 1. The solvents were purified by ordinary methods.

Synthesis and Polymerization of Phenanthryl Methacrylate(PhMA). 9-Phenanthrol was prepared from the purified phenanthrene according to the literature.[17] The PhMA was synthesized by reacting methacryl chloride with the 9-phenanthrol by the route similar to naphthyl methacrylate.[18] The monomer was extracted with benzene, washed with water, and dried over Na_2SO_4. The PhMA was isolated by column chromatography

(silica gel, benzene); mp 53.5—55.0 °C, IR (KBr-disk); 1715 ($\nu_{C=O}$), 1615 ($\nu_{C=C}$), 920 ($\delta_{C=CH_2}$) cm^{-1}, NMR ($CDCl_3$); 1.35—1.61 τ (quartet, two ring protons); 2.03—2.32 τ (multiplet, two ring protons); 2.03—2.32 τ (multiplet, two ring protons); 2.36—2.62 τ (multiplet, five ring protons); 3.54 τ (singlet, terminal vinyl proton(*cis*)); 4.22 τ (singlet, terminal vinyl proton(*trans*)); 7.86 τ (singlet, methyl protons). This monomer was very labile and was polymerized often during the purification. The PPhMA used for spectral measurements was prepared by a thermal polymerization and was reprecipitated from the chloroform solution with methanol. This polymer was insoluble in some organic solvents, but soluble in chloroform. Found: C, 81.31; H, 5.40%. Calcd for $C_{18}H_{14}O_2$; C, 82.41; H, 5.39%.

Method. The sample of PPhEVE (No. 5 in Table 1), which had the highest value of $\overline{DP}$(87) was used for spectral measurements. All of the solvents used (tetrahydrofuran (THF), 2-methyltetrahydrofuran (MTHF), chloroform, and 1,4-dioxane) were purified by the usual methods. Solutions were completely degassed by freeze-pump-thaw cycles. The emission spectra and fluorescence decay times were measured with the apparatus described in the previous paper.[8]

Results and Discussion

Polymerization of PhEVE. The cationic polymerization results are shown in Table 1. The PPhEVE is obtained in fairly good yields at or below 0 °C. The yield decreases with an increase in the polymerization temperature above 0 °C. PhEVE is also polymerized by $AlEtCl_2$ in high yields. The PPhEVE is soluble in some organic solvents, such as tetrahydrofuran and 1,2-dichloroethane.

The PPhEVE prepared in the present study has a comparatively high molecular weight (22000, $\overline{DP}$=87). This value of $\overline{DP}$ for PPhEVE is higher than the values for PCzEVE, PPyMVE, and PNMVE (33, 10, and 22, respectively).[16,19] The rather low softening point (SP) of the PPhEVE suggests the enhanced flexibility of the skeletal chain as compared with the cases of PVPh (SP: 209—218 °C, $\overline{DP}$=18), PPyMVE (SP: 220—230 °C, $\overline{DP}$=10) and PCzEVE (SP: 137—148 °C, DP=33).[16,19] The reason why the PPhEVE with the comparatively high $\overline{DP}$ has the low SP value is that phenanthryl chromophores, being less bulky than carbazolyl and pyrenyl chromophores, are widely spaced on the skeletal chain.

Emission Spectra. 1,3-Di(*N*-carbazolyl)propane and *N*-vinylcarbazole oligomer ($\overline{DP}$=4), of which the monomer compound (ECz) shows no excimer fluorescence, show excimer fluorescence in dilute solution at room temperature.[7,20-22] Therefore, the PVPh(DP=18) sample has sufficient molecular weight to be used in order to examine the possibility of excimer formation.

Fluorescence spectra of PVPh, PPhMA, PPhEVE, and EPh in solutions at room temperature are shown in Fig. 1. The fluorescence spectrum of the concentrated EPh solution indicated that EPh does not form an excimer, as is the case of phenanthrene. The fluorescence spectrum of PPhEVE is similar to that of EPh. Although the fluorescence spectra of PVPh and PPhMA are broad as compared with those of EPh and PPhEVE, no clear excimer fluorescence in the longer-wavelength region is observed for PVPh and PPhMA. Therefore, it is suggested that the interaction between neighboring chromophores in these polymers is much weaker than that observed for other aromatic vinyl polymers.

Fluorescence spectra of PVPh, PPhEVE, and EPh in rigid glasses at 77 K are shown in Fig. 2. The fluorescence band shifts to lower frequencies in the order of EPh, PPhEVE, and PVPh. The clear vibrational structure bands observed for PVPh and PPhEVE are similar to that for EPh and the fluorescence lifetimes of PVPh and PPhEVE are also much the same as that of

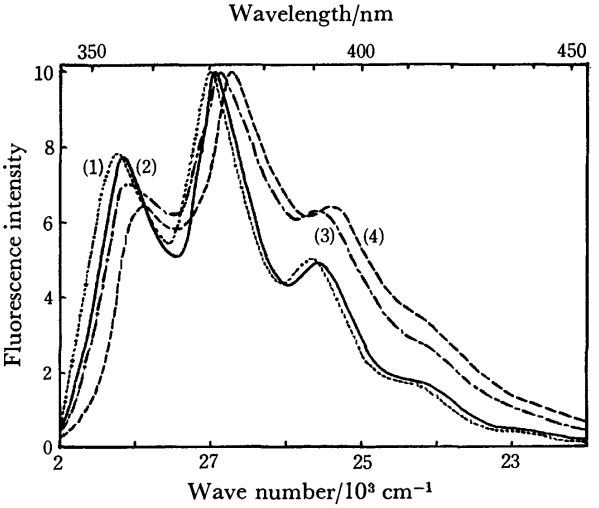

Fig. 1. Normalized fluorescence spectra of (1) ·····; EPh, (2) ——; PPhEVE, (3) ·-·-; PPhMA, and (4) ------; PVPh in solutions at room temperature. Solvents; (1), (2), (3); MTHF-THF (3: 2) mixture, (3); chloroform containing 1.0% ethanol. Excitation wavelength; 345 nm.

Table 1. Polymerization of PhEVE[a]

No.	Cat. (BF_3OEt_2) mol % to monomer	Temp °C	Time h	Conversion %	SP[b] °C	Mol wt[c]
1	1	55	9	28	115—125	
2	1	20	9	52	88—100	
3	1	0	9	73	103—110	
4	1	−15	4	88	100—110	
5	1	−40	4	92	115—120	22000
6	5	−45	4	87	100—118	
7	2	−60	4	90	110—115	18000
8	1	−78	9	84	100—110	

a) PhEVE, 0.2—0.5 g; monomer concentration, No. 6: 0.16 M, the others: 0.2 M; solvent, toluene. b) SP, softening point. c) Measured by a vapor pressure osmometer.

TABLE 2. SPECTROSCOPIC DATA OF VINYL POLYMERS WITH PENDANT PHENANTHRYL CHROMOPHORES IN MTHF–THF

Polymer	Relative yield at 20°C	Fluorescence lifetime[b] /ns				Phosphorescence lifetime/s
		77 K	−40°C	24 °C	50 °C	
EPh	1.00	59	50	50	48	4.4
PPhEVE	0.85	59	49	47	46	3.4
PPhMA[a]	0.15	—	—	16[c]	15[c]	—
PVPh	0.17	58	40	21[c]	20[c]	2.8

a) Solvent: chloroform containing 1.0% ethanol. b) The fluorescence was observed through Toshiba UV-DIC and UV-35 filters. Error is ±2 ns. c) The initial fast decay component was observed.

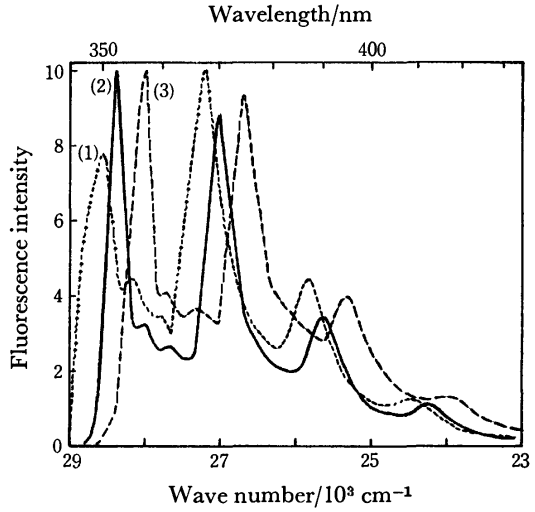

Fig. 2. Normalized fluorescence spectra of (1) EPh, (2) PPhEVE, and (3) PVPh in MTHF–THF rigid glasses at 77 K. Excitation wavelength; 330 nm.

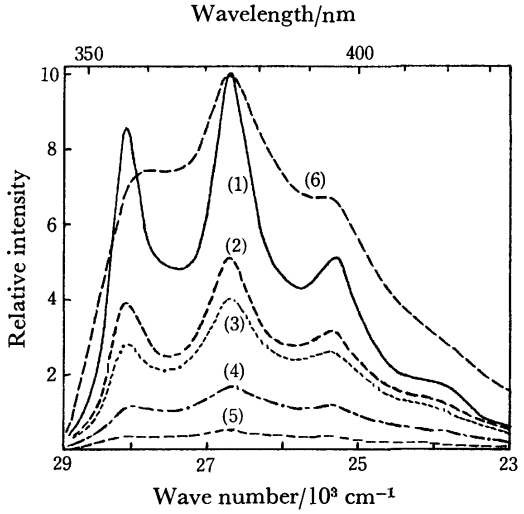

Fig. 3. Temperature dependence of fluorescence spectra of PVPh (5.1×10^{-4} M) in MTHF–THF solution. Excitation wavelength; 310 nm. (1) −130, (2) −86.5, (3) −37.7, (4) 6, and (5) 63.5 °C. The fluorescence (6) is 1.95 times the fluorescence (5).

EPh at 77 K (Table 2). These facts suggest that there is little interaction between neighboring Ph chromophores in PPhEVE and PVPh in rigid glasses at 77 K.

Table 2 shows the relative fluorescence quantum yields, taking the value of EPh as unity, and the fluorescence lifetimes. The fluorescence quantum yields and lifetimes of PVPh and PPhMA at room temperature are much lower than those of EPh and PPhEVE. The decay curve of PVPh has an initial fast component. The fluorescence spectra of PVPh in MTHF–THF solution at various temperatures are shown in Fig. 3. The fluorescence intensity decreases and the vibrational bands broaden with an increase in temperature. Temperature dependences of the fluorescence yields are shown in Fig. 4. The changes observed for EPh, PPhEVE, and PPhMA are small and they show a similar tendency. On the other hand, only PVPh shows a large decrease. The same tendency is observed for the temperature dependence of the fluorescence lifetimes (Table 2). Namely, the fluorescence lifetimes of EPh, PPhEVE, and PVPh in rigid glasses at 77 K are all equal. Only the lifetime of PVPh, however, decreases unusually with an increase in temperature.

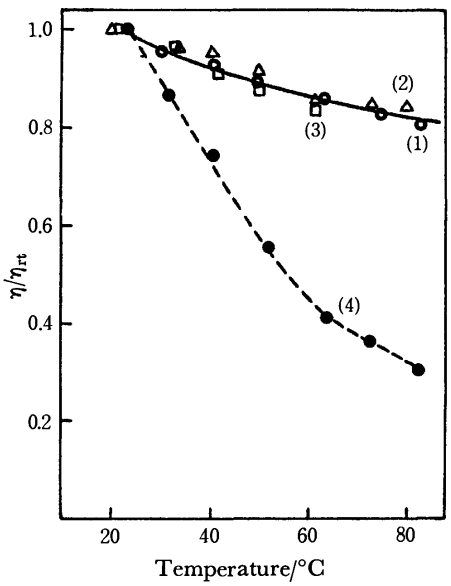

Fig. 4. Temperature dependence of the fluorescence yields. The value of η/η_{rt} exhibits the ratio of the fluorescence yield at some temperature to that at room temperature. (1) ○; EPh, (2) △; PPhEVE, (3) □; PPhMA, and (4) ●; PVPh. Solvent: (1), (2), (4); 1,4-dioxane, (3); chloroform containing 1.0% ethanol. These values were uncorrected for decrease in density of solvents with an increase in temperature.

As mentioned above, the vibrational structure of fluorescence and its lifetimes of PVPh and PPhEVE are similar to those of EPh in rigid solutions at 77 K. How-

ever, the phosphorescence of PVPh and PPhEVE is markedly different from that of EPh, as is shown in Fig. 5. The phosphorescence band shifts to lower frequency and the vibrational structure broadens in the order of EPh, PPhEVE, and PVPh. The phosphorescence lifetime shortens in the same order (Table 2). The red shift of the phosphorescence band is much larger than that of the fluorescence. These facts indicate that an interaction between neighboring Ph chromophores in the triplet state is much larger than that in the singlet state in rigid glasses at 77 K.

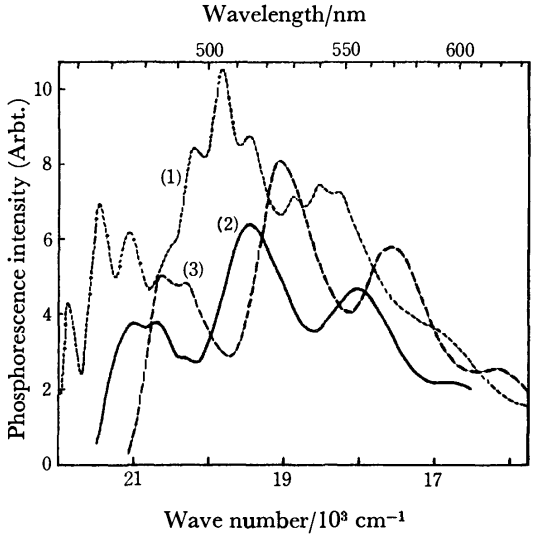

Fig. 5. Phosphorescence spectra of (1) EPh, (2) PPhEVE, and (3) PVPh in MTHF–THF rigid glasses at 77 K. Excitation wavelength; 310 nm.

The delayed emission, of which the position and profile are the same as those observed for the normal fluorescence at 77 K, is observed for PVPh and PPhEVE in rigid glasses at 77 K. The emission intensity depends quadratically on the phosphorescence intensity. The lifetime of this emission of PPhEVE is about 30 ms, while that of PVPh could not be determined because of the extremely low intensity. These facts indicate that this emission band can be assigned to the delayed fluorescence resulting from a T-T annihilation between two migrating triplet excitons.

PPhEVE resembles EPh very closely in fluorescence properties, forms no excimer, and does not show the anomalous fluorescence observed for PCzEVE.[9] The fluorescence spectra of PPhMA is markedly different from that of EPh and its lifetime is very short. The temperature dependence of the fluorescence yield, however, is similar to those of EPh and PPhEVE. This indicate that PPhMA forms no excimer. The fluorescence properties observed for PPhMA seems to be more likely to be affected by the substituent groups (-O-CO-). On the other hand, PPyMVE, PNMVE, and PNMA show the excimer fluorescence in dilute solutions at room temperature. Therefore, the failure of PPhEVE and PPhMA to form an excimer is considered to be attributable to the nature of Ph, which forms an excimer only with difficulty.

Emission properties of PVPh indicate clearly that interaction between neighboring Ph chromophores in PVPh is strongest in these polymers studied. It has been reported, from fluorescence yield and decay curve measurements, that phenanthrene does not show concentration quenching of fluorescence at room temperature.[23,24] Therefore, if PVPh forms no excimer, the fluorescence yield of PVPh is expected to be as large as that observed for EPh. The present result is not so. Namely, the fluorescence yield of PVPh is much lower than that of EPh (Table 2) and decreases largely with an increase in temperature (Fig. 4). These facts suggest that PVPh forms an excimer which has a low fluorescence quantum yield. This is reasonable from the fact that the phenanthrene excimer in the crystal state under a high pressure has a low fluorescence quantum yield.[10]

As mentioned above, ECz, EAcr, and EPh show no excimer fluorescence in concentrated solutions at room temperature. PVCz and PVAcr, however, show the excimer fluorescence in dilute solutions at room temperature. It is suggested from the above mentioned results that PVPh forms an excimer, although it does not show clearly an excimer fluorescence. Thus, the following conclusions were drawn: in the case of the vinyl polymers with the aromatic chromophores which form no excimer, an excimer is formed in the vinyl polymers in which the aromatic chromophores are directly connected to the skeletal chains, but it is not formed in the vinyl polymers in which the aromatic chromophores are widely spaced on the skeletal chains. PCzEVE is considered to be rather a special case.

References

1) M. Yokoyama, T. Tamamura, T. Nakano, and H. Mikawa, *Chem. Lett.*, **1972**, 499.
2) J. R. McDonald, W. E. Echols, T. R. Price, and R. B. Fox, *J. Chem. Phys.*, **57**, 1746 (1972).
3) M. T. Vala, J. Haebig, and S. R. Rice, *J. Chem. Phys.*, **43**, 886 (1965).
4) R. B. Fox, T. R. Price, R. F. Cozzens, and J. R. McDonald, *J. Chem. Phys.*, **57**, 534 (1972).
5) Y. Nishijima, M. Yamamoto, S. Katayama, K. Hirata, Y. Sasaki, and M. Tsujisaki, *Rep. Prog. Polym. Phys. Jpn.*, **15**, 445 (1972).
6) T. Yano, M. Yokoyama, and H. Mikawa, 22nd Annual Meeting on Macromolecules, Kyoto, 29C09, May 1973.
7) A. C. Sommersall and J. B. Guillet, *Macromolecules*, **6**, 218 (1973).
8) M. Yokoyama, T. Tamamura, M. Atsumi, M. Yoshimura, Y. Shirota, and H. Mikawa, *Macromolecules*, **8**, 101 (1975).
9) A. Itaya, K. Okamoto, and S. Kusabayashi, *Bull. Chem. Soc. Jpn.*, **49**, 2082 (1976).
10) P. F. Jones and M. Nicol, *J. Chem. Phys.*, **48**, 5440 (1968).
11) J. B. Birks, "Photophysics of Aromatic Molecules," Wiley-Interscience, New York (1970), p. 341.
12) E. A. Chandross and H. T. Thomas, *J. Am. Chem. Soc.*, **94**, 2421 (1972).
13) C. K. Bradsher and S. T. Amore, *J. Am. Chem. Soc.*, **63**, 493 (1941).
14) C. C. Price and B. D. Halpern, *J. Am. Chem. Soc.*, **73**, 818 (1951).
15) E. Bergmann and O. Blum-Bergmann, *J. Am. Chem.*

Soc., **58**, 1678 (1936).
16) K. Okamoto, A. Itaya, and S. Kusabayashi, *Polym. J.*, **7**, 662 (1975).
17) E. Ohta and A. Takemasa, *Yūki Gōsei Kagaku*, **29**, 183 (1971).
18) S. Patai, M. Bentor, and M. E. Reichmann, *J. Am. Chem. Soc.*, **74**, 845 (1952).
19) S. Yoshimoto, K. Okamoto, H. Hirata, S. Kusabayashi, and H. Mikawa, *Bull. Chem. Soc. Jpn.*, **46**, 358 (1973).
20) W. Klöpffer, *Chem. Phys. Lett.*, **4**, 193 (1969).
21) W. Klöpffer and W. Liptay, *Z. Naturforsh.*, **25a**, 1091 (1970).
22) G. E. Johnson, *J. Chem. Phys.*, **61**, 3002 (1974).
23) B. Stevens and J. T. Dubois, *Trans. Faraday Soc.*, **62**, 1525 (1966).
24) J. B. Birks and S. Georghiov, *J. Phys. B*, **1**, 958 (1968).

Reaction of Recoil ^{35}S Atoms with Organic Compounds. Insertion Reaction of Recoil ^{35}S Atoms into the C-H and the C-C Bond

Kazuhiro NIISAWA and Ko TAKI

Faculty of Industrial Hygiene, Kitasato University, Asamizodai, Sagamihara-shi, Kanagawa 228

(Received July 7, 1976)

The insertion reactions of recoil sulfur atoms produced by the nuclear transformation of $^{35}Cl(n,p)^{35}S$ process into the C–H bond of benzothiazole and the C–C bond of 2-methylbenzothiazole have been examined. It has been found that the C–H insertion is a little easier than the C–C insertion by the energetic sulfur atoms, and that in thermal reaction the water used as a solvent seems to have some role in producing the C–H insertion product.

Sulfur atoms generated by the photolysis of COS react with organic compounds to produce insertion and addition products to the C–H and the C=C double bonds, such as the reaction of CH_2, oxygen and other carbenes.[1-4]

Church and Rowland[5] have studied the insertion reaction of recoil sulfur atoms into the primary and the secondary C–H bond in propane molecule to determine the spin states of the recoil sulfur atoms, and they have found that the sulfur atoms in the triplet state have inserted mainly into the secondary C–H bond. However, the insertion of diradicals into the C–C bond has not been reported.

In this study, the possibility of the insertion of recoil sulfur atoms produced by the nuclear transformation of $^{35}Cl(n, p)^{35}S$ process into the C–C bond was examined, with the aim of determining, if possible, the ratio of the insertion rate of the C–H bond to the C–C bond.

For the C–H and C–C bonds, the 2-position bond of benzothiazole (C–H compound) and the 2-position bond of 2-methylbenzothiazole (C–C compound) were respectively used. The insertion product of ^{35}S atoms to the 2-position of benzothiazole as in (1) leads to 2-mercaptobenzothiazole and to the 2-position of 2-methylbenzothiazole as in (2) leads to 2-(methylthio)benzothiazole. These compounds are well-known and stable substances.

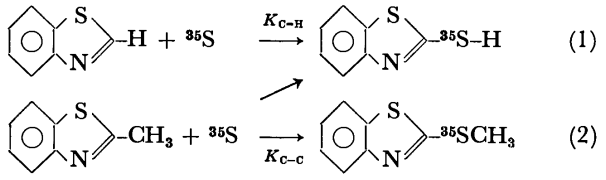

(1)

(2)

Experimental

Materials. After the vacuum distillation of bezothiazole and 2-methylbenzothiazole (Tokyo Kasei Co.), hydrochloric acid was added. Then the hydrochlorides thus produced were purified by sublimation for benzothiazole and by recrystallization for 2-methylbenzothiazole. These starting materials were used as either an aqueous solution or a solid. Oxygen and nitrogen oxide (Takachiho Chem. Co.) were used as additives without further purification.

Thermal Neutron Irradiation. Thermal neutron irradiation of the starting material was performed in a quartz ampoule (about 0.5 ml) at a neutron flux of 3×10^{13} or 7×10^{13} n/cm^2/s for 20 min with JRR-2 or JRR-3 of the Japan Atomic Energy Research Institute.

Separation, Purification, and Radioactivity Measurement of the Reaction Products. The separation and the purification were performed chromatographically and the radioactivity measurements of the products were carried out as previously described.[6]

Nearly all the experimental data are averages of three runs; the errors are about 30% through all runs.

Results and Discussion

When the recoil sulfur atoms react with organic compounds, many reaction products labeled with ^{35}S may be produced by either the energetic process or the thermal one.[7] In order to distinguish between the two processes, radical scavengers such as O_2 and NO are added to the sample; thus the thermal atoms and their reactions may be eliminated.[7]

In this experiment, the total organic yield in aqueous solution was about 70%.[8]

The Effect of Scavengers. From Tables 1 and 2, the yield of the C–^{35}S–H product from the C–H compound in the aqueous solution is clearly inhibited in the presence of NO or O_2. However, the yield of the C–^{35}S–C product from the C–C compound was not affected in the presence of the scavenger. From these results, it may be said that the C–H insertion takes place in both the thermal and energetic reaction, but the C–C insertion takes place only in the energetic reaction. This experi-

TABLE 1. RADIOCHEMICAL YIELD OF THE C–^{35}S–H PRODUCT FROM THE C–H COMPOUND IN THE PRESENCE OF SCAVENGERS IN THE AQUEOUS SOLUTION

Concentration (weight %)		6.0			50.0					75.0	
Scavenger (Torr)	O_2	None			None	15	94	116	150	None	
	NO	None	10	300	None					None	51
Yield (%)		0.6	0.3	0.2	1.0	0.8	0.3	1.1[a] 2.7[b]	0.3	3.3	0.3

a) and b) show the yield obtained by the annealing after the thermal neutron irradiation. Annealing condition was at 95 °C for 1 h (a), or 120 °C for 1 h (b).

Table 2. Radiochemical yield of the C-^{35}S-H and the C-^{35}S-C product from the C-C compound in the presence of scavenger at the concentration of 50%

Scavenger (Torr)		O_2	None	80	100	150
Yield (%)	C-^{35}S-H	0.6	0.3	—	0.3	
	C-^{35}S-C	0.2	0.3	0.3	0.2	

mental fact may not conflict with the results of the reactions of the carbenes produced by the photochemical and thermal processes.[1,2]

The Effect of Solvents and Their Concentrations. The yield of the C-^{35}S-C from the C-C compound shows a constant value in various concentrations of the aqueous solution and the solid. On the other hand, the yields of the C-^{35}S-H product from the C-H and the C-C compounds are affected by the concentration of the aqueous solution, as shown in Fig. 1. But in the presence of scavengers, the yield is no longer affected by the solution concentration. Higher concentration of the C-H compound give higher yields of the C-^{35}S-H product. However, the energetic reaction is not affected by the concentration of the C-H compound.

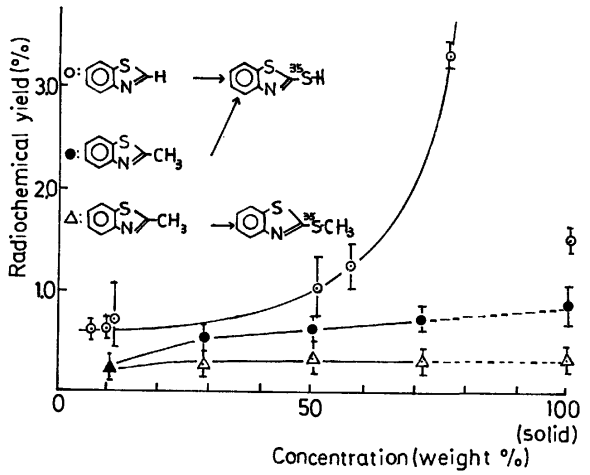

Fig. 1. Yields of the C-^{35}S-H and the C-^{35}S-C product from the C-H and the C-C compound in the aqueous solution.

Organic Solutions.[9] To elucidate the role of the solvent, various solvents such as methanol, benzene, and hexane were used. The results show that the yield of the C-^{35}S-H and the C-^{35}S-C were not affected in the presence of the scavenger nor by the variation of the concentration.

From these results, it seems that only the energetic reaction occurs in the organic solution; in this case thermal sulfur atoms may react easily with the organic solvent to give some other products.[3,4] Therefore, it is not suitable for the thermal reaction of recoil sulfur atoms to use the organic compounds as a solvent. Sulfur atoms seem to be more stable in water than the organic solutions.

The Annealing Effect on the Formation of the C-^{35}S-H Product.[10] After the neutron irradiation of the sample, the yield of the C-^{35}S-H products from the C-H compound in the aqueous solution increases by annealing. The result is shown in Table 1. Although the mechanism of this effect is not clear, it may be considered that the sulfur atoms give some other intermediate with the C-H compound or with water, and then it becomes the C-^{35}S-H product rather easily as a result of the annealing. It seems that the water plays some role in the reaction, because the annealing effect is found only in the aqueous solution and not in the organic solutions.

Table 3. Radiochemical yields of the C-^{35}S-C and the C-^{35}S-H products from the C-C and the C-H compound in various organic solutions

Solvent	Concentration (wt %)	Scavenger NO (Torr)	Yield (%) C-^{35}S-C product
Benzene	9.0	None	0.3
	51.0	None	0.3
	74.0	None	0.2

Solvent	Concentration (wt %)	Scavenger NO (Torr)	Yield (%) C-^{35}S-H product
Benzene	17.0	None	0.5
	38.0	None	0.4
	79.0	None	0.5
Hexane	61.0	None	0.3
		85	0.3
Methanol	32.0	None	0.2
		16	0.3
		180	0.2

p-Dichlorobenzene was used as a chlorine source of the nuclear transformation in these organic systems.

The Radiation Effect on the Formation of the Products. Thiols are easily decomposed by the radicals induced by radiation in aqueous solution, as follows:[11]

$$H_2O \rightsquigarrow H + OH \quad (3)$$

$$R\text{-}SH + OH \longrightarrow RS + H_2O \quad (4)$$

$$R\text{-}SH + H \longrightarrow RS + H_2 \quad (5)$$

The contribution of radiation to the formation and the decomposition of the product during the thermal neutron irradiation could not be estimated exactly. But from the comparison of the rate constant for the decomposition (k_6)[12] with that for the formation (k_7)[13] and the comparison of the number of the sulfur atoms produced (8×10^{12} atoms) by the nuclear transformation with the number of the hydrogen and hydroxyl radicals (4×10^{19} species)[14] formed, the insertion product may quite influenced by the radiation.[15]

$$R\text{-}H + S \xrightarrow{k_6} R\text{-}SH \quad (6)$$

$$R\text{-}SH + H \text{ and } OH \xrightarrow{k_7} \text{decomp} \quad (7)$$

The rate of the R-SH formation may be roughly estimated as the difference of reactions 6 and 7 by the following equation: $d[R\text{-}SH]/dt = k_6[R\text{-}H][S] - k_7[R\text{-}SH][H \text{ and } OH]$

The ratio of the rate constant of the decomposition to that of the formation (k_7/k_6) is about 10^4.

So, if the radiation effect can be neglected, the yield of the C-^{35}S-H compound in the reaction of the recoil sulfur atoms may be about 10 times larger than the ex-

perimental results of the C-^{35}S-H yield. This assumption may be supported by the experimental result that the sulfur atoms produced by the photolysis of $CO^{35}S$ reacted with the C-H compound in the aqueous solution to give about 13% insertion product, based on the carbon monoxide produced.

The Ratio of the Rate Constant for the C-H to the C-C Insertion. Because of the low conversion of the reaction product, it can be considered that the ratio of the rate constant for the C-H to the C-C insertion may be equal to the ratio of the C-^{35}S-H to the C-^{35}S-C product yield.

The ratio of the rate constant of insertion (K_{C-H}/K_{C-C}) is about 1.5 in the energetic process. There are direct and indirect insertion reactions in the reaction of recoil sulfur atoms. One of the indirect insertion reaction is the addition to the -N=C- double bond to form -N-C(S·)-H as described by Grovenstein.[16] The other is the formation of C-^{35}S· intermediate by the reaction of energetic sulfur atoms with the C-H compound; this intermediate abstracts hydrogen from the surrounding molecules to form the C-^{35}S-H product.

The evidence for this reaction is shown by the formation of the C-^{35}S-H product from the C-C compound, as is shown in Table 2 and Fig. 1. Moreover, the hydrogen dissociation in the aqueous solution may be concerned with the production of the C-^{35}S-H, because the yield shows a higher value at the concentration of 75% than that of the solid state. In the reaction of carbon atoms using accelerated $^{14}C^+$ ions with benzene, toluene and cycloheptatriene were formed as synthetic products.[17] It was assumed that the energetic methylene must be involved in this reaction and gives C-H and C-C insertion products. The C-H insertion yield is higher than the C-C insertion in their experiments.

However, the photolytically generated $^{14}CH_2$ reacts with benzene to give toluene in which the methyl group is exclusively labeled (C-H insertion product).[18] And naturally it is possible that the relative populations of the spin states of the recoil sulfur atoms may decide the yield and radioactivity distribution of the insertion product.

From these considerations, it may be concluded that the formation of the C-^{35}S-C is a direct insertion, but the C-^{35}S-H formation involves both direct and indirect insertion.

The C-^{35}S-H product gives a slightly higher yield than the C-^{35}S-C in the aqueous solutions.

The authors wish to express their appreciation to Dr. M. Matsui for his helpful discussion and suggestions on the effects of radiation.

References

1) H. E. Gunning and O. P. Strausz, *Adv. Photochem.*, **4**, 143 (1966).
2) W. Kirmse, "Carbene Chemistry," Academic Press, New York and London (1964).
3) K. Gollnick and E. Leppin, *J. Am. Chem. Soc.*, **92**, 2271 (1970).
4) E. Leppin and K. Gollnick, *J. Am. Chem. Soc.*, **92**, 2221 (1970).
5) L. B. Church and F. S. Rowland, *Radiochim. Acta*, **16**, 55 (1971).
6) K. Taki, *Bull. Chem. Soc. Jpn.*, **43**, 2626 (1970).
7) F. Schmidt-Bleek and F. S. Rowland, *Angew. Chem., Int. Ed. Engl.*, **3**, 769 (1964).
8) This value was estimated from the inorganic yield (mainly SO_4^{2-}, about 30%).
9) In this case, free benzothiazole or 2-methylbenzothiazole and *p*-dichlorobenzene were used as chlorine source.
10) This experimental fact was found in the use of an impure quartz tube; it was estimated that the irradiation temperature rose up about 120 °C in this case.
11) J. E. Pecker, "The Chemistry of Thiol Groups," Wiley-Interscience, New York (1974), p. 481.
12) The rate constant of decomposition of various thiols by radicals induced by radiation is of the order of 10^{10} M^{-1} s^{-1}.[11]
13) The rate constant of the insertion into the C-H bond of sulfur atoms generated by the photolysis of COS is 5×10^7 M^{-1} s^{-1} in liquid phase.[3]
14) During thermal neutron irradiation in the nuclear reactor, the radiation dose may not be less than 10^6rad. The *G*-value of hydrogen atoms and hydroxyl radical is 3.65 and 2.95 respectively in the acidic aqueous solution.[15]
15) M. Haïssinsky, *J. Chim. Phys., Phys.-Chim. Biol.*, **62**, 224 (1965).
16) E. Grovenstein, Jr. and A. J. Mosher, *J. Am. Chem. Soc.*, **92**, 3810 (1970).
17) J. Lintermans, E. Erwin, and R. M. Lemmon, *J. Phys. Chem.*, **76**, 2521 (1972).
18) T. H. Lin, Ph. D. Thesis UCRL-19335, University of California, Berkeley (1969).

The Infrared Band Shapes of Methyl Iodide in Solutions

Shun-ichi IKAWA, Kohji FUKUSHI, Kenji FUJIWARA,* and Masao KIMURA
Department of Chemistry, Faculty of Science, Hokkaido University, Sapporo 060
(Received July 7, 1976)

The infrared band shapes of methyl iodide in solutions were simulated by the superposition of the Lorentzian functions. The a_1-type band was well repoduced by a single Lorentzian function. Its half-width was reasonably explained by the reorientational and vibrational relaxations. The e-type band was reproduced by two Lorentzian functions; one represents the central main peak of the band, while the other is much broader and appears like a background. The half-width of the former was nearly proportional to the Q-branch line spacing in the gas spectrum, while that of the latter seems to be related to the A_1-E-type Coriolis coupling.

The infrared band shape of a molecule in the liquid phase contains information about the rotational diffusion of the molecule.[1-12] However, in order to get insight into the details, it is necessary to take into account the vibrational relaxation of the resonant-exchange[9,10] and translational-diffusion types,[11,12] and the vibration-rotation interaction[6] as well. The effect of other overlapping vibrational transition can not be neglected, either.[11]

It is well-known that the e-type bands of methyl halides in the liquid phase have considerably greater widths than the a_1-type bands. Jones and Sheppard[13] attributed this fact to a large difference between the two kinds of moments of inertia of the molecules. They also suggested that the Coriolis interaction between the degenerate vibration and the rotation about the three-fold axis was operative on the e-type band widths, since a considerable degree of rotational freedom about the three-fold axis remained in solutions. On the other hand, Glass and Pullin[14] and also Bulanin and Tonkov[15] reported that no clear correlation was observed between various half-widths of the e-type bands and the Coriolis constants. Bulanin and Tonkov proposed that the broadening of the e-type band was caused, rather, by the splitting of the degenerate level as a result of the intermolecular force field. However, the observed splittings in a crystal[16] resulting from the intermolecular force field are too small to explain the various half-widths of the e-type bands in the liquid phase. Under these circumstances, more detailed analyses of the bands are necessary in order to clear up the character of the infrared band shape. In a previous paper we reported on the ν_3 band of methyl iodide.[11] In the present work, the simulation of the observed band shape by means of analytical functions has been extended to the eight a_1-type transitions and the five e-type transitions of the same molecule in solutions.

Experimental

The infrared transmission was measured at room temperature with a JASCO DS-701G Spectrophotometer. The spectral slit widths were set at 1.0—1.5 cm^{-1} and about 2 cm^{-1} in the measurement of the a_1- and e-type bands respectively. Under these conditions, no correction is needed for the effect of the finite slit width on the observed band-widths.[17] Uncertainties in the observed band-width were estimated, in the manner described in the previous report,[11] to be ± 0.3 cm^{-1} and ± 1 cm^{-1} for the a_1- and e-bands respectively. The concentrations of methyl iodide in solutions were arranged between 0.4 and 2.3 mol/l. They are in the same concentration range as was employed in the previous work,[11] where the observed band shapes in the ν_3 region were almost independent of the concentrations. Therefore, the concentration-dependence of band shapes was also ignored in the present work. Carbon disulfide and carbon tetrachloride were used as solvents. The two kinds of solutions yielded almost the same band-width wherever both solvents can be used for measurements.

* Present address: Canon Inc., Torite, Ibaragi.

Decomposition of Bands

The observed intensity was obtained by means of this equation:

$$I(\nu) = \ln (\mathbf{T}_0/\mathbf{T})_\nu [\nu(1-\exp(-hc\nu/kT))]^{-1}, \quad (1)$$

where $(\mathbf{T}/\mathbf{T}_0)_\nu$ is the transmittance at wavenumber ν and where T is the absolute temperature. The observed values are indicated by small circles in Figs. 1—5. If the random-reorientation model is adopted for the ensemble of molecules, the band-shape function (1) for a single vibrational transition centered at ν^0 is given by:[1]

$$I(\nu) \sim \sum_{i,f} \rho_i |\langle i|\boldsymbol{\varepsilon}\cdot\boldsymbol{m}^\nu|f\rangle|^2 \delta[(E_f-E_i)/hc-(\nu-\nu^0)] \quad (2)$$

From this equation, one can easily derive the following relationship:

$$I(2\nu^0-\nu) = \exp(-hc(\nu-\nu^0)/kT)\cdot I(\nu) \quad (3)$$

This is nothing but the condition of the detailed balance.[18] Such a function, $I(\nu)$, can be represented in terms of a symmetric function, $I_s(|\nu-\nu^0|)$, as follows:

$$I(\nu) = \exp(hc(\nu-\nu^0)/2kT)\cdot I_s(|\nu-\nu^0|) \quad (4)$$

Here, $I_s(|\nu-\nu^0|)$ represents the Fourier transform of a real autocorrelation function of the transition dipole moment. It is widely accepted that the dipole correlation function should show an exponential decay at a long time in the liquid phase. It follows from this that the central part of the infrared band should be described by a Lorentzian profile. Thus, $I_s(|\nu-\nu^0|)$ was assumed to be Lorentzian. The observed intensity in a given region is, then, expressed in general by:

$$I(\nu) = \sum_i \exp(hc(\nu-\nu_i^0)/2kT)\frac{p_i(\omega_i/2)^2}{(\nu-\nu_i^0)^2+(\omega_i/2)^2}, \quad (5)$$

where ν_i^0, ω_i, p_i denote the band center, the half band-width, and the peak height respectively for the i-th vibrational transition. The right-hand side of Eq. 5 is divergent on the high-frequency side. However, since the absorption regions in question were limited near the

Table 1. Band parameters of the a_1-type vibrations of methyl iodide

	Solvent	Concn mol/l	ν^0 cm^{-1}	cm^{-1}
ν_1	CS_2	1.0	2952.4	10.8
	CCl_4	1.0	2958.0	10.7
$2\nu_2$	CCl_4	1.5	2841.0	20.0
$\nu_3+\nu_5+\nu_6$	CCl_4	1.5	2818.0	18.3
$2\nu_2(0\rightarrow2)$	CS_2	1.6	2464.2	9.1
$2\nu_2(1\rightarrow3)$	CS_2	1.6	2453.0	9.0
ν_2	CS_2	0.4	1239.5	7.7
$2\nu_3$[a]	CS_2	2.3	1046.7	13.2
$\nu_3(0\rightarrow1)$[a]	CS_2	1.5	526.8	8.3
	CCl_4	1.5	527.6	8.3
$\nu_3(1\rightarrow2)$[a]	CS_2	1.5	520.2	7.7
	CCl_4	1.5	521.0	8.3

a) Reproduced from Ref. 11.

band centers, no difficulty occurred in the band analysis. The parameter values fitted are summarized in Tables 1 and 2. Practically, the parameter values adjusted for bands with half-widths smaller than 30 cm^{-1} did not depend upon whether or not the exponential factor in Eq. 5 was ignored. Therefore, the values for the ν_3 band in Table 1 are taken from the previous report, in which this factor was ignored.[11]

Results and Discussion

a_1-Type Bands. The band shape of the fundamental a_1-type vibration is well reproduced by a single Lorentzian function, except for slight deviations from the Lorentzian functions in the lower-frequency wings, as may be seen in Fig. 1. A similar deviation was also found for the ν_3 fundamental band.[11] These deviations may be attributed to the vibration-rotation interaction, as was mentioned in the previous report on the ν_3 band.

The doublet in the region from 2740 to 2900 cm^{-1} was observed as parallel bands in the gas phase and was assigned to the Fermi doublet, $2\nu_5$ and $\nu_3+\nu_5+\nu_6$, by Matsuura and Shimanouchi.[19] The decomposition of the doublet was performed after subtracting the wings of the ν_1 and ν_4 bands from the total absorption. The results are shown in Fig. 2a.

In the absorption region of the $2\nu_2$ band, a small band is observed in the lower-frequency wing, as is shown in Fig. 2b. The best-fit parameter values of the two Lorentzian functions are $\nu_a^0=2464.2$ cm^{-1}, $\nu_b^0=2453.0$ cm^{-1}, $\omega_a=9.1$ cm^{-1}, and $\omega_b=9.0$ cm^{-1}, and the ratio of band areas, $p_b\omega_b/p_a\omega_a$, is 0.095, where the subscripts a and b denote the $2\nu_2$ and the small band respectively. The small band may be assigned to the hot band transition, $2\nu_2+\nu_3-\nu_3$, since its half-width is nearly equal to that of $2\nu_2$ and since the area ratio is in agreement with the theoretical values, $\exp(-hc\nu_3/kT)=0.081$, at $T=300$ K. The anharmonicity constant was estimated using the relation $x_{23}=(\nu_b^0-\nu_a^0)/2$ to be -5.6 cm^{-1}. This value is nearly equal to the value of -5 cm^{-1} obtained by using another relation, $x_{23}=(\nu_2+\nu_3)-\nu_2-\nu_3$, in a CCl_4 solution.[20] Although such a non-zero x_{23} should produce the $\nu_2+\nu_3-\nu_3$ hot band at the frequency lower than that of the ν_2 fundamental by about 5 cm^{-1}, it is impossible to resolve the observed band into the two components. However, the effect of the hot band on the parameter values obtained for the ν_2 fundamental band may be small and need not be taken into account in the following discussion.

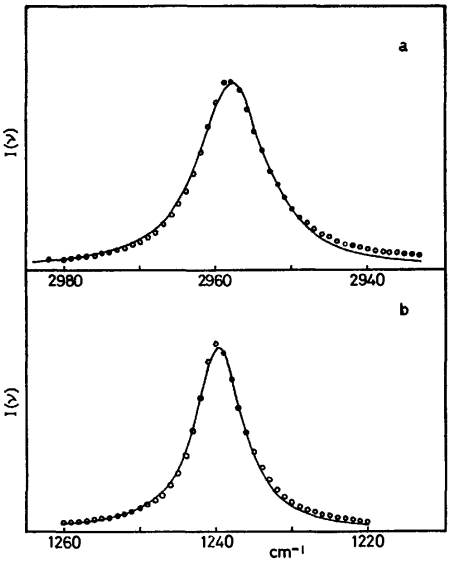

Fig. 1. The infrared bands of methyl iodide in solutions: (a) ν_1 in CCl_4, (b) ν_2 in CS_2.
••••••: Observed; ——: calculated.

The band width of the overtone, $2\nu_2$, is larger than that of the fundamental, ν_2. This is probably due to the difference between contributions from the vibrational relaxation of the translational-diffusion type,[12] as was pointed out in the case of the ν_3 transition.[11] If there is no other cause of the band broadening, the width due to the vibrational relaxation is estimated to be $\omega_2\ (0\rightarrow2)-\omega_2(0\rightarrow1)=1.4$ cm^{-1}; accordingly the width due to the reorientational relaxation becomes $\omega_2(0\rightarrow1)-1.4$ cm^{-1}

Table 2. Band parameters of e-type vibrations of methyl iodide[a]

	Solvent	Concn mol/l	$\nu^0(L_1)$	$\omega(L_1)$	$\nu^0(L_2)$	$\omega(L_2)$	ω(ap)	ζ	$\omega(L_1)/(1-\zeta)$
ν_4	CS_2	1.5	3046	29	3029	200	76	0.060[b]	31
	CCl_4	1.5	3051	27	3042	202	76		29
$\nu_2+\nu_6$	CCl_4	2.3	2126.3	28					
ν_5	CCl_4	1.5	1430.0	31	1418	171	43	-0.016[c]	30
$\nu_3+\nu_6$	CCl_4	1.5	1400.3	30					29
ν_6	CS_2	1.5	881.3	24	882	80	30	0.210[d]	30

a) Frequencies in cm^{-1} unit. b) Taken from Ref. 27a. c) Average of $\zeta_5=-0.242$ and $\zeta_{36}=0.210$, see text.
d) Taken from Ref. 27d.

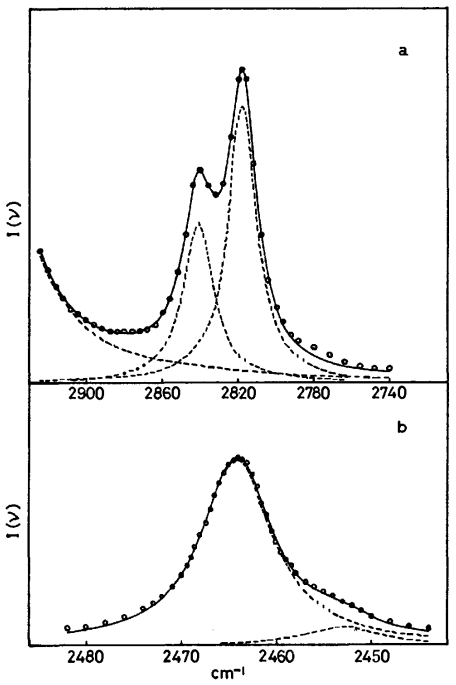

Fig. 2. The infrared bands of methyl iodide in solutions: (a) the region of the doublet $2\nu_5$ and $\nu_3+\nu_5+\nu_6$ in CCl_4, (b) the region of the $2\nu_2$ band in CS_2.
•••••: Observed; ——: calculated, total; ------: calculated, components.

$=6.3\ cm^{-1}$. In order to estimate the reorientational relaxation for the ν_1 band, some Raman data is available. The width of the isotropic component of the Raman ν_1 band has been found to be $3.5\ cm^{-1}$ in CS_2 solutions (1.7 mol/l).[21] This width may be considered to be due to the vibrational relaxation and to be transferable to the infrared-band width.[11,22-25] Then, the band-width of the infrared ν_1 vibration due to the reorientational relaxation is estimated to be $\omega_1(0\rightarrow1)-3.5\ cm^{-1}=7.3\ cm^{-1}$. The widths of the ν_3 band due to the reorientational and vibrational relaxations have previously been estimated to be 6.3 and $2.0\ cm^{-1}$ respectively.[11]

The vibrational species of the same symmetry have transition dipole moments in the same direction in the molecular framework. Therefore, their band-widths based upon the reorientational relaxation should be identical to one another only if the effect of the vibration-rotation interaction is negligible. This is the case for the a_1-type band of CH_3I. The estimated band-widths due to the reorientational relaxation, 7.3, 6.3, and $6.3\ cm^{-1}$ for the ν_1, ν_2, and ν_3 vibrations respectively, agree approximately with one another in spite of a scattering of the observed total widths, 10.8, 7.7, and $8.3\ cm^{-1}$.[26]

The band-widths of the Fermi doublet, $2\nu_5$ and $\nu_3+\nu_5+\nu_6$, are much larger than those of the other a_1-type bands. Matsuura and Shimanouchi[19] have pointed out that the unperturbed $(\nu_3+\nu_5+\nu_6)^0$ band behaves as a quasi-perpendicular band with an effective Coriolis constant of -0.47, whereas the unperturbed $(2\nu_5)^0$ band has the normal profile of a parallel band. The band-widths observed in solutions are intermediate between those of the a_1-type and the e-type bands. It is probable that the vibration-rotation interaction is operative in solutions and that, as a result, the broadenings of the components of this doublet are much larger than those of the other a_1-type bands.

e-Type Bands. The absorption region of the e-type vibration is, as a rule, well reproduced by two Lorentzian functions. The narrower Lorentzian, designated as $\nu(L_1)$, and the broader one, designated as $\nu(L_2)$, represent the shape near the band center and a background-like absorption of a greater width respectively.

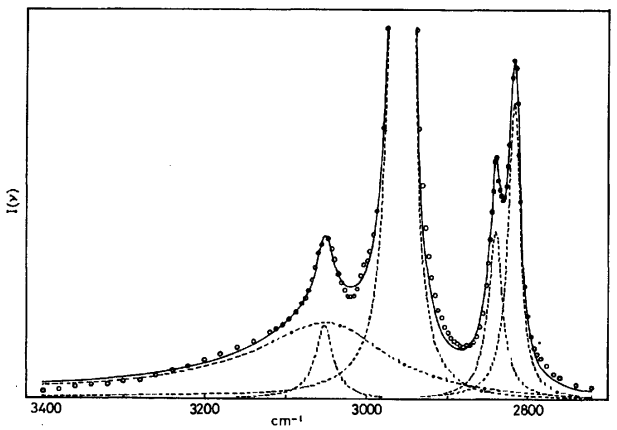

Fig. 3. The infrared absorption in the region from 2720 to 3400 cm^{-1} of methyl iodide in the carbon tetrachloride solution.
•••••: Observed; ——: calculated, total; ------: calculated, components.

Figure 3 shows the absorption ranging from 2720 to 3400 cm^{-1}, of methyl iodide in carbon tetrachloride. In addition to the e-type ν_4 band, there appear three a_1-type bands, ν_1, $2\nu_5$, and $\nu_3+\nu_5+\nu_6$. The absorption in this region is well reproduced by five Lorentzian functions. It should be noted that $\nu_4(L_2)$ is much broader than the others and spreads all over the region.

In the absorption region of ν_5, the combination band $\nu_3+\nu_6$ also appears. This region is well reproduced by three Lorentzian functions, as is shown in Fig. 4. It has

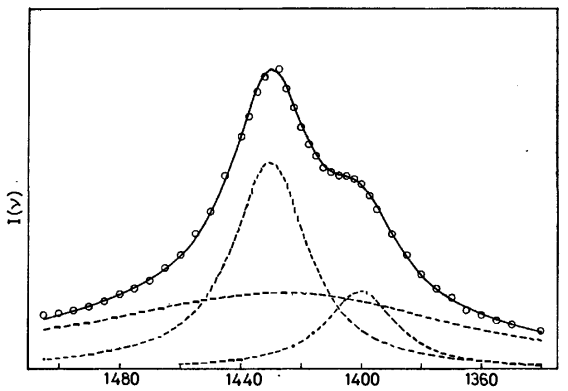

Fig. 4. The infrared absorption in the region of the Fermi doublet ν_5 and $\nu_3+\nu_6$ of methyl iodide in the carbon tetrachloride solution.
•••••: Observed; ——: calculated, total; ------: calculated, components.

been established that the Fermi-resonance occurs between the ν_5 and $\nu_3+\nu_6$ bands.[27] If the value of the Fermi-resonance parameter, $W=K_{356}/\sqrt{2}$, in the solution is assumed to be equal to that in the gas phase, 10.4 cm^{-1},[27d] the unperturbed frequencies may be estimated to be 1426.5 and 1403.8 cm^{-1} for ν_5^0 and $(\nu_3+\nu_6)^0$ respectively. The value of the anharmonicity constant, x_{36}, is, then, obtained to be as follows: $x_{36}=(\nu_3+\nu_6)^0-\nu_3-\nu_6=-4.8$ cm^{-1}. This value agrees with those obtained in the gas phase, -5.6[27d] and -5 cm^{-1}.[27b] Both the values of K_{356} and x_{36} seem to be almost unchanged on going from gas to solution.

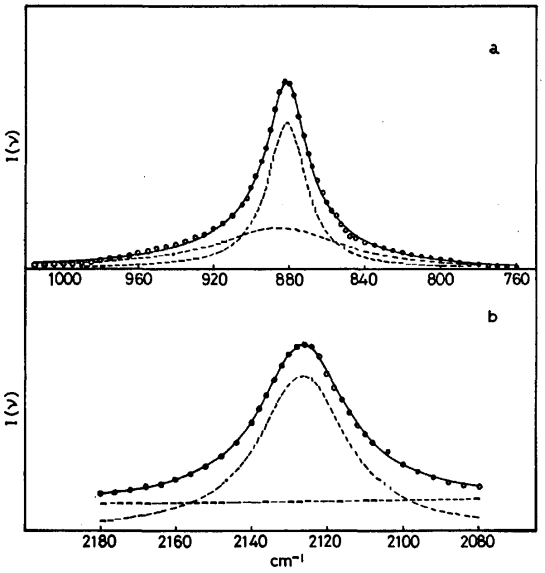

Fig. 5. The infrared bands of methyl iodide in solutions: (a) ν_6 in CS_2, (b) $\nu_2+\nu_6$ in CCl_4.
•••••: Observed; ——: calculated, total; ------: calculated, components.

The region of the ν_6 vibration is simply reproduced by two Lorentzian functions, as is shown in Fig. 5a. The combination band, $\nu_2+\nu_6$, is much weaker than the other e-type bands studied in the present work. The background-like absorption in Fig. 5b looks nearly constant throughout the region. This is probably because of the overlap of the wings of the neighboring bands. It is impossible to extract the $\nu(L_2)$ from the whole background.

The shapes of ν_4, ν_5, and ν_6 fundamental bands, each of which is composed of $\nu(L_1)$ and $\nu(L_2)$, are compared in Fig. 6. Their band-widths, ω(ap), are very different

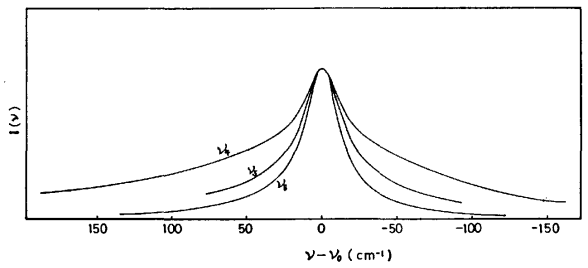

Fig. 6. Comparison of the normalized shapes of the ν_4, ν_5, and ν_6 bands, each of which is composed of $\nu(L_1)$ and $\nu(L_2)$.

from each other, as is shown in Table 2. Nevertheless, the half-widths of $\nu(L_1)$, $\omega(L_1)$, are much less dispersive and in the order of $\omega_5(L_1)>\omega_4(L_1)>\omega_6(L_1)$, in accordance with that of the Q-branch line spacings in the gas phase. The Q-branch line spacing of methyl iodide in the gas phase is nearly proportional to $1-\zeta$, where ζ is the Coriolis coupling constant. The values of ζ have been reported to be 0.060,[27a] -0.242,[27d] and 0.210[27d] for ν_4, ν_5, and ν_6 respectively. If a strong Fermi resonance occurs, the Q-branch line spacing of each Fermi component may be related to the mean value of ζ for the unperturbed vibrations, at least in the region near the band center. Therefore, we tentatively adopted the value of $\zeta=(\zeta_5+\zeta_6)/2$ for the Fermi doublet, by using ζ_6 in place of ζ_{36}. The values of $\omega(L_1)$ divided by $1-\zeta$ are given in the last column in Table 2. They are constant; in other words, $\omega(L_1)$ is proportional to the Q-branch line spacing.

The absorptions specified by $\nu(L_2)$ serve for the broadening of the observed bands; the percentage of each $\nu(L_2)$ occupying the band area and the broadening are much larger for ν_4 than ν_5 and ν_6. No definite conclusion can be drawn about their origin and precise shape at present. However, the $\nu(L_2)$ parts of the e-type bands seem to be related to the A_1-E-type Coriolis coupling, with the intense nondegenerate band in the neighborhood. The intensity perturbation due to the A_1-E-type Coriolis coupling is approximately proportional to $[J(J+1)-K(K+1)]$ in the gas phase.[28] This type of coupling probably intensifies the band-wing, even in the solutions. For methyl iodide, the separations between the degenerate bands and their nondegenerate intense neighbors are $\nu_4-\nu_1\approx90$ cm^{-1}, $\nu_5-\nu_2\approx170$ cm^{-1}, $\nu_2-\nu_6\approx360$ cm^{-1}, and $\nu_6-\nu_3\approx350$ cm^{-1}. Therefore, the A_1-E-type Coriolis coupling may affect the ν_4 band most strongly and the ν_6 band most weakly. This is consistent with the observed order of the magnitudes for $\omega(L_2)$.

The authors wish to thank Professors Osamu Yonemitsu and Kozo Tanabe of Hokkaido University for their permission to use the JASCO DS-701G infrared spectrophotometers.

References

1) R. G. Gordon, *J. Chem. Phys.*, **43**, 1307 (1965).
2) H. Shimizu, *J. Chem. Phys.*, **43**, 2453 (1965); *Bull. Chem. Soc. Jpn.*, **39**, 2385 (1966).
3) J. T. Shimozawa and M. K. Wilson, *Spectrochim. Acta*, **22**, 1609 (1966).
4) a) C. F. Favelukes, A. A. Clifford, and B. L. Crawford, Jr., *J. Phys. Chem.*, **72**, 962 (1968); b) T. Fujiyama and B. L. Crawford, Jr., *ibid.*, **73**, 4040 (1969); c) W. G. Rothschild, *J. Chem. Phys.*, **51**, 5187 (1969); *ibid.*, **52**, 6453 (1970).
5) W. G. Rothschild, *J. Chem. Phys.*, **53**, 990 (1970).
6) M. Kakimoto and T. Fujiyama, *Bull. Chem. Soc. Jpn.*, **45**, 3021 (1972).
7) G. Lévi and M. Chalaye, *C. R. Acad. Sci. Ser. B*, **271**, 1093 (1970).
8) K. Koga, Y. Kanazawa, and H. Shimizu, *J. Mol. Spectrosc.*, **47**, 107 (1973).
9) M. Kakimoto and T. Fujiyama, *Bull. Chem. Soc. Jpn.*, **45**, 2970 (1972).
10) K. A. Valiev, *Opt. Spektrosk.*, **11**, 253 (1961).

11) K. Fujiwara, K. Fukushi, S. Ikawa, and M. Kimura, *Bull. Chem. Soc. Jpn.*, **48**, 3464 (1975).
12) S. Bratož, J. Rios, and Y. Guissani, *J. Chem. Phys.*, **52**, 439 (1970).
13) W. J. Jones and N. Sheppard, *Trans. Faraday Soc.*, **56**, 625 (1960).
14) W. K. Glass and A. D. E. Pullin, *Trans. Faraday Soc.*, **59**, 25 (1963).
15) M. O. Bulanin and M. V. Tonkov, *Opt. Spektrosk.*, **16**, 234 (1964).
16) D. A. Dows, *J. Chem. Phys.*, **29**, 484 (1958). The splittings are described as site-group splittings. Their magnitudes are 13, 6, and 7 cm^{-1} for the ν_4, ν_5, and ν_6 bands respectively, taking account of the Fermi resonance between ν_5 and $\nu_3+\nu_6$. See the text.
17) D. A. Ramsay, *J. Am. Chem. Soc.*, **74**, 72 (1952).
18) B. J. Berne, J. Jortner, and R. G. Gordon, *J. Chem. Phys.*, **47**, 1600 (1967).
19) H. Matsuura and T. Shimanouchi, Lecture in Symposium on Molecular Structure, Tokyo (1974).
20) $\nu_2+\nu_3=1767$ cm^{-1}, $\nu_2=1244$ cm^{-1}, $\nu_3=528$ cm^{-1} in the CCl_4 solution.
21) K. Fukushi, unpublished data.
22) G. P. Buyan, I. I. Kondilenko, and V. E. Pogorelov, *Opt. Spektrosk.*, **27**, 132 (1969); I. I. Kondilenko, V. E. Pogorelov, and K. Khue, *ibid.*, **28**, 367 (1970).
23) S. Bratož and E. Marechal, *Phys. Rev. A*, **4**, 1078 (1971).
24) F. J. Bartoli and T. A. Litovitz, *J. Chem. Phys.*, **56**, 404, (1972).
25) H. S. Goldberg and P. S. Pershan, *J. Chem. Phys.*, **58**, 3816 (1973).
26) Recently, T. Fujiyama, M. Kakimoto, and T. Suzuki [*Bull. Chem. Soc. Jpn.*, **49**, 606 (1976)] pointed out that half-widths in solutions depend on the solvent shifts from the point of view of the concentration fluctuation in a liquid. However, the present results show that, while the ν_1 bands in CS_2 and CCl_4 solutions have almost the same half-widths, nevertheless the peak frequencies differ by about 6 cm^{-1} from each other.
27) a) Y. Morino and J. Nakamura, *Bull. Chem. Soc. Jpn.*, **38**, 443 (1965); b) Y. Morino, J. Nakamura, and S. Yamamoto, *J. Mol. Spectrosc.*, **22**, 34 (1967); c) Y. Morino and C. Hirose, *ibid.*, **22**, 99 (1967); d) H. Matsuura and J. Overend, *J. Chem. Phys.*, **55**, 1787 (1971).
28) C. DI Lauro and I. M. Mills, *J. Mol. Spectrosc.*, **21**, 386 (1966).

Statistical Thermodynamic Theory of Liquid Water

Kiyoshi ARAKAWA, Kazuo TOKIWANO,* and Kazumitsu KOJIMA

Research Institute of Applied Electricity, Hokkaido University, Sapporo 060

** Faculty of Engineering, Hokkaido University, Sapporo 060*

(Received July 12, 1976)

A new statistical thermodynamic theory is presented for a model of liquid water, which consists of two components, *i.e.*, tetrahedrally-coordinated pentamers and non-hydrogen-bonded monomers. In the model the two components are assumed to be immersed in a uniform background potential which results from electrostatic, induction, and dispersion forces between water molecules. A partition function is given without assuming any specified lattice. A translational partition function is written into a simple and explicit expression which is derived from the Lebowitz solution of the Percus-Yevick equation for hard sphere mixtures. The mole fraction of each component and the density are determined by solving two equations, *i.e.*, the condition of free energy minimization and the equation of state derived from the partition function, simultaneously. Various thermodynamic quantities are calculated and the values determined are compared with those observed. Some discussions are carried out, together with the criticism of the earlier theories.

Various kinds of statistical thermodynamic theories of liquid water[1-3] have been proposed for about a decade since the presentation of the earlier theory by Némethy and Scheraga (1962). Many new experimental results have also been accumulated for nearly the same period of time and added a great deal of contributions to the knowledge of the structure of liquid water,[4] though no decisive conclusion about it has been obtained at present.[5]

Concerning the structure theories of liquid water, the situations are diversified nowadays certainly, but, as to the theoretical methods and models used, several distinguishable features are found in the studies carried out recently. Those are classified into three groups: 1) lattice and cell theories, 2) applications of the recent progress in the theory of liquids, *i.e.*, the Percus-Yevick and HNC equations *etc.*, 3) results in computer experiments, *i.e.*, molecular dynamics and Monte Carlo calculations.

Among the first group of studies we find lattice theories presented by Bell and others[6] and by Fleming and Gibbs,[7] a cell theory by Weissmann and Blum,[8] and an order-disorder theory by the authors.[9] Some of these theories[6,7,9] treated the theme of the cooperative character in the structure of liquid water, that is, the cooperative formation and breakage of the hydrogen-bonded structure, but the success of those is only qualitative, subjected to the limitation which is associated with the essential nature of the lattice theory. The studies in line with the second group are mainly promoted by Ben-Naim and others.[10] There seems to be a fair prospect of success of these theories, but the greatest problem lies in mathematical difficulties of solving integral equations for correlation functions. The most remarkable results in the third group are those of molecular dynamics given by Rahman and Stillinger.[11] They have made important contributions to the determination of the structure model for water. All the results described above give new possibilities, surely, to solve the important but difficult problem of the liquid structure of water. However, their successes remain to be qualitative and limited ones on the whole.

From the quantitative view-point of results, recent two theories presented by Weres and Rice[12] and by Scheraga and coworkers[13] are intensely interesting. The former one is a kind of lattice theory and the latter one is based on a mixture model (cluster model). They made a further forward step to the quantitative explanation of the equilibrium behavior of water. However, they are too solid-like. For example, it has been found in the calculation by Weres and Rice that the value of configurational entropy with respect to the arrangement of water molecules in basic cells remains quite unchanged throughout the temperature range from 0 to 100 °C. In the calculation by Scheraga *et al.* also, it has been found that $U_{\text{vib.}}$, the internal energy resulting from the intermolecular vibrational structure, increases from the value of 3.33 kcal/mol to 3.87 kcal/mol throughout the same range of temperature while $U_{\text{trans.}}$, the energy for translational motion, is very small, being within the range from 0.18 to 0.28 kcal/mol. These features of the two theories clearly show the too solid-like character, though it is found to be more intense in the theory by Weres and Rice than in the one by Scheraga *et al.*

Thus, the authors have attempted to propose a statistical thermodynamic theory of liquid water based on the recent progress in studies of liquids, in order to give the more adequate explanation of the properties of water. Details of the results are reported in the following sections.

Description of the Model

Since the proposition by Bernal and Fowler in 1933, the tetrahedral coordination has been considered to dominate in the local structure in liquid water. The results of X-ray studies from Morgan and Warren's (1938) to the recent Narten, Danford, and Levy's[14] has ascertained that the average coordination number in liquid water is slightly larger than four at ordinary temperatures, indicating the predominance of the local tetrahedral geometry. Recent spectroscopical studies by Walrafen[15] and others has also confirmed that the tetrahedrally-coordinated hydrogen-bonded configurations with C_{2v} symmetry constitute most of the structures present in water. This feature should be taken into consideration firstly in the formulation of the theoretical model for water.

In the recent presentation of a statistical thermodynamic theory for water, Lentz, Hagler, and Scheraga

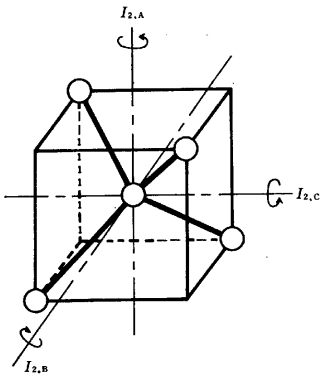

Fig. 1. Tetrahedrally-coordinated pentamer.

have used a model consisting of a distribution of small clusters from 1 to 9,[13] admitting the criticisms against the earlier theory of Némethy and Scheraga[16] (1962) that it used a model with very large clusters.

It is desirable that the basic model underlying a theory is as simple as possible if the theory can explain the behavior of the substance as objects with a sufficient accuracy. Thus, the authors assume that liquid water consists of two species which are tetrahedrally hydrogen-bonded pentamers (Fig. 1) and unbonded monomers. The character of the structure supposed to be intrinsic of water is attributed to the presence of the pentamers, and liquid water is regarded as an equilibrium mixture of the monomers and the pentamers.

In the formulation of the total partition function, we assume that attractive forces between molecules give rise to a uniform background potential, taking into consideration the treatment made first by Longuet-Higgins and Widom for liquid Argon,[17] by Scheraga and others for water,[13,18] and by the authors for normal liquid.[19] The magnitude of the background potential is determined by a direct calculation as described in later sections, while it was treated as an adjustable parameter in the calculation of Scheraga and others.

In order to give a translational partition function we regard the two species as hard spheres with diameters R_1 and R_2 ($R_1<R_2$), respectively, which are immersed in the background potential, and the translational partition function is derived from the analytical solution of the Percus-Yevick equation for hard sphere mixtures. Its details are described later.

The Partition Function

For the model used the total partition function is expressed as a product,

$$Z = Q_{\text{trans.}} Q_{\text{rot.}} Q_{\text{int.}} Q_{\text{BG}}, \tag{1}$$

in terms of the translational, rotational, internal, and background potential contribution, respectively.

i) Translational Partition Function. We can write the translational partition function $Q_{\text{trans.}}$ at given V and T for an assembly of N_1 non-hydrogen-bonded monomers (the mass m_1 and the diameter R_1) and N_2 pentamers (the mass m_2 and diameter R_2). The formula is derived from the analytical and explicit solution of the generalized Percus-Yevick equation given first by Lebowitz.[20,21] The details of the derivation are described in Appendix I.

$Q_{\text{trans.}}$ is expressed as

$$Q_{\text{trans.}} = \left[\left(\frac{2\pi m_1 kT}{h^2}\right)^{3/2} e v_1 f\right]^{N_1} \left[\left(\frac{2\pi m_2 kT}{h^2}\right)^{3/2} e v_2 f\right]^{N_2}, \tag{2}$$

and

$$f = (1-\xi)\exp\left[-\frac{9}{\pi}\frac{V}{N_1+N_2}\frac{1}{(1-\xi)^2}(2XY-2XY\xi+X^3)\right], \tag{3}$$

where

$$v_1 = V/N_1 = \rho_1^{-1},\ v_2 = V/N_2 = \rho_2^{-1},$$

$$X = \frac{\pi}{6}\rho_1 R_1^2 + \frac{\pi}{6}\rho_2 R_2^2,\ Y = \frac{\pi}{6}\rho_1 R_1 + \frac{\pi}{6}\rho_2 R_2,$$

and the packing fraction is

$$\xi = \frac{\pi}{6}\rho_1 R_1^3 + \frac{\pi}{6}\rho_2 R_2^3.$$

The Eqs. 2 and 3 are a generalization of Eqs. 4 and 6 in the previous paper[19] for an one component fluid into the formulas for a mixture of hard spheres, where ξ corresponds to y in the paper. Equation 2 is seen to have a form identical with that given in the free volume theory in general. Thus, $f \equiv$ Eq. 3 is defined as a generalized equivalent free volume fraction, which is similar to the case of an one component fluid.[19] This is extended to the general case for an m-component fluid as described in Appendix I. In the presentation of our theory no lattice is assumed, and the theory derived is free from the criticism against the lattice theory in general in its application to liquids.

ii) Rotational Partition Function. The contribution $Q_{\text{rot.}}$ from the rotational motions to the total partition function becomes

$$Q_{\text{rot.}} = \left[\frac{\pi^{1/2}}{\sigma_1}\left(\frac{8\pi^2 kT}{h^2}\right)^{3/2}(I_{1,A}I_{1,B}I_{1,C})^{1/2}\right]^{N_1} \times \left[\frac{\pi^{1/2}}{\sigma_2}\left(\frac{8\pi^2 kT}{h^2}\right)^{3/2}(I_{2,A}I_{2,B}I_{2,C})^{1/2}\gamma\right]^{N_2}, \tag{4}$$

where $I_{i,A}$, $I_{i,B}$, $I_{i,C}$, and σ_i are the moment of inertia and symmetry factor, respectively, of an i-th particle. γ is a reduction factor which results from the restriction of the over-all free rotation for a larger particle such as a pentamer. Though this factor γ is expected to be smaller than 1 for the pentamer, we take it as 1, for it is impossible to compute the reduced number of rotational configurations. Symmetry factors σ_1 and σ_2 are taken to be 2, as usual.

iii) Internal Partition Function. The internal partition function $Q_{\text{int.}}$ is

$$Q_{\text{int.}} = Q_{\text{vib.}} \exp\left(\frac{-4N_2\varepsilon}{kT}\right), \tag{5}$$

where $Q_{\text{vib.}}$ is the contribution from the vibrational degrees of freedom from N_2 pentamers and ε is the energy of hydrogen bonding within pentamers. In each pentamer four hydrogen bonds are formed between the central molecule and four tetrahedrally-coordinated molecules. We write the vibrational contribution $Q_{\text{vib.}}$ as

$$Q_{\text{vib.}} = \left[\prod_{j=1}^{24}\left\{\frac{\exp(-h\nu_j/2kT)}{1-\exp(-h\nu_j/kT)}\right\}\right]^{N_2}, \tag{6}$$

where ν_j is the frequency of intermolecular vibrational mode within a pentamer. $24(=6\times5-6)$ degrees of freedom are considered for the modes.

iv) Backbround Potential. The contribution Q_{BG} from the uniform background potential term to the total partition function becomes

$$Q_{BG} = \exp(-U_{BG}/kT) \tag{7}$$

As described in the previous section, each hard sphere molecule is assumed to be immersed in a uniform background potential U_{BG}, and no specific interactions are considered between hard spheres. U_{BG} for a molecule is considered to result from the dipole-dipole, dipole-induced dipole, and dispersion interactions between the molecule and all the other molecules as its medium. U_{BG} is expressed as inversely proportional to the volume of the liquid in the same way as Longuet-Higgins and Widon assumed,[17] and is written into a simple form as $U_{BG}=aN^2/V$, where a is a constant. This presupposes that, concerning electrostatic, induction, and dispersion interactions, water molecules behave similarly with each other, whether they are within pentamers or in unbonded state.

The dipolar interaction between permanent point dipoles is expressed as

$$U_{\mu\mu} = \frac{\mu^2}{\tilde{R}^3}[\sin\theta_A \sin\theta_B \cos(\phi_A-\phi_B) - 2\cos\theta_A\cos\theta_B], \tag{8}$$

where $\tilde{R}$ is the separation between a dipole A and a dipole B, θ_A and θ_B the polar angles for A and B (the line connecting A and B is regarded as a polar axis), and ϕ_A and ϕ_B the angles formed by the plane including the dipole and the polar axis with a reference plane. $U_{\mu\mu}$ is averaged for all configurations of two dipoles A and B with respects to angles θ_A, θ_B, ϕ_A, and ϕ_B, and the averaged value $\langle U_{\mu\mu}\rangle$ becomes a function of $\tilde{R}$ only.

$$\langle U_{\mu\mu}\rangle = \int U_{\mu\mu}\exp(-U_{\mu\mu}/kT)d\Omega \Big/ \int \exp(-U_{\mu\mu}/kT)d\Omega, \tag{9}$$

where $d\Omega=\sin\theta_A \sin\theta_B\, d\theta_A\, d\theta_B\, d\phi_A\, d\phi_B$.

The dipole-induced dipole interaction $U_{\mu\alpha}$ becomes

$$U_{\mu\alpha} = -\frac{2\mu^2\bar{\alpha}}{\tilde{R}^6}, \tag{10}$$

where $\bar{\alpha}$ is a average molecular polarizability, and the dispersion interaction between two molecules is

$$U_{disp.} = -\frac{c}{\tilde{R}^6}, \tag{11}$$

The background potential U_{BG} is determined by integration of the sum of Eqs. 9, 10, and 11 multiplied by $g(\tilde{R})$. The $g(\tilde{R})$ is a molecular correlation function[22] obtained from the observed radical distribution function by substracting intramolecular contributions.

Then, U_{BG} is written as

$$U_{BG} = \frac{N^2}{2V}\int[\langle U_{\mu\mu}\rangle + U_{\mu\alpha} + U_{disp.}]g(\tilde{R})4\pi\tilde{R}^2 d\tilde{R}. \tag{12}$$

A Monte Carlo method is used in the calculation of $\langle U_{\mu\mu}\rangle$. The details in the procedure of calculation of U_{BG} are described in Appendix II.

Thermodynamic Variables

In the present model the following equilibrium at given T is established in water,

$$5(H_2O) \rightleftarrows (H_2O)_5, \tag{13}$$

where the total number of water molecules N remains constant,

$$N = N_1 + 5N_2. \tag{14}$$

The free energy F is obtained from the total partition function Z (Eq. 1).

$$F = -kT\ln Z, \tag{15}$$

where N_1, N_2, and molar volume V^0 (density ρ) at equilibrium are determined at given T and N from the condition of Z maximization and the equation of state derived from Z. Under the association equilibrium condition (Eqs. 13 and 14), the following relation holds.[23]

$$\left(\frac{\partial F}{\partial T}\right)_{V,N} = \left(\frac{\partial F}{\partial T}\right)_{V,N_1,N_2}, \quad \left(\frac{\partial F}{\partial V}\right)_{T,N} = \left(\frac{\partial F}{\partial V}\right)_{T,N_1,N_2}. \tag{16}$$

This relation simplifies the formulas for various thermodynamic variables which are derived from Eq. 15.

The equation of state is given as

$$pV = \frac{kT}{(1-\xi)^3}\left[(N_1+N_2)(1+\xi+\xi^2) - \frac{\pi N_1 N_2}{2V}(R_2-R_1)^2 \times\left\{R_1+R_2+\frac{\pi}{6}\left(\frac{N_1R_1^2+N_2R_2^2}{V}\right)R_1R_2\right\}\right] + \frac{aN^2}{V}, \tag{17}$$

where the first term in the right of Eq. 17 is the same as that derived by Lebowitz[20] for hard sphere mixtures, and the second term comes from the background potential term.

The entropy S is expressed[24] as

$$S = S_{trans.} + S_{rot.} + S_{int.}, \tag{18}$$

$$S_{trans.} = k\ln Q_{trans.} + \frac{3}{2}(N_1+N_2)k$$

$$S_{rot.} = k\ln Q_{rot.} + \frac{3}{2}(N_1+N_2)k$$

$$S_{int.} = k\ln Q_{vib.} + kT\frac{\partial \ln Q_{vib.}}{\partial T} = S_{vib.}$$

The internal energy $U=F+TS$ is obtained from F and S as

$$U = 3(N_1+N_2)kT + 4N_2\varepsilon + kT^2\left(\frac{\partial \ln Q_{vib.}}{\partial T}\right) + \frac{aN^2}{V}. \tag{19}$$

$$U_{trans.} = U_{rot.} = \frac{3}{2}(N_1+N_2)kT$$

$$U_{kin.} = U_{trans.} + U_{rot.}$$

$$U_{vib.} = kT^2\left(\frac{\partial \ln Q_{vib.}}{\partial T}\right)$$

$$U_{HB} = 4N_2\varepsilon$$

$$U_{BG} = \frac{aN^2}{V}.$$

The heat capacity at constant pressure, C_p, is derived as follows,

$$C_p = \left(\frac{\partial U}{\partial T}\right)_p + p\left(\frac{\partial V}{\partial T}\right)_p$$
$$= \left(\frac{\partial U}{\partial T}\right)_{p,N_1,N_2} + \left(\frac{\partial U}{\partial N_2}\right)_{p,T}\left(\frac{\partial N_2}{\partial T}\right)_{p,N} + p\left(\frac{\partial V}{\partial T}\right)_p$$
$$= 3(N_1+N_2)k + 2kT\left(\frac{\partial \ln Q_{\text{vib.}}}{\partial T}\right) + kT^2\left(\frac{\partial^2 \ln Q_{\text{vib.}}}{\partial T^2}\right)$$
$$+ \left(\frac{\partial U_{\text{BG}}}{\partial T}\right)_p + \left[-12kT + 4\varepsilon + kT^2\left(\frac{\partial \ln q_{\text{vib.}}}{\partial T}\right)\right]$$
$$\times \left(\frac{\partial N_2}{\partial T}\right)_{p,N} + p\left(\frac{\partial V}{\partial T}\right)_p, \qquad (20)$$

where $(q_{\text{vib.}})=(Q_{\text{vib.}})^{1/N_2}$ is a molecular vibrational partition function for a pentamer.

Numerical Computations

i) Determination of Molecular Parameters. For the purpose of calculating thermodynamic quantities, the following values of molecular parameters are used, which have been determined from various sources. The magnitudes of hard sphere diameters and moments of inertia are tabulated in Table 1.

TABLE 1. MOLECULAR PARAMETERS

	Unbonded monomers	Pentamers
Diameter of hard spheres		
	$R_1=3.10$ Å	$R_2=5.50$ Å 5.55 Å
Polarizability $\bar{\alpha}$	1.44×10^{-24} cm^3	O-H···O distance 2.82 Å
Dipole moment μ	1.84 D	
Moments of inertia (10^{-40} g cm^2)		
	$I_{1,A}=1.0220$ $I_{1,B}=1.9187$ $I_{1,C}=2.9376$	$I_{2,A}=I_{2,B}$ $=I_{2,C}=634.332$

The R_1 is considered to correspond to the van der Waals diameter for water, which is used in the molecular dynamics calculation by Stillinger and Rahman.[11] The magnitudes of moments of inertia for monomers are those determined by Benedict and others[25] and cited by Eisenberg and Kauzmann.[26] Those of moments of inertia for a pentamer are calculated for the configuration shown in Fig. 1, where the hydrogen-bonded distance in liquid water is taken to be 2.82 Å[14,27] and the mass of four tetrahedrally-bonded molecules is assumed to be concentrated at their centers of mass. Calculated values of the moments of inertia for three rectangular axes shown in Fig. 1, *i.e.*, $I_{2,A}$, $I_{2,B}$, and $I_{2,C}$ are all equal in their magnitudes. This equality of these three moments of inertia shows high degree of symmetry of that configuration, which supports the idea that the pentamer is treated as a sphere in this work. Some uncertainly attaches to the determination of R_2. Lentz, Hagler and Scheraga[13] used about 5.3—5.4 Å as the values of R_2 for a pentamer. They determined the value by measuring the displaced volume of "foil-wrapped space-filling models" (by immersion of the models into liquid). Their values are those for "clusters as compact as possible, consistent with a maximum value of hydrogen bonding", and supposed to be a little smaller than that for the pentamer shown in Fig. 1. Thus, we have carried out calculations for two values of R_2, *i.e.* 5.50 and 5.55 Å.

As to the energy of the formation of hydrogen-bonding, the value of 2.5 kcal per mole of hydrogen bonds is used, various experimental sources of which are given in Table 2. This value of ε is assumed to correspond to the energy for the process of hydrogen-bond breakage during which the separation of the hydrogen-bonded pair of molecules remains nearly unchanged. The values determined by various different experimental techniques are seen to agree with each other. Davis and Litovitz used the value of 2.55 kcal/mol in their calculation.[27]

TABLE 2. THE ENERGY OF HYDROGEN-BONDING
ε (kcal/mol)

	ε	Authors	Bonding
R[a]	2.5_5	Walrafen[15]	O-H···O
IR[b]	2.5	Worley and Klotz[28]	O-H···O
R	2.4—2.5	Lindner[15]	O-D···O
IR	2.3	Senior and Verrall[29]	O-D···O
N[c]	≈2.5	Safford[15]	O-H···O
Average	2.5		

a) R: Raman. b) IR: infrared. c) N: neutron scattering.

Concerning the assignment of the frequency ν_j, there is still some uncertainty. We have assigned the values tabulated in Table 3 to each normal mode frequency $\nu_j(j=1—24)$, which are grouped as seen in the table. These values are taken from the sources[13,15,30,31] cited in Table 3 and are used as rounded-up values.

TABLE 3. NORMAL MODE FREQUENCIES
ν_j FOR PENTAMERS

	ν_j (cm^{-1})	Number of modes[a]
ν_L[b]	700	3
ν_L'	550	4
ν_L''	450	4
ν_T	200	3
ν_T'	150	3
$\nu_{tor.}$	100	2
ν_b	60	3
ν_b'	40	2

a) Refs. 13, 15, 30, 31. b) Suffix L, L', L'' are those for librational modes, T and T' for translational ones, tor. for torsional one, and b and b' for bending modes.

ii) Determination of Mole Fraction x for Hydrogen-Bonded Molecules and the Density of Liquid Water. In advance of calculating various thermodynamic quantities we must determine the equilibrium distribution for N_1 and N_2 at given T and V for a given total number N of molecules (Eq. 14). This can be carried out using the condition of the maximization of Z with respect to N_2, where the number of independent variables is only one under the condition of Eq. 14 for a given value of N and we take N_2 for the independent variable for convenience.

Thus,

$$\left(\frac{\partial F}{\partial N_2}\right)_{V,T} = \left(\frac{\partial F}{\partial N_2}\right)_{N_1,V,T} + \left(\frac{\partial F}{\partial N_1}\right)_{N_2,V,T}\left(\frac{\partial N_1}{\partial N_2}\right)_{V,T} = 0.$$

From Eq. 14 for a constant value of N,

$$\left(\frac{\partial N_1}{\partial N_2}\right)_{V,T} = -5.$$

Inserting this into the equation described above, we obtain

$$\left(\frac{\partial F}{\partial N_2}\right)_{N_1,V,T} = 5\left(\frac{\partial F}{\partial N_1}\right)_{N_2,V,T} \tag{21}$$

or $$\mu_2 = 5\mu_1, \tag{21'}$$

where μ_1 and μ_2 is the chemical potential for each species, respectively. Eq. 21 (*i.e.* Eq. 21') is the condition of thermodynamic equilibrium between pentamers and unbonded monomers.

In order to determine the density for the liquid theoretically, the equation of state, which is expressed as Eq. 17, is used, where the left hand side (pV) is safely regarded as zero under ordinary pressures (the so-called "vanishing external pressure condition"[19,32]).

The two procedures for the determination of the mole fraction and the density (*i.e.* molar volume) must be carried out simultaneously, because the two kinds of values to be determined are interrelated to each other in the two equations.

We use $x=5N_2/N$ as an independent variable instead of N_2, which is the mole fraction for hydrogen-bonded molecules in water. The following two equations are used in the determination of x and V for practical use. Eq. 21 becomes

$$\begin{aligned}
&-\left[\ln\left\{\left(\frac{2\pi m_2 kT}{h^2}\right)^{3/2}\frac{V}{N}\frac{5}{x}\right\} + \ln(1-\xi)\right.\\
&-\frac{1}{(1-\xi)}\frac{\pi}{6}\frac{N}{V}\left(1-\frac{4}{5}x\right)R_2^3 - \frac{3}{(1-\xi)}(R_2^2Y+R_2X)\\
&\left.-\frac{3}{(1-\xi)^2}\left(R_2^3XY+\frac{3}{2}R_2^2X^2\right) - \frac{3R_2^3X^3}{(1-\xi)^3}\right]\\
&-\left[\ln\left\{\frac{\pi^{1/2}}{\sigma_2}\left(\frac{8\pi^2kT}{h^2}\right)^{3/2}(I_{2,A}I_{2,B}I_{2,C})^{1/2}\gamma\right\}\right.\\
&\left.+\ln\left\{\prod_{j=1}^{24}\frac{\exp(-h\nu_j/2kT)}{1-\exp(-h\nu_j/kT)}\right\} - \frac{4\varepsilon}{kT}\right]\\
&+5\left[\ln\left\{\left(\frac{2\pi m_1 kT}{h^2}\right)^{3/2}\frac{V}{N}\frac{1}{(1-x)}\right\} + \ln(1-\xi)\right.\\
&-\frac{1}{(1-\xi)}\frac{\pi}{6}\frac{N}{V}\left(1-\frac{4}{5}x\right)R_1^3 - \frac{3}{(1-\xi)}(R_1^2Y+R_1X)\\
&\left.-\frac{3}{(1-\xi)^2}\left(R_1^3XY+\frac{3}{2}R_1^2X^2\right) - \frac{3R_1^3X^3}{(1-\xi)^3}\right]\\
&+5\left[\ln\left\{\frac{\pi^{1/2}}{\sigma_1}\left(\frac{8\pi^2kT}{h^2}\right)^{3/2}(I_{1,A}I_{1,B}I_{1,C})^{1/2}\right\}\right] = 0,
\end{aligned} \tag{22}$$

$$\xi = \frac{\pi}{6}\frac{N}{V}\left[R_1^3(1-x)+R_2^3\frac{x}{5}\right]$$

$$X = \frac{\pi}{6}\frac{N}{V}\left[R_1^2(1-x)+R_2^2\frac{x}{5}\right]$$

$$Y = \frac{\pi}{6}\frac{N}{V}\left[R_1(1-x)+R_2\frac{x}{5}\right],$$

and, from Eq. 17 with the vanishing external pressure condition, we obtain

$$\begin{aligned}
&\frac{kT}{(1-\xi)^3}\left[N\left(1-\frac{4}{5}x\right)(1-\xi)^2\right.\\
&\left.+\frac{18}{\pi}V\{XY(1-\xi)+X^3\}\right] + U_{BG} = 0
\end{aligned} \tag{23}$$

after some calculations (see Appendix I). For given values of various molecular parameters, the two simultanious equations are solved numerically to determine the values of x and V (*i.e.*, the density ρ).

iii) Numerical Calculations of Thermodynamic Variables. The computations of thermodynamic variables, F, U, S, C_p are carried out for each temperature, using the values of U_{AB} given in Appendix II as well as those of x and V determined according to the procedures in the previous section. The values of F, U, S, C_p are tabulated in Table 4 for the case of R_2=5.50 Å, including observed values. The calculated values of x and ρ also are given in Table 5.

We have taken the state of ice at 0 K in its ground intermolecular and intramolecular vibrational levels as the thermodynamic standard states. The values of U_{BG} have been calculated employing the state of infinitely dilute vapor at 0 K as the zero of energy. Then, we have added the value of 11.3−1.4=9.9 kcal/mol to those of U and F calculated from Eqs. 15 and 19, where

Table 4. Calculated and experimental thermodynamic properties of water

Temp (°C)	F (kcal/mol)		U (kcal/mol)		S (cal/deg mol)		C_p (cal/deg mol)	
	Calcd	Obsd[a)]	Calcd	Obsd[a)]	Calcd	Obsd[a)]	Calcd	Obsd[b)]
0	−1.07	−1.44	3.30	2.71	16.0_5	15.2	29.6	18.2
10	-1.16_5	−1.59	3.60_5	2.89	16.8_5	15.8	29.1	18.1
20	−1.34	−1.75	3.89_5	3.07	17.9	16.4	28.4	18.0
30	−1.59	−1.92	4.17_5	3.25	19.0	17.1	26.9	18.0
40	-1.95_5	−2.09	4.42	3.43	20.3	17.6	25.2	18.0
50	−2.35	−2.27	4.68	3.61	21.7	18.2	25.3	18.0
60	-2.65_5	−2.46	4.95_5	3.79	22.8	18.8	26.2	18.0
70	-2.89_5	−2.65	5.23	3.97	23.7	19.3	27.3	18.0
80	-3.09_5	−2.84	5.50	4.15	24.3_5	19.8	27.8	18.1
90	−3.28	−3.04	5.77_5	4.33	24.9_5	20.3	28.0	18.1
100	−3.47	−3.25	6.03_5	4.52	25.4_5	20.8	28.1	18.2

a) Ref. 13 and N.E. Dersey "Properties of Ordinary Water Substances," ACS Monograph, No. 81, Reinhold, New York (1940). b) G.S. Kell, *J. Chem. Eng. Data*, **12**, 66 (1967).

Table 5. Mole fraction of hydrogen-bonded molecules x and density ρ

Temp (°C)	x	ρ (g/cm³)	
		Calcd	Obsd
0	0.790	1.147	0.9998
10	0.729	1.121	0.9997
20	0.645	1.089	0.9982
30	0.529	1.049	0.9957
40	0.362	0.996	0.9922
50	0.200	0.943	0.9880
60	0.091	0.901	0.9832
70	0.040	0.870	0.9778
80	0.019	0.847	0.9718
90	0.009	0.826	0.9653
100	0.005	0.808	0.9584

11.3 kcal/mol is the value of sublimation energy from ice at 0 K[33] and 1.4 kcal/mol is the shift in intramolecular zero-point energy[34] for the process of sublimation.

Results and Discussion

i) Temperature Dependence of x *and* ρ. Values of x calculated are plotted against temperature in Fig. 2, where the two calculations for R_2=5.50 Å (Table 5) and for R_2=5.55 Å are given. The curves given in Fig. 2 shows that magnitude of x, which is regarded as a measure of the "structure" in liquid water, is large at lower temperatures (about 80% for R_2=5.50 Å and about 60% for R_2=5.55 Å) and decreases rapidly with increase of temperature. The inflection point where $\partial^2 x/\partial T^2=0$ and the decreasing rate is maximum is about 40 °C for R_2=5.50 Å. This supports the idea that the structure of water varies a great deal at about 40—50 °C. It is observed experimentally that compressibility becomes minimum near about the temperatures and also that the third peak of the radial distribution curve nearly disappeares above the temperatures.[14,35] The rapid decrease of x at the temperatures is supposed to be associated with those observed facts. The calculation for R_2=5.50 Å is expected to give a more adequate result than that for R_2=5.55 Å.

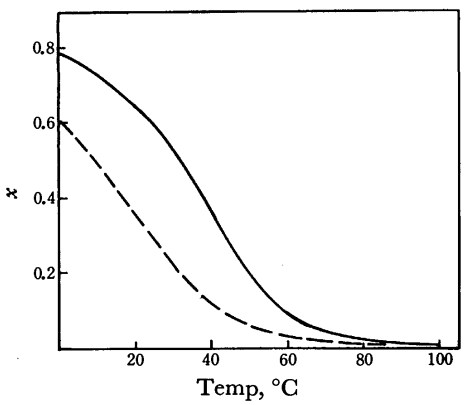

Fig. 2. The temperature dependence of mole fraction of hydrogen-bonded molecules.
——: R_2=5.50 Å,
------: R_2=5.55 Å.

The mole fraction of unbroken hydrogen bonds, x_{HB}, which is calculated from the value of x, is given in Table 6, and is compared with the values of Lentz, Hagler and Scheraga[13] (LHS) and those of Weres and Rice[12] (WR). Our values decrease more rapidly and are found to be smaller than those of LHS and WR. The values of WR are seen to be constant throughout the range of temperature from 0 to 100 °C, and those of LHS also are nearly constant. This is unreasonable, considering from the variation of various properties of water with temperature, *i.e.*, the disappearance of some features in the radial distribution curve at higher temperatures, *etc.* The temperature dependence of x_{HB} found in our work may be reasonably accepted as showing the behavior of water, though the magnitudes are too small at higher temperatures.

Table 6. Mole fraction of unbroken hydrogen bonds x_{HB}

Temp (°C)	This work (R_2=5.50 Å)	LHS	WR
0	0.32	0.47	0.68[a]
20	0.26	0.46	
40	0.14_5	0.45	
100	0.00_2	0.43	

a) Nearly constant from 0 to 100 °C.

Values of ρ calculated are plotted against temperature in Fig. 3 in comparison with observed values. The temperature dependence in the calculated ρ *vs.* T curve is seen to be too large compared with that observed. The curve becomes fairly flat at about 0—10 °C range (R_2= 5.50 Å), though the temperature of maximum density (TMD) is not observed.

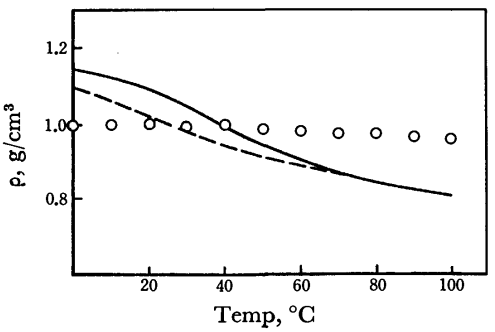

Fig. 3. The temperature dependence of density ρ.
——: R_2=5.50 Å,
------: R_2=5.55 Å,
○: observed values.

In the recent study by Lentz, Hagler, and Scheraga[13] they did not calculate the density and used the observed values as given ones in their calculation. Weres and Rice gave a calculated ρ *vs.* T curve (in Fig. 6 in their paper[12]), but their values of ρ is determined only semi-empirically as a direct result of their assumption that "the dimensions of the basic cell vary linearly with temperature."

In our calculation the density is determined theoretically without any additive assumptions by solving directly a simultaneous equation (Eqs. 22 and 23). The

agreement of the calculated values of ρ with observed ones is fairly good on the whole, which proves the essential usefulness of the procedures for the determination of ρ in this work.

Fleming and Gibbs[7] have presented a lattice gas theory of water and carried out a theoretical determination of ρ. Their values are found to be too large by a factor of 1.4. They also have not succeeded in giving TMD in the range of temperatures from 0 to 100 °C, though a possibility of the presence of TMD below 0 °C has been stated. To give TMD in the calculated ρ *vs.* T curve is the problem of further studies.

ii) Temperature Dependence of Thermodynamic Variables. The values of F, U, and S are plotted against temperature in Figs. 4, 5, and 6, including the values calculated for the case of R_2=5.55 Å and those observed for comparison. The calculated F *vs.* T curve is seen to be in good agreement with the observed curve. Concerning the S *vs.* T given in Fig. 6, the deviation from the observed curve is small at lower temperatures, and it ascends more rapidly with temperature, being above the observed curve through all the range of temperatures from 0 to 100 °C. The behavior is similar to the U *vs.* T curve as given in Fig. 5. As clearly seen in Figs. 2—5, the calculation for R_2=5.50 Å gives better results than that for R_2=5.55 Å.

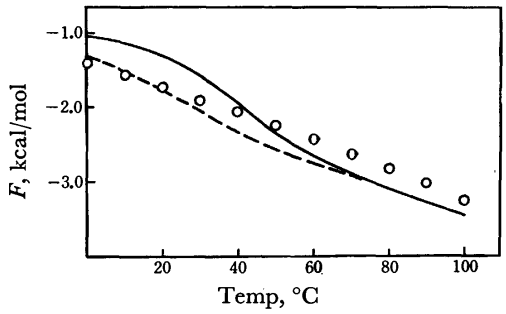

Fig. 4. The temperature dependence of free energy F.
——: R_2=5.50 Å,
------: R_2=5.55 Å,
○: observed values.

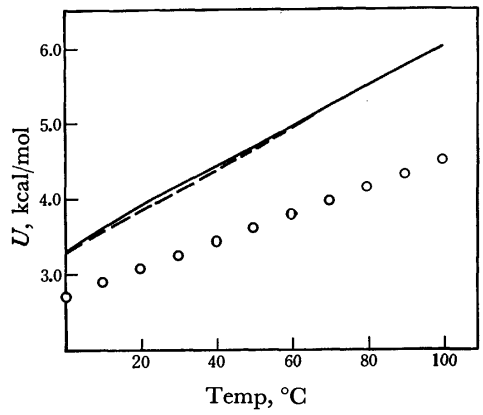

Fig. 5. The temperature dependence of internal energy U.
——: R_2=5.50 Å,
------: R_2=5.55 Å,
○: observed values.

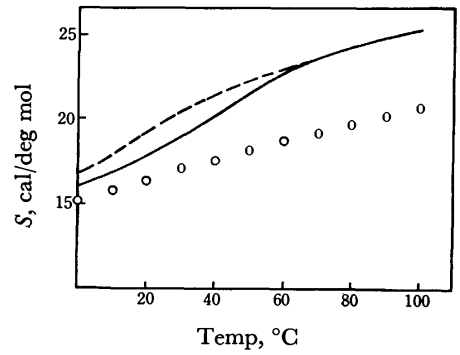

Fig. 6. The temperature depencence of entropy S.
——: R_2=5.50 Å,
------: R_2=5.55 Å,
○: observed values.

As expressed in Eqs. 18 and 19, the thermodynamic quantities calculated are regarded as consisting of several terms which are attributed to various kinds of degrees of freedom. Those are tabulated in Tables 7 and 8. It is very interesting to investigate the variation of the contribution from each degree of freedom with temperature, in order to compare the features of various theories.

Thus, our results (Tables 7 and 8) are compared with those of LHS[13] (Table 9) and WR[12] (Table 10) in

Table 7. Values of various terms in Eq. 18 (cal/deg mol)

Temp (°C)	$S_{trans.}$	$S_{rot.}$	$S_{int.}$[a]	S_{total}
0	1.9	6.5	7.6_5	16.0_5
10	2.7_5	6.8_5	7.2_5	16.8_5
20	4.0_5	7.3	6.5_5	17.9
30	5.6	7.9	5.5	19.0
40	7.7	8.7_5	3.8_5	20.3
50	9.8_5	9.6_5	2.2	21.7
60	11.5	10.3	1.0	22.8
70	12.6	10.6_5	0.4_5	23.7
80	13.3	10.8_5	0.2	24.3_5
90	13.8_5	11.0	0.1	24.9_5
100	14.3_5	11.0_5	0.0_5	25.4_5

a) In our calculation $S_{int.}$ is identical with $S_{vib.}$.

Table 8. Values of various terms in Eq. 19 (kcal/mol)

Temp (°C)	$U_{kin.}$	$U_{vib.}$	U_{HB}	U_{BG}	U_{total}
0	0.60	2.70	−1.58	−8.32	3.30
10	0.70_5	2.54_5	-1.45_5	−8.09	3.60_5
20	0.84_5	2.30	−1.29	−7.86	3.89_5
30	1.04_5	1.92_5	-1.05_5	−7.64	4.17_5
40	1.32_5	1.35	-0.72_5	−7.41	4.42
50	1.62	0.76	−0.40	−7.20	4.68
60	1.84	0.35_5	−0.18	−6.96	4.95_5
70	1.98	0.16	−0.08	−6.73	5.23
80	2.07_5	0.07_5	−0.04	−6.51	5.50
90	2.15	0.03_5	−0.02	−6.29	5.77_5
100	2.21_5	0.02	−0.01	−6.09	6.03_5

a) 9.9 kcal/mol has been added to the sum in order to obtain U_{total}.

Table 9. Thermodynamic properties calculated by Lentz, Hagler, and Scheraga[13]

	0 °C	100 °C
U (kcal/mol)		
$U_{kin.}$ [a]	0.542	0.868
$U_{vib.}$	3.331	3.866
U_{HB}	2.541	3.096
U_{total} [b]	2.914	4.331
S (cal/deg mol)		
$S_{trans.}$	4.16	5.54
$S_{rot.}$	2.50	3.14
$S_{vib.}$	8.73	10.81
S_H	0.63	0.53
S_{total}	16.02	20.02

a) $U_{kin.}=U_{trans.}+U_{rot.}$. b) The intermolecular zero point energy, 3.500 kcal/mol, has been substracted from the sum to obtain U_{total}.

Table 10. Thermodynamic properties calculated by Weres and Rice[12]

	0 °C	100 °C
$H=U$ (kcal/mol)		
Lattice	−8.296	−8.088
Translational vib.	1.729	2.290
Librational	2.517	2.858
Nonbonded neighbor	−1.325	−1.271
Long range	−1.190	−1.166
Intramolecular zero point	−0.900	−0.694
Total[a]	3.835	4.509
S (cal/deg mol)		
Configurational	4.48	4.48
Orientational	1.70	1.69
Translational vib.	7.12	9.28
Librational	2.00	3.44
Nonbonded neighbor	−1.17	−0.95
Vibrational	0.26	0.26
Total	14.39	18.20

a) The sublimation energy at 0 K, 11.3 kcal/mol, has been added to the sum to obtain U_{total}.

details. It is noticed that as to the entropy, each term in our theory corresponds to that in LHS theory when $S_{int.}$ of ours is regarded as equivalent to $(S_{vib.}+S_H)$ in LHS, and also noticed that it is not the case in the comparison with WR theory.

It is easily seen that the temperature dependence of entropy in our results is greater than that in WR and LHS theories. In the case of WR the calculated values of S_{total} are smaller than observed, being in sharp contrast to the authors' values. At lower temperatures the largest contribution to S_{total} comes from the vibrational motion in all three theories, but the behaviors are different at higher temperatures. In the authors calculation, $S_{trans.}$ increases fairly rapidly and amounts to about a half of the total entropy at about 50—60 °C, while $S_{trans.}$ in LHS theory increases only slightly with increasing temperature. As to the internal energy, the similar behavior is observed in the comparison between $U_{kin.}$ in our calculation and that in LHS.

We can see another noticeable feature in the comparison of $S_{vib.}$ and $U_{vib.}$, the contributions from the vibrational degrees of freedom. They both decrease with increasing temperature in our calculation, while in the calculations by LHS as well as WR they increase on the contrary.

From the two features described above, it is tentatively said that the theory of LHS as well as that of WR is possessed of too solid-like character so far as the temperature dependence of thermodynamic variables is concerned.

In the calculation of WR, the configurational entropy which is attributed to the number of ways for the arrangement of molecules within a basic unit cell is kept constant throughout the range of temperatures from 0 to 100 °C. This is unreasonable, because it shows that the local structure in liquid water remains thoroughly unchanged with the variation of temperatures.

In our calculation the magnitudes of $U_{vib.}$, $S_{int.}=S_{vib.}$, $U_{HB.}$, and $S_{trans.}$ vary most rapidly at 40—50 °C with increasing temperature. This is ascribed to the rapid decrease of the mole fraction of water molecules forming pentamers, as seen in Fig. 2, at the temperatures.

iii) Heat Capacity. In using Eq. 20 for the calculation of C_p, the term $p(\partial V/\partial T)_p=pV\alpha$ has been safely ignored in comparison with the term $(\partial U/\partial T)_p$, where $pV<1$ cal/mol and the thermal expansion coefficient $\alpha\lesssim 10^{-3}$ deg.$^{-1}$. Among the remaining terms in Eq. 20, the temperature derivatives of $x=5N_2/N$ and U_{BG} are determined graphically using the curves given in Figs. 2 and AII-2, respectively, and the terms including $Q_{vib.}$ are calculated using Eq. 6.

Our values (the eighth column in Table 4) becomes 27.3_5 cal/deg mol in the average throughout the range of temperatures, 0—100 °C, which is about 9 cal/deg mol larger than the average of $C_{p.obsd.}$. This is in sharp contrast to the feature found in the calculations of LHS[13] and WR,[12] where $C_{p.calcd}$ is smaller than $C_{p.obsd.}$

It is noted that a shallow minimum is observed at about 40 °C in the $C_{p.calcd}$ *vs.* T relation in this work. This corresponds to the presence of a minimum at about 35 °C in the $C_{p.obsd}$ *vs.* T relation. In the calculation of LHS and WR, $C_{p.calcd}$ *vs.* T curves are monotonously increasing throughout the range of temperatures, 0—100 °C. The contribution to C_p from each degree of freedom can be determined from the corresponding values of internal energy (Eq. 19) given in Table 8. Each contribution averaged in the range 0—100 °C is shown in Table 11.

Table 11. Average contributions to the total heat capacity C_p (cal/deg mol)

Kinetic	16.1_5
Vibrational	−26.8
Hydrogen-Bonding	15.7
Background Potential	22.3
$C_{p.total}$	27.3_5

iv) Equivalent Free Volume Fraction f. In the formulation of our theory we have used Eq. 2 as the translational partition function. The partition function

has a form which is similar in its appearance to the formula used in cell theories of fluid mixtures. Then, we have defined f (Eq. 3) as an equivalent free volume fraction, which is a generalization of the authors' proposition[19] with respect to a pure liquid into multi-conponent fluids. In our theory no lattice which is necessary for cell theories is assumed.

The translational partition function for hard sphere mixtures is shown as a comparatively simple explicit expression similar to usual free volume theories. This is expected to give a good promise for further use.

We have calculated the values of f according to Eq. 3 and the values are compared with those calculated by Weissmann and Blum[8] for water using the Monte Carlo method. The values are given in Table 12. Our values are found to be larger than those of Weissmann and Blum. However, in their calculations, the contribution from the rotational degree of freedom is included, and the magnitude of f is expected to be of nearly the same order compared with ours if that contribution to the phase integral is substracted as stated in their paper.

Table 12. Free volume fraction f and packing fraction ξ

Temp (°C)	f		ξ	
	This work	Weissmann-Blum[8]	R_2=5.50 Å	5.55 Å
4	5.80×10^{-5}	0.60×10^{-7}	0.64_5	0.61
50	7.14×10^{-3}	0.34×10^{-6}	0.50	0.48
100	2.95×10^{-2}	1.19×10^{-6}	0.42	0.42

As for the magnitudes of the packing fraction ξ given together in Table 12, the large value of ξ at 4 °C is supposed to result from the too large value of ρ_{calcd} obtained at the temperature.[19,36]

Concluding Remarks

The purpose of this paper has been to formulate a statistical thermodynamic theory for liquid water without using adjustable parameters to obtain the best fit with observed data as ordinarily carried out. We have used a model consisting of tetrahedrally hydrogen-bonded pentamers and unbonded monomers which are immersed in a uniform background potential. The feature in the theory and its results are outlined as follows: (a) the translational partition function for the model has been derived from the analytical solution of the Percus-Yevick equation for hard sphere mixtures, (b) U_{BG} has been calculated directly as the sum of dipole-dipole, dipole-induced dipole, and dispersion interactions, (c) the mole fraction x of hydrogen-bonded species and the density ρ have been determined by solving a simultaneous equation numerically, and calculated values of ρ are found to be of the right order in their magnitudes, compared with observed values, though the TMD is not observed, (d) the magnitude of x is found to be large (about 80%) at 0 °C which shows the predominance of the "structure" in liquid water at lower temperatures, (e) calculated thermodynamic properties are found to vary rapidly at 40—50 °C with increase in temperature, which is attributed to the rapid decrease of x at the range of temperatures, (f) the magnitude of x becomes very small above about 60 °C (Table 5).

The success in the present theory, though it is qualitative and limited, has put a support to the so-called small cluster model, and the better fit of results with observed data is expected through making some improvements of the model used. The first of those is an introduction of one more species, *i.e.* "hydrogen-bonded ring hexamer" as a structure unit. In that model, water is assumed to be a mixture of unbonded monomers, tetrahedrally-coordinated pentamers, and ring hexamers immersed in a uniform background potential. This three-component model is expected to improve the results.

Appendix I. An Analytical Expression of the Partition Function for the Mixture of Hard Spheres

For a system consisting of m components with number densities ρ_i, $i=1,\cdots\cdots m$,

$$F = G - pV = \sum_{i=1}^{m} N_i\mu_i - pV, \tag{AI-1}$$

where μ_i is the chemical potential of the i-th species and $N_i = \rho_i V$. The exact analytical solution of the generalized Percus-Yevick equation for the mixture of hard spheres was given by Lebowitz, and the μ_i becomes, following Lebowitz and Rowlinson,[20]

$$\beta\mu_i = \ln\left[\frac{\rho_i h^3}{(2\pi m_i kT)^{3/2}}\right] - \ln(1-\xi) + \frac{\pi}{6}\beta p R_i^3 + \frac{3}{(1-\xi)}(R_i^2 Y + R_i X) + \frac{9}{2}\frac{R_i^2 X^2}{(1-\xi)^2}, \tag{AI-2}$$

where R_i is the diameter of a particle of the i-th species and $\beta = 1/kT$, and

$$\xi = \sum_{i=1}^{m}\frac{\pi}{6}\rho_i R_i^3, \quad X = \sum_{i=1}^{m}\frac{\pi}{6}\rho_i R_i^2, \quad Y = \sum_{i=1}^{m}\frac{\pi}{6}\rho_i R_i.$$

Substitution of Eq.AI-2 into Eq.AI-1 gives

$$F = \beta^{-1}\sum_{i=1}^{m}\ln\left[\frac{\rho_i h^3}{(2\pi m_i kT)^{3/2}}\right]^{N_i} - \beta^{-1}\ln(1-\xi)^{\sum N_i} + \frac{9}{\pi}\beta^{-1}V\frac{1}{(1-\xi)^2}\left[-\frac{\pi}{9}\beta p(1-\xi)^3 + 4XY - 4XY\xi + 3X^3\right]. \tag{AI-3}$$

The equation of sate (Eq. 2.8 in Ref. 20) which was given associated with the generalized compressibility relation is

$$\beta p = \frac{1}{(1-\xi)^3}\left[(\sum_{i=1}^{m}\rho_i)(1+\xi+\xi^2) - \frac{\pi}{2}\sum_{i<j}\rho_i\rho_j(R_i-R_j)^2(R_i+R_j+R_iR_jX)\right]. \tag{AI-4}$$

Using the relations,

$$\frac{\pi}{2}\sum_{i<j}\rho_i\rho_j(R_i-R_j)^2(R_i+R_j) = 3\xi(\sum_i\rho_i) - \frac{18}{\pi}XY$$

and

$$\frac{\pi}{2}\sum_{i<j}\rho_i\rho_j(R_i-R_j)^2R_iR_j = \frac{18}{\pi}(Y\xi - X^2),$$

we obtain from Eq. AI-4

$$\beta p = \frac{1}{(1-\xi)^3}\left[(\sum_i\rho_i)(1-\xi)^2 + \frac{18}{\pi}(XY - XY\xi + X^3)\right]. \tag{AI-5}$$

Inserting Eq. AI-5 into Eq. AI-3, we obtain

$$F = \beta^{-1}\sum_i \ln\left[\frac{\rho_i h^3}{(2\pi m_i kT)^{3/2}}\right]^{N_i} - \beta^{-1}\ln(1-\xi)^{\sum_i N_i} - \beta^{-1}\sum_i N_i + \frac{9}{\pi}\beta^{-1}V\frac{1}{(1-\xi)^2}(2XY - 2XY\xi + X^3). \quad \text{(AI-6)}$$

From Eq. AI-6 we give the following partition function Z which is expressed as a form with the equivalent free volume fraction f for an m-component mixture of hard spheres,

$$Z = \exp(-\beta F) = \prod_{i=1}^{m}\left[\left(\frac{2\pi m_i kT}{h^2}\right)^{3/2} e v_i f\right]^{N_i} = \frac{(\sum_i N_i)!}{\prod_i N_i!}\prod_{i=1}^{m}\left[\left(\frac{2\pi m_i kT}{h^2}\right)^{3/2} e v f\right]^{N_i} \quad \text{(AI-7)}$$

where f has the form

$$f = (1-\xi)\exp\left[-\frac{9}{\pi}\frac{v}{(1-\xi)^2}(2XY - 2XY\xi + X^3)\right], \quad \text{(AI-8)}$$

and $v_i = V/N_i, v = V/\sum_i N_i$.

For a one-component system, Eqs. AI-7 and AI-8 lead us to the same analytical expression as given in the previous paper by the two of the authors,[19] in which the concept of an equivalent free volume was proposed on the basis of Wertheim's solution for the Percus-Yevick equation of pure liquid.

Appendix II. The Calculation of the Background Potential

Two steps of numerical integrations are required in carrying out the calculation of the background potential U_{BG}. The first step is the integration in obtaining $\langle U_{\mu\mu}\rangle$ (Eq. 9), as follows,

$$\langle U_{\mu\mu}\rangle = \int_0^{\pi}\int_0^{\pi}\int_0^{2\pi}\int_0^{2\pi} d\theta_A d\theta_B d\phi_A d\phi_B \exp\left[-\frac{U_{\mu\mu}(\theta_A,\theta_B,\phi_A,\phi_B)}{kT}\right] \times U_{\mu\mu}\sin\theta_A \sin\theta_B \Big/ \int_0^{\pi}\int_0^{\pi}\int_0^{2\pi}\int_0^{2\pi} d\theta_A d\theta_B d\phi_A d\phi_B \times \exp\left[-\frac{U_{\mu\mu}(\theta_A,\theta_B,\phi_A,\phi_B)}{kT}\right]\sin\theta_A \sin\theta_B, \quad \text{(AII-1)}$$

where

$$U_{\mu\mu} = \frac{\mu^2}{\bar{R}^3}[\sin\theta_A \sin\theta_B \cos(\phi_A - \phi_B) - 2\cos\theta_A \cos\theta_B].$$

The numerical evaluation of multidimentional integral such as Eq. AII-1 is usually carried out by means of the Monte Carlo method which gives as an estimate for the integral the sum,

$$\langle U_{\mu\mu}\rangle = \frac{1}{M}\sum_{i=1}^{M}\exp\left[-\frac{U_{\mu\mu}(\theta_{Ai},\phi_{Ai},\theta_{Bi},\phi_{Bi})}{kT}\right]U_{\mu\mu}\sin\theta_{Ai}\sin\theta_{Bi} \Big/ \frac{1}{M}\sum_{i=1}^{M}\exp\left[-\frac{U_{\mu\mu}(\theta_{Ai},\phi_{Ai},\theta_{Bi},\phi_{Bi})}{kT}\right]\sin\theta_{Ai}\sin\theta_{Bi}, \quad \text{(AII-2)}$$

where M is the number of the points X_i (θ_{Ai}, ϕ_{Ai}, θ_{Bi}, ϕ_{Bi}), and θ_{Ai}, ϕ_{Ai}, θ_{Bi}, and ϕ_{Bi} are chosen at random in the range of integration.

The error of such an estimate is of the order of $M^{-1/2}$ as a standard deviation. In carrying out the evaluation we have used the Monte Carlo method using the technique devised by Haselgrove.[37] It is shown that the error in the method is convergent asymptotically to the order of $O(M^{-1})$ and $O(M^{-2})$ under certain conditions, and also shown that the method is superior to the usual Monte Carlo method. The magnitude of M has been taken as 15000, when the convergence in the integration is very well.

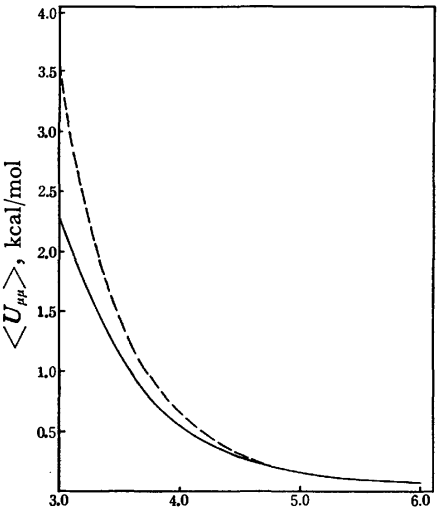

Fig. AII-1. $\langle U_{\mu\mu}\rangle$ *vs.* R curves at 25 °C.
——: Exact, ------: approximated (Eq. AII-3).

The calculated values of $\langle U_{\mu\mu}\rangle$ for 25 °C are plotted against the separation $\bar{R}$ in Fig. AII-1, including the values calculated from the following approximate formula which should be used under the condition that kT is much greater than the difference of the maximum and minimum value of $U_{\mu\mu}$.

$$\langle U_{\mu\mu}\rangle = -\frac{2}{3kT}\frac{\mu^4}{\bar{R}^6} \quad \text{(AII-3)}$$

The curve for this approximate formula is observed to deviate from the exact curve discriminately within the range of $\bar{R}$ smaller than 4—5 Å.

The second step is the numerical evaluation of the integral in Eq. 12, where the magnitudes of $\bar{\alpha}$ and μ are given in Table 1 and the value of c is taken to be 60×10^{-60} erg cm^6.[38]

Then, the background potential is

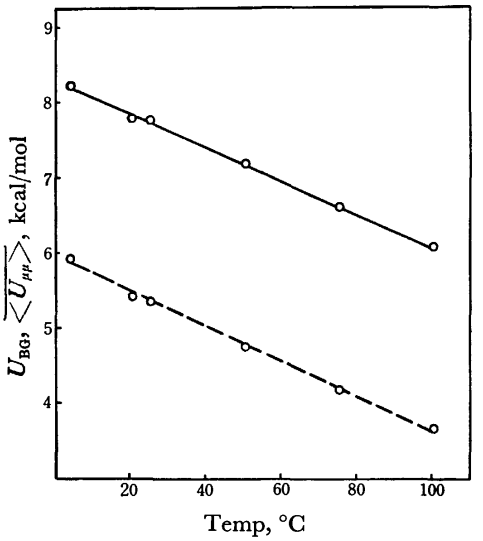

Fig. AII-2. The temperature dependence of U_{BG} and $\overline{\langle U_{\mu\mu}\rangle}$.
——: U_{BG}, ------: $\overline{\langle U_{\mu\mu}\rangle}$.

$$U_{BG} = \frac{N^2}{2V}\int_{\tilde{R}_0}^{\infty}[\langle U_{\mu\mu}\rangle + U_{\mu\alpha} + U_{disp.}]g(\tilde{R})4\pi\tilde{R}^2 d\tilde{R}$$
$$= \overline{\langle U_{\mu\mu}\rangle} + \bar{U}_{\mu\alpha} + \bar{U}_{disp.}, \quad \text{(AII-4)}$$

where the value of $\tilde{R}_0$ is taken to be 3.1 Å.[3,11] We have estimated the integral by means of the Simpson rule. The values of U_{BG} and $\overline{\langle U_{\mu\mu}\rangle}$ thus calculated are given in Fig. AII-2. Throughout the range of temperatures from 0°C to 100 °C, the values of $\bar{U}_{\mu\alpha}$ and $\bar{U}_{disp.}$ are found to remain constant within the range of 0.34 ± 0.01 and 2.05 ± 0.05 kcal/mol, respectively.

References

1) R. A. Horne, Ed., "Water and Aqueous Solution," Wiley-Interscience, New York (1972).
2) F. H. Stillinger, *Adv. Chem. Phys.*, **31**, 1 (1975).
3) K. Arakawa, *Kagaku No Ryoiki Zokan*, No. **106**, 15 (1974); *Kagaku Sosetsu*, No. **11**, 35 (1976).
4) F. Franks, Ed., "Water" Vol. 1—5, Plenum, New York (1972—1975).
5) H. S. Frank, "Water" (Ed., F. Franks) Vol. 1, Plenum, New York (1972) Chapt. 14.
6) G. M. Bell, *J. Phys.*, **C**, **5**, 889 (1972).
7) P. D. Fleming and J. H. Gibbs, *J. Statist. Phys.*, **10**, 157, 351 (1974).
8) M. Weissmann and L. Blum, *Trans. Faraday Soc.*, **64**, 2605 (1968).
9) K. Arakawa and K. Sasaki, *Bull. Chem. Soc. Jpn.*, **40**, 3048 (1970).
10) A. Ben-Naim, *J. Chem. Phys.*, **52**, 5531 (1970); **57**, 3605 (1972); "Water and Aqueous Solutions," Plenum, New York (1974).
11) A. Rahman and F. H. Stillinger, *J. Chem. Phys.*, **55**, 3336 (1971); F. H. Stillinger and A. Rahman, *ibid.*, **57**, 1281 (1972); **60**, 1545 (1974); **61**, 4973 (1974); A. Rahman and F. H. Stillinger, *J. Am. Chem. Soc.*, **95**, 7943 (1973).
12) O. Weres and S. A. Rice, *J. Am. Chem. Soc.*, **94**, 8983 (1972).
13) B. R. Lentz, A. T. Hagler, and H. A. Scheraga, *J. Phys. Chem.*, **78**, 1531 (1974).
14) A. H. Narten, M. D. Danford, and H. A. Levy, *Discuss. Faraday Soc.*, **43**, 97 (1967).
15) G. E. Walrafen, "Water," ed by F. Franks, Vol. 1. Chapt. 5; "Hydrogen-Bonded Solvent Systems," ed by A. K. Covington and P. Jones, Taylor and Francis, London (1968), p. 9.
16) G. Némethy and H. A. Scheraga, *J. Chem. Phys.*, **36**, 3382 (1962).
17) H. C. Longuet-Higgins and B. Widom, *Mol. Phys.*, **8**, 549 (1964).
18) A. T. Hagler, H. A. Scheraga, and G. Némethy, *J. Phys. Chem.*, **76**, 3229 (1972).
19) K. Arakawa and K. Kojima, *Bull. Chem. Soc. Jpn.*, **48**, 26 (1975).
20) J. L. Lebowitz, *Phys. Rev.*, **133A**, 895 (1964); J. L. Lebowitz and J. S. Rowlinson, *J. Chem. Phys.*, **41**, 133 (1964).
21) Scheraga and coworkers used the results of the studies by Lebowitz and Rowlinson only numerically and could not give an analytical expression of $Q_{trans.}$ described in the present text.
22) A. H. Narten and H. Levy, *J. Chem. Phys.*, **55**, 2263 (1971).
23) δF is written as
$$\delta F = \left(\frac{\delta F}{\delta T}\right)_{V,N_1,N_2}\delta T + \left(\frac{\delta F}{\delta V}\right)_{T,N_1,N_2}\delta V + \left(\frac{\delta F}{\delta N_1}\right)_{V,T,N_2}\delta N_1 + \left(\frac{\delta F}{\delta N_2}\right)_{V,T,N_1}\delta N_2,$$
for small variations δT, δV, δN_1, and δN_2. We obtain $\delta N_1 + 5\delta N_2 = 0$ from Eq. 14 for a given N. Then, at the equilibrium condition of Eq. 13 for a given N,
$$(\delta F)_N = \left(\frac{\delta F}{\delta T}\right)_{V,N_1,N_2}(\delta T)_N + \left(\frac{\delta F}{\delta V}\right)_{T,N_1,N_2}\delta(V)_N.$$
Thus, we obtain Eq. 16.
24) In Eq. 18, the contribution from the temperature variation of a is ignored. The magnitude of a was determined from the values of U_{BG} (Table 8) and those of V° obtained from ρ_{calcd} (Table 4). It was found to be $-(1.35\pm0.03)\times10^5$ cal cm^3/mole^2 throughout the range of temperatures, 0—100 °C. Thus, the assumption, $\partial a/\partial T = 0$ is considered to be adequate.
25) W. S. Benedict, N. Gailar, and E. K. Plyler, *J. Chem. Phys.*, **24**, 1139 (1956).
26) D. Eisenberg and W. Kauzmann, "The Structure and Properties of Water," Oxford Univ. Press, New York (1969).
27) C. Davis and T. Litovitz, *J. Chem. Phys.*, **42**, 2563 (1965).
28) J. D. Worley and I. M. Klotz, *J. Chem. Phys.*, **45**, 2868 (1966).
29) W. A. Senior and R. E. Verrall, *J. Phys. Chem.*, **73**, 4242 (1969).
30) B. R. Lentz, A. T. Hagler, and H. A. Scheraga, *J. Phys. Chem.*, **78**, 1844 (1974).
31) J. C. Owicki, L. L. Shipman, and H. A. Scheraga, *J. Phys. Chem.*, **79**, 1794 (1975).
32) K. Arakawa and O. Kiyohara, *Bull. Chem. Soc. Jpn.*, **43**, 975 (1970).
33) Ref. 26, p. 101.
34) E. Whalley, *Trans. Faraday Soc.*, **53**, 1578 (1957).
35) Ref. 26, p. 157.
36) J-P. Hansen and L. Verlet, *Phys. Rev.*, **184**, 151 (1969); D. J. Adams and A. J. Matheson, *J. Chem. Phys.*, **56**, 1989 (1972).
37) C. B. Haselgrove, *Math. Comput.*, **15**, 323 (1961).
38) Ref. 26, p. 44.

ENDOR Studies of Alkylated Biphenyl Anion Radicals in Solution. Relation between Molecular Size and Optimum Temperature of ENDOR Enhancement

Kazuhiko Ishizu, Masayoshi Ohnishi, and Hideo Shikata*

Department of Chemistry, Faculty of Science, Ehime University, Matsuyama 790

* *Laboratory of Chemistry, Faculty of General Education, Ehime University, Matsuyama 790*

(Received July 12, 1976)

The ENDOR spectra of several alkylated biphenyl anions with *para*- and *meta*-substitutions were observed, and the relation between the molecular size and the optimum temperature of *ortho*-proton ENDOR were investigated in terms of the electron-nuclear dipole-dipole interaction. On the basis of the Stokes-Einstein model, a linear relation was found between the inverse of the effective radius and the cubic root of the η/T value at the optimum temperature of the *ortho*-proton ENDOR, under the assumption that the radical anion undergoes rotation accompanied by the solvent shell. In this situation, the separation between the radical anion and the counter cation thus estimated is more than 8.3 Å and the ion pair exists as a solvent-separated ion pair.

It is known that the optimum ENDOR enhancement in a solution can usually be observed in the temperature region close to the freezing point of the solvent. In identical physico-chemical environments, the optimum temperature varies with the proton species, *e.g.*, the aromatic protons and the aliphatic protons; the electron-nuclear hyperfine interaction affects a shift of the optimum temperature. A larger spin density on aromatic carbon usually displaces the optimum enhancement toward higher temperatures. Such an effect is successfully interpreted under the assumption that the electron-nuclear dipole-dipole interaction (END) plays the dominant role in the relaxation process, when the Heisenberg spin-exchange interaction in negligible in dilute solution systems;[1] that is, the desaturation of the ESR by NMR exciation is most effectively established when the lattice-induced nuclear-spin transition probability, W_n, has a certain value comparable to the lattice-induced electron-spin transition probability, W_e. W_n is proportional to the molecular rotational correlation time, τ_R, and the square of spin density. The τ_R value can be also related to the molecular volume and, therefore, the molecular volume, as well as the spin density, should affect the optimum temperature for ENDOR enhancement.

Alkylated biphenyls with *meta*- or *para*-substituents are some of the most suitable systems for investigating this point, because the spin densities at the *ortho*-position are only slightly perturbed by alkyl substitution,[2] and ENDOR observation has already been established.[3-5] In the present paper, the relation between the molecular radius and the temperature dependence of the ENDOR enhancement is investigated for anion radicals such as biphenyl (BP), 4,4′-bitolyl (*p*-Me), 4,4′-diethylbiphenyl (*p*-Et), 4,4′-di-*t*-butylbiphenyl (*p*-Bu), 3,3′,5,5′-tetramethylbiphenyl (*m*-Me), and 3,3′,5,5′-tetra-*t*-butylbiphenyl (*m*-Bu). The effective radii of the solvated radical anions are estimated and the structures of the ion-pairs are discussed.

Experimental

Commercial biphenyl was recrystallized from ethanol and the alkylbiphenyls employed was synthesized and purified in the manner described in a previous paper.[6]

The anion radicals were prepared by reduction with potassium metal in 1,2-dimethoxyethane (DME). The ENDOR spectra were recorded using a JEOL-type ES-EDX-1 spectrometer for a constant rate of microwave output (3.2 mW) from a JES-ME3-ESR spectrometer. The operating power of NMR excitation was maintained constant (120 W). The viscosity of the solvent for all temperatures was calculated using the formula given in the table.[7]

Results and Discussion

Hyperfine Coupling Constants and Optimum Temperature of the ENDOR Signal Intensity. Figure 1 shows the ENDOR spectra of biphenyl and the 3,3′,5,5′-tetra-*t*-butylbiphenyl anion radical. With reference to the previous work, the signals for the biphenyl anion radical observed at 14.43, 17.63, and 21.46 MHz can be easily assigned to the *meta*-, *ortho*-, and *para*-ring protons. The ENDOR spectrum of the 3,3′,5,5′-tetra-*t*-butylbiphenyl anions clearly resolved the *t*-butyl proton splittings, which have never been detected in previous ESR studies.[8] The proton hyperfine splittings for the alkylbiphenyls determined in the same manner are summarized in Table 1, where it is seen that the magnitude of the *ortho*-ring proton splitting more or less close to that of the biphenyl anion radicals. A typical example of the temperature dependence of the ENDOR intensities (F) are shown in Fig. 2. For biphenyl anion radicals, the maximum ENDOR signals for the *meta*-, *ortho*-, and *para*-ring protons appear at −95, −90, and −80 °C, respectively, in order of increasing spin densities; that is, $\rho_m < \rho_o < \rho_p$.

For 9,10-anthraquinone, similar effects due to the different spin densities have already been studied by Kotake and Kuwata, who demonstrated the importance

Table 1. Proton hyperfine coupling constants for alkylbiphenyl anion radicals (in G)

	o	*m*	*p*
BP	2.66	0.41	5.31
p-Me	2.73	0.47	5.76[a]
p-Et	2.70	0.44	3.76[b]
p-Bu	2.71	0.46	0.11[c]
m-Me	2.53	0.31[a]	4.90
m-Bu	2.59	0.06[c]	5.14

a) Methyl proton. b) Ethyl proton. c) Butyl proton.

of the END mechanism.[9] A similar tendency was also seen for the *para*- and *ortho*-positions of the 3,3′,5,5′-tetra-*t*-butylbiphenyl anion radical, except for the anomalous optimum temperature of the *t*-butyl proton, which has often been reported for the hindered phenoxyl radicals.[10] In the case of 3,3′,5,5′-tetra-*t*-butylbiphenyl, however, the optimum temperatures for both the *para*- and *ortho*-positions (−40 °C, −73 °C) were displaced to higher temperatures in comparison with those (−80 °C, −95 °C) for biphenyl. Actually, the ENDOR of the *para*-ring proton of biphenyl anion radicals was clearly recorded at −78 °C, but that of 3,3′,5,5′-tetra-*t*-butylbiphenyl could hardly be detected and the signal intensity gradually increased with elevation of the observing temperature, up to −40 °C.

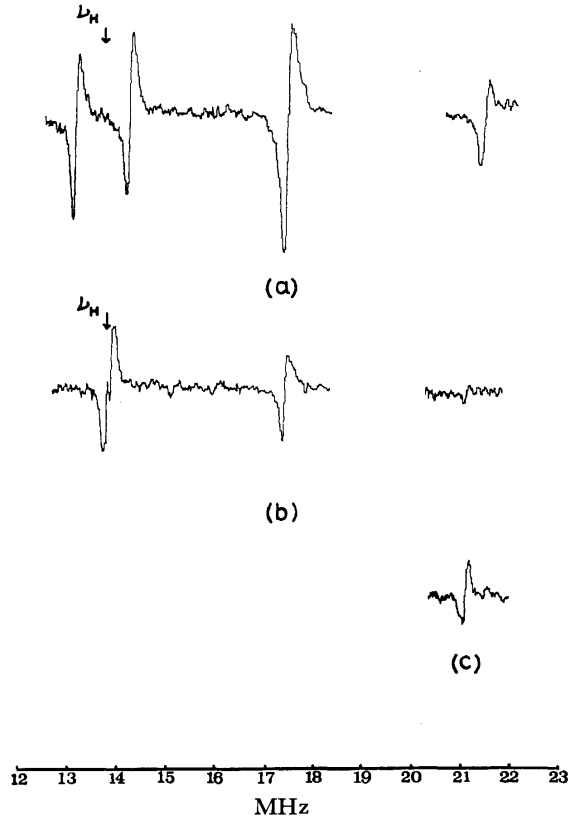

Fig. 1. The ENDOR spectra of biphenyl (a) and 3,3′,-5,5′-tetra-*t*-butylbiphenyl anion radical (b). (a) and (b) were observed at −78 °C. (c) is the ENDOR of *para*-protons of 3,3′,5,5′-tetra-*t*-butylbiphenyl observed at −40 °C.

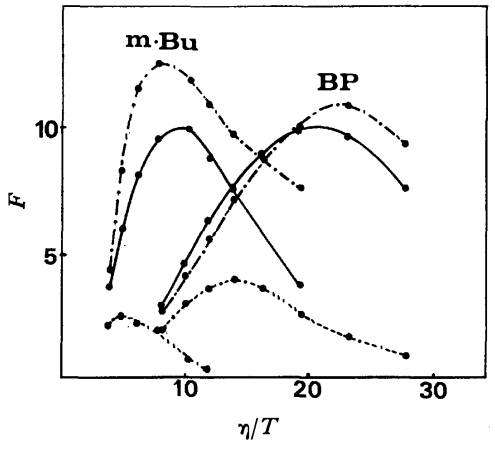

Fig. 2. Temperature dependence of the ENDOR enhancement for biphenyl and 3,3′,5,5′-tetra-*t*-butylbiphenyl anion radicals.
------: *para*, ——: *ortho*, -·-·-: *meta*.
F denotes the ENDOR enhancement calculated to be $F=I_{ENDOR}/I_{ESR}$, where I_{ENDOR} and I_{ESR} are the peak height of the ENDOR and ESR signal at any temperature.

Because the spin densities on the *para*- and the *ortho*-positions are close together in both radicals, alterations of the optimum temperature could be attributed to the differences of the molecular radii. This is true, because the optimum temperature of the *ortho*-proton ENDOR increases with an increase in the number of substituents and their spherical bulkiness as shown in Table 2.

Table 2. Optimum temperatures (°C) of *ortho*-proton ENDOR

BP	*p*-Bu	*p*-Me	*m*-Me	*p*-Et	*m*-Bu
−95	−79	−87	−86	−86	−73

Molecular Radius and Optimum Temperature. Under ordinary ENDOR conditions in solution, the electron-spin transition probability, W_e, and that of the nuclear spin, W_n, can be expressed as functions of the rotational correlation time, τ_R, as follows:[1]

$$W_e = A(1/\tau_R), \quad (1)$$

$$W_n = B\tau_R \quad (2)$$

Where A is the constant related to the magnitude of the g-factor and hyperfine anisotropies, and B is related to that of hyperfine anisotopy only. According to the END approximation, optimum ENDOR enhancement is observed when the ratio

$$b = W_n/W_e = (B/A)\tau_R^2 \quad (3)$$

has a certain value. Because B is proportional to the expectation value of the END term over the molecular wave function, the rotational correlation time at the optimum ENDOR enhancement, τ_R^{opt}, should become shorter for an increase of the spin density on the carbon atom to which the observing proton is bonded. In alkylbiphenyl anion radicals studied here, τ_R^{opt}, corresponding to the optimum ENDOR of the *ortho*-ring proton may have a constant value for each anion radical, because the spin densities, ρ_2^{π}, at the *ortho*-position have more or less the same values regardless of the alkyl substitutions. On the other hand, τ_R^{opt}, can be expressed by the Stokes-Einstein relationship:

$$\tau_R^{opt} = \frac{4\pi r^3}{3k}(\eta/T)_{opt}. \quad (4)$$

One may thus expect that a linear relation holds between the inverse of the effective radius, $1/r$, and the cubic root of the (η/T) value calculated for the optimum temperature of the *ortho*-proton ENDOR. If the radical ions are subject to a tumbling motion accompanied by the solvent shell, which has an averaged thickness, r_s, the following relation can be derived;

$$(r'+r_s)/(r+r_s) = (\eta'/T')^{-1/3}/(\eta/T)^{-1/3}, \quad (5)$$

Where r and r' are the averaged radius of the alkylbiphenyl and the biphenyl anion radical, respectively, and η and η' are the viscosity coefficient at the optimum ENDOR temperature for the derivative (T') and for the biphenyl anion radical (T). The averaged radii, r, of the alkylated biphenyl, which is regarded to be an ellipsoid, were calculated by taking the geometrical average of the three axes a, b, and c. The length of each axis was estimated using the following interatomic bond distances R and bond angles θ:[11]

R_{C-C}(aromatic) = 1.40 Å, $R_{C_1-C_1'}$(bridgehead) = 1.49 Å,
R_{C-C}(aliphatic) = 1.54 Å, R_{C-H} = 1.08 Å,
θ_{sp^2} = 120° and θ_{sp^3} = 109°.

The total length of each shorter and longer axes a and b was estimated by summing the Van der Waals radii of the ring, the aliphatic (1.20 Å) and terminal methyl protons (2.00 Å), and the thickness of the phenyl group, c, was assumed to be 3.40 Å. As is shown in Fig. 3, a

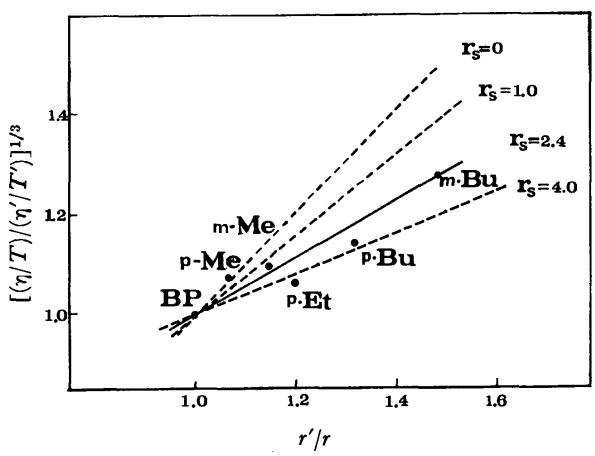

Fig. 3. Relation between the molecular radii and the cubic root of η/T value.

linear rotation can be seen between the (r/r') and the $[(\eta/T)/(\eta'/T')]^{1/3}$ values of each derivative, and r_s is thus estimated to be 2.4 Å, as calculated from the slope of the plot. The rotational correlation times of the anions at the optimum ENDOR, τ_R^{opt}, calculated using the effective radius $r+r_s$ have more or less constant values, which are close to 1.0×10^{-9} s, as summarized in Table 3.

Table 3. Molecular radii, molecular volumes and rotational correlation times at optimum ENDOR enhancement

	BP	*p*-Me	*p*-Et	*p*-Bu	*m*-Me	*m*-Bu
r (10^{-8} cm)	3.16	3.36	3.79	4.16	3.60	4.69
V (10^{-24} cm)	132	159	228	307	200	432
τ_R^{opt} (10^{-9} s)	1.08	0.98	1.28	1.19	1.05	1.07

The τ_R^{opt} values were calculated assuming that the thickness of the solvent shell is 2.4 Å

Since the τ_R^{opt} value thus determined may contain inaccuracies attributable to the crude estimation of the molecular volume and neglect of the contribution due to the anisotropic rotational diffusion,[12] the numerical values cannot be taken too seriously. Nevertheless, the large effective radius of the anion radical demonstrated here, is quite interesting, because this suggests that the distance between the radical anion and the alkali metal cation should be large, at least 8.3 Å in the case of biphenyl$^-$–K$^+$ system, in which case the radius of K$^+$ is assumed to be 1.5 Å.[13] Previous NMR studies of the biphenyl$^-$–K$^+$ system confirmed that the interaction between the anion and the cation is rather weak in DME, and the ion pair is considered to be a solvent separated ion pair.[14] According to conductance studies of biphenyl$^-$–Na$^+$ ion pairs in DME, the dissociation energy is reduced by lowering the temperature, that is, $\Delta H_{20°C} = -2.5$ kcal and $\Delta H^-_{55°C} = 0$ kcal.[15] This means that the cation and the anion are completely separated by the solvent molecules at low temperature. Indeed, no important change was observed in the temperature dependence of the ENDOR enhancement for the biphenyl anion radical, even through the alkali metal cation is replaced by sodium in the present investigation.

References

1) J. H. Freed, *J. Phys. Chem.*, **72**, 38 (1967).
2) K. Ishizu, K. Mukai, H. Hasegawa, K. Kubo, H. Nishiguchi, and Y. Deguchi, *Bull. Chem. Soc. Jpn.*, **42**, 2808 (1969).
3) A. Lagendijki, N. F. M. Tromp, M. Glassbeek, and J. D. W. Voost, *Chem. Phys. Lett.*, **6**, 152 (1970).
4) K. Ishizu, F. Nemoto, K. Mukai, M. Kohno, and H. Hasegawa, *Bull. Chem. Soc. Jpn.*, **48**, 1635 (1975).
5) F. Nemoto, F. Shimoda, and K. Ishizu, *Bull. Chem. Soc. Jpn.*, **48**, 2627 (1975).
6) M. S. Kharasch and E. K. Frelds, *J. Am. Chem. Soc.*, **63**, 2316 (1941).
7) "Technique of Organic Chemistry," Vol. VII, Interscience Publishers, Inc., New York (1955), p. 25.
8) K. Ishizu, Y. Inui, K. Mukai, H. Shikata, and H. Hasegawa, *Bull. Chem. Soc. Jpn.*, **43**, 3956 (1970).
9) Y. Kotake and K. Kuwata, *Bull. Chem. Soc. Jpn.*, **47**, (1974).
10) R. D. Allendoerfer and A. H. Maki, *J. Mag. Resonance*, **3**, 296 (1970).
11) L. Pauling, "The Nature of the Chemical Bond," 3rd ed, Cornell University Press, Ithaca, N. Y. (1960).
12) R. E. D. McClung and D. Kivelson, *J. Chem. Phys.*, **49**, 3380 (1968).
13) M. Szwarc, "Ion and Ion Pairs in Organic Reactions," Vol. I, Wiley-Interscience, N. Y. (1972).
14) G. W. Canter and E. de Boer, *Mol. Phys.*, **26**, 1185 (1973).
15) P. Chang, R. V. Slates, and M. Szwarc, *J. Phys. Chem.*, **70**, 3180 (1966).

Hydrocracking of Tetralin on Supported Nickel-Tungsten Catalysts

Shoko YAMADAYA, Masaaki OBA, and Yasuo MIKI

National Chemical Laboratory for Industry, Mita, Meguro-ku, Tokyo 153

(Received July 16, 1976)

The hydrocracking of tetralin was carried out over supported nickel-tungsten (NiO 3%, WO_3 20%) on silica-alumina, alumina, and silica catalysts at a hydrogen pressure of 100 atm and in the temperature range from 325 to 375 °C. The total conversion of tetralin and the product composition of hydrocracking were measured for the catalysts. The influence of pretreatment of the catalysts with H_2 and H_2S on the conversion and product composition was investigated for each catalyst. The hydrocracking of decalin was also carried out under the same conditions. It is found that the hydrocracking of tetralin proceeds along two reaction paths: (A) hydrogenation to decalin followed by conversion to methylperhydroindenes and C_{10}-naphthenes, (B) isomerization to methylindans followed by cracking to butylbenzene. The selectivity of each reaction path and the catalytic properties are discussed.

Catalytic hydrocracking is of considerable importance in petroleum refining. In the course of the commercial growth of the petroleum industry, the chemistry of hydrocracking over various catalysts has been studied with pure hydrocarbons. Most hydrocracking catalysts of commercial interest are of dual nature, consisting of both a hydrogenation-dehydrogenation component and an acidic support.

Recently, the chemistry of hydrocracking of typically pure hydrocarbons has been reviewed by Langlois and Sullivan,[1] and the mechanism for hydrocracking of polynuclear aromatic hydrocarbons on silica-alumina based dual-functional catalysts (CoS, MoS_2, NiS, WS_2, *etc.*) has been investigated by Qader.[2] Hydrocracking is found to proceed through sequential hydrogenation, isomerization and cracking reactions. Also, the reaction is found to follow first-order kinetics and the data are found compatible with the dual-site mechanism of Langmuir-Hinshellwood.

Sullivan *et al.*[3] have found considerable cyclization of the side chain when certain aromatic hydrocarbons (phenanthrene, anthracene, pyrene, *etc.*) are hydrocracked over a nickel sulfide on silica-alumina catalyst. The product is found to be predominantly tetrahydronaphthalene (tetralin) of lower moleculer weight than that of the reactant.

In this paper, the hydrocracking of tetralin was carried out as a test reaction to clarify the selectivity of hydrocracking catalysts. Supported nickel-tungsten on silica-alumina, alumina and silica catalysts were used. Effect of the carrier in the supported catalysts on the selectivity of hydrocracking was observed to significant extent. Also, the product composition changed extensively with catalyst pretreatment. On sulfiding the silica-alumina supported catalyst with H_2S, the principal reaction was found to be the hydrogenation to perhydronaphthalene (decalin), which was further converted to methylperhydroindenes and C_{10}-naphthenes. While for the catalysts pretreated with H_2, isomerization to methylindans and cracking to butylbenzene occurred predominantly.

The selectivity of each reaction path seems to depend on the relative strength of the acidic and hydrogenation components on the catalysts.

Experimental

Equipment. The experiments were performed in a continuous flow system with a fixed bed reactor, a flow diagram of which is shown in Fig. 1. The catalyst (16—32 mesh, 5 ml) was supported inside a 12 mm i.d. by 680-mm long stainless-steel tube which was surrounded by an electric furnace. The catalyst temperature was measured by a chromel-alumel thermocouple located in a thermowell in the catalyst bed.

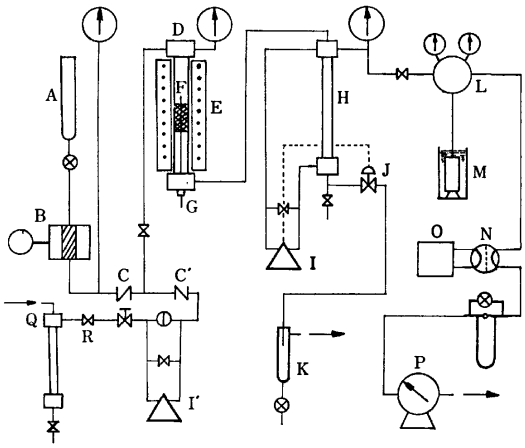

Fig. 1. Reaction apparatus.
A: Reactant vessel, B: plunger pump, C,C': non return valve, D: reactor, E: furnace, F: catalyst bed, G: thermocouple, H: separator, I,I': D.P. cell, J: level control valve, K: reservoir, L: pressure control valve, M: standard pressure vessel, N; six way valve, O: gas chromatograph, P: gas meter, Q: gas purifier, R: flow control valve.

Tetralin or decalin was fed by a plunger pump, and purified hydrogen was fed through a needle valve. The effluent from the reactor was taken to a gas-liquid separator. The liquid from the separator was automatically effluent by a revel control valve. The gas, passing through a six-way valve, was measured with a gas meter. Both the gas and liquid were analyzed by a gas chromatograph.

The reaction was carried out in the temperature range from 325 to 375 °C at a pressure of 100 atm. The liquid hourly space velocity (LHSV) was 8 per h and the molar ratio of hydrogen to the hydrocarbon was 10. In order to collect products representative of steady-state reaction conditions, the first hour was taken as off-stream time for bringing the reaction system to a steady state.

Analysis. The products were analyzed with a Hitachi Model K-53 gas chromatograph with flame-ionization detectors and with a squalan capillary column (90 m × 0.25 mm) at 90 °C. In the identification of each product on the chromatogram, the information[4,5] from the capillary gas chromatographic method for determining the C_3–C_{12} hydrocarbons in full-range moter gasolins was applied.

The peak areas in the chromatograms were measured with a Hewlett-Packerd Model 3380A reporting integrator.

Catalysts and Chemicals. The catalysts consisted of supported nickel-tungsten (3% NiO, 20% WO_3) on commercial alumina (Ketjenfine pure alumina), silica-alumina (25% Al_2O_3, Nikki Kagaku N 633H) and silica carriers. These catalysts were prepared by impregnating the carriers with a solution of nickel nitrate and ammonium paratungstate. The impregnated materials were oven-dried and calcined in air at 500 °C for 10 h.

Prior to reaction, they were reduced in flowing hydrogen at 500 °C for 16 h. In some experiments, they were sulfided with 10% H_2S in H_2 after the reduction.

Surface areas, determined by the standard BET method, were 226 m^2/g for the silica-alumina supported catalyst, 186 m^2/g for the alumina-supported catalyst, 156 m^2/g for the silica-supported catalyst.

Tetralin and decalin were commercial extra-pure reagents (Kokusan Kagaku, 99% purity) and were used without further purification. The decalin consisted of 54% *trans*-decalin and 45% *cis*-decalin.

Results and Discussion

Product Composition and Reaction Path. The total conversions of tetralin and the product compositions for hydrocracking on a nickel-tungsten-silica-alumina catalyst pretreated with H_2S are shown in Table 1. At

TABLE 1. HYDROCRACKING OF TETRALIN ON A SULFIDED NICKEL–TUNGSTEN–SILICA–ALUMINA CATALYST

Hydrogen pressure, 100 atm; LHSV, 8; H_2/Tetralin, 10.

Temperature °C	325	350	375
Total conversion mol %	9.8	13.2	22.6
Product composition mol/100 mol charge			
C_6-Compounds	0.2	0.8	2.2
C_{10}-Naphthenes	0.8	1.9	7.3
Methylperhydroindenes	2.2	2.4	3.4
Butylbenzene	0.6	0.9	1.7
Methylindans	0.3	0.7	1.7
Decalin	4.4	5.2	4.5
Tetralin	90.2	87.4	77.4
Naphthalene	0.8	1.3	1.5

a temperature of 325 °C, the main product is decalin, and the other products are divided into methylindans, methylperhydroindenes, C_{10}-naphthenes, C_6-compounds,[6] butylbenzene, and naphthalene. The selectivities of each product (the ratio of the yield to the total conversion) were calculated from this table and are shown in Fig. 2. At higher temperatures,[7] the selectivity for decalin and methylperhydroindenes decreased, whereas both the yields and selectivities of other products increased.

In Table 2, the conversions and the product compositions for the hydrocracking of decalin are shown under

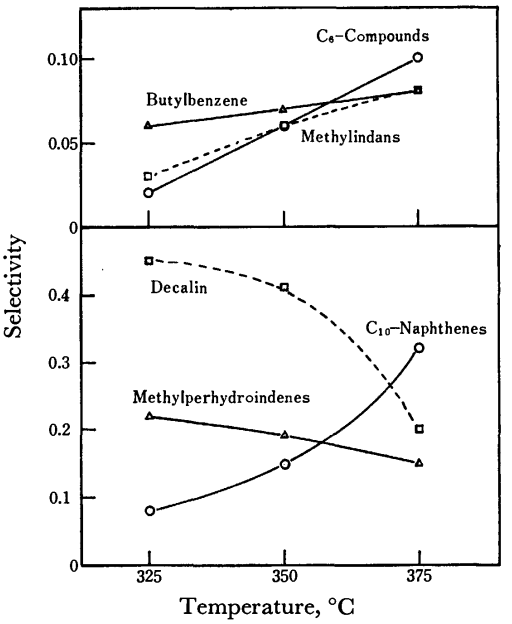

Fig. 2. Selectivity for hydrocracking of tetralin.

TABLE 2. HYDROCRACKING OF DECALIN ON A SULFIDED NICKEL–TUNGSTEN–SILICA–ALUMINA CATALYST

Hydrogen pressure, 100 atm; LHSV, 8; H_2/Decalin, 10.

Temperature °C	325	350	375
Total conversion mol %	6.3	18.2	33.5
Product composition mol/100 mol charge			
C_{10}-Naphthenes	2.6	10.8	22.5
Methylperhydroindenes	3.7	7.4	11.0
Decalin	93.7	81.2	66.5

the same conditions and catalyst as for the tetralin reaction (in Table 1). The principal products are methylperhydroindenes and C_{10}-naphthenes.

From a comparison of the above product compositions for the hydrocracking of tetralin and decalin, it is suggested that hydrogenation to decalin occurred predominantly in the first step during the reaction at a lower temperature and then the isomerization of decalin to methylperhydroindenes occurred in the second step. Then the methylperhydroindenes were further converted to C_{10}-naphthenes in the third step. At higher temperatures, the isomerization to methylindans and cracking to butylbenzene also occurred to a significant extent.

These data indicate that the hydrocracking of tetralin is divided into two types of reaction paths as shown in

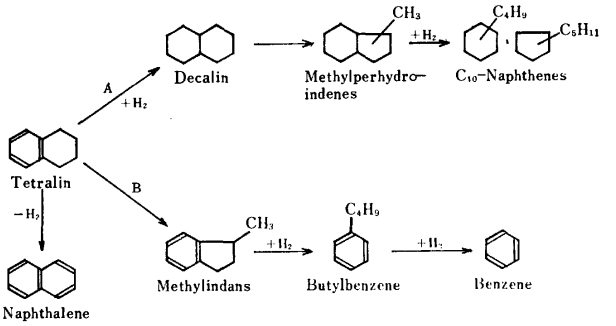

Fig. 3. Mechanism of hydrocracking of tetralin.

Table 3. Hydrocracking of tetralin on supported nickel-tungsten catalysts
Hydrogen pressure, 100 atm; Temperature, 350 °C; LHSV, 8; H_2/Tetralin, 10.

Catalysts	Nickel-Tungsten-Silica-Alumina		Nickel-Tungsten-Alumina		Nickel-Tungsten-Silica		Silica-Alumina
Pretreatment	H_2S	H_2	H_2S	H_2	H_2S	H_2	H_2
Total conversion mol %	13.2	7.6	35.4	17.5	24.0	0.4	4.0
Product composition mol/100 mol charge							
C_6-Compounds	0.8	2.0	—	1.2	—	—	—
C_{10}-Naphthenes	1.9	0.5	0.9	3.2	—	—	—
Methylperhydroindenes	2.4	0.5	—	2.5	—	—	—
Butylbenzene	0.9	0.7	—	2.6	—	—	0.6
Methylindans	0.7	1.2	—	1.9	—	—	1.7
Decalin	5.2	1.7	34.2	5.3	23.8	0.2	—
Tetralin	87.4	92.4	64.6	82.1	76.0	99.6	96.0
Naphthalene	1.3	1.1	0.3	0.8	0.2	0.2	1.8

Fig. 3: (A) hydrogenation to decalin followed by conversion to methylperhydroindenes and C_{10}-naphthenes, and (B) isomerization to methylindans and cracking to butylbenzene followed by conversion to benzene.

Effect of Pretreatment and Carriers of Catalysts. In the hydrocracking of tetralin, the influence of pretreatment of the supported nickel-tungsten catalysts with H_2 and H_2S on the product composition was investigated. In Table 3, the conversions of tetralin and the product compositions on three supported catalysts, silica-alumina-, alumina-, and silica-supported catalysts, were measured at 350 °C. The conversion of tetralin and the product composition for each sulfided catalyst were quite different from those of the reduced catalyst. The conversion on the reduced catalyst was lower than that on the sulfided catalyst in each case.

The decalin yield on the silica-alumina supported catalyst treated with H_2S was higher than that on the reduced catalyst, and the yield of methylperhydroindenes and C_{10}-naphthenes were also higher. However, the yield of methylindans and C_6-compounds on the reduced catalyst were higher than those on the sulfided catalyst.

In the hydrocracking of decalin, the influence of the pretreatment of these catalysts on the decalin conversion was investigated. In Table 4, the conversions on the silica-alumina- and alumina-supported catalysts treated with H_2 and H_2S are compared. The conversion on the silica-alumina-supported catalyst treated with H_2 was about seven times that on the catalyst treated with H_2S. On the alumina-supported catalyst, the reaction was extensively inhibited by the sulfidation. The conversion for the silica-alumina catalyst alone was comparable to that on the sulfided silica-alumina-supported catalyst.

Table 4. Hydrocracking of decalin on supported nickel-tungsten catalysts
Hydrogen pressure, 100 atm, Temperature, 350 °C, LHSV, 8, H_2/Decalin, 10.

Catalysts	Nickel-Tungsten-Silica-Alumina		Nickel-Tungsten-Alumina		Silica-Alumina
Pretreatment	H_2S	H_2	H_2S	H_2	H_2
Total conversion mol %	6.3	42.4	—	36.2	7.0
Product composition mol/100 mol charge					
C_{10}-Naphthenes	2.6	29.0		23.8	2.0
Methyl-perhydroindenes	3.7	13.2	No reaction	12.3	5.0
Decalin	93.7	57.6		63.8	93.0

From the above observation for hydrocracking on these catalysts, the selectivity of catalysts is discussed in relation to several recent reports.

Selectivity of Hydrocracking Catalysts. Some data have been reported on tetralin hydrocracking over nickel sulfide on silica-alumina catalysts.

Flinn *et al.*[8] have reported that ring opening and hydrogenation are the predominant reactions at 68 atm and 412 °C, and light alkanes are produced with a high ratio of branched to unbranched alkanes.

Sullivan *et al.*[3] have reported that the fused bicyclic cycloalkanes as main products are produced by the hydrocracking of tetralin at 288 °C and 82 atm.

However, the reaction path of the hydrocracking was not discussed in these reports.

Table 5. Selectivity for hydrocracking of tetralin on supported nickel-tungsten catalysts

Catalysts	Nickel-Tungsten-Silica-Alumina		Nickel-Tungsten-Alumina		Nickel-Tungsten-Silica
Pretreatment	H_2S	H_2	H_2S	H_2	H_2S
Total conversion mol %	13.2	7.6	35.4	17.5	24.0
Selectivity					
Path A	*0.74*	*0.36*	*0.98*	*0.64*	*0.99*
C_{10}-Naphthenes	0.15	0.07	0.02	0.18	—
Methyl-perhydroindenes	0.19	0.07	—	0.15	—
Decalin	0.40	0.22	0.96	0.31	0.99
Path B	*0.17*	*0.50*	—	*0.31*	—
C_6-Compounds	0.06	0.26	—	0.06	—
Methylindans	0.05	0.15	—	0.10	—
Butylbenzene	0.06	0.09	—	0.15	—
Naphthalene	*0.09*	*0.14*	*0.02*	*0.05*	*0.01*

In the present paper, it was demonstrated that the hydrocracking of tetralin proceeds along two reaction paths (A and B) as shown in Fig. 3. According to the mechanisms, the selectivity calculated from the product composition in Table 3 are shown in Table 5. The selectivity for all naphthenes produced for path A was 0.74 on the sulfided silica-alumina supported catalyst, whereas it was 0.36 on the reduced catalyst. On the alumina-supported catalyst treated with H_2S and H_2, the selectivities were 0.98 and 0.64, respectively. The selectivity for the sulfided silica-supported catalyst was 0.99.

The total conversion of tetralin on each catalyst treated with H_2S was generally higher than that on the reduced catalyst. As shown in Table 4, the activity of the sulfided catalyst for decalin hydrocracking was lower than that of the reduced catalyst.

It is suggested from the above observations that the active sites for hydrogenation of tetralin on the catalyst are produced by means of sulfidation, while the acid sites producing isomerization and the cracking of tetralin and decalin are decreased upon sulfidation.

Langlois *et al.*[9] have found that, with sulfiding a nickel on silica-alumina catalyst, the total conversion of decane hydrocracking greatly increased and the predominant reaction changed from isomerization to cracking. They postulated that the catalyst before sulfidation contained both nickel metal and nickel salts at the silica-alumina acid site, and upon sulfidation the nickel metal was converted to nickel sulfide, and the H_2S reacted with the nickel-silica-alumina salt to regenerate the original strong acid sites of the silica-alumina support.

In this paper, it is suggested that on the silica-alumina supported catalyst treated with H_2S, the original acid sites of the silica-alumina carrier are effective for the isomerization and cracking of tetralin. Also, by reducing the catalyst, acidic sites are formed on the surface of the supported tungsten oxide. Upon sulfidation of the alumina supported catalyst, no hydrocracking of decalin occurs. However, the hydrocracking activity of the reduced catalyst is higher. Therefore, the acidic properties of the catalyst are assumed to be formed by reduction with H_2.

The sulfidation of tungsten oxide supported on silica-alumina catalysts has been studied by Massoth and Bidlack.[10] Supported catalysts and bulk WO_3 were sulfided with mixture of H_2S and H_2 at temperatures between 260 and 594 °C and at a H_2S partial pressure of 0.1—5 atm. Studies of partially reacted samples show the sulfided species to be WS_2 and the unconverted oxide to be $W_{20}O_{58}$, suggesting that partial reduction precedes sulfidation. The salient findings of their study are: (1) reduction of bulk WO_3 by H_2 proceeds rapidly to $W_{20}O_{58}$ and then more slowly to W metal, (2) the sulfidation of bulk WO_3 by H_2S–H_2 mixtures proceeds rapidly through the formation of $W_{20}O_{58}$, followed by a slower reaction to WS_2, and (3) the mechanisms of sulfidation for bulk and supported WO_3 are similar.

The catalytic structure of nickel-tungsten sulfide as a hydrogenation catalyst has been investigated by Voorhoeve[11] using the ESR technique. It was concluded that the active sites for benzene hydrogenation in a wide variety of tungsten-disulfide based catalysts are tungsten ions, probably in the trivalent state. Nickel appears to have an indirect influence on the hydrogenation activity in Ni-W-S rather than acting as the active center.

It is apparent that the state of tungsten on the sulfided catalyst surface in the present study is probably attributable to WS_2. According to the above conclusions reported by Voorhoeve,[11] it is apparent that the active sites for the hydrogenation of tetralin are the tungsten ions of tungsten disulfide crystals on the catalyst.

On the reduced alumina-supported catalyst, the acidic catalyzed isomerization and cracking activity is attributed to the acidic hydroxyl groups over the partially-reduced surface of tungsten oxide supported on alumina.

Appreciation is expressed to Dr. T. Kabe for a significant contribution to this work and to Mr. T. Hasegawa for assistance with the experimental work.

References

1) G. E. Langlois and R. F. Sullivan, "Advances in Chemistry Series No. 97, Refining Petroleum for Chemicals," ACS (1970), Chap. 3, p. 38.
2) S. A. Qader, *J. Inst. Petroleum*, **59**, 178 (1973).
3) R. F. Sullivan, C. J. Egan, and G. E. Langlois, *J. Catal.*, **3**, 183 (1964).
4) W. N. Sanders and J. B. Maynard, *Anal. Chem.*, **40**, 527 (1968).
5) P. Merchant, *Anal. Chem.*, **40**, 2153 (1968).
6) Contains 90% benzene.
7) Only small amounts of butane were observed at 375 °C.
8) R. A. Flinn, O. A. Larson, and H. Beuther, *Ind. Eng. Chem.*, **52**, 153 (1963).
9) G. E. Langlois, R. F. Sullivan, and C. J. Egan, *J. Phys. Chem.*, **70**, 3666 (1966).
10) F. E. Massoth and D. L. Bidlack, *J. Catal.*, **16**, 303 (1970).
11) R. J. H. Voorhoeve, *J. Catal.*, **23**, 236 (1971).

The Distribution of Higher Alcohols in Aqueous Micellar Solutions

Kohji HAYASE and Shigeo HAYANO

Institute of Industrial Science, The University of Tokyo, Roppongi, Minato-ku, Tokyo 106

(Received July 22, 1976)

The distribution coefficients, K, for 1-butanol, 1-pentanol, 1-hexanol, and 1-heptanol between the sodium dodecyl sulfate (SDS) micellar and aqueous phases were measured directly, with the gas chromatographic technique was used to measure the vapor pressure of the alcohols. The standard free energy change of penetration, ΔG_p°, of the alcohol from the aqueous to the micellar phase was obtained using the equation: $\Delta G_p^\circ = -RT\ln K$. There is a linear relation between ΔG_p° and the carbon number of the alcohol.

The change in the standard free energy of an alcohol for a transition from the aqueous to the micellar phase, ΔG_p°, is indispensable to the study of solubilization of additives in surfactant solutions. In spite of the necessity of evaluating ΔG_p°, no values of ΔG_p° have yet been reported for an aqueous alcohol solution. Though Kaufman[1] and Dalen, Gerritsma, and Wijkstra[2] have reported the solubilization of organic additives in organic solvents, they were unable to calculate the distribution coefficient because of a lack of an accurate knowledge of the critical micelle concentration (CMC) in the organic solvent.

Concerning the effect of alcohol on decreasing the CMC, Ward[3] and Herzfed, Corrin, and Harkins[4] have pointed out the importance of evaluating ΔG_p°. Shirahama and Kashiwabara[5] have discussed thermodynamically the relation between ΔG_p° and the CMC decrease of systems containing alcohol. However, since the ΔG_p° were not measured but were estimated values deduced from the physical constants of the alcohols, the theoretical equation does not correspond to their experimental results. Thus, an experimental determination of the ΔG_p° values would be useful in their thermodynamical discussion.

In this paper, experimental work on the distribution coefficients is reported. These experiments are thought to be very important for the discussion of the interaction of surfactants and additives. The distribution coefficients were evaluated by measuring the vapor pressure of the alcohol in an aqueous alcohol solutions both in the presence and absence of sodium dodecyl sulfate (SDS) employing a gas chromatograph. This technique, to the best of the authors' knowledge, has not yet been applied to this kind of problem.

Experimental

Method. 5 ml vapor samples equilibrated with alcohol solutions were introduced from a gas loop by means of a six-way sampling valve into a Shimadzu GC-3BF gas chromatograph equipped with a flame ion detector. Helium was used as the carrier gas at flow rates of 50, 80, and 100 ml/min through a 3 mm×2 m column. The column packing was 5 or 10% polyethylene glycol 6000 on a 30—60 mesh Flusin T support, and 5% Versamid 900 on a 60—80 mesh Uniport KS support. The operating temperature was 120—160 °C.

The experimental arrangement for the gas chromatographic measurements is shown in Fig. 1. The measuring process was similar to the reported by Kaufman.[1] To prevent foam from overflowing to the outer part of the bottle, the helium was passed for four minutes in order to saturate the vapor, which

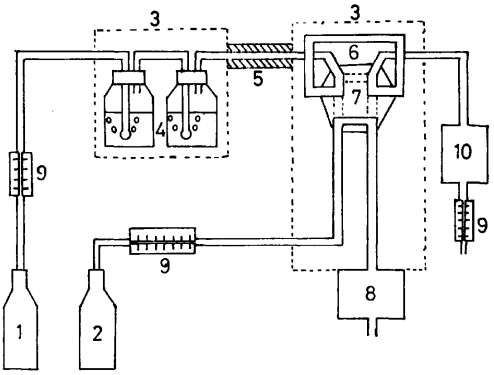

Fig. 1. Experimental arrangement for measuring vapor pressure by gas chromatograph.
(1): Helium cylinder for saturator, (2): helium cylinder for gas chromatograph, (3): thermostat, (4): saturator, (5): ribbon heater, (6): sampling loop, (7): sampling valve, (8): gas chromatograph, (9): flow meters, (10): ballast.
(Solid lines in the sampling valve denote a standby position; dotted lines denote a sampling position.)

was then introduced into the gas chromatograph. The helium flow was stopped for twelve minutes in order to reduce the quantity of foam. The sampling procedure was standardized to allow a uniform 1.5 min period for the valve in the sampling position.

The 1-butanol, 1-pentanol, 1-hexanol, and 1-heptanol peaks were well-resolved, symmetrical and only slightly tailed.

The measurement of the electric conductivity of the SDS solution was made using a Towa Denpa Co., Ltd. Model CG-201PL universal bridge. An electric conductivity cell of the dip type was bright-platinized and immersed in a 100-ml polyethylene beaker which was maintained at 25 °C in a thermostat.

The SDS concentration was varied by adding portions of a concentrated SDS solution containing an alcohol.

Materials. Wako Pure Chemical Industries, Ltd. SDS for biochemical use was carefully dried in a vacuum for twenty hours. The 1-butanol, 1-pentanol, 1-hexanol, and 1-heptanol of high purity (higher than 99%) were used. The water used was passed through a Nihon Millipore Co., Ltd. Milli-Q2 Systems until its specific conductivity fell below 10^{-7} Ω^{-1} cm^{-1}.

Results and Discussion

Figure 2 displays two curves obtained directly from the gas chromatographic measurements. In Fig. 2, 1-heptanol is shown as an example. The upper or calibration curve represents the data taken from a series

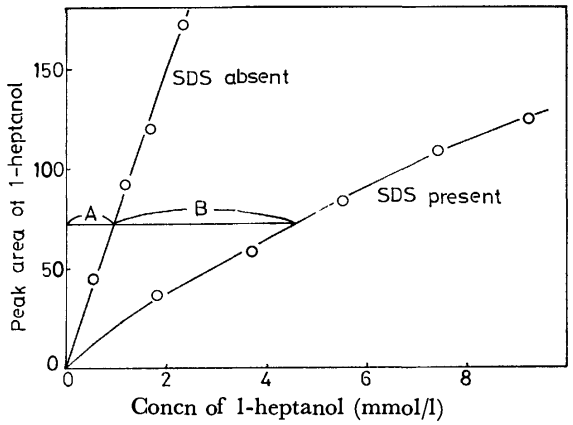

Fig. 2. Calibration curve for the aqueous 1-heptanol solution and typical results for the same solution in the presence of SDS (at 25 °C).
(A): 1-Heptanol fraction remaining in the aqueous phase, (B): 1-heptanol fraction existing in the micellar phase.

of solutions without SDS, while the lower curve shows the data for a similar solution to which a specific amount of SDS was added.

For the purposes of this study, it is unnecessary to know the absolute concentration of the alcohol in the vapor phase, provided that a relationship between the peak area and the compositions of the solutions has once been established. Owing to the self association of the alcohol in the solution, the slopes of the curves decrease as the concentration of the alcohol increases.

The horizontal separation between the two curves at any ordinate represents A and B. B corresponds to the alcohol fraction existing in the micellar phase and A to the alcohol fraction remaining in the aqueous phase. From these curves, the distribution coefficient was calculated from the following equations:

$$Y_a = (18 \times A)/1000, \quad (1)$$

$$X_a = B/(S - \mathrm{CMC}(C_a) + B), \quad (2)$$

and

$$K = X_a/Y_a, \quad (3)$$

where Y_a is the molar fraction of the alcohol in the aqueous phase, X_a the molar fraction of the alcohol in the micellar phase, S the total concentration of SDS added, C_a the concentration of the alcohol in the solution, CMC (C_a) the CMC of SDS in the presence of the alcohol, and K the distribution coefficient of the alcohol (the ratio of the concentration in the micellar phase to that in the aqueous phase).

In Fig. 3, the molar fractions of the alcohol(1-heptanol, for example) in the micellar phase are plotted against the mole fractions of the alcohol in the aqueous phase. The amount of SDS was 40 mmol/l. From these results, we evaluated the distribution coefficients using the least-squares method.

The values of K and ΔG_p° calculated from

$$\Delta G_p^\circ = -RT \ln K \quad (4)$$

are shown in Table 1.

Some work[1,2] has been reported on the solubilization of organic additives by surfactant micelles in organic solvents. Kaufman[1] has given the solubilization ratios

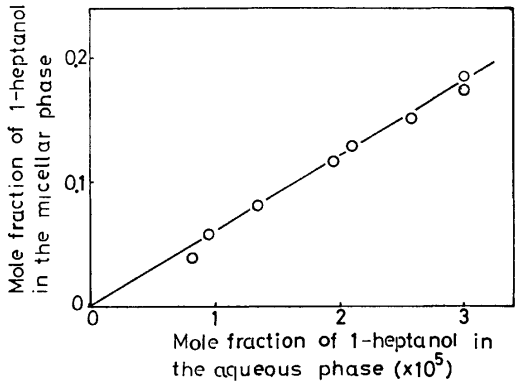

Fig. 3. Distribution of 1-heptanol between the aqueous and the micellar phases (at 25 °C).

Table 1. The distribution coefficients (K) of alcohol between the aqueous and micellar phases and the standard free energy changes of penetration of the alcohols (ΔG_p°) (at 25 °C)

	1-Butanol	1-Pentanol	1-Hexanol	1-Heptanol
K	3.00×10^2	7.22×10^2	2.25×10^3	6.02×10^3
ΔG_p° (kcal/mol)	−3.38	−3.90	−4.57	−5.16

computed for the sodium, cesium, barium, magnesium, and zinc salts of 1,8- dinonyl-4-naphthalene sulfonic acid as a function of methanol, propylamine, and acetic acid in toluene. However, because an accurate value of the CMC was inacessible for organic solvents containing organic additives, no concentration of micellized surfactant was reported. Therefore, an accurate distribution coefficient could not be obtained, because the total surfactant concentration was employed instead of the micellized surfactant concentration.

Table 2. CMC values for SDS in water to which a small amount of alcohol was added (at 25 °C)

Alcohol concn (mmol/l)		CMC (mmol/l)
Pure water		8.01
1-Butanol	43.74	6.96
	116.9	5.32
	204.4	4.18
1-Pentanol	15.41	6.86
	31.15	5.70
	64.45	4.17
1-Hexanol	2.683	7.32
	5.584	6.61
	9.227	5.89
1-Heptanol	0.7354	7.54
	1.918	6.89
	3.178	6.45

Since, in this experiment, accurate values of the CMC using the conductivity method were obtained, as given in Table 2, it is now possible to evaluate the distribution coefficients. Our results for the CMC values both in pure water and in the presence of 1-butanol agree ap-

proximately with those of Shirahama and Kashiwabara.[5]

As shown in Table 1, ΔG_p° is a linear function of the carbon number of the alcohol. As the carbon number of the alcohol increases, the ΔG_p° decreases. Similarly, the standard free energy change of micellization, ΔG_m°, decreases as the carbon number of the surfactant increases.[6] This can be understood since an increase in the carbon number of the alcohol is expected to result in an increased hydrophobic interaction with the surfactant micelles. In other words, penetration of the alcohol into the micellar phase becomes more favorable for an increase in the carbon number of the alcohol. Thus, it is reasonable that this tendency of the ΔG_p° to decrease parallels the tendency of solubility of the alcohol in water to decrease.

ΔG_p° is linearly related to the carbon number of the alcohol as follows:

$$\Delta G_p^\circ = -0.60n - 0.95, \quad (5)$$

where n is the carbon number of the alcohol.

The increment of ΔG_p° per methylene group is -0.60 kcal/mol. Kresheck and Hargraves[6] have investigated the ΔG_m° of the sodium octyl-, decyl-, and dodecyl sulfate series and found that the increment of the ΔG_m° per methylene group was approximately from -0.55 to -0.32 kcal/mol. The absolute value of the increment of the ΔG_p° per methylene group is a little larger than that of the ΔG_m° per methylene group.

Mankowich[7] has reported on the solubilization of Orange OT in aqueous sodium dodecyl benzene sulphonate solutions. In his paper, the standard free energy changes of the solubilization of Orange OT from the non-micellar phase to the micellar phase were reported to be from -5.4 to -5.8 kcal/mol in the range 25—50 °C. In his method, the solubilities of Orange OT both above the CMC and at the CMC were measured. The concentration (mol/l) of Orange OT in the micellar phase was calculated from the solubility of Orange OT above the CMC, and the concentration (mol/l) of Orange OT in the non-micellar phase was calculated from the solubility of Orange OT at the CMC. Then, the standard free energy change was computed from these two concentrations. However, his method is inconvenient for evaluating ΔG_p°, because the solubilities of 1-butanol, 1-pentanol, 1-hexanol, and 1-heptanol are much higher than that of Orange OT, and the CMC values are altered in the presence of the alcohols.

Aveyard and Lawrence[8] and Larsen and Magid[9] reported the standard enthalpy change of penetration, ΔH_p°, of the alcohol from the aqueous phase to the micellar phase obtained using the calorimetric method. If the ΔH_p° of their results (1-butanol: 0.5 kcal/mol, 1-pentanol: 0.4 kcal/mol, 1-hexanol: 0.4 kcal/mol) are employed, it is possible to estimate the standard entropy change of penetration, ΔS_p°, of the alcohol using the following equation:

$$\Delta G_p^\circ = \Delta H_p^\circ - T\Delta S_p^\circ. \quad (6)$$

The results are 13.0, 14.4, and 18.7 cal/mol K for 1-butanol, 1-pentanol, and 1-hexanol, respectively. From these results, it may be considered that penetration of the alcohol from the aqueous to the micellar phases exhibits entropy dependence rather than enthalpy dependence. This is similar to the case of micellization of surfactants, namely, penetration of the alcohol from the aqueous to the micellar phases may be attributed to the release of the compact iceberg structure of water molecules around the hydrophobic parts of the alcohol.

References

1) S. Kaufman, a) *J. Colloid Sci.*, **17**, 231 (1962); b) *J. Phys. Chem.*, **68**, 2814 (1964); c) *J. Colloid Interface Sci.*, **25**, 401 (1967).

2) A. V. Dalen, K. W. Gerritsma, and J. Wijkstra, *J. Colloid Interface Sci.*, **48**, 127 (1974).

3) A. F. H. Ward, *Proc. R. Soc. London, Ser. A*, **176**, 412 (1940).

4) S. H. Herzfed, M. L. Corrin, and W. D. Harkins, *J. Phys. Colloid Chem.*, **54**, 271 (1950).

5) K. Shirahama and T. Kashiwabara, *J. Colloid Interface Sci.*, **36**, 65 (1971).

6) G. C. Kresheck and W. A. Hargraves, *J. Colloid Interface Sci.*, **48**, 481 (1971).

7) A. M. Mankowich, *J. Am. Oil. Chem. Soc.*, **42**, 185 (1965).

8) R. Aveyard and A. S. C. Lawrence, *Trans. Faraday Soc.*, **60**, 2265 (1964).

9) J. W. Larsen and L. J. Magid, *J. Phys. Chem.*, **78**, 834 (1974).

Acidic Properties of SiO_2–MoO_3 and MoO_3, and Their Catalytic Activities

Kazumasa MARUYAMA, Hideshi HATTORI, and Kozo TANABE

Department of Chemistry, Faculty of Science, Hokkaido University, Sapporo 060

(Received August 9, 1976)

MoO_3, SiO_2, and SiO_2–MoO_3 of different compositions were prepared and their surface and catalytic properties examined. A large number of acid sites were generated by mixing SiO_2 with MoO_3, while each component oxide by itself did not exhibit any appreciable acidic properties. The oxidizing property of MoO_3 was enhanced by mixing with SiO_2. No new compounds were detected in the oxide mixture by X-ray diffraction. The activity for depolymerization of 2,4,6-trimethyl-1,3,5-trioxane correlated well with the surface acidity. In the isomerization of 1-butene, both MoO_3 and SiO_2–MoO_3 were active. The active sites on MoO_3 were poisoned by CO_2 but not by NH_3, while those on SiO_2–MoO_3 were poisoned by NH_3 but not by CO_2.

Among the metal oxides most widely used as a component of the multicomponent metal oxide catalysts is MoO_3, which is usually mixed with other oxides such as SiO_2, Al_2O_3, Bi_2O_3, and SnO_2. Many metal oxides are known to exhibit acidic properties when they are mixed with other oxides.[1,2] The acidic sites play an important role not only in reactions recognized as acid-base catalyzed reactions, but also in those of other types. For instance, the selectivity in the oxidation of olefins depends strongly on the surface acid-base properties.[3–6] However, the acid-base properties of the catalysts containing MoO_3 as a component oxide have not been subjected to extensive study except for MoO_3–Al_2O_3.[7]

We have prepared SiO_2–MoO_3 in various molar ratios and examined their acid-base properties. Two typical acid-base catalyzed reactions, depolymerization of 2,4,-6-trimethyl-1,3,5-trioxane and isomerization of butenes, were studied.

Experimental

Catalyst Preparation. SiO_2 and MoO_3 were prepared by precipitation from an isopropanol solution of ethyl orthosilicate and an aqueous solution of ammonium molybdate, respectively, with nitric acid followed by aging at 70—80 °C for 16 h and drying at 110 °C for 24 h.

SiO_2–MoO_3 was prepared as follows. A mixture of ethyl orthosilicate and 10% aqueous solution of ammonium molybdate was dissolved in isopropanol. To the solution was added dilute nitric acid (pH=1) and the solution was heated at 70—80 °C for 16 h to facilitate gelation. The resulting gel was dried at 110 °C for 24 h. Amounts of the reagents are given in Table 1.

Table 1. Amounts of reagents used for the preparation of MoO_3–SiO_2 with different compositions

Composition mol ratio (MoO_3: SiO_2)	$(C_2H_5)_4SiO_4$ ml	$(NH_4)_6Mo_7O_{24}\cdot 4H_2O$ g	$(CH_3)_2CHOH$ ml
MoO_3	0	160	0
9: 1	13.2	159	14
1: 1	167	129	170
1: 9	402	35.3	400
SiO_2	400		400

Acidity and Basicity Measurements. Acidity was measured at 55 °C by titration of the suspension in benzene with 0.1 N butylamine benzene solution. The indicators used were dicinnamilideneacetone ($pK_a=-3.0$), *p*-(phenylazo)diphenylamine (1.5), Dimethyl Yellow (3.3), Methyl Red (4.8), and Neutral Red (6.8). The existence of basic sites was monitored by dropping a series of benzene solutions of nitroaniline indicators onto a sample.

Surface Area, X-Ray Analysis, DTA, and TG, ESR Measurements. Specific surface areas were determined by applying the BET equation to nitrogen adsorption isotherms at −196 °C. X-Ray diffraction patterns were recorded on a Toshiba ADG-301 with a powdered sample over the range of $2\theta=10°$—$60°$. Cu$K\alpha$ was used as the radiation source.

DTA and TG were performed on a Rigakudenki standard model over the range from room temperature to 720 °C. The rate of temperature rise was 20 °C/min.

For ESR measurements, 20 mg of the sample in a cell with a breakable seal was evacuated at the desired temperature for 3 h and sealed off. ESR spectra of these samples were measured at −196 °C and room temperature. After recording the spectra, samples were exposed to butene, oxygen, nitrobenzene or a benzene solution of perylene through a breakable seal. All the spectra were measured on a Varian E-4 ESR spectrometer.

Reaction Procedure. The benzene solution of 2,4,6-trimethyl-1,3,5-trioxane (paraldehyde) (0.0495 mol/l) was used as a reactant for the depolymerization of paraldehyde. Powdered catalyst was calcined at 500 °C for 3 h in air. To 40 ml of the reactant in a 100 ml flask with a cap was added 0.24 g of catalyst followed by magnetic stirring at 30 °C. Portions of the reaction mixture were periodically withdrawn from the system and subjected to analysis of acetaldehyde by the following method. Excess amount of 0.1 N $NaHSO_3$ was added to 10 ml of reaction mixture to form a complex with acetaldehyde. After titration of residual $NaHSO_3$ with I_2, the $NaHSO_3$–acetaldehyde complex was dissociated by the addition of $NaHCO_3$. The amount of $NaHSO_3$ required for the formation of the complex was determined by titration with I_2.

A microcatalytic pulse reactor was employed for the isomerization of butenes. The catalyst was sieved to 20—35 mesh and calcined at 500 °C for 3 h. A quarter grams of the catalyst was placed in the reactor and pretreated at 500°C under a helium stream for 1 h prior to reaction. All the reactions were carried out at 250 °C. Butene (*ca.* 40μ mol) was introduced into a helium carrier ahead of the catalyst by manipulating a stop cock. Effluent products were directly introduced into a gas chromatographic column for analysis. The flow rate of the carrier was kept constant (1.1 ml/s). In some experiments, CO_2 or NH_3 was introduced in order to examine a poisoning effect after reaching a steady activity, which was usually attained after 7 or 8 injections.

Results

Surface Area, X-Ray, DTA, and TG. The specific

Table 2. Specific surface area (m^2/g) of MoO_3–SiO_2 after calcination at various temperatures[a)]

Composition (MoO_3: SiO_2)	Calcination temperature, °C			
	300	400	500	600
MoO_3	4.5	4.8	4.3	2.8
9: 1	5.4	4.5	4.0	2.2
1: 1	143	92	81	40
1: 9	440	376	240	93
SiO_2	—	—	520	375

a) Before measurement, sample was evacuated at 150—170 °C for 1 h.

surface areas ot catalysts are given in Table 2. They decrease with an increase in percentage of MoO_3 and with a rise in calcination temperature.

X-Ray diffraction patterns show that all the peaks obtained for SiO_2–MoO_3 of different compositions calcined at 400, 500, and 600 °C are due to those of MoO_3, strong peaks being observed at $2\theta=10.17$, 19.90, and 29.80°. The samples calcined at 300 °C did not show this set of peaks. The peak intensity increases with a rise in calcination temperature and with an increase in MoO_3 content in SiO_2–MoO_3. No peaks other than those ascribed to MoO_3 were found.

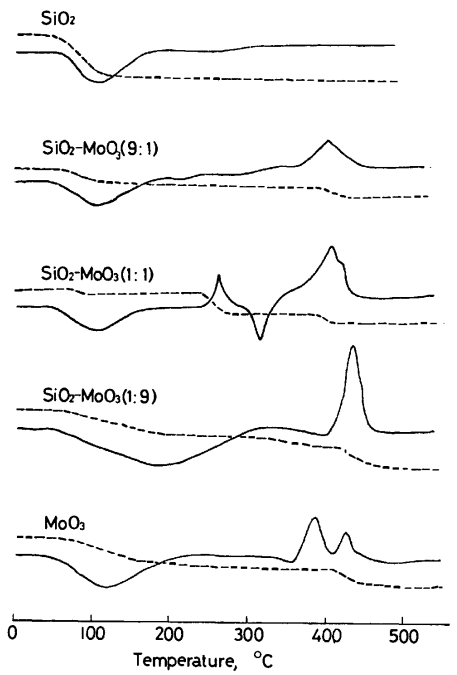

Fig. 1. DTA-TG curves of catalysts. DTA, solid line; TG, broken line.

DTA-TG curves are shown in Fig. 1. All the samples show endothermic peaks by DTA around 50—200 °C with loss of weight. These peaks can be ascribed to desorption of physically adsorbed water. The samples containing MoO_3 show exothermic peaks around 400 °C also accompanied a weight loss.

ESR. SiO_2–MoO_3 and MoO_3 show ESR signals assigned to Mo^{5+}. The signal for SiO_2–MoO_3 (9: 1) after evacuation at 500 °C is shown in Fig. 2. On exposure to nitrobenzene, the amplitude of the signal decreased considerably but no signal for nitrobenzene anion radical was observed. On admission of a benzene solution of perylene, a strong signal appeared which could be assigned to perylene cation radical. The signals observed for SiO_2–MoO_3 9: 1 and 1: 1 showed hyperfine splitting into nine peaks. On the other hand, the signals for SiO_2–MoO_3 (1: 9) and MoO_3 were broad singlets. The variation of the integrated signal amplitude of perylene cation radicals with composition is shown in Fig. 3.

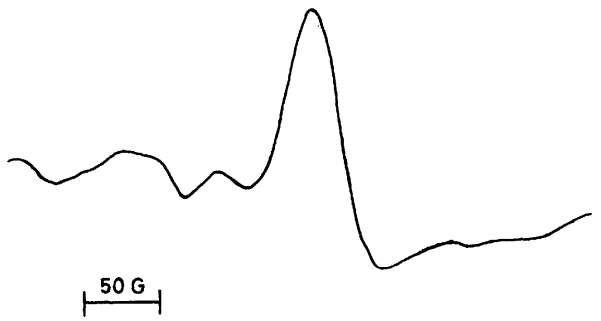

Fig. 2. ESR signal of SiO_2–MoO_3 (9: 1) evacuated at 500 °C.

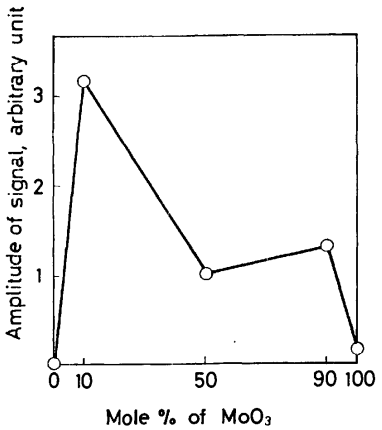

Fig. 3. Numbers of perylene cation radicals on SiO_2–MoO_3 of different composition. Catalysts had been evacuated at 500 °C.

Admission of butene at 200 °C to SiO_2–MoO_3 (9: 1) evacuated at 500 °C resulted in an increase in the signal amplitude of Mo^{5+}, and the successive admission of O_2 after the excess butene had been trapped in liquid nitrogen resulted in a decrease in the amplitude of the Mo^{5+} signal and the production of O^{2-}.

Acidity. Figure 4 shows the acidity of SiO_2–MoO_3 having compositions of 9: 1, 1: 1, and 1: 9 as well as that of SiO_2 and MoO_3, when calcined at 500 °C in air. Although SiO_2 and MoO_3 showed negligible amounts of acid sites stronger than $H_0=3.3$, SiO_2–MoO_3 with composition 9: 1 and 1: 1 showed considerable amounts of these acid sites. Change in calcination temperature caused no great change in acidity. An example is shown in Fig. 5 for SiO_2–MoO_3 (9: 1).

Depolymerization of 2,4,6-Timethyl-1,3,5-trioxane. The reaction rate equation was of first order in concen-

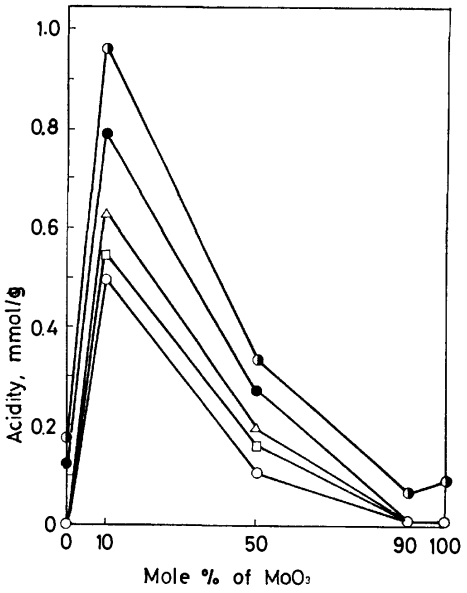

Fig. 4. Acidity of SiO_2–MoO_3 of different composition. $H_0 = -3.0$ (○), $+1.5$ (□), $+3.3$ (△), $+4.8$ (●), $+6.8$ (◑).

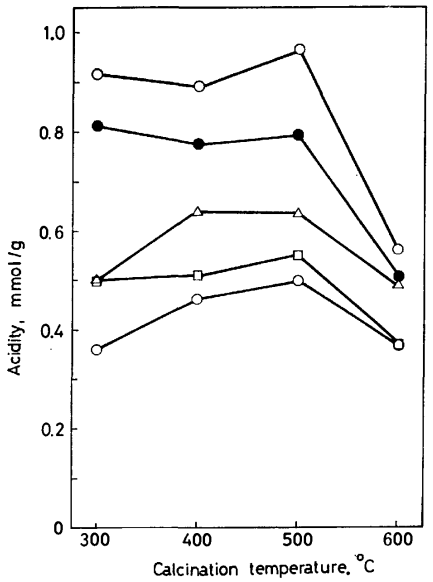

Fig. 5. Changes in acidity of SiO_2–MoO_3 (9: 1) with calcination temperature $H_0 = -3.0$ (○), $+1.5$ (□), $+3.3$ (△), $+4.8$ (●), $+6.8$ (◑).

tration of reactant. Activity of the catalyst was expressed by a first order rate constant, k, per unit weight of catalyst. The variation of the activity with composition is shown in Fig. 6, where the catalysts are calcined at 500 °C in air. A similarity in the change in activity to that in acidity with composition of the catalyst suggests that the acid sites are active sites for the decomposition of 2,4,6-trimethyl-1,3,5-trioxane to produce acetaldehyde. The activity of the catalysts is more than 10 times greater than that of $NiSO_4$ and $CuSO_4$.[7]

Isomerization of Butene. The conversion of *cis*-2-butene over MoO_3 and SiO_2–MoO_3 (9: 1) is plotted against the pulse number in Figs. 7 and 8. The decrease in conversion with the pulse number is greater for MoO_3 than SiO_2–MoO_3 (9: 1). After the conversion had

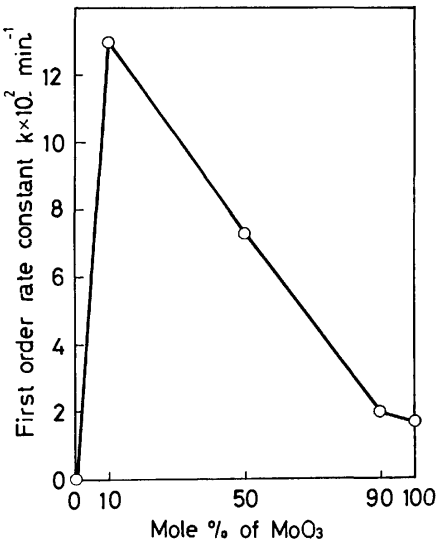

Fig. 6. Variation of activity for depolymerization of 2,4,6-trimethyl-1,3,5-trioxane with composition.

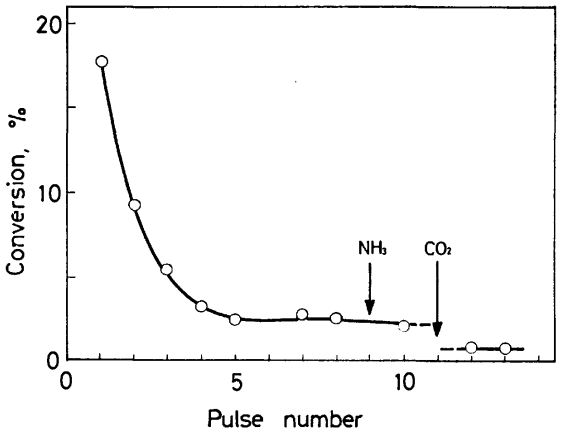

Fig. 7. Activity decrease in isomerization of *cis*-2-butene with pulse number and with NH_3 or CO_2 addition over MoO_3.

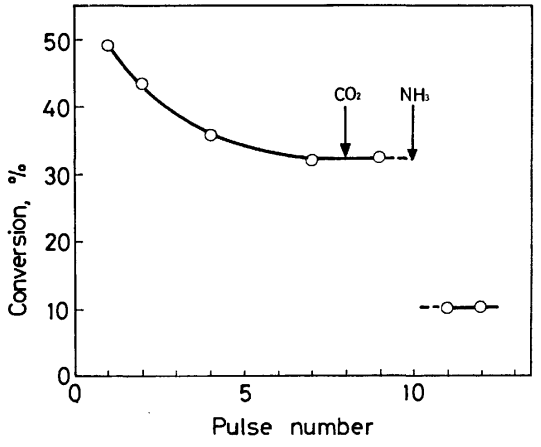

Fig. 8. Activity decrease in isomerization of *cis*-2-butene with pulse number and with NH_3 or CO_2 addition over SiO_2–MoO_3 (9: 1).

attained a constant value, CO_2 or NH_3 was introduced. The active sites of MoO_3 were poisoned by CO_2, but not substantially by NH_3. On the other hand, the active

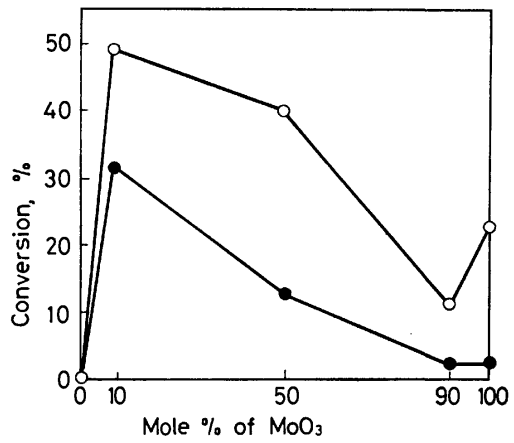

Fig. 9. Initial activity (○) and steady state activity (●) for isomerization of *cis*-2-butene.

sites of SiO_2–MoO_3 were poisoned by NH_3, but not by CO_2.

The conversion at the first pulse and that after several pulses (the constant conversion) are shown in Fig. 9. Except for MoO_3, the change in conversion with the composition of catalyst is similar to that in acidity.

Discussion

Mixing of SiO_2 and MoO_3 gave rise to new surface and catalytic properties not found in either component oxide, though X-ray and DTA-TG data showed no formation of a new compound. Of these properties acidity is important. A good correlation of acidity with activity for depolymerization of 2,4,6-trimethyl-1,3,5-trioxane indicates that the active sites for the reaction are the acid sites generated by mixing SiO_2 and MoO_3.

For the isomerization of butene, MoO_3 showed considerable activity though it had no acidic sites stronger than $H_0=4.8$. The catalyst was not poisoned by NH_3. Thus, the active sites are not acidic. Since CO_2 is an acidic molecule and can be adsorbed on basic sites, and CO_2 actually poisons the catalyst, the active sites on MoO_3 for the butene isomerization seem to be basic. On the other hand, the activity of the mixed oxides correlates with the acidity and NH_3 poisons the active sites. Thus, the active sites on SiO_2–MoO_3 are suggested to be acidic sites and the reaction proceeds *via* a carbenium ion mechanism.

An increase in the amplitude of the ESR signal for Mo^{5+} by the admission of butene to SiO_2–MoO_3 (9: 1) indicates that reduction occurred during the course of isomerization of butene. The activity also decreased with successive pulses. It seems that the active sites become less active by reduction. The mechanism of generation of acid sites in a mixed oxide was proposed by one of the authros,[1,2] and the concept can be applied to the SiO_2–MoO_3 system. Acid sites are caused by the excess positive charge on Si^{4+} in the SiO_2–MoO_3. The reduction of Mo^{6+} reduces the excess positive charge on Si^{4+} by the transfer of negative charge to Si^{4+} through oxygen bridging. This weakens the strength of acid sites or eliminates the acid sites.

References

1) K. Shibata, T. Kiyoura, J. Kitagawa, T. Sumiyoshi, and K. Tanabe, *Bull. Chem. Soc. Jpn.*, **46**, 2985 (1973).

2) K. Tanabe, T. Sumiyoshi, K. Shibata, and J. Kitagawa, *Bull. Chem. Soc. Jpn.*, **47**, 1064 (1974).

3) P. H. Batist, P. C. M. Heihden, and G. C. A. Schuit, *J. Catal.*, **22**, 411 (1971).

4) Y. Takita, A. Ozaki, and Y. Morooka, *J. Catal.*, **27**, 185 (1974).

5) T. Seiyama, M. Egashira, T. Sakamoto, and I. Aso, *J. Catal.*, **24**, 76 (1972).

6) M. Ai and T. Ikawa, *J. Catal.*, **40**, 203 (1975); M. Ai, *ibid.*, **40**, 327 (1975); M. Ai, *Bull. Chem. Soc. Jpn.*, **49**, 1328 (1976).

7) T. Kabe, M. Yamadaya, Y. Miki, and M. Oba, *Shokubai*, **17**, 23 (1975).

8) K. Tanabe and A. Aramata, *J. Res. Inst. Catal., Hokkaido Univ.*, **8**, 43 (1960).

Complexes between Nucleotide Base and Amino Acid. III. Crystal Structure of 5-Bromocytosine:Phthaloyl-DL-glutamic Acid Complex Hemihydrate

Minoru OHKI, Akio TAKENAKA, Hirotaka SHIMANOUCHI, and Yoshio SASADA

Laboratory of Chemistry for Natural Products, Tokyo Institute of Technology, Ookayama, Meguro-ku, Tokyo 152

(Received August 25, 1976)

5-Bromocytosine and phthaloyl-DL-glutamic acid co-crystallize from their aqueous solution in space group $P\bar{1}$, with dimensions of $a=10.578(2)$, $b=19.640$ (4), $c=9.890$ (3) Å, $\alpha=88.13$ (2), $\beta=107.86$ (3), $\gamma=104.26$ (1)°. Two molecular complexes and one water molecule are in an asymmetric unit. The structure was solved by the heavy atom method and refined by a block-diagonal least-squares method. The 5-bromocytosine molecule binds with γ-carboxyl group of the amino acid through NH···O and OH···O hydrogen bonds. In spite of largely different molecular environment in the crystal from that of 5-bromocytosine:*N*-tosyl-L-glutamic acid complex, the mode of interaction between the nucleotide base and the amino acid is the same. Thus, it is suggested that the present geometry is a typical binding mode between cytosine and acidic side group of amino acid.

The present structure determination is a part of the serial studies on specific binding patterns of nucleotide base-amino acid interactions.

As reported in Part II on the 5-bromocytosine:*N*-tosyl-L-glutamic acid complex (BCTG),[1] we have found a specific hydrogen bond of cytosine with γ-carboxyl group of glutamic acid, not with α-carboxyl group. In cytidine:*N*-benzyloxycarbonyl-L-glutamic acid complex dihydrate,[2] on the other hand, cytosine binds with α-carboxyl group of glutamic acid. As α-carboxyl group is used for peptide bond formation in protein except for its C-terminal, the hydrogen bonds between cytosine and γ-carboxyl group may represent a more general mode of interaction. So, it must be examined whether the interaction mode found in BCTG complex is preserved or not, when the molecular environment in a crystal is altered. We have investigated this by the structure analysis of the title complex which has a different *N*-protective group of glutamic acid from BCTG.

Experimental

Plate crystals were obtained from an aqueous solution containing equimolar quantities of the two components. The complex formation was confirmed by IR spectroscopy and an elementary analysis of these crystals. Found: C, 43.12; H, 3.39; N, 12.28%. Calcd for $C_4H_4N_3OBr\cdot C_{13}H_{11}NO_6\cdot 1/2H_2O$: C, 42.87; H, 3.39; N, 11.77%. Diffraction pattern of the crystal indicated the crystal system to be triclinic. The unit-cell dimensions were determined by least-squares calculations from 89 reflexions recorded on equator Weissenberg photographs about the three different axes, calibration being made with superposed silicon lines ($a=5.43075$ Å). These results are listed in Table 1.

Table 1. Crystal data

5-Bromocytosine: phthaloyl-DL-glutamic acid hemihydrate
$C_4H_4N_3OBr\cdot C_{13}H_{11}NO_6\cdot \frac{1}{2}H_2O$
F.W.=476.2
Crystal system: triclinic
Space group: $P\bar{1}$
$a=10.578$ (2) Å $b=19.640$ (4) Å $c=9.890$ (3) Å
$\alpha=88.13$ (2)° $\beta=107.86$ (3)° $\gamma=104.26$ (1)°
$U=1893.3$ (7) Å^3 $Z=4$
$D_x=1.671$ g cm^{-3} $D_m=1.69$ g cm^{-3}
μ (Cu$K\alpha$)=38.11 cm^{-1}

Diffraction data were collected on equi-inclination Weissenberg photographs (0*kl*-7*kl* and *hk*0-*hk*7) using Ni-filtered Cu$K\alpha$ radiation and the intensities were measured by a TV densitometer.[3] The crystals used for the a- and c-axis rotations were $0.1\times0.2\times0.3$ mm and $0.07\times0.19\times0.36$ mm in size, respectively. Corrections were made for Lorentz and polarization effects and spot size, but not for absorption. A total of 7649 independent reflexions was obtained, of which zero-reflexions numbered 3908. The $N(z)$ test[4] indicated the crystal to be centro-symmetric; this is reasonable because the amino acid derivatives is racemic, thus the space group being decided to be $P\bar{1}$. The density, measured by flotation in a $CHBr_3$–CCl_4 mixture, indicated that there are two molecular complexes and one water molecule in an asymmetric unit.

Structure Determination and Refinement

The structure was solved by the heavy atom method, and refined by a block-diagonal least-squares method, the minimized function being $\sum w\Delta F^2$ where $\Delta F=|F_o|-|F_c|$. In this refinement, the zero-reflexions were assumed to have the value of $|F_o|_{min}$ (=4.31). The zero-reflexions for which $|F_c|$ values were smaller than $|F_o|_{min}$ were omitted in each cycle of refinement. The weight function used was as follows: $w=\exp(-as^2-bt^2-cst-ds-et-f)$ for $|F_o|>|F_o|_{min}$, where $s=|F_o|$ and $t=\sin\theta/\lambda$; $w=1/\langle\Delta F^2\rangle$ for $|F_o|=|F_o|_{min}$. The coefficients, *a*—*f*, were evaluated by least-squares at each cycle of the structure refinement so that $\langle w\Delta F^2\rangle=1$. The refinement was terminated when the maximum shift of parameters was less than 0.04σ and 0.06σ for positional and thermal parameters, respectively. At the final cycle, the coefficients of weight function were 0.00006012, 23.72, −0.05158, 0.04557, −21.35, and 5.304, respectively, and weight for $|F_o|_{min}$ was 0.0763. The final value of *R* is 0.13 ($R_w=0.11$). For reflexions of $|F_o|>3\sigma$ ($\sigma=1/\sqrt{w}$), *R* is 0.078. The comparison between observed and calculated structure factors is given in Table 2.[5] Atomic scattering factors used were taken from "International Tables for X-Ray Crystallography."[6] The final positional and thermal parameters are given in Table 3.

TABLE 3. FINAL POSITIONAL AND THERMAL PARAMETERS

Standard deviations are given in parentheses. The temperature factor has the form $\exp[-(\beta_{11}h^2+\beta_{22}k^2+\beta_{33}l^2+\beta_{12}hk+\beta_{13}hl+\beta_{23}kl)]$. All parameters have been multiplied by 10^4.

Atom	x	y	z	β_{11}	β_{22}	β_{33}	β_{12}	β_{13}	β_{23}
N(1A)	−5030(7)	732(3)	6337(8)	85(7)	26(2)	162(11)	31(6)	84(14)	48(7)
C(2A)	−4185(8)	332(4)	7115(9)	80(8)	20(2)	139(11)	14(6)	61(15)	21(7)
N(3A)	−3009(6)	337(3)	6883(8)	77(6)	24(2)	134(9)	18(5)	68(13)	30(6)
C(4A)	−2623(7)	753(4)	5895(9)	80(8)	23(2)	129(11)	24(6)	58(15)	20(7)
C(5A)	−3498(8)	1153(4)	5043(8)	90(8)	24(2)	100(10)	18(6)	54(14)	25(7)
C(6A)	−4695(8)	1125(4)	5285(10)	100(9)	26(2)	131(11)	30(7)	49(16)	27(8)
O(2A)	−4612(5)	−54(3)	8042(7)	90(6)	28(2)	159(8)	29(5)	101(12)	52(6)
N(4A)	−1408(7)	777(4)	5741(9)	89(7)	34(2)	174(11)	39(7)	106(15)	54(8)
Br(5A)	−2979(1)	1711(0)	3616(1)	124(1)	27(0)	123(1)	27(1)	91(2)	32(1)
N(1B)	2738(7)	−278(3)	8361(8)	91(7)	26(2)	148(10)	33(6)	98(14)	39(7)
C(2B)	1906(8)	120(4)	7563(9)	98(8)	20(2)	140(11)	29(6)	78(16)	34(8)
N(3B)	631(6)	26(3)	7603(8)	86(7)	24(2)	145(9)	35(6)	82(13)	49(7)
C(4B)	147(8)	−469(4)	8427(9)	88(8)	27(2)	126(11)	24(7)	87(16)	28(8)
C(5B)	992(8)	−896(4)	9241(9)	95(8)	42(2)	107(10)	32(7)	42(15)	19(7)
C(6B)	2277(8)	−790(4)	9184(9)	102(9)	24(2)	131(11)	30(7)	75(16)	27(8)
O(2B)	2412(6)	574(3)	6810(7)	111(6)	27(2)	179(9)	38(5)	129(13)	76(6)
N(4B)	−1124(7)	−543(4)	8446(9)	97(8)	33(2)	185(12)	46(7)	121(16)	62(8)
Br(5B)	324(1)	−1569(0)	10424(1)	116(1)	30(0)	165(1)	33(1)	117(2)	58(1)
O(3A)	−6109(7)	−4305(3)	8387(8)	138(8)	26(2)	171(10)	−3(6)	120(14)	−6(6)
O(4A)	−4113(7)	−3543(3)	8568(9)	111(7)	32(2)	222(12)	10(6)	136(15)	−4(8)
C(7A)	−5336(8)	−3740(4)	8744(9)	94(8)	27(2)	111(10)	19(7)	57(15)	23(8)
C(8A)	−5644(8)	−3147(4)	9482(9)	77(8)	27(2)	129(11)	7(7)	69(15)	21(8)
C(9A)	−4460(9)	−2769(4)	10761(10)	116(10)	24(2)	129(11)	15(7)	39(17)	12(8)
C(10A)	−3510(9)	−2135(5)	10386(12)	98(9)	30(3)	192(15)	20(8)	51(19)	34(10)
C(11A)	−4175(8)	−1537(4)	9923(10)	83(8)	26(2)	153(12)	25(7)	44(16)	19(8)
O(5A)	−3493(7)	−1074(4)	9235(10)	117(7)	35(2)	287(14)	52(6)	188(17)	88(9)
O(6A)	−5212(7)	−1475(4)	10126(9)	109(7)	41(2)	251(13)	60(7)	138(16)	53(9)
N(5A)	−6893(7)	−3428(3)	9846(8)	94(7)	20(2)	137(9)	22(5)	77(13)	40(6)
C(12A)	−8141(9)	−3236(4)	9241(10)	108(9)	24(2)	134(11)	29(7)	78(17)	28(8)
C(13A)	−7027(8)	−3963(4)	10794(9)	95(8)	22(2)	127(11)	22(7)	57(15)	21(8)
O(7A)	−8303(7)	−2807(4)	8333(8)	128(8)	39(2)	176(10)	54(7)	99(14)	94(8)
O(8A)	−6090(6)	−4208(3)	11459(7)	108(6)	26(2)	157(9)	40(5)	83(12)	60(6)
C(14A)	−9106(8)	−3649(4)	9944(8)	96(8)	24(2)	101(10)	21(7)	60(15)	18(7)
C(15A)	−10423(9)	−3643(5)	9801(9)	100(9)	33(3)	111(11)	30(8)	48(16)	14(8)
C(16A)	−11105(9)	−4105(5)	10616(10)	109(10)	37(3)	128(12)	38(8)	70(17)	9(9)
C(17A)	−10458(9)	−4549(5)	11532(9)	102(9)	32(3)	111(11)	23(8)	64(16)	4(8)
C(18A)	−9101(8)	−4552(4)	11675(9)	106(9)	25(2)	99(10)	15(7)	65(15)	10(7)
C(19A)	−8448(8)	−4097(4)	10854(9)	92(8)	22(2)	114(10)	24(6)	68(15)	11(7)
O(3B)	3892(6)	4443(3)	5505(8)	110(7)	35(2)	169(10)	−15(6)	110(14)	8(7)
O(4B)	2956(6)	4386(3)	7247(7)	110(7)	31(2)	136(8)	9(5)	88(12)	−2(6)
C(7B)	3077(7)	4145(4)	6086(8)	77(7)	26(2)	94(9)	18(6)	25(13)	14(7)
C(8B)	2148(7)	3414(4)	5626(9)	74(7)	25(2)	128(10)	33(6)	79(14)	42(7)
C(9B)	2112(8)	3148(4)	4179(9)	103(9)	23(2)	115(10)	6(7)	63(16)	21(7)
C(10B)	1299(9)	2384(4)	3827(10)	115(10)	24(2)	134(11)	26(7)	49(17)	19(8)
C(11B)	1970(8)	1894(4)	4817(10)	92(8)	25(2)	163(13)	23(7)	113(17)	37(8)
O(5B)	1096(6)	1303(3)	4943(8)	95(6)	26(2)	209(11)	14(5)	111(13)	51(7)
O(6B)	3177(6)	2014(3)	5451(10)	70(6)	31(2)	294(14)	26(5)	53(15)	50(8)
N(5B)	780(6)	3392(3)	5681(7)	79(6)	21(2)	118(8)	23(5)	69(12)	33(6)
C(12B)	113(8)	2932(4)	6508(9)	89(8)	19(2)	121(10)	7(6)	76(15)	18(7)
C(13B)	1(8)	3838(4)	4945(9)	93(8)	24(2)	125(11)	34(7)	48(15)	23(7)
O(7B)	594(6)	2505(3)	7264(7)	131(7)	31(2)	180(10)	51(6)	147(14)	74(7)
O(8B)	373(7)	4296(3)	4203(8)	140(8)	34(2)	179(10)	57(6)	119(15)	72(7)
C(14B)	−1251(7)	3087(4)	6217(9)	72(7)	26(2)	135(11)	1(6)	75(15)	−17(8)
C(15B)	−2345(10)	2769(5)	6711(11)	108(10)	39(3)	156(14)	−13(9)	125(20)	−49(10)
C(16B)	−3528(10)	3040(7)	6202(13)	91(10)	54(4)	188(16)	33(10)	85(20)	−52(13)
C(17B)	−3562(10)	3576(7)	5297(12)	90(10)	61(5)	168(16)	54(11)	45(20)	−6(14)
C(18B)	−2459(10)	3906(6)	4833(12)	92(10)	52(4)	174(15)	62(10)	25(19)	−7(12)
C(19B)	−1307(8)	3631(4)	5289(9)	80(8)	28(2)	121(11)	32(7)	25(15)	8(8)
O(9)	3512(6)	4493(3)	2602(7)	127(7)	29(2)	147(8)	37(6)	76(13)	22(6)

Results and Discussions

Bond lengths and angles of the two independent molecules are listed in Table 4. The values for corresponding bonds are in good agreement, and their averages are given in Fig. 1. The effects of bromine substitution on the bond lengths and angles of pyrimidine ring is not so large; somewhat longer C(2)-O(2) bond and shorter C(2)-N(3) bond are observed as compared with the authentic values of neutral cytosine,[7] but these should be attributable partly to the effects of strong hydrogen bonds involving O(2) (Table 5), which are also observed in BCTG complex.[1] The crystallographically independent molecules are shown in Fig. 2.

The molecules are arranged in layers parallel to the (021) plane (Fig. 3). As shown in Fig. 4, four α-carboxyl groups and two water molecules constitute a 14-membered ring around the center of symmetry at 1/2, 1/2, 1/2 by hydrogen bonds, O(4A)H···O(9), O(9)H···O

Table 4. Bond lengths and angles of the two independent molecules
Standard deviations are given in parentheses.

Bond lengths (l/Å)	Molecule A	Molecule B		Molecule A	Molecule B
N(1)-C(2)	1.38(1)	1.37(1)	C(2)-N(3)	1.33(1)	1.33(1)
N(3)-C(4)	1.35(1)	1.35(1)	C(4)-C(5)	1.42(1)	1.43(1)
C(5)-C(6)	1.35(1)	1.34(1)	C(6)-N(1)	1.36(1)	1.36(1)
C(2)-O(2)	1.29(1)	1.27(1)	C(4)-N(4)	1.33(1)	1.32(1)
C(5)-Br(5)	1.891(8)	1.887(8)			
C(7)-O(3)	1.19(1)	1.20(1)	C(7)-O(4)	1.32(1)	1.31(1)
C(7)-C(8)	1.54(1)	1.52(1)	C(8)-N(5)	1.45(1)	1.46(1)
C(8)-C(9)	1.53(1)	1.53(1)	C(9)-C(10)	1.51(1)	1.53(1)
C(10)-C(11)	1.50(1)	1.50(1)	C(11)-O(5)	1.32(1)	1.32(1)
C(11)-O(6)	1.21(1)	1.20(1)			
N(5)-C(12)	1.41(1)	1.41(1)	N(5)-C(13)	1.40(1)	1.39(1)
C(12)-C(14)	1.48(1)	1.49(1)	C(13)-C(19)	1.48(1)	1.48(1)
C(14)-C(19)	1.39(1)	1.39(1)	C(14)-C(15)	1.36(1)	1.39(1)
C(15)-C(16)	1.41(1)	1.42(2)	C(16)-C(17)	1.38(1)	1.36(2)
C(17)-C(18)	1.40(1)	1.39(2)	C(18)-C(19)	1.39(1)	1.40(1)
C(12)-O(7)	1.21(1)	1.21(1)	C(13)-O(8)	1.21(1)	1.21(1)

Bond angles (ϕ/°)	Molecule A	Molecule B		Molecule A	Molecule B
C(2)-N(1)-C(6)	120.4(7)	121.4(7)	C(8)-N(5)-C(12)	125.4(7)	124.1(7)
N(1)-C(2)-O(2)	116.5(7)	117.2(8)	C(8)-N(5)-C(13)	123.3(7)	123.5(7)
N(1)-C(2)-N(3)	120.9(7)	120.4(8)	C(12)-N(5)-C(13)	111.2(7)	112.4(7)
O(2)-C(2)-N(3)	122.6(8)	122.5(8)	N(5)-C(12)-C(14)	106.0(7)	105.4(7)
C(2)-N(3)-C(4)	119.5(7)	119.8(7)	N(5)-C(12)-O(7)	123.7(8)	124.8(8)
N(3)-C(4)-C(5)	120.6(7)	120.5(8)	C(14)-C(12)-O(7)	130.3(8)	129.8(8)
N(3)-C(4)-N(4)	118.2(8)	117.9(8)	N(5)-C(13)-C(19)	106.1(7)	105.5(7)
C(5)-C(4)-N(4)	121.2(8)	121.7(8)	N(5)-C(13)-O(8)	123.3(8)	124.8(8)
C(4)-C(5)-C(6)	118.4(8)	118.6(8)	C(19)-C(13)-O(8)	130.4(8)	129.7(8)
C(4)-C(5)-Br(5)	120.4(6)	120.1(6)	C(12)-C(14)-C(15)	130.3(8)	129.9(8)
C(6)-C(5)-Br(5)	121.2(6)	121.2(6)	C(12)-C(14)-C(19)	108.1(7)	107.8(7)
C(5)-C(6)-N(1)	120.1(8)	119.3(8)	C(15)-C(14)-C(19)	121.7(8)	122.3(8)
			C(13)-C(19)-C(14)	108.4(7)	108.9(7)
O(3)-C(7)-O(4)	124.6(8)	124.2(8)	C(13)-C(19)-C(18)	130.2(8)	129.7(9)
O(3)-C(7)-C(8)	123.9(8)	123.7(8)	C(14)-C(19)-C(18)	121.4(8)	121.4(9)
O(4)-C(7)-C(8)	111.4(7)	111.9(7)	C(14)-C(15)-C(16)	117.7(8)	115.6(9)
C(7)-C(8)-N(5)	108.8(7)	109.8(6)	C(15)-C(16)-C(17)	121.2(9)	121.2(11)
C(7)-C(8)-C(9)	114.8(7)	113.8(7)	C(16)-C(17)-C(18)	120.9(9)	123.2(11)
N(5)-C(8)-C(9)	112.1(7)	111.7(7)	C(17)-C(18)-C(19)	117.2(8)	116.1(10)
C(8)-C(9)-C(10)	114.0(8)	112.3(7)			
C(9)-C(10)-C(11)	112.8(8)	111.8(8)			
C(10)-(11)-O(5)	111.8(8)	113.1(8)			
C(10)-C(11)-O(6)	125.5(9)	124.7(9)			
O(5)-C(11)-O(6)	122.8(8)	122.2(9)			

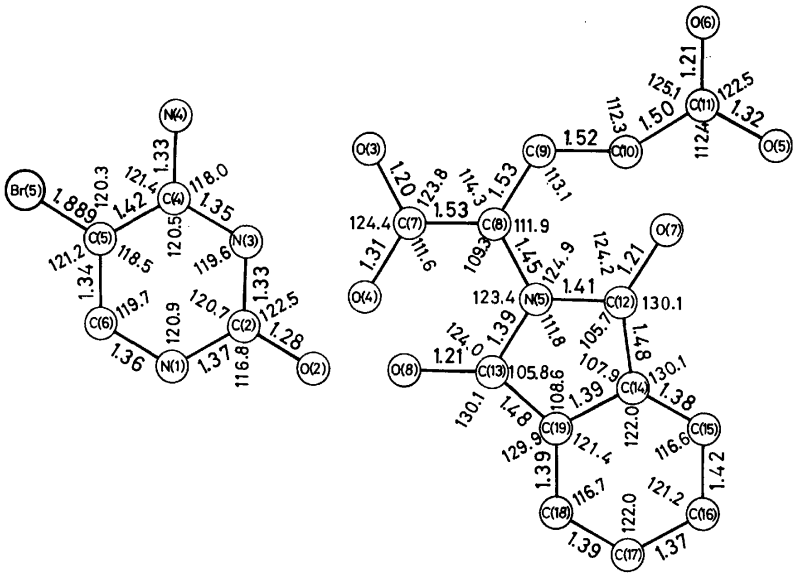

Fig. 1. The average bond lengths (l/Å) and angles (ϕ/°) of the two independent 5-bromocytosine and phthaloylglutamic acid molecules.

Table 5. Distances and angles of hydrogen bonds
(CH···O contacts are also listed in this table.)

Distance (l/Å)					
N(1A)···O(2B)[a]	2.83	N(1B)···O(2A)[b]	2.84	N(4A)···N(3B)[c]	3.03
N(4B)···N(3A)[c]	3.00	N(4A)···O(5B)[c]	2.93	N(4B)···O(5A)[c]	2.80
O(5A)···O(2A)[c]	2.64	O(5B)···O(2B)[c]	2.58	O(4B)···O(3A)[d]	2.67
O(9)···O(3B)[e]	2.78	O(4A)···O(9)[e]	2.53	O(9)···O(8A)[f]	2.75
C(6A)···O(6B)[a]	3.21	C(6B)···O(6A)[b]	3.14		
Angle (ϕ/°)					
N(1A)···O(2B)[a]–C(2B)[a]	126.1	C(2A)–N(1A)···O(2B)[a]	117.2	C(6A)–N(1A)···O(2B)[a]	122.0
N(1B)···O(2A)[b]–C(2A)[b]	125.5	C(2B)–N(1B)···O(2A)[b]	116.6	C(6B)–N(1B)···O(2A)[b]	121.8
N(4A)···N(3B)[c]–C(2B)[c]	123.7	N(4A)···N(3B)[c]–C(4B)[c]	116.3	C(4A)–N(4A)···N(3B)[c]	124.0
N(4B)···N(3A)[c]–C(2A)[c]	123.4	N(4B)···N(3A)[c]–C(4A)[c]	117.0	C(4B)–N(4B)···N(3A)[c]	125.3
N(4A)···O(5B)[c]–C(11B)[c]	141.8	N(4A)···O(5B)[c]···O(2B)[c]	92.0	C(4A)–N(4A)···O(5B)[c]	159.3
N(4B)···O(5A)[c]–C(11A)[c]	149.6	N(4B)···O(5A)[c]···O(2A)[c]	92.8	C(4B)–N(4B)···O(5A)[c]	158.0
O(5A)···O(2A)[c]–C(2A)[c]	122.1	O(5A)···N(4B)[c]···N(3A)[c]	76.7	O(5A)···O(2A)[c]···N(1B)[a]	109.1
C(11A)–O(5A)···O(2A)[c]	117.5	O(5B)···O(2B)[c]–C(2B)[c]	126.2	O(5B)···N(4A)[c]···N(3B)[c]	75.2
O(5B)···O(2B)[c]···N(1A)[b]	106.1	C(11B)–O(5B)···O(2B)[c]	108.4	O(4B)···O(3A)[d]–C(7A)[d]	158.0
C(7B)–O(4B)···O(3A)[d]	128.2	O(9)···O(3B)[e]–C(7B)[e]	127.4	C(7A)–O(4A)···O(9)[e]	113.4
O(9)···O(8A)[f]–C(13A)[f]	122.8	C(6A)···O(6B)[a]–C(11B)[a]	127.9	N(1A)–C(6A)··· O(6B)[a]	88.2
C(5A)–C(6A)···O(6B)[a]	145.2	C(6B)···O(6A)[b]–C(11A)[b]	147.0	N(1B)–C(6B)···O(6A)[b]	99.7
C(5B)–C(6B)···O(6A)[b]	140.6				

a: at $-1+x, y, z$. b: at $1+x, y, z$. c: at x, y, z. d: at $1+x, 1+y, z$. e: at $-x, -y, 1-z$. f: at $1+x, 1+y, -1+z$.

(3B), and O(4B)H···O(3A). Distance of O(4A)··· O(9) is fairly shorter than those of the other OH···O hydrogen bonds (Table 5). Similar short O···O distances are also observed in oxalic acid dihydrate (2.512 Å)[8] and pyromellitic acid dihydrate (2.549 Å).[9] Furthermore, this ring is connected with those in the neighboring unit-cells by the hydrogen bond between water molecule and O(8) atom of phthaloyl group in the A molecule, to complete a three-dimensional network. The structure is further stabilized by the overlapping of the phthaloyl groups; the dihedral angle between the mean planes of the two independent phthaloyl groups is 5.1° and the spacing is about 3.4 Å.

The hydrogen bonding arrangements in the layer is illustrated in Fig. 5, relevant distances and angles being listed in Table 5. The 5-bromocytosine molecules are linked by the hydrogen bonds, N(1A)H···O(2B), N (1B)H···O(2A), N(4A)H···N(3B), and N(4B)H···N (3A), to form a ribbon elongated along [100] direction. To the ribbon, γ-carboxyl group of a glutamic acid is bound through hydrogen bonds in which O(5) atom is a donor to O(2) of 5-bromocytosine and at the same time an acceptor from N(4) of the neighboring base. In addition, O(6) seems to make a CH···O type interaction with C(6) of the base A′. The other crystallographically independent glutamic acid also interacts to the ribbon

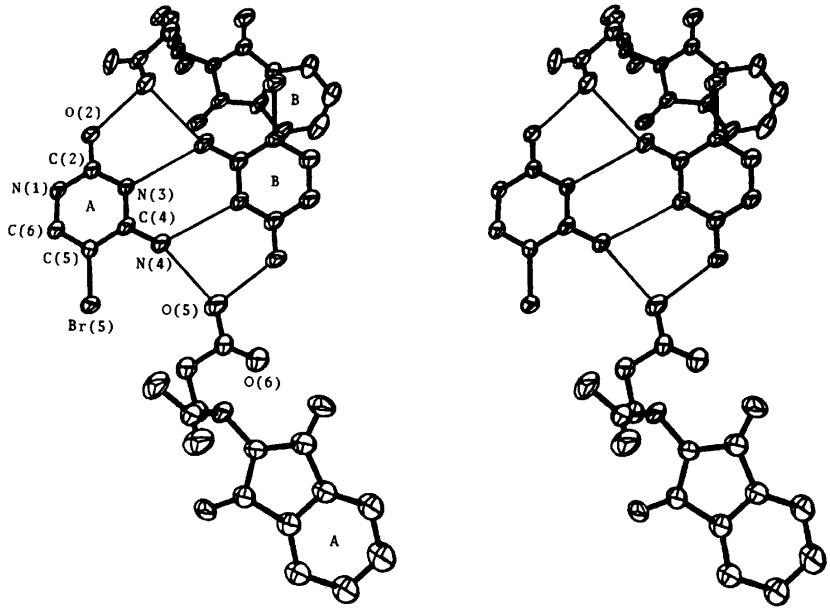

Fig. 2. A stereoscopic view of 5-bromocytosine: phthaloylglutamic acid.
Thermal ellipsoids are drawn at the 50% probability level.

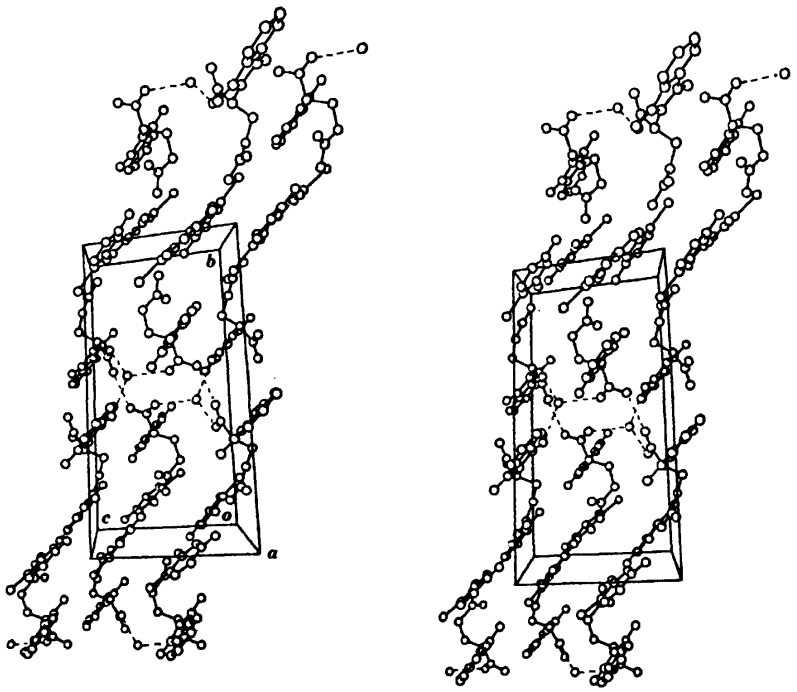

Fig. 3. A stereoscopic view of the crystal structure.

in the same way. It is interesting to note that amino acids bound to one cytosine's ribbon are the same optical isomers.

As seen from the hydrogen bond scheme described above, the N(3) atom of cytosine is not protonated; the C(2)–N(3)–C(4) bond angle of cytosine 119.6° is close to unprotonated form,[7] and the distances and angles of α- and γ-carboxyl groups of glutamic acid correspond to those of undissociated acid.

Each pyrimidine ring is planar within 0.02 Å and each bromine atom also lies in the plane. The dihedral angle between these mean planes is 11.5°.

The conformations of two glutamic acids A and B are different to each other mainly in torsions around the C(7)–C(8) and C(8)–C(9) bonds, as shown in Table 6. In the molecule A, the C(8)–N(5) bond is nearly parallel to α-carboxyl plane and the torsion angle of C(7)–C(8)–C(9)–C(10) is a nearly right angle, while in the molecule B, the C(8)–C(9) bond is parallel to α-carboxyl plane and C(7), C(8), C(9), and C(10) are nearly coplanar.

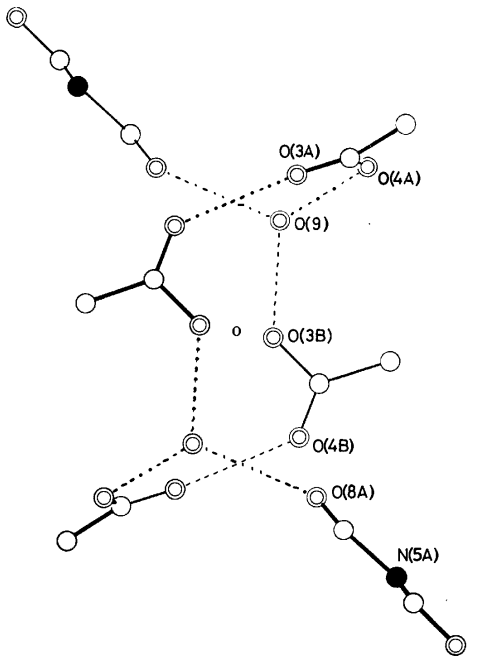

Fig. 4. The hydrogen bonding network around the center of symmetry at 1/2, 1/2, 1/2 viewed along the a axis.

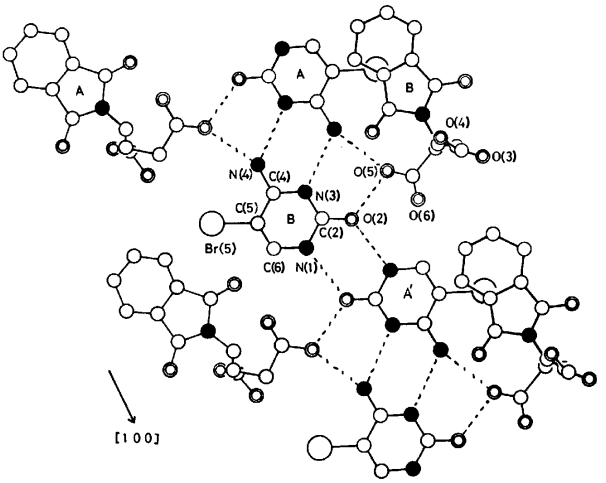

Fig. 5. A projection of one layer of 5-bromocytosine: phthaloyl-DL-glutamic acid onto the (021) plane. This illustrates the hydrogen bonding arrangement in the complex. The crystallographically independent molecules are labeled as A and B.

The side chains of glutamic acids are folded by the rotations around C(9)–C(10) bonds, in contrast to the extended form found in BCTG complex.[1]

As described above, the present crystal structure is different from that of BCTG in a mode of interlayer interaction, in hydrogen bonds of the α-carboxyl groups, and in the conformations of glutamic acids. In spite of these differences, binding scheme between 5-bromocytosine and γ-carboxyl group of glutamic acid is the same as that of BCTG, suggesting that this binding is a typical mode between 5-bromocytosine and the acidic amino acid.

The other type of complex formation between cytosine and glutamic acid has been reported for cytidine: *N*-benzyloxycarbonyl-L-glutamic acid complex dihydrate,[2] in which cytosine moiety interacts with dissociated α-carboxyl group. Such a difference may be attri-

Table 6. Torsion angles of the two independent glutamic acid

	Molecule A	Molecule B
O(3)–C(7)–C(8)–N(5)	8.8°	−138.3°
O(4)–C(7)–C(8)–N(5)	−171.1	46.4
C(7)–C(8)–N(5)–C(12)	−113.0	−121.4
C(7)–C(8)–N(5)–C(13)	62.8	56.9
C(9)–C(8)–N(5)–C(12)	119.0	111.4
C(9)–C(8)–N(5)–C(13)	−65.2	−70.3
O(3)–C(7)–C(8)–C(9)	135.0	−12.3
O(4)–C(7)–C(8)–C(9)	−44.6	172.4
N(5)–C(8)–C(9)–C(10)	−144.8	−61.3
C(7)–C(8)–C(9)–C(10)	90.4	173.7
C(8)–C(9)–C(10)–C(11)	69.0	−65.5
C(9)–C(10)–C(11)–O(5)	−162.4	154.3
C(9)–C(10)–C(11)–O(6)	16.9	−25.4

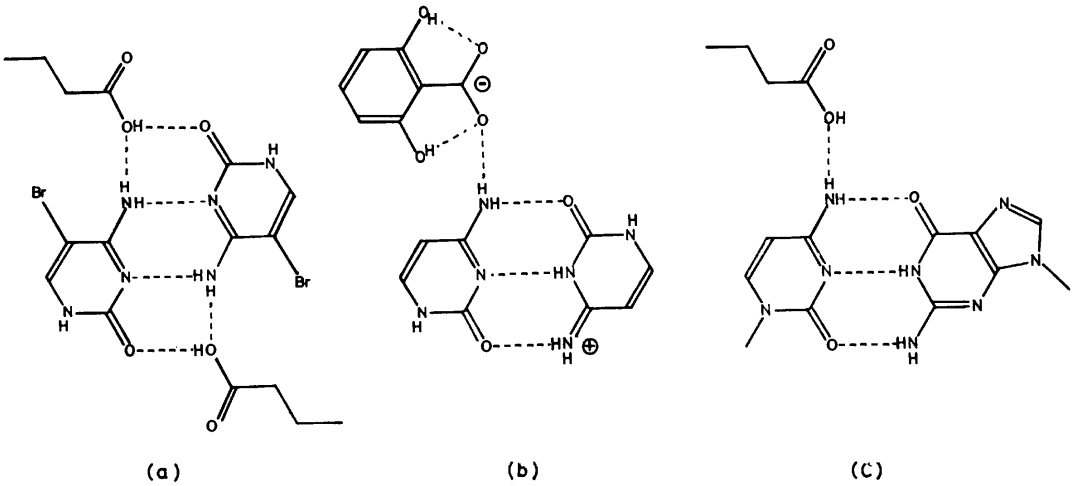

Fig. 6. The hydrogen bond scheme of (a) present and BCTG complexes, (b) cytosine: resorcylic acid 2: 1 complex monohydrate, and (c) a model of interaction between acidic side group of amino acid and the Watson-Crick G: C pair.

buted to the bromine substitution at C(5) of cytosine. Bromine at C(5) decreases the basicity of cytosine, so that a protonation to N(3) is inhibited; pK_a of 5-bromocytosine is 3.04 while those of cytosine and cytidine are 4.61 and 4.1,[10] respectively. In cytidine:*N*-benzyloxycarbonyl-L-glutamic acid, cytosine base is protonated and then hydrogen-bonded with stronger acid, α-carboxyl group of glutamic acid, while in the present and BCTG complexes, the protonation of the base is inhibited so that it becomes possible to interact with milder γ-carboxyl group. This argument is supported by the recent structure analysis of cytosine:phthaloyl-DL-glutamic acid complex,[11] in which cytosine binds with α-carboxyl group of glutamic acid.

Schematic drawing of complex molecules found in the present and BCTG complexes in Fig. 6(a) shows that the mode of three parallel hydrogen bonds of cytosine resembles the triple hydrogen bond in the Watson-Crick guanine:cytosine pair. A similar feature is also found in cytosine: resorcylic acid 2: 1 complex monohydrate[12] (Fig. 6(b)), in which the triple hydrogen bond is formed between neutral and protonated cytosines; furthermore, dissociated carboxyl group of resorcylic acid binds through a hydrogen bond to cytosine in the same geometry as those in the present and BCTG complexes. Thus, if the base on the right side in Fig. 6 (a) and (b) is replaced by guanine as in Fig. 6(c), it might provide a model of interaction between paired cytosine and acidic side group of amino acid. Recently, some model building[13,14] concerning mutual recognition between double helical nucleic acid and protein have been reported, but the present model is the first one based on the observed interaction between nucleotide base and amino acid in the crystal. It is known that elongation factors T_u and G, and initiation factor F_2 in protein synthesis are all acidic protein. Therefore, the present structure might be effected if some acidic side groups of these factors would interact with tRNA, mRNA, and rRNA.

Part of the cost of this research was met by a Scientific Research Grant from the Ministry of Education to which the authors' thanks are due.

References

1) M. Ohki, A. Takenaka, H. Shimanouchi, and Y. Sasada, *Bull. Chem. Soc. Jpn.*, **49**, 3493 (1975).
2) T. Hata, M. Yoshikawa, S. Sato, and C. Tamura, *Acta Crystallogr., Sect. B*, **31**, 312 (1975).
3) T. Izumi, *Jpn. J. Appl. Phys.*, **10**, 1724 (1971).
4) E. R. Howells, D. C. Phillips, and D. Rogers, *Acta Crystallogr.*, **3**, 210 (1950).
5) Table 2 has been deposited at the Chemical Society of Japan (Document No. 7701).
6) "International Tables for X-Ray Crystallography," Vol. III, Kynoch Press, Birmingham (1962), p. 201.
7) R. J. McClure and B. M. Craven, *Acta Crystallogr., Sect. B*, **29**, 1234 (1973).
8) R. G. Delaplane and J. A. Ibers, *Acta Crystallogr., Sect. B*, **25**, 2423 (1969).
9) F. Takusagawa, K. Hirotsu, and A. Shimada, *Bull. Chem. Soc. Jpn.*, **44**, 1274 (1971).
10) I. Wempen and J. J. Fox, *J. Am. Chem. Soc.*, **86**, 2474 (1964).
11) A. Takenaka, M. Ohki, and Y. Sasada, to be published.
12) C. Tamura, S. Sato, and T. Hata, *Bull. Chem. Soc. Jpn.*, **46**, 2388 (1973).
13) K. Adler, K. Beyreuther, E. Fanning, N. Geisler, B. Gronenborn, A. Klemm, B. Muller-Hill, M. Pfahl, and A. Schmitz, *Nature*, **237**, 322 (1972).
14) N. C. Seeman, J. M. Rosenberg, and A. Rich, *Proc. Natl. Acad. Sci. U. S. A.*, **73**, 804 (1976).

The Molecular-Symmetry Reduction in Open-Shell Conjugated Hydrocarbons

Azumao Toyota and Takeshi Nakajima*

Department of Chemistry, Faculty of General Education, Yamagata University, Yamagata 990

** Department of Chemistry, Faculty of Science, Tohoku University, Sendai 980*

(Received September 20, 1976)

On the basis of the second-order Jahn-Teller theorem, we propose a criterion for predicting the stable ground-state geometrical structures of open-shell conjugated hydrocarbons. It is found that in contrast with the cases of the parent closed-shell hydrocarbons no molecular symmetry reduction occurs in the ion radicals of the C_mH_{m-2} cata-condensed nonalternant hydrocarbons, such as pentalene and heptalene. On the other hand, it is revealed that the ion radicals of fulvalene systems suffer the molecular symmetry reduction from D_{2h} to C_{2v}. In addition, the electronic spectra were calculated using the stable geometrical structures obtained by use of the semiempirical open-shell SCF MO method.

It is well known that the ground states of odd cyclic polyene radicals, *e.g.* the cyclopentadienyl radical, and ion radicals of even cyclic polyenes, *e.g.* the benzene positive ion, are unstable in the fully symmetrical nuclear arrangements and undergo the first-order Jahn-Teller distortions.[1] Further, the closed-shell C_mH_{m-2} cata-condensed nonalternant hydrocarbons, considered to be formed by the introduction of a cross-link between the two carbon atoms of like parity in even cyclic polyenes with $4n$ π-electrons, such as pentalene and heptalene, are found to suffer the second-order (pseudo) Jahn-Teller effects in the fully symmetrical nuclear arrangements and to be unstable with respect to the nuclear deformation of bond alternation type.[2] Our present interest is to examine whether the second-order Jahn-Teller distortions occur or not in the ground states of the ion radicals of C_mH_{m-2} cata-condensed nonalternant systems.

In order to predict the stable molecular shapes of closed-shell conjugated hydrocarbons, we have proposed a symmetry rule on the basis of the so-called pseudo Jahn-Teller theorem,[3-5] assuming that only the lowest-lying excited state plays a dominant role for the problem of a molecular symmetry reduction. In spite of the very drastic approximation, this rule has been shown to hold for a large number of conjugated hydrocarbons.[2,3,6-8]

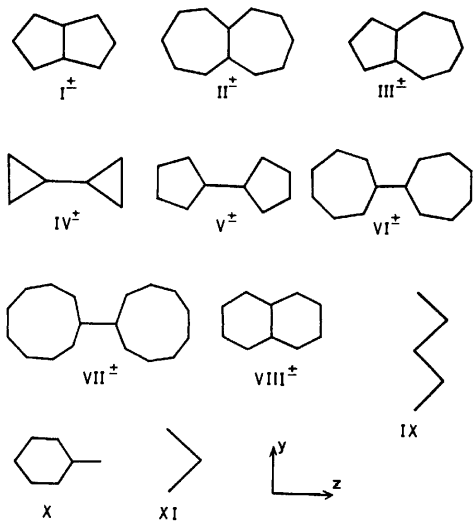

Fig. 1. Carbon skeletons and choice of axes for some open-shell conjugated hydrocarbons. The + or − sign of the superscript refers to the cation or the anion radical, respectively. I: Pentalene, II: heptalene, III: azulene, IV: triafulvalene, V: pentafulvalene, VI: heptafulvalene, VII: nonafulvalene, VIII: naphthalene, IX: pentadienyl radical, X: benzyl radical, XI: allyl radical.

In this paper, we derive a criterion for a molecular symmetry reduction in open-shell conjugated systems, and examine the stable molecular shapes of some ion radicals of (a) C_mH_{m-2} cata-condensed nonalternant systems, (b) $C_{4n+2}H_{4n}$ fulvalene systems, and (c) alternant systems (Fig. 1). Moreover, we calculate the electronic spectra using the stable geometrical structures obtained by use of the open-shell SCF MO method.

Theoretical

The Second-order Jahn-Teller Effect. The method for predicting the stable molecular shapes of conjugated hydrocarbons is based on the second-order Jahn-Teller theorem. First we assume a fully symmetrical nuclear arrangement as the unperturbed nuclear configuration for an open-shell conjugated hydrocarbon. We further assume that in the unperturbed nuclear configuration all the fully symmetrical bond distortions take place until the first-order energy equilibrium is reached. The unperturbed doublet electronic wavefunctions ϕ_0, ϕ_1, $\cdots$, ϕ_n, $\cdots$ and the corresponding eigenvalues E_0, E_1, $\cdots$, E_n, $\cdots$ are assumed to be known. We now distort the nuclei from the fully symmetrical (first-order) nuclear arrangement by means of the ith normal coordinate of nuclear motion Q_i. On the basis of the same approximation as used previously,[3] the energy of the ground state after the deformation may be written as

$$E(Q_i) = E_0 + \frac{1}{2}\left\{k - 2\sum_{n(\neq 0)} \frac{|\langle\phi_n|(\partial v/\partial Q_i)_0|\phi_0\rangle|^2}{(E_n - E_0)}\right\} Q_i^2$$

where k and v represent the force constant for an sp^2 hybridized C–C σ-bond and the operator of one electron nuclear-electron potential energy, respectively.

According to the above equation, the curvature of $E(Q_i)$ with respect to the nuclear deformation Q_i, that is, $\{k - 2\sum_{n(\neq 0)}|\langle\phi_n|(\partial v/\partial Q_i)_0|\phi_0\rangle|^2/(E_n - E_0)\}$, can be identified as the force constant for the nuclear deformation Q_i. If a given matrix element $\langle\phi_n|(\partial v/\partial Q_i)_0|\phi_0\rangle$ is nonvanishing and the associated energy gap $E_n - E_0$ is sufficiently small, the force constant can be negative and the initial nuclear configuration would be unstable with respect to the nuclear deformation Q_i.

Such a nuclear deformation is called the pseudo, or the second-order Jahn-Teller effect.

Criterion for a Molecular Symmetry Reduction. In order to estimate the value of the force constant, we make the following approximation: the infinite sum over the excited states is replaced by one term corresponding to the lowest excited state, ϕ_1. It has been shown that this approximation is amply justified at least in the closed-shell conjugated hydrocarbons.[2,3,6-8]

We now focus our attention on the matrix element, $\langle\phi_1|(\partial v/\partial Q_i)_0|\phi_0\rangle$, called the relaxability of the molecule along the nuclear displacement Q_i.[9] It is obvious from the symmetry argument that this integral is nonvanishing, only if the symmetry of the direct product $\Gamma(\phi_0)\times\Gamma(\phi_1)$ is identical with that of the nuclear deformation Q_i. We can thus determine the symmetry of nuclear deformation effective for the molecular symmetry reduction. It should be noted that in the closed-shell systems the ground state is, in principle, totally symmetric, the symmetry of nuclear deformation Q_i is identical with that of the lowest excited singlet state.

In order to calculate electronic states of open-shell conjugated hydrocarbons, we employ Longuet-Higgins and Pople's method.[10] According to their method, a doublet ground state wavefunction is written as

$$\phi_0 = |\varphi_1\bar{\varphi}_1 \cdots \varphi_{m-1}\bar{\varphi}_{m-1}\varphi_m|$$

where φ_m is the molecular orbital of an odd α electron. As the main electron configuration of the lowest excited doublet state, the following two types of electron excitation are possible:

(i) The excitation of the β electron in φ_{m-1} to φ_m, which gives rise to the doublet wavefunction

$$\phi_A = |\varphi_1\bar{\varphi}_1 \cdots \varphi_{m-1}\bar{\varphi}_m\varphi_m|$$

(ii) The excitation of the odd electron to φ_{m+1}, which gives rise to the doublet wavefunction

$$\phi_B = |\varphi_1\bar{\varphi}_1 \cdots \varphi_{m-1}\bar{\varphi}_{m-1}\varphi_{m+1}|$$

Since $(\partial v/\partial Q_i)_0$ is the one-electron operator, the matrix element $\langle\phi_1|(\partial v/\partial Q_i)_0|\phi_0\rangle$ is reduced to $\int\rho_{01}\cdot(\partial v/\partial Q_i)_0 d\tau$, where ρ_{01} is the so-called transition density. The value of this integral may become very large if the transition density is localized in the regions near nuclei which are involved in the motion. The transition density between the ground and the lowest excited doublet state is given by $\varphi_{m-1}\varphi_m$, if the latter state is ϕ_A, or $\varphi_m\cdot\varphi_{m+1}$ if it is ϕ_B.

It should be noted in this connection that for closed-shell systems the transition density between the ground and the lowest excited singlet state corresponding to the orbital jump $\varphi_i\rightarrow\varphi_j$, in which φ_i and φ_j are respectively the highest occupied and the lowest vacant molecular orbitals, is given by $\sqrt{2}\,\varphi_i\varphi_j$. Therefore, in so far as the transition densities for both open and closed-shell systems are assumed not to vary significantly according to the molecular orbitals concerned, the square of the matrix element, $|\langle\phi_1|(\partial v/\partial Q_i)_0|\phi_0\rangle|^2$, for open-shell systems should be about one half as that for closed-shell systems. As for closed-shell systems, it should be kept in mind that the following criterion[3] for the molecular symmetry reduction holds for a variety of molecules: if the lowest excitation energy of a molecule, calculated assuming the full molecular symmetry, is smaller than *ca.* 1.2 eV, the force constant for a certain antisymmetrical nuclear vibration should be negative, and the molecule would be distorted into a less symmetrical nuclear arrangement.

From the above arguments, we may now draw a criterion for a molecular symmetry reduction in open-shell conjugated hydrocarbons, which states: if the lowest doublet excitation energy of a given molecule, calculated assuming the full molecular symmetry, is smaller than a critical value, *ca.* 0.6 eV, the initial nuclear arrangement is unstable with respect to a certain antisymmetrical C–C nuclear deformation, and the molecule would be distorted into a less symmetrical nuclear arrangement. As to the actual type of nuclear deformation Q_i, it is predicted by examining the distributions of the transition density ρ_{01}.

Since it is based on the second-order Jahn-Teller theorem, the above criterion gives only the type of the most favorable bond distortion. In order to obtain the equilibrium C–C bond-length at which the nuclei of the real molecule will settle, we use the semiempirical open-shell SCF MO method in conjunction with the variable bond-length technique.[11,12]

Results and Discussion

In Table 1 are listed the lowest excitation energies, calculated by using the semiempirical open-shell SCF

Table 1. The lowest excitation energies and symmetries of the ground and the lowest excited doublet states of open-shell conjugated hydrocarbons

Molecule (Point group and ground state symmetry)	Lowest Excited State	
	ΔE (eV)	Symmetry
Pentalene$^+$ (D_{2h}, B_{3u})[a]	1.50	A_u
Pentalene$^-$ (D_{2h}, A_u)	1.77	B_{3u}
Azulene$^+$ (C_{2v},A_2)	1.31	B_1
Azulene$^-$ (C_{2v}, B_1)	1.18	A_2
Heptalene$^+$ (D_{2h}, B_{2g})	1.19	B_{1g}
Heptalene$^-$ (D_{2h}, B_{1g})	1.02	B_{2g}
Nonalene$^+$ (D_{2h}, B_{3u})	0.78	A_u
Nonalene$^-$ (D_{2h}, A_u)	0.99	B_{3u}
Triafulvalene$^+$ (D_{2h}, B_{3u})	1.55	A_u
Triafulvalene$^-$ (D_{2h}, B_{1g})	0.44	A_u
Pentafulvalene$^+$ (D_{2h}, A_u)	0.47	B_{1g}
Pentafulvalene$^-$ (D_{2h}, B_{2g})	1.22	B_{1g}
Heptafulvalene$^+$ (D_{2h}, B_{3u})	1.22	A_u
Heptafulvalene$^-$ (D_{2h}, B_{1g})	0.35	A_u
Nonafulvalene$^+$ (D_{2h}, A_u)	0.31	B_{1g}
Nonafulvalene$^-$ (D_{2h}, B_{2g})	1.17	B_{1g}
Odd linear polyene radicals		
C_3H_5 (C_{2v}, A_2)	3.05	B_1
C_5H_7 (C_{2v}, B_1)	2.10	A_2
C_7H_9 (C_{2v}, A_2)	1.95	B_1
C_9H_{11} (C_{2v}, B_1)	1.59	A_2
$C_{11}H_{13}$ (C_{2v}, A_2)	1.49	B_1
$C_{17}H_{19}$ (C_{2v}, B_1)	1.37	A_2
Benzyl radical(C_{2v}, B_1)	2.54	B_1
Naphthalene$^+$ (D_{2h},A_u)	0.90	B_{3u}
Naphthalene$^-$ (D_{2h}, B_{2g})	0.90	B_{1g}

a) The + or − sign refers to the cation or the anion radical, respectively.

MO CI method and the symmetries of the ground and the lowest excited doublet states at the fully symmetrical nuclear arrangements.

The Ion Radicals of C_mH_{m-2} Cata-condensed Nonalternant Systems. It is found in a previous paper[2] that in the $C_{4n}H_{4n-2}$ closed-shell systems which has a cross-link between the two carbon atoms of like parity all the lowest excitation energies calculated assuming the fully symmetrical structures are significantly smaller than the critical value, which results in the molecular symmetry reduction accompanied by a marked double-bond fixation in the peripheral carbon skeleton. On the other hand, in $C_{4n+2}H_{4n}$ with a cross-link between the two carbon atoms of like parity the lowest excitation energies are predicted to be considerably larger than the critical value for small members and a molecular symmetry reduction would not occur until the number of carbon atoms increases to a certain value. Pentalene (1-methylpentalene) and heptalene, both having $4n$ carbon atoms, have successfully been synthesized by Bloch *et al.*[13] and Dauben and Bertelli,[14] respectively, and are known to exhibit the polyolefinic characters. The theoretical studies on both molecules revealed that at the fully symmetric D_{2h} configuration the lowest excited singlet state (B_{3g}) is nearly degenerate with the ground state (A_g) and therefore the stable geometrical structure is predicted to be of C_{2h} symmetry, showing a marked double-bond fixation in the periphery.

In the cation radicals of pentalene, heptalene, and nonalene, the distributions of the transition densities are of b_{3g} symmetry and they have a tendency to distort into a skew structure corresponding to one of the Kekulé type structures (Fig. 2). However, since the energy gaps of these radicals are considerably larger than the critical value, *ca.* 0.6 eV, we cannot expect such a molecular symmetry reduction as observed in the parent closed-shell hydrocarbons.

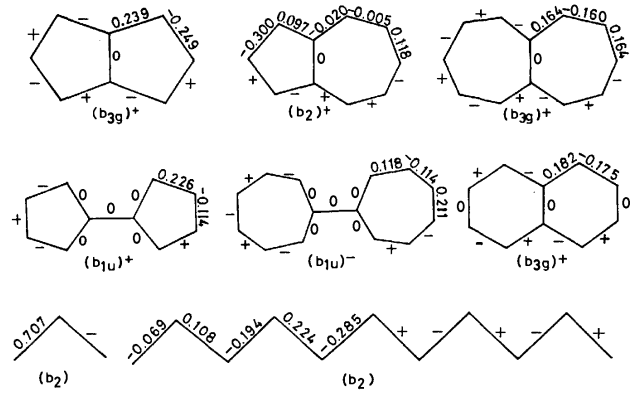

Fig. 2. Symmetries and distributions of the two-center components of transition densities (ρ_{01}). The + or − sign of the superscript written after the parentheses refers to the cation or the anion radical, respectively.

Moreover, in the anion radicals of the above molecules, the situation is the same as that seen in the cation radicals, *i.e.*, no molecular symmetry reduction occurs.

In the cation and anion radicals of azulene belonging to $C_{4n+2}H_{4n}$ system, there is no possibility of a molecular symmetry reduction from C_{2v} to C_s through the nuclear deformation of b_2 symmetry, because of the relatively large energy gap.

Results of SCF MO calculations agree that all these ion radicals, independent of the number of carbon atoms, undergo no molecular symmetry reduction (Fig. 3).

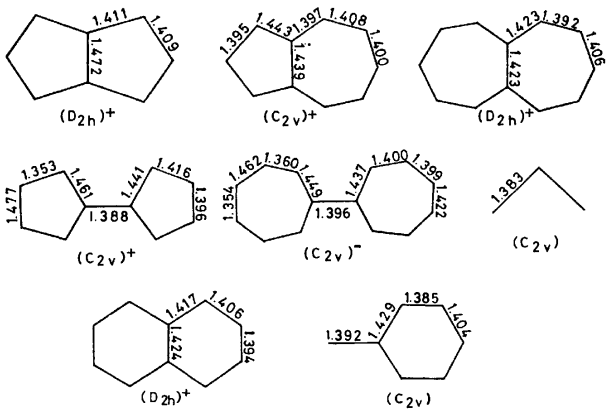

Fig. 3. Molecular symmetry groups and C-C bond lengths (in Å unit).

TABLE 2. TRANSITION ENERGIES AND INTENSITIES

Molecule (Point group)	Transition Symmetry	ΔE (eV)	f (c.g.s)	Obsd (eV)
Azulene$^+$ (C_{2v})	B_1	1.31	0.002	1.40[a]
	A_2	2.37	0.002	2.60
	B_1	2.42	0.003	
	B_1	3.23	0.036	3.37
	A_2	3.83	0.088	
	A_2	4.34	0.012	
Azulene$^-$ (C_{2v})	A_2	1.18	0.003	1.41[a]
	A_2	2.49	0.014	
	B_1	2.82	0.003	2.80
	B_1	2.99	0.091	
	B_1	3.56	0.002	
	B_1	3.93	0.000	
	A_2	4.18	0.031	4.25
	A_2	4.53	0.023	
Benzyl radical (C_{2v})	B_1	2.54	0.000	2.74 (0.003)[b]
	A_2	2.63	0.000	
	B_1	4.21	0.000	3.90 (0.025)
	A_2	4.32	0.127	
	B_1	5.33	0.675	
Naphthalene$^+$ (D_{2h})	B_{3u}	0.90	forb.	
	B_{1g}	1.74	0.097	1.74[a]
	B_{2u}	2.35	0.005	2.51
	B_{2u}	3.30	0.185	3.16
	B_{3u}	3.50	forb.	
	B_{1g}	4.27	0.175	4.00
	B_{1g}	4.96	0.487	
Naphthalene$^-$ (D_{2h})	B_{1g}	0.90	forb.	1.10[a]
	B_{3u}	1.74	0.097	1.49
	A_u	2.35	0.005	2.64
	A_u	3.30	0.185	3.32
	B_{1g}	3.50	forb.	
	B_{3u}	4.27	0.175	3.79 4.21
	B_{3u}	4.96	0.487	

a) Ref. 15. b) Refs. 21 and 22.

It should be noted that using the fully symmetric C_{2v} geometrical structures obtained, we can well reproduce the observed electronic spectra[15] for both ion radicals of azulene (Table 2).

The Ion Radicals of Fulvalene Systems. Of fulvalene systems, $C_{4n+2}H_{4n}$, pentafulvalene ($n=2$), heptafulvalene ($n=3$), and the ion radicals of heptafulvalene have been prepared, and their UV and ESR spectra have been reported.[16,17] Sevilla *et al.* have found that in the cation radical of heptafulvalene the unpaired spin density is delocalized throughout the molecule, while in the anion radical, the spin density is localized essentially on a single seven-membered ring. In a previous paper[18] we have explained the origin of the sharp contrast between the spin density distributions of the cation and anion radicals of heptafulvalene, by examining the energetically favorable molecular symmetry groups and C–C nuclear arrangements, using the open-shell SCF MO method (Fig. 3).

In the cation radicals of triafulvalene ($n=1$) and heptafulvalene ($n=3$), the ground state is of B_{3u} symmetry and the lowest excited doublet state is of A_u one in the fully symmetric D_{2h} configuration. The associated energy gaps of interest (1.55 and 1.22 eV, respectively) are considerably larger than the critical value, so that we cannot expect the molecular symmetry reduction to occur from D_{2h} to C_{2h} through the nuclear deformation of b_{3g} symmetry. On the other hand, in the anion radicals for both molecules, the ground state is of B_{1g} symmetry and the lowest excited state, nearly degenerate with the ground state, is of A_u one. It is therefore expected that in the anion radicals the molecular symmetry reduction occurs from D_{2h} to C_{2v} through the nuclear deformation of b_{1u} symmetry. Of the several nuclear deformation with the b_{1u} symmetry, the one actually effective for the molecular symmetry reduction is predicted by examining the distributions of the transition density shown in Fig. 2.

Further, in the cation radicals of pentafulvalene ($n=2$) and nonafulvalene ($n=4$), the lowest excited state (B_{1g}) is very close to the ground state (A_u). Both ion radicals are predicted to undergo the second-order Jahn-Teller distortions from D_{2h} to C_{2v} through the nuclear deformation of b_{1u} symmetry, whereas in the anion radicals, the situation is found to be the same as that seen in the cation radicals of triafulvalene and heptafulvalene.

From the above results, we can deduce the following rules concerning the molecular symmetry reduction in the ion radicals of $C_{4n+2}H_{4n}$ fulvalene systems: (i) When n is odd, a molecular symmetry reduction occurs in the anion radicals, while (ii) when n is even, it occurs in the cation radicals. These rules are interpreted in terms of Hückel MO energy level diagrams as follows: if n is odd, the lowest vacant molecular orbitals of fulvalene systems, whose symmetries are b_{1g} and a_u, are accidentally degenerate with each other. On the other hand, if n is even, the highest occupied molecular orbitals of b_{1g} and a_u symmetries are also accidentally degenerate. Hence for anion radicals of case (i), there are two ways of assigning one electron to the doubly degenerate molecular orbitals, which results in the degeneracy of the ground state in the simple one-electron picture. If we take into account the electron repulsion, this degeneracy is removed, but the energy gap between the two split states is still small as can be seen in Table 1. In a similar manner, for cation radicals of case (ii), there also occurs the degeneracy of the ground state in the one-electron approximation.

The Odd Alternant and Other Ion Radicals. As to $C_{2n+1}H_{2n+3}$ odd linear polyene radicals, we deal with those with $n=1$ to 8. In smaller systems, the energy gaps are significantly larger than the critical value, and there would be no possibility for the molecular symmetry reduction to occur. However, since as n increases, the energy gap tends to decrease and since in the hypothetical infinite odd cyclic polyene radical, which is mathematically equivalent to the infinite odd linear polyene radical,[19,20] the nuclear distortion of bond alternation type should certainly occur, it may be expected that in molecules with n larger than a certain limiting value there is a possibility of the second-order Jahn-Teller distortions to take place through the nuclear deformation of bond alternation type (Fig. 2).

In benzyl radical, the symmetry of the lowest excited state is the same as that of the ground state and the second excited state is located at the appreciably higher region, *i.e.*, 2.63 eV, so that there is no possibility for the molecular symmetry reduction to occur.

In the cation and anion radicals of naphthalene, they undergo no molecular symmetry reduction, since the calculated energy gaps are larger than the critical value.

Results of SCF MO calculations support the above predictions, and the transition energies calculated at the fully symmetric D_{2h} configurations for both ion radicals of naphthalene and those at the fully symmetric C_{2v} configuration of benzyl radical reproduce well the respective observed transition energies (Table 2).[15,21,22]

Conclusion

The problem of a molecular symmetry reduction in the open-shell conjugated systems are discussed on the basis of the second-order Jahn-Teller theorem. In contrast with the cases of the parent closed-shell hydrocarbons, the ion radicals of C_mH_{m-2} cata-condensed nonalternant hydrocarbons having $4n$ carbon atoms undergo no pseudo Jahn-Teller distortions. In the ion radicals of fulvalene systems, $C_{4n+2}H_{4n}$, a molecular symmetry reduction from D_{2h} to C_{2v} occurs in the cation radicals if n is even, and in the anion radicals if n is odd. It is found further that in odd linear polyene radicals, $C_{2n+1}H_{2n+3}$, with n larger than a certain critical value the nuclear configuration with the full molecular symmetry group should be unstable with respect to the nuclear deformation of bond alternation type.

Finally, it should be noted that the success of the predictions based on the energy-gap law is due to the assumption that the transition density does not vary significantly according to the molecular orbitals concerned, *i.e.*, the value of the matrix element, $\langle\phi_1|(\partial v/\partial Q_i)_0|\phi_0\rangle$, called the relaxability of the molecule along the nuclear displacement is almost constant from molecule to molecule. In view of the good agreement between theory and experiment obtained in this paper, we believe

that this assumption does hold at least for a variety of conjugated hydrocarbons considered in this paper.

The numerical calculation was carried out at Tohoku University with an NEAC 2200-700 electronic computer.

References

1) L. Salem, "The Molecular Orbital Theory of Conjugated Systems," Benjamin, New York (1966), p. 466.
2) A. Toyota and T. Nakajima, *Bull. Chem. Soc. Jpn.*, **46**, 3681 (1973).
3) T. Nakajima, A. Toyota, and S. Fujii, *Bull. Chem. Soc. Jpn.*, **45**, 1022 (1972).
4) R. G. Pearson, *J. Am. Chem. Soc.*, **91**, 1252, 4947 (1969).
5) R. G. Pearson, *J. Chem. Phys.*, **52**, 2167 (1970).
6) T. Nakajima, "Topics in Current Chemistry," Vol. 32, Spring-Verlag, Heidelberg (1972), p. 1.
7) A. Toyota and T. Nakajima, *Bull. Chem. Soc. Jpn.*, **46**, 2284 (1973).
8) A. Toyota, *Bull. Chem. Soc. Jpn.*, **48**, 1152 (1975).
9) L. Salem, *Chem. Phys. Lett.*, **3**, 99 (1969).
10) H. C. Longuet-Higgins and J. A. Pople, *Proc. Phys. Soc. (London)*, **A68**, 591 (1955).
11) T. Nakajima and A. Toyota, *Chem. Phys. Lett.*, **3**, 272 (1969).
12) H. Yamaguchi, T. Nakajima, and T. L. Kunii, *Theor. Chim. Acta*, **12**, 349 (1968).
13) R. Bloch, R. A. Marty, and P. de Mayo, *J. Am. Chem. Soc.*, **93**, 3071 (1971).
14) H. J. Dauben and D. J. Bertelli, *J. Am. Chem. Soc.*, **83**, 4659 (1973).
15) T. Shida and S. Iwata, *J. Am. Chem. Soc.*, **95**, 3473 (1973).
16) W. von E. Doering, "Theoretical Organic Chemistry," (Kekulé Symposium), Butterworths Sci. Publ. (1958), p. 44.
17) M. D. Sevilla, S. H. Flajser, G. Vincov, and H. J. Dauben, *J. Am. Chem. Soc.*, **91**, 4139 (1969).
18) A. Toyota and T. Nakajima, *Chem. Phys. Lett.*, **6**, 144 (1970).
19) H. Labhart, *J. Chem. Phys.*, **27**, 957 (1957).
20) M. Tsuji, S. Huzinaga, and T. Hasino, *Rev. Mod. Phys.*, **32**, 425 (1960).
21) G. Porter and E. Strachan, *Spectrochim. Acta*, **12**, 299 (1958).
22) S. Leach, in "Luminescence of Organic and Inorganic Materials," (H. P. Kallmann and G. M. Spruch, eds.), Wiley, New York (1962), p. 126.

Vibration Spectra and Rotational Isomerism of Chain Molecules. II.[1] Butane, Pentane, Hexane, Pentane-d_{12}, and Hexane-d_{14}

Issei HARADA, Hideo TAKEUCHI,* Masaaki SAKAKIBARA, Hiroatsu MATSUURA, and Takehiko SHIMANOUCHI

Department of Chemistry, Faculty of Science, University of Tokyo, Hongo, Bunkyo-ku, Tokyo 113

(Received July 26, 1976)

The Raman spectra of butane, pentane, hexane, pentane-d_{12}, and hexane-d_{14} and infrared spectra of pentane-d_{12} and hexane-d_{14} were measured for the liquid and solid states. The rotational isomerism of normal paraffins was studied on the basis of the spectral observations and the normal coordinate calculations. The spectra of the deuterated compounds were useful in the confirmation of the less stable isomers and the establishment of the local symmetry force field of normal paraffins. The enthalpy differences among the rotational isomers were studied on pentane and hexane, which yielded some important data for the study of the conformations and properties of longer hydrocarbons.

The study of the vibrational spectra and rotational isomerism of normal paraffins was started by Mizushima and coworkers[2] and Sheppard and coworkers[3] about thirty years ago.

More recently, Snyder *et al.*[4] treated this problem by the use of the newly observed infrared data and normal coordinate analysis and obtained the refined valence force field that could correlate the calculated frequencies with the observed frequencies satisfactorily for various isomers of normal paraffins. As the result, it has become clear that some bands that had been used for the determination of the enthalpy differences are possibly assigned to more than one vibrations of one form or different forms. The enthalpy difference between the *trans-gauche* (TG) and the *trans-trans* (TT) forms and that between the *gauche-gauche* (GG) and the TG forms of pentane have been estimated to be 600±100 cal/mol and 670±100 cal/mol, respectively.[4c]

Verma *et al.*[5] studied the temperature dependence of the Raman spectra of gaseous butane, 2-methylbutane and 2,3-dimethylbutane. They could resolve the Raman bands which had been observed as single bands and obtained the enthalpy difference of 966±54 cal/mol between the G and T forms of butane.

In pursuit of the studies on the vibration spectra and rotational isomerism of chain molecules,[1,6,7] we investigated the vibration spectra of normal paraffins and perdeuterated normal paraffins and obtained the refined local symmetry force field that explained the frequencies

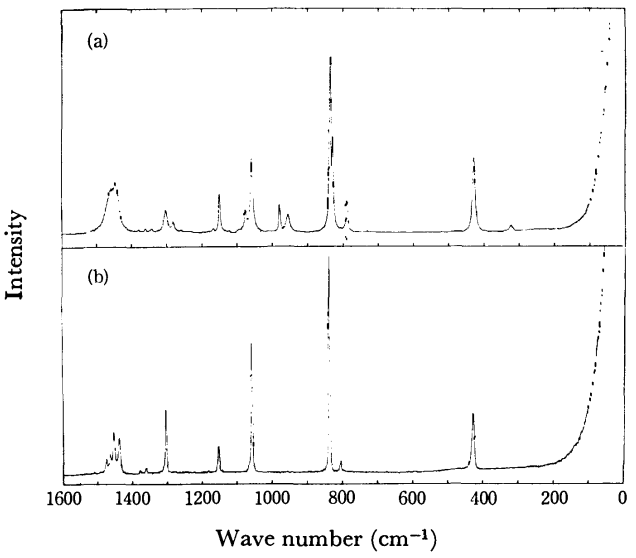

Fig. 1. Raman spectra of butane.
(a) Liquid (−70 °C), b) solid.

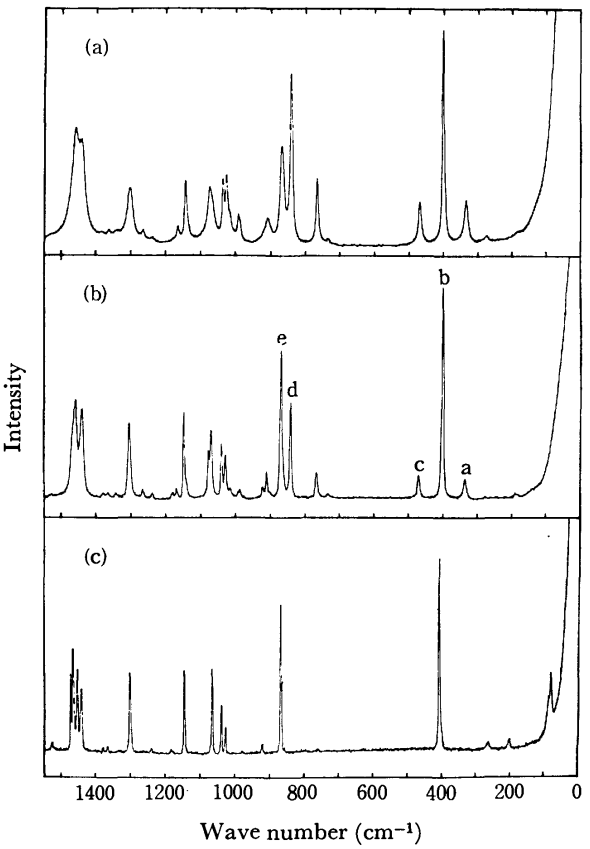

Fig. 2. Raman spectra of pentane.
(a) Liquid (25 °C), (b) liquid (−106 °C), (c) solid (−176 °C).
The temperature dependence of the intensities of the bands a through e was examined (see text and Tables 6 and 7).

* Present address: Department of Chemical Engineering and Chemical Technology, Imperial College, London SW7 2BY, England.

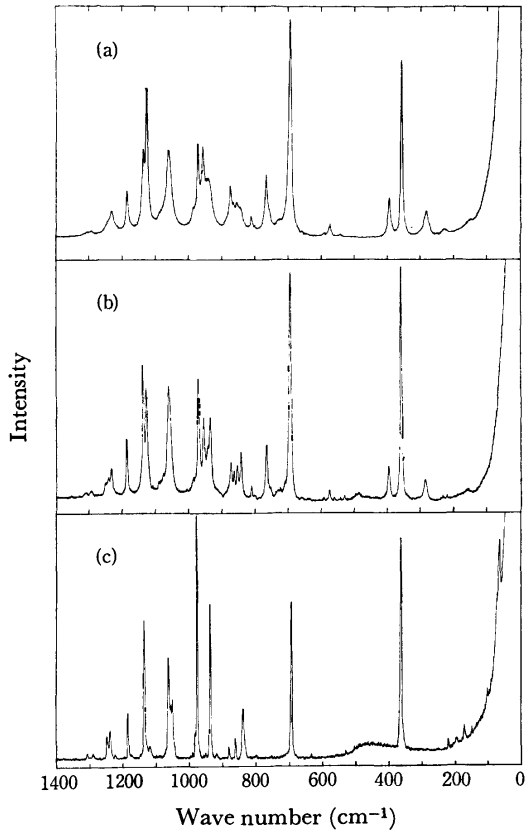

Fig. 3. Raman spectra of pentane-d_{12}.
(a) Liquid (23 °C), (b) liquid (−100 °C), (c) solid.

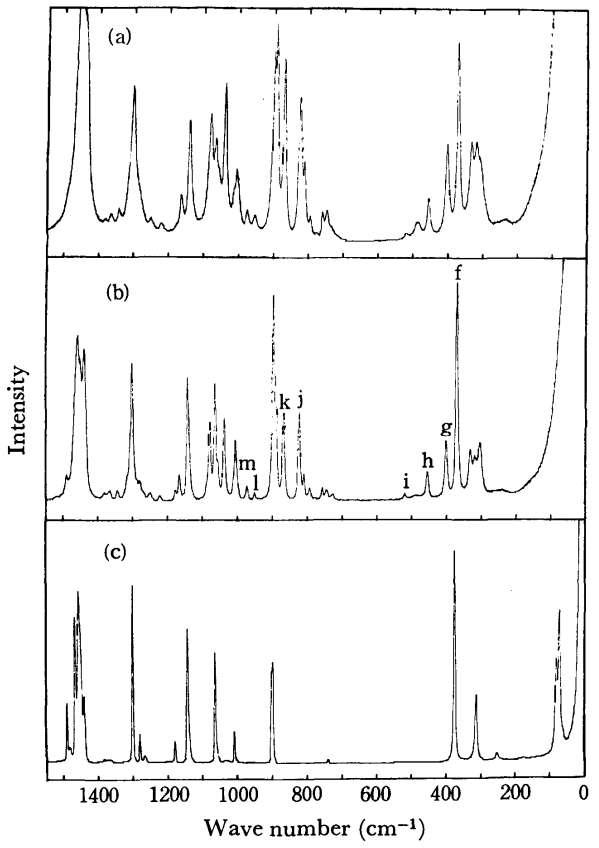

Fig. 4. Raman spectra of hexane.
(a) Liquid (23 °C), (b) liquid (−88 °C), (c) solid (−153 °C).
The temperature dependence of the intensities of the bands f through m was examined (see text and Tables 6 and 7).

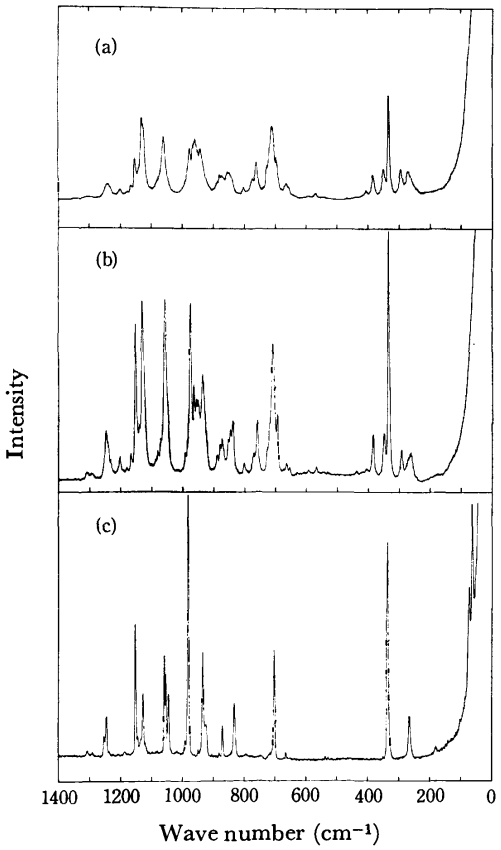

Fig. 5. Raman spectra of hexane-d_{14}.
(a) Liquid (23 °C), (b) liquid (−95 °C), (c) solid.

of both species. In the course of the research, several new findings including the identification of the less stable rotational isomers and the determination of the enthalpy differences among the isomers of pentane and hexane in the liquid state have been obtained. The present paper describes the rotational isomerism and vibrational assignments of butane, pentane, hexane, pentane-d_{12}, and hexane-d_{14}.

Experimental

Butane (stated purity of 98%) was supplied by Tokyo Kasei Kogyo Co., Ltd. and was used without further purification. Highly pure samples (stated purity of 99.9%) of pentane and hexane were purchased from Tokyo Kagaku Seiki Co., Ltd. and were distilled prior to the measurements. Pentane-d_{12} and hexane-d_{14} (stated purity of 98%) were obtained from Merck, Sharp, and Dohme of Canada and were transferred to ampoule Raman cells by the use of a vacuum system. The spectrometers used are the same as those in the previous study.[1]

The Raman spectra were recorded in the region below 1600 cm^{-1}. The measurements of the spectra at low temperatures were performed in the same way as that in a previous study.[8] Liquid nitrogen and liquid-nitrogen cooled ethanol were used as the cooling agent. For the determination of the enthalpy difference, the Raman spectra were recorded twice

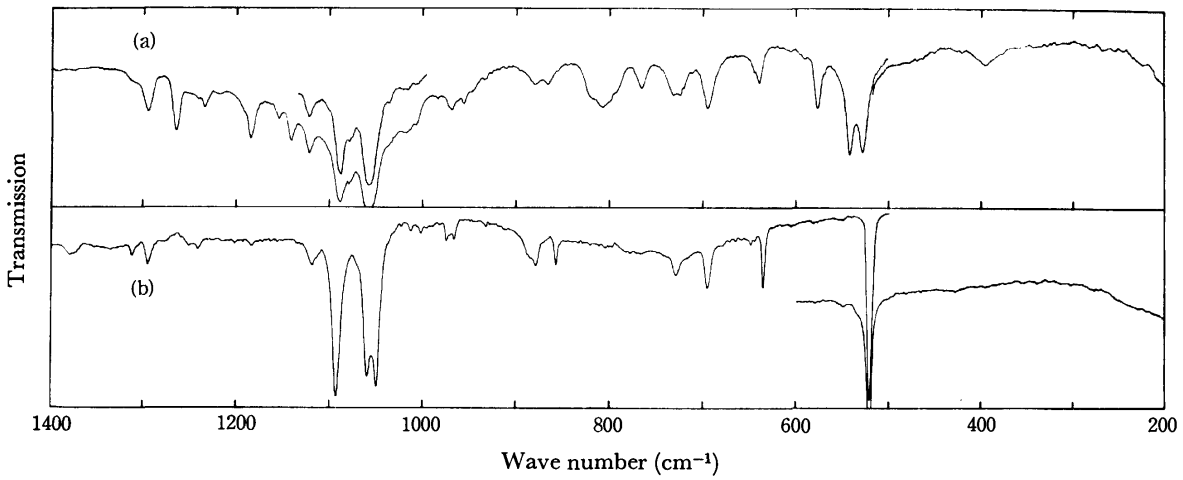

Fig. 6. Infrared spectra of pentane-d_{12}.
(a) Liquid, (b) solid.

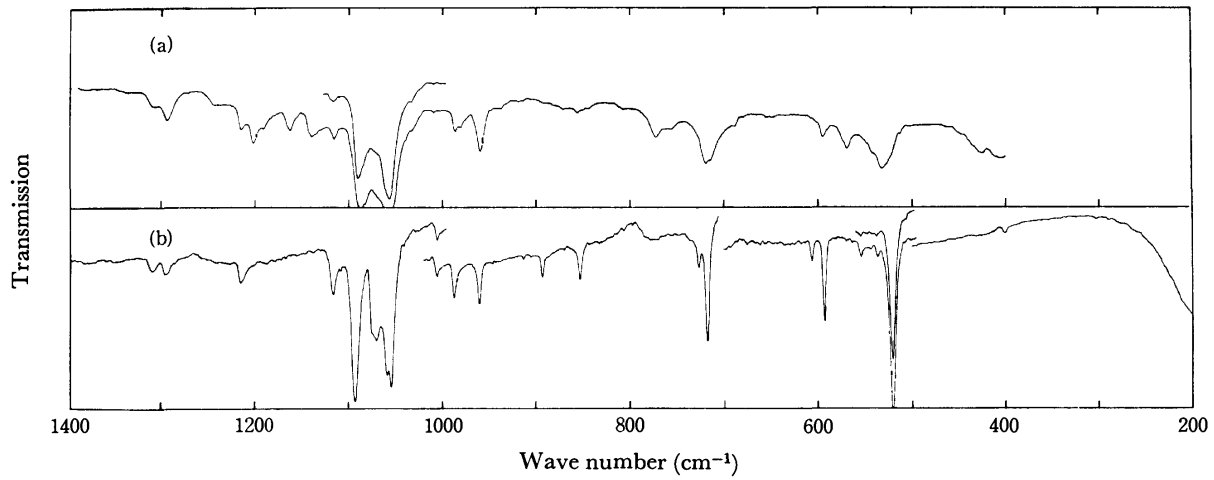

Fig. 7. Infrared spectra of hexane-d_{14}.
(a) Liquid, (b) solid.

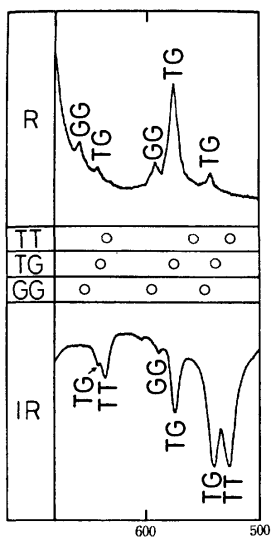

Fig. 8. Comparison of the observed spectra and calculated frequencies of pentane-d_{12}.

at each of ten different temperatures between −111 and 23 °C for pentane and at each of eight different temperatures between −89 and 23 °C for hexane.

Infrared spectra of pentane-d_{12} and hexane-d_{14} in the solid and liquid states were measured in the region 1600—400 cm⁻¹.

Normal Coordinate Treatment

The normal coordinate treatment of normal paraffin molecules was carried out in a way similar to the case of the ethers.[1] The molecules treated are: butane, pentane, hexane, pentane-d_{12}, hexane-d_{14}, poly(ethylene), and poly(ethylene-d_4). Detailed results including structural parameters, symmetry coordinates, and force constants are reported in a separate paper.[9]

A total of 45 force constants of normal paraffins were determined from 254 Raman and infrared frequencies of 14 forms of the seven molecular species.**

** Some of the observed frequencies were assigned to more than one vibrations of the same isomer or different isomers. However each of these frequencies was counted as one.

Table 1. Observed Raman frequencies of butane in cm^{-1} and assignments[a)]

Liquid (−70 °C)	Solid	Assignment
1474 VW, sh[b,c)]	1475 VW[b)]	CH_3 ip-d-deform (**T**)
1463 VW, sh[b,c)]	1464 VW[b)]	
1455 W	1454 VW	CH_3 op-d-deform (**T**, G)
1441 W	1438 VW	CH_2 scis (**T**), CH_3 ip-d-deform (G)
	1377 VW	CH_3 s-deform (**T**)
1360 VW	1360 VW	CH_2 wag (**T**)
1343 VW		CH_2 wag (**G**)
1303 VW	1304 W	CH_2 twist (**T**)
1281 VW		CH_2 twist (**G**)
1181 VW	1182 W	CH_2 rock (**T**)
1168 VW		CH_2 rock (**G**)
1150 W	1153 VW	CH_3 ip-rock (**T**)
1076 VW		CC stretch (**G**)
1058 M	1059 S	CC stretch (**T**)
979 VW		CH_3 ip-rock (**G**)
956 VW		CC stretch (**G**)
837 VS	838 VS	CC stretch (**T**)
829 M		CC stretch (**G**)
	805 VW	CH_3 op-rock (**T**)
789 VW		CH_3 op-rock (**G**)
430 M	428 W	CCC deform (**T**)
323 VW		CCC deform (**G**)

a) There is a possibility that the bands observed only in the solid state are components of crystal field splittings. For the notation and definition of the local symmetry coordinates, see Ref. 10. VS: very strong, S: strong, M: medium, W: weak, VW: very weak, sh: shoulder. b) The two Raman bands are due to the Fermi resonance between the CH_3 ip-d-deform vibration (a_g) and the overtone of the CH_2 rocking vibration (a_u). c) Observed at −140 °C.

Table 2. Observed Raman frequencies of pentane in cm^{-1} and assignments[a)]

Liquid (−106 °C)	Solid (−176 °C)	Assignment
1526 VW	1527 VW	$2\times CH_2$ rock (a_g) (**TT**)
	1473 M	CH_2 scis (**TT**)
1465 W, sh	1467 M	CH_3 op-d-deform (**TT**)
1458 M	1454 M	CH_3 ip-d-deform (**TT**)
1450 W, sh[b)]		CH_3 ip-d-deform (**TG**)
1438 M	1442 W	CH_2 scis (**TT**)
1379 VW	1378 VW	CH_3 s-deform (**TT**, TG)
1365 VW	1365 VW	CH_2 wag (**TT**, TG)
1343 VW		CH_2 wag (**TG**)
1303 W	1303 M	CH_2 twist (**TT**), CH_2 wag (TG)
1265 VW		CH_2 twist (**TG**)
1238 VW	1239 VW	CH_2 twist (**TT**, TG)
1179 VW	1182 VW	CH_2 rock (**TT**)
1167 VW		CH_2 rock (**TG**)
1146 M	1146 M	CH_3 ip-rock (**TT**)
1140 VW, sh		CH_3 ip-rock (**TG**)
1075 W		CC stretch (**TG**)
1068 W	1066 M	CC stretch (**TT**)
1038 W	1039 W	CC stretch (**TT**)
1027 W	1027 VW	CC stretch (**TT**, TG)
1015 VW		CH_3 op-rock (**TG**)
992 VW		CC stretch (**TG**)
986 VW	982 VW	CH_3 op-rock (**TT**)
920 VW	921 VW	CC stretch (**TT**)
909 VW		CH_3 ip-rock (**TG**)
900 VW		CH_3 ip-rock (**GG**)
868 S	870 S	CH_3 ip-rock (**TT**), CH_3 op-rock (TG)
	857 VW	CH_3 op-rock (**TT**)
841 M		CC stretch (**TG**)
766 W	760 VW	CH_2 rock (**TT**, TG)
733 VW		CH_2 rock (**TG**)
471 W		CCC deform (**TG**)
403 VS	409 VS	CCC deform (**TT**)
337 W		CCC deform (**TG**)
276 VW[b)]		CCC deform (**TG**)
190 VW	265 VW, 203 VW	CCC deform, torsions
	86 VW, sh, 80 W	Lattice vibrations

a) The observed bands are assigned to the individual vibrations of the TT and TG forms. The vibration of the GG form is identified in the table when the band is assigned only to this form. There is a possibility that the bands observed only in the solid state are components of crystal field splittings. For the notation and definition of the local symmetry coordinates, see Ref. 10. VS: very strong, S: strong, M: medium, W: weak, VW: very weak, sh: shoulder. b) Observed at room temperature.

Results and Discussion

Figures 1—7 show the Raman and infrared spectra in the liquid and solid states of the molecules. In Figs. 2 and 4, the comparatively isolated bands for which the dependence of the relative intensities on temperature has been examined are identified by letters a through e for pentane and f through m for hexane. The observed frequencies and the assignments based on the calculated potential-energy distributions are listed in Tables 1—5. In the column of assignment in each table, the conformation symbol given by boldface indicates that the corresponding frequency is definitely assigned to the rotational isomer based solely on the experimental result or almost definitely assigned based on the combined results of the experiments and normal vibration calculations. The apparent enthalpy differences calculated by assuming that the intensity of each of the bands is due to one rotational isomer are tabulated in Table 6 and possible assignments of the bands a through m are listed in Table 7. Part of the observed spectra and calculated frequencies of pentane-d_{12} are compared in Fig. 8.

Butane (See Fig. 1 and Table 1). Verma *et al.*[5)] studied the Raman spectra of this molecule in the gaseous and solid states for the purpose of determining the enthalpy difference between the rotational isomers, but reported only the spectra in the regions 900—750 cm^{-1} and 450—300 cm^{-1}. Figure 1 and Table 1 give the Raman frequency data below 1600 cm^{-1} obtained in the present measurements and the assignments. The band

at 421 cm^{-1} observed and assigned to the G form by Verma *et al.*[5] is missing in the spectrum in the liquid state at −70 °C. By comparison of the relative intensities of the band and other *gauche* bands, this band is assigned to a hot band or combination band of the T form. The two bands at 842 and 833 cm^{-1} observed in the gaseous state[5] are also resolved at 837 and 829 cm^{-1} in the liquid state at −70 °C. The bands at 1475 and 1464 cm^{-1} observed in the solid state may be due to the Fermi resonance between the CH_3 ip-d-deformation vibration (a_g) and the overtone of the CH_2 rocking vibration (a_u).

Pentane and Pentane-d_{12} *(See Figs. 2, 3, 6 and 8, and Tables 2 and 3).* The possible conformations are TT, TG, GG, and GG′, of which GG′ may be the least stable because of the steric hindrance. The spectra in the solid state are consistent with the calculated frequencies for the TT form. The spectra in the liquid state are mostly explained by the coexistence of the TT and TG forms. The intensities of the bands at 659 and 592 cm^{-1} of pentane-d_{12} observed at room temperature decrease significantly on cooling compared with those of the TG

TABLE 3. OBSERVED FREQUENCIES OF PENTANE-d_{12} IN cm^{-1} AND ASSIGNMENTS[a]

Liquid		Solid		Assignment
Raman (−100 °C)	Infrared	Raman	Infrared	
1307 VW[b]	1310 VW, sh[b]	1307 VW[b]	1312 VW[b]	
1292 VW[b]	1294 VW[b]	1290 VW[b]	1295 VW[b]	
1247 VW, sh[b]	1254 W[b]	1247 VW[b]	1252 VW[b]	
1238 VW		1238 VW	1242 VW	CC stretch (**TT**)
1230 VW	1233 VW			CC stretch (**TG**)
1184 W	1185 W	1184 VW	1184 VW	CC stretch (**TT**, TG)
	1156 VW			CC stretch (**GG**)
1142 VW, sh	1143 VW			CC stretch (**TG**)
1135 M		1135 M		CC stretch (**TT**)
1125 M	1124 W			CD_2 scis (**TG**)
		1119 VW	1119 VW	CD_2 scis (**TT**)
1088 VW, sh	1090 VS		1092 VS	CD_2 scis (**TT**)
1074 VW, sh	1079 VW, sh			CD_2 scis (**TG**)
1057 M	1057 VS	1062 M	1059 VS	CD_3 s-deform (**TT**, TG)
		1055 W, sh		CD_3 s-deform (**TT**)
		1050 W	1049 VS	CD_3 d-deform (**TT**)
	1036 VW, sh			CD_2 wag (**TG**)
	1020 VW[b]			
	1008 VW, sh		1013 VW	CD_2 wag (**TT**)
			1002 VW[b]	
984 VW, sh		982 VW, sh		CD_2 rock (**TT**, TG)
968 M	970 VW	976 VS	975 VW	CD_2 scis (**TT**), CD_3 op-rock (**TT**, TG)
			967 VW	CD_2 twist (**TT**)
953 M	957 VW			CD_2 twist (**TG**)
942 VW, sh				CD_2 scis (**TG**)
934 W		937 VS		CD_2 twist (**TT**, TG)
			896 VW, sh[b]	
	881 VW	882 VW	879 VW	CC stretch (**TT**)
873 VW	867 VW			CC stretch (**TG**)
863 VW		862 VW	857 VW	CD_2 wag (**TT**)
853 VW				CD_2 wag (**TG**)
842 W		838 W		CD_2 wag (**TT**)
	820 VW, sh[b]			
810 VW[b]	808 W, b[b]			
802 VW	794 VW, sh			CD_2 twist (**GG**)
764 W	767 VW			CD_2 wag (**TG**)
753 VW, sh				CD_2 twist (**TG**)
730 VW	732 VW		728 VW	CD_3 ip-rock (**TT**)
723 VW	726 VW			CD_3 ip-rock (**TG**)
629 VS	695 W	693 S	695 VW	CD_3 ip-rock (**TT**, TG)
659 VW, sh				CD_2 rock (**GG**)
641 VW	643 VW, sh			CD_3 op-rock (**TG**)
	638 VW	635 VW	635 W	CD_3 op-rock (**TT**)
592 VW	589 VW			CD_3 op-rock (**GG**)

Table 3. (Continued)

Liquid		Solid		Assignment
Raman (−100 °C)	Infrared	Raman	Infrared	
575 VW	576 VW			CD_2 rock (**TG**)
			550 VW	CD_2 rock (**TT**)
542 VW	542 M			CD_2 rock (**TG**)
530 VW	528 M	529 VW	522 VS	CD_2 rock (**TT**)
397 VW				CCC deform (**TG**)
358 VS		362 VS		CCC deform (**TT**)
287 VW				CCC deform (**TG**)
233 VW				CCC deform (**TG**)
		195 VW		CCC deform, torsions
		172 VW		
157 VW				
		69 W		Lattice vibration

a) The observed bands are assigned to the individual vibrations of the TT and TG forms. The vibration of the GG form is identified in the table when the band is assigned only to this form. There is a possibility that the bands observed only in the solid state are components of crystal field splittings. For the notation and definition of the local symmetry coordinates, see Ref. 10. VS: very strong, S: strong, M: medium, W: weak, VW: very weak, sh: shoulder, b: broad. b) Assigned to the partially deuterated compounds or origin unknown.

Table 4. Observed Raman frequencies of hexane in cm^{-1} and assignments[a)]

Liquid (−88 °C)	Solid (−153 °C)	Assignment
1489 VW	1489 W	CH_2 scis (**TTT**, TTG, TGT)
	1480 VW	$2\times CH_2$ rock (b_g) (**TTT**)
	1466 S	CH_3 op-d-deform (**TTT**)
1457 S	1456 S	CH_3 ip-d-deform (**TTT**, TTG), CH_2 scis (TGT)
1450 VW, sh	1450 VW, sh	$2\times CH_2$ rock (a_u) (**TTT**)
1438 S	1440 W	CH_2 scis (**TTT**, TTG), CH_3 ip-d-deform (TGT)
1380 VW	1383 VW	CH_3 s-deform (**TTT**, TTG, TGT)
1365 VW	1370 VW	CH_2 wag (**TTT**, TTG, TGT)
1343 VW		CH_2 wag (**TTG**)
1315 VW, sh		CH_2 wag (GTG)
1302 S	1301 VS	CH_2 twist (**TTT**, TTG), CH_2 wag (**TTT**, TGT)
1280 VW	1280 VW	CH_2 twist (**TTT**, TTG)
	1265 VW[b)]	
1250 VW		CH_2 wag (**TTG**)
1222 VW		CH_3 op-rock (TTG, TGT)
1178 VW	1179 VW	CH_2 rock (**TTT**)
1167 VW		CH_2 rock (TTG, TGT)
1143 M	1143 S	CH_3 ip-rock (**TTT**), CC stretch (TGT)
1080 W		CC stretch (TTG, TGT)
1065 M	1064 M	CC stretch (**TTT**)
1057 VW, sh		CC stretch (**TTG**)
1039 W		CC stretch (TTG), CH_3 ip-rock (TGT)
1007 W	1008 W	CC stretch (**TTT**, TGT), CH_2 twist (TTG)
975 VW		CC stretch (**TTG**)
952 VW		CC stretch (GTG, GTG′)
	900 VW, sh	CH_3 ip-rock (**TTT**)
899 VS	898 M	CH_3 op-rock (**TTT**, TTG, TGT)
891 M		CH_3 ip-rock (**TTG**)
870 M		CC stretch (**TTG**)
824 M		CC stretch (**TGT**)
811 VW		CH_2 rock (**TGT**)
794 VW		CH_2 rock (**TTG**)
758 VW		CH_2 rock (**TTG**)
746 VW		CH_2 rock (**TGT**)
	739 VW	CH_2 rock (**TTT**)
727 VW		CH_2 rock (TTG, TGT)
520 VW		CCC deform (**TGT**)
488 VW, b		CCC deform (TGG, GTG)
456 VW		CCC deform (**TTG**)
402 W		CCC deform (**TTG**)
372 VS	376 VS	CCC deform (**TTT**)
332 W		CCC deform (**TGT**)
320 VW		CCC deform (**TTG**)
305 VW	313 W	CCC deform (**TTT**)
240 VW, b	251 VW	Torsions
	175 VW, b	
	81 M	Out-of-plane rotatory lattice vibration[c)]
	72 S	In-plane rotatory lattice vibration[c)]

a) The observed bands are assigned to the individual vibrations of the TTT, TTG, and TGT forms. The vibrations of the TGG, GTG, and GTG′ forms are identified in the table when the bands are assigned to these forms but not to the TTT, TTG, or TGT form. The crystal structure of hexane is P1 (C_i^1), $Z=1$ [N. Norman and H. Mathisen, *Acta Chem. Scand.*, **15**, 1755 (1961)]. Accordingly, no crystal field splitting is expected in the spectrum of the solid state. For the notation and definition of the local symmetry coordinates, see Ref. 10. VS: very strong, S: strong, M: medium, W: weak, VW: very weak, sh: shoulder, b: broad. b) Origin unknown. c) H. Takeuchi, T. Shimanouchi, M. Tasumi, G. Vergoten, and G. Fleury, *Chem. Phys. Lett.*, **28**, 449 (1974).

TABLE 5. OBSERVED FREQUENCIES OF HEXANE-d_{14} IN cm^{-1} AND ASSIGNMENTS[a)]

Liquid		Solid		Assignment
Raman (−95 °C)	Infrared	Raman	Infrared	
1309 VW[b)]	1306 VW[b)]	1307 VW[b)]	1309 VW[b)]	
1293 VW[b)]	1293 W[b)]	1290 VW[b)]	1294 VW[b)]	
		1252 VW[b)]		
1246 W		1245 VW		CC stretch (**TTT**)
1241 VW	1242 VW			CC stretch (**TTG**)
1232 VW				CC stretch (**TGT**)
	1214 W		1214 VW	CC stretch (**TTT**, TGT)
1201 VW	1201 M			CC stretch (**TTG**)
	1190 W[b)]	1186 VW[b)]		
1179 VW				CC stretch (TGG, GTG, GTG′)
1166 VW	1162 W			CC stretch (**TTG**)
1152 S		1151 M		CC stretch (**TTT**), CD_2 scis (TGT)
		1144 VW[b)]		
1138 VW	1139 W			CD_2 scis (**TTG**)
		1135 VW, sh[b)]		
1130 S		1127 W		CD_2 scis (**TTT**, TGT), CC stretch (TTG, TGT)
		1118 VW, sh[b)]		
	1115 W		1115 W	CC stretch (**TTT**)
	1090 VS		1092 VS	CD_2 scis (**TTT**)
1080 VW				CD_2 scis (TTG, TGT)
1070 VW[b)]	1070 W, sh[b)]		1070 S[b)]	
1057 S	1057 VS	1058 M	1059 VS	CD_2 scis (**TTT**, TTG, TGT), CD_3 s-deform (**TTT**, TTG, TGT)
			1054 VS	CD_3 d-deform (**TTT**)
		1053 W		CD_3 s-deform (**TTT**)
		1045 W		CD_3 d-deform (**TTT**)
	1042 VW			CD_3 d-deform (**TTG**, TGT)
		1017 VW[b)]		
	1004 VW[b)]		1005 VW[b)]	
991 VW		992 VW		CD_2 rock (**TTT**)
	987 W		988 W	CD_2 wag (**TTT**), CD_2 rock (TTG)
	981 W		980 VW, sh	CD_2 rock (**TTT**, TGT)
975 S		982 VS		CD_2 scis (**TTT**), CD_2 twist (**TTT**), CD_2 rock (TTG, TGT)
964 M				CD_2 twist (TTG, TGT)
			960 W	CD_2 twist (**TTT**)
957 M	959 M			CD_2 twist (**TGT**)
951 M				CD_2 twist (TTG, TGT), CD_2 scis (TTG)
936 M	933 VW	935 M		CD_2 twist (**TTT**, TTG, TGT)
		925 VW[b)]		
889 VW	892 VW		893 VW	CD_2 wag (**TTT**), CC stretch (TGT)
		881 VW[b)]		
880 VW				CC stretch (**TTG**)
873 VW	872 VW	871 VW		CC stretch (**TTT**), CD_2 wag (TTG)
854 VW	856 VW		853 W	CD_2 wag (**TTT**, TGT)
846 W				CD_2 wag (**TGT**)
839 W		833 W		CD_2 wag (**TTT**, TTG)
803 VW[b)]				
		795 VW[b)]		
771 VW	773 W			CD_2 wag (**TGT**)
760 W	760 W			CD_2 wag (**TTG**)
	752 VW, sh			CD_2 twist (TTG, TGT)
727 VW, sh				CD_2 wag (**GTG′**)
			726 W	CD_2 twist (**TTT**)
	719 M		717 S	CD_3 ip-rock (**TTT**, TTG)
709 S		704 M		CD_3 ip-rock (**TTT**, TTG, TGT)
695 W				CD_3 ip-rock (**TGT**)

Table 5. (Continued)

Liquid		Solid		Assignment
Raman (−95 °C)	Infrared	Raman	Infrared	
665 VW		666 VW		CD_3 op-rock (**TTT**, TTG)
655 VW				CD_3 op-rock (**TGT**)
638 VW				CD_3 op-rock (**TGT**)
			605 VW[b]	
594 VW	595 W		592 M	CD_3 op-rock (**TTT**, **TTG**)
570 VW	569 M			CD_2 rock (**TTG**)
			553 VW[b]	
	540 W, sh			CD_2 rock (**TGT**)
		538 VW		CD_2 rock (**TTT**)
			536 VW[b]	
	532 S			CD_2 rock (**TTG**)
	524 S		520 VS	CD_2 rock (**TTT**)
438 VW				CCC deform (**TGT**)
	425 W			CCC deform (**TGG**)
408 VW	405 W		401 VW	CCC deform (**TTT**, GTG, GTG′)
385 VW				CCC deform (**TTG**)
350 VW				CCC deform (**TTG**)
335 VS		338 VS		CCC deform (**TTT**)
294 VW				CCC deform (**TGT**)
270 VW, sh				CCC deform (**TTG**)
263 VW		266 VW		CCC deform (**TTT**)
179 VW, b		176 VW		Torsion
		73 W		Out-of-plane rotatory lattice vibration[c]
		63 M		In-plane rotatory lattice vibration[c]

a) The observed bands are assigned to the individual vibrations of the TTT, TTG, and TGT forms. The vibrations of the TGG, GTG, and GTG′ forms are identified in the table when the bands are assigned to these forms but not to the TTT, TTG, or TGT form. The crystal structure of hexane is P1 (C_i^1), $Z=1$ [N. Norman and H. Mathisen, *Acta Chem. Scand.*, **15**, 1755 (1961)]. Accordingly, no crystal field splitting is expected in the spectra of the solid state. For the notation and definition of the local symmetry coordinates, see Ref. 10. VS: very strong, S: strong, M: medium, W: weak, VW: very weak, sh: shoulder, b: broad. b) Assigned to the partially deuterated compounds or origin unknown. c) H. Takeuchi, T. Shimanouchi, M. Tasumi, G. Vergoten, and G. Fleury, *Chem. Phys. Lett.*, **28**, 449 (1974).

Table 6. Apparent enthalpy differences in cal/mol

Molecule	Band pair x	Band pair y	ΔH_{x-y}[a]
Pentane	b	a	581(28)
	b	c	574(31)
	a	c	17(34)
	e	d	619(20)
Hexane	f	g	600(11)
	f	h	370(50)
	h	i	3(56)
	j	k	52(18)
	m	l	661(51)

a) $\Delta H_{x-y}=H_x-H_y$. The value in parentheses is the standard deviation.

bands. These bands are explained only by the calculated frequencies of the GG form. Hence, it is certain that the GG form exists at room temperature to some extent.

Hexane and Hexane-d_{14} (See Figs. 4, 5, and 7 and Tables 4 and 5). The spectra in the solid state are explained

Table 7. Possible assignments of the bands used in the calculation of enthalpy differences

Molecule	Raman band	Frequency (cm^{-1})	Possible assignments
Pentane	a	337	TG
	b	403	TT, GG
	c	471	TG, GG
	d	841	TG, GG
	e	868	TT, TG, GG
Hexane	f	372	TTT, GTG[a]
	g	402	TTG, TGG[a]
	h	456	TTG
	i	520	TGT
	j	824	TGT, TGG
	k	870	TTG, GTG, GTG′
	l	952	GTG, GTG′
	m	975	TTG, TGG

a) The value of the enthalpy difference between the TTT and TTG forms depends on the relative amounts of the contributions from these forms to the intensities of the bands f and g (see text).

by the calculated frequencies for the TTT form. Among the liquid-state bands that are due to forms other than the TTT form, the bands at 456 and 520 cm^{-1} of hexane and the bands at 350 and 294 cm^{-1} of hexane-d_{14} are assigned only to the TTG and TGT forms, respectively. The temperature dependence of the intensity of the Raman band at 952 cm^{-1} of hexane is much more significant than those of the above bands. Since this frequency matches the calculated frequencies for the GTG and GTG′ forms, the existence of one or both of these forms is evident.

Enthalpy Differences (See Figs. 2 and 4 and Tables 6 and 7). *Pentane*: As the intensity of the band b in the solid state is very strong, the contribution, if any, from the vibration of the GG form to this band in the liquid state may be small. Hence, the apparent enthalpy difference obtained for the band pair of b and a, 581 cal/mol, may be a good approximate value of the enthalpy difference between the TG and TT forms.

Hexane: It is evident from the value of ΔH_{i-h} that the TGT form is as stable as the TTG form. The great difference between the values of ΔH_{g-f} and ΔH_{h-f} indicates the fair amount of the contribution from the TGG form to the band g. From these values, it is apparent that the enthalpy difference between the TTG and TTT forms lies in the range between 400 and 600 cal/mol. However, since the relative amount of the contribution from the GTG form to the band f is considered to be far less than that from the TGG form to the band g, it may be safely concluded that the enthalpy difference between the TTG and TTT forms is on the side of 400 cal/mol. Moreover, by assuming that the TGG, GTG, and GTG′ forms are approximately of the same stability, it may be concluded from the value of ΔH_{l-m} that the GTG form is less stable than the TTG form by 650 cal/mol.

In conclusion, the present study shows that the TGT form is as stable as the TTG form in the liquid state of hexane and that $\Delta H_{TTG-TTT}$ (400 cal/mol) of hexane is less than ΔH_{TG-TT} (600 cal/mol) of pentane. These results add to the data for the understanding of the stable structure and properties of longer hydrocarbon molecules. It is to be noted that these enthalpy-difference values are appreciably smaller than ΔH_{G-T} (966 cal/mol) reported for gaseous butane.[5]

References

1) Part I: T. Shimanouchi, Y. Ogawa, M. Ohta, H. Matsuura, and I. Harada, *Bull. Chem. Soc. Jpn.*, **49**, 2999 (1976).

2) S. Mizushima, Y. Morino, and S. Nakamura, *Sci. Pap. Inst. Phys. Chem. Res. Tokyo*, **37**, 205 (1940); T. Shimanouchi and S. Mizushima, *ibid.*, **40**, 467 (1943); S. Mizushima and T. Shimanouchi, *Proc. Imp. Acad. Tokyo*, **20**, 86 (1944); S. Mizushima and T. Shimanouchi, *J. Am. Chem. Soc.*, **71**, 1320 (1949); S. Mizushima and H. Okazaki, *ibid.*, **71**, 3411 (1949).

3) N. Sheppard and G. J. Szasz, *J. Chem. Phys.*, **17**, 86 (1949).

4) a) R. G. Snyder and J. H. Schachtschneider, *Spectrochim. Acta*, **19**, 85 (1963); b) J. H. Schachtschneider and R. G. Snyder, *ibid.*, **19**, 117 (1963); c) R. G. Snyder, *J. Chem. Phys.*, **47**, 1316 (1967).

5) A. L. Verma, W. F. Murphy, and H. J. Bernstein, *J. Chem. Phys.*, **60**, 1540 (1974).

6) M. Sakakibara, H. Matsuura, I. Harada, and T. Shimanouchi, *Bull. Chem. Soc. Jpn.*, **50**, 111 (1977).

7) M. Ohta, Y. Ogawa, H. Matsuura, I. Harada, and T. Shimanouchi, *Bull. Chem. Soc. Jpn.*, in press.

8) M. Sakakibara, F. Inagaki, I. Harada, and T. Shimanouchi, *Bull. Chem. Soc. Jpn.*, **49**, 46 (1976).

9) T. Shimanouchi, H. Matsuura, Y. Ogawa, and I. Harada, *J. Phys. Chem. Ref. Data*, to be published.

10) T. Shimanouchi, "Tables of Molecular Vibrational Frequencies," Consolidated Vol. 1, U.S. Govt. Printing Office, No. C13.48: 39 (1972).

Vibration Spectra and Rotational Isomerism of Chain Molecules. III.[1] Ethyl Methyl Sulfide and Deuterium Compounds

Masaaki SAKAKIBARA, Hiroatsu MATSUURA, Issei HARADA, and Takehiko SHIMANOUCHI

Department of Chemistry, Faculty of Science, University of Tokyo, Hongo, Bunkyo-ku, Tokyo 113

(Received July 26, 1976)

The Raman spectra of ethyl methyl sulfide and its three deuterated compounds $CD_3SC_2H_5$, $CH_3SCH_2CD_3$, and $CH_3SC_2D_5$ were measured for the liquid and crystalline states. The Raman spectra of the undeuterated species in the gaseous state were measured at different temperatures. The normal vibration frequencies were calculated by using a consistent set of force constants for aliphatic sulfides. The combination of the spectral observations of the deuterated compounds and the normal vibration calculations showed that only the *gauche* form exists in the crystalline state and the *trans* and *gauche* forms coexist in the liquid and gaseous states. The enthalpy difference between the *gauche* and *trans* forms in the gaseous state, ΔH_{G-T}, was obtained as -30 ± 50 cal/mol.

Ethyl methyl sulfide is the simplest sulfide with one internal rotation axis associated with the rotational isomerism. It has long been accepted that this molecule takes the *trans* form in the crystalline state and the *trans* and *gauche* forms in the liquid and gaseous states, although some ambiguities have been left out.[2]

Recently, Nogami *et al.*[3] compared the spectra of ethyl methyl sulfide with those of related molecules and reached the conclusion that the crystalline ethyl methyl sulfide takes the *gauche* form but not the *trans* form as had been thought.

In the series of studies to establish the intramolecular force field as well as to clarify the existing rotational isomers of chain molecules,[1,4-6] we have investigated the Raman spectra of ethyl methyl sulfide and its deuterium compounds of $CD_3SC_2H_5$, $CH_3SCH_2CD_3$, and $CH_3SC_2D_5$ and determined the rotational isomerism and vibrational assignments for these molecules. The temperature dependence of the Raman spectra of the undeuterated species in the gaseous state has also been examined. The results are reported in the present paper.

Experimental and Calculation

The deuterium compounds were prepared from sodium salts of appropriate thiols and deuterium compounds of methyl iodide or ethyl bromide and the undeuterated compound was purchased from Tokyo Kasei Kogyo Co., Ltd. All of the samples were purified by fractional distillations. The Raman spectra were recorded on a JEOL JRS-400D spectrometer. The Raman spectra in the gaseous state were measured at five different temperatures between 21 and 112 °C. Temperature measurements of the vapor in the laser beam were made by using nitrogen gas as a thermometer.[7]

The Raman spectra in the liquid and crystalline states in the region below 1500 cm^{-1} are shown in Figs. 1—4. The Raman spectra and the calculated frequencies in the 400—150 cm^{-1} region are compared in Fig. 5.* The gaseous-state Raman spectrum of the undeuterated species is shown in Fig. 6. The

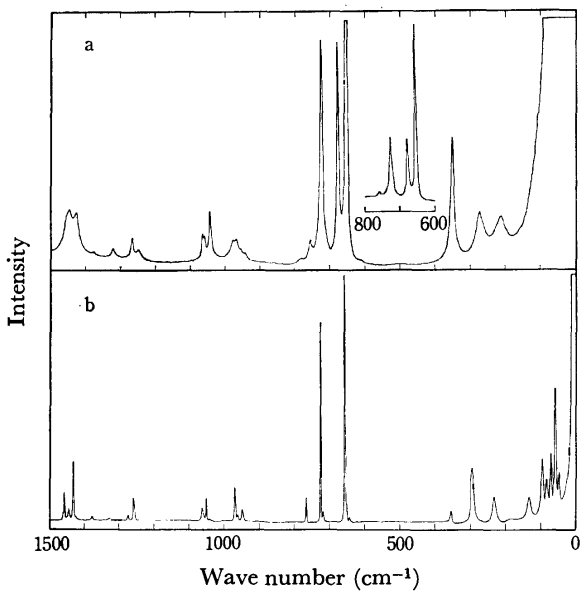

Fig. 1. Raman spectra of $CH_3SC_2H_5$.
a: Liquid, b: crystal.

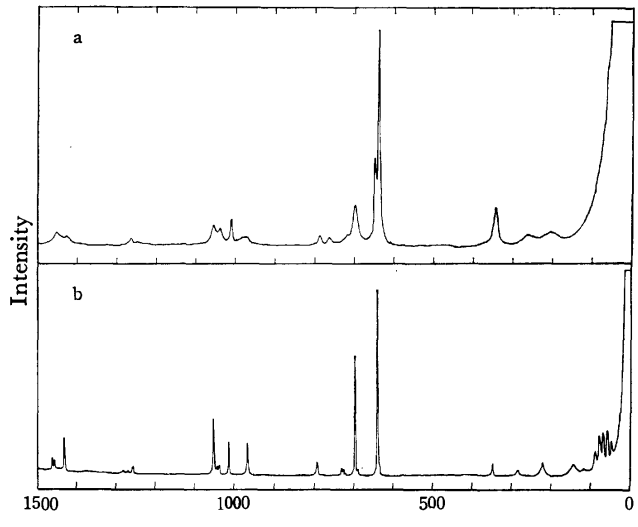

Fig. 2. Raman spectra of $CD_3SC_2H_5$.
a: Liquid, b: crystal.

* The relative intensities of the low-frequency bands (below 400 cm^{-1}) in the crystalline-state spectra are often found to vary depending on the condition of solidification (compare Figs. 1—4 and 5). It is certain that only one isomer exists in the crystalline state as is evident from the complete disapperance of some of the bands in the CS stretching vibration region. One possible explanation of the above observations is that the sample is composed of partially oriented crystallites and gives different intensity patterns due to the different orientation with respect to the polarization direction of the incident light.

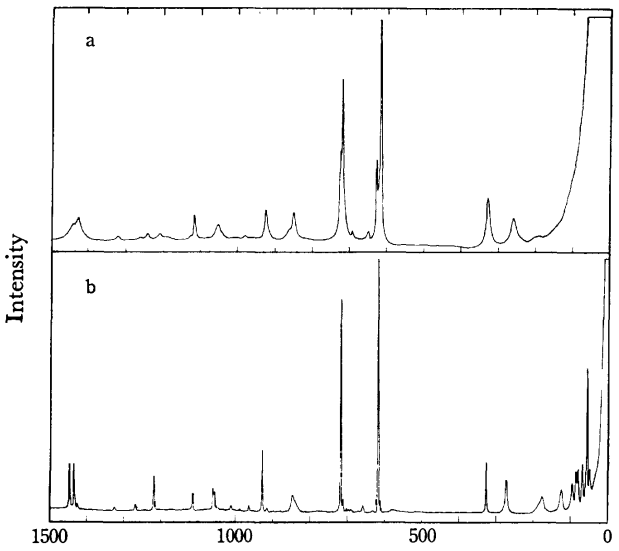

Fig. 3. Raman spectra of $CH_3SCH_2CD_3$.
a: Liquid, b: crystal.

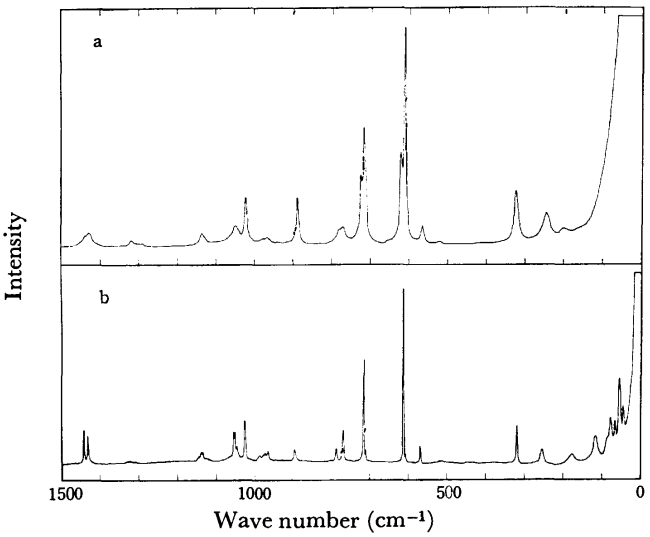

Fig. 4. Raman spectra of $CH_3SC_2D_5$.
a: Liquid, b: crystal.

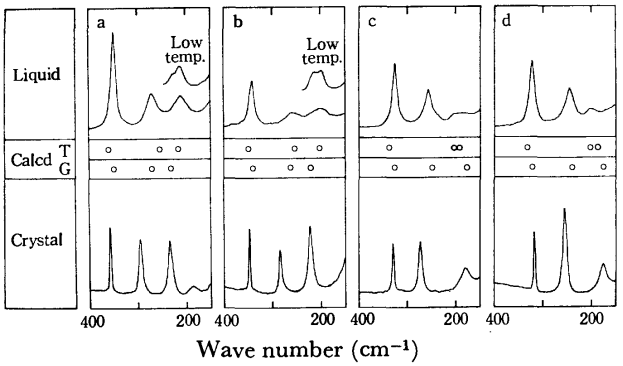

Fig. 5. Raman spectra and calculated frequencies in the 400—150 cm^{-1} region.
a: $CH_3SC_2H_5$, b: $CD_3SC_2H_5$, c: $CH_3SCH_2CD_3$, d: $CH_3SC_2D_5$.

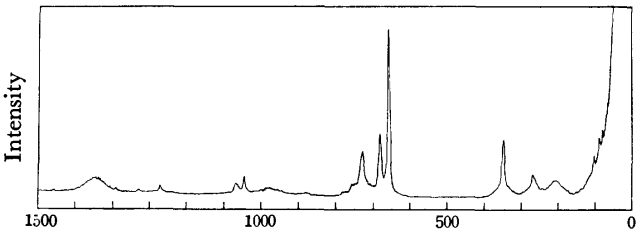

Fig. 6. Raman spectrum of $CH_3SC_2H_5$ in the gaseous state (120 Torr).

TABLE 1. OBSERVED RAMAN FREQUENCIES AND VIBRATIONAL ASSIGNMENTS OF $CH_3SC_2H_5$

Observed Raman frequency (cm^{-1})[a]		Assignment[b]
Liquid	Crystal	
	1461 VW, sh	CH_3 ip-d-deform
1455 VW, sh	1457 VW	CH_3 op-d-deform
1444 VW	1444 VW	CH_3 ip-d-deform
1427 VW	1431 VW	CH_3 op-d-deform, CH_2 scis
1377 VW	1376 VW	CH_3 s-deform
1320 VW	1326 VW	CH_3 s-deform
1267 VW	1272 VW	CH_2 wag
1251 VW	1257 VW	CH_2 twist
1065 VW		CH_3 ip-rock (T)
1060 VW, sh	1060 VW	CH_3 ip-rock (G)
1044 VW	1049 VW	CH_3 op-rock (G, T)
982 VW		CC stretch (T)
973 VW	968 VW	CC stretch (G)
960 VW, sh	962 VW	CH_3 ip-rock (G, T)
955 VW, sh		CH_3 op-rock (T)
948 VW, sh	948 VW	CH_3 op-rock (G)
785 VW		CH_2 rock (T)
758 VW	764 VW	CH_2 rock (G)
725 M	723 S 717 VW	CH_3–S stretch (G, T)
678 M		S–CH_2 stretch (T)
653 VS	656 VS 651 VW	S–CH_2 stretch (G)
353 W	355 VW	SCC deform, CSC bend (G, T)
273 VW	294 W	CSC bend, CC torsion (G), CC torsion (T)
232 VW, sh	232 VW	CC torsion, CSC bend (G)
211 VW		CSC bend, SCC deform (T)
	184 VW	Torsions (G) and lattice vibrations
	133 VW	
	95 W	
	83 VW	
	71 W	
	59 M	
	47 VW	

a) VS: very strong, S: strong, M: medium, W: weak, VW: very weak, sh: shoulder. b) For the notation and definition of the local symmetry coordinates, see Ref. 8.

Table 2. Observed Raman frequencies and vibrational assignments of $CD_3SC_2H_5$

Observed Raman frequency (cm^{-1})[a]		Assignment[b]
Liquid	Crystal	
	1462 VW	CH_3 ip-d-deform
1454 VW	1457 VW	CH_3 op-d-deform
1426 VW	1431 VW	CH_2 scis
1378 VW	1376 VW	CH_3 s-deform
1278 VW	1282 VW	CH_2 wag
1266 VW	1268 VW	CH_2 twist
1063 VW, sh		CH_3 ip-rock (T)
1056 VW	1056 VW, sh	CH_3 ip-rock (G)
1049 VW, sh	1052 W	CD_3 ip-d-deform (G, T)
1040 VW	1042 VW	CD_3 op-d-deform (G, T)
	1038 VW	CD_3 s-deform (G), CH_3 op-rock (T)
1013 VW	1014 VW	CH_3 op-rock (G), CD_3 s-deform (T)
983 VW		CC stretch (T)
971 VW	968 VW	CC stretch (G)
789 VW	793 VW	CH_2 rock (G, T)
761 VW		CD_3 ip-rock (T)
728 VW, sh	731 VW	CD_3 ip-rock (G)
720 VW	726 VW	CD_3 op-rock (G, T)
698 W	698 M	CD_3–S stretch (G, T)
648 M		S–CH_2 stretch (T)
639 VS	641 VS	S–CH_2 stretch (G)
345 VW	349 VW	SCC deform, CSC bend (G, T)
263 VW	285 VW	CC torsion, CSC bend (G), CC torsion (T)
215 VW, sh	221 VW	CSC bend, CC torsion (G)
200 VW		CSC bend, SCC deform (T)
	142 VW	Torsions (G) and lattice vibrations
	116 VW	
	88 VW	
	77 VW	
	68 VW	
	57 VW	
	46 VW	

a), b) See a and b, respectively, of Table 1.

observed frequencies and assignments on the basis of the calculated potential-energy distributions are listed in Tables 1—4.

The normal vibration frequencies were calculated by using a consistent set of force constants for aliphatic sulfides.[5] Detailed results of the calculations and the force constants are reported in a separate paper.[6]

Results and Discussion

Spectra below 400 cm^{-1} and Rotational Isomerism. In the frequency region below 400 cm^{-1}, five normal vibrations are expected for each isotopic species, two skeletal deformation (bending) and three torsional vibrations. As seen from Fig. 5, the frequencies calculated for the *trans* and *gauche* forms of $CH_3SC_2H_5$ or $CD_3SC_2H_5$ are not much different from each other. On the other hand, $CH_3SCH_2CD_3$ and $CH_3SC_2D_5$ give the frequencies which are distinctly different between the two forms.

Table 3. Observed Raman frequencies and vibrational assignments of $CH_3SCH_2CD_3$

Observed Raman frequency (cm^{-1})[a]		Assignment[b]
Liquid	Crystal	
1444 VW	1446 VW	CH_3 ip-d-deform
1432 VW	1431 VW	CH_3 op-d-deform
1425 VW	1425 VW	CH_2 scis
1321 VW	1326 VW	CH_3 s-deform
1263 VW	1269 VW	CH_2 wag (G)
1244 VW		CH_2 wag (T)
1210 VW	1219 VW	CH_2 twist (G, T)
1127 VW		CD_3 s-deform (T)
1115 VW	1115 VW	CD_3 s-deform (G)
	1060 VW	CD_3 ip-d-deform (G)
1052 VW	1054 VW	CD_3 op-d-deform (G, T), CD_3 ip-d-deform (T)
985 VW	988 VW	CH_3 ip-rock (G)
955 VW	963 VW	CH_3 op-rock (G, T), CH_3 ip-rock (T), CH_2 rock (T)
932 VW, sh		CC stretch (T)
924 VW	928 W	CH_2 rock (G)
917 VW, sh	915 VW	CC stretch (G)
863 VW, sh		CD_3 ip-rock (T)
851 VW	848 VW	CD_3 ip-rock (G)
724 M, sh		CH_3–S stretch (T)
719 S	719 S	CH_3–S stretch (G)
	712 VW	
692 VW		Origin unknown
651 VW	657 VW	CD_3 op-rock (G, T)
628 M		S–CH_2 stretch (T)
617 VS	618 VS	S–CH_2 stretch (G)
329 W	327 W	CSC bend, SCC deform (G, T)
258 VW	272 VW	CSC bend, SCC deform (G)
200 VW		CSC bend, SCC deform (T), CC torsion (T)
	176 VW	CC torsion (G)
	125 VW	Torsions (G) and lattice vibrations
	95 VW	
	85 VW	
	80 VW	
	67 VW	
	56 M	
	48 VW	

a), b) See a and b, respectively, of Table 1.

The comparison between the observed and calculated frequencies of these isotopic species shows clearly that the crystalline-state spectra are explained only by the *gauche* form and the liquid-state spectra by the *trans* and *gauche* forms. Thus, the Raman spectra of the deuterium compounds are found to be important in studying the rotational isomerism of ethyl methyl sulfide.

As shown in Tables 1—4, the SCC deformation and CSC bending modes are highly coupled in all of the isotopic species. Such vibrational couplings are known to yield conformation-sensitive frequencies. However, the frequencies of the *trans* and *gauche* forms of $CH_3SC_2H_5$ or $CD_3SC_2H_5$ resemble each other (Fig. 5). This is explained by a further coupling of the CSC bending

TABLE 4. OBSERVED RAMAN FREQUENCIES AND VIBRATIONAL ASSIGNMENTS OF $CH_3SC_2D_5$

Observed Raman frequency (cm^{-1})[a]		Assignment[b]
Liquid	Crystal	
1442 VW, sh	1442 VW	CH_3 ip-d-deform
1430 VW	1431 VW	CH_3 op-d-deform
1320 VW	1325 VW	CH_3 s-deform
1140 VW, sh		CC stretch (T)
1138 VW	1135 VW	CC stretch (G)
1067 VW, sh	1067 VW, sh	CD_2 scis (G, T)
1050 VW	1055 VW 1052 VW	CD_3 op-d-deform (G, T)
1044 VW	1046 VW	CD_3 ip-d-deform (G, T)
1025 VW	1025 VW	CD_3 s-deform (G, T)
978 VW	982 VW	CH_3 ip-rock (G)
968 VW	975 VW 970 VW	CH_3 op-rock (G), CH_3 ip-rock (T)
960 VW, sh	962 VW	CD_3 op-rock (G, T), CH_3 op-rock (T)
887 W	894 VW	CD_3 ip-rock (G, T)
786 VW, sh	786 VW	CD_2 twist (G, T)
770 VW	767 VW	CD_2 wag (G, T)
723 W		CH_3-S stretch (T)
716 M	714 S 711 VW	CH_3-S stretch (G)
622 M		S-CD_2 stretch (T)
612 VS	613 VS 607 VW	S-CD_2 stretch (G)
564 VW	569 VW	CD_2 rock (G)
322 W	319 W	CSC bend, SCC deform (G, T)
244 VW	254 VW	CSC bend, SCC deform(G)
200 VW		CSC bend, SCC deform (T), CC torsion (T)
	178 VW	CC torsion (G)
	117 VW	
	85 VW, sh	Torsions (G) and lattice vibrations
	78 W	
	66 VW	
	55 M	
	45 VW	

a), b) See a and b, respectively, of Table 1.

mode with the CH_2-CH_3 torsional mode in the *gauche* form of these isotopic species. This coupling is removed, however, in $CH_3SCH_2CD_3$ or $CH_3SC_2D_5$ owing to the downward frequency shift of the CH_2-CD_3 or CD_2-CD_3 torsional vibration.

The calculated frequencies of the CH_3-S torsion (160—150 cm^{-1}), the CD_3-S torsion (120—110 cm^{-1}) and the S-CH_2 or S-CD_2 torsion (lower than 100 cm^{-1}) do not differ between the *trans* and *gauche* forms.

It is noted for all of the isotopic species that the Raman band at 270—250 cm^{-1} shifts appreciably to higher frequency in going from the liquid to the crystalline state. The magnitude of the shift is larger for the vibration with a larger contribution from the C-C torsional mode. This large difference between the frequencies of the two states have led previously to misinterpretation of the spectra.[2b] The shifting of this band is confirmed in the present study by observing the Raman spectra of the liquid state at several low temperatures; namely the observed frequency is higher at lower temperature and approaches the crystalline-state value. It is also noted that the *gauche* bands of $CH_3SC_2H_5$ at 232 cm^{-1} and of $CD_3SC_2H_5$ at 215 cm^{-1} are clearly resolved in the low-temperature spectra (Fig. 5).

Sectra in Higher-Frequency Regions. In the 800—600 cm^{-1} region, the bands due to the C-S stretching, CH_2 rocking and CD_3 rocking vibrations are expected. The C-S stretching vibration is known to give rise to much stronger Raman bands than the rocking vibrations.

In the crystalline state, all of the isotopic species exhibit two strong Raman bands separated by 70—100 cm^{-1} (Figs. 1—4). The results of the normal coordinate treatment indicate that the higher-frequency band is assigned to the CH_3-S (CD_3-S) stretching vibration and the lower-frequency band to the S-CH_2 (S-CD_2) stretching vibration, respectively, of the *gauche* isomer.

The 678 cm^{-1} Raman band of liquid $CH_3SC_2H_5$ which disappears on crystallization is assigned to the S-CH_2 stretching vibration of the *trans* isomer. On the other hand, the CH_3-S stretching vibration of the *trans* form has been considered to overlap with the *gauche* band at 725 cm^{-1}.[3] This assignment is confirmed by the present experimental observation that the corresponding bands for $CH_3SCH_2CD_3$ and $CH_3SC_2D_5$ are split into two components in the liquid state. It is seen from the observed spectra of the various isotopic species that the C-S stretching frequencies of the *trans* form are slightly higher than those of the *gauche* form.

The vibrational assignments in other frequency regions have also been established in this study on the basis of the systematic treatment of normal coordinates (see Tables 1—4). The observed Raman frequencies of the deuterated species were found to be important in determining the force field of aliphatic sulfides.[5]

Enthalpy Difference in the Gaseous State. The enthalpy difference between the *gauche* and *trans* forms in the gaseous state, ΔH_{G-T}, has been determined to be -30 ± 50 cal/mol through the analysis of the temperature dependence of the intensities of the band pairs at 682 (*trans*) and 657 cm^{-1} (*gauche*) of the undeuterated species. It is of interest to compare the ΔH_{G-T} values of butane, ethyl methyl ether, and ethyl methyl sulfide. They are 966 ± 54,[7] 1500 ± 200,[9] and -30 ± 50 cal/mol, respectively. The differences in the bond nature of CC-XC (X=C, O, S) groups, as is evident from the above values of enthalpy difference together with those of XC-CY (Y=C, O, S) groups, yield a variety of the structures and properties of longer chain molecules.

References

1) Part II: I. Harada, H. Takeuchi, M. Sakakibara, H. Matsuura, and T. Shimanouchi, *Bull. Chem. Soc. Jpn.*, **50**, 102 (1977).

2) a) D. W. Scott, H. L. Finke, J. P. McCullough, M. E. Gross, K. D. Williamson, G. Waddington, and H. M. Huffman, *J. Am. Chem. Soc.*, **73**, 261 (1951); b) M. Hayashi, *Nippon Kagaku Zasshi*, **77**, 1692 (1956); **78**, 627 (1957); M. Hayashi, T. Shimanouchi, and S. Mizushima, *J. Chem. Phys.*, **26**, 608 (1957); c) D. W. Scott and M. Z. El-Sabban, *J. Mol. Spectrosc.*, **30**, 317 (1969); d) M. Ohsaku, Y. Shiro, and

H. Murata, *Bull. Chem. Soc. Jpn.*, **45**, 954 (1972); **46**, 1399 (1973).

3) N. Nogami, H. Sugeta, and T. Miyazawa, *Bull. Chem. Soc. Jpn.*, **48**, 3573 (1975).

4) T. Shimanouchi, Y. Ogawa, M. Ohta, H. Matsuura, and I. Harada, *Bull. Chem. Soc. Jpn.*, **49**, 2999 (1976).

5) M. Ohta, Y. Ogawa, H. Matsuura, I. Harada, and T. Shimanouchi, *Bull. Chem. Soc. Jpn.*, in press.

6) T. Shimanouchi, H. Matsuura, Y. Ogawa, and I. Harada, *J. Phys. Chem. Ref. Data*, to be published.

7) A. L. Verma, W. F. Murphy, and H. J. Bernstein, *J. Chem. Phys.*, **60**, 1540 (1974).

8) T. Shimanouchi, "Tables of Molecular Vibrational Frequencies," Consolidated Vol. 1, U. S. Govt. Printing Office, No. C13.48: 39 (1972).

9) T. Kitagawa and T. Miyazawa, *Bull. Chem. Soc. Jpn.*, **41**, 1976 (1968).

The Effect of Axial Ligands on the Reductions of Co(III) Complexes with a Macrocyclic Schiff-base Ligand by $Fe(edta)^{2-}$

Yoshimi KURIMURA, Hiroshi SAITO, Ikuko NAKAJIMA, and Yuki FUJII

Department of Chemistry, Ibaraki University, Bunkyo, Mito, Ibaraki 310

(Received March 11, 1976)

The second-order rate constants for the reduction of cobalt(III) complexes with a macrocylic Schiff-base ligand, $Co(dop)L_2^{2+}$ (dop=*N,N'*-bis(2-hydroxyimino-1-methylpropylidene)-1,3-propanediamine and L=primary amine), by Fe (edta)$^{2-}$ are very sensitive to the nature of the axial ligands. The rate increases with a decreases in the basicity of the axial ligands: the order is methylamine, ethylamine, 2-aminoethanol, toluidine, aniline, and bromoaniline derivatives. It is shown that there is a linear relationship between the logarithmic second-order rate constant and the pK_a of the axial primary amine ligand. Among the series of primary amine derivatives, the differences in the free energy of the activation for the reduction can be considered to be mainly dependent upon those in the enthalpy of the activation for the bond stretching of the Co–N (axial ligand) prior to the electron-transfer.

Various kinetic and thermodynamic properties of cobalt(III) complexes with macrocyclic Schiff-base ligands have been well studied in view of the similarities of numerous chemical properties of these with those of the derivatives of coenzyme B_{12}.[1–16] In the ligand-substitution process of such complexes it is demonstrated that the reactive sites are essentially those in the axial ligand resulting from a very high stability of the coordination bonds between the cobalt(III) ion and the equatorial ligands.[15]

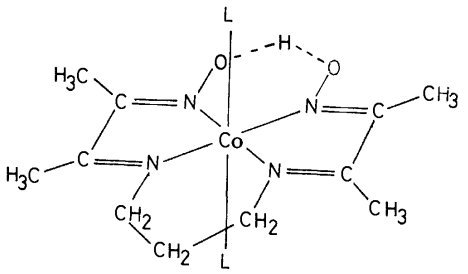

Fig. 1. $Co(dop)L_2^{2+}$.

In the redox process of the cobalt(III)–macrocyclic-ligand complexes, a linear relationship has been found between the polarographic halfwave potential of the first reduction wave and the pK value of the axial Lewis base ligands of the $Co(salen)L_2^+$(salen=*N,N'*-disalicylidene-ethylenediamine) and $Co(dop)L_2^{2+}$ (dop =*N,N'*-bis(2-hydroxyimino-1-methylpropylidene)-1,3-propanediamine).[14] The rate constants for the outer-sphere oxidation of $Co^{II}(N_4)X_2$(N_4=a tetradentate macrocyclic ligand) have been shown to be experimentally correlated to the standard free energy of the reactions.[17] There have been few investigations concerning the effect of the nature of the axial and equatorial ligands on the rate of the reductions of the cobalt(III) complexes with a macrocyclic Schiff-base ligand.

We wish now to report and discuss the influence of axial ligands on the reduction rate of the cobalt(III) complex ions of the $Co(dop)L_2^{2+}$ type by Fe(edta)$^{2-}$. The Fe(edta)$^{2-}$ has been shown to be a good reducing agent for several cobalt(III) complexes in the neutral pH region, and the mechanisms of these reductions have been investigated.[18]

Experimental

Materials. $[Co(dop)Cl_2]$ was prepared after the literature procedure.[19] Complexes of the $[Co(dop)L_2](ClO_4)_2$ type were synthesized by a manner similar to that used in the preparation of $[Co(dop)(NH_3)_2](ClO_4)_2$ described elesewhere.[19] The analytical data of the cobalt(III) chelates prepared are presented in Table 1. The NMR spectra were recorded in DMSO-d_6, with tetramethylsilane as the internal standard. The *trans*-structure of all the chelates were confirmed by their NMR spectra (Table 2). The buffer components, inorganic salts, and disodium salt of ethylenediamine-*N,N,N',N'*-tetraacetic acid were of a guaranteed grade and were used without further purification. The iron(II) chelate solution was prepared by a manner similar to that described previously.[18] The solutions of the iron(II) chelate and the cobalt(III) complexes were adjusted to the described pH and ionic strength by the use of acetate-buffer and potassium-chloride solutions respectively.

Kinetic Measurements. The reduction of the cobalt(III)

Table 1. Analytical data of $[Co(dop)L_2](ClO_4)_2$

L	Found (Calcd) %		
	C	H	N
$Cl^{-a)}$	35.78(35.73)	5.20(4.98)	15.18(15.07)
CH_3NH_2	27.55(27.92)	5.16(5.23)	14.79(15.03)
$C_2H_5NH_2$	30.33(30.68)	5.79(5.66)	14.01(13.63)
$HOC_2H_4NH_2$	29.18(29.09)	5.39(5.38)	13.58(13.57)
$C_6H_5NH_2$	40.08(40.42)	5.27(4.87)	12.24(12.30)
$CH_3C_6H_4NH_2$	42.03(42.21)	5.41(5.24)	11.79(11.81)
$BrC_6H_4NH_2$	39.94(32–84)	3.36(3.72)	9.89 (9.99)

a) $[Co(dop)Cl_2]$.

Table 2. NMR spectral data of $[Co(dop)L_2](ClO_4)_2$ in DMSO-d_6

L	δ /ppm		
	$(-CH_2-)_3$ [a)]	$CH_3C{=}N{-}O-$	$CH_3C{=}N{-}C-$
CH_3NH_2	≈3.85	2.58	2.48
$C_2H_5NH_2$	≈3.9	2.58	2.48
$HO(CH_2)_2NH_2$	≈3.9	2.60	2.48
$C_6H_5NH_2$	≈4.0	2.55	2.24
$CH_3C_6H_4NH_2$	≈4.0	2.54	2.24
$BrC_6H_4NH_2$	≈4.1	2.64	2.32

a) Broad signal.

complexes by the iron(II) chelate were carried out under an atmosphere of nitrogen which had been purified by passing it through acidic chromium(II) ion solutions. Kinetic runs were made under pseudo-first-order conditions in which the concentration of the iron(II) calculate was at least twenty times that of cobalt(III). For relatively slow reactions, the rate was monitored by the measurement of the absorption change (≈500 nm) of the reaction mixture in a thermostated cell compartment of a Union Giken SM-101 spectrophotometer. The cobalt(III) and the iron(II) chelate solutions were mixed by means of a Union Giken MX-7 mixing apparatus. Reaction which were too rapid to be followed by the conventional technique were studied with a Yanagimoto SPS-1 stopped-flow spectrophotometer. The spectral change of the reaction mixture, shown in Fig. 2, was observed by means of a Union Giken RA-1300 rapid-scan spectrophotometer.

Results and Discussion

It was estimated from the known values of the formation constants of the iron(II) chelate species[20] that the predominant species of the iron(II) chelate in the reaction mixture was the normal form of Fe(edta)$^{2-}$ under the conditions employed. The iron(III) chelate species produced in the reaction mixture by the oxidation of Fe(edta)$^{2-}$ could also be estimated to be the normal form of Fe(edta)$^{-}$.[20] A gradual increase in the absorbance at about 510 nm due to the cobalt(II) chelate was observed upon the addition of a solution of the iron(II) chelate to that of the cobalt(III) chelate under a nitrogen atmosphere. In the wave-length region between 500 and 600 nm, the molar extinction coefficients of the cobalt(III), iron(II), and iron(III) in the reaction mixture were very small compared with that of the cobalt(II) chelate under the present conditions. An example of the spectral change for Co(dop)$(HOC_2H_4NH_2)_2^{2+}$ is presented in Fig. 2. It is considered that the reductions of cobalt(III) chelates by Fe(edta)$^{2-}$ all give a product of the cobalt(II) which has a square planar configuration. It has been reported that the cobalt(II)-macrocyclic Schiff-base complexes with a square planar configuration have one or two absorption peaks (log ε= 10^3-10^4) in the visible region.[22,23]

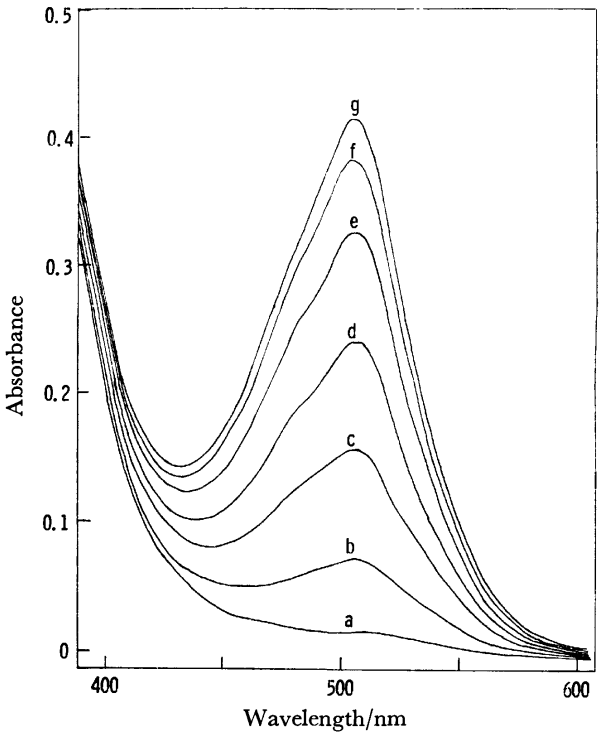

Fig. 2. Spectral change of the reaction mixture.
Initial concentrations: $[Co(dop)L_2^{2+}]_0=1.0\times10^{-4}$ M, L=2-aminoethanol, $[Fe(edta)^{2-}]_0=1.0\times10^{-3}$ M, pH=5.0, μ=0.2, room temp, Scan time: 20 nm/s, a: initial stage, b: 110 s, c: 240 s, d: 420 s, e: 720 s, f: 1200 s, g: final stage.

Table 3. Rate constants for the Fe(edta)$^{2-}$ reductions of $Co(dop)L_2^{2+}$ at μ=0.2 and 25°C[a]

L	k/M^{-1} s^{-1}
CH_3NH_2	$(6.8\pm0.5)\times10^{-2}$
	7.1×10^{-2} [b]
$C_2H_5NH_2$	$(1.4\pm0.06)\times10^{-1}$
$HOC_2H_4NH_2$	1.9 ± 0.04
	1.9[c]
	2.0[d]
$C_6H_5NH_2$	$(3.4\pm0.05)\times10^3$
	3.1×10^3 [e]
	3.2×10^3 [f]
$CH_3C_6H_4NH_2$	$(1.3\pm0.04)\times10^3$
$BrC_6H_4NH_2$	$(5.3\pm0.5)\times10^3$

a) Unless otherwise stated, the experimental conditions were $[Co(dop)L_2^{2+}]_0=1.0\times10^{-4}$M, $[Fe(II)]_0=2.0\times10^{-3}$M, $[X]_f$=0M ($[X]_f$ is the concentration of free amine), and pH=5.0. b) $[X]_f/[Co(III)]_0$= 100. c) pH=4.5. d) pH=5.4. e) $[Fe(II)]_0/[Co(III)]_0$=48. f) $[Fe(II)]_0/[Co(III)]_0$=98.

Plots of $\log(A_\infty-A_t)$ *vs.* time were linear for at least three half-lives for the saturated amine derivatives and two half-lives for the aromatic amine derivatives, where A_∞ is the absorbance when the reaction is completed and A_t, that at time t. The second-order rate constants can be calculated by means of this equation: $k=2.303\times m/[Fe(II)]$, where m is the value of the slope of the straight line. The second-order rate constants for the primary amine derivatives are summarized in Table 3. The second-order rate constants were kept essentially constant by varying the initial concentration of the iron(II) chelate from 2.0×10^{-3} to 1.0×10^{-2} M; they were independent of the hydrogen-ion concentration in the pH region between 4.5 and 5.4. A rate law consistent with the experimental results is given by:

$$d[Co(II)]/dt = k[Co(III)][Fe(edta)^{2-}] \quad (1)$$

where k is the second-order rate constant.

It may safely be assumed that the rate constants obtained correspond to those of Reaction 2, because the reaction is first-order with respect to the concentration of the iron(II) chelate and the rate is not affected by the initial addition of the corresponding free amine to the reaction mixture:

$$Co(dop)L_2^{2+} + Fe(edta)^{2-} \rightleftharpoons Co(dop)L_2^{+} + Fe(edta)^{-} \quad (2)$$

$$Co(dop)L_2^{+} \rightleftharpoons Co(dop)^{+} + 2L \quad (3)$$

That is, the rate-determining step of the reaction is Reaction 2, not the ligand-substitution process represented by 3.

The rate data summarized in Table 3 show that the rate is very sensitive to the nature of the axial ligands: the value of the rate constants vary from 6.8×10^{-2} M^{-1} s^{-1} for methylamine to 5.3×10^{3} M^{-1} s^{-1} for bromoaniline. The reduction rate is enhanced by a decrease in the donor ability of the axial Lewis-base ligand. For a series of runs while varying the axial ligands, a linear relationship between the logarithmic rate constant and the pK_a of the amines was found to hold for the reactions investigated (Fig. 3).

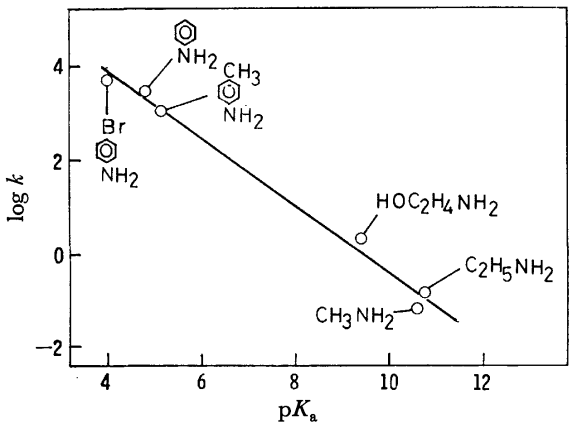

Fig. 3. Relationship between pK_a of axial amine ligand and logarithmic rate constant of the reduction of Co(dop)L_2^{2+} by Fe(edta)$^{2-}$.

Based on the Franck-Condon principle, for the reductions of the cobalt(III) complexes, the reorganization of the cobalt(III) complex would occur prior to the electron-transfer to lower the energy level of the acceptor orbital, which may be d_{z^2} one.[24-26] In the present case, the amounts of free energy for the reorganization may be considered to be dependent upon that for stretching the axial ligands, since the free energy for the reorganization of these ligands would be small as compared with that of the equatorial tetradentate ligand, which is tightly coordinated to the cobalt(III) ion. Such bond stretching energy may increase with an increase in the bond strength between the cobalt(III) ion and the donor atom of the primary amine. It is considered that the Co–N (axial ligand) bond is strengthened when the value of pK_a of the amine increases, since it has substantially the σ bonding nature. It might be concluded that the linear relationship shown in Fig. 3 holds in the electron-transfer reactions, since the predominant factor controlling the activation free energy is the free energy for the reorganization of the axial ligands.

Table 4. Activation parameters for the reduction of Co(dop)L_2^{2+}

L	$\Delta H^{\ddagger}$/kcal mol^{-1}	$\Delta S^{\ddagger}$/e.u.
CH_3NH_2	22.9	8.6
$C_2H_5NH_2$	23.9	18.0
$HOC_2H_4NH_2$	18.4	13.2
$C_6H_5NH_2$	16.2	12.0
$CH_3C_6H_4NH_2$	17.5	13.7
$BrC_6H_4NH_2$	15.0	10.0

The activation parameters for the reactions obtained from the temperature dependence of the rate constant are presented in Table 4. The relatively small variation in the activation entropy as compared with that in the activation enthalpy seems to indicate that the large change in the rate constant upon the variation in the axial ligands is mostly attributable to the relatively large variation in the activation enthalpy.

References

1) G. N. Schrauzer and R. G. Windgassen, *J. Am. Chem. Soc.*, **88**, 3738 (1966).
2) G. N. Schrauzer and R. J. Windgassen, *J. Am. Chem. Soc.*, **89**, 143 (1967).
3) G. N. Schrauzer and R. J. Windgassen, *J. Am. Chem. Soc.*, **89**, 1999 (1967).
4) G. N. Schrauzer and L. Lee, *J. Am. Chem. Soc.*, **89**, 3607 (1967).
5) G. N. Schrauzer, E. Deutsch, and R. J. Windgassen, *J. Am. Chem. Soc.*, **90**, 2441 (1968).
6) G. N. Schrauzer and L. Lee, *J. Am. Chem. Soc.*, **90**, 6541 (1968).
7) G. N. Schrauzer, J. W. Sibert, and R. J. Windgassen, *J. Am. Chem. Soc.*, **90**, 6681 (1968).
8) G. N. Schrauzer, *Acc. Chem. Res.*, **1**, 97 (1968).
9) G. Costa, A. Paxeddu, and G. Tauzer, *Inorg. Nucl. Chem. Lett.*, **4**, 319 (1968).
10) G. N. Schrauzer and E. Deutsch, *J. Am. Chem. Soc.*, **91**, 3341 (1969).
11) G. N. Schrauzer, L. Lee, and J. W. Sibert, *J. Am. Chem. Soc.*, **92**, 2997 (1970).
12) J. W. Siebert and S. N. Schrauzer, *J. Am. Chem. Soc.*, **92**, 1421 (1970).
13) G. N. Schrauzer and J. W. Siebert, *J. Am. Chem. Soc.*, **92**, 1022 (1970).
14) G. Costa, G. Mestroni, A. Paxeddu, and E. Reissenhofer, *J. Chem. Soc., A*, **1970**, 2870.
15) G. Costa, *Coord. Chem. Rev.*, **8**, 63 (1972).
16) K. L. Brown and R. G. Kallen, *J. Am. Chem. Soc.*, **94**, 1894 (1972).
17) D. Rillema and J. F. Endicott, *J. Am. Chem. Soc.*, **94**, 8711 (1972).
18) Y. Kurimura, *Bull. Chem. Soc. Jpn.*, **46**, 2093 (1973).
19) G. Costa and G. Mestroni, *Tetrahedron Lett.*, **41**, 4005 (1967).
20) The pK values of EDTA are $pK_1=1.99$, $pK_2=2.67$, $pK_3=6.16$, and $pK_4=10.26$, while the formation constants are log $K_{Fe^{II}HL}=2.8$, log $K_{Fe^{II}L}=14.3$, log $K_{Fe^{II}HL}=1.4$, log $K_{Fe^{III}L}=25.1$, and log $K_{Fe^{III}OHL}=6.5$.[21] The definitions used here are $K_{Fe^{II}L}=[FeY^{2-}]/[Fe^{2+}][Y^{4-}]$(Y=edta), $K_{Fe^{II}LH}=[FeHY^{-}]/[FeY^{2-}]\,[H^{+}]$, $K_{Fe^{III}L}=[FeY^{-}]/[Fe^{3+}][Y^{4-}]$, $K_{Fe^{III}HL}=[FeHY]/[FeY^{-}][H^{+}]$, and $K_{Fe^{III}OHL}=[Fe(OH)Y^{2-}]/[FeY^{-}][OH^{-}]$.
21) A. Ringbom, "Complexation in Analytical Chemistry," John Wiley and Sons Inc, New York (1963).
22) H. Aoi and S. Yoshikawa, *Bull. Chem. Soc. Jpn.*, **48**, 1019 (1975).
23) C. J. Hipp and W. A. Baker, Jr., *J. Am. Chem. Soc.*, **92**, 792 (1970).
24) L. Orgel, "Report of the Tenth Solvey Conference," Brussels (1956), p. 289.
25) H. Taube, *Adv. Inorg. Chem. Radiochem.*, **1**, 1 (1959).
26) Y. Kurimura, K. Ohashi, T. Ohtsuki, and K. Yamamoto, *Bull. Chem. Soc. Jpn.*, **44**, 1293 (1971).

Synthesis and Magnetic Properties of Iron(III) Complexes with Several Quadridentate Schiff Bases[1)]

Yuzo NISHIDA, Shuhei OSHIO, and Sigeo KIDA

Department of Chemistry, Faculty of Science, Kyushu University, Fukuoka 812

(Received May 29, 1976)

New iron(III) complexes containing quadridentate Schiff bases, $[Fe(L)AB]^{n+}$, were prepared, where H_2L represents a quadridentate Schiff base, and A and B, unidentate ligands, such as imidazole, pyridine derivatives, and cyanide ions. The magnetic moments of the complexes are in the range of 1.9—6.0 B.M. at room temperature. Based on the magnetic susceptibilities at various temperatures (90—295 K), these compleses were classified into four types: (1) high-spin ($S=5/2$), (2) low-spin ($S=1/2$), (3) intermediate spin ($S=3/2$), and (4) cross-over complexes, the last of which have a ligand-field strength near the cross-over point of high-spin and low-spin types. From the ESR spectra obtained, the existence of a spin-equilibrium was established for the cross-over complexes.

Iron(III) complexes have a $(3d)^5$ electronic configuration and the energy levels in the octahedral ligand field have been calculated by Tanabe and Sugano.[2)] According to their diagram, three types of iron(III) complexes can be expected in the octahedral field, depending upon the strength of the ligand field, that is, high-spin ($S=5/2$), low-spin ($S=1/2$), and cross-over complexes, the last of which have a ligand-field strength near the cross-over point of high-spin and low-spin types. In fact, complexes of these types are known for six-coordinated iron(III) complexes.[3)]

For the iron(III) complexes of porphyrin derivatives (abbreviated as H_2por), $[Fe(por)AB]^{n+}$, the magnetic moments depend greatly upon the axial ligands, A and B, and fall in the range of 2.2—5.9 B.M. at room temperature. In seeking to explain the variation in magnetic moments, some authors have claimed the existence of a spin-equilibrium of two spin states in these porphyrin derivatives.[4)] However, Harris has carried out numerous calculations on the magnetic properties of iron(III) complexes with tetragonal symmetry and concluded that the anomalous magnetic behavior of heme derivatives should be elucidated in terms of "spin-mixed states."[5,6)] For the interpretation of the magnetic properties of the cross-over complexes in more detail, systematic data on many other complexes are necessary. Accordingly, we have attempted to prepare iron(III) complexes with a tetragonal symmetry, by the use of quadridentate Schiff bases (abbreviated as H_2L) as the planar ligands. The prepared complexes have the general formula of $[Fe(L)AB]^{n+}$, where A and B are unidentate ligands, such as imidazole, pyridine derivatives, and cyanide ions.

The Schiff bases and other ligands used in this study are listed in Tables 1 and 2 with their abbreviations, while the structural formulas of their representative Schiff bases are shown in Fig. 1.

Table 1. Abbreviations of the Schiff bases
(Skeletal structures are depicted in Fig. 1.)

Type	X	R	Y	Abbreviation (L)
(a)	H	$-CH_2CH_2-$		salen
	H	$1,2-C_6H_4$		salphen
	$3-CH_3O$	$-CH_2CH_2-$		vanen
(b)		$-CH_2CH_2-$	CH_3	acen
		$-CH_2CH_2-$	C_6H_5	bzacen

Table 2. Abbreviations of the unidentate ligands

Ligands	Abbreviation
Imidazole	im
Pyridine	py
4-Aminopyridine	apy
β-Picoline	β-pic
γ-Picoline	γ-pic

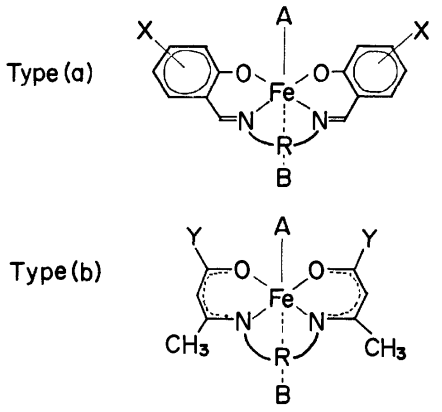

Fig. 1. Iron(III) Schiff base complexes (*cf.* Table 1).

Experimental

Preparations. The quadridentate Schiff bases used in this study were prepared according to the methods described in the literatures.[7)]

[Fe(salen)Cl]: This complex was prepared according to the method of Pfeiffer *et al.*[8)]

[Fe(acen)Cl]: The H_2acen ligand (1.1 g) dissolved in absolute methanol (20 ml), was added to anhydrous iron(III) chloride (0.8 g) dissolved in absolute methanol (20 ml). To this mixture, triethylamine (1.0 g) was then added. The resulting solution was warmed at 60 °C for ten minutes and subsequently allowed to stand for five hours at room temperature. The purple crystals yielded were filtered and washed with cold absolute methanol.

$[Fe(salen)(im)_2]B(ph)_4$: The [Fe(salen)Cl] complex was suspended in absolute methanol (40 ml), and then imidazole (0.6 g) was added to this solution. The solution was warmed at 60 °C for ten minutes and then filtered. Sodium tetraphenylborate (0.7 g) dissolved in absolute methanol (10 ml) was added to the filtrate, and the solution was allowed to

stand overnight at room temperature. The reddish-brown crystals separated were filtered and washed with cold ethanol.

[Fe(vanen)(im)$_2$]B(ph)$_4$ and [Fe(salphen)(im)$_2$]B(ph)$_4$: These complexes were prepared according to a procedure similar to that described for [Fe(salen)(im)$_2$]B(ph)$_4$.

[Fe(acen)(im)$_2$]B(ph)$_4$, [Fe(acen)(py)$_2$]B(ph)$_4$, [Fe(acen)(β-pic)$_2$]B(ph)$_4$, [Fe(acen)(apy)$_2$]ClO$_4$, and [Fe(acen)(γ-ipic)$_2$]ClO$_4$: These complexes were prepared according to a method similar to that described above, except that [Fe(acen)Cl] was used, instead of [Fe(salen)Cl], and $NaClO_4$ instead of NaB(ph)$_4$.

[Fe(salen)CN]·CH$_3$OH: Sodium cyanide (0.05 g) dissolved in absolute methanol (15 ml) was added to an absolute methanol solution (15 ml) of [Fe(salen)(im)$_2$]B(ph)$_4$(0.8 g). This solution was allowed to stand five hours at room temperature. The black precipitate thus yielded was filtered and washed with absolute methanol.

Na[Fe(salen)(CN)$_2$]·CH$_3$OH: Sodium cyanide (0.1 g) dissolved in absolute methanol (15 ml) was added to an absolute methanol solution containing 0.55 gram of [Fe(salen)Cl], and then the solution was warmed at 60 °C for ten minutes. The solution was evaporated under reduced pressure, and the dicyano complex thus separated was recrystallized from hot absolute methanol. The green crystals thus obtained were filtered and washed with absolute ethanol.

Na[Fe(acen)(CN)$_2$] and [Fe(bzacen)(im)CN]: These complexes were prepared by methods similar to those described for Na[Fe(salen)(CN)$_2$] and [Fe(salen)CN]·CH$_3$OH respectively.

[Fe(bzacen)(im)$_2$]B(ph)$_4$: To a hot absolute methanol solution (40 ml) of anhydrous ferric chloride (0.85 g), H_2bzacen (1.73 g) and imidazole (2.00 g) were added, the solution was then warmed at 60 °C for ten minutes and filtered. To this filtrate, NaB(ph)$_4$ (1.0 g) was added, and the solution was allowed to stand for five hours. The dark green crystals thus precipitated were filtered and washed with cold absolute methanol.

Measurements. Magnetic susceptibilities were measured over the range from the temperature of liquid nitrogen to room temperature by the Faraday method, Pascal's constants being used for diamagnetic correction. Mercury(II) tetrathiocyanatocobaltate(II), $HgCo(NCS)_4$ was employed as the standard for magnetic susceptibility. The effective magnetic moments at room temperature were calculated from the expression:

$$\mu_{eff} = 2.828\sqrt{T \cdot \chi_A}$$

where χ_A is the susceptibility per gram atom of iron.

The ESR spectra of polycrystalline samples and DMSO-frozen solutions were measured with a JEOL ESR spectrometer model, JES-ME-3X using an X-band. DPPH was used as the standard marker.

The absorption spectra were measured with a recording spectrophotometer model, Hitachi EPS-2, at room temperature.

Results and Discussion

Characterization of New Complexes. Table 3 gives the analytical data, color, and magnetic moments of the complexes. The structures of the new complexes are assumed to be *trans* (A, B)-[Fe(L)AB]$^{n+}$, because the quadridentate Schiff bases used in this study prefer the planar coordination, furthermore, Na[Fe(salen)(CN)$_2$] shows only one sharp band, at 2105 cm^{-1}, in the infrared spectrum.

The magnetic moments of the complexes depend greatly on the Schiff bases and axial ligands; they fall in the range of 1.9—6.0 B.M. at room temperature. On the basis of magnetic susceptibilities at various temperatures (90—295 K), the **1**—**3** and **4**—**8** complexes are high-spin and low-spin types, respectively. The **9**—**13** complexes show intermediate magnetic moments (2.5—5.0 B.M.) between high-spin and low-spin values; accordingly, they may be assumed to be cross-over complexes. The interpretation of the magnetic data on the assumption of a dimeric structure such as [Fe(salen)Cl]$_2$[9] is impossible, because all the complexes can assume six-coordination without any bridged structure.

Judging from the magnetic data of the series [Fe(L)(im)$_2$]$^{n+}$ complexes shown in Table 3, the spin-pairing abilities of planar Schiff bases appear to be of the following order: H_2acen>H_2bzacen>H_2salen≈H_2salphen. Thus, it was revealed that a small change in the planar

Table 3. Analytical data and magnetic moments

No.	Complexes	C Calcd (Found)	H Calcd (Found)	N Calcd (Found)	Color	Magnetic moments (B.M.) 295 K	80 K
(**1**)	[Fe(salen)(im)$_2$]B(ph)$_4$	71.06(71.57)	5.44(5.50)	10.81(10.84)	brown	5.89	5.37
(**2**)	[Fe(salphen)(im)$_2$]B(ph)$_4$	72.74(72.42)	5.13(5.04)	10.18(10.06)	brown	5.97	5.58
(**3**)	[Fe(acen)Cl]	45.96(45.84)	5.79(5.79)	8.93(8.89)	purple	5.85	5.56
(**4**)	Na[Fe(salen)(CN)$_2$]·CH$_3$OH	53.17(53.24)	4.23(4.21)	13.05(13.22)	green	1.87	1.74
(**5**)	Na[Fe(acen)(CN)$_2$]	47.61(46.65)	5.14(5.26)	15.86(15.40)	green	2.11	2.00
(**6**)	[Fe(acen)(im)$_2$]B(ph)$_4$	68.77(68.35)	6.32(6.36)	11.46(11.46)	green	2.17	1.91
(**7**)	[Fe(acen)(apy)$_2$]ClO$_4$	46.70(46.22)	5.34(5.29)	14.85(14.68)	green	2.29	2.14
(**8**)	[Fe(bzacen)(im)CN]	62.91(62.56)	5.28(5.31)	14.11(13.84)	green	1.99	1.80
(**9**)	[Fe(vanen)(im)$_2$]B(ph)$_4$	68.83(68.65)	5.54(5.61)	10.03(10.03)	dark purple	5.03	3.57
(**10**)	[Fe(bzacen)(im)$_2$]B(ph)$_4$	72.82(72.31)	5.88(5.88)	9.80(9.87)	brownish green	4.79	2.23
(**11**)	[Fe(acen)(py)$_2$]B(ph)$_4$	73.12(72.36)	6.40(6.35)	7.42(7.38)	green	3.31	2.30
(**12**)	[Fe(acen)(β-pic)$_2$]ClO$_4$	51.13(50.52)	5.72(5.66)	9.94(9.87)	brownish green	2.51	1.93
(**13**)	[Fe(acen)(γ-pic)$_2$]B(ph)$_4$	73.56(73.09)	6.69(6.62)	7.16(7.11)	brownish green	3.64	2.04

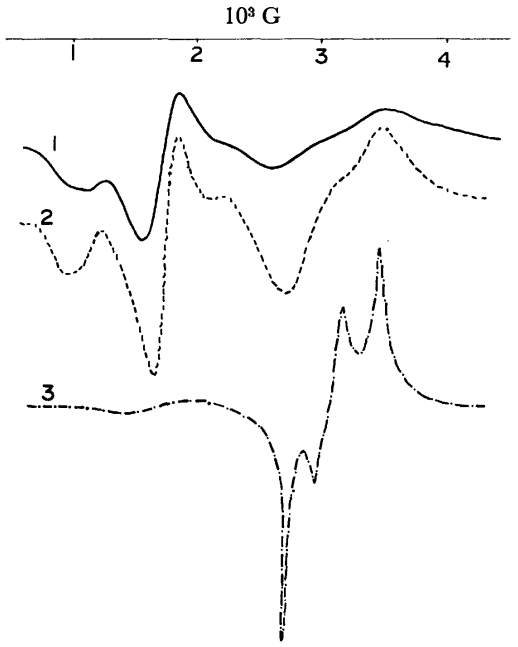

Fig. 2. Powder ESR spectra of [Fe(vanen)(im)$_2$]B(ph)$_4$ (X-band).
1: 244 K, 2: 184 K, 3: 77 K.

ligands exerts a large effect on the electronic configuration of the ground state of the iron(III) ion. From the magnetic data of the series of acen complexes shown in Table 3, the order of spin-pairing ability is: CN> imidazole>apy>β-pic>py>γ-pic. The order of the pyridine derivatives agrees with neither the order of basicity of pyridine nitrogen nor the spectrochemical series. These facts suggest that the choice of the spin state of [Fe(L)AB]$^{n+}$ depends not only on the ligand field strength, but also on the crystal lattice energy and the steric effect of the ligands.

Cross-over Complexes. In Fig. 2, the ESR spectra of [Fe(vanen)(im)$_2$]B(ph)$_4$ at various temperatures are shown. In Fig. 3, the ESR spectra of [Fe(salen)(im)$_2$]-B(ph)$_4$(high-spin type) and Na[Fe(salen)(CN)$_2$](low-spin type) are shown. In the ESR spectrum of [Fe-(salen)(im)$_2$]B(ph)$_4$, some absorptions are observed over the wide range of 1000—3000 G. This is characteristic of high-spin complexes.[10,11] On the other hand, in the case of Na[Fe(salen)(CN)$_2$], some peaks are observed at about 3000 gauss. The small anisotropy of g-values suggests that the electronic configuration of the ground state is $(d_{xz})^2(d_{yz})^2(d_{xy})^1$.[12]

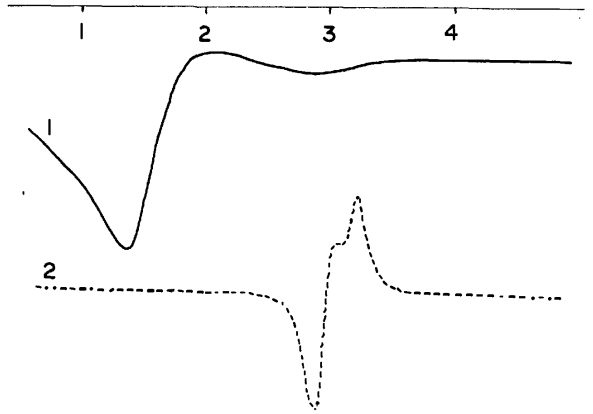

Fig. 3. Powder ESR spectra (X-band, at 244 K).
1: [Fe(salen)(im)$_2$]B(ph)$_4$ (high-spin complex),
2: Na[Fe(salen)(CN)$_2$] (low-spin complex).

In the ESR spectra of [Fe(vanen)(im)$_2$]B(ph)$_4$ and [Fe(bzacen)(im)$_2$]B(ph)$_4$,[1] some peaks are observed at about 3000 gauss and in the range of 1000—2700 G. As the temperature is lowered, the relative intensities of the absorptions change dramatically, as may be seen in Fig. 2, although the positions of the absorptions do not change. This fact indicates two or more spin states exists in these complexes in the temperature range investigated; undoubtedly one of them is $S=1/2$.

Harris[5,6] investigated the magnetic properties of heme derivatives and concluded that the magnetic behavior of complexes with intermediate magnetic moments at room temperature should be explained in terms of "spin-mixed states." However, the presently obtained ESR spectra are not compatible with his prediction. Rather, the magnetic behavior of the **9—13** complexes should be interpreted in terms of a spin-equilibrium between two or more spin states. We further attempted to confirm the spin-equilibrium by the use of the Mössbauer spectra. However, clear peaks were not observed for high-spin complexes; therefore, the existence of spin-equilibrium could not be verified by the Mössbauer spectra.

Absorption Spectra. As shown in Table 3, the colors of the low-spin complexes differ from those of the high-spin complexes. In general, the Lambert-Beer law can not be applied to solutions of these complexes, probably because of the partial dissociation of axial ligands. Therefore, a small excess of axial ligands was added to the methanol solutions of the complexes. In Fig. 4, the absorption spectra of [Fe(salen)(im)$_2$]B(ph)$_4$, Na[Fe(acen)(CN)$_2$], and [Fe(bzacen)(im)$_2$]B(ph)$_4$ are shown. The low-spin Schiff base complexes are generally green or blue, perhaps because of the absorptions at

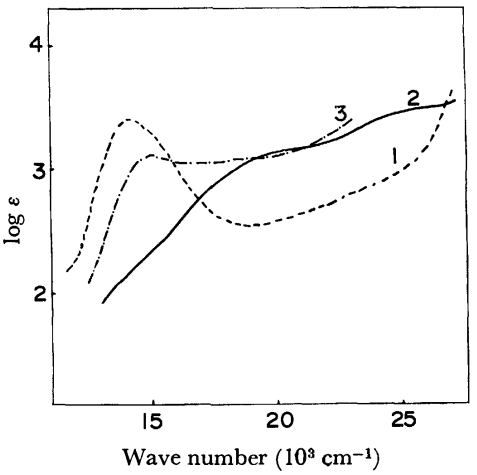

Fig. 4. Absorption spectra of iron(III) Schiff base complexes (at 295 K, in methanol solution).
1: Na[Fe(acen)(CN)$_2$] (low-spin type, 1.9×10^{-4} M),
2: [Fe(salen)(im)$_2$]B(ph)$_4$ (high-spin type, 2.7×10^{-4} M),
3: [Fe(bzacen)(im)$_2$]B(ph)$_4$ (cross-over complex, 4.4×10^{-4} M).

14—16 $\times 10^3$ cm^{-1} (log $\varepsilon \approx 3$). Such absorptions are not observed for high-spin complexes. These bands may be attributed to the charge-transfer transitions between metal and Schiff bases, because this absorption is independent of axial ligands. On the other hand, the absorption spectrum of $[Fe(bzacen)(im)_2]B(ph)_4$ seems to be a superposition of high-spin and low-spin types; this is consistent with the results of the ESR spectra.

References

1) A part of this work has already been reported: Y. Nishida, S. Oshio, and Kida, *Chem. Lett.*, **1975**, 79.
2) Y. Tanabe and S. Sugano, *J. Phys. Soc. Jpn.*, **9**, 753, 766 (1954).
3) S. A. Cotton, *Coord. Chem. Rev.*, **8**, 184 (1972).
4) P. George, J. Beetlestone, and J. S. Griffith, *Rev. Mod. Phys.*, **1964**, 441.
5) G. Harris, *Theor. Chim. Acta*, **10**, 119 (1968).
6) G. Harris, *Theor. Chim. Acta*, **10**, 155 (1968).
7) R. H. Holm, G. W. Everett, and A. Charkravorty, *Prog. Inorg. Chem.*, **7**, 83 (1965).
8) P. Pfeiffer and T. Tsumaki, *Ann.*, **503**, 83 (1933).
9) M. Gerloch, J. Lewis, F. E. Mabbs, and A. Richards, *Nature*, **212**, 809 (1966); J. Lewis, F. E. Mabbs, and A. Richards, *Nature*, **212**, 809 (1966); M. Gerloch and F. E. Mabbs, *J. Chem. Soc., A*, **1967**, 1598.
10) R. D. Dowsing and J. F. Gibson, *J. Chem. Phys.*, **50**, 294 (1969).
11) R. Aasa, *J. Chem. Phys.*, **52**, 3919 (1970).
12) Y. Nishida, S. Oshio, and S. Kida, submitted to *Inorg. Chim. Acta*.

Gas Chromatographic Studies of the Thermal Decompositions of Hexaammine-, Chloropentaammine-, and *trans*-Dichlorotetraammine-cobalt(III) Chloride in the Solid State

Sukeo ONODERA*

Department of Chemistry, Faculty of Science, Tokyo University of Science, Kagurasaka, Shinjuku-ku, Tokyo 162

(Received June 2, 1976)

This paper will describe gas chromatographic studies of the thermal decomposition of cobalt(III) ammine complexes in the solid state. The sample is pyrolyzed in a chamber in a helium atmosphere at a heating rate of 1 °C/min. The evolved products are directly led into a chromatographic separation column at periodic intervals of 10 °C. The preliminary gaseous product for these compound is ammonia. The gas evolution(GE) curves for each compound could be made as function of the temperature on the basis of the various gas chromatograms. These GE curves show two maximum peaks; the first is a sharp peak at about 250 °C, while the second is a broad peak in the 280—340 °C temperature range. The combination of these GE curves with the results of TG and DTA studies allows more complete interpretations of the thermal-decomposition reactions of the cobalt(III) ammine complexes.

Thermogravimetric analysis(TG) and differential thermal analysis (DTA) have been widely used by earlier investigators for studying the thermal-decomposition reactions of some transition metal complexes. These techniques gives information concerning the weight loss or the thermal changes in the compounds during the thermal reactions, but they do not give information on the species and the composition of the produced gases.

When the metal complexes are heated under various experimental conditions, volatile ligands or their gaseous decomposition product are usually liberated from the compounds. Thus, gas evolution analysis (GEA) is required for the above reactions in order to obtain exact information on the decomposition processes of the compounds. The combination of GEA with a TG or DTA apparatus allows more complete interpretations of their curves.

The simultaneous measurements of TG and DTA have been reported by Logers, Yamada and Zinn,[1] and, those of DTA and GEA, by Ayres and Bens,[2] Langer and Gohlke,[3] and Wendlandt *et al.*[4]

In earlier studies by Wendlandt *et al.*,[4] GEA curves were obtained by the use of a thermister thermal conductivity cell, and the composition of the pyrolyzed gases was determined by such conventional techniques as mass spectrometry, gas chromatography, and infrared absorption spectroscopy. Further works by Wendlandt *et al.*[3] have reported the method of leading the evolved product gases directly into a mass spectrometer for studying the thermal decomposition reactions of $[Cu(NH_3)_4]SO_4 \cdot H_2O$, some metal-cupferron chelates, and halogenopentaamminecobalt(III) complexes.

This paper will describe a method of leading the evolved product gases directly into a gas chromatograph, the so-called pyrolysis-gas chromatograph, for studying the thermal decomposition reactions of some chloroammine cobalt(III) complexes in the temperature range of 25—400 °C; on the basis of the GEA curves, the stoichiometries of the thermal-decomposition reactions of these compounds will be presented.

* Present adress: Faculty of Pharmaceutical Science, Tokyo University of Science, Ichigaya-funagawara, Shinjuku-ku, Tokyo 162.

Experimental

Materials. The hexaammine-,[6] chloropentaammine-,[7] and *trans*-dichlorotetraamminecobalt(III) chloride[8] were prepared according to the methods given in the literature. They were identified by the measurements of the infrared absorption spectra. Sample ranging in perticle size between 100—200 mesh were used in these studies. These chloroammine cobalt(III) chlorides were selected because they are the ammine complexes most extensively studied by earlier workers.

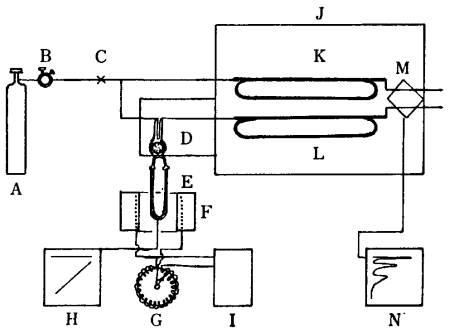

Fig. 1. Schematic diagram of pyrolysis-gas chromatographic apparatus.
A: Helium cylinder. B: Pressure regulator. C: Stop valve. D: Gas sampler. E: Pyrolysis chamber. F: Furnace. G: Slide transformer. H: Temperature recorder. I: AC voltage stabilizer. J: Gas chromatograph. K: Reference column. L: Separation column. M: Thermistor thermal conductivity cell. N: Gas chromatogram recorder.

GEA Apparatus. A schematic diagram of the GEA apparatus is given in Fig. 1, while the pyrolysis part of the apparatus is illustrated in Fig. 2.

The GEA apparatus consisted of a pyrolysis chamber(E), a furnace(F), a furnace temperature controller(G), a sample temperature recorder (H), and a Shimadzu model GC-2C gas chromatograph (J) with a thermal conductivity detector (M). Helium from a cylinder (A) and a pressure regulator (B) was passed through into reference column (K), into the pyrolysis chamber (E), and then into a separation column(L) packed with a 20% Silicon oil SF-96 on Fluoro Pack-80 (60—80 mesh) in a Teflon tube 5 m long by 0.3 cm in diameter.

The pyrolysis chamber consisted of a U-type Pyrex glass tube 15 cm long by 0.4 cm in diameter, which was terminated

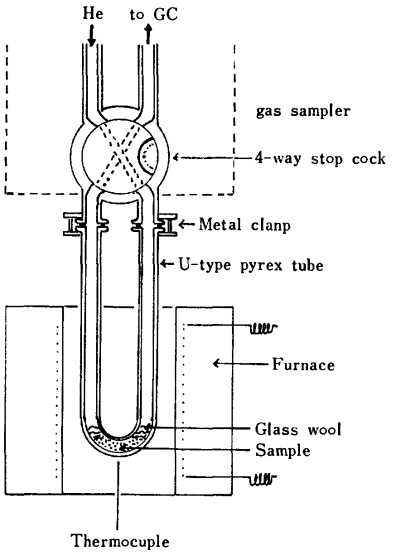

Fig. 2. Pyrolysis part of the apparatus.

on both ends by a 0.4-cm-inner-diameter "O"-ring joint (silicon gem). Two "O" -ring joints were attached to the joint of the gas sampler of the gas chromatograph by means of a metal clamp. The Pyrex tube was electrically heated by Nichrom wire enclosed in the furnace. The furnace was made by an asbestos tube, 15 cm long by 4.0 cm in diameter, which was wound by Nichrom heater wire and then insulated by additional asbestos paper so as to make a layer about 1.0 cm thick. The temperature of the wall of the Pyrex tube was measured by means of a chromel–alumel thermocouple. The pyrolysis temperature rise was controlled by means of the transformer(G).

The glass tubing from the pyrolysis chamber to the gas sampler of the gas chromatograph was maintained at about 60 °C by means of external heating jackets.

Procedure for Pyrolysis of Sample. Twenty mg of a sample was placed in the Pyrex tube and fixed with glass wool. The air in the system was swept out with a helium gas at a flow rate of 40 ml/min for about 30 min. During this time, gas-chromatographic conditions were allowed to be stabilized.

After the flow of helium had been directly passed through into the gas sampler by the changing of the stop cock, the heating of the furnace was begun. Usually, a furnace heating rate of 1 °C/min was employed, but this could be varied at will. The temperature-rising curve was recorded on the strip-chart recorder (H).

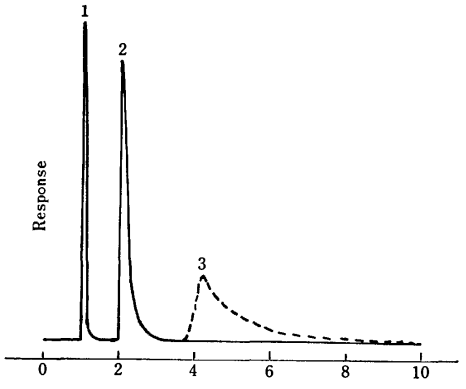

Fig. 3. Gas chromatogram of nitrogen (1), ammonia (2) and water (3) using 20% silicon SF-96 on fluoro Pack-80.

Procedure for the Analysis of the Gaseous Products. The gaseous products evolved during the above pyrolysis procedure were quickly swept into the chromatographic separation column at periodic intervals of 10 °C by changing the stop cock. Thus, the various gas-chromatographic patterns for the evolved gases could be obtained as a function of the temperature.

The peaks appearing on the gas chromatograms were identified by the use of the retention times of various pure substances which may be expected to be formed during the decomposition of the sample. From the peak areas of the various peaks, the amount of the decomposition product could be ascertained as a function of the temperature. The chromatographic patterns for various pure substances are shown in Fig. 3.

Results and Discussion

The GEA curves of the cobalt(III) ammine complexes in the temperature range of 25—400 °C in a helium atmosphere are given in Fig. 4, while the data on gaseous decomposition products are summarized in Table 1. These results were reproducible under the experimental conditions employed in the present work.

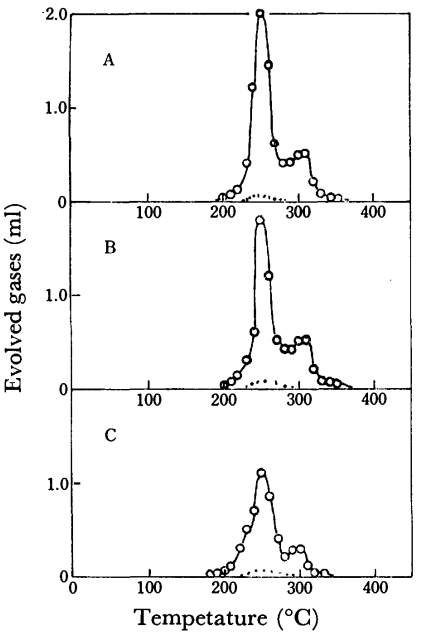

Fig. 4. Gas evolution curves for $[Co(NH_3)_6]Cl_3$ (A), $[CoCl(NH_3)_5]Cl_2$(B) and *trans*-$[CoCl_2(NH_3)_4]Cl$(C) in helium atmosphere.
N_2; ·····, NH_3; -•-•-•-.

Table 1. Data on gaseous decomposition products

Compound	Moles of NH_3/mol of compound	Moles of N_2/mol of compound
$[Co(NH_3)_6]Cl_3$	4.75	0.18
$[CoCl(NH_3)_5]Cl_2$	3.80	0.15
$[CoCl_2(NH_3)_4]Cl$	2.70	0.15

$[Co(NH_3)_6]Cl_3$. Clark, Quick, and Harkins[9] have reported that the evolution of ammonia from this compound *in vacuo* began at about 173 °C, while a sublimate of ammonium chloride was observed at 181 °C.

They also confirmed, on the basis of an analysis of a solid mixture and the gaseous products (for ammonia only), that the stoichiometry of the thermal dissociation of this compound given as;

$$6[Co(NH_3)_6]Cl_3 \longrightarrow 6CoCl_2 + 6NH_4Cl + N_2 + 28NH_3 \quad (1)$$

The TG curves of this compound in a nitrogen atmosphere reported by Watt[10] and by Tanaka and Nanjo[11] indicated that the first mass-loss (evolution of ammonia) began at about 250 °C. On the other hand, the DTA curves of this compound in a helium or nitrogen atmosphere reported by Wendlandt[12] and Watt[10] show that the endothermic peak began at about 200 °C, resulting in a peak with a ΔT_{min} of 280 °C, and that this was followed by a second broad endothermic peak in the 300—375 °C temperature range.

The GEA curve given in Fig. 4A shows that the evolution of ammonia from this compound began at about 200 °C, the maximum intensity for gas evolution being obtained at 250 °C, and that this was followed by a second broad peak in the 280—340 °C temperature range. These temperature ranges and the number of peaks observed in this curve are in agreement with those appearing on the DTA curves reported by Watt[10] and Wendlandt,[12] but the first and second peak maxima were somewhat lower than those appearing on the DTA curves.[10,12]

The stoichiometry of the thermal decomposition of this compound, based on the data given in Table 1, agrees with that previously proposed by Clark *et al.*,[9] Watt,[10] and Wendlandt,[12] as given in Eq. 1.

$[CoCl(NH_3)_5]Cl_2$. The TG curves of this compound have been reported by a number of investigators. Wendlandt[13] found that the compound began to loss mass at 180 °C. However, the TG curves reported by Kawakubo[14] and Watt[10] indicated that the mass-loss of this compound began at 200 °C.

The DTA curves for this compound have been reported by Lavanov *et al.*,[15] Kawakubo,[14] Watt[10] and Wendlandt and Smith.[16] The DTA curves in a nitrogen atmosphere reported by the above investigators contained two endothermic peaks; the first began at about 200 °C, with a ΔT_{min} value of about 280 °C, while second began with a ΔT_{min} value of about 320 °C.

Watt[10] confirmed, from his TG and DTA curves and an analysis of the gaseous decomposition products, that the over-all reaction leading to the formation of $CoCl_2$ is:

$$6[CoCl(NH_3)_5]Cl_2 \longrightarrow 6CoCl_2 + 6NH_4Cl + N_2 + 22NH_3 \quad (2)$$

The GEA curve given in Fig. 4B shows that the evolution of ammonia from this compound began at about 200 °C, the corresponding maximum intensity for gas evolution being found at about 250 °C, and that this was followed by a second broad peak in the 280—320 °C temperature range. These temperature ranges and the number of peaks observed in this curve are in agreement with those appearing on the DTA curves reported by Watt[10] and Wendlandt and Smith.[16]

The stoichiometry of the thermal decompositions of this compound, based on the data given in Table 1, agrees with that previously proposed by Watt[10] and Wendlandt and Smith[16] as given in Eq. 2.

trans-*$[CoCl_2(NH_3)_4]Cl$.* Ocone *et al.*[17] have reported the TG curves for *cis*- and *trans*-types of this compound in a nitrogen atmosphere. The curve for the *trans*-type indicated that the mass-loss began at 181 °C, corresponding to the loss of three moles of ammonia in the over all reaction. Also, the curve for the *trans*-type of this compound was essentially in agreement with that obtained by Watt.[10]

The DTA curve for the *trans*-type of this compound in nitrogen reported by Watt[10] was very similar to that for $[CoCl(NH_3)_5]Cl_2$, exhibiting well-defined endothermal minima at 283 and 347 °C. Watt[10] also confirmed, from his TG and DTA curves, and based on an analysis of the gaseous decomposition products, that the stoichiometry of the thermal dissociation reaction of this compound given as:

$$6[CoCl_2(NH_3)_4]Cl \longrightarrow 6CoCl_2 + 6NH_4Cl + N_2 + 16NH_3 \quad (3)$$

The GEA curve given in Fig. 4C shows that the thermal decomposition of this compound begins with the evolution of ammonia at about 180 °C, the maximum intensity of the gas evolution appearing at 250 °C, and that this followed by a second broad peak in the 280—340 °C temperature range. These temperature ranges and the number of the peaks observed in this curve are in agreement with those appearing on the DTA curves reported by earlier researchers.[10,11]

The stoichiometry of the thermal dissociation of this compound, based on the data given in Table 1, agrees with that previously proposed by Watt[10] given in Eq. 3.

From the GEA curves in Fig. 4 and the results obtained by earlier investigators,[10,11,18-20] it may be seen that the starting of the thermal decomposition reactions of chloroammine cobalt(III) chlorides in a helium atmosphere at a slow heating rate takes place by means of the following competition reactions:

$$[Co^{III}(NH_3)_6]Cl_3 \longrightarrow \begin{cases} [Co^{III}Cl(NH_3)_5]Cl_2 + NH_3 \\ \text{low ammine cobalt(II) complexes} \end{cases}$$

$$[Co^{III}Cl(NH_3)_5]Cl_2 \longrightarrow \begin{cases} [Co^{III}Cl_2(NH_3)_4]Cl + NH_3 \\ \text{low ammine cobalt(II) complexes} \end{cases}$$

$$[Co^{III}Cl_2(NH_3)_4]Cl \longrightarrow \begin{cases} [Co^{III}Cl_3(NH_3)_3] + NH_3 \\ \text{low ammine cobalt(II) complexes} \end{cases}$$

Although the peak maximum temperature is dependent upon the furnace heating rate, the sample size, the carrier gas flow rate, the furnace atmosphere, and so on, the use of simultaneous GEA-gas chromatographic analysis gives exact data concerning the thermal decomposition reactions of metal complexes.

The author wishes to thank Professor Masaakira Iguchi, Tokyo University of Science, for his valuable advice.

References

1) R. N. Rogers, S. K. Yamada, and J. Zinn, *Anal. Chem.*, **32**, 672 (1960).

2) W. M. Ayres and E. M. Bens, *Anal. Chem.*, **33**, 568 (1961).
3) H. G. Langer and R. S. Gohlke, *Anal. Chem.*, **35**, 1301 (1963).
4) W. W. Wendlandt, *Anal. Chim. Acta*, **27**, 309 (1962); W. W. Wendlandt, S. I. Ali, and C. H. Stembrige, *ibid.*, **30**, 84 (1964); W. W. Wendlandt and E. Sturm, *J. Inorg. Nucl. Chem.*, **25**, 535 (1963).
5) W. W. Wendlandt, S. I. Ali, and C. H. Stembrige, *Anal. Chim. Acta*, **31**, 501 (1964); W. W. Wendlandt and T. M Southern, *ibid.*, **32**, 405 (1965).
6) J. Bierrum and J. P. McReynolds, *Inorg. Synth.*, **2**, 216 (1946).
7) W. A. Hynes, L. K. Yanowsky, and M. Schiller, *J. Am. Chem. Soc.*, **60**, 3253 (1938).
8) S. M. Jorgensen, *Z. Anorg. Chem.*, **14**, 404 (1897).
9) G. L. Clark, A. J. Quick, and W. D. Harkins, *J. Am. Chem. Soc.*, **42**, 2483 (1920).
10) G. W. Watt, *Inorg. Chem.*, **3**, 325 (1964).
11) N. Tanaka and M. Nanjo, *Bull. Chem. Soc. Jpn.*, **37**, 1330 (1964).
12) W. W. Wendlandt, *J. Inorg. Nucl. Chem.*, **25**, 545 (1963).
13) W. W. Wendlandt, *Texas J. Sci.*, **10**, 271 (1958).
14) S. Kawakubo, *Nippon Kagaku Zasshi*, **83**, 274 (1962).
15) N. I. Labanov, I. R. Rassonskaya, and A. V. Ablov, *Zh. Neorg. Khim.*, **3**, 1355 (1958).
16) W. W. Wendlandt and J. P. Smith, *J. Inorg. Nucl. Chem.*, **25**, 843 (1963).
17) L. R. Ocone, J. R. Soulen, and B. P. Block, *J. Inorg. Nucl. Chem.*, **15**, 76 (1960).
18) W. W. Wendlandt and J. P. Smith, *J. Inorg. Nucl. Chem.*, **25**, 1267 (1963).
19) E. L. Simmons and W. W. Wendlandt, *J. Inorg. Nucl. Chem.*, **28**, 2183, 2437 (1966).
20) N. Tanaka and K. Nagase, *Bull. Chem. Soc. Jpn.*, **40**, 546 (1967).

Binuclear Metal Complexes. XVI.[1] Hetero Metal Binuclear Complexes with *N,N'*-Bis(3-carboxysalicylidene)ethylenediamine[2]

Hisashi OKAWA, Yuzo NISHIDA, Mitsunori TANAKA,* and Sigeo KIDA

Department of Chemistry, Faculty of Science, Kyushu University, Hakozaki, Higashi-ku, Fukuoka 812
**Faculty of Education, Kagawa University, Takamatsu, Kagawa 760*

(Received June 17, 1976)

Hetero metal binuclear complexes, MM' (fsaen)·nH_2O (M=Cu(II) and Ni(II); M'=Cu(II), Ni(II), Co(II), Fe(II), and Mn(II); n=1—3), with *N,N'*-bis(3-carboxysalicylidene)ethylenediamine (H_4fsaen) have been synthesized and characterized, where M and M' denote the metal ion coordinated by the N_2O_2-coordinating atoms and the O_4-coordinating atoms, respectively. The magnetism of CuNi(fsean)·$3H_2O$ and CuCo(fsaen)·$3H_2O$ is explained in terms of the Heisenberg model. The magnetism of NiCu(fsaen)·H_2O, NiCo(fsaen)·$2H_2O$, and NiMn(fsaen)·$2H_2O$ obeys the Curie-Weiss law, demonstrating the binuclear structure to be composed of one diamagnetic nickel(II) and one paramagnetic M'(II) ions. CuFe(fsaen)·$2H_2O$, NiFe(fsaen)·$2H_2O$, and CuMn(fsaen)·H_2O each shows unusual magnetic property.

Binuclear metal complexes containing two different metal ions are of interest in connection with spin-exchange and charge-transfer between metal ions and in the domain of metalloenzymes and homogeneous catalysis. One method for the synthesis of hetero metal binuclear and polynuclear complexes is to use the reaction of a simple metal salt with a metal chelate ligand such as a quadridentate Schiff base complex[3-5] or a sulfur-ligand complex.[6,7] Binuclear and polynuclear complexes such as V(IV)O-Cu(II)[3,4] and Cu(II)-M(II)-Cu(II)[5] have been obtained by this method. The success in synthesizing hetero metal binuclear complexes depends on the stability of the starting metal chelate and the solubility of the hetero metal complex. Thus, application of this method to other hetero metal polynuclear complexes is limited.

Another method for obtaining hetero metal binuclear complexes is to use a step-wise reaction of two different metal ions with a coordinatively selective binucleating ligand, in which two coordinating sites differ from each other in the ligand field strength or in the stereochemistry of coordination. A few such ligands have recently been reported.[1,8,9]

In previous papers of this series,[1,8] it was shown that the Schiff bases derived from 3-formylsalicylic acid and diamines are binucleating ligands with coordinative selectivity. They formed a hetero metal complex of Cu(II)-Ni(II)[8] and binuclear nickel(II) complexes with one diamagnetic and one paramagnetic nickel(II) ions.[1] This report deals with the synthesis and characterization of hetero metal binuclear complexes with *N,N'*-bis(3-carboxysalicylidene)ethylenediamine (abbreviated to H_4 fsaen). The complexes are represented by MM'(fsaen)·nH_2O (M(II)=Cu(II) and Ni(II); M'=Cu(II), Ni(II), Co(II), Fe(II), and Mn(II); n=1—3),

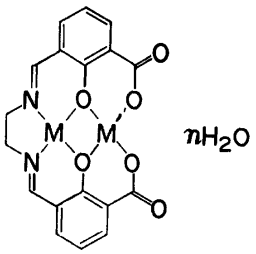

Fig. 1.

where M is an "inside" metal ion coordinated by the N_2O_2-coordinating atoms and M' is an "outside" metal ion coordinated by the O_4-coordinating atoms (Fig. 1). A part of this work has been reported,[8] which is the first report on hetero metal binuclear complexes with H_4 fsaen. Recently some hetero metal binuclear complexes such as Cu(II)-U(VI)O_2 and Ni(II)-Th(IV) were obtained using H_4 fsaen.[10] However, no hetero metal binuclear complexes with first transition metal ions have been obtained.

Experimental

Syntheses. The syntheses of mononuclear complexes, Cu(H_2fsaen)·$0.5H_2O$ and Ni(H_2fsaen)·$0.5H_2O$, have been described in the previous paper.[1]

CuNi(fsaen)·$3H_2O$. Cu(H_2fsaen)·$0.5H_2O$ (107 mg) was dissolved in an aqueous solution (50 ml) of lithium hydroxide monohydrate (21 mg) by warming. A small amount of insoluble particles was separated by filtration. To this solution was added an aqueous solution (10 ml) of nickel(II) chloride hexahydrate (60 mg) and the resulting red-purple solution was left to stand overnight at room temperature to give reddish purple prisms, which were collected, washed with water, and dried over P_2O_5 in a vacuum desiccator.

Found: C, 40.65; H, 3.45; N, 5.27; Cu, 12.27; Ni, 10.74%. Calcd for $C_{18}H_{12}N_2O_6CuNi·3H_2O$: C, 40.90; H, 3.43; N, 5.30; Cu, 12.02; Ni, 11.10%.

CuCo(fsaen)·$3H_2O$. To an aqueous solution prepared from Cu(H_2fsaen)·$0.5H_2O$ (107 mg) and lithium hydroxide monohydrate (21 mg), was added an aqueous solution (10 ml) of cobalt(II) chloride hexahydrate (80 mg) to give a red-purple solution. After the reaction mixture was left to stand overnight at room temperature, purple prisms separated were collected, washed with water, and dried over P_2O_5 *in vacuo*.

Found: C, 40.94; H, 3.58; N, 5.32; Co, 11.41; Cu, 12.28%. Calcd for $C_{18}H_{12}N_2O_6CoCu·3H_2O$: C, 40.88; H, 3.43; N, 5.30; Co., 11.14; Cu, 12.02%.

CuFe(fsaen)·$2H_2O$. This complex was obtained as yellowish brown prisms by reacting Cu(H_2fsaen)·$0.5H_2O$ (107 mg) with iron(II) sulfate heptahydrate (70 mg) in the presence of lithium hydroxide monohydrate (21 mg).

Found: C, 42.25; H, 3.18; N, 5.50; Cu, 12.60; Fe, 10.65%. Calcd for $C_{18}H_{12}N_2O_6CuFe·2H_2O$: C, 42.58; H, 3.18; N, 5.52; Cu, 12.52; Fe, 11.00%.

CuMn(fsaen)·H_2O. This complex was obtained as pink-purple prisms by reacting Cu(H_2fsaen)·$0.5H_2O$ (107 mg)

with manganese(II) sulfate hexahydrate (65 mg) in the presence of lithium hydroxide monohydrate (21 mg).

Found: C, 44.06; H, 2.63; N, 5.72; Cu, 12.52; Mn, 11.51%. Calcd for $C_{18}H_{12}N_2O_6CuMn \cdot H_2O$: C, 44.23; H, 2.89; N, 5.73; Cu, 13.00; Mn, 11.24%.

NiCu(fsaen)·H_2O. $Ni(H_2fsaen) \cdot 0.5H_2O$ (106 mg) was dissolved in an aqueous solution (60 ml) of lithium hydroxide monohydrate (21 mg) by warming. To the resulting red solution was added an aqueous solution (10 ml) of copper(II) chloride dihydrate (34 mg). Immediately pinkish orange prisms separated. After the reaction mixture had been warmed at 50 °C for 10 min, the product was isolated, washed with water, and dried over P_2O_5 *in vacuo*.

Found: C, 43.53; H, 2.52; N, 5.62; Cu, 12.72; Ni, 12.30%. Calcd for $C_{18}H_{12}N_2O_6CuNi \cdot H_2O$: C, 43.89; H, 2.86; N, 5.69; Cu, 12.90; Ni, 11.92%.

NiCo(fsaen)·$2H_2O$. This complex was obtained as yellowish brown micro-crystals from $Ni(H_2fsaen) \cdot 0.5H_2O$ (106 mg), cobalt(II) chloride hexahydrate (65 mg) and lithium hydroxide monohydrate (21 mg).

Found: C, 43.13; H, 2.92; N, 5.67; Co, 11.98; Ni, 12.16%. Calcd for $C_{18}H_{12}N_2O_6CoNi \cdot 2H_2O$: C, 42.73; H, 3.19; N, 5.54; Co, 11.65; Ni, 11.60%.

NiFe(fsaen)·$2H_2O$. This complex was obtained as reddish orange micro-crystals from $Ni(H_2fsaen) \cdot 0.5H_2O$ (106 mg) and iron(II) sulfate heptahydrate (70 mg) in the presence of lithium hydroxide monohydrate (21 mg).

Found: C, 43.24; H, 2.75; N, 5.49; Fe, 11.46; Ni, 12.02%. Calcd for $C_{18}H_{12}N_2O_6FeNi \cdot 2H_2O$: C, 42.99; H, 3.21; N, 5.57; Fe, 11.11; Ni, 11.67%.

NiMn(fsaen)·$2H_2O$. This complex was obtained as yellow needles from $Ni(H_2fsaen) \cdot 0.5H_2O$ (106 mg), manganese(II) sulfate hexahydrate (65 mg) and lithium hydroxide monohydrate (21 mg).

Found: C, 42.74; H, 2.82; N, 5.45; Mn, 10.91; Ni, 11.31%. Calcd for $C_{18}H_{12}N_2O_6MnNi \cdot 2H_2O$: C, 43.07; H, 3.22; N, 5.58; Mn, 10.95; Ni, 11.70%.

Measurements. C, H, and N elemental analyses were carried out at the Service Center of Elemental Analysis, Kyushu University. Metal analyses were carried out with a Shimadzu Atomic Absorption-Flame Spectrophotometer Model AA-610S. The aqueous solution for the measurement was prepared by thermally decomposing a complex in the presence of sulfuric acid and dissolving the resulting metal sulfate in dilute hydrochloric acid or sulfuric acid. Infrared spectra were measured with a Hitachi Infrared Spectrophotometer Model 215 on a KBr disk. Electronic spectra were measured with a Shimadzu Multipurpose Spectrophotometer Model MSP-5000 by the reflection on a powder sample. Magnetic susceptivility was measured by the Faraday method, where diamagnetic correction was carried out by means of Pascal's constants.

Results and Discussion

Infrared spectra of the complexes resemble each other and are similar to those of $Cu_2(fsaen) \cdot 3H_2O$ and $Ni_2(fsaen) \cdot 3H_2O$, whose binuclear structures have been characterized.[1] No band was found in the region 1750—1650 cm^{-1}. Instead a broad and strong band was found around 1550 cm^{-1}, which is attributable to the coordinated carboxylate group.

Because of the low solubility of the complexes in most solvents, the electronic spectra were measured by reflection on a solid sample. The electronic spectra are given in Figs. 2 and 3. The room temperature magnetic moments of the complexes are given in Table 1.

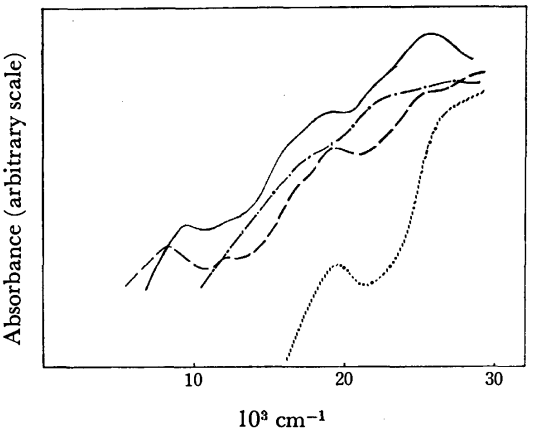

Fig. 2. Electronic spectra of (——)CuNi(fsaen)·$3H_2O$, (— —)CuCo(fsaen)·$3H_2O$, (—·—)CuFe(fsaen)·$2H_2O$, and (·····)CuMn(fsaen)·H_2O.

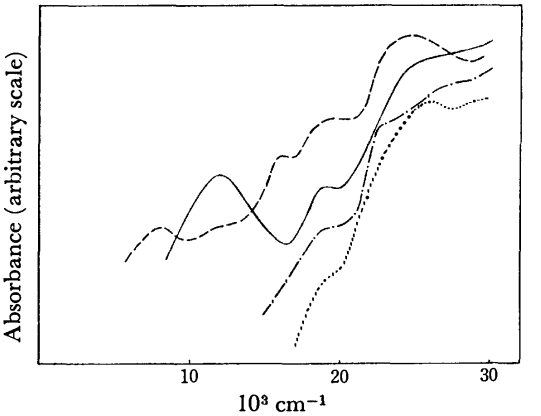

Fig. 3. Electronic spectra of (——)NiCu(fsaen)·H_2O, (— —)NiCo(fsaen)·$2H_2O$, (—·—)NiFe(fsaen)·$2H_2O$, and (·····)NiMn(fsaen)·$2H_2O$.

Table 1. Magnetic moments of complexes at room temperature

	μ_{eff} (T(K)) (Bohr magneton)	
CuNi(fsaen)·$3H_2O$	3.05[a] (292.6)	$N\alpha = 200 \times 10^{-6}$ e.m.u.
CuCo(fsaen)·$3H_2O$	4.76[a] (295.4)	$N\alpha = 450 \times 10^{-6}$ e.m.u.
CuFe(fsaen)·$2H_2O$	2.76[b] (297.8)	
CuMn(fsaen)·H_2O	5.17[b] (293.2)	
NiCu(fsaen)·H_2O	1.87[a] (294.7)	$N\alpha = 60 \times 10^{-6}$ e.m.u.
NiCo(fsaen)·$2H_2O$	5.15[a] (293.1)	$N\alpha = 400 \times 10^{-6}$ e.m.u.
NiFe(fsaen)·$2H_2O$	2.29[b] (297.8)	
NiMn(fsaen)·$2H_2O$	5.71[b] (293.0)	

a) Magnetic moment was calculated by the equation $\mu_{eff} = 2.828\sqrt{(\chi_M - N\alpha)T}$ using the estimated $N\alpha$ given in the Table. b) Calculated by the equation $\mu_{eff} = 2.828\sqrt{\chi_M T}$.

The electronic spectrum of CuNi(fsaen)·$3H_2O$ possesses ligand field bands (9500, 16000, and 19000 cm^{-1}) in the visible region. The band at 19000 cm^{-1} seems substantially the same as the band found for $Cu(H_2fsaen) \cdot 0.5H_2O$ and tentatively assigned to the "inside" copper(II). The bands at 9500 and 16000 cm^{-1}, on the other hand, may be assigned to the nickel(II) in an

octahedral environment. The molar magnetic moment of this complex is subnormal (3.05 Bohr magnetons (μ_B)). It has been shown[1] that this magnetic behavior can be explained on the basis of the Heisenberg model by the equation,

$$\chi_M = \frac{Ng^2\beta^2}{4kT}\cdot\frac{10+\exp(-3J/kT)}{2+\exp(-3J/kT)} + N\alpha \qquad (1)$$

where J is the exchange integral, k the Boltzmann constant, N the Avogadro number, β the Bohr magneton and g the Lande g-factor. The magnetic parameters, J, g_{ave}, and $N\alpha$(temperature-independent paramagnetism), determined from the best fit of the experimental χ_M values to the Eq. 1 are -75 cm^{-1}, 2.19 and 200×10^{-6} e.m.u./mol, respectively.[1]

The electronic spectrum of CuCo(fsaen)·3H$_2$O shows the ligand field bands at 8300, 11000, 17000, and 19200 cm^{-1}. The band at 19200 cm^{-1} is attributed to the copper(II) in the "inside" coordination site. The remaining bands may be assigned to the cobalt(II) ion. The spectrum resembles that of hexaaquacobalt(II). Therefore, coordination of water molecule to the cobalt(II) from an apical direction is presumed. On assuming an octahedral configuration around the cobalt(II), the band at 8300, 11000, and 17000 cm^{-1} are assigned to the $^4T_{2g}\leftarrow{}^4T_{1g}$, $^2E_g\leftarrow{}^4T_{1g}$, and $^4A_{2g}\leftarrow{}^4T_{1g}$ transitions, respectively. The transition $^4T_{1g}$ (P)$\leftarrow{}^4T_{1g}$ (F) can be superposed by the band of the copper(II) ion.

The magnetic moment for a cobalt(II) ion under octahedral symmetry is, in general, larger than the spin-only value because of the contribution from an orbital angular momentum, and is in the range 4.3—5.2 μ_B. The magnetic moment of CuCo(fsaen)·3H$_2$O is 4.76 μ_B which seems common to a magnetically noninteracting Cu(II)-Co(II) system if we take into account the 1.85 μ_B of Cu(H$_2$fsaen)·0.5H$_2$O. However, the magnetic moment of this complex markedly depends on temperature, indicating the spin-spin exchange interaction between the metal ions (Fig. 4). Based on the Heisenberg model, spin-spin coupling between copper(II) ($s_1=1/2$) and cobalt(II) ($s_2=3/2$) would result in two spin states, $s=1$ and $s=2$. The spin-quintet state is separated by $-4J$ from the supposed spin-triplet ground state, where J is the exchange integral. The molar magnetic susceptibility for this system is expressed by the equation,

$$\chi_M = \frac{Ng^2\beta^2}{kT}\cdot\frac{10+2\exp(-4J/kT)}{5+3\exp(-4J/kT)} + N\alpha \qquad (2)$$

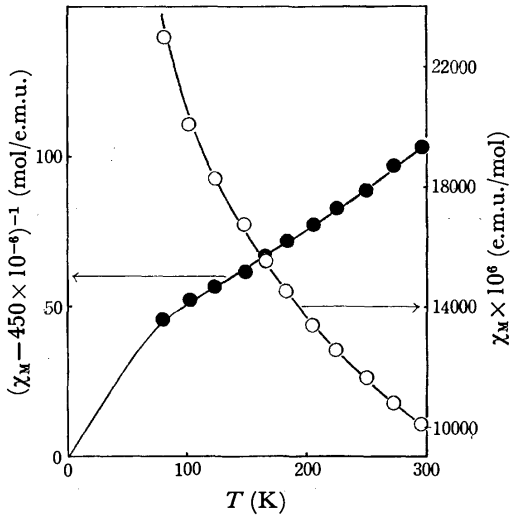

Fig. 4. Variations of molar susceptibility and inverse molar susceptibility for CuCo(fsaen)·3H$_2$O as a function of temperature.

As is seen in Fig. 4, the magnetic susceptibility (and the inverse magnetic susceptibility) is in accordance with the theoretical value when average g-value, J and $N\alpha$ are estimated at 2.45, -35 cm^{-1} and 450×10^{-6} e.m.u./mol, respectively. It is likely that the orbital contribution from the cobalt(II) to the total magnetic susceptibility is small. This implies that the geometry around the cobalt(II) is not exactly octahedral. The $^4T_{1g}$ ground state of cobalt(II) in an octahedral environment should split into two or three states under a low symmetry. If the first excited state were thermally accessible, the temperature dependence of magnetic susceptibility would become much complicated, and could not be interpreted in terms of Eq. 2. Thus, the ground state for the cobalt(II) in CuCo(fsaen)·3H$_2$O is orbitally singlet and the first excited state is above the ground state more than 1000 cm^{-1}. According to Sinn[11] the orbital contribution to magnetic susceptibility of a poly-nuclear cluster, in general, can be ignored. Thus the geometry around the cobalt in CuCo(fsaen)·3H$_2$O is pseudo-octahedral; it is supposed that the water molecules in the apical positions are elongated.

Electronic spectrum of CuFe(fsaen)·2H$_2$O shows a band at 22000 cm^{-1} in addition to the band (19000 cm^{-1}) attributable to the "inside" copper(II). In general, high-spin iron(II) in an octahedral crystal field should show the spin-allowed transition $^5E_g\leftarrow{}^5T_{2g}$ around 11000 cm^{-1}. However, such a band could not be found for CuFe(fsaen)·2H$_2$O. The molar magnetic moment decreases with lowering of temperature from 2.76 μ_B at 297.8 K to 1.90 μ_B at 79.9 K (Table 2). This behavior can not be explained in terms of the spin-exchange interaction between a copper(II) and a high-spin iron(II). It might be possible to explain the magnetism in terms of a spin-equilibrium between high-spin (or intermediate-spin) and low-spin states of iron(II). Based on this assumption, the band at 22000 cm^{-1} is attributable to a low-spin iron(II). However, most iron(II) cross-over complexes are restricted to those containing imine-nitrogen ligands[12–18] and no iron(II) cross-over complex with only oxygen-ligands has yet been obtained.

In the spectrum of CuMn(fsaen)·H$_2$O no characteristic band was found except the band at 19400 cm^{-1}, which is attributable to the "inside" copper(II). This seems natural since a high-spin manganese(II) shows no spin-allowed d-d transition. The molar magnetic moment is 5.17 μ_B which is much lower than the value expected for only high-spin manganese(II). This indicates an antiferromagnetic spin-exchange interaction between copper(II) and manganese(II).

In composition, color, infrared spectrum, electronic spectrum and magnetic property NiCu(fsaen)·H$_2$O differs from CuNi(fsaen)·3H$_2$O. The reflectance spec-

Table 2. Temperature dependence of molar susceptibility(e.m.u./mol) and effective magnetic moment (μ_B) for CuFe(fsaen)·$2H_2O$ and NiFe(fsaen)·$2H_2O$

CuFe(fsaen)·$2H_2O$												
T(K)	79.7	102.2	122.3	146.4	167.2	188.1	207.6	226.0	246.1	265.2	284.1	297.8
$\chi_M \cdot 10^6$	5678	5202	4780	4455	4221	4018	3821	3660	3510	3401	3304	3203
μ_{eff}	1.90	2.06	2.16	2.28	2.38	2.46	2.52	2.57	2.63	2.69	2.74	2.76
NiFe(fsaen)·$2H_2O$												
T(K)	80.6	100.1	119.2	128.9	147.2	167.9	188.3	208.1	227.7	247.8	268.0	297.8
$\chi_M \cdot 10^6$	3384	3048	2810	2684	2606	2547	2483	2401	2349	2295	2256	2198
μ_{eff}	1.48	1.56	1.64	1.66	1.75	1.85	1.93	2.00	2.07	2.13	2.20	2.29

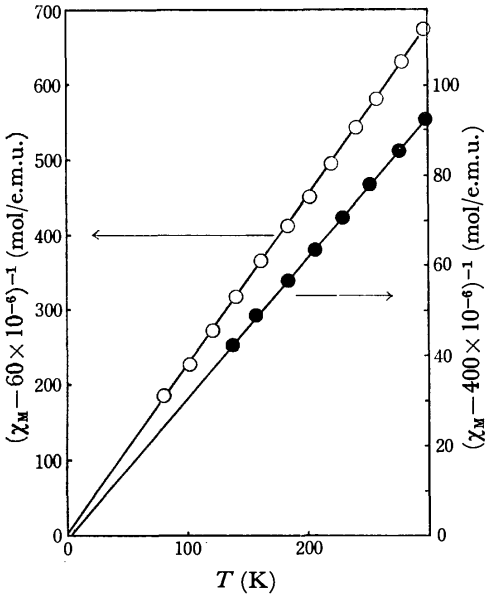

Fig. 5. The inverse magnetic susceptibilities for (○) NiCu(fsaen)·H_2O and (●) NiCo(fsaen)·$2H_2O$.

trum of NiCu(fsaen)·H_2O possesses two ligand field bands at 12000 and 19000 cm^{-1}. The first band seems to be essentially the same as the band (13400 cm^{-1}) found for Cu_2(fsaen)·$2H_2O$. The bands at 12000 and 19100 cm^{-1} are tentatively assigned to the "outside" copper(II) and the "inside" nickel(II), respectively. The molar magnetic moment at room temperature is 1.87 μ_B and the inverse magnetic susceptibility obeys the Curie-Weiss law in the temperature range 78—300 K. Spectral and magnetic properties indicate that NiCu(fsaen)·H_2O is composed of one diamagnetic nickel(II) and one copper(II) ions.

The electronic spectrum of NiCo(fsaen)·$2H_2O$ resembles that of CuCo(fsaen)·$3H_2O$. Therefore, the assignment of the ligand field bands was tentatively done by an assumption of a pseudo-octahedral configuration around the cobalt(II); 8100 ($^4T_{2g} \leftarrow {}^4T_{1g}$), 12000 ($^2E_g \leftarrow {}^4T_{1g}$), 16200 ($^4A_{2g} \leftarrow {}^4T_{1g}$), and 19500 cm^{-1} ($^4T_{1g}(P) \leftarrow {}^4T_{1g}(F)$). The band at 19500 cm^{-1} may be overlapped by the band due to the "inside" nickel(II). The supposed structure of planar nickel(II)-octahedral cobalt(II) is supported by magnetic measurements. The magnetic moment at room temperature is 5.15 μ_B, which is common to high-spin cobalt(II) complexes. The plot of the inverse magnetic susceptibility against temperature obeys the Curie-Weiss law as is shown in Fig. 5.

NiFe(fsaen)·$2H_2O$ resembles CuFe(fsaen)·$2H_2O$ in spectral and magnetic properties. The magnetic susceptibility and magnetic moments at various temperature are given in Table 2. Since the electronic spectrum indicates that the nickel(II) has a planar configuration, unusual magnetic property of this complex is attributed to the iron(II).

From the electronic spectrum it is apparent that the configuration around the nickel(II) in NiMn(fsaen)·$2H_2O$ is also planar. The fact that the room temperature magnetic moment is 5.71 μ_B which is common to high-spin manganese(II) supports the binuclear structure composed of planar nickel(II) and high-spin manganese(II).

Consequently the nickel(II) in NiM'(fsaen)·nH_2O is always planar. This finding is compatible with the fact that the "inside" nickel(II) is always diamagnetic in Ni_2(fsaen)·$3H_2O$ and its homologues. The ligand field band due to the "inside" metal ion in the present complexes shifts to higher energy as compared with the band of the corresponding monomeric complex. This implies that the binuclear complex formation enhances the coplanarity of the "inside" metal plane.[19]

References

1) Part XV. M. Tanaka, M. Kitaoka, H. Okawa, and S. Kida, *Bull. Chem. Soc. Jpn.*, **49**, 2469 (1976).
2) This work was presented at 24th Symposium of Coordination Chemistry, Kanazawa, October 9, 1974.
3) J. Selbin and L. Ganguly, *Inorg. Nucl. Chem. Lett.*, **5**, 815 (1969).
4) H. Okawa and S. Kida, unpublished data.
5) S. J. Gruber, C. M. Harris, and E. Sinn, *J. Inorg. Nucl. Chem.*, **30**, 1805 (1968).
6) D. C. Jicha and D. H. Busch, *Inorg. Chem.*, **1**, 872, 878, 884 (1962).
7) D. Coucouvanis and D. Piltingsrud, *J. Am. Chem. Soc.*, **95**, 5556 (1973).
8) H. Okawa, M. Tanaka, and S. Kida, *Chem. Lett.*, **1974**, 987.
9) B. Tomlonovic, R. L. Hough, M. D. Glick, and R. L. Lintvedt, *J. Am. Chem. Soc.*, **97**, 2925 (1975).
10) M. Vidali, P. A. Vigato, and U. Gasellato, *Inorg. Chim. Acta*, **17**, L5 (1976).
11) E. Sinn, *Coord. Chem. Rev.*, **5**, 313 (1970).
12) Y. Nishida, S. Oshio, and S. Kida, *Chem. Lett.*, **1975**, 79.
13) E. König, G. Ritter, H. Spiering, S. Kremer, K. Madeja, and A. Rosenkrauz, *J. Chem. Phys.*, **56**, 3139 (1972).
14) G. Ritter and H. A. Goodwin, *Chem. Phys.*, **1**, 17 (1973).

15) E. König and K. Madeja, *Inorg. Chem.*, **6**, 48 (1968).
16) E. König, K. Madeja, and K. J. Watson, *J. Am. Chem. Soc.*, **90**, 1146 (1968).
17) C. M. Harris and E. Sinn, *Inorg. Chim. Acta.*, **2**, 296 (1968).
18) A. J. Cunningham, J. E. Fergusson, H. K. J. Powell, E. Sinn, and H. Wong, *J. Chem. Soc., Dalton*, **1972**, 2155.
19) S. J. Gruber, C. M. Harris, and E. Sinn, *J. Inorg. Nucl. Chem.*, **30**, 1805 (1968); *Inorg. Nucl. Chem. Lett.*, **4**, 107 (1968).

A New Spectrophotometric Method for the Determination of Some Reducible Compounds by the Reduction with Chromium(II) Ion

Kikuo TERADA, Hiromi HONNAMI,* and Toshiyasu KIBA

Department of Chemistry, Faculty of Science, Kanazawa University, Kanazawa 920

(Received July 6, 1976)

A number of reducible compounds, such as nitrates, nitrites, nitro, nitroso, azoxy compounds, aldehydes, carbon tetrachloride, oximes, and chloramine T, can be determined by reducing them with chromium(II) ion prepared in an aqueous solution in a special vessel and measuring the absorbance of the resulting chromium(III) in the solution. In this reducing process, nitrate and nitrite are reduced to hydroxylamine quantitatively in hydrochloric acid at room temperature; carbon tetrachloride, nitrobenzene, and chloramine T each consume definite amounts of chromium(II) in an acidic medium at room temperature; propionaldehyde and azoxybenzene react with the reagent only in a basic solution; dimethylglyoxime and 1-nitroso-2-naphthol react only under heating at 80 °C in an basic medium. The absorbance of the resulting chromium(III) ion in the presence of the excess chromium(II) is found to obey Beer's law at the wavelengths of 410—425 nm over the range of 4×10^{-3}—8×10^{-2} mol/l of chromium(III). This concentration range corresponds to about 10^{-5}—10^{-4} mol of the reducible compounds mentioned above. A rapid and precise method has been established with few disadvantages.

Although the spectrophorometric method for nitrite with Griess-Romijin reagent[1] is strikingly simple and accurate, for nitrate we have few methods of accurate determination. Most of the spectrophotometric methods for nitrate are based on the nitration of some organic reagents; these are often difficult to perform, since some methods are only applicable to a solid nitrate sample (*e.g.*, the phenoldisulfonic acid method[2-6]) and others give hardly linear calibration curves at the wavelengths of maximal absorption of the colored compound (*e.g.*, the brucine method[7-8]). This may be caused by the fact that nitration is apt to be affected by the presence of chloride, bromide, or nitrite, and also by other experimental conditions.

On the other hand, both nitrate and nitrite were also found to be readily reduced to hydroxylamine by low valence ions such as Cr(II).[9] It has also been known that some organic compounds containing nitro,[10-12] nitroso,[11] and diazo groups[11] react with some low valence ions such as Cr(II), Ti(III), and V(II); furthermore, chloroform, carbon tetrachloride,[13] and oximes[14] are also reducible with these ions. In the titrimetric process a sample is put into a solution containing an excess of these ions and allowed to react perfectly under an optimum condition of acidity or temperature; then the unconsumed reducing agent is back-titrated with iron(III) standard solution using thiocyanate as an indicator. In this case, however, the color change at the end point was not precisely detectable. Chromium(II) ions are preferred as a reducing agent because the blue color changes to green by the oxidation, so if we can measure the absorbance of the green color of chromium(III) resulting after the reduction of the sample, even minute amounts of the above inorganic and organic compounds could be determined spectrophotometrically.

This paper describes a rapid and simple method based on the above principle with some devices to prevent the oxidation of the remaining chromium(II) by air: we use a new air-shielded vessel that resembles the ordinary reductor vessel with liquid amalgam. The vessel is also useful for pipetting an aliquot of the solution for measuring the absorbance of chromium(III). The absorbance at the wavelength of 420 nm gives the concentration of chromium(III) and is not affected by the excess chromium(II). Beer's law is obeyed over the range of 4×10^{-3}—8×10^{-2} mol/l of chromium(III).

Experimental

Reagents. Potassium dichromate standard solution (0.1 M): Potassium dichromate of the guaranteed reagent grade (29.422 g) was dissolved in 1000 ml of 1.5 M hydrochloric acid. This solution was diluted again with 1.5 M hydrochloric acid to prepare 0.01 M solution.

Standard Nitrate Stock Solution (0.03 M): Potassium nitrate of the guaranteed reagent grade was dried, weighed (3.033 g), and dissolved in 1000 ml of distilled water. A standard nitrate solution in desired concentration was prepared by diluting the stock solution appropriately.

Standard Nitrite Stock Solution (0.18M): In distilled water 12.42 g of sodium nitrite of the guaranteed reagent grade was dissolved and the solution was diluted to 1000 ml. A 100 ml portion of the solution was diluted again to 1000 ml with distilled water and standardized as follows:[15] 50 ml of the 0.05 M potassium permanganate solution, 1 ml of concentrated sulfuric acid, and 50.00 ml of the sodium nitrite solution were taken in a glass-stoppered bottle. The reaction was made to proceed completely under occasional shaking for 15 min, then 2 g of potassium iodide were put into the solution. The liberated iodine was titrated with 0.025 M sodium thiosulfate standard solution using starch as an indicator. From the amount of potassium permanganate consumed by the sodium nitrite the concentration of the standard solution of nitrite was determined. A standard solution of a suitable concentration was prepared by diluting the stock standard solution.

Zinc Amalgam: 3—4 g of mossy zinc metal were washed with 1 M sulfuric acid and the metal pieces were put into 100 g of mercury placed in a porcelain casserole; then they were covered with 20 ml of 1 M sulfuric acid. The casserole was placed on a boiling water-bath to amalgamate the zinc with the mercury under occasional stirring; the liquid zinc amalgam thus prepared was separated from the solid by means of a separating funnel. The liquid zinc amalgam was stored in a glass stoppered bottle which contained 1 M sulfuric acid, enough to cover the amalgam.

* Present address: Department of Chemistry, Faculty of Science, Tokyo Metropolitan University, Setagaya-ku, Tokyo 158.

Organic Compounds: Carbon tetrachloride, chloroform, nitrobenzene, and propionaldehyde, all of the guaranteed reagent grade, were submitted to analysis without any purification.

Chloramine T: 0.845 g of chloramine T (guaranteed reagent grade) was dissolved in 10 ml of distilled water.

Dimethylglyoxime: 0.363 g of dimethylglyoxime was dissolved in 20 ml of 3 M sodium hydroxide.

1-Nitroso-2-naphthol: 0.733 g of 1-nitroso-2-naphthol (guaranteed reagent grade) was dissolved in 20 ml of benzene.

Other Chemicals: Sulfuric acid, sodium hydrogensulfide, and amidosulfuric acid were of the guaranteed reagent grade.

Apparatus. A Hitachi 239 type digital spectrophotometer and Hitachi 323 type recording spectrophotometer with 1 cm glass cells were used.

The devised reductor is shown in Fig. 1, where (A) is a 300-ml glass vessel similar to a separating funnel, with the glass stopcock (E), fitted with a 10-ml glass reservior (C) through a rubber tube (B). (F) is the sample inlet.

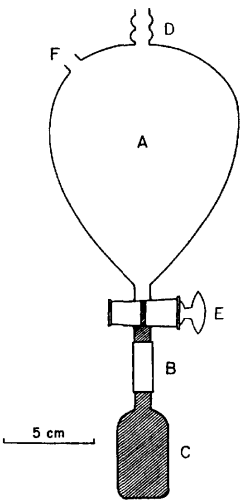

Fig. 1. Amalgam reductor.
A: Amalgam reductor, B: rubber tube, C: glass reservior, D: N_2-gas inlet, E: stopcock, F: sample inlet and outlet.

Procedure. The liquid zinc amalgam was introduced into the vessel (A) through the inlet (D) and dropped into the reservoir to fill out (C) up to the upper level of the stopcock (E). After the stopcock (E) was closed, and excess of the amalgam was rejected through (D) by turning the vessel upside down. The vessel was then returned to the normal position. For the determination of nitrate and nitrite, 10 ml of 0.02 M potassium dichromate solution (in 1.5 M hydrochloric acid) was pipetted into the reductor. Nitrogen gas was introduced through an alkaline pyrogallol washing solution into the reductor for 2—3 min to displace the air in the vessel completely; the gas flowed through the vessel from (D) to (F); (F) and (D) were then closed respectively with small silicon rubber stoppers. The zinc amalgam in the reservoir (C) was transferred back to the reductor by turning the vessel upside down, the stopcock (E) was closed, and the reductor was shaken for about 5 min till the orange color of the solution completely changed to sky blue. After the vessel was returned to normal, the zinc amalgam was completely restored to the reservoir through the cock (E) by pushing on the side of the rubber tube (B) with one's fingers; then the stopcock (E) was sclosed. Ten milliliters of a sample solution were introduced through the inlet (F), under the passage of nitrogen gas from (D) through the vessel. The reductor was shaken for about 5 min. About 5 ml of the solution were carefully sucked up into a 10-ml injector through the silicone rubber stopper and transferred into a 1-cm glass cell placed in a newly designed enclosed vessel, in Fig. 2, which was filled with nitrogen gas from the continuous passage of the gas. The cell was closed with a glass cover plate to protect it from the air. The absorbance of chromium(III) in the solution was measured at 420 nm with distilled water as the reference.

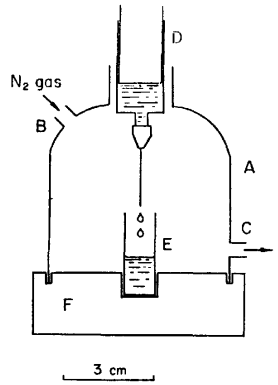

Fig. 2. New designed air-shielded vessel.
A: Air-shielded vessel made of 500 ml polyethylene bottle, B: N_2-gas inlet, C: N_2-gas outlet, D: 10 ml glass injector, E: absorption cell, F: base, made of wood.

Carbon tetrachloride, nitrobenzene, and chloramine T were found to react with chromium(II) ion in 1.5 M hydrochloric acid solution at room temperature. A suitable amount of the sample was introduced to the chromium(II) solution by means of a microsyringe through the inlet rubber stopper (F). After the reductor was shaken for 30 min, the absorbance of the resulting chromium(III) was measured.

Propionaldehyde and azoxybenzene were reduced very slowly in acidic solution at room temperature, whereas they react smoothly in a weak alkaline solution. Five milliliters of 3 M sodium hydroxide solution were slowly introduced with a pipette through (F) into the reductor containing 10 ml of 0.02 M chromium(II) under nitrogen gas flow, and at that time a greyish blue precipitate appeared in the solution. A suitable amount of the sample solution was injected into the reductor with a microsyringe through the rubber stopper (F). After the reductor was shaken for about 30 min, the solution was made acidic by adding 5 ml of 6 M hydrochloric acid with a pipette through (F) under nitrogen gas flow. The absorbance of the resulting chromium(III) was measured in the same way as described above.

Dimethylglyoxime and 1-nitroso-2-naphthol react with chromium(II) ions in a weak alkaline solution at 80 °C. After 5 ml of 3 M sodium hydroxide was introduced into the reductor which contained chromium(II) solution, a suitable amount of the sample was injected with a microsyringe in the same way as above. Then, the reductor was warmed at 80 °C in a thermostat for about 30 min. After the reductor was cooled to room temperature, the solution was made acidic with 5 ml of 6 M hydrochloric acid, and the absorbance of the resulting chromium(III) was measured.

Results and Discussion

Absorption Curves of Chromium(II) and Chromium(III). Twenty milliliters of 0.01 M potassium dichromate solution were reduced to chromium(II) with zinc amalgam

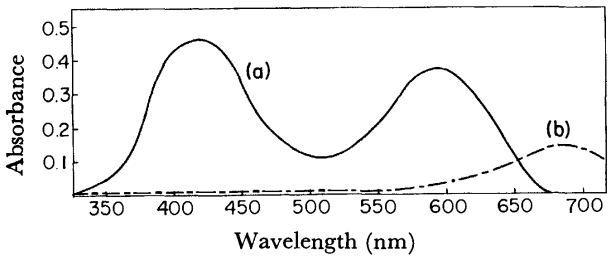

Fig. 3. Absorption spectra of chromium(II) and chromium(III) (0.02 M of metals in 1.5 M hydrochloric acid).
(a): Chromium(III), (b): chromium(II).

in the reductor according to the above procedure, and the absorption spectrum of a portion of the resulting chromium(II) solution was measured using a recording spectrophotometer. The solution which remained in the reductor was allowed to come in contact with air in order to change chromium(II) to chromium(III) completely; then the absorption spectrum of this solution was measured. As shown in Fig. 3, the absorption spectra exhibit the absorption maxima at 420 nm and 590 nm for chromium(III) and at 690 nm for chromium (II). From this figure it can be seen that the absorption maxima of the chromium(III) are isolated from that of chromium(II) and the spectrophotometric determination of the former is unaffected by the latter. These absorption curves almost coincide with those determined by Kranz and Duczmal[16] in 0.5 M sulfuric acid. Although it has been pointed out that chromium(III) forms a wide variety of complex ions, depending on the concentration of chromium, pH, and other ionic species present, the complication due to polynuclear compounds of chromium(III) is minimized in an acidic solution such as 1.0—1.5 M and the chromium(III) ion species seem rather invariable.

Calibration Curve for Chromium(III). The chromium(III) solutions in various concentrations were prepared in a similar way to that described above: chromium(VI) of varying concentrations was reduced to chromium(II) with zinc amalgam and oxidized to chromium(III) by exposing the solution to air. The absorbances of the resulting solutions were measured at 420 nm with a spectrophotometer. Beer's law was obeyed over the range of 4×10^{-3}—8×10^{-2} mol/l of chromium(III), with notably higher precision in the range of 4×10^{-3}—2×10^{-2} mol/l.

TABLE 1. RELATIONSHIP BETWEEN ABSORBANCE OF Cr(III) AT 420 nm AND CONCENTRATION OF NITRATE AND NITRITE

Nitrate taken[a] 10^{-5} mol	Absorbance	Cr(III) produced 10^{-5} mol	Nitrite taken[a] 10^{-5} mol	Absorbance	Cr(III) produced 10^{-5} mol
2.4	0.159	14.1	3.6	0.158	14.0
3.6	0.238	21.2	5.4	0.243	21.7
4.8	0.318	28.2	7.2	0.318	28.4
6.0	0.399	35.7	9.0	0.403	36.0
6.5	0.435	38.9			

a) Both nitrate and nitrite ions are present in 30 ml of the solution, respectively.

Nitrate and Nitrite. In Table 1 are shown the relations between the concentration of nitrate and nitrite ions and the absorbances measured. From this data it is found that 1 mol of nitrate oxidized exactly 6 mol of chromium(II) to chromium(III), and nitrite exactly 4 mol. Therefore, the reactions can be written as follows:

$$NO_3^- + 6Cr^{2+} + 7H^+ \longrightarrow NH_2OH + 6Cr^{3+} + 2H_2O$$

$$NO_2^- + 4Cr^{2+} + 5H^+ \longrightarrow NH_2OH + 4Cr^{3+} + H_2O$$

Hydroxylamine may be the final product, because no further reduction was found when an aqueous solution of hydroxylamine was put in the chromium(II) solution.

Determination of nitrate and nitrite in their mixture: From the above equations, under the present conditions 6.67×10^{-4}—3.3×10^{-3} mol/l of nitrate and 1.00×10^{-3}—5.00×10^{-3} mol/l of nitrite will be determined by measuring the absorbance of the resulting chromium(III). Therefore, if both nitrate and nitrite are present in a sample solution, their sum can be determined by the method. Then, if the nitrite can be removed from the sample by an appropriate reagent, the nitrate alone may be determined by this method. Thus the nitrite could be calculated as the difference between the total and the nitrate. Brasted[17] reported that nitrite was decomposed by amidosulfuric acid in the following process:

$$NaNO_2 + HSO_3NH_2 \longrightarrow N_2 + NaHSO_4 + H_2O$$

In the present study this reaction was employed. A definite volume of a sample solution containing both nitrate and nitrite was put into an Erlenmeyer flask and a suitable amount of amidosulfuric acid(solid) was added to decompose the nitrite. When the violent evolution of gas bubbles ceased, an aliquot of the solution was submitted to the reduction with chromium(II) ions, followed by the spectrophotometric measurement of the resulting chromium(III) ions. When the reaction between nitrite and amidosulfuric acid was performed in the air, the value of the resulting nitrate was often higher than the theoretical one, and was subject to wide fluctuations in every case. This fact is assumed to be caused by the following side reactions:

$$2NO_2^- + 2H^+ \longrightarrow N_2O_3 + H_2O$$

$$2N_2O_3 + O_2 \longrightarrow 4NO_2$$

$$2NO_2 + H_2O \longrightarrow NHO_3 + HNO_2$$

Thus, an appreciable amount of nitrate may be produced and consumes chromium(II) ions, yielding a higher value in the determination of the nitrate. The decomposable percentage of sodium nitrite varies with the concentration of the salt taken initially: about 2% of nitrite for 0.1—0.3 mol/l and about 10% for above 0.5 mol/l are decomposed in the way described above. In order to overcome this difficulty, the nitrite was decomposed under a nitrogen atmosphere in a glass-stoppered Erlenmeyer flask. The results indicated that satisfactory analyses were possible with solutions containing as much as 0.4 g sodium nitrite, but the concentration should not exceed 0.25 mol/l NO_2^-. Moreover, it was found that the amidosulfuric acid treatment did not affect nitrate ions in the range of concentration between 6.67×10^{-4} and 3.33×10^{-3} mol/l, and the chromium(II) reduction process could also be carried out without any trouble.

Table 2. Determination of nitrate and nitrite in their mixture

No.	NO_3^- taken 10^{-5} mol	NO_2^- taken 10^{-5} mol	Absorbance for $(NO_3^-+NO_2^-)$	Absorbance for (NO_3^-)	NO_3^- found 10^{-5} mol	NO_2^- found 10^{-5} mol
1	1.80	1.80	0.203	0.122	1.82	1.78
2	1.80	2.70	0.242	0.125	1.85	2.61
3	2.40	3.60	0.320	0.165	2.44	3.49
4	1.80	2.01	0.105	0.126	1.85	2.05
5	1.80	1.96	0.102	0.123	1.83	2.22

Therefore, one part of nitrate can be determined in the presence of about 350 parts of nitrite. The results for samples containing various amounts of nitrate and nitrite are shown in Table 2. Samples 4 and 5 in the table were diluted 10 and 100 times, respectively, prior to the determination of nitrite. A small amount of nitrite ions can be removed by the amidosulfuric acid method even in the air.

Determination of Nitrate Ions Present as Impurities in a Commercial Sodium Nitrite Reagent: It is well known that bulk nitrite reagents being used in the laboratory are not so stable and always contain some nitrate after the exposure to the air. By the method proposed so far, it is impossible to determine a small amount of nitrate contained in such a large amount of nitrite, since nitrite interferes with the determination of nitrate in many cases. Hence there have not been any reports on this subject. As described above, it seems possible to determine the nitrate impurity in a commercial sodium nitrite by the present method.

0.345 g of dried, ground sodium nitrite was weighed accuralately and dissolved in 20 ml of distilled water in a 200-ml glass-stoppered Erlenmeyer flask. After nitrogen gas was introduced into the flask sufficiently to replace the air, about 2 g of amidosulfuric acid were put in the flask. After 2—3 min the flask was warmed on a water bath (about 60 °C) for 5—10 min to make the reaction complete. The solution was diluted to 25 ml with distilled water in a measuring flask. Ten milliliters of an aliquot was taken in the reductor containing 10 ml of 0.04 M chromium(II) solution and the procedure was carried out as described in the Procedure section.

Table 3. Determination of nitrate ions in a commercial sodium nitrite reagent

$NaNO_2$ taken g	NO_3^- found g	NO_3^- content %
0.34503	0.00333	0.97
0.34493	0.00341	0.99
0.34514	0.00336	0.97
0.34544	0.00324	0.94

The results obtained are shown in Table 3. It was found that the nitrite reagent contained about 0.97% of nitrate. These results agree with that obtained by the gravimetric method with nitron carried out as follows: 1.380 g of sodium nitrite was dissolved in 100 ml of distilled water. 1.80×10^{-4} mol of nitrate was also added in order to obtain the precipitate of nitron which was filterable in the conventional manner. The solution was divided into four nearly equal portions (*ca.* 25 ml), which were put in four separate Erlenmeyer flasks. Two grams of amidosulfuric acid were added in each flask. After the nitrite was removed, each solution was collected together in a beaker, 10% nitron solution (in 5% acetic acid) was added in the solution, and the beaker was cooled in an ice bath to precipitate the nitron nitrate completely. The precipitate was filtered off onto a previously weighed glass-fiber filter paper (Toyo Roshi, GB-100), washed, dried at 110 °C for about 3 h, and weighed. This value coincided with that obtained by the recommended reduction method; the latter method is accurate and more simple and rapid than the former gravimetric one.

Interferences: Some oxidizing salts, such as chlorate, bromate, periodate, iodate, selenate, and selenite, oxidize chromium(II) to chromium(III) and thus interfere with this method; perchlorate, chloride, bromide, iodide, sulfate, and arsenate ions do not (Table 4). Some metal ions, such as copper(II) and iron(III), also interfere. Chlorate, bromate, and periodate and iodate ions are reduced to chloride, bromide, and iodide with chromium(II) ion, while selenate and selenite and copper(II) ions are reduced to their metals and iron(III) ion to iron(II) ion. However, periodate and iodate can be reduced by the addition of a small amount of hydrogensulfite to their 0.01 M hydrochloric acid solution; excess hydrogensulfite can be removed by gently boiling the solution. In this case, however, if the sample solution is

Table 4. Effect of diverse substances

Substance	Concentration, ppm	Effect
Cu^{2+}	100	positive
Fe^{3+}	40	positive
K^+, Na^+	large amount	none
AsO_4^{3-}	2000	none
Cl^-, Br^-, I^-	large amount	none
Cl_2	small amount	positive
ClO_3^-, BrO_3^-, IO_3^-	400	positive
ClO_4^-	large amount	none
CO_3^{2-}	large amount	none
IO_4^-	70	positive
SeO_3^{2-}, SeO_4^{2-}	10	positive
SO_3^{2-}	small amount	positive
SO_4^{2-}	large amount	none
PO_4^{3-}	large amount	none
Carbon tetrachloride	small amount	positive
Nitrobenzene	small amount	positive
Chloramine T	small amount	positive
Alcohol	large amount	none
Ester	large amount	none
Ketone	large amount	none
Aldehyde	large amount	none
Sufamic acid	large amount	none
Urea	large amount	none

more acidic than 0.1 M, a loss of nitrite occurs along with the evolution of gaseous nitric oxide. Nitrite and nitrate are not affected at all by the hydrogensulfite treatment under the present conditions. Some interfering metal ions, such as copper(II) and iron(III), can be removed by passing the sample solution through a column of cation exchange resin, Dowex 50 W×8 in hydrogen form, 100—200 mesh. Chlorate, selenate, and selenite ions can not be removed by any treatment, but as these ions seem to exist in commerical nitrites in only trace concentrations, and therefore except for some special cases, they may not give a serious error to the determination on a semi-micro scale.

Determination of Organic Compounds. The recommended procedures were carried out as described in the Procedure section. In the case of azoxybenzene, it is reduced with chromium(II) ions and gives azobenzene as a precipitate. Then, after acidifying the solution, the solution must be filtered through a dried absorbent cotton on the funnel to remove the precipitate, the filtrate is then received in a photometric cell. The results obtained are shown in Table 5 (1)—(7) together with the wavelength at which the measurement of the absorbance should be made.

TABLE 5. DETERMINATION OF ORGANIC COMPOUNDS

Sample taken 10^{-4} mol	Cr(III) produced 10^{-4} mol	Mol ratio of Cr(III)/ Sample	Wavelength used for abs. meas., nm
(1) Carbon tetrachloride			
0.21	0.85	4.05	410
0.31	1.25	4.03	
0.52	2.05	3.94	
0.63	2.57	4.08	
0.94	3.74	3.98	
(2) Nitrobenzene			
0.20	0.90	4.50	420
0.29	1.33	4.51	
0.39	1.75	4.49	
0.49	2.23	4.55	
0.64	2.88	4.50	
(3) Chloramine T			
0.30	0.62	2.07	425
0.61	1.24	2.03	
0.91	1.83	2.01	
1.21	2.38	1.97	
1.51	2.90	1.92	
(4) Propionaldehyde			
0.55	1.01	1.84	420
0.96	1.93	2.01	
1.37	2.71	1.98	
1.78	3.58	2.00	
(5) Azoxybenzene			
0.39	0.77	1.97	410
0.79	1.65	2.09	
0.98	2.11	2.35	
1.38	3.82	2.04	
(6) Dimethylglyoxime			
0.16	1.33	8.31	410
0.31	2.48	8.00	
0.39	3.06	7.85	
0.47	3.55	7.77	
(7) 1-Nitroso-2-naphthol			
0.21	0.97	4.63	420
0.42	2.05	4.88	
0.63	3.13	4.97	
0.74	3.38	4.57	

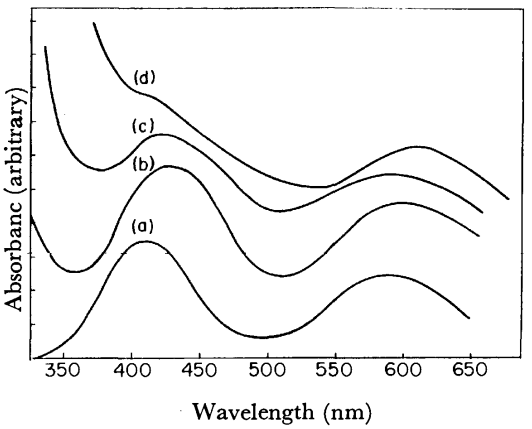

Fig. 4. Absorption spectra of chromium(III) complexes resulted by reaction between chromium(II) and some organic compounds.
(a): Carbon tetrachloride, nitrobenzene, and chloramine T, (b): propionaldehyde, azoxybenzene, and dimethylglyoxime, (c): 1-nitroso-2-naphthol, (d): *p*-benzoquinone and propiophenone oxime.

The absorption spectra of the resulting chromium(III) complex solutions are shown in Fig. 4. The spectra for carbon tetrachloride, nitrobenzene, and chloramine T (a) are very close to the standard one (Fig. 3), while those for propionaldehyde, azoxybenzene, and dimethylglyoxime (b) somewhat deviate from the standard one. On the other hand, the absorption spectra for 1-nitroso-2-naphthol (c) and *p*-benzoquinone and propiophenone oxime (d) exhibit another strong absorption peak at a wavelength shorter than 400 nm, which contributes to the absorption of chromium(III) at 420 nm. This absorption may be attributed to the reaction product in the solution. Consequently, the determined values are higher than the theoretical one, but in the case of 1-nitroso-2-naphthol an approximately linear relationship exists between the concentration of the sample and the absorbance of the resulting solution. Therefore, the determination of 1-nitroso-2-naphthol can be performed satisfactorily (Table 5(7)). However, in the case of *p*-benzoquinone and propiophenone oxime, the absorbance at about 420 nm is difficult to measure because the absorption peak is hindered by a strong absorption at a wavelength shorter than 400 nm. The absorption at 420 nm very quickly decreases, so the determination is impossible.

According to Kiba and Terada,[13] carbon tetrachloride and chloroform were assumed to be reduced to methane by chromium(II) ions. However, in the present study, as the results of the gaschromatographic measurement of the resulting aqueous solution and of the gas phase remained after the reaction in the reductor, it was found that tetrachloroethylene could be detected in the solution and carbon monooxide in the gas phase, but not any methane at all. The mechanism for this reac-

tion remains still obscure.

Carbon tetrabromide also can be determined in the same way, while chloroform reacts completely with chromium(II) under heating at 80 °C.

From the results in Table 5, which shows the mol number of chromium(III) produced by oxidation of chromium(II) with 1 mol of the sample, the reaction stoichiometry can be speculated about:

Nitrobenzene:

$$C_6H_5NO_2 + 6Cr^{2+} + 6H^+ \longrightarrow C_6H_5NH_2 + 6Cr^{3+} + 2H_2O$$

Although 1 mol of nitrobenzene oxidized only 4.5 mol of chromium(II), aniline was detected as a reaction product by gaschromatographic measurements. Consequently, it may be assumed that this reaction will proceed to the extent of 75% under these conditions. However, as an exact linear relationship was obtained between the concentration of the sample and the absorbance of the resulting chromium(III) solution, determination of nitrobenzene should be carried out satisfactorily in the range of 10^{-5}—2×10^{-4} mol.

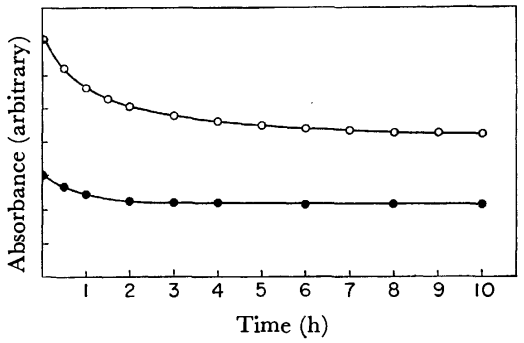

Fig. 5. Change of the absorbance of chromium(III) at 410 nm on the elapse of time.
—○—: 1-Nitroso-2-naphthol, —●—: azoxybenzene.

Chloramine T:

$$CH_3C_6H_4SO_2N\cdot ClNa + 2Cr^{2+} + 2H^+ \longrightarrow CH_3C_6H_4SO_2NH_2 + 2Cr^{3+} + Na^+ + Cl^-$$

Propionaldehyde:

$$CH_3CH_2CHO + 2Cr(OH)_2 + 2H_2O \longrightarrow CH_3CH_2CH_2OH + 2Cr(OH)_3$$

Azoxybenzene:

$$C_6H_5N(O)=NC_6H_5 + Cr(OH)_2 + H_2O \longrightarrow C_6H_5N=NC_6H_5 + 2Cr(OH)_3$$

Dimethylglyoxime:

$$[(CH_3)C=NOH]_2 + 8Cr(OH)_2 + 6H_2O \longrightarrow [(CH_3)CHNH_2]_2 + 8Cr(OH)_3$$

1-Nitroso-2-naphthol:

$$C_{10}H_6(OH)NO + 4Cr(OH)_2 + 3H_2O \longrightarrow C_{10}H_6(OH)NH_2 + 4Cr(OH)_3$$

As shown in Fig. 5, the reaction of the last three compounds is not fast, so the contents must be kept standing for about 3, 1, and 6—7 h, to obtain invariable results for azoxybenzene, dimethylglyoxime, and 1-nitroso-2-naphthol, respectively.

References

1) F. D. Snell and C. T. Snell, "Colorimetric Method of Analysis," Vol. I, Van Nostrand, New York (1944), p. 644.
2) W. Horwitz, Ed., "A. O. A. C. Official Methods of Analysis," 11th ed, Association of Official Agricultural Chemists, Washington D. C. (1970), pp. 565, 684.
3) M. J. Taras, A. E. Greenberg, R. D. Hoak, and M. C. Rand, Ed., "Standard Methods for the Examination of Water and Wastewater," 13th ed, American Public Health Association, Washington D. C. (1955), p. 234.
4) E. M. Chamot and D. S. Pratt, *J. Am. Chem. Soc.*, **31**, 922 (1909).
5) E. M. Chamot, D. S. Pratt, and H. W. Redifield, *J. Am. Chem. Soc.*, **33**, 366 (1911).
6) M. J. Taras, Nitrogen, in D. F. Boltz, Ed., "Colorimetric Determination of Nonmetals," Interscience, New York, N. Y. (1958), p. 135.
7) C. A. Noll, *Ind. Eng. Chem., Anal. Ed.*, **17**, 426 (1945).
8) F. L. Fisher, E. R. Ibert, and H. F. Beckman, *Anal. Chem.* **30**, 1972 (1958).
9) H. Honnami (née Okazaki), Thesis for M. S. degree of Kanazawa University (1975), p. 45.
10) T. Kiba, *Nippon Kagaku Kaishi*, **60**, 1073 (1939).
11) S. Musha, *Nippon Kagaku Kaishi*, **67**, 49 (1946).
12) S. Emi, *Nippon Kagaku Kaishi*, **65**, 713 (1944).
13) T. Kiba and K. Terada, *Nippon Kagaku Kaishi*, **75**, 78 (1954).
14) T. Kiba and Y. Yamazaki, *Nippon Kagaku Kaishi*, **74**, 808 (1953).
15) F. J. Welcher Ed., "Standard Methods of Chemical Analysis," Vol. II B, Van Nostrand, Princeton (1963), p. 2448.
16) M. Kranz and W. Duczmal, *Chem. Anal. (Warsaw)*, **18**, 413 (1973).
17) R. C. Brasted, *Anal. Chem.*, **24**, 1111 (1952).

Synthesis and X-Ray Structure of Triethylenetetraminepalladium(II) Complex

Fumio Hori, Keiji Matsumoto, Shun'ichiro Ooi, and Hisao Kuroya
Department of Chemistry, Faculty of Science, Osaka City University, Sumiyoshi-ku, Osaka 558
(Received July 12, 1976)

The triethylenetetraminepalladium(II) perchlorate and the potassium triethylenetetraminepalladium(II)tris-(hexafluorophosphate) were prepared; the X-ray structure analysis has been carried out for the latter compound. The crystal of $[Pd(trien)](PF_6)_2 \cdot KPF_6$ is orthorhombic, with space group Pbca: $a=21.645$ (5), $b=20.873$ (5), $c=9.541$ (2) Å, and $Z=8$. The structure has been determined from X-ray diffractometer data and refined to $R=0.091$ (1166 reflections). The Pd atom has a planar coordination of 4N atoms disposed in a somewhat trapezoidal form. The complex cation has a pseudo symmetry plane which is perpendicular to the 4 N plane and bisects the H_2N–Pd–NH_2 angle. In the quadridentate triethylenetetramine ligand, each of the terminal H_2N–CH_2–CH_2–NH– fragments forms a 5-membered chelate ring with the asymmetric envelope conformation, whereas the chelate ring formed by the middle –NH–CH_2–CH_2–NH– fragment has the symmetric envelope conformation. The electronic spectrum of $[Pd(trien)]^{2+}$ is presented.

A number of metal chelates, in particular Co(III) chelates, of the triethylenetetramine (trien) have been prepared and characterized as regards various properties. In 1949 Jonassen *et al.* synthesized the Magnus-type $[Pd(trien)][PdCl_4]$, which was the first isolated salt of the $[Pd(trien)]^{2+}$ ion.[1] However, no detailed studies have yet been made of the complex cation. We report here the synthesis, electronic spectrum, and X-ray structure of the Pd(II) chelate of the trien.

Experimental

Preparation of the Compounds. *$[Pd(trien)](PF_6)_2 \cdot KPF_6$*: Triethylenetetramine (58 mg) was added with stirring to a solution of K_2PdCl_4 (107 mg) in 10 ml of water. An orange precipitate was formed but it dissolved immediately. The yellow solution was warmed at 50 °C for 1 h, then $AgPF_6$ (345 mg) dissolved in 5 ml of water was added to the solution. The mixture was stirred for another 0.5 h in the dark and then filtered to remove AgCl. The filtrate was evaporated to dryness under reduced pressure and the residue was dissolved in 10 ml of ethanol. After filtering off the precipitated KPF_6, the filtrate was concentrated to 2 ml, to which 5 ml of water was added. The resulting solution was allowed to stand for 5 days at room temperature. It turned pasty, and yellow needle-like crystals separated out. These crystals were washed with small amounts of cold ethanol and water. Recrystallization was made from ethanol-water solution. Yield, 33%.

Found: C, 9.84; H, 2.40; N, 7.48%. Calcd for $C_6H_{18}N_4PdKP_3F_{18}$: C, 9.92; H, 2.50; N, 7.71%.

$[Pd(trien)](ClO_4)_2$: Triethylenetetramine (202 mg) was added to a solution of $[Pd(NH_3)_4](ClO_4)_2$ (515 mg) in 10 ml of water. The solution was stirred at 50 °C for 2 h and then filtered. The filtrate was evaporated to 5 ml under reduced pressure and the concentrated solution was allowed to stand for 5 days at room temperature. Yellow needle-like crystals were obtained and these were recrystallized from water. Yield, 55%.

Found: C, 15.57; H, 4.12; N, 12.18%. Calcd for $C_6H_{18}N_4PdO_8Cl_2$: C, 15.96; H, 4.03; N, 12.41%.

X-Ray Data Measurement. *Crystal Data*: $C_6H_{18}N_4PdKP_3F_{18}$, F.W.=726.7, Orthorhombic, $a=21.645$ (5), $b=20.873$ (5), $c=9.541$ (2) Å, $U=4311$ (3) Å^3, $D_m=2.18$, $Z=8$, $D_c=2.23$ g cm^{-3}. μ(Mo$K\alpha$)=15.0 cm^{-1}, Mo$K\alpha$ radiation ($\lambda=0.71069$ Å), Space group Pbca. The space group and the approximate cell dimensions were determined from oscillation and Weissenberg photographs taken with Cu$K\alpha$ radiation. The cell dimensions were refined by the least-squares analysis of 38 θ values accurately measured on a Philips PW 1100 four circle diffractometer with Mo$K\alpha$ radiation.

Data Collection: Intensity data for one octant of the reciprocal space were collected by the ω-2θ scan technique with graphite-monochromated Mo$K\alpha$ radiation; the dimensions of the specimen used were $0.13\times0.10\times0.11$ mm. A scan speed of 0.017° s^{-1} in ω, a scan width $(0.8+0.2\tan\theta)$°, and stationary background measurements of 20 s were chosen. A total of 1166 reflections having intensity $I_t-2\sqrt{I_t}>I_b$ was collected in the range of $6°\leq2\theta\leq50°$ (I_t: intensity (counts/s) measured at the peak of reflection during the scan; I_b: mean background intensity (counts/s) obtained from preliminary background measurements of 5 s at each side of the scan). The number of the reflections collected is no more than *ca.* 27% of that of the reciprocal lattice points investigated in the data collection. Three standard reflections (10 0 0, 0 8 0, 0 0 2), monitored every 4 h throughout the data collection, showed no significant variation in intensity. Intensity data were processed by the use of the computer program of Hornstra and Stubbe.[2] No absorption correction was applied.

Structure Determination and Refinement. The crystal structure was solved by the heavy atom technique. The positional and thermal parameters were refined by the block-diagonal least-squares method, with anisotropic temperature factors used for Pd, K, and P atoms. The minimized function was $\sum w(|F_o|-|F_c|)^2$. A weighting scheme of the type suggested by Hughes[3] was applied using $w=0.70$ for $F_o<F_{min}$, $w=1$ for $F_{min}\leq F_o\leq F_{max}$, and $w=(F_{max}/F_o)^2$ for $F_o>F_{max}$; $F_{min}=11.0$ and $F_{max}=31.2$ were found to be optimum. The final R was 0.091 ($R'=[\sum w(|F_o|-|F_c|)^2/\sum wF_o^2]^{1/2}=0.117$). The temperature factors for lighter atoms, especially those for F atoms, are rather high. This is indicative of the disorder in the arrangment of those atoms. In the final cycle of the refinement all parameter shifts were $<(1/5)\sigma$. The atomic coordinates and the temperature factors are listed in Table 1, along with their estimated standard deviations. A complete list of the observed and calculated structure factors is preserved by the Chemical Society of Japan (Document No. 7702).

Atomic scattering factors of neutral Pd, P, F, N, and C, and K^+ were taken from Ref. 4. The real part of the anomalous dispersion correction was applied for the Pd atom. Computer programs used in the calculations were as follows: RSSFR-4 (Fourier synthesis), HBLS-4 (least-squares calculation), and DAPH (interatomic distances and angles, least-squares

Table 1. The atomic coordinates and temperature factors

	x	y	z	B/Å^2
Pd	0.1521(1)	0.1000(1)	0.1658(3)	a)
N(1)	0.222(1)	0.122(1)	0.026(3)	5.0(5)
N(2)	0.139(1)	0.022(1)	0.048(3)	5.3(6)
N(3)	0.088(1)	0.065(1)	0.286(3)	5.7(6)
N(4)	0.156(1)	0.173(1)	0.315(3)	5.5(5)
C(1)	0.226(1)	0.063(2)	−0.077(3)	6.0(8)
C(2)	0.197(1)	0.006(2)	−0.012(4)	6.1(8)
C(3)	0.103(2)	−0.025(2)	0.124(4)	7.1(9)
C(4)	0.072(2)	0.001(2)	0.245(4)	8.0(1.0)
C(5)	0.098(2)	0.087(2)	0.428(4)	8.2(1.0)
C(6)	0.110(1)	0.157(2)	0.430(4)	6.0(8)
K	0.4121(3)	0.2526(4)	0.3696(7)	a)
P(1)	0.0313(3)	0.1700(3)	−0.1442(9)	a)
P(2)	0.2781(4)	0.3037(4)	0.1424(9)	a)
P(3)	0.4008(5)	0.0898(5)	0.1602(11)	a)
F(1)	−0.009(1)	0.223(1)	−0.085(3)	13.4(9)
F(2)	−0.022(1)	0.146(1)	−0.240(3)	10.0(6)
F(3)	0.019(1)	0.117(1)	−0.039(3)	13.3(9)
F(4)	0.088(1)	0.191(1)	−0.053(3)	10.3(6)
F(5)	0.048(1)	0.219(1)	−0.263(3)	10.1(6)
F(6)	0.073(2)	0.120(2)	−0.210(4)	16.5(1.1)
F(7)	0.240(1)	0.263(1)	0.033(2)	8.6(5)
F(8)	0.258(1)	0.367(1)	0.076(3)	11.7(7)
F(9)	0.338(1)	0.294(1)	0.064(3)	12.0(7)
F(10)	0.295(1)	0.237(1)	0.221(3)	12.0(7)
F(11)	0.217(1)	0.307(1)	0.240(3)	9.7(6)
F(12)	0.315(1)	0.338(1)	0.253(3)	11.2(7)
F(13)	0.451(1)	0.058(1)	0.071(2)	9.3(6)
F(14)	0.424(1)	0.047(1)	0.290(3)	12.0(8)
F(15)	0.351(1)	0.119(1)	0.256(3)	13.8(8)
F(16)	0.374(1)	0.131(2)	0.038(3)	14.2(9)
F(17)	0.447(1)	0.143(1)	0.200(3)	14.7(9)
F(18)	0.353(1)	0.036(1)	0.128(3)	13.0(8)

a) Anisotropic temperature factors ($\times 10^4$) in the form $\exp[-(B_{11}h^2+B_{22}k^2+B_{33}l^2+B_{12}hk+B_{13}hl+B_{23}kl)]$, with parameters:

	B_{11}	B_{22}	B_{33}	B_{12}	B_{13}	B_{23}
Pd	27.5(5)	21.5(4)	139(3)	−13(1)	29(3)	−14(3)
K	27(2)	35(2)	117(10)	−7(4)	15(7)	34(9)
P(1)	22(2)	17(2)	122(11)	4(3)	7(9)	17(8)
P(2)	21(2)	31(2)	115(11)	8(4)	1(9)	−34(9)
P(3)	43(2)	37(3)	158(13)	20(5)	26(13)	−14(13)

planes, and coordinates of H atoms), all of which were adapted to the FACOM 270—30 computer at Osaka City University.

In order to confirm the structure, further least-squares calculations were carried out by the use of the anisotropic temperature factors for all atoms, here the weighting scheme $w=(7.6+F_o+0.013F_o^2)^{-1}$ was employed. The R and R' reached 0.054 and 0.072, respectively. The difference Fourier map calculated at this point showed no peaks>0.55 e Å^{-3}. Of the residual peaks, nine could be identified as H atoms.

Electronic Spectra and Electric Conductivity. The absorption spectra were recorded at room temperature using a Hitachi EPS-3T Recording Spectrophotometer. The electric conductivity was measured in water by means of an MY-8 apparatus of the Yanagimoto Seisakusho, Ltd.

Results and Discussion

The projection and elevations of the complex cation are shown in Figs. 1 and 2, respectively. The Pd atom is surrounded by 4 N atoms disposed in trapezoidal form. The complex has a pseudo mirror plane which is perpendicular to the plane defined by the 4 N atoms and bisects the N(1)-Pd-N(4) angle. The 5-membered chelate rings A and C assume the asymmetric envelope conformation, whereas the middle ring B has the symmetric one: the -NH-CH_2-CH_2-NH- fragment in B has an almost eclipsed conformation, with the torsional angle of 9°. This conformation of the trien ligand is essentially identical with that found in [Cu(SCN)(trien)](NCS),[5] though the corresponding torsional angle in the Cu complex (49°) is rather large as compared with that of the Pd complex. In the present $[Pd(trien)]^{2+}$ all C atoms lie on the upper side of the 4 N plane, while the Pd atom deviates slightly downward from the plane, by 0.06 Å. The F(4) atom is in close contact with the Pd atom, at a distance of 3.15 Å. The equations of some least-squares planes are given in Table 2.

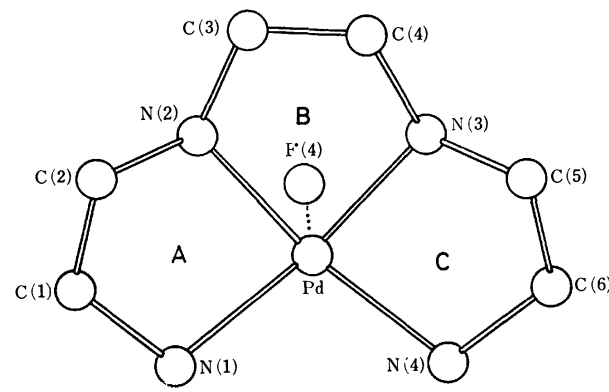

Fig. 1. Projection of the $[Pd(trien)]^{2+}$.

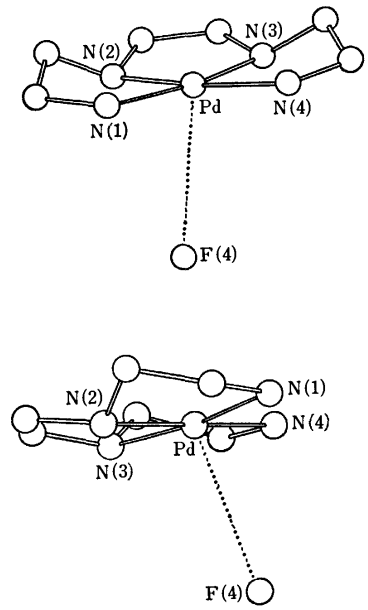

Fig. 2. Elevations of the $[Pd(trien)]^{2+}$.

Table 2.

1) Equations of planes in the form $AX+BY+CZ=D$[a]				
	A	*B*	*C*	*D*
Plane (1)				
N(1), N(2), N(3), N(4)	−0.668	0.514	−0.538	−2.03
Plane (2)				
N(1), C(1), C(2)	−0.884	0.260	−0.389	−3.68
Plane (3)				
N(2), C(2), C(1)	−0.452	−0.209	−0.867	−1.85
Plane (4)				
N(2), C(3), C(4)	−0.800	0.211	−0.563	−2.56
Plane (5)				
N(3), C(4), C(3)	−0.727	0.355	−0.588	−2.56
Plane (6)				
N(3), C(5), C(6)	−0.980	0.163	0.112	−1.33
Plane (7)				
N(4), C(6), C(5)	−0.751	0.135	−0.646	−3.99

2) Deviations (l) of atoms from the plane (1)			
	l/Å		l/Å
N(1)	−0.01	C(1)	−0.16
N(2)	0.01	C(2)	−0.69
N(3)	−0.01	C(3)	−0.37
N(4)	0.01	C(4)	−0.26
Pd	0.05	C(5)	−0.66
		C(6)	−0.08

3) Torsional angles (ϕ) in N–C–C–N fragments	
	ϕ/°
N(1)–C(1)–C(2)–N(2)	47
N(2)–C(3)–C(4)–N(3)	9
N(3)–C(5)–C(6)–N(4)	47

a) The *X*, *Y*, and *Z* coordinates in Å are referred to the crystallographic axes.

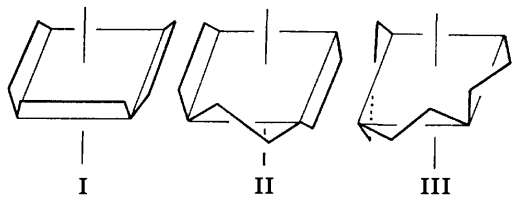

Fig. 3. Possible conformers for a planar disposition of the trien ligand.

Bosnich *et al.* studied the strain energy in the metal chelates of the trien which has a planar disposition. They suggested that the most stable conformations of the ligand are those shown in Figs. 3 I and II.[6] The conformer I has C_s symmetry, while the symmetries of the conformers II and III are C_2. The conformations of trien in the Pd and Cu complexes can be classified as I. The conformation II has not yet been found in the crystal structures of the trien complexes. Although the conformer III was predicted to be less stable than I and II, it is believed that in $(+)_D$-*trans*-$[CoCl_2(trien)]^+$ the chelating ligand assumes the conformation III.[7]

The bond lengths and angles are given in Table 3. The N(1)–Pd–N(4) bond angle is somewhat larger than 90°, showing considerable strain in the complex. However, it is comparable to those in the [Cu(SCN)(trien)](NCS) (98.9°)[5] and $(-)_D$-*trans*-$[Co(NO_2)_2(L\text{-}3,8\text{-dimetrien})](ClO_4)$ (101.6°).[8] The bond length of Pd–N (primary amino group) seems to be somewhat longer than that of the Pd–N (secondary): the mean value of the former is 2.08 Å, whereas that of the latter is 1.98 Å. However, such a difference in metal–nitrogen bonds is less pronounced in the Co complex,[8] and is not found in the Cu one.[5]

Table 3. Bond lengths (l) and angles (ϕ)

	l/Å		ϕ/°
Pd–N(1)	2.07(2)	N(1)–Pd–N(2)	86(1)
Pd–N(2)	2.00(3)	N(2)–Pd–N(3)	85(1)
Pd–N(3)	1.95(3)	N(3)–Pd–N(4)	85(1)
Pd–N(4)	2.08(2)	N(4)–Pd–N(1)	104(1)
N(1)–C(1)	1.57(4)	Pd–N(1)–C(1)	105(2)
N(2)–C(2)	1.42(4)	Pd–N(2)–C(2)	107(2)
N(2)–C(3)	1.44(4)	Pd–N(2)–C(3)	110(2)
N(3)–C(4)	1.43(5)	Pd–N(3)–C(4)	111(2)
N(3)–C(5)	1.45(5)	Pd–N(3)–C(5)	108(2)
N(4)–C(6)	1.53(4)	Pd–N(4)–C(6)	108(2)
C(1)–C(2)	1.49(5)	N(1)–C(1)–C(2)	111(3)
C(3)–C(4)	1.44(6)	N(2)–C(2)–C(1)	110(3)
C(5)–C(6)	1.48(5)	N(2)–C(3)–C(4)	113(3)
		N(3)–C(4)–C(3)	117(3)
Pd···F(4)	3.15(3)	N(3)–C(5)–C(6)	111(3)
		N(4)–C(6)–C(5)	108(3)
P–F	1.51—1.62(4)		

The crystal structure viewed down the c axis is shown in Fig. 4. A K^+ ion is surrounded octahedrally by 6 PF_6^- ions, 10F atoms of which are in contact with the K^+ ion at distances varying from 2.64 to 3.27 Å. There are some weak N–H···F hydrogen bonds in the crystal. The N···F distances are listed in Table 4, along with some important interatomic distances. Both of the NH_2

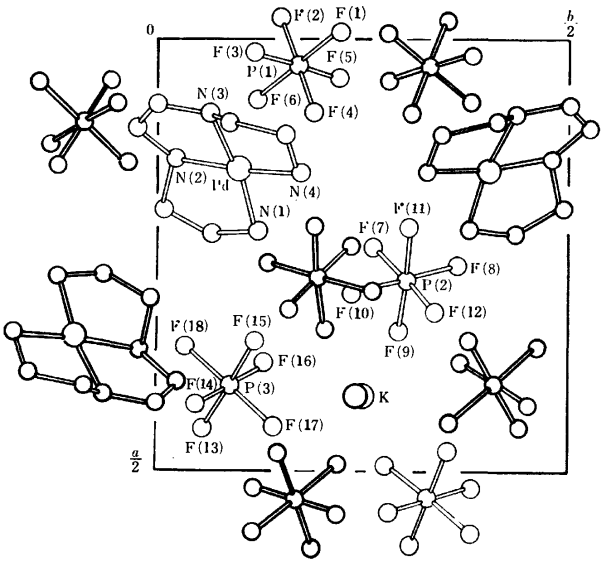

Fig. 4. Crystal structure of the $[Pd(trien)](PF_6)_2 \cdot KPF_6$ viewed down the c axis. Atoms drawn by thin lines are those of the equivalent position (x, y, z), while those shown by the thick lines belong to $(x, 1/2-y, 1/2+z)$.

Table 4. Selected interatomic distances (l)

Atom A	Atom B	l/Å of A B	l/Å of H···B	Positions[a] of A	Positions[a] of B
N(1)-H[b]	F(7)	2.97(3)	2.24	1	1
N(1)-H	F(11)	3.12(3)	2.30	1	4
N(4)-H	F(7)	3.07(3)	2.29	1	4
K	F(1)	3.24(3)		1	2
K	F(1)	2.74(3)		1	3
K	F(2)	2.84(3)		1	2
K	F(5)	3.16(3)		1	2
K	F(9)	2.64(3)		1	4
K	F(10)	2.93(3)		1	1
K	F(12)	2.98(3)		1	1
K	F(15)	3.27(3)		1	1
K	F(16)	3.02(3)		1	4
K	F(17)	2.90(3)		1	1

a) Numerals refer to the following equivalent positions: 1: (x, y, z); 2: $(1/2+x, 1/2-y, -z)$; 3: $(1/2+x, y, 1/2-z)$; 4: $(x, 1/2-y, 1/2+z)$. b) The coordinates of the H atoms were calculated on the assumption that the N-H bond length is 1.03 Å.

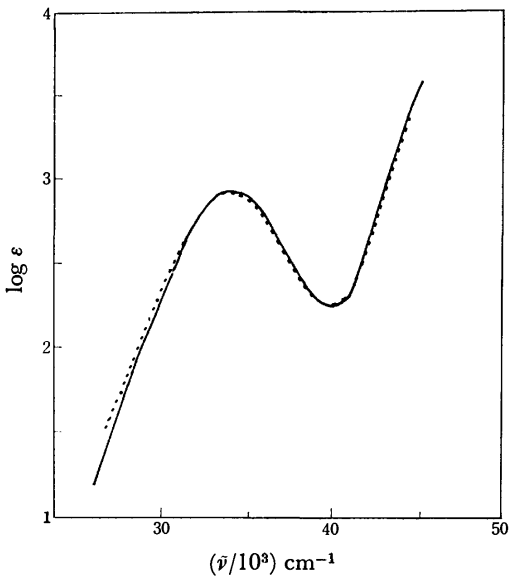

Fig. 5. Absorption spectra of the Pd(II) complexes of trien in aqueous solutions. $[Pd(trien)](PF_6)_2 \cdot KPF_6$: ——; $[Pd(trien)](ClO_4)_2$: ------.

groups participate in the hydrogen bonding, while none of the –NH– groups do.

Figure 5 shows the electronic spectra of the triethylenetetraminepalladium(II) perchlorate and the potassium triethylenetetraminepalladium(II) tris(hexafluorophosphate) in an aqueous solution. These spectra agree with each other and indicate that the species in the solution are identical. The spectra of these compounds resemble those of $[Pd(NH_3)_4](ClO_4)_2$[9] and $[Pd(R\text{-pn})_2]Cl_2$.[10] Accordingly, on the basis of D_{4h} symmetry the absorption band at 33.7×10^3 cm^{-1} may be assigned to the transitions $^1A_{1g} \rightarrow {}^1A_{2g}$, ^1E_g, and $^1B_{1g}$.[9] The peak position of the trien complex is almost equal to that of the ammine complex, but is displaced to a slightly lower energy relative to the band maximum of the R-pn complex. However, the absorption in the present complexes is about three times as intense as those in the complexes cited for comparison. The ion pairing which gives a 5-coordinate complex sometimes results in an enhancement of the absorption intensity.[11] The molar conductance of the perchlorate is 250 ohm^{-1} cm^2 mol^{-1} at 25 °C in 5.90×10^{-4} M aqueous solution. The concentration of this solution is almost equal to those of the solutions used for the measurements of the spectra. The value of conductance is typical for a 1:2 electrolyte: there seems to be no appreciable interaction between the cation and the anion in 10^{-3}—10^{-4} M solution.

The PdN_4 chromophore in the $[Pd(NH_3)_4]^{2+}$ and $[Pd(R\text{-pn})_2]^{2+}$ have an effective symmetry of D_{4h}, and therefore the d→d transition is Laporte-forbidden. On the other hand, the configuration of 4 N atoms in the $[Pd(trien)]^{2+}$ is trapezoidal and the symmetry of the chromophore can be regarded as C_{2v}. Since this group contains no inversion center, Laporte's rule is relaxed. Furthermore, symmetry considerations imply that the C_{2v} symmetry is favorable to the mixing of d→d transitions with some allowed transitions through configuration interaction, as compared with the case of D_{4h} symmetry. Some of these might be responsible for the enhancement of the intensities in the ligand fields bands. The orbitals in the plane of the ligator atoms are most sensitive to the change of the disposition of these atoms. Consequently, the intensity of the $a_1(d_{xy}) \rightarrow b_1(d_{x^2-y^2})$ transition may be the most enhanced of the d→d transitions.

This research was supported by a Grant-in-Aid for Scientific Research from the Ministry of Education.

References

1) H. B. Jonassen and N. L. Cull, *J. Am. Chem. Soc.*, **71**, 4097 (1949).
2) J. Hornstra and B. Stubbe, PW 1100 Data Processing Program, Philips Research Laboratories, Eindhoven, Holland.
3) E. W. Hughes, *J. Am. Chem. Soc.*, **63**, 1737 (1941).
4) "International Tables for X-Ray Crystallography," Vol. 3, Kynoch Press, Birmingham (1962), p. 202.
5) G. Marongiu, E. C. Lingafelter, and P. Paoletti, *Inorg. Chem.*, **8**, 2763 (1969).
6) B. Bosnich, R. D. Gillard, E. D. McKenzie, and G. A. Webb, *J. Chem. Soc., A*, **1966**, 1331.
7) D. A. Buckingham, P. A. Marzilli, A. M. Sargeson, S. F. Mason, and P. G. Beddoe, *Chem. Commun.*, **1967**, 433.
8) M. Ito, F. Marumo, and Y. Saito, *Acta Crystallogr., Sect. B*, **28**, 463 (1972).
9) W. R. Mason, III and H. B. Gray, *J. Am. Chem. Soc.*, **90**, 5721 (1968).
10) H. Ito, J. Fujita, and K. Saito, *Bull. Chem. Soc. Jpn.*, **40**, 2584 (1967).
11) C. Furlani, *Coord. Chem. Rev.*, **3**, 141, (1968).

Studies on Mixed Chelates. VI. Mixed Copper(II) Chelates with *N,N,N',N'*-Tetraethylethylenediamine and Various β-Diketones

Yutaka FUKUDA, Yukiko MIURA, and Kozo SONE

Department of Chemistry, Faculty of Science, Ochanomizu University, Otsuka, Tokyo 112

(Received July 27, 1976)

Ten new mixed copper(II) chelates containing *N,N,N',N'*-tetraethylethylenediamine and various β-diketones were prepared and the cause of the large variations of ν_{max} values observed in the visible absorption spectra of their organic solutions was discussed in comparison with similar variations of the corresponding tetramethyl chelates.

In previous papers,[1,2] the authors reported on the mixed copper(II) chelates containing *N,N,N',N'*-tetramethylethylenediamine(tmen) and various β-diketonate ions. It was found that the position of the d-d band of such chelates depends remarkably upon the coordination ability of the solvent and counter anion, and upon the nature of the substituent groups in the diketonate ions. The present study on the preparation and spectra of the corresponding chelates containing *N,N,N',N'*-tetraethylethylenediamine(teen) was undertaken to see how the bulkiness of the *N*-alkyl groups affects the structure and spectra of these types of chelates.

Experimental

Preparation of the Chelates. *(I) [Cu(teen)aca]ClO_4*: Acetone solutions of $Cu(ClO_4)_2 \cdot 6H_2O$ and aca* (10 mmol each) were mixed together with teen** (15 mmol) with vigorous stirring. After the mixture had been filtered and concentrated, an excess of diethyl ether was added. Crystals of the chelate began to separate out when the vessel wall was scratched with a glass rod. They were washed with an acetone–diethyl ether mixture and dried in a vacuum.

(II) Other Chelates: Acetone solutions of $Cu(ClO_4)_2 \cdot 6H_2O$ (or $Cu(NO_3)_2 \cdot 3H_2O$) and a β-diketone (10 mmol each) were mixed together with teen (15 mmol) as in (I), and the filtered mixture was evaporated to dryness. The raw chelate thus obtained was purified by repeated crystallization from 1,2-dichloroethane, and dried in a vacuum.

The colors, magnetic moments, and analytical data of the new chelates are listed in Table 1. All the chelate perchlorates and nitrates are apparently similar to the tmen chelates reported before; however it was impossible to prepare [Cu(teen)hfa]NO_3, and a green chelate [Cu(teen)hfa_2] was obtained instead. For the physical measurements *cf.* previous papers.[1,2]

Discussion

Electronic Spectra. As in the case of the corresponding tmen chelates, all the teen chelates obtained are fairly soluble in a variety of organic solvents. Measurements of the visible absorption spectra in solution, and the reflection spectra in the solid state, revealed a close resemblance between these spectra and those of the corresponding tmen chelates. Here again it seems that the position of the d-d band depends on two factors, (1) the nature of the substituent groups in the β-diketonate ions, which controls the magnitude of the in-plane ligand field strength, and (2) the strength of the axial bonds formed between the central copper(II) and the counter anions or solvent molecules.

The data in organic solutions are of special interest. Fig. 1 shows some examples of the obtained spectra, *i.e.*, the spectra of [Cu(teen)aca]ClO_4 in five solvents. The variations of the ν_{max} value of the d-d band of each chelate in organic solutions are summarized in Fig. 2.

The spectral variations among the chelate perchlorates are especially similar to those of the corresponding tmen chelates. Thus the ν_{max} value for each chelate decreases in the following order of solvent,

$$1,2\text{-}C_2H_4Cl_2 > \text{acetone} > \text{MeOH} > \text{DMF} > \text{DMSO}$$

and the ν_{max} value in one particular solvent decreases in the following order of the β-diketonate ion,

$$\text{dpm} > \text{aca} > \text{bza} > \text{dbm} \gg \text{hfa}$$

just as in the case of the tmen chelates.

TABLE 1. COLORS, ANALYTICAL DATA,[a] MAGNETIC MOMENTS AND MOLAR CONDUCTIVITIES OF THE CHELATES

No.	Chelate	Color	C%	H%	N%	μ_{eff} (B.M.)	Λ_M[b]
1	[Cu(teen)dpm]ClO_4	Wine	47.64(48.54)	8.37(8.54)	5.49(5.39)	1.71	32.3
2	[Cu(teen)aca]ClO_4	Wine	41.24(41.47)	7.01(7.19)	6.42(6.45)	1.76	34.4
3	[Cu(teen)bza]ClO_4	Wine	47.75(48.28)	6.81(6.69)	5.67(5.63)	1.77	31.6
4	[Cu(teen)dbm]ClO_4	Wine	52.90(53.65)	6.37(6.31)	4.98(5.01)	1.71	31.2
5	[Cu(teen)hfa]ClO_4	Blue	33.29(33.16)	4.94(4.82)	5.01(5.16)	1.73	9.3
6	[Cu(teen)dpm]NO_3	Blue	52.68(52.31)	9.37(9.20)	8.88(8.72)	1.79	25.1
7	[Cu(teen)bza]NO_3	Green	52.25(52.33)	7.07(7.25)	9.38(9.15)	1.76	20.2
8	[Cu(teen)dbm]NO_3	Wine	57.41(57.62)	6.78(6.78)	8.14(8.06)	1.77	21.9
9	[Cu(teen)tfa]NO_3	Blue	39.67(39.95)	6.10(6.26)	9.15(9.32)	1.81	6.6
10	[Cu(teen)hfa_2]	Green	37.12(36.95)	3.69(4.04)	4.14(4.31)	1.81	—

a) Calculated values in parentheses. b) 1×10^{-3}M solution in 1,2-dichloroethane at 25 °C.

* Abbreviations for the names of the diketonate ions are the same as those given in Part V of this series.[3]

** Aldrich Chemical Co., Milwaukee, USA.

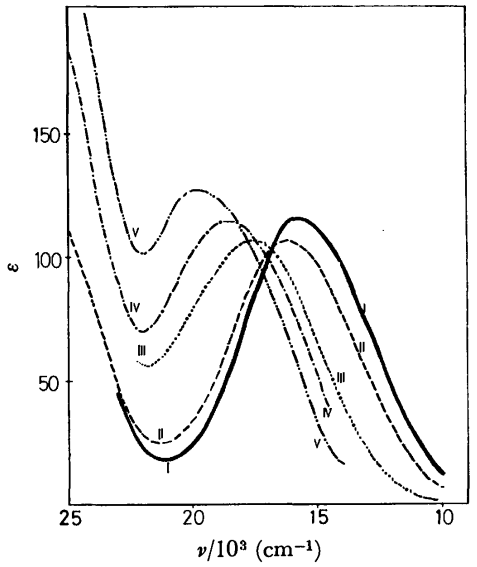

Fig. 1. Electronic absorption spectra of [Cu(teen)aca]-ClO_4 in various solvents. (*Cf.* also Fig. 2).

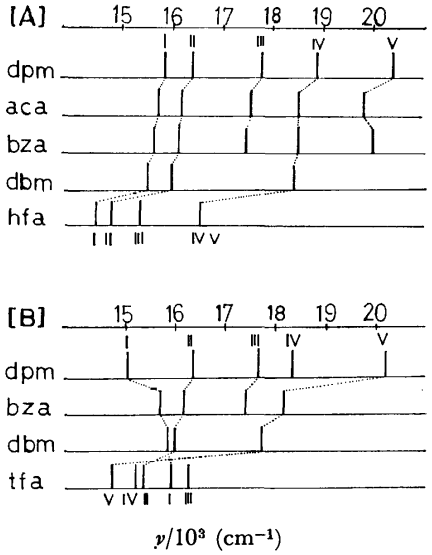

Fig. 2. Variations of the ν_{max} values of the chelates [Cu(teen)β-dik]X in various solvents. [A]: X=ClO_4, [B]: X=NO_3. The solvents studied in Figs. 1 and 2 are: DMSO(I), DMF(II), MeOH(III), acetone (IV) and 1,2-dichloroethane (V); concn ≈5 mM.

The variations among the chelate nitrates seem to be more complicated, poor solubility and the appearance of shoulder-like curves sometimes hindering the correct locating of the bands. However, it can be recognized that the ν_{max} in 1,2-dichloroethane and acetone decrease drastically in going from dpm to tfa, probably for the same reason as that for a similar spectral anomaly observed among the spectra of the tmen chelates in 1,2-dichloroethane, *i.e.*, the coordination of NO_3^- to the chelate cation.

The general features shown in Fig. 2 are thus fairly similar to the corresponding figure of the tmen chelates,[2] but the spectra of the teen chelates seem to be more sensitive to the changes of solvent, anion and substituent groups. For example, in going from DMSO to 1,2-dichloroethane, the ν_{max} of [Cu(tmen)dpm]ClO_4 changes from 16600 to 18900 cm^{-1}, while that of [Cu(teen)dpm]ClO_4 changes from 15800 to 20400 cm^{-1}. One can also compare the complicated pattern of Fig. 2 [B] with the corresponding figure of the tmen chelates, which looks more regular except for the above-mentioned anomaly of 1,2-dichloroethane solutions.

This spectral sensitivity of the teen chelates seems strange, since the four bulky *N*-ethyl groups in teen can be expected to hinder the approach of the solvents and anions more strongly than the *N*-methyl groups of tmen, so that the electronic structure of the teen chelate should be more insensitive to the changes of environment. In fact, the mixed nickel(II) chelates of teen and β-diketonate ions were found to be much more reluctant to combine with solvent molecules and change from square planar to octahedral than the corresponding tmen chelates.[3]

The cause of this spectral sensitivity might be found in the fact that copper(II), unlike nickel(II), tends to form axial bonds even with ligands lying far away from it, and even when they lie considerably outside the z-axis. That is, the axial bonds are considerably elastic or flexible in nature.[4]

It is thus conceivable that the above-mentioned steric hindrance in the teen chelates works only when the coordination ability of the solvent or anion is very low and the in-plane l.f.s. is sufficiently large; in such a case a highly planar chelate structure will result, and its ν_{max} may be higher than that of its tmen analogue. On the other hand, when the coordination ability of the solvent or anion becomes higher and the in-plane l.f.s. lower, the steric hindrance will be readily overcome, and a more or less deformed tetragonal structure will result. The effective l.f.s. in such a structure may be somewhat weaker, and its ν_{max} lower, than that of its tmen analogue, because there will be larger interligand repulsions and structural deformations in the teen system. The observed larger spectral variations among the teen chelates may be a reflection of all these effects.

It should be added that the chelate [Cu(teen)hfa_2] shows only a small variation of ν_{max} in various solvents

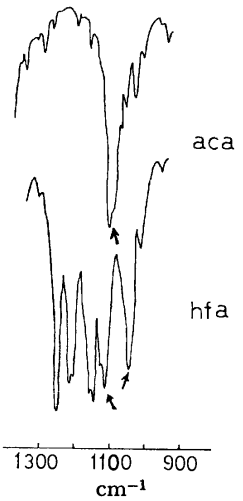

Fig. 3. IR spectra of [Cu(teen)β-dik]ClO_4 in Nujol mulls.

(14080 to 14580 cm^{-1} in DMSO, methanol and 1,2-dichloroethane) probably owing to its 6-coordinate structure which somewhat resembles the chelate [Cu bip hfa_2] reported by Veidis *et al.*[5]

Evidence of Perchlorate Coordination. The data in Fig. 2 suggest that, in 1,2-dichloroethane with very poor coordination ability, and with hfa with the weakest l.f.s. among the diketonate ions used, even ClO_4^- gets coordinated to some extent, since the ν_{max} of [Cu(teen)-hfa]ClO_4 in this solvent is remarkably low and nearly the same as that of the same chelate in acetone. This leads further to the supposition that the same kind of perchlorate coordination will also occur in the crystals of this chelate. The conductivity data in Table 1, and the fact that the IR main peak of ClO_4^- which appears single in other chelates is apparently split in the spectrum of this chelate (Fig. 3) support these suppositions. Similar observations have been made on the tmen system.[2]

The authors are grateful to Dr. Ichiro Fujita and Mrs. Etsuko Fujita, Georgia Institute of Technology (Atlanta, USA), for the supply of a sample of teen.

References

1) Y. Fukuda and K. Sone, *Bull. Chem. Soc. Jpn.*, **45**, 465 (1972).
2) Y. Fukuda, A. Shimura, M. Mukaida, E. Fujita, and K. Sone, *J. Inorg. Nucl. Chem.*, **36**, 1265 (1974).
3) Y. Fukuda, R. Morishita, and K. Sone, *Bull. Chem. Soc. Jpn.*, **49**, 1017 (1976).
4) B. J. Hathaway, *Structure and Bonding*, **14**, 49 (1973).
5) M. V. Veidis, G. H. Schreiber, T. E. Gough, and G. J. Palenik, *J. Am. Chem. Soc.*, **91**, 1859 (1969).

Optical Resolution and Ternary System Solubility Isotherms of Cobalt(III) Complex Salts

Yoichi SHIMURA and Katsuyuki TSUTSUI

Department of Chemistry, Faculty of Science, Osaka University, Toyonaka, Osaka 560

(Received July 28, 1976)

The characteristics of three-component phase diagrams consisting of water and a pair of enantiomeric or diastereomeric cobalt(III) complex salts have been clarified experimentally by constructing the solubility isotherms of the following 6 ternary systems at 25 °C: H_2O–Δ-[Co(ox)$(en)_2$]X–Λ-[Co(ox)$(en)_2$]X, where X stands for Cl^-, I^-, (*R,R*)-$C_4H_5O_6^-$, Δ-[Co(edta)]$^-$, $^1/_2[Sb_2\{(R,R)\text{-}C_4H_2O_6\}_2]^{2-}$ or *d*-$C_{10}H_{14}OBrSO_3^-$. It has been found that the latter two anions form an active racemate, *rac*-[Co(ox)$(en)_2]_2[Sb_2\{(R,R)\text{-}C_4H_2O_6\}_2]\cdot 5H_2O$ and *rac*-[Co(ox)$(en)_2$]-(*d*-$C_{10}H_{14}OBrSO_3)\cdot H_2O$, respectively. Solubility of the [Co(ox)$(en)_2]^+$ salts containing optically active counter-ions was determined at 5—60 °C in water.

The solubility isotherm for a multi-component system consisting of an optically inactive solvent and a pair of enantiomers or diastereomers seems to give useful information on optical resolution.[1,2] However, no such isotherm seems to have been reported for the system of metal complexes and water. The present paper deals with some solubility isotherms for the ternary systems, H_2O–Δ-[Co(ox)$(en)_2$]X–Λ-[Co(ox)$(en)_2$]X, where X stands for univalent anions such as (a) Cl^-, (b) I^-, (c) (*R,R*)-$C_4H_5O_6^-$, (d) Δ-[Co(edta)]$^-$, (e) $^1/_2[Sb_2\{(R,R)\text{-}C_4H_2O_6\}_2]^{2-}$ or (f) *d*-$C_{10}H_{14}OBrSO_3^-$. The monohydrate and tetrahydrate of the chloride (a) are spontaneously resolved,[3–5] but the iodide (b) forms a solid racemic compound.[4] Anions (c) and (d) represent the successful cases of optical resolution, and (e) and (f) the unsuccessful ones.

Experimental

Materials. *[Co(ox)$(en)_2$]I*: Racemic chloride monohydrate was prepared by the method of Dwyer *et al.*[6] and was optically resolved by two kinds of resolving agents: $(+)_{589}$-(*R,R*)-tartrate(1−) ion (abbreviated to *d*-$C_4H_5O_6^-$), which gave the $\Lambda(+)_{589}$ iodide through the less soluble diastereomer Λ-[Co(ox)$(en)_2$](*d*-$C_4H_5O_6)\cdot H_2O$,[7] and $\Delta(+)_{546}$-[Co(edta)]$^-$, which gave the $\Delta(-)_{589}$ iodide through the less soluble diastereomer Δ-[Co(ox)$(en)_2]\cdot\Delta$-[Co(edta)]$\cdot H_2O$. The $\Lambda(+)_{589}$ iodide showed $\Delta\varepsilon_{523}=+2.55$ (lit,[7] $\Delta\varepsilon_{520}=+2.64$), and the $\Delta(-)_{589}$ iodide −2.53.

[Co(ox)$(en)_2$]Cl·H_2O: The recemic complex was also prepared by the method of Dwyer *et al.* The $\Lambda(+)_{589}$ and $\Delta(-)_{589}$ isomers were obtained from the corresponding iodides by treating with AgCl; $\Delta\varepsilon_{523}=+2.57$ and −2.60, respectively.

[Co(ox)$(en)_2$](d-$C_4H_5O_6)\cdot nH_2O$: The Λ-complex salt monohydrate was obtained by the method of Jordan *et al.*,[7] and recrystallized from water; $\Delta\varepsilon_{523}=+2.60$ (lit,[7] $\Delta\varepsilon_{520}=+2.65$). Found: C, 27.46; H, 5.36; N, 12.89%. Calcd for Λ-[Co(ox)$(en)_2$](*d*-$C_4H_5O_6)\cdot H_2O$: C, 27.65; H, 5.35; N, 12.90%. The Δ-complex salt 2.5-hydrate was separated by the method of Froebe[8] from the filtrate from the Λ-complex diastereomer in the procedure of Jordan *et al.*[7] and purified by repeated recrystallizations from hot water; $\Delta\varepsilon_{523}=-2.67$, the yield was almost 1/10 of the corresponding Λ-complex diastereomer. Found: C, 26.20; H, 5.67; N, 11.95%. Calcd for Δ-[Co(ox)$(en)_2$](*d*-$C_4H_5O_6)\cdot 2.5H_2O$: C, 26.03; H. 5.69; N, 12.15%.

[Co(ox)$(en)_2]_2[Sb_2$(d-$C_4H_2O_6)_2]\cdot nH_2O$: The diastereomers were obtained by the reaction of an aqueous suspension (0.1 mol, 50 °C) of $\Lambda(+)_{589}$- or $\Delta(-)_{589}$-[Co(ox)$(en)_2$]I, or *rac*-[Co(ox)$(en)_2$]Cl·H_2O with freshly prepared silver antimony(III) $(+)_{589}$-tartrate, which was precipitated in advance from a cold aqueous solution of tatar emetic $K_2[Sb_2(d\text{-}C_4H_2O_6)_2]\cdot 3H_2O$ (0.05 mol) by adding the equivalent amount of silver nitrate solution. Recrystallization was carried out from warm water; $\Delta\varepsilon_{523}$ per the complex cation was +2.59, −2.48, and 0 for the Λ-, Δ-, and *rac*-complex diastereomers, respectively. Found: C, 19.82; H, 4.04; N, 9.58%. Calcd for Λ-[Co(ox)-$(en)_2]_2[Sb_2(d\text{-}C_4H_2O_6)_2]\cdot 6H_2O$: C, 20.39; H, 4.12; N, 9.51%. Found: C, 20.56; H, 3.85; N, 9.56%. Calcd for Δ-[Co(ox)-$(en)_2]_2[Sb_2(d\text{-}C_4H_2O_6)_2]\cdot 4H_2O$: C, 21.03; H, 3.89; N, 9.81%. Found: C, 20.21; H, 4.02; N, 9.76%. Calcd for *rac*-[Co-(ox)$(en)_2]_2[Sb_2(d\text{-}C_4H_2O_6)_2]\cdot 5H_2O$: C, 20.71; H, 4.00; N, 9.66%.

[Co(ox)$(en)_2$](d-$C_{10}H_{14}OBrSO_3)\cdot nH_2O$: Ammonium $(+)_{589}$-(1*R*,3*S*,4*S*,7*R*)-3-bromocamphor-9-sulfonate (the anion is abbreviated to *d*-$C_{10}H_{14}OBrSO_3^-$) was converted into silver salt by treatment with silver nitrate in a cold aqueous solution. The $\Lambda(+)_{589}$- or $\Delta(-)_{589}$-[Co(ox)$(en)_2$]I, or *rac*-[Co(ox)$(en)_2$]-Cl·H_2O was suspended in warm water and treated with Ag-(*d*-$C_{10}H_{14}OBrSO_3$). The diastereomers obtained were recrystallized from warm water; $\Delta\varepsilon_{523}=+2.54$, −2.58, and 0 for the Λ-, Δ-, and *rac*-complex diastereomers, respectively. Anal. Found: C, 31.56; H, 5.42; N, 9.83%. Calcd for Λ-[Co(ox)-$(en)_2]$(*d*-$C_{10}H_{14}OBrSO_3)\cdot H_2O$: C, 32.27; H, 5.43; N, 9.41%. Found: C, 30.74; H, 5.66; N, 9.01%. Calcd for Δ-[Co(ox)-$(en)_2]$(*d*-$C_{10}H_{14}OBrSO_3)\cdot 2.5H_2O$: C, 30.87; H, 5.68; N, 9.00%. Found: C, 32.00; H, 5.46; N, 9.52%. Calcd for *rac*-[Co(ox)$(en)_2]$(*d*-$C_{10}H_{14}OBrSO_3)\cdot H_2O$: C, 32.27, H, 5.43; N, 9.41%.

[Co(ox)$(en)_2]\cdot\Delta$-[Co(edta)]$\cdot nH_2O$: The less soluble diastereomer was obtained by the method of Dwyer *et al.*;[6] $[\alpha]_{589}=-550°$ (lit,[6] +550° for the enantiomer trihydrate). Found: C, 30.30; H, 4.77; N, 13.35%. Calcd for Δ-[Co-(ox)$(en)_2]\cdot\Delta$-[Co(edta)]$\cdot H_2O$: C, 30.39; H, 4.78; N, 13.29%.

The more soluble diastereomer was prepared from Λ-[Co-

Table 1. Absorption and circular dichroism maximum values of [Co(ox)$(en)_2$]X salts used for calculation of solubility

X	ε at 497 nm	$\Delta\varepsilon$ at 523 nm
Cl^-	117	±2.60
I^-	122	±2.55
d-$C_4H_5O_6^-$	123	±2.67
$1/2[Sb_2(d\text{-}C_4H_2O_6)_2]^{2-}$	116	±2.59
d-$C_{10}H_{14}OBrSO_3^-$	119	±2.58
Δ-[Co(edta)]$^-$	398[a]	—

a) at 524 nm.

TABLE 2. SOLUBILITY OF THE $[Co(ox)(en)_2]^+$ SALTS CONTAINING OPTICALLY ACTIVE COUNTER-IONS (grams of anhydrous salt in 100 grams of water)

Temp (°C)	No. of salt[a]										
	1	2	3	4	5	6	7	8	9	10	11
5	0.98	2.93	1.21	0.291	3.59	2.58	0.907	3.88	—		3.00
10	1.14	3.46	1.46	0.341	4.12	2.73	1.04	4.25	1.76[b]		3.20
15	1.37	4.10	1.86	0.403	4.80	3.00	1.20	4.67	2.13		3.52
20	1.62	4.79	2.21	0.475	5.43	3.30	1.35	5.09	2.49		3.78
25	1.87	5.60	2.79	0.556	6.25	3.67	1.53	5.53	2.97		4.23
30	2.16	6.57	3.47	0.657	7.15	3.92	1.75	6.09	3.50		4.58
35	2.54	7.74	4.24	0.766	8.21	4.40	2.03	6.86	4.02		5.09
40	3.05	8.92	5.26	0.864	9.50	4.76	2.30	7.54		4.39	5.57
45	3.47	10.5	6.38	1.01	10.98	5.27	2.57	8.33		4.83	6.10
50	4.01	—	7.97	1.14	12.66	5.85	2.94	9.19		5.31	6.82
55	4.59	13.5	9.58	1.26	14.54	6.50	3.35	10.3		5.76	7.59
60	5.21	15.5	11.2	1.35	16.78	7.17	3.79	11.7		6.42	8.36

a) 1: Λ-$[Co(ox)(en)_2](d\text{-}C_4H_5O_6)\cdot H_2O$, 2: Δ-$[Co(ox)(en)_2](d\text{-}C_4H_5O_6)\cdot 2.5H_2O$, 3: Λ-$[Co(ox)(en)_2]\cdot\Delta$-$[Co(edta)]\cdot 2.5H_2O$, 4: Δ-$[Co(ox)(en)_2]\cdot\Delta$-$[Co(edta)]\cdot H_2O$, 5: Λ-$[Co(ox)(en)_2]_2[Sb_2(d\text{-}C_4H_2O_6)_2]\cdot 6H_2O$, 6: Δ-$[Co(ox)(en)_2]_2[Sb_2(d\text{-}C_4H_2O_6)_2]\cdot 4H_2O$, 7: *rac*-$[Co(ox)(en)_2]_2[Sb_2(d\text{-}C_4H_2O_6)_2]\cdot 5H_2O$, 8: Λ-$[Co(ox)(en)_2](d\text{-}C_{10}H_{14}OBrSO_3)\cdot H_2O$, 9: Δ-$[Co(ox)(en)_2](d\text{-}C_{10}H_{14}OBrSO_3)\cdot 4H_2O$, 10: Δ-$[Co(ox)(en)_2](d\text{-}C_{10}H_{14}OBrSO_3)\cdot 2.5H_2O$, 11: *rac*-$[Co(ox)(en)_2](d\text{-}C_{10}H_{14}OBrSO_3)\cdot H_2O$. b) At 8 °C.

$(ox)(en)_2]I$ and Δ-$Ag[Co(edta)]$, the latter being obtained by the method given by Maricondi and Douglas.[9] Recrystallization was carried out from warm water; $\Delta\varepsilon_{538}=+2.25$. Found: C, 28.42; H, 5.07; N, 12.53%. Calcd for Δ-$[Co(ox)(en)_2]\cdot\Delta$-$[Co(edta)]\cdot 3H_2O$: C, 28.75; H, 5.13; N, 12.57%.

Measurements. Mutual solubility of the Δ and Λ complex salts in water was measured at 25 °C as follows: A mixed aqueous solution of the Δ and Λ complex salts containing an excess of the solid complex salt(s) in a conical flask was stirred mechanically for about 2 h at 25 °C in a thermostat regulated within ±0.1 °C. After the resulting saturated solution had been left to stand for a while, a portion of the supernatant solution was sucked into a weighing bottle through a cotton plug and then weighed. This was diluted to a known volume, and its optical density and CD were measured at the wave lengths 497 and 523 nm, respectively, except for the case of X=Δ-$[Co(edta)]^-$. The optical density value is related to the total amount of enantiomers (or diastereomers) and the CD value the difference in amounts of Δ and Λ complexes, since no counter ions influence the absorption or CD spectra in the visible region regardless of whether they are optically active or not. Thus, the absorption and CD maximum values of the complex salts (Table 1) enable us to calculate the amounts of both Δ and Λ complexes separately.

In the case of X=Δ-$[Co(edta)]^-$, the total amount of diastereomers was calculated from the observed optical density at 524 nm, where the absorption maximum of $[Co(ox)(en)_2]$-$[Co(edta)]$ salt lies, and the difference in the amount of diastereomers from the observed CD at 538 nm, where the CD curve of Δ-$[Co(edta)]^-$ ion intersects the zero line; the complex salt has a value of $\Delta\varepsilon=\pm 2.25$ at this wavelength. The observed CD value at 561 nm, where the CD curve of Λ-$[Co(ox)(en)_2]\cdot\Delta$-$[Co(edta)]$ diastereomer intersects the zero line, was also used for calculation of the dissolved amount of the Δ-$[Co(ox)(en)_2]\cdot\Delta$-$[Co(edta)]$ diastereomer.

The solid phases were identified from the elemental analyses and measurements of CD or optical rotation (solvent: H_2O). The solubility of complexes in water at 5—60 °C (Table 2) was determined in the same way as previously reported.[4] Optical densities were measured with a Jasco UVIDEC-1 spectrophotometer, CD with a Jasco MOE-1 spectropolarimeter, and optical rotation with a Jasco DIP-4 digital polarimeter.

Results and Discussion

The ternary system data obtained are given in Table 3 and Figs. 1—6. In the triangular isotherms the top part (H_2O corner) is enlarged for the sake of convenience and the tie lines omitted.

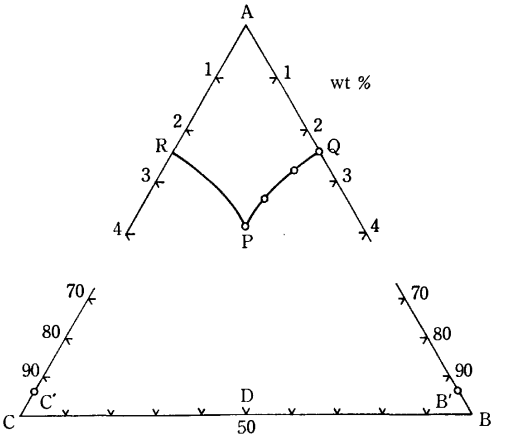

Fig. 1. Solubility isotherm of the ternary system H_2O-(A)-Δ-$[Co(ox)(en)_2]Cl$(B)-Λ-$[Co(ox)(en)_2]Cl$(C) at 25 °C. The solid phase B′ or C′ is monohydrate of B or C, respectively.

Spontaneous Resolution. *$[Co(ox)(en)_2]Cl$*: Figure 1 shows the ternary phase diagram at 25 °C for the system consisting of Δ and Λ isomers of chloride and water. One invariant point P is found. The triangular area PB′C′ represents the compositions consisting of Δ chloride monohydrate, Λ chloride monohydrate and a saturated solution of composition P, which is identical to a saturated solution of the racemic complex. This is the case of spontaneous resolution. The molar solubility in point P should be identical to or larger than $\sqrt{2}/2$ of that in point Q or R.[4]

Table 3. Solubility in the ternary systems, H_2O-Δ-[Co(ox)$(en)_2$]X-Λ-[Co(ox)$(en)_2$]X, at 25 °C

X	Liquid phase composition (wt %) Δ-salt	Λ-salt	Solid phase
Cl^-	2.43	0	Δ-[ ]X·H_2O
	2.17	0.62	Δ-[ ]X·H_2O
	1.99	1.36	Δ-[ ]X·H_2O
	1.91	1.91	Δ-[ ]X·H_2O+Λ-[ ]X·H_2O
I^-	0.41	0	Δ-[ ]X
	0.40	0.01	Δ-[ ]X+*rac*-[ ]X
	0.21	0.02	*rac*-[ ]X
	0.13	0.06	*rac*-[ ]X
	0.08	0.10	*rac*-[ ]X
	0.05	0.15	*rac*-[ ]X
	0.02	0.24	*rac*-[ ]X
	0.01	0.34	*rac*-[ ]X
	0.01	0.40	Δ-[ ]X+*rac*-[ ]X
	0	0.41	Λ-[ ]X
d-$C_4H_5O_6^-$	5.29	0	Δ-[ ]X·2.5H_2O
	5.07	0.64	Δ-[ ]X·2.5H_2O
	4.99	1.06	Δ-[ ]X·2.5H_2O+ Λ-[ ]·H_2O
	3.79	1.09	Λ-[ ]X·H_2O
	2.73	1.23	Λ-[ ]X·H_2O
	1.43	1.48	Λ-[ ]X·H_2O
	0.03	1.92	Λ-[ ]X·H_2O
Λ-[Co(edta)]$^-$	0.52	0.04	Λ-[ ]X·H_2O
	0.41	0.39	Λ-[ ]X·H_2O
	0.36	0.67	Λ-[ ]X·H_2O
	0.29	1.26	Λ-[ ]X·H_2O
	0.26	1.70	Λ-[ ]X·H_2O
	0.20	2.68	Λ-[ ]X·H_2O+ Λ-[ ]X·2.5H_2O
	0	2.72	Λ-[ ]X·2.5H_2O
1/2[Sb_2(*d*-$C_4H_2O_6)_2$]$^{2-}$	3.51	0.04	Δ-[ ]X·2H_2O
	3.51	0.20	Δ-[ ]X·2H_2O+ *rac*-[ ]X·2.5H_2O
	2.46	0.24	*rac*-[ ]X·2.5H_2O
	1.45	0.39	*rac*-[ ]X·2.5H_2O
	0.89	0.68	*rac*-[ ]X·2.5H_2O
	0.61	0.90	*rac*-[ ]X·2.5H_2O
	0.48	1.25	*rac*-[ ]X·2.5H_2O
	0.17	3.51	*rac*-[ ]X·2.5H_2O
	0.12	5.08	*rac*-[ ]X·2.5H_2O
	0.12	5.73	Λ-[ ]X·3H_2O+ *rac*-[ ]X·2.5H_2O
	0	5.75	Λ-[ ]X·3H_2O
d-$C_{10}H_{14}$-$OBrSO_3^-$	2.88	0	Δ-[ ]X·4H_2O
	2.78	1.18	Δ-[ ]X·4H_2O
	2.70	1.48	Δ-[ ]X·4H_2O+ *rac*-[ ]X·H_2O
	2.35	1.81	*rac*-[ ]X·H_2O
	1.90	2.33	*rac*-[ ]X·H_2O
	1.40	2.98	*rac*-[ ]X·H_2O
	1.10	3.65	*rac*-[ ]X·H_2O
	0.88	4.35	*rac*-[ ]X·H_2O
	0.92	4.70	Λ-[ ]X·H_2O+ *rac*-[ ]X·H_2O
	0.06	5.12	Λ-[ ]X·H_2O

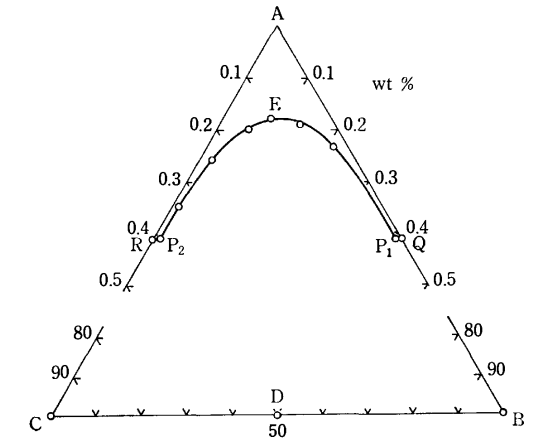

Fig. 2. Solubility isotherm of the ternary system H_2O-(A)-Δ-[Co(ox)$(en)_2$]I(B)-Λ-[Co(ox)$(en)_2$]I(C) at 25 °C.

Formation of Racemic Compound. [*Co(ox)(en)*$_2$]*I*: Figure 2 shows the case of Δ and Λ isomers of iodide and water. Two invariant points P_1 and P_2 appear, the curve P_1EP_2 representing the solubility of the racemic compound Δ-[Co(ox)$(en)_2$]I·Λ-[Co(ox)$(en)_2$]I (D). The solubility curve of the Δ or Λ complex, QP_1 or RP_2, is greatly suppressed in the diagram.

Optical Resolution by Solubility Difference between Diastereomers. [*Co(ox)(en)*$_2$]*X*(*X*=d-$C_4H_5O_6^-$ *and* Δ-[*Co(edta)*]$^-$): The optically active [Co(ox)$(en)_2$]$^+$ ion was first obtained by the substitution reaction[10] of optically active *cis*-[$CoCl_2(en)_2$]$^+$ with oxalate ion, or by preferential crystallization by seeding[11] some optically active complex salts into a concentrated aqueous solution of the racemic bromide [Co(ox)$(en)_2$]Br. The optical resolution through its diastereomer was first performed by Dwyer *et al.*[6] with the use of optically active [Co(edta)]$^-$ ion as the resolving agent. Later, Jordan *et al.*[7] reported a fine procedure of resolution through the $(+)_{589}$-tartrate(1—) diastereomer, [Co(ox)$(en)_2$]-(*d*-$C_4H_5O_6$).

Figure 3 shows the isotherm for the complex of X= *d*-$C_4H_5O_6^-$. Invariant point P appears near the right

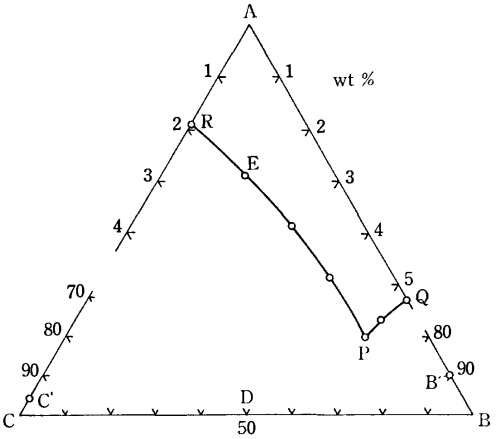

Fig. 3. Solubility isotherm of the ternary system H_2O-(A)-Δ-[Co(ox)$(en)_2$](*d*-$C_4H_5O_6$)(B)-Λ-[Co(ox)$(en)_2$](*d*-$C_4H_5O_6$) (C) at 25 °C. The solid phase B′ is 2.5 hydrate of B, and C′ monohydrate of C.

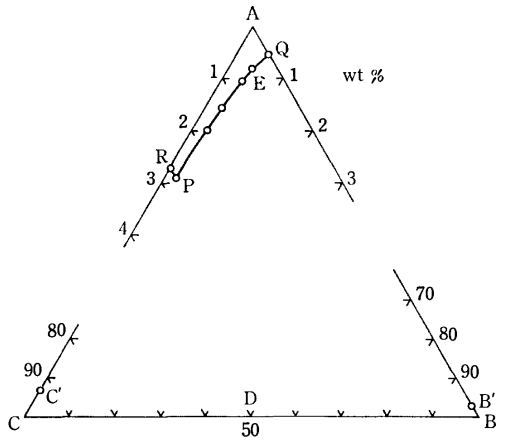

Fig. 4. Solubility isotherm of the ternary system H_2O-(A)-Δ-[Co(ox)(en)$_2$]·Δ-[Co(edta)](B)-Λ-[Co(ox)(en)$_2$]·Δ-[Co(edta)](C) at 25 °C. The solid phase B′ is monohydrate of B, and C′ 2.5 hydrate of C.

hand side. If an aqueous solution of equimolar mixture of the two diastereomers is concentrated at this temperature, the less soluble diastereomer Λ-[Co(ox)(en)$_2$](*d*-$C_4H_5O_6$)·H_2O would crystallize out first and the solution composition would change along the solubility curve EP. The solid phase consists of both the diastereomers at P. Figure 4 shows the case of X=Δ-[Co(edta)]$^-$, the invariant point P appearing near the left hand side. It is expected that the nearer the invariant point to the right or left hand side, the higher the relative yield of the less soluble diastereomer. The relative composition of the saturated solution at point P is Δ: Λ=3.75: 50 and 50: 10.6 for the X=Δ-[Co(edta)]$^-$ and X=*d*-$C_4H_5O_6^-$, respectively.

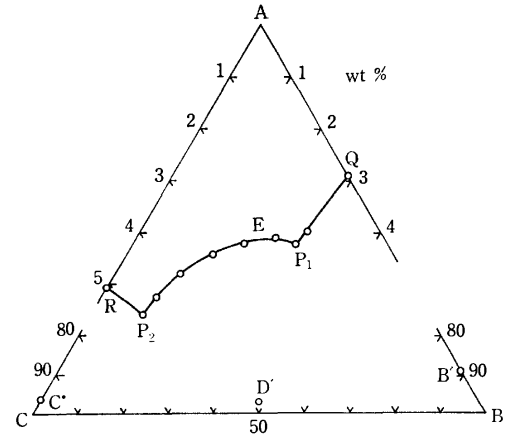

Fig. 5. Solubility isotherm of the ternary system H_2O-(A)-Δ-[Co(ox)(en)$_2$](*d*-$C_{10}H_{14}OBrSO_3$)(B)-Λ-[Co(ox)-(en)$_2$](*d*-$C_{10}H_{14}OBrSO_3$)(C) at 25 °C. The solid phase B′ is tetrahydrate of B, C′ monohydrate of C, and D′ *rac*-[Co(ox)(en)$_2$](*d*-$C_{10}H_{14}OBrSO_3$)·H_2O.

Optically Active Racemate Formed between Diastereomers. [*Co(ox)(en)*$_2$]*X* (*X*=$^1/_2$[*Sb*$_2$(d-$C_4H_2O_6$)$_2$]$^{2-}$ *and* d-$C_{10}H_{14}OBrSO_3^-$): Figure 5 shows the isotherm for the system consisting of Δ and Λ diastereomers of the $(+)_{589}$-(1*R*,3*S*,4*S*,7*R*)-3-bromocamphor-9-sulfonate salt and water. Two invariant points P_1 and P_2 appear, the curve P_1EP_2 representing the solubility of a new solid compound formed between the two diastereomers. This solid compound was isolated from the system and characterized by elemental analysis, visible and ultraviolet absorption, CD, ORD, and IR spectra. It was confirmed that the compound is an optically active racemate, Δ-[Co(ox)-(en)$_2$](*d*-$C_{10}H_{14}OBrSO_3$)·Λ-[Co(ox)(en)$_2$](*d*-$C_{10}H_{14}O$-$BrSO_3$)·$2H_2O$ = *rac*-[Co(ox)(en)$_2$](*d*-$C_{10}H_{14}OBrSO_3$)·H_2O. The same compound was obtained by treating *rac*-[Co(ox)(en)$_2$]Cl·H_2O with silver *d*-bromocamphorsulfonate (see Experimental). If an aqueous solution of this active racemate is concentrated at 25 °C, its composition would change along AE (Fig. 5) and the racemate monohydrate (D′) would crystallize out at point E. Thus the separation of Δ and Λ diastereomers by fractional crystallization is impossible, though the solubility of the two diastereomers in water differs greatly (Table 2).

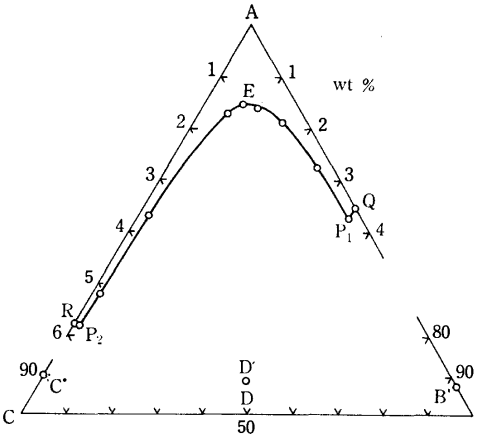

Fig. 6. Solubility isotherm of the ternary system H_2O-(A)-Δ-[Co(ox)(en)$_2$]$_2$[Sb$_2$(*d*-$C_4H_2O_6$)$_2$](B)-Λ-[Co(ox)-(en)$_2$]$_2$[Sb$_2$(*d*-$C_4H_2O_6$)$_2$](C) at 25 °C. The solid phase B′ is tetrahydrate of B, C′ hexahydrate of C, and D′ *rac*-[Co(ox)(en)$_2$]$_2$[Sb$_2$(*d*-$C_4H_2O_6$)$_2$]·$5H_2O$.

Figure 6 shows the case of X=$^1/_2$[Sb$_2$(*d*-$C_4H_2O_6$)$_2$]$^{2-}$. Here, the solubility curve of the active racemate is spread over a wide region and those of the pure Δ and Λ diastereomers are much suppressed. The racemate has the composition Δ-[Co(ox)(en)$_2$]·Λ-[Co(ox)(en)$_2$]·[Sb$_2$(*d*-$C_4H_2O_6$)$_2$]·$5H_2O$=*rac*-[Co(ox)(en)$_2$]$_2$[Sb$_2$(*d*-$C_4H_2O_6$)$_2$]·$5H_2O$.

It is generally thought that the so-called inadequate resolving agent is the one which gives a pair of diastereomers with a smaller difference in solubility. The present solubility data, however, show that the formation of an optically active racemate is also an important cause for unsuccessful optical resolution. A few such active racemates have been reported: a *d*-tartrate(2−) racemate, *rac*-[Co(en)$_2$(1,10-phenanthroline)]$_2$(*d*-$C_4H_4O_6$)$_3$·$9H_2O$, which has been named by Jaeger[12] a "partial racemoid."

Temperature Dependence of Solubility in Water. Table 2 shows temperature dependence of solubility of the [Co(ox)(en)$_2$]$^+$ salts containing optically active counter ions in water. Most of the salts show a temperature dependence similar to that of the halide salts.[4] Thus the solubility at 25 and 60 °C is 1.5—2 and 3—5 times larger than that at 5 °C, respectively. An exceptional

case is found in Λ-[Co(ox)$(en)_2$]·Δ-[Co(edta)]·2.5H_2O, its solubility at 60 °C being about 9 times greater than that at 5 °C. The solubility difference between the Δ and Λ diastereomers of Δ-[Co(edta)]$^-$ salt becomes very large at higher temperatures.

The solubility curve of Δ-[Co(ox)$(en)_2$](d-$C_{10}H_{14}OBrSO_3$) has an inflection point at about 35 °C, where the solid phase changes from 4-hydrate (below 35 °C) to 2.5-hydrate (above 35 °C). However, no such inflection was found in the corresponding Λ diastereomer or the active racemate. The solid phases of both salts consist of the monohydrate in 5—60 °C.

References

1) H. W. B. Roozeboom, *Z. Phys. Chem. (Leipzig)*, **28**, 494 (1899).
2) R. M. Secor, *Chem. Rev.*, **63**, 297 (1963).
3) D. G. Brewer and K. T. Kan, *Can. J. Chem.*, **49**, 965 (1971).
4) K. Yamanari, J. Hidaka, and Y. Shimura, *Bull. Chem. Soc., Jpn.*, **46**, 3724 (1973).
5) K. Yamasaki, H. Igarashi, Y. Yoshikawa, and H. Kuroya, *Inorg. Nucl. Chem. Lett.*, **4**, 491 (1968).
6) F. P. Dwyer, I. K. Reid, and F. L. Garvan, *J. Am. Chem. Soc.*, **83**, 1285 (1961).
7) W. T. Jordan, B. J. Brennan, L. R. Froebe, and B. E. Douglas, *Inorg. Chem.*, **12**, 1827 (1973).
8) L. R. Froebe, Ph. D. Thesis, Univ. of Pittsburgh (1970), p. 90.
9) C. W. Maricondi and B. E. Douglas, *Inorg. Chem.*, **11**, 688 (1972).
10) A. Werner and T. P. McCutcheon, *Ber.*, **45**, 3281 (1912).
11) A. Werner and J. Bosshart, *Ber.*, **47**, 2171 (1914).
12) F. M. Jaeger, *Proc. R. Acad. Amsterdam*, **29**, 559 (1926).

Kinetic Studies of the Inversion of η^2-*trans*-2-Butene in Platinum(II) Complexes Containing Various Amino Carboxylates

Yoshiro TERAI, Hiroaki KIDO, Kazuo KASHIWABARA,* Junnosuke FUJITA,* and Kazuo SAITO

Chemistry Department, Faculty of Science, Tohoku University, Sendai 980

(Received August 9, 1976)

Platinum(II) complexes containing *S,S*- or *R,R*-*trans*-2-butene and various L-amino carboxylate, *i.e.* *cis*(*N*, olefin)[PtCl (L-prolinate)(*S,S*-*trans*-2-butene)] and *trans*(*N*,olefin)[PtCl (L-am)(*S,S*- or *R,R*-*trans*-2-butene)], were synthesized (L-am=L-prolinate, *N*-methyl-L-prolinate, *N*-benzyl-L-prolinate, L-alaninate and L-valinate). The kinetics of the inversion reaction of the coordinated *S,S*- or *R,R*-*trans*-2-butene was investigated in acetone in the presence of an excess of *trans*-2-butene at 8.0 °C. Second order rate law was obeyed with respect to the concentrations of the complex and free olefin, and no solvent path was observed. In the *trans*(*N*,olefin) complexes, interactions steric around the coordinated nitrogen atoms seems to be responsible in determining the ease of inversion *via* an associative mechanism. On the other hand, smaller rate for the *cis*(*N*,olefin) complex than the corresponding trans isomer seems to be due to the trans effect.

The substitution reaction of various olefins for the η^2-*trans*-2-butene in [PtCl(L-pro)(*S,S*-*trans*-2-butene)] (L-pro=L-prolinate) in acetone gave a variety of rate and activation entropy,[1,2] and we pointed out the importance of the steric effect between the nucleophilic olefin and the coordinated amino carboxylate and/or olefin.[1] This paper deals with further kinetic studies of the exchange of *trans*-2-butene with inversion of configuration by use of *cis*(*N*,olefin)[PtCl(L-pro)(*S,S*-*trans*-2-butene)] and various *trans*(*N*,olefin)[PtCl(L-am)(*S,S*- or *R,R*-*trans*-2-butene)] in acetone, where L-am stands for various amino carboxylates, *i.e.* L-prolinate, *N*-methyl-L-prolinate (*N*-Me-L-pro), *N*-benzyl-L-prolinate (*N*-Bz-L-pro), L-alaninate (L-ala), and L-valinate (L-val).

Experimental

Materials. *N*-Methyl- and *N*-benzyl-L-proline were prepared from L-proline.[3] Guaranteed grade L-proline, L-alanine and L-valine and pure grade *trans*-2-butene (Nihon Tokushu Gas Co.) were used without further purification.

Preparation of the Complexes: The *trans*(*N*, olefin) complexes, *trans*(*N*, olefin)[PtCl(L-am)(olefin)] (olefin=ethylene and *trans*-2-butene) were synthesized by the reported methods.[4] The cis complex *cis*(*N*, olefin)[PtCl(L-pro)(C_2H_4)] was prepared by a new method with tin(II) chloride as a catalyst. Three mol dm^{-3} hydrochloric acid (15 cm^3) and K[$PtCl_2$(L-pro)](2 g)[5] were sealed in a 50 cm^3 flask with a rubber stopper, and nitrogen was bubbled for 30 min. A suspension of *ca.* 30 mg tin(II) chloride dihydrate in deoxygenated water (2—3 cm^3) was added with a syringe and ethylene was bubbled slowly with a vigorous stirring. Colorless crystals precipitated within 20 min. After 30 min the flask was cooled by ice, and the precipitate was filtered off, washed with water, air-dried at room temperature, and recrystallized from *N,N*-dimethylformamide (DMF) or acetonitrile (AN). Yield *ca.* 67%.
cis(*N*, olefin)[PtCl(L-pro)(*trans*-2-butene)] was obtained by replacing the coordinated ethylene by *trans*-2-butene in AN, and recrystallized from AN by adding diethyl ether.

All the *trans*-2-butene complexes were resolved by repeated fractional recrystallization until the CD spectra remained unchanged in a mixture of acetone and petroleum ether (trans complex) or of AN and diethyl ether (cis complex).

Identification of Geometrical Isomers: Elemental analysis of carbon, hydrogen, and nitrogen of all the new complexes agreed with the calculated values as shown in Table 1. It was claimed that the *trans*(*N*, olefin) complexes are pale-yellow and *cis*(*N*, olefin) complexes are colorless.[4] The present new complexes seem to obey this empirical rule, when the geometrical isomerism of the prepared complexes is assigned on the basis of the route of synthesis (for the formation of the cis complexes *vide infra*). The pale-yellow and colorless [PtCl(L-pro)(*trans*-2-butene)] gave IR absorption at 350 and 340 cm^{-1}, respectively, which can be assigned to Pt-Cl stretching vibration. This correspondence is also in accord with the empirical rule.[4] The trans complexes are soluble in acetone, AN, and DMF, whereas the cis complexes are very sparingly soluble in acetone and AN and soluble in DMF. Thus the geometrical

TABLE 1. ANALYTICAL DATA OF THE NEW COMPLEXES, *trans*(*N*, olefin) [PtCl(L-am)(olefin)]

L-am	Olefin	C/%		H/%		N/%	
		Calcd	Found	Calcd	Found	Calcd	Found
L-ala	*trans*-2-Butene	22.43	22.51	3.77	3.72	3.74	3.71
L-val	Ethylene	22.43	22.46	3.77	3.83	3.74	3.76
	trans-2-Butene	26.84	26.74	4.50	4.48	3.48	3.51
N-Me-L-pro	Ethylene	24.84	24.81	3.65	3.65	3.62	3.59
	trans-2-Butene	28.95	28.84	4.37	4.48	3.38	3.35
N-Bz-L-pro	Ethylene	36.33	36.30	3.93	3.91	3.03	2.85
	trans-2-Butene	39.15	39.17	4.52	4.50	2.85	2.63
L-pro *cis*(*N*, olefin)	Ethylene	22.56	22.41	3.25	3.25	3.76	3.82
	trans-2-Butene	26.97	26.74	4.02	3.97	3.50	3.39

* Present Address: Department of Chemistry, Faculty of Science, Nagoya University, Nagoya 464.

isomers can be distinguished by the color of crystals, synthetic route, IR absorption, and solubility.

Kinetic Runs. The decrease in CD strength of the complexes with time was recorded in acetone by the following method. The complexes were dissolved in acetone to give *ca.* 10^{-3} mol dm^{-3} solution, cooled and mixed with cold *trans*-2-butene in acetone (10^{-2} to 1 mol dm^{-3}). The solution was placed in a cell box of a spectrometer, which had been cooled to 8.0±0.3 °C, and the decrease in CD strength at the CD peak (360—385 nm) was continuously recorded. The rate of decrease obeyed the first order kinetic law and the observed rate constant k_{obsd} is expressed by Eq. 1.

$$k_{obsd} = -\ln[(\alpha_t-\alpha_\infty)/(\alpha_0-\alpha_\infty)]/t \quad (1)$$

Where α's are the CD strength at the time denoted by the suffices. The concentrations of the complex and free olefin at 8.0 °C were calculated by taking the density of acetone into consideration.

Measurements. The CD spectra were recorded with a JASCO Model ORD/UV-5 Spectrometer with CD attachment. Visible and UV spectra and IR spectra were recorded with a Hitachi 323 and a JASCO DS-403 G, respectively, A Komatsu-Yamato Coolnics thermostat was used for keeping the temperature at 8.0 °C.

Results and Discussion

Preparation of cis(N,*olefin*)[*PtCl*(L-*pro*)(trans-*2-butene*)]. *cis*(*N*, olefin)-complexes of platinum(II) containing prochiral olefin have been known only for the type [$PtCl_2$(*S*- or *R*-α-methylbenzylamine)(*S,S*- or *R,R*-*trans*-2-butene)].[6] We have succeeded in preparing *cis*(*N*, olefin)[PtCl(L-pro)(*trans*-2-butene)] by the substitution of *trans*-2-butene for the ethylene in *cis*(*N*,olefin)[PtCl(L-pro)(C_2H_4)] in AN. Several *cis*(*N*,olefin)[PtCl(am)-(C_2H_4)] had been prepared by the reaction of amino carboxylate with $[PtCl_4]^{2-}$ followed by the action of concentrated hydrochloric acid and ethylene in aqueous solution. However, the corresponding L-prolinate complex was not obtained by this method.[4]

We have found that tin(II) chloride was a useful catalyst for the synthesis of *cis*(*N*,olefin)[PtCl(L-pro)-(C_2H_4)]. Belluco *et al.* studied the mechanism of the catalytic action of tin(II) chloride in the substitution of aquo-soluble olefins for the chloride in $[PtCl_4]^{2-}$ in hydrochloric acid.[7] They considered the formation of some reactive intermediates containing $SnCl_3^-$ ligand. In the present synthesis, $[PtCl_3$(L-proH)$]^-$ (L-proH is coordinated as a unidentate on nitrogen) may have been formed from $[PtCl_2$(L-pro)$]^-$,[5] and reacted with tin(II) chloride in deoxygenated concentrated hydrochloric acid solution, to give *cis*-$[PtCl_2$(L-proH)(C_2H_4)$]^-$ *via* similar intermediates containing $SnCl_3^-$. This *cis* complex must be in equilibrium with *cis*(*N*,olefin)-[PtCl(L-pro)(C_2H_4)] in aqueous solution and the less soluble latter complex was precipitated as colorless crystals. The corresponding L-alaninato complex *cis*(*N*, olefin)[PtCl(L-ala)(C_2H_4)] was not obtained by this method, presumably because of its solubility in aqueous solution.

UV Absorption and CD Spectra. Spectral data of UV absorption of all the trans complexes give d-d transition absorption around 25000 cm^{-1}, whereas the cis complexes at *ca.* 28000 cm^{-1} (Table 2). The CD maxima of all the trans complexes in this region are 26.0—27.0×10^3 cm^{-1}, and that of the cis complex is at 27.8×10^3 cm^{-1}. The diastereoisomers with plus CD in this region are assigned to *S,S*- and those with minus CD to *R,R*-configuration of coordinated *trans*-2-butene, in accordance with Scott and Wrixon's empirical rule.[8]

Table 2. The UV absorption spectral data of *trans*- and *cis*(*N*, olefin) [PtCl(L-am)(olefin)] in ethanol

	Olefin	Absorption maxima/10^3 cm^{-1} (logε)		
trans-Complex	C_2H_4	*ca.* 25* (1.6—1.8)	*ca.* 33.5 (≈3)	37—38 (3.2—3.3)
	trans-2-Butene	*ca.* 25* (1.5)	35—36* (≈3)	*ca.* 39* (3.1—3.3)
cis-Complex	C_2H_4	*ca.* 28* (1.5)	*ca.* 35* (2.9)	*ca.* 38 (3.3)
	trans-2-Butene	*ca.* 28* (1.5)	*ca.* 33.5* (2.4)	*ca.* 39* (3.3)

* shoulder

Table 3. The Δε values of CD maxima in d-d region of the completely resolved *trans* (*N*, olefin)[PtCl(L-am)(*S,S*- or *R,R*-*trans*-2-butene)] and that of the corresponding ethylene complexes in ethanol

L-am	ν (CD max) 10^{3}cm^{-1}	Δε(C_4H_8) (a,c)	Δε(C_2H_4) (b,c)	δΔε[d]	C_4H_8[e]
L-ala	27.0	+1.13	0	+1.13	*S,S*
L-val	26.7	−1.0	0	−1.0	*R,R*
L-pro	27.0	+1.05	−0.05	+1.10	*S,S*
N-Me-L-pro	26.3	−1.06	+0.02	−1.08	*R,R*
N-Bz-L-pro	26.0	+1.00	−0.19	+1.19	*S,S*
L-pro[f]	27.8	+1.14	+0.12	+1.02	*S,S*

a) Δε value of the *trans*-2-butene complex b) Δε value of the ethylene complex, c) at the CD maxima of the *trans*-2-butene complexes at *ca.* 27000 cm^{-1}, d) Δε (*trans*-2-butene complex)-Δε(C_2H_4 complex), e) absolute configuration of coordinated *trans*-2-butene, f) *cis* (*N*, olefin)[PtCl(L-pro)(olefin)].

Table 3 gives the CD strength of all the completely resolved complexes at the peak of the *trans*-2-butene complexes in the d-d transition band region. These complexes are the diastereoisomers first crystallized on fractional crystallization. It also shows the difference in CD strength between the *trans*-2-butene- and the ethylene complexes at the wave length mentioned above. The δΔε is almost equal for all the complexes, suggesting that the contribution of asymmetrically coordinated *trans*-2-butene to the CD strength is not affected by the variety of the coordinated amino carboxylates.

Kinetics of the Inversion of trans-*2-Butene.* When *trans*-2-butene was added to the *trans*- and *cis*(*N*,olefin)-[PtCl(L-am)(*S,S*- or *R,R*-*trans*-2-butene)] complexes in acetone at 8.0 °C, the UV absorption remained unchanged for at least two days, whereas the CD strength at the peak in 360—385 nm region decreased obeying Eq. 1. This reaction should be the substitution with inversion of *trans*-2-butene ligand, *i.e.* the epimerization of the complex on the substitution.

The k_{obs} increased linearly with increase in free *trans*-2-butene concentration to give Eq. 2.

$$k_{obsd} = k_2[\textit{trans}\text{-2-butene}] \quad (2)$$

The k_2 is related to the rate constant of the inversion reaction, k_2^{inv}, by the relation $k_2=2k_2^{inv}$. However, the k_2 values are used in the following discussion. By use of *cis*-2-butene in place of *trans*-2-butene as nucleophile the same relation holds. Absence of intercept on the k_{obsd} *vs.* free ligand concentration diagram indicates no participation of the solvent molecule in the rate determining process.

trans(N,*olefin*) *Complexes*: The second order rate constant decreases in the following sequence as the amino carboxylate was changed. (Table 4).

TABLE 4. RATE CONSTANTS OF THE EPIMERIZATION REACTION OF *trans*(*N*, olefin)[PtCl(L-am)(*S,S*- or *R,R-trans*-2-butene)] IN ACETONE AT 8.0 °C

L-am	Config.[a]	Added olefin	$k_2/10^{-3}$ s^{-1} mol^{-1} dm^3
L-ala	*S,S*	*trans*-2-Butene	30 ± 3
L-val	*R,R*	*trans*-2-Butene	39 ± 4
L-pro	*S,S*	*trans*-2-Butene	9.7 ± 0.6[b,c]
L-pro	*R,R*	*trans*-2-Butene	7.6 ± 0.3
L-pro	*S,S*	*cis*-2-Butene	350 ±13[b,d]
N-Me-L-pro	*R,R*	*trans*-2-Butene	0.54± 0.01
N-Me-L-pro	*R,R*	*cis*-2-Butene	26 ± 5[d]
N-Bz-L-pro	*R,R*	*trans*-2-Butene	<0.01
L-pro[e]	*S,S*	*trans*-2-Butene	<0.3

a) Configuration of coordinated *trans*-2-butene. b) Ref. 1. c) The datum was obtained by the different method (see Ref. 1). d) The rate is not epimerization, but substitution rate. e) *cis*(*N*, olefin)[PtCl(L-pro)(*S,S-trans*-2-butene)].

$$\text{L-val, L-ala} > \text{L-pro} > \textit{N}\text{-Me-L-pro} > \textit{N}\text{-Bz-L-pro} \quad (3)$$

No appreciable difference is seen between the rate for the L-alaninato and L-valinato complex, indicating little influence of the substituents on the asymmetric carbon atoms. Hence, the discussion is to be made among complexes containing various substituents on the coordinated nitrogen atom.

The difference among k_2 values can be interpreted either by the electronic or the steric effect brought about by the amino carboxylates. The most important electronic effect affecting the rate of substitution reaction around square planar complexes is the trans effect. Various factors can give influence upon this effect, but the basicity of the nitrogen atom should be looked upon as predominating in the present complexes. L-Proline has larger pK_a (10.64 at 25 °C) than L-alanine and L-valine (9.64 and 9.72, respectively), and the L-prolinato complex gives much smaller k_2 than the L-alaninato- and L-valinato complexes do. On the other hand, *N*-methyl-L-proline can be expected to be more basic than *N*-benzyl-L-proline (because pK_a of methylamine and benzylamine are 10.68 and *ca.* 9.6, respectively at 25 °C), but the k_2 value of *N*-methyl-L-prolinato complex is larger than that of *N*-benzyl-L-prolinato complex. Thus no regular relationship is observed between the basicity of the amino nitrogen and the second order rate constant, suggesting that the electronic effect is not very important in determining the ease of inversion of *trans*-2-butene.

Parametrization of steric effect is far more difficult. We will use the overall bulkiness of ligands around the platinum(II) ion as influencing the ease of formation of the transition state with coordination number 5 containing two moles of *trans*-2-butene. The k_2 values do not differ much by use of a pair of diastereomers containing *R,R*- and *S,S-trans*-2-butene. Thus, our tentative representation of the overall bulkiness by molecular model studies would not be very inappropriate. Studies with molecular models indicate that the bulkiness of the coordinated amino carboxylate around the platinum(II) ion increases in the sequence of Fig. 1. This sequence is equal to the sequence (3). Thus, presence of bulky substituents on the nitrogen atom may hinder the formation of the transition state with coordination number 5, to result in slower substitution of the olefin.

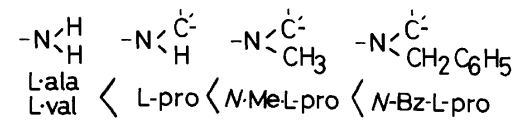

Fig. 1. Sequence of the bulkiness of the coordinated amino nitrogen.

Moreover, Table 4 includes the rate of substitution of *cis*-2-butene for the coordinated *trans*-2-butene. *cis*-2-Butene is not prochiral and its substitution always brings about decrease in CD strength,[1] so that the rate indicates the ease of substitution. When the L-prolinato and the *N*-methyl-L-prolinato complexes are compared, the ratio of their k_2 values is almost equal for both the substitution of *cis*-2-butene and the inversion of *trans*-2-butene. This fact suggests that the bulkiness of the coordinated amino carboxylate affects the rate of the substitution of *cis*-2-butene in a similar manner.

cis(N,*olefin*) *Complex*: Studies with molecular models suggest no significant difference in overall bulkiness around the platinum(II) ion between the *cis*(*N*,olefin)- and the *trans*(*N*,olefin)-L-prolinato complexes. On the other hand, a significant difference in electronic effect is expected, since the pK_a value of the carboxylate oxygen (1.99 at 25 °C) is far smaller than that of the nitrogen (*loc. cit.*). Such a difference is reflected in the frequency of Pt–Cl streching vibration; *i.e.* the *cis*(*N*,-olefin) complex with nitrogen trans to chloride gives an IR absorption peak at 340 cm^{-1}, whereas *trans*(*N*,olefin) with the oxygen trans to chloride at 350 cm^{-1}. Thus a basic ligand at the trans position seems to make the Pt–Cl bond loose. The nature of metal–ligand bond between Pt(II) and η^2-olefin should be significantly different from that between Pt(II) and chloride. However, the ease of exchange of olefins in [PtCl(L-am)(olefin)] seems to be mainly governed by the strength of σ-bond between Pt(II) and olefin.[2] *trans*-2-Butene–Pt(II) bond can be made loose by the trans influence of basic nitrogen in the *trans*(*N*,olefin) complex, so that the k_2 value becomes greater than that of the *cis*(*N*,olefin) complex.

The authors' thanks are due to the Takeda Science Foundation for financial support.

References

1) Y. Terai, H. Kido, J. Fujita, and K. Saito, *Bull. Chem. Soc. Jpn.*, **48**, 1233 (1975).
2) K. Konya, H. Kido, J. Fujita, and K. Saito *Bull. Chem. Soc. Jpn.*, **45**, 2161 (1972).
3) P. Quitt, J. Hellerbach, and K. Vogler, *Helv. Chim. Acta*, **46**, 327 (1963); A. B. Mauger and B. Witkop, *Chem. Rev.*, **66**, 47 (1966).
4) J. Fujita, K. Konya, and K. Nakamoto, *Inorg. Chem.*, **9**, 2794 (1970).
5) H. Ito, *Thesis*(Tohoku University) (1967).
6) G. Paiaro and A. Panunzi, *J. Am. Chem. Soc.*, **86**, 441 (1965).
7) R. Pietropaolo, G. Dolcetti, M. Giustiniani, and U. Belluco, *Inorg. Chem.*, **9**, 549 (1970).
8) A. I. Scott and A. D. Wrixon, *Tetrahedron*, **27**, 2339 (1971).

Studies on Mixed Chelates. VII. Mixed Nickel(II) Chelates Containing *N,N'*- or *N,N*-Dialkylethylenediamines and Acetylacetone

NGUYEN Thi Nga, Yutaka FUKUDA, and Kozo SONE

Department of Chemistry, Faculty of Science, Ochanomizu University, Otsuka, Bunkyo-ku, Tokyo 112

(Received August 19, 1976)

Twelve mixed nickel(II) chelates with *N,N'*- or *N,N*-dimethyl (or diethyl)ethylenediamines and acetylacetonate ion (acac) were prepared, and their properties were compared with those of the similar chelates with *N,N,N',N'*-tetramethyl(or tetraethyl)ethylenediamine. With the decrease of the number and bulkiness of the *N*-alkyl groups in the diamine, the tendency of forming 6-coordinated mixed chelates remarkably increases. The chelates of the type [Ni(diamine)(acac)]X, formed when X is $B(Ph)_4$, which are essentially similar to the corresponding chelates with *N,N,N',N'*-tetraalkylethylenediamines, but more apt to combine with solvent molecules and to go over into 6-coordinated structures than the latter.

In the previous papers,[1,2] the authors reported that *N,N,N',N'*-tetramethylethylenediamine (tmen) and various β-diketonate ions form two kinds of nickel(II) chelates, *i.e.*, the blue, 6-coordinate, high-spin $[Ni(tmen)(\beta\text{-dik})(OH_2)_2]ClO_4$, $[Ni(tmen)((\beta\text{-dik})NO_3]$ and $[Ni(tmen)(\beta\text{-dik})_2]$ and red, planar 4-coordinate, low-spin $[Ni(tmen)(\beta\text{-dik})]ClO_4$ and $[Ni(tmen)(\beta\text{-dik})]B(Ph)_4$, and an equilibrium is established in organic solutions of the latter chelates:

$$\underset{\text{Red}}{[Ni(tmen)(\beta\text{-dik})]^+} + 2Solv. \rightleftarrows \underset{\text{Blue}}{[Ni(tmen)(\beta\text{-dik})(Solv.)_2]^+}$$

(Solv.=solvent molecule). They also studied the chelates containing *N,N,N',N'*-tetraethylethylenediamine (teen) instead of tmen and found generally similar results, but here the planar chelates are more reluctant to go over into 6-coordinate structures, owing to the increased steric hindrance of the larger N-alkyl groups.

In this paper the authors will report on the preparation and properties of similar mixed chelates containing *N,N'*-dimethyl, *N,N*-dimethyl, *N,N'*-diethyl, and *N,N*-diethylethylenediamines (abbreviated as sym-dmen, unsym-dmen, sym-deen and unsym-deen,[3] respectively) and acetylacetonate ion (acac).

Experimental

Preparation of the Chelates. Chelates of the Type [Ni(diamine)(acac)$_2$] (No. I—No. IV in Table 1): To an aqueous solution of $Ni(ClO_4)_2 \cdot 6H_2O$ (10 mmol), acetylacetone (20 mmol) and an aqueous solution of Na_2CO_3 (5 mmol) are added with stirring. The precipitate formed is dissolved in methanol, and dmen or deen (10 mmol) is added. A blue solution is obtained, from which blue crystals separate out upon concentration and standing. They are recrystallized from 1,2-dichloroethane.

The sym-dmen and sym-deen chelates prepared in this way contain one molecule of crystal water, but the unsym-dmen and unsym-deen chelates are anhydrous.

Chelates of the Type [Ni(diamine)$_2$(acac)]ClO$_4$ (No. V—No. VIII): To a methanolic solution of $Ni(ClO_4)_2 \cdot 6H_2O$ (10 mmol), acetylacetone (10 mmol), Na_2CO_3 (5 mmol), and dmen or deen (10 mmol) are added in succession. The blue solution is filtered, concentrated and let stand, until crystals separate out, which are recrystallized from 1,2-dichloroethane.

Chelates of the Type [Ni(diamine)(acac)]B(Ph)$_4$ (No. IX—No. XII): To a methanolic solution of $Ni(NO_3)_2 \cdot 6H_2O$ (10 mmol), acetylacetone (10 mmol), Na_2CO_3 (5 mmol) and sym- or unsym-dmen (10 mmol) are added with stirring in succession. The blue solution is evaporated to driness, and the residue is dissolved in 1,2-dichloroethane and filtered. To this solution, which is expected to contain $[Ni(dmen)(acac)NO_3]$ (*cf.* the preparations of $[Ni(tmen)(acac)NO_3]$ and $[Ni(teen)(acac)NO_3]$ reported before[1,2]), $NaB(Ph)_4$ (14 mmol) is added. A red solution is obtained, which is filtered, concentrated and let stand, until red crystals separate out, which are recrystallized from 1,2-dichloroethane.

The chelates with sym- and unsym-deen are more difficult to prepare. Their 1,2-dichloroethane solutions can be obtained in the same way, but they become syrupy upon concentration. Precipitating with diethyl ether, powder-like mixed chelates can be obtained from them.

Physical Measurements. The methods and instruments used in this study were the same as those in the previous studies of this series.[1,2]

Results and Discussion

The formulas, colors, compositions, and effective magnetic moments of the obtained chelates are shown in Table 1. It is clear that the blue chelates, No. I—No. VIII, are all high-spin, and the red ones, No. IX—No. XII, are all low-spin, and each of them should be formulated as shown. The small magnetic moments of the red chelates are probably due to impurities, since all of them were rather difficult to prepare and purify, and may contain small amounts of high spin chelates.

Formation and Preparation of the Chelates. Although it was tried to get all kinds of mixed chelates corresponding to those obtained before,[1,2] it was found that, with the four dialkyl diamines used in this study, the formation of the chelate species $[Ni(diamine)(acac)_2]$ and $[Ni(diamine)_2(acac)]^+$, *i.e.*, blue, 6-coordinate, high-spin chelates containing three typical chelating ligands, seems to be strongly favored in the reaction mixtures, even when their compositions differ considerably from those of such chelates (*cf.* Experimental), so that only these chelates (the latter in the form of the perchlorates) could be obtained readily in crystalline state. Only in the case where the counter anion is tetraphenylborate, red, planar 4-coordinate and low-spin chelates $[Ni(diamine)(acac)]B(Ph)_4$ were obtained with some

TABLE 1. COLORS, COMPOSITIONS[a], AND MAGNETIC MOMENTS OF THE CHELATES OBTAINED

No.	Chelate	Color	C%	H%	N%	μ_{eff}(B.M.)
I	[Ni(sym-dmen)(acac)$_2$]·H_2O	Blue	46.11(46.30)	8.10(7.79)	7.64(7.72)	3.09
II	[Ni(unsym-dmen)(acac)$_2$]	Blue	48.48(48.73)	7.78(7.59)	8.08(8.12)	3.37
III	[Ni(sym-deen)(acac)$_2$]·H_2O	Blue	49.51(49.12)	8.31(8.26)	7.36(7.16)	3.13
IV	[Ni(unsym-deen)(acac)$_2$]	Blue	51.87(51.50)	8.03(8.10)	7.59(7.51)	3.13
V	[Ni(sym-dmen)$_2$(acac)]ClO_4	Bluish Violet	36.07(36.01)	7.40(7.22)	12.93(12.92)	3.05
VI	[Ni(unsym-dmen)$_2$(acac)]ClO_4	Blue	35.68(36.01)	7.44(7.22)	12.32(12.92)	3.10
VII	[Ni(sym-deen)$_2$(acac)]ClO_4	Blue	41.86(41.70)	8.45(8.03)	11.35(11.44)	3.12
VIII	[Ni(unsym-deen)$_2$(acac)]ClO_4	Blue	41.28(41.70)	8.28(8.03)	11.11(11.44)	3.12
IX	[Ni(sym-dmen)(acac)]$B(Ph)_4$	Red	69.41(70.13)	6.80(6.96)	4.96(4.95)	0.34
X	[Ni(unsym-dmen)(acac)]$B(Ph)_4$	Red	69.14(70.13)	6.87(6.96)	4.69(4.72)	0.52
XI	[Ni(sym-deen)(acac)]$B(Ph)_4$	Red	70.02(70.86)	7.46(7.31)	4.60(4.72)	0.75
XII	[Ni(unsym-deen)(acac)]$B(Ph)_4$	Red	68.14(70.86)	7.25(7.31)	4.53(4.72)	0.32

a) Calculated values in parentheses.

difficulty.*

It may be noted that the chelates of the type [Ni(diamine)$_2$(acac)]X can be prepared with dmen's and deen's but not with tmen and teen, while those of the type [Ni(diamine)(acac)$_2$] can be prepared with any of these diamines. This is undoubtedly due to the fact that the stability of a former type chelate depends critically on the magnitude of the large steric repulsion between two bulky diamines in it, while that of a latter type chelate does not depend so strongly on the bulkiness of the diamine since acac is a ligand of much smaller steric requirement.

Electronic Spectra. As in the case of the tmen and teen chelates, all these chelates are soluble in most organic solvents. The ν_{max} and ε_{max} values in the electronic spectra of such solutions, and the ν_{max} values in the reflection spectra of the solid chelates, are summarized in Tables 2 and 3.

The features of these spectra are in general very similar to those of the tmen- and teen-containing chelates.[1,2] All the high-spin chelates show two weak bands in the visible and near infrared regions, which move only little in going from the solid to the solutions

TABLE 2. $\nu_{max}/(10^3 cm^{-1})$ AND ε_{max}[a] OF THE HIGH-SPIN CHELATES OBTAINED

No.	Solid	$ClCH_2CH_2Cl$	Ethanol	DMF
I		10.00(12.8)	10.13(10.8)	10.05(11.8)
	16.81	16.53(7.8)	16.84(7.4)	16.75(7.7)
II		9.80(14.8)	9.83(10.8)	9.80(12.3)
	16.56	16.47(11.1)	16.50(7.4)	16.42(8.5)
III		9.85(12.4)	9.97(10.7)	9.90(11.8)
	16.56	16.53(7.8)	16.64(7.4)	16.56(7.7)
IV		9.62(11.1)	9.57(9.7)	9.62(10.1)
	16.61	16.31(7.1)	16.26(6.9)	16.29(7.0)
V		10.59(10.6)	10.49	10.58(11.2)
	17.24	17.35(8.4)	17.21	17.30(8.7)
VI		9.70(11.5)	9.76(11.2)	9.80(11.7)
	17.01	17.18(7.6)	16.84(7.2)	16.81(7.6)
		20.49(7.9)		
VII		10.34(10.9)	10.26	10.21(11.8)
		17.09(9.2)	16.92	16.95(8.5)
VIII		8.42(13.1)	8.46	8.66(9.8)
	16.92	16.95(5.7)	16.72	16.61(6.2)
		20.53(3.5)	20.92 vw	

a) In parentheses.

TABLE 3. $\nu_{max}/(10^3 cm^{-1})$ AND ε_{max}[a] OF THE LOW-SPIN CHELATES OBTAINED

No.	Solid	$ClCH_2CH_2Cl$	Acetone	Ethanol	DMF
IX			10.00 (9.6)	10.12(8.5)	10.18(9.4)
			16.61 (9.0)	16.47(6.5)	16.64(7.6)
	20.58	20.88(113)	20.70 (8.4)		
X			9.39 (8.0)	9.80(11.5)	9.83(9.9)
			16.08 (10.5)	16.39(9.2)	16.34(7.7)
	20.36	20.75(120)	21.37 (13.4)		
XI			9.90 (8.1)	9.90(8.7)	9.98(8.8)
			16.56 (9.6)	16.13(9.5)	16.64(8.7)
	20.66	20.79(110)	20.62 (19.6)	20.58 sh	20.49 vw
XII			7.38[b](10.0)	9.40(7.0)	9.62(8.1)
			15.72[b](16.1)	16.23(7.1)	16.29(7.6)
	20.70	20.62(122)	20.92 (36.0)	20.88 sh	

a) In parentheses. b) These very low values may be taken as an indication for the large interligand repulsion in the chelate [Ni(unsym-deen)(acac)(acetone)$_2$] which weakens the Ni–acetone bonds so much.

* The possibility that the chelates X and XII with unsym-diamines are, in fact, Schiff base chelates, *e.g.*, [Ni{NR_2-$(CH_2)_2$N=C(CH_3)CHCOCH_3}(OH_2)]$B(Ph)_4$ with the same compositions as the mixed chelates, can be ruled out, because the NMR spectra of these chelates are clearly in support of the mixed chelate formulation.[4]

in various solvents.** This fact shows that the structures of these 6-coordinate chelates are stable enough in solution and not influenced sensitively by the solvents used.

Comparison of the spectra in 1,2-dichloroethane, in which the interaction with the solutes will be the least, shows that, in each of the two series of the 6-coordinate chelates, the ν_{max} of the two bands decrease in the order (1) of the diamines:

$$\text{sym-dmen} > \text{sym-deen} \gtrsim \text{unsym-dmen} > \text{unsym-deen} \quad (1)$$

indicating that the ligand field strength (l.f.s.) in these chelates also decreases in this order. It may also be noted that, among the chelates of the type $[Ni(diamine)_2(acac)]X$, the decrease in ν_{max} is quite large (10590 cm^{-1} to 8420 cm^{-1} in ν_1, which is a direct measure of 10Dq), while among those of the type $[Ni(diamine)(acac)_2]$ it is much smaller (10000 to 9620 in ν_1), showing that the l.f.s in a former type chelate is much more sensitive to the steric change of its diamine than that in a latter type one, in comformity with the view on their ease of formation mentioned above.

On the other hand, the spectra of the red, 4-coordinate and low-spin chelates are influenced strongly by the solvent, but the mode of the spectral change observed is essentially the same as that observed among the corresponding chelates of tmen or teen, indicating that here again the equilibrium

$$\underset{\text{I}}{[Ni(diamine)(acac)]^+} + 2Solv. \rightleftarrows \underset{\text{II}}{[Ni(diamine)(acac)(Solv.)_2]^+}$$

is established in solution, which is shifted from the left hand side to the right as follows (Figs. 1 and 2):

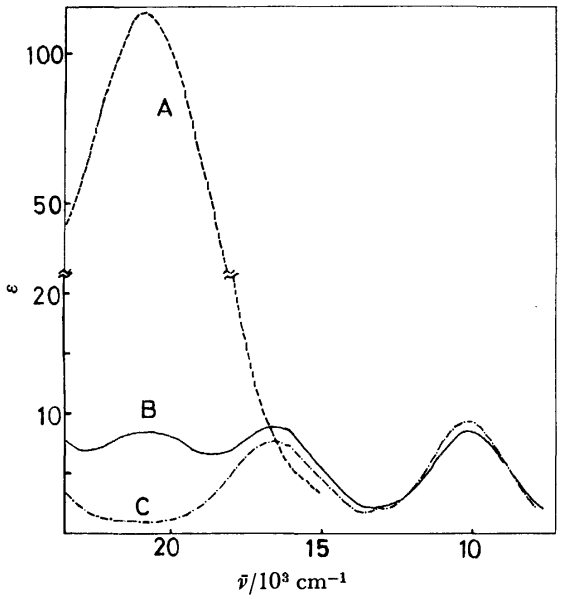

Fig. 1. Electronic spectra of the chelate IX in three solvents.
A: 1,2-Dichloroethane; B: acetone; C: DMF.

** The solid reflection spectra could be measured only up to 700 nm so that the first band is lacking in them.

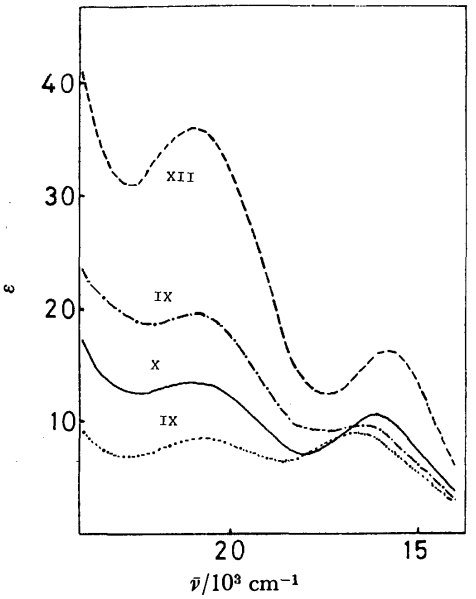

Fig. 2. Comparison of the electronic spectra of the chelates IX—XII in acetone.

TABLE 4. PERCENTAGES OF $[Ni(diamine)(acac)]^+$, REMAINING UNSOLVATED IN THE EQUILIBRIUM MIXTURES PRODUCED BY DISSOLVING THE CHELATES IX—XII AND THEIR tmen- AND teen- CONTAINING ANALOGUES IN ACETONE

IX	7.5%	$[Ni(tmen)(acac)]B(Ph)_4$ [a]	21%
X	11.0	$[Ni(teen)(acac)]B(Ph)_4$ [a]	82
XI	18.0		
XII	30.4		

a) *Cf.* Ref. 2.

$$\underset{\approx 100\%\ \text{I}}{\text{1,2-dichloroethane}} \longrightarrow \underbrace{\text{Acetone} \longrightarrow \text{Ethanol}}_{\text{I+II}} \longrightarrow \underset{\approx 100\%\ \text{II}}{\text{DMF}}$$

Increase in II (dearease in I) $\longrightarrow$

As in the case of the teen chelates,[2] it is possible to calculate the percentages of I in the equilibrium mixtures. From the data in Fig. 1, the values in Table 4 are obtained. The values for the corresponding tmen and teen chelates are also shown. It can be seen that the tendencies of these chelates to combine with solvent molecules and to go over into 6-coordinate structures decrease in the order:

$$\text{sym-dmen} > \text{unsym-dmen} > \text{sym-deen} \approx \text{tmen} > \text{unsym-deen} \gg \text{teen} \quad (2)$$

It is interesting to note that this order (2) is nearly the same as the order (1) of the decreasing l.f.s. in octahedral chelates.*** The relative positions of tmen and teen in the order (1), which can be found by comparing the data of the chelates of the type $[Ni(diamine)(acac)_2]$ with those of $[Ni(tmen)(acac)_2]$ and $[Ni(teen)(acac)_2]$,[1,2] are also nearly the same as their positions in the order (2), except that tmen lies between teen and unsym-deen.

*** In fact, there is also a slight shift of ν_{max} values of the planar $[Ni(diamine)(acac)]B(Ph)_4$ chelates in 1,2-dichloroethane in the order (1), showing that here too the l.f.s. decreases in this order.

These facts can be understood as follows: the total volume of the *N*-alkyl groups in a diamine increase naturally in the order:

teen > unsym-deen, sym-deen > unsym-dmen, sym-dmen

The position of tmen in this series will be somewhere near the deen's. Now if it is assumed that the amount of steric hindrance, which a neighboring ligand suffers from such groups in an unsym-diamine chelate, is somewhat larger than that in its sym-diamine analogue, the order (1) or (2) can be taken as the inverse order of such steric hindrance in each case. Thus the order (1) indicates that the l.f.s. in an octahedral chelate is weakened owing to the increasing interligand repulsion, and the order (2) that the coordination of solvent molecules above and below a planar chelate is hindered more and more owing to the increasing ligand-solvent repulsion.

It is also of interest to note that a weak band at 20000 to 21000 cm^{-1} is observed in some spectra of the chelates VI and VIII, indicating the formation of the species $[Ni(diamine)(acac)]^+$, or, in other words, the dissociation of a diamine molecule from the chelate cation, in solvents of lower coordination ability. Only the chelates of the type $[Ni(diamine)_2(acac)]X$ (and not those of the type $[Ni(diamine)(acac)_2]$) show such a band, and only the unsym-diamine chelates do so,

Table 5. Examples of ν_{CO}, $\nu_{C=C}$, and $\Delta\nu$ in the two types of chelates (cm^{-1})

Chelate	ν_{CO}	$\nu_{C=C}$	$\Delta\nu$	Spin type
II	1604	1514	90	High Spin
IV	1596	1516	80	
V	1597	1525	72	
VI	1586	1507	79	
XI	1578	1528	50	Low Spin
XII	1570	1525	45	

suggesting that here also interligand repulsion is playing a role.

Infrared Spectra. As in the case of the tmen and teen chelates, there are two strong bands at 1500—1600 cm^{-1}, which are ascribed to the C=C and C=O vibrations of acac, and their separations ($\Delta\nu$) are much larger in the 6-coordinate chelates than in 4-coordinate ones (Table 5). It was also found that ClO_4^- ions are not coordinated. In addition, there is N-H stretching absorption at *ca.* 3200 cm^{-1}, which is a single peak in the sym-, but split into two or three peaks in unsym-diamine chelates. The hydrated chelates show also O-H stretching absorption superposed on it, broadening the peak considerably.

In conclusion it can be said that, in going from tmen and teen to the dmen's and deen's, both the l.f.s. in octahedral chelates and their ease of formation (either from component ligands, or from a planar chelate and solvent molecules) remarkably increase, owing to the decrease in steric hindrance caused by the *N*-alkyl groups.

Sincere thanks of the authors are due to Prof. Hiroshi Kakizawa of Tokyo Kyoiku University, for his kind permission to use the Hitachi spectrophotometer in his laboratory. The present work was partially supported by a Grant-in-Aid for Scientific Research from the Ministry of Education.

References

1) Y. Fukuda and K. Sone, *J. Inorg. Nucl. Chem.*, **34**, 2315 (1972); **37**, 455 (1975).

2) Y. Fukuda, R. Morishita, and K. Sone, *Bull. Chem. Soc. Jpn.*, **49**, 1017 (1976).

3) Recently, Fabbrizzi *et al.* (L. Fabbrizzi, M. Micheloni, and P. Paoletti, *Inorg. Chem.*, **13**, 3019 (1974)) reported some interesting observations on the thermochromic Cu(II) and Ni(II) chelates of this ligand.

4) Y. Fukuda, unpublished work.

Fundamental Studies on the Ion-Exchange Separation of Boron Isotopes

Hidetake KAKIHANA, Masahiro KOTAKA, Shohei SATOH, Masao NOMURA, and Makoto OKAMOTO

Research Laboratory for Nuclear Reactors, Tokyo Institute of Technology, Ookayama, Meguro-ku, Tokyo 152

(Received August 20, 1976)

The single-stage separation factors for boron isotopes between an ion-exchange resin and an external solution were determined, using an ion-exchange breakthrough operation. The lighter isotope boron-10 was considerably enriched in the anion-exchange resin phase. The separation factor was very much influenced by the boric acid concentration in the external solution, but not as much influenced by the kind of the anion exchange resin used and operation temperature. The separation factor increased with a decrease in the boric acid concentration of external solution from 1.008 (0.501 mol/l)to 1.016 (0.010 mol/l). The value of the separation factors obtained experimentally were compared with those estimated on the basis of the theory of the two-phase distribution of isotopes.

Naturally occurring boron contains 19.8% boron-10 and 80.2% boron-11. The absorption cross section of natural boron for thermal neutrons is 752 barns; for pure boron-10 and boron-11, the corresponding values are 3837 and 0.005 barns, respectively.[1] This means that isotopically pure boron-10 is five times more effective as a neutron shield than natural boron. The large cross section of boron-10 for thermal neutrons and the α particle emission subsequent to neutron capture have suggested the possible use of boron compounds (enriched in boron-10) for neutron therapy of malignant tissue. This kind of nuclear approach is being actively pursued in the world, especially for treatment of brain tumors[2] and melanotic cancer.[3] In view of this characteristic of boron-10, it is not surprising that a demand for the separation of boron isotopes arose in very early stage of the nuclear era.

The first experiment on ion-exchange separation of boron isotopes had been done by Makishima and coworkers in 1959.[4] In this experiment, boric acid solution was passed through a column packed with a strong-base anion exchange resin (Amberlite CG-400-I) in hydroxide form. The boric acid concentration and the atomic fraction of boron-10 in each fraction of the effluent were measured. It was found that the lighter isotope boron-10 was enriched in the resin phase. and that the values of the single-stage separation factors were 1.010 for aqueous 0.03 mol/l boric acid, and 1.016 for 0.1 mol/l boric acid in 8% glycerol–water solution. Large-scale experiments stimulated by Makishima's work were carried out in France[5] and Spain.[6] Nowadays, at the Isobor company in France isotopically pure boron-10 and 11 are being produced from natural boron by means of ion-exchange chromatography, using a strong-base anion exchange resin.

The present authors have pointed out that this process can be greatly improved by using a weak-base resin in free-base form or a strong-base resin in fluoride form, and thus dispensing with regeneration of the resin in the column.[7-9] In these experiments, a high porosity type weak-base anion exchange resin (Diaion WA 21) in the free-base form, and a gel type strong-base anion exchange resin (Diaion SA 20A) in the fluoride form were used. An aqueous solution containing 5 mmol of boric acid was passed through columns packed with these resins, and the borate band formed in the column was eluted with pure water. It was found that:

(1) Boron-10 was considerably enriched in the rear part of the band, and depleted in the frontal part.

(2) The boric acid charged to the column was completely eluted with pure water.

The remarkable feature of this separation system is that it is scarcely necessary to regenerate the resin in the column. Recently, one of the authors has discussed the further possibility of ion-exchange separation of isotopes, giving the case of boron isotopes as an example.[10]

The purpose of the present research is to determine the effects of temperature, the concentration of boric acid charged to the column, and the kind of resin used, on the single-stage separation factor of boron isotopes between the resin and the external solution phases.

Experimental

The ion-exchange resins used were Diaion WA 21, WA 30, WA 10, PA 312, SA 20A, and PK 224. Diaion WA 21 is a high porosity type weak-base anion exchange resin with primary and secondary amine groups. Diaion WA 30 is a high porosity type weak-base anion exchange resin with tertiary amine groups. Diaion WA 10 is a gel type weak-base anion exchange resin with tertiary amine groups. Diaion PA-312 is a porous type strong-base anion exchange resin with quaternary amine groups. Diaion SA 20A is a gel type strong-base anion exchange resin with quaternary amine groups. Diaion PK 224 is a porous type strong-acid cation exchange resin with sulfonic groups. It is known that the increasing order of resin-basicity is as follows:

$$\text{Diaion WA 21} < \text{Diaion WA 10} < \text{Diaion WA 30} < \text{Diaion SA 20A} < \text{Diaion PA 312}$$

The boric acid used in these experiments was recrystallized twice from aqueous solution. The other chemicals were analytical grade materials used without further purification.

Equilibrium Experiment. The columns used were about 20 cm in length and 1 cm in diameter, surrounded by a jacket through which water from a thermostat was circulated so that the columns were maintained at constant temperature within ± 0.2 °C. The resins described above were packed in the columns, and subjected to chloride–hydroxide or sodium–hydrogen cycles in a usual manner to ensure regeneration and uniform packing. The columns were thoroughly washed with distilled water after converting the resins into the hydroxide or the hydrogen forms. A boric acid solution was placed in a reservoir above the columns which was connected to the columns with a polyolefin tube. In order to establish isotopic equilibrium between the resin in the column and the boric acid solution, the amount of boric acid charged to the column

was more than 50 times the total exchange capacity of the column. The flow rate of the boric acid solution was controlled with a screw cock at the bottom of the column.

After equilibrium was established between the resin and the external solution phases, some samples of the resin in the column were extracted with a pipette, filtered through a sintered glass disk with suction for 10 min, and weighed. Then the boric acid absorbed by the resin was eluted with pure water or other suitable eluting agents, and the concentration of boric acid in the effluent was measured with a Varian Tectron Model 1100 flame photometer and the amount of boric acid absorbed by the resin was calculated. The resin was weighed after being dried in an air bath with autometic controller at 50—60 °C for about 48 h and kept in a desiccator (with silica gel as a drying agent) for 24 h.

The isotopic analysis of boric acid absorbed by the resin was carried out using a Varian Mat CH 5 mass spectrometer by means of the surface ionization method.[11] The mass peaks used were those at *m/e* 88 ($Na_2{}^{10}BO_2^+$) and 89 ($Na_2{}^{11}BO_2^+$). This mass region was repeatedly scanned about 40 times for each sample, and the ratio of peak heights at *m/e* 88 to *m/e* 89 was calculated as an average of these scans. The atomic fraction of boron-10 was determined from the ratio of the peak-heights. The standard deviation of the isotopic analysis of boron-10 was less than ± 0.0002 in every case. Some other samples of the resin in the column, in equilibrium with the external solution of boric acid, were pipetted together with the external solution into eight test tubes. A few drops of an indicator were added to each of these test tubes. The indicators used were methyl red, phenol red, thymol blue, phenolphthalein, cresolphthalein, thynolphthalein, alizarin yellow R. and the Kolthoff's universal indicator. The pH of the resin phase was roughly estimated by comparing the color of the resin with that of standard buffer solutions.

Breakthrough Experiment. A boric acid solution was passed through the same column as used in the equilibrium experiment. The superficial velocity of the boric acid solution was 13 ml h^{-1} cm^{-2}. A number of 20 ml fractions of the effluent were successively collected in 20 ml measuring flasks, and the boric acid concentration and the atomic fraction of boron-10 in these fractions were determined by the methods used in the equilibrium experiment.

Results and Discussion

The results obtained from the equilibrium and breakthrough experiments are summarized in Table 1 along with the experimental conditions. Some examples of the elution graphs obtained from the breakthrough experiment are shown in Figs. 1 through 4. The ${}^{10}_{11}S$ shown in Table 1 is the single-stage separation factor for boron isotopes between the resin and the external solution phases, defined in the following equation:

$$ {}^{10}_{11}S = \frac{\text{Total amount of boron-10 in the resin phase}}{\text{Total amount of boron-11 in the resin phase}} \times \frac{\text{Total amount of boron-11 in the external solution phase}}{\text{Total amount of boron-10 in the external solution phase}} \quad (1) $$

In the case of the equilibrium experiment, the first term of the right hand side of Eq. 1 is the value of isotope ratio measured for the boric acid absorbed by the resin at the equilibrium, and the second term is that of the external solution which is simply the natural isotope ratio. In the case of the breakthrough experiment, ${}^{10}_{11}S$ can be calculated from the experimental data by means of the following equation,[12]

$$ {}^{10}_{11}S = 1 + \frac{1}{Q} \cdot \frac{1}{R_0(1-R_0)} \cdot (R_0 - R_i) \cdot f_i \quad (2) $$

where Q is the total amount of boron in the resin phase (mmol), R_0 the atomic fraction of boron-10 in the feed solution, R_i the atomic fraction of boron-10 in fraction i of the effluent, and f_i the total amount of boron

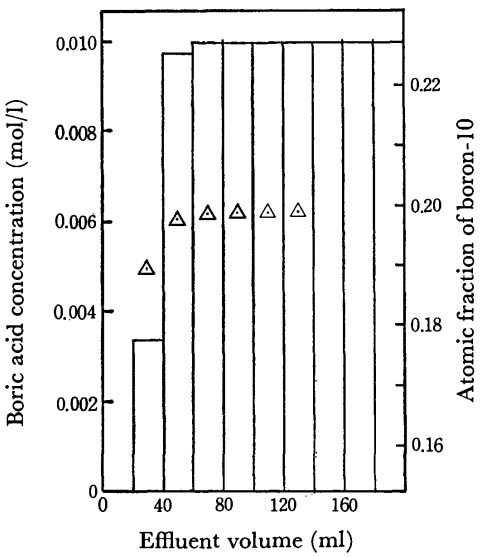

Fig. 1. Breakthrough graph.
Column: Diaion WA 21, free-base form, 20—50 mesh, 1 cm × 10 cm bed.
Load: 0.00999 mol/l boric acid.
Temperature: 25 °C.
Flow rate: 13 ml h^{-1} cm^{-1}.
□: Boric acid concentration in each effluent fraction (mol/l).
△: Atomic fraction of boron-10 in each effluent fraction.

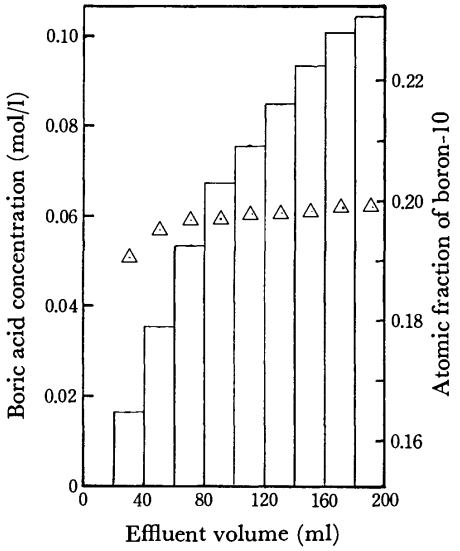

Fig. 2. Breakthrough graph.
Column, temperature, flow rate, □, and △: same as shown in Fig. 1.
Load: 0.105 mol/l boric acid.

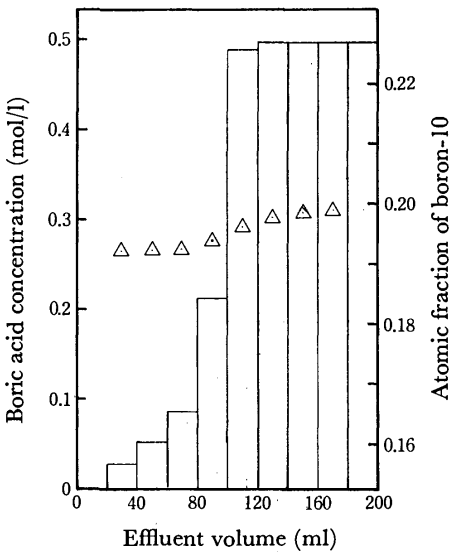

Fig. 3. Breakthrough graph.
Column, temperature, flow rate, □, and △: same as shown in Fig. 1.
Load: 0.496 mol/l boric acid.

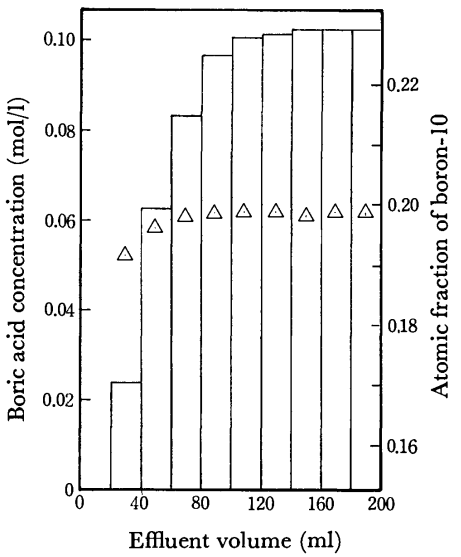

Fig. 4. Breakthrough graph.
Column, flow rate, □, and △: same as shown in Fig. 1.
Temperature: 40 °C
Load: 0.102 mol/l boric acid.

isotopes in fraction i (mmol). In some cases of Diaion WA 21 and Diaion WA 10, both equilibrium and breakthrough experiments were carried out. The values of $^{10}_{11}S$ obtained from the equilibrium experiment agreed well with those obtained from the breakthrough experiment. The values of $^{10}_{11}S$ shown in Table 1 are average values of $^{10}_{11}S$ obtained from both experiments. In other

TABLE 1. EXPERIMENTAL RESULTS AND CONDITIONS
T: Temperature, $^{10}_{11}S$: single-stage separation factor, q: amount of boron absorbed in resin phase, W: weight fraction of water in resin phase, M: boric acid concentration in resin phase.

Run	Resin	T (°C)	Load $B(OH)_3$ (mol/l)	$^{10}_{11}S$ Experimental value	$^{10}_{11}S$ Calculated value (pH)	q (mmol/g-dry resin)	W	M (mol/l)	pH of resin phase
1	Diaion WA 21	40	0.00945	1.014	1.0184(11.0), 1.0185(11.5)	0.03	0.39	0.05	11—11.5
2			0.102	1.011	1.0126(10.0)	0.69	0.43	0.91	10
3			0.494	1.008	1.0073 (8.5), 1.0080 (9.0)	8.3	0.49	8.6	8.5—9
4		25	0.0107	1.017	1.0192(11.0)	0.06	0.40	0.09	11
5			0.102	1.013	1.0094 (9.5), 1.0122(10.0)	1.6	0.43	2.1	9.5—10
6			0.518	1.011	1.0061 (8.0), 1.0065 (8.5)	10.0	0.47	11.0	8—8.5
7		5	0.0104	1.023		0.08	0.47	0.09	10.5—11
8			0.106	1.014		3.4	0.47	3.8	9.5
9			0.511	1.011		11.0	0.49	11.0	8
10	Diaion WA 10	40	0.00945	1.014	1.0185(11.5), 1.0186(12.0)	0.10	0.66	0.05	11.5—12
11			0.105	1.011	1.0132(10.0), 1.0161(10.5)	1.6	0.69	0.72	10—10.5
12			0.496	1.008	1.0080 (9.0)	17.0	0.69	7.6	9
13		25	0.0101	1.016	1.0192(11.0), 1.0193(11.5)	0.08	0.63	0.05	11—11.5
14			0.0991	1.013	1.0131(10.0)	2.5	0.68	1.2	10
15			0.501	1.009	1.0065 (8.5), 1.0072 (9.0)	19.0	0.69	8.5	8.5—9
16		5	0.511	1.013		20.0	0.70	8.6	8.5
17	Diaion WA 30	25	0.00999	1.017	1.0193(11.5)	0.20	0.50	0.20	11.5
18			0.493	1.009	1.0072 (9.0)	7.8	0.56	6.1	9
19	Diaion PA 312	25	0.0104	1.019	1.0176(12.0), 1.0190(13.0)	5.7	0.57	4.3	>12
20			0.109	1.010	1.0107(10.0)	9.9	0.51	9.5	10
21			0.501	1.007	1.0062 (8.0), 1.0065 (8.5)	13.0	0.48	14.0	8—8.5
22	Diaion SA 20A	25	0.106	1.011	1.0177(12.0), 1.0190(13.0)	7.1	0.64	4.0	12
23			0.511	1.010	1.0107(10.0)	16.0	0.65	8.6	10
24	Diaion PK224	25	0.106	1.000	1.000 (3.0), 1.000 (4.0)	0.05	0.45	0.06	<4
25			0.498	1.000	1.000 (3.0), 1.000 (4.0)	0.25	0.43	0.33	<4

cases using Diaion WA 21, Diaion WA 10, and other resins, the values of ${}^{10}_{11}S$ were determined from the equilibrium experiment only. Of the other symbols in Table 1, q is the mass concentration of boron absorbed in the resin phase (mmol/g-dry resin), and W is the weight fraction of water in the resin phase, defined as

$$W = \frac{W_w}{W_r + W_w} \tag{3}$$

where W_r is the weight of the dry resin, and W_w the weight of water in the resin. M is the molar concentration of boric acid in the resin phase, which can be calculated by means of the following equation:

$$M = \frac{1-W}{W} \times q \tag{4}$$

The following can be seen from Table 1 and Figs. 1—4 under the present experimental conditions:

(1) The lighter isotope boron-10 is considerably enriched in the anion exchange resin phase, while in the case of the cation exchange resin no isotope effect is found within our limits of experimental accuracy.

(2) The separation factor is very much influenced by the boric acid concentration in the external solution, but not so much influenced by the kind of anion exchange resins used nor by the operating temperature. The separation factor increases with a decrease in the boric acid concentration.

(3) The amount of boron absorbed in the weak-base anion exchange resins (Diaion WA 21 and 10) increases with a decrease in temperature at a certain concentration of boric acid in the external solution.

(4) The amount of boron absorbed in the weak-base anion exchange resins (Diaion WA 21, 10, and 30) increases remarkably with an increase of the boric acid concentration in the external solution, while in the case of the strong-base anion exchange resins (Diaion PA 312 and SA 20A) it reaches the maximum value at the relatively low concentration of boric acid.

(5) The boric acid concentration in the anion exchange resin phase is very high; that is, at an operating temperature of 25 °C, when the boric acid concentration in external solution is 0.5 mol/l its value reaches about 10 mol/l in the resin.

(6) The pH of the anion exchange resin phase in equilibrium with the external solution shows a considerably higher value (8—12) than that of boric acid solutions; 4.9 at 0.01 mol/l, 4.7 at 0.1 mol/l, 4.3 at 0.5 mol/l.

(7) The breakthrough graph is influenced effectively by the boric acid concentration of the external solution and operating temperature: Its features become sharper with a decrease in the boric acid concentration of the external solution and with an increase in the operating temperature.

The values of the separation factor obtained from the present research agree closely with those obtained for a strong-base anion exchange resin by Rosset and coworkers[5]: 1.018 at 0.0098 mol/l; 1.014 at 0.103 mol/l; 1.011 at 0.249 mol/l; 1.009 at 0.555 mol/l boric acid. This would seem to confirm the correctness of the present results.

The boron-isotope exchange reaction,

$$^{10}B(OH)_3 + {}^{11}B(OH)_4^- = {}^{11}B(OH)_3 + {}^{10}B(OH)_4^-, \tag{5}$$

occurs in aqueous solutions of boric acid. The isotope effect between a trigonal planar structure ($B(OH)_3$) and a tetrahedral structure[13,14] ($B(OH)_4^-$) as calculated from spectroscopic data on molecular vibrations, based on statistical mechanics with quantum corrections, is remarkable.[7,15,16]

The value of equilibrium constant is 1.0194 at 298.1 K as shown in Table 2. This means that boron-10 is enriched in the anionic species $B(OH)_4^-$.

It has been reported by Ingri[17] that the main species formed in aqueous solutions of boric acid are $B(OH)_3$, $B(OH)_4^-$, $B_3O_3(OH)_4^-$, $B_3O_3(OH)_5^{2-}$. That is, the following equilibria exist in the solutions:

$$B(OH)_3 + OH^- \overset{K_1}{=} B(OH)_4^- \tag{6}$$

$$3B(OH)_3 + OH^- \overset{K_2}{=} B_3O_3(OH)_4^- + 3H_2O \tag{7}$$

$$3B(OH)_3 + 2OH^- \overset{K_3}{=} B_3O_3(OH)_5^{2-} + 3H_2O \tag{8}$$

where K_1, K_2, and K_3 are the stability constants; the respective values at 25 °C are $\log K_1 = 5.27$, $\log K_2 = 7.41$, and $\log K_3 = 11.67$. The distribution of the hydrolyzed

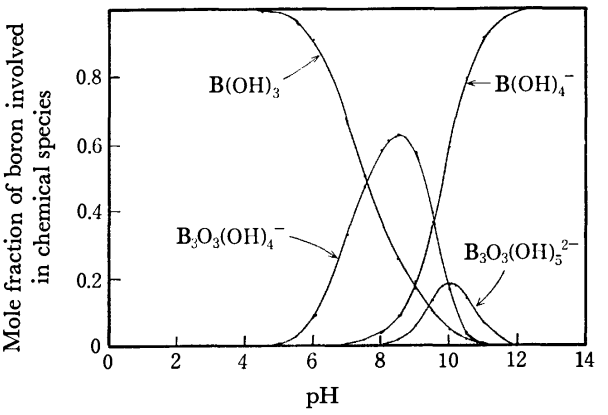

Fig. 5. The calculated distribution of the hydrolyzed species in aqueous solution of boric acid.
Total boron concentration: 0.5 mol/l.
Temperature: 25 °C.

Table 2. Calculated reduced partition function ratios for $B(^{16}OH)_3$ and $B(^{16}OH)_4^-$, and equilibrium constants for boron isotope exchange reaction between $B(^{16}OH)_3$ and $B(^{16}OH)_4^-$

$f_{B(^{16}OH)_3}$: Reduced partition function ratio for $B(^{16}OH)_3$.
$f_{B(^{16}OH)_4}$: Reduced partition function ratio for $B(^{16}OH)_4$.
${}^{10}_{11}K$: Equilibrium constant for boron isotope exchange reaction between $B(^{16}OH)_3$ and $B(^{16}OH)_4^-$.

Temperature (K)	$f_{B(^{16}OH)_3}$	$f_{B(^{16}OH)_4^-}$	${}^{10}_{11}K$
273.1	1.2315	1.2066	1.0206
278.1	1.2248	1.2003	1.0204
288.1	1.2123	1.1887	1.0199
298.1	1.2008	1.1780	1.0194
313.1	1.1852	1.1635	1.0187
323.1	1.1758	1.1549	1.0181
333.1	1.1671	1.1468	1.0177

species in the boric acid solution, calculated at the total boron concentration of 0.5 mol/l from the values of the stability constants described above, is represented graphically in Fig. 5. Figure 5 shows that the main species are $B(OH)_3$ at pH less than 6, $B(OH)_3$ and $B_3O_3(OH)_4^-$ in the pH range 7—8, $B(OH)_3$, $B_3O_3(OH)_4^-$, and $B(OH)_4^-$ in the pH range 8—9, $B(OH)_3$, $B_3O_3(OH)_4^-$, $B(OH)_4^-$, $B_3O_3(OH)_5^{2-}$ in the pH range 9—10, and $B(OH)_4^-$ at pH greater than 10. As mentioned above, in aqueous solution $B(OH)_3$ has a trigonal planar structure and $B(OH)_4^-$ has a tetrahedral structure. It has been also reported[18] that polyborate ions, $B_3O_3(OH)_4^-$ and $B_3O_3(OH)_5^{2-}$, have both trigonal planar and tetrahedral structure: $B_3O_3(OH)_4^-$ is composed of two triangular groups and a tetrahedral group joined by three common oxygen atoms; $B_3O_3(OH)_5^{2-}$ is composed of a triangular group and two tetrahedral groups joined by three common oxygen atoms (Fig. 6).

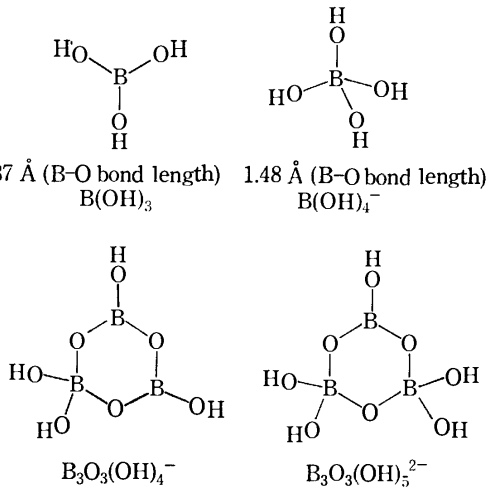

Fig. 6. Structure of boron species.

From the facts mentioned above, the main species present in the anion exchange resin phase in equilibrium with the external solution, could be $B(OH)_4^-$, $B_3O_3(OH)_4^-$, and $B_3O_3(OH)_5^{2-}$, while the main species in the external solution phase is $B(OH)_3$ only. Consequently, the high value of the separation factor for boron isotopes between the two phases is caused by the structure change between boron species existing in the two phases: from trigonal planar structure to tetrahedral structure. The high concentration of boric acid in the resin phase may be caused by the formation of polyborate anions. In the case of the cation exchange resin, the only species present in the two phases is $B(OH)_3$, and therefore, the value of the separation factor is approximately unity.

The separation factor (${}^{10}_{11}S$) for boron isotopes between the anion exchange resin and the external solution phases can be estimated on the basis of the theory of the two phase distribution of isotopes proposed by Kakihana,[19,20] that is, expressed by the following equation,[7]

$$
\begin{aligned}
{}^{10}_{11}S &= \{({}^{10}\overline{[B(OH)_3]} + {}^{10}\overline{[B(OH)_4^-]} + {}^{10}\overline{[B_3O_3(OH)_4^-]} \\
&\quad + {}^{10}\overline{[B_3O_3(OH)_5^{2-}]})/({}^{11}\overline{[B(OH)_3]} + {}^{11}\overline{[B(OH)_4^-]} \\
&\quad + {}^{11}\overline{[B_3O_3(OH)_4^-]} + {}^{11}\overline{[B_3O_3(OH)_5^{2-}]})\} \\
&\quad \times ({}^{11}[B(OH)_3]/{}^{10}[B(OH)_3]) \qquad (9)
\end{aligned}
$$

$$
\begin{aligned}
&= [\bar{X}_{{}^{11}B(OH)_3} + \bar{f}_{B(OH)_3} \cdot \bar{f}^{-1}_{B(OH)_4^-} \cdot \bar{X}_{{}^{11}B(OH)_4^-} \\
&\quad + \bar{f}_{B(OH)_3} \cdot \bar{F}^{-1}_{B_3O_3(OH)_4^-} \cdot \bar{X}_{{}^{11}B_3O_3(OH)_4^-} \\
&\quad + \bar{f}_{B(OH)_3} \cdot \bar{F}^{-1}_{B_3O_3(OH)_5^{2-}} \cdot \bar{X}_{{}^{11}B_3O_3(OH)_5^{2-}}] \\
&\quad \times f^{-1}_{B(OH)_3} \cdot f_{B(OH)_3} \qquad (10)
\end{aligned}
$$

where the bracket [ ] denotes the molar concentration of boron isotopes involved in the corresponding species, the symbol $\bar{}$ the resin phase, X the atomic fraction of a given boron isotope in the form of the specified chemical species, f the reduced partition function ratio, and F the reduced partition function ratio of polyborate anion. Since the difference of the reduced partition function ratios of the same chemical species between the resin and the external solution phase is very small, we can make the approximations $\bar{f}_{B(OH)_3} = f_{B(OH)_3}$, $\bar{f}_{B(OH)_4^-} = f_{B(OH)_4^-}$, $\bar{F}_{B_3O_3(OH)_4^-} = F_{B_3O_3(OH)_4^-}$, $\bar{F}_{B_3O_3(OH)_5^{2-}} = F_{B_3O_3(OH)_5^{2-}}$.

The atomic fraction of boron isotope in a chemical species can be approximated by the mole fraction of the corresponding chemical species.[21] As mentioned above, $B_3O_3(OH)_4^-$ is composed of two triangular groups and a tetrahedral group joined by three common oxygen atoms, while $B_3O_3(OH)_5^{2-}$ a triangular group and two tetrahedral groups joined by three common oxygen atoms. Therefore, the reduced partition function ratios can be approximated by the following equations,

$$F_{B_3O_3(OH)_4^-} = \frac{2f_{B(OH)_3} + f_{B(OH)_4^-}}{3} \qquad (11)$$

$$F_{B_3O_3(OH)_5^{2-}} = \frac{f_{B(OH)_3} + 2f_{B(OH)_4^-}}{3} \qquad (12)$$

Equation 10 is reduced to

$$
\begin{aligned}
{}^{10}_{11}S &= \bar{X}_{B(OH)_3} + f_{B(OH)_3} \cdot f^{-1}_{B(OH)_4^-} \cdot \bar{X}_{B(OH)_4^-} \\
&\quad + f_{B(OH)_3} \cdot \left\{\frac{2f_{B(OH)_3} + f_{B(OH)_4^-}}{3}\right\}^{-1} \cdot \bar{X}_{B_3O_3(OH)_4^-} \\
&\quad + f_{B(OH)_3} \cdot \left\{\frac{f_{B(OH)_3} + 2f_{B(OH)_4^-}}{3}\right\}^{-1} \cdot \bar{X}_{B_3O_3(OH)_5^{2-}} \qquad (13)
\end{aligned}
$$

Thus, ${}^{10}_{11}S$ is calculated as a function of pH and boric acid concentration in the resin phase from Eq. 13, using the stability constants of boron species determined by Ingri and the calculated reduced partition function ratios for $B(OH)_3$ and $B(OH)_4^-$ (Fig. 7 and Table 1). It is apparent from Fig. 7 and the calculated values of ${}^{10}_{11}S$ in Table 1 *i.e.*:

(1) The calculated separation factor increases with an increase of the boric acid concentration in the resin at pH below 8.7, but has the contrary tendency at pH above 8.7, and is independent of the boric acid concentration in the resin at pH 8.7. The formation of polyborate anions containing the tetrahedral groups may contribute to the high values of the separation factor at pH below 8.7.

(2) The calculated separation factors show roughly agreement with those obtained experimentally. The discrepancy between the calculated values and the

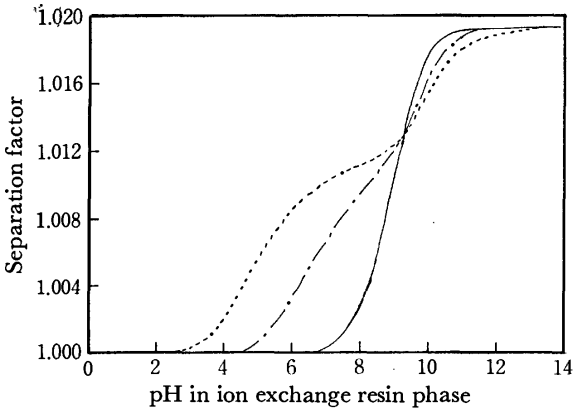

Fig. 7. Separation factor of boron isotopes calculated as a function of pH and boric acid concentration in resin phase at 25 °C.
——: The total boron concentration of 0.05 mol/l.
-•---: The total boron concentration of 1.20 mol/l.
------: The total boron concentration of 8.50 mol/l.

experimental values may be caused mainly by the insufficient accuracy of the resin-phase pH measurement and the use of the stability constants in such a high concentration range (up to 10 molarity), and subsidiarily by the use of the approximate values of the reduced partition function ratio for the polyborate ion. ${}^{10}_{11}S$ was also calculated at 40 °C by the use of the stability constants of boron species determined by Mesmer[22] (Table 1), and the values had a same tendency as these of ${}^{10}_{11}S$ at 25 °C.

The separation system of boron isotopes by means of weak-base anion exchange resins such as Diaion WA 21 may indeed be one of the best separation systems, because the separation factor is as high as that for the system using a strong-base anion exchange resin, the boric acid charged to the column is absorbed in the resin to a high concentration, and it can be completely eluted with pure water. The advantages of the boric acid charged to the column being easily eluted with pure water are that it is scarcely necessary to regenerate the resin in the column, and that the boric acid is free from contamination by any other chemicals.

The authors would like to express their thanks to Professor Y. Marcus of the Hebrew University of Jerusalem for his valuable discussions and to Professor I. Okada for his kind comments and to Mr. D. Dickeson of the University of Washington of the U. S. A. for reading the manuscript.

References

1) D. Hunghes and J. Harvey, "U.S.At. Energy Comm. Rpt. BNL-325" 2nd ed (1964).
2) H. Hatanaka and T. Watanabe, *Igaku No Ayumi*, **76**, 181 (1971).
3) Y. Mishima, *Pigment Cell.* **1**, 215 (1973).
4) Y. Yoneda, T. Uchijima, and S. Makishima, *J. Phys. Chem.*, **63**, 2057 (1956).
5) R. Rosset, H. Fould, M. Chemla, H. Labrousse, J. Hure, and B. Tremillon, *Bull. Soc. Chim. Fr.*, **1964**, 607.
6) M. M. Urgell, J. Iglesias, J. Casas, J. M. Saviron, and M. Quintanilla, Third United Nations International Conference on the Peaceful Uses of Atomic Energy, A/CONF, 28/Spain May (1964), p. 491.
7) The doctorate thesis of M. Kotaka, "Chromatographic Separation of Boron and Nitrogen Isotopes Using Pure Water as Eluent," Tokyo Institute of Technology, 1973.
8) T. Hirao, M. Kotaka, and H. Kakihana, *Nippon Kagaku Kaishi*, **1973**, 1477.
9) M. Kotaka, K. Murayama, and H. Kakihana, *Nippon Kagaku Kaishi*, **1973**, 1482.
10) H. Kakihana, *J. Chromatogr.*, **102**, 47 (1974).
11) M. Nomura, M. Okamoto, and H. Kakihana, *Shituryo Bunseki*, **21**, 277 (1973).
12) H. Kakihana and T. Kanzaki, *Bull. Tokyo Inst, Tech.*, **90**, 77 (1969).
13) W. H. Zachariasen, *Acta Crystallogr.*, **7**, 305 (1954).
14) W. H. Zachariasen, *Acta Crystallogr.*, **16**, 385 (1963).
15) The doctorate thesis of Y. Yato, "Isotope Effects in Isotope-Exchange Reaction and Equilibrium between Two Phases," Tokyo Institute of Technology, 1971.
16) M. Kotaka and H. Kakihana, manuscript in preparation.
17) N. Ingri, *Svensk Kemisk Tidskift*, **75**, 4 (1963).
18) E. Muetterties, "The Chemistry of Boron and Its Compounds," John Wiley and Sons, Inc., New York (1967).
19) H. Kakihana, K. Takahashi, and Y. Yato, *J. Nucl. Sci. Tech.*, **5**, 93 (1968).
20) H. Kakihana and M. Aida, *Bull. Tokyo Inst. Tech.*, **116**, 39 (1973).
21) H. Kakihana, *Nippon Kagaku Zasshi*, **89**, 734 (1968).
22) R. E. Mesmer, C. F. Base, Jr., and F. H. Sweeton, *Inorg. Chem.*, **11**, 537 (1972).

The Conformations of Nickel(II) Complexes with edda-Type Optically Active Polyamino Carboxylic Acids in Aqueous Solutions

Tasuku MURAKAMI, Ichiro HIRAKO, and Masahiro HATANO

Chemical Research Institute of Non-Aqueous Solutions, Tohoku University, 2-1-1 Katahira, Sendai 980

(Received August 30, 1976)

Circular dichroism (CD) and proton magnetic resonance (PMR) spectra of nickel(II) complexes containing a series of ethylenediamine-*N*,*N*′-diacetic acid(H_2edda)-type optically active quadridentate ligands were measured in aqueous solutions. The epro complex which is an edda-type optically active ligand containing L-proline residues is found to exhibit the same CD spectrum as complexes of other edda-type ligands containing L-alanine, L-valine, L-phenylalanine, and L-serine residues. The CD and PMR spectra of the mixed complexes of these edda-type ligands having an oxalate ion was also measured. From the CD and PMR spectral data, it is concluded that these complexes stereospecifically take the *Δ-s-cis* form in solution. The large contact shift observed for the a protons of the amino acidate moieties indicates that the substituent groups become axial to the chelate plane.

In a previous paper,[1] we reported the preparation and solid state character of nickel(II) complexes having a series of ethylenediamine-*N*,*N*′-diacetic acid (H_2edda)-type optically active polyamino carboxylic acids, as is shown in Fig. 1;[2] the stretching frequencies of the coordinated carboxylate groups and the thermal stability suggested that the structure of the edda-type complexes in the solid state is different from that of bis(amino acidato) complexes. In this paper, we wish to report the circular dichroism (CD) and proton magnetic resonance (PMR) spectra measured in order to obtain information about the structure of the nickel(II) complexes with the edda-type optically active ligands in aqueous solutions.

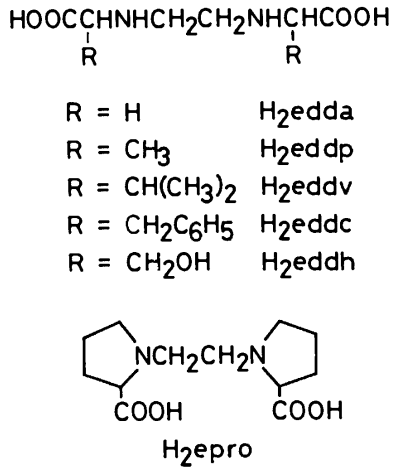

Fig. 1. The edda-type polyamino carboxylic acids. Except for H_2edda these acids possess two asymmetric carbon atoms with the *S* configuration.

Since the investigation of Milner and Pratt,[4] PMR studies have been found to be very useful for the conformational analysis of chelate rings in paramagnetic nickel(II) complexes.[5–9] However, most of subsequent work has involved optically inactive nickel(II) complexes. As is well-known, CD is an effective technique for the conformational analysis of optically active complexes. The combination of PMR and CD should lead to a more detailed understanding of the stereochemistry of paramagnetic nickel(II) complexes with optically active ligands.

Cobalt(III) complexes containing edda and its analogs have been extensively studied.[10–13] Schoenberg *et al.*,[14] have prepared cobalt(III) complexes with eddp, which is an optically active edda-type acid (see Fig. 1), and obtained the *Δ-s-cis* and *Λ-s-cis* isomers as main products and a small amount of the *Δ-uns-cis* isomer.[15,16] Since the yields of the two *s-cis* isomers were nearly equal, the stereospecificity of eddp does not appear to be very large. In the case of the nickel(II) ion, however, eddp-type quadridentate ligands may form only the most stable isomer in solution due to the labile characteristic of the nickel(II) ion. Thus, there is the possibility of displaying their essential stereospecificity by forming labile complexes. One of the purposes of this paper is to clarify this problem. Especially, the epro ion has two pyrrolidinyl groups in its interior (Fig. 1) and hence is expected to coordinate to a metal ion with a large stereospecificity. Even for the copper(II) ion, the epro ion is reported to coordinate with an *uns-cis* configuration.[3] The conformations of the nickel(II) complexes with these edda-type ligands are discussed on the basis of the CD and PMR spectra.

Experimental

Materials. The edda-type optically active polyamino carboxylic acids shown in Fig. 1 and their nickel(II) complexes were prepared as described in a previous paper.[1] Mixed ligand complexes of these acids having an oxalate ion were prepared by adding an amount of sodium oxalate two times in excess to the complex solutions.[17] Sodium 3-(trimethylsilyl)-1-propanesulfonate (TMS*) was used as an internal reference for the chemical-shift measurements for the PMR.

Samples for PMR measurements were prepared as follows. The isolated complex was dissolved in D_2O (99.75%). To reduce the size of the HDO signal, the solution was evaporated to dryness at 50 °C, and dried solid was again dissolved in D_2O. After this procedure had been repeated, the dried solid was dissolved in D_2O containing TMS*. The final concentration of each solution was about 0.02 M. In the case of complexes mixed having an oxalate ion, the complex solutions containing amount of sodium oxalate two times in excess were similarly treated. The concentration was about 0.2 M.

Measurements. Absorption spectra from the near-infrared to the near-ultraviolet regions were measured with a Hitachi EPS-3T spectrophotometer. CD spectra from 250 to 1200 nm were measured with a Jasco J-20A recording

spectropolarimeter (250—1000 nm) and a Jasco J-200 grating spectropolarimeter (900—1200 nm). The PMR spectra were obtained with a Varian CFT-20 spectrometer at 80 MHz. To obtain high signal-to-noise ratios for PMR, each signal was repeatedly accumulated using a Fourier transform (FT) technique or a water-eliminated FT technique.

Results and Discussion

Figure 2 shows the absorption and CD spectra of [Ni(eddp)(H_2O)$_2$], [Ni(eddh)(H_2O)$_2$], and [Ni(epro)-(H_2O)$_2$] in the region of 7000 to 38000 cm^{-1}. These complexes exhibit CD curves with similar shapes, which have a large negative band in the first (lowest energy) absorption band region, two negative bands in the second absorption region, and two bands of oppsite sign in the third absorption region. The diaquanickel-(II) complexes of eddv and eddc also exhibit analogous CD spectra. Of the diaquabis(L-amino acidato)nickel-(II) complexes, on the other hand, it has been reported that only the L-prolinato complex exhibits a quite different CD spectrum from those of other L-amino acidato complexes in methanol[18] and water.[19] This is considered to be due mostly to the large contribution of the asymmetric secondary nitrogen atom of proline to the optical activity. Therefore, the fact that the CD spectrum of the epro complex containing the two proline residues is the same as those of other eddp-type complexes is very interesting. This will be significant in the discussion of the structure of these complexes.

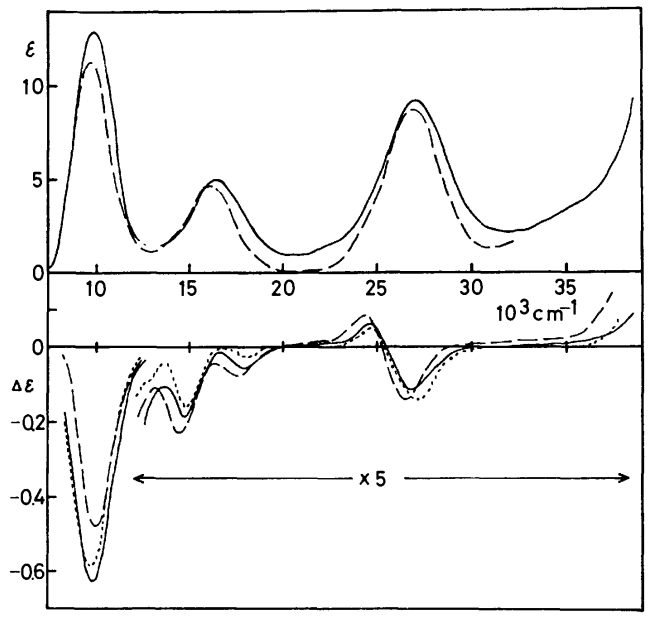

Fig. 2. Absorption and CD spectra of [Ni(eddp)(H_2O)$_2$] (——), [Ni(eddh)(H_2O)$_2$] (------), and [Ni(epro)(H_2-O)$_2$] (----) in aqueous solutions.

For the edda-type complexes, three geometrical isomers, *trans*, *s-cis*, and *uns-cis*, are possible and further there are two optical isomers of Δ and Λ for both the *s-cis* and *uns-cis* forms. Considering the asymmetry of chelate rings, the number of possible conformations increases to many more. Contributions to the CD spectrum observed for the octahedral nickel(II) complexes having edda-type optically active quadridentate ligands arise from (i) the configurational effect based on the arrangement of chelate rings around the nickel ion, (ii) the vicinal effect of the asymmetric nitrogen, (iii) the conformational effect of the central ethylenediamine(en)-type chelate ring, (iv) the conformational effect of the amino acidate chelate ring, and (v) the vicinal effect of the asymmetric carbon. Of these five effects, the contributions from the absolute configuration around the nickel ion and the asymmetric nitrogen are expected to be much more significant. Therefore, the similarity of the CD spectra observed for all the edda-type complexes suggests that these complexes have at least the same absolute configuration and an asymmetric nitrogen atom with the same configuration.

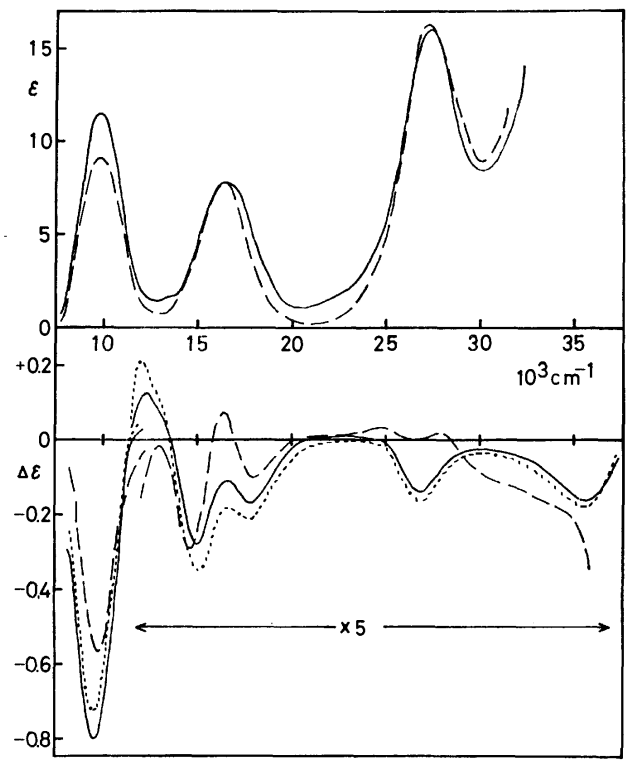

Fig. 3. Absorption and CD spectra of [Ni(eddp)(ox)]$^{2-}$ (——), [Ni(eddh)(ox)]$^{2-}$ (------), and [Ni(epro)(ox)]$^{2-}$ (----) in aqueous solutions.

The edda-type polyamino carboxylic acids appear primarily to have the particular character that they hardly coordinate to a metal ion in a plane.[12] For example, so far, no cobalt(III) complex with an edda-type acid in the planar configuration has been reported. Only *s-cis* and *uns-cis* isomers have actually been obtained.[10-14,20-22] This also appears to be the case for the nickel(II) complexes. The fact that the CD spectra of the nickel(II) complexes are not so greatly influenced when mixed complexes having an oxalate ion are formed (Fig. 3) indicates that these complexes are of the *cis*-type form to which the oxalate ion can coordinate without changing the configuration of the quadridentate ligands.

Among the edda-type ligands, especially the epro ion which has two pyrrolidinyl rings is expected to coordinate with large stereospecificity. Even to the copper(II)

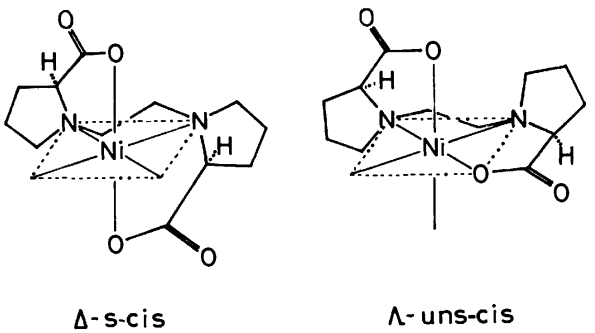

Fig. 4. Schematic drawing of the *Δ-s-cis* and *Λ-uns-cis* forms possible for the epro complex.

ion, which is generally thought to form planar complexes, epro appears to coordinate with a *Λ-uns-cis* configuration.[3] In addition, some tetraamines, which have two pyrrolidinyl groups in their interior as well as epro, do not form planar species of nickel(II) ions, but form only octahedral species.[23-25] An examination of the molecular models shows that the possible *cis* forms for epro are only two, *Δ-s-cis* and *Λ-uns-cis*, because of the rigid pyrrolidine rings. These two forms are illustrated in Fig. 4. The configuration of all the tertiary nitrogen atoms is *R*.[26] The central en-like chelate ring is a *δ gauche* in the *Δ-s-cis* form, while it appears to be an envelope in the *Λ-uns-cis* form. The epro complex will exist in either the *Δ-s-cis* or the *Λ-uns-cis* form in solution. Therefore, other eddp-type complexes are also considered to have a structures similar to either of these two forms on the basis of the similarity of the CD spectra.

The PMR spectra of $[Ni(eddp)(H_2O)_2]$ and $[Ni(eddh)(H_2O)_2]$, and complexes of these mixed with oxalate ions in D_2O are shown in Fig. 5. The signal due to the residual HDO of the solvent is not shown. The large peak at about −5.5 ppm observed for the eddp complex is assigned to the methyl protons on the basis of its relative area. The methylene protons in the hydroxymethyl group of the eddh complex appear at −7.2 ppm. Three other broad peaks, with almost the same intensity, observed at lower fields for each complex correspond to the central ethylene protons and the α protons in the amino acidate moieties, assuming the assignments for the edda complex.[6] Since the protons of the ethylene linkage of the edda complex were found to appear at −26 and −116 ppm, the α proton of the eddp complex could be assigned to either of the two bands at −126 and −103 ppm. Similarly, the α proton of the eddh complex corresponds to either of the two peaks at −121 and −102 ppm. The other of these two peaks is assigned to the equatorial protons of the ethylene linkage. In any case, the α protons of the eddp and eddh complexes would appear at a field lower than −100 ppm. This is significant when examining the ring conformation, as will be described below.

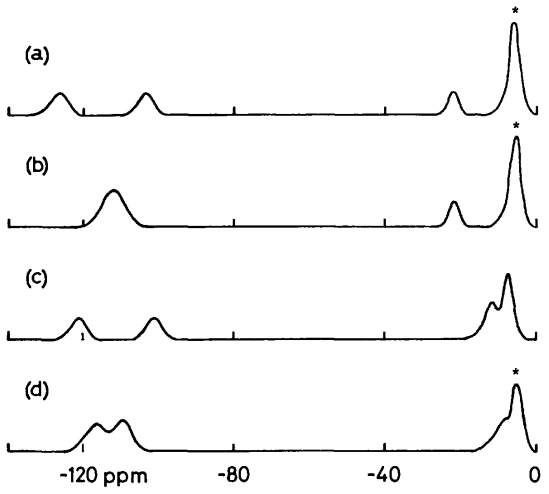

Fig. 5. PMR spectra of (a) $[Ni(eddp)(H_2O)_2]$, (b) $[Ni(eddp)(ox)]^{2-}$, (c) $[Ni(eddh)(H_2O)_2]$, and (d) $[Ni(eddh)(ox)]^{2-}$ in D_2O at 34 °C. The chemical shift is relative to the internal standard, TMS*. The signal from the residual HDO of the solvent is not shown. The signals with the sign (*) overlap with the signal of HDO.

The coordination of an oxalate ion appears to have some influence on the contact shifts of the ethylene and α protons (Fig. 5); in the eddh complex the signal of the equatorial proton of the ethylene moiety and that of the α proton approach each other, and in the eddp complex the two signals overlap to become a single broad band. Since the coordination of an oxalate ion does not change the configuration of the quadridentate ligand, this finding suggests that the coordinated oxalate ion might change the magnetic environment around the protons, or might even affect detailed conformations of the chelate rings.

The simplicity of the PMR spectra suggests that the eddp and eddh complexes exist not as equilibrium mixtures, but almost all in *s-cis* form. In the *s-cis* form, there is a C_2-symmetry axis passing through the central ethylene linkage and the nickel atom which makes the two chelate rings of the amino acidate equivalent. Consequently, it may be concluded that the nickel(II) complexes of edda-type optically active ligands are of *Δ-s-cis*-type absolute configuration. The CD spectra observed for mixed complexes having an oxalate ion afford some evidence to support this conclusion. As can be seen in Fig. 3, a new positive CD band emerges at higher wavenumbers in the first adsorption-band region when mixed complexes are formed. This CD pattern in the first absorption region, with negative and positive components from low wavenumbers, is characteristic of the absolute *Δ* configuration.[27-29] That the mixed complexes clearly indicate the *Δ*-type CD spectra is probably attributable to an increase in *Δ*-type ring pairing due to the addition of the oxalate chelate ring. That is to say, the contribution of the *Δ*-type configurational effect to the optical activity becomes relatively greater.

As described above, the PMR and CD spectral data indicate that these edda-type optically active ligands should stereospecifically ccordinate to a nickel(II) ion to form only the *Δ-s-cis* isomer in solution. Then, the steric factor for which ligands other than epro are forced to coordinate with the *Δ-s-cis* form must be examined. The four possible *s-cis* forms for the eddp-type complexes are depicted in Fig. 6. The symbols *δ* and *λ* represent the *gauche* form of the central en-type

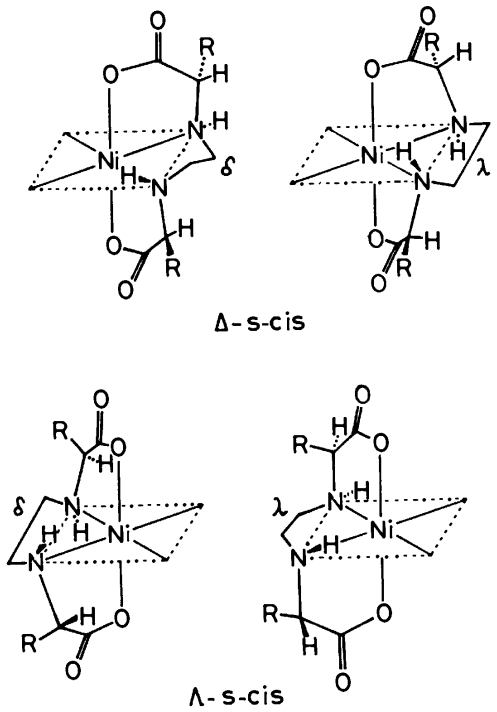

Fig. 6. Schematic drawing of the *cis*-type structures possible for the eddp-type complexes.

chelate ring. The substituent groups are denoted by R. The configuration of the secondary nitrogen atoms is *R* in the *Δ-s-cis* forms and *S* in the *Λ-s-cis* forms.

In the *Δ-s-cis* forms, both substituent groups are axial to the N-Ni-O chelate plane but point away from the central en-like chelate ring(*exo*), while in the *Λ-s-cis* forms, they point toward the central chelate ring(*endo*). Since the interaction between the non-bonding atoms is probably smaller in the *exo*-form than in the *endo*-form,[30] the *Δ-s-cis* form is considered to be thermodynamically more stable than the *Λ-s-cis* form. This may be the reason why these quadridentate ligands coordinate to a labile nickel(II) ion to form stereospecifically the *Δ-s-cis* isomer. For the cobalt(III) complex of eddp, however, both *Δ-s-cis* and *Λ-s-cis* isomers are obtained with almost the same yield, and hence the stereospecificity of eddp is not so large toward the inert cobalt(III) ion.[14] Thus, it can be said that the eddp-type ligands display their essential stereospecificity by forming labile nickel(II) complexes.

As has been pointed out by many other investigators,[4-7,31-33] the contact shift of the α protons in the amino acidate chelate ring depends on the relative axial-equatorial nature of the protons, that is, on the dihedral angle between the planes of the Ni-N-C and N-C-H groups; the equatorial proton appears at a very low value of the field (*ca.* −100 ppm) while the axial proton appears at a field higher than −40 ppm. The α protons of the eddp and eddh complexes are observed at fields lower than −100 ppm, indicating that the α protons are equatorial and hence the substituent groups are axial. Thus, this PMR finding supports the expectation that these complexes should be of Δ-*s-cis* form.

From an empirical correlation between the dihedral angle and the contact shift,[5] the α protons observed at

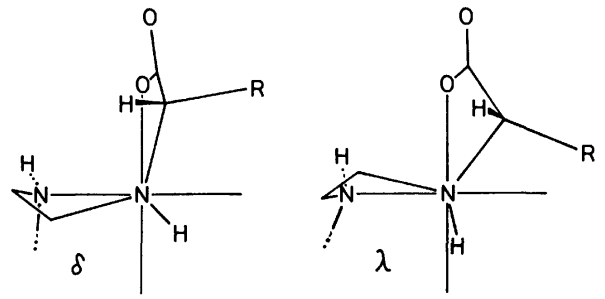

Fig. 7. The ring conformations in the *Δ-s-cis* forms as viewed from the Ni-N bond axis. δ and λ represent the conformations of the central en-type chelate ring. R designates the substituent groups. Another amino acidate chelate ring is not shown for clarity.

about −100 ppm for the eddp and eddh complexes are considered to be on a pseudo-*gauche* form of the amino acidate chelates. Figure 7 shows the ring conformations of the two *Δ-s-cis* forms illustrated in Fig. 6 as viewed from the Ni-N bond axis. The lower amino acidate chelate ring is omitted for clarity. The δ and λ symbols represent the conformation of the central en-type chelate ring. In the case of the λ conformation, the amino acidate ring becomes a highly strained envelope and, moreover, the substituent group designated as *R* closely approaches the neighboring coordination site. Therefore, the λ form is considered to be very unstable. In the δ form, on the other hand, the amino acidate ring is pseudo-*gauche* (λ). The observed contact shift is indicative of the δ form, in fair agreement with the relative stability expected for the two forms.

In conclusion, the eddp-type ligands would stereospecifically coordinate to the nickel(II) ion to form the *Δ-s-cis* isomer, in which the secondary nitrogen atoms are in an *R* configuration and the central en-type chelate ring is *δ-gauche*. This structure is exactly the same as the *Δ-s-cis* form expected for the epro complex except for the minor difference between the secondary and tertiary nitrogens. Thus, it can be said that the stereospecificity of eddp-type ligands is identical to that of epro containing L-proline residues.

The authors wish to thank Dr. K. Aoki of the NEC-Varian Co., Ltd., for the PMR measurements. The authors also acknowledge the Mitsubishi Foundation for the gift of the Jasco J-200 grating spectropolarimeter used in these studies.

References

1) I. Hirako, T. Murakami, and M. Hatano, *Bull. Chem. Soc. Jpn.*, **49**, 147 (1976).

2) The systematic and common names for these edda-type optically-active acids are described in previous papers.[1,3]

3) T. Murakami and M. Hatano, *Bull. Chem. Soc. Jpn.*, **49**, 3037 (1976).

4) R. S. Milner and L. Pratt, *Discuss. Faraday Soc.*, **34**, 88 (1962).

5) L. Pratt and B. B. Smith, *Trans. Faraday Soc.*, **65**, 915 (1969).

6) F. F. -L. Ho, L. E. Erickson, S. R. Watkins, and C. N. Reilley, *Inorg. Chem.*, **9**, 1139 (1970).

7) L. E. Erickson, F. F. -L. Ho, and C. N. Reilley, *Inorg.*

Chem. **9**, 1148 (1970).
8) R. V. Snyder and R. J. Angelici, *Inorg. Chem.*, **13**, 14 (1974).
9) D. S. Everhart and R. F. Evilia, *Inorg. Chem.*, **14**, 2755 (1975).
10) J. I. Legg and D. W. Cooke, *Inorg. Chem.*, **4**, 1576 (1965).
11) J. I. Legg, D. W. Cooke, and B. E. Douglas, *Inorg. Chem.*, **6**, 700 (1967).
12) G. R. Brubaker, D. P. Schaefer, J. H. Worrell, and J. I. Legg, *Coord. Chem. Rev.*, **7**, 161 (1971).
13) K. Igi and B. E. Douglas, *Inorg. Chem.*, **13**, 425 (1974).
14) L. N. Schoenberg, D. W. Cooke, and C. F. Liu, *Inorg. Chem.*, **7**, 2386 (1968).
15) *Δ* and *Λ* refer to the absolute configurations according to the IUPAC rules, as described in *Inorg. Chem.*, **9**, 1 (1970).
16) The nomenclature, *trans*, *s-cis*, and *uns-cis*, used here is employed in order to express three geometrical isomers of edda-type complexes. This was suggested by J. H. Worrell and D. H. Busch, *Inorg. Chem.*, **8**, 1563 (1969).
17) Excess amounts of sodium oxalate were added in order to change the edda-type complexes completely into mixed complexes. Since the absorption and CD spectra observed for the complex solutions containing 2 and 5 times excessive amounts of oxalate ions were exactly the same, the addition of amounts of sodium oxalate 2 times in excess would complete the formation of the mixed complexes.
18) R. A. Haines and M. Reimer, *Inorg. Chem.*, **12**, 1482 (1973).
19) I. Hirako, T. Murakami, and M. Hatano, unpublished data.
20) P. J. Garnett, D. W. Watts, and J. I. Legg, *Inorg. Chem.*, **8**, 2534 (1969).
21) P. F. Coleman, J. I. Legg, and J. Steele, *Inorg. Chem.*, **9**, 937 (1970).
22) K. D. Gailey, K. Igi, and B. E. Douglas, *Inorg. Chem.*, **14**, 2956 (1975).
23) S. Kitagawa, T. Murakami, and M. Hatano, *Chem. Lett.*, **1974**, 925.
24) S. Kitagawa, T. Murakami, and M. Hatano, *Inorg. Chem.*, **14**, 2347 (1975).
25) T. Murakami, S. Kitagawa, and M. Hatano, *Inorg. Chem.*, **15**, 1953 (1976).
26) *R* and *S* refer to the configurations about the asymmetric carbon or nitrogen atom of the ligands, according to the sequence rules of R. S. Cahn, C. K. Ingold, and V. Prelog, *Angew. Chem. Int. Ed. Engl.*, **5**, 385 (1966).
27) R. S. Treptow, *Inorg. Chem.*, **7**, 1229 (1968).
28) F. Woldbye, "Studies over Optisk Aktivitet," Polyteknisk Forlag, Copenhagen (1969).
29) J. Hidaka and Y. Shimura, *Bull. Chem. Soc. Jpn.*, **43**, 2999 (1970).
30) B. Bosnich and A. T. Phillip, *J. Am. Chem. Soc.*, **90**, 6352 (1968).
31) F. F.-L. Ho and C. N. Reilley, *Anal. Chem.*, **41**, 1835 (1969).
32) F. F. -L. Ho and C. N. Reilley, *Anal. Chem.*, **42**, 600 (1970).
33) L. E. Erickson, D. C. Young, F. F.-L. Ho, S. R. Watkins, J. B. Terrill, and C. N. Reilley, *Inorg. Chem.*, **10**, 441 (1971).

The Synthesis of Several Octose Derivatives Related to Octosyl Acids A and B

Kentaro ANZAI and Tsuneo SAITA

The Institute of Physical and Chemical Research, Wako-shi, Saitama 351

(Received May 10, 1976)

Starting from 1,2: 5,6-di-*O*-isopropylidene-α-D-allofuranose (**3a**), the sugar portion of octosyl acids **A** and **B** (**1a** and **1b**) was synthesised, though with some protecting groups. Compound **7a**, thus obtained, was found to be acid-liable, and treatment of **7a** in a dilute hydrochloric acid in methanol resulted in furanose-ring opening, affording an isopropylidene compound **8**.

Octosyl acids **A**, **B**, and **C**, which have been isolated from the fermentation broth of a polyoxin-producing microorganism *Streptomyces cacaoi* var. asoensis,[1] have been reported to have the structures **1a**, **1b**, and **2** by Isono, Crain, and McClosky.[2]

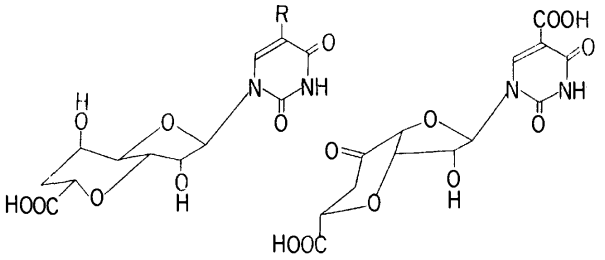

1a R=COOH
1b R=CH_2OH

2

These compounds are considered to be carbo-analogues of cyclic AMP,[2] and exploitation of a synthetic route to them may also contribute to the synthesis of other cyclic AMP analogues. We wish to report here the synthesis of the sugar portion of octosyl acids **A** and **B** with some protecting groups.

1,2: 5,6-Di-*O*-isopropylidene-α-D-allofuranose(**3a**)[3] was chosen as the starting material. Reaction of **3a** with methyl bromoacetate in the presence of sodium hydride in tetrahydrofuran afforded the methyl ester **3b**. Similarly, the ethyl ester **3c** was prepared.

To construct the bicyclic skeleton of octosyl acids, bond formation between the carbon at 3-O and C_6 in **3c** is necessary; for this purpose, an attempt was made to convert **3c** to a malonic acid derivative **3d** in order to activate the carbon atom at 3-O in **3c**.

Reaction of the ester **3c** with diethyl carbonate in the presence of one equivalent of sodium hydride in refluxing tetrahydrofuran afforded two products, which were separated by silica gel chromatography. The less polar compound, which was indistinguishable from the starting material on TLC, was actually found to be the required malonic acid derivative **3d**, showing two carbonyl bands at 1770 and 1740 cm^{-1} in the IR spectrum, a mass fragment ion at *m/e* 403 corresponding to M^+-CH_3, and a singlet a δ 4.78 in the NMR spectrum corresponding to one methine proton at 3-O-C. The more polar compound was found to be a Claisen condensation product **4**, showing a mass fragment ion at *m/e* 631 corresponding to M^+-CH_3. Though **4** was homogeneous on TLC, and the NMR spectrum showed a methine proton singlet at δ 4.78, the anomeric proton signal appeared as a multiplet (δ 5.68—5.88), suggesting that **4** was a mixture of the stereoisomers at the carbon atom flanked by two carbonyl groups. The yield ratio of **3d** to **4** varied markedly in several experiments, though the latter was predominant in every case. However, if the reaction was carried out in refluxing diethyl carbonate (bp 127 °C) instead of refluxing tetrahydrofuran (bp 66 °C), the formation of **3d** was predominant and the ratio of **3d** to **4** was found constantly to be 9: 1. On the contrary, **4** was formed exclusively when the reaction was carried out at 0 °C.

Treatment of **3d** in 70% acetic acid at 37 °C for 3 h was effective in obtaining the monoacetonated compound **5a** in a good yield. Reaction of **5a** with an equimolar amount of tosyl chloride afforded the 6-*O*-tosylate **5b** almost exclusively; a small amount of the ditosylate **5d** as well as the starting material were also isolated from the reaction mixture. With excess tosyl chloride, the ditosylate **5d** was formed exclusively. Reaction of **5b** with acetic anhydride in pyridine afforded the acetyl tosyl compound **5c**, whose proton signal at C-5 appeared in a lower field (δ 5.31) than that of **5b** (δ 3.8), showing the correctness of the assignment of **5b** as the 5-hydroxy compound.

The monotosylate **5b** was treated with an equimolar amount of sodium hydride in tetrahydrofuran at room temperature to give two products, which were separated by silica gel chromatography. The less polar one was the epoxy compound **6a**, the NMR spectrum of which still showed a singlet at δ 4.68, corresponding to one methine proton of the malonic acid moiety. The shifts of the proton signals at C_5 and C_6 in **6a** to higher fields showed the formation of an epoxide ring. The mass spectrum of **6a** showed intense peaks at *m/e* 345, 302, and 169 corresponding to M^+-CH_3, $M^+-CH_3-CH_2CH(-O-)$, and $M^+-CH_3-(C_2H_5OOC)_2CHO-H$.

The more polar one was found to have the same molecular formula as **6a** (M^+-CH_3 *m/e* 345) and was identified as the required **7a**, which showed an IR absorption at 3500 cm^{-1} corresponding to a hydroxyl group. The methine proton signal at δ 4.68 in the NMR spectrum in **5b** was lost **7a**, showing the bond formation between 3-O-C and C_6. The yield ratio of **6a** to **7a** was 1/2 to 1/3 throughout several experiments. Attempts at the conversion of **6a** to **7a** in the presence of varying amounts of sodium hydride (0.1 to 1.0 equivalent) failed, suggesting that the reaction to **6a** and **7a** from **5b** proceeded independently.

Similarly, the ditosylate **5d** and the acetyl tosylate **5c** were converted into two ring-formation compounds, **7c** and **7b**. In the latter case, the reaction conditions were

more vigorous (under reflux in tetrahydrofuran for 2 days) than in the former case (at room temperature in tetrahydrofuran for 20 h).

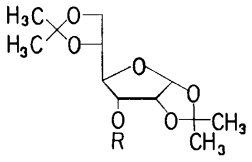

3a R=H
3b R=CH_3OOCH_2
3c R=$C_2H_5OOCH_2$
3d R=$(C_2H_5OOC)_2CH$
3e R=$NCCH_2$

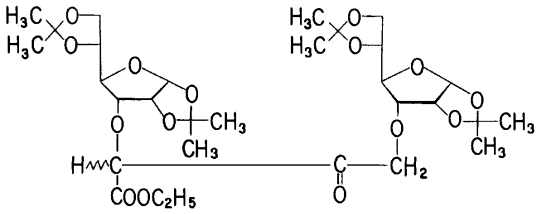

4

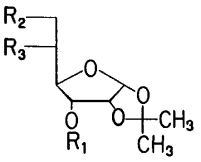

5a R_1=$(C_2H_5OOC)_2CH$, R_2, R_3=OH
5b R_1=$(C_2H_5OOC)_2CH$, R_2=*p*-$CH_3C_6H_4SO_3$, R_3=OH
5c R_1=$(C_2H_5OOC)_2CH$, R_2=*p*-$CH_3C_6H_4SO_3$, R_3=CH_3CO_2
5d R_1=$(C_2H_5OOC)_2CH$, R_2, R_3=*p*-$CH_3C_6H_4SO_3$
5e R_1=$C_2H_5OOCCH_2$, R_2, R_3=OH
5f R_1=$C_2H_5OOCCH_2$, R_2=*p*-$CH_3C_6H_4SO_3$, R_3=OH
5g R_1=$C_2H_5OOCCH_2$, R_2=*p*-$CH_3C_6H_4SO_3$, R_3=$C_6H_5CO_2$
5h R_1=$C_2H_5OOCCH_2$, R_2, R_3=*p*-$CH_3C_6H_4SO_3$
5i R_1=$C_2H_5OOCCH_2$, R_2=I, R_3=$C_6H_5C_3O_2$
5j R_1=$NCCH_2$, R_2, R_3=OH
5k R_1=$NCCH_2$, R_2=*p*-$CH_3C_6H_4SO_3$, R_3=OH
5l R_1=$NCCH_2$, R_2, R_3=*p*-$CH_3C_6H_4SO_3$

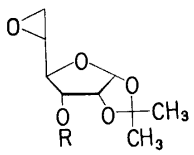

6a R=$(C_2H_5OOC)_2CH$
6b R=$C_2H_5OOCCH_2$
6c R=$NCCH_2$

Attempts were made to construct the bicyclic system of octosyl acids by intramolecular cyclization of the monocarboxylic acid ethyl ester **5f** and its cyanomethyl analogue **5k**. As in the case of the tosylate **5b**, the tosylate **5f** was prepared from the partially deacetonated product **5e** of **3c**; **5e** was also converted into the ditosylate **5h** with excess tosyl chloride.

The cyanomethyl derivative **3e** was obtained in a moderate yield on treatment of **3a** with chloroacetonitrile or bromoacetonitrile in the presence of sodium hydride. Partial deacetonation of **3e** in 70% acetic acid afforded **5j**, which was then converted to the mono- and ditosylate, **5k** and **5l**.

The ester **5f** and the nitrile **5k** gave exclusively the epoxy compounds **6b** and **6c**; the required products were not obtained.

The benzoyl tosylate **5g**, the ditosylate **5h** and the iodo compound **5i**, which had been prepared from **5h** by treatment with sodium iodide in ethyl methyl ketone, were found to be inert to sodium hydride or lithium bis(trimethylsil)amide at room temperature or under reflux. These results were somewhat surprising, because, as has been mentioned previously, the diacetonated compound **3c** was converted into **4** even at 0 °C by treatment with sodium hydride.

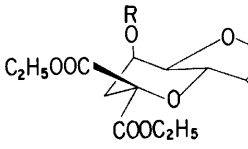

7a R=H
7b R=CH_3CO
7c R=*p*-$CH_3C_6H_4SO_2$

Attempts at acetolysis of **7a**, followed by reaction with bis(trimethylsilyl)uracil using a $SnCl_4$ catalyst[4] to obtain a nucleoside related to octosyl acids, failed. The failure may be attributable to the susceptibility of the 3,7-anhydrooctose skeleton of **7a** to acids, which was also shown by the following results: in a dilute methanolic solution of hydrochloric acid (0.01 M) **7a** was converted into the ring-opened acetonate **8**, and under more vigorous conditions (0.5 M) the deacetonated product **9** was obtained. We feel now that the binding of the aglycon should be prior to the formation of the bicyclic system of the sugar portion in the synthesis of octosyl acids.

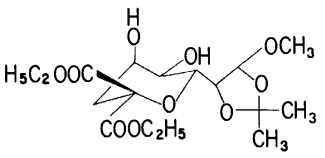

8

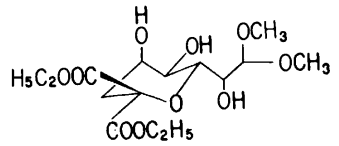

9

Experimental

1,2:5,6-Di-O-isopropylidene-3-O-ethoxycarbonylmethyl-α-D-allofuranose (3c). Sodium hydride (550 mg, 23 mmol), freshly prepared from a commercially available oil-coated product (NaH content, 50%) by washing with hexane, was added to a solution of **3a** (5.2 g, 20 mmol) in dry tetrahydrofuran (20 mmol). After the evolution of hydrogen had ceased, the mixture was cooled to 0 °C and ethyl bromoacetate (5 g, 30 mmol) was added dropwise. The mixture was stirred overnight at room temperature. The remaining sodium hydride was quenched by adding ethanol at 0 °C, and a few drops of acetic acid were added to keep the mixture acidic during processing. After the mixture had been concentrated, it was distributed between ethyl acetate and water. The organic layer was washed with water and then concentrated to dryness to give a crude product, which was crystallized from hexane; yield, 5.8 g (84%); mp 89—90 °C; ν_{CO}^{KBr} 1750 cm^{-1}; M^+-CH_3 *m/e* 331; NMR (100 MHz, $CDCl_3$) δ: 1.30 (t, 3H, ethyl ester J=7 Hz), 1.38 and 1.46 (2s, 6H, two

methyls of one isopropylidene group), 1.38 and 1.58 (2s, 6H, two methyls of one isopylropyidene group), 4.78 (t, 1H, H-2, $J_{1,2}$=4 Hz, $J_{2,3}$=4 Hz), 5.76 (s, 1H, H-1, $J_{1,2}$=4 Hz).

Found: C, 55.87; H, 7.69%. Calcd for $C_{16}H_{26}O_8$: C, 55.48; H, 7.57%.

*1,2:5,6-Di-O-isopropylidene-3-O-methoxycarbonylmethyl-α-D-allofuranose (**3b**).* Compound **3a** (5.2 g, 20 mmol) was treated with methyl bromoacetate (4.6 g, 30 mmol) and sodium hydride (550 mg, 23 mmol) in dry tetrahydrofuran (50 ml) as has been described in the preceding section. The product was crystallized from hexane; yield, 4.7 g (70%). Silica gel chromatography, developed with a mixture of benzene and ethyl acetate (2: 1), gave an analytically pure sample; mp 80—81 °C; ν_{CO}^{KBr} 1760 cm^{-1}; M$^+$−CH_3 *m/e* 317; NMR (100 MHz, $CDCl_3$) δ: 1.36 and 1.46 (2s, 6H, two methyls of one isopropylidene group), 1.36 and 1.58 (2s, 6H, two methyls of one isopropyridene group), 3.75 (s, 3H, methyl ester), 4.76 (t, 1H, H-2, $J_{1,2}$=4 Hz, $J_{2,3}$=4 Hz), 5.76 (d, 1H, H-1, $J_{1,2}$=4 Hz).

Found: C, 54.06; H, 7.16%. Calcd for $C_{15}H_{24}O_8$: C, 54.21; H, 7.28%.

*3-O-Bis(ethoxycarbonyl)methyl-1,2:5,6-di-O-isopropylidene-α-D-allofuranose (**3d**).* A suspension of sodium hydride (500 mg, 20 mmol) in diethyl carbonate (150 ml) previously dried over sodium was heated to reflux, and then the reaction vessel was taken off from the heater. Immediately, the ester **3c** (6.92 g, 20 mmol) was added portionwise. The mixture was further heated under reflux for 2 h and cooled to −15 °C. Ethanol (10 ml) and then acetic acid (2 ml) were added and the mixture was concentrated below 35 °C.

Silica gel chromatography of the ethyl acetate extracts, developed with mixtures of benzene and ethyl acetate (2—1: 1), afforded 6.6 g (80%) of the main product as a syrup, which was subsequently crystallized from ether and hexane; yield, 5.50 g; mp 50—51 °C; 1770 and 1740 cm^{-1}; M$^+$−CH_3 *m/e* 403; NMR (100 MHz, $CDCl_3$) δ: 4.70 (t, 1H, H-2, $J_{1,2}$=4 Hz, $J_{2,3}$=4 Hz), 4.80 (s, 1H, $H_5C_2OOCC\underline{H}COOC_2H_5$), 5.80 (d, 1H, H-1, $J_{1,2}$=4 Hz).

Found: C, 54.71; H, 7.19%. Calcd for $C_{19}H_{30}O_{10}$: C, 54.53; H, 7.23%.

From the reaction mixture was also isolated the Claisen condensation product **4**, which was more polar than **3d**; yield, 0.70 g.

*The Claisen Condensation Product **4**.* The ester **3c** (500 mg, 1.45 mmol) was treated with sodium hydride (40 mg, 1.65 mmol) in tetrahydrofuran (30 ml) first at 0 °C for 8 h and at room temperature for 16 h. The mixture was cooled again at 0 °C. After ethanol (1 ml) and a few drops of acetic acid had been added, it was concentrated and the product was extracted with ethyl acetate. Silica gel chromatography developed with a mixture of benzene and ethyl acetate (1: 1) afforded 310 mg (70%) of a syrup, which was fractionally precipitated from ethyl acetate and hexane for analysis; ν_{CO}^{KBr} 1740 cm^{-1}; M$^+$−CH_3 *m/e* 631; NMR (100 MHz, $CDCl_3$) δ: 4.72 (s, 1H, $OC\underline{H}COOC_2H_5$), 5.68—5.88 (m, 2H, two anomeric protons).

Found: C, 55.72; H, 7.17%. Calcd for $C_{30}H_{46}O_{15}$: C, 55.73; H, 6.98%.

The same reaction was carried out in a mixture of tetrahydrofuran and diethyl carbonate (9: 1) at room temperature. However, no trace of **3d** could be detected as was shown by IR. Note that the separation of **3d** from **3c** on TLC was unsucessful by any combination of solvents.

*3-O-Bis(ethoxycarbonyl)methyl-1,2-O-isopropylidene-α-D-allofuranose (**5a**).* A solution of **3d** (1.9 g) in 70% acetic acid (100 ml) was allowed to stand at 37 °C for 3 h and was evaporated to dryness keeping the temperature below 37 °C. To the residue was added an ice-cooled solution of sodium hydrogencarbonate, and the products were extracted with chloroform. TLC showed the presence of trace amounts of the starting material as well as one major and one minor product, the latter presumably being the di-deacetonated product, 3-*O*-bis(ethoxycarbonyl)methyl-D-allose.

The major one was isolated by silica gel chromatography, developed first with a mixture of benzene and ethyl acetate (1: 1) and then with ethyl acetate; yield, 1.4 g (82%). For further purification it was fractionally precipitated from benzene and hexane to give a syrup, which, on standing, was gradually converted into a solid melting at 53 °C; ν_{CO}^{KBr} 1773 and 1738 cm^{-1}; M$^+$−CH_3 *m/e* 363; NMR (100 MHz, $CDCl_3$) δ: 1.32 (t, 6H, ethyl ester, J=7 Hz), 1.35 and 1.56 (two s, 6H, two isopropylidene methyls), 4.64 (t, 1H, H-2, $J_{1,2}$=4 Hz, $J_{2,3}$=4 Hz), 4.74 (s, 1H, $H_5C_2OOCC\underline{H}COOC_2H_5$), 5.80 (d, 1H, H-1, $J_{1,2}$=4 Hz).

Found: C, 51.07; H, 6.58%. Calcd for $C_{16}H_{26}O_{10}$: C, 50.79; H, 6.93%.

*3-O-Bis(ethoxycarbonyl)methyl-1,2-O-isopropylidene-6-O-tosyl-α-D-allofuranose (**5b**).* Tosyl chloride (0.8 g, 4.2 mmol) was added all at once to a solution of **5a** (1.4 g, 3.7 mmol) in pyridine (50 ml) cooled at −15 °C, after which the mixture was allowed to stand at room temperature overnight. An ice-cooled solution of sodium hydrogencarbonate was added and the products were extracted with ethyl acetate. The main product was isolated by silica gel chromatography, developed with a mixture of benzene and ethyl acetate (2: 1); yield, 1.35 g (70%); M−CH_3 *m/e* 517; NMR (100 MHz, $CDCl_3$) δ: 1.30 (t, 6H, ethyl ester, J=7 Hz), 1.32 and 1.52 (two s, 6H, two isopropylidene methyls), 2.44 (s, 3H, one methyl of the tosyl group), 4.67 (s, 1H, $H_5C_2OOCC\underline{H}COOC_2H_5$), 5.72 (d, 1H, H-1, $J_{1,2}$=4 Hz), 7.33 and 7.82 (two d, 4H, four aromatic protons of the tosyl group, J_{ortho}=9 Hz).

Found: C, 51.93; H, 6.00; S, 5.97%. Cacld for $C_{23}H_{32}O_{12}S$: C, 51.87; H, 6.06; S, 6.02%.

*3-O-Bis(ethoxycarbonyl)methyl-5,6-di-O-tosyl-1,2-O-isopropylidene-α-D-allofuranose (**5d**).* Treatment of **5a** (500 mg) with tosyl chloride (1 g) in pyridine (20 ml) at 37 °C for 2 days afforded a single product. The pyridine was removed by evaporation, and an ice-cooled solution of sodium hydrogencarbonate was added. Extraction with ethyl acetate and silica gel chromatography, developed with a mixture of benzene and ethyl acetate (4: 1), gave a syrup; yield, 700 mg; NMR (100 MHz, $CDCl_3$) δ: 1.23 and 1.28 (two t, 6H, ethyl ester), 1.27 and 1.43 (two s, 6H, two isopropylidene methyls), 2.41 (s, 6H, two methyls of the tosyl group), 4.51 (t, 1H, H-2), 4.59 (s, 1H, $H_5C_2OOCC\underline{H}COOC_2H_5$), 5.11 (m, 1H, H-5), 5.46 (d, 1H, H-1, $J_{1,2}$=4 Hz).

Found: C, 53.05; H, 5.49; S, 9.01%. Calcd for $C_{30}H_{38}O_{14}S_2$: C, 52.47; H, 5.58; S, 9.34%.

*5-O-Acetyl-3-O-bis(ethoxycarbonyl)methyl-1,2-O-isopropylidene-6-O-tosyl-α-D-allofuranose (**5c**).* A solution of **5b** (700 mg) in a mixture of acetic anhydride (5 ml) and pyridine (2 ml) was allowed to stand at 37 °C for 3 h; after it was evaporated to dryness, the product was precipitated from ether and hexane to give a syrup; yield, 650 mg; NMR (100 MHz, $CDCl_3$) δ: 1.30 (t, 6H, ethyl ester, J=7 Hz), 1.32 and 1.52 (two s, 6H, two isopropylidene methyls), 2.03 (s, 3H, acetyl), 2.44 (s, 3H, one methyl of the tosyl group), 4.62 (t, 1H, H-2, $J_{1,2}$=4 Hz, $J_{2,3}$=4 Hz), 4.64 (s, 1H, $H_5C_2OOCC\underline{H}COOC_2H_5$), 5.31 (q, 1H, H-5), 5.70 (d, 1H, H-1, $J_{1,2}$=4 Hz), 7.35 and 7.82 (two d, 4H, four aromatic protons of the tosyl group, J_{ortho}=9 Hz).

Found: C, 52.36; H, 6.11; S, 5.56%. Calcd for $C_{25}H_{34}O_{13}S$: C, 52.25; H, 5.96; S, 5.58%.

5,6-Anhydro-3-O-bis(ethoxycarbonyl)methyl-1,2-O-isopropylidene-

*α-D-allofuranose (**6a**) and 3,7-Anhydro-7-bis(C-ethoxycarbonyl)-6-deoxy-1,2-O-isopropylidene-α-D-allo-heptose (**7a**).* To a solution of **5b** (700 mg, 1.3 mmol) in dry tetrahydrofuran (20 ml), cooled at −15 °C, has been added sodium hydride (34 mg, 1.4 mmol). After the mixture had been stirred for 20 h at room temperature, it was cooled again to −15 °C. Ethanol (1 ml) was added to quench the remaining sodium hydride, and acetic acid (1 ml) was added to keep the reaction mixture acidic during processing. Concentration, extraction with ethyl acetate, and developing on a silica gel column with mixtures of benzene and ethyl acetate (4—1: 1) afforded two products.

The less polar compound (132 mg) was identified as the epoxide **6a** and was obtained as a syrup by precipitation from benzene and hexane; MS (75 eV) *m/e*: 345 (M^+-CH_3), 302 ($M^+-CH_3-CH_2CH(-O-)$), 169 ($M^+-CH_3-H_5C_2OOCCH(O)COOC_2H_5-H$), 127 ($M^+-CH_3-H_5C_2OOCCH(O)COOC_2H_5-CH_2CH(-O-)$); NMR (100 MHz, $CDCl_3$) δ 1.31 and 1.38 (two t, 6H, ethyl ester, J=7 Hz), 1.36 and 1.56 (two s, 6H, two isopropylidene methyls), 2.82 (t, 1H, H_a-6, J_{gem}=4.5 Hz, $J_{5,6a}$=4.5 Hz), 3.10 (q, 1H, H_b-6, J_{gem}=4.5 Hz, $J_{5,6b}$=3 Hz), 3.32 (m, 1H, H-5), 3.81 (q, 1H, H-3, $J_{3,4}$=8 Hz, $J_{2,3}$=4 Hz), 4.28 and 4.29 (two q, 4H, two methylenes of the ester groups, J=7 Hz), 4.41 (q, 1H, H-4, $J_{3,4}$=8 Hz, $J_{4,5}$=2 Hz), 4.63 (t, 1H, H-2, $J_{1,2}$=4 Hz, $J_{2,3}$=4 Hz), 4.68 (s, 1H, $H_5C_2OOCCHCOOC_2H_5$), 5.80 (d, 1H, H-1, $J_{1,2}$=4 Hz).

Found: C, 53.10; H, 6.48%. Calcd for $C_{16}H_{24}O_9$: C, 53.33; H, 6.71%.

The more polar compound (387 mg) was obtained as a syrup by precipitation from benzene and hexane and was identified as **7a**: IR (KBr) cm^{-1}: 3500 (OH), 1770, sh and 1743 (CO); M^+-CH_3 *m/e* 345 (intense); NMR (100 MHz, $CDCl_3$) δ: 1.27 and 1.29 (two t, 6H, ethyl ester), 1.37 and 1.59 (two s, 6H, two isopropylidene methyls), 2.15 (broad, 1H, OH), 2.31 and 2.77 (two dd, 2H, H_a-6 and H_b-6, $J_{5,6a}$=3 Hz, $J_{5,6b}$=4 Hz, J_{gem}=15 Hz), 3.92 (dd, 1H, H-4, $J_{3,4}$=12 Hz, $J_{4,5}$=3 Hz), 4.29 (q, 4H, two methylenes of the ester groups, J=7 Hz), 4.35 (dd, 1H, H-3, $J_{2,3}$=4 Hz, $J_{3,4}$=12 Hz), 4.49 (broad, 1H, H-5), (4.79 (t, 1H, H-2, $J_{1,2}$=4 Hz, $J_{2,3}$=4 Hz), 5.77(d, 1H, H-1, $J_{1,2}$=4 Hz).

Found: C, 53.64; H, 6.67%. Calcd for $C_{16}H_{24}O_9$: C, 53.33; H, 6.71%.

*5-O-Acetyl-3,7-anhydro-7-bis(C-ethoxycarbonyl)-6-deoxy-1,2-O-isopropylidene-α-D-allo-heptose (**7b**).* A mixture of **5c** (535 mg, 0.93 mmol) and sodium hydride (30 mg, 1.3 mmol) in dry tetrahydrofuran (10 ml) was refluxed for 2 days and cooled to −15 °C. Ethanol (0.5 ml) and a few drops of acetic acid were added, and the mixture was concentrated. The product was extracted with ethyl acetate and purified by silica gel chromatography, developed with a mixture of benzene and ethyl acetate (2: 1); yield, 255 mg. For analysis it was fractionally precipitated from ethyl acetate and hexane to give a syrup; M^+-CH_3 *m/e* 387 (intense): NMR (100 MHz, $CDCl_3$) δ: 1.26 and 1.30 (two t, 6H, ethyl ester, J=7 Hz), 1.35 and 1.58 (two s, 6H, two isopropylidene methyls), 2.00 (s, 3H, acetyl), 2.39 and 2.90 (two dd, 2H, H_a-6 and H_b-6, $J_{5,6a}$=3 Hz, $J_{5,6b}$=4 Hz, J_{gem}=15 Hz), 3.95 (dd, 1H, H-4, $J_{3,4}$=10 Hz, $J_{4,5}$=3 Hz), 4.1—4.5 (m, 5H, H-3 and four methylene protons of the ester groups), 4.80 (t, 1H, H-2, $J_{1,2}$=4 Hz, $J_{2,3}$=4 Hz), 5.52 (m, 1H, H-5), 5.78 (d, 1H, H-1, $J_{1,2}$=4 Hz).

Found: C, 53.91; H, 6.55%. Calcd for $C_{18}H_{26}O_{10}$; C, 53.72; H, 6.51%.

*3,7-Anhydro-7-bis(C-ethoxycarbonyl)-6-deoxy-1,2-O-isopropylidene-6-O-tosyl-α-D-allo-heptose (**7c**).* A mixture of **5d** (710 mg, 1.03 mmol) and sodium hydride (38 mg, 1.5 mmol) in dry tetrahydrofuran (20 ml) was stirred at room temperature overnight and was treated as has been described in the preceding section. Silica gel chromatography, developed with a mixture of benzene and ethyl acetate (4: 1) followed by crystallization from ethyl acetate and hexane, afforded 318 mg of **7c**; mp 146—147 °C; MS (75 eV) *m/e*: 499 (M^+-CH_3), 427 ($M^+-CH_3-COOC_2H_5+H$), 342 ($M^+-CH_3C_6H_4SO_3H$); NMR (100 MHz, $CDCl_3$) δ: 1.26 and 1.31 (two t, 6H, ethyl ester), 1.33 and 1.52 (two s, 6H, two isopropylidene methyls), 2.42, (s, 3H, tosyl), 2.46 and 3.06 (two dd, 2H, H_a-6 and H_b-6, $J_{5,6a}$=3 Hz, $J_{5,6b}$=4 Hz, J_{gem}=15 Hz), 3.82 (dd, 1H, H-4, $J_{3,4}$=10 Hz, $J_{4,5}$=3 Hz), 4.1—4.5 (m, 5H, H-3 and four methylene protons of the ester groups), 4.72 (t, 1H, H-2, $J_{1,2}$=4 Hz, $J_{2,3}$=4 Hz), 5.09 (broad, 1H, H-5), 5.54 (d, 1H, H-1, $J_{1,2}$=4 Hz).

Found: C, 53.61; H, 5.83; S, 6.33%. Calcd for $C_{23}H_{30}O_{11}S$: C, 53.68, H, 5.88; S, 6.23%.

*3-O-Ethoxycarbonylmethyl-1,2-O-isopropylidene-α-D-allofuranose (**5e**).* A solution of **3c** (5 g, 14.5 mmol) in 70% acetic acid (100 ml) was allowed to stand at 37 °C for 3 h and was evaporated to dryness. An ice-cooled solution of sodium hydrogencarbonate was added, and the product was extracted with chloroform. TLC showed the presence of one major product as well as a small amount of the starting material and a by-product, the latter being presumably the di-deacetonated product, 3-*O*-ethoxycarbonylmethyl-D-allose.

Silica gel chromatography, developed with a mixture of ethyl acetate and methanol (9: 1), afforded 2.51 g (8.2 mmol, 57%) of **5e**, which was fractionally precipitated from benzene and hexane for analysis; M^+-CH_3 *m/e* 291; NMR (100 MHz, $CDCl_3$) δ: 1.30 (t, 3H, ethyl ester, J=7 Hz), 1.36 and 1.58 (2s, 6H, two isopropylidene methyls), 4.68 (t, 1H, H-2, $J_{1,2}$=4 Hz, $J_{2,3}$=4 Hz), 5.77 (d, 1H, H-1, $J_{1,2}$=4 Hz).

Found: C, 50.99; H, 7.18%. Calcd for $C_{13}H_{22}O_8$: C, 50.97; H, 7.24%.

*3-O-Ethoxycarbonylmethyl-1,2-O-isopropylidene-6-O-tosyl-α-D-allofuranose (**5f**).* Compound **5e** (828 mg, 2.7 mmol) was treated with tosyl chloride (420 mg, 2.7 mmol) much as in the preparation of **5b**. The main product was isolated by silica gel chromatography, developed with mixtures of benzene and ethyl acetate (2—1: 1); it was obtained as a syrup from ethyl acetate and hexane; yield, 810 mg; IR (KBr) cm^{-1}: 3470 (OH), 1735 (ester); M^+-CH_3 *m/e* 445; NMR (100 MHz, $CDCl_3$) δ: 1.26 (t, 3H, ethyl ester, J=7 Hz), 1.33 and 1.52 (2s, 6H, two isopropylidene methyls), 2.42 (1s, 3H, methyl of the tosyl group), 5.71 (d, 1H, H-1, $J_{1,2}$=4 Hz), 7.32 and 7.80 (two d, 4H, four aromatic protons of the tosyl group).

Found: C, 52.23; H, 5.95; S, 6.95%. Calcd for $C_{20}H_{28}O_{10}S$: C, 52.16; H, 6.13; S, 6.96%.

*5,6-Di-O-tosyl-3-O-ethoxycarbonylmethyl-1,2-O-isopropylidene-α-D-allofuranose (**5h**).* Compound **5e** (306 mg, 1 mmol) was treated with tosyl chloride (760 mg, 4 mmol) much as in the preparation of **5d**. Silica gel chromatography, developed with mixtures of benzene and ethyl acetate (4—1: 1), afforded 450 mg of the product, which was crystallized from ethyl acetate and hexane; mp 115—116 °C; NMR (100 MHz, $CDCl_3$) δ: 1.26 (t, 3H, ethyl ester, J=7 Hz), 1.31 and 1.48 (2s, 6H, two isopropylidene methyls), 2.44 (s, 6H, two methyls of the tosyl group), 4.58 (t, 1H, H-2, $J_{1,2}$=4 Hz, $J_{2,3}$=4 Hz), 5.07 (m, 1H, H-5), 5.47 (d, 1H, H-1, $J_{1,2}$=4 Hz), 7.33 and 7.72 (two d, 4H, four aromatic protons of one tosyl group, J_{ortho}=8 Hz), 7.33 and 7.76 (two d, 4H, four aromatic protons of one tosyl group, J_{ortho}=8 Hz).

Found: C, 52.79; H, 5.56; S, 10.42%. Calcd for $C_{27}H_{34}O_{12}S_2$: C, 52.75: H, 5.58; S, 10.43%.

*5-O-Benzoyl-3-O-ethoxycarbonylmethyl-1,2-O-isopropylidene-6-O-tosyl-α-D-allofuranose (**5g**).* To a solution of **5f** (3 g,

6.6 mmol) in pyridine (50 ml), cooled at −15 °C, was added benzoyl chloride (3 g, 21 mmol), after which the solution was stirred for 1 h at room temperature. An ice-cooled solution of sodium hydrogencarbonate was added, and the product was extracted with ethyl acetate. Precipitation from ether and hexane afforded 3.10 g of a syrup (83%); M^+-CH_3 *m/e* 549; NMR (100 MHz, $CDCl_3$) δ: 1.20 (t, 3H, ethyl ester, J=7 Hz), 1.32 and 1.55 (2s, 6H, two isopropylidene methyls), 2.34 (s, 3H, methyl of the tosyl group), 4.68 (t, 3H, H-2, $J_{1,2}$=4 Hz, $J_{2,3}$=4 Hz), 5.5—5.7 (m, 2H, H-1 and H-5), 7.18 and 7.72 (2d, 4H aromatic protons of the tosyl group, J_{ortho}=8 Hz), 7.3—7.6 (m, 3H, *meta* and *para* protons of the benzoyl group), 7.94 (dd, 2H, *ortho* protons of the benzoyl group, J_{ortho}=8 Hz, J_{meta}=1.5 Hz).

Found: C, 57.51; H, 5.73; S, 5.48%. Calcd for $C_{27}H_{32}O_{11}S$: C, 57.43; H, 5.71; S, 5.68%.

5-O-Benoyl-z6-deoxy-3-O-ethoxycarbonylmethyl-6-iodo-1,2-O-isopropylidene-α-D-allofuranose (5i). A solution of **5g** (2.46 g, 4.6 mmol) and sodium iodide (3 g, 20 mmol) in ethyl methyl ketone (50 ml) was refluxed for 17 h. After the solvent had been evaporated to dryness, the residue was distributed between water and ethyl acetate. The organic layer was washed with an aqueous solution of sodium hydrogensulfite. TLC showed the formation of a sigle product, which was isolated by silica gel chromatograpy developed with mixtures of benzene and ethyl acetate (9—4: 1) yield, 1.65 g. For analysis it was fractionally precipitated from ether and hexane. It gradually decomposed at 56 °C *in vacuo*; MS (75 eV) *m/e*: 505 (M^+-CH_3), 393 (M^+-1); NMR (100 MHz, $CDCl_3$) δ: 1.20 (t, 3H, ethyl ester, J=7 Hz), 1.34 and 1.59 (two s, 6H, two isopropylidene methyls), 4.71 (t, 1H, H-2, $J_{1,2}$=4 Hz, $J_{2,3}$=4 Hz), 5.35 (q, 1H, H-5, $J_{4,5}$=6 Hz, $J_{5,6}$=6 Hz), 5.71 (d, 1H, H-1, $J_{1,2}$=4 Hz), 7.3—7.7 (m, 3H, *meta* and *para* protons of the benzoyl group), 8.08 (dd, 2H, *ortho* protons of the benzoyl group, J_{ortho}=8 Hz, J_{meta}=1.5 Hz).

Found: C, 46.98; H, 4.95; I, 23.76%. Calcd for $C_{20}H_{25}O_8I$: C, 47.20; H, 5.09; I, 32.75%.

5,6-Anhydro-3-O-ethoxycarbonylmethyl-1,2-O-isopropylidene-α-D-allofuranose (6b). A mixture of **5f** (689 mg, 1.5 mmol) and sodium hydride (36 mg, 1.5 mmol) in dry terahydrofuran (10 ml) was refluxed for 2 h and then cooled to −15 °C. Ethanol (1 ml) and a few drops of acetic acid were added, and the mixture was concentrated to dryness. The product was extracted with chloroform, and crystallized from ether and hexane; yield, 227 mg; mp 55—57 °C; ν_{CO}^{KBr} 1755 cm^{-1}; MS (75 eV) *m/e*: 273 (M^+-CH_3), 169 ($M^+-CH_3-C_2H_5OOCCH_2O-H$), 127 ($M^+-CH_3-C_2H_5OOCCH_2O-CH_2CH(-O-)$); NMR (100 MHz, $CDCl_3$) δ: 1.32 (t, 3H, ethyl ester, J=7 Hz), 1.39 and 1.60 (2s, 6H two isopropylidene methyls), 2.84 (t, 1H, H_a-6, $J_{5,6a}$=5 Hz, J_{gem}=5 Hz), 3.01 (q, 1H, H_b-6, $J_{5,6b}$=3 Hz, J_{gem}=5 Hz), 3.26 (m, 1H, H-5), 3.82 (q, 1H, H-4, $J_{3,4}$=9 Hz, $J_{4,5}$=5 Hz), 4.71 (t, 1H, H-2, $J_{1,2}$=4 Hz, $J_{2,3}$=4 Hz), 5.79 (d, 1H, H-1, $J_{1,2}$=4 Hz).

Found: C, 54.28; H, 6.81%. Calcd for $C_{13}H_{20}O_7$; C, 54.16; H, 6.99%.

3-O-Cyanomethyl-1,2:5,6-di-O-isopropylidene-α-D-allofuranose (3e). To a stirred mixture of **3a** (19.5 g, 7.5 mmol) and sodium hydride (1.8 g, 7.5 mmol) in dry tetrahydrofuran (200 ml), cooled at −15 °C, was added bromoacetonitrile (10 g, 8.3 mmol) dropwise. The mixture gradually became dark and was stirred at room temperature for 3 h. Ethanol (10 ml) was added at 0 °C to quench any remaining sodium hydride. After concentration of the mixture, the products were extracted with ethyl actate. TLC showed the presence of one major product as well as a few minor ones. Silica gel chromatography, developed with mixtures of benzene and ethyl actate (4—2: 1), and crystallization from ethyl actate and hexane, afforded 7.5 g (33%) of **3e**: mp 109 °C. Similarly, from 13 g of **3a** and 10 g of chloroacetonitrile, 5.1 g of **3e** was obtained; M^+-CH_3 *m/e* 284 (base peak); NMR (100 MHz, $CDCl_3$) δ: 1.36 and 1.49 (2s, 6H,two methyls of one isopropylidne group), 1.36 and 1.57 (2s, 6H two methyls of one isopropylidene group), 4.41 and 4.54 (two d, 2H, OCH_2CN, J_{gem}=16 Hz), 5.81 (d, 1H, H-1, $J_{1,2}$=4 Hz).

Found: C, 55.78; H, 6.96; N, 4.56%. Calcd for $C_{14}H_{21}O_6N$: C, 56.17; H, 7.07; N, 4.68%.

3-O-Cyanomethyl-1,2-O-isopropylidene-α-D-allofuranose (5j). A solution of **3e** (1 g) in 70% acetic acid (50 ml) was allowed to stand at room temperature overnight and was concentrated below 37 °C to dryness. The residue was well dried over phosphorous pentoxide and sodium hydroxide; it was subsequently chromatographed on silica gel developed with ethyl acetate and with a mixture of ethyl acetate and methanol (9: 1) to give a syrup; yield, 730 mg (76%); MS (75 eV) *m/e*: 244 (M^+-CH_3), 198 (M^+-HOCH_2CHOH); NMR (100 MHz, $CDCl_3$) δ: 1.36 and 1.55 (two s, 6H, two isopropylidene methyls), 5.84 (d, 1H, H-1, $J_{1,2}$=4 Hz).

Found: C, 50.68; H, 6.52; N, 5.21%. Calcd for $C_{11}H_{17}NO_6$: C, 50.96; H, 6.61; N, 5.40%.

3-O-Cyanomethyl-1,2-O-isopropylidene-6-O-tosyl-α-D-allofuranose (5k) and 3-O-Cyanomethyl-5,6-di-O-tosyl-1,2-O-isopropylidene-α-D-allofuranose (5l). A mixture of **5j** (1.84 g, 7.1 mmol) and tosyl chloride (2.6 g, 13.6 mmol) in pyridine (30 ml) was allowed to stand at room temperature overnight, and ice water was added. TLC of the chloroform extract showed the formation of two products, which were separated by silica gel chromatography developed with mixtures of benzene and ethyl acetate (4—1: 1).

The less polar compound, identified as the ditosylate **5l**, was obtained as a syrup (1.3 g) by precipitation from benzene and hexane; M^+-CH_3 *m/e* 552; NMR (100 MHz, $CDCl_3$) δ: 1.32 and 1.49 (2s, 6H, two isopropylidene methyls), 2.43 (s, 6H, methyls of two tosyl groups), 4.35 (s, 2H, OCH_2CN), 4.69 (t, 1H, H-2, $J_{1,2}$=4 Hz, $J_{2,3}$=4 Hz), 4.90 (m, 1H, H-5), 5.55 (d, 1H, H-1, $J_{1,2}$=4 Hz).

Found: C, 52.72; H, 5.15; N, 2.48; S, 11.11%. Calcd for $C_{25}H_{29}O_{10}NS_2$: C, 52.90; H, 5.15; N, 2.47; S, 11.30%.

The more polar compound, identified as the monotosylate **5k**, was obtained as a syrup by precipitation from benzene and hexane; M^+-CH_3 *m/e* 398; NMR (100 MHz, $CDCl_3$) δ: 1.34 and 1.52 (two s, 6H, two isopropylidene methyls), 2.44 (s, 3H, methyl of the tosyl group), 4.35 and 4.43 (two d, 2H, OCH_2CN, J=16 Hz), 4.72 (t, 1H, H-2, $J_{1,2}$=4 Hz, $J_{2,3}$=4 Hz), 5.77 (d, 1H, H-1, $J_{1,2}$=4 Hz), 7.34 and 7.80 (2d, 4H four aromatic protons of the tosyl group, J_{ortho}=8 Hz).

Found: C, 52.26; H, 5.63; N, 3.23; S, 7.53%. Calcd for $C_{18}H_{23}O_8NS$: C, 52.29; H, 5.61; N, 3.39; S, 7.76%.

5,6-Anhydro-3-O-cyanomethyl-1,2-O-isopropylidene-α-D-allofuranose (6c). A mixture of **5k** (306 mg, 0.74 mmol) and sodium hydride (21 mg, 0.87 mmol) in dry tetrahydrofuran (10 ml) was stirred at room temperature for 20 h. TLC showed the formation of a single product. Ethanol (1 ml) and a few drops of acetic acid were added, and, after the mixture had been concentrated, the product was extracted with ethyl acetate. Precipitation from ether and hexane afforded 152 mg of a syrup; MS (75 eV) *m/e*: 226 (M^+-CH_3), 169 ($M^+-CH_3-CNCH_2O-H$), 127 ($M^+-CH_3-CNCH_2O-CH_2CH(-O-)$), NMR (100 MHz, $CDCl_3$ δ: 1.35 and 1.54 (2s, 6H two isopropylidene methyls), 2.73 (q, 1H, H_a-6, $J_{5,6a}$=3 Hz, J_{gem}=5 Hz), 2.88 (t, 1H, H_b-6, $J_{5,6b}$=5 Hz, J_{gem}=5 Hz), 3.20 (q, 1H, H-5), 3.88 (q, 1H, H-3, $J_{2,3}$=4 Hz, $J_{3,4}$=8 Hz), 4.08 (q, 1H, H-4, $J_{3,4}$=8 Hz, $J_{4,5}$=3.5 Hz), 4.38

and 4.47 (two d, 2H, OCH_2CN, $J_{gem}=16$ Hz), 4.72 (t, 1H, H-2, $J_{1,2}=4$ Hz, $J_{2,3}=4$ Hz), 5.82 (d, 1H, H-1, $J_{1,2}=4$ Hz).

Found: C, 54.65; H, 6.25; N, 5.71%. Calcd for $C_{11}H_{15}NO_5$: C, 54.76; H, 6.27; N, 5.81%.

Methyl 3,7-Anhydro-7-bis(C-ethoxycarbonyl)-6-deoxy-1,2-O-isopropylidene-D-allo-heptoside (8). A solution of **7a** (270 mg) in methanol containing dry HCl (0.01 M, 10 ml) was allowed to stand at room temperature for 7 h and concentrated while keeping the temperature below 40 °C. An ice-cooled solution of sodium hydrogencarbonate was added, and the product was extracted with ethyl acetate. Silica gel chromatography, developed with a mixture of benzene and ethyl acetate (1:1), and crystallization from benzene and hexane afforded 177 mg of **8**; mp 90 °C; MS (75 eV) *m/e*: 377 (M^+-CH_3), 361 (M^+-OCH_3); NMR (100 MHz, $CDCl_3$) δ: 1.23 and 1.29 (two t, 6H, ethyl ester $J=7$ Hz), 1.47 and 1.49 (two s, 6H, two isopropylidene methyls), 2.23 and 2.76 (two dd, 2H, H_a-6 and H_b-6, $J_{5,6a}=3$ Hz, $J_{5,6b}=4$ Hz, $J_{gem}=15$ Hz), 3.41 (s, 3H, OCH_3), 5.33 (d, 1H, H-1, $J_{1,2}=1$ Hz).

Found: C, 50.61; H, 7.08%. Calcd for $C_{17}H_{28}O_{10}$: C, 50.29; H, 6.63%.

3,7-Anhydro-7-bis(C-ethoxycarbonyl)-6-deoxy-D-allo-heptose Dimethyl Acetal (9). A solution of **7a** (193 mg) in methanol containing dry HCl (0.5 M, 10 ml) was allowed to stand at room temperature overnight; subsequently it was concentrated while keeping the temperature below 40 °C. An ice-cooled solution of sodium hydrogencarbonate was added, and the product was extracted with ethyl acetate. Silica gel chromatography, developed with ethyl acetate followed by a mixture of ethyl acetate and methanol (9:1), afforded 60 mg of an amorphous solid. For analysis it was fractionally precipitated from ethyl acetate and hexane. It showed no definite mp; NMR (100 MHz, $CDCl_3$) δ: 1.25 and 1.29 (two t, 6H, ethyl ester, $J=7$ Hz), 2.21 and 2.77 (two dd, 2H, H_a-6 and H_b-6, $J_{5,6a}=3$ Hz, $J_{5,6b}=4$ Hz, $J_{gem}=15$ Hz), 3.44 and 3.76 (two s, 6H, $2OCH_3$).

Found: C, 49.11; H, 6.90%. Calcd for $C_{15}H_{26}O_{10}$: C, 49.17; H, 7.15%.

References

1) K. Isono, K. Asahi, and S. Suzuki, *J. Am. Chem. Soc.*, **91**, 7490 (1969); K. Isono, J. Nagatsu, Y. Kawashima, and S. Suzuki, *Agric. Biol. Chem.*, **29**, 848 (1965).

2) K. Isono, P. F. Crain, and J. A. McCloskey, *J. Am. Chem. Soc.*, **97**, 943 (1975).

3) R. L. Whistler, and J. N. Beniller, "Methods in Carbohydrate Chemistry," Vol. 6, Academic Press, (1972), p. 123; D. C. Baker, D. Horton, and C. G. Tindall, Jr., *Carbohydr. Res.*, **24**, 192 (1972).

4) H. Vorbrüggen, K. Krolikiewicz, and U. Niedballa, *Ann. N. Y. Acad. Sci.* **255**, 82 (1975); H. Vorbrüggen and U. Niedballa, *Angew. Chem.*, **83**, 729 (1971).

Direct Measurement of the Rates of Ionic Dissociation by Dynamic NMR Technique. Dissociation of α-Chlorodibenzyl Sulfides

Kazutaka ARAI and Michinori ŌKI*

Department of Chemistry, Faculty of Science, The University of Tokyo, Tokyo 113

(Received May 15, 1976)

Exchange processes of diastereotopic protons of α-chlorodibenzyl sulfides were observed by means of dynamic nuclear magnetic resonance. Polar effects of solvents and substituent effects on the ease of the exchange process of protons in *p,p'*-disubstituted α-chlorodibenzyl sulfides indicate that the process occurs with the dissociation of the compounds into benzylic cations and chloride ion. It is possible to measure the rates of ionic dissocation by observing the change in the line shape of signals in ^{1}H NMR spectra. The scope of the method is discussed.

In a previous paper a report was given on the observation of ionic dissociation of 2-chloropolythianes (**1**) by dynamic nuclear magnetic resonance technique.[1] In this case, inversion of the six-membered ring is the required process to average the chemical shifts of the protons in question. Thus, the energetics of the ring inversion might be included in the energetics of ionic dissociation, when the compound requires small energy for the dissociation.

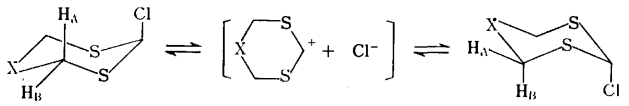

(*1*) (*1'*)

We have undertaken an extension of the above technique in order to generalize the method for determination of the rates and/or energetics for ionic dissociation of certain organic compounds. Since the ionic dissociation is a crucial step in S_N1 reactions, a knowledge of the rates of ionization would help understand such reactions.

For application of dynamic NMR technique, the compound should satisfy the following three conditions. a) It can produce a stable cation since NMR technique can detect neither very slow nor very fast exchange processes. b) It possesses a pair of diastereotopic protons. c) It is desirably an acyclic compound, direct measurement of the rates of ionization being possible, since ring inversion is not necessary for the averaging of protons.

Suitable samples are α-chloro sulfides since they produce stable cations due to the presence of sulfur atoms, as confirmed for chloropolythianes. After several trials we found that α-chlorodibenzyl sulfides (**2**) satisfy the conditions: the cation produced receives additional stabilization due to the presence of a benzene ring. This paper describes the determination of free energies for ionic dissociation of these compounds and discusses the effects of substituents and solvents on ionic dissociation.

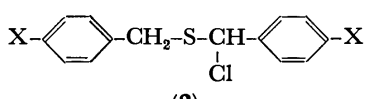

(**2**)

Experimental

Syntheses. The compounds required for the measurements were prepared by chlorination of substituted dibenzyl sulfides (**3**) with *N*-chlorosuccinimide. All the sulfides were known compounds but two were prepared by modified methods.

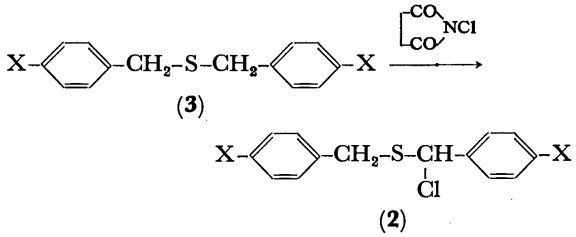

(**3**) (**2**)

*Bis(*p*-chlorobenzyl) Sulfide (**3**, X=Cl).* To a methanolic solution of sodium methoxide prepared from 4.0 g (0.17 mol) of sodium and 150 ml of methanol was added 25 g (0.16 mol) of *p*-chlorophenylmethanethiol and then 25 g (0.16 mol) of *p*-chlorobenzyl chloride during a 10 min period with stirring. The resulting mixture was heated under reflux for 3 h and the solvent was evaporated under reduced pressure. The residue was taken up in benzene and washed with 6 M sodium hydroxide and then with water. After drying over magnesium sulfate, the solvent was evaporated *in vacuo* and the residue was kept overnight at —5 °C to induce crystallization. Washing twice with small amounts of hexane gave pure **3** (X=Cl), mp 42 °C (lit,[2] mp 42 °C), in 90% yield.

*Bis(*p*-methylbenzyl) Sulfide (**3**, X=CH$_3$)*, mp 77 °C (lit,[3] mp 76 °C), was prepared similarly in 90% yield.

^{1}H NMR spectral data of the sulfides are summarized in Table 1.

Table 1. ^{1}H NMR spectral data of *p,p'*-disubstituted dibenzyl sulfides (**3**) in carbon tetrachloride (δ)

Substituent (X)	Benzylic CH_2	Aromatic H	Others
H[4]	3.49	7.18(10H, s)	
CH_3	3.44	7.05 (8H, s)	2.31(6H, s)
Cl	3.46	7.18 (8H, s)	
NO_2[5,a]	3.69	7.44 and 8.21 (J=9.0 Hz)	

a) Data with a $CDCl_3$ solution.

Chlorination of p,p'*-Disubstituted Dibenzyl Sulfides.* To a solution of 1.0 g of a *p,p'*-disubstituted dibenzyl sulfide in 10 ml of carbon tetrachloride was added 1.1 equivalents of powdered *N*-chlorosuccinimide at 35 °C with stirring during a 5 min period under nitrogen atmosphere. Stirring was continued for 1—2 h after completion of the addition. The reaction mixture was filtered in order to remove insoluble materials, contact with moisture being avoided as completely as possible. From ^{1}H NMR spectral data of the filtrate, the

purity and yield of *p,p'*-disubstituted α-chlorodibenzyl sulfides were estimated to be 90—95% and 85—90%, respectively.

The nitro compound, being sparingly soluble in carbon tetrachloride, was chlorinated in benzene by essentially the same procedure.

^{1}H NMR spectral data of the *p,p'*-disubstituted α-chlorodibenzyl sulfides are given in Table 2.

Table 2. ^{1}H NMR spectral data of *p,p'*-disubstituted α-chlorodibenzyl sulfides (**2**) in carbon tetrachloride (δ)

Substituent (X)	Benzylic δ	CH_2 J	Methine H	Aromatic H	Others
H[6]	3.88 3.98	15	5.69	7.30 (10H, m)	
CH_3	3.79 3.93	*ca.* 13	5.67	6.9—7.4 (8H, m)	2.39(3H, s) 2.32(3H, s)
Cl	3.80 3.99	13.5	5.63	7.29 (8H, s)	
NO_2[a]	4.07 4.20	13.5	5.87	7.50—7.70[b] 8.15—8.35 (8H, double q)	

a) Data with a $CDCl_3$ solution. b) It was impossible to determine which of the two pairs at the higher field forms the AB quartet with a pair of signals at the lower field. The coupling constants for the two AB quartets were 9.0 Hz.

Benzenethiolyses of p,p'*-Disubstituted α-Chlorodibenzyl Sulfides.* The solutions of *p,p'*-disubstituted α-chlorodibenzyl sulfides obtained above were treated with 2—3 equivalents of benzenethiol at room temperature for 8—10 h and the resulting mixture was evaporated *in vacuo* Chromatography of the residue on silica gel afforded pure *p,p'*-disubstituted α-phenylthiodibenzyl sulfides (**4**). The pertinent data are summarized in Table 3.

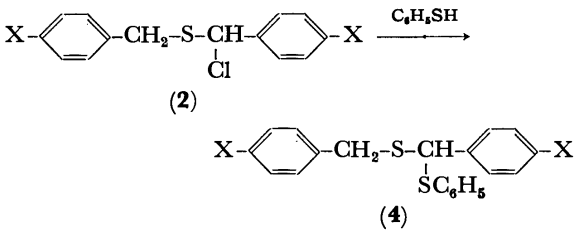

^{1}H NMR Measurement. ^{1}H NMR spectra were recorded on a Hitachi R 20B spectrometer, operating at 60 MHz, with a temperature variation accessory. The temperature reading was calibrated by measuring the chemical shift difference between methylene and hydroxy protons of ethylene glycol for the higher temperatures and that between methyl and hydroxy protons of methanol for the lower temperatures.

Kinetic Parameters. The rate constants of the exchange processes at the coalescence temperature were obtained by application of the following equation,[7] where J_{AB} is the coupling constant of the diastereotopic protons and $\Delta\nu_{AB}$ the chemical shift difference of these protons.

$$k_c = \frac{\pi}{\sqrt{2}}\sqrt{6J_{AB}^2+\Delta\nu_{AB}^2} \quad (1)$$

Free enrgies of activation at the coalescence temperature were obtained by substituting k_c into the following equation.

$$\Delta G_c^{\ddagger} = 4.57T_c\left\{10.319+\log\frac{T_c}{k_c}\right\} \quad (2)$$

Results and Discussion

Confirmation of the Structure of p,p'*-Disubstituted α-Chlorodibenzyl Sulfides.* Since the *p,p'*-disubstituted α-chlorodibenzyl sulfides (**2**), key compounds in this paper, are reactive toward moisture, their structures must be confirmed by other means. This is accomplished by a) the chemical method and b) ^{1}H NMR spectral data. In a), since the method of preparation is generally applied to α-chlorination of sulfides,[8] a chlorine atom is expected to enter at a benzylic position. The ease of reaction of these compounds with benzenethiol is supporting evidence for the structure, since other normal halides would not be so reactive as these compounds. The substituted α-phenylthiodibenzyl sulfides (**4**) are analyzed correctly. In b) the two benzylic protons turn to a methine proton

Table 3. Melting points, ^{1}H NMR data (CCl_4, δ), and analytical data of *p,p'*-disubstituted α-phenylthiodibenzyl sulfides (**4**)

Substituent (X)	Mp (°C)		Found (%)	Calcd	^{1}H NMR data CH_2	CH	Arom. H	Others
H	Oil	C	74.56	74.49			7.11(5H, s)	
		H	5.62	5.63	3.66	4.74	7.15(5H, bs)	
		S	19.99	19.88	3.85		7.21(5H, bs)	
					(J=13.0)			
CH_3	Oil	C	75.08	75.38	3.67			2.28(3H, s)
		H	6.25	6.33	3.83	4.75	7.0 —7.3	2.30(3H, s)
		S	18.00	18.29	(J=13.0)		(13H, m)	
Cl	61 — 62	C	61.16	61.38				
		H	4.03	4.12	3.65	4.70	7.15—7.25	
		Cl	18.17	18.12	3.83		(13H, m)	
		S	16.27	16.38	(J=13.0)			
NO_2	136.5—137	C	57.97	58.24			7.24(5H, s)	
		H	4.17	3.91	3.89	4.88	7.30—7.55[a]	
		N	6.87	6.79	4.08		8.05—8.30[a]	
		S	15.45	15.55	(J=13.5)		(8H, double q)	

a) See Table 2, footnote b. The coupling constants for the two AB quartets were 9.0 Hz.

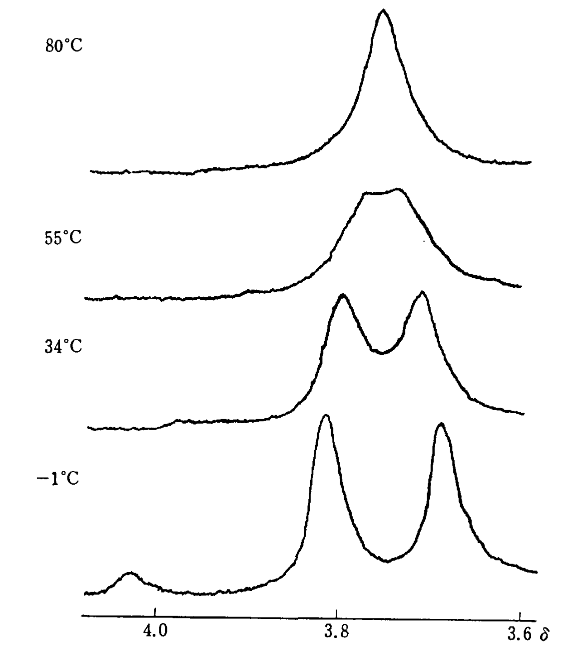

Fig. 1. Temperature dependence of the signals at δ *ca.* 4 in the spectrum of α-chlorodibenzyl sulfide in 1-chloronaphthalene.

which gives a signal at a low field. In addition, the benzylic protons in the chloro compounds **2** and in phenylthio compounds **4** give AB quartets: it would not be possible to explain if a chiral center were not present in the proximity of these protons.

Dynamic NMR and the Rate Process. The ^{1}H NMR spectra of the chlorides **2** were found to be dependent on solvents and temperature. Typical examples of temperature-dependence of the spectra are shown in Fig. 1. Since a quartet signal of a diastereotopic pair of protons does not usually coalesce below 200 °C, the temperature-dependent spectra suggest that a certain exchange process involving bond breaking takes place under these conditions. The process should be such that chirality due to asymmetric carbon is lost.

Survey of solvent and substituent effects on the coalescence temperature and free energies of activation will shed light on the nature of the process. The temperature dependence of the spectra of α-chlorodibenzyl sulfide was investigated in various solvents. The results are given in Table 4. Nitrobenzene showed no tendency of line broadening even at 0 °C. The coalescence temperature is lower when the solvent is more polar, the free energies of activation being lower. The cases of chloroform and deuteriochloroform are exceptions. We wish to attribute this anomaly to the hydrogen bond effect. Chloroform is known to form hydrogen bond[9] which should stabilize an anion.[10] No such stabilization is expected in the other solvents used. Deuteriochloroform would stabilize the anion to a greater extent, since deuterium compounds are known to form a stronger hydrogen bond than the corresponding ^{1}H compounds.[11]

TABLE 4. SOLVENT EFFECTS ON THE EXCHANGE PROCESS OF PROTONS IN α-CHLORODIBENZYL SULFIDE (**2**, X=H)

Solvent	ε	T_C (°C)	J_{AB} (Hz)	$\Delta\nu_{AB}$ (Hz)	$\Delta G^{\neq}_C$ (kcal/mol)
CCl_4	2.24	>80	13.5	5.5	>17.8
C_6H_6	2.27	>70	13.5	16	>17.2
$CHCl_3$	4.81	37	14	6	15.5
$CDCl_3$	—	17	14	6	14.5
m-$Cl_2C_6H_4$	5.04	82	14	7	17.8
$C_{10}H_7Cl$[a)]	5.04	55	13	10	16.5
C_6H_5Cl	5.62	55	13	8	16.5
o-$Cl_2C_6H_4$	9.93	42	13.5	5	15.8
$C_6H_5NO_2$	34.8	<0	(13)	(8)	(<13.6)[b)]

a) 1-Chloronaphthalene. b) J_{AB} and $\Delta\nu_{AB}$ in chlorobenzene are diverted.

The results obtained by changing the solvent are consistent with the idea that the loss of the chiral center is of polar nature. Heterolysis of the C–S bond requires much energy. Then, in principle, the following two modes of dissociation are possible.

$$\mathrm{ArCH_2S\underset{\displaystyle Cl}{\underset{|}{C}}HAr \rightleftarrows ArCH_2S\overset{+}{C}HAr + Cl^-} \qquad (3)$$

$$\mathrm{ArCH_2S\underset{\displaystyle Cl}{\underset{|}{C}}HAr \rightleftarrows ArCH_2S\underset{\displaystyle Cl}{\underset{|}{\bar{C}}}Ar + H^+} \qquad (4)$$

Although it may seem that Eq. 3 is a more plausible process, Eq. 4 may not be ruled out without convincing evidence. Such evidence should be provided when the substituent effect is examined: if the process is represented by Eq. 3, electron-releasing groups should facilitate the exchange, and the reverse is true if the process is represented by Eq. 4.

The results of changing the substituent are given in Table 5, in which σ_m values are included as a measure of electron-donating or electron-withdrawing ability. The results are in line with the idea that the electron-donating substituent facilitates the process. Thus the exchange of proton spins occurs following Eq. 3.

Rate Constants of the Ionic Dissociation. Although the planar cation itself erases the non-equivalency of the CH_2 protons due to its planar structure, we observe no NMR spectra of the cation because of its transient nature. Thus the equivalency of the methylene protons at a higher temperature is caused by the rapid mixing of one stereoisomer with another. The mixing or interconversion of one stereoisomer with another can occur in one or more of the following steps. If the compound dissociates into a free cation and a free anion, recombination to produce the mother compound would proceed from either side of the plane of the cation, thus producing a 1 : 1 mixture of the enantiomers. If the cation undergoes internal rotation about the S–C$^+$ axis while the anion remains immobile, the stereoisomer is formed, or else, the anion will recombine with the cation from the other side than that where the former departed. These cases are possible when the ions form a loose ion pair. If the ions form a tight ion pair, it is not possible to invert the stereochemistry directly. However, we might consider the cation to be of pyramidal shape and inversion of the pyramid followed by recombination with an anion derived from another molecule leads to the formation of a stereoisomer.

It is difficult to determine to what extent the above

Table 5. Free energy of activation for the exchange process and for the ionic dissociation of *p,p'*-disubstituted α-chlorodibenzyl sulfides (**2**)

Substituent	o-$Cl_2C_6H_4$ solution				$C_6H_5NO_2$ solution		
	σ_m	T_c (°C)	$\Delta G^{\neq}_c$ (kcal/mol) (Eachange)	$\Delta G^{\neq}_c$ (kcal/mol) (Ionic dissociation)	T_c (°C)	$\Delta G^{\neq}_c$ (kcal/mol) (Exchange)	$\Delta G^{\neq}_c$ (kcal/mol) (Ionic dissociation)
CH_3	−0.07	−21	12.5	12.2	$\ll 0$[a]	$\ll 13.6$[a]	$\ll 13.4$
H	0.00	42	15.8	15.4	< 0[a]	< 13.6[a]	< 13.4
Cl	0.37	101	18.8	18.3	40	15.7	15.3
NO_2	0.71	—	—	—	100	18.8	18.3

a) The signal due to benzyl protons of *p,p'*-dimethyl-α-chlorodibenzyl sulfide was sharper than that of α-chlorodibenzyl sulfide.

factors are responsible. To a first approximation, however, we may take a model in which the probability of the ion pairs returning to the original stereochemistry and forming the other stereochemistry are 50: 50 as a result of many factors. The rate of the dissociation of the chloride **2** must then be twice the rate of the exchange process. The results are included in Table 5.

It is of interest that the barriers to the ionic dissociation of these compounds are comparable to or smaller than that of triphenylmethyl chloride. The enthalpy and the entropy of activation for the reaction of triphenylmethyl chloride in aqueous acetone were reported to be 12.5 kcal/mol and −17 e.u. at temperatures between −34 °C and −14 °C.[12] The free energy of activation is then calculated to be *ca.* 17 kcal/mol at about −20 °C. If we assume this to be the pure S_N1 reaction, the energy should correspond to that for ionic dissociation. Since the polarity of the solvent is high in this case, the ionic dissociation of the chloro compound **2** may be taken as an easy one. The enthalpy and entropy of activation for the exchange process of chloride ion in benzene are reported to be 12.4 kcal/mol and −39 e.u. respectively, at 50 °C for triphenylmethyl chloride[13] and the free energy is calculated as 25 kcal/mol at that temperature.

Conclusion. The method described here for determining the rates of ionic dissociation seems to be of value in kinetic studies. For the tranditional chemical method, racemization or isotope exchange had to be used. This necessitates an optically active compound or isotopically enriched ions. As an example, the rate of ionization of triphenylmethyl chloride was estimated from the exchange of the chloro group with isotopically labelled tetraalkylammonium chloride,[13] but the method is hampered by the fact that the concentration of the ammonium chloride affects the rates. The method described here needs no expensive isotopes, optical isomers nor a nucleophile to react. Thus the rate of ionization can be obtained without perturbation of the excess of other materials. Since the ionization of an organic compound into a stable cation and an anion is an important step in S_N1 reactions and many stable cations show substantial barriers for reaction with another anion,[14] dynamic NMR method provides an important means for understanding such a reaction.

If a compound possesses a good leaving group at a chiral or prochiral center and diastereotopic protons close to the center, and produces a fairly stable carbonium ion, then the rates of the dissociation can be determined by dynamic NMR technique.[15] As one example, the case of α-chlorodibenzyl sulfides is presented.

References

1) K. Arai and M. Öki, *Bull. Chem. Soc. Jpn.*, **49**, 553 (1976).
2) Z. Martynowicz, *Chem. Z.*, **1910, II**, 1048.
3) C. L. Jackson and J. F. White, *J. Am. Chem. Soc.*, **2**, 166 (1880).
4) Preparation of this compound was reported previously: C. Märcker, *Ann. Chem. Pharm*, **136**, 75 (1865).
5) Preparation of this compound was reported previously: O. Fischer, *Ber.*, **28**, 1338 (1895); T. S. Price and D. F. Twiss, *J. Chem. Soc.*, **95**, 1728 (1909).
6) Preparation of this compound by other methods was briefly reported as an intermediate: H. Böhme, *Ann. Chem.*, **563**, 54 (1949); K. C. Schreiber and V. P. Fernandez, *J. Org. Chem.*, **26**, 2910 (1961).
7) J. A. Pople, W. G. Schneider, and H. J. Bernstein, "High Resolution Nuclear Magnetic Resonance," McGraw-Hill Book Co. Inc., New York (1959), p. 218; J. W. Emsley, J. Feeney, and C. H. Sutcliff, "High Resolution Nuclear Magnetic Resonance Spectroscopy," Pergamon Press, Oxford (1965), p. 481.
8) D. L. Tuleen R. H. Bennett, *J. Heterocycl. Chem.*, **6**, 115 (1969).
9) G. C. Pimentel and A. L. McClellan, "The Hydrogen Bond," W. H. Freeman and Co., San Francisco (1960), p. 197.
10) S. Y. Lam, C. Louis, and R. L. Benoit, *J. Am. Chem. Soc.*, **98**, 1156 (1976).
11) L. N. Ferguson, "The Modern Structural Theory of Organic Chemistry," Prentice-Hall, Inc., Englewoods Cliff, New Jersey (1963), p. 128; G. Dahlgren, Jr. and F. A. Lay, *J. Am. Chem. Soc.*, **82**, 1303 (1960).
12) C. G. Swain and C. B. Scott, *J. Am. Chem. Soc.*, **75**, 246 (1953).
13) C. G. Swain and M. M. Kreevoy, *J. Am. Chem. Soc.*, **77**, 1122 (1955).
14) C. K. Ingold, "Structure and Mechanism in Organic Chemistry," Cornell University Press, Ithaca, N. Y. (1953), p. 360.
15) For references of DNMR spectroscopy, see for example, L. M. Jackman and A. Cotton, "Dynamic Nuclear Magnetic Resonance Spectroscopy," Academic Press, Inc., New York (1975).

The Intramolecular OH---π Bonding in [n]Paracyclophanols[1)]

Nobuo MORI, Tetsuo TAKEMURA, and Takayoshi OHKUMA

Department of Chemistry, Science University of Tokyo, Kagurasaka 1-3, Shinjuku-ku, Tokyo 162

(Received June 3, 1976)

The intramolecular OH···π bonding, the probable conformations, and the internal rotation in two series of [n]-paracyclophanols, I (**1**—**4**) and II (**5**—**8**), are investigated by means of IR, UV, and PMR spectroscopies. The IR results indicate that (1) there is the OH···π bonding in **1**, **2**, **3**, **5**, and **7** in CCl_4, and (2) the integrated intensity ratio of the π-bonded OH species to the free OH, (A_b/A_f), hardly changes in going from **1** to **3**, while it decreases in going from **5** to **7**. The ratio is, then, related to both ΔH and ΔS. In the PMR spectra, aliphatic-proton signals are assigned by means of the spin-decoupling and/or the shift-reagent technique; the results agree with those predicted, with a few exceptions. In the aromatic region, **3**, **4**, and **8** show singlets, while the others show AB-like quartets. These results are discussed in relation to the internal rotation of the benzene ring and/or the alkylene chain.

Intramolecular hydrogen bondings have been observed in many systems of open chains and medium-size rings,[2)] and the spectral shifts of the bonded OH bands have been measured. There have, though, been surprisingly few reports on thermodynamic measurements for the intramolecular hydrogen-bond formations, and these have been for only a few acylic systems of β-phenylalkanols,[3)] 1,3-diols,[4)] and ω-methoxyalkanols.[5)] Only the last system has been examined in relation to the alkylene-chain length. In this system, the loss of entropy accompanying the hydrogen-bond formation increases greatly with the increasing chain length, but the enthalpy term hardly changes at all.

In the present work, we will examine the intramolecular OH···π bonding in two series of [n]paracyclophanols, I and II, by means of IR spectroscopy, and thermodynamic parameters, ΔH and ΔS, for the hydrogen-bond formation will be obtained from measurements of the temperature dependence of the ν_{OH} spectra.

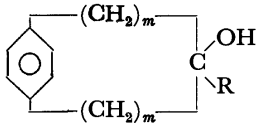

m = 4—7
Series I: R=H
Series II: R=CH_3

The reasons why paracyclophanols are selected are that their conformations are partially fixed around the benzene rings and that at least some of them are expected to be internally hydrogen-bonded with a relatively slight loss of entropy.

On the other hand, there have been presented several experimental or theoretical approaches to estimate the probable conformations of [5]—[12]paracyclophane compounds. These include an examination of molecular models,[6)] a free-electron model calculation,[7)] X-ray diffraction,[8,9)] and a force-field calculation.[10)]

In the present work concerning probable conformations in Series I and II, the degrees of bending of the benzene rings are predicted by a comparison of the UV spectral shifts with the theory,[11)] and the magnitudes of magnetic shielding for the aliphatic protons are estimated by a calculation using the Johnson and Bovey method.[12)] Furthermore, the PMR spectra of the aromatic protons are simulated by assuming an A_2B_2 type of proton system, and the internal rotation of the benzene rings and/or the alkylene chains is discussed.

Experimental

Samples. All the paracyclophanols examined were unknown compounds, except for [9]paracyclophane-5-ol,[13)] **1**. [11]Paracyclophane-6-ol, **2**, and its 6-methyl derivative, **6**, were prepared by the $LiAlH_4$ reduction or by the Grignard reaction of the corresponding ketone, which had itself been obtained by the Dieckmann reaction[14)] of dimethyl benzene-1,4-dihexanoate. The others were similarly obtained from the corresponding known ketones.[13,14)] The alcohols thus obtained were purified by recrystallization from hexane; their melting points and analytical results are summarized in Table 1.

IR Spectra. The ν_{OH} spectra were recorded on a JASCO DS-403G spectrometer; the solvent used was CCl_4, and the concentrations selected were *ca.* 0.003 mol/l or less so as to give apparent peak intensities of *ca.* 1.4 and to avoid an intermolecular association (cell length: 50 mm). The tem-

Table 1. Melting points and analytical data of the paracyclophanols

	Compound No.	m	R	Mp, °C (Uncorrected)	Calcd (%) C	Calcd (%) H	Found (%) C	Found (%) H
I	**1**	4	H	111 —111.5				
	2	5	H	60.0— 61.0	82.87	10.64	83.33	10.76
	3	6	H	51.5— 52.0	83.15	11.02	83.09	10.95
	4	7	H	79.6— 80.2	83.38	11.33	83.49	11.18
II	**5**	4	CH_3	43.2— 43.7	82.70	10.41	82.68	10.32
	6	5	CH_3	101.0—101.6	83.02	10.84	83.38	11.00
	7	6	CH_3	*ca.* 76[a)]	83.27	11.18	83.25	11.16
	8	7	CH_3	88.0— 89.0	83.48	11.47	83.14	11.37

a) A waxy solid which was homogeneous according to its GC and TLC and according to its PMR spectrum,

perature dependence of the spectra was also examined at different temperatures ranging from 10 to 60 °C (error: ±1 °C in each case); correction was made for the thermal expansion of the solvent at each temperature. The calculated spectral slit width was 1.5 cm^{-1} at about 3600 cm^{-1}.

UV Spectra. Measured in concentrations of *ca.* 0.002 mol/l in hexane, using a Hitachi EPS-3T spectrometer.

PMR Spectra. Recorded in concentrations of 5—10 w/v% in CCl_4 on a JEOL JNM4H-100 spectrometer operating at 100 MHz; TMS was used as an internal reference and a lock signal. Dilution experiments were carried out in the concentration range of 1—20 w/v%, and the chemical shifts for concentration-dependent protons were obtained at an infinite dilution. Lanthanoid-induced shift measurements were performed by the step-by-step addition of either $Pr(fod)_3$ or $Eu(fod)_3$ to $CDCl_3$ solutions of substrates in the molar-ratio ranges of 0—0.6, until enough magnitudes of the induced shifts were obtained to assign the proton signals. The temperature dependence of the aromatic proton spectra was examined in dimethyl-d_6 sulfoxide or acetone-d_6 which proved to be suitable for obtaining an appropriately high resolution at the higher or lower temperatures examined.

The above measurements were carried out at room temperature (*ca.* 25 °C) unless otherwise noted.

Results and Discussion

IR Spectra. Three paracyclophanols, **4**, **6**, and **8**, show single, unsymmetric or symmetric OH bands characteristic of the monomers of ordinary secondary or tertiary alkanols.[15] The other paracyclophanols show doublets, which are ascribed to the presence of at least two OH species, free and internally bonded, but to other causes such as Fermi resonance, overtone, conformational heterogeneity, or intermolecular association. If the latter causes were predominant, **4**, **6**, and **8** could be expected to show similar doublets. Each doublet can be graphically separated into two almost symmetric bands; the higher-frequency band corresponds to the free OH group, so the lower-frequency one should then be assigned to the π-bonded one. The integrated intensity of each band is calculated using the following equation:

$$A = (\pi/2cl) \ln (I_0/I)_{max} \Delta\nu_{1/2} \quad (\text{in l mol}^{-1}\,\text{cm}^{-2})$$

The spectra of **1**, **4**, and **5** are shown in Fig. 1 as typical examples, and the results are summarized in Table 2.

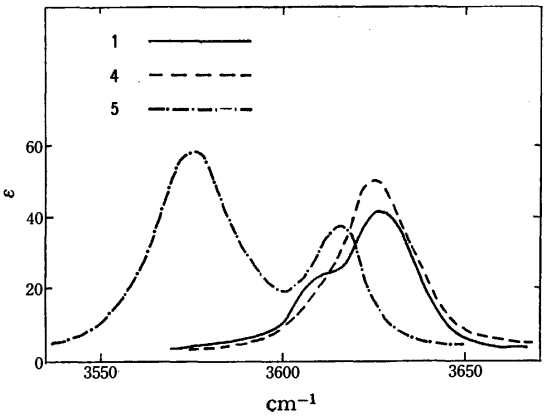

Fig. 1. OH spectra of **1**, **4**, and **5** in CCl_4 at room temperature.

Table 2. IR data of the paracyclophanols at *ca.* 25 °C

	Compound No.	ν_{max} (cm^{-1})	$\Delta\nu_{1/2}$ (cm^{-1})	$A \times 10^{-3}$ (l mol^{-1} cm^{-2})	A_b/A_f [a]
I	**1**	3628.0	19.6	2.850	0.27
		3608.0	12.6	0.769	
	2	3627.5	20.7	2.802	0.23
		3606.8	15.1	0.645	
	3	3630.0	21.3	2.443	0.33
		3609.0	16.6	0.805	
	4	3625.0	21.0	3.833	
III	**5**	3616.3	17.1	2.068	2.5
		3578.0	26.1	5.178	
	6	3616.9	14.4	2.876	
	7	3616.9	17.0	2.634	0.13
		3566.9	18.7	0.354	
	8	3616.9	15.5	3.022	

a) A_b and A_f denote the integrated intensities of bonded and free OH bands respectively.

The A values for **1**, **2**, and **3** may be less accurate than those for the others, because their doublet-components so overlap that it is not easy to separate them. On raising the temperature, ν_{OH} becomes slightly higher and the sum of A_b and A_f becomes smaller, as is usually observed.[16] From these data, the thermodynamic parameters can then be calculated using the following equation:[16]

$$\ln A_b/A_f = -\Delta H/RT + (\Delta S/R - \ln a)$$

where a is the ratio of the true molecular extinction coefficients of the bonded and the free OH groups. Good linear relationships are obtained between $\ln A_b/A_f$ and $1/T$, as Fig. 2 shows. The results are summarized in Table 3.

It can be seen in Table 2 that, in Series I (**1**—**3**), the shifts ($\Delta\nu_{OH}$) of the π-bonded OH frequencies from the

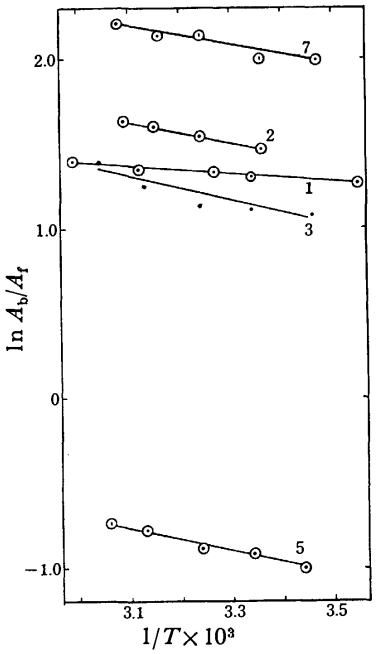

Fig. 2. Linear relationship between $\ln A_b/A_f$ and $1/T$.

corresponding free OH ones are almost the same, *ca.* 20 cm^{-1}, comparable to those in α-phenylalkanols.[17] In Series II (**5** and **7**), $\Delta\nu_{OH}$ is *ca.* 40 or 50 cm^{-1}; these values correspond to those in β- and γ-phenylalkanols.[3,18] The difference in $\Delta\nu_{OH}$ must be related to the distance (r) between the π-bonded OH group and the π-site.[2] However, the relationship between $\Delta\nu_{OH}$ and r can not be examined in the present case, because the paracyclophanols are in very complicated conformations with sterically unfavorable dihedral and bond angles[9,10] and the geometries of the internally bonded conformations can not be estimated.

As an approximate measure of the r, one may assume a magnitude of magnetic shielding for the OH proton. However, the observed magnitude ($\Delta\delta_{OH}=\delta_{ref.OH}-\delta_{OH}$) is not related to the $\Delta\nu_{OH}$, probably because each δ is the weight-average for all the OH species in all conformations.

An inspection of Table 3 reveals that, in Series I, both $-\Delta H$ and $-\Delta S$ tend to increase in going from **1** to **3** and are, therefore, contributable to the A_b/A_f ratio. In Series II also, the ratio is related to ΔH and ΔS, because $-\Delta H$ decreases in going from **5** to **7**, while $-\Delta S$ increases. In this connection, it is noteworthy in Table 2 that, in I and II, the A_b/A_f ratios alternate with m. The alternation in I is noticeable and is attributable to the ΔH's, but not to the ΔS's, because $-\Delta H$ in **5** is greater than that in **1** and $-\Delta H$ in **7** is less than that in **3**, while the ΔS's in **5** and **7** are almost the same as those in **1** and **3**. In **6**, ΔS is expected to be not greatly different from the ΔS in **3**; therefore, the absence of hydrogen bonding should be attributable to ΔH, which would be negligibly small or be positive in sign.

Table 3. Thermodynamic data for the internally bonded paracyclophanols

	Compound No.	$-\Delta H$ (kcal/mol)	$-(\Delta S/R-\ln a)$	$-\Delta S$[a] (e.u.)	$-AI$ (kcal/mol)	RI (kcal/mol)
I	**1**	0.4±0.1	2.1±0.1	4.2	0.94	0.54
	2	1.2±0.1	3.6±0.1	7.2	0.95	−0.25
	3	1.3±0.2	3.3±0.1	6.6	0.95	−0.35
II	**5**	1.4±0.1	1.5±0.1	3.0	1.22	−0.18
	7	0.5±0.1	3.8±0.2	7.6	1.42	0.92

a) Approximate values, assuming $a=1$.[16]

We will now discuss the ΔH by separating it into its two components: the interaction between the OH group and the π-site (AI) and the combined interactions between the other non-bonded atoms (RI). AI can be approximately estimated from $\Delta\nu_{OH}$, using the Joesten and Drago equation[19] for intermolecular hydrogen bonds:

$$-AI \pm 0.5(\text{kcal/mol}) = 0.016\,\Delta\nu_{OH} + 0.63$$

The values of AI and RI calculated in this manner are also listed in Table 3. The accuracy of these values is considerably poor, but it is at least possible to ascertain the tendency of their change through the whole series. Of interest is the fact that, in I and II, $-\Delta H$ is inversely proportional to RI. In other words, the OH···π bond formation is less exothermic in **1**, but more exothermic in **2** and **3**, than expected, because RI increases in **1** but decreases in **2** and **3**. This means that, the longer the alkylene chain is, the more feasible it is for the conformational change in forming the hydrogen bond to occur; this could be a reflection of the theoretical results[10] that, in [5]—[10]paracyclophanes, the conformation is less strained when the alkylene chain is longer.

In Series II, the reverse is true and the OH···π bond formation is more exothermic in **5**, but much less exothermic in **7**, than expected. This may be explained in terms of the flexibility of the alkylene chain being more decreased in II than in I. Because of the methyl group attached to the central bridge atom, the alkylene chains in II are more rigid than those in I. Taking this expectation together with the A_b/A_f ratios into consideration, it seems reasonable that the conformation of **5** is so fixed that the OH···π bond formation is accompanied by only a slight change in RI and that the conformation of **6** is so fixed that the hydrogen-bond formation requires an excessively large increase in RI. The large RI in **7**, as compared to that in **3**, may similarly be explained in terms of the less flexible conformation. This is supported by the observation that the internal rotation of the benzene ring and/or the alkylene chain is more restricted in **7** than in **3**, as will be described later. An examination of molecular models indicates that the C–OH bond in **5** is situated inside the alkylene loop, with its O–H toward the face of the benzene ring, while the C–OH bonds in the other paracyclophanols must be in such conformations as to be less favorable for the OH···π interaction.

Table 4. UV data in hexane solutions

	Compound No.	m	λ_{max} (log ε)	
I	**1**	4	270.8(2.57)	225.5(2.85)
	2	5	268.0(2.56)	222.5(2.85)
	3	6	266.2(2.65)	220.5(2.89)
	4	7	266.0(2.66)	220.5(2.88)
II	**5**	4	271.5(2.54)	—[a]
	6	5	267.3(2.57)	—[a]
	7	6	265.3(2.61)	—[a]
	8	7	265.5(2.57)	—[a]
	9[b]		271 (3)	224 (3)
	10[c]		268 (2)	223 (3)
	12[d]		265 (2)	214 (3)

a) Not observed. b) [9]Paracyclophane. c) [10]-Paracyclophane. d) *p*-Diethylbenzene. The data for b), c), and d) are taken from Ref. 9.

UV Spectra. The spectra of **1**—**8** are quite similar to those of the corresponding [n]paracyclophanes;[20,21] hence, the OH and/or CH_3 substituents at the central bridge carbon and also the OH···π bonding involved seem to have no detectable effect on the electronic transitions. Table 4 lists the spectral properties of the 1st and 2nd electronic transitions. As m decreases from 7 to 4, the absorption maxima shift toward longer wavelengths with lower intensities. This tendency is associated with an increasing bending of the benzene ring from planarity,[9,20] the extent of which is related to the magnitude of

Table 5. Chemical shifts for the aliphatic protons of paracyclophanols in CCl_4 at room temperature (in ppm from TMS downfield)[a]

No.	OH	CH	CH_3	CH_2 at the position of						
				1	2	3	4	5	6	7
1	0.26	2.70		2.57 (t, 4H)	1.45 (m, 4H)	1.00 (m, 4H)	0.60 (m, 4H)			
	0.04	2.55		2.61	1.44	0.95	0.55			
2	0.53	2.80		2.60 (t, 4H)	1.61 (m, 4H)	1.23 (m, 4H)	0.82 (m, 8H)			
	0.09	2.72		2.59	1.49	1.12	0.90	0.80		
3	0.54	3.00		2.58 (t, 4H)	1.60 (m, 4H)	1.10 (range: 0.95—1.30) (bm, 16H)				
	0.53	2.98		2.57	1.62	1.12	1.13	1.15	1.19	
4	0.63	3.40		2.59 (t, 4H)	1.60 (m, 4H)	1.15 (range: 0.9—1.4) (bm, 20H)				
	0.68	3.48		2.59	1.56	1.23	1.25	1.18	1.17	1.33
5	0.37		0.74	2.60 (t, 4H)	1.52 (m, 4H)	0.99 (m, 4H)	0.40 (m, 4H)			
	−0.55		0.77	2.61	1.44	0.95	0.45			
6	0.41		0.88	2.60 (t, 4H)	1.63 (m, 4H)	1.22 (m, 4H)	0.45 (m, 4H)	0.82 (m, 4H)		
	0.49		0.89	2.56	1.52	1.28	0.36	0.82		
7	0.50		0.90	2.58 (t, 4H)	1.60 (m, 4H)	1.12 (bm, 8H)		1.00 (bm, 8H)		
	0.33		0.93	2.57	1.55	1.08	1.27	1.22	1.08	
8	0.57		1.00	2.58 (t, 4H)	1.60 (m, 4H)	1.12 (range: 0.75—1.38) (bm, 20H)				
	0.50		0.91	2.60	1.57	1.24	1.30	1.28	1.08	1.16
9[b]				2.58 (t, 4H)	1.42 (m, 4H)	0.96 (m, 4H)	0.60 (m, 4H)	0.33 (m, 2H)		
				2.61	1.44	0.95	0.55	0.44		
11[c]				2.55	1.55	1.18	0.79	0.79	0.68	
				2.59	1.49	1.12	0.90	0.80	0.65	
13[d]	0.76	3.68		1.50[e]	1.33[f]					
14[g]	0.67		1.08	1.40[e]	1.33[f]					

a) The numerical data in the upper row: observed; those in the lower row: predicted. In parentheses, t=triplet, m=multiplet, bm=broad multiplet, and the number of protons are cited. b) [9] Paracyclophane. c) [11]-Paracyclophane; the observed values are taken from the data presented at the 8th symposium on Structural Organic Chemistry, Kyoto, October 1975, No. 1A03 (T. Kamata, T. Inoue, and S. Misumi). d) Cyclooctadecanol. e) CH_2 at the α-position to OH. f) CH_2's other than e). g) 1-Methylcyclooctadecanol.

the red shift from the λ_{max} of *p*-diethylbenzene.[11] According to this relationship, the angles of bending of the benzene rings in I and II are equal to those in the parent hydrocarbons[11] and may be less than 5 degrees with $m=6$ and 7, equal to *ca.* 5° with $m=5$, and *ca.* 15° with $m=4$.[22]

PMR Spectra. In the aliphatic region, the OH, CH, and CH_3 signals could easily be confirmed by their characteristic patterns, chemical shifts, relative intensities, and/or concentration-dependence. For the CH_2 signals, **1** and **2** (and also **9**, for comparison) were first examined by spin-decoupling. The signals thus assigned showed lanthanoid-induced shifts (LIS) obeying the general rule[23] that, in alkanols, CH_2 groups at greater distances from their positions of attachment to an OH group have smaller LIS values. For this reason, the CH_2 signals of the other paracyclophanols were assigned by means of the shift-reagent technique. The results are summarized in Table 5, while the spectra of **1**, **3**, and **5** are shown in Fig. 3 as typical examples.

A calculation was then made using the Johnson and Bovey method[12] in order to estimate the probable conformations. The magnitudes of chemical shielding for the 1-CH_2 and the other protons were assumed to be equal to the averaged chemical shifts (δ: 2.11 ppm) for the 3-CH_2 groups of cycloheptene and cyclooctene and to those for the corresponding protons in **13** and **14** respectively. The magnitudes of shielding for all the aliphatic protons by the π-current were predicted by constructing molecular models[24] to establish the probable conformation of the alkylene bridge and by measuring the positions of the protons involved. After this procedure has been repeated several times, the average positions were finally obtained. The angles of bending of the benzene rings were taken as 15 and 5 degrees for only $m=4$ and 5 respectively. However, the Johnson

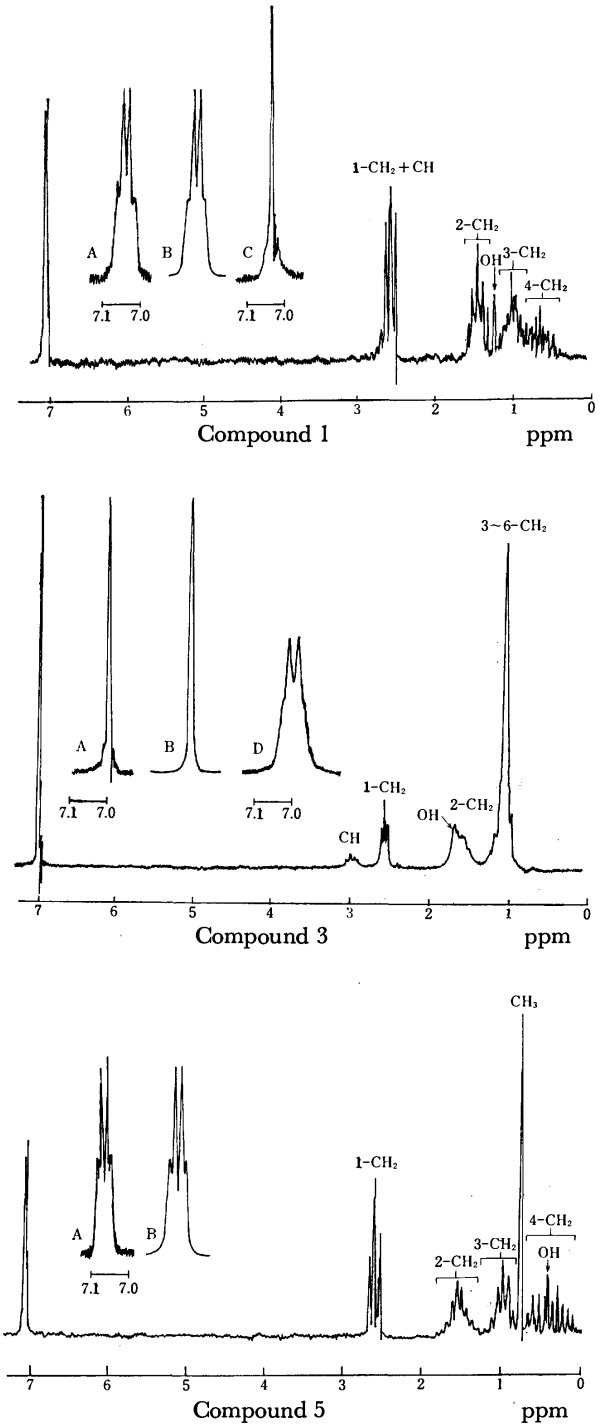

Fig. 3. PMR spectra of **1**, **3**, and **5** in CCl_4 at room temperature. A: five-fold expanded spectrum; B: calculated spectrum; C: in DMSO-d_6 at 130 °C; D: in acetone-d_6 at —60 °C.

and Bovey method was employed with no modification, because there was no appreciable effect of the ring bending upon the aromatic proton resonance (see Table 6). Furthermore, the three possible rotamers of the OH group around the C–O axis were assumed to be equal in population, but the proportion of the rotamers which would be able to interact with the π-site was taken to be equal to the $A_b/(A_b+A_f)$ ratio, when the paracyclophanol in question was internally bonded. The values thus

Table 6. PMR data of the aromatic protons in paracyclophanols in CCl_4 and the parameters used in simulation

No.	δ (ppm)	$\Delta\delta_{A-B}$ (Hz)	J_{AB} (*para*) (Hz)	J_{AB} (*meta*) (Hz)
1	7.03(q)	2.6	0.2	1.2
2	7.01(q)	7.0	0.2	1.2
3	6.99(s)	0	0.2	1.2
4	6.98(s)	—	—	—
5	7.05(q)	2.8	0.2	1.2
6	7.01(q)	2.2	0.2	1.2
7	6.97(q)	2.0	0.2	1.2
8	6.97(s)	0	0.2	1.2
9[a)]	7.07(s)			
11[b)]	7.03(s)			
15[c)]	6.99(s)			

a), b) The same compounds as those in Table 5.
c) *p*-Diethylbenzene.

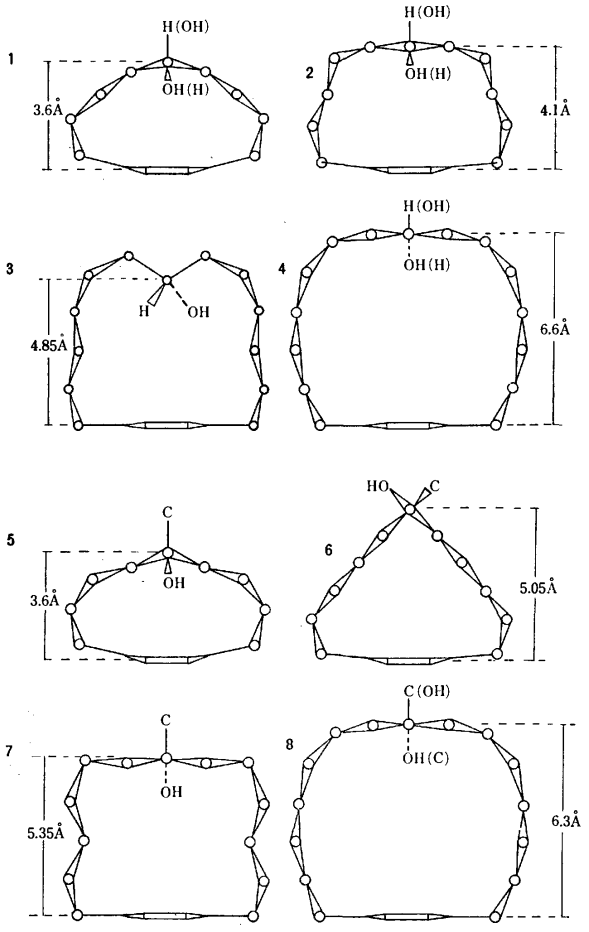

Fig. 4. Projection of the least-crowded conformations of **1**—**8** (shown by means of alkylene-bridge frameworks).

predicted are summarized in Table 5. They are in fairly good agreement with the observed ones, except for the OH protons of **1**, **2**, and **5**. Figure 4 shows the conformations constructed in the above manner, where **1**, **2**, **4**, and **8** each have two conformers with respect to the positions of OH and H or CH_3, while the others have only one conformer. The conformations of **1** and **2** were used in the calculation of **9** and **11** for comparison.

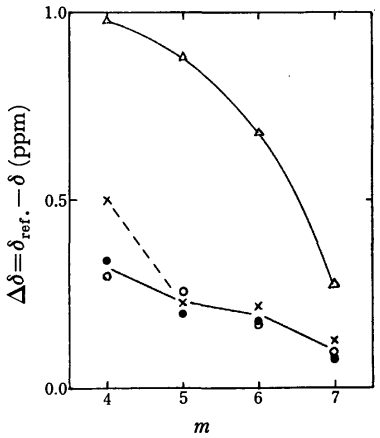

Fig. 5. Plots of m *vs.* $\Delta\delta$. △: CH; ●: CH_3; ×: OH in Series I; ○: OH in Series II.

Of particular interest in Table 5 are the π-current shieldings ($\Delta\delta=\delta_{ref}-\delta$) for OH, CH, and CH_3 at the central bridge carbons. Figure 5 indicates the plots of $\Delta\delta$ *vs.* m. In both Series I and II, except for the pair with $m=4$, the $\Delta\delta_{OH}$'s and $\Delta\delta_{CH_3}$ lie on almost the same curve; therefore, $\Delta\delta_{OH}$ is not related to the population of the π-bonded OH species involved. In other words, a possible deshielding for the OH proton by the π-bonding is not detectable,[25] probably because of the relatively low population of the π-bonded OH species. In the case of $m=4$, however, the $\Delta\delta_{OH}$ for **5** is less by 0.2 ppm than that for **1** (0.5 ppm). The reason for this is not clear, but the much higher population of the π-bonded OH species in **5** might be, at least in part, responsible for it.

In the aromatic region, simple AB-like quartets were observed for the lower paracyclophanols, but not for the higher homologs which showed sharp singlets, as could be confirmed by their five- or ten-fold expanded spectra. The results are listed in Table 6. In order to elucidate the difference, the temperature dependence of the spectra of **1** and **3** was examined in dimethyl-d_6 sulfoxide and acetone-d_6 respectively. On warming, the quartet of **1** changed to a broad triplet and coalesced into a relatively broad singlet at 130 °C (T_c), which thereafter further changed to a sharp singlet. On the other hand, the singlet of **3** changed, in the course of cooling down to −65 °C, to a broad singlet at −47 °C (T_c) and then split into a broad doublet which was further transformed to a broad quartet at −60 °C. These phenomena may be associated with the internal rotation of the benzene ring and/or the alkylene chain, as in substituted paracyclophanes,[26] paracyclophenes,[27] and similar heteraphanes.[28] That is, the signal splitting may be due to the spin-coupling of the aromatic protons rendered distinguishable on the NMR time scale by the slow rotation of the benzene ring and/or the alkylene chain (or by inhibition of the rotation). In the case of **1**, the rotation is slow at room temperature because of the shorter alkylene bridge, but on warming it becomes so fast as to render the protons indistinguishable. Contrary, in **3** the rotation is fast at room temperature because of the longer alkylene bridge, while on cooling it becomes so slow as to render them distinguishable. The internal rotation is expected to be more restricted in II than in I, because the methyl group at the central bridge carbon in II will play a role in restricting the rotation. In fact, **3** shows a singlet, while **7** shows a quartet. The free energy barriers, $\Delta G^{\ddagger}$, to rotation are 22.4 in **1** and 12.3 kcal/mol in **3**, as can be estimated by putting the observed $\Delta\delta$ (2.6 for **1** and 3 Hz for **3**) and T_c into the Calder and Garratt equation;[29] they are reasonable compared with those in other cyclophanes.[26,28]

The cause of the simple AB-like splitting is the closer approach of the C–O bond to the protons on one side of the benzene ring, as is shown below:

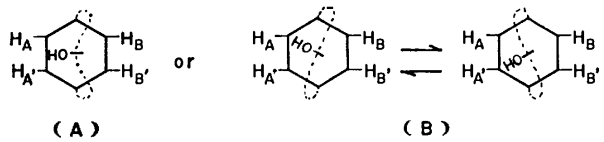

Here, two forms of B interconvert so fast as to render the two pairs of H_A/H_B and $H_{A'}/H_{B'}$ indistinguishable on the NMR time scale. In A and B, if H_A and $H_{A'}$ are immersed in the deshielding cone of the C–O bond, they may be expected to be slightly deshielded compared with H_B and $H_{B'}$. It is, then, safe to assume that the aromatic proton system is an A_2B_2 type, and that the two J_{AB}'s (meta and para) have small, but significant, values. These assumptions may explain the observed resonance pattern, because a rather complicated AA'BB' pattern would otherwise be expected. A computer simulation, performed under these assumptions, gave a good agreement with the observed results. The three typical examples are shown in Fig. 3, and the chemical-shift differences ($\Delta\delta_{A-B}$) and the J values used are listed in Table 6.

The authors wish to thank Dr. Shoichi Kondo of our university for his valuable suggestions and assistance in the computer simulation and also Messrs Mitsuo Yoshifuji and Yasuo Ishitomo of our university for their assistance in the synthesis of the compounds.

References

1) Parts of this work were presented at the 28th Annual Meeting of the Chemical Society of Japan, Tokyo, April 1973 and at the 8th Symposium of Structural Organic Chemistry, Kyoto, October 1975.

2) M. Tichy, "Advances in Organic Chemistry," Vol. 5, ed by R. A. Raphael, E. C. Taylor, and H. Wynberg, Interscience Publishers, New York (1965), p. 115.

3) P. von R. Schleyer, C. Winter, D. S. Trifan, and R. Bacskai, *Tetrahedron Lett.*, **1959**, 1; M. Ōki and H. Iwamura, *Bull. Chem. Soc. Jpn.*, **33**, 427, 1600 (1960).

4) H. Buc and J. Neel, *C. R. Acad. Sci.*, **255**, 2947 (1962).

5) L. P. Kuhn and R. A. Wires, *J. Am. Chem. Soc.*, **86**, 2161 (1964).

6) D. J. Cram and M. Goldstein, *J. Am. Chem. Soc.*, **85**, 1063 (1963).

7) J. S. Waugh and R. W. Fessenden, *J. Am. Chem. Soc.*, **79**, 846 (1957).

8) N. G. Newton, T. J. Walter, and N. L. Allinger, *J. Am. Chem. Soc.*, **95**, 5652 (1973).

9) N. L. Allinger, T. J. Walter, and N. G. Newton, *J.*

Am. Chem. Soc., **96**, 4588 (1974).
10) N. L. Allinger, J. T. Sprague, and T. Liljetors, *J. Am. Chem. Soc.*, **96**, 5100 (1974).
11) N. L. Allinger, L. A. Freiberg, R. B. Hermann, and M. A. Miller, *J. Am. Chem. Soc.*, **85**, 1171 (1963).
12) C. E. Johnson and F. A. Bovey, *J. Chem. Phys.*, **29**, 1012 (1958).
13) D. J. Cram and M. F. Anter, *J. Am. Chem. Soc.*, **80**, 3109 (1958).
14) C. W. Schimelpfenig, Ying-Tsung Lin, and J. F. Waller, *J. Org. Chem.*, **28**, 805 (1963).
15) M. Ōki and H. Iwamura, *Bull. Chem. Soc. Jpn.*, **32**, 950 (1959).
16) M. Ōki and H. Iwamura, *Bull. Chem. Soc. Jpn.*, **33**, 717 (1960).
17) M. Ōki and H. Iwamura, *Bull. Chem. Soc. Jpn.*, **32**, 955 (1959); **35**, 1552 (1962).
18) M. Ōki and H. Iwamura, *Bull. Chem. Soc. Jpn.*, **32**, 1135 (1959).
19) M. D. Joesten and R. S. Drago, *J. Am. Chem. Soc.*, **84** 3817 (1962).
20) D. J. Cram, N. L. Allinger, and H. Steinberg, *J. Am Chem. Soc.*, **76**, 6132 (1954).
21) D. J. Cram, C. S. Montgomery, and G. R. Knox, *J. Am. Chem. Soc.*, **88**, 515 (1966).
22) A force-field calculation indicated the bending angle of 8.5 degrees in the most stable conformation of [9]paracyclophane.[10]
23) A. F. Cockerill, G. L. O. Davis, R. C. Harden, and D. M. Rackhan, *Chem. Rev.*, **73**, 553 (1973).
24) Using HGS models of the Maruzen Co., Ltd., Japan.
25) N. Mori and K. Morioka, *Bull. Chem. Soc. Jpn.*, **48**, 2213 (1975).
26) M. Nakazaki, K. Yamamoto, and S. Okamoto, *Tetrahedron Lett.*, **1969**, 4597; *Bull. Chem. Soc. Jpn.*, **45**, 1562 (1972).
27) G. M. Whitesides, B. A. Pawson, and A. C. Cope, *J. Am. Chem. Soc.*, **90**, 639 (1968).
28) K. Sakamoto and M. Ōki, *Bull. Chem. Soc. Jpn.*, **48**, 497 (1975) and their papers cited therein.
29) I. C. Calder and P. J. Garratt, *J. Chem. Soc., B*, **1967**, 660.

A Reductive Elimination of Steroidal Diol Monoesters with Zinc Giving the Corresponding Olefins

Giichi GOTO

Central Research Division, Takeda Chemical Industries, Ltd., Yodogawa-ku, Osaka 532

(Received June 5, 1976)

Steroidal *cis*-diol monoacetates (**1, 9, 11,** and **13**) were refluxed with zinc powder in acetic acid to give the corresponding olefins (**2, 10, 12,** and **14**) in good yield. Under the reaction conditions, no reaction occurred with diol diacetates (**1b**: $R_1=R_2=H$, $R_3=R_4=Ac$ and **1m**: $R_1=C_6H_5$, $R_2=H$, $R_3=R_4=Ac$) and *trans*-diol monoacetates (**15** and **16**). Acyclic erythro and threo diol monoacetates (**17** and **19**) underwent highly stereoselective reduction affording **18** and **20**, respectively. The olefin-forming elimination proceeded with *syn*-elimination of a cyclic orthoacetate intermediate (**21**). The effect of some metals on the reduction and the behavior of a number of esters (**26**) and orthoesters (**27**) were also investigated.

In connection with mechanistic studies on the Serini reaction,[1,2] the addition of a catalytic amount of acetic acid accelerate was reported to the Serini rearrangement.[2] During the course of an investigation of the effect of acetic acid on the rearrangement, it was found that increase in the amount of acetic acid resulted in the formation of olefinic products. Thus, treatment of 16,-17-dihydroxy steroid monoacetates (**1**) with zinc powder in toluene in the presence of an excess acetic acid at 130 °C for 8 h gave the olefinic compounds (**2**) as a major product and a trace of the Serini rearrangement products (**3**). The finding has led to an investigation of the reductive elimination of diol monoesters to olefins. This paper describes the scope of this new reaction using a variety of steroidal diol monoesters.

Results and Discussion

The solution of steroidal 16,17-*cis*-diol monoacetates (**1**)[2] in acetic acid was refluxed with freshly activated zinc powder[3] under nitrogen for 4—6 h. After removal of the zinc by filtration, the filtrates were extracted with ether to give the corresponding steroidal 16-enes (**2**). Of various *cis*-diol monoacetates, secondary-tertiary diol monoesters were smoothly converted into olefins in high yields, together with a small amount (<5%) of the dehydrated compounds (**4**) as a by-product. Secondary-secondary diol monoacetates were reduced in lower yield and a large amount of diacetate (**1b**: $R_1=R_2=H$, $R_3=R_4=Ac$) was formed.[4] The corresponding diacetates (**1b** and **1m**: $R_1=C_6H_5$, $R_2=H$, $R_3=R_4=Ac$) were not affected under the reaction conditions.[6]

In order to investigate the participation of the neighbouring double bond, 16α-vinyl-16β,17β-diol 17-monoacetate (**1i**)[2] was heated with zinc in acetic acid to afford 16-vinyl-16-ene (**2i**) in 25% yield, coupled with 16β-vinyl-17β-acetate (**5**), its 16α-isomer (**6**) and (*E*)-16-ethylidene-17β-acetate (**7**) in 22, 26, and 17% yields, respectively. The (*E*)-configuration of 16-ethylidene group in **7** was confirmed by the conversion (hydrolysis and then oxidation) of **7** into the known (*E*)-16-ethylidene-17-one derivative.[2] An allenium ion intermediate (**8**) leading to the formation of **5, 6,** and **7** may be involved in this reaction. The results are summarized in Table 1 and the spectral data of **2** are given in Table 2.

In the androstane series, *cis*-diol monoacetates **9**[2] and **11**[8] were treated with zinc in acetic acid to give the corresponding steroidal olefins **10** and **12**, respectively, without elimination of the 3β-acetyl group. Diol monoacetate (**13**)[2] having a 4-en-3-one system was refluxed with zinc in acetic acid to give 3,16-diene (**14**) accompanied by concomitant Clemmensen type reduction[9] of the system.

On the other hand, when *trans*-diol monoacetates (**15** and **16**)[2] were refluxed with zinc in acetic acid for a prolonged reaction time, most of the starting materials were recovered unchanged, along with a small amount (<5%) of the olefinic products (**2e**: $R_1=H$, $R_2=Me$, and **2l**: $R_1=C_6H_5$, $R_2=H$) even after 56 h.

The following results demonstrate that the olefin-

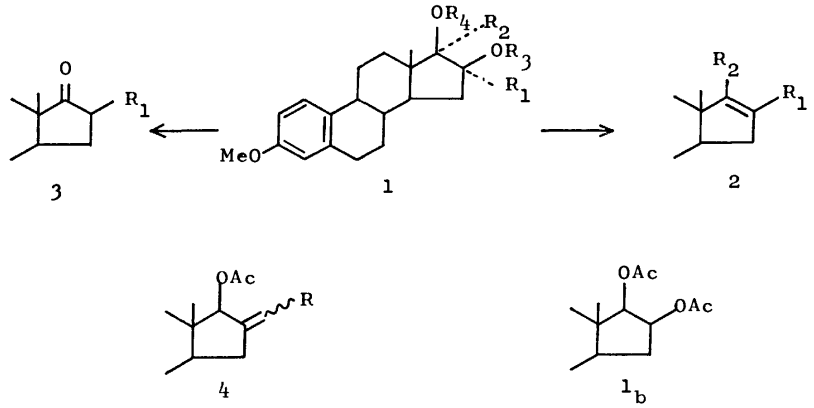

3 1 2 4 1b

Scheme 1.

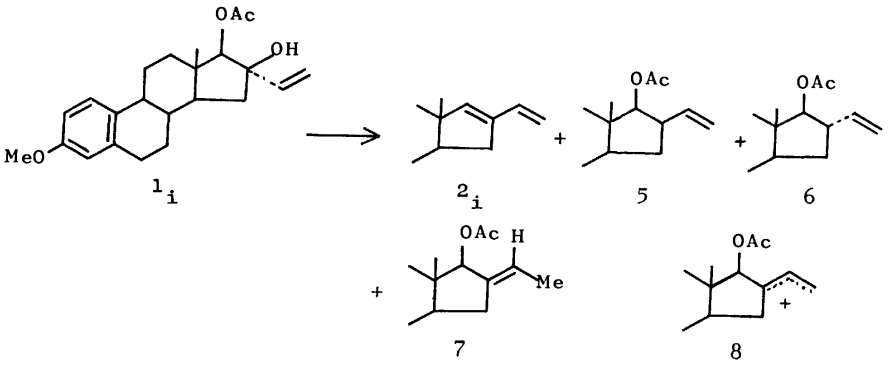

Scheme 2.

Table 1. Reductive elimination of 16,17-dihydroxysteroid monoacetates (**1**) to Δ^{16}-steroids (**2**)

Acetates **1**[a]	R_1	R_2	R_3	R_4	Reaction time (h)	Products **2**	Mp (°C)	Yield[b] (%)
a	H	H	Ac	H	6	**a**[c]	63	7
b	H	H	Ac	Ac	56	—	—	—
c	D	H	Ac	H	6	**c**	63	19
d[d]	Me	H	H	Ac	4	**d**	100	85
e	H	Me	Ac	H	4	**e**	123	88
f	Et	H	H	Ac	4	**f**	74	92
g	Et	H	Ac	H	4	**f**	74	74
h	Et	D	H	Ac	6	**h**	74	83
i	$CH=CH_2$	H	H	Ac	2	**i**	111	25
j	$CH_2CH=CH_2$	H	H	Ac	4	**j**	48	86
k	$(CH_2)_2CH=CH_2$	H	H	Ac	4	**k**	oil[e]	88
l	C_6H_5	H	H	Ac	4	**l**	154	87
m	C_6H_5	H	Ac	Ac	56	—	—	—

a) Ref. 2. b) The yields given are based on recrystallized products from CH_3OH. c) L. Cagliati and M. Magi, *Tetrahedron*, **19**, 1127 (1963). d) H. Mori and K. Yasuda, *Yakugaku Zasshi*, **80**, 330 (1960). e) Crystallization was unsuccessful.

Table 2. Spectral data of Δ^{16}-steroids (**2**)

Δ^{16}-Steroids **2**	R_1	R_2	IR (KBr) $\nu\Delta^{16}$ (cm^{-1})	^{1}H-NMR ($CDCl_3$) δ (ppm) 18-Me (3H, s)	O-Me (3H, s)	17-H (1H, s)	Ar-H (3H, m)	Others	MS (*m/e*) M^+	Others
d	Me	H	1625	0.78	3.77	5.50	6.6—7.3	1.73(3H, s, 16-Me)	282	267, 253
e	H	Me	1625	0.74	3.72	—	6.6—7.3	1.65(3H, s, 17-Me), 5.27(1H, m, 16-H)	282	267, 253
f	Et	H	1630	0.78	3.77	5.52	6.6—7.3	1.02(3H, t, J=7 Hz, Me)	296	281, 267
h	Et	D	1635	0.78	3.77	—	6.6—7.3	1.02(3H, t, J=7 Hz, Me)	297	282, 268
i[a]	$CH=CH_2$	H	1630[b]	0.81	3.70	5.78	6.6—7.3	4.96(1H, d, J=11 Hz, =CH), 5.04(1H, d, J=17 Hz, =CH), 6.2—6.6(1H, m, -CH=)[c]	294	279, 265
j	$CH_2CH=CH_2$	H	1625	0.80	3.77	5.53	6.6—7.3	4.8—6.4(3H, m, $-CH=CH_2$)	308	293, 267
k	$(CH_2)_2CH=CH_2$	H	1630[b]	0.79	3.78	5.55	6.6—7.3	4.8—6.4(3H, m, $-CH=CH_2$)	322	307, 281
l[d]	C_6H_5	H	1625	0.91	3.73	6.25	6.6—7.3	7.26(5H, m, Ar)	344	329, 213

a) UV (EtOH) λ_{max} nm (ε): 221 (12000), 231 (16500), 236 (14000). b) Overlapped with terminal olefinic band. c) Overlapped with aromatic protons. d) UV (EtOH) λ_{max} nm (ε): 220 (13000), 258 (9800).

forming elimination of acyclic erythro and threo diol monoacetates proceeded stereoselectively and in good yield. 17α,20α-Diol monoacetate (**17**), when treated with zinc in acetic acid for 8 h at 120 °C, afforded stereoselectively (93%) (*Z*)-17-ethylidene derivative (**18**)[10] in 92% yield, whereas 20β-epimer (**19**) gave stereoselectively (94%) (*E*)-17-ethylidene isomer (**20**)[11] in 93% yield.

The results suggest that the dideoxygenation reaction proceeds with reductive *cis*-elimination of a cyclic ortho-

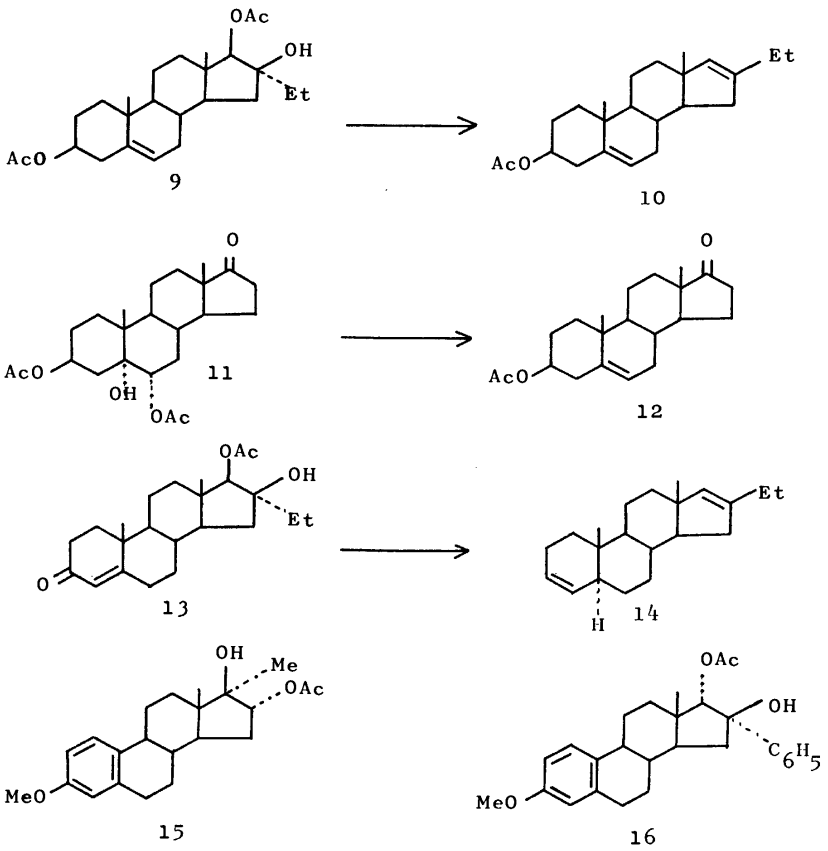

Scheme 3.

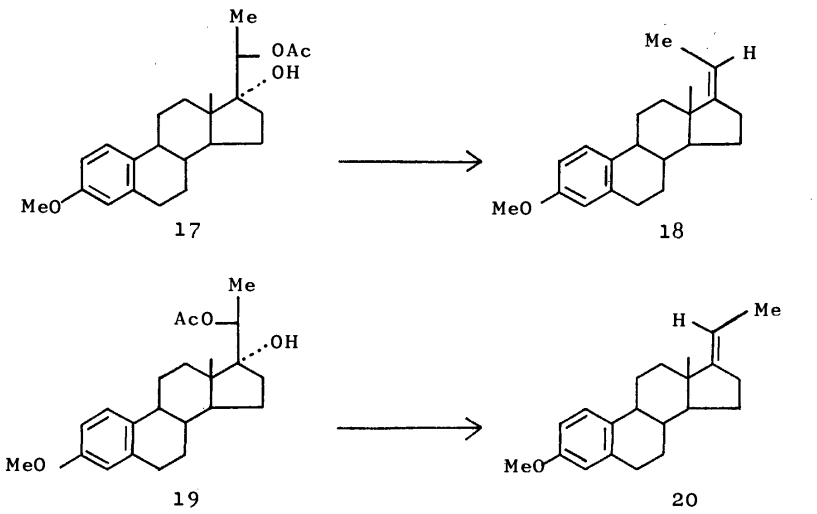

Scheme 4.

acetate intermediate (**21**),[2] which is in accord with the recent *syn*-elimination[12-14] of 1,3-dioxolan derivatives.

The explanation is supported by the following results. The cyclic orthoacetate (**23**), prepared from diol (**22**)[2] and trimethyl orthoacetate,[15] was refluxed with zinc in acetic acid to yield **2f** in 93% yield. It should be noted that heating of **23** with acetic acid gave (*Z*)-16-ethylidene-17β-acetate (**24**)[16] *via trans*-elimination of methanol quantitatively. Furthermore, treatment of **23** under the conditions of the Serini reaction (zinc in toluene)[1] gave 16β-ethyl-17-one (**25**) and **24** in 83% yield with a ratio of 1 : 5. Assignment of the configuration of 16-ethylidene group in **24** was made by comparison of the NMR spectrum with that of (*E*)-16-ethylidene isomer (**7**).

In order to investigate the behavior of esters other than acetates, several esters were subjected to the reaction conditions. The esters (**26**) were smoothly converted into the olefin (**2f**) in a range of 70—90% yield. This means that the reaction is not restrict-

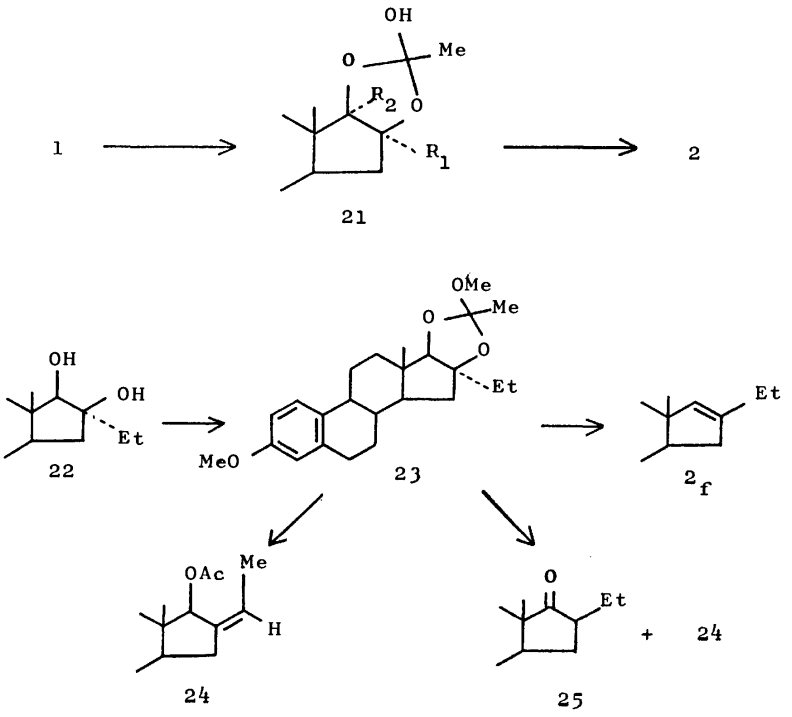

Scheme 5.

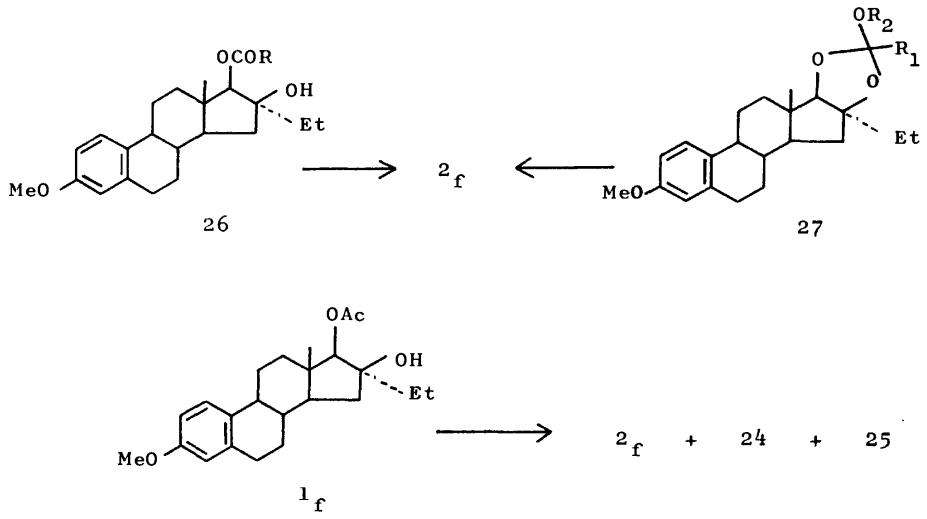

Scheme 6.

Table 3. Reductive elimination of 16,17-dihydroxysteroid monoesters (**26**) and the corresponding orthoesters (**27**) to Δ^{16}-steroid (**2f**)

Esters **26**	R	Mp (°C)	Reaction time (h)	Yield[a] (%)	Ortho-esters[b] **27**	Mp (°C)	R_1	R_2	Reaction time (h)	Yield[1] (%)
a	H	133—134	4	67	**a**	116—118	H	Me	4	69
b	Et	89	6	91	**b**	104—106	H	Et	4	70
c	C_6H_5	137—138	6	83	**c**	oil	Me	Et	4	92
					d	oil	Et	Et	4	90
					e	oil	C_6H_5	Et	6	86

a) The yields given are based on recrystallized product from CH_3OH. b) Isomeric mixture of 1,3-dioxolan derivatives was used.

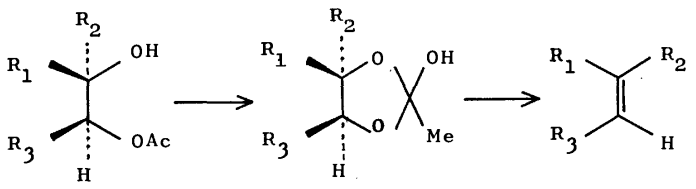

28 29

Scheme 7.

Table 4. Effect of metal on the reduction of 16,17-dihydroxysteroid monoacetate (**1f**)

Metal used	Solvent	Reaction time (h)	Products (%)[c]		
			2f	**24**	**25**
Zn	AcOH	4	92	2	trace
Sn[a]	AcOH	6	24	17	40
Mg[b]	AcOH–Toluene (1: 3)	2	trace	3	7
Al[2]	AcOH–Toluene (1: 3)	2	7	5	12

a) Sn dust was activated by washing with 5% HCl. b) Mg and Al powders were washed with 3% NaOH and then water. c) Isolated yield.

ed to acetate. The corresponding orthoesters (**27**) were also reduced into the olefin (**2f**) in a good yield. The results are summarized in Table 3.

The olefin-forming elimination of diol monoesters was also effected by the use of activated tin powder, but considerable amount of by-products were formed. Other metal powders such as magnesium and aluminium gave no satisfactory results. The effect of metals on the reduction is shown in Table 4. We see that zinc is the most suitable reducing agent in this reaction.

The new dideoxygenation reaction is restricted to the case in which one hydroxyl group is tertiary. However, the reaction may be of general applicability to the stereoselective synthesis of trisubstituted olefins (**29**) from diastereomeric trisubstituted 1,2-glycol monoesters (**28**).

Experimental

All melting points were determined on a micro hot-stage apparatus and were uncorrected. UV spectra were measured in EtOH on a Hitachi EPS-3T spectrophotometer, IR spectra on a Hitachi 215 spectrophotometer. NMR spectra were determined on a Varian HA-100 spectrometer using $CDCl_3$ as a solvent, chemical shifts (δ) being given in ppm relative to internal TMS. The mass spectra were determined on a Hitachi RMU-6D mass spectrometer equipped with a direct inlet system. Silicagel GF_{254} (E. Merck) was used for TLC analysis.

Reaction of Diol Monoacetates with Zinc in Acetic Acid. General Procedure: To a solution of **1** in acetic acid was added a 5—10 fold mol. of freshly activated zinc powder. The mixture was refluxed on an oil bath (at 150 °C) with stirring under nitrogen for 2—6 h. After cooling, ether was added and the solid was removed by filtration. The ether was successively washed with satd $NaHCO_3$ aq solution, water and satd NaCl aq solution, followed by drying, and then concentrated to give crude crystals. Recrystallization from MeOH afforded pure **2**. The mother liquor was treated with column chromatography using silica gel (E. Merck); eluted with benzene: ether (5: 1) to give **4** in 2—5% yield. The mps of **2** are given in Table 1 and IR, UV and NMR spectral data in Table 2. The results of elemental analyses are as follows.

*16-Methyl-3-methoxyestra-1,3,5(10),16-tetraene (**2d**).* Found: C, 85.09; H, 9.29%. Calcd for $C_{20}H_{26}O$: C, 85.05; H, 9.28%.

*17-Methyl-3-methoxyestra-1,3,5(10),16-tetraene (**2e**).* Found: C, 85.01; H, 9.30%. Calcd for $C_{20}H_{26}O$: C, 85.05; H, 9.28%.

*16-Ethyl-3-methoxyestra-1,3,5(10),16-tetraene (**2f**).* Found: C, 85.07; H, 9.63%. Calcd for $C_{21}H_{28}O$: C, 85.08; H, 9.52%.

*16-Ethyl-17-deuterio-3-methoxyestra-1,3,5(10),16-tetraene (**2h**).* Found: C, 84.81; H, 9.80%. Calcd for $C_{21}H_{27}DO$: C, 84.79; H, 9.83%.

*16-Vinyl-3-methoxyestra-1,3,5(10),16-tetraene (**2i**).* Found: C, 85.58; H, 8.90%. Calcd for $C_{21}H_{26}O$: C, 85.66; H, 8.90%.

*16-Allyl-3-methoxyestra-1,3,5(10),16-tetraene (**2j**).* Found: C, 85.70; H, 9.23%. Calcd for $C_{22}H_{28}O$: C, 85.66; H, 9.15%.

*16-(3-Butenyl)-3-methoxyestra-1,3,5(10),16-tetraene (**2k**).* Found: C, 85.80; H, 9.40%. Calcd for $C_{23}H_{30}O$: C, 85.66; H, 9.38%.

*16-Phenyl-3-methoxyestra-1,3,5(10),16-tetraene (**2l**).* Found: C, 87.14; H, 8.20%. Calcd for $C_{25}H_{28}O$: C, 87.16; H, 8.19%.

*Reaction of **1i** with Zinc in Acetic Acid.* To a solution of **1i** (2.4 g) in acetic acid (25 ml) was added activated zinc powder (4.8 g). The mixture was refluxed under nitrogen for 2 h with stirring. Work-up of the reaction mixture in the same way as for **2** gave a mixture of the products which were separated by preparative TLC impregnated with $AgNO_3$ (developed with hexane: ether 5: 1). The product with R_f value 0.89 was **2i** (477 mg). The other products with R_f values 0.47, 0.43 and 0.33 were **5** (505 mg), **7** (390 mg) and **6** (597 mg), respectively.

*17β-Acetoxy-16β-vinyl-3-methoxyestra-1,3,5(10)-triene (**5**).* Mp 107—108 °C (from petroleum ether); IR (KBr) 1730, 1640, 1610 cm^{-1}; NMR 0.83 (3H, s, 18-Me), 1.96 (3H, s, OAc), 3.73 (3H, s, OMe), 4.72 (1H, d, J=9 Hz, 17α-H),[16] 5.0—6.2 (3H, m, vinyl H), 6.6—7.3 (3H, m, Ar); MS *m/e* 354 (M^+), 312, 294. Found: C, 77.90; H, 8.62%. Calcd for $C_{23}H_{30}O_3$: C, 77.93; H, 8.53%.

*17β-Acetoxy-16α-vinyl-3-methoxyestra-1,3,5(10)-triene (**6**).* Mp 109 °C; IR (KBr) 1730, 1640, 1610 cm^{-1}; NMR 0.86 (3H, s, 18-Me), 1.98 (3H, s, OAc), 3.73 (3H, s, OMe), 4.50 (1H, d, J=7 Hz, 17α-H),[16] 4.9—6.2 (3H, m, vinyl H), 6.6—7.3 (3H, m, Ar); MS *m/e* 354 (M^+), 312, 294. Found: C, 77.99; H, 8.52%. Calcd for $C_{23}H_{30}O_3$: C, 77.93; H, 8.53%.

*17β-Acetoxy-(E)-16-ethylidene-3-methoxyestra-1,3,5(10)-triene (**7**).* Mp 99—100 °C; IR (KBr) 1730 cm^{-1}; NMR 0.75

(3H, s, 18-Me), 1.50 (3H, d, J=7 Hz, =CMe), 2.14 (3H, s, OAc), 3.75 (3H, s, OMe), 5.27 (1H, s, 17α-H), 5.2—5.3 (1H, m, =CH), 6.6—7.3 (3H, m, Ar); MS *m/e* 354 (M^+), 312, 294. Found: C, 77.85; H, 8.31%. Calcd for $C_{23}H_{30}O_3$: C, 77.93; H, 8.53%.

*3β-Acetoxy-16-ethylandrosta-5,16-diene (**10**).* Reaction of **9** (3.5 g) with zinc powder (8 g) in acetic acid (25 ml) was carried out by the same procedure as for **2**: **10** (2.6 g), mp 128 °C; IR (KBr) 1730, 1625 cm^{-1}; NMR 0.78 (3H, s, 18-Me), 1.00 (3H, t, J=6 Hz, Me), 1.05 (3H, s, 19-Me), 2.01 (3H, s, OAc), 4.4—4.8 (1H, m, 3α-H), 5.3—5.5 (2H, m, 6-H and 16-H); MS *m/e* 342 (M^+), 327, 282, 267. Found: C, 80.60; H, 10.01%. Calcd for $C_{23}H_{34}O_2$: C, 80.65; H, 10.01%.

*Stereoselective Conversion of 17α,20-Dihydroxy Monoacetates (**17** and **19**) into (Z)- and (E)-17-Ethylidene Derivatives (**18** and **20**).* Reaction of diol monoacetates (**17** and **19**) with zinc in acetic acid was carried out by the same procedure as for **1**. The purity of the products was estimated by gas chromatography on a column with 10% OV-17 (2 m, 265 °C).

Preparation of Orthoesters.[15] *General Procedure*: To a solution of diol (**22**) in CH_2Cl_2 was added trialkyl orthoester and a catalytic amount of *p*-TsOH. After being stirred at room temperature for 2 h, the reaction mixture was poured into 5% $NaHCO_3$ aq solution and extracted with CH_2Cl_2. The extracts were washed with water, dried, and concentrated to give a resinous material. Recrystallization from petroleum ether gave the steroidal orthoesters. The following compounds were prepared.

*Methyl Orthoacetate of **22** (**23**).* Mp 63 °C; IR (KBr) 1610 cm^{-1}; NMR 0.86 (3H, s, 18-Me), 1.04 (3H, t, J=7 Hz, Me), 1.57 (3H, s, Me), 3.25 (3H, s, OMe), 3.73 (3H, s, OMe), 3.84 (1H, s, 17α-H), 6.6—7.3 (3H, m, Ar); MS *m/e* 386 (M^+), 354, 312. Found: C, 74.60; H, 8.80%. Calcd for $C_{24}H_{34}O_4$: C, 74.57; H, 8.87%.

*Methyl Orthoformate of **22** (**27a**).* IR (KBr) 1610 cm^{-1}; NMR 0.83 (3H, s, 18-Me), 1.01 (3H, t, J=7 Hz, Me), 3.27 (3H, s, OMe), 3.71 (3H, s, OMe). 3.86 (1H, s, 17α-H), 5.74 (1H, s, -OCHO-), 6.6—7.3 (3H, m, Ar); MS *m/e* 372 (M^+), 344, 341. Found: C, 74.20; H, 8.60%. Calcd for $C_{23}H_{32}O_4$: C, 74.16; H, 8.66%.

*Ethyl Orthoformate of **22** (**27b**).* IR (KBr) 1610 cm^{-1}; NMR 0.82 (3H, s, 18-Me), 1.00 (3H, t, J=6 Hz, Me), 1.20 (3H, t, J=7 Hz, Me), 3.52 (2H, q, J=7 Hz, $-CH_2-$), 3.73 (3H, s, OMe), 3.78 (1H, s, 17α-H), 5.73 (1H, s, -OCHO-), 6.6—7.3 (3H, m, Ar); MS *m/e* 386 (M^+), 357, 341. Found: C, 74.59; H, 8.90%. Calcd for $C_{24}H_{34}O_4$: C, 74.57; H, 8.87%.

*Ethyl Orthoacetate of **22** (**27c**).* IR (Neat) 1610 cm^{-1}; NMR 0.87 (3H, s, 18-Me), 3.56 (2H, q, J=7 Hz, $-CH_2-$), 3.72 (3H, s, OMe), 3.80 (1H, s, 17α-H), 6.6—7.3 (3H, m, Ar); MS *m/e* 400 (M^+, $C_{25}H_{36}O_4$ requires: 400), 385, 354.

*Ethyl Orthopropionate of **22** (**27d**).* IR (Neat) 1610 cm^{-1}; NMR 0.86 (3H, s, 18-Me), 3.60 (2H, q, J=7 Hz, $-CH_2-$), 3.71 (3H, s, OMe), 3.84 (1H, s, 17α-H), 6.6—7.3 (3H, m, Ar); MS *m/e* 414 (M^+, $C_{26}H_{38}O_4$ requires: 414), 399, 368.

Ethyl Orthobenzoate[17] *of **22** (**27e**).* IR (Neat) 1615, 1610 cm^{-1}; NMR 0.90 (3H, s, 18-Me), 3.70 (3H, s, OMe), 3.72 (2H, q, J=7 Hz, $-CH_2-$), 3.93 (1H, s, 17α-H), 6.6—7.6 (8H, m, Ar); MS *m/e* 462 (M^+, $C_{30}H_{38}O_4$ requires: 462), 447, 434.

Treatment of Orthoesters with Zinc in Acetic Acid. General Procedure: To a solution of orthoester (0.4 g) in acetic acid (5 ml) was added activated zinc powder (1.3 g). The mixture was refluxed under nitrogen for 4—6 h with stirring. Work-up of the reaction mixture gave **2f** which was crystallized from MeOH.

*17β-Acetoxy-(Z)-16-ethylidene-3-methoxyestra-1,3,5(10)-triene (**24**).* A solution of **23** (0.34 g) in acetic acid (10 ml) was heated under reflux for 30 min. The solvent was evaporated under reduced pressure to give crude crystals. Recrystallization from ether: hexane (5: 1) afforded **24** (0.3 g), mp 161—162 °C; IR (KBr) 1730, 1610 cm^{-1}; NMR 0.81 (3H, s, 18-Me), 1.56 (3H, d, J=7 Hz, =CMe), 2.11 (3H, s, OAc), 3.75 (3H, s, OMe), 5.24 (1H, s, 17α-H), 5.49 (1H, m, =CH), 6.6—7.3 (3H, m, Ar); MS *m/e* 354 (M^+), 312, 297, 294. Found: C, 77.85; H, 8.31%. Calcd for $C_{23}H_{30}O_3$: C, 77.93; H, 8.53%.

*Treatment of **23** under the Conditions of the Serini Reaction.* To a solution of **23** (0.77 g) in dried toluene was added freshly activated zinc powder. The mixture was refluxed for 6 h with stirring. Zinc was removed by filtration. The filtrates were evaporated under vacuum to give a residue which was separated by preparative TLC (developed with benzene: ether 10: 1). The product with higher R_f value (0.42) was **24** (490 mg). The other product with R_f value (0.33) was 16β-ethyl-3-methoxyestra-1,3,5(10)-trien-17-one (**25**)[2] (86 mg).

*17β-Formyloxy-16β-hydroxy-16α-ethyl-3-methoxyestra-1,3,5(10)-triene (**26a**).* Formylation of **22** with Ac_2O-HCOOH gave **26a**: IR (KBr) 3500, 1720, 1610 cm^{-1}; NMR 0.97 (3H, s, 18-Me), 3.71 (3H, s, OMe), 4.59 (1H, s, 17α-H), 6.6—7.3 (3H, m, Ar), 8.15 (1H, s, CHO); MS *m/e* 358 (M^+), 312. Found: C, 73.76; H, 8.43%. Calcd for $C_{22}H_{30}O_4$: C, 73.71; H, 8.44%.

*17β-Propionyloxy-16β-hydroxy-16α-ethyl-3-methoxyestra-1,3,5-(10)-triene (**26b**).* Treatment of **22** with propionic anhydride in pyridine gave **26b**: IR (KBr) 3500, 1730, 1610 cm^{-1}; NMR 0.98 (3H, s, 18-Me), 3.75 (3H, s, OMe), 4.58 (1H, s, 17α-H), 6.6—7.3 (3H, m, Ar); MS *m/e* 386 (M^+), 357, 312. Found: C, 74.59; H, 8.80%. Calcd for $C_{24}H_{34}O_4$: C, 74.57; H, 8.87%.

*17β-Benzoyloxy-16β-hydroxy-16α-ethyl-2-methoxyestra-1,3,5-(10)-triene (**26c**).* Treatment of **22** with benzoyl chloride in pyridine afforded **26c**: IR (KBr) 3350, 1695, 1610, 1600 cm^{-1}; NMR 0.95 (3H, t, J=7 Hz, Me), 1.08 (3H, s, 18-Me), 3.74 (3H, s, OMe), 4.85 (1H, s, 17α-H), 6.6—7.3 (3H, m, Ar), 7.4—8.3 (5H, m, Ar); MS *m/e* 434 (M^+), 312. Found: C, 77.40; H, 7.80%. Calcd for $C_{28}H_{34}O_4$: C, 77.39; H, 7.89%.

*Reaction of **26** with Zinc in Acetic Acid. General Procedure*: To a solution of **26** in acetic acid was added freshly activated zinc powder. The mixture was refluxed under nitrogen for 4—6 h with stirring. Work-up by the usual procedure gave **2f**.

*Reaction of **1f** with Tin in Acetic Acid.* To a solution of **1f** (1.2 g) in acetic acid (15 ml) was added tin powder (3 g) which had been washed with acid. The mixture was heated under reflux for 6 h. To the cooled solution was added ether (200 ml) and the solid was removed by filtration. The filtrate was washed with satd $NaHCO_3$ aq, satd NaCl aq solution in succession and then dried. The ether was concentrated to give a residue which was separated by preparative TLC using benzene: ether (10: 1) as an eluent. The product with R_f value 0.86 was **2f** (229 mg). The other products with R_f values 0.42 and 0.33 were **24** (194 mg) and **25** (403 mg), respectively.

The author would like to thank Drs. E. Ohmura, H. Morimoto, T. Miki, and K. Hiraga of this Division for their advice and encouragement.

References

1) a) A. Serini, W. Logemann, and W. Hildebrand, *Ber.*, **72**, 391 (1939); b) T. Goto and L. F. Fieser, *J. Am. Chem. Soc.*, **83**, 251 (1961); c) E. Ghera, *Chem. Commun.*,

1968, 1639; F. Ghera, *J. Org. Chem.*, **35**, 660 (1970).

2) G. Goto, K. Yoshioka, and K. Hiraga, *Tetrahedron*, **30**, 2107 (1974).

3) Zinc powder was treated with dil HCl, followed by washing with distilled water and then dried over P_2O_5 at 100 °C.

4) The facile formation of the diacetate (**1b**) is due to a neighbouring group particitipation[5] of the 16β-acetoxyl group.

5) a) R. Boschan and S. Winstein, *J. Am. Chem. Soc.*, **78**, 4921 (1956); b) J. F. King and A. D. Allbutt, *Tetrahedron Lett.*, **1967**, 49.

6) Reductive elimination of cholestane diacetates by lithium (or calcium) in liquid ammonia was known[7] to occur only when one ester is tertiary and both ester groups are *trans*-diaxial.

7) D. H. R. Barton, P. G. Sammes, and M. Silva, *Tetrahedron Suppl.*, **7**, 57 (1966).

8) J. S. Baran, *J. Org. Chem.*, **25**, 257 (1960).

9) a) J. McKenna, J. K. Norymberski, and R. D. Stubbs, *J. Chem. Soc.*, **1959**, 2502; b) G. M. L. Cragg, C. W. Davey, D. N. Hall, G. D. Meakins, E. E. Kichards, and T. L. Whateley, *J. Chem. Soc., C*, **1966**, 1266; c) B. R. Davis and P. D. Woodgate, *ibid.*, **1966**, 2006.

10) A. M. Krubiner and E. P. Oliveto, *J. Org. Chem.*, **31**, 24 (1966).

11) H. Schick, *Pharmazie*, **30**, 30 (1975).

12) a) E. J. Corey and R. A. E. Winter, *J. Am. Chem. Soc.*, **85**, 2677 (1963); b) E. J. Corey, F. A. Carey, and R. A. E. Winter, *ibid.*, **87**, 934 (1965); c) E. J. Corey and R. A. E. Winter, *Chem. Commun.*, **1965**, 208; d) D. Horton and W. N. Turner, *Tetrahedron Lett.*, **1964**, 2531; e) R. Hull and R. Farrand, *Chem. Commun.*, **1965**, 164; f) E. J. Corey and J. I. Shulman, *Tetrahedron Lett.*, **1968**, 3655; g) M. Tichy and J. Sicher, *ibid.*, **1969**, 4609; h) M. F. Semmelhack and R. D. Stauffer, *ibid.*, **1973**, 2667.

13) a) G. Crank and F. W. Eastwood, *Aust. J. Chem.*, **17**, 1392 (1964); b) J. S. Josan and F. W. Eastwood, *Carbohydr. Res.*, **7**, 161 (1963); c) G. I. Moss, G. Crank, and F. W. Eastwood, *J. Chem. Soc., D*, **1970**, 206; d) J. W. Scheeren, A. P. M. van der Veek, and W. Stevens, *Recl. Trav. Chim. Pays-Bas*, **88**, 165 (1969); e) A. P. M. van der Veek and F. H. Putten, *Tetrahedron Lett.*, **1970**, 3951; f) T. Hiyama and H. Nozaki, *Bull. Chem. Soc. Jpn.*, **46**, 2248 (1973); g) R. A. Braun, *J. Org. Chem.*, **31**, 1147 (1966); h) F. W. Eastwood, K. J. Harrington, J. S. Josan, and J. J. Pura, *Tetrahedron Lett.*, **1970**, 5223.

14) a) P. S. Wharton, G. A. Hiegel, and S. Ramaswami, *J. Org. Chem.*, **29**, 2441 (1964); b) J. S. Josan and F. W. Eastwood, *Aust. J. Chem.*, **21**, 2013 (1968); c) J. N. Hines, M. J. Peagran, G. H. Whitham, and M. Wright, *Chem. Commun.*, **1968**, 1593; d) J. N. Hines, M. J. Peagran, E. J. Thomas, and G. H. Whithan, *J. Chem. Soc. Perkin Trans. 1*, **1973**, 2332.

15) R. H. DeWolfe, "Carboxylic Ortho Acid Derivatives," Academic Press, New York and London (1970).

16) G. Goto, K. Yoshioka, K. Hiraga, and T. Miki, *Chem Pharm. Bull.*, **21**, 1393 (1973).

17) a) L. G. S. Brooker and F. L. White, *J. Am. Chem. Soc.*, **57**, 2480 (1935); b) A. Kiprianov, Z. P. Suitnik, and E. D. Suich, *Zh. Obshch. Khim.*, **6**, 42 (1936).

A New Synthesis of 9-Xanthenones by the Reaction of 2-Hydroxybenzophenones with Metal Salts

Shuichi UEDA* and Kazu KUROSAWA

Department of Chemistry, Faculty of Science, Kumamoto University, Kurokami-2-39-1, Kumamoto 860

(Received June 10, 1976)

Seven 2-hydroxy-4-methoxybenzophenones were oxidized with manganese(III) acetate to give 9-xanthenones (24—65%). 2-Hydroxy-3',4,4',6-tetramethoxybenzophenone gave 1,3,6,7-tetramethoxy-9-xanthenone in a 5% yield. 2-Hydroxy-3',4,4',5-tetramethoxybenzophenone yielded 2,5-dihydroxy-3',4,4'-trimethoxybenzophenone (9%). The oxidation of the 2-hydroxybenzophenones with lead tetraacetate also gave the 9-xanthenones, but in poor yields.

In a previous paper,[1] it has been reported that the reactions of 2-hydroxy-4-methoxy- and 2-hydroxy-4,4'-dimethoxybenzophenones with metal salts gave rise to dimeric compounds and 2,5-dihydroxybenzophenones. It was also reported that 2-hydroxy-2',4,4'-trimethoxy- and 2-hydroxy-3',4,4'-trimethoxybenzophenones yielded 3,6-dimethoxy- and 2,3,6-trimethoxy-9-xanthenones respectively. We have now continued our investigation of the reaction in the hope that this can lead to a new synthesis of 9-xanthenones.

The 2-hydroxybenzophenones were prepared by the known method,[2] while the reactions of the 2-hydroxybenzophenones with manganese(III) acetate and lead tetraacetate were carried out in boiling acetic acid. The structures of the reaction products were determined by examining their IR, NMR, and mass spectra, and by elemental analyses.

When 2-hydroxy-2',4,5'-trimethoxybenzophenone (Ie) was oxidized with manganese(III) acetate, 2,6-dimethoxy-9-xanthenone (IIb) (65%) was obtained. This indicates that an intramolecular coupling between the hydroxyl group and the carbon (2') in Ie took place and that the 2'-methoxyl group on that position was removed.

When Ie was oxidized with lead tetraacetate, 2,6-dimethoxy-1-methyl-9-xanthenone (IIe) (3%) and 1-acetoxymethyl-2,6-dimethoxy-9-xanthenone (IIIe) (6%) were obtained, together with IIb (11%). The NMR spectrum of IIe in CF_3COOH showed the presence of a methyl group {δ 2.96 (s, 3H)}, two methoxyl groups {δ 4.10 (s, 3H) and δ 4.15 (s, 3H)}, three aromatic protons {δ 7.24 (d, J=2 Hz), δ 7.34 (dd, J=9, 2 Hz) and δ 8.45 (d, J=9 Hz)}, and two aromatic protons {δ 7.78 (d) and 7.99 (d), AB system, J=9 Hz}. The methyl group at δ 2.96 can be located at the 1-position on the basis of its extraordinary lower shift[3] and on the basis of the presence of the lower-field doublet at δ 8.45 (J=9 Hz) as a result of the hydrogen adjacent to the carbonyl group. The presence of the aromatic AB system (J=9 Hz) further confirmd the IIe structure. A similar methylation of aromatic compounds and the acetoxylation of an aromatic methyl group have been reported in the reaction of lead tetraacetate.[4] The oxidation of 2-hydroxy-2',4-dimethoxybenzophenone (Ia) and 2-hydroxy-2',4,4'-trimethoxybenzophenone (Ic), both with a 2'-methoxyl group, gave 3-methoxy-9-xanthenone (IIa) (49% with $Mn(OAc)_3$ and 16% with $Pb(OAc)_4$) and 3,6-dimethoxy-9-xanthenone (IIc) (45% with $Mn(OAc)_3$ and 12% with $Pb(OAc)_4$, with the loss of the 2'-methoxyl group, respectively. In the oxidation of Ic with manganese(III) acetate, IV (9%) was isolated; however, its structure could not be determined.

When 2-hydroxy-3',4,4',5'-tetramethoxybenzophenone (If) was subjected to oxidation with manganese(III) acetate, 2,3,4,6-tetramethoxy-9-xanthenone (IIf) was obtained in a 48% yield, whereas the oxidation of If with lead tetraacetate afforded IIf in only a 7% yield, plus 1-acetoxymethyl-2,3,4,6-tetramethoxy-9-xanthenone (IIIf) (6%). 2-Hydroxy-3',4-dimethoxybenzophenone (Ib) and 2-hydroxy-3',4,4'-trimethoxybenzophenone (Id) gave IIb (24%) and 2,3,6-trimethoxy-9-xanthenone (IId) (40%) respectively, showing that the coupling occurred preferentially at the less hindered position.

When 2,4'-dihydroxy-3',4,5'-trimethoxybenzophenone (Ig) was oxidized with manganese (III) acetate, 2,6-dimethoxy-*p*-benzoquinone (V) (13%) was the only isolable product. There were many unidentified compounds in the reaction mixture, suggesting that the oxidation of dihydroxybenzophenones is not useful for the synthesis of 9-xanthenone. A monoacetate of Ig, 2-hydroxy-4'-acetoxy-3',4,5'-trimethoxybenzophenone (Ih), did, however, give 3-acetoxy-2,4,6-trimethoxy-9-xanthenone (IIh) (31%). This may indicate that hydroxy-9-xanthenones can be prepared from dihydroxybenzophenones *via* their acetate.

The manganese (III) acetate oxidation of 2-hydroxy-3',4,4',6-tetramethoxybenzophenone (Ii), which possesses a phloroglucinol nucleus, yielded 1,3,6,7-tetramethoxy-9-xanthenone (IIi) (5%) and 2,6-dimethoxy-3-(3,4-dimethoxybenzoyl)-*p*-benzoquinone (VIi) (5%). The lead tetraacetate oxidation of Ii afforded IIi in a better yield (11%), plus VIi (7%) and 2,6-dimethoxy-3-(3,4-dimethoxybenzoyl)-5-methyl-*p*-benzoquinone(VIi') (7%). A similar methylation is often observed in the reaction of a quinone with lead tetraacetate.[4]

Finally, we examined the oxidation of 2-hydroxy-3',4,4',5-tetramethoxybenzophenone (Ij). 2,5-Dihydroxy-3',4,4'-trimethoxybenzophenone (Ik) (9%) was obtained, together with many unidentified products.

Although 9-xanthenones have been synthesized in a number of ways, *i.e.*, by the dehydration of 2,2'-dihydroxybenzophenones,[2] the base-catalysed cyclization of 2-hydroxy-2'-methoxybenzophenones,[5] the cyclization of *o*-phenoxybenzoic acids,[6] and the oxidative couplings

* Present address: Tokushima Factory, Taiho Co., Ltd., Hiraishi, Kawauchi-machi, Tokushima 771-01.

TABLE 1. THE REACTION OF 2-HYDROXYBENZOPHENONES WITH MANGANESE(III) ACETATE AND LEAD TETRAACETATE IN BOILING ACETIC ACID

Substrate	Reaction conditions			Products (yield, %)				
	Reagent	Molar ratio	Time (min)	9-Xanthenone	Acetoxymethyl-9-xanthenone	Quinone	Benzophenone	*etc.*
Ia	$Mn(OAc)_3$	1:4	180	IIa[10] (49)				
Ia	$Pb(OAc)_4$	1:3	120	IIa (16)				
Ib	$Mn(OAc)_3$	1:4	120	IIb[11] (24)				
Ic[1]	$Mn(OAc)_3$	1:4	180	IIc[1] (45)				IV(9)
Ic	$Pb(OAc)_4$	1:3	120	IIc (12)				
Id[1]	$Mn(OAc)_3$	1:4	90	IId[1] (40)				
Ie	$Mn(OAc)_3$	1:5	180	IIb (65)				
Ie	$Pb(OAc)_4$	1:3	150	IIb (11), IIe(3)	IIIe(6)			
If	$Mn(OAc)_3$	1:5	240	IIf (48)				
If	$Pb(OAc)_4$	1:3	120	IIf (7)	IIIf(6)			
Ig	$Mn(OAc)_3$	1:5	240			V (13)		
Ih	$Mn(OAc)_3$	1:4	120	IIh (31)				
Ii	$Mn(OAc)_3$	1:5	60	IIi (5)		VIi (5)		
Ii	$Pb(OAc)_4$	1:3	100	IIi[12] (11)		VIi (7), VIi'(7)		
Ij[9]	$Mn(OAc)_3$	1:4	120				Ik(9)	

of polyhydroxybenzophenones with potassium permanganate,[6] potassium ferricyanide[7] and dichlorodicyano-*p*-benzoquinone,[8] it is now demonstrated that 9-xanthenones can be synthesized from 2-hydroxy-4-methoxy- and 2-hydroxy-4,6-dimethoxybenzophenones in moderate yields, by the reaction of manganese(III) acetate, but not from 2-hydroxy-4,5-dimethoxybenzophenone. Acetoxy-9-xanthenones, which could not be obtained by the previous methods, can also be prepared by the oxidation of 2-hydroxyacetoxybenzophenones.

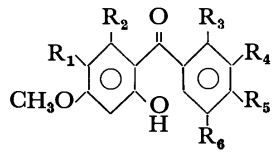

Ia $R_1=R_2=R_4=R_5=R_6=H$, $R_3=OCH_3$
Ib $R_1=R_2=R_3=R_5=R_6=H$, $R_4=OCH_3$
Ic $R_1=R_2=R_4=R_6=H$, $R_3=R_5=OCH_3$
Id $R_1=R_2=R_3=R_6=H$, $R_4=R_5=OCH_3$
Ie $R_1=R_2=R_4=R_5=H$, $R_3=R_6=OCH_3$
If $R_1=R_2=R_3=H$, $R_4=R_5=R_6=OCH_3$
Ig $R_1=R_2=R_3=H$, $R_4=R_6=OCH_3$, $R_5=OH$
Ih $R_1=R_2=R_3=H$, $R_4=R_6=OCH_3$, $R_5=OAc$
Ii $R_1=R_3=R_6=H$, $R_2=R_4=R_5=OCH_3$
Ij $R_2=R_3=R_6=H$, $R_1=R_4=R_5=OCH_3$
Ik $R_2=R_3=R_6=H$, $R_1=OH$, $R_4=R_5=OCH_3$

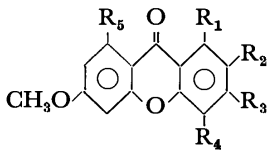

IIa $R_1=R_2=R_3=R_4=R_5=H$
IIb $R_1=R_3=R_4=R_5=H$, $R_2=OCH_3$
IIc $R_1=R_2=R_4=R_5=H$, $R_3=OCH_3$
IId $R_1=R_4=R_5=H$, $R_2=R_3=OCH_3$
IIe $R_3=R_4=R_5=H$, $R_1=CH_3$, $R_2=OCH_3$
IIf $R_1=R_5=H$, $R_2=R_3=R_4=OCH_3$
IIh $R_1=R_5=H$, $R_2=R_4=OCH_3$, $R_3=OAc$
IIi $R_1=R_4=H$, $R_2=R_3=R_5=OCH_3$
IIIe $R_3=R_4=R_5=H$, $R_1=CH_2OAc$, $R_2=OCH_3$
IIIf $R_2=R_3=R_4=OCH_3$, $R_1=CH_2OAc$, $R_5=H$

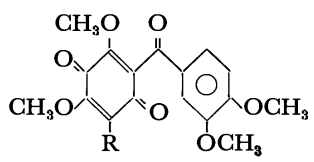

VIi R=H
VIi' R=CH_3

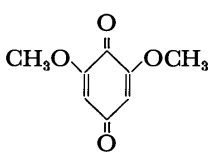

V

Experimental

All the ^1H NMR spectra were recorded for the deuteriochloroform solution, unless otherwise stated, with a Hitachi R 24 NMR spectrometer, with tetramethylsilane as the internal reference. The IR spectra were recorded for the chloroform solution with a JASCO IRA-1 grating spectrometer, while the UV spectra were measured for the methanol solution with a Hitachi EPS-3T spectrophotometer. The mass spectrum was recorded with a Hitachi RMU-6M spectrometer. The melting points were determined with a Yanagimoto hot-stage apparatus and were uncorrected.

Preparations of 2-Hydroxybenzophenones (Ia,Ib,Ie—Ii). The 2-hydroxybenzophenones (Ia Ib, Ie, and Ig) were prepared by the reaction of 3-methoxyphenol (8 mmol) and a benzoic acid (8 mmol) with phosphoryl chloride (7 ml) containing fused zinc chloride (3 g), with heating at 65—70 °C for 2 h. The reaction mixture was poured into water and extracted with chloroform. After the removal of the chloroform, the crude 2-hydroxybenzophenone was purified on a silica gel column (Wakogel C 100) (100 g), eluting with benzene, followed by recrystallization from methanol.

2-Hydroxy-2',4-dimethoxybenzophenone (Ia): Mp 88.5—89 °C, 68%, ν_{max}: 1630 cm^{-1} (C=O), λ_{max} (ε): 286 (14400) and 325 nm (9550), δ: 3.75 (s, OCH_3), 3.81 (s, OCH_3), 6.15—6.5 (m, 2H), 6.8—7.6 (m, 5H), and 12.6 (s, OH). Found: C, 69.68; H, 5.37%. Calcd for $C_{15}H_{14}O_4$: C, 69.75; H, 5.46%.

2-Hydroxy-3',4-dimethoxybenzophenone (Ib): $Bp_{0.3}$ 165—170 °C (bath temp), 54%, ν_{max}: 1630 cm^{-1} (C=O), λ_{max} (ε): 292 (8970) and 325 nm (6780), δ: 3.81 (s, $2\times OCH_3$), 6.2—6.5 (m, 2H), 6.9—7.6 (m, 5H) and 12.4 (s, OH). Found: C, 69.55; H, 5.47%. Calcd for $C_{15}H_{14}O_4$: C, 69.75; H, 5.46%.

2-Hydroxy-2',4,5'-trimethoxybenzophenone (Ie): Mp 110 °C, 21%, ν_{max}: 1628 cm^{-1} (C=O), λ_{max} (ε): 230 (s) (12300), 287 (15000) and 327 nm (9700), δ: 3.66 (s, OCH_3), 3.72 (s, OCH_3), 3.79 (s, OCH_3), 6.2—6.5 (m, 2H), 6.7—7.3 (m, 4H) and 12.5 (broad s, OH). Found: C, 66.65; H, 5.57%. Calcd for $C_{16}H_{16}O_5$: C, 66.66; H, 5.59%.

2,4'-Dihydroxy-3',4,5'-trimethoxybenzophenone (Ig): Ig was prepared by the reaction of 3-methoxyphenol (8 mmol) and

3,4,5-trimethoxybenzoic acid (8 mmol) with phosphoryl chloride (7 ml) containing fused zinc chloride (3 g); mp 142—143 °C, 32%, ν_{max}: 1620 cm^{-1} (C=O), λ_{max} (ε): 241 (s) (10900), 920 (11400) and 344 nm (14600), δ: 3.79 (s, OCH_3), 3.84 (s, $2\times OCH_3$), 6.0 (broad s, OH), 6.2—6.45 (m, $H_{(3)}$ and $H_{(5)}$), 6.84 (s, $H_{(2')}$ and $H_{(6')}$), 7.45 (d, J=8.5 Hz, $H_{(6)}$) and 12.5 (broad s, OH). Found: C, 63.24; H, 5.36%. Calcd for $C_{16}H_{16}O_6$: C, 63.15; H, 5.30%.

2-Hydroxy-3',4,4',5'-tetramethoxybenzophenone (If): A mixture of Ig (6 g), dimethyl sulfate (3 ml), potassium carbonate (5 g), and acetone (50 ml) was heated under reflux for 30 min. After the removal of the acetone, the resulting mixture was extracted with benzene. The benzene was evaporated *in vacuo*, and the resulting liquid was allowed to crystallize from methanol to give If (3.6 g, 57%); mp 106—107 °C, ν_{max}: 1630 cm^{-1} (C=O), λ_{max} (ε): 293 (16300) and 328 nm (15200), δ: 3.81 (s, OCH_3), 3.84 (s, $2\times OCH_3$), 3.88 (s, OCH_3), 6.25—6.55 (m, $H_{(3)}$ and $H_{(5)}$), 6.83 (s, $H_{(2')}$ and $H_{(6')}$), 7.50 (d, J=8.5 Hz, $H_{(6)}$) and 12.50 (s, OH). Found: C, 64.11; H, 5.77%. Calcd for $C_{17}H_{18}O_6$: C, 64.14; H, 5.74%.

2-Hydroxy-4'-acetoxy-3',4,5'-trimethoxybenzophenone (Ih): A mixture of Ig (1.30 g), acetic anhydride (480 mg), and pyridine (8 ml) was kept at room temperature for 24 h. The reaction mixture was then poured into water, and the resulting precipitates were collected and recrystallized from ethanol to give Ih (1.18 g, 80%); mp 124—125 °C, ν_{max}: 1630 (C=O) and 1770 cm^{-1} (OAc), λ_{max} (ε): 294 (13500) and 325 nm (11100), δ: 2.37 (s, OAc), 3.88 (s, $3\times OCH_3$), 6.3—6.8 (m, $H_{(3)}$ and $H_{(5)}$), 6.93 (s, $H_{(2')}$ and $H_{(6')}$), 7.65 (d, J=8.5 Hz, $H_{(6)}$) and 12.40 (s, OH). Found: C, 62.24; H, 5.51%. Calcd for $C_{18}H_{18}O_7$: C, 62.42; H, 5.24%.

2-Hydroxy-3',4,4',6-tetramethoxybenzophenone (Ii): A mixture of 3,5-dimethoxyphenol (4 g), 3,4-dimethoxybenzoyl chloride (5.5 g), aluminium chloride (12 g), and ether (50 ml) was stirred at room temperature for 48 h. By working up in a similar manner to the above, Ii (4.0 g, 49%) was obtained; mp 134 °C, ν_{max}: 1625 cm^{-1} (C=O), λ_{max} (ε): 233 (21900), 286 (11900) and 313 nm (12600), δ: 3.55 (s, OCH_3), 3.86 (s, OCH_3), 3.90 (s, OCH_3), 3.95 (s, OCH_3), 5.99 (d, 1H) and 6.19 (d, 1H) (AB system, J_{AB}=2.0 Hz), 6.19 (d, J=8.5 Hz, $H_{(5')}$), 6.75—6.90 (m, $H_{(2')}$ and $H_{(6')}$), and 11.60 (s, OH). Found: C, 64.22; H, 5.75%. Calcd for $C_{17}H_{18}O_6$: C, 64.14; H, 5.70%.

Oxidation of 2-Hydroxybenzophenones (Ia—Ii) with Manganese (III) Acetate. A mixture of 2-hydroxybenzophenone (1 mmol), manganese(III) acetate dihydrate[13] (4 or 5 mmol), and acetic acid (30 ml) was heated under reflux for the period of time shown in the Table. After the removal of the acetic acid *in vacuo*, the resulting solid was triturated with water and extracted with chloroform. The chloroform was removed *in vacuo* and the resulting products were purified on TLC (Wakogel B 10) and by recrystallization.

Ia gave 3-methoxy-9-xanthenone (IIa); mp 125—126 °C (EtOH) (lit,[10] mp 128—129 °C), 49%, ν_{max}: 1660 cm^{-1} (C=O), λ_{max} (ε): 239 (44100), 270 (12000) and 303 nm (17300), δ: 3.85 (s, OCH_3), 6.7—7.0 (m, 2H), 7.1—7.85 (m, 3H) and 8.1—8.45 (m, 2H).

Ib yielded 2,6-dimethoxy-9-xanthenone (IIb); mp 162 °C (EtOH) (lit,[11] mp 163.5—164.5 °C), 24%, ν_{max}: 1650 cm^{-1} (C=O), λ_{max} (ε): 243 (36500) and 312 nm (15700), δ: 3.88 (s, $2\times OCH_3$), 6.7—7.0 (m, $H_{(5)}$ and $H_{(7)}$), 7.0—7.5 (m, $H_{(3)}$ and $H_{(4)}$), 7.63 (d, J=2 Hz, $H_{(1)}$) and 8.20 (d, J=8 Hz, $H_{(8)}$).

Ic gave 3,6-dimethoxy-9-xanthenone (IIc) [mp 185 °C (EtOH) (lit,[1] mp 182—183 °C), 45%) and IV (mp 157 °C (benzene), 9%, ν_{max}: 1650, 1698 and 1758 cm^{-1}, λ_{max} (ε): 229 (24500), 267 (17400) and 290 nm (9670), δ: 3,75 (s, OCH_3), 3.82 (s, OCH_3), 5.50 (d, J=2 Hz, 1H), 6.16 (dd, J=10, 2 Hz, 1H), 6.40 (d, J=2 Hz, 1H), 6.64 (dd, J=8.2 Hz, 1H), 6.80 (d, J=10 Hz, 1H) and 7.81 (d, J=8 Hz, 1H). *m/e*: 288 (M^+), 150, 122 and 107. Found: C, 62.45; H, 4.21%. Calcd for $C_{15}H_{12}O_6$: C, 62.50; H, 4.20%].

Id yielded 2,3,6-trimethoxy-9-xanthenone (IId); mp 216—217 °C (EtOH) (lit,[1] mp 216—217 °C), 40%.

Ie gave IIb; mp 162 °C, 65%.

If yielded 2,3,4,6-tetramethoxy-9-xanthenone (IIf); mp 130 °C (EtOH), 48%, ν_{max}: 1655 cm^{-1} (C=O), λ_{max} (ε): 246 (38600), 272 (14000) and 313 (21100), δ: 3.92 (s, $2\times OCH_3$), 4.00 (s, OCH_3), 4.02 (s, OCH_3), 6.75—7.05 (m, $H_{(5)}$ and $H_{(7)}$), 7.46 (s, $H_{(1)}$) and 8.14 (d, J=8.5 Hz, $H_{(8)}$). Found: C, 64.35; H, 5.02%. Calcd for $C_{17}H_{16}O_6$: C, 64.55; H, 5.10%.

Ig yielded 2,6-dimethoxy-*p*-benzoquinone (V); mp 255 °C (EtOH) lit,[14] mp 255—256 °C), 12%, ν_{max}: 1660 and 1720 cm^{-1}, δ: 3.82 (s, $2\times OCH_3$) and 5.87 (s, $H_{(3)}$ and $H_{(5)}$).

Ih gave 3-acetoxy-2,4,6-trimethoxy-9-xanthenone (IIh); mp 166—167 °C (EtOH), 31%, ν_{max}: 1660 (C=O) and 1772 cm^{-1} (OAc), λ_{max} (ε): 247 (34000), 274 (12900) and 312 nm (16100), δ: 2.43 (s, OAc), 3.93 (s, $2\times OCH_3$), 4.08 (s, OCH_3), 6.9—7.1 (m, $H_{(5)}$ and $H_{(7)}$), 7.57 (s, $H_{(1)}$) 8.22 (d, J=8.5 Hz, $H_{(8)}$). Found: C, 62.74; H, 4.59%. Calcd for $C_{18}H_{16}O_7$: C, 62.79; H, 4.68%.

Ii yielded 1,3,6,7-tetramethoxy-9-xanthenone (IIi) (mp 202 °C (benzene) (lit,[12] mp 185—190 °C), 5%, ν_{max}: 1650 cm^{-1} (C=O), λ_{max} (ε): 256 (33100), 270 (s) (7100), 305 (11300) and 351 nm (9000), δ: 3.86 (s, OCH_3), 3.94 (s, $3\times OCH_3$), 6.30 (d, 1H) and 6.42 (d, 1H) (AB system, J=2 Hz, $H_{(2)}$ and $H_{(4)}$), 6.76 (s, $H_{(5)}$), and 7.62 (s, $H_{(8)}$)], and 2,6-dimethoxy-3-(3,4-dimethoxybenzoyl)-*p*-benzoquinone (VIi) [mp 161 °C (benzene), 5%, ν_{max}: 1655, 1688 and 1718 cm^{-1}, λ_{max} (ε): 236 (17600) and 289 nm (16200), δ: 3.85 (s, $2\times OCH_3$), 3.95 (s, $2\times OCH_3$), 5.90 (s, $H_{(5)}$), 6.85 (d, J=8.5Hz, $H_{(5')}$), 7.38 (dd, J=8.5, 2 Hz, $H_{(6')}$) and 7.55 (d, J=2 Hz, $H_{(2')}$). Found: C, 61.15; H, 4.89%. Calcd for $C_{17}H_{16}O_7$: C, 61.44; H, 4.85%].

Ij gave 2,5-dihydroxy-3',4,4'-trimethoxybenzophenone (Ik); mp 208—209 °C (EtOH), 9%, ν_{max}: 1630 cm^{-1} (C=O), λ_{max} (ε): 239 (14800), 253 (14600), 287 (10600), and 372 nm (9850), δ: 3.95 (s, OCH_3), 3.97 (s, $2\times OCH_3$), 5.24 (s, OH), 6.58 (s, $H_{(3)}$), 6.95 (d, J=8.5 Hz, $H_{(5')}$), 7.23 (s, $H_{(6)}$), 7.2—7.45 (m, $H_{(2')}$ and $H_{(6')}$) and 12.30 (s, OH). Found: C, C, 63.06; H, 5.30%. Calcd for $C_{16}H_{16}O_6$: C, 63.15; H, 5.30%.

Oxidation of 2-Hydroxybenzophenones (Ia, Ic, Ie, If, and Ii) with Lead Tetraacetate. A mixture of a 2-hydroxybenzophenone (5 mmol), lead tetraacetate[15] (15 mmol), and acetic acid (30 ml) was heated under reflux for the period of time shown in the Table. After the removal of the acetic acid *in vacuo*, the resulting products were triturated with 2M-hydrochloric acid and then extracted with chloroform. The chloroform solution was washed with aqueous sodium hydrogencarbonate, and the chloroform was evaporated again *in vacuo* to give crude products which were purified on TLC (Wakogel B 10) and by recrystallization. Ia gave IIa; mp 125—126 °C (EtOH), 16%. Ic yielded IIc; mp 185 °C (EtOH), 12%. Ie gave IIb (mp 162 °C (EtOH), 11%), 2,6-dimethoxy-1-methyl-9-xanthenone (IIe) [mp 173 °C (EtOH), 3%, ν_{max}: 1655 cm^{-1} (C=O), λ_{max} (ε): 244 (34300), 273 (s) (12200), 309 (13300), and 355 nm (4600), Found: C, 70.92; H, 5.25%. Calcd for $C_{16}H_{14}O_4$: C, 71.10; H, 5.22%], and 1-acetoxymethyl-2,6-dimethoxy-9-xanthenone (IIIe) [mp 196 °C (benzene–light petroleum), 6%, ν_{max}: 1660 (C=O) and 1745 cm^{-1} (OAc), λ_{max} (ε): 242 (38200), 271 (s) (8900), 314 (14200) and 359 nm (5700), δ: 2.05 (s, OAc), 3.87 (s, $2\times OCH_3$), 5.85 (s, 2H, $-CH_2-$), 6.75 (d, J=2 Hz, $H_{(5)}$), 6.85 (dd, J=8.5, 2 Hz, $H_{(7)}$), 7.30 (d, 1H) and 7.43 (d, 1H) (AB system, J_{AB}=

8 Hz, $H_{(3)}$ and $H_{(4)}$), and 8.12 (d, J=8.5 Hz, $H_{(8)}$). Found: C, 65.88; H, 4.93%. Calcd for $C_{18}H_{16}O_6$: C, 65.85; H, 5.19%]. If gave IIf [mp 130 °C (EtOH), 7%] and 1-acetoxymethyl-2,3,4,6-tetramethoxy-9-xanthenone (IIIf) [mp 120—121 °C (benzene), 6%, ν_{max}: 1660 (C=O) and 1745 cm^{-1} (OAc), λ_{max} (ε): 248 (36500), 275 (10200), and 311 nm (17500), δ: 2.05 (s, OAc), 3.86 (s, 2×OCH_3), 4.03 (s, OCH_3), 4.06 (s, OCH_3), 5.72 (s, $-CH_2-$), 6.80 (d, J=2 Hz, $H_{(5)}$), 6.80 (dd, J=8.5, 2 Hz, $H_{(7)}$) and 8.00 (d, J=8.5 Hz, $H_{(8)}$). Found: C, 61.58; H, 5.21%. Calcd for $C_{20}H_{20}O_8$: C, 61.85; H, 5.19%]. Ii yielded IIi (mp 202 °C (benzene), 11%), VIi (mp 161 °C (benzene), 7%), and 2,6-dimethoxy-3-(3,4-dimethoxybenzoyl)-5-methyl-*p*-benzoquinone (VIi') [mp 118—120 °C (benzene), 7% ν_{max}: 1650 and 1690 cm^{-1}, λ_{max} (ε): 236 (17800) and 288 nm (19000), δ: 1.95 (s, CH_3), 3.82 (s, OCH_3), 3.94 (s, 2×OCH_3), 4.01 (s, OCH_3), 6.86 (d, J=8.5 Hz, $H_{(5')}$), 7.35 (dd, J=8.5, 2 Hz, $H_{(6')}$) and 7.65 (d, J=2 Hz, $H_{(2')}$). Found: C, 62.44; H, 5.34%. Calcd for $C_{18}H_{18}O_7$: C, 62.42; H, 5.24%].

References

1) K. Kurosawa, Y. Sasaki, and M. Ikeda, *Bull. Chem. Soc. Jpn.*, **46**, 1498 (1973).
2) P. K. Grover, G. D. Shah, and R. C. Shah, *J. Chem. Soc.*, **1955**, 3982.
3) K. K. Chexal, J. S. E. Holker, T. J. Simpson, and K. Young, *J. Chem. Soc., Perkin Trans. 1*, **1975**, 543.
4) R. Criegee, "Oxidation in Organic Chemistry," Part A, ed by K. S. Wiberg, Academic Press, New York and London (1965), p. 277.
5) G. H. Stout and W. J. Balkenhol, *Tetrahedron*, **25**, 1949 (1969).
6) J. W. A. Findlay, P. Gupta, and J. R. Lewis, *J. Chem. Soc., C*, **1969**, 2761.
7) J. R. Lewis and B. H. Warrington *J. Chem. Soc.*, **1964**, 5074.
8) J. W. A. Findlay, P. Gupta, and J. R. Lewis, *J. Chem. Soc., D*, **1969**, 207.
9) B. J. Donnelly, D. M. X. Donnelly, and A. M. O'Sullivan, *Tetrahedron*, **24**, 2617 (1968).
10) *Chem. Abstr.*, **63**, 1484b (1965).
11) P. D. McDonald and G. A. Hamilton, *J. Am. Chem. Soc.*, **95**, 7752 (1973).
12) H. D. Locksley and J. G. Murray, *Phytochemistry*, **10**, 3179 (1971).
13) P. J. Andrulis, Jr., M. J. S. Dewar, R. Dietz, and R. L. Hunt, *J. Am. Chem. Soc.*, **88**, 5473 (1966).
14) F. Wessely and J. Koltan, *Monatsh. Chem.*, **84**, 291 (1953).
15) L. F. Audrieth, "Inorganic Syntheses," Vol. 3, McGraw-Hill, New York (1950), p. 47.

The Reactions of Sodium 1-Benzyl-1,4-dihydronicotinamide-4-sulfinate with Halogen Compounds

Hiroo INOUE, Nobuaki INOGUCHI, and Eiji IMOTO

Department of Applied Chemistry, College of Engineering, University of Osaka Prefecture, Sakai, Osaka 591

(Received June 18, 1976)

Sodium 1-benzyl-1,4-dihydronicotinamide-4-sulfinate (BNA-SO_2Na) reacts with various halogen compounds, YZCHBr, through the cleavage of the carbon-sulfur bond to give sulfones, $(YZCH)_2SO_2$, in Y=Ph or PhCH=CH and Z=H; *trans*-stilbene in Y=Ph and Z=CH(Br)Ph or $CH(OCH_3)Ph$; and the reduction products, $YZCH_2$ and $(YZCH)_2$, in Y=Ph, Z=Br, and Y=H, Z=PhCO. The BNA-SO_2Na is converted to 1-benzylnicotinamide bromide, while sulfur dioxide or sulfite ions are formed.

Sodium 1-benzyl-1,4-dihydronicotinamide-4-sulfinate (BNA-SO_2Na) is a bright-yellow intermediate isolated in the course of the reduction of 1-benzylnicotinamide chloride (BNA^+Cl^-) with sodium dithionite to 1-benzyl-1,4-dihydronicotinamide (BNAH).[1] The BNA-SO_2Na was characterized by NMR spectroscopy as an addition compound with the sulfinate group at the 4-position of BNAH.[2]

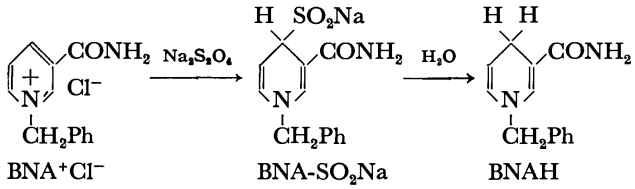

The reaction of BNA-SO_2Na with organic compounds has not yet been reported except for the reduction of pyridinium salts to dihydropyridines.[1] On the other hand, the reducing agents with a sulfinate group, such as sodium dithionite,[3] sodium hydroxymethanesulfinate,[4] and thiourea dioxide,[5] are well known. In view of the reducing action of these agents and BNAH, BNA-SO_2Na might also serve as a reducing agent with the cleavage of the carbon-sulfur bond of BNA-SO_2Na. Our interest in the reactivity of BNA-SO_2Na has led us to examine the reactions of BNA-SO_2Na with organic halogen compounds, of which the carbon-halogen bond reductions with metals[6] and metal complexes[7] and by electrolysis[8] have been studied extensively. In this paper, we wish to report on the reactions of BNA-SO_2Na with halogen compounds which have a phenyl, cinnamyl, or carbonyl group at the same carbon position as that of the halogen atom.

Results and Discussion

Formation of Sulfones. As Table 1 shows, the reaction of BNA-SO_2Na with benzyl bromide (**1**) in methanol or *N,N*-dimethylformamide (DMF) at 60 °C afforded dibenzyl sulfone, together with BNA^+Br^-. This reaction did not occur at 25 °C. The reduction products, such as toluene and 1,2-diphenylethane, were not obtained at all. Thus, the carbon-sulfur bond of BNA-SO_2Na was cleaved by the action of **1** to form BNA^+Br^-. The production of dibenzyl sulfone with BNA^+Br^- in equimolar amounts indicates that the Na^+ or BNA^+ salt of phenylmethanesulfinic acid (**2**) is formed as an intermediate, and that it then reacts with **1** to give dibenzyl sulfone:

$$PhCH_2Br + BNA\text{-}SO_2Na \longrightarrow$$
1

$$PhCH_2SO_2^-Na^+ \text{ (or } BNA^+) + BNA^+ \text{ (or } Na^+)Br^-$$
2

$$\xrightarrow{1} PhCH_2SO_2CH_2Ph + BNA^+Br^- + NaBr$$

A substitution by the sulfinate group was found to take place in the reaction of BNA-SO_2Na with 1,3-dibromo-1-phenylpropane (**3**). As Table 1 shows, a cyclic sulfinate (**4**) was produced by ring-closure in amounts corresponding approximately to those of BNA^+Br^-:

$$PhCHCH_2CH_2Br + BNA\text{-}SO_2Na \longrightarrow$$
3

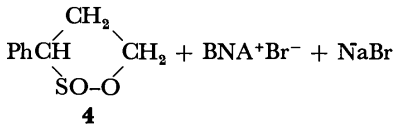

+ BNA^+Br^- + NaBr

4

Cinnamyl bromide (**5**) also reacted with BNA-SO_2Na in 80 vol% aqueous acetone or DMF, even at 25 °C, to give dicinnamyl sulfone in a high yield, together with BNA^+Br^-, as Table 1 shows.

TABLE 1. REACTIONS OF BNA-SO_2Na WITH **1**, **3**, AND **5**[a]

Halogen compd	Reaction conditions	$-SO_2-$ or $-SO-O-$ %[b]	BNA^+Br^- %[b]
1	MeOH, 60 °C, 6 h	67	62
1	DMF, 60 °C, 3 h	69	—[c]
3	EtOH, 60 °C, 3 h	55	64
3	DMF, 60 °C, 3 h	64	71
5	$(CH_3)_2CO$-H_2O (4:1) 25 °C, 3 h	83	86
5	DMF, 25 °C, 3 h	99	96

a) BNA-SO_2Na; 5—5.1 mmol. Solvent; 50 cm^3. BNA-SO_2Na/halogen compd molar ratio; 1. b) Based on the halogen compound (2 × product or BNA^+Br^- (mol)/halogen compd (mol) × 100). The products obtained from **1**, **3**, and **5** are dibenzyl sulfone, **4**, and dicinnamyl sulfone respectively. c) Identified, but not quantified.

Formation of Olefins. When a solution of *dl* or *meso*-1,2-dibromo-1,2-diphenylethane (*dl* or *meso*-**6**) in ethanol containing BNA-SO_2Na was heated at 60 °C, the *dl* and *meso*-**6** were converted to *trans*-stilbene in high yields, as Table 2 shows. On the other hand, *cis*-stilbene was not obtained at all. The BNA-SO_2Na was converted to BNA^+Br^- with the generation of sulfur dioxide. The addition of water to the reaction system

(80 vol% aqueous ethanol) did not affect the yield of *trans*-stilbene. When DMF was used as the solvent, the reaction occurred rapidly, even at 20 °C. Furthermore, the isomerization of *cis*-stilbene to *trans*-stilbene was not observed under the reaction conditions.

threo-1-Bromo-2-methoxy-1,2-diphenylethane (*threo*-**7**) reacted also with BNA-SO_2Na in ethanol and DMF at 60 °C to give, selectively, *trans*-stilbene, although the reaction took place slowly (Table 2). Thus, BNA-SO_2Na underwent the debromination of the *dl* and *meso*-**6** and *threo*-**7**, resulting selectively, in *trans*-stilbene, with BNA$^+$Br$^-$ and sulfur dioxide also formed.

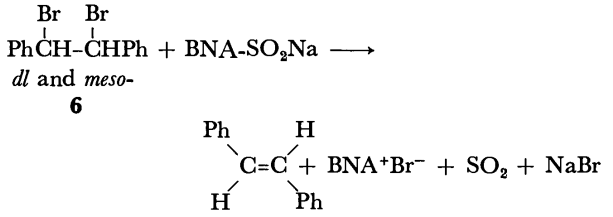

Table 2. Reactions of BNA–SO_2Na with *dl* and *meso*-**6** and *threo*-**7**[a]

6 or **7**	Molar ratio[b]	Solvent	Product, % PhCH=CHPh	Product, % BNA$^+$Br$^-$	Product, % SO_2
dl[c]	1	EtOH	73[e]	80	57
dl	1	DMF	76	78	—[f]
meso	2	EtOH	94	—[f]	50
meso	2	DMF	99	—[f]	—[f]
threo[d]	2	EtOH	48[g]	—	—
threo	1	DMF	39[g]	—	—

a) **6** or **7**; 3 mmol. Solvent; 50 cm^3. Reaction time; 2 h. Temperature; 60 °C. The yields were calculated by means of product (mol)/**6** or **7** (mol) × 100. b) BNA-SO_2Na/**6** or **7**. c) In the case of the molar ratio of 2, *trans*-stilbene was obtained in a 100% yield. d) Reaction time; 3 h. e) Recovery % of *dl*-**6**; 27%. f) Identified, but not quantified. g) Recovery % of *threo*-**7**; 40% (EtOH) and 55% (DMF).

In order to investigate whether or not the existence of the phenyl group in *vic*-dibromides is required for debromination, the reactions of BNA-SO_2Na with *trans*-1,2-dibromocyclohexane (**8**) and *trans*-1-phenyl-1,2-dibromocyclohexane (**9**) in ethanol at 60 °C were carried out. The **8** was recovered unchanged after a reaction of 6 h, but the **9** was converted to 1-phenylcyclohexene in a 77% yield after 2 h. BNA$^+$Br$^-$ was obtained in a 86% yield, together with 90% of the sulfur dioxide. Thus, the phenyl group attached to the carbon atom with the bromine atom favors the debromination of *vic*-dibromides by BNA-SO_2Na.

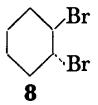

8

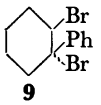

9

The debromination of *dl* and *meso*-**6** by many dehalogenating agents has been studied extensively.[9] Among these reagents, the benzenesulfinate ion has been known to undergo the debromination of *dl*-**6** to give *cis*-stilbene as the major product.[9] Thus, the reactivity of BNA-SO_2Na to *dl*-**6** would differ essentially from that of the benzenesulfinate ion.

Reduction. Benzylidene dibromide (**10**) was converted to *dl*-**6** and *trans*-stilbene by the action of BNA-SO_2Na in water-free DMF at 20 °C, as Table 3 shows. This reaction was accompanied by the conversion of BNA-SO_2Na to BNA$^+$Br$^-$ and sulfur dioxide. When the molar ratio of BNA-SO_2Na to **10** was 2, *trans*-stilbene was obtained as the only product. The *trans*-stilbene must be produced by the debromination of *dl*-**6** by BNA-SO_2Na, as has been described above. In 80 vol% aqueous methanol, however, dibenzyl sulfone was obtained without any formation of *dl*-**6** or *trans*-stilbene. Thus, it is possible that the formation of **1** is the intervening process in the conversion of **10** to dibenzyl sulfone and that, in the process, BNA-SO_2Na undergoes the two-electron reduction of **10** to give **1**. In an aprotic solvent, the PhCHBr produced by the two-electron reduction could react with **10** to give *dl*-**6**.

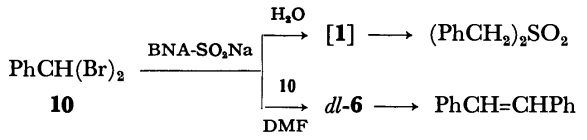

Table 3. Reaction of BNA-SO_2Na with **10**[a]

Reaction conditions[b]	Product, %[c]
DMF, 20 °C, 3 h (1)	*dl*-**6** (26); PhCH=CHPh (36)
DMF, 20 °C, 3 h (2)	PhCH=CHPh (69)
MeOH–H_2O (80%), 60 °C, 3 h (2)	$(PhCH_2)_2SO_2$ (36)

a) **10**; 5—6 mmol. Solvent; 50 cm^3. b) The parentheses represent the molar ratio of BNA-SO_2Na to **10**. c) Based on **10** (2 × product (mol)/**10** (mol) × 100. BNA$^+$Br$^-$ and sulfur dioxide were identified, but not quantified.

α-Bromoacetophenone (**11**) was reduced with BNA-SO_2Na in 80 vol% aqueous methanol at 30 °C to give acetophenone in a good yield, as Table 4 shows. In the reaction, BNA$^+$Br$^-$ and a sulfite ion were produced from BNA-SO_2Na in amounts corresponding to those of acetophenone. No further reduction of acetophenone with BNA-SO_2Na occurred at all. As BNA-SO_2Na is known to be converted to BNAH and a sulfite ion by the action of water, there is a possibility that BNAH acts as a reducing agent. Therefore, the reduction of **11** with BNAH was carried out under similar conditions. Consequently, it was found that the rate of the reduction by BNAH is much slower than that by BNA-SO_2Na: the reduction of **11** with BNAH in 80 vol% aqueous methanol at 25 °C gave acetophenone in a 16% yield after a reaction of 24 h. Furthermore, the reaction of **11** with BNA-SO_2Na was carried out using water-free DMF as the solvent. As Table 4 shows, 1,2-dibenzoylethane was obtained as the reduction product in a high yield, without any formation of 2,4-diphenylfuran, which is produced in the dehalogenation of **11** with Cr(II) or Cu(I) salt[10] in DMF or DMSO. BNA-SO_2Na was converted to BNA$^+$Br$^-$ with the generation of sulfur dioxide. The selective formation of acetophenone or 1,2-dibenzoylethane suggests that the reaction of **11** with BNA-SO_2Na proceeds *via* the formation of **12**, which reacts as a carbanion, PhCO-

Table 4. Reactions of BNA-SO_2Na with α-bromo carbonyl compounds[a]

YZCHBr Y	YZCHBr Z	Reaction conditions[b]	Reduction product, %	BNA^+Br^- %	SO_3^{2-}, SO_2 %
H	PhCO	M-W, 30 °C, 6 h	$PhCOCH_3$ (67)	67	61
H	PhCO	DMF, 30 °C, 3 h	$(PhCOCH_2)_2$ (80)	86	—[c]
Ph	PhCO	M-W, 20 °C, 3 h	$PhCOCH_2Ph$ (82)	89	—[c]
Ph	EtOCO	M-W, 25 °C, 6 h	$PhCH_2CO_2Et$ (82)	88	84
EtOCO	EtOCO	M-W, 20 °C, 6 h	$CH_2(COOEt)_2$ (81)	79	75

a) YZCHBr; 3—5 mmol. Solvent; 50 cm^3. BNA-SO_2Na/YZCHBr molar ratio=1. b) M-W represents 80 vol% MeOH-H_2O. c) Identified, but not quantified.

CH_2^-, followed by a reaction with water to give acetophenone or with **11** in DMF to give 1,2-dibenzoylethane.

$$PhCOCH_2Br \xrightarrow{BNA\text{-}SO_2Na} \underset{\mathbf{11}}{}$$

$$[PhCOCH_2\text{-}SO_2Na] \quad \mathbf{12} \quad \begin{cases} \xrightarrow{H_2O} PhCOCH_3 \\ \xrightarrow[DMF]{\mathbf{11}} (PhCOCH_2)_2 \end{cases}$$

α-Bromodeoxybenzoin, ethyl α-bromophenylacetate, and diethyl α-bromomalonate were all reduced with BNA-SO_2Na in 80 vol% aqueous methanol at 20 °C to the corresponding parent carbonyl compounds in high yields. These reactions were accompanied by the formation of equimolar amounts of BNA^+Br^- and a sulfite ion. Thus, the carbonyl group attached to the carbon atom with a bromine atom favors the reductive debromination by BNA-SO_2Na.

Experimental

Materials. All the halogen compounds, except for **1**, were prepared according to the methods described in the literature.[11] The BNA-SO_2Na was prepared from BNA^+Cl^- and sodium dithionite (85—90% purity) according to the method reported by Biellmann and Callot,[1] and was purified in the following manner: BNA-SO_2Na was dissolved in a 1 M sodium hydroxide solution at 40 °C, and the solution was allowed to cool to 0 °C to give yellow crystals. After the mixture had then been filtered under nitrogen, the crystals were washed with cold water and dried under a reduced pressure of 1 Torr for 4—6 h. All the procedures were carried out in an atmosphere of nitrogen. The purified BNA-SO_2Na was immediately submitted to the reactions with halogen compounds. The UV and NMR spectra (1 M sodium hydroxide solution) of the BNA-SO_2Na used here were identical with those reported by Caughey and Schellenberg.[2]

*Reactions of BNA-SO_2Na. Benzyl Bromide (**1**)*: To a solution of 5.05 mmol of **1** in 50 cm^3 of methanol, we added 5.13 mmol of BNA-SO_2Na. The suspension was stirred under nitrogen at 60 °C for 6 h. After the methanol had then been removed *in vacuo*, the residue was suspended in 150 cm^3 of benzene, and heated under reflux, and the mixture was filtered. The benzene solution was concentrated to 10—15 cm^3. The concentrate was submitted to chromatography on silica gel. Elution with benzene gave 0.42 g (67%) of dibenzyl sulfone; mp 149—150 °C (lit, [12] 149.5—150 °C). Its IR spectrum was identical with that of the authentic specimen. IR (KBr): 1110 and 1300 cm^{-1} (SO_2). The precipitate was then added to 50 cm^3 of methanol, and heated under reflux, and the mixture was filtered. After methanol removal *in vacuo*, the residue was again added to 50 cm^3 of acetone containing a small amount of ethanol and refluxed. The insoluble material was separated from the solution by filtration. The removal of the solvent *in vacuo* gave 0.45 g (62%) of BNA^+Br^-; mp 207—209 °C. Its melting point and IR spectrum were identical with those of the authentic specimen prepared from **1** and nicotinamide. Similar procedures were used in the experiment employing DMF as a solvent.

*1,3-Dibromo-1-phenylpropane (**3**)*: The reaction of BNA-SO_2Na (5.05 mmol) with **3** (5.11 mmol) was carried out, employing ethanol (50 cm^3) as the solvent, under conditions similar to those used in the case of **1**. The reaction products were isolated in a manner similar to that described above to yield 0.5 g (55%) of **4** and 0.93 g (64%) of BNA^+Br^-. The **4** exhibited NMR (CCl_4) signals at δ=2.6 (m, 2H, CH_2), 4.3 (m, 2H, CH_2O), 4.9 (m, 1H, CH), and 7.3 ppm (s, 5H, aromatic protons), and an IR (KBr) peak at 1120 cm^{-1} (SO_2). MS, *m/e*, 182 (parent peak).

Found: C, 59.02; H, 5.66%. Calcd for $C_9H_{10}SO_2$: C 59.33; H, 5.53%.

*Cinnamyl Bromide (**5**)*: A solution of 5.03 mmol of **5** and 5.09 mmol of BNA-SO_2Na in 50 cm^3 of DMF was stirred under nitrogen at 25 °C for 3 h. The reaction mixture was then poured into 300 cm^3 of water to give 0.74 g (99%) of dicinnamyl sulfone; mp 199—200 °C: NMR (CCl_4) δ=3.72 (d, CH_2SO_2) (total 4H), 6.40 (m, =CH) (total 2H), and 7.14 ppm (s, C_6H_5CH=) (total 12H); IR (KBr) 970 (HC=CH) and 1050 and 1180 cm^{-1} (SO_2); MS, *m/e*; 64 (SO_2), 117 (C_6H_5-CH=$CHCH_2$), and 234 [$(C_6H_5CH$=$CHCH_2)_2$].

Found: C, 72.53; H, 6.17%. Calcd for $C_{18}H_{18}SO_2$: C, 72.46; H, 6.08%.

After the water and DMF had been removed *in vacuo*, the residue was extracted with methanol to yield 0.71 g (96%) of BNA^+Br^- in a manner similar to that described above.

vic-*Dibromides (*dl *and* meso-***6***, **8**, *and* **9**) *and* threo-**7**: A typical experiment was as follows: to a solution of 3 mmol of *dl*-**6** in 50 cm^3 of ethanol, we added 3.04 mmol of BNA-SO_2Na. The mixture was stirred at 60 °C for 2 h while nitrogen was being bubbled through the solution. The sulfur dioxide thus evolved was absorbed by 50 cm^3 of a 1 M sodium hydroxide solution. To the alkaline solution we added 20 cm^3 of a 30% hydrogen peroxide solution, and then an excess of a barium chloride solution. The precipitate of barium sulfate was obtained by filtration. Yield: 0.4 g (57%). After the ethanol had been removed *in vacuo*, the residue was extracted with ether. The material, which was insoluble in ether, was then added to methanol. BNA^+Br^- was isolated from the methanol solution by procedures similar to those used in the case of **1**. Yield: 0.71 g (80%). The crude product obtained by the evaporation of the ethereal phase was chromatographed on silica gel to yield *trans*-stilbene (0.394 g, 73%) (mp 118—120 °C), and *dl*-**6** (0.28 g, 27% recovery). Similar procedures were used for

the reactions of BNA-SO_2Na with *meso*-**6**, *threo*-**7**, **8**, and **9**.

*Benzylidene Dibromide (**10**).* *DMF Solvent*: To a solution of 6.06 mmol of **10** in 50 cm^3 of DMF, we added 6.07 mmol of BNA-SO_2Na. The solution was stirred under nitrogen for 3 h at 20 °C, poured into 300 cm^3 of water, and extracted with ether. After the removal of the water and DMF from the aqueous layer, BNA^+Br^- was isolated in a 75% yield by procedures similar to those used in the case of **1**. The ethereal extract was dried on magnesium sulfate, and the ether was removed. The residue was submitted to chromatography on alumina. Elution with hexane and benzene gave 0.195 g (36%) of *trans*-stilbene and 0.26 g (26%) of *dl*-1,2-dibromo-1,2-diphenylethane respectively.

80 Vol% Aqueous Methanol: To a solution of 5.04 mmol of **10** in 50 cm^3 of 80 vol% aqueous methanol, we added 10.1 mmol of BNA-SO_2Na. The solution was then stirred under nitrogen for 3 h at 60 °C. After methanol removal *in vacuo*, 50 cm^3 of water was added to the concentrate. The resulting solution, containing the precipitate, was extracted with ether. The ethereal extract was dried over magnesium sulfate. The subsequent removal of the ether gave 0.22 g (36%) of dibenzyl sulfone.

α-Halo Ketones and Esters: A typical experiment was as follows: A solution of a mixture of 3.02 mmol of **11** and 3.01 mmol of BNA-SO_2Na in 50 cm^3 of 80 vol% aqueous methanol was stirred under nitrogen at 30 °C for 6 h. Then water (200 cm^3) was added, and the resulting solution was extracted with benzene. The benzene phase was dried over magnesium sulfate, and the benzene was then removed. The residue was chromatographed on silica gel to yield 0.244 g (67%) of acetophenone. The aqueous phase, containing a sulfite ion, was acidified by means of 30 vol% hydrobromic acid to bring about the evolution of sulfur dioxide. The sulfur dioxide thus evolved was absorbed by a 1 M sodium hydroxide solution and determined in a manner similar to that described above. Yield of sulfite ions: 61%. The crude product obtained by solvent evaporation was determined by the method described above to contain 0.59 g (67%) of BNA^+Br^-.

Similar procedures were used for the reactions of BNA-SO_2Na with α-bromodeoxybenzoin, ethyl α-bromophenylacetate, and ethyl α-bromomalonate.

The reaction of BNA-SO_2Na (5.05 mmol) with **11** (5 mmol) in DMF (50 cm^3) at 30 °C for 3 h yielded 0.48 g (80%) of 1,2-dibenzoylethane (mp 143—144 °C (lit,[13] 145 °C)), and 0.62 g (86%) of BNA^+Br^-. 1,2-Dibenzoylethane exhibited an IR (KBr) peak at 1675 cm^{-1} (C=O). (Found: C, 80.88; H, 5.88%. Calcd for $C_{16}H_{14}O_2$: C, 80.64; H, 5.92%).

References

1) J. F. Biellmann and H. J. Callot, *Bull. Soc. Chim. Fr.*, **1968**, 1154.

2) W. S. Caughey and K. A. Schellenberg, *J. Org. Chem.*, **31**, 1978 (1966).

3) F. A. Cotton and G. Wilkinson, "Advanced Inorganic Chemistry," 2nd ed, Interscience Publishers, New York (1967), p. 551.

4) R. Kerber and W. Gestrich, *Chem. Ber.*, **106**, 798 (1973).

5) K. Nakagawa and K. Minami, *Tetrahedron Lett.*, **1972**, 343; J. E. Herz and L. A. Márquez, *J. Chem. Soc. Perkin Trans. 1*, **1973**, 2633.

6) S. J. Cristol and R. W. Gleason, *J. Org. Chem.*, **34**, 1762 (1969); D. B. Lelie and S. Maclean, *ibid.*, **34**, 1123 (1969).

7) R. E. Erickson and R. K. Holmquist, *Tetrahedron Lett.*, **1969**, 4209; J. K. Kochi and J. W. Powers, *J. Am. Chem. Soc.*, **92**, 137 (1970).

8) H. O. House, "Modern Synthetic Reactions," W. A. Benjamin, California (1972), p. 221; J. Casanova and L. Eberson, "Electrochemistry of the Carbon-Halogen Bond," S. Patai, ed, Wiley, New York (1973), p. 979.

9) I. M. Mathai, K. Schug, and S. I. Miller, *J. Org. Chem.*, **35**, 1733 (1970); W. K. Kwok and S. I. Miller, *ibid.*, **35**, 4034 (1970); *J. Am. Chem. Soc.*, **92**, 4599 (1970); W. Adam and J. Arce, *J. Org. Chem.*, **37**, 507 (1972).

10) T. Shirafuji, Y. Yamamoto, and H. Nozaki, *Tetrahedron Lett.*, **1969**, 4097.

11) L. Claisen and E. Tietze, *Ber.*, **58**, 275 (1925); L. S. Heble, D. R. Nadkarni, and T. S. Wheeler, *J. Chem. Soc.*, **1938**, 1322; R. E. Buckles, W. E. Steinmetz, and N. G. Wheeler, *J. Am. Chem. Soc.*, **72**, 2496 (1950); L. I. Smith and H. H. Hoehn, *ibid.*, **63**, 1180 (1941); H. O. House and R. S. Ro, *ibid.*, **80**, 182 (1958); H. R. Snyder and L. A. Brooks, *Org. Synth.*, Coll. Vol. II, 171 (1943); R. M. Cowper and L. H. Davidson, *ibid.*, **480** (1943); T. F. Corbin, R. C. Hahn, and H. Shechter, *ibid.*, Vol. V, 328 (1973); I. J. Borowitz, P. E. Rusek, and R. Virkhaus, *J. Org. Chem.*, **34**, 1595 (1969); E. Schwenk and D. Papa, *J. Am. Chem. Soc.*, **70**, 3626 (1948).

12) R. L. Shriner H. C. Struck, and W. J. Jorison, *J. Am. Chem. Soc.*, **52**, 2060 (1930).

13) P. S. Bailey and R. E. Lutz, *J. Am. Chem. Soc.*, **70**, 2412 (1948).

Synthesis of Corticotropin Peptides. XIV. The Synthesis of Two Octadecapeptides Corresponding to the Amino Acid Sequence 22—39 of Porcine and Human Corticotropins*

Kunio WATANABE and Ken INOUYE

Shionogi Research Laboratory, Shionogi & Co., Ltd., Fukushima-ku, Osaka 553

(Received June 29, 1976)

The syntheses are described of two octadecapeptides, H-Val-Tyr-Pro-Asn-Gly-Ala-Glu-Asp-Glu-Leu-Ala-Glu-Ala-Phe-Pro-Leu-Glu-Phe-OH (Ip) and H-Val-Tyr-Pro-Asn-Gly-Ala-Glu-Asp-Glu-Ser-Ala-Glu-Ala-Phe-Pro-Leu-Glu-Phe-OH (Ih), corresponding to a tryptic fragment (positions 22—39) of porcine corticotropin (α_p-ACTH) and that of human hormone (α_h-ACTH), respectively. The porcine peptide and the corresponding human peptide are prepared simultaneously by an identical synthetic procedure except for the introduction of amino acid residue in position 31. Synthetic peptide Ip is compared with the authentic α_p-ACTH (22—39), which has been isolated from a tryptic hydrolysate of natural α_p-ACTH, in terms of chemical and physicochemical properties to establish their identity. These data as well as those obtained with human peptide Ih prove the satisfactory synthesis of the two octadecapeptides.

In corticotropin (ACTH) lysine 21 is the only basic amino acid residue in the C-terminal half of the hormone molecule (Fig. 1). Thus, the tryptic hydrolysis of ACTH yields a peptide fragment comprising the amino acid residues 22—39 of the hormone;[7] H-Val-Tyr-Pro-Asn-Gly-Ala-Glu-Asp-Glu-Leu-Ala-Glu-Ala-Phe-Pro-Leu-Glu-Phe-OH (Ip) from porcine ACTH (α_p-ACTH)[8] and H-Val-Tyr-Pro-Asn-Gly-Ala-Glu-Asp-Glu-Ser-Ala-Glu-Ala-Phe-Pro-Leu-Glu-Phe-OH (Ih) from human ACTH (α_h-ACTH).[8] The present paper describes the synthesis of octadecapeptides Ip and Ih, which has been performed as a step of our total synthesis of α_p-ACTH and α_h-ACTH.[9] The porcine peptide and the corresponding human peptide were prepared in parallel and there was employed an identical synthetic procedure except for the introduction of the amino acid residue in position 31, which makes the only structural difference between the two mammalian hormones.

	1	2	3	4	5	6	7	8
α_p-ACTH:	H-Ser-	Tyr-	Ser-	Met-	Glu-	His-	Phe-	Arg-
α_h-ACTH:	H-Ser-	Tyr-	Ser-	Met-	Glu-	His-	Phe-	Arg-

	9	10	11	12	13	14	15	16	17
α_p-ACTH:	Trp-	Gly-	Lys-	Pro-	Val-	Gly-	Lys-	Lys-	Arg-
α_h-ACTH:	Trp-	Gly-	Lys-	Pro-	Val-	Gly-	Lys-	Lys-	Arg-

	18	19	20	21	22	23	24	25	26
α_p-ACTH:	Arg-	Pro-	Val-	Lys-	Val-	Tyr-	Pro-	Asn-	Gly-
α_h-ACTH:	Arg-	Pro-	Val-	Lys-	Val-	Tyr-	Pro-	Asn-	Gly-

	27	28	29	30	31	32	33	34	35
α_p-ACTH:	Ala-	Glu-	Asp-	Glu-	**Leu**-	Ala-	Glu-	Ala-	Phe-
α_h-ACTH:	Ala-	Glu-	Asp-	Glu-	**Ser**-	Ala-	Glu-	Ala-	Phe-

	36	37	38	39
α_p-ACTH:	Pro-	Leu-	Glu-	Phe-OH
α_h-ACTH:	Pro-	Leu-	Glu-	Phe-OH

Fig. 1. Primary structures of porcine corticotropin (α_p-ACTH)[1-4] and human corticotropin (α_h-ACTH).[4-6]

* All the amino acid residues mentioned in this communication are of the L-configuration. Abbreviations used are those recommended by the IUPAC-IUB Commission of Biochemical Nomenclature [*Biochemistry*, **5**, 2485 (1966); *ibid.*, **6**, 362 (1967); *ibid.*, **11**, 1726 (1972)].

Z-Ala-Glu(OBu^t)-Ala-Phe-Pro-Leu-Glu(OBu^t)-Phe-OBu^t (VIII)[10]

↓ H_2/Pd

↓ Z-Leu-ONp or Z-Ser-N_3

Z-R-Ala-Glu(OBu^t)-Ala-Phe-Pro-Leu-Glu(OBu^t)-Phe-OBu^t (IXp: R=Leu, IXh: R=Ser)

↓ H_2/Pd

↓ Z-Glu(OBu^t)-ONp

Z-Glu(OBu^t)-R-Ala-Glu(OBu^t)-Ala-Phe-Pro-Leu-Glu(OBu^t)-Phe-OBu^t (Xp: R=Leu, Xh: R=Ser)

↓ H_2/Pd

↓ Z-Asp(OBu^t)-ONp

Z-Asp(OBu^t)-Glu(OBu^t)-R-Ala-Glu(OBu^t)-Ala-Phe-Pro-Leu-Glu(OBu^t)-Phe-OBu^t (XIp: R=Leu, XIh: R=Ser)

↓ H_2/Pd

↓ Z-Glu(OBu^t)-ONp

Z-Glu(OBu^t)-Asp(OBu^t)-Glu(OBu^t)-R-Ala-Glu(OBu^t)-Ala-Phe-Pro-Leu-Glu(OBu^t)-Phe-OBu^t (XIIp: R=Leu, XIIh: R=Ser)

Fig. 2. Synthesis of amino acid sequence 28—39 of α_p-ACTH and α_h-ACTH.

Protected dodecapeptides XIIp and XIIh, corresponding to positions 28—39 of α_p-ACTH and α_h-ACTH, respectively, were synthesized as shown in Fig. 2, in which the carboxyl groups were protected as their *t*-butyl esters and the α-amino function was temporarily blocked by a benzyloxycarbonyl group in combination with the subsequent deblocking by catalytic hydrogenolysis. The coupling reactions to lead to the production of porcine peptide XIIp were carried out in a step-by-step manner by the *p*-nitrophenyl ester method throughout, following the strategy employed by Schwyzer and Sieber[10] in their synthesis of the originally proposed amino acid sequence of porcine ACTH.[1,2] This was also applied to our present synthesis of human peptide XIIh with an exception of serine 31 which was introduc-

ed by the azide procedure rather than the active ester method. Among the intermediate compounds involved in the synthesis of XIIp and XIIh, compounds II, III, IV and VII (for structures see Experimental) were obtained in crystalline form. Compounds VIII and IXh separated out of the medium during the coupling reaction. They were amorphous but easily purified by reprecipitation. In the other cases the coupling product had to be chromatographed on a silica gel column for purification, in which methanol-chloroform systems were successfully employed as solvent.

A further extension of the peptide chain at the N-terminal of XIIh produced a tridecapeptide Z-Ala-Glu-(OBu^t)-Asp(OBu^t)-Glu(OBu^t)-Ser-Ala-Glu(OBu^t)-Ala-Phe-Pro-Leu-Glu(OBu^t)-Phe-OBu^t, but its low solubility did not allow us to perform chromatographic purification. Therefore, we synthesized a hexapeptide derivative corresponding to the amino acid residues in positions 22—27 and combined it with dodecapeptides XIIp and XIIh to obtain the desired octadecapeptides. The synthesis of this hexapeptide, Z-Val-Tyr-Pro-Asn-Gly-Ala-NHNH$_2$ (XIX), was carried out as illustrated in Fig. 3. Starting with the dicyclohexylcarbodiimide (DCC)-mediated coupling of Z-Ala-OH with *t*-butyl carbazate, the step-by-step lengthening of peptide chain yielded a tetrapeptide *t*-butoxycarbonyl (Boc)-hydrazide (XVI). The benzyloxycarbonyl (Z) group of XVI was removed by catalytic hydrogenolysis and the resulting N^{α}-free compound was coupled with Z-Val-Tyr-N_3, derived from the corresponding hydrazide[11,12] by the treatment with an alkyl nitrite in an anhydrous acid solution,[13] to give a crystalline hexapeptide derivative (XVIII) in a moderate yield. The subsequent treatment of XVIII with hydrogen chloride in acetic acid to remove the Boc group gave the hydrazide hydrochloride (XIX).

Z-Ala-OH
↓ Boc-NHNH$_2$, DCC
Z-Ala-NHNH-Boc (XIII)
↓ H_2/Pd
↓ Z-Gly-OH, DCC
Z-Gly-Ala-NHNH-Boc (XIV)
↓ H_2/Pd
↓ Z-Asn-ONp
Z-Asn-Gly-Ala-NHNH-Boc (XV)
↓ H_2/Pd
↓ Z-Pro-ONp
Z-Pro-Asn-Gly-Ala-NHNH-Boc (XVI)
↓ H_2/Pd
↓ Z-Val-Tyr-NHNH$_2$[11,12]
Z-Val-Tyr-Pro-Asn-Gly-Ala-NHNH-Boc (XVIII)
↓ HCl/AcOH (+anisole)
Z-Val-Tyr-Pro-Asn-Gly-Ala-NHNH$_2$·HCl (XIX)

XVI $\xrightarrow{\text{HCl/AcOH}}$ Z-Pro-Asn-Gly-Ala-NHNH$_2$·HCl (XVII)

Fig. 3. Synthesis of amino acid sequence 22—27 of ACTH.

Hydrazide XIX obtained above was treated with an alkyl nitrite,[13] and the resulting azide was allowed to react with the N^{α}-free dodecapeptides, derived from XIIp and XIIh by catalytic hydrogenolysis, to give the protected octadecapeptides (XXIp and XXIh). The partially purified preparations of XXIp and XXIh were submitted to catalytic hydrogenolysis and the products were purified on silica gel columns with ethyl acetate–acetic acid–water (4: 1: 1) as solvent to give the N^{α}-free octadecapeptides H-Val-Tyr-Pro-Asn-Gly-Ala-Glu(OBu^t)-Asp(OBu^t)-Glu(OBu^t)-Leu-Ala-Glu(OBu^t)-Ala-Phe-Pro-Leu-Glu(OBu^t)-Phe-OBu^t (XXIIp) and H-Val-Tyr-Pro-Asn-Gly-Ala-Glu-(OBu^t)-Asp(OBu^t)-Glu(OBu^t)-Ser-Ala-Glu(OBu^t)-Ala-Phe-Pro-Leu-Glu(OBu^t)-Phe-OBu^t (XXIIh). Compounds XXIIp and XXIIh have proved to serve as intermediates for the total synthesis of α_p-ACTH and α_h-ACTH, respectively.[9]

Octadecapeptide XXIIh was also synthesized by an alternative route, in which dodecapeptide XIIh was acylated consecutively with Z-Pro-Asn-Gly-Ala-N_3, derived from XVII (Fig. 3), and Z-Val-Tyr-N_3 in combination with the removal of the N^{α}-Z group by catalytic hydrogenolysis. The azides were prepared from the corresponding hydrazides by means of the alkyl nitrite procedure.[13]

Partially protected peptides XXIIp and XXIIh obtained above were deprotected with trifluoroacetic acid in the presence of 2-mercaptoethanol followed by treatment with Amberlite CG-400 (acetate form) to liberate the free octadecapeptides α_p-ACTH(22—39) (Ip) and α_h-ACTH(22—39) (Ih), respectively. The crude preparations of Ip and Ih were purified by partition chromatography on a column of Sephadex LH-20 with 1-butanol–acetic acid–water (4: 1: 2) as solvent. The synthetic octadecapeptides thus obtained were found to be homogeneous in TLC and their acid hydrolysates contained the constituent amino acids in the ratios predicted by theory except for tyrosine, whose recovery was 70—80% as compared with the other amino acids.

In order to obtain the authentic sample of α_p-ACTH-(22—39), a purified preparation of natural α_h-ACTH[9] was submitted to tryptic hydrolysis at pH 8.2 and 37 °C for 60 min. The desired octadecapeptide was isolated from the hydrolysate by chromatography on a column of silica gel with ethyl acetate–acetic acid–water (4: 1: 1) as solvent. This was further purified by partition chromatography on a Sephadex LH-20 column with 1-butanol–acetic acid–water (4: 1: 2) as solvent. Thin-layer chromatography and amino acid analysis revealed the homogeneity of the preparation obtained above, although the tyrosine content was found to be considerably lower than the theoretical value. The low tyrosine content was also observed with the synthetic peptides as described above.[14] The synthetic porcine peptide (Ip) was found to be identical with this authentic octadecapeptide in TLC and in optical rotation within the precision of measurement. It is known that asparagine 25 is the only site of alkaline deamidation in the

ACTH molecule; the Asn-Gly bond (positions 25—26) being transformed into the Asp-α/β-Gly bond by way of the formation of a succinimide intermediate.[15] Upon treatment with 0.1 M ammonia at 37 °C overnight, the authentic α_p-ACTH(22—39) and synthetic peptide Ip yielded an identical product which was clearly distinguished from the intact peptide in TLC with 1-butanol-acetic acid-water (4: 1: 2) as solvent. Thus, the identity between the synthetic peptide and the authentic sample from natural origin has now been established on a sound basis. This would also prove the satisfactory synthesis of human peptide Ih, since peptide Ih was prepared in parallel with Ip using the identical synthetic procedure and conditions except for the introduction of serine 31 in place of leucine 31 in Ip.

Human peptide Ih was found to be more soluble in aqueous acetic acid than porcine peptide Ip and also found to be distinguishable from Ip in TLC with 1-butanol-acetic acid-water (4: 1: 2) as solvent (Ip, R_f= 0.27; Ih, R_f=0.22). These observations may be explained as a reflection of the structural difference between Ip and Ih.

Experimental

Thin-layer chromatography (TLC) was performed on silica gel plates (Kieselgel GF_{254} or precoated Kieselgel $60F_{254}$, Merck) with the following solvent systems: A, chloroform-methanol (8: 2); B, chloroform-methanol-acetic acid (95: 5: 3); C, chloroform-methanol-acetic acid (90: 10: 3); D, ethyl acetate-acetic acid-water (4: 1: 1); E, 1-butanol-acetic acid-water (4: 1: 2).

Z-Glu(OBu^t)-Phe-OBu^t (II). Z-Glu(OBu^t)-OH [derived from the dicyclohexylamine salt (14.3 g, 27.6 mmol) in the usual manner][16] and H-Phe-OBu^t (6.1 g, 27.6 mmol)[17] were coupled with dicyclohexylcarbodiimide (DCC; 5.7 g, 27.6 mmol) in ethyl acetate-dichloromethane (1: 1) to give II, which was crystallized from ether-petroleum ether; yield 12.4 g (83%), mp 132—134 °C, $[\alpha]_D^{22}$ −17.5±0.3° (*c* 2.0, methanol), −14.1±0.3° (*c* 2.0, 95% ethanol). TLC: a single component (sulfuric acid) in system B. Found: C, 66.43; H, 7.42; N, 5.41%. Lit, mp 131.5—132.5 °C, $[\alpha]_D$ −14.0±0.5° (*c* 2, 95% ethanol);[10] mp 131.0—131.5 °C, $[\alpha]_D^{22}$ −11.2° [*c* 0.99, *N,N*-dimethylformamide (DMF)].[18]

Z-Leu-Glu(OBu^t)-Phe-OBu^t (III). Compound II (11.5 g, 21.2 mmol) was hydrogenolyzed over palladium in methanol containing acetic acid to give the N^α-free dipeptide ester, which was coupled with Z-Leu-ONp (8.2 g, 21.2 mmol) in DMF. The product was crystallized from ethyl acetate-ether; yield 13.1 g (94%), mp 109—110 °C, $[\alpha]_D^{22}$ −25.5±0.4° (*c* 2.0, 95% ethanol). TLC: a single component (sulfuric acid) in system C. Found: C, 65.98; H, 7.82; N, 6.52%. Lit, mp 116—117.5°C, $[\alpha]_D$ −26.3±0.6° (*c* 2.0, 95% ethanol);[10] mp 113—115 °C, $[\alpha]_D^{22}$ −14.3° (*c* 1.04, DMF).[18]

Z-Pro-Leu-Glu(OBu^t)-Phe-OBu^t (IV). Compound III (7.60 g, 11.6 mmol) was hydrogenolyzed to give the N^α-free tripeptide ester, which was coupled with Z-Pro-ONp (4.30 g, 11.6 mmol) in DMF. The product was crystallized from ether; yield 8.00 g (92%), mp 160—161°C, $[\alpha]_D^{23}$ −58.7±0.5° (*c* 2.0, 95% ethanol). TLC: a single component (sulfuric acid) in system C. Found: C, 65.68; H, 7.79; N, 7.38%. Lit, mp 152—153 °C, $[\alpha]_D$ −56.8±0.6° (*c* 2, 95% ethanol).[10]

Z-Phe-Pro-Leu-Glu(OBu^t)-Phe-OBu^t (V). Compound IV (12.4 g, 16.5 mmol) was hydrogenolyzed to give the N^α-free tetrapeptide ester, which was coupled with Z-Phe-ONp (6.94 g, 16.5 mmol) in DMF. The crude product was purified on a column of silica gel (100 g, Kieselgel H, Merck) with 2% methanol in chloroform as solvent; yield 14.75 g (97.5%), $[\alpha]_D^{23}$ −54.8±1.0° (*c* 1.0, methanol). TLC: a single component (sulfuric acid) in system C. Found: C, 66.76; H, 7.53; N, 7.87%. Lit, $[\alpha]_D$ not given.[10]

Z-Ala-Phe-Pro-Leu-Glu(OBu^t)-Phe-OBu^t (VI). Compound V (14.1 g, 15.7 mmol) was hydrogenolyzed to give the N^α-free pentapeptide ester, which was coupled with Z-Ala-ONp (5.40 g, 15.7 mmol) in DMF. The crude product was purified on a silica gel column with 1% methanol in chloroform as solvent; yield 11.9 g (77%), $[\alpha]_D^{22}$ −67.9±1.1° (*c* 1.0, methanol). TLC: a single component (sulfuric acid) in system C. Found: C, 64.74; H, 7.55; N, 8.60%. Lit, $[\alpha]_D$ not given;[10] $[\alpha]_D^{22}$ −38.6° (*c* 1.01, DMF).[18]

Z-Glu(OBu^t)-Ala-Phe-Pro-Leu-Glu(OBu^t)-Phe-OBu^t (VII). Compound VI (5.80 g, 5.9 mmol) was hydrogenolyzed to give the N^α-free hexapeptide ester, which was coupled with Z-Glu(OBu^t)-ONp (2.74 g, 5.9 mmol) in DMF. The product was crystallized from ethyl acetate-ether; yield 5.30 g (78%), mp 178—180 °C, $[\alpha]_D^{24}$ −64.8±1.1° (*c* 1.0 methanol). TLC: a single component (sulfuric acid) in system C. Found: C, 64.01; H, 7.73; N, 8.51%. Lit, mp 172—173 °C, $[\alpha]_D$ not given;[10] mp 168—170 °C decomp., $[\alpha]_D^{21}$ −34.4° (*c* 1.03, DMF).[18]

Z-Ala-Glu(OBu^t)-Ala-Phe-Pro-Leu-Glu(OBu^t)-Phe-OBu^t (VIII). Compound VII (4.0 g, 3.64 mmol) was hydrogenolyzed to give the N^α-free heptapeptide ester, which was coupled with Z-Ala-ONp (1.25 g, 3.64 mmol) in ethyl acetate. The product which had separated was filtered off and reprecipitated from ethyl acetate-ether; yield 4.02 g (90%), mp 145—147 °C, $[\alpha]_D^{24}$ −63.8±1.0° (*c* 1.0, methanol). TLC: a single component (sulfuric acid) in system C. Found: C, 62.82; H, 7.68; N, 9.30%. Lit, no data given;[10] mp 185—186 °C decomp., $[\alpha]_D^{23}$ −34.9° (*c* 1.05, DMF).[18]

Z-Leu-Ala-Glu(OBu^t)-Ala-Phe-Pro-Leu-Glu(OBu^t)-Phe-OBu^t (IXp). Compound VIII (2.45 g, 2.0 mmol) was hydrogenolyzed to give the N^α-free octapeptide ester, which was coupled with Z-Leu-ONp (0.85 g, 3.3 mmol) in DMF-ethyl acetate (1: 2). The crude product was purified on a silica gel column (70 g) with 3% methanol in chloroform as solvent; yield 2.40 g (90%), mp 125—130 °C, $[\alpha]_D^{28}$ −60.0 ±1.0° (*c* 1.0, methanol). TLC: a single component (sulfuric acid) in system C. Found: C, 63.17; H, 7.73; N, 9.29%. Lit, no data given.[10]

Z-Ser-Ala-Glu(OBu^t)-Ala-Phe-Pro-Leu-Glu(OBu^t)-Phe-OBu^t (IXh). The N^α-octapeptide ester, derived from VIII (2.65 g, 2.2 mmol) as above, and Z-Ser-N_3 [derived from the corresponding hydrazide (0.84 g, 3.3 mmol) by the treatment with nitrous acid in the usual manner] were coupled in ethyl acetate at 4 °C overnight. The product which had separated was filtered off and reprecipitated from ethyl acetate-ether; yield 2.60 g (90%), mp 187—189 °C, $[\alpha]_D^{24}$ −55.9 ±1.0° (*c* 1.0, methanol). TLC: a single component (sulfuric acid) in system C. Found: C, 61.99; H, 7.63; N, 9.45%. Lit, no data given;[15] mp 181—183 °C decomp., $[\alpha]_D^{28}$ −32.9° (*c* 1.04, DMF).[18]

Z-Glu(OBu^t)-Leu-Ala-Glu(OBu^t)-Ala-Phe-Pro-Leu-Glu-(OBu^t)-Phe-OBu^t (Xp). Compound IXp (2.37 g, 1.8 mmol) was hydrogenolyzed over palladium in acetic acid to give the N^α-free nonapeptide ester. This was then coupled with Z-Glu(OBu^t)-ONp (0.82 g, 1.8 mmol) in DMF in the presence of triethylamine (0.25 ml, 1.8 mmol) at 4 °C overnight. The crude product was purified on a silica gel column (70 g) with 3% methanol in chloroform as solvent; yield 2.32 g (86%), mp 185—190 °C, $[\alpha]_D^{25}$ −57.4±0.9° (*c* 1.0, methanol).

TLC: single component (sulfuric acid) in system C.

Found: C, 62.71; H, 7.79; N, 9.03%. Calcd for $C_{80}H_{118}N_{10}O_{19}$: C, 63.05; H, 7.81; N, 9.19%.

Z-Glu(OBu^t)-Ser-Ala-Glu(OBu^t)-Ala-Phe-Pro-Leu-Glu(OBu^t)-Phe-OBu^t (Xh). Compound IXh (2.62 g, 2.0 mmol) was hydrogenolyzed to give the N^{α}-free nonapeptide ester, which was coupled with Z-Glu(OBu^t)-ONp (0.92 g, 2.0 mmol) in DMF. The crude product was purified on a silica gel column with 3—5% methanol in chloroform as solvent; yield 2.60 g (90%), mp 135—137 °C, $[\alpha]_D^{24}$ −48.9 ±0.9° (*c* 1.0, methanol). TLC: a single component (sulfuric acid) in system C. Found: C, 61.20; H, 7.48; N, 9.45%. Lit, no data given;[15] mp 189—190 °C decomp., $[\alpha]_D^{23}$ −29.7° (*c* 0.98, DMF).[18]

Z-Asp(OBu^t)-Glu(OBu^t)-Leu-Ala-Glu(OBu^t)-Ala-Phe-Pro-Leu-Glu(OBu^t)-Phe-OBu^t (XIp). Compound Xp (2.00 g, 1.32 mmol) was hydrogenolyzed over palladium in acetic acid to give the N^{α}-free decapeptide ester. This was then coupled with Z-Asp(OBu^t)-ONp (0.59 g, 1.32 mmol) in DMF in the presence of triethylamine (0.20 ml, 1.43 mmol) at 4 °C for 2.5 days. The crude product was purified on a silica gel column (70 g) with 3% methanol in chloroform as solvent; yield 2.10 g (94%), mp 224—225 °C decomp., $[\alpha]_D^{26}$ −48.9±0.9° (*c* 1.0, methanol).

Found: C, 61.91; H, 7.67; N, 8.84%. Calcd for $C_{83}H_{131}H_{11}O_{22}$: C, 62.35; H, 7.79; N, 9.09%.

Z-Asp(OBu^t)-Glu(OBu^t)-Ser-Ala-Glu(OBu^t)-Ala-Phe-Pro-Leu-Glu(OBu^t)-Phe-OBu^t (XIh). Compound Xh (2.80 g, 1.87 mmol) was hydrogenolyzed to give the N^{α}-free decapeptide ester, which was coupled with Z-Asp(OBu^t)-ONp (0.84 g, 1.87 mmol) in DMF. The crude product was purified on a silica gel column with 5% methanol in chloroform as solvent; yield 2.98 g (96%), mp 193—195 °C decomp., $[\alpha]_D^{28}$ −48.1±0.5° (*c* 1.0, methanol). TLC: a single component (sulfuric acid) in system C. Found: C, 60.80; H, 7.65; N, 8.94%. Lit, no data given;[15] mp 194—195 °C decomp., $[\alpha]_D^{28}$ −29.8° (*c* 1.05, DMF).[18]

Z-Glu(OBu^t)-Asp(OBu^t)-Glu(OBu^t)-Leu-Ala-Glu(OBu^t)-Ala-Phe-Pro-Leu-Glu(OBu^t)-Phe-OBu^t (XIIp). Compound XIp (2.00 g, 1.18 mmol) was hydrogenolyzed over palladium in acetic acid to give the N^{α}-free undecapeptide ester. This was then coupled with Z-Glu(OBu^t)-ONp (0.55 g, 1.20 mmol) in DMF in the presence of triethylamine (0.20 ml, 1.43 mmol) at 4 °C for 2.5 days. The crude product was purified on a silica gel column (50 g) with 3% methanol in chloroform as solvent; yield 2.10 g (95%), mp 230 °C decomp., $[\alpha]_D^{28}$ −41.2±0.8° (*c* 1.0, methanol). Amino acid ratios in acid hydrolysate (theoretical values are given in parentheses): Asp 0.92 (1), Glu 3.89 (4), Pro 0.92 (1), Ala 1.95 (2), Leu 2.00 (2), Phe 1.82 (2).

Found: C, 61.55; H, 7.82; N, 8.91%. Calcd for $C_{97}H_{146}N_{12}O_{25}$: C, 61.96; H, 7.83; N, 8.94%.

Z-Glu(OBu^t)-Asp(OBu^t)-Glu(OBu^t)-Ser-Ala-Glu(OBu^t)-Ala-Phe-Pro-Leu-Glu(OBu^t)-Phe-OBu^t (XIIh). Compound XIh (2.10 g, 1.26 mmol) was hydrogenolyzed to give the N^{α}-free undecapeptide ester, which was coupled with Z-Glu(OBu^t)-ONp (0.58 g, 1.27 mmol) in DMF. The crude product was purified on a silica gel column with 4% methanol in chloroform as solvent; yield 2.10 g (94%), mp 220—221 °C decomp., $[\alpha]_D^{24.5}$ −26.9±0.7° (*c* 1.0, DMF). TLC: a single component (sulfuric acid) in system C. Amino acid ratios in acid hydrolysate: Asp 1.00 (1), Ser 0.91 (1), Glu 4.11 (4), Pro 1.07 (1), Ala 2.04 (2), Leu 1.00 (1), Phe 1.89 (2). Found: C, 60.77; H, 7.55; N, 8.97%. Lit, no data given;[15] mp 215—216 °C decomp., $[\alpha]_D^{23}$ −27.2° (*c* 1.07, DMF).[18]

Z-Ala-NHNH-Boc (XIII). Z-Ala-OH (11.15 g, 50 mmol) and *t*-butyl carbazate (6.60 g, 50 mmol) were dissolved in ethyl acetate (100 ml) and to this was added DCC (10.35 g, 50 mmol) at 0 °C with ethyl acetate as solvent. The mixture was stirred at 4 °C overnight followed by evaporation *in vacuo*. The residue was submitted to a silica gel column (150 g) with 2% methanol in chloroform as solvent. The fractions (17 g/tube) were examined by TLC in system C and those containing the desired compound as a single component (tubes 39—70) were combined and evaporated *in vacuo* to give a residue which was crystallized from ether-petroleum ether; yield 15.9 g (94%), mp 93—95 °C, $[\alpha]_D^{28}$ −48.2±0.9° (*c* 1.0, methanol).

Found: C, 55.84; H, 6.60; N, 12.34%. Calcd for $C_{16}H_{23}N_3O_5$: C, 56.96; H, 6.87; N, 12.46%.

Z-Gly-Ala-NHNH-Boc (XIV). Compound XIII (3.37 g, 10 mmol) was hydrogenolyzed over palladium in methanol. The resulting N^{α}-free compound and Z-Gly-OH (2.09 g, 10 mmol) were coupled with DCC (2.06 g, 10 mmol) in ethyl acetate (40 ml) at 4 °C overnight. The reaction mixture was worked up in the usual manner to isolate the crystalline product, which was recrystallized from aqueous methanol; yield 4.10 g (99%), mp 110—112 °C, $[\alpha]_D^{22}$ −45.8 ±0.9° (*c* 1.0, methanol).

Found: C, 52.60; H, 7.00; N, 13.38%. Calcd for $C_{18}H_{26}N_4O_6\cdot H_2O$: C, 52.42; H, 6.84; N, 13.59%.

Z-Asn-Gly-Ala-NHNH-Boc (XV). Compound XIV (3.94 g, 9.6 mmol) was hydrogenolyzed over palladium in methanol. The resulting N^{α}-free dipeptide derivative was then coupled with Z-Asn-ONp (3.87 g, 10 mmol) in DMF (10 ml) at 4 °C overnight. The product isolated as amorphous solid was reprecipitated from methanol-ether; yield 4.50 g (92%), mp 146—149 °C decomp., $[\alpha]_D^{28}$ −24.6±0.7° (*c* 1.0, methanol).

Found: C, 52.13; H, 6.52; N, 15.89%. Calcd for $C_{22}H_{32}N_6O_8$: C, 51.96; H, 6.34; N, 16.53%.

Z-Pro-Asn-Gly-Ala-NHNH-Boc (XVI). Compound XV (4.30 g, 8.5 mmol) was hydrogenolyzed over palladium in methanol containing acetic acid to give the N^{α}-free tripeptide derivative, which was coupled with Z-Pro-ONp (3.13 g, 8.5 mmol) in DMF. The product, dissolved in water-saturated 1-butanol-ethyl acetate (1: 1), was washed with 1M acetic acid followed by evaporation *in vacuo*. The residue was precipitated from ethyl acetate-ether (2: 1) and then from methanol-ethyl acetate (1: 3) to give XVI in pure form; yield 4.40 g (83%), mp 145—147 °C, $[\alpha]_D^{24.5}$ −68.1±1.1° (*c* 1.0, methanol). TLC: a single component (sufuric acid) in system A.

Found: C, 51.52; H, 6.63; N, 15.53%. Calcd for $C_{27}H_{39}N_7O_9\cdot H_2O$: C, 52.00; H, 6.63; N, 15.72%.

Z-Pro-Asn-Gly-Ala-NHNH$_2$·HCl (XVII). Compound XVI (4.70 g) was treated with 1M hydrogen chloride in acetic acid (50 ml) at room temperature for 60 min followed by evaporation *in vacuo*. The residue was triturated with ethyl acetate-ether (1: 1) and the resulting precipitates were filtered off and reprecipitated from ethanol (30 ml) two times; yield 2.75 g (65%), mp 145—147 °C decomp., $[\alpha]_D^{24}$ −63.9 ±1.5° (*c* 0.7, methanol).

Found: C, 47.83; H, 6.15; N, 17.28; Cl, 5.71%. Calcd for $C_{22}H_{31}N_7O_7\cdot HCl\cdot H_2O$: C, 47.18; H, 6.12; N, 17.51; Cl, 6.33%.

Z-Val-Tyr-Pro-Asn-Gly-Ala-NHNH-Boc (XVIII). Compound XVI (2.33 g, 3.7 mmol) was hydrogenolyzed over palladium in methanol to give H-Pro-Asn-Gly-Ala-NHNH-Boc (1.96 g) as amorphous solid.

A solution of Z-Val-Tyr-NHNH$_2$ (1.76 g, 4.1 mmol)[11,12] in DMF (18 ml) was chilled to −15—−20 °C and 3.66 M hydrogen chloride in dioxane (4.5 ml) was introduced. To this was added dropwise isopentyl nitrite (0.59 ml, 4.5 mmol)

and the mixture was stirred at the same temperature for 10 min. The resulting azide solution was chilled to −40——50 °C and there were added triethylamine (2.9 ml, 20.6 mmol) and the N^{α}-free tetrapeptide derivative obtained above with DMF (20 ml) as solvent. The bath was removed and the temperature was allowed to rise to 4 °C at which the reaction mixture was stirred for 20 h followed by evaporation *in vacuo*. The residue was shaken with a mixture of 1-butanol–ethyl acetate (1: 1, 20 ml) and 1M acetic acid (20 ml). The organic phase separated was further washed with 1M acetic acid three times followed by evaporation *in vacuo*. The residue was then chromatographed on a silica gel column (70 g) with 15% methanol in chloroform as solvent. The fractions (7 g/tube) were examined by TLC (system A) and those containing the desired compound as a single component were combined and evaporated *in vacuo* to give a residue which was crystallized from ethyl acetate; yield 1.8 g (56%), mp 166—167 °C decomp., $[\alpha]_D^{24}$ −66.4±1.0° (*c* 1.0, methanol).

Found: C, 55.89; H, 6.85; N, 14.34%. Calcd for $C_{41}H_{57}N_9O_{12}$: C, 56.74; H, 6.62; N, 14.53%.

Z-Val-Tyr-Pro-Asn-Gly-Ala-NHNH$_2$·HCl (XIX). Compound XVIII (1.80 g) was treated with 1M hydrogen chloride in acetic acid at room temperature for 60 min in the presence of anisole (0.2 ml) as scavenger. The solvent was evaporated *in vacuo* to give a residue which was triturated with ether; yield 1.70 g, mp 143—145 °C. Amino acid ratios in acid hydrolysate: NH_3 0.99 (1), Asp 1.04 (1), Pro 0.89 (1), Gly 1.04 (1), Ala 1.04 (1), Val 1.00 (1), Tyr 0.87 (1).

Z-Pro-Asn-Gly-Ala-Glu(OBu^t)-Asp(OBu^t)-Glu(OBu^t)-Ser-Ala-Glu(OBu^t)-Ala-Phe-Pro-Leu-Glu(OBu^t)-Phe-OBu^t (XX). Compound XIIh (1.20 g, 0.65 mmol) was hydrogenolyzed over palladium in acetic acid to give the N^{α}-free dodecapeptide ester. A solution of XVII (0.56 g, 1.0 mmol) in tetrahydrofuran containing 1M hydrochloric acid (1.5 ml) was chilled in an ice bath and 2 M sodium nitrite (0.55 ml) was added. The mixture was stirred at 0 °C for 4 min. To this were then introduced ice-cold ethyl acetate (20 ml) and ice-cold 50% potassium carbonate (8 ml). The organic phase separated was dried over magnesium sulfate at 0 °C and was combined with a DMF solution of the dodecapeptide ester obtained above. The mixture was concentrated *in vacuo* at a bath temperature of 5—10 °C to remove ethyl acetate and was stirred at 4 °C for 20 h. The product which was precipitated by the addition of ether and petroleum ether was lyophilized from acetic acid. The resulting soft powder was suspended in aqueous ethanol and the insoluble precipitates were filtered off (1.1 g). Reprecipitation from a mixture of methanol (40 ml) and water (20 ml) afforded hexadecapeptide XX; yield 0.88 g (62%), $[\alpha]_D^{24.5}$ −20.6±0.6° (*c* 1.0, DMF). TLC: almost homogeneous (ninhydrin, after pretreatment with hydrobromic acid) in systems A and E. Amino acid ratios in acid hydrolysate: NH_3 0.93 (1), Asp 1.94 (2), Ser 0.95 (1), Pro 1.96 (2), Glu 4.01 (4), Gly 0.98 (1), Ala 3.00 (3), Leu 1.07 (1), Phe 2.15 (2).

H-Val-Tyr-Pro-Asn-Gly-Ala-Glu(OBu^t)-Asp(OBu^t)-Glu(OBu^t)-Leu-Ala-Glu(OBu^t)-Ala-Phe-Pro-Leu-Glu(OBu^t)-Phe-OBu^t (XXIIp). Compound XIIp (0.98 g, 0.52 mmol) was hydrogenolyzed over palladium in acetic acid to give the N^{α}-free dodecapeptide ester.

A solution of XIX (0.45 g, 0.57 mmol) in DMF (5 ml) was chilled to −20——30 °C and 3.66 M hydrogen chloride in dioxane (0.47 ml) was introduced. To this was added dropwise isopentyl nitrite (0.082 ml, 0.63 mmol) and the mixture was stirred at the same temperature for 10 min. The azide solution thus obtained was chilled to −40——50 °C and triethylamine (0.4 ml, 2.87 mmol) was added. This was then combined with a DMF solution of the N^{α}-free dodecapeptide obtained above and the mixture was stirred for 24 h, while the temperature was allowed to rise to 4 °C. After the solvent had been removed by evaporation *in vacuo* the residue was triturated and washed with water and lyophilized from acetic acid. The resulting powder was suspended in 50% ethanol and the insoluble precipitates were filtered off, washed and dried to give the protected octadecapeptide (XXIp, 1.09 g, 84%), which was almost homogeneous in TLC in system A; mp 232—233 °C decomp.

Compound XXIp (1.40 g) prepared as described above was hydrogenolyzed over palladium in acetic acid. The resulting N^{α}-free peptide was purified on silica gel columns (150—250 g, Kieselgel 60, Merck) with ethyl acetate–acetic acid–water (4: 1: 1) as solvent. The resulting pure material was lyophilized from acetic acid; yield 1.09 g (67%), $[\alpha]_D^{23.5}$ −37.0 ±0.7° (*c* 1.0, acetic acid). TLC: a single component (ninhydrin) in system D. Amino acid ratios in acid hydrolysate: NH_3 0.90 (1), Asp 1.90 (2), Glu 3.95 (4), Pro 1.96 (2), Gly 1.04 (1), Ala 2.97 (3), Val 0.95 (1), Leu 2.00 (2), Tyr 0.86 (1), Phe 1.90 (2).

H-Val-Tyr-Pro-Asn-Gly-Ala-Glu(OBu^t)-Asp(OBu^t)-Glu(OBu^t)-Ser-Ala-Glu(OBu^t)-Ala-Phe-Pro-Leu-Glu(OBu^t)Phe-OBu^t (XXIIh). *a) By (22—23)+(24—39):* Compound XX (0.83 g, 0.38 mmol) was hydrogenolyzed over palladium in acetic acid to give the N^{α}-free hexadecapeptide ester. This was then coupled with Z-Val-Tyr-N_3 [derived from the corresponding hydrazide (0.21 g, 0.5 mmol)[11,12] by the treatment with nitrous acid in the usual manner] in DMF at 4 °C for 2.5 days. The product was repeatedly precipitated from ethanol–water to give a partially purified preparation of the protected octadecapeptide (XXIh, 0.77 g).

Compound XXIh obtained above was hydrogenolyzed over palladium in acetic acid and the resulting N^{α}-free peptide was purified on silica gel columns in the manner described above for XXIIp. The pure material was lyophilized from acetic acid; yield 0.39 g (43%). TLC: a single component (ninhydrin) in system D.

b) By (22—27)+(28—39). Compound XIIh (1.06 g, 0.57 mmol) was hydrogenolyzed over palladium in acetic acid to give the N^{α}-free dodecapeptide ester. This was then coupled with the acyl hexapeptide azide [derived from XIX (0.52 g, 0.65 mmol) in exactly the same manner as described above] in DMF in the presence of triethylamine (0.45 ml, 3.25 mmol) at 4 °C for 24 h. The crude product was lyophilized from acetic acid and the resulting powder was suspended in 50% ethanol and the insoluble material was collected to give XXIh (1.20 g, 87%), which was almost homogeneous in TLC in system A; mp 224—225 °C decomp.

Compound XXIh (2.20 g) prepared as described above was hydrogenolyzed over palladium in acetic acid. The resulting N^{α}-free peptide was purified on silica gel columns as described above; yield 1.71 g (70%), $[\alpha]_D^{23.5}$ −34.3±0.7° (*c* 1.0, acetic acid). TLC: a single component (ninhydrin) in system D. Amino acid ratios in acid hydrolysate: NH_3 0.91 (1), Asp 1.99 (2), Ser 0.87 (1), Glu 4.01 (4), Pro 1.78 (2), Gly 1.04 (1), Ala 3.09 (3), Val 0.99 (1), Leu 1.00 (1), Tyr 0.90 (1), Phe 1.98 (2).

H-Val-Tyr-Pro-Asn-Gly-Ala-Glu-Asp-Glu-Leu-Ala-Glu-Ala-Phe-Pro-Leu-Glu-Phe-OH (Ip). *a) Synthetic Preparation:* Compound XXIIp (100 mg) was dissolved in trifluoroacetic acid (1 ml) together with 2-mercaptoethanol (0.1 ml) and the mixture was kept at room temperature for 60 min. The precipitates which formed upon addition of ether were filtered off and dissolved in 3 M acetic acid (5 ml). The aqueous solution was passed through a column (0.9×7 cm) of Amberlite CG-400 (acetate form) with additional portions

of 3 M acetic acid and the eluates combined were lyophilized. The product was then submitted to partition chromatography on a column of Sephadex LH-20 (3.0×70 cm) with 1-butanol–acetic acid–water (4: 1: 2) as solvent. Five-ml fractions were collected and their absorption at 275 nm was measured. The fractions corresponding to a main peak (tubes 36—60) were pooled and evaporated *in vacuo* at a bath temperature of 45 °C. Lyophilization of the residue from acetic acid afforded Ip; yield 60 mg, $[\alpha]_D^{22}$ −41.6±2.0° (*c* 0.4, acetic acid) TLC: a single component (ninhydrin) in system E. Amino acid ratios in acid hydrolysate: NH_3 1.24 (1), Asp 2.00 (2), Glu 3.83 (4), Pro 2.09 (2), Gly 1.12 (1), Ala 2.99 (3), Val 0.93 (1), Leu 2.03 (2), Tyr 0.70 (1), Phe 2.00 (2).

b) Isolation from Natural α_p-ACTH. To a solution of the purified natural α_p-ACTH (*ca.* 15 mg)[9] in 0.2 M ammonium hydrogencarbonate (pH 8.2, 3.75 ml) was added 0.51 ml of 0.2% trypsin (chymotrypsin-free, in 0.001 M hydrochloric acid) and the mixture was incubated at 37 °C for 60 min. After addition of acetic acid (0.25 ml) the mixture was lyophilized. The tryptic hydrolysate thus obtained was submitted to chromatography on a column of silica gel (5 g, Kieselgel H, Merck) with ethyl acetate–acetic acid–water (4: 1: 1) as solvent. One half-ml fractions were collected and their absorption at 275 nm was measured. The fractions corresponding to a peak (tubes 16—22) were combined, evaporated *in vacuo* at a bath temperature of 40 °C and lyophilized from acetic acid (5 mg). This was further purified on a Sephadex LH-20 column (3.0×74 cm) with 1-butanol–acetic acid–water (4: 1: 2) as solvent. Five-ml fractions were collected and their absorption at 275 nm was measured to reveal the presence of a single component. The fractions corresponding to the peak (tubes 25—29) were combined and evaporated *in vacuo*, and the residue was lyophilized from acetic acid; yield 4 mg, $[\alpha]_D^{22}$ −42.7±3.5° (*c* 0.2, acetic acid). TLC: a single component (ninhydrin) in system E. Amino acid ratios in acid hydrolysate: NH_3 1.11 (1), Asp 2.01 (2), Glu 3.90 (4), Pro 1.91 (2), Gly 1.05 (1), Ala 2.95 (3), Val 0.96 (1), Leu 2.00 (2), Tyr 0.81 (1), Phe 1.83 (2).

H-Val-Tyr-Pro-Asn-Gly-Ala-Glu-Asp-Glu-Ser-Ala-Glu-Ala-Phe-Pro-Leu-Glu-Phe-OH (Ih). Compound XXIIh (100 mg) was treated with trifluoroacetic acid (1 ml) at room temperature for 60 min in the presence of 2-mercaptoethanol (0.1 ml). The precipitates which formed upon addition of ether were passed through an Amberlite CG-400 column with 1M acetic acid as solvent, followed by purification on a Sephadex LH-20 column with 1-butanol–acetic acid–water (4: 1: 2) as solvent in exactly the same manner as described above for Ip; yield 70 mg, $[\alpha]_D^{22}$ −41.4±1.6° (*c* 0.5, acetic acid). TLC: a single component (ninhydrin) in system E. Amino acid ratios in acid hydrolysate: NH_3 1.31 (1), Asp 2.03 (2), Ser 0.93 (1), Glu 3.98 (4), Pro 2.20 (2), Gly 1.08 (1), Ala 3.00 (3), Val 0.95 (1), Leu 1.00 (1), Tyr 0.78 (1), Phe 2.03 (2).

References

1) P. H. Bell, *J. Am. Chem. Soc.*, **76**, 5565 (1954).
2) R. G. Shepherd, S. D. Wilson, K. S. Howard, P. H. Bell, D. S. Davies, S. B. Davis, E. A. Eigner, and N. E. Shakespeare, *J. Am. Chem. Soc.*, **78**, 5067 (1956).
3) L. Gráf, S. Bajusz, A. Patthy, E. Barát, and G. Cseh, *Acta Biochim. Biophys. Acad. Sci. Hung.*, **6**, 415 (1971).
4) B. Riniker, P. Sieber, W. Rittel, and H. Zuber, *Nature New Biol.*, **235**, 114 (1972).
5) T. H. Lee, A. B. Lerner, and V. Buettner-Janusch, *J. Biol. Chem.*, **236**, 2970 (1961).
6) H. P. J. Bennett, *Biochem. J.*, **133**, 11 (1973).
7) W. F. White and W. A. Landmann, *J. Am. Chem. Soc.*, **77**, 1711 (1955).
8) Abbreviations for the ACTH preparations accord with the system of terminology proposed by Li [C. H. Li, *Science*, **129**, 970 (1959)].
9) K. Inouye, K. Watanabe, and H. Otsuka, *Bull. Chem. Soc. Jpn.*, **50**, 211 (1977).
10) R. Schwyzer and P. Sieber, *Helv. Chim. Acta.*, **49**, 134 (1966).
11) H. Schwarz, F. M. Bumpus, and I. H. Page, *J. Am. Chem. Soc.*, **79**, 5697 (1957).
12) K. Inouye, Y. Sumitomo, and M. Shin, *Bull. Chem. Soc. Jpn.*, **49**, 3620 (1976).
13) J. Honzl and J. Rudinger, *Coll. Czech. Chem. Commun.*, **26**, 2333 (1961).
14) In this connection, we should mention that in the amino acid analysis of the full-length ACTH preparations the recovery of tyrosine was excellent.[9] Thus, the extent of decomposition of tyrosine during acid hydrolysis seems to depend on the amino acid composition of a peptide to be hydrolyzed, and some amino acid (*e.g.* methionine) may play a role to protect tyrosine from its decomposition.
15) P. Sieber, W. Rittel, and B. Riniker, *Helv. Chim. Acta.*, **55**, 1243 (1972).
16) R. Schwyzer and H. Kappeler, *Helv. Chim. Acta*, **44**, 1991 (1961).
17) G. W. Anderson and F. M. Callahan, *J. Am. Chem. Soc.*, **82**, 3359 (1960).
18) O. Nishimura, C. Hatanaka, and M. Fujino, *Chem. Pharm. Bull.*, **23**, 1212 (1975).

Synthesis of Corticotropin Peptides. XV. The Synthesis of an Undecapeptide and a Nonapeptide Derivatives Related to the Amino Acid Sequence 11—21 of Corticotropin*

Ken INOUYE and Kunio WATANABE
Shionogi Research Laboratory, Shionogi & Co., Ltd., Fukushima-ku, Osaka 553

(Received June 29, 1976)

An undecapeptide derivative, Z-Lys(Mhoc)-Pro-Val-Gly-Lys(Mhoc)-Lys(Mhoc)-Arg-Arg-Pro-Val-Lys-(Mhoc)-$NHNH_2$, corresponding to the amino acid sequence 11—21 of corticotropin (ACTH) is synthesized. In the course of the synthesis a key intermediate H-Arg(NO_2)-Arg(NO_2)-Pro-OH is derived from Z-Arg(NO_2)-Arg-(NO_2)-Pro-OBzl by the treatment with hydrogen bromide in acetic acid. This procedure eliminates the danger of racemization associated with the use of alkali for saponification. The synthesis is also described of a nonapeptide derivative, Z-Lys(Mhoc)-Pro-Val-Gly-Lys(Mhoc)-Lys(Mhoc)-Arg(NO_2)-Arg(NO_2)-Pro-OH (amino acid sequence 11—19 of ACTH), in which a new protecting group, 9-methyl-9-fluorenyloxycarbonyl (Mfoc), is utilized for the temporary protection of an α-amino function.

In the preceding paper[1] we described the syntheses of the amino acid sequence 22—39 of porcine corticotropin (α_p-ACTH) and that of the human hormone (α_h-ACTH). In the present communication we wish to report the synthesis of an undecapeptide derivative, Z-Lys(Mhoc)-Pro-Val-Gly-Lys(Mhoc)-Lys(Mhoc)-Arg-Arg-Pro-Val-Lys(Mhoc)-$NHNH_2$ (VII), and a nonapeptide derivative, Z-Lys(Mhoc)-Pro-Val-Gly-Lys(Mhoc)-Lys(Mhoc)-Arg(NO_2)-Arg(NO_2)-Pro-OH (XI), corresponding to the amino acid sequences 11—21 and 11—19, respectively, of ACTH which has been performed as a step of the total synthesis of α_p-ACTH and α_h-ACTH.[2]

Synthesis of Undecapeptide Derivative VII. The synthetic procedure of undecapeptide VII is outlined in Fig. 1. The ε-amino function of lysines and the guanidino function of arginines were protected by the 1-methylcyclohexyloxycarbonyl (Mhoc) group and by the nitro group, respectively. The Mhoc group is much the same as the *t*-butoxycarbonyl (Boc) group in susceptibility toward acid reagents.[3] The dicyclohexylcarbodiimide (DCC)-mediated coupling of Boc-Arg(NO_2)-OH with proline benzyl ester yielded a dipeptide (I), which was purified on a silica gel column with a chloroform–methanol system as solvent. Compound I was treated with trifluoroacetic acid and the resulting N^{α}-free peptide was allowed to react with the pentachlorophenyl ester[4] of Z-Arg(NO_2)-OH. The product was purified by chromatography to give a tripeptide (II) in a 70% yield. Compound II was treated with hydrogen bromide in acetic acid for the simultaneous removal of benzyloxycarbonyl (Z) and benzyl ester groups to yield III. This was then coupled with Z-Lys(Mhoc)-OSu[5] to give a tetrapeptide (IV) in an 82% yield after chromatographic purification on a silica gel column with a chroloroform–methanol–acetic acid system as solvent.

A dipeptide derivative Z-Val-Lys(Mhoc)-OMe[5] was hydrogenolyzed to remove its Z group and the product was coupled with IV by the DCC method in the presence of 1-hydroxybenzotriazole (HOBt)[6] to produce a hexapeptide (V) in an excellent yield. Catalytic hydrogenolysis of V yielded H-Lys(Mhoc)-Arg-Arg-Pro-Val-Lys(Mhoc)-OMe. This compound, which was found to be homogeneous in TLC and found to have no appreciable absorption owing to the presence of nitro group, was allowed to react with the azide derived from Z-Lys(Mhoc)-Pro-Val-Gly-Lys(Mhoc)-$NHNH_2$[5] in

H-Pro-OBzl
↓ Boc-Arg(NO_2)-OH, DCC
Boc-Arg(NO_2)-Pro-OBzl (I)
↓ CF_3COOH
H-Arg(NO_2)-Pro-OBzl
↓ Z-Arg(NO_2)-OPcp[4]
Z-Arg(NO_2)-Arg(NO_2)-Pro-OBzl (II)
↓ HBr/AcOH
H-Arg(NO_2)-Arg(NO_2)-Pro-OH (III)
↓ Z-Lys(Mhoc)-OSu[5]
Z-Lys(Mhoc)-Arg(NO_2)-Arg(NO_2)-Pro-OH (IV)
↓ H-Val-Lys(Mhoc)-OMe, DCC (+HOBt)
Z-Lys(Mhoc)-Arg(NO_2)-Arg(NO_2)-Pro-Val-Lys(Mhoc)-OMe (V)
↓ H_2/Pd
H-Lys(Mhoc)-Arg-Arg-Pro-Val-Lys(Mhoc)-OMe
↓ Z-Lys(Mhoc)-Pro-Val-Gly-Lys(Mhoc)-N_3[5]
Z-Lys(Mhoc)-Pro-Val-Gly-Lys(Mhoc)-Lys(Mhoc)-Arg-Arg-Pro-Val-Lys(Mhoc)-OMe (VI)
↓ NH_2NH_2
Z-Lys(Mhoc)-Pro-Val-Gly-Lys(Mhoc)-Lys(Mhoc)-Arg-Arg-Pro-Val-Lys(Mhoc)-$NHNH_2$ (VII)

Fig. 1. Synthesis of amino acid sequence 11—21 of ACTH.
Mhoc: 1-methylcyclohexyloxycarbonyl; HOPcp: pentachlorophenol.

* All the amino acid residues mentioned in this communication are of the L-configuration. Abbreviations used are those recommended by the IUPAC-IUB Commission of Biochemical Nomenclature [*Biochemistry*, **5**, 2485 (1966); *ibid.*, **6**, 362 (1967); *ibid.*, **11**, 1726 (1972)], and include Mhoc: 1-methylcyclohexyloxycarbonyl, Mfoc: 9-methyl-9-fluorenyloxycarbonyl, and HOPcp: pentachlorophenol.

the usual manner. The product was purified on a silica gel column with chloroform–methanol–acetic acid systems as solvent to give an undecapeptide ester (VI) in a pure form. The hydrazinolysis of ester VI yielded the desired undecapeptide hydrazide (VII) whose sufficient purity was confirmed by TLC and elemental analysis. The acid hydrolysates of VI and VII were also found to contain the constituent amino acids in the correct ratios expected by theory.

In the above synthesis of VII the three peptide subunits, which were respectively synthesized in the step-by-step manner from their C-terminal, were connected by the azide procedure and the DCC–HOBt method[6] to form a Lys–Lys bond and a Pro–Val bond, respectively. In addition, there was not employed any alkaline treatment throughout the synthesis. Thus, the cause of racemization associated with chemical processes was fully eliminated. Compound VII has successfully been employed as an intermediate in the total synthesis of α_p-ACTH and α_h-ACTH.[2]

Synthesis of Nonapeptide Derivative XI. The synthetic route to XI was illustrated in Fig. 2. In introducing a lysine residue to position 16, its N^{α}-protecting group was required to be the one selectively removable in the presence of the N^{ε}-Mhoc and the N^{G}-nitro groups. A purpose of the present synthesis is to examine if a new protecting group 9-methyl-9-fluorenyloxycarbonyl (Mfoc), which has been introduced by us recently,[3] meets this requirement.

Z–Arg(NO_2)–Arg(NO_2)–Pro–OMe[5]
↓ HBr/AcOH
H–Arg(NO_2)–Arg(NO_2)–Pro–OMe
↓ Mfoc–Lys(Mhoc)–ONp (VIII)
Mfoc–Lys(Mhoc)–Arg(NO_2)–Arg(NO_2)–Pro–OMe (IX)
↓ 20% HCOOH/AcOH
H–Lys(Mhoc)–Arg(NO_2)–Arg(NO_2)–Pro–OMe
↓ Z–Lys(Mhoc)–Pro–Val–Gly–Lys(Mhoc)–N_3[5]
Z–Lys(Mhoc)–Pro–Val–Gly–Lys(Mhoc)–Lys(Mhoc)–Arg(NO_2)–Arg(NO_2)–Pro–OMe (X)
↓ OH^-
Z–Lys(Mhoc)–Pro–Val–Gly–Lys(Mhoc)–Lys(Mhoc)–Arg(NO_2)–Arg(NO_2)–Pro–OH (XI)

Fig. 2. Synthesis of amino acid sequence 11—19 of ACTH.
Mhoc: 1-methylcyclohexyloxycarbonyl; Mfoc: 9-methyl-9-fluorenyloxycarbonyl.

First, H–Lys(Mhoc)–OH[3] was acylated with 9-methyl-9-fluorenyl azidoformate[3] in the presence of Triton B (benzyltrimethylammonium hydroxide) as base and under anhydrous conditions[7] to give Mfoc–Lys(Mhoc)–OH, from which the *p*-nitrophenyl ester (VIII) was derived by the DCC method in the usual manner. A tripeptide derivative Z–Arg(NO_2)–Arg(NO_2)–Pro–OMe[5] was treated with hydrogen bromide in acetic acid and the resulting N^{α}-free compound isolated in the form of acetic acid salt was allowed to react with VIII. The product was purified on a silica gel column with a chloroform–methanol system as solvent to give a tetrapeptide (IX) in pure form. The subsequent treatment of IX with 20% formic acid in acetic acid achieved the selective removal of the N^{α}-Mfoc group. The removal was complete within 7 h, in which any appreciable cleavage of the Mhoc group was not observed. The N^{α}-free tetrapeptide thus obtained was then coupled with the pentapeptide azide, derived from Z–Lys(Mhoc)–Pro–Val–Gly–Lys(Mhoc)–$NHNH_2$[5] by the treatment with nitrous acid in the usual manner, to give a protected nonapeptide ester (X) in an excellent yield. In the final step ester X was saponified with alkali under the same conditions as those employed for the saponification of Z–Lys(Mhoc)–Arg(NO_2)–Arg(NO_2)–Pro–OMe, in which no appreciable racemization seemed to occur,[5] and the product was purified on a silica gel column with a chloroform–methanol system as solvent to give the desired compound (XI). The purity of XI was confirmed by TLC and elemental analysis. Nonapeptide XI has been utilized as an intermediate in our first synthesis of α_h-ACTH.[2]

Experimental

Thin-layer chromatography (TLC) was performed on silica gel plates (Kieselgel GF_{254} or precoated Kieselgel $60F_{254}$, Merck) with the following solvent systems: A, chloroform–methanol (85: 15); B, chloroform–methanol (3: 1); C, chloroform–methanol–acetic acid (90: 10: 3); D, chloroform–methanol–acetic acid (80: 20: 3); E, ethyl acetate–acetic acid–water (4: 1: 1); F, 1-butanol–acetic acid–water (4: 1: 2).

Boc–Arg(NO_2)–Pro–OBzl (I). An aqueous solution of H–Pro–OBzl·HCl (2.42 g, 10 mmol) was treated with 50% potassium carbonate (5 ml) at 0 °C in the presence of dichloromethane. The organic phase separated was dried over magnesium sulfate and evaporated *in vacuo* at a bath temperature of 20 °C. The resulting proline ester free base and Boc–Arg(NO_2)–OH (3.19 g, 10 mmol) were coupled with dicyclohexylcarbodiimide (DCC; 2.06 g, 10 mmol) in *N,N*-dimethylformamide (DMF)–ethyl acetate in the presence of 1-hydroxybenzotriazole (HOBt; 1.35 g, 10 mmol) at 4 °C; for 20 h. The crude product was purified on a column of silica gel (100 g, Kieselgel H, Merck) with chloroform–methanol (93: 7) as solvent. The fractions (10 g/tube) were examined by TLC in system A and those containing the desired compound as a single component (tubes 62—70) were combined and evaporated *in vacuo* to afford I as a sirupy residue.

Z–Arg(NO_2)–Arg(NO_2)–Pro–OBzl (II). Compound I obtained above was treated with trifluoroacetic acid (10 ml) at room temperature for 60 min. The precipitates which separated upon addition of ether were dissolved in DMF (30 ml) together with HOBt (1.3 g, 10 mmol) and triethylamine (1.4 ml, 10 mmol) and to this was added Z–Arg(NO_2)–OPcp (6.0 g, 10 mmol)[4] at 0 °C. The mixture was stirred at 4 °C overnight followed by evaporation *in vacuo* at a bath temperature of 45 °C. The oily residue was dissolved in aqueous ethyl acetate and the solution was washed with 1M acetic acid and evaporated *in vacuo*. The crude product thus obtained was submitted to a silica gel column (140 g, Kieselgel H, Merck) with chloroform–methanol (90: 10) as solvent. The fractions (12 g/tube) were examined by TLC in system A and those containing the desired product as a single component (tubes 41—60) were combined and evaporated *in vacuo*. The residue was precipitated from ethyl acetate–ether; yield 5.35 g (70%), $[\alpha]_D^{26}$ $-48.4\pm0.9°$

(*c* 1.0, methanol).

Found: C, 51.79; H, 6.04; N, 20.17%. Calcd for $C_{33}H_{43}N_{11}O_{11}$: C, 51.49; H, 5.63; N, 20.02%.

Z-Lys(Mhoc)-Arg(NO_2)-Arg(NO_2)-Pro-OH (IV). Compound II (1.49 g, 1.93 mmol) was treated with 25% hydrogen bromide in acetic acid (20 ml) at room temperature for 3 h. The precipitates which separated upon addition of ether were dissolved in DMF (10 ml) together with triethylamine (1.33 ml, 9.7 mmol) and to the resulting solution was added Z-Lys(Mhoc)-OSu[5] prepared from the dicyclohexylamine salt of Z-Lys(Mhoc)-OH (1.16 g, 1.93 mmol).[3] The mixture was kept at 4 °C for 2.5 days followed by evaporation *in vacuo*. To the residue were added 1-butanol-ethyl acetate (1: 1, 20 ml) and 1M acetic acid (20 ml), and the mixture was shaken vigorously. The organic phase separated was evaporated *in vacuo* (1.6 g). This was purified on a column of silica gel (70 g, Kieselgel H, Merck) with chloroform-methanol-acetic acid (80: 20: 3) as solvent to give IV in pure form; yield 1.50 g (82%), mp 138—140 °C, $[\alpha]_D^{25}$ −37.5 ±0.8° (*c* 1.0, methanol).

Z-Lys (Mhoc)-Arg (NO_2)-Arg (NO_2)-Pro-Val-Lys (Mhoc)-OMe (V). A solution of Z-Val-Lys(Mhoc)-OMe (0.54 g, 1 mmol)[5] in 10% acetic acid in methanol was submitted to hydrogenolysis over palladium for 2 h followed by evaporation *in vacuo*. The residue was dissolved in dichloromethane and the solution was shaken with 50% potassium carbonate at 0 °C. The organic phase was dried over magnesium sulfate at 0 °C and evaporated *in vacuo* at a bath temperature of 20 °C. The resulting dipeptide ester free base and IV (0.94 g, 1 mmol) were coupled with DCC (0.41 g, 2 mmol) in DMF in the presence of HOBt (0.27 g, 2 mmol). The reaction was allowed to proceed at 4 °C for 2.5 days. The crude product was repeatedly precipitated from methanol-ether to give a pure preparation of V; yield 1.26 g (95%), mp 125—130 °C, $[\alpha]_D^{28}$ −55.6±0.9° (*c* 1.0, methanol). TLC: homogeneous (sulfuric acid) in system D.

Found: C, 53.63; H, 7.48; N, 17.13%. Calcd for $C_{59}H_{96}N_{16}O_{17}\cdot H_2O$: C, 53.70; H, 7.49; N, 16.99%.

Z-Lys(Mhoc)-Pro-Val-Gly-Lys(Mhoc)-Lys(Mhoc)-Arg-Arg-Pro-Val-Lys(Mhoc)-OMe (VI). Compound V (0.90 g, 0.69 mmol) was hydrogenolyzed over palladium in acetic acid to give the partially deblocked hexapeptide ester (acetate); no appreciable absorption at 275 nm. TLC: homogeneous (ninhydrin and Sakaguchi reagents) in system F.

An ethyl acetate solution of the azide, derived from Z-Lys(Mhoc)-Pro-Val-Gly-Lys(Mhoc)-$NHNH_2$ (0.73 g, 0.76 mmol) in the same manner as described previously,[5] was combined with a solution of the hexapeptide ester obtained above and triethylamine (0.5 ml, 3.5 mmol) in DMF (3 ml). The mixture was, after removal of ethyl acetate by evaporation at a bath temperature of 5 °C, stirred at 4 °C for 2.5 days. After addition of another quantity of the pentapeptide azide, freshly prepared from the hydrazide (0.33 g, 0.35 mmol), the mixture was stirred for one more day followed by evaporation *in vacuo*. The residue was dissolved in aqueous ethyl acetate and the solution was washed with 1M acetic acid and evaporated. The crude product thus obtained (1.50 g) was then purified on a silica gel column (50 g, Kieselgel 60, Merck) with chloroform-methanol-acetic acid system (90: 10: 3, 100 ml; 80: 20: 3, 100 ml; 60: 40: 3, 200 ml) as solvent to give a pure preparation of VI; yield 1.04 g (76%), mp 129—130 °C, $[\alpha]_D^{24}$ −58.7±1.0° (*c* 1.0, methanol). TLC: a single component (ninhydrin, after preheating at 150 °C) in systems D, E, and F. Amino acid ratios in acid hydrolysate (theoretical values are given in parentheses): Lys 4.00 (4), Arg 1.92 (2), Pro 1.84 (2), Gly 1.00 (1), Val 2.01 (2).

Z-Lys (Mhoc)-Pro-Val-Gly-Lys (Mhoc)-Lys (Mhoc)-Arg-Arg-Pro-Val-Lys(Mhoc)-$NHNH_2$ (VII). Compound VI (0.98 g, 0.49 mmol) was treated with hydrazine hydrate (0.25 ml) in DMF (5 ml) at 37 °C for 40 h. The solvent was evaporated *in vacuo*. To the resulting residue were added 1M acetic acid (15 ml) and 1-butanol-ethyl acetate (1: 1, 15 ml) and the mixture was shaken vigorously. The organic phase was separated and evaporated *in vacuo* (0.95 g). A 0.85 g portion of this product was dissolved in aqueous ethyl acetate and the solution was repeatedly extracted with 1 M acetic acid. The aqueous solutions combined were lyophilized to afford VII; yield 0.79 g (90%), $[\alpha]_D^{24.5}$ −55.4 ±1.1° (*c* 0.9, methanol). TLC: almost homogeneous (ninhydrin, after preheating at 150 °C) in system F. Amino acid ratios in acid hydrolysate: Lys 4.07 (4), Arg 2.01 (2), Pro 1.95 (2), Gly 1.00 (1), Val 2.10 (2).

Found: C, 55.49; H, 8.41; N, 14.78%. Calcd for $C_{97}H_{165}N_{23}O_{21}\cdot 2CH_3COOH\cdot 4H_2O$: C, 55.60; H, 8.36; N, 14.77%.

Mfoc-Lys(Mhoc)-ONp (VIII). N^{ϵ}-Mhoc-lysine (1.43 g, 5 mmol)[3] and 40% benzyltrimethylammonium hydroxide in methanol (Triton B, 2.4 ml) were dissolved in DMF (4 ml) and the solvent was evaporated *in vacuo* at a bath temperature of 45 °C. The residue was redissolved in DMF (10 ml) and 9-methyl-9-fluorenyl azido-formate (1.85 g, 7 mmol)[3] was added. The reaction mixture was stirred at 4 °C for 24 h followed by evaporation *in vacuo*. The residue was dissolved in ethyl acetate and the solution was washed with 1M citric acid and water, dried over magnesium sulfate and evaporated *in vacuo*. The residue was purified on a column of silica gel (50 g, Kieselgel H, Merck) with chloroform-methanol (95: 5) as solvent to give Mfoc-Lys(Mhoc)-OH as an oil; yield 1.65 g (59%).

The diacyllysine thus obtained was dissolved in ethyl acetate along with *p*-nitrophenol (0.42 g, 3 mmol) and to this was added DCC (0.62 g, 3 mmol). The mixture was stirred at 4 °C for 20 h followed by evaporation *in vacuo*. The resulting oily residue was precipitated from methanol-petroleum ether to give VIII; yield 1.95 g (97%). This was used for the subsequent coupling reaction without further purification.

Mfoc-Lys(Mhoc)-Arg(NO_2)-Arg(NO_2)-Pro-OMe (IX). Z-Arg(NO_2)-Arg(NO_2)-Pro-OMe (2.05 g, 3 mmol)[5] was treated with 28% hydrogen bromide in acetic acid (10 ml) at room temperature for 60 min. The precipitates which formed upon addition of ether (1.40 g) were dissolved in water (10 ml) and Amberlite CG-400 (acetate form, wet vol. 10 ml) was added. The mixture was shaken for 30 min and then filtered off. The filtrate was evaporated to give a residue which was dried over sodium hydroxide pellets and phosphorus pentoxide *in vacuo* (1.30 g).

The tripeptide methyl ester obtained above was allowed to react with VIII (1.95 g, 2.88 mmol) in DMF (5 ml) in the present of triethylamine (0.6 ml, 4.4 mmol) at 4 °C for 24 h. The crude product was chromatographed on a column of silica gel (70 g, Kieselgel H, Merck) with chloroform-methanol (95: 5) as solvent to give IX in pure form; yield 2.10 g (92%) mp 135—140 °C decomp., $[\alpha]_D^{25}$ −60.9±1.0° (*c* 1.0, methanol). TLC: homogeneous (sulfuric acid) in system A.

Found: C, 54.55; H, 6.66; N, 17.15%. Calcd for $C_{47}H_{67}N_{13}O_{13}\cdot H_2O$: C, 54.27; H, 6.69; N, 17.51%.

Z-Lys(Mhoc)-Pro-Val-Gly-Lys(Mhoc)-Lys(Mhoc)-Arg-(NO_2)-Arg(NO_2)-Pro-OMe (X). Compound IX (0.52 g, 0.5 mmol) was dissolved in 20% formic acid in acetic acid (6 ml) and the solution was allowed to stand at room temperature for 7 h. The solvent was evaporated and the residue was triturated with ether. The resulting precipitates were filtered off and dried over potassium hydroxide pellets *in vacuo*. To this were added ethyl acetate (15 ml) and 1M

acetic acid (15 ml) and the mixture was shaken vigorously. The organic phase was extracted again with 1M acetic acid. The combined aqueous solution was washed with ethyl acetate, concentrated *in vacuo* and lyophilized.

The N^{α}-free tetrapeptide obtained above was dissolved in DMF and triethylamine (0.07 ml, 0.5 mmol) was added. To this was added an ethyl acetate solution of Z-Lys(Mhoc)-Pro-Val-Gly-Lys(Mhoc)-N_3, derived from the corresponding hydrazide (0.72 g, 0.75 mmol),[5] and the mixture was concentrated *in vacuo* at a bath temperature of 0—5 °C to remove ethyl acetate. The resulting solution was stirred at 4 °C for 20 h followed by evaporation *in vacuo*. The precipitates which formed upon addition of ether were reprecipitated from ethyl acetate to yield X in pure form; yield 0.83 g (96%), mp 130—135 °C, $[\alpha]_D^{23}$ $-52.7\pm0.9°$ (*c* 1.0, methanol). TLC: homogeneous (ninhydrin, after pretreatment with hydrobromic acid) in system A.

Found: C, 55.71; H, 7.68; N, 15.37%. Calcd for $C_{80}H_{130}N_{20}O_{22}$: C, 55.73; H, 7.60; N, 16.25%.

Z-Lys(Mhoc)-Pro-Val-Gly-Lys(Mhoc)-Lys(Mhoc)-Arg-(NO_2)-Arg(NO_2)-Pro-OH (XI). Compound X (0.83 g, 0.48 mmol) in methanol (2 ml) was treated with 2 M sodium hydroxide (0.48 ml) at room temperature for 2 h. The mixture was neutralized by the addition of ice-cold 1M hydrochloric acid (0.96 ml) and then diluted with water. This was repeatedly extracted with 1-butanol–ethyl acetate (1: 1). The organic solutions were combined, washed three times with water and evaporated *in vacuo*. The residue was chromatographed on a column of silica gel (30 g, Kieselgel 60, Merck) with chloroform–methanol (95: 5) as solvent for the first 20 fractions (10 ml/tube) and with chloroform–methanol (80: 20) for the rest. The fractions containing the desired product as a single component (tubes 37—55), as examined by TLC in system B, were combined and evaporated *in vacuo*. The residue was solidified by tritutation with ether to afford XI; yield 0.43 g (50%), mp 160—170 °C, $[\alpha]_D^{24.5}$ $-35.5\pm0.8°$ (*c* 1.0, methanol). TLC: homogeneous (ninhydrin, after pretreatment with hydrobromic acid) in system B.

Found: C, 53.12; H, 7.53; N, 15.40%. Calcd for $C_{79}H_{128}N_{20}O_{22}\cdot 4H_2O$: C, 53.24; H, 7.69; N, 15.72%.

References

1) K. Watanabe and K. Inouye, *Bull. Chem. Soc. Jpn.*, **50**, 201 (1977).
2) K. Inouye, K. Watanabe, and H. Otsuka, *Bull. Chem. Soc. Jpn.*, **50**, 211 (1977).
3) K. Inouye, K. Watanabe, and K. Namba, unpublished data.
4) J. Kovacs, M. Q. Ceprini, C. A. Dupraz, and G. N. Schmit, *J. Org. Chem.*, **32**, 3696 (1967).
5) K. Inouye, Y. Sumitomo, and M. Shin, *Bull. Chem. Soc. Jpn.*, **49**, 3620 (1976)
6) W. König and R. Geiger, *Chem. Ber.*, **103**, 788 (1970).
7) P. Sieber and B. Iselin, *Helv. Chim. Acta*, **51**, 622 (1968).

Synthesis of Corticotropin Peptides. XVI. The Total Syntheses of Porcine and Human Corticotropins*

Ken INOUYE, Kunio WATANABE, and Hideo OTSUKA

Shionogi Research Laboratory, Shionogi & Co., Ltd., Fukushima-ku, Osaka 553

(Received June 29, 1976)

The syntheses are described of two nonatriacontapeptides corresponding to the primary structure of porcine corticotropin (α_p-ACTH) and that of human hormone (α_h-ACTH). The porcine peptide is synthesized by assembling three fragment peptides corresponding to ACTH(1—10), ACTH(11—21) and α_p-ACTH (22—39). The Synthetic product is compared with natural α_p-ACTH in terms of chemical, physicochemical, and biological properties to establish their identity. The human peptide is synthesized *via* two different routes, one of which is the same as that employed for the synthesis of porcine peptide. The two synthetic preparations of human peptide are not only indistinguishable from each other, but also very similar to α_p-ACTH in various items of physicochemical measurements and in the *in vivo* steroidogenesis assay. The collected data prove the satisfactory synthesis of α_h-ACTH as well as α_p-ACTH.

The thirty-nine amino acid sequence of porcine corticotropin (α_p-ACTH) was first proposed by Shepherd *et al.*[1] in 1956 and its total synthesis was accomplished by Schwyzer and Sieber[2] in 1963. The primary structure tentatively proposed for the human hormone (α_h-ACTH)[3] was synthesized by Bajusz *et al.*[4] in 1967.

Natural α_p-ACTH was known to be deamidated upon mild alkaline treatment.[5] Recently, it has also been found by Gráf *et al.*[6] and Riniker *et al.*[7] that the natural preparations of α_p-ACTH and α_h-ACTH undergo deamidation at the same rate in dilute aqueous ammonia. However, the synthetic product of α_p-ACTH[2,7] and that of α_h-ACTH[4,6] were stable under the same conditions. These synthetic peptides contained a single amide group in the form of Gln 30. The inconsistency observed between the natural and the synthetic preparations prompted them to reexamine the structures of these two mammalian hormones. As a result, the primary structure of α_p-ACTH was revised in 1971.[6,7] At the same time, the correct amino acid sequence 22—39 (a tryptic fragment) of α_h-ACTH was also presented.[7] Subsequent to the above revisions, the 1—20 sequence of α_h-ACTH, which had been proposed only on the homology with the hormones from other species, was confirmed by Bennett *et al.*[8] Figure 1 shows the amino acid sequences of porcine and human hormones thus established; note that the only structural difference between the two mammalian hormones resides in position 31, Leu in α_p-ACTH and Ser in α_h-ACTH, and that these structures contain a single amide group in the form of Asn 25. The synthesis of the revised structure of α_h-ACTH was reported by Sieber *et al.*[9] Kisfaludy *et al.*[10] and Nishimura *et al.*[11] A solid-phase synthesis was described by Yamashiro and Li.[12] Very recently Yajima *et al.* have accomplished the synthesis of α_p-ACTH.[13] We wish now to report the total syntheses of α_p-ACTH and α_h-ACTH performed on the basis of our own strategy.

	1	2	3	4	5	6	7	8
α_p-ACTH (Ip):	H-Ser-	Tyr-	Ser-	Met-	Glu-	His-	Phe-	Arg-
α_h-ACTH (Ih):	H-Ser-	Tyr-	Ser-	Met-	Glu-	His-	Phe-	Arg-

	9	10	11	12	13	14	15	16	17
(Ip):	Trp-	Gly-	Lys-	Pro-	Val-	Gly-	Lys-	Lys-	Arg-
(Ih):	Trp-	Gly-	Lys-	Pro-	Val-	Gly-	Lys-	Lys-	Arg-

	18	19	20	21	22	23	24	25	26
(Ip):	Arg-	Pro-	Val-	Lys-	Val-	Tyr-	Pro-	Asn-	Gly-
(Ih):	Arg-	Pro-	Val-	Lys-	Val-	Tyr-	Pro-	Asn-	Gly-

	27	28	29	30	31	32	33	34	35
(Ip):	Ala-	Glu-	Asp-	Glu-	**Leu**-	Ala-	Glu-	Ala-	Phe-
(Ih):	Ala-	Glu-	Asp-	Glu-	**Ser**-	Ala-	Glu-	Ala-	Phe-

	36	37	38	39
(Ip):	Pro-	Leu-	Glu-	Phe-OH
(Ih):	Pro-	Leu-	Glu-	Phe-OH

Fig. 1. Primary structures of porcine corticotropin (α_p-ACTH)[1,6,7] and human corticotropin (α_h-ACTH).[3,7,8]

In the preceding papers, we described the synthesis of an undecapeptide derivative corresponding to ACTH-(11—21),[14] and that of octadecapeptides, α_p-ACTH-(22—39) and α_h-ACTH(22—39).[15] The two octadecapeptides were obtained simultaneously with an identical synthetic procedure, except for the introduction of the amino acid residue in position 31. The fully deblocked porcine peptide was identified with the α_p-ACTH(22—39) isolated from a tryptict digest of

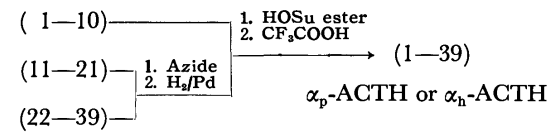

(1—10): Boc-Ser-Tyr-Ser-Met-Glu(OBu^t)-His-Phe-Arg-Trp-Gly-OH (II)[16]

(11—21): Z-Lys(Mhoc)-Pro-Val-Gly-Lys(Mhoc)-Lys(Mhoc)-Arg-Arg-Pro-Val-Lys(Mhoc)-$NHNH_2$ (III)[14]

(22—39): H-Val-Tyr-Pro-Asn-Gly-Ala-Glu(OBu^t)-Asp(OBu^t)-Glu(OBu^t)-R-Ala-Glu(OBu^t)-Ala-Phe-Pro-Leu-Glu(OBu^t)-Phe-OBu^t (IVp: R=Leu, IVh: R=Ser)[15]

Fig. 2. Outlined route for the synthesis of α_p-ACTH and α_h-ACTH (route A). Z: benzyloxycarbonyl, Boc: *t*-butoxycarbonyl, Bu^t: *t*-butyl, Mhoc: 1-methylcyclohexyloxycarbonyl, HOSu: *N*-hydroxysuccinimide.

* All the amino acid residues mentioned in this communication are of the L-configuration. Abbreviations used are those recommended by the IUPAC-IUB Commission of Biochemical Nomenclature [*Biochemistry*, **5**, 2585 (1966); *ibid.*, **6**, 362 (1967); *ibid.*, **11**, 1726 (1972)], and include Mhoc: 1-methylcyclohexyloxycarbonyl.

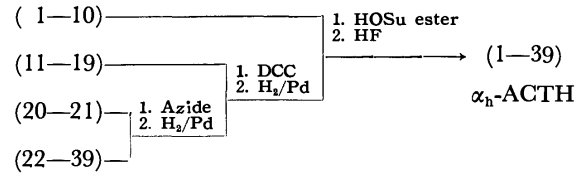

(11—19): Z-Lys(Mhoc)-Pro-Val-Gly-Lys(Mhoc)-Lys(Mhoc)-Arg(NO_2)-Arg(NO_2)-Pro-OH (V)[14]
(20—21): Z-Val-Lys(Mhoc)-$NHNH_2$[19c]

Fig. 3. Alternative synthesis of α_h-ACTH (route B). Z: benzyloxycarbonyl, Mhoc: 1-methylcyclohexyloxycarbonyl, HOSu: *N*-hydroxysuccinimide, DCC: dicyclohexylcarbodiimide.
For (1—10) and (22—39), see Fig. 2.

natural α_p-ACTH.[15] This proved the satisfactory synthesis of porcine peptide and that of human peptide as well. The synthesis of the decapeptide derivative corresponding to ACTH(1—10) was reported previously.[16] The present paper describes the formation of the nonatriacontapeptides, corresponding to α_p-ACTH and α_h-ACTH, from these fragment peptides according to the route illustrated in Fig. 2. An alternative synthesis of α_h-ACTH is also described, in which a nonapeptide derivative corresponding to ACTH(11—19)[14] is utilized as an intermediate (Fig. 3).

Synthesis of Porcine Hormone, α_p-ACTH (Ip). The synthesis started with the coupling of the C-terminal octadecapeptide derivative (IVp, Fig. 2) and the undecapeptide azide, derived from III (Fig. 2) by the treatment with an alkyl nitrite in an anhydrous acid solution,[17] to give a nonacosapeptide Z-Lys(Mhoc)-Pro-Val-Gly-Lys(Mhoc)-Lys(Mhoc)-Arg-Arg-Pro-Val-Lys(Mhoc)-Val-Tyr-Pro-Asn-Gly-Ala-Glu(OBu^t)-Asp(OBu^t)-Glu(OBu^t)-Leu-Ala-Glu(OBu^t)-Ala-Phe-Pro-Leu-Glu(OBu^t)-Phe-OBu^t (IXp). The crude preparation of IXp was purified by partition chromatography on a column of Sephadex LH-20 with 1-butanol-acetic acid-water (4: 1: 2) as solvent. The sufficient purity was confirmed by TLC and by amino acid analysis of the acid hydrolysate. The yield was 64%. Compound IXp thus obtained was then submitted to catalytic hydrogenolysis and the product was chromatographed on a silica gel column with ethyl acetate-acetic acid-water (4: 1: 1) as solvent to give the N^{α}-free nonacosapeptide (Xp) corresponding to α_p-ACTH-(11—39).

The protected decapeptide (II, Fig. 2) corresponding to ACTH(1—10) was synthesized as reported previously,[16] except that in the azide couplings involved Boc-Ser-Tyr-$NHNH_2$ and Boc-Ser-Tyr-Ser-Met-$NHNH_2$ were converted into the corresponding azides by the treatment with an alkyl nitrite,[17] instead of nitrous acid formerly used, to improve the coupling yields significantly. The crude preparation of II was purified on a silica gel column with ethyl acetate-acetic acid-water (4: 1: 1) as solvent. The final reaction connecting the N-terminal decapeptide with the rest of the molecule of α_p-ACTH was performed by the *N*-hydroxysuccinimide (HOSu) ester method.[18] The same procedure had been employed in our synthesis of the ACTH peptides with shorter chain lengths.[19] The decapeptide active ester derived from II was allowed to react with Xp obtained above to give a protected nonatriacontapeptide Boc-Ser-Tyr-Ser-Met-Glu(OBu^t)-His-Phe-Arg-Trp-Gly-Lys(Mhoc)-Pro-Val-Gly-Lys(Mhoc)-Lys(Mhoc)-Arg-Arg-Pro-Val-Lys(Mhoc)-Val-Tyr-Pro-Asn-Gly-Ala-Glu(OBu^t)-Asp(OBu^t)-Glu(OBu^t)-Leu-Ala-Glu(OBu^t)-Ala-Phe-Pro-Leu-Glu(OBu^t)-Phe-OBu^t. The crude product was, without purification, deprotected with trifluoroacetic acid in the presence of anisole and 2-mercaptoethanol as scavengers, followed by the treatment with Amberlite CG-400 (acetate form). Purification of the product was achieved by repeated chromatography on a carboxymethyl cellulose column using an ammonium acetate buffer with a linear concentration gradient of 0—0.4 M (Figs. 4 and 5). The synthetic α_p-ACTH (Ip) thus obtained was found to be homogeneous in TLC and its acid hydrolysate contained the constituent amino acids in the ratios predicted by theory with an exception of tryptophan. The Tyr/Trp ratio in intact Ip was 2.06,

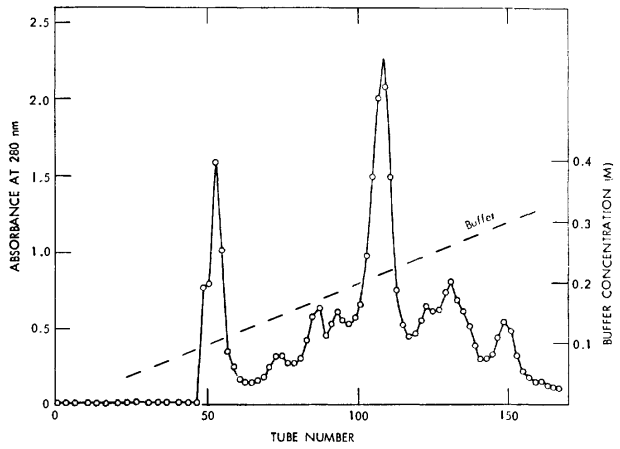

Fig. 4. Carboxymethyl cellulose column chromatography of crude synthetic α_p-ACTH: sample, 0.46 g; column, CM-52 (Whatman), 2.1×22 cm; buffer, 0—0.4 M ammonium acetate (pH 6.5), 1800 ml; fractionation, 9 ml/tube.

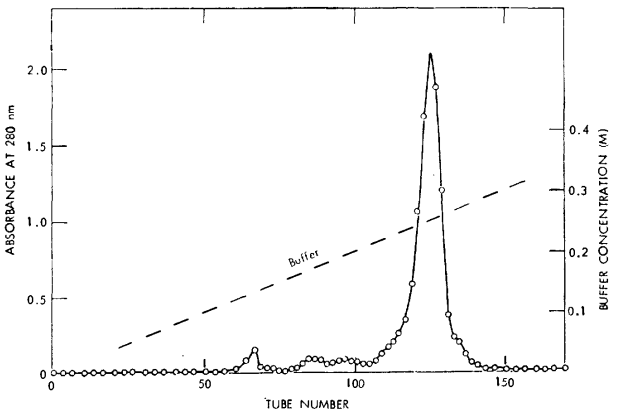

Fig. 5. Rechromatography of partially purified synthetic α_p-ACTH on a carboxymethyl cellulose column: sample, 0.15 g, derived from Fig. 4 (for details see Experimental); column, CM-52 (Whatman), 2.8×22 cm; buffer, 0—0.4 M ammonium acetate (pH 6.5), 1800 ml; fractionation, 9 ml/tube.

as determined spectrophotometrically.[20] The overall yield of Ip for the final coupling, deprotection and purification processes was 26%, when the molecular weight of 5050, estimated from ultraviolet absorption on the assumption that $E^{1\%}_{1cm}=17.7$ (at $\lambda^{0.1MHCl}_{max}=276$ nm) for 100% peptide content,[9] was employed.

An authentic sample of α_p-ACTH to be compared with the synthetic peptide was obtained by purification of a commercial preparation from porcine origin. The crude preparation (Sigma)[21] was submitted to chromatography on a column of carboxymethyl cellulose, in which 0.1 M sodium acetate (pH 6.2) was used as a buffer and the elution of peptide was effected by increasing the concentration of sodium chloride added to the buffer. The fractions containing the desired material were combined and passed through an Amberlite XAD-2 column to remove inorganic salts. The peptide remained on the column was eluted with a mixture of ethanol–0.1 M acetic acid (1: 1) quantitatively. The purified porcine hormone was found to be homogeneous in TLC and amino acid analysis also confirmed its sufficient purity. The Tyr/Trp ratio in intact peptide was 1.94, as determined spectrophotometrically.[20]

The synthetic peptide (Ip) and the natural hormone, obtained as described above, were indistinguishable from each other by electrophoresis on polyacrylamide gel at pH 4.0 (Fig. 6)[22] and pH 9.4 (Fig. 7)[23] and by TLC (cellulose) with 1-butanol–acetic acid–pyridine–water (30: 6: 20: 24) as solvent. The ultraviolet absorption spectra of the synthetic and natural preparations were identical within the precision of measurements. The optical rotatory dispersion and circular dichroism spectra of the synthetic peptide were virtually identical with those of the natural hormone as shown in Tables 1 and 2.[24]

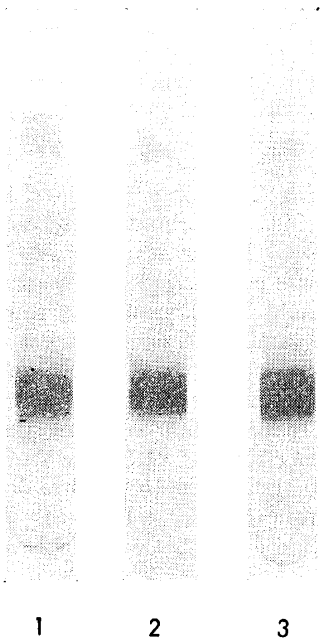

Fig. 6. Electrophoresis of α_p-ACTH and α_h-ACTH preparations on 15% polyacrylamide gel at pH 4.0: 1, natural α_p-ACTH, 60 μg; 2, synthetic α_p-ACTH, 60 μg; 3, synthetic α_h-ACTH, 60 μg. Detection, by staining with Amido-Black 10B.

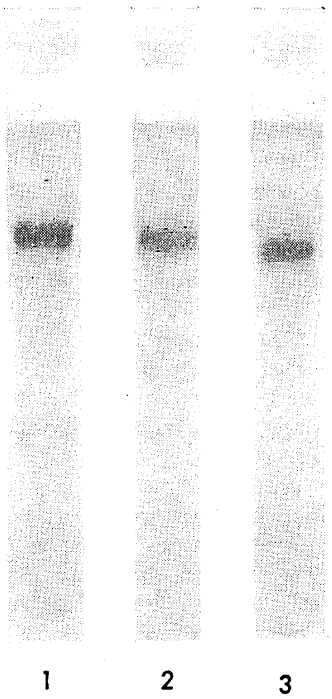

Fig. 7. Electrophoresis of α_p-ACTH and α_h-ACTH preparations on 7.5% polyacrylamide gel at pH 9.4: 1, natural α_p-ACTH, 20 μg; 2, synthetic α_p-ACTH, 20 μg; 3, synthetic α_h-ACTH, 20 μg. Detection, by staining with Amido-Black 10B.

Table 1. Optical rotatory dispersion of natural and synthetic corticotropins[24]

λ (nm)	$[\alpha]^{25}_{\lambda}$		
	Natural α_p-ACTH	Synthetic α_p-ACTH	Synthetic α_h-ACTH
450	−211	−216	−219
400	−309	−313	−296
350	−407	−433	−389
300	−722	−753	−692
250	−1660	−1760	−1560
240	−2160	−2330	−1940
230	−2920	−3050	−2790

Table 2. Circular dichroism of natural and synthetic corticotropins[24]

λ (nm)	$[\theta]^{25}_{\lambda}$		
	Natural α_p-ACTH	Synthetic α_p-ACTH	Synthetic α_h-ACTH
310	0	0	0
287	−37	−43	−33
260	0	0	0
239	−280	−283	−210
233	—	—	0
232	0	0	—

Electrophoretic patterns of a tryptic hydrolysate of the synthetic material were identical with those obtained with the natural hormone. The tryptic digestion

[substrate: enzyme=50 (w/w)] was carried out at pH 8.2 and 37 °C for 60 min and the electrophoresis on a cellulose plate (Cellulose F, Merck) was performed at pH 6.9 in 0.1 M collidine acetate. Recently, it has been shown that natural α_p-ACTH undergoes alkaline deamidation at the asparagine residue in position 25 to form the corresponding aspartyl-α/β-peptide[6,7] which can be distinguished from the intact hormone by electrophoresis on polyacrylamide gel at pH 9.[6] This was equally observed with our synthetic and natural preparations of porcine ACTH, when they were treated with 0.1 M ammonia at 37 °C according to Gráf *et al.*[6] Their electrophoretic patterns are not shown here, since they were virtually the same as those obtained with our synthetic human hormone which are shown in Fig. 12.

Finally, the synthetic material and the authentic porcine hormone were compared for the *in vivo* steroidogenic activity to demonstrate that the former was as active as the latter, when the assays were performed by a method based on the elevated levels of 11-hydroxycorticosteroids in the adrenal venous blood of the hypophysectomized rat in response to intravenous administration of a test sample (Table 3).[25]

TABLE 3. *In vivo* STEROIDOGENIC ACTIVITY OF NATURAL AND SYNTHETIC CORTICOTROPINS[25]

Peptide		Activity[a] (units/mg)
α_p-ACTH	Natural	94.2
	Synthetic	98.1
α_h-ACTH	Synthetic (route A)[b]	98.6
	Synthetic (route B)[c]	98.7

a) The Third USP Corticotropin Reference Standard was used as reference. b) See Fig. 2. c) See Fig. 3.

In view of the correspondence between our synthetic α_p-ACTH and the natural hormone in terms of chemical, physicochemical and biological properties, we conclude that their identity has now been established.

Synthesis of Human Hormone, α_p-ACTH (Ih). The human hormone was synthesized by two different routes A (Fig. 2) and B (Fig. 3). Route A is exactly the same as that employed for the synthesis of the porcine hormone, except that the octadecapeptide derivative (IVh, Fig. 2) was used as a starting material. The intermediate nonacosapeptide, Z-Lys(Mhoc)-Pro-Val-Gly-Lys(Mhoc)-Lys(Mhoc)-Arg-Arg-Pro-Val-Lys(Mhoc)-Val-Tyr-Pro-Asn-Gly-Ala-Glu(OBu^t)-Asp(OBu^t)-Glu(OBu^t)-Ser-Ala-Glu(OBu^t)-Ala-Phe-Pro-Leu-Glu(OBu^t)-Phe-OBu^t (IXh), corresponding to α_h-ACTH(11—39) was obtained in a 63% yield after purification on a Sephadex LH-20 column. Catalytic hydrogenolysis of IXh yielded the N^α-free peptide, which was coupled with the decapeptide (II) by the HOSu ester method[18] to give a protected nonatriacontapeptide Boc-Ser-Tyr-Ser-Met-Glu(OBu^t)-His-Phe-Arg-Trp-Gly-Lys(Mhoc)-Pro-Val-Gly-Lys(Mhoc)-Lys(Mhoc)-Arg-Arg-Pro-Val-Lys(Mhoc)-Val-Tyr-Pro-Asn-Gly-Ala-Glu(OBu^t)-Asp(OBu^t)-Glu(OBu^t)-Ser-Ala-Glu(OBu^t)-Ala-Phe-Pro-Leu-Glu(OBu^t)-Phe-OBu$_t$. The crude product was deblocked with trifluoroacetic acid

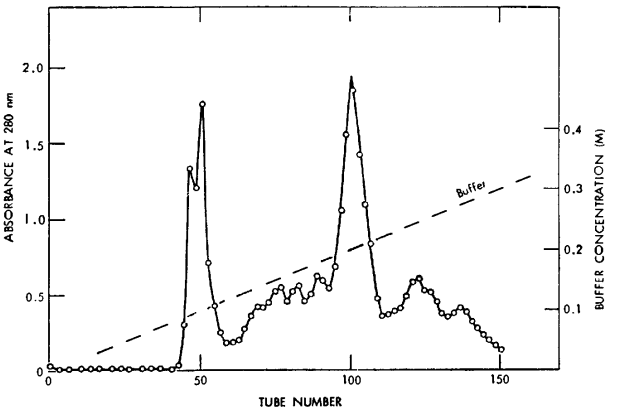

Fig. 8. Carboxymethyl cellulose column chromatography of crude α_h-ACTH synthesized *via* route A: sample, 0.45 g; column, CM-52 (Whatman), 2.1×22 cm; buffer, 0—0.4 M ammonium acetate (pH 6.5), 1800 ml; fractionation, 9 ml/tube.

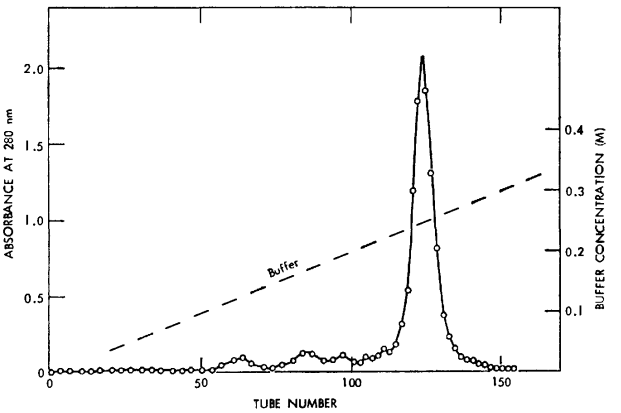

Fig. 9. Rechromatography of partially purified synthetic α_h-ACTH on a carboxymethyl cellulose column: sample, 0.13 g, derived from Fig. 8 (for details see Experimental); column, CM-52 (Whatman), 2.8×22 cm; buffer, 0—0.4 M ammonium acetate (pH 6.5), 1800 ml; fractionation, 9 ml/tube.

and the resulting free peptide isolated in the form of acetate was purified on carboxymethyl cellulose columns (Figs, 8 and 9). The synthetic α_h-ACTH (Ih) thus obtained by route A behaved as a single component in TLC and its acid hydrolysate was found to contain the constituent amino acids in correct ratios with an exception of tryptophan. The Tyr/Trp ratio in intact Ih was 1.98, as determined spectrophotometrically,[20] The overall yield of Ih for the final coupling, deprotection and purification processes was 21.5%, when the molecular weight of 4960, estimated from ultraviolet absorption on the assumption that $E^{1\%}_{1cm}=17.7$ (at $\lambda^{0.1MHCl}_{max}=276$ nm) for 100% peptide content,[9] was employed.

Route B, shown in Fig. 3, represents an alternative synthesis of α_h-ACTH. First, the N^α-free octadecapeptide (IVh, Fig. 2) was acylated with Z-Val-Lys(Mhoc)-N_3, derived from the corresponding hydrazide (Fig. 3)[19c] by the treatment with nitrous acid in the usual manner, to give a protected eicosapeptide (VI) in a 91% yield. Compound VI was submitted to catalytic hydrogenolysis and the resulting N^α-free eicosapeptide was coupled

with nonapeptide V (Fig. 3) corresponding to ACTH-(11—19) by means of DCC in the presence of 1-hydroxybenzotriazole.[26] The product was purified on a silica gel column with chloroform–methanol (9: 1) as solvent to afford a nonacosapeptide, Z-Lys(Mhoc)-Pro-Val-Gly-Lys (Mhoc) - Lys (Mhoc) - Arg (NO_2) - Arg (NO_2)-Pro-Val-Lys (Mhoc)-Val-Tyr-Pro-Asn-Gly-Ala-Glu-(OBu^t)-Asp (OBu^t) -Glu (OBu^t) -Ser-Ala-Glu (OBu^t)-Ala-Phe-Pro-Leu-Glu(OBu^t)-Phe-OBu^t (VII), in a 47% yield. Simultaneous removal of the benzyloxycarbonyl (Z) and two nitro groups from VII was attempted by catalytic hydrogenolysis. However, the reaction gave a product which was reactive to ninhydrin but not to the Sakaguchi reagent. The product was also found to have a maximum absorption at 270 nm ($E^{1\%}_{1cm}$=62.3). These observations strongly suggest that the nitro groups had remained almost intact even after extensive hydrogenolysis. The N^{α}-free nonacosapeptide (VIII) thus obtained was then allowed to react with the HOSu ester of decapeptide II (Fig. 2) to give a protected nonatriacontapeptide Boc-Ser-Tyr-Ser-Met-Glu-(OBu^t)-His-Phe-Arg-Trp-Gly-Lys (Mhoc)-Pro-Val-Gly-Lys (Mhoc) - Lys (Mhoc) - Arg (NO_2) - Arg (NO_2) - Pro-Val-Lys (Mhoc)-Val-Tyr-Pro-Asn-Gly-Ala-Glu-(OBu^t) - Asp(OBu^t) - Glu(OBu^t) - Ser-Ala - Glu(OBu^t)-Ala-Phe-Pro-Leu-Glu(OBu^t)-Phe-OBu^t. The crude product was deprotected by the hydrogen fluoride treatment in the presence of anisole as scavenger[27] to liberate α_h-ACTH as the hydrofluoride. This was treated with Amberlite CG-400 (acetate) in the usual manner. The crude material was purified by chromatography on a carboxymethyl cellulose column using an ammonium acetate buffer (Figs. 10 and 11). The purity of α_h-ACTH (Ih) thus synthesized by route B was confirmed by TLC and by amino acid analysis. The overall yield of Ih for the final coupling, deprotection and purification processes was 29%, as based on the molecular weight of 4960 which was determined spectrophotometrically.

The two synthetic preparations of α_h-ACTH obtained above were indistinguishable from each other by chromatographic and electrophoretic behavior. Their ultraviolet absorption spectra and optical rotations were virtually identical. In addition, they exhibited an identical adrenal-stimulating potency, when assayed for the *in vivo* steroidogenic activity, as shown in Table 3.[25]

Figures 6 and 7 exhibit the electrophoretic patterns of the synthetic human hormone on polyacrylamide gel at pH 4.0 and pH 9.4, respectively, in which those of the porcine hormone preparations are also shown for comparison. There is no significant difference between the two mammalian hormones. Our synthetic preparations of α_h-ACTH obtained above were treated with 0.1 M ammonia at 37 °C according to Gráf *et al.*[6] and the product was submitted to polyacrylamide gel electrophoresis at pH 9. A typical result is shown in

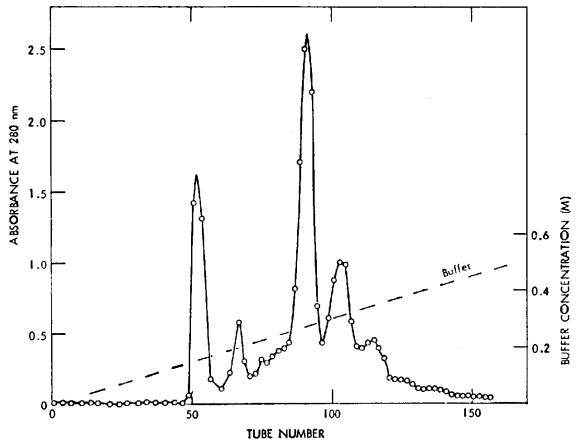

Fig. 10. Carboxymethyl cellulose column chromatography of crude α_h-ACTH synthesized *via* route B: sample, 0.34 g; column, CM-52 (Whatman), 2.1×28 cm; buffer, 0—0.6 M ammonium acetate (pH 6.5), 2000 ml; fractionation, 10 ml/tube.

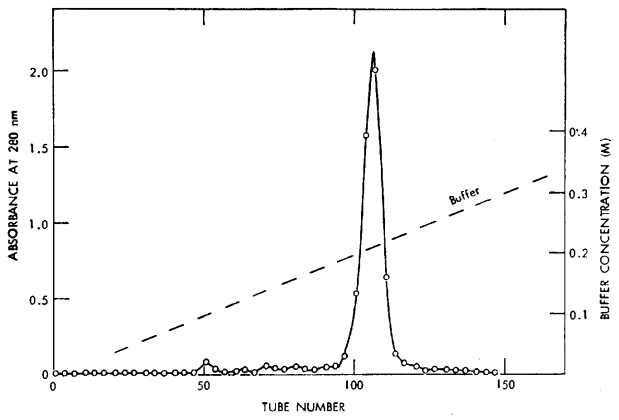

Fig. 11. Rechromatography of partially purified synthetic α_h-ACTH on a carboxymethyl cellulose column: sample, 0.13 g, derived from tubes 75—87 in Fig. 10; column, CM-52 (Whatman), 2.1×28 cm; buffer, 0—0.4 M ammonium acetate (pH 6.5), 2000 ml; fractionation, 10 ml/tube.

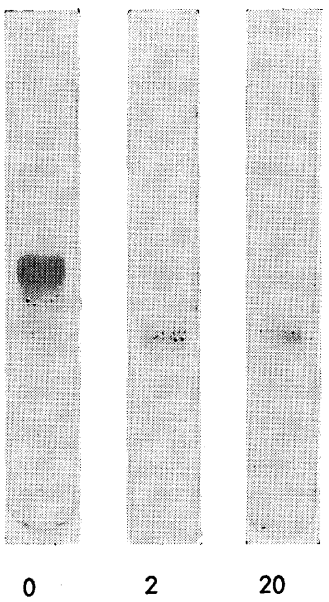

Fig. 12. Electrophoretic patterns of synthetic α_h-ACTH after 0, 2, and 20 h of incubation in 0.1 M ammonia at 37 °C: electrophoresis, on 7.5% polyacrylamide gel at pH 9.4; detection, by staining with Amido-Black 10B.

Figure 12, in which the electrophoretic patterns demonstrate that the synthetic hormone is mostly converted into the deamidated form in 2 h and the complete conversion is attained within 20 h. Virtually the same patterns were obtained with our synthetic as well as natural preparations of α_p-ACTH as described above. These results clearly indicate that the labile Asn 25 is present intact in our synthetic preparations of both α_p-ACTH and α_h-ACTH. The optical rotatory dispersion and circular dichroism of synthetic α_h-ACTH were very similar to those of the α_p-ACTH preparations as shown in Tables 1 and 2.[24] In addition, the *in vivo* steroidogenic potencies of the synthetic α_h-ACTH preparations were identical with those of the natural and synthetic preparations of porcine hormone (Table 3). These close similarities observed between the synthetic α_h-ACTH and the porcine hormone are consistent with the fact that the primary structure of α_h-ACTH is identical with that of α_p-ACTH except for Ser 31 (Fig. 1). Although there is no direct evidence to support the identity of our synthetic α_h-ACTH with the natural human hormone, the above observations may allow us to conclude that our synthesis of α_h-ACTH has been accomplished satisfactorily.

Experimental

Thin-layer chromatography was performed on "silica gel" plates (Kieselgel GF_{254} or precoated Kieselgel $60F_{254}$, Merck) or "cellulose" plates (precoated Cellulose G_{254}, Merck) with the following solvent systems: A chloroform–methanol (85: 15); B, ethyl acetate–acetic acid–water (4: 1: 1); C, 1-butanol–acetic acid–water (4: 1: 2); D, 1-butanol–acetic acid–pyridine–water (30: 6: 20: 24).

Z–Val–Lys(Mhoc)–Val–Tyr–Pro–Asn–Gly–Ala–Glu(OBu^t)–Asp(OBu^t)–Glu(OBu^t)–Ser–Ala–Glu(OBu^t)–Ala–Phe–Pro–Leu–Glu(OBu^t)–Phe–OBu^t (VI). Compound IVh (Fig. 2; 0.39 g, 0.016 mmol)[15] was dissolved in dimethyl sulfoxide (DMSO)–*N,N*-dimethylformamide (DMF) (4: 1, 2.5 ml) and to this was added a solution of Z–Val–Lys(Mhoc)–N_3 [derived from the corresponding hydrazide (Fig. 3; 0.22 g, 0.4 mmol)[19c] by the treatment with nitrous acid in the usual manner] in ethyl acetate (10 ml). The mixture was concentrated *in vacuo* at a bath temperature of 5—10 °C to remove ethyl acetate and then stirred at 4 °C overnight. The precipitates which formed upon addition of water were filtered off, washed thoroughly with water and lyophilized from acetic acid. The resulting powder was suspended in ethyl acetate (30 ml) and the suspension was kept at room temperature overnight. The insoluble precipitates were filtered off and dried *in vacuo* to give VI; wt 0.41 g (91%), $[\alpha]_D^{24.5}$ $-16.3\pm1.5°$ (*c* 0.4, DMF). TLC (silica gel): almost homogeneous (ninhydrin, after pretreatment with hydrobromic acid) in system A. Amino acid ratios in acid hydrolysate (theoretical values are presented in parentheses): Asp 2.00 (2), Ser 0.69 (1), Glu 3.89 (4), Pro 2.23 (2), Gly 1.09 (1), Ala 2.98 (3), Val 2.01 (2), Leu 1.00 (1), Tyr 0.61 (1), Phe 1.90 (2).

Z–Lys(Mhoc)–Pro–Val–Gly–Lys(Mhoc)–Lys(Mhoc)–Arg–(NO$_2$)–Arg(NO$_2$)–Pro–Val–Lys(Mhoc)–Val–Tyr–Pro–Asn–Gly–Ala–Glu(OBu^t)–Asp(OBu^t)–Glu(OBu^t)–Ser–Ala–Glu(OBu^t)–Ala–Phe–Pro–Leu–Glu(OBu^t)–Phe–OBu^t (VII). Compound VI (0.40 g, 0.14 mmol) was hydrogenolyzed palladium in water-saturated 1-butanol for 20 h. The solvent was removed by evaporation *in vacuo* at a bath temperature of 45 °C and the residue was treated with ether to yield the N^{α}-free eicosapeptide derivative as an amorphous powder. This was dissolved in DMF (5 ml) along with V (Fig. 3; 0.25 g, 0.14 mmol)[14] and 1-hydroxybenzotriazole (0.080 g, 0.6 mmol), and dicyclohexylcarbodiimide (DCC, 0.12 g, 0.6 mmole) was added. The reaction mixture was stirred at 4 °C for 2 days followed by evaporation *in vacuo*. The residue was treated with ethyl acetate and the insoluble material was filtered off and dried *in vacuo* (0.53 g). The crude product thus obtained was chromatographed on a column of silica gel (30 g, Kieselgel H, Merck) with chloroform–methanol (90: 10) as solvent. Five-g fractions were collected and they were examined by TLC (silica gel, in system A, and sulfuric acid for detection). Tubes 21—50 were pooled and rechromatographed in almost the same manner as above. The fractions containing the desired product as a single component were combined and evaporated *in vacuo* to give a residue which was solidified by trituration with ether; wt 0.30 g (47%), mp 200—205 °C decomp., $[\alpha]_D^{25}$ $-50.5\pm1.8°$ (*c* 0.5, acetic acid).

H–Lys(Mhoc)–Pro–Val–Gly–Lys(Mhoc)–Lys(Mhoc)–Arg–(NO$_2$)–Arg(NO$_2$)–Pro–Val–Lys(Mhoc)–Val–Tyr–Pro–Asn–Gly–Ala–Glu(OBu^t)–Asp(OBu^t)–Glu(OBu^t)–Ser–Ala–Glu(OBu^t)–Ala–Phe–Pro–Leu–Glu(OBu^t)–Phe–OBu^t (VIII). Compound VII (0.30 g) was hydrogenolyzed over palladium in acetic acid (10 ml) for 24 h. The catalyst was filtered off and the filtrate was lyophilized to give the product which was almost homogeneous in TLC (silica gel, in system B, and ninhydrin as reagent for detection). The product was unreactive to the Sakaguchi reagent wt. 0.29 g, λ_{max}^{MeOH} 270 nm ($E_{1cm}^{1\%}$ 62.3). Amino acid ratios in acid hydrolysate: Lys 4.50 (4),[28] Arg 1.67 (2),[28] Asp 1.99 (2), Ser 0.91 (1), Glu 3.94 (4), Pro 4.23 (4), Gly 2.06 (2), Ala 3.02 (3), Val 3.00 (3), Leu 0.94 (1), Tyr 0.74 (1), Phe 1.93 (2).

Z–Lys(Mhoc)–Pro–Val–Gly–Lys(Mhoc)–Lys(Mhoc)–Arg–Arg–Pro–Val–Lys(Mhoc)–Val–Tyr–Pro–Asn–Gly–Ala–Glu(OBu^t)–Asp(OBu^t)–Glu(OBu^t)–Leu–Ala–Glu(OBu^t)–Ala–Phe–Pro–Leu–Glu(OBu^t)–Phe–OBu^t) (IXp). Compound III (Fig. 2; 0.33 g, 0.15 mmol)[14] was dissolved in a mixture of DMSO–DMF (1: 3, 4 ml). The solution was chilled to −20——30 °C and 3.66 M hydrogen chloride in dioxane (0.41 ml) was added. To this was then added isopentyl nitrite (0.022 ml, 0.165 mmol) and the mixture was stirred at −20—−30 °C for 15 min. The resulting azide solution was neutralized with triethylamine (0.23 ml, 1.65 mmol) at −40—−50 °C and combined with a solution of IVp (Fig. 2; 0.24 g, 0.1 mmol)[15] in DMSO–DMF (1: 4, 2.5 ml). The reaction mixture was stirred at 4 °C for 2 days and then evaporated *in vacuo* at a bath temperature of 45 °C to give a residue which was triturated with water. The crude product (0.54 g) was submitted to partition chromatography on a column (2.8×75 cm) of Sephadex LH-20 with 1-butanol–acetic acid–water (4: 1: 2) as solvent. Three-ml fractions were collected and those containing the desired product as a single component (tubes 46—56), as examined by TLC (silica gel, in system C), were combined, evaporated *in vacuo* at a bath temperature of 45 °C and lyophilized from acetic acid (0.21 g). Tubes 57—61 were combined and rechromatographed in the same manner as above to give an additional quantity of the pure peptide (0.08 g). Thus, the total yield of IXp amounted to 0.29 g (64%); $[\alpha]_D^{23.5}$ $-49.6\pm1.0°$ (*c* 0.9, acetic acid). Amino acid ratios in acid hydrolysate: Lys 3.94 (4), NH_3 1.50 (1), Arg 2.00 (2), Asp 1.90 (2), Glu 4.07 (4), Pro 4.01 (4), Gly 1.94 (2), Ala 2.96 (3), Val 2.89 (3), Leu 2.00 (2), Tyr 0.87 (1), Phe 1.96 (2).

Z–Lys(Mhoc)–Pro–Val–Gly–Lys(Mhoc)–Lys(Mhoc)–Arg–Arg–Pro–Val–Lys(Mhoc)–Val–Tyr–Pro–Asn–Gly–Ala–Glu(OBu^t)–Asp(OBu^t)–Glu(OBu^t)–Ser–Ala–Glu(OBu^t)–Ala–Phe–Pro–Leu–Glu(OBu^t)–Phe–OBu^t (IXh). Compound III (Fig.

2; 0.33 g, 0.15 mmol)[14] was converted into the corresponding azide by the treatment with isopentyl nitrite in an acid solution in the same manner as described above. The azide solution [in DMSO–DMF (1: 3, 4 ml)] was neutralized with triethylamine (0.23 ml, 1.65 mmol) at −40—−50 °C and combined with a solution of IVh (Fig. 2; 0.23 g, 0.1 mmol)[15] in DMSO–DMF (1: 3, 4 ml). The reaction was allowed to proceed at 4 °C for 2 days. The crude product (0.53 g) was purified by partition chromatography on a column of Sephadex LH-20 with 1-butanol–acetic acid–water (4: 1: 2) as solvent, in the manner described above for IXp, to give IXh; wt 0.28 g (63%), $[\alpha]_D^{28.5}$ −47.3±1.0° (*c* 0.8, acetic acid). Amino acid ratios in acid hydrolysate: Lys 3.98 (4), NH_3 1.48 (1), Arg 2.00 (2), Asp 1.99 (2), Ser 0.86 (1), Glu 4.03 (4), Pro 4.11 (4), Gly 2.04 (2), Ala 3.06 (3), Val 3.09 (3), Leu 1.00 (1), Tyr 0.91 (1), Phe 1.92 (2).

H–Lys(Mhoc)–Pro–Val–Gly–Lys(Mhoc)–Lys(Mhoc)–Arg–Arg–Pro–Val–Lys(Mhoc)–Val–Tyr–Pro–Asn–Gly–Ala–Glu(OBu^t)–Asp(OBu^t)–Glu(OBu^t)–Leu–Ala–Glu(OBu^t)–Ala–Phe–Pro–Leu–Glu(OBu^t)–Phe–OBu^t (Xp). Compound IXp (0.53 g) was hydrogenolyzed over palladium in acetic acid for 2 days. The catalyst was filtered off and the filtrate was lyophilized. The product was chromatographed on a column of silica gel [50 g, Kieselgel 60 (100—230 mesh), Merck] with ethyl acetate–acetic acid–water (4: 1: 1) as solvent. Three-ml fractions were collected and examined by TLC (silica gel, in system C). The fractions containing the desired product as a single component (tubes 33—40) were combined, evaporated *in vacuo* and lyophilized from acetic acid (0.20 g). Tubes 13—32, containing the starting material which had remained intact, were combined, evaporated *in vacuo* and hydrogenolyzed for 24 h. This was combined with tubes 41—47 and chromatographed in the same manner as described above to give an additional quantity of Xp from tubes 44—60 (0.14 g). The total yield amounted to 0.34 g (65%); $[\alpha]_D^{21}$ −46.8±1.4° (*c* 0.6, acetic acid). Amino acid ratios in acid hydrolysate: Lys 4.00 (4), NH_3 1.38 (1), Arg 2.08 (2), Asp 2.00 (2), Glu 4.24 (4), Pro 3.99 (4), Gly 2.08 (2), Ala 3.07 (3), Val 2.94 (3), Leu 2.00 (2), Tyr 0.96 (1), Phe 2.00 (2).

H–Lys(Mhoc)–Pro–Val–Gly–Lys(Mhoc)–Lys(Mhoc)–Arg–Arg–Pro–Val–Lys(Mhoc)–Val–Tyr–Pro–Asn–Gly–Ala–Glu(OBu^t)–Asp(OBu^t)–Glu(OBu^t)–Ser–Ala–Glu(OBu^t)–Ala–Phe–Pro–Leu–Glu(OBu^t)–Phe–OBu^t (Xh). Compound IXh (0.45 g) was hydrogenolyzed over palladium in acetic acid for 2 days. The product was chromatographed on a silica gel column [70 g, Kieselgel 60 (100—230 mesh), Merck] in exactly the same manner as described above for Xp. The desired product was obtained from tubes 56—77 (0.12 g). Tubes 11—55 combined were evaporated and the residue was hydrogenolyzed again. This was rechromatographed as above to give an additional quantity of Xh (0.24 g). The total yield amounted to 0.36 g (82%); $[\alpha]_D^{25.5}$ −41.5±1.6° (*c* 0.5, acetic acid). Amino acid ratios in acid hydrolysate: Lys 3.89 (4), NH_3 1.17 (1), Arg 1.97 (2), Asp 2.09 (2), Ser 0.98 (1), Glu 4.28 (4), Pro 4.36 (4), Gly 2.13 (2), Ala 3.13 (3), Val 3.03 (3), Leu 1.00 (1), Tyr 0.96 (1), Phe 2.06 (2).

H–Ser–Tyr–Ser–Met–Glu–His–Phe–Arg–Trp–Gly–Lys–Pro–Val–Gly–Lys–Lys–Arg–Arg–Pro–Val–Lys–Val–Tyr–Pro–Asn–Gly–Ala–Glu–Asp–Glu–Leu–Ala–Glu–Ala–Phe–Pro–Leu–Glu–Phe–OH, α_p-ACTH (Ip). A solution of II (Fig. 2; 0.15 g, 0.09 mmol) in DMF (2 ml) was chilled in an ice-bath and 1M hydrochloric acid (0.2 ml) was added. This was introduced into an ice-cold mixture of ethyl acetate–ether (1: 1, 50 ml) and the resulting precipitates were collected by filtration, washed with ether and dried *in vacuo*. The decapeptide hydrochloride thus obtained was dissolved in DMF (3 ml) together with *N*-hydroxysuccinimide (0.041 g, 0.36 mmol) and DCC (0.080 g, 0.39 mmol) was added. The mixture was stirred at 4 °C for 20 h, after which it was introduced into ethyl acetate–ether (1: 1, 70 ml). The precipitates which formed were filtered off, washed with ethyl acetate and ether, and dried *in vacuo* to give the decapeptide active ester hydrochloride.

Compound Xp (0.30 g, 0.069 mmol) was dissolved in DMF (5 ml) and to this was added the active ester obtained above. The mixture was stirred at room temperature for 20 h. Removal of the solvent by evaporation *in vacuo* followed by treatment with ether yielded a crude preparation of the protected nonatriacontapeptide (0.46 g). The crude product obtained above was then treated with trifluoroacetic acid (5 ml) at room temperature for 90 min in the presence of anisole (0.46 ml) and 2-mercaptoethanol (0.46 ml). The precipitates which formed upon addition of ether were filtered off, washed with ether and dried *in vacuo*. The crude deblocked peptide thus obtained was dissolved in water and the solution was passed through a column (1.5×11 cm) of Amberlite CG-400 (acetate). The column was washed with additional portions of water. The aqueous solutions combined were lyophilized to give a crude preparation of Ip (0.46 g).

The crude peptide was submitted to chromatography on a column of carboxymethyl cellulose with an ammonium acetate buffer (Fig. 4). The fractions corresponding to a major peak (tubes 98—117) were combined, evaporated *in vacuo* at a bath temperature of 45 °C and lyophilized to a constant weight (0.12 g). Tubes 81—97 and 118—140 were combined and rechromatographed in the same manner as above. The fractions corresponding to the peak of desired peptide were combined, evaporated and lyophilized (0.03 g). These preparations were combined (0.15 g) and chromatographed again on a carboxymethyl cellulose column (Fig. 5). The fractions corresponding to a major peak (tubes 119—130) were combined, evaporated and lyophilized to give a pure preparation of Ip; wt 0.090 g (26%), $[\alpha]_D^{25}$ −88.0±2.4° (*c* 0.5, 2% acetic acid). Lit, $[\alpha]_D^{27}$ −80.2° (*c* 0.3, 1% acetic acid).[13] $\lambda_{max}^{0.1M\ HCl}$ 276 nm ($E_{1cm}^{1\%}$ 16.0), $\lambda_{shoulder}^{0.1M\ HCl}$ 289 nm ($E_{1cm}^{1\%}$10.3); $\lambda_{max}^{0.1M\ NaOH}$ 282.5 nm ($E_{1cm}^{1\%}$ 17.7), 289 nm ($E_{1cm}^{1\%}$ 18.2). TLC (cellulose): homogeneous to ninhydrin and the Ehrlich reagent in system D. Amino acid ratios in acid hydrolysate: Lys 3.73 (4), His 1.09 (1), Arg 2.79 (3), Asp 1.97 (2), Ser 1.91 (2), Glu 5.26 (5), Pro 4.53 (4), Gly 3.11 (3), Ala 3.00 (3), Val 3.02 (3), Met 1.04 (1), Leu 2.00 (2), Tyr 2.08 (2), Phe 3.07 (3). The Tyr/Trp ratio in intact Ip was 2.06, as determined spectrophotometrically.[20]

H–Ser–Tyr–Ser–Met–Glu–His–Phe–Arg–Trp–Gly–Lys–Pro–Val–Gly–Lys–Lys–Arg–Arg–Pro–Val–Lys–Val–Tyr–Pro–Asn–Gly–Ala–Glu–Asp–Glu–Ser–Ala–Glu–Ala–Phe–Pro–Leu–Glu–Phe–OH, α_h-ACTH (Ih). *a) From Compound Xh*: In the same manner as described above for α_p-ACTH (Ip), the *N*-hydroxysuccinimide ester hydrochloride, derived from II (Fig. 2; 0.16 g, 0.1 mmol), was coupled with Xh (0.33 g, 0.075 mmol) in DMF (5 ml) at room temperature for 20 h to give the protected nonatriacontapeptide (0.46 g). This was submitted to deprotection with trifluoroacetic acid (5 ml) at room temperature for 90 min in the presence of anisole (0.46 ml) and and 2-mercaptoethanol (0.46 ml) and the product was treated with Amberlite CG-400 (acetate) in water to give a crude preparation of Ih (0.45 g).

The crude peptide was chromatographed on a carboxymethyl cellulose column using an ammonium acetate buffer (Fig. 8). The fractions corresponding to a major peak (tubes 93—111) were combined, evaporated *in vacuo* and lyophilized (0.11 g). Tubes 81—92 and 112—140 were combined and rechromatographed in the same manner as above to afford an additional quantity of the desired peptide

(0.02 g). These preparations combined (0.13 g) were chromatographed again on a carboxymethyl cellulose column (Fig. 9) and the fractions corresponding to a major peak (tubes 119—130) were combined, evaporated and lyophilized to give a pure preparation of Ih; wt 0.080 g (21.5%), $[\alpha]_D^{25}$ $-87.2\pm2.8°$ (*c* 0.5, 2% acetic acid). Lit, $[\alpha]_D^{24}$ $-87.6°$ (*c* 0.26, 2% acetic acid).[11] $\lambda_{max}^{0.1M\ HCl}$ 276 nm ($E_{1cm}^{1\%}$ 16.2), $\lambda_{shoulder}^{0.1M\ HCl}$ 289 nm ($E_{1cm}^{1\%}$ 10.6); $\lambda_{max}^{0.1M\ NaOH}$ 282.5 nm ($E_{1cm}^{1\%}$ 17.3), 289 nm ($E_{1cm}^{1\%}$ 18.0). TLC (cellulose): homogeneous to ninhydrin and the Ehrlich reagent in system D. Amino acid ratios in acid hydrolysate: Lys 4.02 (4), His 1.00 (1), Arg 3.23 (3), Asp 2.04 (2), Ser 2.84 (3), Glu 5.08 (5), Pro 4.42 (4), Gly 3.14 (3), Ala 3.05 (3), Val 3.13 (3), Met 0.98 (1), Leu 1.00 (1), Tyr 2.01 (2), Phe 3.03 (3). The Tyr/Trp ratio in intact Ih was 1.98, as determined spectrophotometrically.[20]

b) From Compound VIII. To a solution of VIII (0.31 g, 0.069 mmol) in DMF (5 ml) was added the *N*-hydroxysuccinimide ester hydrochloride, derived from II (0.14 g, 0.089 mmol) in the same manner as described above. The mixture was stirred at room temperature for 20 h and then introduced to ethyl acetate–ether (1: 1, 50 ml) to afford a crude preparation of the protected nonatriacontapeptide (0.43 g). This was then treated with being hydrogen fluoride (20 ml) at 0 °C for 60 min in the presence of anisole (0.5 ml) in the usual manner.[27] Hydrogen fluoride was evaporated *in vacuo* at 0 °C. The resulting residue was dissolved in ice-cold water and the solution was, after being washed with chloroform, passed through a column (1.4×14 cm) of Amberlite CG-400 (acetate). The column was washed with additional portions of water. The aqueous solutions combined were lyophilized to give a crude preparation of Ih (0.34 g).

The crude product thus obtained was chromatographed on a column of carboxymethyl cellulose using an ammonium acetate buffer (Fig. 10). The fractions corresponding to a major peak (tubes 75—87) were combined, concentrated and lyophilized (0.13 g). This was again chromatographed on a carboxymethyl cellulose column in almost the same manner as above (Fig. 11). The fractions corresponding to a single peak (tubes 101—112) were combined and evaporated *in vacuo*. Repeated lyophilization of the residue yielded the desired Ih as colorless fluffy powder: wt 0.100 g (29%), $[\alpha]_D^{24}$ $-86.5\pm4.0°$ (*c* 0.3, 2% acetic acid). $\lambda_{max}^{0.1M\ HCl}$ 276 nm ($E_{1cm}^{1\%}$ 16.0), $\lambda_{shoulder}^{0.1M\ HCl}$ 289 nm ($E_{1cm}^{1\%}$ 10.0); $\lambda_{max}^{0.1M\ NaOH}$ 282.5 nm ($E_{1cm}^{1\%}$ 17.0), 289 nm ($E_{1cm}^{1\%}$ 17.6). TLC (cellulose): homogeneous to ninhydrin and the Ehrlich reagent in system D. Amino acid ratios in acid hydrolysate: Lys 3.75 (4), His 1.14 (1), Arg 2.88 (3), Asp 1.96 (2), Ser 2.51 (3), Glu 4.91 (5), Pro 4.10 (4), Gly 3.12 (3), Ala 2.87 (3), Val 2.97 (3), Met 0.97 (1), Leu 1.00 (1), Tyr 1.99 (2), Phe 2.96 (3). The Tyr/Trp ratio in intact Ih was 1.97, as determined spectrophotometrically.[20]

Purification of Natural α_p-ACTH. A commercial preparation of α_p-ACTH (45 mg)[21] was chromatographed for purification on a column (1.7×10 cm) of carboxymethyl cellulose (CM-52, Whatman) with a 0.1 M sodium acetate buffer (pH 6.2, 1000 ml). The elution was performed by increasing the sodium chloride concentration of buffer linearly from 0 to 0.2 M. Five-ml fractions were collected and their absorption at 280 nm was measured. The fractions corresponding to a major peak (tubes 63—75) were combined and passed through a column (1.1×7 cm) of Amberlite XAD-2, which had been equilibrated with 0.1 M acetic acid, at a flow rate of 35 ml/h. The column was washed with 0.1 M acetic acid (100 ml) and the peptide adsorbed on the column was then eluted with ethanol–0.1M acetic acid (1: 1). Ten ml-fractions were collected and those corresponding to a single peak (tubes 19—33) were combined, evaporated *in vacuo* at a bath temperature of 45 °C and lyophilized; wt 18 mg (recovery 40%),[29] $[\alpha]_D^{21}$ $-84.6\pm3.5°$ (*c* 0.4, 2% acetic acid). $\lambda_{max}^{0.1M\ HCl}$ 276 nm ($E_{1cm}^{1\%}$ 15.5), $\lambda_{shoulder}^{0.1M\ HCl}$ 289 nm ($E_{1cm}^{1\%}$ 10.3); $\lambda_{max}^{0.1M\ NaOH}$ 282.5 nm ($E_{1cm}^{1\%}$ 16.8), 289 nm ($E_{1cm}^{1\%}$ 17.2). TLC (cellulose): homogeneous to ninhydrin and the Ehrlich reagent in system D. Amino acid ratios in acid hydrolysate: Lys 3.84 (4), His 1.05 (1), Arg 2.90 (3), Asp 2.05 (2), Ser 1.79 (2), Glu 4.96 (5), Pro 3.82 (4), Gly 3.11 (3), Ala 3.04 (3), Val 3.00 (3), Met 1.02 (1), Leu 2.06 (2), Tyr 1.98 (2), Phe 3.00 (3). The Tyr/Trp ratio in intact hormone was 1.94 as determined spectrophotometrically.[20]

The authors wish to thank Dr. Akira Tanaka and Mr. Kunihiro Odaguchi for biological assays and Dr. Kaoru Kuriyama and Mr. Tatsuo Iwata for the measurements of optical rotatory dispersion and circular dichroism spectra. They also thank Miss Yoshie Sumitomo for able technical assistance.

References

1) R. G. Shepherd, S. D. Wilson, K. S. Howard, P. H. Bell, D. S. Davies, S. B. Davis, E. A. Eigner, and N. E. Shakespeare, *J. Am. Chem. Soc.*, **78**, 5067 (1956); P. H. Bell, *ibid.*, **76**, 5565 (1954).

2) R. Schwyzer and P. Sieber, *Helv. Chim. Acta*, **49**, 134 (1966); *Nature*, **199**, 172 (1963).

3) T. H. Lee, A. B. Lerner, and V. Buettner-Janusch, *J. Biol. Chem.*, **236**, 2970 (1961).

4) S. Bajusz, K. Medzihradszky, Z. Paulay, and Zs. Láng, *Acta Chim. Acad. Sci. Hung.*, **52**, 335 (1967).

5) R. G. Shepherd, K. S. Howard, P. H. Bell, A. R. Cacciola, R. G. Child, M. C. Davies, J. P. English, B. M. Finn, J. H. Meisenhelder, A. W. Moyer, and J. van der Scheer, *J. Am. Chem. Soc.*, **78**, 5051 (1956).

6) L. Gráf, S. Bajusz, A. Patthy, E. Barát, and G. Cseh, *Acta Biochim. Biophys. Acad. Sci. Hung.*, **6**, 415 (1971).

7) B. Riniker, P. Sieber, W. Rittel, and H. Zuber, *Nature New Biol.*, **235**, 114 (1972); B. Riniker, In: Structure-Activity Relationships of Protein and Polypeptide Hormones, Proceedings of the 2nd International Symposium, Liège 1971, Excerpta Medica, Amsterdam, p. 519.

8) H. P. J. Bennett, *Biochem. J.*, **133**, 11 (1973).

9) P. Sieber, W. Rittel, and B. Riniker, *Helv. Chim. Acta*, **55**, 1243 (1972).

10) L. Kisfaludy, M. Löw, T. Szirtes, I. Schön, M. Sárközi, S. Bajusz, A. Turan, A. Juhász, R. Beke, L. Gráf, and K. Medzihradszky, in: Chemistry and Biology of Peptides, Proceedings of the 3rd American Peptide Symposium, Boston 1972, J. Meienhofer (ed), Ann Arbor Science, Ann Arbor, Michigan (1972), p. 299.

11) O. Nishimura, C. Hatanaka, and M. Fujino, *Chem. Pharm. Bull.*, **23**, 1212 (1975).

12) D. Yamashiro and C. H. Li, *J. Am. Chem. Soc.*, **95**, 1310 (1973).

13) H. Yajima, K. Koyama, Y. Kiso, A. Tanaka, and M. Nakamura, *Chem. Pharm. Bull.*, **24**, 492 (1976).

14) K. Inouye and K. Watanabe, *Bull. Chem. Soc. Jpn.*, **50**, 207 (1977).

15) K. Waranabe and K. Inouye, *Bull. Chem. Soc. Jpn.*, **50**, 201 (1977).

16) H. Otsuka, K. Inouye, F. Shinozaki, and M. Kanayama, *Bull. Chem. Soc. Jpn.*, **39** 1171 (1966).

17) J. Honzl and J. Rudinger, *Coll. Czech. Chem. Commun.*, **26**, 2333 (1961).

18) G. W. Anderson, J. E. Zimmerman, and F. M. Callahan, *J. Am. Chem. Soc.*, **86**, 1839 (1964); *ibid.*, **85**, 3039 (1963).

19) a) K. Inouye, A. Tanaka, and H. Otsuka, *Bull. Chem. Soc. Jpn.*, **43**, 1163 (1970); b) K. Inouye, F. Shinozaki, M. Kanayama, and H. Otsuka, **49**, 3615 (1976); c) K. Inouye, Y. Sumitomo, and M. Shin, *ibid.*, **49**, 3620 (1976).

20) D. H. Beaven and E. R. Holiday, *Adv. Protein Chem.*, **7**, 319 (1952); T. W. Goodwin and R. A. Morton, *Biochem. J.*, **40**, 628 (1946).

21) Porcine ACTH (Grade II), Lot No. 113C-0520, 88 IU/mg, Sigma Chemical Co., St. Louis, Mo., U. S. A.

22) R. A. Reisfelt, U. J. Lewis, and D. E. Williams, *Nature*, **195**, 281 (1962).

23) B. J. Davis, *Ann. N. Y. Acad. Sci.*, **121**, 404 (1964).

24) Optical rotatory dispersion and circular dichroism spectra were obtained on solutions of natural α_p-ACTH, synthetic α_p-ACTH and synthetic α_h-ACTH at concentrations of 0.497, 0.517 and 0.866 mg/ml, respectively, in 0.02% acetic acid. Peptide concentrations were determined from their ultraviolet absorption spectra with the assumption that $E^{1\%}_{1cm} = 17.7$ (at λ_{max} 276 nm).[9] These measurements were performed by Dr. Kaoru Kuriyama and Mr. Tatsuo Iwata of this laboratory on JASCO spectropolarimeters Model ORD/UV-5 and Model ORD/UV-6 for optical rotatory dispersion and circular dichrosium, respectively.

25) These assays were performed by Dr. Akira Tanaka and Mr. Kunihiro Odaguchi of this laboratory.

26) W. König and R. Geiger, *Chem. Ber.*, **103**, 788 (1970).

27) S. Sakakibara, Y. Shimonishi, Y. Kishida, M. Okada, and H. Sugihara, *Bull. Chem. Soc. Jpn.*, **40**, 2164 (1967).

28) Upon acid hydrolysis nitroarginine will decompose to give arginine and ornithine. The latter amino acid overlaps the lysine peak under the conditions used.

29) There were found two major peaks, tubes 18—40 and tubes 63—75, in CM-52 column chromatography of the commercial α_p-ACTH preparation. The desired pure hormone was obtained from tubes 63—75, as described avobe. Tubes 18—40 afforded an adrenocorticotropically inactive material (15 mg) and its amino acid ratios in acid hydrolysate were found to be greatly different from those expected for α_p-ACTH.

The Efficient Oxidation of Thiols to Disulfides with Thallium(III) Acetate

Sakae UEMURA,* Sakuya TANAKA, and Masaya OKANO
Institute for Chemical Research, Kyoto University, Uji, Kyoto 611
(Received July 2, 1976)

The treatment of various kinds of alkane- and arenethiols with thallium(III) acetate in chloroform at 20—30 °C readily affords the corresponding disulfides almost quantitatively, without affecting other functional groups, such as the hydroxyl, amino, and carboxyl in the thiols. Under similar conditions, the reaction of thiobenzoic *S*-acid with thallium(III) acetate gives thallium(III) thiobenzoate, while that of thioacetic *S*-acid yields diacetyl disulfide and thallium(I) thioacetate.

It is generally known that a large variety of metal ions and oxides oxidize thiols to disulfides.[1] However, although the oxidation with lead(IV) acetate has been fully studied,[2,3] there have been no reports on that with thallium(III) salt, which is also a good oxidizing reagent and which shows some resemblance to lead(IV) salt in many organic reactions.[4] We wish now to describe a facile oxidation of thiols to disulfides with thallium(III) acetate.

Table 1. The oxidation of butanethiol with various oxidants in chloroform[a]

Oxidant (mmol)		*n*-BuSH (mmol)	Temp (°C)	Time (h)	Yield (%)[b] of *n*-BuSS-*n*-Bu
$Tl(OAc)_3$	10	30	25—35	1	104[c,d]
$Tl(OAc)_3$	5	10	20—27	1	100[e]
Tl_2O_3	5	15	26—34	1	61
TlOAc	10	10	25—27	5	30
$Hg(OAc)_2$	5	20	20—27	1	32
$Pb(OAc)_4$	5	20	20—27	1	74
—		10	20	2	trace

a) $CHCl_3$ (15 ml). b) Based on the amount of oxidant charged and determined by GLC. c) Isolated yield. d) TlOAc (91%) was isolated. e) TlOAc (95%) was isolated as TlCl by the addition of aq NaCl to the reaction mixture.

First, the oxidation of 1-butanethiol was examined with various thallium salts and lead(IV) and mercury(II) acetate as oxidants in chloroform. The results are shown in Table 1. It is clear that thallium(III) acetate is a more effective reagent than lead(IV) and mercury(II) acetate for disulfide formation, and also that the stoichiometric reduction of thallium(III) acetate to thallium(I) one occurs thus (Scheme 1):

$$2RSH + Tl(OAc)_3 \longrightarrow RSSR + TlOAc + 2AcOH \quad (1)$$

Since thallium(III) acetate was revealed to be a good oxidizing reagent for disulfides, the reaction was applied to various alkane- and arenethiols. It was found that the oxidation proceeded almost quantitatively without affecting other functional groups, such as the hydroxyl, amino, and carboxyl in the thiols. Some typical results are summarized in Table 2, together with some data obtained using lead(IV) acetate. In the case of 2-methyl-2-propanethiol, the oxidation with thallium(III) acetate gave disulfide selectively, while a further oxidized compound, sulfone, was obtained as the major product

Table 2. The oxidation of thiol with thallium(III) and lead (IV) acetates[a]

RSH R	Time (h)	Yield (%) of RSSR[b] oxidant $Tl(OAc)_3$	$Pb(OAc)_4$
n-Bu	1	100[c]	74[c]
t-Bu	2	73	
t-Bu	5	100[c]	37[c,d] (46)
i-Pr	2	100[c]	(76)
$HOCH_2CH_2$	2	80	(91)
EtO_2CCH_2	1	76	66
Ph	1	100	(88)
o-$H_2NC_6H_4$	1	100	(29)
o-$HO_2CC_6H_4$	3	100	(95)
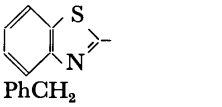	1	100	(81)
$PhCH_2$	1	89	(89)
(L)-$HO_2CCH(NH_2)CH_2$	5	68	4[e]

a) RSH (10 mmol), $M(OAc)_n$ (5 mmol), $CHCl_3$ (15 ml) at 20—30 °C. b) Isolated yield unless otherwise stated. The values in parentheses are from Ref. 2. c) Determined by GLC. d) Other product: *t*-$BuSO_2S$-*t*-Bu (50% yield). e) More than 90% of the lead (IV) salt was recovered (by iodometry).

by the use of lead(IV) acetate. In the case of *o*-aminobenzenethiol, it has been reported that the oxidation with lead(IV) acetate gave disulfide in a low yield, probably because of the oxidation of the amino group by lead(IV) salt.[2] The oxidation with thallium(III) acetate, however, yielded only disulfide quantitatively. In the case of L-cysteine, the oxidation by lead(IV) acetate was very slow compared to that by thallium(III) acetate under nearly the same reaction conditions.

In the oxidation of arenethiols, when the reaction was carried out in the presence of more than two equivalents of thiols to one of thallium(III) acetate, yellow thallium(I) thiolate was formed as well as disulfide, as has previously been reported in the cases with lead(IV) acetate[3] (See Experimental section). The stoichiometry (using three mol of thiols) is shown in Scheme 2. On the other hand, in the cases of alkanethiols, no such thiolate was formed and thallium(I) salt was obtained as the acetate.

$$3ArSH + Tl(OAc)_3 \longrightarrow ArSSAr + TlSAr + 3AcOH \quad (2)$$

Although thiocarboxylic *S*-acids have reacted with lead(IV) acetate to yield diacetyl disulfides,[2,3] the reaction of them with thallium(III) acetate gave slightly different results. That is, the reaction of thiobenzoic

* To whom correspondence should be addressed.

S-acid with thallium(III) acetate in chloroform at room temperature resulted in the formation of thallium(III) thiobenzoate in a good yield (Scheme 3), while that of thioacetic *S*-acid gave diacetyl disulfide and thallium(I) thioacetate (Scheme 4). In the latter case, unstable thallium(III) thioacetate seemed to be formed at first; it then decomposed to give the products. In fact, thallium(III) thiobenzoate also decomposed to thallium-(I) salt and dibenzoyl disulfide upon heating in chloroform or carbon tetrachloride, or even upon standing at room temperature for several days.

$$3PhCOSH + Tl(OAc)_3 \longrightarrow Tl(SCOPh)_3 + 3AcOH \quad (3)$$

$$3CH_3COSH + Tl(OAc)_3 \longrightarrow TlSCOCH_3 + (CH_3COS)_2 + 3AcOH \quad (4)$$

Experimental

The NMR spectra were taken with a Varian EM-360 spectrometer, using $CDCl_3$ as the solvent. The IR and mass spectra were recorded on Hitachi EPI-S2 and JEOL JMS-01SG spectrometers respectively. The GLC analyses were carried out on a Shimadzu 4BMPF apparatus, using an EGSS-X (30%)-Chromosorb W (1 m or 3 m) column. Commercial organic and inorganic materials were used without further purification. The thallium(III) acetate was prepared from thallium(III) oxide and acetic acid.[5]

Reaction of Thiols with $Tl(OAc)_3$. The following is a typical example. To a stirred chloroform (15 ml) solution of 1-butanethiol (2.7 g, 30 mmol) we added solid thallium(III) acetate (3.81 g, 10 mmol) in several portions at 25 °C over a 10-min period. The reaction was exothermic, and the temperature rose to 35 °C during the addition. The resulting yellowish orange mixture was stirred for 1 h. The subsequent evaporation of the chloroform by means of a vacuum evaporator at room temperature left white thallium(I) acetate (2.4 g, 9.1 mmol; mp 130 °C) and organic products, the latter of which was distilled to afford acetic acid (0.5 g, 8.3 mmol; bp 25—35 °C/22 Torr) and dibutyl disulfide (1.85 g, 10.4 mmol; bp 110—118 °C/22 Torr).

Reaction of Benzenethiol with $Tl(OAc)_3$. To a chloroform (15 ml) solution of benzenethiol (3.3 g, 30 mmol) we added several portions of solid thallium(III) acetate (3.81 g, 10 mmol) at 25 °C over a 10-min period. The temperature of the mixture rose to 30 °C during the addition, and a yellow solid of thallium(I) benzenethiolate was precipitated. After 1 h, the solid was filtered off [C_6H_5STl, 2.90 g, 9.3 mmol, 93% yield; mp 255—260 °C (lit,[6] mp 258—260 °C)] and the filtrate was concentrated to give diphenyl disulfide [2.18 g, 10 mmol, 100% yield; mp 59—60 °C (lit,[2] mp 59—61 °C)]. When benzenethiol (20 ml) was added, drop by drop, to a suspension of thallium(III) acetate (10 mmol) in chloroform (15 ml), diphenyl disulfide and thallium(I) acetate were obtained quantitatively. The further addition of the thiol in this case resulted in the formation of thallium(I) benzenethiolate instead of the acetate.

Reaction of Thiobenzoic S-Acid with $Tl(OAc)_3$. The addition of thallium(III) acetate (1.15 g, 3 mmol) to a chloroform (8 ml) solution of thiobenzoic *S*-acid (1.38 g, 10 mmol) at 20—25 °C readily afforded a yellow heterogeneous mixture. After 20 mins' stirring a yellow solid was filtered off and washed with ether. It was revealed to be thallium-(III) thiobenzoate [1.55 g, 2.5 mmol, 84% yield; mp (decomp) 113—114 °C]. IR (hexachlorobutadiene and paraffin mulls), 3070 (w), 1660 (s), 1630 (m), 1590 (m), 1575(m), 1445 (m), 1310 (w), 1195 (s), 1170 (s), 1000 (w), 900 (s), 890 (s), 765 (m), and 675 (s) cm^{-1}. Found: C, 41.10; H, 2.51%. Calcd for $C_{21}H_{15}O_3S_3Tl$: C, 40.95; H, 2.45%. Dibenzoyl disulfide was not detected in the organic extract.

By heating thallium(III) thiobenzoate (0.61 g, 1 mmol) in CCl_4 (15 ml) under reflux for 3 h, dibenzoyl disulfide [0.24 g, 0.88 mmol, mp 125 °C (lit,[3] mp 125—127 °C)] and thallium-(I) thiobenzoate (0.33 g, 0.97 mmol) were isolated. The latter thallium(I) salt was also prepared by the reaction of equimolar amounts of thallium(I) acetate and thiobenzoic acid in ethanol at room temperature for 2 h: mp (decomp) 200—202 °C; Found: C, 24.52; H, 1.30%. Calcd for C_7H_5OSTl: C, 24.60; H, 1.46%.

Reaction of Thioacetic S-Acid with $Tl(OAc)_3$. To a stirred chloroform (10 ml) solution of thioacetic *S*-acid (1.14 g, 15 mmol), we added several portions of solid thallium(III) acetate (1.90 g, 5 mmol) at 25—30 °C. The color of the mixture soon became bright yellow and then gradually changed to pale yellow. After 5 h, a pale yellow solid was filtered off. It was revealed to be thallium(I) thioacetate (1.35 g, 4.82 mmol, 96% yield; mp 76—78 °C). IR (hexachlorobutadiene and paraffin mulls), 1645 (s), 1638(s), 1565 (s), 1545 (sh), 1410 (w), 1348 (m), 1150 (w), 1130 (m), 1110 (s), 950 (m), and 865 (m) cm^{-1}. Found: C, 8.64; H, 1.21%. Calcd for C_2H_3OSTl: C, 8.60; H, 1.08%. The evaporation of chloroform from the organic filtrate left 0.4 g of a residue which was revealed by NMR to consist of almost pure diacetyl disulfide. The distillation of the residue, accompanied by a slight decomposition, gave diacetyl disulfide (0.2 g, 1.33 mmol, 27% yield; bp 40—65 °C/3 Torr), the NMR and IR spectra being identical with those of an authentic sample prepared by the oxidation with $Pb(OAc)_4$.[2]

Reaction of 2-Methyl-2-propanethiol with $Pb(OAc)_4$. The oxidation of 2-methyl-2-propanethiol (0.9 g, 10 mmol) with lead(IV) acetate [2.46 g (90% purity), 5 mmol] in chloroform (15 ml) was carried out at 25—30 °C for 5 h, as in the case with thallium(III) acetate. The lead(II) acetate thus formed (1.40 g, 4.31 mmol) was filtered off, and the subsequent GLC analysis of the filtrate revealed the presence of di-*t*-butyl disulfide (1.85 mmol, 37% yield) and *S*-*t*-butyl 2-methyl-2-propanethiosulfonate, *t*-$BuSO_2S$-*t*-Bu (2.50 mmol, 50% yield). Even when the reaction was stopped within 1 h, the yield of each compound was nearly the same to that described above. The reaction with PbO_2 in place of $Pb(OAc)_4$ was sluggish, and only disulfide was formed. Pure thiosulfonate was isolated by the distillation of the filtrate after the solvent had been removed. Thiosulfonate: bp 122 °C/35 Torr; NMR δ 1.37 (s); MS, (*m/e*) 210 (M^+); IR 1362 (s, ν_{as} SO_2), 1165 (s, ν_s SO_2); Found: C, 45.59; H, 8.92%. Calcd for $C_8H_{18}O_2S_2$: C, 45.68; H, 8.62%. Disulfide: NMR δ 1.30 (s); MS, (*m/e*) 178 (M^+).

References

1) G. Capozzi and G. Modena, "The Chemistry of the Thiol Group," Part 2, ed by S. Patai, John Wiley and Sons, London (1974), p. 801.

2) L. Field and J. E. Lawson, *J. Am. Chem. Soc.*, **80**, 838 (1958).

3) T. Mukaiyama and T. Endo, *Bull. Chem. Soc. Jpn.*, **40**, 2388 (1967).

4) For example, R. J. Ouellette, "Oxidation in Organic Chemistry," ed by W. S. Trahanovsky, Academic Press, London (1973). Part B, Chap. III.

5) K. Ichikawa, S. Uemura, T. Nakano, and E. Uegaki, *Bull. Chem. Soc. Jpn.*, **44**, 545 (1971).

6) H. Gilman and R. K. Abbott, Jr., *J. Am. Chem. Soc.*, **71**, 659 (1949).

Formose Reactions. II. The Photochemical Formose Reaction

Yoshihiro SHIGEMASA, Yoshinobu MATSUDA, Chikahiro SAKAZAWA, and Teruo MATSUURA*

Department of Industrial Chemistry, Faculty of Engineering, Tottori University, Tottori 680
**Department of Synthetic Chemistry, Faculty of Engineering, Kyoto University, Kyoto 606*

(Received July 5, 1976)

Under UV irradiation in the presence of an inorganic base, aqueous formaldehyde was found to give pentaerythritol and 2-hydroxymethylglycerol as the main products, accompanied by the concomitant formation of a mixture of sugars and sugar alcohols. The results indicate that this photochemical formose reaction is considerably different in product distribution from the thermal formose reaction using the $Ca(OH)_2$ catalyst. The detailed examination of the photochemical formose reaction was carried out in the presence of Na_2CO_3, and a possible scheme for the formation of pentaerythritol and 2-hydroxymethylglycerol is proposed.

The formose reaction, which is essentially the autocondensation of formaldehyde by a base catalyst, resulting in the formation of a complex mixture of monosaccharides, has been studied by many investigators. Among various inorganic and organic bases, $Ca(OH)_2$ has been recognized as an excellent catalyst, for this reaction,[1-4] while the mechanism of the sugar formation has been discussed mainly in terms of the aldol condensation between formaldehyde and lower saccharide intermediates.[4-7] In the majority of the reports, the complexity of this reaction has been emphasized. The number of products amounts to more than 30,[8] and this complexity has made it difficult to utilize the method for common carbohydrate resources.

Formose can also be synthesized photochemically. The photochemical sugar formation from formaldehyde was found by Moore *et al.*,[9] who observed the sugar formation under sunlight or irradiation by a mercury lamp in the presence of $FeCl_3$ or uranium compounds as sensitizer. Since Baly *et al.*[10,11] reported that the irradiation of 40% formalin with ultraviolet light in the presence of $CaCO_3$ gives reducing sugars in *ca.* an 8% yield, no significant report on the photochemical formose reaction has appeared. The purpose of the present work is to obtain further information on the effect of additives on the product distribution in the photochemical formose reaction as well as to contribute to the elucidation of the mechanism.

Experimental

Materials. Aqueous formaldehyde solutions were prepared from paraformaldehyde (Merck Co.).[12] All of the inorganic bases used as catalysts were of an analytical grade.

Irradiation Procedure. An aqueous formaldehyde solution (230 ml) containing 15 g of a basic catalyst was irradiated internally with a 450-W high-pressure mercury lamp in a Pyrex tube equipped with a water jacket under stirring in air. The temperature of the solution was maintained at 28—30 °C. After irradiation, the reaction mixture was slightly acidified with 1 M HCl. The formaldehyde consumption and the sugar yield were determined by the methods described in an earlier paper.[12] The amount of the organic acids was determined for acidified 10 ml aliquots by back titration with 2 M KOH.

Thermal Formose Reaction. The reaction was carried out by the method previously described.[12] The sugar products were trimethylsilylated and analyzed by gas chromatography (Fig. 1).

Gas Chromatography. The reaction mixture was evaporated to dryness *in vacuo* at 40 °C by the repeated addition and concentration of water in order to remove formaldehyde as possible. The residue was trimethylsilylated in the usual manner[13] and extracted with chloroform. A Shimadzu GC-5A chromatograph, equipped with a hydrogen-flame ionization detector, was used under the following conditions: coiled glass column of 3 m by 0.3 in. o.d., adsorber, 5% silicon gum SE-30 on 60—80 mesh Chromosorb-W; nitrogen flow rate, 60 ml/min; temperature, 100—250 °C, rising at the rate of 4 °C/min.

Separation and Identification of Products. An aqueous solution (230 ml) containing formaldehyde (55.2 g) and Na_2CO_3 (15.0 g) was irradiated as above for 50 h. The consumption of formaldehyde, the sugar yield, and the yield of organic acid (as formic acid) were determined to be 42.8, 7.5, and 2.5% respectively, based on the starting formaldehyde. The reaction mixture was then passed through columns of Amberlite IR120(H) (120 ml) and Amberlite IRA400 (OH) (500 ml) successively, after which the columns were washed with water (200 and 500 ml respectively). The whole eluate was concentrated *in vacuo* to dryness by the repeated addition and concentration of water in order to remove the formaldehyde. The residue was dissolved in water (50 ml) and diluted with acetone (50 ml) to separate pentaerythritol(I), corresponding to the GLC peak 9 (Fig. 2) (8.8 g; 38% based on the consumed formaldehyde) as colorless crystals (mp 255—256 °C), which were identical with an authentic sample (IR).

The mother liquor was evaporated to a sirup which was chromatographed in 2 g portions as follows. On the top of a column (20 cm by 2.8 cm o.d.) packed with dry cellulose powder, the sample, which had been mixed with a small amount of cellulose powder (Whatman CF-11) and dried in a desiccator, was placed; it was eluted successively with the following solvents: acetone, 500 ml; acetone–methanol (9: 1, v/v), 300 ml; acetone–methanol (8: 2, v/v), 300 ml; acetone–methanol (7:3, v/v), 200 ml; acetone–methanol (5: 5, v/v), 200 ml; methanol, 100 ml. The eluate was then collected in 50 ml portions and was analyzed by GLC and PPC. All the eluates were then divided into two fractions. Fraction A consisted of products corresponding to GLC peaks 1, 2, 3, 4, 5, 6, and 10 (Fig. 2) and amounted to 3.0 g (13%, based on the consumed formaldehyde); the second fraction consisted mainly of a product corresponding to the GLC peak 7 (2.8 g; 12%, based on the consumed formaldehyde). Part of the latter fraction was purified by paper chromatography as follows: Toyo filter paper No. 50; the upper layer of a mixture of 1-butanol–acetic acid–water (4: 1: 5) as the developing solvent; detection by an ammoniacal silver nitrate solution.[14] The chromatogram was extracted with methanol to give 2-hydroxymethylglycerol(II) (GLC peak 7) as a colorless sirup; it was identified from its spectral and analytical data: IR (KBr)

3400, 2950, 1460, 1120, 1040, 910 cm^{-1}; MS 122, 91, 73, 61, 45 *m/e*; Found: C, 39.43; H, 8.16%. Calcd for $C_4H_{10}O_4$: C, 39.34; H, 8.25%. The acetate of 2-hydroxymethylglycerol, NMR ($CDCl_3$) 2.07 (9H, s), 2.08 (3H, s), 4.13 (6H, s).

Amberlite IRA400 (OH) which had been treated with the total reaction mixture was washed with 0.2 M HCl (1 liter), and the washings was concentrated *in vacuo* (Fraction B), (8.5 g; 37%, based on the consumed formaldehyde). Fraction B consisted of products corresponding to GLC peaks (Fig. 2) 8, 14, 15, 20, 21, 23, 24, 27, 29, and organic acids.

Formation of 2-Hydroxymethylglycerol(II) from Glycolaldehyde and Formaldehyde. An aqueous formaldehyde solution (30 ml; 1.7 g) containing 0.75 g of glycolaldehyde and 0.48 g of Na_2CO_3 was stirred at 30 °C without irradiation. At intervals an aliquot was taken up and slightly acidified (pH, 5—6) with 1 M HCl to stop the reaction. The reaction mixture was evaporated to dryness as above, and the residue was trimethylsilylated and analyzed by gas chromatography. The results are shown in Fig. 6.

Photochemical Formation of Pentaerythritol (I). To 20 ml of an aqueous solution of 2-hydroxymethylglycerol (II), concd formalin, Na_2CO_3, and water were added so as to bring the concentrations of II, formaldehyde, and Na_2CO_3 to 0.1 M, 6M, and 0.62 M respectively, and the final volume to 25 ml. A quartz tube containing the solution was irradiated externally with a 450-W high-pressure mercury lamp at 30 °C. At intervals an aliquot was taken up and analyzed as above. The results are shown in Fig. 7.

Results and Discussion

The sugar yields in the photochemical formose reactions with various catalysts are summarized in Table 1.

Table 1. Effect of inorganic base catalyst on the photochemical formose reaction[a)]

Inorganic base	Concentration of base (M)	Sugar yield as glucose (%)
$CaCO_3$	0.86	5.8
$Ca(OH)_2$	0.88	5.2
Na_2CO_3	0.62	8.7
$NaHCO_3$	0.78	4.5
NaOH	1.63	2.0
$Mg(OH)_2$	1.12	6.4

a) Light source, 450-W high-pressure mercury lamp (Pyrex); irradiation time, 72 h; [HCHO]=12.3M; temperature, 30 °C.

In the absence of a basic catalyst, the consumption of formaldehyde became negligible under UV irradiation for 50 h. When $CaCO_3$ was used as the catalyst, the sugar yield (5.8%) was lower than that (8%) reported by Baly.[11)] The discrepancy between these two experimental results might be attributed to differences in the irradiation conditions. The sugar yield was relatively high when Na_2CO_3 was used. The gas chromatogram of the trimethylsilylated products obtained by the use of the Na_2CO_3 catalyst is shown in Fig. 2. It is apparent that the product distribution of the photochemically synthesized formose is simpler than that of the formose prepared by the usual thermal method (Fig. 1). In experiments with the other catalysts listed in Table 1, the GLC patterns were similar to that of Fig. 2, but the product corresponding to peak 9 was obtained in the highest yield in case of the Na_2CO_3 catalyst. Therefore, the detailed studies of the photochemical formose reactions were made using the Na_2CO_3 catalyst.

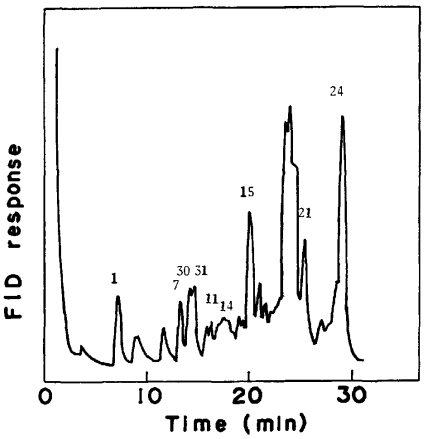

Fig. 1. Gas chromatogram of TMS derivatives of thermosynthesized formose.
[HCHO]=2.0 M; [$Ca(OH)_2$]=0.2 M; Temp, 60 °C; Total volume; 880 ml.[12)]

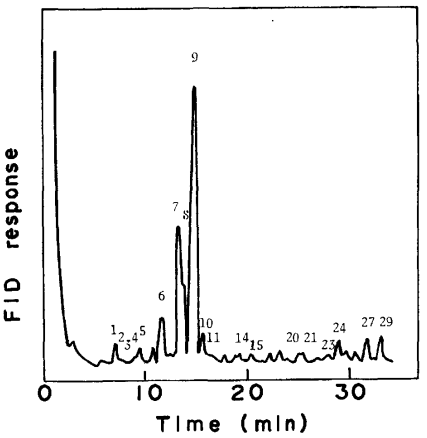

Fig. 2. Gas chromatogram of TMS derivatives of photochemically synthesized formose.
[HCHO]=8.0 M; [Na_2CO_3]=0.62 M; Temp, 30 °C; Light source, 450-W high-pressure mercury lamp; Irradiation time, 50 h; Total volume, 230 ml.

The main products, corresponding to GLC peaks 7 and 9 of Fig. 2, were separated and identified as 2-hydroxymethylglycerol (II) and pentaerythritol (I) respectively. The compound I formed amounts to *ca.* 40% of the total products (by GLC), and the II, to 13%. Fractions A and B are most probably sugar alcohols and sugars respectively, judging from their behavior in the Benedict test (A: negative; B: positive) and the adsorption on the IRA400(OH) resin.

The formaldehyde consumption and the sugar yield in the photochemical formose reaction were found to depend on the formaldehyde concentration, which is shown in Fig. 3. At higher formaldehyde concentrations, both the formaldehyde consumption and the sugar yield increase. At concentrations less than 3 M, the reaction proceeded very slowly under a high-pressure mercury lamp (Pyrex), resulting in a formaldehyde consumption of less than 10% and a negligible formation of the sugars. However, when a 10-W low-pressure mercury

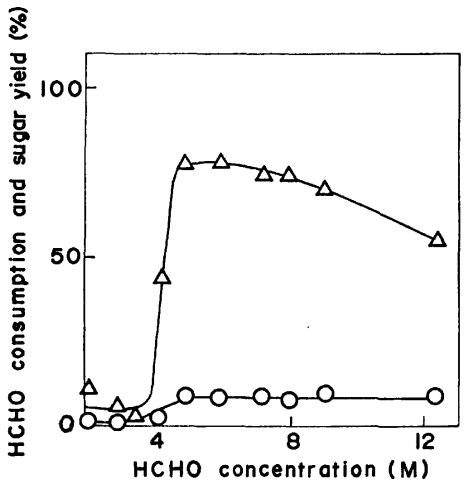

Fig. 3. Effect of HCHO concentrations on the HCHO consumption and the sugar yield.
$[Na_2CO_3]=0.62$ M; Temp, 30 °C; Light source, 450-W high-pressure mercury lamp; Irradiation time, 72 h; Total volume, 230 ml; △, HCHO consumption; ○, Sugar yield.

lamp (quartz tube) was used at a 2 M formaldehyde concentration, the consumption of formaldehyde and the sugar yield were raised to 70 and 5.4% respectively. The gas chromatogram of the products exhibited more than 30 peaks, and no selective formation of I and II was observed.

The sugar yield (usually *ca.* 50%) in the $Ca(OH)_2$-catalyzed formose reaction, in which the Cannizzaro reaction competes with the sugar formation,[5,6] is known to improve upon the addition of methanol because of its inhibitory action on the Cannizzaro reaction.[15] The fact that the sugar yield was low regardless of the formaldehyde concentrations in the photochemical formose reaction (Fig. 3) may be ascribed to the accumulation of formic acid resulting from the Cannizzaro reaction, as may be seen in the decrease in the pH in the course of the reaction (Fig. 5). However, the addition of methanol to the photochemical reaction system

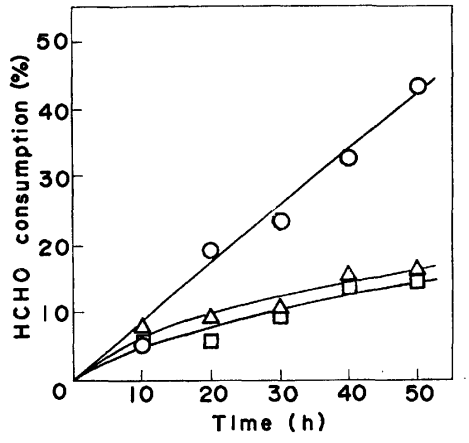

Fig. 4. Effect of methanol addition on the HCHO consumption.
[HCHO]=8.0 M; $[Na_2CO_3]=0.62$ M; Temp, 30 °C; Light source, 450-W high-pressure mercury lamp; [MeOH] (v/v): ○, 0%; △, 50%; □, 100%.

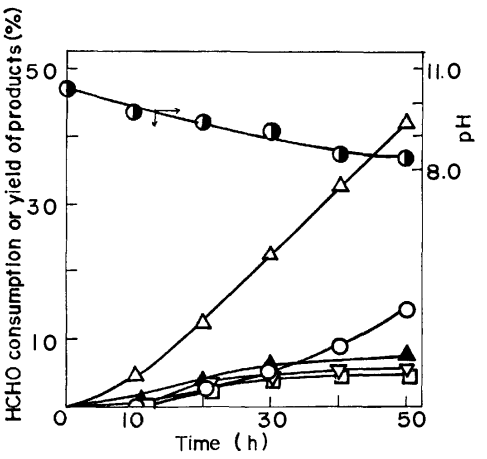

Fig. 5. Time course of the photochemical formose reaction.
[HCHO]=8.0 M; $[Na_2CO_3]=0.62$ M; Temp, 30 °C; Light source, 450-W high-pressure mercury lamp; Total volume, 230 ml; ◑, pH; △, HCHO consumption; ▽, Organic acid (as formic acid); ○, Pentaerythritol; □, 2-hydroxymethylglycerol; ▲, HCHO consumption by dark reaction.

resulted in a decrease in the formaldehyde consumption rate (Fig. 4), and the sugar yield became negligible. This shows that methanol has rather an inhibitory effect on the photochemical formose reaction.

The time course of a typical run of the photochemical formose reaction is shown in Fig. 5. In the earlier stages of the reaction, the yield of pentaerythritol (I) is equal to that of 2-hydroxymethylglycerol (II), but after 40 h the former appreciably exceeds the latter. A lowering of the pH due to the formation of organic acids was also observed. In a control experiment without UV irradiation, formaldehyde was consumed only to a small extent, and it was converted into organic acids nearly quantitatively by the Cannizzaro reaction.

Mechanistic Consideration. The compound I is usually prepared by treating acetaldehyde with about five equivalents of formaldehyde in an aqueous $Ca(OH)_2$ suspension. The reactions proceeds *via* the addition of three molecules of formaldehyde to acetaldehyde, followed by the Cannizzaro reaction of tris(hydroxymethyl)acetaldehyde, leading to I.[16] An attempt was made to detect acetaldehyde in the present photoreaction mixture with morpholine and sodium nitroprusside,[17] but acetaldehyde could not be detected in any stage of the reaction. The gaseous material evolved during the reaction was found by GLC analysis to be O_2 and CO_2 derived from the Na_2CO_3 catalyst.

On the basis of the facts that glycolaldehyde is a product of the first step of the thermal formose synthesis using basic catalysts,[18] and that 2-hydroxymethylglycerol is detected in the final products by GC-MS,[19] the photochemical formose reaction must be: formaldehyde→glycolaldehyde (III)→2-hydroxymethylglycerol (II)→pentaerythritol (I). The following experiments support this sequence.

When an aqueous solution of glycolaldehyde (0.42 M), formaldehyde (1.9 M), and Na_2CO_3 (0.15 M) was allowed to stand at 30 °C, II was formed in *ca.* a 30%

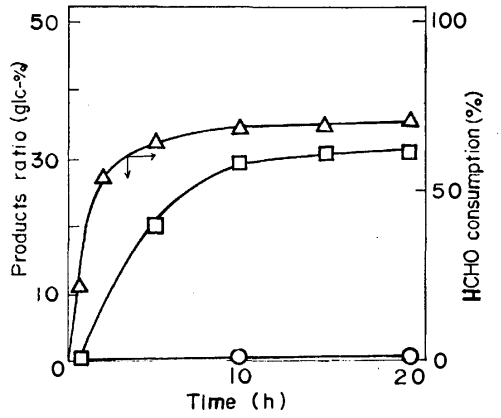

Fig. 6. Formation of 2-hydroxymethylglycerol from glycolaldehyde and formaldehyde.
[HCHO]=1.9 M; [Glycolaldehyde]=0.42 M; [Na_2CO_3]=0.15 M; Temp, 30 °C; Total volume, 30 ml; △, HCHO consumption; □, 2-hydroxymethylglycerol; ○, Pentaerythritol; Products analysis, GLC of TMS derivatives.

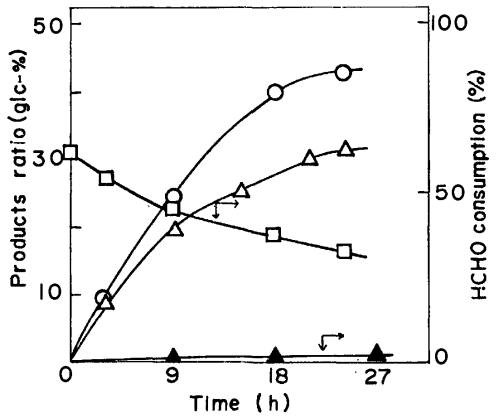

Fig. 7. Photochemical formation of pentaerythritol from 2-hydroxymethylglycerol and formaldehyde.
[HCHO]=6.0 M; [2-hydroxymethylglycerol]=0.1 M; [Na_2CO_3]=0.62 M; Temp, 30 °C; Light source, 450-W high-pressure mercury lamp; Total volume, 25 ml; △, HCHO consumption; ○, Pentaerythritol; □, 2-hydroxymethylglycerol; ▲, HCHO consumption in the absence of Na_2CO_3 (pH=6.6); Product analysis, GLC of TMS derivatives.

yield (by GLC), while formaldehyde was consumed, but no formation of I was detected (Fig. 6). The compound III disappeared rapidly at an early stage of this reaction and was no longer detectable by GLC analysis after 30 min. On the other hand, when an aqueous solution of glycolaldehyde and formaldehyde at the same concentrations was irradiated for 20 h in the absence of Na_2CO_3, the consumption of formaldehyde was less than that in the thermal Na_2CO_3-catalyzed reaction (*ca.* 30%), and neither II nor I was formed. These results indicate that, in the presence of a base and formaldehyde, glycolaldehyde (III) smoothly gives rise to 2-hydroxymethylglycerol (II) by means of a reaction in the dark.

The lack of pentaerythritol formation in the experiment shown in Fig. 6 suggests that the step of pentaerythritol formation in the photochemical formose reaction might require UV irradiation. This was shown by a photochemical formation from II (0.1 M) in the presence of formaldehyde (6 M) and Na_2CO_3 (0.62 M) (Fig. 7). In the course of irradiation, pentaerythritol (I) increases with a decrease in the formaldehyde and II; when UV irradiation was omitted or when the reaction was carried out at pH 5, little formaldehyde was consumed and the formation of I was not observed. At a low concentration of formaldehyde (0.6 M), the yield of I decreases dramatically under a 20 h irradiation.

Now, the pathway of the formation of I and II from formaldehyde under UV irradiation in the presence of a base catalyst can be formulated as is shown in the following scheme:

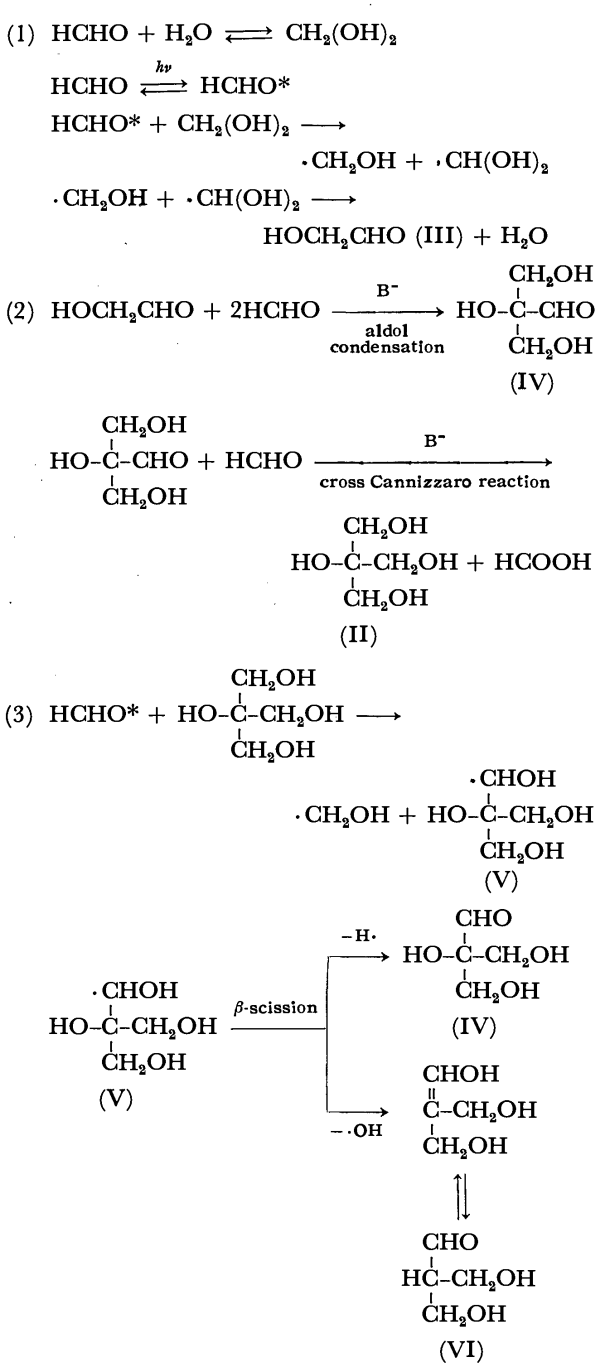

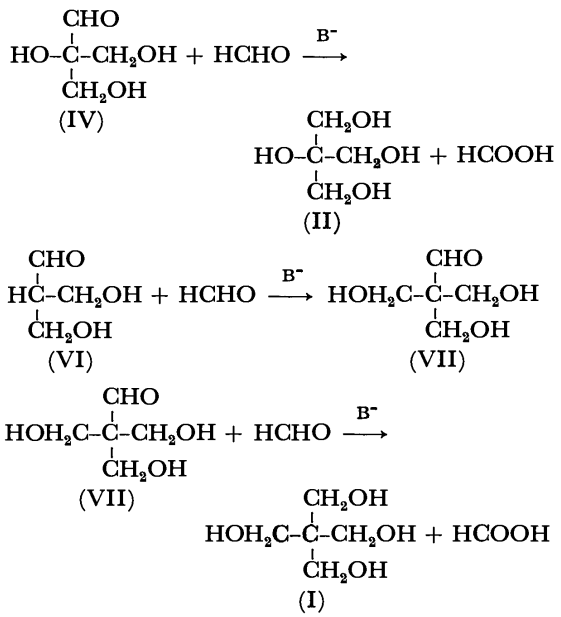

(1) The first step is the formation of glycolaldehyde (III) from formaldehyde with light, as has already been reported by Pribram.[20] An n-π^* excited state of formaldehyde [$\lambda_{max}^{H_2O}$ 288 nm (log ε 1.13)[21]] abstracts hydrogen from its hydrated form,[22] methanediol; this is followed by the coupling of the two radical species.

(2) The second step may consist of thermal processes. In the presence of a base, glycolaldehyde (III) smoothly undergoes aldol condensation with formaldehyde, followed by a cross-Cannizzaro reaction between 2-formylglycerol (IV) and formaldehyde to yield 2-hydroxymethylglycerol (II).

(3) The final step probably involves a photochemical process. An excited state of formaldehyde may abstract hydrogen from a methylene group of II, giving a substituted hydroxymethyl radical (V). The radical may then undergo β-scission to yield either 2-formylglycerol (IV) or bis(hydroxymethyl)acetaldehyde (VI). The oxygen evolved during the reaction may come from the hydroxyl radicals. In the presence of a base and formaldehyde, the former (IV) undergoes a cross-Cannizzaro reaction to revert back to II. The latter (VI) undergoes an aldol condensation with formaldehyde, followed by a cross-Cannizzaro reaction of the tris(hydroxymethyl)-acetaldehyde (VII) thus formed, to yield, finally, pentaerythritol (I).

References

1) H. Franzen and L. Hauck, *J. Prakt. Chem.*, **91**, 261 (1915).
2) R. Mayer and L. Jäschke, *Justus Liebigs Ann. Chem.*, **635**, 145 (1960).
3) T. Mizuno, T. Mori, N. Shiomi, and H. Nakatsuji, *J. Agric. Chem. Soc. Jpn.*, **44**, 324 (1970).
4) A. H. Weiss and T. John, *J. Catal.*, **32**, 216 (1974).
5) H. Tambawala and A. H. Weiss, *J. Catal.*, **26**, 388 (1972).
6) K. Fujino, J. Kobayashi, and I. Higuchi, *Nippon Kagaku Kaishi*, **1972**, 2292.
7) H. Ruckert, E. Pfeil, and G. Scharf, *Chem. Ber.*, **98**, 2558 (1965).
8) T. Mizuno, M. Asai, A. Misaki, and Y. Fujita, *J. Agric. Chem. Soc. Jpn.*, **45**, 344 (1971).
9) B. Moore and T. A. Webster, *Proc. R. Soc. London, Ser. B*, **90**, 168 (1918); *Chem. Zentr.*, **1**, 278 (1919).
10) E. C. C. Baly, I. M. Heilbron, and W. F. Barker, *J. Chem. Soc.*, **1921**, 1025.
11) E. C. C. Baly, *Ind. Eng. Chem.*, **16**, 1016 (1924).
12) Y. Shigemasa, M. Shimano, C. Sakazawa, and T. Matsuura, *Bull. Chem. Soc. Jpn.*, **48**, 2099 (1975).
13) C. C. Sweeley, R. Bentley, M. Makita, and W. W. Wells, *J. Am. Chem. Soc.*, **85**, 2497 (1963).
14) S. M. Partridge and R. G. Westall, *Biochem.*, **42**, 238 (1948).
15) E. Pfeil and G. Schroth, *Chem. Ber.*, **85**, 293 (1952).
16) H. Gilman and A. H. Blatt, *Org. Synth.*, Coll. Vol. I, 425 (1941).
17) L. Lewin, *Ber.*, **32**, 3388 (1899).
18) H. V. Euler and A. Euler, *Ber.*, **39**, 50 (1906).
19) R. D. Partride, A. H. Weiss, and D. Todd, *Carbohyd. Res.*, **24**, 29 (1972).
20) R. Pribram and A. Franke. *Ber.*, **44**, 1035 (1911).
21) R. Bieber and G. Trumpler, *Helv. Chim. Acta*, **30**, 1860 (1947).
22) F. Auerbach and H. Barshall, *Arbb. Kaisarl. Gesundheitsamt.*, **22**, 508 (1905).

The Synthesis of Dimethyl *dl*-3-Ethyl-4-methyl-1,2-cyclopentanedicarboxylates[1]

Shosuke Ito and Yoshimasa Hirata

Department of Chemistry, Faculty of Science, Nagoya University, Chikusa-ku, Nagoya 464

(Received July 6, 1976)

The four 3,4-*cis*-stereoisomers of dimethyl *dl*-3-ethyl-4-methyl-1,2-cyclopentanedicarboxylates (**1a**, **1b**, **1c**, and **1d**) have been synthesized and their configurations established. A comparison of the spectral data and the GLC behaviors has shown that the corresponding ester, one of the key degradation products of ikarugamycin, has the *r*-1, *t*-2, *c*-3, *c*-4-configuration (**1a**). The *r*-1, *t*-2, *c*-3, *t*-4-stereoisomer (**1f**) has also been prepared.

Ikarugamycin[2] is an antibiotic with a unique *as*-hydrindacene skeleton. On permanganate oxidation followed by esterification it yielded a monocyclic ester **1**, $C_8H_{14}(CO_2Me)_2$, along with a number of esters.[2b] The structure of the ester **1** was determined as dimethyl 3-ethyl-4-methyl-1,2-cyclopentanedicarboxylate by spectral data and the concomitant formation of dimethyl 2-ethyl-3-methylglutarate.[2b] Furthermore, the *r*-1, *t*-2, *c*-3, *c*-4 stereochemistry was suggested by the facts: the configuration of the ethyl and methyl groups in the isolated dimethyl 2-ethyl-3-methylglutarate was *erythro*, and the base-catalyzed equilibration of the ester **1** resulted in the recovery of **1** as the major product.[2b]

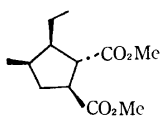
1a

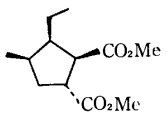
1b

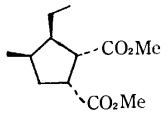
1c

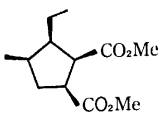
1d

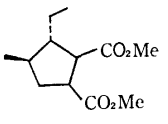
1e

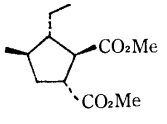
1f

Since the ester **1** contained four of the nine asymmetric carbons in ikarugamycin, it became necessary to unequivocally confirm the relative configuration of the ester **1** through its synthesis. We describe here the synthesis and the stereochemistry of the four isomeric 3,4-*cis*-3-ethyl-4-methyl-1,2-cyclopentanedicarboxylates (**1a**, **1b**, **1c**, and **1d**). Two 3,4-*trans*-stereoisomers (**1e** and **1f**) were also prepared.

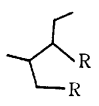

2a: R=CO_2H
2b: R=CH_2OH
2c: R=CH_2OTs
2d: R=CH_2CN
2e: R=CH_2CO_2H
2f: R=$CHBrCO_2Me$

There have been extensive works on the synthesis of nepetic acids, 3-methyl-1,2-cyclopentanedicarboxylic acids.[3] However, none of them seemed applicable for the synthesis of 3,4-disubstituted 1,2-cyclopentanedicarboxylic acids. The cyclization reaction by McDonald and Reitz[4] appeared to be the most convincing method for our purpose. As the starting material was chosen 2-ethyl-3-methylglutaric acid (**2a**) which was prepared by a known method[5] as a mixture (1: 2 ratio) of *erythro*- and *threo*-isomers.

Lithium aluminum hydride reduction of the acid **2a** gave a diol **2b**. The corresponding ditosylate (**2c**) was treated with sodium cyanide in dimethyl sulfoxide to yield a dinitrile **2d**, which was then hydrolyzed with potassium hydroxide in aqueous ethylene glycol to give a dicarboxylic acid **2e**. Bromoesterification[6] of **2e** yielded a dibromo diester **2f**, whose structure was confirmed by the mass spectrum and elemental analysis (see Experimental). The cyclization of **2f** with sodium hydride in *N*,*N*-dimethylformamide[4] proceeded smoothly, giving the two expected cyclopentene derivatives **3a** and **3b** in 5: 7 ratio. They were separated without difficulty by chromatography on silver nitrate impregnated silica gel followed by preparative gas-liquid chromatography (GLC). In order to confirm the relative configurations of the ethyl and methyl groups in the esters (**3a** and **3b**), the latter (**3b**) was submitted to ozonolysis and yielded *threo*-2-ethyl-3-methylglutaric acid.[7]

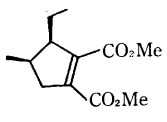
3a

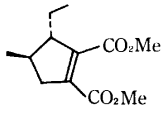
3b

Hydrogenation of the unsaturated 3,4-*cis*-ester (**3a**) proved to be very difficult. However, this was overcome by repeating hydrogenation in acetic acid over platinum oxide. The products, free of unsaturated esters, were separated by preparative GLC, giving three saturated esters **1d**, **1a**,[8] and **1e**[8] in 33, 7, and 13% yields, respectively.

On equilibration by heating with methanolic sodium methoxide, the ester **1d** disappeared to give the isomeric ester **1a** as the major product, along with two new esters **1b** and **1c** (ratio of **1a**, **1b**, and **1c**; 89: 2: 9). This indicates that the isomer **1a** has the most stable *r*-1, *t*-2, *c*-3, *c*-4-configuration.[9]

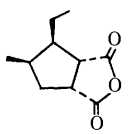
4a

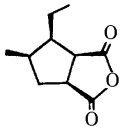
4b

The two isomeric 1,2-*cis*-esters (**1c** and **1d**) were also prepared *via* their anhydrides (**4a** and **4b**) as follows. The ester **1d** was equilibrated, hydrolyzed, and then

treated under reflux with acetic anhydride containing *p*-toluenesulfonic acid. Preparative GLC of the product afforded the 2,3-*trans*-anhydride (**4a**) and the 2,3-*cis*-anhydride (**4b**) in 4: 1 ratio. Methanolysis of **4a** and **4b** followed by esterification with diazomethane gave the corresponding esters (**1c** and **1d**), respectively. Thus, the second most stable isomer **1c** must have the *r*-1, *c*-2, *t*-3, *t*-4-configuration and the least stable isomer **1d** the *r*-1, *c*-2, *c*-3, *c*-4-configuration.

The remaining isomer whose configuration was to be confirmed was then the *r*-1, *t*-2, *t*-3, *t*-4-ester (**1b**). It was prepared from the anhydride **4b** by essentially the same method as used for the preparation of *t*-3-methyl-*r*-1, *t*-2-cyclopentanedicarboxylic acid.[10] The anhydride (**4b**) was converted to a mixture of half methyl esters, which was equilibrated with base and esterified. The product consisted mostly of the ester **1b** which was isolated in 50% yield by preparative GLC.

Thus, all of the four stereoisomers of dimethyl 3,4-*cis*-3-ethyl-4-methyl-1,2-cyclopentanedicarboxylates were prepared with high purities and their stereochemistry established.

Consequently, the isomer **1e**, obtained by the catalytic hydrogenation of **3a** (described above), must have 3,4-*trans*-configuration.[8] In fact, equilibration of **1e** yielded predominantly the sixth isomer **1f** whose stereochemistry was most likely *r*-1, *t*-2, *c*-3, *t*-4.

A comparison of the IR and NMR spectra and retention times on GLC showed that the ester **1**, obtained from ikarugamycin, was identical with the synthetic sample of dimethyl *c*-3-ethyl-*c*-4-methyl-*r*-1,*t*-2-cyclopentanedicarboxylate (**1a**).

Experimental

The IR spectra were taken on a JASCO IR-S spectrophotometer and the UV spectra on a Perkin-Elmer 202 UV-VIS spectrophotometer. The NMR spectra were recorded on Nihondenshi JNM-C60H and 4H-100 spectrometers using CCl_4 as the solvent; the chemical shifts are given in ppm relative to the internal TMS, and the coupling constants given in Hz. The mass spectra were obtained with a Hitachi RMU-6D spectrometer, operating with an ionization energy of 70 eV. The preparative gas-liquid chromatography (GLC) were carried out on a Varian 1828-4 instrument, using a column packed with 10% OV-17 on Chromosorb W at 170 °C.

Synthesis of Dimethyl 2,6-Dibromo-3-ethyl-4-methylpimelate (2f). *(a) 3-Ethyl-4-methyl-1,5-pentanediol (2b)*: A solution of 2-ethyl-3-methylglutaric acid (**2a**: 17.4 g) in ether (100 ml) was added dropwise during 2 h to a stirred suspension of lithium aluminum hydride (11.2 g) in ether (200 ml) at 0 °C. The mixture was stirred at room temperature for an additional 4 h. After cooling to 0 °C ethyl acetate (20 ml) and then water were carefully added. After 1 h a mixture of ice-water (150 ml) and concd sulfuric acid (45 ml) was added and the mixture was extracted with ether (600 ml). The ether extract was washed with saturated sodium hydrogen carbonate solution and saturated sodium chloride solution, and dried over magnesium sulfate. Evaporation of the solvent afforded 12.2 g (83%) of a colorless oil, $\nu_{max}^{CHCl_3}$ 3670, 3600—3200 cm^{-1}.

(b) Ditosylate (2c) of 2b: To a stirred solution of *p*-toluenesulfonyl chloride (38.2 g) in pyridine (70 ml) at 0 °C was added dropwise a solution of the diol **2b** (12.1 g) in pyridine (20 ml) during 20 min. After standing at 5 °C for 18 h the mixture was poured into ice-water (200 ml) and extracted with chloroform (500 ml). The chloroform extract was washed with concd hydrochloric acid (100 ml) and water, and then dried over sodium sulfate. Evaporation of the solvent gave 31.9 g (84%) of a colorless oil, $\nu_{max}^{CHCl_3}$ 1603, 1360, 1170 cm^{-1}. The crude ditosylate was immediately used for the next experiment without a further purification.

(c) 3-Ethyl-4-methylpimelonitrile (2d): A mixture of the ditosylate **2c** (31.9 g) and sodium cyanide (10.3 g) in dimethyl sulfoxide (350 ml) was heated with stirring at 100 °C for 2 h under an atmosphere of nitrogen. After cooling the mixture was poured into a solution of ammonium chloride (40 g) in water (400 ml) and extracted with dichloromethane (800 ml). The dichloromethane extract was washed throughly with water and dried over sodium sulfate. Removal of the solvent gave a reddish residue, which was distilled to furnish 8,7 g (76%) of **2d** as a pale pink oil: bp 132—155 °C/3 mmHg; $\nu_{max}^{CCl_4}$ 2260, 1427 cm^{-1}; *m/e* 165 (M^++1), 163 (M^+−1). Found: C, 73.22; H, 10.27; N, 17.06%. Calcd for $C_{10}H_{16}N_2$: C, 73.12; H, 9.82; N, 17.06%.

(d) 3-Ethyl-4-methylpimelic Acid (2e): A mixture of the nitrile **2d** (9.8 g) and potassium hydroxide (32 g) in ethylene glycol (225 ml)–water (25 ml) was heated with stirring at 110 °C for 16 h. After cooling the mixture was poured into ice-water (200 ml) and extracted with benzene (200 ml). The aqueous layer was acidified with concd hydrochloric acid (60 ml) and extracted throughly with chloroform (600 ml). The chloroform extract was washed with water and dried over sodium sulfate. Evaporation of the solvent left 7.3 g (62%) of **2e** as a pale yellow viscous oil, $\nu_{max}^{CHCl_3}$ 1713 cm^{-1}. which was used for the next experiment without a further purification.

(e) Dimethyl 2,6-Dibromo-3-ethyl-4-methylpimelate (2f): The dicarboxylic acid **2e** (8.7 g) was heated with thionyl chloride (20 ml) under reflux for 2 h and then bromine (5 ml) was added dropwise to the mixture at 90 °C during 1 h. After heating the mixture for 17 h at 90 °C, it was cooled, poured into methanol (60 ml), and kept for 1 h at room temperature. The mixture was then diluted with water and extracted with ethyl acetate (250 ml). The ethyl acetate extract was washed successively with saturated sodium hydrogen sulfite solution, saturated sodium hydrogencarbonate solution, water, and then saturated sodium chloride solution. The extract was dried over sodium sulfate and the solvent evaporated under reduced pressure. The reddish residue was distilled to give 12.3 g of a pale brown oil, bp 153—171 °C/4 mmHg, which was then chromatographed on silica gel (200 g). Elution with hexane–ether (6: 1) gave 9.4 g (38%) of **2f** as a pale yellow oil: $\nu_{max}^{CCl_4}$ 1753 cm^{-1}; *m/e* 359, 357, 355 (M^+−OMe), 309, 307 (M^+−Br). Found: C, 37.18; H, 4.29%. Calcd for $C_{12}H_{16}O_4Br_2$: C, 37.52; H, 4.20%.

Dimethyl cis- *and* trans-*3-ethyl-4-methyl-1-cyclopentene-1,2-dicarboxylates (3a and 3b).* To a stirred solution of sodium hydride (55% mineral oil dispersion; 445 mg) in *N,N*-dimethylformamide (8 ml) at 0 °C was added dropwise a solution of the dibromodiester **2f** (1.97 g) in *N,N*-dimethylformamide (8 ml). The mixture was stirred at 0 °C for 1 h and at room temperature for another 2 h. Aqueous 10% potassium hydroxide (10 ml) was then added and the mixture was stirred at 0 °C for 1 h and at room temperature for 14 h. The mixture was extracted with ether to remove the mineral oil and the ether extract was washed with water. The combined aqueous layer was acidified with 6M hydrochloric acid and extracted with ethyl acetate (200 ml). The ethyl acetate extract was washed throughly with water, saturated sodium chloride solution, and dried over sodium sulfate. Evaporation of the solvent gave a mixture of dicarboxylic acid, which was then

esterified with diazomethane and the product distilled to yield a mixture (966 mg) of **3a** and **3b**, bp 150 °C/6 mmHg. The unsaturated esters were roughly separated by column chromatography on 13% silver nitrate impregnated silica gel (18 g) with hexane–ethyl acetate (6: 1) as an eluent. Further purification by preparative GLC furnished 283 mg (25%) of **3a** and 392 mg (35%) of **3b** as colorless oil.

*Unsaturated 3,4-*cis*-Dimethyl Ester (3a)*: $\nu_{max}^{CCl_4}$ 1728, 1642 cm^{-1}; λ_{max}^{MeOH} 235 nm (ε 6300); *m/e* 226 (M$^+$), 195, 166; δ 0.91 (3H, t, 6.8), 1.01 (3H, d, 6.3), 1.5 (2H, m), 2.2—3.1 (4H, m), 3.65 (3H, s), 3.68 (3H, s). Found: C, 63.40; H, 8.14%. Calcd for $C_{12}H_{18}O_4$: C, 63.70; H, 8.02%.

*Unsaturated 3,4-*trans*-Dimethyl Ester (3b)*: $\nu_{max}^{CCl_4}$ 1727, 1646 cm^{-1}; λ_{max}^{MeOH} 235 nm (ε 5700); *m/e* 226 (M$^+$), 195, 166; δ 0.90 (3H, t, 6.8), 1.10 (3H, d, 6.9), 1.3—2.7 (6H, m), 3.64 (3H, s), 3.65 (3H, s). Found: C, 63.84; H, 7.93%. Calcd for $C_{12}H_{18}O_4$: C, 63.70; H, 8.02%.

*Ozonolysis of Unsaturated 3,4-*trans*-Dimethyl Ester (3b).* The ester **3b** (72 mg) in dichloromethane (4 ml) was saturated with ozone (5 min) at −70 °C. To it 10% sodium hydroxide (2 ml) and 35% hydrogen peroxide (2 ml) were added, and the mixture was vigorously stirred for 20 hr at room tem perature. After extraction with ether the aqueous layer was acidified with 6 M hydrochloric acid and extracted with ether (30 ml). The crude acid (49 mg) obtained was crystallized from ether–hexane, giving 21 mg (38%) of *threo*-2-ethyl-3-methylglutaric acid, mp 98—99 °C. The IR spectrum of this acid was identical with that of an authentic sample, mp 99—100 °C.[7]

*Catalytic Hydrogenation of Unsaturated 3,4-*cis*-Dimethyl Ester (3a): Preparation of Dimethyl Esters 1a, 1d, and 1f.* A solution of **3a** (123 mg) in acetic acid (5 ml) was hydrogenated for 40 h in the presence of platinum oxide (57 mg). The catalyst was filtered and the acetic acid was evaporated under reduced pressure. Although the oil obtained was free of the starting material **3a** (GLC), it contained isomeric unsaturated ester(s) (IR and mass spectra). Therefore, it was again hydrogenated for 12 h in acetic acid (4 ml) over platinum oxide (54 mg). The resulting mixture of saturated esters was separated by preparative GLC into three dimethyl esters, **1a**, **1d**, and **1e**.

Dimethyl c-*3-Ethyl*-c-*4-methyl*-r-*1*, t-*2-Cyclopentanedicarboxylate (1a)*: 8.8 mg (7%); $\nu_{max}^{CCl_4}$ 1742 cm^{-1}; *m/e* 228 (M$^+$), 168,109; δ 0.87 (3H, d, 6.8), 0.90 (3H, t, 7.0), 1.2—2.4 (6H, m), 2.81 (1H, t, 8.0), 3.11 (1H, ddd, 9.0, 8.0, 7.2), 3.61 (3H, s), 3.62 (3H, s). Found: C, 62.73, H, 9.20%. Calcd for $C_{12}H_{20}O_4$: C, 63.13; H, 8.83%.

Dimethyl c-*3-Ethyl*-c-*4-methyl-r-1*, c-*2-Cyclopentanedicarboxylate (1d)*: 40.9 mg (33%); $\nu_{max}^{CCl_4}$ 1746 cm^{-1}; *m/e* 228 (M$^+$), 168, 109; δ 0.93 (3H, d, 5.8), 0.95 (3H, t, 7.5), 1.4 (2H, m), 1.9—2.5 (4H, m), 2.82 (1H, m), 3.10 (1H, t, 6.6), 3.60 (6H, s).

*3,4-*trans*-Dimethyl Ester (1e)*: 16.2 mg (13%); $\nu_{max}^{CCl_4}$ 1742 cm^{-1}; *m/e* 228 (M$^+$), 168, 109; δ 1.02 (3H, d, 5.9), 1.02 (3H, t, 7.1), 1.0—2.5 (6H, m), 3.2 (2H, m), 3.62 (6H, s).

Base-catalyzed Equilibration of 1d Formation of Dimethyl Esters 1a, 1b, and 1c. A solution of **1d** (72 mg) in 1 M sodium methoxide–methanol (5 ml) was heated under reflux for 8 h. The methanol was removed under reduced pressure, the residue was acidified with 6 M hydrochloric acid and extracted with ethyl acetate (30 ml). The ethyl acetate extract was dried over sodium sulfate and concentrated to give an oil, from which three dimethyl esters, **1a**, **1b**, and **1c**, were isolated by preparative GLC.

r-*1*, t-*2*, c-*3*,c-*4-Dimethyl Ester (1a)*: 36.9 mg (51%).

r-*1*, t-*2*, t-*3*, t-*4-Dimethyl Ester (1b)*: 0.8 mg (1%) (described later).

Dimethyl t-*3-Ethyl*-t-*4-methyl*-r-*4*,c-*2-cyclopentanedicarboxylate (1c)*: 3.8 mg (5%): $\nu_{max}^{CCl_4}$ 1747 cm^{-1}; *m/e* 228 (M$^+$), 168, 109; δ 0.85 (3H, d, 7.0), 0.93 (3H, t, 7.2), 1.2—1.7 (3H, m), 2.0—2.5 (3H, m), 2.72 (1H, dd, 10.0, 8.4), 3.10 (1H, dt, 10.0, 8.0), 3.58 (3H, s), 3.59 (3H, s).

Acid Anhydrides 4a and 4b. Preparation of Dimethyl Esters 1c and 1d. The diester **1d** (40 mg) was heated with 1 M sodium methoxide–methanol (5 ml) under reflux for 12 h. Water (1 ml) was added and the mixture was heated under reflux for an additional 2 h. The methanol was evaporated, the aqueous solution was acidified with 6 M hydrochloric acid and extracted with ethyl acetate (50 ml). The ethyl acetate extract was dried over sodium sulfate and evaporated to dryness, yielding a mixture of dicarboxylic acids (33 mg). The oily mixture was dissolved in xylene (1 ml), to which acetic anhydride (1 ml) and *p*-toluenesulfonic acid (3 mg) were added. The mixture was heated at 140 °C for 14 h and then concentrated under reduced pressure. The residue was subjected to preparative GLC, giving two isomeric acid anhydrides **4a** and **4b**

t-*3-Ethyl*-t-*4-methyl*-r-*1*, c-*2-Cyclopentanedicarboxylic Anhydride (4a)*: 11.2 mg (35%); $\nu_{max}^{CCl_4}$ 1865, 1791 cm^{-1}; *m/e* 182 (M$^+$), 154, 140, 110, 81; δ 0.96 (3H, d, 5.6), 1.02 (3H, t, 6.0), 1.0—2.5 (6H, m), 2.9—3.6 (2H, m).

c-*3-Ethyl*-c-*4-methyl*-r-*1*, c-*2-Cyclopentanedicarboxylic Anhydride (4b)*: 2.5 mg (8%); $\nu_{max}^{CCl_4}$ 1865, 1790 cm^{-1}; *m/e* 182 (M$^+$), 154, 140, 110, 81; δ 0.82 (3H, d, 6.3), 1.05 (3H, t, 7.0), 1.1—2.6 (6H, m), 2.9—3.8 (3H, m).

The *r*-1, *c*-2, *t*-3, *t*-4-acid anhydride (**4a**; 9.7 mg) was treated with methanol followed by diazomethane. Purification by preparative GLC gave 8.4 mg (69%) of the corresponding dimethyl ester (**1c**). A similar treatment of the *r*-1, *c*-2, *c*-3, *c*-4-anhydride (**4b**) yielded the corresponding ester (**1d**).

Preparation of r-*1*, t-*2*, t-*3*, t-*4-Dimethyl Ester (1b).* A solution of *r*-1, *c*-2, *c*-3, *c*-4-acid anhydride (**4b**; 27.3 mg) in methanol (1 ml) was heated under reflux for 1 h. Evaporation of the methanol gave a mixture of monocarboxylic acids, $\nu_{max}^{CCl_4}$ 1744, 1706 cm^{-1}. It was heated with 1 M sodium methoxide–methanol (2 ml) under reflux for 2 h. The methanol was evaporated, the residue was acidified with dil hydrochloric acid, and extracted with ethyl acetate. The extract was dried over sodium sulfate and evaporated to dryness, leaving an oil, which was esterified with diazomethane. A mixture of the dimethyl esters **1a** and **1b** was formed, which was separated by preparative GLC, yielding 17.2 mg (50%) of *dimethyl* t-*3-ethyl*-t-*4-methyl*-r-*1*, t-*2-cyclopentanedicarboxylate (1b)* in 97% purity (contaminated by 3% of **1a**): $\nu_{max}^{CCl_4}$ 1742 cm^{-1}; *m/e* 228 (M$^+$), 168, 109; δ 0.89 (3H, t, 6.8), 0.92 (3H, d, 6.8), 1.3 (2H, m), 1.85 (2H, m), 2.2 (2H, m), 3.3 (2H, m), 3.64 (3H, s), 3.66 (3H, s). A mixture (3.4 mg) of **1a** and **1b** was also obtained.

Base-catalyzed Equilibration of 1e: Preparation of Dimethyl Ester 1f. The 3,4-*trans*-dimethyl ester **1e** (11.3 mg) was equilibrated in the same way as used for the equilibration of **1d**. Preparative GLC of the resulting mixture gave 5.3 mg (47%) of *dimethyl* c-*3-ethyl*-t-*4-methyl*-r-*1*, t-*2-cyclopentanedicarboxylate (1f)*: $\nu_{max}^{CCl_4}$ 1743 cm^{-1}; *m/e* 228 (M$^+$), 168, 109; δ 0.90 (3H, t, 6.8), 1.02 (3H, d, 6.0), 1.1—2.2 (6H, m), 2.5—3.3 (2H, m), 3.63 (3H, s), 3.64 (3H, s). A mixture (0.8 mg) of **1f** and other isomers was also obtained.

References

1) A brief accout of this research has appeared in Ref. 2c.

2) a) S. Ito and Y. Hirata, *Tetrahedron Lett.*, **1972**, 1181; b) *ibid.*, **1972**, 1185; c) *ibid.*, **1972**, 2557.

3) E. J. Eisenbraun, P. G. Hanel, K. S. Schorno, Sr. St. F. Dilgen, and J. Osiecki, *J. Org. Chem.*, **32**, 3010 (1967), and

references cited therein.

4) R. N. McDonald and R. R. Reitz, *J. Chem., Soc. Chem. Commun.*, **1971**, 90; *J. Org. Chem.*, **37**, 2418 (1972).

5) H. R. Snyder and R. E. Putnam, *J. Am. Chem. Soc.*, **76**, 33 (1954).

6) P. C. Gupta and D. K. Sankaran, *Org. Synth.*, Coll. Vol. III, 623 (1955).

7) S. Ito and Y. Hirata, *Bull. Chem. Soc. Jpn.*, **46**, 672 (1973).

8) The double bond isomerization and the formation of the *trans*-isomer have many precedents; for examples see a) H. O. House, "Modern Synthetic Reaction," W. A. Benjamin, Inc., New York, N. Y. (1965). p. 19; b) T. Sakan, F. Murai, Y. Hayashi, Y. Honda, T. Shono, N. Nakajima, and M. Kato, *Tetrahedron*, **23**, 4635 (1967).

9) Among the four isomeric 3-methyl-1,2-cyclopentanedicarboxylic acids the *r*-1, *t*-2, *c*-3-isomer is the most stable one; see Ref. 10.

10) R. B. Bates, E. J. Eisenbraun, and S. M. McElvain, *J. Am. Chem. Soc.*, **80**, 3413 (1958).

Studies of Peptide Antibiotics. XXXIV.[1] Syntheses of Tyrocidine A and Its Analogs Containing Glycine

Kouji OKAMOTO,* Kazuhiko NONAKA, and Nobuo IZUMIYA

Laboratory of Biochemistry, Faculty of Science, Kyushu University, Hakozaki, Higashi-ku, Fukuoka 812

(Received July 15, 1976)

The synthesis of Tyrocidine A (TA), an antibiotic cyclic decapeptide, was achieved by a revised conventional method. Two analogs of TA, 6-glycine-TA and 7-glycine-TA, were synthesized by a similar method to investigate the contribution of L-phenylalanine[6] and D-phenylalanine[7] residues in TA to its antibacterial activity. The properties of synthetic TA were identical to natural TA. The antibacterial activities of the two analogs were weaker when compared with TA; the activity of 6-glycine-TA being weaker than 7-glycine-TA. The three cyclic peptides synthesized were subjected to droplet countercurrent chromatography (DCCC) and optical rotatory dispersion (ORD), and the elucidation of the difference in the activities between the two analogs was followed with DCCC and ORD.

Tyrocidine A (TA) is an antibiotic cyclic peptide isolated from *Bacillus brevis* and its structure has been proposed to be that of **18a** (Fig. 1). It is of interest to note that the pentapeptide sequence, L-Val-L-Orn-L-Leu-D-Phe-L-Pro, is found in gramicidin S (GS). In 1966, Ohno *et al.* synthesized a cyclic peptide corresponding to the sequence of TA by a conventional solution-phase method, and showed the synthetic peptide to be identical to natural TA.[2] Recently, we synthesized TA and its analogs by a solid-phase method.[3] As has been generally recognized for a solid-phase method, we observed that the procedure to synthesize the cyclic peptides, including TA, was easier compared with a solution-phase method; however the purity of the TA synthesized was inferior to that synthesized by the solution-phase method.[3] In the present study, therefore, we selected the solution-phase method for peptide synthesis.

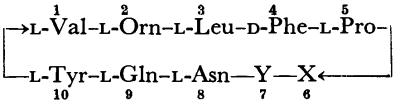

	X	Y
TA (**18a**)	L-Phe	D-Phe
[Gly[6]]-TA (**18b**)	Gly	D-Phe
[Gly[7]]-TA (**18c**)	L-Phe	Gly

Fig. 1. Structure of TA and its analogs.

First we intended to synthesize pure TA through a revised route in a solution-phase method. In the previous paper,[2] Ohno *et al.* cyclized a decapeptide active intermediate, H-Phe[6]-D-Phe-Asn-Gln-Tyr-Val-Orn(Z)-Leu-D-Phe-Pro[5]-ONp,[4] as the key step. Recently, we carried out the cyclization reaction of a pentapeptide *via* several active intermediates and observed that the azide and *N*-hydroxysuccinimide intermediates were excellent ones in regards to high yield, experimental simplicity and absence of racemization.[5] By applying a mechanism of biosynthetic cyclization, Tanaka *et al.*[6] and Abe *et al.*[1] indicated that GS and its analogs could be obtained in excellent yields by the cyclization reaction of linear peptides. In *B. brevis*, TA is biosynthesized with the cyclization of a linear decapeptide (H-D-Phe[4]-Pro-Phe-D-Phe-Asn-Gln-Tyr-Val-Orn-Leu[3]-OH).[7] Considering the facts previously mentioned, a route of TA synthesis was chosen which would place a L-Leu[3] residue at the C-terminal and which would activate the carboxyl as an azide as shown in Fig. 2. As described later, the route was effective, giving pure TA in good yield.

Second, we intended to clarify the contribution of L-Phe[6] and D-Phe[7] residues in the TA molecule to its biological activity. For this purpose, we designed the following syntheses of two analogs, [Gly[6]]-TA and [Gly[7]]-TA (Fig. 1). The route for syntheses of these analogs was similar to that of TA synthesis shown in Fig. 2. The present paper reports the syntheses, and physicochemical and antibacterial properties of TA and its analogs.

For the syntheses of the three cyclic peptides (**18a—c**), a hexapeptide ester (**13**) was prepared by stepwise elongation from the carboxyl toward the amino end, and this same component (**13**) was used throughout the syntheses (Fig. 2). Boc-tetrapeptide-hydrazides

Table 1. Antibacterial activity of cyclic peptides (Minimum inhibitory concentration, μg/ml[a])

Compound	*Escherichia coli*	*Staphylcoccus aureus*	*Bacillus subtilis*	*Mycobacterium Takeo*
GS	>50 (>50)	5 (10)	5 (5)	>50 (>50)
Natural TA	>50 (>50)	20 (50)	10 (10)	>50 (>50)
Synthetic TA (**18a**)	>50 (>50)	20 (20)	10 (10)	>50 (>50)
[Gly[6]]-TA (**18b**)	>50 (>50)	>50 (>50)	50 (50)	>50 (>50)
[Gly[7]]-TA (**18c**)	>50 (>50)	50 (50)	20 (20)	>50 (>50)

a) The assays were carried out with a bouillon agar medium. Numbers in parentheses represent the concentration with a synthetic agar medium.

* Present address: Laboratory of Molecular Biophysics, University of Alabama, Birmingham, Alabama, U. S. A.

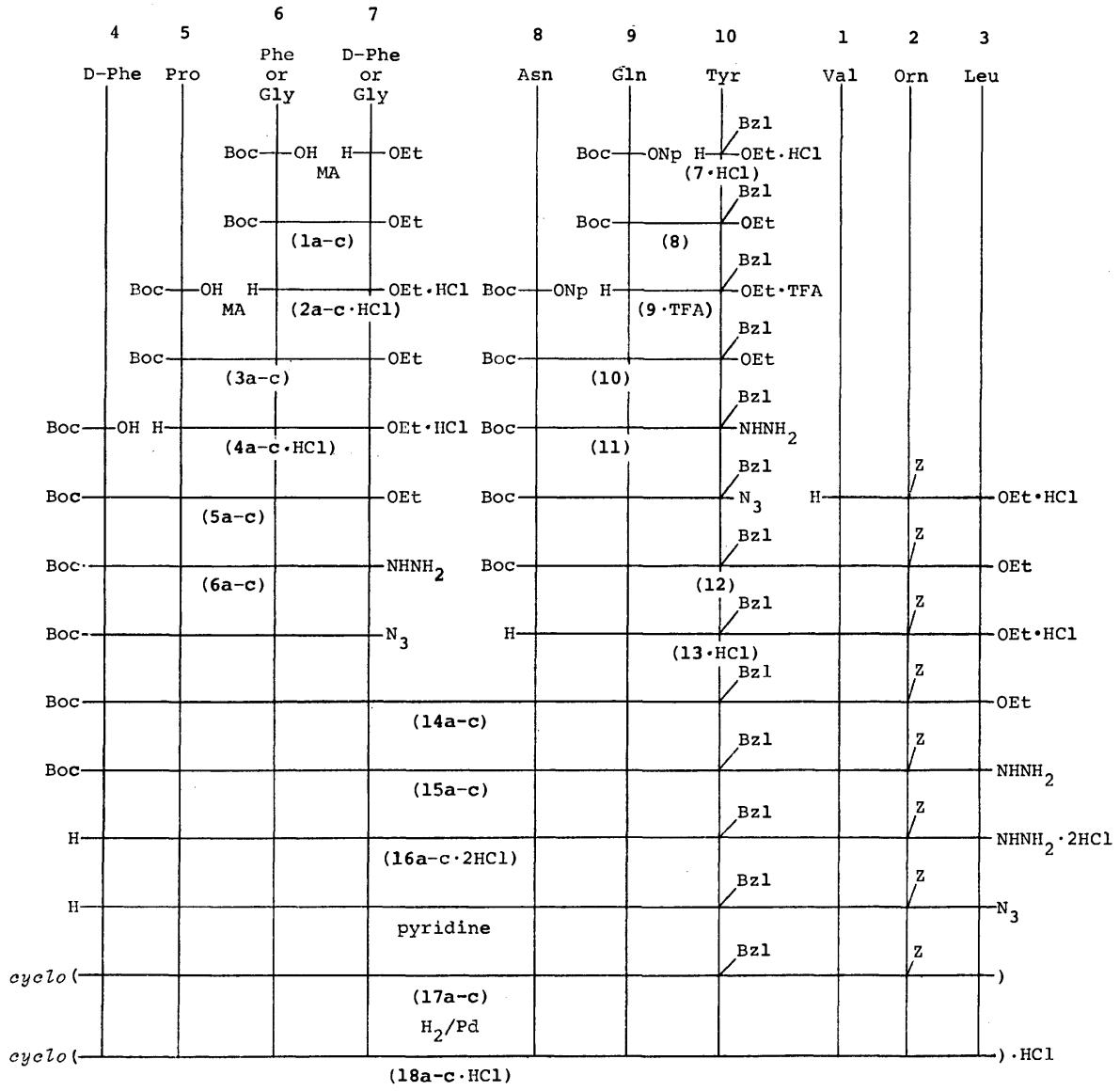

Fig. 2. Synthesis of TA and its analogs. **a**, -Phe^6-D-Phe^7-; **b**, -Gly^6-D-Phe^7-; **c**, -Phe^6-Gly^7-.

(**6a**—**c**) were also prepared by stepwise elongation. Boc-decapeptide ester (**14a**—**c**) was prepared by the coupling of **13** and each azide derived from **6a**—**c**; and a protected cyclic decapeptide (**17a**—**c**) was prepared by the cyclization reaction of each decapeptide azide derived from **16a**—**c**.

For the syntheses of TA (**18a**) and its analogs (**18b**—**c**), **17a**—**c** were subjected to hydrogenolysis, and the cyclic peptides were obtained as crystalline hydrochlorides (**18a**—**c**·HCl). In a previous paper,[8] we indicated that droplet countercurrent chromatography (DCCC) was very effective in the isolation of a desired peptide in a mixture of compounds of similar structures. Here, we applied DCCC for the detection of possible impurities in synthetic TA and the analogs. As shown in Fig. 3, each cyclic peptide (**18a**—**c**) gave a single peak without any additional peaks due to impurities.[9] The synthetic TA gave a single peak at the same position as natural TA. It is of interest to note that **18c** eluted faster than **18b** because **18c** is more hydrophobic in the organic phase in DCCC in spite of the fact that **18b** or **18c** is an analog which replaced only one Phe residue (position 6 or 7) with a Gly residue. The homogeneity of **18a**—**c** was further ascertained by paper and thin-layer chromatographies, paper electrophoresis, and elemental and amino acid analyses.

The antibacterial activities of **18a**—**c** toward several microorganisms were tested, the results shown in Table 1. It was proved that the specific activity of synthetic TA was identical to that of natural TA. Both analogs (**18b**—**c**) exhibited weak activity against *S. aureus* and *B. subtilis*; the results indicating that the aromatic side chain of Phe residue at position 6 and 7 was important for full activity, but not quite essential. At the beginning of this study, we expected that [Gly^7]-TA (**18c**) which the D-Phe^7 residue is replaced might possess weaker activity than [Gly^6]-TA (**18b**) which the L-Phe^6 is replaced because we assumed that the D-configuration at position 7 was more meaningful than L at position 6. Contrary to our expectation, the activity of **18c** was

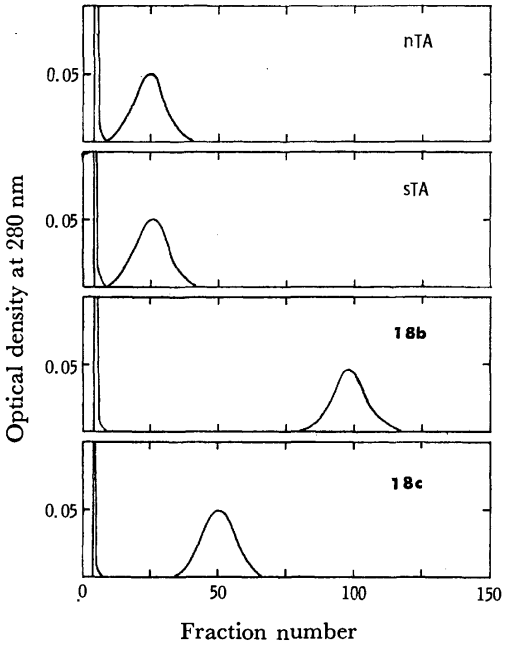

Fig. 3. Droplet countercurrent chromatography of the cyclic peptides. nTA, natural TA; sTA, synthetic TA (**18a**).

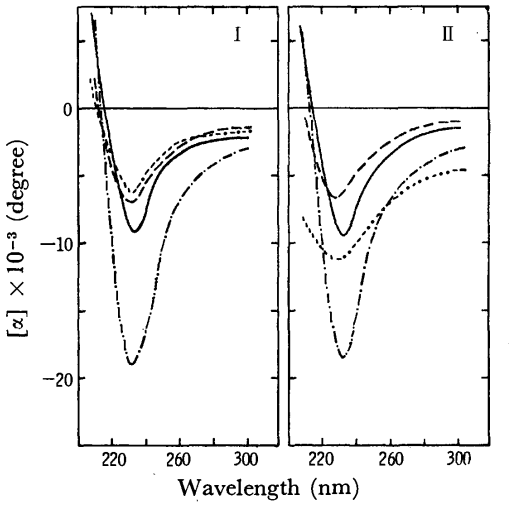

Fig. 4. ORD curves of the cyclic peptides. Solvent: I, 50% EtOH; II, 6 M urea in 50% EtOH. ——, nTA and sTA; – – –, [Gly⁶]-TA (**18b**); ------, [Gly⁷]-TA (**18c**); ·····, GS.

slightly greater than **18b** (Table 1). We can give no definite explanation for the difference of specific activities between **18b** and **18c** from the standpoint of molecular structure, but we can show by the DCCC results that hydrophobicity of **18c** is greater than **18b** and is close to TA (Fig. 3).

The ORD curves of the peptides in 50% ethanol are shown in Fig. 4-I. The curve of synthetic TA was identical with that of natural TA. The negative troughs of the two analogs were shallower than that of TA, but the position at 233 nm was similar to TA and GS. In a solution of 6 M urea, causing denaturation of some polypeptides, the position of the troughs of the two analogs shifted slightly to 229 nm while that of TA and GS remained constant. We showed that conformations of the analogs are different (Fig. 4-I) from TA and more flexible (Fig. 4-II) than TA, and consequently the biological activities of the two analogs are lower than TA.

Experimental

Melting points were uncorrected. TLC was performed on Merck silica gel G with the following solvent systems: R_f^1, BuOH–AcOH–pyridine–H_2O (15: 3: 10: 12, v/v); R_f^2, $CHCl_3$–MeOH (5: 1, v/v); R_f^3, BuOH–AcOH–H_2O (4: 1: 5, v/v). Paper chromatography was performed on Toyo Roshi No. 52 with the following solvent systems: R_f^4, same solvent as that used for R_f^1; R_f^5, BuOH–formic acid–H_2O (15: 3: 2, v/v). Optical rotations were determined with a Union high sensitivity polarimeter PM-71.

*Boc–Phe–D-Phe–OEt (**1a**).* To a chilled solution of Boc–Phe–OH (3.98 g, 15 mmol) and Et_3N (2.1 ml, 15 mmol) in THF (22 ml) was added isobutyl chloroformate (1.97 ml, 15 mmol) at −5 °C. After 10 min, a chilled solution of H–D-Phe–OEt·HCl (3.45 g, 15 mmol) and Et_3N (2.1 ml, 15 mmol) in $CHCl_3$ (22 ml) was added. The mixture was left to stand at room temperature overnight, evaporated *in vacuo*, and the oily residue was dissolved in AcOEt. The solution was washed successively with 4% $NaHCO_3$, 10% citric acid and water, dried (Na_2SO_4), and evaporated. The resulting solid was recrystallized from EtOH–ether–petroleum ether; yield, 4.82 g (73%); mp 91—93 °C; $[\alpha]_D^{25}$ +1.6° (*c* 1, MeOH); R_f^1 0.98, R_f^2 0.90.

Found: C, 68.34; H, 7.35; N, 6.35%. Calcd for $C_{25}H_{32}O_5N_2$: C, 68.16; H, 7.32; N, 6.36%.

*Boc–Gly–D-Phe–OEt (**1b**).* This was prepared from Boc–Gly–OH (3.50 g) and H–D-Phe–OEt·HCl (4.59 g) as described for the preparation of **1a**; yield of oil, 6.42 g (92%); R_f^1 0.89, R_f^2 0.69.

*Boc–Phe–Gly–OEt (**1c**).* This was prepared from Boc–Phe–OH (3.90 g) and H–Gly–OEt·HCl (2.05 g) as described for the preparation of **1a**; yield, 3.64 g (71%); mp 100—101 °C (lit, mp 89.5—90 °C,[10] 88—89.5 °C[11]); $[\alpha]_D^{25}$ −5.0° (*c* 2, EtOH) (lit, $[\alpha]_D^{25}$ −4.3°,[10] −4.2°[11]); R_f^1 0.86, R_f^2 0.62.

*H–Phe–D-Phe–OEt·HCl (**2a**·HCl).* Compound **1a** (4.41 g, 10 mmol) was dissolved in 0.1 M hydrogen chloride in formic acid (120 ml). After being left to stand at room temperature for 20 min, the solution was evaporated to dryness, and the resulting solid was collected by filtration with the aid of ether–petroleum ether. The product was recrystallized from EtOH–ether–petroleum ether; yield, 3.56 g (94%); mp 103—106 °C; $[\alpha]_D^{25}$ +14.0° (*c* 0.5, MeOH); R_f^1 0.87, R_f^2 0.86.

Found: C, 63.40; H, 6.72; N, 7.37%. Calcd for $C_{20}H_{25}O_3N_2Cl$: C, 63.74; H, 6.69; N, 7.43%.

*H–Gly–D-Phe–OEt·HCl (**2b**·HCl).* Compound **1b** (3.68 g, 10.5 mmol) was treated with 0.1 M hydrogen chloride in formic acid (126 ml) as described for the preparation of **2a**·HCl; yield, 2.60 g (86%); mp 131—134 °C; $[\alpha]_D^{25}$ −11.2° (*c* 1, MeOH); R_f^1 0.72, R_f^2 0.24.

Found: C, 54.25; H, 6.71; N, 9.62%. Calcd for $C_{13}H_{19}O_3N_2Cl$: C, 54.45; H, 6.68; N, 9.77%.

*H–Phe–Gly–OEt·HCl (**2c**·HCl).* This was prepared from **1c** (3.50 g) as described for the preparation of **2a**·HCl; yield of oil, 2.80 g (98%); R_f^1 0.75, R_f^2 0.25.

*Boc–Pro–Phe–D-Phe–OEt (**3a**).* Boc–Pro–OH (1.94 g, 9 mmol) and **2a**·HCl (3.39 g, 9 mmol) were coupled by the mixed anhydride method as described for the preparation of **1a**. The product was recrystallized from AcOEt–ether–petro-

leum ether; yield, 2.95 g (61%); mp 103—105 °C; $[\alpha]_D^{25}$ −48.0° (*c* 1, MeOH): R_f^1 0.96, R_f^2 0.81.

Found: C, 66.83; H, 7.40; N, 7.86%. Calcd for $C_{30}H_{39}O_6N_3$: C, 67.02; H, 7.31; N, 7.82%.

*Boc-Pro-Gly-D-Phe-OEt (**3b**).* This was prepared from Boc-Pro-OH (1.72 g) and **2b**·HCl (2.29 g) as described above; yield, 2.81 g (78%); mp 117—119 °C; $[\alpha]_D^{25}$ −45.0° (*c* 1, MeOH); R_f^1 0.88, R_f^2 0.76.

Found: C, 62.12; H, 7.43; N, 9.42%. Calcd for $C_{23}H_{33}O_6N_3$: C, 61.72; H, 7.43; N, 9.39%.

*Boc-Pro-Phe-Gly-OEt (**3c**).* This was prepared from Boc-Pro-OH (2.0 g) and **2c**·HCl (2.66 g); yield, 2.88 g (69%); mp 109—111 °C; $[\alpha]_D^{25}$ −54.4° (*c* 0.25, MeOH); R_f^1 0.82, R_f^2 0.50.

Found: C, 61.42; H, 7.22; N, 9.32%. Calcd for $C_{23}H_{33}O_6N_3$: C, 61.72; H, 7.43; N, 9.39%.

*H-Pro-Phe-D-Phe-OEt·HCl (**4a**·HCl).* Compound **3a** (2.16 g, 4.02 mmol) was dissolved in 3.5 M hydrogen chloride in dioxane (34.3 ml). After being left to stand at room temperature for 2 h, the solution was evaporated, and the resulting hygroscopic solid was collected by filtration with the aid of ether-petroleum ether. The product was recrystallized from EtOH-ether-petroleum ether; yield, 1.37 g (72%); mp 93 °C; $[\alpha]_D^{25}$ −23.0° (*c* 0.5, MeOH); R_f^1 0.72, R_f^2 0.52.

Found: C, 63.74; H, 7.07; N, 8.56%. Calcd for $C_{25}H_{32}O_4N_3Cl$: C, 63.35; H, 6.81; N, 8.87%.

*H-Pro-Gly-D-Phe-OEt·HCl (**4b**·HCl).* Compound **3b** (2.51 g, 5.6 mmol) was treated with 3.5 M hydrogen chloride in dioxane (48.0 ml) as described above; yield of oil, 2.0 g (93%); R_f^1 0.78, R_f^2 0.30.

*H-Pro-Phe-Gly-OEt·HCl (**4c**·HCl).* This was prepared from **3c** (2.73 g) as described above; yield of oil, 1.96 g (84%); R_f^1 0.79, R_f^2 0.52.

*Boc-D-Phe-Pro-Phe-D-Phe-OEt (**5a**).* Boc-D-Phe-OH (0.76 g, 2.86 mmol) and **4a**·HCl (1.36 g, 2.86 mmol) were coupled by the mixed anhydride method as described for the preparation of **1a**; yield of oil, 1.81 g (92%); R_f^1 0.94, R_f^2 0.70.

*Boc-D-Phe-Pro-Gly-D-Phe-OEt (**5b**).* This was prepared from Boc-D-Phe-OH (1.38 g) and **4b**·HCl (2.0 g) as described above. The product was recrystallized from AcOEt-ether-petroleum ether; yield, 2.08 g (67%); mp 128—130 °C; $[\alpha]_D^{25}$ −36.2° (*c* 1, MeOH); R_f^1 0.82, R_f^2 0.53.

Found: C, 63.86; H, 7.02; N, 9.39%. Calcd for $C_{32}H_{42}O_7N_4 \cdot 1/2\ H_2O$: C, 63.66; H, 7.18; N, 9.28%.

*Boc-D-Phe-Pro-Phe-Gly-OEt (**5c**).* This was prepared from Boc-D-Phe-OH (1.35 g) and **4c**·HCl (1.96 g) as described above; yield, 2.28 g (75%); mp 139—141 °C; $[\alpha]_D^{25}$ −72.6° (*c* 1, MeOH); R_f^1 0.86, R_f^2 0.66.

Found: C, 63.29; H, 7.29; N, 9.35%. Calcd for $C_{32}H_{42}O_7\ N_4 \cdot 1/2H_2O$: C, 63.66; H, 7.18; N, 9.28%.

*Boc-D-Phe-Pro-Phe-D-Phe-NHNH$_2$ (**6a**).* A solution of **5a** (0.685 g, 1 mmol) and hydrazine hydrate (2.9 ml, 60 mmol) in MeOH (12 ml) was allowed to stand at 36 °C for 12 h. The solution was evaporated, water was added, and the resulting solid was collected. The product was recrystallized from MeOH-water; yield, 0.302 g (45%); mp 117—120 °C; $[\alpha]_D^{25}$ −67.0° (*c* 0.2, MeOH); R_f^1 0.89, R_f^2 0.83.

Found: C, 64.20; H, 6.85; N, 11.93%. Calcd for $C_{37}H_{46}O_6N_6 \cdot H_2O$: C, 64.51; H, 7.02; N, 12.20%.

*Boc-D-Phe-Pro-Gly-D-Phe-NHNH$_2$ (**6b**).* Compound **5b** (0.357 g) was treated with hydrazine hydrate (0.58 ml) in MeOH (5 ml) as described above. The solution was evaporated, and the residue was dissolved in AcOEt. The solution was washed with a small volume of water, dried (Na_2SO_4), and evaporated. The residual oil was crystallized by the addition of ether-petroleum ether; yield, 0.264 g (76%); mp 100—102 °C; $[\alpha]_D^{25}$ −6.0° (*c* 1, MeOH); R_f^1 0.87, R_f^2 0.74.

Found: C, 60.39; H, 6.97; N, 14.32%. Calcd for $C_{30}H_{40}O_6N_6 \cdot H_2O$: C, 60.18; H, 7.07; N, 14.04%.

*Boc-D-Phe-Pro-Phe-Gly-NHNH$_2$ (**6c**).* This was prepared from **5c** (0.357 g) and hydrazine hydrate (0.58 ml) as described above; yield, 0.284 g (82%); mp 110—113 °C; $[\alpha]_D^{25}$ −73.0° (*c* 1, MeOH); R_f^1 0.94, R_f^2 0.69.

Found: C, 60.01; H, 6.92; N, 13.89%. Calcd for $C_{30}H_{40}O_6N_6 \cdot H_2O$: C, 60.18; H, 7.07; N, 14.04%.

*H-Tyr(Bzl)-OEt·HCl (**7**·HCl).* To a solution of H-Tyr(Bzl)-OH[12] (2.71 g, 10 mmol) in EtOH (20 ml) was added $SOCl_2$ (0.872 ml, 12 mmol). The reaction mixture was stirred at 40 °C for 0.5 h and at room temperature overnight, and evaporated. The resulting oil was crystallized by the addition of ether-petroleum ether; yield, 2.34 g (70%); mp 190—192 °C; $[\alpha]_D^{25}$ +7.1° (*c* 1, MeOH); R_f^1 0.75, R_f^2 0.74.

Found: C, 63.95; H, 6.68; N, 4.17%. Calcd for $C_{18}H_{22}O_3NCl$: C, 64.37; H, 6.60; N, 4.17%.

*Boc-Gln-Tyr(Bzl)-OEt (**8**).* To a solution of **7**·HCl (2.02 g, 6 mmol) and Et_3N (0.924 ml, 6.6 mmol) in DMF (70 ml) were added Boc-Gln-ONp (2.20 g, 6 mmol) and 1-hydroxybenzotriazole (0.081 g, 0.6 mmol). After being left to stand at room temperature for 12 h, several drops of 1-(2-aminoethyl)piperazine[13] were added. The solution was diluted with water (2 l), and the resulting solid was collected, washed with 10% citric acid, 4% $NaHCO_3$, and water; yield, 2.82 g (89%); mp 138—141 °C; $[\alpha]_D^{25}$ −3.9° (*c* 1, DMF); R_f^1 0.96, R_f^2 0.80.

Found: C, 63.56; H, 7.16; N, 7.85%. Calcd for $C_{28}H_{37}O_7N_3$: C, 63.74; H, 7.07; N, 7.97%.

*H-Gln-Tyr(Bzl)-OEt·TFA (**9**·TFA).* A solution of **8** (1.58 g, 3 mmol) in TFA (30 ml) was allowed to stand at room temperature for 10 min and evaporated. The resulting oil was solidified by the addition of ether-petroleum ether. The product was recrystallized from EtOH-ether-petroleum ether; yield, 1.48 g (91%); mp 112—116 °C; $[\alpha]_D^{25}$ +14.6° (*c* 1, MeOH), R_f^1 0.80, R_f^2 0.57.

Found: C, 55.37; H, 5.75; N, 7.52%. Calcd for $C_{25}H_{30}O_7N_3F_3$: C, 55.45; H, 5.58; N, 7.76%.

*Boc-Asn-Gln-Tyr(Bzl)-OEt (**10**).* Boc-Asn-ONp (0.897 g) was coupled with **9**·TFA (1.38 g), Et_3N (0.391 ml), and 1-hydroxybenzotriazole (0.034 g) as described for the preparation of **8**. The product was recrystallized fromDMF-ether; yield, 1.31 g (80%); mp 240—241 °C (dec); $[\alpha]_D^{25}$ −22.0° (*c* 0.6, DMF); R_f^1 0.91, R_f^2 0.72.

Found: C, 59.70; H, 6.88; N, 10.91%. Calcd for $C_{32}H_{43}O_9N_5$: C, 59.89; H, 6.75; N, 10.91%.

*Boc-Asn-Gln-Tyr(Bzl)-NHNH$_2$ (**11**).* A solution of **10** (1.28 g, 3 mmol) and hydrazine hydrate (1.94 ml, 40 mmol) in DMF (40 ml) was allowed to stand at room temperature overnight. The solution was evaporated, water (1000 ml) was added, and the resulting solid was collected; yield, 1.09 g (87%); mp 215—216 °C (dec); $[\alpha]_D^{25}$ −41.0° (*c* 1, DMF); R_f^1 0.72, R_f^2 0.16.

Found: C, 56.54; H, 6.70; N, 15.35%. Calcd for $C_{30}H_{41}O_8N_7 \cdot 1/2H_2O$: C, 56.59; H, 6.65; N, 15.40%.

*Boc-Asn-Gln-Tyr(Bzl)-Val-Orn(Z)-Leu-OEt (**12**).* To a solution of **11** (1.06 g, 1.69 mmol) in DMF (15 ml) was added 3.5 M hydrogen chloride in dioxane (1.49 ml) and isopentyl nitrite[14] (0.262 ml, 1.86 mmol) at −50 °C. After being left to stand at −20 °C for 10 min, the solution was cooled to −60 °C and neutralized with Et_3N (0.731 ml, 5.22 mmol). To this solution was added a chilled solution of H-Val-Orn(Z)-Leu-OEt·HCl (1.10 g, 2.02 mmol)[1] and Et_3N (0.283 ml, 2.02 mmol) in DMF (8 ml). The reaction mixture was allowed to stir at 0 °C for 3 days and evaporated. After the addition of 0.02 M citric acid (300 ml), the solid was

collected and washed with water; yield, 1.59 g (85%); mp 279—281 °C (dec); $[\alpha]_D^{25}$ −41.0° (*c* 0.2, DMF); R_f^1 0.84, R_f^2 0.67.

Found: C, 60.37; H, 7.30; N, 11.28%. Calcd for $C_{56}H_{79}O_{14}N_9 \cdot 1/2H_2O$: C, 60.52; H, 7.26; N, 11.34%.

H-Asn-Gln-Tyr(Bzl)-Val-Orn(Z)-Leu-OEt·HCl (**13**·HCl). Compound **12** (1.70 g, 1.54 mmol) was treated with 0.1 M hydrogen chloride in formic acid (23 ml) as described for the preparation of **2a**·HCl; yield, 1.48 g (92%); mp 265—267 °C (dec); $[\alpha]_D^{25}$ −29.0° (*c* 0.2, DMF); R_f^1 0.81, R_f^2 0.34.

Found: C, 58.01; H, 6.95; N, 11.78%. Calcd for $C_{51}H_{72}O_{12}N_9Cl \cdot H_2O$: C, 57.97; H, 7.06; N, 11.93%.

Boc-D-Phe-Pro-Phe-D-Phe-Asn-Gln-Tyr(Bzl)-Val-Orn(Z)-Leu-OEt (**14a**). Compound **6a** (0.257 g, 0.383 mmol) and **13**·HCl (0.437 g, 0.421 mmol) were coupled by the azide method as described for the preparation of **12**; yield, 0.522 g (83%); mp 243—245 °C (dec); $[\alpha]_D^{25}$ −29.0° (*c* 0.5, AcOH); R_f^1 0.98, R_f^2 0.58.

Found: C, 61.33; H, 6.80; N, 10.54%. Calcd for $C_{88}H_{113}O_{18}N_{13} \cdot 4H_2O$: C, 61.70; H, 7.12; N, 10.63%.

Boc-D-Phe-Pro-Gly-D-Phe-Asn-Gln-Tyr(Bzl)-Val-Orn(Z)-Leu-OEt (**14b**). This was prepared from **6b** (0.222 g) and **13**·HCl (0.418 g) as described above; yield, 0.482 g (81%); mp 253—255 °C (dec); $[\alpha]_D^{25}$ −27.0° (*c* 1, AcOH); R_f^1 0.98, R_f^2 0.63.

Found: C, 60.26; H, 6.92; N, 11.36%. Calcd for $C_{81}H_{107}O_{18}N_{13} \cdot 3H_2O$: C, 60.62; H, 7.10; N, 11.35%.

Boc-D-Phe-Pro-Phe-Gly-Asn-Gln-Tyr(Bzl)-Val-Orn(Z)-Leu-OEt (**14c**). This was prepared from **6c** (0.222 g) and **13**·HCl (0.418 g); yield, 0.505 g (85%); mp 252—254 °C (dec); $[\alpha]_D^{25}$ −43.0° (*c* 0.5, AcOH); R_f^1 0.98, R_f^2 0.64.

Found: C, 61.26; H, 7.01; N, 11.51%. Calcd for $C_{81}H_{107}O_{18}N_{13} \cdot 2H_2O$: C, 61.31; H, 7.05; N, 11.47%.

Boc-D-Phe-Pro-Phe-D-Phe-Asn-Gln-Tyr(Bzl)-Val-Orn(Z)-Leu-NHNH$_2$ (**15a**). Compound **14a** (0.523 g, 0.319 mmol) was treated with hydrazine hydrate (1.55 ml, 31.9 mmol) as described for the preparation of **11**; yield, 0.42 g (81%); mp 252—254 °C (dec); $[\alpha]_D^{25}$ −28.0° (*c* 0.5, AcOH); R_f^1 0.91, R_f^2 0.41.

Found: C, 60.51; H, 6.81; N, 12.22%. Calcd for $C_{86}H_{111}O_{17}N_{15} \cdot 4H_2O$: C, 60.79; H, 7.06; N, 12.37%.

Boc-D-Phe-Pro-Gly-D-Phe-Asn-Gln-Tyr(Bzl)-Val-Orn(Z)-Leu-NHNH$_2$ (**15b**). This was prepared from **14b** (0.183 g) and hydrazine hydrate (0.572 ml) as described above; yield, 0.162 g (90%); mp 254—255 °C (dec); $[\alpha]_D^{25}$ −27.0° (*c* 1, AcOH); R_f^1 0.90, R_f^2 0.30.

Found: C, 59.41; H, 6.93; N, 13.55%. Calcd for $C_{79}H_{105}O_{17}N_{15} \cdot 3H_2O$: C, 59.65; H, 7.03; N, 13.21%.

Boc-D-Phe-Pro-Phe-Gly-Asn-Gln-Tyr(Bzl)-Val-Orn(Z)-Leu-NHNH$_2$ (**15c**). This was prepared from **14c** (0.476 g) and hydrazine hydrate (1.49 ml); yield, 0.437 g (93%); mp 254—256 °C (dec); $[\alpha]_D^{25}$ −29.0° (*c* 0.5, AcOH); R_f^1 0.92, R_f^2 0.36.

Found: C, 60.02; H, 6.86; N, 13.38%. Calcd for $C_{79}H_{105}O_{17}N_{15} \cdot 2H_2O$: C, 60.33; H, 6.99; N, 13.36%.

H-D-Phe-Pro-Phe-D-Phe-Asn-Gln-Tyr(Bzl)-Val-Orn(Z)-Leu-NHNH$_2$·2HCl (**16a**·2HCl). Compound **15a** (0.163 g, 0.1 mmol) was treated with 0.1 M hydrogen chloride in formic acid (1.5 ml) as desctibed for the preparation of **2a**·HCl; yield, 0.147 g (92%); mp 235—237 °C (dec); $[\alpha]_D^{25}$ −35.0° (*c* 0.5, AcOH); R_f^1 0.85, R_f^2 0.38.

Found: C, 59.81; H, 6.75; N, 12.83%. Calcd for $C_{81}H_{105}O_{15}N_{15}Cl_2 \cdot H_2O$: C, 60.14; H, 6.67; N, 12.99%.

H-D-Phe-Pro-Gly-D-Phe-Asn-Gln-Tyr(Bzl)-Val-Orn(Z)-Leu-NHNH$_2$·2HCl (**16b**·2HCl). This was prepared from **15b** (0.141 g) as described above; yield, 0.129 g (93%); mp 237—240 °C (dec); $[\alpha]_D^{25}$ −15.0° (*c* 0.2, AcOH); R_f^1 0.83, R_f^2 0.38.

Found: C, 57.99; H, 6.72; N, 13.37%. Calcd for $C_{74}H_{99}O_{15}N_{15}Cl_2 \cdot H_2O$: C, 58.18; H, 6.66; N, 13.75%.

H-D-Phe-Pro-Phe-Gly-Asn-Gln-Tyr(Bzl)-Val-Orn(Z)-Leu-NHNH$_2$·2HCl (**16c**·2HCl). This was prepared from **15c** (0.17 g) as described above; yield, 0.148 g (88%); mp 238—241 °C (dec); $[\alpha]_D^{25}$ −63.0° (*c* 0.5, AcOH); R_f^1 0.87, R_f^2 0.44.

Found: C, 58.12; H, 6.65; N, 13.40%. Calcd for $C_{74}H_{99}O_{15}N_{15}Cl_2 \cdot H_2O$: C, 58.18; H, 6.66; N, 13.75%.

cyclo(-D-Phe-Pro-Phe-D-Phe-Asn-Gln-Tyr(Bzl)-Val-Orn(Z)-Leu-) (**17a**). Compound **16a**·2HCl (146 mg, 0.091 mmol) was dissolved in a mixture of DMF (4 ml), AcOH (0.2 ml) and 1 M HCl (0.19 ml). To the solution at −10 °C was added 1 M $NaNO_2$ (0.096 ml). After being left to stand at −10 °C for 15 min, the solution was added into pyridine (100 ml) at −5 °C. The solution was allowed to stir at −5 °C for 3 h and at 0 °C for 45 h, and evaporated. The residue was dissolved in a mixture (100 ml) of MeOH–dioxane–water (5: 3: 1), an insoluble material being removed by filtration. The filtrate was passed successively through columns (1.5×12 cm) of Amberlite IRC-50 (H^+ form) and Amberlite IR-45 (OH^- form). The effluent (250 ml) was evaporated, and the resulting solid was collected by filtration with the aid of water; yield, 68 mg (50%); mp 245—248 °C (dec); $[\alpha]_D^{25}$ −95° (*c* 0.1, DMF); R_f^1 0.98, R_f^2 0.70, R_f^3 0.74.

Found: C, 62.57; H, 6.78; N, 12.01%; mol wt, 1493.[15] Calcd for $C_{81}H_{99}O_{15}N_{13} \cdot 3H_2O$: C, 62.81; H, 6.83; N, 11.76%; mol wt, 1549.

cyclo(-D-Phe-Pro-Gly-D-Phe-Asn-Gln-Tyr(Bzl)-Val-Orn(Z)-Leu-) (**17b**). This was prepared from **16b**·2HCl (133 mg) as described above; yield, 65 mg (52%); mp 236—239 °C (dec); $[\alpha]_D^{25}$ −83° (*c* 0.1, DMF); R_f^1 0.95, R_f^2 0.64, R_f^3 0.74.

Found: C, 60.90; H, 6.92; N, 12.32%; mol wt, 1475. Calcd for $C_{74}H_{93}O_{15}N_{13} \cdot 3H_2O$: C, 60.93; H, 6.84; N, 12.48%; mol wt, 1459.

cyclo(-D-Phe-Pro-Phe-Gly-Asn-Gln-Tyr(Bzl)-Val-Orn-(Z)-Leu-) (**17c**). This was prepared from **16c**·2HCl (156 mg); yield, 83 mg (57%); mp 232—235 °C (dec); $[\alpha]_D^{25}$ −85° (*c* 0.1, DMF); R_f^1 0.98, R_f^2 0.64, R_f^3 0.79.

Found: C, 61.23; H, 6.69; N, 12.50%; mol wt, 1445. Calcd for $C_{74}H_{93}O_{15}N_{13} \cdot 3H_2O$: C, 60.93; H, 6.84; N, 12.48%; mol wt, 1459.

cyclo(-D-Phe-Pro-Phe-D-Phe-Asn-Gln-Tyr-Val-Orn-Leu-)·HCl (**18a**·HCl). A solution of **17a** (60 mg, 0.04 mmol) in 0.43 M hydrogen chloride (0.14 ml) in MeOH was hydrogenated in the presence of Pd black. After 20 h, the filtrate was evaporated, and the resulting crystals were collected by filtration with the aid of ether; yield of air-dried product (**18a**·HCl·7H_2O), 48 mg (92%); mp 240—243 °C (dec); $[\alpha]_D^{25}$ −111° (*c* 0.14, 50% EtOH) (lit. $[\alpha]_D^{25}$ −111°,[16] −112°[8]); R_f^1 0.78, R_f^2 0.03, R_f^4 0.98, R_f^5 0.87. Amino acid ratios in acid hydrolysate; Asp 1.02, Glu 1.00, Pro 0.93, Val 0.99, Leu 1.02, Tyr 0.92, Phe 3.19, Orn 0.96.

Found: C, 55.78; H, 6.79; N, 12.25%. Calcd for $C_{66}H_{87}O_{13}N_{13} \cdot HCl \cdot 7H_2O$: C, 55.32; H, 7.17; N, 12.71%.

cyclo(-D-Phe-Pro-Gly-D-Phe-Asn-Gln-Tyr-Val-Orn-Leu-)·HCl (**18b**·HCl). This was prepared from **17b** (56 mg) as described above; yield of air-dried product (**18b**·HCl·8H_2O), 46 mg (94%); mp 232—234 °C (dec); $[\alpha]_D^{25}$ −95° (*c* 0.17, 50% EtOH); R_f^1 0.77, R_f^2 0.03, R_f^4 0.96, R_f^5 0.85. Amino acid ratios in acid hydrolysate; Asp 1.00, Glu 1.00, Pro 0.97, Gly 1.03, Val 1.05, Leu 1.04, Tyr 1.04, Phe 1.93, Orn 1.02.

Found: C, 51.74; H, 6.96; N, 13.74%. Calcd for $C_{59}H_{81}$-

$O_{13}N_{13}\cdot HCl\cdot 8H_2O$: C, 52.07; H, 7.26; N, 13.38%.

*cyclo(-D-Phe-Pro-Phe-Gly-Asn-Gln-Tyr-Val-Orn-Leu-)·HCl (**18c**·HCl).* This was prepared from **17c** (70 mg); yield of air-dried product (**18c**·HCl·$7H_2O$), 56 mg (92%); mp 230—232 °C (dec); $[\alpha]_D^{25}$ −98° (*c* 0.14, 50% EtOH); R_f^1 0.97, R_f^2 0.03, R_f^4 0.97, R_f^5 0.85. Amino acid ratios in acid hydrolysate; Asp 1.03, Glu 1.00, Pro 1.06, Gly 1.06, Val 1.11, Leu 1.09, Tyr 1.00, Phe 1.93, Orn 1.06.

Found: C, 52.31; H, 6.93; N, 13.95%. Calcd for $C_{59}H_{81}O_{13}N_{13}\cdot HCl\cdot 7H_2O$: C, 52.76; H, 7.21; N, 13.56%.

Droplet Countercurrent Chromatography. An apparatus made by Seikagaku Kogyo Co., Tokyo, was used. It consists of 300 columns of glass tubing (0.24×60 cm) connected by teflon tubing (I. D., 0.05 cm). The solvent used was $CHCl_3$–MeOH–0.1 M HCl (19: 19: 12, v/v).[17] The upper phase of the solvent was loaded into 150 glass columns as the stationary phase. The 5 mg samples each of **18a—c** and natural TA were dissolved in the lower phase (1 ml) and placed at the top of first column. The lower phase, as the moving phase, was pumped with nitrogen pressure through the top of the first column at a flow rate of 15 ml/h. Fractions (4 g) from the last column were collected and their absorbances were determined at 280 nm. The results are shown in Fig. 3.

Paper Electrophoresis. This was carried out with Toyo Roshi No. 52 and a solvent system of formic acid–ACOH–MeOH–water (1: 3: 6: 10, v/v; pH 1.8) for 2.5 h at 500 v/30 cm. Fig. 5. showed that each of **18a—c** revealed a single spot.

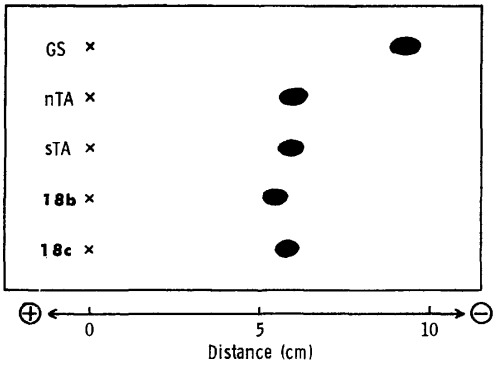

Fig. 5. Paper electrophoresis of the cyclic peptides.

Microbiological Assays,[18] *ORD Measurements.* These were carried out as described in a previous paper,[1] the results being shown in Table 1 and Fig. 4.

The authors wish to express their thanks to Dr. T. Kato, Dr. M. Ohno, Dr. M. Waki, and Mr. K. Sato of this laboratory for their helpful discussions and assistances.

References

1) Part XXXIII of this series: H. Abe, K. Sato, T. Kato, and N. Izumiya, *Bull. Chem. Soc. Jpn.*, **49**, 3113 (1976).

2) M. Ohno and N. Izumiya, *J. Am. Chem. Soc.*, **88**, 376 (1966); M. Ohno, T. Kato, S. Makisumi, and N. Izumiya, *Bull. Chem. Soc. Jpn.*, **39**, 1738 (1966).

3) K. Okamoto, M. Waki, T. Kato, and N. Izumiya, *Mem. Fac. Sci. Kyushu Univ., C*, **8**, 297 (1973).

4) Abbreviations according to IUPAC-IUB commission, *J. Biol. Chem.*, **247**, 977 (1972), are used throughout. Additional abbreviations: BuOH, 1-butanol; DMF, *N,N*-dimethylformamide; MA, mixed anhydride; ONp, *p*-nitrophenyl ester; THF, tetrahydrofuran; TFA, trifluoroacetic acid. Amino acid symbols except Gly and D-Phe denote the L-configuration.

5) S. Matsuura, H. Takiguchi, M. Waki, and N. Izumiya, *Mem. Fac. Sci. Kyushu Univ., C*, **9**, 277 (1975).

6) K. Tanaka, A. Shichiho, and S. Sakakibara, The 20th Natl. Meeting of Chem. Soc. Japan, Tokyo, April, Abst. III, p. 661 (1967).

7) F. Lipmann, *Acc. Chem. Res.*, **6**, 361 (1973).

8) K. Okamoto, H. Yonezawa, and N. Izumiya, *J. Chromatogr.*, **92**, 147 (1974).

9) As seen in Fig. 3, each of **18a—c** gave an additional peak at fraction 10. As reported in Ref. 8, pure natural TA and related cyclic peptides gave also the additional same peak. We assume that a product showing absorption at 280 nm exists in a system of DCCC and the product is eluted at the fraction 10.

10) G. W. Anderson and A. C. McGregor, *J. Am. Chem. Soc.*, **79**, 6180 (1975).

11) G. W. Anderson and R. Paul, *J. Am. Chem. Soc.*, **80**, 4423 (1958).

12) E. Wünsch, G. Fries, and A. Zwick, *Chem. Ber.*, **91**, 542 (1958).

13) E. Wünsch and P. Thamm, *Chem. Ber.*, **104**, 2454 (1971).

14) J. Honzl and J. Rudinger, *Collect. Czech. Chem. Commun.*, **26**, 2333 (1961).

15) Molecular weight was determined on a Hitachi Osmometer, type 115, using DMF as a solvent.

16) A. R. Battersby and L. C. Craig, *J. Am. Chem. Soc.*, **74**, 4019 (1952).

17) Natural TA used in this study was prepared following Ref. 8. In Ref. 8, we reported the use of a solvent system, benzene–$CHCl_3$–MeOH–0.1 M HCl=11: 5: 10: 4, for the separation of gramicidin A and tyrocidine family, and recognized a mistake of the description after the publication of Ref. 8. We wish to correct that the solvent system used was benzene–$CHCl_3$–MeOH–0.1 M HCl=5: 10: 11: 4.

18) We are indebted to the staff of Takeda Chemical Industries, Ltd. for the assay.

The Reaction of Nucleophilic Reagents at the β-Position of 3-Bromo-4-nitropyridine *N*-Oxides

Eizo MATSUMURA and Masahiro ARIGA

Department of Chemistry, Osaka Kyoiku University, Tennoji-ku Osaka 543

(Received July 16, 1976)

The reactions of 3-bromo-4-nitro-2-R_1-6-R_2-5-X-pyridine *N*-oxides (**1a**: R_1=H, R_2=Me, X=H; **1b**: R_1=R_2=Me, X=H; **1c**: R_1=R_2=H, X=Br) with diethyl sodiomalonate, ethyl sodiocyanoacetate, and ethyl sodioacetoacetate have been carried out. The treatment of **1a**, **1b**, and **1c** with diethyl sodiomalonate gives 3-[bis(ethoxycarbonyl)methyl]-4-nitro-2-R_1-6-R_2-5-X-pyridine *N*-oxides (**2a**, **2b**, and **2c**) and 4-[bis(ethoxycarbonyl)methyl]-3,5-dibromopyridine *N*-oxide (**3c**). With ethyl sodiocyanoacetate, 3-[cyano(ethoxycarbonyl)methyl]-4-nitro-2-R_1-6-R_2-pyridine *N*-oxides (**4a** and **4b**) and 4-[cyano(ethoxycarbonyl)methyl]-3,5-dibromopyridine *N*-oxide (**5c**) are obtained. With ethyl sodioacetoacetate, **1a** and **1c** give 3-[acetyl(ethoxycarbonyl)methyl]-6-methyl-4-nitropyridine *N*-oxide (**6a**) and/or 3-ethoxycarbonyl-2-methyl-6-R_1-7-X-furo[3,2-*c*]pyridine *N*-oxides (**7a** and **7c**), but **1b** is unaffected by ethyl sodioacetoacetate under the given conditions. The electronic and steric effects of methyl and bromo groups for the reactions are discussed.

The nucleophilic substitution reactions of pyridine homologues and their *N*-oxides have widely been studied for a long time,[1-4] but these studies dealt almost exclusively with the α or γ-position of the ring, with only a few exceptions.[5-7]

In the previous paper[8] of this series, the authors reported the nucleophilic substitution at the β-position of the pyridine ring. Thus, 3-bromo-4-nitropyridine *N*-oxide reacted with diethyl sodiomalonate, ethyl sodiocyanoacetate, and ethyl sodioacetoacetate to yield 3-[bis(ethoxycarbonyl)methyl]-4-nitropyridine *N*-oxide, 3-[cyano(ethoxycarbonyl)methyl]-4-nitropyridine *N*-oxide, and 3-[acetyl(ethoxycarbonyl)methyl]-4-nitropyridine *N*-oxide, respectively, and with ethyl sodioacetoacetate, when treated at a higher temperature, to yield 3-ethoxycarbonyl-2-methylfuro[3,2-*c*]pyridine *N*-oxide; the ring closure reaction was assumed to occur at the γ-position of the pyridine ring by the intramolecular nucleophilic attack of the mesomeric *O*-anion, which was produced by the loss of a proton from the substituted 3-methyl group of the intermediate, 3-[acetyl(ethoxycarbonyl)methyl]-4-nitropyridine *N*-oxide.

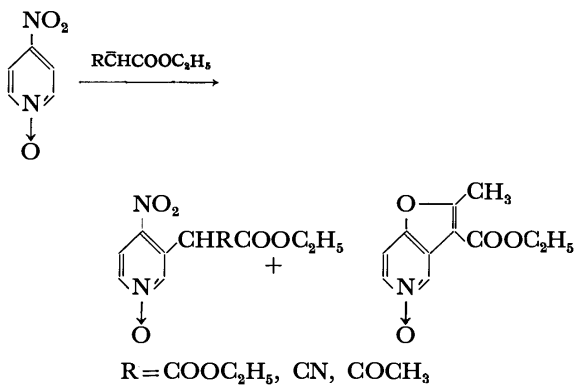

R=$COOC_2H_5$, CN, $COCH_3$

It seems of interest to investigate further the scope of this reaction. This paper deals with the reactions of the above nucleophiles with 3-bromo-6-methyl-4-nitropyridine *N*-oxide (**1a**), 3-bromo-2,6-dimethyl-4-nitropyridine *N*-oxide (**1b**), and 3,5-dibromo-4-nitropyridine *N*-oxide (**1c**). With the former two, the reactivity may be weakened by the inductive effects of the methyl groups located *ortho* and/or *para* to the site of the substitution, and the steric effect of the 2-methyl group also should be taken into consideration in the case of **1b**. With the latter, the resonance effect of the nitro group may be enfeebled by steric compression, and it is supposed that the nitro group, itself, may also be displaced by a nucleophilic substitution reaction.

Results and Discussion

On the treatment of 3-bromo-6-methyl-4-nitropyridine *N*-oxide (**1a**), 3-bromo-2,6-dimethyl-4-nitropyridine *N*-oxide (**1b**), and 3,5-dibromo-4-nitropyridine *N*-oxide (**1c**) with diethyl sodiomalonate in diethyl carbonate at 50 °C, 3-substituted products, 3-[bis(ethoxycarbonyl)methyl]-6-methyl-4-nitropyridine *N*-oxide (**2a**), 3-[bis(ethoxycarbonyl)methyl]-2,6-dimethyl-4-nitropyridine *N*-oxide (**2b**), and 3-[bis(ethoxycarbonyl)methyl]-5-bromo-4-nitropyridine *N*-oxide (**2c**), respectively, were obtained in good yields. These were analogous to the results of the reaction of 3-bromo-4-nitropyridine *N*-oxide with diethyl sodiomalonate in our previous paper.[8] Besides, in the case of the reaction of **1c**, a small amount of **3c** was isolated in addition to **2c**. The compound, **3c**, had the empilical formula $C_{12}H_{13}NO_5Br_2$. The NMR spectra of **3c** showed nearly the same pattern as that of **2c** with exception of the paramagnetic shift of the methin proton in 0.68 ppm. The IR spectra of **3c** indicated the existence of a carbonyl group (1746 cm^{-1}) and an *N*-oxide (1260 cm^{-1}), and the lack of a nitro group. On the basis of these data, **3c** was proved to be 4-[bis(ethoxycarbonyl)methyl]-3,5-dibromopyridine *N*-oxide (**3c**).

The fact that the 4-substituted product, **3c**, was given, though in poor yield, indicated that the potential ability of the 4-nitro group as a leaving group was promoted by the inductive effect of the two bromine atoms, seated in both ortho places, on the nitro group.

The reactions of **1a**, **1b**, and **1c** with ethyl sodiocyanoacetate were performed at different temperature in pyridine. At 5 °C, 3-[cyano(ethoxycarbonyl)methyl]-6-methyl-4-nitropyridine *N*-oxide (**4a**) was obtained from **1a** in a good yield, but at this temperature, **1b** gave 3-[cyano(ethoxycarbonyl)methyl]-2,6-dimethyl-4-nitropyridine *N*-oxide (**4b**) in only 32% yield, and **1c** was

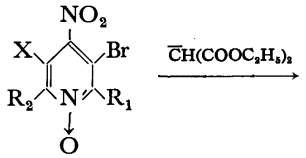

1 (a, b, c)

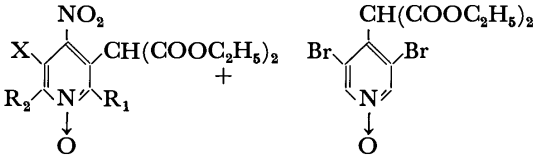

2 (a, b, c) 3c

a: R_1=H, R_2=Me, X=H
b: R_1=R_2=Me, X=H
c: R_1=R_2=H, X=Br

TABLE 1. REACTIONS WITH DIETHYL SODIOMALONATE

Substrates	Temp °C	Time h	Solvent	Products (Yields %)
1a	50	5	Diethyl carbonate	**2a** (97.3)
1b	50	5	Diethyl carbonate	**2b** (87.1)
1c	50	5	Diethyl carbonate	**2c** (88.9) **3c** (2.2)

recovered intact. At 50 °C **1b** was converted to **4b** in a satisfactory yield, but **1c** was still unaffected, **1c** berely underwent the reaction at 75 °C to give 3,5-dibromo-4-[cyano(ethoxycarbonyl)methyl]pyridine *N*-oxide (**5c**). However, 5-bromo-3-[cyano(ethoxycarbonyl)methyl]-4-nitropyridine *N*-oxide (**4c**), analogous to **4a** and **4b**, was not obtained. The yield of **5c** was not enhanced even if the reaction temperature was raised.

With ethyl sodioacetoacetate, **1a** gave 3-[acetyl-(ethoxycarbonyl)methyl]-6-methyl-4-nitropyridine *N*-oxide (**6a**) at the lower temperature (35 °C), and when the reaction was followed by further treatment at the higher temperature (75 °C), the anticipated 3-ethoxycarbonyl-2,6-dimethylfuro[3,2-*c*]pyridine *N*-oxide (**7a**) was obtained. The identity of both products was confirmed by the IR, NMR, and elemental analytical data, and by analogy with the results in the previous paper.[8] Similarly, 7-bromo-3-ethoxycarbonyl-2-methylfuro[3,2-*c*]pyridine *N*-oxide (**7c**) was easily obtained by treatment of **1c** with ethyl sodioacetoacetate at 35 °C, and 5-bromo-3-[acetyl(ethoxycarbonyl)methyl]-4-nitropyridine *N*-oxide (**6c**), analogous to **6a**, was not isolated even under the mild conditions in which a part of **1c** was recovered. The reaction of **1b** with ethyl sodioacetoacetate was examined under several conditions, but resulted in either the recovery of the starting material or the formation of resinous matters.

Examination of the above results as a whole reveals that **1a** is more liable to undergo the reaction with the anions than **1b**. Thus, whereas **1a** can be allowed to react under as mild conditions as 3-bromo-4-nitropyridine *N*-oxide[8] allows, **1b** required more severe conditions to give the same results. These facts are consistent with the results which are expected by considering the electronic effects of the second substituents (2 and/or 6-methyl groups). The inductive and steric effects of the 2-methyl group of **1b** appear to play an important role in preventing the formation of the 3-substituted product on treatment with ethyl sodioacetoacetate. The nucleophilicity of ethyl sodioacetoacetate is intermediate between those of ethyl sodiomalonate and ethyl sodiocyanoacetate (the pK_a value of these esters are about 11, 13, and 9, respectively). The steric requirement of ethyl sodioacetoacetate is also located between those for the other (stericaly favorable -CN,>-$COCH_3$,>-$COOC_2H_5$). Taking into account the operation of these characters a and effects, the lower reactivity of **1b** with ethyl sodioacetoacetate may be reasonable.

It appears that **7a** and **7c** are formed *via* **6a** and **6c**, as shown in the following scheme. This is quite analogous to the formation of 3-ethoxycarbonyl-2-methylfuro[3,2-*c*]pyridine *N*-oxide in the previous paper.[8] This account is supported by the facts that 3-[acetyl(ethoxycarbonyl)-methyl]-4-nitropyridine *N*-oxide was converted to

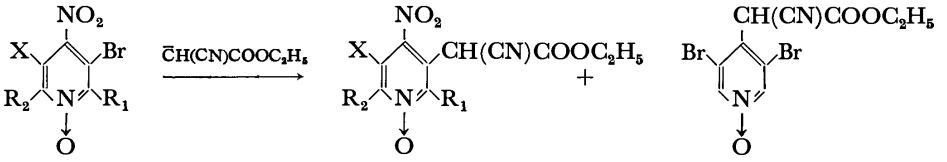

1 (a, b, c) 4 (a, b) 5c

a: R_1=H, R_2=Me, X=H; b: R_1=R_2=Me, X=H; c: R_1=R_2=H, X=Br

TABLE 2. REACTIONS WITH ETHYL SODIOCYANOACETATE

Substrates	Temp °C	Time h	Solvents	Products (Yields %)		
1a	5	5	Pyridine	**4a** (91.5)		
1b	5	5	Pyridine	**4b** (32.1)		**1b** (59.0)
1b	5	10	Pyridine	**4b** (48.8)		**1b** (43.0)
1b	50	5	Pyridine	**4b** (93.0)		
1c	5	5	Pyridine			**1c** (88.0)
1c	50	5	Pyridine			**1c** (84.0)
1c	75	10	Pyridine		**5c** (14.1)	**1c** (78.0)
1c	95	5	Pyridine		**5c** (13.2)	**1c** (48.0)
1c	75	5	DMF		**5c** (12.0)	**1c** (69.0)

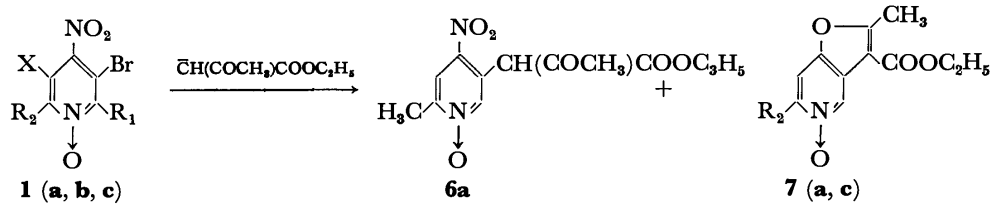

1 (a, b, c) **6a** **7 (a, c)**

a: R_1=H, R_2=Me, X=H; b: R_1=R_2=Me, X=H; c: R_1=R_2=H, X=Br

Table 3. Reactions with ethyl sodioacetoacetate

Substrates	Temp °C	Time h	Solvents	Products (Yield %)		
1a	35	5	Diethyl carbonate	**6a** (86.8)		
1a	35 75	5 5	Diethyl carbonate		**7a** (94.2)	
1b	35	5	Diethyl carbonate			**1b** (89.0)
1b	60	5	Diethyl carbonate			**1b** (78.0)
1b	90	10	Diethyl carbonate			**1b** (74.0)
1b	90	10	Pyridine			**1b** (75.0)
1b	110	10	Pyridine			**1b** (54.0)
1b	130	10	DMF			**1b** (38.0)
1c	35	5	Diethyl carbonate		**7c** (68.6)	**1c** (5.0)
1c	50	5	Diethyl carbonate		**7c** (94.4)	
1c	5—10	5	Diethyl carbonate		**7c** (41.2)	**1c** (43.0)
1c	35	5	Pyridine		**7c** (63.6)	**1c** (6.0)

3-ethoxycarbonyl-2-methylfuro[3,2-*c*]pyridine *N*-oxide either by treating with dilute ethanolic sodium ethoxide or only the prolonged storage.

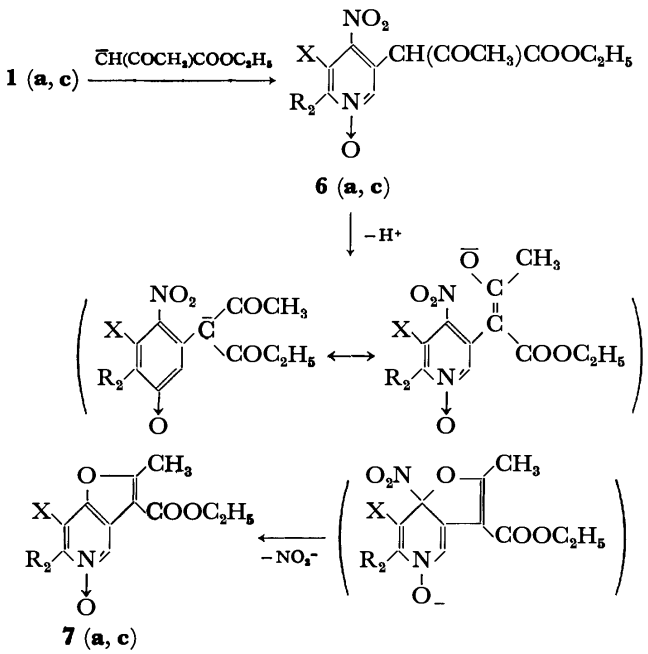

7 (a, c)

a: R_2=Me, X=H; b: R_2=H, X=Br

On reaction of **1c** with ethyl sodioacetoacetate, an anticipated **6c** as an intermediate for **7c** was not isolated even under the mild conditions in which the starting material was recovered as shown in Table 3. This result may be interpreted as follows. The nitro group in the anticipated product, **6c**, was not coplanar with the pyridine ring on account of the steric hindrance by a bromine atom and newly introduced group situated at both *ortho* positions to the nitro group, and **6c**, even if formed, becomes labile and converts to **7c** as soon as it is formed.

Experimental

All the melting points were uncorrected. The IR spectra were obtained on a Hitachi Infrared Spectrophotometer, EPI-S2, as Nujol mulls with the exception of some liquid samples. The NMR spectra were recorded on a Hitachi High Resolution NMR Spectrometer, 20-B, with TMS as the internal standard.

3-Bromo-6-methyl-4-nitropyridine N-*Oxide (1a).* 3-Bromo-6-methylpyridine[9] was treated according to the manner described in our paper[8] to give 3-bromo-6-methylpyridine *N*-oxide (mp 117.5—118 °C) in 86.8% yield. 3-Bromo-6-methyl-4-nitropyridine *N*-oxide (**1a**) (mp 137.5—138 °C) was obtained from 3-bromo-6-methylpyridine *N*-oxide by application of Jujo's method[10] in 76.3% yield.

3-Bromo-2,6-dimethyl-4-nitropyridine N-*Oxide (1b).* 3-Bromo-2,6-dimethylpyridine[11] was managed in the same manner as above to give 3-bromo-2,6-dimethyl-4-nitropyridine *N*-oxide **1b** (mp 111.5—113 °C) in 64.8% total yield.

3,5-Dibromo-4-nitropyridine N-*Oxide (1c).* 3,5-Dibromopyridine[12] was treated as above to give 3,5-dibromopyridine *N*-oxide in 93.5% yield. The *N*-oxide was treated as reported in the literature[13] to give 3,5-dibromo-4-nitropyridine *N*-oxide **1c** in 91.3% yield.

General Procedure of the Reaction of 1a, 1b, and 1c. To a solution of the pyridine **1** in a three necked flask were added three equimolar amounts of sodium salt in appropriate solvents dropwise over a period of an hour, at 15—20 °C with few exceptions, then the mixture were stirred at the required temperature for 5—10 h. The solvent was evaporated under reduced pressure, and the solution were neutralized with dil hydrochloric acid to pH 3—4; when diethyl carbonate is used as a solvent, the evaporation of the solvent may be omitted. The resulting mixture was extracted with chloroform. After drying over anhydrous sodium sulfate the solvent was distilled off, and the residual oil disolved in a small

amount of chloroform and refined through a silica gel (Wakogel C-300) column.

The Reaction of ***1a*** *with Diethyl Sodiomalonate.* A diethyl carbonate solution of 1.0 g of 3-bromo-6-methyl-4-nitropyridine *N*-oxide (**1a**) was treated as general procedure with a solution of diethyl sodiomalonate which had been formed from 0.3 g of sodium and 2.2 g diethyl malonate in 50 ml of diethyl carbonate. After the elution of diethyl malonate with chloroform on the chlomatograph, evaporation of the ethereal elute gave 1.30 g of 3-[bis(ethoxycarbonyl)methyl]-6-methyl-4-nitropyridine *N*-oxide (**2a**) as an oily syrup. Found: C, 49.90; H, 4.92; N, 8.37%; Calcd for $C_{13}H_{16}N_2O_7$: C, 50.00; H, 5.16; N, 8.97%. IR: 1750 cm^{-1} (C=O), 1525 and 1345 (NO_2), 1240 (N→O). NMR ($CDCl_3$): δ 1.27 (6H, t) 4.25 (4H, q), 2.52 (3H, s), 5.26 (1H, s), 8.02 (1H, s), 8.25 (1H, s).

The Reaction of ***1b*** *with Diethyl Sodiomalonate.* From 1.0 g of 3-bromo-2,6-dimethyl-4-nitropyridine *N*-oxide (**1b**), 1.15 g of 3-[bis(ethoxycarbonyl)methyl]-2,6-dimethyl-4-nitropyridine *N*-oxide (**2b**) was obtained as an oily syrup. Found: C, 51.66; H, 5.70; N, 8.19%. Calcd for $C_{14}H_{18}N_2O_7$: C, 51.38; H, 5.54, N. 8.56%. IR: 1745 cm^{-1} (C=O), 1530 and 1340 (NO_2), 1245 (N→O). NMR ($CDCl_3$): δ 1.26 (6H, t), 4.24 (4H, q), 2.54 (3H, s), 2.58 (3H, s), 5.21 (1H, s), 7.84 (1H, s).

The Reaction of ***1c*** *with Diethyl Sodiomalonate.* From the reaction of 1.0 g of **1c** with diethyl sodiomalonate, 1.12 g of 3-[bis(ethoxycarbonyl)methyl]-5-bromo-4-nitropyridine *N*-oxide (**2c**) was obtained from ethereal elution; mp 79—80 °C (acetone–diisopropyl ether). Found: C, 38.08; H, 3.37; N, 7.16%. Calcd for $C_{12}H_{13}N_2O_7Br$: C, 38.22; H, 3.47; N, 7.43%. IR: 1760 cm^{-1} (C=O), 1560 and 1355 (NO_2), 1240 (N→O). NMR ($CDCl_3$): δ 1.29 (6H, t), 4.26 (4H, q), 5.64 (1H, s), 8.37 (2H, s). From the succesive acetone–ether elution was obtained 0.03 g of 4-[bis(ethoxycarbonyl)methyl]-3,5-dibromopyridine *N*-oxide (**3c**); mp 124—125 °C (diisopropyl ether). Found: C, 34.72; H, 3.04; N, 3.16%; Calcd for $C_{12}H_{13}NO_5Br_2$: C, 35.02; H, 3.16; N, 3.40%. IR: 1746 cm^{-1} (C=O), 1254 (N→O). NMR ($CDCl_3$): δ 1.28 (6H, t), 4.26 (4H, q), 5.32 (1H, s), 8.40 (2H, s).

The Reaction of ***1a*** *with Ethyl Sodiocyanoacetate.* From 1.0 g of **1a**, 1.04 g of 3-[cyano(ethoxycarbonyl)methyl]-6-methyl-4-nitropyridine *N*-oxide (**4a**) was obtained: mp 177—177.5 °C (ethanol). Found: C, 49.62; H, 4.01; N, 15.63%. Calcd for $C_{11}H_{11}N_3O_5$: C, 49.81; H, 4.18; N, 15.84%. IR: 2230 cm^{-1} (CN), 1746 (C=O), 1260 (N→O). NMR ($CDCl_3$): δ 1.33 (3H, t), 4.32 (2H, q), 2.52 (3H, s), 5.51 (1H, s), 8.13 (1H, s) 8.43 (1H, s).

The Reaction of ***1b*** *with Ethyl Sodiocyanoacetate.* Under the suitable conditions, 50 °C, 3-[cyano(ethoxycarbonyl)-methyl]-2,6-dimethyl-4-nitropyridine *N*-oxide (**4b**) was obtained in 93.0% yield: mp 118.5—119.0 °C (acetone–diisopropyl ether). Found: C, 51.53; H, 4.46; N, 14.80%. Calcd for $C_{12}H_{13}N_3O_5$: C, 51.61; H, 4.69; N, 14.80%. IR: 2224 cm^{-1} (CN), 1745 (C=O), 1530 and 1342 (NO_2), 1270 (N→O). NMR ($CDCl_3$): δ 1.32 (3H, t), 2.54 (3H, s), 2.60 (3H, s), 4.30 (3H, q), 6.50 (1H, s), 7.97 (1H, s). The starting material, **1b**, when it was recovered, was obtained from chloroform elution following after the reagemt.

The Reaction of ***1c*** *with Ethyl Sodiocyanoacetate.* In this case ethyl sodiocyanoacetate was added at 75 °C over a period of 5 h, then the mixture was managed according to the general procedure. From 1.0 g of 3,5-dibromo-4-nitropyridine *N*-oxide (**1c**), after the collection of unreacted **1c** from ether–acetone elution 0.18 g of 4-[cyano(ethoxycarbonyl)methyl]-3,5-dibromopyridine *N*-oxide (**5c**) was obtained: mp 182—183 °C (ethanol). Found: C, 33.14; H, 2.29; N, 7.84%. Calcd for $C_{10}H_8N_2O_3Br_2$: C, 33.00; H, 2.22; N, 7.70%. IR: 2235 cm^{-1} (CN), 1745 (C=O), 1246 (N→O). NMR ($CDCl_3$): δ 1.33 (3H, t), 4.32 (2H, q), 5.52 (1H, s), 8.30 (1H, s).

The Reaction of ***1a*** *with Ethyl Sodioacetoacetate at 35 °C.* One gram of **1a** was treated with ethyl sodioacetoacetate according to the general procedure; the reaction temperature was kept at 35 °C for 5 h, and from ethereal elution 1.05 g of 3-[acetyl(ethoxycarbonyl) methyl]-6-methyl-4-nitropyridine *N*-oxide (**6a**) was obtained as yellow leaflets; mp 106—107 °C (diethyl ether). Found: C, 51.18; H, 4.87; N, 9.78%. Calcd for $C_{12}H_{14}N_2O_6$: C, 51.08; H, 5.00; N, 9.93%. IR: 1720 cm^{-1} (C=O), 1730 (C=O), 1560 and 1335 (NO_2), 1260 (N→O). NMR ($CDCl_3$): δ 1.12 (3H, t), 1.93 (3H, s), 2.54 (3H, s), 4.11 (2H, m), 7.96 (1H, s), 8.04 (1H, s), 12.98 (1H, s).

The Reaction of ***1a*** *with Ethyl Sodioacetoacetate at 75 °C.* The reaction mixture of the above reaction was further heated at 75 °C for an additional 5 h. The resulting mixture was treated by the same procedure, and from the alcoholic elute, 0.9 g of 3-ethoxycarbonyl-2,6-dimethylfuro[3,2-*c*]-pyridine *N*-oxide (**7a**) was obtained as colorless prisms; mp 120—121 °C (ethanol). Found: C, 61.44; H, 5.58; N, 5.57%. Calcd for $C_{12}H_{13}NO_4$: C, 61.27; H, 5.58; N, 5.95%. IR: 1720 cm^{-1} (C=O), 1246 (N→O). NMR ($CDCl_3$): δ 1.42 (3H, t), 2.58 (3H, s), 2.74 (3H, s), 4.38 (2H, q), 7.28 (1H,s), 8.83 (1H, s).

The Reaction of ***1c*** *with Ethyl Sodioacetoacetate.* When the reaction was carried out at 50 °C, 7-bromo-3-ethoxycarbonyl-2-methylfuro[3,2-*c*]pyridine *N*-oxide (**7c**) was obtained from ethanol elution as colourless prisms; mp 194—195 °C (acetone). Found: C, 44.07; H, 3.24; N, 4.48%. Calcd for $C_{11}H_{10}NO_4Br$: C, 44.02; H, 3.36; N, 4.67%. IR: 1705 cm^{-1} (C=O), 1250 (N→O). NMR ($CDCl_3$): δ 1.43 (3H, t), 2.83 (3H, s), 4.42 (2H, q), 8.28 (1H, s), 8.70 (1H, s).

3-Ethoxycarbonyl-2-methyl[3,2-c]pyridine N-Oxide. The mixture of 0.5 g of 3-[acetyl(ethoxycarbonyl)methyl]-4-nitropyridine *N*-oxide and 0.2 g of sodium ethoxide in 100 ml of ethanol was heated at 50 °C for 5 h. The deep violet color of the mixture faded with time. The solvent was evaporated, and the residue was neutralized with dil hydrochloric acid to pH 4, then extracted with chloroform. After drying over anhydrous sodium sulfate, evaporation of the solvent gave 0.22 g (53.4%) of 3-ethoxycarbonyl-2-methylfuro-[3,2-*c*]pyridine *N*-oxide, semihydrate; mp 150 °C, which was identified by mixed melting point determination and by comparing the IR and NMR spectra data with those of an authentic sample.[8]

References

1) H. S. Mosher, "Heterocyclic Compounds," Vol. 1, Chap. 8, ed. by R. C. Elderfield, John Wiley & Sons, New York (1950).

2) E. Ochiai, "Aromatic Amino Oxides," Elsevier Publishing Co., Amsterdam (1967).

3) A. R. Katritzky and J. M. Lagowski, "Chemistry of the Heterocyclic *N*-Oxides," Academic Press, London (1970).

4) For example, M. Hamana, "The Chemistry of the Heterocycles," Vol. 3, ed by Y. Kitahara, T. Kametani, and T. Kato, Nankodo and Co., Tokyo (1971).

5) S. M. McElvain and M. A. Goese, *J. Am. Chem. Soc.*, **63**, 2283 (1943); W. T. Caldwell, F. T. Tyson, and L. Lauer, *ibid.*, **66**, 1479 (1944).

6) H. J. Richter and N. E. Rustad, *J. Org. Chem.*, **29**, 3381 (1964).

7) J. Himeno, K. Noda, M. Yamazaki, *Chem. Pharm. Bull.*, **18**, 2138 (1970).

8) E. Matsumura and M. Ariga, *Bull. Chem. Soc. Jpn.*, **46**,

1344 (1973).
9) D. E. Peason, W. W. Hergrove, Judith K. T. Chow, and B. R. Suthers, *J. Org. Chem.*, **26**, 789 (1961).
10) R. Jujo, *Yakugaku Zasshi*, **66** (**B**), 49 (1946).
11) W. Drzeniek and P. Tomasik, *Rocz. Chem.*, **43**, 1865 (1969), *cf. Chem. Abst.*, **72**, 66755t (1970).
12) S. M. McElvain and M. A. Goese, *J. Am. Chem. Soc.*, **65**, 2227 (1943).
13) H. J. den Hertog, C. H. Henkens, and K. Dilz, *Recl. Trav. Chim. Pays-Bas*, **72**, 296 (1953).

New Method for Synthesis of Various Types of Substituted 2(5*H*)-Furanones

Kiyoshi IWAI, Hiroshi KOSUGI, Hisashi UDA, and Mikio KAWAI

Chemical Research Institute of Non-Aqueous Solutions, Tohoku University, Katahira-2, Sendai 980

(Received July 20, 1976)

A combination of the reaction of dianions of (phenylthio) acetic acid and its homologs with epoxides, the conjugate addition reaction of 3-phenylthio-2-(5*H*)-furanones with carbanion species, and the α-alkylation reaction of α-phenylthio-γ-butyrolactones is shown to provide a general method for the synthesis of a variety of substituted α-phenylthio-γ-butyrolactones. Oxidation of these α-phenylthiolactones to the corresponding sulfoxides, followed by pyrolysis furnishes all the types of substituted (3-, 4-, and 5-mono-; 3,4-, 3,5- 4,5-, and 5,5-di-; 3,4,5-tri-) 2(5*H*)-furanones in good overall yields.

Recently a number of methods for the synthesis of 2(5*H*)-furanones (γ-crotonolactones, 2-buten-4-olides, $\Delta^{\alpha,\beta}$-butenolides) have been reported,[1] in view of their abundance in nature[2] and usefulness as synthetic intermediates.[1d,3] Concerning the synthesis of natural products by the application of photocycloaddition reactions of 2(5*H*)-furanones to olefins,[3f] we became interested in the development of a convenient method for the synthesis of a variety of 2(5*H*)-furanones.[4]

Results

The method includes α-phenylthio-γ-butyrolactones **1** as the key intermediate. (Phenylthio)acetic acid (**2a**) might be suitable as the starting material for the construction of the C-2, 3 unit in 2(5*H*)-furanones (indicated by a dotted line in **1**). The phenylthio group was chosen since it appears (1) to facilitate the generation of the adjacent carbanion species which would have sufficient nucleophilicity to react with epoxides or alkyl

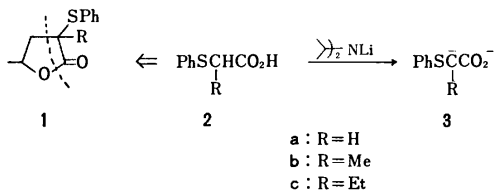

halides before or after the construction of γ-lactone ring, and (2) to be oxidized easily to the sulfinyl group which would be further transformed into other useful intermediary functional groups (vinyl sulfide or sulfoxide) through the Pummerer rearrangement and serve as a facile eliminating group to produce a double bond in the final products.

The dianion **3a** was easily prepared by treating **2a** with lithium diisopropylamide, and reacted smoothly with methyl iodide and ethyl bromide to give α-(phenylthio)propionic acid (**2b**) and -butyric acid (**2c**) in quantitative yields, respectively.[5] The homologous acids **2b** and **2c** also produced the corresponding dianions **3b** and **3c** in the same manner.

The reactions of the dianions **3** with epoxides **4** and subsequent transformation into 5-mono- and 3,5-disubstituted 2(5*H*)-furanones are shown in Scheme 1. The reactions of **3** with propylene oxide (**4a**), 1-hexene oxide (**4b**), or styrene oxide (**4c**) proceeded smoothly to give the corresponding phenylthiobutyrolactones **5** in excel-

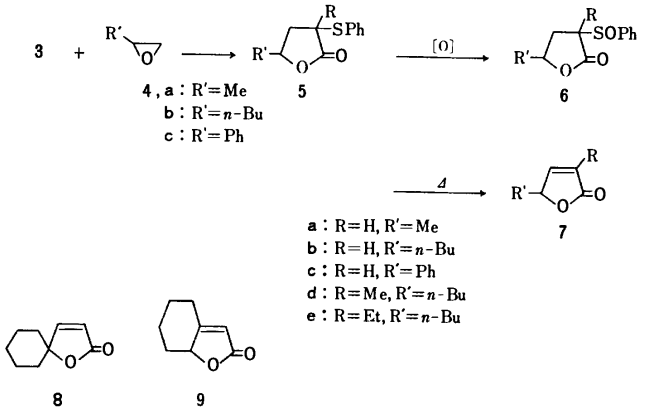

Scheme 1.

lent yields. Each lactone **5** was obtained as a mixture of stereoisomers. On treatment of **5** with *m*-chloroperbenzoic acid, hydrogen peroxide, or sodium periodate, the corresponding sulfoxides **6** were obtained quantitatively and were pyrolyzed (at *ca.* 110 °C for **6a—c** and *ca.* 70 °C for **6d**, **e**) to give 5-mono- and 3,5-disubstituted 2(5*H*)-furanones **7** in high yields. It should be noted that, in the cases of **6d** and **6e**, a double bond was exclusively introduced into an endocyclic position, neither α-methylene- nor α-ethylidene- γ-butyrolactone being detected.[1g]

In a similar way, the use of methylenecyclohexane oxide (1,1-disubstituted epoxide) or cyclohexene oxide (symmetrical 1,2-disubstituted epoxide) gave 5,5-pentamethylene-2(5*H*)-furanone (**8**) (5,5-disubstituted) and 4,5-tetramethylene-2(5*H*)-furanone (**9**) (4,5-disubstituted), respectively.

An attempt to use the anion of the ester of **2a**, PhS-$\bar{C}$HCO$_2$Et, for the reaction with **4a** gave an unsatisfactory result, **5a** being obtained in a low (30%) yield. Thus, the present α-phenylthio carboxylic acid dianion procedure would be very useful for the synthesis of 5-mono, 3,5-di, 5,5-di, and 4,5-di (the same substituents)-substituted 2(5*H*)-furanone derivatives, because of ready availability of the starting materials, simple operation of the reactions, and high yield of the products.

Among the number of methods for the synthesis of 2(5*H*)-furanones,[1] the procedure for 4-substituted derivatives has so far been very limited. Thus the development of a convenient synthetic method for them would be of considerable interest.

In order to introduce a substituent to the C-4 position

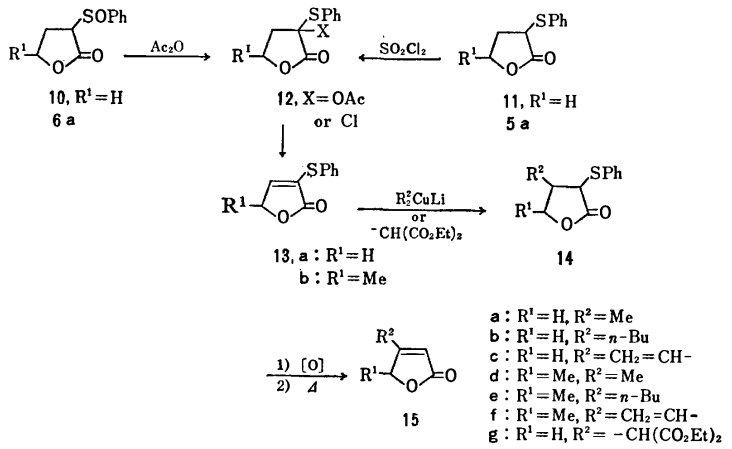

Scheme 2.

of 2(5*H*)-furanone system, we adopted the 1,4-conjugate addition reaction of 3-phenylthio- (**13**) or 3-phenylsulfinyl-2(5*H*)-furanones (**18**). The preparation of **13** was satisfactorily accomplished in two ways through the intermediates **12**: one by the Pummerer rearrangement[6] of α-phenylsulfinyl-γ-butyrolactones (**10** and **6a**) and the subsequent elimination of acetic acid by heating in acetic anhydride (60—70 °C and then 150 °C) (86 and 93% overall) and the other by the chlorination of α-phenylthio-γ-butyrolactones (**11** and **5a**) with sulfuryl chloride, followed by dehydrochlorination (93 and 88% overall) (Scheme 2). Phenylthiofuranones **13** thus obtained underwent conjugate addition with lithium dialkylcuprates (dialkyl=dimethyl, dibutyl, or divinyl) to give the adducts **14a—f** in good yields. These could be converted into the expected 4-mono- and 4,5-disubstituted 2(5*H*)-furanones **15a—f** in good yields. Combined use of the Grignard reagent and cuprous iodide for the conjugate addition gave an unsatisfactory result (low yields of **14** due to formation of a considerable amount of by-products).

In contrast to the successful addition of dialkylcuprate to **13**, the reaction of **13a** with other enolates (diethyl malonate, ethyl valerate, or cyclopentanone) did not necessarily give good results, the low yields of the adducts: 60% for **14g**, 11% for **16**, and 57% for **17**, presumably because of an unfavorable equilibrium (Scheme 3). Hence, the more effective stabilization of the α-anion in the adducts would favor the equilibration to the adduct side, facilitating the conjugate addition reaction of enolates. In fact, 3-phenylsulfinyl-2(5*H*)-furanone (**18**) underwent smoothly the conjugate addition with the enolates of ethyl valerate and cyclopentanone to give the desired adducts **19** and **20**, respectively, in good yields.[7] Unlike **13a**, **18** also reacted with ethyl 2-oxocyclohexanecarboxylate to afford a 30% yield of the adduct **21**. Pyrolysis of **19** and **21** furnished the 4-substituted 2(5*H*)-furanones **22** and **23**, respectively, in good yields, but the 2(5*H*)-furanone **24** derived from **20** was extremely unstable, polymerizing during the course of isolation. The reaction of **13a** with ethyl 2-oxocyclohexanecarboxylate produced only the polymers of **13a** itself, which would arise from self-addition of the 5-anion of **13a** (such as **25**). Actually, the dimer **26** was isolated in the reaction of **13b** in 38% yield.

The preferential abstraction of the 5-hydrogen atom

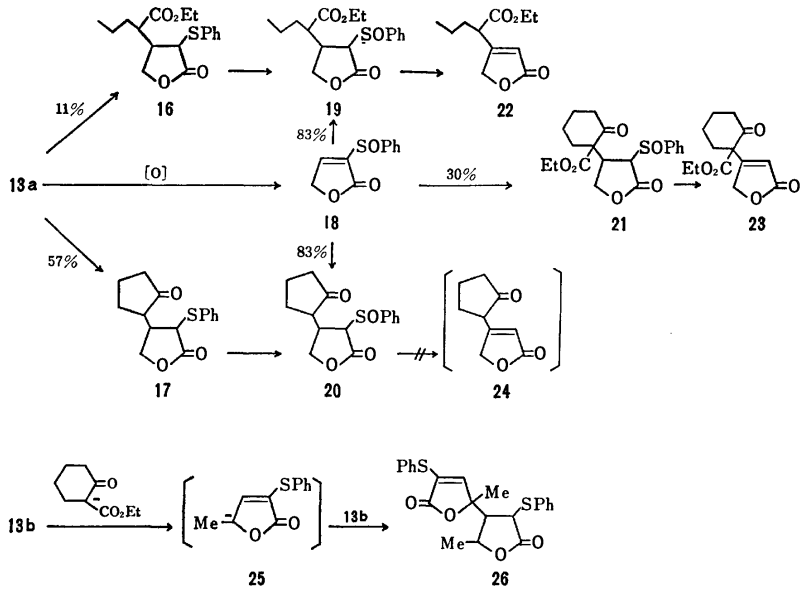

Scheme 3.

was also observed in the reaction of **13a** with an enamine. The reaction of **13a** with 1-morpholino-1-cyclopentene gave, in addition to a 22% yield of **17**, 5-cyclopentylidene-3-phenylthio-2(5*H*)-furanone (**27**) (30%), which would be formed through the reaction of the 5-anion of **13a** with the protonated enamine and the subsequent elimination of morpholine as depicted in Scheme 4. The 5-methyl derivative **13b** gave only the conjugate addition product **28** in low yield.

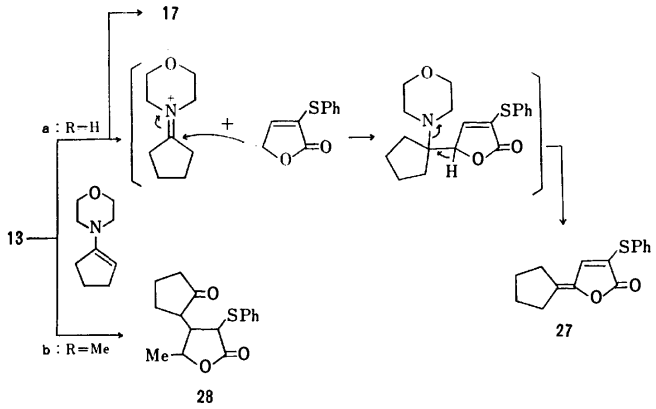

Scheme 4.

Finally, the application of α-alkylation to the α-phenylthio-γ-butyrolactones,[1g] through the subsequent oxidation and dehydrosulfenylation, led to the remaining 3-mono-, 3,4-di-, and 3,4,5-trisubstituted 2(5*H*)-furanone derivatives. Typical examples are shown in Scheme 5.

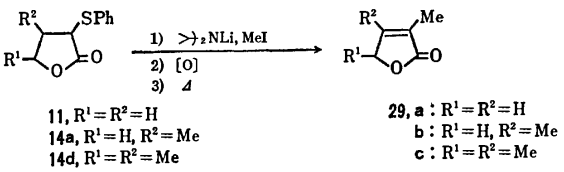

Scheme 5.

The procedures we gave provide useful methods for the synthesis of all types of substituted 2(5*H*)-furanones starting from readily available substances through simple and high-yield operations.

Experimental

All the melting points were taken on a Yamato melting point apparatus and are uncorrected. Distillation of the liquid products was usually carried out evaporatively using a modified sublimation apparatus and the oil bath temperatures were recorded. IR spectra were taken on a Hitachi EPI-S2 or G2 spectrometer. NMR spectra were obtained on a JEOL C-60HL (60 MHz) instrument using TMS as an internal standard. Reported values are given in the δ scale. Both spectra were recorded in CCl_4 solution unless otherwise stated. Elementary analyses were carried out in the microanalytical laboratory of this Institute. Progress of all the reactions was followed by TLC, silica gel (Merck GF_{254} Typ 60). The developing solvent system was petroleum ether–ether mixture, visualization being effected with a fluorescent lamp or concd H_2SO_4 spray.

Generation of the Dianion (3) of (Phenylthio)acetic Acid and its Homologs (2). To a solution of freshly prepared lithium diisopropylamide (0.02 mol) in THF–ether was added dropwise a solution of (phenylthio)acetic acid (**2a**)[8] (1.68 g, 0.01 mol) in THF (7 ml) at 0 °C under nitrogen. The mixture was stirred at 0—4 °C for 1 h. An aliquout (3 ml) was taken with a syringe and quenched with D_2O. Incorporation of one deuterium atom at the α-position in the recovered **2a** (acidification and extraction) was confirmed from the NMR spectrum: δ 3.58 (1H, s).

In the same manner, solutions of the dianions (**3b**) and (**3c**) of the propionic (**2b**) and butyric acid derivatives (**2c**) could be prepared.

Alkylation of the Dianion (3a). A solution of excess methyl iodide (17.6 g) in THF (5 ml) was added dropwise at −60——70 °C to a solution of the dianion (**3a**) (0.01 mol) under nitrogen, and the mixture was stirred overnight and warmed gradually to room temperature. A saturated solution of NH_4Cl and then 30% H_2SO_4 (to Congo Red) were added, and the mixture was extracted with $CHCl_3$. The combined extracts were washed with saturated brine and freed from the solvent. A small amount of ether was added to the residue and the insoluble material was removed by filtration. Evaporation of the solvent, and distillation (100—140 °C/<1 Torr) of the pale yellow oil remaining afforded 1.70 g (93%) of α-(phenylthio)propionic acid (**2b**). NMR 1.50 (3H, d, J=7 Hz, $-CHC\underline{H}_3$), 3.60 (1H, q, J=7 Hz, $-C\underline{H}CH_3$), 7.10—7.60 (5H, m, Ph), and 12.0 (1H, s, COOH).

In the same manner, the alkylation of **3a** with ethyl bromide gave α-(phenylthio)butyric acid (**2c**) in 99% yield. Bp 100—140 °C/<1 Torr; NMR 1.55 (3H, t, J=7.5 Hz, $-CH_2C\underline{H}_3$), 1.60—2.15 (2H, m, $-\dot{C}HC\underline{H}_2CH_3$), 3.47 (1H, t, J=7.2 Hz, $-\dot{C}\underline{H}CH_2-$), 7.10—7.60 (5H, m, Ph), and 11.4 (1H, s, COOH).

Compound **2b** was also prepared by the reaction of ethyl α-bromopropionate with sodium thiophenolate as in the preparation of **2a**. To a stirred slurry of sodium thiophenolate (1.4 g) in THF (20 ml) was added a solution of ethyl α-bromopropionate (1.18 g) in THF (10 ml) at 0 °C, and the mixture was stirred at room temperature for 6 h. After the removal of inorganic salt and solvent, distillation of the residual oil gave 2.0 g (95%) of ethyl α-(phenylthio)propionate. A mixture of this ester (1.8 g) and aqueous potassium hydroxide (720 mg in 10 ml) was heated under reflux for 3 h. At this stage the mixture became homogeneous. The cooled mixture was acidified with 30% H_2SO_4 turing to Congo Red and extracted with ether. The combined extracts were washed with saturated brine and dried. After evaporation of the solvent, distillation of the residue afforded 1.56 g (99%) of **2b**.

General Procedure for Reaction of the Dianions (3) with Epoxides. To a solution of dianion **3** was added a solution of the freshly purified epoxide (a slightly excess molar amount except propylene oxide) in dry THF at *ca.* −60 °C under nitrogen, and the reaction mixture was stirred at this temperature for 1 h and then gradually warmed to room temperature within a period of *ca.* 15 h. For 1 g of an epoxide, *ca.* 3 ml of THF was used. Aqueous NH_4Cl was added to the mixture and the solvent was then removed under reduced pressure. The residue was poured into a mixture of ether and dil H_2SO_4 (sufficient amount for neutralization), and the water layer was thoroughly extracted with ether. The combined ether layers were washed with water and saturated brine, and dried. After removal of the solvent, the residual oil was heated in benzene (*ca.* 10 ml for 1 g) containing a trace of concd H_2SO_4 under reflux for 3 h using a water-separator. The cooled reaction mixture was diluted with ether and successively washed with dil NaOH, water, and saturated brine. Removal of the solvent gave a mixture of *cis* and *trans* γ-substituted α-phenylthio-γ-butyrolactones (**5**) in 70—94% yield, which

were usually separable by chromatography on silica gel using petroleum ether–ether as an eluting agent. In the cases of **5d** and **5e**, the extraction was carried out with $CHCl_3$, and the concentration of the extracts at 80 °C under ordinary pressure resulted in complete lactonization.

General Procedure for Oxidation of α-Phenylthio-γ-butyrolactones. To a solution of the α-phenylthiolactone derivative in CH_2Cl_2 (*ca.* 20 ml for 1 g of the lactone) was added a solution of *m*-chloroperbenzoic acid (MCPBA, 85%, 1.0—1.2 equiv) in CH_2Cl_2 (*ca.* 30 ml for 1 g of the peracid) at 0 °C. The reaction mixture was stirred at 0 °C for 0.5—1 h, diluted with CH_2Cl_2, successively washed with dil $NaHCO_3$ solution and saturated brine, and dried. Evaporation of the solvent under reduced pressure left the α-phenylsulfinyl-γ-butyrolactone derivative in nearly quantitative yield.

The α-phenylthiolactone derivative was treated at room temperature with either $NaIO_4$ (*ca.* 1.2 equiv) in 40—50% methanol (*ca.* 20 ml for 1 g of the lactone) for 12 h or 30% hydrogen peroxide (*ca.* 2 ml) in 50% methanol for 4 days, and the usual work-up (extraction with CH_2Cl_2) gave also the α-phenylsulfinyllactone derivative (**6**) in excellent yield. In all cases, the sample thus obtained was sufficiently pure for the subsequent pyrolysis.

General Procedure for Pyrolysis of α-Phenylsulfinyl-γ-butyrolactones. A solution of the α-phenylsulfinyllactone derivative in toluene (10—20 ml for 1 g of the lactone) or in pyridine (*ca.* 5 ml) was heated under reflux for 0.5—1 h. After removal of the solvent under reduced pressure, the residue was chromatographed on silica gel using petroleum ether–ether as an eluting agent to give the 2(5*H*)-furanone derivative, which was purified by evaporative distillation.

*α-Phenylthio-γ-butyrolactone (**11**).* A solution of α-bromo-γ-butyrolactone[9] (15.1 g) in THF (30 ml) was added dropwise to a suspension of sodium thiophenolate (12.1 g) in THF (70 ml) at room temperature, and the reaction mixture was stirred for 2 days. After the removal of insoluble material and solvent, distillation (165—175 °C/1 Torr) of the residual oil afforded 17.1 g (96%) of **11**. Found: C, 61.56; H, 5.20%. Calcd for $C_{10}H_{10}O_2S$: C, 61.85; H, 5.15%.

*α-Phenylsulfinyl-γ-butyrolactone (**10**)*, yield 86% ($NaIO_4$): mp 100—104 °C from $CHCl_3$–CCl_4. Found: C, 57.11; H, 4.82%. Calcd for $C_{10}H_{10}O_3S$: C, 57.14; H, 4.80%.[10]

*3-Phenylthio-2(5H)-furanone (**13a**).* (a) A solution of **10** (4.4 g) in acetic anhydride (25 ml) was heated at 60—70 °C overnight and then refluxed for 2 h. After the removal of acetic anhydride and acetic acid under reduced pressure, the residue was recrystallized from ethanol to give 3.3 g (86%) of **13a**; mp 57.5—59 °C; IR ($CHCl_3$) 1760 and 1600 cm^{-1}; NMR ($CDCl_3$) 4.84 (2H, d, J=2.2 Hz), 6.75 (1H, t, J=2.2 Hz), and 7.40—7.80 (5H, m). Found: C, 62.57; H, 4.05%. Calcd for $C_{10}H_8O_2S$: C, 62.50; H, 4.20%. When the reaction was stopped at the stage of 70 °C heating, a small amount of α-acetoxy-α-phenylthio-γ-butyrolactone (**12**, R^1=H, X=OAc) was isolated.

(b) A solution of sulfuryl chloride (9.8 g) in CCl_4 (30 ml) was added dropwise (1 h) to a solution of **11** (11.9 g) in CCl_4 (70 ml) at 0 °C under nitrogen. The reaction mixture was stirred at 0 °C for 2 h, poured into aqueous $NaHCO_3$, and extracted with CH_2Cl_2. The combined extracts were successively washed with $NaHCO_3$ solution, water, and saturated brine, and dried. Evaporation of the solvent under reduced pressure left 13.2 g of α-chloro-α-phenylthio-γ-butyrolactone (**12**, R^1=H, X=Cl). The crude product, dissolved in THF (60 ml), was added to a mixture of LiBr (17 g) and Li_2CO_3 (13 g) in THF (60 ml) at room temperature. The reaction mixture was refluxed for 30 min under nitrogen. After the removal of inorganic salts and solvent, the residue was dissolved in CH_2Cl_2, and the solution was washed with $NaHCO_3$ solution and saturated brine, and dried. Evaporation of the solvent gave 9.94 g (93%) of **13a**.

*5-Methyl-3-phenylthio-2(5H)-furanone (**13b**).* This compound was prepared from either of **6a** or **5a** as in the preceding experiment. (a) from **6a**. Yield 93%; (b) from **5a**. Yield 88%. Bp 160—170 °C/1 Torr; IR 1770 and 1600 cm^{-1}; NMR 1.35 (3H, d, J=6.8 Hz), 4.98 (1H, dq, J=1.5 and 6.8 Hz), 6.60 (1H, d, J=1.5 Hz), and 7.20—7.80 (5H, m). Found: C, 63.71; H, 5.15%. Calcd for $C_{11}H_{10}O_2S$: C, 64.07; H, 4.89%.

*General Procedure for the Reaction of **13** with Lithium Dialkylcuprates.* To a freshly prepared solution of lithium dimethyl, dibutyl, or divinylcuprate[11] (2 equiv) in ether or ether–hexane was added dropwise a solution of **13** in ether (60 ml for *ca.* 1.5 g) under nitrogen. The reaction temperature and time for each cuprate are as follows: 0 °C for 2—3 h for dimethylcuprate; −78 °C for 3—4 h for dibutylcuprate; −60—−50 °C for 1.5—2 h for divinylcuprate. The reaction mixture was poured into a cold NH_4Cl solution and thoroughly extracted with ether. The combined extracts were washed with water and saturated brine, and dried. After removal of the solvent, the residual oil was chromatographed on silica gel using petroleum ether–ether as an eluting agent. Yields of **14** were 75—100%.

*β-[Bis(ethoxycarbonyl)methyl]-α-phenylthio-γ-butyrolactone (**14g**).* A mixture of diethyl malonate (350 mg) and lithium hydride (25 mg) in THF (15 ml) was stirred at room temperature for 30 min under nitrogen. To this solution was added a solution of **13a** (384 mg) in THF (10 ml) at room temperature, and the reaction mixture was stirred for 2 h and then refluxed for 30 min. The cooled mixture was poured into a cold NH_4Cl solution and the solvent was removed under reduced pressure. The organic residue was extracted with ether. The extract was washed with saturated brine and evaporated. The oil remaining was chromatographed on silica gel (10 g) using petroleum ether–ether to give 423 mg (60%) of **14g**.

*β-(1-Ethoxycarbonylbutyl)-α-phenylthio-γ-butyrolactone (**16**).* To a solution of lithium diisopropylamide (1 equiv) in THF (10 ml) was added a solution of ethyl valerate (390 mg) in THF (10 ml) at −78 °C under nitrogen, and the mixture was stirred at −78 °C for 1 h. A solution of **13a** (576 mg) in THF (10 ml) was added to this solution, and the reaction mixture was stirred at −78 °C for 20 h and then warmed to room temperature within a period of 8 h. A cold NH_4Cl solution was added, and the mixture was extracted with CH_2Cl_2. The extracts were washed with water and saturated brine, and dried. After removal of the solvent, chromatography of the residual oil on silica gel (100 g) using 1: 1 petroleum ether–ether as an eluent gave 110 mg (11%) of **16** accompanied by the recovery of 140 mg of **13a**.

*β-(2-Oxocyclopentyl)-α-phenylthio-γ-butyrolactone (**17**).* A solution of cyclopentanone (280 mg) in THF (10 ml) was added to a solution of lithium diisopropylamide (1 equiv), and the mixture was stirred for 1 h. To this solution was added a solution of **13a** (576 mg) in THF (15 ml), and the reaction mixture was stirred for 4 h. All the operations were carried out at −78 °C under nitrogen. A cold NH_4Cl solution was added to the mixture, and the solvent was removed under reduced pressure. The residue was extracted with CH_2Cl_2. The combined extracts were washed with saturated brine. After removal of the solvent, the residual oil was chromatographed on silica gel (100 g) using 2: 1 petroleum ether–ether as an eluent to give 500 mg (57%) of **17**.

*γ-Methyl-β-(2-oxocyclopentyl)-α-phenylthio-γ-butyrolactone (**28**).* The reaction of **13b** with cyclopentanone or its morpholine enamine was carried out in the same manner as **13a**. Yields:

64% (cyclopentanone) and 31% (enamine).

3-Phenylsulfinyl-2(5H)-furanone (18). Oxidation of **13a** was carried out using MCPBA (−20—−10 °C for 1 h) and work-up was carried out as described earlier. Yield. 80%. Mp 86—88 °C from ether. IR ($CHCl_3$) 1770 cm^{-1}; NMR ($CDCl_3$) 5.00 (2H, br. s), 7.50—8.00 (5H, m), and 8.10 (1H, br. s). Found: C, 57.62; H, 4.01%. Calcd for $C_{10}H_8O_3S$: C, 57.69; H, 3.87%.

β-(1-Ethoxycarbonylbutyl)-α-phenylsulfinyl-γ-butyrolactone (19). The reaction of **18** with ethyl valerate was carried out in the same manner as for **13a** except for quenching at −78 °C Yield 83%. The compound was also obtained by MCPBA oxidation of **16**.

β-(2-Oxocyclopentyl)-α-phenylsulfinyl-γ-butyrolactone (20). The reaction of **18** with cyclopentanone was carried out in the same manner as for **13a**. Yield 82%.

β-(1-Ethoxycarbonyl-2-oxocyclohexyl)-α-phenylsulfinyl-γ-butyrolactone (21). To a solution of lithium diisopropylamide (1 equiv) in THF (15 ml) was added a solution of ethyl 2-oxocyclohexanecarboxylate (425 mg) in THF (15 ml), and the mixture was stirred for 1 h. A solution of **18** (520 mg) in THF (15 ml) was added to the above enolate solution, and the reaction mixture was stirred for 3 h. All the operations were carried out at −78 °C under nitrogen. A cold NH_4Cl solution was added, and the solvent was removed under reduced pressure. The residue was extracted with CH_2Cl_2, and the combined extracts were washed with saturated brine. After removal of the solvent under reduced pressure, the residue was chromatographed on silica gel (80 g) using 1: 5 petroleum ether–ether as an eluent to give 280 mg (30%) of **21**.

Reaction of 13b with Ethyl 2-Oxocyclohexanecarboxylate. To a solution of the enolate of ethyl 2-oxocyclohexanecarboxylate (374 mg) in THF, prepared according to the manner described earlier, was added a solution of **13b** (412 mg) in THF (10 ml) at −50 °C under nitrogen, and the reaction mixture was gradually warmed to −20 °C within a period of 3 h under stirring. Aqueous NH_4Cl was added, and the solvent was removed under reduced pressure. The organic residue was extracted with ether, and the extracts were washed with saturated brine and dried. After removal of the solvent, the residue was chromatographed on silica gel (60 g) using 1: 1 petroleum ether–ether as an eluent to give 155 mg (38%) of 2,2′-dimethyl-4,4′-bis(phenylthio)-2,2′,3′,4′,5,5′-hexahydro-2,3′-bifuran-5,5′-dione (**26**), bp 200 °C/1 Torr; IR ($CHCl_3$) 1760 cm^{-1}; NMR ($CDCl_3$) 1.20 (3H, d, J=6.8 Hz), 1.43 (3H, s), 2.30 (1H, dd, J=6.8 and 8.2 Hz), 3.35 (1H, d, J=8.2 Hz), 4.48 (1H, quint, J=6.8 Hz), 6.05 (1H, s) and 7.20—7.80 (10H, m). Found: C, 63.88; H, 5.01%. Calcd for $C_{22}H_{20}O_4S_2$: C, 64.07; H, 4.89%.

5-Cyclopentylidene-3-phenylthio-2(5H)-furanone (27). To a solution of 1-morpholino-1-cyclopentene (306 mg)[12] in MeCN (5 ml) was added a solution of **13a** (384 mg) in MeCN (5 ml) at room temperature under nitrogen, and the reaction mixture was stirred at room temperature for 5 h. Dilute HCl (2 M, 10 ml) was added, and the resulting solution was stirred for 1 h, then poured into water, and extracted with ether. The combined extracts were washed with water several times and then saturated brine. After removal of the solvent, the residue was chromatographed on preparative TLC of silica gel with 1: 1 petroleum ether–ether to give 120 mg (22%) of **17** and 165 mg (30%) of **27**, mp 138—139 °C from ethanol; IR ($CDCl_3$) 1750 cm^{-1}; NMR ($CDCl_3$) 1.40—2.00 (4H, m), 2.20—2.80 (4H, m), 6.85 (1H, s), and 7.50 (5H, m). Found: C, 69.55; H, 5.48%. Calcd for $C_{15}H_{14}O_2S$: C, 69.75; H, 5.46%.

Methylation of α-Phenylthio-γ-butyrolactones. A solution of the α-phenylthiobutyrolactone derivative (**11**, **14a**, **14d**) in THF (10 ml for 1 g) was added to a solution of lithium diisopropylamide (1.3 equiv) in THF at −60 °C under nitrogen. After being stirred for 1 h, methyl iodide (large excess) was added, and the mixture was stirred at −60 °C overnight. The usual work-up (quenching, extraction, distillation) gave the α-methylated product in quantitative yield.

α-Phenylthio-γ-butyrolactones. All the α-phenylthio-γ-butyrolactones (**5**, **14**, **16**, **17**, the γ,γ-pentamethylene-, β,γ-tetramethylene-, α-methyl, α,β-dimethyl-, and α,β,γ-trimethyl-derivatives) gave satisfactory analytical and spectral results.

Yield (from the corresponding α-phenylthio-γ-butyrolactones), Bps (Torr), ν_{CO}, Proton Chemical Shifts, and Analytical Data of 2-(5H)-Furanones.

5-Methyl- (7a) (β-Angelica Lactone). 74%. Identified with the authentic sample.[13]

5-Butyl- (7b). 82%. 130—140 °C/2. 1770 cm^{-1}. δ 0.70—2.00 (9H, m), 4.80—5.20 (1H, m), 6.00 (1H, dd, J= 1.5 and 6 Hz), and 7.55 (1H, dd, J=1.5 and 6 Hz). Found: C, 67.94; H, 8.28%. Calcd for $C_8H_{12}O_2$: C, 68.54; H, 8.63%.

5-Phenyl- (7c). 57%, in addition to 23% of 2(3*H*)-isomer, after chromatographic separation. 90—120 °C/1. 1790, 1760, and 1700 cm^{-1}. δ 5.90 (1H, t, J=2.3 Hz), 6.10 (1H, dd, J=2.3 and 6 Hz), 7.30 (5H, s), and 7.45 (1H, dd, J=2.3 and 6 Hz). Found: C, 75.15; H, 5.01%. Calcd for $C_{10}H_8O_2$: C, 74.99; H, 5.03%.

5-Butyl-3-methyl- (7d). 63%. 90—110 °C/1. 1760 cm^{-1}. δ 0.70—1.80 (9H, m), 1.87 (3H, t, J=2.3 Hz), 4.65—5.00 (1H, m), and 7.15 (1H, m). Found: C, 70.27; H, 9.01%. Calcd for $C_9H_{14}O_2$: C, 70.10; H, 9.15%.

5-Butyl-3-ethyl- (7e). 78% (in this case the pyrolysis was carried out in boiling CCl_4 containing 2-mercaptobenzothiazole).[14] 70—90 °C/1. 1760 cm^{-1}. δ 0.70—2.00 (9H, m), 1.13 (3H, t, J=7.5 Hz), 2.25 (2H, tq, J=1.6 and 7.5 Hz), 4.65—5.00 (1H, m), and 7.05 (1H, dt, J=1.6 and 1.6 Hz). Found: C, 71.49; H, 9.49%. Calcd for $C_{10}H_{16}O_2$: C, 71.39; H, 9.59%.

5,5-Pentamethylene- (8). 83%. 130—140 °C/4. 1770 cm^{-1}. δ 1.70 (10H, br. s), 5.92 (1H, d, J=6 Hz), and 7.52 (1H, d, J=6 Hz). Found: C, 71.24; H, 7.68%. Calcd for $C_9H_{12}O_2$: C, 71.02; H, 7.95%.

4,5-Tetramethylene- (9). 82%. 70—90 °C/1. 1780 and 1760 cm^{-1}. δ 0.90—3.10 (8H, m), 4.40—4.90 (1H, m), and 5.60 (1H, m). Found: C, 69.68; H, 7.08%. Calcd for $C_8H_{10}O_2$: C, 69.54; H, 7.30%.

4-Methyl- (15a). 87%. Identified with the authentic sample.[15]

4-Butyl- (15b). 80%. 140 °C/1. 1780 and 1750 cm^{-1}. δ 0.95 (7H, m), 2.45 (2H, br. t, J=7.2 Hz), 4.75 (2H, br. s), and 5.75 (1H, br. s). Found: C, 68.51; H, 8.79%. Calcd for $C_8H_{12}O_2$: C, 68.54; H, 8.63%.

4-Vinyl- (15c).[16] 51%. 1780 and 1760 ($CHCl_3$) cm^{-1}. δ ($CDCl_3$) 5.06 (2H, br. d, J=1.5 Hz), 5.70 (1H, d, J=10.5 Hz), 5.70 (1H, d, J=18 Hz), 6.05 (1H, br. t, J= 1.5 Hz), and 6.82 (1H, dd, J=10.5 and 18 Hz). This compound is unstable, and decomposed partially on distillation. The sample, which was chromatographically and spectroscopically homogeneous, did not give satisfactory analytical results.

4,5-Dimethyl- (15d). 87%. 85 °C/1. 1780 and 1760 cm^{-1}. δ 1.40 (3H, d, J=7.1 Hz), 2.08 (3H, br. s), 4.95 (1H, br. q. J=7.1 Hz), and 5.75 (1H, br. s). Found: C, 64.59; H, 6.80%. Calcd for $C_6H_8O_2$: C, 64.27; H, 7.19%.

4-Butyl-5-methyl- (15e). 82%. 140 °C/1. 1770 cm^{-1}. δ 0.95—1.19 (7H, m), 1.36 (3H, d, J=6.8 Hz), 2.10—2.60 (2H, m) 4.90 (1H, br. q, J=6.8 Hz), and 5.67 (1H, br. s). Found: C, 69.87; H, 8.98%. Calcd for $C_9H_{14}O_2$: C, 70.10;

H, 9.15%.

*5-Methyl-4-vinyl- (**15f**).* 89%. 1780 and 1760 cm^{-1}. δ 1.55 (3H, d, J=7.5 Hz), 5.30 (1H, q, J=7.5 Hz), 5.72 (1H, d, J=18 Hz), 5.75 (1H, d, J=10.5 Hz), 6.07 (1H, s), and 6.73 (1H, dd, J=10.5 and 18 Hz). The thermal property of **15f** is similar to that of **15c**.

*4-[Bis(ethoxycarbonyl)methyl]- (**15g**).* 68%. 140—160 °C/1. 1780, 1750, and 1740 cm^{-1}. δ 1.30 (6H, t, J=7 Hz), 4.30 (4H, q, J=7 Hz), 4.70 (1H, br. s), 5.02 (2H, d, J=2.3 Hz), and 6.20 (1H, br. s). Found: C, 54.68; H, 5.72%. Calcd for $C_{11}H_{14}O_6$: C, 54.54; H, 5.83%.

*4-(1-Ethoxycarbonylbutyl)- (**22**).* 90%. 140—150 °C/1. 1780, 1750, and 1735 cm^{-1}. δ 0.70—2.10 (7H, m), 1.30 (3H, t, J=7.2 Hz), 3.50 (1H, br. t, J=7.5 Hz), 4.15 (2H, q, J=7.2 Hz), 4.80 (2H, br. d, J=1.9 Hz), and 5.87 (1H, br. s). Found: C, 62.22; H, 7.75%. Calcd for $C_{11}H_{16}O_4$: C, 62.25; H, 7.60%.

*4-(1-Ethoxycarbonyl-2-oxocyclohexyl)- (**23**).* 83%. 160 °C/1. 1780, 1750, and 1720 ($CHCl_3$) cm^{-1}. δ ($CDCl_3$) 1.30 (3H, t, J=7.5 Hz), 1.10—3.00 (8H, m), 4.32 (2H, q, J=7.5 Hz), 4.80 (1H, dd, J=18 and 2.1 Hz), 5.10 (1H, dd, J=18 and 2.1 Hz), and 6.00 (1H, m). Found: C, 61.48; H, 6.45%. Calcd for $C_{13}H_{16}O_5$: C, 61.89; H, 6.39%.

*3-Methyl- (**29a**).* 65%. Identified with the authentic sample.[1g,17]

*3,4-Dimethyl- (**29b**).* 75%, in addition to 8% of the *exo*-methylene isomer. 70 °C/1. 1760 cm^{-1}. δ 1.75 (3H, br. s), 2.02 (3H, br. s), and 4.60 (2H, br. s). Found: C, 64.18; H, 7.51%. Calcd for $C_6H_8O_2$: C, 64.27; H, 7.19%.

*3,4,5-Trimethyl- (**29c**).* 93%. 60—80 °C/1. 1760 cm^{-1}. δ 1.38 (3H, d, J=6.8 Hz), 1.77 (3H, br. s), 2.00 (3H, br. s), and 4.78 (1H, br. q, J=6.8 Hz). Found: C, 66.73; H, 8.03%. Calcd for $C_7H_{10}O_2$: C, 66.64; H, 7.99%.

References

1) (a) A review: Y. S. Rao, *Chem. Rev.*, **64**, 353 (1964); (b) *via* fused pyrazoline γ-butyrolactone thermolysis: H. Franck-Neumann, *Angew. Chem.*, **80**, 42 (1968); S. W. Pelletier, Z. Djarmati, S. D. Lajšić, I. V. Nićović, and D. T. C. Yang, *Tetrahedron*, **31**, 1659 (1975); (c) *via* ynoic ester hydrogenation: A. Nobuhara, *Agr. Biol. Chem.*, **34**, 1745 (1970); (d) *via* organocopper-ynoic ester addition: E. J. Corey, C. U. Kim, R. H. K. Chen, and M. Takeda, *J. Am. Chem. Soc.*, **94**, 4395 (1972); (e) *via* β-keto sulfoxide condensation: M. Kurono, K. Imagi, Y. Tanikawa, and M. Watanabe, Abstracts of Papers of the 26th Annual Meeting of the Chemical Society of Japan, Hiratsuka, April 1972, Series III, p 1623; (f) *via* yne diol ketone acetal rearrangement: D. K. Black, Z. T. Fomum, P. D. Landor, and S. R. Landor, *J. Chem. Soc., Perkin Trans. 1*, **1973**, 1349; G. Bennett, *Chem. Lett.*, **1975**, 939; (g) *via* sulfenylation-dehydrosulfenylation: B. M. Torst and T. N. Salzmann, *J. Am. Chem. Soc.*, **95**, 6840 (1973); B. M. Trost and K. K. Leung, *Tetrahedron Lett.*, **1975**, 4197; (h) *via* selenylation-dehydroselenylation: K. B. Sharpless, R. F. Lauer, and A. Y. Teranishi, *J. Am. Chem. Soc.*, **95**, 6137 (1973); (i) *via* sultone photoelimination: B. Gorewit and N. Rosenblum, *J. Org. Chem.*, **38**, 2257 (1973); (j) *via* acetylenic aldehyde or ketone condensation: Y. S. Rao and R. Filler, *Tetrahedron Lett.*, **1975**, 1457; (k) *via* α-bromo aldehyde substitution: A. Padwa and D. Dehm, *J. Org. Chem.*, **40**, 3139 (1975).

2) P. G. Marshal, "Rodd's Chemistry of Carbon Compounds," 2nd ed, Vol. II, Part D, ed by S. Coffey, Elsevier Publishing Co, New York (1970), p. 369; E. Demole and D. Berthet, *Helv. Chim. Acta*, **55**, 1866 (1972).

3) (a) H. Minato and T. Nagasaki, *Chem. Commun.*, **1965**, 377; H. Minato and T. Nagasaki, *J. Chem. Soc., C*, **1966**, 1866; *ibid.*, **1968**, 621; (b) J. L. Herrmann, M. H. Berger, and R. H. Schlessinger, *J. Am. Chem. Soc.*, **95**, 7923 (1973); (c) R. E. Damon and R. H. Schlessinger, *Tetrahedron Lett.*, **1975**, 4551; (d) F. Kido, T. Fujishita, K. Tsutsumi, and A. Yoshikoshi, *J. Chem. Soc., Chem. Commun.*, **1975**, 337; (e) S. A. M. T. Hussain, W. D. Ollis, C. Smith, and J. F. Stoddart, *J. Chem. Soc., Perkin Trans. 1*, **1975**, 1480; (f) H. Kosugi, S. Sekiguchi, R. Sekita, and H. Uda, *Bull. Chem. Soc. Jpn.*, **49**, 520 (1976).

4) Three preliminary reports have been published: (a) K. Iwai, M. Kawai, H. Kosugi, and H. Uda, *Chem. Lett.*, **1974**, 385; (b) K. Iwai, H. Kosugi, and H. Uda, *ibid.*, **1974**, 1237; (c) *ibid.*, **1975**, 981.

5) For the dialkylation of **3a** and the subsequent transformation into vinyl, oxiranyl, or acyl derivatives see P. A. Grieco and C. -L. J. Wang, *J. Chem. Soc., Chem. Commun.*, **1975**, 714.

6) R. Pummerer, *Ber.*, **42**, 2282 (1909); **43**, 1401 (1910); L. Horner and P. Kaiser, *Ann.*, **626**, 19 (1959); W. E. Parham and L. D. Edwards, *J. Org. Chem.*, **33**, 4150 (1968); C. R. Johnson and W. G. Phillips, *J. Am. Chem. Soc.*, **91**, 682 (1969); T. Durst, "Advances in Organic Chemistry," Vol. 6, ed. by E. C. Taylor and H. Wynberg, Interscience, New York, N. Y. (1966), p. 356.

7) An alternative preparation and the Micheal reaction of **18** has recently been reported. M. Watanabe, K. Shirai, and T. Kumamoto, *Chem. Lett.*, **1975**, 855.

8) S. Gabrier, *Ber.*, **12**, 1639 (1879); Beilstein, H. Band VI, p. 313.

9) C. C. Price and J. M. Judge, *Org. Synth.*, Coll. Vol. V, 255 (1973).

10) For an alternative preparation and the Pummerer rearrangement of **10** ($MeSO_3H$–CH_2Cl_2) see H. J. Monteiro and J. P. de Souza, *Tetrahedron Lett.*, **1975**, 921; H. J. Monteiro and A. L. Gemal, *Synthesis*, **1975**, 437.

11) E. J. Corey and R. L. Carney, *J. Am. Chem. Soc.*, **93**, 7318 (1971).

12) S. Hünig and W. Lendle, *Chem. Ber.*, **93**, 909 (1960).

13) Beilstein, H. Band XVII, p. 253.

14) T. Kamiya, T. Teraji, Y. Saito, M. Hashimoto, O. Nakaguchi, and T. Oku, *Tetrahedron Lett.*, **1973**, 3001.

15) F. Fleck and H. Schinz, *Helv. Chim. Acta*, **33**, 146 (1950).

16) For an alternative synthesis of **15c** see Ref 3d.

17) Prepared by dehydration (Py–$SOCl_2$) of α-hydroxy-α-methyl-γ-butyrolactone.[18]

18) C. J. Cavallito and T. H. Haskell, *J. Am. Chem. Soc.*, **68**, 2332 (1946).

Formations and Reactions of Cation Radicals from Compounds Possessing a *p*-Dimethylaminophenyl Group by Reactions with *o*-Sulfobenzoic Anhydride

Toshikazu NAGAI, Tadao SHINGAKI, and Hirokazu YAMADA*

Institute of Chemistry, College of General Education, Osaka University, Toyonaka, Osaka 560

(Received July 26, 1976)

It was found that cation radicals were formed from a number of substrates bearing a *p*-dimethylaminophenyl group, such as *N,N,N',N'*-tetramethyl-*p*-phenylenediamine (TMPD) and *N,N,N',N'*-tetramethylbenzidine (TMB), by reactions with *o*-sulfobenzoic anhydride (*o*-AH). The systems, bis(*p*-dimethylaminophenyl)methane (BMM) and tris (*p*-dimethylaminophenyl)methane (TMM) with *o*-AH, gave their cations in the presence of oxygen, showing that the oxygen eliminates the hydrogen atoms of the cation radicals derived from BMM and TMM. The reactions of *N,N*-dimethylaniline (DMA) with *o*-AH gave rise to isolations of BMM and *N*-methylaniline, along with the formations of the cation radical of TMB and the crystal violet cation (TMM^+). The mechanisms of the reactions are proposed.

Cation radicals are familiar as transient species in mass spectrometry or anodic oxidation.[1] However, the chemical behaviors of cation radicals have not, until recently, received much attention.[2] Previously, we reported that the radical cations of some aromatic hydrocarbons, triethylamine, triphenylamine or *N*-vinylcarbazole arose in liquid sulfur dioxide in the presence of oxygen; in these cases, the existence of the radical cations was proved from the electronic or ESR spectra and from the chemical follow-up reactions.[3] The values of the electron affinity and the dielectric constant of liquid sulfur dioxide are not so much higher than those of the usual acceptors or polar solvents. Hence, sulfur dioxide probably plays a role of a polarizable electrophilic reagent, using the available 3d orbitals of the sulfur atom, rather than that of a polar solvent. Keeping these consideration in mind, we have examined the reaction of some sulfones with substrates possessing a *p*-dimethylaminophenyl group. It was found that mixed sulfonic-carboxylic anhydrides provided a convenient means of generating cation radicals from the substrates.

Results and Discussion

Formation of Cation Radicals and Cations. In the reactions of *N,N,N',N'*-tetramethyl-*p*-phenylenediamine (TMPD), *N,N,N',N'*-tetramethylbenzidine (TMB) and tetrakis(*p*-dimethylaminophenyl)ethylene (TMPE) with *o*-sulfobenzoic anhydride (*o*-AH) in acetonitrile, the formations of their cation radicals were investigated spectrophotometrically. The absorption maxima in the 340—1400 nm range for the cation radicals or dication are summarized in Table 1, being compared with those reported by some authors.

These values were in fair agreement with those reported,[4-11] though the peak positions for TMPE shifted slightly. The reaction of TMPE with *o*-AH in acetonitrile underwent double electron transfer to form the diamagnetic dication ($TMPE^{2+}$), whose absorption band was in essential agreement with that observed in the reaction of TMPE with iodine in acetonitrile.[11] These results are coincident with those reported by Foster and Thomson:[12] that the ease of the complete

Table 1. Absorption maxima of cation species

Cation species	λ_{max} (nm)	Medium	Method of prepn.	Ref.
$(Me_2N\text{-}C_6H_4\text{-}NMe_2)^+$ ($TMPD^+$)	566 615	CH_3CN	Chem	This work
	569 619	CH_3CN	Chem[c]	4
	575 625	$(C_2H_5)_2CHCH_3$[a]	Photo	5
	575 635	CCl_4[a]	γ.	6
	560 606	H_2O	Chem[d]	7
	575 615	EPA[a,b]	Photo	8
$(Me_2N\text{-}C_6H_4\text{-}C_6H_4\text{-}NMe_2)^+$ (TMB^+)	438 458 472 910 1050	CH_3CN	Chem	This work
	436 458 472 900 1050	$(C_2H_5)_2O$	Chem[e]	9
		CCl_4[a]	γ.	6
	435 458 472	CH_3CN	Anodic	10
$[(Me_2N\text{-}C_6H_4)_2C{=}C(C_6H_4\text{-}NMe_2)_2]^{+2}$ ($TMPE^{+2}$)	489 534 640—900	CH_3CN	Chem	This work
	469 540 650—900	CH_3CH_2Cl	Chem	11

a) These experiments were carried out at −196 °C. b) Mixture solvent; ether: isopentane: ethanol 5: 5: 2 (volume ratio). c—f) In the preparations, c) tetrachloro- or tetrabromo-*o*-benzoquinone, d) perchloric acid, e) tris (*p*-bromophenyl)ammonium perchlorate, and f) iodine were used as acceptors.

* Present address: Dai Nippon Ink and Chemicals Industrial Co., Ltd., Takaishi, Osaka 592.

Table 2. Absorption maxima of cations

Cation	Solvent	λ_{max} (nm)	Ref.
$(Me_2N-C_6H_4)_2CH^+$ (BMM$^+$)	CH_3CN	560(sh) 607	This work
	H_2O	608	15
	acid C_2H_5OH	560(sh) 610	16
	C_2H_5OH	605	17
$(Me_2N-C_6H_4)_3C^+$ (TMM$^+$)	CH_3CN	550(sh) 592	This work
	H_2O	542(sh) 590	18
	dil HCl	599	15
	C_2H_5OH	545(sh) 591	16
	CH_3OH	550(sh) 590	19

electron transfer is TMPE>TMPD>TMB.

An investigation by ESR also was undertaken for the reaction of TMPD with *o*-AH in acetonitrile. The hyperfine coupling constants of TMPD$^+$ were assigned as follows: a_{CH_3}=6.65 G; a_N=6.85 G; $a_{ring H}$=1.98 G. These couplings are very similar to those reported by Carrington[13] and Taft.[14]

The reactions of bis(*p*-dimethylaminophenyl)methane (BMM) and tris(*p*-dimethylaminophenyl)methane (TMM) with *o*-AH were investigated spectrophotometrically in acetonitrile. The absorption maxima observed are due to those of bis(*p*-dimethylaminophenyl)methyl cation (BMM$^+$) and tris(*p*-dimethylaminophenyl)methyl cation (TMM$^+$, Crystal Violet cation) by reference to the literature values (Table 2). These cations are to be derived from the corresponding cation radicals (BMM$^+$ and TMM$^+$): the cation radicals are then able to release a hydrogen atom to afford highly stabilized BMM$^+$ and TMM$^+$ respectively.

Table 3. Effect of oxygen on formation of cation species

Amine	Cation species	Yield (mol %)[a] undegassed	degassed
TMPD	TMPD$^+$	20	18
TMM	TMM$^+$	59	29

a) Calculated from molar extinction coefficients. TMPD$^+$: 1.1×10^4 at 615 nm.[7] TMM$^+$: 1.1×10^5 at 592 nm.[18,19]

An intervention of oxygen, here, was considered important for the elimination of the hydrogen atoms. Influences of oxygen on the formation of such cation species have not been investigated to date, though they have been mentioned in Refs. 2b and 9. And so, the reactions with *o*-AH were carried out under a degassed condition. As shown in Table 3, the reaction of TMM with *o*-AH gave a decreased yield of the cation under a degassed atmosphere, in contrast to that of TMPD. Effects of oxygen on the formation rates of the cation species were also studied for the reactions of TMPD, BMM, and TMM with *o*-AH in acetonitrile (Fig. 1). The formation rates of the cations were remarkably accelerated in the presence of oxygen, in contrast to those of the cation radical (TMPD$^+$). These results show that the cations are formed from the cation radicals, which are derived from BMM and TMM which have some available hydrogen atoms, by hydrogen

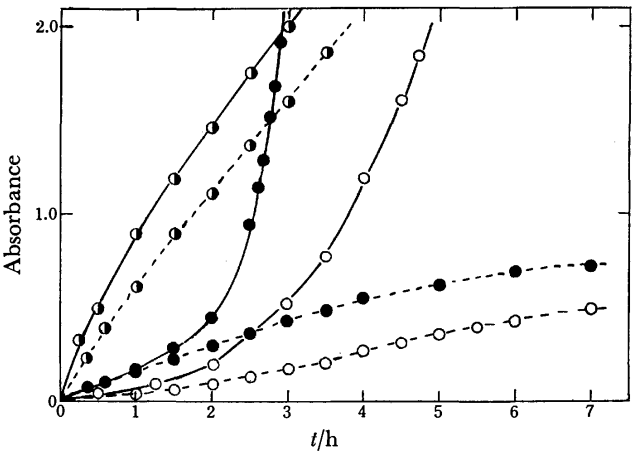

Fig. 1. Effect of oxygen on the rate of formation of cation species in acetonitrile at 8 °C. [TMPD], [BMM], and [TMM]: 7.6×10^{-3} M, [*o*-AH]: 1.3×10^{-3} M. ◑: TMPD$^+$, ○: BMM$^+$, ●: TMM$^+$. ——: under undegassed, ------: under degassed.

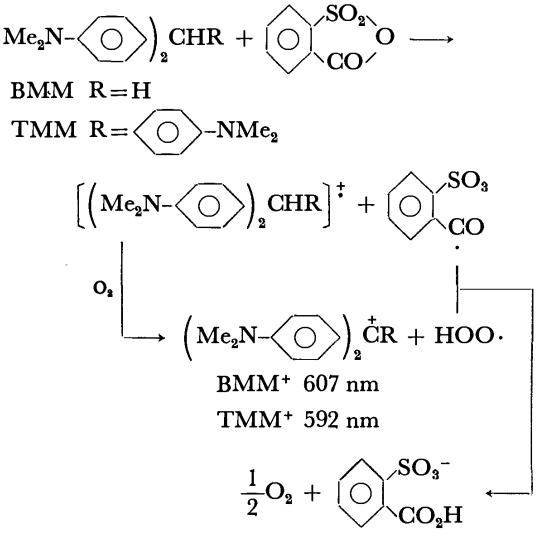

Scheme 1.

abstraction with oxygen (Scheme 1). To explain the retarded formation of the cations under the degassed atmosphere, a following alternative pathway can be considered: the cation radicals (BMM$^+$ and TMM$^+$) give their protons to the counter anion radical shown in Scheme 1, and are transformed into the radicals (BMM· and TMM·), which are then oxidized by *o*-AH to the highly stabilized cations (BMM$^+$ and TMM$^+$).

Reaction of N,N-*Dimethylaniline with* o-*AH.* *N,N*-Dimethylaniline (DMA) has no blocked *para*-position in contrast to the amines used so far. Studies of the cation radical (DMA^+) formation from DMA have been done by many researchers.[2b,9,19-23] In their studies,[2b,19] it was recognized that the cation radical converted to tris(*p*-dimethylaminophenyl)methyl cation (Crystal Violet cation). However, none of the reports clarified the reaction path to the Crystal Violet cation from the cation radical (DMA^+) at all.

TABLE 4. EQUIMOLECULAR REACTIONS BETWEEN DMA AND ANHYDRIDES

Amine	Anhydride	Medium		Yield (%)[a] BMM	Yield (%)[a] C_6H_5-$NHCH_3$
DMA	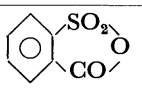	CH_3CN	O_2	49	20
		CH_3CN	N_2	10	6
		C_6H_6	O_2	20	4
DMA	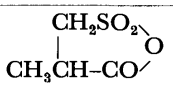	CH_3CN	O_2	45	12
			O_2	13	7

a) Calculated based on triple the molar quantity of the amine used.

An equimolar amount of DMA and *o*-AH was allowed to react in a solvent. Table 4 shows the results. These products are the same as those obtained from the gamma-radiolysis[20] of DMA. This fact and the formation of TMB^+, as described below in detail, suggest that DMA^+ is formed in this reaction. A reaction of DMA with *β*-sulfoisobutyric anhydride (*β*-AH) also gave the same products as the reaction with *o*-AH (Table 4).

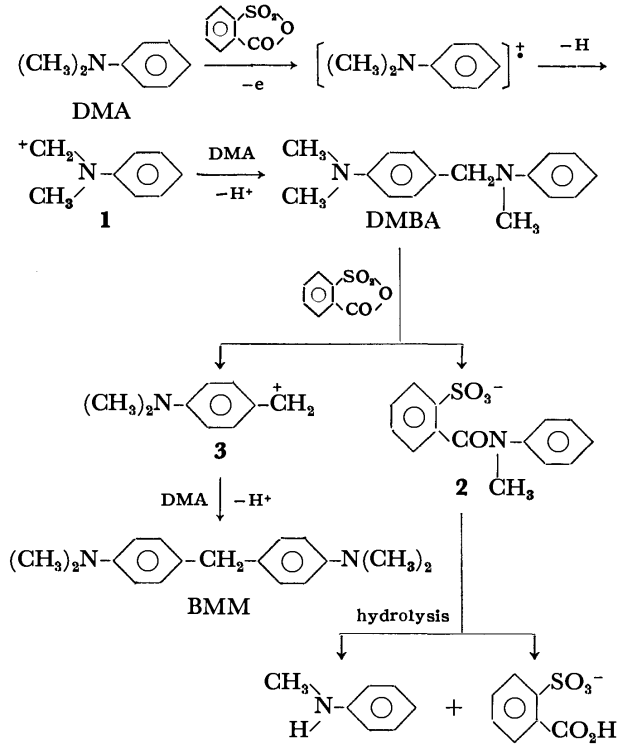

Scheme 2.

The mechanism for this reaction, outlined in Scheme 2, is similar to that reported previously by Grodowski and Latowski[21] from the study of the photoxidation of DMA with bromobenzene. A hydrogen atom of the cation radical derived from DMA is abstracted by oxygen to give *N*-methylanilinomethyl cation (**1**). This cation attacks the *para*-position of unoxidized DMA to afford *N*-(*p*-dimethylaminobenzyl)-*N*-methylaniline (DMBA). In a subsequent reaction step, DMBA is decomposed by sulfonic carboxylic anhydride giving the anilide derivative (**2**) and *p*-dimethylaminobenzyl cation (**3**). This carbocation (**3**), in the presence of DMA, forms the isolated product BMM. The anilide derivative **2** is hydrolyzed by treatment in an alkali solution to yield *N*-methylaniline. On the other hand, when DMA was treated with *o*-AH in the presence of authentic DMBA, the same products, BMM and *N*-methylaniline, were also obtained. In this reaction, it was confirmed by means of NMR and thin-layer chromatography that the DMBA used had been consumed completely. These results support the reaction mechanism shown in Scheme 2.

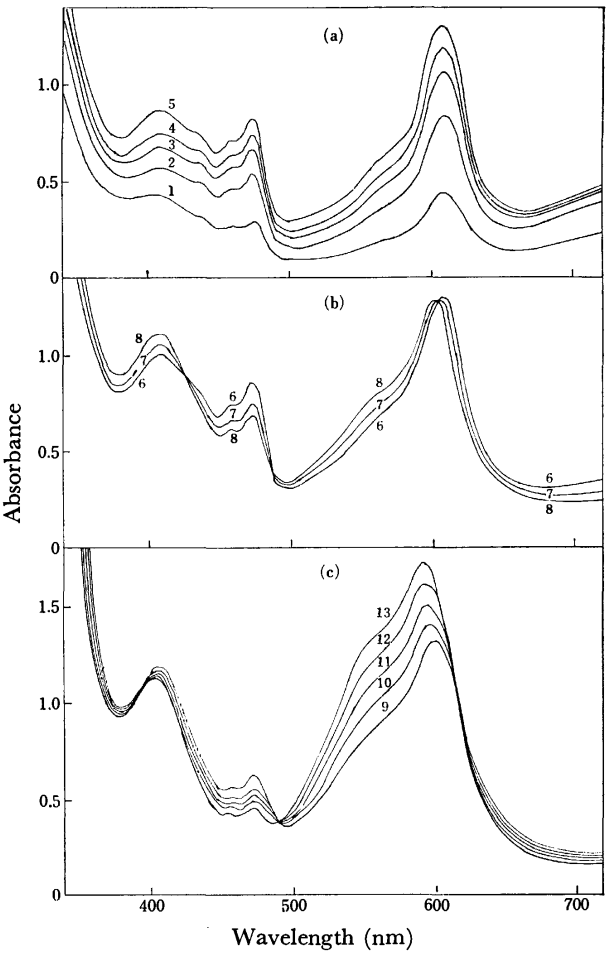

Fig. 2. Spectroscopic course of the reaction of DMA with *o*-AH in acetonitrile. [DMA]=4.1×10^{-2} M, [*o*-AH]=4.1×10^{-2} M. After mixing:
(a) 1, 10 min; 2, 20 min; 3, 30 min; 4, 40 min; 5, 60 min;
(b) 6, 110 min; 7, 160 min; 8, 210 min;
(c) 9, 300 min; 10, 420 min; 11, 540 min; 12, 660 min; 13, 900 min.

Reaction Course from DMA to TMM⁺. In the reaction of DMA with *o*-AH, it was confirmed by the optical spectra that *N,N,N′,N′*-tetramethylbenzidine cation radical (TMB†) and Crystal Violet cation (TMM⁺) were formed. When an acetonitrile solution of DMA was mixed with an acetonitrile solution of *o*-AH, the reaction mixture rapidly assumed a yellowish-green color, then turned to a green color (stage 1). The green color gradually changed to a bluish-green color (stage 2) and finally to a purple color (stage 3). Figure 2 shows the absorption spectra of the reaction mixture of DMA and *o*-AH corresponding to stages 1, 2, and 3.

The addition of an acetonitrile solution of *o*-AH to an acetonitrile solution of DMA gave rise to a new series of absorptions in the visible region at 438, 458, and 472 nm, due to the TMB†, and at 607 nm due to BMM⁺. In addition, a new absorption at 408 nm was also observed. This band was assigned to a dication (**4**) protonated at one nitrogen atom of BMM⁺, because the same absorption band was also obtained by the addition of *o*-sulfobenzoic acid to an acetonitrile solution of BMM⁺, which had been prepared by the reaction of BMM and *o*-AH.

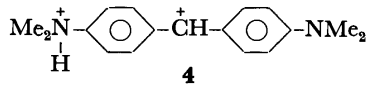

4

In stage 1, each of these absorptions due to TMB†, BMM⁺, and the dication (**4**) increased in intensity over a period of one hour, as shown in Fig. 2a. In stage 2 (Fig. 2b), it was observed that the intensity of the absorption at 592 nm due to TMM⁺ increased while those of TMB† and BMM⁺ decreased, showing the isosbestic points at 426, 490, and 602 nm. In stage 3 (Fig. 2c), the absorption of TMM⁺ showed further increased intensity, with an isosbestic point at 490 nm, with the lapse of time, while the absorptions in the 430—480 nm region, on the contrary, decreased in intensity. Such spectral changes were observed as well by the use of *β*-AH instead of *o*-AH.

From these changes of the absorption spectra, it is suggested that the oxidation of DMA to TMM⁺ by the sulfonic carboxylic anhydrides proceeds through BMM⁺ and TMB†. On the other hand, the addition of DMA to the solution of BMM⁺, which had been prepared by the reaction of BMM with *o*-AH in acetonitrile, showed a new absorption band at 592 nm due to TMM⁺, together with a decrease in the intensity of the absorption at 607 nm due to BMM⁺. The presence of the isosbestic point at 490 nm, in Fig. 2c, shows that a one-electron transfer reaction occurs between TMM and TMB†. This was confirmed also from the result that the spectrum of a mixture of TMM and TMB†, which had come from the reaction of TMB with *o*-AH in acetonitrile, changed with the isosbestic point at 492 nm, as shown in Fig. 3.

Finally, we here propose a mechanism for the oxidation of DMA to TMM⁺ by the sulfonic carboxylic anhydrides, as shown in Scheme 3, which is different

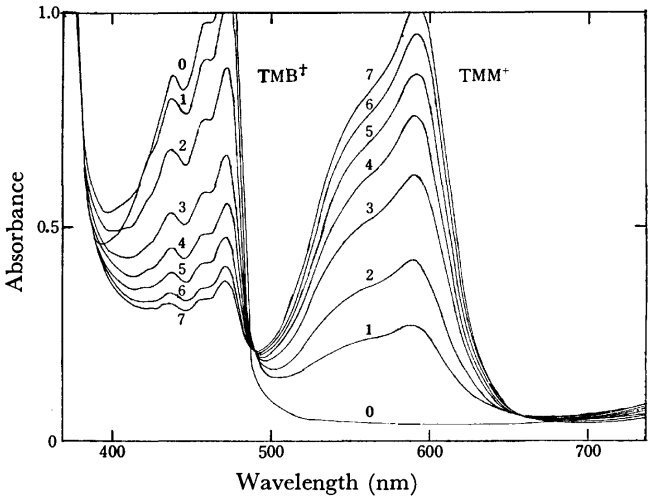

Fig. 3. Spectroscopic course of the reaction of TMB† with TMM in acetonitrile. 0, TMB† alone. After addition of TMM: 1, immediately; 2, 10 min; 3, 20 min; 4, 30 min; 5, 40 min; 6, 50 min; 7, 60 min.

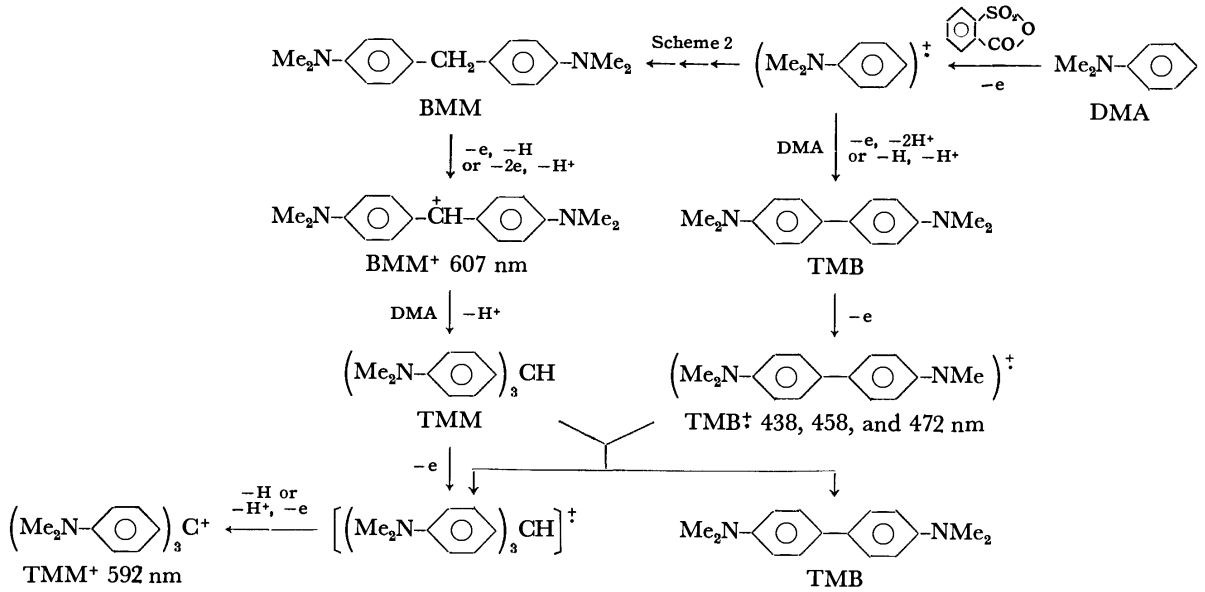

Scheme 3.

from the mechanism proposed in the system of DMA and chloranil.[24] The BMM^+ derived from BMM attacks the *para*-position of the unoxidized DMA, giving TMM. Alternatively, the cation radical of DMA dimerizes or reacts with the parent to form TMB^+. Then, the one-electron transfer reaction between TMM and TMB^+ occurs to afford TMM^+.

Reaction of Triphenylamine with o-*AH.* A reaction of triphenylamine with *o*-AH was studied spectrophotometrically in a similar manner. An absorption band appeared at 480 nm. This broad band is apparently due to the *N,N,N',N'*-tetraphenylbenzidine cation radical (**5**), whose spectral assignment has been reported by Hasegawa,[25] Dollish, and Hall.[26]

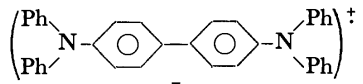

5

Triphenylamine is not blocked at the *para*-positions and doesn't contain a labile hydrogen atom such as the *N*-methyl group of DMA. Thus, the cation radical derived from triphenylamine recombines or reacts with the parent exclusively at the *para*-position to give the cation radical **5**.

Experimental

The optical absorption spectra in the 340—740 nm and 650—1400 nm ranges were recorded on a Union SM-401 and a Shimadzu MPS-50L recording spectrophotometer. The quartz cell used was 1.0 cm in length. If necessary, each of the sample solutions of an electron donor and an acceptor was mixed into the cell after repeated freeze-pump-thaw-cycles. The NMR spectra were obtained on a Varian EM-360 (60 MHz) analytical spectrometer with tetramethylsilane as an internal standard. The IR and ESR spectra were taken on an Hitachi EP-S and a JEOL JES-NE2X instrument. Gas chromatography was done on a Yanagimoto GCG-5DH unit, employing as adsorbent 10% Apiezon Grease M on Celite (60—80 mesh).

Solvents. Acetonitrile, benzene, and dioxane were used after the commercial reagents were purified according to the published directions.[27]

Materials. *o*-Sulfobenzoic anhydride (*o*-AH) was prepared from acid ammonium *o*-sulfobenzoate,[28] which had been obtained by the hydrolysis of *o*-sulfobenzoic imide (saccharin insoluble);[29] mp 127 °C (lit,[28] 128 °C). The preparation of *β*-sulfoisobutyric anhydride (*β*-AH) was the same as that reported by Kharasch *et al.*[30] *N,N,N',N'*-Tetramethyl-*p*-phenylenediamine (TMPD) was obtained by alkalizing an aqueous solution of its dihydrochloride salt with a potassium hydroxide aqueous solution. The amine was purified by means of sublimation; mp 51 °C (lit,[31] 51 °C). The white crystalline solid thus obtained was kept at about −20 °C in the dark until used. *N,N,N',N'*-Tetramethylbenzidine (TMB) was recrystallized twice from 1-pentanol; mp 196 °C (lit,[12] 196 °C). Tetrakis(*p*-dimethylaminophenyl)ethylene (TMPE) was prepared according to the method given in the literature,[32] and recrystallized from a benzene–ligroin mixture; mp 314.5—315.0 °C (lit,[32-33] 314—316 °C). Bis and tris(*p*-dimethylaminophenyl)methanes (BMM and TMM) respectively were recrystallized twice from ethanol. BMM: mp 90 °C (lit,[34] 91 °C). TMM: mp 176 °C (lit,[35,36] 177—178 °C). *N,N*-Dimethylaniline (DMA) was refluxed with acetic anhydride, followed by neutralization, separation of the organic layer, and repeated distillation under reduced pressure. The colorless oil was dried over pellets of sodium hydroxide, and distilled *in vacuo* before use. Triphenylamine was recrystallized from absolute ether, followed by recrystallization from ethanol; mp 127 °C (lit,[37] 128 °C). *N*-(*p*-Dimethylaminobenzyl)-*N*-methylaniline (DMBA) was prepared in the following way. A solution of benzoyl peroxide (12 g) in benzene (100 ml) was added dropwise to a solution DMA (24 g) in benzene (20 ml) with stirring, keeping the temperature at 25 °C. The reaction mixture was refluxed for 14 h. The benzene solution was washed with a sodium hydroxide solution, followed by washing with water and drying with sodium sulfate. Then the benzene and unchanged DMA were removed by distillation under a pressure of 2 Torr. The residue (6 g) was chromatographed on alumina (90 g), and DMBA (1.5 g) was eluted with light petroleum ether. The white crystal was recrystallized from ethanol; mp 67.5—68.0 °C (lit,[23] 68 °C). NMR (CCl_4, δ): 2.80 (s, 6H, $-CH_3$), 2.85 (s, 3H, $-CH_3$), 4.30 (s, 2H, $-CH_2-$) and 6.50—7.20 (m, 9H, aromt.).

Reaction of DMA with Sulfonic Carboxylic Anhydrides. A solution of 3 g of DMA in an absolute solvent (25 ml) was added to an equimolecular solution of sulfonic carboxylic anhydride in the absolute solvent (25 ml). The reaction mixture, protected in the usual way from atmospheric moisture, was stirred for a week in the dark at room temperature. The reaction mixture was evaporated to a deep green syrup under reduced pressure. A sodium hydroxide solution was added to the residue and an insoluble oily substance was extracted with ether; the ether extract was dried over sodium hydroxide. Removal of the solvent gave a brown crystalline residue, which was recrystallized from ethanol. The IR, NMR, and mass spectra of this product were identical with those of the authentic sample, BMM. On the other hand, after the alkali aqueous solution was heated at about 90 °C for 6 h, the solution was extracted with ether. Concentration of the ether solution gave an oily substance, which was analyzed by the use of gas chromatography. The IR and NMR spectra of the product were identical with those of the authentic sample, *N*-methylaniline.

Reaction of DMA with o-*AH in the Presence of DMBA.* A solution of *o*-AH (38.5 mg) in anhydrous acetonitrile (2 ml) was added to a solution of DMA (20 mg) and DMBA (8.6 mg) in absolute acetonitrile (2 ml). The reaction mixture was introduced into a cell and then sealed. The visible spectrum of the final product was identical to that of TMM^+, whose yield was five times that of the reaction in the absence of DMBA. A procedure similar to that described above was carried out.

References

1) E. T. Kaiser and L. Kevan, Ed., "Radical Ions," Wiley Interscience, London (1968).

2) a) Z. Rappoport and A. Horowitz, *J. Chem. Soc.*, **1964**, 1348. b) J. W. Eastman, G. Engelsman, and M. Calvin, *J. Am. Chem. Soc.*, **84**, 1399 (1962). c) R. Foster, "Organic Charge-Transfer Complex," Academic Press, London (1969). d) A. Ledwith, *Acc. Chem. Res.*, **5**, 133 (1972).

3) T. Nagai, T. Miyazaki, Y. Sonoyama, and N. Tokura, *J. Polym. Sci., Part A-1*, **6**, 3087 (1968). b) T. Nagai, T. Miyazaki, and N. Tokura, *J. Polym. Sci., Part B*, **6**, 345 (1968). c) T. Nagai, K. Katayama, and N. Tokura, *Chem. Lett.*, **1973**, 919.

4) R. Foster and T. J. Thomson, *Trans Faraday Soc.*, **58**, 860 (1962).

5) W. C. Meyer and A. C. Albrecht, *J. Phys. Chem.*, **66**,

1168 (1962).
6) T. Shida and W. H. Hamill, *J. Chem. Phys.*, **44**, 2369 (1969).
7) L. Michaelis, M. P. Schubert, and S. Granick, *J. Am. Chem. Soc.*, **61**, 1981 (1939).
8) G. N. Lewis and D. Kipkin, *J. Am. Chem. Soc.*, **64**, 2801 (1942).
9) F. A. Bell, P. Beresford, L. J. Kricka, and A. Ledwith, *J. Chem. Soc., Perkin. Trans. 1*, **1974**, 1788.
10) A. Yamagishi, *Bull. Chem. Soc. Jpn.*, **48**, 3474 (1975).
11) E. H. Anderson, *J. Am. Chem. Soc.*, **83**, 3157 (1961).
12) R. Foster and T. J. Thomson, *Trans Faraday Soc.*, **59**, 1059 (1963).
13) J. R. Bolton, A. Carrington, and J. dos. Santos-Veiga, *Mol. Phys.*, **5**, 615 (1962).
14) B. M. Latta and R. W. Taft, *J. Am. Chem. Soc.*, **89**, 5172 (1967).
15) S. Dutt, *J. Chem. Soc.*, **1926**, 1171.
16) E. R. Watson and D. B. Meek, *J. Chem. Soc.*, **107**, 1567 (1915).
17) "International Critical Tables," Vol. VII, McGraw-Hill Book Co., New York and London (1930), p. 205.
18) R. C. Merril and R. W. Spencer, *J. Am. Chem. Soc.*, **76**, 3683 (1948).
19) H. Sato, *Bull. Chem. Soc. Jpn.*, **38**, 1719 (1965).
20) G. A. Swan and J. M. Fayadh, U. S. Govt., *Res. Develop. Rep.*, **69** (20), 70 (1969).
21) M. Grodowski and T. Latowski, *Tetrahedron*, **30**, 767 (1974).
22) T. Mizoguchi and R. N. Adams, *J. Am. Chem. Soc.*, **84**, 2058, 2061, 2065 (1962). N. L. Weinberg and T. B. Reddy, *ibid.*, **90**, 91 (1968). F. T. Naylor and B. C. Saunders, *J. Chem. Soc.*, **1950**, 3519.
23) J. M. Fayadh, D. M. Jessop, and G. A. Swan, *J. Chem. Soc., C*, **1966**, 1605.
24) E. M. Kosowar, "Reactions through Charge-Transfer Complexes," in "Progress in Physical Organic Chemistry," Vol. 3, ed. by S. G. Cohen, A. Streitwieser, Jr., and R. N. Taft, Interscience Publishers, New York, N. Y. (1965), p. 81.
25) H. Hasegawa, *J. Phys. Chem.*, **66**, 834 (1962).
26) F. R. Dollish and W. K. Hall, *J. Phys. Chem.* **69**, 2124 (1965).
27) J. A. Riddic and W. B. Bunger, "Organic Solvent," in "Techniques of Organic Chemistry," Vol. VII, ed by A. Weissberger, Wiley-Interscience, New York. N. Y. (1970).
28) H. T. Clarke and E. E. Dreger, *Org. Synth.*, Coll. Vol. I, 495 (1956).
29) H. T. Clarke and E. E. Dreger, *Org. Synth.*, Coll. Vol. I, 14 (1956).
30) M. S. Kharasch, T. H. Chao, and H. C. Brown, *J. Am. Chem. Soc.*, **62**, 2393 (1940).
31) I. Isenberg and S. L. Baird, Jr., *J. Am. Chem. Soc.*, **84**, 3803 (1962).
32) R. Willstater and M. Goldmann, *Ber.*, **39**, 3775 (1906).
33) E. H. Rodd and F. W. Linch, *J. Chem. Soc.*, **1927**, 2179.
34) J. Pinnow, *Ber.*, **27**, 3166 (1894).
35) I. Tanaseseu and A. Silberg, *Bull. Soc. Chim. Fr.*, **1932**, 1357.
36) O. Hinsberg, *Ber.*, **50**, 471 (1917).
37) I. Goldberg, *Ber.*, **40**, 2448 (1907).

Synthesis of Alanyl-1-aminoethanesulfonic Acid[1)]

Tetsuo SHIBA, Kenichi MIYOSHI, and Shoichi KUSUMOTO
Department of Chemistry, Faculty of Science, Osaka University, Toyonaka, Osaka 560
(Received August 14, 1976)

For the purpose of the verification of an expectation that the structural analogs of D-alanyl-D-alanine which participates in the biosynthesis of cell wall peptides might inhibit the growth of microorganisms, alanyl-1-aminoethanesulfonic acid was synthesized by the mixed anhydride method. Four diastereomers were separated and their absolute configurations were deduced on the basis of X-ray analysis. None of these dipeptide analogs and their benzyloxycarbonyl or *t*-butoxycarbonyl derivatives showed appreciable activity against *E. coli*.

α-Amino sulfonic acids can often act as antagonists of α-amino carboxylic acids. In 1941, McIlwain[2)] prepared several α-amino sulfonic acids which were found to possess antimicrobial activities. Thereafter, another author reported antivial activity of some amino sulfonic acids.[3)] The analogy between amino carboxylic acid and amino sulfonic acid in biological effect was also proved in meaty taste of γ-sulfonic acid analog of L-glutamic acid.[4)] In this line, an activity as antagonist will be expected in a structural analog of a biologically significant peptide where one of the component amino acids is replaced with the corresponding amino sulfonic acid.

From studies on the biosynthesis of bacterial cell wall,[5)] it has been revealed that D-alanyl-D-alanine is incorporated as a dipeptide unit into a peptidoglycan precursor in an early step and the C-terminal D-alanine residue finally splits off for completion of the network structure of the peptidoglycan through transpeptidation. If an amino sulfonic acid peptide acts as an antagonist of D-alanyl-D-alanine, it may possibly inhibit either the incorporation of the dipeptide or the formation of the cross linkage of the peptide chain.[6)]

On the basis of above consideration, we planned to prepare the compounds in which one alanine residue of the dipeptide is replaced with 1-aminoethanesulfonic acid (Aes) (**1**).[7)] In this paper, the synthesis and separation of four stereoisomers of alanyl-1-aminoethanesulfonic acid (**4** and **6**) are described.

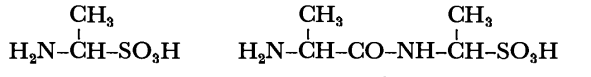

1 **4, 6**

Although Frankel and Moses[8)] reported the preparation of some (*N*-benzyloxycarbonylglycyl)amino sulfonic acids, problems remained to be solved on the stereochemistry of amino sulfonic acids. Mild conditions for deprotection also seemed to have to be investigated.

Results and Discussion

As a preliminary experiment, benzyloxycarbonyl derivative of 1-aminoethanesulfonic acid (**1**) was prepared in order to examine the chemical properties of acylated α-amino sulfonic acid and to investigate the method of deprotection. 1-(Benzyloxycarbonylamino)-ethanesulfonic acid (**2**) was isolated as crystalline anilinium salt which was readily characterized.[9)] Isolation of this sulfonic acid (**2**) as its sodium salt was not preferable since removal of inorganic salt from it became very difficult because of the similar solubilities in water. When benzyloxycarbonyl derivative was hydrogenolyzed in the presence of palladium catalyst, free 1-aminoethanesulfonic acid (**1**) was obtained, though in a low yield (12%). This indicates that the amino sulfonic acid structure can survive more or less through hydrogenolysis depending on the reaction conditions. Thus, the benzyloxycarbonyl group could be used as appropriate protecting group for the synthesis of the amino sulfonic acid peptides.

In a similar manner to the usual peptide synthesis, benzyloxycarbonyl-D-alanine was coupled with sodium salt of 1-aminoethanesulfonic acid (**1**) using ethyl chloroformate to afford benzyloxycarbonyl-D-alanyl-1-aminoethanesulfonic acid (**3**), which was isolated as crystalline anilinium salt. Since racemic **1** was employed as the starting material, the product (**3**) should be a mixture of diastereomers, *i.e.*, benzyloxycarbonyl-D-alanyl-D-1-aminoethanesulfonic acid and its D-L isomer.[10)] However, this product showed no sign of heterogenity either on TLC or on recrystallization.

Catalytic hydrogenolysis of **3** gave free D-alanyl-1-aminoethanesulfonic acid (**4**) by removal of the benzyloxycarbonyl group in a good yield. This product (**4**) showed two ninhydrin positive spots on TLC or paper chromatography (PC). Both components (**4a** and **4b**) which were separated each other by preparative PC had the same molecular formula and thus could be assigned to be the diastereoisomers of D-alanyl-1-aminoethanesulfonic acid, though the configurations of the amino sulfonic acid residues were not clarified at this stage.

In order to confirm this result, the same reactions were carried out starting from benzyloxycarbonyl-L-alanine. Thus, deprotection of benzyloxycarbonyl-L-alanyl-1-aminoethanesulfonic acid (**5**) followed by separation with preparative PC afforded the diastereomers of L-alanyl-1-aminoethanesulfonic acid (**6a** and **6b**). Purities of **6a** and **6b** were well monitored by means of NMR spectra, since slight but distinct differences of chemical shifts between the two compounds are observed at the protons of L-alanine residues (see experimental section). The NMR spectrum of the deprotection product (**6**) before separation corresponds to that expected for a 1 : 1 mixture of **6a** and **6b**.

X-Ray analysis of **6a**[11)] established the *R* configuration for the asymmetric carbon atom of the 1-aminoethanesulfonic acid residue in this diastereomeric form by taking account of the *S* configuration of the L-alanine residue in the same molecule as reference. If D, L re-

Table 1. Physical constants and stereochemistry of diastereomers of alanyl-1-aminoethanesulfonic acid

	Mp (dec) °C	Rf on PC[a]	$[\alpha]_D^{26}$ [b]	Configuration of	
				Ala	Aes[c]
4a	230	0.23	+134°	*R* (D)	*S* (D)[d]
4b	213	0.27	−175°	*R* (D)	*R* (L)
6a	234	0.23	−128°	*S* (L)	*R*[e] (L)
6b	213	0.27	+171°	*S* (L)	*S* (D)

a) Toyo No. 51 filter paper, 1-butanol–acetic acid–water 4: 1: 2. b) *c* 0.5 in 0.5 M HCl. c) Aes: 1-aminoethanesulfonic acid. d) See Ref. 10 in the text. e) Determined by X-ray analysis.

presentation for amino acid is applied to the configuration of aminoethanesulfonic acid, **6a** should be termed as L-alanyl-L-1-aminoethanesulfonic acid. Accordingly, the stereostructures of the other three "dipeptides" were unequivocally assigned by comparison of their physical constants each other. These results are summarized in Table 1.

Consequently, we could thus obtain two pairs of optically active alanyl-1-aminoethanesulfonic acids and determine their absolute configurations. Furthermore, it was also revealed that the configuration of the α-carbon atom in an α-amino sulfonic acid residue is retained stable if its amino group is acylated, although it is generally accepted that α-amino sulfonic acids are unstable, thus being readily dissociated to the parent aldehydes, ammonia and bisulfite in aqueous solution. There has been reported only one case of securing an optically active α-amino sulfonic acid derivative by Neelakantan so far.[12] On reaction of ephedrine with sodium hydrogen sulfite adduct of benzaldehyde, he obtained one of the two possible diastereomers of the amino sulfonic acid derivative and another isomer could not be obtained which was immediately transformed *via* intramolecular cyclization. Therefore, our result in this investigation would be the first and significant example in the determination of stereochemistry of α-amino sulfonic acid.

For further synthesis of more complex peptide analogs containing amino sulfonic acid, applicability of other protecting groups should be examined. *t*-Butoxycarbonyl group was shown to be satisfactorily useful. Thus, *t*-butoxycarbonyl-D and L-alanines were condensed with 1-aminoethanesulfonic acid (**1**) to yield *t*-butoxycarbonyl-D and L-alanyl-1-aminoethanesulfonic acids (**7** and **8**) respectively. Removal of *t*-butoxycarbonyl group was carried out by means of dry hydrogen chloride in ethyl acetate. From the anilinium salt of **8** was obtained free L-alanyl-1-aminoethanesulfonic acid (**6**), which was identified by means of TLC and IR spectra with the sample obtained above by hydrogenolysis of benzyloxycarbonyl-L-alanyl-1-aminoethanesulfonic acid (**5**). When the anilinium salt of the benzyloxycarbonyl derivative (**5**) was treated with anhydrous hydrogen bromide in acetic acid, the protecting group was readily removed and the product was identified with **6** by TLC. However, separation of pure substance from contaminating anilinium bromide was hardly effected.

Finally, antimicrobial activity was tested for the four diastereomers of alanyl-1-aminoethanesulfonic acid (**4a**, **4b**, **6a**, and **6b**) and sodium salts of benzyloxycarbonyl- as well as *t*-butoxycarbonyl-D and L-alanyl-1-aminoethanesulfonic acids (**3**, **5**, **7**, and **8**). Unfortunately, none of them showed appreciable activity against *E. coli* in a modified Henderson-Snell medium free from alanine even in high concentrations of 500—1000 μg/ml.

Experimental[13]

1-Aminoethanesulfonic Acid (1). This compound was prepared through the reaction of acetaldehyde either with ammonium sulfite[2a] or with sodium hydrogen sulfite and ammonia;[14] mp 171—172 °C dec. Use of the former reagent was more convenient though the yield was somewhat lower than the latter. The product was used to the following coupling reaction without recrystallization because of its lability toward decomposition on heating or even on standing at room temperature in an aqueous solution.

1-(Benzyloxycarbonylamino)ethanesulfonic Acid (2) Anilinium Salt. To an ice-cooled solution of **1** (1.25 g, 10 mmol) and Na_2CO_3 (1.17 g, 11 mmol) in water (10 ml), there was added benzyloxycarbonyl chloride (2.1 g, 12 mmol) dropwise with stirring. Stirring was continued at room temperature overnight and excess of the chloride was extracted with ether. After the aqueous layer was concentrated *in vacuo*, aniline (0.93 g, 10 mmol) was added and the mixture was adjusted to pH 6 with 6 M HCl under ice cooling. The crystalline anilinium salt of **2** was collected by filtration; yield 1.35 g (38%). Recrystallization was effected from methanol–ether; mp 164—166 °C dec.

Found: C, 54.34; H, 5.68; N, 7.91; S, 9.09%. Calcd for $C_{16}H_{20}O_5N_2S$: C, 54.53; H, 5.72; N, 7.95; S, 9.10%.

Hydrogenolytic Deprotection of 2. The anilinium salt of **2** (0.70 g, 2 mmol) was dissolved in methanol (20 ml), and hydrogenolyzed in the presence of Pd black and acetic acid (0.12 ml, 2 mmol) at room temperature. After 3 h, the catalyst and the white precipitates formed were filtered and the latter were extracted with water at 40 °C. The aqueous extract was concentrated *in vacuo* and allowed to stand in a refrigerator to form colorless crystals; yield, 30 mg (12%); mp 170—172 °C dec. The IR spectrum of this product was completely identical with that of **1**.

Benzyloxycarbonyl-D-alanyl-DL-1-aminoethanesulfonic Acid (3) Anilinium Salt. Ethyl chloroformate (0.24 ml, 2.5 mmol) was added to a solution of benzyloxycarbonyl-D-alanine (0.53 g, 2.4 mmol) and *N*-methylmorpholine (0.29 ml, 2.6 mmol) in anhydrous tetrahydrofuran (5 ml) at −13 °C with stirring. After 10 min, a solution of **1** (0.45 g, 3.6 mmol) in 2 M aqueous NaOH (1.8 ml) was added dropwise during 5 min, while the mixture was stirred at −13 °C. Stirring was continued at this temperature for further 3 h. After tetrahydrofuran was evaporated *in vacuo*, the mixture was diluted with water, treated with aniline (0.35 ml, 3.8 mmol) and adjusted to pH 6 with 2 M HCl under ice cooling. The crystals of anilinium salt of **3** were filtered; yield, 0.47 g (46%). Recrystallization was effected from methanol–ether; mp 201—204 °C dec.

Found: C, 53.88; H, 5.94; N, 9.93; S, 7.67%. Calcd for $C_{19}H_{25}O_6N_3S$: C, 53.88; H, 5.95; N, 9.92; S, 7.57%.

D-Alanyl-DL-1-aminoethanesulfonic Acid (4). The anilinium salt of **3** (1.27 g, 3.0 mmol) was dissolved in methanol and hydrogenolyzed in the presence of Pd black at room temperature. After the catalyst was filtered off and solvent

was evaporated *in vacuo*, the residue was recrystallized from water–methanol–ether; yield, 0.46 g (77%); mp 220—224 °C dec; R_f 0.23, 0.27 (Toyo No. 51 filter paper, 1-butanol–acetic acid–water 4: 1: 2).

Separation of D-*Alanyl*-D *and* L-*1-aminoethanesulfonic Acids (**4a** and **4b**).* The mixture (400 mg) of the diastereomers (**4**) obtained above was dissolved in a small amount of water and subjected to a preparative PC on Toyo No. 50 filter paper (40×40 cm, 4 pieces) by developing twice with 1-butanol–acetic acid–water (4: 1: 2). The three portions of a ninhydrin positive band were extracted with water separately. From each extract, pure **4a** (75 mg), pure **4b** (40 mg), and a mixture of them (105 mg) were obtained respectively by crystallization from water–methanol–ether.

D-*Alanyl*-D-*1-aminoethanesulfonic Acid (**4a**)*: Physical constants; see Table 1.

Found: C, 27.70; H, 6.62; N, 13.07; S, 14.85%. Calcd for $C_5H_{12}O_4N_2S \cdot H_2O$: C, 28.03; H, 6.59; N, 13.08; S, 14.97%.

D-*Alanyl*-L-*1-aminoethanesulfonic Acid (**4b**)*: Physical constants; see Table 1.

Found: C, 29.91; H, 6.11; N, 13.98; S, 15.86%. Calcd for $C_5H_{12}O_4N_2S \cdot 1/4H_2O$: C, 29.92; H, 6.28; N, 13.96; S, 15.97%.

Benzyloxycarbonyl-L-*alanyl*-DL-*1-aminoethanesulfonic Acid (**5**) Anilinium Salt.* Ethyl chloroformate (1.60 ml, 17 mmol) was added to a solution of benzyloxycarbonyl-L-alanine (3.40 g, 15 mmol) and *N*-methylmorpholine (1.80 ml, 16 mmol) in anhydrous tetrahydrofuran (35 ml) at −9 °C with stirring. After 8 min, there was added a solution of **1** (2.50 g, 20 mmol) in 1.5 M aqueous NaOH (13 ml) with stirring at −9 °C. The mixture was stirred at room temperature for 3 h. The product was converted into its anilinium salt as described above for **3** and recrystallized from methanol–ether; yield 1.90 g (30%); mp 193—194 °C dec. Its IR spectrum was identical with that of the anilinium salt of **3**.

Found: C, 53.51; H, 5.82; N, 9.92; S, 7.56%. Calcd for $C_{19}H_{25}O_6N_3S$: C, 53.88; H, 5.95; N, 9.92; S, 7.57%.

L-*Alanyl*-DL-*1-aminoethanesulfonic Acid (**6**).* The anilinium salt of **5** (1.27 g, 3.0 mmol) was hydrogenolyzed as described above for **4** and the product was recrystallized from water–methanol–ether; yield 0.58 g (97%); mp 224—226 °C dec. NMR[15]: δ 1.51 (3H, d, J=7, CH_3 of Aes), 1.55 and 1.57 (each 1.5H, d, J=7, CH_3 of Ala), 4.11 and 4.12 (each 0.5H, q, J=7, CH of Ala), 5.02 (1H, q, J=7, CH of Aes). The IR spectrum was identical with that of **4**.

Found: C, 29.99; H, 6.23; N, 13.88; S, 16.10%. Calcd for $C_5H_{12}O_4N_2S \cdot 1/4H_2O$: C, 29.92; H, 6.28; N, 13.96; S, 15.97%.

Separation of L-*Alanyl*-L *and* D-*1-aminoethanesulfonic Acids (**6a** and **6b**).* The mixture (400 mg) of the diastereomers obtained above was subjected to preparative PC as described for **4a** and **4b**, affording pure **6a** (130 mg), pure **6b** (130 mg), and a mixture of them (90 mg).

L-*Alanyl*-L-*1-aminoethanesulfonic Acid (**6a**)*: Physical constants; see Table 1. NMR[15]: δ 1.51 (3H, d, J=7, CH_3 of Aes), 1.57 (3H, d, J=7, CH_3 of Ala), 4.12 (1H, q, J=7, CH of Ala), 5.02 (1H, q, J=7, CH of Aes).

Found: C, 27.88; H, 6.66; N, 13.01; S, 14.72%. Calcd for $C_5H_{12}O_4N_2S \cdot H_2O$: C, 28.03; H, 6.59; N, 13.08; S, 14.97%.

L-*Alanyl*-D-*1-aminoethanesulfonic Acid (**6b**)*: Physical constants; see Table 1. NMR[15]: δ 1.51 (3H, d, J=7, CH_3 of Aes), 1.55 (3H, d, J=7, CH_3 of Ala), 4.11 (1H, q, J=7, CH of Ala), 5.02 (1H, q, J=7, CH of Aes).

Found: C, 29.95; H, 6.24; N, 14.11; S, 15.97%. Calcd for $C_5H_{12}O_4N_2S \cdot 1/4H_2O$: C, 29.92; H, 6.28; N, 13.96; S, 15.97%.

t-*Butoxycarbonyl*-D-*alanyl*-DL-*1-aminoethanesulfonic Acid (**7**).* Ethyl chloroformate (0.53 ml, 5.5 mmol) was added to a solution of *t*-butoxycarbonyl-D-alanine (0.95 g, 5.0 mmol) and *N*-methylmorpholine (0.60 ml, 5.5 mmol) in anhydrous tetrahydrofuran (15 ml) at −8 °C with stirring. After 10 min, there was added a solution of **1** (0.95 g, 7.6 mmol) in 1 M aqueous NaOH (7.5 ml) dropwise with stirring at −8 °C. Stirring was continued at this temperature for 1 h and at room temperature for further 3 h. Tetrahydrofuran was removed *in vacuo* and the product was isolated as its anilinium salt as described for **3** and recrystallized from methanol–ether; yield, 0.84 g (43%); mp 163 °C dec. An analytical sample was further recrystallized from the same solvents; mp 179—181 °C dec.

Found: C, 49.09; H, 7.02; N, 10.77; S, 8.22%. Calcd for $C_{16}H_{27}O_6N_3S$: C, 49.34; H, 6.99; N, 10.79; S, 8.23%.

t-*Butoxycarbonyl*-L-*alanyl*-DL-*1-aminoethanesulfonic Acid (**8**).* This compound was prepared as described above for **7** by using *t*-butoxycarbonyl-L-alanine (0.95 g, 5.0 mmol) in place of *t*-butoxycarbonyl-D-alanine. The product was isolated as its anilinium salt; yield, 0.50 g (26%); mp 162—166 °C dec. Its IR spectrum was identical with that of the anilinium salt of **7**.

*Deprotection of **8**.* To a suspension of anilinium salt of **8** (100 mg, 0.26 mmol) in ethyl acetate (3 ml), there was added a saturated solution of dry hydrogen chloride in ethyl acetate (2 ml). While the mixture was stirred at room temperature for 90 min, the initial crystals dissolved and the product separated out. The latter was collected by filtration and recrystallized from water–methanol–ether; yield, 20 mg (40%); mp 220—223 °C dec. Its IR spectrum was identical with that of **6**.

*Sodium Salts of **3**, **5**, **7**, and **8**.* These compounds were prepared by dissolving the corresponding anilinium salt in water containing one equivalent of NaOH, followed by extraction with ether and evaporation of the aqueous phases *in vacuo*.

The authors are deeply indebted to Prof. M. Kakudo and his coworkers, Protein Research Institute, Osaka University for X-ray analysis and to Daiichi Seiyaku Co., Ltd. for the test of antimicrobial activity.

References

1) This work was presented at 34th Annual Meeting of the Chemical Society of Japan, Kanagawa, April 1976; p. 695.

2) a) H. McIlwain, *J. Chem. Soc.*, **1941**, 75. b) H. McIlwain, *Brit. J. Expt. Path.*, **22**, 148 (1941).

3) R. L. Thompson, *J. Immunol.*, **55**, 345 (1947).

4) T. Kaneko, R. Yoshida, and I. Takano, The 14th Annual Meeting of the Chemical Society of Japan, 1961; p. 305.

5) E. Ito and J. L. Strominger, *J. Biol. Chem.*, **237**, 2696 (1962).

6) In this connection, we also synthesized D-alanyl-D-cycloserine and their derivatives. S. Kusumoto, Y. Tarumi, and T. Shiba, Proceeding of the 11th Symposium on Peptide Chemistry (Tokyo, Japan, November, 1973), p. 68.

7) Huber *et al.*, recently synthesized *N*-D-alanyl-1-aminoethylphosphonic acid, a phosphonic acid analog of D-alanyl-DL-alanine, and found weak antimicrobial activity in it. J. W. Huber, III, W. F. Gilmore, and L. W. Robertson, *J. Med. Chem.*, **18**, 106 (1975).

8) M. Frankel and P. Moses, *Tetrahedron*, **9**, 289 (1960). P. Moses, L. Mager, and M. Frankel, *Bull. Res. Counc. Israel*, **9A**, 46 (1960).

9) All the *N*-protected amino sulfonic acids in this work formed crystalline anilinium salts, which were much more easily handled than sodium or potassium salts.

10) The configurations of α-amino sulfonic acids are represented with analogy to α-amino acids for convenience (see the

following text).

11) M. Kakudo and Y. Matsuura, unpublished.
12) L. Neelakantan, *J. Org. Chem.*, **36**, 2253, 2256 (1971).
13) All melting points are uncorrected.
14) F. Raschig and W. Prahl, *Justus Liebigs Ann. Chem.*, **448**, 265 (1926).

15) NMR spectra were determined for D_2O solutions on a Varian XL-100 spectrometer at 100 MHz using TMS as external standard. The chemical shifts and coupling constants were recorded in δ values and Hz.

Deacylations and Syntheses of Some 9-Acylfluorenes

Takao KIMURA, Masahiro MINABE,* Motohiro TSUBOTA, and Kazuo SUZUKI

Department of Industrial Chemistry, Faculty of Engineering, Utsunomiya University, Ishiicho, Utsunomiya 321-31

(Received August 14, 1976)

Deacylations of substituted 9-acetyl-, 9-propionyl-, 9-benzoyl-fluorene, and 9-fluorenyl 9-methyl-9-fluorenyl ketones were studied; the reactivity of deacylation was enhanced by the substitution of the 9-hydrogen atom on 9-acetylfluorene. The reaction of 9-acetylfluorene with ethyl nitrate afforded 9-*aci*-nitrofluorene.

Deacylation promoted by a base has been known already to occur in the active methylene to which an acyl group is attached. In fluorene derivatives, 9-benzoylfluorene (**1**) gave fluorene (**2**) and benzoic acid,[1] and 9-chloro-9-acetylfluorene (**3**) afforded 9,9′-bifluorenyl (**4**).[2] The present work deals with the deacylation of 9-acylfluorenes in order to clarify the reactivities on the 9-carbon atom of fluorenes.

Deacetylation of 9-acetylfluorene (**5**)[3] yielded **2** and ethyl acetate; the yield of **2** increased (28—96%) with the increase of base concentration (1—20%) and with the extension of the reaction time (1—10 h). The deacetylation may be explained by the nucleophilic attack of ethoxide anion on the cationic carbon atom of carbonyl in **5** to form the intermediary carbanion (A) as the reverse-Claisen-type condensation (Scheme 1).

The deacylation of some 9-acylfluorenes was carried out as shown in Table 1. The substituent effect in the deacylation of 9-propionyl- (**6**),[4] 2-ethyl-9-acetyl- (**7**), and 2-bromo-9-acetylfluorene (**8**) was observed to be less significant in comparison with that of **5**. The reaction of 9,9-dibenzoylfluorene (**9**)[5] with base afforded **1**, which was further converted to **2** by debenzoylation.

The elimination was accelerated remarkably in the deacetylation of **3**, 9-methyl- (**10**),[6] and 9-hydroxy-9-acetylfluorene (**11**).[7] The ethoxide anion may be able to attack on the two positions of **5**, that is, the 9-carbon and the carbonyl carbon atoms. The 9-acetylfluoren-9-ide anion would be stabilized by resonance as enolate anion and **5** is less reactive under these conditions. The substitution on the 9-position of **5** prevents the attack on this position and results in the significant formation of the elimination product.

The reaction of **5** with ethyl nitrate in the presence of sodium ethoxide gave pure 9-*aci*-nitrofluorene[8] in good yield. The ethoxide anion removes a proton from the 9-position on the **5**. The resulting carbanion may afford the intermediary 9-nitro-9-acetylfluorene by an attack of ethyl nitrate, and this was converted to 9-*aci*-nitrofluorene by the action of a second ethoxide anion and by the tautomeric effect of the nitro group (Scheme 2).

The deacetylation of the substrate containing an electron-attracting group proceeds more readily than that having an electron-releasing group. Actually, the progress of the deacylations for **3** and also for **10** was followed by means of gas chromatography; the **10** still remained in a considerable amount (37%) at the reaction step in which all the **3** had been consumed. Chloride **3** gave 9,9′-bifluorenylidene (46%) and **4** (trace), and the ethylene was reduced to **4** under similar conditions.

The reactivity of the carbonyl group in 9-*t*-butyl-9-acetylfluorene (**12**) is hindered by the bulky substituent

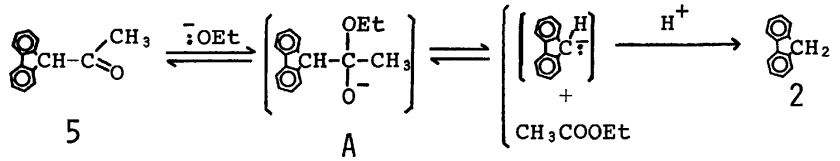

Scheme 1.

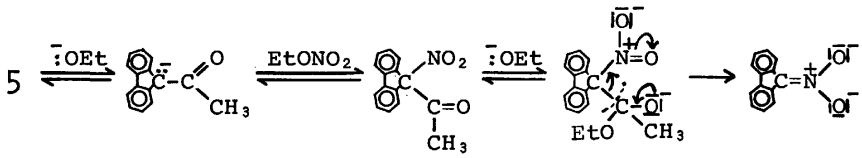

Scheme 2.

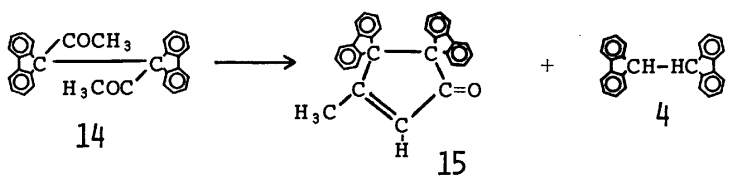

Scheme 3.

* To whom inquiries should be addressed.

Table 1. Characterization and deacylation of 9-acylfluorenes

Compound	Characterization		Deacylation	
	^{1}H-NMR chemical shift[a] δ(ppm); J (Hz)	ν(C=O) on IR spectrum (cm^{-1})	Fluorene %	Recovd %
5	1.60 ($-CH_3$); 4.78 (>CH–)	1698	42 (**2**)	45
6	0.78 ($-CH_3$, J=6.3); 1.75($-CH_2-$); 4.64 (>CH–)	1700	42 (**2**)	38
7	1.26 ($-CH_3$, J=6.0); 1.46 ($-COCH_3$); 2.67 ($-CH_2-$); 4.59 (>CH–)	1701	45 (2-Ethyl-)	45
8	1.65 ($-CH_3$); 4.75 (>CH–)	1698	55 (2-Bromo-)[b]	
9		1680	23(**1**); 26(**2**)	
1	5.37 (>CH–)	1681	66 (**2**)	26
10	1.37 ($-CH_3$); 1.57 ($-COCH_3$)	1702	94 (9-Methyl-)	trace
11	1.54 ($-CH_3$); 4.78 (–OH)	1700	96 (9-Hydroxy-)	trace
12	0.99 ($-CH_3$); 1.36 ($-COCH_3$)	1699	34 (9-*t*-Butyl-)	57
13	2.19 ($-CH_3$); 2.87 ($-CH_2-$, J=4.8); 4.45 (>CH–)	1707		99

a) Measured in $CDCl_3$ or CCl_4. b) In addition, 2-bromo-9-acetyl-9-hydroxyfluorene (2%, mp 154—155 °C, IR: (OH) 3460; (C=O) 1704 cm^{-1}) and 2,2′-dibromo-9,9′-diacetyl-9 9′-bifluorenyl (0.3%, mp 238—240 °C, IR: (C=O) 1705 cm^{-1}) were isolated.

Table 2. Characterization and deacylation of 9-acylfluorenes

Compound	Characterization		Deacylation	
	^{1}H-NMR chemical shift δ (ppm) (Solvent)	ν (C=O) on IR spectrum (cm^{-1})	Time h	Products (%)
16	1.78 ($-CH_3$); 4.52 (>CH–) (Pyridine-d_5)	1700	1	**2** (31); **17** (10); **18** (31); 9-Methylfluorene (9); Recovd (42)
16			10	**2** (58); **17**(22); **18** (30); 9-Methylfluorene (41)
18	1.69 ($-CH_3$); 1.04 ($-CH_3$, J=7.0 Hz);3.97 ($-CH_2-$) (CCl_4)	1721	10	9-Methylfluorene (18); **17** (14); Recovd (67)
19	3.63 ($-CH_3$); 4.71 (>CH–) (CCl_4)	1729	10	**2** (8); **20** (57); Ethyl ester of **20** (10)

from the approach of an attacking ethoxide ion, therefore, the yield of 9-*t*-butylfluorene[9] decreased. No deacetylation was observed in the cases of 9-acetonylfluorene (**13**)[10] and 2-acetylfluorene.[11] This finding shows that deacylation occurs when the acyl group is attached directly to the active 9-position of fluorenes. The anomalous lower field (2.19 ppm) of the methyl chemical shift of **13** compared with that (1.60 ppm) of **5** is ascribed to the predominant conformation of **13** and **5**; the mobile methyl group of **13** may be located further away from the shield zone of the aromatic rings than that of **5**.

The reaction of 9,9′-diacetyl-9,9′-bifluorenyl (**14**)[2] afforded dehydrate compound **15** accompanied by **4** (Scheme 3); **15** would be formed by the intramolecular aldol-type condensation.

The same reaction of 9-fluorenyl 9-methyl-9-fluorenyl ketone (**16**) yielded **2**, 9-methylfluorene, 9-methylfluorene-9-carboxylic acid (**17**),[12] and its ethyl ester (**18**),[13] as summarized in Table 2. The ester **18** gave 9-methylfluorene and **17**. Similarly, methyl fluorenyl-9-carboxylate (**19**) yielded **2**, the corresponding carboxylic acid (**20**), and its ethyl ester. The ratio of the yields of these products indicates that **16** cleaves into 9-fluorenide anion and **18**, but not into 9-methylfluoren-9-ide anion and an ester of **20**; this may be attributed to the stability of the 9-fluorenide anion formed, which is greater than that of the methyl derivative.

Experimental

All the melting points are uncorrected. The instruments used in this experiment have been described elsewhere.[11]

Deacylation of 9-Acylfluorene. General Procedure: Sodium metal (1.15 g) was treated with 33 ml of dry ethanol, then 5 mmol of substrate was added, and the mixture was refluxed for 10 h under an atmosphere of dry nitrogen. Upon cooling, the reaction mixture was poured into 150 ml of 3% hydrochloric acid and the resulting precipitate was purified by a combination of alumina-column chromatography, vacuum sublimation, and recrystallization.

*Reaction of **14** with Sodium Ethoxide.* A 2.070 g portion of **14** was refluxed with 3.4 g of sodium ethoxide in 330 ml of dry benzene for 10 h to give 0.450 g of 3-methyl-4,5-bis(2,2′-biphenylylene)-2-cyclopenten-1-one (**15**), 0.012 g of **4**, and 0.010 g of fluorenone. Mp of **15**: 233.5—234.5 °C. IR: (C=O) 1694 cm^{-1}. Mass: *m/e* 396 (M^+), 381, and 352. NMR (benzene-d_6): δ 1.29 (3H, s), 6.47 (1H, s), and 6.65—7.35 (16H, m) ppm. Found: C, 90.96; H, 5.17%. Calcd for $C_{30}H_{20}O$: C, 90.88; H, 5.09%.

*Reaction of **5** with Ethyl Nitrate.* A soln of 2.08 g of **5**, 1.82 g of ethyl nitrate, and 0.68 g of sodium ethoxide in 20 ml of dry ethanol was refluxed for 2 h. Upon cooling, 100 ml of

benzene and 150 ml of water were added to the reaction mixture and the aqueous layer was neutralized with hydrochloric acid to yield 1.53 g of 9-*aci*-nitrofluorene, mp 154 °C (dec). IR: (OH) 2770; (NO_2) 1653, 1441 cm^{-1}.

2-Ethyl-9-acetylfluorene (7). Compd **7** was prepared by means of the same procedure as used for **5** in a 34% yield, bp 142—144 °C/2 Torr (uncorr.). Mass: *m/e* 236 (M^+).

2,4-Dinitrophenylhydrazone, mp 200—202 °C. IR: (NH) 3320; (NO_2) 1614, 1589 cm^{-1}. Found: C, 66.68; H, 4.95; N, 13.58%. Calcd for $C_{23}H_{20}O_4N_4$: C, 66.33; H, 4.84; N, 13.46%.

2-Bromo-9-acetylfluorene (8). The title compd was obtained by the same method as described above, yield 30%, mp 66—67 °C. Mass: *m/e* 288, 286 (M^+), 245, 243, and 207. Found: C, 62.95; H, 3.64%. Calcd for $C_{15}H_{11}OBr$: C, 62.74; H, 3.86%.

9-t-Butyl-9-acetylfluorene (12). Compd **12** was obtained by a procedure similar to that of **10** in a 39% yield, mp 76.5—77 °C. Mass: *m/e* 264 (M^+), 249, 221, 208, 206, 191, and 165. Found: C, 86.73; H, 7.77%. Calcd for $C_{19}H_{20}O$: C, 86.32; H, 7.63%.

9-Acetonylfluorene (13). This compd was synthesized by the reaction of α-(9-fluorenyl)acetyl chloride with methylmagnesium iodide in the presence of cadmium chloride: yield 58%, mp 62—63 °C (lit,[10] mp 57 °C). Mass: *m/e* 222 (M^+), 179, and 165.

9-Fluorenyl 9-Methyl-9-fluorenyl Ketone (16). To a soln of 9-methyl-9-lithiofluorene (prepared from 0.96 g of lithium chips, 9.4 g of butyl bromide, and 10.3 g of 9-methylfluorene in 100 ml of xylene) was added dropwise 12.0 g of 9-fluorenylcarbonyl chloride in 60 ml of xylene at 0 °C with stirring for 30 min, then the mixture was boiled for 1 h to afford 6.45 g of **16**, mp 226—227.5 °C. Mass: *m/e* 372 (M^+), 179, and 165. Found: C, 90.27; H, 5.57%. Calcd for $C_{28}H_{20}O$: C, 90.29; H, 5.41%.

References

1) P. Pfeiffer and E. Lübbe, *Ber.*, **63**, 762 (1930).
2) E. J. Greenhow, A. S. Harris, and E. N. White, *J. Chem. Soc.*, **1954**, 3116.
3) I. Von and E. C. Wagner, *J. Org. Chem.*, **9**, 155 (1944).
4) S. Wawzonek and E. Dufek, *J. Am. Chem. Soc.*, **78**, 3530 (1956).
5) G. W. H. Scherf and R. K. Brown, *Can. J. Chem.*, **39**, 1613 (1961).
6) E. J. Greenhow, D. McNeil, and E. N. White, *J. Chem. Soc.*, **1952**, 986.
7) G. F. Hennion and B. R. Fleck, *J. Am. Chem. Soc.*, **77**, 3253 (1955).
8) C. D. Nenitzescu and D. A. Isăcescu, *Ber.*, **63**, 2484 (1930).
9) F. A. L. Anet and P. M. G. Bavin, *Can. J. Chem.*, **34**, 991 (1956).
10) J. A. Gautier, M. Miocque, and H. Moskowitz, *Bull. Soc. Chim. Fr.*, **1965**, 1740; *Chem. Abstr.*, **63**, 8280 (1965).
11) M. Minabe, M. Yoshida, M. Fujimoto, and K. Suzuki, *J. Org. Chem.*, **41**, 1935 (1976).
12) E. J. Greenhow, E. N. White, and D. McNeil, *J. Chem. Soc.*, **1953**, 3099.
13) P. M. G. Bavin, *Anal. Chem.*, **32**, 554 (1960).

Oxidation of Cinnamyl Alcohol with Peracetic Acid in Acidic Solvents[1)]

Yoshiro OGATA* and Kohtaro TOMIZAWA

Department of Applied Chemistry, Faculty of Engineering, Nagoya University, Chikusa-ku, Nagoya 464

(Received April 25, 1976)

Peracetic acid oxidation of cinnamyl alcohol(**1**) in tetrahydrofuran(THF) at room temperature has been found to give phenylacetic acid(**2**), benzaldehyde(**4**) and cinnamyl acetate(**5**) as major products. A probable first-formed intermediate, 2,3-epoxy-3-phenyl-1-propanol(**7**), was detected as its derivative (1-phenyl-1,2,3-propanetriol), and also a probable second intermediate, 1-hydroxy-3-phenyl-2-propanone (**3**), was detected. **3** was found to be converted to **2** by the Baeyer-Villiger reaction. On the other hand, the peracetic acid oxidation of **1** in methanol gave a methanolysis product of oxirane ring, 3-methoxy-3-phenyl-1,2-propanediol (**6a**), a small amount of a rearrangement product and benzaldehyde. The peracid oxidation of **1** in various solvents was also studied. A probable reaction mechanism is discussed.

We have previously reported that peracid oxidation of vitamin A alcohol, $Me_3C_6H_6$-CH=CH-CMe=CH-CH=CH-CMe=CH-CH_2OH, yielded 11,12-epoxy-vitamin A aldehyde, $Me_3C_6H_6$-CH=CH-CMe=CH-$\overset{O}{\overset{/\backslash}{CH-CH}}$-CMe=CH-CHO, *via* oxidation of primary alcohol group to aldehyde as well as epoxidation of an ethylenic bond.[2)] In the present paper, we intended to study the peracetic acid oxidation of cinnamyl alcohol (**1**), which have an α,β-unsaturated alcohol group.

The present study showed that the peracid oxidation of **1** had a behaviour different from that of vitamin A alcohol. In this paper we wish to report the mechanism of peracid oxidation of **1** which was speculated from the products of an assumed intermediary epoxide, 2,3-epoxy-3-phenyl-1-propanol (**7**).

It was reported that the perbenzoic acid oxidation of in $CHCl_3$ at 0 °C gave **7**, which could be converted to phenylacetaldehyde, formaldehyde and 1-hydroxy-3-phenyl-2-propanone (**3**) on pyrolysis in the presence of kieselguhr,[3-5)] but resinous material on pyrolysis in the presence of H_2SO_4 or $ZnCl_2$.[3,4)] The pyrolysis products of **7** and the migratory aptitude of the epoxide rearrangement were studied only in the absence of peracid at high temperature[3,6-8)] and little was known on the peracid oxidation of **1** and the subsequent reactions in solution and at lower temperature.

Also peracid oxidation of α,β-unsaturated secondary alcohol was reported to yield the epoxides and its derivative,[9,10)] but no report is available on the mechanism of formation of these derivatives.

Results and Discussion

Oxidation of cinnamyl alcohol(**1**) with an equivalent of peracetic acid in tetrahydrofuran(THF) and in some solvents containing acetic acid at room temperature gave a distribution of products as shown in Table 1. In addition of products listed in the table, a trace of cinnamaldehyde, PhCH=CHCHO, and significant amounts of unknown products were formed but the expected products, 2,3-epoxy-3-phenylpropanal, Ph$\overset{O}{\overset{/\backslash}{CH-CH}}$CHO(**8**), was not detected. Most of these products were identified by the comparison of IR and NMR spectra and GLC peaks with those of the corresponding authentic specimens.

A trace of cinnamaldehyde formed during this oxidation cannot be the precursor to **8**, because the peracetic acid oxidation of cinnamaldehyde did not proceed under these conditions. Furthermore, we observed that **8** was very unstable, thus **8** could not be synthesised by oxidation of cinnamaldehyde by H_2O_2 or *t*-BuOOH even according to the reported procedure in alkaline media[11)] as described in Experimental part. In the case of oxidation of vitamin A alcohol, the steric selectivity of attacking site seems to play an important role,[2)] thus the observed oxidation of unsaturated alcohol to epoxy aldehyde can occur because of the chemical driving force for the formation of its α,β-unsaturated aldehyde in acidic media. Whereas, the peracetic acid oxidation of cinnamyl alcohol (**1**) to **8** is unfavourable because of the

TABLE 1. SOLVENT EFFECT ON THE YIELDS OF PRODUCTS IN THE PERACETIC ACID OXIDATION OF CINNAMYL ALCOHOL (**1**)

Solvent	Reaction time h	Conversion %	Product %					
			2	**3**[b)]	**4**	**5**	**6a**	**6b**
THF	66	65.2	19.2	6.2	16.0	17.0	—	—
Ether	54	61.5	13.9	1.8	14.6	16.3	—	—
Benzene	54	60.3	24.1	7.9	13.4	14.1	—	—
Cyclohexane[a)]	54	70.4	trace	—	4.6	39.7	—	—
CH_2Cl_2	24	75.4	28.9	6.7	15.3	14.3	—	—
Methanol	24	52.7	3.4	—	1.2	5.2	63.5	trace

a) Heterogeneous system. b) The yield of **3** was the value corrected for the amounts of **3** derived from GLC pyrolysis of **7**.

2; $PhCH_2CO_2H$. **3**; $PhCH_2COCH_2OH$. **4**; PhCHO. **5**; $PhCH{=}CHCH_2OAc$. **6a**; PhCH(OMe)-CH(OH)CH_2OH. **6b**; PhCH(OH)CH(OMe)CH_2OH.

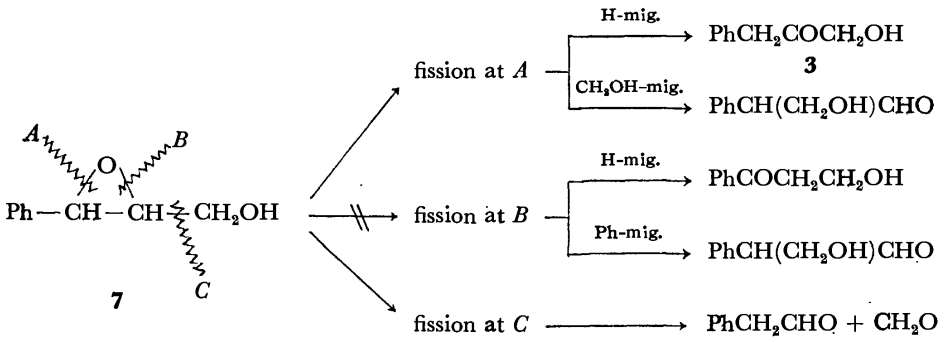

Scheme 1.

faster ring opening of its intermediate epoxide **7** as discussed below.

1-Hydroxy-3-phenyl-2-propanone (**3**) should be a rearrangement product of the initially formed 2,3-epoxy-3-phenyl-1-propanol (**7**) from **1** as shown in Eq. (1a). The epoxide (**7**) may afford by fissions at *A* and *B* three isomers, and by fission at *C*, products of cleavage at C–C as shown in Scheme 1, but actually the catalytic pyrolysis of **7** was reported to give phenylacetaldehyde, formaldehyde and **3**, which may be products of radical reactions.[3,4] Also our pyrolysis of alternatively synthesised **7** at 200—250 °C at the injection temperature of GLC yielded phenylacetaldehyde (25%) and **3** (29%) and unknown products. On the other hand, during the column chromatography with silica gel ($SiO_2 \cdot xH_2O$), **7** was completely changed to give 1-phenyl-1,2,3-propanetriol, $PhCH(OH)CH(OH)CH_2OH$, and no phenylacetaldehyde and **3** was detected by GLC. The present peracetic acid oxidation of **1** gave **3** and a little phenylacetaldehyde, which were identified by GLC, but 1-phenylpropane-1,2,3-triol was obtained instead of phenylacetaldehyde by the column chromatography with silica gel. The above fact suggests that **7** is a primary intermediate formed in this oxidation and that **7** is converted to **3** by the following ionic path (Eq. 1a) which involves no radical species.

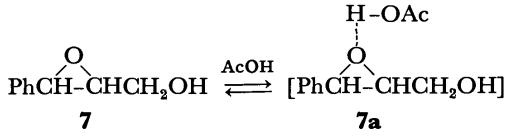

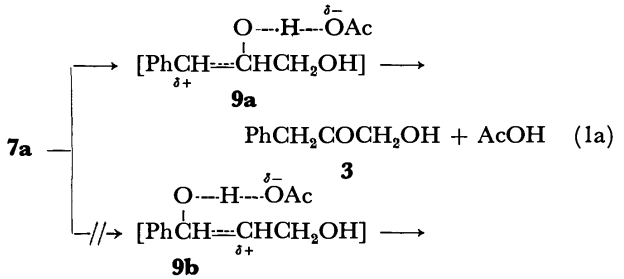

On account of the more resonance delocalization of the positive charge in **9a**, the pathway (Eq. 1a) *via* **9a** leading to **3** should be favoured rather than the pathway (Eq. 1b) *via* **9b** leading to *β*-hydroxypropiophenone.

The authentic **3**, which was prepared alternatively,[4,12] gave phenylacetic acid (**2**) on the peracetic acid oxidation under similar conditions. Hence, **3** may be an intermediate in the formation of **2** from **1**. Three paths from **3** (Eqs. 3a—c) are conceivable for this oxidation, but the Baeyer-Villiger reaction of Eq. 3a is negligible because of the formation of little benzyl alcohol which is fairly stable under these conditions as evidenced in Experimental part. Further, the autoxidation of **3**(Eq. 3c) is less probable, because peracetic acid is necessary for this reaction forming **2** which proceeds even under N_2. Hence, **2** is probably formed *via* Eq. 3b alone, where the preferential migration of methylol group of **10** occurs. The Taft σ^* values are 0.225 for benzyl group and 0.555 for hydroxymethyl group.[13] In

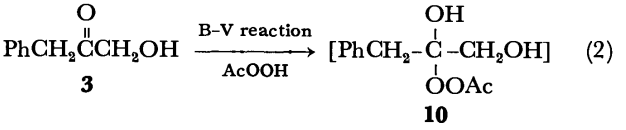

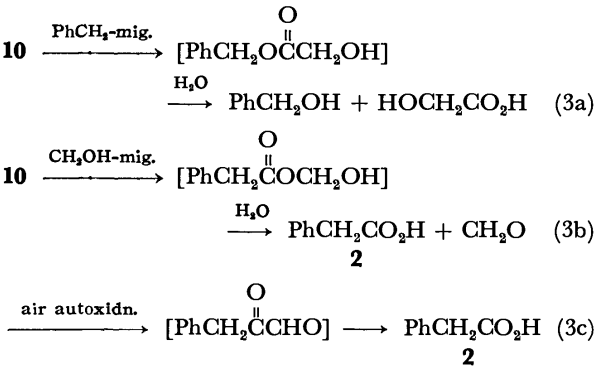

most Baeyer-Villiger reactions, a more electron-releasing group tends to migrate preferentially, but in this case the more electron-attracting hydroxymethyl group must migrate. This migration of methylol group may be due to the formation of hydrogen bonding which facilitates O–O fission in the transition state of migration as shown in **11**. The similar migration of an electron-attracting phenyl group was reported for acetophenone, where

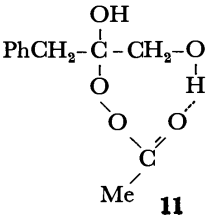

Table 2. Effect of molar ratio of reactants ($PhCH=CHCH_2OH$: AcOOH)

Solvent	Mole ratio[a]	Reaction time h	Conversion %	Product % 2	3[b]	4	5
THF	1:1	66	65.2	19.2	6.2	16.0	17.0
THF	1:2	35	75.4	38.5	5.2	5.3	14.0
Ether	1:1	54	61.5	13.9	1.8	14.6	16.3
Ether	1:2	24	78.6	29.7	4.3	8.7	16.8
Benzene	1:1	54	60.3	24.1	7.9	13.2	14.1
Benzene	1:2	24	73.5	32.4	10.5	10.2	13.2

a) Ratio of cinnamyl alcohol (**1**) and peracetic acid. b) The value for **3** was determined in the same way as Table 1.

bridged phenonium ion assists the migration.[14]

The formation of benzaldehyde (**4**) can also be explained by assuming the H-bonded neutral intermediate **7a**, which is cleaved to give **4** by the addition of peracetic acid to its oxirane ring (Eq. 4) in view of the acid catalysis as will be discussed below. The similar mechanism was reported for the peracetic acid oxidation of ketene.[15]

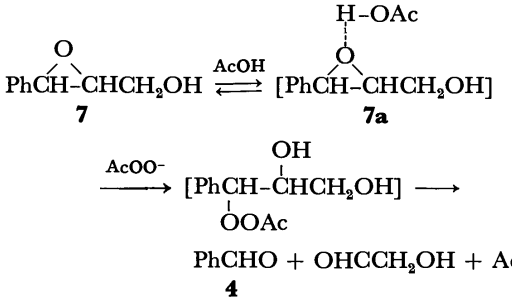

Observed products and pathways in various solvents for the oxidation of **1** are shown in Scheme 2. The structure of **6a** was supported by comparison with 1,3-dimethoxy-1-phenyl-2-propanol (**14**) which was prepared by peracid oxidation of cinnamyl methyl ether (**13**) in MeOH.

The yield of phenylacetic acid (**2**) from **1** increases with increasing amount of peracetic acid, while the yield of benzaldehyde (**4**) decreases (Table 2). On the other hand, when a small amount of mineral acid is added to a mixture of **7** and peracetic acid, the yield ratio [**4**]/[**2**] increases significantly. The above facts may be explained as follows: (i) In the presence of mineral acid, benzaldehyde (**4**) should be obtained as a major product *via* **12** (Eq. 7b), because the greater electro-

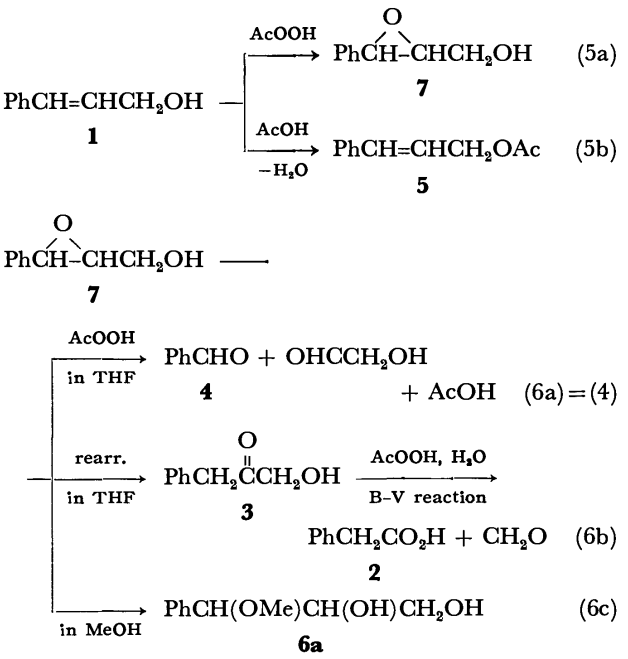

Scheme 2.

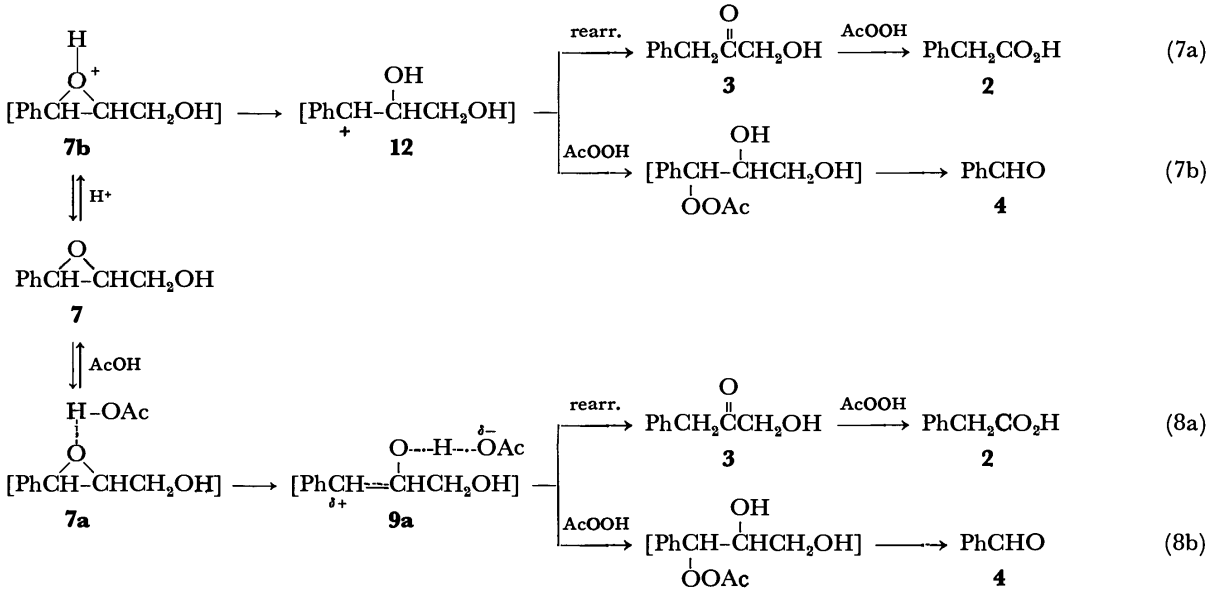

philicity of **12** than that of **7a** accelerates an attack of nucleophiles on **12** and thus favours this addition (Eq. 7b) rather than the rearrangement (Eq. 7a). (ii) In the absence of mineral acid, the precursor of **2**, $PhCH_2COCH_2OH$(**3**), is probably formed as a main product via neutral intermediate **7a** (Eq. 8a), because the carbonium ion from **7a**, if formed, is very unstable and hence the rearrangement (Eq. 8a) is preferred to an attack of nucleophiles ($AcOO^-$, AcOOH) on **9a**. The decrease of the yield of **4** with increasing amount of peracid seems to be curious, but the increase would accelerate the Baeyer-Villiger reaction (Eq. 8a) more than the C–C cleavage (Eq. 8b), which does not involve peracid in the rate-determining step. The increase of acidity on addition of mineral acid promotes the formation of **7b** and increases the yield of **4** by the acceleration of an attack of peracid on **12**. Whereas, in the absence of mineral acid, there is formed no **7b** but H-bonded **7a**, which is much weaker electrophile and thus the rate of Eq. (8a) going to **3** is much faster than the rate of Eq. (8b) going to **4**, and then the increase of concentration of peracid increases the ratio of [**2**]/[**4**].

Experimental

Mps were measured by a Yanagimoto micro-melting point apparatus and they were corrected. IR spectra were measured by a Perkin-Elmer Model 337 grating infrared spectrophotometer. GLC analysis was carried out by a Yanagimoto gas chromatograph with FID, Model GCG-550F, employing two sorts of 2 m×2.5 mm columns(one of which was packed with 2.5% PEG-20 M on Chamelite CS of 80—100 mesh and another packed with 13% DEGS on Chromosorb W of 80—100 mesh), using N_2 as a carrier gas. NMR spectra were recorded by a Japan Electron Optic Laboratory Co., C60 HL NMR instrument. The yield of products are listed in Table 1.

Materials. Peracetic acid was prepared by the reaction of Ac_2O (205 g) with 60% aq. H_2O_2 (50 g) added with concd H_2SO_4 (0.5 ml) at 35—40 °C.[16] The peracid concentration was 3.0—3.1 M in average. THF was purified by distillation over Na, bp 66 °C/760 Torr. 2,3-Epoxy-3-phenyl-1-propanol, PhCH(O)CHCH$_2$OH (**7**), was obtained by the oxidation of cinnamyl alcohol (**1**) (0.105 mol) with perbenzoic acid (0.105 mol) in $CHCl_3$ at 0 °C in a yield of 38%: bp 117.5—118.5 °C/1.5 Torr (lit,[17] 117—118 °C/1.5 Torr), IR (liquid film): 3450—3350, 2920, 2860, 1240, 1025, 880, 750, and 700 cm^{-1}; NMR (CCl_4): δ 3.17 (1H, m, 2-H), 3.65 (1H, s, OH), 3.80 (1H, d, J=6 Hz, 3-H), 3.88 (2H, d, J=3 Hz, 1-H), and 7.40 (5H, s, aromatic). 1-Hydroxy-3-phenyl-2-propanone, $PhCH_2COCH_2OH$ (**3**), was synthesised by the reaction of $HOCH_2CN$ (19.7 g) with $PhCH_2MgCl$ in ether and recrystallized from ethanol–petroleum ether,[4,12] in a yield of 5% based on the used nitrile, mp 49.5—50.5 °C (lit,[4] mp 47—48 °C), IR (KBr disk): 3450—3350, 1720, 750, and 695 cm^{-1}; NMR ($CDCl_3$): δ 3.08 (1H, s, OH), 3.35 (2H, s, 3-H), 4.18 (2H, s, 1-H), and 7.17 (5H, s, aromatic). Cinnamyl methyl ether, $PhCH{=}CHCH_2OMe$ (**13**), was obtained by the reaction of cinnamyl alcohol (**1**) (25 g) with Me_2SO_4 and $NaNH_2$ in ether in a yield of 78%, bp 115—117 °C/20 Torr (lit,[18] 111—112.5 °C/15 Torr), IR (liquid film): 2815, 965, 742, and 690 cm^{-1}; NMR (CCl_4): δ 3.26 (3H, s, OMe), 3.97 (2H, d, J=7 Hz, 1-H), 6.10 (1H, m, 2-H), 6.55 (1H, d, J=16 Hz, 3-H), and 7.20 (5H, s, aromatic). Cinnamyl acetate, $PhCH{=}CHCH_2OAc$ (**5**), was prepared by the acetylation of **1** with Ac_2O, (68%), bp 104—106 °C/3 Torr (lit,[19] 141 °C/18 Torr).

Oxidation of Cinnamyl Alcohol (1). Product Isolation. For the reaction of **1** with peracetic acid, **1** (4.33×10^{-2} mol) was treated with peracetic acid (4.31×10^{-2} mol) in THF (100 ml) at room temperature. The produced solution was condensed under vacuum (50 °C at 30 Torr), and the residue was chromatographed on a 60×2 cm column slurry packed with silica gel (benzene and benzene–ethyl acetate). The first substance eluted was benzaldehyde (**4**) and the second was cinnamyl acetate (**5**). The third was colourless crystals, 1-hydroxy-3-phenyl-2-propanone (**3**), and the fourth was recovered **1** and the fifth was colorless crystals, phenylacetic acid (**2**), mp and mmp 77—78 °C. The sixth was a colourless liquid, which was identified to be 1-phenyl-1,2,3-propanetriol, IR (liquid film): 3400—3300, 2920, 2860, 1460, 1100, 1025, 760, and 695 cm^{-1}; NMR ($CDCl_3$): δ 3.30 (1H, m, 2-H), 3.58 (2H, d, 1-H), 4.25 (3H, s, OH), 4.62 (1H, d, 3-H), and 7.25 (5H, s, aromatic).

Oxidation of 1 in Methanol. Product Isolation. The similar oxidation of **1** in MeOH and the similar work up gave products which were chromatographed through a 60×2 cm column of silica gel and developed by the gradient method of benzene–ethyl acetate. The first eluted substance was benzaldehyde (**4**) (trace). The second one was cinnamyl acetate (**5**) and the third was recovered **1** and the fourth was phenylacetic acid (**2**). The fifth was 3-methoxy-3-phenyl-1,2-propanediol (**6a**) which was identified by IR and NMR spectra, IR (liquid film): 3450—3350, 2820, 1200, 760, and 700 cm^{-1}; NMR (CCl_4): δ 3.06 (3H, s, OMe), 3.47 (2H, s, 1-H), 3.58 (1H, m, 2-H), 3.89 (2H, s, OH), 4.00 (1H, d, J=7 Hz, 3-H), and 7.20 (5H, s, aromatic). Found: C, 66.21; H, 7.74%. Calcd for $C_{10}H_{14}O_3$: C, 65.91; H, 7.74%. The sixth was 2-methoxy-1-phenyl-1,3-propanediol (**6b**) which was identified by IR and NMR spectra, IR (liquid film): 3450—3400, 2815, 1210, 760, and 700 cm^{-1}; NMR (CCl_4): δ 3.15 (3H, s, OMe), 3.30 (2H, d, 1-H), 3.66 (1H, m, 2-H), 3.83 (2H, s, OH), 4.19 (1H, d, 3-H), and 7.30 (5H, s, aromatic).

The peracetic acid oxidation of cinnamyl methyl ether (**13**) in MeOH affords 1,3-dimethoxy-1-phenyl-2-propanol (**14**). The comparison of NMR spectra of $PhCH(OMe)CH(OH)CH_2OH$ (**6a**) with those of $PhCH(OH)CH(OMe)CH_2OH$ (**6b**) and **14** confirms the structure of **6a** and **6b**.

In addition, the structure of **6a** was assured by the structure of product (**15**) by H_2SO_4-catalysed dehydration of **6a**; *i.e.*, **15** was identified to be 1-methoxy-1-phenyl-2-propanone, PhCH(OMe)COMe, IR (liquid film): 1715, 755, and 700 cm^{-1}; NMR (CCl_4): δ 2.05 (3H, s, 3-H), 3.35 (3H, s, OMe), 4.48 (1H, s, 1-H), and 7.27 (5H, s, aromatic).

Oxidation of Cinnamyl Methyl Ether (13) in Methanol. The similar oxidation of **13** and the similar work up afforded 1,3-dimethoxy-1-phenyl-2-propanol (**14**), which was identified by IR and NMR spectra, IR (liquid film): 3450—3400, 2820, 1200, 1140, 755, and 695 cm^{-1}; NMR (CCl_4): δ 2.60 (1H, s, OH), 3.16 (3H, s, 3-OMe), 3.27 (3H, s, 1-OMe), 3.30 (2H, d, J=7 Hz, 1-H), 3.76 (1H, m, 2-H), 4.08 (1H, d, J=7 Hz, 3-H), and 7.22 (5H, s, aromatic).

Oxidation of 1-Hydroxy-3-phenyl-2-propanone (3). Two THF solutions of **3**, one of which contained peracetic acid but the other no peracid, were warmed to 20 °C for 24 h and the resulting solutions were analysed similarly by GLC. In this experiment, the former gave phenylacetic acid (**2**) but the latter did not. Also two THF solutions of **3** and peracetic acid, one of which was filled with air and the other filled with N_2 after deaerated under −78 °C, were warmed to 20 °C for 24 h and the products were analysed similarly. Both of them gave **2** in a good yield. Therefore, **2** was formed from the reaction of **3** with peracetic acid and no autoxidation occurs during the reaction.

Pyrolysis of 2,3-Epoxy-3-phenyl-1-propanol (7). **7** was pyrolysed at 200—250 °C at the injection temperature of GLC. Phenylacetaldehyde and **3** were obtained in yields of 25 and 29%, respectively, together with two unknown products. In the present pyrolysis, neither phenylacetic acid (**2**) nor benzaldehyde (**4**) was formed. Further, phenylacetaldehyde was not oxidised to form **2** during this pyrolysis.

Column Chromatography of 2,3-Epoxy-3-phenyl-1-propanol (7). **7** was chromatographed on a 60×2 cm column slurry packed with silica gel. A large portion of the substance eluted with benzene–ethyl acetate (50: 50) was a colourless liquid and it was identified to be 1-phenyl-1,2,3-propanetriol by IR and NMR spectra. In this column chromatography **7** was not recovered and a small amount of unknown material was obtained. Further, neither phenylacetaldehyde nor **3** was obtained.

Oxidation of 2,3-Epoxy-3-phenyl-1-propanol (7). **7** was oxidised similarly with peracetic acid in THF at room temperature for 24 h and the formation of **2** and **4** established by GLC, since the pyrolysis of **7** at 200—250 °C gave neither **2** nor **4** thus their contamination could be avoided. By the reaction with an equivalent of peracetic acid **7** yielded **2** and **4** in yields of 16 and 12%, respectively. Whereas the reaction with two equivalents of peracid gave **2** and **4** in yields of 24 and 13%, respectively. On addition of a small amount of mineral acid, the peracid oxidation of **7** gave **2** (8%) and **4** (32%).

Oxidation of Benzyl Alcohol in THF. Benzyl alcohol was treated with peracetic acid in THF at room temperature by a work up similar to the oxidation of **1**, the resulting products were identified by GLC using two columns by comparing those of authentic samples. The products and their yields were shown in Table 3.

Table 3. The peracetic acid oxidation of benzyl alcohol in THF

Reaction time h	Conversion %	Product %		
		PhCHO (**4**)	$PhCO_2H$	$PhCH_2OAc$
24	23.8	8.8 (1.5)[a)]	2.4	88.7
48	34.0	10.3 (1.7)[a)]	2.5	87.2

a) Yield by autoxidation.

Oxidation of Cinnamaldehyde. Cinnamaldehyde was oxidised with method (1) H_2O_2 in aq. MeOH at pH 8—8.5 and method (2) *t*-BuOOH in MeOH at pH 10.5±0.2, where pH was controlled with a glass electrode pH meter. The reaction solution was condensed under N_2 *in vacuo* and distilled. In both methods 1 and 2, a considerable amount of cinnamaldehyde was recovered and unknown products were obtained. Further, an attempt to oxidise cinnamaldehyde with peracetic acid in THF under conditions similar to that for **1** gave mostly recovered starting material.

The authors are grateful to Dr. K. Takagi for his helpful discussions.

References

1) Contribution No. 221.
2) Y. Ogata, K. Tomizawa, and K. Takagi, *Tetrahedron*, **29**, 47 (1973).
3) P. Weill and M. Darmon, *C. R. Acad. Sci.*, **194**, 977 (1932).
4) M. Darmon and P. Weill, *Bull. Soc. Chim. Fr.*, **8**, 405 (1941).
5) E. C. Jahn and H. Hibbert, *Can. J. Res.*, **8**, 199 (1933); *Chem. Abstr.*, **27**, 2945[2] (1933).
6) M. Tiffeneau, J. Lévy, and P. Jullian, *Bull. Soc. Chim. Fr.*, **49**, 1788 (1931).
7) J. Lévy and J. Sfiras, *Bull. Soc. Chim Fr.*, **49**, 1823 (1931).
8) M. Tiffeneau, A. Oryekhov, and J. Lévy, *Bnll. Soc. Chim. Fr.*, **49**, 1840 (1931).
9) U. I. Pansevich-Kolyada and T. A. Galysheva, *Otd. Obshchi Tekhn. Khim.*, **1965**, 23; *Chem. Abstr.*, **64**, 6595f (1966).
10) H. B. Henbest and R. A. L. Wilson, *Chem. Ind.* (London), **1956**, 659.
11) G. B. Payne, *J. Org. Chem.*, **25**, 275 (1960).
12) E. C. Kendall and B. McKenzie, *Org. Synth.*, Coll. Vol. I, 256 (1956).
13) Y. Ogata, "Yuki-Hannoron," Maruzen, Tokyo (1972), p. 142.
14) C. H. Hassall, *Org. React.*, **9**, 73 (1957).
15) J. K. Crandall and S. A. Sojka, *Tetrahedron Lett.*, **1972**, 1641.
16) Y. Ogata and K. Aoki, *J. Org. Chem.*, **31**, 4181 (1966).
17) T. Suami, I. Uchida, and S. Umezawa, *Bull. Chem. Soc. Jpn.*, **29**, 417 (1956).
18) B. Gredy, *Bull. Soc. Chim. Fr.*, (5) **3**, 1093 (1936).
19) K. Hess and W. Wustrow, *Justus Liebigs Ann. Chem.*, **437**, 256 (1924).

Synthesis of Taxodione, Royleanone, Cryptojaponol, and Methyl 11-Hydroxy-12-methoxy-7-oxoabieta-8,11,13-trien-18-oate

Takashi MATSUMOTO, Yasuo OHSUGA, Shogo HARADA, and Kenji FUKUI

Department of Chemistry, Faculty of Science, Hiroshima University, Higashisenda-machi, Hiroshima 730

(Received August 30, 1976)

Oxidation at the C-11 position of methyl 12-hydroxyabieta-8,11,13-trien-18-oate (II) and ferruginol (XXXII) were successfully carried out using benzoyl peroxide, and the resulting phenols (VII and XXXVII) were further converted into taxodione (III), royleanone (IV), cryptojaponol (V), and methyl 11-hydroxy-12-methoxy-7-oxoabieta-8,11,13-trien-18-oate (VI).

There have been reported the isolation and structural elucidation of many naturally-occurring tricyclic diterpenes possessing an abietane skeleton. As a part of our synthetic studies on natural terpenes, we attempted the conversion of (—)-abietic acid (I) which was easily obtained from pine rosin, into several 11-oxygenated tricyclic diterpenes. This paper[1] describes the conversion of methyl 12-hydroxyabieta-8,11,13-trien-18-oate (II)[2] prepared from I into taxodione (III)[3,4] which has shown significant tumor-inhibiting activity, royleanone(IV),[3-7] cyptojaponol (V),[4,8,9] and methyl 11-hydroxy-12-methoxy-7-oxoabieta-8,11,13-trien-18-oate (VI).[10] Since (—)-abietic acid (I) has already been synthesized, the present conversion can be regarded as the total syntheses of these natural compounds (III, IV, V, and VI).

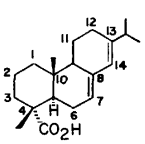
I

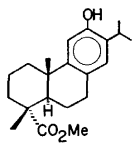
II

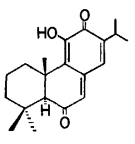
III

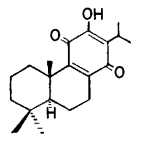
IV

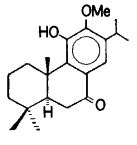
V

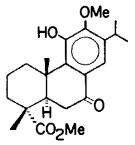
VI

The oxidation of II with benzoyl peroxide in refluxing chloroform afforded a phenol (VII), with three dienones (VIII, IX, and X) as minor products. The structures of these products (VII—X) were assigned on the basis of the following evidence. The phenol (VII) responded positively to the Gibbs test[15] which suggested the presence of an aromatic proton para to a phenolic hydroxyl group. The oxidation of VII with *m*-chloroperbenzoic acid gave a benzoyloxy-*p*-benzoquinone (XI) which was hydrolyzed to give the corresponding hydroxy-*p*-benzoquinone (XII). The NMR spectrum of VII showed a signal at δ 6.57 ppm due to C_{14}–H, while for those of XI and XII no corresponding signal was observed. Thus, the structure of VII was identified to be methyl 12-benzoyloxy-11-hydroxyabieta-8,11,13-trien-18-oate.[16] The treatment of VIII, IX, and X with lithium aluminum hydride in refluxed ether gave the same product, abieta-8,11,13-trien-12,18-diol (XIII).[17,18] This suggests that each of these dienones has an oxygen-function at the C-12 position. From the IR and UV spectra (see Experimental section) of these dienones, it is obvious that IX and X were ortho-substituted dienones,[19] while VIII was a para-substituted dienone.[19] The NMR spectrum of IX was also very similar to that of X, and both IX and X showed two non-equivalent secondary methyl group signals at δ 0.93 and 1.15 ppm and at δ 0.92 and 1.15 ppm, respectively. On the other hand, VIII showed an equivalent signal at δ 1.05 ppm due to the methyls of the isopropyl group. Thus, IX and X should be epimeric isomers with respect to the C-13 position. Hydrolysis of the para-dienone VIII in aqueous methanol with potassium carbonate under reflux gave the corresponding alcohol (XIV). In the NMR spectrum of XIV, the downfield shift of the signal (δ 1.42 ppm) due to the methyl group at the C-10 position relative to the corresponding signal (δ 1.12 ppm) for VIII (or δ 1.17 ppm for II) suggested a 1,3-diaxial-*cis*-relationship between the methyl group and the hydroxyl group at the C-8 position. Thus, the benzoyloxyl group in VIII was stereochemically assigned to be the β-configuration. In order to determine the stereochemistry of the benzoyloxyl group at the C-13 position in the ortho-dienones IX and X, the following thermal rearrangements were carried out. A solution of X in toluene was refluxed for 2 h to give VII (18%) together with the starting substance (X: 80%). However, a similar treatment of IX gave VII (14%) and VIII (16%) along with IX (67%). From this rearrangement of IX into VIII, the stereochemical structure of the benzoyloxyl group in IX was assigned to be the β-configuration, and therefore, that in X to be the α-configuration. The methylation of VII in refluxing methanol with dimethyl sulfate in the presence of aqueous potassium hydroxide gave a monomethyl ether (XV) which responded positively to the Gibbs test. XV was further methylated with dimethyl sulfate and anhydrous potassium carbonate in refluxing methyl ethyl ketones to give methyl 11,12-dimethoxyabieta-8,11,13-trien-18-oate (XVI) which was oxidized with chromium trioxide in acetic acid to afford the corresponding 7-oxo compound (XVII) along with a small amount of methyl 12-methoxy-11,14-dioxoabieta-8,12-dien-18-oate (XVIII). This quinone (XVIII) was also obtained by the oxidation of XV with *m*-chloroperbenzoic acid in a moderate yield. The demethylation of XVIII with hydrochloric acid afforded XII. Subsequently, the conversion of a methoxycarbonyl group at the C-4 position in XVI into a methyl group was carried out in the following manner. The ester XVI was reduced with lithium aluminum hydride to give the

corresponding alcohol (XIX) which by oxidation with a chromium trioxide–pyridine complex gave an aldehyde (XX). Huang-Minlon reduction of XX gave 11,12-dimethoxyabieta-8,11,13-triene (XXI).[3,11,20] The conversion of XXI into taxodione (III) *via* 11,12-dimethoxyabieta-6,8,11,13-tetraene (XXIV) has been achieved by Mori and Matsui.[11] In the present study, XXIV was prepared by an alternate method. The oxidation of XXI with chromium trioxide gave 11,12-dimethoxyabieta-8,11,13-trien-7-one (XXII)[8,9] together with a small amount of royleanone methyl ether (XXIII)[5] which was demethylated to give royleanone (IV). The reduction of XXII with lithium aluminum hydride gave the corresponding alcohol which was immediately dehydrated with *p*-toluenesulfonic acid in refluxing toluene to give XXIV.[11] The conversion of VII and XV into VI was also carried out as follows. Acetylation of VII with isopropenyl acetate in the presence of *p*-toluenesulfonic acid gave an acetate (XXV),[16] which was then submitted to oxidation with chromium trioxide in acetic acid to give the corresponding 7-oxo derivative (XXVI).[16] Alkaline hydrolysis of XXVI, followed by methylation with diazomethane gave VI. This phenol (VI) was also obtained from XV by a similar treatment *via* an acetate (XXVII) and a ketone (XXVIII). Methyl 11-hydroxy-6,12-dioxoabieta-7,9(11),13-trien-18-oate (XXIX), a taxodione analogue, was also synthesized from XXVI. The reduction of a carbonyl group in XXVI with sodium borohydride and subsequent dehydration of the resulting alcohol gave a tetraene derivative (XXX) which was then oxidized with *m*-chloroperbenzoic acid to give a 6-oxo derivative (XXXI). Alkaline hydrolysis of XXXI followed by oxidation gave XXIX.

Next, the above benzoyl peroxide oxidation was applied to ferruginol (XXXII) which was prepared in the following manner. The treatment of II with benzyl chloride in refluxing *N,N*-dimethylformamide in the presence of anhydrous potassium carbonate gave a benzyl ether (XXXIII), which, on reduction with lithium aluminum hydride followed by oxidation of the resulting alcohol (XXXIV) with a chromium trioxide–pyridine complex, yielded a formyl derivative (XXXV). Huang-Minlon reduction of XXXV gave ferruginol benzyl ether (XXXVI) which was then hydrogenolyzed using Pd–C in acetic acid to give ferruginol (XXXII). The oxidation of XXXII with benzoyl peroxide in chloroform at room temperature gave a phenol (XXXVII) and three dienones (XXXVIII-XL), whose structures were also assigned on the basis of spectral and chemical studies (see Experimental section), as in the case of VII—X. The phenol XXXVII was easily converted into royleanone (IV) by *m*-chloroperbenzoic acid oxidation and subsequent alkaline hydrolysis *via* royleanone benzoate (XLII). Further, acetylation of XXXVII gave an acetate (XLIII) and this was then oxidized with chromium trioxide in acetic acid to give the corresponding 7-oxo compound (XLIV). The hydrolysis of XLIV followed by methylation with diazomethane gave cryptojaponol (V). Finally, taxodione (III) was also synthesized from the ketone XLIV *via* a tetraene (XLV), an epoxide (XLVI), and a 6-oxo compound (XLVII), and from the phenol XXXVII *via* a dibenzoate (XLVIII),[21] a 7-oxo compound (XLIX), a tetraene (L), and a 6-oxo compound (LI).

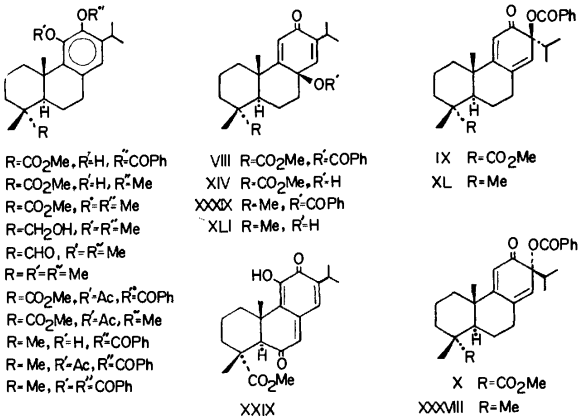

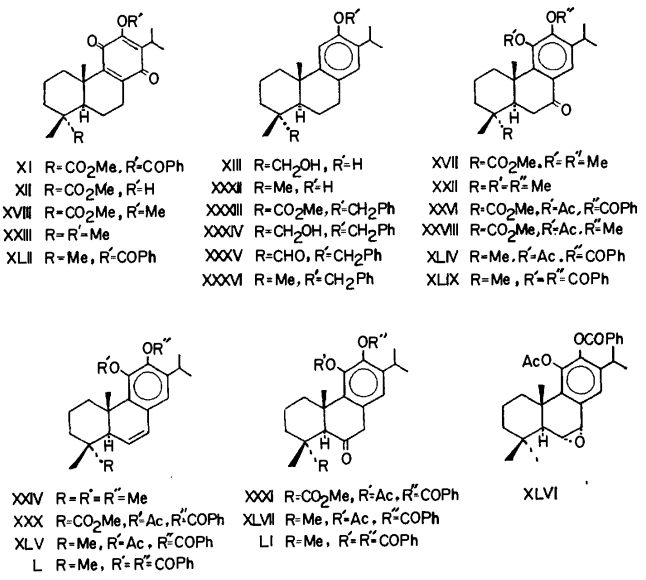

Experimental

All melting points are uncorrected. The IR and UV spectra were taken in chloroform and ethanol, respectively. The NMR spectra were obtained in carbon tetrachloride at 60 MHz with tetramethylsilane as an internal standard, unless otherwise stated. The chemical shifts are presented in the δ values; s: singlet, bs: broad singlet, d: doublet, bd: broad doublet, dd: double doublet, t: triplet, m: multiplet. The optical rotations were measured in chloroform using a Yanaco OR-50D. Column chromatography was performed using Merck silica gel (0.063 mm).

Oxidation of Methyl 12-Hydroxyabieta-8,11,13-trien-18-oate (II) with Benzoyl Peroxide. A solution of the phenol II (5.00 g) and benzoyl peroxide (3.70 g) in chloroform (60 ml) was gently refluxed for 2 h in a stream of nitrogen. The solution was diluted with ether containing a small amount of acetic acid, and washed successively with aqueous potassium iodide, aqueous sodium thiosulfate, aqueous sodium hydrogencarbonate, and water. After drying over sodium sulfate, the solvent was evaporated and the residue was chromatographed on silica gel using benzene and benzene–ether (97: 3 and 95: 5) as eluents, giving four products (VII—X).

a): Methyl 12-benzoyloxy-11-hydroxyabieta-8,11,13-

trien-18-oate (VII: 61%), which responded positively to the Gibbs test;[15] mp 155—157 °C (from methanol), $[\alpha]_D$ +83.1°, IR: 3575, 3375, 1735, 1718 cm^{-1}, NMR: 1.16 and 1.19 (each d and J=7 Hz, $-CH(C\underline{H}_3)_2$), 1.29 (s, C_4-CH_3), 1.38 (s, $C_{10}-CH_3$), 3.64 (s, $-CO_2CH_3$), 5.26 (s, -OH), 6.57 (s, $C_{14}-H$), 7.4—8.2 (m, $-C_6H_5$). Found: C, 74.86; H, 7.71%. Calcd for $C_{28}H_{34}O_5$: C, 74.64; H, 7.61%.

b): Methyl 8β-benzoyloxy-12-oxoabieta-9(11),13-dien-18-oate (VIII: 2%); mp 157—158.5 °C (from methanol), $[\alpha]_D$ −81.8°, IR: 1722, 1668, 1638 cm^{-1}, UV: λ_{max} 236 nm (ε 18600), NMR: 1.05 (d, J=7 Hz, $-CH(C\underline{H}_3)_2$), 1.12 (s, $C_{10}-CH_3$), 1.22 (s, C_4-CH_3), 3.65 (s, $-CO_2CH_3$), 6.11 and 6.25 (each s, $C_{11}-H$ and $C_{14}-H$), 7.2—8.1 (m, $-C_6H_5$). Found: C, 74.46; H, 7.67%. Calcd for $C_{28}H_{34}O_5$: C, 74.64; H, 7.61%.

c): Methyl 13β-benzoyloxy-12-oxoabieta-8(14),9(11)-dien-18-oate (IX: 6%); mp 140—141 °C (from methanol), $[\alpha]_D$ −196°, IR: 1715, 1663 cm^{-1}, UV: λ_{max} nm (ε) 232 (19800), 321 (2280), NMR ($CDCl_3$): 0.93 and 1.15 (each d and J=7 Hz, $-CH(C\underline{H}_3)_2$), 1.28 (s, C_4-CH_3 and $C_{10}-CH_3$), 3.68 (s, $-CO_2CH_3$), 5.92 (bs, $C_{14}-H$), 6.07 (s, $C_{11}-H$), 7.2—8.2 (m, $-C_6H_5$). Found: C, 74.37; H, 7.65%. Calcd for $C_{28}H_{34}O_5$: C, 74.64; H, 7.61%.

d): Methyl 13α-benzoyloxy-12-oxoabieta-8(14),9(11)-dien-18-oate (X: 11%); mp 167—168 °C (from methanol), $[\alpha]_D$ +280°, IR: 1715, 1663 cm^{-1}, UV: λ_{max} nm (ε) 232 (19700), 321 (2740), NMR ($CDCl_3$): 0.92 and 1.15 (each d and J=7 Hz, $-CH(C\underline{H}_3)_2$), 1.23 and 1.29 (each s, C_4-CH_3 and $C_{10}-CH_3$), 3.67 (s, $-CO_2CH_3$), 5.90 (bs, $C_{14}-H$), 6.07 (s, $C_{11}-H$), 7.2—8.2 (m, $-C_6H_5$). Found: C, 74.34; H, 7.75%. Calcd for $C_{28}H_{34}O_5$: C, 74.64; H, 7.61%.

Methyl 12-Benzoyloxy-11,14-dioxoabieta-8,12-dien-18-oate (XI). A solution of VII (360 mg) and *m*-chloroperbenzoic acid (290 mg) in dichloromethane (15 ml) was allowed to stand at room temperature for 22 h and then diluted with ether. The solution was washed successively with aqueous potassium iodide, aqueous sodium thiosulfate, aqueous sodium hydrogencarbonate, and water. After drying over sodium sulfate, the solvent was evaporated and the crude product was purified by column chromatography on silica gel using benzene as the eluent producing the recovered VII (104 mg: 29%) and a quinone (XI) (166 mg: 45%), which was recrystallized from ethanol; mp 121—123 °C, $[\alpha]_D$ +32.4°, IR: 1740, 1720, 1658, 1646 sh, 1602 cm^{-1}, UV: λ_{max} nm (ε) 235.5 (17300), 264.5 (17700), NMR: 1.22 (s, C_4-CH_3), 1.22 and 1.25 (each d and J=7 Hz, $-CH(C\underline{H}_3)_2$), 1.30 (s, $C_{10}-CH_3$), 3.64 (s, $-CO_2CH_3$), 7.4—8.3 (m, $-C_6H_5$). Found: C, 72.39; H, 7.02%. Calcd for $C_{28}H_{32}O_6$: C, 72.39; H, 6.94%.

Methyl 12-Hydroxy-11,14-dioxoabieta-8,12-dien-18-oate (XII). *a)*: A mixture of XI (110 mg), sodium hydrogencarbonate (500 mg), water (4 ml), and methanol (20 ml) was refluxed for 1 h. After removal of the solvent, the residue was extracted with ether, washed with water, and then dried over sodium sulfate. The crude product was chromatographed on silica gel (20 g) using benzene–ether (99: 1) as the eluent to give XII (53 mg; 62%), which was recrystallized from petroleum ether; mp 149—150 °C, $[\alpha]_D$ +93.1°, IR: 3375, 1720, 1640, 1633, 1603 cm^{-1}, NMR: 1.20 (d, J=7 Hz, $-CH(C\underline{H}_3)_2$), 1.22 (s, C_4-CH_3), 1.28 (s, $C_{10}-CH_3$), 3.66 (s, $-CO_2CH_3$), 7.15 (s, -OH). Found: C, 69.95; H, 7.77%. Calcd for $C_{21}H_{28}O_5$: C, 69.97; H, 7.83%.

b): A mixture of methyl 12-methoxy-11,14-dioxoabieta-8,12-dien-18-oate (XVIII: 113 mg) and concentrated hydrochloric acid (5 ml) in methanol (15 ml) was refluxed for 15 h. After the usual work-up, the product was purified using column chromatography and subsequent crystallization to give XII (mp 149—150 °C) which was shown to be identical to a sample of *a)* from a comparison of the IR and NMR spectra.

Reductions of Dienones (VIII, IX, and X) with Lithium Aluminum Hydride. *a)*: A mixture of VIII (100 mg) and lithium aluminum hydride (100 mg) in dry ether (15 ml) was refluxed for 1.5 h. After the usual work-up, the product was recrystallized from a mixture of acetone and petroleum ether to give abieta-8,11,13-trien-12,18-diol (XIII: 60 mg),[17,18] mp 180—181 °C, $[\alpha]_D$ +72.1° (ethanol), which was identical to an authentic sample prepared from II by lithium aluminum hydride reduction. Found: C, 79.71; H, 10.05%. Calcd for $C_{20}H_{30}O_2$: C, 79.42; H, 10.00%.

b): Each of the benzoates (IX and X) was also reduced with lithium aluminum hydride as described in *a)* above producing XIII.

Methyl 8β-Hydroxy-12-oxoabieta-9(11),13-dien-18-oate (XIV). A mixture of VIII (65 mg), potassium carbonate (200 mg), water (2 ml), and methanol (8 ml) was refluxed for 2 h. After the usual work-up, the crude product was chromatographed on silica gel (20 g) using benzene–ether (9: 1) as the eluent to give XIV (46 mg: 92%) which was recrystallized from a mixture of ether and petroleum ether; mp 74—77 °C, $[\alpha]_D$ −60.0°, IR: 3588, 3413, 1720, 1665, 1635 cm^{-1}, UV: λ_{max} 241 nm (ε 12900), NMR: 1.00 and 1.04 (each d and J=7 Hz, $-CH(C\underline{H}_3)_2$), 1.27 (s, C_4-CH_3), 1.42 (s, $C_{10}-CH_3$), 3.64 (s, $-CO_2CH_3$),5.81 and 6.28 (each s, $C_{11}-H$ and $C_{14}-H$).

Thermal Rearrangement of Dienones (IX and X). *a)*: A solution of IX (100 mg) in toluene (3 ml) was refluxed for 2 h and the crude product, after evaporation of the solvent, was purified by column chromatography on silica gel (20 g) using benzene–ether (99: 1) as the eluent giving VII (14 mg: 14%), VIII (16 mg: 16%), and the recovered IX (67 mg: 67%).

b): A solution of X (130 mg) in toluene (3 ml) was refluxed for 2 h. Chromatographic purification gave VII (23 mg: 18%) and the recovered X (103 mg: 80%).

Methyl 11-Hydroxy-12-methoxyabieta-8,11,13-trien-18-oate (XV). A mixture of VII (2.5 g), 30% aqueous potassium hydroxide (4.5 ml), and methanol (50 ml) was refluxed for 10 min in a stream of nitrogen. To the cold solution, dimethyl sulfate (4.5 ml) was added and the mixture was refluxed for 4.5 h. The reaction mixture was further treated with 30% aqueous potassium hydroxide under reflux for 20 min, cooled, acidified with dilute hydrochloric acid, and then extracted with ether. After the usual work-up, the product was chromatographed on silica gel (300 g) using benzene as the eluent and recrystallized from methanol giving XV (1.6 g: 80%), mp 146—147 °C, $[\alpha]_D$ +68.8°, IR: 3500, 1720 cm^{-1}, NMR: 1.20 (d, J=7 Hz, $-CH(C\underline{H}_3)_2$), 1.24 (s, C_4-CH_3), 1.32 (s, $C_{10}-CH_3$), 3.61 (s, $-CO_2CH_3$), 3.69 (s, $-OCH_3$), 5.85 (s, -OH), 6.30 (s, $C_{14}-H$). Found: C, 73.07; H, 8.96%. Calcd for $C_{22}H_{32}O_4$: C, 73.30; H, 8.95%. The phenol XV responded positively to the Gibbs test.[15]

Methyl 11,12-Dimethoxyabieta-8,11,13-trien-18-oate (XVI). A mixture of XV (136 mg), anhydrous potassium carbonate (5 g), dimethyl sulfate (0.6 ml), and methyl ethyl ketone (20 ml) was refluxed for 24 h. After the usual work-up, the product was chromatographed on silica gel (30 g) using benzene as the eluent and recrystallized from methanol giving XVI (134 mg: 95%), mp 92—92.5 °C, $[\alpha]_D$ +82.8°, NMR: 1.16 and 1.18 (each d and J=7 Hz, $-CH(C\underline{H}_3)_2$), 1.24 (s, C_4-CH_3), 1.30 (s, $C_{10}-CH_3$), 3.60 (s, $-CO_2CH_3$), 3.68 and 3.79 (each s, 2-OCH_3), 6.46 (s, $C_{14}-H$). Found: C, 73.80; H, 9.14%. Calcd for $C_{23}H_{34}O_4$: C, 73.76; H, 9.15%.

Methyl 12-Methoxy-11,14-dioxoabieta-8,12-dien-18-oate (XVIII). A solution of XV (210 mg) and *m*-chloroperbenzoic acid (220 mg) in dichloromethane (10 ml) was treated as described above for XI. The crude product was purified by column chromatography on silica gel (20 g) with benzene giving XVIII (128 mg: 59%) which was recrystallized from

petroleum ether; mp 139—140 °C, $[\alpha]_D$ −70.7°, IR: 1718, 1653, 1638, 1600 cm^{-1}, NMR: 1.16 (bd, J=7 Hz, $-CH(C\underline{H}_3)_2$), 1.20 (s, C_4-CH_3), 1.30 (s, $C_{10}-CH_3$), 3.58 (s, $-CO_2CH_3$), 3.82 (s, $-OCH_3$). Found: C, 70.85; H, 8.16%. Calcd for $C_{22}H_{30}O_5$: C, 70.56; H, 8.08%.

Oxidation of XVI with Chromium Trioxide. A mixture of XVI (183 mg) and chromium trioxide (90 mg) in acetic acid (4 ml) was allowed to stand at room temperature for 18 h and then diluted with ether. The mixture was washed successively with water, aqueous sodium hydrogencarbonate, and water. After removal of the solvent, the residue was chromatographed on silica gel (20 g) using benzene–ether (97: 3) as the eluent to give a quinone (29 mg: 16%) which was shown to be identical to XVIII from IR and NMR spectral comparisons. Further elution gave a ketone (XVII) (147 mg: 77%) which was recrystallized from petroleum ether; mp 101.5—102 °C, $[\alpha]_D$ +48.1°, IR: 1720, 1675 cm^{-1}, NMR: 1.22 and 1.26 (each d and J=7 Hz, $-CH(C\underline{H}_3)_2$), 1.30 (s, C_4-CH_3), 1.39 (s, $C_{10}-CH_3$), 3.62 (s, $-CO_2CH_3$), 3.77 and 3.78 (each s, 2-OCH_3), 7.60 (s, C_{14}–H). Found: C, 70.84; H, 8.53%. Calcd for $C_{23}H_{32}O_5$: C, 71.10; H, 8.30%.

11,12-Dimethoxyabieta-8,11,13-trien-18-ol (XIX). A mixture of XVI (393 mg) in dry ether (10 ml) and lithium aluminum hydride (80 mg) was refluxed for 2 h. After the usual work-up, the product was chromatographed on silica gel (40 g) using benzene–ether (99: 1) as the eluent to give an alcohol (XIX: 380 mg), $[\alpha]_D$ +79.7°, IR: 3620, 3450 cm^{-1}, NMR: 0.81 (s, C_4-CH_3), 1.13 and 1.18 (each d and J=6.5 Hz, $-CH(C\underline{H}_3)_2$), 1.28 (s, $C_{10}-CH_3$), 3.65 and 3.75 (each s, 2-OCH_3), 6.42 (s, C_{14}–H).

11,12-Dimethoxyabieta-8,11,13-triene (XXI). a): A solution of XIX (380 mg) in pyridine (6 ml) was added to the Sarett reagent prepared from chromium trioxide (450 mg) and pyridine (6 ml). The mixture was stirred at room temperature for 50 min and then filtered. The filtrate was acidified with dilute hydrochloric acid, extracted with ether, and the extract was washed with brine. The crude product was purified by column chromatography on silica gel (40 g) using hexane–benzene (1: 9) as the eluent to give an aldehyde (XX) (234 mg: 62%), $[\alpha]_D$ +73.5°, IR: 1718 cm^{-1}, NMR: 1.13 (s, C_4-CH_3), 1.16 and 1.18 (each d and J=7 Hz, $-CH(C\underline{H}_3)_2$), 1.32 (s, $C_{10}-CH_3$), 3.68 and 3.78 (each s, 2-OCH_3), 6.47 (s, C_{14}–H), 9.17 (s, –CHO).

b): A mixture of XX (234 mg) in diethylene glycol (6 ml) and 80% hydrazine hydrate (0.6 ml) was refluxed for 2 h and powdered sodium hydroxide (0.6 g) was then added. The mixture was heated at 200 °C for 3 h, cooled, extracted with ether, and the extract was washed with brine. Removal of the solvent and subsequent chromatography on silica gel (20 g) using hexane–benzene (1: 9) as the eluent gave XXI (179 mg: 80%); mp 89.5—90.5 °C, $[\alpha]_D$ +92.0° (EtOH), NMR ($CDCl_3$): 0.93 (s, $-C(CH_3)_2$), 1.18 and 1.21 (each d and J=7 Hz, $-CH(C\underline{H}_3)_2$), 1.30 (s, $C_{10}-CH_3$), 3.70 and 3.78 (each s, 2-OCH_3), 6.55 (s, C_{14}–H). Found: C, 79.74; H, 10.25%. Calcd for $C_{22}H_{34}O_2$: C, 79.95; H, 10.37%.

Oxidation of XXI with Chromium Trioxide. A solution of XXI (570 mg) and chromium trioxide (300 mg) in acetic acid (20 ml) was allowed to stand at room temperature for 48 h. After the mixture had been treated as described above, the product was chromatographed on silica gel (150 g) and eluted with benzene to give a small amount of royleanone methyl ether (XXIII)[5] (19 mg: 3%) which was recrystallized from methanol; mp 117.5—118.5 °C, $[\alpha]_D$ −113°, IR: 1654, 1643, 1602 cm^{-1}, NMR: 0.92 (s, $-C(CH_3)_2$), 1.17 and 1.19 (each d and J=7 Hz, $-CH(C\underline{H}_3)_2$), 1.30 (s, $C_{10}-CH_3$), 3.86 (s, $-OCH_3$).

Further elution with benzene–ether (98: 2) gave 11,12-dimethoxyabieta-8,11,13-trien-7-one (XXII)[8,9] (406 mg: 64%); $[\alpha]_D$ +35.5°, IR: 1672 cm^{-1}, NMR: 1.00 (s, $-C(CH_3)_2$), 1.21 and 1.27 (each d and J=7 Hz, $-CH(C\underline{H}_3)_2$), 1.38 (s, $C_{10}-CH_3$), 3.80 (s, 2-OCH_3), 7.60 (s, C_{14}–H).

11,12-Dimethoxyabieta-6,8,11,13-tetraene (XXIV). A mixture of XXII (203 mg) in dry ether (10 ml) and lithium aluminum hydride (40 mg) was refluxed for 2 h. After the usual work-up, the crude alcohol was further treated under reflux with *p*-toluenesulfonic acid (20 mg) in toluene (20 ml) for 3 h, and then cooled. After the addition of sodium hydrogencarbonate, the mixture was stirred for 30 min, filtered, and the filtrate was evaporated. The crude product was chromatographed on silica gel (50 g) using hexane–benzene (1: 1) as the eluent producing XXIV[11] (165 mg: 85%), $[\alpha]_D$ −99.6°, NMR ($CDCl_3$): 0.96 and 1.03 (each s, $-C(CH_3)_2$), 1.13 (s, $C_{10}-CH_3$), 1.18 and 1.22 (each d and J=7 Hz, $-CH(CH_3)_2$), 2.19 (t, J=3 Hz, C_5–H), 3.77 (s, 2-OCH_3), 5.86 (dd, J=3 and 9 Hz, C_6–H), 6.41 (dd, J=3 and 9 Hz, C_7–H), 6.63 (s, C_{14}–H). Found: C, 80.18; H, 9.88%. Calcd for $C_{22}H_{32}O_2$: C, 80.44; H, 9.83%.

Methyl 11-Acetoxy-12-benzoyloxyabieta-8,11,13-trien-18-oate (XXV). A mixture of VII (300 mg) in toluene (4 ml), *p*-toluenesulfonic acid (30 mg), and isopropenyl acetate (0.6 ml) was refluxed for 5 h. After the usual work-up, the product was recrystallized from methanol containing a small amount of acetone producing XXV (300 mg: 92%), mp 191—192 °C, $[\alpha]_D$ +88.7°, IR: 1763, 1740, 1720 cm^{-1}, NMR: 1.78 (s, $-OCOCH_3$). Found: C, 72.92; H, 7.36%. Calcd for $C_{30}H_{36}O_6$: C, 73.14; H, 7.37%.

Methyl 11-Acetoxy-12-benzoyloxy-7-oxoabieta-8,11,13-trien-18-oate (XXVI). A mixture of XXV (700 mg) and chromium trioxide (350 mg) in acetic acid was allowed to stand at room temperature for 26 h. The crude product was chromatographed on silica gel (70 g) and eluted with benzene–ether (95: 5) giving XXVI (586 mg: 82%), mp 178—180 °C (from methanol), $[\alpha]_D$ +72.0°, IR: 1765, 1738, 1720, 1682 cm^{-1}, NMR: 7.95 (s, C_{14}–H). Found: C, 70.85; H, 6.71%. Calcd for $C_{30}H_{34}O_7$: C, 71.13; H, 6.77%.

Methyl 11-Hydroxy-12-methoxy-7-oxoabieta-8,11,13-trien-18-oate (VI). a): A mixture of XXVI (135 mg) in methanol (7 ml) and 30% aqueous potassium hydroxide (0.6 ml) was refluxed for 2 h in a stream of nitrogen. After removal of the solvent, the residue was acidified, extracted with ether, and the extract was washed with water. The crude product was methylated with diazomethane and then chromatographed on silica gel (20 g) using benzene–ether (99: 1) as the eluent giving VI[10] (68 mg: 68%), which was recrystallized from petroleum ether containing a small amount of acetone; mp 202.5—203.5 °C, $[\alpha]_D$ +33.8°, IR (CCl_4): 3500, 1730, 1685, 1607 cm^{-1}, NMR ($CDCl_3$): 1.25 (d, J=7 Hz, $-CH(C\underline{H}_3)_2$), 1.32 (s, C_4-CH_3), 1.41 (s, $C_{10}-CH_3$), 3.62 (s, $-CO_2CH_3$), 3.78 (s, $-OCH_3$), 6.13 (s, –OH), 7.59 (s, C_{14}–H). Found: C, 70.51; H, 8.12%. Calcd for $C_{22}H_{30}O_5$: C, 70.56; H, 8.08%.

b): Similarly, XV (109 mg) was acetylated with isopropenyl acetate (0.1 ml) and *p*-toluenesulfonic acid (10 mg) in toluene (5 ml) giving the corresponding acetate (XXVII) (94 mg: 77%), IR: 1760, 1720 cm^{-1}.

Oxidation of XXVII (94 mg) with chromium trioxide (50 mg) in acetic acid (3 ml) gave methyl 11-acetoxy-12-methoxy-7-oxoabieta-8,11,13-trien-18-oate (XXVIII) (71 mg: 73%), IR: 1760, 1720, 1680 cm^{-1}, which was then hydrolyzed under reflux for 2 h with 30% aqueous potassium hydroxide (0.3 ml) in methanol (7 ml) yielding VI (44 mg: 69%). IR and NMR spectra of the synthetic VI were identical with those of a natural sample.

Methyl 11-Acetoxy-12-benzoyloxyabieta-6,8,11,13-tetraen-18-oate (XXX). A mixture of XXVI (1.26 g) in methanol

(20 ml) and sodium borohydride (190 mg) was allowed to stand at 0 °C for 3.5 h. After the usual work-up, the crude alcohol (1.26 g) was refluxed with *p*-toluenesulfonic acid (130 mg) in toluene (40 ml) for 1.5 h. The product was chromatographed on silica gel (120 g) using benzene–ether (99: 1) as the eluent giving XXX (1.11 g: 91%), which was recrystallized from ethanol; mp 128—129 °C, $[\alpha]_D$ +29.3°, IR: 1758, 1735, 1720 cm^{-1}, NMR: 3.03 (t, J=2.5 Hz, C_5–H), 5.59 (dd, J=2.5 and 9.5 Hz, C_6–H), 6.42 (dd, J=2.5 and 9.5 Hz, C_7–H). Found: C, 73.36; H, 6.99%. Calcd for $C_{30}H_{34}O_6$: C, 73.45; H, 6.99%.

Methyl 11-Acetoxy-12-benzoyloxy-6-oxoabieta-8,11,13-trien-18-oate (XXXI). A mixture of XXX (210 mg) in dichloromethane (20 ml) and *m*-chloroperbenzoic acid (88 mg) was allowed to stand at 0 °C for 4 h, and then extracted with ether. The ether extract was washed with aqueous sodium hydrogencarbonate and water. Evaporation of the solvent and subsequent chromatography on silica gel (20 g) using benzene–ether (98: 2) as the eluent gave XXXI (46 mg: 22%), which was recrystallized from a mixture of acetone and methanol; mp 253—255 °C, $[\alpha]_D$ +164°, IR: 1760, 1732, 1725, 1710 sh cm^{-1}, NMR ($CDCl_3$): 1.23 and 1.25 (each d and J=7 Hz, $-CH(C\underline{H}_3)_2$), 1.28 and 1.47 (each s, C_4–CH_3 and C_{10}–CH_3), 1.96 (s, $-OCOCH_3$), 3.48 (s, C_5–H), 3.65 (s, $-CO_2CH_3$), 3.71 (s, $-COCH_2-$), 7.00 (s, C_{14}–H), 7.3—8.4 (m, $-C_6H_5$). Found: C, 70.85; H, 6.81%. Calcd for $C_{30}H_{34}O_7$: C, 71.13; H, 6.77%.

Methyl 11-Hydroxy-6,12-dioxoabieta-7,9(11),13-trien-18-oate (XXIX). A mixture of XXXI (298 mg) in methanol (54 ml), sodium hydrogencarbonate (200 mg), and water (6 ml) was refluxed for 40 min, and then extracted with ether. The extract was washed with water, dried over sodium sulfate, and evaporated. The crude product was chromatographed on silica gel (20 g) using benzene–ether (99: 1) as the eluent giving XXIX (127 mg: 61%), which was recrystallized from methanol; mp 57.5—59 °C, $[\alpha]_D$ −80.3°, IR: 3345, 1723, 1667, 1642, 1627, 1617, 1600 cm^{-1}, UV: λ_{max} nm (ε) 325 (20000), 335 (21400), 405 (3020), NMR: 1.22 (d, J=7 Hz, $-CH(C\underline{H}_3)_2$), 1.32 (s, C_4–CH_3), 1.46 (s, C_{10}–CH_3), 3.49 (s, C_5–H), 3.66 (s, $-CO_2CH_3$), 6.21 (s, C_7–H), 6.92 (s, C_{14}–H), 7.62 (s, –OH).

Methyl 12-Benzyloxyabieta-8,11,13-trien-18-oate (XXXIII). A mixture of II (500 mg) in *N,N*-dimethylformamide (2 ml), benzyl chloride (250 mg), and anhydrous potassium carbonate (2 g) was refluxed with stirring for 1 h, cooled, diluted with ether, and then acidified with dilute hydrochloric acid. The ether solution was washed with brine, dried over sodium sulfate, and evaporated. The residue was chromatographed on silica gel using benzene as the eluent giving XXXIII (617 mg: 97%), which was recrystallized from ethanol, mp 76.5—77 °C, $[\alpha]_D$ +70.4°. Found: C, 80.13; H, 8.57%. Calcd for $C_{28}H_{36}O_3$: C, 79.96; H, 8.63%.

12-Benzyloxyabieta-8,11,13-trien-18-one (XXXV). A mixture of XXXIII (4.60 g) in dry ether (50 ml) and lithium aluminum hydride (1.0 g) was refluxed for 4 h. After the usual work-up, the crude alcohol XXXIV (4.05 g) in pyridine (40 ml) was oxidized at room temperature for 1.5 h with Sarett reagent prepared from chromium trioxide (3.09 g) and pyridine (30 ml). The product was recrystallized from ethanol giving XXXV (2.13 g: 69%), mp 135—136.5 °C, $[\alpha]_D$ +73.9°, IR: 1720 cm^{-1}, NMR: 9.15 (s, –CHO). Found: C, 82.83; H, 8.64%. Calcd for $C_{27}H_{34}O_2$: C, 83.03; H, 8.78%.

12-Benzyloxyabieta-8,11,13-triene (Ferruginol Benzyl Ether) (XXXVI). A mixture of XXXV (2.06 g) in diethylene glycol (62 ml) and 80% hydrazine hydrate (8.2 ml) was refluxed for 2 h. After the addition of powdered sodium hydroxide (8.2 g), the mixture was further heated at 195—200 °C for 3 h. After the usual work-up, the product was purified by column chromatography on silica gel (200 g) using hexane–benzene (1: 3) as the eluent giving XXXVI (1.82 g: 92%), which was recrystallized from ethanol, mp 63—64 °C, $[\alpha]_D$ +68.2°. Found: C, 86.37; H, 9.80%. Calcd for $C_{27}H_{36}O$: C, 86.11; H, 9.64%.

Ferruginol (XXXII). A mixture of XXXVI (2.26 g) in acetic acid (150 ml), 5% Pd-C (750 mg), and concentrated hydrochloric acid (1.0 ml) was stirred at room temperature for *ca.* 3 h in an atmosphere of hydrogen. After the usual work-up, the product was chromatographed on silica gel (150 g) using hexane–benzene (2: 3) as the eluent giving XXXII (1.69 g: 98%), $[\alpha]_D$ +57.5°, IR: 3605, 3350 cm^{-1}, NMR: 0.90 and 0.92 (each s, $-C(CH_3)_2$), 1.08 (s, C_{10}–CH_3), 1.17 (d, J=7 Hz, $-CH(C\underline{H}_3)_2$), 5.18 (s, –OH), 6.37 and 6.65 (each s, C_{11}–H and C_{14}–H).

Oxidation of Ferruginol (XXXII) with Benzoyl Peroxide. A solution of XXXII (5.73 g) and benzoyl peroxide (5.60 g) in chloroform (30 ml) was allowed to stand at room temperature for 4 h. The crude product was purified by column chromatography on silica gel giving four products (XXXVII-XL).

a): 12-Benzoyloxyabieta-8,11,13-trien-11-ol (XXXVII: 44%), which responded positively to Gibbs test;[15] mp 132.5—133 °C, (from petroleum ether), $[\alpha]_D$ +81.2°, IR: 3575, 3350, 1740 cm^{-1}, NMR: 0.97 (s, $-C(CH_3)_2$), 1.17 and 1.19 (each d and J=7 Hz, $-CH(C\underline{H}_3)_2$), 1.33 (s, C_{10}–CH_3), 5.17 (s, –OH), 6.50 (s, C_{14}–H), 7.4—8.3 (m, $-C_6H_5$). Found: C, 80.02; H, 8.56%. Calcd for $C_{27}H_{34}O_3$: C, 79.76; H, 8.43%.

b): 12-Oxoabieta-8(14),9(11)-dien-13α-yl benzoate (XXXVIII: 6%); mp 134.5—135.5 °C (from methanol), $[\alpha]_D$ +270°, IR: 1714, 1664 cm^{-1}, UV: λ_{max} nm (ε) 233 (15400), 321 (2230), NMR: 0.90 and 1.11 (each d and J=7 Hz, $-CH(C\underline{H}_3)_2$), 0.96 (s, $-C(CH_3)_2$), 1.19 (s, C_{10}–CH_3), 5.81 and 5.89 (each s, C_{11}–H and C_{14}–H), 7.2—8.1 (m, $-C_6H_5$). Found: C, 79.56; H, 8.55%. Calcd for $C_{27}H_{34}O_3$: C, 79.76; H, 8.43%.

c): 12-Oxoabieta-9(11),13-dien-8β-yl benzoate (XXXIX: 2%); mp 139—140 °C (from methanol), $[\alpha]_D$ −119°, IR: 1721, 1665, 1630 cm^{-1}, UV: λ_{max} 235 nm (ε 20900), NMR: 0.92 (s, $-C(CH_3)_2$), 1.05 (d, J=7 Hz, $-CH(C\underline{H}_3)_2$), 1.11 (s, C_{10}–CH_3), 6.09 and 6.26 (each s, C_{11}–H and C_{14}–H). Found: C, 79.60; H, 8.51%. Calcd for $C_{27}H_{34}O_3$: C, 79.76; H, 8.43%.

d): 12-Oxoabieta-8(14),9(11)-dien-13β-yl benzoate (XL: 3%); mp 135—136 °C (from methanol), $[\alpha]_D$ −214°, IR: 1715, 1663 cm^{-1}, UV: λ_{max} nm (ε) 233 (17000), 321 (2350), NMR: 0.88 and 1.11 (each d and J=7 Hz, $-CH(C\underline{H}_3)_2$), 0.94 and 0.97 (each s, $-C(CH_3)_2$), 1.27 (s, C_{10}–CH_3), 5.80 and 5.88 (each s, C_{11}–H and C_{14}–H), 7.2—8.1 (m, $-C_6H_5$). Found: C, 80.03; H, 8.63%. Calcd for $C_{27}H_{34}O_3$: C, 79.76; H, 8.43%.

Reduction of XXXVIII, XXXIX, and XL with Lithium Aluminum Hydride. A mixture of XXXVIII (83 mg) in dry ether (5 ml) and lithium aluminum hydride (100 mg) was refluxed for 1.5 h. After the usual work-up, the product was purified by column chromatography to give ferruginol (XXXII) (53 mg: 91%).

By similar treatments, XXXIX and XL were also converted to XXXII.

Thermal Rearrangement of Dienones (XXXVIII and XL).

a): A solution of XXXVIII (119 mg) in toluene (5 ml) was refluxed for 2 h, and then evaporated. The residue was chromatographed on silica gel to give XXXVII (8 mg: 7%) and the recovered XXXVIII (106 mg: 89%).

b): A similar treatment of XL (129 mg) in refluxing toluene (5 ml) for 2 h gave XXXVII (22 mg: 17%), XXXIX (15 mg: 12%), and the recovered XL (86 mg: 67%).

8β-Hydroxyabieta-9(11),13-dien-12-one (XLI). A mixture of XXXIX (90 mg) in methanol (16 ml), anhydrous potassium carbonate (200 mg), and water (2 ml) was refluxed

for 2 h and the solvent was removed in a vacuum. After the residue had been extracted with ether, the extract was washed with water, dried, and then evaporated. The crude product was chromatographed on silica gel (20 g) using benzene–ether (95: 5) as the eluent to give the recovered XXXIX (14 mg: 16%) and an alcohol (XLI) (56 mg: 83%), which was recrystallized from methanol, mp 181—182.5 °C, $[\alpha]_D$ −142°, IR: 3580, 3400, 1662, 1630 cm^{-1}, UV: λ_{max} 242 nm (ε 12700), NMR ($CDCl_3$): 0.90 and 0.95 (each s, $-C(CH_3)_2$), 1.05 (d, J=7 Hz, $-CH(C\underline{H}_3)_2$), 1.38 (s, $C_{10}-CH_3$), 1.86 (s, -OH), 5.98 and 6.38 (each s, C_{11}-H and C_{14}-H). Found: C, 79.40; H, 10.12%. Calcd for $C_{20}H_{30}O_2$: C, 79.42; H, 10.00%.

12-Benzoyloxyabieta-8,12-dien-11,14-dione (Royleanone Benzoate) (XLII). A solution of XXXVII (205 mg) and *m*-chloroperbenzoic acid (155 mg) in dichloromethane (7 ml) was allowed to stand at room temperature for 25 h. After the usual work-up, the crude product was chromatographed on silica gel (30 g) using hexane–benzene (1: 1) as the eluent to give the recovered XXXVII (78 mg: 38%) and XLII (100 mg: 45%), which was recrystallized from ethanol; mp 196—197 °C, $[\alpha]_D$ +52.3°, IR: 1740, 1659 cm^{-1}, UV: λ_{max} nm (ε) 235 (15900), 265 (16400), NMR: 0.93 (s, $-C(CH_3)_2$), 1.24 (d, J=7 Hz, $-CH(C\underline{H}_3)_2$), 1.28 (s, $C_{10}-CH_3$), 7.4—8.2 (m, $-C_6H_5$). Found: C, 76.88; H, 7.66%. Calcd for $C_{27}H_{32}O_4$: C, 77.11; H, 7.67%.

Royleanone (IV). *a)*: A mixture of the benzoate XLII (96 mg) in methanol (40 ml), sodium hydrogencarbonate (300 mg), and water (7 ml) was refluxed for 1 h. After removal of the solvent under vacuum, the residue was extracted with ether and the extract was washed with water, dried, and then evaporated. The crude product was chromatographed on silica gel using benzene as the eluent to give royleanone (IV)[5] (62 mg: 84%), which was recrystallized from hexane; mp 181.5—183 °C, $[\alpha]_D$ +137°, IR: 3375, 1674, 1636, 1602 cm^{-1}, UV: λ_{max} nm (ε) 277 (14100), 403 (440), NMR: 0.95 (s, $-C(CH_3)_2$), 1.20 (d, J=7 Hz, $-CH(C\underline{H}_3)_2$), 1.26 (s, $C_{10}-CH_3$), 7.16 (s, -OH). Found: C, 76.21; H, 9.04%. Calcd for $C_{20}H_{28}O_3$: C, 75.91; H, 8.92%.

b): A solution of the methyl ether XXIII (31.8 mg) in methanol (5 ml) and 10% hydrochloric acid (1.0 ml) was refluxed for 16 h. After the usual work-up, the product was purified by column chromatography to give royleanone (IV) (11.7 mg: 38%), mp 180.5—182 °C. The IR and NMR spectra of the synthetic royleanone were identical to those of a natural sample.

11-Acetoxy-12-benzoyloxyabieta-8,11,13-triene (XLIII). A solution of XXXVII (710 mg) in dry toluene (10 ml), *p*-toluenesulfonic acid (40 mg), and isopropenyl acetate (2 ml) was refluxed for 5 h. After the usual work-up, the crude product was chromatographed on silica gel (70 g) using benzene as the eluent to give XLIII (730 mg: 93%), which was recrystallized from methanol; mp 179—179.5 °C, $[\alpha]_D$ +80.0°, IR: 1760, 1738 cm^{-1}, NMR: 0.91 and 0.96 (each s $-C(CH_3)_2$), 1.18 and 1.20 (each d and J=7 Hz, $-CH(C\underline{H}_3)_2$), 1.26 (s, $C_{10}-CH_3$), 1.81 (s, $-OCOCH_3$), 6.82 (s, C_{14}-H), 7.2—8.3 (m, $-C_6H_5$). Found: C, 77.36; H, 8.01%. Calcd for $C_{29}H_{36}O_4$: C, 77.64; H, 8.09%.

11-Acetoxy-12-benzoyloxyabieta-8,11,13-trien-7-one (XLIV). A solution of XLIII (985 mg) in acetic acid (20 ml) was oxidized with chromium trioxide (450 mg) at room temperature for 22 h. The product was purified by column chromatography on silica gel (100 g) using benzene–ether (99: 1) as the eluent to give XLIV (833 mg: 82%), which was recrystallized from ethanol; mp 160—162 °C, $[\alpha]_D$ +56.9°, IR: 1768, 1740, 1680 cm^{-1}, NMR: 0.98 (s, $-C(CH_3)_2$), 1.25 and 1.29 (each d and J=7 Hz, $-CH(C\underline{H}_3)_2$), 1.34 (s, $C_{10}-CH_3$), 1.87 (s, $-OCOCH_3$), 7.5—8.3 (m, $-C_6H_5$), 7.98 (s, C_{14}-H). Found: C, 75.54; H, 7.44%. Calcd for $C_{29}H_{34}O_5$: C, 75.30; H, 7.41%.

Cryptojaponol (V). A mixture of XLIV (250 mg) in methanol (18 ml), sodium hydrogencarbonate (600 mg), and water (2 ml) was refluxed for 1 h. After the usual work-up, the crude product was methylated with diazomethane and then purified by column chromatography on silica gel (20 g) using benzene–ether (99: 1) as the eluent to give cryptojaponol (V)[8,9] (145 mg: 81%), which was recrystallized from methanol; mp 205—206.6 °C, $[\alpha]_D$ +20.0°, IR: 3505, 1670, 1605 cm^{-1}, NMR: 0.98 (s, $-C(CH_3)_2$), 1.26 (d, J=7 Hz, $-CH(C\underline{H}_3)_2$), 1.39 (s, $C_{10}-CH_3$), 3.77 (s, $-OCH_3$), 6.02 (s, -OH), 7.48 (s, C_{14}-H). Found: C, 76.09; H, 9.13%. Calcd for $C_{21}H_{30}O_3$: C, 76.32; H, 9.15%.

11-Acetoxy-12-benzoyloxyabieta-6,8,11,13-tetraene (XLV). A solution of XLIV (263 mg) and sodium borohydride (120 mg) in methanol (7 ml) was allowed to stand at 0 °C for 4 h. After the usual work-up, the product (251 mg) was dehydrated with *p*-toluenesulfonic acid (90 mg) in dry toluene (15 ml) under reflux for 3.5 h to afford a tetraene derivative along with the corresponding 11-hydroxy-12-benzoyloxy derivative. The above mixture was then acetylated with isopropenyl acetate (1 ml) in the presence of *p*-toluenesulfonic acid (20 mg) in refluxing toluene (10 ml) and chromatographed on silica gel to give XLV (148 mg: 56%), which was recrystallized from methanol; mp 157—158 °C, $[\alpha]_D$ −80.8°, IR: 1758, 1737 cm^{-1}, NMR: 0.98 and 1.02 (each s, $-C(CH_3)_2$), 1.15 (s, $C_{10}-CH_3$), 1.20 and 1.24 (each d and J=7 Hz, $-CH(C\underline{H}_3)_2$), 1.84 (s, $-OCOCH_3$), 2.32 (t, J=2.5 Hz, C_5-H), 5.92 (dd, J=2.5 and 9.5 Hz, C_6-H), 6.48 (dd, J=2.5 and 9.5 Hz, C_7-H), 6.84 (s, C_{14}-H), 7.4—8.3 (m, $-C_6H_5$). Found: C, 78.15; H, 7.59%. Calcd for $C_{29}H_{34}O_4$: C, 77.99; H, 7.67%.

11-Acetoxy-12-benzoyloxyabieta-8,11,13-trien-6-one (XLVII). A solution of XLV (589 mg) and *m*-chloroperbenzoic acid (320 mg) in dichloromethane (10 ml) was allowed to stand at room temperature for 24 h. After the usual work-up, the crude epoxide was chromatographed on silica gel (60 g) using benzene–ether (99: 1) as the eluent to give XLVII (475 mg: 78%), which was recrystallized from methanol; 222—224 °C, ($[\alpha]_D$ +111°, IR: 1762, 1740, 1717 cm^{-1}, NMR: 1.05 and 1.30 each s, $-C(CH_3)_2$), 1.19 and 1.23 (each d and J=7 Hz, $-CH(C\underline{H}_3)_2$), 1.30 (s, $C_{10}-CH_3$), 1.87 (s, $-OCOCH_3$), 2.64 (s, C_5-H), 3.60 (bs, $-COCH_2-$), 6.90 (s, C_{14}-H), 7.5—8.3 (m, $-C_6H_5$). Found: C, 75.06; H, 7.54%. Calcd for $C_{29}H_{34}O_5$: C, 75.30; H, 7.41%.

The above crude epoxide was recrystallized from a mixture of acetone and petroleum ether giving pure epoxide (XLVI), mp 199—201 °C, $[\alpha]_D$ +6.5°, IR: 1765, 1740 cm^{-1}, NMR ($CDCl_3$): 1.13 (s, $-C(CH_3)_2$), 1.21 and 1.26 (each d and J=7 Hz, $-CH(C\underline{H}_3)_2$), 1.33 (s, $C_{10}-CH_3$), 1.93 (s, $-OCOCH_3$), 3.54 (t, J=4.5 Hz, C_6-H), 3.92 (d, J=4.5 Hz, C_7-H), 7.38 (s, C_{14}-H), 7.4—8.3 (m, $-C_6H_5$). Found: C, 75.45; H, 7.49%. Calcd for $C_{29}H_{34}O_5$: C, 75.30; H, 7.41%.

11,12-Bis(benzoyloxy)abieta-8,11,13-triene (XLVIII). A solution of XXXVII (244 mg), benzoyl chloride (0.2 ml), and pyridine (4 ml) was heated at 80—100 °C for 2 h. The product was purified by column chromatography on silica gel using benzene as the eluent to give XLVIII[21] (279 mg: 91%), which was recrystallized from a mixture of acetone and petroleum ether; mp 207—208 °C, $[\alpha]_D$ +76.2°, IR: 1735 cm^{-1}, NMR: 0.92 and 0.97 (each s, $-C(CH_3)_2$), 1.22 (d, J=7 Hz, $-CH(C\underline{H}_3)_2$), 1.28 (s, $C_{10}-CH_3$), 6.90 (s, C_{14}-H), 7.0—8.1 (m, 2-C_6H_5). Found: C, 79.82; H, 7.53%. Calcd for $C_{34}H_{38}O_4$: C, 79.97; H, 7.50%.

11,12-Bis(benzoyloxy)abieta-8,11,13-trien-7-one (XLIX). A solution of XLVIII (8.40 g) in acetic acid (300 ml) was oxidized at room temperature for 24 h with chromium trioxide

(7.0 g). The crude product was purified by chromatography on silica gel (300 g) using benzene as the eluent to give XLIX (6.15 g: 69%), which was recrystallized from methanol; mp 150—151 °C, $[\alpha]_D$ +23°, IR: 1742, 1682 cm^{-1}, NMR: 8.03 (s, C_{14}-H). Found: C, 77.56; H, 6.94%. Calcd for $C_{34}H_{36}O_5$: C, 77.83; H, 6.92%.

11,12-Bis(benzoyloxy)abieta-6,8,11,13-tetraene (L). A solution of XLIX (5.55 g) in methanol (120 ml) was reduced at 0 °C for 4 h with sodium borohydride (1.2 g). The crude alcohol was then dehydrated for 2 h with *p*-toluenesulfonic acid (1.8 g) in refluxing toluene (100 ml). The product was purified by chromatography on silica gel (300 g) using hexane–benzene (1: 9) as the eluent to give L (4.40 g: 76%), which was recrystallized from a mixture of acetone and methanol; mp 182.5—183 °C, $[\alpha]_D$ −308°, IR: 1740 cm^{-1}, NMR: 2.33 (t, J=3 Hz, C_5-H), 5.96 (dd, J=3 and 9.5 Hz, C_6-H), 6.52 (dd, J=3 and 9.5 Hz, C_7-H). Found: C, 80.55; H, 7.24%. Calcd for $C_{34}H_{36}O_4$: C, 80.28; H, 7.13%.

11,12-Bis(benzoyloxy)abieta-8,11,13-trien-6-one (LI). A solution of L (501 mg) in chloroform (5 ml) was treated at room temperature for 3 h with *m*-chloroperbenzoic acid (207 mg). The epoxide was chromatographed on silica gel (50 g) using benzene–ether (98: 2) as the eluent to give LI (340 mg: 66%), which was recrystallized from a mixture of acetone and methanol; mp 207—208 °C, $[\alpha]_D$ +58.3°, IR: 1740, 1718 cm^{-1}, NMR: 1.04 and 1.30 (each s, $-C(CH_3)_2$), 1.25 (d, J=7 Hz, $-CH(C\underline{H}_3)_2$), 1.30 (s, C_{10}-CH_3), 2.65 (s, C_5-H), 3.64 (bs, $-COCH_2-$), 6.93 (s, C_{14}-H), 7.0—8.1 (m, 2-C_6H_5). Found: C, 78.12; H, 7.03%. Calcd for $C_{34}H_{36}O_5$: C, 77.83; H, 6.92%.

Taxodione (III). *a)*: A mixture of XLVII (150 mg) in methanol (10 ml), sodium hydrogencarbonate (450 mg), and water (1 ml) was refluxed for 1 h. The crude phenol was chromatographed on silica gel (20 g) using benzene as the eluent to give taxodione (III) (62 mg: 60%), which was recrystallized from petroleum ether; mp 97.5—98 °C, $[\alpha]_D$ +40°, IR: 3345, 1671, 1642, 1626, 1614, 1598 cm^{-1}, UV: λ_{max} nm (ε) 323 (23400), 335 (24500), 405 (3240), Mass: *m/e* 314 (M^+), NMR ($CDCl_3$): 1.12 and 1.27 (each s, $-C(CH_3)_2$), 1.18 (d, J=7 Hz, $-CH(C\underline{H}_3)_2$), 1.27 (s, C_{10}-CH_3), 2.61 (s, C_5-H), 2.96 (m, $-CH(C\underline{H}_3)_2$), 6.20 (s, C_7-H), 6.87 (s, C_{14}-H), 7.57 (s, -OH). Found: C, 76.23; H, 8.39%. Calcd for $C_{20}H_{26}O_3$: C, 76.40; H, 8.34%.

b): A mixture of LI (340 mg) in methanol (25 ml), sodium hydrogencarbonate (1.0 g), and water (7 ml) was treated as described under *a)* above to give taxodione (III) (120 mg: 59%). The IR and NMR spectra of the synthetic taxodione were identical with those of a natural sample.

The authors are grateful to Arakawa Rinsan Kogyo Co., Ltd. for a generous gift of rosin. Thanks are also due to Professor S. Morris Kupchan, University of Virginia, to Professor O. E. Edwards, National Research Council, Ottawa, and to Professor J. F. Biellmann, Institute of Louis Pasteur, for kindly supplying the natural samples and their spectra.

References

1) A part of this work has been reported in preliminary form: T. Matsumoto, Y. Ohsuga, and K. Fukui, *Chem. Lett.*, **1974**, 297.

2) R. C. Cambie and R. A. Franich, *Aust. J. Chem.*, **24**, 117 (1971).

3) S. M. Kupchan, A. Karim, and C. Marcks, *J. Am. Chem. Soc.*, **90**, 5923 (1968); *J. Org. Chem.*, **34**, 3912 (1969).

4) Taxodione,[11,12] royleanone,[5,13,14] and cryptojaponol[9] have previously been synthesized by different methods as optically-active or racemic forms.

5) O. E. Edwards, G. Feniak, and M. Los, *Can. J. Chem.*, **40**, 1540 (1962).

6) J. H. Gough and M. D. Sutherland, *Aust. J. Chem.*, **19**, 329 (1966).

7) C. H. Eugster, *Palette*, **1968**, 25; *Chem. Abstr.*, **69**, 54262e (1968).

8) T. Kondo, M. Suda, and M. Teshima, *Yakugaku Zasshi*, **82**, 1252 (1962).

9) E. Wenkert, J. D. McChesney, and D. J. Watts, *J. Org. Chem.*, **35**, 2422 (1970).

10) J. F. Biellmann, G. Branlant, M. Gero-Robert, and M. Poiret, *Tetrahedron*, **29**, 1237 (1973).

11) K. Mori and M. Matsui, *Tetrahedron*, **26**, 3467 (1970).

12) T. Matsumoto, Y. Tachibana, J. Uchida, and K. Fukui, *Bull. Chem. Soc. Jpn.*, **44**, 2766 (1971).

13) *a)* T. Matsumoto, Y. Tachibana, and K. Fukui, *Chem. Lett.*, **1972**, 321; *b)* Y. Tachibana, *Bull. Chem. Soc. Jpn.*, **48**, 298 (1975).

14) T. Matsui, *J. Sci. Hiroshima Univ. Ser. A*, **40**, 129 (1976).

15) F. E. King, T. J. King, and L. C. Manning, *J. Chem. Soc.*, **1957**, 563.

16) In a previous communication,[1] these substances were formulated as 11-benzoyloxy derivatives. This should now be revised to 12-benzoyloxy compounds.

17) I. Fukushima, Y. Sayama, K. Kyogoku, and H. Murayama, *Agric. Biol. Chem.*, **32**, 1103 (1968).

18) L. F. Fieser and W. P. Campbell, *J. Am. Chem. Soc.*, **61**, 2528 (1939).

19) D. H. R. Barton, P. D. Magnus, and M. J. Pearson, *J. Chem. Soc., C*, **1971**, 2231.

20) C. H. Brieskorn, A. Fuchs, J. B. Bredenberg, J. D. McChesney, and E. Wenkert, *J. Org. Chem.*, **29**, 2293 (1964).

21) C. P. Falshaw, A. W. Johnson, and T. J. King, *J. Chem. Soc.*, **1963**, 2422.

The Temperature and Solvent Effects on the $AlCl_3$-catalyzed Cyclization of 3,3′-Diphenyl-2,2′-biindenyl-1,1′-dione

Fumio Toda and Yozo Todo

Department of Industrial Chemistry, Faculty of Engineering, Ehime University, Matsuyama 790

(Received August 30, 1976)

Upon the $AlCl_3$-catalyzed cyclization of the title biindenone (**1**) into benz[*c*]indeno[2,1-*a*]fluorene-13,14-dione (**2**) and 3,3′: 3,3′-di(*o*-phenylene)-2,2′-biindenylidene-1,1′-dione (**3**), the **2**: **3** ratio increased when the reaction temperature was raised and decreased when the polarity of the solvent was increased.

During the course of our study of the $AlCl_3$-catalyzed cyclization of the title biindenone (**1**) into benz[*c*]-indeno[2,1-*a*]fluorene-13,14-dione (**2**) and 3,3′:3,3′-di-(*o*-phenylene)-2,2′-biindenylidene-1,1′-dione (**3**), we found that the **2**: **3** ratio is remarkably affected by the reaction temperature and the polarity of the solvent.

Results

The yields of the products under various reaction conditions are summarized in Table 1. Of the products, **2**—**6**, **2**[1] and **6**[2] are known compounds. The spectral and analytical data of **3**, 3,3′-(*o*-phenylene)-3,3′-diphenyl-2,2′-biindenylidene-1,1′-dione (**4a**), and its halo derivatives (**4b**—**c** and **5b**—**c**) are summarized in Table 2.

Table 1. Reaction conditions and yields of products[a]

Reaction conditions			Yields (%) of products				
Solvent	Dielectric constant	Reaction temperature (°C)	**2**	**3**	**4**	**5**	**6**
C_6H_6	2.3	20	38		37 (**4a**)		
		80	74				
CS_2	2.6	20	22	6			28
		46	49				28
C_6H_5Br	5.4	20	20	8	19 (**4b**)	12 (**5b**)	
		80	49	14	15 (**4b**)		
C_6H_5Cl	5.6	20	12	8	24 (**4c**)	22 (**5c**)	
		80	30	16	16 (**4c**)		
CH_2Cl_2	8.9	20		70			
		40	89				
$C_6H_5NO_2$	34.8	20		60			
		80		60			

a) The yields are based on the product of the reaction which was carried out for 3 h; within this period all the reactions were completed.

Table 2. Melting points, and spectral and analytical data of **3**, **4**, and **5**[a]

Compound	Mp (°C)	ν_{max}^{Nujol} (cm^{-1})	$\lambda_{max}^{CHCl_3}$ nm ($\varepsilon \times 10^{-2}$)	*m/e* (rel intensity)	Found (Calcd) (%) C	H
3	292	1710 (C=O) 1640 (C=C)	296(375), 308(70), 409(91), 464(16)	408 (M^+, 100), 380 (M^+-CO, 30), 332 ($M^+-C_6H_4$, 85), 176 ($C_{14}H_8^+$, 30)	87.95 (88.22	3.87 3.95)
4a	>310	1710 (C=O) 1645 (C=C)	298(196)	486(M^+, 100), 409 (M^+-Ph, 33), 381 (409−CO, 40), 332 (409−Ph, 10)	88.63 (88.86	4.36 4.56)
4b	276—277	1720 (C=O) 1640 (C=C) 820 (1,4-C_6H_4)	296(191)	564 (M^+, 100), 566 ($(M+2)^+$, 98), 485 (M^+-Br, 50), 409 ($M^+-C_6H_4Br$, 20), 381 (409−CO, 40),	76.24 (76.46	3.55 3.74)
4c	295—296	1720 (C=O) 1640 (C=C) 820 (1,4-C_6H_4)	298(176)	520 (M^+, 100), 522 ($(M+2)^+$, 33), 485 (M^+-Cl, 45), 409 ($M^+-C_6H_4Cl$, 20)	82.79 (82.99	3.82 4.06)
5b	>310	1720 (C=O) 1640 (C=C)	297(194)	564 (M^+, 100), 566 ($(M+2)^+$, 98), 485 (M^+-Br, 50), 409 ($M^+-C_6H_4Br$, 20), 381 (409−CO, 20)	76.31 (76.46	3.66 3.74)
5c	>310	1720 (C=O) 1640 (C=C)	294(182)	520 (M^+, 100), 522($(M+2)^+$, 33) 485 (M^+-Cl, 45), 409 ($M^+-C_6H_4Cl$, 20)	82.71 (82.99	3.97 4.06)

a) All the melting points are uncorrected. The mass spectra were measured with an ionization energy of 75 eV. The NMR spectra showed aromatic protons only.

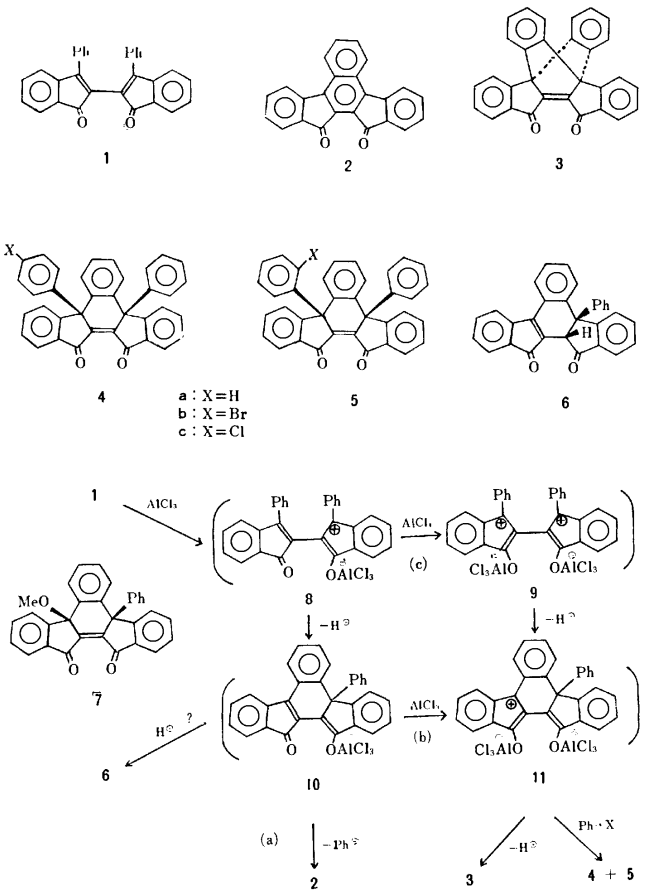

The structures of **4** and **5** were characterized by comparing their spectral data with those of **7**.[2] The structure of **3** was mainly characterized by means of the mass spectrum, which showed the fragmentation of the benzyne from the molecular ion and the formation of an anthracene cation radical (Table 2). The UV spectral bands of **3** in the remarkably longer-wave length region are presumably due to its internal strain. Of the halogen-substituted products (**4b—c** and **5b—c**), **4b** and **4c** were identified as 4-halo derivatives on the basis of their IR bands of 1,4-disubstituted benzene (820 cm^{-1}). Therefore, **5b** and **5c** are probably 2-halo derivatives.

Discussion

Temperature Effect. In the cases of all the reactions except in nitrobenzene with an extremely high dielectric constant, the **2**: **3** ratio increased when the reaction temperature was raised. This was remarkable in dichloromethane, the products at 20 and 40 °C being **3** and **2** respectively. Of course, no thermal conversion of **3** into **2** under the conditions described in Table 1 was observed. The temperature effect can be interpreted as follows: there are two competing reaction pathways, leading to **2** and **3** respectively. One of them proceeds through the elimination of the benzenide anion and $AlCl_3$ from **10**, which was formed by an intramolecular cyclization of the $AlCl_3$-coordinated intermediate (**8**), giving **2** (Path (a)). Another one proceeds through the further coordination of $AlCl_3$ to **10** (Path (b)); cyclization followed by the ketonization of the resulting intermediate (**11**) finally affords **3**. Such a dehydrogenating ketonization of vinyl alcohol has long been known to occur under the influence of $AlCl_3$.[3] At higher temperatures, Path (a) would be much more accelerated than would Path (b). Because of the increase in the steric and then the electrostatic repulsions at higher temperatures, **11** is less favored and Path (b) is relatively retarded. A similar interpretation has recently been reported with regard to the $AlCl_3$-catalyzed dimerization of indenone in boiling dichloromethane (40 °C) and ethylene chloride (83 °C), which afford endo and exo head-to-tail dimers respectively.[4]

The formation of **4** and **5** can be interpreted in terms of arylation on **11**. At 80 °C, the yields of **4** and **5** decreased. Again, this is due to the retardation of Path (b) for the reason presented above. In addition, the approach of the 2-position of halobenzene to the cationic center of **11** is fully inhibited at 80 °C because of the large steric repulsion.

The additional pathway which proceeds *via* **9** (Path (c)) could also be applied to the interpretation of the formation of **3**—**5**. However, this would be unreasonable, because the cyclization of **9** to **11** should overcome large electrostatic and steric repulsions in a transition state. The pathway of the formation of **6** is not clear. Although the ketonization of **10** can give **6**, this consideration disagrees with the finding that the yield of **6** is not affected by the reaction temperature. If **6** is derived directly from **10**, the yield of **6** should decrease at higher temperatures, because the yield of **2** increases when the temperature is raised.

Solvent Effect. Both the **2**: **3** ratio and the ratio of **2** to the total of **3**, **4**, and **5** at 20 °C decreased as the polarity of the solvent increases. This is remarkable in the cases of the reactions in dichloromethane and nitrobenzene; in both cases **3** was the sole isolable product. Especially, nitrobenzene of an extremely high dielectric constant strongly controlled the reaction causing it to proceed through Path (b) even at 80 °C and to produce **3** only. In a polar solvent, **11** would be stabilized by solvation, and thus Path (b) would be enhanced. If **9** is formed in this reaction, **9** would also be stabilized by the polar solvent. Nevertheless, there still remains the question of why **6** was formed only in the reaction in carbon disulfide.

Experimental

Preparation of 1. A mixture of 2,3-bis(diphenylmethylene)succinyl chloride[5] (10 g), benzene (50 ml), ether (50 ml), and $AlCl_3$ (5 g) was stirred at room temperature for 3 h. The reaction mixture was decomposed with water, and then extracted with benzene. The benzene solution was washed with water and dried over anhyd Na_2SO_4. The crude crystals left after the evaporation of the solvent were recrystallized from AcOEt to afford **1** as red prisms; 7 g (82%): mp 214 °C (lit,[6] mp 213—214 °C).

General Procedure of the $AlCl_3$-catalyzed Cyclization of 1. A mixture of **1** (0.5 g), the solvent (50 ml), and $AlCl_3$ (2 g) was stirred for 3 h. The reaction mixture was decomposed with water and then extracted with benzene. During the extraction, **2** was crystallized out as orange needles; it was then recrystallized from AcOEt to afford a pure sample of **2**; mp

306—308 °C (lit,[1] mp 309—310 °C). The benzene solution was washed with water and dried over anhyd Na_2SO_4. The crude crystals left after the evaporation of the solvent were recrystallized from AcOEt to afford **3** or **4**. In the cases of the reaction in halobenzene, **3**, **4**, and **5** were separated by fractional recrystallization from AcOEt. In the cases of the reaction in carbon disulfide, **3** and **6** were separated mechanically.

References

1) A. LeBerre, *Ann. Chim.* (*Paris*), **2**, 371 (1957).
2) F. Toda and Y. Todo, *J. Chem. Soc., Chem. Commun.*, **1976**, 848.
3) A. T. Balaban and C. D. Nenitzescu, "Friedel-Crafts and Related Reactions," Vol. II, Part 2, ed. by G. A. Olah, John Wiley & Sons, New York (1964), p. 979.
4) G. Jammaer, H. Martens, and G. Hoornaert, *Tetrahedron*, **31**, 2293 (1975).
5) F. Toda, F. Monden, and M. Ohi, *Bull. Chem. Soc. Jpn.*, **47**, 316 (1974).
6) J. C. Eck and C. S. Marvel, *J. Am. Chem. Soc.*, **57**, 1898 (1935).

Studies on the Nitration of *m*-Cresol. A New Selective Method for the Preparation of 3-Methyl-6-nitrophenol

Mitsuru SASAKI, Katsuji NODERA, Kunio MUKAI, and Hirosuke YOSHIOKA

Research Department, Pesticides Division, Institute for Biological Science, Sumitomo Chemical Co., Ltd., Takatsukasa, Takarazuka, Hyogo 665

(Received August 30, 1976)

A new selective method for the nitration of *m*-cresol has been established. 3-Methyl-6-nitrophenol was most efficiently prepared by nitration of 3-methyl-4-sulfophenyl carbonate or phosphate and subsequent hydrolysis and desulfonation. Steric effects on the attacks of sulfonium or nitronium ion to the phosphate are discussed.

Certain mononitro derivatives of *m*-cresol are important intermediates for the preparation of organophosphorus pesticides such as Fenitrothion (*O,O*-dimethyl *O*-(3-methyl-4-nitrophenyl) phosphorothioate)[1] and herbicide Metacrephos (*O*-ethyl *N*-*s*-butyl *O*-(3-methyl-6-nitrophenyl) phosphoramidothioate).[2] The preparative value of direct nitration of *m*-cresol is limited due to a number of side reactions, *i.e.*, non-selective isomer formation together with oxidation with nitric acid and poor yield.[3] Various modifications were studied in order to overcome the defects of direct nitration.[4-7] Nitration after the introduction of a suitable protecting functional group to the hydroxyl group was the most common procedure. As an example, tri-*m*-tolyl phosphate was nitrated with a mixed acid, followed by hydrolysis, to yield 3-methyl-4-nitrophenol selectively.[6] 4-Hydroxy-6-methyl-1,3-benzenedisulfonic acid was nitrated and the subsequent desulfonation gave 3-methyl-2-nitrophenol in a good yield.[7] However, no report seems to have been given on an efficient method for selective preparation of 3-methyl-6-nitrophenol in a high yield.

This paper describes the formation of the three isomers of mononitro-3-methylphenols under various conditions, establishing a new selective method for the preparation of 3-methyl-6-nitrophenol. The mechanism of the formation of the product is also discussed.

Results

Syntheses of the Three Isomers of Mononitro-3-methylphenol. The results are given in Table 1. When *m*-cresol was sulfonated at 120 °C for 2 h with a slight excess of sulfuric acid, nitrated with a mixed acid and then desulfonated with diluted sulfuric acid, 3-methyl-6-nitrophenol(6-nitro isomer) was obtained as the major product and 3-methyl-2-nitrophenol (2-nitro isomer) as

TABLE 1. DISTRIBUTION OF ISOMERS OF NITRO-3-METHYLPHENOLS OBTAINED FROM SEVERAL STARTING MATERIALS BY SULFONATION AND NITRATION UNDER VARIOUS CONDITIONS

No.	Substrate	Sulfonation conditions: 96% H_2SO_4	Temp (°C)	Time (h)	Yield (%): Total	2-Isomer	4-Isomer	6-Isomer	Dinitro isomer
1	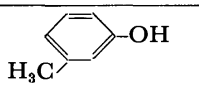	1.10	120	2	62.0	14.6	4.4	33.0	8.7
2	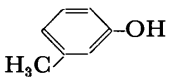	6.80	20—30	24	86.7	72.8	4.8	4.0	5.7
3	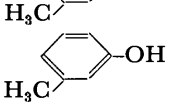	6.80	Direct nitration		50.7	8.7	18.2	9.1	12.0
4	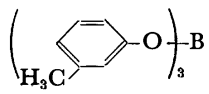	6.80	20—30	24	76.8	59.4	1.5	11.2	3.0
5	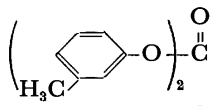	6.80	Direct nitration		80.0	3.2	66.4	10.4	—
6	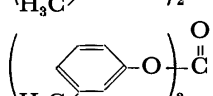	6.80	20—30	24	92.5	6.7	1.8	67.2	6.4
7	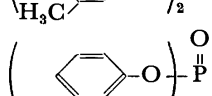	6.80	Direct nitration		95.0	1.9	86.5	6.6	—
8	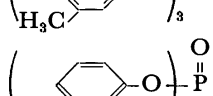	6.80	20—30	24	89.6	7.6	3.7	76.7	1.0

Table 2. Nitro isomer distribution undre different sulfonation conditions

No.	Sulfonating reagent (molar ratio)[a]	Temp (°C)	Time (h)	Yield (%)			
				Total	2-Isomer	4-Isomer	6-Isomer
1	90% H_2SO_4 (6.8)	70	4	81.3	11.8	4.7	61.8
2	96% H_2SO_4 (6.8)	70	5	86.5	8.6	2.7	72.2
3	100% H_2SO_4 (6.8)	70	1	87.3	7.5	3.3	71.6
4	110% H_2SO_4 (6.8)	25	0.5	85.6	8.1	3.0	69.8
5	96% H_2SO_4 (3.0)	30	20	60.7	6.8	5.4	43.9
6	96% H_2SO_4 (4.0)	30	20	81.3	8.7	4.1	65.4
7	96% H_2SO_4 (5.0)	30	20	84.3	9.7	3.7	68.3
8	96% H_2SO_4 (6.8)	30	20	89.5	8.7	3.6	74.4
9	96% H_2SO_4 (10.0)	30	20	90.0	9.1	2.5	74.4
10	96% H_2SO_4 (6.8)	80	0.5	81.7	8.5	2.5	66.9
11	96% H_2SO_4 (6.8)	100	0.5	86.9	9.7	4.2	69.8
12	96% H_2SO_4 (6.8)	120	0.5	72.1	16.9	1.6	52.3

a) Molar ratio; sulfuric acid/tri-*m*-tolyl phosphate.

Table 3. Nitro isomer distribution in sulfonation followed by nitration of tri-*m*-tolyl phosphate under different ratio of nitric acid[a]

No.	Molar ratio[b]	Yield (%)					
		Total	2-Isomer	4-Isomer	6-Isomer	2,6-Isomer	4,6-Isomer
1	3.00	81.7	9.2	2.0	67.7	0.1	0.2
2	3.15	87.3	8.9	3.3	71.8	0.4	1.1
3	3.30	90.1	7.4	2.8	73.9	2.0	2.1
4	3.60	87.1	2.5	2.3	73.1	5.0	3.6

a) A mixture of tri-*m*-tolyl phosphate (0,5 mol) and 96% H_2SO_4 (10 mol) was kept at 20—30 °C for 24 h. The resulting solution was divided into 4 portions. Mixed acid (70% HNO_3, calculated amount plus 96% H_2SO_4, 2 equiv. weight) was added dropwise to each portion at −5—0 °C. b) Molar ratio; 70% HNO_3/tri-*m*-tolyl phosphate.

a minor one. The ratio of formation of the 2- to the 6-nitro isomer was about 1 : 2. When a large excess of sulfuric acid was used, the 2-nitro isomer was obtained as the major product. Direct nitration of *m*-cresol with a mixed acid at −5—0 °C yielded about 50% of nitro-3-methylphenols and dinitro isomers accounted for 12%. Although tri-*m*-tolyl borate appeared to be a poor substrate owing to its rapid hydrolytic nature, the yield of the nitro isomers was 76.8%, the 2-nitro isomer being a main product.[8] Direct nitration of di-*m*-tolyl carbonate or tri-*m*-tolyl phosphate gave 3-methyl-4-nitrophenol (4-nitro isomer) as the major product (Nos. 5 and 7). In contrast, when both compounds were sulfonated, nitrated and followed by hydrolysis and desulfonation, the 6-nitro isomer was a predominant product (Nos. 6 and 8). The yield of the 6-nitro isomer from tri-*m*-tolyl phosphate was higher in comparison with that of the carbonate.

Selective Synthesis of the 6-Nitro Isomer. We see from Table 1 that tri-*m*-tolyl phosphate is the most favorable substrate for the preparation of the 6-nitro isomer. The following optimum conditions for selective preparation of the 6-nitro isomer were selected (Table 2). 96% Sulfuric acid was a better sulfonating reagent than 90% sulfuric acid or 10% oleum. We see from Table 3 that a small excess of nitric acid to the tolyl phosphate was effective for the most selective formation of the 6-nitro isomer (for No. 4, the ratio of the mono-nitro isomer was 1 : 1 : 28). Pure 6-nitro isomer was obtained from the crude mixture by dissociation extraction with a dilute alkaline solution.[9]

Identification of the Sulfonated Intermediates. All attempts to isolate the intermediates such as sulfo-*m*-tolyl phosphate or nitro-sulfo-*m*-tolyl phosphate after sulfonation or nitration were unsuccessful since they hydrolyze too easily. After nitration, the reaction mixture was poured onto ice and allowed to stand at room temperature for 48 h to give a yellow solid product. The product was extremely soluble in water and identical (mp and NMR) with an authentic specimen of 4-hydroxy-2-methyl-5-nitrobenzenesulfonic acid.[10] Desulfonation of the sulfonated nitrophenol with 60% sulfuric acid gave the 6-nitro isomer. 4-Hydroxy-2-methyl-5-nitrobenzenesulfonic acid (87.2%) and 4-hydroxy-2-methyl-3-nitrobenzenesulfonic acid (10.7%) were also detected by HLC analysis. 3-Methyl-4-nitrophenol was detected in the dephosphorylated solution by TLC on silica gel and quantitatively determined by GLC.

Discussion

The 4-nitro isomer was a dominant product of direct nitration of di-*m*-tolyl carbonate and tri-*m*-tolyl phosphate.[4,6] Haworth and Lapworth reported that the 4-position of *m*-cresol was predominantly sulfonated at 120 °C.[11] This was confirmed by the fact that the *o*-nitro isomers, *viz.*, 2- and 6-nitro isomers, occurred after subsequent nitration in a 1 : 2 ratio.

The use of a large excess of sulfuric acid at low temperature resulted in the selective formation of the 2-nitro isomer. This seems to be due to the formation of 4-hydroxy-6-methyl-1,3-benzenedisulfonic acid as an intermediate.

On the other hand, when the carbonate or the phosphate was monosulfonated, nitrated and followed by hydrolysis and desulfonation, the 6-nitro isomer was selectively obtained.

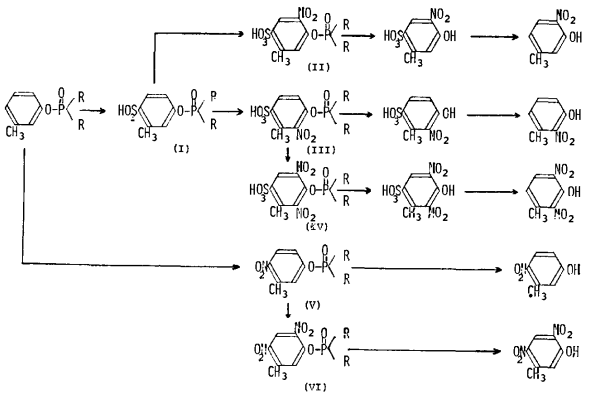

R: *m*-tolyl, nitro-*m*-tolyl, or nitro-sulfo-*m*-tolyl group

Fig. 1.

Selective formation of the 6-nitro isomer from tri-*m*-tolyl phosphate can be illustrated by the reaction sequence shown in Fig. 1. Tri-*m*-tolyl phosphate is sulfonated to give the 4-sulfo derivative (I), which is nitrated to yield the corresponding 6-nitro derivative (II) and 2-nitro derivative (III). It appears that attack of a nitronium ion takes place predominantly at the 6-position of I, since the 2-position of I is apparently hindered by the bulky ditolyloxyphosphinyl group and the 3-methyl group which may be inclined toward the 2-position by a buttressing effect from the 4-sulfonyl group. The higher selectivity of the nitration at the 6-position in the 4-sulfonated intermediates may be due to the peculiar geometry. A small excess of nitronium ion predominantly attacks the 6-position of the intermediate (III) to give the dinitro derivative (IV). IV is hydrolyzed, followed by desulfonation, to yield 2,6-dinitro-3-methylphenol. The unaffected *m*-tolyl group of the phosphate is directly nitrated to give the 4-nitro derivative (V), which undergoes nitration to give the 4,6-dinitro derivative (VI). Hydrolysis of VI produces 4,6-dinitro-3-methylphenol.

In conclusion, the present method of nitration after the specifically controlled sulfonation to the phosphate or the carbonate of *m*-cresol can provide the respective *o*-nitro derivatives in high yields in a convenient "one-pot-procedure." 3-Methyl-6-nitrophenol in particular can be efficiently prepared.

Experimental

Materials. Di-*m*-tolyl carbonate and tri-*m*-tolyl borate were prepared according to the procedures previously reported.[4,8] Tri-*m*-tolyl phosphate (99% pure) and *m*-cresol (98% pure) were prepared at Sumitomo Chemical Co. Ltd., Oita Works and used without further purification. Authentic specimens of 3-methyl-2-nitrophenol, 3-methyl-4-nitrophenol, 3-methyl-6-nitrophenol, 4,6-dinitro-3-methylphenol, 2,6-dinitro-3-methylphenol and 2,4,6-trinitro-3-methylphenol were prepared by the method given in the respective references.[3,10] 2,4-Dinitro-3-methylphenol was prepared by nitration of 3-methyl-2-nitrophenol in acetic acid, whose melting point was quite different from that in the literature.[10] Mp 130 °C (lit, 74 °C). Found: C, 42.56; H, 3.25; N, 14.20%. Calcd for $C_7H_6N_2O_5$: C, 42.43; H, 3.06; N, 14.14%. Physical and spectral data of these nitrophenols are given in Table 4. The following sulfonated nitro-3-methylphenols were prepared.[10] 4-Hydroxy-2-methyl-5-nitrobenzenesulfonic acid, mp 131—132 °C, NMR (D_2O): 2.60 (3H, s, CH_3), 7.10 (1H, S, H-5), and 8.50 (1H, s, H-2). 4-Hydroxy-2-methyl-3-nitrobenzenesulfonic acid, mp 78—79 °C, NMR (D_2O): 2.50 (3H, s, CH_3), 7.00 (1H, d, H-6, J=9.0 Hz), and 7.90 (1H, d, H-5, J=9.0 Hz).

TABLE 4. PHYSICAL AND SPECTRAL DATA OF NITRO-3-METHYLPHENOLS

Compound	Mp[a] (°C)	pK_a	UV in EtOH λ max (nm)	log ε
3-Methyl-2-nitrophenol	41 (39)	7.20	212 235 270	4.08 3.29 3.25
3-Methyl-4-nitrophenol	129 (129)	7.08	208 232 308	4.02 3.93 3.96
3-Methyl-6-nitrophenol	55 (54)	7.63	213 283 351	4.17 3.83 3.55
2,4-Dinitro-3-methylphenol	130 (74)[b]	4.81	207 291 370	4.16 3.84 3.55
4,6-Dinitro-3-methylphenol	65 (64)	4.60	212 260 310	4.13 4.12 3.71
2,6-Dinitro-3-methylphenol	100 (101)	4.00	211 278 337	4.22 3.80 3.52
2,4,6-Trinitro-3-methylphenol	110 (110)[c]	3.73[c]	212 254 348	4.22 3.98 4.02

a) ( ) value cited from Ref. 10. b) See Experimental.
c) Determined in 5% EtOH.

Analysis. Identification and quantitative analysis of the nitro isomers were carried out on a GLC(Yanagimoto G-80 or Yanagimoto GCG-550 F, FID detecter) and a GC-Mass spectrometer (Shimadzu LKB-9000). Products were identified with authentic samples by GC retention time on at least two different columns (2% XE-60 on chromosorb W, 3 mm × 1.5 m, glass column programmed at 110—220 °C; 10% PEG-20M on Chromosorb W, 3 mm × 1.0 m, glass column programmed at 150—200 °C; 2% FFAP on Shimalite TPA, 3 mm × 1.0 m, glass column programmed at 170—200 °C). Neither 2,4-dinitro-3-methylphenol nor 2,4,6-trinitro-3-methylphenol were detected under the conditions described above. Mass spectra of peaks obtained from GLC were determined at 70 eV as follows; 3-methyl-6-nitrophenol (*m/e* 153 M^+), 3-methyl-2-nitrophenol (*m/e* 153 M^+), 3-methyl-4-nitrophenol (*m/e* 153 M^+), 2,6-dinitro-3-methylphenol (*m/e* 198 M^+) and 4,6-dinitro-3-methyl-phenol (*m/e* 198 M^+). 4-Methyl-3-nitrophenol (*m/e* 153 M^+) was obtained among other minor products by the nitration of *p*-cresol, a major impurity in the starting material. The sulfonated nitro-3-methylphenols formed as intermediates were analyzed as follows. The

reaction mixture occurring after nitration was poured onto ice and then neutralized with aqueous sodium hydroxide to pH 7.40. One μl of the solution was subjected to HLC. Operating conditions are follows; instrument, Shimadzu Du Pont 830 liquid chromatograph; column SAX 2 mm × 1.0 m; column temp, 40 °C; column pressure, 70 kg/cm²; mobile phase, distilled water at pH 7.40 with 0.2 M $NaNO_3$; detector, UV photometer at 254 nm; flow rate, 1 ml/min; retention time 4-hydroxy-2-methyl-5-nitrobenzenesulfonic acid (4.0 min', 4-hydroxy-2-methyl-3-nitrobenzenesulfonic acid (6.0 min). Concentrations of sulfuric acid and nitric acid were determined by alkaline titration or specific gravity. pK_a values of the nitro isomers were measured by alkaline titration on a pH meter. UV was recorded with a Shimazu double beam spectrophotometer UV-200. NMR was recorded on a Hitachi NMR spectrometer R-20B (60 Mz).

Preparation of the Mononitro-3-methylphenols. A typical procedure for preparation of the mononitro-3-methylphenols is as follows (see No. 8, Table 1). A mixture of 96% sulfuric acid (200 g, 2.0 mol) and tri-*m*-tolyl phosphate (36.8 g, 0.1 mol) was kept under stirring at 20—30 °C for 24 h. A mixed acid consisting of 70% nitric acid (28.0 g, 0.315 mol) and 96% sulfuric acid (50.0 g 0.5 mol) was added to the solution at −5—0 °C. After 2 h, the reaction mixture was poured onto ice (150 g). The resulting solution was heated and distilled with steam at 140—170 °C until no oily distillate was detected in the steam condensate. The distillate was extracted 3 times with 50 ml portions of chloroform. The combined chloroform extract dried over anhydrous sodium sulfate, chloroform was evaporated *in vacuo*. The yellow residue (41.0 g) was subjected to GLC for analysis. The crude mixture was again distilled with steam at 100 °C. The distillate dissolved in 100 ml of toluene was washed 3 times with 100 ml portions of 0.8% aqueous sodium hydroxide. Removal of toluene gave pure 3-methyl-6-nitrophenol (26.0 g). In experiments Nos. 3, 5, and 7 in Table 1 the mixed acid was added to the reaction mixture immediately after the starting material had been mixed with 96% sulfuric acid. The reaction conditions are summarized in Tables 1, 2, and 3.

References

1) Y. Nishizawa, *Bull. Agr. Chem. Soc. Jpn.*, **24**, 744 (1960).
2) A. Mine, K. Mukai, T. Satomi, S. Hino, and K. Tateishi, Japanese patent, 49-028977 (1974).
3) A. W. Hofmann and W. V. Miller, *Ann. Chem.*, **271**, 51.
4) F. Falis, G. Wagner, and N. Adler, *Ber.*, **77**, 692 (1944).
5) A. E. Tchtchibabine, *Bull. Soc. Chim. Fr.*, **4**, 439 (1937).
6) R. Mersch and D. Delfs, German patent, 1024978 (1958).
7) G. B. Gibson, *J. Chem. Soc.*, **1923**, 1269.
8) H. Steinberg and D. L. Hunter, *Ind. End. Chem.*, **49**, 174 (1957).
9) G. H. Twing, *Nature*, **163**, 1006 (1949).
10) Beilstein, Organische Chemie Band VI, Seite 385.
11) R. D. Haworth and H. Lapworth, *J. Chem. Soc.*, **1924**, 125, 1299.

Synthesis of a Peptide Lactone, *N*-(3-Hydroxypicolinyl)-threonyl-D-leucyl-prolylsarcosyl-leucyl-alanyl-alanine Threonine Lactone

Hideki KINOSHITA and Hiroshi KOTAKE

Department of Chemistry, Faculty of Science, Kanazawa University, Kanazawa 920

(Received September 3, 1976)

The synthesis of a peptide lactone, *N*-(3-hydroxypicolinyl)-threonyl-D-leucyl-prolylsarcosyl-leucyl-alanyl-alanine Threonine Lactone (**21**) is described. The *t*-butoxycarbonyl group of *t*-butyl *O*-(*t*-butoxycarbonyl-alanyl)-*N*-benzyloxycarbonyl-threonyl-D-leucyl-prolylsarcosinate (**12**) was deblocked selectively with formic acid in good yield. The coupling of **12** with the azide derived from *t*-butoxycarbonyl-leucyl-alanine hydrazide (**15**) with isopentyl nitrite gave a heptapeptide ester **17**. Deblocking, cyclization, and hydrogenation gave a heptapeptide lactone **20** which was coupled with 3-hydroxypicolinic acid yielding **21**.

In a previous paper,[1] it was reported that the *t*-butoxycarbonyl group was cleaved selectively in the presence of the *t*-butyl ester group using 85% formic acid and the application of this selective deprotection method for the synthesis of peptides.

In this paper, the usefulness of this method for the synthesis of the peptide lactone[2] is reported.

In the past several years, the structures of a number of new antibiotics have been reported in the literature with the common feature of a lactone that is formed from the carboxyl function of an amino acid with the hydroxyl group of an amino acid. Moreover, in most of the cases, the amino function of the latter is acylated by a heterocyclic acid.[3-6] Examples of this class of compounds are the antibiotic actinomycin,[7] etamycin,[5] echinomycin,[8] *etc.* Synthetic approaches in this field of naturally occurring peptide lactone antibiotics have been limited only to actinomycin[9-11] and etamycin.[12]

Because of the difficulties of synthesis, the authors are interested in finding a new method of synthesizing this class of peptides in the utility of the selective deblocking method[1] described previously. For this purpose an attempt was made to synthesize a peptide lactone **21** as a model (Fig. 1).

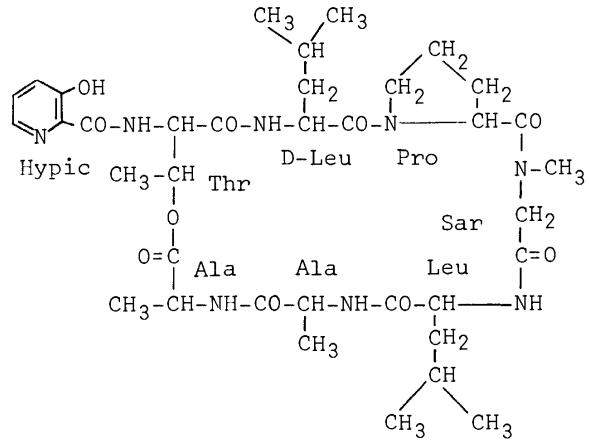

Fig. 1.

In the synthesis of a peptide lactone, it is usual to prepare initially the ester bond followed by cyclization by the formation of an amide bond. For example, in the case of 6-proline-staphylomycin S[13] and etamycin,[12] initially the linear peptide ester containing a 3-hydroxypicolinic acid moiety was prepared and then cyclization was provided by the amide bond formation. However a new route was designed in which the formation of peptide lactone **19** is obtained by cyclization of the linear peptide ester **18** and finally a 3-hydroxypicolinic acid moiety is introduced into the amino group of threonine, as illustrated in Scheme 2. This synthetic approach has not been reported in the literature to date as far as the present authors are aware, because it is necessary to use various protecting groups in this case.

The amide bond between sarcosine and leucine was selected for the cyclization step because of the stability of sarcosine toward racemization. For this approach, it was necessary to synthesize a chain that would include the desired ester bond between alanine and threonine (Scheme 2).

The preparation of the deprotected tripeptide (*t*-butyl D-leucyl-prolylsarcosinate (**10**)) was attempted in two different ways. Catalytic hydrogenation of *t*-butyl benzyloxycarbonyl-D-leucyl-prolylsarcosinate (**3**) derived from the coupling of benzyloxycarbonyl-D-leucyl-proline (**2**) with *t*-butyl sarcosinate, gave a tripeptide ester **10**, but D-leucyl-proline anhydride (**4**) was always produced as a by-product (Scheme 1). Therefore, it was

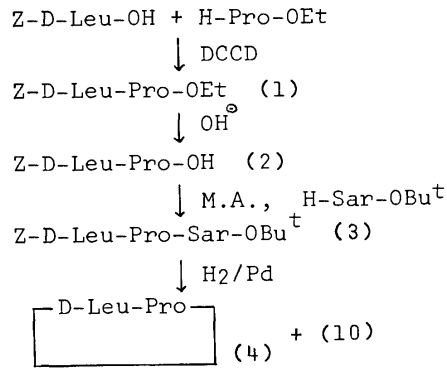

Scheme 1.

thought that the selective deblocking method[1] may be superior for this purpose. The cleavage of the *t*-butoxycarbonyl group of the protected dipeptide ester **7** by formic acid gave a dipeptide ester **8** in a 90% yield, which was condensed with *t*-butoxycarbonyl-D-leucine to give the desired protected tripeptide ester **9** in a 96% yield. Alternatively, compound **9** was obtained only in the low yield of 59% by coupling of *t*-butoxycarbonyl-D-leucyl-proline (**6**) with *t*-butyl sarcosinate. The cleav-

age of the *t*-butoxycarbonyl group of the protected tripeptide ester **9** by formic acid gave a tripeptide ester **10** in an 86% yield with no by-products such as anhydride.

The formation of the ester bond between alanine and threonine was mediated by the mixed anhydride method. The product was separated from the reaction mixture by gel filtration on Sephadex LH-20 to give the desired ester **11** in a 64% yield, which was isolated as dicyclohexylammonium salt. The coupling of the peptide **11** with the tripeptide *t*-butyl ester **10** using the mixed anhydride method gave the pentapeptide ester **12** in an 80% yield.

The selective cleavage of compound **12** by formic acid, a key step in the elongation of the peptide bond to the *N*-terminus, was realized successfully to give the desired deprotected pentapeptide ester **13** in good yield of 87%, which was condensed with the azide **16** derived from *t*-butoxycarbonyl-leucyl-alanine hydrazide (**15**) with isopentyl nitrite[14] to give a 91% yield of the desired heptapeptide ester **17**. A short treatment of the linear heptapeptide ester **17** with anhydrous trifluoroacetic acid is sufficient to remove both of the amino- and the carboxyl-protecting groups to give a trifluoroacetate **18** in a 93% yield. After neutralization with triethylamine, cyclization of the deprotected peptide ester was achieved in a highly dilute solution using five times excess amounts of EDCI and *N*-hydroxysuccinimide,[15] followed by separation of the reaction mixture by preparative TLC to give the desired peptide lactone **19** in good yield (45%). A mass spectrum of compound **19** showed the expected molecular weight. Debenzyloxycarbonylation of the heptapeptide lactone **19** was carried out in an acidic medium containing hydrogen chloride to avoid intramolecular acylation, the so-called O→N acyl

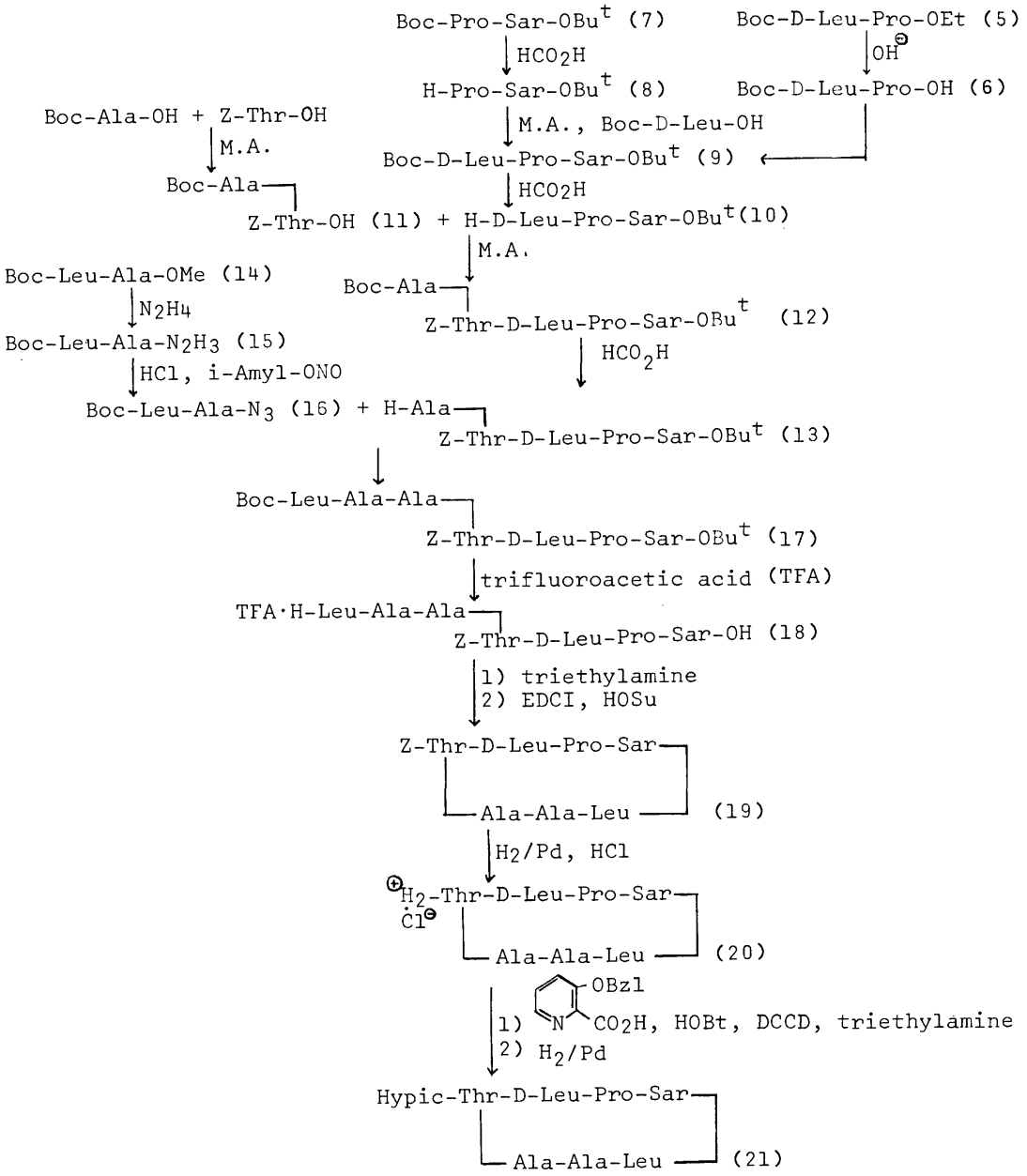

Scheme 2. Synthesis of Peptide Lactone.

migration.[16-18]

The introduction of a 3-hydroxypicolinic acid moiety to the *N*-terminus was at first carried out by the reaction of the deprotected cyclic peptide **20** with the 3-benzyloxypicolinic acid *p*-nitrophenyl ester[19] with slow neutralization, followed by catalytic hydrogenation giving only a poor yield of the desired acylated peptide lactone (20%). Alternatively, condensation of the heptapeptide lactone **20** with the active ester, derived from 3-benzyloxypicolinic acid[19] and HOBt using dicyclohexylcarbodiimide under the same reaction conditions (as described above) gave the desired cyclic octapeptide ester **21** in good yield (68%). The presence of 3-hydroxypicolinic acid was confirmed by spectroscopically[12,13] and by the color reaction[20] of the hydrolysate with an aqueous ferric chloride solution.

As mentioned above, the selective deblocking method has proved useful for the synthesis of a peptide lactone.

Experimental

All melting points are uncorrected. The NMR, IR, and UV spectra were recorded on a JEOL JNH-60, a JASCO IRA-1 spectrometer and a Union Giken SM-401 spectrometer, respectively. The optical rotation values were measured with a JASCO DIP-SL polarimeter.

Z-D-Leu-Pro-OEt (1). To a solution of benzyloxycarbonyl-D-leucine (13.3 g, 0.05 mol) and ethyl prolinate hydrochloride (7.57 g, 0.05 mol) in chloroform (80 ml), triethylamine (5.5 g, 0.055 mol) was added at 0 °C, followed, after 1 h, by dicyclohexylcarbodiimide (10.3 g, 0.05 mol). The reaction mixture was stirred for 3 h below 0 °C and allowed to stand overnight at room temperature. After a precipitate of dicyclohexylurea was filtered off, the filtrate was concentrated to dryness under reduced pressure. The residue was dissolved in ethyl acetate and the organic layer was washed with 1M-hydrochloric acid, 10% sodium hydrogencarbonate and water, and dried over anhydrous sodium sulfate. The solvent was removed *in vacuo* to give an oily product. Yield, 16.3 g (83.6%).

Z-D-Leu-Pro-OH (2). To a solution of **1** (16.3 g, 41.8 mmol) in EtOH (50 ml), 46 ml of 1M-aqueous sodium hydroxide was added with stirring at 0 °C for 3 h, followed by standing overnight at room temperature. The EtOH was removed *in vacuo* and water was added to the reaction mixture. The aqueous residue was extracted with ethyl acetate, and the alkaline aqueous layer was adjusted to pH 3 to afford a crude crystalline product (12.9 g, 81.2%) with a melting point of 98—102 °C, which was recrystallized from ethyl acetate–hexane. Yield, 10.81 g (68%); mp 103—104 °C; $[\alpha]_D^{27}$ −21.3° (1.05, abs EtOH). Found: C, 60.03; H, 7.38; N, 7.21%. Calcd for $C_{19}H_{26}O_5N_2 \cdot H_2O$: C, 59.98; H, 7.38; N, 7.36%.

Z-D-Leu-Pro-Sar-OBu^t (3). To a solution of **2** (7.24 g, 0.02 mol) in dry tetrahydrofuran (40 ml) was added triethylamine (2.02 g, 0.02 mol), followed, after 2 min, by isobutyl chloroformate (2.73 g, 0.02 mol) at −15 °C with stirring. A solution of *t*-butyl sarcosinate (2.90 g, 0.02 mol) in dry tetrahydrofuran (20 ml) was added. The solution was stirred for 2 h below 0 °C and allowed to stand overnight. The solvent was evaporated under reduced pressure and the residual oil was partitioned between ethyl acetate and water. The organic layer was washed with 1M-hydrochloric acid, 10% sodium hydrogencarbonate and water, and dried over anhydrous sodium sulfate. The ethyl acetate was evaporated *in vacuo* to give an oily product. Yield, 8.30 g (84.9%). M^+ 489.

Boc-D-Leu-Pro-OEt (5). *t*-Butoxycarbonyl-D-leucine monohydrate (8.34 g, 33.5 mmol) was dissolved in ethyl acetate (30 ml) and dry tetrahydrofuran (15 ml), and then to this solution was added dicyclohexylcarbodiimide (6.89 g, 33.5 mmol) at 0 °C. After 20 min, a solution of ethyl prolinate (4.97 g, 33.5 mmol) in ethyl acetate (10 ml) was added for a period of 20 min and the reaction mixture was stirred for 2 h at 0 °C and allowed to stand overnight at room temperature. After dicyclohexylurea was filtered off, the filtrate was concentrated to dryness *in vacuo* and the residue was dissolved in ethyl acetate. The organic layer was washed with 1M-hydrochloric acid, 10% sodium hydrogencarbonate and water, and dried over anhydrous sodium sulfate. The solvent was removed *in vacuo* to give an oily product. Yield, 10.8 g (90.6%).

Boc-D-Leu-Pro-OH (6). To a solution of **5** (10.8 g, 30.3 mmol) in EtOH (31 ml) was added 32 ml of 1M-aqueous sodium hydroxide (32 mmol) for a period of 40 min with stirring at −2 °C. The solution was stirred for 2.5 h below 0 °C and allowed to stand overnight. The EtOH was removed *in vacuo* and water was added to the reaction mixture. The aqueous residue was treated with ethyl acetate, and the alkaline aqueous layer was adjusted to pH 3 to afford an oily product, which was extracted with ethyl acetate. The ethyl acetate was removed *in vacuo* to give an oily product in quantitative yield, which was isolated in the form of a crystalline substance, dicyclohexylammonium salt, from ethyl acetate–hexane; 12.58 g (81.6%); mp 168.0—170.5 °C. Recrystallization from ethyl acetate gave a pure crystalline product with a melting point of 172—173 °C; yield, 11.98 g (77.7%); $[\alpha]_D^{31}$ −23.0° (1.02, abs EtOH). Found: C, 65.91; H, 9.92; N, 8.17%. Calcd for $C_{28}H_{51}O_5N_3$: C, 65.97; H, 9.92; N, 8.24%.

For the conversion to the free acid, the dicyclohexylammonium salt 3.50 g (6.87 mmol) was dissolved in a mixture of water and ethyl acetate. After the acidification with 1M-hydrochloric acid (8 ml) the precipitate of dicyclohexylammonium hydrochloride was filtered off. The ethyl acetate extract was dried over anhydrous sodium sulfate and concentrated to dryness *in vacuo*. Yield, 2.24 g (99.6%).

Boc-Pro-Sar-OBu^t (7). To a solution of *t*-butoxycarbonyl proline (1.29 g, 6 mmol) in dry tetrahydrofuran (5 ml) and ethyl acetate (10 ml) were added *t*-butyl sarcosinate (870 mg, 6 mmol) and dicyclohexylcarbodiimide (1.24 g, 6 mmol) with stirring at 0 °C. The reaction mixture was allowed to stand overnight at room temperature. The dicyclohexylurea precipitate was filtered off and the filtrate was concentrated to dryness *in vacuo*. The residue was dissolved in ethyl acetate and the organic layer was washed with 1M-hydrochloric acid, 10% sodium hydrogencarbonate and water. After drying over anhydrous sodium sulfate, the solvent was removed *in vacuo*. A crude crystalline substance (1.66 g, 80%) with a melting point of 70—75 °C was obtained, which was recrystallized from heptane. Yield, 1.48 g (72.7%); mp 73—75 °C. The second crop was obtained from the main solution, 60 mg; mp 72—73 °C. Total yield, 1.54 g (76.8%); $[\alpha]_D^{28}$ −52.1° (1.06, abs EtOH); NMR (CCl_4): δ 1.37 (s, 9H), 1.44 (s, 9H). Found: C, 59.63; H, 9.02; N, 8.08%. Calcd for $C_{17}H_{30}O_5N_2$: C, 59.62; H, 8.83; N, 8.18%.

H-Pro-Sal-OBu^t (8). Compound **7** (300 mg, 0.877 mmol) was dissolved in 7 ml of 85% formic acid, and after the solution had been maintained for 4.5 h at 19 °C, the solvent was removed *in vacuo*. The residual oil was dissolved in chloroform and ammonia was passed through the solution. The precipitate of ammonium formate was filtered off and the filtrate was concentrated to dryness *in vacuo*. The residue was dissolved in ethyl acetate and an insoluble material was filtered off. The organic layer was dried over anhydrous sodium sulfate and removed *in vacuo* to give an oily product.

Yield, 190 mg (89.6%); NMR (CCl_4): δ 1.45 (s, 9H).

Boc-D-Leu-Pro-Sar-OBu^t (9). *Method A*: To a solution of **6** (2.24 g, 6.84 mmol) in dry tetrahydrofuran (15 ml) was added triethylamine (690 mg, 6.84 mmol) and the mixture was cooled to −15 °C. To the solution, isobutyl chloroformate (934 mg, 6.84 mmol) was added followed, after 5 min, by a solution of *t*-butyl sarcosinate (1.00 g, 6.89 mmol) in dry tetrahydrofuran (1 ml). The reaction mixture was stirred for 2 h at 0 °C and allowed to stand overnight at room temperature. The solvent was removed *in vacuo* and the residue was partitioned between ethyl acetate and water, the organic layer was washed with 1 M-hydrochloric acid, 10% sodium hydrogencarbonate and water, and then dried over anhydrous sodium sulfate. The ethyl acetate was removed *in vacuo* to give a crude oil, which was subjected to column chromatography on silica gel using hexane-ethyl acetate (2: 1 v/v). Yield, 1.83 g (58.8%). NMR (CCl_4): δ 1.38 (s, 9H), 1.43 (s, 9H); M^+ 455.

Method B: To a stirred solution of *t*-butoxycarbonyl-D-leucine monohydrate (195 mg, 0.783 mmol) in dry tetrahydrofuran (2 ml) at −10 °C, was added triethylamine (79 mg, 0.783 mmol) followed by isobutyl chloroformate (107 mg, 0.783 mmol). After 5 min a solution of **8** (190 mg, 0.783 mmol) in dry tetrahydrofuran (1 ml) was stirred for 3.5 h below 0 °C and allowed to stand overnight at room temperature. The solvent was evaporated *in vacuo* and the residue was partitioned between ethyl acetate and water. The ethyl acetate layer was washed with 1 M-hydrochloric acid, 10% sodium hydrogencarbonate and water. After drying over anhydrous sodium sulfate, the ethyl acetate was removed *in vacuo* to give a pure oil. Yield, 340 mg (95.7%). The physical properties of this oil were similar to those of the product obtained according to method A.

H-D-Leu-Pro-Sar-OBu^t (10). *Catalytic Hydrogenation Method*: Catalytic hydrogenation of **3** (1.00 g, 2.04 mmol) with palladium (50 mg) in EtOH (25 ml) afforded the desired tripeptide (**10**) contaminated with a ninhydrin-negative compound. It was found that this compound was D-leucylproline anhydride (**4**), which was confirmed by its IR spectrum and elemental analysis. mp 148—149 °C; $[\alpha]_D^{21}$ −105.5° (0.50, abs EtOH). Found: C, 62.67; H, 8.44; N, 13.04%. Calcd for $C_{11}H_{18}O_2N_2$: C, 62.83; H, 8.63; N, 13.32%.

Selective Cleavage Method: Compound **9** (3.36 g, 7.41 mmol) was dissolved in 100 ml of 85% formic acid, and after the solution had been maintained for 3.5 h at 18 °C, the solvent was removed *in vacuo*. The residual oil was dissolved in chloroform, and ammonia was passed through it. After a short cooling, the precipitate was filtered off and the filtrate was evaporated *in vacuo*. The residual oil was dissolved in ethyl acetate and an insoluble material was filtered off. The organic layer was dried over anhydrous sodium sulfate. The solvent was removed *in vacuo* to give an oily product. Yield, 2.24 g (85.9%). NMR (CCl_4): δ 1.44 (s, 9H); M^+ 355.

Boc-Ala—┐

Z-Thr-OH (11). *t*-Butoxycarbonyl-alanine (7.56 g, 40 mmol) and triethylamine (4.04 g, 40 mmol) were dissolved in dry tetrahydrofuran (12 ml), and the solution was cooled to −5 °C. Isobutyl chloroformate (5.44 g, 40 mmol) was added, followed, after 5 min of stirring in the cold bath, by a solution of benzyloxycarbonyl threonine (20.24 g, 80 mmol) and triethylamine (12.12 g, 120 mmol) in dry tetrahydrofuran (80 ml). The reaction mixture was allowed to stand with stirring at room temperature. The salt was filtered off and washed well with ethyl acetate. The filtrate was concentrated to dryness, and the residual oil was partitioned between ethyl acetate and water. The ethyl acetate layer was washed with 1 M-hydrochloric acid and water and dried over anhydrous sodium sulfate. The ethyl acetate was evaporated *in vacuo* to afford an oily product. The crude reaction mixture so obtained was separated by gel filtration on Sephadex LH-20, using chloroform as the elution solvent to give the desired product (16 g), which was isolated in the form of a crystalline product, dicyclohexylammonium salt, from ethyl acetate. Yield, 15.45 g (63.8%) with a melting point of 165—166 °C; $[\alpha]_D^{32}$ −10.5° (1.04, abs EtOH). Found: C, 63.15; H, 8.62; N, 6.83%. Calcd for $C_{32}H_{51}O_8N_3$: C, 63.45; H, 8.49; N, 6.93%.

Boc-Ala—┐

Z-Thr-D-Leu-Pro-Sar-OBu^t (12). Triethylamine (674 mg, 6.67 mmol) and **11** (2.83 g, 6.67 mmol) were dissolved in dry tetrahydrofuran (30 ml) and the solution was cooled to −15 °C with stirring. Isobutyl chloroformate (911 mg, 6.67 mmol) was added, followed, after 5 min of stirring in the cold bath, by a solution of **10** (2.24 g, 6.36 mmol) in dry tetrahydrofuran (20 ml). The reaction mixture was kept at −10 °C for 1 h, then at 0 °C for 1.5 h and allowed to stand overnight at room temperature. The residual oil was partitioned between ethyl acetate and water. The ethyl acetate layer was washed with 1 M-hydrochloric acid, 10% sodium hydrogencarbonate and water and dried over anhydrous sodium sulfate. Evaporation afforded a crude oily product (4.51 g) and this oil was subjected to column chromatography on silica gel using ethyl acetate-hexane (2: 1 v/v) to give an 80% yield of the desired product (3.88 g); $[\alpha]_D^{28}$ −36.4° (1.20, abs EtOH); NMR (CCl_4): δ 1.37 (s, 9H), 1.47 (s, 9H); M^+ 761. Found: C, 59.60; H, 7.91; N, 8.95%. Calcd for $C_{38}H_{59}O_{11}N_5 \cdot 1/2H_2O$: C, 59.20; H, 7.84; N, 9.06%. Amino acid analysis showed the presence of threonine, sarcosine, proline, leucine and alanine in ratios of 0.8: 1.2: 1.3: 0.8: 1.0.

Boc-Leu-Ala-OMe (14). Methyl alaninate hydrochloride (3.14 g, 25 mmol) was suspended in chloroform (30 ml), followed by the addition of triethylamine (2.78 g, 27.5 mmol) at 0 °C. To the solution, dicyclohexylcarbodiimide (5.15 g, 25 mmol) were added. After cooling in a cold bath for 2 h, the reaction mixture was allowed to stand overnight. Dicyclohexylurea was filtered off and the organic layer was washed with 1 M-hydrochloric acid, 10% sodium hydrogencarbonate and water and dried over anhydrous sodium sulfate. The solvent was removed *in vacuo* to give a crystalline substance, (6.80 g, 86%) with a melting point of 113—115 °C, which was recrystallized from benzene-hexane. Yield, 6.36 g (80.5%); mp 113—115 °C; $[\alpha]_D^{28}$ −48.3° (1.20, abs MeOH). Found: C, 57.10; H, 8.84; N, 8.67%. Calcd for $C_{15}H_{28}O_5N_2$: C, 56.94; H, 8.92; N, 8.85%.

Boc-Leu-Ala-N_2H_3 (15). To a solution of **14** (3.9 g, 12.3 mmol), was added hydrazine monohydrate (2.4 g, 48 mmol) in MeOH (10 ml), and the solution was allowed to stand overnight at room temperature. Evaporation *in vacuo* afforded the crude product (3.77 g, 96.7%) with a melting point of 175—177 °C, which was recrystallized from ethyl acetate. Yield, 3.46 g (88.7%); mp 178—179 °C; $[\alpha]_D^{24}$ −51.9° (0.94, abs MeOH). Found: C, 52.90; H, 8.89; N, 17.37%. Calcd for $C_{14}H_{28}O_4N_4$: C, 53.14; H, 8.92; N, 17.74%.

H-Ala—┐

Z-Thr-D-Leu-Pro-Sar-OBu^t (13). Compound **12** (1.20 g, 1.58 mmol) was dissolved in 60 ml of 85% formic acid and then the solution was maintained for 2 h at 18—19 °C. The solvent was removed *in vacuo* and the residual oil was partitioned between ethyl acetate and water. Sodium hydrogencarbonate was added to the aqueous layer producing alkaline solution, and the isolated oil was extracted with ethyl acetate. After drying the solvent was removed *in vacuo* to give the desired product. Yield, 900 mg (86.5%); NMR (CCl_4):

δ 1.47 (s, 9H); M^+ 661.

Boc–Leu–Ala–Ala–Z–Thr–D-Leu–Pro–Sar–OBu^t (**17**). To a solution of **15** (1.062 g, 3.36 mmol) in dry *N,N*-dimethylformamide (18 ml) was added 2.18 ml of 4.62 M-HCl in dioxane (10.08 mmol) at −50 °C, followed by isopentyl nitrite (0.47 ml, 3.36 mmol). After the temperature had been raised to −20 °C and kept there for 30 min, the solution was again cooled to −50 °C, and triethylamine (1.01 g, 10.08 mmol) was added. A solution of **13** (2.22 g, 3.36 mmol) in dry *N,N*-dimethylformamide (10 ml) was added dropwise at −20 °C. After stirring at 0 °C for 70 h, the solvent was removed *in vacuo* and the residual oil was partitioned between ethyl acetate and water. The ethyl acetate layer was washed with 1M-hydrochloric acid, 10% sodium hydrogencarbonate and water. The solvent was evaporated to dryness under reduced pressure to give a crude product. The crude oil was subjected to column chromatography on silica gel using benzene-MeOH (20: 1 v/v) to afford a 90.5% yield of the desired pure product (2.88 g); $[\alpha]_D^{28}$ −37.5° (1.04, abs EtOH); NMR (CCl_4): δ 1.38 (s, 9H), 1.44 (s, 9H). Found: C, 59.05; H, 8.03; N, 10.53%. Calcd for $C_{47}H_{75}O_{13}N_7 \cdot 1/2H_2O$: C, 59.09; H, 7.92; N, 10.27%. Amino acid analysis showed the presence of threonine, sarcosine, proline, alanine and leucine in ratios of 0.8: 0.7: 1.0: 2.0: 1.5.

Z–Thr–D-Leu–Pro–Sar–Ala–Ala–Leu (**19**). Compound **17** (1.10 g, 1.16 mmol) was dissolved in 15 ml of trifluoroacetic acid and allowed to stand for 1 h at room temperature. Excess trifluoroacetic acid was removed *in vacuo* and the residue was triturated with dry ether to give a salt (**18**) in a 92.3% yield (975 mg). The salt (600 mg, 0.664 mmol) was suspended in dry dichloromethane (10 ml) and triethylamine (133 mg,1.32 mmol) was added with ice cooling, after 50 min, followed by evaporation and drying under reduced pressure. The residue was taken up in 1.2 l of dry dichloromethane and cooled to 0 °C. *N*-Hydroxysuccinimide (381 mg, 3.32 mmol) was added and after a short delay, a solution of EDCI (515 mg, 3.32 mmol) in dry dichloromethane (10 ml) was added. The reaction mixture was stirred for 30 h at 0 °C and then the stirring was continued for 60 h at 5 °C. The solution was evaporated *in vacuo* and the residue was partitioned with ethyl acetate and water. The organic layer was washed with 0.1 M hydrochloric acid, 10% sodium hydrogencarbonate and water, dried over anhydrous sodium sulfate, and evaporated. The product was subjected to preparative TLC first using ethyl acetate–EtOH (6: 1 v/v) and once more using benzene–EtOH (5: 2 v/v). The desired product was obtained in a 44.5% yield (233 mg) which was recrystallized from ethyl acetate–hexane to give a crystalline product with a melting point of 176—178 °C. Yield, 224 mg; $[\alpha]_D^{24}$ +59.7° (1.17, abs EtOH); M^+ 771. Found: C, 58.01; H, 7.60; N, 12.41%. Calcd for $C_{38}H_{57}O_{11}N_7 \cdot H_2O$: C, 57.78; H, 7.27; N, 12.41%.

Hypic–Thr–D-Leu–Pro–Sar–Ala–Ala–Leu (**21**). Compound **19** (70 mg, 0.09 mmol) was dissolved in abs EtOH (15 ml) containing 0.04 ml of 4.62 M-HCl in dioxane and hydrogenated for 1 h over 10% palladium on charcoal (30 mg). The catalyst was filtered off and the solution was evaporated *in vacuo* to give a salt (**20**). 3-Benzyloxypicolinic acid sesquihydrate hydrochloride[19] (30 mg, 0.1 mmol) was suspended in 2 ml of dichloromethane followed by the addition of triethylamine (40 mg) with ice cooling. After 1 h the solution was evaporated *in vacuo* and dried. The residue was taken up in 1 ml of dry tetrahydrofuran followed by the addition of HOBt (13.5 mg, 0.1 mmol) and dicyclohexylcarbodiimide (20.6 mg, 0.1 mmol) and stirring for 1 h at 0 °C. To the solution prepared above was added a solution of **20** in tetrahydrofuran (1 ml) and a solution of triethylamine (9.1 mg, 0.09 mmol) in dry tetrahydrofuran (5 ml) was added dropwise over a 2.5 h period. The reaction mixture was stirred for 5 h at room temperature and evaporated. The residue was subjected to preparative TLC using benzene–EtOH (100: 35 v/v) to give the protected product in a 68.1% yield (52 mg), which was hydrogenated for 1 h over 10% palladium on charcoal (40 mg). After filtration of the catalyst the solvent was evaporated *in vacuo* to give the desired product in a 64.5% yield (44 mg); $[\alpha]_D^{22}$ +40.8° (0.98, CH_2Cl_2); IR (KBr): 1740, 1630, 1520 cm^{-1}; λ_{max} 304 nm (log ε 3.77).[12,13] Found: C, 54.87; H, 7.12; N, 14.44%. Calcd for $C_{36}H_{54}O_{10}N_8 \cdot 3/2H_2O$: C, 55.01; H, 7.31; N, 14.25%. The product showed a single spot using various solvents with TLC. Amino acid analysis showed the presence of threonine, sarcosine, proline, leucine, and alanine in ratios of 0.9: 1.0: 1.0: 1.9: 2.0.

References

1) H. Kinoshita and H. Kotake, *Chem. Lett.*, **1974**, 631.

2) The abbreviations used in this work are those recommended by the IUPAC-IUB commision on Biochemical Nomenclature, as published in *J. Biol. Chem.*, **247**, 977 (1972): EDCI for 1-ethyl-3-(3-dimethylaminopropyl) carbodiimide, M. A. for mixed anhydride method, HOBt for 1-hydroxybenzotriazole, and Hypic for 3-hydroxypicolinyl.

3) H. Vanderhaeghe and G. Parmentier, *J. Am. Chem. Soc.*, **82**, 4414 (1960).

4) M. Bodanszky and M. A. Ondetti, *Antimicro. Agents Chemother.*, **1963**, 360.

5) J. C. Sheehan, H. G. Zachau, and W. B. Lawson, *J. Am. Chem. Soc.*, **80**, 3349 (1958).

6) H. Otsuka and J. Shoji, *Tetrahedron*, **21**, 2931 (1965).

7) H. Brockmann, G. Bohnsack, B. Franck, H. Groene, H. Muxfeldt, and C. Sueling, *Angew. Chem.*, **68**, 70 (1956).

8) W. Keller-Schierlein, M. L. Mihailovic, and V. Prelog, *Helv. Chim. Acta*, **42**, 305 (1959).

9) H. Brockmann and H. Lackner, *Naturwissenschaften*, **47**, 230 (1960).

10) H. Brockmann and H. Lackner, *Naturwissenschaften*, **51**, 381, 407, 435 (1964).

11) J. Meienhofer, *J. Am. Chem. Soc.*, **92**, 3771 (1970).

12) J. C. Sheehan and S. L. Ledis, *J. Am. Chem. Soc.*, **95**, 875 (1973).

13) M. A. Ondetti and P. L. Thomas, *J. Am. Chem. Soc.*, **87**, 4375 (1965).

14) J. Honzl and J. Rudinger, *Collect. Czech. Chem. Commun.*, **26**, 2333 (1961).

15) T. Wieland, C. Birr, and F. Flor, *Ann.*, **727**, 130 (1969).

16) S. Guttmann and R. A. Boissonnas, *Helv. Chim. Acta*, **41**, 1853 (1958).

17) D. Theodoropoulos, H. Bennich, G. Foelsh, and O. Mellander, *Nature*, **184**, 270 (1959).

18) H. Kinoshita and H. Kotake, *Bull. Chem. Soc. Jpn.*, **43**, 3609 (1970).

19) J. C. Sheehan, *J. Org. Chem.*, **31**, 636 (1966).

20) Nippon Bunseki Kagaku Kai, "Bunseki Kagaku Binran," Maruzen, Tokyo (1961), p. 553.

Reactions of Benzyne with Substituted Benzenes

Iwao TABUSHI, Hidenori YAMADA, Zenichi YOSHIDA,* and Ryohei ODA*

Department oe Pharmaceutical Sciences, Kyashu University, Fukuoka 812

* *Department of Synthetic Chemistry, Faculty of Engineering, Kyoto University, Kyoto 606*

(Received April 26, 1976)

The reactions of benzyne with substituted benzenes(anisole, chlorobenzene, methyl benzoate, benzylidyne trifluoride and toluene) giving the Diels-Alder adducts were investigated, where two positionally isomeric adducts were possible, *i.e.*, a geminal-para adduct (1,4-adduct with respect to the substituent) and an ortho-meta adduct (2,5-adduct). From the competition reactions, relative reactivities of benzyne to substituted benzenes were estimated for the 1,4-addition and 2,5-addition. Markedly different substituent effects were observed. For the 1,4-addition, large negative ρ value (−1.79) was observed, but for the 2,5-addition, substituent effect was small. From benzyne and toluene, *o*-benzylbiphenyl (**13**) and 2-benzyl-3-phenylbenzo[5,6]bicyclo[2.2.2]octatriene (**14**) were obtained as the successive "ene" products together with the normal Diels-Alder adducts.

Reactions of halogenated benzynes with substituted benzenes were studied well where the Diels-Alder adducts were obtained in good yield.[1] But the reactions of benzyne with substituted benzenes have been scarcely studied probably because of the low reactivity. Only the reactions of benzyne, generated from the thermolysis of benzenediazonium-2-carboxylate, with benzene[2,3] and some alkylbenzenes[4] and that, generated from the pyrolysis of phthalic anhydride, with *o*-dichlorobenzene[5] have been reported. Stiles reported that the reaction of benzyne with benzene gave three one to one adducts, biphenyl, benzocyclooctene and benzobicyclo-[2.2.2]octatriene, together with a two to one adduct **15**.[2] Friedman, however, showed that the former two products were formed only in the presence of a catalytic amount of silver cation and their formations were reduced to near zero in the reaction where the starting benzenediazonium-2-carboxylate was prepared from anthranilic acid(**1**) and pentyl nitrite in the absence of a silver salt.[3,6] We also reported that the addition of several metal salts changed the products of the reaction of benzyne with benzene.[7]

In this paper we report the products and the relative reactivities of substituted benzenes treated with benzyne, generated from benzenediazonium-2-carboxylate, in the absence of a metal salt.

Results

The thermolysis of benzenediazonium-2-carboxylate (**2**) was carried out in a substituted benzene(anisole, chlorobenzene, methyl benzoate, benzylidyne trifluoride or toluene). The products are shown in Scheme 1 and their compositions are listed in Table 1.[8]

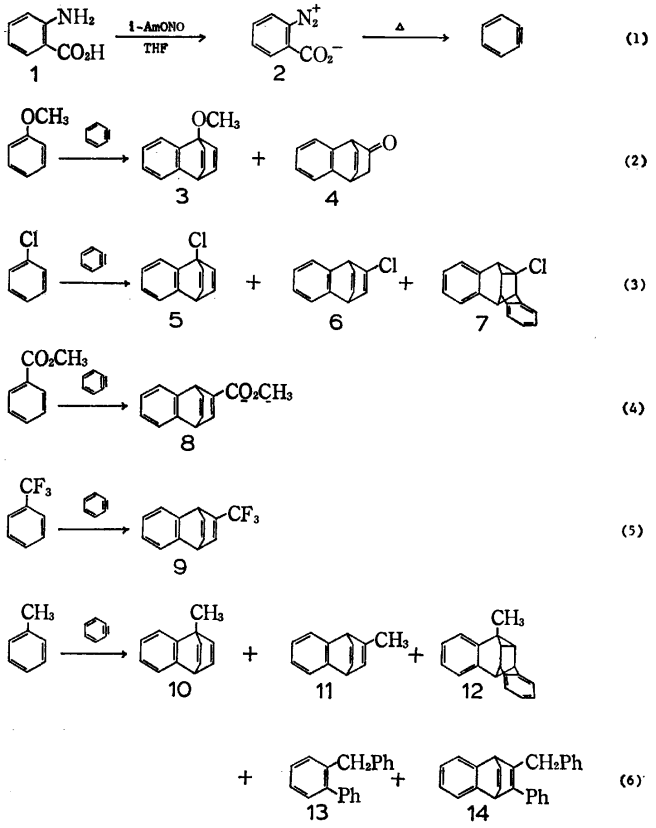

Scheme 1. The products of the reactions of benzyne with substituted benzenes.[9]

Table 1. THE PRODUCT COMPOSITIONS OF THE REACTIONS OF BENZYNE WITH SUBSTITUTED BENZENES[a]

Substrate (ml)	1 (g)	Product compositions (%)				
Anisole (500)	10	**3** 82.9	**4** 17.1			
Chlorobenzene (500)	3	**5** 17.8	**6** 44.4	**7** 37.8		
Methyl benzoate (225)	3	**8** ≈100				
Benzylidyne trifluoride (75)	3	**9** ≈100				
Toluene (500)	3	**10** 13.9	**11** 28.4	**12** 4.1	**13** 37.1	**14** 16.5

a) The product compositions were determined by means of gas chromatography (PEG 20M and Silicon DC 550 columns) and/or NMR spectroscopy.

The reaction of benzyne with anisole gave 1-methoxybenzo[2,3]bicyclo[2.2.2]octatriene(**3**) and benzobicyclo-[2.2.2]octadienone(**4**) in 25(32) and 6(8)% yields, respectively, on the basis of anthranilic acid used (yields in the parentheses were based on benzyne generated).[10] **4** was determined on the basis of its IR spectrum identical with that reported in literature[11] in every detail.

Chlorobenzene gave 1-chlorobenzo[2,3]bicyclo-[2.2.2]octatriene(**5**), 2-chlorobenzo[5,6]bicyclo[2.2.2]-octatriene (**6**) and compound **7** together with biphenylene(19% of the total products)[9] and phenyl benzoate

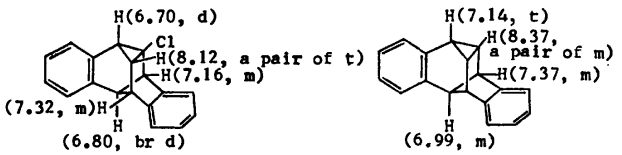

7 15

Fig. 1. H^1 NMR spectra of **7** and **15** (τ-value). Abbreviations are: d, doublet; t, triplet; m, multiplet; br, broad.

(4% of the total products).[9] The molecular peak of mass spectrum of **7** was observed at 264 (*m/e*) with relative intensity 12, indicating that **7** was the two to one adduct of benzyne and chlorobenzene. The 60 MHz NMR spectrum of **7** in CCl_4 consisted of aromatic absorptions as a multiplet at 2.55—3.05 τ (8H) and aliphatic absorptions at 6.70 τ(doublet, 1H), 6.80 τ(broad doublet, 1H), 7.16 τ(multiplet, 1H), 7.32 τ(multiplet, 1H), and 8.12 τ(a pair of triplet, 1H). No olefinic proton was observed. The 60 MHz spin-decoupling experiments showed that the original signal at 8.12 τ was coupled with the signal at 6.70 τ with J value of 7.2 Hz and also coupled with the signal at 6.80 τ with J value of 1.8 Hz. The NMR spectrum of **7** compared with that of unsubstituted compound **15**[2b] is shown in Fig. 1. Observed NMR spectrum of **7** was fully interpreted on the basis of the assigned structure.

Methyl benzoate gave 2-methoxycarbonylbenzo[5,6]bicyclo[2.2.2]octatriene (**8**), biphenylene and phenyl benzoate. No 1-substituted benzobicyclo[2.2.2]octatriene was obtained in a detectable amount.

From benzylidyne trifluoride, 2-trifluoromethylbenzo[5,6]bicyclo[2.2.2]octatriene (**9**), biphenylene and phenyl benzoate were obtained.

From toluene, three products, 1-methylbenzo[2,3]bicyclo[2.2.2]octatriene (**10**), 2-methylbenzo[5,6]bicyclo[2.2.2]octatriene (**11**) and *o*-benzylbiphenyl (**13**) were obtained as was reported elswhere.[4] In addition, unknown compounds **12** and **14** were obtained. Structure of **12** was tentatively determined as shown in Scheme 1 on the basis of NMR spectrum which consisted of the signals at 8.95 τ(singlet), 7.4 τ(broad singlet), and 7.0 τ(broad singlet). The molecular peak of the mass spectrum of **14** was observed at 320 (*m/e*) indicating **14** to be the three to one adduct of benzyne and toluene. Its NMR spectrum showed the olefinic multiplet at 3.06—3.25 τ(2H) and aliphatic signals at 4.99 τ (doublet of doublet, 1H), 5.50 τ (doublet of doublet, 1H), and 6.40 τ (AB quartet, 2H). According to the decoupling experiment, no appreciable coupling was observed between the signals at 4.99 and 5.50 τ. The most probable structure of **14** and NMR assignment are shown in Fig. 2.

The NMR spectra of other benzobicyclo[2.2.2]octatriene derivatives are summarized in Table 2.

Competition reactions were carried out to estimate the relative reactivities of benzyne toward substituted benzenes. In each run, 0.5 g of anthranilic acid and 20—30 g of substituted benzenes were used. Results are shown in Table 3.

TABLE 2. ^{1}H NMR SPECTRA OF BENZOBICYCLO[2.2.2]OCTATRIENE DERIVATIVES[a]

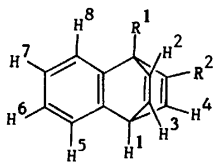

Compounds	R^1	R^2	τ-value									
			R^1	H^1	R^2	H^2	H^3	H^4	H^5	H^6	H^7	H^8
3	OCH_3	H	6.25 (s)	5.35 (tt)				2.95—3.45 (m)				2.65—2.83 (m)
5	Cl	H	—	5.21 (m)				2.90—3.40 (m)				2.40—2.60 (m)
6	H	Cl	5.13—5.45 (m)		—	2.75—3.25 (m)		3.76 (m)		2.75—3.25 (m)		
8	H	CO_2CH_3	4.50—4.73 (m)	4.95—5.24 (m)	6.30 (s)	2.65—3.40 (m)		3.27 (dd)		2.65—3.40 (m)		
9	H	CF_3	4.95—5.23 (m)		—			2.65—3.25 (m)				
10	CH_3	H	8.04 (s)	5.26 (m)	3.58 (dd)				2.80—3.30 (m)			
11	H	CH_3	5.46—5.72 (m)	5.24—5.46 (m)	8.12 (m)	2.85—3.35 (m)		3.65—3.90 (m)		2.85—3.35 (m)		

a) With 1% TMS as an internal standard, 5—10% in CCl_4, 60 MHz. Abbreviations are: s, singlet; d, doublet; dd, doublet of doublet; tt, triplet of triplet; m, multiplet.

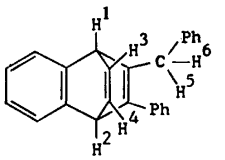

Aromatic H: 2.65—3.06 τ (m, 14H)
H^3, H^4: 3.06—3.25 τ (m, 2H)
H^2: 4.99 τ (dd, 1H), J_{H^1,H^4}=5.4 Hz, J_{H^1,H^3}=2.8 Hz
H^1: 5.50 τ(dd, 1H), J_{H^1,H^3}=5.4 Hz, J_{H^1,H^2}=2.6 Hz
H^5, H^6: 6.40 τ (center, AB quartet, 2H), J_{H^5,H^6}=16.5 Hz

Fig. 2. The NMR spectrum of **14**. With 1% TMS as an internal standard, 10% in CCl_4, 60 MHz. Abbreviations are: dd, doublet of doublet; m, multiplet.

Table 3. Competition reactions of a series of substituted benzene toward benzyne[a]

Run	Substrate (g)	Ratio of products derived from two substrates	k_R/k_H[b]
1	{Benzene (30) {Anisole (20)	1 3.82	1 7.93
2	{Benzene (25) {Toluene (25)	1 3.61	1 4.25
3	{Benzene (20) {Chlorobenzene (30)	1 0.862	1 0.794
4	{Benzene (20) {Benzylidyne trifluoride (30)	1 0.466	1 0.580
5[c]	{Chlorobenzene (20) {Methyl benzoate (30)	1 1.45	0.794 0.993

a) The products from benzene were benzobicyclo[2.2.2]-octatriene (**16**) and **15**. b) Relative reactivities of substituted benzenes to benzene. c) Product compositions derived from chlorobenzene were slightly changed from those shown in Table 1 to **5**, 6.1% and **6**+**7**, 93.9%. The cause of these differences was not clear but it may be due to solvent effect.

Discussion

Regioselectivity of the Diels-Alder Addition. The reaction of benzyne with substituted benzene gave the Diels-Alder adducts[12] where two positional isomers were possible, a geminal-para adduct(1,4-addition; Eq. 7) and an ortho-meta adduct(2,5-addition; Eq. 8) with respect to a substituent.

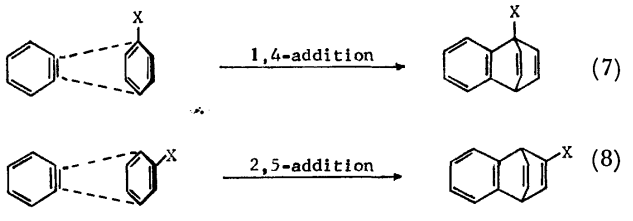

The isomer compositions are shown in Table 4.[13] As shown in the table, the predominant product was systematically changed from the 1,4-adduct for anisole to the 2,5-adduct for methyl benzoate or benzylidyne trifluoride depending on the electron-donating(withdrawing) property of substituent.[14] If the steric factor alone is important, it should reduce the amount of the 1,4-adduct relative to the 2,5-adduct.[15] But our results indicated that the regioselectivity of the Diels-Alder addition could not be so simply explained as only the steric repulsion in the transition state was important (*vide infra*).

Table 4. The isomer compositions of the Diels-Alder adducts (%)

Substrate	1,4-Adduct	2,5-Adduct
Anisole	82.9	17.1
Toluene	28.6	71.4
Chlorobenzene	17.8	82.2
Methyl benzoate	≈0	≈100
Benzylidene trifluoride	≈0	≈100

Table 5. The relative reactivities of benzyne toward substituted benzenes with respect to 1,4-addition and 2,5-addition[a]

Substituent	OCH_3	CH_3	H	Cl	CO_2CH_3	CF_3
1,4-Addition	19.1	2.32	1	0.436	≈0	≈0
2,5-Addition	2.36	2.90	1	0.973	1.49	0.870

a) Statistical factors are corrected.

The Relative Reactivities of Benzyne toward Substituted Benzenes. The relative reactivities of benzyne toward substituted benzenes were estimated from the competition experiments. In Table 5, the relative reactivities of benzyne toward substituted benzenes with respect to 1,4-addition and 2,5-addition are shown. The reactivity of 1,4-addition changed more than 40-fold with changing a substituent, while that of 2,5-addition changed only 3.5-fold. Hammett plots of the relative reactivities of 1,4-addition and 2,5-addition of benzyne toward substituted benzenes are shown in Figs. 3 and 4, respectively. For 1,4-addition, the plot of the logarithms of the relative reactivities *vs.* σ_p^+ gave a straight line and the reaction constant, ρ, was estimated to be −1.79. A comparison of ρ values for several reactions is made in Table 6. As is seen, the absolute value of the present ρ is much smaller than that for the nitration of substituted benzenes but slightly larger than that for cationic phenylation of substituted benzenes.[19] This fact indicates that some positive charge may be induced in benzyne in the transition state of 1,4-addition.

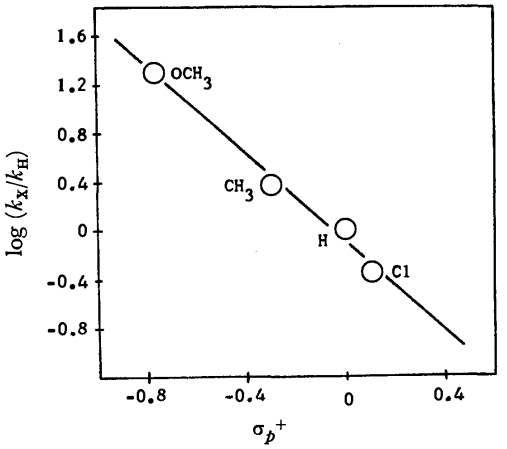

Fig. 3. Hammett plots for 1,4-addition.

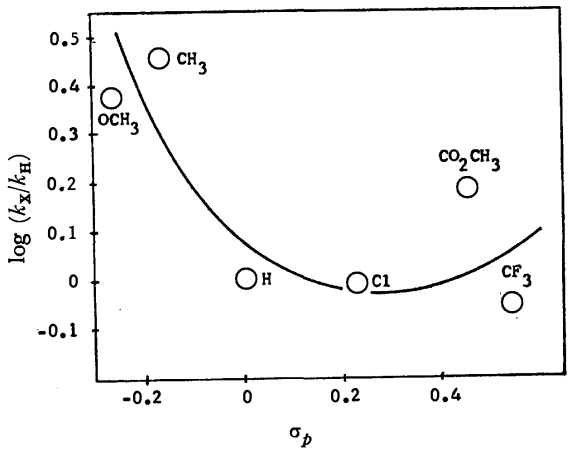

Fig. 4. Hammett plots for 2,5-addition.

TABLE 6. REACTION CONSTANTS FOR SEVERAL REACTIONS OF SUBSTITUTED BENZENES

Reagent	Product	Kind of substituent constant	ρ	Reference
HNO_3–H_2SO_4 (in CH_3NO_2 or Ac_2O, 25 °C)	O_2N–C$_6$H$_4$–X	σ^+	−6.53	16
$PhN_2^+BF_4^-$ (40 °C)	Ph–C$_6$H$_4$–X	σ^+	−1.0	17
$(PhCO_2)_2$ (80 °C)	Ph–C$_6$H$_4$–X	σ_m	0.05	18
Benzyne (≈45 °C)		σ_p^+	−1.79	this work

To a marked contrast, for 2,5-addition, no clear correlation was observed between logarithms of the relative reactivities and σ_p, although some electrophilic nature of benzyne may be seen from Fig. 4. And present substituent effect seems to be similar to that of the radical decomposition of symmetrically disubstituted benzoyl peroxide.[20]

A possible explanation of these results can be made by a concerted mechanism of benzyne with substituted benzenes. Most stable electronic state of benzyne is considered to be a nonbonding diradical.[21] But benzyne is also considered to be strongly polarized in the transition state of the reactions with the nucleophiles[22] as shown for the case of alcohol (Eq. 9). In the transition state of

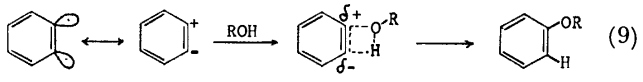

(9)

1,4-addition, because of the steric repulsion between substituent of substituted benzene and hydrogen of benzyne, two bond formations may be unequal. Therefore, the charges are induced in benzyne in the transition state as shown in Fig. 5 and the large substituent effect is observed. On the contrary, for 2,5-addition, this steric repulsion can be negligible, and two bond formations may be equal. Therefore, relatively small charges are

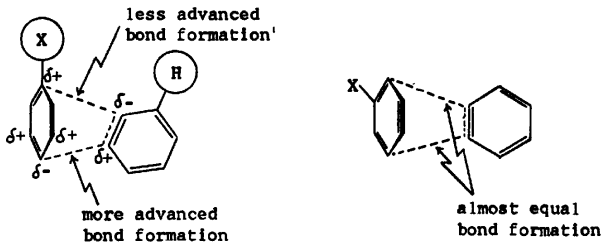

Fig. 5. Unequal bond formations of 1,4-addition and almost equal bond formations of 2,5-addition in the transition states.

induced in benzyne in the transition state (Fig. 5) and the substituent effect appears small. This mechanism also explains the substituent effect of 2,5-addition to be similar to those of the radical reactions. Radical or cationic two step mechanism can neither explain both substituent effects of 1,4- and 2,5-additions satisfactorily at the same time, nor explain no formation of 1,2-adduct(benzocyclooctene derivative).

Double "Ene" Reaction of Benzyne with Toluene. Toluene gave, together with the normal Diels-Alder adducts, the abnormal products *o*-benzylbiphenyl (**13**) and 2-benzyl-3-phenylbenzo[5,6]bicyclo[2.2.2]octatriene (**14**). The formation of **13** was explained by the successive "ene" reactions of two benzyne molecules to one toluene molecule[4] as shown in Eq. 10. The forma-

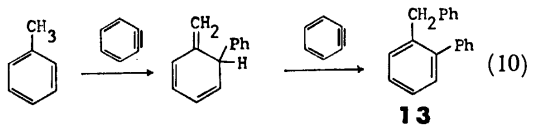

(10)

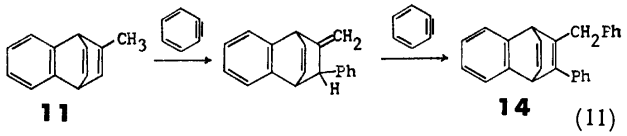

(11)

tion of **14** can be also explained by the successive "ene" reactions of two benzyne molecules to one molecule of **11** (Eq. 11).[23] The fact that intermediates proposed here could not be isolated may be due to the fast second "ene" reactions. The reactions of halogenated benzynes with toluene gave exclusively the Diels-Alder adducts.[1] Thus, there is a remarkable difference between benzyne and halogenated benzyne.

Experimental

Benzenediazonium-2-carboxylate (2). Benzenediazonium-2-carboxylate (**2**) was prepared by the Friedman's method.[3] To a stirring soln of 3 g of anthranilic acid (**1**) in 20 ml of tetrahydrofuran (THF) in the presence of a catalytic amount of trichloroacetic acid was added dropwise 5 g of isopentyl nitrite. The mixture was stirred for 1 h and then cooled with ice bath. After the pale yellow solid of **2** was precipitated, upper liquid was carefully pipetted out, and immediately cold THF was added to the ppt. The mixture was stirred for a moment and kept standing with external cooling until the ppt was settled. Then, the upper THF layer was again removed from the ppt this procedure was repeated until the THF layer became prac-

tically colorless (3—4 times). Then the ppt was similarly washed with dichloromethane twice to remove THF.[10] The ppt, benzenediazonium-2-carboxylate (**2**), thus obtained was used directly for the reaction.

General Procedure of the Reaction of Benzyne with a Substituted Benzene. A mixture of benzenediazonium-2-carboxylate (**2**), prepared from 3—10 g of anthranilic acid (**1**), and 75—500 ml of a substituted benzene was stirred at about 45 °C. After gas evolution had ceased (20—48 h), the mixture was washed with aq sodium hydrogencarbonate soln and water, dried and then concd. The residue was analyzed by gas chromatography (Silicon DC 550, PEG 20M and Golay column of silicon oil). After distillation of the mixture, products were separated by preparative gas chromatography and identified by means of their IR, NMR, and mass spectra.

Reaction of Benzyne with Anisole. Anisole used for the reaction was dried on sodium. Gas chromatographic analysis of the concd crude mixture showed the presence of two products, 1-methoxybenzo[2,3]bicyclo[2.2.2]octatriene (**3**) and benzobicyclo[2.2.2]octadienone (**4**). Distillation of the concd crude mixture at 55—66 °C/0.7 Torr afforded the mixture of **3** and **4**. They were separated by preparative gas chromatography (PEG 20 M). **3** was a colorless oil, n_D^{16} 1.5840; MS, *m/e* (rel intensity) 184 (M^+, 90), 169 (100), 158 (24), 141 (87), 115 (84), and 94 (37); IR (neat), 1330, 1080, 1015, 860, 745, 695, and 680 cm^{-1}. Calcd for $C_{13}H_{12}O$: C, 84.75; H, 6.57%. Found: C, 84.52; H, 6.82%.

4 was the known compd and its IR spectrum was completely consistent with the reported one.[11]

Gas evolution was measured in the reaction of **2**, prepared from 1 g (7.30 mmol) of **1**, with 200 ml of anisole at 48 °C for 9 h, which amounted to 268 ml on water at 16.2 °C, indicating that 5.62 mmol of benzyne to be generated (77% based on **1** used). Gas chromatographic analysis of the crude mixture calibrated with the weighed internal standard (biphenyl) showed that the yields of **3** and **4** were 25 (32) and 6 (8)%, respectively based on **1** used (yields in the parentheses were based on benzyne generated).

Reaction of Benzyne with Chlorobenzene. The concd crude mixture was analyzed by gas chromatography on PEG 20 M which revealed the presence of 1-chlorobenzo[2,3]bicyclo[2.2.2]octatriene (**5**), 2-chlorobenzo[5,6]bicyclo[2.2.2]octatriene (**6**) and a compd **7** together with phenyl benzoate (4% of the total products), biphenylene (19% of the total products) and a small amount of ester not yet characterized. The distillate of the mixture at 70—73 °C/7 Torr consisted of **5**, **6**, biphenylene and phenyl benzoate. Isolations of **5** and **6** were carried out by preparative gas chromatography. **5** was obtained as white crystals, mp 47—48 °C, from ether; MS, *m/e* (rel intensity) 190 (M+2, 12), 188 (M^+, 35), 162 (14), 154 (18), 153 (100), 152 (39), 151 (19), 127 (16), and 126 (10); IR (neat), 1450, 1320, 990, 830, 750, and 685 cm^{-1}. Calcd for $C_{12}H_9Cl$: C, 76.40; H, 4.81; Cl, 18.79%. Found: C, 76.24; H, 5.08; Cl, 18.59%.

6 was obtained as white crystals, mp 47 °C, from ether; MS, *m/e* (rel intensity) 190 (M+2, 17), 188 (M^+, 41), 154 (27), 153 (100), 152 (100), 151 (27), 128 (14), 127 (18), and 126 (13); IR (neat), 1460, 1305, 1005, 820, 810, 750, and 710 cm^{-1}. Calcd for $C_{12}H_9Cl$: C, 76.40; H, 4.81; Cl, 18.79%. Found: C, 76.20; H, 4.77; Cl, 18.58%.

The distillate of the mixture at 116—130 °C/0.9 Torr afforded **7** which was further purified through a column of silica gel (eluted with petroleum ether) and with recrystallization from hexane, mp 128 °C; MS, *m/e* (rel intensity) 266 (M+2, 4), 264 (M^+, 12), 230 (23), 229 (100), 228 (53), 227 (13), 226 (23), 114 (24), 113 (18), 102 (12), and 101 (14); IR (neat), 1490, 1460, 1290, 1250, and 750 cm^{-1}. Calcd for $C_{18}H_{13}Cl$: C, 81.66; H, 4.95; Cl, 13.39%. Found: C, 81.95; H, 5.13; Cl, 13.67%.

Reaction of Benzyne with Methyl Benzoate. Gas chromatographic analysis (Silicon DC 550) of the concd crude mixture showed the presence of 2-methoxycarbonylbenzo[5,6]bicyclo[2.2.2]octatriene (**8**) together with biphenylene (21% of the total products) and phenyl benzoate (25% of the total products). Distilled **8** at 82—90 °C/4 Torr was further purified by preparative gas chromatography, followed by recrystallization from hexane, mp 63.5 °C; MS, *m/e* (rel intensity) 212 (M^+, 58), 169 (12), 154 (20), 153 (100), 152 (70), 151 (19), 128 (20), and 127 (20); IR (neat), 1700, 1240, 1200, 1060, 725, and 690 cm^{-1}. Calcd for $C_{14}H_{12}O_2$: C, 79.23; H, 5.70; O, 15.08%. Found: C, 78.94; H, 5.62; O, 14.79%.

Reaction of Benzyne with Benzotrifluoride. Gas chromatographic analysis (PEG 20 M) of the concd crude mixture showed the presence of 2-trifluoromethylbenzo[5,6]bicyclo[2.2.2]octatriene (**9**) together with biphenylene (45% of the total products) and phenyl benzoate (18% of the total products). Preparative gas chromatography of the distillate at 64—67 °C/3 Torr afforded **9** as a colorless oil, n_D^{16} 1.5092; MS, *m/e* (rel intensity) 222 (M^+, 100), 201 (17), 196 (16), 154 (31), 153 (95), 152 (76), 151 (28), 146 (22), 128 (44), and 127 (19); IR (neat), 1465, 1340, 1260, 1150, 1110, 1015, 740, and 685 cm^{-1}. Calcd for $C_{13}H_9F_3$: C, 70.27; H, 4.08; F, 25.65%. Found: C, 70.81; H, 4.35; F, 25.27%.

Reaction of Benzyne with Toluene. The mixture of **2**, prepared from 3 g of **1**, and 500 ml of toluene in 500 ml of dichloromethane was refluxed for 2 days. After usual work-up, gas chromatographic analysis (PEG 20 M) of the concd crude mixture showed the presence of 1-methylbenzo[2,3]bicyclo[2.2.2]octatriene (**10**), 2-methylbenzo[5,6]bicyclo[2.2.2]octatriene (**11**), small amounts of biphenylene (9% of the total products) and phenyl benzoate (4% of the total products), together with *o*-benzylbiphenyl (**13**) and **12**. The distillate at 68—69 °C/17 Torr consisted of **10** and **11** which were separated by preparative gas chromatography. **10** and **11** were reported elsewhere but their properties were not described.[4] **10** was a colorless oil; MS, *m/e* (rel intensity) 168 (M^+, 96), 167 (68), 165 (36), 153 (100), 152 (49), 149 (81), 141 (45), 128 (73), and 115 (41); IR (neat), 1460, 1445, 1330, 1010, 920, 740, 700, and 680 cm^{-1}. **11** was a colorless oil; MS, *m/e* (rel intensity) 168 (M^+, 100), 167 (71), 155 (38), 153 (97), 152 (54), 149 (62), 141 (45), 128 (85), and 115 (84); IR (neat), 1460, 1310, 805, 735, and 670 cm^{-1}.

The distillate at 64—74 °C/8 Torr consisted of biphenylene, phenyl benzoate and small amounts of **10** and **11**.

The distillate at 70—110 °C/0.8 Torr consisted of **12**, **13**, and **14** in a ratio of 1 : 9 : 4. The mixture was chromatographed through a column of silica gel. Elution with hexane gave a mixture of **12** and **13**. **13** was purified by recrystallization from carbon tetrachloride, melted at 54—55 °C (lit,[24] 54—56 °C). Although **12** was not purified, its structure was tentatively determined on the basis of the NMR spectrum of the mixture of **12** and **13** (**12** was isolated satisfactorily neither by gas chromatography nor by column chromatography). Further elution with a mixture of hexane and benzene gave **14**, recrystallized from hexane; mp 69—71 °C; MS, *m/e* (rel intensity) 320 (M^+, 41), 229 (100), 228 (25), 129 (37), 128 (98), 116 (40), 115 (40), and 105 (28); IR (neat), 1460, 1450, 740, and 690 cm^{-1}. Calcd for $C_{25}H_{20}$: C, 93.71; H, 6.29%. Found: C, 93.53; H, 6.07%.

Even if dichloromethane as a solvent was not used, the products and product composition were scarcely changed.

Competition Reactions of a Series of Substituted Benzenes toward Benzyne. Competition reactions of a series of substituted benzenes toward benzyne were carried out using **2**, prepared

from 0.5 g of **1**, and the following combinations of substituted benzenes: A) benzene 25 g, toluene 25 g; B) benzene 30 g, anisole 20 g; C) benzene 20 g, chlorobenzene 30 g; D) benzene 20 g, benzylidyne trifluoride 30 g; E) chlorobenzene 20 g, methyl benzoate 30 g. Relative reactivities were estimated from the calibrated gas chromatographic analysis and/or NMR analysis of the crude mixtures.

References

1) a) J. P. N. Brewer, I. F. Eckhard, H. Heaney, and B. A. Marples, *J. Chem. Soc., C*, **1968**, 664; b) J. P. N. Brewer and H. Heaney, *Tetrahedron Lett.*, **1965**, 4709; c) D. D. Callander, P. L. Coe, and J. C. Tatlow, *Chem. Commun.*, **1963**, 143; d) D. D. Callander, J. C. Tatlow, and A. J. Uff, *Tetrahedron*, **25**, 25 (1969); e) H. Heaney and J. M. Jablonski, *Tetrahedron Lett.*, **1966**, 4529; f) N. N. Vorozhtsov, V. A. Barkasch, N. G. Ivanova, and A. K. Petrov, *ibid.*, **1964**, 3575; g) J. L. M. Pohlmann and F. E. Brinckman, *Z. Naturforsch*, **20**, 5 (1965); h) R. Harrison and H. Heaney, *J. Chem. Soc., C*, **1968**, 889. i) H. Heaney, K. G. Mason, and J. M. Sketchley, *ibid.*, **1971**, 567.

2) a) R. G. Miller and M. Stiles, *J. Am. Chem. Soc.*, **85**, 1794 (1963); b) M. Stiles, U. Burckhardt, and G. Freund, *J. Org. Chem.*, **32**, 3718 (1967).

3) L. Friedman, *J. Am. Chem. Soc.*, **89**, 3071 (1967).

4) J. M. Brinkley and L. Friedman, *Tetrahedron Lett.*, **1972**, 4141.

5) S. Meyerson and E. K. Field, *Chem. Ind.*, **28**, 1230 (1966).

6) M. Stiles, R. G. Miller, and U. Bruckhardt, *J. Am. Chem. Soc.*, **85**, 1792 (1963).

7) I. Tabushi, K. Fujita, K. Okazaki, H. Yamada, and R. Oda, *Kogyo Kagaku Zasshi*, **72**, 1677 (1969).

8) The products **10**, **11**, and **13** from toluene were already reported by L. Friedman, see Ref. 4.

9) In each case except anisole, biphenylene (9—45% of the total products) and phenyl benzoate (4—25% of the total products) were obtained. But obviously they are not the reaction products of benzyne with substituted benzenes.

10) Anisole distilled on sodium metal was used. In a run where anisole distilled on phosphorus pentoxide was used, diphenyl ether and *o*-hydroxybiphenyl were obtained together with **3** and **4**, and in the presence of tetrahydrofuran, 1,4-diphenoxybutane was also obtained. These products seem to be formed from phenol as follows.

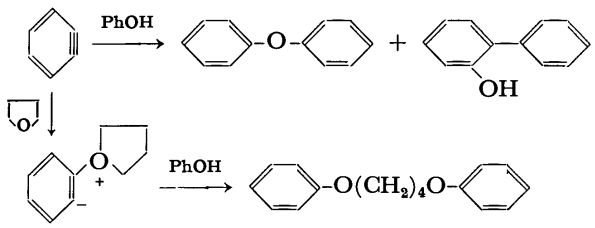

Wolthuis *et al.* reported that from benzyne, tetrahydrofuran and water, 1,4-diphenoxybutane was also obtained. See, E. Wolthuis, B. Bouma, J. Modderman, and L. Sytsma, *Tetrahedron Lett.*, **1970**, 407.

11) K. Kitahonoki and Y. Takano, *Tetrahedron Lett.*, **1963**, 1597. We wish to thank Dr. Takano for his showing us the NMR spectrum of **4** for comparison.

12) In the presence of a silver salt, the reactions of benzyne with substituted benzenes gave mainly biphenyl and/or benzocyclooctene derivatives. See, I. Tabushi, H. Yamada, Z. Yoshida, and R. Oda, *Bull. Chem. Soc. Jpn.*, **50**, 291 (1977).

13) As for toluene, the product **14** was included in 2,5-adduct and the product **12** was included in 1,4-adduct. Similarly for chlorobenzene, the product **7** was included in 2,5-adduct.

14) For anisole and toluene, the results of benzyne were very similar to those of halogenated benzynes. For example, in the case of tetrafluorobenzyne, 86% of 1,4-adduct and 14% of 2,5-adduct from anisole, and 23% of 1,4-adduct and 77% of 2,5-adduct from toluene were obtained. See Ref. 1a.

15) Actually the ratios of 1,4-adducts to 2,4-adducts in reactions of tetrahalogenated benzynes with *t*-butylbenzene were reported to be markedly affected by the bulkiness of halogens. See Ref. 1i.

16) Y. Okamoto and H. C. Brown, *J. Am. Chem. Soc.*, **79**, 1913 (1957).

17) M. Kobayashi, H. Minato, and N. Kobori, *Bull. Chem. Soc. Jpn.*, **43**, 219 (1970).

18) a) D. H. Hey, S. Orman, and G. H. Williams, *J. Chem. Soc.*, **1961**, 565 and the references cited in it; b) R. Ito, T. Migita, N. Morikawa, and O. Simamura, *Tetrahedron*, **21**, 955 (1965).

19) However, some doubt on cationic mechanism have been casted. See Ref. 17.

20) A. T. Blomquist and A. J. Buselli, *J. Am. Chem. Soc.*, **73**, 3883 (1951).

21) a) H. E. Simmons, *J. Am. Chem. Soc.*, **83**, 1657 (1961); b) R. Hoffmann, A. Imamura, and W. J. Hehre, *ibid.*, **90**, 1499 (1968); c) T. Yonezawa, H. Konishi, and H. Kato, *Bull. Chem. Soc. Jpn.*, **41**, 1031 (1968); d) I. Tabushi, R. Oda, and K. Okazaki, *Tetrahedron Lett.*, **1968**, 3743.

22) R. W. Hoffman, "Dehydrobenzene and Cycloalkynes," Academic Press, New York, N. Y. (1967).

23) There is a some possibility of the formation of **14** by the cycloaddition of benzyne to **13**. But, under the experimental condition, that possibility may be small, because the concentration of **13** was much lower than that of toluene and the reactivity of benzyne toward **13** is estimated to be similar to that toward toluene from the result of the substituent effect.

24) J. P. Freeman, *J. Am. Chem. Soc.*, **80**, 1926 (1958).

Reactions of Benzyne-Silver Cation Complex with Substituted Benzenes

Iwao TABUSHI, Hidenori YAMADA, Zenichi YOSHIDA,* and Ryohei ODA*

Department of Pharmaceutical Sciences, Kyushu University, Fukuoka 812

**Department of Synthetic Chemistry, Faculty of Engineering, Kyoto University, Kyoto 606*

(Received April 26, 1976)

The presence of silver perchlorate changed the products in the reaction of benzyne with substituted benzene (anisole, toluene, chlorobenzene or methyl benzoate) to increase biphenyl and/or benzylidyne trifluoride derivatives by the sacrifice of benzobicyclo[2.2.2]octatriene derivatives. In the case of toluene, *o*-methylbiphenyl (**15**) and 6-methylbenzocyclooctene (**14**) were considered to be formed *via* common intermediate. These results were well explained by an assumption of benzyne-silver cation complex. From competition experiments, it was concluded that benzyne·silver cation complex assumed here had a stronger electrophilicity than benzyne itself.

In the previous paper, we reported the reactions of benzyne with substituted benzenes in the absence of a silver salt to yield benzobicyclo[2.2.2]octatriene derivatives.[1] Stiles *et al.* reported the reaction of benzyne with benzene giving biphenyl (**1**), benzocyclooctene (**2**), benzobicyclo[2.2.2]octatriene (**3**) and one two to one adduct **4**.[2] The addition of Ag^+ in the reaction of benzyne with benzene was reported by Friedman to increase **1** and **2** by the sacrifice of **3**.[3] We also reported that the addition of Hg^+, Hg^{2+}, Sn^{2+}, Co^{2+}, or V^{3+} changed the product distribution in the reaction of benzyne with benzene.[4] Friedman proposed a cationic mechanism of benzyne-silver cation complex to explain the change of the product distribution in the reaction of benzyne with benzene in the presence of a silver salt (Eq. 1).[3] Vedejs

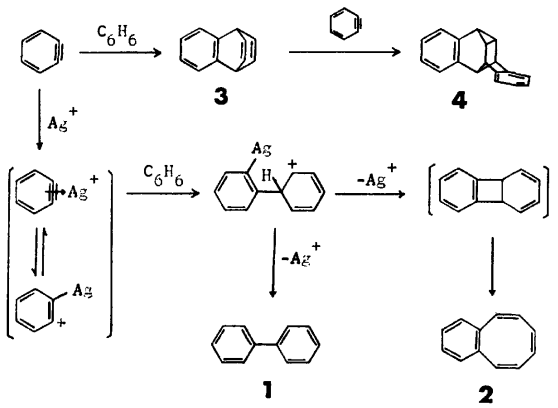

(1)

et al. supported the cationic nature of benzyne-silver cation complex from the result of the reaction of benzyne with cyclooctatetraene in the presence of a silver salt.[5]

In this paper, we wish to report the products and the relative reactivities of substituted benzenes treated with benzyne in the presence of silver perchlorate and to discuss the nature of benzyne in the presence of silver cation.

Results

The thermolysis of benzenediazonium-2-carboxylate (**6**), prepared from anthranilic acid (**5**), was carried out in an excess of substituted benzene (anisole, toluene, chlorobenzene, methyl benzoate or benzylidyne trifluoride) in the presence of silver perchlorate. The products are shown in Scheme 1 and the product compositions in the typical runs are summarized in Table 1.

The reaction of benzyne with anisole in the presence of silver perchlorate gave methoxybiphenyls (**9**—**11**), 1-methoxybenzo[2,3]bicyclo[2.2.2]octatriene (**7**) and benzobicyclo[2.2.2]octadienone (**8**) but did not give benzocyclooctene derivatives.

Toluene gave methylbiphenyls (**15**—**17**), 1-methylbenzo[2,3]bicyclo[2.2.2]octatriene (**12**), 2-methylbenzo[5,6]bicyclo[2.2.2]octatriene (**13**) and hydrocarbon **14**. **14** was a colorless oil and the molecular peak of its mass spectrum was observed at 168 (*m/e*), indicating **14** to be an one to one adduct of benzyne and toluene. IR spectrum of this compound was similar to that of benzocyclooctene (**2**)[6] in the range of 850—650 cm^{-1}. NMR spectrum of **14** in CCl_4 with 100 MHz showed the ratio of aromatic, olefinic and aliphatic protons to be 4: 3: 3. These observations may indicate **14** to be one of methylbenzocyclooctenes. For comparison, NMR spectra of **14** and **2**[7] are shown in Table 2. Only 6-methylbenzocyclooctene can well explain the NMR spectrum of **14**.

TABLE 1. THE PRODUCT COMPOSITIONS OF THE REACTIONS OF BENZYNE WITH SUBSTITUTED BENZENES IN THE PRESENCE OF SILVER PERCHLORATE[a]

Substrate (ml)	**5**(g)	$AgClO_4$ (mg)	Product composition (%)					
Anisole(500)	3	75.0	**7** 10.3	**8** 2.7	**9** 74.5	**10** 1.4	**11** 11.1	
Toluene(170)	3	35.7	**12** 3.3	**13** 7.8	**14** 7.7	**15** 54.3	**16** 18.6	**17** 8.1
Chlorobenzene(200)	1	166	**18** 1.5	**19** 11.1	**20** 68.0	**21** 15.8	**22** 1.0	**23** 2.6
Methyl benzoate(50)	1	115.7	**24** 7.5	**25** 59.6	**26** 32.9			
Benzylidyne trifluoride(50)	1	301	**27** 100					

a) The product compositions were determined by means of gas chromatography (PEG 20M and Silicon DC 550).

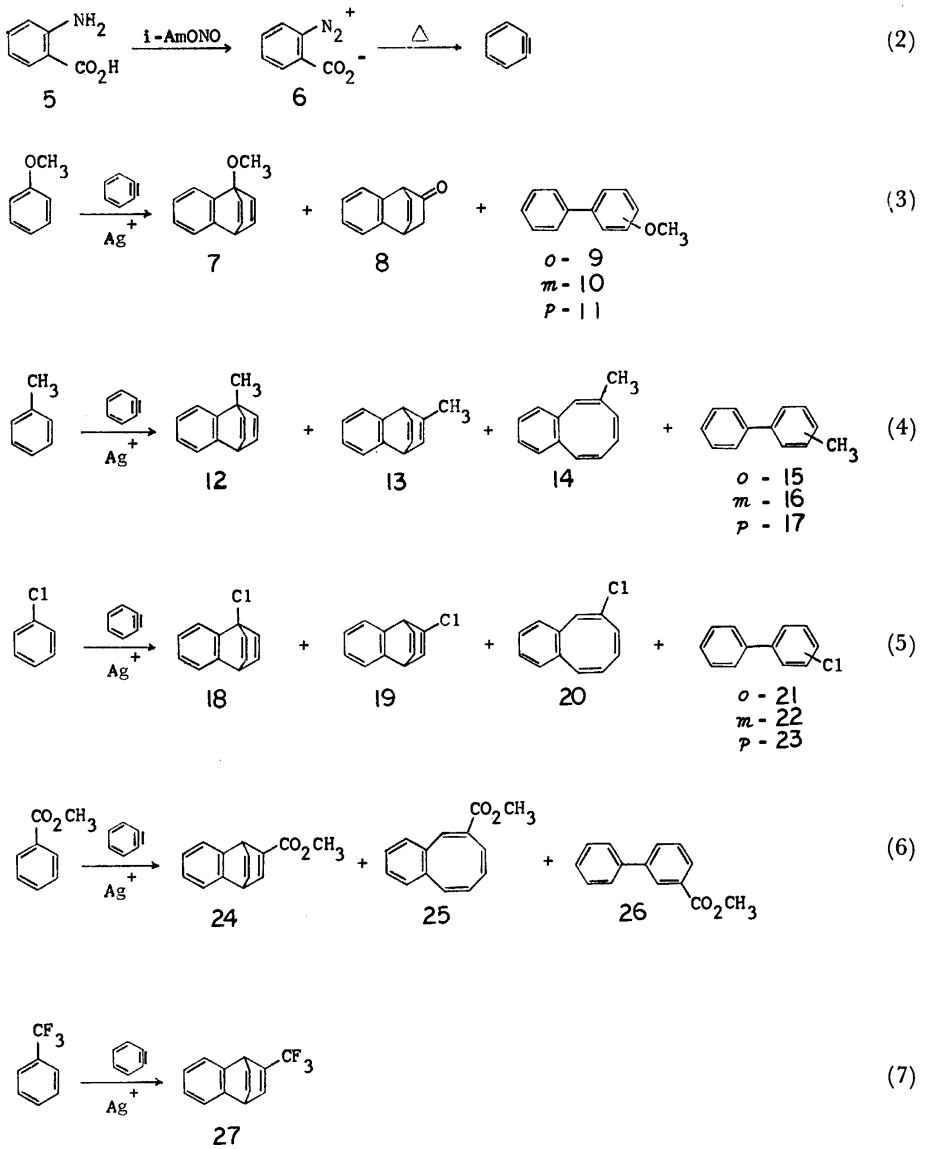

Scheme 1. The products of the reactions of benzyne with substituted benzenes in the presence of silver perchlorate.

The yields of **12**+**13**, **14**, **15**, **16**, and **17** were 2, 4, 31, 10, and 5%, respectively, based on benzyne generated.

From chlorobenzene, 1-chlorobenzo[2,3]bicyclo-[2.2.2]octatriene (**18**), 2-chlorobenzo[5,6]bicyclo[2.2.2]-octatriene (**19**), chlorobiphenyls (**21**—**23**) and compound **20** were obtained. On the basis of the NMR spectrum (Table 2), **20** was determined to be 6-chlorobenzocyclooctene.

In the case of methyl benzoate, the decomposition of benzenediazonium-2-carboxylate (**6**) was markedly retarded by silver perchlorate. Heating of a mixture of **6** prepared from 1 g of **5**, 50 ml of methyl benzoate and 115 mg of silver perchlorate at 55 °C for 13 h did not decompose the precipitates of **6** appreciably and additional heating of the mixture at 90 °C for 9 h gave only small amounts of products. Gas chromatographic analysis of the reaction mixture showed the presence of six products, methylbenzo[5,6]bicyclo[2.2.2]octatriene-2-carboxylate (**24**), methyl 3-biphenylcarboxylate (**26**), compound **25**, one undetermined compound, phenyl benzoate and phenyl salicylate.[2] The latter two products were not the products from benzyne and methyl benzoate,[1] and the undetermined compound was not considered to be a one to one adduct of benzyne and methyl benzoate because of its long retention time in gas chromatography. Compound **25** was considered to be benzocyclooctene derivative based on the NMR and IR spectra, and we determined **25** to be methyl 6-benzocyclooctenecarboxylate, tentatively (Table 2).

From benzylidyne trifluoride, only 2-trifluoromethylbenzo[5,6]bicyclo[2.2.2]octatriene (**27**), biphenylene and phenyl benzoate were obtained, but biphenyl or benzocyclooctene derivatives were not obtained.

The effects of the concentration of silver perchlorate on the distributions of the products of biphenyl and/or benzocyclooctene derivatives were examined, in the cases of anisole, toluene and chlorobenzene. The results

Table 2. NMR spectra of **14**,[a] **20**,[a] **25**,[8] and **2**[b]

Compound	Proton	Chemical shift (τ)
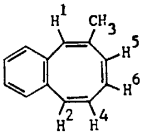 **14**	Aromatic H	2.95—3.3 (m, 4H)
	H^1	3.74 (d, J_{H^1,CH_3}=1.2 Hz, 1H)
	H^2	3.52 (d, J_{H^1,H^2}=11.7 Hz, 1H)
	H^4	4.03 (br d, 1H)
	H^5, H^6	4.24 (br s, 2H)
	CH_3	8.12 (d, 3H)
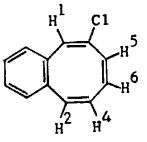 **20**	Aromatic H	2.7—3.2 (m, 4H)
	H^1	3.29 (s, 1H)
	H^2	3.40 (d, J_{H^1,H^2}=10.9 Hz, 1H)
	H^4	3.92 (br d, 1H)
	H^5, H^6	4.10 (br s, 2H)
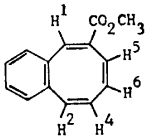 **25**	Aromatic H	2.7—3.2 (m, 4H)
	H^1	2.30 (s, 1H)
	H^2	3.45 (d, J_{H^1,H^2}=11.6 Hz, 1H)
	H^4, H^5, H^6	3.8—4.15 (m, 3H)
	CH_3	6.21 (s, 3H)
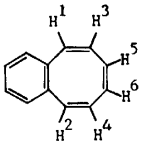 **2**	H^1, H^2	3.39, 3.51
	H^3, H^4	3.94, 4.06
	H^5, H^6	4.13

a) With 1% TMS as an internal standard in CCl_4, 60 MHz (**14** and **20**) or 100 MHz (**25**). Abbreviations are: s, singlet; d, doublet; m, multiplet; br, broad. b) The values reported in Ref. 7, 100 MHz.

Table 3. The effect of the concentration of silver perchlorate on the distribution of methoxybiphenyls in the reaction of benzyne with anisole

Run	**5** g	Anisole ml	$AgClO_4$/**5** mg/g	Distribution (%)		
				o-(**9**)	*m*-(**10**)	*p*-(**11**)
1	3	500	25	85.7	1.6	12.7
2[a]	1	33	28	86.4	1.3	12.3
3[a]	1	25	47	91.6	0	8.4

a) Result from competition reaction with benzene.

are shown in Tables 3—5.

Competition reactions were carried out to investigate the relative reactivities of benzyne toward substituted benzenes in the presence of silver perchlorate. The relative reactivities were calculated from the amounts of biphenyl and benzocyclooctene derivatives produced, since they were considered to be the products concerned with silver perchlorate (*vide infra*). The results are shown in Table 6.

Discussion

In the presence of silver perchlorate, the reactions of benzyne with anisole, toluene, chlorobenzene and methyl benzoate, as well as benzene,[3] gave predominantly biphenyl and/or benzocyclooctene derivatives, in marked contrast to the results in the absence of silver perchlorate where the main products were benzobicyclo[2.2.2]octatriene derivatives.[1] In the case of benzylidyne trifluoride having a strong electron-withdrawing

Table 4. The effect of the concentration of silver perchlorate on the distribution of methylbiphenyls and 4-methyl-1,2-benzocyclooctene in the reaction of benzyne with toluene

Run	**5** g	Toluene ml	$AgClO_4$/**5** mg/g	Distribution (%)				
				14	*o*-(**15**)	**14**+**15**	*m*-(**16**)	*p*-(**17**)
1	3	170	11.9	8.6	61.3	69.9	20.9	9.3
2[a]	1	100	16.2	16.9	55.0	71.9	19 2	8.9
3	3	500	18.3	27.9	43.4	71.3	19.4	9.4
4	1	200	21	18.8	56.2	75.0	15.1	9.9
5	2	200	27	7.2	62.4	69.6	19.5	10.9
6[a]	1	50	40	9.4	61.2	70.6	20.0	9.4

a) Result from competition reaction with benzene.

Table 5. The effect of the concentration of silver perchlorate on the distribution of chlorobiphenyls and 6-chlorobenzocyclooctene in the reaction of benzyne with chlorobenzene

Run	**5** g	Chlorobenzene ml	$AgClO_4$/**5** mg/g	Distribution (%)				
				20	*o*-(**21**)	**20**+**21**	*m*-(**22**)	*p*-(**23**)
1	1	150	9.1	73.3	25.0	98.3	0	1.7
2	3	400	29	68.4	28.4	96.8	1.1	2.1
3	1	150	53	78.3	18.9	97.2	0.9	1.9
4	1	150	165.3	82.0	18.0	100	0	0
5[a]	1	400	329	77.8	18.0	95.8	1.2	3.0

a) Result from competition reaction with benzene.

TABLE 6. RELATIVE REACTIVITIES OF SUBSTITUTED BENZENES TO BENZENE TOWARD BENZYNE IN THE PRESENCE OF SILVER PERCHLORATE

Substituted benzene	ml	Benzene ml	5	$AgClO_4$ mg	k_H/k_R [a]
$PhOCH_3$	25	100	1	47.3	5.17
$PhOCH_3$	33	99	1	28.0	5.26
$PhCH_3$	100	100	1	16.2	2.39
$PhCH_3$	25	100	1	40.0	3.10
PhCl	400	20	1	329	0.0662
PhCl	200	10	1	166	0.0711

a) Relative reactivity of substituted benzene to benzene.

group, silver perchlorate did not change the product. Thus, it is concluded that silver cation catalyzes the formations of biphenyl and/or benzocyclooctene derivatives in the reactions of benzyne with substituted benzenes, unless the substituent is a strong electron-withdrawing group such as CF_3.

For toluene, the distribution of 6-methylbenzocyclooctene (**14**) and *o*-methylbiphenyl (**15**) was affected by the concentration of silver perchlorate, but the sum of **14** and **15** was almost constant (Table 4). This may indicate that 6-methylbenzocyclooctene and *o*-methylbiphenyl are formed *via* a common intermediate. Similar situation was observed in the distribution of 6-chlorobenzocyclooctene (**20**) and *o*-chlorobiphenyl (**21**) in the case of chlorobenzene (Table 5). These observations can be well explained by benzyne-silver cation complex proposed by Friedman[3] (Eq. 1). Namely benzyne-silver cation complex attacks ortho position of a substituted benzene(toluene or chlorobenzene) forming the common intermediate **28** and then leaving of silver cation together with carbon-carbon bond formation gives 6-substituted benzocyclooctene (Eq. 9) or leaving of silver cation together with proton transfer gives *o*-substituted biphenyl (Eq. 8). In this mechanism the formation of 5-substituted benzocyclooctene is also possible, but it may be inhibited by the steric effect of a substituent. There is no satisfactory explanation of the effect of the concentration of silver perchlorate on the distribution of **14** and **15**.

Orientations of Benzyne-Silver Cation Complex to Substituted Benzenes. In the case of toluene, both of 6-methylbenzocyclooctene (**14**) and *o*-methylbiphenyl (**15**) should be included in ortho oriented products, since they were considered to be formed *via* the common intermediate. Similar situation was present in 6-chlorobenzocyclooctene (**20**) and *o*-chlorobiphenyl (**21**) from chlorobenzene. Table 7 shows the orientations of benzyne-silver cation complex to anisole, toluene and chlorobenzene, together with those of phenyl cation[8] and phenyl radical.[9-11] Obviously, the orientations of benzyne-silver cation complex were mostly ortho and very different from those of phenyl cation and phenyl radical. Therefore, we can not discuss the nature of benzyne-silver cation complex only from the distribution of the products from substituted benzene, although Friedman suggested that the distribution of isomeric methylbiphenyls should reveal the nature of benzyne–silver cation complex.[3]

TABLE 8. THE RELATIVE REACTIVITIES OF BENZYNE–SILVER CATION COMPLEX TOWARD THE ORTHO POSITIONS OF SUBSTITUTED BENZENES (F_o)

Substituent	OCH_3	CH_3	H	Cl
F_o	16.5	7.6	1	0.247

Relative Reactivities of Benzyne-Silver Cation Complex toward Substituted Benzenes. From Tables 6 and 7, the relative reactivities of benzyne-silver cation complex toward the ortho positions of substituted benzenes (partial rate factor, F_o) were estimated (Table 8).[12] As is seen, F_o changed about 65-fold with changing substituent from Cl to OCH_3. Hammett plots of log F_o *vs.* σ_p^+ are shown in Fig. 1. A linear relationship was roughly observed between log F_o and σ_p^+, and the reaction constant, ρ, was estimated to be -2.0. A comparison of ρ values for several reactions is made in Table 9. The absolute value of the present ρ is much smaller than that for nitration of substituted benzenes but twice as large as that for cationic phenylation of substituted benzenes and slightly larger than that for 1,4-addition of

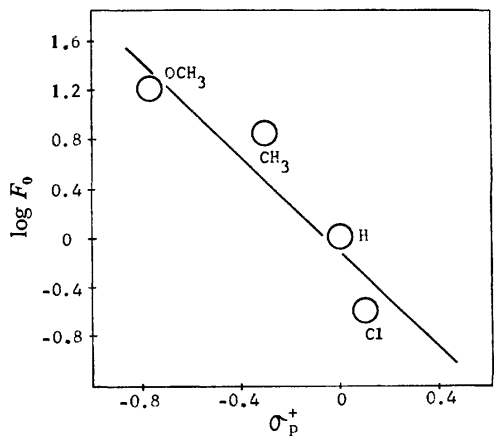

Fig. 1. The Hammett plots for ortho addition reactions of benzyne–silver cation complex to substituted benzenes.

TABLE 7. ORIENTATIONS OF BENZYNE–SILVER CATION COMPLEX, PHENYL CATION AND PHENYL RADICAL

Reagent	$PhOCH_3$			$PhCH_3$			PhCl		
	o	*m*	*p*	*o*	*m*	*p*	*o*	*m*	*p*
Benzyne–Ag^+ (45 °C)[a]	88	1	11	71	19	10	98	0.5	1.5
$PhN_2^+BF_4^-$ (in DMSO, 40 °C)[b]	56.4	12.1	31.8	47.3	21.1	31.6	42.8	24.0	27.8
$(PhCO_2)_2$ (80 °C)	67[c]	28[c]	5[c]	66.5[d]	19.2[d]	14.3[d]	50.1[e]	31.6[e]	18.3[e]

a) This work. b) Ref. 8. c) Ref. 9). d) Ref. 10. e) Ref. 11.

Table 9. Reaction constants for several reactions of substituted benzenes

Reagent	Product	Kind of substituent constant	ρ	Reference
HNO_3–H_2SO_4 (in CH_3NO_2 or Ac_2O, 25 °C)	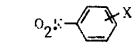	σ^+	−6.53	13
$PhN_2^+BF_4^-$ (40 °C)	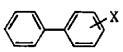	σ^+	−1.0	14
$(PhCO_2)_2$ (80 °C)	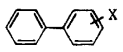	σ_m	0.05	9, 15
Benzyne (≈45 °C)		σ_p^+	−1.79	1
Benzyne–Ag^+ (≈45 °C)	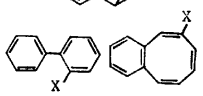	σ_p^+	−2.0	This work

Table 10. Percentages of the formations of 6-substituted benzocyclooctene (6-BCOT) and *o*-substituted biphenyl (*o*-BP) in the reaction of benzyne–silver cation complex with substituted benzene

Substituent	OCH_3	CH_3	H[a]	Cl
4-BCOT	0	10—39	29—46[b]	70—92
o-BP	100	90—61	71—54[c]	30— 8

a) Refs. 2 and 3. b) Benzocyclooctene (**2**).
c) Biphenyl (**1**).

benzyne to substituted benzenes. Thus, it is concluded that benzyne-silver cation complex has a larger electrophilicity than phenyl cation and benzyne itself. This supports the cationic mechanism proposed by Friedman (Eq. 1).[3]

Substituent Effect on the Formation of Benzocyclooctene vs. Biphenyl Derivatives. Table 10 shows the percentages of 6-substituted benzocyclooctene (6-BCOT) and *o*-substituted biphenyl (*o*-BP) from the reactions of benzyne–silver cation complex with substituted benzenes, together with those of benzocyclooctene and biphenyl from benzene. Obviously, the formation of 6-BCOT or *o*-BP depends on the electron-donating (or electron-withdrawing) nature of a substituent of a substituted benzene. Namely, anisole having an electron-donating substituent gave exclusively *o*-methoxybiphenyl, while chlorobenzene having an electron-withdrawing substituent gave predominantly 6-chlorobenzocyclooctene. These results can be explained by the following way.

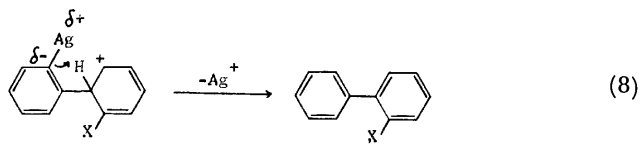

(8)

28

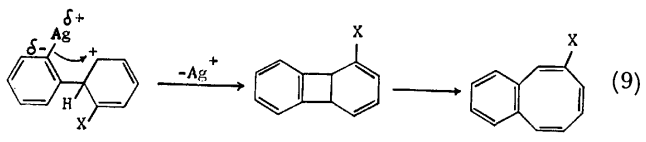

(9)

28

An electron-donating substituent stabilizes the intermediate cyclohexadienyl cation **28** and may reduce the electrophilicity of the cation to the carbon attached to silver. Thus, elimination of silver cation with proton transfer becomes predominant to increase the formation of *o*-substituted biphenyl (Eq. 8). On the other hand, an electron-withdrawing substituent may be reduce the electrophilicity of the cation **28** and elimination of silver cation with cyclization becomes more predominant to increase the formation of 6-substituted benzocyclooctene (Eq. 9). A very strong electron-withdrawing substituent like CF_3 destabilizes the intermediate cyclohexadienyl cation and the cation may not be formed. Thus, the fact that benzylidyne trifluoride did not give biphenyl or benzocyclooctene derivatives could be understood.

Experimental

General Procedure of the Reaction of Benzyne with Substituted Benzene in the Presence of Silver Perchlorate. Benzenediazonium-2-carboxylate (**6**), prepared from 1—3 g of anthranilic acid (**5**) by the method described elsewhere,[1] was stirred in 25—500 ml of a substituted benzene in the presence of a proper amount of silver perchlorate at about 45 °C. After gas evolution had ceased (20—64 h), the mixture was washed with aq sodium hydrogencarbonate soln and water, and dried on calcium chloride. After removal of the most of substituted benzene, the residue was analyzed by gas chromatography (PEG 20 M, Silicon DC 550).

Reaction of Benzyne with Anisole in the Presence of Silver Perchlorate. After the treatment as described above, gas chromatographic analysis (PEG 20 M, Silicon DC 550) of the concd crude mixture showed the presence of 1-methoxybenzo[2,3]bicyclo[2.2.2]octatriene (**7**), benzobicyclo[2.2.2]octadienone (**8**), methoxybiphenyls (**9**—**11**) and a small amount of phenyl benzoate (6% of the total products). All products were consistent with the authentic samples on the basis of the IR spectra and the retention times on gas chromatography, respectively.

Reaction of Benzyne with Toluene in the Presence of Silver Perchlorate. After the treatment as described above, gas chromatographic analysis (PEG 20 M, Silicon DC 550) of the concd crude mixture revealed the presence of 1-methylbenzo[2,3]bicyclo[2.2.2]octatriene (**12**). 2-methylbenzo[5,6]bicyclo[2.2.2]octatriene (**13**), methylbiphenyls (**15**—**17**) and 4-methyl-1,2-benzocyclooctene (**14**). **14** was isolated by preparative gas chromatography (PEG 20 M) from the distillate of the crude mixture at 57 °C/8 Torr. **14** was a colorless oil: MS, *m/e* (rel intensity) 168 (M^+, 92), 167 (49), 165 (28), 153 (100), 152 (50), 141 (21), 128 (44), and 115 (30); IR (neat), 1490, 1430, 830, 790, 760, 725, and 690 cm^{-1}.

Other products were all consistent with the authentic samples on the basis of the IR spectra and the retention times on gas chromatography (PEG 20 M, Silicon DC 550), respectively.

In another experiment using **6** prepared from 2 g (14.6 mmol) of **5**, 200 ml of toluene and 54 mg of silver perchlorate, evolution of 14.4 mmol of gases (N_2 and CO_2, 50% yield of benzyne based on **5** used) was observed. Gas chromatographic analysis of the crude mixture added with weighed diphenylmethane indicated the yields of **12**+**13**, **14**, **15**, **16**, and **17** to be 2, 4, 31, 10, and 5%, respectively, based on benzyne generated.

Reaction of Benzyne with Chlorobenzene in the Presence of Silver Perchlorate. Gas chromatographic analysis (PEG 20 M) of the concd crude mixture indicated the presence of 1-chloro-

benzo[2,3]bicyclo[2.2.2]octatriene (**18**), 2-chlorobenzo[5,6]-bicyclo[2.2.2]octatriene (**19**), 6-chlorobenzocyclooctene (**20**) and chlorobiphenyls (**21**—**23**) together with phenyl benzoate (10—20% of the total products). After distillation of the crude mixture at 47—53 °C/3 Torr, **20** was isolated by preparative gas chromatography (PEG 20 M) as a pale yellow oil: n_D^{16} 1.6226; MS, *m/e* (rel intensity) 190 (M+2, 16), 188 (M^+, 47), 154 (28), 153 (100), 152 (58), 151 (36), 150 (14), 128 (11), 127 (14), and 126 (13); IR (neat), 1495, 1100, 830, 795, 770, and 725 cm^{-1}. Calcd for $C_{12}H_9Cl$: C, 76.40; H, 4.81; Cl, 18.79%. Found: C, 76.38; H, 4.74; Cl, 18.52%.

Other products were all consistent with the authentic samples on the basis of the IR spectra and the retention times on gas chromatography (PEG 20 M), respectively.

Reaction of Benzyne with Methyl Benzoate in the Presence of Silver Perchlorate. A mixture of **6** prepared from 1 g of **5**, 116 mg of silver perchlorate and 50 ml of methyl benzoate was heated at 55 °C for 13 h and then 90 °C for 9 h, but only small amount of **6** was decomposed. The most of methyl benzoate was distilled off at 100 °C using 10 cm of packed column and then the residue was dissolved in ether. The ether soln was washed with aq ammonia and sat sodium chloride soln and dried on sodium sulfate, and then concd. Gas chromatographic analysis (Silicon DC 550) of the residue showed six peaks. First three peaks were due to phenyl benzoate (29% of the total products), 2-methoxycarbonylbenzo[5,6]bicyclo-[2.2.2]octatriene (**24**) (3% of the total products) and phenyl salicylate (13% of the total products), in the order of retention time. These products were all consistent with the authentic samples on the basis of the IR spectra and the retention times on gas chromatography (Silicon DC 550), respectively. The fourth peak (22% of the total products) was tentatively determined to be that of methyl 6-benzocyclooctenecarboxylate (**25**) which was isolated by preparative gas chromatography (Silicon DC 550) after column chromatography through silica gel with benzene. **25** was a pale yellow oil: IR (neat), 1715, 1240, 1065, 800, 755, 730, and 710 cm^{-1}. The fifth peak was that of methyl 3-biphenylcarboxylate (**26**) which was consistent with authentic sample on the basis of the IR spectrum and the retention time on gas chromatography. The last peak (20% of the total products) had a 2—3 times longer retention time than the other five peaks. This compd had a IR absorption at 1730 cm^{-1} but the structure was uncertain.

Reaction of Benzyne with Benzylidyne Trifluoride in the Presence of Silver Perchlorate. Reaction of **6** prepared from 1 g of **5**, with 50 ml of benzylidyne trifluoride in the presence of 301 mg of silver perchlorate gave 2-trifluoromethylbenzo[5,6]bicyclo-[2.2.2]octatriene (**27**) (30% of the total products), biphenylene (38% of the total products) and phenyl benzoate (32% of the total products). All products were consistent with authentic samples based on the IR spectra and the retention times on gas chromatography (PEG 20 M, Silicon DC 550).

Competition Reactions of a Series of Substituted Benzenes toward Benzyne in the Presence of Silver Perchlorate. Competition reactions of a series of substituted benzenes toward benzyne in the presence of silver perchlorate were carried out under usual conditions. Relative reactivities of substituted benzenes were estimated from the calibrated gas chromatographic analyses (PEG 20 M, Silicon DC 550) of the crude reaction mixtures. The results are shown in Table 6.

References

1) I. Tabushi, H. Yamada, Z. Yoshida, and R. Oda, *Bull. Chem. Soc. Jpn.*, **50**, 285 (1977).
2) a) R. G. Miller and M. Stiles, *J. Am. Chem. Soc.*, **85**, 1794 (1963); b) M. Stiles, U. Burckhardt, and G. Freunt, *J. Org. Chem.*, **32**, 3718 (1967).
3) L. Friedman, *J. Am. Chem. Soc.*, **89**, 3701 (1967).
4) I. Tabushi, K. Fujita, K. Okazaki, H. Yamada, and R. Oda, *Kogyo Kagaku Zasshi*, **72**, 1677 (1969).
5) E. Vedejs and R. A. Shepherd, *Tetrahedron Lett.*, **1970**, 1863.
6) G. Wittig, H. Eggers, and P. O. Duffner, *Ann. Chem.*, **619**, 10 (1958).
7) J. A. Elix, M. V. Sargent, and F. Sondeheimer, *Chem. Commun.*, **1966**, 510.
8) M. Kobayashi, H. Minato, E. Yamada, and N. Kobori, *Bull. Chem. Soc. Jpn.*, **43**, 215 (1970).
9) R. Ito, T. Migita, N. Morikawa, and O. Simamura, *Tetrahedron*, **21**, 955 (1965).
10) D. H. Hey, B. W. Dengilly, and G. H. Williams, *J. Chem. Soc.*, **1956**, 1463.
11) E. C. Shih, D. H. Hey, and G. H. Williams, *J. Chem. Soc.*, **1957**, 2600.
12) As yields of meta and para addition products were very low, it is dangerous to discuss about F_m and F_p.
13) Y. Okamoto and H. C. Brown, *J. Am. Chem. Soc.*, **79**, 1913 (1957).
14) M. Kobori, H. Minato, and N. Kobori, *Bull. Chem. Soc. Jpn.*, **43**, 219 (1970).
15) D. H. Hey, S. Orman, and G. H. Williams, *J. Chem. Soc.*, **1961**, 565 and references cited in it.

NOTES

BULLETIN OF THE CHEMICAL SOCIETY OF JAPAN, VOL. 50 (1), 297—298 (1977)

Fluorescence of 9-Aminoacridine Bound to Polynucleotides

Yukio KUBOTA and Yasuo FUJISAKI
Department of Chemistry, Yamaguchi University, Yamaguchi 753

(Received August 26, 1976)

Synopsis. The fluorescence of 9-aminoacridine is completely quenched when bound to poly (dG)·poly (dC), the quantum yield of fluorescence being nearly equal to that of free dye when bound to poly d(A–T). The dye bound to DNA shows a weak fluorescence for which the AT pair is responsible.

The interaction of 9-aminoacridine (9-AA) with DNA is of special interest because of its strong mutagenic activity.[1] In a previous paper,[2] it was reported that the fluorescence of 9-AA bound to DNA is almost completely quenched. In order to elucidate the interaction between 9-AA and the binding sites, fluorescence properties of 9-AA bound to DNA, poly d(A–T) and poly (dG)·poly (dC) were examined as a function of nucleotide to dye (P/D) ratio.

Experimental

9-AA (Tokyo Kasei) was purified by repeated crystallization and chromatography. Calf thymus DNA (Worthington Biochemical Corporation), poly d(A–T) and poly (dG)·poly (dC) (Miles Laboratories) were used.

Fluorescence and fluorescence-excitation (FE) spectra were measured with a Hitachi MPF-2A fluorescence spectrophotometer. Both spectra were corrected for the sensitivity of the detector system and the spectral-energy distribution of the exciting light. The fluorescence quantum yields were measured according to the method of Parker and Rees.[3] Fluorescence lifetimes were determined by the phase-shift measurements.[2] All the measurements were carried out in a 0.005 M phosphate buffer (pH 6.9) at 25 °C.

Results and Discussion

The results of fluorescence lifetimes (τ) and quantum yields (Φ_F) of 9-AA bound to DNA, poly d(A–T) and poly (dG)·poly (dC) are summarized in Table 1. The fluorescence of 9-AA is remarkably quenched when bound to DNA or poly (dG)·poly (dC), whereas the fluorescence quantum yield is approximately equal to that of free dye when bound to poly d(A–T). The fluorescence and FE spectra of 9-AA bound to polynucleotides were examined to obtain information on the fluorescing species. The fluorescence spectra of 9-AA bound to DNA and poly d(A–T) are almost the same, showing a red shift when compared to that of free dye (Fig. 1). We see that the fluorescence and FE spectra of 9-AA bound to poly (dG)·poly (dC) are superimposable on the corresponding fluorescence and FE spectra of free dye, respectively. Each FE spectrum was the same as the corresponding absorption spectrum except for 9-AA–poly (dG)·poly (dC) system. The fluorescence lifetimes of 9-AA–poly (dG)·poly (dC) system are almost the same as the lifetime of free dye (Table 1). In view of these findings, the following

Table 1. Fluorescence lifetimes (τ) and quantum yields (Φ_F) of 9-AA bound to polynucleotides

P/D	DNA		Poly d(A–T)		Poly (dG)·poly (dC)	
	τ(ns)	Φ_F	τ(ns)	Φ_F	τ(ns)	Φ_F
0	17.5	0.98	17.5	0.98	17.5	0.98
590	14.9	0.03				
250			34	0.82		
200	15.1	0.03				
100	15.4	0.03	37	0.81	15.3	0.00_6
50	14.8	0.03_5	38	0.81	15.7	0.01
20	15.0	0.03_5	38	0.77	17.0	0.04_5
10[a]	15.5	0.07	29	0.74	17.5	0.14

a) The contribution of free dye is not negligible.

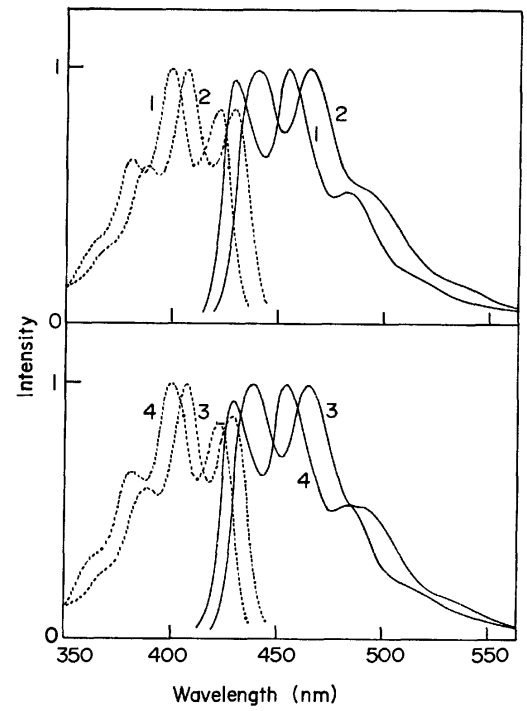

Fig. 1. Normalized corrected fluorescence (——) and FE (------) spectra of 9-AA (6.0×10^{-6} M) in 0.005 M phosphate buffer (pH 6.9) at 25 °C: (1) free, (2) bound to DNA (P/D=590), (3) bound to poly d(A–T) (P/D=250) and (4) bound to poly (dG)·poly (dC) (P/D=50). The excitation and emission wavelengths were 390 and 460 nm, respectively.

conclusions can be drawn: (1) the fluorescence of 9-AA–poly (dG)·poly (dC) system originates from free dye present in solutions;[4] the GC pair completely quenches the fluorescence of bound dye; (2) the AT pair is responsible for a weak fluorescence of 9-AA bound to DNA.

On the other hand, the fluorescence lifetime (34—38 ns) of 9-AA bound to poly d(A-T) is about twice that of free dye (Table 1). Our value is in agreement with the value obtained by nanosecond pulse fluorometry.[5] Such a long lifetime, however, seems to be reasonable on the basis of the strong hypochromicity of bound dye. The area under the absorption spectrum of bound dye plotted against wave number is reduced to about half the corresponding value of free dye. According to the method of Strickler and Berg,[6] the radiative lifetimes (τ_0) of free 9-AA and 9-AA bound to poly d(A-T) were calculated to be 17 and 37 ns, respectively. The τ/τ_0 value is approximately equal to the corresponding Φ_F value for both free and bound dye.

The results of 9-AA bound to DNA are somewhat surprising when compared to those of proflavine (PF). If PF is intercalated between adjacent AT pairs of DNA, the fluorescence quantum yield is nearly equal to that of PF bound to poly d(A-T).[2,7-9] However, the GC pair in the vicinity of bound PF gives rise to an almost complete quenching of the fluorescence.[2,7-9] From the results, it seems that 9-AA behaves similarly to PF with respect to the fluorescence properties. If this is the case, the fluorescence quantum yield of 9-AA bound to DNA should be about 0.3 in the case of calf thymus DNA (GC content of 42%).[2,10] Contrary to expectation, the observed quantum yield is much smaller (Table 1). The reason why the behavior of 9-AA is different from that of PF is not clear.

References

1) A. Albert, "The Acridines," Arnold, London (1966), p. 493.
2) Y. Kubota, *Chem. Lett.*, **1973**, 299.
3) C. A. Parker and W. T. Rees, *Analyst*, **85**, 587 (1960).
4) The absorption spectra suggest that the mole fraction of free dye is below 1% for $P/D>20$.
5) J. P. Schreiber and M. P. Daune, *J. Mol. Biol.*, **83**, 487 (1974).
6) S. J. Strickler and R. A. Berg, *J. Chem. Phys.*, **37**, 814 (1962).
7) J. C. Thomes, G. Weill, and M. Daune, *Biopolymers*, **8**, 647 (1969).
8) L. M. Chan and J. A. McCarter, *Biochim. Biophys. Acta*, **204**, 252 (1970).
9) Y. Kubota and R. F. Steiner, to be published.
10) Φ_F (bound to adjacent AT pairs)$=\Phi_F$ (bound to poly d(A-T))$\times$(mole fraction of AT: AT pair). The mole fraction of AT: AT pair is 0.3364 on the assumption that the base pairs are randomly distributed. Then the fluorescence quantum yield of 9-AA bound to adjacent AT pairs can be estimated to be about 0.3 (0.82×0.3364) by assuming that the bound dye molecules are randomly distributed.

BULLETIN OF THE CHEMICAL SOCIETY OF JAPAN, VOL. 50 (1), 299—300 (1977)

Excited-State Dipole Moments of Picrates of Pyridine, 2-Methylpyridine, 3-Methylpyridine, and 4-Methylpyridine

Osamu SEDOYAMA, Miwako HIGASHI, Yoshinori AKIMOTO, and Hiroyuki YAMAGUCHI*

Department of Chemistry, Kumamoto University, Kumamoto 860

(Received May 13, 1976)

Synopsis. Measurements of the excited-state dipole moments for picrates of pyridine and methylpyridines have been carried out by spectrophotometry. The contribution of the dative structure $\Psi(D^+A^-)$ in the excited state of these picrates is larger than the contribution of $\Psi(D^+A^-)$ in the ground state.

The excited-state dipole moments of electron donor–acceptor (EDA) complexes provide valuable information on the nature of binding in the excited state of the complexes. Recently, Rao and Dwivedi[1] have investigated the excited-state dipole moments of several EDA complexes by using the expression of McRae[2] to describe solvent shifts of electronic spectra. In the case of weak EDA complexes, they have observed red shifts of the CT bands and have concluded that the excited-state dipole moments μ_e are larger than the ground-state dipole moments μ_g. In the case of strong EDA complexes, they have observed solvent blue shifts and $\mu_e < \mu_g$. A lower μ_e compared to μ_g in strong EDA complexes was indeed a new observation.

Under these circumstances, it seems important to obtain experimental knowledge concerning the excited-state dipole moments of strong EDA complexes. We used picrates of pyridine, 2-methylpyridine, 3-methylpyridine, and 4-methylpyridine as strong EDA complexes. The purpose of our research was to determine the μ_e of these picrates from solvent shifts of electronic spectra and to investigate the contribution of the dative structures $\Psi(D^+A^-)$ and $\Psi(D^-A^+)$ in the excited-states of such strong EDA complexes.

Experimental

Materials and Their Purification. According to the procedure described by Raman and Soundararajan,[3] picrates of pyridine, 2-methylpyridine, 3-methylpyridine, and 4-methylpyridine were synthesized. All four picrates were recrystallized from ethyl alcohol three times. The 1:1 complexes precipitated from the solution.[4] The solvents used were carefully purified according to the descriptions in Ref. 5.

Measurements. The dielectric contants were determined with a home-made resonance-method apparatus. The refractive indices were measured by means of a Pulfrich refractometer. The dielectric constant (ε) and the refractive index (n_D) at the sodium D line of the solvents agreed with the values cited in Ref. 5. The densities of the solutions were measured by the use of a pycnometer for volatile liquids. The absorption spectra were taken with a Shimadzu UV-200 recording spectrophotometer equipped with a thermostated cell holder. Matched pairs of stopped silica cells of 1 cm path lengths were used. All measurements were made on deaerated samples at 20 °C.

Determination of Excited-state Dipole Moments. When two polar solvents I and II of similar n_D are used, the solvent shifts ($\Delta\nu$) of electronic spectra can be simplified from the expression of McRae[2] in the following manner:

$$\Delta\nu = \nu_{max}(\mathrm{I}) - \nu_{max}(\mathrm{II}) = C\{[(\varepsilon-1)/(\varepsilon+2)]_\mathrm{I} - [(\varepsilon-1)/(\varepsilon+2)]_\mathrm{II}\} \quad (1)$$

The constant C is given by Eq. 2:

$$C = (2/hc)[\mu_g(\mu_g-\mu_e)/a^3] \quad (2)$$

where a is the cabity radius in Onsager's theory[6] of the reaction field and is estimated from the molal volume on the assumption of the spherical radius of the complexes.

Rao and Dwivedi[1] have shown that the acetonitrile-diethyl ether solvent system can be used to obtain μ_e of EDA complexes from Eq. 1. When we used this solvent system, all four picrates dissociated completely into their donor and acceptor components in acetonitrile.[7] Instead of the acetonitrile-diethyl ether solvent system, we employed the acetone-diethyl ether solvent system. The validity of this solvent system was confirmed from the fact that the μ_e value, 9.8 D, for the hexamethylbenzene–chloranil complex was almost identical to the value, 10.0 D[1], obtained in the acetonitrile-diethyl ether solvent system.

Results and Discussion

The absorption spectra of pyridine picrate are shown in Fig. 1. The absorption band around 410 nm was assigned as the CT band of the picrate. The method of continuous variation was employed at 410 nm to establish the stoichiometry of the complex in the solvent. When the sum of the pyridine and picric acid concentrations was kept constant at 6.70×10^{-3} M, the Job curves showed a distinct maximum for equal concentrations of donor and acceptor, characteristic of a 1:1 complex (see Fig. 2). The results thus obtained for the picrates of three methylpyridines were the same as the above results for pyridine picrate. Since the IR spectra of the four picrates are the same as the IR spectra of the complexes between 2,4,6-trinitroanisole and pyridine and the three methylpyridines, and the complexes show the CT bands at almost the same

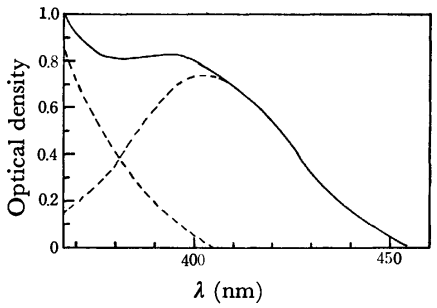

Fig. 1. The absorption spectra of pyridine picrate in diethyl ether at 30 °C. The dashed line shows the best fit of Gauss-curve for the CT band.

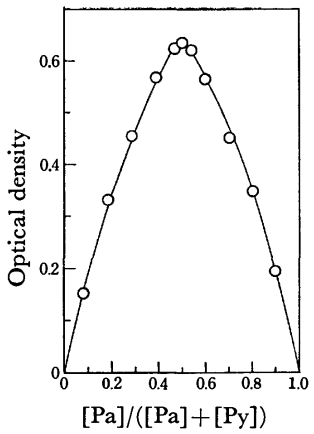

Fig. 2. The continuous variation of pyridine picrate in diethyl ether at 410 nm. The sum of the pyridine (Py) and picric acid (Pa) concentrations was kept constant at 6.70×10^{-3} M.

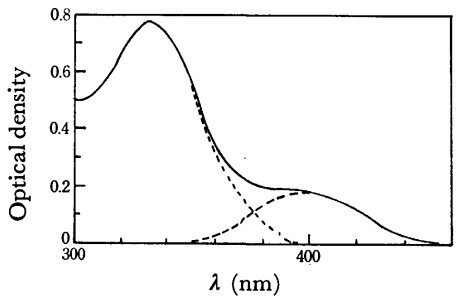

Fig. 3. The absorption spectra of 2,4,6-trinitroanisole-pyridine in diethyl ether at 30 °C. The dashed line shows the best fit of Gauss-curve for the CT band.

wavelength as the CT band of pyridine picrate (*e.g.*, see Figs. 1 and 3), all four picrates are not proton-transfer-typed complexes but EDA complexes. The CT bands of all four picrates were analyzed assuming Gauss-type absorption bands with the method described by Badoz *et al.*[8] (*e.g.*, see Fig. 1). The results are summarized in Table 1.

Table 1. Excited state dipole moments

Complex	ν_{CT}(cm^{-1}) (in ether)	C (cm^{-1})	a (Å)[a]	μ_g (D)[b]	μ_e (D)
Pyridine picrate	24750	−542	4.30	8.70	9.6
2-Methylpyridine picrate	24670	−476	4.25	9.25	10.1
3-Methylpyridine picrate	24650	−610	4.41	9.55	10.4
4-Methylpyridine picrate	24690	−596	4.33	9.60	10.4

a) Estimated from the apparent molal volume in 1,4-dioxane. b) Measured in 1,4-dioxane. See Ref. 3.

As the wave function Ψ_e for the excited state is given by Eq. 3,[1]

$$\Psi_e = C_1\Psi(DA) + C_2\Psi(D^+A^-) + C_3\Psi(D^-A^+) + C_4\Psi(D^*A) + C_5\Psi(DA^*) \quad (3)$$

the μ_e of the complex is proportional to $|C_2^2-C_3^2|$.

It is concluded from the μ_e thus obtained that the contribution of the dative structure $\Psi(D^+A^-)$ in the excited state of the present picrates is larger than the contribution of $\Psi(D^-A^+)$ is negligible even in the excited state of strong complexes such as the present complexes.

The differences of the ground state dipole moments between pyridine picrate and the picrates of 2-methylpyridine, 3-methylpyridine, and 4-methylpyridine are 0.55, 0.85, and 0.90 D, respectively. The differences of the excited-state dipole moments between pyridine picrate and the three picrates of methylpyridines are 0.5, 0.8, and 0.8 D, respectively. From these facts, it is concluded that the methyl groups of methylpyridines do not play any decisive role in the excited state on CT excitation.

The authors are greatly indebted to Professor Hitoshi Takeshita of Kyushū University for the elemental analysis. One of the present authors (H. Y.) especially wishes to thank Professor F. Yoneda of Kumamoto University for the supply of 2,4,6-trinitroanisole.

References

1) C. N. R. Rao and P. C. Dwivedi, *J. Chem. Phys.*, **59**, 1555 (1973).
2) E. G. McRae, *J. Phys. Chem.*, **61**, 562 (1957).
3) R. Raman and S. Soundararajan, *Proc. Indian Acad. Sci., Sect. A*, **54**, 41 (1961).
4) Found: C, 42.68; H, 2.68; N, 18.03; O, 36.61%. Calcd for $C_{11}H_8N_4O_7$: C, 42.86; H, 2.62; N, 18.18; O, 36.34%. Found for 2-methylpyridine picrate: C, 44.21; H, 3.13; N, 17.29; O, 35.37%; for 3-methylpyridine picrate: C, 44.57; H, 3.08; N, 17.32; O, 35.03%; and for 4-methylpyridine picrate: C, 44.61; H, 3.09; N, 17.36; O, 34.94%. Calcd for $C_{12}H_{10}N_4O_7$: C, 44.73; H, 3.13; N, 17.39; O, 34.75%.
5) J. A. Riddick and W. B. Bunger, "Organic Solvent," Vol. II, ed by A. Weissberger, John Wiley & Sons, Inc., New York (1970).
6) L. Onsager, *J. Am. Chem. Soc.*, **58**, 1486 (1936).
7) R. Foster, "Organic Charge-Transfer Complexes," Academic Press Inc., New York, N. Y. (1969), p. 309.
8) J. Badoz, M. Billardon, A. C. Boccare, and B. Briat, *Symp. Faraday Soc.*, **3**, 27 (1969).

BULLETIN OF THE CHEMICAL SOCIETY OF JAPAN, VOL. 50 (1), 301—302 (1977)

Selective Hydrogen Atom Abstraction by Hydrogen Atoms in Photolysis of Cyclohexane-Pentane Mixtures at 77 K

Tetsuo MIYAZAKI,*, Selma M. L. GUEDES, Leonardo G. de A. e SILVA, and Lizete FERNANDES

Instituto de Energia Atômica, C.P. 11049 (Pinheiros), 01000 São Paulo, SP, Brazil

(Received August 9, 1976)

Synopsis. The reaction of H atoms, produced by the photolysis of HI, has been studied in *c*-C_6H_{12}–*n*-C_5H_{12} mixtures at 77K. H atoms in *c*-C_6H_{12} matrix react more effectively with solute *n*-C_5H_{12} than with solvent *c*-C_6H_{12}, while H atoms in *n*-C_5H_{12} matrix react more effectively with solute *c*-C_6H_{12} than with solvent *n*-C_5H_{12}.

Recently, quite interesting phenomena have been reported concerning the hydrogen atom abstraction reaction by H atoms in the solid alkane at 77 K.[1)] When H atoms are produced at 77 K by the photolysis of a hydrogen halide or the radiolysis of a solvent alkane, such as neopentane, the H atoms react selectively with the solute alkane which exists in the neopentane matrix as an additive. The experimental bases of the selective hydrogen atom abstraction reaction by H atoms were described fully in a previous paper.[1b)] The same selective reaction has been found also in the matrices of 2,2,3,3-tetramethylbutane, isobutane, and cyclopropane.[1c)] The selective hydrogen atom abstraction reaction by H atoms has proposed new problems in reaction kinetics in the solid phase at 77 K. When H atoms are hot, we must assume that they migrate a long distance at 77 K through the alkane crystal without losing their kinetic energies. When H atoms are thermal, we must assume that the activation energy for the hydrogen atom abstraction reaction is nearly zero in the alkane matrix at 77 K, though the value amounts to 7—10 kcal/mol in the gas phase.[2,3)]

The previous examples of this reaction have the following characteristics: H atoms react selectively with the solute alkane, denoted as B, in the solvent alkane, denoted as A, where the combination of B in A is fixed. The selective reaction was not observed in the reverse combination, *i.e.* A in B. Here we will report a new type of combination in the case of cyclohexane and normal pentane mixtures. When A contains a small amount of B, H atoms react selectively with B. On the contrary, when B contains A, H atoms react selectively with A.

Experimental

Experimental procedures were identical with those described in the previous studies.[1)] Cyclohexane, >99.7 mol%, and pentane, >99 mol%, were passed through a 1-m column packed with freshly activated alumina and then distilled on a vacuum line before use. UV illumination was provided by a Toshiba medium-pressure mercury lamp at 77 K. The esr measurement was done at 77 K on a JES-ME-3 esr spectrometer.

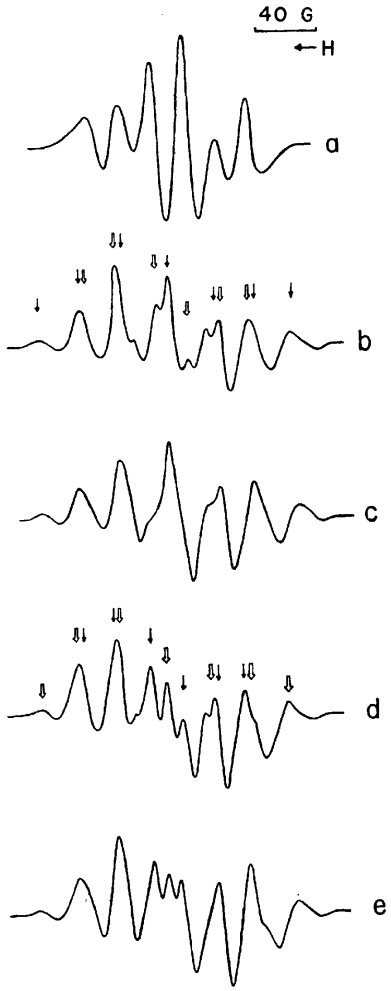

Fig. 1. a: ESR spectrum of UV-illuminated *c*-C_6H_{12}–HI (0.5 mol %) at 77 K. b: ESR spectrum of UV-illuminated *c*-C_6H_{12}–*n*-C_5H_{12} (5%)–HI (0.5%) at 77 K. c: ESR spectrum of UV-illuminated *n*-C_5H_{12}–HI (0.5%) at 77 K. d: ESR spectrum of UV-illuminated *n*-C_5H_{12}–*c*-C_6H_{12} (5%)–HI(0.5%) at 77 K. e: Simulated ESR spectrum of a mixture of C_5H_{11} radicals (60%) and *c*-C_6H_{11} radicals (40%). The relative sensitivities of the spectrometer for a, b, c, and d are approximately the same. The microwave power is 0.2 mW and the modulation width is 5 G. The area of double integration of the first-derivative ESR signal of each radical was used for simulation of the mixed spectra of the two radicals.

* Correspondence should be sent to Tetsuo Miyazaki. His present address is Department of Synthetic Chemistry, Faculty of Engineering, Nagoya University, Chikusa-ku, Nagoya 464.

Results and Discussion

Figure 1a is the ESR spectrum obtained by UV-illumination of c-C_6H_{12}–HI (0.5 mol%) at 77 K. The spectrum is consistent with the reported spectrum for cyclohexyl radical.[4] The H atom produced by the photolysis of HI abstracts the hydrogen atom from cyclohexane to produce a cyclohexyl radical. When c-C_6H_{12} containing n-C_5H_{12} (5 mol%) and HI (0.5 mol %) is illuminated at 77 K by ultraviolet light, quite a different esr spectrum is obtained (Fig. 1b). Figure 1c shows the esr spectrum obtained by the photolysis of n-C_5H_{12}–HI (0.5 mol %) at 77 K. The H atom produced by the photolysis of HI abstracts the H atom from n-C_5H_{12} to produce a C_5H_{11} radical. The spectrum of Fig. 1c is ascribed to a pentyl radical.[5] It is clear that the spectrum of Fig. 1b contains largely the spectrum due to the C_5H_{11} radical. The spectrum of Fig. 1b is ascribed to a mixture of C_5H_{11} radicals, indicated by ↓, and c-C_6H_{11} radicals, indicated by ⇩. Therefore the H atoms produced by the photolysis of HI in cyclohexane react effectively with solute pentane to form C_5H_{11} radicals.

When n-C_5H_{12} containing c-C_6H_{12} (5 mol %) and HI (0.5 mol %) is illuminated at 77 K by ultraviolet light, the esr spectrum of Fig. 1d is obtained. This spectrum is different from that of Fig. 1c which is obtained by the photolysis of n-C_5H_{12}–HI (0.5 mol %). The simulated spectrum of a mixture of C_5H_{11} radical (60%) and c-C_6H_{11} radical (40%) is shown in Fig. 1e. The spectrum of Fig. 1d is approximately similar to that of Fig. 1e. ⇩ and ↓ in Fig. 1d represent C_5H_{11} and c-C_6H_{11} radicals respectively. Therefore H atoms produced by the photolysis of HI in n-C_5H_{12} react effectively with the solute cyclohexane to form cyclohexyl radicals.

In order to obtain the ratio of the solute radical yield to the total radical yield, the esr spectrum in the photolysis of c-C_6H_{12}–n-C_5H_{12}–HI mixture is compared with the simulated spectrum of the mixture of c-C_6H_{11} and C_5H_{11} radicals. The formations of the solute radicals in c-C_6H_{12} and n-C_5H_{12} matrices are shown in Fig. 2 and 3 respectively. In both cases the fraction of solute radical yield is much higher than the concentration of the solute. Therefore, it is concluded that H atoms in the c-C_6H_{12} matrix react more effectively with solute n-C_5H_{12} than with solvent c-C_6H_{12} (Fig. 2), while H atoms in the n-C_5H_{12} matrix react more effectively with solute c-C_6H_{12} than with solvent n-C_5H_{12} (Fig. 3).

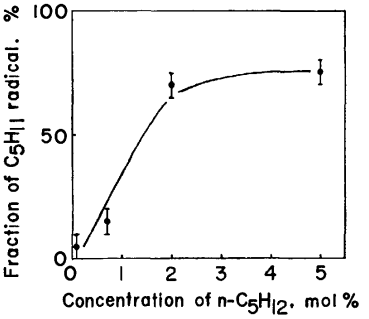

Fig. 2. Formation of solute pentyl radical in the photolysis of c-C_6H_{12}–HI (0.5 mol %) against concentration of n-C_5H_{12}.

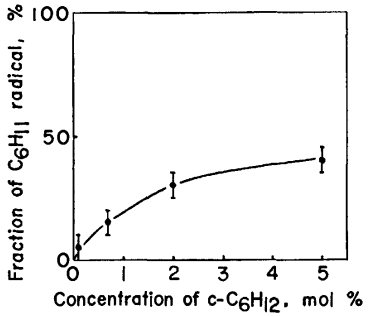

Fig. 3. Formation of solute cyclohexyl radical in the photolysis of n-C_5H_{12}–HI (0.5 mol %) against concentration of c-C_6H_{12}.

The solute alkane may form some active sites in the solid alkane at 77 K and be subjected selectively to H atom attack.

References

1) a) T. Wakayama, T. Miyazaki, K. Fueki, and Z. Kuri, *J. Phys. Chem.*, **77**, 2365 (1973); b) T. Miyazaki and T. Hirayama, *ibid.*, **79**, 566 (1975); c) T. Miyazaki, K. Kinugawa, M. Eguchi, and S. M. L. Guedes, *Bull. Chem. Soc. Jpn.*, **49**, 2970 (1976).

2) B. A. Thrush, *Prog. React. Kinet.*, **3**, 89 (1965).

3) T. Kagiya, Y. Sumida, I. Inoue, and F. S. Dyachkovskii, *Bull. Chem. Soc. Jpn.*, **42**, 1812 (1969).

4) a) B. Smaller and M. S. Matheson, *J. Chem., Phys.*, **28**, 1169 (1958); b) R. W. Fessenden and R. H. Schuler, *ibid.*, **39**, 2147 (1963).

5) R. S. Alger, T. H. Anderson, and L. A. Webb, *J. Chem. Phys.*, 30, 695 (1959).

BULLETIN OF THE CHEMICAL SOCIETY OF JAPAN, VOL. 50 (1), 303—304 (1977)

Calculation of Directly-Bonded Nuclear Spin-Spin Coupling Constants with Localized Orbitals

Kimihiko HIRAO and Hiroshi KATO*

Department of Chemistry, Shiga University of Medical Science, Seta, Otsu 520-21
**Department of General Education, Nagoya University, Chikusa-ku, Nagoya 464*

(Received August 28, 1976)

Synopsis. The directly-bonded nuclear spin-spin coupling constants were calculated by a perturbation method involving the summing over singly-excited states using localized orbitals. It is shown that a localized representation of orbitals in the perturbation expansion can be of considerable value both for interpretative purposes and for assessing the rate at which the pertubation expansion converges.

Although the Hartree-Fock (HF) variational condition selects the occupied and virtual manifolds, it does not completely determine the individual orbitals belonging to each manifold.[1] This orbital ambiguity yields the possibility of obtaining a new set of orbitals, within unitary transformations, which may be more suitable for the investigation of a particular physical problem than the original set of canonical molecular orbitals (CMO). The most interesting case is that of a transformation in which the orbitals are localized as much as possible.

One can employ the perturbation theory starting with a wave function constructed from localized molecular orbitals (LMO) as easily as CMO constructed wave functions. There is a theoretical advantage in using LMO- rather than CMO-based wave functions, since the LMO can often be chosen to be localized in a particular region of space, whereas the CMO are usually delocalized. If the perturbation can be expressed as a series of local perturbations which affect only a relatively small region of space, then there may be some advantages in choosing the original orbitals to reflect this localization.[2,3]

The second-order property of a system may be calculated in the perturbation approach employing a summing over excited states from the second-order energy $E^{(2)}$ or the first-order wave function $\Psi^{(1)}$:

$$E^{(2)} = \langle \Psi_0 | H' | \Psi^{(1)} \rangle$$

$$\Psi^{(1)} = \sum_n{}' C_n \Psi_n, \quad C_n = \langle \Psi_0 | H' | \Psi_n \rangle / (E_0 - E_n) \qquad (1)$$

where H' is the operator describing the perturbation and $\{\Psi_n\}$ is a complete set of eigenfunctions of the zeroth-order Hamiltonian H_0 with the set of eigenvalues $\{E_n\}$

$$H_0 \Psi_n = E_n \Psi_n \quad (n=0, 1, \cdots). \qquad (2)$$

Here the sum in Eq. 1 is over an infinite number of excited states. However, since it is impossible to obtain a set of exact wave functions satisfying Eq. 2, some approximation must be introduced. The most frequent approximation to Eq. 1 is to replace Ψ_0 by the HF wave function and Ψ_n by singly-excited configurations, cutting off from the sum other excited configurations. To this approximation, $E^{(2)}$ depends on the unitary transformation of the singly-excited configurations. It would be expected that an LMO set would guarantee a more rapid convergence of the perturbation expansion than a CMO set.

TABLE 1. RESULTS OF J_{AB} (Hz) FOR THE DIRECTLY-BONDED NUCLEI IN SOME HYDROCARBONS FOR INDO-MO CALCULATIONS

Molecule		Fermi	Spin dipolar	Orbital	Total	Exptl.[a]
CH coupling						
CH_4	CMO[b]	64.6	0.0	0.0	64.6	
	LMO[c]	117.1	0.0	0.0	117.1	125
	FPM[d]	121.0	0.0	0.0	121.0	
C_2H_6	CMO	57.8	0.0	0.0	57.8	
	LMO	112.2	0.0	0.0	112.2	125
	FPM	119.8	0.0	0.0	119.8	
C_2H_4	CMO	80.1	0.0	0.0	80.1	
	LMO	132.8	0.0	0.0	132.8	156.2
	σ-π[e]	133.3	0.0	0.0	133.3	
	FPM	150.2	0.0	0.0	150.2	
C_2H_2	CMO	141.9	0.0	0.0	141.9	
	LMO	186.1	0.0	0.0	186.1	249
	σ-π	189.4	0.0	0.0	189.4	
	FPM	226.4	0.0	0.0	226.4	
CC coupling						
C_2H_6	CMO	6.6	0.4	−0.8	6.2	
	LMO	27.2	0.2	−1.3	26.2	34.6
	FPM	18.6	0.6	−1.0	18.3	
C_2H_4	CMO	20.8	1.4	−5.4	16.8	
	LMO	71.6	0.5	−3.2	68.9	67.6
	σ-π	45.6	1.9	−2.6	43.1	
	FPM	36.7	2.4	−3.4	35.7	
C_2H_2	CMO	56.1	4.2	6.1	66.5	
	LMO	141.1	2.2	1.4	144.7	171.5
	σ-π	75.8	4.5	7.0	87.3	
	FPM	73.4	4.6	7.4	85.4	

a) R.M.Lynden Bell and N. Sheppard, *Proc. R. Soc. London, Ser. A*, **269**, 385 (1962). b) CMO-SOSP results. c) unconstrained LMO-SOSP results. d) FP results. e) σ-π constrained LMO-SOSP results.

In order to test the LMO effects, model calculations were made of nuclear spin-spin coupling constants using INDO-MO[4] and the sum-over-singly excited-state perturbation (SOSP) method. Computational details have been described in a previous paper.[5] The LMO are obtained by minimizing the off-diagonal exchange energy according to the Edminton-Ruedenberg procedure.[6] The virtual orbitals were also transformed in the same manner. The calculated nuclear spin-spin coupling constants are summarized in Table 1. In the table, LMO denotes the SOSP values with a complete LMO set (*i.e.*, banana-type CC bonding orbitals are obtained for C_2H_4 and C_2H_2) and σ-π denotes the results of σ-π constrained LMO. In order to examine the refinement of LMO perturbation approximation, the coupling constants calculated with the SOSP method using CMO and those using the finite perturbation (FP) method[7] are also listed. It is to be noted here that the FP treatment which is equivalent to the coupled HF perturbation theory is the most accurate of the three different approaches, since in the FP approximation some doubly-excited states, in addition to the singly-excited states, can be included in the perturbed wave function.[8]

The LMO and σ-π results for CH coupling constants show a significant shift towards the FP results. Especially LMO values for CH_4 and C_2H_6 (saturated molecules) are in good agreement with the FP values. The Fermi

contributions calculated using the FP method are always larger than those obtained using the SOSP method. It has been suggested that the difference in the second-order properties calculated by the FP method and those by the SOSP method is essentially due to the fact that in the FP treatment one cannot introduce singly-excited states without introducing at the same time doubly-excited states in a restricted manner.[8] That is, if we take the Ψ_n to be singly-excited triplet states, ${}^3\Psi_{i\to a}$, for spin-dependent perturbations like the Fermi interaction, the approximate equation for C_{ia} in Eq. 1 is

$$C_{ia} = -\langle\Psi_0|H'|{}^3\Psi_{i\to a}\rangle/({}^3\Delta E_{i\to a}) \quad (3)$$

in the SOSP method. Here ${}^3\Delta E_{i\to a}$ is the triplet excitation energy. On the other hand, in the FP approximation, C_{ia} takes the first-order form

$$C_{ia} = -\langle\Psi_0|H'|{}^3\Psi_{i\to a}\rangle/({}^3\Delta E_{i\to a} - K_{ia}), \quad (4)$$

where the exchange integral K_{ia} comes from the doubly-excited configuration. Taking this into consideration, the reproduced trend in the CH coupling which is that the LMO-SOSP results are shifted from the CMO-SOSP results toward the FP values, would indicate that an LMO set gives a more rapid convergence of the perturbation expansion than a CMO set.

In CC couplings, σ-π constrained LMO results are also shifted towards the FP results, although the former exceed the latter in magnitude, while unconstrained LMO values are somewhat too large.

A comparison with the FP results indicates that better results would be obtained for C_2H_4 and C_2H_2 with σ-π constrained LMO than those obtained with banana-type LMO, although the latter agree well with the experimental results. In view of the energy localization criterion, the banana-type LMO are more localized than the σ-π constrained LMO. Nevertheless, maintaining the σ-π constraint and hence using less localized orbitals appears to be a better starting point of the perturbation expansion based on HF wave functions.

Next, let us examine the electronic origin of the coupling mechanisms. In the conventional perturbation theory with delocalized orbitals, the calculated result are determined by a very complicated cancellation of a number of large values and hence it is not easy to interpret the results. However, the LMO perturbation theory allows an easier qualitative interpretation of the results. As summarized in Table 2, the Fermi term for the CH couplings are determined by only one transition from the localized CH bonding orbital to the corresponding antibonding orbital. That is, the CH coupling can be expressed as a "local" contribution. The same is true for CC couplings. In the σ-π constrained LMO perturbation method, the transition from a localized CC bonding orbital to an antibonding orbital determines the Fermi term of the CC coupling. For the perturbation with banana-type orbitals, the transitions from banana-type CC bonding orbitals to the corresponding antibonding orbitals play an important role. Moreover, each contribution has the same sign, implying that there is no partial cancellation. Thus, the results can always be expressed as the sum of "local" contributions. Namely, the LMO perturbation results are useful for describing local properties and are of conceptual simplicity. This is an essential advantage in employing LMO perturbation theory. From this point of view, the σ-π constrained LMO appear to be more suitable than the unconstrained LMO.

Table 2. Contributions of "local" transitions to the Fermi term

Molecule		Local transitions[a]	Transition energy (eV)	Contribution of local transition (Hz)	Total Fermi term (Hz)
CH coupling					
CH_4	LMO	ω (2.67)[b] $\to\omega^*$ (3.38)	16.74	117.3	117.1
C_2H_6	LMO	ω (2.81) $\to\omega^*$ (3.40)	16.95	112.3	112.2
C_2H_4	LMO	ω (2.09) $\to\omega^*$ (2.77)	17.44	130.0	132.8
	σ-π	ω (1.95) $\to\omega^*$ (2.61)	17.61	134.8	133.3
C_2H_2	LMO	ω (1.19) $\to\omega^*$ (1.69)	18.21	176.5	186.1
	σ-π	ω (0.97) $\to\omega^*$ (1.43)	18.49	193.2	189.4
CC coupling					
C_2H_6	LMO	σ (2.67) $\to\sigma^*$ (2.73)	22.92	31.8	27.2
C_2H_4	LMO	λ_1 (3.60) $\to\lambda_1^*$ (4.05)	18.59	23.1	
		λ_1 (3.60) $\to\lambda_2^*$ (4.05)	19.93	21.5	
		sum[c]		89.2	71.6
	σ-π	σ (1.47) $\to\sigma^*$ (1.68)	28.84	52.2	45.6
C_2H_2	LMO	λ_1 (3.75) $\to\lambda_1^*$ (4.64)	18.29	20.3	
		λ_1 (3.75) $\to\lambda_2^*$ (4.64)	19.55	19.0	
		sum		174.6	141.1
	σ-π	σ (0.72) $\to\sigma^*$ (1.09)	33.09	86.4	75.8

a) Explanation of notation: $\omega\to\omega^*$ the transition from a CH bonding orbital to the corresponding antibonding orbital, $\sigma\to\sigma^*$ the transition from a CC bonding orbital to an antibonding orbital in $\sigma\to\pi$ constrained LMO form, $\lambda\to\lambda^*$ the transition from CC banana type orbitals to the corresponding antibonding orbitals in unconstrained LMO form. b) Carbon atom hybrids of CH and CC bonds (sp*) are shown in parenthesis. c) The sum denotes the sum over local transitions (*i.e.*, sum$=2\{(\lambda_1\to\lambda_1^*)+(\lambda_1\to\lambda_2^*)\}$ in C_2H_4 and sum$=3\{(\lambda_1\to\lambda_1^*)+2(\lambda_1\to\lambda_2^*)\}$ in C_2H_2).

The authors are indebted to Professor T. Yonezawa for his interest in this work.

References

1) K. Hirao, *J. Chem. Phys.*, **61**, 3247 (1974).
2) A. T. Amos, J. I. Musher, and H. G. Ft Roberts, *Chem. Phys. Lett.*, **4**, 93 (1969).
3) A. T. Amos and J. I. Musher, *J. Chem. Phys.*, **54**, 2380 (1971).
4) J. A. Pople, D. L. Beveridge, and P. A. Dobosh, *J. Chem. Phys.*, **47**, 2026 (1967).
5) K. Hirao, H. Nakatsuji, H. Kato, and T. Yonezawa, *J. Am. Chem. Soc.*, **94**, 4078 (1972).
6) C. Edmiston and K. Ruedenberg, *Rev. Mod. Phys.*, **34**, 457 (1963).
7) H. Nakatsuji, K. Hirao, H. Kato, and T. Yonezawa, *Chem. Phys. Lett.*, **6**, 541 (1970).
8) R. Ditchfield, N. S. Ostlund, J. N. Murrell, and M. A. Turpin, *Mol. Phys.*, **18**, 433 (1970).

BULLETIN OF THE CHEMICAL SOCIETY OF JAPAN, VOL. 50 (1), 305—306 (1977)

The C-Se Stretching Vibrations and Molecular Conformations of Dialkyl Selenides

Keiichi OHNO, Takeshi HIROKAWA, Seiro AONO, and Hiromu MURATA
Department of Chemistry, Faculty of Science, Hiroshima University, Higashisenda-machi Hiroshima 730
(Received September 16, 1976)

Synopsis. The Raman spectra of dialkyl selenides were measured in the liquid and solid states. The most intense Raman lines observed in the 500—700 cm^{-1} region were assigned to the C–Se stretching vibrations. Correlations of the C–Se stretching frequencies to the molecular conformations were found.

Recently, the rotational isomers about the C–Se bond have been confirmed in our laboratory to exist in ethyl methyl selenide and isopropyl methyl selenide.[1] For dialkyl disulfides[2] and dialkyl sulfides[3] of a homologous series, useful correlations of the C–S stretching frequencies to the molecular conformations about the C–C bonds adjacent to the C–S bond have been found, similar to the C–Cl stretching frequencies of alkyl chlorides.[4]

In the present note, therefore, we will study the C–Se stretching frequencies of dialkyl selenides in relation to their molecular conformations.

Results and Discussion

The Raman spectra of dimethyl selenide, ethyl methyl selenide, isopropyl methyl selenide, diethyl selenide, methyl propyl selenide, and *s*-butyl methyl selenide are measured in the liquid and solid states. For these selenides, the C–Se stretching vibrations are expected in the region of 600 cm^{-1} on the basis of the assignments of dimethyl selenide.[5] The most intense Raman lines assigned to the C–Se stretching vibrations are observed in the 500—700 cm^{-1} region; the other vibrations are not expected in this region. Figure 1 shows the liquid and solid spectra in this region, together with the results of the corresponding dialkyl sulfides.[6–8] Although only two Raman lines are expected for one isomer, too many Raman lines are observed in the liquid state for these selenides except for dimethyl selenide. Rotational isomers, therefore, coexist in the liquid state, and only one isomer persists in the solid state. For ethyl methyl selenide, isopropyl methyl selenide, and diethyl selenide, the patterns of the spectral changes from the liquid to the solid states are the same as those of the sulfides. It is estimated that the *gauche* (G) form for ethyl methyl selenide, the molecular form with the C_1 symmetry for isopropyl methyl selenide, and the TT form for diethyl selenide persist in the solid state, in analogy with the cases of the corresponding sulfides.[6–8] For methyl propyl selenide, the CH_3–Se stretching vibrations of all the isomers may be assigned to the Raman line at 591 cm^{-1}. The CH_3–Se stretching vibration is considered to be less affected by a residual part of a molecule, because the frequency difference between the C–Se stretching vibrations of dimethyl selenide (14 cm^{-1}) is considerably smaller than that of dimethyl sulfide (53 cm^{-1})[5] and for methyl propyl selenide the Raman intensity at 591 cm^{-1} is relatively strong, in comparison with that of methyl propyl sulfides.[9] For methyl propyl selenide, by analogy with the case of methyl propyl sulfide pre-

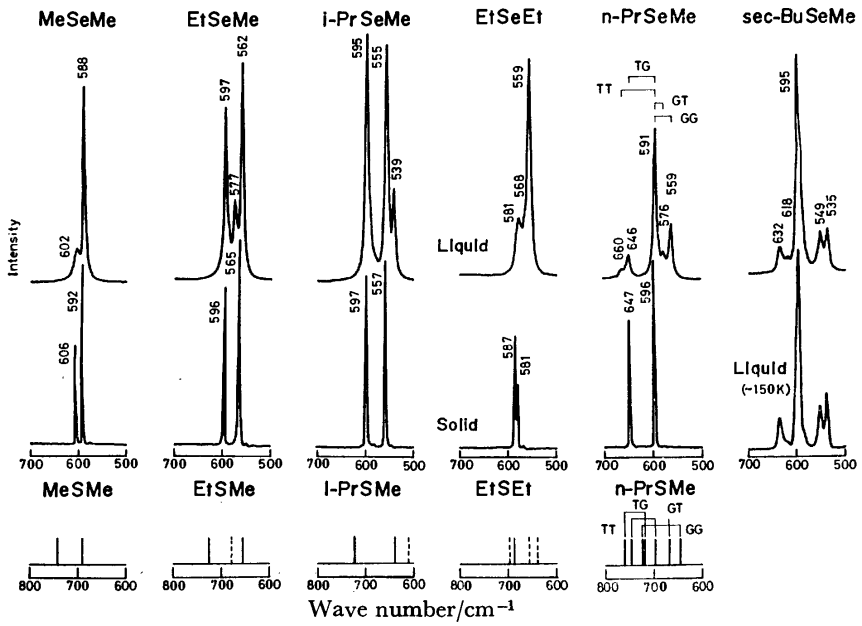

Fig. 1. The Raman spectra of the C–Se stretching vibrations of the dialkyl selenides in the liquid and solid states, together with the results of the dialkyl sulfides. Solid and dotted lines indicate the Raman lines persisting and disappearing in the solid state respectively.

Table 1. Characteristic C–Se stretching frequencies (cm^{-1}) of dialkyl selenides

Molecules	ν (CH_3–Se)	ν (–CH_2–Se)				ν (>CH–Se)				ν (>C–Se)
		P_H–P_H	P_H–P_C	P_C–P_H	P_C–P_C	S_{HH}–P_H	S_{HH}–P_C	S_{CH}–P_H	S_{CH}–P_C	T_{HHH}
CH_3SeCH_3	588*, 602*	—	—	—	—	—	—	—	—	—
$CH_3SeCH_2CH_3$	597*	562*	577	—	—	—	—	—	—	—
$(CH_3CH_2)_2Se$	—	559, 568	581*	—	—	—	—	—	—	—
$CH_3SeCH_2CH_2CH_3$	591*	559	576	646*	660	—	—	—	—	—
$CH_3SeCH(CH_3)_2$	595*	—	—	—	—	539	555*	—	—	—
$CH_3SeCH(CH_3)CH_2CH_3$	595	—	—	—	—	535	549	618	632	—
$((CH_3)_3C)_2Se$[12]	—	—	—	—	—	—	—	—	—	527
	588—602	559—581		646—660		535—555		618—632		527
Alkyl bromides[10]	611	557—617		635—649		529—588		608—617		506—524

viously investigated in detail,[9] it is estimated that the TG (-CH–CH–Se-) form persists in the solid state and that the TT, TG, GT, and GG forms coexist in the liquid state. At present, the solid spectrum of *s*-butyl methyl selenide is not obtained. However, the rotational isomers may coexist in the liquid state, since the changes in the Raman intensities are observed at different temperatures. The most intense Raman line at 595 cm^{-1} may be assigned to the CH_3–Se stretching vibrations of all the isomers, in a manner similar to that used for methyl propyl selenide.

Table 1 summarizes the observed frequencies of the Raman lines due to the C–Se stretching vibrations of the dialkyl selenides in the liquid state; asterisks indicate the Raman lines persisting in the solid state. The P_H, P_C, S_{HH}, S_{CH}, and T_{HHH} values in this table are the same as those used in previous papers.[2,4] For the notation of the molecular form, the first symbol refers to the internal rotation about the C–C bond adjacent to the C–Se bond, and the second symbol, to that about the C–Se bond. The frequency differences in the C–Se stretching vibrations caused by the conformation about the C–C bond adjacent to the C–Se bond (83—85 cm^{-1}) are larger than those caused by the conformation about the C–Se bond (14—22 cm^{-1}). On the other hand, for the C–S stretching vibrations, the frequency differences about the C–C bond have been reported to be 51—105 cm^{-1}, which are similar in magnitude to those in the case of the selenides; those about the C–S bond are 26—35 cm^{-1}, a little larger than those of the selenides.[2,3] The characteristic CH_3–Se stretching vibrations are observed in the 588—602 cm^{-1} region of dimethyl selenide. In the case of the primary selenides, the C–Se stretching vibrations due to the P_H and P_C forms about the C–C bond lie in the regions of 559—581 cm^{-1} and 646—660 cm^{-1} respectively. For the secondary selenides, the C–Se stretching vibrations due to the S_{HH} and S_{CH} forms about the C–C bond lie in the regions of 535—555 cm^{-1} and 618—632 cm^{-1} respectively. The observed frequencies for the dialkyl selenides, in general, correspond very well to the C–Br stretching frequencies of alkyl bromides,[10] much as in the case between dialkyl sulfides and alkyl chlorides.[3]

Experimental

The samples were prepared according to the methods previously reported[11] and were purified by fractional distillation. The resulting purities were estimated to be higher than 98%, as confirmed by gas-chromatographic analysis. All the boiling points are uncorrected. CH_3SeCH_3: bp 57 °C (reported bp[11] 56—57 °C); NMR (CCl_4): δ 1.93 (6H, s, Se ($C\underline{H}_3$)$_2$). $C_2H_5SeCH_3$: bp 85 °C; NMR (CCl_4): δ 1.37 (3H, t, J=7 Hz, $CH_2C\underline{H}_3$), 1.91 (3H, s, $SeC\underline{H}_3$), 2.48 (2H, q, J=7 Hz, $SeC\underline{H}_2$). $(C_2H_5)_2Se$: bp 108 °C (reported bp[11] 107—108 °C); NMR (CCl_4): δ 1.38 (6H, t, J=7 Hz, Se ($CH_2C\underline{H}_3$)$_2$), 2.52 (4H, q, J=7 Hz, Se ($C\underline{H}_2CH_3$)$_2$). *i*-$C_3H_7SeCH_3$: bp 103 °C; NMR (CCl_4): δ 1.40 (6H, d, J=7 Hz, $CH(C\underline{H}_3)_2$), 1.92 (3H, s, $SeC\underline{H}_3$), 2.96 (1H, quintet, J=7 Hz, $SeC\underline{H}$). $C_3H_7SeCH_3$: bp 113 °C; NMR (CCl_4): δ 0.99 (3H, t, J=7 Hz, $CH_2C\underline{H}_3$), 1.65 (2H, sex, J=7 Hz, $C\underline{H}_2CH_3$), 1.90 (3H, s, $SeC\underline{H}_3$), 2.46 (2H, t, J=7 Hz, $SeC\underline{H}_2$). *s*-$C_4H_9SeCH_3$: bp 128 °C; NMR (CCl_4): δ 0.97 (3H, t, J=7 Hz, $CH_2C\underline{H}_3$), 1.36 (3H, d, J=7 Hz, $CHC\underline{H}_3$), 1.57 (2H, quintet, J=7 Hz, $C\underline{H}_2CH_3$), 1.87 (3H, s, $SeC\underline{H}_3$), 2.75 (1H, sex, J=7 Hz, $SeC\underline{H}$).

The Raman spectra were recorded on a JEOL Raman Spectrometer (Model JRS-400D) with an argon-ion laser. For measurements of the solid spectra, samples in ampoules were held on a copper block cooled with liquid nitrogen in a vacuum.

The authors are grateful to Dr. Sachihico Imai of Hiroshima University for the NMR measurements.

References

1) K. Ohno, T. Hirokawa, S. Aono, and H. Murata, *Chem. Lett.*, **1976**, 1221.
2) H. Sugeta, A. Go, and T. Miyazawa, *Chem. Lett.*, **1972**, 83.
3) M. Ohsaku, *Bull. Chem. Soc. Jpn.*, **48**, 707 (1975).
4) J. J. Shipman, V. L. Folt, and S. Krimm, *Spectrochim. Acta*, **18**, 1603 (1962).
5) J. R. Allkins and P. J. Hendra, *Spectrochim. Acta*, **22**, 2075 (1966).
6) N. Nogami, H. Sugeta, and T. Miyazawa, *Bull. Chem. Soc. Jpn.*, **48**, 3573 (1975).
7) M. Ohsaku, Y. Shiro, and H. Murata, *Bull. Chem. Soc. Jpn.*, **45**, 3480 (1972).
8) M. Ohsaku, Y. Shiro, and H. Murata, *Bull. Chem. Soc. Jpn.*, **46**, 1399 (1973); M. Hayashi, *Nippon Kagaku Zasshi*, **77**, 1804 (1956).
9) N. Nogami, H. Sugeta, and T. Miyazawa, *Chem. Lett.*, **1975**, 147.
10) F. F. Bentley, N. T. McDevitt, and A. L. Rozek, *Spectrochim. Acta*, **20**, 105 (1964).
11) T. Hashimoto, M. Sugita, H. Kitano, and K. Fukui, *Nippon Kagaku Zasshi*, **88**, 991 (1967); F. Challenger and M. L. Bird, *J. Chem. Soc.*, **1942**, 570.
12) R. Gaufrés, A. Perez, and J. L. Bribes, *Bull. Soc. Chim. Fr.*, **1971**, 2898.

BULLETIN OF THE CHEMICAL SOCIETY OF JAPAN, VOL. 50, (1) 307—308 (1977)

Studies of Nitrogen-Phosphorus Compounds. XXVIII.[1] The Thermal Decomposition and Fireproofing Effect of Trimeric and Tetrameric Phosphorus Diamide Nitride

Etsuro KOBAYASHI and Tadao KANAYAMA

National Chemical Laboratory for Industry, Hon-machi, Shibuya-ku, Tokyo 151

(Received June 25, 1976)

Synopsis. The thermal decomposition of $N_3P_3(NH_2)_6 \cdot H_2O$ and $N_4P_4(NH_2)_8 \cdot H_2O$ and their fireproofing effects for cellulose have been investigated by means of DTA and TG. These compounds dehydrated at 113 and 124 °C and deammonated at 265 and 271 °C. The activation energies of the dehydration and deammonation were 27 and 42 kcal/mol in the trimer, and 37 and 40 kcal/mol in the tetramer. The cellulose impregnated with either of these compounds flamed up at lower temperatures than did the pure cellulose, but its carbonized product remakably resisted combustion.

The amidated derivatives of the lower polymers of phosphorus dichloride nitride have drawn interest as fireproof materials.[2,3] The present authors had prepared $N_3P_3(NH_2)_6$[4] and $N_4P_4(NH_2)_8$[5] and investigated their hydrolysis behaviors under various conditions.[5-7] In this study, the thermal decomposition of $N_3P_3(NH_2)_6 \cdot H_2O$ and $N_4P_4(NH_2)_8 \cdot H_2O$ was investigated by means of the differential thermal analysis (DTA) and thermogravimetric (TG) measurements; the incombustibility of the cellulose impregnated with either of these compounds was also examined and compared with that of the pure cellulose.

Experimental

$N_3P_3(NH_2)_6 \cdot H_2O$ and $N_4P_4(NH_2)_8 \cdot H_2O$ for the DTA and TG measurements were prepared by the procedures reported previously.[4,5] DTA and TG were performed simultaneously by the use of macro-type and micro-type thermal analysers. The conditions of the thermal analysis are indicated along with Figs. 1 and 3. The cellulose impregnated with $N_nP_n(NH_2)_{2n}$ (n=3,4) was formed as follows: a filter paper (Toyo Roshi Co., Ltd. No. 5B) was immersed in an aqueous solution of $N_nP_n(NH_2)_{2n}$ (n=3,4). It was drawn up, pressed, and dryed. The incombustibility was also examined by using the micro-thermal analyser.

Results and Discussion

The DTA and TG curves for trimeric and tetrameric phosphorus diamide nitride are shown in Fig. 1. In the DTA curve for $N_3P_3(NH_2)_6 \cdot H_2O$, endothermic peaks appeared at 113 and 265 °C: these seemed to be due to the dehydration of the water of crystallization and the deammonation from the amido-groups. In the DTA curve for $N_4P_4(NH_2)_8 \cdot H_2O$, two endothermic peaks also appeared. The height of the first peak was lower than that of the trimer variety, and was shifted to the higher temperature side. Therefore, it may be expected that the water of crystallization of the tetramer is bound more strongly than in the case of the trimer. On the other hand, the weight losses in two steps, which

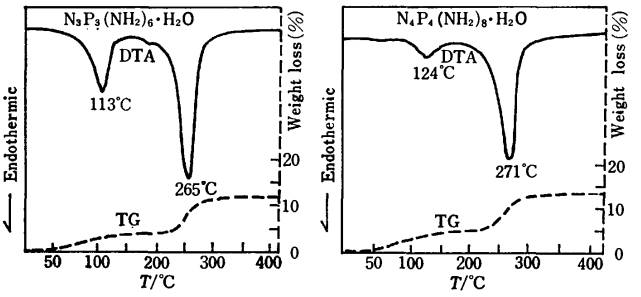

Fig. 1. DTA and TG curves for trimeric and tetrameric phosphorus diamide nitride.
Sample: 100 mg, heating rate: 5 °C/min, DTA: ±250 μV, current gas: N_2 gas 0.3 l/min.

proved the dehydration and deammonation, were recognizable on each TG curve. The activation energies in these reactions were calculated in accordance with Kissinger's method.[8] The peak temperatures (T_{max}) related to the reactions were measured at the heating rates (ϕ) of 5, 10, 20, and 40 °C/min. The activation energies, which were obtained from the relation between the reciprocal of the T_{max} and the log ϕ/T_{max}^2 shown in Fig. 2, were 27 and 37 kcal/mol for the dehydrations in $N_3P_3(NH_2)_6 \cdot H_2O$ and $N_4P_4(NH_2)_8 \cdot H_2O$, and 42 and 40 kcal/mol for their deammonations. It had already been known that the lower polymers of phosphorus diamide nitride decomposed at the elevated temperatures, and then were converted into phospham $(PN_2H)_n$.[4] In this study, it was confirmed by the use of the thermal analyser that a heating product of $N_nP_n(NH_2)_{2n} \cdot H_2O$ (n=3, 4) lost weight quickly at 800 °C, melted at about 900 °C, and immediately sublimed in nitrogen gas, although it burned in air.

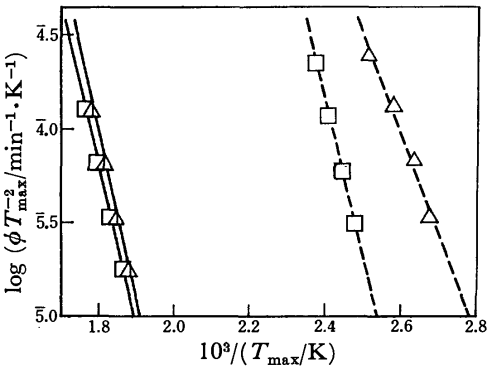

Fig. 2. Relation between $1/T_{max} \cdot 10^3$ and log $(\phi \cdot T_{max}^{-2})$.
△: $N_3P_3(NH_2)_6 \cdot H_2O$, □: $N_4P_4(NH_2)_8 \cdot H_2O$.
——: Dehydration, ——: deammonation.

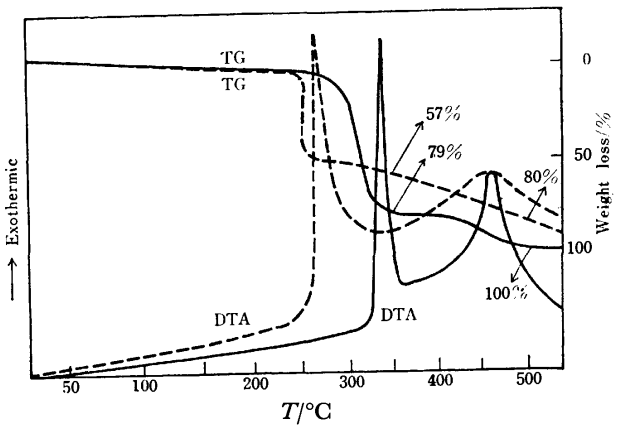

Fig. 3. DTA and TG curves for cellulose and cellulose including $N_4P_4(NH_2)_8$.
Sample: 20 mg, heating rate: 10 °C/min, DTA: ±100 μV, current gas: air 150 ml/min, ——: cellulose, – – –: cellulose impregnated with $N_4P_4(NH_2)_8$ (P: 2.9%).

The DTA and TG curves for the filter paper of pure cellulose and that treated with the aqueous solution of $N_4P_4(NH_2)_8$ are shown in Fig. 3. In the DTA curve for the pure cellulose, exothermic peaks appeared at 333 and 461 °C. The cellulose flamed up at the temperature of the first peak. The weight loss reached 79% at 350 °C, and a carbonized product was incinerated completely at 500 °C. In the DTA curve for the cellulose including $N_4P_4(NH_2)_8$, two exothermic peaks also appeared at 261 and 461 °C. The first peak shifted to the lower temperature side compared with that of the pure cellulose. In this case, the weight of the carbonized residue increased with the increase of the content of phosphorus in it. When the samples of cellulose including 2.0, 2.9, and 3.7% P were heated at 500 °C, the weight % of the residues were 11, 20, and 25%, respectively. The fireproofing effects of the trimer and tetramer varieties were almost the same. From the present results, it may be concluded that these compounds effectively retard the combustion of the cellulose.

References

1) Presented at the 34th National Meeting of the Chemical Society of Japan, Tokyo, April 1976.
2) C. A. Redfarn and H. Coates (Albright and Wilson Ltd.), Brit. Patent 788 785 (1958).
3) Erik R. Nielsen and William L. Stepp (I I T Research Institute), U. S. Patent 3 348 926 (1967).
4) E. Kobayashi, *Nippon Kagaku Kaishi*, **1972**, 38, *J. Nat. Chem. Lab. Ind.*, **68**, 19 (1973).
5) E. Kobayashi, *Bull. Chem. Soc. Jpn.*, **49**, 3524 (1976).
6) E. Kobayashi, *Chem. Lett.* **1976**, 479.
7) E. Kobayashi, *Nippon Kagaku Kaishi*, **1973**, 1437; *J. Nat. Chem. Lab. Ind.*, **67**, 470 (1974).
8) H. E. Kissinger, *Anal. Chem.*, **29**, 1702 (1957).

BULLETIN OF THE CHEMICAL SOCIETY OF JAPAN, VOL. 50 (1), 309—310 (1977)

The Formation and Properties of Solid Solutions in the $PbTiO_3$–$Pb(Ni_{1/2}W_{1/2})O_3$ System

Yasuyoshi Torii

Government Industrial Research Institute, Nagoya, Hirate-machi, Kita-ku, Nagoya 462

(Received July 5, 1976)

Synopsis. By usual and high-pressure techniques, a series of $PbTiO_3$–$Pb(Ni_{1/2}W_{1/2})O_3$ solid solution was formed with a perovskite structure. With an increase in the $Pb(Ni_{1/2}W_{1/2})O_3$ content, the Curie point shifted to lower temperatures and the degree of tetragonality decreased. The thermal-expansions were also measured, showing anomalies at the Curie point.

$PbTiO_3$ is a ferroelectric perovskite with a high Curie point of 490 °C.[1] However, its inability to produce dense $PbTiO_3$ ceramics and the relatively high conductivity of pure $PbTiO_3$ ceramics have restricted its usefulness.[2] On the other hand, $Pb(Ni_{1/2}W_{1/2})O_3$ has been synthesized only by high-pressure technique, and it has been suggested that it exhibits an antiferroelectric behavior.[3] The corresponding perovskites, $Pb(Mg_{1/2}W_{1/2})O_3$ and $Pb(Co_{1/2}W_{1/2})O_3$, have been prepared by usual solid-state reactions, and solid-solution series were formed over the whole composition range in the $PbTiO_3$–$Pb(Mg_{1/2}W_{1/2})O_3$ and $PbTiO_3$–$Pb(Co_{1/2}W_{1/2})O_3$ systems.[4,5] Much attention has been paid, from the physical and crystallographic points of view, to how solid solutions between $PbTiO_3$ and $Pb(Ni_{1/2}W_{1/2})O_3$ are formed. The present paper will report on the structural, dielectric, and thermal-expansion properties of this system.

Experimental

For the sample preparations, PbO, TiO_2, NiO, and WO_3 of high purities were used. Prefiring was done at 800 °C for 3 h in air. When the samples were then fired at temperatures of 850—1000 °C for 2 h, dense bodies were obtained. For samples which were not obtained as a single phase, high-pressure and high-temperature experiments (850 °C, 30 kb, 1 h) were made using a tetrahedral anvil apparatus. The sample was sealed by thin platinum foil to avoid contamination of the sample during the run. The sample container also served as a heating element. The room-temperature structure and the lattice constants of the samples were determined by the X-ray diffraction technique. The dielectric properties were measured on an universal bridge at 1 kHz. The thermal expansions of the sintered 0.7 cm-diameter specimen were measured with an automatic-plotting fused-quartz dilatometer.

Results and Discussion

In the $PbTiO_3$–$Pb(Ni_{1/2}W_{1/2})O_3$ system, tetragonal perovskite solid solutions were formed as a single phase up to the composition containing 50 mol% $Pb(Ni_{1/2}W_{1/2})O_3$, although $Pb(Ni_{1/2}W_{1/2})O_3$ was not synthesized by usual solid-state reaction. Superstructural lines were not observed in powder X-ray patterns. The lattice constants and the tetragonality $(c/a-1)$ are

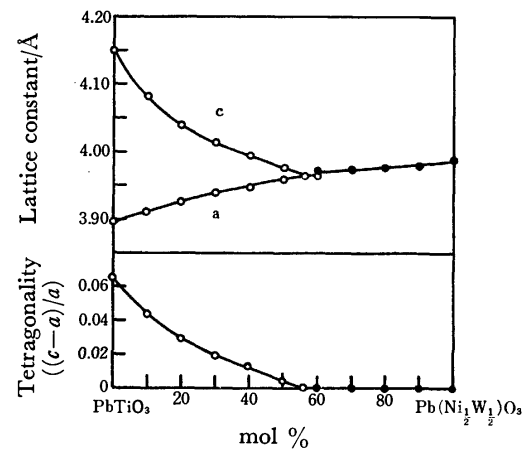

Fig. 1. Lattice constants and the tetragonality in the $PbTiO_3$–$Pb(Ni_{1/2}W_{1/2})O_3$ system.
○: sample obtained by usual solid state reaction.
●: sample obtained by high pressure reaction.

shown in Fig. 1. The tetragonality is continuously decreased by the substitution of the 1/2Ni+1/2W ions for the Ti ions. In a 60 mol% $Pb(Ni_{1/2}W_{1/2})O_3$ sample, other phases were observed to be formed in small amounts besides a cubic perovskite phase. The substitutional limitation of $Pb(Ni_{1/2}W_{1/2})O_3$ for $PbTiO_3$, as estimated from the dependence of the tetragonality on the composition, was *ca.* 56 mol%. In fact, a sample with this composition showed a single-phase pattern with the cubic perovskite structure, and its lattice constant was in good agreement with that in the sample with 60 mol% $Pb(Ni_{1/2}W_{1/2})O_3$. For samples contain-

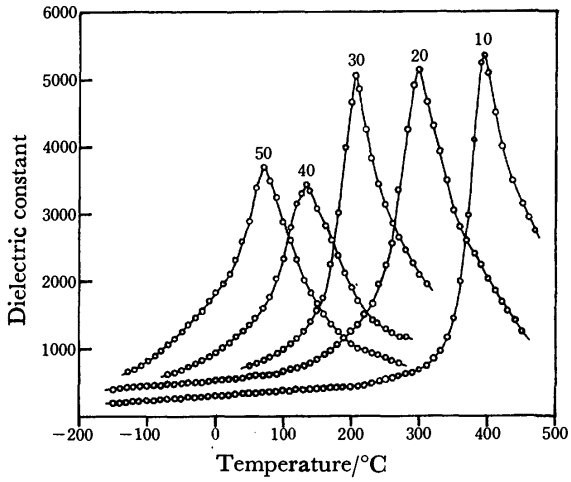

Fig. 2. Temperature dependence of dielectric constant in the $PbTiO_3$–$Pb(Ni_{1/2}W_{1/2})O_3$ system. Numbers on curves refer to $Pb(Ni_{1/2}W_{1/2})O_3$ content in mole percent.

ing more than 60 mol% $Pb(Ni_{1/2}W_{1/2})O_3$, a high-pressure technique was applied. Consequently, all the samples showed single-phase patterns of cubic perovskite. The lattice constant gradually increases with the increase in $Pb(Ni_{1/2}W_{1/2})O_3$, as is shown in Fig. 1. Superstructural lines indicating the NaCl-type ordering were observed for samples containing 70 mol% $Pb(Ni_{1/2}W_{1/2})O_3$.

Figure 2 shows the temperature dependence of the dielectric constant from −190 to 500 °C. High values of the dielectric constant are noticeable in these samples. A dielectric-constant peak characteristic of the ferroelectric substance was observed for each sample. With the increase in $Pb(Ni_{1/2}W_{1/2})O_3$, the sharp peak shifted to lower temperatures. This is attributed to the decrease in tetragonal distortion. The loss tangent for these samples was less than 0.05 below 200 °C and then rapidly increased with the temperature.

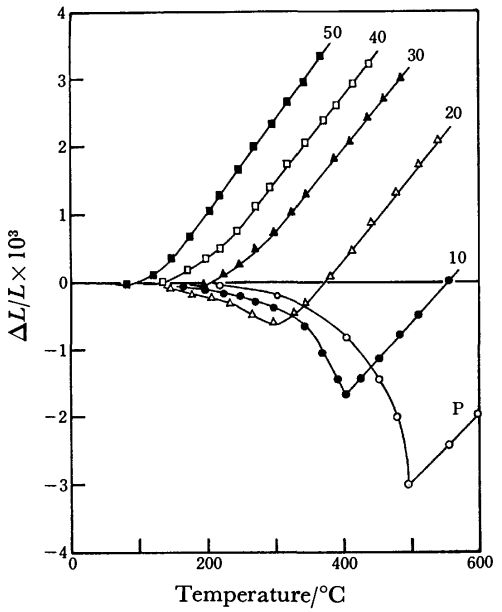

Fig. 3. Linear thermal-expansion curves in the $PbTiO_3$–$Pb(Ni_{1/2}W_{1/2})O_3$ system. Numbers on curves refer to $Pb(Ni_{1/2}W_{1/2})O_3$ content in mole percent and the symbol P means a sample of $PbTiO_3$ with 0.1 mol % CaF_2.

The thermal-expansion curves are shown in Fig. 3. Tien and Carlson have reported that $PbTiO_3$ with a 0.1 mol% addition of CaF_2 shows a net length expansion through a net length contraction at the Curie point.[6] Such a tendency appeared in these samples. With an increase in the $Pb(Ni_{1/2}W_{1/2})O_3$ content, the dilatometric anomaly also shifted to lower temperatures and the total quantity of contraction at the transition temperature became significantly lower. The phase-transition temperature obtained by dielectric and dilatometric measurements agree well. The linear thermal-expansion coefficients above the transition temperature were of the same order of magnitude, 10^{-5} per °C, for all the samples.

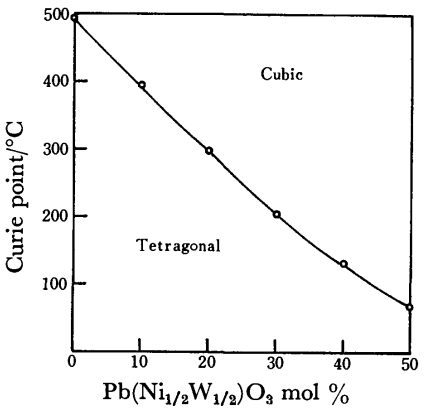

Fig. 4. Dependence of the Curie point on composition of $PbTiO_3$–$Pb(Ni_{1/2}W_{1/2})O_3$ solid solutions.

It may be concluded from these results that solid solutions containing less than 50 mol% $Pb(Ni_{1/2}W_{1/2})O_3$ are transformed from a tetragonal(ferroelectric) to a cubic(paraelectric) structure at the transition temperature. In this range of compositions, the arrangements of the cations in the octahedrally coordinated positions are at random, and the combination of Ni^{2+} and W^{6+} ions lowers the Curie point as is shown in Fig. 4. In samples containing more than 70 mol% $Pb(Ni_{1/2}W_{1/2})O_3$, the Ni^{2+} and W^{6+} ions show a partial ordering of the same type as in $Pb(Ni_{1/2}W_{1/2})O_3$.[3] With the increase in $Pb(Ni_{1/2}W_{1/2})O_3$, the intensities of the superstructural lines increase and the lattice expands. This expansion is probably due to an increase in the mean size of the cations occupying oxygen octahedra (according to Shannon *et al.*,[7,8] the ionic sizes of Ti^{4+}, Ni^{2+}, and W^{6+} ions being 0.605 Å, 0.69 Å, and 0.60 Å respectively). The dielectric anomaly would exist below room temperature, since perovskite solid solutions obtained by high-pressure technique are cubic at room temperature.

The structural and dielectric properties of this system have a tendency similar to those of the $PbTiO_3$–$Pb(Mg_{1/2}W_{1/2})O_3$ and $PbTiO_3$–$Pb(Co_{1/2}W_{1/2})O_3$ systems.[4,5]

References

1) S. Nomura and S. Sawada, *J. Phys. Soc. Jpn.*, **5**, 279 (1950).
2) E. C. Subbarao, *J. Am. Ceram. Soc.*, **43**, 119 (1960).
3) S. Nomura, T. Nakagawa, O. Fukunaga, and S. Saito, *J. Phys. Soc. Jpn.*, **24**, 957 (1968).
4) A. I. Zaslavskii and M. F. Bryzhina, *Soviet Phys. Cryst.*, **7**, 577 (1963).
5) N. Ichinose and K. Kurihara, *J. Phys. Soc. Jpn. Suppl.*, **28**, 321 (1969).
6) T. T. Tien and W. G. Carlson, *J. Am. Ceram. Soc.*, **45**, 567 (1962).
7) R. D. Shannon and C. T. Prewitt, *Acta Crystallogr.*, **B25**, 925 (1969).
8) R. D. Shannon and C. T. Prewitt, *Acta Crystallogr.*, **B26**, 1046 (1970).

BULLETIN OF THE CHEMICAL SOCIETY OF JAPAN, VOL. 50, (1) 311—312 (1977)

Quantitative Analysis of Polybutadiene by Means of Pulse FT Carbon-13 NMR

Chizuko SHIBATA, Mitsuru YAMAZAKI,* and Tsugio TAKEUCHI

Department of Synthetic Chemistry, Faculty of Engineering, Nagoya University, Chikusa-ku, Nagoya 464
**Department of Medical Analysis, School of Pharmacy, Hokuriku University, Kanagawa-cho, Kanazawa 920-11*

(Received July 9, 1976)

Synopsis. ^{13}C NMR was applied to the determination of the vinyl content in polybutadiene by means of the internal standard method. Under optimum experimental conditions, it was found that ^{13}C NMR is applicable to the quantitative analysis of polymer by use of acetonitrile as an internal standard.

Experimental

^{13}C NMR spectra were obtained at 25.2 MHz on a Varian XL-100-15 spectrometer equipped with a VFT-100 Fourier Transform accessory. All the samples had natural isotopic abundance. Noise decoupling of the proton was achieved with a V-3508 decoupler modified to hold its frequency in a field to the frequency of the master crystal of the spectrometer. 1,2-addition polybutadiene and the blends of 1,2-addition polybutadiene and 1,4-*cis* polybutadiene were used as samples (supplied by Asahi Chemical Co., Ltd.). The sample temperature was maintained at about 37 °C. The samples were dissolved in $CDCl_3$ (analytical grade) for field/frequency in 12 mm tubes. TMS and acetonitrile were added to the polymer solution (1—6 wt%) as a chemical shift and an internal standard, respectively. Acetonitrile was selected as an internal standard from the fact that the peak height of methyl carbon of acetonitrile added is comparable to that of the carbon in question and the error in weighing acetonitrile is small. The optimum conditions for polymer analysis were determined by changing pules width, pulse delay and dynamic range, so as to get the best signal to noise ratio (s/n).

Results and Discussion

The peaks were assigned by comparison of the decoupled and coupled spectra.

In order to select the optimum conditions for analysis, first only the pulse width was changed to see the pulse width effect on s/n, the other conditions being kept constant. The results are shown in Fig. 1. s/n decreased rapidly above 130 μs pulse width where spins would flip over 90 degree. 100 μs was therefore taken as the appropriate pulse width.[2]

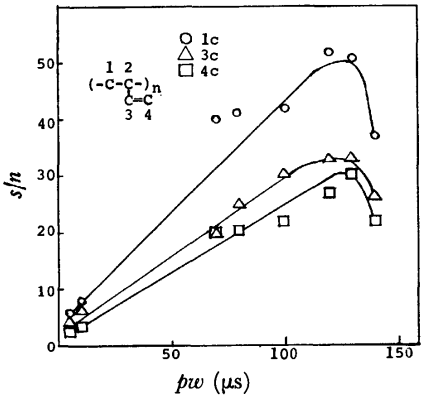

Fig. 1. Effect of pulse width on s/n.

The pulse delay effect on s/n measured is shown in Fig. 2. We see that a 2.4 s pulse delay is long enough to relax the methylene carbon in the main chain, but not the vinyl carbon. In this study, 2.4 s pulse delay was used for pulse delay.

The dynamic range effect on s/n is shown in Fig. 3. It was found that s/n has a maximum around 1 V/cm. This (1 V/cm) was used for dynamic range. The other conditions are follows: sweep width 5000 Hz, acquisition time 0.4 s, data points 4096. Three factors can be

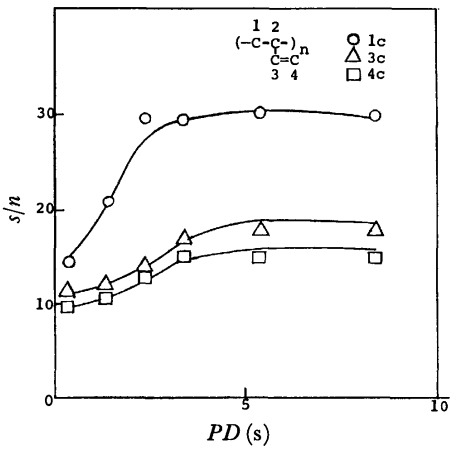

Fig. 2. Effect of pulse delay on s/n.

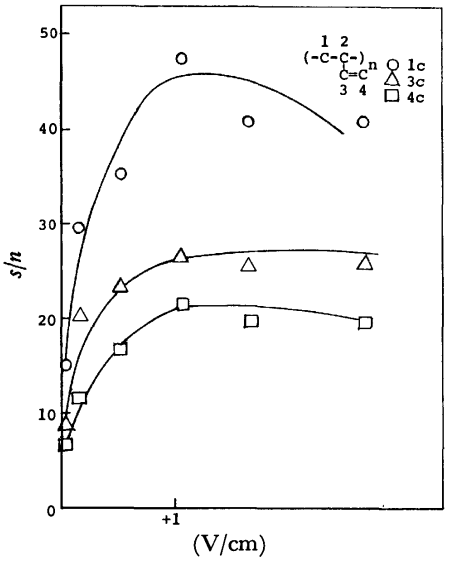

Fig. 3. Effect of dynamic range on s/n.

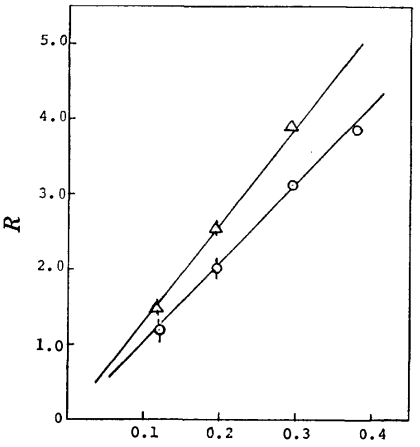

Fig. 4. Relation of ^{13}C NMR signal intensity to sample weight.
$R=I_1/I_S$, I_3/I_S (R_1: ○, R_3: △)
I: $(-\overset{1}{C}-\overset{2}{C}-)_n$ (C=C: 3 4), I_S: $(\overset{*}{C}H_3CN)$

Table 1. Results of ^{13}C NMR method applied to 1,2-addition polybutadiene in blend

Vinyl content		Sample number 1	2	3	4
Calcd (%)		56.1	68.4	78.7	81.6
^{13}C NMR (%)	C_m	56.5	73.4	77.4	86.0
	C_v	55.4	74.6	77.4	94.0
Relative error (%)	C_m	0.71	7.31	1.65	5.39
	C_v	1.24	9.06	1.65	15.2

considered to effect ^{13}C signal intensity. They are relaxation time, Nuclear Overhauser Effect and polymer concentration. Relaxation time in the case of polymer is generally so short[3] that it can be neglected. The plots of intensity ratio (I_{C_1}/I_{CH_3CN} and I_{C_3}/I_{CH_3CN}) observed *vs.* polybutadiene weight are given in Fig. 4. By calculating the error statistically, standard deviations were found to be 0.10 except for the sample having the lowest concentration with standard deviation 0.15. The plots of the intensity ratio are linear. If the degree of NOE depends upon the polymer concentration, the relation (Fig. 4) would not be linear. It can be concluded that NOE is independent of polymer concentration at least in the range of the concentration examined. Since signal intensity is now known to depend upon only polymer concentration, quantitative analysis of polybutadiene can be expected.

Results of the determination of vinyl content in the physical blends between 1,2-addition polybutadiene and 1,4-*cis* polybutadiene are summarized in Table 1. Each sample is determined on the basis of two different relations, one obtained by the plots of intensity ratio $R_1(I_{C_1}/I_{CH_3CN}$, C_1; methylene carbon) and the other by the plots of $R_3(I_{C_3}/I_{CH_3CN}$, C_3; vinyl carbon) in Fig. 4. The result determined by means of methylene carbon is found to be applicable to quantitative analysis, but not that by means of vinyl carbon. This might be explained in terms of experimental conditions suitable for methylene carbon described under pulse delay conditions. It was confirmed that the internal standard method using acetonitrile is applicable to quantitative analysis by ^{13}C NMR under suitable conditions, since NOE is independent of polymer concentration.

References

1) Y. Fujiwara and P. J. Flory, *Mecromolecules*, **3**, 43 (1970).
2) G. C. Levy and G. L. Nelson, "Carbon 13 Nuclear Magnetic Resonance for Organic Chemistry," John Wiley & Sons, New York (1972).
3) Jacob Schafer and David F. S. Natusch, *Macromolecules*, **5**, 416 (1972).

BULLETIN OF THE CHEMICAL SOCIETY OF JAPAN, VOL. 50 (1), 313—314 (1977)

Studies on Mixed Chelates. VIII. Mixed Copper(II) Chelates with *N,N'*- and *N,N*-Dialkylethylenediamines and Acetylacetone

Yutaka FUKUDA, Hiroko OKAMURA, and Kozo SONE

Department of Chemistry, Faculty of Science, Ochanomizu University, Otsuka, Tokyo 112

(Received August 20, 1976)

Synopsis. Mixed chelates [Cu(diamine)(acac)]X (diamine: *N,N'*- and *N,N*-dialkylethylenediamines) were studied. Two such chelates with diethyl ligands were obtained in crystalline state, while the formation of chelate cations $[Cu(diamine)(acac)]^+$ in 80% dioxane was studied with dimethyl ligands, and their formation constants estimated. The importance of steric effect in the bis-diamine chelates on the ease of formation of this type of chelate was pointed out.

The authors have studied the mixed chelates of the type [Cu(diamine)(acac)]X, with diamines such as 2,2'-bipyridine, 1,10-phenanthroline, and *N,N,N',N'*-tetramethyl- and tetraethylethylenediamines (bpy, phen, tmen and teen; acac=acetylacetonate ion)[1-4] and observed that (i) they are formed quite easily in appropriate organic solutions, *i.e.*, their formation constants are quite high; (ii) the ν_{max} values of their d-d band often do not obey the rule of Kida[5], which says that the ν_{max} of a mixed chelate CuAB is the mean of the values of its parent chelates CuA_2 and CuB_2; and (iii) the ν_{max} of the tmen and teen chelates are influenced strongly by the nature of the solvents used.

Extending these studies, the authors studied similar mixed chelates with *N,N'*-dimethyl, *N,N*-dimethyl-, *N,N'*-diethyl- and *N,N*-diethylethylenediamines (abbreviated as sym-dmen, unsym-dmen, sym-deen and unsym-deen, respectively).

Experimental

Preparation of the Chelates. [Cu(sym-deen)(acac)]ClO_4 and [Cu(unsym-deen)(acac)]ClO_4 are prepared as follows. $Cu(ClO_4)_2 \cdot 6H_2O$ (5 mmol) is dissolved in ethanol, and acetylacetone (5 mmol), Na_2CO_3 (2.5 mmol) and deen (5 mmol) are added successively. The crystals which separate out from the mixture are recrystallized from ethanol.

Physical Measurements. The methods and instruments used in this work were the same as those in the previous papers of this series.[1-4]

Results and Discussions

Crystalline Chelates. Although it was tried to prepare the chelates with all the four diamines, using several anions of low coordination power, it was found that many of such chelates are very hard to crystallize, and only the two in Table 1 could be obtained with sufficient purity, which are apparently very similar to the chelate [Cu(tmen)(acac)]ClO_4 studied before.

The values of ν_{max} in their electronic spectra (Table 2) show a strong solvent effect, which is comparable to that observed with [Cu(tmen)(acac)]ClO_4,[1,2] and that the unsym-deen chelate is a little more sensitive than the sym-deen chelate toward solvent change.

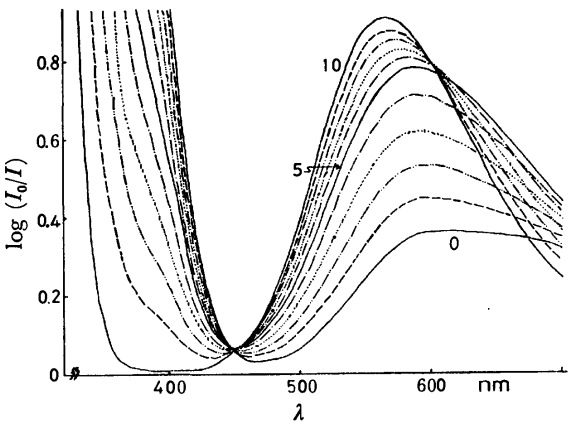

Fig. 1. Electronic spectra of the mixtures of [Cu(sym-dmen)$_2$](ClO_4)$_2$(CuA_2) and [Cu(acac)$_2$](CuB_2) in 80% dioxane at 18 °C. Total chelate concentration 0.91×10^{-2} M, cell thickness 1 cm. The ratio [CuA_2]: [CuB_2] in each sample is 10: 0 (Curve 10), 9: 1, 8: 2, 7: 3, 6: 4, 5: 5 (Curve 5), 4: 6, 3: 7, 2: 8, 1: 9, and 0: 10 (Curve 0).

TABLE 1. COLORS, COMPOSITIONS[a] AND MAGNETIC MOMENTS OF THE CHELATES

No.	Chelate	Color	C %	H %	N %	μ_{eff} (B.M.)
I	[Cu(sym-deen)(acac)]ClO_4	Reddish violet	35.46 (34.92)	6.58 (6.13)	7.52 (7.40)	1.83
II	[Cu(unsym-deen)(acac)]ClO_4	Reddish violet	34.79 (34.92)	6.18 (6.13)	7.39 (7.40)	1.81

a) Calculated values in parentheses.

TABLE 2. $\nu_{max}/10^3$ cm^{-1} AND ε_{max} (IN PARENTHESES) OF THE CHELATES IN VARIOUS SOLVENTS

No.	CH_3NO_2	$ClCH_2CH_2Cl$	CH_3CN	H_2O	80%-Dioxane	DMF	DMSO
I	18.18(87)	17.79(83)	17.12 (92)	16.69 (85)	16.69 (93)	16.56 (92)	16.37 (98)
II	18.28(95)	17.64(98)	17.09(106)	16.50(103)	16.47(108)	16.39(108)	16.05(117)

Stability Studies in Solution. The formation of the mixed chelates were also studied in solution. [Cu(sym-(or unsym-)dmen)$_2$](ClO$_4$)$_2$ and [Cu(acac)$_2$] were dissolved in 80% dioxane (v/v), and the method of continuous variation was applied to the visible spectra of their mixtures (Fig. 1). The plots clearly indicate the formation of 1 : 1 mixed chelates in solution, with formation constant $K([CuAB]^2/[CuA_2][CuB_2])$ estimated to be 500—600 at 18 °C. The same method applied to the system [Cu(sym-deen)$_2$](ClO$_4$)$_2$–[Cu(acac)$_2$] yielded similar results with a still higher value of K(*ca.* 2500 at 18 °C).

Although the accuracy of this estimation is not high,[6] comparison of these values with the K of [Cu(en)(acac)]$^+$ in 75% dioxane reported formerly by Kida (2.6)[5] clearly shows that K increases strongly with the increase in the bulkiness of the *N*-alkyl groups in the diamine.* Now the expression for K can be written as follows:

$$K = (k_{AB} \cdot k_{BA})/(k_{2A} \cdot k_{2B})$$

Here $k_{AB}=[CuAB]/[CuA][B]$, $k_{BA}=[CuAB]/[CuB][A]$, $k_{2A}=[CuA_2]/[CuA][A]$, and $k_{2B}=[CuB_2]/[CuB][B]$.

If A and B are identified with a diamine (en, dmen or deen) and acac, respectively, the data in the literature (*cf.* Table 3) show that k_{2A} decreases remarkably in going from en to dmen's and deen's (to *ca.* 1/150 and 1/3500 of the original value, respectively), owing to the increasing interligand repulsion in the bis-chelate. On the other hand, k_{2B} is naturally independent of A, and model study indicates that the interligand repulsion in CuAB will be nearly absent, so that the changes of k_{AB} and k_{BA} accompanying the change in A will be small. Thus it can be expected that the value of K is determined chiefly by $1/k_{2A}$, which increases about 150 and 3500 times in going from en to dmen's and deen's, respectively. The changes observed among the experimental values of K given above (*ca.* 200 and 1000 times) are not far from this expectation. These considerations thus give further support to the previously expressed view that the stability of the bpy-, phen- and tmen-containing mixed chelates is, to a large part, due to such an effect.[1]

Table 3. Values of k_2 for various diamines (25 °C, $I \rightarrow 0$)[7]

Diamine	k_{2A}	Diamine	k_{2A}
en	9.07	sym-deen	5.57
sym-dmen	6.94	unsym-deen	5.47
unsym-dmen	6.83		

It may be added that, if it is assumed that the spectra of the solutions containing the parent chelates in 1 : 1 ratio are very nearly those of the mixed chelates themselves (the fairly large K values support this view), their ν_{max} values satisfy Kida's rule approximately, indicating that the interligand repulsion in the bis-diamine chelates is not so strong to distort them remarkably from common tetragonal symmetry** (Table 4).

Table 4. $\nu_{max}/10^3$ cm^{-1} of the chelates [Cu(diamine)$_2$]$^{2+}$ and [Cu(diamine)-(acac)]$^+$ in 80% dioxane

Diamine	ν_{max} (bis-chelate)	ν_{max} (mixed chelate)
sym-dmen	17.61	16.98(16.87[a])
unsym-dmen	17.73	16.75(16.93)
sym-deen	17.24	16.69(16.69)
unsym-deen	17.04	16.50(16.59)

a) Values calculated with Kida's rule (ν_{max} for [Cu(acac)$_2$]: 16130 cm^{-1}) are in parentheses.

References

1) Y. Fukuda and K. Sone, *Bull. Chem. Soc. Jpn.*, **45**, 465 (1972).
2) Y. Fukuda, A. Shimura, M. Mukaida, E. Fujita, and K. Sone, *J. Inorg. Nucl. Chem.*, **36**, 1265 (1974).
3) Y. Fukuda, Y. Miura, and K. Sone, *Bull. Chem. Soc. Jpn.*, **50**, 142 (1977).
4) Y. Fukuda and K. Sone, *Bull. Chem. Soc. Jpn.*, **43**, 556 (1970).
5) S. Kida, *Bull. Chem. Soc. Jpn.*, **29**, 809 (1956).
6) H. L. Schläfer, "Komplexbildung in Lösung," Springer, Berlin (1961), p. 238.
7) Data of R. Näsänen taken from "Stability Constants of Metal-Ion Complexes" (Compiled by L. G. Sillén and A. E. Martell), Supplement No. 1, The Chemical Society, London (1971).

* K for [Cu(unsym-deen)(acac)]$^+$ could not be estimated with reasonable accuracy, possibly owing to the errors introduced by the smaller stability of [Cu(unsym-deen)$_2$]$^{2+}$ than those of the other bis-chelates. On the other hand, the values of K for the [Cu(diamine)(acac)]$^+$-type chelates with *N*-methyl- and *N*-ethylethylenediamines were found to be 9—10 (75% dioxane, 20 °C), lying between those of [Cu(en)(acac)]$^+$ and [Cu(dmen)(acac)]$^+$ (Y. Kuma, unpublished study).

** *Cf.*, *e.g.*, the data of [Cu(bpy)$_2$]$^{2+}$, [Cu(phen)$_2$]$^{2+}$ and their mixed chelates studied before.[4]

BULLETIN OF THE CHEMICAL SOCIETY OF JAPAN, VOL. 50 (1), 315—316 (1977)

Synthetic Photochemistry. VII.[1] The Addition Reaction of Acenaphthenequinone and 1,2-Naphthoquinone to Cycloheptatriene

Hitoshi TAKESHITA, Akira MORI, Mitsuru FUNAKURA, and Hiroaki MAMETSUKA
Research Institute of Industrial Science, Kyushu University, Hakozaki, Fukuoka 812

(Received May 31, 1976)

Synopsis. The photoaddition reaction of acenaphthenequinone and 1,2-naphthoquinone to cycloheptatriene was investigated. In contrast to acyclic α-diketones, various cycloadducts were formed from both quinones; the former giving the (2+2)π-, and (2+6)π-cycloadducts together with the ene-product, and the latter the (2+6)π-, (4+2)π-, and (4+4)π-cycloadducts.

A report was given on the results of the photoaddition reaction of cycloheptatriene (tropylidene, **1**) to some acyclic α-diketones.[2] The adduct solely isolated was found to be 7-tropyl-α-ketol derivative, an ene-product in every case. The absence of any cycloadducts is of interest. For comparison, we have examined the reaction of **1** to another type of 1,2-diketo derivatives, cyclic α-diketones.

Irradiation of a dioxane solution of acenaphthenequinone (**2**) and **1** by means of a 500 W tungsten lamp gave three products (**3**, **4**, and **5**) which were isolated by silica gel column chromatography. The first product (**3**, 18% yield) was shown to be a (6+2) π-adduct from the NMR[3] [δ: 2.69 (Ha, d, J=12.0 Hz), 2.96 (Hd, dd, J=7.6, 6.0 Hz), 3.61 (Hb, ddd, J=12.0, 8.0, 6.0 Hz), 4.90 (Hc, ddm, J=8.0, 6.0 Hz), 5.48 (He, dm, J=7.6 Hz), 6.00 (3H, m), and 7.85 (6H, m)] spectral analysis; the coupling patterns of the protons Ha, Hb, Hc and Hd ruled out other possibilitits. Furthermore, the appearance of an isolated signal due to He from the rest of the olefinic proton signals provided an evidence for its stereochemistry.[4]

The second product (**4**, 37%), colorless crystals, was a (2+2) π-adduct since the NMR [δ: 2.73 (Ha, ddm, J= 11.5, 4.5 Hz), 3.18 (Hb, tdm, J=11.5, 2.5 Hz), 4.14 (Hd, dt, J=8.0, 2.0 Hz), 5.31 (He, dd, J=11.5, 2.0 Hz), 5.57 (Hc, ddd, J=11.5, 8.0, 4.5 Hz), 5.6—6.1 (3H, m), and 7.6—8.1 (6H, m)] spectrum showed a signal ascribable to the proton of ethereal carbon (Hc), being spin-coupled to methylene protons (Ha and Hb) and also to Hd. The signal for He appearing in a higher field than for the rest of the protons is utilized to deduce the stereochemistry.

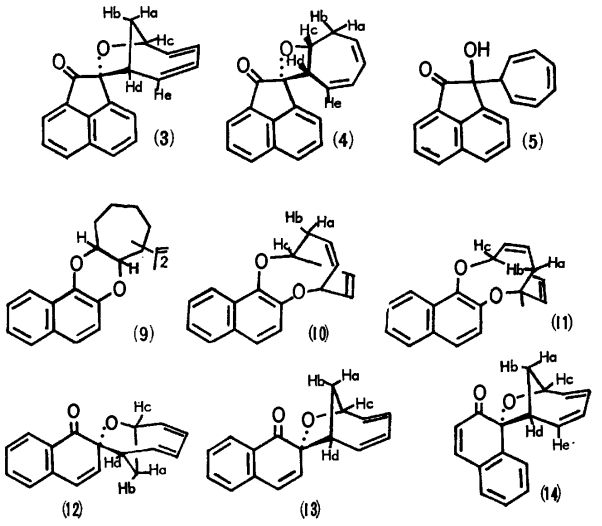

The third product (**5**, 38%), yellow crystals, was found to be the ene-product by the NMR [δ: 2.26 (1H, t, J=6.0 Hz), 5.01 (1H, dd, J=9.5, 6.0 Hz), 5.57 (1H, dd, J=9.5, 6.0 Hz), 6.17 (2H, m), 6.62 (2H, t, J=3.0 Hz), and 7.4—8.3 (6H, m)] spectrum.

When irradiation was carried out under aerial conditions, the products were formed in nearly the same ratio as above, although the main product in this case was 1,8-naphthalenedicarboxylic anhydride (31.3%).

These products must be formed independently, since **3** and **4** were quite stable for further irradiation, but **5** gradually decomposed into 7,7′-bitropyl (**6**),[5] 2-hydroxyacenaphthenenone (**7**),[6] and the starting material (**2**). A similar transformation has been observed in the irradiation of the ene-products derived from **1** and some benzil derivatives.[2] No interconversion of the products (**3**, **4**, and **5**) occurred.

1,2-Naphthoquinone (**8**) and **1** were similarly irradiated in benzene by use of a 500 W tungsten lamp, the products isolated after the column chromatography being a (4+2) π-adduct (**9**, colorless crystals), a pair of (4+4) π-isomers (**10** and **11**, pale yellow oils), a pair of (6+2) π-adducts (**12** and **13** yellow oils) and another (6+2) π-adduct (**14**, a yellow oil). No ene-product was detectable.

9, **10**, and **11** showed neither ν_{OH} nor $\nu_{C=O}$ in their IR spectra, indicating them to be cyclic ethers. The splitting patterns of the proton signals of sp^3-carbon in the NMR of **9** [δ: 2.74 (2H, m), 4.24 (1H, td, J=8.0, 4.6 Hz), 4.66 (1H, d, J=8.0 Hz), 5.95 (4H, m), 7.03 (1H, dd, J=8.0, 3.8 Hz), 7.28 (3H, m), 7.64 (1H, dd, J=8.0, 2.5 Hz), and 8.01 (1H, dd, J=8.0, 2.5 Hz)] was compatible to a (4+2) π-structure. **10** and **11** were stereoisomers which could be separated by high-pressure liquid chromatography. By catalytic reduction, they were converted into the same tetrahydro derivative (**15**) which differs from the tetrahydro derivative (**16**) of **9**. Thus, **10** and **11** were deduced to be the (4+4) π-adducts. Although the NMR spectra of **10** [δ: 2.55 (Ha, dm, J=16.0 Hz), 2.92 (Hb, dddd, J=16.0, 9.0, 3.0, 1.5 Hz), 4.63 (Hc, dt, J=9.0, 3.0 Hz), 4.81 (1H, br. s), 5.93 (4H, m), 6.94 (1H, d, J=9.5 Hz), 7.32 (3H, m), and 7.5—8.0 (2H, m)] and **11** [δ: 2.48 (Ha, dm, J=16.0 Hz), 2.83 (Hb, ddm, J=16.0, 8.0 Hz), 4.51 (Hc, dt, J=8.0, 3.0 Hz), 4.85 (1H, br. s), 5.88 (4H, m), 6.97 (1H, d, J=9.5 Hz), 7.28 (3H, m), and 7.5—8.1 (2H, m)] closely resembled each other, locations of the methylene group were tentatively assigned as depicted from the difference in chemical shifts of Ha, Hb, and Hc.

The NMR spectra of **12** and **13** were considerably different: **12** [δ: 2.53 (Ha, d, J=11.5 Hz), 2.71 (Hb, dt, J=11.5, 6.0 Hz), 2.88 (Hd, td, J=6.0, 1.5 Hz), 4.78 (Hc, tm, J=6.0 Hz), 5.40 (He, m), 5.84 (3H, m), 6.32 (2H, s), and 7.42 (4H, m)] revealed a high field shift for one of the olefinic protons (He); in contrast, **13** [δ: 2.35 (Ha, dt, J=12.0, 3.0 Hz), 2.96 (Hb and Hd, overlapped m), 4.86 (Hc, ddm, J=7.0, 6.5 Hz), 5.90 (4H, m), 6.50 (2H, s), and 7.40 (4H, m)] revealed combined signals for olefinic protons. The absence of α,β-unsaturated carbonyl group was also clear from the chemical shifts of the vinylic protons. Furthermore, the difference in chemical shift between each proton of methylene groups, $\delta_{Ha}-\delta_{Hb}$: 0.18 for **12**, and 0.61 for **13**, was interpreted in terms of the magnetic anisotropy of the carbonyl group on Hb. Thus, the stereochemistry for **12** and **13** was determined as depicted.

The structure of another type of (6+2) π-adduct (**14**) was also clarified from the NMR [δ: 2.41 (1H, d, J=12.0 Hz), 2.86 (1H, dt, J=12.0, 5.8 Hz), 3.24 (1H, dd, J=8.0, 5.8 Hz), 4.88 (1H, tm, J=6.0 Hz), 4.98 (He, tm, J=8.0 Hz), 5.7—6.2 (3H, m), 6.01 (1H, d, 10.0 Hz), 7.36 (1H, d, J=10.0 Hz), and 7.0—8.4 (4H, m)] spectrum. The presence of α,β-unsaturated carbonyl group in **14** is clear from the signals appearing at δ: 6.01 and 7.36. The isolated signal for He, revealing a high field shift, suggests the stereochemistry as depicted.

Formation of the (6+2) π-adducts resembles the mode of reaction of **1** with p-quinones. However, no cycloaddition took place at the C=C part of the quinones in contrast to the case with p-quinones. It is of interest that conjugated olefins, generally regarded to be good triplet quenchers, afforded various types of cycloadducts by irradiations with visible light.[1]

Experimental

*Photoaddition Reaction of Cycloheptatriene (**1**) with Acenaphthenequinone (**2**): Formation of the Cycloadducts (**3**, and **4**) and the Ene-Product (**5**).* A dioxane solution (30 ml) of **1** (2 ml) and **2** (220 mg) was externally irradiated by means of a 500 W tungsten lamp under nitrogen atmosphere for 18 h. After evaporation of the solvent, the residue was fractionated by silica gel column chromatography; **6** was obtained as colorless crystals from the least polar fractions, mp 61—63 °C (lit,[5] 61—62 °C), 17 mg. With the use of benzene as an eluent, three products were obtained consecutively. First, pale yellow crystals (**3**) were eluted, mp 123—125 °C (from ethanol), 23.2 mg [Found: C, 83.12; H, 5.17%. Calcd for $C_{19}H_{14}O_2$: C, 83.20; H, 5.15%. λ_{max}^{MeOH}: 225 nm (ε: 55600), 255.5 (sh., 13800), 308 (6600), 348 (4700)]. Then, colorless crystals (**4**), mp 163—164 °C (from methanol), 47.6 mg [Found: C, 82.91; H, 5.15%. λ_{max}^{MeOH}: 227 nm (ε: 29000), 285 (2700), 319 (2500), 347 (2200)], and pale yellow crystals (**5**), mp 146—147 °C (from methanol), 48.6 mg [Found: C, 83.29; H, 5.10%. λ_{max}^{MeOH}: 223 nm (ε: 47500), 256 (14700), 321 (5100), 345 (4700). ν: 3570, 1735 cm^{-1}] were obtained along with recovered **2** (134 mg).

*Photoaddition Reaction of **1** with **2** in the Presence of Oxygen.* A dioxane solution (16 ml) of **1** (0.5 ml) and **2** (464 mg) was irradiated with a tungsten lamp as above but under aerial conditions for 18.5 h. After evaporation of the solvent, the mixture was washed with a small amount of cold chloroform to recover unreacted **2** (278 mg) from the less soluble portion. Silica gel column chromatography of the soluble portion afforded **3** (38.2 mg), **4** (74.0 mg), colorless crystals, mp 274—275 °C (identified as 1,8-naphthalenedicarboxylic anhydride, 64.5 mg), and **5** (50.1 mg).

*Further Irradiation of **3** and **4**.* **3** (25 mg/3 ml of dioxane) and **4** (33 mg/4 ml of dioxane) were separately irradiated with a tungsten lamp for 9 h. No reaction took place according to the NMR analysis.

*Further Irradiation of **5**.* **5** (15 mg) was dissolved in benzene (10 ml) and irradiated with a tungsten lamp for 17 h. By preparative thin layer chromatography, regenerated **2** ($\approx$1 mg) and **7** ($\approx$1 mg, mp 236—238 °C (lit,[6] 238—239 °C)) were isolated together with **6** which was characterized by gas-liquid chromatographic analysis.

*Photoaddition Reaction of **1** and 1,2-Naphthoquinone (**8**): Formation of Cycloadducts (**9**, **10**, **11**, **12**, **13**, and **14**).* A benzene solution (25 ml) of **1** (1 ml) and **8** (780 mg) was irradiated by means of a 500 W tungsten lamp for 70 h. The product mixture was then separated by silica gel column chromatography. After elution of **6** (9 mg), **9** (colorless crystals, mp 93—94 °C from methanol, 113 mg) [Found: C, 81.29; H, 5.74%. Calcd for $C_{17}H_{14}O_2$: C, 81.58; H, 5.64%. λ_{max}^{MeOH}: 242 nm (ε: 38200)], an oily mixture of **10** and **11** (233 mg), **12** (a colorless oil, bp 120 °C/0.5 Torr (bath temp), 14 mg) [Found: m/e: 250.09509 (M^+). Calcd for $C_{17}H_{14}O_2$: m/e: 250.09938. λ_{max}^{MeOH}: 238 nm (ε: 24200), 275 (sh., 7100)]. **13** (a colorless oil, bp 120 °C/0.5 Torr (bath temp), 72.2 mg) [Found: m/e: 250.09987. λ_{max}^{MeOH}: 240 nm (ε: 40800), 275 (7290)], and **14** (a colorless oil, bp 120 °C/0.5 Torr (bath temp), 47.5 mg) [Found: m/e: 250.10205. λ_{max}^{MeOH}: 238 nm (ε: 14000)] were obtained by elution with benzene.

*Preparative Liquid Chromatographic Separation of a Mixture of **10** and **11**.* The mixture was fractionated by Micropolasil column (2 m) with chloroform: hexane (5: 95) using ALC 202/401 Model of Waters Co., from less polar fractions, a colorless oil (**10**) [Found: m/e: 250.09433. λ_{max}^{MeOH}: 220.5 nm (ε: 24600), 241.5 (38400)] was obtained and from more polar fractions a colorless oil (**11**) [Found: m/e: 250.10009. λ_{max}^{MeOH}: 219.5 nm (ε: 25500), 241.7 (43000)].

*Catalytic Reduction of **10**.* **10** (12 mg) was dissolved in ethyl acetate (2 ml) and reduced by palladium carbon (5%, 4 mg). After the usual work-up, a tetrahydro-derivative (**15**, 8 mg) was obtained as a colorless oil [Found: m/e=254.13292. Calcd for $C_{17}H_{18}O_2$: 254.13068.], whose homogeneity was confirmed by liquid chromatographic analysis.

*Catalytic Reduction of **11**.* Similarly, **11** (25.8 mg) was reduced to give a colorless oil (26 mg) which was identical with **15** in IR and liquid chromatographic comparison.

*Catalytic Reduction of **9**.* **9** (25.6 mg) was dissolved in ethanol (4 ml) and dioxane (1 ml) and reduced by palladium carbon (5%, 7.5 mg). Isolation by the usual work-up afforded colorless crystals, mp 120—121 °C (from methanol) (**16**), 17 mg [Found: C, 79.79; H, 7.18%. Calcd for $C_{17}H_{18}O_2$: C, 80.28; H, 7.13%].

References

1) Part VI of this series: H. Takeshita, A. Mori, and Y. Toyonaga, *Bull. Chem. Soc. Jpn.*, **48**, 307 (1915).
2) A. Mori, T. Fujita, N. Yamamoto, and H. Takeshita, Abstract Papers of 7th Symposium on the Chemistry of Non-Benzenoid Aromatic Compounds, (Oct. 1974, Tokyo) p. 183.
3) The NMR spectra were taken in $CDCl_3$ solution.
4) A. Mori, and H. Takeshita, *Chem. Lett.*, **1975**, 599.
5) W. von E. Doering, and L. H. Knox, *J. Am. Chem. Soc.*, **79**, 352 (1957).
6) Unpublished results of Prof. O. Tsuge, Kyushu Univ.

BULLETIN OF THE CHEMICAL SOCIETY OF JAPAN, VOL. 50 (1), 317—318 (1977)

Absolute Rate Constants for Hydrogen Abstraction from Some Aromatic Hydrocarbons by *p*-Chlorophenylthiyl Radical

Tokuji MIYASHITA, Masashi IINO, and Minoru MATSUDA
Chemical Research Institute of Non-Aqueous Solutions, Tohoku University, Katahira, Sendai 980

(Received June 25, 1976)

Synopsis. The absolute rate constants for hydrogen abstraction from cumene, *p*-cymene, and tetralin by *p*-chlorophenylthiyl radical have been determined by means of flash-photolysis and kinetic absorption spectrophotometry. The results are discussed in comparison with those reported for other types of free radicals.

Thiyl radical can abstract hydrogen atom from hydrocarbons[1,2] containing reactive hydrogen atom and also from compounds containing functional groups such as aldehyde and alcohol.[1] However, few kinetic studies on these reactions have been carried out because of the difficulty of elimination of the reverse reaction under the usual steady state reaction conditions:

$$RS\cdot + R'H \underset{k_{-H}}{\overset{k_H}{\rightleftharpoons}} RSH + R'\cdot \qquad (1)$$

This difficulty has been overcome by using tritium-labeled thiol as a solvent[2] for obtaining the relative rate constants for hydrogen abstraction in the case of the cyclohexylthiyl radical.

We have determined the absolute rate constants for hydrogen abstraction from some hydrocarbons by *p*-chlorophenylthiyl radical by following the decay of a short-lived and a very small amount of the free thiyl radical by means of flash-photolysis and kinetic absorption spectrophotometry;[3] this can effectively eliminate such a reverse reaction. The flash apparatus delivered a flash with an energy of 125 J from xenon-filled lamps. The flash exhibited a half-peak duration of 10 μs.

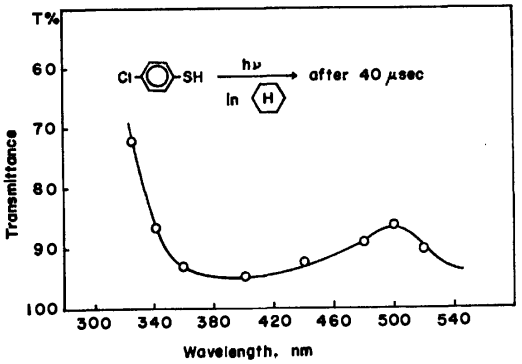

Fig. 1. Electronic spectrum of *p*-chlorophenylthiyl radical produced by flash photolysis of *p*-chlorophenylthiol.

Figure 1 shows the absorption spectrum of *p*-chlorophenylthiyl radical in cyclohexane recorded after 40 μs of the flash. The same spectrum has been reported by Thyrion,[4] and Tagami *et al.*[5] The decay of the *p*-chlorophenylthiyl radical has been followed by monitoring the absorbance at 500 nm. The behavior of the decay observed for *p*-chlorophenylthiyl radical in solutions can be divided into the following three patterns. (a) In cyclohexane and toluene solutions the thiyl radical decays according to second-order kinetics, indicating the occurrence of recombination of the thiyl radical in both the solvents:

$$2RS\cdot \xrightarrow{k_t} RS\text{-}SR \qquad (2)$$

Table 1. Decay kinetics of *p*-chlorophenylthiyl radical in various hydrocarbons (23 °C)

Solvent	Decay order	Rate constant (1 mol^{-1} s^{-1})
Cyclohexane	2 nd	$2k_t/\varepsilon = 4.1 \times 10^{6}$ [a]
		$2k_t = 1.4 \times 10^{9}$ [a]
Cyclohexane	2 nd	$2k_t/\varepsilon = 4.1 \times 10^{6}$
		$2k_t = 1.2 \times 10^{9}$ [b]
Toluene	2 nd	$2k_t/\varepsilon = 4.8 \times 10^{6}$
		$2k_t = 1.4 \times 10^{9}$ [b]
Ethylbenzene	2 nd—1 st	—
Tetralin	1 st	$k_H = 1.50 \times 10^{2}$
Cumene	1 st	$k_H = 1.20 \times 10^{3}$
p-Cymene	1 st	$k_H = 1.42 \times 10^{3}$

a) Ref. 4, the rate constant for the phenylthiyl radical. b) Calculated by using the reported ε[5] (280 dm^3/mol cm at 510 nm) for the *p*-chlorophenylthiyl radical.

The relevant second-order rate constants determined are given in Table 1. A similar recombination rate constant was reported for phenylthiyl radical in cyclohexane[4] (Table 1). (b) The decay in large excess of tetralin, cumene, and *p*-cymene, obeys pseudo first-order kinetics. (c) In the ethylbenzene solution, competitive reactions between the pseudo first-order reaction (hydrogen abstraction from the solvent, the forward reaction in Eq. 1) and recombination take place. The pseudo first-order rate constants were reduced to absolute second-order rate constants per reactive hydrogen atom. These results are also given in Table 1.

Ingold gave the absolute rate constants for hydrogen

Table 2. Absolute rate constants for hydrogen abstraction from cumene by short-lived radicals

Radical	Absolute rate constant k_H (1 mol^{-1} s^{-1})
OH·	Diffusion controlled[a]
Br·	1.2×10^{7} (40 °C)[a]
C_6H_5·	$\simeq 10^{7}$ (60 °C)[a]
t-C_4H_9O·	4.3×10^{4} (40 °C)[a]
p-ClC_6H_4S·	1.2×10^{3} (23 °C)[b]
Cl_3C·	1.3×10^{2} (40 °C)[a]
t-C_4H_9OO·	3.3×10^{-1} (30 °C)[a]
$-CH_2(C_6H_5)CH$·[c]	1.3×10^{-3} (60 °C)[a]

a) Ref. 6. b) This work. c) Polystyryl radical.

abstraction by a variety of radicals.[6] These absolute rate constants for α-hydrogen atom abstraction from cumene by various types of free radicals are summarized together with ours in Table 2. We see that the *p*-chlorophenylthiyl radical abstracts about 30 times faster than the trichloromethyl radical, and about 20 times slower than the *t*-butoxyl radical at 23 °C. Activation energies[6] of 6 kcal/mol and 12 kcal/mol, in the abstraction of *t*-butoxyl and trichloromethyl radicals, respectively, from toluene, were used in the calculation of the rate constants at 23 °C. Zwet and Kooyman reported that the triphenylmethylthiyl radical is more reactive in hydrogen abstraction reactions than the trichloromethyl radical, but less reactive than the *t*-butoxyl radical or chlorine atom.[8] Their findings agree with ours. The slightly greater reactivity toward *p*-cymene than cumene (Table 1) is reasonable in the light of electrophilicity of the thiyl radicals.[2,7]

The authors wish to thank Asst. Prof. Dr. H. Kokubun and Dr. K. Kikuchi, Tohoku University, for their introduction to flash photolysis technique and for the use of the apparatus.

References

1) R. M. Kellogg, "Methods in Free-Radical Chemistry," Vol. II, ed by E. S. Huyser, Marcel Dekker, New York (1969), p. 101.
2) W. A. Pryor, G. Gojon, and J. P. Stanley, *J. Am. Chem. Soc.*, **95**, 945 (1973).
3) G. Porter, "Technique of Organic Chemistry," Vol. VIII, Part 2, ed by A. Weissberger, Interscience Publishers, New York (1963), p. 1055.
4) F. C. Thyrion, *J. Phys. Chem.*, **77**, 1478 (1973).
5) M. Tagami, T. Takakura, M. Okuyama, and H. Kamata, 8th Symposium on High Speed Reactions, 1973, p. 45.
6) K. U. Ingold, "Free Radicals," Vol. I, ed by J. K. Kochi, John Wiley & Sons, New York (1973), p. 74.
7) C. Walling, D. Seymour, and K. B. Wolfstirn, *J. Am. Chem. Soc.*, **70**, 2559 (1948).
8) Ref. 1, p. 104.

BULLETIN OF THE CHEMICAL SOCIETY OF JAPAN, VOL. 50 (1), 319—320 (1977)

Synthesis of New Heptacyclic Propellanes

Yoshito TOBE, Hirofumi OMURA, Atsutaka KUNAI, Koji KIMURA, and Yoshinobu ODAIRA

Department of Petroleum Chemistry, Faculty of Engineering, Osaka University, Suita-shi, Osaka 565

(Received June 28, 1976)

Synopsis. The heptacyclic propellanes, **8** and **9**, having two propellane rings in each molecule, were synthesized by the stepwise photocycloaddition of bicyclo[4.3.0]non-1(6)-en-7-one (**1**) to cyclohexadiene or cyclooctadiene followed by the Wolff-Kishner reduction of the resulting propellanones **6** and **7**. The photosolvolytic behavior of some of the cycloadducts is also described.

As part of a study of the synthesis of polycyclic propellanes,[1] we report that the tetracyclic *trans*-fused cycloadduct (**4** or **5**) was easily derived from the photocycloaddition of bicyclo[4.3.0]non-1(6)-en-7-one (**1**) to cyclohexene or cyclooctene.[2] The present investigation was undertaken to synthesize some new heptacyclic propellanes, having two propellane rings in each molecule, by a similar but stepwise photocycloaddition between the enone (**1**) and two kinds of alicyclic dienes.

First, **1** was irradiated in the presence of 10 molar excess of 1,4-cyclohexadiene or 1,5-cyclooctadiene through a Pyrex filter, until it was almost consumed, giving the sole cycloadduct, **2** or **3**, respectively in 74% or 80% yield. Catalytic hydrogenation of **2** and **3** over Pd/C led to the formation of **4** and **5**, respectively, compounds identical with the cycloadducts. The stereochemistry around the junction of the cyclobutane ring in the compounds **2**, **3**, and **4** has been determined to be *trans* by means of X-ray analysis.[3] Next, the cycloadduct (**2** or **3**) was irradiated with 4 molar excess of the enone (**1**), under similar conditions to those described above, to afford the heptacyclic cycloadduct, **6** or **7**, respectively in 25% or 31% yield. Thus, it seems reasonable to assume that the stereochemistry about the second cyclobutane ring in **6** and **7** is also *trans*, though the stereochemical relation between two bicyclo[4.3.0]-nonan-7-one skeltons in each molecule is still uncertain. Finally, the heptacyclic propellanes (**8** and **9**), having two propellane rings in each molecule, were obtained by the Wolff-Kishner reduction of the corresponding propellanones (**6** and **7**), in 37% and 56% yields, respectively.[4]

Photolyses of the propellanones **2**, **4**, **6**, and **7** were carried out, in an attempt to transform the cycloadducts of [4.3.2]propellane system into polycyclic compounds of another system. Photolyses of **2** and **4** in aqueous dioxane gave the acids, **10** and **11**, respectively, almost quantitatively. Irradiation of **4**, **6**, and **7** in methanol gave the esters **12**, **13**, and **14**, respectively.

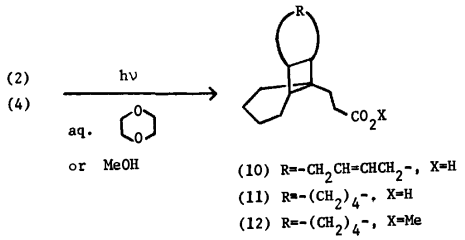

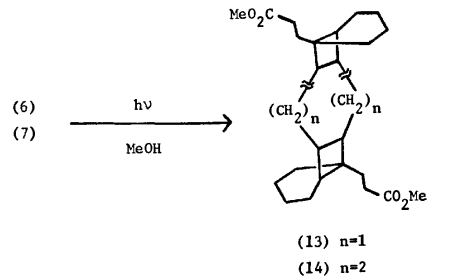

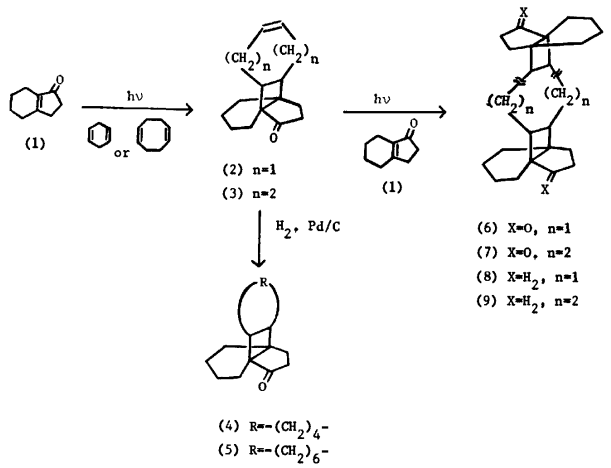

Experimental

Bicyclo[4.3.0]non-1(6)-en-7-one(1). Enone (**1**) was prepared according to the procedure of Dev.[5]

Photocycloaddition of 1 with 1,4-Cyclohexadiene. A solution of **1** (0.800 g, 5.88 mmol) in 1,4-cyclohexadiene (59 mmol) was irradiated through a Pyrex filter under nitrogen at room temperature until enone (**1**) was almost comsumed. After removal of the diene, distillation gave 0.938 g of the cycloadduct (**2**) (74%), as the sole adduct (GLPC). Recrystallization from methanol gave an analytical sample, mp 80—81 °C; ν_{max} 1725, 660 cm^{-1}; δ (CCl_4) 0.60—2.65 (m, 18H), 6.55 (s, 2H); *m/e* 216 (M^+), 137; 2,4-dinitrophenylhydrazone, mp 174—175 °C; Found: C, 63.47; H, 6.03; N, 14.30%. Calcd for $C_{21}H_{24}O_4N_4$: C, 63.62; H, 6.10; N, 14.13%.

Photocycloaddition of 1 with 1,5-Cyclooctadiene. A solution of **1** (0.493 g, 3.62 mmol) in 1,5-cyclooctadiene (36 mmol) was irradiated and work-up as above gave 0.711 g of the cycloadduct (**3**) (80%), mp 88—89.5 °C; ν_{max} 1715, 725 cm^{-1}; δ (CCl_4) 0.60—1.75 (m, 14H), 1.90—2.50 (m, 8H), 6.40—6.65 (m, 2H); *m/e* 244 (M^+), 137; Found: C, 83.59; H, 9.95%. Calcd for $C_{17}H_{24}O$: C, 83.55; H, 9.90%.

Photocycloaddition of 1 with 2. A solution of **1** (2.825 g, 28.1 mmol) and **2** (1.355 g, 6.27 mmol) in 50 ml of pentane

was irradiated as above. After removal of the solvent, the residue was chromatographed on silica gel. The benzene eluate was collected and recrystallized from ethanol to give 0.55 g of the cycloadduct (**6**) (25% based on **2** used), mp 265—267 °C; ν_{max} 1720 cm^{-1}; δ (CCl_4) 0.60—2.40 (m, 28H), 2.40—2.70 (m, 4H); *m/e* 352 (M^+), 137; Found: C, 81.41; H, 9.05%. Calcd for $C_{24}H_{32}O_2$: C, 81.77; H, 9.15%.

*Photocycloaddition of **1** with **3**.* A solution of **1** (5.20 g, 38.2 mmol) and **3** (2.39 g, 9.80 mmol) in 50 ml of pentane was irradiated and work-up as above gave 1.15 g of the cycloadduct (**7**) (35% based on **3** used), mp 239—240 °C; ν_{max} 1715 cm^{-1}; δ ($CDCl_3$) 0.40—2.30 (m, 32H), 2.30—2.70 (m, 4H); *m/e* 380 (M^+), 137; Found: C, 81.79; H, 9.56%. Calcd for $C_{26}H_{36}O_2$: C, 82.06; H, 9.54%.

*Wolff-Kishner Reduction of **6** and **7**.* The Wolff-Kishner reduction of **6** and **7** was carried out according to the procedure of Huang-Minlon.[6] The products were isolated by vacuum distillation and purified by preparative GLPC. They showed no carbonyl absorption in infrared spectra. Reduction of **6** gave **8** (37%), mp 173—175 °C; δ (CCl_4) 0.70—2.30 (m): *m/e* 324 (M^+), 122; Found: C, 88.81; H, 11.43%. Calcd for $C_{24}H_{36}$: C, 88.82; H, 11.18%. Reduction of **7** gave **9** (56%), mp 132—134 °C; δ (CCl_4) 0.70—2.00 (m); *m/e* 352 (M^+), 122; Found: C, 88.16; H, 11.77%. Calcd for $C_{26}H_{40}$: C, 88.56; H, 11.44%.

*Photolysis of **2** and **4** in Aqueous Dioxane.* A solution of **2** or **4** in 90% aq dioxane irradiated in a quartz vessel until the ketone was almost consumed. After removal of the solvent, distillation gave the acid, **10** or **11**, respectively. Recrystallization from hexane gave an analytical sample. **10** (78%); mp 97—99 °C; ν_{max} 3050, 1700, 660 cm^{-1}; δ (CCl_4) 0.80—2.50 (m, 19H), 5.65 (s, 2H), 10.30—11.60 (broad s, 1H); *m/e* 234(M^+). **11** (84%); mp 100—101 °C; ν_{max} 3050, 1700 cm^{-1}; *m/e* 236 (M^+); Found: C, 76.10; H, 10.25%. Calcd for $C_{15}H_{24}O_2$: C, 76.22; H, 10.24%. Catalytic hydrogenation of **10** over Pd/C gave **11**.

*Photolysis of **4**, **6**, and **7** in Methanol.* A solution of **4** or **6** or **7** in methanol was irradiated as above. After removal of the solvent, the ester (**12**) was isolated by distillation, and esters (**13** and **14**) were isolated by column chromatograph on silica gel. **12** (86%); ν_{max} 1740 cm^{-1}; δ (CCl_4) 0.80—2.30 (m, 23H), 3.55 (s, 3H); *m/e* 250 (M^+); Found: C, 77.06; H, 10.75%. Calcd for $C_{16}H_{26}O_2$: C, 76.75; H, 10.74%. **13** (43%); mp 159—161 °C; ν_{max} 1730 cm^{-1}; δ (CCl_4) 0.90—2.40 (m, 34H), 3.60 (s, 6H); *m/e* 416 (M^+); Found: C, 74.81; H, 9.72%. Calcd for $C_{26}H_{40}O_4$: C, 74.96; H, 9.68%. **14** (35%); ν_{max} 1740 cm^{-1}; δ (CCl_4) 0.80—2.40 (m, 38H), 3.60 (s, 6H); *m/e* 444 (M^+).

We are grateful to Prof. N. Kasai and co-workers for the X-ray analysis.

References

1) A. Kunai, T. Omori, T. Miyata, K. Kimura, and Y. Odaira, *Tetrahedron Lett.*, **1974**, 2517; A. Kunai, T. Omori, K. Kimura, and Y. Odaira, *Bull. Chem. Soc. Jpn.*, **48**, 731 (1975); A. Kunai, K. Kimura, and Y. Odaira, *ibid.*, **48**, 1677 (1975).

2) A. Kunai, K. Yorihiro, T. Hirata, and Y. Odaira, *Tetrahedron*, **29**, 1679 (1973); unpublished data, Y. Tobe, A. Doi, K. Kimura, and Y. Odaira.

3) M. Harada, Y. Kai, N. Yasuoka, and N. Kasai, *Acta Crystallogr., Sect. B* **32**, 625 (1976).

4) The propellanones (**2**)—(**5**) were also converted into the corresponding propellanes in similar yields.

5) S. Dev, *J. Indian Chem. Soc.*, **34**, 169 (1957).

6) Huang-Minlon, *J. Am. Chem. Soc.*, **68**, 2487 (1946).

BULLETIN OF THE CHEMICAL SOCIETY OF JAPAN, VOL. 50 (1), 321—322 (1977)

A Convenient Two-Step Synthesis of Bis(polyalkylphenyl) Disulfides from Polyalkylbenzenes[1)]

Hitomi SUZUKI and Misao SHINODA*

Department of Chemistry, Faculty of Science, Hiroshima University, Higashi-sendamachi, Hiroshima 730
**Department of Industrial Chemistry, Faculty of Engineering, Toyama University, Nakagawa-sonomachi, Takaoka 933*

(Received June 30, 1976)

Synopsis. Heating of polyalkyliodobenzenes with copper(I) thiocyanate in phosphoric tris-dimethylamide at 180—190 °C for a short period of time gives the corresponding bis(polyalkylphenyl) disulfides in high yields.

Although the reaction of aryl halides with copper(I) thiocyanate was reported as early as in 1920 to yield a mixture of aryl cyanide, arenethiol, diaryl sulfide, and diaryl disulfide rather than the expected aryl thiocyanates,[2)] no attempts seem to have been made so far to extend the original work to synthetic purpose. This is probably due to the incomplete conversion coupled with the tedious work-up involved in the separation of the products.[3)]

We have found, however, that this reaction can be modified to provide a simple two-step method for the conversion of polyalkylbenzenes into the corresponding diaryl disulfides, which are otherwise less easy of access. Reported preparation of bis(polyalkylphenyl) disulfides is based on the mild oxidation of polyalkylbenzenethiols,[4)] the action of sulfur monochloride on polyalkylbenzenes,[5)] and the reaction of the diazonium compounds of polyalkylanilines with sodium polysulfide.[6)] Almost all these procedures, however, suffer from either difficulty of access to appropriate starting materials or the lack of generality.

A mixture of a polyalkyliodobenzene and copper(I) thiocyanate (mole ratio, *ca.* 1.0: 1.1) in phosphoric tris-dimethylamide was heated in an oil bath and kept at 180—190 °C for a short period of time until the mixture turned dark and homogeneous. After cooling, the thick mixture was diluted with water and the precipitate was filtered off and extracted with hexane or benzene, giving the corresponding diaryl disulfides in good yields. Neither the replacement of iodoarene by bromoarene nor the use of other dipolar aprotic solvents such as *N*-methyl-2-pyrrolidone and *N*,*N*-dimethylformamide gave better results.

This method of preparation of diaryl disulfides has certain advantages, complementing the existing methods for disulfide synthesis: 1) It is a two-step synthesis from hydrocarbon. Each operation is quite simple and overall process can be carried out in half a day. 2) Starting materials are easily available and reagents are cheap. 3) Products are pure and yields are good, although no attempts have yet been made to optimize them.

TABLE 1. PHYSICAL PROPERTIES OF SOME BIS (POLYMETHYLPHENYL) DISULFIDES

Disulfide	Mp (°C)	Yield[a)] (%)	PMR spectra (δ)[b)] CH_3	PMR spectra (δ)[b)] Aromatic H	IR[c)] spectra (cm^{-1})	Elemental analysis (%) Found C	Found H	Calcd C	Calcd H
Bis(2,3,4-trimethylphenyl) disulfide	128—130	91	2.19(1) 2.27(1) 2.38(1)	6.91(d) 7.32(d) J=7.5 Hz	795 812 1005 1148	71.3	7.4	71.5	7.3
Bis(2,4,6-trimethylphenyl) disulfide	126—128 (lit, 125)[4)]	89	2.23(2) 2.25(1)	6.82	715 850 862 1032 1298	71.8	7.5	71.5	7.3
Bis(2,3,4,6-tetramethylphenyl) disulfide	90—91	83	2.10(1) 2.17(2) 2.24(1)	6.84	718 862 1012 1290	72.8	8.0	72.7	7.9
Bis(2,3,5,6-tetramethylphenyl) disulfide	99—101 (lit, 100—101)[4)]	81	2.12(2) 2.15(2)	6.90	718 872 1000	72.7	8.0	72.7	7.9
Bis(pentamethylphenyl) disulfide	190—193	87	2.16(2) 2.22(3)		1008 1062 1285	73.6	8.5	73.7	8.4

a) Based on the isolated product. b) Numerals in parentheses refer to the number of methyl groups.
c) Principal peaks in the region 650—1350 cm^{-1}.

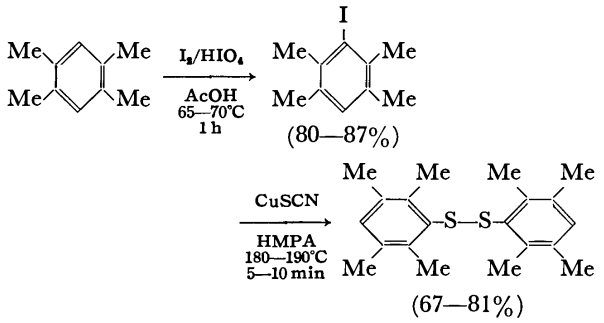

Experimental

All melting points were determined on a hot stage and are uncorrected. The PMR spectra were recorded on a Varian T-60 spectrometer using deuteriochloroform solutions and TMS as internal standard. The IR spectra were measured in Nujol mulls with a Hitachi 215 spectrophotometer.

Iodoarenes were prepared by the direct iodination of arenes with iodine/periodic acid.[7] The structures of all the products were characterized by PMR and IR spectroscopy and elemental analysis. Physical properties and yields of some bis(polymethylphenyl) disulfides obtained are given in Table 1.

The general procedure is illustrated below with the preparation of *bis(2,3,4-trimethylphenyl) disulfide* from 4-iodo-1,2,3-trimethylbenzene:

A mixture of 4-iodo-1,2,3-trimethylbenzene (3.8 g), copper (I) thiocyanate (2.0 g), and phosphoric tris-dimethylamide (6 ml) was stirred and heated in an oil bath. At 180—190 °C the mixture rapidly turned dark and homogeneous. Heating was then stopped and the mixture was allowed to cool with stirring. The black viscous mixture was diluted with water and the precipitated solid was collected by filtration and washed thoroughly with water. It was sucked as dry as possible and then placed in a filter thimble and extracted with hexane with a Soxhlet extractor. The extract was evaporated and the residue was crystallized from ethanol to give bis(2,3,4-trimethylphenyl) disulfide as fine prisms, mp 127—129 °C. Yield, 2.12 g (91%).

References

1) The reaction of polysubstituted aromatics. Part XLV; Part XLIV: H. Suzuki, H. Yoneda, and T. Hanafusa, *Bull. Inst. Chem. Res., Kyoto Univ.*, **54**, 176 (1976).
2) K. W. Rosenmund and H. Harms, *Chem. Ber.*, **53**, (1920).
3) R. G. R. Bacon and H. A. O. Hill, *J. Chem. Soc.*, **1964**, 1097.
4) R. M. Pierson, A. J. Costanza, and A. H. Weinstein, *J. Polym. Sci.*, **17**, 221 (1955); A. J. Costanza, R. J. Coleman, R. M. Pierson, C. S. Marvel, and C. King, *ibid.*, **17**, 319 (1955).
5) Z. S. Ariyan and L. A. Wiles, *J. Chem. Soc.*, **1961**, 4510.
6) W. Rundel, *Chem. Ber.*, **101**, 2956 (1968).
7) H. Suzuki, *Org. Synth.*, **51**, 94 (1971).

BULLETIN OF THE CHEMICAL SOCIETY OF JAPAN, VOL. 50 (1), 323—324 (1977)

Photochemical Ethoxycarbonylmethylation of Toluene with Ethyl Chloroacetate[1]

Yoshiro OGATA and Eiji HAYASHI

Department of Applied Chemistry, Faculty of Engineering, Nagoya University, Chikusa-ku, Nagoya 464

(Received July 30, 1976)

Synopsis. UV irradiation of a toluene solution of ethyl chloroacetate under N_2 gave an isomeric mixture of ethyl tolylacetates: ortho, 5.2%, meta, 9.6%, para, 0.9% and a trace of diethyl succinate. The reaction under air increased the yields of all the products. Addition of $AlCl_3$ also increased the yields, especially that of ortho; *i. e.*; 17.9%; meta, 26.5%; para, 10.6%.

In the ordinary aromatic Friedel-Crafts reaction of carboxylic acids and esters, the site of electrophilic reagents is a carbonyl carbon atom because of the addition of $AlCl_3$ to carbonyl; thus the aromatic substitution by CH_2COOH or CH_2COOR is usually difficult and only a few reports are available on this sort of reaction.[2] However, UV irradiation can overcome this difficulty, the following examples being reported; ethoxycarbonylmethylation of benzene (PhH) giving $PhCH_2COOEt$[3] and carbamolymethylation of phenols (ArH) giving $ArCH_2CONH_2$.[4] The present note deals with the ethoxycarbonylmethylation of toluene with ethyl chloroacetate and a disccussion on its orientation.

Results and Discussion

Irradiation of 0.3 M ethyl chloroacetate solution in toluene under N_2 atmosphere for 40 h gave ethyl tolylacetates, the yields being ortho (I), 5.2%; meta (II), 9.6% and para (III), 0.9%. A trace of diethyl succinate (IV) and an unidentified product were also observed by GLC. Consumption of the chloroacetate was 25%.

$$\underset{\text{excess}}{C_6H_5CH_3} + ClCH_2CO_2Et \xrightarrow{h\nu}$$

$$o\text{-}CH_3C_6H_4CH_2COOEt\ (\text{I}),\quad m\text{-}CH_3C_6H_4CH_2COOEt\ (\text{II})$$

$$p\text{-}CH_3C_6H_4CH_2COOEt\ (\text{III}),\quad \underset{\underset{CH_2COOEt}{|}}{CH_2COOEt}\ (\text{IV}),\quad \textit{etc.}$$

The same reaction under air gave higher yields; I, 16.5%; II, 18.8%; III, 13.8%; IV, 4.5%. Consumption of $ClCH_2COOEt$ was 35%. This effect of oxygen suggests the acceleration of the radical fission of $ClCH_2COOEt$ to Cl· and $\cdot CH_2COOEt$ radicals by Cl· atom abstraction by molecular oxygen or other radicals. This indicates that molecular oxygen itself and/or radicals derived from the photo-oxidation of organic materials can induce the radical abstraction of Cl atom as suggested from the alkyl-halogen fission of some alkyl halides[5] and from the behavior in the SO_2Cl_2 chlorination in the presence of these radicals.[6]

Addition of $AlCl_3$ (3.0 g) to the same mixture of $ClCH_2COOEt$ (5.5 g) and toluene (150 ml) under N_2 for 40 h increased the yields of tolylacetates, especially ortho and para: I, 17.9%; II, 26.5%; III, 10.6%; IV, trace, where 72% of $ClCH_2COOEt$ was photolyzed. Unidentified products in these cases seem to be the same one in view of its GLC peak. Hydrogen chloride was detected in all cases by silver nitrate test.

The yields with toluene were much higher than the reported yield with benzene affording $PhCH_2COOEt$ (2.5% without $AlCl_3$ and 11.5% with $AlCl_3$).[3] In a previous paper[3] it was postulated that the attacking species may be a radical $\cdot CH_2COOEt$ in the absence of $AlCl_3$ and a cation-like species $Al^{\delta-}Cl_3\cdots Cl\cdots C^{\delta+}H_2$-COOEt in the presence of $AlCl_3$ for this type of reaction. The observed effect of CH_3 may imply the stabilization of the transition state by hyperconjugation, which can delocalize both odd electron (V) and positive charge (VI).

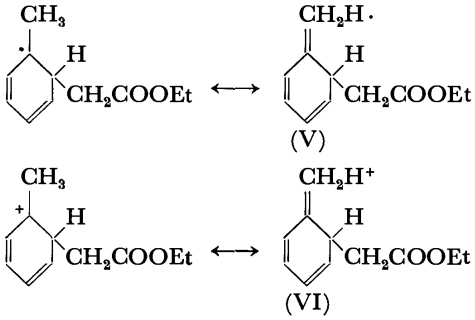

However, the yield of III (para) is much lower, and the yield of II (meta) much higher than that expected from the hyperconjugation. This suggests the different charge distribution in the π-π^* singlet excited aromatics as evidenced in the H-D exchange reaction of aromatics,[7] which prefers ortho and meta substitution of radical and electrophilic reagents to para substitution; The negative charge is more localized at ortho and meta position to CH_3. The observed increase of contents of III and IV under oxygen can be explained in terms of the tendency to statistical orientation due to higher concentration of radical $\cdot CH_2COOEt$, while the increase of III by addition of $AlCl_3$ can be ascribed to the leveling of isomer distribution to the thermodynamic equilibrium in the presence of $AlCl_3$ as observed in ordinary Friedel-Crafts alkylation.[8]

Experimental

Materials. Ethyl *o*-, *m*- and *p*-tolylacetates were prepared by H_2SO_4-catalyzed esterification of the corresponding tolylacetic acids. Boiling points: *o*, 103—104 °C/5 Torr (lit,[9] bp 236—238 °C); *m*, 104—105 °C/6 Torr (lit,[9] bp 228—229 °C); *p*, 98—99 °C/4 Torr (lit,[9] bp 240 °C). Diethyl succinate, bp 104—105 °C/15 Torr (lit,[3] bp 108 °C/19 Torr). Commercial ethyl chloroacetate of guaranteed grade was

used, bp 52—53 °C/21 Torr.

A Typical Procedure. A mixture of ethyl chloroacetate (5.5 g) and toluene (150 ml) was irradiated with a 300 W high pressure Hg lamp in a quartz tube (3×30 cm) for 40 h at 20 °C. The tube and the lamp were immersed in a water bath at a distance of 5 cm.

Identification of the products was carried out by comparison of GLC peaks with those of the authentic samples. GLC analysis was carried out with a column (4 mm×1.2 m) packed with Apiezon Grease L (15 wt%) on Celite 545 of 80—100 mesh and a column (4 mm×1.5 m) packed with PEG (10 wt%) on Chromosorb WAN using N_2 as a carrier gas (40 ml/min) at 80—250 °C (8 °C/min). Ethyl acetate was used as an internal standard.

References

1) Contribution No. 232.

2) a) Y. Ogata and J. Ishiguro, *J. Am. Chem. Soc.*, **72**, 4302 (1950); b) Y. Ogata, J. Ishiguro, and Y. Kitamura, *J. Org. Chem.*, **16**, 239 (1951); c) R. L. Lehmann and J. Linter, U. S. Patent 2 617 822 (1952); *Chem. Abstr.*, **48**, 725 (1954).

3) Y. Ogata, T. Itoh, and Y. Izawa, *Bull. Chem. Soc. Jpn.*, **42**, 794 (1969).

4) O. Yonemitsu and S. Naruto, *Tetrahedron Lett.*, **1969**, 2387.

5) a) M. S. Kharasch and W. H. Urry, *J. Am. Chem. Soc.*, **69**, 1100 (1947); b) M. S. Kharasch and W. H. Urry, *ibid.*, **69**, 1105 (1947); c) M. S. Kharasch and P. Fisher, *ibid.*, **70**, 1055 (1948).

6) M. S. Kharasch and H. C. Brown, *J. Am. Chem. Soc.*, **61**, 3432 (1939).

7) a) D. A. de Bie and E. Havinga, *Tetrahedron*, **21**, 2359 (1965); b) J. P. Colpa, C. Mclean, and E. L. Mackor, *ibid.*, **19**, Suppl. 2, 65 (1963).

8) a) D. V. Nightingale, *Chem. Rev.*, **25**, 329 (1939); b) C. C. Price, *Org. React.*, **3**, 8 (1949); c) G. Baddeley, G. Holt, and D. Voss, *J. Chem. Soc.*, **1952**, 100; d) G. A. Olah *et al.*, *J. Org. Chem.*, **29**, 2313, 2315 (1964).

9) "Beilsteins Handbuch, Hauptwerk," **9**, 527 (1926).

BULLETIN OF THE CHEMICAL SOCIETY OF JAPAN, VOL. 50 (1), 325—326 (1977)

Various Acceleration Conditions of Pummerer Reaction Observed in the Total Synthesis of Illudins[1)]

Takeshi MATSUMOTO, Haruhisa SHIRAHAMA, Fujio SAKAN,* and Kazuko TAKIGAWA*

Department of Chemistry, Faculty of Science, Hokkaido University, Sapporo 060

**Chemical Laboratory, Faculty of Education, Fukui University, Fukui 910*

(Received August 2, 1976)

Synopsis. Pummerer reaction of highly functionalized sulfoxides were examined under various modified conditions. The results indicated that added base and/or neighboring acetoxyl group accelerated the reaction.

In the course of our synthetic work on illudins,[2)] we found a base catalyzed and a neighboring group participated acceleration of Pummerer reaction whose utility for organic synthesis increased recently.[3)]

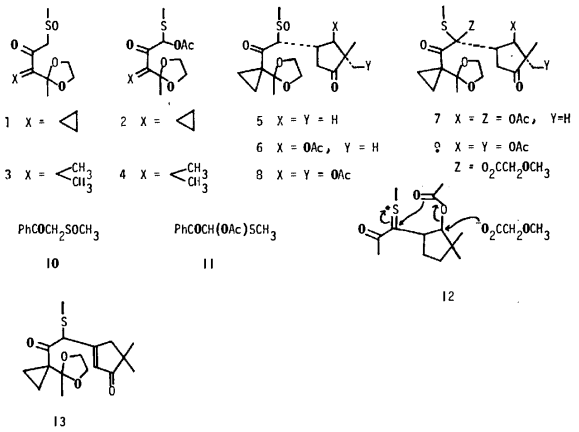

According to the mechanism proposed by Oae and Kise,[4)] the acceleration of the reaction by base was expected and in fact effect of pyridine on simple sulfoxides was recently reported.[5)] In our work highly functionalized sulfoxides, **1**, **3**, **6**, and **8** smoothly underwent Pummerer reaction by addition of pyridine, while without pyridine they did not undergo the reaction under mild reaction conditions or gave no normal reaction products, which were key intermediates for our synthesis,[2)] even under more drastic conditions.

Another new observation is an acceleration of the reaction by neighboring group participation. The reaction with sulfoxides **5** and **6** showed clearly the effect of acetoxyl group on their cyclopentane rings. The mode of participation is not clear at present but migration of acetoxyl group through transition like **12** was excluded by the experiment employing methoxyacetic anhydride (**8**→**9**). The results were summarized in Table 1.

Further study revealed that the Pummerer reaction was markedly accelerated by the addition of mercuric chloride as shown in the Table 1.[6)]

Experimental

Sulfoxide (**10**) was obtained from ethyl benzoate according to Corey's procedure[11)]. Other sulfoxides were synthesized during our synthetic work and their physical and analytical data appeared in the references indicated.

NMR spectra were measured at 100 MHz on a JEOL Model JNM-4H-100 spectrometer using TMS as an internal standard. IR spectra were taken on a HITACHI Model EPI-G3 spectrometer with NaCl optics.

Acetic anhydride used in this work was purified by fractional distillation. Pyridine was dried over potassium hydroxide and distilled before use.

Pummerer Reaction without Pyridine. A mixture of 100 mg of sulfoxide and 2.8 ml of acetic anhydride was heated to reflux for 2 h. The mixture was concentrated in vacuo and the residue was dissolved in chloroform. The solution was washed with saturated sodium hydrogencarbonate solution and brine and dried over anhydrous sodium sulfate. Removal of the solvent gave a practically pure product,—**2**, **4**, and **11**.

The Reaction with Pyridine. A mixture of 100 mg of sulfoxide, 2.8 ml of acetic anhydride and 4.0 ml of pyridine was allowed to stand for 1 week at room temperature. The mixture was concentrated in vacuo at ambient temperature and the residue was stirred with water for 30 min and extracted three times with chloroform. The combined extracts were washed with sodium hydrogencarbonate solution and brine and dried over sodium sulfate. After removal of

TABLE 1. VARIOUS CONDITIONS OF THE PUMMERER REACTION

Sulfoxides	Products	Yields (%) under various conditions			
		Ac_2O/r.t./1 week	Ac_2O/reflux/2 h	Ac_2O–Py/r.t./1 week	Ac_2O–$HgCl_2$/r.t./3 h
1[7)]	**2**[7)]	recovered	79[a)]	85[a,g)]	75[a)]
3[8)]	**4**	recovered	>95[b)]	>90[b,g)]	>90[b)]
5[2b)]	—	recovered	complex mixture[9)]	recovered	—
6[2c)]	**7**[2c)]	recovered	complex mixture	70[a,g)]	—
8[2e)]	**9**[2e)]	—	—	65[a,c,d)]	—
10	**11**	recovered[f)]	>95[b)]	>95[b,e)]	95[b)]

a) Isolated yield (by column chromatography on silica gel). b) Based on NMR analysis. c) Methoxyacetic anhydride was used instead of Ac_2O. d) The reaction was completed in 2 days. e) The reaction was completed in 3 days. f) After 3 days. g) The starting sulfoxide remained in shorter reaction time (TLC analysis).

the solvent the product obtained was practically pure.—**2**, **4**, and **11**.

In the case of the reactions with **6** and **8** the product was purified by chromatography on silica gel.

In the reaction with sulfoxide **8** methoxyacetic anhydride was used instead of acetic anhydride and in this case the reaction was completed in 2 days. The reaction time was 3 days with **10**.

The Reaction with Mercuric Cholride. A mixture of 100 mg of sulfoxide, 2.8 ml of acetic anhydride and 180 mg of mercuric chloride was stirred at room temperature for 3 h. The mixture was then poured into large volume of water with vigorous stirring and extracted with chloroform. The extracts were washed with 2% aqueous EDTA solution and water and dried over sodium sulfate. Removal of the solvent gave a practically pure product.—**4** and **11**.

A pure sample of **2** was obtained through chromatography on silica gel.

1-Methylthio-1-acetoxy-3,3-dimethyl-4-ethylenedioxy-2-pentanone (4). IR(neat) 1745, 1705, 1220, and 1035 cm^{-1}; NMR δ (CCl_4) 1.18, 1.19 (each 3H, s., $C(CH_3)_2$), 1.31 (3H, s., $OCCH_3$), 2.05, 2.09 (each 3H, s., SCH_3, and $OCOCH_3$), 3.94 (4H, b.s., OCH_2CH_2O), and 6.56 (1H, s., SCHO); Anal. Found: C, 52.37; H, 7.26%. Calcd for $C_{12}H_{20}O_5S$: C, 52.16; H, 7.30%.

2-Methylthio-2-acetoxyacetophenone (11). IR (neat) 3050, 1745, 1685, 1595, 1580, 1225, 750, and 690 cm^{-1}; NMR δ (CCl_4) 2.01, 2.13 (each 3H, s., SCH_3 and $OCOCH_3$), 6.70 (1H, s., SCHO), centered at 7.45 and 7.95 (3H, and 2H respectively, m., arom. H); Anal. Found: C, 58.93; H, 5.35%. Calcd for $C_{11}H_{12}O_3S$: C, 58.93; H, 5.40%.

Physical and analytical data of other compounds appeared in the references indicated.

References

1) Large part of this work was read at Winter Meeting of Hokkaido Division of Chemical Society of Japan, Feb. 1, 1971, Sapporo.

2) a) Total synthesis of illudin M; T. Matsumoto, H. Shirahama, A. Ichihara, H. Shin, S. Kagawa, F. Sakan, S. Matsumoto, and S. Nishida, *J. Am. Chem. Soc.*, **90**, 3286 (1968); b) Synthesis of illudane skeleton; T. Matsumoto, H. Shirahama, A. Ichihara, H. Shin, S. Kagawa, N. Ito, T. Hisamitsu, T. Kamada, and F. Sakan, *Tetrahedron Lett.*, **1967**, 4097; c) Synthesis of functionalized illudane; T. Matsumoto, H. Shirahama, A. Ichihara, H. Shin, S. Kagawa, N. Ito, T. Hisamitsu, T. Kamada, F. Sakan, K. Saito, S. Nishida, and S. Matsumoto, *Tetrahedron Lett.*, **1968**, 1925; d) Alternative synthesis of illudin M; T. Matsumoto, H. Shirahama, A. Ichihara, H. Shin, S. Kagawa, and F. Sakan, *Tetrahedron Lett.*, **1970**, 1171; e) Total synthesis of illudin S; T. Matsumoto, H. Shirahama, A. Ichihara, H. Shin, S. Kagawa, F. Sakan, and K. Miyano, *Tetrahedron Lett.*, **1971**, 2449.

3) a) G. A. Russell and G. J. Mikol, *J. Am. Chem. Soc.*, **88**, 5498 (1966); b) R. B. Morin, B. G. Jackson, R. A. Mueller, E. R. Lavagnino, W. B. Scanlon, and S. L. Andrews, *ibid.*, **91**, 1401 (1969); c) Y. Oikawa, and O. Yonemitsu, *Tetrahedron Lett.*, **1972**, 3393; *J. Org. Chem.*, **41**, 1118 (1976); D. Connor and M. von Strardtmann, *J. Org. Chem.*, **39**, 1549 (1974); d) K. Ogura, and G. Tsuchihashi, *J. Am. Chem. Soc.*, **96**, 1960 (1974); S. Iriuchijima, K. Maniwa, and G. Tsuchihashi, *ibid.*, **96**, 4280 (1974); e) H. Kosugi, H. Uda, and S. Yamagiwa, *J. Chem. Soc., Chem. Commun.*, **1975**, 192; **1976**, 71.

4) M. Kise, and S. Oae, *Bull. Chem. Soc., Jpn.*, **43**, 1421 (1970).

5) G. E. Wilson, and G. J. Strong, *J. Org. Chem.*, **37**, 2376 (1972). More recently Uda *et al.* observed acceleration effect of pyridine in Pummerer type reaction.[3e]

6) K. Takigawa, Graduation Thesis, Fukui Univ., 1974.

7) T. Matsumoto, H. Shirahama, A. Ichihara, H. Shin, S. Kagawa, T. Hisamitsu, T. Kamada, and F. Sakan, *Bull. Chem. Soc., Jpn.*, **45**, 1136 (1972).

8) T. Matsumoto, H. Shirahama, A. Ichihara, H. Shin, and S. Kagawa, *Bull. Chem. Soc., Jpn.*, **45**, 1144 (1972).

9) From the complex products only enone **13** could be isolated.[10]

10) T. Matsumoto, H. Shirahama, A. Ichihara, H. Shin, S. Kagawa, N. Ito, T. Hisamitsu, T. Kamada, F. Sakan, K. Saito, S. Nishida, and S. Matsumoto, 11th Symposium on the Chemistry of Natural Products, Kyoto, Oct., 1967, Symposium Paper, p. 120.

11) E. J. Corey, and M. Chaykovsky, *J. Am. Chem. Soc.*, **87**, 1345 (1965).

BULLETIN OF THE CHEMICAL SOCIETY OF JAPAN, VOL. 50 (1), 327—328 (1977)

The Direct Chlorination of Anthraquinone Oxime. The Regioselective Chlorination of Anthraquinone

Takehiko Ito, Koichi Sadakata, Yoshiaki Kindaichi, and Yasuo Takami
National Chemical Laboratory for Industry, Hon-machi, Shibuya-ku, Tokyo 151

(Received August 13, 1976)

Synopsis. The reaction of anthraquinone oxime with chlorine in the presence or absence of a catalyst was investigated. In concentrated sulfuric acid, the direct chlorination of anthraquinone oxime takes place easily at 100 °C. The chlorination occurs selectively in the β-position in the absence of a catalyst and in the α-position in the presence of palladium acetate.

Selective aromatic substitution is an important subject in organic synthetic chemistry. In the case of anthraquinone, there have been much investigations of selective sulfonation, whereas few investigations have been made of direct chlorination. It has been generally impossible to carry out the direct chlorination of anthraquinone selectively.[1,2]

In the present paper, we will report that the chlorination of anthraquinone proceeds selectively when anthraquinone is used as a form of its oxime, and that the chlorination occurs selectively in the α-position in the presence of palladium acetate and in the β-position in the absence of a catalyst.

Results and Discussion

The reaction of anthraquinone oxime with chlorine in sulfuric acid, followed by the hydrolysis of the product, led to the formation of chloroanthraquinones without any accompanying Beckmann-type rearrangement. Table 1 shows the results obtained from reactions in the presence of various kinds of catalysts. In experiments using palladium salt catalysts at 100 °C, with palladium acetate chlorination occurred predominantly in the α-position of anthraquinone, whereas with palladium sulfate in the β-position, and with palladium chloride the chlorination proceeded with a low selectivity. The activity of palladium sulfate and chloride was, probably because of their lower solubility in sulfuric acid, always lower than that of palladium acetate. In the reaction without a catalyst it is noteworthy that β-substitution was predominant. From this fact, it may be assumed that most of the β-substitution observed in the experiments with palladium sulfate and chloride occurred independently of the catalysts. Ferric chloride, which is known to be a useful catalyst for chlorination, was not effective in the present reactions. Iodine showed a catalytic activity, but the chlorination proceeded with a low selectivity.

Table 1. Direct chlorination of anthraquinone oxime
(Anthraquinone oxime, 4.48 mmol; Chlorine, 10 ml/min; H_2SO_4, 10 ml; Reaction temp, 100 °C; Reaction time, 2 h)

AQ-oxime	Catalyst		Yield[a] of AQs	Composition of the product[b] %			
		g	g	AQ[e]	1-Cl[f]	2-Cl[g]	Others
mono[c]	$Pd(OAc)_2$	0.20	0.85	84	15	1	0
mono	$PdSO_4$[h]	0.20	0.92	85	1	11	3
mono	$PdCl_2$	0.20	0.85	91	3	6	0
mono	$FeCl_3$	0.20	0.89	96	1	3	0
mono	I_2	0.10	0.94	72	17	7	4
di[d]	I_2	0.10	0.86	97	2	1	0
mono	none	—	0.90	92	1	6	1

a) Yield of free anthraquinone and chlorinated anthraquinones obtained by the hydrolysis of the product of the chlorination of anthraquinone oxime. b) Product obtained by the hydrolysis of the product of the chlorination of anthraquinone oxime. c) Monoxime. d) Dioxime. e) Anthraquinone. f) 1-Chloroanthraquinone. g) 2-Chloroanthraquinone. h) Reaction time, 6 h.

Table 2. Chlorination of anthraquinone oxime in the presence of palladium acetate
(Anthraquinone oxime, 4.48 mmol; Chlorine, 10 ml/min; $Pd(OAc)_2$, 0.20 g)

Run No.	AQ-oxime	Reaction temp °C	Reaction time h	H_2SO_4 ml	Yield[a] of AQs g	Composition of product[b] %								
						AQ[e]	1-[f]	2-	1,4-	1,5-	1,8-	1,6-	1,7-	1,2-
1	mono[c]	100	2	5	0.81	73.0	24.3	0.8	1.2	0.7	+			
2[g]	mono	100	4	5	0.95	52.4	40.3	0.6	2.2	2.2	1.0	+	+	+
3	mono	120	2	5	0.83	60.3	33.5	1.8	1.5	0.5	0.6	+	+	
4	mono	150	2	5	0.87	24.6	36.3	3.3	3.9	3.9	6.3	1.9	4.8	1.0
5[g]	mono	100	12	5	0.95	29.2	35.5	2.2	5.3	4.6	4.5	1.5	3.4	1.7
6	mono	100	4	10	0.85	69.1	28.4	1.5	+	+				
7	di[d]	100	4	10	0.61	83.2	15.9	0.7	+	+				
8	AQ[e]	100	4	10	1.10	58.2	23.8	4.4	2.7	2.7	2.3	0.9	2.0	0.7
9	mono	100	4	10[h]	0.83	93.8	6.2	+						

a)—e) The symbols are the same as in Table 1. f) 1-Chloroanthraquinone. The other chloroanthraquinones are shown similarly. The numerical symbol indicates the position of the chlorosubstituent. g) As the catalyst 0.40 g of $Pd(OAc)_2$ was used. h) Tetrachloroethylene was used instead of sulfuric acid.

Table 3. Chlorination of anthraquinone oxime without a catalyst
(Anthraquinone oxime, 4.48 mmol; H_2SO_4, 10 ml; Chlorine, 10 ml/min)

Run No.	AQ-oxime	Reaction temp °C	Reaction time h	Yield[a] of AQs g	Composition of product[b] %								
					AQ[e]	1-Cl[f]	2-Cl	1,6-	1,7-	1,2-	2,6-	2,7-	2,3-
10	mono[c]	100	2	0.90	92.1	0.6	6.2						
11	mono	100	6	0.92	71.5	1.5	19.1				0.9	0.8	0.3
12	mono	100	12	0.94	53.2	3.5	30.2	0.5	0.5	0.6	2.1	2.5	1.1
13	mono	150	2	0.89	46.5	7.2	27.2	1.8	1.9	1.3	1.9	2.5	1.1
14	di[d]	100	6	0.88	72.0	+	19.1				2.3	3.7	0.9
15	di	150	2	0.71	50.8	0.9	32.4		+		4.8	6.2	2.1
16[g]	mono	100		0.94	41.3	23.4	14.2	2.3	4.6	1.6	0.9	0.9	+
17	AQ[e]	100	4	0.92	97.5	2.0	0.5						

a)—e) The symbols are the same as in Table 1. f) The same as in Table 2. g) The reaction was carried out without a catalyst for 6 hours, and then 0.20 g of palladium acetate was added to the reaction mixture and the reaction was continued for a further 4 h.

More detailed research was done in order to elucidate the difference between reactions in the presence of palladium acetate and in the absence of a catalyst. Table 2 shows the results of the chlorination using palladium acetate as the catalyst. As is clear from the comparison of the results of Run No. 6 with those o No. 8, the α-selectivity of the chlorination of anthraquinone oxime is much higher than that of the chlorination of free anthraquinone. The chlorination of the oxime, as may be seen from the results of No. 2, tends to stop at the stage of monochlorination to give 1-chloroanthraquinone with a high selectivity, and this greatly differs from the chlorination of free anthraquinone.[3] As to the effect of the temperature, the selectivity for α-substitution decreases with the rise in the reaction temperature. Anthraquinone dioxime (No. 7) shows a similar selectivity for α-substitution, although the reactivity of the dioxime is lower than that of the monoxime.

It is well known that palladium coordinates with nitrogen more strongly than with oxygen.[4] In the reaction with palladium acetate, it seems reasonable, therefore, to think that palladium interacts with the nitrogen of the oxime and, because of this interaction, chlorination occurs selectively in the α-position neighboring the C=N-OH group.

The results of the chlorination in the absence of a catalyst are shown in Table 3. In the reaction of anthraquinone monoxime and chlorine without a catalyst at 100 °C chlorination occurred predominantly in the β-position; this is in contrast to the reaction with palladium acetate and the reaction of free anthraquinone without a catalyst (No. 17). As for the dioxime, chlorination occurred exclusively in the β-position at 100 °C, and a similar result was obtained even at 150 °C. In the reaction of the monoxime at 150 °C, however, an increase in α-chlorinated products was observed. The α-chlorination in this case, in view of the results described above, seems to have occurred at the opposite side of the C=N-OH group.

In the experiment of Run No. 16, β-chlorination was at first carried out in the absence of a catalyst, and then α-chlorination was carried out in the presence of palladium acetate. As a result, the formation of a comparatively great amount of 1,7-dichloroanthraquinone was observed. This result seems to suggest that the β-chlorination in the absence of a catalyst tends to occur on the same side of the C=N-OH group. Although the mechanism in which the chlorination of anthraquinone oxime in the absence of a catalyst occurs selectively in the β-position is not clear at present, the contribution of the *meta*-orientation of $=N^+-$ formed in the C=N-OH group in sulfuric acid seems to be possible.

Experimental

Anthraquinone mono and dioxime were prepared according to the methods described in the literature.[5,6] Reagent-grade concd sulfuric acid (95%) was used without further treatment. The products were analyzed by means of high-speed liquid chromatography in a manner similar to that described in a preceding paper:[2] column, Zorbax-Sil 25 cm; eluent, pentane (containing 0.02% MeOH); flow rate, 100 ml/h, (90 kg/cm²); temperature, 20 °C; detector, UV-254 nm.

Chlorination of Anthraquinone Oxime. Anthraquinone monoxime (1 g, 4.48 mmol) was dissolved in 5 ml of concd sulfuric acid, and then 0.20 g of palladium acetate was added, the mixture was thereafter heated for two hours at 100 °C with stirring under a flow of chlorine (10 ml/min). The reaction mixture was then poured into ice water and filtered. The precipitate was treated with a mixture of 7 ml of concd hydrochloric acid and 10 ml of formalin for 5 h on a water bath in order to hydrolyze the oxime. The mixture was filtered, and the residue was washed repeatedly with water and dried at 100 °C. The product was passed through a short active alumina column, using dichloromethane as the eluent, in order to separate the undecomposed oxime and by-products. A part of the product was analyzed by HLC.

References

1) There are several patents relating to the preparation of tetrachloroanthraquinone, *e.g.*, U. S. Patent, 2378745 (1945).

2) T. Ito, Y. Kindaichi, and Y. Takami, *Nippon Kagaku Kaishi*, **1977**, 82.

3) In our previous study, we observed that the reactivity of 1-chloroanthraquinone toward chlorine is greater than that of anthraquinone; consequently, the chlorination of free anthraquinone does not stop at the stage of monosubstitution.[2]

4) F. Basolo and R. G. Peason, "Mechanisms of Inorganic Reactions," John Wiley & Sons (1965), pp. 23, 60.

5) M. A. Haq, J. N. Ray, and M. T. Malkana, *J. Chem. Soc.*, **1934**, 1326.

6) J. Meisenheimer and E. Mahler, *Ann.*, **508**, 185 (1935).

BULLETIN OF THE CHEMICAL SOCIETY OF JAPAN, VOL. 50 (1), 329—330 (1977)

Reactions of Perfluoro-2,5-dimethyl-3,4-hexanedione with Amines

Seiji SHIN-YA and Nobuo ISHIKAWA

Department of Chemical Technology, Tokyo Institute of Technology, Ookayama, Meguro-ku, Tokyo 152

(Received August 23, 1976)

Synopsis. Perfluoro-2,5-dimethyl-3,4-hexanedione and aromatic or aliphatic amines gave the respective 1: 1 adducts in good yields. With excess amounts of aliphatic amines or basic aromatic amines such as *p*-anisidine, the perfluorodiketone gave oxamides. With *o*-phenylenediamine, it gave 2,3-dihydroxyquinoxaline.

In an earlier communication,[1] we reported on the nucleophilic reactions of heptafluoro-1-methylethyl phenyl ketone, which resulted in the formation of benzoic acid derivatives and heptafluoropropane. This made a contrast to trifluoromethyl and pentafluoroethyl phenyl ketones, which are known to form 1: 1 adducts with nucleophiles.

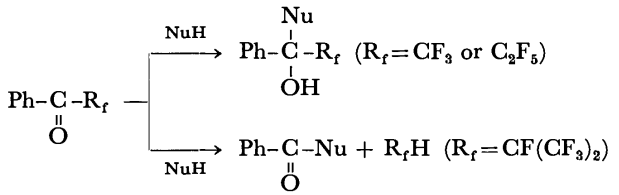

The above fact reveals the enhanced leaving ability of the heptafluoro-1-methylethyl group. This characteristic is presumably ascribable to the high stability of the heptafluoro-1-methylethanide anion as a leaving group and to the bulkiness of that group as a substituent. In this paper we wish to report on similar reactions of perfluoro-2,5-dimethyl-3,4-hexanedione, **1**, an α-diketone carrying two heptafluoro-1-methylethyl groups on both sides.

The reaction of **1** with an equimolar amount of aniline in diethyl ether easily gave a 1: 1 adduct, **2** (R=Ph). When a solution of this adduct in chloroform was heated, a dehydrated product, an imine, **3**, was formed; this substance is, however, very hygroscopic and is readily reconverted into **2**.

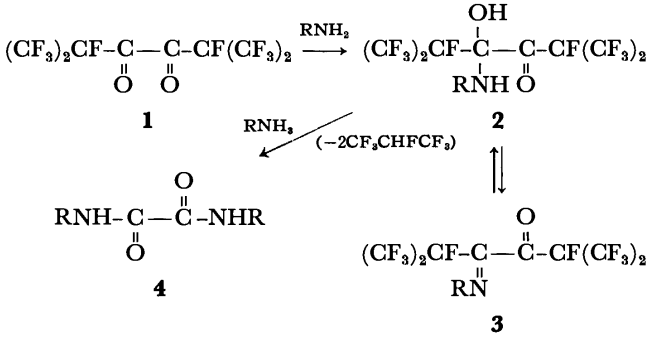

Other aromatic amines, such as *p*-toluidine, *p*-chloroaniline, *p*-anisidine, and α-naphthylamine, as well as aliphatic amines, such as butylamine and benzylamine, all gave the corresponding 1: 1 adducts (Table 1).

Whereas perfluorobiacetyl is known to form both 1: 1 and 2: 1 adducts with nucleophiles,[2] **1** did not give a 2: 1 adduct even when an excess of aniline was used. With more basic aromatic amines, however, it gave oxamides, **4**, by releasing two molecules of heptafluoropropane. For example, when 3.3 equivalents of *p*-anisidine were allowed to react with **1** at room temperature for 48 h, *N*,*N*′-bis(*p*-methoxyphenyl)oxamide was obtained quantitatively.

While neither bis(heptafluoro-1-methylethyl) ketone[3] nor heptafluoro-1-methylethyl phenyl ketone[1] forms an addition product such as hydrate or hemiacetal, probably because of their steric effect, **1** is enough released from that effect, as is shown above. The addition of the additional molecule of the amines to the carbonyl group

TABLE 1. PREPARATION AND PROPERTIES OF 1: 1-ADDUCTS (**2**)

R-NH_2	Preparation				Properties of **2**								
					IR (cm^{-1})			^{19}F NMR (δ ppm)[a]			Found (Calcd) (%)		
	Mole ratio of RNH_2/1	Time (h)	Yield (%)	Mp (°C)	NH	OH	C=O	CF_3	CF_3	CF	C	H	N
$PhNH_2$	1.0	3	93	133—134	3390	3150—3250	1710	−9.75	−7.80	+95.7	34.72 (34.52)	1.39 (1.45)	2.80 (2.88)
	2.0	3	97										
p-$MeC_6H_4NH_2$	1.0	1.5	100	127.5—128	3390	3150—3250	1710	−9.90	−7.80	+95.4	36.24 (35.94)	1.56 (1.81)	2.90 (2.79)
p-$ClC_6H_4NH_2$	2.2	5.5	81	123—124	3390	3300—3400	1720	−9.90	−7.80	+95.4	32.17 (32.24)	1.24 (1.16)	2.70 (2.69)
p-$MeOC_6H_4NH_2$	1.0	0.75	100	127 (dec)	3390	3150—3250	1710	−9.50	−7.70	+95.6	35.08 (34.83)	1.69 (1.75)	2.68 (2.70)
α-$C_{10}H_7NH_2$	2.2	3	90	139 (dec)	3380	3200—3300	1710	−10.20	−8.30	+94.7	40.38 (40.24)	1.70 (1.69)	2.60 (2.61)
n-$BuNH_2$	1.0	2	88	69.5—70.0	3435	3200—3300	1700	−11.25	−8.25	+95.1	30.94 (30.85)	2.56 (2.37)	3.14 (3.00)
$PhCH_2NH_2$	1.0	1	79	91—93	3400	3150—3250	1700	−9.90	−7.95	+94.8	35.83 (35.95)	1.67 (1.81)	3.02 (2.99)

a) The chemical shifts are given in δ ppm upfield from ext. CF_3CO_2H.

of **2**, however, brought about C–C bond cleavage to afford oxamides. Naturally, aliphatic amines, such as methyl, butyl and benzylamines, reacted much faster than aromatic amines, and when an excess amount was used, they gave oxamides directly (Table 2).

Table 2. Preparation of oxamides, **4**

RNH_2	Mole ratio of RNH_2/1	Time (h)	Yield[a] (%)	Mp (°C)
p-$MeOC_6H_4NH_2$	3.3	48	100	256—257
$MeNH_2$	large excess[b]	2	86	215—217
n-$BuNH_2$	2.2	2	84	152—154
$PhCH_2NH_2$	2.2	2	100	220—221

a) All the products were identified with authentic compounds by a comparison of the mps and IR spectra. b) Methylamine gas was bubbled into an ethereal solution of **1**.

A similar reactivity of the perfluoro diketone **1** was also observed in the cyclization reaction with *o*-phenylenediamine. Perfluorobiacetyl[2] and perfluorooctane-4,5-dione[4] are known to react with *o*-phenylenediamine to give 2,3-bis(perfluoroalkyl)quinoxalines.

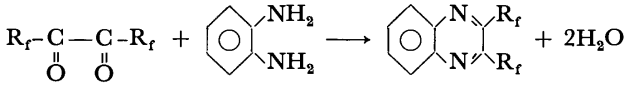

$R_f = CF_3$ or *n*-C_3F_7

In contrast to these diones, we found that the reaction between **1** and *o*-phenylenediamine provides a 1 : 1 adduct, which is then converted into 2,3-dihydroxyquinoxaline by heating in a solvent.

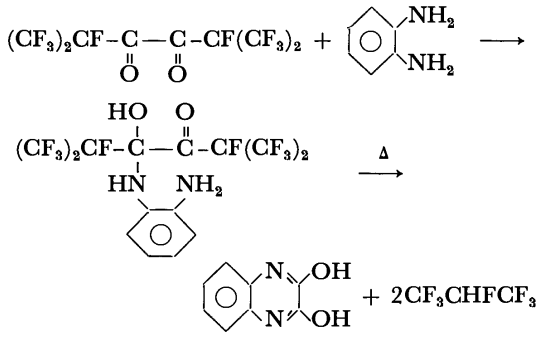

This result indicates again the leaving ability of the heptafluoro-1-methylethyl group as an anion, characterizing the reaction mode of heptafluoro-1-methylethyl ketones.

Experimental

Perfluoro-2,5-dimethyl-3,4-hexanedione (1). This compound was prepared by a modification of the method of Smith *et al.*[3] They made hexafluoropropene to react directly with oxalyl difluoride, which had been prepared from oxalyl dichloride. The difluoride, however, is a poisonous gas and can not be handled safely. Therefore, we used oxalyl dichloride as the starting material and made the difluoride generate *in situ*. Oxalyl dichloride (7.4 g, 58.3 mmol), finely ground dry potassium fluoride (33.8 g, 583 mmol), and acetonitrile (60 ml) were put into a glass tube vessel equipped with a mechanical stirrer. Liquefied hexafluoropropene (175 mmol) was added to the vessel at −70 °C. After having been sealed, the vessel was brought to room temperature. The whole was then heated for 9 h under mechanical stirring in an oil bath kept at 75—80 °C. Thereafter, the lower layer of the reaction contents was separated and subjected to distillation to give **1** (6.0 g, 26%) (bp 91—93 °C) and bis(perfluoro-1-methylethyl) ketone (4.3 g, 20%) (bp 72—73 °C).

Reaction of the Perfluoro Diketone 1 with Aniline. A solution of aniline (0.12 g, 1.3 mmol) in diethyl ether (1 ml) was added, drop by drop, to the diketone **1** (0.5 g, 1.3 mmol) at 0 °C. After 3 h of stirring at room temperature, the crystals which had come out were collected, giving the 1 : 1 adduct **2** (R=Ph) (0.57 g, 93%). Recrystallization from chloroform afforded the pure material (mp 133—134 °C). Reactions with other aromatic amines were carried out in similar manners.

Reaction of 1 with Excess Butylamine. A solution of butylamine (0.16 g, 2.2 mmol) in diethyl ether (4 ml) was added, drop by drop, to perfluoro diketone **1** (0.4 g, 1.0 mmol) at 0 °C. After 2 h of stirring at room temperature, the separated crystals were collected to give *N,N'*-dibutyloxamide (0.17 g, 85%), **4** (R=*n*-Bu). Reactions with other amines to give oxamides, **4**, were carried out in similar manners. The products thus obtained were identified with the authentic samples by a comparison of the melting points and IR spectra.

Reaction of 1 with o-Phenylenediamine. A solution of *o*-phenylenediamine (0.076 g, 0.7 mmol) in acetonitrile (0.5 ml) was added to perfluoro diketone **1** (0.25 g, 0.64 mmol) at 0 °C. After 30 min of stirring at room temperature, it was filtered to give a 1 : 1 adduct (0.27 g, 85%) (mp >300 °C). IR: 3400—3500 (OH), 3350, 3300 (NH), 1705 (C=O) cm^{-1}.

A solution of the 1 : 1 adduct in ethanol was refluxed for 1 h, and the separated crystals were collected to give 2,3-dihydroxyquinoxaline (mp >300 °C), in an 84% yield. This product was identified with an authentic sample by means of its IR spectrum.

References

1) N. Ishikawa and S. Shin-ya, *Chem. Lett.*, **1976**, 673.
2) L. O. Moore and J. W. Clard, *J. Org. Chem.*, **30**, 2472 (1965).
3) R. D. Smith, F. S. Fawcett, and D. D. Coffman, *J. Am. Chem. Soc.*, **84**, 4285 (1962).
4) J. J. Drysdale and D. D. Coffman, *J. Am. Chem. Soc.*, **82**, 5111 (1960).

Solvent Effects upon Dynamic Behavior of Intramolecular Heteroexcimers

Tadashi OKADA, Takashi SAITO, Noboru MATAGA, Yoshiteru SAKATA,* and Soichi MISUMI*

Department of Chemistry, Faculty of Engineering Science, Osaka University, Toyonaka, Osaka 560

**The Institute of Scientific and Industrial Research, Osaka University, Suita, Osaka 565*

(Received April 27, 1976)

Solvent effects upon fluorescence quantum yields, fluorescence rise and/or decay curves of p-$(CH_3)_2NC_6H_4$-$(CH_2)_n$-(9-anthryl) (n=1, 2, 3) and p-$(CH_3)_2NC_6H_4$-$(CH_2)_n$-(1-pyrenyl) (n=1, 2, 3) have been investigated in detail. It is concluded that the sandwich structure is not necessary for the intramolecular charge transfer in polar solvents and that the mechanism of intramolecular heteroexcimer formation in polar solvents is different from that in nonpolar solvents.

Studies on the structures and dynamic behavior of electron donor–acceptor systems in excited states are important for understanding primary processes of photochemical reactions. We have examined the intramolecular exciplex (heteroexcimer and excimer) systems in order to clarify the electronic structures and mechanisms of the dynamic behavior of exciplex systems, such as fluorescence quenching due to the electron transfer reaction as well as the fluorescent exciplex formation. In a previous paper,[1] solvent shifts of the fluorescence bands and an analysis of results by a theoretical method were reported for the following intramolecular heteroexcimer systems: p-$(CH_3)_2NC_6H_4$-$(CH_2)_n$-(1-pyrenyl) (n=1, 2, 3, abbreviated as P_n) and p-$(CH_3)_2NC_6H_4$-$(CH_2)_n$-(9-anthryl) (n=1, 2, 3, abbreviated as A_n).

We have measured the solvent effects upon fluorescence quantum yields as well as fluorescence rise and/or decay curves of these compounds. From the results the mechanisms of intramolecular charge transfer and the fluorescent heteroexcimer formation will be discussed in the following.

Experimental

Absorption spectra were measured with a Cary 15 spectrophotometer. Fluorescence quantum spectra were measured with an Aminco-Bowman spectrophotofluorometer calibrated by using a standard tungsten lamp. The fluorescence rise and decay curves as well as the time resolved fluorescence spectra were observed on an apparatus consisting of a Bausch & Lomb high intensity monochromator, 1P28 photomultiplier, Tektronix 661 sampling oscilloscope, and a pulsed nitrogen gas laser of *ca.* 1 kW peak power.

The preparation of A_n and P_n will be reported elsewhere. Spectrograde hexane, decalin, dibutyl ether, tetrahydrofuran (THF), 2-propanol, acetone, and acetonitrile were used without further purification. Butylacetate and isobutyl alcohol (chromatographic reagents) were used without purification. GR-grade diethyl ether and methanol were used without further purification. 1-Pentanol was dried over calcium oxide and distilled. Butyronitrile was dried over calcium hydride and distilled carefully with phosphorus pentoxide. All solutions were deaerated by freeze-pump-thaw cycles. For the measurement of temperature effects upon the fluorescence rise and decay curves and the time resolved fluorescence spectra as well as the steady state fluorescence spectra, the temperature of a solution in a cuvette placed in a metal dewar with quartz windows was controlled by a constant flow of cold nitrogen gas. The temperature of the sample was measured with a thermocouple placed in the sample tube.

Results and Discussion

A. Solvent Effects upon Fluorescence Quantum Yields. Absorption spectra of A_1, A_2, A_3, P_1, P_2, and P_3 show no indication of the ground state interaction. Excitation for the fluorescence measurements was made at the absorption band of the pyrene or anthracene moiety. For the evaluation of relative fluorescence yields of A_n and P_n in various solvents, their fluorescence quantum spectra were measured using solutions with equal absorbance (0.45) at the wavelengths of the excitation, 345 nm for P_n and 368 nm for A_n. Since the LE (local excited state) fluorescence band of pyrene or anthracene moiety frequently overlaps the intramolecular HE (heteroexcimer) fluorescence band, it is necessary to subtract the LE band from the observed spectra for the evaluation of the HE fluorescence yield. For this purpose, LE fluorescence spectra of hexane solutions of A_1, A_2, 9-ethylanthracene, P_1 and 1-ethylpyrene were used, respectively, for the spectra of A_1, A_2, A_3, P_1, and P_2 as well as P_3 in various solvents. We have employed this procedure instead of using the same LE spectra throughout the P_n or A_n series, since the vibrational structures of the spectra appear to depend a little upon the number of methylene chains as indicated in Fig. 1 for A_1 and A_2. A continued ultraviolet irradiation of solutions of A_n and P_n brings out a decrease in the absorption intensity of the aromatic hydrocarbon moiety as well as an increase in the LE fluorescence intensity and a decrease in the HE fluorescence intensity. Accordingly, freshly prepared solutions were used always for quantitative measurements. Practically no change in absorption and fluorescence intensities was observed during the course of measurements. Fluorescence quantum yields were determined, using 9,10-diphenylanthracene as a standard.[2] The values obtained are given in Table 1, where Φ_{LE} is the quantum yield of the LE fluorescence and Φ_{HE} that of the HE fluorescence.

A_1, A_2, and P_1 in nonpolar solvents such as hexane and decalin show the LE fluorescence of anthracene or pyrene part, and the HE fluorescence can be observed only in polar solvents.[1,3,4] The result is explained as follows.[1] Because of the large separation between donor and acceptor groups, the stabilization energy of the charge transfer state due to the coulomb interaction between the pair in these compounds may be smaller than in the case of A_3 or P_3 where the sandwich type conformation is possible. However, since their dipole moments in the charge transfer state are much larger

Table 1. Fluorescence quantum yield of intramolecular HE systems

Solvent	P_1		P_2		P_3		A_1		A_2		A_3	
	Φ_{LE}	Φ_{HE}	Φ_{LE}	Φ_{HE}	Φ_{LE}	Φ_{HE}	Φ_{LE}	Φ_{HE}	Φ_{LE}	Φ_{HE}	Φ_{LE}	Φ_{HE}
Hexane	0.61	—	0.13	0.13_3	0.01_0	0.40_3	0.2_5	—	0.4_3	—	0.1_3	0.3_2
Decalin	0.60	—	0.09_1	0.10_3	0.007_3	0.24_4	0.1_9	—	0.5_2	—	0.2_5	0.2_5
Dibutyl ether	0.09	0.17	0.01_8	0.09_6	0.003_8	0.26_1	0.02	0.02_2	0.3_4	0.3_4	0.1_4	0.2_3
Diethyl ether	0.006	0.07_0	0.02_1	0.12_1	0.004_7	0.26_3	0.004	0.008	0.09	0.1_2	0.03_1	0.2_2
Butyl acetate	0.003	0.05_0	0.01_0	0.15_4	0.001_0	0.15_4	0.0004	0.004	0.01_3	0.06_5	0.01_6	0.1_6
THF	0.005	0.04_0	0.01_7	0.15_7			0.0005	0.001	0.01_1	0.07	0.004	0.1_1
Isobutyl alcohol	0.002	0.03_0	0.01_0	0.03_1	0.003_8	0.08_3	0.0005	0.0005	0.01_7	0.004	0.01_4	0.01_5
Acetone	0.006	0.02_0	0.01_0	0.001	0.003_5	0.03_4	0.0005	0.0008	0.009	0.003_0	0.01_7	0.003
Methyl alcohol	0.002	0.004_3	0.009		0.001_1	0.005_2						
Aceto-nitrile	0.002	0.004_0	0.008	0.0001	0.001_7	0.004_0	0.0003	0.0003	0.006	0.0004	0.007	≈ 0

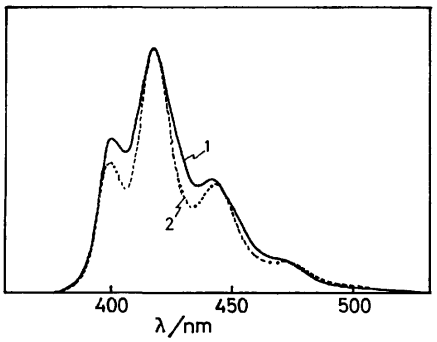

Fig. 1. Fluorescence spectra of A_1 (1) and A_2 (2) in hexane at room temperature.

than those of the sandwich type heteroexcimers, the solvation in a polar solvent may be very effective for the stabilization of the charge transfer state. Thus, the level inversion between the LE and the charge transfer state may arise and the HE fluorescence will compete with the LE fluorescence in polar solvents.

Roughly speaking, Φ_{LE} as well as Φ_{HE} decrease with increasing solvent polarity. Presumably, deactivation processes leading to the ground state or to some non-fluorescent products are considerable in strongly polar solvents. In the case of A_1, both Φ_{LE} and Φ_{HE} are much smaller than those of the other systems in polar solvents. Thus the deactivation processes competing with the HE formation are predominant in the case of A_1 in polar solvents.

Although the fluorescence yields decrease with increase in solvent polarity, Φ_{HE} values of the present intramolecular HE systems in polar solvents are much larger as compared with the intermolecular case. As an example, Φ_{HE} of P_3 in pyridine is 0.07[3] as compared with 0.015 of pyrene-*N*,*N*-dimethylaniline (DMA) intermolecular HE.[5] The observed values of P_3 in acetone and acetonitrile are 0.034 and 0.004, respectively, while no HE fluorescence can be observed in these solvents in the case of the intermolecular system.

The above results were explained[3,4] as due to the fact that it is difficult for ionic dissociation from the nonrelaxed electron transfer state, which is a dominant process in the case of the intermolecular HE system in

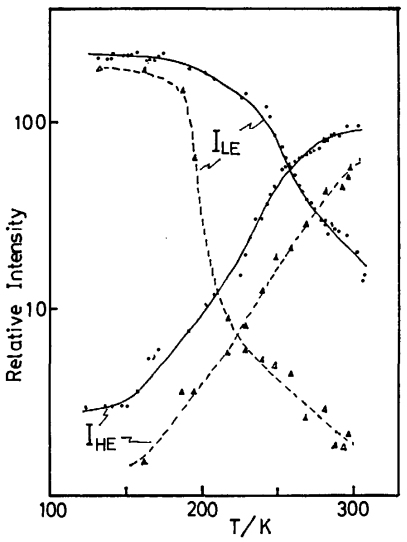

Fig. 2. Temperature dependence of I_{LE} and I_{HE} of P_3 in decalin (solid line) and 2-propanol (dotted line).

polar solvents,[6,7] to occur in the case of the intramolecular HE.

Although the ionic "dissociation" is not possible, the formation of non-fluorescent intramolecular ion-pairs from the LE state or the non-relaxed electron transfer state may not be prohibited in polar solvents. This seems to result in the decrease of HE fluorescence yield with increasing solvent polarity as described above.

For detailed studies of the intramolecular HE formation processes, it is necessary to confirm, especially in the case of the system capable of forming sandwich type of HE, whether the HE is formed by the dynamic process or not. It is possible that weak intramolecular complexes are formed at low temperature in the ground state leading to immediate formation of fluorescent HE state under excitation.[8]

For this purpose, temperature effects upon fluorescence intensity of P_3 were examined. As indicated in Fig. 2, the intensity of the LE fluorescence (I_{LE}) increases with decreasing temperature, approaching a constant value at sufficiently low temperature both in decalin and isopropanol. This suggests that the

TABLE 2. FLUORESCENCE RISE AND DECAY TIMES OF INTRAMOLECULAR HE SYSTEMS (in units of ns)

Solvent	P_1		P_2		P_3		A_1		A_2		A_3	
	τ_{LE}	τ_{HE}	τ_{LE}	τ_{HE}	τ_{LE}	τ_{HE}	τ_{LE}	τ_{HE}	τ_{LE}	τ_{HE}	τ_{LE}	τ_{HE}
Hexane	156	—	120	101	4.5 & 86	87	4.8	—	9.5	—	3.3	130
Decalin	120	—	5.6 & 92	3.3[a], 101	7.5 & 90	7.5[a], 90	6.7	—	12	—	4.8	130
Dibutyl ether	19.3	20.8	3.9	80	6	116	7.0	7.5	≈3 & 48	48	≈3	121
Diethyl ether	9.3	9.3	3.8 & 85	82	3	141	7.3	8.9	≈3 & 112	120	<2	200
Butyl acetate	3.1	10.8	3.8	76	4	134						
THF	4	11	4.4	72			7.5[b]	11	51	83		150
Isobutyl alcohol	4	9	4.2	21	5	4.5, 86	3	4.5	<2	≈2		40
Acetone	3.6	10	4.3	8.5	4.4	63	7.5[b]	4	8.5[b]	5		9
Methyl alcohol	3	4.5	3.5	≈2	3	23.5						
Acetonitrile	4	7.5	3.9	3.5	5	≈2	8.5[b]	≈5	8.8[b]	≈3	9[b]	≈3

a) Rise time of the HE fluorescene detected by the present apparatus. b) The values might be the lifetimes of the photoproducts.

intramolecular donor-acceptor interaction arises mainly by the dynamic process in the excited state. In accordance with this behavior of LE fluorescence, the intensity of the HE fluorescence (I_{HE}) decreases with temperature lowering.

B. Effects of Solvent Polarity and Temperature upon Fluorescence Rise and Decay Processes. Fluorescence rise and decay curves were measured at both wavelengths of LE and HE fluorescence bands. Typical two-component decay curve measured at the LE band and corresponding rise and decay curves measured at the HE band were confirmed in the case of several systems in nonpolar or slightly polar solvents. These kind of rise and decay curves are common in the case of intermolecular excimer and HE systems.

A possible kinetic scheme for the formation and decomposition processes of an intramolecular HE in nonpolar solvents can be written as follows.

$$\begin{array}{ccc} A^*\cdots D & \underset{k_2}{\overset{k_1}{\rightleftharpoons}} & (A^-\cdot D^+) \\ {\scriptstyle k_1}\big\downarrow \quad \big\downarrow{\scriptstyle k_f} & & {\scriptstyle k_1'}\big\downarrow \quad \big\downarrow{\scriptstyle k_f'} \\ A\cdots D & \longleftarrow & (A\cdot D) \end{array} \qquad (1)$$

Assuming a δ-function excitation, the time dependences of the LE and HE fluorescence intensities are given by the following equations.

$$I_{LE}(t) = \frac{I_0}{(\lambda_2-\lambda_1)}\{(\lambda_2-X)\exp(-\lambda_1 t) + (X-\lambda_1)\exp(-\lambda_2 t)\} \qquad (2)$$

$$I_{HE}(t) = \frac{I_0 k_1}{(\lambda_2-\lambda_1)}\{\exp(-\lambda_1 t) - \exp(-\lambda_2 t)\} \qquad (3)$$

where

$$\left.\begin{matrix}\lambda_1 \\ \lambda_2\end{matrix}\right\} = 1/2[X+Y \mp \{(Y-X)^2+4k_1k_2\}^{1/2}] \qquad (4)$$

$$X = k_1 + k_f + k_l$$

$$Y = k_2 + k_f' + k_l'$$

$$I_0 = I_{LE}(0)$$

By means of Eqs. 2 and 3, the short lived component in the decay curve of the LE fluorescence and the rise time of HE fluorescence were evaluated graphically from the semilogarithmic plots of $I(t)$ as indicated in Fig. 3. However, in moderately as well as strongly polar solvents, it was difficult to observe the two-component decay of the LE fluorescence or the rise curve of the HE fluorescence. The results of fluorescence rise and decay times at room temperature are given in Table 2.

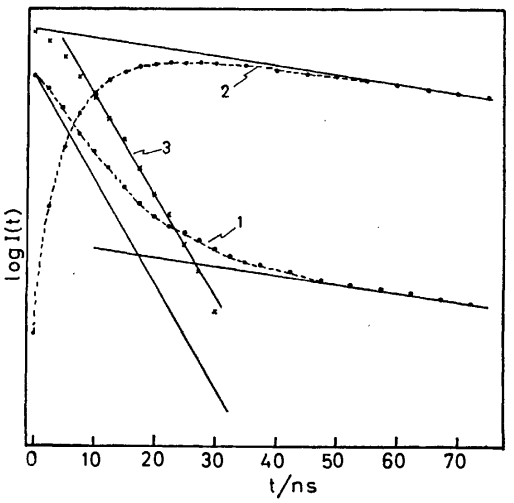

Fig. 3. Semilogarithmic plots of $I_{LE}(t)$ and $I_{HE}(t)$ of P_3 in decalin at room temperature.
(1): $I_{LE}(t)$ (2): $I_{HE}(t)$
(3): $\frac{I_0 k_1}{\lambda_2-\lambda_1}\cdot\exp(-\lambda_1 t) - I_{HE}(t)$

In the case of A_1, A_2, and P_1, although the fluorescence spectrum of hexane solution is identical with that of the decalin solution, the fluorescence lifetime of hexane solution differs from that of the decalin solution. This seems to suggest that, even in the case of these systems in nonpolar solvents, the HE state is attained transiently from the thermally excited LE state, but will decompose immediately by the back charge transfer process of k_2.

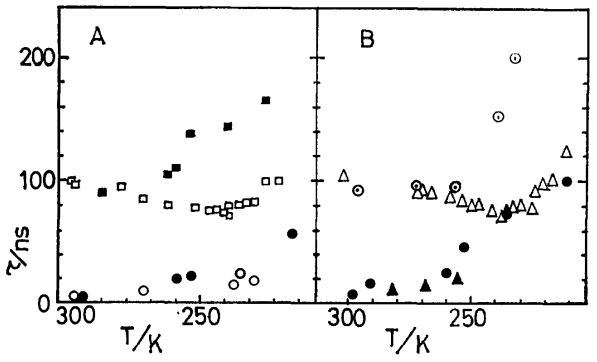

Fig. 4. Temperature effects upon fluorescence rise and decay times of P_2 and P_3 in decalin.
A. Rise and decay times of HE fluorescence.
○: Rise time of P_2, ●: rise time of P_3, □: decay time of P_2, ■: decay time of P_3.
λ_{obsd} for P_2: 500 nm, λ_{obsd} for P_3: 550 nm.
B. Decay times of two-component LE fluorescence.
△: Long life component of P_2, ⊙: long life component of P_3, ▲: short life component of P_2, ●: short life component of P_3.
$\lambda_{obsd}=400$ nm for both P_2 and P_3.

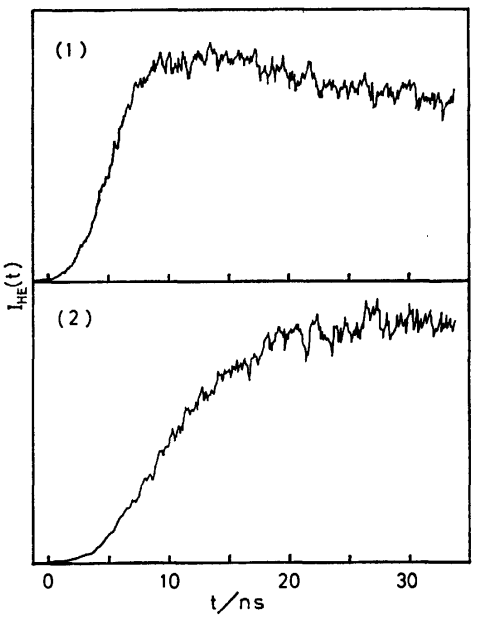

Fig. 5. Fluorescence rise curves of P_3 HE in 1-pentanol (1) and decalin (2) at room temperature.

Lewis and Ware[9] reported a special case of the HE system where the quenching process of the LE fluorescence could not be explained without assuming the transient HE formation though no HE emission was obseved as in the above case. They estimated the lifetime of the transient HE by analyzing the effect of the quencher concentration upon the decay process of the LE fluorescence. In the present case, however, it is not possible to examine such a concentration effect.

With the increase in solvent polarity, the HE state may be stabilized and the rate constant k_1 will increase. When the HE state is placed at the same energy as the LE state of pyrene or anthracene part and no extensive change of the geometrical structure is necessary, it is plausible that the HE formation and decomposition reaction becomes so rapid that the equilibrium between LE and HE state is attained approximately. If the equilibrium is attained, both the LE and HE fluorescence will show the single exponential decay with the same decay time. The behavior of A_1 as well as P_1 in ethers seems to correspond to this case.

Typical two-component decay represented by Eq. 2 was observed in cases of P_2 and P_3 in hexane as well as decalin, and A_2 in ethers at room temperature. The rise and decay times of P_3 HE in decalin were $\lambda_2^{-1}=7.5$ ns and $\lambda_1^{-1}=90$ ns, agreeing respectively with those obtained by measuring the two-component decay of the LE fluorescence. The temperature effect on the rise and decay curves of P_2 and P_3 in decalin was examined, the results being shown in Fig. 4. The observed decay curves can be reproduced by Eq. 2 in the temperature range 300—210 K. Thus, it has been confirmed that the HE's of P_2 and P_3 in decalin are formed by the dynamic process in the excited state even at low temperatures. Although λ_2 is a function of various rate constants, it seems to be close to k_1. Thus, the formation process of the HE state does not seem to be so fast as in the case of the intermolecular HE. The result may be due to the hindered rotations about CH_2–CH_2 bonds which are necessary to form a sandwich type HE, and also due to somewhat large solvent viscosity of decalin. As an example, values $\lambda_2^{-1}=25$ ns at 263 K, and 58 ns at 223 K were obtained in the case of P_3 in decalin. Thus, the temperature lowering makes the process of conformational change very slow. It is possible that both the hindered rotation itself and the solvent viscosity can be affected by the change of temperature. It is not clear which of these is more effective for retarding the conformational change.

In contrast to the above results, the rise time of P_3 HE fluorescence at room temperature is shorter than 2 ns (the rise time of the exciting laser pulse) both in 1-pentanol and 2-propanol, though these solvents are more viscous than decalin. The rise curve of P_3 HE in 1-pentanol is shown in Fig. 5 together with that in decalin. The result suggests that the mechanism of HE formation in polar solvents differs from that in nonpolar solvents. Presumably, orientational fluctuations of surrounding solvent dipoles and a slight approach of the two moieties of P_3 may induce the electron transfer without taking the sandwich type of structure.

In order to clarify the behavior of HE in polar solvents, temperature effects upon the fluorescence rise and decay curves of P_1, P_2, and P_3 in 2-propanol have been examined. The results are shown in Fig. 6. The rise times of HE fluorescence in the range from room temperature to *ca.* 160 K are much shorter than those of P_2 and P_3 HE's in decalin solution. Thus, the HE formation process in 2-propanol is much faster than that in decalin not only at room temperature but also at low temperatures. The decay time of the HE fluorescence of P_1 and P_2 is *ca.* 10 ns at room temperature, slightly increasing at low temperatures.

In the case of P_3 HE, the decay of HE fluorescence above 250 K can be represented by a single exponential curve, but not so below 250 K. By subtracting the slow component from the decay curve, the residual part

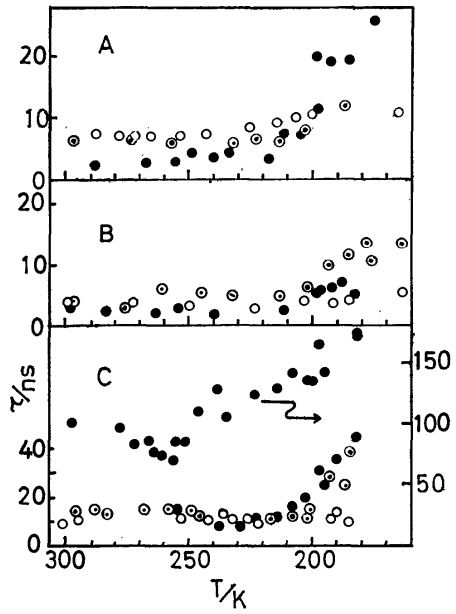

Fig. 6. Temperature effects upon fluorescence rise and decay times of P_1, P_2 and P_3 in 2-propanol.
○: P_1, ⊙: P_2, ●: P_3.
A. Decay times of LE fluorescence. $\lambda_{obsd}=400$ nm.
B. Rise times of HE fluorescence. $\lambda_{obsd}=550$ nm.
C. Decay times of HE fluorescence. $\lambda_{obsd}=550$ nm.
The time scale for the long life component of P_3 is indicated on the right hand side ordinate.

can be represented approximately by an exponential decay, as indicated in Fig. 7. Moreover, below 220 K, it was possible to observe the rise time of the HE fluorescence in 2-propanol with the present apparatus. The observed decay time of the fast component of the LE fluorescence at low temperatures does not agree with the rise time of the HE fluorescence. Similar results were obtained in 1-pentanol and butyronitrile.

As indicated in Fig. 6-C, the decay time of the fast component of the HE fluorescence of P_3 observed below 250 K shows a temperature dependence similar to that of the fluorescence decay times of P_1 and P_2 HE's. The result suggests that, at low temperatures, there are two kinds of HE's of P_3 which have decay times differing from each other, one of which seems to have a structure similar to that of P_1 or P_2 HE.

On the other hand, according to the result of recent laser photolysis studies,[10] the absorption spectrum of P_2 HE in 2-propanol was very close to the superposition of the absorption bands of pyrene anion and *N,N*-dimethylaniline cation, while a very broad absorption band with peak around 500 nm was observed in the case of the P_3 HE in 2-propanol. As regards the above argument concerning two kinds of HE's, we have measured time-resolved absorption spectra of P_3 HE in 2-propanol at 210 K. Corresponding to the result of fluorescence measurements, the short-life and long-life components of the time-resolved absorption spectra were similar respectively to the spectrum of P_2 HE and P_3 HE in 2-propanol at room temperature. Thus, the existence of two kinds of HE's of P_3 at low temperatures, one similar to P_1 or P_2 HE and the other analogous to the P_3 HE at room temperature, has been confirmed.

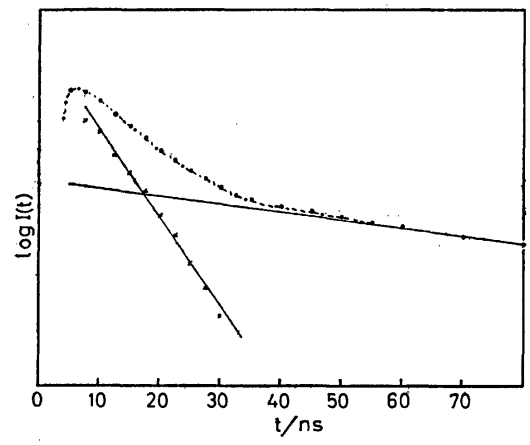

Fig. 7. Fluorescence decay function of P_3 HE observed at 550 nm in 2-propanol at 223 K.

However, according to our measurement of the time-resolved fluorescence spectra of P_3 HE, the spectrum of the slow component of the decay curve was approximately the same as that of the fast component. The result seems to indicate that these HE states with different lifetimes emit fluorescence at approximately the same wavelength region. Actually, the fact that the fluorescence band maxima of P_1, P_2, and P_3 in 2-propanol at room temperature are *ca.* 585, 585, and 590 nm, respectively,[1] indicates that a small difference in the geometrical structure of the HE does not appreciably affect the wavelength of the HE fluorescence in these polar solvents. Therefore, there seems to be a possibility that many kinds of HE's with different geometrical structures in polar solvents have similar fluorescence spectra and the HE fluorescence decay curve consists of many exponential curves with different decay times, which might be revealed by a more accurate measurement.

In the above interpretation, the non-fluorescent ion-pair does not play an important role in the formation process of the HE state. Nevertheless, it seems plausible that some non-fluorescent ion-pairs are formed in polar solvents, as discussed in *A* in relation to the solvent effect upon the HE fluorescence yield. Namely, several kinds of HE's as well as the non-fluorescent ion-pairs may be formed from the LE state or the non-relaxed CT state in polar solvents. Actually, formation of a species which might be identified with the non-fluorescent ion-pair was observed in the case of P_3 in acetonitrile.[3]

We see from the tables that both the HE fluorescence yield and decay time of the present systems decrease with increase of the solvent polarity, the extent of the decrease of the yield being a little larger. The result is comprehensible on the basis of the above discussion. The formation of the non-fluorescent ion-pair from the LE state or the non-relaxed CT state may be enhanced with increase of the solvent polarity. The result can also be interpreted by assuming the solvent-induced change of electronic and geometrical structures of the HE.[3,5] However, the interpretation does not seem to

be supported by the above results of fluorescence decay curve measurements at low temperatures and their explanation.

It is described in *A* that the fluorescence yields of the present intramolecular HE's are much higher as compared with those of the intermolecular systems. However, the difference between the intra- and intermolecular systems is not restricted to the fluorescence yield. The fluorescence lifetimes of these intramolecular HE's are much longer than those of the intermolecular systems. As an example, the fluorescence lifetime of P_3 HE in pyridine is 100 ns[3] as compared with the value 30 ns of the pyrene-DMA intermolecular HE.[5] Although the fluorescence of the pyrene-DMA intermolecular HE cannot be observed in acetone probably due to the predominant ionic dissociation from both the non-relaxed CT state and the HE state, the HE fluorescence of P_3 with lifetime of 63 ns can be observed easily in the same solvent. Thus, once the HE of P_3 is formed, it seems to be difficult for the quenching process to the non-fluorescent ion-pair to take place even in such a strongly polar solvent as acetone. A more or less analogous circumstance can be observed in the other systems.

In view of the above results, it should be noted that the exceptionally high fluorescence quantum yield and long lifetime of the intermolecular HE systems in alcohol solutions[11] can be ascribed to some mechanism involving the hydrogen bonding between the surrounding solvent molecules which prevents the ionic dissociation.

The authors' thanks are due to Mr. Tadashi Tokuda for his assistance in the measurements of the fluorescence spectra of P_n.

References

1) S. Masaki, T. Okada, N. Mataga, Y. Sakata, and S. Misumi, *Bull. Chem. Soc. Jpn.*, **49**, 1277 (1976).

2) I. B. Berlman, "Handbook of Fluorescence Spectra of Aromatic Molecules," 2nd ed, Academic Press, New York (1971).

3) N. Mataga, T. Okada, H. Masuhara, N. Nakashima, Y. Sakata, and S. Misumi, *J. Luminescence*, **12/13**, 159 (1976).

4) T. Okada, T. Fujita, M. Kubota, S. Masaki, N. Mataga, R. Ide, Y. Sakata, and S. Misumi, *Chem. Phys. Lett.*, **14**, 563 (1972).

5) N. Mataga, T. Okada, and N. Yamamoto, *Chem. Phys. Lett.*, **1**, 119 (1967).

6) Y. Taniguchi, Y. Nishina, and N. Mataga, *Bull. Chem. Soc. Jpn.*, **45**, 764 (1973); Y. Taniguchi and N. Mataga, *Chem. Phys. Lett.*, **13**, 596 (1972).

7) H. Masuhara, T. Hino, and N. Mataga, *J. Phys. Chem.*, **79**, 994 (1975)

8) (a) M. Itoh, T. Mimura, H. Usui, and T. Okamoto, *J. Am. Chem. Soc.*, **95**, 4388 (1973); M. Itoh and T. Mimura, *Chem. Phys. Lett.*, **24**, 551 (1974); M. Itoh, *ibid.*, **26**, 505 (1974); (b) T. Okada and N. Mataga, *Bull. Chem. Soc. Jpn.*, **49**, 2190 (1976).

9) C. Lewis and W. R. Ware, *Mol. Photochem.*, **5**, 261 (1973).

10) J. Hinatsu, H. Masuhara, and N. Mataga, to be published. Absorption Spectra of Some Intramolecular Exciplexes.

11) H. Knibbe, Thesis, Free University of Amsterdam (1969); N. Orbach and M. Ottolenghi, *Chem. Phys. Lett.*, **35**, 175 (1975).

Water Vapor Affinity of Potassium Bromide Coated with Potassium Oleate[1)]

Masatoshi CHIKAZAWA, Fujio YAMAMOTO, Eiko SAITA, Mamoru KAIHO,* and Takafumi KANAZAWA

Department of Industrial Chemistry, Faculty of Technology, Tokyo Metropolitan University, Fukazawa, Setagaya-ku, Tokyo 158

(Received May 14, 1976)

The amounts of adsorbed water and the isosteric heats for water vapor adsorption on fine crystals of KBr treated with various amounts of potassium oleate (KOl) were measured. In the adsorption isotherm of untreated KBr, a slight stepped rise of the amount adsorbed was observed, and this step is considered to be due to the two-dimensional condensation of water molecules adsorbed on the uniform surfaces of KBr particles. The monolayer capacity, determined from the adsorption isotherm of KBr by the point B method, agreed with the value calculated according to an adsorptive structure based on the two assumptions that all the surfaces of the KBr particles consist of (100) planes and that one water molecule is adsorbed per regularly distributed Br^- site.

A small amount of pre-adsorbed KOl was recognized to prevent the water vapor adsorption on KBr, and conversely, this effect disappeared with increasing KOl content while the hygroscopicity of the sample increased markedly. This abnormal increase in the adsorbed amount suggests that the adsorbed water molecules penetrate into the multilayer films of KOl on the KBr.

In order to change the surface properties of powder particles, the surface is often modified by coating with some material such as surfactants. Studies of the effect of the coating on surface properties and of the mechanism of the coating are instructive in many powder industries. In the present paper, data of the water vapor adsorption isotherms and isosteric heats of adsorption on KBr powders coated with various amounts of potassium oleate (KOl) are described, and the relationship between the water vapor affinity of KBr and the KOl concentration, the amount adsorbed on the surface per unit KBr surface area, was investigated to clarify the surface properties of the bromide. These experimental results will be available for research on the moisture-proofing and caking of powder materials.

Experimental

Materials. A potassium bromide sample was prepared by twice recrystallizing special-grade reagent KBr using distilled water. An aqueous solution of KBr (30 wt%, *ca.* 100 ml) was poured with stirring into ethyl alcohol (*ca.* 500 ml) cooled to −80——90 °C. The bromide thus obtained was filtered and washed four times with absolute ethyl alcohol and then dried at a reduced pressure of 10^{-3} Torr. This precipitate was observed by microscopy to be very small cubic crystals (2—7 μ).

Ground powders of KBr were prepared by pulverization of the recrystallized KBr in a ball-mill for 1 h.

Potassium oleate (special-grade reagent) was purified twice with absolute ethyl alcohol and also dried at reduced pressure.

Potassium Oleate Coating. A mixed solvent of CCl_4–C_2H_5OH in a volume ratio of 5 : 1 (50 ml) including an adequate amount of KOl was stirred for 5—6 min after KBr (30 g) had been added to the solvent, and the salt thus treated was filtered and dried at reduced pressure. A standard sample was prepared by immersing KBr in a mixed solvent which was free of KOl. The amount of KOl adsorbed on the surface of KBr particles was estimated by measuring the UV absorbance at 250 mμ after the adsorptive measurement had been completed. Ethyl alcohol and carbon tetrachloride were dehydrated with metal Mg and silica-gel, respectively, and then distilled prior to use.

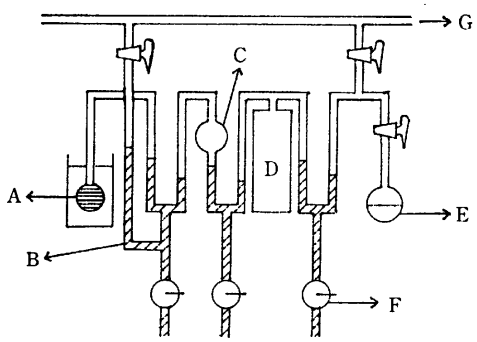

Fig. 1. Schematic diagram of apparatus for measurement of water vapor and nitrogen adsorptions.
A: Sample tube, B: mercury manometer, C, D: water vapor or nitrogen reservoir, E: water reservoir, F: greaseless cock, G: vacuum line.

Adsorption Measurement. Figure 1 shows the schematic diagram of a volumetric apparatus for water vapor and nitrogen adsorption. The equilibrium pressure of the water vapor and nitrogen were measured using a mercury manometer and a reading magnifier having a resolution of 10^{-2} mm.

Surface Area. The specific surface areas of the samples were determined by applying the BET equation to the nitrogen-adsorption data obtained at 77 K, assuming the cross-sectional area of a nitrogen molecule to be 16.2 $Å^2$.

Results and Discussion

Water Vapor Adsorption. The specific surface area of the standard sample was estimated to be *ca.* 0.24 m^2/g, and this value agreed roughly with the surface area measured for KBr powder untreated with the above solvent. The water vapor adsorption isotherms for this standard and the ground powders of KBr are illustrated in Fig. 2. In the adsorption isotherms, slight stepped rises of the amount of adsorbed water are observed in the relative vapor pressure range of 0.075 to 0.13, excepting the case of ground KBr. More remarkable steps in the water adsorption isotherms have been observed for NaCl, KCl,[2,3)] and NaBr.[4)] The relative pressures, at which the steps appear in the

* Present address: National Research Institute for Pollution and Resources; Kawaguchi, Kawaguchi-shi, Saitama 332.

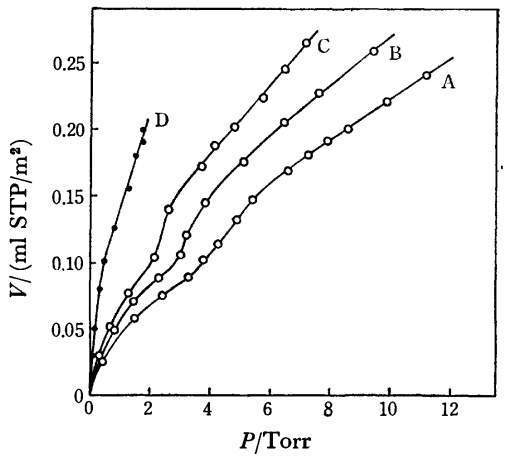

Fig. 2. Water vapor adsorption isotherms of KBr.
A: at 35 °C, B: at 30 °C, C: at 25 °C, D: Ground KBr at 20 °C.

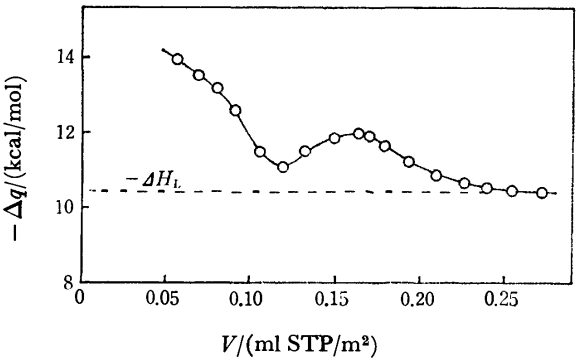

Fig. 3. Isosteric heat of water vapor adsorption on KBr.
$-\Delta H_L$: Heat of liquefaction of water vapor.

isotherms described previously, are higher than that determined for KBr. Disagreements in the relative pressures at which the step appears may be ascribable to the difference in the adsorption mechanisms of water molecules between the above salts and KBr.

Isosteric Heat of Adsorption. Figure 3 indicates the isosteric heats of adsorption calculated from the isotherms given in Fig. 2. A peak is seen in the isosteric heat curve at $V=0.17$ ml STP/m². This value corresponds closely to the monolayer capacity estimated by the point B method. On the other hand, the BET plot for the isotherm in Fig. 2 was found to be linear in the relative pressure range of 0.03 to 0.3, and it gave a monolayer capacity which is 1.3_7 times the value obtained at point B. However, no changes which are expected to suggest monolayer completion were observed in the isotherm and the isosteric heat curve at about $V=0.17\times1.3_7$ ml STP/m². If the surfaces of all KBr particles consist of (100) planes and one water molecule is adsorbed on one Br^- site of the surface, the amount of monolayer adsorption is calculated to be 0.171 ml STP/m². This value is almost equal to that obtained by the point B method. From these results, the adsorption mechanism of water vapor on a KBr surface and the characteristics of the adsorption isotherm and isosteric heat curves will be interpreted as follows. Water molecules are adsorbed on Br^- sites in a ratio of 1 : 1. An interaction force induced by hydrogenbonding among the adsorbed water molecules increases with the amount adsorbed, and reaches a maximum value at a coverage of $\theta=1$. The peak in the isosteric heat curve appears due to the effect of hydrogenbonding. Moreover, the slight stepped rise observed in the adsorption isotherm of the recrystallized KBr is considered to be due to the two-dimensional condensation of water molecules adsorbed on the uniform surfaces of the salt, since monolayer adsorption was formed at the end of the step. On the other hand, the stepped rise disappears in the isotherm of ground KBr owing to the inhomogeneity of its surface.

Lad[5] has obtained a water vapor adsorption isotherm on cleaved NaCl crystals, and its isotherm suggests an adsorptive structure, which is a hydrogen-bonded first layer with one molecule of water for two Cl^- sites. According to this result, two hydrogen atoms in a water molecule are considered to attach to two adjacent Cl^- sites. Therefore, the adsorption characteristics of water vapor on an alkali halide are considerably affected by the distance between the two adjacent anions, the electronegativities and the ionic radii of the chemical elements involved. The difference between the water vapor adsorption mechanisms of NaCl and KBr may be mainly due to the differences in their lattice spacings and in the electronegativities of the elements of which the surface is composed. The distance between the two Br ions is larger than that between Cl ions, and the electronegativity of bromine is smaller than that of chlorine. Hence, the two hydrogen atoms in a water molecule do not fit onto the two adjacent Br^- sites of KBr.

Effect of Potassium Oleate Coating. The effects of the concentration of the pre-adsorbed KOl on the water adsorption isotherm and the isosteric heat of adsorption are shown in Figs. 4 and 5, respectively. The slight stepped rise declined gradually with increasing KOl concentration. Moreover, no peak which was expected to appear for a coverage $\theta=1$ was observed in the heat curve of adsorption on KBr coated with KOl. Therefore, the disappearance of the step is thought to be due to increasing inhomogeneity of the component and the geometric structure of the solid surface containing adsorbed KOl. This interpretation is compatible with the result obtained using ground

TABLE 1. WATER VAPOR AFFINITIES OF KBr SAMPLES COATED WITH POTASSIUM OLEATE

Sample[a]	Oleate concentration (mg/m²)	V_m (ml STP/m²)	C	S_{H_2O}/S_{N_2}
A	0	0.236	8.46	0.69
B	0.472	0.238	6.11	0.69
C	0.576	0.225	7.36	0.65
D	0.579	0.209	9.11	0.60
E	0.597	0.231	8.58	0.67
F	1.193	0.269	9.17	0.78
H	5.25	0.35	25.6	1.0

a) The symbols are the same as those in Fig. 4.

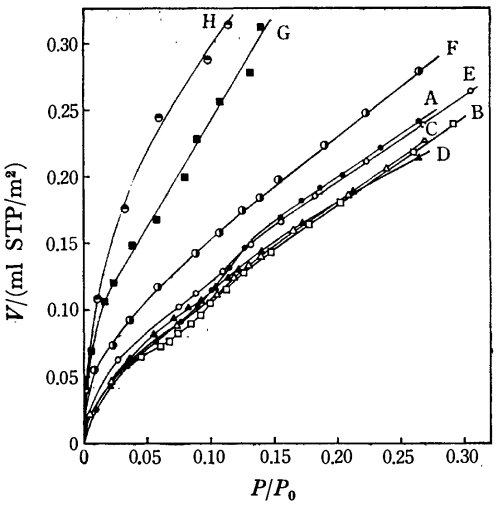

Fig. 4. Water vapor adsorption isotherms of KBr coated with KOl at 35 °C.
KOl concentration (mg/m²): A; Zero, B; 0.463, C; 0.576, D; 0.579, E; 0.597, F; 1.19, G; 2.99, H; 5.25, G, H at 30 °C.

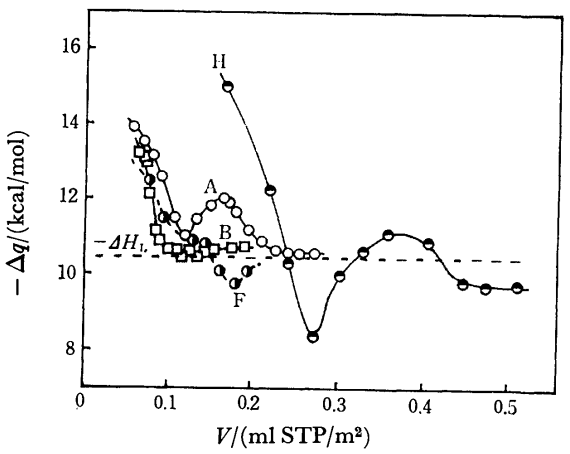

Fig. 5. Isosteric heat of water vapor adsorption on KBr coated with KOl.
KOl concentration (mg/m²): A; Zero, B; 0.463, F; 1.19, H; 5.25.

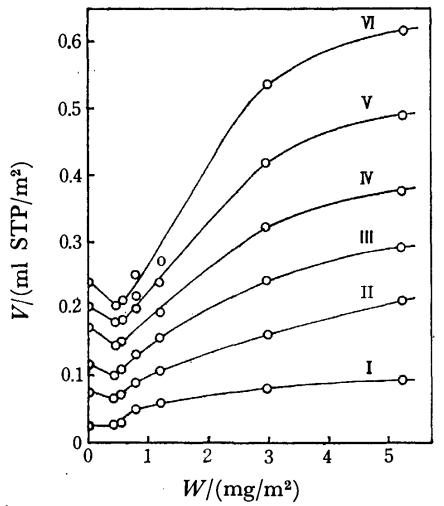

Fig. 6. Effect of KOl concentration on the amount of adsorbed water measured under fixed relative water vapor pressures.
P/P_0: I; 0.01, II; 0.05, III; 0.10, IV; 0.15, V; 0.20, VI; 0.25.

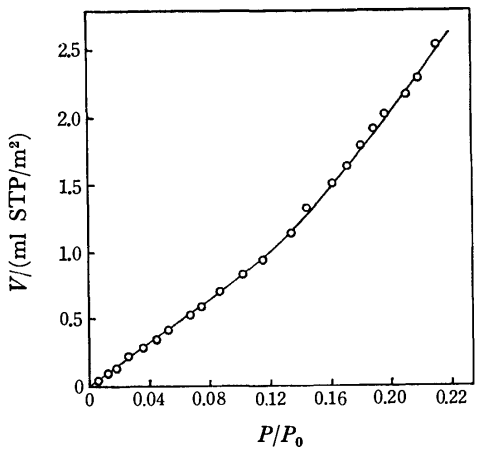

Fig. 7. Water vapor adsorption isotherm of KOl particles at 20 °C.

KBr. In addition, the pre-adsorbed KOl is believed to prevent the interaction between the adsorbed water molecules induced by the hydrophobic property of KOl and to eliminate a peak in the isosteric heat curves.

Pre-adsorption of KOl, in a certain concentration range and for a given surface coverage, weakened slightly the subsequent adsorption of water vapor, whereas at higher concentrations this trend was reversed and the amount adsorbed began to increase markedly.

Water vapor affinity, one of the surface properties of solids, is often expressed by the ratio S_{H_2O}/S_{N^2}, where S_{H_2O} and S_{N_2} are surface areas determined using H_2O and N_2 as adsorbates, respectively, assuming cross-sectional areas of 10.6 Å² for H_2O and 16.2 Å² for N_2. These values for KBr at various concentrations of pre-adsorbed KOl and C values obtained from the water vapor BET plots are summarized in Table 1. The slight effect of the pre-adsorbed KOl on the prevention of water vapor adsorption is observed for low concentrations of KOl, whereas at higher concentrations the water vapor affinity increases. The change in the isosteric heats of adsorption with increasing KOl concentration prove this tendency.

The relationship between the KOl concentration and the amount of adsorbed water at a fixed water vapor pressure is given in Fig. 6. The KOl concentration available for preventing water vapor adsorption is determined from the curve in Fig. 6 to be about 0.46 mg/m². If the amount of pre-adsorbed KOl required to cover the surfaces of KBr particles with a complete monolayer corresponds to a value of 0.46 mg/m², the resulting cross-sectional area of KOl is calculated to be 120 Å². However, this value is larger than the 45—50 Å² obtained by Adam[6] based on the structure of the liquid condensed film formed on the surface of an aqueous solution. The former value can probably be explained under the assumption that a hydrocarbon chain in the KOl molecule lies across the KBr surface. In such a case, the cross-sectional area of KOl is estimated from

the molecular structure to be 130—150 Å^2. This value is close to the above-stated value (120 Å^2).

Table 1 indicates that at higher KOl concentrations the hygroscopicity of the sample increases with the KOl concentration, and this tendency seems ascribable to the penetration of water molecules into the ionic layers of KOl films adsorbed in a multilayer which may be of laminar form. A similar effect of KOl[7] has been observed in the case of adsorption on $CaCO_3$ pre-adsorbed KOl. The water-vapor adsorption isotherm on KOl powder itself is illustrated in Fig. 7. The amount of adsorbed water per unit KOl surface area is considerably larger than that estimated to be the physical adsorption of water vapor on a KOl surface. Therefore, most of the adsorbed water molecules are thought to penetrate into KOl particles. A similar observation was reported by Gross and Bauer[8] in their study of water-vapor adsorption on aluminum soaps. They concluded that water molecules penetrate into the soap crystallites and undergo hydrogen bonding at recurring Al-O linkages.[8] On the basis of these results, the abnormal increase in hygroscopicity of the sample can be reasonably explained by assuming the penetration of the adsorbed water molecules into KOl films on the surface of KBr.

References

1) A part of this paper was presented at the 31st National Autumn Meeting of the Chemical Society of Japan, Sendai, October 1974.

2) M. Kaiho, M. Chikazawa, and T. Kanazawa, *Nippon Kagaku Kaishi*, **1974**, 233.

3) P. B. Barraciough and P. G. Hall, *Surf. Sci.*, **46**, 393 (1974).

4) M. Chikazawa, M. Kaiho, and T. Kanazawa, *Nippon Kagaku Kaishi*, **1976**, 410.

5) R. A. Rad, *Surf. Sci.*, **12**, 37 (1968).

6) N. K. Adam and J. W. W. Deyer, *Proc. R. Soc. London, Ser. A*, **106**, 694 (1924).

7) P. G. Hall, V. M. Lovell, and N. P. Finkelstein, *Trans. Faraday Soc.*, **66**, 2629 (1970).

8) J. H. Gross and W. H. Bauer, *J. Phys. Chem.*, **58**, 877 (1954).

Pressure Effect of the Nondispersive Infrared Gas Analyser

Tsutomu YONEZAWA and Eiji NIKI

Department of Industrial Chemistry, Faculty of Engineering, Tokyo University, Hongo, Tokyo 113

(Received June 9, 1976)

Based on the Elsasser model, a formula for the mean absorption applicable to the pressure effect of the nondispersive infrared gas analyser has been derived. The formula is generalized by removing the assumption in the Elsasser model that the total absorption coefficient, the half width and the spectral distance are constant.

In previous papers,[1,2] a formula was given for the mean absorption corresponding to the screening percent for the infrared ray due to the null balance shutter of the analyser as a function of the partial pressure of absorber p_a, the total pressure P and the cell length l. Many similar formulas, often empirical, have been reported,[3-6] but it is difficult to determine the coefficients in the formulas either experimentally or theoretically. There are two theories concerning the derivation of the formulas: total absorption by Ladenburg and Reiche,[7] and mean absorption by Elsasser.[8] The Lorentz type absorption coefficient is assumed in both theories. However the method for approximate evaluation of the following integral,

$$\int\{1-\exp(-k(\nu)l)\}\mathrm{d}\nu$$

viz. total absorption, is different.

The Elsasser theory is based on the three assumptions that the following are constant: i) the total absorption coefficient α_m, ii) the half width of the line δ_m and the spectral distance of the vibrational rotational line d_m. When assumption i) was removed, it was possible to obtain a good quantitative comparison between the theory and experiment.[2] In this paper, the formula is generalized by removing the remaining assumptions.

Apparatus

The apparatus and the principle of measurement have been reported.[2]

Theoretical

Half Width of Absorption Lines. According to the classical kinetic theory of gases, the collision width of the line is given by[2]

$$\delta = \frac{1}{4\pi}\sum_i N_i(D_{a,i})^2\left[[2\pi kT\left(\frac{1}{m_a}+\frac{1}{m_i}\right)\right]^{1/2} \quad (1)$$

where N_i is the number density of a molecule of the gas of ith type, $D_{a,i}$ the sum of the optical collision diameters of the absorbing molecule and the molecule of the ith type, m_a the mass of the absorbing molecule and m_i the mass of the ith type of molecule. For binary mixtures, Eq. 1 becomes

$$\delta = \frac{1}{4\pi}(2\pi kT)^{1/2}\left[N_a(D_{a,a})^2\left(\frac{2}{m_a}\right)^{1/2} + N_b(D_{a,b})^2\left(\frac{m_a+m_b}{m_a m_b}\right)^{1/2}\right]. \quad (2)$$

It is not necessarily correct that the half width is common to all the lines according to Eqs. 1 and 2. It was found that each line differs slightly in half width.[9] From quantum mechanics[10] the half width of the line is not constant since the colliding molecules exert different interaction due to the intermolecular force on each vibrational rotational energy level of the absorbing molecule.

Taking the above situation into consideration, it is better to express Eq. 2 as follows.

$$\delta_m = \frac{1}{4\pi}(2\pi kT)^{1/2}\left[N_a(D_{a,a})_m^2\left(\frac{2}{m_a}\right)^{1/2} + N_b(D_{a,b})_m^2\left(\frac{m_a+m_b}{m_a m_b}\right)^{1/2}\right]. \quad (3)$$

where the subscript m is the number of the line. $(D_{a,a})_m$ and $(D_{a,b})_m$ should be determined quantum mechanically. The first term of Eq. 3 explains the effect the collisions between absorbing molecules exert on the half width of the mth line, and the second the effect the collisions between the foreign and absorbing molecules exert on the mth line. Expressing N_i in term of partial pressure, Eq. 3 becomes

$$\delta_m = \frac{1}{4\pi}\left(\frac{2\pi}{kT}\right)^{1/2}[(C_{a,a})_m P_a + (C_{a,b})_m P_b] = \frac{1}{4\pi}\left(\frac{2\pi}{kT}\right)^{1/2}(C_{a,a})_m\left[P_a+\frac{(C_{a,b})_m}{(C_{a,a})_m}P_b\right] \quad (4)$$

where

$$(C_{a,a})_m = (D_{a,a})_m^2(2/m_a)^{1/2}$$

and

$$(C_{a,b})_m = (D_{a,b})_m^2(m_a+m_b/m_a m_b)^{1/2} \quad (5)$$

Here the notation δ_{0m} is defined by

$$\delta_{0m} = \frac{1}{4\pi}\left(\frac{2\pi}{kT}\right)^{1/2}(C_{a,a})_m. \quad (6)$$

δ_{0m} is the constant independent of pressure if the temperature is constant. Though it is not necessarily obvious that the ratio of $(D_{a,a})_m$ to $(D_{a,b})_m$ is constant, its ratio is assumed to be constant according to the method in the previous papers.[1,2] Then the following relation can be assumed

$$\frac{(C_{a,a})_m}{(C_{a,b})_m} = \left(\frac{2m_b}{m_a+m_b}\right)^{1/2}\left\{\frac{(D_{a,a})_m}{(D_{a,b})_m}\right\}^2 = B(=const)$$

where B is the so-called self-broadening coefficient. As a result, the half width of the line can be expressed by

$$\delta_m = \delta_{0m}P_e \quad (7)$$

where P_e is the effective pressure defined by

$$P_e = p_a + (1/B)p_b. \quad (8)$$

The difference in the half width of each line is taken

consideration by Eq. 7. Namely δ_m should be understood for δ of Eq. 2 to be extended. The theoretical expressions obtained in the previous papers,[1,2] however, must not be altered, except that $\delta_0\left(=\frac{1}{4\pi}\left(\frac{2\pi}{kT}\right)^{1/2}(C_{a,a})\right)$ in the definition of k_{0m} is simply replaced by δ_{0m} of Eq. 6.

Total Absorption Coefficient of the Line, α_m. The total absorption coefficient of the mth line is determined by means of the integral of the absorption coefficient which is ordinarily approximated by the following Lorentz type function in the infrared region.

$$k_m(\nu) = \frac{4\pi N_a}{3\hbar C}\nu_m|\mu_m|^2\frac{\delta_m}{(\nu-\nu_m)^2+\delta_m^2} \tag{9}$$

where μ_m is the matrix element of the dipole moment. The total absorption coefficient is, therefore,

$$\alpha_m = \int_0^\infty k_m(\nu)\mathrm{d}\nu = \int_0^\infty \frac{4\pi N_a}{3\hbar C}\nu_m|\mu_m|^2\frac{\delta_m}{(\nu-\nu_m)^2+\delta_m^2}\mathrm{d}\nu \tag{10}$$

It is evident that α_{0m} is proportional to the number density of absorber N_a. N_a is rewritten by the partial pressure p_a and we have

$$\alpha_m = \alpha_{0m}P_a. \tag{11}$$

α_{0m} is directly related to the Einstein transition probability except for the numerical constant.

By substituting $N_a=p_a/kT$ into Eq. 10, α_{0m} is expressed by the molecular constants as follows.

$$\alpha_{0m} = \frac{4\pi^2\nu_m|\mu_m|^2}{3\hbar ckT} \tag{12}$$

It was assumed that $\alpha_m=const$ in the Elsasser model. However, α_m is not constant in this paper.

Extension of the Definition of k_{0m} and the Approximate Expression for the Parameter t Determinable from the True Slit Function. If we denote the product of α_{0m} and δ_{0m} by l_{0m}

$$\alpha_{0m}\delta_{0m} \equiv l_{0m}, \tag{13}$$

it is determined from Eqs. 6 and 12 with use of the molecular constants as follows.

$$l_{0m} = \frac{1}{4\pi}\left(\frac{2\pi}{kT}\right)^{1/2}(D_{a,a})_m^2(2/m_a)^{1/2}\frac{4\pi^2\nu_m|\mu_m|^2}{3\hbar ckT} \tag{14}$$

On the other hand, t is approximately connected with the maximum extinction E_m as follows.[2]

$$E_m = t(\alpha_m\delta_m l)^{1/2}/a \tag{15}$$

where a is the slit width in cm^{-1} and l the cell length. For the simple component of the absorbing gas, Eq. 15 becomes

$$E_m = t(\alpha_{0m}\delta_{0m}l)^{1/2}P_a/a. \tag{16}$$

From Eqs. 13 and 16, we have

$$t = \frac{aE_m}{(l_{0m}l)^{1/2}P_a} \tag{17}$$

Here the quantity k_{0m} should be defined by

$$k_{0m} = E_m^2/\{4(d_m/a)^2P_a^2l\} \tag{18}$$

which can be evaluated from the maximum intensity of the absorption spectrum corresponding to the conditions of measurement. d_m is the spectral distance of the mth line. k_{0m} was defined with use of the mean spectral distance instead of d_m.[1,2] From Eqs. 17 and 18, the parameter t can be determined by the following approximate relation.

$$t = 2d_m\sqrt{\frac{k_{0m}}{l_{0m}}}. \tag{19}$$

Theoretical Extension of the Mean Absorption to the Molecules with Two Absorption Regions. The mean absorption of the molecules with a single absorption region should be extended to the molecules with weak bands such as the combination or the overtone band other than the fundamental one. In this case, the intensity of the infrared source I_ν and the mean spectral distance differ between both band regions. The expression for the mean absorption to be evaluated is as follows.

$$x = \frac{\sum_{m=1}^{n}\int_{u'}^{v'} I_f\{1-\exp(-k_m(\nu)l)\}\mathrm{d}\nu + \sum_{m'=1}^{n'}\int_{u''}^{v''} I_c\{1-\exp(-k_{m'}(\nu)l)\}\mathrm{d}\nu}{I_f nd' + I_c n'd''} \tag{20}$$

x corresponds to the screening percent of the incident light due to the null balance shutter of the infrared gas analyser. v', u', v'' and u'' are $\nu_m+d'/2$, $\nu_m-d'/2$, $\nu_{m'}+d''/2$ and $\nu_{m'}-d''/2$. d' and d'' are the widths of rectangles in each region by which the shape of absorption lines of the condenser microphone detector is approximated. By putting $I_c/I_f=r$ (the ratio of the intensity of the infrared source in both regions) and $n=n'$, the following expression is obtained for the high pressure near atmospheric pressure.

$$x = \frac{\sum_{n=0}^{\infty}(-P_e w)^n/n!\cdot\{\langle k_{0m}/D^2)^n\rangle_{av} + r'\langle(k_{0m'}/D'^2)^n\rangle_{av}\}}{1+r'} \tag{21}$$

where

$$1/D = (2/t)\cdot(d/d'),\quad 1/D' = (2/t)\cdot(d/d''),\quad r' = rd''/d' \text{ and } w=p_a l. \tag{22}$$

k_{0m} and $k_{0m'}$ are determined with use of the mean spectral distance d over both regions.

$$k_{0m} = E_m^2/\{4(d/a)^2p_a l\}$$

and

$$k_{0m'} = E_{m'}^2/\{4(d/a)^2p_a l\}.$$

$\langle\ \rangle_{av}$ denotes the normal average over m or m'.

When $d'=d''$, Eq. 20 is simplified as follows for the low pressure,

$$x = 2\left(\frac{\langle k_{0m}^{1/2}\rangle_{av} + r\langle k_{0m'}^{1/2}\rangle_{av}}{(1+r)D}\right)P_e^{1/2}w^{1/2} \tag{23}$$

and for the high pressure in the exponential form,

$$x = 1 - \exp\left[-(2\pi/D^2)\cdot\left(\frac{\langle k_{0m}\rangle_{av} + r\langle k_{0m'}\rangle_{av}}{1+r}\right)P_e w + \frac{(2\pi/D^2)^2}{2!}\left\{\left(\frac{\langle k_{0m}^2\rangle_{av} + r\langle k_{0m'}^2\rangle_{av}}{1+r}\right)\right.\right.$$

$$-\left(\frac{\langle k_{0m}\rangle_{av}+r\langle k_{0m'}\rangle_{av}}{1+r}\right)^2\Big\}(P_e w)^2$$
$$-\frac{(2\pi/D^2)^3}{3!}\Big\{\left(\frac{\langle k^3_{0m}\rangle_{av}+r\langle k^3_{0m'}\rangle_{av}}{1+r}\right)$$
$$-3\left(\frac{\langle k^2_{0m}\rangle_{av}+r\langle k^2_{0m'}\rangle_{av}}{1+r}\right)\cdot\left(\frac{\langle k_{0m}\rangle_{av}+r\langle k_{0m'}\rangle_{av}}{1+r}\right)$$
$$+2\left(\frac{\langle k_{0m}\rangle_{av}+r\langle k_{0m'}\rangle_{av}}{1+r}\right)^3\Big\}(P_e w)^3+\cdots\cdots\Big]. \quad (24)$$

Eqs. 23 and 24 explain the mean absorption of the molecules with two absorption regions, and are reduced to the expressions for the single absorption region if r approaches 0.

Extension to the Case in which the Assumption that the Spectral Distance is Constant is Removed. The present study is based on the Elsasser model. However the spectral distance is actually assumed to vary quadratically according to the number of the line m. Taking this situation into consideration, a more precise expression for the mean absorption is obtained as follows.[2)]

$$y=\frac{\sum_{m=1}^{n}\int_u^v\{1-\exp(-k_m(\nu)l)\}d\nu}{\sum_m d_m} \quad (25)$$

where v is $\nu_m+d_m/2$, and u is $\nu_m-d_m/2$. With use of the extended mean fractional transmission

$$T_m=\frac{1}{d_m}\int_u^v\exp\left\{-\frac{(\alpha_m/\pi)\delta_m}{(\nu-\nu_m)^2+\delta_m^2}l\right\}d\nu, \quad (26)$$

y is given by

$$y=1-\frac{\sum_m T_m d_m}{\sum_m d_m}$$
$$=1-\langle T_m\rangle \quad (27)$$

where $\langle T_m\rangle$ should be interpreted as $\sum T_m d_m/\sum d_m$. For the region of low pressure, T_m is

$$T_m=1-2(\alpha_m\delta_m l)^{1/2}/d_m \quad (28)$$

and then

$$y=2\cdot\frac{\sum(\alpha_m\delta_m l)^{1/2}}{\sum d_m}$$
$$=2\cdot\frac{\sum(\alpha_m\delta_m l/d^2)^{1/2}}{n}. \quad (29)$$

Thus y is reduced to the normal average. On the other hand, we have for the region of high pressure

$$y=1-\frac{\sum\exp(-2\pi\alpha_m\delta_m l/d_m^2)\cdot d_m}{\sum d_m}$$
$$=\frac{\sum\{(2\pi\alpha_m\delta_m l/d_m^2)-(2\pi\alpha_m\delta_m l/d_m^2)^2/2+\cdots\}}{\sum d_m} \quad (30)$$

Thus the value of y can be obtained when the following expressions are calculated

$\sum(\alpha_m\delta_m/d_m^2)/\sum d_m$, $\sum(\alpha_m\delta_m/d_m^2)^2 d_m/\sum d_m$, *etc.*

For the sake of convenience, g_{0m} is defined by

$$g_{0m}\equiv\frac{\alpha_{0m}\delta_{0m}}{\delta_m^2} \quad (31)$$

g_{0m} is a constant characteristic of each line. g_{0m} is connected with k_{0m} of Eq. 18 by the relation

$$g_{0m}=(2/t)^2 k_{0m}.$$

With use of g_{0m}, Eq. 30 becomes

$$y=1-\exp\Big\{-2\pi\langle g_{0m}\rangle P_e w$$
$$+\frac{(2\pi)^2}{2!}(\langle g^2_{0m}\rangle-\langle g_{0m}\rangle^2)(P_e w)^2$$
$$-\frac{(2\pi)^3}{3!}(\langle g^3_{0m}\rangle-3\langle g^2_{0m}\rangle\langle g_{0m}\rangle+2\langle g_{0m}\rangle^3)(P_e w)^3+\cdots\Big\} \quad (33)$$

where

$$\langle g^n_{0m}\rangle=\frac{\sum g^n_{0m}d_m}{\sum d_m}. \quad (34)$$

Eq. 33 was obtained without the three assumptions in the Elsasser model.

Application to the Infrared Gas Analyser. The above method can immediately be applied to the infrared gas analyser. The shape of the spectral lines of the condenser microphone detector is approximated by the rectangular lines with unit height and the width $d_{m'}$, which is not necessarily constant. The following expression corresponds to the absorption intensity of the sample gas in the nondispersive infrared gas analyser, and is of the same form as that of mean absorption.

$$x=\frac{\int_0^\infty I_\nu\{1-\exp(-\sum_{m=1}^{n}k_m(\nu)l)\}\{1-\exp(-\sum_{m=1}^{n}k'_m(\nu)l')\}d\nu}{\int_0^\infty I_\nu\{1-\exp(-\sum_{m=1}^{n}k_{m'}(\nu)l')\}d\nu}. \quad (35)$$

According to the above approximation, x is reduced to Eq. 25 if d_m is regarded as $d_{m'}$. x becomes

$$x=2\langle g'^{1/2}_{0m}\rangle P_e^{1/2}w^{1/2} \quad (36)$$

for low pressure, and

$$x=1-\exp\{-2\pi\langle g'_{0m}\rangle P_e w$$
$$+\frac{(2\pi)^2}{2!}(\langle g'^2_{0m}\rangle-\langle g'_{0m}\rangle^2)(P_e w)^2\}$$
$$-\frac{(2\pi)^3}{3!}(\langle g'^3_{0m}\rangle-3\langle g'^2_{0m}\rangle\langle g'_{0m}\rangle+2\langle g'_{0m}\rangle^3)(P_e w)^3+\cdots\Big\} \quad (37)$$

for high pressure, where

$$g'_{0m}=\frac{\alpha_{0m}\delta_{0m}}{d_m'^2}\quad\text{and}\quad\langle g'^n_{0m}\rangle=\frac{\sum g'^n_{0m}d_m'}{\sum d_m'}. \quad (38)$$

Usually g'_{0m} can not be calculated if the value of d'_m is not known. However, g'_{0m} can be calculated if $d'_m/d_m=const.$ If we put $(d'_m/d_m)\cdot(t/2)=D$, x agrees with the results[2)] which are obtained when r approaches 0 in Eqs. 23 and 24.

When $d_{m'}/d_m$ is not constant, x can not be expressed with use of the correction factor D because of the following relation

$$\langle g'^n_{0m}\rangle=\frac{\sum g'^n_{0m}d_m'}{\sum d_m'}=\frac{\sum g^n_{0m}(d_m/d_m')^{2n}d_m'}{\sum d_m'}$$
$$\neq\frac{D2^n\sum k^n_{0m}d_m'}{\sum d_m'}. \quad (39)$$

It is possible to extend Eqs. 36 and 37 to the cases of molecules with more than two absorption regions if $\langle g'^n_{0m}\rangle$ is regarded as

$$\langle g'^{n}_{0m} \rangle = \frac{\sum g'^{n}_{0m} d'_m + r \sum g''^{n}_{0m'} d''_{m'} + \cdots}{\sum d'_m + r \sum d''_{m'} + \cdots} \tag{40}$$

where

$$g''_{0m'} = \frac{\alpha_{0m'} \delta_{0m'}}{d''^{2}_{0m'}}. \tag{41}$$

Conclusion

It was found that the original expressions[2] hold good even if the assumption that δ_0 is constant is removed. However k_{0m} $(=\alpha_{0m}\ \delta_0/d^2)$ should be regarded as $\alpha_{0m}\delta_{0m}/d^2$. The ambiguous parameter t[2] was approximately determined in the explicit form with use of the molecular constants. It is concluded that the molecules with more than two absorption regions have the same pressure dependence as the molecules with a single absorption region. A more general formula was obtained for the mean absorption with use of the constant g_{0m} without the three assumptions in the Elsasser model. It can be concluded that in general x can not be expressed with use of a correction factor D.

References

1) T. Yonezawa and E. Niki, *Trans. Soc. Instr. Cont. Eng.*, **7**, 236 (1970).
2) E. Niki and T. Yonezawa, *Bull. Chem. Soc. Jpn.*, **46**, 3757 (1973).
3) L. D. Gray, *Appl. Opt.* **4**, 1494 (1965).
4) J. N. Howard, D. E. Burch, and D. Williams, *J. Opt. Soc. Am.*, **46**, 237 (1956).
5) U. P. Oppenheim and Y. Ben-Aryeh, *J. Quant. Spectrosc. Radiat. Transfer*, **4**, 559 (1964).
6) D. E. Burch, D. A. Gryvnak, and D. Williams, *Appl. Opt.*, **1**, 759 (1962).
7) R. Ladenburg and F. Reiche, *Ann. Phys.*, **38**, 249 (1912).
8) W. M. Elsasser, *Phys. Rev.*, **54**, 126 (1938).
9) S. Chen and M. Takeo, *Revs. Modern Phys.*, **29**, 20 (1957).
10) P. W. Anderson, *Phys. Rev.*, **76**, 647 (1949).

Electronic Structures and Spectra of Azulenophenalenes

Tsuguo KOYANAGI, Yuko SHIN, and Hiroyuki YAMAGUCHI
Department of Chemistry, Kumamoto University, Kumamoto 860

(Received July 3, 1976)

The ground-state electronic properties and electronic spectra of azuleno [5, 6, 7-*cd*] phenalene (I) and azuleno-[1, 2, 3-*cd*]phenalene(II), which are isomers of the potent carcinogen benzo[*a*]pyrene (III), have been investigated by using the SCF screened potential MO CI method in combination with the variable bond-length technique. From the calculated C–C bond lengths and the position dependence of the SCF screened potential, it may be concluded that molecules I, II, and III are all both aromatic and polyolefinic. The electronic spectra of I, II, and III predicted using the screened potential are in better agreement with the experimental values than those calculated using the bare potential.

Since the molecular geometries of azuleno[5,6,7-*cd*]phenalene (I) and azuleno[1,2,3-*cd*]phenalene (II) resemble that of the potent carcinogen benzo[*a*]pyrene (III), the electronic structures and spectra of I, II, and III have been of interest. Molecule I, which was recently synthesized by Jutz and Kirchlechner,[1] was found to be carcinogenic.[2] Very recently, Murata *et al.*[3] have synthesized molecule II.

Fischer and Ege[4] have applied the SCF MO method based on the Pariser-Parr-Pople approximation to I and have calculated its electronic structures and spectra. Using the LCI-SCF MO method, Zahradnik[5] has investigated the electronic spectra of I and II. Germer and Becker[6] and Pancir and Zahradnik[7] have studied theoretically the electronic spectra of III, but they did not mention the aromaticities and carcinogenicities of I, II, or III. Recently, Thulstrup *et al.*[8] have measured the magnetic circular dichroism (MCD) spectrum of I and assigned its absorption spectrum. Very recently, Tajiri *et al.*[9] have measured the MCD spectrum of II and interpreted its complicated absorption bands.

The purpose of this paper is to investigate theoretically the ground-state electronic properties and electronic spectra of I, II, and III by using the SCF screened potential MO CI method in combination with the variable bond-length technique,[10,11] which is known to reproduce well the electronic structures of large conjugated molecules. It is possible to use the results of such calculations to deepen our understanding of the aromatic characteristics and carcinogenicities of I, II, and III.

Method of Calculation

A procedure that combines the SCF screened potential with the variable bond-length technique[11] is used in the Pariser-Parr-Pople SCF MO CI method.[12,13] At each step of the SCF calculation, the new bond lengths are obtained from the corresponding bond orders.[14] The screened potential is evaluated by using the bare potential obtained from the new bond lengths. The bare potential is calculated using the Mataga-Nishimoto formula.[15] This screened potential is used in the calculation of the next step. The calculation is repeated until self-consistency is reached. The screened potential for the CI calculation of the five low-lying singlet excitations is calculated by omitting the low-lying subset of configurations in Eq. 8 of Ref. 10. The SCF calculation of the ground state is made by using the full effective interaction.

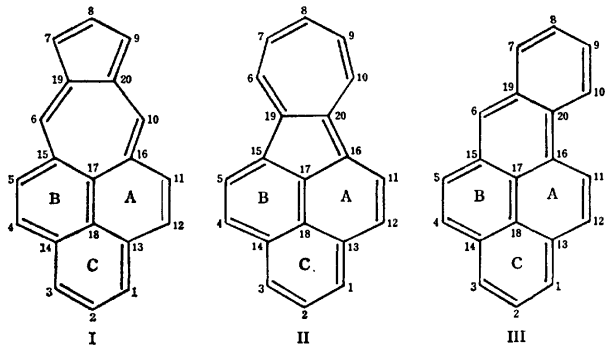

Fig. 1. Numbering of atoms.

Results and Discussion

Ground-state π-Electronic Properties. The calculated charge densities, free valence, and bond lengths are summarized in Table 1. The greatest nucleophilic reactivity is predicted at the 6 and 10 atoms in I and the 6 and 10 atoms in II. The greatest electrophilic reactivity is expected at the 7 and 9 positions in I and the 15 and 16 positions in II. The results for I agree with those of Fischer and Ege[4] and Thulstrup *et al.*[8] The calculated charge densities for III indicate that the Coulson-Rushbrooke theorem,[16] which states that, in alternant hydrocarbons, the π-electron densities for all the carbon atoms are unity, does not hold for III, when the screened potential is used. The technique of ^{13}C-NMR and ESCA[17] is capable of resolving the small charge differences in III.

From the viewpoint of carcinogenic activity, let us discuss the reactivity for the addition reactions of I, II, and III. The sum of the free valences for the two positions of the K-region,[18] $F_4+F_5=F_{11}+F_{12}=0.942$ in II, is smaller than $F_4+F_5=0.983$ in III, which is the strong carcinogen, but is comparable to the sum $F_4+F_5=F_{11}+F_{12}=0.948$ in I, which has carcinogenicity.

As for the bond lengths, it is of interest to note that the bond lengths of the azulene nucleus of I and II are almost the same as those of the free azulene molecule and that the bond lengths of the naphthalene nucleus of III are almost the same as those of the free naphthalene molecule. Two isolated C–C double

TABLE 1. CHARGE DENSITIES, FREE VALENCE NUMBERS, AND BOND LENGTHS

Molecule	Atom	Charge density	Free valence	Bond	Bond length (Å)	Molecule	Atom	Charge density	Free valence	Bond	Bond length (Å)
I	1	1.017	0.440	1— 2	1.396	III	1	1.016	0.441	1— 2	1.388
	2	0.977	0.395	1—13	1.404		2	0.988	0.396	1—13	1.411
	4	0.993	0.480	13—18	1.415		3	1.021	0.439	2— 3	1.404
	5	0.986	0.470	4—14	1.447		4	0.993	0.491	3—14	1.396
	6	0.927	0.493	4— 5	1.361		5	0.994	0.492	4—14	1.454
	7	1.135	0.478	5—15	1.445		6	1.034	0.491	4— 5	1.355
	8	1.010	0.421	15—17	1.419		7	1.001	0.448	5—15	1.454
	14	0.980	0.152	17—18	1.433		8	0.993	0.418	15—17	1.432
	15	0.994	0.171	6—15	1.406		9	1.001	0.422	6—15	1.383
	17	0.951	0.177	6—19	1.403		10	0.994	0.442	6—19	1.426
	18	1.004	0.140	19—20	1.461		11	0.992	0.455	7—19	1.428
	19	0.997	0.188	7—19	1.409		12	0.998	0.468	7— 8	1.373
				7— 8	1.398		13	0.992	0.139	8— 9	1.423
II	1	1.042	0.443	1— 2	1.396		14	0.988	0.166	9—10	1.374
	2	0.984	0.394	1—13	1.405		15	0.983	0.171	19—20	1.407
	4	1.038	0.480	13—18	1.415		16	1.001	0.178	10—20	1.426
	5	0.977	0.462	4—14	1.445		17	1.005	0.158	11—12	1.364
	6	0.894	0.461	4— 5	1.362		18	1.002	0.145	11—16	1.439
	7	1.010	0.440	5—15	1.442		19	0.994	0.158	12—13	1.441
	8	0.909	0.148	15—17	1.417		20	1.008	0.145	16—17	1.399
	14	0.983	0.148	17—18	1.434					16—20	1.433
	15	1.103	0.198	6—19	1.404					14—18	1.419
	17	1.008	0.160	6— 7	1.399					13—18	1.410
	18	0.999	0.142	7— 8	1.400					17—18	1.436
	19	1.004	0.213	19—20	1.457						
				15—19	1.416						

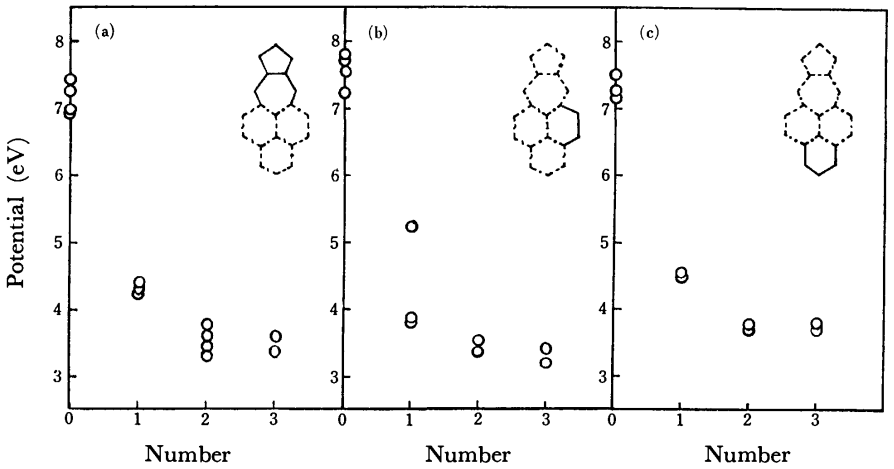

Fig. 2. The SCF screened potentials in azuleno[5,6,7-*cd*]phenalene plotted *versus* the number; (a) the azulene nucleus, (b) the benzene ring (A or B), and (c) the benzene ring (C).

bonds exist in the benzene rings (A and B) of the phenalenyl moiety for I, II, and III. The bond lengths of the benzene ring (C) in I, II, and III are composed of two vinyl molecules and 6-phenylazulene, 2-phenylazulene, and 2-phenylnaphthalene, respectively.

Position Dependence of SCF Screened Potential. Terasaka *et al.*[11] divided the SCF screened potentials V into the following groups: V_{11}, V_{12}, V_{13},⋯; V_{22}, V_{23}, V_{24},⋯;⋯. In Fig. 2, the SCF screened potentials in each group of I are plotted *versus* a number that indicates the kinds of screened potential, that is, 0: one-center potentials V_{11}, V_{22}, V_{33},⋯; 1: the nearest two-center potentials V_{12}, V_{23}, V_{34},⋯; *etc.* The results in II and III are shown in Figs. 3 and 4, respectively. In the azulene nucleus of I and II, at each of the numbers the various screened potentials are almost the same as those of the free azulene molecule (see Fig. 9 of Ref. 11). In the naphthalene nucleus of III, a tendency similar to that in the free naphthalene molecule appears (see Fig. 8 of Ref. 11). In the free naphthalene molecule, there is a fairly clear double-

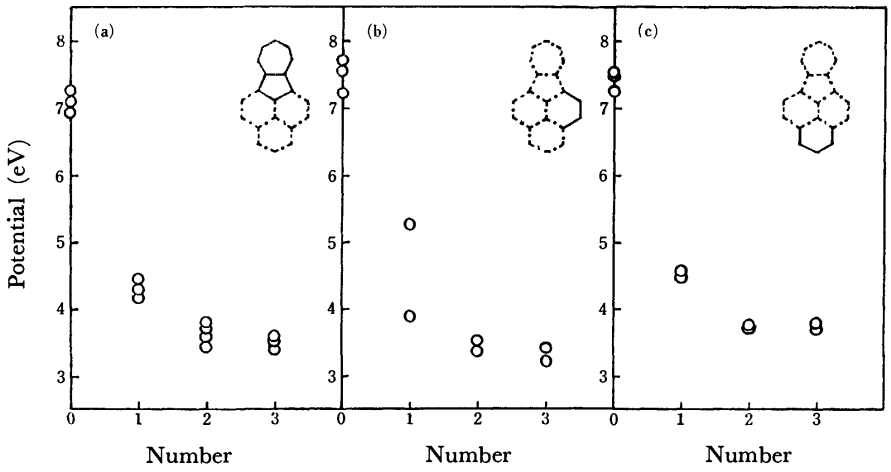

Fig. 3. The SCF screened potentials in azuleno[1,2,3-*cd*]phenalene plotted *versus* the number; (a) the azulene nucleus, (b) the benzene ring (A or B), and (c) the benzene ring (C).

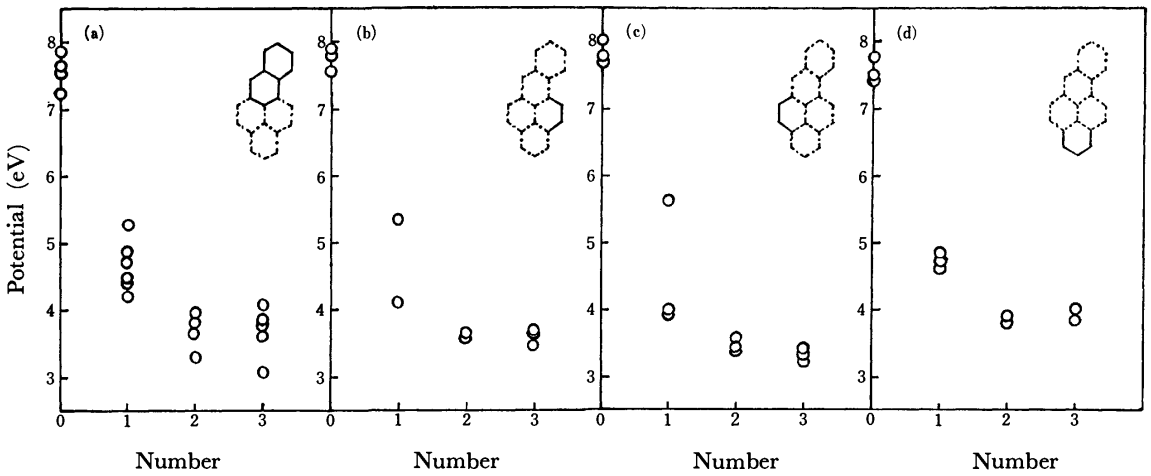

Fig. 4. The SCF screened potentials in benzo[*a*]pyrene plotted *versus* the number; (a) the naphthalene nucleus, (b) the benzene ring (A), (c) the benzene ring (B), and the benzene ring (C).

bond fixation, so that the characteristics of the screened potential are the same as those of the polyene ($n=10$) (see Fig. 8 of Ref. 11). The SCF screened potential is very sensitive to a bond alternation. There are two kinds of screening (screening and anti-screening) at the odd numbers in molecules such as polyene, in which there exists a strong bond alternation.[11] The characteristics of the screened potential of the benzene rings (A and B) in the phenalenyl moiety of I, II, and III presented in Figs. 2(b), 3(b), 4(b), and 4(c) shows trends similar to those of the polyene. The screened potential of the benzene ring (C) of I, II, and III shows a tendency similar to that of the free azulene molecule. From the above results, it may be concluded that the azulene nucleus of I and II and the benzene ring (C) in the phenalenyl moiety of I, II, and III are aromatic, but the naphthalene nucleus of III and the benzene rings (A and B) in the phenalenyl moiety of I, II, and III are polyolefinic. Molecules I, II, and III may have both aromatic and polyolefinic characters.

Electronic Spectra. Table 2 shows the transition energies and oscillator strengths calculated by using the SCF screened potential (SP) in combination with the variable bond-length SCF technique, along with those calculated assuming the bare potential (BP). It may be noted that the calculated excitation energies and oscillator strengths using the screened potential are in better agreement with the experimental values than those calculated using the bare potential. The spectral results calculated for I by Fischer and Ege[4] and by Thulstrup *et al.*,[8] for I and II by Zahradnik,[5] for II by Tajiri *et al.*,[9] and for III by Germer and Becker[6] and by Pancir and Zahradnik[7] are in fairly good agreement with the present results obtained using the SCF screened potential.

One of the present authors (H. Y.) especially wishes to thank Professor I. Murata of Osaka University for providing him with copies of the ultraviolet absorption spectra of azuleno[1,2,3-*cd*]phenalene and to thank Dr. Y. Fujimura of Tohoku University for his fruitful discussions.

TABLE 2. TRANSITION ENERGIES (ΔE(eV)) AND INTENSITIES (f)

Molecule	Theoretical				Experimental
	BP		SP		
	ΔE	f	ΔE	f	ΔE
I	1.98	0.035	1.83	0.031	1.65 ($f=0.01$)[a]
	2.82	0.52	2.72	0.37	2.75 ($f=0.4$)[a]
	3.66	0.044	3.49	0.021	3.35[a]
	4.15	0.26	3.78	0.25	3.66 ($f=0.3$)[a]
	4.16	2.16	3.88	1.89	3.84 ($f=1.6$)[a]
II	1.91	0.022	1.74	0.033	1.63 ($\log\varepsilon=2.52$)[b]
	2.81	0.57	2.54	0.68	2.60 ($\log\varepsilon=4.69$)[b]
	3.76	0.075			
	3.89	1.99	3.60	1.58	3.53 ($\log\varepsilon=4.85$)[b]
III	3.46	0.89	3.18	0.000	3.07 ($\log\varepsilon=3.61$)[c]
	3.49	0.000	3.39	0.68	3.22 ($\log\varepsilon=4.44$)[c]
	4.42	0.000	4.30	0.006	
	4.52	0.088	4.39	0.030	4.18 ($\log\varepsilon=4.76$)[c]
	4.68	1.26	4.62	1.16	4.67 ($\log\varepsilon=4.64$)[c]

a) Taken from Ref. 8. b) Taken from Ref. 3. c) Taken from Ref. 6.

References

1) Ch. Jutz and R. Kirchlechner, *Angew. Chem. Int. Ed. Engl.*, **5**, 516 (1966).

2) N. P. Buu-Hoi, N. B. Giao, and Ch. Jutz, *Naturwissenschaften*, **57**, 499 (1970).

3) I. Murata, K. Nakasuji, K. Yamamoto, T. Nakazawa, Y. Kayane, A. Kimura, and O. Hara, *Angew. Chem.*, **87**, 170 (1975).

4) H. Fischer and G. Ege, *Chem. Ber.*, **100**, 395 (1967).

5) R. Zahradnik, "Nonbenzenoid Aromatics," Vol. II, ed by J. P. Snyder, Academic Press Inc., New York, N. Y. (1971), p. 1.

6) H. A. Germer, Jr. and R. S. Becker, *Theor. Chim. Acta*, **28**, 1 (1972).

7) J. Pancir and R. Zahradnik, *J. Phys. Chem.*, **77**, 121 (1973).

8) E. W. Thulstrup, J. Michl, and C. Jutz, *J. Chem. Soc. Faraday Trans. 2*, **9**, 1618 (1975).

9) A. Tajiri, M. Hatano, I. Murata, and K. Nakasuji, *Chem. Lett.*, **1976**, 543.

10) H. Gutfreund and W. A. Little, *J. Chem. Phys.*, **50**, 4468 (1969).

11) T. Terasaka, T. Iijima, Y. Fujimura, and T. Nakajima, *Bull. Chem. Soc. Jpn.*, **46**, 1301 (1973).

12) R. Pariser and R. G. Parr, *J. Chem. Phys.*, **21**, 446, 767 (1953).

13) J. A. Pople, *Trans. Faraday Soc.*, **49**, 1375 (1953).

14) T. Nakajima and S. Katagiri, *Mol. Phys.*, **7**, 149 (1964).

15) N. Mataga and K. Nishimoto, *Z. Phys. Chem.*, **13**, 140 (1957).

16) C. A. Coulson and G. S. Rushbrooke, *Proc. Cambridge Phil. Soc.*, **36**, 1963 (1940).

17) A. Fablman, K. Hamrin, J. Hedman, R. Nordberg, C. Nordling, and K. Siegbahn, *Nature*, **210**, 4 (1966).

18) B. Pullman, *C. R. Acad. Sci.*, **238**, 1935 (1954).

Thermal Dissociation of *N,N*-Dimethylformamide–Tetracyanoethylene and Dimethyl Sulfoxide–Tetracyanoethylene Complexes into Ions

Nobuo KUSHIBIKI and Hiroshi YOSHIDA

Faculty of Engineering, Hokkaido University, Kita-ku, Sapporo 060

(Received July 10, 1976)

Ionic dissociation of *N,N*-dimethylformamide (DMF)-tetracyanoethylene (TCNE) and dimethyl sulfoxide (DMSO)-TCNE electron donor-acceptor (EDA) complexes was studied by means of optical absorption and electron spin resonance measurements. Upon dissolving TCNE into DMF or DMSO, essentially all the TCNE became complexed with the electron-donationg solvent; charge-transfer bands with maxima at 310 and 380 nm were found for DMF-TCNE and DMSO-TCNE complexes, respectively. The CT bands were transformed slowly in the dark into the band of $TCNE^-$. This transformation proceeded quantitatively and indicated the dissociation of the EDA complexes into ions. The rate of the ionic dissociation was determined by following a first-order growth of the ESR spectrum of $TCNE^-$ at various temperatures: $k=10^{8.9}\exp(79/RT)$ for the DMF-TCNE complex and $k=10^{6.3}\exp(59/RT)$ for the DMSO-TCNE complex, in units of s and kJ/mol. Dissolved oxygen was found not only to react chemically with the complex to form a new stable species, but also to quench physically the ionic dissociation. Upon evacuating the oxygen, the survival fraction of the complex was found to start dissociation again. It is suggested that the ionic dissociation arises from a long-lived precursor state, probably the triplet state of the complex.

Since the very early work of Kainer and Uberle showing the formation of ions on dissolving *N,N,N',N'*-tetramethyl-*p*-phenylenediamine-chloranil solid complex in acetonitrile,[1] the role of electron donor–acceptor (EDA) complexes in chemical reactions has been subject of spectroscopic study.[2] The role in photoinduced reactions has been extensively studied mostly by a flash photolysis technique: selective excitation at charge-transfer (CT) band or bands of constituent molecules has facilitated the elucidation of the molecular mechanism in the reactions. The photoinduced formation of ions from donor–acceptor pairs in solution has been shown to occur through an excited state of the EDA complexes and/or through an exciplex.[3] However, ion formation without light has been studied comparatively little, and its molecular mechanism has not been fully elucidated.[4–9]

TCNE, one of the strongest organic acceptors, has been known to form readily its radical anion ($TCNE^-$) when photoilluminated in fluid or rigid etherial solvents such as tetrahydrofuran (THF) which have an electron-donating nature.[7,10–13] Stewart *et al.* further found the formation of $TCNE^-$ in the absence of light upon mixing TCNE in more polar solvents such as dimethyl sulfoxide (DMSO) and *N,N*-dimethylacetamide (DMA).[6,7] The concentration of $TCNE^-$ was found to reach a maximum within a few minutes, before starting the measurements, and then to decay slowly. They proposed, in adopting the mechanism presented by Calvin for the THF-TCNE complex,[12] that the "prompt ESR signal of $TCNE^-$" arises from the thermal population of the CT triplet state, which then decays to give the ground state EDA complex between solvent and TCNE or to give ions. The slow decay was explained by recombination of ions to give the complex. These authors seem to have assumed that the observed $TCNE^-$ is the precusor of the complex rather than its product. Later, Keys and Carper found that in degassed solutions $TCNE^-$ was very stable and its concentration increased slowly after its prompt formation.[8] These observations were again interpreted on the basis of Stewart's view.

Recently, we also studied the formation without light of $TCNE^-$ in DMSO by the ESR method[14] and found a difference in its kinetical features from those reported previously.[6,7] We found no prompt formation of $TCNE^-$. Its concentration increased following a first-order kinetics during the whole period of reaction in the dark. The result suggested, in contrast to Stewart's view, the thermal dissociation of DMSO-TCNE complex into ions which is unexpectedly slow. The previous investigation is extended here and the formation of $TCNE^-$ is studied in either DMSO or *N,N*-dimethylformamide (DMF) by means of not only the ESR technique but also optical absorption measurements.

Experimental

TCNE of analytical grade was purified by recrystallization from anhydrous methylene dichloride and by sublimation under vacuum several times. DMF of spectroscopic grade was dried under vacuum with calcium hydride and then with barium oxide baked beforehand at *ca.* 650 K overnight, degassed by a freezing-pumping-thawing technique, and kept in the dark. DMSO of spectroscopic grade was dried with calcium hydride, degassed and treated with molecular sieves baked beforehand under vacuum, and kept in the dark.

TCNE was dissolved in DMF or DMSO within a closed glass system with an optical absorption cell or an ESR sample tube through a break seal under vacuum better than 1×10^{-5} Torr, and subjected to measurements. These procedures were carried out cautiously in total darkness. The optical absorption spectrum of the solution was recorded with a conventional recording spectrophotometer (Hitachi, Model EPS-3T) at room temperature (298±1 K) between intermittent warmings at a fixed temperature. Electron spin resonance (ESR) measurements were carried out with a conventional X-band spectrometer (JEOL, Model JES-ME-2X) equipped with a variable temperature accessary (Model JES-VT). The reaction temperature in the ESR resonant cavity was thus controlled within an uncertainty of 0.5 K. Absolute concentrations of $TCNE^-$ formed in the solutions were determined from their ESR spectral intensities, as compared with the intensity of the $TCNE^-$ authentically

generated by reducing TCNE with sodium metal in acetonitrile.[15]

Results

Optical Absorption Studies. Immediately after dissolving TCNE into DMF, an optical absorption band with a broad structureless shape was observed at about 310 nm, as shown in Fig. 1, where neither TCNE nor DMF gives an absorption. A similar band was observed at about 380 nm for DMSO solvent, as shown in Fig. 2. The shift of absorption maximum from 310 to 380 nm seems to correspond to the difference in ionization potential and in dielectric constant between DMF and DMSO. These bands are attributed to a charge-transfer transition and indicate the formation of EDA complexes between solvents and TCNE. The CT band of the DMSO-TCNE complex was reported to have an absorption maximum at 372 nm in carbon tetrachloride.[6] The band of the DMF-TCNE complex has not been reported. The 310 nm band in Fig. 1 is very similar to that of the DMA-TCNE complex, which shows an absorption maximum at 298 nm.[7]

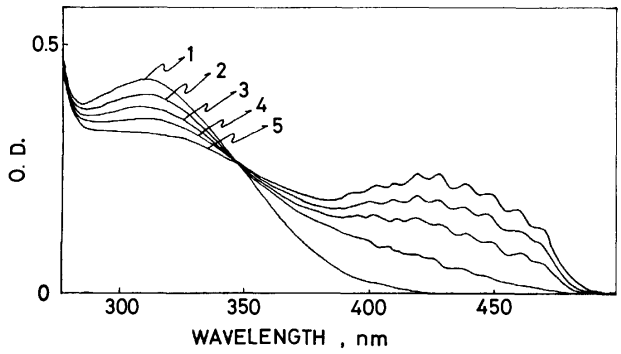

Fig. 1. Optical absorption spectra of DMF-TCNE observed at 298 K (1) immediately after mixing TCNE (3.0×10^{-4} mol dm^{-3}) in DMF under vacuum and after warming at 323 K for (2) 90, (3) 150, (4) 250 (5) 350 min. Optical path: 0.5 cm.

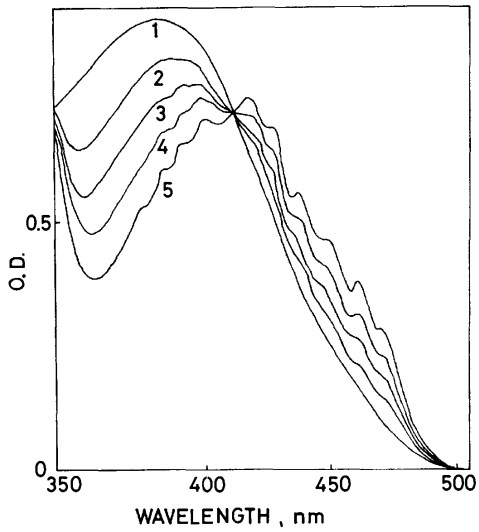

Fig. 2. Optical absorption spectra of DMSO-TCNE observed at 298 K (1) immediately after (2) 15, (3) 50, (4) 110 and (5) 280 min after mixing TCNE (6.0×10^{-4} mol dm^{-3}) in DMSO under vacuum. Optical path: 0.2 cm.

Figure 1 shows changes in the absorption spectrum when the solution of TCNE in DMF was warmed to 323 K: the CT band of the DMF-TCNE complex decayed slowly, while a new band appeared, extending from 350 to 500 nm. The new band has a vibrational structure which is essentially the same as that previously attributed to $TCNE^-$ which was chemically generated in acetonitrile.[15] The isosbestic point at 350 nm very probably indicates that ionic dissociation of the EDA complex proceeds quantitatively to give negative and positive ions, though no positive ions could be detected. Figure 2 shows similar results observed for the TCNE–DMSO system. An isosbestic point at 410 nm indicates the ionic dissociation of the DMSO-TCNE complex into ions. For this complex, the dissociation was found to be accelerated even by the analyzing light.

The growth of the absorption band of $TCNE^-$ was completely inhibited in the solution prepared in an open cell or in the presence of oxygen in a sealed cell, but an absorption band at about 300 nm was found to grow instead. This is clearly demonstrated in Fig. 3 for a solution of TCNE in DMSO under the pressure controlled to be 1×10^{-3} Torr, higher than that for the usual sample preparation. An isosbestic point at 340 nm indicates the quantitative transformation, in the presence of oxygen, of the EDA complex into another unidentified product. Although this transformation is as slow as the ionic dissociation observed in the absence of oxygen (see Fig. 2), the EDA complex does not dissociate into ions but is transformed exclusively into the unidentified product. Upon evacuating oxygen (or air), a survival fraction of the EDA complexes was found to start the dissociation into ions, but the unidentified product, once formed, was too stable to revert to the original complex.

ESR Studies. The formation of $TCNE^-$ in DMF or DMSO was evidenced also by the ESR method. The signal recorded from the solutions was exclusively due to the ESR spectrum of $TCNE^-$, which was essentially the same as that of $TCNE^-$ generated by reducing TCNE with alkali metal.[16,17] The spectrum

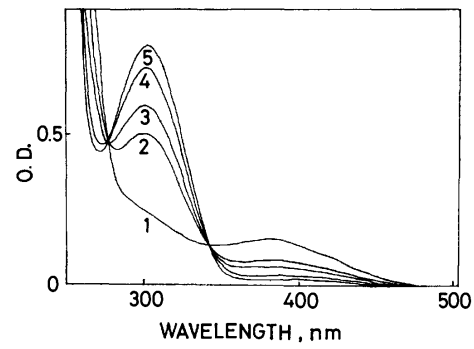

Fig. 3. Optical absorption spectra of unidentified product prepared by mixing TCNE (1.0×10^{-4} mol dm^{-3}) in DMSO under atmospheric pressure of 1×10^{-3} Torr and observed at 298 K (1) 5, (2) 35, (3) 60, (4) 100 and (5) 140 min after the mixing. Optical path: 0.2 cm.

consisted of 11 hyperfine lines equally spaced with a separation of 0.165 mT. Each hyperfine line was very narrow with a width, ΔH_{msl}, of 0.008 mT. The kinetical features of the formation of $TCNE^-$ were followed by observing the intensity of its spectrum at several temperatures. The advantage of ESR studies is that quantitative measurements can be readily made for $TCNE^-$ without any effect from light.

Figure 4 shows the formation of $TCNE^-$ in DMF. The $TCNE^-$ concentration increased slowly at a temperature-dependent rate and then tended to an asymptotic value, which was identical with the concentration of TCNE added in the solution. The observed time-concentration curves agreed well with a first order reaction, and the rate constant was independent of the concentration of TCNE. $TCNE^-$ was very stable in the dark and no decay was observed during a few weeks. Nor was any decay found even when the solution was exposed to air. The observed first order rate constant, k, is shown as a function of reciprocal temperature in Fig. 5, which gives a good Arrhenius relation with an activation energy of 79 kJ/mol and frequency factor of $10^{8.9}\,s^{-1}$.

The time-concentration curves for the formation of $TCNE^-$ in DMSO were already reported.[14] The observed kinetical features were essentially the same as those in DMF, except that the rate of the anion formation was larger in DMSO. The dashed curve in Fig. 6 shows the formation at 303 K under white light from a tungsten lamp, which is much quicker than that in the dark at the same temperature, as shown by a solid curve. It was found that even room light gives a large amount of $TCNE^-$ during the procedure of dissolving TCNE into DMSO. The activation energy and the frequency factor in DMSO in the dark were previously reported to be 59 kJ/mol and $10^{6.3}\,s^{-1}$,

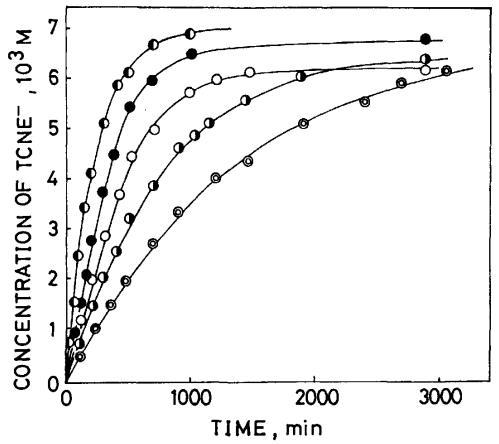

Fig. 4. Increase of the concentration at various temperatures of $TCNE^-$ formed from TCNE (7.0×10^{-3} mol dm^{-3}) mixed in DMF under vacuum determined by ESR. ◑, 318 K; ●, 313 K; ○, 308 K; ◑, 308 K; ◑, 303 K; ◎, 298 K.

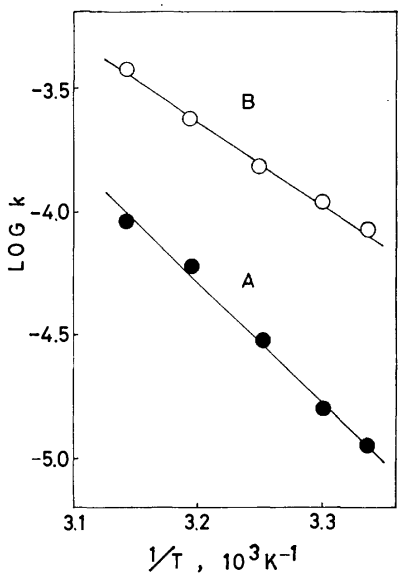

Fig. 5. Arrhenius plot of the first-order rate constant, k, for the formation of $TCNE^-$ (A) in DMF-TCNE, and (B) DMSO-TCNE systems in the dark determined by ESR.

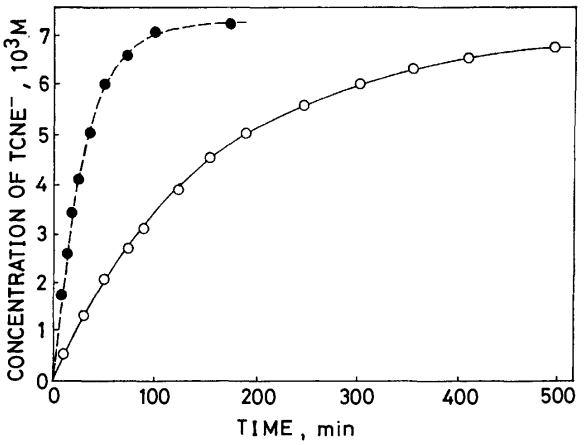

Fig. 6. Growth of the concentration of $TCNE^-$ formed from TCNE (7.0×10^{-3} mol dm^{-3}) in DMSO (solid line) in the dark and (dashed line) under light from an incandescent lamp both at 303 K determined by ESR.

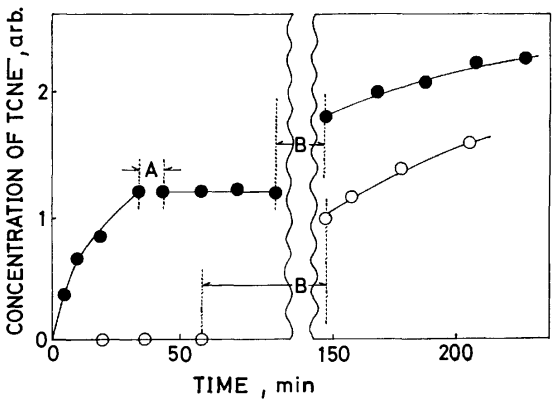

Fig. 7. Growth of the concentration of $TCNE^-$ ● in DMSO-TCNE prepared under vacuum and ○ in DMSO-TCNE prepared under 760 Torr of oxygen both at 303 K determined by ESR. A indicates the period of introducing 760 Torr of oxygen into the solution and B indicates the period of evacuating oxygen from the solution. The concentration of added TCNE was 7.0×10^{-3} mol dm^{-3}.

respectively.[14]

Figure 7 shows the effect of oxygen studied by ESR. When oxygen was introduced into the solution during ESR measurements, the formation of $TCNE^-$ became inhibited, as shown by closed circles. On re-evacuating the oxygen, the formation started again, but the formation rate was smaller than before. The solution prepared under 1 atm of oxygen gave no $TCNE^-$, but it was found to form when the dissolved oxygen was removed by evacuation, as shown by the open circles. These results indicate the physical quenching of the $TCNE^-$ formation and the chemical elimination of the precursor of the radical anion by the oxygen dissolved in the solution.

Discussion

Formation of EDA Complexes. CT bands have been studied for the EDA complexes between several electron donors and TCNE.[6,7,18,19] The molar extinction coefficient at the absorption maximum at 372 nm and the equilibrium constant were reported for the complex formation for the DMSO–TCNE system in carbon tetrachloride to be 973 $mol^{-1}\,dm^3\,cm^{-1}$ and 95.4 $dm^3\,mol^{-1}$, respectively, at 298 K. The CT band of the DMSO–TCNE complex was found in the present investigation to develop before starting the measurements of the absorption spectrum (see Fig. 2). Its absorption maximum lay at a slightly longer wavelength, 380 nm. The shift in wavelength is attributed to a larger dielectric constant for the present donor-solvent, DMSO, compared with that of carbon tetrachloride. Adopting the reported equilibrium constant, the uncomplexed fraction of TCNE is estimated to be as small as 7.5×10^{-4}. Thus, it is concluded that essentially all the TCNE becomes complexed with DMSO immediately after mixing the former into the latter. It should be noted that the present results, shown in Fig. 2, indicate an extinction coefficient of 7500 $mol^{-1}.\,dm^3\,cm^{-1}$ for the DMSO–TCNE complex (in DMSO solution), much larger than that reported previously. This large extinction coefficient is substantiated by the isosbestic point at 410 nm and the reported extinction coefficient of 6200 $mol^{-1}\,dm^3\,cm^{-1}$ at 407 nm for $TCNE^-$.[6] Nevertheless, the conclusion of complete complex formation is tenable, even if the equilibrium constant is presumed to be one-tenth as small as that reported. As a matter of fact the equilibrium constant was reported to be 83.5 $dm^3\,mol^{-1}$ for the DMA–TCNE complex,[7] which seems to be very similar in nature to the DMSO–TCNE complex.

Although the spectroscopic data have not been reported for the DMF–TCNE pair, DMF is a rather strong electron donor.[22] Therefore, all the TCNE may safely be assumed to form initially the complex with DMF. Assuming a complete complex formation, the molar extinction coefficient is estimated from spectral curve 1 in Fig. 1 for the DMF–TCNE complex to be 2900 $mol^{-1}\,dm^3\,cm^{-1}$ at 310 nm.

Ionic Dissociation of EDA Complex. The present optical absorption studies reveal the growth of an absorption band at 350—500 nm due to $TCNE^-$ simultaneously with the decay of the CT band due to the EDA complexes (see Figs. 1 and 2). The ESR observation (Figs. 4 and 6) also indicates the slow formation of $TCNE^-$. It is concluded that the DMF–TCNE and DMSO–TCNE complexes dissociate into ions in the dark. It should be emphasized that the formation of $TCNE^-$ occurs after the completion of complex formation between TCNE and solvent. The observation of an isosbestic point appeared in the optical absorption studies and the asymptotic value of the $TCNE^-$ concentration indicate that the complexes dissociate quantitatively into ions.

The radical cation of DMSO and also that of DMF should be formed simultaneously with the $TCNE^-$ formation, but no cationic species could be detected either by the optical absorption measurements or by the ESR technique, as reported previously.[6–8,10–14] Absence of an ESR spectrum due to $DMSO^+$ has been interpreted as due to a rapid spin exchange between $DMSO^+$ and the remaining DMSO.[6] However, such an interpretation seems highly inconceivable, because it turns out that such a rapid exchanging spin (positive hole) has a lifetime as long as that of $TCNE^-$, which was found to be more than several weeks in the present investigation. $DMSO^+$ might be transformed readily into a stable diamagnetic cation, which no longer reacts with $TCNE^-$ and causes the stability of $TCNE^-$, as suggested by Achiba and Kimura for 2-methyltetrahydrofuran–TCNE system.[20] Both acceptor radical anion and donor radical cation were observed by ESR for 2,3-dichloro-5,6-dicyano-*p*-benzoquinone and *p*-phenylendiamine and *N,N,N',N'*-tetramethyl-*p*-phenylenediamine in acetonitrile.[21]

The formation of $TCNE^-$ in DMSO and DMA in the dark was studied previously by ESR, but the observed kinetical features differ from those in the present investigation. Stewart *et al.* reported that the formation is completed promptly before starting the measurements (within a few minutes).[6,7] Keys and Carper observed that, in addition to the prompt development of the ESR spectrum of $TCNE^-$, its intensity still increases slowly to an asymptotic value, though they gave no interpretation for the difference between these two modes of the formation of $TCNE^-$.[8] The present investigation indicates no prompt formation of $TCNE^-$. Taking account of the striking effect of light in accelerating the $TCNE^-$ formation (see Fig. 6), the prompt formation reported previously seems to result from this light effect.

On the basis of the observed total participation of TCNE in the EDA complexes and the subsequent exponential growth of the concentration of $TCNE^-$, the formation of $TCNE^-$ is attributed simply to dissociation of the complexes into ions. The apparent activation energy was found to be as large as 0.82 eV (79 kJ/mol) and 0.61 eV (59 kJ/mol) for the dissociation of the DMF–TCNE and the DMSO–TCNE complexes, respectively. As far as we know, this is the first example where the thermal ionic dissociation of EDA complex has been evidenced and its rate constant determined. Recently, Farrell and Ngô studied the spontaneous formation of $TCNE^-$ in *N,N*-dimethylaniline–TCNE system and found it apparently slow.[23]

However, they interpreted this slow formation by assuming the competition between an essentially fast formation of $TCNE^-$ and its fast disappearance. The ionic dissociation of EDA complex in the dark is really a slow process, at least in the DMF-TCNE and DMSO-TCNE systems.

Effect of Dissolved Oxygen. Stewart *et al.* observed the slow decay of the ESR signal of $TCNE^-$ by a second-order process and explained it by a recombination of ions.[6,7] Later, Keys and Carper found that careful exclusion of oxygen affects the ESR signal and that it persists for a period as long as a month in the dark. They also observed that introduction of oxygen kills the signal.[8] However, the present observations indicate that $TCNE^-$ is stable either in the absence or in the presence of oxygen, if it is once generated. The reason is not known for the difference in the observed stability of $TCNE^-$ when oxygen is introduced.

An important finding here is the reversible inhibition of the ionic dissociation of the complexes by the introduction of oxygen. Figure 3 indicates that the DMSO-TCNE complex is transformed by a trace of oxygen into another species giving an absorption band at about 300 nm, which is not identified but presumed to be a ternary complex of DMSO, TCNE, and oxygen. Although this unidentified species develops as slowly as the $TCNE^-$ formation in the absence of oxygen, the latter does not proceed at all in the presence of oxygen. This indicates that dissolved oxygen not only chemically reacts with the DMSO-TCNE complex but also physically quenches the precursor of $TCNE^-$. The formation of $TCNE^-$ on re-evacuation, shown in Fig. 7, also indicates the quenching of the precursor by oxygen in the closed cell.

Assuming that oxygen at low pressure (10^{-3} Torr) is totally dissolved in the solution, the concentration of oxygen is roughly estimated to be 10^{-6} mol dm^{-3}. If one further assumes that the quenching is a diffusion-controlled process with a rate constant of 10^{10} mol^{-1}. dm^3 s^{-1}, the lifetime of the precursor is estimated to be as long as 10^{-4} s or more. The efficient quenching by a trace of oxygen supports the view that the thermal ionic dissociation of the complexes occurs through their lowest triplet state. It would be inconceivable that there exists any long-lived transient intermediate other than the triplet state complex, which is thermally accessible, is quenched by oxygen, and acts as a precursor of $TCNE^-$.

Based on the kinetic features of formation and decay of $TCNE^-$, Ilten and Calvin proposed a molecular mechanism for the photoinduced ionic dissociation of the THF-TCNE complex, where $TCNE^-$ results from a long-lived triplet state of the complex populated by intersystem crossing from a photoexcited singlet state.[12] Later, the involvement of the triplet state has been reported for the photoinduced ionic dissociation of other EDA complexes as well.[13,24-26] Stewart *et al.* proposed a similar triplet state mechanism for the formation of $TCNE^-$ in the dark from DMSO-TCNE and DMA-TCNE pairs, on the basis of experimental observations different from those in the present investigation.[6-8] They assumed that the high enthalpy of complex formation leads to an appreciably populated triplet state of the complexes, during complex formation, from which the ionic dissociation occurs. In contrast, the present investigation reveals that the triplet state is populated by a slow thermal process long after the complex formation.

In conclusion, we can formulate the simplified reaction scheme for the thermal ionic dissociation of the DMF-TCNE and DMSO-TCNE complexes as

$$\mathrm{D.A} \underset{k_{-1}}{\overset{k_1}{\rightleftharpoons}} {}^3(\mathrm{D.A})^* \xrightarrow{k_2} \mathrm{D}^+ + \mathrm{A}^-, \qquad (1)$$

on the basis of the present observation, where D and A denote the electron donor (DMF or DMSO) and the acceptor (TCNE), respectively. Naturally k_1 is much smaller than k_{-1}. If $k_{-1} \ll k_2$, the observed first-order rate constant, k, for the formation of acceptor anion is given by k_1 and the thermal activation to ^{3}(D. A)* is the rate-determinant step of the anion formation. The observed activation energy (see Fig. 5) corresponds to the energy separation between ^{3}(D. A)* and D. A. If $k_{-1} \gg k_2$ on the other hand, k is given by k_1k_2/k_{-1}, and the rate-determinant step is the dissociation of ^{3}(D. A)*. In this case, the activation energy seems to give the upper limit of the energy separation. The most crucial question which might arise about the triplet state of the EDA complexes is whether it lies so low as to be populated thermally. Unfortunately, there appear to be no results, either experimental or theoretical, in the literature which could answer this question, and there is an obvious need for data (in particular energy and lifetime) on ^{3}(D. A)* to substantiate the above reaction scheme.

References

1) H. Kainer and A. Uberle, *Chem. Ber.*, **88**, 1147 (1955).
2) See for example, R. Foster, "Molecular Association I," Academic Press, London (1975).
3) M. Ottolenghi, *Acc. Chem. Res.*, **6**, 153 (1972).
4) J. W. Eastman, G. Engelsma, and M. Calvin, *J. Am. Chem. Soc.*, **84**, 1339 (1962).
5) I. Isenberg and S. L. Baird, Jr., *J. Am. Chem. Soc.*, **84**, 3803 (1962).
6) F. E. Stewart, M. Eisner, and W. R. Carper, *J. Chem. Phys.*, **44**, 2866 (1966).
7) F. E. Stewart and M. Eisner, *Mol. Phys.*, **12**, 173 (1967).
8) R. T. Keys and W. R. Carper, *J. Chem. Phys.*, **47**, 3682 (1967).
9) T. Yamaoka and S. Nagakura, *Bull. Chem. Soc. Jpn.*, **44**, 1780 (1971).
10) M. Sofue and S. Nagakura, *Bull. Chem. Soc. Jpn.*, **38**, 1048 (1965).
11) R. L. Ward, *J. Chem. Phys.*, **39**, 852 (1963).
12) D. F. Ilten and M. Calvin, *J. Chem. Phys.*, **42**, 3760 (1965).
13) Y. Achiba, S. Katsumata, and K. Kimura, *Bull. Chem. Soc. Jpn.*, **45**, 1272 (1972); *Chem. Phys. Lett.*, **13**, 213 (1972).
14) N. Kushibiki and H. Yoshida, *J. Am. Chem. Soc.*, **98**, 268 (1976).
15) O. W. Webster, W. Mahles, and R. E. Benson, *J. Am. Chem. Soc.*, **84**, 3678 (1962).
16) W. D. Phillips, J. C. Rowel, and S. I. Weissman, *J. Chem. Phys.*, **33**, 626 (1960).

17) M. Ogasawara, H. Yoshida, and K. Hayashi, *Bull. Chem. Soc. Jpn.*, **47**, 1611 (1974).
18) R. E. Merrifield and W. D. Phillips, *J. Am. Chem. Soc.*, **80**, 2778 (1958).
19) R. Vars, L. A. Tripp, and L. W. Pickett, *J. Phys. Chem.*, **66**, 1754 (1962).
20) Y. Achiba and K. Kimura, *Chem. Phys. Lett.*, **39**, 515 (1976).
21) N. H. Kolodny and K. W. Bowers, *J. Am. Chem. Soc.*, **94**, 1113 (1972).
22) R. S. Drago, B. Wayland, and R. L. Carlson, *J. Am. Chem. Soc.*, **85**, 3125 (1963).
23) P. G. Farrell and P. N. Ngô, *J. Chem. Soc. Perkin Trans. 2*, **1974**, 552.
24) R. Potashnik, C. R. Goldschmidt, and M. Ottolenghi, *J. Phys. Chem.*, **73**, 3170 (1969).
25) M. Irie, H. Masuhara, K. Hayashi, and N. Mataga, *J. Phys. Chem.*, **78**, 341 (1974).
26) M. Shimada, H. Masuhara, and N. Mataga, *Bull. Chem. Soc. Jpn.*, **46**, 1903 (1973).

Oxidation Activity and Acid-base Properties of Mixed Oxide Catalysts Containing Titania. II. The TiO_2–V_2O_5–P_2O_5 System

Mamoru Ai

Research Laboratory of Resources Utilization, Tokyo Institute of Technology, Ookayama, Meguro-ku, Tokyo 152

(Received August 4, 1976)

The acidity and basicity of a series of TiO_2–V_2O_5–P_2O_5(atomic ratio Ti : V : P=9 : 1 : x)catalysts with different P_2O_5 contents (x=0—18), were measured by studying the adsorption of the basic and acidic molecules in the gas phase, using both the static and pulse methods. TiO_2–V_2O_5(V/Ti=1/9) is rather basic, but this catalyst can be modified from basic to acidic by the introduction of P_2O_5. The vapor-phase oxidation of butadiene and 1-butene, which were chosen as electron-donor-type reactants, and that of acetic acid, as an acidic reactant, were carried out in the presence of an excess of air, and then the relationship between the catalytic behavior and the acid-base properties was investigated. The results support an earlier proposal that the activity and selectivity in mild oxidation can be interpreted in terms of the acid-base properties of the catalyst and the reactant.

TiO_2 is an amphoteric oxide and its acid-base properties are significantly modified by the introduction of a small quantity of additive.[1,2] The acidic sites and electron donating sites of TiO_2 and their variation with pretreatment or in combination with several oxides have also been studied, in connection with active sites for the isomerization of butene, by Tanabe *et al.*[3-5]

In a preceding report,[6] the acid-base properties of TiO_2–V_2O_5 and TiO_2–MoO_3 binary systems and their correlation with oxidation activities were studied. It was found that the basic character of the systems is greatly enhanced by the addition of a small amount of such acidic elements as MoO_3 and V_2O_5 to TiO_2 and, therefore, the binary systems are sufficiently basic at Mo<20 or V<10 atom%. On the other hand, it has been reported that (1) the addition of P_2O_5 to TiO_2 sharply increases the acidity,[1] unlike the case in which P_2O_5 is added to SnO_2,[7] and that (2) TiO_2–P_2O_5 catalysts containing a large amount of P_2O_5 are highly acidic and are active as polymerization catalysts.[8]

This evidence led to the prediction that the acid-base character of TiO_2-containing mixed oxide catalysts can be modified by controlling the amounts of either the V_2O_5 or the P_2O_5 added.

The present paper is the second part of an investigation of the oxidation activity of the TiO_2-based catalysts. An attempt was made to ascertain how the addition of various amounts of P_2O_5 to TiO_2–V_2O_5 (amount ratio V/Ti=1/9) modifies the acid-base properties and how these properties are correlated with the oxidation activity and selectivity.

Experimental

Catalysts. The catalysts used in this study were of the TiO_2–V_2O_5–P_2O_5 series (atomic ratio Ti : V : P=9 : 1 : x), with eight different amounts of P_2O_5 (x=0—18). They were prepared by the procedures described in a preceding report.[6]

Procedures. The acidity of the TiO_2–V_2O_5–P_2O_5 catalysts were determined both by the amount of NH_3 irreversibly adsorbed (static method) and by that of the pyridine required to completely poison the isomerization activity for 1-butene (pulse method). The basicity was determined by the amount of CO_2 irreversibly adsorbed, using the static method. The technique used in these measurements has also been described earlier.[6,7,9]

The vapor-phase oxidation of 1-butene, 1,3-butadiene, and acetic acid and the isomerization of 1-butene were carried out in the presence of an excess of air, in an ordinary continuous-flow-type reaction system. The reactor and the experimental procedures were the same as those employed previously.[1,6,7,9]

Results

Surface Areas. The surface areas of the TiO_2–V_2O_5–P_2O_5 catalysts were checked by the BET method using nitrogen at −196 °C. The results are shown in Table 1. The surface area increases gradually for an increase in the P_2O_5 content (x), but decreases when the P_2O_5 content becomes too high (x=18).

Acidity. The acidity per unit surface area of the TiO_2–V_2O_5–P_2O_5 catalysts, as determined by the amounts of NH_3 irreversibly adsorbed at 20, 200, and 250 °C, are plotted in Fig.1 as a function of the P_2O_5 content (x). These results indicate that the P_2O_5-poor catalysts have a fair amount of acidic sites of weak acid strength, as has been pointed out in a previous paper.[6] The acidity obtained by the amount of pyridine required to completely poison the isomerization activity for 1-butene at 160 °C is also plotted in Fig. 2. Parallels were found between the amounts of NH_3 obtained by means of the static method and those of pyridine obtained by means of the pulse method, which proves the validity of these results.

It is found, as was expected, that the acidity of TiO_2–V_2O_5–P_2O_5 catalysts increases for an increase in the P_2O_5 content.

Basicity. The basicity per unit surface area of the TiO_2–V_2O_5–P_2O_5 catalysts, as determined by the amount of CO_2 irreversibly adsorbed at 20 °C, is plotted in Fig. 3 as a function of the P_2O_5 content (x). It is also demonstrated that the basicity of the catalysts

Table 1. Surface area of the TiO_2–V_2O_5–P_2O_5 (atomic ratio Ti : V : P=9 : 1 : x) catalysts used

P_2O_5 content x	Surface area (m^2/g)	P_2O_5 content x	Surface area (m^2/g)
0	23.8	2.0	39.1
0.2	24.0	4.0	42.4
0.5	35.0	9.0	46.2
1.0	37.3	18.0	25.3

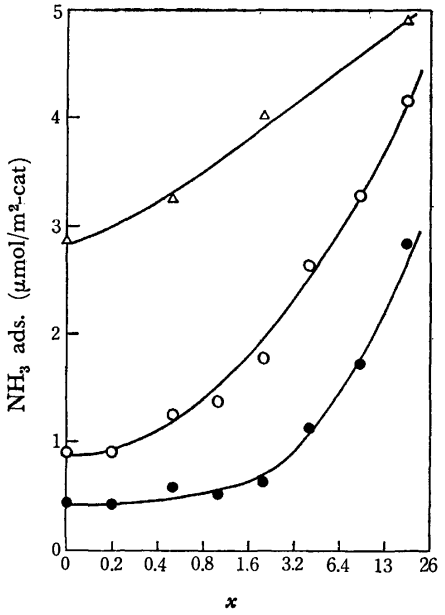

Fig. 1. Acidity of TiO_2-V_2O_5-P_2O_5 (9 : 1 : x) as a function of the P_2O_5 content (x). I. Irreversible adsorption of NH_3 at 20 °C: △, at 200 °C: ○, at 250 °C: ●.

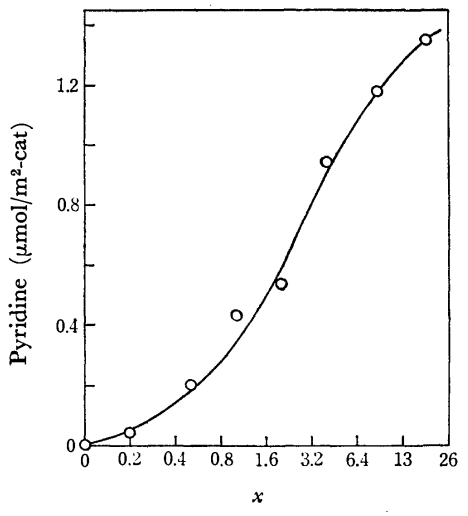

Fig. 2. Acidity of TiO_2-V_2O_5-P_2O_5 (9 : 1 : x) as a function of the P_2O_5 content (x). II. Pyridine required to poison the isomerization activity for 1-butene at 160 °C (pulse method).

gradually decreases for an increase in the P_2O_5 content.

Isomerization Activity for Butene. The relationship between the catalytic activity for isomerization and the acid-base properties was investigated. The reaction was carried out at 0.67 mol% 1-butene in air and at 250 °C by changing the catalyst amounts in the range of 1.0 to 10 g. As a measure of the isomerization activity, the ratio of (*cis*-2-butene+*trans*-2-butene)/(1-butene+*cis*-2-butene+*trans*-2-butene) corresponding to 1 m² of the catalyst, I, was adopted, much as in the cases reported previously.[6,7,9]

The results are plotted in Fig. 4 as a function of the acidity of the catalyst, *i. e.*, the amount of pyridine required to poison the isomerization activity. A rough-

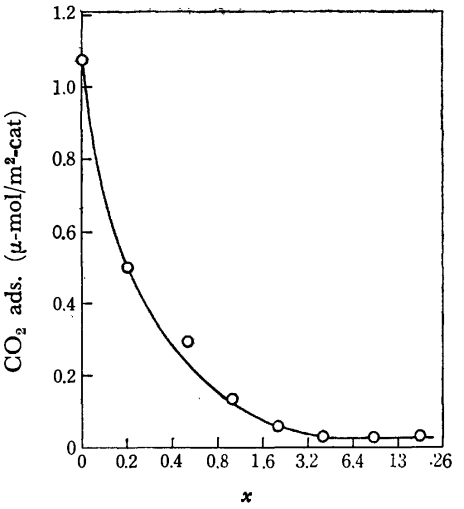

Fig. 3. Basicity of TiO_2-V_2O_5-P_2O_5 (9 : 1 : x) as a function of the P_2O_5 content (x). Irreversible adsorption of CO_2 at 20 °C.

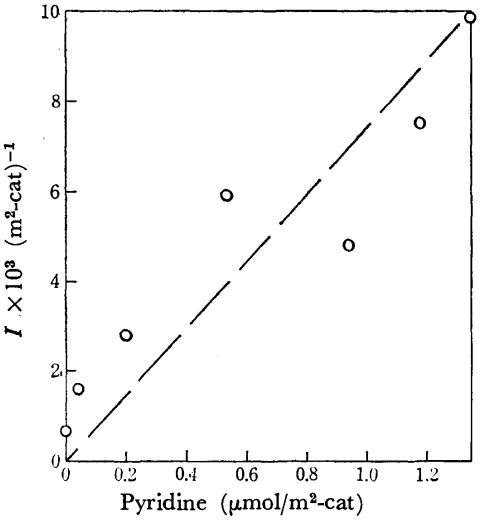

Fig. 4. Relation between the isomerization activity for 1-butene (I) and the acidity (amount of pyridine required to poison the isomerization of 1-butene). I=(*cis*-2-C_4H_8 + *trans*-2-C_4H_8)/(1-C_4H_8 + *cis*-2-C_4H_8 + *trans*-2-C_4H_8) corresponding to 1 m² of the catalyst, T=250 °C, 1-C_4H_8=0.67 mol% in air.

ly proportional relationship was obtained between the isomerization activity and acidity.

Oxidation Activity for Olefin. Butadiene was chosen as an electron-donor-type (basic) reactant and was oxidized in an excess of air (0.67 mol% of butadiene in air) by changing the amounts of the catalyst from 3 to 20 g. The initial rate of the overall consumption of butadiene at 295 °C, r_B (mol/h m²-cat), was adopted as a measure of the oxidation activity, much as in the cases reported previouly.[6,7,9] This is plotted in Fig. 5 as a function of the P_2O_5 content (x).

The activity first increases with the P_2O_5 content, reaches a maximum at about x=0.4, and then decreases again to a very low value.

Oxidation Activity for an Acidic Compound. Acetic acid was chosen as the acidic reactant, and it was oxidized in an excess of air (1.5 mol% of acetic acid

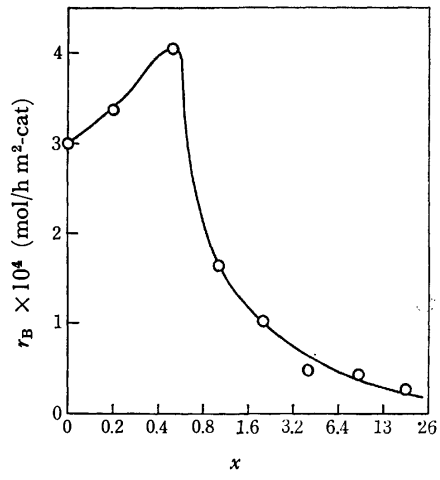

Fig. 5. The oxidation activity for butadiene (r_B) as a function of the P_2O_5 content (x).
Butadiene=0.67 mol% in air, T=295 °C.

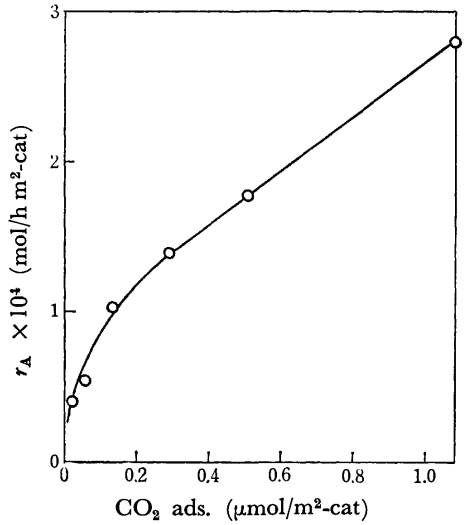

Fig. 6. Relation between the oxidation activity for acetic acid (r_A) and the basicity (amount of CO_2 irreversibly adsorbed).
Acetic acid=1.5 mol% in air, T=325 °C.

in air). The initial rate of oxidation to CO_2 at 325 °C, r_A (mol/h m^2-cat), was adopted as a measure of the oxidation activity. It is plotted in Fig. 6 as a function of the basicity of the catalyst, *i. e.*, the amount of CO_2 irreversibly adsorebed. The activity steadily increases with an increase in the basicity of the catalyst.

Selectivity in the Oxidation of an Olefin. The partial oxidation reactions are divided into two types in terms of the acid-base properties of the products:[1,6,7,9,10]

Type 1: Basic reactant→acidic product
Type 2: Basic reactant→basic product

Both the selectivity of butadiene to maleic anhydride at 40—50% conversion and that of 1-butene to butadiene at 30—40% conversion, which were chosen as model reactions of Types 1 and 2, respectively, are plotted in Fig. 7 as a function of the P_2O_5 content (x).

The results indicate that the "base-formation" reaction is favored by a rather basic catalyst and that the "acid-formation" reaction is favored by an acidic catalyst, as expected on the basis of earlier studies.[1,6,7,9,10]

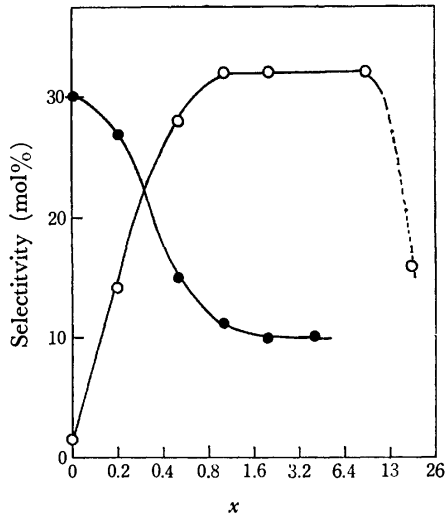

Fig. 7. Selectivity as a function of the P_2O_5 content (x).
○: Selectivity of butadiene to maleic anhydride, ●: selectivity of 1-butene to butadiene.

Discussion

Generally speaking, to be active in oxidation reactions, a catalyst must participate in the following two processes:

(1) activation of reactant molecules, and
(2) activation of oxygen.

When a catalyst is potent in the activation of oxygen, *i. e.*, has an oxidizing power which depends on two factors: (a) the number of oxidizing sites, and (b) the mobility of oxygen at a site, the oxidation reaction takes place without requiring activation of the reactant, therefore, the catalytic activity is controlled only by the activation of oxygen and the reaction proceeds non-selectively toward CO_2 and H_2O. This is the case of deep oxidation over such metal oxides as NiO, Co_3O_4, Cr_2O_3, MnO_2, and CuO. On the other hand, when the oxidizing power of a catalyst is not so strong, the reaction requires activation of the reactant as well as of oxygen, and, therefore, the difference in the mode or degree of this reactant-activation brings about the selectivity of the catalyst. Thus, it can be said that a requirement for an effective catalyst for any selective oxidation is a "moderate" oxidizing power, as has been pointed out by Sachtler *et al.*[11]

In studies on selective oxidations, many attempts have been made to disclose the active component in mixed oxide catalysts and to interpret the catalytic behaviors in connection with a particular structure (including electronic structure) of the metal oxides, as has been reviewed.[12]

Recently, the present author has proposed, from a different point of view, that it is the acid-base properties of the catalyst as well as the oxygen mobility which are directly responsible for the catalytic actions, although a change in the structure may naturally cause a change in these properties.[6,7,9,10] The acidic sites,

probably consisting of metal ions with a particularly high electron affinity, play a role in electron transfer from the reactant of the sites, resulting in the formation of a cationic intermediate and a reduced metal ion,[13] *i. e.*, the acidic sites contribute to the activation of the reactant. On the other hand, the basic sites, owing to their ability to donate electron to oxygen, contribute to adsorb and activate the gaseous oxygen and also to reoxidize the reduced metal ions, that is, the basic sites are connected with the oxidizing sites, probably consisting of lattice oxygen, O^{2-}.[9,10] Explanations of the role of each component in the catalytic action of such binary oxide systems as Cu–Sb,[14] Bi–Mo,[13,15] and others[16,17] appear to be based essentially on the same notion as that stated above, although the structure and generation of acidic and basic sites cannot be explained at present.

Let us now discuss the experimental results from this viewpoint. TiO_2–V_2O_5 (V/Ti=1/9) is rather basic, although it has a fair amount of acidic sites of weak acid strength. The addition of P_2O_5 to TiO_2–V_2O_5 gradually decreases the basicity and increases the acidity. Therefore, the ternary system containing a large amount of P_2O_5 is highly acidic but scarcely basic.

The oxidation activity for basic compounds, such as butadiene, is maximum at x=about 0.4 and is not correlated with the acidity of the catalyst, unlike MoO_3- or V_2O_5-based catalysts.[6,7,9,10] These results can be interpreted as follows. When the P_2O_5 content is low and the basic sites which are connected with the oxidizing sites, are sufficiently numerous, the oxidation activity is dependent mainly on the activation of the basic reactant (olefin) over the acidic sites. However, when, the P_2O_5 content is high and the oxidizing sites are strongly extinguished by the P_2O_5, the oxidation activity is then limited by the activation of oxygen but not by that of the reactant. It should be noted that the TiO_2–P_2O_5 system containing a large amount of P_2O_5 is inactive as an oxidation catalyst, due to the lack of oxidizing power, though it is highly acidic.[18] The same phenomenon was observed in the case of WO_3–P_2O_5–X_nO_m (X_nO_m=different metal oxides) catalysts, where the high oxidizing power of NiO, Co_3O_4, and MnO_2 is completely extinguished by WO_3–P_2O_5.[19]

On the other hand, in the case of the oxidation of an acidic compound, such as acetic acid, the activation of the reactant as well as of oxygen takes place on the basic sites, owing to the electron-donating ability to the electron-acceptor-type compounds, acetic acid and oxygen.[9,10] This view is consistent with the experimental results shown in Fig. 6.

As regards the selectivity, the results obtained from the TiO_2–V_2O_5–P_2O_5 system also support an earlier proposal that a requirement for an effective catalyst in "acid-formation" reactions is an acidic character and that a requirement for a catalyst to be effective in "base-formation" reactions is a moderate character both as an acid and a base.[1,6,7,9,10]

Conclusion

The character of the TiO_2–V_2O_5–P_2O_5 ternary catalysts can be modified from basic to acidic by controlling the P_2O_5 content.

The catalytic behavior of the TiO_2–V_2O_5–P_2O_5 system supports an earlier proposal that the activity and selectivity in mild oxidations can be interpreted in terms of the acid-base properties of the catalyst and the reactant. The acidic sites contribute to the activation of electron-donor-type reactants, while the basic sites are connected with the oxidizing sites and they also contribute to the activation of acidic reactants.

References

1) M. Ai and S. Suzuki, *Shokubai*, **15**, 159 (1973).
2) S. Okazaki and A. Kurosaki, Preprint of 37th Shokubai (Catalyst) Meeting (Fukuoka) (1975), p. 14.
3) M. Itoh, H. Hattori, and K. Tanabe, *J. Catal.*, **35**, 225 (1974).
4) H. Hattori, M. Itoh, and K. Tanabe, *J. Catal.*, **38**, 172 (1975).
5) K. Morishige, H. Hattori, and K. Tanabe, *Shokubai*, **17**, 29 (1975).
6) M. Ai, *Bull. Chem. Soc. Jpn.*, **49**, 1328 (1976).
7) M. Ai, *J. Catal.*, **40**, 318, 327 (1975).
8) T. Kagiya, T. Sano, T. Shimizu, and K. Fukui, *Kogyo Kagaku Zasshi*, **66**, 1893 (1963).
9) M. Ai and T. Ikawa, *J. Catal.*, **40**, 203 (1975).
10) M. Ai, Preprint of 9th Sanka-hanno (Oxidation reaction) Meeting (Tokyo) (1975), p. 1: *Shokubai*, **18**, 17 (1976).
11) W. M. H. Sachtler and N. H. de Boer, *Proc. Intern. Congr. Catal. 3rd*, (Amsterdam, 1964), **I**, 252 (1965).
12) D. J. Hucknall, "Selective Oxidation of Hydrocarbons," Academic Press, London/New York (1974).
13) J. M. Peacock, M. J. Sharp, A. J. Parker, P. G. Ashmore, and J. A. Hockey, *J. Catal.*, **15**, 379 (1969).
14) N. Kominami, K. Shibata, and S. Minekawa, *Kogyo Kagaku Zasshi*, **65**, 1510 (1962).
15) I. Matsuura and G. C. A. Schuit, *J. Catal.*, **20**, 19 (1970).
16) T. G. Alkhazov, M. S. Belenky, and R. I. Alekseyeva, Reprints of papers Intern. Congr. Catal. 4th, **I**, 293 (1968).
17) M. Niwa and Y. Murakami, *J. Catal.*, **26**, 359 (1972).
18) M. Ai, Preprint of 37th Shokubai (Catalyst) Meeting (Fukuoka) (1975), p. 58.
19) M. Ai, Preprint of 39th Shokubai (Catalyst) Meeting (Sapporo), in press (1976).

Vibrational Spectra of Ethyleneurea and Its *C,C'*- and *N,N'*-Deuterated Derivatives

Yutaka SAITO and Katsunosuke MACHIDA

Faculty of Pharmaceutical Sciences, Kyoto University, Sakyo-ku, Kyoto 606

(Received August 28, 1976)

Infrared and Raman spectra of ethyleneurea and its *C,C'*- and *N,N'*-deuterated compounds have been measured. The fundamental frequencies have been assigned by referring to isotopic frequency shifts and Raman depolarization ratios. A normal coordinate analysis has been carried out for the infrared active vibrations of a planar C_{2v} molecular model. A Urey-Bradley potential function supplemented by valence type constants for the out-of-plane deformation and the torsional coordinates has been used. The calculated frequencies based on a refined set of force constants agree well with the observed.

As a part of our serial studies on the vibrational spectra and the force field of urea derivatives,[1,2] the present work has been undertaken to deal with the infrared and Raman spectra of ethyleneurea and its *C,C'*- and *N,N'*-deuterated derivatives. It has been known that the group vibrations of monosubstituted amides, R-CONH-R', are quite sensitive to the relative positions of the CO and the NH bonds.[3] The CN stretching and the NH in-plane deformation vibrations in the *trans* structure couple appreciably with each other, giving rise to the characteristic amide II and III frequencies, while those in the *cis* structure do not. An analogous coupling has been found for *N*-alkyl- and *N,N'*-dialkylureas which have at least one NH bond at the *trans* position of the CO bond.[4] In this respect, the behavior of the CN stretching and the NH in-plane deformation vibrations in the absence of the *trans* -CONH- structure in ethyleneurea is of interest as a clue to the correlation between the vibrational spectra and the structure of urea derivatives.

Experimental

Materials. Ethyleneurea (EU-d_0) was obtained from Tokyo Kasei Co. and was recrystallized twice from ethanol and then once from ethylacetate. For the preparation of the *C,C'*-deuterated ethyleneurea (EU-d_4), 1 ml of ethylene glycol-d_4 (Merck AG., 99%) was heated gradually with *ca.* 4 g of urea from 150 to 240 °C during 4 h.[5] The resulting resinous solid was pyrolized at 240—270 °C under reduced pressure, and EU-d_4 was distilled from the solid as it decomposed. The crystallization from ethylacetate gave *ca.* 0.21 g of EU-d_4. No indication of the re-exchange of deuterium by hydrogen in this process was detected in the infrared and the Raman spectra of this sample. The *N,N'*-undeuterated compounds were converted into the corresponding *N,N'*-deuterated compounds (EU-d_2 and EU-d_6) by the exchange reaction with heavy water.

Measurements. The infrared spectra were recorded on a JASCO IR-A2 grating infrared spectrophotometer (4000—400 cm^{-1}). The measurements were made for Nujol and hexachlorobutadiene mulls, and the observed absorption frequencies were calibrated with the standard absorptions of indene, polystyrene and ammonia. The Raman spectra were recorded on a JEOL S-1 laser Raman spectrophotometer by using the excitation line 488.0 nm of a Coherent 52G Ar^+ laser. The measurements were made for fine crystalline powder sealed in 1 mm capillary tubes, and the observed Raman frequencies were calibrated with the spontaneous emission lines of the Ar^+ laser. The depolarization measurements were made for the aqueous solutions of EU-d_0 and EU-d_4 and for the solutions of EU-d_2 and EU-d_6 in heavy water. The spectral slitwidth was 12.7 cm^{-1} for all the measurements.

The infrared spectra are shown in Figs. 1 and 2, and the Raman spectra in Figs. 3 and 4. The observed frequencies are listed in Table 1 together with approximate band intensities and assignments.

Vibrational Assignments

The crystal structure of ethyleneurea has not been determined to date. We may assume, however, that ethyleneurea takes the planar C_{2v} configuration in the crystal, since the X-ray analysis has shown that an analogous compound, ethylenethiourea, takes approximately this configuration.[6] On this assumption, EU-d_0 and its deuterated compounds should contain 30 normal vibrations which are classified as $10a_1+5a_2+6b_1+9b_2$.

In the infrared spectrum, the NH stretching band of EU-d_0 appears as a doublet but that of EU-d_4 does not. Contrarily, the ND stretching band splits for EU-d_6 but not for EU-d_2. This result indicates that the splittings observed for EU-d_0 and EU-d_6 can be attributed neither to the presence of two NH or ND bonds nor to the crystal field splitting but to anharmonic resonances. Possible candidates of the summation tones participating mainly in the weaker components of the doublets are $1423+2\times991$ (or $1376+991+1041$) ≈3415 cm^{-1} for EU-d_0 and $1243+1169\approx2415$ cm^{-1} for EU-d_6.

In the Raman spectra of EU-d_0 and EU-d_2 in aqueous solution, two strong and polarized bands appear at 3005 and 2908 cm^{-1}. These bands are attributed to the a_1 CH_2 stretching vibration and the overtone of the a_1 CH_2 bending vibration involved in a Fermi resonance. Similarly, aqueous solutions of EU-d_4 and EU-d_6 show two strong Raman bands at 2185 and 2145 cm^{-1} attributable to a resonance diad involving the a_1 CD_2 stretching vibration. The b_1 and the b_2 CH_2 stretching vibrations of EU-d_0 seem to g ve weak Raman bands at 2980 and 2915 cm^{-1}, respectively, observed only when the incident and the scattered lights are polarized perpendicularly to each other. These bands are hidden by the strong a_1 bands in the ordinary Raman spectrum.

The strong infrared band around 1660 cm^{-1} observed for EU-d_0 and EU-d_4 arises obviously from the C=O stretching vibration. The corresponding Raman band is polarized in the solution spectra as expected from the

Table 1. Observed frequencies (cm^{-1}) and assignments

IR	Raman			Assignments	IR	Raman			Assignments
Solid	Solid	Solution			Solid	Solid	Solution		
		EU-d_0					EU-d_2		
3285 s	3310 m	—		$\nu NH(a_1, b_2)$	3000 vw	—	3005 s	p	$2\times b_2\beta CH_2(A_1)$
3000 sh	—	3005 s	p	$2\times b_2\beta CH_2(A_1)$	—	—	2980 vw	dp	$\nu CH_2(b_1)$
—	—	2980 vw	dp	$\nu CH_2(b_1)$	2955 m	2972 m	—		$2\times a_1\beta CH_2(A_1)$
2960 m	2972 s	—		$2\times a_1\beta CH_2(A_1)$	—	—	2915 vw	dp	$\nu CH_2(b_2)$
—	—	2915 vw	dp	$\nu CH_2(b_2)$	2900 sh	2913 vs	2908 s	p	$\nu CH_2(a_1)$
2900 m	2913 s	2908 s	p	$\nu CH_2(a_1)$	2460 s	2487 w	—		$\nu ND(a_1, b_2)$
1668 vs	1662 m	1665 w	p	$\nu CO+\nu CN(a_1)$	1652 vs	1647 m	1645 m	p	$\nu CO+\nu CN(a_1)$
1502 s	1522 m	—		$\beta CH_2(b_2)$	1502 s	1522 m	—		$\beta CH_2(b_2)$
1485 m	1493 w	1495 vw		$\beta CH_2(a_1)$	1485 m	1494 m	1498 m	p	$\beta CH_2(a_1)$
1451 s	1450 vw	—		$\nu CN(b_2)$	1445 s	1438 w	1445 w	dp	$\nu CN(b_2)$
1423 m	—	1420 sh		$\delta NH(b_2)$	1274 vs	1273 w	—		$\omega CH_2(b_2)$
—	1385 w	—		$\delta NH(a_1)$	1250 sh	—	—		$\omega CH_2+\delta ND(a_1)$
1274 vs	—	—		$\omega CH_2(b_2)$	1202 vw	1209 vw	1210 vw	p	$\omega CH_2(a_1)$, $tCH_2(b_1)$
1207 vw	1207 m	1215 w	dp	$\omega CH_2(a_1)$, $tCH_2(b_1)$	1178 m	1190 sh	—		$\delta ND+\nu C'N(b_2)$
1105 m	1112 w	1101 w	p	$\nu C'N(a_1)$	1017 vw	1025 m	1015 w	dp	$\nu C'C'+\nu C'N(a_1)$
1041 w	1045 m	—		$\nu C'N(b_2)$	925 vw	933 vs	939 vs	p	$\nu CN+\nu C'C'(a_1)$
991 vw	1000 s	1000 m	p	$\nu CN(a_1)$	897 vw	908 m	—		$\delta ND+\nu C'N(b_2)$, $\rho CH_2(b_1)$
933 vw	934 vs	934 vs	p	$\nu C'C'(a_1)$					
768 m	—	—		$\pi CO(b_1)$	850 vw	875 sh	—		$\delta ND+\nu C'C'(a_1)$
703 s	712 m	717 m	p	$\delta NCN+\nu C'N(a_1)$, $\pi NH+\tau CN(b_1)$	764 s	—	—		$\pi CO(b_1)$
					694 s	693 s	695 m	p	$\delta NCN+\nu C'N(a_1)$
660 sh	—	—		$\delta NC'C'+\delta CNC'(b_2)$	650 sh	—	—		$\delta NC'C'+\delta CNC'(b_2)$
511 m	502 w	—		$\delta CO(b_2)$	510 sh	—	—		$\pi ND+\tau CN(b_1)$
—	250 sh	230 vw	dp	$\tau CN+\pi NH(b_1)$	497 s	—	—		$\delta CO(b_2)$
					—	250 vw	230 w	dp	$\tau CN+\pi ND(b_1)$
		EU-d_4					EU-d_6		
3303 vs	3300 w	—		$\nu NH(a_1, b_2)$	2472 s	2513 w	—		$\nu ND(a_1, b_2)$
—	—	2250 w	dp	$\nu CD_2(b_1)$	—	—	2250 w	dp	$\nu CD_2(b_1)$
2215 w	2230 s	2185 m	p	$2\times b_2\omega CD_2(A_1)$	2213 m	2230 s	2185 m	p	$2\times b_2\beta CD_2(A_1)$
—	2140 vs	2145 s	p	$\nu CD_2(a_1)$	—	2143 m	2145 s	p	$\nu CD_2(a_1)$
2125 w	—	—		$\nu CD_2(b_2)$	2125 w	—	2135 vw	dp	$\nu CD_2(b_2)$
2090 sh	2100 vw	2120 sh	p	$2\times a_1\nu CN(A_1)$	2088 w	2098 m	2105 w	p	$2\times b_2\omega CD_2(A_1)$
1660 vs	1654 w	1665 w	p	$\nu CO+\nu CN(a_1)$	1637 vs	1636 m	1640 m	p	$\nu CO+\nu CN(a_1)$
1425 s	—	—		$\nu CN(b_2)$, $\delta NH(b_2)$	1410 vs	1420 vw	—		$\nu CN(b_2)$
1377 m	1376 m	1360 vw		$\delta NH(a_1)$	1243 m	1248 w	1242 m	p	$\delta ND+\nu C'N(a_1)$
1176 m	—	1175 vw		$\beta CD_2+\nu C'N(b_2)$	1169 m	1165 vw	1165 vw		$\nu C'N+\delta ND(b_2)$
1145 vw	1140 m	1130 w	p	$\beta CD_2(a_1)$	1134 vw	1130 m	1120 m	p	$\beta CD_2+\nu C'C'(a_1)$
1122 w	—	—		$\nu C'N+\nu C'C'(a_1)$	1098 m	1089 m	1087 m	dp	$\beta CD_2(b_2)$, $\nu C'N(a_1)$
1088 m	1082 sh	1090 sh	dp	$\omega CD_2(b_2)$	1051 m	—	—		$\omega CD_2(b_2)$
1053 w	1069 m	1070 m	p	$\nu CN(a_1)$	911 sh	928 s	928 vs	p	$\nu CN(a_1)$
924 m	928 vs	925 vs	p	$\nu C'C'+\nu CN(a_1)$	901 w	—	—		$tCD_2(b_1)$
901 w	—	—		$\omega CD_2(b_2)$, $tCD_2(b_1)$	850 vw	863 m	862 m	p	$\delta ND+\omega CD_2(a_1)$
785 sh	791 m	787 w	p	$\omega CD_2+\nu C'C'(a_1)$	830 w	840 m	835 sh	dp	$\omega CD_2+\delta ND(b_2)$
771 m	—	—		$\pi CO(b_1)$	—	786 m	778 w	p	$\omega CD_2+\nu C'C'(a_1)$
688 s	703 w	707 w	p	$\delta NCN+\nu C'N(a_1)$, $\pi NH+\tau CN(b_1)$	766 m	740 vw	—		$\pi CO(b_1)$
					689 m	687 s	690 s	p	$\delta NCN+\nu C'N(a_1)$
660 sh	—	—		$\rho CD_2(b_1)$	650 sh	—	—		$\rho CD_2(b_1)$
619 vw	595 vw	—		$\delta NC'C'+\delta CNC'(b_2)$	595 w	592 vw	—		$\delta NC'C'+\delta CNC'(b_2)$
503 m	490 vw	490 w		$\delta CO(b_2)$	505 sh	—	—		$\pi ND+\tau CN(b_1)$
—	225 vw	—		$\tau CN+\pi NH(b_1)$	491 s	475 vw	485 vw		$\delta CO(b_2)$
					—	225 sh	210 vw		$\tau CN+\pi ND(b_1)$

a) vs, very strong; s, strong; m, medium; w, weak; vw, very weak; sh, shoulder. b) p, polarized; dp, depolarized. c) ν, stretching; β, bending; ω, wagging; t, twisting; ρ, rocking; δ, in-plane deformation; π, out-of-plane deformation; τ, torsion.

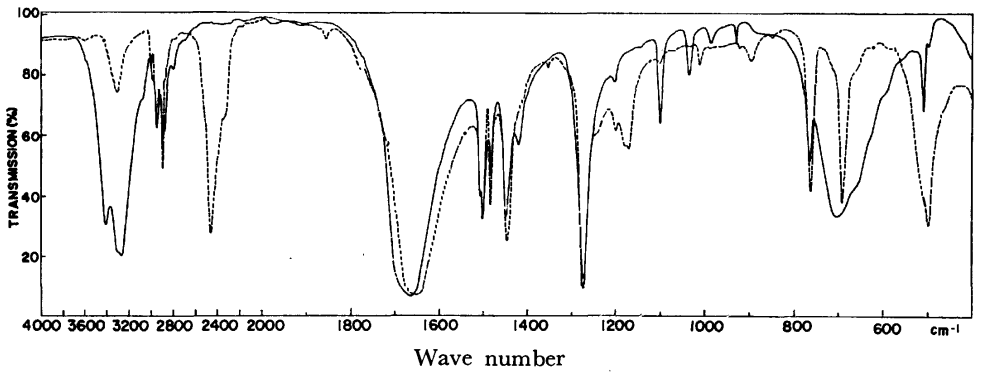

Fig. 1. Infrared spectra of EU-d_0 (——) and EU-d_2 (----).

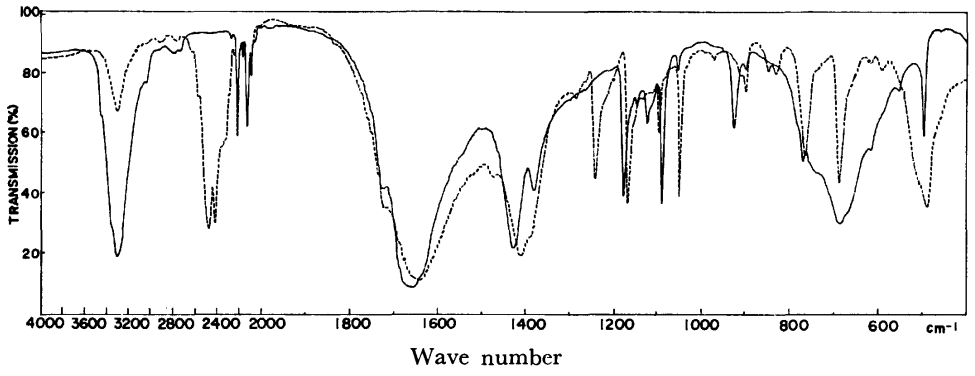

Fig. 2. Infrared spectra of EU-d_4 (——) and EU-d_6 (----).

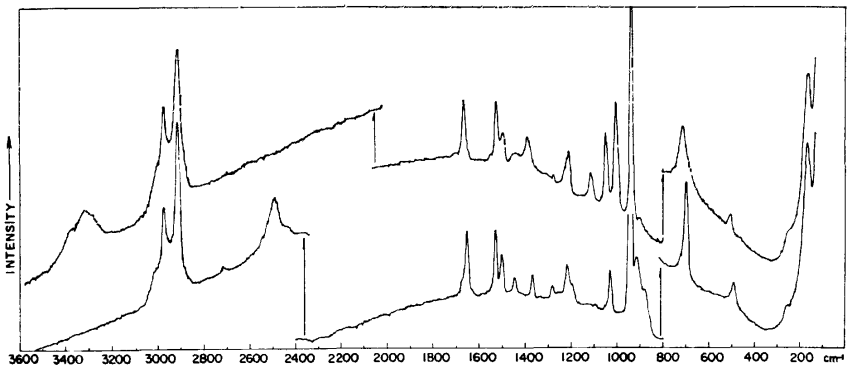

Fig. 3. Raman spectra of EU-d_0 (above) and EU-d_2 (below).

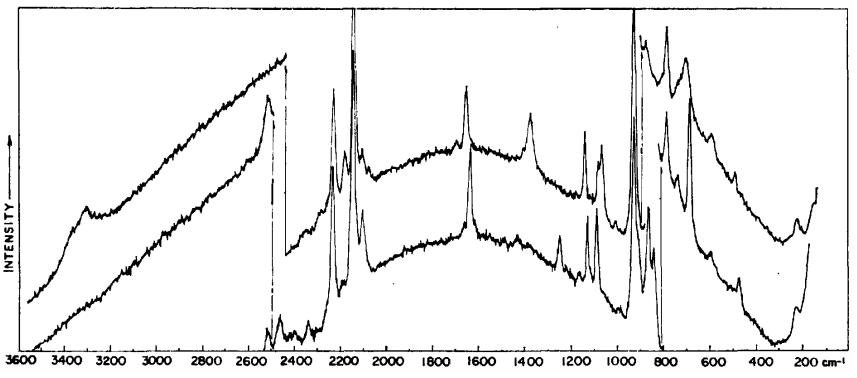

Fig. 4. Raman spectra of EU-d_4 (above) and EU-d_6 (below).

assignment. A slight low-frequency shift was observed for this band on the *N,N'*-deuteration, revealing a small coupling between the C=O stretching and the a_1 NH in-plane deformation vibrations.

In the infrared and Raman spectra of EU-d_0 and EU-d_2, the bands due to the CH_2 bending vibrations around 1500 cm^{-1} and those due to the CH_2 wagging vibrations around 1270 and 1200 cm^{-1} were easily assigned because they disappeared on the *C,C'*-deuteration. According to the normal coordinate analysis, the b_1 CH_2 twisting vibration may also contribute to the bands around 1200 cm^{-1}. The infrared and the Raman bands due to the CH_2 rocking vibrations of EU-d_0 and EU-d_2, and those due to the CD_2 bending, wagging, twisting and rocking vibrations of EU-d_4 and EU-d_6 were not obvious and we picked them up tentatively by referring to the calculated frequencies for the initial force constants.

In contrast to the cases of methylurea[2,7] and *N,N'*-dimethylurea,[8] EU-d_0 and EU-d_4 show no infrared bands in the region between 1550 and 1510 cm^{-1} where the amide II frequency is expected. Instead, EU-d_0 shows a strong infrared band at 1451 cm^{-1}, which persists on the *N,N'*-deuteration with a small low-frequency shift, and a weak band at 1423 cm^{-1} which disappears on the *N,N'*-deuteration. From analogy with urea[1,9] and *cis*-monosubstituted amides,[3,10] the 1451 cm^{-1} and the 1423 cm^{-1} bands are assigned to the CN stretching and the NH in-plane deformation vibrations, respectively, in the b_2 species. The a_1 NH in-plane deformation vibration is thought to give rise to the Raman band at 1385 cm^{-1}. For EU-d_4, the infrared absorptions due to the CN stretching and the NH in-plane deformation vibrations in the b_2 species seem to overlap at 1425 cm^{-1}, and the a_1 NH in-plane deformation band appears around 1377 cm^{-1} both in the infrared and the Raman spectra. For EU-d_2, and EU-d_6, the a_1 and the b_2 ND in-plane deformation vibrations are likely to contribute to the Raman band around 900 cm^{-1} and the infrared band around 1200 cm^{-1}, respectively. A weak Raman band was observed at 1360 cm^{-1} for EU-d_2 but was left unassigned since no fundamental frequencies were expected around this frequency.

In the infrared spectrum, EU-d_0 shows four bands at 1105, 1041, 991, and 933 cm^{-1} attributable to the skeletal stretching vibrations. From intensities and depolarization ratios of the corresponding Raman bands, the 1105, 991, and 933 cm^{-1} bands are assigned to the a_1 species and the 1041 cm^{-1} band to the b_2 species. Shifts of these bands on the *N,N'*- and the *C,C'*-deuterations suggest that the skeletal stretching vibrations couple complicatedly with the CD_2 and the ND deformation vibrations. Particularly, one of the a_1 skeletal stretching vibrations couples strongly with the a_1 ND in-plane deformation vibration, and gives rise to an infrared band around 1240 cm^{-1} for EU-d_2 and EU-d_6.

In the Raman spectrum between 800 and 400 cm^{-1}, EU-d_0 shows two bands at 712 and 502 cm^{-1} which persist on both the *N,N'*- and the *C,C'*-deuterations without large frequency shifts. Based on the depolarization ratio, the 712 cm^{-1} and the 502 cm^{-1} bands were assigned to skeletal vibrations in the a_1 and the b_2 species, respectively. In the infrared spectra, the corresponding bands around 700 cm^{-1} of EU-d_0 and EU-d_4 and around 500 cm^{-1} of EU-d_2 and EU-d_6 are markedly broadened and intensified by overlapping absorptions due to the NH and the ND out-of-plane deformation vibrations, respectively, in the b_1 species. EU-d_0 shows an infrared band at 768 cm^{-1} which is almost insensitive to both the *N,N'*- and the *C,C'*-deuterations and is assigned to the C=O out-of-plane deformation vibration. The weak Raman band at 250 cm^{-1} of EU-d_0 and EU-d_2 is depolarized in the solution spectra and shifts to 225 cm^{-1} on the *C,C'*-deuteration. This band is thus assigned reasonably to the b_1 skeletal torsional vibration. Throughout whole the investigated region of infrared and Raman spectra, no bands assignable to the a_2 species are observed for any of EU-d_0, EU-d_2, EU-d_4, and EU-d_6.

Table 2. Product and Sum rules

Product rule[a]		d_0/d_2	d_0/d_4	d_0/d_6
a_1	theor.	1.975	2.761	5.458
	obsd[b]	1.988	2.626	5.304
b_2	theor.	1.934	2.653	5.139
	obsd[b]	1.957	2.609	5.249
b_1	theor.	1.396	2.625	3.665
	obsd[b]	1.394[c]	2.683	3.678
Sum rule[d]		$\Delta\lambda(d_0-d_2)$	$\Delta\lambda(d_4-d_6)$	$\Delta\lambda(d_0-d_4)$	$\Delta\lambda(d_2-d_6)$
a_1[b]		3.443	3.434	3.290	3.294
b_2[b]		3.452	3.493	3.356	3.385
b_1[b]		0.150[c]	0.133		

a) $d_i/d_j=\Pi\nu(\text{EU-}d_i)/\Pi\nu(\text{EU-}d_j)$. b) The observed frequencies in Table 5 were used. c) The unobserved fundamental frequency in the b_1 species was replaced by the calculated frequency, 898 cm^{-1}. d) $\Delta\lambda(d_i-d_j)=10^{-5}\times4\pi^2c^2\{\sigma(\text{EU-}d_i)-\sigma(\text{EU-}d_j)\}/N$ (10^{-5} s^{-2}), where c is the velocity of light and N is the Avogadro number.

In order to check isotopic consistency in the assignment, the product rule[11] and the sum rule[12] were applied to the observed fundamental frequencies after correcting a few for anharmonic resonances. The results are given in Table 2. Denoting the sum of the squared frequencies of the isotope A over the species Γ by $\sigma(A, \Gamma)$, we may write the sum rule relations as

$$\sigma(\text{EU-}d_0, a_1) - \sigma(\text{EU-}d_2, a_1) = \sigma(\text{EU-}d_4, a_1) - \sigma(\text{EU-}d_6, a_1)$$

and similar expressions for the b_2 and the b_1 species. According to the modified sum rule for symmetrical isotopic molecules,[13] one more independent relation

$$\sigma(\text{EU-}d_0, a_1) - \sigma(\text{EU-}d_2, a_1) = \sigma(\text{EU-}d_0, b_2) - \sigma(\text{EU-}d_2, b_2)$$

holds provided that the force field includes no interaction terms between the two NH groups, and similarly we have

$$\sigma(\text{EU-}d_0, a_1) - \sigma(\text{EU-}d_4, a_1) = \sigma(\text{EU-}d_2, b_2) - \sigma(\text{EU-}d_6, b_2)$$

in the absence of interaction terms between the two

CH_2 groups. In support of the assignments, all these relations are satisfied fairly well by the observed frequencies.

Normal Coordinate Analysis

Based on the assumed symmetry of the point group C_{2v}, the G matrices were set up by using structure parameters transferred from the crystallographic data for urea[14] and ethylenethiourea,[6] the former being referred to only with respect to the C=O bond-length. They are shown in Fig. 5. The tetrahedral redundancy around each CH_2 group was eliminated analytically by introducing an orthogonal set of local symmetry coordinates.[15] The out-of-plane vibrations of the -NHCONH- group were described by the NH and the CO out-of-plane deformation coordinates and the internal rotation coordinates[16] around the C-N and the N-C′ bonds (Table 3). The redundant coordinates associated with the ring (2 in a_1, 1 in b_2 and 2 in b_1) were eliminated numerically on diagonalizing the G matrices.[17]

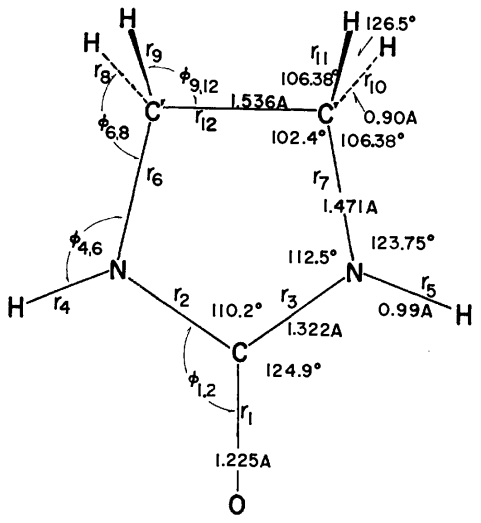

Fig. 5. Structural parameters and internal coordinates.

TABLE 3. OUT-OF-PLANE INTERNAL COORDINATES OF THE -NHCONH- GROUP

Coordinate	description[a]
$S_1=\Delta\pi_1$[b]	πCO
$S_2=\Delta\pi_4$[b]	πNH
$S_3=\Delta(\tau_{124}+\tau_{126}+\tau_{324}+\tau_{326})/4$	τCN
$S_4=\Delta\sum_{j=8,9,12}(\tau_{46j}+\tau_{26j})/6$	τNC′
$S_5=\Delta\pi_5$[b]	πNH
$S_6=\Delta(\tau_{135}+\tau_{137}+\tau_{235}+\tau_{237})/4$	τCN
$S_7=\Delta\sum_{j=10-12}(\tau_{57j}+\tau_{37j})/6$	τNC′

a) See footnote c), Table 1. b) The out-of-plane deformation coordinates were defined to be positive when the end atoms (O for S_1 and H for S_2 and S_5) move toward the observer from the plane of Fig. 5.

A simple Urey-Bradley force field including 25 force constants was employed for the a_1 and the b_2 vibrations. The initial values of the force constants were transferred from methylurea.[2] On refining the force constants, the observed frequencies were mostly taken from the infrared data. In the first step of the refinement, the stretching and the bending constants were adjusted by referring to the Jacobian matrix elements, and then by the least squares method in which K(NH) and K(CH) were fixed. In the next step, the stretching and the bending constants were fixed at the final values in the above process, and the repulsion constants were refined by the least squares method. Finally, the force constants except K(NH), K(CH), H(NC′C′) and F(HC′H) were refined by the least squares method, the last two being fixed because of large uncertainties.

The potential function for the b_1 vibrations was written as the sum of a simple Urey-Bradley type force field for the CH_2 group and a valence type force field for the torsional and the out-of-plane deformation vibrations. The values of the Urey-Bradley type constants were transferred from the converged set obtained in the treatment of the a_1 and the b_2 vibrations. The values of the diagonal constants were taken initially to be the observed frequency parameters divided by the corresponding G matrix elements for EU-d_0. These diagonal constants were adjusted first by referring to the Jacobian matrix elements and then by the least squares method. The off-diagonal constants $f(\pi$NH, τC′N) and $f(\pi$NH, πCO), were then added with the initial values zero, and all the constants were refined by the least squares method.

TABLE 4. FORCE CONSTANTS

Urey-Bradly type constants (in mdyn/Å)							
K(NH)	5·50	K(CH)	4.44	K(CN)	$5.059_0(0.127_8)$[a]	K(NC′)	$2.734_0(0.172_5)$
K(C′C′)	$2.307_0(0.170_8)$	K(C=O)	$5.892_0(0.444_3)$	H(HC′H)	$0.382_1(0.006_3)$	H(C′C′H)	$0.201_4(0.028_2)$
H(NC′H)	$0.175_7(0.037_7)$	H(NC′C′)	0.308_1	H(C′NH)	$0.200_6(0.046_3)$	H(CNH)	$0.275_8(0.070_0)$
H(CNC′)	$0.092_9(0.091_8)$	H(NCN)	$1.108_0(0.271_7)$	H(NCO)	$0.171_3(0.060_3)$	F(HC′H)	0.084_7
F(C′C′H)	$0.340_2(0.031_3)$	F(NC′H)	$0.482_4(0.041_8)$	F(NC′C′)	$0.421_0(0.084_2)$	F(C′NH)	$0.358_0(0.079_7)$
F(CNH)	$0.492_0(0.141_2)$	F(CNC′)	$0.849_0(0.277_4)$	F(NCN)	$0.669_0(0.216_0)$	F(NCO)	$1.644_0(0.186_8)$
κ(C′)	$0.013_6(0.033_9)$ mdyn Å						
Valence type constants (in mdyn Å/rad²)[b]							
$f(\pi$NH, πNH)	$0.123_4(0.022_2)$[a]	$f(\tau$NC′, τNC′)	$0.046_8(0.033_0)$	$f(\pi$CO, πCO)	$0.796_1(0.014_4)$		
$f(\tau$CN, τCN)	$0.473_9(0.077_2)$	$f(\pi$NH, τNC′)	$0.034_0(0.013_2)$	$f(\pi$NH, πCO)	$0.081_3(0.008_1)$		

a) ( ); dispersion. b) The relevant internal coordinates are shown in the parentheses; π, out-of-plane deformation coordinate; τ, internal rotation coordinate.

Table 5. Fundamental frequencies of ethyleneurea and its deuterated derivatives

	$(CH_2NH)_2CO$		$(CH_2ND)_2CO$		$(CD_2NH)_2CO$		$(CD_2ND)_2CO$	
	Obsd	Calcd	Obsd	Calcd	Obsd	Calcd	Obsd	Calcd
a_1	3303[a]	3299	2900	2916	3303	3299	2460[b]	2415
	2900	2915	2460	2415	2125	2096	2125	2096
	1668	1669	1652	1645	1660	1667	1637	1643
	1485	1496	1485	1494	1377	1375	1243	1239
	1385	1376	1250	1261	1145	1146	1134	1135
	1207	1212	1202	1187	1122	1123	1098	1093
	1105	1111	1017	1022	1053	1049	911	905
	991	1000	925	929	924	910	850	862
	933	928	850	857	785	787	786	783
	703	703	694	697	688	685	689	681
b_2	3303[a]	3296	2915	2925	3303	3296	2460[b]	2406
	2915	2925	2460	2406	2125	2110	2125	2110
	1502	1499	1502	1498	1425	1433	1410	1427
	1451	1438	1445	1430	1425	1417	1169	1201
	1423	1417	1274	1279	1176	1158	1098	1104
	1273	1277	1178	1177	1088	1073	1051	1050
	1041	1029	897	917	901	894	830	830
	660	653	650	643	619	620	595	612
	511	512	497	500	503	502	491	492
b_1	2980	3006	2980	3006	2250	2243	2250	2243
	1207	1160	1202	1160	901	852	901	852
		898	897	896	771	765	766	764
	768	770	764	769	688	707	650	664
	703	699	510	503	660	655	505	502
	250	243	250	243	225	231	225	230

a) The value for EU-d_4 was used as the unperturbed frequency. b) The value for EU-d_2 was used as the unperturbed frequency.

The final values of the force constants are listed in Table 4. The magnitudes of the stretching constants are reasonable in comparison with the corresponding constants of urea,[1,9] methylurea[2] and diketopiperazine,[17,18] being correlated well with the assumed bond-lengths. For the b_1 vibrations, both the diagonal and the off-diagonal force constants are of comparable magnitudes with the corresponding constants of methylurea.[2] The frequencies calculated from the final set of force constants are shown in Table 5. The agreement between the observed and the calculated frequencies is excellent throughout the four isotopic ethyleneureas.

It is well known for amide and urea derivatives containing a *trans* -CONH- group that the NH in-plane deformation and the CN stretching vibrations couple strongly with each other and give rise to the amide II and III bands in infrared spectra.[3,4] According to the present calculation, such a coupling does not occur for EU-d_0 and EU-d_4 which contain a -NHCONH- group in the *cis-cis* conformation (Table 1).

The authors wish to thank Mrs. Yuko Inamoto for her technical assistance. The calculation in this work was performed on a FACOM 230-60 computer at the Data Processing Center, Kyoto University.

References

1) Y. Saito, K. Machida, and T. Uno, *Spectrochim. Acta*, **27A**, 991 (1971).
2) Y. Saito, K. Machida, and T. Uno, *Spectrochim. Acta*, **31A**, 1237 (1975).
3) T. Miyazawa, T. Shimanouchi, and S. Mizushima, *J. Chem. Phys.*, **24**, 408 (1956).
4) Y. Mido, *Spectrochim. Acta*, **28A**, 1503 (1972).
5) C. E. Schweitzer, *J. Org. Chem.*, **15**, 475 (1950).
6) P. J. Wheatley, *Acta Crystallogr.*, **6**, 369 (1953).
7) Y. Mido and H. Murata, *Nippon Kagaku Zasshi*, **90**, 254 (1969).
8) Y. Mido and H. Murata, *Bull. Chem. Soc. Jpn.*, **42**, 3372 (1969).
9) A. Yamaguchi, T. Miyazawa, T. Shimanouchi, and S. Mizushima, *Spectrochim. Acta*, **10**, 170 (1957).
10) K. Fukushima, Y. Ideguchi, and T. Miyazawa, *Bull. Chem. Soc. Jpn.*, **36**, 1301 (1963).
11) O. Redlich, *Z. Phys. Chem.*, **B28**, 371 (1935).
12) J. C. Decius and E. B. Wilson, Jr., *J. Chem. Phys.*, **19**, 1409 (1951).
13) K. Machida, *J. Chem. Phys.*, **38**, 1360 (1963).
14) J. E. Worham, Jr., H. A. Levy, and S. W. Peterson, *Acta Crystallogr.*, **10**, 319 (1957).
15) T. Onishi and T. Shimanouchi, *Spectrochim. Acta*, **20**, 325 (1964).
16) T. Miyazawa and K. Fukushima, *J. Mol. Spectrosc.*, **3**, 308 (1965).
17) K. Fukushima, Y. Ideguchi, and T. Miyazawa, *Bull. Chem. Soc. Jpn.*, **37**, 349 (1964).
18) M. Asai, K. Noda, and A. Sado, *Spectrochim. Acta*, **30A**, 1147 (1974).

Electron-Capture Reaction of Halogenated Benzenes in MTHF Glass at 77 K

Toshinari SHIMOKAWA and Takeshi SAWAI

Tokyo Metropolitan Isotope Research Center, Fukazawa, Setagaya, Tokyo 158

(Received August 30, 1976)

The relative electron-capture efficiency of a number of halogenated benzenes was determined by means of competition with biphenyl as a reference material in glassy MTHF at 77 K. It was observed that the efficiency increased as the number of chlorine-atom substitutions on the benzene ring increased. Similar results were obtained for brominated benzenes. An excellent linear correlation is found between the logarithm of the efficiency and the polarographic reduction potential of a series of chlorinated benzenes. Moreover, a semilog plot of the efficiency *vs.* electron affinity of monohalogenated benzenes is apparently linear. The mechanisms of the electron-capture reaction are also discussed.

The study of the radiolysis of organic halogen compounds has advanced greatly in the last decade. These compounds have often been used as electron scavengers, because there is an effective way for examining ionic reactions in irradiated glass. Knowledge of the reactivity of organic halogen compounds with electrons is necessary for understanding and formulating the kinetics of the reaction process.

In spite of the many investigations on electron-capture reactions, the effect of halogen atom substitution in benzene is not fully understood.

In the present work, the relative efficiencies of electron capture by halogenated benzenes were determined in terms of the decrease in OD at 410 nm for biphenyl anions in glassy MTHF at 77 K.

Experimental

Reagents of special and guaranteed grade from Tokyo Kasei Co., Ltd. were used as received, except for 2-methyltetrahydrofuran (MTHF). The MTHF was purified by passage through a column of activated alumina. An MTHF solution of about 0.04 M biphenyl containing various halogenated benzenes was placed into a spectrosil vessel (10×10 mm) and dissolved oxygen was purged by bubbling nitrogen gas prior to irradiation. The sample was immersed in liquid nitrogen during the irradiation with ^{60}Co γ-ray. Measurement of the optical absorption was carried out at 77 K with a Cary 14R spectrophotometer.

The dose rate was determined by the Fricke dosimetry method to be 2.0×10^{18} eV/g h and the irradiation dose was about 5.0×10^{17} eV/g for all samples.

Results and Discussion

It is well known that biphenyl is an appropriate scavenger for the electrons generated by irradiation in organic glasses at 77 K, because its reactivity with electrons is very fast, $k=4\times10^{9}$ M^{-1} s^{-1}, and moreover, the biphenyl anion is identifiable in an absorption spectrum by a high absorption coefficient in the near-UV region. Hamill and his coworkers have used biphenyl as a reference material for determining the reactivity of some solutes with electrons in glassy media.[1] The competitive reaction of biphenyl with the solute for electrons is, in general, as follows:

$$e^- + C_{12}H_{10} \longrightarrow C_{12}H_{10}^-$$

$$e^- + \text{Solute} \longrightarrow \text{Product}$$

Assuming that the electron capture reaction is a simple competitive process, the biphenyl-anion optical density in various solute concentration is given by the following expression:

$$\frac{OD^\circ}{OD} = 1 + \frac{K_s}{K_{\phi_2}}\frac{[s]}{[\phi_2]} \quad (1)$$

where OD° and OD represent the optical densities of the biphenyl anion (410 nm) in the absence and in the presence of the solute, respectively, K_s and K_{ϕ_2} are the electron-capture coefficients of a given solute and of biphenyl, respectively, [s] and [ϕ_2] are the concentrations of a given solute and of biphenyl, respectively. The OD at 410 nm decreased with an increase in the concentration of chlorinated benzenes.

Arai *et al.* have shown recently by the low-temperature pulse radiolysis of halogenated compounds in ethanol glass that a strong absorption based on product negative ions appears in the visible to UV region.[2] In 1,2,3-trichlorobenzene, for example, there is no absorption for $\lambda>380$ nm, but below *ca.* 360 nm a strong absorption is observed ($\lambda_{max}\approx320$ nm). If the absorption of negative ions of the halogenated benzenes used in our experiments affects that of biphenyl (especially at $\lambda_{max}=410$ nm), then Eq. 1 is not suitable.

Then, competitive experiments were carried out after confirming that no absorption of solute anions was observed in the region around 410 nm.

The plot of OD°/OD for constant biphenyl concentration (0.04 M) should be a straight line as a function of the solute concentration. Figure 1 shows a plot of OD°/OD *vs.* [s]/[ϕ_2] obtained in an MTHF solution of monochlorobenzene, 1,2-dichlorobenzene, and 1,2,4-trichlorobenzene at 77 K. The slope of the line in Fig. 1 corresponds to the relative electron-

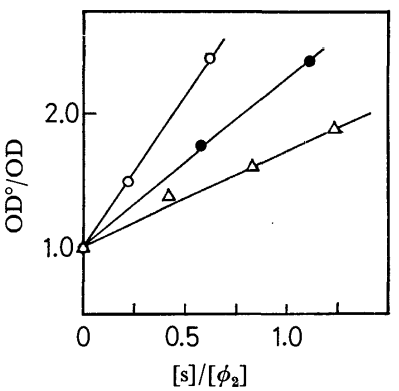

Fig. 1. Plot of OD°/OD *vs.* [s]/[ϕ_2] in irradiated MTHF glass at 77 K.
-○-: 1,2,4-$C_6H_3Cl_3$, -●-: 1,3-$C_6H_4Cl_2$, -△-: C_6H_5Cl.

TABLE 1. THE RELATIVE ELECTRON CAPTURE EFFICIENCIES OF HALOGENATED BENZENES, γ-BHC, AND HEXACHLOROETHANE

No.	Material	K_s/K_{ϕ_2}
1	C_6H_5Cl	0.49
2	1,2-$C_6H_4Cl_2$	1.12
3	1,3-$C_6H_4Cl_2$	1.09
4	1,4-$C_6H_4Cl_2$	1.03
5	1,2,4-$C_6H_3Cl_3$	1.88
6	1,2,3-$C_6H_3Cl_3$	2.02
7	1,3,5-$C_6H_3Cl_3$	2.55
8	1,2,3,4-$C_6H_2Cl_4$	3.42
9	1,2,3,5-$C_6H_2Cl_4$	2.90
10	1,2,4,5-$C_6H_2Cl_4$	3.62
11	C_6HCl_5	6.60
12	C_6Cl_6	4.42
13	C_6H_5Br	0.84
14	1,4-$C_6H_4Br_2$	1.30
15	1,3,5-$C_6H_3Br_3$	2.78
16	C_6H_5F	0.05
17	C_6H_5I	0.88
18	γ-BHC	3.39
19	C_2Cl_6	4.04

capture efficiency (K_s/K_{ϕ_2}). Such competitive experiments were carried out for a number of chlorinated and brominated benzenes, as well as fluorobenzene and iodobenzene. The results are tabulated in Table 1. As can be seen in Table 1, the electron-capture coefficient (K_s) increases generally with an incraese in the number of chlorine or bromine atoms substituted on the benzene ring. While, no difference in the efficiency of the di-, tri-, and tetrachlorobenzene isomers was observed, the order of the reactivity for monohalogenated benzene is fluoro≪chloro<bromo<iodobenzene, which is the same as that for hydrated electrons in aqueous solutions.[3]

The electron-capture reaction for an aromatic compound is shown in the following scheme as formulated for monohalogenated benzene.[4]

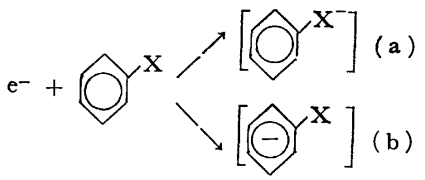

The initial addition of an electron to the aromatic compound appears to occur predominantly by reaction process (b).[5] Therefore, the initial process for chlorinated benzenes is preferably the interaction of the π-orbital system of the benzene ring with the electron. Studier and Hart have suggested that the reaction of benzene with the electron is similar to reaction process (b).[6] However, the direct interaction for the substituent halogen atom on the benzene ring, which corresponds to reaction process (a), may be possible. In the case of monohalogenated benzene, the order of the relative electron-capture efficiencies may be explained by the effect of net electron-withdrawing, which is estimated from Hammett's parameters, σ_I and σ_R, of substituent halogen atoms on the benzene ring. σ_I and σ_R represent Hammett's parameters for inductive and resonant (mesomeric) effects, respectively.[7]

The decrease in the relative electron-capture efficiency for hexachlorobenzene in comparison with pentachlorobenzene would be attributed to a great extent to shielding of the π-orbital system by substituent chlorine atoms on the benzene ring. The value of the efficiency for hexachlorobenzene is similar to that of aliphatic hexachloro-compounds, such as hexachloroethane and γ-BHC. This fact indicates that the π-orbital system of hexachlorobenzene provides a lower contribution to electron capture than that of other chlorinated benzenes.

Christodouleas and Hamill have found that the relative electron-capture efficiency of aromatic hydrocarbons, such as phenanthrene, is correlated to the polarographic reduction potential.[8] It was found that the relative electron-capture efficiencies in the present results can also be roughly correlated with the reduction potential of the various monohalogenated benzene derivatives, which have been determined in aprotic solvents by Sease *et al.*[9] Recently, Tsuji has determined the reduction potential of a series of chlorinated benzenes by the differential pulse polarographic method and shown that the value increased proportionally with the number of substituted chlorine atoms on the benzene ring from mono- to hexachlorobenzene.[10] And also no difference in the reduction potential for isomers of polychlorinated benzenes was observed.[11] The results of the relative electron-capture efficiencies for isomers are in accord with the trend of the polarographic reduction potential.

Figure 2 shows a semilogarithmic plot of the relative electron-capture efficiency *vs.* the reduction potential of chlorinated benzenes. Interestingly, the plot, as shown in Fig. 2, is very linearly from mono- to pentachlorobenzene, except for hexachlorobenzene.

The relationship between the logarithm of the electron-capture efficiency and the reduction potential from mono- to pentachlorobenzene can be expressed by

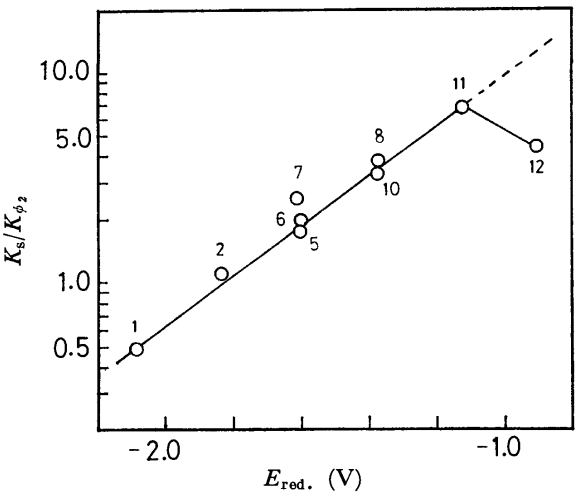

Fig. 2. Plot of $\log K_s/K_{\phi_2}$ *vs.* reduction potential ($E_{red.}$) of a series of chlorinated benzenes. The values of reduction potential for penta- and monochlorobenzene estimated from the secondary peak of hexachlorobenzene and 1,2-dichlorobenzene measurements, respectively. Key is shown in Table 1.

following equation, which is plotted in Fig. 2:

$$\log K_s/K_{\phi_2} = a E_{red.} + b \quad (2)$$

where $E_{red.}$ is the reduction potential, and a and b are constants. Nenner and Schulz have accurately measured the electron affinity using electron transmission spectroscopy.[12] They indicated that a good correlation between the polarographic reversible electrode potential and the electron affinity was observed. The reversible electrode potential for halogenated benzenes cannot be obtained from the usual polarographic measurement, because dissociation preferentially occurs prior to the reversible reaction. However, it is clear that the reversible electrode potential is related to the reduction potential of halogenated compounds.[12] Thus, the logarithm of the relative electron-capture efficiency may be linear as a function of the quasi-electron affinity which is estimated from the polarographic reduction potential. Therefore, a similar relation to that shown in Fig. 2 can be expected for accurate electron affinities. A semilog plot of the relative electron capture efficiency *vs.* the electron affinity[12] of monohalogenated benzenes is shown in Fig. 3. Figure 3 shows that the relative electron-capture efficiencies for halogenated benzenes are given as a function of the electron affinity as has been mentioned for the reactivity of many compounds with hydrated electrons by Anbar and Hart.[13]

Wentworth and his coworkers have proposed that the relation between the electron-capture coefficient and the electron affinity in gas phase can be shown to be[14]

$$\log KT^{3/2} = \log A + \log k_L/k_M + EA/RT \quad (3)$$

where A is composed fundamental constants, including the mass of the electron, k_L and k_M are the rate constant for neutralization of negative ions and electrons, respectively and EA is the electron affinity. Thus, the relative electron-capture efficiency would be given by following expression:

$$\log K_s/K_{\phi_2} = \log(k_L)_s - \log(k_L)_{\phi_2} + (EA)_s/RT - (EA)_{\phi_2}/RT \quad (4)$$

where the subscripts ϕ_2 and s refer to biphenyl and solute, respectively. Assuming that the rate of neutralization is very slow at a low temperature of 77 K, Eq. 4 can be rewritten as follows:

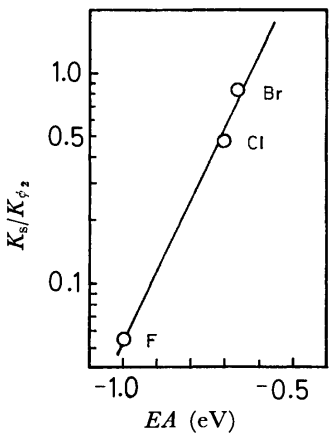

Fig. 3. Plot of $\log K_s/K_{\phi_2}$ *vs.* electron affinity of monohalogenated benzenes.

$$\log K_s/K_{\phi_2} = (EA)_s/RT - (EA)_{\phi_2}/RT, \quad (5)$$

where $(EA)_{\phi_2}/RT$ is constant at 77 K. Equation 5 indicates that a linear relationship between $\log K_s/K_{\phi_2}$ and $(EA)_s$, and that the slope is dependent on the temperature. The semilog-linearity in Fig. 3 can apparently be explained by Eq. 5. According to Eq. 5, the slope is given by $1/RT$, which has a value of 150. However, the slope of the line in Fig. 3 is about 3.5. Since such a great difference between the observed slope (Fig. 3) and the slope calculated from Eq. 5 is observed, a treatment similar to that in the gas phase may not be applicable at low temperatures.

On the other hand, Miller has emphasized that the tunneling mechanism for the electron-capture reaction is of importance in glassy media and has suggested that the electron affinity is a predominant factor in determining whether or not the tunneling reaction can occur.[15] Namiki *et al.* have pointed out that the scavenging efficincy is linear as a function of the adiabatic electron affinity of the acceptor in alcoholic glasses.[16] They discussed the electron-capture process on the basis of the tunneling model. This consideration is interesting, but until recently only limited data had been available on accurate electron affinities of a series of halogenated benzenes in order to conform the relationship between the relative electron-capture efficiency and the electron affinity. For a more detailed explanation on this relationship, measurements of the efficiencies for many kinds of substituted benzenes will be necessary.

The authors indebted to Dr. Keiichi Tsuji, The Institute of Physical and Chemical Research, for providing the polarographic data on the polychlorinated benzenes and for useful advice. The authors are also grateful to Dr. Teruko Sawai for helpful discussions.

References

1) W. H. Hamill, "Radical Ions," ed by E. T. Kaises and L. Kevan, John Wiley & Sons, New York (1968), p.301.
2) S. Arai, S. Tagawa, and M. Imamura, *J. Phys. Chem.*, **78**, 519 (1974).
3) M. Anbar and P. Neta, *Int. J. Appl. Radiat. Isotopes.*, **18**, 439 (1967).
4) R. Koster and K. D. Asmus, *J. Phys. Chem.*, **77**, 749 (1973).
5) E. J. Fendler and J. H. Fendler, *Prog. Phys. Org. Chem.*, **7**, 229 (1970).
6) M. H. Studier and E. J. Hart, *J. Am. Chem. Soc.*, **91**, 4068 (1969).
7) C. D. Johnson, "The Hammett Equation," the Cambridge University press (1973), p. 11.
8) N. Christodouleas and W. H. Hamill, *J. Am. Chem. Soc.*, **86**, 5413 (1964).
9) J. W. Sease, F. G. Burton, and S. L. Nickol, *J. Am. Chem. Soc.*, **90**, 2595 (1968).
10) K. Tsuji, *Rev. Polarog.*, **21**, 57 (1975).
11) K. Tsuji, private communication.
12) I. Nenner and G. J. Schulz, *J. Chem. Phys.*, **62**, 1747 (1975).
13) E. J. Hart and M. Anbar, "The Hydrated Electron," Wiley Interscience, New York (1970), p. 179.
14) W. E. Wentworth, L. W. Kao, and R. S. Becker, *J. Phys. Chem.*, **79**, 1161 (1975).
15) J. R. Miller, *J. Phys. Chem.*, **79**, 1070 (1975).
16) A. Namiki, M. Noda, and T. Higashimura, *Bull. Chem. Soc. Jpn.*, **48**, 3073 (1975).

The Interaction of Bovine Plasma Albumin with Cationic Detergent. Studies by Binding Isotherm, Optical Rotation and Difference Spectrum

Koichi HIRAMATSU, Chiaki UEDA, Koji IWATA, Kinichi ARIKAWA, and Koichiro AOKI

Department of Synthetic Chemistry, Faculty of Engineering, Gifu University, Kagamigahara, Gifu 504

(Received September 17, 1976)

Binding isotherms were determined at pH 6.9 for systems of bovine plasma albumin (BPA) and cationic detergents at 25° C and 5 °C. Detergents used were: hexadecyltrimethylammonium bromide (HTAB), tetradecyltrimethylammonium bromide (TTAB), dodecyltrimethylammonium bromide (DTAB) and decyltrimethylammonium bromide (DeTAB). Binding affinity of the cationic detergent to BPA increased with the increase in the carbon number of the detergent, and with the increase in temperature. The first five detergent ions were bound to BPA statistically at 25 °C, and succeeding detergent ions were bound cooperatively. Thermodynamic parameters indicated that the statistical binding was caused mainly by the hydrophobic bonding. Measurements of $-[\alpha]_{233}$ and $-[\alpha]_{313}$ at pH 5.2 revealed that the conformation of BPA changed when it complexed with the cationic detergent. The conformation of BPA changed slightly when 5—8 HTAB or TTAB's were bound, and a second large conformational change occurred when 15—20 of these detergent ions were bound. DTAB and DeTAB caused only the first conformational change. Thus HTAB and TTAB are stronger unfolders of BPA than DTAB and DeTAB. The UV difference spectrum of the complex BPA–TTAB showed a red shift of the peak of Try residue (*e. g.* 292 nm), being in contrast to the blue shift of the same peak in the complex BPA–sodium dodecyl sulfate. It is suggested that BPA is unfolded, at least, in the NH_2 terminal half by binding with cationic detergent.

In a previous paper,[1] it was reported that the binding of cationic detergent to BPA (bovine plasma albumin) at pH 9 induced the SH–S-S exchange reaction of BPA, forming a series of aggregates of BPA. The exchange reaction occurred at lower concentration of the detergent, when the carbon number of detergent was higher. It was suggested that the first step of the reaction is the unfolding of BPA by the cationic detergent.

This time studies were made on the binding behavior of cationic detergents to BPA and on the conformational change of BPA caused by the cationic detergent. Studies were made by equilibrium dialysis, by measuring the optical rotations at 233 and 313 nm, and by measuring the UV difference spectrum. Some aspects of the unfolding of BPA by the cationic detergent were made clear at pH 5.2 and 6.9. Cationic detergents used were:

hexadecyltrimethylammonium bromide (HTAB),
tetradecyltrimethylammonium bromide (TTAB),
dodecyltrimethylammonium bromide (DTAB), and
decyltrimethylammonium bromide (DeTAB).

So far, several works have been made on the interaction between BPA and cationic detergents.[1-5]

Experimental

Materials. Crystallized BPA (Armour, Lot No. M-72603) was used. A part of the experiment was performed using BPA whose SH group was blocked by iodoacetamide. The blocking was made at room temperature and pH 8.0 (in 0.1M KCl+KOH) for 3 h. Then the solution was dialyzed against the deionized water at 5 °C for more than 24 h or passed through the Sephadex G-25 gel (Pharmacia Fine Chemicals, Lot No. 0063) column. Frequently, contaminants were removed by filtering the solution through Millipore filter (HATF, 02500). The concentration of BPA was determined spectrophotometrically using the value $E^{1\%}_{1cm}=6.67$ at 279 nm.

Buffers used were: phosphate buffer at pH 6.9 and ionic strength 0.1, and $Na_2B_4O_7$–HCl buffer at pH 9.0 and ionic strength 0.025 (sometimes the ionic strength was raised to 0.1 by adding KCl). BPA was also dissolved in 0.1 M KCl; the isoionic point was pH 5.2.

Cationic detergents used were the same samples as those described in a previous paper.[1]

Equilibrium Dialysis. The Visking tube (20/30) was heated in a half saturated solution of $NaHCO_3$ at 90 °C for 1 h, then the tubings were rinsed well with deionized water. Five ml of 0.5% BPA was dialyzed against 25 ml of detergent solution. The dialysis was conducted for 65 h at 5 and 25 °C.

Determination of the Cationic Detergent. The determination was carried out following the method of Few and Ottewill.[6] The method involves the procedure to extract the detergent–Orange II complex in the aqueous phase by the organic solvent. In the present work, the extraction solvent was dichloromethane instead of chloroform. The optimum conditions for the extraction were: concentration of the complex is to be in the range 9×10^{-6} and 3×10^{-5} mol/l, and the mol ratio of Orange II to detergent is to be in the range 1—3. When the concentration of the detergent in the sample solution was higher than the optimum value, the solution was diluted by the same buffer as was used for the sample solution. The extinction coefficient of the complex at 485 nm was 1.80×10^4 mol^{-1} cm^{-1} in presence or absence of ethanol (antifoaming agent), and was 2.20×10^4 mol^{-1} cm^{-1} in aqueous phase. The extinction coefficient of the complex in distilled water was equal to that of Orange II.

Optical Rotation. The optical rotation was measured using 0.2% BPA at various concentrations of detergent. The 1 mm cell and 10 mm cell were used to measure the optical activity at 233 and 313 nm, respectively. To increase the sensitivity of the measurements, compensation by means of sucrose was employed.[7] The temperature was kept constant at 25±0.2 °C. The apparatus was a Jasco spectropolarimeter, model ORD/CD/UV-5.

Difference Spectrum. The difference spectrum was measured using 0.15% BPA in presence of various amounts of detergent. Using 10 mm cell, the spectrum was recorded in the range 275—350 nm. The temperature of the cell was kept constant at 25±0.2 °C. The apparatus was a Hitachi EPS-3 spectrophotometer.

Results and Discussion

Equilibrium Dialysis. *a) Binding Isotherms at pH 6.9*: In Fig. 1 are shown binding isotherms of the systems of BPA and each one of the detergents, HTAB, TTAB, DTAB, or DeTAB at pH 6.9 and 25 °C. All of the curves consist of two parts: one of which lies in the lower concentration of the detergent and has a small slope and the other is the curve having a large slope. It is known later that the binding of the detergent to BPA is statistical in the lower concentration region of the detergent, and that it is cooperative in the higher concentration region. The whole binding isotherm shifts to the left with the increase in the carbon number of the detergent. In other words, the binding occurs at lower concentrations of detergent, when the detergent with higher carbon number is used. This suggests that the hydrophobic group of the detergent is more effective than the charged group for the BPA–cationic detergent interaction.

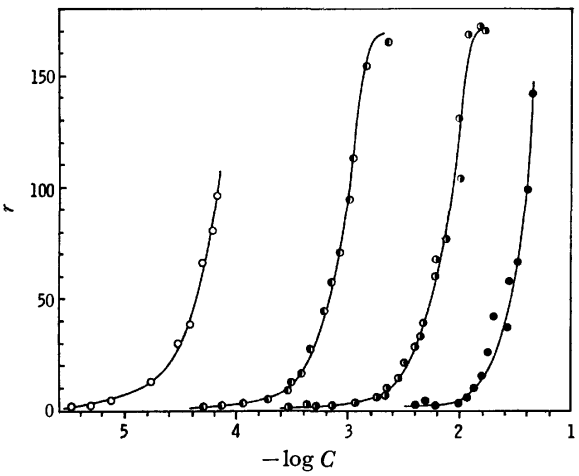

Fig. 1. Binding isotherms of the systems of BPA and cationic detergents at pH 6.9, ionic strength 0.1 and 25 °C. C: equilibrium concentration of detergent (mol/l), r: number of detergents bound to BPA. ○: HTAB-BPA, ◐: TTAB-BPA, ◑: DTAB-BPA, ●: DeTAB-BPA.

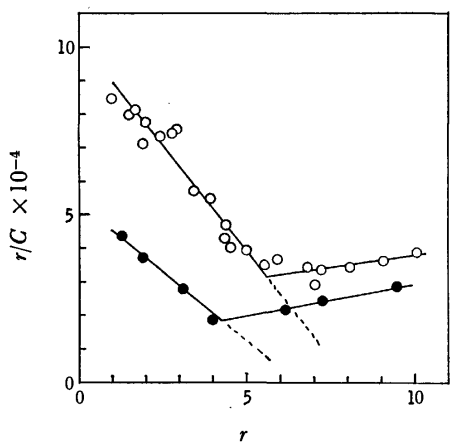

Fig. 2. Scatchard plot for the system BPA-TTAB. ○: 25 °C, ●: 5 °C.

When the temperature is increased, the binding isotherm shifts to the left, indicating that the binding is increased with the increase in temperature, *i.e.*, the binding is endothermic. The result agrees with that by calorimetric measurement by Jones *et al.*[5] The effect of temperature is shown in Fig. 2.

The binding isotherm was analyzed by the Scatchard equation.[8]

$$r/C = k_0 n - k_0 r \qquad (1)$$

where, C: equilibrium concentration of detergent, n: maximum number of the binding sites, r: average number of the detergent ions bound and k_0: intrinsic binding constant. The application of the equation to the system BPA-TTAB, as an example, is given in Fig. 2. There are two straight lines with a break. The one is that for 25 °C, and the other is that for 5 °C. The straight line with a negative slope satisfies the Eq. 1, meaning that the binding is statistical. The straight line with a positive slope gives a negative value of k_0; the meaning is that the binding is cooperative.

Figure 2 shows that $r_{s,max}$ is 5.5 at 25 °C.* If the straight line with a negative slope is extended, it is found that the maximum number of sites n should be 8. The value of $r_{s,max}$ is 4 at 5 °C. Values of $r_{s,max}$ for other detergents are given in Table 1. It was difficult to find accurate values for DeTAB. This might be due to the difficulty in analytical procedure.

b) Statistical Binding: As is seen in Table 1, $r_{s,max}$ does not depend on the carbon number of the detergent, *i.e.*, it is 4 at 5 °C and 5 at 25 °C. The value agrees with the value 4 by Nozaki *et al.*[4] for tetradecyltrimethylammonium chloride at pH 5.6 and 24 °C within the experimental error, and agrees also with the value 6 by Few *et al.*[2] at the isoionic point and 20 °C for DTAB. When 4 or 5 cationic detergent ions are bound to BPA, slight unfolding occurs in BPA as is described later, thus $r_{s,max}$ is constant, *i. e.*, more binding sites with high affinity are destroyed when unfolding occurs. If the unfolding does not occur before all the n sites are occupied, $r_{s,max}$ would be equal to n.

The value of $r_{s,max}$ is 4—5 for the cationic detergents with C_{12} and C_{14}, but it is 8—10 for the anionic detergents with C_{12} and C_{14}.[9,10] (Decker and Foster[9] reported that $r_{s,max} \fallingdotseq n = 10$ for sodium dodecylbenzenesulfonate.) Such a difference in numericals exists between the cationic and anionic detergent bindings. It is well known that the BPA unfolds when the number of anionic detergents bound exceeds the value of $r_{s,max}$.[10]

c) Thermodynamic Properties of Statistical Binding: In Table 1 are given values of k_0 and thermodynamic parameters $-\Delta F$, ΔS, and ΔH for the interactions. It is seen that $H>0$ and $\Delta S>0$, and that $T\Delta S>\Delta H$. This indicates that the binding of the cationic detergent

* The notation $r_{s,max}$ means the maximum number of the detergent ions bound statistically. As is known from Eq. 1, the crossing point of the straight line with a negative slope and the abscissa gives the value of n. The break of the straight line in Fig. 2 is named $r_{s,max}$ to distinguish it from n.

Table 1. Thermodynamic parameters for BPA-cationic detergent interactions

Detergent	Temp °C	$r_{s,max}$	k_0 l/mol	$-\Delta F$ kcal/mol	ΔH kcal/mol	ΔS e. u.
HTAB	25	5	8.7×10^4	6.7	4.0	36
	5	4	5.2×10^4	5.8		
TTAB	25	5.5	1.3×10^4	5.5	3.5	30
	5	4	8.2×10^3	5.0		
DTAB	25	5	9.7×10^2	3.9		

to BPA is entropic. This means that the interaction between the detergent and the solvent molecule is replaced by the interaction between the detergent and BPA, *i. e.*, that hydrophobic bonds are formed. It is known from Table 1 that $-\Delta F$ is 600—800 cal/mol per CH_2 residue of the detergent. The value agrees with 700 cal/mol per CH_2 residue, which is obtained when CH_2 is transferred from the aqueous phase to the organic solvent.[11]

Literature survey[10,12-14] indicates that the free energy change $-\Delta F$ is larger when the anionic detergent (with sulfate or sulfonate) or fatty acid is bound to BPA than when the cationic detergent is bound, if the length of the hydrocarbon chain is the same in the range C_{10}—C_{16}. Tanford[15] has pointed out that both the ionic and hydrophobic interactions take part in the anionic detergent binding at pH 6.8, and attributed half of $-\Delta F$ to the ionic interaction. If $-\Delta F$ for the anionic detergent with C_{12} is compared with that for the cationic detergent with C_{12}, there is a difference by 3—4 kcal, which is almost the same as $-\Delta F$ estimated for ionic interaction.[15] Thus, it is concluded that the contribution of the ionic interaction is smaller in the cationic detergent binding than in the anionic detergent binding. In other words, the hydrophobic bonding is the main force in the cationic detergent binding.[16]

d) Cooperative Binding: It is clear in Fig. 1 that the cooperative binding also depends on the length of the hydrocarbon chain of the detergent. The change in the standard free energy accompanying the cooperative binding is given by the equation $\Delta F=RT \ln X$, where X is the mid-point of the two extreme equilibrium concentrations for the region in which the cooperative binding occurs.[15] The value of $-\Delta F$ was calculated for TTAB and DTAB at 25°C using the equilibrium concentration at which 85 detergent ions were bound.[17] The highest number of detergent ions bound was 170 for these two detergents (Fig. 1). It was found that $-\Delta F$ was 2.9 kcal/mol for DTAB binding and that it was 4.2 kcal/mol for TTAB binding. These figures lead to the conclusion that the free energy change was 650 cal/mol per CH_2 residue; the value is almost the same as that for the statistical binding. Thus, the hydrophobic bonding is also the main force in the cooperative binding.

e) Binding Isotherm at the Isoionic Point: The binding isotherm of the system BPA-DTAB at 25° C and pH 5.2 (in 0.1M KCl) was the same as that at pH 6.9; $r_{s,max}$ was 5 and k_0 was also the same within the experimental error. When r was less than 70, the isotherm at pH 5.2 lay on that at pH 6.9. When it was more than 70, the isotherm at pH 5.2 located upper than that at pH 6.9. The highest number of the detergent ions bound was slightly less, *i. e.*, 140.

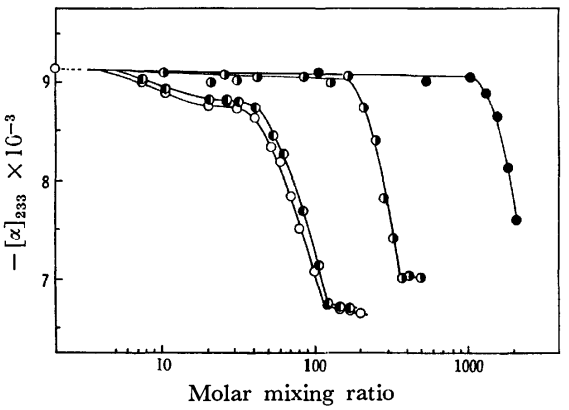

Fig. 3. $-[\alpha]_{233}$ *vs.* molar mixing ratio (detergent/BPA). pH 5.2 in 0.1 M KCl and 25 °C. ○: HTAB-BPA, ◐: TTAB-BPA, ◑: DTAB-BPA, ●: DeTAB-BPA.

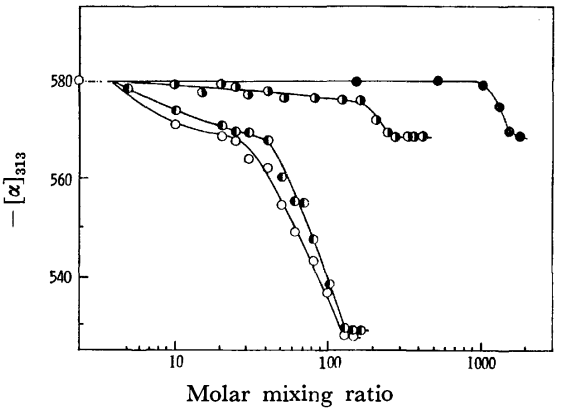

Fig. 4. $-[\alpha]_{313}$ *vs.* molar mixing ratio (detergent/BPA). pH 5.2 in 0.1 M KCl and 25 °C. ○: HTAB-BPA, ◐: TTAB-BPA, ◑: DTAB-BPA, ●: DeTAB-BPA.

Optical Rotation. *a) Unfolding of BPA by Cationic Detergent at pH 5.2*: Optical rotations were measurcd at the isoionic point of BPA in 0.1 M KCl (pH 5.2). Values of $-[\alpha]_{233}$ and $-[\alpha]_{313}$ are given as a function of the molar mixing ratio (detergent/BPA) in Figs. 3 and 4, respectively. It is clear in these figures that the BPA is disorganized by the binding of particular numbers of the detergent. Figure 3 shows how the helix content[18] in BPA decreases by the binding of the detergent. Detergent with higher carbon number is more effective in the range C_{10}—C_{14}; TTAB and

HTAB seem to have almost the same ability to unfold the BPA. Figure 4 shows how the tertiary structure[19] of BPA is disorganized by the cationic detergent.

In Figs. 3 and 4, it is seen that $-[\alpha]_{233}$ and $-[\alpha]_{313}$ are constant in the region of TTAB/BPA=20—40. If the data of equilibrium dialysis are combined, the complexes formed in this region are found to be AD_5—AD_{15} (A: BPA and D: cationic detergent). When the molar mixing ratio exceeds 40, both of the rotations decrease remarkably and continuously, attaining to a constant. Since $-[\alpha]_{233}$ is 6700 at the molar mixing ratio 120, *i.e.*, for AD_{60}, it is found that the helix of BPA was destructed by 40% by binding of 60 cationic detergents.[20] In the region of HTAB/BPA=10—25, $-[\alpha]_{233}$ and $-[\alpha]_{313}$ are constant. The compositions of the complexes are AD_8—AD_{20}. When the mixing ratio exceeds 25, values begin to decrease.

For DTAB, $-[\alpha]_{233}$ begins to decrease at AD_7 and attains constant at AD_{40}: $-[\alpha]_{313}$ drops at AD_7 and attains constant at AD_{20}. This means that the helix content of BPA decreases, keeping the tertiary structure constant, when r is more than 20. Almost the same is true for DeTAB. When 7 DeTAB are bound to BPA, both the helical content and the tertiary structure begin to decrease.

In conclusion, the ability for the cationic detergent to destruct BPA is in the order: HTAB≧TTAB>DTAB>DeTAB.[21]

b) Unfolding of BPA at pH 6.9 and 9.0: Changes in $-[\alpha]_{233}$ and $-[\alpha]_{313}$ with the molar mixing ratio TTAB/BPA were measured for SH blocked BPA at pH 6.9 and 9.0. Results are given in Fig. 5 by the expression $-[\alpha]_{233}$ *vs.* $-[\alpha]_{313}$. Measurements were made using SH blocked BPA at these pH's to prevent the SH-S-S exchange reaction.

Difference Spectra. In Fig. 6 are shown difference spectra of SH blocked BPA in presence of TTAB at pH 6.9. When the concentration of TTAB is low, peaks are observed at 275, 283, 292, and 298 nm, and troughs at 277, 287, 295, and 305 nm, *i.e.*, the red shift occurs. Especially, peak at 292 nm is large. Peaks increase their magnitudes with the increase in the amount of TTAB. Peak at 292 nm is caused by Try, those at 275 and 283 nm are caused by Try and Tyr, and peak at 298 nm would be caused by Try. The environment of Try residue, and probably that of Tyr residue also, seem to change when some detergents are bound to BPA.

Generally, the blue shift occurs when the protein is denatured, or when the buried chromophore in the protein is exposed to the aqueous solvent. The binding of alkyl sulfate, whose carbon number is more than 12, to BPA causes conformational change in BPA. The blue shift of peak at 292 nm (Try residue) occurs when smaller number of detergents are bound, and the blue shift of peak at 288 nm (Tyr residue) occurs when larger number of detergents are bound.[22,23] In the present study, however, the red shift was observed in a wider range of molar mixing ratio. This suggests that the cationic detergent unfolds BPA in such a way as to prevent the Try residue from exposing to the aqueous phase.

The same red shift was observed also at the isoionic point.

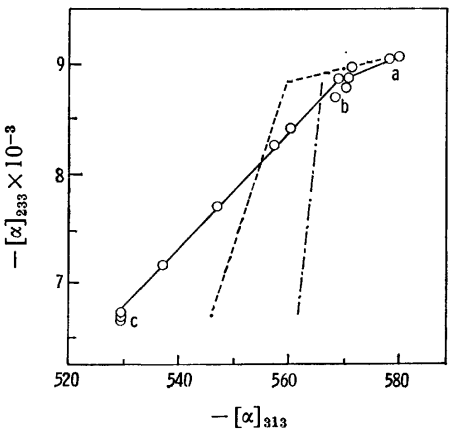

Fig. 5. Relations between $-[\alpha]_{233}$ and $-[\alpha]_{313}$. O: BPA-TTAB complexes at pH 5.2 in 0.1 M KCl. a: AD_0, b: AD_{15}, and c: AD_{60}. (AD_x means the composition of the complex.) ----: SH blocked BPA-TTAB complexes at pH 6.9. —·—: SH blocked BPA-TTAB complexes at pH 9.

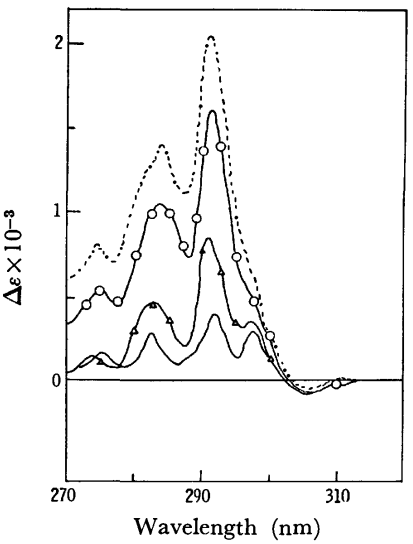

Fig. 6. UV difference spectrum of BPA-TTAB complexes. pH 6.9, ionic strength 0.1 and 25 °C. Sample: SH blocked BPA plus TTAB. Reference: SH blocked BPA. Molar mixing ratio are 20 (——), 30 (-△-), 50 (-O-) and 60 (·····).

General Discussion. As was described above, TTAB and HTAB were bound to BPA statistically up to $r=5$ at pH 6.9 and 5.2. When r was more than 5, the cooperative binding occurred accompanying a conformational change in BPA. Measurements of optical rotation revealed that the second unfolding begins to occur at $r=20$.

Studying the BPA solution by the small angle X-ray scattering, Luzzati *et al.*[24] suggested that the BPA is composed of the NH_2 terminal half which is compact and the COOH terminal half which is rather loose. Recently, Hilak *et al.*[25] supported this model by studying the fragments of BPA produced by the pepsin digestion and by measuring the optical rotation of each fragment in the N-F transition region. It is known that two Try residues are involved in the com-

pact NH_2 terminal half.[26] This time it has been found that the cationic detergent binding changes the environment of Try residue. This suggests that the compact NH_2 terminal half, at least, is unfolded by binding with the cationic detergent.

In the previous paper.[1] it was reported that the SH–S-S exchange reaction begins to occur between BPA molecules when 5 mol of TTAB are added to 1 mol of BPA at pH 9. In the present study, it has been found at pH 6.9 that the BPA is unfolded when r is more than 5. The BPA at pH 9 is unfolded by the N–B transition and by the binding of cationic detergent.[27]

The SH group is also in the compact NH_2 terminal half,[25] and locates in the crevice, its depth being at least 9.5 A.[29] If the BPA is unfolded, some of the S–S bond will be exposed,[30] and the crevice will be broken to expose the SH group. Thus the SH–S-S exchange reaction will take place easier at the alkaline pH in presence of the cationic detergent. In a recent study in our laboratory, it was deduced that the S–S bond is more reactive when it is surrounded by the cationic detergent.[32]

This work was supported by Grant of the Ministry of Education, Japan.

References

1) K. Aoki and K. Hiramatsu, *Anal. Biochem.*, **60**, 213 (1974).
2) A. V. Few, R. H. Ottewill, and H. C. Parreira, *Biochim. Biophys. Acta*, **18**, 136 (1955).
3) S. Kaneshina, M. Tanaka, T. Kondo, T. Mizuno, and K. Aoki, *Bull. Chem. Soc. Jpn.*, **46**, 2735 (1973).
4) Y. Nozaki, J. A. Reynolds, and C. Tanford, *J. Biol. Chem.*, **249**, 4452 (1974).
5) M. N. Jones, H. A. Skinner, and E. Tipping, *Biochem. J.*, **147**, 229 (1975).
6) A. V. Few and R. H. Ottewill, *J. Colloid Sci.*, **11**, 34 (1956).
7) B. J. M. Harmsen, S. H. De Bruin, L. H. M. Janssen, J. F. Rodrigues de Miranda, and G. A. J. Van Os, *Biochemistry*, **10**, 3217 (1971).
8) G. Scatchard, *Ann. N. Y. Acad. Sci.*, **51**, 660 (1949).
9) R. V. Decker and J. F. Foster, *Biochemistry*, **5**, 1243 (1966).
10) J. A. Reynolds, S. Herbert, H. Polet, and J. Steinhardt, *Biochemistry*, **6**, 937 (1967).
11) C. Tanford, *J. Am. Chem. Soc.*, **84**, 4240 (1962).
12) J. Reynolds, S. Herbert, and J. Steinhardt, *Biochemistry*, **7**, 1357 (1968).
13) D. S. Goodman, *J. Am. Chem. Soc.*, **80**, 3892 (1958).
14) A. A. Spector, J. E. Fletcher, and J. D. Ashbrook, *Biochemistry*, **10**, 3229 (1971).
15) C. Tanford, "The Hydrophobic Effect," Wiley International Publication, New York (1973), p. 135.
16) Tanford[15] insisted that the free energy change for the interaction between BPA and the anionic detergent is constant when the carbon number of the detergent is more than 10. His explanation for the interaction is that the hydrophobic part of the detergent binds to a hydrophobic surface patch or patches of BPA. In contrast, the free energy change for the present interaction increased with the increase in the carbon number of cationic detergent up to the carbon number 16. Thus the above explanation by Tanford can not be applied. Our explanation is that the hydrocarbon part of the cationic detergent is buried into the hydrophobic crevice of BPA.
17) The equilibrium concentration of the detergent at the highest number of binding is equal to its critical micelle concentration (CMC) in phosphate buffer of pH 6.9, ionic strength 0.1 and 25 °C. The CMC is 1.6×10^{-3} mol/l for TTAB and 1.2×10^{-2} mol/l for DTAB. When the equilibrium concentration of the detergent is higher than the CMC, the micelle is formed in the solution.
18) B. Jirgensons, "Optical Activity of Proteins and Other Macromolecules," 2nd ed, Springer-Verlag, Berlin, Heidelberg, New York (1973), p. 67.
19) W. J. Leonard, Jr. and J. F. Foster, *J. Biol. Chem.*, **236**, 2662 (1961).
20) In Fig. 3, it is seen that the conformational change of BPA by TTAB finishes almost completely at AD_{60}. However, the complex AD_{60} is formed around the mid-point of the binding isotherm in the region of cooperative binding in Fig. 1. This means that binding of more than 60 TTAB does not induce additional unfolding in BPA. The same is true for other detergents. A similar result to this was obtained by Nozaki *et al.*[4]
21) Raynolds *et al.*[10] studied the conformational change of BPA caused by a series of anionic detergents whose carbon numbers are different. They stated that the detergent whose carbon number is less than 10 binds to BPA cooperatively without the conformational change in BPA, and that the detergent whose carbon number is more than 12 binds to BPA cooperatively inducing the conformational change in BPA. In the present study, cationic detergents induced the conformational change, when the carbon number was more than 10.
22) C. C. Bigelow and M. Sonenberg, *Biochemistry*, **1**, 197 (1962).
23) J. Steinhardt, J. G. Leidy, and J. P. Mooney, *Biochemistry*, **11**, 1809 (1972).
24) V. Luzzati, J. Witz, and A. Nicolaieff, *J. Mol. Biol.*, **3**, 379 (1961).
25) M. C. Hilak, B. J. M. Harmsen, W. G. M. Braam, J. J. M. Joordens, and G. A. J. Van Os, *Int. J. Pept. Prot. Res.*, **6**, 95 (1974).
26) W. G. M. Braam, M. C. Hilak, B. J. M. Harmsen, and G. A. J. Van Os, *Int. J. Pept. Prot. Res.*, **6**, 21 (1974).
27) When TTAB is added to BPA at pH 9.0, $-[\alpha]_{233}$ changes remarkably and $-[\alpha]_{313}$ changes slightly, giving almost perpendicular straight line without a break in Fig. 6. This is because the BPA in the B form unfolds.[28]
28) W. J. Leonald, Jr., K. K. Vijai, and J. F. Foster, *J. Biol. Chem.*, **238**, 1984 (1963).
29) H. H. Hall, R. Chang, and L. J. Kaplan, *Biochim. Biophys. Acta*, **400**, 132 (1975).
30) Kolthoff and Tan[31] state that a few S–S bonds are on the surface of BPA molecule at pH 7.
31) I. M. Kolthoff and B. H. Tan, *J. Am. Chem. Soc.*, **87**, 2717 (1965).
32) K. Hiramatsu, *Biochim. Biophys. Acta*, in press. "Cleavage of the S–S bond in 5,5′-dithiobis-(2-nitrobenzoic acid) in presence of cationic detergent. An approach to the cleavage of S–S bond in bovine plasma albumin."

Molecular Structure of Molybdenum Tetrafluoride Oxide Studied by Gas Electron Diffraction

Kinya IIJIMA

Department of Chemistry, Faculty of Science, Shizuoka University, Oya, Shizuoka 422

(Received September 29, 1976)

The molecular structure of molybdenum tetrafluoride oxide was determined to be square-pyramidal by a sector-microphotometer method of gas electron diffraction. The following molecular parameters were obtained by a least-squares method: r_g(Mo–F)=1.836±0.003 Å, r_g(Mo–O)=1.650±0.007 Å, and r_g(F···F(s))=2.522± 0.005 Å. The molecular structure is similar to those of WCl_4O and $MoCl_4O$, but significantly different from those of XeF_4O and IF_5. The molecular intensities calculated using the TFD or RHFS phase angle for molybdenum atom were in disagreement with the observed ones.

The molecular structures of WCl_4O,[1] $MoCl_4O$,[2] XeF_4O,[3,4] IF_5,[4,5] BrF_5,[4] and ClF_5[4] were reported to be square-pyramidal in gas phases, but the oxygen-metal-chlorine angles in WCl_4O and $MoCl_4O$ differ significantly from the corresponding angles in the other compounds. Although the MoF_4O molecule in the solid state is octahedral in consequence of bridging through fluorine atoms,[6] the molecule in the gas phase is monomeric with C_{4v} symmetry as predicted from spectroscopic studies.[6–8] The present study was undertaken in order to determine the structure of gaseous MoF_4O by means of gas electron diffraction. It is interesting to compare the molecular structure of MoF_4O with those of $MoCl_4O$ and other square-pyramidal molecules. Seip and Seip noted from the electron diffraction analysis of MoF_6[9] that the observed cut-off point for Mo–F pair disagrees with the theoretical value. This problem was also checked in the present study.

Experimental

The chlorine atoms in molybdenum tetrachloride oxide which was prepared by the method described before[10] were substituted with fluorine atoms by the reaction with anhydrous hydrogen fluoride.[11] The sample was purified by repeated sublimations *in vacuo*. It was vaporized at 70—80 °C, and electron-diffraction photographs were taken with an r^3-sector at the camera distance of 144 mm. The accelerating voltage was 40 kV, the exposure time 30 s, and the electron-beam current 0.8 μA. The pressure of the diffraction chamber was below 3×10^{-5} Torr during a photographic exposure. The electron wavelength was calibrated by gold powder patterns. The lattice constant of gold was calibrated by means of X-ray diffraction, and checked by electron diffraction studies of thallium chloride[12] and carbon disulfide.[13] Photographs were recorded on Fuji process hard plates, and the photographic densities of four plates were measured with a digital microphotometer at intervals of 0.4 mm. The intensities of each plate were used independently for the structure analysis. The electron diffraction unit and digital microphotometer used in the present study were described elsewhere.[14]

Analysis

Intensities were leveled by the theoretical background which was calculated by using the elastic scattering factors of Kimura *et al.*[15] and the inelastic scattering factors of Cromer and Mann.[16] The leveled intensities were obtained in a range s=5.3—32.0 Å^{-1} at intervals $\Delta s=\pi/10$.

The radial distribution curve is shown in Fig. 1. The N_{ij} functions which fit μ_{ij}[1,17] in a whole range of scattering angle were as follows;

$$N_{Mo-F} = 1.097 + 0.104\exp(-0.0034\,s^2)$$
$$N_{Mo-O} = 1.118 + 0.153\exp(-0.0089\,s^2)$$
$$N_{F\cdots F} = 1.355 + 0.713\exp(-0.0057\,s^2)$$
$$N_{F\cdots O} = 1.380 + 0.814\exp(-0.0072\,s^2)$$

The radial distribution curve suggests that the molecular structure of MoF_4O is square-pyramidal.

The index of resolution, r(Mo–F), r(Mo–O), r(F···F(s)), and five root-mean-square amplitudes l(Mo–F), l(Mo–O), l(F···F(s)), l(F···F(l)), and l(F···O) were determined by the least-squares calculations[2,18,19] with the assumption of C_{4v} symmetry. Asymmetry parameters for bonded distances were estimated by a diatomic molecule approximation[20] to be 1.2×10^{-6} and 0.6×10^{-6} Å^3 for Mo-F and Mo–O, respectively. The parameter, a, in the Morse function was assumed to be 2.0 Å^{-1}. The asymmetry parameters for non-bonded distances were ignored.

At the first stage of analysis a large difference between the observed and theoretical molecular intensities was found in the range s=22—32 Å^{-1}, as shown in Fig. 2. The cut-off point for Mo–F pair is observed at s=23.2 ±0.6 Å^{-1}, but the theoretical value is s=27.0 Å^{-1}.

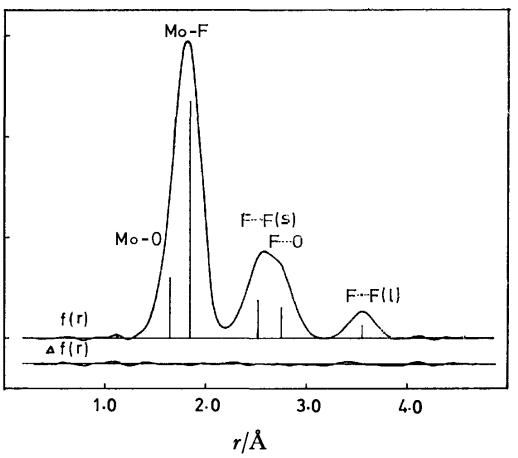

Fig. 1. Experimental radial distribution, $f(r)$, and the difference between the experimental and theoretical ones, $\Delta f(r)$. A damping function of $\exp(-0.0020\,s^2)$ was used.

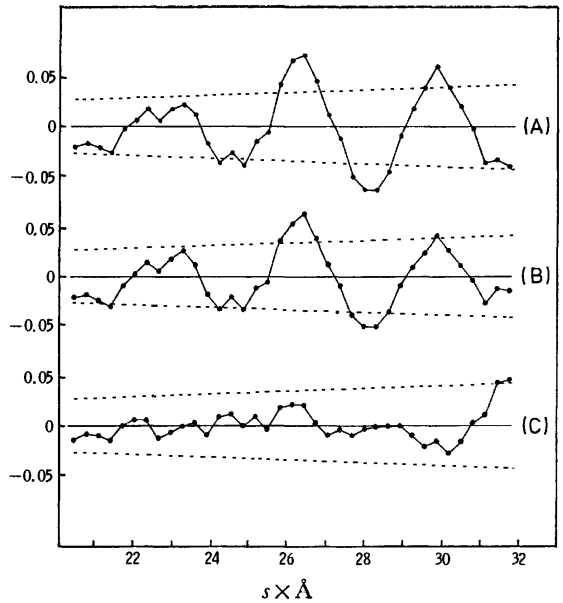

Fig. 2. The observed minus theoretical molecular intensities. The observed values were an average of intensities from four plates, and the theoretical ones in (A), (B), and (C) curves were calculated by using parameters of (A), (B), and (C) in Table 1, respectively. The broken curves show the limits of error in the $sM(s)$.

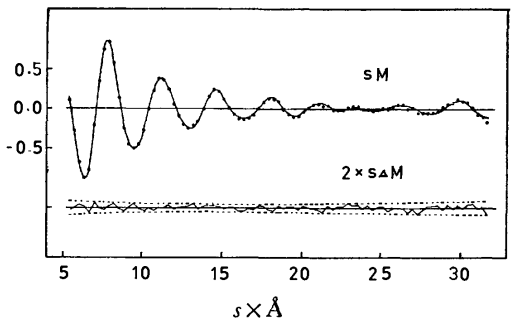

Fig. 3. Observed and theoretical molecular intensities. Typical observed values are shown in dots, and the best-fit theoretical ones are shown in the solid curve. The lower solid and broken curves represent the residuals and the limits of error, respectively, in the $sM(s)$.

The phase angles, η, obtained from the Thomas-Fermi-Dirac (TFD) and Hartree-Fock (HF) potentials[15] were used for molybdenum and fluorine atoms, respectively. The phase angle from the relativistic Hartree-Fock-Slater (RHFS) potential[21] was also used for molybdenum atom, and the theoretical cut-off point is $s=26.1$ Å^{-1}. The disagreement between the observed and theoretical molecular intensities may be due to the uncertainty in molybdenum phase angle, η_{Mo}, used in the anlysis. The theoretical cut-off point for Pd-F pair calculated using the TFD phase angle for palladium atom is $s=23.7$ Å^{-1}, in agreement with the observed value for the Mo-F pair. Since the absolute value of atomic scattering factor, $|f|$, for molybdenum atom had a negligible effect on molecular parameters, the analysis using $|f_{Mo}|$ and η_{Pd} for molybdenum atom was carried out, and the calculated intensities gave the best fit to the observed ones. The results of least-squares analyses, where the TFD and RHFS phase angles of molybdenum and the TFD phase angle of palladium were used, are listed in Table 1.

Table 1. Results of least-squares analyses (in Å)

	(A)[b]	(B)[b]	(C)[b]
r_g(Mo-F)	1.838 (2)	1.836 (1)	1.836 (1)
r_g(Mo-O)	1.654 (7)	1.649 (6)	1.650 (5)
r_g(F···F(s))	2.524 (4)	2.519 (4)	2.522 (3)
l(Mo-F)	0.059 (3)	0.057 (3)	0.046 (3)
l(Mo-O)	0.045(21)	0.040(16)	0.034(10)
l(F···F(s))	0.098 (8)	0.100 (7)	0.098 (5)
l(F···F(l))	0.084(14)	0.086(12)	0.084 (9)
l(F···O)	0.101(10)	0.104 (8)	0.101 (7)
R[a]	0.978(36)	1.019(43)	0.979(38)

Estimated random errors (2.5σ) are shown in parentheses ($\times 10^3$). a) The index of resolution, R, is dimensionless. b) (A), (B), and (C) are the results of analyses using TFD f_{Mo}, RHFS f_{Mo}, and TFD $|f_{Mo}|$ and η_{Pd}, respectively, for molybdenum atom.

Table 2. Distances and mean amplitudes (in Å)

	r_g	l
Mo-F	1.836±0.003	0.046±0.013
Mo-O	1.650±0.007	0.034±0.015
F···F(s)	2.522±0.005	0.098±0.005
F···F(l)	3.563±0.008	0.084±0.009
F···O	2.752±0.009	0.101±0.008
∠OMoF	103.8±0.6°	
∠FMoF	86.7±0.3°	

The final results of the analysis are given in Table 2, where parameter values were obtained from the analysis using palladium phase angle for molybdenum atom. Random errors were given by 2.5 times the larger of σ_1 and σ_2.[19,22] The uncertainty in phase angle for molybdenum atom was taken into account as systematic errors in bond distances and amplitudes. The error in lattice constant of a reference material (0.06%) and the errors in measurements of diffraction patterns of the reference (0.09%) and of the camera distance (0.04%) were also taken into account as systematic errors in bond distances. The correlation matrix[23] is given in Table 3, and the best-fit theoretical intensity curve is shown in Fig. 3.[24] The least-squares calculations were carried out by use of a FACOM 230-60 computer at the Nagoya University Computing Center.

Discussion

The phase angle for molybdenum was not sensitive to the distances of the atomic pairs relating to molybdenum, but was considerably sensitive to the amplitudes as shown in Table 1. The Mo-F and Mo-O amplitudes obtained using η_{Pd} in place of η_{Mo} were in fair agreement with 0.040 and 0.035 Å calculated from the Mo-F and Mo-O vibrational frequencies,[7,25] respectively. The analysis using η_{Pd} gave the smallest

Table 3. Correlation matrix for molecular parameters of MoF_4O[a)]

	r(Mo-F)	r(Mo-O)	r(F···F(s))	l(Mo-F)	l(Mo-O)	l(F···F(s))	l(F···F(1))	l(F···O)	R
r(Mo-F)	1.0	0.13	0.38	0.05	−0.26	0.04	0.02	0.08	0.13
r(Mo-O)		1.0	0.54	−0.11	−0.07	−0.21	−0.07	−0.12	−0.50
r(F···F(s))			1.0	−0.16	−0.16	−0.05	−0.06	0.03	−0.36
l(Mo-F)				1.0	0.34	0.24	0.09	0.19	0.65
l(Mo-O)					1.0	0.06	0.01	0.04	0.15
l(F···F(s))						1.0	0.06	0.62	0.39
l(F···F(1))							1.0	0.04	0.15
l(F···O)								1.0	0.30
R									1.0

a) The elements are defined as $\rho_{ij}=B_{ij}^{-1}/(B_{ii}^{-1}\times B_{jj}^{-1})^{1/2}$.

standard deviations for parameters. The cut-off point for Mo-F pair, s=23.2 Å^{-1}, obtained at the accelerating voltage of 40 kV in the present study is estimated to be equivalent to about 22 Å^{-1} at 35 kV by use of the formula.[26)] This value is in good agreement with 22.2±0.4 Å^{-1} from the experiment of MoF_6 at 35 kV.[9)]

The molecular structure of MoF_4O is square-pyramidal in the gas phase, but in the crystal state[6)] it is distorted by bridging of fluorine to another molecule and forms a nearly octahedral arrangement around a molybdenum atom. The Mo-F and Mo-O distances in the crystal, 1.81—1.84 and 1.62—1.65 Å, respectively, are in agreement with the corresponding distances in the gas phase. However, the average OMoF (terminal) angle in the crystal, 100.4°, is a little smaller than that in the gas phase because of an octahedral arrangement.

The gaseous MoF_4O has the same structure as the gaseous WCl_4O[1)] or $MoCl_4O$,[2)] but it is apparently distinguished from those of XeF_4O[3,4)] and IF_5[4,5)] with respect to the XMY angle, where M is a central atom. The angles of the latter molecules are about 90° or less, and can be explained by considering the repulsions between bonding electron pairs and a nonbonding electron pair of central atoms.[27)]

There are only small differences between MoF_4O and $MoCl_4O$ with respect to Mo–O distance and OMX angle. However, the Mo-F distance, 1.836±0.003 Å, is shorter than the Mo-Cl distance, 2.279±0.003 Å, by about 0.44 Å. The force constant for the Mo–O bond in MoF_4O is estimated to be 8.6 mdyn/Å from the frequency of Mo–O stretching vibration in the gas phase[7)] and is nearly equal to that in $MoCl_4O$, 8.29 mdyn/Å.[2)] The distance and force constant for the Mo–O bond in gaseous MoF_4O give a good fit to the correlation curve between them,[28)] and its bond order is estimated to be 3. The Mo-F distance in MoF_4O is greater than that in MoF_6 (1.820±0.003 Å[9)]) by about 1%. The lengthening of the Mo-F distance may be interpreted as the effect of the Mo–O multiple bond.

The author thanks Professor Shuzo Shibata for his kind advice and helpful discussions. He is also indebted to Dr. Shunji Nagase of the Government Industrial Research Institute for preparation of the sample.

References

1) K. Iijima and S. Shibata, *Bull. Chem. Soc. Jpn.*, **47**, 1393 (1974).
2) K. Iijima and S. Shibata, *Bull. Chem. Soc. Jpn.*, **48**, 666 (1975).
3) E. J. Jacob, H. B. Thompson, and L. S. Bartell, *J. Mol. Struct.*, **8**, 383 (1971).
4) G. M. Begun, W. H. Fletcher, and D. F. Smith, *J. Chem. Phys.*, **42**, 2236 (1965).
5) G. R. Jones, R. D. Burbank, and N. Bartlett, *Inorg. Chem.*, **9**, 2264 (1970).
6) A. J. Edwards and B. R. Steventon, *J. Chem. Soc., A*, **1968**, 2503.
7) B. G. Ward and F. E. Stafford, *Inorg. Chem.*, **7**, 2569 (1968).
8) I. R. Beattie, K. M. S. Livingston, D. J. Reynolds, and G. A. Ozin, *J. Chem. Soc., A*, **1970**, 1210.
9) H. M. Seip and R. Seip, *Acta Chem. Scand.*, **20**, 2698 (1966).
10) R. Colton, I. B. Tomkins, and P. W. Wilson, *Aust. J. Chem.*, **17**, 496 (1964).
11) O. Ruff and F. Eisner, *Ber.*, **40**, 2931 (1907).
12) W. Witt, *Z. Naturforsch.*, **19a**, 1363 (1964).
13) Y. Morino and T. Iijima, *Bull. Chem. Soc. Jpn.*, **35**, 1661 (1962).
14) S. Shibata, K. Iijima, R. Tuni, and I. Nakamura, *Rep. Fac. Sci. Shizuoka Univ.*, **9**, 33 (1974).
15) M. Kimura, S. Konaka, and M. Ogasawara, *J. Chem. Phys.*, **46**, 2599 (1967); M. Ogasawara, S. Konaka, and M. Kimura, *ibid.*, **50**, 1488 (1969).
16) D. T. Cromer and J. B. Mann, *J. Chem. Phys.*, **47**, 1892 (1967); D. T. Cromer, *ibid.*, **50**, 4857 (1969).
17) R. M. Gavin and L. S. Bartell, *J. Chem. Phys.*, **48**, 2460 (1968).
18) S. Shibata, *Bull. Chem. Soc. Jpn.*, **45**, 1631 (1972).
19) Y. Morino, K. Kuchitsu, and Y. Murata, *Acta Crystallogr.*, **18**, 549 (1965).
20) K. Kuchitsu, *Bull. Chem. Soc. Jpn.*, **40**, 505 (1967).
21) L. Schäfer, A. C. Yates, and R. A. Bonham, *J. Chem. Phys.*, **55**, 3055 (1971).
22) S. Konaka, Y. Murata, K. Kuchitsu, and Y. Morino, *Bull. Chem. Soc. Jpn.*, **39**, 1134 (1966).
23) O. Bastiansen, L. Hedberg, and K. Hedberg, *J. Chem. Phys.*, **27**, 1311 (1957).
24) Numerical experimental data of the leveled total intensity and the background have been deposited with the Chemical Society of Japan (Document No. 7703).
25) H. H. Claassen, G. L. Goodman, J. H. Hoolloway, and H. Selig, *J. Chem. Phys.*, **53**, 341 (1970).
26) J. A. Ibers and J. A. Hoerni, *Acta Crystallogr.*, **7**, 405 (1954).
27) R. J. Gillespie, *J. Chem. Educ.*, **40**, 295 (1963); *ibid.*, **47**, 18 (1970).
28) F. A. Cotton and R. M. Wing, *Inorg. Chem.*, **4**, 867 (1965).

An INDO-UHF Molecular Orbital Study of the Conformations and Electronic Structures of Some σ-Type Radicals

Katsutoshi OHKUBO and Hiroyuki SATO

Department of Synthetic Chemistry, Faculty of Engineering, Kumamoto University, Kurokami, Kumamoto 860

(Received October 4, 1976)

The equilibrium geometric parameters determined for XC=Y radicals (HC=O, CH_3C=O, NH_2C=O, and HC=CH_2) are not characterized by their bond lengths but by their X–C–Y angles, which are wide compared with the angles in their parent molecules (XHC=Y). The %s character of the σ orbitals on the C atom in XHC=Y was found to be conserved in the %s character and the s-orbital spin density of the same atom in XC=Y radicals: there are linear relationships between them. Some notable features of the unpaired-electron distribution on the frameworks of XC=Y radicals are also discussed in connection with the electronic properties of the σ radicals.

The conformations and electronic structures of paramagnetic species containing an odd electron in their σ orbitals (*e.g.*, σ-type radicals such as vinyl, formyl, and phenyl) have been the object of only limited experimental and MO-theoretical investigations. Concerning the conformations of the σ radicals, the equilibrium geometric parameters have hitherto been given only for simple σ radicals such as HC=O,[1] even though, in connection with the electronic structures of the σ radicals, the nuclear hyperfine constants of several σ radicals (C_6H_5, CH_2=CX, or XC=O, where X=H, CH_3, OCH_3, *etc.*) have already been obtained by ESR observations.[2]

On the other hand, the distribution of unpaired electrons on the frameworks of σ radicals such as vinyl, formyl, and phenyl has been discussed on the basis of their electronic structures obtained by the EHMO,[3] CNDO,[4] or INDO[5] computations with assumed bond lengths and angles; but the first two methods are not capable of giving a proper account of the contribution of spin polarization to the unpaired electron density because they neglect interelectron repulsions (in the EHMO) or about atomic exchange integrals (in the CNDO).

In the present paper, using the semiempirical INDO method,[6] the conformations of some σ radicals of XC=Y (HC=O, CH_3C=O, NH_2C=O, and HC-CH_2) are characterized by comparing them with those of the parent molecules of XHC=Y; the unpaired electron distributions are also discussed in connection with their conformations and electronic properties.

Method of Calculation

The integrations and parametrizations involved in the INDO method, which is relatively reliable for bond angles but less so for bond lengths,[6,7] have been described in detail in Ref. 6, so they will not be repeated here. In the INDO-UHF computations the annihilation procedure was not carried out, because the annihilation has little effect on the electron density distribution[8] and because, in the conventional evaluation of the hyperfine splitting constants (a_N), the best fitting proportionality constants to the experimental a_N values have been determined on the basis of the computed spin densities without the annihilation.[5]

The geometric parameters of XC=Y radicals (HC=O, CH_3C=O, NH_2C=O, and HC=CH_2) shown in Fig. 1 were first determined by changing them in turn so as to minimize the total energy until they become identical; then, the optimized conformations of the XC=Y radicals were recalculated by changing all their geometric parameters in the magnitude of $\pm$0.01 Å and $\pm$1° as a check on the reliability of the optimization results. In the above optimizations, some assumed bond lengths (r_{NH}=1.0 Å in NH_2C=O and r_{CH}=1.08 Å in CH_3C=O) and angles ($\angle$CNH=120° in NH_2C=O and $\angle$HCH=109.5° in CH_3C=O) were used to shorten the computation time.

Results and Discussion

Optimized Conformations. The computed equilibrium geometric parameters of the XC=Y radicals (HC=O, CH_3C=O, NH_2C=O, and HC=CH_2) are summarized in Table 1, together with those (obtained by the INDO calculations) of the parent molecules of XHC=Y (HCHO, CH_3CHO, NH_2CHO, and H_2C=CH_2). The difference in the bond lengths between XC=Y and XHC=Y was very small (within 0.04 Å) in their respective frameworks, but the computed bond angles (θ) of the former were too large (by 7.42—37.4°) as compared with those of the latter. The optimized bond angle (θ) of XC=Y seems to be overestimated. The experimental θ value, for example, for HC=O (θ=119.5°[1]) is too small as compared with the calculated one (θ=131°), even though some overestimations of the bond angle (θ) of XHC=Y have been seen, ranging from 2.1° in NH_2CHO (exptl=121.5°[9]) to 3° in

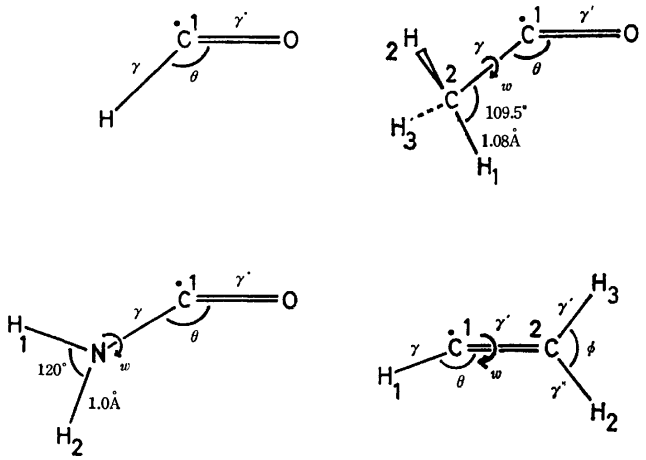

Fig. 1. Geometric parameters for the conformational optimization.

Table 1. Optimized geometric parameters for the XC=Y radicals

XC=Y	γ/Å	γ'/Å	θ/deg	ω/deg	γ''/Å	ϕ/deg
HC=O	1.12	1.23	131			
	(1.12)	(1.25)	(115)			
CH_3C=O	1.44	1.23	142	0		
	(1.44)	(1.26)	(124)	(0)		
NH_2C=O	1.35	1.26	131	0		
	(1.343)	(1.243)	(123.6)	(0)		
HC=CH_2	1.10	1.27	161.7	0	1.12	107.4
	(1.11)	(1.31)	(124.3)	(0)	(1.11)	(111.4)

Values in parentheses are those for the parent XHC=Y molecules, and the underlined values are the ones fixed (taken from Ref. 9) for the calculations.

CH_3CHO (exptl=121°[9]) and H_2C=CH_2 (exptl=121.3°[10]). At any rate, the INDO computations tend to give overestimated bond angles (θ) for the XC=Y radicals, because the widening of the bond angle (θ) unilaterally decreases the electron and nuclear repulsions. For example, the widening of the bond angle in HC=O from θ=115° (corresponding to that in HCHO) to 131° (corresponding to that in HC=O) monotonously decreased the electron and nuclear repulsions (E_{II} and E_N respectively) from 28.827 to 28.724 a. u. in E_{II} and from 13.816 to 13.700 a. u. in E_N, with a monotonous decrease in the one-electron attraction (E_I) from −67.441 to −67.229 a. u. The balance in the repulsions and the attraction energies, therefore, gave the rather large bond angle (θ=131°) for HC=O. In this sense, it can be said that the underestimation of the electron repulsions, which is the usual trend of the INDO calculations,[5,11] gave bond angles (θ) to the XC=Y radicals which were too large.

Next we discuss the change in the energetical stability of the XC=Y radicals by the internal rotation of the X or Y group around the C–C bond in CH_3C=O or HC=CH_2 and around the C–N bond in NH_2C=O. The rotation angle (ω) for the energetically most stable and unstable conformations are given in Fig. 2, together with the rotation barriers. In the most stable or unstable conformations of XHC=Y and XC=Y, the rotation angles (ω) were just the same between the respective parent molecules and the σ radicals, but the rotation barriers of the XC=Y radicals were rather low in comparison with those of the XHC=Y molecules (0.345 kcal/mol for CH_3CHO, 23.11 kcal/mol for NH_2CHO, and 105.22 kcal/mol for H_2C=CH_2). The INDO computations without polycenter interelectron repulsions usually result in low rotation barriers (for instance, the calculated barrier (0.345 kcal/mol) for CH_3CHO was too low as compared with the experimental value of 1.16 kcal/mol[13]), but the number (105.22 kcal/mol) for H_2C=CH_2 (r_{CC}=1.31 Å at ω=0° was stretched to r_{CC}=1.38 Å in the triplet state conformation at ω=90°) was computed to be too high in comparison with the experimental number of 65.0 kcal/mol.[12] The overestimated rotation barrier for H_2C=CH_2 is probably due to the incomplete optimization of its geometric parameters, such as r_{CH} and ∠CCH, at ω=90°. The decrease in the E_I term by the rotation

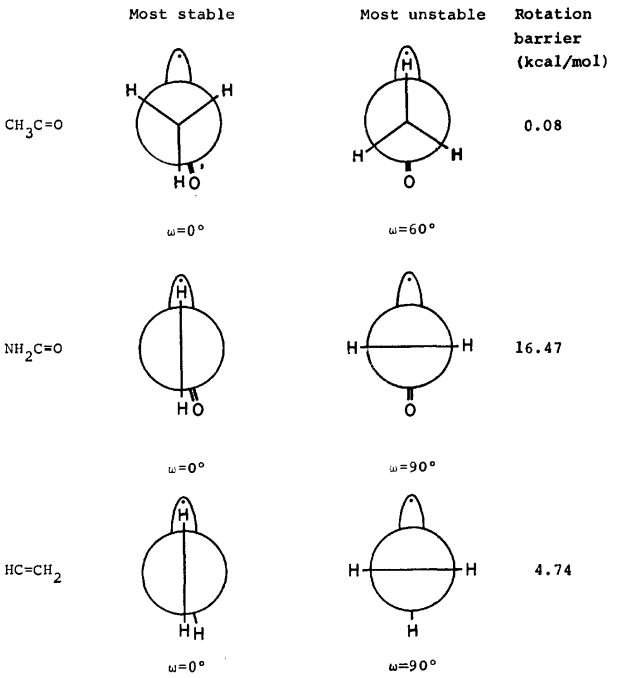

Fig. 2. The most stable and unstable conformers of CH_3C=O, NH_2C=O, and HC=CH_2.

from ω=0° to ω=90° (or ω=60° in CH_3C=O and CH_3CHO) made both species (XC=Y and XHC=Y) more unstable, and this seems to be directly related to the decrease in the contribution of the π conjugation (including the pseudo one in CH_3C=O or CH_3-CHO) between the C–C or C–N bond to the stabilization of XC=Y or XHC=Y (see Table 2).

Electron Distribution and Spin Density. The polarization (charge distribution) in the XC=Y radicals was not so markedly different from that in the XHC=Y molecules, as seen from the computed atomic charge densities and dipole moments of XC=Y and XHC=Y in Table 3, but one slight difference is that XC=Y have a less positively charged C^1 atom and a less negatively charged O, C, or N atoms attached to the C^1, in comparison with XHC=Y. This was mainly caused by the electron shift from the neighboring atoms to the C^1 through the π-bonding orbitals during the widening of the bond angle (θ) in the XC=Y radicals. The hybridizations (sp^n) of the σ orbitals on the C^1 atom, n=1.35 (HC=O) —1.75 (HC=CH_2)

Table 2. Energy contribution terms and overlap populations for the most stable and unstable conformers of the XC=Y radicals

XC=Y	Conformer	E_I/a.u.	E_{II}/a.u.	E_N/a.u.	Total/a.u.	Overlap population of π conjugation	
						C-C(or C-N)	C=O
$CH_3C=O$	a	−119.781	52.270	34.228	-33.282_5	0.0632	0.1866
		(−130.451)	(57.100)	(39.156)	(-34.195_4)	(0.0641)	(0.1851)
	b	−119.774	52.265	34.226	-33.282_4	0.0634	0.1863
		(−130.440)	(57.094)	(39.151)	(-34.194_9)	(0.0642)	(0.1850)
$NH_2C=O$	a	−127.473	56.225	34.439	−36.809	0.1204	0.1462
		(−139.746)	(61.780)	(40.247)	(−37.719)	(0.1081)	(0.1706)
	b	−127.430	56.237	34.410	−36.783	0.0571	0.1779
		(−139.558)	(61.683)	(40.194)	(−37.681)	(0.0578)	(0.1899)
$HC=CH_2$	a	−53.617	22.122	15.891	−15.604	0.3018	
		(−61.445)	(25.507)	(19.370)	(−16.568)	(0.2835)	
	b	−53.612	22.125	15.891	−15.596	0.2770	
		(−60.446)	(25.145)	(18.901)	(−16.400)	(0.0978)	

Values in parentheses are those for the parent XHC=Y molecules.

Table 3. Charge and spin distributions and physicochemical constants for the XC=Y radicals

HC=Y	Atom	Charge density	Dipole moment (D)	ρ_s	ρ_p	Total	a_N(G)	
							calcd	obsd
HC=O	C^1	3.846(3.789)	1.49(2.10)	0.1726	0.3932	0.5658	141.58	134.5
	O	6.152(6.188)		0.0051	0.2742	0.2793	4.54	
	H	1.002(1.011)		0.1549		0.1549	83.63	136.5
$HC=CH_2$	C^1	4.085(4.003)	0.33(0.0)	0.0661	0.8171	0.8832	54.24	107.57
	C^2	3.965(4.003)		−0.0368	−0.2059	−0.2427	−30.15	−8.55
	H^1	0.948(0.999)		−0.0281		−0.0281	−15.16	13.39
	H^2	1.007(0.999)		0.2245		0.2245	121.20	65.0
	H^3	0.995(0.999)		0.1630		0.1630	87.99	37.0
$CH_3C=O$	C^1	3.861(3.674)	2.59(2.86)	0.1276	0.4918	0.6194	104.67	
	C^2	3.973(4.011)		0.0080	0.0007	0.0087	6.56	5.3
	O	6.210(6.286)		0.0062	0.2747	0.2809	5.48	
	H^1	1.002(0.995)		0.0796		0.0796	42.99	
	H^2	0.977(0.985)		0.0057		0.0057	3.05	
	H^3	0.977(0.985)		0.0057		0.0057	3.05	
$NH_2C=O$	C^1	3.809(3.550)	3.71(3.90)	0.1647	0.3034	0.4681	135.06	
	N	5.163(5.236)		0.0308	0.0151	0.0459	11.67	21.6
	O	6.270(6.384)		0.0058	0.4124	0.4182	5.18	
	H^1	0.876(0.876)		−0.0026		−0.0026	−1.40	1.15
	H^2	0.882(0.871)		0.0704		0.0704	38.01	30.45

Values in parentheses are those for the XHC=Y molecules.

in XC=Y and n=1.62 (HCHO) —1.80 ($H_2C=CH_2$) in XHC=Y, were also almost the same magnitude in the radicals and the parent molecules. Strictly speaking the order of the %s character of the C^1 σ-orbitals in XC=Y, HC=O(42.50%) > $NH_2C=O$(41.43%) > $CH_3C=O$(38.69%)>$HC=CH_2$(37.62%), was well reflected in that in XHC=Y, HCHO(38.10%)> NH_2CHO(37.50%) > CH_3CHO(36.76%) > $H_2C=CH_2$ (35.69%), and there is a completely linear correlation between the above %s characters of XC=Y and XHC=Y (Fig. 3). Thus, the %s chracter of the σ-orbitals on the C^1 atom in XHC=Y was conserved in the same C^1 atom of XC=Y, and this is in harmony with the fact that the %s character of the C atom in XYZCH molecules (X, Y, or Z=substituent) is conserved in the same atom of XYZC radicals.[14]

In regard to the spin distribution in the XC=Y radicals, the total spin densities (Table 3) chiefly spread over the C^1 atom (46.6% in $NH_2C=O$ —61.9% in $CH_3C=O$) and the C^1-bound oxygen or carbon (C^2) atom (15.7% in $HC=CH_2$ —41.6% in $NH_2C=O$). Such a spin distribution was predominantly recognized on the p orbitals (especially, on the p orbital conjugating with the C^1 unpaired-electron orbital) of the O or C^2 atom or of the C^1 atom *per se*, and the spin densities on the C^1 p-orbitals, ρ_p, follow the order of $HC=CH_2$ >$CH_3C=O$>HC=O>$NH_2C=O$. The above order is just the same as that in the bond order of the

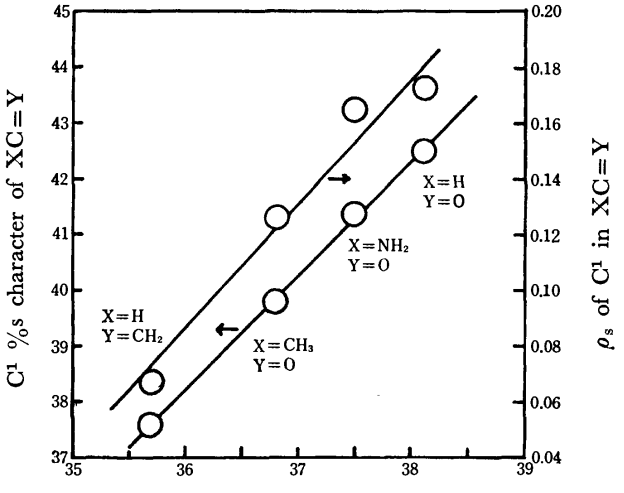

Fig. 3. Linear relationship of the C^1 %s character of XHC=Y with the C^1 %s character of XC=Y and with the ρ_s of C^1 in XC=Y.

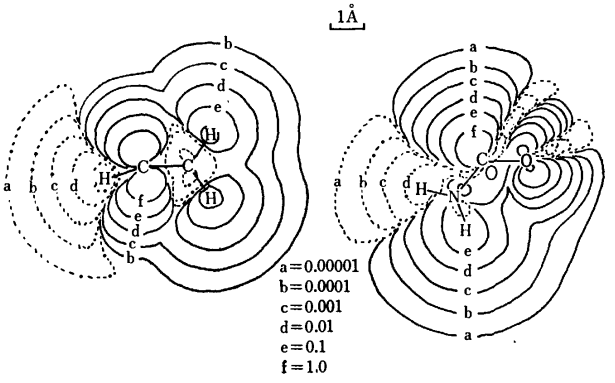

Fig. 4. Spin density contour maps for $HC{=}CH_2$ and $NH_2C{=}O$.

pseudo π-orbital between the C^1 and O (or C^2) p-orbitals; that is, $HC{=}CH_2(0.472) > CH_3C{=}O(0.375) > HC{=}O(0.359) > NH_2C{=}O(0.352)$, where the values in parentheses are the bond orders. This suggests that the direct spin polarization from the C^1 atom to the neighboring one through the π-type bonding decreases with increasing the bond order. In this respect, the internal rotation increasing the bond order of the pseudo π-conjugation in the C^1–C^2 ($HC{=}CH_2$) or C^1–N ($NH_2C{=}O$) bond resulted in the increase of the spin density of the C^1 atom (especially, that on the C^1 p-orbital).

On the other hand, the spin density of the C^1 s-orbital, ρ_s, was directly related to the hybridization on the C^1 σ-orbitals. Specifically, the ρ_s values show a linear dipendence on the %s character of the C^1 σ-orbitals (Fig. 3) and follow the order of $HC{=}O > NH_2C{=}O > CH_3C{=}O > HC{=}CH_2$. This is also in harmony with the fact that the hyperfine splitting constant, a_N, (reflecting the ρ_s value) of the carbon atom in the XYZC radical correlates linearly with the $J_{C^{13}H}$ coupling constant (reflecting the %s character of the C^{13} atom) of the XYZCH molecule.[14]

It should be noted that the computed spin density of the hydrogen *trans* to the site of the unpaired-electron orbital on the C^1 atom in $HC{=}CH_2$, $CH_3C{=}O$, or $NH_2C{-}O$ was considerably larger than that of the hydrogen *cis* to the above orbital. This trend was also seen in the ESR observations: the a_N value of the *trans* hydrogen in $HC{=}CH_2$, $NH_2C{=}O$, or $H_2C{=}CCH_3$ (*trans* H=(+) 57.89 G[15]) and *cis* H=(+)32.92 G[15]) is larger than that of the *cis* hydrogen. In view of the fact that the internal rotation from $\omega=0°$ to $\omega=90°$ monotonously decreased the spin density of the *trans* hydrogen in $HC{=}CH_2$ or $NH_2C{=}O$, with equivalent spin densities for H^2 and H^3 in $HC{=}CH^2H^3$ or for H^1 and H^2 in $NH^1H^2C{=}O$ at $\omega=90°$, the predominant interaction of the C^1 unpaired-electron orbital with the *trans* H s-orbital rather than with the *cis* H s-orbital presumably caused the spin polarization to be stronger for the *trans* H atom. Such circumstances of the spin polarization (or of the spin delocalization) may also be understandable from the contour map of the spin distribution in $HC{=}CH_2$ or $NH_2C{=}O$ (Fig. 4).

Finally, we will briefly point out the hyperfine splitting constants, a_N, of the present XC=Y radicals (Table 3). The a_N values computed with the best proportionality constants[5] did not show satisfactorily good coincidence with the observed a_N values, and those for ^1H, ^{13}C, ^{14}N, and ^{17}O had almost the same accuracy of agreement with the observed ones. Here, no characteristic feature of the calculated a_N values for the present XC-Y radicals was recognized in terms of a coincidence between the INDO computation results and the ESR observations.

References

1) G. Herzberg and D. A. Ramsay, *Proc. R. Soc. London, Ser. A*, **233**, 34 (1955); D. A. Ramsay, *Adv. Spectrosc.*, **1**, 1 (1959).
2) For instance, see J. K. Kochi, Ed., "Free Radicals," Vol. II, John Wiley & Sons, New York (1973), p. 435.
3) G. A. Petersson and A. D. McLachlan, *J. Chem. Phys.*, **45**, 628 (1966); W. T. Dixon, *Mol. Phys.*, **6**, 201 (1965).
4) N. M. Atherton and A. Hinchliffe, *Mol. Phys.*, **12**, 349 (1967).
5) J. A. Pople, D. L. Beveridge, and P. A. Dobosh, *J. Am. Chem. Soc.*, **90**, 4201 (1968).
6) J. A. Pople and D. L. Beveridge, "Approximate Molecular Orbital Theory," McGraw-Hill, New York (1970).
7) M. D. Newton, W. A. Lathan, W. J. Hehre, and J. A. Pople, *J. Chem. Phys.*, **52**, 4064 (1970).
8) A. T. Amos and L. Snyder, *J. Chem. Phys.*, **41**, 1773 (1964).
9) L. E. Sutton, Ed., "Tables of Interatomic Distances," Chem. Soc., London, Special Publications, No. 11 (1958) and No. 18 (1965).
10) H. C. Allen and E. K. Plyler, *J. Am. Chem. Soc.*, **80**, 2673 (1958).
11) H. Fisher, H. Kollmar, and H. O. Smith, *Tetrahedron Lett.*, **1968**, 5821.
12) M. J. S. Dewar and E. Haselbach, *J. Am. Chem. Soc.*, **92**, 590 (1970).
13) R. W. Kilb, C. C. Lin, and E. B. Wilson, *J. Chem. Phys.*, **26**, 1695 (1957).
14) N. Muller and D. E. Pritchard, *J. Chem. Phys.*, **31**, 768 (1959).
15) R. W. Fessenden and R. H. Schuler, *J. Chem. Phys.*, **39**, 2147 (1963).

Vibration Spectra and Rotational Isomerism of Chain Molecules. IV.[1] Diethyl Sulfide, Ethyl Propyl Sulfide, and Butyl Methyl Sulfide

Masahiro OHTA, Yoshiki OGAWA, Hiroatsu MATSUURA, Issei HARADA, and Takehiko SHIMANOUCHI

Department of Chemistry, Faculty of Science, University of Tokyo, Hongo, Bunkyo-ku, Tokyo 113

(Received October 26, 1976)

The Raman and infrared spectra of diethyl sulfide, ethyl propyl sulfide and butyl methyl sulfide were measured for the gaseous, liquid, glassy and crystalline states. The normal vibration frequencies were calculated, a consistent set of force constants explaining the frequencies of basic aliphatic sulfides being assumed. The rotational isomerism was studied and the following conclusions were obtained. (1) Only the all-*trans* form exists in the crystalline state. (2) Many forms coexist in the liquid state and most of them persist in the glassy state even at the liquid nitrogen temperature. (3) In the liquid state, the *gauche* conformation about the S–C axis is more stable than the *trans* conformation, and the *gauche* conformation about the C–C axis directly adjoining the S–C axis is as stable as the *trans* conformation. These results confirm that the repulsive force between nonbonded hydrogen atoms is one of the important factors influencing the stability of molecualr conformations. The stable conformations of the sulfide molecules were correlated with those of polythioether chains.

In previous papers,[1-3] we compared the Raman and infrared spectra of unbranched ethers, paraffins and ethyl methyl sulfide in the crystalline, glassy, liquid and gaseous states with the results of normal vibration calculations and determined the rotational isomers existing in each state.

In the present paper, the same method is applied to unbranched sulfide molecules. The results also show that the method is useful in the study of rotational isomerism. The stable forms of these sulfide molecules do not always correspond to those of the ethers. The factors stabilizing the isomers will be discussed.

The stable conformations of some sulfides[1,4-12] and polythioethers[13-15] have already been studied. The present results will be correlated with the former conclusions.

Experimental

Diethyl sulfide, ethyl propyl sulfide and butyl methyl sulfide were purchased from Tokyo Kasei Kogyo Co., Ltd. and were distilled prior to the measurements. The Raman spectra were measured for the liquid, glassy and crystalline states and the infrared spectra for the gaseous, liquid, glassy and crystalline states. The spectrometers described in the previous study[2] are used.

The Raman spectra were recorded in the region below 1600 cm^{-1}. The spectra in the liquid state were measured at room and lower temperatures. The glassy state for the Raman measurements was obtained by putting into liquid nitrogen the sample enclosed in an ampoule and cooling it rapidly, and the crystalline state by cooling the sample slowly with liquid nitrogen. The crystallization of diethyl sulfide was very rapid and the Raman spectra in the glassy state could not be measured.

The infrared spectra in the gaseous state were measured with a 10 cm gas cell in the region 1600—600 cm^{-1}. For the measurements of the infrared spectra in the liquid state, 0.05 and 0.025 mm fixed cells with KBr windows were used in the region 1600—400 cm^{-1}, and a variable thickness cell with KRS-5 windows in the region 700—250 cm^{-1}. The glassy state for the infrared measurements were obtained by depositing the sample onto a cooled window of KBr or KRS-5, and the crystalline state by annealing the glass several times. For the measurements in the region 700—250 cm^{-1}, the spectrometer was flushed with dry air to get rid of water vapor absorptions.

Normal Coordinate Treatment

The normal coordinate treatment of the unbranched sulfides was carried out in a way similar to the case of the ethers.[2] Detailed results including structural parameters, symmetry coordinates and force constants are reported in a separate paper.[16]

A total of 70 force constants associated with the sulfide group were determined from 446 Raman and infrared frequencies of 31 forms of 11 molecular species. Table 1 shows the procedure of the least-squares refinement of the force constants.

Results

Figures 1—9 show the Raman and infrared spectra of the sulfides in the various states. The observed frequencies and the assignment based on the calculated potential-energy distributions are listed in Tables 2—4.

The observed spectra were analyzed with reference to the results of the normal coordinate treatment. The following spectral features are observed for the three sulfides studied in this work. (1) The spectra in the various states are distinctly different, especially in the 500—200 cm^{-1} region of the skeletal deformation vibrations and in the 800—600 cm^{-1} region of the C–S stretching and the methylene rocking vibrations. (2) The spectral pattern of the crystalline state is the simplest and the number of the observed bands is the smallest. (3) In the glassy state, many bands are observed in addition to those which persist in the crystalline state. (4) The liquid-state spectra have essentially the same numbers of bands as those in the glassy-state spectra. However, their relative band intensities and widths are considerably different between the two states.

In the following subsections, the rotational isomerism of the individual sulfides is described.

Diethyl Sulfide. Since this molecule has two C–S axes associated with the rotational isomerism, there are four possible isomers, TT, TG, GG, and GG′, as given in Table 1 of Part I of this series.[2] The observed and calculated frequencies in the 900—200 cm^{-1} region are compared in Fig. 3.

The spectra in the crystalline state show that only

TABLE 1. PROCEDURE OF THE LEAST-SQUARES CALCULATION

Step	$CH_3SC_2H_5$[a]	$C_2H_5SC_2H_5$[b]	$CH_3SC_3H_7$[c]	$C_2H_5SC_3H_7$[b]	$CH_3SC_4H_9$[b]	$CH_3SC_2H_4SCH_3$[d]
1	T (7)	TT (27)	TT (25)	TTT (32)	TTT (30)	
	G (20)					
2		TG (8)	TG (4)			
		GG (4)	GT (25)			
			GG (16)			
3				TGT (17)	GTT (9)	
4						GTG′(26)
5				GTT (5)	TGT (9)	TTT (3)
				GGT (9)	GGT (9)	TTG (9)
				GGG (7)		TGG (7)
						GGG (8)
6	$CD_3SC_2H_5$[e] T (5), G (20)			$CH_3SCH_2CD_3$[e] T (7), G (20)		
	$CH_3SC_2D_5$[f] T (5), G (20)					
7	$(-SCH_2CH_2SCH_2CH_2-)_n$[g] GTG′G′TG (28)			$(-SCD_2CD_2SCD_2CD_2-)_n$[g] GTG′G′TG (25)		

The least-squares calculation begins with the simplest sulfides given in the first step and the first set of force constants is determined so as to give the best fit between the observed and calculated frequencies. This set of force constants gives the definite vibrational assignments of the sulfides given in the second step and the second set of force constants is subsequently determined from the observed frequencies in this step in addition to those in the first step. By repeating this procedure, the final set of force constants is obtained. The figures in parentheses give the numbers of observed frequencies used for the least-squares calculation. The observed frequencies of the CH and CD stretching vibrations are not included in the calculation and accordingly the force constants associated with these vibrations are not refined. The results of the following references are utilized in the least-squares calculation. a) Refs. 1, 5, and 17. b) This study. c) Refs. 8 and 12. d) Ref. 18. e) Ref. 1. f) Refs. 1 and 6. g) Ref. 13.

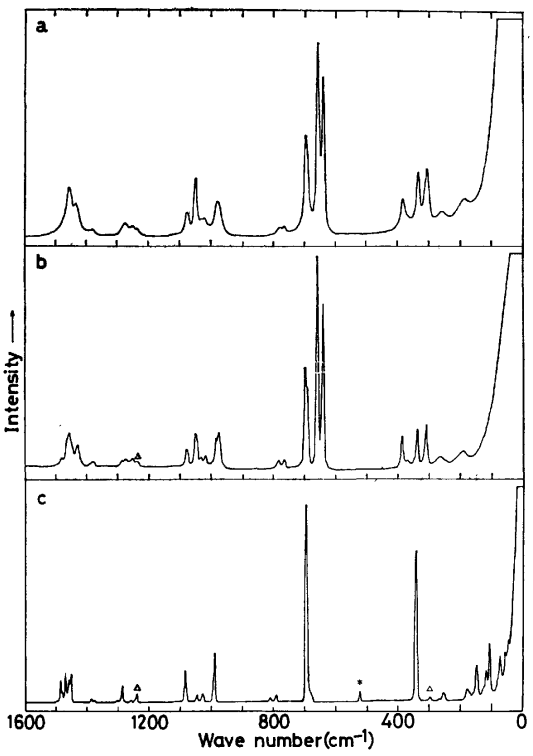

Fig. 1. Raman spectra of diethyl sulfide.
a: Liquid (room temperature), b: liquid (−100 °C), c: crystal (liquid nitrogen temperature).
Following symbols are used in Figs. 1—9.
*: Emission line of Ar^+, □: librational infrared band of H_2O, ×: impurity, △: origin unknown.

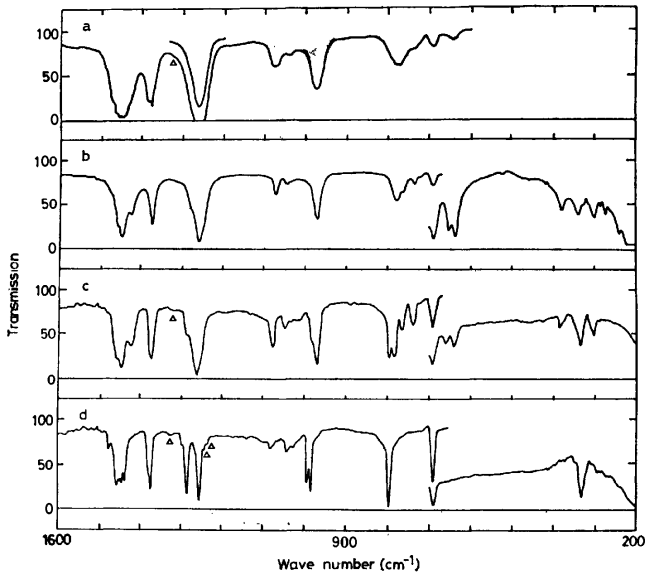

Fig. 2. Infrared spectra of diethyl sulfide.
a: Gas, b: liquid, c: glass, d: crystal.
The symbol is explained in the caption of Fig. 1.

the TT form exists. The number of the observed bands is just what is expected for one form. The frequencies of the skeletal deformation bands, 343 and 332 cm^{-1}, can only be explained by the TT form.

The glassy- and liquid-state spectra show that the TT, TG, and GG forms coexist. The temperature dependence of the liquid-state Raman spectra, combined with the results of the normal vibration calculations,

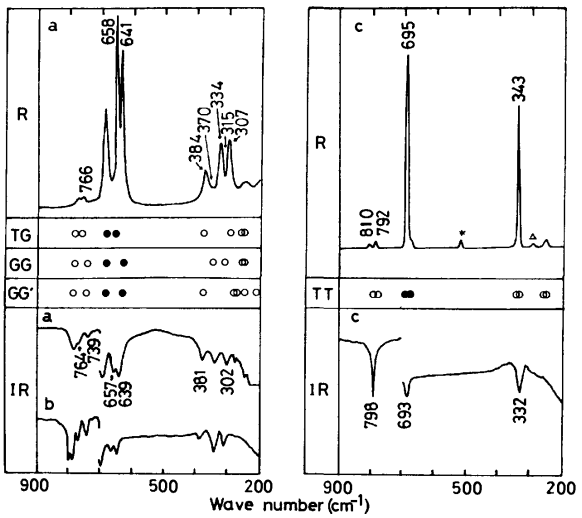

Fig. 3. Comparison of the calculated and observed frequencies of diethyl sulfide in the 900—200 cm^{-1} region.
a: Liquid, b: glass, c: crystal.
The filled circles denote the CS stretching vibrations.
The symbols in the Raman spectrum of the crystalline state are explained in the caption of Fig. 1.

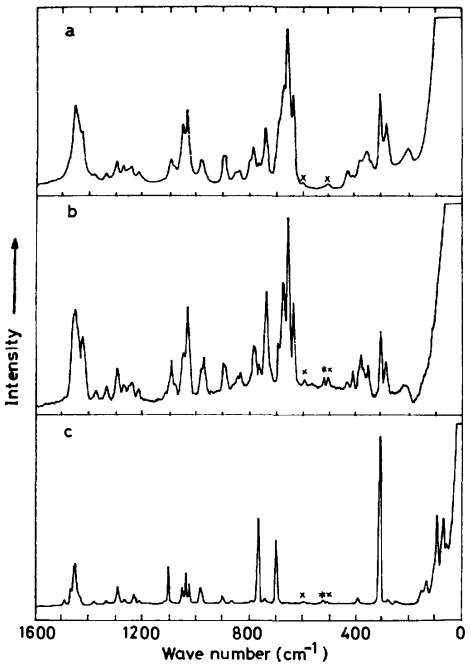

Fig. 4. Raman spectra of ethyl propyl sulfide.
a: Liquid (room temperature), b: glass (liquid nitrogen temperature), c: crystal (liquid nitrogen temperature).
The symbols are explained in the caption of Fig. 1.

indicates that the bands at 766, 658, 384, and 307 cm^{-1} are assigned to the TG form and those at 739, 641, 370 (a shoulder of the 384 cm^{-1} band), and 315 cm^{-1} (a shoulder of the 307 cm^{-1} band) are assigned to the GG form. It should be noted that the assignment of the 739 cm^{-1} band, which has not been made clearly in previous studies, is now established.

Existence of the GG′ form is uncertain, since all of

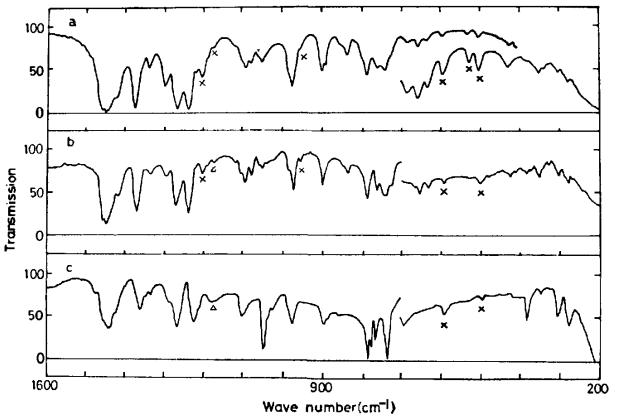

Fig. 5. Infrared spectra of ethyl propyl sulfide.
a: Liquid, b: glass, c: crystal.
The symbols are explained in the caption of Fig. 1.

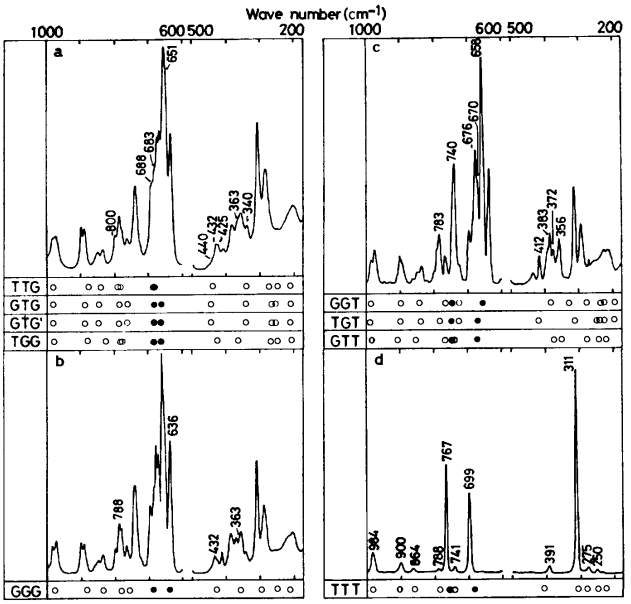

Fig. 6. Comparison of the calculated and observed Raman frequencies of ethyl propyl sulfide in the 1000—600 and 500—175 cm^{-1} regions.
a: Liquid (room temperature), b: liquid (−90 °C), c: glass (liquid nitrogen temperature), d: crystal (liquid nitrogen temperature).
The filled circles denote the CS stretching vibrations.

the calculated frequencies of this form are almost coincident with those of the other forms, TT, TG, and GG. However, the distance between the two terminal methyl groups seems to be too short for this form to be stable. In fact, for methyl propyl sulfide, the GG′ form is found to be very unlikely as will be described later.

The enthalpy differences between the GG and TG forms and between the TT and TG forms in the liquid state were determined from the relative Raman intensities at eight different temperatures between −90 and 23 °C. The intensity ratios of the 641 and 658 cm^{-1} bands and of the 334 and 384 cm^{-1} bands gave the enthalpy differences $\Delta H_{GG-TG}=40\pm50$ cal/mol and

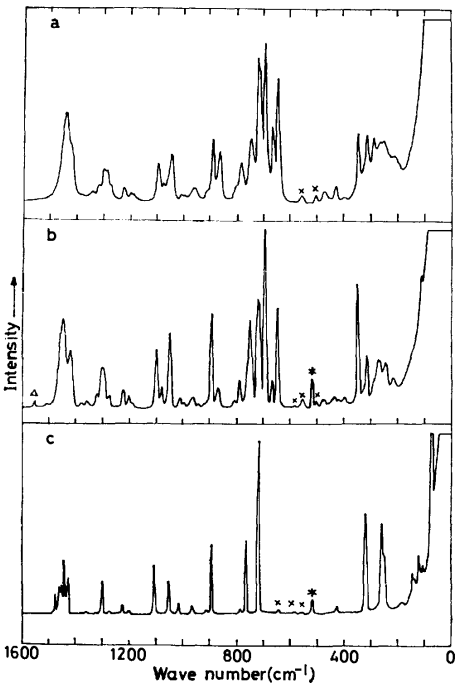

Fig. 7. Raman spectra of butyl methyl sulfide.
a: Liquid (room temperature), b: glass (liquid nitrogen temperature), c: crystal (liquid nitrogen temperature).
The symbols are explained in the caption of Fig. 1.

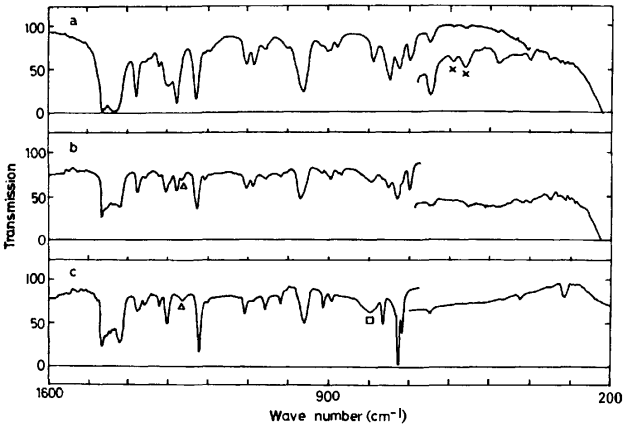

Fig. 8. Infrared spectra of butyl methyl sulfide.
a: Liquid, b: glass, c: crystal.
The symbols are explained in the caption of Fig. 1.

$\Delta H_{TT-TG}=460\pm100$ cal/mol, respectively.

The infrared spectrum of gaseous diethyl sulfide is essentially the same as that of the liquid. This observation suggests that the TT, TG, and GG forms coexist in the gaseous state.

Ethyl Propyl Sulfide. This molecule has fourteen possible rotational isomers as listed in Table 1 of Part I.[2] Of these, TGG', GG'T, GGG', GG'G, and GG'G' are rejected because of the same reason as stated above for diethyl sulfide.

Figure 6 shows that the observed Raman spectrum in the crystalline state is explained by the TTT form only. The spectra in the glassy and liquid states exhibit much more bands than those in the crystalline

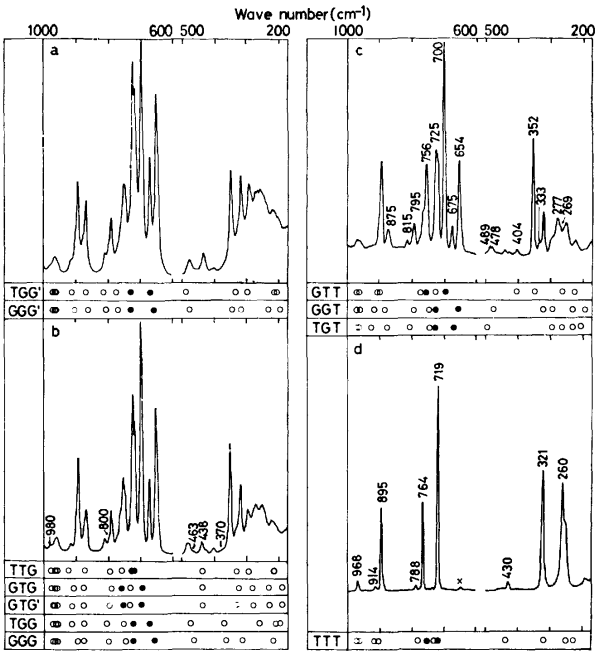

Fig. 9. Comparison of the calculated and observed Raman frequencies of butyl methyl sulfide in the 1000—600 and 500—175 cm^{-1} regions.
a: Liquid (room temperature), b: liquid (−90 °C), c: glass (liquid nitrogen temperature), d: crystal (liquid nitrogen temperature).
The filled circles denote the CS stretching vibrations.
The symbol in the spectrum of the crystalline state is explained in the caption of Fig. 1.

state, suggesting the coexistence of many rotational isomers. The temperature dependence of the Raman intensities and the comparison with the calculated results indicate that the observed spectra in these states are explained by the TTT, GGT, TGT, GTT, GGG, TTG, and TGG forms and either one or both of the GTG, and GTG' forms.

The comparison of the Raman spectrum in the glassy state and that in the liquid state at room temperature shows that the intensities of the bands at 783, 740, 658, 412, 383, 372, and 356 cm^{-1} are enhanced in the glassy state. In the liquid state, these bands are also stronger at lower temperatures. Examinations of the experimental and calculated results indicate that the bands at 658 and 383 cm^{-1} are assigned to the GGT form, those at 783 and 412 cm^{-1} to the TGT form, those at 372 and 356 cm^{-1} to the GTT form, and that at 740 cm^{-1} to the GGT, TGT, and GTT forms. The bands at 676 and 670 cm^{-1} are assigned to the TGT and GTT forms, respectively, on the basis of the facts that the intensity of the former band increases at lower temperatures relative to the intensity of the latter band and that corresponding intensity variations are observed for the band pair of the 412 cm^{-1} band (TGT form) and the 372 or 356 cm^{-1} band (GTT form).

The observed spectra show that the intensities of some other bands such as those at 800, 788, 688, 683, 651, 440, 432, 425, 363, and 340 cm^{-1} decrease in the glassy state as compared with the liquid state at room

TABLE 2. OBSERVED FREQUENCIES AND VIBRATIONAL ASSIGNMENTS OF DIETHYL SULFIDE

Observed frequency (cm^{-1})[a]						
Gas[c]	Liquid		Glass	Crystal		Assignment[b]
IR	R	IR	IR	R	IR	
			1478 VW	1483 VW	1478 VW	CH_3 ip-d-deform
		1463 S, sh		1466 VW	1458 S	CH_3 ip-d-deform
1450 S, vb	1456 W, b	1456 VS, b	1459 VS, sh 1448 VS	1455 VW 1449 VW	1454 S, sh 1450 S	CH_3 op-d-deform CH_3 op-d-deform
					1444 S	CH_2 scis
	1431 VW	1436 M	1424 M		1438 S	CH_2 scis
1382 M, b	1382 VW			1382 VW	1380 S, sh	CH_3 s-deform
		1375 S	1372 S	1372 VW	1375 S	CH_3 s-deform
1324 VW, sh			1322 VW		1326 VW, b	Origin unknown
1287 M, sh	1273 VW, b	1278 M, sh	1285 W, sh	1298 VW 1284 VW	1299 VW 1286 VS	CH_2 wag (**TT**, TG, GG) CH_2 wag (**TT**, TG, GG)
1260 VS, b		1260 VS	1262 VS		1264 W, sh	CH_2 twist (**TT**, TG, GG)
	1252 VW	1248 M, sh	1254 S, sh	1255 VW	1256 VS	CH_2 twist (**TT**, TG, GG)
					1244 W	Origin unknown
1236 VW, sh	1236 VW, sh			1235 VW	1238 VW	Origin unknown
1076 W, b	1077 VW	1076 W	1079 M	1082 VW	1080 VW	CC stretch (**TT**, TG)
1044 VW, b	1047 W	1048 VW	1048 W	1044 VW	1042 VW	CH_3 ip-rock (**TT**, TG, GG), CH_3 op-rock (**TT**), CC stretch (GG)
			1032 VW			CH_3 op-rock (TG, GG)
				1026 VW	1028 VW	CH_3 op-rock (**TT**)
	1018 VW		1014 VW			CH_3 op-rock (TG, GG)
			994 VW, sh		993 S	CH_3 ip-rock (**TT**)
976 M, b	979 VW	980 M, sh	982 M, sh	988 W	986 S	CC stretch (**TT**, GG), CH_3 ip-rock (TG)
967 M, sh		973 S	971 VS			CC stretch (TG), CH_3 ip-rock (GG)
			797 VS	810 VW	798 VW	CH_2 rock (**TT**)
784 W	782 VW	783 M	784 VS	792 VW		CH_2 rock (**TT**, TG, GG)
773 W	766 VW	764 W	765 M			CH_2 rock (**TG**)
735 VW, sh		739 VW	739 W			CH_2 rock (**GG**)
698 VW, sh	695 M	695 VW	692 M	695 VS	693 S	CS stretch (**TT**, TG, GG)
691 VW	689 W, sh	689 VW, sh		683 VW, sh		CS stretch (**TT**)
648 VW	658 VS	657 VW	656 W			CS stretch (**TG**)
639 VW	641 VS	639 VW	639 W			CS stretch (**GG**)
	384 VW	381 VW	384 VW			SCC deform (**TG**)
	370 VW, sh					SCC deform (**GG**)
	349 VW, sh	342 VW	349 VW		348 VW	SCC deform (**TT**)
	334 W	328 VW	335 W	343 S	332 W	SCC deform (**TT**)
	315 VW, sh					SCC deform (**GG**)
	307 W	302 VW	303 VW			SCC deform (**TG**)
				294 VW	294 VW	Origin unknown
		275 VW		267 VW	273 VW	CH_3 torsion (**TT**, TG, GG)
	260 VW	263 VW		253 VW	262 VW	CH_3 torsion (**TT**)
		243 VW				CH_3 torsion (TG, GG)
	187 VW					CSC bend (TG, GG)
				178 VW		CSC bend (**TT**), torsions (**TT**) and lattice vibrations
				171 VW		
				147 VW		
				126 VW, sh		
				116 VW		
				104 W		
				72 VW		
				55 VW		
				48 VW		

TABLE 2. (Continued)

a) VS: very strong, S: strong, M: medium, W: weak, VW: very weak, vb: very broad, b: broad, sh: shoulder. The broadness of the band shapes in the liquid state does not always allow us to correlate the individual bands in the glassy or crystalline state to those in the liquid state. Only approximate correlations are made in such cases. b) The band is assigned preferentially to the isomer(s) given by boldface. For the notation and definition of the local symmetry coordinates, see Ref. 19. c) Some of the infrared bands in the gaseous state have rotational structures. However, only the frequencies of the band centers are listed in the table.

TABLE 3. OBSERVED FREQUENCIES AND VIBRATIONAL ASSIGNMENTS OF ETHYL PROPYL SULFIDE

Observed frequency (cm^{-1})[a]						Assignment[b]
Liquid		Glass		Crystal		
R	IR	R	IR	R	IR	
	1473 W, sh		1472 VW, sh	1489 VW	1474 W	CH_2 scis
	1457 VS	1465 VW, sh	1464 VS, sh	1465 VW	1463 VS, sh	CH_3 ip-d-deform
1452 M, vb	1451 VS	1457 W, b	1457 VS	1452 W	1456 VS	CH_3 op-d-deform
		1449 W, sh	1446 VS	1449 W	1446 VS, sh	CH_3 ip-d-deform
	1440 S, sh			1440 VW, sh	1440 VS	CH_2 scis
1430 M, sh	1423 M, sh	1424 W, sh	1434 M, sh 1417 S	1431 VW	1424 S, sh	CH_2 scis (**TTT**, GTT, GGG) CH_2 scis (TGT, GGT)
1381 VW	1375 VS	1375 VW	1374 M, sh 1370 S	1379 VW, sh 1376 VW	1366 S	CH_3 s-deform CH_3 s-deform, CH_2 wag (**GGG**)
1335 VW	1339 W	1335 VW	1335 VW	1332 VW	1333 VW	CH_2 wag (**TTT**, TGT, GTT, GGT)
1298 W	1298 M	1293 VW	1295 VW	1290 VW	1286 W	CH_2 twist (**TTT**, TGT, GTT, GGT, GGG)
1270 VW 1266 VW, sh	1269 S	1269 VW	1271 S	1263 VW	1266 VS	CH_2 wag (TGT, GTT, GGT, GGG) CH_2 twist (**TTT**, TGT, GTT, GGT, GGG), CH_2 wag (**TTT**)
1250 VW, sh		1248 VW				CH_2 wag (TGT, GGT)
1239 VW	1238 S	1237 VW	1237 VS	1231 VW 1225 VW, sh	1224 M	CH_2 wag (**TTT**, GTT)
	1219 W	1220 VW, sh	1222 VW, sh			CH_2 twist (TGT, GTT, GGT), CH_2 wag (GGG)
1213 VW		1213 VW		1210 VW	1212 VW, sh	CH_2 twist (**TTT**)
1120 VW, sh	1116 VW	1122 VW	1118 VW			CC stretch (**TTG**)
1100 VW, sh	1100 VW, sh	1100 VW, sh	1101 W	1100 W	1100 M	CH_3 ip-rock (**TTT**, GTT)
1092 VW	1090 VW	1093 W	1093 M			CH_3 ip-rock (TGT, GGT), CC stretch (GGG)
1080 VW	1076 VW	1079 VW	1078 W	1078 VW	1073 VW	CH_2 rock (**TTT**, TGT, GTT, GGT)
1056 VW, sh	1056 VW, sh	1056 VW, sh	1056 VW, sh			CH_3 ip-rock (TGT, GTT, GGT, GGG)
1047 M	1049 VW	1047 W	1050 VW	1047 VW	1049 VS	CH_3 ip-rock (**TTT**, GGG)
	1036 VW, sh		1038 VW	1036 VW	1039 W, sh	CC stretch (**TTT**), CH_3 op-rock (TGT)
1030 M	1030 VW, sh	1030 S	1030 VW, sh			CC stretch (TGT, GTT, GGT, GGG)
1022 VW, sh	1023 VW, sh	1020 VW, sh	1021 VW	1023 VW	1024 W	CH_3 op-rock (**TTT**, GTT, GGT, GGG)
981 VW, sh	981 VW, sh	982 W	982 M	984 VW	983 M, sh 976 M	CC stretch (**TTT**, TGT)
972 VW	972 M	972 W	972 S			CC stretch (GTT, GGT, GGG)
	954 VW, sh		954 VW			Origin unknown
899 VW	898 W	900 VW	899 S	900 VW	898 W	CC stretch (**TTT**, GTT, GGT)
892 VW	890 W, sh	892 VW, sh	890 VW, sh			CC stretch (TGT, GGG)
862 VW, sh		863 VW, sh	860 VW, sh	864 VW	860 VW	CH_3 op-rock (**TTT**)
852 VW	849 VW, sh	847 VW	846 VW, sh			CH_3 op-rock (**GTT**)
836 VW	835 VW	835 VW	833 W			CH_3 op-rock (TGT, GGT, GGG)
800 VW, sh	800 VW, sh	800 VW, sh	800 VW, sh			CH_2 rock (TTG, GTG or GTG')
788 W 780 VW, sh	786 W	788 VW, sh 783 W	786 S	788 VW	788 VS 778 S	CH_2 rock (**TTT**, GGG) CH_2 rock (**TGT**)
764 VW	760 VW	765 VW	762 M	767 M	766 S	CS stretch (**TTT**), CH_2 rock (GTT, GGT, GGG)

Table 3. (Continued)

Observed frequency (cm^{-1})[a]						Assignment[b]
Liquid		Glass		Crystal		
R	IR	R	IR	R	IR	
740 M	740 W	740 S	740 S, b	741 VW	747 M, sh 736 VS	CH_2 rock (**TTT**, GTT), CS stretch (TGT, GTT, GGT)
723 VW, sh	724 VW, sh	723 VW, sh	723 M			CH_2 rock (TGT, GGT)
693 M, sh		695 W	690 VW	699 M	694 W	CS stretch (**TTT**, GGG)
688 M, sh		688 W, sh				CS stretch (TTG, TGG, GTG or GTG')
683 M, sh	685 VW, b	683 W, sh				CS stretch (**TTG**)
675 S		676 S	675 VW			CS stretch (**TGT**)
670 S		670 M				CS stretch (**GTT**)
658 VS	657 VW	658 VS	657 VW			CS stretch (**GGT**)
651 VS, sh		651 M, sh				CS stretch (TGG, GTG or GTG')
636 S	634 VW	636 M	634 VW			CS stretch (**GGG**)
440 VW, sh	440 VW, sh	442 VW, sh				CCC deform (GTG or GTG')
432 VW	428 VW, b	433 VW	424 VW, b			CCC deform (GGG, TTG)
425 VW, sh		425 VW, sh				CCC deform (**TGG**)
411 VW	411 VW, sh	412 VW				CSC bend (**TGT**)
392 VW, sh		392 VW, sh		391 VW	385 VW	CCC deform (**TTT**)
383 W	385 VW, sh	383 W	384 VW, b			CSC bend (**GGT**)
372 W, sh 363 W, sh	366 VW, sh	372 VW 363 VW, sh				CSC bend (**GTT**) CSC bend (GGG, TGG)
355 W	351 VW	356 W	351 VW			CCC deform (**GTT**)
340 W		340 VW, sh				SCC deform (TTG, GTG or GTG')
321 VW, sh		321 VW, sh				SCC deform (**GGT**)
307 S	302 VW	309 M	303 VW	311 VS	307 VW	SCC deform (**TTT**), CCC deform (TGT)
295 W, sh		295 W, sh				SCC deform (**GGG**)
285 M		288 W				CCC deform (GGT), SCC deform (GTT)
277 VW, sh	277 VW	277 VW, sh	277 VW	275 VW	279 VW	SCC deform (**TTT**)
		255 VW				CH_3 torsion (TGT, GGG)
		245 VW, sh	244 VW	250 VW	243 VW	CH_3 torsion (**TTT**, GTT), SCC deform (TGT)
		240 VW, sh				CH_3 torsion (**GGT**)
225 W, sh		225 VW, b				CH_3 torsion (**TTT**, TGT, GTT, GGT)
		213 VW, b				CH_3 torsion (**GGG**)
200 W, b		200 VW, sh				CH_3 torsion (TGT, GGT)
				148 VW 132 VW 107 VW, sh 92 M 70 W 58 VW		CSC bend (**TTT**), torsions (**TTT**) and lattice vibrations

a), b) See a) and b), respectively, of Table 2.

temperature. Of these, the band at 788 cm^{-1} is assigned to the GGG form, that at 683 cm^{-1} to the TTG form, that at 425 cm^{-1} to the TGG form, that at 440 cm^{-1} to either one or both of the GTG and GTG' forms, that at 432 cm^{-1} to both of the GGG and TTG forms, and that at 363 cm^{-1} to both of the GGG and TGG forms. The existence of the GGG form is evident from the result that the band at 636 cm^{-1} is assigned exclusively to this form. The following bands are assigned to all or any of the molecular forms given in parentheses: 800 and 342 cm^{-1} (TTG, GTG, and GTG'), 688 cm^{-1} (TGG, GTG, GTG', and TTG), and 651 cm^{-1} (TGG, GTG, and GTG').

The relative stabilities of the rotational isomers existing in the liquid state are determined from the dependence of the band intensities on temperature (Fig. 6) and the band assignment mentioned above; (1) the GGT and TGT forms have almost the same stability and are the most stable, (2) the third stable isomer is the GTT form, which is followed by the TTT and GGG forms having nearly equal stability to each other, and (3) the TTG, GTG, GTG', and TGG forms are less stable than the forms given above, but the relative stabilities among these forms are not clear.

The above conclusion obtained from the Raman spectra is also consistent with the change of the infrared

TABLE 4. OBSERVED FREQUENCIES AND VIBRATIONAL ASSIGNMENT OF BUTYL METHYL SULFIDE

Observed frequency (cm^{-1})[a]						Assignment[b]
Liquid		Glass		Crystal		
R	IR	R	IR	R	IR	
		1555 VW				Origin unknown
		1470 VW, sh		1476 VW	1476 VW, sh	CH_2 scis
1462 VW, sh	1464 VS	1457 W, sh	1465 VS	1461 VW	1464 M	CH_2 scis
	1458 VS, sh		1458 VS, sh	1454 VW	1458 M, sh	CH_3 op-d-deform
1445 M, sh	1452 VS, sh	1448 M	1452 VS	1446 VW, sh	1451 M	CH_3 ip-d-deform
	1435 VS	1443 W, sh	1436 S	1441 W	1442 M	CH_3 ip-d-deform
	1432 VS		1432 VS	1429 W	1432 W	CH_3 op-d-deform
1429 W, sh			1428 S			CH_3 op-d-deform (**GTT**)
	1424 VS	1422 W	1422 S			CH_2 scis (**GTT**)
	1418 S, sh		1419 S		1424 M, sh 1418 M	CH_2 scis
1381 VW	1378 S	1380 VW	1375 M	1380 VW	1376 W 1372 W, sh	CH_3 s-deform, CH_2 wag (TGT, GGT)
1360 VW	1354 VW	1360 VW	1356 VW	1359 VW	1356 VW	CH_2 wag (**TTT**, GTT)
1345 VW	1341 VW					CH_2 wag (TGG or GGG)
1324 VW	1321 VW	1323 VW	1323 VW	1325 VW	1320 VW	CH_3 s-deform, CH_2 wag (TGT)
1305 VW	1302 W	1305 VW	1304 M			CH_2 twist (**TTT**, GTT, TGT, GGT), CH_2 wag (GGT)
1296 VW	1296 W	1297 VW, sh	1297 W, sh	1301 VW	1302 W	CH_2 wag (**TTT**, GTT)
1278 VW	1276 S	1278 VW	1277 M	1276 VW		CH_2 twist (**TTT**, GTT, TGT, GGT)
			1264 W		1263 VW	Origin unknown
1228 VW	1227 S	1229 VW	1226 VS	1225 VW	1220 S	CH_2 wag (**TTT**, GTT)
1203 VW	1204 VW	1206 VW	1208 W	1201 VW	1201 VW	CH_2 rock (**TTT**, GTT, TGT)
1193 VW	1193 VW	1194 VW, sh				CH_2 rock (**GGT**)
1169 VW, sh	1169 VW					CH_2 wag (TGT, GGT)
1125 VW, sh		1126 VW				CC stretch (TGG or GGG)
	1108 VW, sh	1110 W, sh	1108 W, sh	1106 W	1107 W	CC stretch (**TTT**)
1101 W	1100 W	1104 W	1101 M			CC stretch (GTT, TGT, GGT)
1082 VW	1083 W	1086 VW	1086 M			CH_2 twist (**TTT**, GTT, TGT, GGT)
1058 VW, sh	1058 W	1061 VW, sh	1059 W			CC stretch (TTG, GTG or GTG′)
1053 W	1051 W	1053 W	1051 W	1054 VW	1056 W	CC stretch (**TTT**, GTT, TGT, GGT)
1012 VW	1012 VW, sh	1015 VW	1014 VW	1017 VW	1017 VW	CC stretch (**TTT**, GTT)
1001 VW, sh	998 VW	1002 W	995 VW			CC stretch (TGT, GGT)
980 VW, sh	980 W, sh	978 VW, sh	978 VW, sh			CH_3 ip-rock (TGG, GGG, TTG, GTG or GTG′)
966 VW, b	968 M, sh	970 VW	968 S	968 VW	964 W, sh	CH_3 ip-rock (**TTT**, GTT, TGT, GGT)
	959 S	962 VW	963 S 956 S		957 W	CH_3 op-rock (**TTT**, TGT, GGT) CH_3 op-rock (**GTT**)
918 VW, sh	916 VW	918 VW, sh	916 VW	914 VW	910 VW	CH_3 op-rock (**TTT**), CH_3 ip-rock (TGT, GGT)
903 VW, sh	901 W	903 VW, sh	899 W, sh			CH_3 op-rock (**GTT**)
897 W	894 W	896 M	894 W	895 M	892 VW	CH_3 ip-rock (**TTT**, GTT)
878 VW, sh 872 W	877 VW 870 VW, sh	875 VW	873 VW 867 VW			CH_3 op-rock (**GGT**) CH_3 op-rock (**TGT**)
813 VW	812 VW	815 VW				CH_2 rock (**TGT**)
800 VW, sh	800 VW, sh	800 VW, sh				CH_2 rock (TTG, GTG, GTG′ or GGG)
793 VW	788 VW	795 VW	794 VW	788 VW		CH_2 rock (**TTT**, GGT)
		775 VW, sh	776 VW			CH_2 rock (**GTT**)
765 VW, sh		765 VW, sh	766 W	764 M	764 W	CS stretch (**TTT**)
753 M	756 VW, sh	756 M	756 W, sh			CS stretch (**GTT**)
	748 M		749 M			CH_2 rock (TGT, GGT)

TABLE 4. (Continued)

Observed frequency (cm^{-1})[a]						Assignment[b]
Liquid		Glass		Crystal		
R	IR	R	IR	R	IR	
725 VS	729 W, sh 724 M	725 M	729 S	735 VW	726 VS	CS stretch (TGT, GGT) CH_2 rock (**TTT**, GTT)
719 VS, sh	718 W, sh	720 M, sh	720 M, sh	719 VS	716 M	CS stretch (**TTT**)
697 VS	697 W	700 VS	699 M			CS stretch (**GTT**)
672 M	671 VW	675 VW	672 VW			CS stretch (**TGT**)
654 S	650 VW	654 M	651 VW			CS stretch (**GGT**)
489 VW, sh 481 VW	480 VW	489 VW 478 VW				CCC deform (**TGT**) CCC deform (GGT, TGG)
463 VW	460 VW	463 VW				CCC deform (**GGG**)
438 VW		443 W				CCC deform (TTG, GTG or GTG′)
425 VW, sh	430 VW	425 VW	420 VW	430 VW	426 VW	CCC deform (**TTT**)
406 VW	402 VW	404 VW	399 VW			CCC deform (**GTT**)
370 VW, sh	366 VW					CCC deform (TGG or GGG)
353 M	350 VW	352 M	352 VW			SCC deform (**GTT**)
333 W, sh	328 VW	333 VW, sh				CSC bend (**GGT**)
320 W	316 VW	319 W		321 M	316 VW	CCC deform (**TTT**)
295 W	303 VW	295 VW, sh				CCC deform (TGT, GGT)
277 W, sh		277 W				CSC bend (**GTT**)
267 W		269 VW, sh				CSC bend (**TGT**)
258 W		258 VW, sh				CSC bend (**TGG**)
250 W, sh		250 VW		260 M 253 W, sh		CSC bend (**TTT**)
220 VW		221 VW				CH_3 torsion
				205 VW 189 VW 159 VW, sh 147 VW 137 VW 124 VW 108 VW 75 VW 64 VW		SCC deform (**TTT**), torsions (**TTT**) and lattice vibrations

a), b) See a) and b), respectively, of Table 2.

spectra in the various states.

Butyl Methyl Sulfide. This molecule has fourteen possible rotational isomers. The existence of the GG′T, GG′G, and GG′G′ forms are unlikely, but the TGG′ and GGG′ forms are not ruled out, since unlike the GG′ sequence of the CS–C–CC part in ethyl propyl sulfide, the GG′ sequence of the SC–C–CC part is not expected to give rise to very large steric hindrance.

Figure 9 shows that only the TTT form exists in the crystalline state. In the glassy and liquid states, the spectra exhibit many bands to be assigned to various rotational isomers. It is evident, however, that the GTT and TTT forms exist in these states. The relative intensities of the bands at 756, 700, 404, 352, and 277 cm^{-1} increase in going from the liquid state at room temperature to the glassy state. These bands are all explained by the calculated frequencies of GTT form.

The remaining many bands in the glassy and liquid states imply the coexistence of additional isomers. However, the assignment of the observed bands to individual isomers is not always straightforward, because each of the observed Raman bands corresponds to calculated frequencies of two or more isomers. It is likely that the *trans* conformation about the CH_2CH_2–CH_2CH_3 axis in this molecule is appreciably more stable than the *gauche* conformation as suggested from the conformational stabilities of normal paraffin molecules.[3] The molecular forms with the *trans* conformation about this axis are the TGT and GGT form besides the TTT and GTT forms mentioned above Most of the bands which persist in the glassy state but are not assigned to the GTT and TTT forms are explained by the calculated frequencies of the TGT and GGT forms; namely the bands at 815, 675, 489, and 269 cm^{-1} are assigned to the TGT form, those at 795, 654, 478, and 333 cm^{-1} to the GGT form and those at 875 and 725 cm^{-1} to both of the TGT and GGT forms.

TABLE 5. ROTATIONAL ISOMERISM OF THE SULFIDES

	$CH_3SC_2H_5$[a]	$C_2H_5SC_2H_5$	$CH_3SC_3H_7$[b]	$C_2H_5SC_3H_7$	$CH_3SC_4H_9$
Liquid	**G** **T**	**TT** **TG** **GG**	**TT** **GT** **TG** **GG**	**TTT** **GGT** **TGT** **GTT** **GGG** TTG TGG GTG GTG′	**TTT** **GTT** **TGT** **GGT** TTG TGG GGG GTG GTG′ (TGG′) (GGG′)
Glass	—	**TT** **TG** **GG**	**TT** **GT** **TG** **GG**	**TTT** **GGT** **TGT** **GTT** **GGG** TTG TGG GTG GTG′	**TTT** **GTT** **TGT** **GGT** TTG TGG GGG GTG GTG′ (TGG′) (GGG′)
Crystal	**G**	**TT**	**TT**[c] **GT**[c] **GG**[c]	**TTT**	**TTT**

The isomers given by boldface are confirmed to exist. The existence of the isomers in parentheses is uncertain. For more details, see text. a) Refs. 1 and 7. b) Ref. 8. c) Three different crystal modifications have been identified. For more details, see Ref. 8.

In addition to the bands mentioned above, the liquid- and glassy-state Raman spectra have several other bands such as those at 980, 800, 463, 438, and 370 cm^{-1}. Spectral observations indicate that the intensities of these bands decrease more sharply than those of the above-mentioned bands when temperature is lowered. With reference to the calculated frequencies, the 463 cm^{-1} band is assigned to the GGG form, the 370 cm^{-1} band to either one or both of the TGG and GGG forms, the 800 and 438 cm^{-1} bands to all or any of the TTG, GTG and GTG′ forms, and the 980 cm^{-1} band to all or any of the TTG, TGG, and GTG forms. The calculated frequencies of the TGG′ and GGG′ forms are almost coincident with those of the other forms. This situation makes it difficult to confirm the existence of these forms in the liquid or glassy state.

As mentioned above, the examinations of the experimental and calculated results show that the relatively strong bands which retain most of their intensities in the low-temperature liquid and glassy states are reasonably explained by the isomers with the *trans* CH_2CH_2–CH_2CH_3 axis and the other bands which lose their intensities largely in these states are explained by the isomers with the *gauche* CH_2CH_2–CH_2CH_3 axis. These interpretations justify the statement made earlier that the *trans* conformation about this axis is more stable than the *gauche* conformation.

The relative stabilities of the rotational isomers existing in the liquid state are found from the temperature dependence of the Raman intensities; (1) the GTT form is the most stable, (2) the TTT, GGT, and TGT forms follow in order, and (3) the forms having the *gauche* CH_2CH_2–CH_2CH_3 axis are less stable than the above-mentioned forms.

The above conclusion is also consistent with the results of the infrared spectra.

Rotational Isomerism. In Table 5, the rotational isomerism of the three sulfides studied in this work and of ethyl methyl sulfide and methyl propyl sulfide is summarized.

Ethyl methyl sulfide has long been accepted to take the T form in the crystalline state and the T and G forms in the liquid state.[4-6,10] However, the recent studies by Nogami *et al.*[7] and by Sakakibara *et al.*[1] showed that the bands of the crystalline state are assigned to the G form but not to the T form.

The rotational isomerism of methyl propyl sulfide was studied by Nogami *et al.*[8] They found three crystal modifications with the molecular conformations of GT, TT, and GG, respectively. In the liquid and glassy states, an additional isomer of the TG form coexists with the three isomers. They obtained no experimental evidence for the existence of the GG′ form. The comparison of their spectra with the present results of the normal coordinate treatment indicates that the existence of this form may safely be ruled out.

The vibrational spectra of diethyl sulfide have been studied by several investigators.[6,9] Their conclusions on the rotational isomerism agree essentially with the present one, although the existence of the GG form in the liquid state has once been questioned.[10]

The rotational isomerism of ethyl propyl sulfide and butyl methyl sulfide has been discussed previously by Ohsaku.[11] He showed that these molecules in the crystalline state take the *trans* conformation about the C–C axis adjacent to the S–C axis, but did not determine whole molecular conformations.

Discussion

The following results were obtained for the three sulfides studied in this work. (1) Only the all-*trans* form exists in the crystalline state. (2) Many forms coexist in the liquid state. Most of them persist in the glassy state even at the liquid nitrogen temperature. (3) In the liquid state, the forms with the *gauche* C–S axes are more stable than those with the *trans* C–S axes. (4) The *gauche* conformation about the C–C axis directly adjoining the S–C axis is appreciably stable and is only slightly less stable than the corresponding *trans* conformation.

For the C–C and C–O axes in unbranched paraffins and ethers, the *trans* conformation has been found to be more stable than the *gauche* conformation.[2,3] However, the above results indicate that the conformational stability about the C–S axis is remarkably different from that of the C–C or C–O axis. For diethyl sulfide, the TG and GG forms were found to be more stable than the TT form by 400—450 cal/mol in the liquid state. The stability of the *gauche* conformation about the C–S axis over that of the *trans* conformation was also observed for ethyl propyl sulfide and butyl methyl sulfide. In addition to these experimental evidences, it has been found that the G

form of ethyl methyl sulfide is more stable than the T form by 140±50 cal/mol in the liquid state[7] and by 30±50 cal/mol in the gaseous state,[1] and that the GT form of methyl propyl sulfide is the most stable isomer in the liquid state.[12] Thus, it is now established that the *gauche* C–S axis in unbranched sulfides is more stable than the *trans* C–S axis but the stability difference between them is not large.

The stable existence of the *gauche* C–S axis contrasts with the *gauche* C–O axis which is far less stable. One of the possible factors making this difference is the longer C–S bond length (about 1.8 Å) than the C–O bond length (about 1.4 Å), as has been discussed by Tadokoro *et al.*[13a] When the C_1S–C_2C_3 axis takes the *gauche* conformation, the distance between nonbonded hydrogen atoms attached to C_1 and C_3 is 2.1—2.2 Å, which is 0.4—0.5 Å longer than the corresponding distance in ethers. This fact suggests that the repulsive forces between the nonbonded hydrogen atoms in the sulfides are much weaker than those in the ethers and that this effect is responsible for making the *gauche* C–S conformation stable.

The relative stability of the *gauche* conformation about the SC–CC axis was found to be much higher than that of the *gauche* conformation about the CC–CC axis. This is explained by less significant nonbonded interactions as in the case of the *gauche* OC–CC axis in the ethers.[2] Indeed, methyl propyl sulfide takes the GG form in a metastable crystal modification.[8]

The above discussions on the conformational stability indicate that the S–C axis and the C–C axis adjacent to the S–C axis are susceptible of taking the *trans* and *gauche* conformations without large stability differences and accordingly the energy differences among various rotational isomers are small. These results are in accord with the experimental facts observed for all of the sulfides so far studied that many isomers coexist in the glassy state and that methyl propyl sulfide has the three crystal modifications with the molecular conformations of GT, TT, and GG.[8]

It is noticed for the three sulfides studied in this work that the most stable isomer in the liquid or glassy state does not exist in the crystalline state. This fact suggests that intermolecular forces play a more important role for stabilizing the molecular conformation in the crystal.

It is of interest to compare the molecular conformations of the unbranched sulfides with the chain conformations of polythioethers. According to the X-ray diffraction studies, poly(thioethylene)$(-SCH_2CH_2-)_n$ takes the GTG'G'TG conformation for the series of S–C–C–S–C–C–S bonds[13] and poly(thiotrimethylene)$(-SCH_2CH_2CH_2-)_n$ takes the GGGG conformation for the series of S–C–C–C–S bonds.[14] It should be noted that S–C axes in these polymers are all in the *gauche* conformation and the C–C axes adjacent to the S–C axes in the latter polymer are in the *gauche* conformation. These chain conformations are consistent with those of the shorter sulfides as described in this paper.

References

1) Part III: M. Sakakibara, H. Matsuura, I. Harada, and T. Shimanouchi, *Bull. Chem. Soc. Jpn.*, **50**, 111 (1977).

2) Part I: T. Shimanouchi, Y. Ogawa, M. Ohta, H. Matsuura, and I. Harada, *Bull. Chem. Soc. Jpn.*, **49**, 2999 (1976).

3) Part II: I. Harada, H. Takeuchi, M. Sakakibara, H. Matsuura, and T. Shimanouchi, *Bull. Chem. Soc. Jpn.*, **50**, 102 (1977).

4) D. W. Scott, H. L. Finke, J. P. McCullough, M. E. Gross, K. D. Williamson, G. Waddington, and H. M. Huffman, *J. Am. Chem. Soc.*, **73**, 261 (1951); M. Hayashi, *Nippon Kagaku Zasshi*, **77**, 1692 (1956), **78**, 627 (1957); M. Hayashi, T. Shimanouchi, and S. Mizushima, *J. Chem. Phys.*, **26**, 608 (1957).

5) M. Ohsaku, Y. Shiro, and H. Murata, *Bull. Chem. Soc. Jpn.*, **45**, 954 (1972).

6) M. Ohsaku, Y. Shiro, and H. Murata, *Bull. Chem. Soc. Jpn.*, **46**, 1399 (1973).

7) N. Nogami, H. Sugeta, and T. Miyazawa, *Bull. Chem. Soc. Jpn.*, **48**, 3573 (1975).

8) N. Nogami, H. Sugeta, and T. Miyazawa, *Chem. Lett.*, **1975**, 147.

9) D. W. Scott, H. L. Finke, W. N. Hubbard, J. P. McCullough, G. D. Oliver, M. E. Gross, C. Katz, K. D. Williamson, G. Waddington, and H. M. Huffman, *J. Am. Chem. Soc.*, **74**, 4656 (1952); M. Hayashi, *Nippon Kagaku Zasshi*, **77**, 1804 (1956); M. Ohsaku, Y. Shiro, and H. Murata, *Bull. Chem. Soc. Jpn.*, **45**, 956 (1972).

10) D. W. Scott and M. Z. El-Sabban, *J. Mol. Spectrosc.*, **30**, 317 (1969).

11) M. Ohsaku, *Bull. Chem. Soc. Jpn.*, **48**, 1037 (1975).

12) N. Nogami, unpublished work.

13) a) Y. Takahashi, H. Tadokoro, and Y. Chatani, *J. Macromol. Sci., Phys.*, **B2**, 361 (1968); b) M. Yokoyama, H. Ochi, A. M. Ueda, and H. Tadokoro, *ibid.*, **B7**, 465 (1973).

14) K. Tai and H. Tadokoro, *Macromolecules*, **7**, 507 (1974).

15) A. C. Angood and J. L. Koenig, *J. Macromol. Sci., Phys.*, **B3**, 321 (1969).

16) T. Shimanouchi, H. Matsuura, Y. Ogawa, and I. Harada, *J. Phys. Chem. Ref. Data*, to be published.

17) K. Oyanagi, T. Fukuyama, and K. Kuchitsu, 32nd Annual Meeting of the Chemical Society of Japan, Tokyo (1975), 1126.

18) Part V: Y. Ogawa, M. Ohta, M. Sakakibara, H. Matsuura, I. Harada, and T. Shimanouchi, *Bull. Chem. Soc. Jpn.*, in press.

19) T. Shimanouchi, "Tables of Molecualr Vibrational Frequencies," Consolidated Vol. 1, U. S. Govt. Printing Office, No. C13.48:39 (1972).

Note added in proof

Erratum in Table 3 of Part II.[3] For 629 listed in the column of Raman (−100°C) of Liquid read 692.

The Preparation and Stereochemistry of Optically Active Cobalt(III) Complexes with 3,3′-Dimethyl-2,2′-bipyridine and Bis(diamines) or Tetramines

Toshishige M. SUZUKI and Tetsuo KIMURA
Government Industrial Research Institute, Tohoku, Nigatake, Haranomachi, Sendai 983

(Received June 15, 1976)

Bis(en), trien, tren and bis(*R*,*R*-chxn) cobalt(III) complexes of 3,3′-dimethyl-2,2′-bipyridine (dmbpy) have been prepared and resolved. The dissymmetric conformation of dmbpy arising from the non-coplanarity of the two pyridine rings is maintained in the inert complexes. 3,3′-Dimethyl-2,2′-bipyridine coordinates to the cobalt(III) ion with a stereospecific conformation depending on the configuration. The absorption and circular dichroism (CD) spectra of the dmbpy complexes were compared with those of the corresponding 2,2′-bipyridine (bpy) complexes.

Although bpy is one of the most extensively studied chelating agents,[1] little work has been done on its 3,3′-dimethyl derivative. On the basis of molecular models, it seems that metal chelate of the dmbpy has considerable strain caused by its puckered conformation. Cagle Jr. and Smith[2] reported that dmbpy forms an iron(II) complex in an aqueous solution, but its absorption intensity of 526 nm is only one-fifth of that of the bpy complex. They explained this by considering a twisted conformation of the dmbpy moiety in contrast with the planar chelate ring of bpy. So far no metal complex of dmbpy has been isolated. We have been succeeded in preparing several cobalt (III) complexes containing this ligand. A part of the study has been reported briefly.[3]

Twisted conformation of dmbpy can give atrope isomerism such as biphenyl derivatives,[4] but the isomers were not isolated presumably because of its rapid racemization. The conformation of the ligand might be fixed by an inert metal complex formation. Only a limited number of metal chelates involving such an isomerism are known.[5,6]

This paper deals with the preparation and resolution of several cobalt(III) complexes of dmbpy. The stereochemistry of the complexes is discussed.

Experimental

Materials. *3,3′-Dimethyl-2,2′-bipyridine*: 3-Methylpyridine was refluxed with sodium amide in xylene[7] and the resulting 2-amino-3-methylpyridine was converted into 2-bromo-3-methylpyridine by means of the Sandmeyer reaction.[8] Condensation of the bromo compound by Ullmann reaction yielded 3,3′-dimethyl-2,2′-bipyridine.[9] Found: C, 78.42; H, 6.65; N, 15.09%. Calcd for $C_{12}H_{12}N_2$: C, 78.23; H, 6.75; N. 15,21%.

2,2′,2″-Triaminotriethylamine (tren). This was prepared according to the method given in literatures.[10,11]

[Co(dmbpy)$_3$](ClO$_4$)$_3$. Air was bubbled through a mixture of $CoCl_2 \cdot 6H_2O$ (2.38 g in 50 ml of water), dmbpy (5.52 g in 10 ml of ethanol) and activated charcoal (1.0 g) for 12 h. The solution was filtered and the filtrate was warmed at 60 °C for 30 min with 10 ml of concentrated hydrochloric acid. Sodium perchlorate (4.0 g in 10 ml of water) was added to the cooled solution. The resulting yellow precipitate was filtered off, washed with a small amount of water, ethanol and ether, and recrystallized from hot water. Found: C, 47.22; H, 3.95; N, 8.94%. Calcd for $C_{36}H_{36}N_6O_{12}CoCl_3$: C, 47.50; H, 3.96; N, 9.24%.

[Co(tren)(dmbpy)](ClO$_4$)$_3 \cdot 4H_2O$. A mixture of [Co(dmbpy)$_3$](ClO$_4$)$_3$ (1.82 g in 50 ml of water), 0.3 g of 2,2′,2″-triaminotriethylamine (tren) and activated charcoal (0.5 g) was warmed at 60 °C for 10 min and filtered. A few drops of concentrated hydrochloric acid was added to the filtrate. The solution was diluted 20 times with water and poured onto a SP-Sephadex C-25 column (ϕ 2.5×25 cm). The adsorbed orange band was washed with water and eluted with 0.2 M hydrochloric acid. The eluate of the orange band was collected, evaporated to dryness, dissolved in 10 ml of water, treated with 1 g of sodium perchlorate in 5 ml of water and stored in a refrigerator overnight. Orange crystals were filtered off and washed with ethanol-water (1 : 1), ethanol and then ether.
Found: C, 28.11; H, 5.03; N, 11.02%. Calcd for $C_{18}H_{38}N_6O_{16}CoCl_3$: C, 28.43; H, 5.00; N, 11.05%.

Partial Resolution of [Co(tren)(dmbpy)](ClO$_4$)$_3 \cdot 4H_2O$.
About 200 mg of [Co(tren)(dmbpy)](ClO$_4$)$_3 \cdot 4H_2O$ was adsorbed on a column containing SP-Sephadex C-25 (ϕ 2.5×75 cm), and the band was eluted with 0.1 M aqueous solution of potassium (+)$_D$-tartratoantimonate (III)for fractionation into thirteen portions. The last fraction was adsorbed again on a SP-Sephadex C-25 column (ϕ 2.5×20 cm) and eluted with 0.2 M hydrochloric acid. The eluate was evaporated to dryness and dissolved in a small amount of water, the circular dichroism spectrum being recorded (Fig. 5). The concentration of the complex ion was determined by visible absorbance of the solution. The circular dichroism curve of the first part of the fractions showed a pattern enantiomeric to that of the last fraction.

[Co(en)$_2$(dmbpy)]Cl(ClO$_4$)$_2 \cdot H_2O$. A mixture of *trans*-[CoCl$_2$(en)$_2$]Cl (4.0 g in 40 ml of water), dmbpy (2.0 g in 10 ml of ethanol) and activated charcoal (0.5 g) was warmed at 60 °C for 1 h, then filtered. To the filtrate was added 20 ml of 1 M hydrochloric acid. The solution was diluted with water and poured onto the SP-Sephadex C-25 column (ϕ 5.5×30 cm). The adsorbed band was washed with water, then eluted with 0.2 M hydrochloric acid. The orange band was eluted off and the eluate was evaporated to dryness. The dried residue was dissolved in 40 ml of water and the solution was filtered. After the addition of sodium perchlorate (5 g in 10 ml of water), the solution was allowed to stand for 1 h at room temperature. Orange crystals obtained were collected, washed with cold water, ethanol and ether, and recrystallized from hot water.
Found: C, 31.25; H, 4.94; N, 13.62%. Calcd for $C_{16}H_{22}N_6O_9CoCl_3$: C, 31.17; H, 4.87; N, 13.64%.

Resolution of [Co(en)$_2$(dmbpy)]Cl(ClO$_4$)$_2 \cdot H_2O$. *Method I*: A mixture of [Co(en)$_2$(dmbpy)]Cl(ClO$_4$)$_2 \cdot H_2O$ (3.0 g in50 ml of water) and K$_3$[Co(L-cysu)$_3$][12] (cysu=cysteinsulfinate) (1.4 g in 20 ml of water)was heated at 80 °C on a water bath for 10 min, filtered, and left to stand for 3 h at room temperature. Needlelike yellow crystals of (+)$_D$-diastereomer which appeared were filtered and washed with water, ethanol and then ether. Yield 2.0 g. (The filtrate free from the (+)$_D$-

isomer was stored in order to obtain $(-)_D$-isomer.) The $(+)_D$-diastereomer was recrystallized twice from hot water. The CD strength at 485 nm did not change on repeated recrystallization. Pure $(+)_D$-diastereomer in 20 ml of water was treated with 10 ml of 2 M hydrochloric acid. Yellow precipitate of $H_3[Co(L\text{-cysu})_3]$ was filtered off, and the solution was treated with 2.0 g of sodium perchlorate in 5 ml of water, and stored in a refrigerator overnight. Needlelike orange crystals were collected and recrystallized from water. Yield 0.8 g. Found: C, 31.24; H, 4.98; N, 13.77%. Calcd for $C_{16}H_{22}N_6O_9CoCl_3$: C, 31.17; H, 4.87; N, 13.64%.

The filtrate free from the $(+)_D$-isomer was evaporated to 10 ml. The precipitate was filtered off, and 2 ml of 6 M hydrochloric acid was added to the filtrate. Yellow precipitate of $H_3[Co(L\text{-cysu})_3]$ was filtered off. The filtrate was treated with sodium perchlorate (2.0 g in 5 ml of water), and stored in a refrigerator. Needlelike orange crystals were collected and recrystallized twice from hot water. Yield 0.3 g.

Found: C, 31.22; H, 4.87; N, 13.66%. Calcd for $C_{16}H_{22}N_6O_9CoCl_3$: C, 31.17; H, 4.87; N, 13.64%.

Method II: An aqueous solution of the racemic complex (about 8 mg) was poured on a SP-Sephadex C-25 column (ϕ 1.3×110 cm) and the adsorbed orange band was eluted with 0.15 M aqueous solution of potassium $(+)_D$-tartratoantimonate(III) at a rate of 0.47 ml per min. The eluate was fractionated into 5 ml portions and the absorption spectrum of each fraction was checked (330 nm). Only two isomers were obtained (Fig. 2a). The $(+)_D$-isomer was eluted faster than the $(-)_D$-isomer.

cis-α-*[Co(trien)(dmbpy)]Cl(ClO$_4$)$_2$*. This complex was prepared according to a method similar to that for $[Co(en)_2(dmbpy)]Cl(ClO_4)_2\cdot H_2O$. A mixture of *cis*-α-$[CoCl_2(trien)]Cl$[13] (4.4 g in 30 ml of water), dmbpy (2.0 g in 5 ml of ethanol) and activated charcoal (1 g) was warmed at 70 °C for 20 min, and filtered. The filtrate was acidified with 1 M hydrochloric acid and treated with 5 g of sodium perchlorate in 10 ml of water. Orange crystals appeared within a minute. They were filtered off after 30 min and washed with a small amount of ice-water, ethanol and then ether, and recrystallized from hot water. Yield 4.8 g.

Found: C, 34.43; H, 4.84; N, 13.03%. Calcd for $C_{18}H_{30}N_6O_8CoCl_3$: C, 34.64; H, 4.85; N, 13.47%.

Resolution of cis-α-*[Co(trien)(dmbpy)]Cl(ClO$_4$)$_2$*. This complex was resolved by a method similar to that for $[Co(en)_2(dmbpy)]Cl(ClO_4)_2\cdot H_2O$ with $K_3[Co(L\text{-cysu})_3]$ as resolving agent. Two optical isomers were obtained. The CD curve showed that they are enantiomeric to each other. A chromatographic method similar to that for $[Co(en)_2(dmbpy)]^{3+}$ was also employed. An aqueous solution of 18 mg of the complex was poured on a SP-Sephadex C-25 column (ϕ 1.3×110 cm) and the adsorbed band was eluted with a 0.15 M potassium $(+)_D$-tartratoantimonate-(III) as the eluent. The eluate was fractionated into 5 ml portions and their absorption spectra (280 nm) was checked. Figure 2b shows that two well separated bands were obtained. The $(+)_D$-isomre was eluted faster than the $(-)_D$-isomer. The CD curves show that these isomers are enantiomeric to each other.

*$(-)_D$[Co(*R,R*-chxn)$_2$(dmbpy)](ClO$_4$)$_3$*. This complex was prepared by a method similar to that for $[Co(en)_2(dmbpy)]Cl(ClO_4)_2\cdot H_2O$. A mixture of *trans*-$[CoCl_2(R,R\text{-chxn})_2]ClO_4$(chxn=cyclohexanediamine) (1.0 g in 20 ml of water), dmbpy (0.5 g in 10 ml of ethanol) and activated charcoal (0.5 g) was warmed at 70 °C for 15 min, filtered and treated with 10 ml of 1 M hydrochloric acid. The solution was diluted with water 10 times in volume and poured on a column of SP-Sephadex C-25 (ϕ 3.0×30 cm). The adsorbed band was eluted with 0.2 M hydrochloric acid. All the fractions showed equal absorption and CD patterns. They were collected and evaporated to dryness. The residue was dissolved in 20 ml of water, filtered, treated with 1.5 g of sodium perchlorate in 10 ml of water and stored in a refrigerator overnight. Orange crystals were filtered off and washed with a small volume of water, ethanol and ether and then air dried.

Found: C, 37.35; H, 5.54; N, 10.97%. Calcd for $C_{24}H_{40}N_6O_{12}CoCl_3$: C, 37.47; H, 5.20; N, 10.97%.

*$(-)_D$[Co(*R,R*-chxn)$_2$(bpy)](ClO$_4$)$_3$*. The procedure was similar to that for the $(-)_D[Co(R,R\text{-chxn})_2(dmbpy)](ClO_4)_3$ using bpy instead of dmbpy. A mixture of 1.2 g of *trans*-$[CoCl_2(R,R\text{-chxn})_2]ClO_4$ in 25 ml of water. 0.5 g of bpy in 10 ml of ethanol and 0.5 g of activated charcoal was heated at 60 °C for 15 min, filtered, acidified with 10 ml of 1 M hydrochloric acid, diluted with water and poured onto a column containing SP-Sephadex C-25. The adsorbed orange band was eluted with 0.2 M hyrochloric acid. Abosrption and CD spectra of the fractions were checked. Fractions giving similar spectral data were collected and evaporated to dryness. The residue was dissloved in 20 ml of water. The solution was filtered, and treated with 1.5 g of sodium perchlorate in 10 ml of water. The orange crystals were filtered off and washed with a small volume of ice-water, ethanol and ether, and recrystallized from water. Yield 0.65 g.

Found: C, 35.59; H, 4.93; N, 11.31%. Calcd for $C_{22}H_{36}N_6O_{12}CoCl_3$: C, 35.62; H, 4.89; N, 11.33%.

Measurements. Absorption and CD spectra were recorded on a Shimadzu Double 40-R spectrophotometer and a Jasco J-20 spectropolarimeter, respectively, at room temperature. PMR spectra were recorded with a JNM-PMX 60 spectrometer using DSS as an internal standard. Infrared specrta were recorded over the NaCl region with a Hitachi Model 285 infrared spectrometer. The complexes, $(+)_D$-$[Co(en)_2(dmbpy)]Cl(ClO_4)_2\cdot H_2O$, $(+)_D[Co(trien)(dmbpy)]$-$Cl(ClO_4)_2$ and $(-)_D[Co(R,R\text{-chxn})_2(dmbpy)](ClO_4)_3$ were converted into their bromide by use of the anion exchanger Dowex 1-X8 in bromide form, for the measurement of PMR and infrared spectra. Most of the measurements were made at 25 °C.

Results and Discussion

Preparation and Stereochemistry. The cobalt(III) complexes, $[Co(dmbpy)_3]^{3+}$, $[Co(tren)(dmbpy)]^{3+}$, $[Co(en)_2(dmbpy)]^{3+}$, $[Co(trien)(dmbpy)]^{3+}$, and $[Co(R,R\text{-chxn})_2(dmbpy)]^{3+}$ were characterized by elemental analysis, absorption, CD and PMR spectra. Among these complexes, the tren complex has no chiral configuration around the cobalt(III) ion and the optical activity in this complex arises exclusively from the twisted conformation of the dmbpy chelate. $[Co(tren)(dmbpy)]^{3+}$ was partially resolved by column chromatography, and the CD spectrum in the visible region remained unchanged at room temperature for several days. This indicates that the dmbpy chelate of this complex is twisted and takes a nonconvertible conformation.

The bis(en), trien, bis(*R,R*-chxn) complexes have two kinds of dissymmetry; the configurational dissymmetry, Δ and Λ, and conformational dissymmetry, δ and λ (Fig. 1). Consequently, four optical isomers

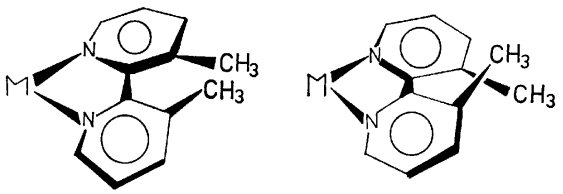

$\lambda(R)$-conformation $\delta(S)$-conformation

Fig. 1. Two conformations of dmbpy chelates.

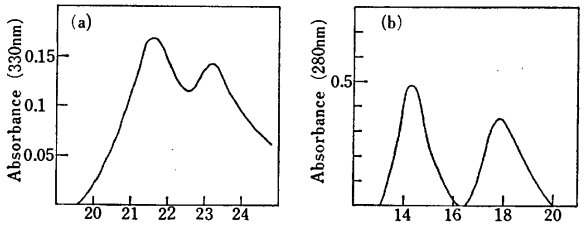

Fig. 2. a) Elution curve of $[Co(en)_2(dmbpy)]^{3+}$ ion. Plots of absorbance at 330 nm (path length = 1.0 cm) *vs.* the ratio of the eluate volume (v) to the bed volume (v_t = 146 ml).
b) Elution curve of *cis*-α-$[Co(trien)(dmbpy)]^{3+}$ ion. Plots of absorbance at 280 nm (path length = 1.0 cm) *vs.* the ratio of the eluate volume (v) to the bed volume (v = 146 ml).

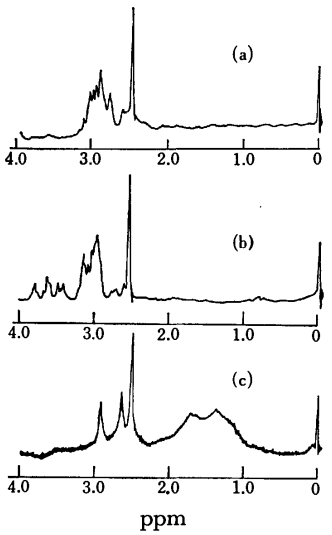

Fig. 3. The PMR spectra of a) $[Co(en)_2(dmbpy)]Br_3$ b) *cis*-α-$[Co(trien)(dmpy)]Br_3$ c) $(-)_D$-$[Co(R,R\text{-chxn})_2(dmbpy)]Br_3$ in D_2O.

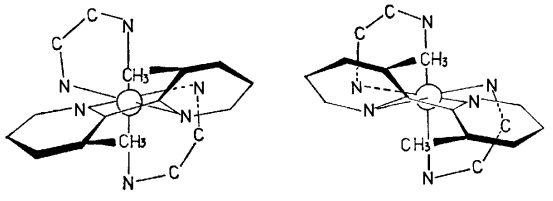

$\Delta(\lambda$-dmbpy) $\Delta(\delta$-dmbpy)

Fig. 4. Schematic structues of Δ-$[Co(en)_2(\lambda\text{-dmbpy})]^{3+}$ and Δ-$[Co(en)_2(\delta\text{-dmbpy})]^{3+}$ ions.

Table 1. Absorption (AB) and circular dichroism (CD) spectral data in 10^3 cm^{-1}, (log ε) and ($\varepsilon_l - \varepsilon_r$)

Complex	AB	CD
$(+)_D[Co(tren)(dmbpy)]^{3+}$	20.83(2.23)	19.80(+ 0.022)
		22.22(− 0.018)
	31.75(3.99)	28.57(+ 0.58)
		31.25(+ 0.20)
	43.86(4.58)	
$(+)_D[Co(en)_2(bpy)]^{3+}$	21.74(1.99)	20.70(+ 3.02)
	ca. 31.25(4.03)	32.47(− 6.64)
	32.46(4.12)	*ca.* 45.87(−24.83)
	45.87(4.68)	49.50(+28.87)
$(+)_D[Co(en)_2(dmbpy)]^{3+}$	21.28(2.21)	21.05(+ 7.45)
	30.30(3.77)	28.17(− 5.84)
	33.67(3.91)	33.78(− 4.72)
		39.37(−21.11)
	44.24(4.73)	47.17(+35.70)
$(+)_D$-*cis*-α$[Co(trien)(dmbpy)]^{3+}$	21.05(2.29)	20.74(+ 7.23)
	30.30(3.67)	28.17(− 4.14)
	34.01(3.91)	30.12(− 6.02)
		31.55(− 6.20)
		40.81(−18.53)
	43.48(4.76)	48.08(+46.30)
$(-)_D[Co(R,R\text{-chxn})_2(bpy)]^{3+}$	21.28(2.07)	20.53(− 3.31)
	32.26(4.11)	32.26(+ 9.29)
		40.98(+42.72)
	45.05(4.64)	48.54(−34.49)
$(-)_D[Co(R,R\text{-chxn})_2(dmbpy)]^{3+}$	21.10(2.17)	20.83(− 7.12)
	ca. 30.49(3.82)	27.78(+ 5.41)
	31.75(3.88)	30.03(+ 5.41)
	32.79(3.90)	33.78(+ 7.33)
		40.48(+51.80)
	44.14(4.72)	46.72(−61.50)

are possible for each complex. In addition to the optical isomers, the trien complex has geometric isomers, *i.e. cis*-α and *cis*-β. They can usually be distinguished by their IR spectra in the 990—1090 cm^{-1} region; while *cis*-α complexes show two strong absorption bands in this region, *cis*-β complexes give four bands.[15] The IR spectrum of $[Co(trien)(dmbpy)]Br_3$ shows two strong band in this region and hence the complex can be assigned to *cis*-α isomer.

The en and trien complexes were resolved by chemical and chromatographic methods. The CD spectra of the two isomers of the chemically resolved en (or trien) complex showed symmetrical curves to each other over all the wavelengths, indicating that they are a pair of enantiomers. The en and trien complexes were adsorbed on a column of SP-Sephadex C-25 and eluted with 0.15 M potassium $(+)_D$-tartratoantimonate(III) solution. Figure 2 shows their elution curves. No indication for the presence of more than two isomers was found in both chemical and chromatographic resolution. On the other hand, $[Co(R,R\text{-chxn})_2(dmbpy)](ClO_4)_3$ yielded only $(-)_D$-isomer stereospecifically (see Experimental). The PMR spectra

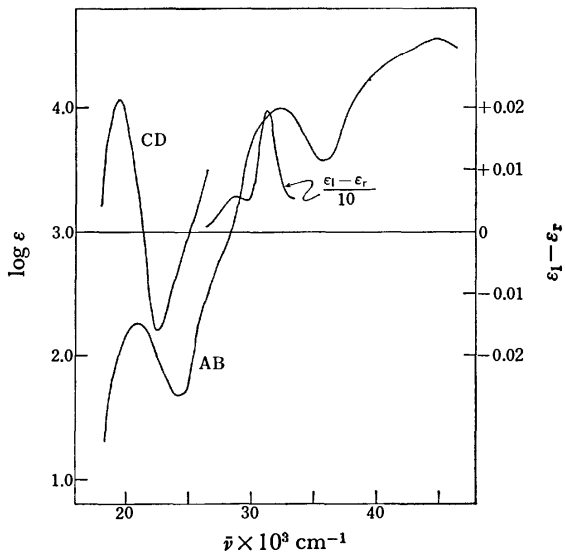

Fig. 5. Absorption (AB) and CD spectra of $(+)_D$-[Co(tren)(dmbpy)]$^{3+}$.

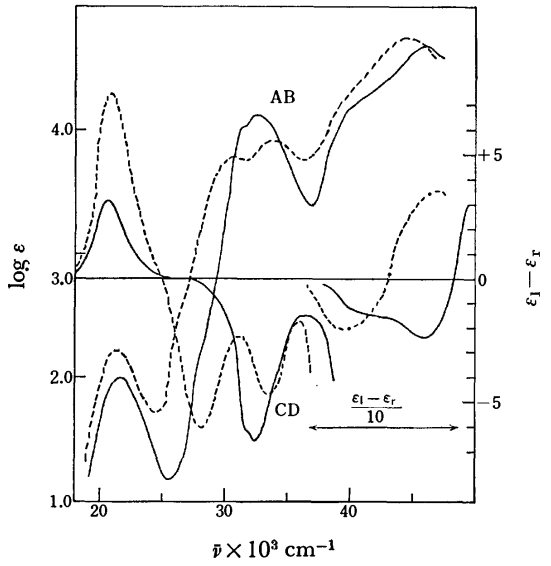

Fig. 6. AB and CD spectra of $(+)_D[Co(en)_2(bpy)]^{3+}$ (——) and $(+)_D[Co(en)_2(dmbpy)]^{3+}$ (----).

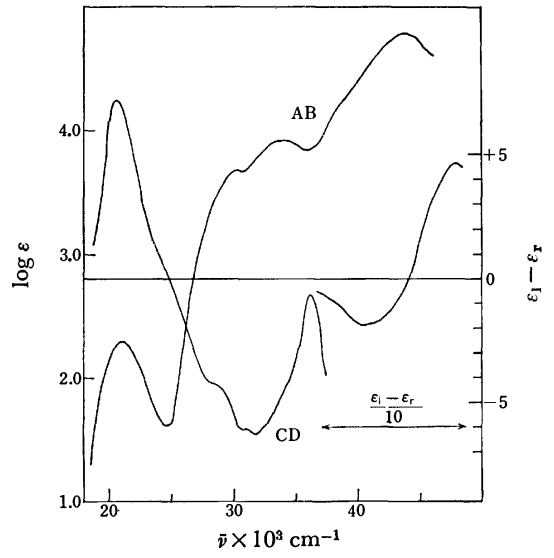

Fig. 7. AB and CD spectra of $(+)_D$-*cis*-α-[Co(trien)-(dmbpy)]$^{3+}$.

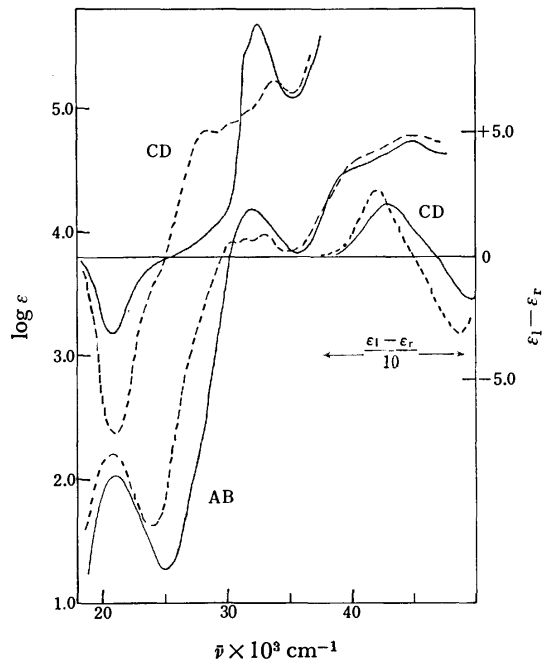

Fig. 8. AB and CD spectra of $(-)_D[Co(R,R\text{-chxn})_2(bpy)]^{3+}$ (——) and $(-)_D[Co(R,R\text{-chxn})_2(dmbpy)]^{3+}$ (----).

of en, trien and *R,R*-chxn complexes show only one methyl signal at *ca.* 2.5 ppm (Fig. 3). The results also support the view that the dmbpy coordinates stereospecifically to the central cobalt(III) ion in the given configuration.

Recently, Douglas *et al.*[5] and Tanimura *et al.*[6] prepared and resolved a series of cobalt(III) complexes of 2,2′-diaminobiphenyl (dabp). The bidentate ligand dabp also takes a non-coplanar conformation upon coordination as dmbpy does. They reported that the conformation of the dabp chelates depends on the configuration of the complexes. The crystal structure of Δ-$[Co(R\text{-pn})_2(dabp)]Cl_3$ has been determined by X-ray analysis, the conformation of the dabp chelate being found to be λ.[6]

Figure 4 gives a schematic representation of the two possible structures of Δ-$[Co(en)_2(dmbpy)]^{3+}$. In the $\Delta(\lambda$-dmbpy) arrangements, the pyridine rings are twisted into open faces of the octahedron, *i.e.*, the faces are not occupied by en chelates. The interaction between π-electron cloud of bipyridine rings and ethylenediamine protons of $\Delta(\lambda$-dmbpy) seems to be less than $\Delta(\delta$-dmbpy). The same relationship holds for $\Lambda(\delta$-dmbpy) and $\Lambda(\lambda$-dmbpy).

R-Diamine such as *R*-pn or *R,R*-chxn takes the *λ-gauche* conformation upon coordination.[15,16] Thus, the structure of the stereospecifically formed $(-)_D[Co(R,R\text{-chxn})_2(dmbpy)]^{3+}$ should be either $\Delta(\lambda\lambda,\delta$-dmbpy) or $\Delta(\lambda\lambda,\lambda$-dmbpy). The absolute configuration was assigned to Δ from the CD sign of the first d-d region.[17] Molecular model studies suggest that the 2C-2C′ bond

in λ-dmbpy chelate is parallel to the pseudo-three fold axis whereas it is oblique in δ-dmbpy. The stability of these two isomers might differ. The tris(*R*-diamine) cobalt(III) complexes have two optical isomers $\Delta(\lambda\lambda\lambda)(lel)$ and $\Lambda(\lambda\lambda\lambda)(ob)$ in which the lel isomer of $[Co(R\text{-pn})_3]^{3+}$ is known to be more stable than the ob isomer.[15] It is likely that the dmbpy chelate takes λ conformation in $(-)_D[Co(R,R\text{-chxn})_2(dmbpy)]^{3+}$. This agrees with the molecular model consideration for the $[Co(en)_2(dmbpy)]^{3+}$ (Fig. 4).

Absorption Spectra. The absorption and CD spectra of all the $[Co(N)_6]^{3+}$ type complexes are shown in Figs. 5—8. Their band locations and intensities are given in Table 1. The first absorption band maxima of the dmbpy complexes have higher intensities and appear at longer wavelength as compared with $(+)_D[Co(en)_2(bpy)]^{3+}$ or $(-)_D[Co(R,R\text{-chxn})_2(bpy)]^{3+}$. The absorption peaks in 25000—35000 cm^{-1} region might be related to the electronic transitions of the coordinated dmbpy or bpy.[18] The intensities of these bands of the dmbpy complexes are always lower and the band patterns are broader as compared with those of the bpy complexes. These effects are presumably due to a torsional strain and inhibition of resonance of the dmbpy chelate.[19]

CD Spectra. Two component Cotton effects, a positive and a negative peaks from longer to shorter wavelength are observed in the visible region of the $(+)_D[Co(tren)(dmbpy)]^{3+}$ (Fig. 5). Two positive Cotton effects are observed in the region 28000—35000 cm^{-1}. The origin of the optical activity of this complex is due to the twisted conformation of the dmbpy chelate. The absolute conformation of the ligand cannot be assigned from the CD spectra at present.

A strong CD band is observed for each $(+)_D[Co(en)_2(dmbpy)]^{3+}$, *cis* α-$(+)_D[Co(trien)(dmbpy)]^{3+}$ and $(-)_D[Co(R,R\text{-chxn})_2(dmbpy)]^{3+}$ in the first absorption region (Figs. 6—8). Their CD magnitudes are greater than those of the bpy complexes. The CD sign of a cobalt(III) complex in the first absorption band is known to depend on the absolute configuration of the complex.[17] Thus, the absolute configurations of $(+)_D[Co(en)_2(dmbpy)]^{3+}$, $(+)_D[Co(trien)(dmbpy)]^{3+}$, and $(-)_D[Co(R,R\text{-chxn})_2(dmbpy)]^{3+}$ are assigned to Λ, Λ and Δ, respectively. While the CD spectra of bpy complexes gave one component Cotton effect in the region 25000—35000 cm^{-1}, the dmbpy complexes showed broad and split peaks. The absolute conformation of the twisted dmbpy can not be assigned at present from the CD patterns in these region.

The authors wish to thank Professor Kazuo Saito of Tohoku University, and Professor Junnosuke Fujita and Dr. Kazuo Kashiwabara of Nagoya University for their helpful suggestions and discussions.

References

1) "Advances in Inorg. Chem. and Radiochem," Academic Press, **12**, 135 (1969).
2) F. W. Cagle Jr. and G. F. Smith, *J. Am. Chem. Soc.*, **69**, 1860 (1947).
3) T. M. Suzuki, *Chem. Lett.*, **93**, 1975.
4) K. Mislow, E. Bunnenberg, R. Record, K. Wellman, and C. Djerassi, *J. Am. Chem. Soc.*, **85**, 1342 (1963).
5) W. T. Jordan, Ching-Yu Lin, and B. E. Douglas, *J. Coord. Chem.*, **3**, 1 (1973).
6) T. Tanimura, H. Ito, J. Fujita, K. Saito, S. Hirai, and K. Yamasaki, *J. Coord. Chem.*, **3**, 161 (1973).
7) O. Seide, *Ber.*, **57**, 1802 (1924).
8) *Org. Synth.* Coll. Vol. 3, 136.
9) F. H. Case, *J. Am. Chem. Soc.*, **68**, 2574 (1946).
10) *Org. Synth.* Coll. Vol. 1, 119.
11) E. Ristenpart, *Ber.*, **29**, 2531 (1896).
12) L. S. Dollimore and R. D. Gillard, *J. Chem. Soc., Dalton Trans.*, **1973**, 933.
13) A. M. Sargeson and G. H. Searle, *Inorg. Chem.*, **6**, 787 (1967).
14) D. A. Buckingham and D. Jones, *Inorg. Chem.*, **4**, 1387 (1965).
15) E. J. Corey and J. C. Bailar, Jr., *J. Am. Chem. Soc.*, **81**, 2620 (1959).
16) S. Yano, H. Ito, K. Koike, J. Fujita, and K. Saito, *Bull. Chem. Soc. Jpn.*, **42**, 3184 (1969).
17) A. J. MacCaffery, S. F. Mason, and B. J. Norman, *J. Chem. Soc.*, 5094 (1965).
18) G. Favini, *Gazz. Chim. Ital.*, **94**, 1287 (1964).
19) B. Williamson and W. H. Rodebush, *J. Am. Chem. Soc.*, **63**, 3018 (1941).

Note added in proof

The structure of $(+)_D[Co(en)_2(dmbpy)]Cl(ClO_4)_2\cdot H_2O$ was determined recently by X-ray crystal analysis. The configuration of the complex and the conformation of dmbpy were found to be Λ and δ, respectively. (S. Sato and Y. Saito, private communication)

We are grateful to Dr. S. Sato and Professor Y. Saito, the University of Tokyo, for providing us with this information prior to publication.

Determination of Chlorine in Rocks, Soils and Organic Materials by Heating Powdered Sample in Strong Phosphoric Acid, and Some Additional Investigations on the Related Reactions

Kikuo TERADA, Saburo HIRAKAWA, and Toshiyasu KIBA

Department of Chemistry, Faculty of Science, Kanazawa University, Kanazawa, Ishikawa 920

(Received July 12, 1976)

The decomposition of several salts in strong phosphoric acid (SPA) was examined. These halides were decomposed and hydrogen halides evolved by heating the samples with SPA at various temperatures. Based on these data an adequate reagent was chosen for the efficient separation of various elements which can form volatile halides. The recommended distillation condition was applied to determine the chlorine content in solid samples, such as rocks, soils or some organic materials. The sample was heated in an SPA medium and a distillate of hydrogen chloride was absorbed in a sodium hydroxide solution. The solution was subjected to volumetric analysis with a silver nitrate solution for chlorine in the range of 10^{-2} to 10^{-4} mol and to spectrophotometric determination with mercury thiocyanate for elements less than 10^{-4} mol. Furthermore, from the results of X-ray diffraction measurements of the original and the SPA-treated samples, it was confirmed that the main crystal structure of a rock sample could be decomposed by heating with SPA. The chlorine analysis was performed for Japan Geological Survey standard rocks, JG-1 and JB-1, and a synthesized complex compound.

It is known that some metallic and ammonium salts of acids of low boiling point could readily be decomposed in strong phosphoric acid by heating and evolve gaseous acid quantitatively.[1] Sulfides and halides fall in this category, and, based on this various applications have been developed for the determination of sulfur.[2-12]

On the other hand, when an element having a volatile halide is present in a sample, an exchange reaction may occur in the strong phosphoric acid medium, if the sample is heated together with the alkali halide in the medium. In the previous papers,[13,14] the present authors reported that when selenium-containing samples of rocks, soils, or sediments are heated with ammonium chloride or ammonium bromide in SPA, selenium(IV) tetrachloride or tetrabromide, respectively, evolve quantitatively from the sample.

The decomposition of metal halides and the evolution of hydrogen halide may be expressed as

$$X^- + H_nP_mO_l \longrightarrow HX + H_{n-1}P_mO_l^- \quad (1)$$

and the succeeding reaction with selenium(IV) and (VI) compounds is

$$H_2SeO_3 + 4HX \longrightarrow SeX_4 + 3H_2O \quad (2)$$

In Eq. 1, the evolved hydrogen halide may be in an extremely reactive gaseous state. To accomplish the two reactions successfully for the quantitative recovery of selenium from a sample, Reaction 1 should proceed concurrently with Reaction 2; Therefore, the forming rate of the active hydrogen halide upon heating of the SPA medium may be the first important practical factor, and the boiling temperature of the selenium halide and the rate of Reaction 2 may be the second.

The present authors investigated the above factors in detail with the aim of extending the SPA-analytical method to the determination of halogens in solid samples such as rocks, soils, and organic materials and to the rapid separation of selenium and arsenic[15] as halides in solid samples.

Experimental

Reagents. *Strong Phosphoric Acid (SPA)*: Commercial ortho-phosphoric acid of extra pure reagent grade was dehydrated as described previously.[13,16] The syrupy liquid obtained was stored in a closed vessel.

Silver Nitrate Standard Solution (M/10). *Mercury Thiocyanate Solution*: Mercury(II) nitrate (5 g) was dissolved in 200 ml of 0.5 M nitric acid; 3 ml of a saturated ammonium iron(III) sulfate solution in 1 M nitric acid was added; the solution was titrated with a 4% potassium thiocyanate solution with continuous shaking until the color changed to pale orange; the white crystalline precipitate thus obtained was filtered through a glass filter, washed well with distilled water and dried in air; 0.3 g of this reagent was dissolved in 100 ml of ethanol and stored in a dark bottle. This solution is stable for several months.

Ammonium Iron(III) Sulfate Solution: Six grams of dodecahydrated salt of guaranteed reagent grade was dissolved in 100 ml of 6 M nitric acid.

Standard Chloride Solution: Sodium chloride of guaranteed reagent grade (2.013 g) was dissolved in distilled water in a 1-liter measuring flask. This solution was diluted for use.

Other Chemicals: Ammonium chloride, bromide, and iodide, potassium chloride, bromide, and iodide, sodium chloride, bromide, and iodide, hydrochloric acid, sodium hydroxide and fluorescein were all of guaranteed reagent grade.

Apparatus. Electric conductivity measurements: a conductivity outfit, Model MY-7 (Yanagimoto Seisakusho Co.) connected to a conductivity cell, Model CDC-121 (M & S Instr. Co., Inc.).

A photo-electric spectrophotometer (Hirama Rika Kenkyujo), Type 6 and 1-cm glass cell.

A Hitachi-Horiba glass electrode pH meter, Model M-3.

The reaction vessel used was the same as that described previously[13] and was connected to an absorption tube or a conductivity cell.

Procedure. Sodium chloride in amounts of 5×10^{-4}—2×10^{-3} mol was placed in the reaction vessel and about 30 g of SPA was added. Twenty milliliters of a sodium hydroxide solution was placed in the absorption tube and all joints were connected as shown in Fig. 1. The air was aspirated slowly from the last outlet tube by means of a suction pump and the reaction vessel was heated on an electric heater to start the reaction. The reaction rate was followed every 2—3 min by measuring the electric conductivity of the absorption solution using a flow-type conductivity cell. The temperature of the reaction medium was recorded at the same time. The evolving hydrogen chloride in the

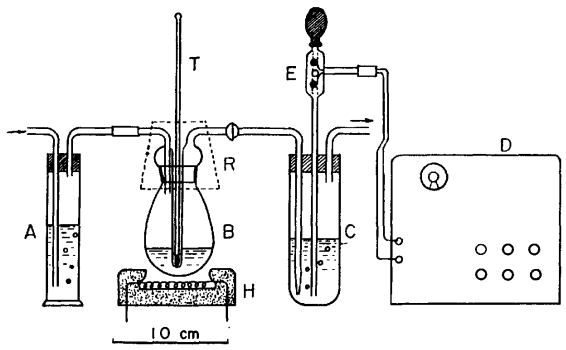

Fig. 1. Apparatus for successive conductivity measurement for SPA-distillate absorbing solution.
A: Washing bottle, B: reaction vessel, C: absorption tube, D: conductivity outfit, E: flow-type conductivity cell, H: electric heater, R: ribbon heater, T: thermometer.

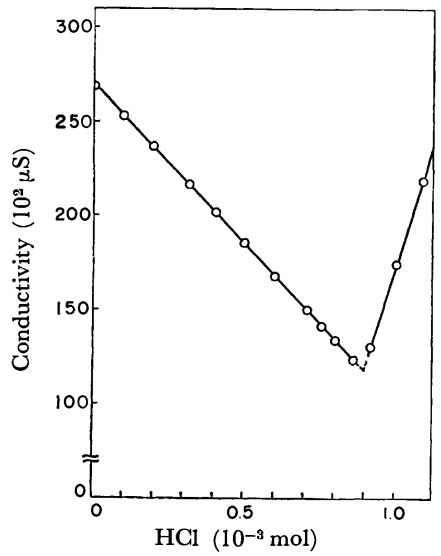

Fig. 2. Conductometric titration curve.
Sodium hydroxide was titrated with hydrochloric acid.

absorption solution was determined from the conductivity value obtained. The relationship between the evolving hydrogen chloride and the electric conductivity was obtained using the titration curve (Fig. 2) which was constructed on the basis of the titration of 20 ml of a M/20 sodium hydroxide solution with 1 M hydrochloric acid. In the case of decomposing bromide or iodide salts, hydrobromic acid or hydroiodic acid were used in place of hydrochloric acid in the above procedure.

Results and Discussion

Decomposition of Various Halide in SPA. Figures 3, 4, and 5 show decomposition curves for several chlorides, bromides and iodides in SPA media. In the figures, the open circles represent the amounts of hydrogen halide trapped in the absorption solution after each heating period as determined by the conductivity measurements and the filled-in circles the temperature of the reaction medium after the same periods. It is clear that the decomposition of chloride salts is initiated at about

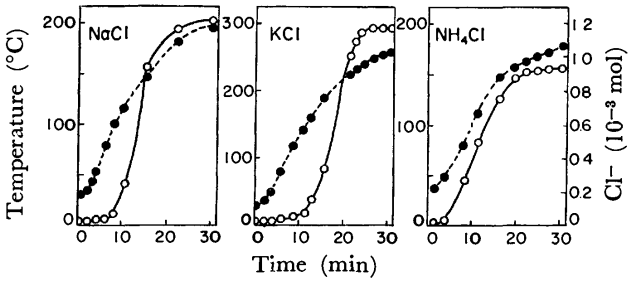

Fig. 3. SPA-decomposition curves for cloride salts.
—○—: Amount of hydrogen chloride in absorption solution, --●--: temperature change of SPA-medium.

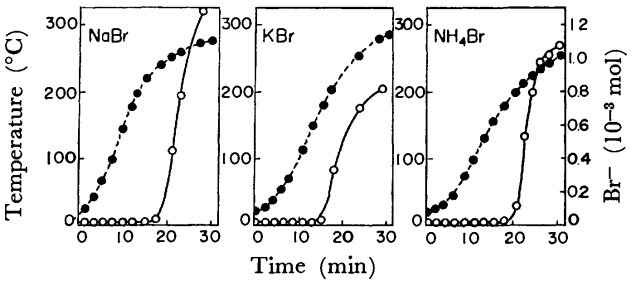

Fig. 4. SPA-decomposition curves for bromide salts.

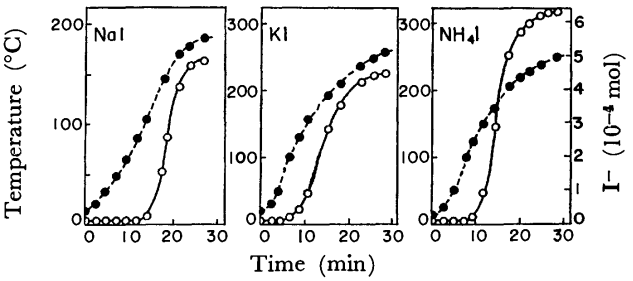

Fig. 5. SPA-decomposition curves for iodide salts.

Table 1. Decomposition temperature of various halide salts in SPA media

Salt	Temperature of decomposition, °C	
	Start	Finish
NaCl	100	200
KCl	50	230
NH_4Cl	50	160
NaBr	230	290
KBr	180	280
NH_4Br	180	260
NaI	180	260
KI	80	230
NH_4I	100	240

110, 50, and 50 °C and the evolution of hydrogen chloride may be completed at 200, 230, and 160 °C, for the sodium, potassium, and ammonium salts, respectively. In the case of the bromides, the sodium salt was most resistant to decomposition, and the ammonium salt reacted with SPA more easily than did the others. For the iodides, again the sodium salt was most resistant to SPA action, whereas the potassium salt was most easily decomposed. The results

are summarized in Table 1. However, it should be noted that there is a certain time lag between the hydrogen halide generation and its arrival in the absorption solution. Furthermore, the present results may fluctuate to some extent depending on the heating time and also on the amounts of halide salts used. The difficulty in detecting halide ions in amounts less than 2×10^{-5} mol in 20 ml of the absorption solution makes it necessary to delay the measurement until the evolved hydrogen halide gas has accumulated in detectable amounts in the solution. Therefore, a delay is unavoidable in the response of the hydrogen halide gas evolution and the completion of the decomposing reaction. Therefore, the data shown in Figs. 3, 4, and 5 are strictly valid only under the present experimental conditions.

But it may be possible to present a discussion based on the present results which may be not differ too much from those obtained for arbitrary experimental conditions. As suggested above, a complete distillation of a certain element in gaseous halide form from the SPA medium would be expected to occur when decomposition of the halide reagent added to the sample in the reaction vessel begins as the increasing temperature approaches the boiling point of the halide of the element concerned and ceases at temperatures above the boiling point. Thus, from the present results it may be possible to predict which reagent is suitable for use in the distillation of a given element by evolution as a gaseous halide from an SPA medium.

Distillation of Selenium and Arsenic as Halides. As previously reported,[13] selenium(IV) and (VI) can be distilled as tetrabromide from bromide-SPA at about 250 °C. The sublimation temperature of the selenium tetrabromide is known to be 196 °C. Therefore, sodium chloride and ammonium chloride are presumed to be unsuitable for the distillation of selenium since hydrogen chloride gas will evaporate off before the temperature reaches the sublimation point of selenium tetrachloride. In fact, ammonium and sodium chlorides distill selenium incompletely (50—80%).

On the other hand, ammonium bromide was found to be the most useful for this purpose, although the sublimation temperature of selenium(IV) tetrabromide is still unknown. This temperature may fall between 200 and 250 °C, because the boiling point of a metal bromide in an aqueous solution is generally higher than that of the corresponding chloride.

For arsenic(III), the boiling point of arsenic(III) chloride and bromide are known to be 130.4 and 221 °C, respectively.[17] Thus the chloride would be expected to be the most adequate form for distillation from the SPA medium. Therefore, sodium and potassium chlorides may be useful for this purpose. As shown in Fig. 6, the distillation of arsenic(III) was complete in the sodium chloride-SPA reagent solution when the temperature reached 180 °C and a slightly lower recovery was observed when potassium chloride was used.[15] On the other hand, the recovery of arsenic by ammonium bromide was incomplete as expected.

Another example is the distillation of germanium. The boiling points of germanium(IV) chloride and bromide are known to be 84 and 185.9 °C, respectively.[17] Therefore, ammonium or potassium chloride may be suitably employed for the distillation of germanium in tetrachloride form, whereas all bromides are useless. Tin(IV) can also be distilled as tin(IV) chloride (bp 114 °C) or bromide (bp 202 °C) from ammonium chloride-SPA and ammonium bromide-SPA media.

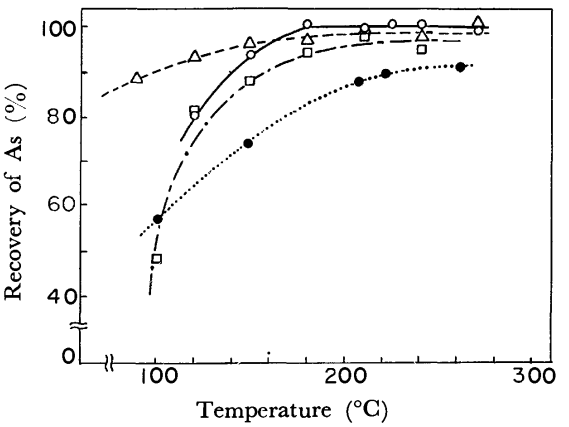

Fig. 6. Recovery of arsenic at various temperatures of various SPA-reagents media.
—○—: NaCl, --△--: KCl, —-□—-: NH_4Cl, ···●···: NH_4Br.

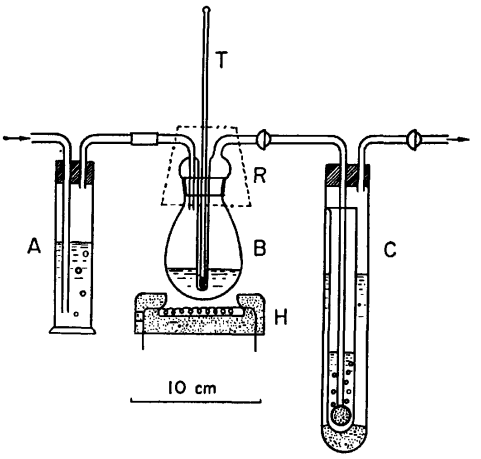

Fig. 7. SPA distillation apparatus for determination of halogen.
A: Washing bottle, B: reaction vessel, C: absorption tube, H: electric heater, R: ribbon heater, T: thermometer.

Further predictions will be made for the distillation of the other volatile metal halides, for example, chromium, niobium, rhenium, and antimony.[18] Further details and applications of the present study will be given elsewhere.

Determination of Chloride in Solid Samples. In general, the analysis of chlorine content in rocks, soils, and minerals requires an alkaline or carbonate fusion treatment of the sample, followed by extraction with hot water or nitric acid. The fusion process is tedious and may cause unexpected losses of the element or contamination of the element from the reagents used and from the instruments. Furthermore, matrix constituents occasionally interfere with the determination

Table 2. Volumetric determination of chloride after SPA distillation

Cl^- added, mol[a)]	Cl^- found, mol
1×10^{-3}	1.01×10^{-3}
	1.00
	1.02
	1.00
1×10^{-4}	1.01×10^{-4}
	0.98
	1.02
	0.99
	0.98

a) Cl^- was added as NaCl.

Table 3. Spectrophotometric determination of chloride after SPA distillation

Cl^- added, mol[a)]	Cl^- found, mol
3.4×10^{-5}	3.2×10^{-5}
	3.1
	3.5
	3.3
5.0×10^{-6}	4.8×10^{-6}
	4.7
	5.2
	4.9

a) Cl^- was added as NaCl.

of chloride in low concentrations. Thus, it is desirable to separate chlorine from the matrix more rapidly and effectively.

As mentioned above, many chloride compounds were quantitatively decomposed and chloride was distilled off as hydrogen chloride from SPA media by heating to about 250 °C. Therefore, the present method seems to be applicable to the determination of chlorine in chloride or other halide form in solid materials, such as rocks, minerals, soils, biological materials, and complex compounds.

The apparatus used is shown in Fig. 7. The procedure is as follows. A suitable amount of the sample (0.5—1.0 g) was placed in the reaction vessel (B), and about 30 g of SPA was added. An accurately-determined amount of 20 ml of a 0.05 M sodium hydroxide solution was put into the absorption tube (C), which was placed in a wider test tube containing cooling water. Then all joints were connected as shown in the figure. (A) is a gas-washing bottle containing a 0.1 M silver nitrate solution. Air was aspirated slowly from the last outlet tube and the reaction vessel was heated with an electric heater until the temperature of the contents reached about 250 °C. Around the cap of the reaction vessel was wound a ribbon heater to avoid trapping of hydrogen chloride at this point during distillation.

After distillation, the absorption and the washing solutions were combined and subjected to chloride measurement. For chlorides in the range of 10^{-3} to 10^{-4} mol, titration was performed with a silver nitrate standard solution using fluorescein as an indicator.

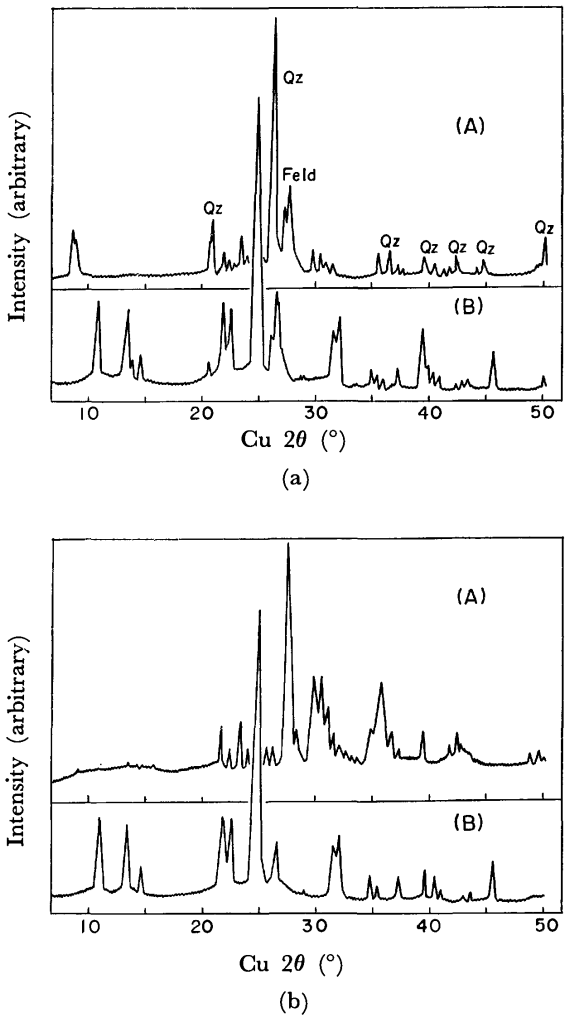

Fig. 8. X-Ray diffraction pattern for standard rocks and SPA treated standard rocks.
a: JG-1, b: JB-1.
A: Original rock sample, B: SPA treated rock sample.

For chlorides less than 10^{-4} mol, the determination was made spectrophotometrically using mercury thiocyanate[19] as follows: after distillation, 4 ml of an ammonium iron(III) sulfate solution and 2 ml of a mercury thiocyanate solution were added to the absorption solution. This solution was mixed well by shaking, and then the absorption was measured at a wavelength of 460 nm. In this case, the volume of the absorption solution during distillation appeared to remain unchanged. From Tables 2 and 3, which indicate the results it is clear that the determination of chlorides in the concentration range of 10^{-6}—10^{-2} mol can be performed very satisfactorily.

Decomposition of Rock Samples in SPA Media. When organic compounds or complex materials, such as complex compounds, hair, or rice, are heated in an SPA medium with decomposition of the materials to carbon, chlorine can be evolved as hydrogen chloride. However, a problem remained as to whether or not rock samples could be decomposed. Therefore, in the present study, experiments were carried out to clarify this problem.

Japan Geological Survey standard rocks, JG-1 and

TABLE 4. CHLORINE CONTENTS OF STANDARD ROCKS, JG-1 AND JB-1

JG-1, ppm	JB-1, ppm	Reference
53	178	
57	160	
50	168	
58	175	
52	164	Present results
av 54±4	169±10	
200	—	Sen Gupta (1971)
57	190	Akaiwa *et al.* (1973)
67 (5)	167 (5)	Terashima (1974)

TABLE 5. DETERMINATION OF CHLORINE IN *trans*-$[CoCl_2en_2]H_5O_2Cl_2$ AFTER SPA DISTILLATION

Sample taken, mg[a)]	Cl, mg	
	Found	Calcd
100.9	38.4	38.7
99.5	38.1	38.3
100.4	38.3	38.5

a) The sample was dried at 100 °C for 1 h.

JB-1, were subjected to treatment with SPA and the remaining white residue were washed with distilled water to remove any phosphoric acid. Then, X-ray diffraction patterns of these crystals was examined and compared with the X-ray diffraction patterns of the original rock samples. The X-ray patterns obtained are shown in Fig. 8. The peaks due to quartz and feldspar in the original JG-1 sample completely disappeared after the treatment, and new peaks appeared. Also, in the case of JB-1, entirely different patterns were observed for the original and the SPA-treated samples. These new X-ray patterns were assigned to $Si_3(PO_4)_4$. From the results, it can be confirmed that the original crystalline structure of silicate minerals in a rock sample is decomposed and then converted into a new crystalline structure whose composition includes SPA and silica. Therefore, it is reasonable to conclude that chlorine can also be completely liberated from a rock sample during decomposition due to heating of the sample in SPA.

In Table 4, the analytical results obtained by the present method for the standard rocks, JG-1 and JB-1, are compared with those reported by Sen Gupta,[20] Akaiwa[21] and Terashima.[22] The present results are in good agreement with those of Akaiwa andTerashima. The value reported by Sen Gupta appears to be too high.

A determination was also carried out for a synthesized complex compound, the structure of which was reported to be $[CoCl_2en_2]H_5O_2Cl_2$.[23] The data are shown in Table 5. The observed chlorine content coincides fairly well with the calculated result.

Support of a part of this work by the Ministry of Education is gratefully acknowledged.

References

1) T. Kiba, T. Takagi, Y. Yoshimura, and I. Kishi, *Bull. Chem. Soc. Jpn.*, **28**, 641 (1955).
2) S. Ohashi, *Bull. Chem. Soc. Jpn.*, **28**, 645 (1955).
3) T. Kiba, I. Akaza, and N. Sugishita, *Bull. Chem. Soc. Jpn.*, **30**, 972 (1957).
4) T. Kiba and I. Akaza, *Bull. Chem. Soc. Jpn.*, **30**, 44 (1957).
5) T. Kiba, I. Akaza, and S. Taki, *Bull. Chem. Soc. Jpn.*, **30**, 482 (1957).
6) S. Akabori and T. Fujiwara, *Bull. Soc. Chim. Biol.*, **40**, 1983 (1958).
7) H. Terada and M. Yoshida, *Kogyo Kagaku Kaishi*, **61**, 1301 (1958).
8) K. Kitagawa and N. Shibata, *Bunseki Kagaku*, **7**, 181 (1958).
9) H. Terada and M. Yoshida, *Kogyo Kagaku Kaishi*, **61**, 1303 (1958).
10) T. Kiba, *Kagaku To Kogyo*, **11**, 730 (1958).
11) K. Tanaka, *J. Res. Inst. for Catalysis, Hokkaido Univ.*, **7**, 87 (1959).
12) T. Kiba, *Bunseki Kagaku*, **9**, 651 (1960).
13) K. Terada, T. Ooba, and T. Kiba, *Talanta*, **22**, 41 (1975).
14) K. Terada, K. Matsumoto, and T. Kiba, *Bull. Chem. Soc. Jpn.*, **48**, 2567 (1975).
15) K. Terada, K. Okuda, and T. Kiba, *J. Radioanal. Chem.*, in press.
16) T. Kiba, K. Terada, T. Kiba, and K. Suzuki, *Talanta*, **19**, 451 (1972).
17) "International Critical Tables of Numerical Data, Physics, Chemistry and Technology," Vol. 1, ed by E. W. Washburn, National Research Council of U. S. A., McGraw-Hill Book Co., New York (1962); "Kagaku Binran (in Japanese)," Chem. Soc. Jpn., 2nd ed, Maruzen Book Co., Tokyo (1975).
18) E. B. Sandell, "Colorimetric Determination of Traces of Metals," 3rd ed, Interscience Publ., New York, N. Y. (1959), p. 72.
19) S. Utsumi, *Nippon Kagaku Kaishi*, **73**, 835 (1952).
20) J. G. Sen Gupta, quoted in A. Ando, H. Kurasawa, T. Ohmori, and E. Takeda, *Geochem. J.*, **8**, 175 (1974).
21) H. Akaiwa, E. Tajima, and A. Todokoro, quoted in A. Ando, H. Kurasawa, T. Ohmori, and E. Takeda, *Geochem. J.*, **8**, 175 (1974).
22) S. Terashima, *Bull. Geol. Surv. Jpn.*, **25**, 175 (1974).
23) *Inorg Synth.*, Vol. 1, 233 (1939).

Spectral Studies on the Interaction between Oxovanadium(IV) β-Diketonates and Organic Solvents

Natumi ADACHI, Yutaka FUKUDA, and Kozo SONE

Department of Chemistry, Faculty of Science, Ochanomizu University, Otsuka, Bunkyo-ku, Tokyo 112

(Received August 14, 1976)

The effect of temperature on the visible absorption spectra of oxovanadium(IV) β-diketonates [VO (β-dik)$_2$] (β-dik=aca, bza, tfa, and dpm*) were studied in organic solvents. The results together with the spectral and thermogravimetric data of the pyridine and dioxane adducts of these chelates lead to the conclusion that the ease of taking up a solvent molecule to form a six-coordinate solvated chelate in solution increases in the order: VO(tfa)$_2$> VO(bza)$_2$≈VO(aca)$_2$>VO(dpm)$_2$. Various proofs for the existence of a polymeric structure of VO(tfa)$_2$, which was formerly indicated on the basis of its IR spectrum, were found.

The visible absorption spectrum of oxovanadium-(IV) acetylacetonate (VO (aca)$_2$) in an organic solvent changes remarkably with solvent.[1-3] This is explained on the assumption that the square pyramidal five-coordinated structure of the original chelate is more or less transformed into an octahedral six-coordinated one by the coordination of a solvent molecure, and that the spectral change observed is the reflection of the degree of this structual change.

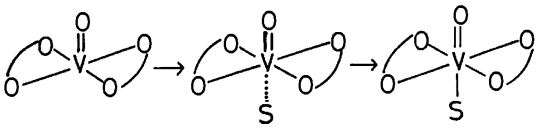

Increase in DN of the solvent (S) →
Increase in $\Delta_{I,II}$ →

According to Selbin *et al.*,[1-3] the difference between the wave numbers of the two visible bands of this chelate ($\Delta_{I,II}$) serves as a good measure of the degree of this change; when the coordination ability of the solvent (which may be expressed by the donor number (DN) of Gutman)[4] is very low (*e.g.*, in 1,2-dichloroethane or nitromethane) and the chelate nearly retains its original structure in solution, $\Delta_{I,II}$ is in the vicinity of 1—2 kK, but it increases with the DN of the solvent used, reaching 4—5 kK in DMSO and pyridine. It was also pointed out that there is a fairly good linear relationship between $\Delta_{I,II}$ and DN.[4]

Although these relations, which we shall call the Selbin-Gutmann rule, were well established in the case of VO(aca)$_2$, published data on other β-diketonates of VO^{2+} seem to be rather scanty. We have tried to confirm the applicability of this rule to three such chelates.

Experimental

Preparations. VO(aca)$_2$ and VO(tfa)$_2$ were prepared by the method of Rowe and Jones,[5] and VO(bza)$_2$ and VO(dpm)$_2$ by that of Selbin *et al.*[6] Their identity was confirmed by means of their IR spectra which agreed well with the data published.

VO(aca)$_2$py and VO(tfa)$_2$py: VO(aca)$_2$ or VO(tfa)$_2$ was dissolved in pyridine and the mixture was evaporated at low temperature (*ca.* 77 K) under reduced pressure. The concentrated solution was then allowed to stand at 0 °C. After 12 h, green microcrystals of the pyridine adduct separated out in the case of VO(aca)$_2$, but it took about a month to get similar crystals of VO(tfa)$_2$py. They were filtered and dried in a vacuum.

VO(bza)$_2$py: VO(bza)$_2$ was dissolved in pyridine and the mixture was refluxed for 2 h, and then allowed to stand at room temp for 12 h. The solution was then evaporated under reduced pressure at 70 °C. The brown microcrystals which separated out were filtered and dried in a vacuum.

VO(aca)$_2$diox, and VO(tfa)$_2$diox: These adducts were prepared as in the case of VO(bza)$_2$py, using dioxane insted of pyridine.

The results of elementary analyses are given in Table 1.

Solvents and Reagents. All the solvents and reagents used were of "Extra Pure" or "Spectro" Grade.

Measurements. The IR spectra between 400 cm^{-1} and 4000 cm^{-1} were determined with Nujol mulls between caesium bromide plates using a JASCO IR-G spectrophotometer. The electronic spectra of the solutions were recorded with a Shimadzu D-40R Spectrophotometer, using 50, 10, and 5 mm quartz cells, and Dewar-equipped cells described by Iwasaki *et al.*[7] The reflectance spectra of solid samples between 300 and 700 nm were recorded with the same spectrophotometer and those between 700 and 800 nm were recorded with a Hitachi EPS-3T spectrophotometer, using reflectance attachments and MgO discs as reference. Thermogravimetric analyses of the adducts were carried out with a Shinku Riko TGD-3000 Differential Thermal Microbalance with a heating rate of 5 °C/min in a nitrogen stream (flow rate: 50 ml/min), using *ca.* 30 mg of the sample in each measurement.

TABLE 1. ELEMENTARY ANALYSES OF THE ADDUCTS

Adduct	Found (Calcd) %		
	C	N	H
VO(aca)$_2$py	52.32(51.74)	4.07(4.19)	5.57(5.49)
VO(bza)$_2$py	62.77(62.56)	3.07(3.15)	4.76(5.23)
VO(tfa)$_2$py	39.21(39.84)	2.85(3.09)	3.22(2.90)
VO(aca)$_2$diox[a]	42.48(47.60)		5.59(6.28)
VO(tfa)$_2$diox[a]	33.59(36.45)		3.36(3.50)

a) These adducts slowly decompose on standing, losing dioxane, and revert to the parent complexes, making agreement with calculation less satisfactory. The values for carbon were deduced from the data of the thermogravimetric analyses.

* Abbreviations; β-dik=a β-diketonate ion, aca=acetylacetonate ion, bza=benzoylacetonate ion, tfa=trifluoroacetylacetonate ion, dpm=dipivaloylmethanate ion, py=pyridine, and diox=dioxane. kK=10^3 cm^{-1}.

Results and Discussion

Thermochromism of VO(β-dik)$_2$ in Organic Solvents. When the four chelates VO(aca)$_2$, VO(bza)$_2$, VO(tfa)$_2$, and VO(dpm)$_2$ are dissolved in various solvents at room temperature, and the observed values of $\Delta_{I,II}$ are plotted against DN of the solvents (Fig. 1), the Selbin-Gutmann relation holds quite well in the case of VO(aca)$_2$ and VO(bza)$_2$, but apparently not for the other two chelates.** For the sake of clarification, the influence of temperature on the spectra (thermochromism) was studied. The results for VO(aca)$_2$ are summarized in Fig. 2. A similar figure is obtained for VO(bza)$_2$. The $\Delta_{I,II}$ values increase with DN at each observed temperature, but decrease more or less distinctly with increasing temperature, showing that the bonding of solvent molecule at the bottom of the pyramid is gradually loosened and the complex becomes more "five-coordinated" on heating. In the course of these spectral changes no distinct isosbestic point was observed,*** so it seems that they are due not to the shift of the simple solvation equilibrium of

$$VO(aca)_2 + S = VO(aca)_2 \cdot S$$

type, but to the gradual structure change of the dissolved species.

Figure 3 shows the results for VO(dpm)$_2$. The curves go down with the rise of temperature, but only the curves for pyridine and DMF, *i.e.*, those for solvents with especially high DN, lie high above, while those for chloroform, nitromethane and acetonitrile lie close to each other near the abscissa. This suggests that the chelate is less easily solvated in solution, and the solvents with lower DN are not bound effectively by it, so that there is only little spectral difference between their solutions. This reluctance for solvation is probably the result of the electron-donating effect of C(CH$_3$)$_3$ groups in dpm, which strengthens the V–O bonds in the chelate rings and reduces the positive charge of vanadium and the steric effect caused by the same groups.

Figure 4 shows the results for VO(tfa)$_2$. Since all the curves flock closely together, the scale for $\Delta_{I,II}$ is expanded twice in comparison with that shown in Figs. 2 and 3. We see that pyridine, DMF, methanol, and acetonitrile form octahedral solvates nearly equally well. Nitromethane also does so at lower temperature, but the solvation becomes remarkably weaker at higher temperature. Thus it is clear that this chelate, in contrast to VO(dpm)$_2$, is more easily solvated, probably owing to the electron-withdrawing effect of tfa which weakens the V–O bonds in the chelate rings.

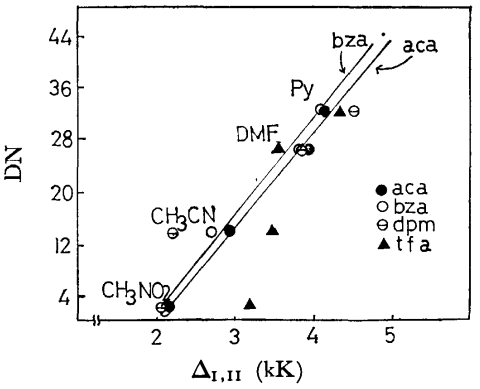

Fig. 1. The relation between DN and $\Delta_{I,II}$ at room temperature; concentration: 1×10^{-2} mol/l.

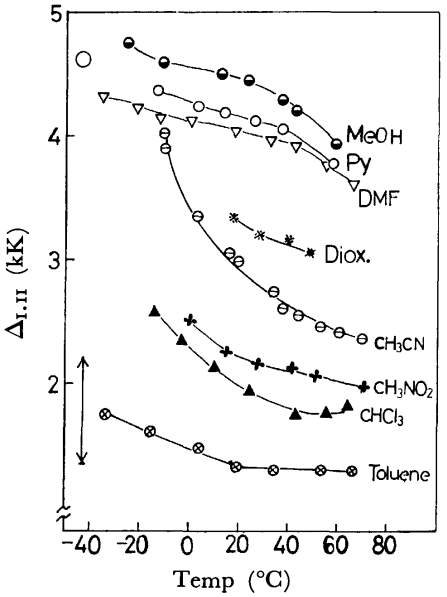

Fig. 2. Thermochromism of VO(aca)$_2$ in some organic solvents; cell thickness: 5 mm, concentration: 1×10^{-2} mol/l.
↔ and ○ on the ordinate axis correspond, respectively, to the $\Delta_{I,II}$ values of the chelate and its pyridine adduct in solid state.

It seems strange that even in chloroform, which is a very poor donor, a six-coordinated complex species seems to be formed with VO(tfa)$_2$. However, the $\Delta_{I,II}$ of VO(tfa)$_2$ in chloroform was found to be notably dependent on its concentration, changing from *ca.* 3.4 to 2.9 in going from 1×10^{-1} to 4×10^{-3} M. This leads one to suppose that there is a monomer-polymer equilibrium (1) in this solution, and the

$$n\ VO(tfa)_2 \underset{\text{heat}}{\overset{\text{cool}}{\rightleftharpoons}} [VO(tfa)_2]_n \qquad (1)$$

Monomer, 5-coordinated — Polymer with O=V←O=V bonds, 6-coordinated

** Alcoholic solutions poses some problems. The $\Delta_{I,II}$-values of VO(aca)$_2$ and VO(bza)$_2$ in methanol are much higher than expected from the DN scale. However, as stated by Gutman concerning values in aqueous solution, this may be explained by the formation of the hydrogen bond (V=O···H–OR), in addition to the coordinate bond to vanadium (O=V···OHR), by the solvent. The values of $\Delta_{I,II}$ in other alcohols at room temperature are nearly the same as that in methanol. On the other hand, all the chelates studied are not stable in alcoholic solutions against oxidation, becoming brownish within several hours. In the case of VO(dpm)$_2$, this color change begins within several minutes, making it impossible to measure the spectra.

*** An apparent isosbestic point was found to appear in acetonitrile and nitromethane at lower temperature. Moreover, a drastic reversible color change from blue to pink took place when VO(aca)$_2$ was dissolved in acetonitrile or nitromethane and frozen in liquid nitrogen, but this was not observed with the other chelates. The nature of these phenomena is not clear.

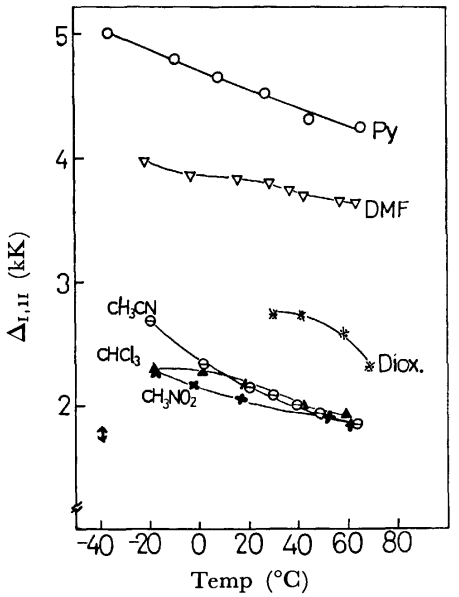

Fig. 3. Thermochromism of $VO(dpm)_2$; the conditions are the same as in the case of $VO(aca)_2$.

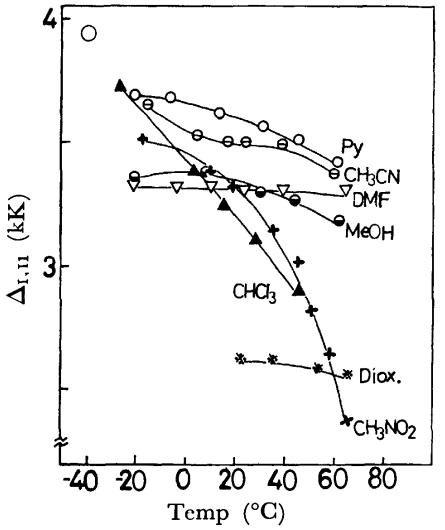

Fig. 4. Thermochromism of $VO(tfa)_2$; the conditions are the same as in the case of $VO(aca)_2$.

observed changes of $\Delta_{I,II}$ with temperature and concentration are, in fact, due to the shifts of this equilibrium.† This view is also supported by the view of Al-Niami *et al.*[13] who observed that the infrared spectrum of $VO(tfa)_2$ indicates its polymeric structure, with the molecules forming chains of O=V←O=V←O=V. Thus it seems possible that a similar kind of association occurs in a non-coordinating solvent like chloroform, to various degrees, according to the temperature and concentration.

In most cases, Band I (*i.e.*, that of the red side) shifts toward blue and Band II toward red with increasing temperature, the first shift being much larger. In terms of the Ballhausen-Gray[8] MO scheme with the assumption that Band I is $^2B_2$-^2E and Band II is $^2B_2$-$^1B_1$,[11,13,15] Band I is due to the excitation of an electron from a nonbonding orbital (b_2) to a π-antibonding one (e_π^*), and its blue shift means the corresponding stabilization of e_π, *i. e.*, that the π-bond formation between the vanadium d_{xz} and d_{yz} and oxygen p_x and p_y orbitals in the V=O group is enhanced with the rise of temperature and in non-coordinating solvents. On the other hand, Band II is due to the excitation of the same electron to a σ-antibonding orbital (b_1^*), its red shift indicating the corresponding instabilization of b_1, leading to the weakening of V-aca coordinate bonds. These relations are all compatible with the view that the complex changes gradually from an octahedral structure to a tetragonal pyramidal one upon heating and with a decrease in solvent polarity.

Comparison of the Thermochromism Data with Some Properties of Solid Adducts. In order to see the difference in the ease of solvation among the chelates, their pyridine, dioxane and DMF adducts were prepared, and a comparison was made between some of their properties and the data of thermochromism. Adducts of the compositions $VO(aca)_2py$, $[VO(aca)_2]_2$-diox, $VO(\beta\text{-dik})_2$·4-methylpyridine *N*-oxide have been reported.[12-14] We have prepared the monopyridine adducts of $VO(aca)_2$, $VO(bza)_2$, and $VO(tfa)_2$ and monodioxane adducts of $VO(aca)_2$, $VO(tfa)_2$, the pyridine adduct of $VO(dpm)_2$, the dioxane adduct of $VO(bza)_2$, and DMF adducts being obtained only paste-like samples. The method of preparation for $VO(aca)_2py$ (*cf.* Experimental) seemed to be better than that given in literature, since a product which was analytically quite pure could be obtained with nearly theoretical yield.

It was pointed out formerly that all the parent chelates show a V=O streching band between 950 and 1000 cm^{-1} in their IR spectra, except for $VO(tfa)_2$ which shows the same band at 925 cm^{-1} owing to its polymeric six-coordinated structure.[6,13] From the data given in Table 2, we see that, on adduct formation, the ν value of this band for $VO(aca)_2$ and $VO(bza)_2$ decreases, but that for $VO(tfa)_2$ increases, approaching from each side. This indicates that the polymeric structure of $VO(tfa)_2$ is destroyed by adduct formation, and the strength of the V–O bond in the resulting adduct becomes nearly the same as that in other adducts. The dioxane in the adducts seems to be held more loosely than pyridine, since the ν values of the dioxane adducts lie between those of the parent chelates and those of the pyridine adducts. The thermal instability of the dioxane adducts (Table 1, footnote) supports this view.

The solid reflectance spectra of the parent chelates and adducts are also of interest. The $\Delta_{I,II}$ of $VO(aca)_2$, $VO(bza)_2$, and $VO(dpm)_2$ are 1.5—2,[6] and in the neighborhood of the values for their chloroform solutions at room temperature. As expected, the $\Delta_{I,II}$ values of the adducts are much higher, Band I shifting to red and Band II to blue. However, the $\Delta_{I,II}$ of $VO(tfa)_2$ is 4.44 and even larger than that for its pyridine adduct (3.9, with Band I shifting to blue). The fact that $VO(tfa)_2$ is six-coordinate in its solid

† No such strong dependence of $\Delta_{I,II}$ on concentration was observed with other solvents.

Table 2. V=O and V-O stretching frequencies (cm^{-1}) and ν_{max} and $\Delta_{I,II}$ from solid reflectance spectra (kK)

Complex	V=O[b]	V-O[a,b]	ν_I^c	ν_{II}^c	ν_{III}^c	$\Delta_{I,II}$
$VO(aca)_2$	992	602	14.59	16.12—16.80 bf	25.00 sh	1.53—2.21
$VO(aca)_2 \cdot py$	962	590	12.84	17.36	25.32 sh	4.52
$VO(aca_2 \cdot diox$	980	598	13.51	16.52—18.98 bf	24.39	3.01—5.47
$VO(bza)_2$	994	565	14.52	15.74—16·26 bf	27.77 sh	1.22—1.74
$VO(bza)_2 \cdot py$	948	550	12.90	17.70	21.14	4.8
$VO(bza)_2 \cdot diox$	(975)	(555)				
$VO(tfa)_2$	925	592	13.03	17.47	23.80 sh	4.44
$VO(tfa)_2 \cdot py$	958	588	13.39	17.27	22.72	3.88
$VO(tfa)_2 \cdot diox$	987	592	13.64	16.20—18.80 bf	22.65	2.56—5.16
$VO(dpm)_2$	1000	648	14.83	16.50	22.00	1.67
$VO(dpm)_2 \cdot py$	(961)	(632)				

a) β-diketonate oxygen. b) Values in parentheses are those obtained with paste-like samples. c) bf: broad or flat, sh: shoulder.

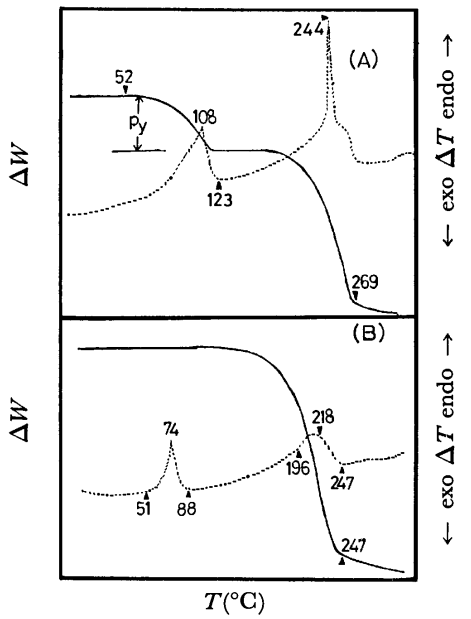

Fig. 5. The TG(——)-DTA(----) curves. A) $VO(aca)_2 \cdot py$, B) $VO(tfa)_2 \cdot py$.

owing to polymerization is evident.

The $\Delta_{I,II}$ values in the solid spectra of the adducts are indicated on the ordinate axis in Figs. 2 and 4. We see that, in each case, this value corresponds approximately to the low-temperature limit of the curve for the corresponding solution, supporting the idea that the chelate in solution tends to be more 6-coordinate with the fall of temperature.

The pyridine adducts were also studied thermogravimetrically. $VO(aca)_2py$ liberates pyridine at 53—120 °C, and the remaining parent chelate sublimes at a higher temperature (>159 °C). A similar result was obtained with $VO(bza)_2py$. On the other hand, $VO(tfa)_2py$ melts at 74 °C without evolution of pyridine, and begins to evaporate only at 196 °C, showing that pyridine is more firmly held in this adduct than in the other two (Fig. 5). The curve for $VO(aca)_2$ is similar to that of $VO(aca)_2py$ after evolution of pyridine, that of $VO(tfa)_2$ differing a great deal. Evaporation takes place at a much higher temperature (>256 °C), and a strong endothermic peak appears at 209 °C, suggesting that the intermolecular O=V←O=V bonds must be broken, or essentially weakened, in advance of evaporation.

From the results it can be concluded that the ease of solvation among the chelates studied increases in the order: $VO(tfa)_2 > VO(bza)_2 \approx VO(aca)_2 > VO(dpm)_2$, and the Selbin-Gutman rule on the relation between $\Delta_{I,II}$ and DN ceases to hold at one or the other end of this series, *i. e.* when the chelate is too apt, or too reluctant, to be solvated and become six-coordinate. The data also offer various new proofs for the polymeric nature of solid $VO(tfa)_2$, which was formerly indicated on the basis of its infrared spectrum by Al-Niami *et al.*

The authors wish to express their sincere thanks to Dr. Kenzo Nagase, Tohoku University, for carring out thermogravimetric measurements, and to Prof. Yukio Kondo, St. Paul's University, for use of the Hitachi EPS-3T spectrophotometer.

References

1) J. Selbin, *Chem. Rev.*, **65**. 153 (1965).
2) J. Selbin and T. R. Ortoland, *J. Inorg. Nucl. Chem.*, **26**, 37 (1964).
3) J. Selbin, H. R. Manning, and G. Cessac, *J. Inorg. Nucl. Chem.*, **25**, 1253 (1963).
4) V. Gutman, "Coordination Chemistry in Non-Aqueous Solution," Springer, Wien (1963).
5) R. Rowe and M. M. Jones, *Inorg. Synth.*, **5**, 115, (1957).
6) J. Selbin, G. Maus, and P. L. Jonson, *J. Inorg. Nucl. Chem.*, **29**, 1735 (1967).
7) N. Iwasaki, K. Sone, and Y. Fukuda, *Z. Anorg. Allg. Chem.*, **412**, 170 (1975).
8) C. J. Ballhausen and H. B. Gray, *Inorg. Chem.*, **2**, 1315 (1963).
9) J. Selbin, T. R. Ortolano, and F. J. Smith, *Inorg. Chem.*, **2**, 1315 (1963).

10) G. Basu, W. A. Yeranous, and R. L. Belford, *Inorg. Chem.*, **3**, 929 (1964).
11) M. H. Valek, W. A. Yeranous, G. Basu, P. K. Hornand, and R. L. Belford, *J. Mol. Spectrosc.*, **37**, 228 (1971).
12) M. R. Caira, J. M. Haigh, and L. R. Nassimbeni, *J. Inorg. Nucl. Chem.*, **34**, 3171 (1972).
13) N. S. Al-Niami, A. R. Al-Karaghouli, S. M. Aliwiand, and M. G. Jolhoom, *J. Inorg. Nucl. Chem.*, **36**, 283 (1974).
14) K. Dichmann, G. Hamer, S. C. Nyburg, and W. F. Reynolds, *Chem. Commun.*, **1970**, 1295.
15) R. L. Farmerand and F. L. Urbach, *Inorg. Chem.*, **13**, 587 (1974).
16) J. Selbin, L. H. Holmes, and S. P. Mcglynn, *J. Inorg. Nucl. Chem.*, **25**, 1539 (1963).
17) R. Larsson, *Acta Chem. Scand.*, **26**, 549 (1972).

A Potentiometric Study on Complex Formation of Cadmium(II) and Lead(II) Ions with Ethylenediaminetetraacetic Acid

Noboru OYAMA, Hiroaki MATSUDA, and Hitoshi OHTAKI

Department of Electronic Chemistry, Tokyo Institute of Technology, O-okayama, Meguro-ku, Tokyo 152

(Received August 23, 1976)

The complex formation of cadmium(II) and lead(II) ions with ethylenediaminetetraacetic acid (EDTA) has been studied potentiometrically in a 1.0 M $NaClO_4$ medium at 25.0 °C by using glass and metal-amalgam electrodes. The results were explained in terms of the formation of the complexes of MH_qL with $q=3$, 2, 1, and 0 for both metals. The corresponding formation constants were determined: for the Cd-EDTA system, log $\beta_{101}=14.25\pm0.02$, log $\beta_{111}=17.41\pm0.02$, log $\beta_{121}=19.71\pm0.02$ and log $\beta_{131}=21.35\pm0.02$; for the Pb-EDTA system, log $\beta_{101}=16.50\pm0.05$, log $\beta_{111}=19.78\pm0.02$, log $\beta_{121}=21.35\pm0.02$ and log $\beta_{131}=22.50\pm0.02$, where $\beta_{pqr}=[M_pH_qL_r^{(2p+q-4r)+}]/[M^{2+}]^p[H^+]^q[L^{4-}]^r$ and L denotes the unprotonated molecule of EDTA. The protonation constants of unprotonated EDTA were found to be log $\beta_{011}=8.63\pm0.02$, log $\beta_{021}=14.99\pm0.02$, log $\beta_{031}=17.63\pm0.02$, log $\beta_{041}=19.87\pm0.02$, log $\beta_{051}=21.54\pm0.02$, and log $\beta_{061}=22.70\pm0.02$.

In a previous work[1] we determined the formation constants of protonated complexes of the type MH_qL with $q=2,1$ and $q=3,2,1$ in the Cd(II)- and Pb(II)-*N*-(2-hydroxyethyl) ethylenediamine - *N*,*N*',*N*' - triacetate (H_3-hedta) systems, respectively. Since HEDTA is regarded as a monohydroxyethyl derivative of EDTA, the formation of complexes similar to the HEDTA complexes is expected in the Cd(II)- and Pb(II)-EDTA systems. The results of studies on electrode reactions in Cd(II)- and Pb(II)-EDTA solutions suggest that the protonated complexes MH_qL($q=1$, 2, and 3) participate in the charge transfer processes at the electrode surface.[2,3] The formation constants of unprotonated and monoprotonated metal-EDTA (1 : 1) complexes have been determined[4] in the bulk of these solutions, but those of diprotonated and triprotonated complexes have not been reported except by Sudmeier and Reilley,[5] who evaluated the formation constant of the diprotonated complex for the Cd(II)-EDTA system.

The present work, as a continuation of the previous study,[1] has been carried out to study the formation of protonated complexes in these systems.

Symbols

h	Concentration of hydrogen ion at equilibrium
m	Concentration of metal ion at equilibrium
H	Analytical excess of hydrogen ion in a test solution
M	Cd(II) or Pb(II)
c_M	Total concentration of M
L	Ethylenediaminetetraacetate anion ($edta^{4-}$)
c_L	Total concentration of L
l	Concentration of free L
X	Degree of neutralization of H_4L: $\dfrac{-H+[H]-[OH]}{c_L}$
p	Number of metal atoms bound to complexes
q	Number of protons bound to complexes
r	Number of ligands bound to complexes
β_{pqr}	Equilibrium constant for the reaction $pM + qH + rL = M_pH_qL_r$
$\bar{n}$	Formation function of the ligand H_nL
E_q, E_m	Emf of the cells defined by the subscripts and Eqs. 1 and 2 in Ref. 1.
$E_j(h,m)$	Liquid junction potential as a function of h and m
[ ]	Concentration

All charges are omitted for the sake of convenience.

Experimental

Reagents. *Disodium ethylenediaminetetraacetate* (reagent grade, Dojindo Laboratories) was recrystallized twice, dried at *ca.* 85 °C and then stored in a desiccator over silica gel. *Cadmium(II) perchlorate, lead(II) perchlorate, sodium hydroxide,* and *perchloric acid* solutions were prepared by the methods described in the preceding paper.[1]

Sodium perchlorate was prepared according to Biedermann and Ciavatta.[6]

Cadmium- and lead-amalgams were prepared from cadmium(II) perchlorate and lead(II) nitrate solutions, respectively, by electrolysis with a Metrohm E211A coulometer. The metal content of the amalgams was about 3% (weight).

Apparatus. *A potentiometric cell* similar to the one previously employed was used. *A digital pH/mV meter* (Orion Research, Model 801) and a *digital voltmeter* (Takeda Riken, Model TR-6656) were used for potentiometric measurements in combination with glass and amalgam electrodes, an Ag-AgCl electrode being used as a reference.

Emf Measurements. The method of emf measurements was essentially the same as that employed previously.[1]

When $c_{Cd}>0.0025$ M, titration was interrupted in the pH range 1.7—2.3, since white precipitates which might be CdH_2L^0 separated out. In such cases no stable emf's could be recorded. The emf of the amalgam electrode usually required 15 min to attain a constant value and was measured within an accuracy of ±0.02 mV in the pH range 1.0—2.0 and ±0.1 mV in the pH range 2.0—3.5. At pH above 3.5 the emf's became unstable. The emf of the glass electrode cell became constant after about 5 min and was determined within an accuracy of ±0.1 mV over the pH range 1.0—10.0.

Results and Discussion

Evaluation of Protonation Constants of EDTA. Overall protonation constants of the EDTA base, β_{0n1}, were determined from the formation function $\bar{n}$. A generalized least squares method was applied in order to make the error squares sum $U=\sum(\bar{n}-\bar{n}_{calcd})^2$ a minimum for the set of overall protonation constants, β_{011}, β_{021}, β_{031}, β_{041}, β_{051}, and β_{061}. This calculation was performed with an electronic computer HITAC 8700. $\bar{n}_{calcd}$ and $\bar{n}$ denote, respectively,

$$\bar{n}_{calcd}=\frac{\sum_{n=1}^{6}n\beta_{0n1}h^n}{1+\sum_{n=1}^{6}\beta_{0n1}h^n} \quad (1)$$

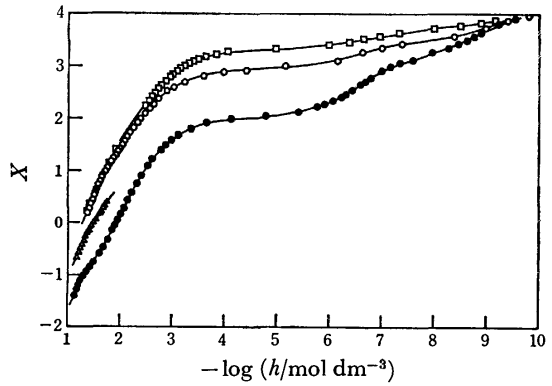

Fig. 1. Degrees of neutralization, X, of ethylenediaminetetraacetic acid (EDTA) solutions for the Cd(II)-EDTA systems.
(●): $c_{Cd}=0.0$ M, $c_L=0.01351$ M,
(○): $c_{Cd}=0.002526$ M, $c_L=0.005002$ M,
(△): $c_{Cd}=0.002408$ M, $c_L=0.009567$ M,
(□): $c_{Cd}=0.008018$ M, $c_L=0.01186$ M.
Solid lines are the values of X calculated by the use of the stability constants in Table 1.

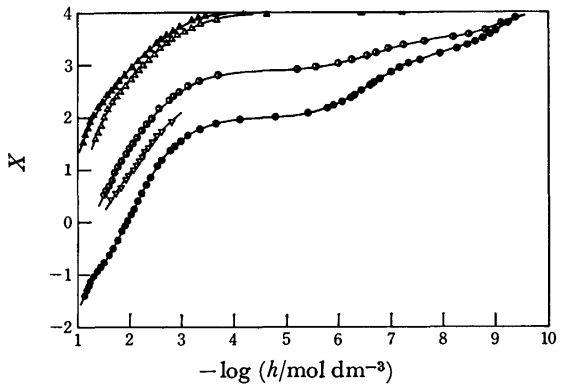

Fig. 2. Degrees of neutralization, X, of EDTA solutions for the Pb(II)-EDTA systems.
(●): $c_{Pb}=0.0$ M, $c_L=0.01351$ M,
(▽): $c_{Pb}=0.001839$ M, $c_L=0.007247$ M,
(◑): $c_{Pb}=0.004601$ M*, $c_L=0.009455$ M*,
(△): $c_{Pb}=0.005067$ M, $c_L=0.005060$ M,
(▲): $c_{Pb}=0.01517$ M*, $c_L=0.007603$ M*.
Solid lines are the values of X calculated by the use of the stability constants in Table 1.
*: c_{Pb} and c_L are the initial concentration of the metal and the ligand, and c_{Pb} and c_L are slightly changed during the course of titration by the addition of the titrants.

and

$$\bar{n}=\frac{4c_L+H-h+(K_w/h)}{c_L} \tag{2}$$

where K_w is the autoprotolysis constant of water in 1.0 M $NaClO_4$ solution, $10^{-13.95}$.[7] The protonation constants thus obtained were $\log \beta_{011}=8.63\pm0.02$, $\log \beta_{021}=14.99\pm0.02$, $\log \beta_{031}=17.63\pm0.02$, $\log \beta_{041}=19.87\pm0.02$, $\log \beta_{051}=21.54\pm0.02$, and $\log \beta_{061}=22.70\pm0.02$. Anderegg reported the values of $\log \beta_{011}=8.85$, $\log \beta_{021}=15.13$, $\log \beta_{031}=17.43$, $\log \beta_{041}=19.63$, $\log \beta_{051}=21.03$, and $\log \beta_{061}=20.19$ in a 1.0 M $NaClO_4$ medium at 20 °C.[7]

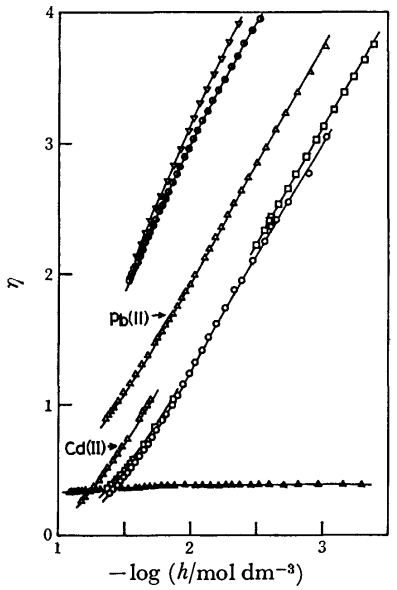

Fig. 3. Relationships between η and $-\log h$ for the Cd(II) and Pb(II) systems.
Symbols are the same as those in Figs. 1 and 2, respectively. Solid lines are curves calculated by the use of the stability constants in Table 1.

Determination of the Composition and the Stability Constants of Complexes. Titration curves of the Cd(II)- and Pb(II)-EDTA solution are shown in Figs. 1 and 2, respectively. In Fig. 3, the quantity $\eta=\log(c_M/m)$, which is a measure of the degree of complexation of the metal ion M, is plotted against $-\log h$. We see that $\eta>0$ at $-\log h=1.2$. This shows that the complex formation reaction takes place between the metal ions and EDTA even in the most acidic solution.

Since EDTA is an analog of HEDTA, the data obtained in the EDTA systems may be treated in the same manner as that used in calculation of the formation constants of the HEDTA complexes. Polynuclear or polyligand complexes may be neglected.[1] As a first approach to analysis of the data, we assume that the complex formation reaction can be written as

$$M^{2+}+qH^{+}+L^{4-}=MH_qL^{(q-2)+} \tag{3}$$

from which we obtain

$$c_M=m+\sum_{q=0}^{Q}[MH_qL] \tag{4}$$

$$c_L=l+\sum_{n=1}^{N}[H_nL]+\sum_{q=0}^{Q}[MH_qL] \tag{5}$$

Insertion of Eq. 4 into Eq. 5 and rearrangement lead to

$$l=(c_L-c_M+m)/(1+\sum_{n=1}^{N}\beta_{0n1}h^n) \tag{6}$$

A function F_0 is defined as follows:

$$F_0=(c_M-m)/ml=\sum_{q=0}^{Q}[MH_qL]/ml=\sum_{q=0}^{Q}\beta_{1q1}h^q \tag{7}$$

The plot of $\log F_0$ against $-\log h$ is shown in Fig. 4 for both systems of Cd(II)- and Pb(II)-EDTA except for the case $c_M \geq c_L$. In each system a single curve was obtained regardless of variations of c_M, c_L and c_M/c_L. This supports the assumption that neither polynuclear nor polyligand species is formed. In the case $c_M \geq c_L$,

Table 1. Stability constants of the Cd(II)- and Pb(II)-EDTA complexes ($\log \beta_{pqr}$)
$\log \beta_{011}=8.63\pm0.02$, $\log \beta_{021}=14.99\pm0.02$, $\log \beta_{031}=17.63\pm0.02$,
$\log \beta_{041}=19.87\pm0.02$, $\log \beta_{051}=21.54\pm0.02$, $\log \beta_{061}=22.70\pm0.02$

Complexes	ML^{2-}	MHL^{-}	MH_2L^{0}	MH_3L^{+}
Cd(II)	14.25±0.02	17.41±0.02	19.71±0.02	21.35±0.02
Pb(II)	16.50±0.05	19.78±0.02	21.35±0.02	22.50±0.02

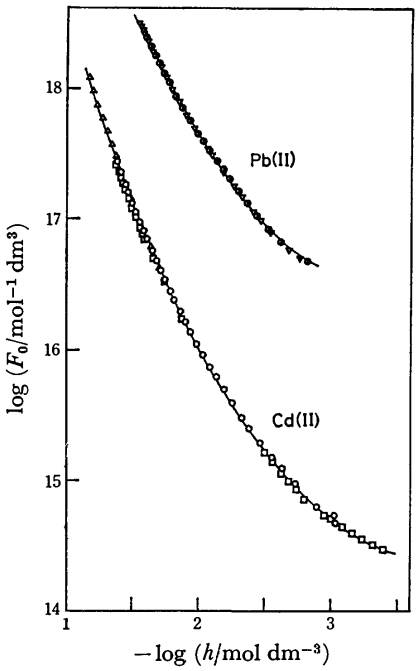

Fig. 4. Plot of $\log F_0$ against $-\log h$ for both systems. Each solid line is the curve calculated with the values of the stability constants in Table 1.

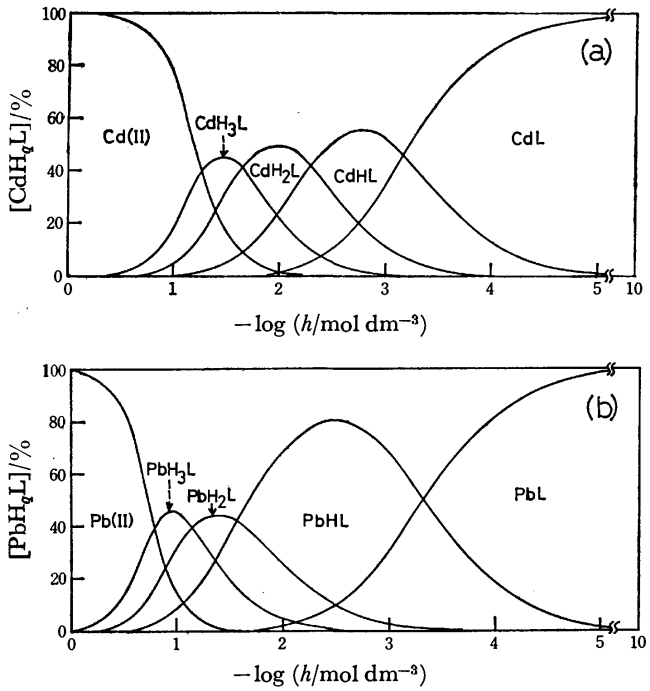

Fig. 5. The distribution of metal-EDTA complexes *vs.* $-\log h$ ($c_M=0.001$ M, $c_L=0.01$ M).
(a): for the Cd(II)-EDTA system.
(b): for the Pb(II)-EDTA system.

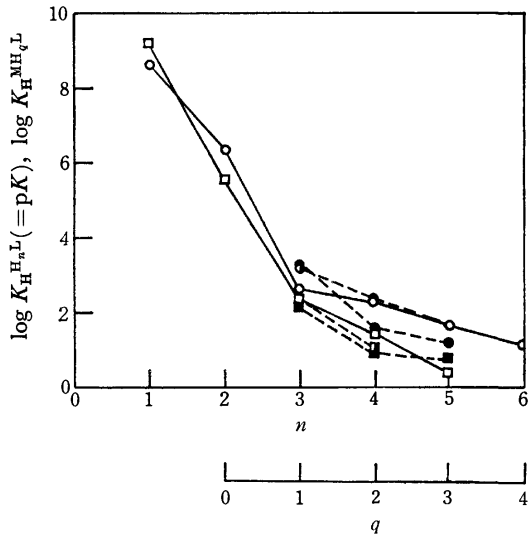

Fig. 6. Plot of $\log K_H^{MH_qL}(=\log\{[MH_qL]/[MH_{q-1}L][H]\})$ and $\log K_H^{H_nL}(=\log\{[H_nL]/[H_{n-1}L][H]\})$ against the number of protons within the complexes q and the ligand n.
○: EDTA, (◑): Cd(II)-EDTA complexes, (●): Pb(II)-EDTA complexes, (□): HEDTA, (◨): Cd(II)-HEDTA complexes, (■): Pb(II)-HEDTA complexes.

the value of the term (c_L-c_M+m) in Eq. 6 becomes too small to use the data for the calculation of F_0.

From the plot of F_0 against h, we obtained the formation constant β_{101}, β_{111}, β_{121}, and β_{131} for both systems according to the procedure reported.[1] By using the values of β_{1q1} thus obtained as the initial values, the formation constants of the complexes were refined by a generalized least squares method. The method was applied to make the error squares sum $U=\Sigma\{\log F_0-\log F_{0,\mathrm{calcd}}\}^2$ minimum for the set of the formation constants over the pH range 1.2—3, where $F_{0,\mathrm{calcd}}$ denotes the value of F_0 calculated for a particular set of the formation constants. The results are given in Table 1.

Since the metal amalgam electrodes did not function well in a high pH range, the data in the high pH range were not analyzed. However, the constants reproduced the experimental results fairly well over the whole pH range (solid lines, Figs. 1 and 2).

The distribution of the Cd(II)- and Pb(II)-EDTA complexes are graphically represented in Fig. 5.

The stepwise protonation constant of the species MH_qL is defined as $K_H^{MH_qL}=[MH_qL]/[MH_{q-1}L][H]$. The values of $\log K_H^{MH_qL}$ are plotted against the number of protons within the complex q, together with the values of $\log K_H^{H_nL}$ $(=\log [H_nL]/[H_{n-1}L][H])$against n(Fig. 6). The values of $\log K_H^{H_nL}$ of the HEDTA and

Table 2. Stability constants of the complexes defined by $\log K_{H_qL}^{MH_qL}=\log\{[MH_qL]/[M][H_qL]\}$

	EDTA				HEDTA			
	$\log K_{L}^{ML}$	$\log K_{HL}^{MHL}$	$\log K_{H_2L}^{MH_2L}$	$\log K_{H_3L}^{MH_3L}$	$\log K_{L'}^{ML'}$	$\log K_{HL'}^{MHL'}$	$\log K_{H_2L'}^{MH_2L'}$	$\log K_{H_3L'}^{MH_3L'}$
Cd(II)	14.25	8.78	4.72	3.72	13.21	6.41	1.96	—
Pb(II)	16.50	11.15	6.36	4.87	14.83	7.77	3.17	1.61

EDTA molecules first steeply decreased with n. According to the NMR and infrared spectrophotometric measurements,[8,9] the first two protons (to form HL and H_2L) are located on the nitrogen atoms of the EDTA and HEDTA molecules. We see that the protonation of the amino groups of the ligands brings about a significant change in the values of the protonation constants. The protonation on the carboxylic groups results in the relatively small change in the $K_H^{H_nL}$ values. The stepwise protonation constants $K_H^{MH_qL}$ ($q=1$, 2, and 3) of the Cd(II)- and Pb(II)-HEDTA and EDTA complexes are close to the values of $K_H^{H_nL}$ with $n=3$, 4, and 5 of the corresponding ligands. Thus we conclude that protonation of the complexes occurs on the acetate groups with the cleavage of the metal-oxygen bonds within the complexes with a decrease in pH, while the strong metal-nitrogen bonds are hardly influenced by the hydrogen-ion concentration over the pH range examined.

Another kind of formation constants of the complexes may be defined as $\log K_{H_qL}^{MH_qL}=\log[MH_qL]/[M][H_qL]$, which is calculated from the values of β_{1q1} and β_{0n1}. The values are given in Table 2. The values of K_L^{ML} of the Cd(II)- and Pb(II)-EDTA complexes are larger than those of the HEDTA complexes, as expected from the simple chelate theory, because the former ligand is sexidentate, whereas the latter quinquidentate. Nevertheless, the K_{HL}^{MHL} values of the EDTA complexes are smaller than the $K_{L'}^{ML'}$ ($L'=$ hedta^{3-} anion) values of the HEDTA complexes, the ligand HL (L=edta^{4-} anion) being expected to act as a quinquidentate ligand. The same tendency was found in the complex formation of the MH_2L of EDTA and the MHL' of HEDTA (Table 2). However, a comparison between the formation constants of the MH_3L complex of EDTA and the MH_2L' complex of HEDTA leads to the opposite result.

The protons within the protonated ligands HL and H_2L are located at the nitrogen atoms of the amino groups of the ligands. On the other hand, the protons of the protonated metal complexes MH_qL are combined with the acetate groups. Thus the free energy change defined by the equation $\Delta G_{MH_qL}=-RT\ln K_{H_qL}^{MH_qL}$ should include the free energy change of the intramolecular rearrangement of protons from the amino groups to the acetate groups. In the MHL complex of EDTA, the free energy change accompanied by the transfer of one proton from a nitrogen atom to an oxygen atom is needed as compared with the corresponding value of the ML' complex of HEDTA. Since the entropy change for the complex formation of MHL from M and HL (L=edta^{4-}) is nearly equal to that of ML' from M and L' (L'=hedta^{3-}) as reported by Brunetti *et al.*,[10] the difference between $K_{L'}^{ML'}$ and K_{HL}^{MHL} is mainly due to the difference in the enthalpy change of the proton transfer reaction from a nitrogen atom to an acetate group in the latter case. In the formation of MH_2L of EDTA, two protons must move from the amino groups to the acetate groups, while the transfer of only one proton is required in the complex formation MHL' with M and HL'. In contrast to the case considered above, the two proton transfer reaction is always accompanied by the complex formation of MH_qL from M and H_qL ($q\geq 2$) of either HEDTA or EDTA molecule. The free energy change of the intramolecular rearrangement of protons in the complex formation of MH_3L of EDTA may not largely differ from that of the MH_2L' complex of HEDTA. The difference between $K_{H_3L}^{MH_3L}$ and $K_{H_2L'}^{MH_2L'}$ (Table 2) cannot be explained in terms of the enthalpy changes in the chelate formation. The contribution of the hydroxyethyl group to the chelate formation might stabilize the MH_2L' complex, and therefore $K_{H_2L'}^{MH_2L'}$ would be larger than $K_{H_3L}^{MH_3L}$. The difference may be attributed to the entropy difference in the intramolecular rearrangement of the protons of the ligands, but we have no evidence to clarify the phenomenon.

References

1) N. Oyama, T. Shirato, H. Matsuda, and H. Ohtaki, *Bull. Chem. Soc. Jpn.*, **49**, 3047 (1976).

2) N. Oyama and H. Matsuda, *J. Electroanal. Chem.*, in press.

3) N. Oyama, T. Shirato, and H. Matsuda, *J. Electroanal. Chem.*, submitted.

4) L. G. Sillén and A. E. Martell, "Stability Constants," Chemical Society, London (1964), Supplement No. 1 (1971).

5) J. L. Sudmeier and C. N. Reilley, *Inorg. Chem.*, **5**, 1047 (1966).

6) G. Biedermann and L. Ciavatta, *Acta Chem. Scand.*, **15**, 1347 (1961).

7) G. Anderegg, *Helv. Chim. Acta*, **50**, 2333 (1967).

8) J. J. Sudmeier and C. N. Reilley, *Anal. Chem.*, **36**, 1698 (1964).

9) N. Nakamoto, Y. Morimoto, and A. E. Martell, *J. Am. Chem. Soc.*, **85**, 309 (1963).

10) A. P. Brunetti, G. H. Nancollas, and P. N. Smith, *J. Am. Chem. Soc.*, **91**, 4680 (1969).

Thermal Behavior of the Clathrate Compounds of the Type $M(diam)M'(CN)_4 \cdot 2C_6H_6$

Jun-ichi OHYAMA, Ryokichi TSUCHIYA, Akira UEHARA, and Eishin KYUNO*

Department of Chemistry, Faculty of Science, Kanazawa University, Kanazawa 920

**Department of Pharmaceutical Science, School of Pharmacy, Hokuriku University, Kanazawa 920*

(Received August 25, 1976)

The thermal behavior of the guest molecule trapped in the clathrate compounds, $M(diam)M'(CN)_4 \cdot 2C_6H_6$, where M and M′ are bivalent metal atoms and diam is two ammonia molecules or one molecule of diamine, and the structural changes of the host lattice upon heating were studied by means of derivatographic and isothermal measurements. In $Cd(NH_3)_2Ni(CN)_4 \cdot 2C_6H_6$, the elimination of guest benzene molecules was found to proceed in two steps. X-Ray powder diffraction patterns suggest that the skeleton of the host is preserved, at least during the first liberation of 1 mol of benzene, but the skeleton collapses after the complete liberation of benzene and ammonia. The host skeleton of $Cd(en)Ni(CN)_4 \cdot 2C_6H_6$ was preserved till the liberation of 75% of benzene. The activation energies were a little larger than the respective enthalpy changes. The replacement of M′=Ni by Pd or of M′=Cd by Hg in the clathrate compounds, if M and diamine are the same, scarcely changes the activation energy for the liberation of the guest molecule, but the replacement of M and diamine by other ones somewhat changes the activation energy.

A well-known clathrate compound, $Ni(NH_3)_2Ni(CN)_4 \cdot 2C_6H_6$, was first prepared by Hofmann and Küspert in 1897.[1] They pointed out that the benzene molecule in this compound is retained firmly as a guest in the host lattice, and its elimination cannot be detected at room temperature under ordinary pressure. Anysley *et al.*[2] reported, however, that the benzene molecule can be removed slowly *in vacuo* even at room temperature without the liberation of ammonia from the lattice. The crystal structure of this clathrate compound was determined by means of X-ray diffraction by Powell and Rayner,[3,4]

By replacing both or either one of the nickel ions in $Ni(NH_3)_2Ni(CN)_4 \cdot 2C_6H_6$ by other bivalent metal ions which can form hexacoordinated, octahedral and tetracoordinated, square planar complexes, various modified compounds have been prepared and their structures were confirmed to be similar to that of $Ni(NH_3)_2Ni(CN)_4 \cdot 2C_6H_6$.[5-10]

In analogous clathrate compounds such as $Cd(en)Ni(CN)_4 \cdot 2C_6H_6$[11] the ethylenediamine molecule links both cadmium ions in upper and lower adjacent layers, forming three-dimensional host lattice network.[12,13]

All the compounds containing the square planar $M'(CN)_4$ (M′=Ni or Pd) moiety may be referred to "Hofmann-type clathrates." Recently, another new type of clathrate compounds containing tetrahedral $M'(CN)_4$ moiety was prepared by Iwamoto and others and the crystal structures were determined.[14-16] These compounds are called "Iwamoto-type clathrates" to distinguish them from the Hofmann-type ones.

Aynsley *et al.* examined the thermal decomposition of $Ni(NH_3)_2Ni(CN)_4 \cdot 2C_6H_6$, and found that the elimination of benzene proceeds in the zeroth order,[2] which indicates that the rate determining step is the escape of benzene molecule from the surface of the clathrate. On the other hand, it is known that the rate of the escape of benzene varies with the kind of metal atom constituting the host lattice.[2] The present study was undertaken (1) to investigate the thermal liberation processes of benzene molecule from the host lattices in the two types of clathrate compound and (2) to see what effect is induced by the variation of the host lattices.

Experimental

Preparation of Clathrate Compounds. The clathrate compounds $M(diam)M'(CN)_4 \cdot 2C_6H_6$, where M is Cd, Ni or Cu, (diam) is $(NH_3)_2$, ethylenediamine or trimethylenediamine and M′ is Ni, Pd, Cd, and Hg, were prepared[5-7,11,14] and their characterization was carried out by measuring both IR spectra and X-ray powder diffraction patterns.

$Cd[Ni(CN)_4]$ was prepared by a method similar to that for $Zn[Ni(CN)_4]$, and dried at 70 °C for 2 h. The compound was used as the reference material to examine the final product by the thermal decomposition of $Cd(NH_3)_2Ni(CN)_4 \cdot 2C_6H_6$.

Found: C, 17.74; N, 20.39%. Calcd for $Cd[Ni(CN)_4]$: C, 17.45; N, 20.35%.

One of the compounds corresponding to the host lattice which has lost the guest molecule $Cu(NH_3)_2Ni(CN)_4$, was obtained by keeping the mother clathrate $Cu(NH_3)_2Ni(CN)_4 \cdot 2C_6H_6$ to stand in an ambient atmosphere for a few days.[17]

Measurements. The derivatograms for these compounds were obtained with a MOM Derivatograph Typ-OD-102. 0.5 or 0.4 g of sample was used in each run. All the measurements were carried out under a constant flow of nitrogen stream with a heating rate of 1 K min^{-1}. The enthalpy changes, ΔH, were evaluated by the analysis of DTA peak in the derivatogram.[18]

The isothermal measurements were carried out with a Shimadzu TM-1A Thermanobalance in static air.

The infrared and far infrared absorption spectra in the Nujol and HCB mull states were measured with JASCO IRA-2 and IR-F infrared spectrophotometers, respectively.

The X-ray powder diffraction patterns were recorded with a Rigaku-denki Geiger-flex X-ray Analyser, using Cu$K\alpha$ ray (λ=1.5405 Å) filtered with a nickel plate.

Results and Discussion

Hofmann-type Clathrate Compounds. Derivatography: The derivatograms of $Cd(NH_3)_2Ni(CN)_4 \cdot 2C_6H_6$ (I), $Cd(NH_3)_2Pd(CN)_4 \cdot 2C_6H_6$ (II), $Cd(en)Ni(CN)_4 \cdot 2C_6H_6$ (III), and $Cd(en)Pd(CN)_4 \cdot 2C_6H_6$ (IV) are shown in Fig. 1. The TG curve of compound I indicates that the mass loss of 1 mol of benzene was observed until 130 °C, and then another 1 mol of benzene and 2

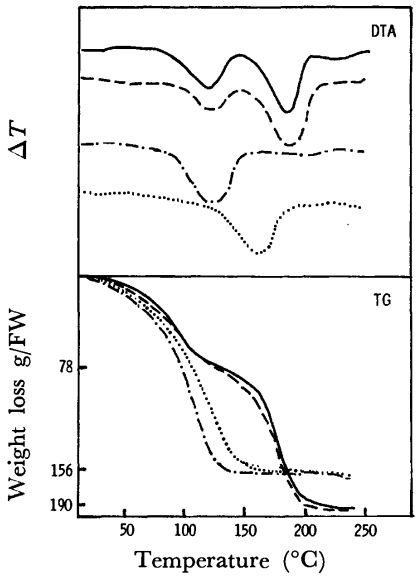

Fig. 1. Derivatograms of compounds (I) Cd(NH$_3$)$_2$-Ni(CN)$_4$·2C$_6$H$_6$ (——), (II) Cd(NH$_3$)$_2$Pd(CN)$_4$·2C$_6$H$_6$ (----), (III) Cd(en)Ni(CN)$_4$·2C$_6$H$_6$ (-·-·-) and (IV) Cd(en)Pd(CN)$_4$·2C$_6$H$_6$ (·····).

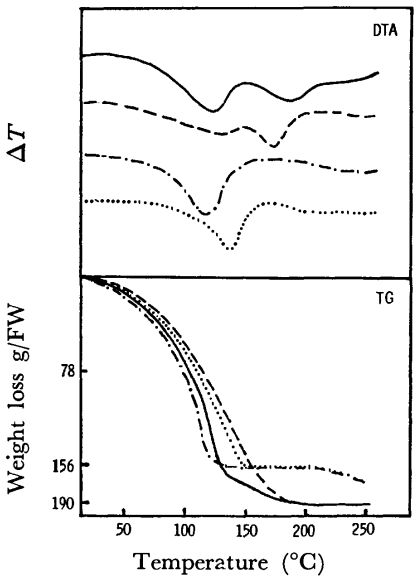

Fig. 2. Derivatograms of compounds (V) Cu(NH$_3$)$_2$-Ni(CN)$_4$·2C$_6$H$_6$ (——), (VI) Cu(NH$_3$)$_2$Pd(CN)$_4$·2C$_6$H$_6$ (----), (VII) Ni(NH$_3$)$_2$Ni(CN)$_4$·2C$_6$H$_6$ (-·-·-) and (VIII) Ni(NH$_3$)$_2$Pd(CN)$_4$·2C$_6$H$_6$ (·····).

mol of ammonia were lost successively in the higher temperature region 135—200 °C, no further mass loss being detectable up to the decomposition point. The elemental analysis for the product obtained by heating I at 200 °C is as follows: Found: C, 17.52; N, 20.00%. Calcd for CdNi(CN)$_4$: C, 17.45; N, 20.35%. The DTA curve gives two endothermic peaks corresponding to the discrete mass loss steps.

Compound II gives only one mass loss step in TG, but shows two split endothermic peaks in DTA. It seems that two benzene molecules are eliminated in two overlapping steps.

On the other hand, compounds III and IV lose the

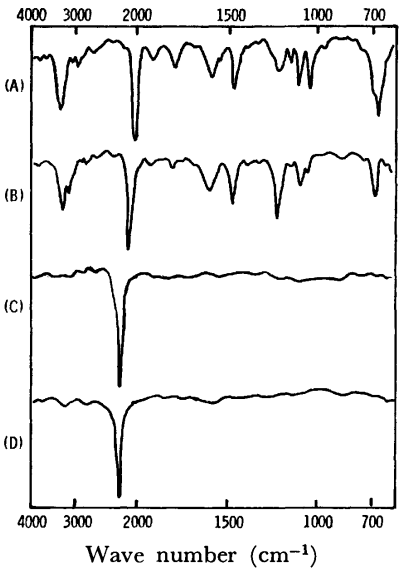

Fig. 3. IR spectra of compound (I) (A), the product obtained by heating (I) at 130 °C (B), that obtained at 200 °C (C) and of Cd[Ni(CN)$_4$] (D).

benzene molecules in one step up to 130 °C and 140 °C, respectively, each giving an endothermic peak at the corresponding region in the DTA curve. Ethylenediamine was not liberated until the decomposition point. The elemental analysis for the product obtained by heating compound III at 140 °C is as follows: Found: C, 21.67; H, 2.49; N, 24.35%. Calcd for Cd(en)-Ni(CN)$_4$: C, 21.48; H, 2.39; 25.06%.

Figure 2 shows the derivatograms of Cu(NH$_3$)$_2$-Ni(CN)$_4$·2C$_6$H$_6$ (V), Cu(NH$_3$)$_2$Pd(CN)$_4$·2C$_6$H$_6$ (VI), Ni(NH$_3$)$_2$Ni(CN)$_4$·2C$_6$H$_6$ (VII) and Ni(NH$_3$)$_2$Pd-(CN)$_4$·2C$_6$H$_6$ (VIII). In compound V, the TG curve shows two steps of mass loss at 130 °C and at 130—175 °C, the corresponding discrete peaks appearing in the DTA curve. From the results of infrared absorption spectral measurements, the first step is considered to correspond to the elimination of 2 mol of benzene and the second to the liberation of ammonia. The total weight loss due to the escape of all the benzene and ammonia is also observed in compound VI, the separation of their two processes not being clear.

Both compounds VII and VIII lost all benzene in one step. The weight remained constant till 250 °C at which the partial liberation of ammonia was observed just before the decomposition point.

IR and Far-IR Spectra. In order to clarify the structural change at several stages upon heating, changes in the infrared and far-infrared absorption spectra and X-ray diffraction patterns were measured for compounds I and III.

The infrared absorption spectra of compound I heated at various temperatures are shown in Fig. 3, together with that of Cd[Ni(CN)$_4$], which is expected to be formed by heating compound I. The spectrum of I in which one mole of benzene is lost at 130 °C is similar to that of the starting compound at room temperature except for the weakened bands assigned to benzene at 3072, 3055, 3019, 1972, 1872, and 1479 cm^{-1}.[14] At 200 °C, however, the bands assigned to

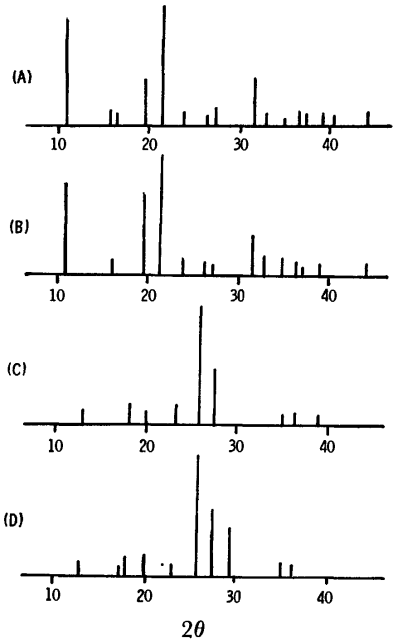

Fig. 4. X-Ray diffraction patterns of compound (I) (A), the product obtained by heating (I) a 130 °C (B), that obtained at 200 °C (C) and of $Cd[Ni(CN)_4]$ (D).

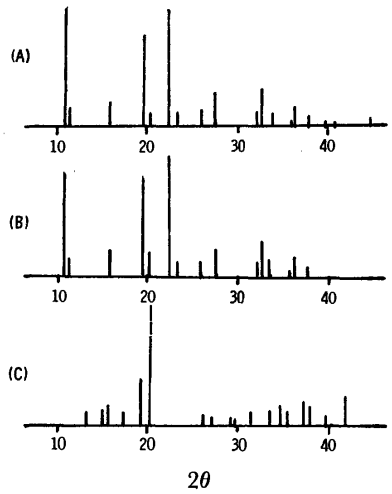

Fig. 5. X-Ray diffraction patterns of compound (III) (A), the product obtained by heating (III) at 120 °C (B) and that obtained at 140 °C (C).

benzene and to ammonia disappear, and the C≡N stretching vibration band is shifted to *ca.* 20 cm^{-1} higher. The spectrum coincides with that of $Cd[Ni(CN)_4]$. This supports the elimination processes of benzene and ammonia.

In compound III, the bands assigned to benzene disappear completely at 140 °C, accompanied by the elimination of benzene at this temperature. So far as the ethylenediamine is concerned, the band due to NH_2 wagging mode (*ca.* 1089 cm^{-1}) disappears and two new bands (*ca.* 1120, 1065 cm^{-1}) appear upon heating. The results suggest that the structure of ethylenediamine molecule bridging between the layers of $M(CN)_4$ network changes to some extent. The fact that the band due to CH_2 rocking vibration at 856 cm^{-1} still remains after heating suggests that the

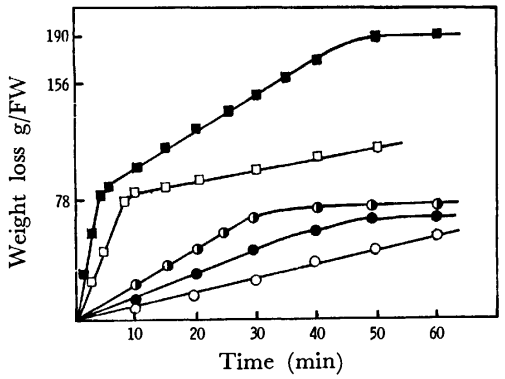

Fig. 6. The plots of weight loss *vs.* time for compound (I).
○: 84 °C, ●: 94 °C, ◑: 104 °C, □: 138 °C, ■: 160 °C.

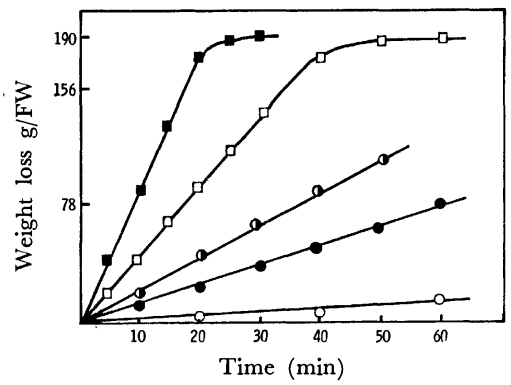

Fig. 7. The plot of weight loss *vs.* time for compound (III).
○: 55 °C, ●: 80 °C, ◑: 89 °C, □: 100 °C, ■: 119 °C.

trans configuration of ethylenediamine remains unchanged.[19]

X-Ray Powder Diffraction Patterns. The X-ray powder diffraction patterns for compound I obtained in each heating step are shown in Fig. 4. The pattern obtained at 130 °C shows no change from that at room temperature, but at 200 °C the pattern completely changes to give a similar one to that of $Cd[Ni(CN)_4]$. This suggests that the crystal lattice of compound I at room temperature is retained even when one mole of benzene is lost but the lattice is deformed at first when another one mole of benzene and ammonia are liberated.

The change in the X-ray patterns for compound III is shown in Fig. 5. The pattern at room temperature remains till 120 °C at which 75% of benzene is removed, but it becomes quite different at 140 °C at which the residual benzene is completely evolved.

Isothermal Kinetics. The weight losses of the compounds *versus* time of heating at various temperatures for compounds I and III are plotted in Figs. 6 and 7, respectively.

In compound I the elimination of 1 mol of benzene proceeds in the zeroth order at least at temperature below 130 °C, but above 130 °C the remaining benzene and ammonia are liberated more slowly also in the zeroth order after 1 mol of benzene is removed,

Table 1. Enthalpy changes ΔH and activation energies E_a in the elimination of benzene molecule from clathrate compounds

Compound		ΔH kJ mol^{-1}	E_a kJ mol^{-1}
I	$Cd(NH_3)_2Ni(CN)_4\cdot 2C_6H_5$	59	75.6 (1st step)
			71.0 (2nd step)
II	$Cd(NH_3)_2Pd(CN)_4\cdot 2C_6H_6$	55	74.8 (1st step)
III	$Cd(en)Ni(CN)_4\cdot 2C_6H_6$		51.2
IV	$Cd(en)Pd(CN)_4\cdot 2C_6H_6$	50	51.7
V	$Cu(NH_3)_2Ni(CN)_4\cdot 2C_6H_6$	50	65.9
VI	$Cu(NH_3)_2Pd(CN)_4\cdot 2C_6H_6$		67.2
VII	$Ni(NH_3)_2Ni(CN)_4\cdot 2C_6H_6$	55	67.2
VIII	$Ni(NH_3)_2Pd(CN)_4\cdot 2C_6H_6$	55	67.6

The results suggest that 2 mol of benzene are liberated in two different mechanisms. However, since the two guest benzene molecules cannot be distinguished from each other in their structure, it is considered that a thermally metastable intermediate might be formed after the loss of one mole of benzene retaining the initial host lattice.

On the other hand, the elimination of benzene from the clathrate III is considered to proceed in the zeroth order up to 80% removal of benzene as seen in Fig. 7.

The rate constant k for the elimination of benzene was obtained from the slope of the lines shown in Figs. 6 and 7. The activation energies E_a were calculated from the Arrhenius plots (Table 1). The enthalpy changes ΔH, calculated by the analysis of the DTA curve, are also given.

The enthalpy changes are about 55 kJ mol^{-1} in all the clathrates and the activation energy values are relatively similar to one another within 66—75 kJ mol^{-1} except for those of III and IV. This suggests that the elimination process is analogous to that of the vaporization of the liquid so that the migration of the benzene molecule within the lattice is comparatively easy and the rate determining step is the escape of the benzene from the surface, giving the zeroth order.

From a comparison of E_a values we see that the replacement of the tetracoordinated metal atom from nickel to palladium causes no appreciable change. On the other hand, replacement of the hexacoordinated metal or amine with others gives rise to some changes in E_a values.

The values for compounds III and IV which contain ethylenediamine as the diamine are slightly smaller than those for other compounds which contain ammonia as the diamine. It can be seen that the steric repulsion between ethylenediamine and the benzene molecule makes it unstable for benzene to exist in the cavity of the host lattice, owing to the replacement of a more bulky ethylenediamine instead of two ammonia molecules.

Iwamoto-type Clathrate Compounds. Derivatography: The derivatograms of $Cd(NH_3)_2Hg(CN)_4\cdot 2C_6H_6$ (IX), $Cd(en)Hg(CN)_4\cdot 2C_6H_6$ (X), $Cd(en)Cd(CN)_4\cdot 2C_6H_6$ (XI), and $Cd(tn)Hg(CN)_4\cdot 2C_6H_6$ (XII) are shown in Fig. 8. IX gives two steps of mass loss up to 120 °C and 120—150 °C in TG and two endothermic peaks corresponding to each step in DTA curve. From the infrared absorption spectra, it seems that the first step of mass loss is due to the elimination of 2 mol of benzene and the second to the liberation of ammonia, resembling the elimination process in compound V.

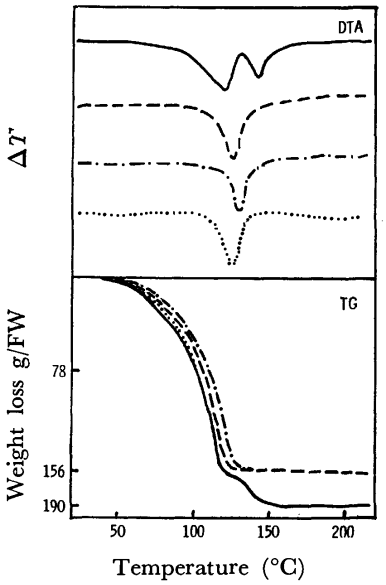

Fig. 8. Derivatograms of compounds (IX) $Cd(NH_3)_2Hg(CN)_4\cdot 2C_6H_6$ (——), (X) $Cd(en)Hg(CN)_4\cdot 2C_6H_6$ (----), (XI) $Cd(en)Cd(CN)_4\cdot 2C_6H_6$ (-·-·-) and (XII) $Cd(tn)Hg(CN)_4\cdot 2C_6H_6$ (·····).

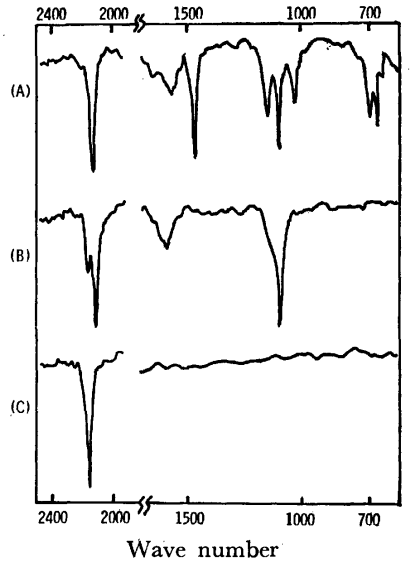

Fig. 9. IR spectra of Compounds (IX) (A), the product obtained by heating (IX) at 120 °C (B) and that obtained at 150 °C (C).

On the other hand, X, XI, and XII lose all benzene molecules in one step until about 135 °C.

IR Spectra. The infrared absorption spectra of compound IX at several heating steps are shown in Fig. 9. The absorption peaks due to benzene at 1479, 1042, 690, and 672 cm^{-1} disappear upon heating at 120 °C and those due to the NH_3 vibration mode at 1592 and 1089 cm^{-1} disappear upon heating at 150 °C with the shift of $\nu_{C\equiv N}$ at 2150 cm^{-1} to about

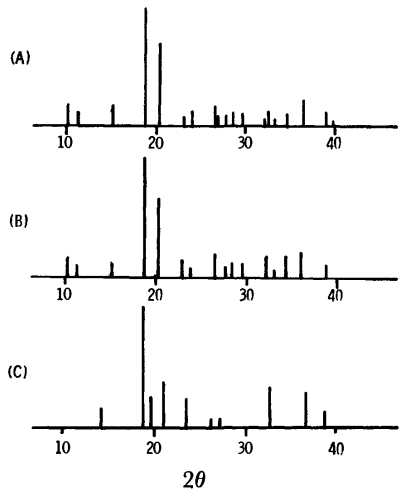

Fig. 10. X-Ray diffraction patterns of compounds (IX) (A), the product obtained by heating (IX) at 120 °C(B) and that obtained at 150 °C(C).

35 cm^{-1} higher.

X-Ray Powder Diffraction Patterns. The X-ray powder diffraction patterns at several heating setps for compound IX are shown in Fig. 10. The pattern obtained by heating at 110 °C where 70% of benzene is removed shows no appreciable change, whereas the one at 150 °C shows a remarkable change. This suggests that the removal of 70% of benzene from the clathrate IX causes no essential change of structure in the host skeleton of the mother clathrate, but the removal of the residual benzene and ammonia gives rise to a structural change. Such a tendency is also observed in compounds X—XII.

Isothermal Kinetics. Isothermal studies were carried out in the same way as those for Hofmann-type clathrates. The enthalpy changes (ΔH) and activation energies (E_a) are given in Table 2.

The value of each activation energy is close to that of the corresponding enthalpy change. The activation energy values of Iwamoto-type clathrates are similar to those of Hofmann-type ones, the elimination of benzene proceeding in one step. There are two different kinds of cavities in Iwamoto-type clathrates. However, they cannot be distinguished from each other as regards thermal behavior of the guest molecules. From this point of view, Iwamoto-type clathrates are analogous to Hofmann-type ones with regard to the state of the guest benzene molecules. The activation energy of compound XII gave a somewhat small value. This might be due to the relatively larger repulsion between bulky trimethylenediamine and benzene than that between ethylenediamine and benzene.

Table 2. Enthalpy changes ΔH and activation energies E_a in the elimination of benzene molecule from clathrate compounds

Compound		ΔH kJ mol^{-1}	E_a kJ mol^{-1}
IX	$Cd(NH_3)_2Hg(CN)_4 \cdot 2C_6H_6$	63	76.4
X	$Cd(en)Hg(CN)_4 \cdot 2C_6H_6$	67	74.3
XI	$Cd(en)Cd(CN)_4 \cdot 2C_6H_6$	67	75.6
XII	$Cd(tn)Hg(CN)_4 \cdot 2C_6H_6$	42	65.1

References

1) K. A. Hofmann and F. Z. Küspert, *Z. Anorg. Allg. Chem.*, **15**, 204 (1897).
2) E. E. Aynsley, W. A. Campbell, and R. E. Dodd, *Proc. Chem. Soc. (London)*, **1957**, 210.
3) H. M. Powell and J. H. Rayner, *Nature*, **163**, 566 (1949).
4) J. H. Rayner and H. M. Powell, *J. Chem. Soc.*, **1952**, 319.
5) R. Baur and G. Schwarzenbach, *Helv. Chim. Acta*, **43**, 842 (1960).
6) T. Iwamoto, T. Miyoshi, T. Miyamoto, Y. Sasaki, and S. Fujiwara, *Bull. Chem. Soc. Jpn.*, **40**, 1174 (1967).
7) T. Nakano, T. Miyoshi, T. Iwamoto, and Y. Sasaki, *Bull. Chem. Soc. Jpn.*, **40**, 1297 (1967).
8) Y. Sasaki, *Bull. Chem. Soc. Jpn.*, **42**, 2412 (1969).
9) T. Miyoshi, T. Iwamoto, and Y. Sasaki, *Inorg. Chim. Acta*, **7**, 97 (1973).
10) R. Kuroda and Y. Sasaki, *Acta Crystallogr., Sect. B*, **30**, 687 (1974).
11) T. Iwamoto, *Inorg. Chim. Acta*, **2**, 269 (1968).
12) T. Miyoshi, T. Iwamoto, and Y. Sasaki, *Inorg. Nucl. Chem. Lett.*, **6**, 21 (1970).
13) T. Miyoshi, T. Iwamoto, and Y. Sasaki, *Inorg. Chim. Acta*, **6**, 59 (1972).
14) T. Iwamoto and D. F. Shriver, *Inorg. Chem.*, **11**, 2570 (1972).
15) T. Iwamoto, *Chem. Lett.*, **1973**, 723.
16) R. Kuroda, *Inorg. Nucl. Chem. Lett.*, **9**, 13 (1974).
17) T. Miyoshi, T. Iwamoto, and Y. Sasaki, *Inorg. Chim. Acta*, **1**, 20 (1967).
18) R. Tsuchiya, Y. Kaji, A. Uehara, and E. Kyuno, *Bull. Chem. Soc. Jpn.*, **42**, 1881 (1969).
19) I. Nakagawa and S. Mizushima, *J. Chem. Phys.*, **21**, 2195 (1953).

Synthesis and PMR Study of Mixed Ligand Cobalt(III) Complexes with Aliphatic α-Hydroxyimino Ketone and Pyridine

Minoru TANAKA, Ryonte RYU, Isao MASUDA,* and Toshiyuki SHONO

Department of Applied Chemistry, Faculty of Engineering, Osaka University, Yamada-kami, Suita, Osaka 565

**Department of Chemistry, Faculty of Science, Fukuoka University, Nanakuma, Nishi-ku, Fukuoka 814*

(Received September 8, 1976)

Cobalt(III) complexes with a series of aliphatic α-hydroxyimino ketone (moH) and pyridine (py) were obtained as fine crystals. The aliphatic α-hydroxyimino ketones used are R-C(=O)-C(=NOH)-R′ where R=CH_3 or C_2H_5 and R′=CH_3, C_2H_5, *i*-C_3H_7, *n*-C_3H_7 or $COCH_3$. These complexes are formulated as $[Co(mo)_2(py)_2]ClO_4$. The PMR spectral investigation shows that the proton resonances of the alkyl group bound to the hydroxyimino group are shifted toward higher fields upon complex formation. This unusual upfield shift is accounted for by consideration of the specific configuration and ring-current of the pyridine in the complex.

The α-hydroxyimino ketones, R-C(=O)-C(=NOH)-R′, abbreviated as moH, are known to react with transition metal ions.[1] The specific cobalt complexes studied have been reported as having the formula $Co^{III}(mo)_3$. In the case where R and/or R′ are saturated alkyl groups, the α-hydroxyimino ketones appear to produce less stable complexes than aromatic α-hydroxyimino ketones with phenyl or 2-furyl groups. Thus, in respect to the aliphatic α-hydroxyimino ketone complexes, their synthesis and characterization appear to remain equivocal.

In the present paper, the method of preparation of the crystalline cobalt(III) complexes of aliphatic α-hydroxyimino ketones having the formula $[Co(mo)_2(py)_2]ClO_4$, where py is pyridine, is described. The PMR spectral behavior is discussed in terms of a specific steric configuration of alkyl groups of the complexes in solution.

Experimental

Preparation. The α-hydroxyimino ketones were prepared by the hydroxyimination reaction of the methylene group of the corresponding ketone with isopentyl nitrite.[2]

Cobalt(III) complexes were obtained by the following general procedure: to 50 ml of a tetrahydrofuran solution of 0.01 mol of α-hydroxyimino ketone and 0.005 mol of $Co(ClO_4)_2 6H_2O$ was added 0.01 mol of pyridine. The mixture was stirred in air at room temperature for 2 h. The precipitate separated was collected on a glass filter, and then recrystallized from ethanol. Table 1 shows the analytical data for the complexes thus obtained. The same procedure using ammonia or aniline as a base resulted in no precipitation of any similar complex.

Measurement. PMR spectra were recorded with a Japan Electron Optics Model JNM-PS-100 spectrometer at a frequency of 100 MHz and/or a JNM-3H spectrometer at 60 MHz, at an ambient probe temperature of 20 °C. The chemical shifts were determined in ppm using TMS as an internal standard.

Results and Discussion

The results of elemental analysis, as listed in Table 1, show that the composition of the complexes corresponds closely to the formula, $[Co\{R-C(=O)-C(=NO)-R'\}_2(py)_2]ClO_4$. These complexes are diamagnetic, which suggests that cobalt(III) complexes were obtained.

The PMR spectra of free biacetyl monoxime (R=R′=CH_3) and its complex are given in Fig. 1. The free ligand exhibits three singlet signals at 2.00, 2.39, and 9.83 ppm; these are readily assigned to the CH_3^a, CH_3^s, and NOH protons on the basis of published data,[3] respectively. The complex has two signals for the CH_3^a singlet and the CH_3^s singlet (at 1.95 and 2.53 ppm, respectively) and no signal for the NOH proton, which indicates that the two biacetyl monoximato ligands are equivalent. It should be noted that upon complex formation, the resonances of the H^a and H^s protons are shifted in opposite directions, that is, the H^a signal is shifted toward higher fields, whereas the H^s signal is shifted toward lower fields.

In general, it is considered that the coordination of the functional group as $>C=NO^-$ or $>C=O$ bound to an alkyl group accompanies either no appreciable or only a small downfield shift of the alkyl proton resonance. This PMR spectral characteristic has been shown in the case of Co^{III}(2,4-pentanedionato)$_3$[4] and *trans*-$[Co^{III}(dimethylglyoximato)_2(py)X]$ (X=NO_2^- or halide ions).[5] The downfield shift of the alkyl proton

TABLE 1. ANALYTICAL DATA OF THE COMPLEXES, $[Co\{R-C(=O)-C(=NO)-R'\}_2(py)_2]ClO_4$[a]

Complex		Found %			Calcd %		
R	R′	C	H	N	C	H	N
CH_3	CH_3	41.71	4.34	10.76	41.85	4.26	10.84
CH_3	CH_2CH_3	44.29	4.85	9.94	44.10	4.77	10.28
CH_3	$CH_2CH_2CH_3$	46.11	5.28	9.80	45.97	5.24	9.77
CH_3	$CH(CH_3)_2$	46.11	5.82	9.46	45.97	5.24	9.77
CH_3	$COCH_3$	41.75	4.06	9.31	41.95	3.84	9.78
CH_3CH_2	CH_3	43.37	4.79	10.17	44.10	4.77	10.28

a) py=pyridine.

TABLE 2. PMR DATA FOR FREE- AND COORDINATED-HYDROXYIMINO KETONES

R	R′	Solvent	Chemical shift, ppm R-C(=O)-C(=NOH)-R′					[Co{R-C(=O)-C(=NO)-R′}$_2$(py)$_2$]ClO$_4$				
			H^a	H^b	H^α	H^β	H^γ	H^a	H^b	H^α	H^β	H^γ
CH_3^a	CH_3^α	$CDCl_3$	2.39 s		2.00 s			2.53 s		1.95 s		
		d_6-DMSO	2.32 s		1.83 s			2.52 s		1.68 s		
		Py	2.45 s		2.15 s			2.54 s		1.90 s		
		H_2O[a]	2.35 s		1.86 s			2.42 s[b]		1.84 s[b]		
CH_3^a	$CH_2^\alpha CH_3^\beta$	$CDCl_3$	2.38 s		2.55 q	1.05 t		2.55 s		2.38 q	0.66 t	
		d_6-DMSO	2.29 s		—[c]	0.91 t		2.55 s		2.29 q	0.54 t	
CH_3^a	$CH_2^\alpha CH_2^\beta CH_3^\gamma$	$CDCl_3$	2.39 s		2.54 t	1.50m	0.93 t	2.54 s		2.34 t	1.13m	0.46 t
		d_6-DMSO	2.29 s		2.40 t	1.38m	0.82 t	2.55 s		2.31 t	1.05m	0.35 t
CH_3^a	$CH^\alpha(CH_3^\beta)_2$	$CDCl_3$	2.38 s		3.45m	1.24d		2.55 s		—[d]	0.93d	
		d_6-DMSO	2.26 s		3.31m	1.13d		2.56 s		3.30m	0.83d	
CH_3^a	$COCH_3^\beta$	$CDCl_3$	2.43 s[e]			2.43 s[e]		2.90 s			2.33 s	
$CH_3^bCH_2^a$	CH_3^α	d_6-DMSO	—	1.15 t	1.98 s			2.83 q	1.17 t	1.89 s		

s=singlet, d=doublet, t=triplet, q=quartet, and m=multiplet.
a) Sodium 3-trimethylsilylpropanesulfonate is used as an external reference. b) Obtained for the sodium salt. c) Obscured by the solvent signal. d) An accurate value is not obtained due to low solubility. e) H^a and H^β are observed as one signal.

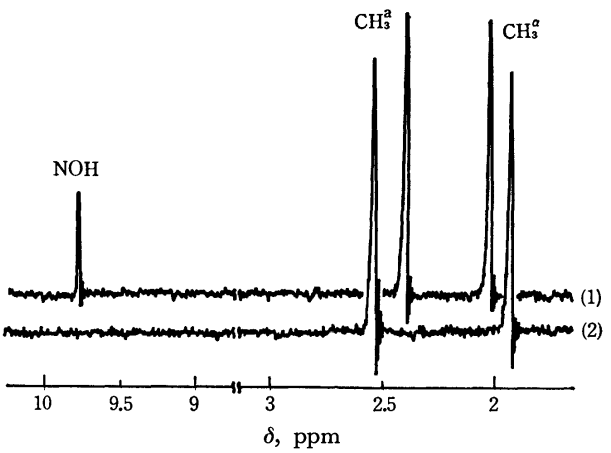

Fig. 1. PMR spectra in $CDCl_3$.
(1): CH_3^a-C(=O)-C(=NOH)-CH_3^α.
(2): [Co{CH_3^a-C(=O)-C(=NO)-CH_3^α}$_2$(py)$_2$]ClO$_4$.

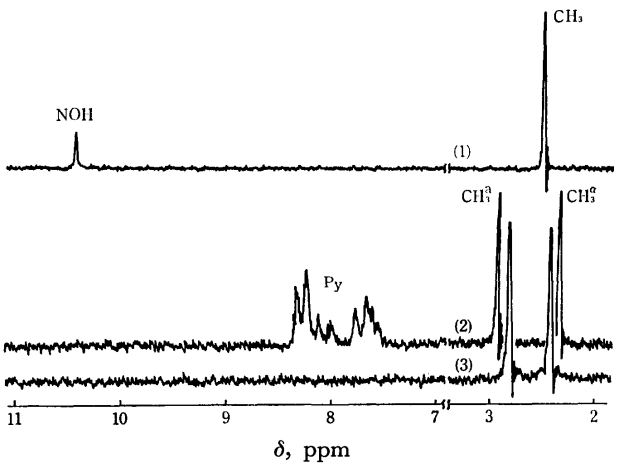

Fig. 2. PMR spectra in $CDCl_3$.
(1): CH_3^a-C(=O)-C(=NOH)-C(=O)-CH_3.
(2): [Co{CH_3^a-C(=O)-C(=NO)-C(=O)-CH_3}$_2$-(py)$_2$]ClO$_4$.
(3): Co{CH_3^a-C(=O)-C(=NO)-C(=O)-CH_3}$_3$.

resonance may be interpreted as follows. The electron density on the coordinated atom decreases, which causes a decrease in the shielding of the alkyl protons. The observed downfield shift of the H^a signal by coordination is consistent with the above interpretation. On the other hand, the upfield shift for the H^α signal is unexpected. There is no appreciable difference between the H^α chemical shift values of biacetyl monoximato anion and the neutral biacetyl monoxime, as shown in Table 2. This fact implies that it is improbable that the unusual upfield shift is caused by the negative charge on the functional group.

The similar spectral behavior of the upfield shift for the R′ proton is also observed in the case of 3-hydroxyimino-2,4-pentanedione (R=CH_3^a and R′=$COCH_3^\beta$). The free 3-hydroxyimino-2,4-pentanedione in $CDCl_3$ has one singlet at 2.43 ppm, as shown in Fig. 2. Patel and Haldar[6] have reported that the signal near 2.43 ppm is split into two peaks in dioxane. Both phenomena stated above can be explained by the rate of bond switching in hydrogen bonding between hydroxyimino-hydrogen and two carbonyl-oxygens. In the solution of $CDCl_3$, the bond switching time is shorter than the measurement time. One resonace signal is then obtained in the present case. The tris-complex, Co^{III}(3-hydroxyimino-2,4-pentanedionato)$_3$, exhibits two singlets at 2.40 and 2.79 ppm and the bis-complex, [Co^{III}(3-hydroxyimino-2,4-pentanedionato)$_2$(py)$_2$]ClO$_4$, also gives rise to two singlets at 2.33 and 2.90 ppm. The singlet at 2.33 ppm for the bis-complex is shifted toward higher fields by 0.1 ppm than that of the free ligand and is assigned to the $COCH_3$ protons considering its similarity to the upfield shift of the H^α proton signal in biacetyl monoxime.

The upfield shift of the R′ proton resonance is also confirmed in the PMR spectra of a series of α-hy-

droxyimino ketones with such R′ groups as C_2H_5, *i*-C_3H_7, and *n*-C_3H_7. From the PMR data presented in Tables 2 and 3, it is found that upon complex formation, the amount of the upfield shift for the R′ proton resonances increases in the following order: $H^\alpha < H^\beta < H^\gamma$. On the other hand, the H^b proton signal in $R=CH_3^bCH_2^a$ is shifted to lower fields upon coordination, as expected.

In order to interpret the above upfield shift for the R′ proton resonances, it is proposed that the R′ group in the complex is situated so as to experience a strong shielding effect due to the magnetic anisotropy—the pyridine ring-current. A similar shielding effect has been pointed out for the methylene proton resonance of 1,4-polymethylenebenzene analogues, where the methylene groups are above the phenyl ring.[7] Hill and Morallee[8] have reported that the resonances of the bridging methylene protons are shifted toward higher fields by the axial coordination of pyridine with RCo(bae), where R=an alkyl group and bae=a bis(acetylacetone)ethylenediiminato anion. This upfield shift is attributed to the ring-current effect of the coordinated pyridine. Abott and Martel[9] have shown that the 2-CH_3 signal of the bis(pyridoxylideneserinato)Al(III) complex is found to be as much as 100 Hz higher than that of the 2-CH_3 of the free Schiff base.

It is beyond the aim of this study to describe the conclusive structure of [Co(mo)$_2$(py)$_2$]ClO$_4$.[10] Figure 3 shows the limiting structure for R′=*n*-C_3H_7, where the alkyl group experiences most strongly the shielding effect of the pyridine. The framework molecular model suggests that the free rotation of the R′ group is not restricted sterically. For the 1,2-dioximato chelates, it has been suggested that the d_π-orbitals of the metal interact with both p_π-orbitals of the chelate ligand and the pyridine which perpendicularly coordinates with the metal-chelate plane.[11] It is also possible to expect a similar interaction of the p_π(pyridine)-, d_π(cobalt)-, and p_π(hydroxyiminato nitrogen)-orbitals for the pyridine conformation in [Co(mo)$_2$(py)$_2$]ClO$_4$ given in Fig. 3. Consequently, the pyridine occupies the position in which the pyridine plane is perpendicular to the Co–N(hydroxyiminato nitrogen) bonding. The pyridine plane then faces the R′ group and an upfield shift of the R′ proton resonances is obtained. Because the carbon atom of the hydroxyimino group is sp^2-hybridized, the CH_2^a carbon atom is drawn on the xy-plane.

It is scarcely possible to evaluate the exact distance between the pyridine and the alkyl group of the complex in solution. The vertical distance of the alkyl carbon from the xy-plane is, therefore, estimated using the molecular model framework and is tentatively plotted versus the amount of upfield shift of the R′=$CH_2^aCH_2^\beta$-CH_3^γ proton resonance caused by coordination (Fig. 4). Figure 4 suggests that the shielding effect by the pyridine increases in the order: $H^\alpha < H^\beta < H^\gamma$. The distance between the CH_3 carbon atom and the center of the pyridine ring is about 2.8 Å at its distance of closest approach, as shown in Fig. 3. In the case of 1,4-polymethylenebenzene analogues,[7] it is seen from the molecular model that the methylene carbons are vertically situated at about 2 Å above the phenyl ring.

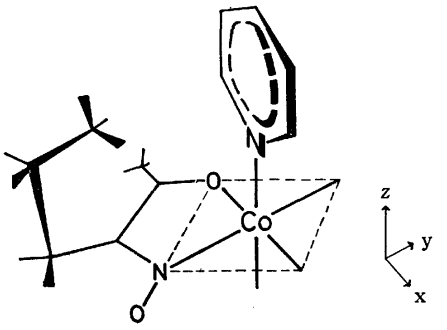

Fig. 3. Proposed limiting structure for [Co{CH_3^a-C(=O)-C(=NO)-$CH_2^aCH_2^\beta CH_3^\gamma$}$_2(py)_2$]ClO$_4$.

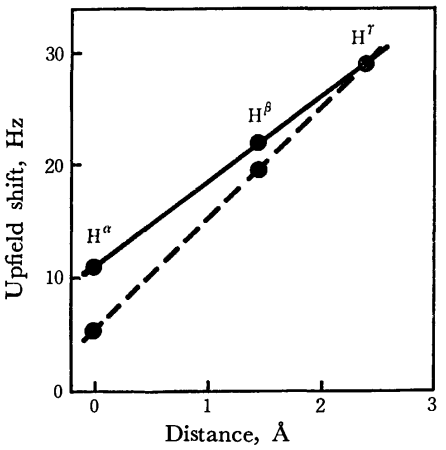

Fig. 4. Amount of the upfield shift caused by coordination and vertical distance of the alkyl carbon atom from the metal-chelate plane for [Co{CH_3^a-C(=O)-C(=NO)-$CH_2^aCH_2^\beta CH_3^\gamma$}$_2(py)_2$]ClO$_4$.
——: in $CDCl_3$, – – –: in d_6-DMSO.

Table 3. Upfield shift of the R′ proton signal from free ligands caused by complex formation

R	R′[a]	Amount of upfield shift in $CDCl_3$, Hz[b]		
		H^α	H^β	H^γ
CH_3^a	CH_3^a	4		
CH_3^a	$CH_2^aCH_3^\beta$	12	24	
CH_3^a	$CH_2^aCH_2^\beta CH_3^\gamma$	11	22	29
CH_3^a	$CH^\alpha(CH_3^\beta)_2$		19	
CH_3^a	$COCH_3^\beta$		6	

a) For the general formula, refer to Table 1.
b) The data were obtained at 60 MHz.

As summarized in Table 3, upon complex formation, the upfield shift of the H^α or H^β signal for R′=$CH_2^aCH_3^\beta$ is nearly equal to that of the corresponding signal for R′=$CH_2^aCH_2^\beta CH_3^\gamma$. On the other hand, the upfield shift of the H^β signal for R′=$COCH_3^\beta$ (6 Hz) is smaller than that of the H^β signal for R′=C_2H_5 or *n*-C_3H_7 (22 to 24 Hz). This result is interpreted as follows. The H^β protons in $COCH_3^\beta$ are farther from the pyridine than in C_2H_5 and *n*-C_3H_7, because the CH_2^β group is bound to the sp^2-carbonyl carbon atom. The small upfield shift of 6 Hz is obtained as a result of the decrease

in the shielding effect by the pyridine. Compared with the upfield shift of the H^{α} signal for $R'=C_2H_5$ or n-C_3H_7, that of the H^{α} signal for $R'=CH_3^{\alpha}$ is rather small.

References

1) References are included in the review by A. Chakravorty, *Coord. Chem. Rev.*, **13**, 1 (1974); J. Bassett, J. Bensted, and R. Grzeskowiak, *J. Chem. Soc., A*, **1969**, 2873.

2) O. Diels and H. Jost, *Ber.*, **35**, 3290 (1902); *Org. React.*, Vol. VII, Ch. 6 (1953).

3) J. W. Emsley, J. Feeney, and L. H. Sutcliffe, "High Resolution Nuclear Magnetic Resonance Spectroscopy," Pergamon Press, New York (1965), p. 1125.

4) Y. Murakami, K. Nakamura, H. Uchida, and Y. Kanaoka, *Inorg. Chim. Acta*, **2**, 133 (1968).

5) H. A. O. Hill and K. G. Morallee, *J. Chem. Soc., A*, **1969**, 554.

6) N. J. Patel and B. C. Haldar, *J. Inorg. Nucl. Chem.*, **29**, 1037 (1967).

7) J. S. Waugh and R. W. Fessenden, *J. Am. Chem. Soc.*, **79**, 846 (1957).

8) H. A. O. Hill and K. G. Morallee, *J. Organometal. Chem.*, **11**, 167 (1968).

9) E. H. Abott and A. E. Martell, *J. Am. Chem. Soc.*, **91**, 6866 (1969).

10) An X-ray study of [Co(3-hydroxyimino-2,4-pentanedionato)$_2$(py)$_2$]ClO_4 indicates the two chelating hydroxyimino ketones are in the *cis*-positions, and that the two nitrogen atoms are also in *cis*-positions. Consequently, two pyridines occupy the residual *cis*-positions. H. Tamura, R. Ryu, I. Masuda, K. Ogawa, and T. Shono presented the details at the 25th Symposium on Coord. Chem., Tokyo (1975).

11) Y. Yamano, I. Masuda, and K. Shinra, *J. Inorg. Nucl. Chem.*, **33**, 521 (1971); *Nippon Kagaku Zasshi*, **92**, 707 (1971).

Stereochemical Studies of the Electrolytic Reactions of Organic Compounds. II. Electrolytic Reduction of Optically Active 6-Chloro-2,6-dimethyloctane to the Corresponding Alkane

Tsutomu NONAKA, Tetsuro OTA,* and Keijiro ODO

Department of Electronic Chemistry, The Graduate School, Tokyo Institute of Technology
Ookayama, Meguro-ku, Tokyo 152

(Received May 1, 1976)

In order to clarify the mechanism of electroreduction of aliphatic halides, optically active 6-chloro-2,6-dimethyloctane(I), in which an (*R*)-(−)-enantiomer was present in excess, was electrolyzed at a mercury cathode in various organic solvents. An (*R*)-(−)-enantiomer was also present in excess in the 2,6-dimethyloctane(II) which was obtained. This result indicates that the reduction of I to II proceeds with an excess of the inversion of the absolute configuration of the starting halide. In this paper, the stereochemistry of a radical intermediate formed at an initial stage in the course of reduction is discussed.

A number of studies of the mechanism of electroreduction of organic halogen compounds have been performed from electrochemical and organic chemical aspects.[1] In recent years there has been a great deal of interest shown in the sterochemistry of the electroreduction of aliphatic halides.[2] Most of studies in this field have dealt with the geometrical isomerism of reactant, intermediate, and/or product, while studies dealing with optical isomerism have been very rare.

Czochralska[3] electrolyzed optically active 2-phenyl-2-chloropropionic acid(III) at a mercury cathode in 90% ethanol containing tertaethylammonium chloride as a supporting electrolyte and obtained optically active 2-phenylpropionic acid, in which the absolute configuration had been inverted, in a high optical yield. At almost the same time, Annino *et al.*[4] also found that the electrolytic reduction of optically active cyclopropyl bromides (IVa—IVd) at a mercury cathode in 95% ethanol are stereochemically controlled by the substituent at the asymmetric carbon. While the reductions of IVa and IVb proceed with the inversion of configuration, the reductions of IVc and IVd proceed with its retention. These facts are very interesting, though the halides used are not typical tertiary alkyl halides.

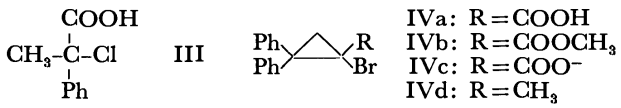

For the first investigation of the substiuent effect, a tertiary halide having as simple as possible substituents should be used. 3-Halo-3-methylhexane is such an alkyl halide, but its optical resolution is very difficult. In this work, (*R*)-(−)-6-chloro-2,6-dimethyloctane(I) derived from natural *l*-linalool was used as the second best sample, because no optical resolution was necessary and the absolute configurations of I and the corresponding alkane were known.

Results and Discussion

Electrolytic results are summarized in Table 1. The electrolytic products consisted of optical isomers of an alkane and a small amount of an optically inactive alkene. The alkane was confirmed to be 2,6-dimethyloctane, in which an (*R*)-(−)-enantiomer is in excess, by its physical properties. On the other hand, although the molecular structure of the alkene(m/e=140) could not be confimed, its retention volume in gas chromatography was equal to that of the dehydration product of tetrahydrolinalool in hot anhydrous formic acid.

The optical rotation of I used in this work was $[\alpha]_D^{23}$ −0.34°. The accurate optical purity could not be estimated because optically pure I has never been prepared. The above value of optical rotation is obtained in the region between 54[5] and 12%[6] of optical purity. On the other hand, the optical rotation of optically pure II is known to be $[\alpha]_D^{20}$ 7.32°.[6] Therefore, the optical yield of II could be shown only by giving its upper and lower limits.

As shown in Table 1, I with $[\alpha]_D^{23}$ −0.34° gave II with minus values of optical rotation, which range from −0.01 to −0.34°, under a variety of electrolytic conditions such as cathode material, solvent, and proton donor. Since I[7] and II[6] with minus values are in (*R*)-configuration, it is concluded that the reduction proceeds with an excess of the inversion of the absolute configuration of I. In the case of a lead cathode, the racemization may be regarded as exclusive.

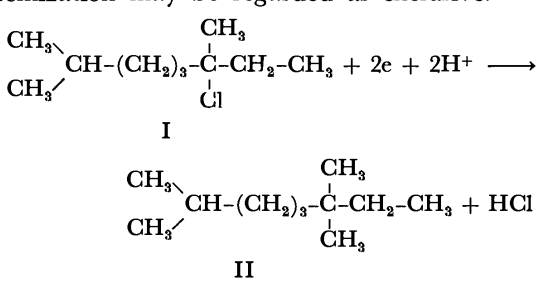

An essential conclusion drawn from the results of Czochralska[3] was that the electrolytic reduction of alkyl halides proceeds in an S_N2 type mechanism initiated by the attack of an electron to a halogen atom. However, the results of Annino *et al.*[4] cannot be explained by such a mechanism. Since the attack on a halogen is also confirmed through the fact that bridgehead bicyclic halides are reducible at a mercury cathode,[8] there would be no doubt about this point at least in the case of a mercury cathode.

Elving and Pullman[9] generalized the reduction

* Present address: Asahi Chemical Industry Co., Ltd., Chemical Administration, Yako 1-3-1, Kawasaki-ku, Kawasaki 210.

TABLE 1. ELECTROLYTIC RESULTS OF 6-CHLORO-2,6-DIMETHYLOCTANE WITH $[\alpha]_D^{23}$ −0.34°

Solvent	Proton donor	Cathode material	Current density A/dm²	Cathode potential V *vs.* Ag/AgCl	Quantity of electricity passed ×10⁶, C/mol	2,6-Dimethyloctane		Optical yield[a,b] %
						Chemical yield, %	$[\alpha]_D^{23}$ deg	
MeO	—	Hg	2.6	−2.20—−2.30	4.4	74	−0.08±0.01	8— 2
EtOH	—	Hg	1.6	−2.15—−2.30	2.9	90	−0.04±0.01	4— 1
EtOH	—	Pb	1.2	−1.85—−2.00	1.7	54	−0.01±0.01	1— 0
EtOH	AcOH	Hg	2.0	−1.55—−2.00	2.7	87	−0.12±0.01	12— 3
EtOH	Et_3NHBr	Hg	0.8	−1.65—−1.95	2.3	47	−0.12±0.02	12— 3
MeCN	—	Hg	2.0	−2.40—−2.45	2.7	96	−0.34±0.01	36— 9
MeCN	—	Hg	0.9	−2.25—−2.35	1.9	84	−0.31±0.04	35— 8
DMF	—	Hg	2.0	−2.20—−2.30	1.9	76	−0.05±0.01	4— 1

a) [(optical purity of product)/(optical purity of reactant)]×100%. b) Upper limit—lower limit.

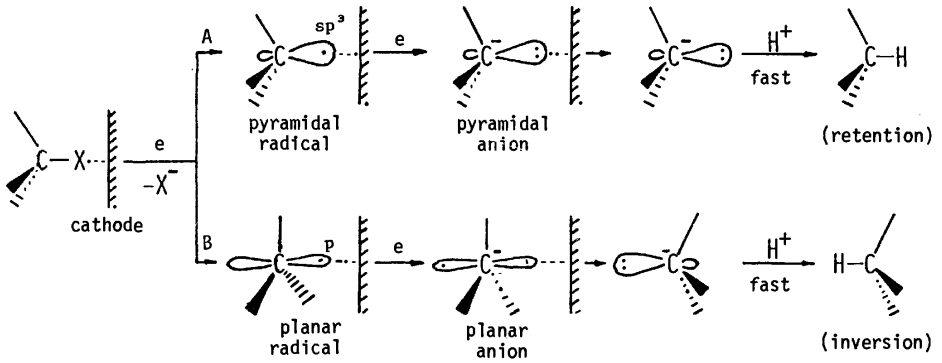

Fig. 1. Schematic mechanisms for the configurational retention and inversion in the electroreduction of alkyl halide to the corresponding alkane.

mechanism of alkyl halides as follows:

$$R\text{-}X \xrightarrow[-X^-]{e} [R\cdot] \xrightarrow{e} [R^-] \xrightarrow{H^+} R\text{-}H$$

where [R·] and [R⁻] represent electrode complexes or adsorbed species on an electrode surface.

The present paper will employ the steric form of a radical derived from a tertiary alkyl halide in order to rationalize the apparently complicated results of the electroreductions of optically active halides such as I, III, and IVa—IVd.

It is well known that the steric form of a carbon radical can vary from being almost completely planar to being pyramidal with the kind of substituent, although the former is energetically more unstable than the latter.[10] While a small alkyl radical, such as the methyl radical, is undoubtedly almost planar,[11] there has been no reliable information about the planarity of a large tertiary alkyl radical such as methylethyl-1-(4-methyl)hexylmethyl radical from I. On the other hand, small cyclic alkyl radicals, especially cyclopropyl radicals, are undoubtedly pyramidal.[12] The planarity of a radical would be favored by substituents having a π-electron system, such as phenyl or carbonyl groups, because of the favorable interaction between the two electron orbitals paralleled to each other: the p orbital of an unpaired electron of the planar radical and the π electron orbital of the substituent.

According to the above viewpoint, the radicals from III, IVa, and IVb would be planar, while the radical from IVd would be pyramidal. The radical from IVc would be planar in a free environment, but it would be pyramidal in the adsorbed state on a cathode surface because of the electrostatic repulsion of a carboxylate anion from a negatively polarized cathode surface. Although the steric form of the radical from I is ambiguous, it may be acceptable that such a radical could be at least a very shallow pyramid, even if not a plane, considering the fact that an optically active staring compound gave a completely racemized product in a homogeneous reaction involving methylethyl-1-(2-methyl)propylmethyl radical, which resembles the radical from I, as an intermediate.[13] The configurational stability of the radical would be increased by the adsorption on an electrode or by the formation of an electrode complex. Generally, a carbanion is configurationally more stable than the corresponding radical. The stability of a carbanion would be increased by a counter cation in the immediate vicinity, while it would be decreased by solvation, especially of the solvent insertion type, to the cation.

As shown in Fig. 1, a pyramidal radical would result in a carbanion which retained its configuration by the introduction of the second electron to the sp^3 orbital of an unpaired electron. On the other hand, the introduction of the second electron to the p orbital of a planar radical would intermediately give a very unstable planar carbanion, which would be immediately converted into an ordinary carbanion having the inverted pyramidal from. This inversion is thought to be due to a steep potential gradient in the immediate

vicinty of the cathode. Figure 1 illustrates extreme cases where either retention or inversion occurs exclusively.

In conclusion, it can be actually supposed that the path "B" is slightly predominant in the reduction of I, since the radical intermediate is not a complete plane but a shallow pyramid. Steric hindrance between the three alkyl groups and a cathode is alleviated in a pyramidal radical. Also, the path "B" is more predominant in the cases of III, IVa, and IVb, since their radicals are almost planar even on a cathode. One reason for being planar may be that the p-π interaction described previously is so strong that the contribution of the steric hindrance is more than canceled. In the cases of IVc and IVd, the path "A" is predominant, since nothing causes the corresponding cyclopropyl radicals to be planar.

While the steric configuration of the alkane formed would be mainly controlled by the steric form of an intermediate radical on a cathode, the optical yield would be controlled not only by the configurational stabilities of the radical and the carbanion intermediates but also by the protonation rate of the latter. The fact that proton donors such as acetic acid and triethylamine hydrobromide added in ethanolic catholyte increased the optical yield may partially support the above discussion.

The solvent effect on the optical yield of II can be explained as due to the difference of the proton-donating force to the carbanion intermediate, except for the case of DMF. The reduction in DMF afforded II with an optical rotation equal to one in the case of methanol, though DMF is not only weaker in proton-donating force but also stronger in solvating force to a counter cation of the carbanion intermediate than methanol. There has been no clear explanation of the solvent effect.

Experimenatl

(R)-(−)-6-Chloro-2,6-dimethyloctane(I). I was prepared from a commercial natural *l*-linalool with $[\alpha]_D^{23}$ −14.0° (lit,[6] $[\alpha]_D^{20}$ −14.47°), by the literature method.[6] Bp 83—84 °C/15 Torr (lit,[6] 90.2—91.3 °C/21 Torr), n_D^{25} 1.4342 (lit,[6] 1.4346), and $[\alpha]_D^{23}$ −0.34° (lit,[6] $[\alpha]_D^{25}$ −0.42°).

Electrolytic Procedure. An H-type cell divided by a sintered glass diaphragm was used. The cathode was a mercury pool (diameter, 4 cm) or a lead plate (4×3 cm). The catholyte and the anolyte were 50 ml of dried organic solvent(methanol, ethanol, DMF, or acetonitrile) containing 9.95 g of tetraethylammonium chloride as a supporting electrolyte. After nitrogen gas was introduced to the catholyte for one hour in order to remove the oxygen in the solvent, 2.65 g (0.015 mol) of I, and also 0.01 mol of a proton donor (acetic acid or triethylamine hydrobromide) if necessary, were added to the catholyte. A constant current was supplied, which was turned off when the cell voltage rose to above 20 V or when vigorous hydrogen evolution was observed. The temperature of the catholyte was maintained below 20 °C during the electrolysis.

Analysis and Isolation of 2,6-Dimethyloctane. After the electrolysis a large volume of water was added to the catholyte. The separating oil was extracted with ether and the ether extract was dried with anhydrous sodium sulfate. The ethereal solution was analyzed by gas chromatography (apeazone grease L, 100 °C). In the gas-chromatogram, three peaks (corresponding to II, alkene, and unreacted I) appeared.

After the gas chromatographic analysis, the ethereal solution was shaken with concentrated sulfuric acid in order to remove the alkene. The ethereal solution was concentrated by evaporation and the residual oil was distilled under reduced pressure. Gas-chromatographically pure II was obtained as the main fraction: bp 60—62 °C/30 Torr (lit,[6] 99—100 °C/121 Torr); n_D^{25} 1.4091 (lit,[6] 1.4087); mass spectrum (*m/e*) 142(M^+); IR spectrum(cm^{-1}) 2880, 1460, and 1375 as principal absorption bands. No absorption band appeared at 1653 or 888 cm^{-1} related to a double bond in terminal position.[6]

The optical rotation was measured in ethanol by Perkin-Elmer Micro-Polarimeter Model 141.

The authors with to express their thanks to Dr. T. Fuchigami of the Tokyo Institute of Technology for his helpful discussion.

References

1) J. Casanova and L. Eberson, "The Chemistry of the Carbon-Halogen Bond," ed by S. Patai, Interscience Publishers, New York (1973), p. 979.
2) K. P. Butin, *Usp. Khim.*, **40**, 1058 (1971); *Russ. Chem. Rev.*, **40**, 525 (1971).
3) B. Czochralska, *Chem. Phys. Lett.*, **1**, 239 (1967).
4) R. Annino, R. E. Erickson, J. Michalovic, and B. McKay, *J. Am. Chem. Soc.*, **88**, 4424 (1966).
5) D. B. Denney and R. Dileone, *J. Org. Chem.*, **26**, 984 (1961).
6) P. E. Verkade, K. S. Vries, and B. M. Wepster, *Recl. Trav. Chim. Pays-Bas*, **83**, 367 (1964).
7) V. Prelog and E. Watanabe, *Justus Liebigs Ann. Chem.*, **603**, 1 (1957).
8) L. Horner and H. Böder, *Chem. Ber.*, **101**, 4179 (1968).
9) P. J. Elving and B. Pullman, *Adv. Chem. Phys.*, **3**, 1 (1961).
10) A. D. Walsh, *J. Chem. Soc.*, **1953**, 2296.
11) G. Herzberg, *Proc. R. Soc. London, Ser. A*, **262**, 291 (1961).
12) R. W. Fessenden and R. H. Shuler, *J. Chem. Phys.*, **39**, 2147 (1963); T. Yonezawa, T. Kawamura, and H. Kato, *Bull. Chem. Soc. Jpn.*, **43**, 74 (1970).
13) W. v. E. Doering, M. Farber, M. Sprecher, and K. B. Wiberg, *J. Am. Chem. Soc.*, **74**, 3000 (1952).

Synthesis of Tuftsin and Its Analogs

Sukekatsu NOZAKI, Kazuhito HISATSUNE, and Ichiro MURAMATSU*

Department of Microbiology, Faculty of Pharmaceutical Sciences, Josai University, Sakado, Saitama 350-02

**Department of Chemistry, College of Science, Rikkyo University, Nishi-Ikebukuro, Tokyo 171*

(Received June 17, 1976)

Tuftsin, a phagocytosis stimulating peptide, was synthesized according to a liquid phase method together with its four analogs, H-Thr-Arg-Pro-Arg-OH (**2**), H-Thr-Lys-Pro-Lys-OH (**3**), H-Thr-Arg-Pro-Lys-OH (**4**), and H-Arg-Pro-Lys-Thr-OH (**5**).

Tuftsin (**1**), a tetrapeptide containing two basic amino acids, lysine and arginine, was isolated from the enzymatic digest of γ-globulin[1] and synthesized according to Merrifield's solid phase method by Nishioka *et al.*[2] They also synthesized two analogs of **1** lacking N- or C-terminal amino acid of the original peptide, *viz.*, H-Lys-Pro-Arg-OH and H-Thr-Lys-Pro-OH, and another analog having an additional proline, H-Thr-Lys-Pro-Pro-Arg-OH.[3] None of these analogs exhibited the phagocytosis stimulating activity, but the pentapeptide, H-Thr-Lys-Pro-Pro-Arg-OH, strongly inhibited tuftsin activity. This indicates that a certain restriction of the primary structure is required for biological activity to appear. However, the relationship between structure and activity is still unclarified. In order to investigate the effect of the replacement of lysine by arginine, or arginine by lysine, we synthesized the following tuftsin analogs (**2**—**5**) as well as **1** by a liquid phase method. **2**, *i.e.*, [2-arginine]-tuftsin, and **3**, *i.e.*, [4-lysine]-tuftsin are analogs in which either one of the two basic amino acids is replaced by the other. **4**, *i.e.*, [2-arginine, 4-lysine]-tuftsin has a sequence in which the positions of lysine and arginine are exchanged. **5**, the analog with the retro sequence of **1**, was also synthesized in order to see the effect of alternation of the primary structure.

The synthesis of **1** and its analogs is summarized in Charts 1—5. Benzyl ester was employed for the protection of carboxyl functions of C-terminal amino acids. In each step of the peptide elongation, *t*-butoxycarbonyl amino acids were used as the acylating reagent except in the final stages of the elongation. The *t*-butoxycarbonyl group was removed by HCl/THF or trifluoroacetic acid treatment prior to the next coupling. The ε-amino group of lysine and the guanidyl group of arginine were protected by benzyloxycarbonyl and nitro group, respectively. A mixed anhydride method was employed for the coupling reaction except at the introduction of N^{α}-*t*-butoxycarbonyl, N^{g}-nitro arginine, when the dicyclohexyl carbodiimide/*N*-hydroxy-1*H*-benzotriazole method[4] was used. Some of the intermediates were obtained as oily substance with a trace of impurities detectable

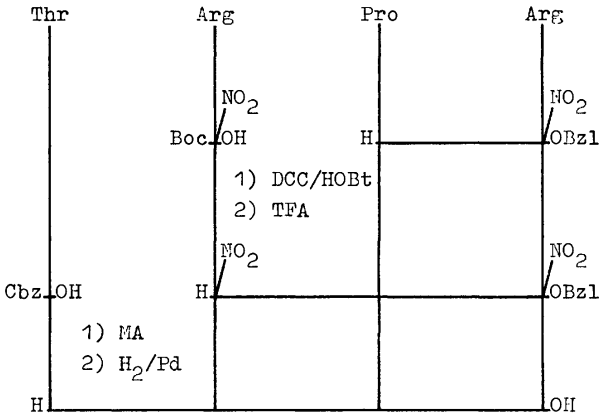

Chart 2. Preparation of **2**.

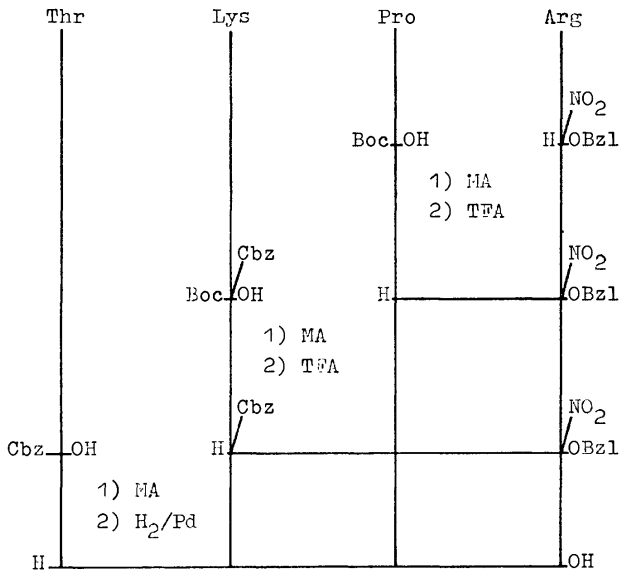

Chart 1. Preparation of **1**.

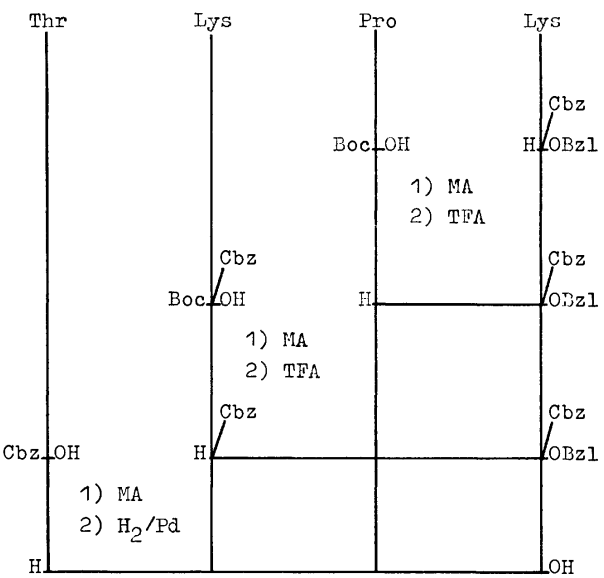

Chart 3. Preparation of **3**.

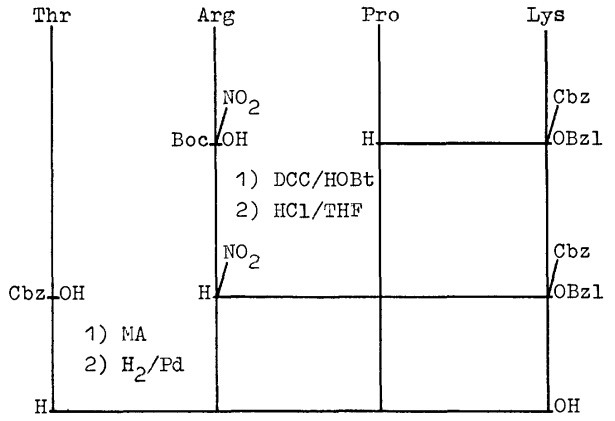

Chart 4. Preparation of **4**.

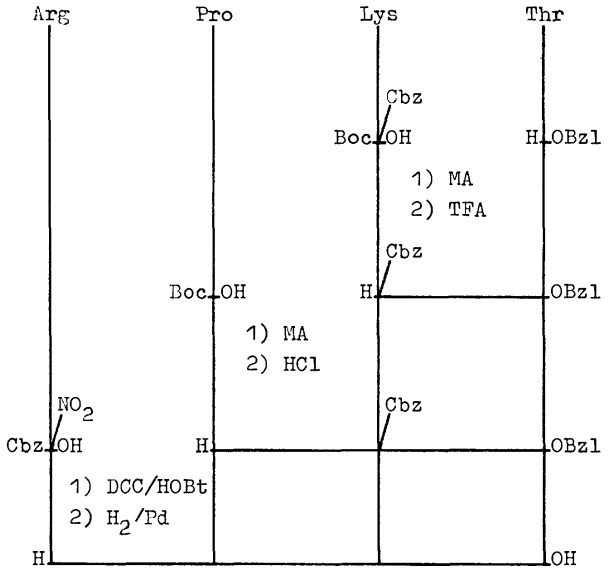

Chart 5. Preparation of **5**.

on TLC. However, no further trials for crystallization nor purification were carried out, since an ion exchange chromatography was expected to be effective for the purification of the basic peptides finally obtained. In the final stages of the construction of the peptides, benzyloxycarbonyl amino acids were used for acylation. The protected tetrapeptides were hydrogenated in the presence of palladium black in order to remove all the blocking groups.

The resulting free peptides were purified by carboxymethyl cellulose (Serva, or Whatman CM-52) chromatography using a linear gradient of ammonium acetate buffer (0—0.4 M, pH 7.0). **2** and **3** could be purified satisfactorily, but not the other analogs or **1**. The latter peptides gave no reasonable results on amino acid analysis after acid hydrolysis, although each of them showed individually a single spot on TLC (Avicel-cellulose, 1-butanol–pyridine–acetic acid–water, 16 : 10 : 3 : 12) and electrophoresis (Avicel-cellulose, pH 1.9, 40 V/cm). All efforts to remove the impurities by the carboxymethyl cellulose column were unsuccessful. Further purification of **4**, **5**, and **1** was successfully carried out on a Dowex 50 W×4 column with a linear gradient of pyridinium acetate buffer (0.6—2.0 M, pH 4.2—6.1). The highly purified products were desalted by a Biogel P-2 column and were lyophilized to give hygroscopic solids.

Phagocytosis stimulating activities of the synthetic peptides were measured according to the literature.[5] Compounds **2**, **3**, **4**, and **1** showed biological activity. For the appearance of biological activity, some alternation might be allowed in the primary structure of tuftsin, where the basic amino acids at positions 2 and 4 are exchangeable with each other without abolishing the biological potency.

Experimental[6]

Amino acid analyses were carried out with a JLC-6AS automatic analyzer (JEOL) after acid hydrolysis in HCl of constant bp (110 °C, 16 h). The theoretical values of amino acid ratios are shown in parentheses after each result. In TLC, Merck silicagel-precoated plate (S) and Avicel cellulose-precoated plate (C) were used with the following solvent systems: chloroform–methanol, 99 : 1 (a), 98 : 2 (b), 95 : 5 (c), 90 : 10 (d); 1-butanol–acetic acid–water 4 : 1 : 1 (e); 2-butanol–7M ammonia–ethanol, 1 : 4 : 2 (f), 1-butanol–pyridine–acetic acid–water, 16 : 10 : 3 : 12 (g). All the R_f values are the results of TLC. The properties and analytical results of the intermediates obtained in solid are as follows: Boc–Arg(NO_2)–Pro–Arg(NO_2)–OBzl: mp 89—111 °C, yield 65%, R_f (S, c) 0.34. $[\alpha]_D^{24}$ −31.1° (*c* 1.00, DMF). Found: C, 48.95; H, 6.64; N, 21.37%. Calcd for $C_{29}H_{45}O_{10}N_{11}$; C, 49.22; H, 6.41; N, 21.77%. Boc–Thr–Arg(NO_2)–Pro–Arg(NO_2)–OBzl (**6**); mp 88—124 °C, yield 92%, R_f(S, d) 0.50. $[\alpha]_D^{19}$ −29.0° (*c* 1.00, DMF). Found: C, 50.50; H, 6.13; N, 19.61%. Calcd for $C_{36}H_{50}O_{12}N_{12}\cdot H_2O$: C, 50.23; H, 6.09; N, 19.52%. The following intermediates were obtained as oily products and were used without crystallization (yield, R_f).

Boc-Pro–Arg(NO_2)–OBzl: 98%, (S, e) 0.44. Boc–Pro–Lys(Cbz)–OBzl: 95%, (S, a) 0.48. Boc–Lys(Cbz)–Pro–Lys(Cbz)–OBzl: 74%, (S, a) 0.19. Cbz–Thr–Lys(Cbz)–Pro–Lys(Cbz)–OBzl (**7**): 85%, (S, b) 0.29, (S, c) 0.82. Boc–Arg(NO_2)–Pro–Lys(Cbz)–OBzl: 100%, (S, c) 0.79. Cbz–Thr–Arg(NO_2)–Pro–Lys(Cbz)–OBzl (**8**): 90%, (S, c) 0.30. Boc–Lys(Cbz)–Thr–OBzl: 99%, (S, b) 0.70. Boc–Pro–Lys(Cbz)–Thr–OBzl: 98%, (S, b) 0.33. Cbz–Arg(NO_2)–Pro–Lys(Cbz)–Thr–OBzl (**9**): 85%, (S, c) 0.36. Boc–Lys(Cbz)–Pro–Arg(NO_2)–OBzl: 68%, (S, c) 0.49. Cbz–Thr–Lys(Cbz)–Pro–Arg(NO_2)–OBzl (**10**): 90%, (S, c) 0.41.

Preparation of **1**. **10** (12.0 g) was hydrogenated in a mixture of DMF (100 ml), water (20 ml) and acetic acid (3.5 ml) in the presence of Pd black. After hydrogenation for 12 h, the mixture was diluted with additional solvent; DMF (200 ml), water (50 ml) and acetic acid (3 ml). Hydrogenation was continued for 17 h more, the catalyst being removed after the addition of DMF (300 ml). The solvent was evaporated *in vacuo* and the residue was dissolved in water. The water-insoluble parts were removed by filtration. A half of the filtrate was applied to a CM-cellulose (Serva) column (3.7×42 cm), which was eluted with a linear gradient of ammonium acetate (pH 7.0, 0—0.4 M, 800 ml each). The fractions from 1092 ml to 1248 ml were combined, concentrated and desalted by means of a Biogel P-2 column (3.5×35 cm, 4% acetic acid). Lyophilization of the desalted fractions gave 1.01 g of the product. A part of the product was applied to a Dowex 50 W×4 column (2.2×30 cm), which was eluted with a linear gradient of pyridinium acetate

(0.6 M pyridine, pH 4.2—2.0 M pyridine, pH 6.1, 800 ml each). The fractions from 954 ml to 1425 ml were combined, desalted by means of Biogel column (3.5×35 cm) and lyophilized. R_f(S, f) 0.28, (C, g) 0.20. $[\alpha]_D^{24}$ −60.5° (*c* 0.95, 5% acetic acid). (lit,[7] $[\alpha]_D^{22}$ −60.8°, 5% acetic acid). Amino acid ratios: Thr 1.01 (1), Pro 0.99 (1), Lys 1.02 (1), Arg 0.97 (1).

Found: C, 47.36; H, 8.00; N, 17.27%. Calcd for $C_{21}H_{40}O_6N_8 \cdot 2CH_3COOH \cdot H_2O$: C, 47.01; H, 7.89; N, 17.54%.

Preparation of ***2***. **6** (0.50 g) was hydrogenated on a mixture of ethanol (60 ml), water (60 ml) and 1 M acetic acid (6 ml) in the presence of Pd black. After removal of the catalyst, the solvent was evaporated *in vacuo*. The crude tetrapeptide obtained was applied to a CM-cellulose (Whatman CM-52) column (2.0×44 cm), which was eluted with a linear gradient of ammonium acetate (pH 7.0, 0—0.4 M, 400 ml each). The fractions from 470 ml to 520 ml were combined and concentrated. After being desalted with Biogel P-2 column (3.5×35 cm) and lyophilized, 0.22 g of the desired peptide was obtained. R_f (S, f) 0.04, (C, g) 0.27, (S, g) 0.12. $[\alpha]_D^{24}$ −56.6° (c 0.90, 5% acetic acid). Amino acid ratios: Thr 1.06 (1), Pro 0.96 (1), Arg 1.98 (2).

Found: C, 45.22; H, 7.83; N, 20.58%. Calcd for $C_{21}H_{40}O_6N_{10} \cdot 2CH_3COOH \cdot H_2O$: C, 45.04; H, 7.56; N, 21.01%.

Preparation of ***3***. **7** was treated in a way similar to that for the preparation of **2**, CM-cellulose (Serva) being used in the ion exchange chromatography. R_f (S, f) 0.57, (C, g) 0.21, (S, g) 0.10. $[\alpha]_D^{24}$ −66.7° (*c* 1.02, 5% acetic acid). Amino acid ratios: Thr 1.01 (1), Pro 0.95 (1), Lys 2.04 (2).

Found: C, 49.30; H, 8.66; N, 13.55%. Calcd for $C_{21}H_{40}O_6N_6 \cdot 2CH_3COOH \cdot H_2O$: C, 49.17; H, 8.25; N, 13.76%.

Preparation of ***4***. **8** was hydrogenated in a mixture of ethanol, water and acetic acid. The product was purified as in the preparation of **1**. R_f (S, f) 0.27, (C, g) 0.19. $[\alpha]_D^{24}$ −62.6° (*c* 0.92, 5% acetic acid). Amino acid ratios: Thr 0.99 (1), Pro 1.00 (1), Lys 1.00 (1), Arg 1.00 (1).

Found: C, 47.02; H, 8.19; N, 17.25%. Calcd for $C_{21}H_{40}O_6N_8 \cdot 2CH_3COOH \cdot H_2O$: C, 47.01; H, 7.89; N, 17.54%.

Preparation of ***5***. **9** was treated as described in the preparation of **4**. R_f (S, f) 0.26, (C, g) 0.25, (S, g) 0.04. $[\alpha]_D^{24}$ −58.0° (*c* 0.87, 5% acetic acid). Amino acid ratios: Thr 0.99 (1), Pro 1.00 (1), Lys 1.02 (1), Arg 0.98 (1).

Found: C, 47.14; H, 7.79; N, 17.56%. Calcd for $C_{21}H_{40}O_6N_8 \cdot 2CH_3COOH \cdot H_2O$: C, 47.01; H, 7.89; N, 17.54%.

The authors are indebted to the members of Research Laboratories of Toyo Jozo Co., Ltd. for the elemental analyses. They also thank Miss Keiko Kobayashi for the biological measurement, Mr. Yoshiaki Motoki for the amino acid analyses and to Mr. Yuji Watanabe for his assistance.

References

1) V. A. Najjar and K. Nishioka, *Nature*, **228**, 627 (1970).
2) K. Nishioka, A. Constantopoulos, P. S. Satoh, and V. A. Najjar, *Biochem. Biophys. Res. Commun.*, **47**, 172 (1972).
3) K. Nishioka, P. S. Satoh, A. Constantopoulos, and V. A. Najjar, *Biochim. Biophys. Acta*, **310**, 230 (1973).
4) W. König and R. Geiger, "Peptides," ed by E. Scoffone, North-Holland Pub. Co., Amsterdam (1969), p. 17.
5) V. A. Najjar and A. Constantopoulos, *J. Reticuloendothel. Soc.*, **12**, 197 (1972).
6) All melting points are uncorrected. Amino acids used are of the L-configuration. The abbreviations for amino acids and peptides are in accordance with the rules of the IUPAC-IBU Commission on Biochemical Nomenclature. Other abbreviations are as follows. Boc=*t*-butoxycarbonyl, Cbz=benzyloxycarbonyl, OBzl=benzyl ester, TFA=trifluoroacetic acid, MA=mixed anhydride method, DCC / HOBt = dicyclohexylcarbodiimide / *N*-hydroxy-1*H*-benzotriazole method.
7) H. Yajima, H. Ogawa, H. Watanabe, N. Fujii, M. Kurobe, and S. Miyamoto, *Chem. Pharm. Bull.*, **23**, 371 (1975).

Carbon-Nitrogen Bond Fission in Ureas and Thioureas. Preparation of Alkyl and Aryl Isothiocyanates Using Carbon Disulfide and Butyllithinm or a Grignard Reagent

Shizuyoshi SAKAI, Tatsuo FUJINAMI, and Toshiyuki AIZAWA

Department of Industrial Chemistry, Faculty of Engineering, Shizuoka University, Hamamatsu 432

(Received July 1, 1976)

The carbon-nitrogen bond in *N,N'*-diaryl- and dialkyl-thioureas or -ureas was easily cleaved by the metallation of thioureas or ureas using butyllithium, followed by the addition of an excess of carbon disulfide or 1,3-dithiolan-2-thione in tetrahydrofuran under reflux, to afford about two mol of the corresponding isothiocyanates per mol of the thioureas or ureas used. Instead of butyllithium, ethylmagnesium bromide was also effective in such a type of carbon-nitrogen bond fission of the (thio)ureas in refluxing tetrahydrofuran, and in this case the addition of carbon disulfide was not required. To explain these results, a six-centered decomposition of the dilithium salt of *N*-dithiocarboxy(thio)urea in the reaction using butyllithium was tentatively proposed, while a four-centered mechanism seems applicable to the reaction using ethylmagnesium bromide.

The carbon-nitrogen bond in ureas or thioureas is difficult to cleave. In many instances, extreme conditions such as thermal decomposition with or without very concentrated acid have been applied. In such cases, the yield of isothiocyanate (**2**) is, in principle, less than one mol from one mol of **1**, and the reported yield of **2** is rather low (based on Eq. 1).[1]

$$\underset{\mathbf{1}}{\mathrm{RNHCSNHR}} \xrightarrow{\Delta} \underset{\mathbf{2}}{\mathrm{RNCS}} + \underset{\mathbf{3}}{\mathrm{RNH_2}} \qquad (1)$$

We have previously established a novel method for the preparation of aryl and alkyl isothiocyanates under moderate reaction conditions using amine, carbon disulfide, and butyllithium or a Grignard reagent.[2,3] The scheme for the reaction was proposed (Eq. 2; X=S)[2]:

$$\underset{\mathbf{3}}{\mathrm{RNH_2}} \xrightarrow[2)\ \mathrm{CSX}]{1)\ \mathrm{BuLi}} \underset{\mathbf{4}}{\mathrm{RNHC(S)XLi}} \xrightarrow{\mathrm{BuLi}} \underset{\mathbf{5}}{\mathrm{RN(Li)C(S)XLi}} \xrightarrow{\mathrm{CS_2}} \mathrm{RNCS} + \mathrm{Li_2CS_2X} \qquad (2)$$

An anologous type of reaction for *N,N'*-substituted thiourea (X=NR in **5**) appear to be an interesting process for carbon-nitrogen bond fission, affording two mol of isothiocyanate from 1 mol of thiourea. In this report, we will describe a new method for the preparation of isothiocyanates by breaking the carbon-nitrogen bond in *N,N'*-disubstituted thioureas or ureas using butyllithium or a Grignard reagent, and carbon disulfide or 1,3-dithiolan-2-thione in anhydrous tetrahydrofuran (THF). Moreover, the reaction using butylithium will be compared with that using ethylmagnesium bromide from several mechanistic points of view.

Results and Discussion

Preparation of Isothiocyanates Using Butyllithium. *N,N'*-Dilithio-*N,N'*-diphenylthiourea (**7**; R=Ph), directly prepared from one mol of thiourea and two mol of butyllithium, was reacted with an excess of carbon disulfide for 3 h under a refluxing temperature of THF to give 1.45 mol of phenyl isothiocyanate (72% yield, based on Eq. 3; Direct Method). The yield of isothiocyanates obtained from various thioureas are summarized in Table 1.

$$\underset{\mathbf{7}}{\mathrm{RN(Li)C(S)N(Li)R}} + \underset{\mathbf{8}}{2\mathrm{CS_2}} \longrightarrow \underset{\mathbf{2}}{2\mathrm{RNCS}} + \underset{\mathbf{9}}{\mathrm{Li_2CS_3}} \qquad (3)$$

The results in Table 1 indicate that aromatic isothiocyanates were easily obtained by the distillation of the reaction mixture of the aryl-substituted ureas (**7**; R=arom.) with **8**. On the contrary, the yields of aliphatic isothiocyanates were low in the corresponding reactions of alkyl-substituted thioureas (**7**; R=aliph.) with **8**, and some amounts of the corresponding carbodiimides were found to be formed under the reaction conditions used.

Furthermore, the yields of isothiocyanates were increased when butyllithium and **8** were added step-by-step to the solution of the thiourea (Step-by-step Method): the *mono*-lithiothiourea formed by the reaction of **1** with one mol of butyllithium reacted with one mol of **8** with a slight exotherm, and the reaction mixture was treated with the second mole of butyllithium, followed by a reaction with **8** under reflux (see Note c in Table 1). The better results were obtained probably because of the higher degree of metallation of **1** needed to form **10a** or **10b**. The

Table 1. Yields of isothiocyanates (RNCS) from the reaction of thioureas ($(RNH)_2CS$), butyllithium, and carbon dislfide[a]

Thiourea R in thiourea	Yield of RNCS %	Bp °C/Torr	$\nu_{N=C=S}$ cm^{-1}
C_6H_5	73 (93)[c]	95—100/ 5	2070
o-$CH_3C_6H_4$	82	104—105/10	2070
p-$CH_3C_6H_4$	73	105—108/10	2070
2,6-$(CH_3)_2C_6H_3$	91	114—116/10	2080
α-Naphthyl	82[c]	108—112/0.1	2090
C_2H_5	40	72— 74/100	2090
$(CH_3)_3C$	43[d]	73— 76/50	2090
Cyclohexyl	41[d]	73— 74/20	2090

a) The *N,N'*-dilithiothiourea, prepared *in situ* using two mol of butyllithium, was reacted with mol of carbon disulfide for 3 h in refluxing THF (Direct Method). b) Based on Eq. 3. c) The yield obtained by the Step-by-step Method (see Experimental). d) Accompanied by the formation of carbodiimide.

results from other thioureas by the Step-by-step Method are shown in Table 1.

To discuss the reaction course, the reaction of *N,N'*-di(*o*-tolyl)thiourea was precisely examined. The thiourea was treated with an equivalent of butyllithium to evolve one mol of butane, suggesting the formation of *N*-lithio-*N,N'*-di(*o*-tolyl)thiourea. The reaction mixture was allowed to react with one mol of carbon disulfide at room temperature with a slight exotherm, followed by a reaction with the second mole of butyllithium to evolve about one mol of butane. The total amount of butane evolved during the metallation reactions was almost twice the amount of **1** used. The reaction mixture was then stirred below room temperature to afford a heterogeneous solution containing the carbodiimide **11** (R=*o*-tolyl) and dilithium trithiocarbonate **9**.[4] The formation of carbodiimide was also observed in the initial stage of the reaction by the Direct Method below room temperature. The carbodiimide (**11**; R=*o*-tolyl) was separated from dilithium trithiocarbonate[4] by filtration. However, without filtration, a heterogeneous reaction mixture containing **11** and **9** was heated under reflux for 3 h to give a homogeneous solution. It showed the characteristic $\nu_{N=C=S}$ band of the isothiocyanate (**2**; R=*o*-tolyl) at 2070 cm^{-1}. The reaction mixture was subsequently distilled to afford **2** (R=*o*-tolyl) and a residue, which reacted with 1,2-dibromoethane in THF to form 2-(*o*-tolylimino)-1,3-dithiolane. The detection of the latter suggests the reaction of **12a** with 1,2-dibromoethane. Compound **12a** (or **12b**) has been reported to react rapidly with **8** below room temperature to afford **2** and **9**.[4]

Judging from these results, it seems that the reaction by the Step-by-step or Direct Method probably proceed *via* **10a** to form **11** and **9** in the initial stage of the reaction below room temperature. However, in the final stage of the reaction at room temperature or under reflux in THF, **11** and **9** will be converted to **2** and **12a** (or **12b**), probably *via* **10a** or **10b**. The unstable intermediates, **10a** and **10b**, could not be characterized, but their identification is supported by the fact that **11** (R=*o*-tolyl) reacted with **9** for 4 h under reflux to give **2** in an almost quantitative yield. In the next step, **12a** (or **12b**) reacted with **8** to afford **2** and **9**. The reaction course are tentatively shown by Eqs. 4, 5, and 6.

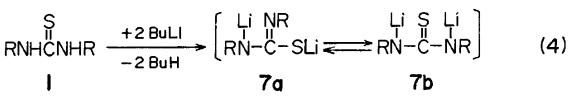

(4)

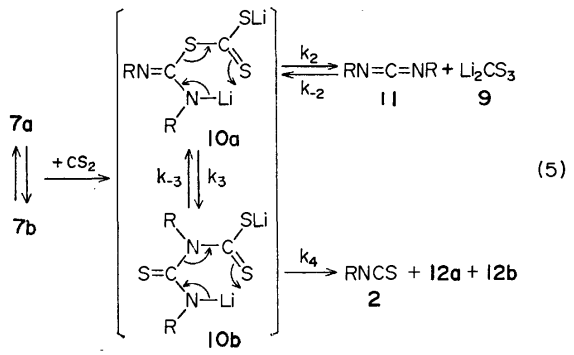

(5)

(6)

The fact that the characteristic $\nu_{N=C=N}$ band appeared in the initial stage of all the reactions using both the Direct and Step-by-step Methods below room temperature suggests that the rate constant, k_2, in Eq. 5 is much larger than k_4 or k_{-2}. From **7a** (or **7b**) with bulky groups, such as *o*-tolyl, 2,6-xylyl, or cyclohexyl, the corresponding carbodiimide, **11**, was isolated, probably because of a steric effect (smaller k_{-2}), while only **2** was isolated in the reaction of **7a** (or **7b**) with less bulky groups, such as phenyl or *p*-tolyl, probably because of the larger k_{-2} value.

In the reaction of Eq. 3, 1,3-dithiolan-2-thione was also used instead of carbon disulfide. It reacted with an equivalent amount of **7** (R=Ph) for 5 h in THF under reflux to afford phenyl isothiocyanate in a 67% yield (Eq. 7).

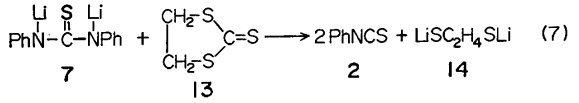

(7)

Preparation of Isothiocyanate Using Ethylmagnesium Bromide. The thermal decomposition of the dilithiothiourea **7**, (R=Ph), did not afford **2** but small amount of diphenylcarbodiimide and a resinous product were found to be formed. On the other hand, *N,N'*-bis(bromomagnesio)-*N,N'*-diphenylthiourea **15** (R=Ph) was thermally decomposed at about 140 °C to afford the isothiocyanate (**2**; R=Ph; 35% yield) and the *N,N'*-bis(bromomagnesio)amine **16**, which reacted exothermically with carbon disulfide to give an additional yield of **2** (38%). Table 2 shows the results of the reaction of **15** with an excess amount of carbon disulfide. The yields were moderate, but the purity of the isothiocyanates obtained was better than when butyllithium was used.

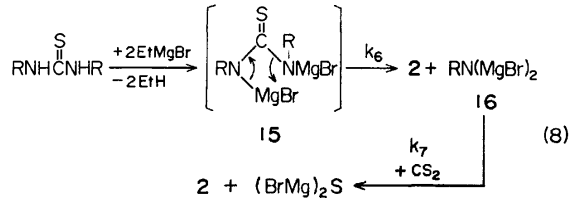

(8)

Table 2. Yields of isothiocyanates from the reaction of thioureas, ($(RNH)_2CS$), ethylmagnesium bromide, and carbon disulfide

Thiourea	Reaction condition		Yield of RNCS
R in thiourea	Temp/°C	Time/h	%[b]
C_6H_5	a	40	65
p-$CH_3C_6H_4$	a	8	51
C_2H_5	a	34	48

a) The *N,N'*-bis(bromomagnesio)thiourea, prepared *in situ* using two mol of EtMgBr, was reacted with an excess of carbon disulfide in refluxing THF. b) Based on Eq. 8.

As has already been mentioned, dilithio-thiourea was easily decomposed by the addition of carbon disulfide, while the thermal decomposition of bis-(bromomagnesio)-compound (k_6 in Eq. 8) was not accelerated by the addition of carbon disulfide. However, the carbon disulfide used in the following step (k_7) is effective in improving the yield of **2**. These results suggest that **15** is thermally decomposed *via* a four-centered mechanism to give **2** and **16**, which is then converted to **2** by the action of the added carbon disulfide, as was shown in Eq. 8.

Carbon-Nitrogen Bond Fission of Urea. Carbon-nitrogen bonds are generally stable. However, we found that these bonds are easily cleaved by the reaction of carbon disulfide and butyllithium or a Grignard reagent in anhydrous THF. For example, *N,N'*-diphenylurea was allowed to react with two mol of butyllithium to form the *N,N'*-dilithio-derivative, **18** (R=Ph), and butane. Compound **18** was treated with an excess of carbon disulfide for 30 min in THF at room temperature. The reaction mixture showed the characteristic band of isothiocyanate at 2090 cm^{-1}. After the reaction mixture had been refluxed for 3 h, phenyl isothiocyanate, **2**, was obtained in an 80% yield (based on Eq. 9).

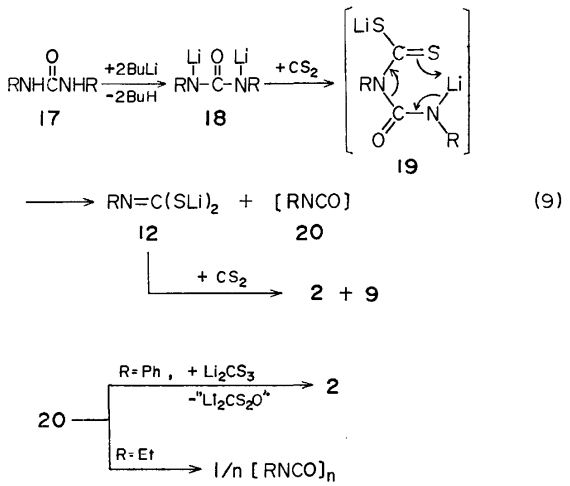

In the reaction of aryl ureas, the corresponding isothiocyanates were formed in good yields, because aryl isocyanates reacted with dilithium trithiocarbonate to form isothiocyanates. Thus, two mol of **2** (R=Ph) was obtained from one mol of *N,N'*-diphenylurea. On the other hand, the yield of ethyl isothiocyanate was low in the reaction of an alkyl-substituted urea, $(EtNH)_2CO$, probably because of the base-catalyzed oligomerization of the ethyl isocyanate formed as an intermediate. At present, the mechanism of carbon-nitrogen bond fission in urea may tentatively depicted analogously to the case of thiourea.

A Grignard reagent, EtMgBr, was sometimes used in the carbon-nitrogen bond fission in alkyl- and aryl-substituted ureas instead of the butyllithium shown in Eq. 9, but the yields of isothiocyanates were low.

Experimental

All the melting and boiling points are uncorrected. The IR and NMR spectra were recorded with a JASCO IRA-1 spectrometer, and a Hitachi Perkin-Elmer R-24 spectrometer, respectively. The *N,N'*-disubstitued thioureas (**1**; $(RNH)_2CS$) used were prepared mainly from amines and carbon disulfide by the reported methods[5-7]; mp (R): 154—155 (Ph), 160—163 (*o*-tolyl), 189—190 (*p*-tolyl), 230—232 (2, 6-xylyl), 206—207 (α-naphtyl), 131—132 (*t*-butyl), and 187—188 °C (cyclohexyl). The 1, 3-dithiolan-2-thione (**13**),[8] butyllithium in petroleum ether, and ethylmagnesium bromide in THF were prepared by the usual methods. The ureas, thioureas, carbon disulfide, 1, 2-dibromoethane, and THF were dried before use. All the reactions were carried out under a dry nitrogen atmosphere.

Reaction of Carbon Disulfide with N,N'-*Dilithio*-N,N'-*diphenylthiourea (7; R=Ph) (Direct Method).* In a flask equipped with a mechanical stirrer, a condencer, a dropping funnel, and a nitrogen inlet, butyllithium (60 mmol) was slowly introduced into a solution of the thiourea (**1**; R=Ph; 6.3 g, 27 mmol) in THF (50 cm^3) under cooling with a water bath to form, directly, **7** (R=Ph). Carbon disulfide (4.5 g; 60 mmol) was then added to the solution and the mixture was refluxed for 3 h. After the evaporation of the solvent, the residue was distilled in a vacuum to afford phenyl isothiocyanate (**2**: R=Ph) in a 72% yield (5.3 g, 39 mmol); bp 95—100 °C/15 Torr. The IR and NMR spectra coincided well with those of an authentic sample.[3] The results for other thioureas are summarized in Table 1.

Step-by-step Reaction of N,N'-*Di*-o-*tolylthiourea (1; R=o-*$CH_3C_6H_4$*) with Butyllithium and Carbon Disulfide (Step-by-step Method).* *N,N'*-Di-*o*-tolylthiourea (**1**; R=*o*-$CH_3C_6H_4$; 6.3 g, 27 mmol in 50 cm^3 of THF) was allowed to react with butyllithium (30 mmol), accompanied by the evolution of butane (28 mmol). To the solution of the *mono*-lithio thiourea thus prepared, carbon disulfide (2.2 g, 30 mmol in 3 cm^3 of THF) was added slowly under cooling with an ice bath. The homogeneous reaction mixture was subsequently treated again with an additional amount of butyllithium (30 mmol) at room temperature, thus evolving more butane (25 mmol). The total amount of butane formed in the metallation reaction was twice the amount of thiourea used. However, the structure of the unstabe intermediate (or trandition state), **10a** or **10b**, could not be established even by spectroscopic methods such as IR and NMR. After the addition of butyllithium for 10 min, the reaction mixture became a heterogeneous solution to form **11** (R=*o*-$CH_3C_6H_4$) and **9**,[4] the former being detected by the $\nu_{N=C=N}$ band at 2145 cm^{-1} in the IR spectrum of the mixture. In the following step, carbon disulfide (2.2 g, 30 mmol) was added to the heterogeneous solution and the mixture was stirred for 30 min at room temperature to give a semi-transparent solution, which showed the $\nu_{N=C=S}$ band of **2** (R=*o*-$CH_3C_6H_4$) at 2070 cm^{-1} and the $\nu_{N=C=N}$ band of **11** at 2145 cm^{-1}. The mixture was heated for further 3 h to convert the **11** to **2**. After the evaporation out of the solvent of THF and petroleum ether the residue was distilled under a vacuum to afford *o*-tolyl isothiocyanate in a 92% yield (6.8 g, 50 mmol).

*Reaction of 8 with 12 (R=*o-$CH_3C_6H_4$*) Prepared* in situ. A heterogeneous solution containing **11** and **9** was prepared from *N,N'*-di-*o*-tolylthiourea (**1**; R=*o*-$CH_3C_6H_4$; 6.3 g; 27 mmol), butyllithium (30+30 mmol), and carbon disulfide (30 mmol) by the Step-by-step Method described above; when it was then heated for 3 h, the mixture became almost homogeneous. After evaporation of the solvent, the mixture was distilled to afford **2** (3.7 g, 25 mmol) and a residue containing **12** (R=*o*-$CH_3C_6H_4$). After the residue had been treated with an excess of carbon disulfide with an exotherm, the distillation of the reaction mixture gave **2** (3.4 g, 23 mmol) and **9**. The latter was detected by the IR method ($\nu_{CS_3}{}^{-2}$

935 cm^{-1}).

Detection of **12** *(R=o-$CH_3C_6H_4$).* The distillation residue containing **12**, prepared by the method described above, was treated with an excess of 1,2-dibromoethane to form 2-(*o*-tolylimino)-1,3-dithiolane, which was identified by a comparison of its IR and NMR spectra with those of an authentic sample.[9]

Reaction of Carbodiimide (R=o-$CH_3C_6H_4$) with **9**. Compound **11** (R=*o*-$CH_3C_6H_4$; 3.4 g) was allowed to react with powders of anhydrous dilithium trithiocarbonate (**9**; 30 mmol, 3.7 g) for 3 h under reflux of THF containing carbon disulfide (20 cm^3); the reaction mixture was then distilled to give **2** (R=*o*-$CH_3C_6H_4$) in an almost quantitative yield (6.1 g, 90%).

Reaction of Carbon Disulfide with N,N'-*Dilithio*-N,N'-*di-t-butyl)thiourea (7; R=$(CH_3)_3C$).* Compound **7** (R=$(CH_3)_3C$); 25 mmol), prepared *in situ* by the Direct Method, was allowed to react with carbon disulfide (4.0 g, 55 mmol) in THF under reflux, after which the mixture was distilled to afford *t*-butyl isothiocyanate (2.5 g, 43%) and di-*t*-butylcarbodiimide (1.0 g, 25%); bp 70—72 °C/10 Torr; IR (neat) 2094 cm^{-1} ($\nu_{N=C=N}$); NMR (CCl_4) δ=1.20 ppm (s, 18, CH_3).

Reaction of Dithiolan-2-thione with N,N'-*Dilithio*-N,N'-*Diphenylthiourea (7; R=Ph).* Compound **7** (R=Ph; 45 mmol) was allowed to react with 1,3-dithiolan-2-thione (**13**; 6.1 g, 45 mmol) for 5 h in THF under reflux, after which the mixture was distilled to afford **2** (R=Ph) in a 67% yield 8.0 g, 60 mmol).

After the treatment of the distillation residue with dilute hydrochloric acid, 1, 2-ethandithiol was detected in the residue by gas-chromatographic analysis.

Thermal Decomposition of N,N'-*Bis(bromomagnesio)*-N,N'-*diphenylthiourea (15; R=Ph).* Compound **15** (R=Ph), prepared from *N,N'*-diphenylthiourea (5.8 g, 25 mmol) and ethylmagnesium bromide (55 mmol) in THF, was pyrolyzed in a flask at about 140 °C; the mixture was then distilled to afford phenyl isothiocyanate in a 35% yield (1.2 g); bp 95—97 °C/10 Torr. The distillation residue was allowed to react exothermically with excess carbon disulfide (6 cm^3) in 20 cm^3 of THF, and then heated for 2 h at 140 °C; The mixture was subsequently distilled to afford phenyl isothiocyanate in a 38% yield (1.3 g); bp 95—99 °C/10 Torr.

Hydrogen sulfide gas was vigorously evolved when the residue of the second distillation was treated with dilute acid.

Reaction of N,N'-*Bis(bromomagnesio)*-N,N'-*di*-p-*tolylthiourea (15; R=p-$CH_3C_6H_4$) in the Presence of Carbon Disulfide.* *(A)* Compound **15** (R=Ph), prepared *in situ* from *N,N'*-di-*p*-tolylthiourea (6.4 g, 25 mmol) and ethylmagnesium bromide (55 mmol), was treated with an excess of carbon disulfide (3.8 g, 50 mmol) in THF for 1 h under reflux; the reaction mixture was then distilled to afford *p*-tolyl isothiocyanate in a 33% yield (2.5 g). The residue was treated again with carbon disulfide (6 cm^3) for 2 h under reflux, and then distilled to afford *p*-tolyl isothiocyanate in a 16% yield (1.2 g). *(B)* Compound **15** (20 mmol), prepared as has been described above, was treated with an excess of carbon disulfide (10 cm^3) in THF under reflux. After the evaporation of the solvent and an excess of carbon disulfide, the residue was distilled in a vacuum to afford the corresponding isothiocyanate. The results are summarized in Table 2.

Reaction of Carbon Disulfide with the N,N'-*Dilithiourea (18).* *(A) Using Butyllithium*: Compound **18** (R=Ph) was prepared *in situ* from *N,N'*-diphenylurea (**17**, R=Ph; 6.4 g, 30 mmol) and butyllithium (66 mmol) in 50 cm^3 of THF under cooling by ice-water, and subsequently reacted with carbon disulfide (6 cm^3) for 30 min at room temperature The reaction mixture showed the $\nu_{N=C=S}$ band at 2070 cm^{-1} in the IR spectrum. After refluxing for 3 h, phenyl isothiocyanate was isolated by distillation in an 80% yield (6.5 g); bp 94—96 °C/15 Torr.

In the same manner described above, ethyl isothiocyanate was obtained in a 44% yield (1.2 g, 13 mmol) from a reaction using *N,N'*-diethylurea (**17**, R=Et; 3.5 g, 30 mmol); 78—91 °C/90 Torr; IR (neat) 2090 cm^{-1} ($\nu_{N=C=S}$); NMR (CCl_4) δ=1.36 (t, 3, J=7.1 Hz, CH_3) and 3.60 ppm (q, 2, J=7.1 Hz, CH_2). The distillation residue showed the band at 1745 ($\nu_{C=O}$) and at 1690 cm^{-1} in the IR spectrum.

(B) Using Ethylmagensium Bromide: *N,N'*-Bis(bromomagnesio)-*N,N'*-diphenylurea prepared *in situ* from the urea (**17**, R=Ph; 6.4 g, 30 mmol) and ethylmagnesium bromide (66 mmol) was allowed to react with an excess of carbon disulfide (12 cm^3) for 1 h at 45 °C; the mixture was then distilled to give phenyl isothiocyanate in a 44% yield (3.5 g).

Reaction of Phenyl Isocyanate with Dilithium Trithiocarbonate. Phenyl isocyanate (2.4 g, 20 mmol) reacted with dilithium trithiocarbonate powders (2.7 g, 22 mmol) in THF (50 cm^3) with stirring for 4 h under reflux; it was subsequently distilled to afford phenyl isothiocyanate in a 65% yield (1.8 g).

The present work was partially suported by a Grant-in-Aid for Sci. Res. from the Ministry of Education (No. 055126).

References

1) J. Cymerman-Craig, *Org. Synth.*, Coll. Vol. IV, 700 (1963).
2) S. Sakai, T. Aizawa, and T. Fujinami, *J. Org. Chem.*, **39**, 1970 (1974).
3) S. Sakai, T. Fujinami, and T. Aizawa, *Bull. Chem. Soc. Jpn.*, **48**, 2982 (1975).
4) S. Sakai, T. Fujinami, N. Otani, and T. Aizawa, *Chem. Lett.*, **1976**, 811.
5) H. S. Fry, *J. Am. Chem. Soc.*, **35**, 1539 (1913).
6) G. M. Dyson, H. J. George, and R. F. Hunter, *J. Chem. Soc.*, **1927**, 436.
7) D. Martin, *Chem. Ber.*, **98**, 2425 (1965).
8) D. J. Martin and C. C. Greco, *J. Org. Chem.*, **33**, 1275 (1968).
9) Y. Ueno, T. Nakai, and M. Okawara, *Bull. Chem. Soc. Jpn.*, **43**, 162 (1970).

12,13-Epoxy-*C*-nor-*D*-homosteroids. III.[1] The Synthesis and Stereochemistry of 17-Oxygenated 12,13-Epoxyetiojervanes[2]

Akio MURAI, Noriaki IWASA, Masami TAKEDA, Hiroshi SASAMORI, and Tadashi MASAMUNE

Department of Chemistry, Faculty of Science, Hokkaido University, Sapporo 060

(Received July 10, 1976)

The synthesis of several 17-oxygenated 12,13-epoxyetiojervanes is described. Jervine (**1**) was degraded by a known procedure into trienone (**10**), which on hydride reduction afforded 11α- and 11β- alcohols (**11** and **12**). The respective alcohols were submitted to the Lemieux-Johnson oxidation to give Δ^{12}-17-oxo-11-alcohols (**13** and **14**), which were reduced under the Birch conditions to yield Δ^{12}-17-ketone (**15**). Epoxidation of these alcohols and ketone produced the aimed epoxides (**18**—**24**). The structure and configuration of these epoxides and the synthetic intermediates were determined on the basis of the chemical and spectral evidence.

In the previous papers[3] we reported the synthesis and reaction of 11-oxygenated 17α-acetyl-12,13-epoxyetiojervanes. As a continuing study aimed at the preparation of biologically active normal steroids from jervine and other available alkaloids, we have been working on the synthesis and reaction of other types of 12,13-epoxyetiojervanes. In this Part we describe the synthesis and stereochemistry of 17-oxygenated 12,13-epoxyetiojervanes.

As the first step for the synthesis, it was undertaken to prepare 17-oxo-Δ^{12}-etiojervanes, important intermediates for the objective epoxy compounds. Jervine (**1**) was degraded by a known procedure, *via* trienone[4] (**2a**), into Δ^{12}-11,17-diketone[5] (**3**), which on treatment with zinc and acetic acid afforded 11,17-diketone[5] (**4**), a known compound with established configurations,[6] in a 67% yield together with a small amount (3%) of 11α-hydroxy-Δ^{12}-17-ketone (**5**), mp 249—250.5 °C. The α-hydroxy configuration at C_{11} of the latter (**5**) was deduced from facile conversion (82%) into its 3,11-diacetate (**5a**), mp 168—170 °C, under mild conditions. The major product (**4**) was then transformed, *via* the corresponding 17-ethylene acetal, amorphous, into a known compound, 3β-hydroxy-11,17-diketone 17-acetal[7] (**6**), in an 81% yield, which on reduction with sodium in isopropyl alcohol gave 3β,11α-diol (**7**), mp 157—159 °C, in a 69% yield.

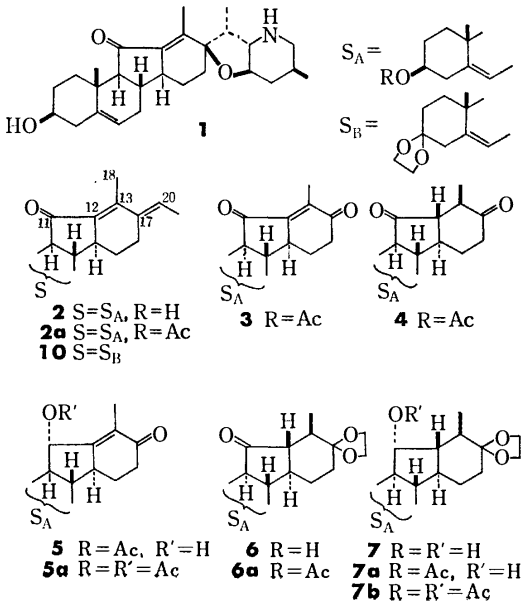

The assigned α-configuration to the 11-hydroxyl group of **7** was based on the chemical shift (δ 0.98) of the 19-methyl protons (δ_{calcd} 0.99 for 11α-OH and 1.26 for 11β-OH).[8] Acetylation of 3β,11α-diol (**7**) under controlled conditions (0 °C, 1.5 h) effected monoacetylation to give, after chromatography, 3-monoacetate (**7a**), mp 235—236 °C, in a 57% yield with 3,11-diacetate (**7b**), mp 172—173 °C (12%), and the starting diol (**7**) (8%). The 3-monoacetate (**7a**) was smoothly deacetalized with *p*-toluenesulfonic acid in aqueous acetone to yield 17-ketone (**8**), mp 216.5—217.5 °C, and was also oxidized with chromic acid to 11-ketone (**6a**), mp 188—190 °C, in good yields, respectively. The latter (**6a**) proved to be identical with a known compound with established configurations,[6,7] indicating that each of compounds **6**—**8** possesses a β-oriented hydrogen atom at C_{12}.

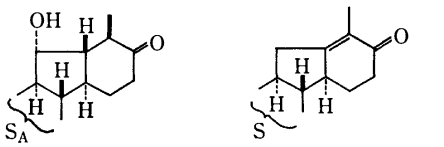

8 R=Ac

9 S=S_A, R=H
9a S=S_A, R=Ac
15 S=S_B

Compound **8**, 17-oxo-11α-alcohol, when treated with phosphoryl chloride and pyridine, underwent dehydration with concomitant double bond migration to give Δ^{12}-17-ketone (**9a**), mp 172—173 °C, in a low yield (38%), which was readily hydrolyzed with base (KOH) to the corresponding 3β-alcohol (**9**), mp 174—175 °C, quantitatively. In accordance with the formula, compound **9a** exhibited absorption maxima at 246 nm (ε 12000) and at 1665 cm^{-1} in the UV and IR spectra and displayed two three-proton singlets due to the 19- and 18-methyl protons at δ 1.04 and 1.73 in the NMR spectrum. This Δ^{12}-17-ketone (**9a**) was also obtained by treatment of 11α-acetoxy-Δ^{12}-17-ketone (**5a**) with zinc and acetic acid in a 73% yield. Likewise, 11α-hydroxy-17-ketone 17-acetal (**7a**), when treated with phosphoryl chloride under the same conditions as 17-ketone (**8**) and then with hydrochloric acid in aqueous dioxane, was converted into Δ^{12}-17-ketone (**9**) in a 74% yield. Compound **9** is one of the most important intermediates for preparation of the aimed 12,13-epoxides. However, the afore-mentioned process involved 11 steps and the over-all yield from jervine

amounted to only 4%. In order to improve the yield of compound **9** or its analogues, we searched an alternate route.

3β-Hydroxy-trienone[4] (**2**) was transformed *via* a known process into 3-oxo-trienone 3-acetal[9] (**10**), which was treated with aluminium hydride in tetrahydrofuran. The reduction proceeded without saturation of the double bonds[10] and, after chromatography, gave the corresponding 11α- and 11β-alcohols (**11** and **12**), mp 142—144 and 138—141 °C, in 59 and 21% yields, respectively. The configurations of C_{11} in these alcohols were assigned as shown in the formulas on the basis of chemical shifts of the protons at C_{19} and C_{11}; 19-CH_3, δ 1.10 for **11** and 1.30 for **12**;[3a,8] H at C_{11}, δ 4.66 (d J=7 Hz) for **11** and 4.90 (d J=7 Hz) for **12**.[3a] The result is interesting in the sense that the hydride reduction has led to predominant formation of 11α-alcohol (**11**), and we have such a precedent.[3a] The 11α-alcohol (**11**) was readily converted into its 11-acetate (**11a**), mp 171—174 °C, quantitatively, which on oxidation with sodium periodate in 75% aqueous dioxane (the Lemieux-Johnson oxidation)[11] afforded 11α-acetoxy-Δ^{12}-17-ketone (**13a**), mp 189—191 °C, in a 71% yield. This 17-ketone (**13a**) was also obtained by the Lemieux-Johnson oxidation of 11α-alcohol (**11**) into 11α-hydroxy-Δ^{12}-17-ketone (**13**), mp 186—188 °C, followed by acetylation in a 70% yield. Likewise, 11β-alcohol (**12**) was oxidized under the same conditions as **11** to give 11β-hydroxy-Δ^{12}-17-ketone (**14**), mp 169—170 °C in a 52% yield. These 11β-alcohols (**12** and **14**) were not converted into the respective 11-acetates under the same conditions as the corresponding 11α-alcohols (**11** and **13**). An attempted reduction to remove the oxygen functions at C_{11} of 11α-acetoxy- or 11β-hydroxy-Δ^{12}-17-ketone (**13a** or **14**) with zinc and acetic acid[12] produced a multi-component mixture containing 3-deacetalized compounds. However, the Birch reduction of these compounds (**13a** and **14**) effected the relevant reduction to give a desirable product, Δ^{12}-17-ketone (**15**), mp 163—165 °C, in 86 and 73% yields, respectively. The over-all yield of **15** amounted to 19%.

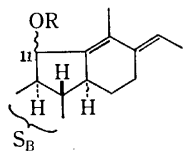

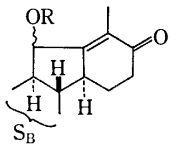

11 11β-H, R=H
11a 11β-H, R=Ac
12 11α-H, R=H

13 11β-H, R=H
13a 11β-H, R=Ac
14 11α-H, R=H

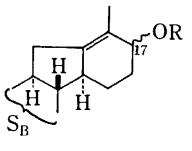

16 17β-H, R=H
16a 17β-H, R=Ac
17 17α-H, R=H
17a 17α-H, R=Ac

Reduction of Δ^{12}-17-ketone (**15**) with sodium borohydride produced Δ^{12}-17α-alcohol (**16**), mp 132—133 °C, in a 95% yield as a sole isolable compound. On the other hand, when aluminium hydride was used as the reduction reagent, its 17-epimer, Δ^{12}-17β-alcohol (**17**), mp 92—94 °C, was obtained in a 6% yield along with the 17α-epimer (**16**) (88%). The configurations of 17-hydroxyl groups were drawn from the optical rotations and spectral patterns of protons at C_{17}; $[\alpha]_D$ −25.7° for **16** and −77.3° for **17**;[13] H at C_{17}, δ 4.12 (br W_H=18 Hz) for **16** and 3.96 (br W_H=8 Hz) for **17**.[14] These Δ^{12}-17-alcohols (**16** and **17**) were readily transformed into the respective 17-acetates (**16a** and **17a**), mp 142—143 and 138—141 °C, quantitatively; H at C_{17}, δ 5.35 for **16a** and 5.21 for **17a**.[14] Prior to epoxidation of the 12,13-double bond, it was desirable to modify the Δ^5-3-ketone 3-acetal grouping into a Δ^4-3-carbonyl system, which leads to decrease of electrophilicity of the 5,6-double bond. However, all attempts to hydrolyze the 3-acetal group under various conditions (with *p*-toluenesulfonic acid in aqueous acetone under reflux or at room temperature, with anhydrous magnesium sulfate in wet benzene,[15] with trityl tetrafluoroborate in dry dichloromethane,[16] and so on) failed, giving complex mixtures. This suggested that the relevant epoxidation must be carried out under carefully controlled conditions.

Epoxidation of Δ^{12}-17α-alcohol (**16**) with perbenzoic acid in benzene afforded 12α,13α-epoxy-17α-alcohol (**18**), mp 158—161 °C, as a main product (75%) with small amounts (3 and 6%) of 12β,13β-epoxy- and 5β,6β,12α,13α-diepoxy-17α-alcohols (**19** and **20**), mp 136—138 and 123—125 °C. The major product (**18**) was also obtained by oxidation of **16** with *t*-butyl hydroperoxide in the presence of bis(acetylacetonato)-oxovanadium(IV) in a 57% yield as a sole compound, which could be isolated from complex mixtures. The 12α,13α- and 12β,13β-epoxy configurations were assigned to compounds **18** and **19** on the premise that (i) peracid epoxidation of olefins takes place by an electrophilic attack mainly from a less-hindered (α) side,[17] and (ii) epoxidation of allyl alcohols in the presence of the transition metal leads to preferential formation of epoxides with the group at the same side as the hydroxyl group.[18] On the other hand, the epoxy-configurations of diepoxide (**20**) were deduced as shown by the formula from the chemical shift of 19-methyl protons; δ_{obsd} 0.99, δ_{calcd} 0.81 for 5α,6α,12α,13α-diepoxide and 1.02 for 5β,6β,12α,13α-diepoxide.[3a,8,19] Compound **18** was then converted into 17-acetate (**18a**), mp 212—213 °C, and oxidized with chromium(VI) oxide in pyridine to 12α,13α-epoxy-17-ketone (**21**), mp 139—140 °C, in good yields.[20] The latter (**21**) was also produced by direct oxidation of Δ^{12}-17-ketone (**15**) with hydrogen peroxide in alkaline aqueous methanol in an 86% yield. Reduction of the 17-ketone (**21**) produced two 17-epimeric alcohols, the original 17α-alcohol (**18**) and 12α,13α-epoxy-17β-alcohol (**22**), mp 144—146 °C, which were isolated in 65 and 25% yields from the mixture. The latter (**22**) readily formed 17-acetate (**22a**), mp 144—147 °C, quantitatively. The NMR spectra of these 17-epimeric alcohols were in good accord with the assigned configurations: H

at C_{17}, δ 3.76 (br W_H=28 Hz) for **18** and 4.06 (br W_H=7 Hz) for **22**; δ 5.04 (do d J=10 and 5 Hz) for **18a** and 5.16 (br W_H=6 Hz) for **22a**.

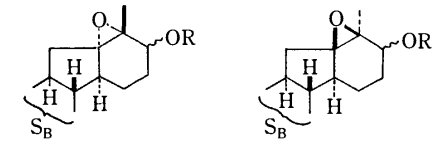

18 17β-H, R=H
18a 17β-H, R=Ac
22 17α-H, R=H
22a 17α-H, R=Ac

19 17β-H, R=H
19a 17β-H, R=Ac
23 17α-H, R=H
23a 17α-H, R=Ac

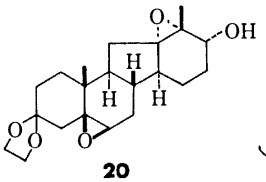

20

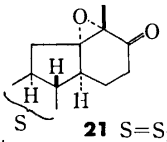

21 S=S_B
25 S=S_A, R=H

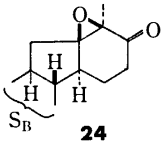

24

Epoxidation of Δ^{12}-17β-alcohol (**17**) with *t*-butyl hydroperoxide in the presence of bis(acetylacetonato)-oxovanadium(IV)[18] proceeded smoothly to give a new epoxide, 12β,13β-epoxy-17β-alcohol (**23**), mp 130—132 °C, in an 83% yield, which formed 17-acetate (**23a**), mp 132—135 °C, in a good yield. Oxidation of **23** with chromium(VI) oxide in pyridine afforded 12β,13β-epoxy-17-ketone (**24**), mp 184—186 °C, in an 80% yield, which was reconverted by treatment with sodium borohydride into the original 17β-alcohol (**23**) only in a 38% yield, the major product being 12β,13β-epoxy-17α-alcohol (50%). The latter was readily converted into 17-acetate (**19a**), mp 142—144 °C, and was naturally identical with the afore-mentioned epoxy-alcohol (**19**). A series of these reactions correlating all 17-hydroxy- and 17-oxo-12,13-epoxides (**18**—**24**) were consistent with the assigned epoxy configurations to the respective compounds. Confirmatory evidence was presented by comparison of the ORD curves of two epoxy-ketones (**21** and **24**), which exhibited negative and positive Cotton effects (a=−119° and +125°), respectively (Fig. 1).

Finally we examined collectively the chemical shifts of 19-methyl protons of etiojervanes described in this paper. We now add the contributions of new functional groups shown in Table 1 to *Table 2 in the Ref. 8.* These data, coupled with those in *Table 1 of the Ref. 3a*, would be valuable in confirming certain stereochemical points as well as promoting the structure determination of new derivatives. For example, 3β-hydroxy-Δ^{12}-17-ketone (**9**) was oxidized with hydrogen peroxide in an alkaline solution to give 12α,13α-epoxy-17-ketone (**25**), mp 173.5—175 °C, in a 57% yield. This epoxide (**25**) exhibited the ORD curve with a negative Cotton effect (a=−99°) and the NMR signal due to the 19-methyl protons at δ 1.02; δ_{calcd} 1.00 for 12α,13α-epoxide and 1.09 for 12β,13β-epoxide.

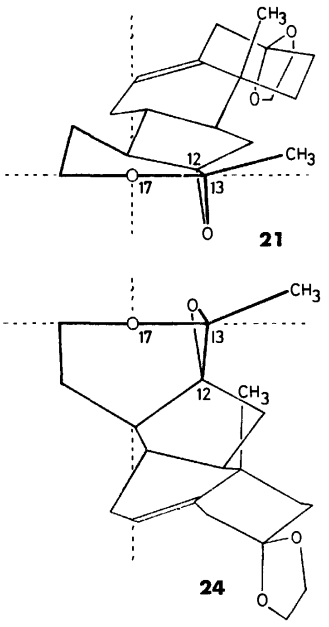

21

24

Fig. 1.

Table 1. The contribution ($\Delta\delta$) of functional groups to the chemical shift of the 19-methyl protons of etiojervanes

Groups	A-T[a]	B-T[a]
Reference shifts	0.74[a]	0.79[a]
Functional groups (No of examples)	$\Delta\delta$[b]	$\Delta\delta$[b]
11β-OH, Δ^{12}, $\Delta^{17(20)}$ (1)	0.32	—
11α-OH, Δ^{12}, $\Delta^{17(20)}$ (1)	0.12	—
11α-OAc, Δ^{12}, $\Delta^{17(20)}$ (1)	0.16	—
11β-OH, Δ^{12}, 17=O (1)	0.34	—
11α-OH, Δ^{12}, 17=O (2)	0.16	—
11α-OAc, Δ^{12}, 17=O (2)	0.20	—
12β,13β-O-[c] (5)	0.06	—
12α,13α-O-[c] (5)	—	−0.01[d]
12β,13β-O-, 17=O (1)	0.12	—
12α,13α-O-, 17=O (2)	—	−0.02[d]

a) *Cf.*, Table 2 in Ref. 8. b) "$\Delta\delta$" means deshielding effect. c) The abbreviations "12β,13β-O- and 12α, 13α-O-" denote "12β,13β-epoxy and 12α,13α-epoxy", respectively. d) The negative sign means "up-field shift".

Experimental

All the mps were uncorrected. The homogenity of each compd was always checked by TLC over silica gel (Wakogel B-5) with various solvent systems, and the spots were developed with cerium(IV) sulfate in dil sulfuric acid and/or iodine. The optical rotations, ORD curves, UV and IR spectra were measured in chloroform, dioxane, ethanol, and Nujol, respectively, unless otherwise stated. The NMR spectra were obtained in chloroform-*d* at 100 MHz, and the chemical shifts were given in δ-values, TMS being used as an internal reference. The abbreviations "s, d, t, q, br, do, and sh" in the NMR and IR spectra denote "singlet, doublet, triplet,

quartet, broad, double, and shoulder," respectively.

3β-Hydroxy-12β-etiojerv-5-ene-11,17-dione 3-Acetate (4), 3β,-11α-Dihydroxyetiojerva-5,12-dien-17-one 3-Acetate (5), and Its 3,11-Diacetate (5a). A soln of 3β-hydroxyetiojerva-5,-12-diene-11,17-dione 3-acetate[5] (**3**, 22 g) in glacial acetic acid (1730 ml) was heated with zinc powder (27.5 g) at 90 °C for 30 min under stirring, when the yellow soln had become colorless. The reaction mixture was worked up according to the known procedure[5] to give crystalline residue (32 g), showing two spots, which was separated by chromatography over alumina (Merck, standard, 340 g). Eluates with benzene–hexane (3 : 1), benzene, and benzene–ether (3 : 1) afforded **4** (14.8 g), mp 164—166 °C (diisopropyl ether) (lit,[4] 171—172 °C). Eluates with chloroform gave **5** (0.65 g), mp 246—248 °C (acetone), which was recrystallized from acetone for analysis; mp 249—250.5 °C and $[\alpha]_D$ −61°; MS, *m/e* 344 (M^+); UV, λ_{max} 249 nm (ε 15000); IR, ν_{max} 3495, 1722, 1648 (br), 1250, 1041, and 1031 cm^{-1}; NMR, δ 1.14, 1.90, and 2.07 (each 3H, s, 19- and 18-C$\underline{H}_3$, and OCOC$\underline{H}_3$), 4.67 (1H, br W_H=24 Hz, $\underline{H}$ at C_3), 4.73 (1H, d J=7 Hz, $\underline{H}$ at C_{11}), and 5.46 (1H, br W_H=10 Hz, $\underline{H}$ at C_6). Found: C, 73.24; H, 8.19%. Calcd for $C_{21}H_{28}O_4$:C, 73.22; H, 8.19%.

A soln of **5** (1.44 g) in acetic anhydride (Ac_2O, 7.2 ml) and pyridine (Py, 14.4 ml) was allowed to stand at room temp for 24 h. The reaction mixture was poured into ice-water and extracted with chloroform. The chloroform soln was washed with 2 M hydrochloric acid, 5% aq sodium hydrogencarbonate and water, dried over anhyd sodium sulfate, and evaporated to leave amorphous residue (2.02 g), which was crystallized from acetone to yield **5a** (1.33 g), mp 167—170 °C. This was recrystallized for analysis from acetone; mp 168—170 °C and $[\alpha]_D$ −93°; MS, *m/e* 326 (M^+−CH_3COOH), 284, 266, and 251; UV, λ_{max} 244 nm (ε 15000); IR ν_{max} 1724, 1670, 1249, 1238, 1042, and 1033 cm^{-1}; NMR, δ 1.19 and 1.68 (each 3H, s, 19- and 18-C$\underline{H}_3$), 2.05 and 2.07 (each 3H, s, 2OCOC$\underline{H}_3$), 4.63, and 5.47 (each 1H, br W_H=22 and 9.5 Hz, 2$\underline{H}$ at C_3 and C_6), and 6.12 (1H, d J=8 Hz, $\underline{H}$ at C_{11}). Found: C, 71.38: H, 7.81%. Calcd for $C_{23}H_{30}O_5$: C, 71.48; H, 7.82%.

3β-Hydroxy-12β-etiojerv-5-ene-11,17-dione 17-Ethylene Acetal (6). A soln of **4** (20 g) in ethylene glycol (80 ml) was refluxed with *p*-toluenesulfonic acid (PTS, 1.0 g) in benzene (1600 ml) for 21 h, water being removed with a Dean-Stark apparatus. After being cooled, the soln was worked up as usual to leave crude acetal (23.7 g), which, without purification, was refluxed in methanol (670 ml) containing potassium hydroxide (70 g) for 1 h under nitrogen. The reaction mixture was worked up as usual to leave crystalline residue, which was recrystallized from hexane–benzene to give **6** (16.3 g), mp 160—162 °C (lit,[7] 165—167 °C).

3β,11α-Dihydroxy-12β-etiojerv-5-en-17-one 17-Ethylene Acetal (7), Its 3-Acetate (7a), and 3,11-Diacetate (7b). To a refluxing soln of **6** (10.0 g) in isopropyl alcohol (1400 ml) was added in small protions sodium metal (51 g) during 2 h. The mixture was further refluxed for 20 min under stirring, when it had become homogeneous. After being cooled, the mixture was combined with water (300 ml) and concentrated under reduced pressure to leave oily residue, which was mixed with water and extracted with chloroform. The extracts were worked up as usual to leave amorphous residue, which on trituration with aq ethanol afforded **7** (6.98 g), mp 156—158 °C. This was recrystallized from the same solvent mixture for analysis; mp 157—159 °C and $[\alpha]_D$ −34°; MS, *m/e* 348 (M^+), 330, 315, 286, and 259; IR, ν_{max} 3370, 1089, and 1050 cm^{-1}; NMR, δ 0.94 (3H, d J=7 Hz, 18-C$\underline{H}_3$), 0.98 (3H, s, 19-C$\underline{H}_3$), 3.48 (1H, br W_H=26 Hz, $\underline{H}$ at C_3), 3.94 (4H, s, OC$\underline{H}_2$C$\underline{H}_2$O), 4.05 and 5.32 (each 1H, br W_H=8 and 10 Hz, 2$\underline{H}$ at C_{11} and C_6). Found: C, 70.65; H, 9.39%. Calcd for $C_{21}H_{32}O_4 \cdot C_2H_5OH$: C, 70.01; H, 9.71%.

Compd **7** (125 mg) was dissolved in Py (1.26 ml) and Ac_2O (0.33 ml) under cooling with ice and then allowed to stand at room temp for 1.5 h. After being poured into ice-water, the mixture was extracted with chloroform. The extracts were worked up as usual to leave oily residue (164 mg), showing three spots on TLC, which was separated by chromatography over silica gel (Merck, 9 g). Eluates with benzene–ether (5 : 1) were crystallized and recrystallized from hexane to give **7b** (18 mg), mp 172—173 °C and $[\alpha]_D$ −15°; MS, *m/e* 432 (M^+), 372, 357, 312, and 297; IR, ν_{max} 1731, 1240 (br), 1086, 1043, and 1018 cm^{-1}; NMR, δ 0.77 (3H, d J=6 Hz, 18-C$\underline{H}_3$), 1.07 (3H, s, 19-C$\underline{H}_3$), 2.00 and 2.02 (each 3H, s, 2OCOC$\underline{H}_3$), 3.92 (4H, s, OC$\underline{H}_2$C$\underline{H}_2$O), 4.53 (1H, br W_H=20 Hz, $\underline{H}$ at C_3), and 5.37 (2H, br W_H= 10 Hz, 2$\underline{H}$ at C_{11} and C_6). Found: C, 69.24; H, 8.27%. Calcd for $C_{25}H_{36}O_6$: C, 69.42; H, 8.39%.

Eluates with benzene–ether (3 : 1) were crystallized and recrystallized from diisopropyl ether to give **7a** (80 mg), mp 235—236 °C and $[\alpha]_D$ −43°; MS, *m/e* 390 (M^+), 330, 268, and 242; IR, ν_{max} 3540, 1725, 1253, 1085, 1035, and 1023 cm^{-1}; NMR, δ 0.95 (3H, d J=6.5 Hz, 18-C$\underline{H}_3$), 1.00 (3H, s, 19-C$\underline{H}_3$), 2.01 (3H, s, OCOC$\underline{H}_3$), 3.94 (4H, s, OC$\underline{H}_2$C$\underline{H}_2$O) 4.10, 4.60, and 5.38 (each 1H, br W_H=9, 22, and 9 Hz, 3H at C_{11}, C_3, and C_6). Found: C, 70.84; H, 8.83%. Calcd for $C_{23}H_{34}O_5$: C, 70.74; H, 8.78%. Eluates with benzene–ether (1 : 1) were crystallized and recrystallized from aq ethanol to give the starting material (**7**, 10 mg), mp 156—158 °C, which was identical with an authentic sample.

To a pasty mixture, prepared by addition of chromium-(VI) oxide (500 mg) into Py (5 ml) at 0 °C under stirring, was added a soln of **7a** (20 mg) in Py (0.8 ml), and the whole mixture was stirred at room temp for 22 h. The reaction mixture was worked up as usual to yield an oily material, which was purified by chromatography over silica gel (Merck, 1 g). Eluates with benzene–ether (5 : 1) afforded 12β-etiojerv-5-en-3β-ol-11,17-dione 3-acetate 17-ethylene acetal (**6a**, 10 mg), mp 188—190 °C (diisopropyl ether), which was identical with an authentic sample[6,7] (IR, NMR, TLC, and mixed mp).

3β,11α-Dihydroxy-12β-etiojerv-5-en-17-one 3-Acetate (8). A soln of **7a** (1.91 g) in acetone (300 ml) and water (30 ml) was refluxed with PTS (150 mg) for 3 h under stirring. The soln was worked up as usual to leave crystalline residue (1.68 g), showing a single spot, which was recrystallized from acetone to give **8** (1.61 g), mp 216.5—217.5 °C and $[\alpha]_D$ −139°; MS, *m/e* 286 (base, M^+ −CH_3COOH), 271, 268, and 253; IR, ν_{max} 3615, 1728, 1696, 1250, and 1036 cm^{-1}; NMR, δ 1.03 (3H, s, 19-C$\underline{H}_3$), 1.11 (3H, d J=6 Hz, 18-C$\underline{H}_3$), 2.06 (3H, s, OCOC$\underline{H}_3$), 4.13 (1H, do d J=4 and 6 Hz, $\underline{H}$ at C_{11}), 4.63 and 5.43 (each 1H, br W_H=23 and 9 Hz, 2$\underline{H}$ at C_3 and C_6). Found: C, 72.97; H, 8.73%. Calcd for $C_{21}H_{30}O_4$: C, 72.80; H, 8.73%.

3β-Hydroxyetiojerva-5,12-dien-17-one 3-Acetate (9a).
(i) Compd **5a** (204 mg), dissolved in glacial acetic acid (14 ml), was stirred vigorously with zinc powder (440 mg) at 90 °C for 30 min. The mixture, after being cooled, was filtered to remove excess of the zinc powder, which was washed with chloroform. The filtrate and chloroform washings were combined, evaporated, diluted with water, and then extracted with chloroform. The extracts were worked up as usual to leave an amorphous substance (172 mg), which was crystallized from acetone to yield **9a** (127mg), mp 172—173 °C. This was recrystallized for analysis from

acetone; mp 172—173 °C and $[\alpha]_D$ −93.4°; MS, *m/e* 328 (M^+), 268, 253; UV, λ_{max} 246 nm (ε 12000); IR, ν_{max} 1731, 1665, 1248, and 1035 cm^{-1}; NMR, δ 1.04, 1.73, and 2.05 (each 3H, s, 19- and 18-C$\underline{H}_3$, and OCOC$\underline{H}_3$), 4.66 and 5.45 (each 1H, br W_H=21 and 9 Hz, 2$\underline{H}$ at C_3 and C_6). Found: C, 76.96; H, 8.52%. Calcd for $C_{21}H_{28}O_3$: C, 76.79; H, 8.59%.

(ii) To a soln of **8** (1.5 g) in dry Py (39 ml), cooled at 0 °C, was added dropwise phosphoryl chloride ($POCl_3$, freshly distilled, 1.95 ml) during 1 min under stirring, and the mixture was kept at room temp for 9 min. The reaction mixture was poured into ice–water (*ca.* 500 ml) and extracted with chlorofrom, and the chloroform soln was worked up as usual to give a crystalline substance, which was recrystallized from acetone to give **9a** (540 mg), mp 172—173 °C, identical with an authentic sample.

*3β-Hydroxyetiojerva-5,12-dien-17-one (**9**).* (i) Compd **9a** (6.49 g) was refluxed in methanol (160 ml) containing 5% potassium hydroxide for 1 h under nitrogen. The reaction mixture was worked up as usual to leave a crystalline substance (6.04 g), which was purified by chromatography over silica gel (Merck, 60 g). Eluates with benzene - ether (1 : 3) afforded **9** (5.07 g), mp 172—174 °C (acetone), which was recrystallized for analysis from acetone; mp 174—175 °C and $[\alpha]_D$ −106°; MS, *m/e* 286 (M^+), 268, and 253; UV, λ_{max} 246 nm (ε 12000); IR, ν_{max} 3440, 1643, and 1065 cm^{-1}; NMR, δ 1.03 and 1.73 (each 3H, s, 19- and 18-C$\underline{H}_3$), 3.57 and 5.42 (each 1H, br W_H=23 and 9 Hz, 2$\underline{H}$ at C_3 and C_6). Found: C, 79.70; H, 9.14%. Calcd for $C_{19}H_{26}O_2$: C, 79.68; H, 9.15%.

(ii) A soln of **7a** (5.68 g) in Py (57 ml) was treated with $POCl_3$ (5.7 ml) at room temp for 12 min (*cf.*, dehydration of **8**). The reaction mixture was worked up as mentioned above to leave an amorphous material (5.62 g), which was dissolved in dioxane (300 ml) and water (110 ml), and treated with concd hydrochloric acid (25 ml) at room temp for 25 h under stirring. The mixture was concentrated to 200 ml below 65 °C under reduced pressure, diluted with water, and then allowed to stand overnight, when crystalline substances (3.75 g) precipitated. These were collected by filtration and recrystallized from acetone to yield **9** (3.09 g), mp 169—170 °C, identical with an authentic sample.

*11α-Hydroxy-17-ethyletiojerva-5,12,17(20)-trien-3-one 3-Ethylene acetal (**11**), Its 11-Acetate (**11a**), and Its 11β-Ol Epimer (**12**).* (i) To an ice-cooled, stirred suspended mixture of lithium aluminium hydride (LAH, 3.40 g) in dry tetrahydrofuran (THF, 120 ml) was added dropwise 95% sulfuric acid (2.3 ml) under a stream of nitrogen, and the mixture was further stirred at room temp for 1 h and then kept in a refrigerator. The supernatant THF soln contained 0.75 M aluminium hydride. To a soln of 17-ethyletiojerva-5,12,17(20)-triene-3,11-dione 3-ethylene acetal[9] (**10**, 5.0 g) in THF (60 ml) cooled with ice was added slowly the above THF soln (25 ml) under stirring, and the whole mixture was stirred at room temp for 3 h. After addition of ethanol and 6 M aq ammonia to decompose excess of the hydride, the reaction mixture was filtered to remove aluminium hydroxide, which was washed with ethanol. The filtrate and ethanol washings were combined, concentrated, diluted with water, and extracted with chloroform. The extracts were washed with water, dried, and evaporated to leave oily residue, which was separated by chromatography over alumina (Merck, 200 g). Eluates with benzene–ether (3 : 1 and 2 : 1) gave the starting trienone (**10**, 77 mg). Eluates with benzene–ether (1 : 1) afforded crystalline substances, which were collected by filtration and recrystallized from benzene–ether to yield **12** (1.06 g), mp 138—141 °C and $[\alpha]_D$ −2.0°; MS, *m/e* 356 (M^+), 341, 338, and 323; UV, λ_{max} 260 (sh), 252, and 244 (sh) nm (ε 7000, 11000, and 10000); IR, ν_{max} 3540, 1110, and 1095 cm^{-1}; NMR, δ 1.30 and 1.93 (each 3H, s, 19- and 18-C$\underline{H}_3$), 1.72 (3H, d J=7 Hz, 21-C$\underline{H}_3$), 3.96 (4H, s, OC$\underline{H}_2$C$\underline{H}_2$O), 4.90 (1H, d J=7 Hz, $\underline{H}$ at C_{11}), 5.30 (1H, br W_H=11 Hz, $\underline{H}$ at C_6), and 5.60 (1H, q J=7 Hz, $\underline{H}$ at C_{20}). Found: C, 77.54; H, 8.99%. Calcd for $C_{23}H_{32}O_3$: C, 77.49; H, 9.05%.

Eluates with ether afforded **11** (2.96 g), mp 142—144 °C and $[\alpha]_D$ +6.9°; MS, *m/e* 356 (M^+), 341, 338, 323, and 239; UV, λ_{max} 258 (sh), 250, and 242 (sh) nm (ε 7000, 10000, and 9000); IR, ν_{max} 3350, 1110, and 992 cm^{-1}; NMR, δ 1.10 and 1.90 (each 3H, s, 19- and 18-C$\underline{H}_3$), 1.72 (3H, d J=7 Hz, 21-C$\underline{H}_3$), 3.96 (4H, s, OC$\underline{H}_2$C$\underline{H}_2$O), 4.66 (1H, d J=7 Hz, $\underline{H}$ at C_{11}), 5.36 (1H, br W_H=11 Hz, $\underline{H}$ at C_6), and 5.56 (1H, q J=7 Hz, $\underline{H}$ at C_{20}). Found: C, 77.58; H, 9.10%. Calcd for $C_{23}H_{32}O_3$: C, 77.49; H, 9.05%.

(ii) Compd **11** (205 mg) was treated with Ac_2O (1 ml) and Py (2 ml) at room temp overnight under stirring. The reaction mixture was worked up as usual to give **11a** (228 mg), mp 171—174 °C (benzene–ether) and $[\alpha]_D$ −37.5°; MS, *m/e* 398 (M^+), 338, and 323; UV, λ_{max} 259 (sh), 250, and 244 (sh) nm (ε 9500, 14800, and 13600); IR, ν_{max} 1720, 1245, 1108, and 1092 cm^{-1}; NMR, δ 1.16 and 1.72 (each 3H, s, 19- and 18-C$\underline{H}_3$), 1.69 (3H, d J=7 Hz, 21-C$\underline{H}_3$), 2.03 (3H, s, OCOC$\underline{H}_3$), 3.96 (4H, s, OC$\underline{H}_2$C$\underline{H}_2$O), 5.37 (1H, br W_H=12 Hz, $\underline{H}$ at C_6), 5.60 (1H, q J=7 Hz, $\underline{H}$ at C_{20}), and 6.10 (1H, d J=7 Hz, $\underline{H}$ at C_{11}). Found: C, 75.01; H, 8.43%. Calcd for $C_{25}H_{34}O_4$: C, 75.34; H, 8.60%.

*11α-Hydroxyetiojerva-5,12-diene-3,17-dione 3-Ethylene Acetal (**13a**) and Its 11-Acetate (**13a**).* (i) A soln of **11a** (850 mg) in 75% aq dioxane (70 ml) was stirred with osmium tetraoxide in dioxane (0.74 ml) (OsO_4 : dioxane=1.0 g : 80 ml) at room temp for 30 min, when the colorless soln gradually became dark-brown. To the soln was added sodium periodate (0.88 g) during 30 min, and the mixture was stirred at room temp for 22 h, when white precipitates separated out and were removed by filtration. The filtrate was concentrated, diluted with water, and extracted with chloroform repeatedly. The chloroform soln was washed with water, dried and evaporated to leave amorphous residue, which was purified by chromatography over silica gel (Merck, 34 g) with mixtures of benzene and ether to give **13a** (584 mg), mp 189—191 °C (benzene–ether) and $[\alpha]_D$ −79.7°; MS, *m/e* 386 (M^+) and 326; UV, λ_{max} 244 nm (ε 11000); IR, ν_{max} 1732, 1658, 1240, and 1093 cm^{-1}; NMR, δ 1.18, 1.66, and 2.06 (each 3H, s, 19- and 18-C$\underline{H}_3$, and OCOC$\underline{H}_3$), 3.97 (4H, s, OC$\underline{H}_2$C$\underline{H}_2$O), 5.40 (1H, br W_H=9 Hz, $\underline{H}$ at C_6), and 6.10 (1H, d J=7 Hz, $\underline{H}$ at C_{11}). Found: C, 71.03; H, 7.38%. Calcd for $C_{23}H_{30}O_5$: C, 71.48; H, 7.82%.

(ii) Compd **11** (2.20 g) was oxidized in the same manner as **11a** to give **13** (1.48 g), mp 186—188 °C (benzene–ether) and $[\alpha]_D$ −44.1°; MS, *m/e* 344 (M^+); UV, λ_{max} 249 nm (ε 12000); IR, ν_{max} 3480, 1665, 1110, and 1095 cm^{-1}; NMR, δ 1.14 and 1.90 (each 3H, s, 19- and 18-C$\underline{H}_3$), 3.98 (4H, s, OC$\underline{H}_2$C$\underline{H}_2$O), 4.78 (1H, d J=7 Hz, $\underline{H}$ at C_{11}), and 5.43 (1H, br W_H=10 Hz, $\underline{H}$ at C_6). Found: C, 73.30; H, 8.10%. Calcd for $C_{21}H_{28}O_4$: C, 73.22; H, 8.19%.

Compd **13** (4.16 g) was treated with Ac_2O (21 ml) and Py (42 ml) at room temp overnight under stirring to give **13a** (4.64 g), which was identical with an authentic sample.

*11β-Hydroxyetiojerva-5,12-diene-3,17-dione 3-Ethylene Acetal (**14**).* The Lemieux-Johnson oxidation of **12** (105 mg) was carried out in the same manner as that of **11** and gave **14** (51 mg), mp 169—170 °C (benzene–ether); MS, *m/e* 344

(M+); UV, λ_{max} 247 nm (ε 10600); IR, ν_{max} 3360, 1640, 1118, and 1100 cm^{-1}; NMR, δ 1.32 and 1.90 (each 3H, s, 19- and 18-C$\underline{H}_3$), 3.98 (4H, s, OC$\underline{H}_2$C$\underline{H}_2$O), 5.00 (1H, d J=7 Hz, $\underline{H}$ at C_{11}), and 5.30 (1H, br W_H=10 Hz, $\underline{H}$ at C_6). Found: C, 73.45; H, 8.40%. Calcd for $C_{21}H_{28}O_4$: C, 73.22; H, 8.19%.

*Etiojerva-5,12-diene-3,17-dione 3-Ethylene Acetal (**15**).*
(i) To a blue-colored soln of lithium (2.0 g) in liquid ammonia (*ca.* 300 ml) cooled with Dry Ice-Acetone was added **13a** (4.7 g) in THF (15 ml), and the mixture was stirred at the temp for 15 min. The reaction mixture, on addition of ammonium chloride (20 g), became colorless and was then allowed to stand at room temp to remove the ammonia. The residue was submitted to filtration to remove ammonium chloride, the latter being washed with ethanol. The filtrate and ethanol washings were combined, concentrated, diluted with water, and extracted with chloroform, repeatedly. The extracts were worked up as usual to give crystalline residue, which on recrystallization from ether yielded **15** (3.43 g), mp 163—165 °C and $[\alpha]_D$ −81.5°; MS, *m/e* 328 (M+); UV, λ_{max} 247 nm (ε 9200); IR, ν_{max} 1658 and 1110 cm^{-1}; NMR, δ 1.06 and 1.73 (each 3H, s, 19- and 18-C$\underline{H}_3$), 3.98 (4H, s, OC$\underline{H}_2$C$\underline{H}_2$O), and 5.42 (1H, br W_H=10 Hz, $\underline{H}$ at C_6). Found: C, 76.65; H, 8.68%. Calcd for $C_{21}H_{28}O_3$: C, 76.79; H, 8.59%.

(ii) The Birch reduction of **14** (8.00 g) was carried out in the same manner as that of **13a** and produced **15** (5.58 g), which was identical with the afore-mentioned sample.

*17α-Hydroxyetiojerva-5,12-dien-3-one 3-Ethylene Acetal (**16**), Its 17β-Ol Epimer (**17**), and Their 17-Acetates (**16a** and **17a**).*
(i) A soln of **15** (1.00 g) in methanol (100 ml) was stirred with sodium borohydride (1.8 g) at room temp for 35 min. After addition of a small amount of acetic acid, the mixture was neutralized with 5% aq sodium hydrogencarbonate, concentrated, diluted with water, and extracted with chloroform, repeatedly. The chloroform soln gave crystalline residue, which was recrystallized from ether to yield **16** (950 mg), mp 132—133 °C and $[\alpha]_D$ −25.7°; MS, *m/e* 330 (M+) and 312; IR, ν_{max} 3360, 1110, and 1090 cm^{-1}; NMR, δ 0.98 and 1.65 (each 3H, s, 19- and 18-C$\underline{H}_3$), 3.94 (4H, s, OC$\underline{H}_2$C$\underline{H}_2$O), 4.12 and 5.35 (each 1H, br W_H=18 and 10 Hz, 2$\underline{H}$ at C_{17} and C_6). Found: C, 75.93; H, 9.12%. Calcd for $C_{21}H_{30}O_3$: C, 76.32; H, 9.15%.

Compd **16** (0.11 g) was treated with Ac_2O (0.7 ml) and Py (1.4 ml) at room temp for 1 d under stirring to give **16a** (0.12 g), mp 142—143 °C (benzene-ether) and $[\alpha]_D$ −10.6°; MS, *m/e* 372 (M+) and 312; IR, ν_{max} 1734, 1237, 1107, 1092, 1019, and 976 cm^{-1}; NMR, δ 0.99, 1.54, and 2.06 (each 3H, s, 19- and 18-C$\underline{H}_3$, and OCOC$\underline{H}_3$), 3.94 (4H, s, OC$\underline{H}_2$C$\underline{H}_2$O), and 5.35 (2$\underline{H}$, br W_H=10 Hz, 2$\underline{H}$ at C_6 and C_{17}). Found: C, 74.05; H, 8.62%. Calcd for $C_{23}H_{32}O_4$: C, 74.16; H, 8.66%.

(ii) To an ice-cooled and stirred soln of LAH (0.8 g) in THF (40 ml) was added dropwise concd sulfuric acid (0.7 ml) under a stream of nitrogen, and the mixture was then kept in a refrigerator. To a soln of **15** (2.00 g) in THF (20 ml) was added slowly the above supernatant THF soln (25 ml) under nitrogen, and the whole mixture was stirred at room temp for 2 h. The mixture, after being worked up as described before, gave amorphous residue, which was separated by chromatography over silica gel (Merck, 65 g). Eluates with benzene-ether (2 : 1) afforded a mixture, showing two spots, which was further separated by preparative TLC over silica gel (Wakogel B-5, 35 plates of 20×20 cm^2) with benzene-ether (2 : 1). A less polar fraction afforded **17** (0.11 g), mp 92—94 °C (benzene-ether) and $[\alpha]_D$ −77.3°; MS, *m/e* 330 (M+), 312, and 297; IR, ν_{max} 3500, 3260, 1190, 1035, 1015, and 970 cm^{-1}; NMR, δ 0.98 and 1.71 (each 3H, s, 19- and 18-C$\underline{H}_3$), 3.94 (5H, s, OC$\underline{H}_2$C$\underline{H}_2$O and $\underline{H}$ at C_{17}), and 5.36 (1H, br W_H=10 Hz, $\underline{H}$ at C_6). Found: C, 75.93; H, 9.34%. Calcd for $C_{21}H_{30}O_3$: C, 76.32; H, 9.15%. A more polar fraction afforded **16** (1.77 g), which was obtained from eluates with benzene-ether (1 : 1) and ether, and proved to be identical with an authentic sample.

Compd **17** (14 mg) was acetylated with Ac_2O (0.4 ml) and Py (0.8 ml) at room temp for 3 d to give **17a** (15 mg), mp 138—141 °C (acetone) and $[\alpha]_D$ −89.7°; MS, *m/e* 372 (M+) and 312; IR, ν_{max} 1738, 1238, 1108, 1090, 1020, and 957 cm^{-1}; NMR, δ 1.00, 1.59, and 2.05 (each 3H, s, 19- and 18-C$\underline{H}_3$, and OCOC$\underline{H}_3$), 3.95 (4H, s, OC$\underline{H}_2$C$\underline{H}_2$O), 5.21 and 5.39 (each 1H, br W_H=8 and 10 Hz, 2$\underline{H}$ at C_{17} and C_6). Found: C, 74.18; H, 8.63%. Calcd for $C_{23}H_{32}O_4$: C, 74.16; H, 8.66%.

*Epoxidation of **16**.* (i) To a soln of **16** (100 mg) in dry benzene (10 ml) was added perbenzoic acid (50 mg, purity 95%), and the mixture was stirred at room temp for 30 min. After addition of 5% aq sodium thiosulfate, the mixture was concentrated and shaken with water and chloroform. The chloroform soln was washed with 5% aq sodium hydrogencarbonate and water, dried and evaporated to leave amorphous residue, which was separated by chromatography over silica gel (Merck, 4.0 g). Eluates with benzene-ether (3 : 1) gave a crystalline substance (4 mg), which was recrystallized from benzene to give 17α-hydroxy-12β,13β-epoxyetiojerv-5-en-3-one 3-ethylene acetal (**19**), mp 136—138 °C and $[\alpha]_D$ −63.8°; MS, *m/e* 346 (M+) and 328; IR, ν_{max} 3500, 1106, and 1022 cm^{-1}; NMR, δ 1.04 and 1.40 (each 3H, s, 19- and 18-C$\underline{H}_3$), 3.96 (5H, s, OC$\underline{H}_2$C$\underline{H}_2$O and $\underline{H}$ at C_{17}), and 5.36 (1H, br W_H=10 Hz, $\underline{H}$ at C_6). Found: C, 72.48; H, 8.75%. Calcd for $C_{21}H_{30}O_4$: C, 72.80; H, 8.73%.

Eluates with benzene-ether (2 : 1) gave the 12α,13α-epoxy epimer (**18**, 75 mg), which was recrystallized for analysis from benzene-ether: mp 158—161 °C and $[\alpha]_D$ −57.0°; MS, *m/e* 346 (M+) and 328; IR, ν_{max} 3440, 1110, 1100, and 1035 cm^{-1}; NMR, δ 1.00 and 1.40 (each 3H, s, 19- and 18-C$\underline{H}_3$), 3.76 (1H, br W_H=28 Hz, $\underline{H}$ at C_{17}), 3.96 (4H, s, OC$\underline{H}_2$C$\underline{H}_2$O), and 5.38 (1H, br W_H=11 Hz, $\underline{H}$ at C_6). Found: C, 72.89; H, 8.74%. Calcd for $C_{21}H_{30}O_4$: C, 72.80; H, 8.73%. Eluates with benzene-ether (1 : 1) afforded the 5β,6β,12α,13α-diepoxide (**20**, 10 mg), mp 123—125 °C (benzene-ether) and $[\alpha]_D$ −28.6°; MS, *m/e* 362 (M+) and 347; IR, ν_{max} 3460, 1100, 1040, and 957 cm^{-1}; NMR, δ 0.99 and 1.38 (each 3H, s, 19- and 18-C$\underline{H}_3$), 3.14 and 3.72 (each 1H, br W_H=5 and 24 Hz, 2$\underline{H}$ at C_6 and C_{17}), and 3.90 (4H, s, OC$\underline{H}_2$C$\underline{H}_2$O). Found: C. 69.44; H, 8.43%. Calcd for $C_{21}H_{30}O_5$: C, 69.58; H, 8.34%.

Compd **18** (300 mg) and **19** (10 mg) were treated with Ac_2O and Py (1.5 and 3 ml, and 0.15 and 0.3 ml) to give the respective acetates (**18a**, 276 mg and **19a**, 8 mg). Compd **18a**, mp 212—213 °C (acetone) and $[\alpha]_D$ −44.7°; MS, *m/e* 388 (M+) and 328; IR, ν_{max} 1737, 1240, 1107, 1092, and 1030 cm^{-1}; NMR, δ 1.00, 1.26, and 2.12 (each 3H, s, 19- and 18-C$\underline{H}_3$, and OCOC$\underline{H}_3$), 3.96 (4H, s, OC$\underline{H}_2$C$\underline{H}_2$O), 5.04 (1H, do d J=5 and 10 Hz, $\underline{H}$ at C_{17}), and 5.37 (1H, br W_H=10 Hz, $\underline{H}$ at C_6). Found: C, 70.82; H, 8.31%. Calcd for $C_{23}H_{32}O_5$: C, 71.10; H, 8.30%. Compd **19a**, mp 142—144 °C (ether) and $[\alpha]_D$ −53.0°; MS, *m/e* 388 (M+) and 328; IR ($CHCl_3$), ν_{max} 1732, 1248, 1110, 1095, and 1025 cm^{-1}; NMR, δ 1.04, 1.29, and 2.06 (each 3H, s, 19- and 18-C$\underline{H}_3$, and OCOC$\underline{H}_3$), 3.96 (4H, s, OC$\underline{H}_2$C$\underline{H}_2$O), 5.04 and 5.37 (each 1H, br W_H=14 and 10 Hz, 2$\underline{H}$ at C_{17} and C_6). Found: C, 70.34; H, 8.83%. Calcd for $C_{23}H_{32}O_5$·

0.5 $(C_2H_5)_2O$: C, 70.56; H, 8.76%.

(ii) To a refluxing, green-colored soln of **16** (200 mg) in dry benzene (3 ml) containing bis(acetylacetonato)-oxovanadium(IV) (2.7 mg) was added rapidly *t*-butyl hydroperoxide (0.12 ml), when the soln became yellow-colored. The soln was then refluxed for 20 min and cooled. The reaction mixture was washed with 5% aq sodium hydrogensulfite, until the mixture became colorless, and then with water, dried and evaporated to leave a resinous material, which was purified by chromatography over silica gel (Merck, 8.0 g) to yield **18** (120 mg), mp 157—159 °C, from eluates with benzene–ether (1 : 2). This was identical with the afore-mentioned sample.

*12α,13α-Epoxyetiojerv-4-ene-3,17-dione 3-Ethylene Acetal (**21**).* (i) A soln of **15** (200 mg) in methanol (14 ml), containing 4 M aq sodium hydroxide (0.4 ml) and 30% aq hydrogen peroxide (0.8 ml), was allowed to stand in a refrigerator for 3 d. The reaction mixture was concentrated and shaken with water and chloroform, and the chloroform soln was washed with 5% aq sodium thiosulfate and water, dried and evaporated to give amorphous residue, which was purified by chromatography over silica gel (Merck, 7.0 g). Eluates with benzene–ether (2 : 1) gave a crystalline substance, which was recrystallized from benzene–ether to give **21** (180 mg), mp 139—140 °C and $[\alpha]_D$ −67.1°; ORD (dioxane), $[\Phi]_{326}^{trough}$ −5600°, $[\Phi]_{280}^{peak}$ +6300°, $a=-119°$; MS, *m/e* 344 (M^+); IR, ν_{max} 1712, 1211, 1117, 1102, 1032, 974, and 943 cm^{-1}; NMR, δ 1.00 and 1.34 (each 3H, s, 19- and 18-C$\underline{H}_3$), 3.96 (4H, s, OC$\underline{H}_2$C$\underline{H}_2$O), and 5.38 (1H, br W_H= 10 Hz, $\underline{H}$ at C_6). Found: C, 73.22; H, 8.25%. Calcd for $C_{21}H_{28}O_4$: C, 73.22; H, 8.19%.

(ii) A soln of **18** (50 mg) in Py (2 ml) was mixed with a suspended mixture of chromium(VI) oxide (0.5 g) in Py (5 ml), and then stirred at room temp for 5 h. The reaction mixture was filtered through Florisil (3.0 g), which was washed with ether. The filtrate was diluted with water and extracted with ether. The ether soln and ether washings were combined and worked up as usual to give **21** (45 mg), mp 139—142 °C (ether), which was identical with the aforementioned sample.

*Reduction of **21** with Sodium Borohydride.* A soln of **21** (330 mg) in methanol (38 ml) was treated with sodium borohydride (660 mg) at room temp for 20 min. The reaction mixture was worked up as usual to give a mixture of alcohols, which was separated into two fractions by chromatography over silica gel (Merck, 10 g). A less-polar fraction eluted with benzene–ether (2 : 1) gave 12α,13α-epoxyetiojerv-5-en-17β-ol-3-one 3-ethylene acetal (**22**, 82 mg), mp 144—146 °C (benzene) and $[\alpha]_D$ −63.1°; MS, *m/e* 346 (M^+) and 328; IR, ν_{max} 3480, 1120, 1103, 1033, 1003, and 970 cm^{-1}; NMR, δ 1.00 and 1.38 (each 3H, s, 19- and 18-C$\underline{H}_3$), 3.94 (4H, s, OC$\underline{H}_2$C$\underline{H}_2$O), 4.06 and 5.37 (each 1H, br W_H=7 and 10 Hz, 2H at C_{17} and C_6). Found: C, 73.03; H, 8.76%. Calcd for $C_{21}H_{30}O_4$: C, 72.80; H, 8.73%. A more-polar fraction eluted with benzene–ether (1 : 1 and 1 : 2) gave 17α-alcohol (**18**, 215 mg), mp 159—162 °C (benzene), which was identical with the sample described above.

Compd **22** (45 mg) was treated with Ac_2O (0.5 ml) and Py (1.0 ml) to give 17-acetate (**22a**, 45 mg), mp 144—147 °C (ether) and $[\alpha]_D$ −39.7°; MS, *m/e* 388 (M^+) and 328; IR, ν_{max} 1742, 1237, 1098, 1028, 1010, and 968 cm^{-1}; NMR, δ 1.02, 1.26, and 2.09 (each 3H, s, 19- and 18-C$\underline{H}_3$, and OCOC$\underline{H}_3$), 3.93 (4H, s, OC$\underline{H}_2$C$\underline{H}_2$O), 5.16 and 5.34 (each 1H, br W_H=6 and 10 Hz, 2H at C_{17} and C_6). Found: C, 71.33; H, 8.20%. Calcd for $C_{23}H_{32}O_5$: C, 71.10; H, 8.30%.

*Epoxidation of **17**.* Compd **17** (80 mg) was oxidized with *t*-butyl hydroperoxide (0.05 ml) in the presence of bis(acetylacetonato)oxovanadium(IV) (2 mg) under reflux for 20 min. The reaction mixture was worked up as described before to yield 12β,13β-epoxyetiojerv-5-en-17β-ol-3-one 3-ethylene acetal (**23**, 55 mg), mp 130—132° C (ether) and $[\alpha]_D$ −58.4°; MS, *m/e* 346 (M^+) and 328; IR ($CHCl_3$), ν_{max} 3570, 1110, 1062, 1024, 990, and 972 cm^{-1};NMR, δ 1.04 and 1.45 (each 3H, s, 19- and 18-C$\underline{H}_3$), 3.81 (1H, br W_H=12 Hz, $\underline{H}$ at C_{17}), 3.96 (4H, s, OC$\underline{H}_2$C$\underline{H}_2$O), and 5.40 (1H, br W_H=10 Hz, $\underline{H}$ at C_6). Found: C, 72.48; H, 8.75%. Calcd for $C_{21}H_{30}O_4$: C, 72.80; H, 8.73%.

Compd **23** (14 mg) was treated with Ac_2O (0.15 ml) and Py (0.3 ml) to give 17-acetate (**23a**, 11 mg), mp 132—135 °C (ether) and $[\alpha]_D$ −38.0°; MS, *m/e* 388 (M^+), 360, 345, and 328 cm^{-1}; IR ($CHCl_3$), ν_{max} 1733, 1245, 1110, 1090, 1025, and 973 cm^{-1}; NMR, δ 1.06, 1.37, and 2.14 (each 3H, s, 19- and 18-C$\underline{H}_3$, and OCOC$\underline{H}_3$), 3.98 (4H, s, OC$\underline{H}_2$C$\underline{H}_2$O), 5.14 and 5.40 (each 1H, br W_H=12 and 10 Hz, 2H at C_{17} and C_6). Found: C, 70.68; H, 7.99%. Calcd for $C_{23}H_{32}O_5$: C, 71.10; H, 8.30%.

*12β,13β-Epoxyetiojerv-5-ene-3,17-dione 3-Ethylene Acetal (**24**).* Compd **23** (30 mg) in Py (2 ml) was oxidized with chromium (VI) oxide (0.35 g) in Py (3.5 ml) at room temp for 4 h. The reaction mixture was worked up as usual to give an amorphous substance, which was purified by preparative TLC over silica gel (Wakogel B-5, 3 plates) with benzene–ether (2 : 1) to give **24** (24 mg), mp 184—186 °C (ether) and $[\alpha]_D$ −13.4°; ORD (dioxane), $[\Phi]_{280}^{trough}$ −8500°, $[\Phi]_{324}^{peak}$ +4000°, a=+125°; MS, *m/e* 344 (M^+); IR ($CHCl_3$), ν_{max} 1706, 1230, 1110, 1090, and 1028 cm^{-1}; NMR, δ 1.10 and 1.42 (each 3H, s, 19- and 18-C$\underline{H}_3$), 3.96 (4H, s, OC$\underline{H}_2$C$\underline{H}_2$-O), and 5.39 (1H, br W_H=10 Hz, $\underline{H}$ at C_6). Found: C, 72.89; H, 8.45%. Calcd for $C_{21}H_{28}O_4$: C, 73.22; H, 8.15%.

*Reduction of **24** with Sodium Borohydride.* Compd **24** (18 mg) was treated with sodium borohyride (36 mg) in methanol (4 ml) at room temp for 30 min. The reaction mixture was worked up as described before to give amorphous residue, which was separated into two fractions by preparative TLC over silica gel (Wakogel B-5, 2 plates) with benzene–ether (5 : 1). Less and more polar fractions gave **23** (9 mg), mp 133—135 °C (ether) and **19** (7 mg), mp 136—138 °C (diisopropyl ether), respectively, which were identical with the corresponding authentic sample.

*3β-Hydroxy-12α,13α-epoxyetiojerv-5-en-17-one (**25**).* A soln of **9** (295 mg) in methanol (28 ml) was mixed with 30% aq hydrogen peroxide (1.64 ml) in 4 M aq sodium hydroxide (0.84 ml), and then allowed to stand in a refrigerator (5 °C) for 46 h. The reaction mixture was concentrated, diluted with water, and extracted with chloroform. The chloroform soln was worked up as usual to leave amorphous residue (249 mg), showing a single spot, which on trituration with acetone crystallized, and was then recrystallized from acetone to give **25** (177 mg), mp 173.5—175 °C and $[\alpha]_D$ −92.3°; ORD (dioxane), $[\Phi]_{326}^{trough}$ −5530°, $[\Phi]_{280}^{peak}$ +4410°, $a=-99.4°$; MS, *m/e* 302 (M^+), 284, and 269; IR, ν_{max} 3480, 1703, and 1062 cm^{-1}; NMR, δ 1.02 and 1.37 (each 3H, s, 19- and 18-C$\underline{H}_3$), 3.59 and 5.43 (each 1H, br W_H=24 and 10 Hz, 2H at C_3 and C_6). Found: C, 75.23; H, 8.61%. Calcd for $C_{19}H_{26}O_3$: C, 75.46; H, 8.67%.

References

1) Part II, A. Murai, H. Sasamori, and T. Masamune, *Chem. Lett.*, **1976**, 975.

2) Part XXIX of "*C*-Nor-*D*-homosteroids and Related

Alkaloids;" Part XXVIII, Ref. 1.

3) a) A. Murai, H. Sasamori, and T. Masamune, *Bull. Chem. Soc. Jpn.*, submitted; b) Ref. 1.

4) S. M. Kupchan and S. D. Levine, *J. Am. Chem. Soc.*, **86**, 701 (1964).

5) J. Fried and A. Klingsberg, *J. Am. Chem. Soc.*, **75**, 4929 (1953).

6) T. Masamune, A. Murai, and S. Numata, *Tetrahedron*, **25**, 3145 (1969).

7) S. M. Kupchan, A. W. By, and M. S. Flom, *J. Org. Chem.*, **33**, 911 (1968).

8) T. Masamune, A. Murai, Nishizakura, T. Orito, S. Numata, and H. Sasamori, *Bull. Chem. Soc. Jpn.*, **49**, 1622 (1976).

9) S. M. Kupchan, T. Masamune, and G. W. A. Milne, *J. Org. Chem.*, **29**, 755 (1964).

10) N. M. Yoon and H. C. Brown, *J. Am. Chem. Soc.*, **90**, 2927 (1968).

11) a) R. Pappo, D. S. Allen, Jr., R. U. Lemieux, and W. S. Johnson, *J. Org. Chem.*, **21**, 478 (1956); b) S. H. Graham and A. J. S. Williams, *J. Chem. Soc., C*, **1966**, 655.

12) R. S. Rosenfeld and T. F. Gallagher, *J. Am. Chem. Soc.*, **77**, 4367 (1955).

13) *Cf.*, J. A. Mills, *J. Chem. Soc.*, **1952**, 4976; A. K. Bose and R. G. Chatterjee, *J. Org. Chem.*, **23**, 1425 (1958); J. H. Brewster, *J. Am. Chem. Soc.*, **81**, 5493 (1959); R. K. Hill and J. W. Morgan, *J. Org. Chem.*, **33**, 927 (1968).

14) *Cf.*, G. F. H. Green, J. E. Page, and S. E. Staniforth, *J. Chem. Soc., B*, **1966**, 807; T. Dahl, Young-Ho Kim, D. Levy, and R. Stevenson, *J. Chem. Soc., C*, **1969**, 2723.

15) *Cf.*, J. J. Brown, R. H. Lenhand, and S. Bernstein, *J. Am. Chem. Soc.*, **86**, 2183 (1964).

16) *Cf.*, H. J. Dauben, Jr., L. R. Honnen, and K. M. Harmon, *J. Org. Chem.*, **25**, 1442 (1960); D. H. R. Barton, P. D. Magnus, G. Smith, G. Streckert, and D. Zurr, *J. Chem. Soc., Perkin Trans. 1*, **1972**, 542.

17) H. O. House, "Modern Synthetic Reactions," W. A. Benjamin Inc., Menlo Park, California (1972), p. 302.

18) K. B. Sharpless and R. C. Michaelson, *J. Am. Chem. Soc.*, **95**, 6136 (1973).

19) N. S. Bhacca and D. H. Williams, "Applications of NMR Spectroscopy in Organic Chemistry," Holden-Day Inc., San Francisco, California (1964), p. 20.

20) *Cf.*, G. I. Poss, G. E. Arth, R. E. Beyler, and L. H. Sarett, *J. Am. Chem. Soc.*, **75**, 422 (1953); H. H. Wasserman and N. E. Aubrey, *ibid.*, **77**, 590 (1955).

12,13-Epoxy-*C*-nor-*D*-homosteroids. IV.[1] The Reaction of 11-Oxygenated 17α-Acetyl-12α,13α-epoxyetiojervanes with Boron Trifluoride Etherate[2]

Akio MURAI, Hiroshi SASAMORI, and Tadashi MASAMUNE
Department of Chemistry, Faculty of Science, Hokkaido University, Sapporo 060
(Received July 10, 1976)

The titled compounds were treated with boron trifluoride etherate in benzene at room temperature. 11α-Hydroxy-12α,13α-epoxide (**1**) underwent rapid cleavage of the epoxy ring at both C_{13} and C_{12} to give 11α-hydroxy-13β-fluoro-12α-alcohol (**2**), 13α-hydroxy-12βH-11-ketone (**3**), 17-deacetyl-Δ^{12}-11-ketone (**4**), and an acetophenone derivative (**5**) in comparative yields. The same acid treatment of 11α-acetoxy-12α,13α-epoxide (**1a**) yielded 11α-acetoxy-13β-fluoro-12α-alcohol (**2a**) as a single isolable product, while that of 11-unsubstituted 12α,13α-epoxide (**16**) afforded 12β-fluoro-13α-alcohol (**17**) besides **5**, a major product. Evidently, compounds **2a** and **17** are products formed by the epoxy ring opening at C_{13} and C_{12}, respectively. Interestingly, compounds **2** and **2a**, when treated with bases, produced a rearranged 13α-pregnane derivative (**12**) *via* 11α,12α-dihydroxy-$\Delta^{13(17)}$-20-ketone (**10**), in good yields. On the other hand, the epoxy cleavage of 11-oxo-12α,13α-epoxide (**13**) led to predominant formation of rearranged products, bicyclo[3.3.1]nonane-2,9-dione and hydrooxepin derivatives (**14** and **15**). It is emphasized that the epoxy cleavage reactions proceeded more slowly and took place at C_{13} rather than at C_{12} with increase of electronegativity of the 11-substituents.

In the previous paper[3] we reported the synthesis and stereochemistry of 17α-acetyl-12,13-epoxyetiojervanes. As a continuing study aimed at the preparation of biologically active normal steroids from jervine, we have examined reactions of several 11-oxygenated 17α-acetyl-12α,13α-epoxyetiojervanes with boron trifluoride etherate, keeping in mind the Coxon and coworkers' result, a low yield of formation of hecogenin acetate by the acid treatment of the corresponding 12α,13α-epoxy-*C*-nor-*D*-homospirostan.[4] Contrary to the expectation, the reactions have not led to the desirable rearrangement but have resulted in formation of many compounds including interesting rearranged products such as bicyclo[3.3.1]nonane-2,9-dione and hydrooxepin derivatives.[5]

Treatment of 17α-acetyl-12α,13α-epoxyetiojerv-4-en-11α-ol-3-one (**1**), the most readily available 12,13-epoxides, with boron trifluoride etherate in benzene at room temperature for 30 s afforded a multi-component mixture, from which four compounds (**2**—**5**) were isolated after careful chromatography in 20, 10, 10, and 11% yields, respectively. The major product (**2**), mp 153—155 °C, was assigned structure **2** on the following evidence. The mass [*m/e* 364 (M^+), 346, 345, 344, 326 (M^+-HF-H_2O), and 301 ($M^+-HF-COCH_3$)] and NMR spectra [δ 2.37 (3H, s, 21-C$\underline{H}_3$), 3.34 (2H, br W_H=28 Hz, $\underline{H}$ at C_{17} and O$\underline{H}$) and 5.96 (1H, s, O$\underline{H}$)] revealed the presence of one fluorine atom, one acetyl (at C_{17}) and two hydroxyl groups. These spectra, as coupled with the UV [λ_{max} 239 nm (ε 10000)] and IR spectral data (ν_{max} 1703 cm^{-1}), indicated that the A ring and 17-side chain remained unchanged. The NMR spectrum also exhibited two three-proton singlets due to the 19- and 18-methyl protons at δ 1.26 and 1.50, a one-proton singlet ($\underline{H}$ at C_4) at δ 5.76 and also one doublet (J=8 Hz) due to a proton on the carbon atom (at C_{11}) bearing the hydroxyl group at δ 4.02. Compound **2**, when acetylated with acetic anhydride at room temperature and also oxidized with the Jones reagent, was converted into the corresponding monoacetate and hydroxy ketone (**2a** and **6**), mp 140—142 and 188—190 °C, in 95 and 85% yields, respectively. The latter (**6**) displayed a strong absorption maximum at 1753 cm^{-1} in the IR spectrum, proving that the secondary hydroxyl group in question existed in a five-membered C ring. These facts were consistent with the assigned formula (**2**) and also with an alternate formula (**2'**). Compound **2** was then treated with periodic acid in aqueous dioxane at room temperature for 18 h, when one mole of the acid had been consumed. The resulting single product, mp 128—130 °C, isolated in a 75% yield, was formulated as lactol (**7**) rather than keto aldehyde (**8**) on the spectral data (Exp). Moreover, compound **2** readily formed the corresponding acetonide (**9**), oil, by treatment with acetone and acid ($HClO_4$) at room temperature in a quantitative yield. All these results indicate that the compound is represented by structure **2** with a *cis*-glycol partial formula, excluding the alternate structure (**2'**), and also establish the previously assigned 12α,13α-epoxy configuration to the starting epoxide (**1**).

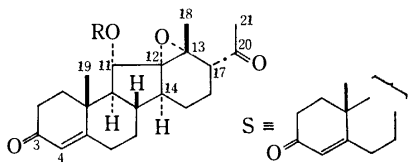

1 R=H
1a R=Ac

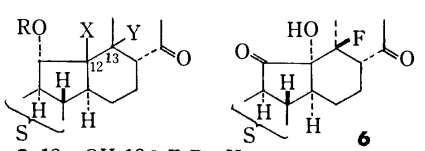

6

2 12α-OH,13β-F, R=H
2a 12α-OH,13β-F, R=Ac
2' 12β-OH,13α-F

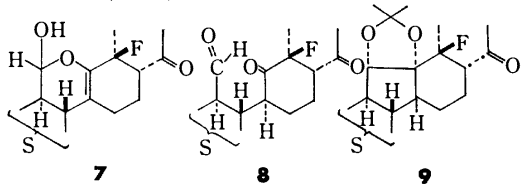

7 **8** **9**

The configuration of the fluorine atom at C_{13} was deduced from analogous examples[4,6] as well as consideration of the 11-carbonyl frequency of hydroxy ketone (**6**) as discussed below. The relevant absorption maximum was observed at a higher wave number (ν_{max} 1753 cm^{-1}) than that (ν_{max} *ca.* 1735 cm^{-1}) of usual 11-oxo-12α-etiojervanes without any substituent at C_{12}. The Dreiding model indicates that the D ring of **6** would probably adopt a half-chair or a twist-boat (bowsprit and flagpole at C_{14} and C_{17}) conformation with both the 17α-acetyl and 13β-fluoro substituents pseudo-equatorial. If the D ring assumes another twist-boat form (bowsprit-flagpole at C_{13} and C_{15}), the pseudo-equatorial 17α-acetyl group would readily form hydrogen-bonding with the 12α-hydroxyl group and show the absorption maximum at a lower wave number than at the observed (ν_{max} 1715 cm^{-1}). With either one of the afore-mentioned conformations with the fluorine atom pseudo-equatorial, the carbon-fluorine and 11-carbonyl bonds were located to be 1,3-diaxial-like and hence the carbonyl absorption would be susceptible to hypsochromic effect owing to the nearby dipole (C–F bond). Furthermore the 12α-hydroxyl group was disposed almost perpendicular to the 11-carbonyl bond and would exert no influence on the frequency in question. This presumption is reasonable and supports the above β-assignment to the fluorine atom. Here we emphasize that fluorohydrin (**2**) would result from a nucleophilic attack of a fluoride anion, probably contained in the reagent,[6b] to the epoxy ring at C_{13}.

11α-Hydroxy-fluorohydrin (**2**) was then treated with potassium carbonate in aqueous methanol at room temperature for 1 h. Contrary to the expectation that the starting epoxide (**1**) would be regenerated, compound **2** underwent dehydrofluorination to give $\Delta^{13(17)}$-20-ketone (**10**), mp 173—174 °C, in a quantitative yield, which on treatment with acetone and acid ($HClO_4$) formed the corresponding acetonide (**11**), oil, in a good yield. The latter (**11**) was also obtained by treatment of acetonide **9** with potassium carbonate under the same conditions as mentioned above. In accordance with the assigned structures, compound **10** exhibited an absorption maximum at 245 nm (ε 17000) and two three-proton singlets due to the 19- and 18-methyl protons at δ 1.20 and 1.87 in the UV and NMR spectra, and compound **11** showed absorption maxima at 1383 and 1372 cm^{-1} and two three-proton singlets due to the acetonide methyl protons at δ 1.50 and 1.56 in the IR and NMR spectra. However, prolonged treatment of fluorohydrin **2** or the α,β-unsaturated ketone (**10**) with the base (K_2CO_3) afforded a new compound (**12**), mp 164—166 °C, in low yields (7—28%) along with the unsaturated ketone (**10**). This new nompound could be obtained from the starting fluorohydrin (**2**), $\Delta^{13(17)}$-20-ketone (**10**) and also 11-acetoxy-fluorohydrin (**2a**) by treatment with potassium hydroxide in ethanol at room temperature for *ca.* 2 h in quantitative yields.

Compound **12** had the same molecular formula $C_{21}H_{28}O_4$ as the α,β-unsaturated ketone (**10**). The mass spectrum suggested the presence of hydroxyl and acetyl groups at *m/e* 344 (M^+), 326 (M^+-H_2O), 311, and 301 (base, M^+-COCH_3). However, the NMR spectrum exhibited three three-proton singlets at δ 1.25, 1.37, and 1.60, the former two singlets being assignable to the 19- and probably 18-methyl protons but the last (δ 1.60) being not attributed to the acetyl methyl protons. This singlet would be ascribed to methyl protons of a partial formula CH_3-(C)(OH)-O-,[7] in which (C) denotes a quarternary carbon. The IR spectrum displayed three absorption maxima at 1714, 1665, and 1614 cm^{-1} in the double bond region and also due to (a) hydroxyl group(s) at 3600 and 3440 cm^{-1}. The above two absorptions (1665 and 1614 cm^{-1}) revealed the existence of the Δ^4-3-carbonyl system, which was supported by the UV [λ_{max} 237 nm (ε 10000)] and NMR spectra [δ 5.69 (1H, s, H at C_4)]. Hence, the remaining oxygen atom would have to constitute a carbonyl group (ν_{max} 1714 cm^{-1}) on a straight chain or a six-membered ring. Moreover, a one-proton singlet was observed at a low field (δ 4.33), which was ascribed to a proton on the carbon atom flanked by a carbonyl group and an oxygen atom. These facts, combined with the chemical shift (δ 1.25 or 1.37) of the 19-methyl protons, indicate that the compound is represented most favorably by the 13α-pregnane formula (**12**) with an oxo group at C_{11} and a hemi-acetal group formed by the 12-hydroxyl and 17-acetyl groups. Presumably, formation of the 13α-pregnane (**12**) (Scheme 1) would take place *via* (i) intramolecular Michael addition of a carbanion at C_{14}, generated by cleavage of the bond at C_{12}–C_{14}, into a partially positive β-carbon at C_{13} of the α,β-unsaturated carbonyl system ($\Delta^{13(17)}$-20-one) and (ii) subsequent tautomerization at C_{11} and C_{12} as well as epimerization at C_{17} of the resulting 13α-pregnane derivative (iii) followed by conversion into the hemi-acetal structure.

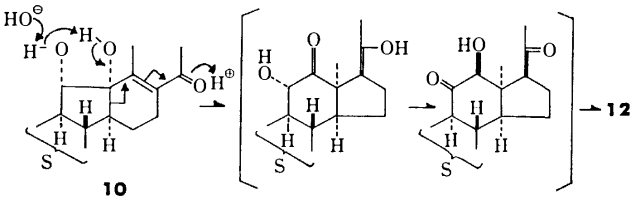

Scheme 1. Pathway for formation of 13α-pregnane (**12**).

The second product (**3**) mp 175.0—176.5 °C, had the same molecular formula $C_{21}H_{28}O_4$ as the starting epoxide (**1**) and was formulated as structure **3**. In good accord with the structure, the IR spectrum revealed the presence of five-membered carbonyl and hydroxyl groups at 1732 and 3480 cm^{-1}, and the NMR spectrum showed two three-proton singlets at δ 1.20 and 1.58, which could be attributed to the 19- and 18-methyl protons. These chemical shifts indicate that the hydroxyl group is attached to the carbon at C_{13},

and also that the C and D rings are *trans*-fused (12βH) (19-CH_3, δ_{obsd} 1.20; δ_{calc} 1.21 for 12βH, and 1.26 for 12αH).[8] In view of the fact that the corresponding 12-epimer (12αH) was not isolated, compound **3** would probably be formed by cleavage of the epoxide ring at C_{12} with concomitant hydride shift of the β-oriented hydrogen at C_{11} to the carbon atom at C_{12}.

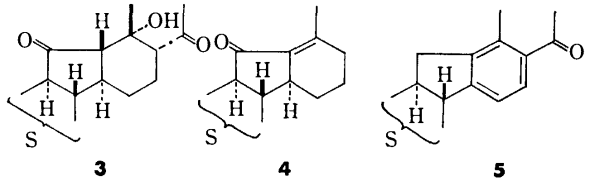

3 **4** **5**

The third product (**4**), mp 112—115 °C, had a molecular formula of $C_{19}H_{24}O_2$, indicative of elimination of a $C_2H_4O_2$ (CH_3CO+OH) moiety from the starting epoxide (**1**) and was assigned formula **4**. Removal of the 17-acetyl group was revealed by the absence of a three-proton singlet near δ 2.3 in the NMR spectrum. The UV and IR specta [λ_{max} 247 nm (ε 13000), and ν_{max} 1708 and 1639 cm^{-1}] showed the presence of a new α,β-unsaturated carbonyl group (Δ^{12}-11-one) besides the Δ^4-3-carbonyl system (ν_{max} 1668 and 1639 cm^{-1}). This was confirmed by appearance of two three-proton singlets due to 19- and 18-methyl protons at δ 1.24 and 2.15 as well as a one-proton singlet (H at C_4) at δ 5.77 in the NMR spectrum. This compound (**4**) was also produced by treatment of hydroxy ketone (**3**) with base (KOH) in refluxing methanol though in a low yield. The transformation of hydroxy ketone (**3**) into Δ^{12}-11-ketone (**4**) evidently takes place by retro-aldol reaction, initiated by attack of hydroxide ion to the acetyl carbonyl group, and subsequent migration of the resulting double bond (at C_{13}–C_{17}). On the other hand, the α,β-unsaturated ketone (**4**) was *not* obtained by the boron trifluoride treatment (including work-up) of hydroxy ketone (**3**) under the same conditions as those for formation of the compround (**4**) from epoxide **1**. Probably, formation of compound **4** would be formed by initial cleavage of the epoxy ring at C_{13} followed by degradation of the resulting cationic glycol *via* several pathways as shown in Scheme 2.

The fourth product (**5**), mp 143—145 °C, was assigned reasonably a substituted acetophenone structure

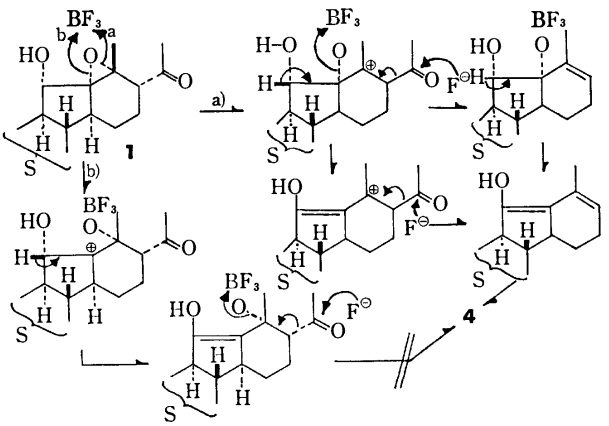

Scheme 2. Pathway for formation of Δ^{12}-11-ketone (**4**).

(**5**) on the basis of the spectral data (Exp). We only mention that the chemical shift (δ 1.32) of 19-methyl protons was in good accord with that of the corresponding veratramine derivatives.[9]

11α-Acetoxy-12α,13α-epoxide (**1a**), 11-acetate of 11α-alcohol **1**, was similarly treated with boron trifluoride etherate in benzene at room temperature. The reaction proceeded slowly and afforded fluorohydrin, as an only isolable product in a 60% yield, after 15 min, when the starting epoxide (**1a**) was recovered unchanged in a 10% yield. The sole product, mp 143—145 °C, was identified as 11-acetate (**2a**) of the 11α-hydroxy-fluorohydrin (**2**) as described before. It should be noted that no product, considered to be formed by initial cleavage of the epoxy ring at C_{12}, was isolated, when the starting epoxide passed from 11α-alcohol (**1**) to 11α-acetate (**1a**).

11-Oxo-12α,13α-epoxide (**13**) was then treated with excess of the Lewis acid under almost the same conditions as mentioned above. The epoxide cleavage proceeded only slowly and, after 140 min, gave a complex mixture, from which three compounds (**6**, **14**, and **15**) were isolated by column chromatogrphy in 25, 20, and 20% yields, respectively. The first product, mp 190.5—191.5 °C, was identified as 11-oxo-fluorohydrin (**6**). The second product (**14**), mp 227—228 °C, had the same molecular formula $C_{21}H_{26}O_4$ as the starting epoxide (**13**). The mass [*m/e* 342 (M^+) and 299(M^+ $-COCH_3$)], UV [λ_{max} 234 nm (ε 14000)], IR [ν_{max} 1667 and 1619 cm^{-1}], and NMR spectra [δ 2.19 (3H, s, 21-CH_3) and 5.72 (1H, s, H at C_4)] indicated that the 17-acetyl and Δ^4-3-carbonyl groups were left unchanged. In view of the absence of a hydroxyl group (no absorption near 3400 cm^{-1}), the remaining two oxygen atoms would have to exist as two carbonyl groups, which were observed as two absorption bands at 1742 and 1716 cm^{-1}, the latter being overlapping with that of the acetyl carbonyl group. The mass spectrum [*m/e* 271 (M^+-CH_3CO-CO)] suggested that one of the two carbonyl groups would be readily removable. The NMR spectrum also exhibited two three-proton singlets due to the 19- and 18-methyl protons at relatively low fields (δ 1.07 and 1.48) as well as a broad one-proton signal (W_H=8 Hz) at δ 3.54 besides that (20 Hz) due to the 17β-proton at δ 3.18. The signal (δ 3.54) would be attributed to a proton on the carbon atom (C_{14}) adjacent to the carbonyl group. All these spectral data revealed the presence of a bicyclo[3.3.1]nonane-2,9-dione[10] moiety and hence the compound was formulated most favorably as structure **14**.

The third product, mp 198—200 °C, also had the same molecular formula $C_{21}H_{26}O_4$ as the starting epoxide (**13**) and was assigned formual **15** on the basis of the following spectral data. The UV spectrum [λ_{max} 245 nm (ε 14000)] showed that an α,β-unsaturated carbonyl or an analogous system was newly formed besides the original Δ^4-3-carbonyl group [δ 5.78 (1H, s, H at C_4)]. The mass spectrum, unlike those of other 17-acetyletiojervanes, displayed a fragmentation peak caused by removal of a CH_2CO moiety at *m/e* 300 instead of that (M^+-CH_3CO) at *m/e* 299, but the NMR spectrum still exhibited a six-proton

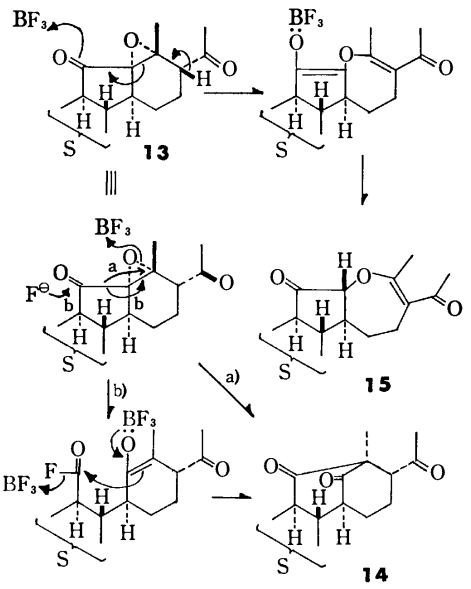

Scheme 3. Pathway for formation of compounds **14** and **15**.

singlet at δ 2.10, which was assignable to the 18-methyl and acetyl-methyl protons. The IR spectrum revealed the presence of two carbonyl groups, besides the Δ^4-3-carbonyl group (ν_{max} 1674 and 1618 cm^{-1}), at higher wave numbers (ν_{max} 1750 and 1714 cm^{-1}) as compared with those of five-membered carbonyl and 17-acetyl groups of usual 17-acetyl-11-oxoetiojervanes (ν_{max} *ca.*, 1735 and 1705 cm^{-1}). These carbonyl absorptions, coupled with an absorption due to a vinyl ether at 1044 cm^{-1}, were ascribed to α-alkoxy five-membered carbonyl and vinylogous ester carbonyl groups, respectively. Moreover, a broad one-proton doublet (J =10 Hz) was observed at δ 5.42 along with a 19-methyl proton singlet at δ 1.23. The relevant low field peak could be assigned to a proton on the carbon atom flanked by a carbonyl group and an oxygen atom. These results indicated the existence of a partial formula O=C(at C_{11})-CH-O-C(CH_3)=C-C(=O)CH_3, which led to assignment of formula **15** to the compound.

The formation of these two compounds (**14** and **15**) was rationalized as described in Scheme 3.[11] While we have analogous precedents[12] regarding the novel elimination-rearrangement involving the C-C bond cleavage of an epoxide ring of the 11-oxo-12,13-epoxide (**13**) to give the seven-membered ether ring compound (**15**), the transformation of epoxide **13** into compound **14**, a rearrangement of α,β-epoxy-carbonyl system into a bicyclo[3.3.1]nonane-2,9-dione system under acidic conditions, is most noteworthy and would probably be the first example as for such rearrangements. It should be emphasized that all these products again resulted from cleavage of the epoxide ring at C_{13}, apart from that whether the respective reactions are concerted or step-wise.

The same treatment of 11-unsubstituted 12α,13α-epoxide (**16**) only for 30 s produced two compounds (**5** and **17**) in 60 and 12% yields, the starting epoxide (**16**) being not detected on TLC. The major product, mp 141—143 °C, was identified as acetophenone (**5**), and would be formed by cleavage of the epoxide ring at C_{13} and/or C_{12} followed by dehydration and dehydrogenation. The minor product (**17**) had a molecular formula of $C_{21}H_{29}O_3F$ and was assigned 12β-fluoro-13α-hydroxy structure (**17**) on the basis of the following facts. (i) The molecular formula and spectral data indicated product **17** to be a fluorohydrin formed by simple cleavage of the epoxy ring. (ii) The product (**17**) underwent no dehydrofluorination, the starting material being recovered unchanged, under the same basic (K_2CO_3) conditions as those under which 13β-fluoro-12α-alcohols (**2** and **2a**) were readily converted into $\Delta^{13(17)}$-20-ketone (**10**). (iii) 13β-Fluoro-12α-hydroxy-etiojervanes and *C*-nor-*D*-homospirostan[4] (**2**, **2a**, **6**, and **18**) exhibited signals due to the 18-methyl protons at δ 1.50, 1.58, 1.47, and 1.58, respectively, which 12α-fluoro-13β-hydroxy-*C*-nor-*D*-homospirostan[4] (**19**) and the product in question displayed the corresponding signals at higher fields, δ 1.27 and 1.29. Moreover, compounds **2**, **2a**, and **6** showed signals due to the protons at C_{17} near δ 3.30 (W_H= 24—20 Hz), δ 3.34, 3.30, and 3.27, respectively, while compound **17** displayed the 17-proton at δ 2.89 (W_H= 18 Hz). All these facts revealed that the substituent at C_{13} in product **17** was not a fluorine atom but a hydroxyl group, and hence the product (**17**) is represented favorably by structure **17**. This structure was also supported by the ORD curves; **17**, a=+90°; 17α-acetyl-12β-etiojervan-3β-ol 3-acetate[13] and its 12α-epimer[14] (**20** and **21**), a=+53° and +34°.[15] Compound **17** evidently resulted from the epoxide ring cleavage at C_{12}. In summary, we again emphasize that the epoxide opening reactions proceeded more slowly and took place at C_{13} rather than at C_{12} with increase of electronegativity of the 11-substituents.

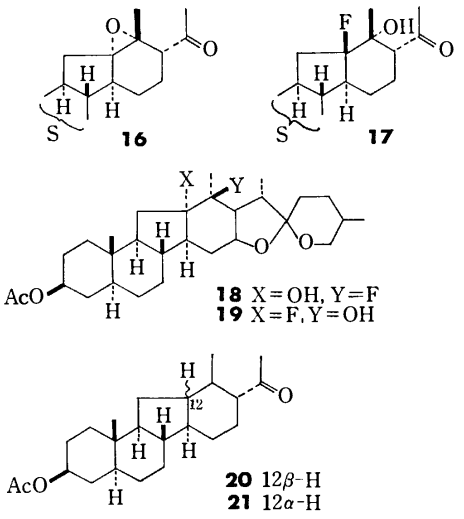

Experimental

All the melting points were uncorrected. The homogenity of each compound was always checked by TLC on silica gel (Wakogel B-5) with various solvent systems, and the spots were developed with cerium(IV) sulfate in dil sulfuric acid and/or iodine. The optical rotations, UV, and IR spectra

were measured in chloroform, ethanol, and chloroform, respectively, unless otherwise stated. The NMR spectra were obtained in deuterochloroform at 100 MHz, and the chemical shifts were given in δ-values, TMS being used as an internal reference. The abbreviations "s, d, and br" in the NMR spectra denote "singlet, doublet, and broad", respectively.

*Treatment of 17α-Acetyl-12α,13α-epoxy-11α-hydroxyetiojerv-4-en-3-one (**1**) with Boron Trifluoride Etherate (BF_3).* A solution of **1** (900 mg) in anhydrous benzene (93 ml) was stirred with BF_3 (2 ml), freshly distilled over calcium hydride, at room temperature (temp.) for 30 s. The solution was mixed with ether (50 ml), washed with 5% aqueous sodium hydrogencarbonate ($NaHCO_3$) and water, dried over anhydrous sodium sulfate, and evaporated to leave amorphous residue (877 mg), which was chromatographed over silica gel (Merck 70—230 mesh, 26 g) with mixtures of benzene and ether. Benzene–ether (5 : 1) eluates gave etiojerva-4,12-diene-3,11-dione (**4**, 74 mg), mp 112—115 °C (from hexane–methanol) and $[\alpha]_D$ +97°; MS, *m/e* 284 (M^+) and 269; UV, IR, and NMR, in the text. Found: C, 79.98; H, 8.58%. Calcd for $C_{19}H_{24}O_2$: C, 80.24; H, 8.51%.

Benzene–ether (3 : 1) eluates gave 17-acetyletiojerva-4,12,14,16-tetraen-3-one (**5**, 92 mg), mp 143—145 °C (from hexane–acetone) and $[\alpha]_D$ +148°; MS, *m/e* 308 (M^+), 293, and 265; UV, λ_{max} 295 nm (ε 4000) and 239 (13000); IR (Nujol), ν_{max} no OH, 1680—1650 (broad), and 1615 cm^{-1}; NMR, δ 1.32, 2.42, and 2.56 (each 3H, s, 19-, 18-, and 21-C<u>H</u>$_3$), and 5.85 (1H, s, <u>H</u> at C_4), 7.04 and 7.56 (each 1H, ABq J=8 Hz, 2<u>H</u> at C_{15} and C_{16}). Found: C, 81.55; H, 7.73%. Calcd for $C_{21}H_{24}O_2$: C, 81.78; H, 7.84%.

Benzene–ether (2 : 1) eluates afforded 17α-acetyl-13α-hydroxy-12β-etiojerv-4-ene-3,11-dione (**3**, 90 mg), mp 175.0—176.5 °C (from isopropyl ether–acetone) and $[\alpha]_D$ +26°; MS, *m/e* 344 (M^+), 326, and 301; UV (MeOH), λ_{max} 236 nm (ε 14,000); IR (Nujol), ν_{max} 3480, 1732, 1692, 1675, and 1610 cm^{-1}; NMR, δ 1.20, 1.58, and 2.25 (each 3H, s, 19-, 18-, and 21-C<u>H</u>$_3$), 4.01 (1H, s, O<u>H</u>), and 5.78 (1H, s, <u>H</u> at C_4). Found: C, 73.06; H, 8.27%. Calcd for $C_{21}H_{28}O_4$: C, 73.22; H, 8.19%.

Benzene–ether (1 : 1) eluates afforded 17α-acetyl-11α,12α-dihydroxy-13β-fluoro-13-epietiojerv-4-en-3-one (**2**, 180 mg), mp 153—155 °C (from ether) and $[\alpha]_D$ +38°; MS and UV (MeOH), in the text; IR (Nujol), ν_{max} 3400—3480 (broad), 1703, 1660, and 1610 cm^{-1}; NMR, in the text. Found: C, 69.53; H, 8.15%. Calcd for $C_{21}H_{29}O_4F$: C, 69.20; H, 8.02%.

Compound **3** (15 mg) was refluxed in methanol containing 5% potassium hydroxide. After being cooled, the mixture was made neutral with 10% aqueous acetic acid, evaporated and shaken with water and chloroform. The chloroform solution was washed with water, dried and evaporated to leave amorphous residue (13 mg), which was separated by preparative TLC over silica gel (Wakogel B-5F, one plate with 20×20 cm^2) with a 3 : 1 mixture of benzene and ether to yield **4** (4 mg), mp 112—114 °C. This was identical with the afore-mentioned sample in IR, NMR, and TLC.

*Treatment of 17α-Acetyl-12α,13α-epoxy-11α-hydroxyetiojerv-4-en-3-one 11-Acetate (**1a**) with BF_3.* A solution of **1a** (196 mg) in anhydrous benzene (18 ml) was stirred with BF_3 (0.4 ml) at room temp for 15 min. The reaction mixture was worked up as described above to leave amorphous residue (206 mg), showing one major and one minor spot, which was separated by chromatography over silica gel (7 g). The major fraction, eluted with benzene–ether (3 : 1) afforded 11-acetoxy-fluorohydrin (**2a**, 103 mg), mp 143—145 °C (from isopropyl ether–acetone) and $[\alpha]_D$ +75°; MS, *m/e* 406 (M^+), 388, 386, 346, 326, and 283; UV, λ_{max} 238 nm (ε 10000); IR, ν_{max} 3420, 1737, 1717, 1663, 1614, and 1243 cm^{-1}; NMR, δ 1.24, 1.58, 2.32, and 2.12 (each 3H, s, 19-, 18-, 21-C<u>H</u>$_3$, and OCOC<u>H</u>$_3$), 3.30 and 5.42 (each 1H, br W_H=24 and 12 Hz, 2<u>H</u> at C_{17} and C_{11}), 5.56 and 5.75 (each 1H, s, O<u>H</u> and <u>H</u> at C_4). The minor fraction, eluted with benzene–ether (1 : 1), gave acetate (20 mg), mp 198—200 °C (from ether), which was identified as the starting epoxide (**1a**) (IR, NMR, TLC, and mixed mp).

*Treatment of 17α-Acetyl-12α,13α-epoxyetiojerv-4-en-3,11-dione (**13**) with BF_3.* Compound **13** (180 mg) in benzene (20 ml) was treated with BF_3 (0.28 ml) at room temp for 140 min. The reaction mixture was worked up as mentioned above to leave amorphous residue (182 mg), which was separated into three fractions by preparative TLC over silica gel (Wakogel B-5F, 9 plates) with a 3 : 1 mixture of benzene and ether. A most mobile fraction gave a crystalline substance, which was recrystallized from isopropyl ether–acetone to yield a bicyclo[3.3.1]nonane-2,9-dione derivative (**14**, 35 mg), mp 227—228 °C and $[\alpha]_D$ +95°; MS, IR (Nujol), and NMR, in the text. Found: C, 73.26; H, 7.66%. Calcd for $C_{21}H_{26}O_4$: C, 73.66; H, 7.66%.

A middle fraction afforded 11-oxo-fluorohydrin (**6**, 47 mg), mp 190.5—191.5 °C (from isopropyl ether–acetone) and $[\alpha]_D$ +182°; MS, *m/e* 362 (M^+), 342, 319, and 299; UV, λ_{max} 234 nm (ε 12,000); IR, ν_{max} 3380, 1753, 1699, 1644, and 1615 cm^{-1}; NMR, δ 1.21, 1.47, and 2.33 (each 3H, s, 19-, 18-, and 21-C<u>H</u>$_3$), 3.24 (1H, br W_H=20 Hz, <u>H</u> at C_{17}), 5.72 and 5.77 (each 1H, s, O<u>H</u> and <u>H</u> at C_4). Found: C, 69.38; H, 7.58%. Calcd for $C_{21}H_{27}O_4F$: C, 69.62; H, 7.51%.

A least mobile fraction gave an oxepin derivative (**15**, 35 mg), mp 198—200 °C (from isopropyl ether) and $[\alpha]_D$ +160.5°; MS, *m/e* 342 (M^+), 300 ($M^+ - CH_2CO$), 282, and 267; UV, IR (Nujol), and NMR, in the text. Found: C, 73.36; H, 7.69%. Calcd for $C_{21}H_{26}O_4$: C, 73.66; H, 7.66%.

*Treatment of 17α-Acetyl-12α,13α-epoxyetiojerv-4-en-3-one (**16**) with BF_3.* Compound **16** (500 mg) in benzene (50 ml) was stirred with BF_3 (0.72 ml) at room temp for 30 s. The reaction mixture was worked up as usual to leave an amorphous material, which was separated into two fractions by chromatography over silica gel (Merck 70—230 mesh, 30 g) with benzene–ether mixtures. Eluates with benzene–ether (5 : 1) gave a crystalline substance (284 mg), mp 141—143 °C (from hexane–acetone), which was identical with acetophenone (**5**) in IR, NMR, TLC, and mixed mp. Eluates with benzene–ether (3 : 1) afforded 17α-acetyl-12β-fluoro-13α-hydroxyetiojerv-4-en-3-one (**17**, 66 mg), mp 157—159 °C (from ether) and $[\alpha]_D$ +83°; ORD, $[\Phi]_{306}^{peak}$ +4750°, $[\Phi]_{282}^{trough}$ −4250°, a=+90°; MS, *m/e* 348 (M^+), 333, 328, and 310; UV, λ_{max} 237 nm (ε 10000); IR, ν_{max} 3460, 1696, 1657, and 1616 cm^{-1}; NMR, δ 1.17, 1.25, and 2.26 (each 3H, s, 19-, 18-, and 21-C<u>H</u>$_3$), 2.89 (1H, br W_H= 18 Hz, <u>H</u> at C_{17}), 4.32 and 5.75 (each 1H, s, O<u>H</u> and <u>H</u> at C_4). Found: C, 72.19; H, 8.54%. Calcd for $C_{21}H_{29}O_3F$: C, 72.38; H, 8.39%.

*Oxidation of Fluorohydrin **2**.* (i) A solution of **2** (20 mg) in dry acetone (3 ml) was stirred with the Jones reagent (0.2 ml) for 2 h under cooling with ice. After addition of ethanol to decompose excess of the reagent, the solution was evaporated and shaken with water and chloroform. The chloroform solution was worked up as usual to leave a crystalline substance, showing a single spot, which was recrystallized from isopropyl ether–acetone to give 11-oxo-fluorohydrin (**6**, 16 mg), mp 188—190 °C, which was identical with the above-mentioned sample in IR, NMR, TLC, and mixed mp.

(ii) A solution of **2** (20 mg) in dioxane (1.5 ml) was stirred with periodic acid (50 mg as $HIO_4 \cdot 2H_2O$) in water (0.5 ml) at room temp for 18 h. The solution was diluted with water, extracted with chloroform, and the chloroform solution, after being worked up as usual, gave a crystalline material, showing a single spot. This was recrystallized from ether to give lactol (**7**, 14 mg), mp 128—130 °C; MS, *m/e* 362 (M^+), 347, and 342; IR, ν_{max} 3570, 3440, 1715, 1665, and 1615 cm^{-1}; NMR, δ 1.24, 1.33, and 2.26 (each 3H, s, 19-, 18-, and 21-C$\underline{H}_3$), 3.70 (1H, s, O$\underline{H}$), 5.40 (1H, d J=8 Hz, $\underline{H}$ at C_{11}), and 5.73 (1H, s, $\underline{H}$ at C_4), and no absorption near δ 1.0.

*11-Acetate (**2a**) and 11,12-Acetonide (**9**) of Fluorohydrin **2**.* (i) Compound **2** (15 mg) was treated with acetic anhydride (0.15 ml) and pyridine (0.3 ml) at room temp for 24 h under stirring. The reaction mixture was worked up as usual to give **2a** (17 mg), mp 140—142 °C (from isopropyl ether–acetone), which was identical with the sample obtained from **1a** (IR, NMR, and mixed mp).

(ii) A solution of **2** (10 mg) in acetone (2 ml) was stirred with 60% aqueous perchloric acid (0.1 ml) for 1.5 h. The solution was made alkaline with 5% aqueous $NaHCO_3$, evaporated and extracted with chloroform. The chloroform solution, after being worked up as usual, gave acetonide (**9**), oil, showing a single spot on TLC; MS, *m/e* 405 (M^++1), 389, and 384; IR, ν_{max} 1715, 1664, 1614, 1384, and 1373 cm^{-1}; NMR, δ 1.23, 1.40, 1.53, and 2.26 (3H, 6H, 3H, and 3H, each s, 19-, 18-, and 21-C$\underline{H}_3$, and acetonide 2C$\underline{H}_3$ or *vice versa*), 4.71 (1H, br W_H=12 Hz, $\underline{H}$ at C_{11}), and 5.76 (1H, s, $\underline{H}$ at C_4).

*Alkali Treatment of 11-Hydroxy-fluorohydrin (**2**), Its 11-Acetate (**2a**), and Its 11,12-Acetonide (**9**).* (i) Compound **2a** (18 mg) was stirred with potassium carbonate (200 mg) in a mixture of methanol (6 ml) and water (2 ml) at room temp for 2 h under nitrogen. The reaction mixture, after being worked up as usual, left amorphous residue (17.5 mg), showing two spots, which was separated into two fractions by preparative TLC over silica gel (Wakogel B-5F, one plate). A less polar fraction gave a crystalline substance, which on recrystallization from hexane–acetone afforded $\Delta^{13(17)}$-20-ketone (**10**, 10 mg), mp 173—174 °C and $[\alpha]_D$ −26°; MS, *m/e* 344 (M^+), 326, 311, and 301; UV, in the text; IR, ν_{max} 3620, 3440, 1680 (shoulder), 1662, and 1613 cm^{-1}; NMR, δ 1.20, 1.87, and 2.29 (each 3H, s, 19-, 18-, and 21-C$\underline{H}_3$), 3.32 (2H, br, s, 2O$\underline{H}$), 3.61 (1H, br W_H=15 Hz, $\underline{H}$ at C_{11}), and 5.78 (1H, s, $\underline{H}$ at C_4). Found: C, 72.89; H, 8.12%. Calcd for $C_{21}H_{28}O_4$: C, 73.22; H, 8.19%. A more polar fraction was identified as 13α-pregnane (**12**, 1 mg), by comparison with the sample described later (MS and TLC).

When compound **2a** (12.8 mg) was treated with the base under the same conditions for 1 h as mentioned above, the product (10 mg), mp 170—172 °C, showed a single spot and was identified as **10**.

Compound **10** (7.3 mg) was stirred with acetone (2 ml) containing perchloric acid (60%, 0.1 ml) at room temp for 1 h. The mixture was worked up as usual to leave oily residue, showing a single spot, which was purified by preparative TLC to yield acetonide (**11**, 8.0 mg), oil and $[\alpha]_D$ −43°; MS, *m/e* 384 (M^+), 369, and 326; UV, λ_{max} 241 nm (ε 16000); IR, ν_{max} no OH, 1664, 1615, 1383, and 1372 cm^{-1}; NMR, δ 1.16, 1.50, 1.56, 1.86 and 2.30 (each 3H, 19-, 18-, and 21-C$\underline{H}_3$, acetonide 2C$\underline{H}_3$, or *vice versa*), 4.18 (1H, d J= 8 Hz, $\underline{H}$ at C_{11}), and 5.80 (1H, s, $\underline{H}$ at C_4). This acetonide (**11**, 16 mg) was obtained by treatment of **9** (17 mg) with potassium carbonate.

(ii) A solution of **2a** (20 mg) in ethanol (5 ml) containing 5% potassium hydroxide was stirred at room temp for 100 min. The solution was made neutral with 10% aqueous acetic acid under cooling, evaporated below 40 °C, and shaken with water and chloroform. The chloroform solution was worked up as usual to leave an oily material, showing a single spot, which was purified by preparative TLC to give a 13α-pregnane derivative (**12**, 13 mg), mp 164—166 °C (isopropyl ether–acetone) and $[\alpha]_D$ +64°; MS, UV, IR, and NMR, in the text; NMR (C_5D_5N), δ 1.30, 1.58, and 1.74 (each 3H, s, 19-, 18-, and 21-C$\underline{H}_3$), 4.50 and 5.76 (each 1H, s, 2$\underline{H}$ at C_{12} and C_4).[16]

Found: C, 73.08; H, 8.12%. Calcd for $C_{21}H_{28}O_4$: C, 73.22; H, 8.19%.

Treatment of **2** (5.3 mg) and **10** (4.7 mg) with potassium hydroxide under almost the same conditions as mentioned above afforded **12** (5.0 and 4.7 mg, respectively), and that of **10** (9.7 mg) with potassium carbonate also gave **12** (2.7 mg) along with the starting material (**10**, 4.7 mg) after preparative TLC.

References

1) Part III, A. Murai, N. Iwasa, M. Takeda, H. Sasamori, and T. Masamune, *Bull. Chem. Soc. Jpn.*, **50**, 429 (1977).

2) Part XXX of "*C*-Nor-*D*-homosteroids and Related Alkaloids," Part XXIX, Ref. 1.

3) A. Murai, H. Sasamori, and T. Masamune, *Bull. Chem. Soc. Jpn.*, to be submitted.

4) J. M. Coxon, M. P. Hartshorn, and D. N. Kirk, *Tetrahedron*, **21**, 2489 (1965).

5) A preliminary communication of this paper, A. Murai, H. Sasamori, and T. Masamune, *Chem. Lett.*, **1976**, 975.

6) a) I. G. Guest and B. A. Marples, *J. Chem. Soc., C* **1970**, 1626, and their previous papers; b) D. N. Kirk and M. P. Hartshorn, "Steroid Reaction Mechanisms," Elsevier Publ. Co., London (1968), p. 353.

7) M. Biollaz, J. Schmidlin, and J. Kalvoda, *Helv. Chim. Acta*, **58**, 1433 (1975).

8) T. Masamune, A. Murai, K. Nishizakura, T. Orito, S. Numata, and H. Sasamori, *Bull. Chem. Soc. Jpn.*, **49**, 1622 (1976).

9) T. Masamune, I. Yamazaki, K. Orito, and M. Takasugi, *Tetrahedron*, **27**, 3387 (1971).

10) *Cf.*, P. W. Hickmott and J. R. Hargreaves, *Tetrahedron*, **23**, 3151 (1967); D. Y. Curtin and R. R. Fraser, *J. Am. Chem. Soc.*, **81**, 662 (1959).

11) After preparation of this manuscript, we received Domagala and coworkers' report on the mechanism of the acid-catalyzed rearrangement of acyl groups to adjacent positive centers; J. M. Domagala, R. D. Bach, and J. Wemple, *J. Am. Chem. Soc.*, **98**, 1975 (1976).

12) J. M. Coxon, R. P. Garland, M. P. Hartshorn, and G. A. Lane, *Tetrahedron Lett.*, **1968**, 1506; *Tetrahedron*, **26**, 1533 (1970); M. Niwa, M. Iguchi, and S. Yamamura, *Tetrahedron Lett.*, **1975**, 3661.

13) A. Murai, T. Nishimura, and T. Masamune, *Bull. Chem. Soc. Jpn.*, **49**, 1602 (1976).

14) N. Sato, Ph. D. Thesis, Hokkaido University, Sapporo, 1969.

15) The ORD data (Ref. 13, p. 1609) of compounds **20** and **21** in Ref. 13 should be revised to those of **21** and **20** in Ref. 13 (because of our error in typing).

16) R. Tschesche, I. Morner, and G. Snatzke, *Justus Liebigs Ann. Chem.*, **670**, 103 (1963).

The Reactions of 1,3-Indandiones and 1,3(2*H*)-Phenalenediones with Lead Tetraacetate

Keiichi Ezoe and Kazu Kurosawa

Department of Chemistry, Faculty of Science, Kumamoto University, Kurokami 2-39-1, Kumamoto 860

(Received July 23, 1976)

The reaction of 1,3-indandione with lead tetraacetate gave phthalic anhydride and 2,2-diacetoxy-1,3-indandione. The reaction of 2,2-dihydroxy-1,3-indandione gave phthalic anhydride. The reactions of 1,3(2*H*)-phenalenedione and 2,3-dihydroxy-1-phenalenone yielded acenaphthenequinone and 1,8-naphthalenedicarboxylic anhydride. The reactions of acenaphthenequinone and 2,2-dihydroxy-1,3-phenalenedione gave 1,8-naphthalenedicarboxylic anhydride with higher yields. The reactions of [2-^{14}C]-labeled compounds showed that the middle carbon atom was lost.

Mckillop and his co-workers[1] have reported that the reaction of chalcones with thallium(III) nitrate gave benzils with the loss of one carbon atom. Roberts *et al.*[2] reported that the decarbonylation of 1,3-diphenyl-1,2,3-propanetrione with cupric acetate in refluxing acetic acid yielded benzil with the loss of the center carbonyl group, as evidenced by the decarbonylation of the ^{14}C-labeled trione. Moriyama[3] also reported that the oxidation of 2-acetoxy-1,3-diphenyl-1,3-propanedione-2-^{14}C with lead tetraacetate gave inactive benzil and active carbon dioxide, again indicating that the middle carbon was lost. However, the oxidation of β-hydroxychalcone-α-^{14}C with lead tetraacetate gave radioactive benzil (the relative specific radioactivity was 0.53) and carbon dioxide (the relative specific radioactivity was 0.06 as barium carbonate), thus suggesting that binary reaction mechanisms may operate in this case. We therefore examined the reactions of 1,3-indandiones and 1,3(2*H*)-phenalenediones with lead tetraacetate, which are cyclic analogues to the 1,3-diphenyl-1,3-propanediones, in the hope of clarifying the reaction pathways.

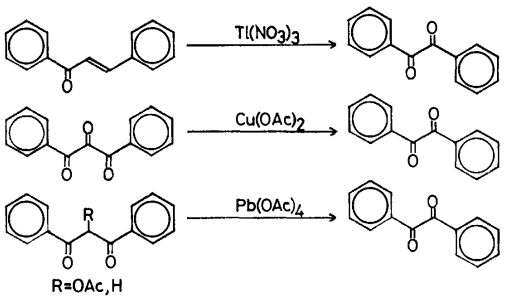

Scheme 1.

Results

When 1,3-indandione (I)[4] was oxidized with lead tetraacetate in boiling benzene, two compounds (III-(7%) and IV(12%)) were obtained. The NMR spectrum of III ($C_{13}H_{10}O_6$; mp 174—175 °C) indicated the presence of two acetoxyl groups [δ 2.14(s, 6H)] and aromatic protons [δ 7.98 (m, 4H)]. The IR spectrum of this compound suggested the presence of two carbonyl groups [ν_{max} 1745 (CO) and 1765 cm^{-1} (OAc)]. These spectroscopic properties indicated that this product has the structure of 2,2-diacetoxy-1,3-indandione. The second compound (IV) was found to be phthalic anhydride, which was identified by comparison of its IR spectrum and its melting point with those of an authentic specimen.

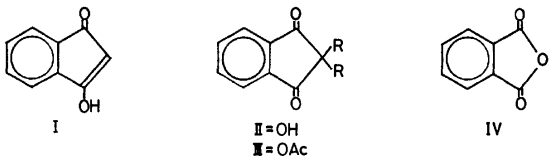

The yields of III and IV were slightly improved by increasing the amount of lead tetraacetate. These results are shown in Table 1.

The reaction of 2,2-dihydroxy-1,3-indandione (II)[5] with lead tetraacetate in boiling benzene gave only IV (43%).

The reaction of 1,3(2*H*)-phenalenedione (VI)[6] with lead tetraacetate in various molar ratios in boiling acetic acid gave two products (IX, mp 272—273 °C and X, mp 259—260 °C). IX and X were shown to be 1,8-naphthalenedicarboxylic anhydride and acenaphthenequinone respectively, by comparison of their melting points and their IR spectra with those of authentic specimens.

When 2,3-dihydroxy-1-phenalenone (VIII)[6] was oxidized with one equivalent of lead tetraacetate in boiling acetic acid, two compounds (IX and X) were obtained. However, when VIII was oxidized with three equivalents of lead tetraacetate, only IX was obtained.

The reaction of 2,2-dihydroxy-1,3-phenalenedione (VII)[7] with lead tetraacetate in boiling acetic acid gave IX as the sole product.

Table 1. Oxidations of 1,3-indandione (I) and 2,2-dihydroxy-1,3-indandione (II) with lead tetraacetate in boiling benzene

Compound	Reaction conditions: Molar ratio	Reaction conditions: Time (min)	Products: (Isolated yield, %) III	IV	CO_2
I	1 : 2	20	4.8	3.4	a)
I	1 : 3	20	5.7	4.1	a)
I	1 : 4	20	6.8	12.0	29.6
II	1 : 1	20		23.4	a)
II	1 : 2	20		37.5	a)
II	1 : 3	20		43.2	17.0

a) Not measured.

Table 2. Oxidation of 1,3(2*H*)-phenalenediones (VI, VII, VIII) and acenapquinone(X) with lead tetraacetate in boiling acetic acid

Compound	Reaction conditions: Molar ratio	Reaction conditions: Time (min)	Products (Isolated yield, %): IX	X	CO_2
VI	1 : 1	10	a)	3.2	6.2
VI	1 : 2	10	a)	2.3	a)
VI	1 : 3	30	a)	1.8	a)
X	1 : 1	20	70		a)
VII	1 : 1	5	68		2.9
VII	1 : 2	5	68		a)
VII	1 : 3	15	62		a)
VIII	1 : 1	5	a)	14	a)
VIII	1 : 2	10	21		a)
VIII	1 : 3	15	62		57

a) Not measured.

The oxidation of acenaphthenequinone with one equivalent of lead tetraacetate in boiling acetic acid gave IX (70%) after 20 min. The yields of the products obtained by the above reactions are summarized in Table 2.

In order to establish the nature of the decarbonylation reaction, the reactions were repeated using [2-^{14}C]-labeled compounds, *i.e.*, [2-^{14}C]-I, [2-^{14}C]-II, [2-^{14}C]-VI, [2-^{14}C]-VII, and [2-^{14}C]-VIII. The results are summarized in Schemes 2 and 3.

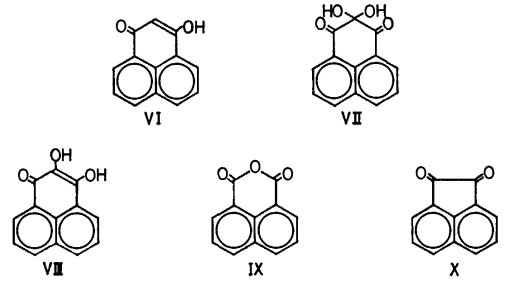

1,3-Indandione-2-^{14}C was synthesized by the reaction of diethyl phthalate with ethyl acetate-2-^{14}C. When 1,3-indandione-2-^{14}C was oxidized with lead tetraacetate, radioactive IV (the relative specific radioactivity was 0.17) and carbon dioxide (the relative specific radioactivity was 0.28 as barium carbonate) were obtained. On the other hand, the oxidation of 2,2-dihydroxy-1,3-indandione-2-^{14}C gave inactive IV and active carbon dioxide (the relative specific radioactivity was 0.71 as barium carbonate) (Scheme 2).

1,3(2*H*)-Phenalenedione-2-^{14}C was synthesized by the reaction of 1,8-naphthalenedicarboxylic anhydride with diethyl malonate-2-^{14}C. When 1,3(2*H*)-phenalenedione-2-^{14}C was oxidized with lead tetraacetate, radioactive X (the relative specific radioactivity was 0.19) and carbon dioxide (the relative specific radioactivity was 0.13 as barium carbonate) were obtained. When 2,3-dihydroxy-1-phenalenone-2-^{14}C was oxidized with lead tetraacetate, radioactive IX (the relative specific radioactivity was 0.13) and carbon dioxide the relative specific radioactivity was 0,60 as barium carbonate) were obtained. The oxidation of 2,2-dihydroxy-1,3-phenalenedione-2-^{14}C gave inactive IX and active carbon dioxide (the relative specific radiocativity was 0.80) (Scheme 3).

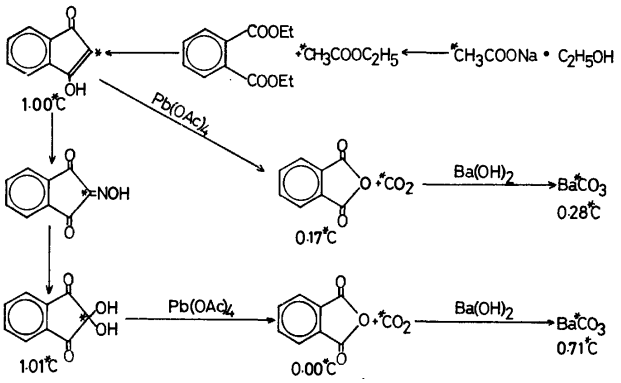

Scheme 2. Synthesis and decarbonylation reactions of 1,3-indandiones[2-^{14}C] (the figures under the formulae refer to the specific activities of the compounds relative to 1,3-indandione).

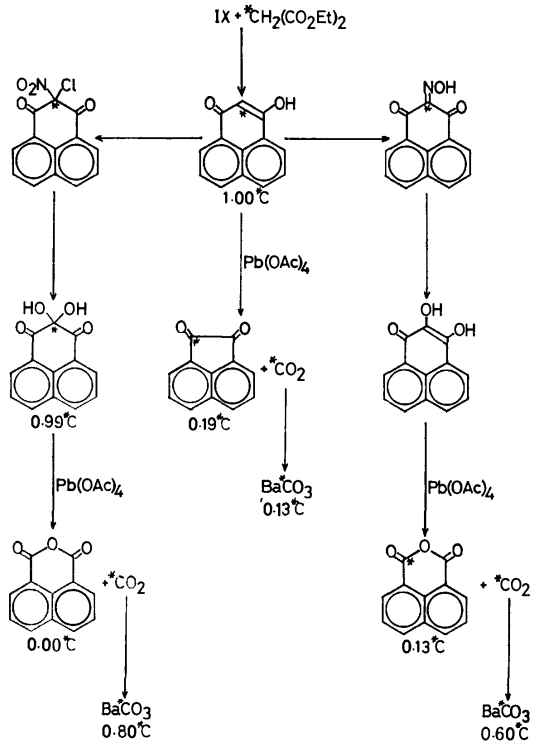

Scheme 3. Synthesis and decarbonylation reactions of 1,3(2*H*)-phenalenediones[2-^{14}C] (the figures under the formulae refer to the specific activities of the compounds relative to 1,3(2*H*)-phenalenedione).

Discussion

The conversion of I to III can readily be explained in terms of successive acetoxylations at the α-carbon adjacent to the carbonyl group. The conversion of I to IV involves the loss of 83% of C(2), suggesting that there may be binary reaction pathways.

In the case of the reaction of II with lead tetraacetate, the yield of IV was increased by increasing the molar

ratio of the oxidant. From the tracer experiment, it was shown that the decarbonylation of C(2) is involved in the oxidation of II with lead tetraacetate, as indicated by the complete loss of the radioactivity.

When VI was oxidized with lead tetraacetate, the yield of X was decreased by increasing the molar ratio of the oxidant. It seems that X is an intermediate, as the oxidation of X with one equivalent of lead tetraacetate gave IX in better yield (70%). However a longer reaction time (20 min) was needed to consume the lead tetraacetate than in the case of VI. Therefore, we must eliminate the possibility that the reaction proceeds *via* X. The experiment on the ^{14}C-labeled compound showed that the reaction pathway involved the decarbonylation of C(2) atoms by 81%.

The oxidation of VIII with one equivalent of lead tetraacetate gave both IX and X, but that with three equivalents of lead tetraacetate gave only IX (62%). The experiment on the ^{14}C-labeled compound again indicated that the decarbonylation of C(2) was involved by 87% in this case.

The oxidation of VII gave IX (68%) without redox disproportionation, which was reported to occur in the reactions of VII[6] in boiling water or at high temperature, and completed by one equivalent of the oxidant. This reaction pathway involved the complete loss of C(2) atoms as shown by the tracer experiment (Scheme 4).

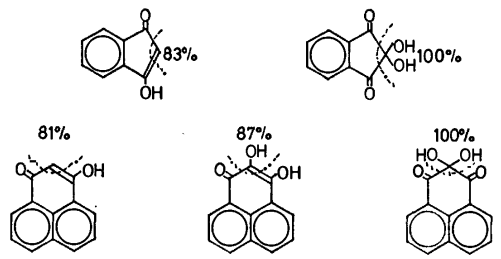

Scheme 4. The loss of the carbon (2-position) in 1,3-diones.

The above data indicate that the reaction pathway for the oxidation of the 1,3-diones and the enediol are fairly complicated ones, as indicated by the presence of the portion of the radioactivity in the product.

In the case of trione, on the other hand, on change in the yields of IV in the oxidation of II was observed when acetic acid was used as a solvent. The oxidations of VIII required only one equivalent of the oxidant and lost the C(2) completely. The above two facts suggest that the radical mechanism is favored in this case. However, no conclusive evidence is available to distinguish the radical and ionic mechanisms which operate in the reaction.

Experimental

The NMR spectra were recorded for the deuteriochloroform and trifluoroacetic acid solutions with a Hitachi R 24 NMR spectrometer, with tetramethylsilane as an internal reference. The IR spectra were recorded for the chloroform solution and KBr disk with a JASCO IRA-1 grating spectrometer. The melting points were determined with a Yanagimoto hot-stage apparatus. The radioactivities were recorded, for samples crystallized to a constant specific radioactivity, with an Aloka liquid scintillation spectrometer. The scintillator consisted of DPO(6 g), POPOP (0.275 g), and naphthalene (Dojin Laboratories, Kumamoto) dissolved in dioxane. Barium carbonate samples were suspended in a gel made up with 4% W/V CAB-O-SIL (Beckmann Instruments Inc., U.S.A.). Sample counts were repeated twice; the maximum observed error was within 0.5%.

Oxidations of 1,3-Indandiones with Lead Tetraacetate. The typical procedure of the oxidation of 1,3-indandiones is as follows. A mixture of 1,3-indandione (2 mmol), lead tetraacetate (4—8 mmol), and benzene (30 ml) was heated under reflux for the period of time shown in Table 1. Nitrogen was passed through the reaction mixture, and the evolved gases were passed into saturated aqueous barium hydroxide, aqueous potassium permanganate, and again saturated aqueous barium hydroxide. The precipitated barium carbonate was collected by centrifugation, washed with water, and dried. After the removal of insoluble materials by filtration, the benzene was evaporated *in vacuo* and the products were purified on TLC with chloroform as an eluting solvent. I gave 2,2-diacetoxy-1,3-indandione (III), mp 174—175 °C, 6.8%, (Found: C, 59.34; H, 3.99%. Calcd for $C_{13}H_{10}O_6$: C, 59.54; H, 3.84%, δ: 7.98 (m, 4H) and 2.14 (s, 6H, OAc), ν_{max}: 1745 and 1750 cm^{-1}), phthalic anhydride (IV) (mp 130—131 °C) and carbon dioxide. II yielded IV (mp 130—131 °C) and carbon dioxide.

Oxidation of 1,3(2H)-Phenalenediones with Lead Tetraacetate. A typical procedure of the oxidation of 1,3(2*H*)-phenalenediones is as follows. A mixture of 1,3(2*H*)-phenalenedione (2 mmol), lead tetraacetate (2—6 mmol), and hot acetic acid (30 ml) was heated under reflux for a period of time shown in Table 2. The carbon dioxide which evolved was converted to barium carbonate as described previously. After the removal of the acetic acid *in vacuo*, the residue was treated with 2M hydrochloric acid (60 ml) and extracted with chloroform. The chloroform solution was dried over sodium sulfate and evapolated under reduced pressure, and the products were separated on TLC with chloroform as an eluting solvent, giving the 1,8-naphthalenedicarboxylic anhydride (IX) (mp 272—273 °C) and/or acenaphthenequinone (X) (mp 259—260 °C). VII yielded IX (mp 272—273 °C) and carbon dioxide. VIII yielded IX (mp 272—273 °C), carbon dioxide and/or X (mp 259—260 °C).

Oxidation of Acenaphthenequinone (X). A mixture of acenaphthenequinone (2 mmol), lead tetraacetate (2 mmol), and acetic acid (30 ml) was heated under reflux for 20 min. After cooling, the crystals which precipitated were collected by filtration, giving IX (mp 272—273 °C).

1,3-Indandione-2-^{14}C. Into a mixture of diethyl phthalate (72 g) and powdered sodium (14.3 g) was dropped ethyl acetate-2-^{14}C (70 g) (which was prepared from acetic-2-^{14}C acid (250 μCi, Radiochemical Centre, Amersham, England) in absolute ethyl alcohol (1.43 g) over a period about 90 min). The material in the flask was refluxed gently during the addition of ethyl acetate mixture. The heating was continued for 6 h, and ether (30 ml) was added after cooling. As much of the sodium salt as possible was collected on a filter and then washed with ether, using as small a volume as possible. The total yield of the dry, yellow sodium salt was 55 g (71%). The sodium salt (55 g) was added to hot water (750 ml). The solution was cooled to 70 °C and under vigorous agitation the sodium salt was decomposed with a sulfuric acid solution (three parts of concentrated sulfuric acid and one part of water) (50 ml). The mixture was cooled to 15 °C and filtered. The 1,3-indandione thus obtained was a pale yellow solid (mp 127—

129 °C, 29 g, 61.3%, specific radioactivity 0.176 μCi/mmol).

2,2-Dihydroxy-1,3-indandione-2-^{14}C. To 1,3-indandione-2-^{14}C (5 g) dissolved in dilute sodium hydroxide (200 ml) was added sodium nitrite (2.5 g); then the mixture was cooled to 0 °C. Hydrochloric acid was added dropwise until the solution became distinctly acidic, whereupon the ice-bath was removed and the mixture was stirred for 30 min at room temperature. The solution was filtered and a yellow amorphous powder (5.9 g, 100%) was obtained. The oxime was recrystallized from acetic acid and formed yellowish green plates; mp 200—201 °C (decomp.). A mixture of selenious acid and the oxime (5 g) was refluxed for 3 h, and the clear solution was cooled to room temperature and saturated with sulfur dioxide. The solid which separated was filtered off and the filtrate was concentrated by distillation to *ca.* 50 ml and filtered. The filtrate was boiled with active carbon, filtered again, concentrated to 20 ml, and allowed to stand at room temperature. The crude 2,2-dihydroxy-1,3-indandione-2-^{14}C was filtered, and the mother liquor was concentrated to obtain a second crop; total yield 3.7 g (73%). It was purified by recrystallization from hot water with the aid of active carbon. Long colorless prisms of 2,2-dihydroxy-1,3-indandione-2-^{14}C were obtained, mp 241—243 °C (decomp.). The specific radioactivity was 0.178 μCi/mmol.

*1,3(2*H*)-Phenalenedione-2-*^{14}C. To a stirred mixture of diethyl malonate-2-^{14}C (75 ml, 250 μCi, Radiochemical Centre, Amersham, England) and 1,8-naphthalenedicarboxylic anhydride (25 g) was added zinc chloride (25 g); then the mixture was heated to *ca.* 170—175 °C for 6 h. The cooled reaction mass, after the addition of hot water (50 ml), was crushed to a powder and filtered. The residue was stirred with aqueous ammonia (one part of ammonia and four parts of water, 250 ml) for 15 min, and filtered. The filtrate was treated with active carbon, again filtered, and acidified with acetic acid. The solution was allowed to stand at room temperature for one hour, and filtered. The crystals obtained were washed with water, mp 254 °C (decomp.) (20.0 g, 81%, specific radioactivity 0.369 μCi/mmol).

2,3-Dihydroxy-1-phenalenone-2-^{14}C. 1,3(2*H*)-Phenalenedione-2-^{14}C (9.8 g) was dissolved in dilute sodium hydroxide (5%, 200 ml). After the addition of sodium nitrite (3.8 g), the mixture was cooled to 0 °C. Hydrochloric acid (17%) was added dropwise until the solution became distinctly acidic, whereupon the ice-bath was removed and the mixture was stirred for 30 min at room temperature. The solution was filtered and then washed with water and dried in *vacuo*, yielding the oxime (11.25 g, *ca.* 100%). The oxime (2.25 g) was dissolved into a mixture of acetic acid (10 ml), formalin (6.5 ml, 40%), and hydrochloric acid (2 ml). The mixture was refluxed for 4 h, and the solution was cooled and water (30 ml) was added. The solution was filtered to obtain 2,3-dihydroxy-1-phenalenone-2-^{14}C (1.7 g, 80%, mp 256 °C (xylene)). The specific radioactivity could not be obtained because of the deep coloration of the sample solution.

2,2-Dihydroxy-1,3-phenalenedione-2-^{14}C. A mixture of 1,3-(2*H*)-phenalenedione-2-^{14}C (1.96 g), sodium chloride (0.7 g), acetic acid (20 ml), and nitric acid (5 ml) was heated at 100 °C and stirred for 10 min. After cooling, the precipitates were collected, washed with ether, and dried. This gave 2-chloro-2-nitro-1,3-phenalenedione-2-^{14}C (1.8 g, 69%). The compound (1.0 g) was heated in nitrobenzene (10 ml) at 140 °C for 15 min; then the solution was cooled and the precipitates were washed with ether. This gave 2,2-dihydroxy-1,3-phenalenedione-2-^{14}C (0.62 g, 81%, mp 263 °C (decomp.), specific radioactivity 0.367 μCi/mmol).

Oxidation of [2-^{14}C]-*Compounds by Lead Tetraacetate.* [2-^{14}C]-Compounds were oxidized by the method described previously for the oxidation of the unlabeled compounds.

1,3-Indandione-2-^{14}C (292 mg) gave phthalic anhydride, mp 129—131 °C (35.6 mg, 12%, specific radioactivity 0.030 μCi/mmol), and carbon dioxide, which was converted to barium carbonate (116.7 mg, 29.6%, specific radioactivity 0.048 μCi/mmol).

2,2-Dihydroxy-1,3-indandione-2-^{14}C (356 mg) gave phthalic anhydride, mp 129 °C (127.7 mg, 43.2%, no radioactivity), and carbon dioxide, which was converted to barium carbonate (67.5 mg, 17%, specific radioactivity 0.124 μCi/mmol).

1,3(2*H*)-Phenalenedione-2-^{14}C (329 mg) gave acenaphthenequinone, mp 260 °C (11.5 mg, 3.2%, specific radioactivity 0.071 μCi/mmol), and carbon dioxide, which was converted to barium carbonate (24.3 mg, 6.2%, specific radioactivity 0.049 μCi/mmol).

2,3-Dihydroxy-1-phenalenone-2-^{14}C (424 mg) gave 1,8-naphthalenedicarboxylic anhydride, mp 274 °C (247.3 mg, 62.4%, specific radioactivity 0.049 μCi/mmol), and carbon dioxide, which was converted to barium carbonate (225.5 mg, 57%, specific radioactivity 0.222 μCi/mmol).

2,2-Dihydroxy-1,3-phenalenedione-2-^{14}C (456 mg) gave 1,8-naphthalenedicarboxylic anhydride, mp 274 °C (270 mg, 68%, no radioactivity), and carbon dioxide, which was converted to barium carbonate (11.47 mg, 2.9%, specific radioactivity 0.299 μCi/mmol).

References

1) A. Mckillop and B. Swan, *Tetrahedron Lett.*, **1970**, 5281.
2) J. D. Roberts, D. R. Smith, and C. C. Lee, *J. Am. Chem. Soc.*, **73**, 618 (1951).
3) K. Kurosawa and A. Moriyama, *Bull. Chem. Soc. Jpn.*, **47**, 2717 (1974).
4) W. O. Teeters and R. L. Shriner, *Ber.*, **55**, 3026 (1933).
5) S. Egashira, *Nippon Kagaku Zasshi*, **75**, 308 (1954).
6) B. Eistert, W. Eifler, and H. Göth, *Chem. Ber.*, **101**, 2162 (1968).
7) B. Eistert and O. Ganster, *Chem. Ber.*, **102**, 198 (1969).

Reaction of Dimethyl Sulfoxide–Trifluoroacetic Anhydride with Anilines, Phenols, and Thiophenols

Yuji HIRAKI, Masahiro KAMIYA, Rikuhei TANIKAGA, Noboru ONO, and Aritsune KAJI

Department of Chemistry, Faculty of Science, Kyoto University, Kitashirakawa, Sakyo-ku, Kyoto 606

(Received July 26, 1976)

The reaction of dimethyl sulfoxide–trifluoroacetic anhydride complex with anilines, phenols, and thiophenols was studied, and the following results were obtained. (1) The yields of a methylthiomethylated product were improved with anilines. The reaction proceeded without significant amount of tar, the unreacted anilines being easily recovered. (2) Selective *ortho*-methylthiomethylation took place with phenols in good yields at lower temperature, *para*-methylthiomethylation occurring at higher temperature. (3) Methylthiomethylation took place with thiophenols on a sulfur atom of thiophenol at room temperature in a simple process.

Sulfides and sulfoxides are activated with electrophiles to produce the reactive sulfonium salts. These electrophiles include dicyclohexylcarbodiimide+acid,[1] acetic anhydride,[2] acetyl chloride,[3] phosphorus pentoxide, polyphosphoric acid,[4] sulfur trioxide–pyridine,[5] diphenylketene–*p*-tolylimine+acid,[6] *etc.*

By employing sulfides activated with chlorine or *N*-chlorosuccinimide, Corey and Kim[7] carried out the mild oxidation of aliphatic alcohols to ketones. Gassman and co-workers[8–10] described *ortho*-methylthiomethylation of anilines by using *N*-chloroanilines and dialkyl sulfide. However, *N*-chloroanilines with electron-donating groups are unstable and easily oxidized to tar. Thus the reaction does not proceed without disturbance even though the improved dimethyl sulfide–chlorine method[11] is employed. Similar difficultics arise with the *ortho*-methylthiomethylation of phenols.

As for the reaction of activated sulfoxides, Claus and coworkers[12,13] reported that dimethyl sulfoxide and phosphorus pentoxide complex reacted with anilines to produce *N*-arylsulfimides. The dimethyl sulfoxide–phosphorus pentoxide system presented difficulties in purification of the product during the course of work-up. Swern and co-workers[14] also succeeded in preparing sulfimides by employing dimethyl sulfoxide–trifluoroacetic anhydride. Burdon and Moffatt[15,16] reported acid-catalyzed *ortho*-methylthiomethylation of phenols with dimethyl sulfoxide, dicyclohexylcarbodiimide, and anhydrous orthophosphoric acid. The yields were moderate, 1,3-benzoxathian and phenyldicyclohexyl urea being produced as by-products.

Dimethyl sulfoxide–trifluoroacetic anhydride system is expected to overcome these difficulties and improve the yields in alkylation of the anilines and the phenols owing to a good leaving group, *i.e.* trifluoroacetate.

No report has been found concerning the reaction of thiophenol with the activated sulfoxide and sulfide, except for the formation of diphenyl disulfide with dimethyl sulfide and dicyclohexylcarbodiimide.[15] The dimethyl sulfoxide–trifluoroacetic anhydride complex reacted with a variety of the substituted thiophenols to give methylthiomethyl phenyl sulfide in good yields.

Results and Discussion

Trifluoroacetic anhydride (TFAA) reacts with dimethyl sulfoxide (DMSO) readily to afford the complex I at low temperature as formulated in Eq. 1. In methylene chloride as solvent, it appears as a white precipitate (see Experimental). Trifluoroacetoxyl group on the sulfur atom facilitates the substitution of sulfur atom being attacked by nucleophiles.

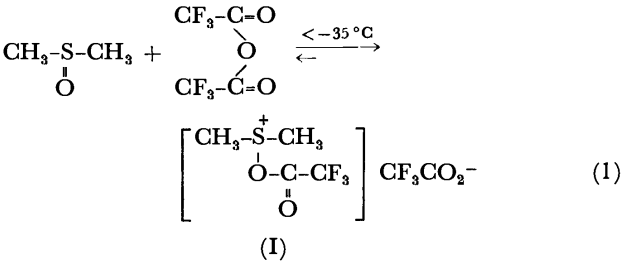

(I) (1)

ortho-*Methylthiomethylation of Aniline.* In general, the 'activated DMSO' reacts with a variety of anilines to afford azasulfonium compounds (**2**) followed by conversion into ylids (**5**) on treatment with base.[10] The ylid rearranges smoothly at lower temperature to the desired *o*-substituted aniline *via* Sommelet-Hauser type rearrangement as shown in Scheme 1. Alternatively, it may also be possible that the treatment of base leads to the abstraction of hydrogen on N atom of compound **2** to afford sulfimide (**3**), which rearranges to the corresponding product (**6**) in base. On the other hand, compound **2** is anticipated to decompose back to the starting aniline (**1**). If this process

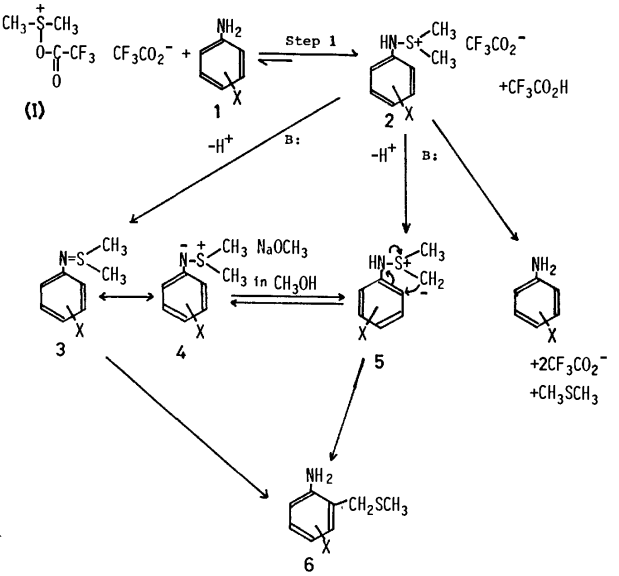

Scheme 1.

is involved, a complete conversion can not be considered to be attained.

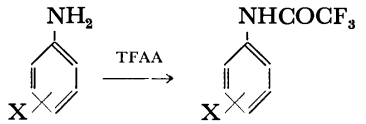

(2)

7

Substituted anilines (X=NO_2, CN, CO_2CH_3, Cl, CH_3, OCH_3) were alkylated on the *ortho* position with 1.2 equivalent of the complex I. In each case, the reaction proceeded without significant amount of tar, the unreacted aniline being easily recovered as shown in Table 1.

TABLE 1. *ortho*-METHYLTHIOMETHYLATION OF *para*-SUBSTITUTED ANILINES

Compd	X	Yield (%)[a] 6	Yield (%)[a] 7	Recovered anilines (%)
1a	NO_2	55	5	40
1b	CN	52	2	46
1c	CO_2CH_3	49	—	33
1d	Cl	67	9	11
1e	H	54	1	45
1f	CH_3	45	16	33
1g	OCH_3	27	7	66

a) Isolated yield based on the starting anilines.

In the case of anilines substituted by the strong electron-withdrawing group (*i.e.* *p*-nitroaniline), sulfimide **3** is preferred to the ylid form, since the hydrogen of the amino group is prone to be abstrated rather than the methyl hydrogen, and required to be refluxed with triethylamine in dry toluene to cause *o*-alkylation. On the other hand, it is enough to keep the reaction mixture below room temperature in the case of the rearrangement of azasulfonium compounds derived from anilines substituted by electron-donating group (*i.e.* *p*-toluidine and *p*-anisidine).

Sodium methoxide in absolute methanol was employed in each rearrangement of the azasulfonium compounds. *N*-Trifluoroacetylation took place instead of the desired rearrangement, when the compound derived from *p*-anisidine was treated with triethylamine. Potassium *t*-butoxide in THF was examined in a similar procedure to give *N*-trifluoroacetylation product, but the yield of *o*-alkylation decreased to a few %. Methanol is presumed to facilitate the protonation and counter anion exchang[12] from **3** to **5** through structure **4**, and **5** rearranges spontaneously even at low temperature below −50 °C.

In step 1, trifluoroacetic acid is generated, and is thought to protonate the aniline, while the protonated aniline is considered not to attack complex I. Attempts were made to remove the acid generated. In the presence of one equivalent of 2,6-lutidine, *p*-chloroaniline was reacted with the complex followed by the usual procedure. GLC analysis shows the formation of *o*-substitution product (20%) and acylation product (27%), and recovery of unreacted aniline (30%), indicating that 2,6-lutidine was not effective. In the same manner, *p*-toluidine was reacted in the presence of potassium carbonate. GLC analysis suggests that acylation predominated. Two equivalent of *p*-chloroaniline to the complex I afforded *o*-substituted product in 45% yield, attempts being unsuccessful.

Trifluoroacetylation took place as the sole side reaction (Eq. 2). However, it was possible to depress it with a choice of solvent system. Trifluoroacetylation is more unfavorable than the alkylation of aniline in a less polar solvent, though the process of alkylation is complicated. Less polar solvent (toluene) was preferred to methylene chloride in the reaction of *p*-anisidine which has higher basicity; Methylene chloride–acetonitrile (1/1=v/v) solvent was preferred in the reaction of *p*-chloroaniline which is less basic (Table 2).

o-Monosubstituted anilines were also alkylated on the *ortho* position in a similar manner. Table 3 gives the yields of *o*-alkylation of the *o*-monosubstituted anilines. Methylene chloride–acetonitrile (1/1=v/v) was used as the solvent, toluene being used in the case of *o*-anisidine. *o*-Anisidine was alkylated in 52% yield in toluene as compared with 24% in methylene chloride.

TABLE 2.

Compd	X	Solvent	Yield(%)[a] of **6**	**7**/(Recovered aniline+**7**) ×100
1d	Cl	CH_2Cl_2	21	24
		CH_2Cl_2-CH_3CN[b]	67	25
		CH_3CN	40	29
1f	CH_3	CH_2Cl_2	39	15
		CH_2Cl_2-CH_3CN[b]	45	33
		CH_3CN	14	37
1g	OCH_3	Toluene	27	10
		CH_2Cl_2	23	9
		CH_2Cl_2-CH_3CN[b]	23	24

a) Isolated yield based on the starting anilines.
b) 1/1=v/v.

TABLE 3. *ortho*-METHYLTHIOMETHYLATION OF *ortho*-SUBSTITUTED ANILINES

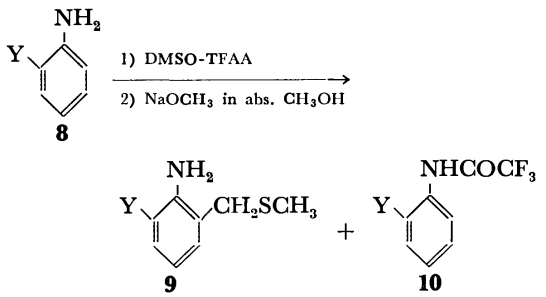

Compd	Y	Yield (%)[a] 9	Yield (%)[a] 10	Recovered anilines (%)
8a	NO_2	41	8	40
8b	Cl	71	19	trace
8c	CH_3	48	15	25
8d	OCH_3	52	11	37

a) Isolated yield based on the starting anilines.

Methylthiomethylation of the Phenols. To a solution of the DMSO-TFAA complex formed below −60 °C was added the substituted phenol **11** to produce oxysulfonium compound **12**, followed by conversion into *ortho*-alkylated phenols **13** and **14** through the ylid intermediate on treatment with base. Scheme 2 shows the reaction path.

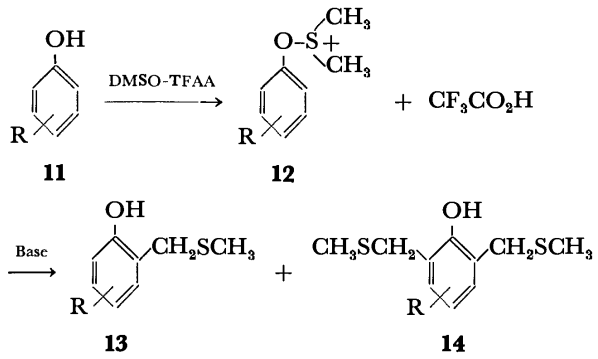

Scheme 2.

Various substituted phenols were alkylated as shown in Table 4, yields higher than those of the precedent works being marked.[15,20]

When the DMSO-TFAA complex and phenol were treated with sodium methoxide in absolute methanol, the desired product **13** was not obtained. Triethylamine was found to be the suitable base. In the reaction quenched 7 min after addition of the base, 0.5 equivalent of complex I to phenol marked a higher yield than one equivalent. This indicates that phenol was protonated and blocked by trifluoroacetic acid generated in the course of the reaction. It was thus necessary to eliminate the acid. 2,6-Lutidine, which has little nucleophilicity and is able to trap proton, was considered to be effective. Table 5 gives the yield from *o*-cresol and the effect of 2,6-lutidine. In the absence of triethylamine, 2,6-lutidine did not work as the base in the rearrangement, but a combination of 2,6-lutidine and triethylamine was recognized to be a good base. Optimum yield was attained in methylene chloride-hexane (1/1=v/v).

On the other hand, phenol reacted with DMSO-TFAA in acetonitrile at room temperature to produce viscous liquid instantaneously. NMR analysis (in $CDCl_3$) showed a singlet (6H) at δ 2.68 and a multiplet (4H) at δ 7.24—7.36. The liquid was refluxed with triethylamine in acetonitrile for 5 h to afford 4-methylthiomethylphenol in 23% yield (Eq. 3): NMR (CCl_4) δ=1.84 (s, 3), 3.44 (s, 2), and 6.44—7.08 ppm (q, 4). Anisol which also produced viscous liquid in a similar procedure was refluxed in acetonitrile with triethylamine to afford 4-methylthiomethylanisol (Eq. 4). The yield was low, but unreacted anisol was recovered: NMR (CCl_4) δ=1.88 (s, 3), 3.46 (s, 2), 3.64 (s, 3), 6.56—7.01 (q, 4).

Table 4. *ortho*-Methylthiomethylation of substituted phenols

Compd	R	Yield (%)[a]	
		13	**14**
11a	4-OCH_3	55	14
11b	4-CH_3	33	5
11c	H	39	—
11d	4-Cl	43	11
11e	2-CH_3	49[b]	
11f	2,4-CH_3	41	

a) Isolased yield based on TFAA.
b) Determined by GLPC.

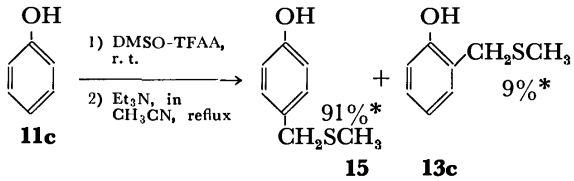

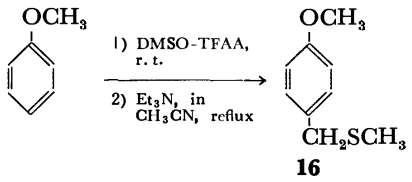

Hirose and Ukai reported on the conversion of dimethyl-*p*-hydroxyphenylsulfonium perchlorate **17** into methyl *p*-hydroxyphenyl sulfide (**18**) by heating in an aqueous saturated potassium chloride solution.[17] The acetonitrile solution of DMSO-TFAA and phenol was refluxed in an aqueous saturated potassium chloride solution for 5 h. No methyl *p*-hydroxyphenyl sulfide was detected. Dimethyl-*p*-hydroxyphenylsulfonium perchlorate was prepared according to the method of Hirose and Ukai,[17] and treated with triethylamine in acetonitrile at room temperature. The sole product was identified with methyl *p*-hydroxyphenyl sulfide **18**. The results exclude the possibility of oxysulfonium intermediate **12** and dimethyl-*p*-hydroxyphenylsulfo-

* Yield was determined as cresol after desulfurization by Raney-Ni.

Table 5.

Compd	R	Reaction time (h)	Base	2,6-Lutidine (equiv)	Solvent	Yield (%) of **13**
11c	H	14	$NaOCH_3$	0	CH_2Cl_2	0
11e	2-CH_3	3	Et_3N	0	CH_2Cl_2	19
11e	2-CH_3	3	Et_3N	1.2	CH_2Cl_2	40
11e	2-CH_3	3	—	1.2	CH_2Cl_2	0
11e	2-CH_3	3	Et_3N	1.2	CH_2Cl_2-Hexane[a]	49

a) 1/1=v/v.

nium intermediate in the *para* alkylation reaction of phenol. It seems that methylmethylenesulfonium cation (Pummerer type intermediate) is the attacking species to phenol and anisol.

Methylthiomethylation on Sulfur Atom of Thiophenols. Complex I reacted with thiophenol below −50 °C under the usual conditions. Thiophenol was oxidized to give diphenyl disulfide, DMSO being reduced to dimethyl sulfide quantitatively. It is assumed that dimethylphenylthiosulfonium species was attacked by unreacted thiophenol along path a as shown in Scheme 3.

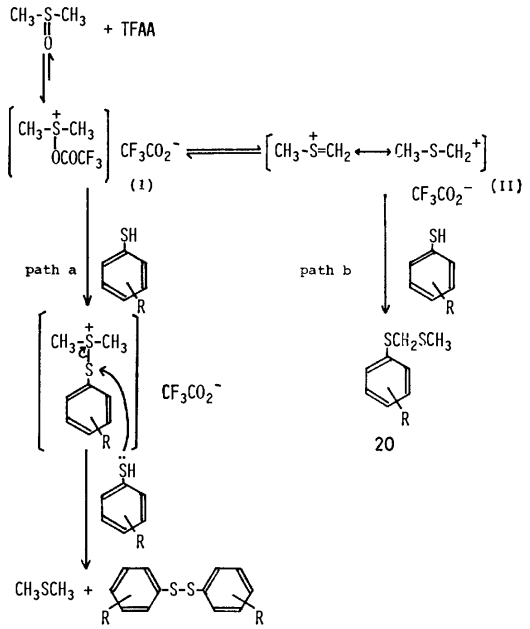

Scheme 3. Generation of the Pummere type intermediate.

On the other hand, complex I is expected to be transformed into carbonium ion following deprotonation (Pummerer type intermediate) (II). Trifluoroacetoxy anion (the counter anion) in the complex I has very weak nucleophilicity. Thus a certain nucleophile is considered to be able to trap this intermediate carbonium ion. *p*-Methylthiophenol gave methylthiomethyl *p*-methylphenyl sulfide **20** in good yield (59% isolated) and bis(*p*-methylphenyl) disulfide (21% yield) in a simple procedure: TFAA and thiophenols were added to an acetonitrile solution of DMSO successively at room temperature, and the reaction mixture was evaporated. The reaction was completed instantaneously, and dimethyl sulfide and trifluoroacetic acid formed were removed by evaporation of the solvent. No additional base was required. The yield decreased from 59 to 21% in the presence of triethylamine, because of the decomposition of complex I.

Table 6. Methylthiomethylation of Thiophenol

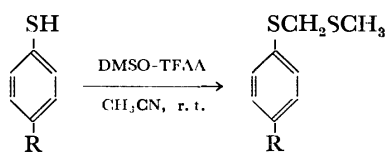

19 **20**

Compd	R	Yield[a] of **20** (%)
19a	Cl	55
19b	H	59
19c	CH_3	59

a) Isolated yield by preparative thin layer chromatography.

Several substituted thiophenols were alkylated (Table 6). DMSO-TFAA complex is the effective reagent for methylthiomethylation.

Experimental

*Preparation of 4-Chloro-2-methylthiomethylaniline (**6d**) from* p-*Chloroaniline. (Procedure A)* Dimethyl sulfoxide (1.4 g, 18 mmol) was dissolved in 20 ml of dry methylene chloride–acetonitrile (1/1=v/v), and the solution was stirred with a magnetic stirrer under nitrogen atmosphere and cooled below −70 °C in a Dry Ice–acetone bath. Trifluoroacetic anhydride (TFAA, 2.5 g, 12 mmol) was added dropwise to the solution maintained below −30 °C. The reaction was exothermic and a white precipitate immediately appeared. To the solution was gradually added *p*-chloroaniline (1.28 g, 10 mmol) in 10 ml of acetonitrile. A white precipitate soon disappeared and the solution which became homogeneous was kept stirring for 5 h. Sodium methoxide (30 mmol) in 15 ml of absolute methanol was added to the reaction mixture dropwise below −50 °C. The solution was allowed to warm to room temperature and was kept overnight (*ca.* 12 h). The resulting mixture was diluted with 40 ml of 10% aqueous sodium hydroxide. The organic layer was separated, the aqueous phase extracted three times with 70 ml portions of methylene chloride, and the organic layers were combined with the original organic phase, dried over anhydrous magnesium sulfate, filtered, and concentrated *in vacuo* to yield yellow oil. The resulting oil was dissolved in 100 ml of acetonitrile with 5 ml of triethylamine, and refluxed for 15 h. The solution was evaporated in order to remove the solvent and triethylamine to give a brown oil. Column chromatography on silica gel gave acylated aniline, *p*-chloroaniline, and 4-chloro-2-methylthiomethylaniline: 1.27 g isolated (eluant: benzene–hexane=1/1, v/v); mp 79—80 °C (lit, mp 78—79 °C[12]); NMR (CCl_4) δ=2.00 (s, 3), 3.62 (s, 2), 4.07 (s, 2), 6.5—7.1 (m, 3) (identical with the lit[12]).

*Preparation of 4-Nitro-2-methylthiomethylaniline (**6a**) from* p-*Nitroaniline. (Procedure B)* DMSO (1.4 g, 18 mmol) in 90 ml of dry methylene chloride–acetonitrile (1/1=v/v) was stirred and kept below −70 °C in a Dry Ice–acetone bath under nitrogen atmosphere. TFAA (2.5 g, 12 mmol) was added dropwise to the solution maintained below −30 °C throughout the course of addition. No white precipitate appeared. To the solution was gradually added *p*-nitroaniline (1.38 g, 10 mmol) and DMSO (3 ml) dissolved in 20 ml of acetonitrile. It was kept stirring for 7 h, and sodium methoxide (50 mmol) in 25 ml of absolute methanol was added dropwise below −40 °C. The reaction mixture was allowed to warm to room temperature and kept overnight (10 h). After the usual workup, yellow crystals and oil were obtained. They were dissolved in 100 ml of dry toluene with 5 ml of triethylamine, and refluxed for two days. This solution was evaporated to give crude solid. Column chromatography on silica gel gave 4-nitro-2-methylthiomethylaniline: 0.99 g isolated (eluant: benzene); mp 75—76 °C (lit, mp 75—

77 °C[12]); NMR ($CDCl_3$) δ=2.06 (s, 3), 3.72 (s, 2), 4.92 (s, 2), 6.64—8.12 (m, 3) (identical with lit[12]). The crystals obtained before reflux were identified with *N*-nitrophenyl dimethyl sulfimide: mp 164—167 °C (lit, mp 166—167 °C[14]); NMR ($CDCl_3$) δ=2.72 (s, 3), 6.66—8.04 (q, 4) (identical with lit[14]).

*Preparation of 4-Methyl-2-methylthiomethylaniline (**6f**) from* p-*Toluidine. (Procedure C)* DMSO–TFAA complex was prepared in 20 ml of methylene chloride and acetonitrile from 18 mmol of DMSO and 12 mmol of TFAA as described in procedure A. *p*-Toluidine (1.07 g, 10 mmol) in 10 ml of acetonitrile was added dropwise below −50 °C. The solution was stirred for 3 h. Sodium methoxide (30 mmol) in absolute methanol 15 ml was added slowly, and the solution was kept overnight at room temperature (*ca.* 10 h). The usual work-up gave a dark oil. Column chromatography on silica gel gave 4-methyl-2-methylthiomethylaniline: 0.752 g isolated (eluant: benzene–hexane=1/1, v/v); mp 43—44 °C (lit, mp 42—45 °C[12]); NMR (CCl_4) δ=1.91 (s, 3), 2.21 (s, 3), 3.58 (s, 2), 3.79 (s, 2), 6.42—6.86 (m, 3) (identical with values in lit[12]).

*Preparation of 2-Methylthiomethylaniline (**6e**) from Aniline.* The reaction was carried out according to procedure A. Methylene chloride (20 ml) solution of the DMSO–TFAA complex (DMSO 36 mmol and TFAA 24 mmol) and 20 ml of methylene chloride solution of aniline (20 mmol) were employed. Column chromatography on silica gel gave 2-methylthiomethylaniline: 0.83 g isolated (eluant: benzene–hexane=1/1, v/v); NMR (CCl_4) δ=1.94 (s, 3), 3.64 (s, 2), 4.01 (s, 2) 6.60—7.12 (m, 4) (identical with lit[12]), and *N*-trifluoroacetylaniline **7e**: MS (20 eV), *m/e*, 189; NMR ($CDCl_3$) δ=7.14—7.50 (m, 5), 7.80 (s, 1); IR (KBr) 1710 cm^{-1}; mp 90.0—90.5 °C.

*Preparation of 4-Methoxy-2-methylthiomethylaniline (**6g**) from* p-*Anisidine.* The reaction was carried out according to procedure C. The DMSO–TFAA complex was prepared in dry toluene. Column chromatography on silica gel gave 4-methoxy-2-methylthiomethylaniline: 0.49 g (eluant: benzene–hexane); NMR (CCl_4) δ=1.92 (s, 3), 3.53 (s, 2), 3.63 (s, 3), 3.68 (s, 2), 6.46 (s, 3) (identical with lit[10]).

*Preparation of 4-Cyano-2-methylthiomethylaniline (**6b**) from* p-*Cyanoaniline.* The reaction was carried out according to procedure B. Column chromatography on silica gel gave 4-cyano-2-methylthiomethylaniline: 0.94 g isolated; mp 84—86 °C; NMR ($CDCl_3$) δ=2.00 (s, 3), 3.68 (s, 2), 4.7 (s, 2), 6.5—7.2 (m, 3) (identical with values in lit[18]).

*Preparation of 4-Carbomethoxy-2-methylthiomethylaniline (**6c**) from* p-*Carbomethoxyaniline.* The reaction was carried out according to procedure B. Column chromatography on silica gel gave starting aniline, acylated aniline, and 4-carbomethoxy-2-methylthiomethylaniline: 1.03 g isolated (eluant: benzene); mp 85—87 °C; NMR ($CDCl_3$) δ=2.00 (s, 3), 3.80 (s, 2), 3.82 (s, 3), 4.80 (s, 2), 7.4—8.0 (m, 3) (identical with values in lit[18]).

*Preparation of 6-Chloro-2-methylthiomethylaniline (**9b**) from* o-*Chloroaniline.* The reaction was carried out according to procedure A. The oil obtained after quenching with 10% aqueous sodium hydroxide was refluxed in 100 ml acetonitrile with 5 ml of triethylamine for 10 h. Column chromatography on silica gel gave 6-chloro-2-methylthiomethylaniline: 1.33 g isolated (eluant: benzene–hexane=1/1, v/v); NMR (CCl_4) δ=1.85 (s, 3), 3.57 (s, 2), 4.48 (s, 2), 6.51—7.18 (m, 4) (identical with values in lit[12]).

*Preparation of 6-Methoxy-2-methylthiomethylaniline (**9d**) from* o-*Anisidine.* DMSO (1.4 g) was dissolved in 100 ml of dry toluene, and the solution was cooled below −70 °C in a Dry Ice–acetone bath under nitrogen atmosphere. TFAA (2,5 g) was added. Methylene chloride solution of *o*-anisidine (10 mmol) was added dropwise. The precipitate soon disappeared, and the solution was kept standing for 5 h. Sodium methoxide (30 mmol) in 15 ml of methanol was added below −50 °C. The cooling bath was removed in order to warm the reaction mixture upto room temperature. After quenching with 10% aqueous sodium hydroxide, the reaction mixture was dissolved in 100 ml of acetonitrile and refluxed for several hours with 5 ml of triethylamine. Preparative thin layer chromatography (Merck Silica gel 60 PE_{254}) gave 6-methoxy-2-methylthiomethylaniline: 0.95 g isolated (eluant: benzene–hexane=1/1, v/v); NMR (CCl_4) δ=1.87 (s, 3), 3.57 (s, 2), 3.76 (s, 3), 4.04 (s, 2), 6.56—7.16 (m, 3); MS (20 eV), *m/e*, 183.

*Preparation of 6-Nitro-2-methylthiomethylaniline (**9a**) from* o-*Nitroaniline.* The reaction was carried out according to procedure B. Column chromatography on silica gel gave 6-nitro-2-methylthiomethylaniline: 0.812 g isolated (eluant: benzene–hexane=1/1, v/v); mp 80—82 °C; NMR ($CDCl_3$) δ=2.00 (s, 3), 3.70 (s, 2), 6.5—7.2 (m, 3), 8.0 (s, 2); MS (20 eV), *m/e*, 198, 151, and 105.

*Preparation of 6-Methyl-2-methylthiomethylaniline (**9c**) from* o-*Toluidine.* The reaction was carried out according to procedure A. Preparative thin layer chromatography (Merck Silica gel 60 PE_{254}) gave 6-methyl-2-methylthiomethylaniline: 0.802 g isolated (eluant: benzene–hexane=1/2, v/v); NMR (CCl_4) δ=1.86 (s, 3), 2.08 (s, 3), 3.53 (s, 2), 3.90 (s, 2), 6.56—7.16 (m, 3) (identical with values in lit[12]).

*Preparation of 2-Methylthiomethylphenol (**13c**) from Phenol. (General Procedure)* DMSO–TFAA complex was prepared from DMSO (28 mmol) and TFAA (14 mmol) in 10 ml of dry methylene chloride below −60 °C. White precipitate appeared immediately. Phenol (2.7 g, 29 mmol) and 2,6-lutidine (1.6 g 15 mmol) dissolved in 4.5 ml of DMSO and 10 ml of methylene chloride was added dropwise, and the solution was stirred for 3 h. After triethylamine (2 ml) had been added, the solution was allowed to warm up to room temperature overnight. The reaction mixture was poured into 70 ml of dil. hydrochloric acid, the organic layers were separated, and the aqueous phase was extracted three times with 50 ml portions of methylene chloride. The organic layers were combined, and dried over magnesium sulfate, filtered, and concentrated *in vacuo*. Column chromatography on silica gel gave 2-methylthiomethylphenol: 0.452 g isolated (eluant: benzene–hexane=1/1, v/v); NMR (CCl_4) δ=1.86 (s, 3), 3.58 (s, 2), 6.40—6.96 (m, 4) (identical with values in lit[19]); IR (neat), 3350 cm^{-1} (O–H).

*Preparation of 4-Methyl-2-methylthiomethylphenol (**13b**) from* p-*Cresol.* The reaction was carried out according to the general procedure. *p*-Cresol (0.99 g), DMSO (0.7 ml), and TFAA (1.04 g) were employed. The resulting oil was purified by preparative thin layer chromatography (Merck Silica gel 60 PF_{254}), which gave 0.28 g of mono substituted cresol and 0.06 g of disubstituted cresol (eluant: benzene–hexane=1/1, v/v). 4-methyl-2-methylthiomethylphenol: NMR (CCl_4) δ=1.88 (s, 3), 2.18 (s, 3), 3.58 (s, 2), 6.52 (m, 3) (identical with values in lit[20]); IR (neat), 3350 cm^{-1} (O–H) 4-methyl-2,6-bismethylthiomethylphenol: NMR (CCl_4) δ= 1.92 (s, 6), 2.20 (s, 3), 3.62 (s, 4), 6.78 (s, 2); IR (neat), 3300 cm^{-1} (O–H).

*Preparation of 4-Chloro-2-methylthiomethylphenol (**13d**) from* p-*Chlorophenol.* The reaction was carried out according to general procedure. DMSO (0.4 ml), TFAA (0.50 g), and *p*-chlorophenol (0.75 g) were employed. The resulting oil was separated by preparative thin layer chromatography (Merck Silica gel PF_{254}, eluant: benzene–hexane=1/1, v/v) to give 0.20 g of 4-chloro-2-methylthiomethylphenol:[21]

NMR (CCl_4) δ=1.96 (s, 3), 3.62 (s, 2), 6.96—7.20 (m, 3); IR (neat), 3310 cm^{-1} (O-H), and 0.06 g of 4-chloro-2,6-bis(methylthiomethyl)phenol: NMR (CCl_4) δ=1.92 (s, 6), 3.60 (s, 4), 6.96 (s, 2); IR (neat), 3290 cm^{-1} (O-H)

*Preparation of 4-Methoxy-2-methylthiomethylphenol (**13a**) from* p-*Methoxyphenol.* The reaction was carried out according to general procedure. DMSO (6 mmol), TFAA (2.3 mmol), and *p*-methoxyphenol (5 mmol) were employed. Preparative thin layer chromatography (Merck Silica gel 60 PF_{254}, eluant: benzene–hexane=1/1, v/v) gave 4-methoxy-2,6-bis(methylthiomethyl)phenol (0.08 g) and 4-methoxy-2-methylthiomethylphenol (0.23 g). Mono-alkylated product:[21] NMR (CCl_4) δ=1.94 (s, 3), 3.64 (s, 2), 3.68 (s, 3), 6.52—6.80 (m, 3); IR (neat), 3340 cm^{-1} (O-H) dialkylated product: NMR (CCl_4) δ=1.98 (s, 6), 3.68 (s, 4), 3.74 (s, 3), 6.60 (s, 2); IR (neat), 3340 cm^{-1} (O-H)

*Preparation of 2-Methyl-6-methylthiomethylphenol (**13e**) from* o-*Cresol.* The reaction was carried out according to general procedure. DMSO (10 mmol), TFAA (6 mmol), and *o*-cresol (5 mmol) were used. Column chromatography on silica gel (eluant: benzene–hexane=1/1, v/v) gave 6-methyl-2-methylthiomethylphenol (0.412 g):[20] NMR (CCl_4) δ=1.92 (s, 3), 2.24 (s, 3), 3.64 (s, 2), 6.56—7.00 (m, 3); IR (neat), 3360 cm^{-1} (O-H).

*Praparation of 2,4-Dimethyl-6-methylthiomethylphenol (**13f**) from 2,4-Xylenol.* According to the general procedure, 2,4-xylenol was converted into methylthiomethylated phenol. DMSO (20 mmol), TFAA (12 mmol), and 2,4-xylenol (10 mmol) were used. The resulting oil was separated by column chromatography on silica gel (eluant: benzene–hexane=1/1, v/v) to give 0.75 g of 4,6-dimethyl-2-methylthiomethylphenol:[2b] NMR (CCl_4) δ=1.88 (s, 3), 2.14 (s, 6), 3.60 (s, 2), 6.24—6.76 (m, 2); IR (neat), 3350 cm^{-1} (O-H).

*Reaction of Dimethyl-*p*-hydroxyphenylsulfonium Perchlorate with Triethylamine.* Dimethyl-*p*-hydroxyphenylsulfonium perchlorate was prepared by the method[17] of Hirose and Ukai; 78% yield, mp 158—159 °C (lit, mp 155—157 °C); NMR (CD_3CN–$CDCl_3$) δ=3.06 (s, 6), 7.00—7.75 (q, 4).

Triethylamine was added to 20 ml acetonitrile solution of dimethyl-*p*-hydroxyphenylsulfonium perchlorate at room temperature. White precipitates appeared instantaneously. After evaporation of the solvent, the reaction mixture was washed with 100 ml of water and extracted three times with 60 ml portions of chloroform. The organic phase was dried over anhydrous magnesium sulfate and concentrated *in vacuo* to yield white crystals which were identified with methyl *p*-hydroxyphenyl sulfide: mp 85—86 °C (lit, mp 86—87 °C[17]); NMR (CCl_4) δ=2.38 (s, 3), 4.18 (s, 1), 6.61—7.17 (q, 4).

*Preparation of Methylthiomethyl Phenyl Sulfide (**20b**) from Thiophenol. (General Procedure)* DMSO (10 mmol) wa dissolved in 10 ml of dry acetonitrile at room temperature. TFAA (2.1 g, 10 mmol) in 5 ml acetonitrile was added to the solution at room temperature with stirring. Thiophenol (10 mmol) was added. The reaction was completed instantaneously, and the reaction mixture was evaporated in order to remove the solvent. The resulting yellow liquid was separated by preparative thin layer chromatography (Merck Silica gel 60 PF_{254}, eluant: hexane) to give methylthiomethyl phenyl sulfide (1.0 g, 59% yield): NMR (CCl_4) δ=2.19 (s, 3), 3.95 (s, 2), 7.12—7.46 (m, 5); MS (20 eV), *m/e*, 170 and 61.

Preparation of Methylthiomethyl p-*Chlorophenyl Sulfide (**20c**) from* p-*Chlorothiophenol.* The reaction was carried out according to general procedure. Preparative thin layer chromatography (Merck Silica gel 60 PF_{254}, eluant: hexane) gave methylthiomethyl *p*-chlorophenyl sulfide: 0.94 g isolated: NMR (CCl_4) δ=2.18 (s, 3), 3.93 (s, 2), 7.30 (s, 4); MS (20 eV), *m/e*, 204 and 61.

Preparation of Methylthiomethyl p-*Methylphenyl Sulfide (**20c**) from* p-*Methylthiophenol.* The reaction was carried out according to general procedure. Preparative thin layer chromatography (Merck Silica gel 60 PF_{254}, eluant: hexane) gave methylthiomethyl *p*-methylphenyl sulfide: 1.1 g isolated; NMR (CCl_4) δ=2.16 (s, 3), 2.31 (s, 3), 3.82 (s, 2), 6.98—7.29 (q, 4); MS (20 eV), *m/e*, 184 and 61.

This work was partially supported by a Grant-in-Aid for Science Research from the Ministry of Education (No. 043017 1975—6).

References

1) K. E. Pfitzner and J. G. Moffatt, *J. Am. Chem. Soc.*, **87**, 5661, 5670 (1965).
2) a) J. D. Albright and L. Goldman, *J. Am. Chem. Soc.*, **87**, 4214 (1965). b) Y. Hayashi and R. Oda, *J. Org. Chem.*, **32**, 457 (1967).
3) K. Anzai and S. Suzuki, *Bull. Chem. Soc. Jpn.*, **40**, 2854 (1967).
4) P. Claus and W. Vycudilik, *Tetrahedron Lett.*, **1968**, 3607.
5) J. R. Parikh and W. von E. Doering, *J. Am. Chem. Soc.*, **89**, 5505. (1967).
6) R. E. Harmon, C. V. Zenarosa, and S. K. Gupta, *Chem. Commun.*, **1969**, 327.
7) E. J. Corey and C. U. Kim, *Tetrahedron Lett.*, **1973**, 919; *ibid.*, **1974**, 287.
8) P. G. Gassman and G. Gruetzmacher, *J. Am. Chem. Soc.*, **95**, 588 (1973).
9) P. G. Gassman and H. R. Drewes, *J. Am. Chem. Soc.*, **96**, 3002 (1974).
10) P. G. Gassman and G. Gruetzmacher, *J. Am. Chem. Soc.*, **96**, 5487 (1974).
11) P. G. Gassman, G. Gruetzmacher, and T. J. Bergen, *J. Am. Chem. Soc.*, **96**, 5512 (1974).
12) P. Claus, W. Vycudilik, and W. Rieder, *Monatsh. Chem.*, **102**, 1571 (1971).
13) P. Claus, W. Rieder, P. Hofbauer, and E. Vilsmair, *Tetrahedron*, **31**, 505 (1975).
14) A. K. Sharma, T. Ku, A. D. Dawson, and D. Swern, *J. Org. Chem.*, **40**, 2758 (1975).
15) M. G. Burdon and J. G. Moffatt, *J. Am. Chem. Soc.*, **88**, 5855 (1966).
16) M. G. Burdon and J. G. Moffatt, *J. Am. Chem. Soc.*, **89**, 4725 (1967).
17) K. Hirose and S. Ukai, *Yakugaku Zasshi*, **86**, 187 (1966).
18) P. Claus and W. Rieder, *Monatsch. Chem.*, **103**, 1163 (1972).
19) J. P. Marino, K. E. Pfitzner, and R. A. Olofson, *J. Am. Chem. Soc.*, **87**, 4658 (1965).
20) J. P. Marino, K. E. Pfitzner, and R. A. Olofson, *Tetrahedron*, **27**, 4181 (1971).
21) P. G. Gassman and D. R. Amick, *Tetrahedron Lett.*, **1974**, 889.

Seven-membered *N*-Heterocycles. XIII.[1] Rearrangement of 7-Benzyl-4-hydroxy-6,7,8,9-tetrahydro-5*H*-pyrimido[4,5-*d*]azepines to 7-Benzyl-4-vinyl-6,7-dihydro-5*H*-pyrrolo[2,3-*d*]pyrimidines

Hiroshi YAMAMOTO, Heizan KAWAMOTO, Shiro MOROSAWA, and Akira YOKOO

Department of Chemistry, Faculty of Science, Okayama University, Tsushima, Okayama 700

(Received July 26, 1976)

The title pyrimidoazepines when treated with phosphoryl chloride underwent rearrangement to the vinylpyrrolo-pyrimidines *via* probable intermediates 5-(2-benzylaminoethyl)-4-chloro-6-vinylpyrimidines. Reduction and subsequent dehydrogenation of the products led to the preparation of 4-ethyl-7*H*-pyrrolo[2,3-*d*]pyrimidines and their 5,6-dihydro derivatives. The structures are discussed on the basis of pK_a values, UV and NMR spectra.

Tetrahydroazepines fused with various heterocycles have been actively synthesized in recent years mainly because of their pharmacological usefulness.[2] We have reported[3] the synthesis of a variety of substituted 4-hydroxy-6,7,8,9-tetrahydro-5*H*-pyrimido[4,5-*d*]azepines (*e.g.* **1**) by the condensation of *N*-substituted 5-ethoxycarbonyl-1-azacycloheptan-4-ones with various formamidine derivatives. These 4-hydroxypyrimidoazepines have been converted to the versatile 4-chloro derivatives by the usual method[4] (*i.e.* with $POCl_3$ in the presence of $PhNEt_2$ as a catalyst), leading to the preparation of 6,7,8,9-tetrahydro-5*H*-pyrimido[4,5-*d*]azepines bearing various substituents at the 2,4,7-positions.[3]

On carrying out the above chlorination without catalyst, however, we had noticed a considerable decrease in the yield of the desired 4-chloro compounds along with the simultaneous formation of a certain by-product. We wish to report here the structure of the by-product which was found to form through a rare type of rearrangement, since such a ring transposition of heterocycles has been a topic of current interest.[5]

The present investigation showed that refluxing **1a** in $POCl_3$ (without $PhNEt_2$) for 2—5 h also gave the expected 4-chloro compound[3] **2a** in a reasonable yield (60—70%). The UV spectra of the monocations of **2a** and its dechlorinated derivative[6] **3** did not differ appreciably from those of the neutral species (see Table 1). This implied that the first protonation took place on the azepine ring nitrogen in **2a** and **3** (*cf.* UV spectra and pK_a values of pyrimidine[7,8] and benzylamine[9,10]).

Prolonged heating of **1a** (*e.g.* for 34 h) with $POCl_3$ and subsequent chromatographic separation of the reaction mixture over alumina, however, resulted in formation of **2a** (40%) and a minor amount of intensely blue-fluorescent (under UV light) colorless prisms. The latter compound had the molecular formula $C_{15}H_{15}N_3$ (thus its yield was 30%). The IR spectrum indicated absence of OH, NH, or C=O group but showed characteristic absorptions at 1635, 980, and 930 cm^{-1}, indicative of the presence of a vinyl group. In contrast to **2a** and **3** the by-product had the longest wavelength UV absorption maximum at 324 nm which, on protonation (pK_a 5.94), showed a hypsochromic shift of *ca.* 20 nm with an increased intensity (Table 1); this is reminiscent of the UV spectra of 4-aminopyrimidines (see below). Since 4-vinylpyrimidine has been reported[11] to exhibit a strong, blue fluoresecnce under UV light, the presence of a vinyl group attached to a 4-aminopyrimidine nucleus was thought to account for the intense fluorescence and the UV of the by-product. The NMR spectrum of the by-product markedly differed from that of **2a** (Table 2) in the following respects: 1) a down-field shift (1.0 ppm) of the benzyl methylene singlet (at δ 4.59) of the by-product and 2) splitting of the complex azepine ring methylene absorptions (8H) of **2a** into a quasi-A_2B_2 methylene signal (4H; centered at δ 3.20) and a typical ABX vinyl signal (at δ 6.60, 6.28, and 5.54). The remaining absorptions in the spectrum of the by-product were two singlets at δ 7.27 (5H; Ph) and 8.39 (1H; pyrimidine ring proton); no deuterium-exchangeable proton was present. Combination of these spectral data led to the structure **4a** 7-benzyl-4-vinyl-6,7-dihydro-5*H*-pyrrolo[2,3-*d*]pyrimidine for the by-product; the assignments of the NMR signals are shown in Table 2.

Heating the 2-methylpyrimido-azepine (**1b**) with $POCl_3$ analogously produced a mixture of the chloro compound[3] (**2b**) and the similar rearranged product (**4b**); yields of **2b** and **4b** (from **1b**) *vs.* reaction time are shown in Table 3. The UV and NMR spectra of **2b** and **4b**, which closely resembled those of **2a** and **4a**, respectively, were consistent with the structures (see Tables 1 and 2). The pK_a of **4b** (6.95) was one unit higher than that of **4a**, while the pK_a difference between **2b** and **2a** was 0.35. This can be explained in terms of the large base-strengthening effect of a methyl group (usually 0.8 unit) when it is α- or γ- to ionizing nitrogen.[12]

The 2-phenyl derivative **1c**, made by the condensation of 1-benzyl-5-ethoxycarbonyl-1-azacycloheptan-4-one with benzamidine, gave only the 4-chloro compound **2c** in good yield when treated with boiling $POCl_3$ for 2—5 h. Heating of **1c** with $POCl_3$ at an elevated temperature (160 °C) in a sealed tube, however, produced the similar rearranged product **4c** in 38% yield; the physical properties of **4c**, recorded in Tables 1 and 2, were in conformity with the structure. The same reaction of the 2-amino compound[3] **1d** with $POCl_3$ yielded a mixture of several intractable products.[13]

The structure **4a** was confirmed by examining the spectra of the hydrogenated derivative **5a** readily obtainable as colorless prisms with the molecular formula of $C_{15}H_{17}N_3$. Its IR and NMR spectra (Table 2) clearly showed the conversion of the vinyl group of **4a** to an ethyl group, indicating the structure 7-benzyl-4-ethyl-6,7-dihydro-5*H*-pyrrolo[2,3-*d*]pyrimidine for **5a**.

TABLE 1. IONIZATION CONSTANTS AND UV SPECTRA[a]

Compound	Species[c]	Ionization in water (20°C)			Spectroscopy[b] in water		
		pK_a	Concn (M)	A.w.l.[d]	λ_{max}(nm)	log ε	pH
2a	+	6.70±0.05	3.9×10^{-5}	230	*252*, 257, *261*	*3.66*, 3.70, *3.62*	3.8
	0				*253*, 258, *263*	*3.69*, 3.73, *3.66*	8.9
3	++	0.65±0.1	6.7×10^{-5}	254	254	3.75	−1.3
	+	7.05±0.05	6.7×10^{-5}	227	251, *255*, 268	3.60, *3.56*, 2.94	4.9
	0				253, *255*, *273*	3.62, *3.61*, *2.99*	9.8
2b	+	7.05±0.04	2.2×10^{-4}	234	261, *267*,	3.67, *3.56*	1.7
	0				262, *268*	3.67, *3.59*	9.1
2c	+	7.0[e]	3.1×10^{-5}	230	262, *267*, *291*	4.30, *4.28*, *3.73*	3.6
	0				265, *268*, *293*	4.38, *4.37*, *3.84*	EtOH[f]
4a	+	5.94±0.03	7.0×10^{-5}	295	*298*, 305, *315*,	*4.12*, 4.13. *4.10*,	
					330, *345*	*3.96*, *3.65*	2.9
	0				225, 229, 270,	4.29, 4.29, 3.90,	
					324, *330*, *349*	3.87, *3.85*, *3.58*	9.0
4b	+	6.95±0.05	4.6×10^{-5}	291	*226*, *235*, 296,	*4.20*, *4.08*, 4.11,	
					305, *315*, *328*	4.12, *4.10*, *3.97*	2.7
	0				220, *227*, *236*,	4.35, *4.32*, *4.27*,	
					249, 265, 325	*4.11*, 3.96, 3.94	9.5
4c	+	5.40±0.03[g]	1.9×10^{-5}	238	*245*, 261, 307	*4.23*, 4.31, 4.07	2.0
	0				240, 291, 338	4.55, 3.89, 3.84	EtOH[f]
5a	+	6.68±0.02	6.2×10^{-5}	280	279	4.23	3.8
	0				*261*, 265, *286*	*4.11*, 4.12, *3.78*	9.8
5b	+	7.75±0.02	4.0×10^{-5}	277	277	4.23	1.5
	0				263, *285*	4.08, *3.87*	10.0
5c	+	6.20±0.02[g]	4.5×10^{-6}	261	258, *275*	4.47, *4.35*	2.0
	0				247, 271, 312	4.41, 4.10, 3.73	EtOH[f]
6b	+	5.10±0.02	6.6×10^{-5}	271	226, 271, 297	4.43, 3.52, 3.37	2.0
	0				221, 273, *283*	4.40, 3.66, *3.62*	8.7
	−	13.3 ±0.1[h]	6.6×10^{-5}	280	231, 279, 313	4.35, 3.71, 3.26	15
7-Deaza-	+	[j]			225, 265, 299	4.44, 3.49, 3.18	1
purine[i]	0				271	3.60	6.8
	−	[j]			273	3.59	NaOH
6d	+	5.91±0.03	5.4×10^{-5}	288	227, 274, 303	4.44, 3.52, 3.35	3.0
	0	[k]			222, *270*, 280	4.42, *3.63*, 3.66	9.0
6e	+	4.24±0.01[g]	1.9×10^{-5}	257	255, 303	4.45, 4.04	2.0
	0				257, 302	4.44, 4.12	EtOH[f]
6f	+	4.88±0.04	2.0×10^{-5}	272	250, 298	4.41, 4.10	2.0
	0				250, 291	4.41, 4.05	7.7
	−	13.4 ±0.1[h]	2.0×10^{-5}	270	263, *332*	4.36, *3.65*	15

a) Measured with a Hitachi EPS 3T Recording Spectrophotometer. b) Inflections in italics. c) Dication (++), monocation (+), neutral species (0), monoanion (−). d) Analytical wavelength in nm (*cf.* Ref. 23). e) Approx. value because the neutral species is hardly soluble in water. f) In 95 v/v% ethanol. g) In 0.01 M buffers containing 25 v/v% ethanol because the neutral species is hardly soluble in the buffers alone. h) Approx. i) From Ref. 16. j) No pK_a values have been reported. k) The acidic $pK_a>14$.

The close resemblance of the UV of **5a** (pK_a 6.68; Table 1) to those of structurally similar 4-dimethylaminopyrimidine (pK_a 6.35)[14] further supported the structure; the longest wavelength absorption maxima of the neutral species of both compounds showed about 7 nm hypsochromic shift (with increased intensities) on protonation. The 2-methyl- and 2-phenyl-4-vinylpyrrolo-pyrimidine **4b** and **4c** were also readily reduced to the 4-ethyl derivatives **5b** and **5c**, respectively. Those spectral properties evidently supported the structures (see Tables 1 and 2 for UV and NMR spectra).

Synthesis of a variety of substituted pyrrolo[2,3-*d*]-pyrimidines ("7-deazapurines") and their 5,6-dihydro derivatives has been drawing an increasing interest in view of their biological importance recently.[15] When our dihydropyrrolopyrimidine **5a** was heated in decalin in the presence of 10% Pd-C, a mixture of 7-benzyl-4-ethyl-7*H*-pyrrolo[2,3-*d*]pyrimidine (**6a**) and the debenzylated derivative (**6b**) (in 27 and 33% yields, respectively) was produced, the latter (**6b**) being presumably derived from **6a** by reduction with the hydrogen absorbed on the catalyst. The fully aromatic structures for **6a** and **6b** were confirmed by

Table 2. ^{1}H-NMR spectra[a]

Compound	δ-Values[b] for H-2	H-4	H_2-5,9	H_2-6,8	H-7
1c	7.25—7.6 m (3H)[c] 8.25 m (2H)[c]	—	2.85—3.20 m	2.05—2.85 m	3.67 s (2H)[d] 7.35 s (5H)[e]
2a[f]	8.59 s	—	2.9 —3.2 m	2.45—2.76 m	3.58 s (2H)[d] 7.25 s (5H)[e]
2b[f]	2.53 s[g]	—	2.85—3.2 m	2.4 —2.75 m	3.56 s (2H)[d] 7.25 s (5H)[e]
2c	7.30—7.56 m (3H)[c] 8.41 m (2H)[c]	—	2.95—3.4 m	2.5 —2.85 m	3.63 s (2H)[d] 7.34 s (5H)[e]
4a	8.39 s	5.54 dd (J=9.1, 3.5)[h] 6.28 dd (J=17.0, 3.5)[i] 6.60 dd (J=17.0, 9.1)[j]	2.8 —3.18 m[k]	3.22—3.7 m[l]	4.59 s (2H)[d] 7.27 s (5H)[e]
4b	2.53 s[g]	5.54 dd (J=10.0, 3.0)[h] 6.27 dd (J=17.0, 3.0)[i] 6.59 dd (J=17.0, 10.0)[j]	2.73—3.13 m[k]	3.25—3.65 m[l]	4.60 s (2H)[d] 7.29 s (5H)[e]
4c	7.30—7.55 m (3H)[c] 8.40—8.65 m (2H)[c]	5.58 dd (J=8.5, 4.5)[h] 6.49 dd (J=16.5, 4.5)[i] 6.70 dd (J=16.5, 8.5)[j]	2.80—3.20 m[k]	3.35—3.75 m[l]	4.72 s (2H)[d] 7.34 s (2H)[e]
5a	8.23 s	1.18 t (J=7.5)[m] 2.42 q (J=7.5)[n]	2.65—3.1 m[k]	3.2 —3.6 m[l]	4.52 s (2H)[d] 7.23 s (5H)[e]
5b	2.38 s[g]	1.18 t (J=7.3)[m] 2.41 q (J=7.3)[n]	2.65—3.1 m[k]	3.2—3.6 m[l]	4.53 s (2H)[d] 7.23 s (5H)[e]
5c	7.30—7.55 m (3H)[c] 8.35—8.55 m (2H)[c]	1.28 t (J=7.5)[m] 2.59 q (J=7.5)[n]	2.75—3.15 m[k]	3.30—3.70 m[l]	4.71 s (2H)[d] 7.34 s (5H)[e]
6a	8.85 s	1.41 t (J=7.5)[m] 3.06 q (J=7.5)[n]	6.58 d[o] J=3.5	7.12 d[p] J=3.5	5.47 s (2H)[d] 7.29 s (5H)[e]
6b	8.88 s	1.44 t (J=7.5)[m] 3.12 q (J=7.5)[n]	6.64 d[o] J=3.5	7.38 bd[q] J=3.5	12.10 m[r]
6c	2.78 s[g]	1.39 t (J=7.5)[m] 3.03 q (J=7.5)[n]	6.50 d[o] J=3.4	6.99 d[p] J=3.4	5.41 s (2H)[d] 7.26 s (5H)[e]
6d	2.85 s[g]	1.40 t (J=7.5)[m] 3.05 q (J=7.5)[n]	6.56 d[o] J=3.4	7.26 bd[q] J=3.4	12.80 m[r]
6e	7.20—7.55 m (3H)[c] 8.45—8.70 m (2H)[c]	1.45 t (J=7.5)[m] 3.04 q (J=7.5)[n]	6.42 d[o] J=3.5	6.94 d[p] J=3.5	5.45 s (2H)[d] 7.23 s (5H)[e]
6f	7.45—7.65 m (3H)[c] 8.35—8.60 m (2H)[c]	1.48 t (J=7.5)[m] 3.15 q (J=7.5)[n]	6.57 dd[o] J=3.5, 1.5	7.14 dd[q] J=3.5, 2.0	12.40 m[r]

a) Measured with a Hitachi High Resolution NMR Spectrometer, R-20A (60 MHz). b) In $CDCl_3$ with TMS as an internal standard, except for compounds **2a**, **2b**, and **6e** (in CCl_4). Suffixes: b, broad; s, singlet; d, doublet; dd, double doublet; t, triplet; q, quartet; m, multiplet; J, coupling constants (Hz). c) For C_6H_5-2. d) For PhCH_2-7. e) For $C_6H_5CH_2$-7. f) Values from Ref. 3 for comparison. g) For Me-2. h, i) For CH_2=CH-4 (*trans* and *cis* with respect to the nucleus, respectively). j) CH_2=C*H*-4. k) For H_2-5. l) For H_2-6. m) For CH_3CH_2-4. n) For CH_3CH_2-4. o) For H-5. p) For H-6. q) For H-6. Becomes doublet on D_2O exchange. r) For H-7; D_2O exchangeable.

the down-field shifts of the coupled doublets (1H each, J=3.5 Hz) due to H-5 and 6 and of the benzyl methylene singlet (in the case of **6a**) in the NMR spectra (see Table 2). The UV spectra of **6b** (Table 1) resembled those of the parent substance[16] (Table 1) and of pyrrolo[2,3-*e*]pyrimidine ("9-deazapurine"),[17] but differed slightly from those of purine[18] by having an extra absorption band in 285—315 nm region. The basic and acidic pK_a values of **6b** were in the similar order to those of 9-deazapurine (pK_a 4.24, 13.16).[17] The 2-methyl compound **5b** also gave a mixture of **6c** and **6d** in 10 and 80% yields, respectively; the physical properties of those products shown in Tables 1 and 2 were similar to those of **6a** and **6b**. The 2-phenyl compound **5c** produced likewise **6e** and **6f** (in 31 and 64% yields, respectively).

A Reaction Pathway for the Formation of the Rearrangement Products ***4***. It was found that the 4-chloro compounds **2a**—**c** also produced mainly **4a**—**c**, when heated with $POCl_3$. The compound **4b** was obtained on heating the monohydrochloride of **2b** at 130 °C in *N*,*N*-dimethylformamide. Thus the rearrangement products **4a**—**c** were most likely formed through the protonated tetrahydropyrimido-azepines **7**, which afforded the ring-opened intermediate 5-(2-benzylaminoethyl)-4-chloro-6-vinylpyrimidines (**8**) through

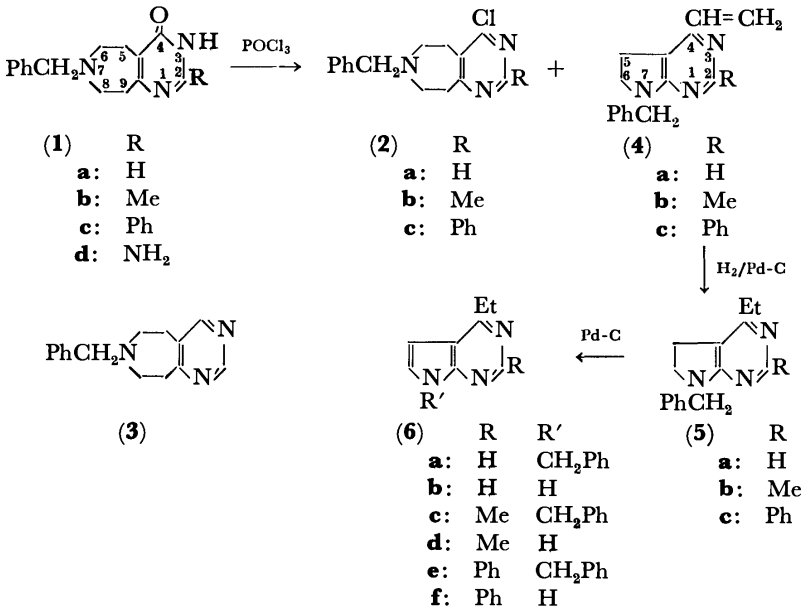

Scheme 1.

TABLE 3. ISOLATED YIELDS OF **2b** AND **4b** FROM **1b**

Chlorinating agents	React. time (h)	**2b** (%)	**4b** (%)
$POCl_3 + PhNEt_2$	2	70	10
$POCl_3$	5	50	20
$POCl_3$	8	25	40
$POCl_3$	13	0	45

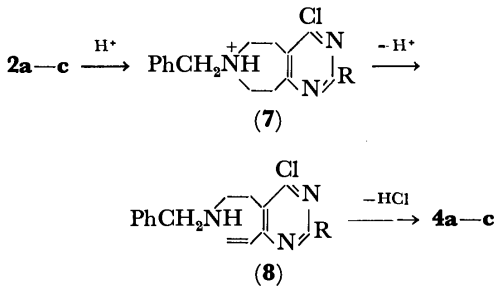

Scheme 2.

Hofmann-type degradation[19] (or retrograde Michael reaction[20]). This ring-opening would preferably take place at the N(7)–C(8) [not N(7)–C(6)] bond of **7**, because the C(9) methylene group (which is α- and γ- to the pyrimidine ring nitrogens) is expected to be more acidic than that of C(5).[21] The intermediate **8** would then yield the final products **4a**—**c** by the intramolecular cyclization between the 5-(2-benzylaminoethyl) and 4-chloro groups of the pyrimidine ring (Scheme 2). 4-Vinylpyrimidines have been reported[11] to polymerize easily. The main reason for the moderate yields thus far of the rearranged products **4a**—**c** appeared to be likewise a facile addition polymerization of the vinyl functional group of the products (or of the intermediate **8**), since a considerable amount of a colorless rubberlike substance always accompanied during the preparation and purification of **4a**—**c**.

Many rearrangements have been known[5] involving fission of a heterocyclic ring and ring closure in the alternative direction catalyzed by base, heat, light or miscellaneous reagents. The present rearrangement seems, to our knowledge, to be a rare example of acid-catalyzed thermal ring transposition of fused heterocycles.[22]

Experimental

The microanalyses were carried out in this department using a Yanagimoto CHN Corder, MT-2. The solid materials for the analysis were dried over P_2O_5 for 2—4 h at 25 °C/20 Torr unless otherwise specified. Each of the analytical samples gave a single spot on thin-layer chromatography (silica gel and alumina). The IR spectra were taken with a JASCO IRA-1 Diffraction Grating IR Spectrophotometer. The measurements of ionization constants were carried out spectrophotometrically in 0.01 M buffers by the usual method.[23]

The Reaction of ***1a*** *with Phosphoryl Chloride.* A mixture of 1.0 g of **1a** and 15 ml of $POCl_3$ was refluxed under N_2 for 34 h. After evaporation of the $POCl_3$ at 40 °C/15 Torr, the residue was triturated with 20 ml of cold water, then diluted with 20 ml of cold chloroform. The aqueous layer was carefully brought to pH 8 with Na_2CO_3 at 5 °C. After separation, the aq. layer was extracted with $CHCl_3$. The combined organic layer was washed with brine, dried over K_2CO_3, and evaporated *in vacuo*, giving 1.14 g of a brown viscous liquid, which consisted mainly of **2a** and **4a** (in a ratio of 3 : 2 by NMR; the ratio was 9 : 1 after 9 hours' refluxing). This was chromatographed over alumina (Merck, Activity I; 60 g) and eluted with benzene (which was gradually changed up to 20% ether/benzene), giving first 0.48 g (40%) of **2a** as colorless prisms (from benzene/light petroleum, bp 30—70 °C), mp 65—67 °C (lit,[3] 67—68 °C), then 0.28 g (30%) of **4a** as colorless prisms (from ether/light petroleum), mp 71—73 °C. IR ($CHCl_3$): 1635, 1592, 1582, 1320, 980, 930, and 855 cm^{-1}. Found: C, 76.02; H, 6.50; N, 17.53%. Calcd for $C_{15}H_{15}N_3$: C, 75.91; H, 6.37; N, 17.71%.

7-Benzyl-6,7,8,9-tetrahydro-5H-pyrimido[4,5-d]azepine (***3***). A suspension of 100 mg of **2a** and 100 mg of sodium acetate in 5 ml of abs. EtOH was hydrogenated over 30 mg of 10%

Pd-C under atmospheric pressure, followed by the usual work-up procedure, giving 65 mg (74%) of **3** as colorless prisms (from light petroleum), mp 65—66 °C (lit,[3] 66.5—67.5 °C).

*The Reaction of **1b** with Phosphoryl Chloride.* One gram of **1b** was refluxed in 15 ml of $POCl_3$ and the same procedure as that described for **1a** was followed; the reaction time and the isolated yields of the products are shown in Table 3. The chloropyrimidoazepine (**2b**) was a colorless liquid (bp 170 °C/0.7 Torr[3]), which gave the monohydrochloride with HCl/ether as colorless flakes (from EtOH), mp 204—205 °C dec. Found (for material dried at 80 °C): C, 59.18; H, 6.09; N, 12.97%. Calcd for $C_{16}H_{18}N_3Cl \cdot HCl$: C, 59.28; H, 5.91; N, 12.96%.

The pyrrolo-pyrimidine **4b** was colorless needles (from benzene/light petroleum), mp 96—97 °C. IR ($CHCl_3$): 1635, 1590, 1390, 1340, 980, and 930 cm^{-1}. Found: C, 76.58; H, 6.92; N, 16.30%. Calcd for $C_{16}H_{17}N_3$: C, 76.45; H, 6.82; N, 16.72%.

*The Reaction of **2b** Hydrochloride with Phosphoryl Chloride.* A suspension of 100 mg of **2b** hydrochloride in 2 ml of $POCl_3$ was refluxed under N_2 for 12 h, followed by the same procedure as above, giving 80 mg of the crude reaction mixture as an amber liquid, which consisted mainly of unreacted **2b** and the rearranged **4b** in a ratio of 8 : 2 (by NMR).

*Heating of **2b** Hydrochloride in* N,N-*Dimethylformamide.* A solution of 0.32 g of **2b** hydrochloride in 10 ml of dry DMF was heated under N_2 at 130 °C for 5 h. The volatile was removed at 80 °C/15 Torr and the residue was dissolved in a cold mixture of $CHCl_3$ and 5% aq $NaHCO_3$ (10 : 10 ml). After separation, the aq layer was extracted with $CHCl_3$. The combined organic layer was dried over K_2CO_3 and evaporated *in vacuo*, giving a pale amber liquid (0.48 g). This was chromatographed over silica gel (40 g) into 15 ml fractions with $CHCl_3$ (which was gradually changed up to 2% MeOH/$CHCl_3$) as an eluent. The fractions 8—22 gave 0.10 g (43%) of a colorless solid which consisted mostly of **4b** (by NMR). Recrystallization from benzene/light petroleum afforded pure **4b** as colorless prisms, mp 94—95 °C.

*7-Benzyl-4-hydroxy-2-phenyl-6,7,8,9-tetrahydro-5*H*-pyrimido[4,5-*d*]azepine (**1c**).* To a cold solution of 1.15 g of sodium in 60 ml of dry MeOH were added 3.12 g of 1-benzyl-5-ethoxycarbonyl-1-azacycloheptan-4-one hydrochloride[24] and 2.62 g of benzamidine hydrochloride (monohydrate). The mixture was refluxed under N_2 for 4.5 h. After evaporation of the solvent *in vacuo*, the residue triturated with 80 ml of cold water was carefully taken to pH 6 with cold 6M-HCl and stirred at 25 °C for 1 h. The precipitate was collected and recrystallized from 80% EtOH, giving 2.50 g (75%) of **1c** as pale yellow needles, mp 197—199 °C. IR ($CHCl_3$): 3400—3000, 1630, 1600, and 1500 cm^{-1}. Found (for material dried at 80 °C): C, 75.41; H, 6.57; N, 12.62%. Calcd for $C_{21}H_{21}N_3O$: C, 75.10; H, 6.39; N, 12.68%.

*7-Benzyl-4-chloro-2-phenyl-6,7,8,9-tetrahydro-5*H*-pyrimido[4,5-*d*]azepine (**2c**).* A mixture of 0.42 g of **1c** and 15 ml of $POCl_3$ was refluxed under N_2 for 5 h. The volatile was removed *in vacuo* and the residue was triturated in 50 ml of cold water. The mixture was taken to pH 9 with Na_2CO_3 at 5 °C and extracted with benzene. The dried (over K_2CO_3) extract was evaporated *in vacuo*, giving 0.37 g (81%) of **2c** as colorless prisms, mp 117—119 °C, after recrystallization from benzene/light petroleum. IR ($CHCl_3$): 1560, 1520, and 1359 cm.$^{-1}$ Found: C, 72.33; H, 6.06; N, 12.03%. Calcd for $C_{21}H_{20}N_3Cl$: C, 72.08; H, 5.76; N, 12.06%.

*7-Benzyl-2-phenyl-4-vinyl-6,7-dihydro-5*H*-pyrrolo[2,3-*d*]pyrimidine (**4c**).* A suspension of 0.33 g of **1c** in 20 ml of $POCl_3$ was heated in a sealed tube at 160—170 °C for 13 h. The same procedure described above for **4a** and **4b** was followed, giving the crude reaction mixture which contained mostly **4c** and a trace of **2c**. Chromatographic purification over alumina (25 g) with $CHCl_3$ as an eluent gave 0.12 g (38%) of **4c** as pale yellow prisms (from benzene/light petroleum), mp 145—146 °C. IR ($CHCl_3$): 1635, 1580, 1560, 1370, 1350, 1320, 980, 930, and 880 cm^{-1}. Found: C, 80.56; H, 6.23; N, 13.16%. Calcd for $C_{21}H_{19}N_3$: C, 80.48; H, 6.11; N, 13.41%.

*7-Benzyl-4-ethyl-6,7-dihydro-5*H*-pyrrolo[2,3-*d*]pyrimidine (**5a**).* The vinyl compound **4a** (60 mg) was hydrogenated in 4 ml of abs. EtOH over 30 mg of 10% Pd-C. The usual work-up procedure yielded 49 mg (81%) of **5a** as colorless prisms (from light petroleum), mp 41—42 °C. Found: C, 75.42; H, 7.20; N, 17.31%. Calcd for $C_{15}H_{17}N_3$: C, 75.28; H, 7.16; N, 17.56%.

*7-Benzyl-4-ethyl-2-methyl-6,7-dihydro-5*H*-pyrrolo[2,3-*d*]pyrimidine (**5b**).* The vinyl compound **4b** (100 mg) was similarly hydrogenated, giving 81 mg (80%) of **5b** as colorless prisms (from light petroleum), mp 72—73 °C. Found: C, 75.46; H, 7.67; N, 16.10%. Calcd for $C_{16}H_{19}N_3$: C, 75.85; H, 7.56; N, 16.59%. The picrate: yellow prisms (from EtOH), mp 138—139 °C. Found: C, 54.65; H, 4.54; N, 16.81%. Calcd for $C_{22}H_{22}N_6O_7$: C, 54.77; H, 4.60; N, 17.42%.

*7-Benzyl-4-ethyl-2-phenyl-6,7-dihydro-5*H*-pyrrolo[2,3-*d*]pyrimidine (**5c**).* The similar hydrogenation of 100 mg of **4c** gave 85 mg (85%) of **5c** as colorless needles (from ether/light petroleum), mp 89—90 °C. Found: C, 79.69; H, 6.84; N, 13.07%. Calcd for $C_{21}H_{21}N_3$: C, 79.96; H, 6.72; N, 13.32%.

*Dehydrogenation of **5a**.* A mixture of 60 mg of **5a** and 30 mg of 10% Pd-C was refluxed in 1 ml of dry decalin under N_2 for 17 h. The catalyst was filtered off and washed with hot benzene. The filtrate combined with washings was concentrated at 20 °C/15 Torr to *ca.* 1 ml and set aside at 0 °C overnight, depositing 8 mg of *4-ethylpyrrolo[2,3-*d*]-pyrimidine (**6b**).* The filtrate was chromatographed over silica gel (5.5 g) and eluted with benzene, then with $CHCl_3$ (which was gradually changed up to 2% MeOH/$CHCl_3$), giving first 17 mg (27%) of *7-benzyl-4-ethylpyrrolo-[2,3-*d*]pyrimidine (**6a**)* as a colorless liquid, then 5 mg of more **6b** as a colorless crystalline powder. Recrystallization of the latter (**6b**; 33% total yield) from benzene/light petroleum gave colorless needles, mp 99—100 °C. IR ($CHCl_3$): 3430, 3200, 3150, 1580, 1345, and 890 cm^{-1}. Found: C, 65.53; H, 6.44; N, 28.55%. Calcd. for $C_8H_9N_3$: C, 65.28; H, 6.16; N, 28.55%. The benzyl compound **6a** gave the picrate as yellow prisms (from EtOH), mp 153—154 °C. Found: C, 54.28; H, 3.92; N, 18.31%. Calcd for $C_{21}H_{18}N_6O_7$: C, 54.08; H, 3.89; N, 18.02%.

*Dehydrogenation of **5b**.* A mixture of 70 mg of **5b**, 40 mg of 10% Pd-C, and 1.2 ml of dry decalin was refluxed under N_2 for 10 h. The similar work-up procedure as above was followed, giving 36 mg (80%) of *4-ethyl-2-methylpyrrolo-[2,3-*d*]pyrimidine (**6d**)* and 7 mg (10%) of the 7-benzyl derivative (**6c**). The latter was a colorless liquid. IR ($CHCl_3$): 2910, 2840, 1580, 1440, and 1400 cm^{-1}. It gave the picrate as yellow prisms (from EtOH), mp 137—138 °C. Found: C, 55.33; H, 4.20; N, 17.63%. Calcd for $C_{22}H_{20}N_6O_7$: C, 55.00; H, 4.20; N, 17.49%.

The former (**6d**) was colorless needles (from benzene/light petroleum), mp 141—142 °C. IR ($CHCl_3$): 3460, 3120, 1580, 1390, and 885 cm^{-1}. Found: C, 67.30; H, 7.22; N, 26.32%. Calcd for $C_9H_{11}N_3$: C, 67.05; H, 6.88; N, 26.07%.

*Dehydrogenation of **5c**.* Fifty milligrams of **5c** upon

similar dehydrogenation gave 15 mg (64%) of *4-ethyl-2-phenylpyrrolo[2,3-d]pyrimidine (6f)* and 10 mg (31%) of the 7-benzyl derivative (**6e**). The latter (**6e**) was colorless needles (from light petroleum), mp 46—47 °C. IR ($CHCl_3$): 1600, 1575, 1560, 1390, and 1370 cm^{-1}. Found: C, 80.11; H, 6.24; N, 13.17%. Calcd for $C_{21}H_{19}N_3$: C, 80.48; H, 6.11; N, 13.41%. The former (**6f**) was colorless needles (from ether/light petroleum), mp 139—140 °C. IR ($CHCl_3$): 3480, 3200, 3140, 1580, 1380, 900, 800, and 690 cm^{-1}. Found: C, 74.91; H, 5.96; N, 18.49%. Calcd for $C_{14}H_{13}N_3$: C, 75.31; H, 5.87; N, 18.82%.

References

1) Part XII. H. Kawamoto, T. Matsuo, S. Morosawa, and A. Yokoo, *Bull. Chem. Soc. Jpn.*, **46**, 3898 (1973).

2) *e.g.* See a) J. B. Hester, Jr., Fr. M. 6699; *Chem. Abstr.*, **75**, 5876 (1971) for 6-alkyl-1,2,3,4,5,6-hexahydroazepino-[4,5-*b*]indoles; b) G. Griss, M. Kleemann, W. Grell, and H. Ballhause, Ger. Offen. 2127267; *Chem. Abstr.*, **79**, 78777 (1973) for 2-amino-4,5,7,8-tetrahydro-6*H*-oxazolo[5,4-*d*]azepines.

3) H. Yamamoto, M. Nakata, S. Morosawa, and A. Yokoo, *Bull. Chem. Soc. Jpn.*, **44**, 153 (1971).

4) *e.g.* See D. J. Brown, "The Pyrimidines," Interscience, New York (1962), p. 162.

5) H. C. van der Plas, "Ring Transformation of Heterocycles," Academic Press, New York (1973).

6) Compound **3**, which has been made from **2a** *via* the 4-hydrazino derivative and subsequent oxidation with Ag_2O (Ref. 3), is now readily available by simple catalytic hydrogenation, see Experimental.

7) a) A. Albert, D. J. Brown, and G. Cheeseman, *J. Chem. Soc.*, **1951**, 474; b) M. P. Boarland and J. F. W. McOmie, *ibid.*, **1952**, 3716. λ_{max} (pH 0) 242 nm (log ε 3.6) λ_{max} (pH 7) 243, 272 nm (log ε 3.4, 2.5).

8) A. Albert, R. J. Goldaere, and J. Phillips, *J. Chem. Soc.*, **1948**, 2240: pK_a 1.30.

9) R. A. Friedel and M. Orchin, "Ultraviolet Spectra of Aromatic Compounds," Wiley, New York (1951).

10) E. J. Robinson and A. K. Kiang, *Trans. Faraday Soc.* **52**, 327 (1956): pK_a 9.35.

11) C. G. Overberger and I. C. Kogon, *J. Am. Chem. Soc.*, **76**, 1879 (1954).

12) A. Albert, "Heterocyclic Chemistry," 2nd ed, Athlone Press, London (1968), p. 437.

13) Conversion of hydroxy groups of pyrimidines into chloro groups in the presence of amino groups frequently encounters difficulties, see Ref. 4.

14) D. J. Brown and L. N. Short, *J. Chem. Soc.*, **1953**, 331: λ_{max} (pH 3.15) 262 nm (log ε 4.31), λ_{max} (pH 9.3) 250, 286 nm (log ε 4.22, 3.56).

15) a) For a review, see V. Amarnath and R. Madhav, *Synthesis*, **1974**, 837; b) H. Wolfers, U. Kraatz, and F. Korte, *Heterocycles*, **3**, 187 (1975); c) H. J. Roth and K. Eger, *Arch. Pharm. (Weinheim, Ger.)*, **308**, 252 (1975); *Chem. Abstr.*, **83**, 97187 (1975); d) D. H. Kim and A. A. Santilli, U. S. 3910913; *Chem. Abstr.*, **84**, 31116 (1976); e) A. A. Santilli, A. C. Scotese, and D. H. Kim, *J. Heterocyclic Chem.*, **13**, 135 (1976).

16) a) Wellcome Foundation Ltd., Brit. 812366; *Chem. Abstr.*, **54**, 592 (1960); b) J. Davoll, *J. Chem. Soc.*, **1960**, 131.

17) A. Albert, *Chem. Ind.*, **1970**, 365.

18) a) S. F. Mason, *J. Chem. Soc.*, **1954**, 2071; b) A. Albert and C. Pendersen, *ibid.*, **1956**, 4683.

19) *e. g.* For a review, see A. C. Cope and E. R. Trumbell, *Org. React.*, **11**, 320 (1960).

20) *e.g.* See H. O. House, "Modern Synthetic Reactions," 2nd ed., Benjamin, 1972, pp. 595—623 and references cited therein.

21) 4-Methyl group of pyrimidines is generally more acidic than 5-methyl group; see W. Pfleiderer and H. Mosthaf, *Chem. Ber.*, **90**, 728 (1957).

22) Applications of this reaction to synthesis of other heterocycles are currently under investigation.

23) A. Albert and E. P. Serjeant, "Ionization Constants of Acid and Base," Methuen, London (1962).

24) T. Moriya, T. Oki, S. Yamaguchi, S. Morosawa, and A. Yokoo, *Bull. Chem. Soc. Jpn.*, **41**, 230 (1968).

Synthesis of Riparіochromene B and C[1]

Masao TSUKAYAMA

Department of Applied Chemistry, Faculty of Engineering, Tokushima University, Minami-Josanjima, Tokushima 770

(Received August 3, 1976)

Condensation of 7-hydroxy-2,2-dimethylchroman with benzoyloxyacetonitrile gave 7-hydroxy-6-benzoyloxyacetyl-2,2-dimethylchroman (**3**) which was converted into 7-hydroxy-6-acetoxyacetyl-2,2-dimethylchroman (**7**) in four steps. Dehydrogenation of **7** with DDQ in dried toluene afforded riparіochromene B (**1**). Riparіochromene B was also synthesized by oxidative cyclization of 2,4-dihydroxy-5-(3-methyl-2-butenyl)-ω-acetoxyacetophenone (**13**) which was prepared from resorcinol and acetoxyacetonitrile in two steps. Riparіochromene C (**2**) was synthesized from resorcinol by the same method as that described above.

Riparіochromene B and riparіochromene C have recently been isolated from Australian *Eupatorium riparium* Regel along with several other chromenes, and these structures have been determined to be respectively 7-hydroxy-6-acetoxyacetyl-2,2-dimethylchromene (**1**) and 7-hydroxy-6-isobutyryloxyacetyl-2,2-dimethylchromene (**2**) which have an acyloxyacetyl substituent at the 6-position on the basis of spectral evidence.[2] In the present paper, the syntheses of **1** and **2** are reported to confirm the proposed structures of natural riparіochromene B and C.

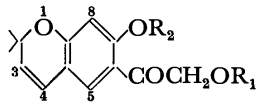

(**1**) $R_1=CH_3CO$ $R_2=H$
(**2**) $R_1=(CH_3)_2CHCO$ $R_2=H$
(**8**) $R_1=R_2=CH_3CO$
(**11**) $R_1=(CH_3)_2CHCO$ $R_2=CH_3CO$

Fig. 1.

The condensation of 7-hydroxy-2,2-dimethylchroman[3] with benzoyloxyacetonitrile in the presence of freshly-fused zinc chloride gave 7-hydroxy-6-benzoyloxyacetyl-2,2-dimethylchroman (**3**), which produced a dark-brown reaction in the ferric chloride color test. Chroman **3** was easily converted into a 7-(benzyloxy) chroman derivative (**4**) upon treatment with benzyl chloride. Compound **4** was hydrolyzed with diluted hydrochloric acid in ethanol to give a 6-(hydroxyacetyl) chroman derivative (**5**) which showed absorption bands attributable to an alcoholic hydroxyl group in the IR spectrum and no proton signals from the benzoyl group in the NMR spectrum. The hydrolysis of **4** with a diluted alkali, however, did not afford the desired chroman derivative **5**. Compound **5**, after being converted into a 6-(acetoxyacetyl)chroman derivative (**6**)

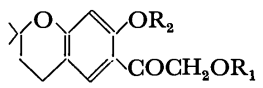

(**3**) $R_1=C_6H_5CO$ $R_2=H$
(**4**) $R_1=C_6H_5CO$ $R_2=C_6H_5CH_2$
(**5**) $R_1=H$ $R_2=C_6H_5CH_2$
(**6**) $R_1=CH_3CO$ $R_2=C_6H_5CH_2$
(**7**) $R_1=CH_3CO$ $R_2=H$
(**9**) $R_1=(CH_3)_2CHCO$ $R_2=C_6H_5CH_2$
(**10**) $R_1=(CH_3)_2CHCO$ $R_2=H$

Fig. 2.

with acetyl chloride in a large quantity of pyridine cooled by ice, was subjected to hydrogenolysis over palladium on charcoal in methanol to afford a 7-(hydroxy)chroman derivative (dihydroriparіochromene B) (**7**), which produced a light-brown reaction in the ferric chloride color test and indicated an intramolecular hydrogen-bonded hydroxyl group in the NMR spectrum. The dehydrogenation[4-6] of **7** with boiling in DDQ (2,3-dichloro-5,6-dicyano-*p*-benzoquinone) in dried toluene afforded the desired chromene (**1**) (mp 146—147 °C) (lit, mp 145—146 °C).[2] This compound was further converted into the acetate of riparіochromene B (**8**).

According to the procedure described above, **5** was treated with isobutyryl chloride to give a 6-(isobutyryloxyacetyl)chroman derivative (**9**). The subsequent hydrogenolysis of **9** afforded a 7-(hydroxy)chroman derivative (dihydroriparіochromene C) (**10**). The dehydrogenation of **10** with DDQ gave the desired chromene (**2**) (mp 109.5—110.5 °C) (lit, mp 109—110 °C).[2] Chromene **2** was also converted into the acetate of riparіochromene C (**11**).

Chromenes **1** and **2** thus synthesized were respectively confirmed to be identical to natural riparіochromene B and C on the basis of a mixed melting-point determination and NMR, IR, and UV spectral comparisons.

In order to provide an alternate approach to the synthesis of chromenes **1** and **2**, another route was investigated. The condensation of resorcinol with acetoxyacetonitrile or isobutyryloxyacetonitrile in the presence of freshly-fused zinc chloride easily gave ω-(acyloxy)acetophenones (**12**) or (**16**), respectively, which showed a positive reaction in the ferric chloride color test and was supported by IR and NMR spectra. The BF_3-catalyzed condensation of 2-methyl-3-buten-2-ol[7] with **12** or **16** afforded 3- or 5-(3-methyl-2-butenyl)-ω-(acyloxy)acetophenones (**13** and **14**) or (**17** and **18**), respectively, which were isolated by column chromatography. All these compounds showed positive reactions in the ferric chloride color test, and these structures were supported by NMR spectra. The major product **13** or **17**, in each condensation, was boiled with DDQ in dried toluene for conversion into chromene **1** or **2**, which was confirmed to be identical with the riparіochromene B or C synthesized above, respectively. The minor products **14** and **18** in the condensation were similary treated to give compounds **15** and **19**, whose structures were revealed by their NMR spectra to be chromenes.

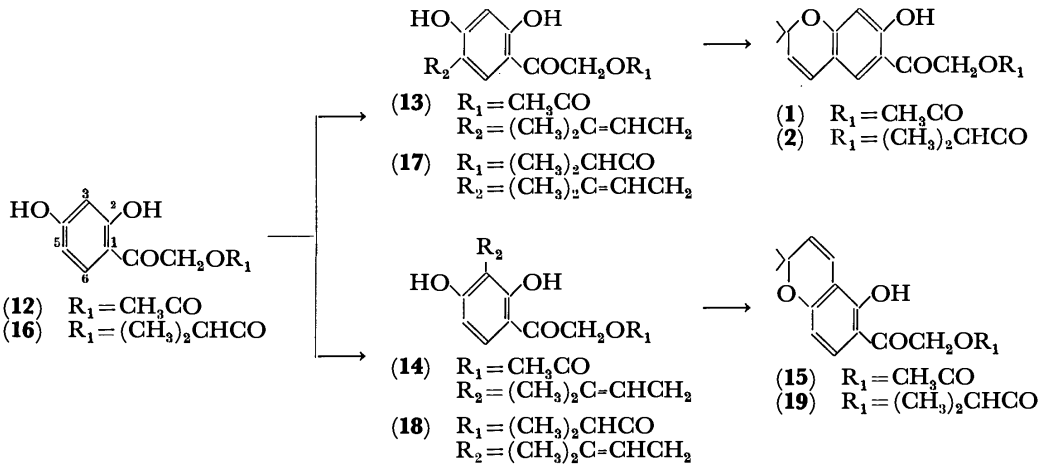

Fig. 3.

Experimental

All the melting points are uncorrected. The IR spectra were taken on a Hitachi 215 Spectrophotometer and the UV spectra on a Hitachi 124 Spectrophotometer. The NMR spectra were measured with a JOEL PS-100 Spectrometer (100 MHz), using tetramethylsilane as an internal standard (δ, ppm). Column chromatography was carried out on Kieselgel 60 (70—230 mesh) (Merck).

7-Hydroxy-6-benzoyloxyacetyl-2,2-dimethylchroman (3). 7-Hydroxy-2,2-dimethylchroman (10.6 g), anhydrous benzoyloxyacetonitrile (14.5 g), and freshly-fused zinc chloride (4 g) were successively added in dried ether (60 ml), and a rapid stream of dried hydrogen chloride was bubbled into the mixture with stirring and cooling in an ice-salt bath for 7 h. The reaction mixture was allowed to stand for 24 h in a refrigerator, and then the solvent was decanted. The residual solid, after being washed with dried ether (80 ml), was boiled in water (80 ml) for 1 h and cooled to give a white precipitate, which was collected and recrystallized from methanol as colorless needles (**3**) (15.2 g, 75%): mp 141—142 °C; IR ν_{max}^{KBr} 1720, 1665 cm^{-1}; NMR ($CDCl_3$) δ 1.36 (s, 6H, 2×CH_3), 1.83 (t, 2H, J=7 Hz, C_3-H), 2.73 (t, 2H, J=7 Hz, C_4-H), 5.48 (s, 2H, CH_2), 6.32 (s, 1H, arom. H), 7.3—7.6 (m, 4H, arom. H), 8.0—8.3 (m, 2H, arom. H), 11.66 (s, OH). Found: C, 70.55; H, 5.85%. Calcd for $C_{20}H_{20}O_5$: C, 70.57; H, 5.92%.

7-Benzyloxy-6-benzoyloxyacetyl-2,2-dimethylchroman (4). Compound **3** (10.2 g), benzyl chloride (7.0 g), potassium iodide (9.0 g), and dried potassium carbonate (15.0 g) were successively added to dried acetone (150 ml). After the mixture was heated under reflux for 7 h, the solvent was evaporated under reduced pressure, and the residual substance was poured into cold water. The white precipitate thus formed was collected and recrystallized from ethanol to give colorless needles (**4**) (11.6 g, 90%): mp 146—147 °C; IR ν_{max}^{KBr} 1725, 1662 cm^{-1}; NMR ($CDCl_3$) δ 1.36 (s, 6H, 2×CH_3), 1.83 (t, 2H, J=7 Hz, C_3-H), 2.73 (t, 2H, J=7 Hz, C_4-H), 5.11 (s, 2H, $C\underline{H}_2C_6H_5$), 5.34 (s, 2H, CH_2), 6.45 (s, 1H, C_8-H), 7.3—7.6 (m, 8H. arom. H), 7.79 (s, 1H, C_5-H), 8.0—8.2 (m, 2H, arom. H). Found: C, 75.36; H, 6.04%. Calcd for $C_{27}H_{26}O_5$: C, 75.33; H, 6.09%.

7-Benzyloxy-6-hydroxyacetyl-2,2-dimethylchroman (5). Compound **4** (8.6 g) with *ca.* 18% hydrochloric acid (80 ml) in ethanol (400 ml) was refluxed for 8 h, and then the organic solvent was removed under reduced pressure. The precipitate was recrystallized from methanol to give colorless needles (**5**) (2.7 g, 40%): mp 142—143 °C; IR ν_{max}^{KBr} 3480, 1643 cm^{-1}; NMR ($CDCl_3$) δ 1.37 (s, 6H, 2×CH_3), 1.83 (t, 2H, J=7 Hz, C_3-H), 2.75 (t, 2H, J=7 Hz, C_4-H), 4.63 (s, 2H, CH_2), 5.05 (s, 2H, $C\underline{H}_2C_6H_5$), 6.43 (s, 1H, C_8-H), 7.36 (s, 5H, arom. H), 7.87 (s, 1H, C_5-H). Found: C, 73.63; H, 6.74%. Calcd for $C_{20}H_{22}O_4$: C, 73.60; H, 6.79%.

7-Benzyloxy-6-acetoxyacetyl-2,2-dimethylchroman (6). To a solution of **5** (1.0 g) in dried pyridine (25 ml) was added acetyl chloride (1.5 ml) drop by drop with stirring and cooling in an ice bath, and the mixture was stirred with cooling for 6 h. The reacted mixture was poured into ice-cold water (20 ml) to give a white precipitate, which was collected and recrystallized from methanol as colorless needles (**6**) (0.76 g, 65%): mp 111—112 °C; IR ν_{max}^{KBr} 1740, 1662 cm^{-1}; NMR ($CDCl_3$) δ 1.32 (s, 6H, 2×CH_3), 1.78 (t, 2H, J=7 Hz, C_3-H), 2.72 (t, 2H, J=7 Hz, C_4-H), 2.14 (s, 3H, CH_3CO), 5.06 and 5.10 (each s, 2H, $C\underline{H}_2C_6H_5$ and $COCH_2O$), 6.41 (s, 1H, C_8-H), 7.41 (s, 5H, arom. H), 7.76 (s, 1H, C_5-H). Found: C, 71.90; H, 6.68%. Calcd for $C_{22}H_{24}O_5$: C, 71.72; H, 6.57%.

7-Hydroxy-6-acetoxyacetyl-2,2-dimethylchroman (Dihydroripariochromene B) (7). Compound **6** (0.74 g) was hydrogenated over palladium on charcoal (10%; 0.18 g) in methanol until the uptake of hydrogen ceased. The solvent was removed under reduced pressure, and the residue was recrystallized from methanol to give colorless plates (**7**) (0.37 g, 70%): mp 131—132 °C; IR ν_{max}^{KBr} 1745, 1645 cm^{-1}; NMR ($CDCl_3$) δ 1.34 (s, 6H, 2×CH_3), 1.81 (t, 2H, J=7 Hz, C_3-H), 2.71 (t, 2H, J=7 Hz, C_4-H), 2.21 (s, 3H, CH_3CO), 5.24 (s, 2H, CH_2), 6.31 (s, 1H, C_8-H), 7.30 (s, 1H, C_5-H), 11.80 (s, OH). Found: C, 64.87; H, 6.59%. Calcd for $C_{15}H_{18}O_5$: C, 64.73; H, 6.52%.

7-Hydroxy-6-acetoxyacetyl-2,2-dimethylchromene (Riparіochromene B) (1). A mixture of **7** (0.11 g) and DDQ (0.10 g) in dried toluene (50 ml) was heated under reflux for 10 h, and then the solvent was removed under reduced pressure. The residual substance was purified by column chromatography over silica gel with chloroform to give chromene **1**, which was recrystallized from carbon tetrachloride as colorless needles (40 mg, 40%): mp 146—147 °C (no depression in a mixed melting-point determination with natural riparіochromene B); IR ν_{max}^{KBr} 1750, 1652 cm^{-1}; UV λ_{max}^{EtOH} nm (log ε) 257 (4.51), 286 (3.95), 347 (3.85). NMR ($CDCl_3$) δ 1.41 (s, 6H, 2×CH_3), 2.20 (s, 3H, CH_3CO), 5.20 (s, 2H, CH_2), 5.54 (d, 1H, J=9 Hz, C_3-H), 6.23 (d, 1H, J=9 Hz, C_4-H), 6.30 (s, 1H, C_8-H), 7.15 (s, 1H, C_5-H), 12.20 (s, OH). Found: C, 65.09; H, 5.79%. Calcd for

$C_{15}H_{16}O_5$: C, 65.21; H, 5.84%.

7-Acetoxy-6-acetoxyacetyl-2,2-dimethylchromene (Acetate of Ripariochromene B) (8). After a mixture of **1** (54 mg), acetic anhydride (1 ml), and pyridine had been allowed to stand over 24 h at room temperature, cold water was added to the mixture and it was again allowed to stand overnight in a refrigerator. The mixture was extracted with ether and the ethereal solution was washed with a saturated aqueous solution of sodium chloride, dried over sodium sulfate, and the solvent was evaporated. The residue was recrystallized from a mixture of benzene and hexane to give colorless needles (**8**) (58 mg, 93%): mp 109—110 °C; IR ν_{max}^{KBr} 1770, 1735, 1675 cm^{-1}; NMR ($CDCl_3$) δ 1.46 (s, 6H, $2\times CH_3$), 2.19 (s, 3H, CH_3CO), 2.35 (s, 3H, C_7-CH_3CO), 5.10 (s, 2H, CH_2), 5.64 (d, 1H, J=10 Hz, C_3-H), 6.29 (d, 1H, J=10 Hz, C_4-H), 6.53 (s, 1H, C_8-H), 7.46 (s, 1H, C_5-H). Found: C, 64.25; H, 5.68%. Calcd for $C_{17}H_{18}O_6$: C, 64.14; H, 5.70%.

7-Benzyloxy-6-isobutyryloxyacetyl-2,2-dimethylchroman (9). Isobutyryl chloride (1.5 ml) was added to a solution of **5** (0.86 g) in dried pyridine (25 ml). After stirring in an ice bath for 10 h, the mixture was worked up in the same manner, as in the case of **6**, to give chroman **9**, which was recrystallized from methanol as colorless needles (0.76 g, 73%): mp 93—94 °C; IR ν_{max}^{KBr} 1740, 1680 cm^{-1}; NMR ($CDCl_3$) δ 1.23 [d, 6H, J=7 Hz, $(CH_3)_2CH$], 1.32 (s, 6H, $2\times CH_3$), 1.77 (t, 2H, J=7 Hz, C_3-H), 2.71 (t, 2H, J=7 Hz, C_4-H), 2.65 [m, 1H, $(CH_3)_2CH$], 5.06 and 5.09 (each s, 2H, $CH_2C_6H_5$ and $COCH_2O$), 6.40 (s, 1H, C_8-H), 7.40 (s, 5H, arom. H), 6.77 (s, 1H, C_5-H). Found: C, 72.86; H, 6.84%. Calcd for $C_{24}H_{28}O_5$: C, 72.70; H, 7.12%.

7-Hydroxy-6-isobutyryloxyacetyl-2,2-dimethylchroman (Dihydroripariochromene C) (10). Compound **9** (0.44 g) was hydrogenated over palladium on charcoal and the reacted mixture was worked up in the same manner, as in the case of **7**, to give colorless plates (**10**) (0.26 g, 70%): mp 113—114 °C; IR ν_{max}^{KBr} 1738, 1640 cm^{-1}; NMR ($CDCl_3$) δ 1.24 [d, 6H, J=7 Hz, $(CH_3)_2CH$], 1.33 (s, 6H, $2\times CH_3$), 1.80 (t, 2H, J=7 Hz, C_3-H), 2.70 (t, 2H, J=7 Hz, C_4-H), *ca.* 2.67 [m, 1H, $(CH_3)_2CH$], 5.22 (s, 2H, CH_2), 6.30 (s, 1H, C_8-H), 7.30 (s, 1H, C_5-H), 11.80 (s, OH). Found: C, 66.62; H, 7.50%. Calcd for $C_{17}H_{22}O_5$: C, 66.65; H, 7.24%.

7-Hydroxy-6-isobutyryloxyacetyl-2,2-dimethylchromene (Ripariochromene C) (2). A mixture of **10** (102 mg), DDQ (85 mg), and dried toluene (30 ml) was heated under reflux for 9 h. The reacted mixture was worked up in the same manner, as in the case of **1**, to give chromene **2**, which was recrystallized from carbon tetrachloride as colorless needles (30 mg, 30%): mp 109.5—110.5 °C (no depression in a mixed melting-point determination with natural ripariochromene C); IR ν_{max}^{KBr} 1740, 1645 cm^{-1}; UV λ_{max}^{EtOH} nm (log ε) 257 (4.39), 287 (3.77), 348 (3.72); NMR ($CDCl_3$) δ 1.26 [d, 6H, J=7 Hz, $(CH_3)_2CH$], 1.45 (s, 6H, $2\times CH_3$), 2.73 [m, 1H, $(CH_3)_2$-CH], 5.24 (s, 2H, CH_2), 5.57 (d, 1H, J=9 Hz, C_3-H), 6.25 (d, 1H, J=9 Hz, C_4-H), 6.33 (s, 1H, C_8-H), 7.18 (s, 1H, C_5-H), 12.05 (s, OH). Found: C, 67.37; H, 6.58%. Calcd for $C_{17}H_{20}O_5$: C, 67.09; H, 6.62%.

7-Acetoxy-6-isobutyryloxyacetyl-2,2-dimethylchromene (Acetate of Ripariochromene C) (11). A mixture of **2** (54 mg), acetic anhydride (1 ml), and pyridine was worked up in the same manner, as in the case of **8**, to give colorless needles (**11**) (56 mg, 91%): mp 124—125 °C; IR ν_{max}^{KBr} 1775, 1740, 1685 cm^{-1}; NMR ($CDCl_3$) δ 1.24 [d, 6H, J=7 Hz, $(CH_3)_2$-CH], 1.46 (s, 6H, $2\times CH_3$), 2.35 (s, 3H, CH_3CO), 2.70 [m, 1H, $(CH_3)_2CH$], 5.07 (s, 2H, CH_2), 5.63 (d, 1H, J=10 Hz, C_3-H), 6.29 (d, 1H, J=10 Hz, C_4-H), 6.52 (s, 1H, C_8-H), 7.48 (s, 1H, C_5-H). Found: C, 65.88; H, 6.32%. Calcd for $C_{19}H_{22}O_6$: C, 65.88; H, 6.40%.

2,4-Dihydroxy-ω-(acetoxy)acetophenone (12). Resorcionl (20 g), acetoxyacetonitrile (26.5 g), and zinc chloride (8 g) were successively added to dried ether (100 ml), and a rapid stream of dried hydrogen chloride was bubbled into the mixture with stirring in an ice-salt bath for 2 h. The mixture, after being treated in the same manner as in the case of **3**, was heated in water–methanol (1 : 9; 300 ml) for 1.5 h at 60 °C, and the solvent was distilled out under reduced pressure. The residue was recrystallized from chloroform to give colorless plates (**12**) (15 g, 40%), producing a light-brown reaction in the ferric chloride color test: mp 167—168 °C; IR ν_{max}^{KBr} 1740, 1610 cm^{-1}; NMR (DMSO) δ 2.13 (s, 3H, CH_3CO), 5.24 (s, 2H, CH_2), 6.30 (bs, 1H, C_3-H), 6.35 [q, 1H, (J=2.5, 9 Hz) C_5-H], 7.68 (d, 1H, J=9 Hz, C_6-H), 10.63 (s, C_4-OH), 11.54 (s, C_2-OH). Found: C, 57.03; H, 4.77%. Calcd for $C_{10}H_{10}O_5$: C, 57.14; H, 4.80%.

5-(3-Methyl-2-butenyl)-2,4-dihydroxy-ω-(acetoxy)acetophenone (13) and 3-(3-Methyl-2-butenyl)-2,4-dihydroxy-ω-(acetoxy)acetophenone (14). To a mixed solution of **12** (5.0 g) and boron trifluoride etherate (3.3 g) in dried dioxane (70 ml) was gradually added a solution of 2-methyl-3-buten-2-ol (2.1 g) in dried dioxane (15 ml) and the mixture was heated at 50—60 °C for 3 h. The reacted mixture was cooled to room temperature, poured into cold water, and taken up in ether. The ethereal solution was washed with an aqueous solution of sodium hydrogen carbonate, dried over sodium sulfate, and the solvent was evaporated to give a yellow oil, which was chromatographed over a silica-gel column with chloroform with separation of compounds A (R_f=0.19) and B (R_f=0.07). Compound B was recrystallized from benzene as colorless needles (**13**) (1.8 g, 20%): mp 129—130 °C; IR ν_{max}^{KBr} 1740, 1630 cm^{-1}; NMR ($CDCl_3$) δ 1.77 (bs, 6H, $2\times CH_3$), 2.23 (s, 3H, CH_3CO), 3.24 (d, 2H, J=7 Hz, CH_2CH=), 5.24[8] (s, 2H, CH_2), *ca.* 5.24[8] [1H, $(CH_3)_2C$=CH], 6.31 (s, 2H, C_3-H, C_4-OH), 7.25 (s, 1H, C_6-H), 11.93 (s, C_2-OH). Found: C, 64.77; H, 6.43%. Calcd for $C_{15}H_{18}O_5$: C, 64.73; H, 6.52%.

Compound A was recrystallized from benzene as colorless needles (**14**) (0.4 g, 6%), producing a positive reaction in the ferric chloride color test: mp 147—148 °C; IR ν_{max}^{KBr} 1725, 1630 cm^{-1}; NMR ($CDCl_3$) δ 1.74 (s, 3H) and 1.80 (s, 3H) [$(CH_3)_2C$=CH], 2.22 (s, 3H, CH_3CO), 3.39 (d, 2H, J=7 Hz, CH_2CH=), 5.22[8] (s, 2H, CH_2), *ca.* 5.22[8] [1H, $(CH_3)_2C$=CH], 6.32 (d, 1H, J=9 Hz, C_5-H), 6.37 (s, C_4-OH), 7.83 (d, 1H, J=9 Hz, C_6-H), 12.45 (s, C_2-OH). Found: C, 64.68; H, 6.41%. Calcd for $C_{15}H_{18}O_5$: C, 64.73; H, 6.52%.

Another Synthesis of Ripariochromene B (1). A mixture of **13** (0.30 g), DDQ (0.32 g), and dried toluene (120 ml) was heated under reflux for 2 h. The reacted mixture was worked up in the same manner as in the case of chromene **1**. The chromene thus obtained was recrystallized from carbon tetrachloride as colorless needles (**1**) (0.18 g, 65%): mp 146—147 °C (no depression in a mixed melting-point determination with the ripariochromene B synthesized above).

5-Hydroxy-6-acetoxyacetyl-2,2-dimethylchromene (15). A mixture of **14** (57 mg), DDQ (68 mg), and dried toluene (20 ml) was worked up in the same manner described above. The chromene thus obtained was crystallized from petroleum ether (35—40 °C) as colorless prisms (**15**) (24 mg, 42%): mp 117—118.5 °C; IR ν_{max}^{KBr} 1755, 1660 cm^{-1}; NMR ($CDCl_3$) δ 1.44 (s, 6H, $2\times CH_3$), 2.21 (s, 3H, CH_3CO), 5.23 (s, 2H, CH_2), 5.56 (d, 1H, J=10 Hz, C_3-H), 6.32 (d, 1H, J=10 Hz, C_4-H), 6.67 (d, 1H, J=10 Hz, C_8-H), 7.38 (d, 1H, J=10 Hz, C_7-H), 12.32 (s, OH). Found: C, 65.10; H,

5.90%. Calcd for $C_{15}H_{16}O_5$: C, 65.21; H, 5.84%.

*2,4-Dihydroxy-ω-(isobutyryloxy)acetophenone (**16**).* A mixture of resorcinol (10.4 g), isobutyryloxyacetonitrile (18 g), and zinc chloride (6 g) in dried ether (200 ml) was worked up in the same manner as in the case of **12** to give colorless prisms (**16**) (10 g, 40%): mp 116—117 °C; IR ν_{max}^{KBr} 1710, 1635 cm^{-1}; NMR (DMSO) δ 1.15 [d, 6H, J=7 Hz, $(CH_3)_2$-CH], 2.63 [m, 1H, $(CH_3)_2CH$], 5.23 (s, 2H, CH_2), 6.28 (bs, 1H, C_3-H), 6.33 [q, 1H, (J=2.5, 9 Hz) C_5-H], 7.68 [d, 1H, (J=9 Hz) C_6-H], 10.57 (s, C_4-OH), 11.46 (s, C_2-OH). Found: C, 60.46; H, 5.74%. Calcd for $C_{12}H_{14}O_5$: C, 60.50; H, 5.92%.

*5-(3-Methyl-2-butenyl)-2,4-dihydroxy-ω-(isobutyryloxy) acetophenone (**17**) and 3-(3-Methyl-2-butenyl)-2,4-dihydroxy-ω-(isobutyryloxy)acetophenone (**18**).* A mixed solution of **16** (8.0 g), boron trifluoride etherate (3.6 g), and 2-methyl-3-buten-2-ol (2.1 g) in dried dioxane (150 ml) was worked up in the same manner as in the case of **13** to give **17** and **18**. Compound **17** was recrystallized from benzene as colorless needles (1.8 g. 20%): mp 122—123 °C; IR ν_{max}^{KBr} 1720, 1650 cm^{-1}; NMR ($CDCl_3$) δ 1.27 [d, 6H, J=7 Hz, $(CH_3)_2$-CH], 1.74 [bs, 6H, $(CH_3)_2C$=CH], 2.74 [m, 1H, $(CH_3)_2CH$], 3.23 [d, 2H, J=7 Hz, CH_2CH=], 5.23[8] (s, 2H, CH_2), *ca.* 5.23[8] [1H, $(CH_3)_2C$=CH], 6.29 (s, 1H, C_3-H), 6.47 (s, C_4-OH), 7.25 (s, 1H, C_6-H), 11.96 (s, C_2-OH). Found: C, 66.88; H, 7.29%. Calcd for $C_{17}H_{22}O_5$: C, 66.65; H, 7.24%.

Recrystallization of **18** from benzene gave colorless needles (0.4 g, 5%): mp 147—148 °C; IR ν_{max}^{KBr} 1713, 1625 cm^{-1}; NMR ($CDCl_3$) δ 1.25 [d, 6H, J=7 Hz, $(CH_3)_2CH$], 1.73 (s, 3H) and 1.79 (s, 3H) [$(CH_3)_2C$=CH], 2.73 [m, 1H, $(CH_3)_2CH$], 3.40 (d, 2H, J=7 Hz, CH_2CH=), 5.24[8] (s, 2H, CH_2), *ca.* 5.24[8] [1H, $(CH_3)_2C$=CH], 6.35 (d, 1H, J=9 Hz, C_5-H), 6.39 (s, C_4-OH), 7.36 (d, 1H, J=9 Hz, C_6-H), 12.45 (s, C_2-OH). Found: C, 66.50; H, 7.12%. Calcd for $C_{17}H_{22}O_5$: C, 66.65; H, 7.24%.

*Another Synthesis of Riparіochromene C (**2**).* A mixture of **17** (0.30 g), DDQ (0.29 g), and dried toluene (120 ml) was worked up in the manner described above to give colorless needles (**2**) (0.18 g, 60%): mp 109.5—110.5 °C (no depression in a mixed melting-point determination with the riparіochromene C synthesized above).

*5-Hydroxy-6-isobutyryloxyacetyl-2,2-dimethylchromene (**19**).* A mixture of **18** (102 mg), DDQ (113 mg), and dried toluene (120 ml) was worked up in the manner described above to give colorless prisms (**19**) (53 mg, 52%): mp 72—73.5 °C; IR ν_{max}^{KBr} 1735, 1640 cm^{-1}; NMR ($CDCl_3$) δ 1.26 [d, 6H, J=7 Hz, $(CH_3)_2CH$], 1.44 (s, 6H, 2×CH_3), 2.73 [m, 1H, $(CH_3)_2CH$], 5.22 (s, 2H, CH_2), 5.55 (d, 1H, J=10 Hz, C_3-H), 6.32 (d, 1H, J=10 Hz, C_4-H), 6.68 (d, 1H, J=10 Hz, C_8-H), 7.38 (d, 1H, J=10 Hz, C_7-H), 12.33 (s, OH). Found: C, 67.36; H, 6.72%. Calcd for $C_{17}H_{20}O_5$: C, 67.09; H, 6.62%.

The author wishes to express his deep gratitude to Professor Shûichi Hayashi and Dr. Mitsuru Nakayama, Hiroshima University, for their guidance and encouragement throughout the course of this work, and also to Dr. Thorleif Anthonsen, Norway Institute of Technology, for supplying the samples of natural riparіochromene B and C.

References

1) Part of this work has previously been reported in preliminary form: M. Nakayama, S. Hayashi, M. Tsukayama, T. Horie, and M. Masumura, *Chem. Lett.*, **1974**, 87.

2) T. Anthonsen, *Acta Chem. Scand.*, **23**, 3605 (1969).

3) R. J. Molyneux and L. Jurd, *Tetrahedron*, **26**, 4743 (1970).

4) M. Nakayama, M. Ohno, S. Hayashi, and K. Fukui, *Bull. Chem. Soc. Jpn.*, **43**, 3311 (1970).

5) M. Nakayama, S. Nishimura, T. Matsui, S. Hayashi and K. Fukui, *Experientia*, **27**, 875 (1971).

6) M. Nakayama, S. Hayashi, M. Tsukayama, T. Horie, and M. Masumura, *Chem. Lett.*, **1972**, 315.

7) M. Nakayama, S. Hayashi, M, Masumura. T. Horie, M. Tsukayama, and T. Yamada, *Chem. Lett.*, **1975**, 315.

8) Methylene protons and a methine proton overlapped.

Skeletal Rearrangement of Furanoeremophilane-6β,10β-diol into Farfugin A, Farfugin B, and 6-[(4*R*)-Chloropentyl]-3,5-dimethylbenzofuran[1]

Masahiro TADA, Yoshiaki TANAHASHI, Yoshihiko MORIYAMA, and Takeyoshi TAKAHASHI

Department of Chemistry, Faculty of Science, The University of Tokyo, Bunkyo-ku, Tokyo 113

(Received August 5, 1976)

Treatment of furanoeremophilane-6β,10β-diol (**1**; R=H) with phosphoryl chloride in pyridine at 110 °C gave farfugin A (**2**; yield: 23%), farfugin B (**3**; y: 34%), and 6-[(4*R*)-4-chloropentyl]-3,5-dimethylbenzofuran (**4**; y: 15%). A mechanism of formation of these three compounds (**2**, **3**, and **4**) is discussed.

Furanoeremophilane-6β,10β-diol (**1**; R=H)[2] is a sesquiterpene of eremophilane-type isolated from *Ligularia japonica* Less., while farfugin A (**2**)[3] and farfugin B (**3**)[3] are benzofuran derivatives contained in *Farfugium japonicum* (L.) Kitam. In connection with a structure investigation of **1** (R=H), we found that farfugin A, farfugin B, and another benzofuran (**4**) were formed on dehydration of **1** (R=H) with phosphoryl chloride. In the present paper we wish to report the mechanism of these skeletal rearrangements.

The diol (**1**; R=H) was treated with phosphoryl chloride in pyridine at 110 °C under nitrogen to give three benzofuran derivatives (**2**, **3**, and **4**). The two products, **2** (yield: 23%), mp 78—79 °C, $[\alpha]_D$+32° (EtOH), and **3** (y: 34%), an oil, proved to be identical with farfugin A (**2**) and farfugin B (**3**), respectively. The molecular formula $C_{15}H_{19}OCl$ of the third product (**4**; y: 15%), an oil, $[\alpha]_D$—20° (EtOH), was determined by elemental analysis and mass spectrometry. The UV spectrum of **4** is superimposable with that of **3**; this suggests the presence of a benzofuran moiety in **4** similar to that in **3**. The IR spectrum of **4** indicates the presence of a C-Cl group (795 cm^{-1}) and the absence of a *trans* -CH=CH- system. The PMR spectrum of **4** shows a doublet (J=7.5 Hz) at δ 1.50 due to a secondary methyl (CH_3-CHCl-) and a multiplet at δ 4.0 due to a proton on the chlorine-bearing carbon (CH_3-CHCl-), while a multiplet at δ 5.45[3b] due to a *trans* olefin system (-CH=CH-) observed for **3** is absent. The other PMR spectral data of **3** are closely related to those of **4**. The observation shown above led to the structure **4** for the third product. The absolute configuration at the chlorine-substituted carbon in **4** (with negative sign of $[\alpha]_D$) was deduced to be (*R*) by application of Brewster rule.[4]

A similar treatment of 10β-hydroxy-6β-methoxyfuranoeremophilane (**1**; R=CH_3)[2] and 6β-acetoxy-10β-hydroxyfuranoeremophilane (**1**; R=Ac)[2] yielded also the three benzofuran derivatives (**2**, **3**, and **4**) (detected by TLC). When **1** (R=H) was treated with trace of hydrochloric acid in acetone at room temperature, the formation of these compounds (**2**, **3**, and **4**) was observed by TLC examination along with tarry products.

The fact that both **2** and **4** are optically active is of interest in view of the mechanism of these skeletal rearrangements. The absolute configuration at $C_{(4)}$ of the diol (**1**; R=H) and the absolute stereochemistry at $C_{(9)}$ of farfugin A (**2**) have recently been reported to be both (*S*).[2b,5] The configuration of the migrating center was thus shown to be retained before and after the transformation. The formation of **2** from **1** would be explained by two successive 1,2-alkyl shifts involving a spiro intermediate (**B**),[6] or by a 1,5-sigmatropic shift[7] *via* **5** and **6** (X=$POCl_2$ or other phosphate esters) (Scheme 1).

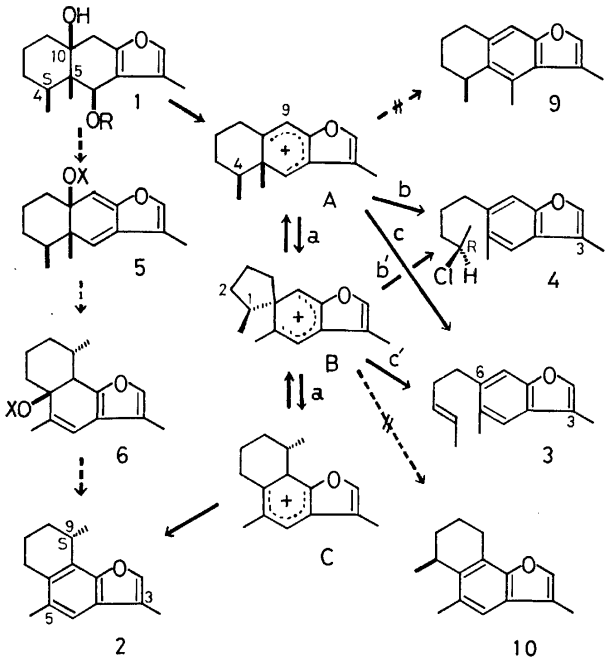

Scheme 1.

Reduction of furanoeremophil-9-en-6-one (**7**)[2b] with lithium aluminium hydride gave the corresponding alcohol (**8**), which was treated with phosphoryl chloride under the same conditions described for **1** (R=H). The three benzofuran derivatives (**2**, **3**, and **4**) were fairly obtained in a similar ratio to that observed for the rearrangement products of **1** (R=H). This fact strongly suggests that these three benzofurans are formed from an intermediate cyclohexadienyl cation (**A**),[8] which could be produced from **8** by elimination of a hydroxyl (or its equivalents). The pathway through the cation **A** would thus be favorable rather than the route involving 1,5-sigmatropic shift.

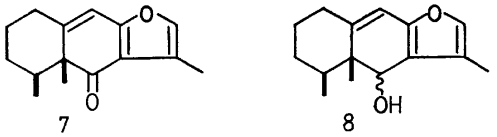

The presence of two stage 1,2-alkyl shifts through a spiro intermediate in the dienone-phenol rearrangement of a cyclohexadienyl cation has elegantly been demonstrated.[9,10] In an acid-catalyzed dienone-phenol rear-

rangement the medium affects the products.[11,12] A preferential migration, especially favored under the anhydrous conditions, of the more highly substituted carbon atom in the rearrangement was demonstrated.[9-12]

The mechanism of the rearrangement of **1** into **2**, **3**, and **4** could therefore be well rationalized as follows. The elimination of hydroxyls (or their equivalents) from **1** would give rise to the cyclohexadienyl cation **A** (depicted as **D**), which would then suffer rearrangements to form the three benzofuran derivatives (**2**, **3**, and **4**). (a) A migration of $C_{(4)}$-$C_{(5)}$ bond in **A** gives a spiro intermediate (**B**)[9-11] which would be further rearranged into another cation (**C**). An elimination of a proton from **C** affords farfugin A (**2**) whose configuration at $C_{(9)}$ is (*S*) (pathway a). Two processes could account for the formation of both **4** and **3**. (b and/or b') A S_N2 type substitution by Cl^- is effected at the secondary methyl carbon of **A** (path b) and/or of **B** (path b') with concomitant aromatization of ring B. These pathway would give the (4*R*)-4-chloropentyl side chain in **4**. (c and/or c') An abstraction of $C_{(3a)}$-H from **A** with aromatization of ring B would lead to a formation of the *trans*-3-pentenyl side chain[3b] in farfugin B (**3**) (path c). An alternative route involving an elimination of $C_{(2)}$-H from **B** accompanied with aromatization could produce a mixture of isomers with the *cis* and *trans* side chains. The *cis*-isomer would then isomerize under the reaction conditions to give **3** (path c'). A choice between the two routes (between b and b', and between c and c') for each formation of **4** and **3**, remained undecided (*cf.* **D** and Scheme 1).

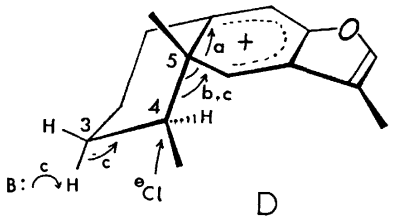

D

In the rearrangement of the diol (**1**; R=H), benzofuran derivatives such as **9**[13] and **10** might be expected to be produced form **A** and **B**, respectively. This was, however, contrary to the observation. This evidence could be interpreted by the preferential migration (or bond-scission) of the more highly substituted carbon atom[9-12] ($C_{(4)}$ of **A**, or $C_{(1)}$ of **B**), whose rearrangement would be especially pronounced in anhydrous conditions ($POCl_3$-pyridine), to afford **2** (**3**, and **4**).

In conclusion, the conversion of **1** into **2**, **3**, and **4** can be best explained by an intermediacy of the cyclohexadienyl cation **A** as in the case of dienone-phenol rearrangement.[14]

Experimental

IR spectra were measured using a Hitachi EPI-G2 spcetrometer. Optical rotation was measured on a JASCO DIL-SL polarimeter. Mass spectra were taken on a Hitachi RMU-6-Tokugata mass spectrometer with a direct inlet system operating at 70 eV. PMR spectra were measured using a JEOL PS-100 (100 MHz). Thin layer chromatography (TLC) was carried out on Kieselgel PF_{254} (E. Merck, Darmstadt). For column chromatography Wakogel 200 (Wako Pure Chemical Co.) was used. All mps were determined on a hot block and reported uncorrected.

Treatment of Furanoermophilane-6β,10β-diol (***1*** : *R=H*) *with Phosphoryl Chloride.* To a solution of the diol (**1** : R=H; 67 mg)[2] in pyridine (2 ml), phosphoryl chloride (0.2 ml) was added dropwise with stirring, and the mixture was heated under nitrogen at 110 °C (bath temperature) for 1 h. The cooled reaction mixture was poured into a mixture of ice and water and extracted with ether. The organic layer was washed with 2 M hydrochloric acid and then with water, dried over anhydrous sodium sulfate, and evaporated to give a residue, which was chromatographed on a column of silica gel. Elution with petroleum ether gave farfugin A (**2**; 13 mg; y: 23%) and farfugin B (**3**; 19 mg; y: 34%) successively. These compounds (**2** and **3**) proved to be identical (by IR, UV, PMR, TLC, and mass spectrometry) with natural farfugin A[3b] and farfugin B[3b] respectively. Further elution with the same solvent yielded 6-[(4*R*)-4-chloropentyl]-3,5-dimethylbenzofuran (**4**; 10 mg; y: 15%), an oil, $[\alpha]_D$ −20° (*c* 1.0, EtOH); IR (liquid) 1630, 1580, 1132, 1090, and 795 cm^{-1}; UV (EtOH) λ_{max} 252 nm (ε 10600), 258 (sh), 276 (sh), 282 (3400), 285 (3300), and 292 (3800); PMR ($CDCl_3$) δ 1.50 (3H, d, J=7.5 Hz; $C\underline{H}_3$-CHCl-), 2.19 (3H, d, J=1.2 Hz; $C_{(3)}$-CH_3), 2.40 (3H, s; $C_{(5)}$-CH_3), *ca.* 4.0 (1H, m; CH_3-C$\underline{H}$Cl-), *ca.* 7.2—7.3 (3H, $C_{(2)}$-H, $C_{(4)}$-H, and $C_{(7)}$-H), and *ca.* 2.5—3.0 [6H, -$(CH_2)_3$-]; mass spectrum *m/e* 252 and 250 (M^+; in an intensity ratio of *ca.* 1 : 3) and 159 (base peak). Found: C, 71.70; H, 7.58; Cl, 14.42%. Calcd for $C_{15}H_{19}OCl$: C, 71.84; H, 7.64; Cl, 14.14%. Other benzofuran derivatives such as **9** and **10** were not obtained.

Gas chromatographic examination before effecting the column chromatographic separation showed that the ratio of these products (**2**, **3**, and **4**) was 1.0 : 1.5 : 0.4 based on the integrated area of the peak for each product [column: Diasolid H-523, 5(mm)×1.5(m); column temperature: 170 °C; detection: FID; carrier gas: N_2, 66 ml/min; instrument: Shimadzu GC-4A PF].

Treatment of 10β-Hydroxy-6β-methoxyfuranoeremophilane (***1*** : *R=*CH_3) *and 6β-Acetoxy-10β-hydroxyfuranoeremophilane* (***1*** : *R=Ac*) *with Phosphoryl Chloride.* A methoxy alcohol (**1**; R=CH_3; 5 mg)[2] or an acetoxy alcohol (**1**; R=Ac; 5 mg)[2] was treated with phosphoryl chloride (0.05 ml) in pyridine (0.5 ml) at 110 °C for 1 h. In each case the reaction mixture gave, after the work-up described above, a residue which was shown to be a mixture of the three benzofuran derivatives (**2**, **3**, and **4**) by TLC examination.

Acid-Catalyzed Rearrangement of the Diol (***1***; *R=H*). To a solution of the diol (**1**; R=H; 5 mg)[2] in dry acetone (0.5 ml) was added a drop of concentrated hydrochloric acid at room temperature. The reaction mixture was treated as usual to give a residue, which was examined by TLC to show the formation of the three benzofurans (**2**, **3**, and **4**) and of tarry products formed probably by degradation of the furan ring.

Reduction of Furanoeremophil-9-en-6-one (***7***) *with Lithium Aluminium Hydride and Successive Treatment with Phosphoryl Chloride.* Lithium aluminium hydride (100 mg) was added to a solution of the ketone (**7**; 40 mg)[2b] in ether (10 ml), and the mixture was stirred under nitrogen at room temperature for 1 h. The excess of lithium aluminium hydride was decomposed with water, and the mixture was extracted with ether. The ethereal layer was washed with water and brine, and then dried over anhydrous sodium sulfate. On

removal of the solvent, an unstable oily alcohol (**8**; ν_{OH} 3500 cm^{-1}; one spot on TLC) was obtained, which without further characterization was dissolved in pyridine (0.5 ml). After addition of phosphoryl chloride (0.1 ml), the resulting mixture was heated under nitrogen at 110 °C for 1 h. The reaction mixture was treated as usual to give a residue, which was subjected to separation by preparative TLC to afford the three benzofurans (**2**, **3**, and **4**). The ratio of these products (**2**, **3**, and **4**) was determined to be 1.0 : 1.3 : 0.3 by gas chromatography (under the same conditions mentioned above) before effecting the TLC separation.

References

1) A preliminary account of this paper: M. Tada, Y. Tanahashi, Y. Moriyama, and T. Takahashi, *Tetrahedron Lett.*, **1972**, 5255.

2) a) M. Tada, Y. Moriyama, Y. Tanahashi, T. Takahashi, M. Fukuyama, and K. Sato, *Tetrahedron Lett.*, **1971**, 4007; b) M. Tada, Y. Moriyama, Y. Tanahashi, and T. Takahashi, *Bull. Chem. Soc. Jpn.*, **47**, 1999 (1974).

3) a) H. Nagano, Y. Moriyama, Y. Tanahashi, T. Takahashi, M. Fukuyama, and K. Sato, *Chem. Lett.*, **1972**, 13; b) H. Nagano, Y. Moriyama, Y. Tanahashi, and T. Takahashi, *Bull. Chem. Soc. Jpn.*, **47**, 1994 (1974).

4) J. H. Brewster, *J. Am. Chem. Soc.*, **81**, 5475 (1959).

5) a) M. Tada, Y. Moriyama, Y. Tanahashi, and T. Takahashi, *Tetrahedron Lett.*, **1972**, 5251; b) M. Tada, Y. Moriyama, Y. Tanahashi, and T. Takahashi, *Bull. Chem. Soc. Jpn.*, **48**, 549 (1975).

6) D. J. Dunham and R. G. Lawton, *J. Am. Chem. Soc.*, **93**, 2075 (1971).

7) R. B. Woodward and R. Hoffmann, "The Conservation of Orbital Symmetry," Verlag Chemie GmbH, Weinheim (1970).

8) *e. g.* V. P. Vitullo and N. Grossman, *J. Am. Chem. Soc.*, **94**, 3844 (1972). *Cf.* Refs. 6, 9—11, and a large number of reports on the dienone-phenol rearrangement in steroids and terpenes.

9) a) R. B. Woodward, in "Perspectives in Organic Chemistry," ed by A. Todd, Interscience, New York (1956), pp. 155, 178; b) R. B. Woodward and T. Singh, *J. Am. Chem. Soc.*, **72**, 494 (1950); c) R. B. Woodward, H. H. Inhoffen, H. O. Larson, and K. Menzel, *Chem. Ber.*, **86**, 594 (1953).

10) S. M. Bloom, *J. Am. Chem. Soc.*, **80**, 6280 (1958).

11) P. J. Kropp, *J. Am. Chem. Soc.*, **85**, 3280 (1963).

12) A. S. Dreiding, W. J. Pummer, and A. J. Tomasewski, *J. Am. Chem. Soc.*, **75**, 3159 (1953); the dienone-phenol rearrangement of androsta-1,4-diene-3,17-dione was also described. *Cf.* A. S. Dreiding and A. Voltman, *ibid.*, **76**, 537 (1964).

13) The structure of **9** is related to those of sesquiterpenes of cacalane-type. *Cf. e. g.* a) H. Kakisawa, Y. Inouye, and J. Romo, *Tetrahedron Lett.*, **1969**, 1929; b) Y. Inouye, Y. Uchida, and H. Kakisawa, *Chem. Lett.*, **1975**, 1317; c) K. Naya, Y. Miyoshi, H. Mori, K. Takai, and M. Nakanishi, *ibid.*, **1976**, 73. And references cited therein.

14) The skeletal structures of farfugin A (**2**) and farfugin B (**3**) can be expressed as 4(5→9)abeo-furanoeremophilane and 4,5-seco-furanoeremophilane, respectively.

Reaction of 1,1-Diiodoethane with Copper Powder in the Presence of Olefins and/or Alkylbenzenes

Nariyoshi KAWABATA,* Nobuyuki YAMAGISHI, and Shinzo YAMASHITA

Department of Chemistry, Kyoto Institute of Technology, Matsugasaki, Sakyo-ku, Kyoto 606

(Received August 13, 1976)

The treatment of 1,1-diiodoethane with copper powder in the presence of 1-heptene gave a 1.3 : 1 mixture of *cis*- and *trans*-1-methyl-2-pentylcyclopropane in 11% yield. The treatment in the presence of cyclohexene gave a 1 : 1.7 mixture of *endo*- and *exo*-7-methylbicyclo[4.1.0]heptane in 32% yield, together with 1-ethylcyclohexene in 8% yield, which was shown to be derived mainly from isomerization of the *endo*-isomer. These reactions were concluded to proceed *via* organocopper intermediate rather than free methylcarbene. The treatment of 1,1-diiodoethane with copper powder in the presence of alkylbenzene gave a mixture of *o*- and *p*-ethyl(alkyl)benzene contrary to the corresponding reaction of methylcarbenoid of zinc which gave cycloheptatriene derivatives.

This paper describes an α-elimination of iodine from 1,1-diiodoethane by the reaction with copper powder. Although α-elimination reactions provide the best route to most classes of carbenes and carbenoids,[1] only a few publications are available on the α-elimination of halogen from 1,1-dihaloalkane. Alkyl- and dialkylcarbenes are distinguished from other classes of carbenes by the predominance of intramolecular reactions leading to olefins and cyclopropane derivatives. Kirmse and Wächtershäuser[2] reported that the treatment of 1,1-diiodoalkane with sodium, lithium, and magnesium afforded predominantly cyclopropane derivatives, whereas the treatment with zinc and copper produced olefins *via* rearrangements of the Wagner-Meerwein type, but these workers did not refer to the α-elimination of 1,1-diiodoethane. The α-elimination of iodine from 1,1-diiodoalkane by zinc-copper couple was reported to give predominantly olefins.[3] The reaction of 1,1-diiodoethane with zinc-copper couple was reported to give ethylene.[4]

The α-elimination reactions of 1,1-dihaloalkanes in the presence of olefins give the corresponding cyclopropane derivatives by intermolecular cycloaddition of alkylcarbene or carbenoid to olefins.[4-6] Previously we have proposed an improved method for preparing methylsubstituted cyclopropane derivatives by the reaction of olefins with 1,1-diiodoethane and diethylzinc.[7]

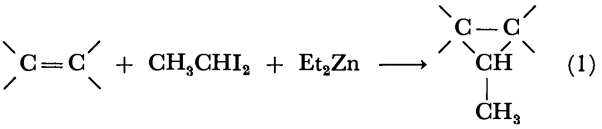

(1)

Recently we found that the reaction of diiodomethane with copper powder in the presence of olefins gave the corresponding cyclopropane derivatives in good yields.[8]

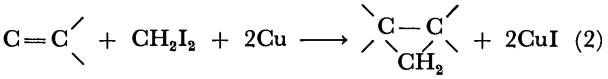

(2)

As an extension of this work, we have investigated the reaction of 1,1-diiodoethane with copper powder in the presence of olefins and/or alkylbenzenes.

Results and Discussion

The reaction of 1,1-diiodoethane with copper powder was carried out in toluene at 75 °C for 24 h. Gas chromatographic analysis of the liquid layer showed that 74% of 1,1-diiodoethane remained unchanged in the reaction mixture under the conditions. In the gaseous products was shown the formation of ethylene in 2% yield, but ethane was not detected. The experimental results indicate that 1,1-diiodoethane reacted with copper powder under the conditions. Methylcarbene or methylcarbenoid of copper would be reactive intermediates. The absence of ethane in the gaseous products indicates that the methylcarbene or carbenoid did not undergo the hydrogen abstraction under the conditions.

The treatment of 1,1-diiodoethane with copper powder in the presence of 1-heptene gave a 1.3 : 1 mixture of *cis*- and *trans*-1-methyl-2-pentylcyclopropane in 11% yield based on the olefin.

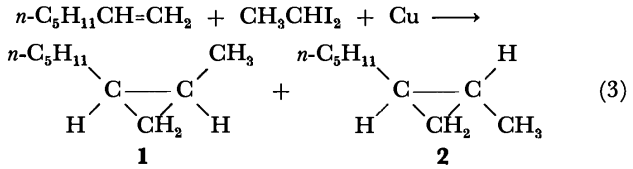

(3)

1 **2**

Isomeric olefins were not detected in the reaction mixture which would be expected from the insertion of free methylcarbene into C–H bonds. Therefore, the α-elimination of iodine from 1,1-diiodoethane by copper powder may proceed *via* an organocopper intermediate (methylcarbenoid of copper) rather than free methylcarbene.

Since the *cis*-isomer **1** was obtained predominantly over the *trans*-isomer **2**, the methylcarbenoid of copper was concluded to show essentially the *syn*-selectivity[9] in the cycloaddition with olefins as the methylcarbenoid of zinc.[7]

1,1-Diiodoethane was allowed to react with copper powder in the presence of cyclohexene to give a 1 : 1.7 mixture of *endo*- and *exo*-7-methylbicyclo[4.1.0]heptane in 32% yield, together with 1-ethylcyclohexene (**5**) in 8% yield based on the olefin.

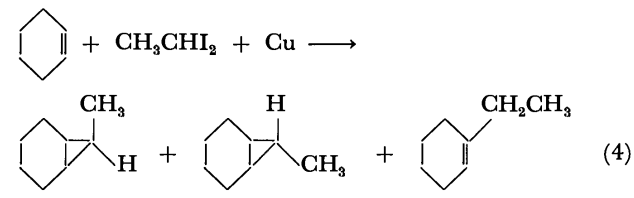

(4)

3 **4** **5**

* To whom correspondence should be addressed.

Table 1. Formatiom of ethyl(alkyl)benzene by reaction (5)

R	Copper (mmol)	Alkylbenzene (ml)	1,1-Diiodoethane (mmol)	Temp (°C)	Time	Yield (%)[a]	Isomer ratio (*p*/*o*)
H	72.0	15.0	32.0	75	17 day	1	—
CH_3	18.0	4.0	8.1	100	95 h	3	2.1
CH_3CH_2	72.0	15.0	31.3	125	40 h	27	2.4

a) Based on 1,1-diiodoethane.

Heating of an isolated mixture (77 : 23) of **3** and **5** in the presence of copper (I) iodide gave a 4 : 96 mixture of **3** and **5**. On the other hand, the *exo*-isomer **4** did not isomerize to **5** under the conditions. Therefore, **5** was concluded to be derived mainly from the isomerization of **3** during the reaction (Eq. 4) rather than the insertion of free methylcarbene into C–H bonds. When **5** was supposed to be completely derived from the isomerization of **3**, the reaction (Eq. 4) was led to give a nearly equimolar amount of **3** and **4**. In any case, the *endo*-isomer **3** did not predominate over the *exo*-isomer **4** in the reaction (Eq. 4), contrary to the corresponding reaction of methylcarbenoid of zinc. The reaction (Eq. 1) with cyclohexene gave a 1.5 : 1 mixture of **3** and **4**.[7]

In order to compare the behavior of the organocopper intermediate (methylcarbenoid of copper) with that of the methylcarbenoid of zinc generated from 1,1-diiodoethane and diethylzinc in the reaction with alkylbenzene, we also studied on the reaction of 1,1-diiodoethane and copper powder in the presence of alkylbenzene.

1,1-Diiodoethane was found to react with copper powder in alkylbenzene to give mixtures of *o*- (**6**) and *p*-ethyl(alkyl)benzene (**7**) as are given in Table 1. *m*-Ethyl(alkyl)benzene was not significantly detected in the reaction mixture (see experimental for details). Cycloheptatriene derivatives were not detected in the above reaction mixtures.

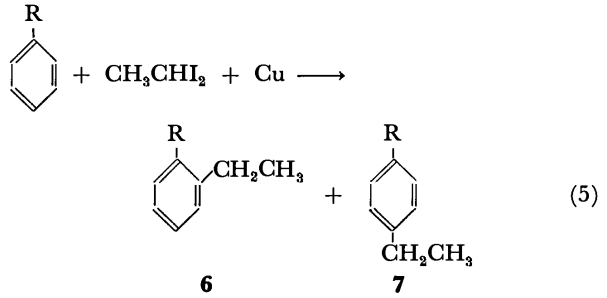

(5)

6 **7**

These experimental results form a sharp contrast with those observed in the reaction of methylcarbenoid of zinc with alkylbenzene. In the latter reaction, the ring expansion reaction was predominant to afford cycloheptatriene derivatives.[10]

The reaction of the methylcarbenoid of zinc with naphthalene gave 7-methyl-2,3-benzobicyclo[4.1.0]-hepta-2,4-diene (**8**).[10] On the other hand, the treatment of 1,1-diiodoethane and copper powder in the presence of naphthalene in ethylbenzene gave α-ethylnaphthalene in 12% yield at 125 °C based on naphthalene together with *o*- and *p*-diethylbenzene. β-Ethylnaphthalene and **8** were not detected in the reaction mixture.

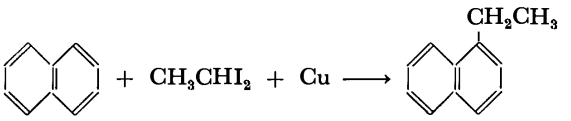

(6)

Since cycloheptatriene derivatives and **8** were not formed by the reactions (Eqs. 5 and 6), the following route should be excluded: the cycloaddition of the methylcarbenoid of copper to the aromatic carbon-carbon unsaturated bond to afford bicyclo[4.1.0]-hepta-2,4-diene derivatives followed by isomerization to ethylbenzene derivatives. The *ortho-para* orientation in the reaction (Eq. 5) and the predominant formation of α-ethylnaphthalene in the reaction (Eq. 6) show the electrophillic nature of the reaction of 1,1-diiodoethane and copper powder with alkylbenzene to afford ethylbenzene derivatives, but further experiments are required to discuss the mechanism of the substitution.

Experimental

Gas chromatographic analyses were carried out on a Shimadzu GC-4A or GC-4B gas chromatograph. NMR spectra were obtained with a Varian Model T-60-A spectrometer using carbon tetrachloride as the solvent and tetramethylsilane as the internal standard. IR spectra were recorded on a Hitachi Model 215 or Japan Spectroscopic Model 402 G spectrophotometer.

Materials. 1,1-Diiodoethane was prepared according to the procedure of Letsinger and Kammeyer.[11] Diethylzinc was prepared according to the procedure of Holler.[12] Active zinc-copper couple was prepared according to the procedure of Shank and Shechter.[13] The ordinary commercial grade of copper powder (particle size was 5—15 μ) provided by Nakarai Chemicals Ltd., Kyoto was used without further purification. Olefins, alkylbenzenes, and solvents were purified by distillation. Nitrogen was purified by being passed through a tube containing copper turnings in a furnace at 170 °C. Authentic samples of ethylene and ethane were prepared by hydrolyses of vinylmagnesium bromide and ethylmagnesium bromide, respectively. Authentic samples of **1**,[14] **2**,[14] **3**,[7] and **4**[7] were prepared by conventional methods, respectively. Commercial authentic samples and other chemicals were used without further purification.

Reaction of 1,1-Diiodoethane with Copper Powder. Copper powder (2.28 g, 36.0 mmol) was allowed to react with a small amount (0.10 g, 0.4 mmol) of iodine in 4.0 ml of toluene at room temperature in a flask equipped with a gas burrette and a magnetic stirrer. After the brown color of iodine disappeared, 1,1-diiodoethane (4.51 g, 16.0 mmol) was added, and the mixture was heated at 75 °C for 24 h with stirring. The total amount of the evolved gas was determined by the gas burrette, and the gaseous products were analyzed by gas chromatography. The liquid layer was also analyzed by gas chromatography after elimination of the inorganic ma-

terials from the reaction mixture by filtration. Results are given in the text.

Reaction of 1,1-Diiodoethane with Copper Powder in the Presence of 1-Heptene. Copper powder (2.28 g, 36.0 mmol) was allowed to react with a small amount (0.10 g, 0.4 mmol) of iodine in 6.0 ml of toluene at room temperature in a flask equipped with a reflux condenser and a magnetic stirrer. After the brown color of iodine disappeared, 1,1-diiodoethane (4.31 g, 15.3 mmol) and 1-heptene (0.88 g, 9.0 mmol) were added, and the mixture was heated at 85 °C for 91 h with stirring. After the reaction, inorganic materials were removed by filtration, and the organic layer was analyzed by gas chromatography. Yields were determined by the gas chromatographic analyses of the reaction mixture. The structures of the products **1** and **2** were determined by comparison of their retention times with those of authentic samples in gas chromatography using two types of different liquid phase, *i.e.*, Silicone DC 550 and Apiezon Grease L. Results are given in the text.

Reaction of 1,1-Diiodoethane with Copper Powder in the Presence of Cyclohexene. Copper powder (3.42 g, 54.0 mmol), iodine (0.15 g, 0.6 mmol), 1,1-diiodoethane (7.03 g, 24.9 mmol), and cyclohexene (1.04 g, 12.7 mmol) were reacted in 9.0 ml of benzene at 75 °C for 304 h in a similar way. Yields were determined by gas chromatographic analyses of the reaction mixture. Products **3**, **4**, and **5** were isolated by collection from the organic layer by gas chromatography. Structures of **3** and **4** were determined by comparison of their IR spectra with those of authentic samples. The structure of **5** was determined by its NMR spectrum. NMR (CCl_4) τ: 4.68 (1 H, m), 7.7—8.8 (8 H, m), 8.09 (2 H, q, J=7 Hz), and 9.01 (3 H, t, J=7 Hz).

A 77 : 23 mixture of **3** and **5** (0.14 g, 1.2 mmol) collected by gas chromatography was heated at 75 °C for 40 h in the presence of copper(I) iodide (0.95 g, 2.5 mmol) in 2.5 ml of benzene. Gas chromatographic analysis of this reaction mixture showed the presence of a 4 : 96 mixture of **3** and **5**, and **4** was not detected in this reaction mixture.

An isolated sample of **4** (0.09 g, 0.8 mmol) collected by gas chromatography was heated at 75 °C for 40 h in the presence of copper(I) iodide (0.65 g, 1.7 mmol) in 1.7 ml of benzene. Gas chromatographic analysis of this reaction mixture showed the presence of **4** without **3** and **5**.

Reaction of 1,1-Diiodoethane with Copper Powder in the Presence of Alkylbenzene. The reaction of 1,1-diiodoethane with copper powder in the presence of alkylbenzene was carried out in a similar way. Products were isolated by collection from the organic layer by gas chromatography. Structures were determined by comparison of their IR spectra with those of authentic samples. Yields were determined by gas chromatographic analyses of the reaction mixture. Results are given in the text.

Reaction of 1,1-Diiodoethane with Copper Powder in the Presence of Naphthalene. The reaction of copper powder (3.82 g, 60.0 mmol), 1,1-diiodoethane (8.12 g, 28.8 mmol), iodine (0.20 g, 0.8 mmol), and naphthalene (2.56 g, 20.0 mmol) was carried out in 10.0 ml of ethylbenzene at 125 °C for 22 h. Gas chromatographic analysis of the reaction mixture showed the formation of α-ethylnaphthalene in 12% yield based on naphthalene, together with *o*- and *p*-diethylbenzene. The sturcture of α-ethylnaphthalene was determined by comparison of the IR spectrum of an isolated sample collected by gas chromatography with that of an authentic sample.

References

1) W. Kirmse, "Carbene Chemistry," 2nd ed, Academic Press, New York, N. Y. (1971).
2) W. Kirmse and G. Wächtershäuser, *Tetrahedron*, **22**, 73 (1966).
3) R. C. Newman, *Tetrahedron Lett.*, **1964**, 2541.
4) H. E. Simmons, E. P. Blanchard, and R. D. Smith, *J. Am. Chem. Soc.*, **86**, 1347 (1964).
5) T. J. Katz and P. J. Garratt, *J. Am. Chem. Soc.*, **86**, 4876 (1964).
6) H. E. Simmons and R. D. Smith, *J. Am. Chem. Soc.*, **81**, 4256 (1959).
7) J. Nishimura, N. Kawabata, and J. Furukawa, *Tetrahedron*, **25**, 2647 (1969).
8) N. Kawabata, M. Naka, and S. Yamashita, *J. Am. Chem. Soc.*, **98**, 2676 (1976).
9) The terms *syn*- and *anti*-selectivity are used in the sense defined by R. A. Moss, *J. Org. Chem.*, **30**, 3261 (1965).
10) J. Nishimura, J. Furukawa, N. Kawabata, and T. Fujita, *Tetrahedron*, **26**, 2229 (1970).
11) R. L. Letsinger and C. W. Kammeyer, *J. Am. Chem. Soc.*, **73**, 4476 (1951).
12) C. R. Holler, *Org. Synth.*, Coll. Vol. II, 269 (1966).
13) R. S. Shank and H. Shechter, *J. Org. Chem.*, **24**, 1825 (1959).
14) C. Asselineau, H. Montrozier, and J. C. Prome, *Bull. Soc. Chim. Fr.*, **1969**, 1911.

The Backbone Rearrangement of 3β,4β-Epoxyfriedelane and the Synthesis of Dendropanoxide[1]

Motoo TORI, Takahiro TORII, Kazuo TACHIBANA, Sachiko YAMADA, Takahiko TSUYUKI, and Takeyoshi TAKAHASHI

Department of Chemistry, Faculty of Science, The University of Tokyo, Bunkyo-ku, Tokyo 113

(Received August 13, 1976)

Dendropanoxide (**1**) was synthesized by the reaction of 3β,4β-epoxyfriedelane (**19**) with boron trifluoride etherate in ether at −10 °C. In the rearrangement reaction, 4α-fluorofriedelan-3β-ol (**20**), D : B-friedo-olean-5(10)-en-3β-ol (**21**), β-amyrin (**22**), and D : B-friedo-olean-5-en-3β-ol (**23**) were also produced.

A triterpene oxide, named dendropanoxide,[2] isolated from *Dendropanax trifidus* Makino (=*Gilibertia trifida* Makino, Araliaceae) is also known as epoxyglutinane[3] and campanulin[4] and distributed in a number of plants of Araliaceae and Ericaceae families.[5] Although two alternative structures, D : B-friedo-olean-3,10-oxide (**1**)[3,4,6] and D : B-friedo-olean-3,5-oxide (**2**),[2,3,5] had been proposed, the D : B-friedo-olean-3β,10β-oxide structure (**1**) was recently assigned for this triterpene oxide by X-ray study.[7]

From an interest in biogenetic relationship between dendropanoxide (**2**) and friedelin (**3**),[8] conversion of **3** into **1** was attempted. Dendropanoxide (**1**) may arise by the following biogenetic pathways.[9] An alunusane (glutinane) type intermediate (**4**) may be derived by a sequence of 1,2-shifts of methyl groups and a hydrogen atom from a protonated β-amyrin type intermediate (**5**) which is originated from squalene. A cationic center at C-10 of the resulting intermediate (**4**) then may suffer an attack by an oxygen atom of the C-3 hydroxyl group from β-side, followed by deprotonation in the last step to give dendropanoxide (**1**).

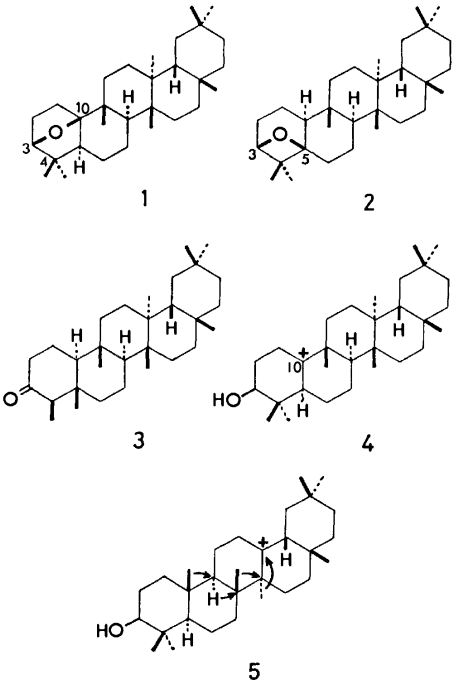

It has been reported that friedel-3-ene (**6**) affords only 3α,4α-epoxyfriedelane (**7**)[10] on epoxydation because of a preferential attack of oxidizing reagents from α-side, and that a treatment of the α-epoxide (**7**) with stannic chloride[10a] or boron trifluoride etherate[10b] gave D : B-friedo-olean-5(10)-en-3α-ol (**8**),[10] olean-12-en-3α-ol (**9**),[10b] 18α*H*-olean-12-en-3α-ol (**10**),[10b] olean-13(18)-en-3α-ol (**11**),[10b] and 18α*H*-A-neo-oleana-3(5),12-diene (**12**).[10b]

Recently Hadley and Halsall[11] reported a boron trifluoride-catalyzed rearrangement of epoxides (**13** and **14**) to give five-membered oxides (**15** and **16**, respectively) in both norlabdane and decalin series. In connection with a study on the rearrangement of tetramethyldecalin derivatives, we found also the formation of a five-membered oxide (**17**) by a similar treatment of an epoxide (**18**).[12] It is therefore suggested that a treatment of 3β,4β-epoxyfriedelane (**19**) with boron trifluoride etherate would produce, by epoxide opening followed by 1,2-methyl shift, the intermediate cation (**4**) (or its equivalent species) which would then afford dendropanoxide (**1**). In the case of shionane derivatives, a conversion of 3β,4β-epoxyshionane into dihydrobaccharis oxide was re-

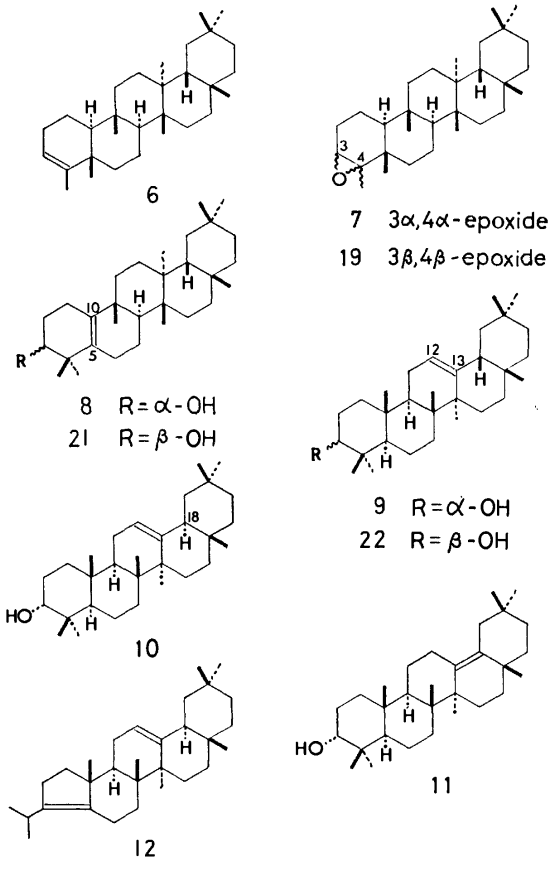

cently achieved.[13] In the present paper, the formation of dendropanoxide (**1**) as well as 4α-fluorofriedelan-3β-ol (**20**), D : B-friedo-olean-5(10)-en-3β-ol (**21**), β-amyrin (**22**), and D : B-friedo-olean-5-en-3β-ol (**23**) by treatment of 3β,4β-epoxyfriedelane (**19**) with boron trifluoride etherate is described.

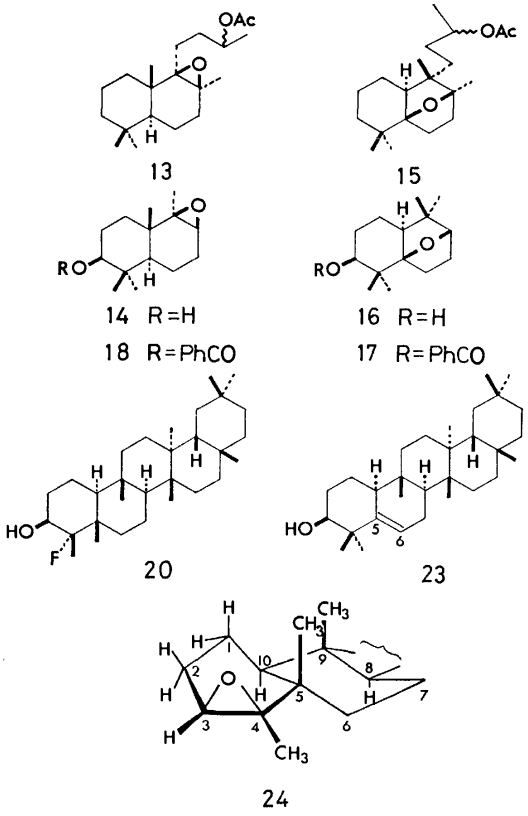

It was reported that 3β,4β-epoxyshionane was formed as a minor product together with 3α,4α-epoxyshionane on epoxidation of shion-3-ene.[14] Friedelin (**3**) was transformed *via* friedelan-3β-ol[8a,b] into friedel-3-ene (**6**)[8a,b] by the known procedures. Epoxidation of **6** with *m*-chloroperbenzoic acid gave two epoxides in a ratio of about 2 : 1. One epoxide, mp 234—236 °C, obtained as a major product, was shown to be identical with 3α,4α-epoxyfriedelane (**7**).[10] The other one, $C_{30}H_{50}O$, mp 237—250 °C,* therefore, is corresponding to 3β,4β-epoxyfriedelane (**19**), whose structure was supported by the spectral data (IR, PMR, and mass spectra) and the elemental analysis. Neither hydroxyl nor carbonyl group was observed in the IR spectrum. The PMR spectrum showed a multiplet ($W_{1/2}$ 3 Hz) signal at δ 2.90[14] due to the methine proton attached to a carbon atom (C-3) on the epoxide ring terminus; the corresponding signal of 3α,4α-epoxide (**7**) appeared at δ 2.86.

Treatment of 3β,4β-epoxyfriedelane (**19**) with boron trifluoride etherate in ether at −10 °C gave a complex mixture, which showed four spots on silver nitrate-impregnated silica gel TLC besides a spot attributed to the starting epoxide (**19**). The reaction mixture was separated by silver nitrate-impregnated silica gel column chromatography and by subsequent separation procedures described below into five components (**a**—**e**).

The least polar component **a** (yield: *ca.* 22%) was an oxide, $C_{30}H_{50}O$, mp 206—208 °C, $[\alpha]_D$ +71°, and was found to be identical in all respects with dendropanoxide (**1**), obtained by isolation from *Dendropanax trifidus* Makino according to Kimura's procedure[2], and with authentic D : B-friedo-olean-3β,10β-oxide (**1**), isolated from *Rhododendron macrophyllum* by Block and Constantine.[5,6] The second component **b** (y: *ca.* 1.7%) was identified to be the starting β-epoxide (**19**).

The third component **c** (y: *ca.* 21%) was a fluoride, $C_{30}H_{51}OF$, mp 223.5—224.5 °C. The presence of a secondary hydroxyl group was shown by the PMR spectrum (δ 3.72, 1H, dt, J=6 and 3 Hz) and by the IR spectrum (3450, 1100, and 1030 cm^{-1}). The fluoro alcohol was treated with potassium hydroxide in ethanol under reflux temperature to generate the starting β-epoxide (**19**). These observations led to the conclusion that the fluoro alcohol should be formulated as 4α-fluorofriedelan-3β-ol (**20**). The formation of a fluorohydrin in the reaction of an epoxide with boron trifluoride etherate is often encountered[15].

The fourth component **d** (y: *ca.* 23%) was found to be a mixture of three compounds. The mixture was subjected to fractional recrystallization from acetone to afford an alcohol, $C_{30}H_{50}O$, mp 236.5—237.5 °C. The physical and spectral data were completely identical with those of authentic D : B-friedo-olean-5(10)-en-3β-ol (**21**),[2-6] prepared by isomerization of dendropanoxide (**1**) with hydrochloric acid in ethanol,[2-6] and of the specimen derived from friedelin (**3**) by the known procedure.[16] On evaporation of the solvent, the mother liquor of the fractional recrystallization gave a residue. Although a separation of the residue by TLC under various conditions was attempted, it was not satisfactorily achieved. Then the residue was examined by high performance liquid chromatography (HPLC) and three peaks were detected at 18.0, 19.7, and 20.5 min, the shortest one of which was shown to be attributed to D : B-friedo-olean-5(10)-en-3β-ol (**21**). In the PMR spectrum of the residue obtained from the mother liquor, two signals due to olefinic protons at δ 5.20 and 4.87 besides tertiary methyl signals at δ 0.76—1.20 were observed. The mass spectrum showed two prominent peaks at *m/e* 218 and 205 with relative intensities 100 and 46%, respectively, together with the molecular ion peak at *m/e* 426. It is well known that a characteristic peak at *m/e* 218 due to a retro-Diels-Alder fragmentation is observed in pentacyclic Δ^{12}-triterpenes such as β- or α-amyrin.[17] From this fact as well as the PMR spectrum, in which an olefin proton of β-amyrin resonates at δ 5.20, it was concluded that one component in the residue must be β-amyrin itself. The validity of the conclusion was verified by direct comparison of the retention time (20.5 min) with that of authentic β-amyrin (**22**) in the HPLC examination. The structure of the third compound present in the residue of the mother liquor is left undetermined because of lack of the material and of difficulty of the separation.

* Due to thermal fragility, no sharp melting point was observed (*Cf.* Experimental).

The most polar component **e** (y: *ca.* 14%), eluted from the column, $C_{30}H_{50}O$, mp 208.5—209.5 °C, $[\alpha]_D$ +63.8°, proved to be identical with the authentic D : B-friedo-olean-5-en-3β-ol (**23**)[3,5,6] prepared by the reaction of 4α-bromofriedelin with silver acetate[16] and also by the isomerization of dendropanoxide (**1**) with boron trifluoride.[5,6]

The A-ring of the β-epoxide (**19**) is suggested to be in a conformation depicted as in **24**. The formation of dendropanoxide (**1**) from **19** can be explained by a mechanism involving a non-concerted process. The conversion of friedelin (**3**) into dendropanoxide (**1**) *via* the β-epoxide (**19**) was thus achieved.

Experimental

General Procedure. Melting points were determined on a Mel-temp capillary melting point apparatus (Laboratory Devices) and are uncorrected. Infrared (IR) spectra were determined on a Hitachi EPI-G2 infrared spectrometer. Mass spectra were measured using a Hitachi RMU-6 mass spectrometer operating at 70 eV with a direct inlet system. High resolution mass spectra were measured using a Hitachi RMH-2 mass spectrometer operating at 70 eV. Proton magnetic resonance (PMR) spectra were measured in a deuteriochloroform solution using a JEOL JNM PS-100 (100 MHz) or a Hitachi R-20B (60 MHz) spectrometer. Chemical shifts are expressed in δ value downfield from TMS as an internal standard and coupling constants in Hz. Optical rotation was measured with a JASCO DIP-SL polarimeter. High performance liquid chromatography (HPLC) analyses were determined on a Waters liquid chromatograph model ALC-GPS 202—401. Analytical and preparative thin layer chromatographies (TLC) were carried out on Kieselgel G nach Stahl (E. Merck) and Kieselgel 60 PF_{254} (E. Merck), respectively. Column chromatography was carried out on Wakogel C-200 (Wako Pure Chem. Ind.).

Preparation of 3β,4β-Epoxyfriedelane (19). To a solution of friedel-3-ene (**6**; 1.97 g) in benzene, *m*-chloroperbenzoic acid (1.74 g) in benzene was added with stirring at room temperature, and the solution was allowed to stand overnight. The reaction was stopped by addition of 10% sodium sulfite solution and the organic layer was washed with saturated sodium hydrogencarbonate solution and then with brine. After drying over sodium sulfate, evaporation of the solvent gave a residue, which was chromatographed on silica gel to afford 3α,4α-epoxide (**7**; 1.06 g), mp 234—236 °C, [IR (KBr) 865 cm^{-1}; PMR δ 0.82, 0.95, 1.07, 1.18, 1.19 (each 3H, s, *t*-CH_3), 1.00 (9H, 3×*t*-CH_3), and 2.86 (1H, t, J=2.5 Hz, $C_{(3)}$-H); mass spectrum *m/e* 426] and 3β,4β-epoxide (**19**; 0.49 g) as colorless needles (crystallized from acetone). The epoxide (**19**) showed no sharp melting point; on heating in a capillary, it began to melt at 237—240 °C and melted completely at 250 °C. In a sealed tube, it sublimed at 245—250 °C. IR (KBr) 1000, 890, 790, and 760 cm^{-1}; PMR δ 0.80, 0.96, 1.07 (each 3H, s, *t*-CH_3), 1.01 (9H, s, 3×*t*-CH_3), 1.18 (6H, s, 2×*t*-CH_3), and 2.90 (1H, m, $W_{1/2}$ 3 Hz, $C_{(3)}$-H); mass spectrum *m/e* 426 (M^+, 42%), 411 (33), 408 (8), 393 (8), 218 (100), and 205 (83); Found: C, 84.54; H, 11.88%. Calcd for $C_{30}H_{50}O$: C, 84.44; H, 11.81%.

Reaction of 3β,4β-Epoxyfriedelane (19) with Boron Trifluoride Etherate. To a solution of 3β,4β-epoxide (**19**; 300 mg) in anhydrous ether (200 ml) kept at −10 °C, boron trifluoride etherate (4 ml) was added with stirring, and the progress of the reaction was monitored by TLC. After 30 min, the starting material was almost consumed and the reaction was stopped by addition of a saturated potassium hydroxide methanolic solution (200 ml). The usual treatment gave a residue, which was subjected to column chromatography on silica gel (70 g) impregnated with silver nitrate (12 g) and the following solvents were used (each fraction 100 ml): frs 1 and 2, petroleum ether; frs 3—5, petroleum ether–benzene (5 : 1); frs 6—8, (4 : 1); frs 9—15, (3 : 1); frs 16—21, (2 : 1); frs 22—41, (1 : 1); frs 42—47, (1 : 2); frs 48—57, benzene; frs 58—63, benzene–ether (3 : 1).

Fractions 9—15, on evaporation of the solvents, afforded dendropanoxide (**1**; component **a**; 65 mg), mp 206—208 °C (recrystallized from acetone), mixed mp 206—208 °C; IR (KBr) 1100, 1010, 995, 980, and 955 cm^{-1}; PMR δ 0.91, 0.95, 0.97, 1.00, 1.02, 1.15, 1.17, 1.20 (each 3H, s, *t*-CH_3), and 3.75 (1H, d, J=4.8 Hz, $C_{(3)}$-H); $[\alpha]_D$ +71° (*c* 0.97, $CHCl_3$); mass spectrum *m/e* 426 (M^+, 15%), 411 (65), 344 (8), 343 (8), 205 (24), and 137 (100). Found: C, 84.64; H, 12.01%. Calcd for $C_{30}H_{50}O$: C, 84.44; H, 11.81%.

Fractions 25 and 27—30 yielded 3β,4β-epoxide (**19**; component **b**; 5 mg) and 4α-fluorofriedelan-3β-ol (**20**; component **c**), respectively, on evaporation of the solvents.

Fractions 31—39 were evaporated to give a mixture, which was separated by column chromatography on silver nitrate-impregnated silica gel (10 g) into the fluoro alcohol (**20**; component **c**) and a component **d**. The fluoro alcohol (**20**) obtained from fractions 27—30 and fractions 31—39 were combined and weighed 64 mg, mp 223.5—224.5 °C (recrystallized from chloroform–methanol); IR (KBr) 3450, 1100, and 1030 cm^{-1}; PMR δ 0.88, 0.96, 1.18 (each 3H, s, *t*-CH_3), 1.00, 1.02 (each 6H, s, 2×*t*-CH_3), and 3.72 (1H, dt, J=6 and 3 Hz, $C_{(3)}$-H); mass spectrum *m/e* 446 (M^+, 15%), 431 (18), 426 (20), 411 (14), 293 (36), 273 (36), and 205 (100); MW 446.3977 (by high resolution mass spectrometry). Calcd for $C_{30}H_{51}OF$: MW 446.3922.

A residue obtained from fractions 40—57 contained component **d** (by TLC examination). This residue and the component **d** from fractions 31—39 were combined (in total, weighed about 70 mg), and fractionally recrystallized from acetone to give D : B-friedo-olean-5(10)-en-3β-ol (**21**; component $\mathbf{d}_1$; 38 mg), mp 236.5—237.5 °C; IR (KBr) 3450, 1630, and 1040 cm^{-1}; PMR δ 0.95, 1.02 (each 9H, s, 3×*t*-CH_3), 1.05, 1.20 (each 3H, s, *t*-CH_3), 3.45 (1H, dd, J=9.5 and 4.5 Hz, $C_{(3)}$-H), and the absence of olefinic proton signal; mass spectrum *m/e* 426 (M^+, 17%), 411 (17), 408 (11), 393 (7), and 205 (100). Found: C, 84.72; H, 12.08%. Calcd for $C_{30}H_{50}O$: C, 84.44; H, 11.81%.

The mother liquors of fractional crystallization were combined and evaporated to give a residue, which was examined by PMR, mass spectrometry, and HPLC: PMR δ 5.20 and 4.87 (olefinic protons); mass spectrum *m/e* 218 (100%) and *m/e* 205 (46%); HPLC (μ-porasil, elution with 10% ether–hexane at flow rate 1.0 ml/min) 18.0, 19.7, and 20.5 min. The retention times of D : B-friedo-olean-5(10)-en-3β-ol (**21**) and β-amyrin (**22**) under the same conditions were 18.0 and 20.5 min, respectively. Therefore, the presence of β-amyrin (**22**; component $\mathbf{d}_2$) in the mother liquor received support. The structure of the third component ($\mathbf{d}_3$; with retention time 19.7 min) contained in the mother liquor remains undetermined.

On evaporation of the solvents, fractions 58—63 gave D : B-friedo-olean-5-en-3β-ol (**23**; 41 mg), mp 208.5—209.5 °C (crystallized from chloroform–methanol); IR (KBr) 3450, 1630, 1095, and 825 cm^{-1}; PMR δ 0.87, 0.97, 1.06, 1.11 1.18 (each 3H, s, *t*-CH_3), 1.02 (6H, s, 2×*t*-CH_3), 3.45 (1H, m, $W_1/_2$ 6 Hz, $C_{(3)}$-H), and 5.63 (1H, dd, J=4 and 1.8 Hz, $C_{(6)}$-H); $[\alpha]_D$ +63.8° (*c* 1.1, $CHCl_3$); mass spectrum

m/e 426 (M^+, 4%), 411 (2), 408 (2), 393 (2), 274 (100), 259 (66), and 205 (45). Found: C, 84.25; H, 11.99%. Calcd for $C_{30}H_{50}O$: C, 84.44; H, 11.81%.

*Treatment of 4α-Fluorofriedelan-3β-ol (**20**) with Base.* 4α-Fluorofriedelan-3β-ol (**20**; 44 mg) in 5% potassium hydroxide ethanolic solution (20 ml) was heated under reflux for 21 h. The usual work-up and recrystallization from acetone gave 3β,4β-epoxyfriedelane (**19**; 17 mg).

*Isomerization of Dendropanoxide (**1**).* *(a) With Hydrochloric Acid in Ethanol*: Dendropanoxide (**1**; 103 mg) was dissolved in ethanol (20 ml) and conc hydrochloric acid (0.8 ml). The solution was heated under reflux for 30 min and then left at room temperature overnight. The reaction mixture, after the usual treatment, was purified by preparative TLC to afford D : B-friedo-olean-5(10)-en-3β-ol (**21**; 55 mg).

(b) With Boron Trifluoride Etherate: Boron trifluoride etherate (1.4 ml) was added to dendropanoxide (**1**; 631 mg) in ether (110 ml) at room temperature and the reaction mixture was allowed to stand at room temperature for 22 h. Work-up in a usual manner and a separation by column chromatography on 20% silver nitrate-impregnated silica gel using benzene as eluent gave D : B-friedo-olean-5(10)-en-3β-ol (**21**; 417 mg) and D : B-friedo-olean-5-en-3β-ol (**23**; 50 mg).

The authors wish to thank Professor J. H. Block and Professor G. H. Constantine, Jr., Oregon State University, for a generous gift of the authentic sample of D : B-friedo-olean-3β,10β-oxide (**1**) and also Dr. Hidehiro Ishizuka and Dr. Kazuyuki Aizawa for the measurements of PMR (100 MHz) spectra and high resolution mass spectra, respectively.

References

1) A part of this work was reported in a preliminary form: T. Torii, K. Tachibana, S. Yamada, T. Tsuyuki, and T. Takahashi, *Tetrahedron Lett.*, **1975**, 2283.

2) K. Kimura, Y. Hashimoto, and I. Agata, *Chem. Pharm. Bull.*, **8**, 1145 (1960).

3) H. R. Arthur and W. H. Hui, *J. Chem. Soc.*, **1961**, 551.

4) S. Rangaswami and K. Sambamurthy, *Proc. Indian Acad. Sci.*, **54A**, 132 (1961).

5) G. H. Constantine, Jr. and J. H. Block, *Phytochemistry*, **9**, 1659 (1970). And references cited therein.

6) J. H. Block and G. H. Constantine, Jr., *Phytochemistry*, **11**, 3279 (1972).

7) J. D. White, J. Fayos, and J. Clardy, *J. Chem. Soc. Chem. Commun.*, **1973**, 357.

8) a) E. J. Corey and J. J. Ursprung, *J. Am. Chem. Soc.*, **78**, 5041 (1956); b) G. Brownlie, F. S. Spring, R. Stevenson, and W. S. Strachan, *J. Chem. Soc.*, **1956**, 2419; c) T. Takahashi and G. Ourisson, *Bull. Soc. Chim. Fr.*, **1956**, 353; d) H. Dulter, O. Jeger, L. Ruzicka, *Helv. Chim. Acta*, **38**, 1268 (1955).

9) *Cf.* A. Eshenmoser, L. Ruzicka, O. Jeger, and D. Arigoni, *Helv. Chim. Acta*, **38**, 1890 (1955).

10) a) J. W. ApSimon, R. R. King, and J. J. Rosenfeld, *Can. J. Chem.*, **47**, 1989 (1969); b) P. Sengupta, B. Roy, S. Chakraborty, J. Mukherjee, and K. G. Das, *Indian J. Chem.*, **11**, 1249 (1973).

11) M. S. Hadley and T. G. Halsall, *J. Chem. Soc. Perkin Trans. 1*, **1974**, 1334.

12) T. Tatee, T. Tsuyuki, and T. Takahashi, *Bull. Chem. Soc. Jpn.*, **48**, 2221 (1975).

13) K. Tachibana and T. Takahashi, *Tetrahedron Lett.*, **1975**, 1857.

14) a) S. Yamada, S. Yamada, Y. Moriyama, Y. Tanahashi, and T. Takahashi, *Tetrahedron Lett.*, **1972**, 5043; b) S. Yamada, S. Yamada, K. Tachibana, Y. Moriyama, Y. Tanahashi, T. Tsuyuki, and T. Takahashi, *Bull. Chem. Soc. Jpn.*, **49**, 1134 (1976). The PMR signals due to a proton on C-3 appeared at δ 2.89 for 3β,4β-epoxyshionane, while those for 3α,4α-epoxyshionane were observed at δ 2.83.

15) Ex. a) L. H. Knox, J. A. Zderic, J. P. Ruelas, C. Djerassi, and H. J. Ringold, *J. Am. Chem. Soc.*, **82**, 1230 (1960); b) J. M. Coxon, M. P. Hartshorn, and D. N. Kirk, *Tetrahedron*, **20**, 2547 (1964); c) J. R. Bull, *Tetrahedron Lett.*, **1968**, 5959; d) P. A. Diassi and J. Fried, U. S. P. 3,364,204 (1964), *Chem. Abstr.*, **69**, 27638a (1968); e) J. W. Blunt, M. P. Hartshorn, and D. N. Kirk, *Tetrahedron*, **21**, 559 (1965); f) J. M. Coxon, M. P. Hartshorn, and D. N. Kirk, *ibid.*, **21**, 2489 (1965).

16) J. M. Beaton, F. S. Spring, R. Stevenson, and J. L. Stewart, *Tetrahedron*, **2**, 246 (1958).

17) H. Budzikiewicz, C. Djerassi, and D. H. Williams, "Structure Elucidation of Natural Products by Mass Spectrometry," Vol. II, Holden-Day, Inc., San Francisco, London, Amsterdam (1964), p. 122.

Mechanism of the Chemiluminescence of Lucigenin. II. The Charge-transfer Structure of Lucigenin and Reduction of 10,10′-Dimethyl-9,9′-biacridinium Dication by Electron Transfer from Nucleophiles

Koko MAEDA, Toshi KASHIWABARA, and Mizue TOKUYAMA

Department of Chemistry, Faculty of Science, Ochanomizu University, Otsuka, Bunkyo-ku, Tokyo 112

(Received August 26, 1976)

Lucigenin (10,10′-dimethyl-9,9′-biacridinium dinitrate, $DBA^{2+}2NO_3^-$) was found to be a CT complex between DBA^{2+} and NO_3^-. In the reaction of lucigenin with several nucleophiles in the absence of molecular oxygen or oxidizing agents the following four types of products were obtained, depending upon the relative power of the nucleophiles to donate electrons to DBA^{2+}: (1) salts of DBA^{2+} ($DBA^{2+}2X^-$) which are the CT complex between DBA^{2+} and the nucleophiles, such as Cl^-, Br^-, SCN^-, and I^-, (2) the cation radical $DBA^{+\cdot}$ produced by one-electron transfer from nucleophiles, such as $C_6H_5COCH_2^-$ and $CH_3COCH_2^-$, to DBA^{2+}, (3) the biradical $DBA^{\cdot}_2$ produced by two-electron transfer from nucleophiles such as OH^-, CN^-, CCl_3^-, and $C_6H_5S^-$ and (4) 10,10′-dimethyl-9,9′-bi(dihydroacridinylidene) produced from $DBA^{\cdot}_2$. Only the nucleophiles of (3), which produced $DBA^{\cdot}_2$ brought about the luminescence of lucigenin in the presence of oxygen, and $DBA^{\cdot}_2$ also showed luminescence in organic solvents in the presence of oxygen. From these findings it was concluded that the first process of the chemiluminescent reaction of lucigenin was the electron transfer reduction of DBA^{2+} by the nucleophiles to form the biradical $DBA^{\cdot}_2$.

Numerous studies concerning the mechanism of the chemiluminescenec of lucigenin($DBA^{2+}2NO_3^-$, **1**) with hydrogen peroxide in an aqueous alkaline solution have been carried out.[1] It has been established that *N*-methylacridone, the end product of the luminescence, is a light emitter.[1g] Totter has suggested a mechanism for the luminescence involving two successive, two equivalent reductions and autoxidation. From the results of an ESR study Janzen and collaborators have proposed[2] the mechanism shown in Scheme 1 involving *N*-methylacridone ketyl, **3**. Maeda and Hayashi have previously reported that crystals of **1** exhibited a weak ESR absorption,[3a] and Maeda, Hayamizu, and Hayashi have shown that an aqueous sodium hydroxide solution of **1** produced a compound[3b] with the same UV and IR spectra as 10,10′-dimethyl-9,9′-bi(dihydroacridinylidene), **5**, but in contrast to **5**, the product exhibited an ESR absorption both in solid state and in solution and luminescence with molecular oxygen in solutions of organic solvents. These findings suggest a radical mechanism of the luminescence involving a reduction process of **1** by a hydroxide ion. In order to obtain further information on the radical mechanism of the chemilumnescence of **1**, its reactions with the various nucleophiles shown in Table 1 were studied. This paper deals with the results of the reactions and discusses the mehanism involving a reduction process of DBA^{2+}.

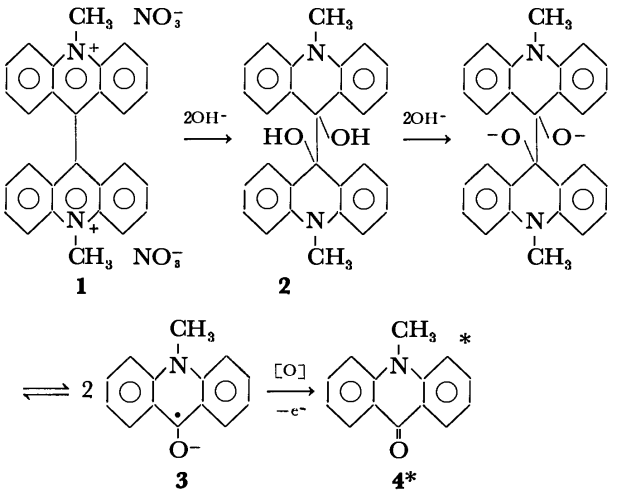

Scheme 1.

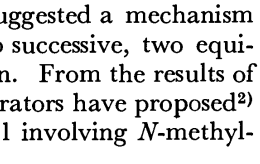

5

Experimental

Measurements. Measurements of electronic absorption spectra were carried out using a Shimadzu UV 200 spectrophotometer with oxygen-free solutions which were purged with prepurified nitrogen. The IR spectra were measured on a JASCO IR-G infrared spectrophotometer. The ESR spectra and spin concentrations were obtained by a JES p-10 type ESR spectrometer (100 kHz modulation) equipped with a JES 1D-2 type integrator with deaerated solutions and solids. The proton NMR spectra were measured with a JEM C-60-HL NMR spectrometer. The fluorescence spectra were obtained with a Hitachi EPF-2A fluorescence spectrophotometer with deaerated solutions.

Materials. Lucigenin, **1**, was synthesized by the method of Decker and Dunnant[4] from *N*-methylacridone which was obtained from acridine. Purification of **1** was achieved by recrystallization from water and then ethanol to give amber crystals. NMR(D_2O); δ 5.07(6H, s, N–CH_3), δ 7.26—8.52 (16H, m, aryl proton). 10,10′-Dimethyl-9,9′-bi(dihydroacridinylidene), **5**, was prepared by the reduction of *N*-methylacridone with zinc and acetic acid, and recrystallized from pyridine to give lemon yellow fine crystals.

Results and Discussion

The addition of aqueous solutions containing the nucleophiles of group (a) in Table 1 to an aqueous

Table 1. The chemiluminescence of an aqueous solution of **1** ($DBA^{2+}2NO_3^-$) upon the addition of aqueous solutions of nucleophiles in the presence of oxygen

Nucleophile (a)	Chemi-luminescence	Nucleophile (b)	Chemi-luminescence
$(C_2H_5)_3N$	+	Cl^-	−
NH_3	+	Cr^-	−
$NH_2NH_2H_2O$	+	SCN^-	−
$CH_3COCH_2^-$	+	I^-	−
$CH_3SOCH_2^-$	+		
CCl_3^-	+		
OH^-	+		
t-BuO^-	+		
CN^-	+		
S^{2-}	+		
$C_6H_5S^-$	+		

+: Chemiluminescent; −: Non-chemiluminescent
Concentration of **1**: 1×10^{-4} mol l^{-1}.

solution of **1** in the presence of oxygen brought about the luminescence of **1**, but the addition of the nucleophiles of group (b) in Table 1 under the same conditions did not result in any luminescence. On the other hand, a DMF solution of **1** exhibited luminescnce in the presence of oxygen with or without the nucleophiles of group (b) in Table 1. In order to obtain some information about the difference in behavior between the nucleophiles of group (a) and (b) of Table 1 for the chemiluminescence of **1**, reactions of these nucleophiles with **1** were studied in oxygen-free solutions in which no luminescence was exhibited. It was found that the following four types of products, $DBA^{2+}2X^-$, $DBA^{+}X^-$, $DBA^{\cdot}$, and DBA, **5**, were produced, depending upon the kind of nucleophiles and reaction conditions, as described below.

I. Salts of 10,10′-Dimethyl-9,9′-biacridinium Dication, DBA^{2+} $2X^-$. When solids of potassium or sodium salts of Cl^-, Br^-, SCN^-, and I^-, the nucleophiles of group (b) in Table 1, were added to an aqueous solution of **1** (1×10^{-2} mol l^{-1}) in amounts equivalent to twice the molar quantity of **1**, salts of DBA^{2+} with the nucleophilic anions added, $DBA^{2+}2Cl^-$(**6**), $DBA^{2+}2Br^-$(**7**), DBA^{2+} $2SCN^-$(**8**), and DBA^{2+} $2I^-$(**9**), as by elemental analysis of Cl, Br, S, and I, were separated out. The colors of salts **1**, **6**, and **7** were amber, while the colors of salts **8** and **9** were orange and dark red, respectively. The deepened colors of salts **8** and **9** caused by the replacement of NO_3^- by SCN^- or I^-, which has a larger nucleophilicity[5] than NO_3^-, suggest the formation of a CT complex between DBA^{2+} and SCN^- or I^-, as has been reported for the salts of pyridinium,[6] tropylium[7] and quinolinium[8] cations.

The crystals of **1** exhibited weak ESR absorption(g= 2.003, the line width was 12.5 G) and those of **6**, **7**, **8**, and **9** also exhibited weak ESR absorption(g=2.003). The spin concentrations of **1**, **8**, and **9** are shown in Table 2. The intensities of these signals increased two or three times upon irradiation with an incandescent lamp for about 1 h and reverted to their original intensities after standing in the dark at room temperature. These findings suggest that lucigenin is also

Table 2. The spin concentrations and colors of the CT complexes $DBA^{2+}2X^-$ measured in the absence of the light

X^-	Spin mol^{-1}	Color
NO_3^-	7×10^{18}	amber
SCN^-	1.5×10^{19}	orange
I^-	1×10^{20}	dark red

the CT complex **1′** shown below, although the degree of charge transfer was less than those in **8** and **9**.

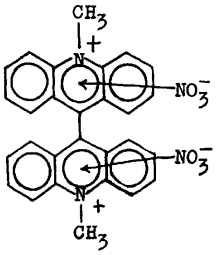

1′

Confirmation of the CT structure of these salts was carried out by measurements of their absorption spectra. For example, the absorption spectra of **9** measured in mixed solvents of DMSO, $CHCl_3$, and CH_2Cl_2 showed a broad band in a longer wavelength region than 500 nm, which was not observed in water, as shown in Fig. 1. The band was attributed to charge transfer from I^- to DBA^{2+}, since the absorbance of the band was intensified for a decrease in the polarity of the mixed solvent and disappeared in water. This fact appears to indicate a shift of equilibrium in solutions, shown in Scheme 2, which favors an ionic species in polar solvents. Comparison of the CT absorption of **1**, **6**, **7**, **8**, and **9** measured in ethanol, DMSO, and DMF,

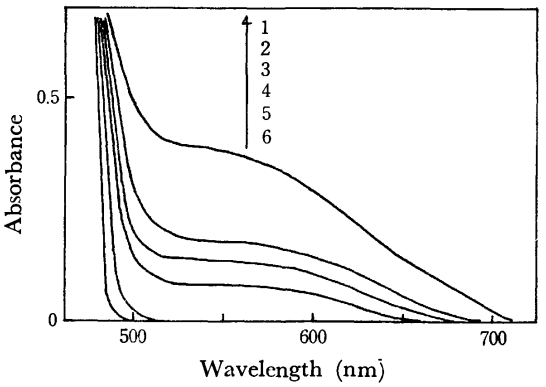

Fig. 1. The variation of the absorption spectrum of **9** with decreasing the polarity of solvents.

	Solvents (vol%)			
	CH_2Cl_2	$CHCl_3$	DMSO	H_2O
1	50	20	30	0
2	50	15	35	0
3	50	10	40	0
4	50	5	45	0
5	0	0	100	0
6	0	0	0	100

Concentration of **9**: 2.0×10^{-4} mol l^{-1}.

←increase of the polarity—

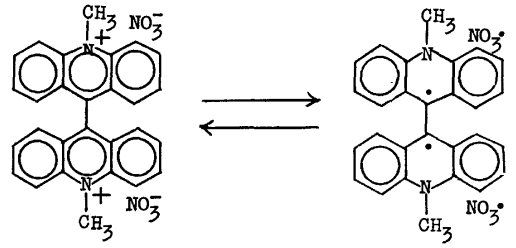

Scheme 2.

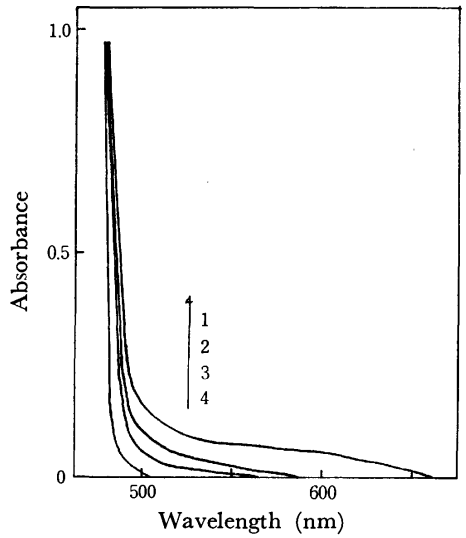

Fig. 2. The absorption spectra of $DBA^{2+}2X^-$.

	X^-		Solvent
1	I^-	**9**	DMF
2	SCN^-	**8**	DMF
3	NO_3^-	**1**	DMF
4	NO_3^-	**1**	H_2O

Concentration of $DBA^{2+}2X^-$: 1.0×10^{-3} mol l^{-1}.

respectively, showed that the degree of charge transfer from the nucleophiles to DBA^{2+} increased in the following order, $NO_3^-<Cl^-\approx Br^-<SCN^-<I^-$ and for a decrease in the Z value[9] of the solvents, $H_2O<$ethanol$<$DMSO$<$DMF. The spectra of the salts of **1**, **8**, and **9** observed in DMF are shown in Fig. 2.

The formation of similar CT complexes of DBA^{2+} was also observed in oxygen-free solutions in reactions of **1** with the nucleophiles of group (a) in Table 1. By the evaporation of a solvent immediately after adding to an aqueous solution of **1** (7.8×10^{-3} mol l^{-1}) the nucleophiles in amounts equivalent to twice the molar quantity of **1**, crystals of various CT complexes of DBA^{2+} containing the added nucleophiles were obtained. After treatment of the crystals with benzene to remove the small quantity of a by-porduct, a reduction product which appeared later, the CT complexes were purified by recrystallization from water and then from ethanol. The absorption spectra of these complexes measured in water agreed with those of **1**, **8**, and **9** in the shorter wavelength region below 500 nm, but showed an additional weak broad band in the longer wavelength region above 500 nm. The broad band is considered to be due to charge transfer between nucleophiles and DBA^{2+}, because the absorbance of

Tabte 3. The spin concentrations and colors of the CT complexes obtained from **1** and nucleophiles

Nucleophile	Spin mol^{-1}	Color	Type of the fine structure of the ESR spectrum in Fig. 3
$(C_2H_5)_3N$	1×10^{20}	brown	B
$CH_3COCH_2^-$	2×10^{20}	brown	B
CCl_3^-	4×10^{20}	brown	B
$C_6H_5COCH_2^-$	4×10^{20}	bluish brown	B
NH_3	6×10^{20}	reddish brown	B
$C_6H_5S^-$	7×10^{20}	reddish brown	A
CN^-	9×10^{20}	orange brown	A
OH^-	4×10^{21}	reddish brown	A
t-BuO^-	2×10^{22}	reddish brown	A

the band measured in water was intensified in DMF. These complexes exhibited strong ESR absorptions (g=2.003) both in solid state (line widths were about 11.4 G) and in oxygen-free solutions of DMF and C_6H_6. The colors and spin concentrations of the ESR abosrption in solid state are shown in Table 3. The intensities of the ESR signals increased upon irradiation and reverted to the original intensities after standing in the dark at room temperature. These properties of the complexes are comparable to those of **1**, **8**, and **9**, although the degrees of charge transfer from the nucleophiles of group (a) in Table 1 to DBA^{2+} are larger than those from SCN^- and I^- (the nucleophiles of group (b) in Table 1) and NO_3^-. ESR spectra of the CT complexes containing the nucleophiles of group (a) in Table 1 measured in oxygen-free solutions showed fine structures which are classified into two groups, A and B, shown in Fig. 3. Although it is now difficult to explain the two types of the fine structures, it is observed that (1) the CT complexes which exhibited a spectrum of type A (the spacing was 1.6 G) had spin concentrations larger than those of the CT complexes which exhibited a spectrum of type B (the spacing was 3.0 G) as shown in Table 3 and (2) fine structure of type A is similar to that of the ESR spectrum[2a] which was attributed to the radical cation of DBA^{2+} produced by the one-electron reduction of DBA^{2+}. From these findings it is conceivable that both in solid state and in less polar solvents, the equilibrium

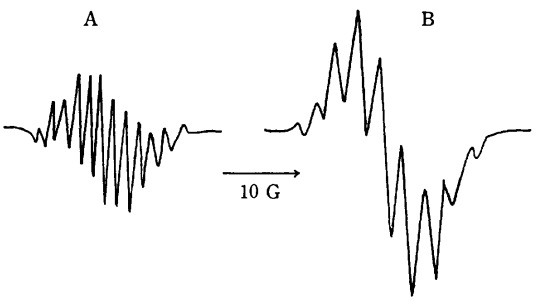

Fig. 3. Two types of ESR spectra of $DBA^{2+}2X^-$ in the oxygen-free DMF solution.
X^- showing type A: $C_6H_5S^-$, CN^-, OH^-, t-BuO^-.
X^- showing type B: $(C_2H_5)_3N$, $CH_3COCH_2^-$, CCl_3^-, $C_6H_5COCH_2^-$, NH_3.

shown in Scheme 2 might be further shifted more to the right-hand side in CT complexes having a fine structure of type A than in CT complexes having a fine structure of type B. Counter anions in CT complexes having a structure of type A, $C_6H_5S^-$, CN^-, OH^-, and *t*-BuO^-, might have a larger electron-donating power than the neutral or anionic nucleophiles in CT complexes having a structure of type B, $(C_2H_5)_3N$, $CH_3COCH_2^-$, CCl_3^-, $C_6H_5COCH_2^-$, and NH_3.

II. 10,10'-Dimethyl-9,9'-bi(dihydroacridinyl) Biradical DBA and 10,10'-Dimethyl-9,9'-bi(dihydroacridinylidene) Produced by Two-electron Transfer from Nucleophiles to DBA^{2+}. Although aqueous solutions of **1**, **8**, and **9** did not exhibit chemiluminescence in the presence of oxygen or hydrogen peroxide, the addition of nucleophiles of group (a) in Table 1 to these solutions produced luminescence. Luminescence of the salts was also observed in aqueous solutions containing organic solvents such as ethanol, DMSO, DMF, and pyridine in the presence of oxygen or hydrogen peroxide. It has already been reported by Janzen[2] that the addition of the potassium or sodium salts of the nucleophiles, CN^-, *t*-BuO^-, and S^{2-}, included in group (a) in Table 1, to solutions of **1** in DMSO, DMF, or aqueous DMSO in the presence of oxygen resulted in luminescence, as in the case of the addition of OH^-, and radical **10** corresponding to ketyl radical **3** was formed as an intermediate. If the mechanism involving **3** or **10** is correct, the nucleophiles

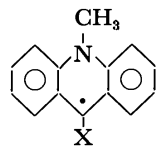

X: CN, *t*-BuO, S^-

10

of group (a) in Table 1 which exhibited luminescence in the presence of oxygen, might produce a radical corresponding to **10** in oxygen-free solutions *via* the addition at the 9,9'-positions of DBA^{2+}. This assumption was examined by measuring the variation of the absorption spectrum of **1** for the addition of the nucleophiles of group (a) in Table 1. When various amounts of the nucleophiles were added to a solution of **1** (1.6×10^{-4} mol l^{-1}) in oxygen-free aqueous ethanol (50 : 50 vol%), a new broad band appeared in the wavelength range longer than 500 nm, and the absorbance of the band increased with an increase in the nucleophile amount. Two examples are shown in Figs. 4 and 5. The broad band can reasonably be attributed to charge transfer in the salts formed between DBA^{2+} and the nucleophiles. When the nucleophiles were added to a more dilute solution of **1** (8×10^{-5} mol l^{-1}) in oxygen-free aqueous ethanol, the mixture gradually turned reddish brown and then became turbid owing to the formation of an insoluble product. The evolution of the absorption spectrum of **1** was followed in dilute solutions of **1** until turbidity appeared. No broad CT band was observed, but each spectrum showed a decrease in the absorbance of the band of DBA^{2+} at 370 nm accompanied by the increase of a band at 423 nm and two isosbestic points near 380 and 480 nm. The time-resolved absorption spectra of mixtures of

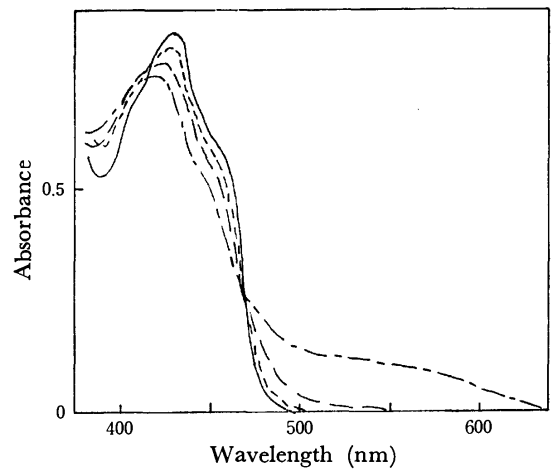

Fig. 4. The variation of the absorption spectrum of **1** with increasing the amount of $(C_2H_5)_3N$ added.
Solvent: C_2H_5OH-H_2O (50 : 50 vol%).
Concentration of **1**: 1.6×10^{-4} mol l^{-1}.
Concentration of $(C_2H_5)_3N$: —— 0, ---- 5.1×10^{-2} mol l^{-1}, — — — 1.0×10^{-1} mol l^{-1}, ——— 2.0×10^{-1} mol l^{-1}.
The spectra were measured immediately after mixing of $(C_2H_5)_3N$.

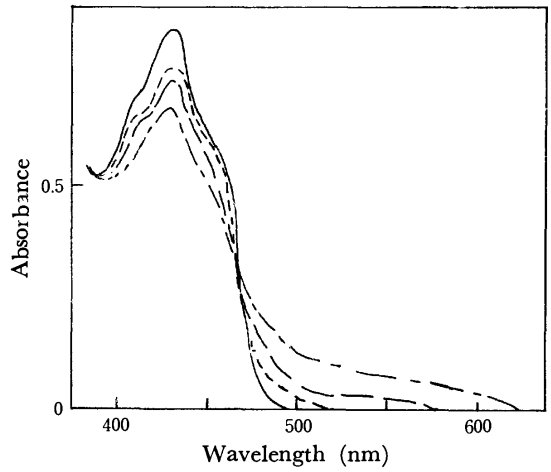

Fig. 5. The variation of the absorption spectrum of **1** with increasing the amount of *t*-BuOK added.
Solvent: C_2H_5OH-H_2O (50 : 50 vol%).
Concentration of **1**: 1.6×10^{-4} mol l^{-1}.
Concentration of *t*-BuOK: —— 0, ---- 1.1×10^{-2} mol l^{-1}, — — — 1.3×10^{-2} mol l^{-1}, ——— 1.6×10^{-2} mol l^{-1}.
The spectra were measured immediately after mixing of *t*-BuOK.

1 and $(C_2H_5)_3N$ and CN^-(NaCN) are shown in Figs. 6 and 7 as examples. A similar variation of the UV spectrum of **1** was also observed by mixing the nucleophiles in aqueous DMF and in aqueous pyridine. The variations in these solvents were faster than those in the aqueous ethanol, although they were similar. The absorption maximum at 423 nm shown in Figs. 6 and 7 agrees with that of 10,10'-dimethyl-9,9'-bi(dihydroacridinylidene), **5**. These facts and the formation of the CT complexes described above appear to show that the reaction of DBA^{2+} with the nucleophiles was the reduction of DBA^{2+} with the nucleophiles by electron

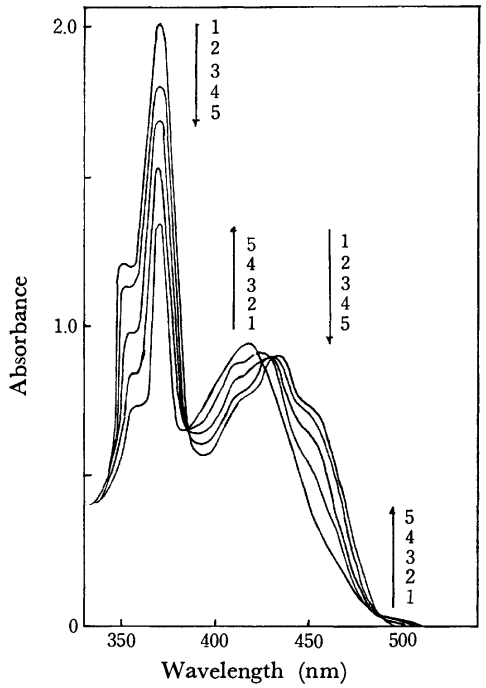

Fig. 6. The time-resolved absorption spectra of a mixture of **1** and $(C_2H_5)_3N$.
Solvent: C_2H_5OH-H_2O (50 : 50 vol%).
Concentration of **1**: 8.0×10^{-5} mol l^{-1}.
Concentration of $(C_2H_5)_3N$: 2.5×10^{-2} mol l^{-1}.
1: Before mixing, 2: 1 min after mixing, 3: 6 min after mixing, 4: 11 min after mixing, 5: 20 min after mixing.

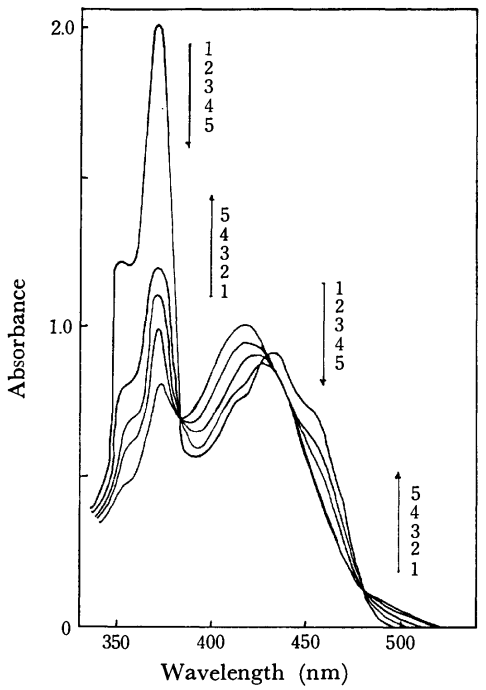

Fig. 7. The time-resolved absorption spectra of a mixture of **1** and NaCN.
Solvent: C_2H_5OH-H_2O (50 : 50 vol%).
Concentration of **1**: 8.0×10^{-5} mol l^{-1}.
Concentration of NaCN: 1.0×10^{-2} mol l^{-1}.
1: Before mixing, 2: 5 min after mixing, 3: 8 min after mixing, 4: 13 min after mixing, 5: 20 min. after mixing.

transfer *via* the formation of CT complexes rather than the formation of a radical **10** *via* the formation of pinacol **2**.[10]

The reduction of DBA^{2+} with the nucleophiles was further confirmed on the basis of the following reaction. When sodium benzenethiolate (8×10^{-4} mol) was added to an aqueous solution of **1** (4×10^{-4} mol in 45 ml) over 2 h with stirring in nitrogen, orange yellow fine crystals of the reduction product (83%) were separated out. The crystals were filtered and diphenyl disulfide (mp 60.5—61.5 °C from ethanol, 82%), the amount of which was comparable to that of the reduction product, was isolated from the filtrate. The crystals showed an absorption spectrum with a maximum at 423 nm in benzene and a green fluorescence in benzene with a maximum at 504 nm. These spectra and the IR spectrum agreed with those of **5**. The crystals decomposed at 360 °C and the results of elemental analysis[11] corresponded to **5**. However, the crystals exhibited an ESR absorption (g=2.003) in both solid state and solution. The spin concentration in solid state was 6×10^{20} spin mol^{-1}. Repeated recrystallization of the crystals from pyridine or benzene eventually gave lemon yellow crystals which exhibited no ESR absorption and were identified to be **5**. From these facts it is believed that the crystals were a mixture of **5** and a radical which is reasonably assumed to be biradical 10,10′-dimethyl-9,9′-bi(dihydroacridinyl), **11**.[12] It appears that **5** was produced from biradical **11** by bonding of the two spins and diphenyl disulfide was produced by dimerization of phenylthiyl radicals formed by one-electron oxidation of benzenethiolate

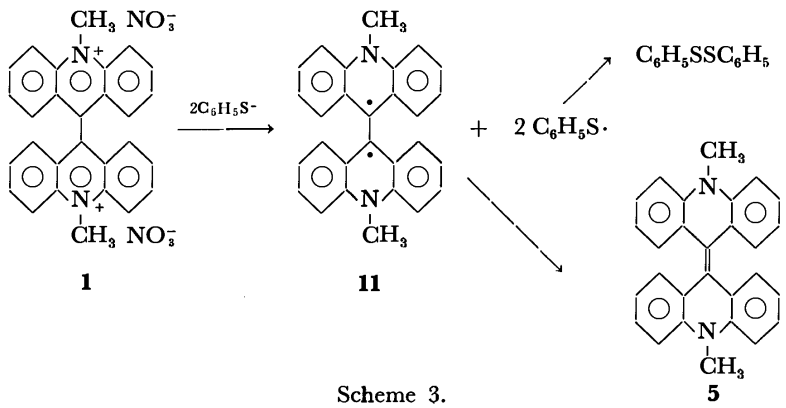

Scheme 3.

TABLE 4. THE YIELDS OF THE REDUCTION PRODUCTS OF DBA^{2+} OBTAINED FROM **1** AND NUCLEOPHILES

Nucleophile	Yield (%)
$(C_2H_5)_3N$	70
$C_6H_5S^-$	83
t-BuO$^-$	84
OH^-	86
S^{2-}	92
CN^-	93

anions by DBA^{2+}, as shown in Scheme 3. Because the ESR spectrum of **11** measured in C_6H_6 showed no signals attributable to a triplet state, it appears that there was little interaction between the two spins, and the two dihydroacridinyl groups in biradical **11** were twisted about the C_9–$C_{9'}$ bond. A similar reduction product of DBA^{2+} was isolated by the addition of other nucleophiles, as shown in Table 4, and it exhibited an ESR absorption which had a spin concentration of $(5—10)\times10^{20}$ spin mol^{-1}, depending upon the kind of nucleophile and the reduction condition. The spin concentration showed that the amount of biradical **11** included in the reduction product was little. Chemiluminescence was visually observed in the reduction product in organic solvents such as ethanol, benzene and pyridine in the presence of oxygen,[13] while no luminescence was observed in a pure sample of **5** under the same conditions. Therefore, when sodium dithionite ($Na_2S_2O_4$) which has a strong reducing power was used as a nucleophile, the reduction product isolated (88%) was mostly **5** and exhibited hardly any ESR absorption or chemiluminescence. Thus, it is reasonable to consider that the chemiluminescence of the reduction products is connected with the oxygenation of biradical **11**.

No reduction of DBA^{2+} in water occurred by NO_3^- and the nucleophiles of group (b) in Table 1, but occurred upon irradiation. When a dilute aqueous solution of **1** ($(5—10)\times10^{-4}$ mol l^{-1}) was irradiated with a high-pressure mercury lamp or an incandescent lamp in a nitrogen atomosphere, a solid product was gradually deposited on the wall of the reaction vessel. For example, the yield of the product was about 10% after irradiation by a 400 watt high-pressure mercury lamp for 25 h. The reduction product obtained photochemically exhibited luminescence in organic solvents in the presence of oxygen in a manner similar to the reduction products obtained by the chemical reduction of DBA^{2+} described above. The reduction of DBA^{2+} under irradiation with NO_3^- and I^- in **1** and **9** in both ethanol and DMSO was followed by observing the variation of the absorption spectra of DBA^{2+}, respectively. The variation of the spectrum of **1** in ethanol shown in Fig. 8 is similar to those shown in Figs. 6 and 7.[14] It is believed that because the electron-donating powers of nucleophiles NO_3^- and I^-(group (b) in Table 1) are weaker than those of nucleophiles of group (a) in Table 1, the former does not reduce DBA^{2+} without irradiation in water, but the latter does reduce DBA^{2+} without irradiation by the electron transfer mechanism. As described above, a DMF solution of

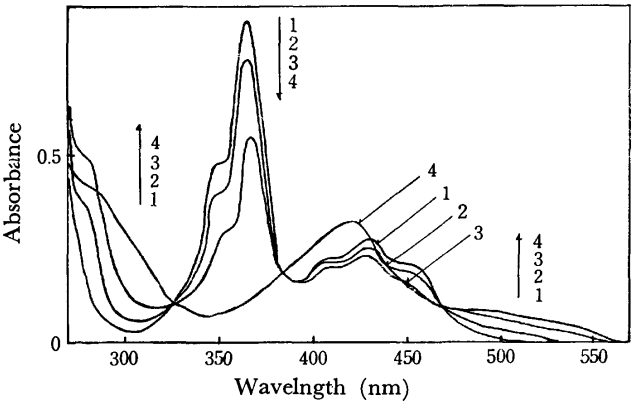

Fig. 8. The variation of the absorption spectrum of **1** in ethanol under irradiation.
Irradiation: A 400 watt high-pressure mercury lamp.
Concentration of **1**: 6.1×10^{-4} mol l^{-1}.
1: Before irradiation, 2: after irradiation for 1 min, 3: after irradiation for 3 min, 4: after irradiation for 5 min.

1 exhibited luminescence in the presence of oxygen without any other nucleophiles. This fact can be explained in terms of the electron-donating power of NO_3^- which is stronger in DMF than in water. Therefore, in the DMF solution of **1** the equilibrium of Scheme 2 was shifted greatly to the right-hand side. This explanation is further supported by the fact that a DMF solution of **1** exhibited a green fluorescence visually similar to that of **1** in water, but, in contrast to the fluorescence in water, the excitation spectrum of the fluorescence in DMF was not consistent with the absorption spectrum of DBA^{2+}, but was consistent with that of **5**, the reduction product of **1**.

III. Cation Radical DBA^{+} Produced by One-electron Transfer from Nucleophiles to DBA^{2+}. It has previously been reported[3b] that an aqueous solution of **1** containing acetone turned blue upon the addition of aqueous sodium hydroxide. It was found that a similar blue color also appeared in aqueous alkaline solutions of **1** containing $RCOCH_3$ in which R was C_6H_5, C_2H_5, and H. It appears that the blue color is due to a substance produced by the reduction of DBA^{2+} with $RCOCH_2^-$ which was formed from $RCOCH_3$ and OH^-. For example, upon the addition of an ethanolic solution of acetophenone (1.74 g in 15 ml) containing aqueous sodium hydroxide (1 ml of 0.3 mol l^{-1}) to an aqueous solution of **1** (0.25 g in 45 ml) with stirring in nitrogen the solution turned blue. After 2 h, the solvent was evaporated under reduced pressure. When the residue was repeatedly extracted with water and washed with a small amount of benzene, a blue compound was obtained. The residue was soluble in benzene, pyridine, DMF, and ethanol and exhibited a strong ESR absorption in both solid state and solution (g=2.003). By evaporating the combined aqueous extracts a salt of DBA^{2+} involving $C_6H_5COCH_2^-$ as a counter ion(0.111 g) was obtained, which was recrystallized from water giving bluish-brown crystals. The salt showed an absorption spectrum having a CT absorption band in the longer wavelength range below 500 nm and showed an ESR

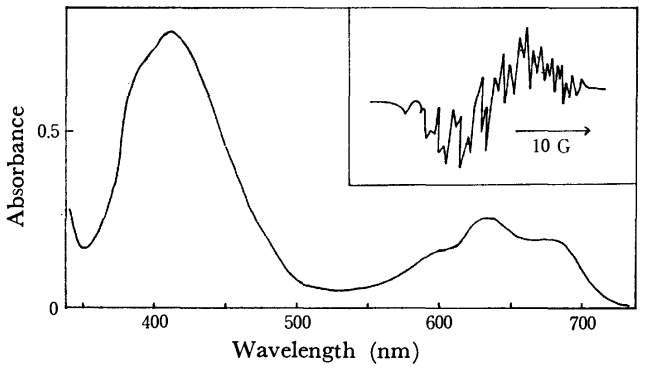

Fig. 9. The absorption spectrum of **12** in benzene and the ESR spectrum in oxygen-free DMF.

absorption both in solid state and solution. The ESR spectrum of the salt measured in an oxygen-free DMF solution was similar to the ESR spectrum of type B shown in Fig. 3.

The absorption spectrum of the blue compound **12** in benzene and the ESR spectrum in oxygen-free DMF are shown in Fig. 9. The absorption spectrum of **12** is different from that of the salt of DBA^{2+}, but resembled those of methylviologen cation radical **13**[15] and biisoquinolinium cation radical **14**,[16] which were one-electron reduction products of the parent dications, methylviologen and biisoquinolinium, respectively, although the absorption maxima of **12** (blue; 600, 630, and 680 nm in benzene) are shifted to wavelengths longer than those of **13** (royal blue; 560, 610, and 670 nm in CH_3CN[15]) and **14** (orange red; 460, 500, and 538 nm in CH_3OH[16]). Similarly to **13** which was reoxidized to the original dication by oxygen or iodine, **12** was also reoxidized to the original dication DBA^{2+} in both DMF and methanol upon the addition of an equimolar amount of iodine, because a residue obtained by evaporation of the solvents showed an absorption spectrum in water which agreed with that of DBA^{2+}. When **12** was chromatographed on silica gel using benzene as the eluent in nitrogen atmosphere, the blue color of **12** on silica gel faded and **5** was isolated as yellow crystals from the eluate. In addition, a small amount of solid which was identified to be a salt of DBA^{2+} by comparing its absorption spectrum with that of DBA^{2+}, was isolated when water was used as the second eluent. From these findings it can reasonably be assumed that the blue compound **12** is the one-electron reduction product of DBA^{2+}, DBA^{+} $C_6H_5COCH_2^-$. The cation radical corresponds to **13** and **14**, which have a common partial structure, **15**. The

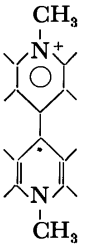

15

results of the elemental analysis of $DBA^{+}C_6H_5COCH_2^-$ (Found: C; 84.84, H; 5.70, N; 5.78%. Calcd for $C_{36}H_{29}N_2O$: C, 85.54, H; 5.74; N; 5.55%) and its IR spectrum, which appears to be the superposed spectra of **5** and acetophenone, also supported the structure of **12** for the blue compound. The formation of **5** and DBA^{2+} from **12** by chromatography on silica gel was considered to be due to the disproportionation reaction shown in Scheme 4. The blue color observed in the reaction of DBA^{2+} with $CH_3COCH_2^-$, $C_2H_5COCH_2^-$, and $HCOCH_2^-$, which were formed from the corresponding ketones or acetaldehyde and hydroxide ion, was also attributed to the formation of the cation radical DBA^{+}.

The rate of formation of **12** in solutions depended upon the reaction conditions, such as the kind of solvents and the concentrations of DBA^{2+} and $C_6H_5COCH_2^-$. When the concentrations of **1** and $C_6H_5COCH_2^-$ were rather high, the absorption spectrum of

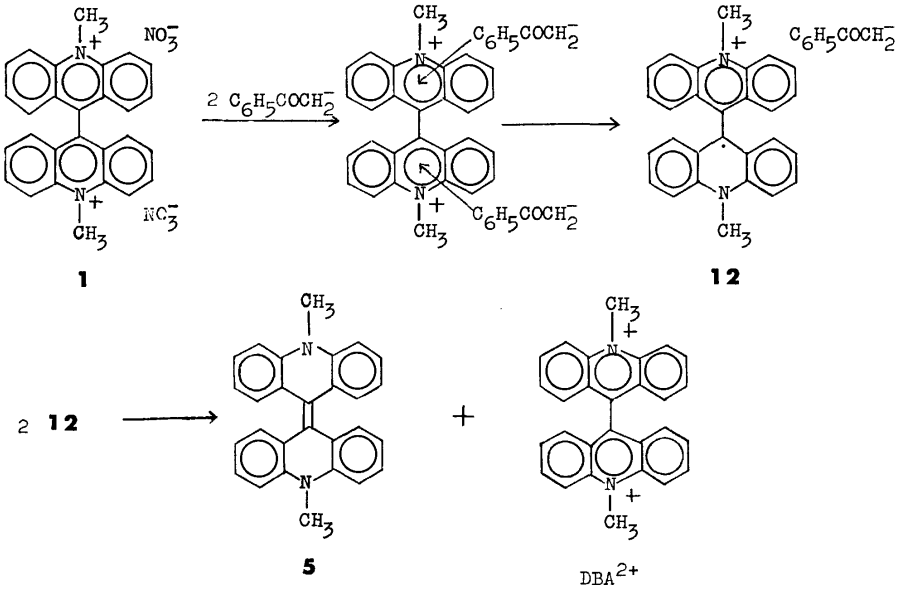

Scheme 4.

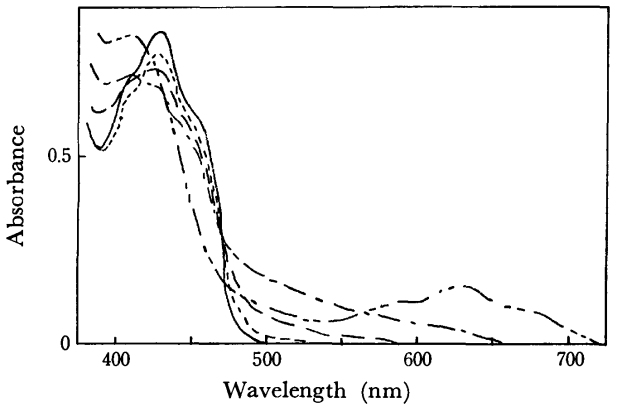

Fig. 10. The variation of the absorption spectrum of DBA^{2+} with increasing the concentration of $C_6H_5COCH_2^-$.
Solvent: C_2H_5OH-H_2O (50 : 50 vol%).
Concentration of **1**: 1.6×10^{-4} mol l^{-1}.
Concentration of $C_6H_5COCH_3$: 8.4×10^{-2} mol l^{-1}.
Concentration of NaOH added into the solution of $C_6H_5COCH_3$:
—— 0, ---- 4.7×10^{-4} mol l^{-1}, — — — 1.8×10^{-3} mol l^{-1}, ——— 2.3×10^{-3} mol l^{-1}, ——— 3.0×10^{-3} mol l^{-1}.
The spectra were measured immediately after mixing of **1** and $C_6H_5COCH_2^-$.

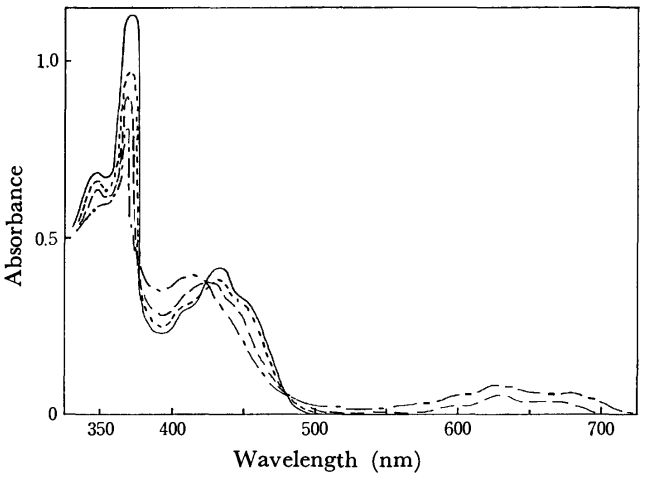

Fig. 11. The time-resolved absorption spectra of the mixture of **1** and $C_6H_5COCH_2^-$.
Solvent: C_2H_5OH-H_2O (50 : 50 vol%).
Concentration of **1**: 8.0×10^{-5} mol l^{-1}.
Concentration of $C_6H_5COCH_3$: 8.4×10^{-2} mol l^{-1}.
Concentration of NaOH added into the solution of $C_6H_5COCH_3$: 5.0×10^{-4} mol l^{-1}.
—— Before mixing, ---- immediately after mixing, — — — 10 min after mixing, ——— 40 min after mixing.

12 immediately appeared after mixing solutions of **1** and the nucleophiles, as shown Fig. 10. However, when the concentration of the nucleophiles was lower, CT absorption appeared immediately after mixing and then the absorption spectrum gradually changed to that of **12**, as is shown in Fig. 11.

In order to explain the fact that only nucleophile $RCOCH_2^-$ formed the cation radical DBA^+, one- and two-electron half-wave reduction potentials of DBA^{2+} in **1**, shown in Scheme 5, were measured polarographically[17] to be −0.035 and −0.43 V, respectively. In a manner similar to methylviologen dication*[18] and biisoquinolinium dication**,[16] the reduction potentials showed that the one-electron reduction in the first step from the dication to the corresponding cation radical **12** occurred more easily than that in the second step from the cation radical, **12**, to **5**. Although most of the oxidation-reduction potentials of the nucleophiles used in the present study are not known, it is reasonable to assume that the electron-donating power of nucleophiles $RCOCH_2^-$ to DBA^{2+} was stronger than those of NO_3^-, SCN^-, and I^- which gave CT complexes in an aqueous solution, but weaker than those of CN^-, OH^-, and CCl_3^- which gave DBA^{2+} as a reduction product. Therefore, the nucleophile $RCOCH_2^-$ formed the cation radical DBA^+ because of the difficulty in the second reduction step from DBA^+ to the two-electron reduction product.

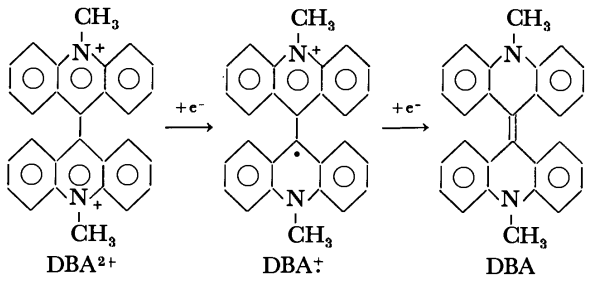

Scheme 5.

The results obtained in I, II, and III are summarized below and the mechanism of the chemiluminescence of lucigenin, **1**, is reasonably concluded to be that described below.

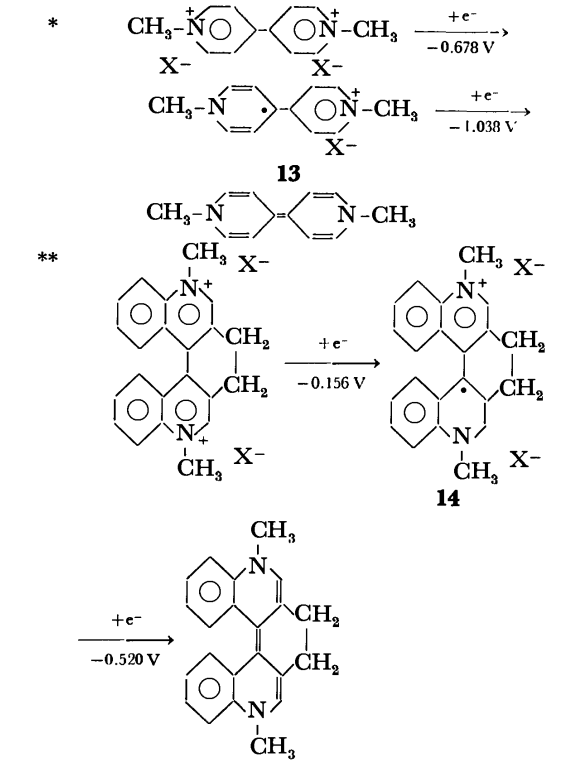

1. Lucigenin($DBA^{2+}2NO_3^-$) is a CT complex between DBA^{2+} and NO_3^-. Nucleophiles, such as Cl^-, Br^-, SCN^-, and I^-, give CT complexes upon their introduction into an aqueous solution of **1**.

2. The first process of the chemiluminescent reaction of **1** in an aqueous solution in the presence of oxygen is a reduction-oxidation reaction in which DBA^{2+} is reduced by two-electron transfer from OH^- to the biradical $DBA^{:}$ *via* the cation radical $DBA^{+\cdot}$. The biradical forms dioxetane[19] by oxygenation and then produces excited *N*-methylacridone, the light emitter. The mechanism of the chemiluminescence of **1** is shown in Scheme 6.

$$\underset{\mathbf{1}}{DBA^{2+}2NO_3^-} \xrightarrow{OH^-} \underset{\text{cation radical}}{(DBA^{+\cdot})} \xrightarrow{OH^-} \underset{\mathbf{11}}{DBA^{:}} \xrightarrow{O_2} \text{dioxetane}$$

$$\longrightarrow \underset{\mathbf{4^*}}{N\text{-methylacridone}^*} \longrightarrow h\nu + \underset{\mathbf{4}}{N\text{-methylacridone}}$$

Scheme 6.

3. Several nucleophiles which have strong electron-donating powers, such as CN^-, $t\text{-}BuO^-$, $C_6H_5S^-$, CCl_3^- and NH_3, also give the biradical which exhibits luminescence in organic solvents in the presence of oxygen. Nucleophiles which have weak electron-donating powers, such as $C_6H_5COCH_2^-$ and $CH_3COCH_2^-$, give cation radicals by one-electron transfer *via* CT complexes, but do not produce the biradical, and consequently exhibit no luminescence in the presence of oxygen.

The authors wish to express their deep gratitude to Professor Emeritus Taro Hayashi of Ochanomizu University for helpful discussions throughout this investigation. They wish also to express their gratitude to Dr. Hiroshi Midorikawa of the Institute of Physical and Chemical Research, Tokyo for his kind help, and to Dr. Kikuko Hayamizu of the National Chemical Laboratory for Industry, Tokyo, and Mrs. Makiko Onishi for their experimental assistance in the early stages of this investigation. This work was partially supported by a grant for Scientific Research from the Ministry of Education (No. 964095).

References

1a) K. Gleu and W. Petsch, *Angew. Chem.*, **45**, 57 (1935); 1b) H. Decker and W. Petsch, *J. Prakt. Chem.*, **143**, 211 (1935); 1c) B. Tamamushi and H. Akiyama, *Trans. Faraday Soc.*, **35**, 491 (1939); 1d) H. Kautsky and K. H. Kaiser, *Naturwissenschaften*, **31**, 505 (1943); 1e) A. V. Kariakin, *Opt. Spektrosk.* **7**, 75 (1959); 1f) J. R. Totter, V. J. Medina, and J. L. Scoseria, *J. Biol. Chem.*, **235**, 238 (1960); 1g) J. R. Totter, *Photochem. Photobiol.*, **3**, 231 (1964); 1h) F. McCapra and P. G. Richardson, *Tetrahedron Lett.*, **1964**, 3167; 1i) J. R. Totter and G. E. Philbrook, *Photochem. Photobiol.*, **5**, 177 (1966); 1j) F. McCapra and R. A. Hann, *Chem. Commun.*, **1969**, 442.

2a) E. G. Janzen, J. B. Pickett, J. W. Happ, and W. DeAngelis, *J. Org. Chem.*, **35**, 88 (1970); 2b) J. W. Happ and E. G. Janzen, *ibid.*, **35**, 96 (1970); 2c) J. W. Happ, E. G. Janzen, and B. C. Rudy, *ibid.*, **35**, 3382 (1970).

3a) K. Maeda and T. Hayashi, *Bull. Chem. Soc. Jpn.*, **40**, 169 (1967); 3b) K. Maeda, K. Hayamizu, and T. Hayashi, The 17th Annual Meeting of the Chemical Society of Japan, Tokyo, April 1964.

4) H. Decker and G. Dunnant, *Ber.*, **42**, 117 (1909).

5) C. G. Swain and C. B. Scott, *J. Am. Chem. Soc.*, **75**, 141 (1953).

6) E. M. Kosower and P. E. Klindinst, *J. Am. Chem. Soc.*, **78**, 3493 (1956).

7) W. von E. Doering and N. H. Knox, *J. Am. Chem. Soc.*, **79**, 352 (1957); K. M. Harmon, F. E. Cummings, D. A. Davic, and D. J. Diestler, *ibid.*, **84**, 120 (1962).

8) S. Sakamoto, Y. Kai, N. Yasuoka, N, Kasai, M. Kakudo, and H. Mikawa, *Chem. Commun.*, **1969**, 176.

9) E. M. Kosower, *J. Am. Chem. Soc.*, **80**, 3253, 3261 (1958).

10) If pinacol **2** were formed in a first process and then changed to *N*-methylacridone ketyl **3**, as shown in Scheme 1, an absorption spectrum due to pinacol **2** must appear in the wavelength region below that of **5**. In fact, the absorption spectrum of 10-methyl-9-phenyl-9,10-dihydro-9-acridinol, which is considered to have an absorption spectrum similar to that of **2**, showed only a maximum at 285 nm in ethanol.

11) Found: C, 86.72, H; 5.66, N; 7.34%. Calcd for **5**, $C_{28}H_{22}N_2$: C; 87.02; H; 5.74; N; 7.24%.

12) It appears that the biradical corresponds to a biradical which was suggested by Tamamushi and Akiyama[1e] in 1939 to be the product in the primary reaction in the proposed reaction mechanism of the chemiluminescence of **1**, on the basis of their finding, *i. e.* the formation of a brownish substance upon the warming or irradiation of a dilute alkaline solution of **1**.

13) Details of the chemilumunescence spectrum will be reported in a future publication.

14) When the photochemical reactions of **1** in both ethanol and DMSO were carried out for 2 h, a new compound which was determined to be a cyclization product of **11** was produced by further photolysis of **11** in the solutions. The new compound will be reported in a future publication.

15) E. M. Kosower and J. L. Cotter, *J. Am. Chem. Soc.*, **86**, 5524 (1964).

16) C. A. Heller, R. A. Henty, and J. M. Fritsch, "Chemiluminescence and Bioluminescence," ed by M. J. Cormier, D. M. Hercules, and J. Lee, Plenum Press, New York, London (1973), p. 249.

17) The measurement of the reduction potentials of **1** by a polarographic method was carried out by Professor Kazuo Nakada of the University of Electro-Communications. The potentials were measured *versus* a mercury electrode in DMF with tetramethylammonium iodide as the supporting electrolyte.

18) R. M. Flofson and R. L. Edsberg, *Can. J. Chem.*, **35**, 646 (1957).

19) F. McCapra and R. A. Hann, *Chem. Commun.*, **1969**, 442.

ESR Studies of Dibenzenesulfenamidyl Radicals[1]

Yozo MIURA, Noboru MAKITA, and Masayoshi KINOSHITA
Department of Applied Chemistry, Faculty of Engineering, Osaka City University, Sumiyoshi-ku, Osaka 558
(Received September 2, 1976)

Dibenzenesulfenamidyl radicals (**2**) were generated by the oxidation of dibenzenesulfenamides (**1**), and their ESR and visible spectra were measured. The ESR spectra were split into a 1 : 1 : 1 triplet by the interaction with the nitrogen nucleus (a_N=11.26—11.49 G); in some spectra, each of the triplet was further split by the interaction with the ring protons ($a_{o\text{-}H}=a_{p\text{-}H}$=0.48—0.70, $a_{m\text{-}H}$=0.18—0.22 G). The *g*-values lay in the range of 2.0080—2.0083. From the results, it was concluded that the unpaired electron is distributed mainly on the nitrogen and the two sulfur atoms. Kinetic studies of the decay of **2** indicated that **2** decays with second-order kinetics and is not sensitive to the atmospheric oxygen.

A number of nitrogen-centered free radicals have so far been prepared, and extensive ESR studies for such radicals have been undertaken.[2] Some of them can be readily isolated as pure crystals: 2,2-diphenyl-1-picrylhydrazyl (DPPH),[3] 3,4-dihydro-2,4,6-triphenyl-2*H*-1,2,4,5-tetrazin-1-yl (1,3,5-triphenylverdazyl),[4] *etc.*

About fifty years ago, Lecher *et al.* reported that dibenzenesulfenamide (**1a**) in benzene gives a purple solution on treatment with lead dioxide or silver oxide.[5] They inferred from the coloration that a new class of nitrogen-centered free radicals, dibenzenesulfenamidyl radical (**2a**), had been generated. This radical possesses an interesting structure in which two divalent sulfur atoms are adjacent to the radical center. Barton *et al.* have recently found that tribenzenesulfenamide (**3a**) affords **2a** on photolysis or pyrolysis.[6] ESR studies on dibenzenesulfenamidyl radicals (**2**), however, have been rare. In this paper, the authors wish to report a detailed ESR investigation of **2**.

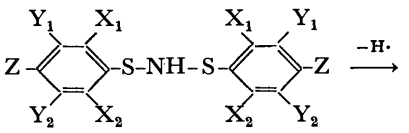

1

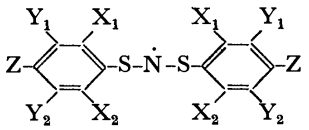

2

a: $X_1=X_2=Y_1=Y_2=Z=H$
b: $X_1=X_2=Y_1=Y_2=H$, $Z=CH_3$
c: $X_1=X_2=Y_1=Y_2=H$, $Z=C(CH_3)_3$
d: $X_1=X_2=Y_1=Y_2=H$, $Z=NO_2$
e: $X_1=X_2=Y_1=Y_2=H$, $Z=F$
f: $X_1=X_2=Y_1=Y_2=H$, $Z=Cl$
g: $X_1=X_2=Y_1=Y_2=H$, $Z=Br$
h: $X_1=X_2=Y_1=Z=H$, $Y_2=Cl$
i: $X_1=X_2=Y_1=Z=H$, $Y_2=Br$
j: $X_1=Y_1=Y_2=Z=H$, $X_2=CH_3$
k: $X_1=Y_1=Y_2=Z=H$, $X_2=Cl$
l: $X_1=Y_1=Y_2=Z=H$, $X_2=Br$
m: $X_1=Y_1=Y_2=H$, $X_2=Z=CH_3$
n: $X_1=Y_1=Y_2=H$, $X_2=CH_3$, $Z=Cl$
o: $X_1=Y_1=Y_2=H$, $X_2=Z=Cl$
p: $X_1=Y_2=Z=H$, $X_2=Y_2=Cl$
q: $X_1=Y_1=Z=H$, $X_2=Y_1=Cl$
r: $X_1=X_2=Z=H$, $Y_1=Y_2=Cl$

Results and Discussion

Generation of Radicals. Eighteen dibenzenesulfenamides (**1**) were prepared according to a procedure similar to that in the literature.[5] The compounds **1** in benzene all afforded immediately a purple solution on treatment with lead dioxide and potassium carbonate, and the solution showed a strong ESR signal. The ESR parameters for the radicals are listed in the table. The radicals are also generated by the photolysis of **1**, with or without the assistance of di-*t*-butyl peroxide. In general, nitrogen-centered free radicals are easily converted to the corresponding nitroxide radicals. However, even if the present radicals were treated under exposure to the atmosphere, the corresponding nitroxide radicals were not detected. The compounds **1** were not oxidized to **2** by the atmospheric oxygen, but they were subject to photolysis under exposure to the sunlight to give **2**.

Visible Spectra of Radicals. It is important to prove that the radicals **2** are responsible for the purple colors. For example, a visible spectrum of **2a** in benzene shows a λ_{max} at 538 nm, which is responsible for the purple color. The absorbance at this point was plotted against the intensity of the ESR signal (Fig. 1). The good linearity of the plot indicates that the purple color is attributable to the radical. The absorption maxima of **2** are summarized in the table.

ESR Spectra of Radicals. The ESR spectra of **2** were recorded in degassed benzene in order to make them well-resolved. The radical **2a** gave a broad 1 : 1 : 1 triplet spectrum, indicating that the splitting is due to the interaction with the nitrogen nucleus. For the radical, the reported value of a_N is 11.4 G (in cyclohexane),[6] which is in good agreement with this experimental value. The *para*-substituted radicals, **2b** and **2d**, also gave a similarly broad 1 : 1 : 1 triplet spectrum. On the other hand, in the cases of **2c**, **2f**, **2g**, and **2o**, each of the triplet was further split by the interaction with the ring protons, although the splittings were not well-resolved (Fig. 2). In the spectra of **2h**, **2i**, **2k**, **2l**, and **2p**—**r**, however, the splittings were well-resolved (Figs. 3 and 4), and thus the values of a_H were easily determined. The spectra of **2e**, **2j**, **2m**, and **2n** were split by the interaction with the fluorine nuclei and the methyl protons, respectively. However, the spectra were complicated due to superposition with the splittings due to the ring protons,

TABLE. ESR AND VISIBLE SPECTRAL DATA OF DIBENZENESULFENAMIDYL RADICALS (2) IN BENZENE AT ROOM TEMPERATURE

Radical	Coupling constant (G)				g-Value	λ_{max} (nm)
	a_N	$a_{o\text{-H}}$	$a_{m\text{-H}}$	$a_{p\text{-H}}$		
2a	11.41				2.0082	538
2b	11.45			—	2.0082	545
2c	11.45	0.48	0.20	—	2.0082	541
2d	11.26			—	2.0080	497
2e	11.49			—	2.0082	531
2f	11.37	0.56		—	2.0082	543
2g	11.37	0.56	0.22	—	2.0083	544
2h	11.40	0.57		0.57	2.0081	535
2i	11.40	0.57		0.57	2.0081	537
2j	11.36				2.0083	557
2k	11.29	0.67	0.21	0.67	2.0081	559
2l	11.27	0.67		0.67	2.0081	558
2m	11.44				2.0083	561
2n	11.36				2.0083	568
2o	11.29	0.62		—	2.0082	569
2p	11.27	0.70	0.21	0.70	2.0080	559
2q	11.30	0.70	0.18	0.70	2.0080	558
2r	11.40	0.58	—	0.58	2.0080	531

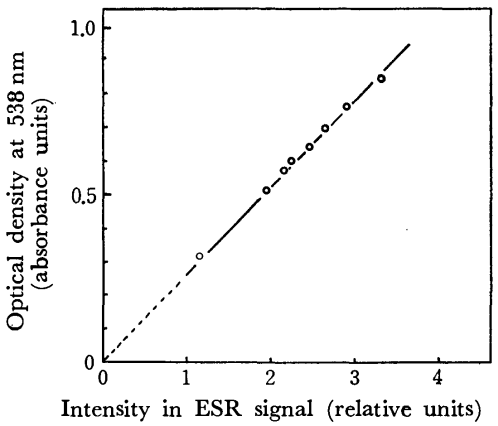

Fig. 1. Plot of ESR signal intensity *vs.* optical density (538 nm) for dibenzenesulfenamidyl radical (**2a**) in benzene at 23 °C.

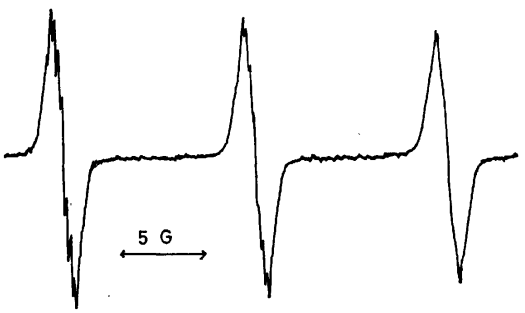

Fig. 2. The ESR spectrum of 4,4′-di-*t*-butyldibenzenesulfenamidyl radical (**2c**) in benzene at room temperature.

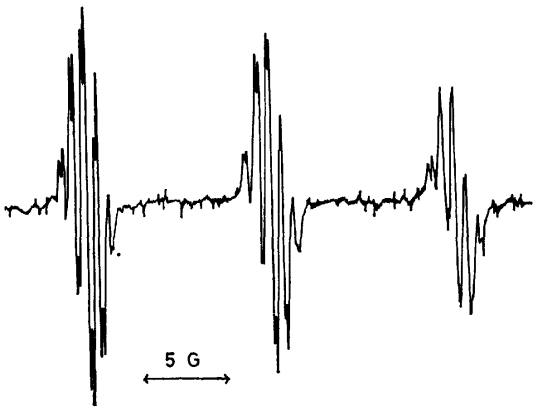

Fig. 3. The ESR spectrum of 2,2′,5,5′-tetrachlorobenzenesulfenamidyl radical (**2q**) in benzene at room temperature.

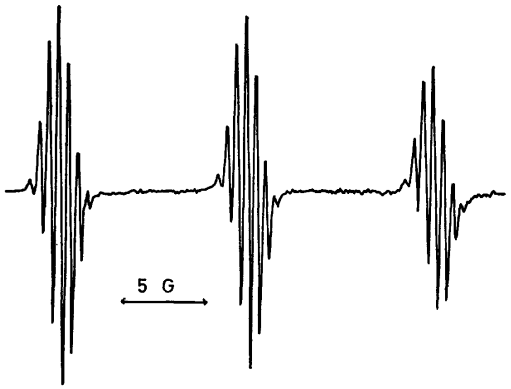

Fig. 4. The ESR spectrum of 3,3′,5,5′-tetrachlorodibenzenesulfenamidyl radical (**2r**) in benzene at room temperature.

and thus poorly resolved. Consequently, the values of a_H and a_N of the radicals could not be determined.

As found in the table, the values of a_N lie in the range of 11.26 to 11.49 G and are almost uninfluenced by the substituents. The values of a_H are very small, indicating that the spin densities of the rings are not large. The unpaired electron is, therefore, distributed mainly on the nitrogen and the two sulfur atoms. The *g*-values of **2** lie in the range of 2.0080 to 2.0083;[7] these are large for a nitrogen-centered free radical.[8] This can be explained in terms of the presence of sulfur atoms possessing a large spin-orbit coupling parameter in the π-system.[9]

Decay Kinetic Studies of Radicals. The radicals **2** are rather long-lived in non-polar solents such as benzene and hexane, and give diaryl disulfide and nitrogen in quantitative yields as final decomposition products. Kinetic studies of the decay of **2** were undertaken at 23 °C in the dark. The results are illustrated in Fig. 5.

According to Barton *et al.*,[6] a small quantity of **3a** is generated by the coupling reaction of **2a** with phenylthiyl radical in the course of decomposition of **2a**. Since **3a** already decomposes at relatively low temperature (78 °C) into the original radicals, **2a** and phenylthiyl radical, if tribenzenesulfenamides (**3**) are

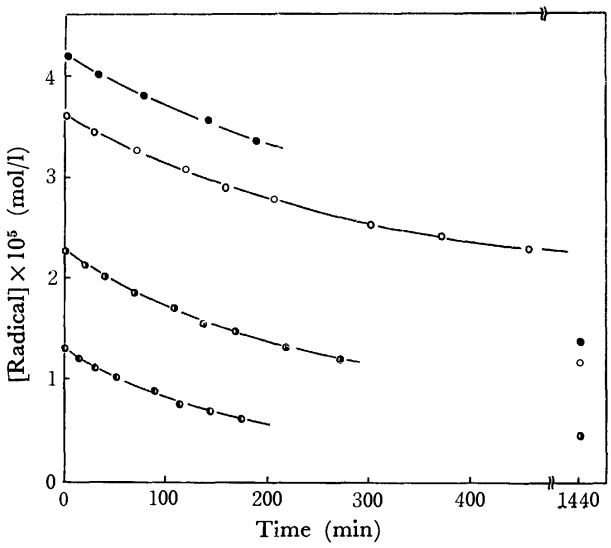

Fig. 5. Decay plots of dibenzenesulfenamidyl radicals at 23 °C.
○; Dibenzenesulfenamidyl radical (**2a**) in degassed benzene, ●; **2a** in benzene exposed to the atmosphere, ◑; 4,4′-dichlorodibenzenesulfenamidyl radical (**2f**) in degassed benzene, ◐; 4,4′-dinitrodibenzenesulfenamidylradical (**2d**) in degassed benzene.

generated in the present kinetic system, the analyses of the kinetic studies may become difficult.

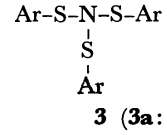

3 (**3a**: Ar=C_6H_5)

In order to examine whether **3** was generated or not in the present system, thin layer chromatographic analysis was performed for every solution after the kinetic measurement was completed. The substance **3**, however, was not detected at all. Furthermore, the benzene solution of 0.015 mol/l of **3a** gave only 3.0×10^{-6} mol/l of **2a** at 23 °C in the dark (the concentration of **1a** used for the kinetic investigation was 0.054 mol/l). From these results, it seems that **3** scarcely affects the present kinetic studies.

From the figure, it was found that the radicals **2** decay with second-order kinetics (the rate constant **2a**: 1.1, **2d**: 6.8, **2e**: 2.0 l/mol s) and are not sensitive to the atmospheric oxygen. The decay rates decrease in the order of **2d**>**2e**>**2a**, indicating that introduction of electron-withdrawing groups destabilizes the radicals.[2] This may be explained as follows: electron-withdrawing groups stabilize the corresponding hydrazines by reducing the dipolar repulsion between the nirogen atoms.[10] The hydrazines have not yet been isolated, in spite of many attempts,[5] probably because they are very unstable.

Experimental

All melting points were uncorrected. IR and visible spectra were recorded on a Jasco Model IR-G Spectrometer and a Hitachi Recording Spectrometer Model ESP-3T, respectively. Thin layer chromatographic analyses were performed on alumina (Merck Art 1064), using hexane as eluent, and detected by UV-irradiation.

ESR Measurement. ESR spectra were recorded with a JES-ME 3X Spectrometer, equipped with 100 kHz field modulation, at room temperature (23 °C).

Sample preparation was performed as follows: a) dibenzenesulfenamide (**1**, 10 mg) was treated with lead dioxide (0.5 g) and potassium carbonate (0.5 g) in benzene (1.0 ml), and the inorganic compounds were removed by filtration. 0.4 ml of the filtrate was placed in an ESR tube and degassed by three freeze-and-thaw cycles, and then sealed; b) a solution of **1** (5 mg) and di-*t*-butyl peroxide (0.02 ml) in benzene (0.4 ml) was placed in an ESR tube and degassed as above, and then sealed. ESR spectra were recorded under UV-irradiation from a distance of 40 cm using a high pressure mercury lamp (JES-UV-1, 100 W).

Kinetic Studies. Sample preparation was performed according to the procedure b (di-*t*-butyl peroxide was not added). The solution was UV-irradiated for *ca.* 3 min as described above, and the lamp was turned off. Decay rates of radicals were measured at 23 °C in the dark by monitoring the intensity of the ESR signals. Integrations of ESR signals were achieved with a Model JES-ID-2 Integrator, using a benzene solution of 3,4-dihydro-2,4,6-triphenyl-2*H*-1,2,4,5-tetrazin-1-yl[4] as a standard.

Materials. The benzene used for the ESR measurements was purified by the usual method: it was shaken with concd sulfuric acid, and washed with dilute potassium carbonate and then water. After drying over anhydrous magnesium sulfate, it was distilled from sodium wire. Commercially available di-*t*-butyl peroxide, benzenethiol, 2-methyl-, 4-methyl-, 4-*t*-butyl-, and 4-chlorobenzenethiols were used without further purification. 4-Fluoro-, 4-bromo-, 2,4-dimethyl-, and 2,4-dichlorobenzenethiols were prepared by treatment of the appropriate benzenes with chlorosulfonic acid, followed by reduction with zinc dust and sulfuric acid.[11,12] 2-Chloro-, 2-bromo-, 3-chloro-, 3-bromo-, 2-methyl-4-chloro-, 2,3-dichloro-, 2,5-dichloro-, and 3,5-dichlorobenzenethiols were prepared from the appropriate diazotized anilines.[13] 4-Nitrobenzenethiol was prepared by the procedure of Price *et al.*[14]

All dibenzenesulfenamides (**1**) except 4,4′-dinitrodibenzenesulfenamide (**1d**) were prepared according to a procedure similar to that in the literature;[15] **1d** was obtained by a modified method. A typical procedure for the preparation of **1** is described below.

Dibenzenesulfenamide (1a). Chlorine gas was passed into dry chlorofrom (200 ml) at −5—0 °C. To the solution was added dropwise benzenethiol (25 g, 0.23 mol) over a period of 1 h, and for an additional 1 h the gas was passed at the same temperature. After chloroform was evaporated, the resulting red oil was distilled, giving pure benzenesulfenyl chloride; 56—57 °C/3 Torr, 24.7 g (0.17 mol). Ammonia gas was passed into dry ether (600 ml) at −40——50 °C under stirring. To the solution was added dropwise the sulfenyl chloride in dry ether (200 ml) over a period of 2 h. After completion of the addition, the passing of ammonia gas was stopped, and the temperature was gradually raised to room temperature. The formed ammonium chloride was filtered off, and ether was evaporated, giving purple crystals, which were recrystallized from hexane; mp 127—128 °C lit,[15] 127—128 °C), 11.8 g (0.051 mol, 60%).

2-Methyl-(87—88 °C/4 Torr), 4-methyl-(76—78 °C/3 Torr), 4-*t*-butyl-(124—126 °C/7 Torr), and 2,4-dimethylbenzenesulfenyl chlorides (76—78 °C/3 Torr) were purified by distillation. On the other hand, the other sulfenyl chlorides

were used for the following steps without any purification after the removal of chloroform.

*4,4'-Ditoluenesulfenamide (**1b**).* Mp 98—100 °C (petroleum ether), 29%. IR (KBr): 3270 cm^{-1} (NH). Found: C, 64.18; H, 5.97; N, 5.55%. Calcd for $C_{14}H_{15}NS_2$: C, 64.37; H, 5.77; N, 5.36%.

*4,4'-Di-t-butyldibenzenesulfenamide (**1c**).* Mp 89—91 °C (petroleum ether), 28%. IR (KBr): 3270 cm^{-1} (NH). Found: C, 69.75; H, 7.67; N, 4.21%. Calcd for $C_{20}H_{27}NS_2$: C, 69.50; H, 7.89; N, 4.05%.

*4,4'-Difluorodibenzenesulfenamide (**1e**).* Mp 127—129 °C (hexane), 54%. IR (KBr): 3270 cm^{-1} (NH). Found: C, 53.33; H, 3.14; N, 5.24%. Calcd for $C_{12}H_9NF_2S_2$: C, 53.51, H, 3.37; N, 5.20%.

*4,4'-Dichlorodibenzenesulfenamide (**1f**).* Mp 132—133 °C (benzene–hexane, lit,[16] 137—140 °C), 71%.

*4,4'-Dibromodibenzenesulfenamide (**1g**).* Mp 138—139 °C (methanol), 53%. IR (KBr): 3270 cm^{-1} (NH). Found C, 36.87; H, 2.37; N, 3.70%. Calcd for $C_{12}H_9NBr_2S_2$: C, 36.85; H, 2.32; N, 3.58%.

*3,3'-Dichlorodibenzenesulfenamide (**1h**).* Mp 122—123 °C (benzene–hexane), 24%. IR (KBr): 3270 cm^{-1} (NH). Found: C, 47.49; H, 2.95; N, 4.83%. Calcd for $C_{12}H_9NCl_2S_2$: C, 47.68; H, 3.01; N, 4.64%.

*3,3'-Dibromodibenzenesulfenamide (**1i**).* Mp 115—117 °C (benzene–hexane), 24%. IR (KBr): 3270 cm^{-1} (NH). Found: C, 37.11; H, 2.23; N, 3.77%. Calcd for $C_{12}H_9NBr_2S_2$: C, 36.85; H, 2.32; N, 3.58%.

*2,2'-Ditoluenesulfenamide (**1j**).* Mp 128—130 °C (petroleum ether), 39%. IR (KBr): 3270 cm^{-1} (NH). Found: C, 64.27; H, 5.72; N, 5.31%. Calcd for $C_{14}H_{15}NS_2$: C, 64.37; H, 5.77; N, 5.36%.

*2,2'-Dichlorodibenzenesulfenamide (**1k**).* After the removal of ether from the filtrate, to the residue (oil) hexane was added, giving crystalline **1k**, which was recrystallized from methanol, and benzene–hexane; mp 167—169 °C, 21%. IR (KBr): 3270 cm^{-1} (NH). Found: C, 47.57; H, 2.95; N, 4.72%. Calcd for $C_{12}H_9NCl_2S_2$: C, 47.68; H, 3.01; N, 4.64%.

*2,2'-Dibromodibenzenesulfenamide (**1l**).* After the removal of ether from the filtrate, to the residue (oil) hexane was added, giving crystalline **1l**, which was recrystallized from methanol, and benzene–hexane; mp 173—174 °C, 31%. IR (KBr): 3270 cm^{-1} (NH). Found: C, 36.86; H, 2.25; N, 3.61%. Calcd for $C_{12}H_9NBr_2S_2$: C, 36.85; H, 2.32; N, 3.58%.

*2,2',4,4'-Dixylenesulfenamide (**1m**).* Mp 116—118 °C (petroleum ether), 49%. IR (KBr): 3270 cm^{-1} (NH). Found: C, 66.33; H, 6.65; N, 5.05%. Calcd for $C_{16}H_{19}NS_2$: C, 66.39; H, 6.62; N, 4.84%.

*2,2'-Dimethyl-4,4'-dichlorodibenzenesulfenamide (**1n**).* Mp 144—146 °C (chloroform), 48%. IR (KBr): 3270 cm^{-1} (NH). Found: C, 50.63; H, 3.90; N, 4.21%. Calcd for $C_{14}H_{13}NCl_2S_2$: C, 50.91; H, 3.98; N, 4.24%.

*2,2',4,4'-Tetrachlorodibenzenesulfenamide (**1o**).* After the removal of ether from the filtrate, the crystalline residue was refluxed in methanol (100 ml) for 10 min (not soluble completely) and cooled. The crystals separated were filtered and recystallized from benzene; mp 185—186 °C, 23%. IR (KBr): 3270 cm^{-1} (NH). Found: C, 38.75; H, 1.86; N, 3.78%. Calcd for $C_{12}H_7NCl_4S_2$: C, 38.83; H, 1.91; N, 3.76%.

*2,2',3,3'-Tetrachlorodibenzenesulfenamide (**1p**).* After the removal of ether from the filtrate, to the oily residue hexane was added, giving crude **1p**, which was filtered, and refluxed in methanol (50 ml) for 10 min (not soluble completely) and cooled. The crystals separated were filtered and recrystallized from benzene–hexane; mp 197—198 °C, 26%. IR (KBr): 3270 cm^{-1} (NH). Found: C, 38.94; H, 1.91; N, 3.76%. Calcd for $C_{12}H_7NCl_5S_2$: C, 38.83; H, 1.91; N, 3.76%.

*2,2',5,5'-Tetrachlorodibenzenesulfenamied (**1q**).* After the removal of ether from the filtrate, to the oily residue hexane was added, giving crude **1q**, which was filtered, and refluxed in methanol (50 ml) for 10 min (not soluble completely) and cooled. The crystals separated were filtered and recrystallized from benzene–hexane; mp 197—198 °C, 20%. IR (KBr): 3270 cm^{-1} (NH). Found: C, 39.06; H, 1.73; N, 3.72%. Calcd for $C_{12}H_7NCl_4S_2$: C, 38.83; H, 1.91; N, 3.76%.

*3,3',5,5'-Tetrachlorodibenzenesulfenamide (**1r**).* Mp 185—186 °C (benzene–chloroform), 16%. IR (KBr): 3270 cm^{-1} (NH). Found: C, 38.75; H, 1.86; N, 3.78%. Calcd for $C_{12}H_7NCl_4S_2$: C, 38.83; H, 1.91; N, 3.76%.

*4,4'-Dinitrodibenzenesulfenamide (**1d**).* By a procedure similar to **1a**, 4-nitrobenzenethiol was treated with chlorine and ammonia gases. After the removal of ether from the filtrate, the obtained residue was recrystallized from benzene–hexane, giving 4-nitrobenzenesulfenamide; mp 104—106 °C (lit,[17] 103 °C), 49%.

4-Nitrobenzenesulfenyl chloride, which was prepared from 5.5 g (0.032 mol) of 4-nitrobenzenethiol, was added dropwise at −10—−5 °C under stirring to a solution of 4-nitrobenzenesulfenamide (5.5 g, 0.032 mol) and triethylamine (4.0 g) in acetonitrile (100 ml). After completion of the addition, the reaction mixture was stirred for an additional 30 min at 0 °C, and filtered. After the removal of acetonitrile, the resulting residue was recrystallized repeatedly from methanol, giving yellow brown needles [it was very difficult to obtain pure crystals of **1d**, because bis (4-nitrophenyl) disulfide was always contaminated]; mp 167—169 °C (lit,[17] 155 °C), 0.30 g (9.3 mmol, 3.2%). IR (KBr); 3270 cm^{-1} (NH). Found: C, 44.64; H, 2.64; N, 12.88%. Calcd for $C_{12}H_9N_3O_4S_2$: C, 44.57; H, 2.89; N, 13.00%.

*Tribenzenesulfenamide (**3a**).* The compound was prepared according to the literature,[6] mp 62—64 °C (lit,[6] 68 °C).

References

1) Presented in part at the 28th Annual Meeting of the Chemical Society of Japan, Tokyo, April 1—4, 1973 (Pref. Abst., p. 1198), and for a preliminary report, see Y. Miura, N. Makita, and M. Kinoshita, *Tetrahedron Lett.*, **1975**, 127.

2) (a) A. R. Forrester, J. M. Hay, and R. H. Thomson, "Organic Chemistry of Stable Free Radicals," Academic Press, New York, N. Y. (1968); (b) S. F. Nelsen, "Free Radicals," Vol. II, ed by J. K. Kochi, John & Wiley, New York, N. Y. (1973), p. 527; (c) W. C. Danen and F. A. Neugebauer, *Angew. Chem.*, **87**, 823 (1975).

3) S. Goldschmidt and K. Renn, *Ber.*, **55**, 628 (1922).

4) R. Kuhn and H. Trischmann, *Monatsh. Chem.*, **95**, 457 (1964).

5) H. Lecher, K. Kökerle, and P. Stöcklin, *Ber.*, **58**, 423 (1925).

6) D. H. R. Barton, I. A. Elair, P. D. Magnus, and R. K. Norris, *J. Chem. Soc., Perkin Trans. 1*, **1973**, 1031.

7) U. Schmidt, K. H. Kabitzke, and K. Markau, *Angew. Chem.*, **76**, 376 (1964).

8) For example, the *g*-value of diphenylamino radical is 2.0032; F. A. Neugebauer and S. Bamberger, *Chem. Ber.*, **107**, 2362 (1974).

9) The spin-orbit coupling parameter of sulfur is 382 cm^{-1}; D. S. McClure, *J. Chem. Phys.*, **20**, 682 (1952).

10) G. N. Lewis and D. Lipkin, *J. Am, Chem. Soc.*, **63**, 3232 (1941).
11) R. Adams and C. S. Marvel, *Org. Synth.*, Coll. Vol. I, 504 (1956).
12) E. H. Huntress and F. H. Carten, *J. Am. Chem. Soc.*, **62**, 511 (1940).
13) D. S. Tarbell and D. K. Fukushima, *Org. Synth.*, Coll. Vol. III, 809 (1955).
14) C. C. Price and G. W. Stacy, *J. Am. Chem. Soc.*, **68**, 498 (1946).
15) H. Lecher, F. Holschneider, K. Köberle, W. Speer, and P. Stöcklin, *Ber.*, **58**, 409 (1925).
16) T. Mukaiyama, T. Taguchi, and M. Nishi, *Bull. Chem. Soc. Jpn.*, **44**, 2797 (1971).
17) T. Zincke and S. Lenhardt, *Justus Liebigs Ann. Chem.*, **400**, 1 (1913).

A Synthesis of 3′-Deoxybutirosin B

Isamu WATANABE, Akio EJIMA, Tsutomu TSUCHIYA, Daishiro IKEDA, and Sumio UMEZAWA

Institute of Bioorganic Chemistry, 1614 Ida, Nakahara-ku, Kawasaki 211

(Received September 9, 1976)

3′-Deoxybutirosin B (**13**) was prepared from 3′-deoxyparomamine (**1**), D-ribose and (*S*)-4-amino-2-hydroxybutyric acid (AHBA). The synthesis involves replacement of the 6′-hydroxyl group of 3′-deoxyparomamine with azido group, 1,6-carbamate ring formation, condensation with tri-*O*-(*p*-nitrobenzoyl)-α,β-D-ribofuranosyl bromide, selective cleavage of the carbamate ring, and acylation of the free amino group at C-1 with AHBA.

In a previous paper,[1] we described the synthesis of 3′-deoxybutirosin B (**13**), a compound having a remarkable activity against resistant bacteria, starting from ribostamycin. In this paper we describe a second synthesis of **13** by condensation of a 3′-deoxyparomamine derivative with a protected ribosyl bromide. The starting material 3′-deoxyparomamine[2] (**1**) is conveniently obtained by hydrolysis of lividomycins,[3] an antibiotic complex produced by *streptomyces lividus*.

For attaining the synthesis, three key steps were required: 1) replacement of the 6′-hydroxyl group with an amino group, 2) selective ribosylation of the 5-hydroxyl group, and 3) selective amidation of the 1-amino group with (*S*)-4-amino-2-hydroxybutyric acid. The step (1) was performed by selective 6′-*O*-tosylation of a paromamine derivative followed by azidation and hydrogenation. For the step (2) the preparation of a 3′-deoxyparomamine derivative having a free hydroxyl group only at C-5 was required. For this purpose cyclic 1,6-carbamate[4] formation was utilized. Ito *et al.*[5] have reported the synthesis of ribostamycin by condensation of an *O*-benzoylribosyl chloride with a neamine derivative bearing two free hydroxyl groups at C-5 and C-6 to give 5-*O*-ribosyl glycoside as the major product. On the other hand, Hanessian *et al.*[6] have obtained a 6-*O*-ribosyl glycoside almost quantitatively by condensation of the ribosyl chloride with a protected paromamine derivative having two free hydroxyl groups at C-5 and C-6. In our experiences,[13] the 6-hydroxyl group is observed to be more reactive than the 5-hydroxyl group, therefore, we designed to protect the 6-hydroxyl group by cyclic 1,6-carbamate formation. The 1,6-carbamate suggested another advantage that the space around the 5-hydroxyl group is extended by the formation of the cyclic carbamate, favouring the 5-*O*-glycosylation, while commonly used 6-*O*-acyl groups may exert steric hindrance on the 5-hydroxyl group. For the step (3), the cyclic 1,6-carbamate was again useful because it is preferentially cleaved[4] to give the free amino group at C-1.

Tri-*N*-benzyloxycarbonyl-3′-deoxyparomamine (**2**) obtained by treatment of 3′-deoxyparomamine[2] (**1**) with benzyl chloroformate was tosylated. In spite of the presence of four hydroxyl groups in **2**, the 6′-*O*-tosyl derivative (**3**) was isolated in a yield of 68%. The position of the group was indicated by the difficulty of tritylation of **3**. Treatment of **3** with sodium azide in *N*,*N*-dimethylformamide (DMF) gave the 6′-azido derivative (**4**) quantitatively. Reaction of **4** with sodium hydride in DMF in a manner as described in previous papers[1,4,7] gave the cyclic carbamate derivative (**5**) in a yield of 80%. The presence of a carbamate group was confirmed by its IR spectrum.[8] Since **5** has two hydroxyl groups at C-5 and 4′, the hydroxyl group at C-4′ was protected in advance. For the purpose we utilized α-naphthoyl group, a bulky one, expecting its regioselective effect. The 4′-*O*-(α-naphthoyl) derivative (**6**) was obtained in a yield of 65%. The structure of **6** was confirmed by acidic hydrolysis of the mesyl derivative (**14**) of **6**. Hydrolysis of **6** gave 2-deoxystreptamine, whereas hydrolysis of **14** did not give 2-deoxystreptamine, indicating that the hydroxyl at C-5 of 2-deoxystreptamine moiety was mesylated.

The 5-*O*-ribosylation of **6** was next studied. Among the protected ribosyl halogenides tested, the anomeric mixture (*ca.* 1 : 1) of 2,3,5-tri-*O*-(*p*-nitrobenzoyl)-D-ribofuranosyl bromide (**8**), which was prepared *via* methyl 2,3,5-tri-*O*-(*p*-nitrobenzoyl)-β-D-ribofuranoside (**7**), was found suitable for the coupling partner to **6**, because **8** is stable to recrystallization from benzene and can be kept for months. The corresponding *O*-acetyl and *O*-benzoyl bromide were less stable. In addition, the presence of the *p*-nitrobenzoyl group at C-2 may be convenient in the glycoside formation in preventing[9] the formation of undesirable orthoester. After completion of our work, Khadem *et al.*[12] have reported the syntheses of **7** and **8** in the β-anomeric form by a method similar to ours. Condensation of **6** with **8** was carried out in dichloromethane in the presence of mercuric cyanide. In this reaction, the use of fairly decreased amount of dichloromethane (7—10 times v/w for **8**) was required to raise the yield of the condensation product (**9**). The use of benzene–dioxane, or nitromethane as the solvent or the use of Ag_2CO_3–$AgClO_4$ as the catalyst also decreased the yield.

Cleavage of the 1,6-carbamate as well as that of *O*-acyl groups was performed by use of a limited amount of barium hydroxide in dioxane, as reported in previous papers,[1,4,7] to give **11**. When, sodium *p*-methoxybenzylate was used as the base in this reaction, the 1,6-carbamate was cleaved to give the 1-*N*-(*p*-methoxybenzyloxycarbonyl) derivative (**10**). The 1-*N*-protecting group was selectively removed by the action of trifluoroacetic acid[10] in methoxybenzene to give **11** in high yield. The use of boiling acetic acid[10] decreased the yield of **11**.

(*S*)-4-Benzyloxycarbonylamido-2-hydroxybutyryl[11] group was then introduced to the free amino group at C-1 by *N*-hydroxysuccinimide ester method. Catalytic hydrogenolysis of the *N*-benzyloxycarbonyl groups

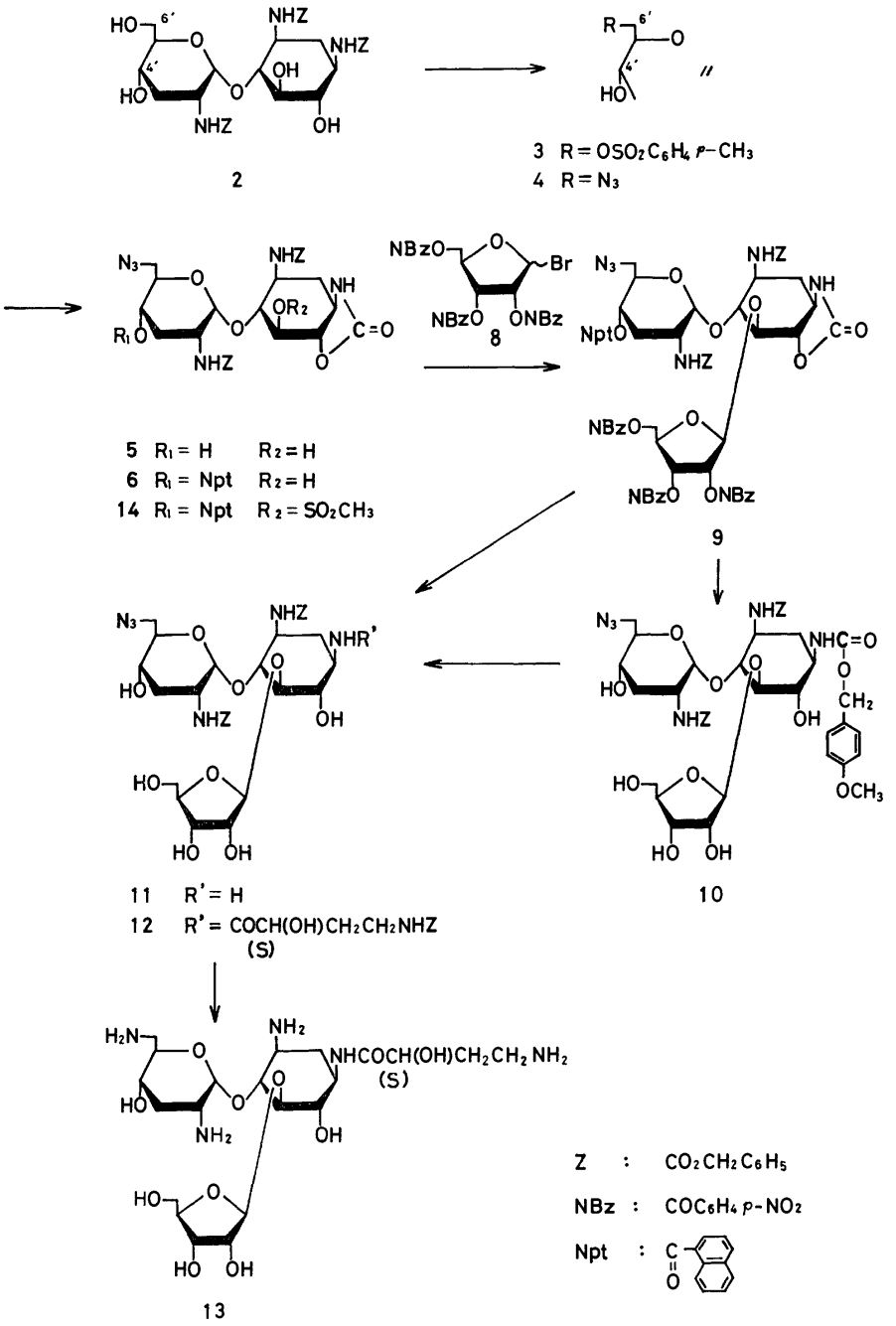

and the 6'-azido group of the amide (**12**) gave the 3'-deoxybutirosin B (**13**) in overall yield of *ca.* 6% based on **1**. The PMR spectrum of **13** was superimposable with that of 3'-deoxybutirosin B prepared[1] from ribostamycin.

Experimental

Thin-layer chromatography (TLC) was carried out on Wakogel B-5 with sulfuric acid spray for detection. For column chromatography, silica gel (Wakogel C-200) was used.

*1,3,2'-Tri-*N*-benzyloxycarbonyl-3'-deoxyparomamine (2).* A sample of 3'-deoxyparomamine[2] (**1**) was treated with benzyl chloroformate in a similar manner as reported[7] in benzyloxycarbonylation of lividomycin A to give a solid of **2** almost quantitatively, $[\alpha]_D^{22}$ +43° (*c* 0.5, dioxane).

Found: C, 60.70; H, 6.06; N, 5.63%. Calcd for $C_{36}H_{43}N_3O_{12}$: C, 60.92; H, 6.11; N, 5.92%.

*1,3,2'-Tri-*N*-benzyloxycarbonyl-3'-deoxy-6'-*O*-tosylparomamine (3).* To an ice-cold solution of **2** (9.78 g) in pyridine (200 ml), anhydrous *p*-toluenesulfonyl chloride (12.7 g, 5 mol equivalent for **2**) was added and the solution was kept at −10 °C overnight. The solution showed, on TLC with chloroform–ethanol (12 : 1), a major spot at R_f 0.53 and other several slight spots. After addition of water (2.5 ml), the solution was concentrated to give a yellow syrup. The chloroform solution (500 ml) of the syrup was washed with aqueous potassium hydrogensulfate, aqueous sodium hydrogencarbonate and water, dried (Na_2SO_4), and concentrated to give a slightly yellow syrup, which was recrystallized from hot dioxane–hexane to give colorless needles, 8.04 g (68%), mp 185—186 °C, $[\alpha]_D^{21}$ +33° (*c* 1, dioxane); PMR ($CDCl_3$–pyridine-d_5) δ: 2.33 (3H s, CH_3(Ts)).

Found: C, 59.89; H, 5.70; N, 4.87; S, 3.72%. Calcd

for $C_{43}H_{49}N_3O_{14}S$: C, 59.78; H, 5.72; N, 4.86; S, 3.71%.

*6'-Azido-1,3,2'-tri-*N*-benzyloxycarbonyl-3',6'-dideoxyparomamine (4).* A mixture of **3** (5.46 g) and sodium azide (4.2 g) in DMF (100 ml) was agitated at 60 °C for 7 h. Either prolonged or shorter reaction at that temperature decreased the yield of **4**. The solution showed, on TLC with chloroform–ethanol (12 : 1), a single spot at R_f 0.50. Filtration followed by concentration of the filtrate with additions of toluene gave a solid, which was dissolved in dioxane and, after filtration, the solution was concentrated to give a solid, 4.51 g (97%), $[\alpha]_D^{22}$ +90° (*c* 0.5, dioxane); IR (KBr): 2100 (N_3), 1690 cm^{-1} (carbamate).

Found: C, 58.87; H, 5.78; N, 11.20%. Calcd for $C_{36}H_{42}N_6O_{11}$: C, 58.85; H, 5.76; N, 11.44%.

*6'-Azido-3,2'-di-*N*-benzyloxycarbonyl-3',6'-dideoxyparomamine 1,6-Carbamate (5).* To an ice-cold solution of **4** (1.11 g) in DMF (22 ml), 50% oily sodium hydride (240 mg) was added and the mixture was vigorously stirred for 2.5 h in the cold under the atmosphere of nitrogen. The solution showed, on TLC with chloroform–ethanol (15 : 1), a single spot at R_f 0.2. After addition of acetic acid (0.35 ml), the resulting pale-brown gelatinous mixture was poured into water (400 ml). After the mixture had been kept in a refrigerator overnight, it was filtered, and the solid was washed with water. After drying, the solid was reprecipitated from dioxane–hexane to give a solid, 0.75 g (80%). $[\alpha]_D^{20}$ +73° (*c* 1, dioxane); IR (KBr): 2100, 1760 (cyclic carbamate), 1700 cm^{-1}.

Found: C, 55.67; H, 5.50; N, 12.91%. Calcd for $C_{29}H_{34}N_6O_{10}$: C, 55.59; H, 5.47; N, 13.41%.

*6'-Azido-3,2'-di-*N*-benzyloxycarbonyl-3',6'-dideoxy-4'-*O*-(α-naphthoyl)paromamine 1,6-Carbamate (6).* To a cold solution of **5** (1.03 g) in dry pyridine (20 ml) in ice–salt bath, α-naphthoyl chloride (370 mg, 1.2 mol equivalent for **5**) was added and the solution was kept at −10 °C overnight. On TLC with chloroform–ethanol (20 : 1), the solution showed spots at R_f 0.12 (slight, **5**), 0.33 (major, **6**), 0.40 (slight, 5-*O*-α-naphthoyl isomer?) and 0.57 (slight, di-*O*-α-naphthoyl isomer?). Working up in a usual manner gave a crude solid, which was chromatographed over silica gel with benzene–ethyl acetate (3 : 2, gradually changed to 1 : 1) to give a solid of **6**, 826 mg (65%), $[\alpha]_D^{23}$ +98° (*c* 1, dioxane); IR (KBr): 2100, 1750, 1730 cm^{-1}.

Found: C, 61.42; H, 5.24; N, 10.49%. Calcd for $C_{40}H_{40}N_6O_{11}$: C, 61.53; H, 5.17; N, 10.76%.

*6'-Azido-3,2'-di-*N*-benzyloxycarbonyl-3',6'-dideoxy-4'-*O*-(α-naphthoyl)-5-*O*-[2,3,5-tri-*O*-(p-nitrobenzoyl)-β-*D*-ribofuranosyl]paromamine 1,6-Carbamate (9).* To a suspension of **6** (108 mg) in dichloromethane (2.0 ml), calcium sulfate (Drierite, 600 mg, reactivated at 250 °C), mercuric cyanide (350 mg, dried at 90 °C *in vacuo*) and **8** (330 mg, 3.85 mol. equivalent for **6**) were added and the mixture was vigorously stirred at room temperature overnight. On TLC with chloroform–ethanol (30 : 1), the solution showed spots of R_f 0.27 (major), 0.23 (slight), and 0.19 (minor, α-anomeric isomer?), which were of all non-reducing ability (checked by triphenyltetrazolium chloride reagent). After filtration, the solution was washed with aqueous sodium hydrogencarbonate and water, dried (Na_2SO_4), and concentrated. The resulting solid was chromatographed over silica gel with chloroform–ethyl acetate (3 : 2) to give a solid of **9**, 119 mg (66%), mp 136—138 °C, $[\alpha]_D^{22}$ +25° (*c* 1, chloroform); IR (KBr): 2100, 1770 (cyclic carbamate), 1730, 1530, and 1350 cm^{-1} (NO_2).

Found: C, 58.04; H, 4.32; N, 8.99%. Calcd for $C_{66}H_{57}N_9O_{24}$: C, 58.28; H, 4.22; N, 9.27%.

*6'-Azido-3,2'-di-*N*-benzyloxycarbonyl-3',6'-dideoxy-1-*N*-(p-methoxybenzyloxycarbonyl)-5-*O*-(β-*D*-ribofuranosyl)paromamine (10).* To a solution of **9** (444 mg) in dioxane (40 ml) containing *p*-methoxybenzylalcohol (8.8 ml dried over Molecular Sieves 4A), 1 M sodium *p*-methoxybenzylate in the same alcohol (1.6 ml) was added and the solution was kept overnight at room temperature. On TLC with chloroform–ethanol (10 : 1), the solution showed a single spot at R_f 0.26. After addition of acetic acid (0.1 ml), the solution was concentrated and the syrup was dissolved in chloroform (150 ml). The solution was washed several times with water and concentrated to give a syrup. Evaporation (110 °C, 0.02 Torr) of the *p*-methoxybenzylalcohol remained in the syrup gave a thick syrup, which was chromatographed over silica gel firstly with chloroform (to elute the alcohol remained) and then with chloroform–ehtanol (12 : 1) to give a colorless solid of **10**, 175 mg (60%), mp 96—98 °C, $[\alpha]_D^{23}$ +38° (*c* 1, chloroform); IR (KBr): 2100, 1695, 1520 cm^{-1}; PMR ($CDCl_3$) δ: 3.69 (3H s, $CH_3O \cdot C_6H_4$).

Found: C, 56.12; H, 5.76; N, 9.08%. Calcd for $C_{42}H_{52}N_6O_{16}$: C, 56.24; H, 5.84; N, 9.37%.

*6'-Azido-3,2'-di-*N*-benzyloxycarbonyl-1-*N*-[(S)-4-benzyloxycarbonylamido-2-hydroxybutyryl]-3',6'-dideoxy-5-*O*-(β-*D*-ribofuranosyl)paromamine (12).* *A. From 9.* To a solution of **9** (94 mg) in dioxane (4.4 ml), 0.05 M barium hydroxide solution (1.5 ml, 1 mol equivalent for **9**) was added and the mixture was stirred at 60 °C for 30 min. To the resulting neutral solution, additional aliquots of the barium hydroxide solution (1.5 ml × 2) were added at intervals and the mixture was treated as above. On TLC with chloroform–ethanol (7 : 2), the solution showed a major spot at R_f 0.15. Introduction of carbon dioxide followed by filtration and concentration of the filtrate gave a residue, which was extracted with dioxane and the dioxane-soluble product (crude **11**, 65 mg) was isolated.

To a solution of the crude **11** in THF (0.8 ml), *N*-hydroxysuccinimide ester[11] (32 mg) of (*S*)-4-benzyloxycarbonylamido-2-hydroxybutyric acid and triethylamine (*ca.* 11 mg) were added and the solution was stirred at 0 °C for 1 h and then kept at room temperature overnight. On TLC with chloroform–methanol (7 : 1), the solution showed a major spot at R_f 0.31 and the spot at R_f 0.05 (**11**) almost disappeared. The solution was concentrated and the chloroform solution of the residue was washed successively with aqueous potassium hydrogensulfate, aqueous sodium hydrogencarbonate and water, dried (Na_2SO_4), and concentrated. The residue was then chromatographed over silica gel with chloroform–methanol (20 : 1) to give **12**, 24 mg (36% based on **9**), mp 94—96 °C, $[\alpha]_D^{22}$ +19° (*c* 0.25, chloroform); IR (KBr): 2100, 1700, 1530 cm^{-1}.

Found: C, 55.62; H, 5.81; N, 9.95%. Calcd for $C_{45}H_{57}N_7O_{17}$: C, 55.84; H, 5.94; N, 10.13%.

B. From 10. To a cold suspension (in ice–salt bath) of **10** (142 mg) in methoxybenzene (0.13 mg), trifluoroacetic acid (0.8 ml) was added and the mixture was stirred in the cold for a while. The resulting clear solution was kept in the cold for further 30 min. On TLC with chloroform–ethanol (7 : 2), the solution showed majorly a ninhydrin-positive spot (**11**, R_f 0.15). Concentration of the solution *in vacuo* followed by addition of methanolic ammonia to the concentrate until weakly alkaline gave a gelatinous mixture, which was chromatographed over silica gel with chloroform–ethanol (10 : 1) to give a solid of **11**, 102 mg (88%). Reaction of the solid with the active ester in a similar manner as described in A gave **12**, 71 mg (58%).

3'-Deoxybutirosin B (13). To a solution of **12** (64 mg) in dioxane (1.2 ml), water (1.0 ml) and a drop of acetic acid was added and the mixture was hydrogenated with

palladium black under an atmospheric pressure of hydrogen. Concentration of the solution gave a solid, which was chromatographed over CM-Sephadex C-25 (NH_4 form) with 0—0.4 M ammonia with gradient increase in concentration to give **13** as monocarbonate, 25 mg (63%), mp 147—149 °C, $[\alpha]_D^{23}$ +29° (*c* 1, water); IR (KBr): 1640, 1565 cm^{-1}.

Found: C, 44.22; H, 7.27; N, 11.71%. Calcd for $C_{21}H_{41}N_5O_{11}\cdot H_2CO_3$: C, 43.92; H, 7.20; H, 11.64%.

Methyl 2,3,5-Tri-O-(p-nitrobenzoyl)-β-D-ribofuranoside (7). To an ice-cold solution of D-ribose (2.0 g) in dry methanol (40 ml), 1 M methanolic hydrogen chloride (4.5 ml) was gradually added and the solution was kept at room temperature for 1 h. On TLC with benzene–ethanol (1 : 1), the solution showed spots at R_f 0.63 (major, β-riboside) and 0.44 (slight) (*cf.* D-ribose, R_f 0.54). Pyridine (12 ml) was added and the solution was concentrated with additions of toluene to give a syrup. To the solution of the syrup in pyridine (44 ml), *p*-nitrobenzoyl chloride (8.15 g) was added and the solution was kept at room temperature overnight. Water (1 ml) was added and the solution was concentrated. The chloroform solution of the syrup was successively washed with aqueous potassium hydrogensulfate, aqueous sodium hydrogencarbonate and water, dried (Na_2SO_4), and concentrated. Recrystallization of the solid from acetone gave pale-yellow needles, 4.9 g (60%), mp 169—170.5 °C, $[\alpha]_D^{27}$ +80° (*c* 1, choroform) [lit,[12]: mp 169.5—170 °C (from acetone–petroleum ether), $[\alpha]_D^{20}$ +79.7° (*c* 1.38, $CHCl_3$)]; IR (KBr): 1735, 1525, 1350 (NO_2) cm^{-1}; PMR ($CDCl_3$) δ: 3.53 (3H s, OCH_3), 5.32 (1H s, H-1).

Found: C, 53.23; H, 3.56; N, 7.03%. Calcd for $C_{27}H_{21}N_3O_{14}$: C, 53.03; H, 3.46; N, 6.87%.

2,3,5-Tri-O-(p-nitrobenzoyl)-α,β-ribofuranosyl Bromide (8). To an ice-cold solution of **7** (210 mg) in dichloromethane (1.1 ml), hydrogen bromide saturated in acetic acid (1.1 ml) was added and the solution was kept at room temperature for 1 h in the dark place. The solution was concentrated *in vacuo* and the resulting syrup was again dissolved in dichloromethane (20 ml). The solution was successively washed, as fast as possible, with water, aqueous sodium hydrogen carbonate, water again, dried (Na_2SO_4) and concentrated to give a pale-yellow solid. Recrystallization from benzene gave almost colorless needles, 170 mg (75%), mp 105—112 °C, $[\alpha]_D^{23}$ +61° (*c* 1, chloroform) [β-anomer:[12] mp 100—105 °C (from CH_2Cl_2), $[\alpha]_D^{20}$ +55.4° (*c* 1.58, $CHCl_3$)]; PMR ($CDCl_3$) δ: 6.56 (*ca.* 0.5 H s, β-H-1), 6.94 (*ca.* 0.5 H d, J= 4.5 Hz, α-H-1), 6.32 (*ca.* 3H s, C_6H_6).

Found: C, 49.85; H, 3.17; N, 5.87; Br, 10.88%. Calcd for $C_{26}H_{18}BrN_3O_{13}\cdot 1/2C_6H_6$: C, 49.80; H, 3.03; N, 6.01; Br, 11.43%.

6'-Azido-3,2'-di-N-benzyloxycarbonyl-3',6'-dideoxy-5-O-mesyl-4'-O-(α-naphthoyl)paromamine 1,6-Carbamate (14). To a solution of **6** (60 mg) in dry pyridine (2 ml), methanesulfonyl chloride (60 mg) was added and the solution was kept at room temperature for 4 h. The solution showed on TLC with chloroform–methanol (30 : 1) an single spot at R_f 0.48. Isolation of the product in a usual manner gave a solid of **14**, 58 mg (88%); $[\alpha]_D^{24}$ +86 ° (*c* 0.5, chlorofrom); IR (KBr): 1180 (ν_sSO_2), 1350 ($\nu_{as}SO_2$), 1770 cm^{-1}; PMR, δ of SO_2-CH_3: 3.10 ($CDCl_3$), 3.21 ($CDCl_3$–CD_3OD=1 : 1), 3.39 (C_5D_5N).

Found: C, 57.11; H, 5.00; N, 9.57; S, 3.44%. Calcd for $C_{41}H_{42}N_6O_{13}S$: C, 57.33; H, 4.93; N, 9.79; S, 3.73%.

The authors are grateful to Professor Hamao Umezawa, Director of Institute of Microbial Chemistry, for his support and encouragement.

References

1) D. Ikeda, F. Nagaki, S. Umezawa, T. Tsuchiya, and H. Umezawa, *J. Antibiot.*, **28**, 616 (1975); D. Ikeda, F. Nagaki, T. Tsuchiya, and S. Umezawa, and H. Umezawa, *Bull. Chem. Soc. Jpn.*, **49**, 3666 (1976).

2) T. Oda, T. Mori, and Y. Kyotani, *J. Antibiot.*, **24**, 503 (1971).

3) T. Oda, T. Mori, Y. Kyotani, and M. Nakayama, *J. Antibiot.*, **24**, 511 (1971).

4) D. Ikeda, T. Tsuchiya, S. Umezawa, and H. Umezawa, *Bull. Chem. Soc. Jpn.*, **47**, 3136 (1974).

5) T. Ito, E. Akita, T. Tsuruoka, and T. Niida, *Antimicrob. Agents Chemother.*, **1970**, 33.

6) T. Ogawa, T. Takamoto, and S. Hanessian, *Tetrahedron Lett.*, **1974**. 4013.

7) I. Watanabe, T. Tsuchiya, S. Umezawa, and H. Umezawa, *Bull. Chem. Soc. Jpn.*, **48**, 2124 (1975).

8) S. Umizawa, Y. Takagi, and T. Tsuchiya, *Bull. Chem. Soc. Jpn.*, **44**, 1411 (1971).

9) P. A. J. Gorin, *Can. J. Chem.*, **40**, 275 (1962).

10) F. Weygand and K. Hunger, *Chem. Ber.*, **95**, 1 (1962).

11) H. Kawaguchi, T. Naito, S. Nakagawa, and K. Fujisawa, *J. Antibiot.*, **25**, 695 (1972).

12) H. S. El Khadem. T. D. Audichya, D. A. Niemeyer, and J. Kloss, *Carbohydr. Res.*, **47**, 233 (1976).

13) For example see: S. Umezawa, S. Koto, K. Tatsuta, and T. Tsumura, *Bull. Chem. Soc. Jpn.*, **42**, 529 (1969).

Photolysis in Rigid Matrixes at Low Temperatures. An Intermediate of Photo-dehydrobromination

Satoshi HIRAYAMA

Faculty of Textile Science, Kyoto Technical University, Matsugasaki, Sakyo-ku, Kyoto 606

(Received March 8, 1976)

The intermediate of the photo-dehydrobromination of 9-(α-bromopropionyl)anthracene (I) to yield 9-anthryl vinyl ketone (IV) was detected by its electronic spectrum upon photolysis in polar solvent matrixes at 77 K. Approximately 80% of the initial photo-products is trapped as the intermediate. The remainder is observed as the final product IV formed directly from I. The intermediate is stable only below *ca.* 83 K in EPA. Above this temperature, it decomposes rapidly to form IV. No intermediate was detected for this reaction in the non-polar solvent matrixes at 77 K. Instead, a conformational change of IV with temperature was noticed. Based on the temperature and solvent effects on the stability of the intermediate, a loose structure where a hydrogen bromide is almost completely eliminated *via* a concerted mechanism is postulated for the intermediate. This is supported by the evidence that the main electrochemical reduction product of I is only 9-propionylanthracene. The temperature effects on the other photochemical reactions of I are also discussed in relation to the allowed molecular motions in rigid matrixes.

According to the previous results reported by the present author *et al.*,[1,2] the mechanisms of the intramolecular photochemical reactions of 9-(α-bromopropionyl)anthracene (I) can be summarized as follows:

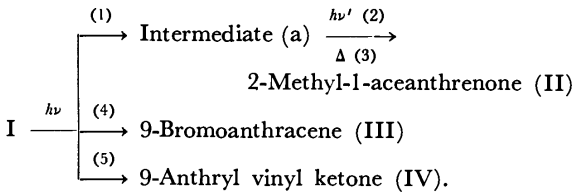

The intermediate (a) to give II was rather stable and was readily detectable by its UV-absorption spectrum.[1,3]

The present detailed study of Reaction (5) in several matrixes at low temperatures has revealed that an intermediate to yield IV can also be detected spectroscopically at 77 K. Its stability is strongly dependent upon not only the temperature but also the nature of the matrix. Although no absorption due to the intermediate to give IV was detected in the non-polar solvent matrixes, an apparently different spectral change from that observed in the polar solvent matrixes was observed upon gradually softening the matrixes after the photolysis. This observation is explicable in terms of the presence of a second elementary process prior to giving IV, implying that Reaction (5) should involve at least one more transient state other than the newly found intermediate. These findings are of significance, since they will give us additional information as to the mechanism of the photo-dehydrohalogenation of α-haloketones.[4-6] A plausible structure of the intermediate will be given below, referring to the evidence demonstrated by the electrolysis of I.

Taken together with the previous results,[1-3] the present results also demonstrate that each of the Reactions (1) to (5) (revised (5), see below) shows a different temperature dependence. This appears to reflect a difference in the ease of the molecular motions which accompany each reaction mentioned above. Since the photochemistry of I involves rather a wide variety of molecular motions, it is expected that the present photochemical reactions will also provide the possibility of predicting what kind of molecular motion is allowed or prohibited in rigid matrixes upon photo-excitation.

Experimental

Materials. The preparation and purification of I have been described elsewhere.[1] Methylcyclohexane (MCH), isopentane (IP), ethanol (ET), diethyl ether, triethylamine (TEA), and 2-methyltetrahydrofuran (MTHF) were of a guaranteed grade from the Nakarai Chem. Co., Ltd. and were used after an ordinary distillation on a 30-cm Widmer column. Acetonitrile (ACN), a solvent used for the electrolysis of I, was repeatedly distilled over anhydrous aluminium chloride, sodium carbonate, and finally calcium hydride according to the method of Walter and Ramaley.[7] Dry tetrabutylammonium perchlorate (TBAP) or potassium perchlorate was used as a supporting electrolyte (*ca.* 0.1 M).

Procedures. The electonic absorption spectra at the controlled low temperatures were recorded in the same way as has previously been described.[8] For photolysis at low temperatures, a glass gas-inlet pipe at the bottom of a transparent Pyrex Dewar vessel, in which a reaction cell was set, was attached directly to the inlet of a metal Dewar vessel which served as a liquid-nitrogen reservoir. From the bottom of the Pyrex Dewar vessel, boiled cold nitrogen gas was admitted by means of a power resister in order to control the temperature in the range of 90—200 K. After the thermal equilibrium had been attained, the temperature was measured with a copper-constantan thermocouple which was directly immersed in the reaction cell. Photolysis at 77 K was performed by immersing the reaction cell directly in a transparent Pyrex Dewar vessel containing liquid nitrogen. The reaction cells were made of quartz and were 1.0 and 0.2 cm in path length. When the matrixes were unstable toward temperature variation, the cells of the smaller path length were employed. The irradiation source was an Ushio 100 W medium-pressure mercury-arc lamp. A Pyrex Dewar vessel or a water-cooled jacket made of Pyrex glass served as a glass cut-off filter. Since the photolysis of I is essentially independent of whether or not the solution is deaerated, the sample solutions were not degassed unless otherwise stated.

A conventional H-shaped electrolysis cell, the center of which was separated into two compartments by means of a sintered glass-plate, was employed to electrolyze I at a constant potential. Working and auxiliary electrodes were platinum plates of 2×2 cm. A reference-electrode (silver wire) compartment was isolated from the solution to be electrolyzed by means of a glass frit. The solutions were

deaerated by bubbling dry nitrogen gas through. To control the potential, a Hokuto Denko Model HA 101 potentiostat and a Hewlett Packard Model 3300 A function generator were used. Electrolysis products were analyzed by column chromatography on silica gel with benzene after removing the solvent and were identified by comparison (IR- and UV-absorption spectra) with the authentic samples.

For the studies of the cyclic voltammograms of I under a thoroughly degassed and dried condition, a cell similar to that which had previously been prepared for ECL observation was used.[9]

Results

Photolysis at Low Temperatures. Figure 1 shows the absorption spectra of I before and after photolysis in EPA (diethyl ether, isopentane, and ethanol, 5 : 5 : 2 by volume) at 77 K. All the spectra were taken at 77 K. As is shown in Fig. 1b, the absorption of I disappears with irradiation and, instead, we obtain the red-shifted broad band superposed upon by the sharp band with peaks at 364 and 384 nm. The absorbances of these broad and sharp bands increase only with irradiation and, after the thorough consumption of the reactant (spectrum (b)), continued irradiation causes no further spectral change at 77 K. Upon warming the matrix, however, the broad band disappears and changes into a sharp spectrum with the 0-0 band at 384 nm (spectrum (c)). Since IV is the sole photolysis product in EPA at 77 K, as has previously been verified,[1,2] the (c) spectrum is solely due to IV.

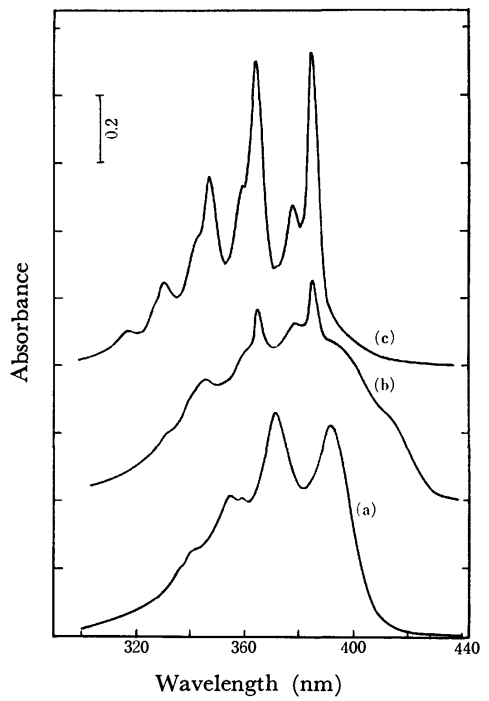

Fig. 1. Photolysis of I (7.1×10^{-5} M) in EPA at 77 K. (a) Before irradiation, (b) after irradiation for 3 h, (c) the spectrum observed at 77 K immediately after warming the sample with the (b) spectrum to room temperature. The (c) spectrum is due to IV. For the sake of clarity, the base line (right-hand side) of each spectrum is shifted by an appropriate amount of absorbance in Figs. 1, 3, 4, and 5.

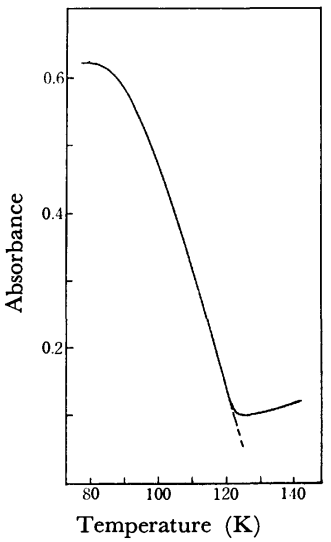

Fig. 2. Change in the absorbance (at 395 nm) of the intermediate with temperature.
A rise in the absorbance at around 123 K is caused by the opacity of the matrix on softening. This figure shows that the intermediate is stable only below 82—83 K. Temperature-rise time: *ca.* 4 min (77—83 K); *ca.* 5 min (83—123 K).

Therefore, the broad band on the longer-wavelength side can reasonably be attributed to an intermediate (hereafter called intermediate (b)) to give IV.

Figure 2 shows how labile the intermediate (b) is against a rise in the temperature. The change in the absorbance of the intermediate formed in EPA was monitored at 395 nm against the temperature by allowing the matrix to grow warmer, and was displayed on an X-Y recorder. From this curve it is apparent that the intermediate (b) is stable only below 82—83 K. In fact, no absorption due to the intermediate (b) was observed during the photolysis of I in EPA at 93 K. At 77 K, however, the intermediate was very stable and no absorption change was observed after allowing the photolyzed solution to stand in the dark at 77 K for several hours. A similar phenomenon was also observed in other transparent-matrix-forming polar (or slightly polar) solvents such as MTHF, ET, and TEA.

The presence of the small sharp peaks before warming the matrix, as is shown in Fig. 1b, implies that a part of the photoeliminated hydrogen bromide molecules can escape from the solvent cage, probably because of excess excitation energy, and that IV is formed directly from I. The percentage of this escape is calculated to be *ca.* 20%[10] in EPA and does not differ significantly in MTHF, ET, TEA, and in EPA.

In contrast, in a non-polar and rather soft MCHIP matrix (methylcyclohexane and isopentane, 3:1 by volume),[11] no absorption similar to that which was observed in EPA was detected, in spite of almost a 100% yield of IV.[2] The results of the spectral change upon photolysis are shown in Fig. 3. The (c) spectrum was obtained at 77 K once after warming the photolyzed solution with the (b) spectrum to room temperature. Although the absorption due to the in-

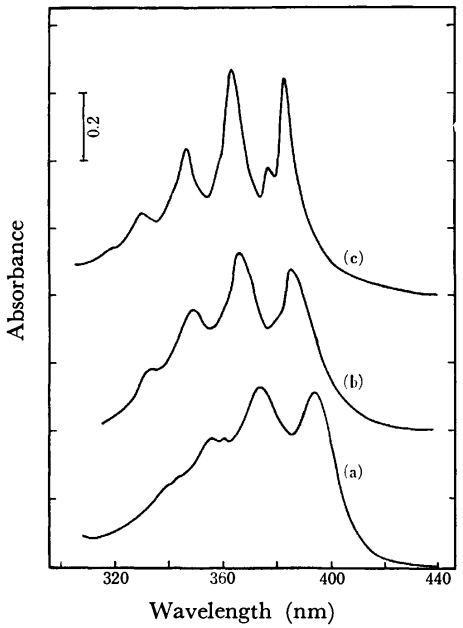

Fig. 3. Photolysis of I (5.3×10^{-5} M) in MCHIP at 77 K.
(a) Before irradiation, (b) after irradiation for 3 h, (c) the spectrum observed at 77 K immediately after warming the sample with the (b) spectrum to room temperature. The (c) spectrum is due to IV. No absorption due to the intermediate (b) is observable.[11,13]

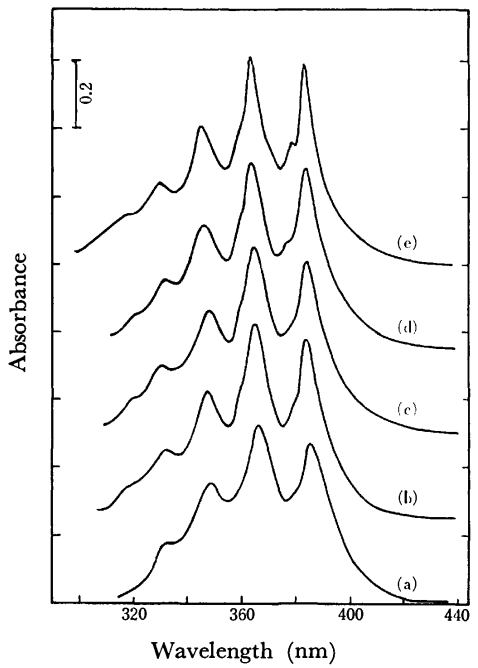

Fig. 4. Temperature dependence of the absorption spectrum of the photo-product formed in MCHIP at 77 K.
(a) 77 K, (b) 98 K, (c) 114 K, (d) 127 K, (e) 144 K. The (e) spectrum apparently differs in the sharpness of the bands from the other spectra.

termediate (b) cannot be observed in MCHIP, the absorption spectra of the photolyzed solution apparently differ between before and after softening the matrix.

Figure 4 shows at what temperature this spectral change occurs. After thorough photolysis in MCHIP at 77 K, the absorption spectra were recorded upon warming the matrix to several constant temperatures. In the neighborhood of 140 K, a rather broad band is seen to change into a sharp band with a greater molar extinction coefficient. Since the medium at these temperatures is fluid enough to allow free molecular motions,[12] the observed spectral change cannot be explained in terms of a change in the rigidity of the matrix with temperature. A possible cause of this spectral change will be discussed later,[13] in relation to a conformational change in IV.

A similar spectral change was also detected during

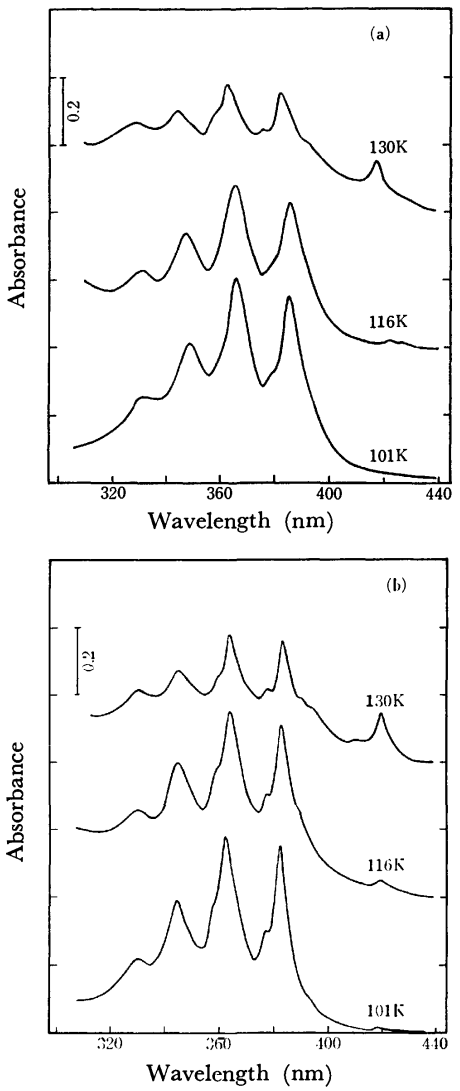

Fig. 5. Absorption spectra of the photo-products of I formed at several low tempratures.
(a) Immediately after photolysis;
(b) after warming to room temperature.
The samples were photolyzed at the indicated temperatures and their spectra were observed at 77 K (Fig. 5a) and were then warmed once to room temperature before the second observation at 77 K (Fig. 5b). All the spectra in Fig. 5b are sharper in shape than the corresponding spectra in Fig. 5a. The small peaks at 418 nm are due to II,[2,8]

the photolysis of I in MCHIP at temperatures higher than 77 K. The results are shown in Fig.5. Comparing Fig.5a with 5b, a difference in the sharpness of the bands can be seen particularly at 383 nm.

In the first instance, a radical species derived from the homolysis of the C–Br bond may be considered as an appropriate candidate for the intermediate (b). However, no ESR signal was observed upon photolysis at 77 K in either polar- or non-polar-solvent matrixes. Thus, Reaction (5) does not appear to involve a radical mechanism but to proceed *via* a concerted elimination mechanism.[6]

In order to confirm this from a different point of view, the electrolysis of I was carried out.

Electrolysis. The cyclic voltammograms of I before and after electrolysis at a constant potential are shown in Fig. 6. A similar result was obtained under a thoroughly degassed and dried condition.

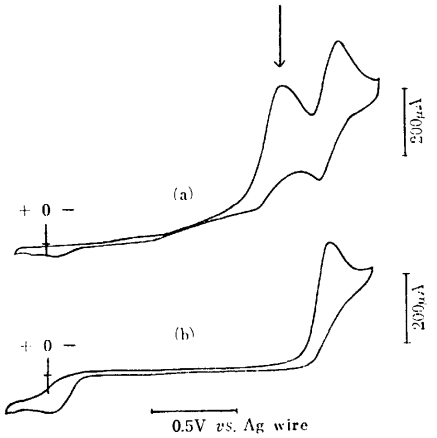

Fig. 6. Cyclic voltammograms of I (2.7×10^{-3} M) and its electrolysis products in ACN.
(a) Before electrolysis;
(b) after electrolysis for 30 min at the constant potential indicated by the arrow. Supporting electrolyte: TBAP, Sweep rate: 86 mV/s.

Based on product analysis by column chromatography, the main electrolysis product was only 9-propionylanthracene (V, 9-CH_3CH_2CO-A, more than 95% of the detected products), a product of bromine atom replacement. Thus, the first and second peaks in Fig.6a correspond to the reduction-wave peaks of I and V respectively.[14] The fact that the loss of a bromide ion from the $[I]^{\cdot-}$ anion radical is rapid is demonstrated by the absence of an anodic wave of the reoxidation of $[I]^{\cdot-}$. This is the case even at low temperatures where the anion radical might be stabilized.[16] Similar results were obtained with both TBAP and potassium perchlorate, the latter of which has no hydrogen atom to donate.

Referring to the previously reported reduction reaction mechanism of organic halides,[17] the present result may be interpreted by the following mechanism;

$$I + e \longrightarrow [I]^{\cdot-} \longrightarrow 9\text{-}CH_3\dot{C}HCO\text{-}A + Br^-,$$

$$9\text{-}CH_3\dot{C}HCO\text{-}A \xrightarrow{\text{solvent}} V,$$

$$V + e \longrightarrow [V]^{\cdot-} \longrightarrow \text{rapid follow-up reactions.}^{15}$$

A 9-$CH_3\dot{C}HCO$-A radical, formed as a result of bromide ion elimination, immediately abstracts a hydrogen atom from the solvent to give V,[18] but not IV. Thus, the intermediacy of the ketonyl radical in the photolysis of I may reasonably be ruled out. In considering the detailed mechanism of Reaction (5), it is noteworthy that none of the main photolysis products[1] was found in the electrolysis products; the photochemistry of I in ACN is essentially the same as that in ET or in MCH.

Discussion

A Postulated Structure of the Intermediate (b). Summarizing the above-mentioned facts, Reaction (5) may be rewritten as follows:

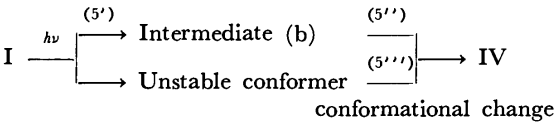

Each process, of course, depends on the nature of the matrix.

We must now consider the structure of the intermediate (b) and the origin of the conformational change indicated in the above scheme. Based on the facts that no ESR signal was detected and that the main electrolysis product was solely V, a radical species such as 9-$CH_3\dot{C}HCO$-A can safely be excluded as an appropriate intermediate to give IV. Taking into account the fact that the intermediate is very labile toward a rise in the temperature from 77 K, completely unstable in soft matrixes, and gives a single product IV upon sofetening the matrix, a structure in which dehydrobromination has almost been completed appears to be most appropriate as a structure of the intermediate (b). A postulated structure is dipicted in Fig. 7a. The dotted-line bonds will be much weaker than the broken-line bonds. This structure is reminiscent of the structure frequently referred to as the four-membered *syn*-elimination transition state in the pyrolytic dehydrohalogenation reactions of organic halides.[6,20] Its loose structure could explain the broad absorption spectrum of the intermediate. Although the intermediacy of a tight radical pair formed as a result of homolysis of the C–Br bond may not be ruled

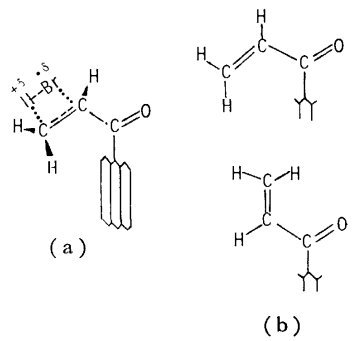

Fig. 7. A plausible conformation of the intermediate (b) (Fig. (a)) and two conformers of IV (Fig. (b)). It is not obvious which conformer is more stable.

out completely, we may expect, in such a case, the formation of V in an appreciable amount.[21] To the author's knowledge, this is the first case where an intermediate of photo-dehydrohalogenation has been detected by its electronic absorption spectrum.

Figure 7b shows two possible conformers of IV. Acrylaldehyde serves as the simplest model compound for the substituent of IV and *s-trans*-acrylaldehyde is reported to be more stable than *s-cis*-acrylaldehyde.[22] Thus, the conformational change in the substituent of IV from *cis* to *trans* or *vice versa* may give rise to the observed spectral change at around 140 K, where the potential barrier of the conformational change will come to be surmounted. The reason for the absence of a similar change in EPA or in MTHF may be that interactions between I or IV and solvent molecules (hydrogen-bonding, *etc.*)[23] can preferentially stabilize one of the conformers.

Allowed Molecular Motions in the Rigid Matrixes. It is very important and instructive to know what kinds of molecular motions are allowed in rigid matrixes, particularly upon photo-excitation. However, there are few such related works, except for detailed studies of *cis-trans* photoisomerization at low temperatures.[24] Fortunately, the present results provide the possibility of investigating a wide variety of allowed molecular motions in matrixes by observing the temperatures at which the photochemical and follow-up dark reactions of I are prohibited. The sequence of the prohibition of the present reactions is as follows, in increasing order:

(5′) (77 K) < (2) (77 K, very slow) < (5″) (85 K) < (4)[1] < (1) (100 K) < (5‴) (140 K) < (3)[1]

In parentheses are given the approximate lowest temperatures where the indicated reactions can still be observed. The first inequality means that the photodehydrobromination from the intermediate (a) is very slow, though detected at 77 K, as compared with Reaction (5′).[25] Reactions (3), (5″), and (5‴) are thermal reactions, the last of which is observed in MCHIP. From the above sequence, it can be said that:

i) The elimination of small molecules (*e.g.*, HX, N_2, CO_2) which is not accompanied by a large structural change will occur readily even at 77 K.[26,27] In the hard matrixes, however, the eliminated molecules cannot be expelled out of the solvent cage, but stay very near to the parent pieces; in a fortunate case, the intermediate(s) will be detected.

ii) A large rotational motion of a group equal to or greater than an acetyl (or propionyl) group is strongly prohibited at 77 K.[2]

iii) Compared with photochemical reactions, the corresponding thermal reactions (*i.e.*, the reaction to yield the same product(s)) are generally retarded much faster upon cooling, as is demonstrated by a comparison of Reactions (2) and (3).[1] This does not mean that the local heating due to irradiation may be of some help to the photolysis of I in the frozen matrixes.

Even for photochemical reactions, some amount of activation energy is necessary, and hence the prohibition of photochemical reactions in frozen matrixes does not always mean the prohibition of the necessary molecular motion due to the matrix rigidity. Hence, if a photolytic reaction which belongs to item i) cannot be detected in frozen matrixes, the activation energy of that reaction may be said to play a dominant role in the prohibition. On the basis of the temperature effect on its reaction, every photochemical reaction reported herewith seems principally rigidity-controlled and Reactions (3) and (5‴) are activation-energy controlled.

References

1) T. Matsumoto, M. Sato, and S. Hirayama, *Bull. Chem. Soc. Jpn.*, **48**, 1659 (1975).
2) T. Matsumoto, M. Sato, and S. Hirayama, *Chem. Phys. Lett.*, **27**, 237 (1974).
3) T. Matsumoto, M. Sato, and S. Hirayama, *Bull. Chem. Soc. Jpn.*, **47**, 358 (1974).
4) K. Schaffner and O. Jeger, *Tetrahedron*, **30**, 1891 (1974).
5) R. S. Givens and L. Strekowski, *J. Am. Chem. Soc.*, **97**, 5807 (1975).
6) P. C. Hiberty, *J. Am. Chem. Soc.*, **97**, 5975 (1975).
7) M. Walter and L. Ramaley, *Anal. Chem.*, **45**, 165 (1973).
8) S. Hirayama, *Bull. Chem. Soc. Jpn.*, **48**, 2653 (1975).
9) T. Matsumoto, M. Sato, and S. Hirayama, *Bull. Chem. Soc. Jpn.*, **46**, 369 (1973).
10) Prolonged irradiation at 77 K did not cause an increase in this percentage, implying that under the present conditions, the temperature rise due to local heating did not exceed 6—7 K.
11) In either MCH or IP, no intermediate was detected upon the photolysis of I at 77 K. In the softer matrixes composed of the higher ratio of IP to MCH (*e. g.*, IP and MCH 3 : 1 or 10 : 1 by volume), the absence of the intermediate (b) can more clearly be demonstrated than is shown in Figs. 3 and 4, since the photolyzed solutions give slightly sharper absorption bands at 77 K before warming.
12) S. Seltzer and S. G. Mylonakis, *J. Phys. Chem.*, **72**, 754 (1968).
13) On the other hand, the spectral change noticed in the range of 77—100 K may arise from a change in the rigidity of the matrix.
14) The electrode reduction reactions of the carbonyl derivatives of anthracene were studied in detail by Fukumoto[15] and V was found to show a chemically irreversible reduction wave.
15) Y. Fukumoto, M. Eng. Thesis, Kyoto Technical University (1975).
16) T. Matsumoto, M. Sato, and S. Hirayama, *Chem. Lett.*, **1972**, 603.
17) J. G. Lawless, D. E. Bartak, and M. D. Hawley, *J. Am. Chem. Soc.*, **91**, 7121 (1969).
18) Another reaction mechanism, $9\text{-}CH_3\dot{C}HCO\text{-}A + e \rightarrow [9\text{-}CH_3\ddot{C}HCO\text{-}A]^- \xrightarrow{[H^+]} V$, may partly participate in giving V.[19] The controlled-potential coulometry of I, however, showed that the number of electrons needed to give V was close to one (0.98).
19) M. R. Rifi and F. H. Covitz, "Introduction to Organic Electrochemistry," Marcel Dekker, Inc., New York (1974), p. 194.
20) A. Maccoll and P. J. Thomas, "Progress in Reaction Kinetics," Vol. 4, ed by G. Porter, Pergamon Press, New York (1967), p. 119.

21) P. J. Kropp, T. H. Jones, and G. S. Poindexter, *J. Am. Chem. Soc.*, **95**, 5420 (1973).
22) E. A. Cherniak and C. C. Costain, *J. Chem. Phys.*, **45**, 104 (1966).
23) S. Iwata and K. Morokuma, *J. Am. Chem. Soc.*, **97**, 966 (1975).
24) (a) T. Wismonski-Knittel, G. Fischer, and E. Fischer, *J. Chem. Soc., Perkin Trans.*, **1974**, 1930; (b) J. Kordas and M. A. El-Bayoumi, *J. Am. Chem. Soc.*, **96**, 3043 (1974).
25) The intermediate (a) was formed in deaerated MCHIP at room temperature in a similar way as before.[1] Then the solution was rapidly cooled to study the photolysis of the intermediate (a) at this temperature.
26) O. L. Chapman, C. L. McIntosh, and J. Pacansky, *J. Am. Chem. Soc.*, **95**, 4061 (1973).
27) C. R. Flynn and J. Michl, *J. Am. Chem. Soc.*, **95**, 5802 (1973).

The Volumetric Behavior of Nitrobenzene in Electron Donating Solvents

Vojtech FRIED, Lewis P. MILLER, and Howard N. WACHTER[1)]

Department of Chemistry, Brooklyn College of the City University of New York, Brooklyn, New York 11210, U.S.A.

(Received April 12, 1976)

The excess volumes of 18 binary solutions containing nitrobenzene as a weak electron acceptor and various mono- and polysubstituted aromatic donors were evaluated at 25 °C. The partial molal volume of nitrobenzene in these solvents was also evaluated. There is no quantitative correlation between the volumetric behavior of the solutions and the electron donor acceptor abilities of the solution constituents. The results, however, clearly prove that isomers of higher cohesive energy affect the volumetric behavior of solutions less than their lower cohesive energy counterparts. An attempt is made to interpret this observation in terms of the steric effect and the cohesive energy of donors.

It is well known that solutions with strong specific interactions, such as H_2O+HCl, $H_2O+H_2SO_4$, H_2O+HNO_3, acetone+chloroform, methylacetate+chloroform, water+hydrazine and many others frequently exhibit negative deviations from ideal behavior ($G^E<0$, $\gamma_1<1$).[2)] There are systems for which the reasons for negative deviations from ideal behavior are not as obvious as in the above mentioned solutions. The 2,3-dimethyl-2-butene+carbon tetrachloride solution is a good example of this kind of a system.[3)] By comparing the negative G^E values of this system with the positive G^E values of the very similar 2,3-dimethyl-2-butene+tetrachloroethylene system one must conclude that the diametrically different thermodynamic behavior of the two solutions is due to charge transfer interactions in the $C_2(CH_3)_4+CCl_4$ system. The chlorines in the CCl_4 molecule have the ability to withdraw π-electrons from the electron rich double bond of the donor molecule $[(CH_3)_2C=C(CH_3)_2]$; this charge transfer interaction may eventually lead to complex formation between the donor and acceptor molecules. The chlorines in the C_2Cl_4 molecule do not possess such ability. These chlorines saturate themselves with electrons by withdrawing them from the double bond of the C_2Cl_4 molecule itself. Consequently, the C_2Cl_4 molecule cannot act as an electron acceptor and is unable to participate in complex formation. The partially double bond character of the C–Cl bond in the C_2Cl_4 molecule (the C–Cl bond is shorter than in the CCl_4 molecule) gives strong support for such interpretation.

Electron charge transfer interactions account for the thermodynamic behavior in far more numerous systems than suspected in the past. Deviations of solutions from ideal behavior is frequently due to charge transfer interactions between the solution constituents. Complex formation in binary mixtures of carbon tetrachloride with aromatic donor molecules has been extensively studied and is well established.[3–10)] The great majority of these systems exhibit positive G^E values in spite of the charge transfer interaction in the solution. This seems to be contradictory and can be explained by the following reasoning. When only charge transfer interactions exist in a solution, or when these interactions control the behavior of a solution, then G^E is expected to be negative. The discrepancy arises from the practical impossibility of separating the specific and nonspecific interactions in solutions from each other. There is no rigorous method, theoretical or experimental, which can quantitively distinguish the contributions to thermodynamic behavior of liquid solutions due to specific and nonspecific interactions. Data appearing recently in the literature[11–13)] indicate that simultaneous thermodynamic and structural investigtions might yield some qualitative insight into this extremely important problem.

This work is concerned with the excess volumes and partial molal volumes of nitrobenzene (electron acceptor) in 18 eletron donating solvents.

Results and Discussion

The purity of the chemicals employed in this investigtion, the experimental technique used for density measurements, and the density *versus* concentration data were reported elsewhere.[14)]

The molar volumes of the solutions, v, evaluated from experimental densities, d, by using the formula

$$v=\frac{x_1M_1+x_2M_2}{d} \tag{1}$$

where M_i and x_i are the molecular weight and mole fraction of the two solution constituents, were fitted by a least-squares method to a polynomial of the form:

$$v=\sum_{i=0}^{i} b_i x_1^i \tag{2}$$

The number of constants necessary to obtain the best fit was chosen so that the deviation of the experimental molar volumes from the correlated volumes was within the limit of experimental error (±0.003 $cm^3\ mol^{-1}$). Most systems required four constants to obtain such accuracy. The constants for the 18 systems are summarized in Table 1. The slight fluctuation in the molar volume of pure nitrobenzene ($v_2\equiv b_0$) is explained by the fact that for each system a freshly distilled and dried sample was used. It was practically impossible to obtain samples exactly of the same purity. The average value of $b_0=102.723$ $cm^3\ mol^{-1}$ is, however, very close to the literature value.[15)]

The assumption was made that in dilute donor solutions the specific interactions control the behavior of the solutions. If this assumption was correct then the constant $b_1\left(\equiv\frac{v-b_0}{x_1}\right)$ could be considered as a measure of charge transfer interactions, at least in dilute solutions. As the data in Table 1 indicate, the systems with little or no specific interactions at all

TABLE 1. COEFFICIENTS OF EQ. 2 EXPRESSING THE DEPENDENCE OF MOLAR VOLUME OF THE SOLUTION ($cm^3\ mol^{-1}$) ON THE DONOR MOLE FRACTION AT 25.00±0.01 °C

System	b_0[a]	b_1	b_2	b_3
Benzene+nitrobenzene	102.722	−13.604	−0.3065	0.5798
Toluene+nitrobenzene	102.731	3.1129	0.4169	0.5852
o-Xylene+nitrobenzene	102.736	17.710	0.2216	0.5180
p-Xylene+nitrobenzene	102.725	20.214	−0.0297	1.0025
m-Xylene+nitrobenzene	102.723	19.646	0.3139	0.7646
Ethylbenzene+nitrobenzene	102.729	19.426	0.2608	0.6382
Styrene+nitrobenzene	102.719	12.531	−0.5439	0.7682
n-Propylbenzene+nitrobenzene	102.722	36.645	0.1057	0.6148
Isopropylbenzene+nitrobenzene	102.719	36.361	−0.0904	0.9898
1,2,4-Trimethylbenzene+nitrobenzene	102.717	34.344	0.0712	0.7207
1,3,5-Trimethylbenzene+nitrobenzene	102.720	35·799	0.7479	0.4975
Butylbenzene+nitrobenzene	102.721	53.405	0.1712	0.4436
Isobutylbenzene+nitrobenzene	102.717	54.365	0.420	0.5387
1,2,3,4-Tetramethylbenzene +nitrobenzene	102.719	46.204	−0.0232	0.3286
Bromobene+nitrobenzene	102.727	2.9179	−0.1823	—
Benzonitrile+nitrobenzene	102.723	−0.0480	0.3749	—
Chlorobenzene+nitrobenzene	102.719	−0.7958	0.0917	0.1892
Aniline+nitrobenzene	102.723	−10.106	−0.8458	−0.2468

a) Average value 102.723 $cm^3\ mol^{-1}$.

have very small b_1 values (bromobenzene+nitrobenzene, chlorobenzene+nitrobenzene, and benzonitrile+nitrobenzene). The small b_1 values of these systems may, however, also result from the fact that their molar volume ratios v_2/v_1 (see Table 2) are very close to unity. Because of this and also because the other 15 systems do not show any obvious correlations between complex formation and the b_1 values, the assumption made above cannot be recommended (see further discussion). The volume of mixing per mole of solution for the 18 systems was calculated from the formula:

$$v_{mix} = v^E = v - x_1v_1 - x_2v_2$$
$$= x_1x_2\left[\left(-b_2-\frac{3}{2}b_3\right)-\frac{b_3}{2}(x_1-x_2)\right] \quad (3)$$

where b_2 and b_3 are the constants listed in Table 1,

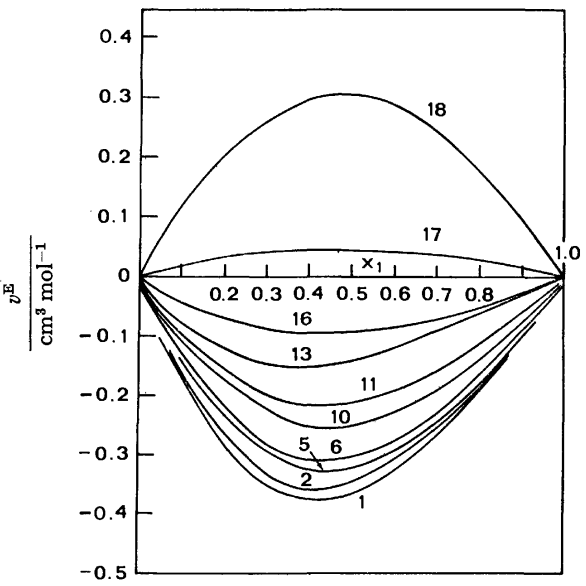

Fig. 1. Excess volume as a function of donor mole fraction at 25 °C. Systems: *p*-xylene(1), 1,3,5-trimethylbenzene(2), toluene(5), isobutylbenzene(6), *o*-xylene (10), *n*-butylbenzene(11), benzene(13), chlorobenzene (16), bromobenzene(17), aniline(18). Nitrobenzene is the acceptor in all the solutions.

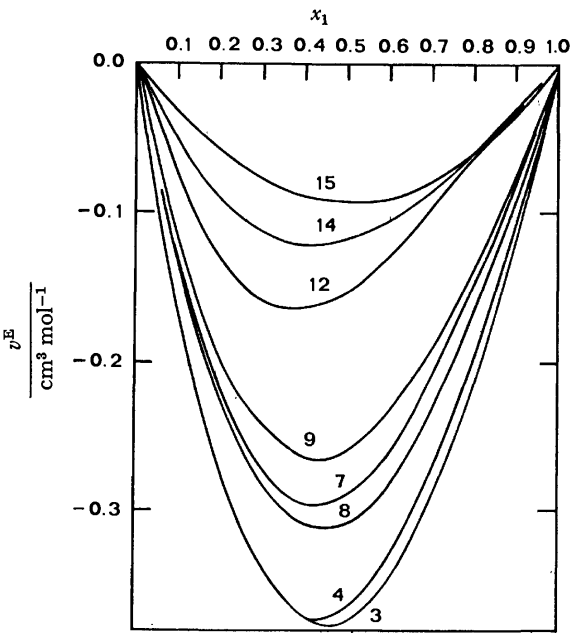

Fig. 2. Excess volume as a function of donor mole fraction at 25 °C. Systems: *m*-xylene(3), isoproylbenzene(4), ethylbenzene(8), 1,2,4-trimethylbenzene (7), *n*-proplybenzene(9), styrene(12), 1,2,3,4-tetramethylbenzene(14), benzonitrile(15). Nitrobenzene is the acceptor in all the solutions.

v_1 and v_2 are the molar volumes of the donor and acceptor respectively, and x_1 and x_2 are their respective mole fractions. The v^E *vs.* x_1 data for 18 systems are shown in Figs. 1 and 2, respectively. The binary systems containing bromobenzene, chlorobenzene and benzonitrile are again readily distinguishable from all the other solutions. The b_3 values of these systems are very small and consequently their v^E *vs.* x_1 curves are symmetrical. The curves representing the other systems, except the one for the aniline system, are more or less skewed, depending on their b_3 values, and have minima between $x_1=0.4$ and $x_1=0.5$. The skewed shape is indicative of specific interactions. The bromobenzene, chlorobenzene and benzonitrile systems seem to be the only solutions within this group with little or no specific interactions at all. The question of how much specific interaction there is in a solution cannot be answered from the shape of the curve alone. Only qualitative observations can be made from these curves and from the data listed in Table 2. Some of them are as follows:

1. The longer the chain of the substituent on the donor the smaller is $|v^E|$. In the series of donors, toluene, ethylbenzene, propylbenzene and butylbenzene, the toluene system exhibits the largest and the butylbenzene system the smallest $|v^E|$. This is just the opposite of the conclusion for NMR studies that the longer the chain of the substituent on the donor the greater the extent of complexation in the solution.

The difference in v^E for the toluene and ethylbenzene systems in 0.020 $cm^3\ mol^{-1}$ at equimolar concentration. For the ethylbenzene and propylbenzene systems the difference amounts to 0.045 $cm^3\ mol^{-1}$ and remains very much the same for the *n*-propylbenzene and butylbenzene systems.

2. The v^E *vs.* mole fraction data indicate that the branched donors have a more profound effect on $|v^E|$ than do the unbranched donors:

$$(v^E_{\text{isopropyl}}-v^E_{\text{propyl}})=(v^E_{\text{isobutyl}}-v^E_{\text{butyl}})=0.095\ \text{cm}^3\ \text{mol}^{-1}$$

3. The monosubstituted ethylbenzene affects v^E less than its disubstituted isomers, *m*- and *p*-xylenes (for *o*-xylene see below). This is in agreement with NMR measurements, according to which polysubstituted donors are superior to their monosubstituted counterparts in complex formation.

4. Donors having substituents in neighboring (*ortho*) positions have in general a smaller effect on v^E than similar donors with substituents in non-neighboring positions. The *o*-xylene system when compared with the other two xylene systems illustrates this fact. This is also seen from comparison of the 1,2,4-trimethylbenzene and the 1,3,5-trimethylbenzene systems. The relatively small $|v^E|$ values of the 1,2,3,4-tetramethylbenzene system very clearly proves the "neighboring substituent effect". The steric effect of the *ortho* substituted donors, as well as their stronger intermolecular forces, indicated by higher enthalpies of vaporization, may be responsible for the diametrically different volumetric behavior of the

Table 2. Comparison of some characteristic properties of the different systems

Donor[a]	v_1 / $cm^3\ mol^{-1}$	l_{vap} / cal g^{-1}	v_1/v_2	$\left(\frac{v^E}{x_1x_2}\right)_{x_1=0.5}$ / $cm^3\ mol^{-1}$	$(\bar{v}_2-v_2)_{x_1\to 1}$[b] / $cm^3\ mol^{-1}$
iso-Butylbenzene	158.041	—	1.538	−1.23	−1.504
n-Butylbenzene	156.741	—	1.526	−0.84	−1.060
1,2,3,4-Tetramethylbenzene	149.228	80.2	1.452	−0.47	−0.638
1,2,3,5-Tetramethylbenzene	—	78.0[c]	—	—	—
iso-Propylbenzene	139.979	77.6	1.362	−1.39	−1.896
n-Propylbenzene	140.088	79.1	1.363	−1.03	−1.337
1,3,5-Trimethylbenzene	139.764	80.6	1.360	−1.49	−1.746
1,2,4-Trimethylbenzene	137.853	81.5	1.342	−1.15	−1.519
1,2,3-Trimethylbenzene	—	83.2[c]	—	—	—
p-Xylene	123.911	84.9	1.206	−1.48	−1.974
m-Xylene	123.448	85.3	1.200	−1.46	−1.843
o-Xylene	121.185	86.5	1.178	−1.00	−1.245
Ethylbenzene	123.054	84.3	1.200	−1.22	−1.539
Styrene	115.475	90.0	1.124	−0.61	−0.996
Toluene	106.846	—	1.040	−1.29	−1.578
Benzonitrile	103.050	—	1.003	−0.38	−0.375
Chlorobenzene	102.204	—	0.998	−0.37	−0.474
Bromobenzene	105.463	—	1.026	+0.18	+0.186
Aniline	91.530	—	0.890	+1.22	+1.343
Benzene	89.391	—	0.870	−0.58	−0.854

a) In all the systems nitrobenzene is the acceptor. b) The average value $v_2=102.723\ cm^3\ mol^{-1}$. c) Given just for comparison. 1,2,3,5-Tetramethylbenzene has lower cohesion energy than 1,2,3,4-tetramethylbenzene. 1,2,4-Trimethylbenzene has lower cohesion energy than 1,2,3-trimethylbenzene. The specific enthalpies of vaporization were evaluated from vapor pressure-temperature data at the respective boiling points of the donors.

ortho substituted donor solutions. The heat of vaporization per gram, l_{vap}, for some of the donors is listed in Table 2. As these data indicate, donors having substituents in neighboring positions exhibit larger l_{vap} values; consequently they must have larger intermolecular forces and exhibit smaller molar volumes.

It may be argued that $|v^E|$ values will depend on both the electron donor ability of the base and the intermolecular forces in the base.

Addition of acceptor molecules to the pure donor will result in charge transfer interaction and consequently in a lowering of the volume of the solution. Due to these interactions it might be reasonable to expect that the distance between the donor and acceptor molecules will be shorter than between two donor molecules. NMR measurements show that the three xylene isomers have approximately the same donor ability and therefore it is expected that the lowering of the molar volume of the solution caused by charge transfer interactions will be the same regardless of whether or not the donor is *ortho* or non *ortho* substituted.

The *ortho* substituted donors, due to their larger cohesive forces, represent more densely packed solvents (see v_1 in Table 2). For donor and acceptor molecules to interact they must approach each other. Molecules of the solvent must separate from each other in order to make space for the approaching nitrobenzene molecule. Because of the closer packing of molecules in the *ortho* substituted donors, relatively larger separation is required. Thus, the volume increase in these solvents will be larger than in the other donors. The charge transfer interaction effect and the separation effect when combined together will therefore result in smaller $|v^E|$ values for the *ortho* substituted solvents.

Similar arguments can also be used for the other systems studied and especially for the ethylbenzene and styrene systems. The relatively high cohesion energy in styrene is probably responsible for the unexpectedly smaller $|v^E|$ value for the styrene-nitrobenzene system.

5. There is no obvious correlation between $|v^E|$ and v_1/v_2. For the three isomeric xylenes v_1/v_2 is approximately the same and yet $|v^E|$ of the *o*-xylene system differs significantly from $|v^E|$ of the other two xylene systems. The chlorobenzene and toluene systems have very close v_1/v_2 values and yet their $|v^E|$ differ substantially. Similar conclusions can be made for the C_9H_{12} isomeric solutions and for the $C_{10}H_{14}$ isomeric solutions (see Table 2).

6. There is no obvious correlation between $|v^E|$ and the polarity of the donor molecules. Systems containing the polar *m*-xylene and the nonpolar *p*-xylene exhibit roughly the same $|v^E|$ values. Solutions of nonpolar 1,3,5-trinitrobezne seem to be more nonideal than solutions of polar 1,2,4-trimethylbenzene.

7. Of the 18 systems presented here only the two containing bromobenzene and aniline exhibit positive v^E values. The large positive values of v^E for the aniline system (0.305 cm^3 mol^{-1} at $x_1=x_2=0.5$) is probably due to some structure breaking in the aniline. Aniline is known as a highly associated liquid. The nitrobenzene molecules break some of the bulky aniline conglomerates into smaller units and separate them from each other. Consequently, there is a volume increase during mixing.

A number of methods have been suggested for the determination of partial molal volumes from density measurements.[16,17] In this investigation we have used a method which establishes an empirical equation to describe the experimental molar volumes of the solution as a function of mole fraction

$$v = b_0 + b_1x_1 + b_2x_1^2 + b_3x_1^3 \quad (2)$$

where $v_2 \equiv b_0$. It is then simple to evaluate the derivatives at any point and therefore to determine the partial molal quantity. In this way we obtain for the partial molal volume of the acceptor (nitrobenzene)

$$\bar{v}_2 = v_2 - b_2x_1^2 - 2b_3x_1^3 \quad (4)$$

The constants b_2 and b_3 are those listed in Table 1.

The function $\bar{v}_2-v_2$ for the 18 systems is plotted against x_1 in Fig. 3. The limiting values of $\bar{v}_2-v_2$ for $x_1\rightarrow 1$, listed in Table 2, are of theoretical significance. Friedman and Sheraga[18] derived a very simple but illustrative theory that evaluates the contribution of nonpolar groups to the partial molal volume in dilute aqueous alcoholic solutions from the limiting values. We were unable to apply this theory to our systems.

The presence of an inflection point on the v^E *vs.* x_1

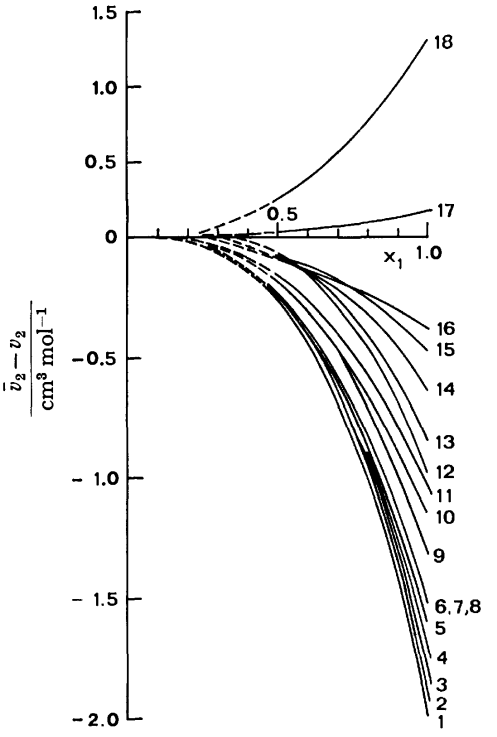

Fig. 3. Partial molal volume of nitrobenzene in electron donating slovents as function of donor mole fraction at 25 °C. Systems: *p*-xylene(1), isopropylbenzene(2), *m*-xylene(3), 1,3,5-trimethylbenzene(4), toluene(5), ethylbenzene(6), 1,2,4-trimethylbenzene (7), isobutylbenzene(8), *n*-propylbenzene(9), *o*-xylene(10), *n*-butylbenzene(11), styrene(12), benzene(13) 1,2,3,4-tertamethylbenzene(14), chlorobenzene(15), benzonitrile(16), bromobenzene(17), aniline(18).

curve indicates the occurrence of extrema on the partial molal volume *vs.* x_1 curves (minimum for one component and maximum for the other component). No such inflection points were observed for our systems. Consequently, no extrema are expected on the $\bar{v}_2$ *vs.* x_1 curves. Frequently, such extrema occur in the limits of low ($x_1 \rightarrow 0$) and high concentrations ($x_1 \rightarrow 1$). We investigaed these regions thoroughly and found no evidence of extrema for these systems.

Since there is direct relationship between v^E and $\bar{v}_2$, all the conclusions drawn from the excess volumes apply equally to the partial molal volumes.

The senior author wishes to thank the Japan Society for the Promotion of Science for the financial support given him during his 3 months stay in Japan.

References

1) This paper is dedicated to the memory of Howard N. Wachter, a graduate student who passed away recently.
2) E. Hála, I. Wichterle, J. Polák and T. Boublik, "Vapor-Liquid-Equilibrium Data," Pergamon Press, Oxford (1968).
3) A. Baghdoyan, F. Hsu, and V. Fried, *J. Chem. Thermodyn*, **7**, 895 (1975).
4) A. Baghdoyan and V. Fried, *J. Chem. Thermodyn*, **7**, 409 (1975).
5) R. Kind, D. Kahnt, D. Schmidt, J. Schomann, and H. J. Bittrich, *Z. Phys. Chem. (Leipzig)*, **11**, 277 (1968).
6) R. Anderson and J. M. Prausnitz, *J. Chem. Phys.*, **39**, 1225 (1963).
7) M. L. McGlashan, D. Stubley, and H. Watts, *J. Chem. Soc., A*, **1969**, 673.
8) G. Scatchard, S. E. Wood, and J. M. Mochel, *J. Am. Chem. Soc.*, **62**, 712 (1940).
9) R. R. Rastogi, J. Nath, and J. Misra, *J. Phys. Chem.*, **71**, 2524 (1967).
10) S. N. Bhattacharyya and A. Mukherjee, *J. Phys. Chem.*, **72**, 56 (1968).
11) F. Smith and I. Brown, *Aust. J. Chem.*, **26**, 705 (1973); *ibid.*, **26**, 691 (1973).
12) K. Nakanishi, N. Kato, and M. Maruyama, *J. Phys. Chem.*, **71**, 814 (1967).
13) I. Nagata, *Z. Phys. Chem. (Leipzig)*, **254**, 273 (1973).
14) L. P. Miller, H. N. Wachter, and V. Fried, *J. Chem. Eng. Data*, **20**, 417 (1975).
15) J. Timmermaus, "Physico-Chemical Constants of Pure Organic Compounds," Elsevier, New York (1950).
16) J. G. Aston and J. J. Fritz, "Thermodynamics and Statistical Thermodynamics," Wiley, New York (1959).
17) H. C. Van Ness, "Classical Thermodynamics of Non-Electrolytic Solutions," Pergamon Press, New York (1964).
18) M. E. Friedman and H. A. Sheraga, *J. Phys. Chem.*, **69**, 3795 (1965).

Condensed State Spectra and Phase Transitions of Charge Transfer Autocomplexes

Jānis FREIMANIS, Andrejs MĀLMANIS, and Jānis DRĒGERIS

Institute of Organic Synthesis, Latvian Academy of Sciences, Riga 226006, U. S. S. R.

(Received January 8, 1976)

The results of a spectroscopic study of super-cooled melts and crystalline layers of charge-transfer autocomplexes are reported. Samples obtained by sublimation *in vacuo* or by melting of the complex between transparent plates undergo a "liquid-solid" phase transition. Amorphous films produce absorption bands identical with those obtained from solutions, whereas crystalline layers are colored depending on intermolecular CT interaction. In some cases transparent crystalline films with pronounced optical anisotropy were obtained.

Vacuum-sublimed solid thin films are widely used for studying optical and electrophysical properties of organic compounds. Difficulties encountered in such studies are connected with the fact that the state of organic matter changes with time. Polychromism and polymorphism in donor–acceptor compounds (also in monomolecular ones) have been reported in a number of cases.[1-11] Only few of these have, however, been analysed from a structural point of view.[3,6,7,10] Another difficulty arises in connection with the fact that thin-layer samples are liable not only to polymorphic transitions of the "crystal-crystal" type, but also to "supercooled amorphous phase - crystal" transitions. Melting has been also found to produce considerable changes in the optical properties of certain donor–acceptor compounds.[12,15]

Polychromic changes of 2,4-dinitro-4′-diethylaminodiphenylamine and 2,4,6-trinitro-4′-diethylaminodiphenylamine have been reported previously.[2] The present work deals with a spectroscopic study of phase states, as well as of charge-transfer phenomena of molecular donor–acceptor autocomplexes (AC), particularly in thin-layer condensed films. Molecular autocomplexes of the naphthoquinone and nitroaryl series I,II,III have been investigated.

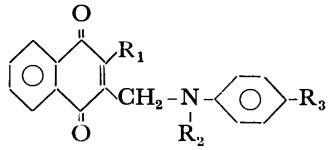

I

a) R_1=Cl; R_2=C_2H_5; R_3=Br.
b) R_1=Cl; R_2=C_2H_5; R_3=H.
c) R_1=Cl; R_2=CH_3; R_3=CH_3.
d) R_1=CH_3; R_2=CH_3; R_3=OCH_3.
e) R_1=CH_3; R_2=CH_3; R_3=CH_3.

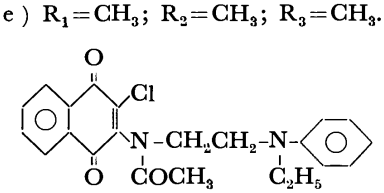

II

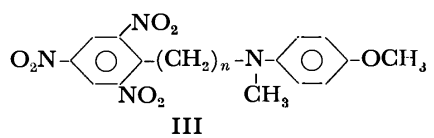

III

a) n=1, b) n=2.

Thin layers of these compounds were obtained by sublimation or melting *in vacuo*.[3] In this procedure the majority of compounds condense on the base in an unstable form, deposited as an amorphous, usually sticky, transparent and homogeneous film. Mechanical interference or standing leads to transition of the layers in to a final, stable form. Both forms have been examined by means of electron diffraction pattern.

Amorphous layers have been recently obtained even for naphthacene,[16] whereas production of so-called specular non-crystalline dye layers from solution is well known. In our case the amorphous layers obtained may be considered as unstable supercooled melts. The optical density and hence the extinction coefficient of such layers can be calculated within a certain error, accounting for a 1.1-fold expansion of most cyclic organic compounds on melting (Ref. 17 as well as calculations based on available data on specific volume changes of many substances on melting).

Amorphous films of complexes I and II crystallize after a certain time. A change of color of the film can be observed with phase transition and formation of fissures. Free parts of the base appearing between crystallites can be observed by means of a microscope. This necessitates in some cases great care in securing conditions for minimum light scattering in the final crystalline layer (*cf.* Experimental).

Let us first consider visible absorption in naphthoquinone AC. Figure 1a and Table 1, as well as the shape of experimental curves[18] show close similarity between the absorption curves of solutions and those of amorphous layers of the substances. It can be inferred that the long wavelength band of amorphous films is most likely due to intermolecular n-π^* or π-π^* (in the case of II) charge transfer, as is in the case for liquid[18,19] or solid[20] solutions of these compounds. There is, however, a general increase in intensity ever the whole visible spectrum in the case of non-crystalline layers.

This is apparently due to the fact that in sublimed layers the molecules are free from a solvent shell and thus may possess a somewhat different donor or acceptor ability of their molecular fragments, as well as different conditions of intermolecular orbital overlap.

The spectra of crystalline naphthoquinone autocomplex films show further increase in visible absorption (Figs. 2—3 and Table 1). X-Ray data on complex Ic[21] and on the prototype of autocomplexes

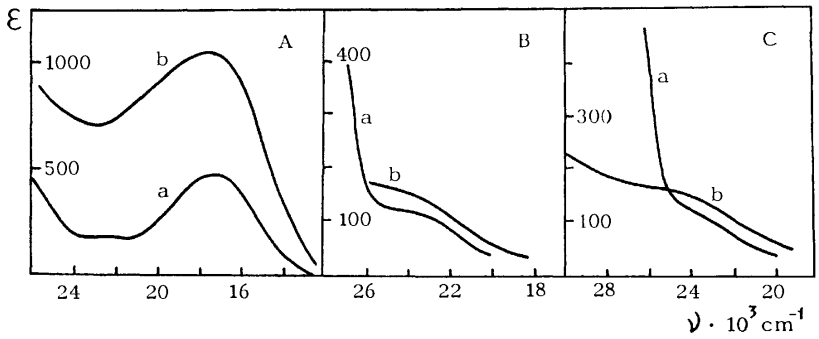

Fig. 1. Absorption of naphthoquinone-type AC Ia and some model compounds.
A, curves: a—Ia in benzene, b—sublimed amorphous film.
B, C—accordingly 2-methyl-1,4-naphthoquinone and 2-chloro-1,4-naphthoquinone, a—in benzene, b—crystalline layer from a melt.

Table 1. Optical characteristics of the solutions and sublimated layers of autocomplexes

Compound	Solution		Amorphous layer		Crystalline layer	
	ν_{max}	ε	ν_{max}	ε	ν_{max}	ε
Ia	17.3	490	17.5	≈1050[a]	of Fig. 3B	
Ib	16.7	410	17.0	≈680	16.0	≈1160
Ic	16.7	410	16.8	≈890	18.7	≈4000
Id	18.4	185	19.0	≈600	19.0	≈850
	≈23.5	150	23.0	≈600		
Ie	18.5	225	19.0	≈550	17.8	≈810
	≈23.5	170	23	≈530		
II	18.8	1700	18.3	≈1850	17.8	≈3650
IIIa	≈27 i	1250	24.0	≈2800		
IIIb	20.6	1490	19.8	≈6060[b]	19.3	≈7070[b]

ν_{max} in $cm^{-1} \times 10^{-3}$, ε—molar extinction coefficient. i—inflexion. Bands with ν_{max} 27×10^3 cm^{-1} are cited only. a) Supercooled melt between two glass plates. b) Sublimed films with a different degree of crystallinity.

Id, e[22] show a packing of molecular donor and acceptor fragments in infinite stacks of type DADADA..., as is usual for binary CTC. This leads to the conclusion that the observed changes in absorption with phase transition of the autocomplexes is due to the appearance of an additional band of intermolecular charge transfer (ICT). A phase transition alone could not have produced such considerable changes in visible absorption. This is seen clearly from a comparison of UV spectra obtained from solutions and from solid layers of 2-chloro- and 2-methyl-1,4-naphthoquinones which correspond to the acceptor fragments of autocomplexes Ia—e (Fig. 3B, C). Some possible differences in simple van der Waals intermolecular interactions in amorphous and crystalline states should not be neglected, but these would be considerably small.

The position of the ICT band of the crystal can be determined from differential spectra and depends only very little on absorption background (Figs. 2 and 3A). The intensity of the ITC band peak which characterizes electronic transitions in the crystal can only be approximately estimated, owing to different light scattering in the crystalline and the corresponding amorphous film. Each sample may also contain, in addition to its basic phase, inclusion of the other phase. Thus the accuracy of intensity measurements is estimated to be within ±5%. Intermolecular charge

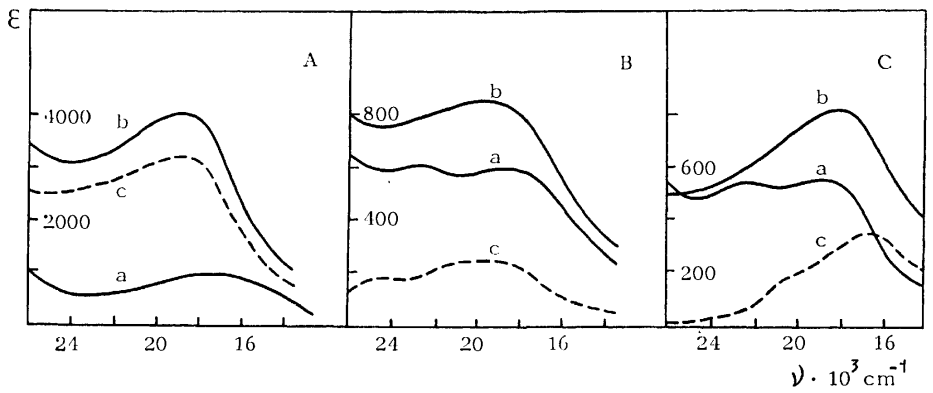

Fig. 2. Absorption of crystalline and amorphous films of naphthoquinone autocomplexes.
A—Ic; B—Id; C—Ie.
Curves: a—amorphous film, b—crystalline layer, c—differential curves "b"—"a". For Ic $\nu_{max} = 19000$ cm^{-1}, $\varepsilon = 3200$; for Id $\nu_{max} = 20000$ cm^{-1}, $\varepsilon = 260$; Ie—$\nu_{max} = 16600$ cm^{-1}, $\varepsilon = 350$. All the samples were obtained by sublimation technique.

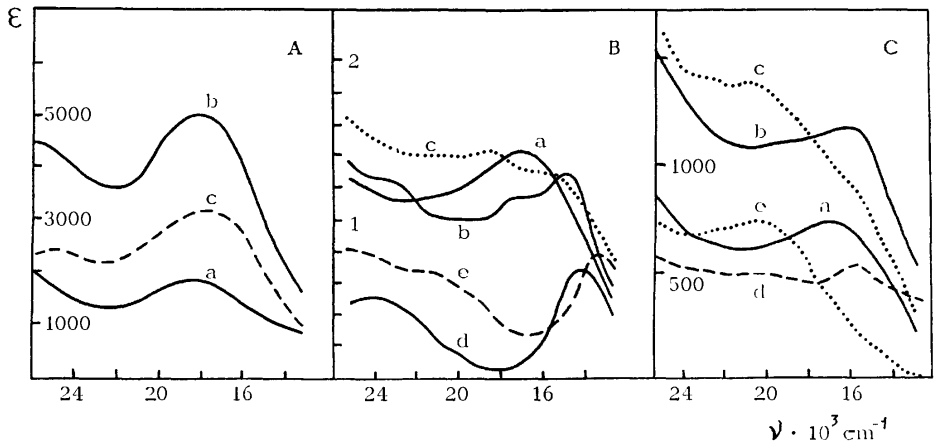

Fig. 3. Absorption of crystalline and amorphous films of naphthoquinone autocomplexes.
A—layers from II obtained by sublimation.
Curves: a—amorphous film, b—crystalline layer, c—differential spectrm "b"—"a", ν_{max} = 17800 cm^{-1}, ε = 3100.
B—from layers Ia obtained by melting.
Curves: a—amorphous film, b—the same film in a day, c—absorption of the large-grained layer, d—differential spectrum "b"—"a", ν_{max} = 14000 cm^{-1}, e—differential spectrum "c"—"a". Ordinate in arbitrary units.
C—layers from Ib.
Curves: a—amorphous sublimed layer, b—fine-crystalline sublimed layer, c—large-grained layer from the melt, d—differential spectrum "b"—"a", $\nu_{max} = \approx 15800$ cm^{-1}, e—differential spectrum "c"—"a". For curves a, b, d on the ordinate—extinction coefficient, for curves c, e the absorption is given in arbitrary units.

transfer in AC Ic is primarily caused crystallographically. It was shown that[23,24] in crystalline autocomplex II we might expect intramoleclar donor-acceptor interaction but the orientation of the nearest planes of donor and acceptor fragments of adjoining molecules in the crystal should not favor intermolecular charge transfer. Hence, the very high intensity of the CTC band in the differential spectrum (Fig. 3A, curve c) may be due either to compression of the horseshoe-shaped molecules II in the process of crystallization of the amorphous phase, or to additional intermolecular interaction within the crystal, *e. g.* through contacts C–O . . . Cl. In the case of Ic and II the interatomic distances of adjacent molecules in the lattice are practically equal to those caused by van der Waals interaction[21,23]; nevertheless distinct n-π^* charge transfer is suggested for analogous halogenquinones by de Gaultier *et al.*[25]

It could be shown in the case of autocomplexes Ia,b that the optical properties of crystalline films largely depend on the mode of preparation. Crystallization of a melt of Ia between glass plates, or fast sublimation of Ib leads to the formation of blue microcrystalline layers. Their spectra clearly show an ICT band in the region of (14—16) $\times 10^3$ cm^{-1} (Figs. 3 B, C, curves b, d).

A crystalline melt of quinone Ia between a quartz and a mica plate, or that of an analogue of Ib between glass plates has much larger crystalline particles. These particles are, in the case of a layer of Ia, distributed non-homogeneously, and the sample is always unevenly colored. Violet and blue patches can be observed simultaneously. The resultant spectrum is shown in Fig. 3Bc. These shades merge into each other on a change in the angle of vision, or on observing the film through a polarizing microscope with a white light source and a rotating object-table. Quinone Ib produces a more homogeneous layer, and change of the angle of vision leads to a change of shade of the whole sample. At the same time, the band in the region (14—16) $\times 10^3$ cm^{-1} is less characteristic of this compound, unlike the other analogue of Ia, as can be seen from curves "c" in Figs. 3B, C and from the corresponding differential spectra "c"—"a".

It follows that in microcrystalline samples of AC Ia,b the orientation of separate single crystals, and, hence, that of the planes of molecular donor-acceptor pairs, with respect to the plane of the base is essentially different from the one in the macrocrystalline sample of quinone Ib. The inhomogeneous macrocrystalline sample of Ia shows a non-uniform distribution of single crystals both with respect to orientation and to location within the area of the film.

The absorption spectrum of a siblimed nitroaryl AC IIIa film has a bathochromically shifted long wave (length) edge, as compared to that of solution (Fig. 4A, curves a, b). Analysis of first Gaussian components shows that the low-frequency absorption edge is shifted towards lower energy values by at least 4×10^3 cm^{-1}. This indicates a high microcrystal inclusion or oligomolecular associate percentage in a "freshly" sublimed film, intermolecular interaction taking place between each part of such inclusions. Thus the well defined 22.5×10^3 cm^{-1} band in the differential spectrum of amorphous phase *vs.* solution indicates not only changes in intermolecular interaction between

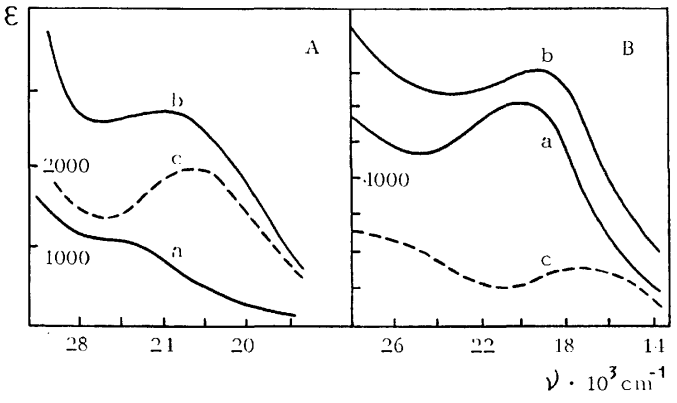

Fig. 4. Absorption of nitroaryl autocomplexes.
A—spectra of IIIa.
Curves: a—in benzene solution, b—"amorphous" sublimed layer, c—differential spectrum "b"—"a".
B—spectra of IIIb.
Curves: a—freshly sublimed film, b—the same sample after a 15 day storage, c—differential spectrum "b"—"a", $\nu_{max} \approx 18000\ cm^{-1}$, $\varepsilon = 1500$.

functional groups in the absence of solvent, but also contribution of the intermolecular charge transfer, as demonstrated by X-ray studies.[24,26]

A freshly sublimed film of the three-member-bridged autocomplex IIIb hardly differs optically from a film that has been kept for several weeks. Only a considerable intensity increase of the CT band and a slight bathochromic peak shift can be observed, as compared with that of solution (Fig. 4B and Table 1). In this case the differential spectrum also shows an absorption component due to intermolecular interaction; both samples are likely to contain both the amorphous and the crystalline phases, only in different proportions. The ICT band is estimated to be in the region $(17—18) \times 10^3\ cm^{-1}$ in this case.

As expected, owing to different polarization values of the molecules and their fragments in the solid phase the variochromic ICT band shift do not always follow the simple Mulliken relations (spectra of pairs of compounds differing only in one structural element, such as IIIa, b; Id, e; Ie, c; Ia, b). This, too, can be easily explained by the fact that the differential spectra can demonstrate only intermolecular CT absorption as a whole, which undoubtedly depends on the different grain orientation at the base for different compounds.

Experimental

Compounds I—III were synthesized according to the methods reported.[27-30] Samples for absorption measurements were prepared by sublimation of AC I—III *in vacuo* on a glass base at room temperature. The sublimation process is controlled visually. The heater of the evaporator is switched off[31] as soon as the melting point of the autocomplex has been reached. A thermogravimetric experiment on Ib demonstrated that this substance is not decomposed by melting. The heating rate of a compound in the evaporator varied from 3 to 20 min, the vacuum being about 10^{-5} Torr, depending on the desired type of film. For the preparation of an amorphous coating, comparatively rapid sublimation is usually necessary; only in the case of complex Ib and amorphous layer could be prepared by slow sublimation. However, in this case the film itself must be sufficiently thick. Microcrystalline layers were obtained immediately in the course of sublimation from substances Ic and II only if the evaporator was heated very slowly. A microcrystalline film from AC Ib is formed only by very rapid sublimation of a small sample.

The method of melting the sample *in vacuo* between transparent windows was used when the vacuum-deposited films turned out to scatter light after crystallization (Ib, and sometimes Ia). For this purpose a supercooled amorphous layer is prepared between two glass plates. In a few hours the melt crystallizes into a microcrystalline (Ia) or a large-grained sample (Ib). Large-grained samples of Ia could be obtained by melting the complex between a glass and a mica plate. Films of AC IIIa, b could not be obtained by the melting procedure owing to decomposition.

The authors express their gratitude to E. Chirkowa and M. Kaminsky for thermographic analysis of AC Ib; to J. Kalnačs for structure analysis by electron diffraction; to L. Berzina, D. Novicka, E. Silinš for their assistance and to Ya. Eiduss for valuable advice.

References

1) J. F. Freimanis and L. E. Berzina, *Dokl. Akad. Nauk SSSR*, **185**, 139 (1969).
2) J. F. Freimanis, J. J. Drēgeris, L. E. Berzina, A. J. Mālmanis, and E. J. Neimanis, *Zh. Obshch. Khim.* **42**, 603 (1972).
3) J. F. Freimanis, A. J. Mālmanis, J. J. Drēgeris, and S. J. Bitte, *Izv. Akad. Nauk Latv. SSR, Ser. Khim.*, **1973**, 333.
4) V. A. Ismailsky and V. I. Stavrovskaya, *Zh. Obshch. Khim.*, **9**, 1006 (1939).
5) V. A. Ismailsky and V. E. Limanov, *Izv. Akad. Nauk SSSR, Ser. Khim.*, **1959**, 1500.
6) R. L. Hansen and J. J. Neumayer, *J. Phys. Chem.*, **71**, 3047 (1967).
7) E. Hertel and M. Schinzel, *Z. Elektrochem.* **45** (5), 51 (1939).
8) Sh. Koizumi and Y. Matsunaga, *Bull. Chem. Soc. Jpn.*, **45**, 423 (1972).
9) Y. Matsunaga, *Bull. Chem. Soc. Jpn.*, **44**, 2868 (1971).
10) J. Aihara, G. Kushibiki, and Y. Matsunaga, *Bull. Chem. Soc. Jpn.*, **46**, 3584 (1973).
11) Y. Matsunaga, VII Molecular Crystal Symposium, NIKKO, Japan, 1975, Abstracts, p. 173.
12) G. Saito and Y. Matsunaga, *Bull. Chem. Soc. Jpn.*, **44**, 3328 (1971).
13) N. Inoue and Y. Matsunaga, *Bull. Chem. Soc. Jpn.*, **46**, 3345 (1973).
14) J. Aihara, A. Sasaki, and Y. Matsunaga, *Bull. Chem. Soc. Jpn.*, **43**, 3323 (1970).
15) J. Aihara, *Bull. Chem. Soc. Jpn.*, **47**, 2063 (1974).
16) Y. Maruyama, K. Machida, and N. Iwasaki, VII Molecular Crystal Symposium, NIKKO, Japan, 1975, Abstracts, p. 49.
17) E. A. Melwyn-Hughes, "Physical Chemistry," (Russ. ed), Moscow (1962), p. 663.
18) J. F. Freimanis, J. J. Drēgers, L. E. Berzina, I. V. Turovsky, S. J. Bitte, L. M. Blynov, and V. G. Rumiancev, *Adv. Mol. Rel. Processes*, **5**, 33 (1973).
19) V. G. Rumiancev, L. M. Blynov, J. F. Freimanis, and J. J. Drēgeris, *Zh. Strukt. Khim.*, **16**, 223 (1975).
20) J. F. Freimanis, S. V. Titarenko, V. A Gailite, and J. J. Drēgeris, *Izv. Akad. Nauk Latv. SSR, Ser. Khim.*, **1975**, 216.

21) A. E. Shvets, J. J. Bleidelis, and J. F. Freimanis, *Zh. Strukt. Khim.*, **16**, 417 (1975).
22) C. K. Prout and E. E. Castellano, *J. Chem. Soc., A*, **1970**, 2775.
23) A. E. Shvets, J. J. Bleidelis, and J. F. Freimanis, *Zh. Strukt. Khim.*, **16**, 640 (1975).
24) A. E. Shvets, J. J. Bleidelis, and J. F. Freimanis, *Acta Crystallogr.*, **A31**, Part S3, p. S129 (1975).
25) J. Gaultier, Ch. Hauw, and M. Schvoerer, *Acta Crystallogr.*, **B27**, 2199 (1971).
26) A. E. Shvets, J. J. Bleidelis, and J. F. Freimanis, *Zh. Strukt. Khim.*, **16**, 98 (1975).
27) J. J. Drēgeris, D. J. Murniece, and J. F. Freimanis, *Zh. Obshch. Khim.*, **42**, 600 (1972).
28) J. J. Drēgeris, S. J. Bitte, J. F. Freimanis, and A. J. Spārina, *Zh. Obshch. Khim.*, **45**, 123 (1975).
29) L. E. Berzina, J. J. Drēgeris, J. F. Freimanis, and I. V. Turovsky, *Zh. Obshch. Khim.*, **42**, 2719 (1972).
30) L. E. Berzina, D. J. Murniece, J. J. Drēgeris, and J. F. Freimanis, *Izv. Akad. Nauk Latv. SSR, Ser. Khim.*, **1971**, 460.
31) A. K. Gailis, A. E. Silinš, and J. F. Freimanis, *Elektrokhimiya*, **1966**(2), 1420.

Kinetic Studies on the Decolorization Reaction of Rosaniline in Aqueous Acidic Medium*

Sudhir K. SINHA** and Sarvagya S. KATIYAR

Department of Chemistry, Indian Institute of Technology, Kanpur, India

(Received March 12, 1976)

The reaction responsible for the decolorization of rosaniline in acid medium has been studied spectrophotometrically. The rate-determining step has been found to be the reaction of the protonated dye cation with water molecule. Kinetic data have been analyzed on the basis of rate equations which were derived considering the complete protolytic scheme involving all the steps of the reaction of rosaniline in acid and alkaline media. The rate constant k_1 for the ion-molecule reaction has been found to be independent of the dye concentration and hydrogen ion concentration. The apparent rate constant k at various hydrogen ion concentrations has been utilized for calculating the equilibrium constant for the fast protonation step. Effect of ionic strength in the range 0—0.27 indicates no substantial effect on the rate constant k_1. Anomalous solvent effects were obtained suggesting the solvated nature of the reactants. The average energy of activation for the reaction of rosaniline in aqueous medium corresponded to 10.52 kcal. Chemical and kinetic evidence has been presented to prove the participation of water molecule in the rate-determining step.

The mechanism for the color fading of the basic triphenylmethane dyes in acidic medium put forward by Biddle and Porter[1] indicates that in the rate-determining step the dye cation reacts with proton giving

$$R_3\overset{+}{C}\text{-}R_2 + H^+ \overset{\text{slow}}{\rightleftharpoons} R_3\text{-}\overset{+}{C}\text{-}R_2H^+$$
(R_1 on the carbon in both)

a protonated product. Later on working with malachite green Katiyar[2] found almost linear dependence of rate constant on the proton concentration as well as increase in rate constant with the increase in ionic strength of the medium and decrease in rate with decrease in dielectric constant of the medium. These data apparently agreed with the mechanism given by Biddle and Porter. However, it was difficult for us to conceive the idea of a protonation rection of an amino group being slower than the reaction of the protonated dye cation with water. A careful analysis of the data on the variation of the rate constant with hydrogen ion concentration in the color fading reaction of rosaniline as well as the earlier data[2] showed that the values of the so-called bimolecular rate constant obtained by dividing the apparent rate constant with $[H^+]$ are not identical. This raised suspicion as to the validity of the ion-ion step as the rate determining step in the reaction-leading to decolorization of triphenylmethane dyes in acid solutions.

In some of the investigations,[3-7] all the possible reactions of the dye with various other species present in the aqueous acidic solutions have been considered in interpreting the observed kinetic data. But in these studies where the reaction was treated as an ion-molecule reaction, the authors did not make any attempt to find out the effect of dielectric constant or ionic strength on the reaction rate. Existing literature also revealed complete absence of such studies on the ion-molecular type reaction of triphenylmethane dyes. Apart from this, no direct chemical evidence has been cited for the suggested mechanism.

In view of the above mentioned facts, we decided to undertake the investigation of the reaction of color fading of rosaniline (C.I. Basic violet 14), a primary member of the triphenylmethane dyes, in acidic medium. These studies have been utilized to establish the nature of the reacting species and to provide a possible explanation for the misleading effect of dielectric constant and ionic strength on the reaction rate.

Experimental

Materials. Rosaniline hydrochloride (C. I. No. 42510, Basic violet-14) was obtained from Eastman Organic Chemicals. Paraffin wax used for coating the inside of the reaction vessels was a B. D. H. laboratory grade material (congealing point 60—62 °C). Dioxane, a B. D. H. analytical grade reagent was purified further[8] before use. All other chemicals needed for buffer solutions were either B. D. H. AnalaR or E. Merck "pro analysi" grade reagents. Deionized all glass distilled water was used for all the experiments.

Methods. Investigations were carried out spectrophotometrically using Beckman DU or Cary model 14 spectrophotometers by the method described earlier.[9]

Rosaniline has an absorption maximum at 546 nm in water solution. It follows Beer's law at 546 nm satisfactorily up to the concentration of 2.5×10^{-5} M ($\varepsilon'=66500$). It was observed that the absorption maximum remains unchanged by the addition of a neutral electrolyte such as 1.0 M solution of KCl. All the measurements, when pure water was used as solvent, were made at 546 nm and the concentration of the dye taken was less than 2.5×10^{-5} M. The decolorization reaction of rosaniline in the presence of acid was found to be reversible in nature. In the presence of small amounts of acid (pH>4), therefore, the fading reaction did not proceed to completion. The backward reaction was minimized by taking the concentration of acid in large excess (pH<2) over that of the dye (2.5×10^{-5} M), which shifted the equilibrium to the side of the product. Further, the kinetic data were recorded in the first few minutes of the reaction.

Fitting of data to straight lines by method of least squares and calculations of the standard derivations to assess the error limits were done with the help of an I. B. M. 7044 digital computer.

* Taken in part from the Ph. D. Thesis of S. K. Sinha, submitted to Indian Institute of Technology, Kanpur.

** Present address: Department of Chemistry, Bihar University, L. S. College, Muzaffarpur, Bihar, India.

Results and Discussion

Chemical and Kinetic Evidence for the Reactant and Product. In order to get a direct chemical evidence for the nature of reactants, we carried out the protonation of rosaniline in complete absence of water. It was observed that when pure dry HCl gas was passed into a solution of rosaniline (4×10^{-4} M) in pure dry acetonitrile, the solution instantaneously changed its color from red to reddish violet. Further passage of dry HCl gas changed the color to yellowish green, which remained stable in the absence of moisture. These colored species are due to the protonation of the first and second amino groups respectively. Earlier spectral investigations[10,11] also indicated that out of three amino groups only two get protonated. That one *p*-amino grouping is never protonated in all these cases is due to the fact that only one of the benzene rings is involved in resonance interactions, thus giving a difference in base strength of one amino group with respect to the other two. It has been also reported that 68% of the carbonium ions from crystal violet add two protons in 1 M hydrochloric acid.[12] These protonations of amino groups in rosaniline may be represented as follows:

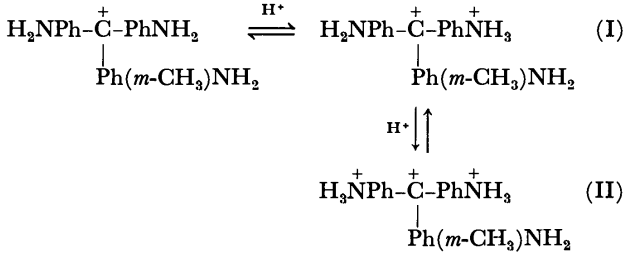

A drop of water in the violet (I) or green (II) solution thus obtained changed them to colorless solution. This demonstrates that colorless product is obtained from the reaction of water with the protonated species and not from the protonation of the dye.

Now in order to establish the rate-determining step, the rate of decolorization of the protonated species in the presence of water was compared with the rate of unprotonated rosaniline in aqueous acidic medium under identical conditions. The overall rate constants, k, for these protonated and unprotonated solutions were found to be 0.207 and 0.202 min^{-1} respectively at pH 1.35. Similarly at pH 2.4, k corresponedd to 0.026 and 0.018 min^{-1} for these protonated and unprotonated rosaniline solutions. It is thus esablished that under the identical conditions of temperature, solvent and hydrogen ion concentration the rates of reaction responsible for the decolorization of protonated and unprotonated dye are the same within reasonable limits. This finding augments the earlier evidence that water is one of the reactants and further proves that the rate-determining step in the decolorization reaction of basic triphenylmethane dye in aqueous-acidic medium is definitely not the protonation process, but is the reaction of water molecule with the protonated dye cation giving protonated carbinol, whose existence is reported in the literature.[13-15]

Rate Expression for the Decolorzation of Rosaniline. Evidence presented above shows that protonation of rosaniline is the fast equilibrium step and subsequent reaction of water molecule with the protonated dye cation is the slow rate-determining step. On the basis of the protolytic scheme given by Cigen[3] and taking into account only the protonation of one amino group, as the concentration of acid used in all the cases was not that much as to cause further protonation, all the steps of the reaction of the rosaniline in acid and alkaline media can be shown as follows. The solid lines in the scheme indicate that the reactions proceed instantaneously whereas broken lines indicate that the reactions take place with measurable velocity.

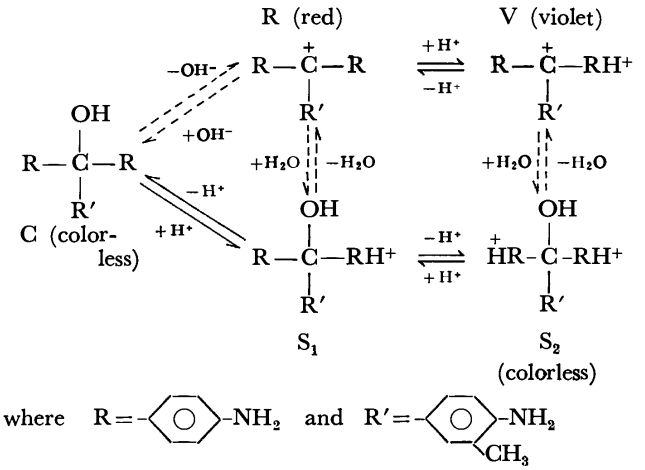

Now let us define the following constants:

$K_1=\dfrac{[V]}{[R][H^+]}$, where [R] is the concentration of rosaniline

k_1 = pseudo first order rate constant for the reaction; $V+H_2O\rightarrow S_2$

k_2 = first order rate constant for the reaction; $S_2\rightarrow H_2O+V$.

The investigations were carried out spectrophotometrically. Therefore, the concentrations of the dye are given in the form of specific absorptions. The following symbols are used:

ε_R, ε_V = The molar absorptivity of R and V respectively.

e_R, e_V = The specific absorbance of a solution containing only R and V respectively.

e_0, e_t, e_∞ = The specific absorbance of the solution at times 0, t and at equilibrium.

C_M = The total concentration of rosaniline.

If protonation equilibrum is achieved instantaneously, one can obtain the following equations by the method of Cigen.

$$\frac{[H^+]}{(e_R-e_0)}=[H^+]\cdot\frac{1}{(e_R-e_V)}+\frac{1}{K_1(e_R-e_V)} \quad (1)$$

And the overall rate constant k at pH<2 is given as

$$k=\frac{1}{t}\ln\frac{e_0-e_\infty}{e_t-e_\infty}=k_1\frac{K_1[H^+]}{1+K_1[H^+]}+k_2 \quad (2)$$

neglecting the other equilibrium terms except the protonation and subsequent water addition step. Thus a plot of $[H^+]/(e_R-e_0)$ against $[H^+]$ will give a straight line. The intercept, C, of this line on the Y axis and its slope, m, give $(e_R-e_V)=1/m$ and thus giving $K_1=m/C$ hence, the value of K_1 can be obtained from Eq. 1.

Table 1.[a] Rate constants at varying concentration of rosaniline

$[H^+] = 1.89 \times 10^{-2}$ M

Rosaniline concn mol/l $\times 10^6$	k, $s^{-1} \times 10^2$
19.6	0.21
17.7	0.20
15.7	0.21
13.7	0.22
11.8	0.21
9.8	0.21
5.9	0.22

a) Temperature=25 °C.

The value of k_1, the rate of hydration, can be obtained from the slope of a plot of k *versus* $K_1[H^+]/(1+K_1[H^+])$ and that of k_2 from the intercept of this plot.

Effect of Rosaniline Concentration on the Reaction Rate. The dependence of rate on the concentration of rosaniline was studied by recording the kinetic runs at varying dye concentrations in the range 19.6×10^{-6} M to 3.9×10^{-6} M and a fixed amount of hydrochloric acid (1.89×10^{-2} M). Value of e_∞ was obtained by measuring the absorbance after the lapse of four hours. Analysis of the results from the graphical method yielded linear first order plots with almost the same slope, giving a constant value of k for all the rosaniline concentrations as shown in Table 1. This indicates that the value of k is independent of the initial concentration of rosaniline. As the equilibrium constant k_1 and the hydrogen ion concentration are constant, the value of k_1, the true rate constant for hydration, will remain unchanged for all rosaniline concentrations in accordance with Eq. 2. Thus, k_1 is independent of initial concentration of rosaniline. Since the concentration of the reactant, namely, water is in great excess as compared to that of the dye, the first order nature of the reaction is in agreement with the suggested mechanism.

Effect of Hydrogen Ion Concentration on Reaction Rate. As in the aqueous solution of the dye there exist more than one species, it is not possible to determine the values of ε_R, ε_V, e_R, e_V directly from the measured absorption curves. For simplicity, aqueous solution of dye of pH 6.5 was taken. In such a solution, the concentration of the red form, R, is about 80—90% of the total dye concentration. If the apparent molar extinction coefficient of such a solution is denoted by ε'_R and the specific extinction by e'_R, then $e'_R/e_R = e'_V/e_V$. From this relation and Eq. 1, the value of K_1 can be determined by substituting e'_R, the measured specific extinction, for e_R and e'_V for e_V. For the determination of equilibrium constant the rates of decolorization of rosaniline were measured at various hydrogen ion concentrations at constant ionic strength. The equilibrium $R + H^+ \rightleftharpoons V$ is reached instantaneously during the mixing, whereupon the color of the solution fades owing to the reaction $V + H_2O \rightleftharpoons S_2$. By determining the fading rate and extrapolating the extinction to $t=0$, e_0 was obtained. The measurements were carried out at the wavelength, 546 nm, where the absorption curve of the red component has a sharp maximum. The plots of $\log(e_t - e_\infty)$

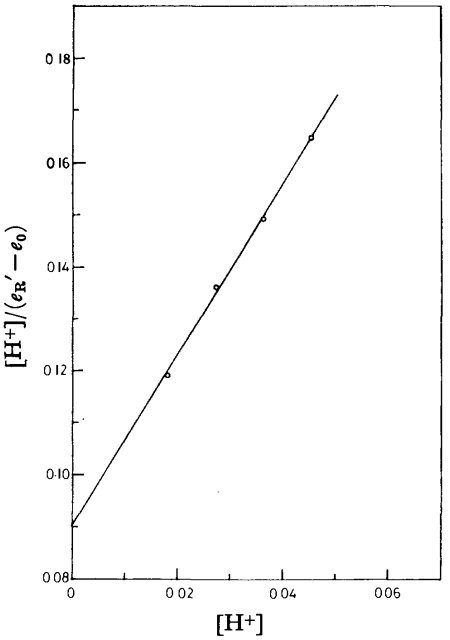

Fig. 1. Variation of $[H^+]/(e_R' - e_0)$ with $[H^+]$ for the reaction of rosaniline in aqueous medium at ionic strength equal to 0.09 at 25 °C.

Table 2.[a] Rates of hydration of rosaniline k_1, k_2, and equilibrium constant K_1 at 25 °C

e_R'	$[H^+]$	$\log(e_0 - e_\infty)$	e_∞	e_0	$e_R' - e_0$	$\frac{[H^+]}{e_R' - e_0}$
0.598	0.0182	1.594	0.052	0.445	0.153	0.119
0.598	0.0272	1.558	0.037	0.398	0.200	0.136
0.598	0.0363	1.513	0.029	0.355	0.243	0.149
0.598	0.0454	1.491	0.015	0.325	0.275	0.165

$K_1 = 18.13 \pm 0.15$ M^{-1}

k, $s^{-1} \times 10^3$	$\frac{K_1[H^+]}{1+K_1[H^+]}$	k_1, s^{-1}	k_2, s^{-1}
3.99	0.248		
5.22	0.330		
6.18	0.397	1.7×10^{-2}	0.4×10^{-3}
7.31	0.452		

a) Ionic_strength=0.09.

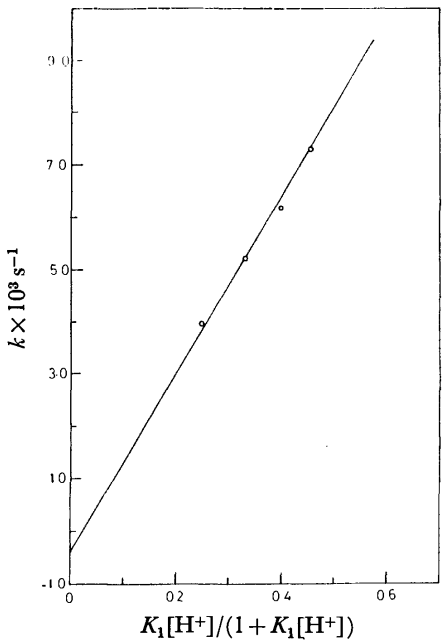

Fig. 2. Plot of k *vs.* $K_1[H^+]/(1+K_1[H^+])$ for the reaction of rosaniline at $\mu=0.091$.

vs. time at various hydrogen ion concentrations were linear indicating the first order nature of the reaction as expected from Eq. 2. The values of apparent rate constants, k, were found to increase with increasing concentration of the acid (Table 2). In order to find out the equilibrium constant K_1 of the protonation step using Eq. 2, a plot of $[H^+]/(e_R'-e_0)$ against $[H^+]$ was made as shown in Fig. 1. The slope and intercept from this graph gave a value of $18.1\pm0.15\ M^{-1}$ for the equilibrium constant K_1. As is evident from Eq. 2, a plot of $K_1[H^+]/(1+K_1[H^+])$ *vs.* k should give a straight line with slope equal to k_1 and intercept k_2. Such plot shows the linear variation of $K_1[H^+]/(1+K_1[H^+])$ with k giving the value of $k_1=1.7\times10^{-2}\ s^{-1}$ and $k_2=0.40\times10^{-3}\pm0.05\times10^{-3}\ s^{-1}$ which are independent of the hydrogen ion concentrations (Fig. 2). It is evident from the values of k_1 and k_2 that the rate of forward reaction is much greater than that of backward reaction under the experimental conditions but still k_2 is quite significant. Hence, in all the measurements of k_1, the backward reaction has been taken into account.

Effect of Ionic Strength on the Rate Constant k_1. Usually for a reaction between an ion and a neutral molecule, the electrostatic effects are small in very dilute solution. If the reacting species in the rate determining step in the present case are ionic type the rate constant should increase with increase in ionic strength.[9,16] The effect of ionic strength ion dipole interaction can be expected from considerations of interactions of the ion atmosphere with the dipole moment of the reactant molecule in the free state and in the complex.[17]

Studies were done taking fixed concentration of the dye ($0.72\times10^{-5}M$) and varying HCl concentration at a constant ionic strength of 0.27. The values of rate constants and equilibrium constants obtained from Eqs. 1 and 2 are reported in Table 3. It is of interest to note that the equilibrium constant K_1 is $34.9\pm0.15\ M^{-1}$ and it is considerably higher that the value obtained at $\mu=0.091$ which is $18.13\pm0.15\ M^{-1}$ (Table 2). The equilibrium constant at higher ionic strength increases as expected, since the effect of ionic strength on the association constant follows the Bjerrum-Brønsted relationship.[18] The values of k_1 at $\mu=0.27$ was found to be $2.08\times10^{-2}\ s^{-1}$. Comparing this value to k_1 obtained at $\mu=0.091$ ($1.7\times10^{-2}\ s^{-1}$), it is evident that it does not change much in accordance with the equation valid for ionic reactions,[9,16] and given below:

$$\ln k = \ln k_0 + \frac{2Z_AZ_BA\sqrt{\mu}}{1+\beta a_1\sqrt{\mu}} \qquad (3)$$

The increase in the value of k_1 even after a three-fold increase in ionic strength is too small to get any meaningful quantitative correlation. In view of the limitation that the acid concentration cannot be decreased above pH 2 and the overall rate becomes faster with increase in ionic strength, the study could not be extended to higher ionic strength. But, the above studies clarifies the cause of apparent increase of the overall rate constant with increase in ionic strength which led to the false inference about the nature of reactants, by previous workers. No doubt the overall rate constant k is markedly dependent on the ionic strength of the medium but this is because of the change in value of K_1 and the rate constant k_1 is only slightly effected. Thus, the above observations further supports the nature of reacting species as given in the protolytic scheme.

Effect of Dielectric Constant on the Rate Constant k_1. Experiments were carried out at different dioxane-water compositions keeping the ionic strength of the solution constant using suitable HCl-KCl mixtures in all the experiments. It was observed that the wavelength of maximum absorption shifted to 543 nm in dioxane-water mixtures, the studies were therefore carried out at 543 nm. The values of e_R' were determined prior to the experiment at each solvent percentage. Rate constants and equilibrium constants at different dixane-water concentrations are sum-

TABLE 3.[a] RATE CONSTANTS AND EQUILIBRIUM CONSTANTS AT CONSTANTS AT $\mu=0.27$

$[H^+]$	k, $s^{-1}\times10^3$	$\frac{[H^+]}{e_R'-e_0}$	K_1	$\frac{K_1[H^+]}{1+K_1[H^+]}$	k_1, $s^{-1}\times10^2$	k_2, $s^{-1}\times10^3$
0.0145	3.46	0.112	$34.91\pm0.25\ M^{-1}$	0.336	2.08 ± 0.06	0.40 ± 0.05
0.0218	5.30	0.131		0.432		
0.0291	6.77	0.151		0.504		
0.0363	8.28	0.169		0.559		

a) Temperature=25 °C.

Table 4. Rate constants and equilibrium constants in dioxane-water mixtures at 25 °C

$[H^+]$	k, $s^{-1}\times10^3$	$\frac{[H^+]}{e_R'-e_0}$	K_1	$\frac{K_1[H^+]}{1+K_1[H^+]}$	k_1, $s^{-1}\times10^2$
			5% (v/v) Dioxane-Water		
0.0908	7.67	0.211		0.509	
0.0726	6.91	0.188		0.453	
			$(11.43\pm0.20)M^{-1}$		(1.58 ± 0.10)
0.0636	6.50	0.180		0.421	
0.0545	5.76	0.168			
			10% (v/v) Dioxane-Water		
0.0908	8.06	0.317		0.620	
0.0817	7.04	0.296		0.595	
			$(18.01\pm0.2)M^{-1}$		(2.80 ± 0.15)
0.0726	6.39	0.275		0.566	
0.0545	4.32	0.237		0.495	
			15% (v/v) Dioxane-Water		
0.0908	5.04	0.404		0.658	
0.0817	4.61	0.376		0.634	
			$(21.23\pm0.20)M^{-1}$		(1.70 ± 0.15)
0.0726	5.06	0.349		0.606	
0.0545	3.20	0.298		0.536	

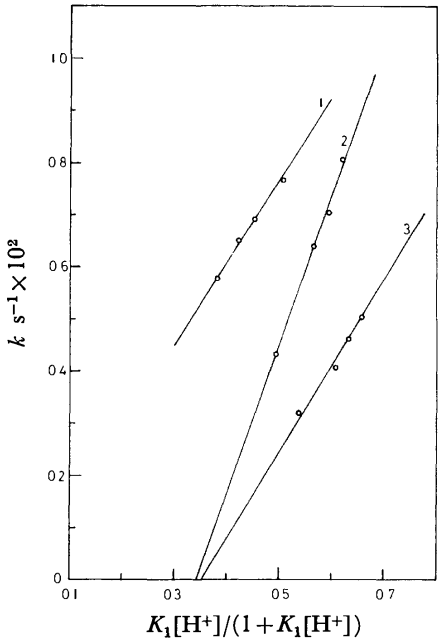

Fig. 3. Plot of $K_1[H^+]/(1+K_1[H^+])$ *vs.* k in dioxane-water media at 25 °C.
1 : 5% dioxane; 2 : 10% dioxane; 3 : 15% dioxane.

marized in Table 4. It is of interest to note that the values of equilibrium constant K_1 increase with increase in solvent percentage or decrease in dielectric constant of the medium. It corresponded to 11.43 M^{-1} in 5%, 18.01 M^{-1} in 10% and 21.23 M^{-1} in 15% dioxane-water mixture. This increase in equilibrium constant with decrease in dieletric constant is understandable and is in accordance with the formulation discussed elsewhere. Figure 2 represents the plot of $K_1[H^+]/(1+K_1[H^+])$ *vs.* k, the total reaction rate. As expected from Eq. 2, the plot is a fairly straight line. It may be seen from Fig. 3 that the slope increases in 5% to 10% and then decreases in 15%, 2.8×10^{-2} s^{-1} in 10% and $1.7\times10^{-2}s^{-1}$ in 15% dioxane-water mixture, even though total rate generally decreases with decrease in dielectric constant of the medium. Several treatments are available for interpreting the influence of the solvent on electrostatic force which modifies the rate process between ion and dipolar molecules. The equation derived by Amis and Jaffe[20] and modified by Amis[21] is as follows:

$$\ln k_D' = \ln k_\infty' + \frac{Z_A m_0 \varepsilon}{kTr^2 D} \qquad (4)$$

where k_D' and k' are specific reaction rates at dielectric constant D and m_0 is the moment at $\mu=0$. Further modification of the Eq. 4 was done by Quinlan and Amis[22] to obtain a relation which also predicts linear dependence of $\ln k'_{\mu=0}$ on $1/D$. Laidler and Landskroener[23] proposed a relation for such type of reaction based on Kirkwood[24] and Kirkwood and Westheimer's[25] theory which also predicts that the dependence of $\ln k'$ on $1/D$ should be linear. Thus,

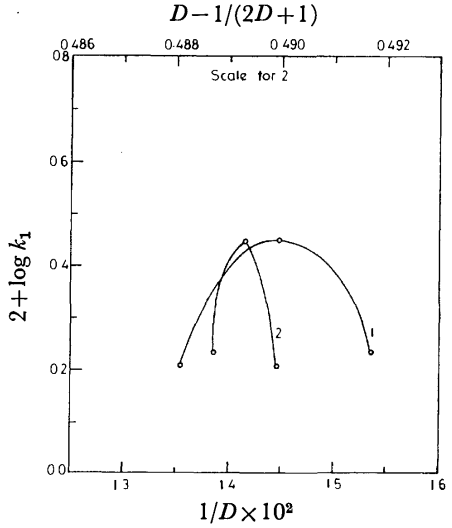

Fig. 4. Variation of $\log k_1$ as a function of dielectric constant (D) of the medium at 25 °C.
1 : $1/D$; 2 : $(D-1)/(2D+1)$.

almost all the models suggest that on the basis of electrostatic considerations the plot of $\ln k'$ *vs.* $1/D$ should be linear with positive slope if the charge on the reacting ion is positive for reaction between an ion and a neutral molecule. Figure 4 represents the dependence of $\log k_1$ on $1/D$. The plot, contrary to expectation, does not show any linear behavior and after 10% dioxane-water composition, the slope also becomes negative. The inconsistency with the predicted behavior can be analyzed on the basis of Laidler and Eyring[26] equation according to which the plot of $\ln k_1$ *vs.* $1/D$ will be straight line only when the Kirkwood term in the equation is only slightly affected with change in dielectric constant of the medium and the change in ϕ's (the non-electrostatic term) is insingnificant. In the present case, since the reacting species are water and protonated triphenylmethane carbonium ion, the effect on Kirkwood term due to change in dielectric constant is apparently significant.

For a bimolecular reaction of dipolar molecule (A) with dipolar molecule (B) the specific velocity constant is given as follows:

$$A + B \rightarrow M^* \rightarrow X + Y$$

$$\ln k' = \ln\left(\alpha\frac{\bar{k}T}{h}K_0^*\right) - \frac{1}{\bar{k}T}\frac{D-1}{2D+1}\left(\frac{\mu_A^2}{a_A^3}+\frac{\mu_B^2}{a_B^3}-\frac{\mu_{M^*}^2}{a_{M^*}^3}\right) + \frac{\phi_A+\phi_B-\phi_{M^*}}{\bar{k}T} \quad (5)$$

where k' is the specific velocity constant, α is the transmission coefficient, $\bar{k}$ is the Boltzmann constant, h is Planck's constant, T is the temperature in degrees Kelvin, D is the dielectric constant of the final solution, and for dilute solutions D is effectively the dielectric constant of the pure solvent. a_B is the average distance of closest approach of B to A, a_A is the average distance of closest approach of A to B, ϕ_A, ϕ_B and ϕ_{M^*} are the sum of the non-electrostatic terms considered by Laidler and Eyring.[26] K_0^* is defined by Laidler and Eyring as $K_0^*=F'_{M^*}/F_AF_B$, where F_A and F_B are the partition function of A and B and F'_{M^*} is the part of the partition function of complex, F_M which refers to the degrees of translational freedom corresponding to decomposition. According to this equation, if the non-electrostatic terms are negligibly small, a plot of $\ln k'$ *vs.* $(D-1)/(2D+1)$ should give a straight line. Laidler and Eyring[26] used Eq. 5 to interpret the solvent effects on the hydrolysis of esters. They plotted $\ln k'$ *vs.* $(D-1)/(2D+1)$ for acid and alkaline hydrolysis of some esters and obtained good straight line plots. Figure 4 (plot 2) represents the variation of $\log k_1$ with $(D-1)/(2D+1)$. It may be seen that this plot is also not linear. There are several reactions[27] where the solvent effect cannot be accounted for satisfactorily by electrostatic considerations only. Basic triphenylmethane dyes, as reported earlier,[9] exhibit specific solvent effect also in the case of carbinol formation in alkaline medium. The explanation of specific effects can be formulated in terms of the non-eletrostatic terms, ϕ's. Probably, the most important factor contributing to these terms is the solvating power of the solvents.

Effect of Temperature on Rate Constant k_1. Kinetic runs were further carried out at 20 and 30 °C maintaining the ionic strength for the solution constant using suitable HCl-KCl mixture. The data obtained are summarized in Table 5. It is interesting to note that increase in temperature decreased the value K_1 from 25.33 M^{-1} at 20 °C to 19.71 M^{-1} at 30 °C. This indicates that the equilibrium is shifted towards the reactants. Thus, even if the total rate increases with increase in temperature, the values of e_0 and e_∞ are also increased. This decrease in equilibrium constant with increase in temperature is well expected for the exothermic reaction of protonation of amino group. From the slopes of the plots of $K_1[H^+]/(1+K_1[H^+])$ *vs.* k at 20 and 30 °C the values of rate constants k_1 were obtained and were found to be 1.12×10^{-2} s^{-1} at 20 °C and 2.03×10^{-2} s^{-1} at 30 °C. Taking the value of k_1 at 25 °C equal to 1.7×10^{-2} s^{-1} as obtained earlier in aqueous medium, although this value is at slightly different ionic strength but the change due to this can be ignored as discussed earlier, dependence of $\log k_1$ on $1/T$ was plotted. This plot shows a fairly good straight line indicating that ΔE remains constant in this narrow temperature range. The average value of apparent ΔE was found to be 10.52 kcal. These studies suggest that the protolytic scheme is valid at higher temperatures also. Raising the temperature has the effect of displacing the equilibrium constant towards

Table 5. Variation of rate constant and equilibrium constant with temperature

$[H^+]$	k, $s^{-1}\times10^2$	$\frac{[H^+]}{e_R'-e_0}$	$\frac{K_1[H^+]}{1+K_1[H^+]}$	k_1, $s^{-1}\times10^2$
		Temperature 20 °C		
0.0908	0.728	0.242	0.697	
0.0726	0.639	0.207	0.647	
				1.12±0.06
0.0545	0.574	0.174	0.579	
0.0363	0.490	0.143	0.479	
		Temperature 30 °C		
0.0908	1.27	0.250	0.642	
0.0726	1.16	0.218	0.589	
				2.03±0.10
0.0545	1.02	0.188	0.518	
0.0363	0.79	0.154	0.417	

the colored, dehydrated form. The dissociation constant increases with temperature if they are defined as acid constants that is, as $1/K_1$. Due to specific solvent effect exhibited by the system, the different contributions to the energy of activation and thereby the true energies and entropies of activation could not be calculated.

References

1) H. C. Biddle and C. W. Porter, *J. Am. Chem. Soc.*, **37**, 1571 (1915).
2) S. S. Katiyar, *Z. Phys. Chem. (Frankfurt)*, **34**, 346 (1962).
3) R. Cigen, *Acta Chem. Scand.*, **12**, 1456 (1958); **13**, 1113 (1959); **14**, 979 (1960).
4) R. Cigen, *Acta Chem. Scand.*, **15**, 1892 (1961); **15**, 1905 (1961); **16**, 192 (1962).
5) R. Cigen and G. Bengtsson, *Acta Chem. Scand.*, **16**, 1837 (1962); **17**, 2091 (1963).
6) R. Cigen and C. G. Ekstrom, *Acta Chem. Scand.*, **17**, 1189 (1963); **17**, 1843 (1963); **17**, 2083 (1963); **18**, 157 (1954).
7) G. Bengtsson and M. Aronsson, *Acta Chem. Scand.*, **22**, 1241 (1968).
8) A. I. Vogel, "A Text Book of Practical Organic Chemistry," 3 rd ed, Longmans Green and Co., London (1957), pp. 169, 171, 177.
9) S. K. Sinha and S. S. Katiyar, *J. Phys. Chem.*, **74**, 1382 (1970).
10) G. E. K. Branch and B. M. Tolbert, *J. Am. Chem. Soc.*, **71**, 781 (1949).
11) M. S. Newman and B. M. Tolbert, *J. Am. Chem. Soc.*, **73**, 3644 (1951).
12) E. Q. Adams and L. Rosenstein, *J. Am. Chem. Soc.*, **36**, 1452 (1914).
13) B. M. Tolbert and G. E. K. Branch, *J. Am. Chem. Soc.*, **69**, 1083 (1947).
14) C. D. Ritchie, W. F. Sager, and E. S. Lewis, *J. Am. Chem. Soc.*, **84**, 2349 (1962).
15) C. C. Barker, G. Hallas, and A. Stamp, *J. Chem. Soc.*, **1960**, 3791.
16) J. C. Turgeon and V. K. LaMer, *J. Am. Chem. Soc.*, **74**, 5988 (1952).
17) S. W. Benson, "The Foundations of Chemical Kinetics," McGraw Hill Book Co., N. Y. (1960), p. 537.
18) N. Bjerrum, *Z. Phys. Chem.*, **108**, 82 (1924); **118**, 251 (1925).
19) E. A. Moelwyn-Hughes, "Kinetics of Reactions in Solution," Oxford University Press, London (1950), pp. 197—198.
20) E. S. Amis and G. Jaffe, *J. Chem. Phys.*, **10**, 598 (1942).
21) E. S. Amis, *J. Chem. Educ.*, **30**, 351 (1953).
22) J. E. Quinlan and E. S. Amis, *J. Am. Chem. Soc.*, **77**, 4187 (1955).
23) K. J. Laidler and P. A. Landskroener, *Trans. Faraday Soc.*, **52**, 200 (1956).
24) J. G. Kirkwood, *J. Chem. Phys.*, **2**, 351 (1934).
25) J. G. Kirkwood and F. H. Westheimer, *J. Chem. Phys.*, **6**, 506 (1938).
26) K. J. Laidler and H. Erying, *Ann. N. Y. Acad. Sci.*, **39**, 303 (1940).
27) E. S. Amis, "Solvent Effects on Reaction Rates and Mechanisms," Academic Press, New York (1966), pp. 56, 258.

Synthesis and Spectra of 3-Benzyl(or *p*-tolyl)-5-methyl-2-(substituted benzothiazol-2′-ylimino)-4-thiazolidones

Radhey SHYAM* and I. C. TIWARI

Department of Chemistry, Faculty of Science, Banaras Hindu University, Varanasi 221005, India

(Received April 8, 1974)

Some 3-benzyl(or *p*-tolyl)-5-methyl-2-(substituted benzothiazol-2′-ylimino)-4-thiazolidones were prepared. Their structures and the purity of the compounds were corroborated by their analytical and spectral data. Screening tests on these compounds showed the 4-chloro and 6-bromo analogues to be the most active as CNS depressants, muscle relaxants and anticonvulsants.

Certain thiocarbamides and their cyclic analogues are known to possess good pharmacological activity.[1] An interesting structural variation is the cyclisation of thiocarbamides to thiazolidones.[2,3] A number of disubstituted 4-thiazolidones have been prepared[4] and it has been observed that many of these compounds inhibit convulsions in cats and rats.[5] Various other Δ^4-thiazolidones have been reported[6] and the greatest effort has been made in the synthesis of heterocyclic analogues of thiazolidones.[7,8]

In extending the work, we synthesized 3-benzyl (or *p*-tolyl)-5-methyl-2-(substituted benzothiazol-2′-ylimino)-4-thiazolidones by the cyclisation of *N*-benzyl (or *p*-tolyl)-*N*′-(substituted)benzothiazol-2-yl thiocarbamides with α-chloropropionic acid under anhydrous conditions. The structures and the purity of the compounds were determined with the help of NMR, IR, and TLC. The compounds were also tested for their pharmacological activity.

Experimental

All melting points were measured by the capillary method and are uncorrected. A *Varian-A60D* was used for recording NMR spectra, a *Perkin-Elmer 257* for IR and a *Coleman Analyzer* for analyses.

N-Benzyl-N′-(4-methyl)benzothiazol-2-yl Thiourea (1). A mixture of 4-methyl-2-aminobenzothiazol (4.1 g), benzyl isothiocyanate (3.7 ml) and dry benzene (40 ml) was refluxed on a water-bath for about 5 h at 80—90 °C. The residue was filtered and washed with ether followed by a little 40% HCl solution. The product was crystallised from 80% ethanol, yield 73%, mp 170 °C. TLC: R_f=0.79 (benzene-ether, 3 : 1). Calcd for $C_{16}H_{15}N_3S_2$: N, 13.42; S, 20.45%. Found: N, 13.41; S, 20.54%. IR ν_{max}^{Nujol} cm^{-1}: 3180(⟩N-H), 3035m(⟩N-H), 1560s(⟩C=N- or ⟩C=C⟨), 1200s(⟩C=S), NMR($CDCl_3$) δ(J=Hz): 2.35(3H, s), 5.08 (2H, d, J=5.0), 7.80(1H, broad), 10.95(1H, broad) and 7.50 for aromatic protons (8H, m).

Similarly, other substituted-2-aminobenzothiazoles were converted into their respective thioureas by treating with benzyl isothiocyanate and *p*-tolyl isothiocyanate.

3-Benzyl-5-methyl-2-(4′-methylbenzothiazol-2′-ylimino)-4-thiazolidone (2). *N*-Benzyl-*N*′-(4-methyl) benzothiazol-2-yl thiourea (3.13 g) was dissolved in absolute alcohol (35 ml) and to this was added α-chloropropionic acid (1.5 ml) and anhydrous sodium acetate (2.5 g). The mixture was refluxed on a water-bath for 8—10 h and poured into cold water. On standing overnight, a solid mass precipitated. It was filtered and recrystallised from 80% ethanol into shining needles of (**2**), yield 67%, mp 149 °C. TLC: R_f= 0.79 (benzene-ether, 3 : 1). Calcd for $C_{19}H_{17}N_3OS_2$: N,

TABLE 1. PHYSICAL DATA AND IR PEAKS OF 3-BENZYL(OR *p*-TOLYL)-5-METHYL-2-(SUBSTITUTED BENZOTHIAZOL-2′-YLIMINO)-4-THIAZOLIDONES

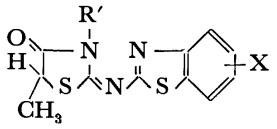

S. No.	Substituent X	Molecular formula	Yield (%)	Mp (°C)	Nitrogen (%) Found	Nitrogen (%) Calcd	Sulfur (%) Found	Sulfur (%) Calcd	Characteristic IR peaks (cm^{-1})	R_f values[a]
					R′=-CH_2·C_6H_5					
1	H	$C_{18}H_{15}N_3OS_2$	87	183	11.85	11.89	18.11	18.13	1725 s, 1565 s, 1530 s	0.68
2	4-Cl	$C_{18}H_{14}N_3OS_2Cl$	58	205	10.81	10.84	16.41	16.52	1722 s, 1648 s, 1635m	0.83
3	6-Br	$C_{18}H_{14}N_3OS_2Br$	68	215	9.62	9.72	14.95	14.81	1640 s, 1535 s, 1470m	0.50
4	4-OCH_3	$C_{19}H_{17}N_3O_2S_2$	54	209	10.84	10.96	16.82	16.71	1642 s, 1665 s, 1530m	0.79
					R′=-C_6H_4·CH_3(*p*)					
5	5-CH_3	$C_{19}H_{17}N_3OS_2$	45	189	11.31	11.44	16.91	17.43	1645 s, 1565 s, 1520 s	0.81
6	6-CH_3	$C_{19}H_{17}N_3OS_2$	78	239	11.15	11.44	17.26	17.43	1665 s, 1555 s, 1520 s	0.78
7	6-Cl	$C_{18}H_{14}N_3OS_2Cl$	83	205	10.59	10.83	16.46	16.51	1735 s, 1575 s, 1515m	0.63
8	6-Br	$C_{18}H_{14}N_3OS_2Br$	89	219	9.45	9.72	14.53	14.81	1735 s, 1595m, 1515 s	0.65

a) R_f values were measured on developing the TLC plates (adsorbent, silica gel BDH) in benzene-ether (3 : 1) mixture. s=sharp, m=medium, and w=weak.

* Present Address: Head, Department of Chemistry, Dig Vijai Nath Degre College, Gorakhpur, India.

Table 2. Pharmacological activity of 3-benzyl(or *p*-tolyl)-5-methyl-2-(substituted benzothiazol-2′-ylimino)-4-thiazolidones

S. No.[a]	Substituted	Pharmacological activity	MED/MIC	Species
2	4-Chloro	CNS Depress.	160 mg/kg po	Mouse
		Muscle Relax.	160 mg/kg po	
3	6-Bromo	CNS Depress.	160 mg/kg po	Mouse
		Muscle Relax.	160 mg/kg po	
		Electr. Shock	80 mg/kg po	
4	4-Methoxy	None	160 mg/kg po	Mouse
5	5-Methyl	None	160 mg/kg po	Mouse

MED=Minimum effective dose. MIC=Minimum inhibitory concentration. CNS=Central Nervous System.
a) S. Nos. correspond to the serial number of the compounds in Table 1.

11.44; S, 17.44%. Found: N, 11.42; S, 17.52%. IR ν_{max}^{Nujol} cm^{-1}: 1720s(>C=O), 1552s(>C=C< or >C=N-). NMR ($CDCl_3$) δ(J=Hz): 1.75(3H, d, J=7.5), 2.75(3H, s), 4.17 (1H, q, J=7.5), 5.21(2H, s) and 8.25 for aromatic protons (8H, m).

Likewise, other substituted benzothiazolyl thiazolidones were synthesised. Their structures were confirmed by their analytical, spectral and R_f values as recorded in Table 1.

Hydrolysis of 3-Benzyl-5-methyl-2-(4′-methylbenzothiazol-2′-ylimino)-4-thiazolidone (2). 3-Benzyl-5-methyl-2-(4′-methylbenzothiazol-2′-ylimino)-4-thiazolidone (1.83 g), concd HCl (2 ml) and ethanol (20 ml) were refluxed on a water-bath for 8—10 h. After distilling off the ethanol, the reaction mixture was poured into cold water and filtered. The residue was washed with water and crystallised from ethanol to afford 3-benzyl-5-methyl-2,4-thiazolidindione (**3**), yield 76%, mp 186 °C. Calcd for $C_{11}H_{11}NO_2S$: N, 6.33; S, 14.47%. Found: N, 6.53; S, 14.58%. IR ν_{max}^{Nujol} cm^{-1}: 1730s(>C=O), 1720(>C=O), 1552s(>C=C< or >C=N-). On neutralisation with ammonium hydroxide the filtrate gave 4-methyl-2-aminobenzothiazole, melting at 136 °C.

3-Benzyl-5-methyl-2,4-thiazolidindione (3). A mixture of *S*-dibenzyl thiourea (6.0 g), α-chloropropionic acid (2.0 ml) and glacial acetic acid (10 ml) was refluxed on a water-bath for 5 h and then allowed to cool. Addition of excess cold water gave a solid mass which was washed with water and dried. It was crystallised from 80% ethanol, yield 69%, mp 186 °C. Calcd for $C_{11}H_{11}NO_2S$: N, 6.33; S, 14.47%. Found: N, 6.21; S, 14.53%. IR ν_{max}^{Nujol} cm^{-1}: 1732s(>C=O), 1716s(>C=O) and 1565s(>C=C< or >C=N-).

Discussion

The structure of 3-benzyl(or *p*-tolyl)-5-methyl-2-(substituted-benzothiazol-2′-ylimino)-4-thiazolidones was assigned on the basis of the elemental analyses, spectral data and the nature of their degradation products. NMR spectrum of compound (**2**) in $CDCl_3$ shows a singlet at δ 2.75 for the benzene ring methyl protons. A doublet (J=7.5Hz) for the thiazolidone ring methyl protons at δ 1.75 and a quartet (J=7.5Hz) for the thiazolidone ring single proton at δ 4.75 were observed. A singlet at δ 5.21 was assigned to >N–$CH_2C_6H_5$ protons. The aromatic protons resonated at δ 8.25 as a multiplet. A strong IR peak at 1720 cm^{-1} for the >C=O group is the characteristic of lactam group.

Actually, the possibility of two isomeric products may be assumed here from the two possible tautomeric forms of thiocarbamides undergoing reactions with α-chloropropionic acid. The compound 3-benzyl-5-methyl-2-(4′-methylbenzothiazol-2′-ylimino)-4-thiazolidone after hydrolysis affords a residue which was identified as 3-benzyl-5-methyl-2,4-thiazolidindione by comparing with an authentic sample of the thiazolidindione (**3**) by the mixed melting point method.

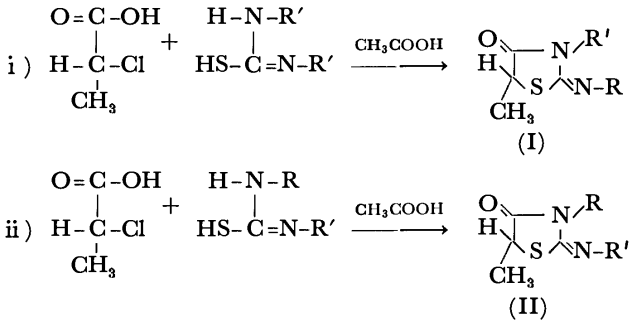

R=(substituted)benzothiazol-2-yl-
R′=benzyl or *p*-tolyl-

The structure of 3-benzyl-5-methyl-2,4-thiazolidindione (**3**) is also supported by its IR spectrum which shows an additional peak at 1730 cm^{-1} for the carbonyl group attached to position-2 of the thiazolidindione ring.

Hence the hydrolysis as well as spectral data show the attachment of 2-amino-(substituted)benzothiazoles residue at position-2 and benzyl or *p*-tolyl residue at position-3, thereby confirming the structure as type I but not as type II. Therefore, these findings agree with structure III for compound (**2**).

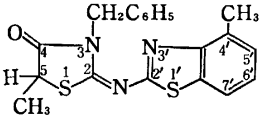

(III)

Screening Results. The selected compounds have been tested for their pharmacological activities at Bristol Laboratories, Syracuse, New York. The com-

pound 3-benzyl-5-methyl-2-(4′-chlorobenzothiazol-2′-ylimino)-4-thiazolidone was found to be active as a CNS depressant and muscle relaxant and 3-benzyl-5-methyl-2-(6′-bromobenzothiazol-2′-ylimino)-4-thiazolidone as a CNS depressant, muscle relaxant and anticonvulsant.

Thanks are due to Prof. P. N. Bhargava, for his keen interest and Prof. G. B. Singh and Dr. R. S. Dwivedi for providing facilities. The financial assistance provided by CSIR, New Delhi to R.S. and by PGIIM, B.H.U. to I.C.T. is gratefully acknowledged.

References

1) L. Doub, L. M. Richardson, D. R. Herbst, M. L. Black, O. L. Stevenson, L. L. Bambas, G. P. Youmans, and A. S. Youmans, *J. Am. Chem. Soc.*, **80**, 2205 (1958).
2) P. N. Bhargava, (Miss) K. Bhargava, and R. C. Kapoor, *J. Ind. Chem. Soc.*, **38**, 23 (1961).
3) P. N. Bhargava and M. R. Chaurasia, *J. Chem. UAR*, **12**, 149 (1969).
4) F. B. Drains, R. Irvin, and C. C. Harvel, *J. Am. Chem. Soc.*, **43**, 613 (1921).
5) H. D. Troutman and L. M. Long, *J. Am. Chem. Soc.*, **70**, 3436 (1948).
6) L. P. Kolomoitsue, N. I. Geonya, B. E. Zhitar, and S. N. Baranov, *Mikrobiol. Zh. (Kiev)*, **33**, 255 (1971).
7) K. S. L. Srivastava, *Ind. J. Appl. Chem.*, **32**, 369 (1969).
8) H. Tripathi, P. N. Dhal, and G. N. Mahapatra, *J. Ind. Chem. Soc.*, **50**, 135 (1973).

Fluorination with Substituted (Difluoroiodo)arenes

Ana GREGORČIČ and Marko ZUPAN*

"*J. Stefan*" *Institute and Department of Chemistry, University of Ljubljana, 61000 Ljubljana, Yugoslavia*

(Received January 21, 1976)

The reaction of substituted (difluoroiodo)arenes with 1-phenyl-1-(*m*-chlorophenyl)ethylene results in 1,1-difluoro-1-(*m*-chlorophenyl)2-phenylethane, with 1-phenyl-1-(*p*-methoxyphenyl)ethylene in 1,1-difluoro-1-phenyl-2-(*p*-methoxyphenyl)ethane, and with 1-phenylcyclopentene and 1-phenylcyclohexene in rearranged *gem*-difluoro compounds. The reaction with norbornene results in three products: fluoronortricyclane (9—12%), 2-*exo*-7-*syn*-difluoronorbornane (75—86%), and 2-*exo*-7-*anti*-difluoronorbornane (5—15%) depending upon the substituent on the phenyl ring in (difluoroiodo)arenes.

The addition of chlorine to olefinic double bonds using (dichloroiodo)benzene as a halogenating agent has received (difluoroiodo)arenes attention from several workers.[2-5] The corresponding received much more limited attention as fluorinating agents, possibly because of the difficulties involved in their preparation and storage. Three methods are of particular interest for the preparation of (difluoroiodo)arenes. The first is the method of Dimroth and Bockemüller[6] or the modified one of Garvey *et al.*[7] in which the appropriate iodosoarene is treated with 46% hydrogen fluoride in acetic acid. The method of Carpenter[8] involves one-step reaction of mercuric oxide and aqueous hydrofluoric acid with (dichloroiodo)benzene in dichloromethane. The dichloromethane solution is then used directly for fluorination. The third procedure[9] involves the electrolysis of an acetonitrile solution of silver(I) fluoride. We developed a method for the synthesis of various (difluoroiodo)arenes, using xenon difluoride as fluorinating agent in dichloromethane solution, in the presence of anhydrous hydrogen fluoride at room temperature.[10] We have recently found that (difluoroiodo)methane reacts with phenylalkenes in the presence of hydrogen fluoride as a catalyst to form the corresponding 1-fluoro-2-iodo-1-phenylalkanes,[11] and not the rearranged *gem*-difluoro compounds observed in similar fluorination reactions with (difluoroiodo)arenes.[8,12] We now report the study of fluorination of various phenylalkenes and norbornene with substituted (difluoroiodo)arenes.

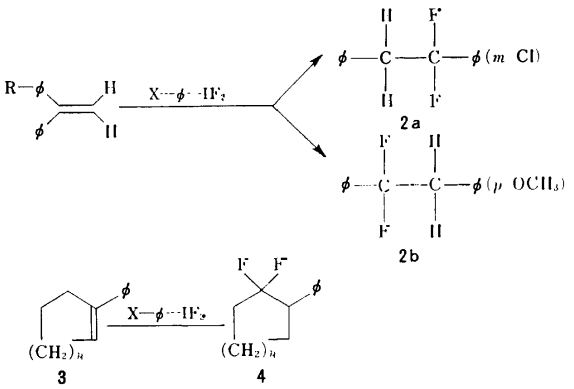

Scheme 1.

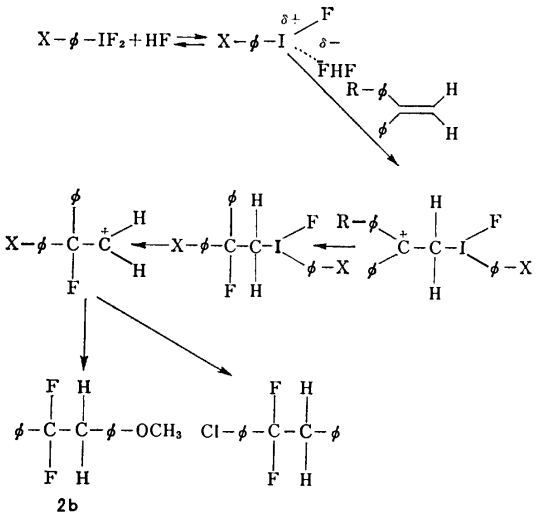

Scheme 2.

Results and Discussion

(Difluoroiodo)arenes have already been used for fluorination of 1,1-diphenylene[12] and styrene[8], giving *gem*-difluoro compunds. Carpenter[8] showed that hydrogen fluoride or some other strong acid such as trifluoroacetic acid is necessary as a catalyst in the fluorination reaction, and proposed an ionic mechanism with the phenonium ion as the intermediate. We obtained evidence which supports the phenonium ion intermediate by the fluorination of 1-phenyl-1-(*m*-chlorophenyl)ethylene (**1a**), 1-phenyl-1-(*p*-methoxyphenyl)ethylene (**1b**) with substituted (difluoroiodo)-arenes (Scheme 1). The reactions resulted in 1,1-difluoro-1-(*m*-chlorophenyl)-2-phenylethane (**2a**) and 1,1-difluoro-1-phenyl-2-(*p*-methoxyphenyl) ethane (**2b**), respectively. The structures of the products were estabished on the basis of their NMR data (δF-100 ppm (t, J_{FH}=15 Hz)) for **2a** and (δF-105.2 ppm (t, J_{FH}=16.5 Hz)) for **2b**, which correspond to those of *gem*-difluoro compounds. In the mass spectrum the fragments for the product **2a** were the tropylium ion *m/e* 91 and the difluorochlorobenzylium ion *m/e* 161, indicating phenyl group migration. On the other hand, product **2b** showed as fragments the methoxytropylium ion *m/e* 121 and the difluorobenzylium ion *m/e* 127, which indicates *p*-methoxyphenyl group migration. The fluorination of the phenyl-substituted cycloolefins, 1-phenylcyclopentene (**3a**) and 1-phenylcyclohexene (**3b**), with (difluoroiodo)arenes also resulted in the formation of *gem*-difluoro compounds (**4**) (Scheme 1), which could be identified by their NMR and mass spectral data. We were unable to detect any trace of

iodofluoro compounds. In the light of these experiments we suggest a mechanism similar to that proposed by Carpenter[8] (Scheme 2). It might be expected that in the presence of hydrogen fluoride, substituted (difluoroiodo)arenes behave as electrophiles (reactions were completely quenched when no hydrogen fluoride was added), adding to an olefin, thus forming a carbonium ion, which is then attacked by the fluoride ion. In the next step, dissociation of the carbon iodine bonds results in the formation of carbonium ion, accompanied by phenyl group or *p*-methoxyphenyl group migration.

The reaction of a bicyclic olefin, norbornene, has been utilized for elucidating the mechanism and stereochemistry of various reactions.[13-18] It is possible (from the identification of the products) to discriminate the three possible mechanistic pathways leading to the products; (i) a concerted *cis*-molecular addition, (ii) a free radical reaction, (iii) a reaction path proceeding *via* cationic intermediates.

We have studied the fluorination reaction of various substituted (difluoroiodo)arenes with norbornene. Reactions resulted in the formation of three products, which could be separated by preparative GLC. The first product shows in its ^{19}F NMR (rel to CCl_3F) spectrum a doublet of triplet at −218.2 ppm, and in H NMR spectrum at $\delta = 5.05$ ppm a doublet of triplet signal which corresponds to the proton bonded on the same carbon atom as the fluorine atom, with the characteristic geminal F-H coupling constant of 69 Hz. The product **6** was synthesised independently by addition of hydrogen fluoride to norbornadiene,[19] which made it possible to determine the structure of the first product as fluoronortricyclane (**6**). Both of the remaining products showed a similar mass spectrum with the molecular peak *m/e* 132, which suggests the structure of the difluoro compounds. The basic peak for both of the products *m/e* 81 corresponds to the splitting off of the fragment $-CHF_2$. In the mass spectra of both compounds, the fragments were *m/e* 99, 86, 85, 72, which correspond to the splitting off of $-CH_2F$, $-C_2H_3F$, $-C_2H_4F$, and C_3H_5F fragments, respectively. From the extraordinary similarity of the mass spectra we concluded that the two compounds are remarkably alike. The product obtained in the lower yield (5—13%), shows in its ^{19}F NMR spectra two signals; one at −176.2 ppm as doublet of multiplet, corresponding to an *exo*-bonded fluorine atom, and the other at −232.3 ppm as doublet of triplet, which corresponds to fluorine bonded at C7. In the proton spectrum we have observed two signals for hydrogen atoms at lower field, the first at $\delta = 4.28$ ppm as doublet of multiplet, corresponding to an *endo*-bonded hydrogen atom, and the second signal at $\delta = 5.48$ ppm as doublet, which corresponds to a hydrogen atom at C7 (see Experimental).

The main product formed in the fluorination of norbornene with substituted (difluoroiodo)arenes shows an NMR spectrum very similar to that of the previously described one.[18] In the ^{19}F spectrum we observed a signal at −179.5 ppm as doublet of multiplet and the second at −223.5 ppm as doublet of multiplet. In the proton NMR we observed two protons at a lower field, one at 5.1 ppm as a doublet of doublet and the other at 5.21 ppm as a doublet. From the data we were unable to decide the stereochemistry at position C7. However, from a detailed comparison of the NMR spectra with the literature ones[18] the stereochemistry on C7 could be confirmed. If we compare the chemical shifts for protons bonded at C7 in various substituted norbornane derivatives[18] we see that the one in the 2-*exo*-7-*anti* isomer is at a lower field than the one in the 2-*exo*-7-*syn* isomer. The chemical shift for the proton at C2 is at a higher field in the 2-*exo*-7-*anti* isomer (but not in all cases) than in the 2-*exo*-7-*syn* isomer. Tanner and Van Bostelen[18] established the stereochemistry at the Carbon 7 also by chemical transformations, *i.e.*, dehydrofluorination and reduction. From the data mentioned above, we can conclude that the main product, formed in 75—86% yield, is 2-*exo*-7-*syn*-difluoronorbornane (**7**), and the third product, obtained in 5—13% yield, is 2-*exo*-7-*anti*-difluoronorbornane (**8**) (Scheme 3).

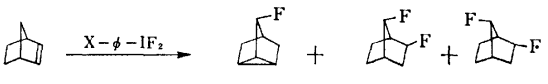

5 6 7 8

Relative yields[a]

X	6	7	8
p-OCH_3	12	75	13
m-OCH_3	18	74	8
H	9	84	7
m-Cl	6	88	6
m-NO_2	9	86	5

a) Determined by GLC.

Scheme 3.

We have studied the effect of groups bonded to benzene ring on the distribution of the products formed in the reaction of norbornene with substituted (difluoroiodo)arenes. The ratios of the products were established by VPC. Each reaction was repeated several times the average data being presented in Scheme 3. We observed no isomerisation of the products under the reaction and isolation conditions or during the course of isomerisation. The data (Scheme 3) show a very high yield (86%) of 2-*exo*-7-*syn*-difluoronorbornane (**7**) formed in the reaction with the *m*-nitro derivative. On the other hand, with electron donating substituents bonded to the benzene ring of (difluoroiodo)arenes, we observed a lower amount of product **7** and a higher amount of compound **8**.

The formation of three products could be explained by the reaction of norbornene with the polarized molecule of (difluoroiodo)arenes with hydrogen fluoride, thus primarily forming the carbonium ion A (Scheme 4) which undergoes the Wagner-Meerwein rearrangement, in turn forming ions B, which could be attacked by the nucleophile, leading to the product F. The S_N2 substitution of the aryliodo function by fluoride anion can produce 2-*exo*-7-*anti*-difluoronorbornane (**8**). Carbonium ion B can undergo the hydride 6—1 shift, thus forming carbonium ion C, followed by nucleophilic attack of fluoride anion and

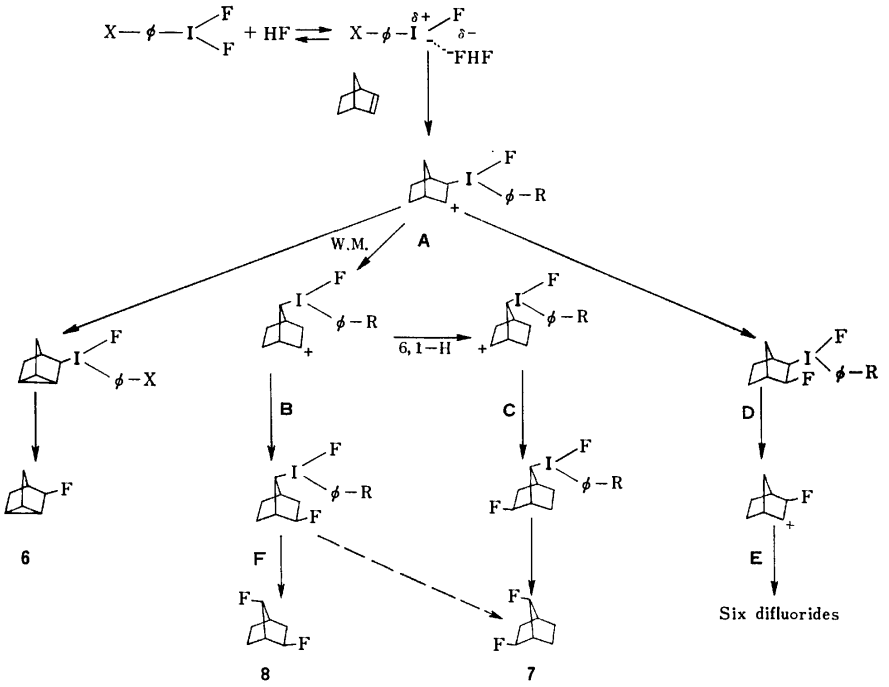

Scheme 4.

S_N2 substitution of aryliodo function, resulting in the formation of 2-*exo*-7-*syn*-difluoronorbornane (**7**). The next possibility for an explanation of the formation of difluoro compounds could be the attack of fluoride anion on the primarily formed carbonium ion A, thus forming the adduct D, and dissociation of carbon–iodine bond leading to formation of fluorocarbonium ion E, which would rearrange by Wagner-Meerwein and hydride shift, resulting in six difluoro compounds. The β-fluorocarbonium ion E formed in the reaction of xenon difluoride with norbornene undergoes rearrangement, thus forming six difluoro compounds[20] after fluoride anion attack. From the results we could eliminate this reaction pathway. However, we suggest another possible explanation for the formation of product **7** in a high yield (Scheme 5). The intermediately formed compound F can be polarized by hydrogen fluoride and *via* the transition state G results in difluoro compounds.

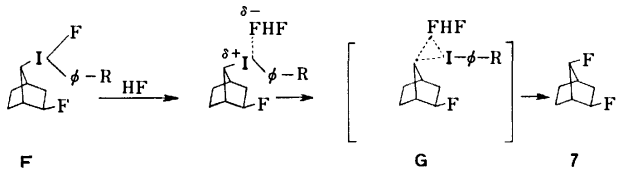

Scheme 5.

Experimental

IR spectra were recorded with a Perkin-Elmer 257 spectrometer, ^1H and ^{19}F NMR spectra with a Jeol JNM-PS-100 from CCl_4 solution with TMS or CCl_3F as an internal reference. Mass spectra and high resolution measurements were taken on a CEC-21-110 spectrometer. Gas-Liquid partition chromatography was carried out on a Varian Aerograph Model 1800 and TLC on Merck PSC-fertigplatten SILICA GEL F-254.

Materials. Pure samples of olefins were prepared by known methods: 1-phenyl-1-(*m*-chlorophenyl)ethylene,[21] 1-phenyl-1-(*p*-methoxyphenyl)ethylene,[21] 1-phenylcyclopentene,[22] 1-phenylcyclohexene.[22] Other commercial olefins were distilled or purified by VPC to conform with published physical and spectral data. Substituted iodobenzenes were prepared by known methods from corresponding amino derivatives and distilled before use. Dichloromethane was purified[23] and stored over molecular sieves. Hydrogen fluoride of Fluka Purum quality was used, and xenon difluoride was prepared by the photosynthetic method[24] with a purity better than 99.5%.

Substituted (Difluoroiodo)benzenes. Substituted iodobenzene (1.1 mmol) was dissolved in dichloromethane (5 ml) at room temperature. Anhydrous HF (1—3 mmol) was introduced into the reaction mixture and pure XeF_2 (1.1 mmol) was added under stirring. After a few second the colourless solution turned dark green, xenon gas being evolved. Gas evolution ceased after 45 min (for *p*-OCH_3, or 3 h for the *m*-NO_2 derivative) and the reaction appeared to be complete. The solution was used for fluorination of olefins.

General Procedure for Fluorination with Substituted (Difluoroiodo)-arenes: To a solution of the previously prepared substituted (difluoroiodo)arenes was added 1 mmol of olefin under stirring at room temperature. After 2 h the reaction mixture was diluted with dichloromethane (15 ml), washed with 10 ml of 5% $NaHCO_3$, dried over anhydrous Na_2SO_4, the solvent being evaporated *in vacuo*. The crude products were separated by preparative TLC or GLC.

1,1-Difluoro-1-(m-chlorophenyl)-2-phenylethane (2): The product was separated by preparative TLC (silica gel, methanol : chloroform = 1 : 9) yield 50% of oily product. NMR δF-100 ppm (t), δH = 3.25 (t), ppm, $\delta\phi$ = 7.2 (m) ppm, J_{FH} = 15 Hz. Mass spectrum: calcd for $C_{14}H_{11}ClF_2$ *m/e* 252.0517, found *m/e* 252.0510, *m/e*: 254 (M^++2,4%), 252 (M^+, 12%), 215 (40), 179 (40), 178 (46), 163 (10), 161 (30), 91 (100), 89 (18), 77 (20), 76 (20), 75 (16), 51 (25).

1,1-Difluoro-1-phenyl-2-(p-methoxyphenyl)ethane (2b): The

product was separated by preparative TLC (silica gel, methanol : chloroform = 1 : 9), yield 55% of yellow oily product. NMR δF-105.0 (t) ppm, δH = 3.3 (t) ppm, δOCH_3 = 3.7 (s) ppm, $\delta\phi$ = 7.2 (m) ppm, J_{FH} = 16.5 Hz. Mass spectrum: calcd for $C_{15}H_{14}F_2O$ *m/e* 248.1008, found *m/e* 248.1008, *m/e*: 248 (100%, M^+), 209 (46), 197 (40), 165 (46), 139 (40), 127 (46), 121 (60), 77 (40).

1-Phenyl-2,2-difluorocyclopentane (***4a***): The product was separated by preparative TLC (silica gel, cyclohexane: chloroform = 4 : 1), yield 60% of yellow oily product. NMR δF-101.3 (m) ppm, $\delta\phi$ = 7.3 (m) ppm, δH = 2 (m) ppm. Mass spectrum: calcd for $C_{11}H_{12}F_2$ *m/e* 182.0902, found *m/e* 182.0911, *m/e*: 182 (M^+, 3%), 155 (14), 154 (100, 153 33 (33), 152 (21), 117 (47), 115 (50), 77 (10), 76 (17).

1-Phenyl-2,2-difluorocyclohexane (***4b***): The product was separated by preparative TLC (silica gel, methanol: chloroform = 1 : 9), yield 63% of yellow oily product. NMR δF-103.5 (m) ppm, $\delta\phi$ = 7.5 (m) ppm, δH = 1.7 (m) ppm. Mass spectrum: calcd for $C_{12}H_{14}F_2$ *m/e* 196.0125, found *m/e* 196.0160, *m/e*: 196 (M^+, 35%), 176 (9), 173 (9), 158 (14), 154 (55), 153 (21), 152 (13), 130 (22), 129 (17), 128 (30), 127 (100), 117 (37), 104 (30), 91 (33), 77 (38), 69 (48), 68 (55), 58 (34).

Products Formed in the Fluorination of Norbornene: Separated by preparative GLC (Chromosorb Regular 100-DDP 10%, ϕ 3/8′ × 2 m, stainless steel column).

Fluoronortricyclane (***6***): Yield 8% of volatile, white waxy solid product, mp (sealed capillary) 44—45 °C, lit,[19] 48—50 °C. NMR (CCl_4): δF-218.2 (dt) ppm, δH = 5.05 (dt) ppm, J_{FH} = 69 Hz. Mass spectrum: calcd for C_7H_9F *m/e* 112.0688, found *m/e* 112.0697.

2-exo-7-syn-Difluoronorbornane (***7***): Yield 68% of volatile, white waxy solid product, mp (sealed capillary) 116—119 °C, lit,[18] 95—97 °C. NMR (CCl_4): δF2-179.5 (dm) ppm, δF7-223.5 (dm) ppm, δH_2 = 5.1 (dd) ppm, δH7 = 5.2 (d) ppm, J_{F2H2} = 60 Hz, J_{F2H} = 40 Hz, J_{F7H7} = 63 Hz, J_{F7H} = 12.6 Hz. Mass spectrum: calcd for $C_7H_{10}F_2$ *m/e* 132.0752. Anal. calcd for $C_7H_{10}F_2$: C, 63.60; H, 7.63; found C, 63.32; 7.40.

2-exo-7-anti-Difluoronorbornane (***8***): Yield 6% of volatile, waxy solid product, mp (sealed capillary) 101—102 °C, lit,[18] 107—110 °C. NMR (CCl_4): δF2-176.2 (dm) ppm, δF7-232.3 (dt) ppm, δH2 = 4.28 (dm) ppm, δH7 = 5.48 (d) ppm, J_{F2H2} = 60 Hz, J_{F2H} = 30 Hz, 7.5 Hz, J_{F7H7} = 65 Hz, J_{F7H} = 3 Hz. Mass spectrum calcd for $C_7H_{10}F_2$ *m/e* 132.0750, found *m/e* 132.0753. Anal. calcd for $C_7H_{10}F_2$: C, 63.60; H, 7.63, found C, 63.44; H, 7.70.

We thank Prof. J. Slivnik for the supply of XeF_2 and Prof. J. Marsel for the use of facilities. Financial assistance from the Boris Kidrič Foundation and the "KRKA" Pharmaceutical Co., Novo mesto, is acknowledged.

References

1) Presented in part at 5 th European Symposium on Fluorine Chemistry, Aviemore, September 1974.
2) D. F. Banks, *Chem. Rev.*, **66**, 243 (1966).
3) D. H. R. Barton and E. Miller, *J. Am. Chem. Soc.*, **72**, 370 (1950).
4) S. J. Cristol, F. R. Stermitz, and P. S. Ramey, *J. Am. Chem. Soc.*, **78**, 4939 (1956).
5) D. D. Tanner and G. C. Gidley, *J. Org. Chem.*, **33**, 38 (1968).
6) O. Dimroth and W. Bockemüller, *Ber.*, **64**, 516, 522, (1931).
7) B. S. Garvey, Jr., L. F. Halley, and C. F, Allen, *J. Am. Chem. Soc.*, **59**, 1827 (1937).
8) W. Carpenter, *J. Org. Chem.*, **31**, 2688 (1966).
9) H. Schmidt and H. Meinert, *Angew. Chem.*, **72**, 109 (1960).
10) M. Zupan and A. Pollak, *J. Fluorine Chem.*, in press.
11) M. Zupan and A. Pollak, *Tetrahedron Lett.*, **1975**, 3576.
12) J. Bornstein, M. R. Borden, F. Nunes, and H. I. Tarlin, *J. Am. Chem. Soc.*, **85**, 1909 (1963).
13) R. C. Fahey, *Top. Stereochem.*, **3**, 237 (1968).
14) J. A. Berson, "Carbonium Ion Rearrangement in Bridged Bicyclic Systems," in Molecular Rearrangements, Vol. 1, Part 2, ed by P. de Mayo, Interscience, New York (1963), p. 111.
15) T. G. Traylor, *Acc. Chem. Res.*, **2**, 152 (1969).
16) D. R. Marshall, P. Reynolds-Warnhoff, E. W. Warnhoff, and J. R. Robinson, *Can. J. Chem.*, **49**, 885, (1971).
17) H. C. Brown and Kwang-Tin Liu, *J. Am. Chem. Soc.*, **97**, 2469 (1975).
18) D. D. Tanner and P. Van Bostelen, *J. Am. Chem. Soc.*, **94**, 3187 (1972).
19) M. Hanack and W. Kaiser, *Justus Liebigs Ann. Chem.*, **1962**, 657, 12.
20) M. Zupan, A. Pollak, and A. Gregorčič, presented in part at Sastanak Kemičara Hrvatske 1975, Zagreb, Yugoslavia. We isolated: 2-*exo*-3-*exo*-, 2-*exo*-3-*endo*-, 2-*exo*-5-*exo*-, 2-*exo*-5-*endo*-, 2-*exo*-7-*syn*- and 2-*exo*-7-*anti*-difluoronorbornane.
21) J. E. Dubois, A. F. Hegarty, and E. D. Bergmann, *J. Org. Chem.*, **37**, 2218 (1972).
22) E. W. Garbisch, *J. Org. Chem.*, **26**, 4165 (1961).
23) J. H. Mathews, *J. Am. Chem. Soc.*, **48**, 562 (1926).
24) S. M. Williamson, *Inorg. Syn.*, **11**, 147 (1968).

NOTES

BULLETIN OF THE CHEMICAL SOCIETY OF JAPAN, VOL. 50 (2), 521—522 (1977)

The Position Dependence of the SCF Screened Potential in Several Pseudo-Jahn-Teller Nonbenzenoid Aromatic Hydrocarbons

Tsuguo KOYANAGI and Hiroyuki YAMAGUCHI

Department of Chemistry, Kumamoto University, Kurokami, Kumamoto 860

(Received August 16, 1976)

Synopsis. The SCF screened potentials of pentalene, heptalene, and *s*-indacene were calculated by using the SCF screened potential MO CI method. The characteristics of the screened potential in the nuclear arrangement belonging to the lower molecular symmetry group, C_{2h}, are similar to those of the polyene.

Recently, Terasaka *et al.*[1] have shown that there are two kinds of screening (screening and anti-screening) in molecules such as polyene in which there exists a strong bond alternation, while there is only one kind of screening in molecules such as benzene and azulene which do not show a clear bond alternation.

The purpose of this paper is to investigate the position dependence of the SCF screened potential in pseudo-Jahn-Teller nonbenzenoid hydrocarbons, such as pentalene (I), heptalene (II), and *s*-indacene (III), by using the SCF screened potential MO CI method in combination with the variable bond-length technique.[1,2] It may be possible to use the results of such calculations to deepen our understanding of the aromatic characteristics of nonbenzenoid aromatic hydrocarbons.

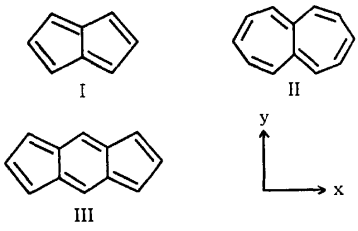

Fig. 1. Numbering of molecules and choice of axes.

Method of Calculation

A procedure that combines the SCF screened potential with the variable bond-length technique[1,2] is used in the Pariser-Parr-Pople SCF MO CI method.[3,4] At each step of the SCF calculation, the new bond lengths are obtained from the corresponding bond orders.[5] The screened potential is evaluated by using the bare potential (Mataga-Nishimoto[6]) obtained from the new bond lengths. This screened potential is thus used in the calculation of the next SCF step. The calculation is repeated until self-consistency is reached. As the starting geometrical structures for iterative calculation, we adopt various distorted structures in which bond lengths are distorted, so that the set of displacement vectors may form a basis for an irreducible representation of the full symmetry group, D_{2h}, of molecules I, II, and III. In the case of I, for example, there are 3, 2, 2, and 2 distinct bond distortions belonging to a_g, b_{1g}, b_{2u}, and b_{3u} respectively. If self-consistency is achieved at two or more different nuclear arrangements, the total energies should be compared with each other in order to determine which one is most favorable. The total energy is assumed to be the sum of the π-electron energy and the σ-electron energy, the latter being calculated by using the harmonic oscillator model, with the force constant equal to 714 kcal/Å.[7] All the singly-excited states are considered in the calculation of the RPA porlarization part.

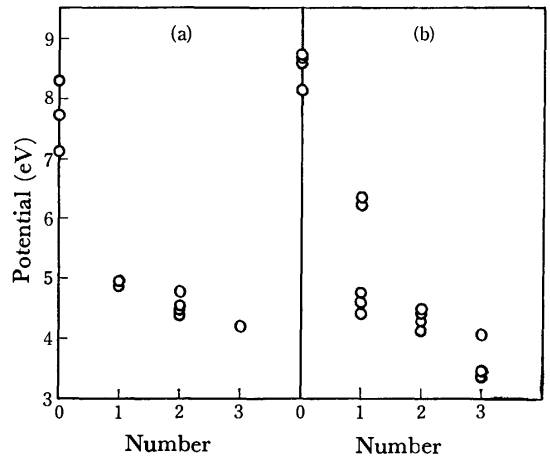

Fig. 2. The SCF screened potentials in pentalene plotted *vs.* the number; (a) the nuclear arrangement D_{2h}, (b) the nuclear arrangement C_{2h}.

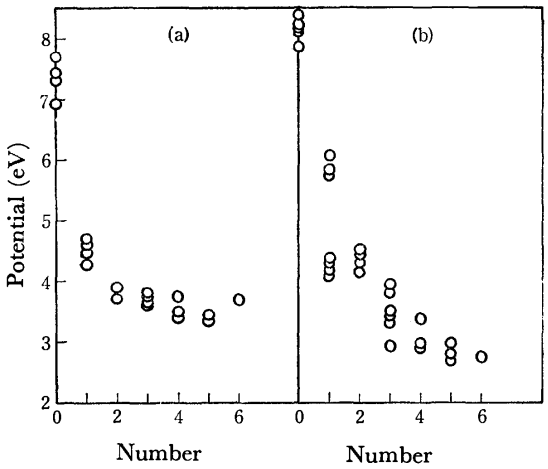

Fig. 3. The SCF screened potentials in heptalene plotted *vs.* the number; (a) the nuclear arrangement D_{2h}, (b) the nuclear arrangement C_{2h}.

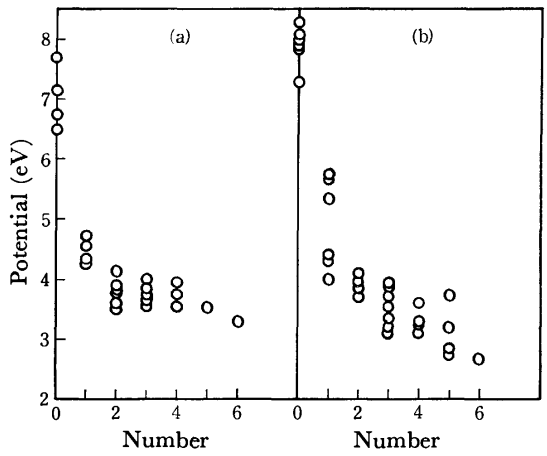

Fig. 4. The SCF screened potentials in *s*-indacene plotted *vs.* the number; (a) the nuclear arrangement D_{2h}, (b) the nuclear arrangement C_{2h}.

Results and Discussion

The starting bond distortions, belonging to the a_g, b_{2u}, and b_{3u} representations, all converge into the unique self-consistent set of bond lengths belonging to the molecular symmetry group D_{2h}, while the distortions belonging to b_{1g} converge into another set of bond lengths belonging to C_{2h}. The nuclear arrangement belonging to C_{2h} is energetically more favored than that belonging to D_{2h}. The stabilization energies for I, II, and III are predicted to be 8.2, 12.0, and 2.2 kcal/mol respectively. There exists a strong bond alternation in the peripheral carbon skeleton of the nuclear arrangement, C_{2h}. There is no bond alternation in the peripheral carbon skeleton of the nuclear arrangement, D_{2h}. The above results are almost the same as the results obtained by using the bare potential SCF CI method.[8]

In Figs, 2, 3, and 4, the SCF screened potentials, V, in the nuclear arrangements, D_{2h} and C_{2h}, of I, II, and III are plotted against a number that indicates the kind of screened potential, that is, 0: one-center potentials V_{11}, V_{22}, V_{33},$\cdots$; 1: the nearest two-center potentials V_{12}, V_{23}, V_{34},$\cdots$, *etc.* There is only one kind of screened potential at each of the numbers in the D_{2h} structures of I, II, and III (*cf.* Fig. 9 of Ref. 1). There is one kind of screened potential at the even numbers in the C_{2h} structures of these molecules. However, under the influence of the bond-length alternation, there are two kinds of screened potentials, screening and anti-screening, at the odd numbers in the C_{2h} structures of I, II, and III. Such characteristics of the screened potentials in the C_{2h} structures of I, II, and III show a tendency similar to those of the polyene shown in Fig. 7 of Ref. 1.

References

1) T. Terasaka, T. Iijima, Y. Fujimura, and T. Nakajima, *Bull. Chem. Soc. Jpn.*, **46**, 1301 (1973).
2) H. Yamaguchi, T. Nakajima, and T. L. Kunii, *Theor. Chim. Acta (Berl.)*, **12**, 349 (1968).
3) R. Pariser and R. G. Parr, *J. Chem. Phys.*, **21**, 446, 767 (1953).
4) J. A. Pople, *Trans. Faraday Soc.*, **49**, 1375 (1953).
5) T. Nakajima and S. Katagiri, *Mol. Phys.*, **7**, 149 (1964).
6) N. Mataga and K. Nishimoto, *Z. Phys. Chem.*, **13**, 140 (1957).
7) L. C. Snyder, *J. Phys. Chem.*, **66**, 2299 (1962).
8) T. Nakajima, "Topics in Current Chemistry," Vol. 32, Spring-Verlag, Heidelberg (1972), p. 1.

BULLETIN OF THE CHEMICAL SOCIETY OF JAPAN, VOL. 50 (2), 523—524 (1977)

Effect of Pressure on Interfacial Tension between Oil and Water

Norihiro MATUBAYASI, Kinsi MOTOMURA, Shoji KANESHINA,
Makoto NAKAMURA, and Ryohei MATUURA
Department of Chemistry, Faculty of Science, Kyushu University, Fukuoka 812

(Received August 23, 1976)

Synopsis. The interfacial tension of hexane, octane, carbon tetrachloride and benzene against water was measured as a function of pressure up to 150 MPa at 303.15 K, using a newly designed apparatus. The interfacial tension showed definite increase with pressure and positive volume change was found on interface formation.

Several experimental studies have been carried out on the effect of pressure on interfacial tension between oil and water, but no coincidence of the results has been exhibited because of the lack of precaution for precise measurement.[1-6] It is necessary for the thermodynamic study of the interface to measure the exact pressure dependence of interfacial tension.

Experimental

A pendant drop method was adopted for measuring interfacial tension. This method is very satisfactory for the accurate evaluation of the interfacial tension between oil and water, but some precaution should be kept for precise measurement. We have newly designed an apparatus suitable for organic liquid/water interface. A schematic diagram of the apparatus designed here is shown in Fig. 1. The pressure vessel is a cylinder of stainless steel (SUS 27) 110 mm in o.d., 25 mm in i.d., and 420 mm in height, in which two quartz windows 12 mm thick and 20 mm in diameter are installed so that we can take the picture of pendant drop profiles by the camera. In order for the pendant drop cell to be free from contamination, which is caused by desorption of surface active impurities from the vessel, the cell is made of quartz, which consists of the syringe, the barrel shaped optical part, the drop forming tip, and the cylinder. The capacity of the cell is about 20 cm^3; the syringe and cylinder are filled out with water and organic liquid, respectively; and the pendant drop is formed by making use of the difference on their isothermal compressibility. Pressure was generated by means of a high pressure hand-pump and measured with a Heise bourdon gauge. Temperature was kept constant at 303.15 K by circulating thermostated water in the jacket of the pressure vessel.

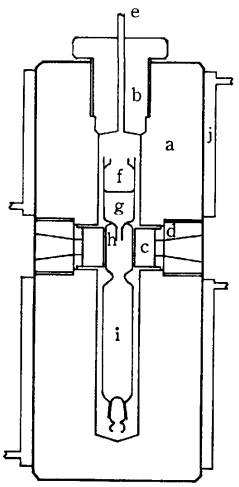

Fig. 1. Schematic diagram of the apparatus. a) Cylinder; b) flange; c) quartz window; d) window plug; e) pressure tubing with which the pressure pump and bourdon gauge are connected; f) plunger; g) syringe in which water is filled; h) drop forming tip; i) cylinder in which oil is filled; j) jacket.

Water used was refluxed with $KMnO_4$ and distilled. Organic liquids were purified by the usual method and the purity was checked by evaluating the interfacial tension at the atmospheric pressure. Water and organic liquids were stored together so that mutual solubilities were attainable.

Since the mutual solubilities of water–organic liquid systems are negligibly small, we used the density and compression data of pure water and organic liquids for the calculation of interfacial tension.[7-11]

The pendant drop cell was filled with water and organic liquid before it was set in the pressure vessel. Measurements of the interfacial tension were made under the condition of increasing pressure. For each rise in pressure, the apparatus was allowed to stand for 30 min so as to remove errors brought about by the adiabatic compression. Then the enlarged photograph of pendant drop was taken by the camera at each pressure. The dimensions of profile were determined to a precision of μm by Nikon Measurescope. The interfacial tension was calculated by using an equation proposed by Andreas *et al.*[12] and Fordham's correction factor was applied within a precision of ± 0.1 mN m^{-1}.[13]

Results and Discussion

The interfacial tension-pressure (γ-p) curves observed for organic liquid–water system are shown in Fig. 2. It is seen that the interfacial tension increases with an

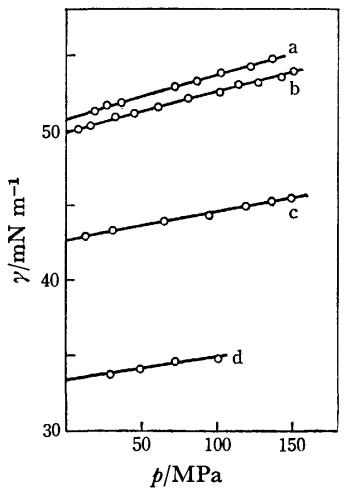

Fig. 2. The variation of the interfacial tension with pressure. a) octane/water; b) hexane/water; c) carbon tetrachloride/water; d) benzene/water.

increase in pressure and the slope of the curve is almost constant all over the pressure range investigated. The experimental equation expressing the interfacial tension as a function of the pressure is then formulated as

$$\gamma = a + bp \quad (1)$$

The constants a and b were determined by the method of least squares. The values of a and b evaluated are given in Table 1. It is apparent that the slope of γ-p curve

Table 1. The constants of the Eq. 1 resulting in the best fit to the experimental data

	a/mN m^{-1}	b/mN m^{-1} MPa^{-1}
Octane	50.89	0.0287
Hexane	49.94	0.0259
Carbon tetrachloride	42.68	0.0188
Benzene	33.42	0.0138

varies regularly with the value of interfacial tension, which is known to be correlated directly with the mutual solubility between organic liquid and water.[14] Some of these systems have been studied by several investigators. For benzene–water system, Hassan *et al.* observed for the slope to be negative,[3] Michaels *et al.* reported that the slope is positive at lower temperatures and negative at higher temperatures,[2] and Harvey observed that the γ-p curve has a minimum when temperature is low.[4] On the other hand, Jennings obtained the linear γ-p which bears a positive but very small slope.[5] The slopes obtained by these investigators are definitely small compared with those given in Table 1. Taking into consideration that they used pendant drop cells made of stainless steel with which water and organic liquids were in contact, it seems likely that the discrepancy among them can be ascribed to contamination by surface-active impurities, because it is found that the slope of γ-p curve is diminished by the adsorption of surface-active substances.[15]

According to the thermodynamics, the variation of interfacial tension with pressure at constant temperature is shown to be given by the equation

$$(\partial\gamma/\partial p)_{T,\sigma} = (\partial V/\partial\sigma)_{T,p} \quad (2)$$

where V is the volume of the organic liquid–water system and σ the interfacial area.[16] The right-hand side of the above equation expresses the volume change ΔV accompanied by the interface formation. Applying this equation to the present data we see ΔV being positive, as shown in Table 1 as b.

References

1) C. J. Linde, *Phys. Rev.*, **22**, 181 (1906).
2) A. S. Michaels and E. A. Hauser, *J. Phys. Chem.*, **55**, 408 (1951).
3) M. E. Hassan, R. F. Nielsen, and J. C. Calhoun, Jr., *Trans. A.I.M.E.*, **198**, 299 (1953).
4) R. R. Harvey, *J. Phys. Chem.*, **62**, 322 (1958).
5) H. Y. Jennings, Jr., *J. Colloid Interface Sci.*, **24**, 323 (1967).
6) M. M. Lin, P. Mansoura, and R. Merigoux, *C. R. Acad. Sci. Ser. B.*, **277**, 325 (1973).
7) R. E. Gibson and J. F. Kincaid, *J. Am. Chem. Soc.*, **60**, 511 (1938).
8) R. E. Gibson and O. H. Loeffler, *J. Am. Chem. Soc.*, **63**, 898 (1941).
9) H. E. Eduljee, D. M. Newitt, and K. E. Weale, *J. Chem. Soc.*, **1951**, 3086.
10) G. S. Kell and E. Whally, *Phil. Trans. R. Soc. London*, **A 258**, 565 (1965).
11) T. Grindley and J. E. Lind, Jr., *J. Chem. Phys.*, **54**, 3983 (1971).
12) J. M. Andreas, E. A. Hauser, and W. B. Tucker, *J. Phys. Chem.*, **42**, 1001 (1938).
13) S. Fordham, *Proc. R. Soc., Ser. A*, **194**, 1 (1948).
14) D. J. Donahue and F. E. Bartell, *J. Phys. Chem.*, **56**, 480 (1952).
15) K. Motomura, N. Matubayasi, M. Aratono, and R. Matuura, unpublished work.
16) G. N. Lewis and M. Landall, "Thermodynamics," 2nd ed, revised by K. S. Pitzer and L. Brewer, McGraw-Hill, New York, (1961).

BULLETIN OF THE CHEMICAL SOCIETY OF JAPAN, VOL. 50 (2), 525—526 (1977)

Electronic States of the 4,4′-Dinitrobiphenyl-Benzidine Complex

Masashi TANAKA

Department of Chemistry, Faculty of Science, Nagoya University, Chikusa, Nagoya 464

(Received August 25, 1976)

Synopsis. The charge transfer complex composed of 4,4′-dinitrobiphenyl and benzidine was studied by measuring and analyzing the UV crystalline spectra. The deep coloration of this complex was found to be due to the charge transfer bands appearing at 21000 and 25000 cm^{-1}, while the long axes of the component molecules are known to be perpendicular to each other.

Common electron donor-acceptor complexes crystallize in the plane-to-plane stacking of the molecules and are much more deeply colored than the component compounds. Nevertheless, 4,4′-dinitrobiphenyl has been known to form a complex with benzidine in a stack in which the 4,4′-dinitrobiphenyl molecules is arranged at right angles to each benzidine molecule and the complex becomes deeply red in color while the component molecules are light yellow.[1,2] Therefore, it is very interesting to determine whether or not the deep coloration of this complex is due to the appearance of broad, weak charge-transfer absorption. The author measured the polarized reflection and absorption spectra of the complex crystal and analyzed them theoretically.

Experimental and Theoretical

Single crystals of the complex were kindly supplied by the Research Institute for Polymers and Textiles. The crystals showed developed planes of (100) and (101). These planes were identified by X-ray examination. The reflection spectra at normal incidence and the transmission spectra were measured with spectrophotometers constructed in this laboratory. The absorption spectra obtained by the Kramers-Kronig[3] transformation of the reflection spectra are shown in Fig. 2 and the polarized transmission spectra in Fig. 3.

As Davydov splitting was not observed in these spectra, exciton treatment was not developed in this study and the electronic energy levels of the complex were calculated assuming a 1: 1 dimer type complex of 4,4′-dinitrobiphenyl and benzidine molecules, although the actual composition is 4: 1. The calculation of the dimer were made by taking into account the configuration interaction between the ground (Φ_0), locally-excited (LE; $\Phi_{at\to aj}$) and charge-transfer (CT; $\Phi_{at\to bj}$) configurations. These matrix elements were estimated in the zero differential overlap approximation, except for the elements between the Φ_0 and $\Phi_{at\to bj}$ configurations,[4]

$$(\Phi_0|H|\Phi_{at\to bj}) = -\sqrt{2}K(\phi_a{}^i|\phi_b{}^j)$$

where K is a constant and was taken to be 10.0. The atomic Coulomb integrals were estimated by the Nishimoto-Mataga method.

The molecular orbitals ϕ_a^i and the orbital energies were given using the PPP approximation. The results of the calculation are shown in Table 1.

The computation was carried out on the Facom 230-60 computer at the Nagoya University Computation Center.

Results and Discussion

Crystals of the 4,4′-dinitrobiphenyl–benzidine complex belong to the C_c space group.[5] The unit cell contains four of the complex groups $[O_2N\cdot C_6H_4\cdot C_6H_4\cdot NO_2]_4\cdot[H_2N\cdot C_6H_4\cdot C_6H_4\cdot NH_2]$. Figure 1 shows a projection of the unit cell along b on to the ac plane. The benzidine molecules lie along b and are thus seen end-on. Each dinitrobiphenyl molecule shown on the projection represents four molecules lying parallel to one another and separated by $(1/4)b$ or 3.7 Å. These dinitrobiphenyl molecules must all lie with their long axes very nearly on the $(40\bar{2})$ planes, while the benzidine molecules must lie almost wholly on these planes.

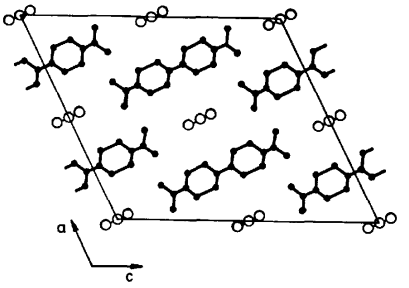

Fig. 1. A projection of the unit cell along b on to the ac plane.

Figure 2 shows the polarized absorption spectra of the crystal obtained by K-K analysis of the reflection spectra. In the b-axis spectrum, the long-axis polarized state of benzidine is located at about 32000 cm^{-1}. The long-axis state of 4,4′-dinitrobiphenyl is observed at

Table 1. Calculated transition energies, intensities and wavefunctions of the 4,4′-dinitrobiphenyl–benzidine complex

Obsd			Calcd
ΔE (cm^{-1})	ΔE (cm^{-1})	f	Wave functions[a]
21000	21870	0.00	$0.9968\ \Phi(\phi_2{}^8\to\phi_1{}^{11}) + 0.0711\ \Phi(\phi_2{}^8\to\phi_1{}^{13}) + \cdots$
25000	24700	0.00	$0.9994\ \Phi(\phi_2{}^8\to\phi_1{}^{12}) - 0.0275\ \Phi(\phi_2{}^6\to\phi_1{}^{12}) + \cdots$
29000	29200	0.27	$0.7532\ \Phi(\phi_1{}^{10}\to\phi_1{}^{11}) + 0.6528\ \Phi(\phi_2{}^7\to\phi_1{}^{11}) + \cdots$
	30300	0.21	$0.6561\ \Phi(\phi_1{}^{10}\to\phi_1{}^{11}) - 0.7368\ \Phi(\phi_2{}^7\to\phi_1{}^{11}) + \cdots$
32000	32400	0.52	$0.9199\ \Phi(\phi_2{}^8\to\phi_2{}^9) + 0.2789\ \Phi(\phi_2{}^6\to\phi_1{}^{12}) - 0.1874\ \Phi(\phi_1{}^8\to\phi_1{}^{12}) + \cdots$

a) $\phi_1{}^i$ indicates the i-th MO of the 4,4′-dinitrobiphenyl molecule and $\phi_2{}^j$ the j-th MO of the benzidine molecule.

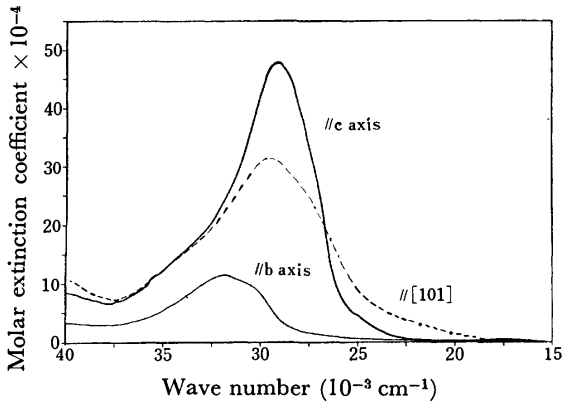

Fig. 2. The polarized absorption spectra of the crystal obtained by the Kramers-Kronig analysis of the reflection spectra.

29000 cm^{-1} in the c- and [101]-axis spectra. Two broad, weak shoulders occur in the vicinity of 17500 to 25000 cm^{-1} in the [101]-axis spectrum.

Figure 3 shows the polarized absorption spectra of the crystal obtained by the transmission method. Two peaks are observed at 21000 and 25000 cm^{-1} in the [101]-axis spectrum.

Table 1 shows that the first and second bands at about 21000 and 25000 cm^{-1} are assigned to the CT bands from the occupied MO of the benzidine molecule

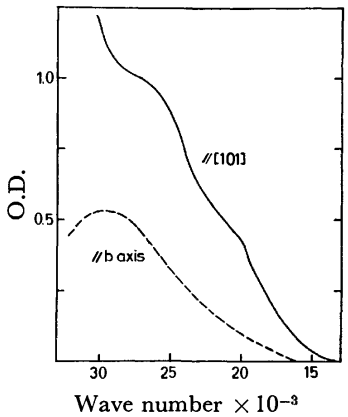

Fig. 3. The polarized absorption spectra of the crystal obtained by the transmission method.

to the vacant MO of the dinitrobiphenyl molecule. As these CT configurations do not mix strongly with the ground and LE configurations, the absorption intensities to these CT states are nearly forbidden and weak, as is shown in Figs. 2 and 3. In the third and fourth states, the large mixing between the LE configuration $\Phi(\phi_1^{10}\rightarrow\phi_1^{11})$ of the dinitrobiphenyl molecule and the CT configuration $\Phi(\phi_2^{7}\rightarrow\phi_1^{10})$ from the occupied MO of benzidine to the vacant MO of dinitrobiphenyl is due to the nearly degenerate configuration energies and the transition moments of these states depend mainly on the transition moments of the LE configuration $\Phi(\phi_1^{10}\rightarrow\phi_1^{11})$ of the dinitrobiphenyl molecule. The LE configuration $\Phi(\phi_1^{10}\rightarrow\phi_1^{11})$ is polarized parallel to the long axis of the dinitrobiphenyl molecule. Therefore, the 29000-cm^{-1} band observed in the c- and [101]-axis spectra may be assigned to the long-axis state of dinitrobiphenyl. The fifth state consists of the LE configuration $\Phi(\phi_2^{8}\rightarrow\phi_2^{9})$ polarized parallel to the long axis of the benzidine molecule and the 32000-cm^{-1} band in the c-axis spectrum can be assigned to the long-axis state of benzidine.

In the ground state, mixing with the charge-transfer configurations is small and the stabilization of the ground state appears to be due to the quadrupole interaction rather than to the charge-transfer and polarization effects. Accordingly, this dinitrobiphenyl–benzidine complex forms an inclusion compound and can be crystallized in various molecular ratios.

The author would like to thank Mr. Kazuaki Harata of the Research Institute for Polymers and Textiles for supplying the crystal of the 4,4′-dinitrobiphenyl–benzidine complex.

References

1) W. S. Rapson, D. H. Saunder, and E. T. Stewart, *J. Chem. Soc.*, **1964**, 1110.
2) K. Abe, Y. Matsunaga, and G. Saito, *Bull. Chem. Soc. Jpn.*, **41**, 2852 (1968).
3) H. J. Bowlden and J. K. Wilmskurst, *J. Opt. Soc. Am.*, **53**, 1073 (1963); D. M. Roesler, *Brit. J. Appl. Phys.*, **16**, 1119 (1965).
4) T. Takabe, M. Tanaka, and J. Tanaka, *Bull. Chem. Soc. Jpn.*, **47**, 1917 (1974).
5) D. H. Saunder, *Proc. R. Soc., Ser. A*, **190**, 508 (1947).

BULLETIN OF THE CHEMICAL SOCIETY OF JAPAN, VOL. 50 (2), 527—528 (1977)

An Improved Gas Circulation Pump

Isao YASUMOTO and Keizo NAGAI*

Department of Chemistry, Yonago Technical College, Yonago 683

**Department of Electrical Engineering, Yonago Technical College, Yonago 683*

(Received September 11, 1976)

Synopsis. A gas circulation pump made of glass has been constructed, which works at less than one atmosphere. The pumping speed of the present pump is approximately 4 l/min.

The study of the gas-solid reactions on the surface of catalysts requires in many cases a technique for circulating gas in a closed system.

This report will describe an improved design of a gas circulation pump[1-4] and present some experimental results performed with this new pump. The design was found to be satisfactory and to have a number of advantages, such as:

(1) The pump works at any pressure less than one atmosphere.

(2) A high pumping speed can be obtained.

(3) Piston overshooting does not occur.

(4) The pump can be baked at 500 °C. The pressure of 1×10^{-5} Torr is obtainable.

(5) Modern electronics can be applied to the switching circuit of the pump.

The pump consists of a cylinder, a piston with a coil, and four sets of valves with coils of the same design (Figs. 1 and 2). The cylinder is a Pyrex tube 18 mm in inside diameter and 66 cm in length and is placed horizontally. The closely fitting piston is a piece of Pyrex tube enclosing a ferrite rod 12 mm wide and 100 mm long.

The coil for the piston consists of 10000 turns of an enamelled copper wire 0.5 mm in diameter and is fixed on a slider, which is driven on rails by means of a reciprocating slider-crank mechanism with a 50 watt DC servomotor. The piston accordingly makes a smooth back-and-forth motion over the distance of about 53 cm

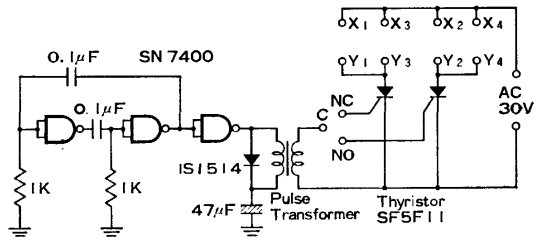

Fig. 2. The switching circuit. C, NC, and NO-terminals of the switch. X_i and Y_i; terminals.

at the repetition rate set at 15 cycle/min without danger of overshooting. The exciting current for the coil was found to be about 0.4 amperes (corresponding to 30 W). The rise in the temperature of the cylinder during a continuous operation was negligibly small.

The valve has a glass bulb which encloses a ferrite rod 4 mm wide and 22 mm long (Fig. 3). The bulb

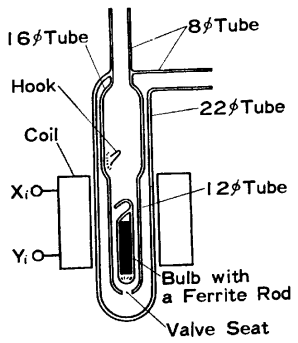

Fig. 3. The schematic sketch of the valve. X_i and Y_i; terminals of the coil.

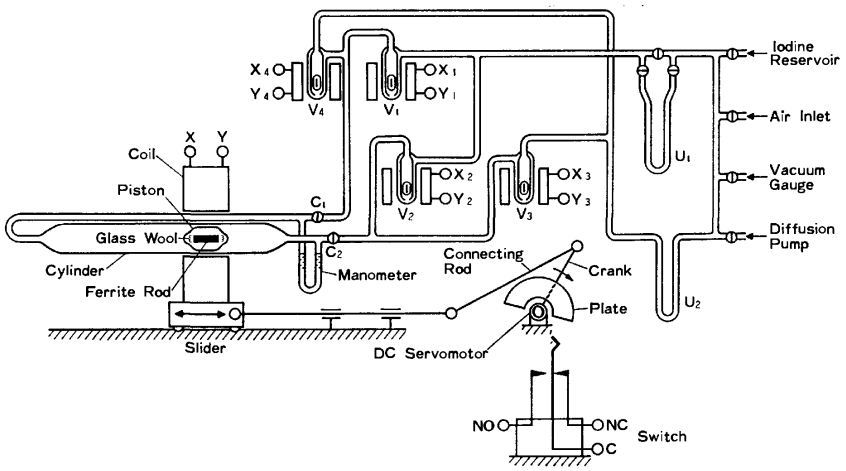

Fig. 1. The circulation pump with the vacuum line.
X, Y, X_i and Y_i; terminals of the coils. C, NC, and NO; terminals of the switch. V_i; valves. U_i; traps. C_i; taps.

end and the valve seat are ground together to form a ball joint of about 7 mm in radius.

The coil for the valve consists of 5000 turns of an enamelled copper wire 0.5 mm in diameter. The proper exciting current was about 0.5 amperes (corresponding to 15 W) and the rise in the temperature around the valve was approximately 5 °C after a prolonged operation.

The concerted action of the valve system with the motion of the piston is achieved by attaching to the crank shaft a semicircular plastic plate which pushes the lever of a switch, owing to its thickness, during one half period of time. A triggering signal turns thyristors on. The current through each thyristor excites alternately two pairs of coils: V_1 and V_3, and V_2 and V_4.

To bake out the pump the bulb is raised with the coil and hung on a hook, and then the five coils are all removed.

The pump works at any pressure of gas in theory, but at low pressure the migration of gaseous molecules by diffusion predominates. For the purpose of investigating this phenomenon, the series of procedures described below were repeated.

Dry air of a certain pressure is admitted into the apparatus (Fig. 1) as a carrier gas for iodine vapor. The apparatus is equipped with two traps, U_1 and U_2: the former is filled with a quantity of sublimed iodine and cooled in a Dry Ice–acetone mixture and the latter is left at room temperature. The U_2-trap is then dipped in another Dry Ice–acetone mixture and cooled. When the refrigerant which cools the U_1-trap is removed, the temperature of iodine in the U_1-trap gradually rises to room temperature. Iodine vapor, flowing from the iodine trap, reaches the U_2-trap, either downstream *via* the circulation pump or directly upstream by diffusion, and condenses there. The lengths of these paths are roughly in the ratio of 8 to 1. Several minutes after, the refrigerant which cools the U_2-trap is removed, and the U_2-trap is photographed (Fig. 4).

Runs 1, 2, 3, and 4 were carried out under the pressures of 300, 100, 15, and 1 Torr of air, and their iodine deposits in the left arm of the trap were denser than in the right one. However, a new deposit appeared in the right arm in run 5, in which the pressure of 0.4 Torr of air was used. It looked as dense as the left arm deposit in run 6, which was done under the pressure of 0.3 Torr of air. The right arm deposit was denser than the left one in run 7, in which the pressure of 0.1 Torr of air was used; the diffusion of gas would have a considerable share in this case.

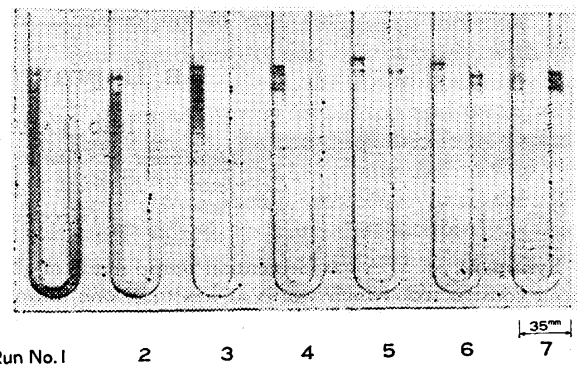

Fig. 4. The photographs of the U_2-trap containing iodine deposit.
Run No. —pressure of air: 1—300 Torr, 2—100 Torr, 3—15 Torr, 4—1 Torr, 5—0.4 Torr, 6—0.3 Torr, 7—0.1 Torr.

To estimate the circulating power of the pump, air was admitted into the apparatus up to 50 Torr. The circulating air was cut off by closing the taps of C_1 and C_2 and the pressure difference between the spaces in the front and the rear of the piston was measured with a manometer, while the piston was pulled slowly in one direction by the coil. The pressure difference was found to be roughly 14 Torr.

References

1) A. Farkas and H. W. Melville, "Experimental Methods in Gas Reactions," McMillan, London (1939), p. 53.
2) O. Mabuchi, *Nippon Kagaku Zasshi*, **63**, 1733 (1942).
3) W. R. Bennett, Jr., *Rev. Sci. Instrum.*, **28**, 1092 (1957).
4) T. Takaishi, *Shokubai*, **9**, 127 (1967).

BULLETIN OF THE CHEMICAL SOCIETY OF JAPAN, VOL. 50 (2), 529—530 (1977)

The Crystallization of $Pb_5Si_3O_{11}$ from the Glass in the PbO-SiO_2 System

Hiroshi HASEGAWA, Masahiko SHIMADA,* Fumikazu KANAMARU,* and Mitsue KOIZUMI*

Department of Chemistry, Faculty of Engineering, Shizuoka University, Hamamatsu, Shizuoka 432

**The Institute of Scientific and Industrial Research, Osaka University, Suita, Osaka 565*

(Received August 16, 1976)

Synopsis. A new compound, $Pb_5Si_3O_{11}$, is prepared by the crystallization of the glass in the PbO–SiO_2 system. $Pb_5Si_3O_{11}$ has an orthorhombic symmetry, and its lattice parameters are determined to be a_0=9.93 Å, b_0=8.31 Å, and c_0=34.4 Å.

During the course of a systematic study of the crystallizing phenomena of lead germanate glasses and of lead germanosilicate glasses,[1,2] it was found that a ferroelectric crystalline phase, $Pb_5Ge_3O_{11}$, was easily obtained from the $5PbO \cdot 3GeO_2$ glass, that the glass-ceramic product was transparent, and that a ferroelectric solid solution, $Pb_5Ge_{3-x}Si_xO_{11}$ ($0 \leq x \leq 2$), was precipitated from the $5PbO \cdot (3-X)GeO_2 \cdot XSiO_2$ glass ($0 \leq X \leq 2$).

Eysel *et al.*[3] reported that the single crystals of the $Pb_5(Ge, Si)_3O_{11}$ solid solution, containing up to 62% of Si replacing Ge, were prepared from the melt. Assuming that Si can be completely substituted for Ge in a nearly ideal fashion, the presence of $Pb_5Si_3O_{11}$ can be expected. As to the PbO–SiO_2 system, Ott and McLaren[4] obtained a corrected phase diagram by means of the crystallization of lead silicate glasses and suggested the existence of five compounds: Pb_4SiO_6, Pb_3SiO_5, Pb_2SiO_4, $Pb_3Si_2O_7$, and $PbSiO_3$. More recently, Smart and Glasser[5] studied the phase equilibria in this system and reported the existence of six compounds: Pb_4SiO_6, Pb_3SiO_5, Pb_2SiO_4, $Pb_3Si_2O_7$, $PbSiO_3$ and $Pb_5Si_8O_{21}$. However, the existence of the $Pb_5Si_3O_{11}$ compound has not been reported.

The purpose of this research is to ascertain the existence of $Pb_5Si_3O_{11}$ by using the crystallization of lead silicate glasses.

Experimental

Pure lead monoxide and silicic acid were carefully mixed. About 50 g of the mixture was preheated at 550 °C for 10 h, and then melted in a platinum crucible at 800 °C. After the melting has been completed, the melt was poured onto a steel mould and formed into a plate glass. The compositon of the glass was checked by chemical analysis. The specimen prepared in this way was placed in a platinum basket, heated in an electric furnace at temperatures from 350 to 650 °C for 1 to 340 h, and then quickly cooled to room temperature. The crystallized phases after the heat-treatment were identified by powder X-ray diffraction analysis.

Results and Discussion

A microcrystalline phase, denoted as "Phase X," was precipitated in the $5PbO \cdot 3SiO_2$ glass by heating at about 400 °C. This phase was stable up to 600 °C, but decomposed at a higher temperature into Pb_2SiO_4 and $PbSiO_3$. According to the phase diagram of this system reported by Ott and McLaren, the major crystalline phase precipitated from the $5PbO \cdot 3SiO_2$ glass might be $Pb_3Si_2O_7$. However, the powder X-ray diffraction pattern of Phase X was similar not to that of lead-barysilite, $Pb_3Si_2O_7$, reported by Billhardt,[6] but to that of ferroelectric $Pb_5Ge_3O_{11}$ as shown in Fig. 1.

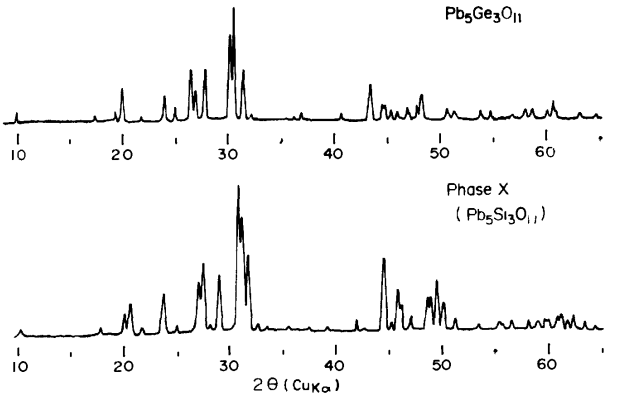

Fig. 1. X-Ray diffraction patterns of Phase X and $Pb_5Ge_3O_{11}$.

On the basis of the crystal structure of $Pb_5Ge_3O_{11}$, the crystal structure of Phase X was determined to be pseud-hexagonal and orthorhombic. Its lattice parameters were calculated to be a_0=9.93 Å, b_0=8.31 Å. and c_0=34.4 Å. The X-ray diffraction data of Phase X are tabulated in Table 1.

TABLE 1. X-RAY DIFFRACTION DATA OF PHASE X

(h k l)	I/I_0	d_{obsd}	d_{calcd}	(h k l)	I/I_0	d_{obsd}	d_{calcd}
1 0 2	5	8.616	8.600	3 2 4	2	2.480	2.479
1 0 6	10	4.962	4.965	3 0 10	2	2.384	2.385
1 0 7	15	4.410	4.404	1 2 12	2	2.300	2.296
2 0 4	30	4.300	4.300	4 0 8	5	2.149	2.150
2 1 2	5	4.111	4.117	1 1 16	40	2.037	2.037
0 2 4	30	3.738	3.741	5 0 0	15	1.982	1.986
1 1 8	10	3.564	3.564	2 0 16	10	1.976	1.973
3 0 0	30	3.294	3.301	5 0 4	10	1.932	1.935
2 0 8	45	3.250	3.250	5 0 6	20	1.877	1.877
1 2 6	2	3.169	3.168	0 1 18	15	1.864	1.862
3 0 4	40	3.076	3.079	4 3 2	30	1.840	1.838
3 1 4	100	2.896	2.896	2 0 18	10	1.783	1.784
3 0 6	75	2.867	2.867	6 0 2	2	1.646	1.647
2 0 10	45	2.821	2.818	6 0 4	5	1.625	1.625
3 0 7	2	2.744	2.745	6 0 6	2	1.589	1.590
0 3 3	2	2.696	2.693	0 0 22	5	1.562	1.562

Orthorhombic; a_0=9.93Å
b_0=8.31Å
c_0=34.4Å ($2\sqrt{3} \cdot a_0$)

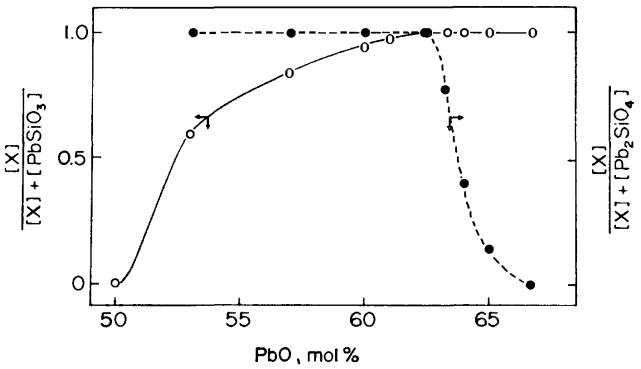

Fig. 2. Relative amounts of products after the crystallization of the glasses as functions of the PbO content of the glass.

Phase X was obtained only through the crystallization of glass. All the attempts to synthesize Phase X by the usual solid-state-reaction methods and by the solidification of the melts failed.

The chemical composition of Phase X was determined by using the following process. Powder glass samples with ten compositions, ranging from 50.1%PbO·49.9%SiO_2 to 66.7%PbO·33.3%SiO_2 in mol, were heat-treated at about 550 °C for 340 h, and the amounts of crystallized products were estimated from the intensities of the most intense peaks of Phase X, Pb_2SiO_4 and $PbSiO_3$. The crystallization of the glasses investigated was completed within about 5 h at 550 °C, so that our experimental conditions—at 550 °C for 340 h—are sufficient to reach the equilibrium state. A microscopic examination of crystallized products showed that the sample was completely crystalline. The relation between the amounts of each phase and the PbO contents of the glass is illustrated in Fig. 2. As is shown in this figure, in the range where the PbO content is less than 62.5%, the yield of Phase X increased with an increase in the PbO content, and in the range where the PbO content is more than 62.5%, mixtures of Phase X and Pb_2SiO_4 were observed. From these results, the chemical composition and the chemical formula of Phase X were determined to be 62.5%PbO·37.5%SiO_2 and $Pb_5Si_3O_{11}$.

In conclusion, in the present research the existence of a new crystalline phase, $Pb_5Si_3O_{11}$, has been confirmed by using the crystallization of lead silicate glasses.

References

1) H. Hasegawa, M. Shimada, and M. Koizumi, *J. Mater. Sci.*, **8**, 1725 (1973).
2) H. Hasegawa, M. Shimada, F. Kanamaru, and M. Koizumi, to be published.
3) W. Eysel, R. W. Wolfe, and R. E. Newnham, *J. Am. Ceram. Soc.*, **56**, 185 (1973).
4) W. R. Ott and M. G. McLaren, *J. Am. Ceram. Soc.*, **53**, 374 (1970).
5) R. M. Smart and F. P. Glasser, *J. Am. Ceram. Soc.*, **57**, 378 (1974).
6) H. W. Billhardt, *Am. Mineral.*, **54**, 510 (1969).

BULLETIN OF THE CHEMICAL SOCIETY OF JAPAN, VOL. 50 (2), 531—532 (1977)

The Crystal Structure of Nitratotriaquo(2,2′-bipyridine)copper(II) Nitrate $[Cu(NO_3)(H_2O)_3(bipy)]NO_3$*

Hisayoshi NAKAI,** Shun'ichiro OOI, and Hisao KUROYA

Department of Chemistry, Faculty of Science, Osaka City University, Sugimoto-cho, Sumiyoshi-ku, Osaka 558

(Received September 21, 1976)

Synopsis. The crystal structure of the title compound has been determined from three-dimensional X-ray data. The crystal is composed of the nitrate anions and the distorted-octahedral $[Cu(NO_3)(H_2O)_3(bipy)]^+$ cations, where the nitrato-groups act as a monodentate ligand and the three coordinated water molecules occupy a facet of the octahedron.

It has been found that the bis(2,2′-bipyridine)copper(II) complexes have a variety of stereochemistries: distorted trigonal bipyramid and *cis*- and *trans*-distorted octahedrons.[1-4] As a part of our structural studies on such complexes, a single crystal X-ray analysis has been carried out on $[Cu(NO_3)(H_2O)_3(bipy)]NO_3$.

Experimental

The crystals of $[Cu(NO_3)(H_2O)_3(bipy)]NO_3$ were easily prepared by adding a methanol solution of 2,2′-bipyridine (8 mmol in 20 cm³ of the solvent) to an aqueous solution of cupric nitrate (10 mmol in 30 cm³ of water), and were recrystallized from a water–methanol mixture. Found: C, 30.29; H, 3.75; N, 14.05%. Calcd for $[Cu(NO_3)(H_2O)_3(bipy)]NO_3$: C, 30.20; H, 3.55; N, 14.09%.

The lattice parameters were obtained by the least-squares refinement of the data from the higher-angle reflections of the (0*kl*), (*h*0*l*) and (*hk*0) Weissenberg photographs, on which aluminum powder lines were superimposed for calibration. Cu*K*α radiation (λ=1.5418 Å) was used throughout the diffraction study. The density was measured by the flotation technique, using a benzene–bromoform mixture. Of the two possible triclinic space groups, $P\bar{1}$ and P1, the former was chosen initially; it was subsequently verified by the successful refinements of the derived structure. Crystal data: $[Cu(NO_3)(H_2O)_3(bipy)]NO_3$, *F.W.*=397.8, triclinic $P\bar{1}$, a=9.52(1), b=7.80(1), c=13.62(2) Å, α=110.4(2), β=124.3(2), γ=77.3(1)°, Z=2, D_m=1.65, D_c=1.69 g·cm^{-3}, μ=25.3 cm^{-1} (for Cu*K*α radiation). The intensity data of 0*kl* to 5*kl*, and *h*0*l* to *h*4*l* were collected by the multiple-film equi-inclination technique from two cylindrically shaped crystals with approximate dimensions of 0.2×0.2×0.8 mm. The intensities of 2890 independent reflections were visually estimated by comparison with a standard scale; 374 of them were too weak to be measured and so were assumed to be zero. After the intensity data have been corrected for Lorentz-polarization, spot-extension, and absorption effects, the structure factors were placed on a common arbitrary scale by the least-squares method.

Structure Determination

The crystal structure was determined by the heavy-atom method. The position of the copper atoms was determined from a three-dimensional Patterson map, and a Fourier synthesis phased with the Cu atoms revealed all the atoms except the hydrogen atoms and those of the uncoordinated NO_3^- ion; the NO_3^- ion was found from the subsequent Fourier and difference Fourier maps. The structure was refined by the block-diagonal least-squares method, using the HBLS-IV program coded by Prof. Ashida. The weighting scheme used was: w=0.2 when F_o=0, and w=1.0 when F_o>0. The atomic scattering curves were taken from the International Tables for X-ray Crystallography,[5] the real part of the anomalous dispersion correction ($\Delta f'$=−2.1) being applied for the neutral copper atom. Refinement of the positional and thermal parameters, at first isotropic and subsequently anisotropic, reduced the R value to 0.124 for 2516 non-zero reflections, and no other significant peak was obtained in the final Fourier and difference Fourier maps. Final atomic coordinates and thermal parameters are listed in Table 1. The observed and calculated structure factors are listed in Table 2.***

Results and Discussion

The crystal is composed of the $[Cu(NO_3)(H_2O)_3(bipy)]^+$ cations and the nitrate anions. Figure 1 shows a schematic drawing of the complex cation. The coordination geometry about the copper atom is a tetragonally distorted octahedron: two nitrogen atoms of the bipy ligand[Cu–N(1)=2.02(1) and Cu–N(2)=1.99(1) Å], and two oxygen atoms of the coordinated water molecules[Cu–O(1)=1.99(1) and Cu–O(2)=

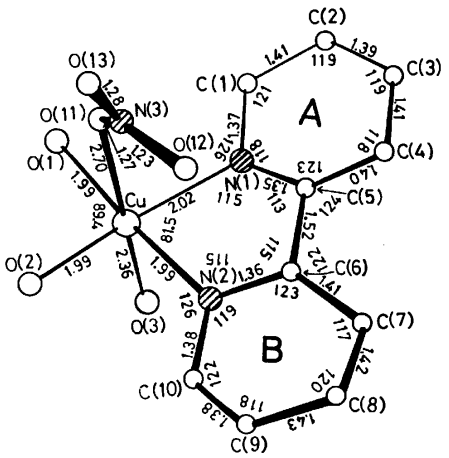

Fig. 1. A schematic drawing of the complex cation $[Cu(NO_3)(H_2O)_3(bipy)]^+$.

* A preliminary report of this work was presented at the 19th Annual Meeting on Coordination Chemistry, Sendai, September 1969, Abstract, p. 169.

** Present address: *Department of Chemistry, Hyogo College of Medicine, Mukogawa-cho, Nishinomiya-shi, Hyogo 663.*

*** Table 2 has been deposited at the Office of the Chemical Society of Japan, Document No. 7704.

Table 1. Atomic parameters ($\times 10^4$) and their standard deviations
The anisotropic thermal factors are of the form
$\exp\{-(h^2B_{11}+k^2B_{22}+l^2B_{33}+hkB_{12}+hlB_{13}+klB_{23})\}$.

Atom	x	y	z	B_{11}	B_{22}	B_{33}	B_{12}	B_{13}	B_{23}
Cu	4761(2)	3832(2)	1949(1)	32(2)	79(3)	14(1)	38(4)	45(2)	14(2)
O(1)	5847(11)	1826(11)	1192(8)	139(16)	115(17)	65(8)	96(27)	164(19)	55(18)
O(2)	2959(10)	4115(11)	277(7)	90(13)	104(16)	33(6)	65(24)	67(15)	37(15)
O(3)	3370(10)	1682(12)	1950(8)	77(13)	124(18)	83(9)	-7(25)	120(18)	54(20)
O(11)	6552(12)	6047(12)	1924(9)	141(16)	94(17)	116(11)	-12(28)	196(23)	86(21)
N(3)	6531(11)	7779(12)	2189(8)	64(13)	88(18)	39(7)	21(26)	63(17)	47(18)
O(12)	6106(15)	8751(14)	2919(9)	273(26)	192(24)	77(10)	65(40)	251(28)	16(24)
O(13)	7004(12)	8498(11)	1709(8)	176(17)	84(16)	71(8)	-8(27)	187(21)	34(18)
N(1)	6723(10)	4068(12)	3706(7)	40(12)	74(16)	36(7)	-3(24)	48(15)	17(17)
C(1)	8170(12)	2982(17)	4083(10)	18(13)	147(25)	45(9)	33(31)	32(18)	62(24)
C(2)	9492(13)	3311(19)	5334(11)	37(15)	206(31)	44(9)	45(36)	28(20)	57(27)
C(3)	9338(14)	4787(19)	6210(10)	51(16)	185(29)	40(9)	-65(36)	29(20)	27(26)
C(4)	7829(14)	5866(18)	5830(10)	82(18)	152(26)	29(8)	-64(36)	50(20)	8(23)
C(5)	6563(12)	5449(14)	4573(9)	36(13)	96(20)	32(8)	22(28)	59(17)	32(20)
C(6)	4869(12)	6487(14)	4044(9)	37(13)	94(20)	31(7)	16(28)	63(17)	23(19)
C(7)	4423(14)	7956(16)	4792(10)	98(18)	95(22)	49(9)	-20(34)	116(23)	-5(22)
C(8)	2794(16)	8814(16)	4192(11)	126(21)	98(23)	63(11)	72(37)	147(26)	35(25)
C(9)	1686(16)	8182(17)	2876(12)	117(20)	115(24)	75(12)	139(38)	147(27)	89(27)
C(10)	2246(13)	6736(17)	2228(10)	62(16)	144(25)	53(10)	103(34)	87(22)	76(25)
N(2)	3826(11)	5906(13)	2796(8)	66(14)	111(19)	31(7)	17(27)	63(17)	24(18)
O(21)	2739(9)	7576(12)	-37(8)	49(11)	152(19)	73(8)	58(24)	77(16)	112(20)
N(4)	1124(12)	7952(13)	-696(9)	76(15)	84(18)	55(8)	22(28)	73(19)	38(20)
O(22)	87(12)	7159(18)	-706(12)	81(15)	332(33)	162(15)	23(37)	106(26)	334(39)
O(23)	624(15)	8961(22)	-1353(16)	137(21)	446(46)	255(24)	152(51)	120(37)	583(59)

1.99(1) Å] define the equatorial plane, while the axial positions are occupied by the O(3) atom of the third coordinated water molecule[Cu-O(3)=2.36(1) Å], and by the O(11) atom of the nitrato-group[Cu-O(11)= 2.70 Å]. The copper atom is 0.12 Å distant from the equatorial plane, towards the O(3) atom. The angles of N(1)-Cu-O(11), N(1)-Cu-O(3), N(2)-Cu-O(11), and N(2)-Cu-O(3) are 84.9(4), 94.0(4), 93.2(4), and 91.7(4)° respectively.

The bipyridine ligand is in the *cis*-planar configuration with the maximum deviation of 0.04 Å, and the "bite" angle, N(1)-Cu-N(2), is 81.5°; the planarities of the two pyridine rings, A and B, are good with the maximum deviations of 0.02 and 0.01 Å respectively, and the dihedral angle between the A and B planes is 3°. The C(5)-C(6) bond length is 1.52(2) Å, and the aromatic C-C(1.38—1.43 Å) and C-N(1.35—1.38 Å) bond lengths are 1.41 and 1.36 Å on the average. It should be noted that the angles of C(4)-C(5)-C(6) and C(5)-C(6)-C(7) are larger than those of N(1)-C(5)-C(6) and C(5)-C(6)-N(2) by 8—10°; the same trend has been observed in the 2,2′-bipyridine[6] and its copper complexes.[1-4,7,8] The dihedral angle between the equatorial plane and the plane of the bipy ligand is 8°.

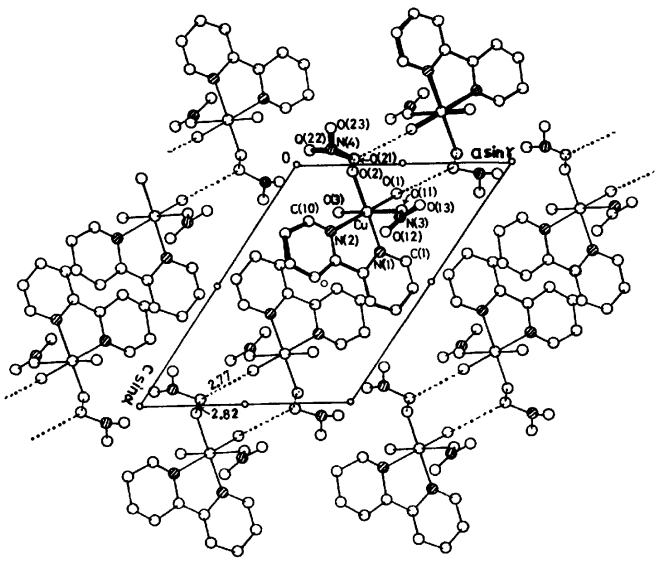

Fig. 2. Projection of the structure along the b axis. Dotted lines are hydrogen bonds.

The nitrato-group is planar and acts as a monodentate ligand. The O(11) is bonded to the copper atom (2.70 Å), while the O(13) is linked to the O(1)′[x,1+ y,z] by a hydrogen bond (2.76 Å). The plane of the nitrato-group makes the dihedral angles of 72° with the equatorial plane and of 79° with the plane of the bipy ligand.

The uncoordinated nitrate ion is also planar and is linked to the two water molecules by hydrogen bonds, which are indicated by the dotted lines in Fig. 2 [O(21) ···O(2)=2.82(2) and O(21)···O(11)″[1−x, 1−y, −z]= 2.77(2) Å]. The bond lengths of N(4)-O(21), N(4)-O(22), and N(4)-O(23) are 1.32(2), 1.27(2), and 1.22(2) Å respectively. The O-N(4)-O angles in the nitrate ion range from 119(1) to 121(1)°. The plane of the nitrate ion makes the angles of 74° with the plane of the coordinated nitrato-group and of 79° with the equatorial plane of the complex cation.

References

1) G. A. Barclay. B. F. Hoskins, and C. H. L. Kennard, *J. Chem. Soc., A*, **1963**, 5691.
2) I. M. Procter and F. S. Stephens, *J. Chem. Soc., A*, **1969**, 1248.
3) H. Nakai, S. Ooi, and H. Kuroya, *Bull. Chem. Soc. Jpn.*, **43**, 577 (1970).
4) H. Nakai, *Bull. Chem. Soc. Jpn.*, **44**, 2412 (1971).
5) "International Tables for X-Ray Crystallography," Vol. III, Kynoch Press, Birmingham (1962), p. 201.
6) L. L. Merritt, Jr., and E. D. Schroeder, *Acta Crystallogr.*, **9**, 801 (1956).
7) F. S. Stephens, *J. Chem. Soc., A*, **1969**, 2081.
8) R. J. Majeste and E. A. Meyers, *J. Phys. Chem.*, **74**, 3497 (1970).

BULLETIN OF THE CHEMICAL SOCIETY OF JAPAN, VOL. 50 (2), 533—534 (1977)

Absorption Spectra of Bis(sulfito) and Bis(thiosulfato) Complexes of Cobalt(III)

Keiji AKAMATSU, Jinsai HIDAKA,* and Yoichi SHIMURA

Department of Chemistry, Faculty of Science, Osaka University, Toyonaka, Osaka 560

(Received September 27, 1976)

Synopsis. It has been shown that the near ultraviolet "specific band" of a *trans* isomer of bis(sulfito) or bis(thiosulfato) cobalt(III) complexes is more bathochromic than the corresponding *cis* isomer. The *cis*-$[Co(SO_3)_2(en)_2]^-$ complex was optically resolved and its circular dichroism spectrum reported.

This note deals with "specific bands" of the *cis-trans* isomers of bis(aniono-*S*) cobalt(III) complexes, *i.e.*, bis(sulfito) and bis(thiosulfato) ones. It has been shown that the "specific bands" due to the aniono-*S* or aniono-*N* ligands such as SO_3^{2-} or NO_2^- are mostly of charge-transfer character,[1,2] but we retain the old name for convenience.

There had been a confusion as to the configuration assignment of tetraamminebis(sulfito)cobaltate(III) complex, but recent crystal structure[3] and other[4] studies of the *cis* isomer have solved the problem; thus the *cis-trans* assignment of Hofmann and Jenny,[5] and of Bailar and Peppard[6] are correct, while that of one of the present authors in 1952[7] incorrect. The isomers of the corresponding bis(ethylenediamine) complexes were assigned by infrared spectral[8] and lability[9] studies, and the result has been confirmed by the optical resolution of the *cis* isomer in the present study.

Results and Discussion

Figure 1 shows the visible and ultraviolet absorption spectra of bis(sulfito) and bis(thiosulfato) complexes, of which those of the *trans* bis(sulfito) complexes were measured in 0.1 M aqueous Na_2SO_3 solution to prevent the aquation due to the strong *trans* effect of sulfito ligand.[4] Table 1 presents the data of specific bands of the bis(aniono-*S*) complexes together with those of bis(aniono-*N*) ones for the purpose of comparison, and shows that the specific band of a *trans* isomer is in a longer wavelength region than that of the *cis* isomer is. It is remarkable that the specific bands of the *cis* isomers of tetraamminebis(sulfito)- and bis(ethylenediamine)-bis(sulfito) complexes split into distinct components. The *cis* isomer of bis(ethylenediamine)bis(thiosulfato) complex also shows a tendency to split in the specific band region (Fig. 1). A probable splitting of the specific band has been suggested for the *cis* isomers of dinitro-, diazido-, or diisothiocyanatobis(ethylenediamine) cobalt(III) complexes from their circular dichroism (CD) measurements.[1] Now, the *cis* isomer of $[Co(SO_3)_2(en)_2]^-$ was optically resolved and the CD spectrum is shown in Fig. 1. Since the major CD component of the first d-d transition in the longer wavelength region is negative for the obtained isomer, the absolute configura-

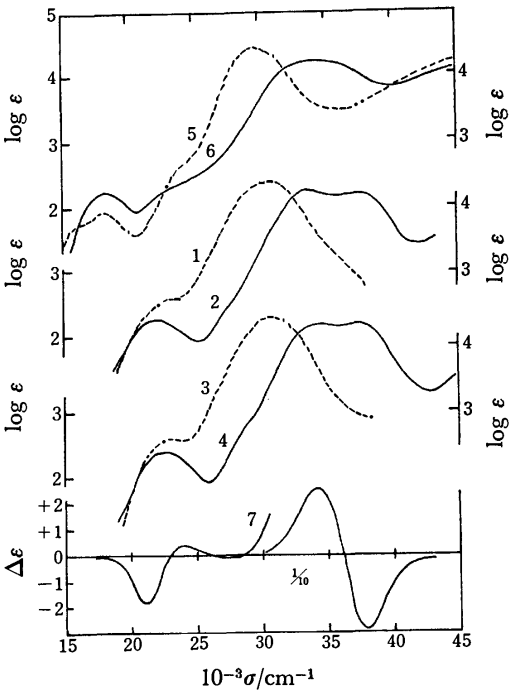

Fig. 1. Absorption spectra of (1) *trans* and (2) *cis* isomers of $[Co(SO_3)_2(NH_3)_4]^-$; (3) *trans* and (4) *cis* isomers of $[Co(SO_3)_2(en)_2]^-$; (5) *trans* and (6) *cis* isomers of $[Co(S_2O_3)_2(en)_2]^-$; and CD spectrum of (7) $(-)^{CD}_{475}$-*cis*-$[Co(SO_3)_2(en)_2]^-$.

Table 1. The specific absorption bands of geometrical isomers of bis(aniono-*S*) and bis(aniono-*N*) cobalt(III) complexes

(Wave numbers are given in 10^3 cm^{-1}, and log ε values in parentheses).

Complex	*cis* isomer	*trans* isomer	Ref.
$[Co(SO_3)_2(NH_3)_4]^-$	34.13(4.21) 37.59(4.19)	30.68(4.38)	
$[Co(SO_3)_2(en)_2]^-$	34.48(4.35) 37.25(4.36)	308.6(4.46)	
$[Co(SO_3)_2(CN)_4]^{5-}$	38.65(4.27)	38.00(4.10)	10
$[Co(S_2O_3)_2(en)_2]^-$	35.34(4.20)	29.94(4.43)	
$[Co(NO_2)_2(NH_3)_4]^+$	30.86(3.62)	28.82(3.68)	11
$[Co(NO_2)_2(en)_2]^+$	31.1 (3.56)	29.5 (3.56)	12
$[Co(NO_2)_2(R,R\text{-chxn})_2]^+$	30.9 (3.65)	29.2 (3.51)	13
$[Co(NO_2)_2(tn)_2]^+$	30.3 (3.67)	28.6 (3.49)	14
$[Co(N_3)_2(NH_3)_4]^+$	32.98(4.01)	29.68(4.14)	15
$[Co(N_3)_2(en)_2]^+$	33.1 (4.06)	30.0 (4.13)	12
$[Co(NCS)_2(en)_2]^+$	32.5 (3.46)	31.6 (3.49)	12
$[Co(NCS)_2(tn)_2]^+$	29.4 (3.44)	28.8 (3.52)	16, 17

tn=trimethylenediamine; *R*, *R*-chxn=(1*R*, 2*R*)-diaminocyclohexane.

* Present address: Department of Chemistry, The University of Tsukuba, Ibaraki 300-31.

tion is Δ from a criterion of McCaffery *et al.*[18] The CD of Δ isomer shows a pattern of positive and then negative in the order of increasing energy in the specific band region. This sign pattern coincides well with those found for dinitro-, diazido-, and diisothiocyanatobis-(ethylenediamine) complexes in this region.[1]

Experimental

Preparations. *(1)* cis- *and* trans-$M[Co(SO_3)_2(NH_3)_4]$ *(M=Na, or* NH_4*)*: The *cis* isomer was prepared by the method of Bailar and Peppard.[6] Absorp. max. 10^{-3} σ/cm^{-1} (log ε): 22.12 (2.27), 34.13 (4.21), 37.59 (4.19). Found: H, 6.01; N, 20.12%. Calcd for *cis*-$NH_4[Co(SO_3)_2(NH_3)_4]\cdot 2.5H_2O$: H, 6.05; N, 19.99%.

To the filtrate from the *cis* isomer was added twice the volume of methanol and the resulting yellowish brown *trans* isomer was recrystallized from 0.1 M aqueous Na_2SO_3 and dried in air. Absorp. max. 10^{-3} σ/cm^{-1} (log ε): 23 sh (2.60), 30.68 (4.38). Found: H, 5.00; N, 14.99; S, 17.42%. Calcd for *trans*-$Na[Co(SO_3)_2(NH_3)_4]\cdot 3H_2O$: H, 4.99; N, 15.38; S, 17.60%.

(2) cis- *and* trans-$Na[Co(SO_3)_2(en)_2]$: The isomers were prepared as in literature.[19] Absorp. max 10^{-3} σ/cm^{-1} (log ε): *cis* 22.73 (2.40), 34.48 (4.35), 37.25 (4.36); *trans* 23.10 (2.62), 30.86 (4.46). Found: C, 9.00; H, 4.23; N, 10.38%. Calcd for *cis*-$Na[Co(SO_3)_2(en)_2]\cdot NaClO_4\cdot 3H_2O$: C, 8.91; H, 4.12; N, 10.40%. Found: C, 13.21; H, 4.63; N, 15.59%. Calcd for *trans*-$Na[Co(SO_3)_2(en)_2]$: C, 13.26; H, 4.46; N, 15.46%.

(3) Optical Resolution of cis-$Na[Co(SO_3)_2(en)_2]\cdot NaClO_4$: The resolving agent $(+)_{589}$-$[Co(ox)(en)_2]I$ (2.7 g, 6.0×10^{-3} mol) was suspended in 10 cm^3 of water, and converted into the acetate by treating with silver acetate (1.0 g, 6.0×10^{-3} mol). This solution was added to a solution of *cis*-$[Co(SO_3)_2(en)_2]\cdot NaClO_4\cdot 3H_2O$ (1.6 g, 3.0×10^{-3} mol) in 10 cm^3 of water. Red crystals, $(+)_{589}$-$[Co(ox)(en)_2]ClO_4$, appeared immediately. After filtration, the filtrate was evaporated at about 20 °C in a rotary evaporator to about half the initial volume. During the process, another crop of the red crystals (perchlorate of the resolving agent) precipitated, and this was filtered off. The filtrate was kept for a week in a refrigerator, when the less soluble reddish brown diastereomer gradually crystallized out. The diastereomer was converted into the sodium salt by using a cation exchanger SP-Sephadex C-25 (Na^+ form), and the eluate was evaporated. Sodium perchlorate was added to the concentrated solution to precipitate the active complex. CD extrema 10^{-3} σ/cm^{-1} ($\Delta\varepsilon$): 21.05 (−1.83), 23.81 (+0.42), 27.66 (−0.07), 34.25 (+25.7), 38.02 (−28.7). Found: C, 10.13; H, 4.46; N, 11.81%. Calcd for $Na[Co(SO_3)_2(en)_2]\cdot 2.5H_2O\cdot 0.5NaClO_4$: C, 10.25; H, 4.53; N, 11.96%.

(4) cis- *and* trans-$M[Co(S_2O_3)_2(en)_2]$ *(M=Na or Li)*: Ammonium thiosulfate (0.5 g) dissolved in 1 cm^3 of water was added to 10 cm^3 of dimethyl sulfoxide. To this solution 1 g of *cis*-$[CoCl_2(en)_2]Cl$ was added and the mixture was stirred for half an hour at about 70 °C; then this was cooled to room temperature. The precipitated dark green crystals were filtered off, and the filtrate was poured into an anion exchanger column (QAE-Sephadex A-25, Cl^- form; ϕ 2.6 cm, l 30 cm). The column was washed with water and eluted with 0.07 M aqueous LiCl or NaCl solution. A dark green (*trans*)[20] and a brownish violet (*cis*) band were eluted in this order. The *cis* eluate was condensed below 20 °C, and isolated as the lithium salt, while the *trans* one as the sodium salt. Absorp. max. 10^{-3} σ/cm^{-1} (log ε): *trans* 16.5 sh (1.76), 18.32 (1.92), 29.94 (4.43); *cis* 18.35 (2.22), 35.34 (4.20). Found: C, 11.17; H, 3.88; N, 13.39%. Calcd for *trans*-$Na[Co(S_2O_3)_2(en)_2]$: C, 11.26; H, 3.78; N, 13.13%. Found: C, 8.50; H, 4.72; N, 9.47%. Calcd for *cis*-$Li[Co(S_2O_3)_2(en)_2]\cdot 6H_2O\cdot 1.6LiCl$: C, 8.21; H, 4.83; N, 9.57%.

Measurements. The absorption spectra were measured by a Shimadzu UV-200 Spectrophotometer in 0.1 M aqueous Na_2SO_3 solution for the *trans*(SO_3) isomers, in 3% aqueous NH_3 solution for the *cis*-$NH_4[Co(SO_3)_2(NH_3)_4]$, and in H_2O for all the other complexes. The CD spectrum was recorded on a JASCO MOE-1 Spectropolarimeter.

References

1) K. Yamasaki, J. Hidaka, and Y. Shimura, *Bull. Chem. Soc. Jpn.*, **49**, 3060 (1976).
2) V. M. Miskowski and H. B. Gray, *Inorg. Chem.*, **14**, 401 (1975).
3) T. Nomura and M. Nakahara, *Bull. Chem. Soc. Jpn.*, **44**, 1233 (1971).
4) K. L. Scott, *J. Chem. Soc., Dalton Trans.*, **1974**, 1486.
5) K. A. Hofmann and A. Jenny, *Ber.*, **34**, 3855 (1901).
6) J. C. Bailar, Jr. and D. F. Peppard, *J. Am. Chem. Soc.*, **62**, 105 (1940).
7) Y. Shimura, *Bull. Chem. Soc. Jpn.*, **25**, 46 (1952).
8) M. E. Baldwin, *J. Chem. Soc.*, **1961**, 3123.
9) D. R. Stranks and J. K. Yandell, *Inorg. Chem.*, **9**, 751 (1970).
10) H. Siebert, C. Siebert, and S. Thym., *Z. Anorg. Allg. Chem.*, **383**, 165 (1971).
11) M. Linhard and M. Weigel, *Z. Anorg. Allg. Chem.*, **267**, 133 (1951).
12) K. Yamasaki, J. Hidaka, and Y. Shimura, to be submitted.
13) B. J. Brenan and B. E. Douglas, *J. Coord. Chem.*, **1**, 297 (1971).
14) M. B. Ćelap, M. J. Malinar, and P. N. Radivojša, *Inorg. Chem.*, **14**, 2965 (1975).
15) M. Linhard and M. Weigel, *Z. Anorg. Allg. Chem.*, **267**, 121 (1951).
16) H. Kawaguchi, N. Yano, and S. Kawaguchi, *Bull. Chem. Soc. Jpn.*, **42**, 136 (1969).
17) H. Kawaguchi and S. Kawaguchi, *Bull. Chem. Soc. Jpn.*, **43**, 2103 (1970).
18) A. J. McCaffery, S. F. Mason, and B. J. Norman, *J. Chem. Soc.*, **1965**, 5094.
19) R. D. Hargens, W. Min, and R. C. Henney, *Inorg. Synth.*, **14**, 77 (1973).
20) J. Hidaka, J. Fujita, Y. Shimura, and R. Tsuchida, *Bull. Chem. Soc. Jpn.*, **32**, 1317 (1959).

BULLETIN OF THE CHEMICAL SOCIETY OF JAPAN, VOL. 50 (2), 535—536 (1977)

The Halogenation and Nitration of the Optical Active Isomer of the α-Acetylacetonato(triethylenetetramine)cobalt(III) Complex

Kashiro KURODA, Kazumi YAMAGUCHI, and Noriko YAMAOKA

Department of Chemistry, Faculty of Science, Ehime University, Matsuyama, Ehime 790

(Received October 4, 1976)

Synopsis. The methylidyne hydrogen of the coordinated acetylacetonate ion in $(+)_D$-α-acetylacetonato(triethylenetetramine)cobalt(III) perchlorate has been replaced with halogens and with a nitro group with a complete retention of the configuration. The order of the molar rotations of the complexes has been found to be: acac-<Clacac-<Bracac-<Iacac-complex and acac-≃O_2Nacac-complex.*

Resolution into the optical-active antipodes from a synthesized metal complex is generally tedious, since we have no common knowledge as to a suitable resolving reagent for the specified complex. Therefore, if an active complex which has been resolved can be converted into its derivatives with a complete retention of the configuration, our labor in the preparation of the active complexes will be greatly reduced. This technique has been used for the preparation of some active complexes of cobalt(III).[1] However, when a substitution of a ligand is involved in the procedure, there is always a possibility of racemization during the reaction, and the verification of the optical purity of the product remains necessary.

We have found that $(+)_D$-$[Co(acac)(en)_2]^{2+}$* reacts with a slight excess of *N*-chlorosuccinimide in water and in a methanol(50%)–water mixture at *ca.* 40 °C with an increase in activity to form $(+)_D$-$[Co(Clacac)(en)_2]^{2+}$. The activity of the solution at t_∞ (practically, after 1 day) was the same as that of the solution with an equal concentration prepared with the isolated and recrystallized $(+)_D$-$[Co(Clacac)(en)_2](ClO_4)_2$. This means that the chlorination proceeds with a complete retention of the configuration under those conditions; accordingly, $(+)_D$-$[Co(acac)(en)_2](ClO_4)_2$ was treated with the other *N*-halogenosuccinimides and active halogenoacetylacetonato complexes have been obtained.[2] In order to make surer the halogenations with a retention of configuration, $(+)_D$-α-$[Co(acac)(trien)](ClO_4)_2$ was newly prepared and was treated with *N*-halogenosuccinimides. Furthermore, the nitration of the ligand in both active complexes was examined using a mixture of copper(II) nitrate trihydrate and acetic anhydride as a nitration reagent. Thus, a series of optically active halogenated and nitrated complexes were isolated as crystals.

Experimental

Preparation of $(+)_D$-α-$[Co(acac)(trien)](ClO_4)_2$. In 10 ml of water, 2.5 g of the racemic perchlorate salt and 1.0 g of potassium acetate were stirred for 10 min, and then the mixture was cooled. The precipitate($KClO_4$) was filtered off. Into the filtrate, 1.3 g (1/2 equiv. to the complex) of $(+)_D$-$NaAsOC_4H_4O_6$ in 3 ml of water was added. Since it took a long time for the first crystal to come out, a few pieces of $(+)_D$-$[Co(acac)(en)_2][(+)_D$-$AsOC_4H_4O_6]_2$[3] were added to induce the crystal growth. Thus, pale red crystals came out gradually. After the mixture had been placed in a refrigerator overnight, the precipitate was separated and washed with ethanol and ether. Yield, 1.8 g.

Into a suspension of 0.5 g of the diastereoisomeric salt in 30 ml of ethanol, 3 ml of aqueous 2 M $NaClO_4$ was added. The mixture was then stirred vigorously for 1 h at *ca.* 45 °C, whereupon the solid phase turned white. The solid($NaAsOC_4H_4O_6$) was subsequently filtered off, and the filtrate was evaporated to dryness. To the residue we added 5 ml of warm water, and, after the removal of a white insoluble material by filtration, a few drops of 6 M $HClO_4$ were added to the filtrate, which was then cooled. The bright red crystals which were thus precipitated were collected and washed with an ethanol(20%)–ether mixture and with ether. Yield, 0.3 g.

Preparation of $(+)_D$-$[Co(acac)(en)_2](ClO_4)_2$. The procedure of the preparation was described in the preceding report.[2]

Chlorination, Bromination, Iodination, and Nitration of the Active Complexes. The halogenations and the nitration of the active isomers were carried out by the methods used for the inactive complexes.[2]

Identification and Measurement of the Optical Rotations. Each complex was identified by making sure its absorption spectrum was identical with that of the respective inactive complex.[2] The rotation of the complexes was counted with a JASCO DIP 180 Polarimeter at 589, 577, 546, 435, and 405 nm, using a 0.1% aqueous solution for the first four wavelengths and a 0.02% solution for the last wavelength.

Results and Discussion

Sodium arsinyl tartrate, which is known as an excellent resolving reagent for $[Co(acac)(en)_2]^{2+}$,[3] is also useful for the resolution of α-$[Co(acac)(trien)]^{2+}$. The conversion of the diastereoisomeric salt into the perchlorate was carried out by utilizing the property of the perchlorate of being soluble in ethanol including a small amount of water.

The molar rotations of the obtained complexes are shown in Table 1. As may be seen in the table, the rotatory characters of the trien complexes as well as of the en complexes are quite similar to each other; therefore, the chirality around the central cobalt must be same, and, since $(+)_D$-$[Co(acac)(en)_2]^{2+}$ has been established as having the *Λ*-configuration,[4] all of the trien complexes as well as the halogenated and nitrated en complexes can be concluded as having the *Λ*-configuration:

* The following abbreviations have been used in this report: en, ethylenediamine; trien, triethylenetetramine; acac, acetylacetonate ion (2,4-pentanedionate ion); Clacac, chloroacetylacetonate ion (3-chloro-2,4-pentanedionate ion); Bracac, bromoacetylacetonate ion; Iacac, iodoacetylacetonate ion; O_2Nacac, nitroacetylacetonate ion.

Table 1. Molar rotations of $(+)_D$-[Co(Xacac)$(en)_2$]-$(ClO_4)_2$ and $(+)_D$-α-[Co(Xacac)(trien)]$(ClO_4)_2$

Complex	$[M]_{589}$	$[M]_{577}$	$[M]_{546}$	$[M]_{435}$	$[M]_{405}$
$(+)_D$-[Co(Xacac)$(en)_2$]$(ClO_4)_2$					
acac	+2280°	+2900°	+3200°	−11500°	−11800°
Clacac	+2590°	+3260°	+3330°	−12700°	−13300°
Bracac	+2630°	+3280°	+3340°	−12800°	−13600°
Iacac	+2770°	+3330°	+3410°	−13500°	−14400°
O_2Nacac	+2090°	+2650°	+3750°	−11500°	−12600°
$(+)_D$-α-[Co(Xacac)(trien)]$(ClO_4)_2$					
acac	+2560°	+3280°	+4630°	−13700°	−13500°
Clacac	+3130°	+3900°	+4990°	−16000°	−15800°
Bracac	+3210°	+4060°	+5270°	−16800°	−16200°
Iacac	+3330°	+4200°	+5350°	−17800°	−16700°
O_2Nacac	+2240°	+2840°	+5050°	−15300°	−14600°

$(+)_D$-α-[Co(Xacac)(trien)]$^{2+}$

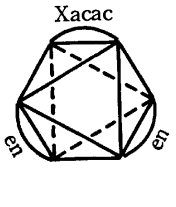

$(+)_D$-[Co(Xacac)$(en)_2$]$^{2+}$

The orders of the activities can be seen as:

acac-<Clacac-<Bracac-<Iacac-complex

and

acac-≃O_2Nacac-complex

in both en and trien complexes. Thus, the increase or the maintenance of rotation by the substitutions indicates that the reactions proceed without any bond rupture between the cobalt and the ligands, as has been verified in the chlorination of $[Co(acac)(en)_2]^{2+}$; hence, the method for obtaining these optical active isomers has been greatly simplified.

References

1) A. M. Sargeson and G. H. Searle, *Inorg. Chem.*, **4**, 45 (1965); B. Bosnich, M. Harrowfield, and H. Boucher, *ibid.*, **14**, 815 (1975); B. Bosnich and M. Harrowfield, *ibid.*, **14**, 836, 853 (1975).

2) K. Kuroda, K. Yoshitani, K. Kunigita, Y. Kamiiba, and K. Watanabe, *Bull. Chem. Soc. Jpn.*, **49**, 2445 (1976).

3) I. K. Reid and A. M. Sargeson, *Inorg. Synth.*, **9**, 167 (1967).

4) A. J. McCaffery, S. F. Mason, and B. J. Norman, *J. Chem. Soc.*, **1965**, 5094.

BULLETIN OF THE CHEMICAL SOCIETY OF JAPAN, VOL. 50 (2), 537—538 (1977)

cis-2-Pentenyl Moiety from 5,6-Dihydro-2*H*-thiopyran. A Convenient Synthesis of *cis*-Jasmone

Sigeru Torii, Hideo Tanaka, and Yoshihisa Tomotaki

Department of Industrial Chemistry, School of Engineering, Okayama University, Okayama 700

(Received June 4, 1976)

Synopsis. A method for the synthesis of *cis*-jasmone from 5,6-dihydro-2*H*-thiopyran is described. Formation of *cis*-2-pentenyl moiety was achieved by reductive desulfurization of the 2*H*-thiopyran derivative obtained by the alkylation of 5,6-dihydro-2*H*-thiopyran with epichlorohydrin.

The construction of *cis*-2-pentenyl moiety has been the subject of jasmonoid syntheses.[1a-c] Preparation of the *cis*-pentenyl group by elaborated routes has been reported, *e.g.*, the partial hydrogenation of carbon-carbon triple bond,[1d] including the formation of 2-pentynyl group,[1e] the Wittig reaction of formylmethyl group with propylidenetriphenylphosphorane under salt-free condition ,[1f] and 1,5-sigmatropic rearrangement of 1-(1-propenyl)spiro[2.5]octan-4-one.[1g]

The dipole inversion (umpolung)[2] of *cis*-2-pentenyl cation (A) derived from *cis*-2-pentenyl halide would be *cis*-2-pentenide ion (B) which promises a novel approach for jasmonoid synthesis. A synthetic equivalent of the carbanion (B) is considered to be 5,6-dihydro-2*H*-thiopyran-2-ide ion (C). From our preliminary experiments, the regioselective alkylation of ambident carbanions (C) and (D) with epichlorohydrin has been found to occur exclusively at C-2 carbon atom.[3] This led us to investigate the novel synthesis of *cis*-jasmone.

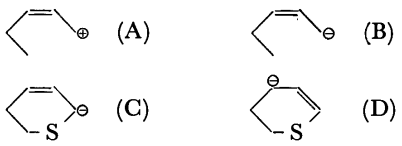

Treatment of 5,6-dihydro-2*H*-thiopyran (**1**)[4] with 1.1 equivalents of *s*-butyllithium in tetrahydrofuran (THF) at −78 °C and subsequent addition of epichlorohydrin gave the 2-alkylated product **2** in 95% yield. Product **2** was contaminated with less than 2% of the corresponding 4-alkylated product. Reduction of **2** in THF at room temperature with lithium aluminum hydride afforded the alcohol **3**. Reductive desulfurization of the corresponding tetrahydropyranyl ether of **3** was performed by a two-step operation: treatment of **4** with lithium metal–ethylamine[5] at *ca.* −25 °C and subsequent reduction of the thiol **5** with Raney nickel (W-2)[6] in methanol at 25—28 °C, giving *cis*-7-tetrahydropyranyloxy-3-octene (**6**) in 84% over-all yield. Acetal exchange reaction of **6**[7] with *p*-toluenesulfonic acid–methanol and subsequent oxidation with chromic acid[8] gave *cis*-5-octen-2-one (**8**)[9] in 85% yield.

The conversion of the ketone **8** into *cis*-jasmone was achieved by Harper and Smith,[10] the preparation of dihydrojasmone from 2-octanone being established.[1] The cross-coupling of enolate anions from 2-octanone and acetone has been found to be promoted by copper(II) chloride in *N*,*N*-dimethylformamide.[11] According to the method of Ito *et al.* **8** could react with acetone to give diketone **9** in 74% yield. Refluxing of **9** in aqueous 2% potassium hydroxide afforded *cis*-jasmone in 86% yield.[12]

The *cis* double bonds of the products **8**, **9**, and **10** were analyzed by comparing their spectral data with those reported.[9,11,12] The results indicate that the *cis* double bonds of the intermediates **6** and **7** are retained during the course of conversion from **4** to **8**.

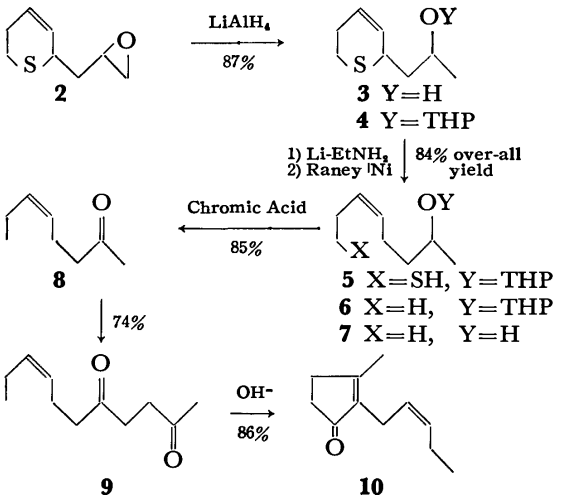

Experimental

Boiling points were indicated by air bath temperature without correction. NMR spectra were recorded on a Hitachi R-24 instrument. IR spectra were taken with JASCO model IRA-1 spectrometer. Analytical TLC was performed on commercial glass plates bearing 0.1—0.2 mm layer of Merck silica gel PF-254.

5,6-Dihydro-2H-thiopyran (1). An Inproved Method: A mixture of 4-hydroxytetrahydrothiopyran[13] (1.30 g, 11 mmol) and a catalytic amount of $KHSO_4$ was heated to 250—300 °C under N_2 for 10 min and then distilled. After work-up in the usual manner, 0.90 g (82%) of **1** was obtained; bp 74—75 °C/60 Torr (lit,[4] bp 35—36 °C/12 Torr); IR (neat) 3020 (HC=), 1652 cm^{-1}; NMR (CCl_4) δ 2.30 (m, 2H, CH_2–C=), 2.65 (m, 2H, CH_2–S), 3.04 (m, 2H, S–CH_2–C=), 5.75 (m, 2H, HC=CH).

2-(2,3-Epoxypropyl)-5,6-dihydro-2H-thiopyran (2). *s*-BuLi in pentane (1.5 M, 2.5 ml, 3.8 mmol) was added dropwise to a solution of **1** (350 mg, 3.5 mmol) in THF (15 ml) with stirring under N_2 at −78 °C for 1 h. To this mixture was added epichlorohydrin (336 mg, 3.6 mmol) with stirring at −78 °C for 1 h and at room temp for an additional 1 h. The reaction was terminated by a few drops of water. The mixture was treated in the usual manner and the residue was subjected to short-path distillation to give **2** (520 mg, 95%): bp 84—86 °C/9 Torr; IR (neat) 3024 (HC=), 1658 cm^{-1} (C=C); NMR (CCl_4) δ 3.38 (m, 1H, HC–S), 5.75 (m, 2H, HC=CH). Found:

C, 61.26; H, 7.82%. Calcd for $C_8H_{12}OS$: C, 61.50; H, 7.74%.

2-(2-Hydroxypropyl)-5,6-dihydro-2H-thiopyran (3). A THF solution (4 ml) of **2** (344 mg, 2.2 mmol) was added to a suspension of $LiAlH_4$ (100 mg, 2.6 mmol) in ether (12 ml) at 0 °C under N_2. The mixture was stirred at 0 °C for 2 h and at room temp for 11 h and quenched with water at 0 °C until a white precipitate formed. The white solid was filtered off and the filtrate was concentrated. The residue was chromatographed over silica gel (2 g) with hexane–THF (10: 1) to give **3** (340 mg, 87%): TLC R_f 0.30 (hexane–THF, 4: 1); IR (neat) 3360 (OH), 3020 (HC=), 1654 cm^{-1}; NMR ($CDCl_3$) δ 1.22 (d, J=6.5 Hz, 3H, CH_3), 1.55—1.94 (m, 2H), 2.29 (m, 2H, CH_2–C=), 2.69 (m, 2H, CH_2–S), 2.98 (s, 1H, OH), 3.41 (m, 1H, CH–S), 3.96 (m, 1H, CH–O), 5.75 (m, 2H, HC=CH). The analytical sample was prepared by short-path distillation at 50—55 °C/0.001 Torr. Found: C, 60.62; H, 9.07%. Calcd for $C_8H_{14}OS$: C, 60.72; H, 8.92%.

2-(2-Tetrahydropyranyloxypropyl)-5,6-dihydro-2H-thiopyran (4) was prepared from **3** (88 mg, 0.56 mmol) and dihydropyran (100 mg, 1.20 mmol) in benzene (2 ml) in the presence of *p*-toluenesulfonic acid (5 mg) in 89% yield: bp 67—72 °C/0.001 Torr; IR (neat) 3015 (HC=), 1652 cm^{-1} (C=C); NMR ($CDCl_3$) δ 1.20 (m, 3H, CH_3), 1.62 (m, 8H), 2.26 (m, 2H, CH_2–C=), 2.67 (m, 2H, CH_2–S), 3.17—4.20 (m, 4H, CH_2–O, CH–O, CH–S), 4.69 (m, 1H, O–CH–O), 5.73 (m, 2H, HC=CH). Found: C, 64.19; H, 9.22%. Calcd for $C_{13}H_{22}O_2S$: C, 64.42; H, 9.15%.

cis-*7-Tetrahydropyranyloxy-3-octene (6).* Lithium metal (11 mg, 1.6 mmol) was added at −25 °C to a solution of **4** (30 mg, 0.12 mmol) in $EtNH_2$ (3 ml), stirring being continued for 1 h. The mixture was quenched with water. After evaporation of the solvent, the residue was extracted with AcOEt, washed with brine, and concentrated, then subjected to column chromatography of silica gel with hexane–THF (10: 1) to give the thiol **5** (28 mg, 93%): TLC R_f 0.35 (hexane–THF, 10: 1); IR (neat) 3000 (HC=), 1654 cm^{-1} (C=C); NMR ($CDCl_3$) δ 1.16 (m, 3H, CH_3), 1.27—2.70 (m, 15H), 3.15—4.10 (m, 3H), 4.67 (m, 1H, O–CH–O), 5.41 (m, 2H, HC=CH). Without further purification a MeOH solution (2 ml) of **5** (28 mg, 0.11 mmol) was added to a suspension of Raney Ni (W-2) (60 mg) in MeOH (1 ml) over a period of 5 min at room temp. The mixture was stirred for 1 h at 25—28 °C, diluted with acetone, filtered and concentrated. The residue was chromatographed on silica gel (2 g) with hexane–THF (50: 1) to give **6** (22 mg, 90%): TLC R_f 0.62 (hexane–THF, 15: 1); IR (neat) 3040 cm^{-1} (HC=); NMR ($CDCl_3$) δ 0.95 (t, J=7.2 Hz, 3H, CH_3), 1.15 (m, 3H, CH_3), 1.30—2.33 (m, 12H), 3.20—4.07 (m, 3H), 4.69 (m, 1H, O–CH–O), 5.37 (m, 2H, HC=CH). The analytical sample was obtained by short-path distillation at 71—75 °C/1.0 Torr. Found: C, 73.36; H, 11.62%. Calcd for $C_{13}H_{24}O_2$: C, 73.54; H, 11.39%.

cis-*5-Octen-2-ol (7).* To a MeOH solution (3 ml) of **6** (50 mg, 0.24 mmol) was added *p*-toluenesulfonic acid (5 mg) at 0 °C. After being stirred for 5 min at 0 °C, then 1.5 h at room temp the mixture was worked up in the usual manner to give the alcohol **7** (30 mg, 99%); bp 62—65 °C/13 Torr; TLC R_f 0.30 (hexane–THF, 10: 1); IR (neat) 3330 (OH), 3000 (HC=), 1652 cm^{-1} (C=C); NMR ($CDCl_3$) δ 0.96 (t, J=7.2 Hz, 3H, CH_3), 1.17 (d, J=6.2 Hz, 3H, CH_3), 1.20—2.35 (m, 7H), 3.76 (m, 1H, CH–O), 5.38 (m, 2H, HC=CH). Found: C, 75.05; H, 12.87%. Calcd for $C_8H_{16}O$: C, 74.97; H, 12.85%.

cis-*5-Octen-2-one (8).* To a solution of **7** (30 mg, 0.23 mmol) in ether (3 ml) was added aqueous chromic acid[8] (1.3 M, 0.1 ml) at 0 °C. The mixture was stirred for 30 min at 0 °C and for 1 h at room temp. The organic phase was separated and worked up in the usual manner to give **8** (25 mg, 85%); bp 110—115 °C/760 Torr (lit,[9] bp 54—57 °C/10 Torr), whose IR and NMR spectra were identical with those of the authentic compound.[9]

cis-*8-Undecen-2,5-dione (9).*[11] The compound **8** (30 mg, 0.24 mmol) was added dropwise to a solution of *i*-Pr_2NLi in THF (0.9 M, 1.3 ml, 1.2 mmol) at −78 °C under N_2. Stirring was continued for 15 min and then acetone (41 mg, 0.47 mmol) was added over a period of 10 min. The mixture was stirred for 15 min at −78 °C and then a solution of copper-(II) chloride (184 mg, 1.1 mmol) in DMF (1 ml) was added at −78 °C. The mixture was kept at −78 °C for 30 min, warmed to room temp, and stored for 30 min. The solution was poured into ice cooled aqueous 5% HCl (5 ml) and extracted with ether. The extract was worked up in the usual manner and the residue was subjected to preparative GLPC[14] to give **9** (32 mg, 74%), whose spectral data were in agreement with those of the authentic sample.[12]

cis-*Jasmone (10).* A solution of diketone **9** (20 mg, 0.11 mmol) in aqueous 2% KOH was refluxed for 3 h. After work-up in the usual manner, 17 mg (86%) of **10** was obtained, bp 105—110 °C/3 Torr (lit,[12] bp 93—97 °C/0.8 Torr), which was identified as *cis*-jasmone by comparison of the IR and NMR spectra of **10** with those reported.[12]

References

1) (a) S. Torii and H. Tanaka, *Koryo*, **114**, 41 (1976); (b) T.-L. Ho, *Synth. Commun.*, **4**, 256 (1974); (c) R. A. Ellison, *Synthesis*, **1973**, 397; (d) H. Lindlar, *Helv. Chim. Acta*, **35**, 446 (1952); (e) K. Sisido, S. Kurozumi, and K. Utimoto, *J. Org. Chem.*, **34**, 2661 (1969); (f) H. Tanaka and S. Torii, *ibid.*, **40**, 462 (1974) and references cited therein; (g) Y. Bahurel and G. Descotts, *C. R. Acad. Sci., Ser. C.*, **275**, 1593 (1973).

2) D. Seebach and M. Kolb, *Chem. Ind. (London)*, **1974** 687.

3) S. Torii, H. Tanaka, and Y. Tomotaki, *Chem. Lett.*, **1974**, 1541.

4) R. F. Naylor, *J. Chem. Soc.*, **1949**, 2749.

5) K. Kondo, A. Negishi, K. Matsui, D. Tunemoto, and S. Masamune, *J. Chem. Soc., Chem. Commun.*, **1972**, 1311.

6) R. Mozingo, *Org. Synth.*, Coll. Vol. III, 181 (1955).

7) P. A. Grieco, N. Marinovic, and M. Miyashita, *J. Org. Chem.*, **40**, 1670 (1975).

8) H. C. Brown, C. P. Garg, and K.-T. Liu, *J. Org. Chem.*, **36**, 387 (1971).

9) L. Crombie, P. Hemesley, and G. Pattenden, *J. Chem. Soc., C*, **1969**, 1016.

10) S. H. Harper and R. J. D. Smith, *J. Chem. Soc., C*, **1955**, 1512.

11) Y. Ito, T. Konoike, and T. Saegusa, *J. Am. Chem. Soc.*, **97**, 2912 (1975).

12) L. Crombie, P. Hemesley, and G. Pattenden, *J. Chem. Soc., C*, **1969**, 1024.

13) W. E. Parhan, L. Christenses, S. H. Groen, and R. M. Dodson, *J. Org. Chem.*, **29**, 2211 (1964).

14) The condition of GLPC: R_t 18 min, 3 m×4 mm column of 10% SE-30 on Chamelite CK 80—100 mesh at 140 °C with a flow rate of 20 ml/min.

BULLETIN OF THE CHEMICAL SOCIETY OF JAPAN, VOL. 50 (2), 539—540 (1977)

Geometrical Isomerism of 2,4-Dinitrophenylhydrazones of Some Pyruvic Esters

Takeo NASHIMA, Fumihide ISHIBASHI, Masayuki IWAMOTO,* Yoko AIHARA,**
Sumiko ANZAI,† and Goro YAMANO††
Department of Chemistry, Osaka Kyoiku University, Tennoji-ku Osaka 543

(Received June 16, 1976)

Synopsis. Visible, IR, and PMR spectra of 2,4-dinitrophenylhydrazones (DNPH) of some pyruvic esters were studied. It is suggested that each α-isomer with a higher R_f-value involves an intramolecular hydrogen bond between the imino hydrogen and the ester carbonyl group, to which the *Z*-structure is assigned. The *E*-structure is assigned to each β-isomer with a lower R_f-value.

Formation of various phenylhydrazones is usually utilized for the identification of pyruvic acid and its esters. The problem of geometrical isomerism of the hydrazones has been studied for many years by a number of investigators. However, only a few investigations deal with the geometrical isomerism of DNPH of pyruvic esters, *cf.* H. van Duin,[1] and P. Juvvik and B. Sundby.[2]

Van Duin[1] prepared DNPH of pyruvic esters by the reaction of the corresponding alcohols with DNPH of pyruvoyl chloride and separated two geometrical isomers of DNPH of each ester by partition column chromatography, and assigned *E*(*anti*)-structure to the isomer with the smaller retention volume (α-isomer) and *Z*(*syn*)-structure to the other (β-isomer). His assignment was based on the fact that the wavelength of the absorption maximum in the visible spectra for each α-isomer is very close to that for DNPH of normal ketones. Recently, Juvvik and Sundby[2] assigned, on the basis of the IR spectra (no data given), *E*-structure to DNPH of ethyl pyruvate obtained from the ester and the hydrazine reagent in an aqueous hydrochloric acid solution, no detail being given except for the UV-visible spectral data for the DNPH.

We report the results of the observations on the visible, IR, and PMR spectra for the geometrical isomers of DNPH of pyruvic esters. It is suggested that van Duin's assignment is inconsistent.

Experimental

Methyl and ethyl pyruvates (Sigma Chemical Co.) were distilled before use. Isopropyl and *t*-butyl pyruvates were prepared by esterification of pyruvic acid. DNPH of diethyl mesoxalate was prepared from 2,4-dinitrophenylhydrazine and the ester which was obtained by the oxidation of diethyl bromomalonate with dimethyl sulfoxide.

When DNPH of pyruvic esters were formed in an alcoholic sulfuric acid solution, followed by separation of the resulting mixture of isomers by means of column chromatography on

TABLE 1. MELTING POINTS, ELEMENTARY ANALYSES, CRYSTALLINE FORMS, AND R_f-VALUES OF DNPH OF PYRUVIC ESTERS (**1**) AND OF DIETHYL MESOXALATE (**2**)

Compd		Mp (°C)[a]	Analysis (%) Found (Calcd) C	H	N	Formula	Crystalline form[f]	R_f-Value[g]
	α	184.5—185	42.56	3.34	20.13		Needles	0.38
1, R=Me			(42.56	3.57	19.85)	$C_{10}H_{10}N_4O_6$		
	β	151.5—152	42.77	3.37	20.04		Prisms	0.11
	α	154.5—155	44.41	3.97	19.08		Prisms	0.42
1, R=Et			(44.60	4.08	18.91)	$C_{11}H_{12}N_4O_6$		
	β	126.5—127[b]	44.37	4.03	19.18		Scales	0.12
	α	159.5—160.5	46.22	4.39	17.93		Scales	0.49
1, R=*i*-Pr			(46.45	4.55	18.06)	$C_{12}H_{14}N_4O_6$		
	β	119.5—120[c]	46.65	4.48	18.33		Prisms	0.14
	α	146—147[d]	48.25	4.73	17.33		Scales	0.61
1, R=*t*-Bu			(48.15	4.97	17.28)	$C_{13}H_{16}N_4O_6$		
	β	148.5—149.5[e]	48.11	4.73	17.37		Prisms	0.19
2		118—118.5	43.86	3.85	16.00		Prisms	0.30
			(44.07	3.98	15.82)	$C_{13}H_{14}N_4O_8$		

a) Uncorrected. b) 115—117°C.[1] c) 115.5 °C.[1] d) 151.5 °C.[1] e) 117.5—119.5 °C.[1] f) Recrystallized from ethanol. g) TLC on silica gel utilizing benzene as the developing solvent.

* Kanan Senior High School of Osaka Prefecture, Tondabayashi, Osaka.
** Yatanishi Elementary School, Higashisumiyoshi-ku, Osaka.
† Amamikita Elementary School, Matsubara, Osaka.
†† Ryuge Junior High School, Yao, Osaka.

silica gel with benzene as an eluting solvent, the main product was the α-isomer with a higher R_f-value. On the other hand, the lower R_f-value was found for the main product of the reaction of pyruvic esters with the hydrazine reagent in a dilute aqueous hydrochloric acid solution with subsequent separation.

Results and Discussion

Melting points, elementary analyses, crystalline forms, and R_f-values of DNPH of pyruvic esters (**1**, α and β) together with those for diethyl mesoxalate (**2**) are summarized in Table 1.

The visible, IR, and PMR spectral data for **1** and, for comparison, for **2** and DNPH of acetone (**3**) are given in Table 2. We see that, (a) absorption maxima in the visible spectra for all the α-isomers lie at the longer wavelengths than those for all the corresponding β-isomers, (b) extinction coefficients at the absorption maxima for all the α-isomers are larger than those for all the corresponding β-isomers, (c) both N–H and C=O stretching bands in the IR spectra appear at wave numbers for all the α-isomers smaller than those for all the corresponding β-isomers, (d) all the α-isomers show NH signals in the PMR spectra at lower magnetic fields than all the corresponding β-isomers.

Table 2. Visible, IR, and PMR spectra for **1**, **2**, and **3**

Compd		Visible (in EtOH)[a]		IR (Nujol mull)[b]		PMR (in $CDCl_3$)[c]
		λ_{max} (nm)	$\varepsilon \times 10^{-4}$	ν_{N-H} (cm^{-1})	$\nu_{C=O}$ (cm^{-1})	δ_{NH} (ppm)
1, R=Me	α	360	2.67	3148	1695	14.0
	β	348	2.37	3304	1727	11.1
1, R=Et	α	360	2.62	3200	1697	14.1
	β	349	2.37	3320	1723	11.1
1, R=*i*-Pr	α	361	2.64	3173	1685	14.0
	β	350	2.52	3316	1706	11.1
1, R=*t*-Bu	α	362	2.71	3220	1696	14.0
	β	351	2.45	3312	1708	11.1
2		349	2.17	3190	1691	14.1
		373	2.34		1724	
3		360	2.03	3305	—	10.9

a) Recorded on a Hitachi Recording Spectrophotometer ESP-3. b) Recorded on a Hitachi-Perkin-Elmer IR-Spectrometer 225. c) Recorded at 60 MHz on a Hitachi-Perkin-Elmer High Resolution NMR-Spectrometer R-20B.

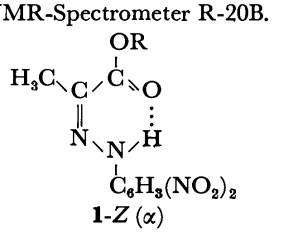

1-*Z* (α)

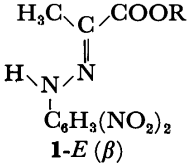

1-*E* (β)

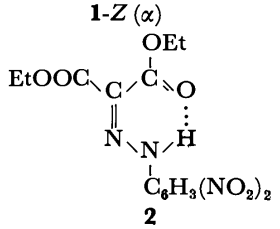

2

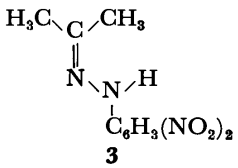

3

R=Me, Et, *i*-Pr, *t*-Bu

Table 3. IR Spectra for **1**, **2**, and **3** in CCl_4 at various concentrations

Compd		0.01 M (cm^{-1})		0.005 M (cm^{-1})		0.001 M (cm^{-1})	
		ν_{N-H}	$\nu_{C=O}$	ν_{N-H}	$\nu_{C=O}$	ν_{N-H}	$\nu_{C=O}$
1, R=Me	α	3200[a]	1707[a]			3205	1708
	β	3316	1725			3315	1720
1, R=Et	α	3206	1700	3205	1696	3205	1701
	β	3316	1714	3316	1713	3315	1714
1, R=*i*-Pr	α	3202	1694			3205	1695
	β	3318	1713			3315	1708
1, R=*t*-Bu	α	3200	1695			3195	1692
	β	3317	1709			3312	1705
2		3195	1695			3195	1695
			1732				1730
3		3320	—			3320	—

a) Saturated solution.

Infrared spectral data for **1**, **2**, and **3** in carbon tetrachloride at various concentrations are given in Table 3. We see that both N–H and C=O stretching bands for all the α-isomers appear at wave numbers smaller than those for all the corresponding β-isomers as in the case with Nujol mull. The observation may suggest that each α-isomer involves an intramolecular hydrogen bond between the imino hydrogen and the ester carbonyl group.

The results suggest that the *Z*-structure (**1**-*Z*) is assigned to the α-isomers and the *E*-structure (**1**-*E*) to the β-isomers. Similar suggestions were reported on the geometrical isomerism of DNPH of α-keto acids,[3,4] and of phenylhydrazones of α-keto acids,[5] pyruvamide,[6] and methyl[6] and ethyl[7] pyruvates. The assignment is just the opposite to that of van Duin. **3** gives an absorption maximum in the visible spectra at the wavelength close to those given by the α-isomers of **1** as was reported by him. However, **2** shows two absorption bands, the stronger band appearing at a longer wavelength than for **3**. Thus, the mere agreement of the wavelength, at which the maximum absorption in the UV-visible spectra occurs, cannot be taken to indicate the coincidence of geometrical structure. The IR and PMR spectral data for **2** and **3** also support our assignment (Tables 2 and 3).

References

1) H. van Duin, *Recl. Trav. Chim. Pays-Bas*, **73**, 78 (1954).
2) P. Juvvik and B. Sundby, *Acta Chem. Scand.*, **27**, 3632 (1973).
3) T. Moriwaki, H. Katsuki, and S. Tanaka, *Nippon Kagaku Zasshi*, **76**, 1367 (1955).
4) H. Katsuki, T. Yoshida, J. Nagai, and S. Tanaka, *Bull. Chem. Soc. Jpn.*, **44**, 3108 (1971).
5) N. Ariga, *Mem. Fac. Sci. Kyoto Univ., Ser. Phys., Astrophys., Geophys. Chem.*, **34**, 183 (1973).
6) R. A. Abramovitch and I. D. Spenser, *J. Chem. Soc.*, **1957**, 3767.
7) J. Elguero, R. Jacquier, and G. Tarrago, *Bull. Soc. Chim. Fr.*, **1966**, 2981.

BULLETIN OF THE CHEMICAL SOCIETY OF JAPAN, VOL. 50 (2), 541—542 (1977)

Pseudohalogen Chemistry. V.[1] Homolytic Addition of Thiocyanogen Chloride to Some Haloalkenes on Irradiation with UV Light

Robert G. Guy and Ian Pearson

School of Natural Sciences, The Hatfield Polytechnic, P.O. Box 109, Hatfield, Hertfordshire, England

(Received July 5, 1976)

Synopsis. When irradiated with UV light, thiocyanogen chloride reacts with haloalkenes containing 1—4 halo substituents yielding α-chloro-β-thiocyanato compounds. Addition to unsymmetrical alkenes is regioselectively anti-Markownikov. A radical-chain mechanism, involving S_H2 displacement on the sulfur atom of thiocyanogen chloride and chlorine atoms as the adding/chain-carrying species, is proposed.

In earlier papers it was shown that, under heterolytic conditions in acetic acid, thiocyanogen chloride ($\overset{\delta-}{Cl}$–$\overset{\delta+}{SCN}$) behaves as an electrophile towards aliphatic alkenes[2] and α-arylalkenes[3] yielding α-chloro-β-thiocyanato compounds and the corresponding α-acetoxy-β-thiocyanato compounds; in the case of unsymmetrical alkenes preferential or exclusive Markownikov addition is observed.[4] Here we describe the homolytic reaction of thiocyanogen chloride with some alkenes previously shown to be unreactive under heterolytic conditions.[2-4]

Results and Discussion

UV irradiation of equimolar amounts of thiocyanogen chloride and *cis*-dichloroethylene under conditions previously shown to lead to homolytic substitution reactions with aralkyl hydrocarbons[5] (acetic acid or carbon tetrachloride solvent, an aerial atmosphere, ambient temperatures) resulted in slow reactions. Faster reactions were achieved, especially in acetic acid, by increasing the intensity of the radiation and, more strikingly, by using a nitrogen atmosphere (see Table 1).

Under these conditions, vinyl bromide, *cis*-dichloroethylene, *trans*-dichloroethylene, 1,1-dichloroethylene, trichloroethylene, and tetrachloroethylene all yielded α-chloro-β-thiocyanato compounds exclusively (see products **1**—**8** in Table 1); unsymmetrical alkenes yielded both regioisomers, with the anti-Markownikov isomer predominating in each case (see products **2**—**7** in Table 1). Reaction times and yields are recorded in Table 1. Neither tetraphenylethylene nor *trans*-1,2-dithiocyanatoethylene added thiocyanogen chloride, but, in the latter case, the recovered alkene consisted of the equilibrium mixture of *cis*- and *trans*-isomers. No telomers or crossed products, *i. e.* dichlorides or dithiocyanates, were observed.

Initiation: $ClSCN \xrightarrow{h\nu} Cl\cdot + \cdot SCN$ (1)

Addition: $Cl\cdot + \rangle C{=}C\langle \rightleftharpoons -\overset{|}{\underset{|}{C}}-\overset{|}{\underset{Cl}{C}}-\cdot$ (2)

Transfer: $-\overset{|}{\underset{Cl}{C}}-\overset{|}{\underset{\cdot}{C}}- + ClSCN \rightarrow -\overset{|}{\underset{Cl}{C}}-\overset{|}{\underset{SCN}{C}}- + Cl\cdot$ (3)

Photochemical induction of the reaction and its inhibition by aerial oxygen point towards a radical chain reaction, albeit of low chain length as indicated by the effect of the radiation intensity and the relatively long reaction times. The chemical results are consistent with the chain reaction shown in Eqs. 1—3 in which a chlorine atom, formed photochemically from thiocyanogen chloride[5] (Eq. 1), is the adding and chain-carrying species. Reversible addition of the chlorine atom to the alkene (Eq. 2), well-established in radical additions of molecular chlorine,[6] accounts for the observed isomerisation of *trans*-dithiocyanatoethylene. The transfer step (Eq. 3) involves S_H2 displacement on the electron-deficient sulfur atom of thiocyanogen chloride by the donor[7] chloroalkyl radical and the generation of a chlorine atom to carry on the chain; this accounts for (a) the exclusive formation of chlorothiocyanato compounds rather than the corresponding, thermodynamically more stable, chloroisothiocyanato compounds, (b) the preferential anti-Markownikov orientation of addition to unsymmetrical alkenes (*via* the more stable of the two possible chloroalkyl radicals), and (c) the lower rates of reaction as the donor characteristics of the chloroalkyl radical are reduced by the electronic and steric effects of further halo, thiocyanato and phenyl substituents.[7]

In contrast, homolytic additions of all other RSCl compounds examined so far have involved either exclusive displacement on the chlorine atom with RS· radicals as the adding/chain-carrying agent (*e. g.* Cl_3CSCl,[8] Cl_3CSO_2Cl,[9] F_5SCl[10]), or concurrent displacements on the chlorine and sulfur atoms with RS· and Cl· radicals respectively as competing adding/chain-carrying agents (*e.g.* F_3CSCl[11]). These differences, also noted in the homolytic substitution reactions of these compounds,[12] are consistent with the steric barrier to displacement at the sulfur atom increasing in the order $NCSCl < F_3CSCl < Cl_3CSCl$, Cl_3CSO_2Cl, F_5SCl.

Experimental

Alkenes. The haloalkenes and tetraphenylethylene were commercial samples purified until their physical constants agreed with those recorded in the literature. *trans*-1,2-Dithiocyanatoethylene was prepared as described.[13]

General Procedure. Reactions were carried out on an ≈0.4 M scale using the procedure described earlier[5] and the modifications recorded in the text and Table 1. Irradiation was continued until iodometric titrations showed at least 70% consumption of thiocyanogen chloride. Products were isolated as described.[5]

Identification of the Products. Adducts of the haloalkenes were identified as before by IR and NMR spectroscopy;[2-4] regioisomers were not separated, but isomer

Table 1. Photo-chlorothiocyanation of haloalkenes

Alkene	Conditions[a]			Time (h)	Product(s)	Yield (%)
	Solvent	Distance[b]	Atmosphere			
cis-CHCl=CHCl	CCl_4	10	air	1	$CHCl_2CH(SCN)Cl$ (**1**)	5
	CCl_4	10	N_2	1	**1**	14
	CCl_4	1	N_2	1	**1**	30
	AcOH	10	air	1	**1**	7
	AcOH	10	N_2	1	**1**	17
	AcOH	1	N_2	1	**1**	60
trans-CHCl=CHCl	AcOH	1	N_2	1	**1**	58
CH_2=CHBr	AcOH	1	N_2	1	$CH_2ClCH(SCN)Br$ (**2**)	61
					$CH_2(SCN)CHClBr$ (**3**)	9
CH_2=CCl_2	AcOH	1	N_2	2.5	$CH_2ClC(SCN)Cl_2$ (**4**)	55
					$CH_2(SCN)CCl_3$ (**5**)	4
CHCl=CCl_2	AcOH	1	N_2	12	$CHCl_2C(SCN)Cl_2$ (**6**)	52
					$CHCl(SCN)CCl_3$ (**7**)	6
CCl_2=CCl_2	AcOH	1	N_2	12	$CCl_3C(SCN)Cl_2$ (**8**)	11

a) During the reactions, the temperature rose from 20 to *ca.* 40 °C. b) Distance (in cm) between UV light source and side of reaction flask.

Table 2. Characterisation data for α-chloro-β-thiocyanato compounds

Product	^{1}H-NMR Spectrum[a]	IR Spectrum (νSCN) (cm^{-1})	Bp (°C/Torr)	Formula	Analysis (%) Calcd C	H	N	Found C	H	N
1	3.88, d, 3.5, $C\underline{H}Cl_2$; 4.23, d, 3.5, $C\underline{H}(SCN)Cl$	2165	115—117/15	$C_3H_2Cl_3NS$	18.9	1.05	7.35	18.65	1.1	7.15
2	4.71, t, 7, $C\underline{H}(SCN)Br$; 5.86, d, 7, $C\underline{H}_2Cl$	2164	50—53/0.1	$C_3H_3BrClNS$	17.95	1.5	7.0	17.95	1.35	6.75
3	4.60, t, 7, $C\underline{H}ClBr$; 6.21, d, 7, $C\underline{H}_2SCN$	2164								
4	5.61, s, —, $C\underline{H}_2Cl$	2165	60—63/0.2	$C_3H_2Cl_3NS$	18.9	1.05	7.35	19.0	1.0	7.0
5	5.90, s, —, $C\underline{H}_2SCN$	2165								
6	3.75, s, —, $C\underline{H}Cl_2$	2165	68—70/0.1	C_3HCl_4NS	16.0	0.45	6.25	16.3	0.6	6.55
7	3.85, s, —, $C\underline{H}Cl(SCN)$	2165								
8	—	2164	61—63/0.05	C_3Cl_5NS	13.9	0.0	5.4	14.0	0.1	5.35

a) τ(ppm in CCl_4), multiplicity (s=singlet, d=doublet, t=triplet), J(Hz), assignment.

ratios were determined from the integral traces of appropriate signals in the NMR spectra of the crude mixtures. Characterisation data are recorded in Table 2.

trans-1,2-Dithiocyanatoethylene was recovered quantitatively as the 80 : 20 equilibrium mixture[13] of *trans*- and *cis*-isomers respectively as shown by IR and NMR spectroscopy. Tetraphenylethylene was recovered quantitatively and identified by its IR spectrum.

We thank Hertfordshire County Council for the award of a Research Assistant ship (to I.P.)

References

1) Part IV: R. Bonnett, R. G. Guy and D. Lanigan, *Tetrahedron*, **32**, 2439 (1976).
2) R. G. Guy and I. Pearson, *J. Chem. Soc., Perkin Trans. 1*, **1973**, 281.
3) R. G. Guy and I. Pearson, *J. Chem. Soc., Perkin Trans. 2*, **1973**, 1359.
4) R. G. Guy and I. Pearson, *Bull. Chem. Soc. Jpn.*, **49**, 2310 (1976).
5) R. G. R. Bacon and R. G. Guy, *J. Chem. Soc.*, **1961**, 2428.
6) P. I. Abell, "Free Radicals," Vol. 2, ed by J. K. Kochi, Wiley, New York (1973), p. 63.
7) E. S. Huyser, "Free-Radical Chain Reactions," Wiley-Interscience, New York (1970), p 77.
8) H. Kloosterziel, *Quart. Rep. Sulfur Chem.*, **2**, 353 (1967).
9) E. S. Huyser, *Mechanisms of Reactions of Sulfur Compounds*, **3**, 87 (1968); H. Goldwhite, M. S. Gibson, and C. Harris, *Tetrahedron*, **20**, 1613 (1964).
10) J. R. Case, N. H. Ray, and H. L. Roberts, *J. Chem. Soc.*, **1961**, 2066, 2070; H. W. Sidebottom, J. M. Tedder, and J. C. Walton, *Trans. Farad. Soc.*, **66**, 2038 (1970).
11) J. F. Harris, Jr., *J. Am. Chem. Soc.*, **84**, 3148 (1962).
12) J. F. Harris, *J. Org. Chem.*, **31**, 931 (1966), and references therein.
13) E. Söderbäck, *Justus Liebings Ann. Chem.*, **443**, 142 (1925).

BULLETIN OF THE CHEMICAL SOCIETY OF JAPAN, VOL. 50 (2), 543—544 (1977)

The Reactions of β-Amino Enones with Hydroxylamine

Choji KASHIMA*, Yasuhiro YAMAMOTO, Yoshimori OMOTE, and Yoshihiko TSUDA

Department of Chemistry, University of Tsukuba, Sakura-mura, Niihari-gun, Ibaraki 300-31

**Department of Chemistry, Tokyo Kyoiku University, Otsuka, Tokyo 113*

(Received August 27, 1976)

Synopsis. The reactions of *N*-substituted β-amino enones with hydroxylamine give two isoxazole isomers. The ratio of these isomers changes with the electron-withdrawing effect of the *N*-substituents.

Previously, we reported the synthesis of β-amino enones, such as 1-substituted 3-amino-2-buten-1-ones, from 3,5-dimethylisoxazole *via* 5-substituted 3-methylisoxazoles by hydrogenolysis.[1] These β-amino enones are isoelectronic with the β-diketones. Although the β-diketones exhibit behavior similar to keto and enol tautomers, the β-amino enones exhibit mainly behavior similar to amino derivatives of enones. Therefore, the reactions of β-amino enones with nucleophiles are quite interesting. Grignard reactions with β-amino enones give β-alkylated enones.[2] Also Kashima *et al.* have reported the regioselective reaction of β-amino enones with *N*-monosubstituted ureas to give 1-substituted 2(1*H*)-pyrimidinones.[3]

In the literature, it has been reported that 3,5-unsubstituted isoxazoles can be prepared from the corresponding β-amino enones and hydroxylamine.[4] However, the regioselectivity of β-amino enones in the reaction with hydroxylamine has never been reported. The reactions of 1-substituted 3-amino-2-buten-1-ones with hydroxylamine to give 3,5-disubstituted isoxazoles are presented here.

When a mixture of 5-amino-4-hexen-3-one (**4**) and hydroxylamine hydrochloride is refluxed in ethanol in the presence of potassium carbonate, two products, 3-ethyl-5-methyl- (**7a**) and 3-methyl-5-ethylisoxazole (**7b**) are expected. However, the only product was **7b** no trace of **7a** was detected in the NMR spectrum. These results suggest that the amino group of the hydroxylamine attacked the C-5 position of the amino enones as in Michael addition, and then the adducts were cyclized to isoxazoles by deamination and dehydration.

Here, the reactivity of the nucleophiles with the enones is considered to reflect the electron density at the reaction site. Fortunately, the electron densities of β-amino enones can be varied due to the electron-withdrawing effect of the acyl group on the nitrogen atom.[5] When 5-(methoxycarbonylamino)-4-hexen-3-one (**5**) and 5-(trichloroacetamido)-4-hexen-3-one (**6**) were treated with hydroxylamine under the same conditions, a mixture of **7a** and **7b** was obtained. The product ratio a/b from **6** is 3.0, while from **5** it is 0.5. From these results, it can be concluded that the product ratio a/b increases with an increase in the electron-withdrawing effect of the *N*-substituents (R').

Furthermore, various β-trichloroacetamido enones, 5-(trichloroacetamido)-1-phenyl-4-hexen-3-one (**8**), 5-(trichloroacetamido)-2,2-dimethyl-4-hexen-3-one (**10**) and 3-trichloroacetamido-1-phenyl-2-buten-1-one (**13**), were treated with hydroxylamine to give the corresponding isoxazoles, **9**, **11**, and **14**, respectively. As shown in Table, the results suggest that as the substituents, R, become more bulky, the product ratio a/b decreases.

TABLE.

β-Amino-eonoes	Isoxazoles	Yield	Ratio a/b
1	3	59	—
2	3	50	—
4	7	47	0
5	7	81	0.50
6	7	45	3.0
8	9	40	0.82
10	11	46	0
12	14	86	0
13	14	43	0

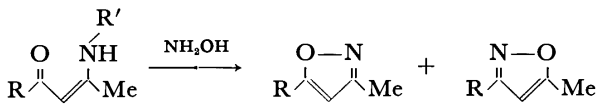

1 R=Me, R'=H
2 R=Me, R'=$COCCl_3$
4 R=Et, R'=H
5 R=Et, R'=COOMe
6 R=Et, R'=$COCCl_3$
8 R=CH_2CH_2Ph, R'=$COCCl_3$
10 R=*t*-Bu, R'=$COCCl_3$
12 R=Ph, R'=H
13 R=Ph, R'=$COCCl_3$

b

3 R=Me
7 R=Et
9 R=CH_2CH_2Ph
11 R=*t*-Bu
14 R=Ph

a

Experimental

Materials. Using known methods, 4-amino-3-penten-2-one (**1**),[6] 3-amino-1-phenyl-2-buten-1-one (**12**)[7] and 5-(methoxycarbonylamino)-4-hexen-3-one (**5**)[5] were prepared. *N*-Acylated derivatived were also prepared from the corresponding β-amino enones and acyl chloride in pyridine.[5]

5-Amino-4-hexen-3-one (4). By hydrogenolysis in ethanol in the presence of platinum, **4** was prepared from 3-methyl-5-ethylisoxazole, recrystallized from hexane, mp 62—63 °C; yield 69%; NMR ($CDCl_3$): δ 1.18 (t, 3H, J=4.0 Hz), 1.91 (s, 3H), 2.26 (q, 2H, J=4.0 Hz), 4.99 (s, 1H), 6.2 ppm (broad s, 1H).

Found: C, 63.78; H, 9.64; N, 12.22%. Calcd for $C_6H_{11}NO$: C, 63.69; H, 9.80; N, 12.38%.

4-(Trichloroacetamido)-3-penten-2-one (2). From **1** and trichloroacetyl chloride, **2** was prepared and recrystallized from hexane, mp 74.5—75.5 °C; yield 64%; IR (KBr): 1740, 1645, 1615, 1480 cm^{-1}: NMR ($CDCl_3$): δ 2.22 (s, 3H), 2.43 (s, 3H), 5.59 (s, 1H), 13.5 ppm (broad s, 1H).

Found: C, 34.32; H, 3.23; N, 5.77%. Calcd for $C_7H_8NO_2Cl_3$: C, 34.39; H, 3.30; N, 5.73%.

5-(Trichloroacetamido)-4-hexen-3-one (6). From **4** and

trichloroacetyl chloride, **6** was prepared and recrystallized from hexane, mp 91—93 °C; yield 47%; IR (KBr): 3445, 1740, 1650, 1620, 1480 cm^{-1}; NMR ($CDCl_3$): δ 1.11 (t, 3H, J=6.8 Hz), 2.42 (s, 3H), 2.43 (q, 2H, J=6.8 Hz), 13.4 ppm (broad s, 1H).

Found: C, 37.33; H, 3.97; N, 5.56%. Calcd for $C_8H_{10}NO_2Cl_3$: C, 37.16; H, 3.90; N, 5.42%.

5-(Trichloroacetamido)-1-phenyl-4-hexen-3-one (8). From 5-amino-1-phenyl-4-hexen-3-one[1] and trichloroacetyl chloride, **8** was prepared, bp 170—176 °C/3 Torr; yield 77%; IR (liquid film): 3050, 1735, 1650, 1615, 1600, 1470 cm^{-1}; NMR ($CDCl_3$): δ 2.42 (s, 3H), 2.5—3.2 (m, 4H), 5.56 (s, 1H), 7.23 (s, 5H), 13.5 ppm (broad s, 1H).

Found: C, 50.79; H, 4.42; N, 4.18%. Calcd for $C_{14}H_{14}NO_2Cl_3$: C, 50.25; H, 4.22; N, 4.19%.

5-(Trichloroacetamido)-2,2-dimethyl-4-hexen-3-one (10). 3-Methyl-5-*t*-butylisoxazole was hydrogenated in ethanol in the presence of platinum to give 5-amino-2,2-dimethyl-4-hexen-3-one, which was recrystallized from hexane, mp 65—66.5 °C; yield; 95%; IR (KBr): 3300, 1620, 1595, 1530 cm^{-1}; NMR ($CDCl_3$): δ 1.15 (s, 9H), 1.98 (s, 3H), 5.2 (broad s, 1H), 5.23 (s, 1H), 9.7 ppm (broad s, 1H).

Found: C, 67.82; H, 10.76; N, 9.92%. Calcd for $C_8H_{15}NO$: C, 68.04; H, 10.71; N, 9.92%. 5-Amino-2,2-dimethyl-4-hexen-3-one was acylated using trichloroacetyl chloride to give **10**, bp 109—113 °C/3 Torr; yield 79%; IR (liquid film): 1740, 1650, 1605, 1470 cm^{-1}; NMR ($CDCl_3$): δ 1.20 (s, 9H), 2.47 (s, 3H), 5.79 (s, 1H), 13.6 ppm (broad s, 1H).

Found: C, 41.93; H, 5.00; N, 4.82%. Calcd for $C_{10}H_{14}NO_2Cl_3$: C, 41.91; H, 4.92; N, 4.89%.

3-(Trichloroacetamido)-1-phenyl-2-buten-1-one (13). From **12** and trichloroacetyl chloride, **13** was prepared and recrystallized from hexane, mp 118—119 °C; yield 63%; IR (KBr): 1730, 1625, 1600, 1470 cm^{-1}; NMR ($CDCl_3$): δ 2.57 (s, 3H), 6.30 (s, 1H), 7.3—8.1 (m, 5H), 10.4 ppm (broad s, 1H).

Found: C, 47.07; H, 3.32; N, 4.46%. Calcd for $C_{12}H_{10}NO_2Cl_3$: C, 47.01; H, 3.29; N, 4.57%.

The Reaction of β-Amino Enones with Hydroxylamine Hydrochloride. A mixture of β-amino enone (3.2 mmol), hydroxylamine hydrochloride (8.0 mmol) and anhydrous potassium carbonate (3.9 mmol) in ethanol (10 ml) was refluxed for 6 h (in the cases of *N*-acyl derivatives, the refluxing time was 20 h). To the mixture, ether was added, and the organic layer was separated. The organic layer was washed with dilute hydrochloric acid and water, and dried over anhydrous sodium sulfate. After the solvent was removed, the product ratios were measured by the NMR spectra of the residual mixture. The products were identified from authentic samples using the spectral data.[1]

References

1) C. Kashima, S. Tobe, N. Sugiyama, and M. Yamamoto, *Bull. Chlm. Soc. Jpn.*, **46**, 310 (1973).
2) G. Kobrich and W. E. Breckoff, *Justus Liebigs Ann. Chem.*, **704**, 42 (1967).
3) C. Kashima, Y. Yamamoto, Y. Omote, T. Otsuka, and Y. Tsuda, *Heterocycles*, **4**, 1387 (1976).
4) H. Bredereck, H. Herlinger, and E. H. Schweizer, *Chem. Ber.*, **93**, 1208 (1960).
5) C. Kashima, Y. Yamamoto, and Y. Tsuda, *J. Org. Chem.*, **40**, 526 (1975).
6) A. Combes and C. Combes, *Bull. Soc. Chim. Fr.*, [3], **7**, 779 (1892).
7) E. Knoevenagel, *Ber.*, **36**, 2180 (1903).

BULLETIN OF THE CHEMICAL SOCIETY OF JAPAN, VOL. 50 (2), 545—546 (1977)

Metal Phosphinylides and Phosphinothioylides. VII.[1] The Structure of [Ph_2PX]M (X=O, S) in Solution and Their Disproportionation

Koshiro GODA, Hideyuki GOMI, Masaaki YOSHIFUJI, and Naoki INAMOTO
Department of Chemistry, Faculty of Science, The University of Tokyo, Hongo, Tokyo 113

(Received August 31, 1976)

Synopsis. The species [Ph_2PO]M in THF were found to exist as Ph_2P–O–M by ^{31}P-NMR, and [Ph_2PS]MgCl as Ph_2P–S–MgCl by Raman spectrum. The species [Ph_2PS]M undergo easy disproportionation by heating.

The species [Ph_2PX]M (X=O, S) have been prepared by the reaction of sodium or magnesium with diphenylphosphinic (**1a**)[2,3] or diphenylphosphinothioic chloride (**1b**)[3] (Method A) and by the reaction of butyllithium[3] or Grignard reagents[4] with diphenylphosphine oxide (**2a**) or sulfide (**2b**) (Method B).

$$\underset{\mathbf{1}}{Ph_2P(X)Cl} + M \longrightarrow \underset{\mathbf{3}}{[Ph_2PX]M} \qquad \text{(Method A)}$$

a, X=O; b, X=S

$$\underset{\mathbf{2}}{Ph_2P(X)H} + R'M \text{ (or M)} \longrightarrow \underset{\mathbf{3}}{[Ph_2PX]M} \qquad \text{(Method B)}$$

a, X=O; b, X=S

The following equilibrium is possible in a solution of **3**.

$$\underset{\mathbf{4}}{Ph_2P\text{–}X\text{–}M} \rightleftarrows \underset{\mathbf{4'}}{Ph_2P(X)M}$$

It was found from ^{31}P-NMR data that [$(EtO)_2PO$]M exists as $(EtO)_2P$–O–M in solution.[5] The present paper describes the results of a reexamination of the reactions of **1** with metals by means of ^{31}P-NMR and the structure of **3** in solution.

The reactions by Methods A and B were carried out in tetrahydrofuran (THF) at room temperature under nitrogen. The ^{31}P-NMR data are given in Tables 1 and 2. The yields of **3** were nearly quantitative based on the ^{31}P-NMR spectra, except for the case of M=MgCl in Method A (Table 1). We see that reactions of **1**, especially **1b**, with metals are very complicated,

TABLE 1. ^{31}P-NMR DATA OF REACTION MIXTURE OF **1** WITH METAL (M) IN THF (METHOD A)

M	X=O δ_P (ppm)	X=O Assignment	X=S δ_P (ppm)	X=S Assignment	Yield (%)[a]
none	−42.8	**1a**	−79.8	**1b**	
Li	−93.8	[Ph_2PO]-Li	16.2	Ph_2PPPh_2	2
			−37.0	$Ph_2P(S)$-$P(S)Ph_2$	20
			−59.8	$Ph_2P(S)SLi$	46
Mg	−17.7	[Ph_2PO]-MgCl	15.9	Ph_2PPPh_2	4
			−37.9	$Ph_2P(S)$-$P(S)Ph_2$	23
			−59.0	$Ph_2P(S)$-SMgCl	46

a) Based on the peak areas in the ^{31}P-NMR spectra.

TABLE 2. ^{31}P-NMR DATA OF [Ph_2PX]M IN THF (METHOD B)

RM or M	X=O δ_P (ppm)	X=O Assignment	X=S δ_P (ppm)	X=S Assignment
none	−22.9 (J=490 Hz)	**2a**	−20.8 (J=468 Hz)	**2b**
n-BuLi	−93.8	[Ph_2PO]-Li	−20.7	[Ph_2PS]-Li
n-BuMgCl	−90.0	[Ph_2PO]-MgCl	−14.3	[Ph_2PS]-MgCl
NaH			−22.3	[Ph_2PS]-Na
K			−25.0	[Ph_2PS]-K

indicating dimerization, desulfurization, and disproportionation of **3b**.[3] Thus, for the preparation of **3**, Method B is preferable to Method A.

The phosphorus atom in **3a** is trivalent (**4** type) in THF (Tables 1 and 2), except for the case of M=MgCl in Method A.[6] However, the structure of **3b** could not be determined, due to δ_P values being similar to those of **2b**. Thus, the Raman spectrum of [Ph_2PS]MgCl prepared by Method B was compared with spectra of some model compounds (Table 3). From the results the structure was determined to be **4** type. In the case of M=Li and Na, no Raman spectra could be obtained because of the emission of fluorescence.

TABLE 3. RAMAN SPECTRA

Compound	$\nu_{P=S}$ (cm^{-1})	ν_{P-S} (cm^{-1})
$Ph_2P(S)H$ (THF)	650	—
$Ph_2P(S)OMe$ (THF)	638	—
$Ph_2P(S)SMe$ (THF)	658	537
$Ph_2P(O)SMe$ (THF)	—	568
Ph_2PSEt (neat)	—	515
[Ph_2PS]MgCl (THF)	—	530

Easy disproportionation of **3b** was confirmed by the following experiments. Reaction of **1b** with lithium in THF at room temperature for 24 h afforded *S*-methyl diphenylphosphinodithioate (**5**) and methyldiphenylphosphine sulfide (**6**) in a ratio of 5:1 after treatment first with methyl iodide and then sulfur.

$$2[Ph_2PS]Li \longrightarrow \underset{\mathbf{5}}{Ph_2P(S)SLi} + Ph_2PLi$$

$$\downarrow MeI \qquad \downarrow MeI \qquad S_8 \downarrow MeI$$

$$\underset{\mathbf{6}}{2Ph_2P(S)Me} \qquad \underset{\mathbf{5}}{Ph_2P(S)SMe} \qquad \mathbf{6}$$

Refluxing of a mixture of **2b** and butyllithium in THF also gave **5** and **6** after a similar treatment (see Experi-

mental).

In this connection, a large contribution of metal diphenylphosphinodithioate is considered to take place in the reactions of $[Ph_2PS]M$ with THF.[7]

Experimental

^{31}P-NMR spectra were measured with a Hitachi R-20B-R-204 PB spectrometer using 85% phosphoric acid as an external standard. Raman spectra were taken with a JEOL-JSP-RS 4000 spectrometer.

Materials. Diphenylphosphinic (**1a**) and diphenylphosphinothioic chlorides (**1b**), diphenylphosphine oxide (**2a**) and sulfide (**2b**) were prepared by the methods described in a previous paper.[3] The following compounds were prepared by the reported methods: *O*-methyl diphenylphosphinothioate,[8] *S*-methyl diphenylphosphinodithioate,[9] and ethyl diphenylphosphinothioate.[10]

Preparation of S-Methyl Diphenylphosphinothioate. To a mixture of 13.4 g (57 mmol) of diphenylphosphinothioic acid and 2.5 g (63 mmol) of sodium hydroxide in 50 ml of THF was added 6 ml of methyl iodide, and the mixture was stirred for 3 h at room temperature. After washing with water and extraction with benzene, the extract was distilled *in vacuo*, bp 190 °C/0.2 Torr yield 13.0 g (92%). The distillate solidified on standing, mp 49.0—50.5 °C (from cyclohexane). IR (KBr): 1435, 1118 (P–Ph), 1202 (P=O), and 565 cm^{-1} (P–S); NMR (CCl_4): δ 2.10 (d, $J_{PSCH}=13$ Hz, 3H, SMe) and 7.2—8.0 (m, 10H, P–Ph); ^{31}P-NMR (THF): $\delta_P-38.6$ ppm.

Found: C, 62.91; H, 5.06; S, 13.05%. Calcd for $C_{13}H_{13}OPS$: C, 62.89; H, 5.28; S, 12.91%.

Disproportionation of $[Ph_2PS]Li$. A mixture of 1.405 g (6.4 mmol) of **2b**, 0.336 g (7.9 mmol) of lithium chloride, 12 mmol of butyllithium in hexane (8 ml), and 30 ml of THF was refluxed for 3 h and 1 ml of methyl iodide was added. The presence of methyldiphenylphosphine, **5**, and **6** was shown by means of gas chromatography (H 523 on Diasolid at 210 °C). Sulfur (0.38 g, 1.5 mmol) was added to the reaction mixture and the mixture was refluxed for several minutes. Only **5** and **6** were observed in the ratio 27: 73.

This work was partly supported by a Grant-in-Aid for Scientific Research from the Ministry of Education. The authors thank Dr. Issei Harada and Mr. Shuji Imazeki for the measurement of Raman spectra.

References

1) For VI see: K. Goda and N. Inamoto, *Bull. Chem. Soc. Jpn.*, **49**, 1175 (1976).
2) L. Horner and P. Beck, *Chem. Ber.*, **93**, 1371 (1960); L. Horner, P. Beck, and V. G. Toscano, *ibid.*, **94**, 1317, 1323 (1961).
3) T. Emoto, H. Gomi, M. Yoshifuji, R. Okazaki, and N. Inamoto, *Bull. Chem. Soc. Jpn.*, **47**, 2449 (1974); K. Goda, H. Gomi, M. Yoshifuji, and N. Inamoto, *ibid.*, **47**, 2453 (1974).
4) R. F. Cann, S. Warren, and M. R. Williams, *J. Chem. Soc, Perkin Trans. 1*, **1972**, 2377.
5) K. Moedritzer, *J. Inorg. Nucl. Chem.*, **22**, 19 (1961).
6) The structure is unknown but a possible one might be of the **4'** type such as $Ph_2P(O)$–MgCl and $[Ph_2P(O)]_2Mg$.
7) K. Goda, M. Yoshifuji, R. Okazaki, and N. Inamoto, *Bull. Chem. Soc. Jpn.*, **48**, 2484 (1975).
8) T. A. Mastryukova, T. A. Melent'eva, and M. I. Kobachnik, *Zh. Obshch. Khim.*, **35**, 1197 (1965); *Chem. Abstr.*, **63**, 11605 (1965).
9) W. A. Higgins, P. W. Vogel, and W. G. Craig, *J. Am. Chem. Soc.*, **77**, 1864 (1955).
10) A. Arbuzov, *J. Russ. Phys. Chem. Soc.*, **42**, 549 (1910).

BULLETIN OF THE CHEMICAL SOCIETY OF JAPAN, VOL. 50 (2), 547—548 (1977)

Ullmann Condensation Reaction of Haloanthraquinone Derivatives with Amines in Aprotic Solvents

Sadao ARAI, Takamichi YAMAGISHI, Satoshi OTOTAKE, and Mitsuhiko HIDA

Department of Industrial Chemistry, Faculty of Technology, Tokyo Metropolitan University, Fukazawa, Setagaya-ku, Tokyo 158

(Received September 17, 1976)

Synopsis. Cuprous catalysts were more effective than cupric ones in the Ullmann condensation of haloanthraquinones with amines in aprotic media. In the presence of Cu(I) catalyst, amines with a hydroxyl group (3-amino-1-propanol and 2-aminoethanol) were more reactive than the higher basic butylamine.

In our previous papers we discussed the mechanism of the Ullmann condensation reaction of haloanthraquinones with amines.[1] The reaction rate and mechanism were found to be largely affected by the chemical structures of haloanthraquinones, amines, and ligands and by the valence state of copper catalysts.

This paper deals with the reactivities of haloanthraquinones, amines, and catalysts in aprotic media under nitrogen atmosphere.

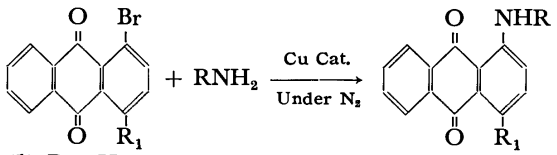

(**1**) R_1=H
(**2**) R_1=NH_2

Results and Discussion

As shown in Table 1, cuprous salts were more effective than cupric ones. The catalytic activities of cuprous salts decreased with the increase of Cu(I)-halogen bond strength[2]: CuCl>CuBr>CuI. The reactivities of 1-bromoanthraquinone (**1**) and 1-amino-4-bromoanthraquinone (**2**) toward some kinds of amines with and without the catalyst are summarized in Table 2. Table 2 suggests that the character of the reaction is largely changed in the presence of the catalyst. Thus in the absence of cuprous catalyst the yields of the condensation products, though very low, increased with increasing basicity of the amines used. This fact can be easily understood by the nucleophilic character of this reaction.

Amines with a hydroxyl group, however, were more reactive than butylamine, stronger as a base, in the presence of cuprous bromide: butylamine<3-amino-1-propanol<2-aminoethanol. It is also noteworthy that 2-aminoethanol was more reactive toward 1-bromoanthraquinone (**1**) than toward 1-amino-4-bromoanthraquinone (**2**) in the absence of cuprous catalyst, but the reverse was found in the presence of the catalyst. Such unexpected results in the presence of the catalyst may be ascribed to the difference in the coordination of haloanthraquinones to cuprous species.

When the reactions of bromoanthraquinones with 2-aminoethanol were carried out in 1,2-dimethoxyethane by use of cuprous catalyst under nitrogen atmosphere, the blue cupric complex deposited. In 1,2-dimethoxyethane-methyl cellosolve solution the blue cupric complex did not deposit very much, since it was more soluble in this solvent. No cupric complex was formed without bromoanthraquinones.

Table 1. Comparison of the catalytic activity in the condensation of 1-bromoanthraquinone with 2-aminoethanol[a]

Catalyst	t/h	Yield (%)	Solvent
CuCl	2	21.6	THF–EtOH 4:1
CuBr	2	17.7	THF–EtOH 4:1
CuI	2	9.3	THF–EtOH 4:1
$CuBr_2$	2	1.3	THF–EtOH 4:1[b]
CuBr	2	12.2	THF[b]
None	3	2.6	THF

a) Reaction temp: 60 °C; [Substrate (**1**)]$_0$=5×10^{-3} mol/l, [Catalyst]$_0$=2×10^{-3} mol/l, [$NH_2CH_2CH_2OH$]$_0$=5×10^{-1} mol/l. b) Heterogeneous system.

Table 2. Comparison of the reactivity in the condensation of haloanthraquinone (**1** or **2**) with amines[a]

Amine	pK_a	Yield (%) at 5h: Substrate (**1**) CuBr	Substrate (**1**) none	Substrate (**2**) CuBr	Substrate (**2**) none
n-$C_4H_9NH_2$	10.60	9.1	6.0	6.0	0.4
$NH_2CH_2CH_2CH_2OH$	9.96	31.3	6.1	30.9	0.4
$NH_2CH_2CH_2OH$	9.51	43.2	4.3	48.8	0.2

a) Reaction temp: 70 °C; Solvent: 1,2-dimethoxyethane–methyl cellosolve 4:1; [Substrate]$_0$=5×10^{-3} mol/l, [Amine]$_0$=5×10^{-1} mol/l, [Catalyst]$_0$=2×10^{-3} mol/l.

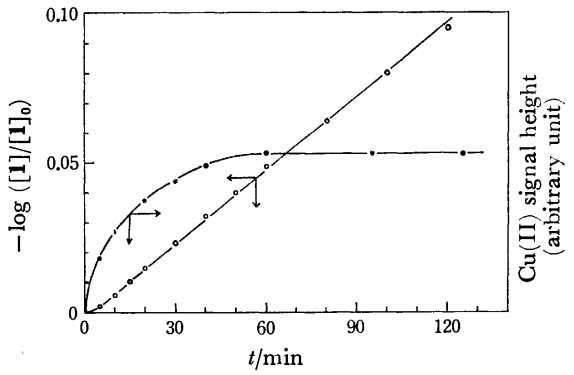

Fig. 1. Pseudo-first order plots and the time dependence of Cu(II) signal height; temp 70 °C under N_2 atmosphere, [substrate (**1**)]$_0$ 5×10^{-3} mol/l, [$NH_2CH_2CH_2OH$]$_0$ 5×10^{-1} mol/l, [CuBr]$_0$ 2×10^{-3} mol/l, solvent 1,2-dimethoxyethane-methyl cellolve 4:1.

The ESR spectra suggested that the Cu(II) species were formed[3] and their concentration increased up to a certain amount as the reaction proceeded (Fig. 1). The formation of the Cu(II) species can be understood by an electron transfer from Cu(I) to the haloanthraquinone. In the reaction system of 1-bromoanthraquinone with 2-aminoethanol using CuBr catalyst, the organic paramagnetic species, assumed to be a radical anion of 1-bromoanthraquinone, was indeed observed. As shown in Fig. 1, however, the reaction rate did not decrease in accordance with the formation of Cu(II) species, which is much less active than Cu(I) species.

The formation and the role of Cu(II) species is a very interesting and important problem of the Ullmann condensation reaction in aprotic media. Further examination of this problem will be reported in the near future.

Experimental

Materials and Solvents. 1-Bromoanthraquinone (**1**) was prepared from 1-aminoanthraquinone by Sandmeyer's bromination and purified by column chromatography on alumina (benzene as developing solvent) followed by recrystallization from benzene: λ_{max} (C_2H_5OH) 336 nm (ε 4980); mp 189.6—189.9 °C(cor) (lit, mp 192 °C[4]) (Found: C, 58.60; H, 2.20%). 1-Amino-4-bromoanthraquinone (**2**) was prepared by desulfonation of sodium 1-amino-4-bromoanthraquinone-2-sulfonate with 80% sulfuric acid. After being separated from the reaction mixture by column chromatography on alumina (benzene as developing solvent), it was recrystallized from acetic acid: λ_{max} ($CH_3OCH_2CH_2OCH_3$) 474 nm (ε 7100); mp 178.5—179.2 °C(cor) (lit, mp 170—176 °C[5]) (Found: C, 55.75; H, 2.56; N, 4.56%). 2-Aminoethanol and 3-amino-1-propanol were dried over sodium hydroxide and distilled under nitrogen atmosphere. Butylamine was dried over sodium and distilled under nitrogen atmosphere. Cuprous halides were prepared by the usual methods.[6] All solvents were purified by the usual methods and stored under nitrogen atmosphere.

Spectral Measurements. The UV and visible spectra were measured using a Shimadzu UV-200 spectrophotometer. The ESR spectra were taken on a JEOL JES-PE-3X instrument.

Reaction Procedure. A typical run is as follows. 1-Bromoanthraquinone and the solvent (THF–EtOH) were mixed in a flask. After this solution was brought to the reaction temp, the reaction was initiated by the addition of a homogeneous ethanol solution containing 2-aminoethanol and cuprous bromide. All above operations were performed under a dry and oxygen-free nitrogen atmosphere. At regular time intervals, 0.5 ml portions of the reaction solution was withdrawn and diluted in 25 ml of ethanol. The yields were determined spectrophotometrically.

Products. Products were obtained from the reaction mixture in a following manner. After the solvent was removed under reduced pressure, the reaction mixture was poured into water. After being filtered, washed with water, and dried, the precipitate was chromatographed. The separated amination product was recrystallized.

1-Amino-4-(β-hydroxyethylamino)anthraquinone: λ_{max} (C_2H_5OH) 616 nm (ε 16700); mp 195.3—196.4 °C(cor) (lit, 195—197 °C[7]) (Found: C, 67.68; H, 4.96; N, 9.63%).

1-(β-Hydroxyethylamino)anthraquinone: λ_{max}(C_2H_5OH) 503 nm (ε 6700); mp 175.6—175.8 °C(cor) (lit, 171—171.5 °C[7]) (Found: C, 71.86; H, 4.70; N, 4.99%).

1-Amino-4-(γ-hydroxypropylamino) anthraquinone: λ_{max} ($CH_3OCH_2CH_2OCH_3$) 615 nm (ε 15300); mp 211.7—212.3°C(cor); Found: C, 68.78; H, 5.43; N, 9.51%. Calcd for $C_{17}H_{16}O_3N_2$: C, 68.91; H, 5.44; N, 9.45%.

1-(γ-Hydroxypropylamino)anthraquinone: λ_{max}($CH_3OCH_2CH_2OCH_3$) 502 nm (ε 6800); mp 184.7—185.4 °C(cor); Found: C, 72.58; H, 5.37; N, 5.03%. Calcd for $C_{17}H_{15}O_3N$: C, 72.58; H, 5.37; N, 4.98%.

1-Amino-4-(butylamino)anthraquinone: λ_{max}(C_2H_5OH) 617 nm (ε 17600); mp 142.6—143.1 °C(cor); Found: C, 73.32; H, 6.01; N, 9.65%. Calcd for $C_{18}H_{18}O_2N_2$: C, 73.45; H, 6.16; N, 9.52%.

1-(Butylamino)anthraquinone: λ_{max}(C_2H_5OH) 507 nm (ε 7090); mp 85.9—86.7 °C(cor) (lit, 80—81 °C[8]); Found: C, 77.57; H, 6.20; N, 4.88%.

References

1) T. D. Tuong and M. Hida, *Bull. Chem. Soc. Jpn.*, **43**, 1763 (1970); *ibid.*, **44**, 756 (1971); *J. Chem. Soc., Perkin Trans. 2*, **1974**, 676.

2) R. G. R. Bacon and H. A. O. Hill, *Quart. Rev.*, **19**, 95 (1965).

3) Very little formation of cupric species was observed in the reaction with butylamine. In the reaction with 3-amino-1-propanol the cupric species were formed in a smaller amount than in the reaction with 2-aminoethanol.

4) Y. Takekawa, S. Kato, M. Mabuchi, and T. Kurano, *Kogyo Kagaku Zasshi*, **60**, 595 (1957).

5) J. Gasparic and J. Marhan, *Collect. Czech. Chem. Commun.*, **27**, 46 (1962).

6) CuBr and CuCl: R. N. Keller and H. D. Wycoff, *Inorg. Synth.*, **2**, 1 (1946); CuI: G. B. Kauffmann and R. P. Pinnell, *ibid.*, **6**, 3 (1960); G. B. Kauffmann, *ibid.*, **11**, 215 (1968).

7) K. Naiki, *Yuki Gosei Kagaku Kyokai Shi*, **12**, 401 (1954).

8) G. D. Wood and A. T. Peters, *J. Chem. Soc.*, **1962**, 3373.

BULLETIN OF THE CHEMICAL SOCIETY OF JAPAN, VOL. 50 (2), 549—550 (1977)

Acyl Cyanide. IV. The Reduction of Phenyl-substituted Carbamoyl Cyanides with Metal Hydrides

Akira Oku,* Jiro Inoue, Hiroyuki Ueda, and Fujio Mashio
Department of Chemistry, Kyoto Institute of Technology, Matsugasaki, Sakyo-ku, Kyoto 606

(Received September 18, 1976)

Synopsis. The reaction of phenylcarbamoyl cyanide with $LiAlH_4$ or $NaBH_4$ gave glycine anilide, *N*-phenylethylenediamine, and *N*-methylaniline. With the latter hydride, 4-amino-1,3-diphenyl-2-imidazolidinone was also formed. The reduction of diphenylcarbamoyl cyanide with $LiAlH_4$ gave *N*-methyldiphenylamine as the only reduction product.

The utilization of acyl cyanides (α-ketonitriles) as useful precursors in organic synthesis has been discussed in a number of literatures.[1] In contrast, carbamoyl cyanides, the nitrogen homologues of acyl cyanide, have not been extensively studied, and only a small quantity of information has accummulated about their chemical properties.[2]

Among the chemical reactions of acyl cyanides it has been known that the reduction by lithium aluminum hydride generally gives β-amino alcohols, β-(acylamino) alcohols, or aldehydes depending on the reaction conditions.[3] Can analogous products be obtained in the reduction of carbamoyl cyanides with metal hydrides? Is there any difference between the reactions of mono- and di-substituted carbamoyl cyanides? In answer to these questions, we would like to present the results obtained from the reduction of phenylcarbamoyl cyanide (**1**) and diphenylcarbamoyl cyanide (**8**) with metal hydrides.

Results and Discussion

When phenylcarbamoyl cyanide (**1**) was treated with lithium aluminum hydride ($LiAlH_4$) in anhydrous ether, the following four products: aniline (**2**), *N*-methylaniline (**3**), glycine anilide (**4**), and *N*-phenylethylenediamine (**5**), were obtained. The time-dependent increase of **5** with a decrease in **4**, as observed by a VPC analysis, indicated that the product, **4**, was the reduction intermediate to produce **5**. In addition, the yield of **3** increased from 6 to 21% as the $[LiAlH_4]/[1]$ ratio increased from 1 to 5.

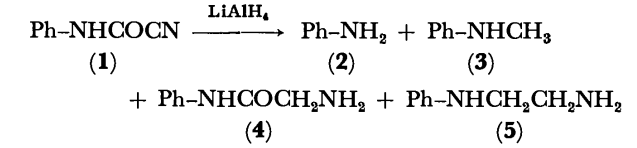

Analogously, when cyanide **1** was treated with sodium borohydride ($NaBH_4$) in tetrahydrofuran, the same products were produced. In addition, 4-amino-1,3-diphenyl-2-imidazolidinone (**6**) was isolated. The same product was also formed when 1,3-diphenyl-5-iminohydrantoin (**7**) was treated with the same hydride. Therefore, the base-induced condensation of cyanide **1** into **7** must occur under the present conditions[2a] competitively with the slow reduction. The yields of

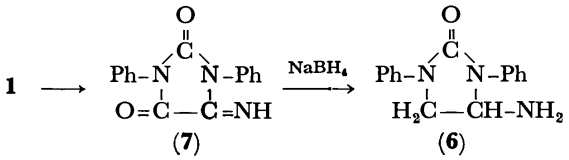

the other products depended significantly upon the reaction conditions, *i.e.*, the amounts of the reductant and additives such as $AlCl_3$,[4] and the time. For example, that the yield of aniline (**2**) decreased upon the lengthening in the reaction period indicates that **2** may be formed mainly by the hydrolysis of the unreacted **1**.[5] Indeed, the alkaline hydrolysis of **1** in aqueous NaOH proceeded very easily. However, the yield of **2** was only 30% at the maximum, and the main product was *N*,*N*′-diphenylurea. We found separately that a number of amines and alcohols induced **1** to undergo facile nucleophilic substitution.[6] Therefore, it seems reasonable that diphenylurea was formed by the reaction of **1** with aniline, which is the primary hydrolysis product of **1**.

Diphenylcarbamoyl cyanide (**8**)[7] seems to be an appropriate compound to examine in order to ascertain the difference in reaction behavior between monosubstituted (*e.g.*, **1**) and disubstituted (*e.g.*, **8**) carbamoyl cyanides. The results obtained from the reduction of **8** with $LiAlH_4$ are listed in Table 1. The only products detected by VPC were diphenylamine (**9**) and *N*-methyldiphenylamine (**10**). The former was apparently produced by the hydrolysis of **8** through the work-up process, as is evidently proved by Run 3. The latter, the only reduction product, must be formed by either Route *a* or Route *b*. Although conclusive evidence has not yet been obtained, it has been reported that

Table 1. Reduction of diphenylcarbamoyl cyanide (**8**) with $LiAlH_4$[a]

Run No.	Solvent	Product yield (%)		**8**
		Ph_2NH	Ph_2NCH_3	
1	Et_2O	38	58	0
2	THF	18	72	0
3	THF[b]	22	0	78

a) $[\mathbf{8}]/[LiAlH_4]=1.0$, 1 h each at −50 and 35 °C.
b) $LiAlH_4$ was hydrolyzed prior to the addition of **8**.

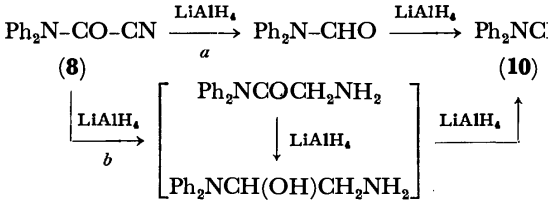

the cyanides, **1** and **8**, undergo a facile displacement of the cyano group by the appropriate nucleophiles.[3,6] Therefore, our tentative preference is Route *a*, where the displacement of the cyano group by the hydride anion takes place, as is evident in the case of acyl cyanides.[3]

Now, let us recall the reduction of **1** where *N*-methylaniline (**3**) was one of the major products. As has been reported recently,[6] cyanide **1** behaves as if it generates the phenyl isocyanate intermediate under various conditions (*i.e.*, it acts as a *carbamoylating reagent*). Also known is the reduction of phenyl isocyanate with $NaBH_4$, where **3** is the main product.[8] Nevertheless, the formation of **10** from **8** seems to present rational evidence in favor of the hypothesis that the derivation of **3** from **1** does not necessarily involve phenyl isocyanate as the intermediate.

In addition, it became evident in our study that amide carbonyl groups can undergo $NaBH_4$ reduction, at least when the vicinal substituent to the carbonyl is an unsaturated group such as CN or C=NH, though it has been our general understanding that amide carbonyls are resistant against that reagent.[9] Also proved is the transformability of the cyanocarbonyl group of carbamoyl cyanides into a methyl group by treatment with such metal hydrides as $LiAlH_4$ or $NaBH_4$.

Experimental

General. The NMR, mass, and IR spectra were taken on JEOL 4H-100, Hitachi RMU-6L, and JASCO IRA-1 spectrometers respectively. Some typical experimental procedures are shown below.

Reduction of Phenylcarbamoyl Cyanide (1) with $LiAlH_4$. To a solution of **1** (4.4 g, 30 mmol) in dry THF (100 ml) was added a suspension of $LiAlH_4$ (2.3 g, 60 mmol) in dry THF (30 ml) over a 40-min period at 5 °C. After stirring for 30 min, a mixture of THF (20 ml) and water (6 ml) was added and the decomposed mixture was filtered. The filtrate was dried over anhyd $MgSO_4$ and distilled under a vacuum. The first fraction (55 °C/3 Torr, 0.8 g) was found by VPC (Apiezon L, 10%, 1 m) to consist of aniline (**2**, 15%) and *N*-methylaniline (**3**, 10%). The third fraction (95—97 °C/1.5 Torr, 1.5 g, 37%) formed a picrate (mp 175—177 °C) which did not show any mp depression when mixed with an authentic picrate of *N*-phenylethyleneadimine. The fifth fraction (145—148 °C/1 Torr, 12 g, 27%) was a solid (mp 98—100 °C) containing a small amount of impurity with a higher mp. Therefore, the fraction was heated with Ac_2O in AcOH to give an acetylated product (98%); mp 195.5—196.5 °C (from ethanol). Found: C, 62.59; H, 6.29; N, 14.61%. Calcd for $C_{10}H_{12}N_2O_2$: C, 62.48; H, 6.29; N, 14.58%.

Reduction of 1 with $NaBH_4$. A mixture of **1** (4.4 g, 30 mmol) and dry $NaBH_4$ (1.2 g, 30 mmol) in dry THF (50 ml) was stirred for 4 h at 40 °C. The reaction mixture was poured into cold 5% NaOH, the solution was extracted with ether, and the extract was dried. After removing the solvent, the residue was analyzed by VPC to find that it consisted of **2**+**3** (22%), **4** (6.2%), and **5** (1%). After these were distilled off, the residue was chromatographed (silica gel, $CHCl_3$) to give a colorless solid of **6** (45%); mp 178 °C; P^+ (*m/e*) 253; IR (cm^{-1}) 1690 (C=O), 3400, and 3330 (NH); NMR (δ, $CDCl_3$) 1.90 (2H, bs), 3.57 (H, q, J_1=10, J_2=5.0 Hz), 4.14 (H, q, J_1=10, J_2=8.5 Hz), 5.23 (H, q, J_1=8.5, J_2=5.0 Hz), 7.0—7.65 (10H, m). Found: C, 71.35; H, 6.01; N, 16.40%. Calcd for $C_{15}H_{15}N_3O$: C, 71.12; H, 5.97; N, 16.60%.

Hydrolysis of 1 by Aq NaOH. A dioxane solution of **1** was hydrolyzed in 5% aq NaOH at 20 °C for 2 h. After a similar work-up, VPC and column chromatographic analysis of the product mixture showed it to consist of **4** (30%) and *N,N'*-diphenylurea (45%).

Reduction of Diphenylcarbamoyl Cyanide (8) with $LiAlH_4$. To a solution of **8** (2.22 g, 10 mmol) in dry ether (20 ml) was added a suspension of $LiAlH_4$ (0.4 g, 10 mmol) in dry ether (10 ml) over 10 min at −50 °C. After stirring the mixture for 1 h each at −50 and 35 °C, the mixture was decomposed under ice cooling by the addition of a cold mixture of THF (20 ml) and water (0.8 g), followed by the addition of a saturated NH_4Cl solution (30 ml). After work-up, the ethereal extract weighed 1.69 g and was analyzed by VPC (Apiezon L, 10%, 1 m, 200—250 °C). Diphenylamine (**9**, 38%, identified with an authentic sample) and *N*-methyldiphenylamine (**10**, 58%, NMR Me at δ 3.28, and by MS P^+ 183) were detectable products. See Table 1.

Treatment of 8 with Water-treated $LiAlH_4$. The same treatment of **8** as described above, but with the $LiAlH_4$ preliminarily decomposed by an equivalent mole of water, was carried out in order to examine the hydrolysis product. After work-up, the VPC of the reaction mixture proved that diphenylamine (**9**) was its only product (22%), together with the recovered **8** (78%).

References

1) a) K. T. Potts, *J. Org. Chem.*, **26**, 4719 (1961); b) V. F. Raaen, *ibid*; **31**, 3310 (1966); c) G. F. Bettinetti, A. Donetti, and P. Gruenanger, *Tetrahedron Lett.*, **1966**, 2933; *Gazz. Chim. Ital.*, **96**, 965 (1966); d) J. A. Settepani and A. B. Borkovic, *J. Heterocyclic Chem.*, **3**, 188 (1966).

2) a) W. Dieckman and H. Kammerer, *Ber.*, **38**, 2981 (1905); b) W. Dieckman and H. Kammerer, *ibid.*, **40**, 3737, 3742 (1907); c) A. Oku, M. Okano, and R. Oda, *Makromol. Chem.*, **78**, 186 (1964); d) A. Oku, T. Shono,and R. Oda, *ibid.*,**100**, 224 (1964).

3) A. Dornow and H. Theidel, *Chem. Ber.*, **88**, 1267(1955).

4) H. C. Brown and B. C. Subba Rao, *J. Am. Chem. Soc.*, **77**, 3164 (1955).

5) F. Hibbert and D. P. N. Satchell, *J. Chem. Soc., B*, **1967**, 755, 653; *ibid., D*, **1966**, 516.

6) A. Oku, T. Suzuki, H. Koura, and F. Mashio, *Bull. Chem. Soc. Jpn.*, **49**, 3578 (1976).

7) R. G. Hisky and F. I. Carroll, *J. Am. Chem. Soc.*, **83**, 4644 (1961).

8) a) W. Ried and F. Muller, *Chem. Ber.*, **85**, 470 (1952); b) A. E. Finholt, C. D. Anderson, and C. L. Agre, *J. Org. Chem.*, **18**, 1388 (1953).

9) a) S. Yamada, *Yuki Gosei Kagaku Kyokai Shi*, **28**, 1083 (1970); b) Y. Ogata, "Sanka To Kangen," Nanko-do, Tokyo (1963), pp. 765—878.

BULLETIN OF THE CHEMICAL SOCIETY OF JAPAN, VOL. 50 (2), 551—552 (1977)

The Palladium-catalyzed Phenylation of Enol Esters with Iodobenzene

Akira KASAHARA, Taeko IZUMI, and Naoki FUKUDA

Department of Applied Chemistry, Faculty of Engineering, Yamagata University, Yonezawa 992

(Received October 12, 1976)

Synopsis. The palladium-catalyzed phenylation of olefins with iodobenzene has been extended to enol esters. In the presence of triethylamine and a catalytic amount of palladium acetate, vinyl acetate is phenylated with iodobenzene to produce, mainly, stilbene, accopanied by small amounts of (*E*)- and (*Z*)-styryl acetates.

Recently, the palladium-catalyzed substitution of vinylic hydrogen by aryl and vinyl halides has received wide attention.[1-5] Meanwhile, Heck[6] has reported the reaction of enol esters with the organo-palladium species generated from an arylmercury(II) compound and palladium salts. We are, therefore, intrigues by the palladium-catalyzed reaction of enol esters with iodobenzene (**1**) and wish to report herein the results of a study of this reaction.

Table 1 shows the results of the phenylation of enol esters with **1**. The reaction of vinyl acetate (**2**) with **1** gave stilbene (**3**) as the main product and (*E*)- and (*Z*)-styryl acetates (**4** and **5**) as the minor products. Since neither styrene nor acetophenone enol ester was found in the reaction mixture and since, in addition, a mixture of **4** and **5** reacted with **1** to give **3** under the same conditions, the compound **3** appears to be formed by the secondary phenylation of **4** and **5**, as despicted in Scheme 1. (Scheme 1).

The phenylation of isopropenyl acetate (**6**) gave three isomers of the diphenylated propene derivatives (**7**, **8**, and **9**) and two isomers of (*E*)- and (*Z*)-2-acetoxy-1-phenyl-1-propene (**10** and **11**). It has been reported[6] that the Heck reaction of **2** with phenylmercury(II) salt gave **4** and **5** as the main products and **3** and styrene as the minor products, while the Heck reaction of **6** afforded a mixture of **10**, **11**, and 2-acetoxy-3-phenyl-1-propene. The results obtained here indicate that the phenylation of **2** and **6** with **1** favors the formation of diphenylated olefin compounds more than the Heck reaction of **2** and **6**.

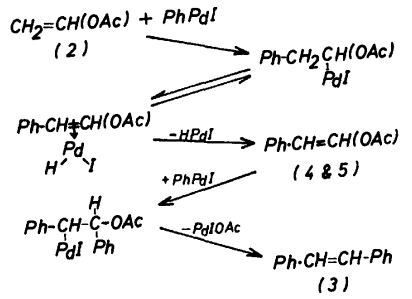

Scheme 1.

A common mechanism has been proposed for the arylation of olefins with aryl halides.[2,3] In the phenylation of **6** with **1**, the formation of 2,3-diphenyl-1-propene (**9**) may require that the phenylpalladium group is added to the double bond in both possible directions

TABLE 1. PHENYLATION OF ENOL ESTERS WITH IODOBENZENE (**1**)

Enol ester	Product, bp or mp°C, (lit)	Yield[a] %
CH_2=CH(OAc) (**2**)	Biphenyl, mp 68—69 (mp 69—70[b])	3
	(*E*)-Stilbene (**3**), mp 124, (mp 123—124[c])	52
	(*E*)-Styryl acetate (**4**)	10
	(*Z*)-Styryl acetate (**5**), bp of the mixture of **4** and **5** 95—120/2.5 Torr (bp 87—112/1.5 Torr[d])	2
Ph-CH=CH(OAc) (**4** and **5**, **4**/**5**=7/1)	Biphenyl	3
	(*E*)-Stilbene (**3**)	58
CH_2=CCH_3(OAc) (**6**)	Biphenyl	24
	(*E*)-2,2-Diphenyl-1-propene (**7**), mp 78—79 (mp 79—79.5[e])	21
	(*Z*)-1,2-Diphenyl-1-propene (**8**), mp 47—48 (mp47—48[e])	8
	2,3-Diphenyl-1-propene (**9**), bp 162—165/14 Torr (bp 81—83/0.12 Torr[e])	2
	(*E*)-2-Acetoxy-1-phenyl-1-propene (**10**), bp 102—105/3 Torr (bp 112—116/5 Torr[f])	10
	(*Z*)-2-Acetoxy-1-phenyl-1-propene (**11**), bp 102—105/3 Torr (bp 112—116/5 Torr[f])	2
CH_2=C(OAc)Ph (**12**)	Biphenyl	36
	(*E*)-Stilbene (**3**)	25
	1,2-Diphenyl-1-acetoxyethene (**13**),mp 104—106, (mp 102—106[g])	20

a) The yields are based upon the iodobenzene (**1**) used are determined by gas chromatography. b) E. Muller and T. Topel *Ber.*, **72**, 273 (1939). c) R. L. Shrine and A. Bergrr, *Org. Synth.*, Coll. Vol. III, 786 (1965). d) R. F. Heck, *Organometal. Chem. Syn.*, **1**, 455 (1972). e) D. H. Hunter and D. J. Cram. *J. Am. Chem. Soc.*, **86**, 5478 (1964). f) H. O. House, L. J. Czuba, M. Gall, and H. D. Olmstead, *J. Org. Chem.*, **34**, 2324 (1969). g) C. V. Gheorghin, *Chem. Abstr.*, **17**, 1559, (1923).

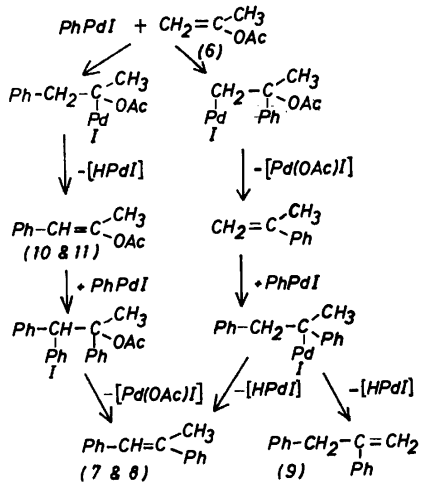

Scheme 2.

(Scheme 2).

The phenylation of acetophenone enol acetate (**12**) gave **3** and 1,2-diphenyl-1-acetoxyethene (**13**). The formation of **3** may require three intermediate steps, namely, the initial elimination, a readdition of the palladium hydride in the reverse direction, and another elimination of Pd(OAc)I, as shown in Scheme 3.

Experimental

Materials. Iodobenzene, vinyl acetate, and isopropenyl acetate of a commercial grade were used without further purification. The preparation of the following compounds has already been reported: (*E*)- and (*Z*)-styryl acetates[7] and acetophenone enol acetate.[9]

General Procedure for The Phenylation of Enol Acetate. A mixture of 2.04 g (10 mmol) of **1**, 12 mmol of enol acetate, 1.21 g (12 mmol) of triethylamine, 0.022 g (0.1 mmol) of palladium acetate, and 0.524 g (0.2 mmol) of triphenylphosphine in acetonitrile (10—15 ml) was heated in a sealed tube flushed with nitrogen at 100 °C for 8 h. The products

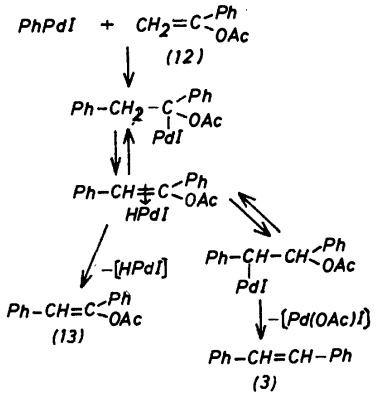

Scheme 3.

were isolated by diluting the cooled reaction mixtures with water and ether. The ether phase was separated, washed several times with water, dried over anhydrous magnesium sulfate, and concentrated. The products were generally analyzed by gas chromatography on a 1 m SE 30 (5% on celite) column with a Hitachi K-53 gas chromatograph, and identified by comparing the retention time on the gas chromatogram and the IR and NMR spectra with those of an authentic sample. The reactions carried out are listed in Table 1.

References

1) T. Mizoroki, K. Mori, and A. Ozaki, *Bull. Chem. Soc. Jpn.*, **44**, 581 (1971); *ibid.*, **46**, 1505 (1973).
2) R. F. Heck and J. P. Nolley, Jr., *J. Org. Chem.*, **37**, 2320 (1972).
3) H. A. Dieck and R. F. Heck, *J. Am. Chem. Soc.*, **96**, 1133 (1974); *J. Org. Chem.*, **40**, 1083 (1975).
4) J. B. Melpolder and R. F. Heck, *J. Org. Chem.*, **41**, 265 (1976).
5) A. J. Chalk and S. A. Magennis, *J. Org. Chem.*, **41**, 273, 1206 (1976).
6) R. F. Heck, *J. Am. Chem. Soc.*, **90**, 5535 (1968).
7) R. F. Heck, *Organometal. Chem. Syn.*, **1**, 455 (1972).
8) R. F. Heck, *J. Am. Chem. Soc.*, **91**, 6707 (1969).
9) P. Z. Bedoukian, *J. Am. Chem. Soc.*, **67**, 649 (1946).

BULLETIN OF THE CHEMICAL SOCIETY OF JAPAN, VOL. 50, (2) 553—554 (1977)

Carbonylation Reaction of Isoprene Catalyzed by Palladium(II) Acetate and Triphenylphosphine

Jiro TSUJI and Hideyuki YASUDA

Department of Chemical Engineering, Tokyo Institute of Technology, Ookayama, Meguro-ku, Tokyo 152

(Received November 4, 1976)

Synopsis. The carbonylation reaction of isoprene in alcohol catalyzed by palladium(II) acetate and triphenylphosphine gave 4-methyl-3-pentenoate selectively in a moderate yield. Unlike butadiene, no dimerization-carbonylation of isoprene to give C_{11} esters took place.

Palladium catalyzed carbonylation of butadiene in alcohol proceeds in two ways depending on the catalytic species. When palladium(II) chloride is used as the catalyst, 3-pentenoate is obtained selectively.[1] On the other hand, when halogen free palladium compounds such as palladium(II) acetate or palladium(II) acetylacetonate are used with triphenylphosphine as the catalyst, the dimerization-carbonylation occurs to give 3,8-nonadienoate exclusively.[2] Carbonylation of isoprene catalyzed by palladium(II) chloride in ethanol gave ethyl 4-methyl-3-pentenoate as the main product.[2]

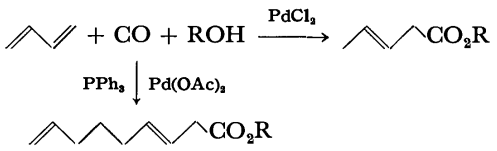

In this paper we report on the carbonylation reaction of isoprene in alcohol which we carried out with use of palladium(II) acetate and triphenylphosphine as the catalyst, expecting the formation of C_{11} esters by the dimerization-carbonylation of isoprene. However, no dimerization took place, the product being a C_6 ester. The C_6 ester was a single compound with no contamination of isomeric C_6 esters. The structure of the ester was determined to be 4-methyl-3-pentenoate based on spectral data. The carbonylation of isoprene proceeded

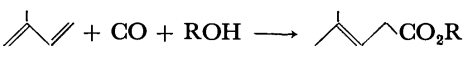

much slower than that of butadiene under the same reaction conditions, taking roughly three times longer a period than that of butadiene. The structure of alcohols used as the reactant and solvent showed crucial effect on the carbonylation. As observed in the carbonylation of butadiene catalyzed by palladium(II) acetate, methanol was not a good solvent, hardly any carbonylation taking place in methanol. In ethanol, the ethyl ester was obtained after 60 h in 37% yield by using 1 mol % of the catalyst. *t*-Butyl alcohol seems to be an effective reactant and *t*-butyl 4-methyl-3-pentenoate was obtained as the sole product in 50% yield with 0.45 mol % of palladium(II) acetate. The ratio of palladium(II) acetate to triphenylphosphine is also an important factor, the ratio of 1: 6—7 giving the best result. With a lower ratio, palladium metal precipitated during the course of reaction. The reaction was carried out at 115 °C. A reaction temperature higher than 130 °C resulted in the decomposition of the catalyst into black palladium metal, no carbonylation taking place above this temperature.

The selective formation of 4-methyl-3-pentenoate can be explained by the following mechanism. At first the π-allyl complex is formed by the reaction of isoprene with palladium–hydride species. The selective attack of carbon monoxide at the unsubstituted side of the π-allylic complex then follows to give 4-methyl-3 pentenoate. Usually the reaction of isoprene with nucleophiles catalyzed by palladium(II) acetate and triphenylphosphine leads to the formation of a mixture of various substituted head-tail and tail-tail dimers.[3-6] It is interesting that in the carbonylation only one π-allylic complex is formed selectively, which is attacked by carbon monoxide, but not by another isoprene to lead to the dimer formation.

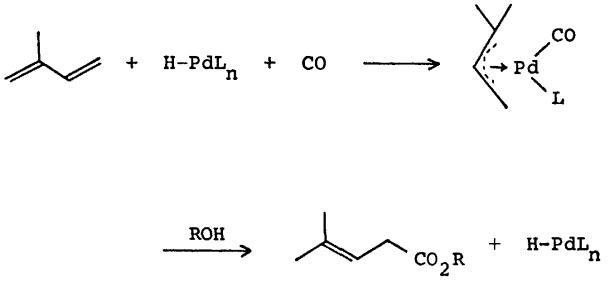

Experimental

A typical carbonylation reaction in *t*-butyl alcohol was carried out in the following way. A mixture of isoprene (2.72 g, 40 mmol), palladium(II) acetate (40 mg, 0.178 mmol, 0.45 mol% based on isoprene), triphenylphosphine (327 mg, 1.245 mmol) and *t*-butyl alcohol (10 ml) was put in a glass cylinder placed in a 50-ml autoclave and then carbon monoxide was introduced until the pressure reached 30 atm. The autoclave was placed in an oil bath kept at 120 °C and stirred with a magnetic stirrer. Gas absorption took place slowly. Gas chromatographic analysis of the reaction mixture showed the exclusive formation of 4-methyl-3-pentenoate and the presence of a very small amount of by-products. After 48 h, the product was subjected to distillation to give 3.40 g (50%) of *t*-butyl 4-methyl-3-pentenoate at 76—78 °C/19 Torr. NMR (CCl_4); 5.25 (m, 1, olefinic), 2.83 (d, 2, J=7 Hz, $-CH_2-CO$), 1.75, 1.64 (s, s, 6, $2CH_3$), 1.4 ppm (s, 9, *t*-Bu), IR (neat); 1715 cm^{-1}.

Similarly the ethyl ester (1.60 g, 37.6%) was obtained by the reaction of isoprene (1.98 g, 30 mmol) in ethanol (10 ml) with use of palladium(II) acetate (67 mg, 0.3 mmol) and triphenylphosphine (393 mg, 1.5 mmol) at 115 °C for 60 h. Bp 62—63 °C/18 Torr.

References

1) J. Tsuji, Y. Mori, and M. Hara, *Tetrahedron*, **28**, 3721 (1972).

2) S. Hosaka and J. Tsuji, *Tetrahedron*, **27**, 3821 (1971).
3) S. Takahashi, T. Shibano, and N. Hagihara, *Shokubai*, **11**, 4 (1969).
4) K. Suga, S. Watanabe, and K. Hijikata, *Aust. J. Chem.*, **24**, 197 (1971).
5) K. Takahashi, G. Hata, and A. Miyake, *Bull. Chem. Soc. Jpn.*, **46**, 600 (1973).
6) A. D. Josey, *J. Org. Chem.*, **39**, 139 (1974).

BULLETIN OF THE CHEMICAL SOCIETY OF JAPAN, VOL. 50 (2), 555—556 (1977)

Gaseous Products from the Plasma Decomposition of Isomeric Xylenes

M. VENUGOPALAN and Thomas W. SCOTT

Department of Chemistry, Western Illinois University, Macomb, Illinois 61455, U. S. A.

(Received July 31, 1976)

Synopsis. The formation of methane and ethane on decomposition of the isomeric xylenes in Siemens-type discharges has been investigated. With increasing voltage the methane yield decreased, while the ethane yield increased; the C_2H_6/CH_4 mole ratios increased continuously but varied in the order *ortho*>*meta*>*para*.

A recent investigation[1] of the plasma decomposition of isomeric xylenes showed that ethane is the major gaseous product and that very little methane is formed in high-frequency (10—2450 MHz) electrical discharges. Under the experimental conditions extensive polymerization occurred.[1,2] Dimerization by elimination of hydrogen has been reported[3] to be the major reaction in low-frequency (50 Hz) electrical discharges in xylene vapors, but there is no published data on the gaseous products from such discharges.

In our preliminary investigations of isomeric xylene plasmas produced by low-frequency Siemens-type discharges significant amounts of methane and ethane were detected among the gaseous products.[4] Since methane was not a significant product in the high-frequency discharges,[1] it was desirable to re-investigate this aspect of the plasma chemistry of xylenes. In this paper we report on the yields of methane and ethane from 50 Hz xylene plasmas.

Experimental

Xylene vapor (99.9 per cent purity, Matheson Company) was pumped at a pressure of 7 Torr and a flow rate of 22 micromole s^{-1} through a 15 cm long Siemens co-axial-type Pyrex reactor with 5 mm inter-electrode separation. The plasma was produced by applying line frequency (50 Hz) high voltage from a transformer to electrodes which were (1) a thick copper wire dipping in salt solution inside the inner glass tube and (2) a thin copper wire wound outside the outer glass tube of the reactor. For the experimental conditions an approximate residence time of 0.75 s was calculated[5] for the xylene in the plasma zone where, depending on the applied voltage, 5—10 per cent of the input xylene was decomposed. The products were trapped at 77 K in a U-trap which was warmed to 215 K prior to the gas chromatographic analysis for CH_4 and C_2H_6. The analysis was performed *in situ* using a Gow-Mac chromatograph in conjunction with a 1.2 m long silica gel column at 273 K.

Results and Discussion

The yields of CH_4 and C_2H_6 found per mole of *o*-xylene entering the discharge tube are shown in Fig. 1. At the lower applied voltages the methane yield increased slightly to a maximum, but it then dereased almost linearly with increasing voltage while the ethane yield increased continuously. This behavior was less dominant in the case of the *meta* and *para* isomers

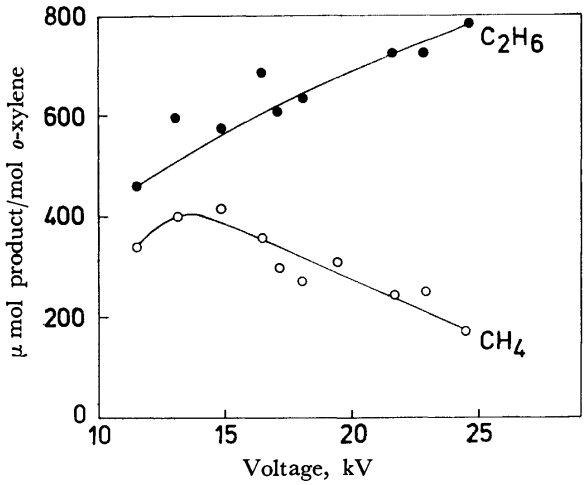

Fig. 1. Methane and ethane yields from *o*-xylene as functions of the applied voltage.

than the *ortho* isomer. The CH_4 and C_2H_6 yields varied in the order *ortho*>*meta*>*para* suggesting that these product yields depend on the proximity of the two methyl groups in the xylene molecule.

Some sort of xylene ion must form as a result of inelastic collisions between the electrons and xylene molecules in the plasma, but whether these ions or some derivative species are the reactive intermediates is not known. The energetics of xylene decomposition[6] suggests that both the C–H (*ca.* 77.5 kcal mol^{-1}) and C–C (87 kcal mol^{-1}) bonds in the xylene molecule may split under plasma conditions:

$$C_6H_4(CH_3)_2 \rightarrow CH_3C_6H_4CH_2^{\cdot} + {}^{\cdot}H \quad (1)$$

$$C_6H_4(CH_3)_2 \rightarrow CH_3C_6H_4^{\cdot} + {}^{\cdot}CH_3 \quad (2)$$

The formation of these free radicals is supported by the evidence from mass spectroscopy[7] and emission spectroscopy[8,9] of the xylene plasmas. If reaction (2) is the CH_3 radical source[10] and is followed only by the recombination reaction to form ethane

$$2\,CH_3^{\cdot} \rightarrow C_2H_6 \quad (3)$$

and the abstraction reaction to form methane

$$CH_3^{\cdot} + C_6H_4(CH_3)_2 \rightarrow CH_3C_6H_4CH_2^{\cdot} + CH_4 \quad (4)$$

then the fate of the methyl radicals produced in the xylene plasmas is somewhat exemplified by the C_2H_6/CH_4 mole ratios[11] shown in Fig. 2. The voltage dependence of the ratio suggests that reactions (2) and (3) are favored and reaction (4) is disfavored as the voltage is increased. The different ratios for the isomers at a given voltage indicate that the proximity of the two interacting methyl groups in the xylene molecule may be significant for methane production *via* reaction (4). This conclusion, however, excludes

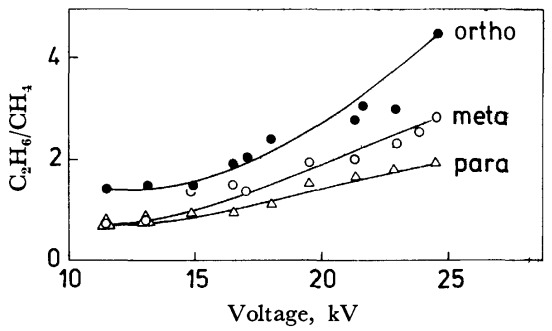

Fig. 2. Variation of the C_2H_6/CH_4 ratios with applied voltage for the three isomeric xylenes.

the loss of CH_3 radicals by their combination with $CH_3C_6H_4CH_2$ radicals to form the isomeric ethyltoluenes.

The authors are grateful to the Research Council, Western Illinois University, for a grant in support of this work.

References

1) H. Taki, *Bull. Chem. Soc. Jpn.*, **43**, 1578 (1970).
2) H. Hiraoka, H. Kamada, and S. Hanai, *Nippon Kagaku Zasshi*, **90**, 1239 (1969).
3) H. Suhr, G. Rolle, and B. Schrader, *Naturwissenschaften*, **55**, 168 (1968).
4) Of course, H_2 is the most abundant gaseous product from xylene plasmas. For a given plasma conditions the product distribution varied in the order $H_2 > C_2H_6 > CH_4$.
5) This is an upper limiting value because the rate of flow through the plasma volume (*ca.* 44 cm^3) was assumed to be the molar rate of input of xylene vapor at room temperature. For the calculation of the residence time, see R. A. Jones, W. Chan, and M. Venugopalan, *J. Phys. Chem.*, **73**, 3695 (1969).
6) T. L. Cottrell, "The Strengths of Chemical Bonds," 2nd ed, Butterworths Publications, London (1958), p. 184.
7) American Petroleum Institute, Res. Proj. 44, Spectrum Nr. 178—180.
8) H. Schueler and L. Reinebeck, *Z. Naturforsch.*, **4a**, 577 (1949).
9) A. N. Singh, D. K. Rai, and I. S. Singh, *Proc. First. Intern. Conf. Spectrosc., Bombay*, 1967, Vol. 1. p. 238.
10) Another source is the exchange reaction $H^{\cdot} + C_6H_4(CH_3)_2 \rightarrow C_6H_5CH_3 + CH_3^{\cdot}$ which is unlikely due to high activation energy requirement.
11) The ratio of product yields is sufficient for the type of comparison attempted here. Absolute considerations would require that the ratio $[C_2H_6]^{1/2}/[CH_4]$ be used.

BULLETIN OF THE CHEMICAL SOCIETY OF JAPAN, VOL. 50 (2), 557—558 (1977)

Magnetic Properties of Oxovanadium(IV) Complexes with Bidentate ON Donor Schiff Bases*

A. SYAMAL†

Department of Chemical Technology, The University of Bombay, Matunga Road, Bombay 400019, India

(Received April 27, 1976)

Synopsis. The magnetic properties of oxovanadium(IV) complexes of Schiff bases(I) are reported. Contrary to an earlier report that these complexes are involved in magnetic exchange, the complexes are found to be magnetically dilute. The complexes display μ_{eff} in the range 1.68—1.71 B. M. at 78—297 K with $\theta=2$—4 K, and exhibit 8 line ESR spectra.

The $3d^1$ oxovanadium(IV) ion belongs to $s=1/2$ system and the coupling of two $s=1/2$ spins of interacting pair of oxovanadium(IV) ions may lead to both antiferromagnetic and ferromagnetic spin-spin coupling. Many terdentate dibasic ONO or ONS donor Schiff base ligands have been utilized for the syntheses of dimeric or polymeric oxovanadium(IV) complexes with antiferromagnetic properties.[1] The terdentate dibasic character of these ligands force the oxovanadium(IV) ion to dimerise or polymerise leading to complexes with subnormal magnetic properties. The oxovanadium(IV) complexes of the bidentate monobasic, terdentate monobasic, quadridentate dibasic Schiff bases are usually magnetically dilute.[2] On the other hand, the copper(II) complexes of terdentate monobasic and quadridentate dibasic Schiff bases are usually involved in magnetic exchange.[3,4] Although most copper(II) complexes with bidentate monobasic Schiff bases are magnetically dilute, several examples of copper(II) complexes of bidentate monobasic Schiff bases involved in magnetic exchange are known.[3,4] This difference in magnetic properties has been attributed to the presence of out-of-plane magnetic interaction in copper(II) complexes. The absence of such out-of plane magnetic interaction in oxovanadium(IV) complexes is due to the non-participation of the vanadyl oxygen atom in magnetic exchange.[1] A recent cryomagnetic study[5] of an oxovanadium(IV) Schiff base complex containing a V=O···V=O··· chain indicates that the vanadyl oxygen bridges (*ca.* 170° exchange) do not contribute to the antiferromagnetic interaction due to the intraionic exchange *via* $\sigma(O_{p_z}-V_{d_{z^2}})$ or $\pi(O_{p_x,p_y}-V_{d_{xz},d_{yz}})$ pathway. In the above light one may expect that the oxovanadium(IV) complexes with bidentate monobasic Schiff bases

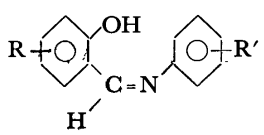

I. R=H, C_4H_4;
R′=H, Cl, SO_2NH_2.

will not exhibit the behaviour of antiferromagnetic exchange. However, the oxovanadium(IV) complexes of ON donor bidentate monobasic Schiff bases(I) have been reported to possess a magnetic moment of 1.54 B.M. at 297 K indicating the presence of antiferromagnetic exchange in these complexes.[6] Kuge and Yamada[7] have also prepared the oxovanadium(IV) complex of I (R=C_4H_4, R′=H) but they believe the complex to be magnetically dilute. Due to this disagreement between these two groups of workers, it was of interest to repeat the work. We report here the detailed magnetic(78—297 K), ESR and molecular weight measurements on the complexes.

Experimental

The oxovanadium(IV) complexes of I were prepared according to the method of Dutta and Sengupta.[6] However, the complexes were not recrystallised, and the complexes without recrystallisation gave satisfactory elemental analyses.

The magnetic susceptibilities of the complexes were determined by the Gouy method using mercury(II) tetrathiocyanatocobaltate(II) as the standard. Diamagnetic corrections of the metal and ligand atoms were calculated using a standard source.[8] The magnetic susceptibilities were corrected for the temperature independent paramagnetism using a value of 40×10^{-6} cgs unit. Electron spin resonance spectra were obtained with a Varian V-4502-12 X-band spectrometer using 100-kHz modulation and a 9-inch electromagnet. A minute polycrystalline sample of diphenylpicrylhydrazil (Aldrich Chemical Co., U. S. A.) free radical was used as a *g*-marker in a dual channel cavity and the frequency was monitored with the help of a frequency meter. Molecular weight measurements were made in $CHCl_3$ using a Hewlett-Packard Mechrolab Model 301 A Vapor Pressure Osmometer operating at 37 °C and calibrated with benzil.

Results and Discussion

The magnetic susceptibities and magnetic moment data of the complexes are presented in Table 1. The room temperature magnetic moments(1.69—1.71 B.M.) of the complexes are close to the spin-only value of 1.73 B.M. expected for a d^1 system. The magnetic data of the complexes indicate that the magnetic moments of the complexes remain almost constant in the temperature range 78—297 K. The complexes obey the Curie-Weiss law** with Weiss constant, θ in the range +2 to +4 K. A typical plot of reciprocal magnetic susceptibility *versus* temperature is given in Fig. 1. Thus the magnetic susceptibility data indicate the absence of magnetic exchange in

* ON represents oxygen and nitrogen donor bidentate Schiff bases(I).

† Present address: Department of Chemistry, Regional Engineeriag College, Kurukshetra 132119, Haryana, India.

** The Curie-Weiss law is used in the form: $\chi_M^{corr}=\frac{C}{T-\theta}$.

Table 1. Magnetic susceptibilities and magnetic moments of oxovanadium(IV) Schiff base complexes[a,b,c]

VO (hydrox-aniline)				VO (hydrox-*p*-chloroaniline)$_2$				VO (sal-salphanilamide)$_2$			
Temp (K)	χ_M^{corr} (10^{-6} cgs unit)	μ_{eff} (B. M.)	θ (K)	Temp (K)	χ_M^{corr} (10^{-6} cgs unit)	μ_{eff} (B. M.)	θ (K)	Temp (K)	χ_M^{corr} (10^{-6} cgs unit)	μ_{eff} (B. M.)	θ (K)
295	1198	1.69		297	1216	1.71		295	1215	1.70	
189	1851	1.68	+4	185	1936	1.70	+2	184	1930	1.69	+2
78	4472	1.68		80	4477	1.70		78	4542	1.69	

a) Abbreviations: hydrox=2-hydroxy-1-naphthaldehyde and sal=salicylaldehyde. The effective magnetic moment was calculated using the Curie equation: $\mu_{eff}=2.84(\chi_M^{corr}\times T)^{1/2}$ B. M. b) TIP=40×10^{-6} cgs units. c) Although the magnetic susceptibilities were determined at seven temperatures (see Fig. 1), the data for only three temperatures are presented for brevity.

these complexes. We synthesized these three complexes by several independent experiments and measured magnetic susceptibilities separately, and found deviation in the magnetic moment seldom greater than ±2%.

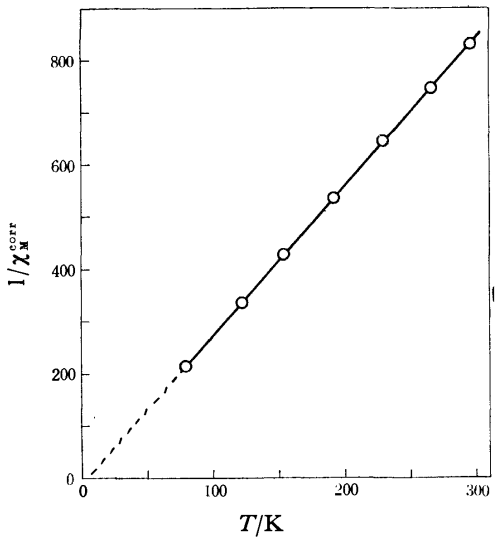

Fig. 1. The inverse magnetic susceptibility *vs.* temperature plot of VO(hydroxynaphthaldehyde-aniline)$_2$.

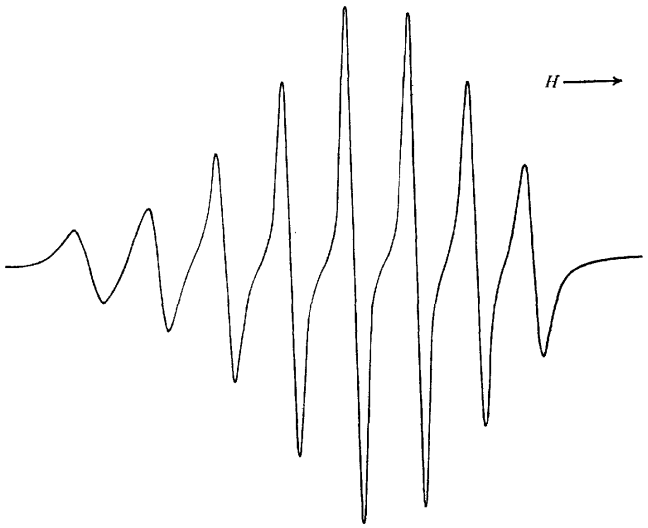

Fig. 2. The ESR spectrum of VO(hydroxynaphthaldehyde-aniline)$_2$ in chloroform.

We recorded the electeon spin resonace spectra of the complexes in dilute chloroform soution. The spectra of the complexes exhibit eight line spectra (^{51}V, I=7/2) with $g_{av}=1.98\pm0.01$ and average hyperfine splittings ⟨A⟩ around 100 gauss. A typical spectrum is presented in Fig. 2. The complexes do not exhibit any triplet state spectra ($\Delta Ms=\pm2$ transition) at around 1600 gauss. The ESR spectra of the complexes are typical of the spectra of magnetically dilute oxovanadium(IV) complexes.[2] The osmometric molecular weight measurements in chloroform solutions indicate the monomeric nature of the complexes. Thus the magnetic, ESR, and molecular weight data of the complexes indicate the absence of magnetic exchange in these complexes and the magnetic moments reported by Dutta and Sengupta[6] are in error. Our work agrees with the work of Kuge and Yamada[7] and proves conclusively that the complexes are spin-doublet species. On the basis of the experimental evdence presented a monomeric square pyramidal structure is suggested to these complexes.

The author is indebted to the Council of Scientific and Industrial Research, New Delhi, the Atomic Energy Commission (Government of India), the University Grants Commission, New Delhi and the faculty research fund of the University of Bombay for support of this work.

References

1) A. Syamal, *Coord. Chem. Rev.*, **16**, 309 (1975).
2) J. Selbin, *Chem. Rev.*, **65**, 153 (1965); *Coord. Chem. Rev.*, **1**, 293 (1966).
3) M. Kato, H. B. Jonassen, and J. C. Fanning, *Chem. Rev.*, **64**, 99 (1964).
4) W. E. Hatfield and R. Whyman, "Transition Metal Chemistry," Vol. 5, Marcel Dekker Inc., New York (1969), p. 47.
5) D. M. L. Goodgame and S. V. Waggett, *Inorg. Chim. Acta*, **5**, 155 (1971).
6) R. L. Dutta and G. P. Sengupta, *J. Indian Chem. Soc.*, **44**, 738 (1967); *ibid.*, **48**, 33 (1971).
7) U. Kuge and S. Yamada, *Bull. Chem. Soc. Jpn.*, **45**, 799 (1972).
8) B. N. Figgis and J. Lewis, "Modern Coordination Chemistry," ed by J. Lewis and R. G. Wilkins, Interscience Publishers New York (1960), p. 403.

BULLETIN OF THE CHEMICAL SOCIETY OF JAPAN, VOL. 50 (2), 559—560 (1977)

Microdetermination of Furfural Using Bromine Monochloride

V. K. S. SHUKLA* and S. SHUKLA
Department of Pharmacology, M. L. N. Medical College, Allahabad, India

(Received January 29, 1976)

Synopsis. A simple micro procedure for the estimation of furfural with bromine monochloride has been presented. A 2—10 mg sample dissolved in distilled water is reacted with a known excess of bromine monochloride in acetic acid in an ice bath, and the excess reagent is back titrated iodometrically. The maximum deviation in the results is ±0.90%.

A number of methods are available for the quantitative determination of furfural depending upon the various analytical principles. Kruglikov and coworker[1] determined furfural titrimetrically with a potassium bromide-potassium bromate mixture. Spiridonova[2] reported a rapid method for the determination of furfural concentrations in non-aqueous solutions by titration with water. Similarly Nikitm and coworker[3] developed a rapid procedure for the determination of furfural by titration with water in the presence of isobutyl alcohol as a turbidity indicator. Larzlo and coworker[4] proposed a bromometric method for the determination of furfural. In the present work a new titrimetric method has been described for the microgram determination of furfural using bromine monochloride in a water-acetic acid medium.

Validity of the Reaction for the Quantitative Determination. Before applying the reaction for the determination of furfural the stoichiometry of the reaction was determined as follows: A 2—10 mg of the sample dissolved in water was reacted with a known amount of bromine monochloride solution in acetic acid. The reaction was allowed to proceed for about 15 min in an ice bath, after which the excess of the reagent was back-titrated iodometrically. Results obtained are presented in Table 1.

TABLE 1. DETERMINATION OF THE STOICHIOMETRY OF THE REACTION

Wt. of sample (mg)	Number of moles of BrCl consumed per mole of furfural
1.999	3.002
4.996	3.000
6.994	3.004
9.992	3.006

These results show that, 3 mol of BrCl are consumed per mole of furfural. The possible explanation for this is that 2 mol of BrCl are probably used for

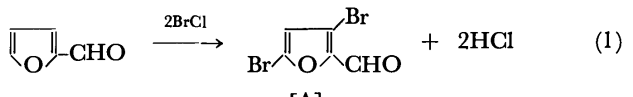

(1)

[A]

substitution, and then this dibromination product (A) acts as diene (just as butadiene) to add one more mole of BrCl.

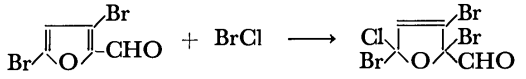

(2)

[A]

This is the 1,4 addition of BrCl, and probably Br will go to the carbon 2 due to the effect of the formyl group. Furan derivatives are known to undergo easy substitution (like (1)) and also to act as diene. The effect of coexistence of impurities such as other furan derivatives has not been examined.

Experimental

Procedure. An aliquot containing 2—10 mg of the sample solution in distilled water was placed in a 100 ml iodine flask. Five ml of glacial acetic acid followed by 5 ml of bromine monochloride[5] were introduced and the flask was stoppered and shaken well. The flask was placed in an ice bath and reaction mixture allowed to cool well for about 15 min. After the reaction was over the stopper was washed with 5 ml of distilled water followed by the same volume of 15% potassium iodide solution, and the liberated iodine was titrated with 0.02 M sodium thiosulfate solution using starch as an indicator. A blank experiment was also run under the identical conditions except for the use of the sample.

Results and Discussion

The proposed method has been applied for the determination of furfural, and the results of the determination are presented in Table 2. Excess of bromine monochloride should be controlled as it leads to higher results. Acetic acid is a good solvent and reaction medium for a large variety of compounds. Cooling of the reaction mixture is necessary for obtaining good results.

TABLE 2. MICRO DETERMINATION OF FURFURAL USING BROMINE MONOCHLORIDE

Sample No.	Taken (mg)	Found (mg)	No. of Determinations	Error (%)
1.	1.999	2.016	4	+0.84
2.	4.996	5.041	4	−0.90
3.	6.994	6.936	4	−0.82
4.	9.992	10.080	4	+0.90

* Present address: c/o Roskilde Universitetscenter, Hus 161, P. O. Box 260, 4000-Roskilde, Denmark.

References

1) L. A. Kuz'mina and A. A. Kruglikov, *Zavod. Lab.*, **32**, 142 (1966).

2) S. I. Spridonova, *Izv. Vyssh. Uchebn. Zavad., Khim. Khim. Tekhnol.*, **9**, 156 (1966) (Russ); *Chem. Abstr.*, **65**, 9736a (1966).

3) I. Ya Gaivoronskaya and E. K. Nikitm, *Zh. Anal. Khim.*, **22**, 461 (1967) (Russ).

4) Margit Szakacs-Pinter and Larzlo Maros, *Magy. Kem. Foly.*, **74**, 77 (1968) (Hung); *Chem. Abstr.*, **68**, 95092x (1968).

5) J. P. Sharma, A. K. Awasthy, and V. K. S. Shukla, *Microchim. Acta*, **1972**, 522.

BULLETIN OF THE CHEMICAL SOCIETY OF JAPAN, VOL. 50 (2), 561—562 (1977)

The Synthesis of 4-Acetylaminoimidazole-5-sulfonamide and 1-Acetyl-5-acetylimidazole-4-sulfonamide

B. Robinson* and M. Uppal Zubair**,*

* *Manchester University, Oxford Street, Manchester, England*

** *Islamabad University, Islamabad, Pakistan*

(Received June 7, 1976)

Synopsis. The synthesis of mono- and di-, *N*-acetyl derivatives of 5-aminoimidazole-4-sulfonamide, from 5-nitroimidazole-4-sulfonamide, as analogues of 5-amino-1'-ribonucleotyl)imidazole-4-carboxamide, is described.

The l-ribonucleotides of several imidazoles are well-established[1] as intermediates in purine ribonucleotide anabolism, but as yet few structurally related compounds have received attention as potential anti-viral or oncolytic agents. Since one of the intermediates in *de novo* nucleic acid synthesis is 5-amino-1-(1'-ribonucleotyl)imidazole-4-carboxamide[2] (I), we have now synthesised the di- and mono-*N*-acetyl-5-amino-4-sulfonamide derivatives (II and III respectively), which by possible *in vivo* hydrolysis of the acetyl group and l-ribonucleotylation would become bioisosteric with the above-mentioned natural ribonucleotide and thereby exibit an antimetabolite relationship.

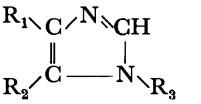

	R_1	R_2	R_3
I	$-CONH_2$	$-NH_2$	-Ribonucleotyl
II	$-SO_2NH_2$	$-NHCOCH_3$	$-COCH_3$
III	$-SO_2NH_2$	$-NHCOCH_3$	-H
IV	$-SO_2NH_2$	$-NO_2$	-H
V	$-SO_2NH_2$	$-NH_2$	-H

Many unsuccessful attempts have been made to introduce a sulfonamide moiety into the 4-position of an imidazole ring and to prepare 5-aminoimidazole-4-sulfonamide. Attempts to prepare 4-sulfonyl chlorides as potential intermediates failed[3] when imidazole-4-sulfonic acid, 2-methylimidazole-4-sulfonic acid and 5-methylimidazole-4-sulfonic acid[4] failed to react with phosphorus pentachloride, phosphorus pentachloride–phosphoryl chloride mixtures, thionyl chloride or chlorosulfuric acid.[5] Attempts to proceed *via* the sulfenamide starting from 1-methyl-4-nitro-5-mercaptoimidazole also failed,[5] as did an attempt[5] to introduce a sulfonyl chloride group directly by chlorosulfonation of 4-acetamidoimidazole. However, 5-bromoimidazole has been successfully chlorosulfonated to give 5-bromo-4-sulfonyl chloride, which was readily converted to the corresponding amide but attempts to subsequently replace the bromo substiuent by an amino group failed.[5] although unfortunately an attempt using sodamide was not made. Attempts to catalytically hydrogenate the nitro group to an amino group in 5-nitroimidazole-4-sulfonamide (IV) led only to the formation of decomposition products,[6] probably because the amino sulfonamide (V) is unstable.

We have repeated this hydrogenation with 5-nitroimidazole-4-sulfonamide (IV), under the catalytic action of platinum, at elevated temperature and pressure, in a solution of glacial acetic acid and acetic anhydride. Instead of isolating the free amine formed, which is unstable, its diacetyl derivative (II) was formed, by boiling under reflux the reaction mixture, under the atmosphere of nitrogen gas. Aqueous hydrolysis of compound (II) afforded the monoacetyl derivative, 5-acetamidoimidazole-4-sulfonamide (III). The structure of II was confirmed by its elemental analysis and by its infrared spectrum which in particular showed two carbonyl functions. The structure of III was established by its high resolution mass spectral analysis and by its infrared spectrum which showed only one carbonyl function.

Experimental

Melting points were determined on a Kofler hot stage apparatus and are uncorrected. The IR spectra were recorded (solids as mulls in Nujol) with a Perkin-Elmer model 237 spectrophotometer, mass spectra were recorded with AEI MS-12 (low resolution) and MS-9 (high resolution) spectrometers.

5-Nitroimidazole-4-sulfonamide (IV). This compound was synthesised by the known method.[6]

5-Acetamido-1-acetylimidazole-4-sulfonamide (II). A mixture of IV (250 mg) and finely divided platinum (100 mg) in glacial acetic acid (5 ml) and acetic anhydride (15 ml), was hydrogenated at 50 p. s. i./50—60 °C. After hydrogen uptake had ceased (4 h), nitrogen was passed through the reaction mixture, the catalyst was rapidly removed by filteration and the filtrate was boiled under reflux for 1.5 h. After decolorisation (charcoal) the excess acetic acid and acetic anhydride were evaporated to afford a pale-yellow oil (50 mg) which crystallised from methanol to afford 5-acetamido-1-acetylimidazole-4-sulfonamide (II), as white prisms mp 250—252 °C; yield, 26 mg (8%).

Found: C, 33.9; H, 3.9; N, 22.7%. Calcd for $C_7H_{10}N_4O_4S$: C, 34.1; H, 4.0; N, 22.7%.

Mass spectrum: *m/e* 246 $(M)^+$; the infrared spectrum indicated the characteristic bands of the two carbonyl groups at 1710 and 1695 cm^{-1}.

5-Acetamidoimidazole-4-sulfonamide (III). A solution of II (25 mg) in water was boiled under reflux for 0.5 h. Evaporation of water and recrystallisation from methanol/ether afforded 5-acetamidoimidazole-4-sulfonamide (III) as white prisms; mp 220—221 °C; yield, 9 mg; 43%. High resolution mass spectral analysis showed a molecular ion at *m/e* 204.0319. Calcd for $C_5H_8N_4O_3S$ 204.031 the infrared spectrum indicated a characteristic band of a carbonyl group at 1675 cm^{-1}. The site of acetylation in this product is based[5] upon the similar partial hydrolysis of 1-

acetyl-4-acetamidoimidazole which affords 4-acetamidoimidazole.

References

1) H. R. Mahler and E. H. Cordes, "Biological Chemistry," Harper & Row, Tokyo (1966), Ch. 17, pp. 714—751.
2) J. M. Buchanan, *Taxas Rep. Biol. Chem.*, **15**, 148 (1957).
3) R. Forsyth, J. A. Moore, and F. L. Pyman, *J. Chem. Soc.*, **125**, 919 (1924).
4) G. R. Barnes and F. L. Pyman, *J. Chem. Soc.*, **1927**, 2711.
5) L. L. Bennett and H. T. Baker, *J. Am. Chem. Soc.*, **79**, 2188 (1957).
6) M. H. Fisher, W. H. Nicholson, and R. S. Stuart, *Can. J. Chem.*, **39**, 501 (1961).

Improvement of Zone-melting Apparatus: A New Apparatus with a High-precision Heater-temperature-controlling Mechanism

Yasuko ISHIZUKA

National Chemical Laboratory for Industry, Honmachi, Shibuya-ku, Tokyo 151

(Received March 31, 1976)

A new zone-melting apparatus with a high-precision heater-temperature-controlling mechanism has been designed and constructed. The apparatus can control the width of several melting zones at an equal temperature and thus can obtain smooth concentration profiles after zone refining. The effect of zone refining with this apparatus was examined with fair success, using phenanthrene and naphthalene as samples.

The zone-melting technique has been recognized as a useful method for purifying organic compounds, and many apparatuses for this purpose have been manufactured. Most of the automatic zone-melting apparatus have several heaters to refine the samples efficiently.[1] However, when the heater temperatures are not precisely controlled, the difference between them causes differences in the widths of the molten zones[2] and, consequently, a difference in the impurity transfer, which results in an inefficient refining. Thus, impurity concentration profiles after zone-refining experiments have bumps and are not smooth. To avoid this disadvantage, the heater temperatures must be controlled so as to have equal values in all operating zones. On the other hand, other causes of differences in the widths of molten zones over a long period of experiment, such as changes in the electric power added to the heaters, the ambient temperature, *etc.*, must also be borne in mind.

In this paper, the design and construction of a new zone-melting apparatus which has precisely controlled heaters, as well as a few results obtained by using it, will be reported.

Experimental

Heaters and their temperature controls: A unit of the heater consists of nichrome wire and the other elements shown in Fig. 1. The nichrome wire (NTK No. 3, 0.23ϕ, 110 cm length, Ishikawa Co., Tokyo) is wound around two Turner rings (22 mm o.d., 12 mm i.d. and 2 mm in thickness), and a sheet of mica is put between these two Turner rings as an electric shield. This part of heater is wound around with a glass wool ribbon and set inside two Turner lids. A chromel alumel thermocouple is inserted through a groove of the Turner lids into the inside so as to touch the glass wool ribbon. The temperature of the heaters thus constructed rise to *ca.* 440 °C if an electric voltage of 50 V is supplied.

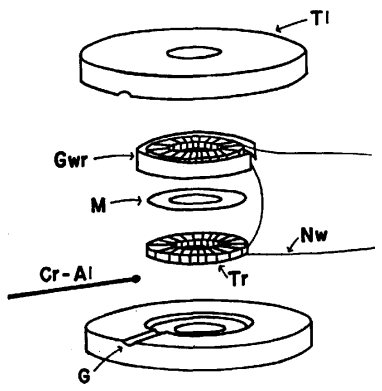

Fig. 1. Composition of a heater.
Tl: Turner lid. Gwr: Glass wool ribbon. Tr: Turner ring. M: Mica sheet. Nw: Nichrome wire. Cr-Al: Cr-Al thermocouple. G: Groove for a thermocouple.

Eighteen heaters are used in this zone-melting apparatus and are connected parallel. They are precisely controlled using eighteen thermocouples and three sets of an automatic temperature controller Model E-500 (Chino Works, Ltd., Tokyo) and a multicontroller Model P-885-6 (Chino Works, Ltd., Tokyo). The temperature of the automatic temperature controller is set 1—2 °C higher than the melting point of the sample. The heater temperature is measured for 12 s every 72 s; the electric voltage applied to the heaters is maintained until the next measurement time by means of a relay circuit memory system included in the multicontroller. When the heater temperature is lower than the setting temperature, the setting voltage which is preliminarily chosen is applied to the heater. On the other hand, when it is higher than the setting temperature, 80% of the setting voltage is applied. With this mechanism, the heater temperature is maintained constant and does decrease rapidly to temperature lower than the setting temperature, particularly for the samples with high melting points. By this mechanism the heater temperature is maintained within 100 ± 3 °C when it is set at 100 °C. This precision is mainly a result of the precision of the automatic temperature controller, Model E-500.

Apparatus: An apparatus with a device to prevent the breakage of the sample tube was previously constructed by the present author and his coworkers.[3] The new apparatus reported here is improved in several points: 1) No buffer is used to prevent the breakage of the sample tube. Instead, a vacant space which is considerably large in the sample tube and which is filled with an inert gas, is regarded as a buffer for the expansion of the sample at melting. 2) The sample tube moves twice the distance of two neighboring heaters to smooth out the difference in the performances of the two neighboring heaters which is caused by a slight difference in the structures of the heaters. 3) The sample tube rotates and the direction of rotation reverses periodically in order to stir the liquid zones vigorously.[4] 4) The sample tube moves in a slant-wise manner so as to prevent the formation of voids in the sample during the purification.[5]

A diagram of the apparatus is shown in Fig. 2. A Pyrex tube (10 mm o.d., 110 cm length) is used as a sample tube (St). 10—50 g of a sample is compactly packed into the tube, and then the tube is sealed with 1/2 atm of an inert gas. The sample tube is set so that the end filled with the sample is supported by a clamp (Cl) and the other end, filled with the inert gas, is supported by a support (S). Eighteen precisely controlled heaters (H1, H2,···, H18) and nineteen coolers (C) are alternately arranged; the distance between neighboring heaters is 5 cm. The part shown by a heavy line in

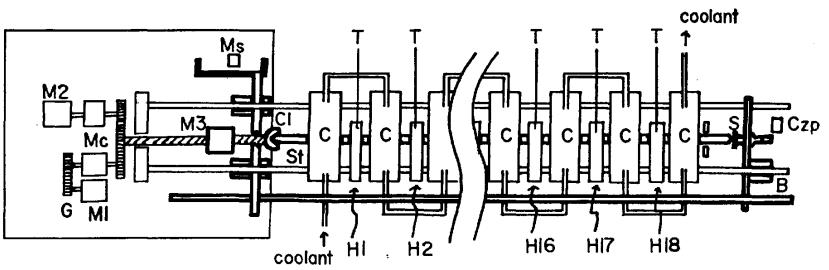

Fig. 2. Diagram of zone melting apparatus.
St: Sample tube. H: Heater. C: Cooler. T: Thermocouple. Cl: Clamp. S: Support. B: Ball bearing. Mc: Magnetic clutch. M1, M2: Motor. M3: Reversible motor. G: Gear. Ms: Microswitch. Czp: Counter for zone passes.

the figure is moved slowly 10 cm to the left by a motor (M1) and then rapidly returned to the initial position by another motor (M2). This alternating movement of the sample tube is controlled automatically by means of a microswitch (MS) and a pusher mechanism. The velocity of moving the tube to the left, which determines the solidifying velocity of the sample, can be selected by changing gears (G) at 150, 75, 50, 37.5, 30, or 18.8 mm/h. The time required for returning to the initial position is several seconds. Starting from H1 and H2, two heaters are switched on in the order of the number of heater every time the reciprocating movement stops. After all heaters are switched on, the sample tube continues the reciprocating movements for the needed time. Then two heaters are turned off in the order of the heater number every time the reciprocating movement stops until all the heaters are turned off. This mechanism of turning off the heaters makes the number of zone passes equal at every point of a refined sample. To stir the melted part of a sample, the sample tube is rotated around the axis of the tube by means of a reversible motor (M3, 100 r.p.m.), and the direction of the rotation is periodically reversed every 1, 1/2, or 1/3 s.

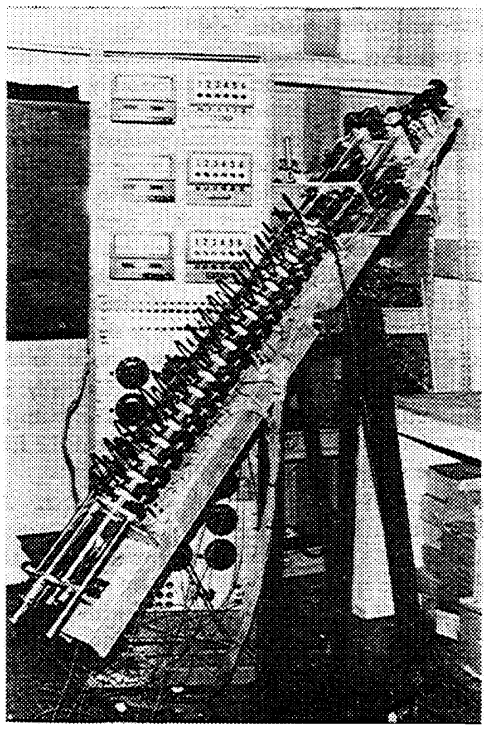

Fig. 3. Zone melting apparatus.

Figure 3 shows the temperature-controlled zone-refining apparatus in the front part and the controlling part in the rear part. The apparatus operates in a slant posture so as to make the vacant space of the sample tube higher than the sample. The slanting angle is continuously changed.

Results and Discussion

The zone-refining performance of the new apparatus was examined with two samples, naphthalene and phenanthrene. In both experiments the solidifying

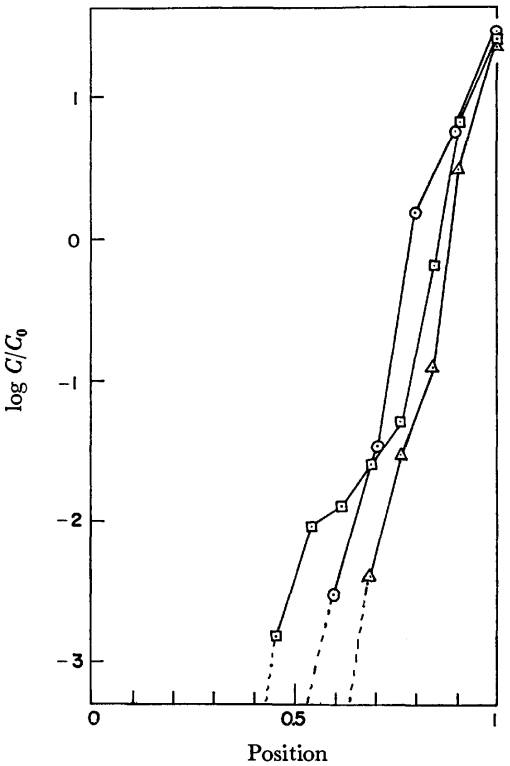

Fig. 4. Concentration (C) of 2-methylnaphthalene in the naphthalene sample after the zone refining. As for the abscissa the total sample length was regarded as 1.0 and each sample position was measured from the vacant space side. Initial concentration (C_0) was 1%. Detectable limit was 5 ppm.
—○—: 9 zone passes with the apparatus reported here.
—△—: 20 zone passes with the apparatus reported here.
—□—: 60 zone passes (33 mm/h solidifying speed) with the apparatus reported previously.[3]

velocity was kept at 50 mm/h, the slanting angle to a vertical line, at 50°, and the reversing cycle of the rotation, at 2 cycle/s.

2-Methylnaphthalene was doped in naphthalene (Kokusan Chemical Works Ltd., Tokyo) as an impurity so that the concentration of the impurity was 1%. The quantity of 2-methylnaphthalene in the refined sample was examined by means of a gas chromatograph equipped with F.I.D. A sample solution for the gas chromatograph was prepared using 200 mg of the refined samples taken every 5 cm starting from the vacant space side. As is shown in Fig. 4, the 2-methylnaphthalene in the naphthalene sample moves in the same direction as the movement of the melting zone. After only 9 zone passes, the concentration of the impurity decreases to less than 5 ppm in the first 40% of the naphthalene sample, starting from the vacant space in the sample tube, and then increases smoothly for the next 60% of the sample. Figure 4 also shows that naphthalene is more effectively refined with the new apparatus than with the apparatus previously reported.[3]

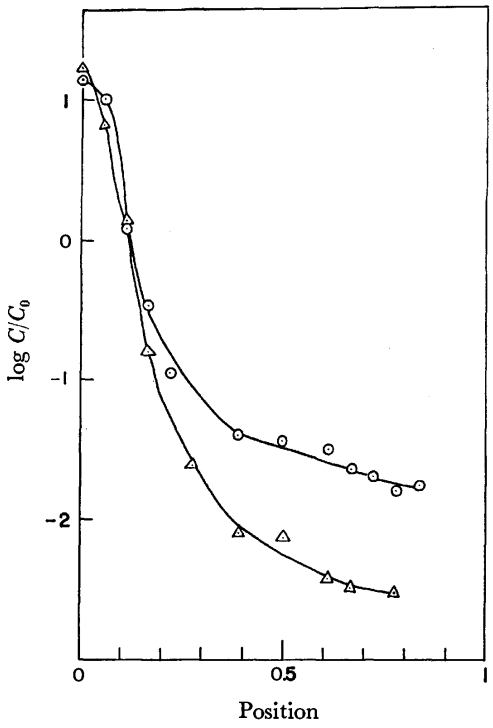

Fig. 5. Concentration (C) of anthracene in the phenanthrene sample after the zone refining. The abscissa is the same as explained in Fig. 4. Initial concentration (C_0) was 1%.
—○—: 304 zone passes, —△—: 774 zone passes.

The phenanthrene sample (Tokyo Kasei Kogyo Co., Ltd., Tokyo) includes 1% anthracene as a major impurity. The concentration of anthracene in the zone-refined sample is examined by means of the absorptivity of a 379 nm band of anthracene in a benzene solution. In this case, 100—250 mg of the refined sample, cut in the same way as the naphthalene sample, is used to make the benzene solution. Figure 5 shows the results after 304 and 774 zone passes. In this case, the impurity moves in the direction opposite to the movement of the melting zone. Both results show that phenanthrene samples are effectively refined and that anthracene as the impurity is smoothly distributed. In the 0.8—1 range in the figure, the phenanthrene samples are colored by other impurities.

The equal widths of the melting zones resulting from the equal temperatures realized by the high-precision controlling mechanism of the heater temperatures and the reverse rotation of a sample tube make the efficient refining possible. With this new apparatus, organic materials with high melting points can be refined effectively without the breakage of the sample tube.

The author wishes to thank Dr. Y. Mashiko, Mrs. N. I. Wakayama, and Mr. I. Takeda of this laboratory for their valuable advice.

The author is also indebted to Mr. K. Tsuji of the Institute for Solid State Physics, the University of Tokyo, for his valuable advice and technical help in the construction of the apparatus.

References

1) W. G. Pfann, "Zone Melting," Wiley, New York (1958); H. Shildknecht, "Zone Melting," Weinheim, Verlag Chemie (1966); M. Zief and W. R. Wilcox, "Fractional Solidification," Marcel Dekker (1967).

2) Unpublished work.

3) N. I. Wakayama, Y. Nakano, and Y. Mashiko, *Bull. Chem. Soc. Jpn.*, **46**, 2277 (1973).

4) W. G. Pfann, C. E. Miller, and J. D. Hunt, *Rev. Sci. Instrum.*, **37**, 649 (1966); N. J. G. Bollen, M. J. van Essen, and W. M. Smit, *Anal. Chim. Acta*, **38**, 279 (1967).

5) S. Maeda, H. Kobayashi, and K. Ueno, *Talanta*, **20**, 653 (1973); E. F. G. Herington, "Zone Melting of Organic Compounds," Blackwell Scientific Publications, Oxford (1963), p. 30.

The Detemination of the Formation Constants of the Triiodide Ion in Water-Alcohol Mixed Solvents at Various Temperatures

Katumitu HAYAKAWA and Sumio NAKAMURA

Department of Chemistry, Faculty of Science, Kagoshima University, Koorimoto, Kagoshima 890

(Received April 26, 1976)

The formation constants of the triiodide ion were determined in water–alcohol mixed solvents by a spectrophotometric method at various temperatures. The formation reaction of the triiodide ion from an iodide ion and an iodine molecule is accompanied by a negative enthalpy change and a positive entropy change at various alcohol contents: $\Delta H°$/kJ mol^{-1}, −15.4 (in water) to −14.3 (in methanol) in the water-methanol system, −15.4 (in water) to −21.4 (in ethanol) in the water-ethanol system; $\Delta S_x°$/J K^{-1} mol^{-1}, 36 (in water) to 57 (in methanol) in the water-methanol system, and about 36 at various ethanol contents in the water–ethanol system. The enthalpy term is the dominant factor in the water-ethanol mixtures, whereas the entropy term is the dominant factor in the water-methanol mixtures. In order to explain the thermodynamic behavior, the changes in the solvation properties as well as the activity coefficients of solutes must be considered in both the mixture systems.

During the course of an investigation of the effect of solvents on the rate of the oxidation of the formate ion by iodine, it became necessary to know the formation constant of the triiodide ion in mixed solvents at various temperatures. Although the formation constant has been determined in some mixed solvents[1,2] and some organic solvents[3,4] at 25 °C, it has not been determined at various temperatures in mixed solvents. The present work was undertaken in order to determine the values of the formation constant in water–alcohol mixed solvents at various temperatures. The formation constant varies with the composition of the solvents, and it has been found that the variation in the solvation properties influences the formation constant of the triiodide ion.

Experimental

Materials. The iodine, potassium iodide, ethanol (99.5%), and methanol (99.5%) were obtained from Wako Pure Chemicals Industries. The ethanol was of Wako's super special grade, while the other chemicals were of a guaranteed grade. The solutions of the iodine were prepared by dissolving exactly weighed amounts of iodine purified by sublimation in the potassium iodide solution. The presence of iodide lowers the reactivities of iodine with solvents. The potassium iodide used was dried at 120 °C overnight, and the solutions were prepared by dissolving exactly weighed amounts of the salt in mixed solvents. The water used was double-distilled from potassium permanganate in an all-glass apparatus.

Measurements. The absorbance at 355 nm was measured by using a Hitachi 101 spectrophotometer with quartz cells with a light-path length of 10 mm in a thermostated holder, and using a Valhalla Scientific digital multimeter, Model 4440, as the digital output at various temperatures. The pH and the ionic strength in the solutions were uncontrolled.

The Determination of the Formation Constant of I_3^-. The formation constant of the triiodide ion was calculated from the dependence of the absorbance at 355 nm on the concentration of the iodide of the solution containing a constant concentration of iodine (*ca.* 25×10^{-6} mol dm^{-3}).

For Reaction 1, the apparent formation constant, K_c, is given by Eq. 2:

$$I_2 + I^- \rightleftarrows I_3^- \quad (1)$$

$$K_c = [I_3^-]/[I_2][I^-] = x/(a-x)(b-x) \quad (2)$$

where the brackets represent the respective concentrations, a and b are the total concentrations of iodine and potassium iodide respectively, and x is the equilibrium concentration of the triiodide ion. As potassium iodide does not absorb the light at 355 nm, the absorption coefficient at 355 nm, $A(\equiv D_1/l)$, is given by Eq. 3:

$$A = \varepsilon_0(a-x) + \varepsilon_1 x \quad (3)$$

where ε_0 and ε_1 are the molar absorption coefficients of iodine and the triiodide ion respectively, at 355 nm. From Eqs. 2 and 3,

$$\bar{\varepsilon} \equiv A/a = \varepsilon_0 + K_c b(\varepsilon_1-\varepsilon_0)/[1+K_c(a-x)+K_c b] \quad (4)$$

As b is much larger than $(a-x)$ in the present measurements, and as ε_1 is much larger than ε_0 at 355 nm,

$$1/\bar{\varepsilon} \approx (1/\varepsilon_1 K_c)(1/b) + 1/\varepsilon_1 \quad (5)$$

Therefore, K_c and ε_1 can be calculated by the intercept and slope of the $1/\bar{\varepsilon}$ *vs.* $1/b$ plot. All the plots were linear in various mixed solvents at $b \gg a$, and the intercept of each line was almost independent of the temperature.

Results and Discussion

The iodine solution in methanol and ethanol has an absorption band with a maximum absorbance near 355 nm.[1,5] However, the absorbance at 355 nm is not proportional to the concentration of iodine. This band is ascribed to a small amount of the triiodide ion formed by the reaction of iodine with alcohol.[5,6] The formations of I_5^-, I_7^-, I_9^-, *etc.* are neglected because of the low concentration of iodine in the present work (for example, $\log([I_5^-]/[I_2]^2[I^-]) = 1.8$ in ethanol[2]).

In aqueous solutions, Reaction 1 is accompanied by Reactions 6 and 7:[7-10]

$$I_2 + H_2O \rightleftarrows HIO + I^- + H^+ \quad (6)$$

$$3I_2 + 3H_2O \longrightarrow IO_3^- + 5I^- + 6H^+ \quad (7)$$

At pH≈7, Equilibrium 6 may be neglected.[9,10] Reaction 7 is sufficiently slow in the presence of excess potassium iodide.[9] In fact, the absorbance at 355 nm did not vary for 24 h in an iodine solution containing an excess of potassium iodide.

Table 1 gives the values of the apparent formation constants of the triiodide ion, K_c. The constant increases when the temperature is lowered and the alcohol content is increased. The values of K_c obtained in the present work are compared with those of other workers in

Table 1. The formation constant, K_c, of the triiodide ion in water–alcohol mixed solvents

Mole fraction of alcohol	$10^{-3} \times K_c$/mol^{-1} dm^3			
Methanol				
0.00	1.01±0.01 (9.5 °C)	0.73±0.00 (25.0 °C)		0.55±0.02 (38.0 °C)
0.10	1.25±0.04 (11.0 °C)	0.98±0.02 (22.1 °C)	0.88±0.00 (30.0 °C)	0.72±0.02 (37.4 °C)
0.18	2.07±0.05 (10.0 °C)	1.69±0.06 (19.5 °C)	1.35±0.04 (29.0 °C)	1.20±0.10 (37.7 °C)
0.31	4.10±0.04 (11.1 °C)	3.25±0.03 (21.2 °C)	2.64±0.04 (30.8 °C)	2.34±0.02 (37.4 °C)
0.47	7.57±0.03 (10.0 °C)	5.98±0.05 (20.8 °C)	5.06±0.20 (29.0 °C)	4.51±0.23 (37.4 °C)
0.64	10.4 ±0.1 (11.3 °C)	8.56±0.03 (21.0 °C)	7.39±0.04 (28.8 °C)	6.29±0.09 (38.1 °C)
0.82	14.1 ±0.0 (10.3 °C)	11.0 ±0.1 (20.9 °C)	9.66±0.01 (28.9 °C)	7.86±0.01 (39.0 °C)
0.99	16.0 ±0.1 (11.8 °C)	13.6 ±0.2 (20.0 °C)	10.9 ±0.1 (31.0 °C)	9.59±0.02 (38.6 °C)
Ethanol				
0.07	2.05±0.08 (12.0 °C)	1.66±0.05 (20.5 °C)	1.34±0.06 (29.5 °C)	1.17±0.04 (37.0 °C)
0.13	5.54±0.02 (11.2 °C)	4.44±0.10 (19.0 °C)	3.63±0.03 (27.0 °C)	2.86±0.03 (37.0 °C)
0.24	12.7 ±0.1 (11.0 °C)	10.8 ±0.2 (18.0 °C)	7.80±0.07 (29.0 °C)	6.26±0.10 (37.2 °C)
0.38	21.4 ±0.5 (11.0 °C)	15.7 ±0.7 (20.0 °C)	12.2 ±0.5 (30.0 °C)	10.0 ±0.3 (37.0 °C)
0.55	27.5 ±0.4 (9.5 °C)	20.0 ±0.2 (18.2 °C)	15.4 ±0.2 (27.5 °C)	11.9 ±0.3 (37.0 °C)
0.76	32.8 ±1.0 (8.0 °C)	22.6 ±0.5 (19.2 °C)	17.0 ±0.4 (30.0 °C)	14.1 ±0.6 (36.0 °C)
0.98	35.1 ±0.8 (10.0 °C)	28.7 ±0.2 (17.0 °C)	20.7 ±0.2 (28.0 °C)	15.1 ±0.2 (39.0 °C)

Fig. 1. Ramadan *et al.*[1] assigned the absorption bands at 360 and 294 nm to the iodine molecule, and obtained the molar absorption coefficient of the iodine molecule, ε_0, from the absorbance of the iodine–alcohol–water systems. However, this assignment is questionable, because the absorbances at 360 and 294 nm are not proportional to the concentration of iodine. The absorption bands may be ascribed to a small amount of the triiodide ion formed by the reaction of iodine with the alcohol.[6] The difference between the present results and those reported by Barraqué *et al.*[2] (Fig. 1) may be attributed to the difference in methods. Barraqué *et al.* used a potentiometric method.

Table 2 gives the values of the standard thermodynamic functions, $\Delta H°$, $\Delta S_c°$, and $\Delta G_c°$, of Reaction 1 and the molar absorption coefficient, ε_1, of the triiodide ion. In order to compare the formation constant in mixed solvents, it is necessary to use a measure which is independent of the conventional scale. For a solute A, the chemical potential, μ(A), is represented by either Eq. 8 or Eq. 9:

$$\mu(\mathrm{A}) = \mu_c°(\mathrm{A}) + RT\ln(C_\mathrm{A}/C°) + RT\ln y_\mathrm{A} \quad (8)$$

$$\mu(\mathrm{A}) = \mu_x°(\mathrm{A}) + RT\ln x_\mathrm{A} + RT\ln f_\mathrm{A} \quad (9)$$

where x_A is the mole fraction of A, C_A is the concentration of A, y_A, and f_A are the activity coefficients in

Table 2. The equilibrium characteristics and the absorption coefficient of the formation of triiodide in water–alcohol mixed solvents at 25 °C

Mole fraction of alcohol	$\Delta H°$ / kJ mol^{-1} (±0.4)	$\Delta G_c°$ / kJ mol^{-1} (±0.6)	$\Delta S_c°$ / JK^{-1} mol^{-1} (±2)	$\Delta G_x°$ / kJ mol^{-1} (±0.5)	$\Delta S_x°$ / JK^{-1} mol^{-1} (±3)	$10^4 \times \varepsilon_1$[a] / mol^{-1} dm^3 cm^{-1} (±0.2)
Methanol						
0.00	−15.4	−16.3	3	−26.3	36	2.5
0.10	−15.0	−17.0	7	−26.7	39	2.7
0.18	−14.8	−18.1	11	−27.6	43	2.7
0.31	−15.7	−19.8	14	−29.0	45	2.7
0.47	−14.0	−21.4	25	−30.3	55	2.8
0.64	−13.9	−22.3	28	−30.9	57	2.6
0.82	−14.8	−22.9	27	−31.2	55	2.7
0.99	−14.3	−23.3	30	−31.3	57	2.8
Ethanol						
0.07	−16.6	−18.1	5	−27.8	38	2.5
0.13	−18.7	−20.4	6	−29.8	37	2.6
0.24	−20.1	−22.5	8	−31.5	38	2.7
0.38	−21.1	−23.6	8	−32.1	37	2.6
0.55	−22.0	−24.1	7	−32.1	34	2.6
0.76	−21.5	−24.5	10	−32.0	35	2.7
0.98	−21.4	−24.8	11	−31.9	35	2.5

a) At 355 nm.

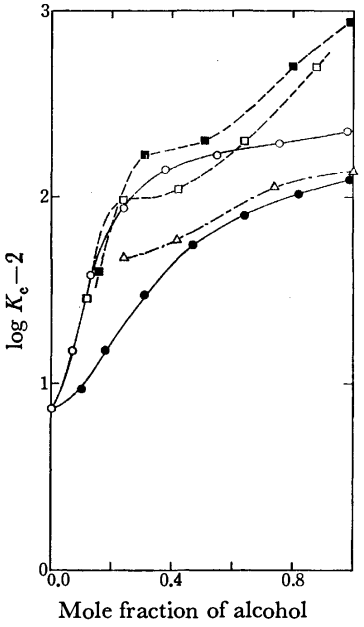

Fig. 1. Effects of the alcohol content on the formation constant of the triiodide ion at 25 °C. Open marks: water–ethanol mixture, closed marks: water–methanol mixture. Circle: the present work, square: by Ramadan *et al.*,[1] Triangle: by Barraqué *et al.*[2]

the respective concentration scale, and C° is the standard concentration, selected as 1 mol dm^{-3} in the present work. At an infinite dilution,

$$\mu_x^\circ(\mathrm{A}) = \mu_c^\circ(\mathrm{A}) + RT\ln\{(C_\mathrm{A}/C^\circ)/x_\mathrm{A}\} \quad (10)$$

Since $x_\mathrm{A} \approx C_\mathrm{A}(x_\mathrm{B}M_\mathrm{B} + x_\mathrm{C}M_\mathrm{C})/\rho$ in the B–C mixed solvents,

$$\mu_x^\circ(\mathrm{A}) = \mu_c^\circ(\mathrm{A}) + RT\ln\{\rho/(x_\mathrm{B}M_\mathrm{B} + x_\mathrm{C}M_\mathrm{C})C^\circ\} \quad (11)$$

where M_B and M_C are the molar masses of B and C respectively, while ρ is the mass of the 1 dm^3 solution. Since $\Delta G_c^\circ = \mu_c^\circ(\mathrm{I_3^-}) - \mu_c^\circ(\mathrm{I_2}) - \mu_c^\circ(\mathrm{I^-})$ for Reaction 1,

$$\Delta G_x^\circ = \mu_x^\circ(\mathrm{I_3^-}) - \mu_x^\circ(\mathrm{I_2}) - \mu_x^\circ(\mathrm{I^-})$$
$$= \Delta G_c^\circ - RT\ln\{\rho/(x_\mathrm{B}M_\mathrm{B} + x_\mathrm{C}M_\mathrm{C})C^\circ\} \quad (12)$$

Since $\Delta H_c^\circ = \Delta H_x^\circ (= \Delta H^\circ)$ and $\Delta S_c^\circ = (\Delta H_c^\circ - \Delta G_c^\circ)/T$,

$$\Delta S_x^\circ = (\Delta H_x^\circ - \Delta G_x^\circ)/T$$
$$= \Delta S_c^\circ + R\ln\{\rho/(x_\mathrm{B}M_\mathrm{B} + x_\mathrm{C}M_\mathrm{C})C^\circ\} \quad (13)$$

Table 2 shows also the values of ΔG_x° and ΔS_x° at 25 °C.

Figure 2 shows the dependence of these quantities on the mole fraction of alcohol. The values of ΔH° are nearly constant in the methanol–water mixtures, whereas in the ethanol–water mixtures they increase remarkably on the addition of the first portions of ethanol and become nearly constant beyond the 0.4 mol fraction. On the other hand, the values of ΔS_x° are nearly constant in the ethanol–water mixtures, while they increase in the methanol–water mixtures. The values of ΔS_c° increase with the ethanol content, whereas those of ΔS_x° are constant (Table 2). The increase in ΔS_c° may be due to the neglect of the entropy change on the mixing of the solvents.

Two factors can explain the variations in ΔS_x° and ΔH° with the alcohol content: one is the variation in the activity coefficients of the solutes with the alcohol content, and the other is the variation in the solvation properties with the alcohol content. The activity

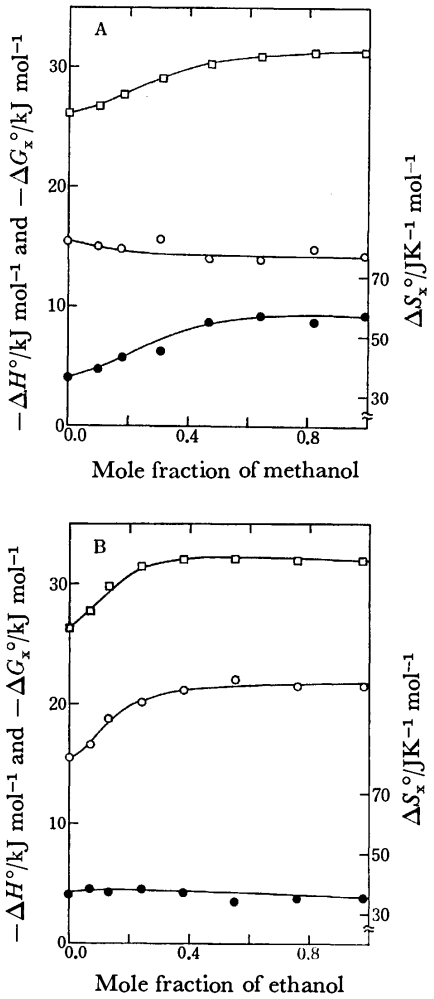

Fig. 2. The standard thermodynamic functions of the formation of the triiodide ion in water–alcohol mixed solvents. A: water–methanol mixtures, B: water–ethanol mixtures. □: ΔG_x°, ○: ΔH°, ●: ΔS_x°.

coefficients of $\mathrm{I_3^-}$ and $\mathrm{I^-}$ are nearly the same in a given solvent, because the two ions are univalent. The activity coefficient of $\mathrm{I_2}$ will be close to unity because it is a neutral molecule. Even if the activity coefficient varied from 1.0 to 0.5 with the alcohol content, the difference in ΔG_x° would be only about 2 kJ mol^{-1}. Thus, the activity coefficients of solutes cannot explain the effects of the solvent on ΔG_x°.

Next, the variation in the solvation properties, such as the structure of the solvation shell and the specific solvation, must be considered in both the mixture systems. ΔH° and ΔS_x° in Fig. 2 reflect the solvation energy of each solute and the structure of the solvation shell of each solute respectively, because μ_x° is based on the infinite dilution. For example, the curves of ΔH° in Fig. 2 indicate that the difference in the solvation energy between the reactants and the product in Reaction 1 is nearly constant in the methanol–water system, while it increases on the addition of a small amount of ethanol to water in the ethanol–water system. Ramadan *et al.*[1] ascribed the marked change in K_c by the addition of a small amount of organic solvents to the rearrangement of the structure of the solvent and a subsequent change in its solvation properties. In order

to make it clear why ΔS_x° is the dominant factor in the methanol–water system, while ΔH° is the dominant factor in the ethanol–water system, we need to know the structure of the solvation shell of each solute and the transfer-free energy of the solutes in various solvents. Thus, in order to explain the thermodynamic behavior of Reaction 1 in the two mixture systems, the changes in the solvation properties as well as the activity coefficients of the solutes must be considered.

References

1) A. A. Ramadan, P. K. Agasyan, and S. I. Petrov, *Zh. Obshch. Khim.*, **44**, 983 (1974).
2) C. Barraqué, J. Vedel, and B. Trémillon, *Anal. Chim. Acta*, **46**, 263 (1969).
3) A. A. Ramadan, P. K. Agasyan, and S. I. Petrov, *Zh. Anal. Khim.*, **28**, 2396 (1973).
4) S. Lormeau and M. H. Mannebach, *Bull. Soc. Chim. Fr.*, **1966**, 2576.
5) F. H. Getman, *J. Am. Chem. Soc.*, **48**, 1877 (1926).
6) "Mellor's Comprehensive Treatise on Inorganic and Theoretical Chemistry," Supplement 2, Part 1, Longmans, Green and Co, London (1956), p. 923.
7) H. D. Murray, *J. Chem. Soc.*, **1925**, 882.
8) E. Angelescu and V. D. Popescu, *Z. Phys. Chem.*, **A156**, 304 (1931).
9) J. D. Burger and H. A. Liebhafsky, *Anal. Chem.*, **45**, 600 (1973).
10) T. L. Allen and R. M. Keefer, *J. Am. Chem. Soc.*, **77**, 2957 (1955).

An ESR Study of the 4,4′-Difluorobiphenyl Cation Radical*

Fujito NEMOTO, Kazuhiko ISHIZU, and Fumio SHIMODA**

Department of Chemistry, Faculty of Science, Ehime University, Bunkyo-cho, Matsuyama 790

(Received May 10, 1976)

The ESR spectra of the 4,4′-difluorobiphenyl cation show resolved second-order splittings and a marked line-broadening attributable to the modulation of the ^{19}F anisotropic hyperfine interactions by the tumbling motion. This dipolar broadening is mainly observed for the lines associated with the triplet state ($I=1$) of the two equivalent ^{19}F nuclei. When the temperature is lowered, the wings of the triplet due to the two ^{19}F and the downfield second-order components become broad and finally disappear. The dipolar contributions to the line widths are calculated as a function of the correlation time for the molecular motion, τ_2. Furthermore, the ESR observation of the ^{13}C hyperfine structures is carried out, and the spin densities on each ring carbon and the fluorine atoms are experimentally determined. From the spin densities thus determined, the parameters in the equation

$$a_F = Q^F_{CF}\rho^\pi_C + Q^F_{F(FC)}\rho^\pi_F,$$

in which the ^{19}F hyperfine coupling constant is correlated to the π spin densities on the fluorine atom and the adjacent carbon atom, are estimated to be $Q^F_{CF}=39$ and $Q^F_{F(FC)}=324$ G.

Recently there have been a number of ESR and NMR studies of fluoro-substituted alkyl and aromatic radicals in solution. The objectives of these studies may mainly be classified as follows; (1) The ESR spectra of fluoro-substituted radicals show a viscosity-dependent selective line-width effect due to a relaxation process brought about by the modulation of the relatively large anisotropic fluorine splitting by the tumbling motion. The information about the motion of molecules in solution was extracted from the analysis of their temperature-dependent selective line width. The fluorinated alkyl radicals ordinarily have simple ESR spectra and show large fluorine hyperfine coupling constants, so that the line width of the spectra can be determined with great precision. Consequently, the temperature dependence and selective variations in line widths were studied in detail for fluorinated alkyl radicals.[1-3] There has been no detailed study of the fluoro aromatic radicals, however, because of the small values of the ^{19}F hyperfine splitting. (2) The hyperfine coupling constants, a_F, of fluorine atoms in fluoro-substituted aromatic radicals depend on both the spin density, ρ^π_C, at the adjacent carbon atom and the spin density, ρ^π_F, at the fluorine atom. There have been numerous investigations of the fluoro aromatic radicals, and a consistent functional relationship between the isotropic fluorine splitting and the π spin densities has been proposed.[11-19] Mainly, two types of equations have been examined;

$$a_F = Q^F_{CF}\rho^\pi_C \quad (1)$$

$$a_F = Q^F_{CF}\rho^\pi_C + Q^F_{F(FC)}\rho^\pi_F \quad (2)$$

Here, Q^F_{FC} is the π–σ contribution analogous to that of the aromatic C–H fragment. $Q^F_{F(FC)}$is the contribution from the π–σ polarization of the 1s and 2s electrons of fluorine by the spin density centered on the $2p_\pi$ orbital of fluorine.

The results of the ESR and NMR investigations indicate that the simple linear relationship, Eq. 1, may be inadequate to describe the data of fluorinated compounds. Equation 2 seems more realistic than Eq. 1 in that it allows for conjugation on the fluorine $2p_\pi$ orbital with the π electrons in the aromatic ring. The previously determined values of Q's in Eq. 2 are, however, scattered over a wide range because the π fluorine spin densities are usually not obtained by solution ESR studies; the simple LCAO MO approach to the calculation of the ρ^π_F is, then, not necessarily valid.

In the present paper, we wish to report the results of ESR studies of the 4,4′-difluorobiphenyl cation radical. The value of the ^{19}F hyperfine coupling constant is quite large (19.20 G) compared with those of the fluoro aromatic radicals, and a second-order splitting of ^{19}F and a temperature-dependent broadening of ^{19}F splitting were observed. Furthermore, the spin densities on each ring carbon and fluorine atom were experimentally determined based on the observation of the ^{13}C hyperfine splittings for ring carbons, and the Q values of Eq. 2 were discussed.

Experimental

4,4′-Difluorobiphenyl (mp 88—89 °C) was synthesized and recrystallized from ethanol. The cation radicals was generated by $SbCl_5$ oxidation in CH_2Cl_2 in a manner described before.[7] The ESR spectrum of the 4,4′-difluorobiphenyl cation radical was observed using a JEOL-ME-3X spectrometer operating with a 100 kHz magnetic field modulation. The magnetic field was calibrated by means of a perylene cation radical prepared in concentrated sulfuric acid.

Results and Discussion

Temperature-dependent Line Broadening of the ^{19}F Splittings. The high-resolution ESR spectrum of the 4,4′-difluorobiphenyl cation radical was observed in the temperature range from −90 to +20 °C. The spectrum observed at +10 °C is shown in Fig. 1-a. This spectrum consists of a large triplet of 19.20 G due to two ^{19}F nuclei (a_F), each line of which splits into a quintet of 2.76 G due to the four ring ortho-protons (a^H_2)[8]; the central component ($I_z=0$ lines) of the triplet further splits, by means of the second-order effect, into a doublet of 250 mG corresponding to the possible values ($I=1$, 0) of the resultant nuclear angular momentum for the two

* A Part of this work has been previously pulbished as a communication: F. Nemoto, F. Shimoda, and K. Ishizu, *Chem. Lett.*, **1975**, 567.

** Present address: Department of Chemistry, Faculty of Science, Hiroshima University, Hiroshima 730.

equivalent ^{19}F nuclei. As is well known, the second-order splitting of the $I_z=0$ component of the first-order triplet is $(a_F)^2/H_0$, where H_0 is the position of the center of the spectrum.[6] The expected value of $(a_F)^2/H_0$ is about 100 mG, taking $a_F=19.20$ and $H_0=3300$ G, but the observed splitting is larger than that theoretically expected. This is probably due to the line broadening attributed to the modulation of the ^{19}F anisotropic hyperfine interactions as a result of the tumbling motion, which makes the accurate measurement of the hyperfine splittings difficult.

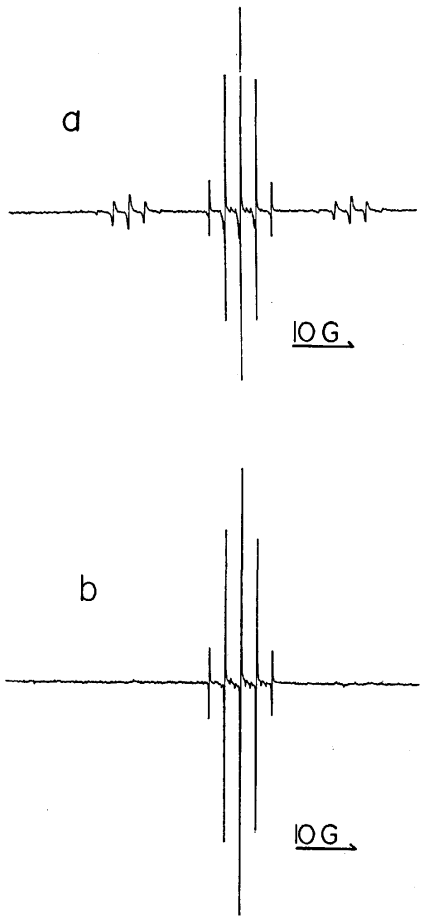

Fig. 1. The ESR spectra of 4,4'-difluorobiphenyl cation radical. a) +10 °C. b) −80 °C.

Upon a lowering of the temperature, the wing lines of the triplet due to the two ^{19}F, and the downfield second-order components ($I=1$, $I_z=0$) become broad and finally disappear, while the central quintet ($I=0$ lines) is unaffected, as is shown in Fig. 1-b.

For organic radicals in solution, it is well known[1-3] that the line width variations in the various second-order components are mainly due to a relaxation process brought about by the modulation of the anisotropic hyperfine coupling tensor by rotational Brownian motion; this theory is well established.[4,5]

The dipolar contribution to the line width of the (I, I_z) hyperfine components can be calculated as a function of the molecular rotational correlation time τ_2, using a spin Hamiltonian for a system undergoing dipolar relaxation.

Assuming a set of completely equivalent ^{19}F nuclei with an axially symmetric hyperfine tensor, the main term of the dipolar contribution to the line width is given by:[4,5]

$$T_{2d}^{-1} = \frac{A_{//}^2}{40}[(3I(I+1)+5I_z^2)J_0+(7I(I+1)-I_z^2)J_1] \quad (3)$$

where $J_0=\tau_2$, $J_1=\tau_2(1+\omega^2\tau_2^2)^{-1}$, and $A_{//}$ is the parallel component of the anisotropic part of the hyperfine tensor. From the line widths of the $I_z=\pm1$ lines, the correlation times, τ_2, are estimated using Lorentzians with line widths given by:

$$[T_2(I, I_z)]^{-1} = [T_{2d}(I, I_z)]^{-1} + T_{20}^{-1} \quad (4)$$

where T_{20} accounts for the other relaxation processes and T_{20}^{-1} is assumed to be 80 mG. The experimental value of $A_{//}$ is not known for the cation radical of 4,4'-difluorobiphenyl. Therefore, the estimation of $A_{//}$ was performed in the following way.

The anisotropic component of the ^{19}F hyperfine tensor for a $\rangle$C–F fragment may be described by the following equation[9,23]:

$$\boldsymbol{B}_F = \boldsymbol{B}_C^\pi\rho_C^\pi + \boldsymbol{B}_F^\pi\rho_F^\pi + \boldsymbol{B}_F^\sigma\rho_F^\sigma \quad (5)$$

where $\boldsymbol{B}_C^\pi$, $\boldsymbol{B}_F^\pi$, and $\boldsymbol{B}_F^\sigma$ are the anisotropic tensors due to the interaction of a fluorine nucleus with carbon $2p_\pi(\rho_C^\pi=1)$, fluorine $2p_\pi(\rho_F^\pi=1)$, and fluorine $2p_\sigma(\rho_F^\sigma=1)$ electrons respectively. The principal values of $\boldsymbol{B}_C^\pi$ and $\boldsymbol{B}_F^\pi$ have been calculated by Cook *et al.*[9] and Morton *et al.*[24] respectively. According to Iwasaki *et al.*,[23] Eq. 5 may be represented in this form:

$$\boldsymbol{B}_F = (\boldsymbol{B}_C^\pi+\boldsymbol{Q}_{CF}^F)\rho_C^\pi + (\boldsymbol{B}_F^\pi+\boldsymbol{Q}_{CF}^F)\rho_F^\pi \quad (6)$$

where $\boldsymbol{Q}_{CF}^F$ and $\boldsymbol{Q}_{FC}^F$ are the tensor polarization factors of the $F_{2p\sigma}$ electrons arising from the unit spin density in C_{2p_π} and F_{2p_π} respectively, and where the parameters, $\boldsymbol{Q}_{CF}^F$ and $\boldsymbol{Q}_{FC}^F$, have been experimentally determined.

Using Eq. 6, the value of $A_{//}$ in Eq. 4 was estimated to be 41 G based on the spin densities, ρ_C^π and ρ_F^π, determined from the ^{13}C hyperfine splittings for the ring carbons (see Table 2 and the following section). The values of τ_2 obtained are 1.5×10^{-10} s at −60 °C and 0.8×10^{-10} s at +10 °C. These correlation times are typical of those found for similar molecules in liquids by a study of the relaxation mechanism of ENDOR.[10]

Estimate of Q Values. As is shown in Fig. 2, four kinds of ^{13}C hyperfine splitting were recorded. The absolute values of these hyperfine coupling constants are much like those of the ring carbon atoms of the 4,4'-bitolyl cation radical, as has already been reported[7] (see Table 1). In previous works, it has been reported that the substitution of fluorine for hydrogen has little effect on the spin-density distribution.[9,11-14] The ^{13}C hyperfine coupling constants, therefore, can more easily be assigned than those of the 4,4'-bitolyl cation radical; $a_1^C=-0.78$, $a_2^C=1.90$, $a_3^C=-3.57$, and $a_4^C=6.92$ G. The experimental values of the ring spin densities were obtained from the ring proton hyperfine splittings, a_2^H, and the ^{13}C hyperfine splittings, a_1^C, based on the Colpa-Bolton[20] and the Karplus-Fraenkel[21] formulae:

$$a_1^H = Q_{CH}^H\rho_1^\pi + K_{CH}^H[\rho_1^\pi]^2 \quad (7)$$

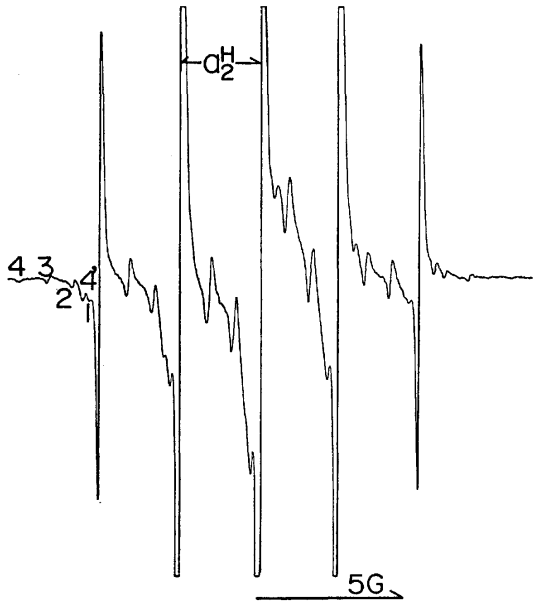

Fig. 2. The ^{13}C splitting of the ring carbon atoms of 4,4′-difluorobiphenyl cation radical. The figures denote the ring position.

$$a_1^C = (S^C + \sum_{k=1}^{3} Q^C_{C_1X_k})\rho_1^\pi + \sum_{k=1}^{3} Q^C_{X_kC_1}\rho_k^\pi \quad (8)$$

The parameters in Eq. 7 were taken as $Q^H_{CH}=-27$ and $K^H_{CH}=-12$ G, while the parameters in Eq. 8 were taken as $S^C=-12.7$ G, $Q^C_{C_1X_k}(Q^C_{C_1H}=19.5$, $Q^C_{C_1C_k}=14.4$ G), and $Q^C_{C_1C_k}=-13.9$ G. The experimental values of the spin density are summarized in Table 2. Here, the fluorine spin densities were obtained by the normalization of the total spin density. For comparison, Hückel- and McLachlan-type calculations were carried out, taking the Coulomb integral and resonance integral to be $\alpha_F=\alpha_C+2.5\beta_C$ and $\beta_{CF}=0.62\beta_C$.[11] The results are summarized in Table 2. As may be seen in Table 2, the values of the spin densities for the 4,4′-difluorobiphenyl cation radical are nearly the same as those for the 4,4′-bitolyl cation radical, and the similarity in the spin densities on the ring carbon atoms shows that the substitution of fluorine for hydrogen does not produce a large perturbation in the overall spin densities.

The evaluation of Q^F_{CF} and $Q^F_{F(CF)}$ in Eq. 2 requires the values of ρ^π_C and ρ^π_F. Nevertheless, there have been few studies in which ρ^π_C and ρ^π_F were experimentally determined, and the simple LCAO MO approach to the estimation of ρ^π_F is not necessarily valid.

Recently Icli and Kreilick[12,13] experimentally determined the values of both ρ^π_C and ρ^π_F for a series of fluorinated phenoxyl radicals based on the measurement of the paramagnetic chemical shift in NMR; they also examined Eq. 2. For a series of fluorinated phenoxyl radicals, the ratios of ρ^π_C to ρ^π_F at the adjacent carbon are nearly constant (0.07). This situation is not feasible for determining the individual values of Q^F_{CF} and $Q^F_{F(FC)}$, because two sets of data on ρ^π_F and ρ^π_C with very different ratios (ρ^π_F/ρ^π_C) should be chosen for obtaining accurate Q values.

On the other hand, for the 4,4′-difluorobiphenyl cation radical the ratio of ρ^π_F to ρ^π_C at the adjacent carbon is much larger (0.27) than those for other fluorinated aromatic radicals, and this situation is very favorable for estimating the values of Q^F_{CF} and $Q^F_{F(FC)}$ accurately. The estimation of the values of Q's was carried out using a_F and the spin densities, ρ^π_C and ρ^π_F, obtained for the 4,4′-difluorobiphenyl cation, together with those for the 4-(*p*-fluorophenyl)-2,6-di-*t*-butylphenoxyl radical.[13] The estimated values of the parameters are $Q^F_{F(FC)}=324$ and $Q^F_{CF}=39$ G.

In order to examine the validity of our parameters, we applied the present Q values to the fluorine coupling constants of several compounds previously studied. In Table 3, the experimental and calculated fluorine coupling constants are summarized. We found that our two-parameter equation, $a_F=324\rho^\pi_F+39\rho^\pi_C$, gives a consistent explanation in every case.

Based on the experimental finding that fluorine substitution has little effect on the ring spin densities except for the at the adjacent carbon,[9,11-14] we assumed that the original spin density, ρ^0_C, on the carbon atom in the parent molecule is shared by the carbon atom and the fluorine atom;

$$\rho^\pi_C + \rho^\pi_F = \rho^0_C \quad (9)$$

By substituting Eq. 9 into Eq. 2, we obtain:

$$a_F = [(Q^F_{F(FC)}-Q^F_{CF})K+Q^F_{CF}]\rho^0_C = Q_{eff}\rho^0_C \quad (10)$$

Table 1. The observed values of the proton and ^{13}C hyperfine coupling constants (G)

		a^H_2	a^H_3	$a^F_4(a^{CH_3}_4)$	a^C_1	a^C_2	a^C_3	a^C_4
4,4′-Difluorobiphenyl	Cation	2.76	—	19.20	−0.78	1.90	−3.57	6.92
	Anion[22]	2.28	—	3.13				
4,4′-Bitolyl	Cation[7]	2.64	—	8.79[a]	—	1.83	−3.59	8.47

a) Methyl proton hyperfine coupling constant.

Table 2. Experimental and theoretical spin densities

Position		1	2	3	4	F
4,4′-Difluorobiphenyl cation	Exptl	0.1171	0.0980	−0.0028	0.1517 (0.1925)[a]	0.0408
Hückel		0.1190	0.0800	0.0269	0.1514	0.0167
McLachlan	$\lambda=1.2$	0.1265	0.0905	−0.0108	0.1975	0.0165
4,4′-Bitolyl cation[7]	Exptl	—	0.0939	0.0172	0.1945	

a) This value is the sum of the $\rho_4{}^\pi$ and $\rho_F{}^\pi$ values experimentally determined.

Table 3. Carbon and fluorine spin densities and calculated and experimenal fluorine coupling constants

	$\rho_C^\pi \times 10^2$	$\rho_F^\pi \times 10^3$	$\left(\frac{\rho_F^\pi}{\rho_C^\pi}\right) \times 10^2$	a_F (G) Exptl	a_F (G) Calcd	Lit
4,4'-Difluorobiphenyl	15.17	40.08	26.9	19.20	19.14	55)
I	−2.45	−1.70	7.0	−1.42	−1.48	13)
II	7.11	5.28	7.4	4.45	4.48	
A	3.64	2.23	6.1	1.66	2.14	12)
B	−1.77	−1.68	9.5	−1.11	−1.23	
C	5.31	4.61	8.6	3.60	3.56	

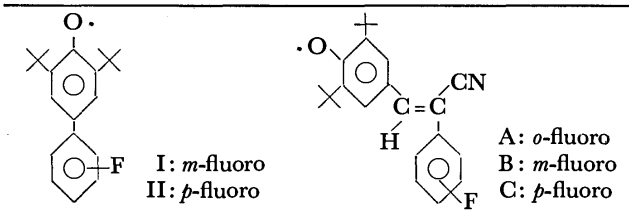

where K is the ratio of ρ_F^π to ρ_C^0 and $Q_{eff}=(285K+39)$ G, using our estimated values. This equation corresponds to Eq. 1.

In respect of Eq. 1, many investigators have reported that the experimentally or semiempirically determined values of Q are scattered over a wide range from molecule to molecule.[11-23] This is not surprising, because the K ratio is certainly not a constant for different molecules. Perhaps the K ratio depends on the double-bond character of the C–F bond, as has previously been proposed by Eaton *et al.*[11] For example, the fluorine hyperfine coupling constant of the 4,4'-difluorobiphenyl cation radical is about six times as large as that of the 4,4'-difluorobiphenyl anion radical,[22] but the spin densities of the anion and cation, based on the LCAO MO calculations, are nearly identical with each other. These results are analogous to the case of the hyperconjugation of the methyl group (see Tables 1 and 2). We can, therefore, consider that the value of Q_{eff} in Eq. 10 is related to the degrees of π-conjugation between the $2p_z$ orbital of fluorine atom and the $2p_z$ orbital of carbon which is adjacent to fluorine. That is, the large value of Q_{eff} represents the strong conjugation of the π system on the C–F fragment. As a result of this strong conjugation, the spin density on the fluorine atom and the K ratio increase. Indeed, the estimated value of Q_{eff} for the 4,4'-difluorobiphenyl cation is very large (100 G), and the corresponding K value reaches 0.21.

The numerical calculations were carried out mainly at the Computing Center of Ehime University.

References

1) J. Cooper, A. Hudson, R. A. Jackson, and M. Townson, *Mol. Phys.*, **23**, 1155 (1972).
2) P. Meakin and P. J. Krusic, *J. Am. Chem. Soc.*, **95**, 8186 (1973).
3) K. S. Chen, P. J. Krusic, P. Meakin, and J. K. Kochi, *J. Phys. Chem.*, **78**, 2014 (1974).
4) J. H. Freed and G. K. Fraenkel, *J. Chem. Phys.*, **39**, 326 (1963).
5) A. D. McLachlan, *Proc. R. Soc. London, Ser. A.*, **280**, 271 (1964).
6) R. W. Fessenden, *J. Chem. Phys.*, **37**, 747 (1962).
7) K. Ishizu, M. Ouchi, F. Nemoto, and M. Suga, *Bull. Chem. Soc. Jpn.*, **46**, 2932 (1973).
8) P. H. Fisher and H. Zimmerman, *Tetrahedron Lett.*, **1969**, 797; M. J. Shaw, J. A. Weil, H. H. Hyman, and R. Filler, *J. Am. Chem. Soc.*, **92**, 5096 (1970).
9) R. J. Cook, J. R. Rowlands, and D. H. Whiffen, *Mol. Phys.*, **7**, 31 (1963).
10) K. Ishizu, M. Ohnishi, and H. Shikata, *Bull. Chem. Soc. Jpn.*, **50** 76 (1977).
11) D. R. Eaton, A. D. Josey, W. D. Phillips, and E. Benson, *Mol. Phys.*, **5**, 407 (1962).
12) W. G. Esperson and R. W. Kreilick, *Mol. Phys.*, **16**, 577 (1969).
13) S. Icli and R. W. Kreilick, *J. Phys. Chem.*, **75**, 3462 (1971).
14) S. V. Kulkarni and C. Trapp, *J. Am. Chem. Soc.*, **92**, 4801 (1970).
15) H. Konishi and K. Morokuma, *J. Am. Chem. Soc.*, **94**, 5603 (1972).
16) J. Sinclair and D. Kivelson, *J. Am. Chem. Soc.*, **90**, 5074 (1968).
17) A. Carrington, A. Hudson, and H. C. Longuet-Higgins, *Mol. Phys.*, **9**, 377 (1965).
18) W. E. Geiger, Jr. and W. M. Gulick, Jr., *J. Am. Chem. Soc.*, **91**, 4657 (1969).
19) W. R. Knolle and J. B. Bolton, *J. Am. Chem. Soc.*, **91**, 5411 (1969).
20) J. P. Colpa and J. R. Bolton, *Mol. Phys.*, **6**, 273 (1963).
21) M. Karplus and G. K. Fraenkel, *J. Chem. Phys.*, **35**, 1312 (1961).
22) A. L. Allred and L. W. Bush, *Tetrahedron*, **24**, 6883 (1968).
23) M. Iwasaki, S. Noda, and K. Toriyama, *Mol. Phys.*, **18**, 201 (1970).
24) J. R. Morton, J. R. Rowlands, and D. H. Whiffen, *Circ. Nat. Phys. Lab.*, No. BPR13 (1962).

Infrared Studies on Water Adsorption Systems with the Use of HDO. I. Molecular Sieves 13X and 4A

Masao HINO

Government Industrial Development Laboratory, Hokkaido, Higashi-Tsukisamu, Toyohira-ku, Sapporo 061-01

(Received July 12, 1976)

It was shown that the use of HDO molecules in IR studies on water adsorption system is advantageous for obtaining information as to whether 1) a band arises from the surface structural hydroxyl groups or from adsorbed water molecules, 2) a band arises from an overtone bending vibration, and 3) water molecules are adsorbed in a state of its two hydroxyl bonds being equivalent. The bands in the spectra of Molecular sieves–H_2O systems were assigned as follows. I) 13X–H_2O system. Bands at 3752, 3685, and 3647 cm^{-1} correspond to surface structural OH, bands at 3697, 3360, and 1650 cm^{-1} to asymmetrically adsorbed water molecules, band at 3230 cm^{-1} to overtone bending vibration of the same molecules. The band at 3590 cm^{-1} was found to arise from some other type of adsorbed water molecules. II) 4A–H_2O system. Bands at 3500, 3400, and 1660 cm^{-1} correspond to symmetrically adsorbed water molecules, band at 3280 cm^{-1} to overtone bending vibration of the same molecules. Another type of adsorbed water was suggested to be present.

Infrared spectroscopy has been widely employed in studies on surface and adsorbed species. However, analysis of the spectra has not always been easy to carry out. This is due to inevitable characteristics of the spectra of adsorption systems, such as the specific complexity of the spectra and the lack of means of spectral observation over a wide frequency range masked by strong absorption by adsorbents.

Thus, additional information from other sources is desirable. As an example, the use of partially deuterated compounds is considered to be effective. The use of this technique has been made for the spectral study on adsorption systems to some extent.[1] A number of investigations have been carried out on water adsorption systems. However, they were restricted to the measurement of the spectra of H_2O or D_2O adsorption systems. No work seems to have been made with the use of HDO.

In the present work, IR absorption spectra of hydroxyls and adsorbed water on Molecular sieves 13X and 4A are analyzed by the use of HDO. Although assignments of the spectral bands of these systems have been made to a certain extent,[2–14] more direct and conclusive evidences for the assignments are obtained by the use of the present technique.

Its applicability to other molecular adsorption systems will be suggested.

Experimental

Materials. Linde molecular sieves 13X and 4A (GASUKURO Ind. Co., Ltd.) were used. The crystallinity and purity of these materials were confirmed to be of a sufficiently high by X-ray diffraction analysis. The surface area of the 13X sieve was 717 m^2/g. In order to obtain extremely fine powder samples for IR experiments, the materials were ground in an agate motor with a small amount of water, and then suspended in deionized water. The particle size of the fine powders was found to be less than 1 μm in diameter by electron microscopic observation. D_2O (E. Merck, Darmstadt) of 99.75% in purity and deionized-distilled H_2O were used for IR experiments after being degassed.

Apparatus and Procedure. A JASCO Model 402-G IR spectrophotometer and a Pyrex glass cell were used for recording the spectra. The cell was essentially similar to that designed by Angell *et al.*[6] In order to prevent the contamination of the sample pieces by grease vapor, a Teflon greaseless valve was fixed directly to the top of the cell. The exchange of sample pieces was made by cutting and re-fixing the arm part of the cell.

The sample powders were pressed into disks under a pressure of 2.5 tons/cm^2, and then the disks were cut into pieces of 1×2 to 2.5 cm to fit the cell windows. The "thickness" was 12—80 mg/cm^2.

After the sample pieces had been set in the cell, they were evacuated at 500 °C for at least 3 h prior to experiments. Before the addition of each type of sample water for IR measurements, the surface of the sample as well as the inner wall of the cell were washed by the following procedure. The sample was exposed at room temperature to the saturated sample water vapor, and then pumped out at 180—200 °C for 10 min. This procedure was repeated five times. Finally, it was evacuated at 500 °C for 3 h. Spectral observation confirmed that the washing was sufficient. In the case of measurements of H_2O-adsorbent systems on a new sample piece, washing was omitted.

The experiments related to HDO were carried out in the presence of H_2O and D_2O. By mixing H_2O with D_2O at a molar ratio of a to b, HDO is obtained under the coexistence of other water in a ratio of about H_2O: HDO: $D_2O=a^2$: $2ab$: b^2.

All the spectra were measured at room temperature. Spectra on the desorption process were observed after the pretreated sample piece was first exposed to the saturated sample water vapor and then evacuated at various temperatures. Spectra on the adsorption process were measured by dosing small amounts of sample water at room temperature successively after the sample piece was evacuated at 500 °C.

The measurements were carried out mainly in the OD stretching region in place of the OH stretching region, since the former is not only higher in transparency but also flatter in background owing to the lack of weak absorption bands arising from the water vapor in the air.

Results

13X–Water System. D_2O, H_2O Systems: The spectra of 13X–D_2O and H_2O systems were measured for a comparison of the results with those of the HDO system (Figs. 1 and 2). The spectra observed were similar to those published.[17] On evacuation at 90 °C six absorption bands were observed at 2756, 2727, 2682, 2645, 2470, and 2395 cm^{-1} in the D_2O system, (these

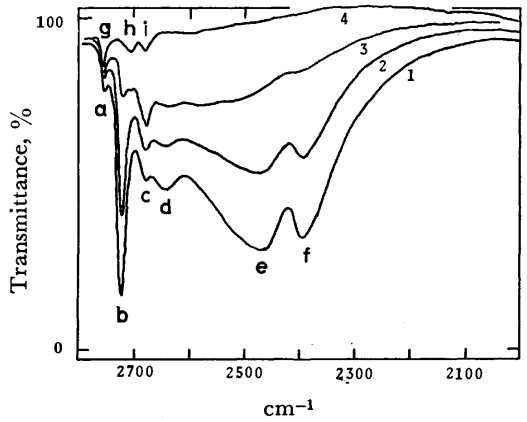

Fig. 1. Spectra of 13 X–D_2O system.
Evacuated for (1) 1 h at 90 °C, (2) 1 h at 120 °C, (3) 20 min at 170 °C, (4) 2 h at 500 °C. "Thickness" of the sample piece was 12 mg/cm².

bands as well as the corresponding bands in other systems will be referred to as a, b, c, d, e, and f). In the H_2O system the six bands corresponding to those in D_2O system were at 3752, 3697, 3645, 3590, *ca.* 3360, and 3230 cm^{-1}. In the latter system a single HOH bending vibration band was observed at 1650 cm^{-1}. Elevation of the evacuation temperature gave rise to a decrease in the intensity of all these bands except for a and c. After the final evacuation at 500 °C, three sharp bands remained at 2756, 2708, and 2683 cm^{-1} in the D_2O system (referred to as g, h, and i, respectively), and in the H_2O system at 3752, 3685, 3647 cm^{-1}.

HDO System: The spectra in OD stretching and bending regions are shown in Fig. 3. In this experiment, an H_2O–D_2O mixture in the ratio 3 to 1 was used except for curve 5, the contents being H_2O 56.3%, HDO 37.5% and D_2O 6.3%. In the number of OD chemical bond, the 75% belongs to HDO and the rest to D_2O. The OH stretching region of this system (Fig. 4) was measured employing another mixture in the ratio H_2O: D_2O = 1 : 5. The spectra of OD and OH stretching regions of this system were compared with those of D_2O and H_2O systems, respectively. All the correlations

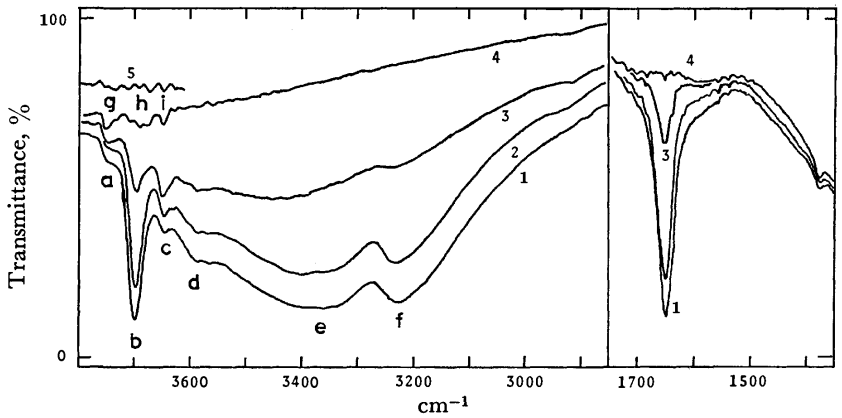

Fig. 2. Spectra of 13X–H_2O system.
Evacuated for (1) 1 h at 100 °C, (2) 1 h at 120 °C, (3) 25 min at 165 °C, (4) 2 h at 500 °C. (5) Empty cell.[16] Sample piece "thickness" 12 mg/cm².

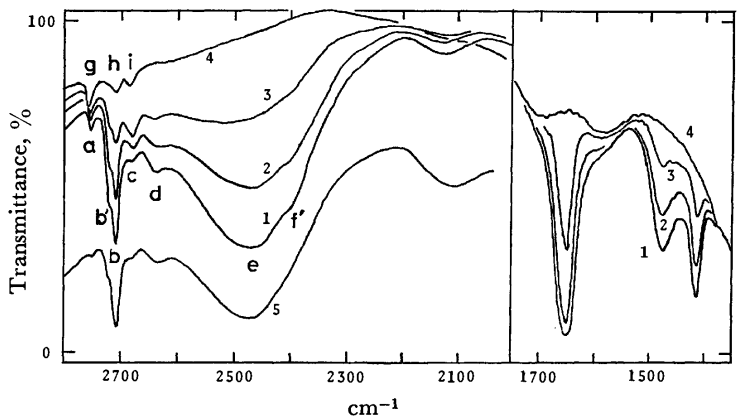

Fig. 3. Spectra of 13X–HDO system in the OD stretching and bending regions.
Evacuated for (1) 1 h at 95 °C, (2) 1 h at 120 °C, (3) 20 min at 165 °C, (4) 2 h at 500 °C after exposure to the vapor of H_2O–D_2O mixture of a molar ratio of 3 to 1, and (5) evacuated for 1 h at 90 °C after exposure to the vapor of H_2O–D_2O 7 to 1 mixture. Sample piece "thickness" 43 mg/cm².

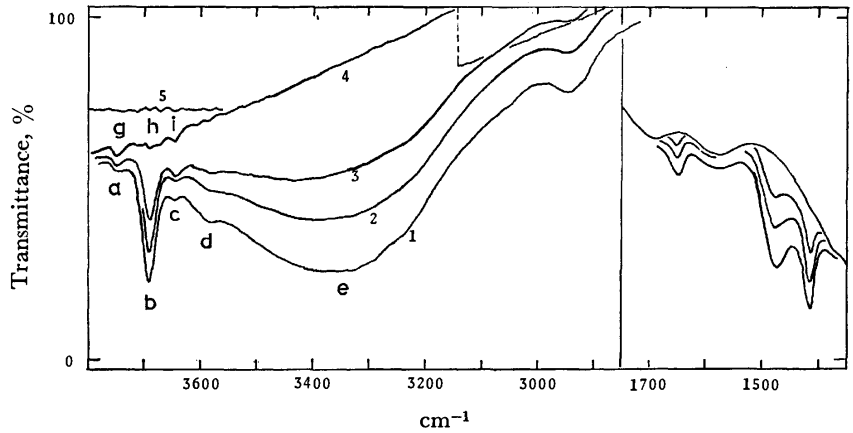

Fig. 4. Spectra of 13X–HDO system in the OH stretching and bending regions. Evacuated for (1) 1 h at 95 °C, (2) 1 h at 120 °C, (3) 20 min at 165 °C, (4) 3 h at 500 °C after exposure to the vapor of H_2O–D_2O 1 to 5 mixture. (5) Empty cell. Sample piece "thickness" 38 mg/cm².

between the spectra in the OH stretching region of HDO system and those of H_2O system were analogous to those between the spectra in the OD stretching region of the HDO system and those of D_2O system. The frequencies of the bands in OH stretching regions are parenthesized.

Bands a, c, and e in the spectra of HDO system appeared in the OD stretching region at 2756, 2680, and 2470 cm^{-1} (3750, 3645, *ca.* 3350 cm^{-1}) which were of nearly the same frequencies as those of the D_2O system. However, band b was observed at a distinctly different frequency from that of D_2O system, namely at 2710 cm^{-1} (3690 cm^{-1}). As for band d, even though the difference in frequency was not very great, *ca.* 7 cm^{-1}, the frequency 2638 cm^{-1} was not equal to that of the band in D_2O system. In the OH region, band d was so broad that the difference could not be detected decisively. It should be noted that no band f appeared in the spectra of this system. The fact that the shoulders at 2725 and 2395 cm^{-1} are due to the D_2O molecules contained in the mixed water as "impurity" was confirmed from another experiment, *viz.* the spectra after the adsorption of sample water followed by evacuation at 100 °C were measured in a series where the D content of the sample water was changed step by step from 0 to 100 atom %. The results showed that the intensities of both shoulders change in proportion to the D content. The spectrum in the OD stretching region obtained by the use of H_2O: D_2O=7.1: 1.0 mixed water is shown in Fig. 3, curve 5. A band somewhat broader and weaker appeared in both stretching regions, at 2945 cm^{-1} in the OH region and at 2120 cm^{-1} in the OD region. The weak absorption bands of g, h, and i were measured in the OD stretching region with a thick sample for the sake of comparison with those in D_2O system. The results showed that the three bands were exactly equal in wavenumber to those in D_2O system, and were 27% in intensity as compared with that of the latter which is almost equal to the D content, 25 atom %, of the mixed water used. In the bending vibration region, three absorption bands were observed at 1650, 1476, and 1415 cm^{-1}. The band at 1650 cm^{-1} is assigned to HOH bending vibration, because its frequency was quite the same as that of pure H_2O system and its intensity decreased with decrease of H_2O content in the mixed water (Figs. 3 and 4). Thus the other two arise from HDO.

The spectra measured on the adsorption process were almost the same as those on the desorption process. However, the intensity of the band d was so weak that the band was hardly observable on the adsorption process in the spectra of any of the systems.

4A-Water System. In this system the spectral measurements were carried out only on the adsorption process.

4A-D_2O, H_2O Systems: In the stretching region of the spectra of D_2O (H_2O) system (Figs. 5 and 6) three main bands were observed at 2578, 2515, and 2427 cm^{-1} (in H_2O system, at 3500, 3400, and 3280 cm^{-1}) and three weak bands at 2760, 2737, and 2645 cm^{-1} (in H_2O system, only the two former bands were detected at 3750 and 3715 cm^{-1}). In H_2O system one bending band was observed at 1660 cm^{-1}. These were similar to those reported by previous authors.[7,8]

4A-HDO System: The spectra obtained in the OD stretching and bending regions employing an H_2O–D_2O

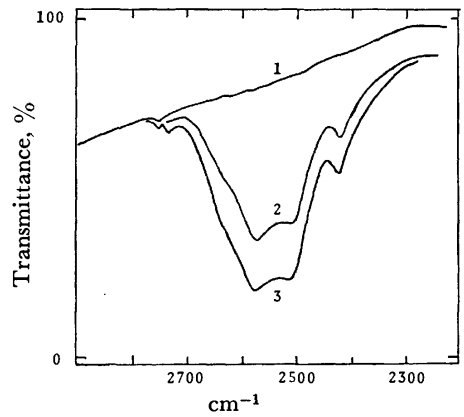

Fig. 5. Spectra of 4A–D_2O system.
(1) Evacuated for 3 h at 500 °C, (2) 9 μmol, (3) 18 μmol of D_2O readsorbed. Sample piece "thickness" 30 mg/cm².

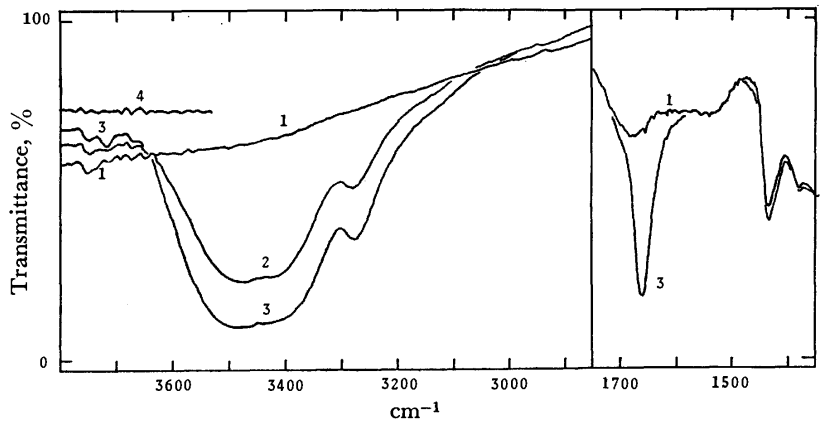

Fig. 6. Spectra of 4A–H_2O system.
(1) Evacuated for 3 h at 500 °C, (2) 9μmol, (3) 18 μmol of H_2O readsorbed.
(4) Empty cell. Sample piece "thickness" 15 mg/cm².

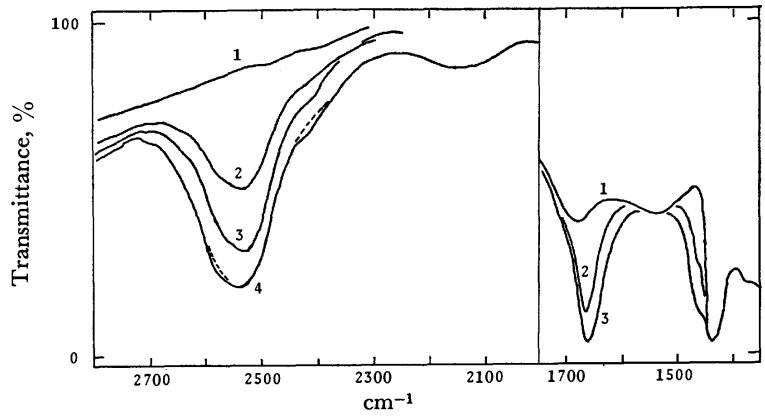

Fig. 7. Spectra of 4A–HDO system in the OD stretching and bending regions.
(1) Evacuated for 3 h at 500 °C, (2) 18 μmol, (3) 36 μmol, (4) 54 μmol of H_2O–D_2O 3 to 1 mixture were readsorbed. Sample piece "thickness" 30 mg/cm².

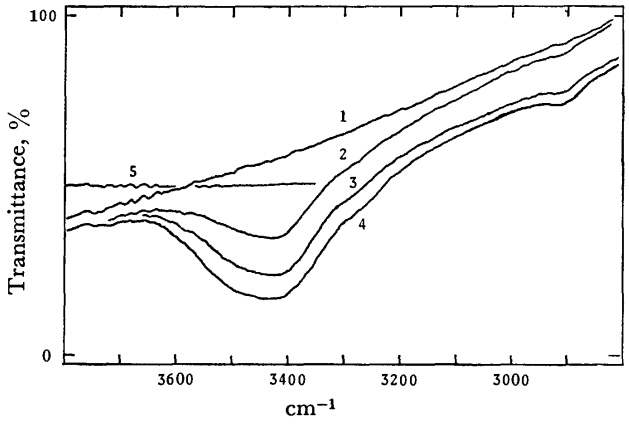

Fig. 8. Spectra of 4A–HDO system in the OH stretching region.
(1) Evacuated for 3 h at 500°C, (2) 18 μmol, (3) 36 μmol, (4) 54 μmol of H_2O–D_2O 1 to 5 mixture were readsorbed. (5) Empty cell. Sample piece "thickness" 30 mg/cm².

mixture in the ratio 3 to 1 and those in the OH stretching region employing another mixture in the ratio 1 to 5 are shown in Figs. 7 and 8, respectively. In each stretching region, a main single OD or OH stretching band of symmetric shape appeared at a frequency of 2530 or 3420 cm^{-1}. Their positions are located between two strong stretching bands appearing in the spectra of D_2O or H_2O system. A weak band was observed at 2705 cm^{-1} in the OD stretching region but not the fitting band in the OH region. As in the case of 13X-water system a new band was observed in each stretching region at 2140 cm^{-1} in the OD region and at 2910 cm^{-1} in OH region. Both bands at 2427 cm^{-1} in D_2O system and 3280 cm^{-1} in H_2O system disappeared from each corresponding region of the spectra of HDO system. Swellings around 2580, 2420 cm^{-1} (Fig. 7) and 3500, 3280 cm^{-1} (Fig. 8) arise obviously from D_2O or H_2O present in the water mixtures. Only one HOD bending band appeared at 1465 cm^{-1}. The 1660 cm^{-1} band corresponds to HOH bending vibration as previously described.

Table 1. Summary of the IR bands of molecular sieves–water systems

Band sign	D_2O system (cm^{-1})	H_2O system (cm^{-1})	HDO s-stem (cm^{-1}) Stretching regions OD	Stretching regions OH	Bending region	Assign
		[13X-water System]				
a (g)	2756	3752	2756	3750		1)
b	2727	3697	2710	3690		2)
c (i)	2682	3645	2680	3645		3)
d	2645	3590	2638	3590		4)
e	2470	3360	2470	3350		5)
f	2395	3230				6)
h	2708	3685	2708	3685		7)
				2945		8)
		2120				9)
		1650			1476, 1415	10)
b′			(2725)		(1650)	11)
f′			(2395)			11)
			(2120)			11)
		[4A-water System]				
	2760	3750				12)
	2737	3715	2705			13)
	2645					13)
	2578	3500	2530	3420		14)
	2515	3400				14)
	2427	3280				15)
				2910		16)
		1660			1465	17)
			(2580)	(3500)	(1660)	18)
			(2420)	(3280)		18)
			(2140)			18)

1), 3), 7), 12) OD(H) stretching of structural deuteroxyl groups. 2), 5), 10) Free OD(H) stretching, hydrogen-bonded OD(H) stretching and HOH (HOD) bending of asymmetrically adsorbed water (Type WX-I), respectively. 4), 13) OD(H) stretching of adsorbed water of Types WX-II and WA-II, respectively. 6), 15) DOD(HOH) overtone bending of Types WX-I and WA-I water, respectively. 8), 16) HOD overtone bending or combination of adsorbed HDO? 9) Combination of adsorbed H_2O. 11), 18) Arising from D_2O or H_2O impurities. 14) OD (H) stretching of symmetrically adsorbed water (Type WA-I). 17) HOH(HOD) bending of Type WA-I water.

The observed bands are summarized with their assignments in Table 1.

Discussion

13X-Water System. Discussion has been made as to whether various absorption bands, especially those of h, i, d, and b, arise from surface hydroxyl groups or from adsorbed water molecules.[15] The use of HDO gives more detailed information. If a band arises from the former, the wavenumbers of the corresponding two OH (or OD) vibration bands, one appearing in the H_2O (or D_2O) adsorption system and the other in the HDO adsorption system, should be exactly the same as each other, and if it arises from the latter the wave numbers would not be equal. Thus, the residual bands g, h, and i can be attributed to the stretching vibrations of surface hydroxyl groups, since their corresponding bands appear at the same frequency in the two systems. Bands a and c are also attributable to hydroxyl groups. They would be the same bands as g and i, respectively, because of equal frequency. However, the origin of band b differs from that of h. The fact that band b in HDO system appears in the OD stretching region at a frequency 16 cm^{-1} lower than that in D_2O system (as well as in the OH stretching region 7 cm^{-1} lower than that in H_2O system) indicates that the band does not arise from structural hydroxyl groups but from adsorbed water molecule. Band e is attributed to the OH stretching vibration of the water molecules hydrogen bonded to the surface. The absorption d was reported by Habgood,[5] Ward[9] and also by Kiselev *et al.*[12] However, no assignment was made. Only Uytterhoeven *et al.*[11] attributed the band to OH groups in ions of the type $Me^+(OH)$. However, the results in the present experiments indicate that its origin is not the structural OH groups but a certain type of adsorbed water molecule. Band f was considered by Ward[9] and Abramov *et al.*[14] to arise from the OH stretching of another type of water molecule adsorbed in a different way from the origin of band e. Kiselev *et al.*[12] attributed it to the overtone bending vibration of the water molecules, which are the origin of band e, enhanced by Fermi resonance. Our results support the assignment by Kiselev *et al.* The frequencies of the overtone bending vibrations of HDO would be near 2952 and 2830 cm^{-1} if they appear, since the fundamentals were observed at 1476 and 1415 cm^{-1}. However, since they differ a great deal from the frequency of any stretching vibration of HDO, no resonance would occur. Thus, if the band arises from the overtone bending vibration it would not appear in the spectra of HDO system, or would be only slightly observable at frequencies near 2952 and 2830 cm^{-1}. There is some uncertainty in the attribution of the observed 2945 cm^{-1} band to the overtone bending of HDO molecules. If we suppose that the 2945 cm^{-1} band is the overtone of 1476 cm^{-1} band, we cannot explain the reason why that of 1415 cm^{-1} band does not appear. However, at least the disappearance of band f from the spectra of HDO system is in line with the assignment by Kiselev *et al.* On the other hand, if Ward's assignment is accepted, no reason can be found for the disappearance of the band.

There were two bending vibrations in the adsorbed HDO molecules, but only one in adsorbed H_2O. This supports the schematic structure of water adsorption originally proposed by Bertsch and Habgood[3] (I). If the structure is adopted, the adsorbed HDO molecules would take either of the two forms onto the surface by equal chance as illustrated in (II)-a and (II)-b, then the adsorbed HDO molecules as well as the H_2O

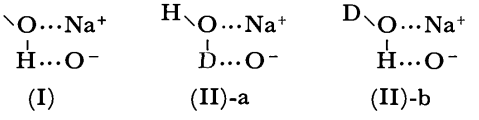

molecules should yield the bending vibrations in accordance with the observed results. This adsorption model also supports the experimental fact on the stretching vibration of the adsorbed molecules. There were two OH (OD) stretching vibration bands, one of free OH (OD, band b) and the other of hydrogen bonded OH (OD, band e), in both spectra of H_2O (D_2O) and HDO systems.

4A-Water System. First, the band at 3280 cm^{-1} in the spectra of H_2O system (at 2427 cm^{-1} in the D_2O system) is assigned to the overtone bending of adsorbed H_2O (D_2O) in the same manner as in the discussion on 13X-water system, although there remains some doubt in attributing the 2910 cm^{-1} band in HDO system to the overtone of 1465 cm^{-1} band in analogy of the case of 13X-water system. Then, the existence of two strong OH (OD) stretching bands, presumably corresponding to the ν_3 and ν_1 vibrations, and one bending band in the spectra of H_2O (D_2O) system suggests that there exists only one adsorbed species with two equivalent hydroxyl bonds. This is also supported by HDO adsorption experiment. If HDO molecule is adsorbed in this manner, OH, OD stretching bands and HOD bending band arising from the adsorbed molecule should all be single. This is in line with the observed results.

The weak bands at 2737 and 2645 cm^{-1} (Fig. 5) are possibly assigned to the ν_3 and ν_1 vibrations of another adsorbed D_2O molecule, which may fit the origin of the weak 2705 cm^{-1} band in HDO system (Fig. 7). However, the reason is not clear why the bands corresponding to them, except for at 3715 cm^{-1} in H_2O system, do not appear in the OH regions.

Bands at 2945, 2120 cm^{-1} in 13X-HDO System and at 2910, 2140 cm^{-1} in 4A-HDO System. The frequency ratios of each couple of bands, 1.39 and 1.36, seem to suggest that they arise from OH and OD stretching vibrations of HDO molecules adsorbed. However, these assignments contradict the fact that the frequencies are too low and no band corresponding to them could be detected in the spectra of H_2O or D_2O adsorption systems. In order to investigate the origin of these bands the spectra of pure H_2O, D_2O and mixtures of D_2O and H_2O were measured in liquid phase. The results show that there is a band at 2140 cm^{-1} in the spectrum of pure H_2O, its intensity decreasing with a decrease in H_2O content. No band around 2945—2910 cm^{-1} was detected in the spectrum of either pure H_2O or D_2O, but a band appeared in the spectra of mixed waters at 2920 cm^{-1}. Simultaneously, an HOD bending band was observed at 1450 cm^{-1} in the latter spectra. From a comparison of the spectra of liquid water with those of adsorption systems, the band at 2120 or 2140 cm^{-1} is considered to arise from a combination band of adsorbed H_2O molecules existing in the mixed water. The band at 2945 or 2910 cm^{-1} can be attributed to a overtone bending or a combination band of adsorbed HDO molecule.

The present technique is widely applicable to spectral analyses of adsorption systems including XH_n type molecules, with the use of partially deuterated $XH_{n-1}D$ or XHD_{n-1} molecules. It is applicable, in some cases, to the compounds including the atomic groups of $-XH_n$ type.

The author thanks Dr. Toshio Sato for his helpful advice and Mr. Okio Nishimura for his assistance in electron microscopic techniques.

References

1) For example: T. Nakata and S. Matsushita, *J. Phys. Chem.*, **72**, 458 (1968); R. J. Kokes, *Acc. Chem. Res.*, **6**, 226 (1973); B. A. Morrow, *J. Chem. Soc., Faraday Trans. 1*, **70**, 1527 (1974).
2) H. A. Szymanski, D. N. Stamires, and G. R. Lynch, *J. Opt. Soc. Am.*, **50**, 1323 (1960).
3) L. Bertsch and H. W. Habgood, *J. Phys. Chem.*, **67**, 1621 (1963).
4) L. Carter, P. J. Lucchesi, and D. J. Yates, *J. Phys. Chem.*, **68**, 1385 (1964).
5) H. W. Habgood, *J. Phys. Chem.*, **69**, 1764 (1965).
6) C. L. Angell and P. C. Schaffer, *J. Phys. Chem.*, **69**, 3463 (1965).
7) S. P. Zhdanov, A. V. Kiselev, V. I. Lygin, M. E. Ovsepyan, and T. I. Titova, *Zh. Fiz. Khim.*, **39**, 2554 (1965).
8) L. H. Little, A. V. Kiselev, and V. I. Lygin, "Infrared Spectra of Adsorbed Species," Academic Press, London & New York (1966), Chap. 14.
9) J. W. Ward, *J. Phys. Chem.*, **72**, 4211 (1968).
10) J. W. Ward, *J. Catal.*, **11**, 238 (1968).
11) J. B. Uytterhoeven, R. Schoonheydt, B. V. Liengme, and W. K. Hall, *J. Catal.*, **13**, 425 (1969).
12) A. V. Kiselev, V. I. Lygin, and R. V. Starodubceva, *J. Chem. Soc., Faraday Trans. 1*, **68**, 1793 (1972).
13) G. Senkyr and H. Noller, *J. Chem. Soc., Faraday Trans. 1*, **71**, 997 (1975).
14) V. N. Abramov, A. V. Kiselev, and V. I. Lygin, *Zh. Fiz. Khim.*, **39**, 123 (1965).
15) Refs. 3—6, 9, 10, 12.
16) The spectrum of the empty cell was measured in order to obtain an accurate background curve including many weak absorptions arising from the water vapor in the air. The background (curve 5) was substructed from the curve 4 for the sake of obtaining net spectrum.
17) Refs. 4, 5, 8, 9, 13.

Radiation-induced Phase Transformations in $NdNb_{1-x}V_xO_4$

Tadao KENJO and Seishi YAJIMA

The Oarai Branch, The Research Institute for Iron, Steel and Other Metals, Tohoku University, Oarai-machi, Ibaraki 311-13

(Received July 12, 1976)

When $NdNb_{1-x}V_xO_4$ compounds were exposed to a fast neutron dose of 6.6×10^{18} *nvt*, their monoclinic-tetragonal transition temperatures were lowered; particularly the transition temperature for the compound with $x=0.3$ was lowered to a temperature below room temperature. The lowering of the transition temperatures was greater for samples containing more V^{5+} ions. Although the present work does not fully reveal why neutron-irradiation lowers the transition temperature, it does show that neither the internal stress due to radiation damage nor the change in valency state of Nb^{5+} or Nd^{3+} lowers the transition temperature.

In previous work it was found that when the $YNbO_4$ compounds containing various impurities were exposed to a fast-neutron dose, the monoclinic $YNbO_4$ lattice approached a tetragonal structure; the *a*/*c* ratio of the monoclinic lattice became closer to unity.[1] This radiation-induced structural change can be explained as being due to (1) the presence of the high-temperature phase (tetragonal form) which is formed by quenching by the thermal spike mechanism, or (2) a lowering of the transition temperature (T_t), as will be described in more detail in a later section. One can expect no changes in T_t from (1), while a lowering of T_t can be expected from (2). Therefore, a measurement of T_t for the irradiated samples would determine which explanation is valid. In previous work, however, the T_t of the irradiated samples could not be measured without recovery of the damage due to radiation because this process begins at a temperature below T_t. This work employed the doping method in order to lower T_t to a temperature below the recovery temperature. Vanadium oxide (V_2O_5) was chosen as a dopant which may lower the T_t of $LnNbO_4$ (Ln=a rare earth) for the reasons described below. (1) Vanadium belongs to the same family of the periodic table as niobium and thus their chemical properties are similar so that the substitution of Nb^{5+} by V^{5+} can be expected to be efficient. (2) The ABO_4 scheelite-type oxides appear to form a tetragonal structure when the ionic potential (Z/r, Z=ionic charge, r=ionic radius) of ions at the A site is small and that at the B site is great, *e.g.*, for $CaWO_4$, $BaMoO_4$ and $NaIO_4$,[2] while they appear to be distorted to a monoclinic structure in the opposite case, *e.g.*, for $LnNbO_4$ and $LnTaO_4$.[2,3] The V^{5+} dopant (Z/r of $Nb^{5+}=7.25$, Z/r of $V^{5+}=8.47$) enhances the mean ionic potential of the Nb^{5+} sites so that, for the above-mentioned reason, V^{5+} can be expected to stabilize the tetragonal structure of $LnNbO_4$ in such a way that the more V^{5+} ions that the $LnNbO_4$ samples contain, the greater will be the T_t lowering.

Neodymium was used as Ln because the T_t of $NdNbO_4$ is one of the lowest of the $LnNbO_4$ family[4] and because it is induced to only a weak radioactivity upon reactor irradiation.

Experimental

Samples were prepared by the usual ceramic technique, as described previously.[1] The oxide mixtures were milled in a mortar and pressed into $15\phi\times3$ mm pellets, which were then heated to 1400 °C in air for 15 h. The samples thus obtained were irradiated in the JMTR (Japan Material Testing Reactor) at a temperature of 150 °C by a fast-neutron flux ($E>1$ MeV) of 1.9×10^{13} *nv* for 4 days, for a total flux of 6.6×10^{18} *nvt*.

The lattice parameters of the irradiated and non-irradiated samples were calculated using the data obtained from X-ray powder patterns using KCl as an internal standard. Since no DTA peaks for the phase transformation were observed, a high-temperature X-ray diffractometer was used for the measurements of T_t.

The magnetic susceptibility was measured using a Gouy balance.

Results and Discussion

The crystal structure of V_2O_5-doped $NdNbO_4$ compounds was identified as a monoclinic-distorted scheelite structure; the X-ray diffraction powder patterns could be indexed according to the known data for monoclinic

Table 1. Lattice parameter changes due to neutron irradiation of $NdNb_{1-x}V_xO_4$ (v=unit cell volume)

x	irr./ nonirr.	Temp	a(Å)	b(Å)	c(Å)	sinβ	a/c	v(Å^3)
0.1	nonirr.	R.T.	5.441	11.333	5.157	0.9979	1.0551	317.29
	irr.	R.T.	5.431	11.331	5.169	0.9982	1.0507	317.49
0.2	nonirr.	R.T.	5.391	11.377	5.172	0.9988	1.0423	316.83
	irr.	R.T.	5.378	11.383	5.195	0.9991	1.0352	317.74
0.3	nonirr.	R.T.	5.346	11.416	5.193	0.9994	1.0295	316.73
	irr.	R.T.	5.276	11.423	5.276	1	1	317.97
	irr.	liq. N_2	5.354	11.383	5.181	0.9995	1.0335	315.55
	irr.	0 °C	5.31	11.42	5.25	0.9999	1.010	318

$LnNbO_4$ structures.[4] Table 1 gives the lattice parameters for the irradiated (irr.) and non-irradiated (nonirr.) $NdNb_{1-x}V_xO_4$ samples. Since the dependence of the lattice parameters of the non-irradiated samples on the V_2O_5 concentration is smooth, the V_2O_5-doped $NdNbO_4$ samples can be regarded as solid solutions. The reduction in the unit cell volume with increasing V_2O_5 content is reasonable because V^{5+} is smaller than Nb^{5+}.

Table 1 indicates that the $NdNb_{1-x}V_xO_4$ compounds approach tetragonal structures (the compound with $x=0.3$ becomes tetragonal) when they are irradiated; a/c and $\sin\beta$ become closer to unity (these parameters become unity for $x=0.3$) with increasing irradiation. These lattice parameter changes due to irradiation can be explained as being due to (1) the presence of the high-temperature phase formed by the thermal spike mechanism, or (2) a lowering of T_t, as mentioned above. The problem to be solved is to determine which explanation is valid.

In the thermal spike process, small regions of the solid are heated for a very short time and followed by very rapid cooling. If the heating process raises the local temperature high enough for transformation to a high-temperature form, the thermal-spiked areas maintain the high-temperature structure, at least when the local temperature is higher than T_t. The high-temperature phase thus formed is quenched as a metastable phase if the cooling rate of the thermal-spiked regions is so high that the high-temperature structure formed cannot return to the low-temperature structure. Due to this thermal spike process the samples irradiated thus consist of a quenching-formed high-temperature phase and an unchanged low-temperature phase and the fractional portion of the former phase present increases with increasing irradiation dose.[3] The thermal-spiked region is expected to be a sphere of approximately a few tens of Å in diameter and the X-ray diffraction patterns for the high-temperature phase thus formed cannot be separated from those for the low-temperature phase, that is, the lattice parameters in this case denote mean values of the above two phases. The presence of the tetragonal structure thus formed renders the mean values of a/c and $\sin\beta$ closer to unity. This is observed in the case of $x=0.1$ and 0.2 (Table 1). When the whole region of the solid has been covered with rapidly-quenched high-temperature phase islands, the radiation-induced phase transformation is completed. This is the case for $x=0.3$. Thus, as far as the lattice parameters at room temperature are concerned, the thermal spike mechanism explains the radiation-induced structural changes in $NdNb_{1-x}V_xO_4$.

The radiation-induced structural changes can also be explained as being due to a lowering of T_t. The values of a/c and $\sin\beta$ for $LnNbO_4$ approach unity with increasing temperature and become unity at T_t, where the $LnNbO_4$ transforms from monoclinic to tetragonal form.[1,3] Therefore, if the T_t of $NdNb_{1-x}V_xO_4$ is lowered due to the irradiation, the a/c and $\sin\beta$ values at room temperature become closer to unity. This is the case for $x=0.1$ and 0.2. If T_t is lowered due to the irradiation to a temperature below room temperature, the crystal structure at room temperature is tetragonal. This is the case for $x=0.3$.

If the lattice parameter changes due to irradiation are ascribable to the fractional portion of the tetragonal phase formed by process (1), the transition temperature is unchanged upon irradiation because the process (1) does not change the T_t for the monoclinic phase and because the tetragonal phase formed by the rapidly-quenching process does not contribute to the T_t shift. On the other hand, if the lattice parameter changes are due to a lowering of T_t, the transition temperature is lowered by the irradiation. Therefore, measuring the T_t of the irradiated samples determines which explanation is valid.

The irradiated $NdNb_{0.7}V_{0.3}O_4$ sample has a tetragonal structure. If the tetragonal structure is ascribed to the thermal spike process, then when the irradiated $NdNb_{0.7}V_{0.3}O_4$ sample is cooled it maintains its tetragonal structure at any temperature below room temperature. On the other hand, if this structure is the result of the lowering of T_t to a temperature below room temperature, the tetragonal form is transformed into a monoclinic structure when the irradiated sample is cooled to a temperature that is lower than T_t but still high enough for the transformation rate. As is shown in the last line of Table 1, the values of $\sin\beta$ and a/c at 0 °C show small deviations from unity, or a slight distortion to the monoclinic form. The values at liquid N_2 temperature (the next to the last line in the same table) show greater deviations from unity. These findings indicate that the tetragonal structure in the irradiated $NdNb_{0.7}V_{0.3}O_4$ sample is due to a lowering of T_t to a temperature below room temperature, that is, explanation (2) is valid.

Figure 1 gives the temperature dependence of the lattice parameters for both irradiated (○) and non-irradiated (●) $NdNb_{0.8}V_{0.2}O_4$. From the figure, the T_t for the irradiated sample is found to be ≈290 °C and that the non-irradiated sample to be ≈330 °C.

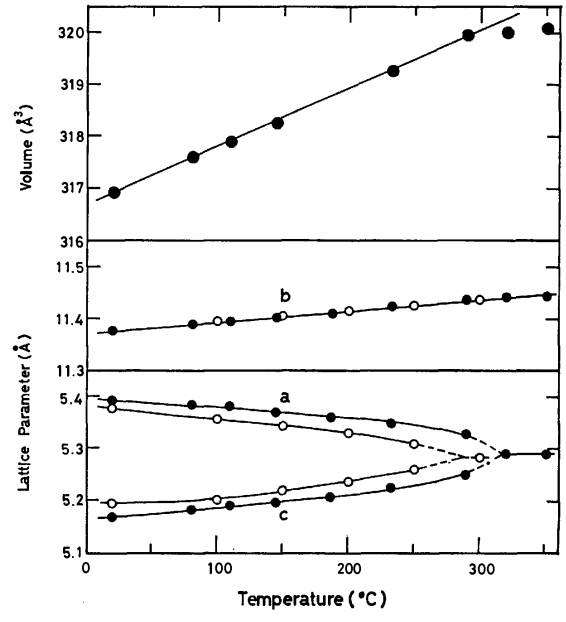

Fig. 1. Temperature dependence of lattice parameters of $NdNb_{0.8}V_{0.2}O_4$.
●: Non-irradiated, ○: irradiated.

TABLE 2. TRANSITION TEMPERATURES (T_t) FOR IRRADIATED AND NON-IRRADIATED $NdNb_{1-x}V_xO_4$

x	irr./nonirr.	T_t(°C)
0.1	nonirr.	520
	irr.	≈510
0.2	nonirr.	330
	irr.	290
0.3	nonirr.	170
	irr.	20

This indicates that the radiation-induced lattice distortion in $NdNb_{0.8}V_{0.2}O_4$ is also due to a lowering of T_t. Similarly, the high-temperature X-ray diffraction data indicate that the T_t of the $NdNb_{0.9}V_{0.1}O_4$ sample is also lowered upon irradiation, although the data are not given. Table 2 summarized the results of T_t for the irradiated and non-irradiated $NdNb_{1-x}V_xO_4$ samples, indicating that their transition temperatures are lowered when they are irradiated. Thus, it has been shown that the radiation-induced structural changes in $NdNb_{1-x}V_xO_4$ are due to a lowering of T_t, and not due to the rapidly-quenched tetragonal phase. Table 2 also indicates that the T_t lowering due to irradiation is greater in samples containing more V_2O_5 dopant. Although this cannot be explained at present, we suppose that the lattice distortion induced by the dopant plays a role in stabilizing the radiation damage.

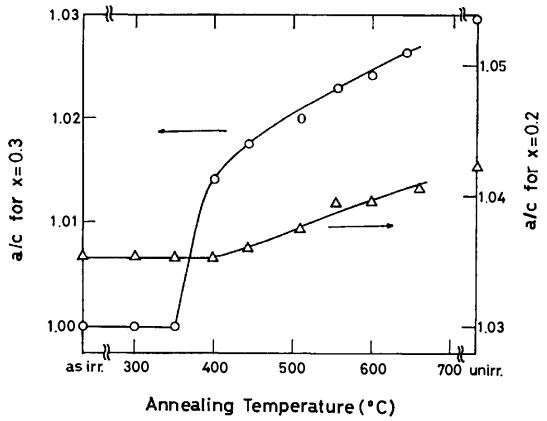

Fig. 2. Variation of a/c with annealing temperature in $NdNb_{0.8}V_{0.2}O_4$ (△) and $NdNb_{0.7}V_{0.3}O_4$ (○) irradiated.

To confirm that the sample does not recover from radiation damage while T_t is being measured, a study of the annealing of the irradiated samples was carried out. The samples were annealed successively at each temperature for 1 h in air. Figure 2 shows the variation of a/c for the irradiated $NdNb_{0.8}V_{0.2}O_4$ and $NdNb_{0.7}V_{0.3}O_4$ samples with the annealing temperature, indicating that the radiation damage recovery begins at ≈350 °C. Neither of the values of T_t for the two samples is higher than that. The data for the annealing of $NdNb_{0.9}V_{0.1}O_4$ could not be obtained because the a/c change due to irradiation is too small. However, the amount of damage recovery during the T_t measurements, if any, could be considered to be very small due to the fact that the lattice parameters of the irradiated sample are essentially the same before heating as those of the same sample after heating to 520 °C (520 °C= the T_t of $NdNb_{0.9}V_{0.1}O_4$). Thus, it has been shown that the T_t values for the irradiated samples involve no recovery effects of the radiation damage.

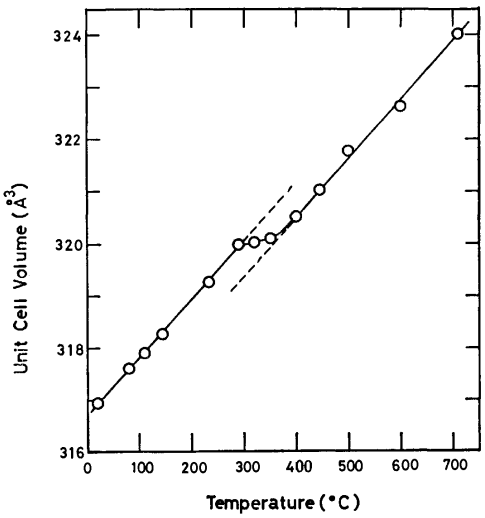

Fig. 3. Temperature dependence of unit cell volume of $NdNb_{0.8}V_{0.2}O_4$.

Several materials undergo similar shifts in transition temperatures when exposed to fast-neutron doses.[5-9,11-13] However, it is not yet clearly understood why their transition temperatures vary due to irradiation. Some workers have attributed this to the internal stress caused by radiation damage; the internal stress acts on T_t as if a pressure had been applied. However, this explanation may not be valid for the reason described below. As is shown in Fig. 3, the unit cell of $NdNb_{0.8}V_{0.2}O_4$, which is an example of $NdNb_{1-x}V_xO_4$, shrinks when it transforms from a monoclinic to a tetragonal structure. Therefore, if such an internal stress lowers T_t, it must act as a positive pressure on T_t, as predicted by the Clausius-Clapeyron equation. When a positive pressure is applied the crystal lattice shrinks. Therefore, such radiation-induced internal stress shrinks the unit cell, that is, the irradiation must result in the shrinking the unit cell. However, on the contrary, the unit cells of $NdNb_{1-x}V_xO_4$ expand when they are irradiated (Table 1). This contradiction strongly suggests that the internal stress due to the radiation damage, if at present at all, is not the dominant cause of the T_t lowering.

The experimental results of the neutron-irradiation of $BaTiO_3$[9] also appear to disprove the "internal stress theory." The $BaTiO_3$ compound is transformed from a tetragonal to a cubic structure at 130 °C. It undergoes T_t lowering when it is irradiated.[9] In a manner similar to the case of $NdNb_{1-x}V_xO_4$, a positive pressure must be assumed[10] as the internal stress to explain the T_t lowering due to the irradiation. However, in reality, the unit cell expands upon irradiation.[9] This contradicts the assumption that the internal stress acts as a positive pressure.

The radiation-induced lowering of T_t may be explained as being due to a change in the valency state. As described in the previous section, the $NdNbO_4$ compound appears to suffer a lowered T_t when replacing the Nb^{5+} ion with ions of greater ionic potential or

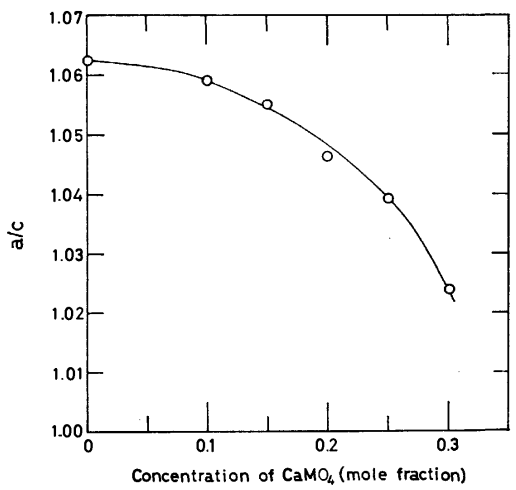

Fig. 4. Variation of a/c with concentration of $CaMoO_4$ in $NdNbO_4$.

when replacing the Nd^{3+} ions with ions of lower ionic potential. In fact, as shown in Fig. 4, the $CaMoO_4$ dopant for which the ionic potential of Ca^{2+} ($Z/r=2.02$) is smaller than that of Nd^{3+}($Z/r=2.88$) and that of Mo^{6+}($Z/r=9.68$) is greater than that of Nb^{5+}($Z/r=7.25$), lowers the a/c ratio of $NdNbO_4$, that is, it lowers the T_t of $NdNbO_4$. A similar effect on T_t occurs for a change in valency state. If electrons are transferred from Nb^{5+} to Nd^{3+} and are trapped there when the $NdNbO_4$ compound is irradiated, the irradiated $NdNbO_4$ compound contains $Nd^{2+}Nb^{6+}O_4$. It can be expected that the ionic potential of Nd^{2+} is smaller than that of Nd^{3+} and that the ionic potential of Nb^{6+} is greater than that of Nb^{5+}. Therefore, if irradiation induces the $Nd^{2+}Nb^{6+}O_4$ compound in the $NdNbO_4$ matrix, the effect on the T_t of $NdNbO_4$ may well be similar to that of the $CaMoO_4$-dopant, that is, the $Nd^{2+}Nb^{6+}O_4$ compound will lower the T_t of $NdNbO_4$.

The $Nd^{2+}Nb^{6+}O_4$ compound may be detected by measuring the magnetic susceptibility of the sample It is reasonable to expect that Nd^{2+} shares 4 Bohr magnetons/mol and Nb^{6+} 1 Bohr magneton/mol while the non-irradiated $NdNbO_4$ compound retains 3 Bohr magnetons/mol.[14] V^{5+} is diamagnetic. Therefore, if $Nd^{2+}Nb^{6+}O_4$ is present in the irradiated sample, the magnetic susceptibility of the irradiated sample will be greater than that of non-irradiated sample by 2 Bohr magnetons per mol due to the $Nd^{2+}Nb^{6+}O_4$ present. The $CaMoO_4$ doping data (Fig. 4) leads to the estimation that, if the radiation-induced $Nd^{2+}Nb^{6+}O_4$ compound lowers the T_t of a $NdNb_{0.7}V_{0.3}O_4$ sample, at least one tenth mole of $Nd^{2+}Nb^{6+}O_4$ must be present in the irradiated $NdNb_{0.7}V_{0.3}O_4$ samples. Such an amount of $Nd^{2+}Nb^{6+}O_4$ can readily be detected using a Gouy balance. Figure 5 gives the temperature dependence of the magnetic susceptibilities of irradiated (○) and non-irradiated (△) $NdNb_{0.7}V_{0.3}O_4$. However, no significant difference in the magnetic susceptibilities between the two is observed. Therefore, the change in the valency state is not an important cause of the radiation-induced lowering of T_t.

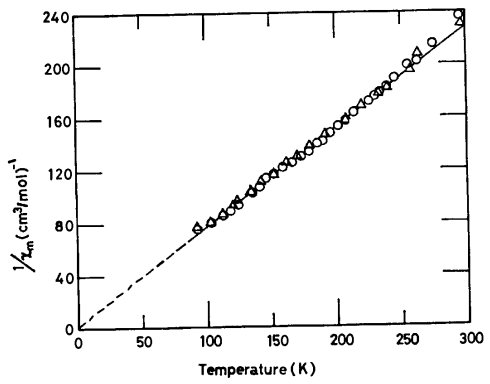

Fig. 5. Temperature dependence of inverse molar susceptibility in irradiated (○) and non-irradiated (△) $NdNb_{0.7}V_{0.3}O_4$ sample.

This study provides no definite explanation of the radiation-induced lowering of T_t, but it is supposed that this may be ascribed to disordering in the crystal lattice.

References

1) T. Kenjo and S. Yajima, *Chem. Lett.*, **1976**, 759.
2) R. W. G. Wyckoff, "Crystal Structures," 2nd ed, Vol. 3, Interscience (1965), p. 21.
3) H. P. Rooksby and E. D. White, *Acta Crystallogr.*, **16**, 888 (1963).
4) MaCarthy, *et al.*, "X-Ray Powder Data File," American Society for Testing and Materials, 22-1175.
5) M. C. Wittels and F. A. Sherrill, *J. Appl. Phys.*, **27**, 643 (1956); M. C. Wittels and F. A. Sherrill, *Phys. Rev. Lett.*, **3**, 176 (1959).
6) O. Krisement and G. Trömel, *Z. Naturforsch.*, **15a**, 634 (1960).
7) R. Roy and C. P. Buhsmer, *Am. Mineral.*, **50**, 1473 (1965).
8) R. Roy and C. P. Buhsmer, *J. Appl. Phys.*, **36**, 331 (1965).
9) O. Hauser and M. Shenk, *Phys. Status Solidi*, **18**, 457 (1966).
10) A pressure of *ca.* 20 kbar is required to lower the T_t of $BaTiO_3$ to room temperature.
11) S. P. Solov'ev, and I. I. Kuz'min, and V. V. Zakurkin, *Ferroelectrics*, **1**, 19 (1970).
12) S. P. Solov'ev and I. I. Kuz'min, *Izv. Akad. Nauk SSSR, Ser. Fiz.*, **34**, 2604 (1970).
13) V. V. Dem'yanov and M. I. Shchedrin, *Fiz. Tved. Tela*, **14**, 3064 (1972).
14) The effective magnetic moment for $NdNbO_4$ is found to be 3.68 Bohr magnetons.[15]
15) J. H. Van Vleck, "Electrical and Magnetic Susceptibilities," Oxford University Press, London (1959), p. 243.

Mössbauer Absorption Spectra of ^{119}Sn in Single Crystals of $(CH_3)_2SnF_2$ and $(CH_3)_2SnCl_2$

Hisao NEGITA, Ryukei BOKU, Makoto NAKAMURA, and Sumio ICHIBA

Department of Chemistry, Faculty of Science, Hiroshima University, Higashisenda-machi, Hiroshima 730

(Received September 2, 1976)

The Mössbauer absorption spectra of ^{119}Sn in single crystals of $(CH_3)_2SnF_2$ and $(CH_3)_2SnCl_2$ have been studied as a function of the orientation angles of the incident unpolarized gamma-ray beam with respect to the crystal axes, taking the absorber thickness effect into account. The analysis of the intensity ratios of the quadrupole splitting doublet yields the asymmetry parameter (η) and the orientation of the principal axes of the electric-field gradient with respect to the crystal axes. The value of η in $(CH_3)_2SnCl_2$ at 135 K was about 0.4, less than the value published previously. The sign of the ^{119}Sn quadrupole coupling constant (e^2qQ) in these compounds was found to be positive, as has been reported before.

Several parameters, such as the electric-field gradient (EFG) and the mean square-displacement (MSD) tensors at the sites of the resonant nuclei, can be obtained by means of the Mössbauer absorption spectra of the single-crystal samples.

Zory has discussed the analysis of the EFG in a single-crystal absorber containing ^{57}Fe and has applied his analysis to $FeCl_2 \cdot 4H_2O$ and evaluated all the EFG parameters.[1] This method has been successfully employed for the complete determination of all the parameters of the EFG tensor in the iron compounds, $Na_2[Fe(CN)_5NO] \cdot 2H_2O$,[2] $FeSO_4 \cdot 7H_2O$,[3] $FeSO_4 \cdot (NH_4)_2 SO_4 \cdot 6H_2O$,[3] *etc.*[4-6]

In these cases, the analysis of the quadrupole hyperfine anisotropy, however, was based on the thin absorber approximation. Unless the absorber is extremely thin, the analysis is complicated by the partial saturation of the absorption intensity in a polarized single crystal.

The general theory of polarization effects given by Housley *et al.*[7] has been developed recently by Gibb,[8] who treated the data of the $FeSO_4 \cdot (NH_4)_2SO_4 \cdot 6H_2O$ single crystal with polarization in the absorption cross section and obtained good results.

So far no Mössbauer experiments with single crystals containing tin have been performed except for $Fe\{(\pi\text{-}C_5H_5)(CO)_2\}_2 SnCl_2$,[9] with which the EFG tensor at tin has been evaluated and discussed by the use of a point-charge model. Therefore, in this paper we wish to report the results for Mössbauer absorption spectra by taking into account the absorber thickness effect in single crystals of $(CH_3)_2SnF_2$ and $(CH_3)_2SnCl_2$.

Experimental

A single crystal of $(CH_3)_2SnF_2$ was grown by the slow evaporation of its HF solution. A thin crystal plate of approximately 0.4×0.4 cm^2 could be obtained over about 8 weeks. The crystal habit has been described in detail.[10] An unusual feature is the dominance of the 001 plane, whose edges coincide with the crystallographic a direction. $(CH_3)_2SnF_2$ is a tetragonal crystal in the space group I4/mmm, with cell dimensions of $a=b=4.24$ Å and $c=14.16$ Å.[11] A unit cell contains two Sn atoms at the 2a positions (0, 0, 0) and (1/2, 1/2, 1/2), with a point symmetry of 4/mmm. The tin atoms are octahedrally surrounded by two methyl groups and four bridging fluorine atoms. These octahedra have the same orientation relative to the crystal axes. The local environment of the tin is shown in Fig. 1(a).

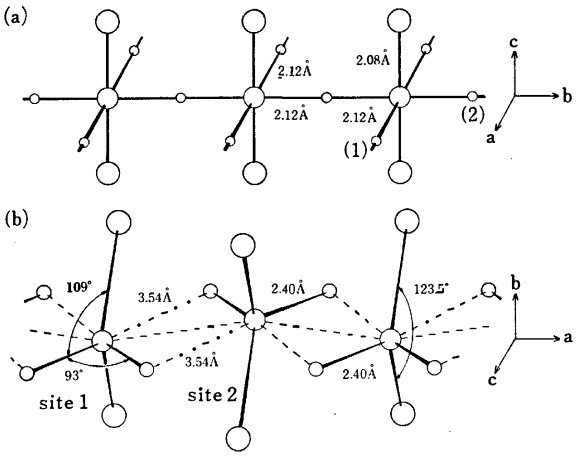

Fig. 1. The structure of (a) $(CH_3)_2SnF_2$ and (b) $(CH_3)_2SnCl_2$.
○: Me, ○: Sn, ○: Cl, and ○: F.

A large crystal of $(CH_3)_2SnCl_2$ was grown by the Bridgman method.[12] After it had been cut with a knife along the habit plane (011 and 01$\bar{1}$), we obtained a thin plate of approximately 0.7×0.7 cm^2 by the hand-polishing technique. $(CH_3)_2SnCl_2$ crystallizes in the orthorhombic space group of Imma, with unit cell dimensions of $a=8.78$, $b=7.75$, and $c=9.25$ Å.[13] The structure consists of a chain of molecules running parallel to the a axis, with the tin atoms in the distorted octahedrals. The tin and chlorine atoms in each chain are coplanar, and the methyl groups are not collinear with the tin atoms joined to their own neighbors by two bridging chlorine atoms (Fig. 1(b)).

The thickness of the crystal samples was determined by means of their weights and areas. The values of $(CH_3)_2SnF_2$ and $(CH_3)_2SnCl_2$ were 29 and 18 mg/cm^2 respectively for Sn. The crystal was mounted on a goniometer head, and the crystal axes were located by the X-ray diffraction method. Then the goniometer head was placed in a liquid nitrogen cryostat so the gamma ray might be incident perpendicularly to the crystal plate. The angle of the plate to the gamma ray was varied by the rotation of the goniometer head.

The Mössbauer spectra were obtained by the use of a constant-acceleration-type spectrometer. The gamma-ray source was 0.7 mCi ^{119}Sn in the barium stannate matrix and was used at room temperature. The absorber temperatures were 135 K for single-crystal samples and 100 K for powder. X-Rays from the source were shut out by a palladium foil 50 micron thick. The velocity scale was calibrated by the use of reference absorbers of $BaSnO_3$ and Sn foil. All the

spectra were analyzed by means of a least-squares computer fitting the Lorentzian-line shapes without constraints on the line positions, widths, and intensities by the use of HUC-III, HITAC-8700.

Method of Calculation

The Absorption Cross Section. The polarization of the absorption cross section can be described in terms of 2×2 density matrices such as:

$$\begin{pmatrix} \rho_{11}^{ij} & \rho_{12}^{ij} \\ \rho_{21}^{ij} & \rho_{22}^{ij} \end{pmatrix}$$

where sites are labeled by j and the hyperfine components of a resonance by i.[7] The normalization conditions are $\sum_i \rho_{11}^{ij} = \sum_i \rho_{22}^{ij} = 1$ and $\sum_i \rho_{12}^{ij} = \sum_i \rho_{21}^{ij} = 0$. The density matrix can always be diagonalized if the direction of observation is in a mirror or glide plane, along a 3-fold or higher rotation or a screw axis, and normal to a suitable 2-, 4-, 6-fold rotation axis. Furthermore, if there is only one resonant site per unit cell, then the density matrix can always be diagonalized for any observation direction.

$(CH_3)_2SnF_2$ has only one resonant site per unit cell, and $(CH_3)_2SnCl_2$ has three 2-fold rotation axes parallel to the a, b, and c axes. In these single crystals, therefore, the density matrix is diagonalized for the observation direction normal to the a axis.

If there are only two absorption lines in the spectrum, as in the case for the $I=1/2\rightarrow3/2$ nuclear transition, appropriate density matrix elements for a single site, j, have been shown to be:

$$\begin{aligned} \rho_{11}^{j} &= 1/2 \pm (1/4)w(1+\eta\cos 2\phi_j) \\ \rho_{22}^{j} &= 1/2 \pm (1/4)w(1-3\sin^2\theta_j - \eta\cos^2\theta_j\cos 2\phi_j) \\ \rho_{12}^{j} &= \rho_{21}^{j} = \pm(\eta/4)w\cos\theta_j\sin 2\phi_j \end{aligned} \quad (1)$$

where $w=[3/(3+\eta^2)]^{1/2}$, where the upper signs correspond to the $\pm1/2\rightarrow\pm3/2$ (π) transitions and the lower to the $\pm1/2\rightarrow\pm1/2$ (σ) transitions, and where θ_j and ϕ_j are polar angles with respect to the principal-axes system (PAS) of the EFG.

Let us transform Relation (1) from the θ_j and ϕ_j coordinates to the Θ and Φ coordinates, which define the crystal axes with respect to the incident radiation beams, as is illustrated in Fig. 2. Since the $\boldsymbol{a}$, $\boldsymbol{b}$, and $\boldsymbol{c}$ directions are orthogonal with one another, the following expressions relate θ_j, ϕ_j to Θ, Φ, and the Euler angles $(\alpha_j, \beta_j, \gamma_j)$ which relate the j site to the axes $(\boldsymbol{a}, \boldsymbol{b}, \boldsymbol{c})$:

$$\begin{aligned} \sin\theta_j\cos\phi_j &= \sin\Theta\cos\Phi(\boldsymbol{b}\cdot\boldsymbol{x}_j) + \sin\Theta\sin\Phi(\boldsymbol{c}\cdot\boldsymbol{x}_j) \\ &\quad + \cos\Theta(\boldsymbol{a}\cdot\boldsymbol{x}_j) \equiv B_j \\ \sin\theta_j\sin\phi_j &= \sin\Theta\cos\Phi(\boldsymbol{b}\cdot\boldsymbol{y}_j) + \sin\Theta\sin\Phi(\boldsymbol{c}\cdot\boldsymbol{y}_j) \\ &\quad + \cos\Theta(\boldsymbol{a}\cdot\boldsymbol{y}_j) \equiv C_j \\ \cos\theta_j &= \sin\Theta\cos\Phi(\boldsymbol{b}\cdot\boldsymbol{z}_j) + \sin\Theta\sin\Phi(\boldsymbol{c}\cdot\boldsymbol{z}_j) \\ &\quad + \cos\Theta(\boldsymbol{a}\cdot\boldsymbol{z}_j) \equiv A_j \end{aligned} \quad (2)$$

where:

$$\begin{aligned} (\boldsymbol{b}\cdot\boldsymbol{x}_j) &= \cos\alpha_j\cos\beta_j\cos\gamma_j - \sin\alpha_j\sin\gamma_j \\ (\boldsymbol{c}\cdot\boldsymbol{x}_j) &= -\cos\alpha_j\cos\beta_j\sin\gamma_j - \sin\alpha_j\cos\gamma_j \\ (\boldsymbol{a}\cdot\boldsymbol{x}_j) &= \cos\alpha_j\sin\beta_j \\ (\boldsymbol{b}\cdot\boldsymbol{y}_j) &= \sin\alpha_j\cos\beta_j\cos\gamma_j + \cos\alpha_j\sin\gamma_j \\ (\boldsymbol{c}\cdot\boldsymbol{y}_j) &= -\sin\alpha_j\cos\beta_j\sin\gamma_j + \cos\alpha_j\cos\gamma_j \\ (\boldsymbol{a}\cdot\boldsymbol{y}_j) &= \sin\beta_j\sin\gamma_j \\ (\boldsymbol{b}\cdot\boldsymbol{z}_j) &= -\sin\beta_j\cos\gamma_j \\ (\boldsymbol{c}\cdot\boldsymbol{z}_j) &= \sin\beta_j\sin\gamma_j \\ (\boldsymbol{a}\cdot\boldsymbol{z}_j) &= \cos\beta_j \end{aligned} \quad (3)$$

From Eq. 2, it may be shown that Eq. 1 has the form of:

$$\begin{aligned} \rho_{11}^{j} &= 1/2 \pm (1/4)w\{1+\eta(B_j^2-C_j^2)/(1-A_j^2)\} \\ \rho_{22}^{j} &= 1/2 \pm (1/4)w\{1-3(1-A_j^2) \\ &\quad -\eta A_j^2(B_j^2-C_j^2)/(1-A_j^2)\} \\ \rho_{12}^{j} &= \rho_{21}^{j} = \mp(\eta/2)wA_jB_jC_j/(1-A_j^2) \end{aligned} \quad (4)$$

Absorption Areas. Since the ^{119}Sn first excited state has a spin of 3/2, as a result of the interaction of the nuclear quadrupole moment with the EFG, the resonance absorption line splits into two components, whose separation is given by:

$$\Delta E = (1/2)e^2qQ(1+\eta^2/3)^{1/2} \quad (5)$$

where eq is the EFG in the z (major-axis) direction, η the asymmetry about the z axis ($0\leq\eta<1$) and eQ the nuclear quadrupole moment of the first excited state of ^{119}Sn.

If the observed spectrum has the form of the individual, completely split components—*i.e.*, if the energy difference between components is larger than the absorption line width, then the absorption area, A_i, for the i-th component of the spectrum of the absorber with the effective cross section of T_a is given by:

$$A_i = \alpha f\pi K(T_{ia}) \quad (6)$$

where:

$$\begin{aligned} K(T_{ia}) &= T_{ia}\exp(-T_{ia}/2)[I_0(T_{ia}/2)+I_1(T_{ia}/2)], \\ T_{ia} &= b_iT_a, \end{aligned}$$

α is the fraction of the resonance quanta in the emission spectrum; f, the recoilless fraction of the source, $I_0(x)$ and $I_1(x)$, the zero- and the first-order Bessel function and imaginary argument respectively, and b_i, the relative intensity of the i-th component.[14] If we are considering a polarized absorber (such as a single crystal) with two independent polarizations of the cross section, ρ_{11}^i and ρ_{22}^i, then the area of the i-th component

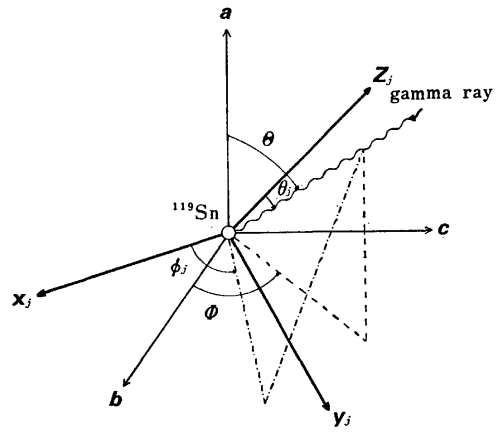

Fig. 2. The orientation of the incident radiation beam relative to the crystal axes (**a**, **b**, **c**) and the EFG axes ($\mathbf{x}_j$, $\mathbf{y}_j$, $\mathbf{z}_j$) of the j-th site in the unit cell.

is given by[8]:

$$A_i = \alpha f\pi[(1/2)K(\rho_{11}^i T_a)+(1/2)K(\rho_{22}^i T_a)] \quad (7)$$

Density Matrix for Two Sites in $(CH_3)_2SnCl_2$. If we let k_j stand for either x_j, y_j, or z_j, the symmetry relation between two sites in the unit cell is a 180° rotation about the a axis and can be written as:

$$\begin{aligned}(b\cdot k_1) &= -(b\cdot k_2)\\ (c\cdot k_1) &= -(c\cdot k_2)\\ (a\cdot k_1) &= (a\cdot k_2)\end{aligned} \quad (8)$$

Consequently, from Eqs. 2 and 8, for observation in the bc plane, *i.e.*, for $\Theta=90°$, the diagonal elements of the density matrix are the same for both sites. The resulting diagonal elements of the density matrix are:

$$\begin{aligned}\rho_{11} &= (1/2) \pm (1/4)w\{1+\eta(B'^2-C'^2)/(1-A'^2)\}\\ \rho_{22} &= (1/2) \pm (1/4)w\{1-3(1-A'^2)\\ &\quad -\eta A'^2(B'^2-C'^2)/(1-A'^2)\}\end{aligned} \quad (9)$$

where:

$$\begin{aligned}A' &= \cos\Phi(b\cdot z) + \sin\Phi(c\cdot z)\\ B' &= \cos\Phi(b\cdot x) + \sin\Phi(c\cdot x)\\ C' &= \cos\Phi(b\cdot y) + \sin\Phi(c\cdot y)\end{aligned}$$

Eq. 9 also holds for observation along the a axis; *i.e.*, $\Theta=0°$, where:

$$A' = (a\cdot z),\quad B' = (a\cdot x),\quad C' = (a\cdot y)$$

Note that these equations are ill-conditioned if $1-A'^2=0$; *i.e.*, $\beta=90°$ and $\alpha=\Phi$ in the first case, and $\beta=0°$ in the second.

Recoilless Fraction. When the recoilless fraction of the absorber is f', the effective cross section can be written as $T_a=\eta f'\sigma_0$, where n is the number of resonant nuclides per cm², and σ_0, a resonant cross section. Therefore, the effective cross section, T_a, depends on f'.

From the elementary theory of the Mössbauer-Lamb fraction, the dependence of the recoilless fraction on the mean-square amplitude of the vibration ($\langle u^2\rangle$) is given by:

$$f' = \exp(-\langle u^2\rangle/\lambda\!\!\!^{-2}) \quad (10)$$

where $2\pi\lambda\!\!\!^{-}=hc/E$, the gamma quatum wavelength, which for ^{119}Sn is 5.190×10^{-9} cm. For an axial-symmetric crystal, using the model for the angular distribution of MSD given by Kündig *et al.*,[15]

$$\langle u^2\rangle(\theta') = \langle u_\perp{}^2\rangle \sin^2\theta' + \langle u_{//}{}^2\rangle \cos^2\theta' \quad (11)$$

where $\langle u_\perp{}^2\rangle$ and $\langle u_{//}{}^2\rangle$ are components of the MSD tensor normal to and parallel to its principal axis, and θ', the polar angle made by the gamma-ray-propagation vector, k, with respect to the PAS of the MSD tensor. From Eqs. 10 and 11, the recoilless fraction for the powder sample is given by:

$$f' = \exp\{-(1\lambda\!\!\!^{-2})(\langle u_{//}{}^2\rangle+2\langle u_\perp{}^2\rangle)/3\} \quad (12)$$

By assuming a Debye model for the phonon spectrum, the temperature dependence of the recoilless fraction is given by the well-known expression[16]:

$$f' = \exp\{-(3E_R/2k\theta_D)[1+4(T/\theta_D)^2\int_0^{\theta_D/T} x\,dx/(e^x-1)]\} \quad (13)$$

in which, within the high-temperature limit, ($T\geq\theta_D/2$) takes the form of:

$$f' = \exp[(-6E_R/k\theta_D{}^2)T] \quad (14)$$

where E_R is the recoil energy of the free nucleus, and θ_D, the Debye temperature. Therefore, if the MSD or the Debye temperature is known, f' can be estimated from Eqs. 10, 12, and 13.

From Eq. 6, if a second spectrum is determined using a similar absorber k times as thick as the original one, the ratio of the intensity is determined as follows:

$$A_i'/A_i = K(kb_i\eta f'\sigma_0)/K(b_i\eta f'\sigma_0) \quad (15)$$

where $k=n'/n$.

Since A_i', A_i, n', and n are measurable, and since $K(x)$ is assumed to be a Lorentzian, the value of f' can be determined from Eq. 15.

Results and Discussion

$(CH_3)_2SnF_2$. The Mössbauer spectra were obtained at 135K for the single-crystal absorber mounted on the a axis normal to the observation axis. Figure 3 shows two typical experimental spectra. The upper spectrum is observed when the angle of the source radiation is 10° from the c axis of the crystal and the crystal thickness is 29.5 mg/cm² for Sn; the lower spectrum is observed when the direction of the radiation is 45° from the c axis and the crystal thickness is 41.0 mg/cm² for Sn.

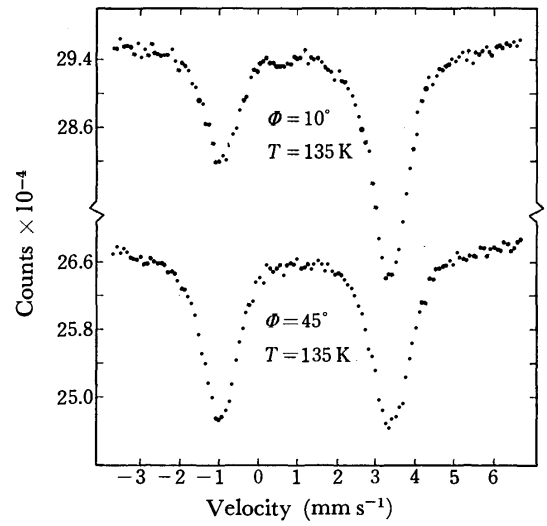

Fig. 3. The Mössbauer absorption spectra of $(CH_3)_2SnF_2$ single crystal absorber with the direction of observation normal to the a axis.

The room-temperature mean-square amplitude of vibration along the a axis, $\langle u_\perp{}^2\rangle$, and that along the c axis, $\langle u_{//}{}^2\rangle$, have been reported to be 0.0188 Å² and 0.0440 Å² respectively.[11] These values were substituted into Eq. 12 in order to estimate the value of f' at room temperature. Using this value of f', it was estimated from Eq. 14 that the Debye temperature, θ_D, is 115.7 K and that f' is 0.17 at 135 K.

Previously it was mentioned that the tin is surrounded by a octahedron composed of four fluorine atoms and two methyl groups. It will be noted that the C–Sn–C bond direction is assuredly a 4-fold axis, because the angles between the axes of the octahedron are 90°. Therefore, the Sn–C direction is taken as the z axis of the EFG, and the Sn–F(1) and Sn–F(2) directions, as the x and y axis respectively. The EFG is thus axially

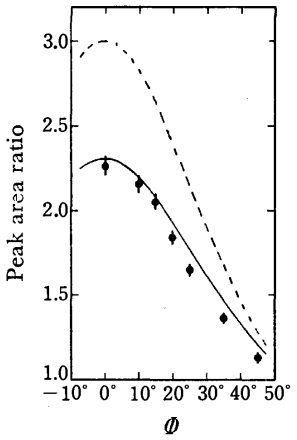

Fig. 4. The area ratio as a function of the observation angle Φ for $(CH_3)_2SnF_2$ single crystal at 135 K. The solid line is computed for $e^2qQ>0$, $\eta=0$, $f'=0.17$, $\alpha=0°$, $\beta=90°$, and $\gamma=90°$. The broken line is computed for neglecting polarization effects.

symmetric ($\eta=0$). Assuming that f' is isotropic, we calculated the area ratio, A_π/A_σ, as a function of the observation angle, Φ, in the bc plane using Eqs. 2, 3, 4, and 7. The assumption that f' is isotropic is supported by the work of Herber and Chandra,[17] who reported that the mean-square amplitudes of vibration of the tin atoms in $(CH_3)_2SnF_2$ were the same in all directions at 140K. The results are shown in Fig. 4. The solid line is the curve computed for $f'=0.17$, $\eta=0$, $\alpha=0°$, $\beta=90°$, and $\gamma=90°$. The broken curve is the line calculated neglecting the effects of polarization, as in Zory.[1] The agreement between the experimental and theoretical results means that the ratio of the high-energy experimental absorption area to the low energy one, A_H/A_L, is equal to A_π/A_σ and not A_σ/A_π. This implies that the $\pm3/2\rightarrow\pm1/2$ transition is higher in energy than the $\pm1/2\rightarrow\pm1/2$ transition, *i.e.*, the sign of the quadrupole interaction (e^2qQ) is positive, which is in accordance with the result obtained by the application of a large external magnetic field.[18]

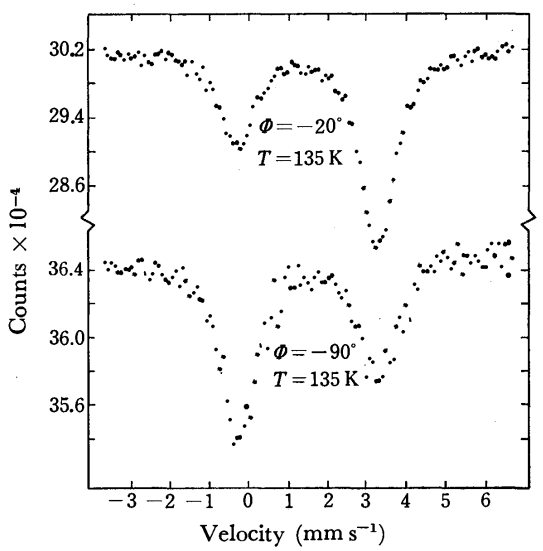

Fig. 5. The Mössbauer absorption spectra of $(CH_3)_2SnCl_2$ single crystal absorber with the direction of observation normal to the a axis.

$(CH_3)_2SnCl_2$. The single-crystal Mössbauer spectra were obtained at 135 K for gamma radiation in the bc plane. The spectra which were obtained for two cases are shown in Fig. 5. In the first case, the gamma ray direction from the b axis was −20° and the thickness was 19.2 mg/cm^2 for Sn, whereas in the second the values are −90° and 28.0 mg/cm^2 respectively.

An approximate value of f' was obtained by the area-ratio method using the powder sample at 100 K. Figure 6 illustrates the results. The low-energy experimental-absorption-area ratios $(A'/A)_L$, are plotted against n'/n. A reasonable fit to the data is obtained for $nf_L'\sigma_0=0.60$, which gives $f'_L=0.10$. A similar analysis for the high-energy experimental-absorption-area ratios $(A'/A)_H$ yields $f'_H=0.11$. Therefore, $f'_L+f'_H=0.21$ is obtained as the recoilless fraction of $(CH_3)_2SnCl_2$ at 100K. Substituting $f'=0.21$ into Eq. 14, the Debye temperature θ_D

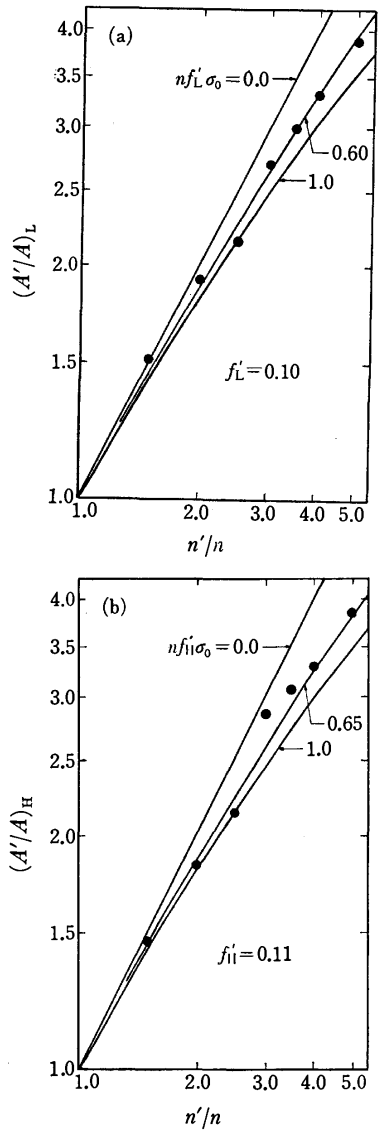

Fig. 6. The absorption area ratio against $(CH_3)_2SnCl_2$ powder absorber thickness ratio at 100 K. (a) The lower energy experimental area ratio $(A'/A)_L$ is plotted against n'/n. (b) The higher energy experimental area ratio $(A'/A)_H$ is plotted against n'/n.

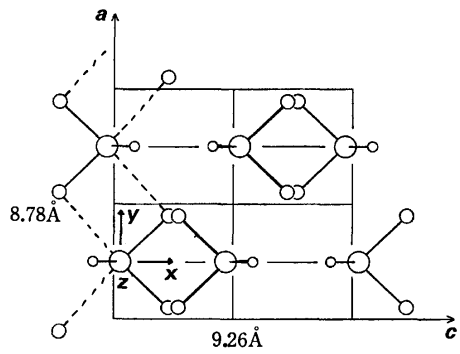

Fig. 7. Projection of the unit cell of $(CH_3)_2SnCl_2$ on the ac plane. ○: Sn, ○: Cl, and o: C.

is derived as 107.1 K, which is in good agreement with the literature value,[19] 108.3 K at 70 K. Using this value of θ_D, the value of f' at 135 K is found to be nearly equal to 0.12.

In the following discussion, we shall refer only to one site because the two sites are related by a 180° rotation about the a axis. The projection onto the crystallographic ac plane of the unit cell of $(CH_3)_2SnCl_2$ is shown in Fig. 7. Since the tin atom in the unit cell lies on the mirror plane parallel to the ac and bc plane and has C_{2v} symmetry, it can be expected that the principal axes of the EFG tensor lie parallel to the crystallographic a, b, and c axes. However, it is unclear which principal axes of the EFG the a, b, and c axes correspond to; furthermore, the value of η can not be determined from the point symmetry of the tin site itself. Erickson has reported that the sign of V_{zz} in $(CH_3)_2SnCl_2$ is negative.[20] The negative sign of V_{zz} (which corresponds to an excess of the negative charge along the z axis) in *trans*-R_2SnX_4 compounds can most logically be interpreted by assuming that tin-carbon bonds have a much larger p-electron density along the bond that do tin-halogen bonds along their bond axes. Therefore, it seems most likely that the V_{zz} direction is along the b axis.

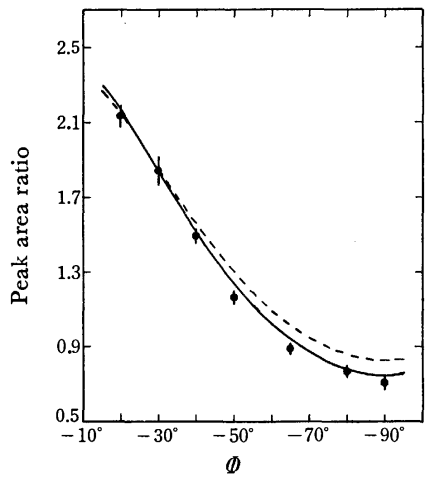

Fig. 8. The area ratio as a function of the observation angle Φ for $(CH_3)_2SnCl_2$ single crystal at 135 K. The dotted curve is computed for $\eta=0.6$, and solid curve for $\eta=0.4$, when $e^2qQ>0, f'=0.12$, $\alpha=0°$, $\beta=90°$, and $\gamma=90°$.

Equations 3, 7, and 9 were evaluated by means of a small computer program to give the density matrix elements for various values of α, β, γ, and η. We assumed that f' was approximately isotropic and that V_{xx} and V_{yy} were parallel to the crystallographic c axis and a axis respectively. The observation angle (Φ) curve for the area ratio was then found using Eq. 7. The results of $\eta=0.4$ and 0.6 are shown, along with the experimental values, in Fig. 8. The dotted curve is computed for $\eta=0.6$, and the solid curve, for $\eta=0.4$, when $f'=0.12$, $\alpha=0°$, $\beta=90°$, and $\gamma=90°$. The agreement between the experimental and calculated values is better when $\eta=0.4$ is used than when $\eta=0.6$ is used. The latter value, which was published previously,[20] must be overestimated. A more detailed value for η may be obtained by comparison with the results of other observations normal to the b axis or the c axis. As we have seen, the thickness of the sample has so profound an effect on the absorption spectra that precise area measurements are necessary to determine the value of η as well as e^2qQ.

We wish to express our sincere gratitude to Assistant Professors Toshihiko Kushi of Hiroshima University and Mitsuo Mishima of Shimane University for their valuable advice in analyzing the data.

References

1) P. Zory, *Phys. Rev.*, **140**, A1401 (1965).
2) J. Danon and L. Iannabrella, *J. Chem. Phys.*, **47**, 382 (1967).
3) K. Chandra and S. P. Puri, *Phys. Rev.*, **162**, 272 (1968).
4) V. K. Garg and S. P. Puri, *J. Chem. Phys.*, **54**, 209 (1971).
5) J. F. Duncan and J. H. Johnston, *Aust. J. Chem.*, **26**, 231 (1973).
6) G. Langonche, M. Van Rossum, K. P. Schmidt, and R. Coussement, *Phys. Rev., B*, **9**, 848 (1974).
7) R. M. Housley, R. W. Grant, and U. Gonser, *Phys. Rev.*, **178**, 514 (1969).
8) T. C. Gibb, *J. Phys. C*, **7**, 1001 (1974).
9) T. C. Gibb, R. Greatrex, and N. N. Greenwood, *J. Chem. Soc., Dalton Trans.*, **1971**, 238.
10) E. O. Schlemper and W. C. Hamilton, *Inorg. Chem.*, **5**, 995 (1966).
11) H. A. Szymwski, "Raman Spectroscopy," Plenum Press, New York (1967), Chap. IV.
12) M. E. Buckley, "Crystal Growth," John Wiley and Sons, New York (1951), p. 35.
13) A. G. Davies, H. J. Milledge, D. C. Puxley, and P. J. Smith, *J. Chem. Soc., A*, **1970**, 2862.
14) G. A. Bykov and Pham zuy Hien, *Sov. Phys.-JETP.*, **16**, 646 (1963).
15) W. Kündig, K. Ando, and H. Bömmel, *Phys. Rev.*, **139**, A889 (1965).
16) V. I. Gol'danskii and R. H. Herber, "Chemical Applications of Mössbauer Spectroscopy," Academic Press, New York (1968), p. 34.
17) R. H. Herber and S. Chandra, *J. Chem. Phys.*, **52**, 6045 (1970).
18) B. A. Goodman and N. N. Greenwood, *J. Chem. Soc., A*, **1971**, 1862.
19) H. A. Stöckler and H. Sano, *Chem. Commun.*, **1969**, 954.
20) N. E. Erickson, *Chem. Commun.*, **1970**, 1349.

Magnetic Circular Dichroism of the Thulium and Erbium Ethyl Sulfate Nonahydrate Crystals

Yoshifumi KATO, Toshikazu NAKAYA, and Toshiyuki NAGAI

Department of Chemistry, Faculty of Science, Kobe University, Nada-ku, Kobe 657

(Received July 26, 1976)

The magnetic circular dichroism and absorption spectra of the thulium and erbium ethyl sulfate nonahydrate crystals have been measured at low temperatures, down to 18 K. The analyses are made for five absorption bands of $Tm(C_2H_5SO_4)_3 \cdot 9H_2O$; the bands from the ground state, $^3H_6$, to the excited states $^3F_3$, $^3F_2$, $^1G_4$, $^1D_2$, and $^3P_1$ of Tm^{3+}, and for four bands of $Er(C_2H_5SO_4)_3 \cdot 9H_2O$; the bands from the ground state, $^4I_{15/2}$, to the excited states $^4S_{3/2}$, $^4F_{5/2}$, $^4F_{3/2}$, and $^2G_{9/2}$ of Er^{3+}. With the aid of the information about energy levels already obtained, the *g* values of the crystal levels relevant to absorptions are derived from the Faraday parameters; these are in good agreement with those obtained by other methods.

A certain amount of crystal field level data for rare earth crystals has been accumulated by the analysis of the absorption and fluorescence spectra and the Zeeman effect for these crystals.[1,2] By using the knowledge of these well established energy levels, it has been pointed out[3-6] that even when optical absorption bands are too broad to give resolved Zeeman patterns, fairly accurate estimates of the spectroscopic splitting factors (*g* value) in the ground and excited states can be obtained from the magnetic circular dichroism (MCD) spectra.

In the present work, the MCD measurements for five absorption bands of thulium ethyl sulfate nonahydrate, $Tm(C_2H_5SO_4)_3 \cdot 9H_2O$ (Tm(ES)), and four absorption bands of erbium ethyl sulfate nonahydrate, $Er(C_2H_5SO_4)_3 \cdot 9H_2O$ (Er(ES)), have been carried out at low temperatures and the *g* values derived from the MCD are compared with those obtained by other methods.

Experimental

The procedure of the preparation of the crystals is described in our previous paper.[6] All the absorption and MCD spectra were obtained by a JASCO J-10 spectrophotometer equipped with a permanent magnet of 3.6 kG. The measurements at low temperatures down to 18 K were performed using a metal Dewar vessel, as showh in Fig. 1. The temperature of the crystal packed into a sample cell attached to the tail of the liquid helium vessel was measured by using an Au-Co *versus* chromel thermocouple with one junction pressed directly against the crystal and found to be 80 ± 1 and 18 ± 2 K at liquid nitrogen and helium temperatures, respectively.

The product of the concentration and path length for a sample was determined from a comparison of the absorption strength of several isolated bands in the crystal with that of the corresponding aqueous solution at room temperature. While this procedure may produce errors in the estimate of the absorption coefficient and the molar ellipticity, this is not a serious matter,[6,7] because the important quantities in our discussion are always the ratios of the Faraday parameters to the dipole strength. The slit width was made as narrow as possible ($\approx$0.01 mm) to resolve an overlapping band, although there was a limitation owing to the characteristic resolving power of the instrument. When the incident light beam was directed along the principal axis of a uniaxial, crystal, no birefringence effect was observed in the present measurement; the base line was flat and well behaved with zero magnetic field. The MCD and absorption data thus obtained are considered to be accurate within 20 percent.

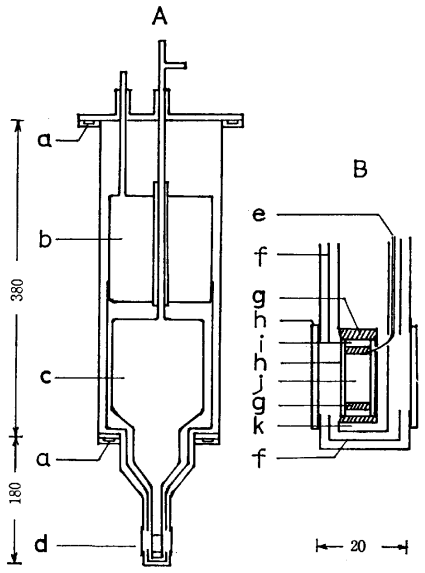

Fig. 1. Metal Dewar vessel for the MCD measurement at liquid helium temperature (A) and the enlarged diagram of its tail part (B). The units are in mm. a: O-ring, b: liquid nitrogen vessel, c: liquid helium vessel, d: sample part, e: thermocouple, f: liquid nitrogen shield, g: indium, h: quartz window, i: sample cell, j: crystal, k: Cu-holder.

Results and Discussion

Energy Levels and Calculated g *Values.* The Tm^{3+} and Er^{3+} ions in ethyl sulfate have $4f^{12}$ and $4f^{11}$ electronic configurations respectively. According to the analysis of the crystal structure of rare earth ethyl sulfates,[8] the space group is $P6_3/m$ (C^2_{6h}) and the local symmetry about a rare earth ion is D_{3h} as far as the nearest-neighbor oxygen atoms of 9 crystalline waters are concerned. An ion state $|JM>$ placed in a crystal field splits into several crystal levels, designated by the crystal quantum numbers η, following Hellwege:[9] *e.g.*, the ground ion state of Tm(ES), $^3H_6$, and that of Er(ES), $^4I_{15/2}$, split into 9 and 8 crystal levels in D_{3h} symmetry, respectively.

In general, it is possible to evaluate theoretically the *g* values of crystal levels. Wong and Richman[10] made

the calculation of the crystal levels of Tm(ES) and their g values. They obtained the root mean square deviation of 118.9 cm^{-1} for 11 ion levels by the operator equivalent method and that of 10.8 cm^{-1} for 21 crystal levels by the first-order perturbation theory. Although the accuracy of the physical quantities calculated depends on that of the wave functions used, the results by Wong and Richman are considered to be fairly reliable. As there has been no calculation for the g values of Er(ES), we have made the crystal field calculation for this crystal[11] in which the configuration interaction for ion levels and complete J-mixing for crystal levels are taken into account by means of the tensor method.[12] This calculation has made it possible to fit 22 ion levels with the root mean square deviation of 78.2 cm^{-1} and to fit 50 crystal levels with that of 3.6 cm^{-1}. The calculated g values will be utilized in the comparison with those from MCD in the following section.

MCD Spectra. The general expressions for the MCD extensively used can be applied to a uniaxial crystal. The ellipticity accompaning an electronic transition is written as

$$\theta = -\frac{4}{3}\gamma N_a[Af_1/\hbar+(B+C/kT)f_0]H, \qquad (1)$$

where the explicit expressions for the Faraday parameters A, B, and C, are given by Stephens.[13,14] The ordinary conditions assumed in the derivation of Eq. 1 (Zeeman energy $\ll$zero-field state separation, line width, and kT) are satisfied in the present measurements. The ratios of the Faraday parameters to the dipole strength D $(=(1/d_a)|\langle a|\boldsymbol{m}|j\rangle|^2)$ are related to the g values of the ground a and excited j states in a transition as

$$|A/D| = |g_j-g_a|, \quad |C/D| = |g_a|, \qquad (2)$$

where the Zeeman splitting is taken as $2g\beta H$, since there are no multiplets except the doublet in the ethyl sulfate crystals. The selection rules in D_{3h} symmetry in case of an even and odd number of electrons are given in

TABLE 1. SELECTION RULES FOR CRYSTAL QUANTUM NUMBER η IN D_{3h} SYMMETRY

Even number electrons.

$\eta''\backslash\eta'$	0	±1	±2	3
0	—	—	σ	π
±1	—	σ	π	σ
±2	σ	π	σ	—
3	π	σ	—	—

Odd number electrons.

$\eta''\backslash\eta'$	$\pm1/2$	$\pm3/2$	$\pm5/2$
$\pm1/2$	—	σ	σ, π
$\pm3/2$	σ	π	σ
$\pm5/2$	σ, π	σ	—

Table 1,[15] while σ polarization can be observed in the present experiment. The energy level diagrams of Tm(ES) and Er(ES) relevant to the present analysis are given in Fig. 2.[1] The MCD and absorption spectra observed are shown in Figs. 3 and 4 for Tm(ES) and Er(ES), respectively. The absorption bands analyzed are five for Tm(ES): $^3H_6 \rightarrow {}^3F_3$, $^3F_2$, $^1G_4$, $^1D_2$, and $^3P_1$, and four for Er(ES): $^4I_{15/2} \rightarrow {}^4S_{3/2}$, $^4F_{5/2}$ $^4F_{3/2}$, and $^2G_{9/2}$.[16] The Faraday parameters derived from the method of moments[14,17] are given in Tables 2 and 3 for Tm(ES) and Er(ES), respectively. We consider that the parameter values by the graphical method by Bodoz *et al.*[18] and the curve fitting method by a least-squares procedure[19] can be also obtained with similar accuracy to those by the moment method when a careful application of these two methods is made.[19]

Discussion for Tm(ES). The lowest crystal level of the $^3H_6$ state of Tm(ES) is a non-degenerate level $\eta=0$. The population of the next level ($\eta=\pm1$), which is 32 cm^{-1} higher than the lowest level, is 8 percent of

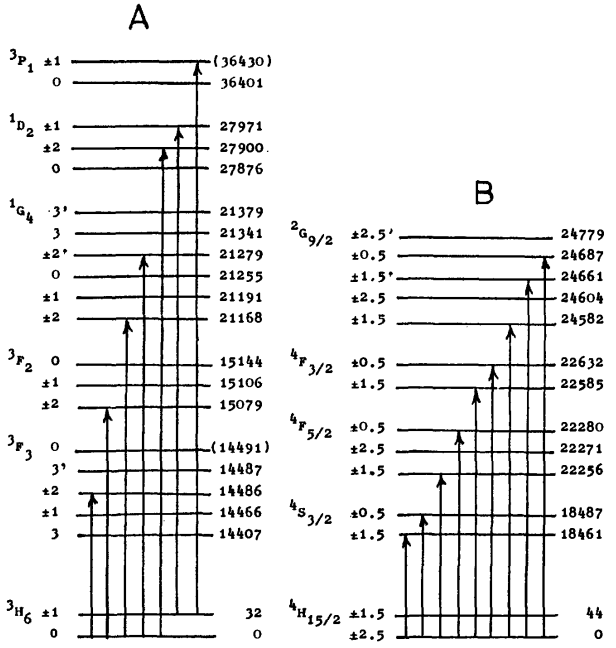

Fig. 2. Energy level diagrams of Tm(ES) (A) and Er(ES) (B) (Ref. 1). The units of energy are in cm^{-1}. The values in parentheses are not yet determined experimentally. Allowed transitions are indicated by arrows.

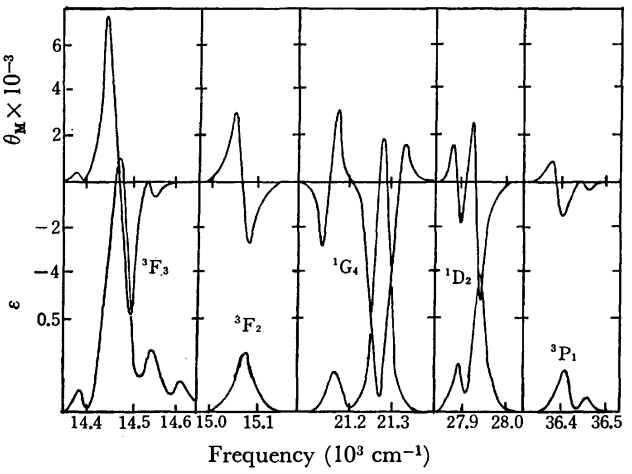

Fig. 3. Absorption and MCD spectra of Tm(ES) at 18 K. θ_M and ε are the MCD in molar ellipticity units (degree deciliter decimeter^{-1} mol^{-1}) per unit gauss and molar extinction coefficient, respectively.

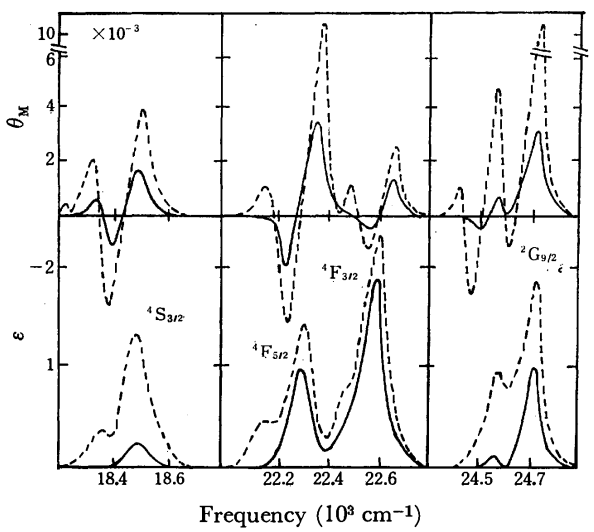

Fig. 4. Absorption and MCD spectra of Er(ES) at 18 K (solid line) and at 80 K (broken line). Notations and units are the same as in Fig. 3.

that of the latter at 18 K. As seen in Fig. 3, the $^3H_6 \rightarrow {}^1D_2$ band splits into two bands: each of these should correspond to the $^3H_6(\eta=0) \rightarrow {}^1D_2(\eta=\pm 2)$ and the $^3H_6(\eta=\pm 1) \rightarrow {}^1D_2(\eta=\pm 1)$ transitions (Fig. 2). Furthermore, the band at about 36400 cm^{-1} is readily seen to be the $^3H_6(\eta=\pm 1) \rightarrow {}^3P_1(\eta=\pm 1)$ transition from the selection rules (Table 1). Thus, the absolute value of g in the $^3H_6(\eta=\pm 1)$ level can be obtained separately from the C/D values in the two transitions from this level; its average value is 1.11 β. The absolute g values for the excited levels of these two bands are also obtained from the corresponding A/D values. However, for the $^3H_6 \rightarrow {}^3F_3$, $^3F_2$, $^1G_4$ bands, no evident transition from the $^3H_6(\eta=\pm 1)$ level is observed in the present measurements (Fig. 3). If it is assumed that these bands arise solely from the lowest level $^3H_6(\eta=0)$, then all the C/D values for these bands turn out to be zero, the B/D values are fixed, and the absolute g values of the excited levels are obtained from the corresponding A/D values. As a result, all the g values of the crystal levels observed are definitely settled. The g values derived from MCD are compared with those of other methods in Table 4; here the agreement among the three methods is fairly good within the accuracy estimated. The g values from MCD seem to be in better agreement with those by Zeeman effect than are the calculated values.

Discussion for Er(ES). All the crystal levels of Er(ES) are doubly degenerate due to the Kramers degeneracy. The lowest crystal level of the $^4I_{15/2}$ state of Er(ES) is $\eta=\pm 5/2$. The population of the next level ($\eta=\pm 3/2$) which is 44 cm^{-1} higher than the lowest level, is 3 percent of that of the latter at 18 K. Thus, we can assume that all the absorption bands at 18 K originate only from the lowest crystal level. However, from the energy level diagram (Fig. 2), each of the bands except the band at about 24580 cm^{-1} should be considered to consist of two transitions to the excited crystal levels ($\eta=\pm 3/2$ and $\pm 1/2$), owing to low dispersion of the instrument used. Therefore, the estimate of g values is not so straightforward. In the $^4I_{15/2} \rightarrow {}^2G_{9/2}$ band consisting of only one transition, the absolute g values for the $^4I_{15/2}(\eta=\pm 5/2)$ and $^2G_{9/2}(\eta=$

Table 2. Faraday parameters divided by dipole strength D, central frequency ν_0, and half-width Δ at $1/e$ of the maximum absorption in Tm(ES) at 18 K

Transition	ν_0[a,b] (cm^{-1})	Δ (cm^{-1})	D (10^{-5} D^2)	A/D (β)	B/D[b] (β/cm^{-1})	C/D (β)
$^3H_6(0) \rightarrow {}^3F_3(\pm 2)$	14486	27	2.51	1.45	−0.0011	0
$^3H_6(0) \rightarrow {}^3F_2(\pm 2)$	15079	25	0.560	−1.34	−0.0037	0
$^3H_6(0) \rightarrow {}^1G_4(\pm 2)$	21168	20	0.254	1.89	−0.0057	0
$^3H_6(0) \rightarrow {}^1G_4(\pm 2')$	21279	23	2.35	0.11	0.0205	0
$^3H_6(0) \rightarrow {}^1D_2(\pm 2)$	27900	13	0.121	−1.23	0.0008	0
$^3H_6(\pm 1) \rightarrow {}^1D_2(\pm 1)$	27939	15	0.487	−0.66	(0)	1.30
$^3H_6(\pm 1) \rightarrow {}^3P_1(\pm 1)$	(36400)	22	0.207	−0.57	(0)	0.91

a) The data from Ref. 1. b) The values in parentheses are assumed ones.

Table 3. Faraday parameters divided by dipole strength D, central frequency ν_0, and half-width Δ at $1/e$ of the maximum absorption in Er(ES)

Excited state[a]	T (K)	ν_0 (cm^{-1})	Δ (cm^{-1})	D (10^{-5} D^2)	A/D (β)	B/D (β/cm^{-1})	C/D (β)
$^4S_{3/2}(\pm 3/2, \pm 1/2)$	80	18470	44	3.36	1.45	0.001	−0.21
	18		40	0.96	1.50		
$^4F_{5/2}(\pm 3/2, \pm 1/2)$	80	22270	54	3.71	1.39	0.013	−0.26
	18		40	1.97	1.02		
$^4F_{3/2}(\pm 3/2, \pm 1/2)$	80	22615	59	4.25	0.22	−0.003	−0.01
	18		42	4.09	0.12		
$^2G_{9/2}(\pm 3/2)$	80	24580	52	0.68	2.62	0.006	−0.86
	18		28	0.16	2.51		
$^2G_{9/2}(\pm 1/2, \pm 3/2')$	80	24670	42	2.89	1.64	−0.009	−0.10
	18		35	1.25	1.22		

a) The ground state is $^4I_{15/2}(\eta=\pm 5/2)$.

TABLE 4. COMPARISON OF THE g VALUES IN Tm(ES)

Level		Energy (cm^{-1})	g value		
Term	η		MCD[a]	Zeeman[b]	Calcd[c]
$^3H_6$	±1	32	1.11	1.00±0.20	0.55
$^3F_3$	±2	14486	1.45	1.88±0.10	2.17
$^3F_2$	±2	15079	1.34	1.46±0.02	1.51
$^1G_4$	±2	21168	1.89	1.80±0.03	1.52
	$\pm2'$	21279	0.11	0.00	0.40
$^1D_2$	±1	27900	1.99	—	2.27
	±2	27971	1.23	—	1.14
$^3P_1$	±1	≈36430	1.48 or 0.34	—	—

a) The absolute values. b) The data from Ref. 21. c) The data from Ref. 10.

$\pm3/2$) levels can be determined from the Faraday parameters. As seen in Table 3, the A/D values for each of the other four bands are almost constant and independent of temperature, but the C/D values over these bands are not consistent with each other and also are considerably different from the value of the $^4I_{15/2}(\eta=\pm5/2)\rightarrow{}^2G_{9/2}(\eta=\pm3/2)$ band. Therefore it will be difficult to extract useful information from these C/D values. When it is assumed that each A/D value of the above four bands is a simple sum of the values from the two transitions which are contained within a band, and the g value of the ground level is taken as 0.75, being the value from the Zeeman experiment,[20] the g values for the excited crystal level can be estimated. The g values thus obtained are compared with those of other methods in Table 5. The agreement between the g values from MCD and those of other methods is satisfactory, considering the above assumption.

TABLE 5. COMPARISON OF THE g VALUES IN Er(ES)

Level		Energy (cm^{-1})	g value		
Term	η		MCD[a]	Zeeman[b]	Calcd[c]
$^4I_{15/2}$	$\pm5/2$	0	0.86	0.75±0.03 0.74±0.02[d]	0.71
$^4S_{3/2}$	$\pm3/2$	18461	(2.47)	2.47±0.09	2.53
	$\pm1/2$	18487	1.00	—	0.84
$^4F_{5/2}$	$\pm3/2$	22256	(1.56)	1.56±0.15	1.57
	$\pm1/2$	22280	0.35	—	0.53
$^4F_{3/2}$	$\pm3/2$	22585	(1.05)	1.05±0.08	1.12
	$\pm1/2$	22632	0.28	—	0.37
$^2G_{9/2}$	$\pm3/2$	24582	1.82	−1.83±0.05	−2.26
	$\pm3/2'$	24661	(1.50)	−1.50±0.25	−0.96
	$\pm1/2$	24687	0.08	0.15±0.10	0.54

a) The absolute values. The values in parentheses are assumed ones. b) The data from Ref. 20. c) The data from Ref. 11. d) The value from paramagnetic resonance (Ref. 22).

In conclusion, it may be stated that with the aid of the knowledge of well-established energy levels, the g values of crystal levels can be estimated with considerable accuracy from MCD, and these values might be better than other calculated ones.

We wish to express our gratitude to Professor T. Kanda and his coworkers at Kobe University for their aid with the experiment at liquid helium temperature.

References

1) G. H. Dieke, "Spectra and Energy Levels of Rare Earth Ions in Crystals," Interscience Publishers, New York (1968). In this article there are the references up to 1967.
2) For Tm crystals: (a) D. N. Olsen and J. B. Gruder, *J. Chem. Phys.*, **54**, 2077 (1971) ($TmCl_3\cdot6H_2O$, Tm^{3+}:$YCl_3\cdot6H_2O$); (b) J. Stohr, D. N. Olsen, and J. B. Gruber, *ibid.*, **55**, 4463, 4472 (1971) and *ibid.*, **60**, 1697 (1974) ($TmCl_3\cdot6H_2O$); (c) E. A. Karlow and J. B. Gruber, *ibid.*, **55**, 4730 (1971) and *ibid.*, **62**, 1606 (1975) ($Tm_2(SO_4)_3\cdot8H_2O$); (d) R. C. Alig, R. C. Duncan, Jr., and B. J. Mokross, *ibid.*, **59**, 5837 (1973) (Tm^{3+}:$SrCl_2$, CaF_2); (e) J. Stohr, E. R. Seidel, and J. B. Gruber, *ibid.*, **61**, 4820 (1974) ($Tm_2(SO_4)_3\cdot8H_2O$). For Er crystals: (f) D. J. Randazzo, *J. Chem. Phys.*, **49**, 1808 (1968) (Er^{3+}:$GdCl_3$); (g) M. R. Brown, H. Thomas, J. S. S. Whiting, and W. A. Shand, *ibid.*, **50**, 881 (1969) (Er^{3+}:SrF_2); (h) M. R. Brown, H. Thomas, J. M. Williams, R. J. Woodward, and W. A. Shand, *ibid.*, **51**, 3321 (1969) (Er^{3+}:SrF_2); (i) E. Bernal, *ibid.*, **55**, 2538 (1971) (Er^{3+}:$CaWO_3$); (j) R. L. Cone, *ibid.*, **57**, 4893 (1972) ($Er(OH)_3$); (k) V. L. Dolan and A. A. Santiago Jr., *ibid.*, **57**, 4717 (1972) (Er^{3+}:$YAlO_3$); (l) W. T. Carnell, P. R. Field, and R. Sarup, *ibid.*, **57**, 43 (1972) (Er^{3+}: LaF_3, $ErCl_3\cdot6H_2O$); (m) J. B. Fenn Jr., J. C. Wright, and F. K. Fong, *ibid.*, **59**, 5591 (1973) (Er^{3+}: CaF_2).
3) J. Margerie, *Physica*, **33**, 238 (1967).
4) A. C. Boccara and B. Briat, *J. Phys. (Paris)*, **30**, 445 (1969).
5) J. Ferre, A. C. Boccara, and B. Briat, *J. Phys. (Paris)*, **31**, 63 (1970).
6) Y. Kato, T. Nagai, and T. Nakaya, *Chem. Phys. Lett.*, **39**, 183 (1976).
7) A. J. McCaffery, P. N. Schatz, and T. E. Lester, *J. Chem. Phys.*, **50**, 379 (1969).
8) D. R. Fitzwater and R. E. Rundle, *Z. Kristallogr.*, **112**, 362 (1959).
9) K. H. Hellwege, *Ann. Phys.*, **4**, 95 (1949).
10) E. Y. Wong and I. Richman, *J. Chem. Phys.*, **34**, 1182 (1961).
11) Y. Kato, T. Nagai, and A. Saika, to be published.
12) G. Racah, *Phys. Rev.*, **62**, 438 (1942); **63**, 367 (1943); **76**, 1352 (1949).
13) A. D. Buckingham and P. J. Stephens, *Ann. Rev. Phys. Chem.*, **17**, 399 (1966).
14) P. J. Stephens, *J. Chem. Phys.*, **52**, 3489 (1970).
15) B. G. Wybourne, "Spectroscopic Properties of Rare Earths," John Wiley & Sons, Inc., New York (1965), p. 207.
16) E. H. Erath (*J. Chem. Phys.*, **34**, 1985 (1961)) and Dieke (Ref. 1) have reported that the ion level which has the center of crystal levels at 24516 cm^{-1} is $^2H_{9/2}$. However, this level should be assigned to $^2G_{9/2}$ according to the present calculation (Ref. 11). The wave function of this level with $J=9/2$ is given by

$$|\Psi\rangle = -0.49152|^4F\rangle+0.43494|^2G(I)\rangle-0.39289|^2G(II)\rangle +0.24835|^4G\rangle+0.26420|^2H(I)\rangle-0.40396|^2H(II)\rangle +0.34670|^4I\rangle.$$

17) P. J. Stephens, *Chem. Phys. Lett.*, **2**, 241 (1968).
18) J. Badoz, M. Billardon, A. C. Boccara, and B. Briat, *Symp. Faraday Soc.*, **3**, 27 (1969).
19) Y. Kato and K. Nishioka, *Bull. Chem. Soc. Jpn.*, **47**, 1047 (1974).
20) K. H. Hellwege, S. Hufner, and H. G. Kahle, *Z. Phys.*, **160**, 149 (1960).
21) U. Johnsen, *Z. Phys.*, **152**, 454 (1958).
22) R. J. Elliott and K. W. Stevens, *Proc. R. Soc. London, Ser. A*, **219**, 387 (1953).

A Semi-empirical NDDO Method for All-valence-electron Systems. I. Hydrocarbons

Osamu KIKUCHI

Department of Chemistry, The University of Tsukuba, Sakura-mura, Ibaraki 300-31

(Received August 5, 1976)

A semi-empirical NDDO method is applied to the evaluation of the molecular geometries and excitation energies of a variety of hydrocarbons, both saturated and conjugated, and of the heats of reactions among these hydrocarbons. Two-center electron repulsion integrals are evaluated by the simple formulae derived from the corresponding theoretical formulae. The off-diagonal core matrix elements and core-core repulsion energies are estimated empirically. It is shown that the method gives good estimates of the molecular geometries and excitation energies and permissible values for the heats of reactions.

The understanding of a chemical reaction process requires a knowledge of the potential energy surfaces for the lowest and excited states. The MO method to be used in the study of a reaction process should well reproduce three quantities at the same time; the molecular geometries, the heats of reaction, and the excitation energies of the molecules. Many semi-empirical methods for all-valence-electron systems have been reported,[1-5] and the recent MINDO/3 version, in which a large number of parameters are introduced, reproduces satisfactorily the ground-state properties of molecules.[3] However, little attention has been paid to the simultaneous evaluation of the above three quantities. This paper will search for a semi-empirical method, which is at the same level of parametrization as in the MINDO/2 method,[4] and which gives good estimates of the above three quantities.

Most of the semi-empirical methods for all-valence electrons are modified versions of the CNDO and INDO approximations, while only a few are those of the NDDO (Neglect of Diatomic Differential Overlap) approximation.[5] The NDDO approximation may be difficult to parametrize or for use in evaluating a large number of additional integrals semi-empirically. However, it represents a more logical solution of the problem[6] than the CNDO and INDO approximations. In this study, the NDDO approximation was used. Two-center integrals were evaluated by the simple formulae which were derived from the corresponding theoretical formulae. Parameters were chosen so as to give, at the same time, well-balanced values for the above three quantities. The method was applied to several hydrocarbons, and the results were compared with the observed values.

Method

The LCAO-MO's for valence electrons are determined from Roothaan's LCAO-SCF equation.[7] The atomic integrals necessary for the calculation are evaluated by the following methods.

One-center electron repulsion integrals are evaluated from the Slater-Condon parameters, F_K and G_K, as in MINDO/2.[4]

Two-center electron repulsion integrals are evaluated from the integrals related to the local diatomic coordinate. Consider the integrals between AO's of two atoms, A and B:

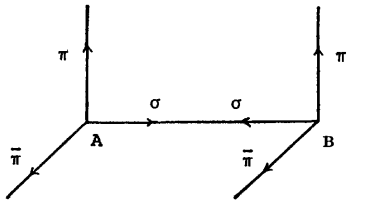

Fig. 1. Local diatomic coordinate and AO's of atoms A and B.

$$(\mu^A\nu^A|\lambda^B\sigma^B) \equiv \int \phi_\mu{}^A(1)\phi_\nu{}^A(1)\frac{1}{r_{12}}\phi_\lambda{}^B(2)\phi_\sigma{}^B(2)\mathrm{d}\tau_1\mathrm{d}\tau_2 \quad (1)$$

First, we transform the AO's, ϕ_μ's, into the local coordinate system of Fig. 1. The repulsion integrals of the original AO's can be expressed in terms of integrals between the transformed AO's. The integrals between the AO's of Fig. 1 are given by Roothaan.[8] In Roothaan's formulae, if the terms higher than the third order in $1/R_{AB}$ (R_{AB} is the distance between two atoms, A and B) are neglected, the integrals between the AO's of Fig. 1 are written as:

$$\begin{aligned}
&(s^As^A|s^Bs^B) \equiv \gamma_{AB}\\
&(\sigma^A\sigma^A|\sigma^B\sigma^B) = \gamma_{AB} + 6I_1\\
&(s^As^A|\sigma^B\sigma^B) = \gamma_{AB} + 3I_1\\
&(\sigma^A\sigma^A|\pi^B\pi^B) = \gamma_{AB} + \frac{3}{2}I_1\\
&(s^As^A|\pi^B\pi^B) = \gamma_{AB} - \frac{3}{2}I_1\\
&(\pi^A\pi^A|\pi^B\pi^B) = (\pi^A\pi^A|\bar{\pi}^B\bar{\pi}^B) = \gamma_{AB} - 3I_1\\
&(s^A\sigma^A|s^Bs^B) = (s^A\sigma^A|\sigma^B\sigma^B) = (s^A\sigma^A|\pi^B\pi^B) = I_2\\
&(s^A\pi^A|s^B\pi^B) = I_3\\
&(s^A\sigma^A|s^B\sigma^B) = I_4\\
&(\sigma^A\pi^A|\sigma^B\pi^B) = (\pi^A\bar{\pi}^A|\pi^B\bar{\pi}^B) = (s^A\pi^A|\sigma^B\pi^B) = 0
\end{aligned} \quad (2)$$

where s^A is the 1s or 2s AO of the A atom and where σ^A and π^A are the $2p\sigma$ and $2p\pi$ AO's of the A atom. They are defined in the local coordinate (Fig. 1). The I_i's are sub-integrals defined by Roothaan:

$$\begin{aligned}
I_1 &= [3S|3D\Sigma]\\
I_2 &= \frac{5}{2\sqrt{3}}[3S|3P\Sigma]\\
I_3 &= \frac{25}{12}[3P\Pi|3P\Pi]\\
I_4 &= \frac{25}{12}[3P\Sigma|3P\Sigma]
\end{aligned} \quad (3)$$

The sub-integral $[3S_a|3D\Sigma_b]$ is different from $[3S_b|3D\Sigma_a]$ when the A and B atoms are of different species. In the above formulae, this difference is neglected, though, and both are written as I_1.

The integrals between s orbitals, γ_{AB}, are calculated by using the Ohno-Klopman expression.[9] The sub-integrals, I_i's, are calculated by means of the following formulae:

$$\begin{aligned} I_1 &= 19.294 f R_{AB}\gamma_{AB}^4 \\ I_2 &= 1481.9 f R_{AB}\gamma_{AB}^3 \\ I_3 &= 0.5 I_4 = 52.263 f R_{AB}\gamma_{AB}^4 \end{aligned} \tag{4}$$

where $f=(F_2^A+F_2^B)/(F_0^A+F_0^B)$[5]. An explanation of these formulae is given in the Appendix. The values of the repulsion integrals calculated from (2) were compared with the theoretical values (Table 1). All two-center repulsion integrals (1) between the original AO's can be evaluated from the above integrals by means of:

$$\begin{aligned} &(s^A s^A|s^B s^B) = \gamma_{AB} \\ &(s^A s^A|s^B p_k^B) = a_{k\sigma} I_2 \\ &(s^A s^A|p_k^B p_l^B) = \delta_{kl}\gamma_{AB} + \frac{3}{2} I_1\{3a_{k\sigma}a_{l\sigma} - \delta_{kl}\} \\ &(s^A p_i^A|s^B p_k^B) = I_3\{\delta_{ik} + 3a_{i\sigma}a_{k\sigma}\} \\ &(s^A p_i^A|p_k^B p_l^B) = \delta_{kl}a_{i\sigma}I_2 \\ &(p_i^A p_j^A|p_k^B p_l^B) = \delta_{ij}\delta_{kl}\gamma_{AB} + \frac{I_1}{2}\{-6\delta_{ij}\delta_{kl} \\ &\qquad + 9\delta_{ij}a_{k\sigma}a_{l\sigma} + 9\delta_{kl}a_{i\sigma}a_{j\sigma}\} \end{aligned} \tag{5}$$

where s represents the s AO, and p_i, one of the $2p_x$, $2p_y$, and $2p_z$ AO's defined in the original coordinate. The $a_{i\sigma}$ is scalar product of two vectors, $\mathbf{e}_i$ and $\mathbf{e}_{AB}$, the unit vector directed along the i-axis and that directed from A toward B respectively. These expressions satisfy the correct transformation condition which ensures the invariance with respect to the rotation of axes.

TABLE 1. VALUES OF CARBON-CARBON TWO-CENTER REPULSION INTEGRALS FOR $R_{CC}=1.50$ Å.

Type	Values of integrals	
	Calcd using Slater AO's	Calcd from (2)—(4)
$(ss\|ss)$	9.21 eV	7.26 eV
$(s\sigma\|s\sigma)$	10.94	8.11
$(ss\|s\sigma)$	9.99	7.68
$(s\sigma\|\pi\pi)$	9.51	7.47
$(ss\|\pi\pi)$	8.82	7.05
$(\pi\pi\|\pi\pi)$	8.56	6.83
$(\pi\pi\|\bar{\pi}\bar{\pi})$	8.38	6.83
$(s\sigma\|ss)$	2.41	1.50
$(s\sigma\|s\sigma)$	2.77	1.50
$(s\sigma\|\pi\pi)$	2.23	1.50
$(s\sigma\|s\sigma)$	0.96	0.76
$(s\pi\|s\pi)$	0.78	0.38

The attraction $(\phi_\mu^A|V_B|\phi_\mu^A)$ between an electron in an AO ϕ_μ on the A atom and the core of the B atom was assumed to be:

$$(\phi_\mu^A|V_B|\phi_\mu^A) = -Z_B(\phi_\mu^A\phi_\mu^A|s^B s^B) \tag{6}$$

where $Z_B e$ is the core charge of the B atom. In the NDDO approximation, the attraction $(\phi_\mu^A|V_B|\phi_\nu^A)$ is also taken into account. This was assumed to be:

$$(\phi_\mu^A|V_B|\phi_\nu^A) = -Z_B(\phi_\mu^A\phi_\nu^A|s^B s^B) \tag{7}$$

by analogy with the diagonal parts. From these approximations, the core matrix elements between AO's on the same atom is written as:

$$H_{\mu\nu} = \delta_{\mu\nu}U_{\mu\mu} - \sum_{B(\neq A)} Z_B(\phi_\mu^A\phi_\nu^A|s^B s^B) \tag{8}$$

where $U_{\mu\mu}$ is the diagonal matrix element of ϕ_μ with respect to the one-electron Hamiltonian containing only the core of its own atom, the values of which are given by Baird and Dewar.[4] The off-diagonal elements between AO's on the different atoms are calculated by means of:

$$H_{\mu\nu} = \frac{1}{2}S_{\mu\nu}(\beta_\mu+\beta_\nu) \tag{9}$$

where $S_{\mu\nu}$ is the overlap integral and β_μ is a parameter which is empirically determined.

The core repulsion energy between the A and B atoms, *i.e.*, E_{core}^{AB}, must be equal to the electron-electron repulsion energy between the neutral atoms when $R_{AB}\to\infty$. $R_{AB}\to 0$, E_{core}^{AB} should tend to infinity. Many parametric expressions for E_{core}^{AB} which satisfy these conditions are possible. The following simple expressions are used in the present study:

$$\begin{aligned} E_{ore}^{AB} &= Z_A Z_B \gamma_{AB} && (R_{AB} > R_0) \\ E_{core}^{AB} &= Z_A Z_B\left\{\frac{b}{R_{AB}^a} + c\right\} && (R_{AB} < R_0) \end{aligned} \tag{10}$$

The constant, c, is determined by fitting values calculated from the two equations at $R_{AB}=R_0$. The a, b, and R_0 parameters are determined empirically.

Results and Discussion

The excitation energies of six hydrocarbons (CH_4, C_2H_6, C_3H_8, C_2H_4, C_4H_6, and C_2H_2) were calculated by the CI method, in which only singly excited configurations were taken into account in the evaluation of the singlet excited states. The relation between the values of β_μ and the excitation energies of these compounds was examined. The values of $\beta_{1s}(H)=-7.3$ eV, $\beta_{2s}(C)=-13.8$ eV, and $\beta_{2p}(C)=-9.5$ eV gave the best fit of the calculated excitation energies with the observed values. These β_μ values, however, were not appropriate for the estimation of the molecular geometries and heats of reactions. A compromise was thus made for the values of β_μ, and the values listed in Table 2 were used in all the calculations in this paper.

TABLE 2. VALUES OF β_μ(eV)

	1s(H)	2s(C)	2p(C)
β_μ	−7.5	−13.2	−9.3

In order to determine the parameters in the core-core repulsion energy (10), the calculated geometries of the above six hydrocarbons and the heats of reactions among them were compared with the observed values. The parameters were determined with the help of the

Table 3. Parameters in core-core repulsion formulae (10)[a]

	a	b	R_0
H-H	10.45	0.7436	2.642
H-C	14.00	0.5034	2.779
C-C	13.16	0.4899	3.621

a) The core-core repulsion energies calculated from the parameters are in eV units.

Davidon-Fletcher-Powell minimization technique.[10,11] They are listed in Table 3.

Molecular Geometry. The molecular geometries of typical hydrocarbons were calculated using the parameters determined above. They are listed in Table 4. The C–C and C=C bond lengths calculated agreed with the observed values within 0.03 Å (mean deviation; 0.01 Å), while the C≡C bond lengths were smaller than the observed values by 0.05 Å. The C–H bond lengths estimated agreed with the observed values within 0.01 Å. The bond angles also agreed well with the observed values (within 1 degree) except for the HCH angles; they were slightly smaller than the observed values. It seems that the present NDDO method predicts the geometries of hydrocarbons correctly.

Table 4. Calculated equilibrium geometries of hydrocarbons[a]

Compound	Type	Expt[12]	Calcd
Methane	C–H	1.091	1.090
Ethane	C–C	1.536	1.517
	C–H	1.107	1.095
	HCC	110.5	110.0
Propane	C–C	1.526	1.528
	C–H	1.091	1.098
	HCC	111.8	111.1
	CCC	112.4	111.4
Ethylene	C=C	1.332	1.315
	C–H	1.084	1.091
	HCH	115.4	112.5
Propene[b]	C–C	1.488	1.517
	C=C	1.353	1.324
	CCC	124.8	123.1
s-trans-Butadiene	C–C	1.483	1.483
	C=C	1.337	1.331
	CCC	122.4	123.9
Acetylene	C≡C	1.205	1.158
	C–H	1.059	1.069
Propyne[b]	C–C	1.459	1.466
	C≡C	1.206	1.162
Allene	C=C	1.308	1.292
	C–H	1.081	1.093
	HCH	116.0	110.8
Cyclopropane	C–C	1.524	1.531
	C–H	1.092	1.104
	HCH	118.2	106.1
Cyclobutane[b]	C–C	1.548	1.548
Cyclopropene[b]	C–C	1.525	1.514
	C=C	1.286	1.311
Cyclobutene[b]	C–C	1.551[c]	1.560
	=C–C	1.523[c]	1.530
	C=C	1.325[c]	1.343

a) Bond lengths in Å; bond angles in degrees. b) Geometries of CH(sp) and CH_2(sp^2, sp^3) groups were assumed to be those of acetylene, ethylene and cyclopropane. c) Estimated from Ref. 13.

Heats of Reactions. The heats of reactions among the above hydrocarbons were estimated by using the geometries obtained in the previous section (Table 5). The energy difference between *s-trans-* and *s-cis-*butadiene was correctly estimated. The agreement of the heats of the hydrogenations of unsaturated hydrocarbons with the observed values was not satisfactory, however, (the mean deviation for 8 examples was 7 kcal/mol). Considerable disagreements were found in the hydrogenations and additions related to ethylene or cyclic compounds. This comes form the fact that the calculated energy of ethylene is high (≈15 kcal/mol unstable) in comparison with other compounds, while those of cyclic compounds are quite low (stable).

Table 5. Calculated heats of reactions[a]

Reactions	Expt[14]	Calcd[b]
Hydrogenations		
acetylene → ethane	74.4	73.6
ethylene → ethane	32.7	47.6
propyne → propane	69.1	54.9
propene → propane	29.7	38.0
cyclopropene → cyclopropane	43.9	46.2
cyclobutene → cyclobutane	31.1	38.2
cyclopropane → propane	37.5	29.9
allene → propene	41.0	33.9
Isomerizations		
s-trans-butadiene → *s-cis*-butadiene	2.2	2.9
allene → propyne	1.6	17.0
cyclopropane → propene	7.8	−8.1
Additions		
acetylene + ethylene → *s-trans*-butadiene	40.4	51.8
acetylene + methane → propene	31.4	34.6
ethylene + methane → propane	30.2	46.6

a) Heats of reactions in kcal/mol. b) The molecular geometries listed in Table 4 were used in the calculation.

Excitation Energy. The excitation energies of several hydrocarbons were calculated by the CI method using their calculated geometries. In the CI calculation, only singly excited configurations were taken into account. The excitation energies are listed in Table 6. The MINDO/2 method, which includes parameters comparable to the present NDDO method and gives good estimates for the molecular ground-state properties, gives poor excitation energies. This is an obstacle to its application to photochemical reactions. The excitation energies obtained by the NDDO method agree with the observed values within 0.5 eV, however; this deviation is permissible in studies of photochemical processes.

Since a properly parametrized version of NDDO should be superior to a similar parametric version of

TABLE 6. LOWER THREE EXCITED SINGLET STATES AND THE LOWEST TRIPLET STATE OF HYDROCARBONS (eV)

Compound	Excited states	Calcd	Obsd[15]	MINDO/2
Methane	$^1T_2$	9.49	9.71	7.41
	$^1T_2$	11.02		
	$^1T_1$	11.27		
	$^3T_2$	8.15		
Ethane	^1E_u	9.01	9.40	6.24
	^1E_g	9.46		
	$^1A_{2u}$	9.70		
	^3E_u	8.42		
Propane	$^1B_1$	8.79	8.89	6.06
	$^1A_1$	9.23		
	$^1B_2$	9.27		
	$^3B_1$	8.03		
Ethylene	$^1A_{2g}(\sigma\rightarrow\pi^*)$	6.37		
	$^1B_{1g}(\pi\rightarrow\sigma^*)$	7.21		
	$^1B_{1u}(\pi\rightarrow\pi^*)$	7.45	7.6	5.32
	$^3B_{1u}(\pi\rightarrow\pi^*)$	3.09		
trans-Butadiene	$^1B_u(\pi\rightarrow\pi^*)$	5.91	6.0	4.93
	$^1A_u(\sigma\rightarrow\pi^*)$	6.03		
	$^1A_u(\pi\rightarrow\sigma^*)$	6.73		
	$^3B_u(\pi\rightarrow\pi^*)$	2.21		
Acethelene	$^1\Sigma_u$	5.73	5.23	4.13
	$^1\Delta_u$	6.29		
	$^1\Pi_u$	7.51		
	$^3\Sigma_u$	4.56		

INDO, it seems that the present NDDO method is not completed in its parametrization. However, it gives good estimates of the molecular geometries and excitation energies of hydrocarbons and permissible values of the heats of reactions among them. It may be fit for the evaluation of potential energy surfaces related to both thermal and photochemical reactions.

The author wishes to express his thanks to Professor Keizo Suzuki for his helpful suggestions.

Appendix

An explanation of Eqs. 4 will be given here. Consider the sub-integral $[3S|3D\Sigma]$ between carbon atoms. When $\rho \gg 1$ ($\rho \equiv R_{AB}(\zeta_A+\zeta_B)/a_0$, and when $R_{CC}=1.0$ Å corresponds to $\rho \simeq 6$), this is approximately expressed by:

$$[3S|3D\Sigma] \simeq \zeta/\rho^3 \qquad \text{(A-1)}$$

This means that the integral is approximated by a function of γ_{CC}^3 from the present semi-empirical point of view:

$$I_1 = c_1 R \gamma_{CC}^4 \qquad \text{(A-2)}$$

where $R\gamma_{CC}$ was introduced so that $I_1 \rightarrow 0$ when $R_{CC} \rightarrow 0$. To determine the coefficient, c_1, the sub-integral, $[3D\Delta|3D\Delta] \lesssim \zeta/\rho^5$, was approximated as a function of γ_{CC}^5:

$$[3D\Delta|3D\Delta] = c_2 \gamma_{CC}^5 \qquad \text{(A-3)}$$

If the present semi-empirical values of $[3D\Delta|3D\Delta]$ (namely$=4/27(pp'|pp') \propto F_2^C$) and γ_{CC} ($=F_0^C$) at $R_{CC}=0$ are used in (A-3), the relation between c_2 and the Slater-Condon parameters is obtained:

$$c_2 \propto (F_2^A+F_2^B)/(F_0^A+F_0^B)^5 \qquad \text{(A-4)}$$

where A and B represent two carbon atoms. The theorcoretical formulae indicate that the $[3S|3D\Sigma] \simeq [3D\Delta|3D\Delta]|\rho^2$ relation holds approximately.[8] Thus, the I_1 integral was expressed as:

$$I_1 = c_3 \frac{F_2^A+F_2^B}{(F_0^A+F_0^B)^5} R_{AB}\gamma_{AB}^4 \qquad \text{(A-5)}$$

The c_3 coefficient was determined by means of the following equation, the integral being evaluated at $R_{CC}=1.50$ Å:

$$(I_1^{theor}/I_1^{emp}) = (\gamma_{AB}^{theor}/\gamma_{AB}^{emp})^3 \qquad \text{(A-6)}$$

Though (A-5) is obtained from the carbon-carbon pair, (A-5) will be used for the integrals between other atomic pairs. The "F_2^H" value was estimated using the I_2 formula of (4) and an equation similar to (A-6); $F_2^H=7.802$ eV was obtained.

References

1) J. A. Pople, D. P. Santry, and G. A. Segal, *J. Chem. Phys.*, **43**, S129 (1965); J. A. Pople and G. A. Segal, *ibid.*, **43**, S136 (1965).
2) J. A. Pople, D. L. Beveridge, and P. A. Dobosh, *J. Chem. Phys.*, **47**, 2026 (1969); H. Fischer and H. Kollmar, *Theor. Chim. Acta*, **13**, 213 (1969); D. R. Salahab and C. Sandorfy, *Theor. Chim. Acta*, **20**, 227 (1971); A. DasGupta and S. Huzinaga, *ibid.*, **35**, 329 (1974); C. W. Eaker and J. Hinze, *J. Am. Chem. Soc.*, **96**, 4048 (1974); J. Del Bene and H. H. Jaffe, *J. Chem. Phys.*, **48**, 1807 (1968).
3) R. C. Bingham, M. J. S. Dewar, and D. H. Lo, *J. Am. Chem. Soc.*, **97**, 1285, 1294, 1302, 1307 (1975); M. J. S. Dewar, D. H. Lo, and C. A. Ramsden, *ibid.*, **97**, 1311 (1975).
4) N. C. Baird and M. J. S. Dewar, *J. Chem. Phys.*, **50**, 1262 (1969); N. Boder, M. J. S. Dewar, A. Harget, and E. Haselbach, *J. Am. Chem. Soc.*, **92**, 3854 (1970).
5) M. J. S. Dewar and G. Klopman, *J. Am. Chem. Soc.*, **89**, 3089 (1967); F. Hirota and S. Nagakura, *Bull. Chem. Soc. Jpn.*, **43**, 1642 (1970).
6) B. Voigt, *Theor. Chim. Acta*, **31**, 289 (1973).
7) C. C. J. Roothaan, *Rev. Mod. Phys.*, **23**, 69 (1951).
8) C. C. J. Roothaan, *J. Chem. Phys.*, **19**, 1445 (1951).
9) K. Ohno, *Theor. Chim. Acta*, **2**, 219 (1964); G. Klopman, *J. Am. Chem. Soc.*, **87**, 3300 (1965).
10) W. C. Davidon, *A. E. C. Res. Develop. Rep.*, ANL-5990 (1959); R. Fletcher and M. J. D. Powell, *Computer J.*, **6**, 163 (1963).
11) G. W. Stewart III, *J. Assoc. for Comput. Machinery*, **14**, 72 (1967).
12) E. Sutton, "Tables of Interatomic Distances," Special Publications No. 11, The Chemical Society, London (1958); see also references cited in Ref. 4.
13) H. Kim and W. D. Gwinn, *J. Chem. Phys.*, **42**, 3728; E. Goldwish, K. Hedberg, and V. Schomaker, *J. Am. Chem. Soc.*, **78**, 2714 (1956).
14) "Selected Values of Physical and Thermodynamic Properties of Hydrocarbons and Related Compounds," Carnegie Press, Pittsburgh (1953); see also references cited in Ref. 4.
15) B. A. Lombos, P. Sauvageau, and C. Sandorfy, *J. Mol. Spectrosc.*, **24**, 253 (1967); P. G. Wilkinson and R. S. Mulliken, *J. Chem. Phys.*, **23**, 1895 (1955); R. Pariser and R. G. Parr, *ibid.*, **21**, 767 (1953).

He I Photoelectron Spectra of Ethylene Carbonate and Related Compounds

Masafumi JINNO,* Iwao WATANABE, Yu YOKOYAMA, and Shigero IKEDA

Department of Chemistry, Faculty of Science, Osaka University, Toyonaka, Osaka 560

(Received August 7, 1976)

He I photoelectron spectra of ethylene carbonate, propylene carbonate, γ-butyrolactone, β-propiolactone and vinylene carbonate have been investigated. Assignments of an oxygen lone pair and nonbonding π orbitals have been made by means of analysis of vibrational structures and molecular orbital calculation. Many vibrational structures could be assigned to appropriate vibrational modes of the corresponding neutral molecules from a comparison with infrared and Raman spectra. Correlation among the orbital energies of the compounds is discussed.

Photoelectron spectral bands originating from the carbonyl oxygen lone pair and the nonbonding π orbitals of carbonyl compounds appear in the lower ionization energy range, lying sometimes close to each other. In the present report we deal with the photoelectron spectra of five heterocyclic carbonyl compounds, that is, ethylene carbonate and related compounds. The related compounds are derived from ethylene carbonate by the following substitution: 1) replacement of a hydrogen atom by a methyl group, 2) replacement of an esteric oxygen by a methylene group, 3) removal of an esteric oxygen, and 4) change of the single bond between the ethylenic carbons into a double bond. Their constitutional formulas are shown in Fig. 1.

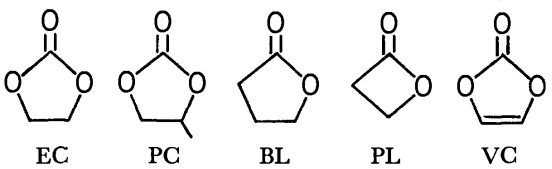

Fig. 1. Structural formulas of compounds investigated. EC: Ethylene carbonate, PC: propylene carbonate, BL: γ-butyrolactone, PL: β-propiolactone, VC: vinylene carbonate.

It has been proved that a comparison of a series of related compounds is useful for the assignment of their spectral bands to a particular molecular orbital, and that analysis of vibrational structures in some bands can be utilized for band assignment. By these means the effects of substitution on orbital energy and also orbital character could be clarified.

Experimental

He I resonance line at 58.4 nm emitted from a direct current discharge tube was used as an excitation light source. The discharge tube was so designed as to intensify the resonance line and to obtain photoelectron spectra of high signal-to-noise ratio. It has two coaxially aligned hollow electrodes and collimator capillaries to introduce the light produced within the whole discharge area into the ionization chamber. The photoelectron energy analyzer used was of a parallel plate type.[1] Xe gas was mixed with sample gas and used as an internal standard. A half width of Xe $2p_{3/2}$ peak was approximately 30 meV. The organic compounds used showed a tendency to broaden Xe peaks, probably due to in homogeneity of the surface potential caused by the adsorption of sample gas onto the analyzer electrodes.

Variation in room temperature caused a drift of the position of peaks, probably due to the variation in adsorption equilibrium caused by a change of the sample pressure. The ionization energy was therefore determined by measuring the sample peak and internal standard peak alternately several times. Coating of the electrode surface with graphite emulsion effectively lowered the background of the spectrum. Better resolution was obtained at a sample pressure above the pressure range in which there is a linear relation between sample pressure and spectral intensity. This might be related to the neutralization of the space charge in the ionization chamber by backscattered electrons and to the saturation of adsorbed sample gas.

Vinylene carbonate was synthesized from chloroethylene carbonate,[2,3] and purified by vacuum distillation. All the other compounds were chemicals of G. R. grade and used without purification. Samples in which residual water was detected were used after dehydration with anhydrous sodium sulfate or phosphorus pentoxide.

Laser Raman spectra of the three carbonates were taken for reference in the vibrational analysis of their photoelectron spectra.

Results and Discussion

Ethylene Carbonate and Propylene Carbonate. The lowest energy overlapping bands in the photoelectron spectra

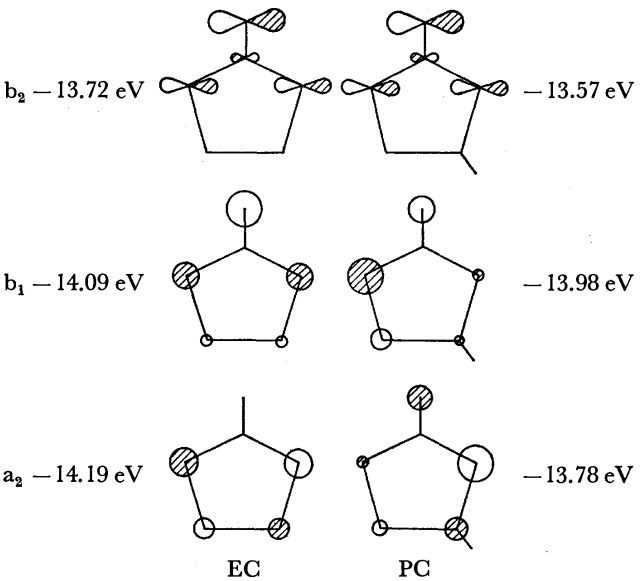

Fig. 2. Orbital energy and electron distribution of ethylene carbonate(EC) and propylene carbonate(PC) obtained from INDO calculation.

* Present address: Shimadzu Seisakusho, Ltd., Kuwabara-cho, Nakagyo-ku, Kyoto 604.

TABLE 1. IONIZATION ENERGY AND VIBRATIONAL FREQUENCY OF ETHYLENE CARBONATE AND PROPYLENE CARBONATE

	Band	Ionization energy, eV		Vibrational frequency, cm^{-1}		Band assignment
		adiabatic	vertical	ion	molecule	
Ethylene carbonate	1 st	10.70	10.89	1530	1765—1790[a]	$n_O(5b_2)$
				910	1065 [b]	
	2 nd		11.38			$\pi(2a_2)$
	3 rd		11.45			$\pi(3b_1)$
Propylene carbonate	1 st	10.52	10.71	1520	1785[a]	$n_O(b_2)$[c]
				820	960[b]	
	2 nd		11.17			$\pi(a_2)$[c]
	3 rd		11.27			$\pi(b_1)$[c]

a) Carbonyl stretching vibration. b) Skeletal stretching vibration. c) Propylene carbonate does not belong to the point group C_{2v}. However, the respective orbitals can be associated with b_2, a_2, and b_1 orbitals of ethylene carbonate from electron distribution.

of ethylene carbonate and propylene carbonate have been assigned to three appropriate molecular orbitals as a result of analysis of vibrational structures and INDO molecular orbital calculation.[4] The ionization energies and vibrational frequencies are given in Table 1. Figure 2 shows the orbital energies and electron distributions of ethylene carbonate and propylene carbonate obtained from the molecular orbital calculation.

Several reports have appeared on the ionization energies of the carbonyl oxygen lone pair orbital of ethylene carbonate.[5-8] However, there are discrepancies among the reported values both for the adiabatic and vertical ionization energies. We pointed out that the vertical ionization energy corresponds not to the highest peak but to the second peak in the main vibrational progression, this conclusion being derived from the reasoning that the second peak should be the most intense if the relative intensity of the peaks in the vibrational progression is not modified by the slope of the adjacent bands.[4]

The adiabatic ionization energy and the frequency of carbonyl stretching vibration we determined are consistent with the results obtained by Sweigart and Turner[5] (10.70 eV and 1500 cm^{-1}), but not with those by McGlynn *et al.*[7,8] (10.40 eV and approx. 1900 cm^{-1}). Variation in room temperature during the course of measurement causes a change of sample pressure in the sample reservoir, leading to apparent drift of ionization energy. Since the lowest energy overlapping bands obtained by McGlynn *et al.* are identical with ours and they used the same energy reference (Xe $2p_{3/2}$ 12.130 eV) as we did, the only possible explanation for the discrepancies seems to be a drift in the ionization energy in their measurement. Contraction of the ionization energy scale with the Xe $2p_{3/2}$ peak as a base point would result in a lowering of the adiabatic ionization energy and at the same time an increase in the vibrational frequency. The direction of the shift of their values relative to ours is in line with the above inference. Contrary to their results, the frequency of the carbonyl stretching vibration of the neutral molecule is usually reduced on ionization from the carbonyl oxygen lone pair orbital.

The vibrational spacing of the subsidiary vibrational progression in the first band is 910 and 820 cm^{-1} for ethylene carbonate and propylene carbonate, respectively.[4] The vibration should correspond to one of the skeletal stretching modes. Two skeletal stretching vibrations appear in the Raman spectra of ethylene carbonate (980 and 1065 cm^{-1}) and propylene carbonate (1125—1150 and 960 cm^{-1}). In many cases the ionization from a molecular orbital with almost the same electron distribution gives nearly the same reduction ratio of vibrational frequency of a neutral molecule to the corresponding cation among different molecules. Thus the vibrational frequencies giving the common reduction ratio, which is calculated to be 0.85, are 1065 cm^{-1} (for ethylene carbonate) and 960 cm^{-1} (for propylene carbonate). Angell[9] denoted the skeletal stretching vibrations of 980 and 1065 cm^{-1} in infrared spectra of ethylene carbonate by ν_4 and ν_5, respectively, which belong to the irreducible representation A_1. Thus the analysis of photoelectron spectra shows that the skeletal stretching vibration of 960 and 1125—1150 cm^{-1} in the Raman spectrum of propylene carbonate should

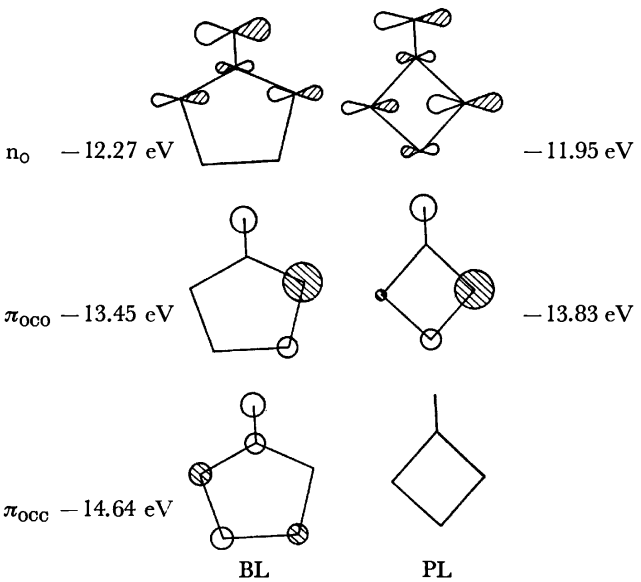

Fig. 3. Orbital energy and electron distribution of γ-butyrolactone(BL) and β-propiolactone(PL) obtained from INDO calculation. The esteric oxygen occupies the same position as shown in Fig. 1.

correspond to ν_5 and ν_4 in ethylene carbonate, respectively, *viz.*, a reversal in magnitude of the vibrational frequency of the two vibrational modes. This result shows that the methyl substituent effect on the frequency of skeletal stretching modes differs for ν_4 and ν_5. This effect could not be revealed by analysis of Raman or infrared spectra alone, even when the spectra for both carbonates were compared with each other.

γ-Butyrolactone and β-Propiolactone. Characteristic bands related to the ionization from the carbonyl oxygen lone pair and the nonbonding π orbitals were also studied for γ-butyrolactone and β-propiolactone in relation to ethylene carbonate. INDO molecular orbital calculation was made for these two lactones on the assumption of planar molecular configuration. The results are given in Fig. 3. The calculation shows that there are considerable differences between these compounds. Firstly, the lone pair orbital of γ-butyrolactone, $n_{O\gamma}$, is localized mainly on the two oxygen and one carbon atoms. On the other hand, that of β-propiolactone, $n_{O\beta}$, is fairly delocalized over all the skeletal atoms so that the electron density on the esteric oxygen atom is almost equal to that on the carbonyl oxygen atom. Secondly, γ-butyrolactone contains two π orbitals which can be thought to have a nonbonding character from the similarity in nodal plane to the nonbonding π orbitals of ethylene carbonate. They will be denoted by π_{OCO} and π_{OCC} according to the electron distribution. On the other hand, only one of the nonbonding π orbitals remains in β-propiolactone, which will be denoted by π'_{OCO}, corresponding to the orbital π_{OCO} in γ-butyrolactone.

The whole photoelectron spectra of γ-butyrolactone and β-propiolactone are shown in Fig. 4. The first band of γ-butyrolactone has several vibrational fine structures, as shown in Fig. 5. There are four main peaks with vibrational spacings of approximately 1530 cm^{-1}, which could be attributed to the excitation of the carbonyl stretching mode of the ion. The first band could be assigned to ionization from the carbonyl oxygen lone pair orbital, $n_{O\gamma}$. These spacings are almost equal to those of the n_O bands of ethylene carbonate and propylene carbonate. The three compounds give four

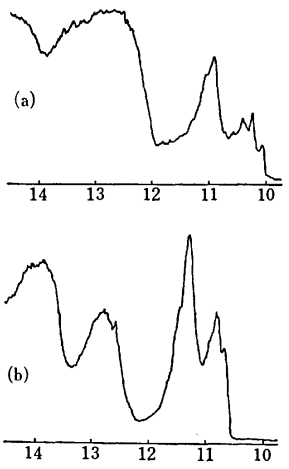

Fig. 4. (a) Photoelectron spectrum of γ-butyrolactone.
(b) Photoelectron spectrum of β-propiolactone.

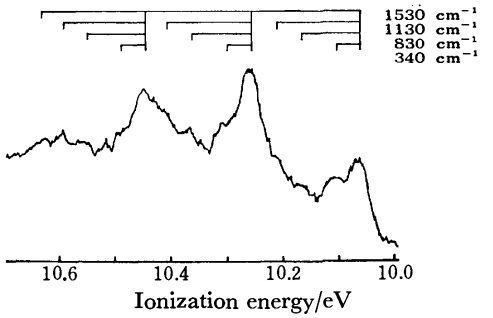

Fig. 5. First band of photoelectron spectrum of γ-butyrolactone.

sharp or prominent main peaks in the first band corresponding to the ionization from the lone pair orbitals. The number of fine structures shows that the change of geometry from neutral molecule to ion or the Franck-Condon factor seems to be almost equal to each other. It would be said that the degrees of localization of the lone pair orbital are almost equal among these molecules. There are further three weak peaks on the higher ionization energy side of each main peak of γ-butyrolactone, which are not seen in the spectrum of ethylene carbonate. Vibrational spacings from each main peak are approximately 340, 830, and 1130 cm^{-1} for the three peaks. From a comparison with the infrared and Raman spectra, the vibrational spacings of 1130 cm^{-1} might be attributed to the excitation of the skeletal stretching mode of the ion, which is 1170 cm^{-1} in the neutral molecule. Appearance of two more vibrational excitations for γ-butyrolactone should be attributed to the substitution of a methylene group for an oxygen atom in ethylene carbonate and, at the same time, change of molecular symmetry. The adiabatic and vertical ionization energies of the first band of γ-butyrolactone are 10.06 and 10.26 eV, respectively. The vertical one is identical to the value reported by Bain and Frost.[6]

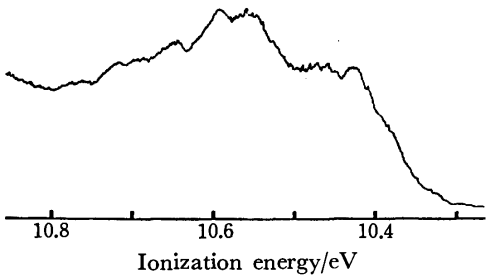

Fig. 6. First band of photoelectron spectrum of β-propiolactone.

The orbitals of the first band in the photoelectron spectrum of β-propiolactone are shown in Fig. 6. There are many peaks, but they are very complex and cannot be attributed to any harmonic vibrational progressions. This tendency has been reported as regards the photoelectron spectra of cycloalkanones.[10] Cyclobutanone gives a complex first band, while cyclopentanone clearly shows some vibrational progressions. The complexity may be due to the change in hybridization of the lone pair orbital of the carbonyl oxygen atom resulting from the strain of the ring. In fact, the results of molecular

orbital calculations shown in Fig. 3 indicate a marked change in electron distribution, *viz.*, the delocalization of $n_{O\beta}$ orbital over all the skeletal atoms. The somewhat unusual aspect of the first band of β-propiolactone seems to be associated with the result of infrared study by Durig,[11] which showed that the vibration of this molecule is very anharmonic.

The second band of γ-butyrolactone can be compared with the second band of β-propiolactone. Each second band has a shoulder on its higher ionization energy side. These peaks are fairly broad as compared with those in the first band. The second bands in the two spectra can be assigned to the ionization from the approximately nonbonding π orbital, π_{OCO} in γ-butyrolactone and π'_{OCO} in β-propiolactone from the results of molecular orbital calculation and the similarity in spectral shapes. Intensity ratios of the π band to the first band are almost equal for the two compounds, indicating that only one orbital is involved in the second band of γ-butyrolactone. The spacing between the shoulder and the main peak could not be attributed to any vibrational progression, since the peak for the adiabatic ionization cannot be distinguished. The vertical ionization energy of π_{OCO} orbital for γ-butyrolactone is 10.93 eV and that of π'_{OCO} orbital for β-propiolactone is 11.20 eV.

The molecular orbital calculation predicts that the second nonbonding π orbital, π_{OCC}, of γ-butyrolactone should exist approximately 1 eV below the first nonbonding π orbital, and that three σ orbitals cluster together with the second nonbonding π orbital in an energy range of approximately 2 eV. As a matter of fact, the photoelectron spectrum of γ-butyrolactone indicates that the third band begins to rise at 12 eV (approximately 1 eV higher than the second band), and that a number of bands overlap in the energy range 12—14 eV, supporting the prediction of the molecular orbital calculation. Thus the adiabatic ionization energy of the π_{OCC} orbital could be estimated to be 12 eV or higher. The results are summarized in Table 2.

Vinylene Carbonate. Vinylene carbonate is a cyclic carbonate ester of the hypothetical enediol and differs from ethylene carbonate in having a double bond in the ring structure. The molecule is considered to have a planar configuration and consequently C_{2v} symmetry in gaseous phase from the results of microwave spectroscopic study by Slayton *et al.*[12] Infrared and Raman spectroscopic studies for this molecule were carried out by Dorris *et al.*[13]

The photoelectron spectrum of vinylene carbonate gives three well separated prominent bands in the lower ionization energy region. Each of the three bands shows distinct vibrational progressions.

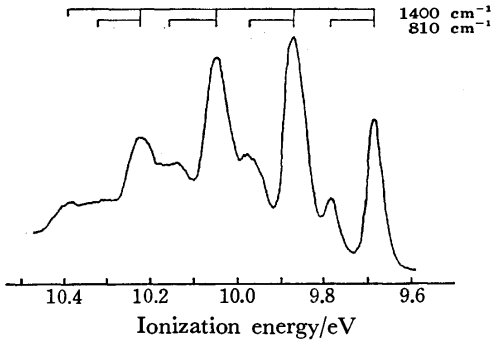

Fig. 7. First band of photoelectron spectrum of vinylene carbonate.

The first band (Fig. 7) has five main peaks with vibrational spacings of approximately 1400 cm^{-1}, each main peak being accompanied by one subsidiary peak. The spacings between the subsidiary and main peaks are approximately 810 cm^{-1}.

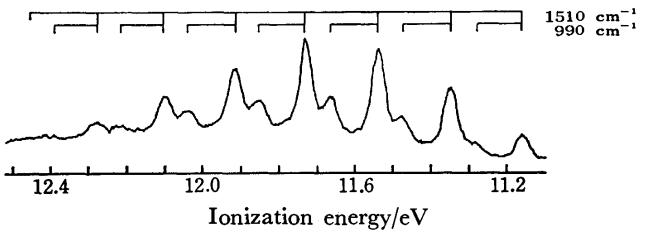

Fig. 8. Second band of photoelectron spectrum of vinylene carbonate.

The second band (Fig. 8) has at least eight main peaks with vibrational spacings of approximately 1510 cm^{-1} and subsidiary peaks approximately 990 cm^{-1} apart from each main peak.

The third band (Fig. 9) is on the slope of the next broad band, having at least four main peaks with vibrational spacings of approximately 1900 cm^{-1}. Each main peak is accompanied by three subsidiary peaks,

TABLE 2. IONIZATION ENERGY AND VIBRATIONAL FREQUENCY OF γ-BUTYROLACTONE AND β-PROPIOLACTONE

	Band	Ionization energy, eV		Vibrational frequency, cm^{-1}		Band assignment
		adiabatic	vertical	ion	molecule	
γ-Butyrolactone	1 st	10.06	10.26	1530		n_O
				1130	1170[a]	
				830		
				340		
	2 nd		10.93			π_{OCO}
	3 rd	>12.0				π_{OCC}
β-Propiolactone	1 st		10.7	anharmonic		n_O
	2 nd		11.20			π_{OCO}

a) Skeletal stretching vibration.

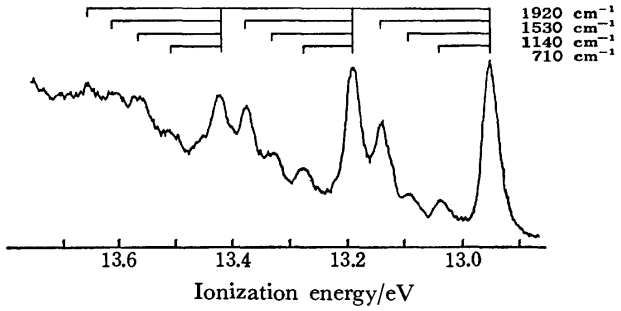

Fig. 9. Third band of photoelectron spectrum of vinylene carbonate.

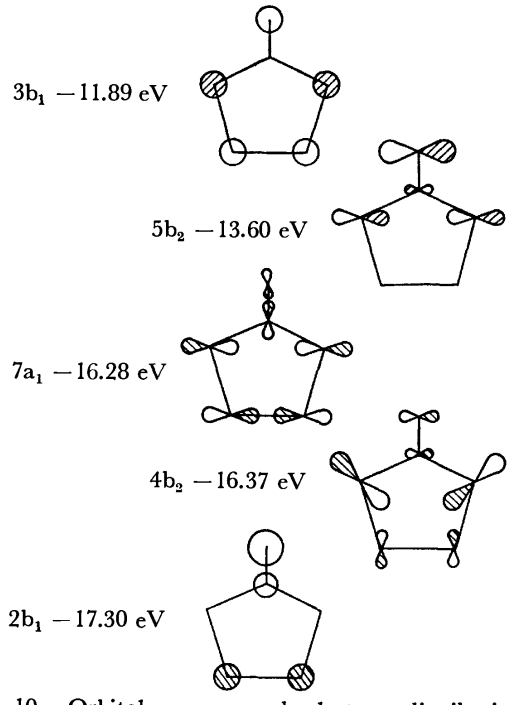

Fig. 10. Orbital energy and electron distribution of vinylene carbonate obtained from INDO calculation.

approximately 1530, 1140, and 710 cm^{-1} apart from each main peak.

INDO molecular orbital calculation shows possible orbitals to be assigned to these three bands (Fig. 10), which are denoted by $3b_1$, $5b_2$, $7a_1$, $4b_2$, and $2b_1$ after the notations for ethylene carbonate. The double bond in the ring structure changes the situations of some orbitals.

The $5b_2$ and $4b_2$ orbitals of vinylene carbonate are almost equal in energy to the $5b_2$ and $4b_2$ orbitals, respectively, of ethylene carbonate. However, introduction of the double bond into the ring structure results in the promotion of the $3b_1$ orbital energy above the $5b_2$ orbital energy. The results of calculation indicate that the $3b_1$ orbital should have the lowest ionization energy. This was confirmed by the following vibrational analysis of the photoelectron spectrum of vinylene carbonate. The vibrational spacings of approximately 1400 cm^{-1} in the first band would correspond to the excitation of the skeletal stretching mode reduced from 1625 cm^{-1} in the neutral molecule. The vibrational mode is mainly dominated by the vibration between the ethylenic carbons. Thus such a reduction suggests the ionization from an orbital having a bonding character between the ethylenic carbons, such as $3b_1$, $7a_1$, and $2b_1$ orbitals. Since the orbital energy of $3b_1$ orbital is raised higher than that of the highest occupied π orbital of ethylene (−10.5 eV) by introduction of vinylene group, the first band could be assigned to $3b_1$ orbital (*cf.* Section "Correlation of Orbital Energies of Five Compounds). The vibrational spacings of approximately 810 cm^{-1} could be ascribed to the skeletal breathing vibration in the ion reduced from 911 cm^{-1} in the neutral molecule. The adiabatic and vertical ionization energies can easily be determined to be 9.68 and 9.87 eV, respectively.

The results of calculation also predict that the second band corresponds to the ionization from the $5b_2$ orbital. The vibrational spacings of approximately 1510 cm^{-1} in the main vibrational progression would correspond to the carbonyl stretching mode in relation to the assignment in the previous sections. Thus the second can be assigned to the ionization from the $n_O(5b_2)$ orbital in accordance with expectation from the calculated orbital energy. The spacings of approximately 990 cm^{-1} would correspond to the skeletal stretching mode reduced from 1100 cm^{-1} in the neutral molecule. The skeletal stretching frequency of the ions is higher than that of ethylene carbonate. The reduction ratio of the frequency is approximately 0.90, indicating that the change in skeletal bonding strength is somewhat smaller than that of ethylene carbonate. The discrepancy would be caused by the existence of the double bond in the ring structure of vinylene carbonate. At least eight components appear in the main vibrational progression ascribed to carbonyl stretching, while there are only four components in the lone pair photoelectron band of ethylene carbonate. This implies that the molecular geometry is rather largely changed by the ionization from the $5b_2$ orbital than in ethylene carbonate. The change in carbonyl oxygen-carbon distance seems similar to that of ethylene carbonate where the reduction ratio is approximately 0.82. Many vibrational components are found in the band corresponding to the ionization accompanied by a drastic change of molecular symmetry, *e.g.* in the first band of ammonia (pyramidal to planar). It could thus be said that not only the carbonyl carbon-oxygen distance but also the C_{2v} symmetry in the neutral molecule change with the photoionization from the $5b_2$ molecular orbital of vinylene carbonate. The adiabatic and vertical ionization energies for the $5b_2$ lone pair orbital of vinylene carbonate are 11.16 and 11.73 eV, respectively. The vertical one differs from the value reported by Bain and Frost[6] by a unit of vibrational spacings, approximately 0.19 eV.

The vibrational spacings of approximately 1900 cm^{-1} in the third band are considerably large compared with the largest possible vibration of the neutral molecule. In this case, it is necessary to refer to the characters of molecular orbitals. From the results of calculation, any of the $7a_1$, $4b_2$, and $2b_1$ orbitals around −16.5 eV could be taken for the third band. Their orbital energies seem to be almost degenerate from molecular orbital calculation alone and it would be impossible to choose

an appropriate one among them. In this case the characteristic vibrational spacings mentioned above could be used as a clue to the assignment of the third band. A possible mode of vibration to be assigned to the vibrational spacings of approximately 1900 cm^{-1} is the carbonyl stretching or the skeletal stretching involving the carbon-carbon double bond stretching. The $7a_1$ molecular orbital has a strong bonding character between the double bond in the ring structure. It has also the same character for the carbon-oxygen double bond of the carbonyl group. If an electron is ionized from this orbital, these bonds would reduce their bonding character. As a result, the vibrational frequencies corresponding to these bonds should be reduced relative to those in the neutral molecule. This orbital is not suitable for explaining the high frequency in the ion. The same discussion can also be applied to the case of the $2b_1$ orbital. The $4b_2$ orbital reveals a bonding character in the carbon-oxygen double bond and an antibonding character in the carbon-carbon double bond. The ionization of an electron from such an orbital would cause a desirable change, *viz.*, carbon-carbon double bond in the ring should be stronger in the ion than in the neutral molecule. The vibrational spacings of approximately 1900 cm^{-1} could be attributed to the skeletal stretching mode of the ion, the wave number of which is 1625 cm^{-1} in the neutral molecule. Thus, the third band could be assigned to the ionization from the $4b_2$ orbital. Necessarily the vibrational spacings of approximately 1530 cm^{-1} could be attributed to the carbonyl stretching mode reduced from 1830 cm^{-1} in the molecule and the spacings of 1140 and 710 cm^{-1} could be attributed to the skeletal breathing and skeletal stretching mode which are 911 and 1100 cm^{-1}, respectively, in the neutral molecule. A study by means of group theory shows that five vibrational modes belonging to an irreducible representation A_1 are possible for six atoms except C–H vibrations. Four of them can be found in the third band showing that the $4b_2$ orbital is actually distributed on the whole skeletal structure. The other one is the carbonyl bending vibration which would not be excited through a photoionization process. The results are summarized in Table 3.

Correlation of Orbital Energies of Five Compounds. The vertical ionization energies of the oxygen lone pair and nonbonding π orbitals of the five compounds are shown in the form of a correlation diagram in Fig. 11. Propylene carbonate, γ-butyrolactone, and β-propiolactone do not belong to the point group C_{2v}. However, the π orbitals of these compounds can be associated with the b_1 or a_2 orbital of ethylene carbonate from a consideration of electron distribution.[4]

Table 3. Ionization energy and vibrational frequency of vinylene carbonate

Band	Ionization energy, eV		Vibrational frequency, cm^{-1}		Band assignment
	adiabatic	vertical	ion	molecule	
1 st	9.68	9.87	1400	1625[b]	$\pi(3b_1)$
			810	911[c]	
2 nd	11.16	11.73	1510	1830[a]	$n_O(5b_2)$
			990	1100[b]	
3 rd	12.95	12.95	1900	1625[b]	
			1530	1830[a]	
			1140	911[c]	$(4b_2)$
			710	1100[b]	

a) Carbonyl stretching vibration. b) Skeletal stretching vibration. c) Skeletal breathing vibration.

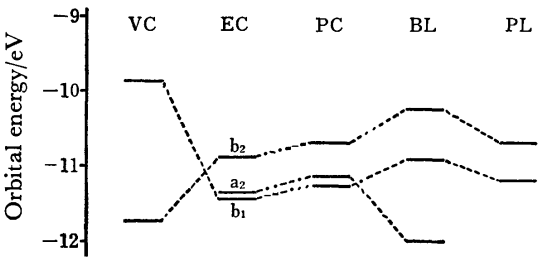

Fig. 11. Correlation diagram of observed orbital energies for ethylene carbonate and related compounds.

Oxygen Lone Pair Orbital n_O: The orbital of propylene carbonate is destabilized (0.18 eV) relative to ethylene carbonate due to the electron releasing effect of methyl group.[4] The orbital of γ-butyrolactone is destabilized (0.63 eV) as a result of the substitution of esteric oxygen with methylene, which is less electronegative than the former. The degree of orbital stabilization of β-propiolactone relative to γ-butyrolactone (0.44 eV) is approximately the same as that of cyclobutanone relative to cyclopentanone (0.36 eV), which was attributed to the hybridization change as well as an inductive effect of a methylene chain.[10] The orbital stabilization of vinylene carbonate relative to ethylene carbonate (0.84 eV) is in line with that of cyclopenten-3-one relative to cyclopentanone (approximately 0.2 eV), which could also be attributed to the greater electronegativity of sp^2-carbons as compared with sp^3-carbons.[14,15]

Nonbonding π Orbitals: The nonbonding π orbitals of propylene carbonate destabilize (approximately 0.2 eV) relative to the corresponding orbitals of ethylene carbonate due to the electron releasing effect of methyl group. γ-Butyrolactone and β-propiolactone belong to the point group C_s in a planar molecular configuration. When the molecular symmetry is lowered from C_{2v} to C_s, the representations B_1 and A_2 are changed to A″, and the b_1 and a_2 orbitals go over into a″ orbitals. Thus the accidentally degenerate b_1 and a_2 orbitals of ethylene carbonate can interact with each other to generate the π_{OCO} and π_{OCC} orbitals in γ-butyrolactone. Inspection into the electron distribution shows that the π_{OCO} orbital is more closely related to the b_1 orbital and the π_{OCC} orbital to the a_2 orbital. Destabilization of the π_{OCO} orbital (0.52 eV) could result from both the substitution of an esteric oxygen with methylene and the interaction, accompanied by the stabilization of the π_{OCC} orbital ($<$0.6 eV). π_{OCC} orbital stabilization of β-propiolactone relative to γ-butyrolactone (0.27 eV) could be explained by an inductive effect of a methylene chain.

In contrast to the n_O orbital the nonbonding $\pi(b_1)$ orbital of vinylene carbonate is destabilized (1.58 eV) relative to the corresponding orbital of ethylene carbonate. The destabilization could be explained by assuming that the two carbonates are a composite

molecule of a localized carbonate and a localized hydrocarbon groups (ethylene and vinylene groups, respectively) and that symmetric π orbitals of the carbonate and hydrocarbon groups combine in a reversed phase to produce the $\pi(b_1)$ orbital. The energy of the symmetric π orbitals of the vinylene group was taken as -10.51 eV from the energy of the highest occupied π orbital of ethylene.[16] That of the ethylene group (-15.4 eV) was adopted from the energy of ethane $1e_u$ orbital which belongs to the pseudo-π molecular orbitals built from e-type methyl orbitals.[17] The energy of the symmetric π orbital of the carbonate group cannot readily be estimated. However, it should be around -12 or -13 eV, since the energy level of an oxygen π orbital is found around this energy range in such molecules as water, formic acid *etc.* Thus, the symmetric π orbital of the vinylene group lies higher than the corresponding one of the carbonate group. In ethylene carbonate the b_1 orbital is somewhat destabilized relative to the orbital energy of the carbonate group due to the interaction between the orbitals of the ethylene and the carbonate groups. In vinylene carbonate, on the other hand, such an interaction leads to the destabilization of the b_1 orbital higher up than the orbital energy of the vinylene group.

References

1) Y. Yokoyama, I. Watanabe, and S. Ikeda, *Bunseki Kagaku*, **20**, 1502 (1971).
2) M. S. Newman and R. W. Addor, *J. Am. Chem. Soc.*, **75**, 1263 (1953).
3) N. D. Field and J. R. Schaefgen, *J. Polym. Sci.*, **58**, 533 (1962).
4) Y. Yokoyama, M. Jinno, I. Watanabe, and S. Ikeda, *J. Electron Spectrosc.*, **5**, 1095 (1974).
5) D. A. Sweigart and D. W. Turner, *J. Am. Chem. Soc.*, **94**, 5592 (1972).
6) A. D. Bain and D. C. Frost, *Can. J. Chem.*, **51**, 1245 (1973).
7) J. L. Meeks, J. F. Arnet, D. Larson, and S. P. McGlynn, *Chem. Phys. Lett.*, **30**, 192 (1975).
8) S. P. McGlynn and J. L. Meeks, *J. Electron Spectrosc.*, **8**, 85 (1976).
9) C. L. Angell, *Trans. Faraday Soc.*, **52**, 1178 (1956).
10) D. Chadwick, D. C. Frost, and L. Weiler, *Tetrahedron Lett.*, **1971**, 4543.
11) J. R. Durig, *Spectrochem. Acta*, **19**, 1225 (1963).
12) G. R. Slayton, J. W. Simmons, and J. H. Goldstein, *J. Chem. Phys.*, **22**, 1678 (1954).
13) K. L. Dorris, J. E. Boggs, A. Danti, and L. L. Altpeter, Jr., *J. Chem. Phys.*, **46**, 1191 (1967).
14) D. Chadwick, D. C. Frost, and L. Weiler, *J. Am. Chem. Soc.*, **93**, 4320 (1971).
15) G. Hentrich, E. Gunkel, and M. Klessinger, *J. Mol. Struct.*, **21**, 231 (1974).
16) A. D. Baker, C. Baker, C. R. Brundle, and D. W. Turner, *Int. J. Mass Spectrosc. Ion Phys.*, **1**, 285 (1968).
17) J. N. Murrell and W. Schmidt, *J. Chem. Soc., Faraday Trans. 2*, **68**, 1709 (1972).

The Sol-Gel Transition of Sodium Deoxycholate Solutions under High Pressures

Gohsuke SUGIHARA, Toshiaki UEDA, Shoji KANESHINA,* and Mitsuru TANAKA

Department of Chemistry, Faculty of Science, Fukuoka University, Nanakuma, Nishi-ku, Fukuoka 814
**College of General Education, Kyushu University, Ropponmatsu, Chuo-ku, Fukuoka 810*

(Received August 11, 1976)

The effect of pressure on the sol-gel transition of sodium deoxycholate (SDC) solutions was investigated by the electric conductivity method up to 2000 atm in the temperature range from 10 to 65 °C. The gelation of SDC solutions is effected more easily at lower temperatures, at higher pressures, and at higher concentrations of SDC. The changes in the volume ($\Delta\bar{V}^{(\alpha\beta)}$), the enthalpy ($\Delta\bar{H}^{(\alpha\beta)}$), and the entropy ($\Delta\bar{S}^{(\alpha\beta)}$) of gelation were calculated thermodynamically. The values for $\Delta\bar{V}^{(\alpha\beta)}$, $\Delta\bar{H}^{(\alpha\beta)}$, and $\Delta\bar{S}^{(\alpha\beta)}$ are all negative under the conditions of this experiment. Therefore, it is concluded that the gel formation of SDC is attributable to intermolecular hydrogen bonds.

One of the most unique characteristics of sodium deoxycholate (SDC) is its specific hydrolysis, *i.e.*, the pH change in aqueous solutions, and another is its polymer-like aggregation. The relation between these two characteristics has been studied by the present authors[1-3] and by Rich and Blow.[4] The micelle formation of SDC in aqueous solutions is well known. The formation of polymer-like aggregates in the aqueous solution of SDC was described for the first time by Rich and Blow.[4,5] Under suitable conditions, the micelles of SDC aggregate secondarily to form a gelatinous complex with macromolecular dimensions in a solution. X-Ray diffraction studies of the fibers of this complex showed that the molecules assume an elongated helical configuration 3.6 nm in diameter. Botré *et al.*[6] have studied the stability of the polymer-like structure and the effect of cations on the sol-gel transition of deoxycholic acid in aqueous solutions. One of the present authors previously suggested that the polymer-like aggregates of SDC were formed by intermolecular hydrogen bonding between the 3α-hydroxyl group and the carboxyl group of SDC.[1] In spite of these studies, however, there remain many problems to be solved with respect to the gelation of bile salt solutions. In order to make clear the mechanism of gelation, it is useful to investigate the sol-gel transition as a function of the pressure as well as of the temperature and concentration, because the study of the pressure effect affords effective thermodynamic information. In this study we will examine the pressure effect on the sol-gel transition of SDC solutions by means of the electric conductivity method.

Experimental

Materials. The SDC (Merck Co.) was recrystallized from a mixed solvent of methanol and ethanol. All the other chemicals used were of a guaranteed reagent grade. The thrice-distilled water used was previously freed from CO_2 gas by passing the air through a soda-lime column.

Apparatus. The high-pressure apparatus used in the present study consists of a pressure generator and a pressure vessel. A screw- and hand-pump (Hikari Kikai Co.) was used as a pressure generator. The pressure vessel was made of stainless steel (SUS 27) so as to withstand pressures up to 3000 atm; 80 mm o.d., 20 mm i.d., and 250 mm height. The pressure generator and vessel were connected with a piece of flexible stainless steel tubing (1/8 in. o.d. and 0.024 in. i.d.). The prevention of oil leakage from the vessel and the connection between conductivity cell and electrical leads are devised in a manner described before.[7] The conductivity cell fitted with platinized platinum electrodes was made by modifying an injector. The specific conductivity of SDC solutions was measured by means of a Yanagimoto conductivity outfit, Model MY-8. The cell constant was checked with a KCl solution before and after applying high pressures; no change was observed. The pressures were measured within an accuracy of ±3.5 atm by means of a Heise pressure gauge. The thermostatted bath in which the pressure vessel was immersed was regulated within ±0.01 °C. The measurement of the conductivity was carried out in the temperature range from 10 to 65 °C, and in the pressure range from 1 to 2200 atm.

Procedure. The preparation of the SDC solution and of the gel was performed according to the method of Botré *et al.*[6] so as to confirm their results. The SDC gel was obtained by dissolving a known amount of SDC in water and by then adjusting the pH value to 6.85 at 20 °C by adding a small amount of HCl under continuous and con-

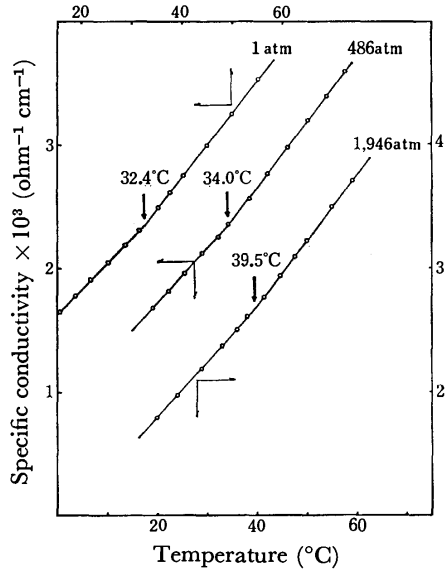

Fig. 1. The specific conductivity of SDC solution (3.180 × 10^{-2} mol/kg) as a function of temperature. The break in the slope indicates a transition.

stant stirring. All the gels obtained were stored at about 5 °C, and the gels used for measurements were permitted to stand for at least 20 h after the preparation.

The temperature of the sol-gel transition was decided as follows. The specific conductivity of an SDC solution with a given concentration was measured at various temperatures and at a desired constant pressure. The temperature was raised or lowered so slowly that the solution reached a sufficient equilibrium. It was confirmed by the constancy of the conductivity that the equilibrium was established after the thermostatted bath had been regulated at a constant temperature.

The specific conductivity measured at a constant pressure and concentration was plotted against the elevating temperature, resulting in the two straight lines which intersect each other at a certain temperature, as is shown in Fig. 1. The temperature corresponding to the break in these lines indicates the exact transition temperature,[6] which can be determined under various pressures as well as under atmospheric pressure. The strict determination of the transition temperature was performed by computing the intersection point of the two straight lines obtained by the least-squares method. The differences between the transition temperatures determined on elevating the temperature and on lowering the temperature were within 1 °C.

Results

Plotting the transition temperature at various concentrations of SDC against the pressure, straight lines are obtained, as is shown in Fig. 2. This figure shows a sol-gel phase diagram of the SDC–HCl solution system at different concentrations of SDC. The phase on the left-hand side of each curve is of a gel, while the phase on the right-hand side is of a sol. On the curves, the sol and gel phases may coexist in equilibrium.

In Fig. 3, the logarithm of the SDC concentration (in mole fraction) on the gelation at given pressures

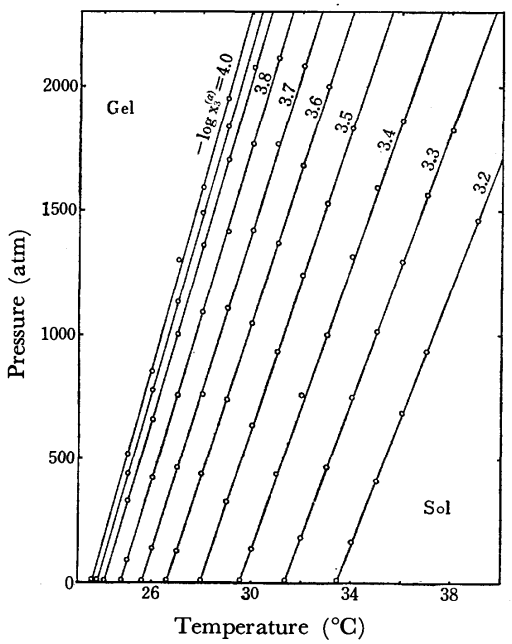

Fig. 2. Sol-gel phase diagram of SDC solutions at various concentrations. Numerical values indicate $-\log X_3^{(\alpha)}$. These relations are of Eq. 13 in the text.

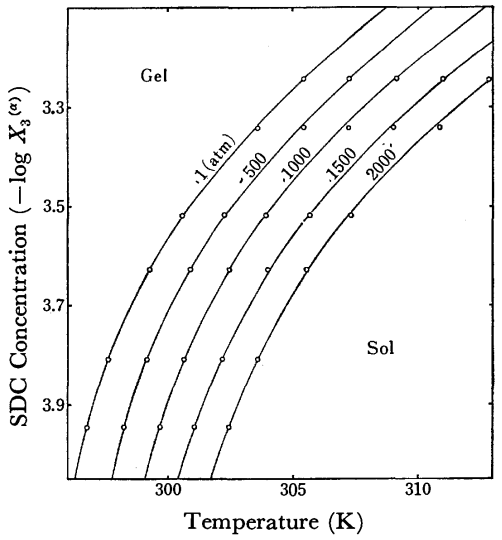

Fig. 3. Sol-gel phase diagram of SDC solutions at various pressures. Numerical values indicate pressure in atm. These relations are of Eq. 14 in the text.

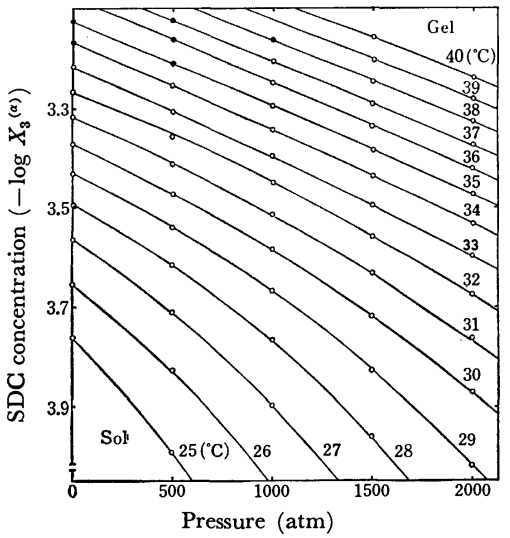

Fig. 4. Sol-gel phase diagram of SDC solutions at various temperatures. Numerical values indicate temperature in °C. These relations are of Eq. 15 in the text. (●: Extrapolated value in Fig. 3).

is plotted against the transition temperatures, which are taken from Fig. 2 by reading interpolated points on the curves. The region above each curve is of a gel, while that below each curve is of a sol.

In Fig. 4 the phase diagram is made by plotting the transition pressure against the logarithm of the SDC mole fraction at given temperatures. The regions above and below each isotherm refer to the gel and the sol phases respectively. It may be seen from Figs. 2, 3, and 4 that the gelation of SDC solutions is caused more easily at the lower temperatures, the higher pressures, and the higher concentrations of SDC.

Discussion

In order to analyze the above results, we will try to treat thermodynamically the gelation of SDC in an

aqueous dilute solution of HCl. The system under given conditions is in equilibrium between the sol phase (α) and the gel phase (β) and consists of three components; water (1), HCl (2), and SDC (3). The Gibbs free energy of each phase is expressed as follows:

$$G^{(\alpha)}[T, P, N_1^{(\alpha)}, N_2^{(\alpha)}, N_3^{s(\alpha)}, N_3^{m(\alpha)}] \quad (1)$$

$$G^{(\beta)}[T, P, N_1^{(\beta)}, N_3^{(\beta)}] \quad (2)$$

where T, P, and N denote the temperature, the pressure, and the number of moles, and where the superscripts, s and m, refer to singly dispersed SDC and micellar SDC respectively.

In the sol phase the Gibbs free energy is expressed by:

$$dG^{(\alpha)} = -S^{(\alpha)}dT + V^{(\alpha)}dP + \sum \mu_i^{(\alpha)} dN_i^{(\alpha)} \quad (3)$$

where $\mu_i^{(\alpha)}$ is the chemical potential of the i component in the sol phase. In the system under consideration, HCl is very diluted and the pH of solutions is adjusted to 6.85 at 20 °C. Since co-ions, *i.e.*, chloride ions, scarcely affect the gelation, the $N_2^{(\alpha)}/N_1^{(\alpha)}$ ratio can be regarded as constant. Hence, the aqueous dilute solution of HCl may be regarded as the solvent, and $N_{12}^{(\alpha)} = N_1^{(\alpha)} + N_2^{(\alpha)}$. Therefore, $X_{12}^{(\alpha)} = (N_1^{(\alpha)} + N_2^{(\alpha)})/(N_1^{(\alpha)} + N_2^{(\alpha)} + N_3^{(\alpha)}) = 1 - X_3^{(\alpha)}$. Here, $N_3^{(\alpha)}$ is the total number of moles of singly dispersed and micellar SDC, and $X_3^{(\alpha)}$ is the mole fraction of total SDC in the sol phase.

At equilibrium,

$$d\mu_3^{s(\alpha)} = d\mu_3^{m(\alpha)} = d\mu_3^{(\alpha)}. \quad (4)$$

Therefore,

$$dG^{(\alpha)} = -S^{(\alpha)}dT + V^{(\alpha)}dP + \mu_{12}^{(\alpha)}dN_{12} + \mu_3^{(\alpha)}dN_3^{(\alpha)} \quad (5)$$

and

$$d\mu_i^{(\alpha)} = -\bar{S}_i^{(\alpha)}dT + \bar{V}_i^{(\alpha)}dP + RT(\partial \ln a_i^{(\alpha)}/\partial \ln X_3^{(\alpha)})_{T,P} d \ln X_3^{(\alpha)} \quad (6)$$

where

$$\mu_i^{(\alpha)} = \mu_i^{\circ(\alpha)} + RT \ln a_i^{(\alpha)}.$$

It may be seen from Eqs. 5 and 6 that the state of solution could be completely defined by three variables, T, P, and $X_3^{(\alpha)}$, because $X_{12}^{(\alpha)} = 1 - X_3^{(\alpha)}$.

Next, in the overall gel phase (β) we obtain Eq. 7 from a consideration of the Gibbs-Duhem equation:

$$\bar{S}^{(\beta)}dT - \bar{V}^{(\beta)}dP + (1 - X_3^{(\beta)})d\mu_1^{(\beta)} + X_3^{(\beta)}d\mu_3^{(\beta)} = 0. \quad (7)$$

By analogy with Eq. 6,

$$d\mu_1^{(\beta)} = -\bar{S}_1^{(\beta)}dT + \bar{V}_1^{(\beta)}dP + RT\left(\frac{\partial \ln a_1^{(\beta)}}{\partial \ln X_3^{(\beta)}}\right)_{T,P} d \ln X_3^{(\beta)}, \quad (8)$$

and

$$d\mu_3^{(\beta)} = -\bar{S}_3^{(\beta)}dT + \bar{V}_3^{(\beta)}dP + RT\left(\frac{\partial \ln a_3^{(\beta)}}{\partial \ln X_3^{(\beta)}}\right)_{T,P} d \ln X_3^{(\beta)}. \quad (9)$$

At an equilibrium between α and β phases,

$$d\mu_{12}^{(\alpha)} = d\mu_1^{(\beta)} \text{ and } d\mu_3^{(\alpha)} = d\mu_3^{(\beta)}.$$

Hence, from Eqs. 7, 8, and 9,

$$\Delta\bar{S}^{(\alpha\beta)}dT - \Delta\bar{V}^{(\alpha\beta)}dP + RT\{(1 - X_3^{(\beta)})(\partial \ln a_{12}^{(\alpha)}/\partial \ln X_3^{(\alpha)})_{T,P} + X_3^{(\beta)}(\partial \ln a_3^{(\alpha)}/\partial \ln X_3^{(\alpha)})_{T,P}\} d \ln X_3^{(\alpha)} = 0. \quad (10)$$

Here, the changes in the entropy ($\Delta\bar{S}^{(\alpha\beta)}$) and volume ($\Delta\bar{V}^{(\alpha\beta)}$) on the gelation are:

$$\Delta\bar{S}^{(\alpha\beta)} = \{\bar{S}^{(\beta)} - (1 - X_3^{(\beta)})\bar{S}_{12}^{(\alpha)} - X_3^{(\beta)}\bar{S}_3^{(\alpha)}\} \quad (11)$$

and

$$\Delta\bar{V}^{(\alpha\beta)} = \{\bar{V}^{(\beta)} - (1 - X_3^{(\beta)})\bar{V}_{12}^{(\alpha)} - X_3^{(\beta)}\bar{V}_3^{(\alpha)}\} \quad (12)$$

If the concentration dependence of the activity coefficient in Eq. 10 is negligible in the vicinity of the equilibrium state, the following equations may be derived; these equations enable us to obtain $\Delta\bar{S}^{(\alpha\beta)}$, $\Delta\bar{V}^{(\alpha\beta)}$, and $\Delta\bar{H}^{(\alpha\beta)}$.

At a constant concentration of SDC,

$$\left[\frac{\partial P}{\partial T}\right]_{\ln X_3^{(\alpha)}} = \frac{\Delta\bar{S}^{(\alpha\beta)}}{\Delta\bar{V}^{(\alpha\beta)}} = \frac{\Delta\bar{H}^{(\alpha\beta)}}{T\Delta\bar{V}^{(\alpha\beta)}}. \quad (13)$$

At a constant pressure,

$$RT\left[\frac{\partial \ln X_3^{(\alpha)}}{\partial T}\right]_P = -\Delta\bar{S}^{(\alpha\beta)}. \quad (14)$$

At a constant temperature,

$$RT\left[\frac{\partial \ln X_3^{(\alpha)}}{\partial P}\right]_T = \Delta\bar{V}^{(\alpha\beta)}. \quad (15)$$

It should be noted that the analytical concentration can be used for the evaluation of the above thermodynamic quantity. The left-hand sides in Eqs. 13, 14, and 15 are experimentally determinable by using the results shown in Figs. 2, 3, and 4 respectively. From the slopes of the P *vs.* T curves in Fig. 2, we first obtained $\Delta\bar{S}^{(\alpha\beta)}/\Delta\bar{V}^{(\alpha\beta)}$ or $\Delta\bar{H}^{(\alpha\beta)}/T\Delta\bar{V}^{(\alpha\beta)}$ by using Eq. 13, *i.e.*, the Clausius-Clapeyron relation. The entropy change in the gelation is obtained from the slope of the $\log X_3^{(\alpha)}$ *vs.* T curve in Fig. 3 based on Eq. 14. The volume change, $\Delta\bar{V}^{(\alpha\beta)}$, is obtained from the slope of the $\log X_3^{(\alpha)}$ *vs.* P curve in Fig. 4. This estimation is based on Eq. 15. Actually, we obtained $\Delta\bar{V}^{(\alpha\beta)}$ by applying Eq. 15 to Fig. 4 and then estimated $\Delta\bar{S}^{(\alpha\beta)}$ and $\Delta\bar{H}^{(\alpha\beta)}$ by the use of Eq. 13 and Fig. 2.

The change in volume on gelation, $\Delta\bar{V}^{(\alpha\beta)}$, is shown as a function of the pressure at various temperatures in Fig. 5. The transition from a sol to a gel is accompanied by a decrease in the volume. The lower the temperature and the higher the pressure, the larger the degree of

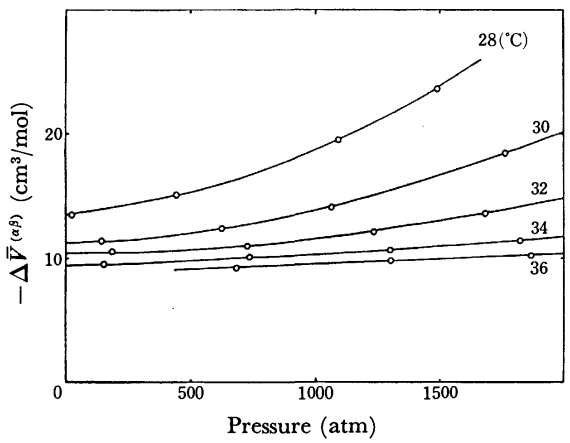

Fig. 5. The volume change of gel formation as a function of pressure at various temperatures. Numerical values indicate temperature in °C.

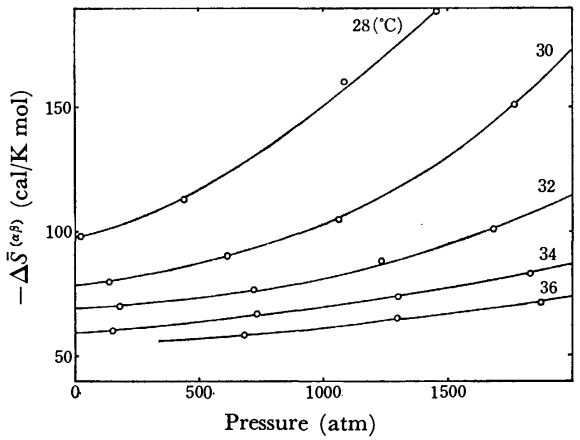

Fig. 6. The entropy change of gel formation as a function of pressure at various temperatures. Numerical values indicate temperature in °C.

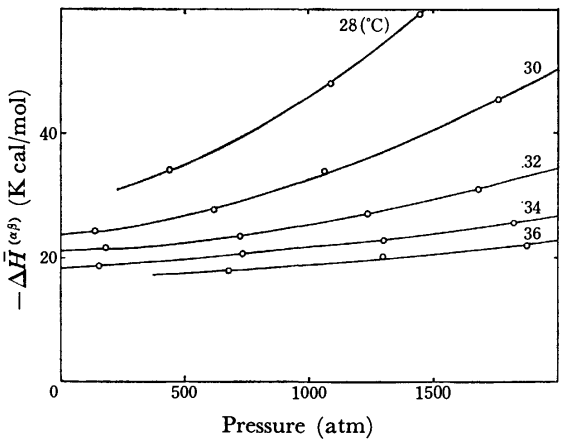

Fig. 7. The enthalpy change of gel formation as a function of pressure at various temperatures. Numerical values indicate temperature in °C.

volume decrease. The changes in the entropy ($\Delta\bar{S}^{(\alpha\beta)}$) and enthalpy ($\Delta\bar{H}^{(\alpha\beta)}$) of gel formation are shown as functions of the pressure at various temperatures in Figs. 6 and 7 respectively. The values of $\Delta\bar{S}^{(\alpha\beta)}$ and $\Delta\bar{H}^{(\alpha\beta)}$ are all negative under the conditions of this study and come to be negatively larger as the temperature is lowered and the pressure is raised.

Suzuki and his co-workers[8] have studied the effect of the pressure on the thermodynamically reversible gelation of gelatin, poly(vinyl alcohol), and methylcellulose in aqueous solutions. They have found that the formation of intermolecular hydrogen-bonded cross-links results in negative values of both the enthalpy and volume change on gelation. Taniguchi and Suzuki[9] have reported the effect of the pressure on the gel formation of 12-hydroxyoctadecanoic acid in CCl_4 and showed the enthalpy and volume changes on gelation to be negative.

In a thermodynamically reversible gel, the cross-links are known to be caused by secondary forces, such as hydrogen bonds, hydrophobic, and electrostatic interactions, rather than by covalent bonds. Of these, the hydrogen-bond formation is characterized by a negative change in the volume and an exothermic change in the enthalpy. On the other hand, the hydrophobic interactions (*i.e.*, the hydrophobic bonds) lead to positive changes in volume and entropy upon the gel formation. Therefore, the negative changes in the thermodynamic quantities on gelation are at least attributable to the cross-links of the intermolecular hydrogen bonds.

The enthalpy change per mole of the hydrogen bond is well known to be within the range from −4 to −4.5 kcal/mol.[10] The volume change per mole of the hydrogen bond has also been found to be −5.5 cm^3/mol in the gel formation of 12-hydroxyoctadecanoic acid in CCl_4,[9] −4.64 cm^3/mol for the association of 1-butanol in CS_2,[11] −3.0 to −3.4 cm^3/mol for the hydrogen-bond formation between phenol and dioxane in hexane,[12] and −7.0 cm^3/mol for the dimerization of formic acid.[13]

A molecule of SDC has, as a maximum, three sites for hydrogen bonds, *i.e.*, the 3α- and 12α-hydroxyl groups and the carboxyl group. Judging from the values of $\Delta\bar{V}^{(\alpha\beta)}$ and $\Delta\bar{H}^{(\alpha\beta)}$ shown in Figs. 5 and 7 and the respective values for hydrogen-bond formation per mole described above, the number of hydrogen bonds per mole of SDC in the gel formation can be roughly estimated to be about 3 or more if the gel formation involves the hydrogen-bond formation alone. The number of hydrogen bonds tends to increase as the temperature is lowered. This is probably attributable to the hydrogen bonds with solvent water.

References

1) G. Sugihara, K. Motomura, and R. Matuura, *Memoirs of Fac. of Sci., Kyushu Univ. Series C. Chem.*, **7**, 103 (1970).
2) G. Sugihara, *Fukuoka Univ. Sci. Reports*, **1**, 23, 29 (1972).
3) G. Sugihara and M. Tanaka, *Bull. Chem. Soc. Jpn.*, **49**, 3457 (1976).
4) A. Rich and D. M. Blow, *Nature*, **182**, 423 (1958).
5) D. M. Blow and A. Rich, *J. Am. Chem. Soc.*, **82**, 3566 (1960).
6) C. Botré, P. A. Ciccnetti, G. Lionetti, and M. Marchetti, *J. Pharm. Sci.*, **56**, 1035, (1967).
7) M. Tanaka, K. Kaneshina, T. Tomida, K. Noda, and K. Aoki, *J. Colloid Interface Sci.*, **44**, 525 (1973).
8) K. Suzuki, Y. Taniguchi, and T. Enomoto, *Bull. Chem. Soc. Jpn.*, **45**, 336 (1972).
9) Y. Taniguchi and K. Suzuki, *J. Phys. Chem.*, **78**, 759 (1974).
10) G. C. Pimentel and A. L. McClellan, "The Hydrogen Bond," W. H. Freeman, San Francisco, Calif. (1960).
11) E. Fishman and G. H. Drickamer, *J. Chem. Phys.*, **24**, 548 (1956).
12) K. Suzuki and M. Tsuchiya, *Bull. Chem. Soc. Jpn.*, **48**, 1701 (1975).
13) K. Suzuki, Y. Taniguchi, and T. Watanabe, *J. Phys. Chem.*, **77**, 1918 (1973).

Reaction of Pyridine Bases with Carboxylic Acids in Benzene

Katsumi HIROSE and Motoharu TANAKA*

Laboratory of Analytical Chemistry, Faculty of Science, Nagoya University, Nagoya 464

(Received August 20, 1976)

The reaction of pyridine bases with aliphatic monocarboxylic acids has been studied by means of the partition method. Partition was carried out at 25 °C between benzene and 0.10 mol dm^{-3} (Na, H) ClO_4 aqueous solution, the total concentration of pyridine base and that of carboxylic acid being less than 2×10^{-2} mol dm^{-3} and 1.0 mol dm^{-3}, respectively. Both (1: 1) and (1: 2) complexes (base to acid ratio) are formed in benzene, (1: 3) complex being additionally formed only for 2,4,6-trimethylpyridine. A linear free energy relationship is observed between the formation of the (1: 1) and (1: 2) complexes and the protonation in water of the corresponding bases except for sterically crowded 2,6-dimethyl derivatives of pyridine. The structure of the (1: 2) and (1: 3) complexes is discussed.

The reaction of bases with carboxylic acids in nonpolar solvents is important for understanding the nature of the acid-base reaction, since a carboxylic acid undergoes association in nonpolar solvents.[1] Several interesting features of the acid-base reaction, such as, the formation of higher hydrogen-bonded complexes and the proton transfer complex have been reported.[2] It was revealed that the hydrogen bond strength is parallel to the acidity and basicity of components.[3]

The system involving pyridine bases and carboxylic acids in organic solvents was initially studied by Barrow with use of IR spectroscopy. He revealed the stoichiometry of reaction products and discussed the extent of the proton transfer in relation to the acid strength of a carboxylic acid.[4] Since then, various physical methods, such as IR, visible, NMR, NQR, thermodynamic method and dipole moment measurement, have been applied to the reaction of the pyridine bases with carboxylic acids in solution or in solid state.[5-10] In the present paper, we describe the reaction of carboxylic acid with pyridines in reference to the effect of substituents. The structure of the (1: 2) and (1: 3) species (base to acid ratio) is discussed.

Experimental

Reagent. All the pyridine bases, *i.e.* pyridine, 3-bromopyridine, 2-methylpyridine, 4-methylpyridine, 2,6-dimethylpyridine and 2,4,6-trimethylpyridine were of G. R. grade. Carboxylic acids, *i.e.* butyric acid, valeric acid and hexanoic acid, were of G. R. grade, while decanoic acid was of chemical pure grade. The purification of pyridine bases, carboxylic acids and benzene (G. R.) as a solvent has been described elsewhere.[11,12]

Procedure. The partition was carried out in an incubator thermostated at (25±0.1) °C. Equilibrium is reached within 1 h. Concentrations were 0.1—1.0 mol dm^{-3} for the carboxylic acids and 2×10^{-3}—2×10^{-2} mol dm^{-3} for the pyridine bases. The ionic strength in the aqueous phase was maintained at 0.10 mol dm^{-3} with sodium perchlorate. Hydrogen ion concentration was measured with a Orion Ionalyzer Model 801 and a Beckman Research pH meter. A 1.00×10^{-2} mol dm^{-3} perchloric acid solution containing 0.09 mol dm^{-3} sodium perchlorate was employed as a standard of hydrogen ion concentration. Hydrogen ion concentration was estimated by correcting for a liquid-junction potential.[13] The total concentration of pyridine base in the aqueous phase was determined by colorimetry for 3-bromopyridine; for the other pyridine bases the total concentration in the organic phase was determined by acid-base titration in glacial acetic acid with Crystal Violet as an indicator.

* To whom correspondence should be addressed.

Results

When a pyridine base, B, is extracted with a carboxylic acid, HA, in benzene, the extraction equilibrium between the organic and aqueous phases is written as

$$mB_w + n(HA)_o \rightleftharpoons (B_m(HA)_n)_o \quad (1)$$

where $B_m(HA)_n$ denotes an extracted species which involves m molecules of pyridine base and n molecules of carboxylic acid, and subscripts w and o refer to the aqueous and organic phases, respectively. Since the activity coefficient of each species in both phases is assumed to be kept constant,[14,15] the concentration equilibrium constant, $K_{ex(mn)}$, for Eq. 1 is kept constant.

$$K_{ex(mn)} = [B_m(HA)_n]_o[B]_w^{-m}[HA]_o^{-n} \quad (2)$$

The association between a pyridine base and a carboxylic acid is negligible in the aqueous phase.

When a pyridine base is extracted with a carboxylic acid in benzene, the total concentration of the pyridine base in the organic phase, $C_{B,o}$, is given by

$$C_{B,o} = \sum_{m=1}\sum_{n=0} m[B_m(HA)_n]_o \quad (3)$$

Substituting this relation into Eq. 2, we have

$$C_{B,o} = \sum_{m=1}\sum_{n=0} mK_{ex(mn)}[B]_w^m[HA]_o^n \quad (4)$$

If only species involving m molecules of pyridine base are present in the organic phase, the total concentration of the pyridine base in the organic phase can be written as

$$C_{B,o} = [B]_w^m\{\sum_{n=0} mK_{ex(mn)}[HA]_o^n\} \quad (5)$$

or

$$\log(C_{B,o}/\text{mol dm}^{-3}) = m\log([B]_w/\text{mol dm}^{-3}) + \log\{\sum_{n=0} mK_{ex(mn)}[HA]_o^n/\text{mol}^{1-m}\,\text{dm}^{3m-3}\} \quad (5')$$

$\log(C_{B,o}/\text{mol dm}^{-3})$ is linearly related with $\log([B]_w/\text{mol dm}^{-3})$ for a given concentration of monomeric carboxylic acid in the organic phase. From the slope of this linear relationship we find the number of the pyridine base involved in the extracted species. The plots of $\log([B]_w/\text{mol dm}^{-3})$ *vs.* $\log(C_{B,o}/\text{mol dm}^{-3})$ for the extraction of the six pyridine bases with decanoic acid are shown in Fig. 1. They give rise to straight lines

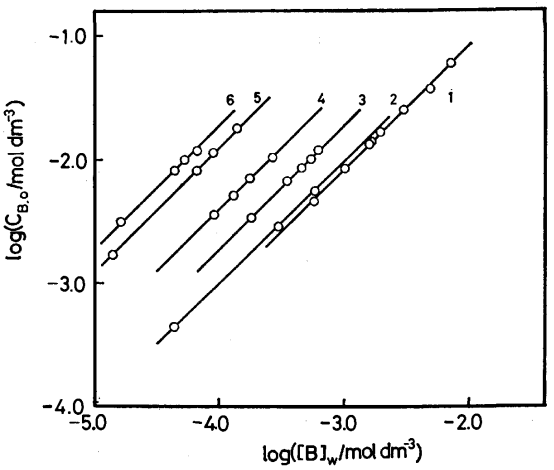

Fig. 1. Determination of the number of pyridine base involved in extracted species.
1: Decanoic acid–pyridine, 2: decanoic acid–3-bromopyridine, 3: decanoic acid–2-methylpyridine, 4: decanoic acid–4-methylpyridine, 5:decanoic acid–2,6-dimethylpyridine, 6: decanoic acid–2,4,6-trimethylpyridine.

with a slope of unity. We thus have extracted species involving only one molecule of pyridine base in benzene.

From Eq. 5 we obtain

$$C_{B,o}[B]_w^{-1} = \sum_{n=0} K_{ex(1n)}[HA]_o^n \quad (6)$$

By use of the distribution ratio, D, and the formation constant of pyridinium in the aqueous solution, K_{HB}, Eq. 6 is rewritten as

$$D\cdot\alpha_B = \sum_{n=0} K_{ex(1n)}[HA]_o^n \quad (7)$$

where α_B is the side reaction coefficient taking into account the protonation of the base:

$$\alpha_B = 1 + K_{HB}[H^+] \quad (8)$$

The $K_{ex(10)}$ in Eq. 7 is identical with the partition constant, $K_{D,B}$, of the pyridine base between benzene and aqueous solution in the absence of a carboxylic acid. In order to determine the number of carboxylic acid involved in the extracted species, $D\cdot\alpha_B$ was plotted against the concentration of the monomeric carboxylic acid in benzene. The latter was calculated from the partition constant and the dimerization constant in benzene[12]:

Acid	Partition constant*	Dimerization constant*
Butyric acid	0.11	182
Valeric acid	0.54	229
Hexanoic acid	1.9_1	251
Decanoic acid	500	260

* Hydration not corrected.

The results for the extraction of 4-methylpyridine with four carboxylic acids are shown in Fig. 2. Non-linearity of the plots indicates the presence of the extracted species involving more than one molecule of the carboxylic acid. Similar results were obtained for the other pyridine bases. Equation 7 can be rewritten as follows:

$$(D\cdot\alpha_B - K_{D,B})[HA]_o^{-1} = K_{ex(11)} + K_{ex(12)}[HA]_o + \cdots \quad (9)$$

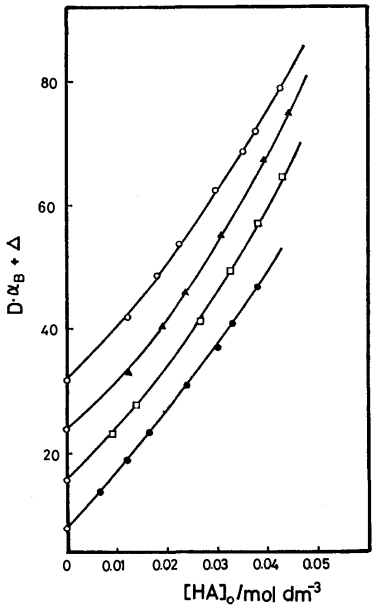

Fig. 2. Determination of the number of carboxylic acid involved in extracted species for 4-methylpyridine. The solid lines represent calculated values.
○: Decanoic acid (Δ=24), ▲: hexanoic acid (Δ=16), □: valeric acid (Δ=8), ●: butyric acid (Δ=0).

If only the first two terms on the right side are important, $(D\cdot\alpha_B - K_{D,B})[HA]_0^{-1}$ should be linearly related to the concentration of monomeric carboxylic acid in the organic phase. The plots of $[HA]_o$ *vs.* $(D\cdot\alpha_B - K_{D,B})$-$[HA]^{-1}$ for the extraction of 4-methylpyridine with the four carboxylic acids are shown in Fig. 3, in which we utilized the partition constants of the pyridine bases determined previously.[16] Straight lines with non-zero intercept (Fig. 3) indicate the presence of 1: 1 and 1: 2 complexes in the organic phase. The extraction constants of 1: 1 and 1: 2 complexes can be obtained from the intercept and the slope, respectively. Similar results were obtained for pyridine and its derivatives except for 2,4,6-trimethylpyridine. The formation of complexes

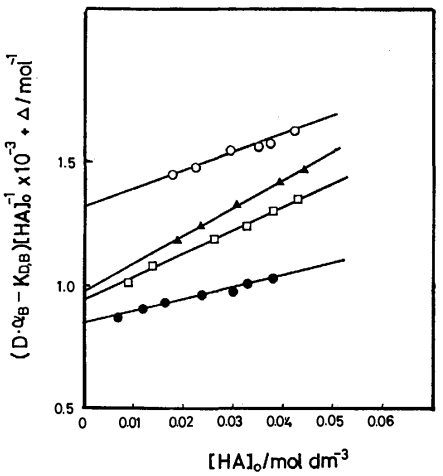

Fig. 3. Determination of the number of carboxylic acid involved in extracted species for 4-methylpyridine.
○: Decanoic acid (Δ=0.6), ▲: hexanoic acid (Δ=0.4), □: valeric acid (Δ=0.2), ●: butyric acid (Δ=0).

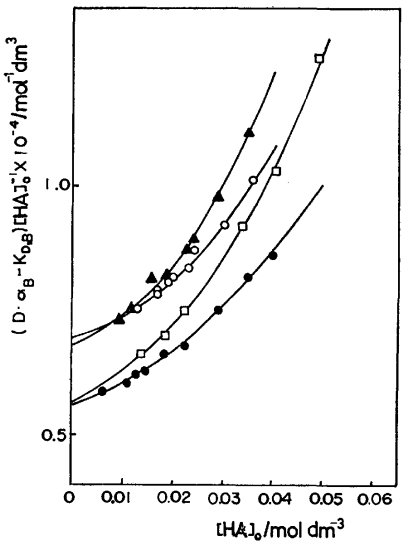

Fig. 4. Determination of the number of carboxylic acid involved in extracted species for 2,4,6-trimethylpyridine. The solid line represent the calculated values. ○: Decanoic acid, ▲: hexanoic acid, □: valeric acid, ●: butyric acid.

with the same compositions in nonpolar solvents such as carbon tetrachloride has been confirmed by IR study for the reaction of pyridine with several carboxylic acids.[4,6,8]

For 2,4,6-trimethylpyridine, the plot of $[HA]_o$ *vs.* $(D\cdot\alpha_B - K_{D,B})[HA]_o^{-1}$ is not linear (Fig. 4). This indicates the presence of higher complexes. Rearranging Eq. 9, we have

$$\{(D\cdot\alpha_B - K_{D,B})[HA]_o^{-1} - K_{ex(11)}\}[HA]_o^{-1} = K_{ex(12)} + K_{ex(13)}[HA]_o + \cdots \quad (10)$$

By plotting the values of the left side of Eq. 10 against $[HA]_o$ for 2,4,6-trimethylpyridine we obtain straight

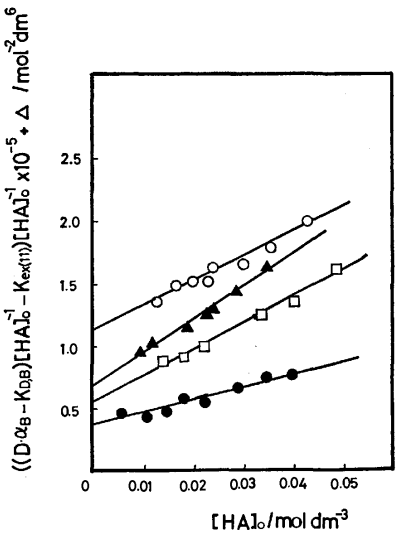

Fig. 5. Determination of the number of carboxylic acid involved in extracted species for 2,4,6-trimethylpyridine. The extraction constants of the 1:2 and 1:3 complexes were obtained from the intercept and slope, respectively. ○: Decanoic acid (Δ=0.9), △: hexanoic acid (Δ=0.4), □: valeric acid (Δ=0.2), ●: butyric acid (Δ=0).

TABLE 1. LOGARITHMIC EXTRACTION CONSTANTS OF $(B\cdot HA)$, $(B\cdot(HA)_2)$ AND $(B\cdot(HA)_3)$ COMPLEXES BETWEEN BENZENE AND AQUEOUS SOLUTION

Base	Acid	log ($K_{ex(11)}$/mol^{-1} dm^3)	log ($K_{ex(12)}$/mol^{-2} dm^6)	log ($K_{ex(13)}$/mol^{-3} dm^9)
3-Bromopyridine	Butyric acid	2.97	3.5_8	
	Valeric acid	3.02	3.8_5	
	Hexanoic acid	2.99	3.9_7	
	Decanoic acid	3.02	3.6_7	
Pyridine	Butyric acid	2.24	3.2_1	
	Valeric acid	2.31	3.2_3	
	Hexanoic acid	2.20	3.3_7	
	Decanoic acid	2.31	3.1_9	
2-Methylpyridine	Butyric acid	2.80	3.7_1	
	Valeric acid	2.70	3.8_6	
	Hexanoic acid	2.77	3.8_3	
	Decanoic acid	2.76	3.7_7	
4-Methylpyridine	Butyric acid	2.93	3.6_9	
	Valeric acid	2.87	3.9_7	
	Hexanoic acid	2.83	4.0_3	
	Decanoic acid	2.91	3.8_7	
2,6-Dimethyl-pyridine	Butyric acid	3.09	4.1_3	
	Valeric acid	3.12	4.1_9	
	Hexanoic acid	3.15	4.2_9	
	Decanoic acid	3.18	4.0_3	
2,4,6-Trimethyl-pyridine	Butyric acid	3.75	4.5_1	6.1
	Valeric acid	3.76	4.5_6	6.3
	Hexanoic acid	3.83	4.4_5	6.4
	Decanoic acid	3.84	4.3_8	6.3

$\log(K_{ex(11)}/\text{mol}^{-1}\,\text{dm}^3)$, $\log(K_{ex(12)}/\text{mol}^{-2}\,\text{dm}^6)$, and $\log(K_{ex(13)}/\text{mol}^{-3}\,\text{dm}^9)$ values are estimated to be accurate to ±0.05, ±0.10, and ±0.2, respectively.

lines (Fig. 5). It is obvious that three species, *i.e.* 1:1, 1:2, and 1:3 complexes are present in benzene for 2,4,6-trimethylpyridine. The extraction constants are summarized in Table 1.

From the results, the equilibria of the pyridine bases with the carboxylic acids in benzene are formulated as follows:

$$B_o + (HA)_o \rightleftarrows (B\cdot HA)_o \qquad K_{11} \quad (11)$$

$$B_o + (HA)_{2,o} \rightleftarrows (B\cdot(HA)_2)_o \qquad K_{12} \quad (12)$$

$$(B\cdot(HA)_2)_o + (HA)_o \rightleftarrows (B\cdot(HA)_3)_o \qquad K_{13} \quad (13)$$

In addition, the dimerization of a carboxylic acid occurs in benzene:

$$2(HA)_o \rightleftarrows (HA)_{2,o}$$

The formation constant of complexes in benzene can be evaluated from the corresponding extraction constant by use of the partition constant of the pyridine base and the dimerization constant of the carboxylic acid.

Polar solutes, *i.e.* carboxylic acids and amines, form hydrates in a nonpolar solvent equilibrated with water.[17] Thus correction for hydration of pyridine base and carboxylic acid should be made in order to evaluate the true formation constant of complexes. We have information on the hydration of pyridine bases and carboxylic acids in benzene.[11,12] The formation constants corrected for the hydration of acids and bases are summarized in Table 2.

Table 2. Logarithmic formation constants of $(B\cdot HA)$, $(B\cdot(HA)_2)$, and $(B\cdot(HA)_3)$ complexes in benzene

Base	Acid	log (K_{11}/mol^{-1} dm^3)	log (K_{12}/mol^{-2} dm^6)	log (K_{13}/mol^{-3} dm^9)
3-Bromopyridine	Butyric acid	1.34	−0.4	
	Valeric acid	1.38	−0.2	
	Hexanoic acid	1.34	−0.1	
	Decanoic acid	1.35	−0.5	
Pyridine	Butyric acid	1.97	0.5_9	
	Valeric acid	2.03	0.5_1	
	Hexanoic acid	1.91	0.6_2	
	Decanoic acid	1.99	0.4_2	
2-Methylpyridine	Butyric acid	2.14	0.7_0	
	Valeric acid	2.04	0.7_4	
	Hexanoic acid	2.10	0.6_9	
	Decanoic acid	2.07	0.6_1	
4-Methylpyridine	Butyric acid	2.18	0.6_0	
	Valeric acid	2.12	0.7_8	
	Hexanoic acid	2.06	0.8_0	
	Decanoic acid	2.12	0.6_2	
2,6-Dimethyl-pyridine	Butyric acid	1.94	0.6_3	
	Valeric acid	1.96	0.5_9	
	Hexanoic acid	1.98	0.6_6	
	Decanoic acid	1.99	0.3_8	
2,4,6-Trimethyl-pyridine	Butyric acid	2.20	0.6_1	$1._7$
	Valeric acid	2.20	0.5_6	$1._9$
	Hexanoic acid	2.26	0.4_2	$2._1$
	Decanoic acid	2.25	0.3_3	$2._0$

$\log(K_{11}/\text{mol}^{-1}\text{ dm}^3)$, $\log(K_{12}/\text{mol}^{-2}\text{ dm}^6)$, and $\log(K_{13}/\text{mol}^{-3}\text{ dm}^9)$ values are estimated to be accurate to ±0.05, ±0.10, and ±0.2, respectively.

Discussion

It has been suggested that the extent of formation of hydrogen-bonded complex between a series of bases and phenols or alcohols is a function of basicity of these bases.[18,19] We have observed the linear free energy relationship between the hydration of pyridine bases in benzene and the formation of the corresponding pyridiniums in aqueous solution,[11] a similar relationship being observed for the hydration of carboxylic acids.[12] The formation constants of 1 : 1, 1 : 2, and 1 : 3 complexes for a given pyridine base remain constant for the carboxylic acids studied (Table 2). This seems reasonable since the acidity of the four carboxylic acids does not differ appreciably from each other.

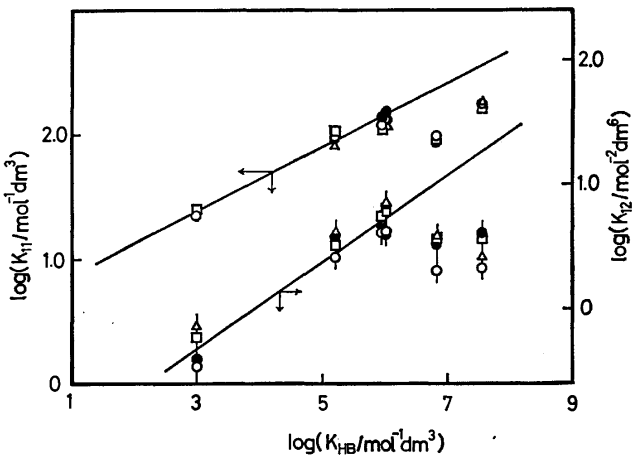

Fig. 6. Correlation between the logarithmic formation constants of the 1:1 and 1:2 complexes and the logarithmic formation constants of pyridinium in aqueous solution. Data of log K_{HB}'s were taken from Ref. 16.

Let us examine the correlation between the formation of 1 : 1 complex and the formation of the corresponding pyridinium. The plot of the logarithmic formation constant of 1 : 1 complex against $\log(K_{HB}/\text{mol}^{-1}\text{ dm}^3)$ is shown in Fig. 6. A linear correlation was obtained between $\log(K_{11}/\text{mol}^{-1}\text{ dm}^3)$ and $\log(K_{HB}/\text{mol}^{-1}\text{ dm}^3)$ except for sterically crowded 2,6-dimethyl derivatives of pyridine. The relationship is written as follows (dimensions are hereafter omitted for the sake of simplicity):

$$\log K_{11} = 0.25 \log K_{HB} + 0.62 \qquad (15)$$

A similar relationship has been obtained for the formation of the monohydrate of pyridines[11]:

$$\log \beta_{11}(\text{hydrate}) = 0.09 \log K_{HB} - 0.37 \qquad (15')$$

The coefficient of $\log K_{HB}$ in Eq. 15 is appreciably larger than that in Eq. 15'. In view of the fact that acidity of the carboxylic acid is much higher than that of water, it is reasonable that the extent of the complex formation of the pyridine bases with the carboxylic acids is greater than that of the hydration. The $\log K_{11}$ values for the sterically crowded 2,6-dimethyl derivatives of pyridine are smaller than that expected from $\log K_{HB}$.

We shall examine the correlation between the reaction of the pyridine base with the dimeric carboxylic acid and the formation of pyridinium. In Fig. 6 the logarithmic formation constant of the 1 : 2 complex for carboxylic acids is plotted against $\log K_{HB}$ of corresponding pyridiniums. The correlation is obviously good except for 2,6-dimethyl derivatives of pyridine. This relationship is expressed by

$$\log K_{12} = 0.35 \log K_{HB} - 1.44 \qquad (16)$$

We see that the formation of the 1 : 2 complex would occur to a negligible extent for the pyridine bases less basic than 3-brompyridine. A comparison of coefficients of $\log K_{HB}$ in Eqs. 15 and 16 suggests that the dimeric carboxylic acid is somewhat more acidic than monomeric carboxylic acid.

Let us consider the structure of the 1 : 2 complex. We have two possible structures of dimeric carboxylic acids:

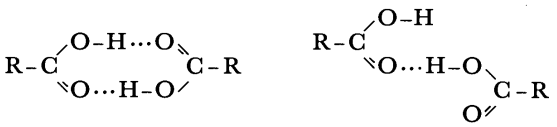

cyclic dimer, c-$(HA)_2$ open dimer, o-$(HA)_2$

The following equilibrium might take place.

$$\text{o-}(HA)_2 \rightleftharpoons \text{c-}(HA)_2 \qquad K_{o-c} \qquad (17)$$

Pyridine bases are assumed to react only with the open dimer:

$$\text{o-}(HA)_2 + B \rightleftharpoons (B\cdot\text{o-}(HA)_2) \qquad K_{OB} \qquad (18)$$

Then the formation constant of the 1 : 2 complex can be written as:

$$K_{12} = [B\cdot\text{o-}(HA)_2][B]^{-1}([\text{o-}(HA)_2] + [\text{c-}(HA)_2])^{-1}$$
$$= K_{OB}(1+K_{o-c})^{-1} \qquad (19)$$

If K_{OB} is approximated as K_{11}, we have

$$K_{o-c} = K_{11}K_{12}^{-1} - 1 \qquad (20)$$

Thus the value of K_{O-C} can be calculated from values of K_{11} and K_{12} given in Table 2. Average values of K_{O-C} for the four carboxylic acids are as follows: butyric, 31; valeric, 28; hexanoic, 26; decanoic, 44. The proportion of the open dimer is roughly estimated to be *ca.* 3% of acid dimer. IR spectroscopic study and the slopes of the LFER given in Fig. 6 suggest strongly that the acidity of the open dimer should exceed the acidity of the monomeric carboxylic acid, *i.e.*

$$K_{OB} > K_{11}$$

Then the proportion of the open dimer should be less than 3%.

Combining Eqs. 16 and 19, we have

$$\log K_{OB} = 0.35 \log K_{HB} - 1.44 + \log(1+K_{o-c}) \qquad (21)$$

K_{OB} should be greater than K_{11} for all bases including a base of which K_{HB} is equal to 1. Then from Eqs. 15 and 21 we obtain

$$-1.44 + \log(1+K_{o-c}) > 0.62$$

or $$K_{o-c} > 119$$

The fraction of the open dimer in the total dimer concentration seems to be a little less than 1%. Since the estimations are consistent with the previous findings,[20] we can conclude that the open dimer of a carboxylic acid reacts with a pyridine base to form a 1 : 2 complex:

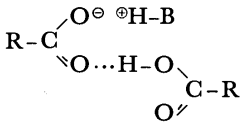

(22)

2,4,6-Trimethylpyridine forms the 1 : 3 complex with the four carboxylic acids in benzene. The formation of 1 : 3 complex in organic solvents has been found in several systems involving more acidic carboxylic acids or more basic amines.[21-24] The stronger the base, the the more extensive the polarization of -OH group in the 1 : 2 complex (formula 22) and the more basic the terminal -C=O becomes. Thus we have the 1 : 3 complex for the stronger bases, the situation being similar for stronger acids.

References

1) G. Allen and E. F. Caldin, *Quart. Rev.*, **7**, 255 (1953).
2) M. M. Davis, "The Chemistry of Non-Aqueous Solvents," Vol. III, ed by J. J. Lagowski, Academic Press, New York (1970), p. 1.
3) D. Hadži, C. Klofutar, and S. Oblak, *J. Chem. Soc., A*, **1968**, 905.
4) G. M. Barrow, *J. Am. Chem. Soc.*, **78**, 5803 (1956).
5) S. L. Johnson and K. A. Rumon, *J. Phys. Chem.*, **69**, 74 (1965).
6) R. Lindemann and G. Zundel, *J. Chem. Soc., Faraday Trans. 2*, **68**, 979 (1972).
7) L. Sobczyk and Z. Pawelka, *J. Chem. Soc., Faraday Trans. 1*, **70**, 832 (1974).
8) G. S. Denisov, Ya. Starosta, and V. M. Shraiber, *Opt. Spectrosck.*, **35**, 447 (1973).
9) H. Chihara and N. Nakamura, *Bull. Chem. Soc. Jpn.*, **44**, 1980 (1971).
10) Z. Dega-Szafran, E. Grech, M. Z. Naskret-Barciszewska, and M. Szafran, *J. Chem. Soc., Perkin Trans. 2*, **1975**, 250.
11) K. Hirose and M. Tanaka, *Bull. Chem. Soc. Jpn.*, **49**, 623 (1976).
12) Y. Fujii and M. Tanaka, *J. Chem. Soc., Faraday Trans. 1*, in press.
13) N. Nakasuka, Y. Mitsuoka, and M. Tanaka, *J. Inorg, Nucl. Chem.*, **36**, 431 (1974).
14) G. N. Vriens and E. C. Medcalf, *Ind. Eng. Chem.*, **45**, 1098 (1953).
15) H. Yamada and M. Tanaka, *J. Inorg. Nucl. Chem.*, **35**, 3307 (1973).
16) K. Hirose and M. Tanaka, *J. Inorg. Nucl. Chem.*, **38**, 2285 (1976).
17) S. D. Christian, A. A. Taha, and B. W. Gash, *Quart. Rev.*, **24**, 20 (1970).

18) R. W. Taft, D. Gurka, L. Joris, P. von R. Schleyer, and J. W. Rakshys, *J. Am. Chem. Soc.*, **91**, 4801 (1969).
19) T. Kitao and C. H. Jarboe, *J. Org. Chem.*, **32**, 407 (1967).
20) N. Tatsumoto, T. Sano, N. Matsunaga, E. Tochigi, and T. Yasunaga, *Bull. Chem. Soc. Jpn.*, **45**, 2083 (1972).
21) F. Kohler, E. Liebermann, G. Miksch, and C. Kainz, *J. Phys. Chem.*, **76**, 2764 (1972).
22) L. Kuca and E. Högfeldt, *Acta Chem. Scand.*, **21**, 1017 (1967).
23) H. Kohara, I. Ishibashi, and S. Fujita, *Bunseki Kagaku*, **17**, 854 (1968).
24) S. Bruckenstein and A. Saito, *J. Am. Chem. Soc.*, **87**, 698 (1965).

A Study of Catalysis by Metal Phosphates. IV.[1] The Alkylation of Phenol with Methanol over Metal Phosphate Catalysts

Fumio Nozaki and Isao Kimura

Department of Industrial Chemistry, Faculty of Engineering, Chiba University, Yayoi-cho, Chiba 280

(Received August 26, 1976)

The catalytic methylation in the vapor phase over various metal phosphates has been investigated using a conventional flow reactor at temperatures ranging from 350 to 500 °C under atmospheric pressure. The $Ca_3(PO_4)_2$ catalyst was excellent in both its activity and its selectivity for ortho-methylation, giving predominantly *o*-cresol and 2,6-xylenol, whereas the BPO_4 or $CaHPO_4$ catalyst simultaneously promoted the formation of anisole. The activity of $Ca_3(PO_4)_2$ was significantly higher than that of the CaO or MgO catalyst. The influences of the reaction temperature, the contact time, and the calcination temperature of the catalyst upon the conversion of phenol, and the yields of the products were investigated in detail over the $Ca_3(PO_4)_2$ catalyst. The activities and the selectivities of various catalysts were discussed in connection with their acid-base properties. The mechanism of the participation of both the acidic and basic sites in the methylation was also discussed.

The alkylation of phenol in the ortho position has been of interest in recent years,[2] and the catalytic process using methanol as an alkylating reagent has been investigated by several workers.[3-7] The alkylation reactions of phenol or cresol using C_2—C_4 olefins or C_1—C_4 alcohols have also been studied over various catalysts.[8-10] However, no study of the phosphate catalyst has been reported.

Our preliminary study has revealed that calcium orthophosphate has a significant activity and an interesting selectivity for the alkylation of phenol with methanol in the vapor phase. The present paper will describe the behavior of metal phosphates as a catalyst. The correlation between the selectivity for the reaction and the acid-base character of the catalysts will also be discussed.

Experimental

Catalysts. The metal phosphate catalysts were obtained from guaranteed commercial reagents by the usual method of pellet-catalyst preparation, which involves wet mixing and extruding in order to mold the catalyst. All the catalysts were in the form of 1—2 mm pellets. The CaO and MgO catalysts used to characterize the phosphate catalysts were prepared by the thermal decomposition of the $Ca(OH)_2$ and $(MgCO_3)_4 \cdot Mg(OH)_2$ reagents respectively. Unless otherwise noted, the catalysts were activated before use by calcining at 500 °C for 3 h in a stream of air.

Apparatus and Procedure. A usual type of flow reactor consisting of a 18 mmϕ glass tube was used to perform the catalytic tests. Unless otherwise specified, the reactor contained 2 g of the catalyst. The reactor was vertically supported and externally heated in an electric furnace. The upper part of the reactor was packed with small glass beads, thereby vaporizing and preheating the reactants. A stream of nitrogen was passed through the catalyst bed at 500 °C for 1 h and then the temperature was lowered to the reaction temperature in a stream of nitrogen. A methanol-phenol mixture of a known composition was fed into the reactor at a constant rate by means of a microfeeder, and then carried by nitrogen to the catalyst bed. The outlet vapor was condensed in a trap cooled with an ice bath, and samples for analysis were collected periodically. The condensed liquid products were analyzed by means of a gas-chromatographic unit containing a 3-m column of Silicone DC-550. The column was operated at 150 °C, with hydrogen as the carrier gas. The products were identified by a comparison of their chromatograms with those of authentic samples. Besides the methylation of phenol, methanol was simultaneously consumed by the gasification which was a side-reaction, giving such non-condensable products as CO, CO_2, and CH_4. However, no detailed measurement of the non-condensable products has been made because they were formed to only a small extent throughout the catalytic tests in which the phosphates were used as catalysts. The conversion of phenol and the yields of the products were expressed in mol%. The liquid products obtained consisted mainly of *o*-cresol, 2,6-xylenol, anisole, 2,4,6-trimethylphenol, 2,4-xylenol, and small amounts of *m*, *p*-cresol. Very small peaks of unknown products were detected in the gas-chromatograms, but their formation was neglected in the calculation of the conversion and the selectivity. The selectivity for the ortho-methylation, S_o, was defined as follows:

$$S_o = \frac{\text{yield of } (o\text{-cresol}+2,6\text{-xylenol})}{\text{total conversion of phenol, } x}$$

The selectivity for anisole formation, S_A, and the selectivity to the other products (*m*- and *p*-cresol+2,4-xylenol+2,4,6-trimethylphenol), S_B, were defined as follows:

$$S_A = \frac{\text{yield of anisole}}{\text{total conversion of phenol, } x}$$

$$S_B = 1 - (S_o + S_A)$$

As an indication of the contact time in the flow reactor, we used W/F, defined as follows:

$$W/F = \frac{\text{catalyst weight (g)}}{\text{feed rate of the sum of reactants and nitrogen (mol/h)}}$$

The powdered catalyst samples calcined at 500 °C for 3 h in air were used for the measurements of their acidity and basicity. The acidities of the catalysts were measured by usual *n*-butylamine titration, using the Hammett indicators. According to the method of Tanabe *et al.*,[11] the basicities of the catalysts were measured by titrating them with a benzoic acid–benzene solution, using bromothymol blue ($pK_a=7.1$) and phenolphthalein ($pK_a=9.3$) as indicators.

Results and Discussion

Catalyst Activity and Change in Activity with the Process Time. The changes in the activity and selectivity during the course of the reaction were generally not serious, although the degree of the change depended on the species of the catalysts. Henceforth, in order to

Table 1. Activities and selectivities of various catalysts

Conditions: reaction temperature (t)=460 °C, W/F=14.5 g h/mol, feed molar ratio (m) of methanol/phenol/N_2=2.0/1.0/1.2.

Catalyst		$Ca_3(PO_4)_2$	$CaHPO_4$	$Ca(H_2PO_4)_2$	BPO_4	CaO	MgO
Conversion of phenol, x (%)		77.7	26.4	1.0	47.0	7.6	48.0
Selectivity, S_o (%)		88	28	0	46	75	80
Yield (%)	anisole	0.6	19.0	1.0	25.4	0.6	1.9
	o-cresol	38.2	7.4	0	17.8	5.7	30.5
	m,p-cresol	0	0	0	0	1.3	4.8
	2,6-xylenol	30.3	0	0	3.8	0	7.9
	2,4-xylenol	3.1	0	0	0	0	1.8
	2,4,6-trimethylphenol	5.5	0	0	0	0	1.1
Conversion of methanol, x_M (%)		42.1	—	—	95.8	4.6	—
Selectivity for methylation, S_M (%)		93	—	—	25	83	—

compare the catalysts, we will use the activity data obtained around 1.5 h after the start of the reaction. The activities and the selectivities of various catalysts are shown in Table 1. It can be seen from Table 1 that the $Ca_3(PO_4)_2$ catalyst is excellent in activity and selectivity for ortho-methylation, leading to *o*-cresol and 2,6-xylenol. Another characteristic of the $Ca_3(PO_4)_2$ catalyst is the fact that it is liable to form highly methylated products, such as xylenol isomers and 2,4,6-trimethylphenol. The ortho-selectivity of the BPO_4 catalyst is far less than that of the $Ca_3(PO_4)_2$, since the BPO_4 gives rise to anisole in a large quantity even though it has a substantial activity. Both the $CaHPO_4$ and $Ca(H_2PO_4)_2$ are somewhat inferior to the other catalysts. The CaO and MgO catalysts have a low activity, though it is high in ortho-selectivity. Tanabe *et al.*[4,5] have already pointed out that the CaO or MgO catalyst has a high selectivity for ortho-methylation. In agreement with their papers, our experiment has also revealed that the CaO and MgO catalysts have a high selectivity, although their activities are far less than that of the $Ca_3(PO_4)_2$. In the cases of the other phosphate catalysts, the catalytic tests gave the following results; $Ni_3(PO_4)_2$: x=8%, S_O=38%, S_A=62%, $AlPO_4$: 9, 56, 44%, $CrPO_4$: 19, 21, 79% and $Zr_3(PO_4)_4$: 6, 33, 67%, respectively. The activities and the ortho-selectivities of these phosphate catalysts were appreciably inferior to those of the $Ca_3(PO_4)_2$; an additional characteristic of their behaviors as catalysts was the fact that scarcely any formation of *m,p*-cresol, 2,4-xylenol, or 2,4,6-trimethylphenol was found. As has been described in previous papers,[1,12] $Cd_3(PO_4)_2$ is an effective catalyst for the dehydrogenation of alcohols, by analogy with the $Ca_3(PO_4)_2$ catalyst. However, $Cd_3(PO_4)_2$ exhibited very little activity for the methylation of phenol. This seems to be the reason for the low thermostability of the $Cd_3(PO_4)_2$ catalyst.[12]

During the course of the methylation, the phenol is not entirely decomposed to form benzene or gaseous compounds. In contrast, methanol is consumed through two simultaneous reactions, the methylation of phenol and the gasification giving such non-condensable products as CO, CO_2, and CH_4. The effectiveness of the catalyst should be discussed not only in terms of the conversion of phenol, but also in terms of the fraction of methanol utilized as an alkylating reagent. An important characteristic of the $Ca_3(PO_4)_2$ catalyst to be noted here is that only a small % of the methanol converted is consumed for gasification. It must be generally accepted that the MO-Fe_2O_3 catalyst developed by Kotanigawa *et al.*[3] is more active than the $Ca_3(PO_4)_2$ catalyst. The MO-Fe_2O_3 catalyst, however, leads to significant amounts of gasification of methanol; hence, it can be said that the $Ca_3(PO_4)_2$ catalyst is more effective in the selectivity of methanol than the MO-Fe_2O_3 catalyst.

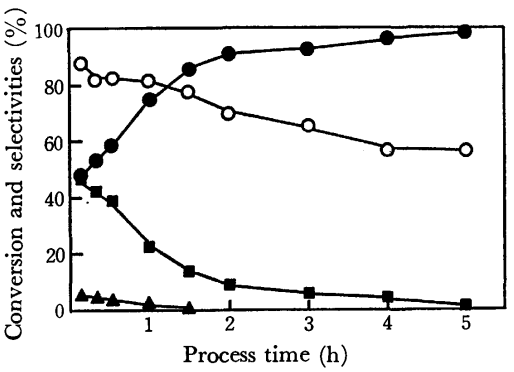

Fig. 1. Changes in activity and selectivity of $Ca_3(PO_4)_2$ catalyst with process time.
Conditions: t=460 °C, W/F=14.5 g h/mol, m=2.0/1.0/1.2.
○: Conversion of phenol (x), ●: selectivity for ortho-methylation (S_O), ▲: selectivity for anisole formation (S_A), ■: selectivity to the other products (S_B).

The change in the activity and selectivity of the $Ca_3(PO_4)_2$ catalyst with the process time are illustrated in Fig. 1. Both the activity and the selectivity change rapidly at the initial period, and then they gradually approach almost constant values. The selectivity for ortho-methylation, S_O, increases with the process time and approaches 100% after the reaction had been continued for 4 h. In contrast, the selectivity to the other products, S_B, decreases rapidly and is lowered to a very small value with an increase in the process time. The selectivity for anisole formation, S_A, is allowed to continue at a small value and then becomes practically negligible around 2 h after the start of the reaction. Consequently, only two products, *o*-cresol and 2,6-xylenol, are obtained after the reaction has been continued for 5 h or more. Such a decrease in activity

and change in selectivity as are shown in Fig. 1 might be due to the disappearance of active sites, leading to the formation of a highly methylated product or anisole by the deposition of a carboneous substance. After the reaction has been continued for several hours, however, the catalyst surface is brought into a situation favorable to ortho-methylation and the subsequent catalytic reaction reaches an almost steady state.

Effects of the Reaction Temperature and Contact Time. The effect of the reaction temperature on the conversion, the selectivity, and the yields of the products was investigated with the $Ca_3(PO_4)_2$ catalyst. The results are shown in Figs. 2 and 3; the data were obtained by using a fresh catalyst in each run and by analyzing the samples collected 1.5 h after the start of the reaction. The higher the reaction temperature, the higher the conversion and the yield of *o*-cresol, 2,6-xylenol, or 2,4,6-trimethylphenol became. The selectivity for ortho-methylation was approximately 80%, regardless

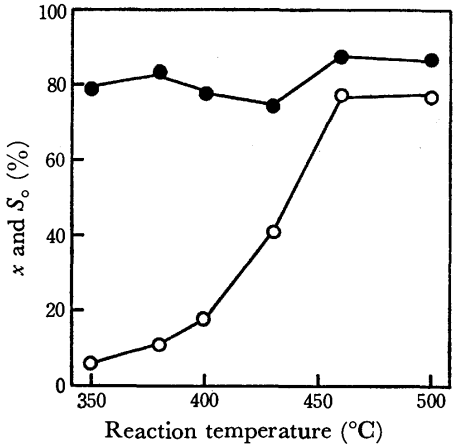

Fig. 2. Effect of reaction temperature on conversion and selectivity.
Conditions: $Ca_3(PO_4)_2$ catalyst, W/F=14.5 g h/mol, m=2.0/1.0/1.2.
○: Conversion of phenol (x), ●: selectivity for ortho-methylation (S_o).

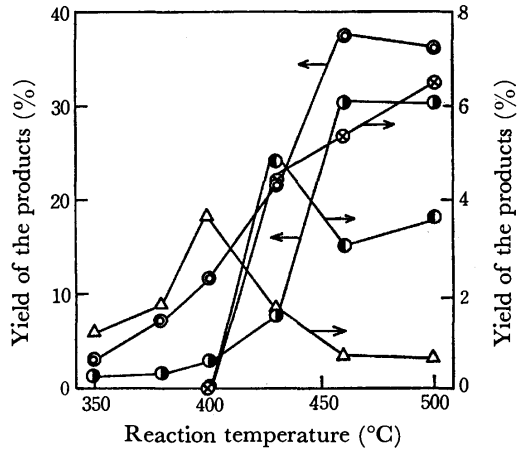

Fig. 3. Correlation between reaction temperature and yield of the products.
Conditions are the same as for Fig. 3.
◎: *o*-Cresol, ◑: 2,6-xylenol, ◐: 2,4-xylenol, ⊗: 2,4,6-trimethylphenol, △: anisole.

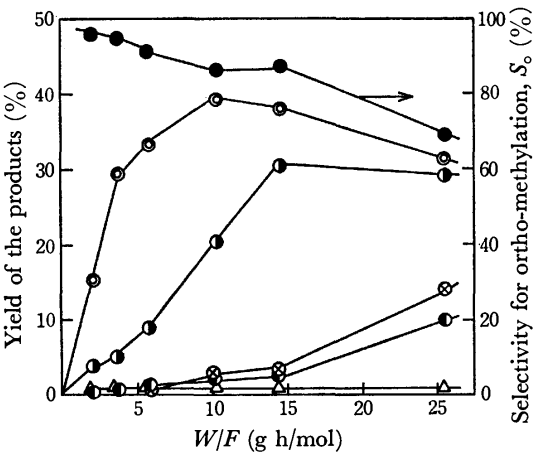

Fig. 4. Yield and selectivity over $Ca_3(PO_4)_2$ catalyst as a function of W/F.
Conditions: t=460 °C, m=2.0/1.0/1.2.
Symbols are the same as those defined in Figs. 2 and 3.

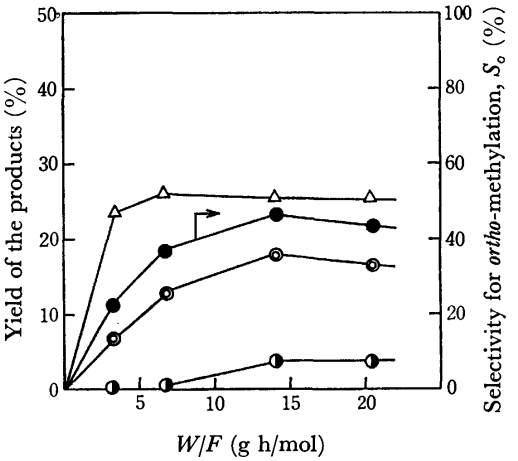

Fig. 5. Yield and selectivity over BPO_4 catalyst as a function of W/F.
Conditions and symbols are the same as for Fig. 4.

of the reaction temperature. The temperature providing the maximal yields of anisole and 2,4-xylenol were about 400 and 430 °C respectively. However, their yields did not exceed 5%.

The effects of W/F on the yields of the products are shown in Figs. 4 and 5. Figure 4 indicates that the $Ca_3(PO_4)_2$ catalyst gives, selectively, *o*-cresol and 2,6-xylenol in the low range of W/F. With an increase in W/F, the consecutive methylation of *o*-cresol to xylenols and trimethylphenol is gradually increased, but the formation of anisole is slight over the entire range of W/F. Figure 5 indicates that, in the case of the BPO_4 catalyst, the increase in W/F does not result in a remarkable increase in the yields of the products or in the selectivity for ortho-methylation. Anisole is predominantly formed over the whole range of W/F, but no definitive maximum in the yield of anisole is perceived throughout the experimental range of W/F. The yields of xylenol isomers were vanishingly small, and such highly methylated products as trimethylphenol were completely missing, even at the highest range of W/F.

Table 2. Acid-base properties of various catalysts

Catalyst	Acidity (mmol/g) $H_0 \leqq 3.3$	$H_0 \leqq 4.8$	$H_0 \leqq 6.8$	Basicity (mmol/g) $H_0 \geqq 7.1$
$Ca_3(PO_4)_2$	0	0	0.132	0.053
$CaHPO_4$	0	0.046	0.073	0
$Ca(H_2PO_4)_2$	0.196	—[b]	—[a]	0
BPO_4	0.220	—[b]	0.370	0
CaO	0	0	0.043	0.066

a) The acidity ($H_0 \leqq 6.8$) of $Ca(H_2PO_4)_2$ could not be measured quantitatively because of the formation of a precipitate. b) The measurements were not carried out.

Acid-Base Property of the Catalyst and the Catalytic Activity. The acid-base properties of the catalysts are shown in Table 2. The strong basic site with $H_0 \geqq 9.3$ was not found in any catalyst. Between the catalytic activities and the acid-base properties of the catalysts, no simple correlation can be observed by comparing Table 1 with Table 2. Excluding the case of the $Ca(H_2PO_4)_2$ catalyst, however, it is likely that anisole is produced over the BPO_4 or $CaHPO_4$ catalyst with acidic sites ($H_0 \leqq 4.8$) but no basic sites, and that the ortho-methylation can occur over the catalysts with both weak acidic sites ($H_0 \leqq 6.8$) and basic sites.

In order to make this aspect clearer, we have investigated the relationship between the catalytic activity and the acid-base property, using a series of $Ca_3(PO_4)_2$ catalysts calcined at various temperatures. The results are shown in Figs. 6 and 7. Both the acidic strength and the basic strength of the $Ca_3(PO_4)_2$ catalyst remained unaltered by a change in the calcination temperature, although either the acidity ($H_0 \leqq 6.8$) or the basicity ($H_0 \geqq 7.1$) varied, as is shown in Fig. 6. Figure 6 indicates that the acidity decreases monotonously with the rise in the calcination temperature, while the basicity has its maximum at the calcination temperature near 550 °C. Figure 7 indicates that the catalyst activity (the conversion of phenol) slightly increases with rise in the calcination temperature from 460 to 500 °C, passes

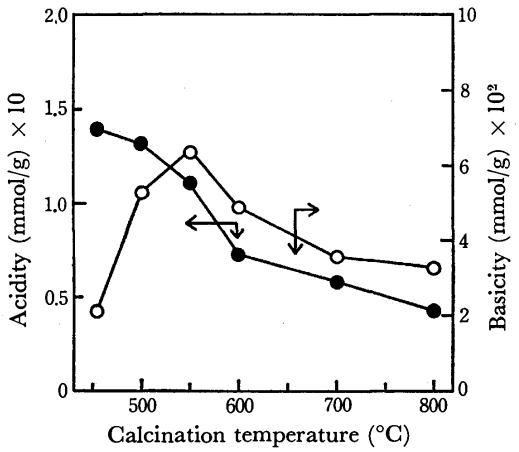

Fig. 6. Acidity and basicity of $Ca_3(PO_4)_2$ calcined at various temperatures.
●: Acidity (measured at $H_0=6.8$), ○: basicity (measured at $H_0=7.1$).

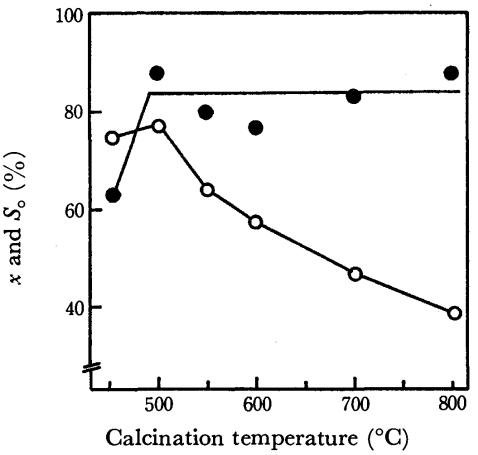

Fig. 7. Activity and selectivity of $Ca_3(PO_4)_2$ catalyst calcined at various temperatures.
Conditions and symbols are the same as for Fig. 2.

through a maximum at about 500 °C, and then significantly decreases. In contrast, the selectivity for ortho-methylation remains almost constant at temperatures ranging from 500 to 800 °C, except for the low selectivity of the catalyst prepared at 460 °C. A comparison of Fig. 6 with Fig. 7 suggests that the catalytic activity may be correlated to both the acidity and basicity, whereas the ortho-selectivity essentially depends on whether or not the basic sites coexist with acidic sites.

Reaction Pathway and Reaction Mechanism. By considering the fact that a maximal yield in the anisole formation is not observed in Fig. 4, the ortho-methylation giving *o*-cresol and 2,6-xylenol is expected to occur through a direct methylation of phenol, not through the formation of phenylethers, such as anisole or *o*-methylanisole, and their subsequent isomerization. In order to make more clear the reaction pathway of methylation, we have carried out additional catalytic tests between anisole, *o*-cresol or xylenols, and methanol. The results are summarized in Table 3. When anisole alone was passed through the $Ca_3(PO_4)_2$ catalyst under

Table 3. Catalytic reactions between anisole, *o*-cresol, 2,4-xylenol, or 2,6-xylenol and methanol over the $Ca_3(PO_4)_2$ catalyst
The conditions are the same as in Table 1, except for the methanol/reactant feed ratio.[a]

Reaction[a]	Anisole–methanol	*o*-Cresol–methanol	2,6-Xylenol–methanol	2,4-Xylenol–methanol
Conversion[b] (%)	48	40	25	66
	Yield of the product (%)			
Phenol	2	3	0	0
o-Methylanisole	6	3	0	0
o-Cresol	8	—	8	4
m,p-Cresol	0	0	0	1
2,6-Xylenol	16	23	—	0
2,4-Xylenol	5	7	0	—
2,4,6-Trimethylphenol	11	4	17	61

a) Feed molar ratio of methanol/anisole, methanol/*o*-cresol, *etc.*=1. b) Conversion of anisole, *o*-cresol, *etc.*

the same conditions as those described in Table 3, the anisole was rearranged, giving a small amount of *o*-cresol (in a 7.5% yield); it was partly demethylated to give phenol (in a 9.8% yield). From a comparison of Table 3 with the results shown in the other tables and figures, the following speculations are possible with respect to the reaction pathway of methylation: (1) the formation of *o*-cresol is due mostly to the direct methylation of phenol; (2) anisole is scarcely methylated at all to form *o*-methylanisole; (3) the isomerization of *o*-cresol to anisole or *m,p*-cresol is not observed; (4) xylenol isomers are formed by a consecutive methylation of *o*-cresol, whereupon it tends to form 2,6-xylenol rather than 2,4-xylenol, and (5) 2,4,6-trimethylphenol is formed by the further methylation of xylenol isomers, whereupon 2,4-xylenol is more readily methylated than 2,6-xylenol. Thus, the reaction pathway of methylation over the $Ca_3(PO_4)_2$ catalyst may be depicted as the following steps:

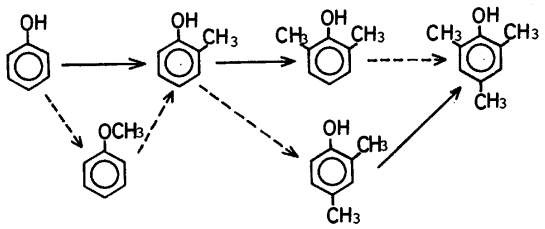

where the(→)arrow shows the main route of the methylation and(⇢), the sub-route. The behavior of $Ca_3(PO_4)_2$ as a catalyst was characterized by a selective formation of the ortho alkylated products. The reaction pathway described above is intrinsically consistent with the result obtained over the basic catalysts by Tanabe *et al.*[4] and by Enomoto *et al.*[7] Tanabe[13] and Enomoto *et al.*[7] have already pointed out that acidic catalysts, such as SiO_2–Al_2O_3 or condensed phosphoric acid, promote the reactions, giving phenylethers or *m*-alkylated products, while basic catalyst, such as MgO or ZnO–Fe_2O_3, promote the direct alkylation, giving the *o*-methylphenols without passing through phenylethers as an intermediate. According to their argument, the $Ca_3(PO_4)_2$ catalyst appears to be characteristically basic. This is not in conflict with our previous reports,[1,12] in which the $Ca_3(PO_4)_2$ has been characterized as a basic catalyst for the dehydrogenation of alcohols. However, it should be noted that the ortho-methylation of phenol depends not only on the basic sites, but also on the acidic sites, as has been mentioned above.

The acid-base properties of the colored phosphates, such as $Ni_3(PO_4)_2$ or $CrPO_4$, are difficult to measure by the titration method using Hammett indicators. Thus, instead of using the experimentally found values of the acid-base properties of the catalysts, the electronegativities (x_i) of the metal ions[14] in the phosphate or oxide catalysts were used as an indication of the acidic or basic strength, according to the theory proposed by Tanaka.[14] The selectivities for the ortho-methylation of various catalysts are shown in Fig. 8 as functions of the parameter, x_i. Figure 8 shows that the correlation between S_0 and x_i has a rough tendency to move towards a low selectivities with the increase in x_i. This

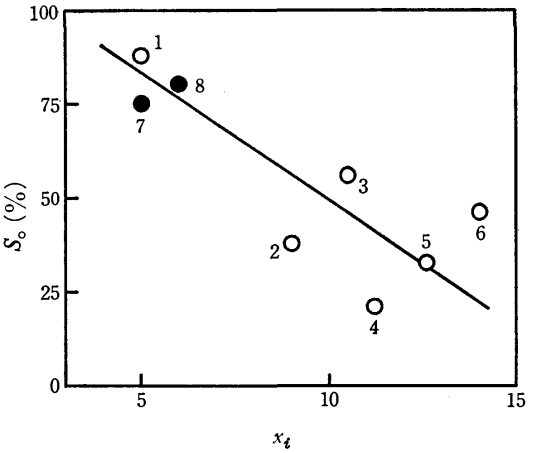

Fig. 8. Correlation between S_0 and x_t.
Catalyst—1: $Ca_3(PO_4)_2$, 2: $Ni_3(PO_4)_2$, 3: $AlPO_4$, 4: $CrPO_4$, 5: $Zr_3(PO_4)_4$, 6: BPO_4, 7: CaO, 8: MgO.

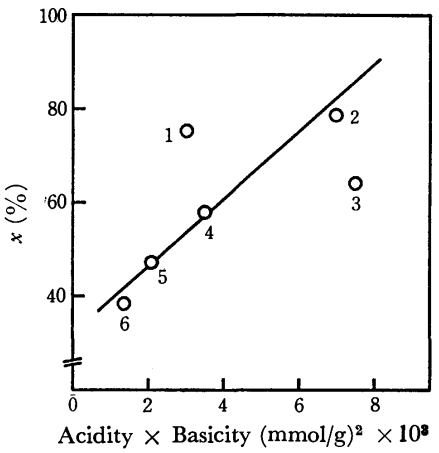

Fig. 9. Correlation between acid-base property and catalytic activity of $Ca_3(PO_4)_2$ calcined at various temperatures.
Calcination temperature—1: 460, 2: 500, 3: 550, 4: 600, 5: 700, 6: 800 °C.

downward trend in the selectivity on x_i is intrinsically the same result as those reported by Tanabe *et al.*[10,13] On the other hand, the change in the activity depending on the variety of catalyst was too complicated to deal with quantitatively. In the limited case of the $Ca_3(PO_4)_2$ catalyst calcined at various temperatures, however, there was a rough correlation between the acid-base property (Fig. 6) and the catalyst activity (the conversion of phenol in Fig. 7), as is shown in Fig. 9. The upward trend in the activity with an increase in the term of (acidity)·(basicity) presumably suggests that the catalytic methylation is attributable to the mechanism involving both the acidic and basic sites. Further details of the reaction scheme and the catalyst structure must remain the subjects of future study.

References

1) Part III of this series: F. Nozaki and Y. Iimori, *Bull. Chem. Soc. Jpn.*, **49**, 567 (1976).
2) A. Tasaka, *Shokubai*, **15**, 155 (1973).
3) T. Kotanigawa, M. Yamamoto, K. Shimokawa, and Y.

Yoshida, *Bull. Chem. Soc. Jpn.*, **44**, 1961 (1971).

4) T. Nishizaki and K. Tanabe, *Shokubai*, **14**, No. 4 (Abstract of the 31st Annual Meeting of Catalysis Society of Japan), p. 138 (1972); *ibid.*, **15**, No. 4 (Abstract of the 33 rd Annual Meeting of Catalysis Society of Japan), p. 94 (1973).

5) H. Hattori, K. Shimazu, N. Yoshii, and K. Tanabe, *Bull. Chem. Soc. Jpn.*, **49**, 969 (1976).

6) N. Takamiya, Y. Nakamura, M. Uomori, and S. Murai, *Nippon Kagaku Kaishi*, **1974**, 1852.

7) M. Inoue and S. Enomoto, *Chem. Pharm. Bull.*, **19**, 2518 (1971); *Shokubai*, **15**, No. 4 (Abstract of the 33 rd Annual Meeting of Catalysis Society of Japan), p. 98 (1973).

8) Y. Ogata and M. Itoh, *Kogyo Kagaku Zasshi*, **70**, 911 (1967).

9) M. Nitta, K. Aomura, and K. Yamaguchi, *Bull. Chem. Soc. Jpn.*, **47**, 2360, 2897 (1974).

10) T. Yamanaka and K. Tanabe, *Shokubai*, **17**, No. 4 (Abstract of the 37 th Annual Meeting of Catalysis Society of Japan), p. 102 (1975).

11) T. Takeshita and K. Tanabe, *Shokubai*, **7**, 467 (1965).

12) F. Nozaki and H. Ohta, *Bull. Chem. Soc. Jpn.*, **47**, 1307 (1974).

13) K. Tanabe, *Shokubai*, **17**, 72 (1975).

14) K. Tanaka, "Shokubai Kogaku Koza," Vol. 10, ed by the Catalysis Society of Japan, Chijin Shokan, Tokyo (1967), p. 752.

Photoemission from Anthracene and Compounds Containing Anthracene-ring Systems

Shojun HINO,† Tomohiko HIROOKA,* and Hiroo INOKUCHI††

The Institute for Solid State Physics, The University of Tokyo, Roppongi, Minato-ku, Tokyo 106
**Department of Chemistry, Faculty of Science, The University of Tokyo, Hongo, Bunkyo-ku, Tokyo 113*

(Received September 16, 1976)

The Photoemission from the organic compounds containing anthracene rings—anthracene, 9-methylanthracene, 9,10-dichloroanthracene and 9,9′-bianthryl—was measured. The photoelectron energetic responses of all these compounds were nearly the same. The resemblance of the photoelectron energy distribution curves and the spectral dependence of the quantum yield revealed the coincidence of the electronic structures of these compounds in a solid. The comparison between solid- and gas-phase photoelectron spectra showed that the optical excitation process is the most characteristic one in photoemission phenomena.

Anthracene is a typical compound in the research field of molecular crystals, like polycyclic aromatic hydrocarbons and solid rare gases. The various physicochemical properties of anthracene have been reported.[1,2] Among them, photoemission has recently been revealed to be a useful method for the investigation of the electronic structures of the solid state.[3–10]

We have measured the photoelectric response of anthracene and aromatic compounds containing anthracene-ring systems. The photoelectron energy distribution curves (EDCs) were obtained with a high accuracy by means of an electrical differentiation circuit.[7,11]

In this paper, we will compare the photoelectric effect among these compounds, and will also discuss the effect of the anthracene-ring on the photoemission behavior. We will also point out the resemblance of the photoelectron spectra between the gaseous and solid phases.

Experimental

Measurement. Monochromatic light obtained by a half-meter Seya-Namioka-type monochromator[12] was admitted into a chamber through a lithium fluoride window, which limited the measurement to $h\nu < 12$ eV. The energy distribution of the photoemitted electrons was measured by means of a spherical retarding electrode coated with colloidal graphite, Aquadag, on the inside. The small ac voltage (200 mV peak to peak, 4 Hz) was superimposed on the retarding potential in order to differentiate the I—V characteristic curves.[7,11] The spectral width of the monochromatized light was between 0.05 eV at 200 nm and 0.13 eV at 120 nm. In all, the experimental error is estimated to be less than 0.2 eV in measuring the EDCs.

As the total photocurrents were about 10^{-10} A or less, a preamplifier, a Cary 31 vibrating reed electrometer, had to be used to amplify the photocurrent. 4 Hz ac was adopted to differentiate the I—V characteristics, since the time response of the electrometer was not fast enough for a higher frequency to be used.

The spectral dependence of the quantum yield (SDQY) were measured by means of the same electrode, applying enough accelerating voltage between the emitter and the collector. The relative light intensity was also measured by means of a photomultiplier tube RCA 5819 with the aid of a coronene wavelength converter. As the stray light of the monochromator easily affects the photocurrent (this effect could not be neglected in the case of a low incident photon energy), filters, mainly a quartz filter (with a cut-off wavelength of 155 nm), were applied.

Samples. The samples used in this study were anthracene, 9-methylanthracene (9MeA), 9,10-dichloroanthracene (DClA), and 9,9′-bianthryl. Anthracene and 9MeA were deposited onto a cooled emitter (copper disk 12 mm in diameter) as a thin film by the sublimation method in a fairly low vacuum (10^{-3}—10^{-4} Torr) in order to prevent sample evaporation. After the preparation of the specimens, the emitter was introduced into the ionization chamber. During this operation, the specimen absorbed oxygen and water on its surface easily. The effect of this contamination will be discussed later.

DClA and 9,9′-bianthryl, on the other hand, were deposited onto the emitters under a pressure of less than 4×10^{-6} Torr by the sublimation method, this was possible because of their low vapor pressures.

The film thickness is an important factor in the quantitative photoemission measurements of organic crystals; a thinner film is not thick enough to prevent the penetration of light to the substrate, and the photocurrent due to the substrate is often observed, while a thicker film causes a charge-up effect which affects the EDCs. The thickness of the evaporated films in this work was from 40 to 100 nm in the first preparation. As the samples were sublimed successively from the surface of the thin film during the measurements, it was difficult to estimate the film thickness at each measurement.

Results

Energy Distribution Curves. Figures 1—4 show the photoelectron energy distribution curves of anthracene and its derivatives. Each EDC is indicated in arbitrary units, plotted as a function of the retarding potential, V; the numerical value beside each EDC is the incident photon energy. A dominant peak was observed in each EDC at about $V=0$ V. This peak position was independent of the incident photon energy. The kinetic energy of the photoejected electrons which are attributed to this dominant peak was less than 1 eV.

On the left side of the dominant peak (a large retardation voltage was applied) several structures were observed. These structures resemble each other. They come from the valence bands of each material as will be discussed later. On the right side of the peak, most EDCs except those of anthracene were cut sharply by

† Present address: Department of Chemistry, Faculty of Science, Josai University, Keyakidai, Sakado, Saitama 350-02.

†† Present address: Institute for Molecular Science, Okazaki 444.

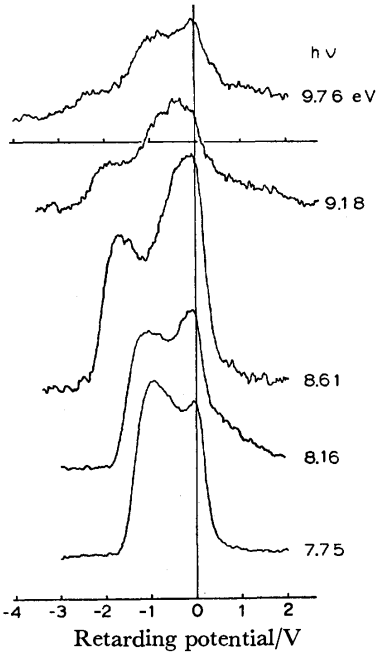

Fig. 1. EDCs of anthracene plotted as a function of retarding potential.

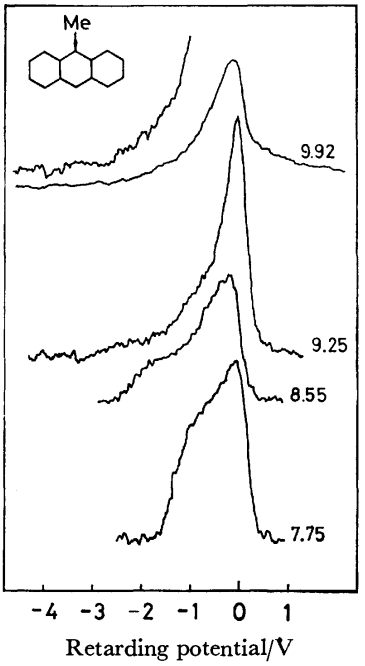

Fig. 2. EDCs of 9MeA plotted as a function of retarding potential.

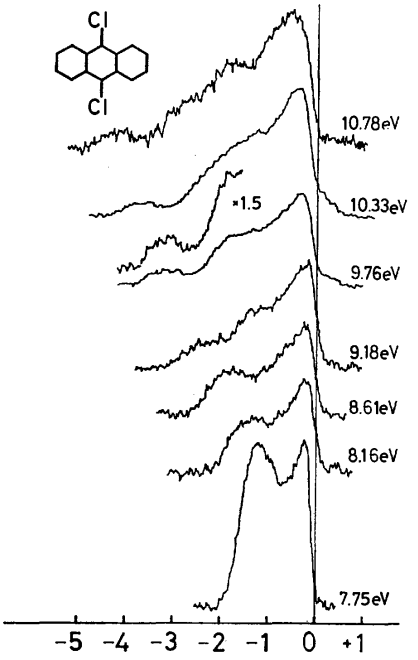

Fig. 3. EDCs of DClA plotted as a function of retarding potential.

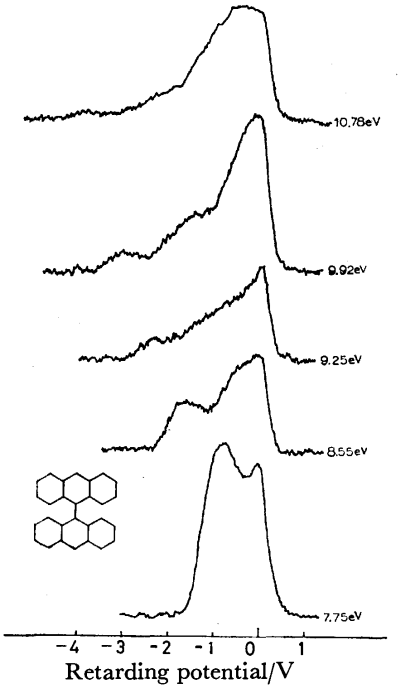

Fig. 4. EDCs of 9,9′-bianthryl plotted as a function of retarding potential.

an effect of the escape function for passing electrons from a solid to a vacuum through the surface. However, long tails were found in some EDCs of anthracene. These long tails were caused by potential drops between the sample surface and the copper disk, since we were sometimes obliged to use thick specimens to avoid quick sample consumption.

The EDCs of 9MeA did not show any distinguishing peaks on the left side of the dominant peak. They showed only shoulders.** These results were perhaps due to the contamination of the specimen surface as will be discussed later, because the deposition of 9MeA was not performed under good conditions.

The threshold energy, E_{th}, can be obtained by using the well-known equation:

$$E_{th} = h\nu - E_w$$

** Moreover, the dominant peaks of 9MeA were much higher than the others.

TABLE 1. THRESHOLD ENERGIES OF THE ORGANIC COMPOUNDS CONTAINING ANTHRACENE-RING SYSTEMS, BOTH OBTAINED FROM THE EDCs AND THE CUBE ROOT PLOT IN eV

	This work		Others	
	E_{th}[a]	E_{th}[b]		
Anthracene	5.7	5.7_5	5.65[c]	5.95[d]
9-Methylanthracene	5.7_5	5.6_8	5.56[e]	5.95[d]
9,10-Dichloroanthracene	5.8	5.7_5		6.10[d]
9,9′-Bianthryl	5.9	5.9_6		—

a) Obtained from the EDCs. b) Obtained from the cube root plot. c) Ref. 3. d) Ref. 6. e) Ref. 9.

where $h\nu$ is the energy of the incident photon and E_w is the band width of the EDCs. The threshold energies of these compounds are collected in Table 1.

Quantum Yield. Figure 5 shows the spectral dependence of the quantum yield of anthracene and its derivatives. All the SDQYs showed steep rises at about 6 eV. This is due to the effect of the escape function, which dominates the photoelectron-escape probability at the solid-vacuum interface. In the region between 6.5 and 7.5 eV, all the SDQYs had almost flat slopes. These flat slopes meant a small probability of photoelectron emission in spite of an increase in the light energy. Above 7.5 eV, the quantum yields increased gradually in accordance with the photon energy.

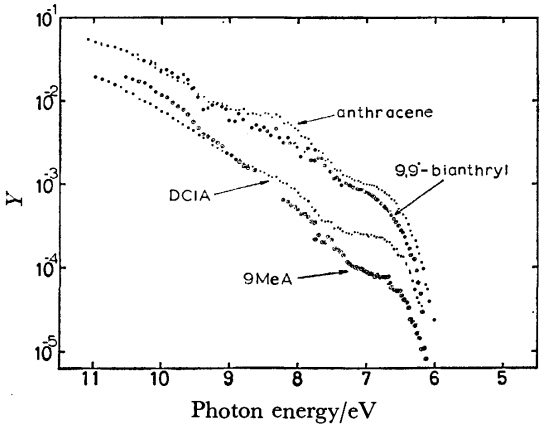

Fig. 5. Spectral dependence of quantum yield of these four compounds.

Anthracene and 9,9′-bianthryl showed the same yields throughout the energy region, while the photoelectric yield of DClA was about a half of that of anthracene. The photoelectric current of 9MeA varied with the exchange of specimens at the same intensity of the exciting light. This phenomenon was probably due to the surface conditions; one specimen was fairly clean and free from the contamination of the surface, while the others were not. As the surface contamination affects the photoelectric quantum yield, the SDQY of 9MeA shown in Fig. 5 is somewhat dubious.

Discussion

Energy Distribution Curves. Figures 6—8 show the replotted EDCs arranged with the first edges of each EDC on the same line. There are fixing peaks in this revised plot which vary the peak position with the incident quanta as shown in Figs. 1—4. These peaks

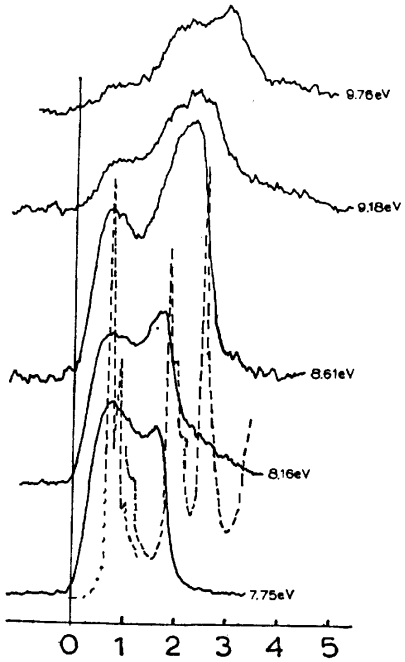

Fig. 6. EDCs of anthracene rewritten so that the first edge of each EDC should coincide. Abscissa is energy measured from threshold energy, 5.7 eV. Broken line indicates a molecular photoelectron spectrum of anthracene.[13] See description of text.

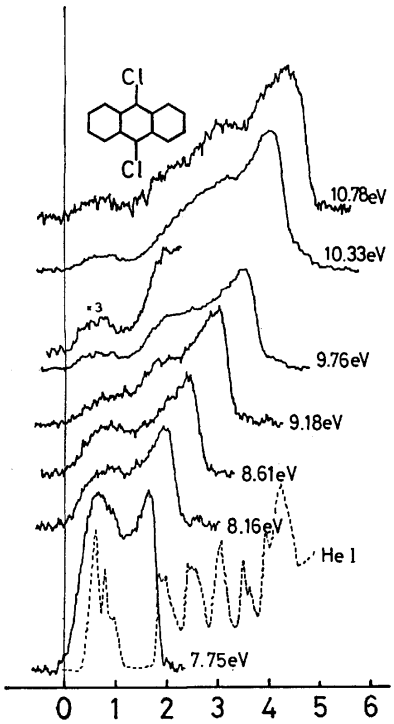

Fig. 7. EDCs (solid line) and molecular photoelectron spectrum (broken line) of DClA.[15] Abscissa is energy measured from threshold energy, 5.8 eV.

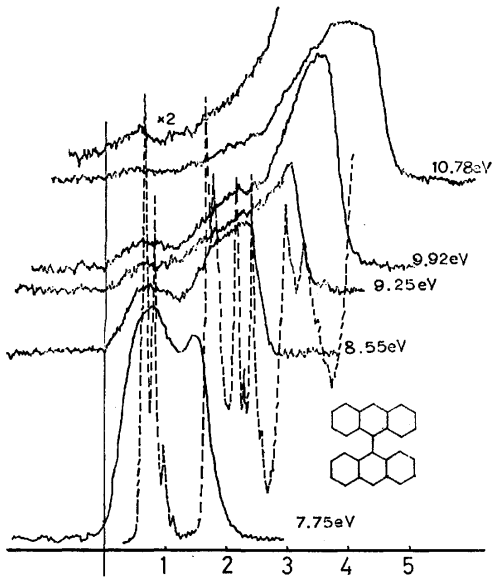

Energy from threshold energy in eV

Fig. 8. EDCs (solid line) and molecular photoelectron spectrum (broken line) of 9,9′-binathryl.[16] Abscissa is energy measured from threshold energy, 5.9 eV.

correspond to the valence electrons of each substance. This can be confirmed by a comparison of the broken lines in each figure;[13–16] this line is the molecular photoelectron spectrum, with a slight shift so that the first peaks of both spectra will coincide. The positions of the peaks or shoulders in the EDCs are in good agreement with the photoelectron spectra indicated by the broken lines. This fact indicates that the EDCs obtained by photoemission measurements reflect the state density of the valence band. The ionization potentials obtained by photoemission measurements (peak position) are collected in Table 2, which also lists the I_p's of gaseous anthracene and its derivatives. Table 3 summarizes the energy differences between the first ionization potential and the others.

On the other hand, the dominant peak, which was at the right side of each EDC and had a kinetic energy nearly 0 eV, has no corresponding photoelectron spectrum in the gas phase. This result suggests two possible explanations: The existence of auto-ionization levels in the conduction band, as Zagrubskii and Vilesov

Table 2. Peak positions of the photoelectron spectra in gaseous and solid phases in eV

	Anthracene		9-Methyl-anthracene		9,10-Dichloro-anthracene		9,9′-Bianthryl	
	Solid	Gas[a]	Solid	Gas[b]	Solid	Gas[c]	Solid	Gas[d]
1 st	6.4	7.47	(6.5)	7.25	6.5	7.58	6.5	(7.24, 7.42)
2 nd	7.6	8.57	(7.8_5)	8.43	7.7	8.88	7.6	(8.23, 8.34)
3 rd	8.2	9.23	—	9.07	8.1	9.42	8.2	(8.73, 9.00)
4 th	—	10.26	—	9.87	8.8	9.91	9.2	(9.55, 9.87)

a) Ref. 13. b) Ref. 14. c) Ref. 15. d) Ref. 16.

Table 3. Energy differences between the first ionization potentials and the others in eV

	Anthracene		9-Methyl-anthracene		9,10-Dichloro-anthracene		9,9′-Bianthryl	
	Solid	Gas	Solid	Gas	Solid	Gas	Solid	Gas[a]
1 st	0.0	0.00	0.0	0.00	0.0	0.00	0.0	0.00
2 nd	1.2	1.10	(1.3_5)	1.18	1.2	1.30	1.1	0.95
3 rd	1.8	1.76	—	1.82	1.6	1.84	1.7	1.53
4 th	—	2.79	—	2.72	2.3	2.33	2.7	2.38

a) Mean values were adopted.

proposed,[8] or a scattering mechanism of photoexcited electrons in the transport process, as estimated by Kochi *et al.*[5] and Schechtman.[10]

As for the first explanation, it is difficult to consider a characteristic level which uniformly results in the creation of electrons of nearly 0 eV in these compounds. According to Zagrubskii and Vilesov,[8] the vibrational excitation, ΔE_j, of the auto-ionizing state, M_j^*, has a dominant role in making the stationary peaks in the low-kinetic-energy region. The probability of auto-ionizing processes becomes more significant and the EDCs become structureless when ΔE_j is large. Moreover, ΔE_j is considerable in large molecules. It is, however, doubtful whether the ΔE_j of these compounds are the same. Moreover, the resemblance between the obtained results of anthracene and 9,9′-bianthryl (twice as large as anthracene) raises a question about their explanation.

The second explanation is more reasonable. In the solid state, there are various scattering processes, and such processes cause a decrease in the kinetic energy of the photoelectrons over a considerably wide energy range. Moreover, the peak ratio of this dominant peak depends strongly on the photon energy. These facts suggest that the scattering mechanism is the origin of the dominant peak.[17]

The result for 9MeA, which did not show any abrupt large peaks except for the dominant peak, can be understood in terms of the contamination of the solid surface especially with water. The effect of the contamination was checked by the use of DClA evaporated films. The film evaporated at room temperature showed several structures, as is shown in Fig. 4. The films prepared at about −30 °C, however, showed dull shapes, and their EDCs changed with the evacuating time; the structure became sharper. Moreover, the total photoelectric current increased. These facts suggest that the contamination mainly caused by the adsorption of water affects the measurements of the photoemission and that continuous evacuation reduces the contamination of the sample surface. Therefore, if we seek to account for the experimental conditions of 9MeA, low vacuum and a thin sample film which were inadequate to evaporate the contaminated layer of the film, it is probable that the intrinsic EDCs of 9MeA are not just like those of Fig. 2: This figure may be somewhat too vague.

When we consider the exceptional situations in the case of 9MeA, anthracene and its derivatives may be said to show the same EDCs, as may easily be seen in

the figures. This finding indicates that the photoelectron energetic responses of these compounds are nearly the same. This fact is useful in considering the mechanism of photoemission from organic crystals. As is well known, photoemission is constituted of three steps: photoelectron generation, electron-transport, and escape from the surface. When electron-transport process is the dominant process in photoemission, the EDCs obtained must be different, unrelated to the photoelectron generation, since the field with which an excited electron is affected differs with the compound. For example, though DClA has a large polarizability and chlorine atoms which have a large electronegativity so as to easily catch the electrons, the EDC patterns of DClA are analogous to those of anthracene. As for the escape process, the resemblance of the EDCs in spite of various experimental conditions may indicate that the electron escape probabilities of these compounds are the same. Therefore, the photoelectron generation process, which is considered to be the same as in the case of gas-phase photoexcitation, plays the dominant role in the photoemission of organic crystals. Electron transport does not affect the shape of the EDCs so much. They are slightly affected by the electron-escape process, mainly by the contamination of the surface, as is 9MeA.

As is shown by the broken lines in Figs. 6 and 8, though the ionization potentials of 9,9′-bianthryl were much more complicated than those of anthracene, the EDCs obtained were almost the same, within the limits of resolution of the analyzer. This result implies an analogy in the electronic states of the two compounds in the solid state. In the gas phase at high temperatures, two anthryl groups may rotate along the C–C axis and may perturb the molecular orbitals of each other. On the other hand, in the solid state the two anthryl groups, mainly π-electron systems, are independent of each other. This phenomenon was also observed in biphenyl derivatives[18] and *p*-terphenyl.[19]

Quantum Yield. The steep rise in SDQYs at about 6 eV is due to the effect of the escape function, which rules the electron transport from the surface into the vacuum. To this region we can apply the following relation in order to obtain the threshold energy;[5]

$$Y \propto (h\nu - E_{th})^3$$

The cube-root plot of these compounds shows linear relation between the photon energy and the cube root of the quantum yield. The threshold energies of the compounds obtained by this method are collected in Table 1; the threshold energies obtained from the EDCs are also listed in that table.

The values obtained from the cube root plot and from the EDCs show a good accordance. As to the comparison with other works, the threshold energy obtained by Lyons and Morris[3] shows a good agreement with our present results. That of 9MeA reported by Vilesov and Sukhov[9] seems somewhat small, though the method of obtaining the threshold energy reported by Marchetti and Kearns[6] gives a slightly large value because it considers the thermal excitation. Therefore, their values, which were larger than our present results by about 0.2 eV, nevertheless show a good agreement with ours in the trend among these compounds.

In the energy region higher than 7.5 eV, the quantum yield increased in accordance with increase in the photon energy. This is probably due to the photoelectrons from deeper levels. There are some dips in the SDQYs. Seki and his co-workers[17] suggested that these dips might be due to the change in the absorption coefficient. The basis of their conclusion was that the electron-attenuation length, L, is much shorter than the reciprocal of the absorption coefficient α, *i.e.*, $\alpha L \ll 1$; the photoelectrons observed might be produced mainly near the surface. Consequently, the SDQYs of this region depend on the spectral response of the absorption coefficient. However, our recent experiment on electron-attenuation length measurement has shown that the $\alpha L \ll 1$ relation does not always hold good. In some cases αL is nearly equal to unity or slightly larger than unity.[20,21] This fact is not always inconsistent with their postulate that the dips are due to the change in the absorption coefficient. However, particularly when αL is larger than unity, all the photoelectrons excited have a high probability of escaping into the vacuum. Therefore, we should conclude that the dips in the SDQYs are due not only to the spectral response of the absorption coefficient, but also to the beginning of the ionization of deeper levels.

The SDQYs of anthracene and 9,9′-bianthryl resembled each other and showed a larger photoelectron efficiency than that of DClA. The resemblance between them is considered in terms of electronic structures, as has previously been discussed. Though the SDQYs of DClA was about half that of anthracene, their inclination was analogous to that of anthracene. This analogy indicates that the skeletal structure of the molecules (the anthracene ring system) influences the SDQYs as in the EDCs. Moreover, the small quantum yield of DClA is probably due to the effect of the chlorine atom.[22]

The SDQY of 9MeA was not parallel with that of anthracene. The ratio of both SDQYs, 9MeA and anthracene, changed from 0.6 ($h\nu \simeq 10$ eV) to 0.1 ($h\nu \simeq 7$ eV). This fact seems inconsistent with previous discussion. However, the experimental conditions for measuring 9MeA were not good. In this case, as the contamination of the surface reduced the photoelectron-escape probability, we could not obtain the same SDQY. Moreover, the quantum yield of 9MeA changed with the evacuation time and with the conditions at sample preparation. Though we chose the largest photocurrent as the true photoelectron efficiency, there was still some probability of contamination due to the adsorption of water or oxygen.

Therefore, in view of the effect described above, all four SDQYs of anthracene and its derivatives show analogous structures. This fact also indicates that the electronic structures and photoelectric responses of these compounds are almost the same.

Conclusion

The external photoelectric responses of anthracene and its derivatives show the same behavior, and their EDCs correspond with the molecular photoelectron

spectra. The coincidence among the EDC of the same skeletal structure (anthracene ring system) implies that the original π-electronic state is the dominant factor in the energy distribution of photoemitted electrons. The resemblance of their SDQYs supports the above conclusion.

The authors wish to thank Professor Werner Schmidt, Institut für Organische Chemie, Universität München, for sending them the photoelectron spectrum of 9,9′-bianthryl.

References

1) F. Gutmann and L. E. Lyons. "Organic Semiconductors," John Wiley and Sons, New York (1967).
2) H. Meier, "Organic Semiconductors," Verlag Chemie, Weinheim (1974).
3) L. E. Lyons and G. C. Morris, *J. Chem. Soc.*, **1960**, 5192.
4) F. I. Vilesov, A. A. Zagrubskii, and D. Z. Garbuzov, *Fiz. Tverd. Tela (Leningrad)*, **5**, 2000, (1963) [*Soviet Physics-Solid State*, **5**, 1460 (1964)].
5) M. Kochi, Y. Harada, T. Hirooka, and H. Inokuchi, *Bull. Chem. Soc. Jpn.*, **43**, 2690 (1970).
6) A. P. Marchetti and D. R. Kearns, *Mol. Cryst. Liq. Cryst.*, **6**, 299 (1970).
7) T. Hirooka, K. Tanaka, M. Fujihira, H. Inokuchi, Y. Harada, and K. Kuchitsu, *Chem. Phys. Lett.*, **18**, 930 (1973).
8) A. A. Zagrubskii and F. I. Vilesov, *Fiz. Tverd. Tela (Leningrad)*, **13**, 2300 (1971) [*Soviet Physics-Solid State*, **13**, 1927 (1972)].
9) F. I. Vilesov and D. A. Sukhov, *Fiz. Tverd. Tela (Leningrad)*, **14**, 2393 (1972) [*Soviet Physics-Solid State*, **14**, 2069 (1973)].
10) B. H. Schechtman, Ph. D. Thesis, Stanford University, 1968.
11) K. A. Kress and G. L. Lapeyre, *Rev. Sci. Instrum.*, **40**, 74 (1969).
12) Y. Harada and H. Inokuchi, *Bull. Chem. Soc. Jpn.*, **39**, 1443 (1960).
13) R. Boschi, J. N. Murrel and W. Schmidt, *Discuss. Faraday Soc.*, **54**, 116 (1972).
14) S. Hino and H. Inokuchi, *Chem. Lett.*, **1974**, 363.
15) D. G. Streets and T. A. Williams, *J. Electron Spectrosc.*, **3**, 71 (1974).
16) W. Schmidt, private communication.
17) K. Seki, T. Hirooka, Y. Kamura, and H. Inokuchi, *Bull. Chem. Soc. Jpn.*, **49**, 904 (1976).
18) J. Daintith, J. P. Maier, D. A. Sweigart, and D. W. Turner, in "Electron Spectroscopy," ed by D. A. Shirley, North-Holland, Amsterdam (1972), p. 289.
19) S. Hino, K. Seki, and H. Inokuchi, *Chem. Phys. Lett.*, **36**, 335 (1975).
20) S. Hino, N. Sato, and H. Inokuchi, *Chem. Phys. Lett.*, **37**, 494 (1976).
21) S. Hino, to be published.
22) S. Hino, T. Hirooka, and H. Inokuchi, *Bull. Chem. Soc. Jpn.*, **48**, 1133 (1975).

The Microwave Spectrum, Structure, Quadrupole Coupling Constants, and Barrier to Internal Rotation of Methyldichlorosilane

Kunihiko ENDO,* Harutoshi TAKEO, and Chi MATSUMURA

National Chemical Laboratory for Industry, Honmachi, Shibuya-ku, Tokyo 151

(Received September 18, 1976)

The microwave spectra of the $^{35}Cl_2$, $^{35}Cl^{37}Cl$, and $^{37}Cl_2$ isotopic species of CH_3SiHCl_2 have been investigated in the frequency region from 12 to 40 GHz. The rotational constants and centrifugal distortion constants have been determined and were used to calculate the structure of the molecule. The structural parameters determined are:

r(Si-C) = 1.850 Å, ∠C-Si-Cl = 109.8°,

r(Si-Cl) = 2.040 Å, ∠Cl-Si-Cl = 108.8°.

A few high-J R-branch transitions are split into doublets because of the methyl internal rotation. These splittings give a barrier to internal rotation of 1.69±0.05 kcal/mol. An analysis of the $^{35}Cl_2$ quadrupole splittings leads to quadrupole coupling constants of $\chi_{aa}=-19.1\pm0.3$ MHz, $\chi_{bb}=5.4\pm1.3$ MHz, $\chi_{cc}=13.7\pm1.4$ MHz, $\chi_{bond}=-41.2\pm2.0$ MHz, and $\eta_{bond}=0.16\pm0.03$.

A comparison of the molecular structures in various substituted fluorosilane molecules reveals that both the Si-C and Si-F bond distances decrease upon the substitution of the fluorine atoms for the hydrogen atoms attached to the silicon.[1-4] Furthermore, it is interesting to note that the barrier to internal rotation decreases markedly with an increase in the number of fluorine atoms, while the barriers to internal rotation of various fluoroethane molecules have almost the same values.[5]

The chloro derivatives of methylsilane also provide a group of molecules that may be used to test the changes in the molecular constants with the substitution of the chlorine atoms for the hydrogen atoms. However, CH_3SiHCl_2 has not been studied by microwave spectroscopy, and only incomplete molecular structures have been determined for CH_3SiH_2Cl and CH_3SiCl_3. CH_3SiCl_3 was first investigated by Mockler *et al.*,[6] and the primitive molecular structure was presented on the basis of an analysis of the spectra of $CH_3Si^{35}Cl_3$ and $CH_3Si^{37}Cl_3$. Although the data for its isotopic species were added by Mitzlaff *et al.*,[7] they did not determine the molecular structure, since they failed to observe the silicon isotopic species. Recently the present authors suceeded in observing the spectrum of the ^{29}Si species, and the molecular structure has been analyzed.[8] Zeil *et al.* investigated the microwave spectrum of CD_3SiH_2Cl and presented the partial r_s structure of Si-Cl.[9] Though they recently reported about normal species, CH_3SiD_2Cl, and CD_3SiD_2Cl,[10] the molecular structure has not yet been determined.

The barrier to internal rotation of CH_3SiCl_3 has been obtained from the intensity measurement of the microwave spectral lines,[7] and that of CH_3SiH_2Cl has been determined by the observation of the far-infrared spectrum,[11] while the barrier height of CH_3SiHCl_2 in the vapor phase has not been obtained. In the present study, we measured the microwave spectrum of CH_3SiHCl_2 and determined the molecular structure and the barrier to internal rotation.

* Present address: College of Science and Engineering, Aoyama Gakuin University, Chitosedai, Setagaya-ku, Tokyo 157.

Experimental

The sample of CH_3SiHCl_2 was obtained from a commercial source and was used without further purification. The $CH_3SiH^{35}Cl^{37}Cl$ and $CH_3SiH^{37}Cl_2$ isotopic apecies were observed in their natural abundances. Since the sample decomposed gradually in the cell, it was continuously introduced into the cell and pumped out during the measurement. The spectrometer used in this reseach was a conventional 100 kHz Stark modulation type, with a 3 m X-band waveguide cell cooled with Dry Ice. The frequency accuracy is estimated to be ±0.1 MHz.

Analysis of the Spectra

The spectrum of CH_3SiHCl_2 was predicted from an approximate structure based on the structures of CH_3SiHF_2[3] and CH_3SiH_2Cl.[9] The χ_{bond} values (quadrupole coupling constants in coordinate system with z axis along the Si-Cl bond) were assumed to be the same as in CH_3SiH_2Cl. The predicted spectrum indicated that the c- and b-type transitions are allowed and that the b-type transitions are stronger if the large bond moments are assumed along the Si-Cl bonds. The prediction also showed that the b-type R-branch transitions with low K_{-1} numbers make the strongest series and have very small splittings due to hyperfine structures, and that they should have large Stark effects because of the nearly degenerate K-type doublet levels which are coupled with the μ_c dipole component. In fact, the clear K-doublet patterns for the $9_{09}\leftarrow8_{18}$ and $9_{19}\leftarrow8_{08}$ transitions were observed first under very small Stark modulation voltages. Between these two K-doublet lines, unusual spectral lines showing only Stark components were observed, as is shown in Fig. 1. These lines were identified as $9_{09}\leftarrow8_{08}$ and $9_{19}\leftarrow8_{18}$. Since this molecule lacks the μ_a component, these transitions are prohibited at the zero-field duration time of the square-wave modulation. On the other hand, the transitions are allowed at the other duration time in which the electric field is applied, because of the breakdown of the selection rule caused by the mixing of the energy levels by the μ_c component. This mechanism is illustrated schematically in Fig. 2. The similar transitions were observed also for $J=8\leftarrow7$, $J=10\leftarrow9$, and

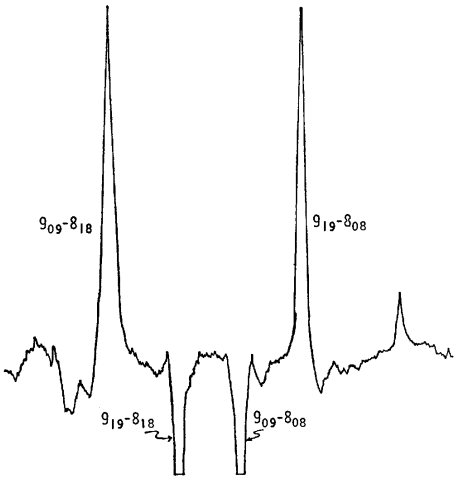

Fig. 1. The $9_{09}\leftarrow 8_{08}$, $9_{19}\leftarrow 8_{18}$ prohibited transitions.

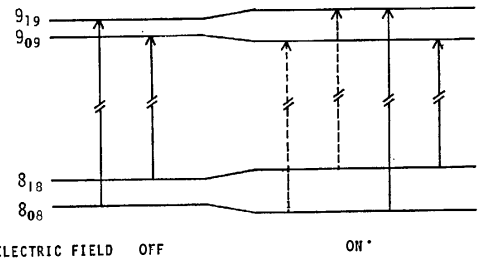

Fig. 2. Schematical illustration for breakdown of the prohibited transitions. Dotted lines represent prohibited transitions which is allowed only when an electric field is applied.

$J=11\leftarrow 10$ R-branch K-type doublets. Subsequently, Q-branch transitions were searched for in the region predicted from the rotational constants roughly determined by the R-branch transitions, and assigned by means of their characteristic hyperfine structures.

The unsplit frequencies of the observed transitions, which were obtained by a method to be described later, are listed in Table 1. The rotational constants and the centrifugal distortion constants of the $CH_3SiH^{35}Cl_2$ species were determined by a least squares fit calculation using the formula presented by Watson.[12] The determined constants are given in Table 2. The rotational constants of the $^{35}Cl^{37}Cl$ and $^{37}Cl_2$ species were determined by assuming the same centrifugal distortion constants as those of the $^{35}Cl_2$ species.

Table 1. Observed and calculated frequencies of methyldichlorosilane (MHz)

Transition		ν_{obsd}	$\nu_{obsd}-\nu_{calcd}$
$CH_3SiH^{35}Cl_2$			
$3_{1\,3}$	$2_{0\,2}$	12583.45	0.23
$4_{4\,0}$	$4_{3\,1}$	15493.42	−0.04
$4_{1\,4}$	$4_{0\,3}$	15620.39	0.07
$4_{0\,4}$	$3_{1\,3}$	14425.55	0.03
$5_{4\,1}$	$5_{3\,2}$	15047.81	0.06
$5_{1\,5}$	$4_{0\,4}$	18744.28	0.07
$5_{0\,5}$	$4_{1\,4}$	18166.36	−0.16
$6_{1\,6}$	$5_{0\,5}$	21993.24	0.07
$6_{0\,6}$	$5_{1\,5}$	21739.76	−0.23
$6_{1\,5}$	$6_{0\,6}$	13596.78	0.12
$6_{2\,5}$	$6_{1\,6}$	14944.88	−0.06
$6_{4\,3}$	$6_{3\,4}$	15824.25	−0.11
$6_{5\,1}$	$6_{4\,2}$	19856.25	0.24
$7_{2\,6}$	$6_{1\,5}$	29175.62	−0.05
$7_{1\,6}$	$7_{0\,7}$	16731.74	0.04
$7_{2\,6}$	$7_{1\,7}$	17444.50	−0.12
$7_{1\,7}$	$6_{0\,6}$	25327.84	0.13
$7_{0\,7}$	$6_{1\,6}$	25223.72	0.00
$8_{1\,7}$	$8_{0\,8}$	19742.98	0.24
$8_{2\,7}$	$8_{1\,8}$	20084.24	−0.26
$8_{1\,8}$	$7_{0\,7}$	28706.38	0.26
$8_{0\,8}$	$7_{1\,7}$	28665.31	0.05
$8_{2\,7}$	$7_{1\,6}$	32058.76	−0.17
$9_{1\,9}$	$8_{0\,8}$	32104.52[a]	0.35
$9_{0\,9}$	$8_{1\,8}$	32088.37[a]	−0.23
$9_{2\,8}$	$8_{1\,7}$	35164.14	−0.04
$9_{1\,8}$	$8_{2\,7}$	34653.72	−0.18
$9_{2\,7}$	$8_{3\,6}$	35141.16	−0.33
$10_{1\,10}$	$9_{0\,9}$	35510.62[a]	0.25
$10_{0\,10}$	$9_{1\,9}$	35504.58[a]	0.00
$10_{1\,9}$	$10_{0\,10}$	25494.36	−0.10
$10_{2\,8}$	$10_{1\,9}$	21067.00	−0.08
$10_{3\,8}$	$10_{2\,9}$	22033.16	−0.21
$10_{4\,6}$	$10_{3\,7}$	11286.27	0.12
$10_{4\,7}$	$10_{3\,8}$	19664.20	0.24
$10_{5\,5}$	$10_{4\,6}$	15931.73	−0.13
$10_{5\,6}$	$10_{4\,7}$	20313.84	0.03
$10_{6\,4}$	$10_{5\,5}$	23090.72	−0.11
$10_{6\,5}$	$10_{5\,6}$	23895.28	−0.11
$10_{7\,3}$	$10_{6\,4}$	28516.92	0.03
$10_{7\,4}$	$10_{6\,5}$	28578.48	0.11
$11_{1\,10}$	$11_{0\,11}$	28306.54	0.22
$11_{2\,10}$	$11_{1\,11}$	28333.20	0.11
$CH_3SiH^{35}Cl^{37}Cl$			
$3_{1\,3}$	$2_{0\,2}$	12388.10	−0.03
$5_{2\,4}$	$5_{1\,5}$	12497.86	−0.12
$6_{1\,5}$	$6_{0\,6}$	13216.84	−0.06
$7_{1\,6}$	$7_{0\,7}$	16313.85	0.00
$7_{2\,6}$	$7_{1\,7}$	17125.19	0.14
$7_{1\,7}$	$6_{0\,6}$	24825.00	0.10
$7_{0\,7}$	$6_{1\,6}$	24703.00	0.05
$8_{1\,8}$	$7_{0\,7}$	28128.80	−0.06
$8_{0\,8}$	$7_{1\,7}$	28079.60	0.09
$9_{1\,9}$	$8_{0\,8}$	31455.00	0.13
$9_{0\,9}$	$8_{1\,8}$	31435.46	−0.05
$10_{1\,10}$	$9_{0\,9}$	34790.28	−0.05
$10_{0\,10}$	$9_{1\,9}$	34782.80	−0.13
$CH_3SiH^{37}Cl_2$			
$6_{0\,6}$	$5_{1\,5}$	20827.10	0.13
$7_{0\,7}$	$6_{1\,6}$	24189.35	−0.12
$7_{1\,7}$	$6_{0\,6}$	24330.39	−0.06
$8_{0\,8}$	$7_{1\,7}$	27502.00	−0.15
$8_{1\,8}$	$7_{0\,7}$	27560.91	0.12
$9_{0\,9}$	$8_{1\,8}$	30791.80	−0.15
$9_{1\,9}$	$8_{0\,8}$	30815.84	0.26
$10_{0\,10}$	$9_{1\,9}$	34072.10	0.17
$10_{1\,10}$	$9_{0\,9}$	34081.00	−0.20

a) "A" component of internal rotation.

TABLE 2. ROTATIONAL CONSTANTS AND CENTRIFUGAL DISTORTION CONSTANTS OF METHYLDICHLOROSILANE (MHz)

	$CH_3SiH^{35}Cl_2$	$CH_3SiH^{35}Cl^{37}Cl$	$CH_3SiH^{37}Cl_2$
A	4342.16(06)	4313.75(09)	4285.39(3.30)
B	2433.28(03)	2370.94(02)	2311.39(0.68)
C	1706.05(02)	1671.23(02)	1636.85(0.87)
d_J	−0.00157		
d_{JK}	−0.02646		
d_K	−0.02027		
d_{WJ}	0.106×10^{-5}		
d_{WK}	0.109×10^{-4}		

The assignment was also confirmed by the observation of the double-resonance effects between the transitions of $7_{25}\leftarrow7_{16}$ and $8_{27}\leftarrow7_{16}$, and between those of $9_{36}\leftarrow9_{27}$ and $9_{27}\leftarrow8_{36}$. The spectral line of $8_{27}\leftarrow7_{16}$ or $9_{27}\leftarrow8_{36}$ was observed on a cathode ray tube, and the transition of $7_{25}\leftarrow7_{16}$ or $9_{36}\leftarrow9_{27}$ was saturated. About 30% of the intensity decrease was observed when the exact pumping frequency was applied.

Hyperfine Structure

The hyperfine structures of the spectrum due to the two chlorine nuclei were analyzed on the basis of the theory presented by Robinson and Cornwell.[13] A typical pattern of the hyperfine structure and an observed spectrum, when the moments of the two chlorine nuclei are identical, are given in Fig. 3. As is shown in the figure, the strongest line, which consists of four degenerate components, always exists at the unsplit value. Therefore, the unsplit values can be determined simply by measuring the strongest lines in the hyperfine structures. Although this degenerate line splits into four components when the two quadrupole coupling constants are not identical, as in the case of the $^{35}Cl^{37}Cl$ species, the strongest lines without splittings were always observed for the spectrum of $CH_3SiH^{35}Cl^{37}Cl$. Therefore, the unsplit frequencies of the spectrum were approximated by the center frequencies of the unresolved lines for this species.

The values of the χ tensor for $CH_3SiH^{35}Cl_2$ were determined from the analysis of the five Q-branch

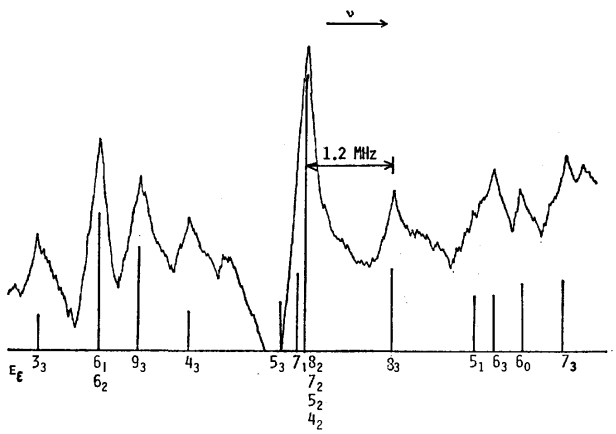

Fig. 3. Recorded spectrum and predicted hyperfine structure for the $6_{51}\leftarrow6_{42}$ transition in $CH_3SiH^{35}Cl_2$.

TABLE 3. QUADRUPOLE COUPLING CONSTANTS OF $CH_3SiH^{35}Cl_2$

χ_{aa}	−19.1±0.3 MHz
χ_{bb}	5.4±1.3 MHz
χ_{cc}	13.7±1.4 MHz
χ_{bond}	−41.2±2.0 MHz
η_{bond}	−0.16±0.03

transitions. The obtained values are listed in Table 3, along with the values of χ_{zz} and η. Since the off-diagonal elements of the tensor in the principal axis system of the molecule were not obtained, χ_{zz} and η were calculated by the use of the transformation coefficients determined from the structure obtained in the present study. In this coordinate system, the z axis is along the Si–Cl bond, the x axis is in the Cl–Si–Cl plane, and the y axis is perpendicular to these two. The obtained values of this χ_{zz} may be compared with that of SiH_3Cl ($eQq=-40.0$ MHz).[14]

Internal Rotation

The low-J lines in the spectrum of this molecule are of rigid asymmetric top. Some of the high-J R-branch transitions, however, shows splittings due to the interaction between the internal rotation and the over-all rotation. These splittings have been analyzed to determine the barrier to internal rotation using the structure shown in Table 5. Table 4 lists the frequencies, ν_A, the frequency differences, $\nu_A-\nu_E$, and the calculated values of V_3 for four transitions in $CH_3SiH^{35}Cl_2$. The splittings due to the quadrupole coupling are very small and are not observed for these transitions.

TABLE 4. BARRIER HEIGHT OF CH_3SiHCl_2

Transition	ν_A(MHz)	$\nu_A-\nu_E$ (MHz)	V_3 (kcal/mol)
$8_{1\,9}\ 8_{0\,8}$	32104.52	0.79	1.70
$9_{0\,9}\ 8_{1\,8}$	32088.37	−0.89	1.68
$10_{1\,10}\ 9_{0\,9}$	35510.62	2.01	1.69
$10_{0\,10}\ 9_{1\,9}$	35504.58	−2.02	1.68

Internal rotation parameters
$I_\alpha=3.2$ amu Å^2 (assumed)
$\lambda_b=0.902585$
$\lambda_c=0.430511$
$F=160.26$ GHz

Results
Average $s=49.16$
Average $V_3=1.69\pm0.05$ kcal/mol

Durig and Hawley measured the vibrational spectra of gaseous and solid CH_3SiHCl_2,[11] and they estimated that the very weak band at 173 cm^{-1} in solid phase arose from the methyl torsion. This value leads to 2.09 kcal/mol as the barrier height; this value is consistent with our value considering that the barrier in the solid phase is always higher than that in the gas phase.[11]

Molecular Structure

Since only three isotopic species ($^{35}Cl_2$, $^{35}Cl^{37}Cl$, and $^{37}Cl_2$) were measured, and since the $^{37}Cl_2$ species gives

essentially the same informations as to the molecular structure as does the $^{35}Cl^{37}Cl$ species, it is necessary to assume some parameters in order to determine the molecular structure. The partial structures of the CH_3 and SiH groups were chosen as those to be assumed, because the probable errors in the assumed structures cause little errors in the other parameters. In principle, it is possible to determine the four parameters of the C-Si and Si-Cl bond lengths and the Cl-Si-Cl and C-Si-Cl angles from six rotational constants. Although this was tried first, the obtained values were changed appreciably by the small deviations of the rotational constants. Therefore, the Si-C length was also assumed for the analysis of the molecular structure. The C-Si bond distances in methylsilane and methylfluorosilanes have been determined precisely by the substitution method. Durig *et al.*[4] have revealed that both the Si-C and Si-F bond distances decrease with a further substitution of the fluorine atoms for the hydrogen atoms attached to the silicon. In Fig. 4 the change in the Si-C bond distances in methylfluorosilanes versus the number of fluorine atoms is plotted. A similar shortening of Si-C distances in methylcholorosilanes can also be expected by the substitution of the chlorine atoms for the hydrogen atoms, while the amount of the shortening

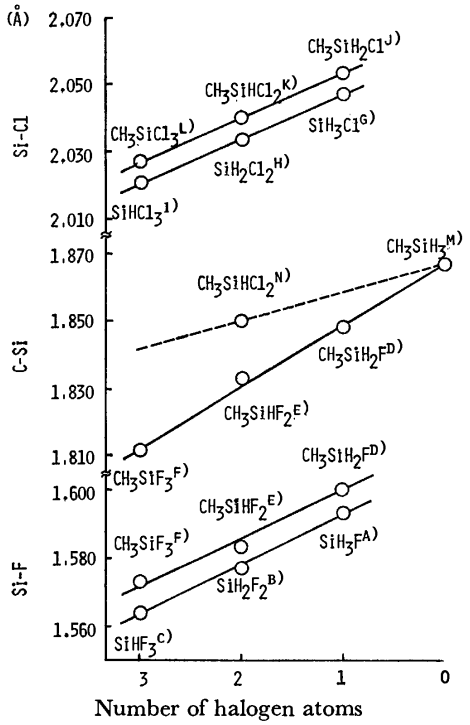

Fig. 4. The change of bond distances due to substitution of the halogen atoms for the hydrogen atoms in halosilanes and methylhalosilanes.
A), G) R. Kewley, P. M. McKinney, and A. G. Robiette, *J. Mol. Spectrosc.*, **34**, 390 (1970). B) V. W. Laurie, *J. Chem. Phys.*, **26**, 1359 (1957). C) G. A. Heath, L. F. Tomas, and J. Sheridan, *Trans. Faraday Soc.*, **50**, 779 (1954). D), E) L. C. Krisher and L. Pierce, *J. Chem. Phys.*, **32**, 1619 (1960). F) Ref. 4. H) R. W. Davis and M. C. L. Gerry, *J. Mol. Spectrosc.*, **60**, 117 (1976). I), L) Ref. 8. J) Ref. 9. K) This work. M) Ref. 1. N) Assumed values: see text.

Table 5. Molecular structure of methyldichlorosilane

Assumed structural parameters			
r Si-C	1.850 Å	∠ Si-C-H	109.5°
r Si-H	1.467 Å	∠ C-Si-H	110.9°
r C-H	1.093 Å		
C_{3v} symmetry for methyl group			
Fitted structural parameters			
r Si-Cl	2.040 Å		
∠ C-Si-Cl	109.8°		
∠ Cl-Si-Cl	108.8°		
Calculated rotational constants (MHz)			
	A	*B*	*C*
$CH_3SiH^{35}Cl_2$	4342.18	2433.62	1706.04
$CH_3SiH^{35}Cl^{37}Cl$	4313.70	2371.20	1671.20
$CH_3SiH^{37}Cl_2$	4283.32	2310.85	1636.90

is expected to be about a half of that in the case of fluorine. Therefore, we estimated that the C-Si bond distance of methyldichlorosilane should be about 1.850 Å, which is the average value of the C-Si bond distances in methylsilane and methyldifluorosilane. This estimation is supported by the results of the structure analysis for the halogen derivatives of hydrocarbones. The Cl-Si length, and the C-Si-Cl and Cl-Si-Cl angles were determined, using this assumed value, by means of a least-squares method. The obtained values are listed in Table 5.

Discussion

The obtained Si-Cl bond distance is compared with those of chlorosilanes and other methylchlorosilanes in Fig. 4. Zeil *et al.* have presented two Si-Cl bond distances, 2.049±0.013 Å and 2.052±0.005 Å by combining the rotational constants of $CD_3{}^{28}SiH_2{}^{35}Cl$, $CD_3{}^{29}SiH_2{}^{35}Cl$, $CD_3{}^{30}SiH_2{}^{35}Cl$, and $CD_3{}^{28}SiH_2{}^{37}Cl$. When we choose 2.052 Å for the plot of Si-Cl bond distances in Fig. 4, it can clearly be seen that the Si-Cl bond distances decrease with the substitution of chlorine atoms for the hydrogen atoms and that the change is quite regular. It should be noted that the slopes of chlorosilanes and methylchlorosilanes have almost the same gradient.

In Table 6, the barrier of CH_3SiHCl_2 determined in this study is compared with a few values of methylsilanes and methylhalosilanes which have been determined by microwave and infrared spectroscopy. In the CH_3SiH_3,

Table 6. Comparison of barriers to internal rotation in methylhalosilane

Molecule	V_3(kcal/mol)	Method
CH_3SiH_3	1.70[a)]	Mw split
CH_3SiH_2F	1.559[b)]	Mw split
CH_3SiHF_2	1.255[c)]	Mw split
CH_3SiF_3	0.93[d)]	Mw intensity
CH_3SiH_2Cl	1.84,[e)] 2.25[e)]	IR gas, IR solid
CH_3SiHCl_2	1.69, 2.09[e)]	This work, IR solid
CH_3SiCl_3	0.58[f)]	Mw intensity

a) Ref. 1. b) Ref. 2. c) Ref. 3. d) Ref. 4. e) Ref. 11. f) Ref. 7.

CH_3SiH_2F, CH_3SiHF_2, CH_3SiF_3 series, it can clearly be observed that the substitution of a fluorine for a hydrogen causes a significant decrease in the barrier to internal rotation. The CH_3SiH_3, CH_3SiH_2Cl, CH_3SiHCl_2, CH_3SiCl_3 series, however, shows that the substitution of a chlorine for a hydrogen does not cause any significant effect on the barrier except CH_3SiCl_3. A similar comparison of the barriers for chloro and fluoroethanes has revealed that the substitution of a chlorine with a hydrogen increases the barrier, while the change in the barrier is small in the case of fluorine. Therefore, one might assume that the nonbonded Cl···H interaction is always larger than the nonbonded F···H interaction. From this point of view, it is very difficult to explain the remarkably low barrier of CH_3SiCl_3. Since the barrier of 0.58 kcal/mol for CH_3SiCl_3 was obtained by the microwave intensity method, it is probable that there was a confusion in the assignment of the tortional state; a careful re-investigation of the microwave spectrum may, therefore, be necessary.

References

1) R. W. Kilb and L. Pierce, *J. Chem. Phys.*, **27**, 108 (1957).
2) L. Pierce, *J. Chem. Phys.*, **29**, 383 (1958).
3) J. D. Swalen and B. P. Stoicheff, *J. Chem. Phys.*, **28**, 671 (1958).
4) J. R. Durig, Y. S. Li, and C. C. Tong, *J. Mol. Struct.*, **14**, 225 (1972).
5) G. Graner and C. Thomas, *J. Chem. Phys.*, **49**, 4160 (1968).
6) R. C. Mockler, J. H. Bailey, and W. Gordy, *J. Chem. Phys.*, **21**, 1710 (1953).
7) M. Mitzlaff, R. Holm, and H. Hartmann, *Z. Naturforsch.*, **22a**, 1415 (1967).
8) H. Takeo and C. Matsumura, *Bull. Chem. Soc. Jpn.*, in press.
9) W. Zeil, R. Gegenheimer, S. Pferrer, and M. Dakkouri, *Z. Naturforsch.*, **27a**, 1150 (1972).
10) W. Zeil, W. Braun, B. Haas, H. Knehr, F. Rückert, and M. Dakkouri, *Z. Naturforsch.*, **30a**, 1441 (1975).
11) J. R. Durig and C. W. Hawley, *J. Chem. Phys.*, **59**, 1 (1973).
12) J. K. G. Watson, *J. Chem. Phys.*, **46**, 1935 (1967).
13) G. W. Robinson and C. D. Cornwell, *J. Chem. Phys.*, **21**, 1436 (1953).
14) B. Bak, J. Bruhn, and J. R. Andersen, *J. Chem. Phys.*, **21**, 753 (1953).

The *cis-trans* Isomerization of 2-Butenes Caused by Sulfur Dioxide Adsorbed on Porous Vycor Glass. The Contribution of the Charge-transfer Complex

Kiyoshi Otsuka, Kiyoshi Eshima, and Akira Morikawa

Department of Chemical Engineering, Tokyo Institute of Technology, Ookayama, Meguro-ku, Tokyo 152

(Received October 8, 1976)

Sulfur dioxide adsorbed on porous Vycor glass enhances the *cis-trans* isomerization of 2-butenes selectively, but it poisons the double-bond migration. The correlation between the *cis-trans* isomerization and the sulfur dioxide–*cis*-2-butene charge-transfer complex observed on the glass were studied under various pressures of the reactants. The kinetic data of the reaction were well explained by the reaction mechanism in which the isomerization occurs *via* the addition and elimination of 2-butene molecules at the terminal of the polysulfone formed from sulfur dioxide and *cis*-2-butene in the adsorbed layer. It has been suggested that the copolymerization is initiated through the charge-transfer complex polarized in the strong electrostatic field of the exposed aluminum ions contained in the glass.

Porous Vycor glass, evacuated at a high temperature (>500 °C), is catalytically inactive for the isomerization of normal butenes at room temperature. However, the addition of a small amount of sulfur dioxide causes a considerably fast *cis-trans* isomerization of 2-butenes very selectively. In the gas phase, of course, sulfur dioxide exerts no effect upon the butene isomerization. Similar specific catalyses of the sulfur dioxide manifested in the adsorbed layer of various solid adsorbents have been reported in previous papers,[1,2] and it has been suggested that the geometrical isomerization of 2-butenes takes place by means of a mechanism in which the addition and subsequent elimination of the *cis*- or *trans*-2-butene molecule at the terminal of the formed polysulfone cause the isomerization. It has been suggested that the polysulfone formation may be initiated by the sulfur dioxide–olefin (1: 1) molecular complex,[2] though the kinetic data obtained over NaX zeolite[2] could not be tested in this point by observing the presence of the complex by means of ultraviolet spectroscopy because of its opacity in the ultraviolet-wavelength region.

In order to carry out a quantitative test of the contribution of the molecular complex, we have chosen porous Vycor glass as the adsorbent because of its good transparency in the wavelength range down to ≈ 210 nm. In the present work, we will first carry out a kinetic investigation of the geometrical isomerization of *cis*-2-butene over porous Vycor glass in the presence of sulfur dioxide. Then, examining the molecular complex in the adsorbed layer of the glass by means of the ultraviolet spectroscopic method, we intend to verify that the complex plays a significant role in the reaction. Finally, the nature of the active site on the glass will be discussed along with the kinetic data obtained over glass evacuated at various temperatures.

Experimental

Materials. The porous Vycor glass used was a glass plate (Corning No. 7930, surface area 150 m^2/g) $30\times8\times0.8$ mm in size. Similar samples were shown to contain ≈3% of B_2O_3, ≈0.4% of Al_2O_3, and less than 0.2% of Na_2O and K_2O inaddition to silica [information supplied by Corning Glass Works]. After having been calcined thoroughly at 700 °C in air, the glass was washed by distilled water and dried at 400 °C; then it was placed in the reactor.

The sulfur dioxide reagent was of an anhydrous grade of the Matheson Chemical Company. The *cis*-2-butene was a high-purity product of the Phillips Petroleum Company. The stated purity of 99.9% for *cis*-2-butene was verified by gas chromatography. Each compound was further purified by trap-to-trap distillation in a vacuum apparatus.

Apparatus. The appratus employed was a conventional mercury-free and grease-free gas-circulating system with a dead volume of 288 ml, capable of achieving a vacuum down to 10^{-6} Torr. A part of the reactor, where the glass was placed, was constructed from a quartz cell ($10\times10\times40$ mm) designed for spectrophotometric use. The pressure readings for the reactants were made with a glass Bourdon gauge.

Procedure. Prior to every run of the experiment, the glass placed in the reactor was calcined at 600 °C in dried oxygen and then evacuated for 2 h in a vacuum below 5×10^{-5} Torr at the same temperature. After introducing sulfur dioxide at 25 °C, the reaction was started by feeding in *cis*-2-butene and circulating the mixture gas through the reactor. A small amount of reacting gas was periodically collected and analyzed by gas chromatography. The temperature of the reactor was controlled within ±0.2 °C by using a water bath. The ultraviolet-spectra measurements were performed by means of a Shimadzu UV-200 spectrometer. The spectra were recorded by placing the glass without any adsorbate on the reference side of the light beam.

Results

The geometrical Isomerization of cis*-2-Butene Enhanced by Sulfur Dioxide.* Porous Vycor glass calcined in a vacuum at 600 °C exhibits a low catalytic activity in the two isomerizations of *cis*-2-butene, *i.e.*, the geometrical isomerization to *trans*-2-butene and the double-bond isomerization to 1-butene, at 25 °C. The initial rates of the former and latter reactions were 7.23×10^{-8} and 15.0×10^{-8} mol/g min respectively, at an initial pressure of *cis*-2-butene of 46 Torr.

The addition of a small amount of sulfur dioxide to the reaction system markedly enhanced the rate of geometrical isomerization, but it stopped the double-bond migration. Furthermore, no double-bond migration in the presence of sulfur dioxide was confirmed by using 100% 1-butene as the starting olefin.

The effects of the pressure of sulfur dioxide and *cis*-2-butene on the initial rate of the *trans*-2-butene

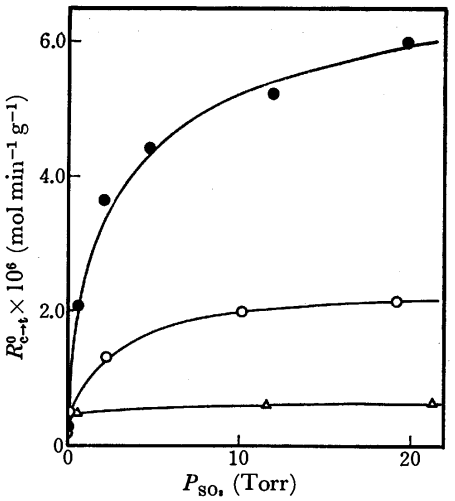

Fig. 1. Effect of the pressure of sulfur dioxide on the rate of geometrical isomerization: The pressure of *cis*-2-butene: (●), 107 Torr; (○), 6.2 Torr; (△), 0.9 Torr.

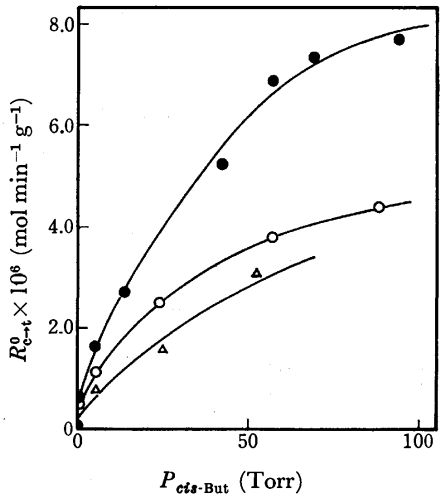

Fig. 2. Effect of the pressure of *cis*-2-butene on the rate of the isomerization: The pressure of sulfur dioxide: (●), 51 Torr: (○), 4.9 Torr; (△), 2.0 Torr.

formation, $R^0_{c\to t}$, at 25 °C are shown in Figs. 1 and 2. These figures exhibit that $R^0_{c\to t}$ can not be expressed by a simple function of the pressures of the two compounds.

The Charge-transfer Complex of Sulfur Dioxide with cis-*2-Butene.* Examples of the ultraviolet spectra of the glass with *cis*-2-butene, sulfur dioxide, and the two compounds adsorbed together on the glass are shown in Fig. 3. The (c)spectrum, taken 3—5 min after the coadsorption of sulfur dioxide and *cis*-2-butene, indicates new absorptions at around 240 and 330 nm. The absorbance of the spectra at wavelengths less than ≈250 nm increases with the time, as can be seen in the figure (Spectra(c)—(f)). After various durations of the coadsorption, the glass was evacuated in a vacuum for 2 h at 25 °C. The spectra of the glass taken after this treatment are shown in Fig. 4. The absorption due to adsorbed sulfur dioxide has disappeared after the evacuation, though a considerable portion of the spectra seen at the wavelengths less than ≈240 nm still remains.

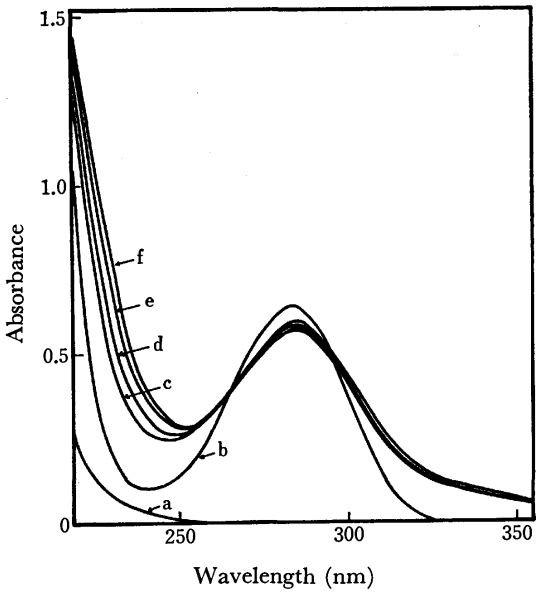

Fig. 3. The UV-spectra of the compounds adsorbed at 25 °C on the porous Vycor glass. (a) *cis*-2-butene (amount of adsorption is 2.40 ml STP/g); (b) sulfur dioxide (0.45 ml STP/g); (c)—(f) sulfur dioxide (0.45 ml STP/g) and *cis*-2-butene (2.4 ml STP/g) coadsorbed. The spectra (c)—(f) were recorded at various times after the addition of the both compounds: (c) 3—5 min, (d) 12—14 min, (e) 40—42 min, (f) 108—110 min. Scanning speed was 100 nm/min, scanning wavelength from 400 to 200 nm.

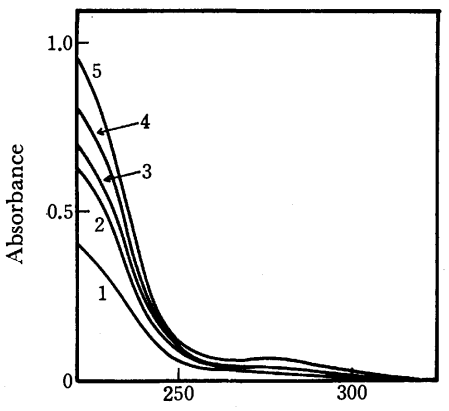

Fig. 4. The UV-spectra of the compound remained on the glass after the evacuation for 2 h: Sulfur dioxide and *cis*-2-butene had been coadsorbed before the evacuation for the following time; (1) 8 min, (2) 20 min, (3) 38 min, (4) 105 min, (5) 930 min.

It is assumed that the increase in the absorbance with the time for the spectra in Fig. 3 results from the accumulation of the unknown compounds, referred to as P_x hereafter, which corresponds to the spectra in Fig. 4. The D_{ctc} at various wavelengths, defined by the following equation (i):

$$D_{ctc} = D_{ob} - D_{SO_2} - D_{But} \quad \text{(i)}$$

are plotted against the duration of coadsorption, where D_{ob}, D_{SO_2}, and D_{But} are the optical density of the total absorption observed in the case of coadsorption

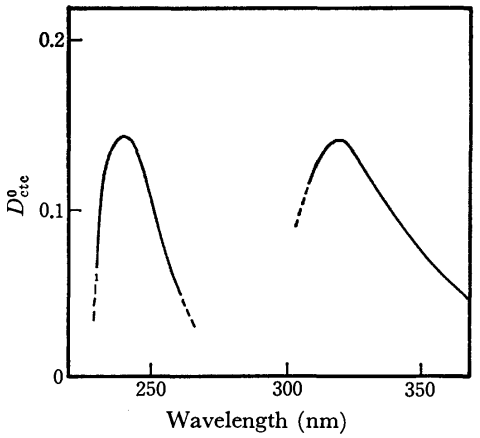

Fig. 5. Plot of D^0_{ctc} against wavelength.

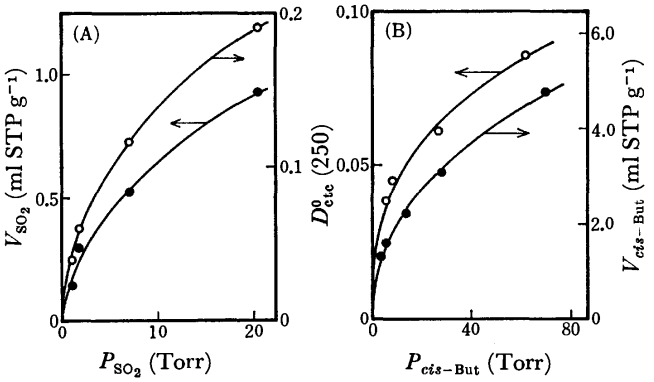

Fig. 6. (A) Plot of D^0_{ctc} (250) (open circles) and the amount of adsorbed sulfur dioxide (V_{SO_2}) (closed circles) against the pressure of sulfur dioxide: $P_{cis\text{-But}}$ =6.2 Torr. (B) Adsorption isotherm of *cis*-2-butene (closed circles) and the plot of D^0_{ctc} (250) against the pressure of *cis*-2-butene (open circles): P_{SO_2}=4.9 Torr.

(Spectra(c)—(f) in Fig. 3), the optical density for the sulfur dioxide (Spectrum(b)), and that for the *cis*-2-butene (Spectrum(a)) respectively. In order to exclude the contribution of P_x, the extrapolated values of D_{ctc} to the zero duration time of adsorption, D^0_{ctc}, were estimated. They are plotted against the wavelengths in Fig. 5.

The effects of the pressures of sulfur dioxide and *cis*-2-butene on D^0_{ctc} at 250 nm are indicated by open circles in Fig. 6. The adsorption isotherm of sulfur dioxide in the presence of *cis*-2-butene is also shown in Fig. 6-(A) by closed circles. The adsorption isotherm of the *cis*-2-butene in Fig. 6-(B) (closed circles) was obtained in the absence of sulfur dioxide.

Effect of the Evacuation Temperature. Following the usual pretreatment of the glass, water vapor was adsorbed at 25 °C under a pressure of 4.6 Torr. Then, the temperature of the glass was raised to a temperature at which the glass was allowed to stand for 1 h; thereafter the system was evacuated for 2 h at the same temperature. With the glass thus treated, the rate of the sulfur dioxide-enhancing isomerization was measured. The data are plotted against the evacuation temperature in Fig. 7.

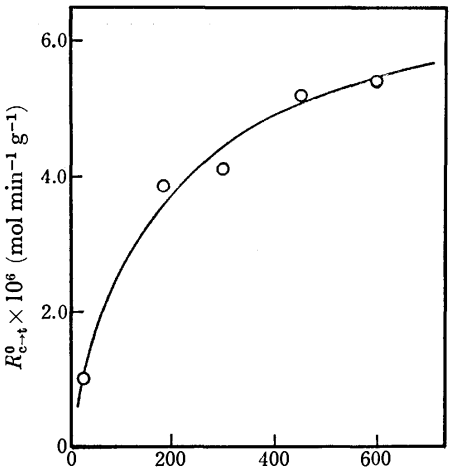

Fig. 7. Effect of evacuation temperature on the rate of the isomerization: reaction at 25 °C; P_{SO_2}=5.0 Torr, $P_{cis\text{-But}}$=90 Torr.

Discussion

The carbonium-ion mechanism, generally accepted for porous glass,[3,4] requires not only the occurrence of the *cis-trans* geometrical isomerization, but also the double-bond migration of normal butenes. The fact that no double-bond migration is observed in the presence of sulfur dioxide suggests that the geometrical isomerization of 2-butenes, enhanced by the addition of sulfur dioxide, proceeds by means of a new mechanism, different from that operative in the absence of sulfur dioxide; sulfur dioxide strongly inhibits the double-bond migration which proceeds on the glass without sulfur dioxide.

D_{SO_2} or D_{But}, the optical density obtained from the data of the individual adsorption of sulfur dioxide or that of *cis*-2-butene, can, in the case of the coadsorption of the two compounds, be used in calculating D_{ctc} by means of equation (i), for the following reasons: (1) The total coverage of the two adsorbates was less than 0.1 under the experimental conditions applied to the data in Fig. 3; (2) a small equilibrium quantity of the charge-transfer complex formed appears in a hexane solution;[5] (3) a much larger extinction coefficient of the complex compared to that of sulfur dioxide has been confirmed.[5]

The two absorption bands at ≈240 and ≈330 nm are seen in Fig. 5; the former was identified as the charge-transfer band of the sulfur dioxide–*cis*-2-butene molecular complex, and the latter, as the enhanced absorption of the sulfur dioxide brought about by the proximity of the π-donating *cis*-2-butene molecule.[2,5] In the following discussion, the D^0_{ctc} at 250 nm, D^0_{ctc} (250), has been adopted as the optical density due to the charge-transfer complex, because it is the most reliable value.

The curves of D^0_{ctc} (250) and the adsorption isotherm in Fig. 6-(A) or those in Fig. 6-(B) indicate a similar dependence on the pressure. Most of the sulfur dioxide or *cis*-2-butene adsorbed on the glass is physically adsorbed; this similar dependence implies that the

complex results from the reaction between the weekly adsorbed sulfur dioxide and *cis*-2-butene.

Role of the Charge-transfer Complex in the Reaction Mechanism. It has been suggested that the selective *cis-trans* isomerization is accompanied by the copolymerization of sulfur dioxide with 2-butenes on the solid surface.[2,6] Since the pressure readings of the reacting gases did not change during the isomerization, the formation of the polymer could not be confirmed in the present work. However, the unknown compound, P_X, giving the tailing spectra in Fig. 4 may possibly be the polysulfone formed from sulfur dioxide and *cis*-2-butene.

In the following discussion, we intend to examine the role of the charge-transfer complex along with the reaction mechanism shown below:[2]

$$SO_2 + \textit{cis}\text{-2-butene} \overset{K}{\rightleftharpoons} CTC \quad (1)$$

$$CTC \longrightarrow P_B + P_S \quad (2)$$

$$P_B \longrightarrow P_S + \textit{trans}\text{-2-butene} \quad (3)$$

$$P_B \longrightarrow P_S + \textit{cis}\text{-2-butene} \quad (4)$$

$$P_S \longrightarrow P_B + SO_2 \quad (5)$$

$$P_B + SO_2 \longrightarrow P_S \quad (6)$$

$$P_S + \textit{cis}\text{-2-butene} \longrightarrow P_B \quad (7)$$

$$P_B \longrightarrow \text{stabilized} \quad (8)$$

$$P_S \longrightarrow \text{stabilized} \quad (9)$$

where the mechanism is considered under a low conversion, using 100% *cis*-2-butene as the starting olefin; *CTC* is the charge-transfer complex, and P_B and P_S represent the terminal group of 2-butyl and sulfonyl radical of the active polysulfone respectively.

The steady-state treatment of P_S and P_B with Eq. 1—9 gives the following rate equation by assuming $k_9/2+k_5 \ll k_7[\textit{cis}\text{-2-butene}]$:

$$R^0_{c\to t} = \frac{2k_2k_3k_7[\textit{cis}\text{-2-butene}][CTC]}{k_7k_8[\textit{cis}\text{-2-butene}]+k_9(k_8/2+k_3+k_4+k_6[SO_2])} \quad \text{(ii)}$$

where the concentration for the each compound is assigned to that on the surface. Since it has been shown that the equilibrium constant of the formation of the charge-transfer complex is small in a hexane solution ($K=0.075\pm0.082$ l mol^{-1} at 25 °C),[5] a low concentration of *CTC* on the glass can reasonably be assumed, and the Lambert-Beer law holds for the optical density:

$$D^0_{ctc} = \varepsilon[CTC]l \quad \text{(iii)}$$

We may then rearrange Eq. ii to Eq. iv to see the effect of the concentration of adsorbed sulfur dioxide:

$$\frac{D^0_{ctc}}{R^0_{c\to t}} = A + B[SO_2] \quad \text{(iv)}$$

where

$$A = \frac{\varepsilon l}{2k_2k_3}\left\{k_8+\frac{k_9(k_8/2+k_3+k_4)}{k_7[\textit{cis}\text{-2-butene}]}\right\}$$

$$B = \frac{\varepsilon l}{2k_2k_3}\left\{\frac{k_6k_9}{k_7[\textit{cis}\text{-2-butene}]}\right\}.$$

Using the data of $R^0_{c\to t}$ in Fig. 1 and those of D^0_{ctc} (250) and V_{SO_2} in Fig. 6 at the *cis*-2-butene pressure of 6.2 Torr, where the concentration of the adsorbed *cis*-2-butene is assumed to be constant because of the low total coverage of the adsorbed compounds ($\theta<0.1$),

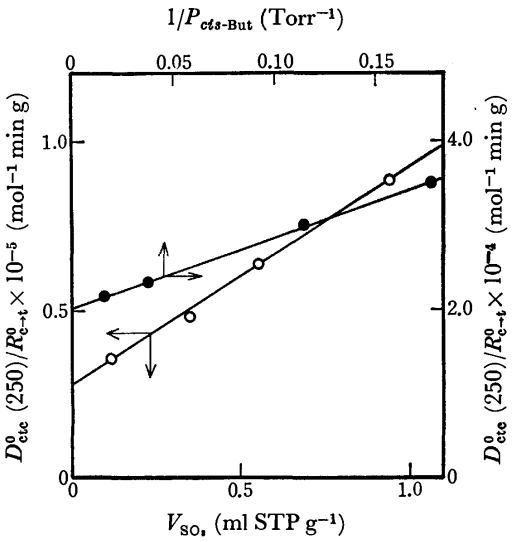

Fig. 8. Plot of (D^0_{ctc} (250)/$R^0_{c\to t}$) against the amount of sulfur dioxide adsorbed (○), or that against the inverse of *cis*-2-butene pressure (●).

$D^0_{ctc}(250)/R^0_{c\to t}$ is plotted against V_{SO_2} in Fig. 8 (open circles). A reasonably good linear relation is obtained between the variables.

Assuming that the *cis*-2-butene in the propagation step (7) is chemically adsorbed on the active site of the glass and that the adsorption isotherm can be represented by a Langmuir-type equation such as:

$$[\textit{cis}\text{-2-butene}] = \frac{b(P_{cis\text{-But}})}{1+b(P_{cis\text{-But}})} \quad \text{(v)}$$

we may rearrange Eq. ii to Eq. vi:

$$\frac{D^0_{ctc}}{R^0_{t\to c}} = C + D(P_{cis\text{-But}})^{-1} \quad \text{(vi)}$$

where

$$C = \frac{\varepsilon l}{2k_2k_3}\left\{k_8+\frac{k_9}{k_7}\left(\frac{k_8}{2}+k_3+k_4+k_6[SO_2]\right)\right\}$$

$$D = \frac{\varepsilon lk_9}{2k_2k_3k_7b}\left(\frac{k_8}{2}+k_3+k_4+k_6[SO_2]\right).$$

$D^0_{ctc}(250)/R^0_{c\to t}$, calculated from the data in Fig. 6 and Fig. 2 at a fixed pressure of sulfur dioxide (=4.9 Torr), is plotted against $1/P_{cis\text{-But}}$ in Fig. 8 (closed circles); the plot confirms the theoretically expected linear relation of the plot.

Consequently, the results in Fig. 8 confirm the previously predicted hypothesis[2] that the charge-transfer complex initiates the reaction by Process (2).

The Nature of the Active Site on the Porous Vycor Glass. Figure 7 shows that the catalytic activity of the glass increases with a rise in the evacuation temperature. In contrast to this result, if sulfur dioxide is absent, the activity of the glass decreases with the evacuation temperature from 400 to 700 °C;[7] this is consistent with the results reported by Blomfield and Little.[8] It has been suggested that the alumina contained in the porous Vycor glass is responsible for the catalytic activity of the glass.[3,4] West, Haller, and Burwell also suspected that most of the reported reactions over silica gel occur at impurity sites, most likely Al^{3+}.[9] In the studies of the isomerization of normal butenes over

silica–alumina, it has been found that the rate of reaction decreases as the concentration of hydroxyl groups on the catalyst is decreased by a rise in the evacuation temperature.[10,11] On the contrary, on an alumina catalyst, the reaction rate is inversely related to the surface density of hydroxyl groups,[10-12] suggesting that the active sites involve the exposure of aluminum ions, creating dual acid-base sites[12] when hydroxyl groups are removed. Hence, if the silica–alumina site on the porous Vycor glass is much more active than the exposed aluminum ion site for the normal butene isomerization in the absence of sulfur dioxide, the opposite dependences of the isomerization rates on the evacuation temperature in the presence and in the absence of sulfur dioxide can be explained by considering that the reaction in the absence of sulfur dioxide occurs on the silica–alumina-type site, while the one in the presence of sulfur dioxide proceeds on similar sites over an alumina catalyst.[11,12] It is probable that sulfur dioxide strongly adsorbs on the silica–alumina site and, accordingly, poisons the double-bond migration of the butenes. If the sulfur dioxide–*cis*-2-butene molecular complex approached the exposed aluminum ions, it would be polarized by the strong electrostatic field surrounding these cations toward the radical-ion structure $\dot{S}O_2CH(CH_3)\overset{+}{C}H(CH_3)$, and this could readily initiate the polysulfone formation and the accompaning geometrical isomerization.

References

1) K. Otsuka and A. Morikawa, *J. Chem. Soc., Chem. Commun.*, **1975**, 218.
2) K. Otsuka and A. Morikawa, *J. Catal.*, in press.
3) L. H. Little, H. E. Klauser, and C. H. Amberg, *Can. J. Chem.*, **39**, 42 (1961).
4) G. A. Blomfield and L. H. Little, *J. Catal.*, **14**, 213 (1969).
5) D. Booth, F. S. Dainton, and K. J. Ivin, *Trans. Faraday Soc.*, **55**, 1293 (1959).
6) K. Otsuka, T. Tanabe, and A. Morikawa, to be published.
7) M. Hattori, K. Otsuka, and A. Morikawa, unpublished data.
8) G. A. Blomfield and L. H. Little, *J. Catal.*, **21**, 139 (1971).
9) P. B. West, G. L. Haller, and R. L. Burwell, Jr., *J. Catal.*, **29**, 486 (1973).
10) H. R. Gerberich and W. K. Hall, *J. Catal.*, **5**, 99 (1966).
11) J. W. Hightower and W. K. Hall, *J. Am. Chem. Soc.*, **89**, 778 (1967).
12) J. B. Peri, Actes Congr. Intern. Catalyse, 2e, Paris, 1960, Vol. **1**, 1333 (1961); *J. Phys. Chem.*, **69**, 211, 220, 231 (1965).

The Microwave Spectrum of Dichlorodifluoromethane

Harutoshi TAKEO and Chi MATSUMURA

National Chemical Laboratory for Industry, Honmachi, Shibuya-ku, Tokyo 151

(Received October 12, 1976)

The microwave spectra of three isotopic species of dichlorodifluoromethane have been observed, and the following rotational constants have been obtained:

$A = 4118.90$ MHz, $B = 2638.70$ MHz, $C = 2233.72$ MHz for $^{12}C^{35}Cl_2F_2$
$A = 4092.07$ MHz, $B = 2582.30$ MHz, $C = 2185.54$ MHz for $^{12}C^{35}Cl^{37}ClF_2$
$A = 4115.73$ MHz, $B = 2638.95$ MHz, $C = 2232.86$ MHz for $^{13}C^{35}Cl_2F_2$.

The bond lengths and angles determined from them are r(C–Cl)=1.744 Å, r(C–F)=1.345 Å, ∠Cl–C–Cl=112°33′, and ∠F–C–F=106°14′. The nuclear quadrupole coupling constants in the C–Cl bond axis system are $\chi_{zz}=-82.7$ MHz and $\eta_{bond}=0.06$.

The chloro and fluoro derivatives of methane have been examined by many investigators,[1] and the molecular structures have been determined by microwave spectroscopy. Lide[2] pointed out that a clear bond shortening occurs upon the substitution of hydrogen atoms by halogen atoms in the series of CH_mCl_n and CH_mF_n, and that the shortening effect is larger in the fluoromethanes than in the chloromethanes. A similar effect can be expected in the series of chlorofluoromethanes, whereas only dichlorodifluoromethane has not been studied of the molecules with the general formula of $CH_lCl_mF_n$. The purposes of this research are to determine the structure of dichlorodifluoromethane precisely and to check the shortening effect in the series of methane derivatives with both fluorine and chlorine atoms.

Experimental

The sample of dichlorodifluoromethane was prepared by the fluorination of tetrachloromethane.[3] Since this reaction also produced trichlorofluoromethane, the sample was purified by gas chromatgraphy. The ^{13}C species was prepared by the same reaction from $^{13}CCl_4$.

The spectrometer used was a conventional Stark modulated type with a 100 kHz square-wave modulation. The X-13 and X-12 klystrons dipped in oil baths were used as 8—18 GHz microwave sources, while 18—36 GHz sources were obtained by the use of harmonic generators. A stability of the microwave frequency of within 0.005 MHz per minute was obtained, and the resolution was about 0.2 MHz with the sample pressure of 5 mTorr. The spectra were all observed with a sample cell cooled with Dry Ice.

Analysis of the Spectra

Hyperfine Structure. The hyperfine structure of the spectrum was predicted and analyzed by using the first-order perturbation theory for the rotational levels of an asymmetric-top molecule containing two nuclei of isotopic spin 3/2 presented by Robinson and Cornwell.[4] The calculated patterns of the hyperfine structures showed that the low-J transitions consist of many weak components with the selection rule of $\Delta F=0, \pm1$ and $\Delta\varepsilon=0, \pm2$, while in the high-$J$ transitions only $\Delta F=\Delta J$ transitions have strong intensities. This makes the hyperfine structures of high-J transitions simple and easy to be observed. Some typical patterns

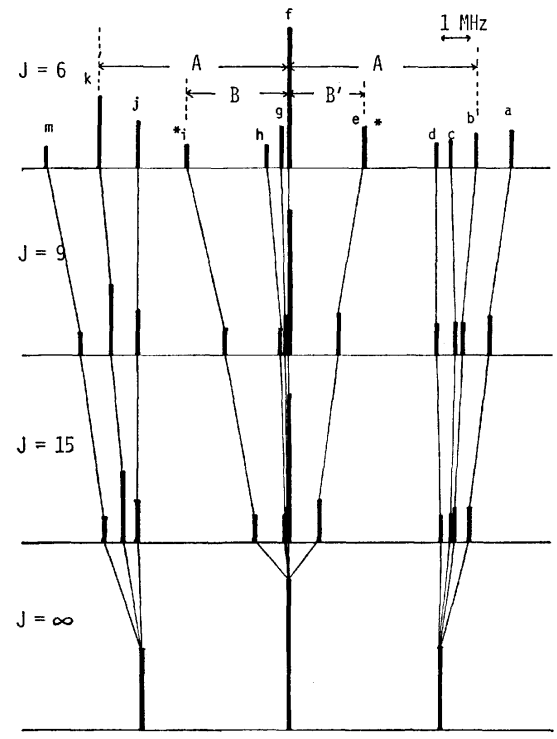

Fig. 1. The J dependance of hyperfine structures with identical nuclei of spin 3/2. The same values of $\langle eqQ \rangle_J$ are used for the calculation. For the notation of the alphabet attached to each component, see Table 1.

of the hyperfine structure in the high-J Q-branch series are shown in Fig. 1. It should be noted that the asterisked components in Fig. 1 shift greatly with the change in the J number, while the ratio of A to B depends only on J, not on the other quantum numbers nor on the quantities of the $\langle eqQ \rangle_J$ values of the upper and lower levels of the transition. The J number in the Q-branch transition can easily be assigned by the measurement of these values, even in the transition with the J number of 15 or more; in fact, $15_{6,10}$—$15_{5,11}$ was assigned without any other information.

The intensity alternation occurs in each hyperfine component depending on the spin weight due to fluorine nuclei. The intensity ratio by spin weight between ε=even and ε=odd components in the $(ee)\leftrightarrow(oo)$ transitions should be 1 to 3, and this ratio should change

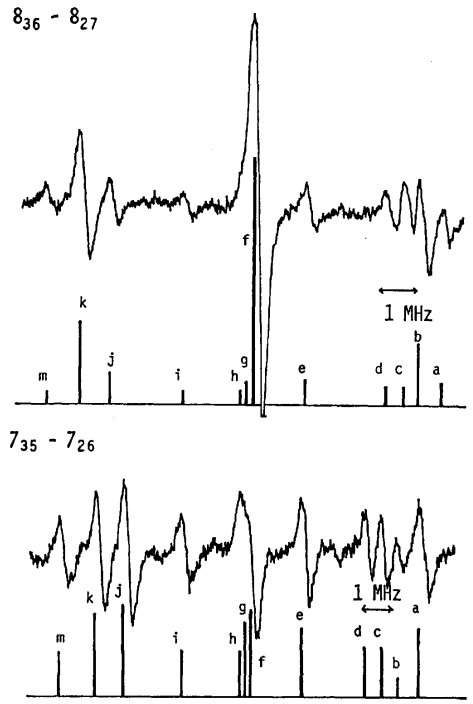

Fig. 2. The recorded and calculated hyperfine structures of $C^{35}Cl_2F_2$.

to 3 to 1 in the $(eo)\leftrightarrow(oe)$ transitions. This phenomenon was also helpful in the assignment of the transitions. The recorded hyperfine structures of the two transitions, which have different spin weights, are shown in Fig. 2. The figures also show that the strong component always exists at the unsplit position, and that it is the strongest in the transition of $(eo)\leftrightarrow(oe)$. Therefore, the measurements of only these components lead to the rotational constants, without any analysis of the hyperfine structures being necessary, if the second-order approximation is correct enough. In the hyperfine structures of the $C^{35}Cl^{37}ClF_2$ species, on the other hand, there are no such components at the exact unsplit positions because the two quadrupole moments are not identical. However, the shifts of the four components which degenerate in the spectrum of the $C^{35}Cl_2F_2$ species are quite small in this case; in fact, the strong sharp lines were always obtained in the hyperfine structure of $C^{35}Cl^{37}ClF_2$ species. It is believed that the difference between the observed peak position of this component and the hypothetical unsplit value is within 0.1 MHz. Therefore, these values were used for the determination of the rotational constants.

Assignment of the Spectrum. The Q-branch series were searched for first in the region predicted by the rotational constants of the assumed structure based on other halogenomethanes, and were assigned by using the method described above. The spectrum of the $C^{35}Cl^{37}ClF_2$ species was assigned first, since the degenerate K-type doubling transitions of this molecule have fairly large Stark effects compared with those of symmetric $C^{35}Cl_2F_2$ species because of the existance of a small μ_a component. The same transitions of the $C^{35}Cl_2F_2$ species were observed with Stark voltages about 1000 V/cm. This suggests that the dipole moment of the molecule is fairly small because of the cancellation of the C–Cl and C–F bond moments. The R-branch transitions were assigned by means of the values calculated from the structure refined by Q-branch transitions. The observed transitions used for the determination of the quadrupole coupling constants are listed in Table 1. The obtained values for the diagonal components of the quadrupole coupling constant tensor along the principal inertial axes are listed in Table 2, along with the diagonalized χ tensor, which was calculated using the molecular structure determined in this study with the assumption that the z axis coincides with the C–Cl internuclear line.

The frequencies of the observed transitions are listed in Table 3. The rotational constants and the centrifugal distortion constants were determined by a least-squares fit of all the transitions listed in Table 3. They are shown in Table 4.

Table 1. Observed quadrupole splitting patterns of $C^{35}Cl_2F_2$ (MHz)

	ε	F	$5_{3\,3}-5_{2\,4}$		$6_{2\,5}-6_{1\,6}$		$6_{5\,1}-6_{4\,2}$	
			Obsd	Δ[a]	Obsd	Δ	Obsd	Δ
a	3	$J+1$	8977.85	0.00				
b	0	J	8976.69	0.04	9575.28	0.02		
c	3	J	8975.32	0.01			14913.98	0.01
d	1	$J-1$	8974.87	−0.03			14913.37	−0.01
e	3	$J+2$	8973.07	0.05	9571.00	−0.06	14910.92	0.03
	2	$J+2$						
	2	$J+1$						
f	2	$J-1$	8969.99	0.01	9568.32	0.02	14908.24	−0.01
	2	$J-2$						
g	1	$J+1$	8969.56	0.02			14907.90	−0.01
h	3	$J-1$	8968.76	0.00			14907.45	0.01
i	3	$J-2$	8965.58	0.00			14904.65	0.04
j	3	$J+3$	8964.89	−0.02	9562.79	0.04	14902.93	0.01
	2	J						
k	1	J	8963.30	0.01	9561.34	0.01	14901.55	0.02
m	3	$J-3$						
	$\Delta\langle eqQ\rangle_J$[b]		−10.15	−0.01	−11.03	0.02	−10.61	0.01

TABLE 1. (Continued)

	ε	F	$7_{3\,5}-7_{2\,6}$ Obsd	Δ[a]	$8_{1\,7}-8_{0\,8}$ Obsd	Δ	$8_{6\,2}-8_{5\,3}$ Obsd	Δ
a	3	$J+1$	10256.88	0.00	12023.67	0.04	18194.15	−0.01
b	0	J	10256.14	0.00	12022.83	0.04	18193.46	−0.03
c	3	J	10255.62	0.00	12022.31	0.02	18193.08	−0.01
d	1	$J-1$	10255.14	0.00	12021.70	0.01	18192.65	0.03
e	3	$J+2$	10253.00	0.01	12018.69	−0.01		
	2	$J+2$						
	2	$J+1$						
f	2	$J-1$			12016.80	−0.02	18188.77	−0.01
	2	$J-2$						
g	1	$J+1$						
h	3	$J-1$						
i	3	$J-2$	10249.12	0.05	12014.45	0.00	18186.92	0.05
j	3	$J+3$	10247.33	0.00	12011.79	−0.03	18184.77	−0.02
k	2	J						
	1	J	10246.43	−0.01	12010.82	−0.03	18184.02	0.00
m	3	$J-3$	10245.38	0.01			18183.08	−0.02
	$\Delta\langle eqQ\rangle_J$[b]		−7.92	0.01	−10.05	−0.04	−7.93	0.00

a) $\Delta=\nu_{obsd}-\nu_{calcd}$. b) The $\langle eqQ\rangle_J$ of upper level minus the $\langle eqQ\rangle_J$ of the lower level.

TABLE 2. QUADRUPOLE COUPLING CONSTANTS OF $C^{35}Cl_2F_2$

χ_{aa}	-43.7 ± 0.2 MHz
χ_{bb}	4.8 ± 0.2 MHz
χ_{cc}	38.9 ± 0.2 MHz
χ_{zz}	-82.7 ± 1.3 MHz
η	0.06 ± 0.01

Molecular Structure

The substitution coordinates of the carbon and chlorine atoms were calculated by means of Kraitchman's equation; they led to the C–Cl bond length and the Cl–C–Cl angle. The C–F distance and the F–C–F angle were determined from the coordinates

TABLE 3. OBSERVED AND CALCULATED FREQUENCIES FOR CCl_2F_2 (MHz)

Transition	$C^{35}Cl_2F_2$ Obsd	Δ[a]	$C^{35}Cl^{37}ClF_2$ Obsd	Δ	$^{13}C^{35}Cl_2F_2$ Obsd	Δ
$2_{1\,2}-1_{0\,1}$	10820.10	0.09			10814.50	0.24
$2_{2\,0}-1_{1\,1}$			14926.96	−0.18	15058.80	−0.11
$2_{2\,1}-1_{1\,0}$	14590.33	−0.04	14461.43	−0.24	14580.00	0.02
$3_{0\,3}-2_{1\,2}$	13194.22	−0.09	12860.45	−0.22		
$3_{3\,0}-2_{2\,1}$	23080.42	−0.10	22891.20	0.03	23064.72	0.00
$4_{3\,1}-3_{2\,0}$					19320.30	0.20
$4_{1\,4}-3_{0\,3}$	31274.68	0.02				
$5_{4\,2}-4_{3\,1}$			35792.38	0.23		
$7_{5\,3}-7_{4\,4}$			15112.84	−0.17		
$7_{5\,2}-7_{4\,3}$	14757.18	0.01			14727.94	−0.06
$8_{3\,6}-8_{2\,7}$	11229.62	0.05			11230.35	−0.05
$8_{5\,4}-8_{4\,5}$	14804.22	0.08	15044.03	−0.15	14776.82	−0.06
$8_{5\,3}-8_{4\,4}$	14484.36	−0.16				
$8_{6\,3}-8_{5\,4}$	18206.20	0.05	18501.98	−0.09		
$8_{6\,2}-8_{5\,3}$	18188.58	−0.12	18487.00	−0.18		
$10_{5\,6}-10_{4\,7}$	14807.40	−0.05			14783.23	0.00
$10_{7\,4}-10_{6\,5}$			21821.06	0.12	21428.02	0.13
$10_{7\,3}-10_{6\,4}$	21459.46	0.03	21813.86	0.09		
$11_{5\,7}-11_{4\,8}$	14973.63	−0.03			14953.17	0.06
$11_{6\,5}-11_{5\,6}$	17456.24	0.08	17813.23	0.02		
$11_{7\,4}-11_{6\,5}$	21317.08	−0.04	21681.01	0.15	21275.32	−0.08
$11_{7\,5}-11_{6\,6}$			21704.20	−0.05	21304.36	−0.02
$12_{7\,6}-12_{6\,7}$	21194.02	0.05	21559.25	0.06	21152.18	0.06
$12_{7\,5}-12_{6\,6}$			21429.57	−0.09	21070.04	−0.02

a) $\Delta=\nu_{obsd}-\nu_{calcd}$.

Table 4. Rotational constants and centrifugal distortion constants of CCl_2F_2 (MHz)

	A	B	C	$I_c-I_a-I_b$[a]
$^{12}C^{35}Cl_2F_2$	4118.90(04)	2638.70(02)	2223.72(02)	87.972(04)
$^{12}C^{35}Cl^{37}ClF_2$	4092.07(07)	2582.30(05)	2185.54(06)	87.973(10)
$^{13}C^{35}Cl_2F_2$	4115.73(03)	2638.95(02)	2232.86(02)	87.962(04)
	d_J = −0.00135(95)			
	d_{JK} = −0.00222(63)			
$^{12}C^{35}Cl_2F_2$	d_K = 0.00165(41)			
	d_{WJ} = 0.0000011(3)			
	d_{WK} = 0 (fixed)			

a) amuÅ².

of fluorine atoms, which were themselves obtained by the use of the first-moment equation for b-coordinates and the value of $I_c-I_a-I_b$ for the c-coordinates. They were also determined by a least-squares fit of all the observed rotational constants, the C–Cl length and the Cl–C–Cl angle being fixed to the previously determined values. The structural parameters obtained by the two methods are in good agreement with each other. They are listed in Table 5.

Table 5. Coordinates of atoms (Å) and the structural parameters determined from them

	Cl	C	F
a	±1.4506(13)	0	0
b	−0.6591(29)	0.3083(20)	1.1158(26)[a]
c	0	0	±1.0759(03)[b]
	r(C–Cl) = 1.744±0.004 Å		
	r(C–F) = 1.345±0.003 Å		
	∠Cl–C–Cl = 112°33′±31′		
	∠F–C–F = 106°14′±23′		

a) Calculated from the first moment equation.
b) Calculated from the value of $I_c-I_a-I_b$.

Discussion

The obtained C–Cl and C–F bond distances are compared with those of other halogenomethanes in Fig. 3. The values indicated by black circles have been determined by using many isotopic data; they seem to be precise enough. On the other hand, the values indicated by white circles may have fairly large ambiguities because they were obtained from few isotopic data. As Lide[2] pointed out, the carbon-halogen distances in the CH_3Cl, CH_2Cl_2, $CHCl_3$ series and the CH_3F, CH_2F_2, CHF_3 series show a quite regular shortening upon further substitution of the hydrogen by the halogen, and the C–F shortening is more marked than the C–Cl shortening. In the figure we can see that the C–Cl shortening occurs as a fluorine is added to the molecule. The C–F shortening is also seen as a chlorine is added. It is interesting to note that the bond shortening upon the substitution of a fluorine is always more marked than that upon the substitution of a chlorine. The irregularities in $CClF_3$ and CCl_3F may be attributed to the improper analyses of their molecular structures, since the assumption of some structural parameters seem to be invalid for the analyses of these molecules. Therefore, the precise re-determination of the molecules

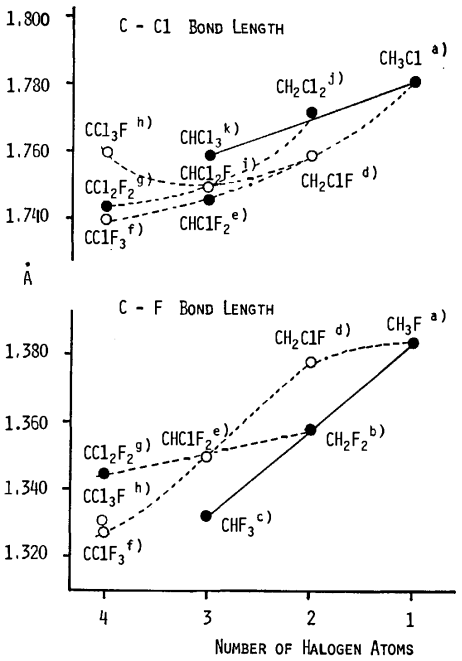

Fig. 3. The plot of carbon-halogen bond lengths versus number of halogen atoms in halogenomethanes.
a) C. C. Costain, *J. Chem. Phys.*, **29**, 864 (1958). b) E. Hirota, T. Tanaka, A. Sakakibara, Y. Ohashi, and Y. Morino, *J. Mol. Spectrosc.*, **34**, 222 (1970). c) S. N. Ghosh, R. Trambarulo, and W. Gordy, *J. Chem. Phys.*, **20**, 605 (1952). d) N. Müller, *J. Am. Chem. Soc.*, **75**, 860 (1953). e) D. B. Mclay and C. R. Mann, *Can. J. Phys.*, **40**, 61 (1962). f) J. Sheridan and W. Gordy, *J. Chem. Phys.*, **20**, 591 (1952). g) This work. h) M. W. Long, Q. Williams, and T. Weatherly, *J. Chem. Phys.*, **33**, 508 (1960). i) D. B. Mclay, *Can. J. Phys.*, **42**, 720 (1964). j) R. J. Myers and W. D. Gwinn, *J. Chem. Phys.*, **20**, 1420 (1952). k) M. Jen and D. R. Lide, Jr., *J. Chem. Phys.*, **36**, 2525 (1962).

indicated by white circles in the figure is necessary for a further detailed discussion.

Gordy and Cook[5] have shown that the change in quadrupole coupling constants obtained by the pure nuclear quadrupole resonance is quite regular in the CCl_4, CCl_3F, CCl_2F_2, $CClF_3$ series and that the change can be interpreted in terms of hyperconjugation. The χ_{zz} obtained in the present study, however, is fairly large compared with the value expected from their figure. As far as we know, this value is the highest in the coupling constants obtained for chlorine nuclei

attached to carbon atoms. For a detailed discussion, it is desirable to determine the χ_{zz} by the analysis of the off-diagonal element of the χ tensor in the principal axis system, which can be obtained from the measurement of the second-order quadrupole effect. However, all the transitions measured in this study fit the calculated values within the limits of experimental errors without the second-order terms.

References

1) See the note in Fig. 3.
2) D. R. Lide, Jr., *J. Am. Chem. Soc.*, **74**, 3548 (1952).
3) H. D. Mallory, *J. Am. Chem. Soc.*, **74**, 839 (1952).
4) G. W. Robinson and C. D. Cornwell, *J. Chem. Phys.*, **21**, 1436 (1953).
5) W. Gordy and R. L. Cook, "Microwave Molecular Spectra," ed by W. West, Interscience Publishers, New York, N. Y. (1970), p. 592.

The Effect of the Deuterium Substituent on the Anomalous Phase Transition of the Crystalline Galvinoxyl Radical

Kazuo MUKAI, Tadashi MISHINA, Kazuhiko ISHIZU, and Yasuo DEGUCHI*

Department of Chemistry, Faculty of Science, Ehime University, Matsuyama 790
**College of Liberal Arts and Science, Kyoto University, Kyoto 606*

(Received October 12, 1976)

Two kinds of deuterium substituents of the galvinoxyl radical have been synthesized, and the effect of the deuterium substitution on the anomalous phase transition of the crystalline galvinoxyl radical at 82 K has been studied. The results, investigated by means of ESR and magnetic susceptibility measurements, indicate that the effect was not strong enough to induce any observable change in the transition.

In the previous papers,[1-3] we have reported that the galvinoxyl radical shows a first-order phase transition accompanying the pairing of magnetic spins at 82 K; the magnetic susceptibility is paramagnetic above the magnetic transition point, 82 K, where the susceptibility drops very sharply on cooling, while it is diamagnetic (weak paramagnetic) below this point. The anomaly at 82 K in the galvinoxyl has disappeared in the bisindophenoxyl radical, in which the centered methylidyne group (-CH=) of galvinoxyl is replaced by a nitrogen atom (-N=).[2] The magnetic susceptibility of the bisindophenoxyl radical exhibits a broad maximum at 54±2 K. This susceptibility can be explained approximately using a model which consists of a singlet ground state and a triplet state lying slightly above the ground state. On the other hand, the deuterated galvinoxyl radical, in which a centered methylidyne proton of galvinoxyl is replaced by a deuteron, showed a quite similar anomaly at 82 K.[4]

It has been reported that the deuterium substitution causes changes in the proton hyperfine splittings at the undeuterated positions of deuterated radicals.[5-9] Karplus *et al.*[10] have successfully analyzed the above results in terms of a model for the effect of the difference in the CH and CD out-of-plane bending motions. This vibration can affect the sigma-pi coupling, the pi-electron spin-density distribution, or both.

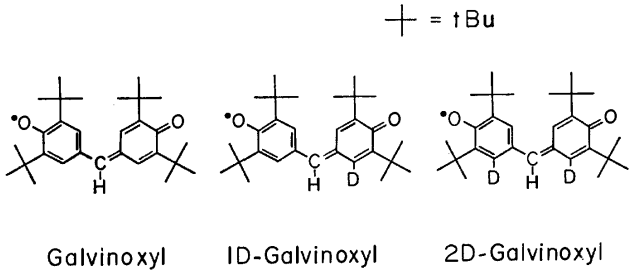

Fig. 1. Molecular structures of the galvinoxyl, 1D-galvinoxyl, and 2D-galvinoxyl radicals.

In the present paper, we have synthesized two mono- and di-deuterium derivatives, in which one and two of four *meta*-ring protons of the galvinoxyl radical are deuterated respectively (hereafter, they will be denoted as 1D- and 2D-galvinoxyl; see Fig. 1) and studied the magnetic properties of these radicals by means of ESR and magnetic susceptibility measurements.

Experimental

Materials. 2,6-Di-*t*-butylphenol and 2,6-di-*t*-butyl-4-methoxymethylphenol are commercially available. The synthesis of 2,6-di-*t*-butyl-3-deuteriophenol (bp 128—132°C/13 Torr) was reported previously.[11] The degree of deuterium substitution was determined as at least 95% from the NMR data of 2,6-di-*t*-butyl-3-deuteriophenol. 3,3′,5,5′-Tetra-*t*-butyldiphenylmethane-4,4′-diol, phenol (I) (mp 157.0—157.5 °C (lit, 154 °C)) was prepared according to the method of Kharash and Joshi.[12] 3,3′,5,5′-Tetra-*t*-butyl-2,2′-dideuteriodiphenylmethane-4,4′-diol, phenol (III), was also similarly prepared from 2,6-di-*t*-butyl-3-deuteriophenol by condensation with formaldehyde in a KOH–ethanol solution. Mp 157.5—158.0 °C. (Found: C, 81.57; H, 10.82%. Calcd for $C_{29}H_{42}D_2O_2$: C, 81.63; H, 10.87%). UV spectrum (λ_{max}=279 nm, logε=3.53 in ethanol). NMR spectrum ($\delta_{C(CH_3)_3}$=1.40 ppm (36), δ_{CH_2}=3.74 (2), δ_{OH}=4.86 (2). $\delta_{m\text{-}H}$=6.85 (2); δ in CCl_4, with TMS as the internal standard). 3,3′,5,5′-Tetra-*t*-butyl-2-deuteriodiphenylmethane-4,4′-diol, phenol (II), was prepared by the reaction of 2,6-di-*t*-butyl-3-deuteriophenol and 2,6-di-*t*-butyl-4-methoxymethylphenol in a KOH–methanol solution, according to the procedure used by Steelink *et al.*[13] to prepare 3,5-di-*t*-butyl-3′,5′-dimethyl-4,4′-dihydroxydiphenylmethane. Mp 156.0—157.0 °C. (Found: C, 82.22; H, 10.72%. Calcd for $C_{29}H_{43}D_1O_2$: C, 81.83; H, 10.66%). UV spectrum (λ_{max} =279 nm, logε=3.51 in ethanol). NMR spectrum ($\delta_{C(CH_3)_3}$ =1.41 ppm (36), δ_{CH_2}=3.76 (2), δ_{OH}=4.88 (2), $\delta_{m\text{-}H}$=6.89 (3); δ in CCl_4, with TMS as the internal standard.

The galvinoxyl (I), 1D-galvinoxyl (II), and 2D-galvinoxyl (III) radicals (see Fig. 1) were prepared according to the methods of Coppinger[14] and of Bartlett and Funahashi.[15] The diphenylmethane precursors, phenols (I)—(III), were oxidized

Table 1. Chemical and physical properties of galvinoxyl, 1D-, and 2D-galvinoxyls

	Mp (°C)	UV		Visible		Calcd (%)		Found (%)	
		λ_{max}	log ε	λ_{max}	log ε	C	H	C	H
Galvinoxyl	151.0—152.5	289nm	4.06	430nm	5.23	82.61	9.80	82.55	9.88
1D-Galvinoxyl	150.5—151.5	289	4.03	430	5.21	82.41	10.02	82.33	9.90
2D-Galvinoxyl	149.0—150.5	289	4.03	429	5.21	82.22	10.23	81.75	10.06

with PbO_2 in diethyl ether, with the temperature kept between 0 and 5°C under nitrogen gas throughout. The PbO_2 was then filtered off carefully, and the diethyl ether solvent was slowly evaporated under nitrogen gas. Very dark blue crystalline compounds of the galvinoxyl (I)—(III) remained in the round-bottomed flask. This flask was connected to a vacuum line (5×10^{-3} Torr) for two hours to remove the diethyl ether solvent completely. The chemical and physical properties of these radicals are summarized in Table 1. All these values show good accordance with each other within the limits of experimental error.

Apparatus. The susceptibility measurements were carried out with a Shimadzu-type MB-2 magnetic torsion balance, equipped with a low-temperature cryostat. The temperatures were measured using an AuCo-Cu thermocouple. Manganese Tutton salt was used for the calibration of the themometers and the field gradient. The ESR measurements were carried out using a JES-ME-3X spectrometer equipped with a Takeda-Riken microwave frequency counter. The ESR hyperfine splittings and g-values were measured relative to those of $(KSO_3)_2NO$ ($a^N=13.05\pm0.03$ G; $g=2.0054$[16]). The NMR spectra were taken on a JEOLCO 4H-100 100 MHz NMR spectrometer.

Results and Discussion

Initial slight oxidations of 3,3′,5,5′-tetra-*t*-butyldiphenylmethane-4,4′-diol and 3,3′,5,5′-tetra-*t*-butyl-2,2′-dideuteriodiphenylmethane-4,4′-diol, (I) and (III) phenols, with PbO_2 in toluene in a sealed, degassed system give ESR spectra consisting of triplet-triplet or triplet-doublet splittings respectively. We assign the spectra to the primary phenoxyl radicals (I-P) and (III-P) formed from the parent phenols by the abstraction of a phenolic hydrogen atom. The large triplet splittings ($a^H=9.58$ G for (I-P) and $a^H=9.57$ G for (III-P) at 15 °C) in the primary radicals are clearly due to the para methylene group, and the triplet or doublet splittings ($a^H=1.65$ G for (I-P) and 1.68 G for (III-P)) can be explained by the meta hydrogens. One group of large triplet splittings of (I-P) and (III-P) is shown in Figs. 2(a) and (b). The spectrum shown in Fig. 2(b) includes also a weak triplet signal arising from undeuterized phenol. The theoretical ratio (a^D/a^H) of the deuteron to the proton splittings expected on the basis of the magnetic moments and spins of the two nuclei is 0.1535; thus, we can expect 0.25 G as the deuteron hyperfine splitting for the (III-P) radical. However, the deuteron hyperfine splitting (a_m^D) due to the *meta*-ring deuteron of the (III-P) primary radical was not resolved, as is shown in Fig. 2(b). On the basis of the relative intensities and line widths of the ESR spectrum consisting of doublet and triplet splittings, it is estimated that the samples contain approximately 8% undeuterized protons. This value shows a good agreement with that of 5% estimated from the NMR spectrum. The spectrum of the primary radical (II-P) obtained by the PbO_2 oxidation of phenol (II) may be explained as resulting from the addition of the spectra from (I-P) and (III-P).

As the oxidation of the phenol (I) solution proceeds, a further absorption due to a secondary radical, galvinoxyl, appeared, and finally the spectrum was completely altered to a doublet-quintet spectrum with hyperfine splittings, $a_{CH}^H=5.77$ G and $a_m^H=1.41$ G.[17] The (II) and (III) phenols also show similar behavior; they give doublet-quartet and doublet-triplet spectra due to 1D- and 2D-galvinoxyl radicals. The deuteron hyperfine splittings were not resolved, as is to be expected from the results obtained for the primary radicals. Recordings of the 1D-galvinoxyl spectrum also include

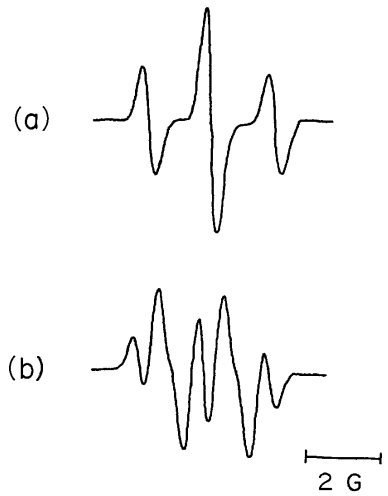

Fig. 2. ESR spectra of the primary radicals, (a) (I-P) and (b) (III-P), obtained by the PbO_2 oxidation of the phenols, (I) and (III), in toluene at 15 °C. One group of the three identical absorption groups is shown in Fig. 2(a) and (b), respectively.

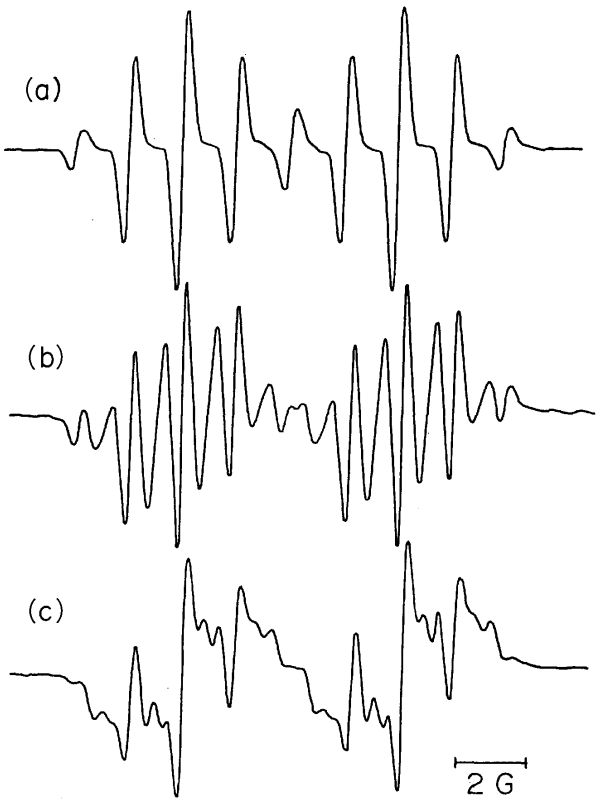

Fig. 3. ESR spectra of (a) galvinoxyl, (b) 1D-galvinoxyl, and (c) 2D-galvinoxyl radicals obtained by the PbO_2 oxidation of the phenols, (I), (II), and (III), in toluene at 20 °C.

Table 2. Hyperfine splittings and G-values of galvinoxyl, 1D-, and 2D-galvinoxyls

	$A^{H}_{-CH=}$ (G)	A^{H}_{m} (G)	G-value
Galvinoxyl	5.77±0.04	1.41±0.04	2.00434±0.00003
1D-Galvinoxyl	5.82±0.04	1.36±0.04	2.00433±0.00003
2D-Galvinoxyl	5.86±0.04	1.35±0.04	2.00431±0.00003

the doublet-quintet spectrum of undeuterated galvinoxyl, because the sample of the monodeuterated diphenylmethane precursor (phenol (II)) contains the diphenylmethane (phenol (I)) as an impurity. Similarly, the spectrum of the 2D-galvinoxyl radical sample also includes signals due to both 1D-galvinoxyl and galvinoxyl radical impurities. These spectra are shown in Fig. 3. The g-values of these radicals in toluene were also measured. All these values are listed in Table 2. Both the hyperfine splittings and the g-values of these radicals remain constant, within the limits of experimental error, indicating that deuterium substitution to the *meta*-ring proton of the phenyl rings does not significantly affect the unpaired electron distribution.

The molar susceptibilities obtained for the galvinoxyl radical are shown in Fig. 4 as a function of the temperature. The data have been corrected for a calculated diamagnetism of -0.276×10^{-3} emu/mol. The susceptibility of galvinoxyl follows the Curie-Weiss law with a Curie constant of 0.358 K emu/mol and a Weiss constant of 13.0±2.0 K in the temperature region between 86 and 300 K. At 85.1±2.0 K, χ_P rapidly decreases by 93% of its maximum value within about three degrees, and afterward falls off gradually until 55 K. The residual paramagnetic radical concentration, calculated from the susceptibility at 55 K assuming Curie law, is only 1.1%. As has been reported before, the anomaly in the galvinoxyl is thought to be a first-order phase transition, accompanied by a pairing of the magnetic spins.[2] It has also been reported before that the magnetic susceptibilities in the low-temperature region (5—50 K) obey the Curie-Weiss law, with different spin concentrations from about 10 to 30 mol % for the three independently-prepared samples; thus, the low-temperature susceptibilities are probably due to the residual unpaired galvinoxyl radicals with a spin of 1/2, the radicals being randomly located in the lattice. In the present work, poly crystals of the galvinoxyl radical were prepared by careful, slow evaporation from a saturated etherial solution under nitrogen throughout in order to decrease the quantity of residual unpaired spins. In fact, the residual radical concentration (1.1%) obtained is much smaller than the values (from about 10 to 30 mol %) reported before for the galvinoxyl.

The 1D- and 2D-galvinoxyl radical samples were similarly prepared. The magnetic susceptibilities of these

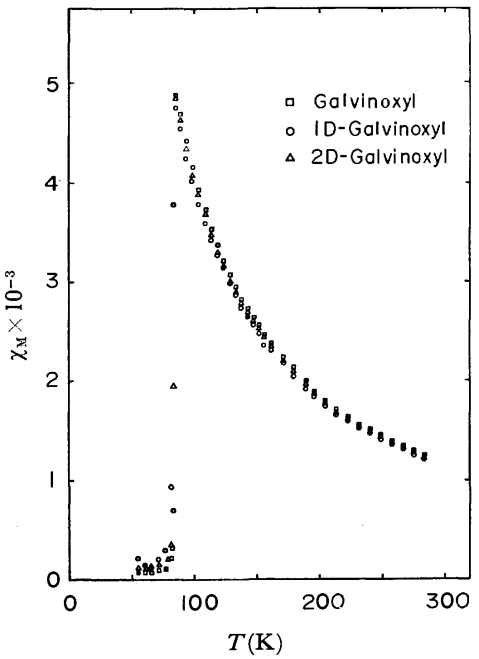

Fig. 4. Molar susceptibilities of the galvinoxyl (open square, □), 1D-galvinoxyl (open circle, ○), and 2D-galvinoxyl (open triangle, △) radicals versus temperature (55—300 K).

radicals between 55 and 300 K are shown in Fig. 4, together with those of the galvinoxyl radical. As is clear from the results shown in Fig. 4, the temperature dependences of the magnetic susceptibilities of the 1D- and 2D-galvinoxyl radicals are very similar to that of the galvinoxyl. The values of the Curie constants (C), the Weiss constants (θ), the radical concentrations, the transition temperatures (T_{max}), and the residual radical concentrations obtained in this work are summarized in Table 3. The small differences observed between these radicals for the radical concentrations above the transition temperature and the residual radical concentrations below it must be due to differences in the sample preparation. On the other hand, the expected change in the phase-transition temperature and the Weiss constant upon the deuterium substitution to the *meta*-ring protons of the galvinoxyl was not observed. It has been reported by ESR studies that the deuterium substitution to aromatic radicals can produce significant modifications in the proton hyperfine splittings (a^H) for ring positions other than that of substitution. The most notable effect is observed in the benzenide anion;[5,6] the equal hyperfine splittings (a^H=3.75 G) obtained at all positions in $C_6H_6^-$ are replaced in the benzenide-1-*d* anion by $a^H_2=a^H_3=3.95$ G, $a^H_4=3.49$ G and in the benzenide-2,6-d_2 anion by

Table 3. Results from susceptibility measurements of galvinoxyl, 1D-, and 2D-galvinoxyls

	C (emu K/mol)	θ (K)	Radical concentration (%)	T_{max} (K)	Residual para (%)
Galvinoxyl	0.358	13.0±2.0	95.0±2.0	85.1±2.0	1.1±0.5
1D-Galvinoxyl	0.343	13.2±2.0	90.9±2.0	84.3±2.0	3.2±0.5
2D-Galvinoxyl	0.347	13.6±2.0	92.1±2.0	84.9±2.0	1.7±0.5

$a_1^H = a_4^H = 4.16$ G, $a_3^H = 3.61$ G. Smaller changes are observed in deuterated naphthalenide anions[7] and in the *N*-deuterated dihydropyrazine cation and its methyl derivatives.[8] However, all the results obtained for the galvinoxyl, 1D-, and 2D-galvinoxyl radicals in the solid state and in solution indicate that the perturbations in electronic and magnetic properties resulting from the deuterium substitution are quite small in these radicals.

References

1) K. Mukai, H. Nishiguchi, and Y. Deguchi, *J. Phys. Soc. Jpn.*, **23**, 125 (1967).
2) K. Mukai, *Bull. Chem. Soc. Jpn.*, **42**, 40 (1969).
3) A. Kosaki, H. Suga. S. Seki, K. Mukai, and Y. Deguchi, *Bull. Chem. Soc. Jpn.*, **42**, 1525 (1969).
4) K. Mukai, M. Iizuka, and K. Ishizu, *Bull. Chem. Soc. Jpn.*, **46**, 3578 (1973).
5) R. G. Lawler, J. R. Bolton, G. K. Fraenkel, and T. H. Brown, *J. Am. Chem. Soc.*, **86**, 520 (1964).
6) R. G. Lawler and G. K. Fraenkel, *J. Chem. Phys.*, **49**, 1126 (1968).
7) R. G. Lawler, J. R. Bolton, M. Karplus, and G. K. Fraenkel, *J. Chem. Phys.*, **47**, 2149 (1967).
8) M. R. Das and G. K. Fraenkel, *J. Chem. Phys.*, **42**, 792 (1965).
9) D. Purins and M. Karplus, *J. Chem. Phys.*, **62**, 320 (1975), and references cited therein.
10) M. Karplus, R. G. Lawler, and G. K. Fraenkel, *J. Am. Chem. Soc.*, **87**, 5260 (1965).
11) K. Mukai, T. Mishina, and K. Ishizu, *J. Chem. Phys.*, **66**, 1680 (1977).
12) M. S. Kharasch and B. S. Joshi, *J. Org. Chem.*, **22**, 1435 (1957).
13) C. Steelink, J. D. Fitzpatrick, L. D. Kispert, and J. S. Hyde, *J. Am. Chem. Soc.*, **90**, 4354 (1968).
14) G. M. Coppinger, *J. Am. Chem. Soc.*, **79**, 501 (1957).
15) P. D. Bartlett and T. Funahashi, *J. Am. Chem. Soc.*, **84**, 2596 (1962).
16) M. T. Jones, *J. Chem. Phys.*, **38**, 2892 (1963).
17) E. Müller, K. Ley, K. Scheffler, and R. Mayer, *Chem. Ber.*, **91**, 2682 (1958).

Charge-transfer Character in the Intramolecular Hydrogen Bond: Electronic Structures and Spectra of Hydrogen Maleate Anion and Related Molecules

Hiroshi MORITA, Kiyokazu FUKE, and Saburo NAGAKURA

The Institute for Solid State Physics, The University of Tokyo, Roppongi, Minato, Tokyo 106

(Received October 18, 1976)

Ultraviolet absorption spectra were measured with aqueous solutions of maleic acid (H_2M) at various pH values and in concentrated sulfuric acid solutions. With the aid of the theoretical calculations of electronic structures by the modified CNDO-CI method, relatively strong bands observed at 193.5 nm for H_2M, at 210.0 nm for the hydrogen maleate anion (HM^-), and at 202.8 and ≈230 nm for the dinegative ion (M^{2-}) are assigned to the π–π^* transition bands. Special attention was paid to the charge-transfer (CT) character (pertinent to the strong intramolecular hydrogen bond) in the excited states of HM^-. Configuration analysis of the wave functions revealed us that the first π–π^* band of HM^- covered by the much stronger 210 nm band is rich in the CT character pertinent to the hydrogen bond.

In some hydrogen-bonded systems (X-H···Y), the charge-transfer (CT) force between a proton donor (X-H) and a proton acceptor (Y) has been recognized to be important as well as the electrostatic and exchange repulsion forces.[1–6] On the basis of the CT mechanism, the CT band characteristic of hydrogen bond is expected to appear in the ultraviolet (UV) or vacuum ultraviolet (VUV) region, and observation of the band is a direct proof of the CT mechanism of hydrogen bond.

The hydrogen maleate anion (HM^-) has a symmetrical intramolecular hydrogen bond ($(O\text{-}H\text{-}O)^-$) as revealed from the X-ray diffraction analysis[7] and from the studies by infrared spectroscopy.[8–10] One of the present authors observed an electronic absorption band of HM^- in aqueous solution at ≈210 nm and determined the direction of the transition moment (being parallel to the O-H-O bond) of the band.[11] From a theoretical calculation based on the π-electron approximation, the 210 nm band was suggested to be the CT band characteristic of the intramolecular hydrogen bond ($(O\text{-}H\text{-}O)^-$) of HM^-. Further theoretical studies have been carried out with the ground and excited states of HM^- by the non-empirical[12] and semi-empirical[13] methods. The potential energy curve of hydrogen bond calculated by the modified CNDO method[13] for HM^- agreed with the experimentally expected one.[8–10]

In the present study, in order to extend the previous works and to elucidate the electronic structures of the excited states of the hydrogen maleate anion, the absorption spectra of the maleic acid cation (H_3M^+), maleic acid (H_2M), HM^-, and maleate dinegative ion (M^{2-}) have been measured and their electronic structures have been calculated and analysed by the modified CNDO-CI method[14] combined with the configuration analysis method.[15] From the comparison between the theoretical and experimental results, the CT character (pertinent to the hydrogen bond) in some lower excited states of HM^- has been discussed in detail.

Experimental

Maleic acid (Wako G. R. grade) was purified by repeated recrystallizations from water. HM^- was prepared[10] by treating aqueous solution of maleic acid with potassium hydrogen carbonate ($KHCO_3$), and recrystallized three times from water. Methanol and acetonitrile (Wako spectrograde) were used as solvents without further purification. A buffer solution with pH=4.4 was prepared from aqueous solutions of acetic acid and sodium acetate.[16]

UV absorption spectra were measured with a Cary recording spectrophotometer model 14, a cell of 0.933 mm light path length being used. VUV absorption spectra were measured with a spectrophotometer constructed in our laboratory[17].

Theoretical

The electronic structures of H_3M^+, H_2M, HM^-, and M^{2-} were calculated by the modified CNDO-CI method presented in a previous paper.[14] The method has the characteristics that the semi-empirical electron repulsion, core resonance, and core potential integrals are separately evaluated for the σ- and π-orbitals. As in the case of formic and acrylic acids reported,[14] the one-center Coulomb repulsion integrals, γ's and bonding parameters, β^0's were commonly used for all the 2s and 2p atomic orbitals (AO) of the two oxygen atoms in the carboxyl group. Furthermore, in order to consider the effect of excess formal charge of the ions, the β^0 and γ values and the effective nuclear charge (Z) of the basis

TABLE 1. EFFECTIVE NUCLEAR CHARGE (Z), ONE-CENTER COULOMB REPULSION INTEGRAL (γ_{AA}(eV)), AND BONDING PARAMETER (β_A^0(eV)) FOR H, C, AND O ATOMS

	H	C		O[a]			
		σ-AO	π-AO	H_3M^+	H_2M	HM^-	M^{2-}
Z	1.2(1.0)[b]	3.25	3.25	4.64	4.55	4.46	4.38
γ_{AA}	12.85	13.22	10.60	18.23	17.89	17.55	17.20
β_A^0	−12.0(−9.0)[b]	−17.9	−12.9	−31.8	−27.0	−23.0	−17.9

a) Value being employed for both the σ- and π-AO's. b) Employed only for HM^-.

AO's of oxygen and the hydrogen-bonded hydrogen atoms were modified from those of the neutral H_2M molecule. The parameters finally used are tabulated in Table 1. In the configuration interaction (CI) calculation, 24 singly excited π-π^* and σ-σ^* configurations and 25 singly excited π-σ^* and σ-π^* configurations were taken into account.

Geometrical structures were taken for H_2M and HM^- from the X-ray crystal analysis data[7,18] and assumed for H_3M^+ and M^{2-} to be the same as those of H_2M and HM^-, respectively, except for the fact that the additional proton was attached or removed.

The configuration analysis[15] was applied to the ground and two excited (B_1 symmetry) states of HM^-. The molecular orbitals (MO) of M^{2-} and 1s orbital of the hydrogen-bonded hydrogen atom were adopted as the reference MO's. The ground state of HM^- was analysed by the ground and 92 singly excited π-π^* and σ-σ^* reference configurations (with A_1 symmetry) and by all the doubly excited reference configurations derived from the above configurations, and the excited states of HM^- were analysed by 93 singly excited π-π^* and σ-σ^* reference configurations (with B_1 symmetry) and 93×92 doubly excited reference configurations.

Results and Discussion

Figure 1 shows the absorption spectra of HM^- in aqueous buffer solution with pH=4.4 and of M^{2-} in aqueous KOH solution with pH=11.0, the spectrum of M^{2-} being tentatively resolved into two components.

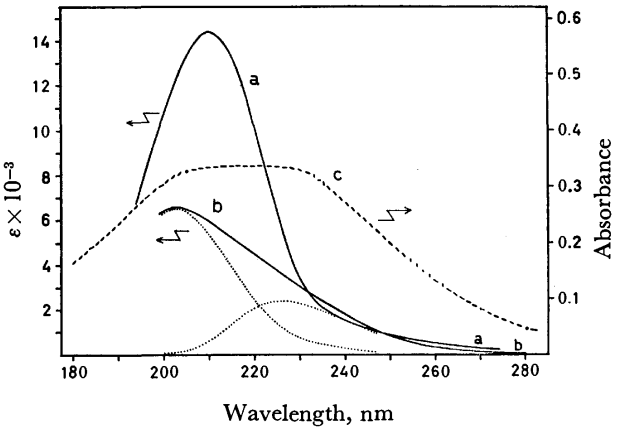

Fig. 1. Near and vacuum UV absorption spectra of (a) HM^- in aqueous buffer solution with pH=4.4, (b) M^{2-} in aqueous KOH solution with pH=11.0, and (c) HM^- crystalline powder. The composite band of M^{2-} is tentatively resolved by dotted lines.

This figure also shows the VUV spectrum observed with HM^- crystalline powder. Table 2 shows the transition energies, oscillator strengths, and directions of transition moments calculated by the modified CNDO-CI method, together with the observed values. Within the molecular (x-y) plane, the x-axis is parallel to the O-H-O hydrogen bond. From the comparison between the observed and calculated results, the 210.0 nm (5.90 eV) band of HM^- in aqueous solution and $\approx$220 nm band of HM^- crystalline powder can safely be assigned to the second

TABLE 2. TRANSITION ENERGIES ($^1\Delta E$ (eV)), OSCILLATOR STRENGTHS (f), AND DIRECTIONS OF TRANSITION MOMENTS OBSERVED AND CALCULATED FOR HM^- AND M^{2-}

HM^-						M^{2-}				
	Obsd		Calcd				Obsd		Calcd	
Assignment	$^1\Delta E$	f	$^1\Delta E$	f	Main config.[a]	Assignment	$^1\Delta E$	f	$^1\Delta E$	f
n-π^*			3.36	0.002(z)[b]	22—23	n-π^*			3.00	0.001(z)[b]
n-π^*			3.98	0	19—23	n-π^*			3.51	0.000(z)
n-π^*			4.17	0.000(z)	21—23	n-π^*			3.57	0
n-π^*			5.77	0	22—24 16—23	n-π^*			3.73	0
						π-π^*			5.31	0.021(x)
n-π^*			6.05	0.002(z)	22—25 19—24	π-π^*	$\approx$5.4	$\approx$0.06	5.38	0.101(y)
π-π^*			6.32	0.063(x)	17—23 22—26	n-π^*			5.73	0.009(z)
						n-π^*			6.06	0
n-π^*			6.71	0	22—24 19—23 19—25	σ-π^*			6.79	0
						π-π^*	6.11	0.18	6.83	0.543(x)
π-π^*	5.90	0.42	6.73	0.626(x)	20—23	n-π^*			6.91	0.000(z)
π-π^*			6.81	0.058(y)	18—23	π-σ^*			7.09	0.000(z)
n-π^*			7.82	0.001(z)	22—25 21—25	π-σ^*			7.09	0
						n-π^*			7.14	0
π-π^*			8.13	0.729(x)	17—23 22—26	π-π^*			7.40	0.439(x)
						π-π^*			7.53	0.166(y)
σ-π^*			8.29	0	16—23 15—23					

a) Main electron configurations of the respective excited states are shown. b) The direction of the transition moment is shown in the parentheses, the x-axis being taken to be parallel to the O-H-O bond within the molecular (x-y) plane.

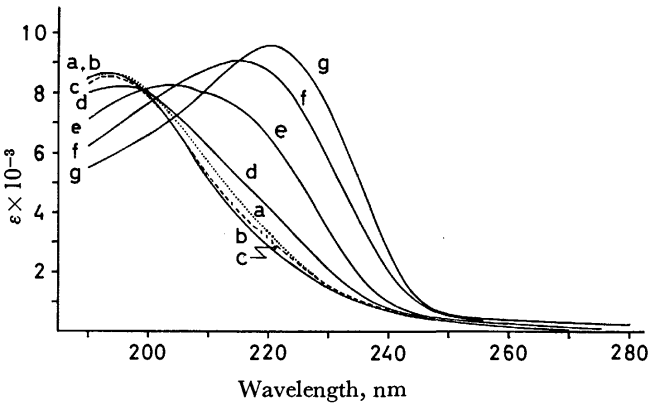

Fig. 2. UV absorption spectra of maleic acid in (a) 1.78% (dotted line), (b) 8.64%, (c) 24.3% (broken line), (d) 42.5%, (e) 62.5%, (f) 78.2%, and (g) 90.9% sulfuric acid.

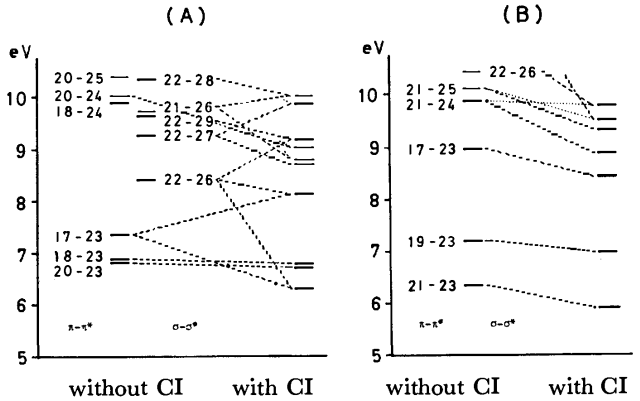

Fig. 3. Energy levels calculated with and without CI treatment for some lower π–π^* and σ–σ^* excited states of (A) HM^- and (B) H_2M.

π–π^* transition (calculated at 6.73 eV), whereas the ≈230 nm (≈5.4 eV) and 202.8 nm (6.11 eV) bands of M^{2-}, to the second and third π–π^* transitions (calculated at 5.38 and 6.83 eV), respectively. The theoretical results indicate that the first π–π^* band is covered by the stronger second (and third) π–π^* band(s) for both HM^- and M^{2-}.

Figure 2 shows the UV absorption spectra measured with the sulfuric acid (H_2SO_4) solutions of maleic acid. From the dependency of the spectrum on the sulfuric acid concentration, spectrum b in 8.6% H_2SO_4 solution can be ascribed to the spectrum of H_2M. The theoretical result in Table 3 shows that the 193.5 nm (6.41 eV) band of H_2M is assigned to the first π–π^* transition (calculated at 5.87 eV). In more concentrated sulfuric acid, the spectrum shifts to longer wavelengths, showing a strong band at 220.5 nm (5.62 eV) (curve g in Fig. 2). The spectra of the concentrated sulfuric acid solutions e, f, and g show practically no change even after 15 days. Moreover, dilution of the 90.9% H_2SO_4 solution of maleic acid (solution g) with water gives a spectrum similar to that of the sulfuric acid solution of the corresponding acidity. These facts indicate that the species having the absorption band at 220.5 nm in concentrated sulfuric acid solution is not a reaction product but a cation in equilibrium with sulfuric acid; H_3M^+ or the acylium ion as observed with the concentrated H_2SO_4 solution of mesitoic acid.[19]

Table 3. Transition energies ($^1\Delta E$(eV)) and oscillator strengths (f) observed and calculated for H_2M and H_3M^+

H_2M					H_3M^+		
Assignment	Obsd $^1\Delta E$	Obsd f	Calcd $^1\Delta E$	Calcd f	Assignment	Calcd $^1\Delta E$	Calcd f
n–π^*			3.28	0.003	n–π^*	3.90	0.003
n–π^*			3.92	0.000_6	π–π^*	6.20	0.335
n–π^*			5.84	0.000_4	n–π^*	6.44	0.001
π–π^*	6.41	0.35	5.87	0.489	σ–π^*	6.84	0.000_1
σ–π^*			6.66	0.000_4	σ–π^*	7.55	0.000_3
π–π^*			6.96	0.013	π–π^*	8.02	0.293
n–π^*			7.01	0.000_7	n–π^*	8.40	0.000
σ–π^*			7.60	0.003	σ–π^*	8.57	0.000_6
π–π^*			8.40	0.415	π–π^*	9.09	0.084
π–π^*			8.84	0.123	π–σ^*	9.25	0.004
π–σ^*			8.85	0.002	π–π^*	9.36	0.576
n–π^*			8.90	0.000_7	σ–π^*	9.99	0.000_8
π–σ^*			9.25	0.028	n–σ^*	10.24	0.040
π–π^*			9.30	0.169			
n–σ^*			9.48	0.069			

Let us investigate the electronic structure of HM^- in more detail. Figure 3 shows the energy levels calculated for some lower π–π^* and σ–σ^* excited states of HM^- compared with those of H_2M. In the figure, a singly excited configuration i–j represents one electron excitation from the i-th occupied MO to the j-th vacant MO. The shapes of MO's of HM^- are schematically shown in Fig. 4. The CT character pertinent to the intramolecular

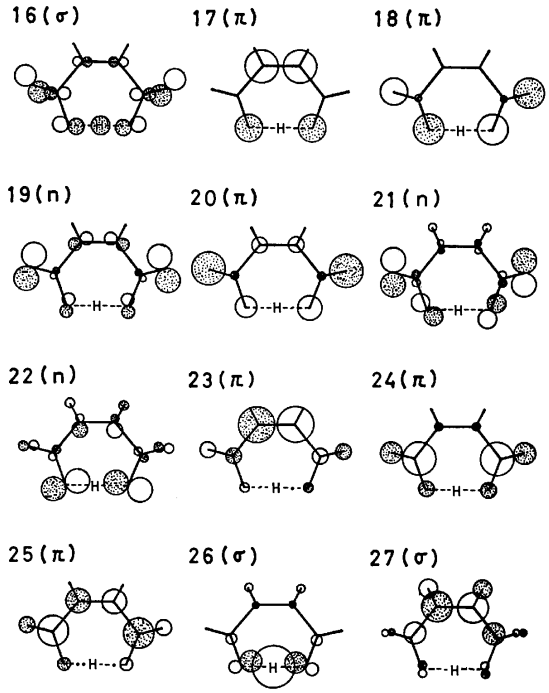

Fig. 4. Schematic shapes of some occupied and vacant MO's of HM^-. The 22th MO is the highest occupied one.

Table 4. Results of the configuration analysis (weights) for the ground and the first and second π–π^* excited states of HM^-

Structure	Reference configuration[a,b]	State		
		Ground	1 st π–π^*	2 nd π–π^*
$(OH^-O^+)^- + (O^+H^-O)^-$[c]	i,j-35, 35	0.1095	—	—
$(OH^-O^+)^- - (O^+H^-O)^-$	i,j-35, 35	—	0.1058 (0.1617)[d]	0.0058 (0.0067)[d]
$(O\text{–}H\cdots O)^- + (O\cdots H\text{–}O)^-$	i-35	0.4093	—	—
	i-35+π–π^*[e]	0.0272	0.2577 (0.1672)	0.4045 (0.3981)
	i-35+σ–σ^*[e]	0.0154	0.0124 (0.0227)	0.0057 (0.0108)
	(Total for sym. covalent structure)	(0.4519)	(0.2701 (0.1899))	(0.4102 (0.4089))
$(O\text{–}H\cdots O)^- - (O\cdots H\text{–}O)^-$	i-35	—	0.1978 (0.3023)	0.0109 (0.0125)
	i-35+π–π^*[e]	—	0.0131 (0.0200)	0.0007 (0.0008)
	i-35+σ–σ^*[e]	—	0.0079 (0.0122)	0.0004 (0.0004)
	(Total for antisym. covalent structure)		(0.2188 (0.3345))	(0.0120 (0.0137))
$O^-H^+O^-$	G^0[f]	0.3825	—	—
	π–π^*[g]	0.0254	0.2408 (0.1562)	0.3780 (0.3721)
	σ–σ^*[g]	0.0172	0.0154 (0.0274)	0.0058 (0.0107)
	i,j–k,l	0.0024	0.0237 (0.0173)	0.0341 (0.0341)
	(Total for $O^-H^+O^-$ structure)	(0.4275)	(0.2799 (0.2009))	(0.4179 (0.4169))
	Total	0.9889	0.8746 (0.8870)	0.8459 (0.8462)

a) i and j denote the 22 occupied MO's of M^{2-}, and k and l, the 12 vacant MO's of M^{2-}. The 1s orbital of hydrogen-bonded hydrogen is numbered as the 35th vacant orbital. b) i–k and i,j–k,l denote the singly and doubly excited reference configurations, respectively. c) The ionic structure, $[(O^+H^-O)^- + (OH^-O^+)]$ is also involved. d) The result for the case where the excitation energies of all the CT and σ–σ^* configurations are lowered by 1.0 eV in the CI treatment is listed in the column (with parentheses). e) Doubly excited configurations, i,j–k, 35. f) The ground reference configuration coincides with the ground state of M^{2-}. g) Singly excited configurations, i–k.

hydrogen bond corresponds to the transition from the nonbonding orbital to the antibonding orbital in the hydrogen bond. The 21—26 and 22—26 configurations are easily seen to have the CT character pertinent to the hydrogen bond. The energy levels of the CT configurations calculated for HM^- are $\approx$3 eV lower than those for the corresponding CT configurations of H_2M. As is illustrated in Fig. 3, the CT configuration 22—26 of HM^- interacts strongly with the 17—23 π–π^* configuration. Consequently, the first and fourth π–π^* excited states of HM^- turn out to be considerably rich in the CT character pertinent to the hydrogen bond.

The conclusion was further clarified by the configuration analysis for the first π–π^* excited state of HM^-; the result is tabulated in Table 4, together with the results for the ground and the second π–π^* excited (assigned to the 210.0 nm band) states. Because of the symmetrical hydrogen bond in HM^-, the CT structure corresponds to the antisymmetric covalent structure, $[(O\text{–}H\cdots O)^- - (O\cdots H\text{–}O)^-]$ and the antisymmetric ionic structure, $[(OH^-O^+)^- - (O^+H^-O)^-]$. As is shown in Table 4, the antisymmetric covalent and ionic structures contribute considerably ($\approx$32%) to the first π–π^* excited state, revealing that the first π–π^* excited state is rich in the CT character in the hydrogen bond. Table 4 shows also the result for the case where the excitation energies of all the CT and σ–σ^* configurations are lowered by 1.0 eV in the CI treatment. The result shows that the quantitative CT character is sensitive to

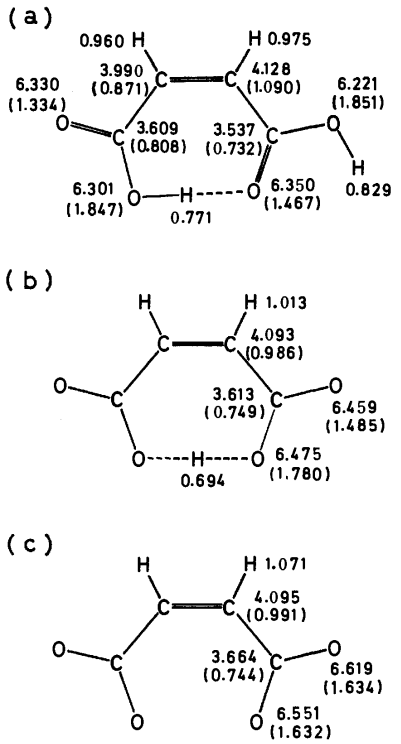

Fig. 5. Total and π-(in parentheses) electron densities calculated for the ground states of (a) H_2M, (b) HM^-, and (c) M^{2-}.

the relative position of the π-π^* (17—23) and CT (22—26) configurations; the CT character of the first π-π^* excited state increases to $\approx$50% by the energy lowering of the CT configuration.

The electron densities for the ground states of H_2M, HM^-, and M^{2-} are shown in Fig. 5. The excess formal charge in HM^- and M^{2-} is mainly distributed on the oxygen atoms.

References

1) C. A. Coulson, *Research (London)*, **10**, 149 (1957).
2) S. Bratož, "Advances in Quantum Chemistry," Vol. 3, ed by P.O. Löwdin, Academic Press, New York (1967), p. 209.
3) H. Tsubomura, *Bull. Chem. Soc. Jpn.*, **27**, 445 (1954); *J. Chem. Phys.*, **23**, 2130 (1955); *ibid.*, **24**, 927 (1956).
4) K. Nukasawa, J. Tanaka, and S. Nagakura, *J. Phys. Soc. Jpn.*, **8**, 792 (1953); S. Nagakura and M. Gouterman, *J. Chem. Phys.*, **26**, 881 (1957).
5) M. Weissmann and N. V. Cohan, *J. Chem. Phys.*, **43**, 119 (1965).
6) F. B. van Duijneveldt and J. N. Murrell, *J. Chem. Phys.*, **46**, 1759 (1967).
7) S. F. Darlow and W. Cochran, *Acta Crystallogr.*, **14**, 1250 (1961); S. F. Darlow, *ibid.*, **14**, 1257 (1961).
8) H. M. E. Cardwell, J. D. Dunitz, and L. E. Orgel, *J. Chem. Soc.*, **1953**, 3740.
9) R. Blinc, D. Hadži, and A. Novak, *Z. Electrochem.*, **64**, 566 (1960).
10) K. Nakamoto, Y. A. Sarma, and G. T. Behnke, *J. Chem. Phys.*, **42**, 1662 (1965).
11) S. Nagakura, *J. Chim. Phys.*, **61**, 217 (1964).
12) K. Morokuma, S. Iwata, and W. A. Lathan, "The World of Quantum Chemistry," ed by R. Daudel and B. Pullman, D. Reidel, Dordrecht, Holland (1974), p. 277.
13) H. Morita and S. Nagakura, *Theor. Chim. Acta*, **27**, 325 (1972).
14) H. Morita, K. Fuke, and S. Nagakura, *Bull. Chem. Soc. Jpn.*, **49**, 922 (1976).
15) H. Baba, S. Suzuki, and T. Takemura, *J. Chem. Phys.*, **50**, 2078 (1969).
16) "International Critical Tables," Vol. 1, National Research Council, McGraw-Hill, New York (1926), p. 84.
17) K. Kaya and S. Nagakura, *J. Mol. Spectrosc.*, **44**, 279 (1972).
18) M. Shahat, *Acta Crystallogr.*, **5**, 763 (1952).
19) H. Hosoya and S. Nagakura, *Spectrochim. Acta*, **17**, 324 (1961).

Vibration Spectra and Rotational Isomerism of Chain Molecules. V.[1] 2,5-Dioxahexane, 2,5-Dithiahexane, and 2-Oxa-5-thiahexane

Yoshiki OGAWA, Masahiro OHTA, Masaaki SAKAKIBARA, Hiroatsu MATSUURA, Issei HARADA, and Takehiko SHIMANOUCHI

Department of Chemistry, Faculty of Science, University of Tokyo, Hongo, Bunkyo-ku, Tokyo 113

(Received November 5, 1976)

The Raman and infrared spectra of 2,5-dioxahexane $CH_3OCH_2CH_2OCH_3$, 2,5-dithiahexane $CH_3SCH_2CH_2SCH_3$ and 2-oxa-5-thiahexane $CH_3OCH_2CH_2SCH_3$ were measured for the gaseous, liquid, glassy and crystalline states and were correlated with the normal-vibration calculations. The rotational isomerism was studied and the following conclusions were obtained. (1) The molecular form existing in the crystalline state is a non-extended form, in contrast with the cases of the unbranched ethers or sulfides containing one oxygen or sulfur atom which take the extended all-*trans* form. (2) Many forms coexist in the gaseous, liquid and glassy states. (3) The form existing in the crystalline state is the most stable in the liquid state. It was found that the repulsive force between non-bonded hydrogen atoms is one of the important factors influencing the conformational stabilities and for 2,5-dioxahexane the dipole-dipole interaction is another important factor. The stable conformations of these molecules were correlated with those of the polyether and polythioether chains. The stable isomers of 2-oxa-5-thiahexane could be explained on the basis of the knowledge of the conformational stabilities of the unbranched ethers and sulfides. The force constants of the ethers and sulfides were satisfactorily transferred to 2-oxa-5-thiahexane.

In previous papers,[1,2] we reported the vibration spectra and the rotational isomerism of the unbranched ethers and sulfides which contain one oxygen or sulfur atom, and obtained information on the conformational stability for these molecules. In the present paper, we extended our studies to 2,5-dioxahexane (ethylene glycol dimethyl ether) $CH_3OCH_2CH_2OCH_3$, 2,5-dithiahexane $CH_3SCH_2CH_2SCH_3$, and 2-oxa-5-thiahexane $CH_3OCH_2CH_2SCH_3$. The Raman and infrared spectra of these molecules in various states were analyzed and the rotational isomers existing in each state were determined on the basis of normal-vibration calculations.

The present results on the rotational isomerism will be discussed together with those previously obtained for the unbranched ethers and sulfides.[1-6] Discussions will also be made in relation to the stable conformations of polyethers[7,8] and polythioethers.[9]

Experimental

2,5-Dioxahexane was purchased from Tokyo Kasei Kogyo Co., Ltd. and was distilled prior to the measurements. 2,5-Dithiahexane was synthesized by the reaction

$$BrCH_2CH_2Br + 2CH_3SNa\ (aq) \xrightarrow{60\ ^\circ C,\ 6\ h} CH_3SCH_2CH_2SCH_3 + 2NaBr.$$

After the organic layer was dried over anhydrous sodium sulfate, 2,5-dithiahexane was obtained by the distillation under reduced pressure. 2-Oxa-5-thiahexane was synthesized by the following reactions

$$2HOCH_2CH_2Cl + (CH_3)_2SO_4 \xrightarrow[120\ ^\circ C,\ 5\ h]{CaCO_3} 2CH_3OCH_2CH_2Cl + H_2SO_4$$

and

$$CH_3OCH_2CH_2Cl + CH_3SNa\ (aq) \xrightarrow[60\ ^\circ C,\ 30\ h]{NaOH} CH_3OCH_2CH_2SCH_3 + NaCl.$$

After the organic layer was dried over anhydrous sodium sulfate, 2-oxa-5-thiahexane was obtained by the distillation (bp 134—135 °C).

The Raman and infrared spectra were measured for the gaseous, liquid, glassy, and crystalline states by the methods reported previously.[1,2] The glassy state for the Raman measurements was obtained by putting into liquid nitrogen the sample enclosed in an ampoule and cooling it rapidly, and that for the infrared measurements by depositing the sample onto a cooled window of KBr or KRS-5.

Normal Coordinate Treatment

Normal coordinate treatment was carried out with a computer program NCTB2[10] and a HITAC 8700/8800 computer system at the Computer Center of the University of Tokyo. The data of 2,5-dioxahexane and 2,5-dithiahexane were included in the least-squares refinement of the force constants of the unbranched ethers and sulfides.[1,2]

For 2-oxa-5-thiahexane, the force constants were transferred from the unbranched ethers and sulfides[1,2] except those for the OCH_2CH_2S part. The force constants for this part were initially transferred from the OCH_2CH_2O part and the stable forms of the rotational isomers were determined. The nine important force constants, the CC stretching and methylene-methylene interactions, were subsequently refined by the least-squares method from 56 Raman and infrared frequencies.

Detailed results of the calculations and the force constants are reported in a separate paper.[10]

Results

Figures 1—10 show the Raman and infrared spectra obtained. The observed frequencies and the vibrational assignments based on the calculated potential-energy distributions are listed in Tables 1—3. The observed spectra were analyzed with reference to the results of the normal coordinate treatment.

In the following subsections, the rotational isomerism

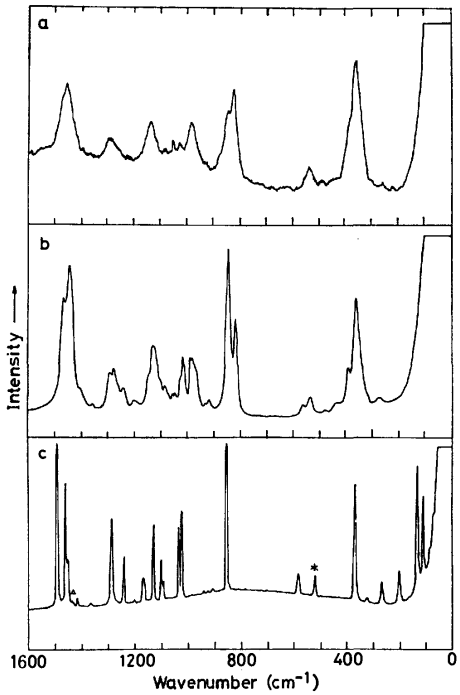

Fig. 1. Raman spectra of 2,5-dioxahexane.
a: Gas (60 °C), b: liquid (room temperature), c: crystal (liquid nitrogen temperature).
Following symbols are used in Figs. 1—10.
*: Emission line of Ar^+, □: librational infrared band of H_2O, ×: impurity, △: origin unknown.

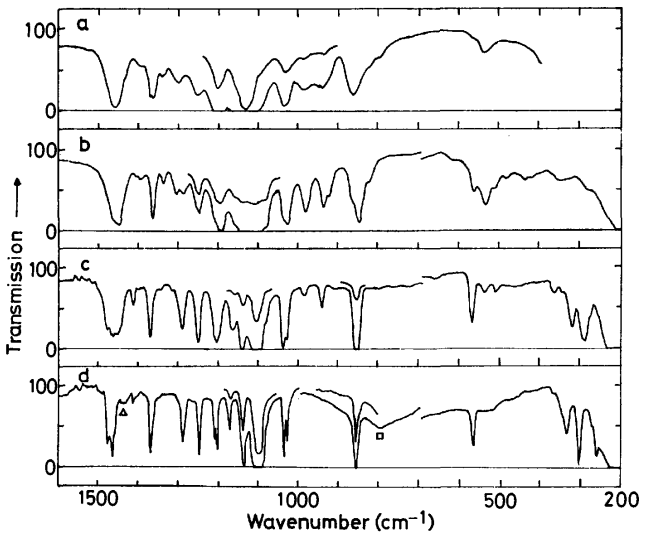

Fig. 2. Infrared spectra of 2,5-dioxahexane.
a: Gas (room temperature), b: liquid (room temperature), c: glass, d: crystal.
The symbols are explained in the caption of Fig. 1.

of the individual molecules is described.

2,5-Dioxahexane $CH_3OCH_2CH_2OCH_3$. Since this molecule has two C–O axes and one C–C axis associated with the rotational isomerism, there are ten possible rotational isomers as given in Table 1 of Part I of this series.[2] Of these, the GG'G form is rejected, because the distance between the two terminal methyl groups is too short for this form to be stable. However, the TGG' and GGG' forms are not simply ruled out, since the

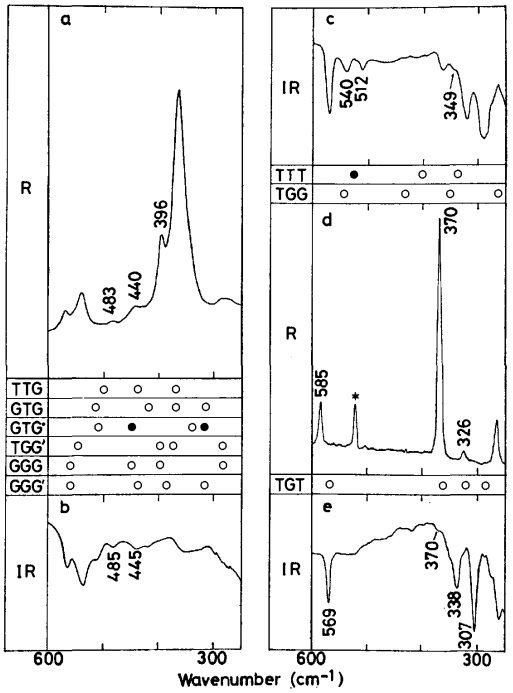

Fig. 3. Comparison of the observed and calculated frequencies of 2,5-dioxahexane in the 600—250 cm^{-1} region.
a: Liquid (R), b: liquid (IR), c: glass (IR), d: crystal (R), e: crystal (IR).
The symbol is explained in the caption of Fig. 1. For the forms which have the center of symmetry, the open and filled circles denote the Raman and infrared active vibrations, respectively.

steric hindrance in the GG' sequence of the OC–C–OC part is expected to be smaller than that in the former case. The observed and calculated frequencies in the 600—250 cm^{-1} region are compared in Fig. 3.

A comparison between the observed spectra and the calculated frequencies indicates that the TGT form exists in the crystalline state. It should be noted that some of the low-frequency vibrations give frequencies depending to some extent on the state and the spectroscopic measurement. Namely, the infrared bands at 338 and 307 cm^{-1} in the crystalline state correspond to the infrared bands at 325 and 295 cm^{-1}, respectively, in the glassy state and the Raman bands at 585 and 326 cm^{-1} in the crystalline state correspond to the infrared bands at 569 and 338 cm^{-1}, respectively.

The infrared spectrum in the glassy state shows that the TGT, TTT, and TGG forms coexist in this state. The glassy state for Raman measurements could not be obtained, since the liquid sample enclosed in an ampoule cell turns quickly into crystal even when it is put into liquid nitrogen for rapid cooling. In the glassy-state infrared spectrum, many bands appear in addition to the bands which have been assigned to the TGT form. Of these, the infrared band at 512 cm^{-1} is also observed in the infrared spectrum of the liquid state, but not observed in the Raman spectrum of this state. On the other hand, the Raman band observed at 396 cm^{-1} in the liquid state is missing in the infrared spectrum of this state. These bands are reasonably assigned to the

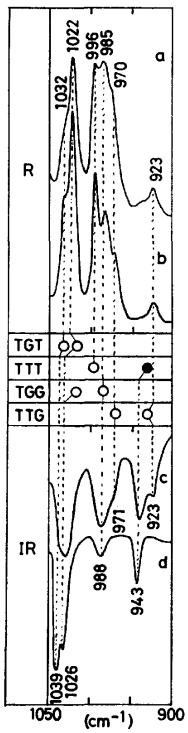

Fig. 4. Liquid-state Raman spectra at room and lower temperatures and liquid- and glassy-state infrared spectra of 2,5-dioxahexane in the 1050—900 cm^{-1} region.
a: Liquid (R, room temperature), b: liquid (R, −60°C), c: liquid (IR, room temperature), d: glass (IR, near liquid nitrogen temperature).
For the TTT form, the open and filled circles denote the Raman and infrared active vibrations, respectively.

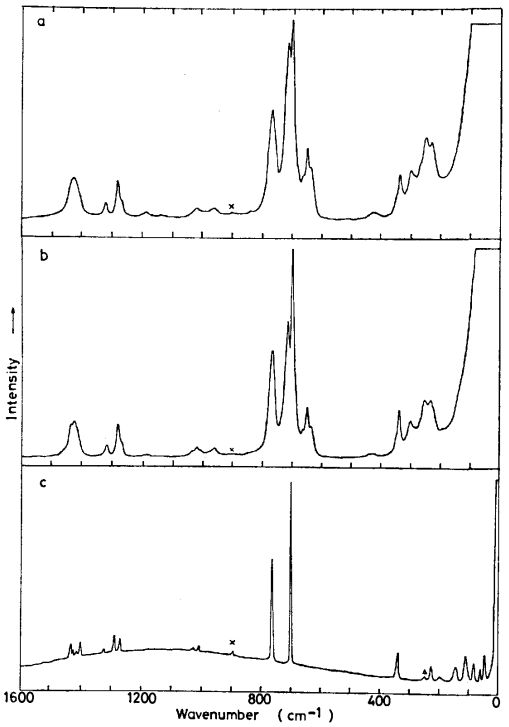

Fig. 5. Raman spectra of 2,5-dithiahexane.
a: Liquid (80 °C), b: liquid (room temperature), c: crystal (liquid nitrogen temperature).
The symbols are explained in the caption of Fig. 1.

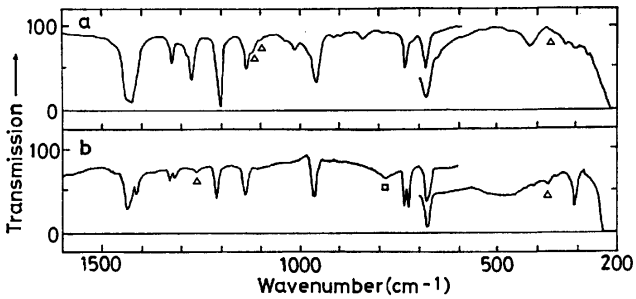

Fig. 6. Infrared spectra of 2,5-dithiahexane.
a: Liquid (room temperature), b: crystal.
The symbols are explained in the caption of Fig. 1.

TTT form which has the center of symmetry. Other additional frequencies such as 540 and 349 cm^{-1} are well explained by the calculated frequencies of the TGG form.

In the liquid state, the observed spectra are explained by the coexistence of the TGT, TTT, TGG, and TTG forms. The Raman bands at 483 and 440 cm^{-1} and the corresponding infrared bands at 485 and 445 cm^{-1} appear in the liquid state. These frequencies agree well with the calculated frequencies of the TTG form. The existence of other forms is not proved, since their frequencies and the Raman and infrared activities are not consistent between the calculated results and the spectral observations.

The liquid-state Raman spectra at room and lower temperatures and the liquid- and glassy-state infrared spectra in the 1050—900 cm^{-1} region are shown in Fig. 4. These spectra also prove the coexistence of the TGT, TTT, and TGG forms in the glassy state and of the TGT, TTT, TGG, and TTG forms in the liquid state. The Raman bands at 1032 and 1022 cm^{-1} and the infrared bands at 1039 and 1026 cm^{-1} in the glassy state are assigned to the TGT form, the Raman band at 996 cm^{-1} and the infrared band at 943 cm^{-1} in the glassy state to the TTT form, the Raman band at 985 cm^{-1} and the infrared band at 988 cm^{-1} to the TGG form, and the Raman bands at 970 and 923 cm^{-1} and the additional infrared bands at 971 and 923 cm^{-1} in the liquid state to the TTG form. The temperature dependence of the liquid-state Raman spectra and the non-existence of the TTG form in the glassy state near the liquid nitrogen temperature indicate that the rotational isomers become less stable in the order of the TGT, TTT, TGG, and TTG forms.

In the gaseous state, the spectra have essentially the same number of bands as in the liquid state (Figs. 1 and 2). However, in contrast with the liquid-state spectra, the Raman intensity of the 822 cm^{-1} band is stronger than that of the 848 cm^{-1} band in the gaseous state. The infrared intensity of the 868 cm^{-1} band, which is observed as a shoulder of the 852 cm^{-1} band in the liquid state, increases in the gaseous state. These spectral changes are related to the polarity of the molecules as will be mentioned later. The gaseous-state spectra are explained by the coexistence of the TGT,

TABLE 1. OBSERVED FREQUENCIES AND VIBRATIONAL ASSIGNMENTS OF 2,5-DIOXAHEXANE

Observed frequency (cm^{-1})[a]							
Gas		Liquid		Glass	Crystal		Assignment[b]
R	IR	R	IR	IR	R	IR	
			1490 VW, sh	1485 W, sh	1492 VS		CH_2 scis
		1470 M, b	1479 W, sh	1478 M	1472 VW	1475 M	CH_2 scis
			1468 M, sh	1468 M		1464 S	CH_3 ip-d-deform
			1460 M, sh	1462 M	1461 S		CH_3 ip-d-deform
1460 M, vb	1460 M, vb			1459 M, sh		1458 M, sh	CH_3 s-deform
			1459 M	1457 M	1453 W, sh		CH_3 s-deform
		1450 VS, b	1451 M, sh	1451 M, sh		1450 VW, sh	CH_3 op-d-deform
			1439 W, sh	1440 W, sh	1438 VW	1435 VW	Origin unknown
		1410 VW, sh	1407 VW	1415 W	1417 VW	1411 VW	CH_2 wag (**TGT**, TTT)
	1396 VW, b						
		1395 VW, sh	1393 VW				CH_2 wag (TGG, TTG)
	1372 W						CH_2 wag (**TGG**)
	1365 W	1365 VW	1365 M	1370 M	1370 VW	1366 S	CH_2 wag (**TGT**)
	1340 VW		1338 VW	1347 VW			CH_2 wag (**TTT**, TTG)
1309 W		1301 W	1306 W	1313 VW			CH_2 twist (**TGG**, TTG)
1285 W	1300 W, b	1285 W	1286 W	1290 M	1288 M	1286 M	CH_2 twist (**TGT**)
1270 VW, sh		1270 VW, sh					CH_2 twist (TTT, TTG)
			1256 W, sh				CH_2 twist (**TGG**)
1255 VW, sh	1256 W	1250 VW	1247 M	1250 S	1244 W	1247 S	CH_2 twist (**TGT**)
	1204 M	1208 VW	1210 S, sh	1204 S	1202 VW	{1208 M 1202 S	CH_3 ip-rock (**TGT**, TTT, TGG, TTG)
	1192 W, sh	1195 VW, sh	1195 VS				CH_3 ip-rock (**TGG**)
						1174 W	CH_3 op-rock (**TGT**, TTT, TGG, TTG)
1160 VW, sh	1155 W, sh	1155 VW, sh	1160 S, sh	1164 M	1171 W		
						1171 W	CH_3 op-rock (**TGT**, TTT, TGG, TTG)
1145 W	1142 VS, sh	1138 W	1140 VS, sh				CC stretch (**TTG**, TTT)
				1140 VS			
1125 VW, sh	1132 VS	1131 W	1130 VS, sh		1131 M	1137 S	CC stretch (**TGT**, TGG)
	1118 VS, sh		1122 VS, sh	1122 W, sh			CO stretch (**TTT**)
	1108 M, sh	1108 VW, sh	1106 VS	1106 VS			CH_2 rock (**TGG**, TTG)
	1095 M, sh	1092 VW	1092 S, sh		{1102 W 1095 VW	1100 VS	CO stretch (**TGT**)
	1080 W, sh	1078 VW, sh	1080 M, sh	1080 W, sh		1080 W	CH_2 rock (**TGT**, TTT), CO stretch (TTG)
		1063 VW					CO stretch (**TTT**)
1058 VW		1053 VW	1055 VW, sh				CO stretch (TGG, TTG)
	1038 M, b						
1035 VW		1032 VW, sh	1037 M, sh	1039 S	1036 M	1037 M	CO stretch (**TGT**)
1020 VW		1022 W	1028 S	1026 M	1026 M	1028 M	CO stretch (**TGT**, **TGG**)
		996 W					CO stretch (**TTT**)
990 M, b	990 W, b	985 W	985 M	988 VW			CO stretch (**TGG**)
		970 W, sh	971 W, sh				CO stretch (**TTG**)
	940 W		938 M	943 VW			CO stretch (**TTT**)
		936 VW					(365 cm^{-1}+ 568 cm^{-1})
		923 VW	923 W				CO stretch (**TTG**)
	868 M		868 M, sh				CO stretch (**TGG**)
848 M	852 W, sh	848 VS	852 S	858 VS	857 VS	858 VS	CO stretch (**TGT**), CH_2 rock (**TGT**, TGG)

Table 1. (Continued)

Observed frequency (cm^{-1})[a]							Assignment[b]
Gas		Liquid		Glass	Crystal		
R	IR	R	IR	IR	R	IR	
822 M	823 W, sh	822 W	823 W	822 VW			CH_2 rock (**TTG**, TTT)
565 VW, sh		568 VW	568 VW	571 VW	585 VW	569 VW	OCC deform (**TGT**)
540 VW	540 VW, b	540 W	539 VW	540 VW			OCC deform (**TGG**)
			513 VW	512 VW			COC bend (**TTT**)
490 VW		483 VW	485 VW				COC bend (**TTG**)
451 VW		440 VW	445 VW				OCC deform (**TTG**)
425 VW, sh		420 VW, sh	420 VW				COC bend (**TGG**)
390 M, sh		396 W					OCC deform (**TTT**)
365 VS		365 S	360 VW	368 VW	370 M	370 VW	COC bend (**TGT**, TTG)
		352 W, sh	352 VW, sh	349 VW			COC bend (**TGG**)
		326 VW, sh		325 VW	326 VW	338 VW	COC bend (**TGT**)
		280 VW, b		295 VW		307 VW	OCC deform (**TGT**)
				275 VW, sh			OCC deform (**TGG**)
					267 VW	262 VW	
					205 W		Torsions (**TGT**) and lattice vibrations
					136 S		
					115 S		
					90 VW		
					76 VW		

a) VS: very strong, S: strong, M: medium, W: weak, VW: very weak, vb: very broad, b: broad, sh: shoulder. The broadness of the band shapes in the gaseous state does not always allow us to correlate the individual bands in the liquid state to those in the gaseous state. Only approximate correlations are made in such cases and in other cases of similar situations. b) The band is assigned preferentially to the isomer(s) given by boldface. For the notation and definition of the local symmetry coordinates, see Ref. 11.

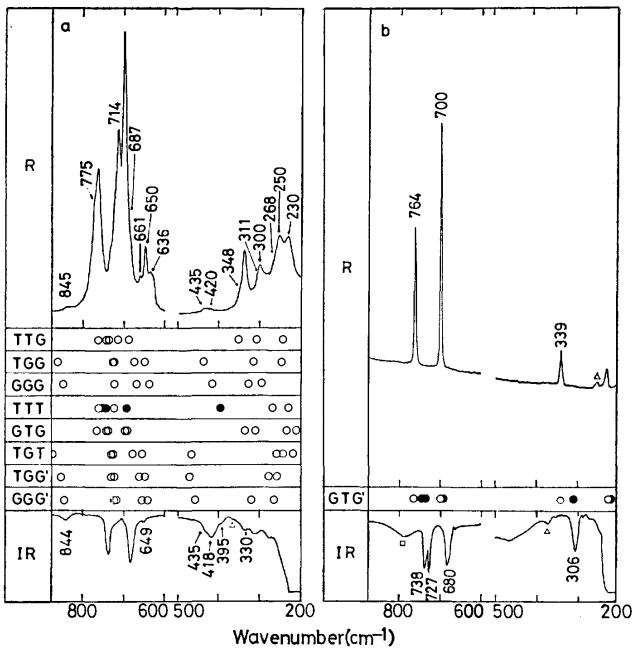

Fig. 7. Comparison of the observed and calculated frequencies of 2,5-dithiahexane in the 875—200 cm^{-1} region.
a: Liquid, b: crystal.
The symbols are explained in the caption of Fig. 1. For the forms which have the center of symmetry, the open and filled circles denote the Raman and infrared active vibrations, respectively.

TTT, TGG, and TTG forms similar to the liquid state.

2,5-Dithiahexane $CH_3SCH_2CH_2SCH_3$. This molecule has ten possible rotational isomers like the case of 2,5-dioxahexane. Of these, the GG'G form is rejected because of the reason stated for 2,5-dioxahexane. The observed and calculated frequencies in the 900—200 cm^{-1} region are shown in Fig. 7.

In the crystalline state, the Raman and infrared spectra are quite different from each other and the mutual exclusion rule holds as shown in Fig. 7. The TTT and GTG' forms are the possible candidates, since they possess the center of symmetry. Figure 7 shows that the calculated frequencies of the GTG' form are in good agreement with the observed frequencies of the crystalline state. The Raman and infrared activities expected for each vibration of this molecular form are also consistent with the spectral observations.

In the liquid state, the observed spectra are explained by the coexistence of the GTG', TTT, TTG, TGG, and GGG forms. Many bands appear in this state in addition to those existing in the crystalline state. As seen from Fig. 7, the Raman band at 268 cm^{-1} and the infrared band at 395 cm^{-1} are assigned to the TTT form, the Raman bands at 714, 348, and 300 cm^{-1} to the TTG form, the Raman bands at 650, 435 and 250 cm^{-1} and the infrared band at 435 cm^{-1} to the TGG form, and the Raman bands at 636 and 420 cm^{-1} and the infrared bands at 418 and 330 cm^{-1} to the GGG form.

The existence of the GTG form is uncertain, since all of its calculated frequencies are almost coincident

TABLE 2. OBSERVED FREQUENCIES AND VIBRATIONAL ASSIGNMENTS OF 2,5-DITHIAHEXANE

Observed frequency (cm^{-1})[a]				Assignment[b]
Liquid		Crystal		
R	IR	R	IR	
			1437 VS	CH_3 ip-d-deform
1439 VW, sh	1436 VS, sh	1436 VW, sh		CH_3 ip-d-deform
			1432 VS, sh	CH_3 op-d-deform
1428 VW	1432 VS	1432 VW		CH_3 op-d-deform
		1425 VW		
	1425 VS		1424 M, sh	CH_2 scis
			1412 M	
1415 VW, sh		1415 VW		CH_2 scis
		1402 VW		
		1325 VW		CH_3 s-deform
1322 VW	1323 W		1326 VW	CH_3 s-deform, CH_2 wag (TGG, GGG)
			1316 VW	
		1290 VW		CH_2 twist (**GTG′**, TTT)
1284 VW	1286 W, sh			CH_2 twist (**TTG**)
		1270 VW		CH_2 wag (**GTG′**, TTT)
1270 VW, sh	1272 S			CH_2 wag (TTG), CH_2 twist (TGG, GGG)
			1262 VW	Origin unknown
	1206 VS		1210 S	CH_2 wag (**GTG′**, TTT)
1209 VW				CH_2 wag (**GTG**)
1190 VW				CH_2 wag (**TTG**)
1181 VW	1181 VW, sh			CH_2 wag (TGG, GGG)
	1134 M		1136 M	CH_2 twist (**GTG′**, TTT)
1135 VW				CH_2 twist (TTG, TGG, GGG)
	1120 W, sh			Origin unknown
	1096 VW, sh			Origin unknown
1045 VW, sh				CC stretch (**TTT**)
1036 VW, sh	1034 VW, sh			CC stretch (**TTG**)
		1026 VW		CC stretch (**GTG′**)
1024 VW		1010 VW		
	1024 VW, sh			CC stretch (**TGG**)
1010 VW	1010 W			CC stretch (**GGG**)
976 VW, sh	976 W, sh			CH_2 rock (TTG, TTT), CH_3 ip-rock (TGG, GGG)
			968 S	CH_3 ip-rock (**GTG′**, TTG, TTT)
970 VW, sh		965 VW		CH_3 ip-rock (**GTG′**, TTG, TGG, GGG, TTT)
	960 S			
960 VW			964 S	CH_3 op-rock (**GTG′**, TTG, TGG, GGG, TTT)
		958 VW		CH_3 op-rock (**GTG′**, TTG, TGG, GGG, TTT)
	915 VW			CH_2 rock (**GGG**)
845 VW	844 VW			CH_2 rock (TGG, GGG)
775 VW, sh				CS stretch (**TTG**)
765 M		764 M, sh		CS stretch (**GTG′**, TTT), CH_2 rock (TTT)
			738 S	CS stretch (**GTG′**, TTT), CH_2 rock (TTG)
	736 M			
735 W, sh				CS stretch (**TTG**)
			727 S	CH_2 rock (**GTG′**)
	727 VW, sh			
725 M, sh				CS stretch (TGG, GGG, TTT)
714 S				CS stretch (**TTG**)
700 VS		700 VS		CS stretch (**GTG′**)
687 W, sh				CS stretch (**TTG**)
	684 M			
			680 S	CS stretch (**GTG′**, TTT)
661 VW				CS stretch (TGG, GGG)
650 W	649 VW			CS stretch (**TGG**)
636 VW				CS stretch (**GGG**)
435 VW	435 VW			SCC deform (**TGG**)
420 VW	418 VW			SCC deform (**GGG**)
	395 VW, sh			CSC bend (**TTT**)
	372 VW, sh		372 VW	Origin unknown
348 VW, sh				CSC bend (**TTG**)

Table 2. (Continued)

Observed frequency (cm^{-1})[a]				Assignment[b]
Liquid		Crystal		
R	IR	R	IR	
		339 VW		CSC bend (**GTG'**)
339 VW	330 VW			CSC bend (**GGG**)
311 VW, sh	309 VW			CSC bend (**TGG**)
			306 VW	CSC bend (**GTG'**)
300 VW				CSC bend (**TTG**)
295 VW, sh	278 VW			CSC bend (**GGG**)
268 VW, sh				SCC deform (**TTT**)
250 W				CSC bend (**TGG**)
		250 VW		Origin unknown
245 VW, sh				SCC deform (**TTG**)
230 W		228 W		SCC deform (**GTG'**), CSC bend (TTT)
		199 VW		
		145 VW		
		112 VW		
		105 VW, sh		Torsions (**GTG'**) and lattice vibrations
		84 VW		
		61 VW		
		46 VW		

a), b) See a) and b), respectively, of Table 1.

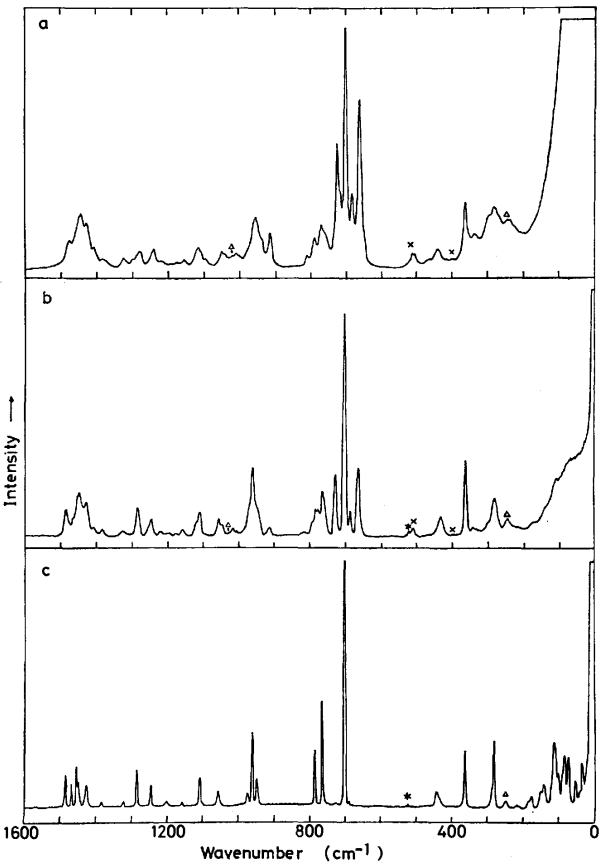

Fig. 8. Raman spectra of 2-oxa-5-thiahexane.
a: Liquid (room temperature), b: glass (liquid nitrogen temperature), c: crystal (liquid nitrogen temperature). The symbols are explained in the caption of Fig. 1.

with those of the GTG' form. However, the existence of the GTG form may not be ruled out, since the spacial

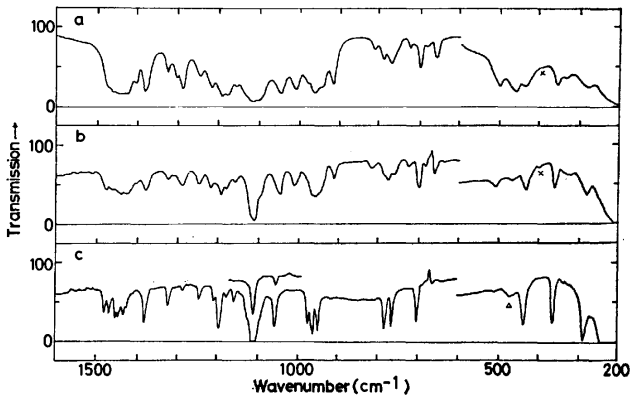

Fig. 9. Infrared spectra of 2-oxa-5-thiahexane.
a: Liquid (room temperature), b: glass, c: crystal. The symbols are explained in the caption of Fig. 1.

steric repulsions in this form are not much larger than those in the GTG' form. It is not probable that the TGT, TGG', and GGG' forms exist in the liquid state, since no bands are observed around their characteristic frequencies in the region 460—475 cm^{-1}.

As temperature is lowered in the liquid state, the Raman intensities of the bands assigned to the GTG' form increase relative to those of other bands (Fig. 5). Thus the GTG' form is found to be the most stable in the liquid state.

2-Oxa-5-thiahexane $CH_3OCH_2CH_2SCH_3$. This molecule has fourteen possible rotational isomers as listed in Table 1 of Part I of this series.[2] The existence of the GG'G form can be again rejected because of the very large steric hindrance. Figure 10 shows the observed and calculated frequencies in the 1000—200 cm^{-1} region.

The spectra in the crystalline state show that the

TABLE 3. OBSERVED FREQUENCIES AND VIBRATIONAL ASSIGNMENTS OF 2-OXA-5-THIAHEXANE

Observed frequency (cm^{-1})[a]						Assignment[b]
Liquid		Glass		Crystal		
R	IR	R	IR	R	IR	
1480 VW	1480 S, sh	1484 W	1477 W	1484 VW	1480 W	CH_2 scis
1465 VW, sh	1465 S, sh	1465 VW, sh	1465 VW	1466 VW	1467 W	CH_3 ip-d-deform
1455 W, sh	1460 VS	1460 VW, sh	1460 W	1453 VW	1453 W	CH_3 s-deform
	1455 VS, sh	1449 W	1449 W, sh	1450 VW, sh	1449 W	CH_3 op-d-deform
1449 M	1449 VS	1444 W, sh	1444 W	1444 VW, sh	1444 VW, sh	CH_3 ip-d-deform
1431 M	1432 VS	1427 VW	1435 W	1431 VW, sh	1432 W	CH_3 op-d-deform
	1420 S, sh		1420 W, sh	1426 VW	1424 VW	CH_2 scis
1410 W	1405 S	1405 VW, sh	1405 VW, sh			CH_2 wag (TGG, TGT)
1390 VW	1382 S	1380 W	1380 W	1383 VW	1381 M	CH_2 wag (**TTG**, TTT)
1375 VW, sh	1373 M, sh		1373 VW, sh			CH_2 wag (GTG or GTG′)
1327 VW	1325 M	1324 VW	1324 W	1322 VW	1321 W	CH_3 s-deform (**TTG**, TGG, TGT, TTT)
1305 VW	1304 M	1301 VW	1307 VW			CH_2 twist (GTG or GTG′)
1290 VW, sh	1290 S	1290 VW, sh	1290 W			CH_2 twist (TGG, TGT)
1283 VW	1281 W, sh	1283 VW	1283 W, sh	1284 W	1286 VW	CH_2 twist (**TTG**, TTT)
1255 VW, sh	1247 M	1249 VW	1246 W			CH_2 wag (**TGG**)
1245 VW				1245 VW	1246 VW	CH_2 wag (**TTG**, TGT, TTT)
1215 VW, sh	1218 S	1218 VW	1218 M	1208 VW, sh	1209 VW	CH_2 twist (**TTG**, TTT), CH_3 ip-rock (TGG, TGT)
1190 VW, sh	1196 VS	1195 VW	1193 M	1198 VW	1196 M	CH_3 ip-rock (**TTG**, TTT)
1180 VW	1180 VS	1176 VW	1178 W			CH_2 twist (TGG, TGT)
1158 VW	1156 VS	1158 VW	1156 W	1160 VW	1158 W	CH_3 op-rock (**TTG**, TTT)
1130 VW, sh	1135 VS		1135 W, sh			CH_3 op-rock (TGG, TGT)
1120 VW	1122 VS	1120 VW, sh	1120 S, sh			CO stretch (TGG, TGT, TTT)
1110 VW, sh	1113 VS	1110 VW	1110 VS	1107 VW	1111 VS	CO stretch (**TTG**)
1100 VW, sh	1098 S	1096 VW, sh	1092 M, sh			CO stretch (GTG or GTG′)
1055 VW	1055 M, sh	1055 VW	1055 W, sh	1056 VW	1055 M	CC stretch (**TTG**, TGT, TTT)
1045 VW, sh	1046 S	1045 VW	1047 M			CC stretch (**TGG**)
1028 VW, sh		1028 VW, sh				Origin unknown
1015 VW	1012 S	1015 VW	1013 M			CH_2 rock (**TGT**)
1005 VW, sh	1000 M, sh	1005 VW	1005 M, sh			CH_2 rock (**TGG**)
980 VW, sh	980 S, sh	980 VW, sh	980 M, sh	974 VW	973 M	CH_2 rock (**TTG**, TTT)
968 VW, sh	968 S	968 VW, sh	970 M, sh			CH_3 ip-rock (TGT), CO stretch (TTT)
	964 S		964 S		962 M, sh	CO stretch (**TTG**, TGT), CH_3 ip-rock (TGG, TTT)
961 VW		959 W		961 M		
	959 S		956 S		960 M	CH_3 ip-rock (**TTG**, TGT, TTT), CO strech (TGG)
945 VW, sh	945 S	945 VW, sh	945 M, sh	948 VW	948 M	CH_3 op-rock (**TTG**, TGG)
920 W	918 S	914 VW	915 W			CO stretch (GTG or GTG′)
815 VW	814 VW	818 VW	816 VW			CH_2 rock (TGT, TTT)
793 VW	792 W	793 VW, sh	792 W, sh	785 W	783 M	CH_2 rock (**TTG**, TGG)
778 VW, sh	773 W	778 VW	778 W			CS stretch (GTG or GTG′)
765 VW, sh	760 VW, sh	762 VW	760 W	764 M	764 M	CS stretch (**TTG**)
758 VW, sh		758 VW, sh				CS stretch (**TTT**)
729 S	727 VW	728 W	726 VW			CS stretch (TGG, TGT)
720 VW	720 VW, sh	720 VW, sh	719 VW, sh			CS stretch (**TTT**)
703 VS	702 W	702 VS	700 W	701 VS	701 M	CS stretch (**TTG**)
685 W	682 VW	687 VW	683 VW			CS stretch (**TGT**)
664 S	661 W	665 W	660 VW			CS stretch (**TGG**)
520 VW	520 VW, sh	520 VW	519 VW, sh			OCC deform (**TGT**)
509 VW	503 VW	509 VW	509 VW			OCC deform (**TGG**)
468 VW	464 VW	470 VW	465 VW			COC bend (**TTT**)
441 VW	438 VW	435 VW	433 VW	441 VW	436 VW	COC bend (**TTG**)
363 W	359 VW	364 W	360 VW	363 W	363 VW	OCC deform (**TTG**)
340 VW, sh	340 VW	340 VW, sh	340 VW, sh			OCC deform (**TTT**)
335 VW	335 VW, sh	335 VW	335 VW			COC bend (TGG, TGT), CSC bend (TGG)

Table 3. (Continued)

Observed frequency (cm^{-1})[a]						Assignment[b]
Liquid		Glass		Crystal		
R	IR	R	IR	R	IR	
303 VW	300 VW, sh	303 VW, sh	300 VW, sh			CSC bend (GTG or GTG')
290 VW, sh	285 VW	285 VW	280 VW			CSC bend (**TGT**)
281 W				281 W	285 VW	CSC bend (**TTG**)
265 VW, sh						CSC bend (**TTT**)
243 W		245 VW		248 VW		Origin unknown
228 VW, sh						CH_3 torsion (TGG, TGT, TTT)
				218 VW		SCC deform (**TTG**), torsions (**TTG**) and lattice vibrations
				184 VW, sh		
				176 VW		
				152 VW, sh		
				144 VW		
				113 W		
				103 VW, sh		
				90 VW, sh		
				85 W		
				73 W		
				54 VW		
				33 VW		

a), b) See a) and b), respectively, of Table 1.

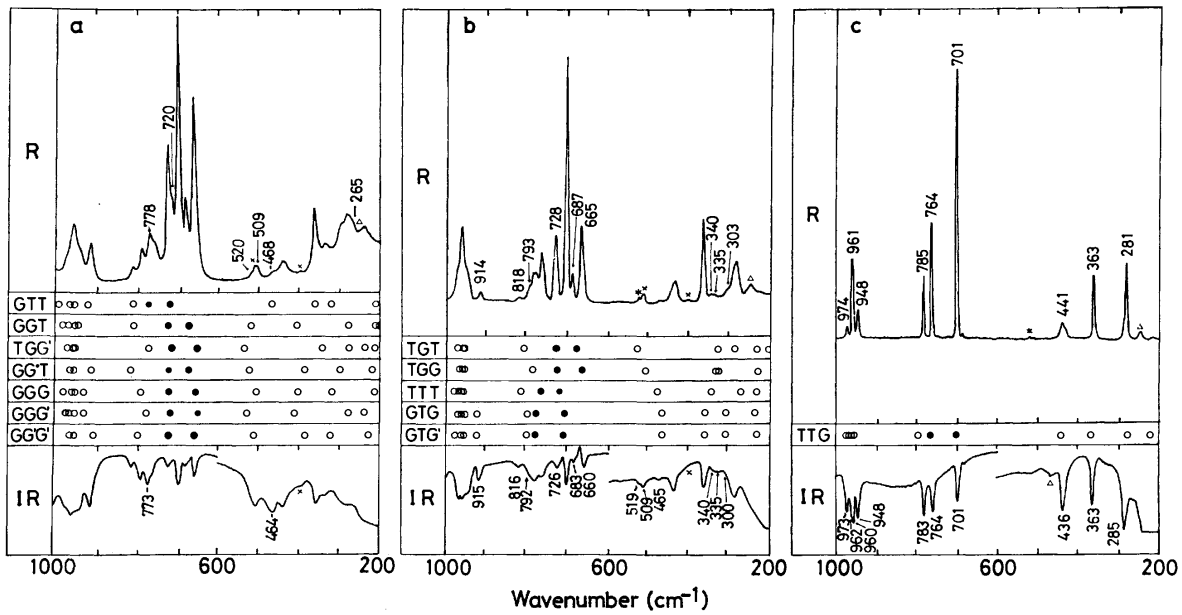

Fig. 10. Comparison of the observed and calculated frequencies of 2-oxa-5-thiahexane in the 1000—200 cm^{-1} region.
a: Liquid, b: glass, c: crystal.
The symbols are explained in the caption of Fig. 1. The filled circles denote the CS stretching vibrations.

TTG form exists. In the liquid state, the spectra have essentially the same number of bands as in the glassy state. The glassy- and liquid-state spectra are explained by the coexistence of the TTG, TTT, TGT, and TGG forms. One or both of the GTG and GTG' forms also exist in these states. In the liquid and glassy states, many bands appear in addition to those existing in the crystalline state. Of these bands observed in the liquid state, the Raman bands at 720, 468, and 265 cm^{-1} and the infrared band at 464 cm^{-1} are assigned to the TTT form, the Raman bands at 687 and 520 cm^{-1} and the infrared bands at 683 and 519 cm^{-1} to the TGT form, the Raman bands at 665 and 509 cm^{-1} and the infrared bands at 660 and 509 cm^{-1} to the TGG form, and the Raman bands at 914 and 303 cm^{-1} and the infrared bands at 915 and 300 cm^{-1} to one or both of the GTG and GTG' forms.

Each of the GGT, GGG, GG'T, GGG', and GG'G' forms has a characteristic frequency in the region 385—410 cm^{-1}. The weak Raman band at 400 cm^{-1} and the

TABLE 4. ROTATIONAL ISOMERISM OF THE MOLECULES TREATED IN THIS WORK

	$CH_3OCH_2CH_2OCH_3$	$CH_3SCH_2CH_2SCH_3$	$CH_3OCH_2CH_2SCH_3$
Gas	**TGT TTT TGG TTG**	—[a]	—[a]
Liquid	**TGT TTT TGG TTG**	**GTG′ TTG TGG GGG TTT** GTG	**TTG TGT TGG TTT** GTG or GTG′ (GTT) (GGT) (TGG′) (GG′T) (GGG) (GGG′) (GG′G′)
Glass	**TGT TTT TGG**	—[a]	**TTG TGT TGG TTT** GTG or GTG′ (GTT) (GGT) (TGG′) (GG′T) (GGG) (GGG′) (GG′G′)
Crystal	**TGT**	**GTG′**	**TTG**

The isomers given by boldface are confirmed to exist. The existence of the isomers in parentheses is uncertain. For more details, see text. a) Spectral measurements were not made.

weak infrared band at 395 cm^{-1} are observed in the liquid-state spectra. However, these bands are attributed at least in part, to an impurity, because the Raman intensity of this band in the liquid state of the distillate with bp 135—136 °C is much stronger than that of the distillate with bp 134—135 °C. Since these bands are much weaker than those assigned to the TTG, TTT, TGT, TGG, and GTG or GTG′ forms, the populations of the GGT, GGG, GG′T, GGG′, and GG′G′ forms, if they exist, are much smaller than those of the former ones. The existence of the GTT and TGG′ forms is uncertain, since all of their calculated frequencies are almost coincident with those of the other forms mentioned above.

As temperature is lowered in the liquid state, the Raman intensities of the bands assigned to the TTG form increase relative to those of the bands assigned to the other forms. Accordingly, the TTG form is the most stable in the liquid state.

Rotational Isomerism. In Table 4, the rotational isomerism of the three compounds treated in this work is summerized.

The vibration spectra of 2,5-dioxahexane have been studied by several investigators.[3-5] Snyder and Zerbi[4] concluded that the TGT form exists in the crystalline state and the TGT, TTT, and other forms in the glassy and liquid states. Iwamoto[5] indicated the existence of the TGG and TTG forms in addition to that of the TGT and TTT forms in the liquid state on the basis of the comparison of the infrared spectra of pure liquid, liquid containing $HgCl_2$ and crystalline complex with $HgCl_2$. In the present work, these conclusions were further confirmed and the relative stabilities among the rotational isomers were determined.

The rotational isomerism of 2,5-dithiahexane has been discussed by Hayashi *et al.*[6] They found that the GTG′ form exists in the crystalline state and the GTG′ and GGG forms in the liquid state. The present work shows that in addition to these two forms the TTT, TTG, and TGG forms also exist in the liquid state. The isomerism of 2-oxa-5-thiahexane has first been studied in the present work.

The following results were obtained for the three compounds studied in this work in common. (1) The molecular form existing in the crystalline state is a non-extended form, in contrast with the cases of the unbranched ethers or sulfides containing one oxygen or sulfur atom which take the extended all-*trans* form.[1,2] (2) Many forms coexist in the gaseous, liquid and glassy states. (3) The form existing in the crystalline state is the most stable in the liquid state.

Discussion

In a previous paper,[2] the following results were reported for unbranched ethers containing one oxygen. (1) About the CO–CC axis, the *trans* conformation is more stable than the *gauche* conformation. (2) About the OC–CC axis, the *gauche* conformation is as stable as the *trans* conformation. (3) The repulsive force between nonbonded hydrogen atoms is one of the important factors influencing the stability of these conformations.

In the crystalline state, 2,5-dioxahexane exists in the TGT form which has the *gauche* conformation about the OC–CO axis. This form is also the most stable in the liquid state. These results are consistent with those obtained for the one-oxygen containing ethers mentioned above.

In addition to the stabilizing factor with regard to the repulsive force between the nonbonded hydrogen atoms in the TGT form, the dipole moment is suggested to be another important factor to stabilize this form in the crystalline and liquid states. For 2,5-dioxahexane, the observed frequencies for the same molecular vibrations are appreciably different between the Raman and infrared spectra in the crystalline state and between the infrared spectra in the crystalline and glassy states. The magnitudes of these frequency differences are much larger than those for the one-oxygen containing ethers.[2] These spectral observations may be due to the effect of dipole moment.

In the liquid state, as compared with the case in the gaseous state, polar molecular forms are more stabilized than non-polar forms.[12] In fact, as shown in Fig. 1, the intensities of the bands assigned to the TGT form (polar form) increase in the liquid state as compared with the gaseous state. However, the details in this point are left to be studied.

In connection with the TGT form of 2,5-dioxahexane in the crystalline state, it is important to examine the structure of polyether.[7,8] It has been shown that poly(oxyethylene) $(-OCH_2CH_2-)_n$ and poly(oxytri-

methylene) $(-OCH_2CH_2CH_2-)_n$ have several crystal modifications. In the most stable crystal modification, the molecule takes the TGT conformation for the series of O-C-C-O bonds in the former polymer and the TGGT conformation for the series of O-C-C-C-O bonds in the latter polymer. In other modifications, the poly(oxyethylene) molecule takes the TTT conformation, and the poly(oxytrimethylene) molecule takes the TTGTTTG'T and $(TTTT)_2$ conformations for the series of O-C-C-C-O-C-C-C-O bonds. The stabilizing factors for the TGT conformation of 2,5-dioxahexane are thus found to be strongly correlated to those of the TGT conformation of poly(oxyethylene) and the TGGT conformation of poly(oxytrimethylene).

In a previous paper,[1] the following results were reported for the one-sulfur containing sulfides. (1) About the CS-CC axis, the *gauche* conformation is slightly more stable than the *trans* conformation. (2) About the SC-CC axis, the *gauche* conformation is as stable as the *trans* conformation. (3) The repulsive force between nonbonded hydrogen atoms is an important factor influencing the conformational stability.

In the crystalline state, 2,5-dithiahexane exists in the GTG' form which has the *gauche* conformation about the two CS-CC axes. This form is also the most stable in the liquid state. These results are consistent with those obtained for the one-sulfur containing sulfides mentioned above.

The 2,5-dithiahexane molecule corresponds to the monomer unit of poly(thioethylene) $(-SCH_2CH_2-)_n$. Accordingly, the conformation of 2,5-dithiahexane in the crystalline state must be closely related to the chain conformation of poly(thioethylene). In fact, the poly(thioethylene) molecule takes the GTG'G'TG conformation for the series of S-C-C-S-C-C-S bonds according to the X-ray diffraction studies by Tadokoro *et al.*[9]

From the results for the unbranched ethers and sulfides stated above, the stable conformations of 2-oxa-5-thiahexane are expected to have the following factors. (1) About the CO-CC axis, the *trans* conformation is more stable than the *gauche* conformation. (2) About the OC-CS axis, the *gauche* conformation is as stable as the *trans* conformation. (3) About the CC-SC axis, the *gauche* conformation is slightly more stable than the *trans* conformation.

In the present study, 2-oxa-5-thiahexane was found to take the TTG form in the crystalline state. Most of the bands observed in the liquid state are explained by the existence of the four forms of TTG, TTT, TGT, and TGG, of which the TTG form is the most stable. These results are in good agreement with the above points for the stable conformations of this molecule.

In the present normal vibration calculations, 107 force constants were used for 2-oxa-5-thiahexane. However, the majority of the force constants was assumed to be the same as the corresponding force constants for the unbranched ethers and sulfides treated previously,[1,2] and only nine force constants characteristic of this molecule were determined by the least-squares method. The vibrational frequencies calculated from these force constants were indeed accurate enough to predict the rotational isomerism of this molecule.

Through the previous[1,2] and present studies on the vibration spectra and rotational isomerism of the unbranched ethers and sulfides, the following conclusions are drawn. (1) The force constants determined in these studies are satisfactorily transferable to similar molecules. (2) The conformational stabilities of the ethers and sulfides are consistently explained and it may be possible to predict stable isomers of similar molecules on the basis of the knowledge obtained in these studies. (3) The combined method of the systematic measurements of vibration spectra and the systematic normal vibration calculations is useful for the studies of the rotational isomerism of chain molecules. The measurement of Raman spectra is more important than that of infrared spectra. The former offers, without much difficulty, information on the low-frequency vibrations which are closely associated with the rotational isomerism. In addition, the temperature dependence of band intensities is more easily measured by the method of Raman spectroscopy.

References

1) Part IV: M. Ohta, Y. Ogawa, H. Matsuura, I. Harada, and T. Shimanouchi, *Bull. Chem. Soc. Jpn.*, **50**, 380 (1977).

2) Part I: T. Shimanouchi, Y. Ogawa, M. Ohta, H. Matsuura, and I. Harada, *Bull. Chem. Soc. Jpn.*, **49**, 2999 (1976).

3) K. Machida and T. Miyazawa, *Spectrochim. Acta*, **20**, 1865 (1964); H. Matsuura, T. Miyazawa, and K. Machida, *Spectrochim. Acta*, **29A**, 771 (1973).

4) R. G. Snyder and G. Zerbi, *Spectrochim. Acta*, **23A**, 391 (1967).

5) R. Iwamoto, *Spectrochim. Acta*, **27A**, 2385 (1971).

6) M. Hayashi, Y. Shiro, T, Oshima, and H. Murata, *Bull. Chem. Soc. Jpn.*, **39**, 118 (1966).

7) T. Miyazawa, K. Fukushima, and Y. Ideguchi, *J. Chem. Phys.*, **37**, 2764 (1962).

8) T. Yoshihara, H. Tadokoro, and S. Murahashi, *J. Chem. Phys.*, **41**, 2902 (1964); H. Tadokoro, Y. Takahashi, Y. Chatani, and H. Kakida, *Makromol. Chem.*, **109**, 96 (1967); Y. Takahashi, I. Sumita, and H. Tadokoro, *J. Polym. Sci. Polym. Phys.*, **11**, 2113 (1973); Y. Takahashi and H. Tadokoro, *Macromolecules*, **6**, 672 (1973).

9) Y. Takahashi, H. Tadokoro, and Y. Chatani, *J. Macromol. Sci.-Phys.*, **B2**, 361 (1968); A. C. Angood and J. L. Koenig, *J. Macromol. Sci.-Phys.*, **B3**, 321 (1969); M. Yokoyama, H. Ochi, A. M. Ueda, and H. Tadokoro, *J. Macromol. Sci.-Phys.*, **B7**, 465 (1973).

10) T. Shimanouchi, H. Matsuura, Y. Ogawa, and I. Harada, *J. Phys. Chem. Ref. Data*, to be published.

11) T. Shimanouchi, "Tables of Molecular Vibrational Frequencies," Consolidated Vol. 1, U. S. Govt. Printing Office, No. C13.48: 39 (1972).

12) S. Mizushima, "Structure of Molecules and Internal Rotation," Academic Press, New York (1954).

V-51 and Mn-55 NMR Studies of Metal Carbonyls

Taku NAKANO*

Department of Chemistry, Faculty of Sciences, The University of Tokyo, Hongo, Bunkyo-ku, Tokyo 113

(Received November 7, 1975)

The metal chemical NMR shifts of metal carbonyls are reported and discussed in relation to the bonding nature characteristic of carbonyl compounds of the $M(CO)_6$- and $Mn(CO)_5X$-types, where M is V or Mn, and X is a halogen or SCN. Theoretically evaluated chemical shift data based upon Ramsey's expression agree well with those observed for the $M(CO)_6$-type carbonyls. Regarding $Mn(CO)_5X$, the variation of the shifts for halogens is elucidated theoretically and revealed to be dependent upon the π-bonding nature between the metal and the halogen atom.

The stability of organometallic complexes in low oxidation states has been interpreted in terms of the formation of the covalent bonding between the metal atom and ligands, such as carbon monoxide and tertiary phosphines. This covalent bonding may be divided into σ-bonding and π-bonding parts; the latter is frequently called "back bonding" or "back donation." The basicity of carbon monoxide is relatively weak[1] and the coordination through a σ-bond is not enough to stabilize the complexes. On the other hand, the formation of the π-bond between the unfilled antibonding π-orbital on the carbon atom and the metal d-orbitals (d_{xy}, d_{yz}, d_{xz}) increases the double-bond character thereby strengthening the bonding between CO and the metal. Simultaneously, the back donation results in the dilution of the negative charge of the central metal, reducing the repulsive energy among the electrons. Cotton and Kraihanzel[2] calculated the force constants of the CO vibrations in a model system of metal carbonyls where both the σ- and π-bonds were taken into consideration. This led Graham[3] to the idea of the σ- and π-parameters in the bonding of metal carbonyls.

^{59}Co and ^{55}Mn NMR of metal carbonyls have been reported by Calderazzo *et al.*,[4] Onaka *et al.*,[5] and Bancroft *et al.*,[6] and ^1H NMR signals have been obtained for hydrides of metal carbonyl complexes.[7] ^{13}C NMR chemical shifts suggest the existence of a strong covalent bond between carbon and metal atoms.[8]

In order to investigate the bonding nature of metal carbonyls from the viewpoint of the magnetic character, $[V(CO)_6]^-$ and $[Mn(CO)_6]^+$ were chosen as typical compounds for the present study; they are highly symmetric and isotropic geometrically, electronically, and furthermore, magnetically. The ^{55}Mn chemical shifts of $Mn(CO)_5X$ with C_{4v} symmetry, as referred to below, are dependent on halogen atoms,[4] reflecting the bonding characters of the metal carbonyl derivatives.

The ^{51}V and ^{55}Mn chemical shifts were calculated using suitable molecular orbitals and the general formula derived by Ramsey;[9,10] the latter has been successfully applied to the calculation of ^{19}F chemical shifts by Saika and Slichter.[11]

Experimental

Metal Carbonyl Compounds. $Mn_2(CO)_{10}$ and $Na[V(CO)_6]$ were obtained from Pressure Chemical Company and Strem Chemicals Inc., respectively. Other metal carbonyl compounds were prepared by methods described in the literature.[12-19]

NMR Measurements. ^{51}V and ^{55}Mn NMR spectra were recorded on a Varian VF-16 spectrometer at 10.55 or 7.35, and 11.20 MHz, respectively.

A tetrahydrofuran or acetone solution, or a neat liquid of the metal carbonyls was sealed in glass tubes 15 mm in diameter. NMR measurements were carried out at 20°C.

The NMR signals of ^{51}V and ^{55}Mn of $KMnO_4$ were obtained in dispersion modes in order to avoid saturation. All other signals were recorded in absorption modes.

For the manganese compounds, potassium permanganate was used as the standard compound for the shifts and for the vanadium compounds, vanadium oxotrichloride was employed.

TABLE 1. CHEMICAL SHIFTS AND LINE WIDTHS OF METAL CARBONYLS

Compound	Solvent	Shift(ppm)	Width(Oe)
$[V(CO)_6]^-$	THF	2010±5	0.1
$[Mn(CO_6)]^+$	acetone	935±5	4.28
$HMn(CO)_5$	neat	2560±10	2.45±0.05
	THF	2630[a]	2.39[a]
	THF	2578[b]	2.28[b]
$Mn(CO)_5Cl$	THF	1003±10	0.30±0.01
	THF	1005[a]	0.182[a]
$Mn(CO)_5Br$	THF	1200±10	0.66
	THF	1160[a]	0.378[a]
$Mn(CO)_5I$	THF	1520±10	0.84±0.02
	THF	1485[a]	0.557[a]
$Mn(CO)_5SCN$	THF	1130±10	3.51

a) Values from Ref. 4. b) Values from Ref. 7.

Chemical Shift Data. The observed ^{51}V and ^{55}Mn chemical shift data are summarized in Table 1, together with those reported in the literature. All compounds examined give signals higher than that of the reference compound.

Calculation of the Chemical Shifts

The symmetries of the $M(CO)_6$- and $Mn(CO)_5X$-type compounds allow their electronic structures to be analyzed with the aid of the molecular orbital theory. The results can be compared with photoelectron and ultraviolet spectra.

The molecular orbitals of $[V(CO)_6]^-$ and $[Mn(CO)_6]^+$, and $Mn(CO)_5X$ reported by Beach and Gray[20] and Fenske and DeKock[21] were applied here to estimate the

* Present Address: Faculty of Pharmaceutical Sciences, University of Toyama, Gofuku, Toyama 930.

chemical shifts in these compounds.

According to Ramsey,[10] the chemical shift is expressed by the following formula,

$$\sigma = e^2/mc^2\langle 0|\sum_k (x_k^2+y_k^2)/r_k^3|0\rangle - 2\sum_n (1/(E_n-E_0))\{\langle 0|\sum_k m_{zk}^0|n\rangle\langle n|\sum_{k'} m_{zk'}^0/r_{k'}^3|0\rangle + \langle 0|\sum_k m_{zk}^0/r_k^3|n\rangle\langle n|\sum_{k'} m_{zk'}^0|0\rangle\}, \quad (1)$$

where

$$m_{zk}^0 = -e\hbar/2mci(x_k\partial/\partial y_k - y_k\partial/\partial x_k) \quad (2)$$

and $|0\rangle$ and $|n\rangle$ denote the ground state and the n th excited state wave functions of the molecule, respectively, with E_0 and E_n being the energies of the corresponding states. The other symbols have their usual meanings.

In order to simplify the system, we assumed that only the d-electrons of the central atoms contribute to the paramagnetic term; the core electrons are assumed not to contribute to the matrix elements $\langle 0|m_{zk}^0|n\rangle$ and $\langle 0|m_{zk}^0/r_k^3|n\rangle$. Contribution from 4p-electrons and the variation of the orbital exponents caused by the bond formation are neglected here.

$M(CO)_6$-type Carbonyls. Applying Eq. 1 to the $M(CO)_6$-type carbonyls, we obtain the following reduced equation for the chemical shift,

$$\sigma = \sigma_P + \sigma_D \quad (3)$$

$$\sigma_P = -8e^2\hbar^2/m^2c^2\langle 1/r^3\rangle_{3d}\sum_{i,j} C_i^2C_j^2/\Delta E(i,j) \quad (4)$$

$$\sigma_D = e^2/3mc^2\{\langle 1/r\rangle_{3d}P_{3d} + \langle 1/r\rangle_{4s}P_{4s} + \langle 1/r\rangle_{4p}P_{4p} + \sum_k^{\text{core}}\langle 1/r\rangle_k\}, \quad (5)$$

where C_i is the coefficient of the i th atomic d-orbital in the molecular orbital of t_{2g} or e_g symmetry and $\langle 1/r\rangle_k$ and $\langle 1/r^3\rangle_k$ are the average values of $1/r$ and $1/r^3$ for the k th orbital, respectively. Here, we assume that the $\langle r^n\rangle_k$ values are those of free atoms. P_i is the electron population of the corresponding orbital defined by Mulliken.[22] $\Delta E(i,j)$ is the transition energy between the i th and j th levels.

TABLE 2. CALCULATED VALUES FOR $\langle 1/r\rangle$, $\langle 1/r^3\rangle$, AND $\langle r^2\rangle$ IN ATOMIC UNITS

	Vanadium complexes	Manganese complexes
$\langle 1/r\rangle_{1s}$	22.395	24.385
$\langle 1/r\rangle_{2s}$	5.018	5.540
$\langle 1/r\rangle_{3s}$	1.507	1.680
$\langle 1/r\rangle_{4s}$	0.322	0.347
$\langle 1/r\rangle_{2p}$	4.625	5.075
$\langle 1/r\rangle_{3p}$	1.237	1.392
$\langle 1/r\rangle_{4p}$	0.191	0.200
$\langle 1/r\rangle_{3d}$	0.849	1.020
$\langle 1/r^3\rangle_{3d}$	2.0755	3.2484
$\langle r^2\rangle_{1s}$	0.0060	0.0050
$\langle r^2\rangle_{2s}$	0.1132	0.0937
$\langle r^2\rangle_{3s}$	1.0441	0.8508
$\langle r^2\rangle_{4s}$	14.7720	12.5757
$\langle r^2\rangle_{2p}$	0.0877	0.0728
$\langle r^2\rangle_{3p}$	1.1978	0.9489
$\langle r^2\rangle_{4p}$	39.0585	36.1045
$\langle r^2\rangle_{3d}$	3.9738	2.7711

On estimating the $\langle r^n\rangle_k$ values, the Richardson wave functions[23] for the radical parts of the metal orbitals were adopted as in the treatments of the calculations of the molecular orbitals.[20,21] The calculated values of $\langle 1/r\rangle_k$ and $\langle 1/r^3\rangle_k$ are listed in Table 2 together with the values of $\langle r^2\rangle_k$ which are used in the Appendix.

For the closure approximation in this system, one should consider that t_{2g} is the highest occupied orbital and e_g is the lowest vacant one, and that only the $\langle t_{2g}|\boldsymbol{m}|e_g\rangle$ and $\langle t_{2g}|\boldsymbol{m}/r^3|e_g\rangle$ components have non-zero values. Thus, the transition energy is between the $^1A_{1g}$ and $^1T_{1g}$ states. Though the electron transition between the t_{2g} and e_g levels is forbidden and is masked in the intensive charge-transfer bands, the values of ΔE_{av} were adopted from the results obtained by Beach and Gray,[20] employing Gaussian analysis of the electronic spectra. These values are 25500 cm^{-1} for $[V(CO)_6]^-$ and 41050 cm^{-1} for $[Mn(CO)_6]^+$.

TABLE 3. ESTIMATED CHEMICAL SHIFT VALUES FOR $[Mn(CO)_6]^+$ AND $[V(CO)_6]^-$

Compound	Calculated value (ppm) σ_D	σ_P	$\sigma=\sigma_D+\sigma_P$	Chemical shift	Experimental value (ppm) *vs.* $KMnO_4$ or K_3VO_4
$[Mn(CO_6)]^+$	1915	−6102	−4187	928	935±5
$KMnO_4$	1900	−7015	−5115		
$[V(CO)_6]^-$	1718	−5993	−4275	612	1480±5
K_3VO_4	1708	−6595	−4887		

The results are summarized in Table 3. The chemical shifts for the reference compounds are estimated in the Appendix.** The calculated values of σ_D are in good agreement with those obtained by Dickinson[24] in the Hartree-Fock approximation. Here, the following values are used: $P_{3d}=6.37$, $P_{4s}=0.00$, $P_{4p}=0.14$ for manganese and $P_{3d}=4.36$, $P_{4s}=0.06$, $P_{4p}=0.19$ for vanadium.[20]

In order to further improve the approximation, one should consider other non-zero matrix elements between the more highly-excited states and the ground state. The transition energies are assumed to be the difference between the orbital energies of the corresponding molecular orbitals, which are partly quoted in Table 4.

Thus, the paramagnetic part of Eq. 1 becomes

$$\sigma_P = -e^2\hbar^2/m^2c^2\langle 1/r^3\rangle_{3d}\{8C_{3e_g}^2C_{2t_{2g}}^2/\Delta E(3e_g, 2t_{2g}) + 4C_{3t_{2g}}^2C_{2t_{2g}}^2/\Delta E(3t_{2g}, 2t_{2g}) + 8C_{3t_{2g}}^2C_{2e_g}^2/\Delta E(3t_{2g}, 2e_g)\}, \quad (6)$$

where C_i is the coefficient of the d-orbital of the molecular orbitals, i denotes the symmetry of the corresponding orbital, and $\Delta E(i,j)$ is the difference in energy between the i and j levels.

The values obtained are given in Table 5, and the non-zero terms are listed with transition energies and calculated σ_P values. The values of σ_P are not very far

** The signal for vanadium oxotrichloride appears at a value 533 ppm below that for potassium vanadate.[25]

Table 4. Molecular orbital coefficients for $M(CO)_6$[a)]

Molecular orbital		Metal orbital			CO orbital			
		3d	4s	4p	σ_1	σ_2	π	π^*
$[Mn(CO)_6]^+$	$2e_g$	−0.45595			0.01381	−0.76603		
	$2t_{2g}$	−0.89269					0.40850	−0.23794
	$3e_g$	1.0173			0.59145	−0.75222		
	$4t_{1u}$			−0.45919	−0.25475	0.23124	0.17384	−0.81047
	$2t_{2u}$						—	—
	$3t_{2g}$	0.50218					−0.03841	−1.0138
$[V(CO)_6]^-$	$2e_g$	0.19191			0.15206	−0.91938		
	$2t_{2g}$	−0.75519					0.39318	−0.44528
	$3e_g$	1.1750			0.55442	−0.62517		
	$4t_{1u}$			−0.46568	−0.22002	0.20197	0.17636	−0.80884
	$2t_{2u}$						−0.06406	−1.0006
	$2t_{1g}$						−0.17892	−1.0040
	$3t_{2g}$	0.76817					−0.17376	−0.97471

a) The values were taken in part from the results of Beach and Gray.[20)]

Table 5. Chemical shift values, σ_P, for $M(CO)_6$

Mixing		$[Mn(CO)_6]^+$		$[V(CO)_6]^-$	
		$\Delta E(i,j)$ (eV)	$-\sigma_P$ (ppm)	$\Delta E(i,j)$ (eV)	$-\sigma_P$ (ppm)
$3e_g$	$2t_{2g}$	8.601	5784	5.442	5577
$3t_{2g}$	$2t_{2g}$	10.984	552	9.614	675
$3t_{2g}$	$2e_g$	17.982	186	18.571	45
Total			6522		6297

from those obtained in the closure approximation.

$Mn(CO)_5X$-type Carbonyls. The chemical shifts of $Mn(CO)_5X$-type carbonyls are evaluated in a similar way. The molecular orbitals adopted here are described partly in Tables 6-1 to 6-3 based in the work of Fenske and DeKock,[21)] who have comfirmed the orbital energies of the highest occupied MOs by photoelectron spectroscopy.

The paramagnetic terms in Eq. 1 are summarized as follows,

Table 6-1. AO Coefficients for MO of $Mn(CO)_5Cl$[a)]

MO	$3d_{z^2}$	$3d_{x^2-y^2}$	$3d_{xy}$	$3d_{xz}$
11e				0.0190
$6b_1$		0.0000		
10e				0.0036
$11a_1$	−0.3272			
9e				−0.5496
$5b_1$		−0.7634		
$3b_2$			0.5997	
$10a_1$	−0.7054			
8e				0.3379
7e				0.7333
$2b_2$			0.7679	
$9a_1$	0.2648			
6e				−0.0111
$8a_1$	0.3886			
$4b_1$		0.4730		

a) The values were taken in part from the molecular orbitals of Fenske and DeKock.[21)]

Table 6-2. AO Coefficients for MO of $Mn(CO)_5Br$

MO	$3d_{z^2}$	$3d_{x^2-y^2}$	$3d_{xy}$	$3d_{xz}$
11e				0.0197
$6b_1$		0.0000		
10e				0.0033
$11a_1$	−0.3098			
9e				−0.5497
$5b_1$		−0.7648		
$3b_2$			0.6013	
$10a_1$	−0.6974			
8e				0.2470
7e				0.7686
$2b_2$			0.7669	
$9a_1$	0.3048			
6e				−0.0113
$8a_1$	0.3887			
$4b_1$		0.4719		

Table 6-3. AO Coefficients for MO of $Mn(CO)_5I$

MO	$3d_{z^2}$	$3d_{x^2-y^2}$	$3d_{xy}$	$3d_{xz}$
11e				0.0202
$6b_1$		0.0000		
10e				0.0029
$11a_1$	−0.2987			
9e				−0.5520
$5b_1$		−0.7665		
$3b_2$			0.6035	
$10a_1$	−0.6865			
8e				0.1897
7e				0.7831
$2b_2$			0.7654	
$9a_1$	0.3401			
6e				−0.0112
$8a_1$	0.1065			
$4b_1$		0.4704		

$$\sigma_P = -e^2\hbar^2/3m^2c^2\langle 1/r^3\rangle_{3d}\{8\sum_{i,j}^{b_1,b_1} C_i^2C_j^2/\Delta E(i,j) + 4\sum_{i,j}^{e,b_1} C_i^2C_j^2/\Delta E(i,j) + 12\sum_{i,j}^{e,a_1} C_i^2C_j^2/\Delta E(i,j) + 4\sum_{i,j}^{e,e} C_i^2C_j^2/\Delta E(i,j) + 4\sum_{i,j}^{e,b_1} C_i^2C_j^2/\Delta E(i,j)\}, \quad (7)$$

where $\sum_{i,j}^{k,l}$ means the summation of matrix elements between the orbitals of k and l symmetries, and $\Delta E(i,j)$ is the transition energy between the i and j levels. All possible excited states for a single electron transition from the ground state are considered. The values of σ_P resulting from the above calculation are listed in Table 7, together with the values of σ_D which are calculated from Eq. 5 for 3d-orbital populations of $P_{3d}(Cl)=5.687$, of $P_{3d}(Br)=5.723$, of $P_{3d}(I)=5.747$, those of the other P_is being unity.[21]

Table 7. Estimated chemical shift values for $Mn(CO)_5X$

Compound	Calculated value (ppm)		Observed (ppm)
	σ_D	σ_P	σ_P
$Mn(CO)_5Cl$	1897	−2722	−6009
$Mn(CO)_5Br$	1898	−2696	−5813
$Mn(CO)_5I$	1899	−2615	−5494

Though the calculated values for σ_P are almost one half of those obtained experimentally, the order of the chemical shifts for the halogen atom series is in agreement with that observed.

Discussion

The calculated values of the shifts of hexacarbonylmetal compounds based upon the molecular orbitals of Beach and Gray[20] agree well with the experimental results. This leads us to conclude that the paramagnetic term contributes dominantly to the shifts, and that the chemical shift directly reflects the nature of the chemical bond. This is more clearly revealed in the case of pentacarbonylmanganese halides and thiocyanate.

Though the calculated chemical shifts of pentacalbonylmanganese halides do not quite agree with the experimental values, it is clear that the dominant change of the shifts is due to the paramagnetic terms, while the diamagnetic terms vary only slightly. In the approximation described above, in which only the matrix elements involving the d-orbitals are taken into account, the calculated values of the paramagnetic terms are about one half of those observed. The paramagnetic terms under consideration involve only with the squares of the coefficients of the metal d-orbitals, so that the calculated values should be somewhat smaller than those obtained experimentally. In order to improve the agreement between the theoretical and experimental results, the cross terms between the d-orbitals of the metal and the orbitals of the ligand should be considered.***

The chemical shifts are linearly correlated with the electronegativity of the halogen and pseudohalogen; the shifts decrease with increasing electronegativity. In plotting the shifts versus the Schwarzenbach bond strength,[25] an appropriately linear relationship is obtained.

*** The theoretical treatmant will be reported elsewhere.

If halogen atoms withdraw electrons from the central metals, the diamagnetic shielding would decrease and the nuclei would be less shielded. However, the fact that the total 3d-orbital populations are essentially constant, as shown by the Fenske molecular orbitals, indicates that a variation in σ_D terms is unlikely. Thus, the order of the shifts for the various halogens can be elucidated using the paramagnetic term. Thus, the next problem is to determine which part should dominantly contribute to the paramagnetic term.

Table 8. Chemical shift values, σ_P, in parts of $Mn(CO)_5X$

Mixing		$Mn(CO)_5Cl$		$Mn(CO)_5Br$		$Mn(CO)_5I$	
		$\Delta E(i,j)$ (eV)	$-\sigma_P$ (ppm)	$\Delta E(i,j)$ (eV)	$-\sigma_P$ (ppm)	$\Delta E(i,j)$ (eV)	$-\sigma_P$ (ppm)
$2b_2$	$5b_1$	12.325	560.7	12.274	563.6	12.229	566.0
$4b_1$	$3b_2$	25.680	63.0	25.595	63.3	25.217	63.5
$2b_2$	9e	13.443	133.2	13.294	134.4	13.129	136.7
7e	$3b_2$	11.835	164.3	11.641	184.5	11.514	195.0
8e	$3b_2$	8.975	46.0	8.057	27.5	7.536	17.5
$9a_1$	9e	13.599	47.0	12.671	66.8	11.806	90.0
$8a_1$	9e	26.066	52.8	25.952	53.1	25.618	4.1
7e	$11a_1$	17.455	99.5	17.211	99.4	16.968	97.3
8e	$11a_1$	14.595	25.3	13.629	13.0	12.990	7.5
7e	$10a_1$	10.414	775.0	10.475	827.4	10.465	833.0
8e	$10a_1$	7.554	226.9	6.891	129.9	6.487	78.9
7e	$5b_1$	11.929	264.1	11.766	295.3	11.681	310.1
8e	$5b_1$	9.090	73.8	8.182	43.9	7.703	27.6
$4b_1$	9e	26.893	25.3	26.741	25.3	26.584	25.5
7e	9e	13.048	125.2	12.786	140.4	12.581	149.3
8e	9e	8.586	40.4	9.202	20.1	8.603	12.8

As shown in Table 8, which gives the parts of the paramagnetic terms, the variations of the paramagnetic shifts are caused mostly by terms involving mixing between the 8e and $10a_1$ levels. The summation of the other parts leads to almost the same values for three halogen derivatives. For the values of $\Delta E(i, j)$, no significant variations are found. On the other hand, the variation of the coefficients of the d-orbitals in the 8e orbitals plays an important role in the evaluation of matrix elements such as $\langle 8e|\boldsymbol{m}|10a_1\rangle$.

While the a_1 symmetric orbitals form the σ-bonds, the e symmetric orbitals form π-bonds between the metal and halogen atoms. Consequently we conclude that the π-bonding between metal and halogen atoms is a dominant cause of the chemical shifts, and the σ-bonding does not vary the values very much. This suggests that the Graham σ-parameter makes almost no contribution to the chemical shifts but that π-parameter must be closely related to these values.

It should be pointed out that the variation of the chemical shifts depends upon the π-bond which has been neglected so far in discussing the nature of halogen-metal bonds. If the ligands have the ability to form π-type bonds with the metal, this effect appears to be larger than that of the halogen ligands.

It should be emphasized that the values of the paramagnetic term increase in the order H<I<Br<Cl<CO; especially we note here that hydrogen has the

least tendency to form π-bond and carbon monoxide has the greatest. The π-bonding which seems to stabilize the low oxidation states in the metalcarbonyl can be estimated from the NMR chemical shifts. The π-bond formation in other halogen compounds can be predicted from these shifts.

For pentacarbonylmolybdenum halides reported by Takano,[26] a similar relation between the chemical shifts and the halogen atoms has been found, although the differences between the chemical shifts are less than those in the case of manganese compounds: 1584 ppm for $Mo(CO)_5Cl$, 1596 ppm for $Mo(CO)_5Br$, and 1709 ppm for $Mo(CO)_5I$ against potassium molybdate.

The author would like to express his sincere thanks to Professor Yukiyoshi Sasaki of The University of Tokyo and Professor Shigeyuki Aono of Kanazawa University for valuable discussions.

Appendix

Evaluation of the Chemical Shifts of $KMnO_4$ and K_3VO_4. The molecular orbitals of the $[MnO_4]^-$ ion have been calculated by several authors, but the computation of the energies is not yet adequate to explain the electronic structure accurately. The bonding between oxygen and manganese is covalent, and the electrons which contribute to the paramagnetism come from ligand oxygen; the d-electron population of the central manganese atom is 6.15 according to the molecular orbitals of Brown.[27]

Since the results of the calculation of the paramagnetism are not satisfactory, the shifts are estimated empirically as follows.

The magnetic susceptibility of $KMnO_4$, $\chi_g=0.175\times10^{-6}$ cm^3/g,[28] is divided into two parts, paramagnetic and diamagnetic terms, which in units of moles, is

$$\chi_M(KMnO_4) = \chi_M^D(KMnO_4) + \chi_M^P(KMnO_4) \quad (1)$$

and

$$\chi_M^D(KMnO_4) = \chi_M^D(Mn) + \chi_M^D(K^+) + \chi_M^D(4O^{2-}) \quad (2)$$

$$\chi_M^D(Mn) = -N(e^2/6mc^2)\sum_i\langle r^2\rangle_i, \quad (3)$$

where

$$\sum_i\langle r^2\rangle_i = \sum_i^{core}\langle r^2\rangle_i + P_{4s}\langle r^2\rangle_{4s} + P_{4p}\langle r^2\rangle_{4p} + P_{3d}\langle r^2\rangle_{3d}, \quad (4)$$

N is the Avogadro number, and P_i is the electron population of the i th orbital; $P_{4s}=0.24$, $P_{4p}=0.16$, $P_{3d}=6.15$.[27]

$\chi_M^D(4O^{2-})$ is estimated to be the difference of the sums of the empirical values for O^{2-} and O ($\chi_M^D(O^{2-})=-13.7\times10^{-6}$ and $\chi_M^D(O)=-5.3\times10^{-6}$ cm^3/mol[28]):

$$\chi_M^D(4O^{2-}) = (8-P_{3d}-P_{4s}-P_{4p}) \times (\chi_M^D(O^{2-})-\chi_M^D(O)) + 4\times\chi_M^D(O). \quad (5)$$

$\chi_M^D(Mn)=-26.82\times10^{-6}$ and $\chi_M^D(K^+)=-14.9\times10^{-6}$ cm^3/mol.[28] From Eq. 2, $\chi_M^D(KMnO_4)=-68.6\times10^{-6}$ cm^3/mol.

Since $\chi_M(KMnO_4)=\chi_g\times$(molecular weight)$=27.7\times10^{-6}$ cm^3/mol, Eq. 1 gives $\chi_M^P(KMnO_4)=96.36\times10^{-6}$ cm^3/mol.

The paramagnetic shift has the following relation to $\chi_M^P(KMnO_4)$:

$$\sigma_P = 2/N\times\langle 1/r^3\rangle_{3d}\chi_M^P(KMnO_4) \quad (6)$$

neglecting the contribution from 4p-electrons. $\sigma_P(KMnO_4)$ is calculated to be 7015 ppm.

For potassium vanadate, the values were calculated similarly using the following data: $P_{4s}=0.0148$, $P_{4p}=0.3519$, $P_{3d}=3.7167$,[30] and $\chi_g=-0.08\times10^{-6}$ cm^3/g.[31]

Thus, we obtain $\chi_M^P(K_3VO_4)=95.9$ cm^3/mol and evaluate the shift for potassium vanadate to be $\sigma_p(K_3VO_4)=6595$ ppm.

The shift of the diamagnetic term is found to be

$$\sigma_D = e^2/3mc^2\sum_i\langle 1/r\rangle_i,$$

where

$$\sum_i\langle 1/r\rangle_i = \sum_i^{core}\langle 1/r\rangle_i + P_{4s}\langle 1/r\rangle_{4s} + P_{4p}\langle 1/r\rangle_{4p} + P_{3d}\langle 1/r\rangle_{3d}. \quad (8)$$

The values in Table 2 are used for $\langle 1/r\rangle_i$s and the values of P_is as above, and we obtain $\sigma_D(KMnO_4)=1900$ ppm and $\sigma_D(K_3VO_4)=1708$ ppm.

References

1) For example, L.E. Orgel, "An Introduction to Transition-Metal Chemistry: Ligand Field Theory," 2nd ed, Muthuen, London (1966), Chap. 9.
2) F. A. Cotton and C. S. Kraihanzel, *J. Am. Chem. Soc.*, **81**, 4432 (1962).
3) W. A. G. Graham, *Inorg. Chem.*, **7**, 315 (1968).
4) P. Carderazzo, E, A. C. Lucken, and D. F. Williams, *J. Chem. Soc.*, **1967**, 154.
5) S. Onaka, T.Miyamoto, and Y. Sasaki, *Bull. Chem. Soc. Jpn.*, **44**, 1851 (1971).
6) G. M. Bancroft, H. C. Clark, R. G. Kidd, A. T. Rake, and H. G. Spinny, *Inog. Chem.*, **12**, 728 (1973).
7) R. M. Stevens, C. W. Kern, and W. N. Lipscomb, *J. Chem. Phys.*, **37**, 279 (1962).
8) For example, E. W. Randall, *Chem. Brit.*, **1971**, 371.
9) N. F. Ramsey, *Phys. Rev.*, **78**, 699 (1950).
10) N. F. Ramsey, *Phys. Rev.*, **86**, 243 (1952).
11) A. Saika and C. P. Slichter, *J. Chem. Phys.*, **22**, 26 (1954).
12) E. W. Abel and G. Wilkinson, *J. Chem. Soc.*, **1959**, 1501.
13) R. B. King, "Organometallic Syntheses," Vol. 1, Transition-metal compounds, Academic Press (1965), p. 174.
14) R. B. King, "Organometallic Syntheses," Vol. 1, Transition-metal compounds, Academic Prsss (1965), p. 149.
15) W. F. Edgell and W. M. Reseny,Jr., *J. Am. Chem. Soc.*, **88**, 5451 (1966).
16) W. Schropp, Jr., *Chem. Ber.*, **94**, 305 (1961).
17) T. Kruck and M. Noack, *Chem. Ber.*, **97**, 1703 (1964).
18) C. G. Barraclough and J. Lewis, *J. Chem. Soc.*, **1960**, 4842.
19) A. Wojicicki and M. F. Farona, *Inorg. Chem.*, **3**, 151 (1963).
20) N. A. Beach and H. B. Gray, *J. Am. Chem. Soc.*, **90**, 5713 (1968).
21) R. F. Fenske and R, L. DeKock, *Inorg. Chem.*, **9**, 1053 (1970).
22) R. S. Mulliken, *J. Chem. Phys.*, **23**, 1833 (1955).
23) J. W. Richardson, W. C. Nieuwpoort, R. R. Powel, and W. F. Edgell, *J. Chem. Phys.*, **36**, 1057 (1962).
24) W. C. Dickinson, *Phys. Rev.*, **80**, 563 (1950).
25) H. E. Walchli and H. W. Morgan, *Phys. Rev.*, **87**, 541 (1952).
26) T. Takano, Dissertation submitted for the degree, Doctor of Philosophy in Chemistry, to The University of Tokyo, 1972.
27) R. D. Brown, B. H. James, M. F. O'Dwyer, and K. R. Roby, *Chem. Phys. Lett.*, **1**, 459 (1967).
28) A. Pacault, J. Hoarau, A. Marchand, "Advances in Chemical Physics," Vol. 3, Interscience (1961), p. 209.
29) V. C. G. Trew, *Trans. Faraday Soc.*, **37**, 476 (1941).
30) R. Kebabcioglu and A Müller, *Chem. Phys. Lett.*, **8**, 59 (1971).
31) G. Wehrmeyer, *Diss. Münster*, **1957**, 91.

Studies of the Ruthenium Complexes. XIII. Kinetic Studies of Electron-transfer Reactions between Aquapentaammineruthenium(II) and Halopentaammineruthenium(III) Comlexes

Akira OHYOSHI, Kenichiro YOSHIKUNI, Hidetoshi OHTSUYAMA, Tomohisa YAMASHITA, and Shigeyoshi SAKAKI

Department of Industrial Chemistry, Faculty of Engineering, Kumamoto University, Kumamoto 860

(Received February 14, 1976)

Kinetic measurements of the electron-transfer reactions from $Ru(OH_2)(NH_3)_5^{2+}$ to $RuX(NH_3)_5^{2+}$, where X=Cl, Br, and I, have been made in aqueous solutions. The reaction rate is independent of the hydrogen-ion concentration, while it is greatly influenced by the ionic strength of the reaction solution. The rate constants were determined to be 147, 172, and 293 $M^{-1}s^{-1}$ for the reaction systems of chloro- bromo- and iodopentaammineruthenium(III) ions respectively at 25 °C in a solution with an ionic strength of 0.0944 M. The activation parameters, (ΔH^* kcal mol^{-1}, ΔS^* cal K^{-1} mol^{-1}), were (19.4, 16), (18.9, 15), and (11.2, −10) respectively, for the same systems. From the facts that the reaction rate decreases in the order of I>Br>Cl and that the ionic strength of the solution strongly affects the reaction rate, it may be concluded that the present electron-transfer reactions proceed by means of an outersphere-type mechanism.

The reduction reactions of ruthenium(III) ammine complexes have been studied by use of such reductants as Cr(II),[1-3] V(II),[3] the Ru(II) complex,[4] and divalent rare earth ions.[3,5] Since the reduced ruthenium(II) ammines are labile, reactions such as aquation and reoxidation proceed successively to complicate the redox reactions. Electron-transfer reactions from aquapentaammineruthenium(II) to halopentaammineruthenium(III) ions are observed in the radiolysis[6] and the electrochemical reactions.[7,8] However, there have been few quantitative investigations with respect to the kinetics and the reaction mechanism.

The present report will deal with the reaction kinetics of halopentaammineruthenium(III) with the aquapentaammineruthenium(II) ion, and an attempt to elucidate the reaction mechanism will be made on the basis of the kinetic sequences. The reaction rate was spectrophotometrically determined in solutions with various hydrogen-ion concentrations and ionic strengths.

Experimental

Materials. The halopentaammineruthenium(III) halides were prepared from ruthenium trichloride by the previously reported procedures.[9] The complex *p*-toluenesulfonates were recrystallized from a saturated *p*-toluenesulfonate solution. The chemical purities of the products were confirmed spectrophotometrically.[9,10] The reductant, the $Ru(OH_2)(NH_3)_5^{2+}$ ion solution, was prepared from iodopentaammineruthium(III) and zinc amalgam in a deaerated solution with high-purity argon gas. The water was triply distilled.

Procedures. The reductant solution was rapidly added to a deoxygenated solution of the halopentaammineruthenium(III) ion. The pH and the ionic strength of this solution were adjusted with *p*-toluenesulfonic acid and its sodium salt. Before mixing, the solutions were thermostated in a water bath at constant temperatures. The reaction rates were determined by measuring the change in the absorbance at given wave numbers[9] as a function of the reaction time—for instance, at 30.5×10^3 cm^{-1} (ε=1930 M^{-1} cm^{-1}) for chloropentaammine, at 25.1×10^3 cm^{-1} (ε=1980 M^{-1} cm^{-1}) for bromopentaammine, and at 18.5×10^3 cm^{-1} (ε=2050 M^{-1} cm^{-1}) for iodopentaammine. The concentrations of reactants were chosen to be $(2—5)\times10^{-4}$ M for $RuX(NH_3)_5^{2+}$ and $(1—5)\times10^{-5}$ M for $Ru(OH_2)(NH_3)_5^{2+}$ in the reaction solution. A Shimadzu UV 200 spectrophotometer was used for all the experiments.

Results and Discussion

The progressive changes in the absorption spectrum are shown in Fig. 1 for the electron-transfer reaction of the chloropentaammine complex. The absorption band at 30.5×10^3 cm^{-1} of the original complexes[9] rapidly decreases as the reaction proceeds. The absorption band at 37.3×10^3 cm^{-1} of the reaction product,[1] $Ru(OH_2)(NH_3)_5^{3+}$, could not be observed since there is an intense absorption of *p*-toluenesulfonate in the region higher than 36×10^3 cm^{-1}. However, this product was identified in a separate experiment[10] in the absence of *p*-toluenesulfonate. Similar changes in the absorption spectrum were observed in the reactions of the other complexes.

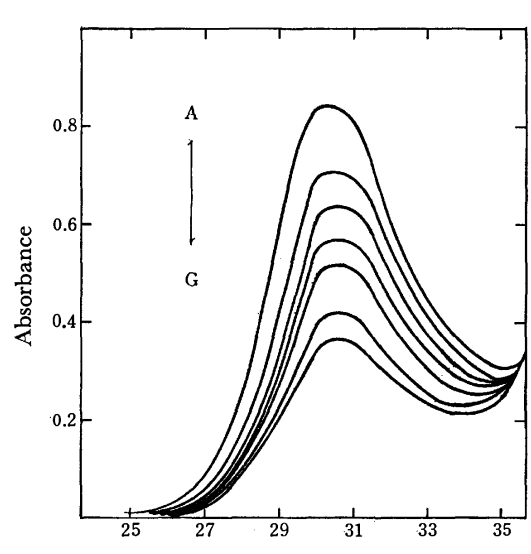

Fig. 1. Changes of absorption spectrum during reduction of $RuCl(NH_3)_5^{2+}$ with $Ru(OH_2)(NH_3)_5^{2+}$ at 30 °C. Curve A is the initial trace followed successively by traces at 25, 50, 85, 125, 180, and 220 (G) sec reaction.

Here, we assumed the following mechanism:

$$Ru^{III}X(NH_3)_5^{2+} + Ru^{II}(OH_2)(NH_3)_5^{2+} \underset{k_{-1}}{\overset{k_1}{\rightleftharpoons}} Ru^{II}X(NH_3)_5^{+} + Ru^{III}(OH_2)(NH_3)_5^{3+} \quad (1)$$

$$Ru^{II}X(NH_3)_5^{+} + H_2O \underset{k_{-2}}{\overset{k_2}{\rightleftharpoons}} Ru^{II}(OH_2)(NH_3)_5^{2+} + X^- \quad (2)$$

The rate constants have been given[8] as $k_2=6.3\ s^{-1}$, $k_{-2}=9.0\ M^{-1}\ s^{-1}$ for the chlorocomplex and $k_2=5.4\ s^{-1}$, $k_{-2}=5.9\ M^{-1}\ s^{-1}$ for the bromocomplex at 25 °C and at an ionic strength of 0.1 M. The rate formula with respect to the ruthenium complex in Reactions 1 and 2 can be expressed by Eqs. 3—6:

$$d[Ru^{III}X(NH_3)_5^{2+}]/dt = -k_1[Ru^{III}X(NH_3)_5^{2+}][Ru^{II}(OH_2)(NH_3)_5^{2+}] + k_{-1}[Ru^{II}X(NH_3)_5^{+}][Ru^{III}(OH_2)(NH_3)_5^{3+}] \quad (3)$$

$$d[Ru^{II}(OH_2)(NH_3)_5^{2+}]/dt = -k_1[Ru^{III}X(NH_3)_5^{2+}][Ru^{II}(OH_2)(NH_3)_5^{2+}] + k_{-1}[Ru^{II}X(NH_3)_5^{+}][Ru^{III}(OH_2)(NH_3)_5^{3+}] + k_2[Ru^{II}X(NH_3)_5^{+}] - k_{-2}[Ru^{II}(OH_2)(NH_3)_5^{2+}][X^-] \quad (4)$$

$$d[Ru^{II}X(NH_3)_5^{+}]/dt = k_1[Ru^{III}X(NH_3)_5^{2+}][Ru^{II}(OH_2)(NH_3)_5^{2+}] - k_{-1}[Ru^{II}X(NH_3)_5^{+}][Ru^{III}(OH_2)(NH_3)_5^{3+}] - k_2[Ru^{II}X(NH_3)_5^{+}] + k_{-2}[Ru^{II}(OH_2)(NH_3)_5^{2+}][X^-] \quad (5)$$

$$d[Ru^{III}(OH_2)(NH_3)_5^{3+}]/dt = k_1[Ru^{III}X(NH_3)_5^{2+}][Ru^{II}(OH_2)(NH_3)_5^{2+}] - k_{-1}[Ru^{II}X(NH_3)_5^{+}][Ru^{III}(OH_2)(NH_3)_5^{3+}] \quad (6)$$

In the initial period of the reaction, the concentration of $RuX(NH_3)_5^{+}$ may be negligibly small, because the rate of aquation (Eq. 2) is large as compared with that of the reverse reaction. In the initial stationary-state period, therefore, Eq. 3 can be simplified to Eq. 7:

$$-d[Ru^{III}X(NH_3)_5^{2+}]/dt = k_1[Ru^{III}X(NH_3)_5^{2+}][Ru^{II}(OH_2)(NH_3)_5^{2+}] \quad (7)$$

The plot of $\log[Ru^{III}X(NH_3)_5^{2+}]$ *vs.* the reaction time shows a good linearity for about 60 s after the initiation. The slope of the first-order plot is independent of the initial concentrations of the complex and the hydrogen ion. The rate constants, k_1 calculated from Eq. 7 as a function of the reactant and the hydrogen-ion concentration and of the ionic strength are listed in Table 1. The second-order rate constant, k_1, is independent of the concentrations of the reactants and the hydrogen ion, but increases with an increase in the ionic strength. Applying the simplified Brønsted-Bjerrum-Christiansen formulation,[11] the dependence of the k_1 value on the ionic strength was investigated. Figure 2 shows the relationship between k_1 and the ionic strength, I. The slope of the straight line is nearly +4; this fact suffices to show that the charge product of the reacting particles is four at the transition state of Reaction 1. This effect is similar to those in the reactions of $Ru(NH_3)_6^{2+}$ with $CoX(NH_3)_5^{2+}$, (X=Br, I) and $CoCl_2(en)_2^{+}$ ions.[2]

Table 1. The rate constants of the electron-transfer reactions of $RuCl(NH_3)_5^{2+}$ with $Ru(OH_2)(NH_3)_5^{2+}$ at (30±1) °C

$[Ru^{III}Cl(NH_3)_5^{+}]$ 10^{-4} M	$[Ru^{II}(OH_2)(NH_3)_5^{2+}]$ 10^{-5} M	I 10^{-2} M	$[H^+]$ 10^{-2} M	k_1 $M^{-1}\ s^{-1}$
3.36	4.77	9.44	9.44	158
3.98	4.77	9.44	9.44	173
5.06	4.77	9.44	9.44	161
4.69	1.14	9.44	9.44	173
4.37	1.97	9.44	9.44	159
4.07	2.79	9.44	9.44	165
2.77	2.99	9.44	9.44	172
3.06	4.44	9.44	3.15	163
5.61	4.44	9.44	6.35	167
				Av 166±6
2.96	3.89	12.10	9.44	179
2.96	3.87	14.00	9.44	199
3.21	3.89	16.10	9.44	216
3.73	3.89	18.80	9.44	250
3.51	3.89	29.10	9.44	265

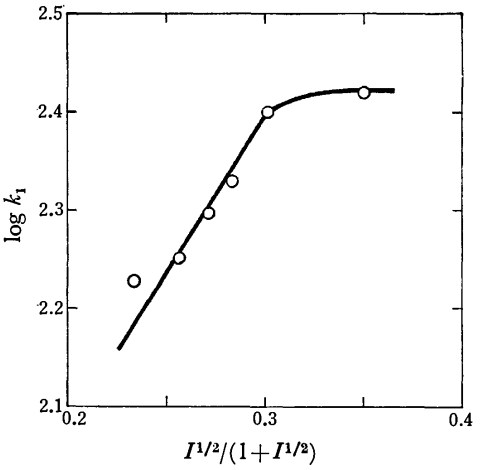

Fig. 2. Effect of ionic strength on the electron transfer reaction rate of $RuCl(NH_3)_5^{2+}$ with $Ru(OH_2)(NH_3)_5^{2+}$ at 30 °C, $[H^+]=0.0944$ M.

The curve-fitting method with various k_{-1} values was applied to the reaction between $RuCl(NH_3)_5^{2+}$ and $Ru(OH_2)(NH_3)_5^{2+}$ using the values of $k_1=147\ M^{-1}\ s^{-1}$, $k_2=6.3\ s^{-1}$, and $k_{-2}=9.0\ M^{-1}\ s^{-1}$. As is shown in Fig. 3, the experimental plot of the concentration variation for the $RuCl(NH_3)_5^{2+}$ species falls on the calculated curve when $k_{-1}\leqq 100\ M^{-1}\ s^{-1}$. The concentration variations of the other species in Reactions 1 and 2 were calculated by means of the numerical integration of Eqs. 3—6 using the same values of the rate constants. The results are also given in Fig. 3. The concentration of the intermediate, $[RuCl(NH_3)_5^{+}]$, is less than those of the other species by a factor of about 10^{-2}—10^{-3}, and it instantly reaches a maximum after the initiation of the reaction. The concentration of $[Ru(OH_2)(NH_3)_5]^{2+}$ decreases momentarily upon initiation, and then it increases very slowly.

The kinetic parameters for the electron-transfer reactions of the halogenopentaammineruthenium(III) complexes are exhibited in Table 2, along with those for the

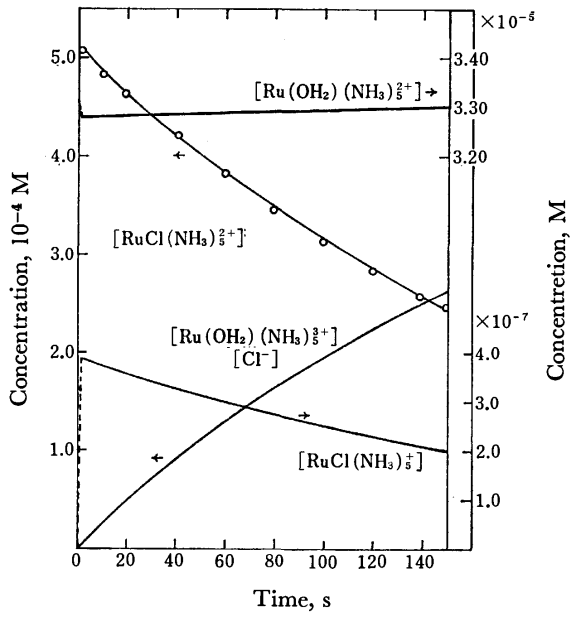

Fig. 3. Concentration variation of chemical species participating in the electron transfer reaction of $RuCl(NH_3)_5^{2+}$ with $Ru(OH_2)(NH_3)_5^{2+}$ at 25 °C, $[RuCl(NH_3)_5^{2+}]_{t=0}=5.10\times10^{-4}$ M, $[RuOH_2(NH_3)_5^{2+}]_{t=0}=3.32\times10^{-5}$ M, $I=[H^+]=0.0944$ M.
○: Experimental, —: calculated.

reference reactions. All the rate constants are determined in the solution with I=0.094 M. The order of the magnitude of the rate constants is chloropentaammine< bromopentaammine<iodopentaammine. This order is not the same as that of 3.5×10^4 M^{-1} s^{-1}>2.2×10^3 M^{-1} s^{-1}>2.6×10^2 M^{-1} s^{-1} estimated on the basis of the analysis of catalytic reactions involved in the process of the electron transfer between halogenopentaammines and Cr(II).[3] The relative rates (chloro: bromo: iodo) are 135: 8: 1 for the Cr(II) reaction and 57: 12: 1 for the reaction with Eu(II). On the other hand, the relative rates are 1: 1.7:—[12] for the V(II) reaction, and 1: 1.2: 2.0 at 25 °C or 1: 1.7: 2.4 at 30 °C for the present reaction with $Ru(OH_2)(NH_3)_5^{2+}$. The reactions of the ruthenium(III) halopentaammines with Cr(II) and Eu(II) are innersphere, while the reactions with V(II) are of the outersphere type.[3] This similarity in the relative reactivity may support the theory that the present reaction has an outersphere mechanism.

An outersphere process often occures when both reactants of the electron-transfer reaction are inert to substitution over the period required for the electron-transfer process. A typical reaction can be found in a homonuclear self-exchange electron transfer such as the reaction between $Ru(NH_3)_6^{3+}$ and $Ru(NH_3)_6^{2+}$ ions.[4] In the present study, all of the oxidants contain halide ligands which can interact with the reducing cation,

Table 2. Kinetic parameters for the electron-transfer reactions of halogenopentaammineruthenium(III) complexes

Reaction system	k_1 M^{-1} s^{-1} (temp °C)	ΔH^* kcal mol^{-1}	ΔS^* cal K^{-1} mol^{-1}
$RuCl(NH_3)_5^{2+}$–$Ru(OH_2)(NH_3)_5^{2+}$ a)	32±2 (16) 147±5 (25) 166±6 (30)	19.4	16
–Cr^{2+} b)	3.5×10^4(25)	1.3	−33
–V^{2+} b)	3.0×10^3(25)	3.8	−30
–Eu^{2+} b,c)	1.5×10^4(25), 2.4×10^4(25)	—	—
–Sm^{2+} c)	1.5×10^8(25)	—	—
–Yb^{2+} c)	1.5×10^7(25)	—	—
–e_{aq} c)	6.0×10^{10}(25)	—	—
$RuBr(NH_3)_5^{2+}$–$Ru(OH_2)(NH_3)_5^{2+}$ a)	52±2 (15) 106±4 (20) 172±8 (25) 286±8 (30)	18.9	15
–Cr^{2+} b)	2.2×10^3(25)	2.8	−34
–V^{2+} b)	5.1×10^3(25)	2.8	−34
–Eu^{2+} b,c)	$\approx3\times10^3$(25), 1.3×10^9(25)	1	−37
–Sm^{2+} c)	1.5×10^8(25)	—	—
–Yb^{2+} c)	3.3×10^7(25)	—	—
–e_{aq} c)	5.0×10^{10}(25)	—	—
$RuI(NH_3)_5^{2+}$–$Ru(OH_2)(NH_3)_5^{2+}$ a)	140±5 (15) 225±8 (20) 293±7 (25) 396±9 (30)	11.2	−10
–Cr^{2+} b)	2.6×10^2(25)	—	—
–Eu^{2+} c)	2.6×10^2(25)	—	—
–Sm^{2+} c)	$\approx10^8$(25)	—	—
–Yb^{2+} c)	$\approx10^8$(25)	—	—
–e_{aq} c)	$\approx6\times10^{10}$(25)	—	—
$Ru(NH_3)_6^{3+}$–$Ru(NH_3)_6^{2+}$ d)	437±51 (15) 843±69 (25)	10.3±1.0	−11±3

a) Present work, $I=[H^+]=0.094$ M. b) Ref. 3. c) Ref. 5. d) Ref. 4.

while the reductant has a water molecule in the coordination sphere which is weakly capable of reacting with the oxidizing cation. The rate constants for the aquation of halogenopentaammineruthenium(III) have been determined to be 3.28×10^{-4} s^{-1} for the chlorocomplex, 3.99×10^{-4} s^{-1} for the bromocomplex, and 1.64×10^{-4} s^{-1} for the iodocomplex at 54.5 °C.[13] These values are smaller than those of the pseudo-first-order rate constants for the correspondings electron-transfer reactions. The rate constants for the anations of the chloride and bromide ions to $Ru(OH_2)(NH_3)_5^{2+}$ have been determined to be 9.0 M^{-1} s^{-1} and 5.9 M^{-1} s^{-1} at 25 °C respectively.[8] These values are also smaller than those for the electron-transfer reactions. Thus, the substitution on either $RuX(NH_3)_5^{2+}$ or $Ru(OH_2)(NH_3)_5^{2+}$ is not rate-determing; hence, the outersphere mechanism is applicable to the present electron-transfer reactions.

In Table 2, the values of both ΔH^* and ΔS^* are practically the same for the reactions of chloro and bromopentaammines, and for the reactions of the $RuI(NH_3)_5^{2+}$-$Ru(OH_2)(NH_3)_5^{2+}$ and $Ru(NH_3)_6^{3+}$-$Ru(NH_3)_6^{2+}$ systems. This suggests that the energy change to form the reaction intermediate is the same for both the reaction systems. The electron-transfer reactions of halopentaammines with the simple metal ions are characterized by small values of ΔH^* and large negative values of ΔS^*. The reactions with Cr_{aq}^{2+} and Eu_{aq}^{2+} are regarded as of the innersphere type,[3,5] while the reaction with V_{aq}^{2+} is accounted for by the outersphere mechanism.[3] Hence, it is inadequate to distinguish the innersphere and outersphere mechanisms by only the aid of the activation parameters.

References

1) J. F. Endicott and H. Taube, *J. Am. Chem. Soc.*, **84**, 4984 (1962).
2) J. F. Endicott and H. Taube, *Inorg. Chem.*, **4**, 437 (1965).
3) J. A. Stritar and H. Taube, *Inorg. Chem.*, **8**, 2281 (1969).
4) T. J. Meyer and H. Taube, *Inorg. Chem.*, **7**, 2369 (1968).
5) M. Faraggi and A. Feder, *Inorg. Chem.*, **12**, 236 (1973).
6) J. H. Baxendale, M. A. Redgers, and M. D. Ward, *J. Chem. Soc., A*, **1970**, 1246.
7) H. S. Lin, D. J. Barclay, and F. C. Anson, *Inorg. Chem.*, **11**, 1460 (1972).
8) G. N. Coleman, J. W. Gesler, and J. R. Kuempel, *Inorg. Chem.*, **12**, 1036 (1973).
9) H. Hartmann and C. Buschbeck, *Z. Phys. Chem.*, **11**, 120 (1957).
10) A. Ohyoshi, A. Jyo, and N. Shin, *Bull. Chem. Soc. Jpn.*, **45**, 2121 (1972).
11) F. Basolo and R. G. Pearson, "Mechnisms of Inorganic Reactions," 2 nd ed, John Wiley and Sons, New York (1967), p. 34.
12) The value for iodopentaammine is not given in Ref. 3.
13) J. A. Broomhead and L. Kane-Maguire, *Inorg. Chem.*, **7**, 2519 (1968).

The Influence of a Co-ion on the Potential of a Liquid Ion-exchnger Membrane Electrode

Akinori Jyo, Kazumi Fukamachi, Wataru Koga, and Nobuhiko Ishibashi

Department of Applied Analytical Chemistry, Faculty of Engineering, Kyushu University, Fukuoka 812

(Received April 8, 1976)

The potential of a liquid ion-exchanger membrane electrode was affected by a co-ion, *i.e.*, an ionic species with the same charge sign as the ion-exchange site in the liquid membrane, when the co-ion in the sample was lipophilic. An aspect of the influence or interference of the co-ion on the response of the electrode is clarified theoretically, based on the three-region concept of the membrane potential. Theoretical predictions of the co-ion interference are illustrated by the measurement of potentials of a nitrate-sensitive nitrobenzene membrane electrode for sample solutions containing sodium nitrate, tetramethylammonium nitrate and the like. The co-ion interference became more important for increased extractability of the co-ion in the nitrobenzene–water system, specifically the order is $Rb^+ < Cs^+ < (CH_3)_4N^+$, and for a decrease in the concentration of the ion-exchanger in the membrane. Co-ion interference appeared for high concentration levels of the ion to be determined and produced a negative error in the activity measurement. The results are in good agreement with the theoretical predictions.

Recently, it has been pointed out both theoretically and experimentally that the interference of an ionic species with the charge sign opposite to that of the ion to be determined, the so-called co-ion, causes problems in the activity measurement of the ion using a liquid membrane electrode of the neutral carrier type.[1-4] According to the Teorell-Meyer-Sievers theory of membrane potentials,[5] the interference of a co-ion is anticipated in the response of a usual liquid ion-exchanger membrane electrode. Nevertheless, studies on the influence of a foreign ion on the response of such an electrode has been heretofore restricted to the interference of an ionic species with the same charge sign as the ion to be determined, the so-called counter ion. Little, therefore, is known about the effects of co-ion interference on the response of a liquid ion-exchanger membrane electrode.

In this report, the membrane potential of a liquid ion-exchanger membrane electrode is discussed theoretically in the case in which the co-ion in the sample solution is not completely rejected by the membrane, and the theoretical predictions are compared with experimental results.

Theoretical

We will analyze the membrane potential of the following membrane system with the help of a three-region concept of the membrane potential, *i.e.*, the regions of the two interfacial potential differences and of the diffusion potential in the membrane. The membrane system consists of a liquid ion-exchanger and two aqueous solutions. The membrane contains an electrolyte S-i, and is denoted by an asterisk. One aqueous solution marked by a prime contains an electrolyte A-i, and corresponds to the inner reference solution of an i ion-sensitive liquid ion-exchanger membrane electrode. The other solution designated by a double prime contains an electrolyte B-i and corresponds to the sample solution. We take the space coordinate x to be in the direction of the membrane thickness. The origin of the x-axis is placed at the membrane-reference solution interface. The x value of the other interface is denoted by d. The following assumptions are made:

(i) All the electrolytes dissociate completely in all phases.

(ii) The ion-exchange site S is confined to the membrane, and the concentration of ion-exchange sites in the membrane C_s^* is constant throughout.

(iii) While co-ion A in the reference solution is completely rejected by the membrane, co-ion B in the sample solution is not completely rejected by the membrane, and dissolves into the membrane with the ion i.

(iv) The concentrations are equal to the activities and vary linearly with x within the membrane.

(v) Electroneutrality holds.

First, the equation which expresses the diffusion potential in the membrane is derived. According to the Nernst-Planck equation, we can write this as:

$$\phi_n^* = -U_n^* C_n^* (\partial \tilde{\mu}_n^*/\partial x), \quad (n: A, B, i, S). \tag{1}$$

Assumptions (ii) and (iii) allow us to write the relation:

$$\phi_A^* = \phi_S^* = 0 \tag{2}$$

When no current flows,

$$I^*/F = \sum_n z_n \phi_n^* = 0 \quad (n: B, i). \tag{3}$$

From Eqs. 1, 2, and 3, the following relation can be obtained:

$$\partial \Psi^*/\partial x = -(RT/F)(\sum_n z_n U_n^* C_n^* \partial \ln C_n^*/\partial x)/(\sum_n z_n^2 U_n^* C_n^*) \quad (n: B, i). \tag{4}$$

Integrating Eq. 4 from $x=0$ to d under the foregoing assumptions, one obtains the relation in the case of $|z_n|=1$:

$$\Psi^*(0) - \Psi^*(d) = ((RT/z_i F)(U_i^* - U_B^*)/(U_i^* + U_B^*)) \times \ln (((U_i^* + U_B^*)C_i^*(d) - U_B^* C_s^*)/U_i^* C_s^*). \tag{5}$$

Next, we consider the interfacial potential differences. From the electrochemical equilibria at the respective boundaries, $x=0$ and $x=d$, we have the relations:

$$\Psi' - \Psi^*(0) = -(\mu^\circ - \mu^{\circ *})/z_i F + (RT/z_i F) \ln (C_i^*(0)/a_i')$$
$$\Psi^*(d) - \Psi'' = (\mu^\circ - \mu^{\circ *})/z_i F + (RT/z_i F) \ln (a_i''/C_i^*(d)) \tag{6}$$

From assumption (v) and the electrochemical equilib-

rium at the membrane-sample solution interface, $x=d$, we obtain the relation:

$$C_i^*(d) = (C_s^* + (C_s^{*2} + 4k_ik_B(a_i'')^2)^{1/2})/2. \quad (7)$$

Adding together Eqs. 5 and 6, and inserting Eq. 7, we obtain the desired equation which expresses the influence of the co-ion on the potential E_M of the liquid ion-exchanger membrane electrode:

$$E_M = \Psi' - \Psi'' = (RT/z_iF) \ln (a_i''/a_i') - (RT/z_iF) \ln ((C_s^* + (C_s^{*2} + 4k_ik_B(a_i'')^2)^{1/2})/2C_s^*) + ((RT/z_iF)(U_i^* - U_B^*)/(U_i^* + U_B^*)) \ln (((U_i^* + U_B^*) \times ((C_s^* + (C_s^{*2} + 4k_ik_B(a_i'')^2)^{1/2})/2) - U_B^*C_s^*)/U_i^*C_s^*). \quad (8)$$

Experimental

The influence of the co-ion on the potential E_M of the i ion-sensitive electrode was examined by EMF measurement of the following electrochemical cells:

+SCE/Reference Solution (A-i)/Liquid Membrane/ Sample Solution (B-i)/SCE− (9)

and

+SCE/Reference Solution (A-i)/Liquid Membrane/ Sample Solution (A-i, B-j)/SCE−, (10)

where j is a foreign ion with the same charge sign as the i ion. The j ion selected scarcely interferes with the activity measurement of the i ion. The interference effects of co-ions were examined for the response of nitrate-sensitive and methylephedrine-sensitive electrodes using cells (9) and (10), respectively. The liquid membrane in cell (9) was a nitrobenzene solution of the nitrate salt of crystal violet, and that in cell (10) was a nitrobenzene solution of the tetraphenylborate (TPB) salt of methylephedrine (MEP). The reference solutions in cells (9) and (10) were 1.00×10^{-2} M(M=mol dm^{-3}) solutions of sodium nitrate and methylephedrine hydrogenchloride, respectively. Electrolytes B-i used in cell (9) were sodium nitrate, rubidium nitrate, cesium nitrate and tetramethylammonium nitrate. Sodium nitrate, sodium iodide and sodium thiocyanate were used as the electrolyte B-j in cell (10). The procedures for the preparation of the membrane solutions and the EMF measurement have been described in detail elsewhere.[6-8]

Results and Discussion

Equation 8 can be reduced to a Nernstian equation, when $4k_ik_B(a_i'')^2$ is sufficiently smaller than the square of the concentration of the ion-exchanger in the membrane, C_s^{*2}. On the other hand, the second and third terms of Eq. 8 may contribute to E_M when $4k_ik_B(a_i'')^2$ is not much smaller than C_s^{*2} and co-ion B thus interferes with the activity measurement of the i ion using the i ion-sensitive electrode with the liquid ion-exchanger membrane. In most liquid ion-exchanger membrane electrodes, the mobilities of ions in the membrane are not so different for the ions of interest, whereas the partition coefficients of the ions differ greatly for these ions.[9-13] Accordingly, the effect of co-ion interference can be discussed in a first approximation, neglecting the contribution of the third term of Eq. 8 to E_M. Since the value of $(C_s^* + (C_s^{*2} + 4k_ik_B(a_i'')^2)^{1/2})/2C_s^*$ is always larger than unity when the co-ion enters the membrane, the observed potential E_M gives a lower activity of the i ion than true value. The co-ion interference thus leads to a negative error in the activity measurement of the i ion, whereas a positive error is measured in the usual interference of a foreign counter-ion species. From Eq. 8 the effect of co-ion interference can be summarized as follows:

(i) Co-ion interference becomes more important with decreasing concentration of the ion-exchanger in the membrane; conversely, the co-ion interference can be reduced by increasing the concentration of the ion-exchanger in the membrane.

(ii) Co-ion interference occurs at high activity levels of the objective ion i, whereas the interference of a foreign counter ion occurs at low activity levels of the i ion.

(iii) Co-ion interference increases with increasing extractability of the co-ion.

To illustrate the theoretical predictions, the nitrate-sensitive membrane electrode system (9) was selected because it is likely to fulfill most of the foregoing assumptions.[9-13]

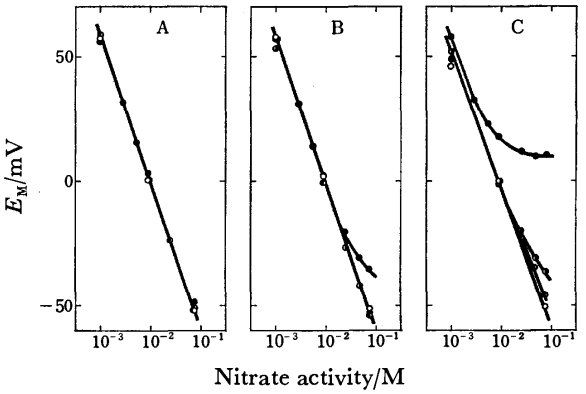

Fig. 1. The interference of a co-ion or cation in the response of the nitrate-sensitive electrode with the nitrobenzene membrane containing the nitrate salt of Crystal Violet as an ion-exchanger.
Concentration of the ion-exchanger in the membrane: (A) 1.0×10^{-3} M, (B) 1.0×10^{-4} M, (C) 1.0×10^{-5} M; Nitrate salt in the sample solution: $NaNO_3$ (○), $RbNO_3$ (◑), $CsNO_3$ (◐), $(CH_3)_4N\,NO_3$ (●); Temp: 24±1 °C.

In Fig. 1, the potentials of the nitrate-sensitive electrode are shown. The potential was stable in the concentration range above 10^{-3} M of the sample salt. Below 10^{-3} M, however, the potential was somewhat unstable in the initial stage of the measurement. In such cases, the stationary values observed after a delay of 15—20 min are used.

A membrane with a 10^{-3} M ion-exchanger showed a Nernstian response to all of nitrate salts up to 10^{-1} M. In the case of a membrane with a 10^{-4} M ion-exchanger, the response for tetramethylammonium nitrate differed from the ideal Nernstian response in the activity level above 10^{-2} M. A negative error was observed in accordance with theoretical predictions. A large deviation from Nernstian response was observed for the response of a membrane with a 10^{-5} M ion-exchanger. Except

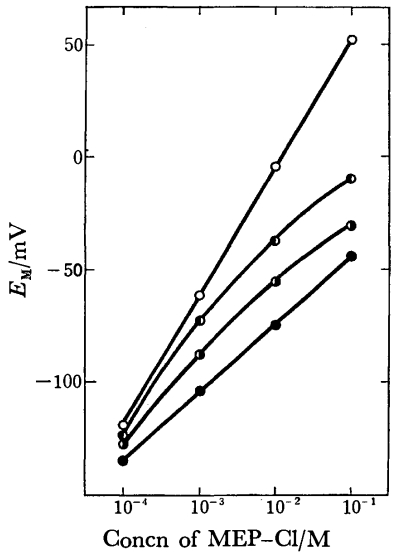

Fig. 2. The response of the methylephedrine-sensitive electrode for sample solutions containing methylephedrine hydrogenchloride (MEP-Cl) and sodium salts of inorganic anions.

Liquid membrane of the electrode: 1.0×10^{-4} M nitrobenzene solution of MEP-TPB; Sample solution: MEP-Cl only (○), MEP-Cl+0.5 M $NaNO_3$ (◐), MEP-Cl+0.1 M NaI (◑), MEP-Cl+0.1 M NaSCN (●); Temp: 20°C.

for the case of sodium nitrate, the responses were no longer Nernstian in the relatively high activity levels of the sample salt. In this case, the extent of the interference is distinguishable for the co-ion species. The order of increasing interference is $Rb^+<Cs^+<(CH_3)_4N^+$. This order is in agreement with the increasing extractability of the ions in the nitrobenzene–water system.[10] The results are thus in good agreement with the theoretical expectations. An example of co-ion interference for electrode response is shown for a sample solution containing mixed electrolytes A-i and B-j (cell (10)) in Fig. 2. The methylephedrine-sensitive electrode showed a nearly Nernstian response for a sample solution containing only methylephedrine hydrogenchloride (MEP-Cl).[8] In the presence of the sodium salt of nitrate, iodide or thiocyanate, the electrode response was no longer Nernstian. A negative error was observed. The order of increasing interference is also in agreement with the increasing extractability of the ions in the nitrobenzene–water system, *i.e.*, $NO_3^-<I^-<SCN^-$.[11]

Usually, it is considered that co-ions do not affect the response potential of a liquid ion-exchanger membrane electrode. As shown by this work, however, co-ions do, in some cases, interfere strongly with the activity measurement of the objective ion of the electrode, especially when a lipophilic ion is contained in the sample as a co-ion. In this connection, the recent study of Llenado on the calcium electrode response in the presence of ionic surfactants is interesting because it is anticipated that ionic surfactants may show this type of interference.[14] In conclusion, *the presented results suggest that co-ion interference should be considered in the analytical use of a liquid ion-exchanger membrane electrode, in addition to the consideration of the usual interference of foreign counter ions.*

The authors greatly acknowledge the financial support of the Ministry of Education.

Symbols

a	:	activity
C	:	concentration
I	:	electric currnt
U	:	mobility of ion
k	:	partition coefficient of ion
Ψ	:	inner potential
ϕ	:	flux of ion
$\tilde{\mu}$	:	electrochemical potential
μ°	:	standard chemical potential in water
$\mu^{\circ *}$	:	standard chemical potential in organic phase
i	:	objective ion of the electrode
A	:	co-ion A
B	:	co-ion B
S	:	ion-exchange site
x	:	distance variable
*	denotes a quantity in the membrane	
′	denotes a quantity in the reference solution	
″	denotes a quantity in the sample solution	

References

1) J. H. Boles and R. P. Buck, *Anal. Chem.*, **45**, 2057 (1973).
2) W. E. Morf, G. Kahr, and W. Simon, *Anal. Lett.*, **7**, 9 (1974).
3) H. Seto, A. Jyo, and N. Ishibashi, *Chem. Lett.*, **1975**, 483.
4) D. Amman, M. Güggi, and W. Simon, *Anal. Lett.*, **8**, 709 (1975).
5) J. Koryta, *Anal. Chim. Acta*, **61**, 329 (1972).
6) N. Ishibashi and H. Kohara, *Anal. Lett.*, **4**, 785 (1971).
7) N. Ishibashi, H. Kohara, and N. Uemura, *Bunseki Kagaku*, **21**, 1072 (1971).
8) K. Fukamachi, R. Nakagawa, M. Morimoto, and N. Ishibashi, *Bunseki Kagaku*, **24**, 428 (1975).
9) A. Jyo, M. Torikai, and N. Ishibashi, *Bull. Chem. Soc. Jpn.*, **47**, 2862 (1974).
10) J. Rais, *Collect. Czech. Chem. Commun.*, **36**, 3253 (1971).
11) Y. Yamamoto, T. Tarumoto, and E. Iwamoto, *Anal. Chim. Acta*, **64**, 1 (1973).
12) Y. Yamamoto, E. Sumimura, K. Miyoshi, and T. Tominaga, *Anal. Chim. Acta*, **64**, 225 (1973).
13) S. Motomizu and K. Toei, *Bull. Chem. Soc. Jpn.*, **42**, 1006 (1969).
14) R. A. Llenado, *Anal. Chem.*, **47**, 2243 (1975).

A Study of the Structures of Aluminum Complexes with Isopropoxy and Methyl Groups Using Pulsed NMR and Chemical Ionization Mass Spectrometry

Masao UETSUKI and Yuzuru FUJIWARA

Central Research Laboratories, Kuraray Co., Ltd., Sakazu 2045, Kurashiki 710

(Received May 17, 1976)

The structures of aluminum complexes formed by the reaction of aluminum isopropoxide with trimethylaluminum was investigated by measuring the spin-lattice relaxation times, T_1 for ^1H and T_1* for ^{27}Al. The motion of the ligand of the complexes reflected upon the value of T_1, which was about twice as long at the terminal position as at the bridge position, and decreased with increasing molecular weight. Coordination symmetry about the aluminum nucleus of the complexes governed the value of T_1*, which was about ten times as long at the center of the tetrameric complexes as at the wing of the dimeric complexes. The ^{13}C NMR signals of the isopropoxy group varied with the configuration of the ligands, while those of the methyl group were either broad or not observable. Chemical ionization mass spectra of the complexes supported the tetrameric and the dimeric structures determined from the results of NMR measurements.

Aluminum alkoxides have a stable structure, while alkylaluminums are so reactive that they are utilized as a reducing reagent in various reactions.[1] A tetrameric structure, T^0, for aluminum isopropoxide was first proposed by Bradley,[2] and a dimeric one, D^2, for trimethylaluminum by Laubengayer *et al.*[3] ^1H NMR has been used effectively for the structure determination of these complexes.[4-6]

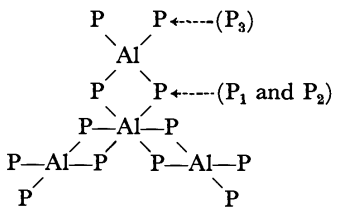

T^0

P=$(CH_3)_2CHO$-

M_w=817

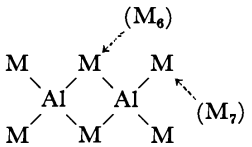

D^2

M=CH_3-

M_w=320

M_w indicates the molecular weight of the complexes. Using ^1H NMR spectroscopy, it has been found that aluminum isopropoxide reacts with trimethylaluminum to produce three kinds of tetranuclear complexes, T^1, T^2 and T^3, and two kinds of binuclear ones, D^0 and D^1.[7] Chemical shifts, spin-spin coupling constants between the protons, signal intensities and relative values of the spin-lattice relaxation times were measured to confirm the structures reported in a previous publication.[7]

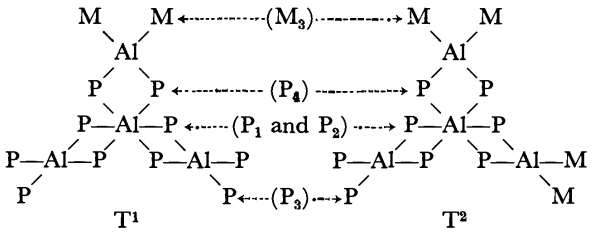

T^1

M_w=729

T^2

M_w=641

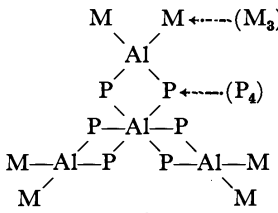

T^3

M_w=553

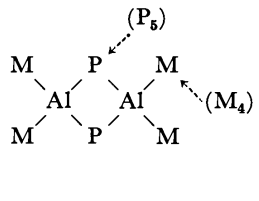

D_0

M_w=409

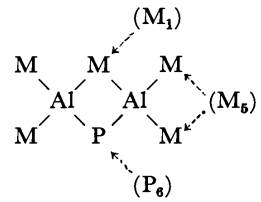

D^1

M_w=364

The remaining problems are summarized as follows. a) When ^1H NMR signals were obtained in the CW (continuous wave) mode, the spin-lattice relaxation time was measured using the progressive saturation method, so that the absolute values for T_1 could not be obtained, and relative values for T_1 could hardly be determined for NMR signals which are close to each other. b) As a result of overlapping of the NMR signals it was impossible to discriminate between the three kinds of tetranuclear complexes, T^1, T^2 and T^3. c) Since the NMR measurements were performed only on the protons of the ligands, no direct information was obtained concerning the aluminum nucleus of the complexes.

In the present work, the absolute values of T_1 for both ^1H and ^{27}Al were measured in the pulsed NMR mode to reconfirm the structures of the aluminum complexes and to study the remaining problems. ^{13}C NMR was also used to study the coordination mode of the ligand. The molecular weight of the complexes was examined using chemical ionization mass spectrometry, which is a useful technique for estimating the molecular size of such unstable compounds.

Experimental

Reagents. All the reagents used were obtained and purified by the same method as that described in Ref. 7.

Preparation of Samples. Aluminum isopropoxide and trimethylaluminum were dissolved separately in benzene, and solutions were mixed at 25 °C in an atmosphere of nitrogen in a dry box. The concentration was set so that the total amount of the solutes was 20 and 5.0 mol % in the solutions used to prepare the samples for pulsed NMR spectroscopy and chemi-

cal ionization mass spectrometry, respectively. Since a trace of oxygen in the solution which reacted with trimethylaluminum showed no observable effect upon the magnetic relaxation time, none of the samples were degassed.

Measurements of NMR and Mass Spectra. NMR spectra were measured with a Bruker SXP 4-100 spectrometer operating at 21.14 kG. Spin-lattice relaxation times for ^{1}H and ^{27}Al nuclei were measured at 28 °C using a partial relaxation technique with π- and $\pi/2$-pulses. The length of the π-pulses were 1.3×10^{-5} and 2.4×10^{-5} s for ^{1}H and ^{27}Al, respectively. Mass spectra were recorded using a Finnigan model 3300F quadrupole mass spectrometer equipped with a chemical ionization system. Methane was used as the reactant gas for the chemical ionization.

Results and Discussion

^{1}H NMR. The ^{1}H NMR spectra of the aluminum complexes showed four types of signals with hyperfine structures characteristic of the functional groups of the ligands; the methyl groups displayed a singlet pattern for τ=9.96—10.53, the isopropoxy methyl groups a doublet for τ=8.31—9.04, the isopropoxy methine groups a heptad for τ=5.27—5.70, and methane, a by-product of the reaction of aluminum isopropoxide with trimethylaluminum, a singlet at τ=9.85. For convenience, the signals of the isopropoxy methyl groups are denoted by P_1, P_2, P_3, P_4, P_5, and P_6 in the order of increasing τ values, and those of the methyl groups by M_1, M_2, M_3, M_4, and M_5 at 28 °C. Below −40 °C, the signal due to trimethylaluminum, M_2, splits into two singlet signals, which are designated as M_6 for the smaller value and as M_7 for the larger. On the basis of considerations of chemical-shifts, spin-spin coupling constants and signal intensities, these signals were assigned in Ref. 7 to T^0, T^1, T^2, T^3, D^0, D^1, and D^2.

In the present work, an attempt was made to reconfirm the signal assignments using the spin-lattice relaxation time, T_1. Typical ^{1}H NMR spectra measured using the partial relaxation technique are shown in Fig. 1, where the molar ratio of added trimethylaluminum and aluminum isopropoxide is 0.40: 0.60. The logarithm of the recovery rate of the signals was plotted against the delay time of the $\pi/2$-pulse after the π-pulse, and the linearity was sufficient to determine the T_1 values to within an accuracy of ±5% as listed in Table 1.

From the observed T_1 values, the isopropoxyl methyl signals can be classified into two groups, I (P_1, P_2, P_3 and P_4), and II (P_5 and P_6), which represent T_1 values of 0.35—0.97 and 3.2—4.0 s, respectively. In a similar manner, the methyl signals can also be classified into two groups, I (M_3), and II (M_2 and M_4), with T_1 values of 1.9 and 3.2—4.6 s, respectively. Since it is known

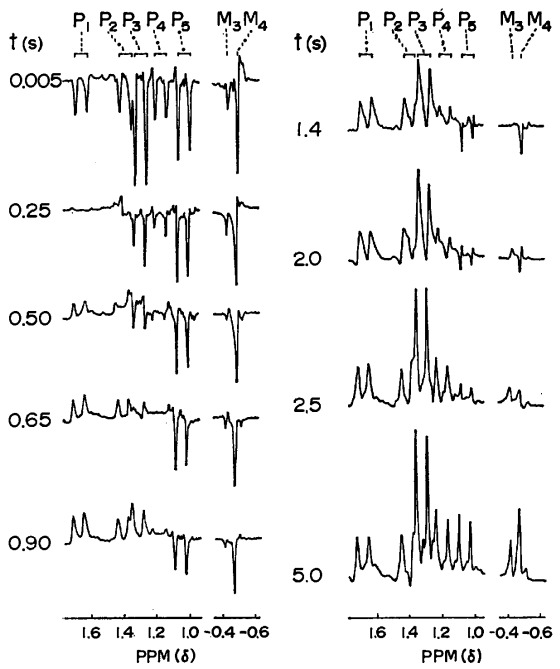

Fig. 1. ^{1}H NMR spectra of the methyl groups of the aluminum complexes in benzene at 28 °C. t is delay time of the $\pi/2$-pulse after the π-pulse. Trimethylaluminum and aluminum isopropoxide were mixed at the molar ratio 0.40: 0.60.

that aluminum isopropoxide and trimethylaluminum are tetrameric[2] and dimeric,[3] respectively, the signals of groups I and II are referred to the ligands of the tetra- and the binuclear aluminum complexes, respectively.

The M_2 signal, which is a singlet due to the rapid exchange of bridging and terminal methyl groups, M_6 and M_7, of dimeric trimethylaluminum D^2, has the longest T_1 value, 4.6 s. The bridging ligand is supposed to be less mobile and have a shorter value of T_1 than the terminal ligand. Since P_5 and M_4 have shorter T_1 values than P_6 and M_5, the former can be assigned to the ligand of D^0, and the latter to that of D^1. The results agree with those obtained from the change in the signal intensity with the ratio of the trimethylaluminum to aluminum isopropoxide concentrations.[7] The T_1 values of P_5 and P_6 show that the T_1 value of the isopropoxyl methyl group increases by about 0.6 s when the neighboring isopropoxyl group is substituted by a methyl group. The increase in the T_1 value is attributable to a decrease in the number of neighboring protons, which play the role of the energy carriers in the spin-lattice relaxation process.

The T_1 values of P_1 and P_2 are *ca.* 0.35 s, and P_3 has a

Table 1. Spin-lattice relaxation times for methyl protons of aluminum complexes in benzene at 28 °C

$Al(CH_3)_3$: $Al(isoPrO)_3$[a)]	Spin-lattice relaxation time (s)								
	P_1	P_2	P_3	P_4	P_5	P_6	M_2	M_3	M_4
0.00 : 1.00	0.35	0.35	0.65						
0.40 : 0.60	0.36	0.36	0.79	0.97	3.2			1.9	3.2
0.80 : 0.20					3.4	4.0	4.6		

a) Molar ratio.

T_1 value about twice as long as the former two. Therefore, P_1 and P_2 are assigned to the bridging isopropoxy group of the tetranuclear complexes, and P_3 to the terminal one. The splitting of the signal of the isopropoxy methyl group into the two signals, P_1 and P_2, suggests that the bridging group is less mobile than the terminal group, P_3. P_4 has a T_1 value *ca.* 0.6 s longer than P_1 or P_2, and is equivalent in molar intensity to M_3, which has a T_1 value about twice as long as P_4. Hence, P_4 and M_3 are assigned to the bridging isopropoxy group and the terminal methyl group, respectively, of one of the substituted wings of the tetranuclear structures, T^1, T^2 or T^3. The T_1 values of P_4 and M_3, as well as those of P_1, P_2 and P_3, become longer with an increase in the amount of trimethylaluminum. This phenomenon shows that the T_1 value increases with decreasing proton number of the neighboring ligands, a fact which supports the assumption that all three structures, T^1, T^2, and T^3, exist in the solution. If, for instance, only T^0 and T^3 existed, the T_1 values of P_1, P_2, P_3, P_4, and M_3 would not change with the ratio of the trimethylaluminum and aluminum isopropoxide concentrations.

As long as similar structures are considered, it is seen that the T_1 value is inversely proportional to the molecular weight. For instance, the ratio of the molecular weight of D^0 to that of D^1 is 0.89, while the ratio of the T_1 values of P_5 and P_6 is 0.85 when trimethylaluminum and aluminum isopropoxide are mixed at a molar ratio of 0.80: 0.20. When the ratio of the trimethylaluminum and aluminum isopropoxide concentrations is 0.40: 0.60, the mean molecular weight of the tetranuclear complexes is calculated from the T_1 value of P_3 to be 672 in comparison with that for a pure solution of aluminum isopropoxide, while from the T_1 values of M_3 and M_4, it is 689. The mean molecular weight decreases with an increase the number of methyl groups.

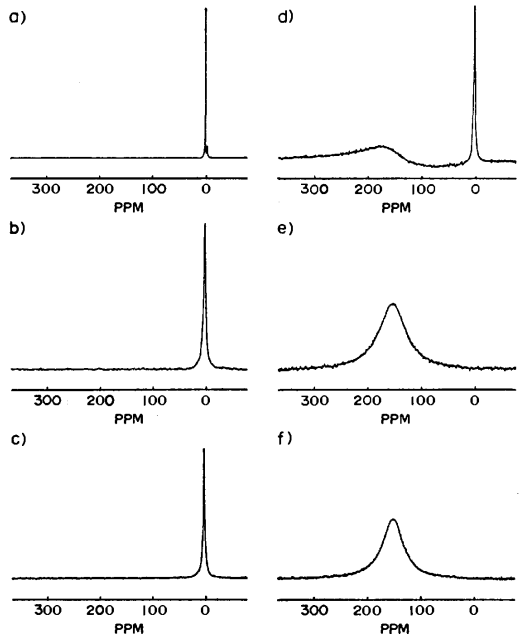

Fig. 2. ^{27}Al NMR spectra of a) aluminum sulfate in water, and the mixture of trimethylaluminum and aluminum isopropoxide at the molar ratios b) 0.00: 1.00, c) 0.40: 0.60, d) 0.60: 0.40, e) 0.80: 0.20, and f) 1.00: 0.00 in benzene at 28 °C.

Table 2. Chemical shifts, ν, half-height widths, $\Delta\nu$, and spin-lattice relaxation times, T_1*, for ^{27}Al NMR signals in benzene at 28 °C

$Al(CH_3)_3$: $Al(isoPrO)_3$[a]	ν (ppm)	$\Delta\nu$ (Hz)	T_1* (s)
$Al_2(SO_4)_3$[b]	0	1.35×10	2.2×10^{-3}
0.00 : 1.00	2.69	1.02×10^2	4.3×10^{-4}
0.40 : 0.60	3.75	8.75×10	4.5×10^{-4}
0.60 : 0.40[c]	2.30	7.19×10	7.2×10^{-4}
0.80 : 0.20	5.37×10^2	1.48×10^3	2.3×10^{-5}
1.00 : 0.00	5.37×10^2	1.04×10^3	3.2×10^{-5}

a) Molar ratio. b) Saturated water solution. c) The narrower of the two signals.

^{27}Al NMR. The aluminum nucleus forms the skelton of the polynuclear complexes, but little work has so far been undertaken on the structure of the complexes based on information about the aluminum nucleus itself. For this reason ^{27}Al NMR spectroscopy is an indispensable technique. However, ^{27}Al NMR signals are usually broad because of the $I=5/2$ spin and the large electric quadrupole moment,[8] so that they are not easily used to obtain detailed information. After the work of O'Reilly,[9] most studies using ^{27}Al NMR, which is a sensitive probe of the environment of the aluminum nucleus, have been developed by measuring line widths instead of direct measurements of the spin-lattice relaxation times.

^{27}Al NMR spectra of the reaction products of aluminum isopropoxide with trimethylaluminum are shown in Fig. 2, where aluminum sulfate dissolved in water is used as a chemical shift standard. Values of the chemical shift, ν, and the half-height width, $\Delta\nu$, are listed in Table 2. Aluminum sulfate shows up as a sharp line with a half-height width of 13.5 Hz indicating the formation of a monomeric structure involving six ligands in water. A single line of aluminum isopropoxide appeared at a frequency 2.69 ppm higher than that of aluminum sulfate with a half-height width of 102 Hz, although the tetrameric structure T^0 contains two kinds of the aluminum nuclei. Trimethylaluminum, the dimeric structure D^2 of which was determined from ^{1}H NMR spectra,[5,6] showed a broad signal with a half-height width of 1042 Hz at a frequency 537 ppm higher than that of aluminum sulfate. No signals other than those corresponding to the tetrameric or the dimeric structures were observed at molar ratios for trimethylaluminum and aluminum isopropoxide of 0.40: 0.60 and 0.80: 0.20, respectively. When trimethylaluminum and aluminum isopropoxide were mixed at a molar ratio of 0.60: 0.40, the ^{27}Al NMR spectrum displayed both narrow and broad lines corresponding to the tetra- and binuclear complexes, respectively. The coordination number of the aluminum nucleus of the tetranuclear complexes is six at the center and four in the wing. Hence, the aluminum nucleus at the latter position should show an NMR signal with a frequency close to that of the binuclear complexes, but no such signal was observed. As a result, the aluminum nuclei that represent the NMR signals are attributable to the

central nucleus of the tetranuclear complexes, T^0, T^1, T^2 and T^3, and to the nuclei forming the binuclear complexes, D^1 and D^2. The spin-lattice relaxation time for the aluminum nuclei situated in the wings of all the tetranuclear complexes and for those of the binuclear complex D^0 is believed to be too short to exhibit this NMR signal because of the low symmetry of the coordination structures.

In order to evaluate the spin-lattice relaxation time from the ^{27}Al NMR data, it is necessary to formulate an equation that describes the nuclear magnetization of aluminum in terms of the time interval t between the π- and $\pi/2$-pulses. The master equations for a nucleus with a spin quantum number I are expressed as

$$dP_1/dt = -W_{12}(P_1-P_2-\delta_{12})$$
$$dP_i/dt = W_{i-1,i}(P_{i-1}-P_i-\delta_{i-1,i}) - W_{i,i+1}(P_i-P_{i+1}-\delta_{i,i+1})$$

and

$$dP_n/dt = W_{n-1,n}(P_{n-1}-P_n-\delta_{n-1,n}), \quad (1)$$

where n is the total number of spin states given by $n=2I+1(=6)$, and i can take any integer between unity and n. P_i and $W_{i,i+1}$ denote the spin population of the i-th state and transition probability of the spin from the i-th state to the next higher state, respectively. $\delta_{i,i+1}$ denotes the difference in the spin populations between the i-th and $(i+1)$-th states at thermal equilibrium. For simplicity, it is assumed that both $W_{i,i+1}$ and $\delta_{i,i+1}$ are constants independent of i, and that the apparent value of the spin-lattice relaxation time is given by T_1^*, one half of the reciprocal of the transition probability. Then, the normalized value of the magnetization M for the ^{27}Al nucleus is given by

$$M = M(t)/M(\infty) = 1 - (2/105)(A+B+C), \quad (2)$$

where $A=\exp(-t/T_1^*)$, $B=2(26+15\sqrt{3})\exp[-(2-\sqrt{3})t/(2T_1^*)]$ and $C=2(26-15\sqrt{3})\exp[-(2+\sqrt{3})t/(2T_1^*)]$. A and C have smaller values than B, so that they are negligible within the practical accuracy of M. Hence Eq. 2 can be simplified to

$$M = 1 - 2\exp[-(2-\sqrt{3})t/(2T_1^*)]. \quad (3)$$

Experimental values of $\log 2(1-M)^{-1}$ lie along a straight line when plotted against the value of t. For a sample composed of a mixture of D^1 and D^2, it was difficult to obtain a straight line as a result of the overlapping of the broad signals, so that the apparent value of T_1^* was determined from the line width upon comparison with that of D^2. The T_1^* values are listed in the last column of Table 2.

Aluminum sulfate dissolved in water provided the longest T_1^* value, 2.2×10^{-3} s, of all the samples. T_1^* of the signal due to the tetranuclear complexes gradually increased with an increase in the amount of trimethylaluminum. This corresponds to a decrease in the molecular weight, as well as to a slight change in the coordination symmetry about the observable aluminum nucleus, supporting the assumption that it is the central nucleus alone that produces the NMR signal of the tetranuclear complexes. The T_1^* value is much shorter for the aluminum nucleus with the coordination number six, as can be seen from the following results of the binuclear complexes. When trimethylaluminum and aluminum isopropoxide were mixed at a molar ratio of 0.80: 0.20, the ^{27}Al NMR spectrum displayed a T_1^* value of 2.3×10^{-5} s, which was shorter than that for a pure solution of trimethylaluminum. This indicates that the aluminum nucleus of the binuclear complex D^1 produces an NMR signal at the same position as dimeric trimethylaluminum D^2. The T_1^* value would be too short to allow detection of the NMR signal of the aluminum nucleus between a pair of bridging isopropoxy groups and a pair of terminal methyl or isopropoxy groups.

^{13}C NMR. The coordination state of the ligand was examined by ^{13}C NMR, too, as is shown in Fig. 3, where tetramethylsilane was used as the chemical shift standard. The isopropoxy methyl and methine carbons produced ^{13}C NMR signals higher in frequency and narrower in width than those of the methyl carbons attached to the aluminum nucleus.

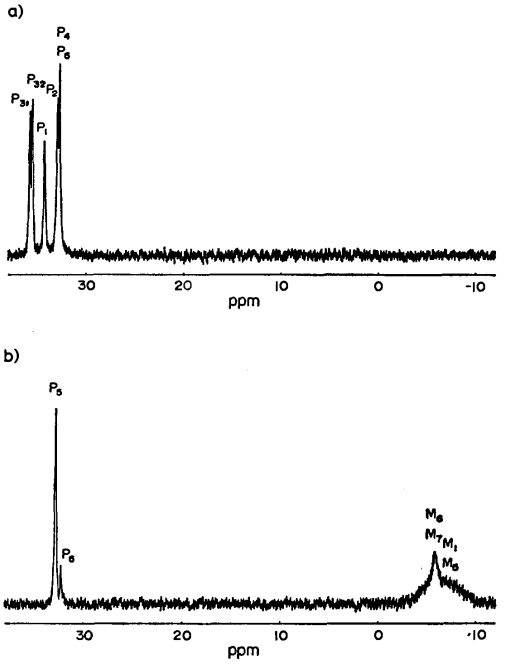

Fig. 3. ^{13}C NMR spectra of the mixture of trimethylaluminum and aluminum isopropoxide at the molar ratios a) 0.40: 0.60, and b) 0.80: 0.20 in benzene at 28 °C.

Four kinds of signals from the isopropoxyl methyl of the benzene carbon at 128.60 ppm, were observed in the ^{13}C NMR spectrum of a pure solution of aluminum isopropoxide. The signals at 34.27 and 33.00 ppm are assigned to the bridging ligand of tetrameric aluminum isopropoxide, T^0, and are designated by P_1 and P_2, respectively, in a similar manner to the case of ^{1}H NMR. The two signals at 35.75 and 35.53 ppm, which are close to each other in comparison with the other two signals, are assigned to the terminal ligand P_3 of T^0, and are indicated by P_{31} and P_{32}, respectively. The ^{1}H NMR signal from P_3 was, however, lower in frequency than the signals from P_1 and P_2, and did not split. On the other hand, the isopropoxy methine

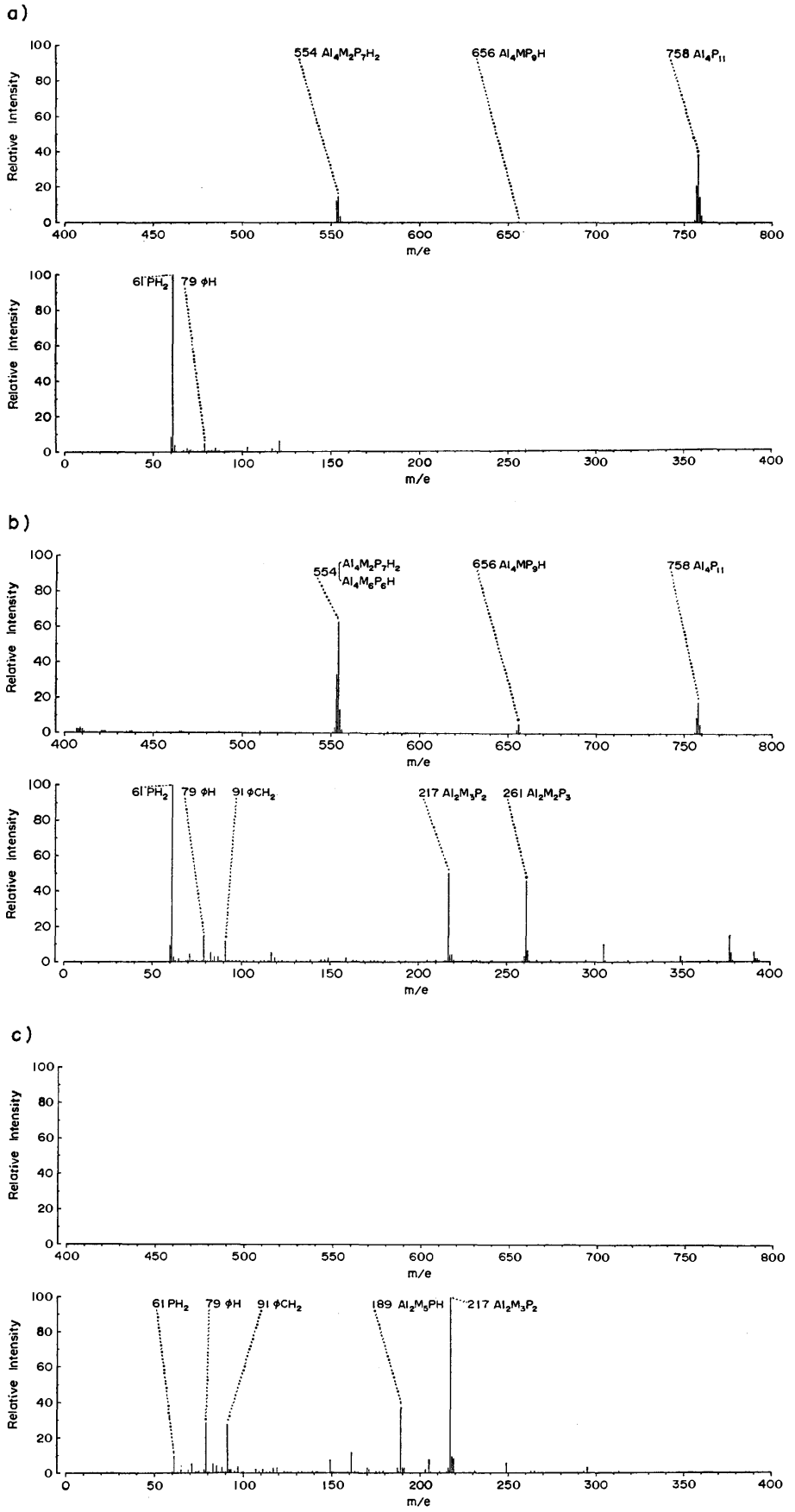

Fig. 4. Chemical ionization mass spectra of the mixture of trimethylaluminum and aluminum isopropoxide at the molar ratios a) 0.00: 1.00, b) 0.30: 0.70, and c) 0.90: 0.10 in benzene.

carbons of aluminum isopropoxide display only the two signals with equimolar intensity at 73.70 and 70.83 ppm, which are assigned to the terminal and bridging ligands respectively, so that splitting of the isopropoxy methyl, signal is attributed to the steric difference of the two methyl groups bonded to a methine carbon.

When trimethylaluminum was added to aluminum isopropoxide in benzene, a new signal from the isopropoxy methyl carbon appeared at 32.80 ppm, which was assigned to a mixture of the bridging ligands, P_4 of the substituted wing of the tetranuclear complexes T^1, T^2, and T^3, and P_5 of the binuclear complex D^0. However, the methyl groups of M_3 and M_4 attached to the aluminum nuclei bearing P_4 and P_5, respectively, produced no ^{13}C NMR signal. This phenomenon coincides with the result of the ^{27}Al NMR experiments that no NMR signal was detected due to these aluminum nuclei.

When the amount of trimethylaluminum exceeded 75.0 mol % in the benzene solution, signals from the tetranuclear complexes diminished to the point of disappearing, and a signal due to the isopropoxy methyl carbon, assigned to P_6 of the binuclear complex D^1, appeared at 32.21 ppm accompanied by the signals from the corresponding to methyl groups M_1 and M_5, which overlapped each other at -7.0 ppm with a half-height width of *ca.* 140 Hz. The methyl groups, M_6 and M_7, of dimeric trimethylaluminum D^2 also displayed an overlapping of the carbon signals at -5.9 ppm with a half-height width of *ca.* 20 Hz. Line broadening of the methyl carbons bonded to the aluminum nucleus corresponds to the exchange of the methyl groups and to the electric quadrupole moment of the adjacent aluminum nucleus, as well as to the spin-spin coupling between the ^{13}C and ^{27}Al nuclei.[10] Since the carbons of the ligands are located at positions closer to the aluminum nucleus in comparison with the protons, the ^{13}C NMR spectrum exhibits an intermediate character between the ^1H NMR and the ^{27}Al NMR data supporting these results.

Chemical Ionization Mass Spectrometry. In order to verify the NMR results mentioned above, it is desirable to determine the molecular weight of the aluminum complexes. However, these complexes are so unstable that it is very difficult to measure their molecular weights using ordinary methods. CIMS (chemical ionization mass spectrometry) is a useful technique for the molecular weight measurements of such unstable compounds, since ions are produced under a milder condition in CIMS than in electron impact mass spectrometry.

CIMS spectra of the reaction products of aluminum isopropoxide with trimethylaluminum are illustrated in Fig. 4. In the CIMS spectrum of aluminum isopropoxide, the large peak at an *m/e* of 758 corresponds to an ion of $[Al_4(isoPrO)_{11}]^+$, which is a fragment from a $Al_4(isoPrO)_{12}$ molecule. This indicates a tetrameric structure for aluminum isopropoxide, although no molecular ion $[T^0H]^+$ was detected at an *m/e* of 818. The peaks at *m/e* of 656 and 554 are assigned to $[Al_4(CH_3)(isoPrO)_9H]^+$ and $[Al_4(CH_3)_2(isoPrO)_7H_2]^+$, respectively, which are produced by the partial substitution of the isopropoxyl groups of T^0 by methyl groups of methane, the reactant gas. The isopropoxyl group of the ligand produces a peak at an *m/e* of 61, which is assigned to $[isoPrOH_2]^+$.

When trimethylaluminum and aluminum isopropoxide were mixed at a molar ratio of 0.30: 0.70, the peaks at *m/e* of 656 and 554 were enhanced indicating the progress of the substitution reaction of the isopropoxyl group by the methyl group for trimethylaluminum. The peak at an *m/e* of 554 might include a molecular ion $[Al_4(CH_3)_6(isoPrO)_6H]^+$ from the tetranuclear complex T^3, but no molecular ions were produced from the tetranuclear complexes, T^1 and T^2, as well as from T^0. The peaks at *m/e* of 261 and 217 are attributable to $[Al_2(CH_3)_2(isoPrO)_3]^+$ and $[Al_2(CH_3)_3(isoPrO)_2]^+$ binuclear ions, respectively. The former corresponds to the reaction product of D^0 with the isopropoxyl ion or to a fragment from T^1, T^2, or T^3, and the latter to a fragment from D^0.

At a molar ratio of trimethylaluminum and aluminum isopropoxide concentrations of 0.90: 0.10, no tetranuclear ions were detected in the CIMS spectrum, which displayed large peaks for binuclear ions at *m/e* of 217 and 189. The peak at an *m/e* of 189 is assigned to the $[Al_2(CH_3)_5(isoPrO)H]^+$ molecular ion from D^1. These results agree with the data obtained in the NMR experiments.

Conclusion

The structure of aluminum complexes formed by the reaction of aluminum isopropoxide with trimethylaluminum was investigated from three different angles: the ligand was examined using ^1H NMR and ^{13}C NMR, the central nucleus using ^{27}Al NMR, and the molecular weight employing chemical ionization mass spectrometry.

The spin-lattice relaxation time of ^1H is sensitive to the motion of the ligand; T_1 was shorter at the bridge position than at the terminal position, and inversely proportional to the molecular weight. This was used to estimate the mean molecular weight of the mixture of tetranuclear complexes, which were indistinguishable from one another using the chemical shift of the ^1H and ^{13}C NMR signals.

The coordination symmetry about the aluminum nucleus was reflected on the spin-lattice relaxation time of ^{27}Al, which was defined as one half of the reciprocal of the transition probability of the spin, T_1^*. The T_1^* value was longer at the center of the tetranuclear complex than at the binuclear complex, and was too short to produce an NMR signal for the aluminum nucleus between a pair of bridging isopropoxy groups and a pair of terminal methyl or isopropoxy groups.

The ^{13}C NMR data for the ligand represented an intermediate character between the data for ^1H NMR and ^{27}Al NMR; the ^{13}C NMR signal due to the isopropoxyl group reflected the configuration of the ligand in a manner similar to the ^1H NMR, while that of the methyl group was broad and was not observed with a methyl group attached to the aluminum nucleus that showed no NMR signal.

The chemical ionization mass spectra of the products of the reaction of aluminum isopropoxide with trimethylaluminum showed fragment ions from both the tetra- and the binuclear complexes as predicted from the NMR study. However, no molecular ions of tetrameric aluminum isopropoxide were observed.

All the results support the conclusions of previous work[7] that the terminal isopropoxy groups of tetrameric aluminum isopropoxide are replaced successively by the methyl groups of dimeric trimethylaluminum to form three kinds of tetranuclear and two kinds of binuclear complexes, and that, after the reactions, the resultant tetranuclear complex undergoes decomposition reactions leading to two kinds of binuclear complexes.

References

1) H. Reinheckel, K. Haage, and D. Jahnke, *Organometal. Chem. Rev., Sect. A*, **4**, 47 (1969).
2) D. C. Bradley, *Advan. Chem. Ser.*, **23**, 10 (1959).
3) A. W. Laubengayer and W. F. Gilliam, *J. Am. Chem. Soc.*, **63**, 447 (1941).
4) V. J. Shiner, Jr., D. Whittaker, and V. P. Fernandez, *J. Am. Chem. Soc.*, **85**, 2318 (1963).
5) N. Muller and D. E. Pritchard, *J. Am. Chem. Soc.*, **82**, 248 (1960).
6) K. C. Ramey, J. F. O'Brien, I. Hasegawa and A. E. Borchert, *J. Phys. Chem.*, **69**, 3418 (1965).
7) M. Uetsuki and Y, Fujiwara, *J. Am. Chem. Soc.*, **95**, 4142 (1973).
8) L. Petrakis and F. K. Dickson, *Appl. Spectrosc. Rev.*, **4**, 1 (1970).
9) D. E. O'Reilly, *J. Chem. Phys.*, **32**, 1007 (1960).
10) O. Yamamoto, *J. Chem. Phys.*, **63**, 2988 (1975).

Chromium(III) Complexes with Amino Acids. II. Chromium(III) Complexes with L-α-Amino Acids

Hisaya Oki

Department of Chemistry, Faculty of Education, Fukui University, Fukui 910

(Received June 4, 1976)

As chromium(III) complexes with L-α-amino acids (alanine, aminobutyric acid, norvaline, norleucine, valine, isoleucine and leucine), $[Cr(ala)_3]$, (+)$[Cr(am\text{-}but)_3]$, $[Cr(OH)(am\text{-}but)_2]_2$, (+) and (−)$[Cr(norval)_3]$, (−)-$[Cr(norleu)_3]$, $[Cr(OH)(norleu)_2]_2$, $[Cr(val)_2(val\text{-}O)(NH_3)]$, (+)$[Cr(isoleu)_3]$, $[Cr(isoleu)_2(isoleu\text{-}O)(NH_3)]$, $[Cr(OH)(isoleu)_2]_2$, (+) and (−)$[Cr(leu)_3]$, and $[Cr(OH)(leu)_2]_2$ were prepared by the matrix method in solid state, and $[Cr(ala)_3]$, $[Cr(am\text{-}but)_3]$, $[Cr(OH)(am\text{-}but)_2]_2$, (−)$[Cr(norval)_3]$, $[Cr(OH)(norval)_2]_2$, (−)$[Cr(norleu)_3]$, $[Cr(OH)(norleu)_2]_2$, (+)$[Cr(val)_3]$, $[Cr(val)_2(val\text{-}O)(NH_3)]$, $[Cr(OH)(val)_2]_2$, (+)$[Cr(isoleu)_3]$, $[Cr(OH)(isoleu)_2]_2$, and a mixture of diasteroisomers of $[Cr(leu)_3]$ were obtained by the usual method in solution. Some differences in the formation of the tris-type and hydroxo-dimer complexes appeared between the two methods. Especially, in the solid reaction, some complexes gave diastereoisomers with optically-active counter structures depending upon the kind of solvents used for preparation. All tris-type chromium(III) complexes with L-α-amino acids were of *fac*-structure.

In a previous paper,[1] systematic studies were reported on the effect of the length of the skeletal carbon chain or the presence of side chains in glycine and racemic amino acids upon the formation of complexes by the isothermal matrix method in solid state and by the usual method in solution in which hexaamminechromium(III) nitrate was used as the starting material. In the present work, attempts were made to prepare chromium(III) complexes with L-α-amino acids (alanine, aminobutyric acid, norvaline, norleucine, valine, isoleucine and leucine) by applying the same methods as described in Ref. 1 with respect to the preparation of racemic amino acids and to study the difference between racemic and L-amino acids in complexation. The studies of the formation of optical isomers of the complexes were also investigated.

Experimental

Preparation of Chromium(III) Complexes. There are two methods for the preparation of chromium(III) complexes with L-α-amino acids depending on the starting technique.

a) Preparation by Solid State Reaction: Hexaamminechromium(III) nitrate was mixed with the respective L-amino acid in a mortar. The mixture was heated at (150±1)°C in a Toyoroshi electronic drying oven. The molar ratio of the amino acids to the starting complexes was 3: 1 and the heating time was 20 min.

The reaction product containing L-alanine was dissolved in water. After removal of the residue by filtration, filtrate was kept standing at room temperature for one or two days. $[Cr(ala)_3]$ was gradually deposited as pink crystals. The main product of the residues was also $[Cr(ala)_3]$. Using a method similar to that described above, the di-μ-hydroxo-tetrakis(amino acidato)dichromium(III) complexes were obtained as light purple crystals, when the amino acid was L-α-aminobutyric acid, L-norleucine or L-leucine. The complex with L-norvaline was, however, obtained as (−) $[Cr(norval)_3]\cdot 3H_2O$. In the case of L-isoleucine, a mixture of pink and purple crystals was gradually deposited. The mixture was dissolved in DMF. After filtration, the filtrate was added dropwise to water, causing instant precipitation of (+)$[Cr(isoleu)_3]\cdot 3H_2O$ as pink crystals. The purple residue obtained by the above filtration was $[Cr(OH)(isoleu)_2]_2\cdot 6H_2O$.

The reaction products containing L-α-aminobutyric acid, L-norvaline, L-norleucine, L-valine, L-isoleucine and L-leucine were dissolved in methanol. After removal of the residues by filtration, the filtrates were kept standing at room temperature for two or three days. (+)$[Cr(am\text{-}but)_3]\cdot H_2O$, (+)$[Cr(norval)_3]\cdot 2H_2O$, $[Cr(norleu)_3]\cdot 3H_2O$, $[Cr(val)_2(val\text{-}O)(NH_3)]\cdot 2H_2O$, $[Cr(isoleu)_2(iaoleu\text{-}O)(NH_3)]\cdot 2H_2O$ and (+)$[Cr(leu)_3]\cdot 3.5H_2O$ were gradually deposited as pink crystals. After filtering the (+)$[Cr(am\text{-}but)_3]\cdot H_2O$ obtained above, the filtrate was kept standing at room temperature until completely dried, another type of $[Cr(am\text{-}but)_3]\cdot H_2O$ also being obtained as pink crystals. The former was soluble, whereas the latter was insoluble in water. The complexes $[Cr(val)_2(val\text{-}O)(NH_3)]\cdot 2H_2O$ and $[Cr(isoleu)_2(isoleu\text{-}O)(NH_3)]\cdot$ were obtained by drying for 30 min the above-mentioned crystals deposited at 50°C.

When ethanol was used as the solvent, tris type complexes were obtained as pink crystals only for L-norvaline, L-norleucine and L-leucine. The CD sign of these optically active tris type complexes was, however, negative, which is opposite to that of the corresponding complexes obtained in methanol. Complexes with L-valine and L-isoleucine were also obtained as $[Cr(val)_2(val\text{-}O)(NH_3)]\cdot 2H_2O$ and $[Cr(isoleu)_2(isoleu\text{-}O)(NH_3)]\cdot 2H_2O$, respectively, although they might have been contaminated by small amounts of tris type complexes. In the case of L-α-aminobutyric acid, only an oily substance was obtained, the crystallization having been unsuccessful. In the case of L-alanine, the reaction product was insoluble in both ethanol and methanol.

The analytical data for the complexes obtained by the above method are shown in Table 1, except for the dimer-complexes with isoleucine and norleucine. The IR spectra of these complexes were coincident with those of the corresponding complexes obtained by the solution method.

b) Preparation by Solution Reaction: Hexaamminechromium(III) nitrate (345 mg) and L-α-alanine (267 mg) were dissolved in hot water (5 ml) and the mixture was heated in a water bath until pink crystals began to appear and then was cooled to room temperature. The pink crystals obtained were $[Cr(ala)_3]$. By applying the method described above, the complexes with L-α-aminobutyric acid, L-norvaline and L-valine were all precipitated as pink crystals. The pink crystals containing L-norvaline were dissolved in DMF or DMSO. After filtration, the filtrate was added dropwise to water, causing instant precipitation of (−)$[Cr(norval)_3]\cdot 3H_2O$. The pink complex containing L-α-aminobutyric acid was washed with water and then with ethanol. In the case of L-valine, the pink crystals were

Table 1. Analytical data (for the solid reaction)

Complexes	C (%)		H (%)		N (%)	
	Calcd	Found	Calcd	Found	Calcd	Found
$[Cr(ala)_3]^{a)}$	34.18	34.12	5.74	5.75	13.29	14.11
$[Cr(am\text{-}but)_3]\cdot H_2O^{b)}$*	38.30	37.92	6.96	6.63	11.17	11.06
$[Cr(am\text{-}but)_3]\cdot H_2O^{b)}$**	38.30	38.40	6.96	6.55	11.17	11.18
$[Cr(norval)_3]\cdot 3H_2O^{a)}$	39.61	39.52	7.92	7.84	9.24	9.19
$[Cr(norval)_3]\cdot 2H_2O^{b)}$	41.28	40.71	7.39	7.14	9.63	9.76
$[Cr(norval)_3]\cdot 3H_2O^{c)}$	39.61	39.63	7.92	7.52	9.24	9.20
$[Cr(norleu)_3]\cdot 3H_2O^{b)}$	43.54	43.75	8.53	8.15	8.46	8.53
$[Cr(norleu)_3]\cdot 3H_2O^{c)}$	43.54	43.43	8.53	8.17	8.46	8.42
$[Cr(isoleu)_3]\cdot 3.5H_2O^{a)}$	42.77	42.51	8.57	8.07	8.31	8.53
$[Cr(leu)_3]\cdot 3.5H_2O^{b)}$	42.77	42.73	8.57	7.99	8.31	8.21
$[Cr(leu)_3]\cdot 2H_2O^{c)}$	45.18	44.90	8.43	8.60	8.78	9.16
$[Cr(val)_2(val\text{-}O)(NH_3)]\cdot 2H_2O^{b)}$	40.00	39.49	7.61	7.75	12.43	12.25
$[Cr(isoleu)_2(isoleu\text{-}O)(NH_3)]\cdot 2H_2O^{b)}$	43.62	44.06	8.74	8.18	11.31	11.19
$[Cr(OH)(am\text{-}but)_2]_2\cdot 1.5H_2O^{a)}$	33.51	33.79	6.45	5.88	9.77	9.90
$[Cr(OH)(leu)_2]_2\cdot 6H_2O^{a)}$	37.59	36.53	8.65	7.96	7.71	7.31

Solvent: a) water, b) methanol, c) ethanol. * dissolved in water, ** not dissolved in water.

Table 2. Analytical data (for the solution reaction)

Complexes	C (%)		H (%)		N (%)	
	Calcd	Found	Calcd	Found	Calcd	Found
$[Cr(ala)_3]$	34.18	33.18	5.74	5.49	13.29	13.17
$[Cr(am\text{-}but)_3]\cdot H_2O$	38.30	38.12	6.96	6.60	11.17	11.10
$[Cr(norval)_3]\cdot 3H_2O$	39.61	40.16	7.92	7.10	9.24	9.35
$[Cr(norval)_3]\cdot 3H_2O$	39.61	39.75	7.92	7.10	9.24	9.09
$[Cr(norleu)_3]\cdot H_2O$	46.95	46.44	8.32	8.27	9.12	8.87
$[Cr(val)_3]\cdot 3H_2O$	39.61	39.60	7.92	7.75	9.24	9.25
$[Cr(isoleu)_3]\cdot 3H_2O$	43.54	43.41	8.53	8.33	8.46	8.41
$[Cr(leu)_3]\cdot 2H_2O$	45.18	46.05	8.43	8.40	8.78	8.93
$[Cr(OH)(am\text{-}but)_2]_2\cdot 1.5H_2O$	33.51	33.44	6.45	6.13	9.77	10.30
$[Cr(OH)(norval)_2]_2\cdot 2H_2O$	37.62	37.39	7.26	7.01	8.77	8.53
$[Cr(OH)(norleu)_2]_2\cdot 4H_2O$	39.45	40.06	8.00	7.67	7.67	7.88
$[Cr(OH)(val)_2]_2\cdot 2H_2O$	37.62	36.91	7.26	6.52	8.77	8.78
$[Cr(OH)(isoleu)_2]_2\cdot 6H_2O$	37.59	37.04	8.65	8.15	7.31	7.32

dissolvaed in ethanol. After filtration, $(+)[Cr(val)_3]\cdot 3H_2O$ was obtained from the residue and when the filtrate was allowed to stand at room temperature for three or four days, $[Cr(val)_2(val\text{-}O)(NH_3)]\cdot xH_2O$ was gradually deposited as red-purple crystals. By heating at 50°C for 30 min, the amount of crystal water contained was determined to be $x=2$. The IR spectrum of this complex was coincident with that of the corresponding complexes obtained for the solid state reaction.

By using a similar method, with the exception that 60 ml of water was employed insteaed of 5 ml of hot water, hydroxo-dimer complexes with L-α-aminobutyric acid, L-norvaline, L-norleucine, L-valine and L-isoleucine were obtained as purple crystals. However, the complexes with L-alanine and L-leucine were of tris-type. When 10 ml of water was employed, hydroxo-dimer complexes were obtained in the case of L-α-aminobutyric acid and L-valine, whereas only tris complexes were obtained for all the other amino acids. The tris complex containing L-norvaline was dissolved in methanol. After filtration, the filtrate was concentrated using a cooling dryer, causing the precipitation of $(-)[Cr(norval)_3]\cdot 3H_2O$. The residue thus obtained was identical to that obtained previously.

The analytical data of these complexes are shown in Table 2.

Apparatus. The UV spectra were measured with a Hitachi 139 spectrophtometer. The IR spectra were measured in a KBr disk with a Hitachi EPI-G3 infrared spectrophtometer. The CD spectra were recoded on a JASCO Model ORD/UV-5 spectrophtometer with a CD attachment.

Results and Discussion

UV Absorption Spectra. The absorption spectra of the chromium(III) complexes with L-α-amino acids of type $[Cr(L)_3]$ and $[Cr(L)_2(L\text{-}O)(NH_3)]$, where L denotes amino acids, were measured in DMSO, except for the complexes with alanine, aminobutyric acid and norleucine which were insoluble in DMSO. The spectra of the chromium(III) complexes with alanine and aminobutyric acid were measured in solid state and in perchloric acid. The spectrum of the tris(norleucinato)-chromium(III) complex was not measured, because the yield of this complexes was very small. Since the color of this complex was pink, the structure may be of facial form.

The numerical data for their absorption maxima are summarized in Table 3. These data suggest that the

Table 3. Absorption maxima of tris- and bis-type chromium(III) complexes

ν: wave number of absorption maximum,
ε: molar absorption coefficient (M^{-1} cm^{-1} M: mol dm^{-3}).

	$\nu_1/10^3$ cm^{-1}	(log ε)	$\nu_2/10^3$ cm^{-1}	(log ε)	Solvent
Solid state reaction					
$[Cr(ala)_3]$	18.7	(1.71)	25.1	(1.62)	20%$HClO_4$
$[Cr(ala)_3]$	19.4		26.0		Reflectance
$[Cr(am\text{-}but)_3]$	19.4	(1.87)	26.0	(1.83)	DMSO
$[Cr(am\text{-}but)_3]$	18.6	(1.70)	25.0	(1.64)	20%$HClO_4$
$[Cr(norval)_3]$[a]	19.5	(2.20)	25.7	(2.09)	DMSO
$[Cr(norval)_3]$[b]	19.2	(2.24)	25.3	(2.11)	DMSO
$[Cr(norval)_3]$[c]	19.5	(2.22)	25.7	(2.10)	DMSO
$[Cr(norleu)_3]$	19.5	(2.25)	25.7	(2.05)	DMSO
$[Cr(isoleu)_3]$	19.2	(2.24)	25.3	(2.14)	DMSO
$[Cr(leu)_3]$[b]	19.2	(2.30)	25.3	(2.20)	DMSO
$[Cr(leu)_3]$[c]	19.4	(2.29)	25.5	(2.20)	DMSO
$[Cr(val)_2(val\text{-}O)(NH_3)]$	19.3	(1.76)	25.7	(1.81)	DMSO
$[Cr(isoleu)_2(isoleu\text{-}O)(NH_3)]$	19.3	(1.75)	25.7	(1.82)	DMSO
Solution state reaction					
$[Cr(ala)_3]$	19.4		26.0		Reflectance
$[Cr(am\text{-}but)_3]$	18.6	(1.70)	25.0	(1.65)	20%$HClO_4$
$[Cr(am\text{-}but)_3]$	19.4		26.0		Reflectance
$[Cr(norval)_3]$	19.5	(2.19)	25.7	(2.08)	DMSO
$[Cr(norleu)_3]$	19.5	(2.27)	25.7	(2.06)	DMSO
$[Cr(val)_3]$	19.1	(2.24)	25.4	(2.08)	DMSO
$[Cr(isoleu)_3]$	19.2	(2.24)	25.4	(2.12)	DMSO
$[Cr(leu)_3]$	19.3	(2.28)	25.4	(2.20)	DMSO

Solvent: a) water, b) methanol, c) ethanol.

complexes with L-alanine and L-α-aminobutyric acid undergo acid hydrolysis or some chemical reaction on dissolution in perchloric acid and that the behavior is similar to that of complexes with *dl*-alanine and *dl*-α-aminobutyric acid. Also it is seen that the absorpiton maxima of the other chromium(III) complexes are almost coincident with those of the corresponding chromium(III) complexes of tris-type with *dl*-amino acids.[1] This suggests that the chromium(III) complexes

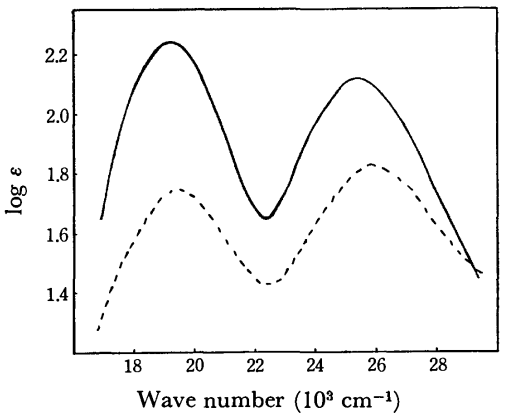

Fig. 1. The absorption spectra of $[Cr(isoleu)_3]$ (——) and $[Cr(isoleu)_2(isoleu\text{-}O)(NH_3)]$ (------) in DMSO solution.
ε: M^{-1} cm^{-1}, M: mol dm^{-3}.

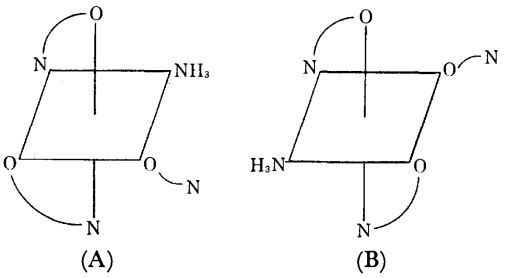

Fig. 2. The possible structures of $[Cr(isoleu)_2(isoleu\text{-}O)(NH_3)]$.

of tris-type are of *fac*-structure.

The spectra of $[Cr(isoleu)_3]$ and $[Cr(isoleu)_2(isoleu\text{-}O)(NH_3)]$ in DMSO are shown in Fig. 1. The absorption curve of the bis-type complex is similar to that of the tris-type, except that the first absorption band has a lower absorption coefficient than the second band of the bis-type complex. Therefore, this uggests that the coordinating structure of the bis-type complex is a cis-cis structure with respect to the nitrogen or oxygen atoms and the symmetry of this complex is lower than the C_{3v} of tris-type complex. Thus, for the bis-type complex, two geometrically possible isomers are considered, as shown in Fig. 2. When the reaction product was dissolved in water, instead of methanol, a mixture of *fac*- and hydroxo-dimer complexes were obtained. This suggests that the coordinating structure of this complex is that of (A) in Fig. 2. The absorption spectrum of $[Cr(val)_2(val\text{-}O)(NH_3)]$ was similar to that of $[Cr(isoleu)_2(isoleu\text{-}O)(NH_3)]$. The structure of the bis(valinato) complex is also coincident with that of the bis(isoleucinato) one.

IR Spectra. Infrared absorption spectra were measured in the range of 4000 to 400 cm^{-1}. The spectra of $[Cr(isoleu)_3]$ and $[Cr(isoleu)_2(isoleu\text{-}O)(NH_3)]$ are shown in Fig. 3. It is seen from this firgure that the absorption peak which is assigned to the NH_2 deformation vibration appears at 1505 cm^{-1} in the bis-type complex, but that in the tris complex in which all amine groups were bonded to the chromium atom, this peak is shifted to 1600 cm^{-1}. Therefore, these results lead to the conclusion that the structure of this bis-type complex is that of (A) in Fig. 2. The bis-type

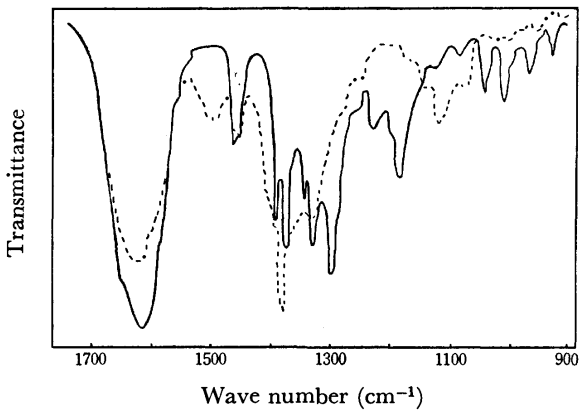

Fig. 3. The IR spectra of $[Cr(isoleu)_3]$ (——) and $[Cr(isoleu)_2(isoleu\text{-}O)(NH_3)]$ (------).

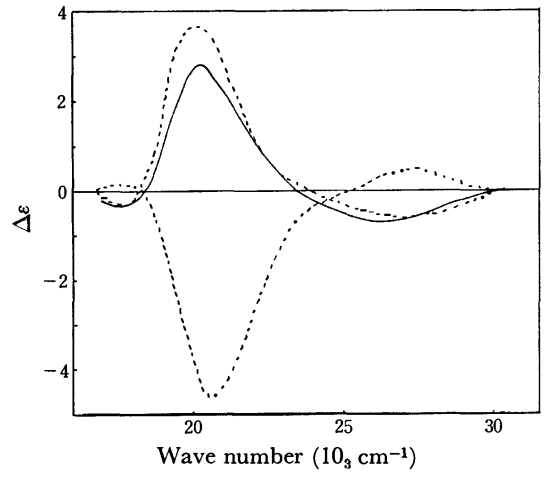

Fig. 4. The CD spectra of (+)[Cr(L-am-but)$_3$] (——) and (+) and (−)[Cr(L-norval)$_3$] (------).
ε: M^{-1} cm^{-1}, M: mol dm^{-3}.

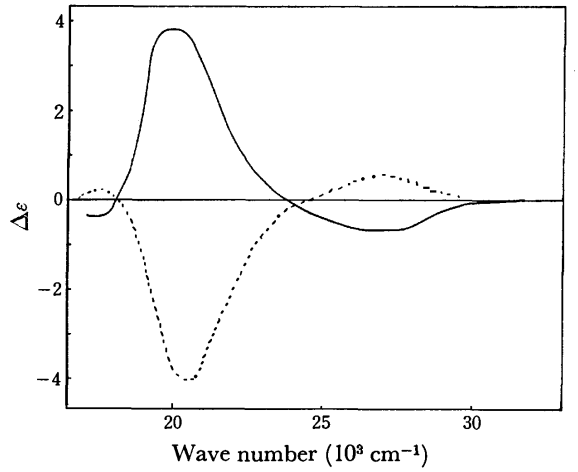

Fig. 5. The CD spectra of (−)[Cr(L-norleu)$_3$] (------) and (+)[Cr(L-val)$_3$]] (——).
ε: M^{-1} cm^{-1}, M: mol dm^{-3}.

complex with L-valine also has an absorption peak at 1505 cm^{-1}. This suggests that the structure of this complex is similar to that of the bis-type complex with L-isoleucine.

CD Spectra. The circular dichroism for (+)[Cr(am-but)$_3$] and (+) and (−)[Cr(norval)$_3$] (Fig. 4), (−)[Cr(norleu)$_3$] and (+)[Cr(val)$_3$] (Fig. 5), and (+)[Cr(isoleu)$_3$] and (+) and (−)[Cr(leu)$_3$] (Fig. 6) were measured in DMSO. Although the separation of these optical isomers was not always perfect, the $\Delta\varepsilon_{(ext)}$ of the major components of the first absorption band were larger than those for the corresponding cobalt(III) complexes.[2] Therfore, it appears that these optical isomers were obtained as complexes with fairly high optical purity. Their configurations can be tentatively identified as *Λ* for (+) and *Δ* for (−) by comparing the CD curves of the present complexes with those of the *Λ*-tris(oxalato)[3] and *Λ*-tris(ethylendiamine)chromium[4] ions, respectively. Gillard *et al.* have reported that [Cr(ala)$_3$] which is insoluble in water is of *Λ*-form.[5] The IR spectrum of [Cr(ala)$_3$] obtained in the present work agrees with that published by the above authors.

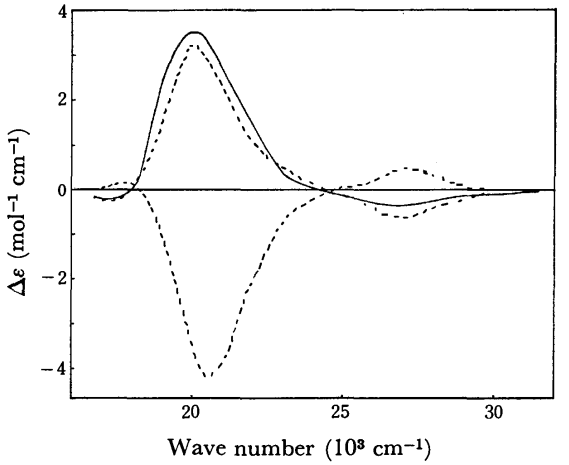

Fig. 6. The CD spectra of (+)[Cr(L-isoleu)$_3$] (——) and (+) and (−)[Cr(L-leu)$_3$] (------).
ε: M^{-1} cm^{-1}, M: mol dm^{-3}.

Douglas and Yamada have reported[6] that the lower solubility of (*β*)-*Λ*[Co(L-ala)$_3$] is not surprising since the molecules of the isomer might be expected to interact strongly through intramolecular hydrogen bonding which would be possible if the molecules were stacked directly above one another. The solubility of (+)[Cr(norval)$_3$] is appreciably lower than that of the corresponding (−) complex. Therefore, the tris(aminobutyrato) and tris(norleucinato)chromium(III) complexes, which are insoluble in both water and DMSO might be also of (+)-form. But, (+)[Cr(am-but)$_3$] which is soluble in water might be different from the other complexes in crystal structure. In general, the solubility of *fac*-(+)chromium(III) complexes with L-amino acids which do not have the side chain is lower than that of the (−) complexes. On the other hand, it is not difficult to understand that the solubility of (+)[Cr(val)$_3$], (+)[Cr(isoleu)$_3$] and (+)[Cr(leu)$_3$] is high, since the interaction through intramolecular hydrogen bonding would become weaker as these amino acids have a methyl group in the *β*- or *γ*-position. Since the spectra of [Cr(val)$_2$(val-O)(NH$_3$)] and [Cr(isoleu)$_2$-(isoleu-O)(NH$_3$)] were not observed, except for the small peaks which are regarded as due to vicinal effects, these complexes are considered to be mixturees of diastereoisomers.

Table 4. Chromium(III) complexes prepared with L-amino acids

Amino acid	[Cr(L)$_3$]	[Cr(L)$_2$-(L–O)(NH$_3$)]	[Cr(OH)-(L)$_2$]$_2$
Alanine	◑		
Aminobutyric acid	◑		◑
Norvaline	◑		○
Norleucine	◑		◑
Valine	○	◑	○
Isoleucine	◑	●	◑
Leucine	◑		●

L=amino acid.
●: Complexes prepared by the solid method.
◑: Complexes prepared by both methods.
○: Complexes prepared by the solution method.

The chromium(III) complexes with various L-α-amino acids of type $[Cr(L)_3]$, $[Cr(L)_2(L\text{-}O)(NH_3)]$ and $[Cr(OH)(L)_2]_2$ were synthesized in solid state and in solution (Table 4). The preparation of chromium(III) complexes with natural L-α-amino acids by the two methods may be characterized as follows.

i) *Solid State Reaction.* The complexes of tris-type structure were prepared for all amino acids, except for L-valine, but the complexes of dimer-structure were prepared only for amino acids other than L-alanine, L-norvaline and L-valine. As far as valine and isoleucine, which have a methyl group in the β-position, are concerned, a new type complex, $[Cr(L)_2(L\text{-}O)(NH_3)]$ was prepared. When water was used as the solvent, the complexes containing alanine and norvaline obtained were of tris-type, while the complexes containing aminobutyric acids and norleucine were of dimer structure. Complexes with L-α-amino acids are predominatly of tris- and dimer-type, alternatively, depending on the length of the carbon skeleton. This is also observed for the complexes with racemic amino acids prepared by the solution method.

Table 5. Optical isomers of the tris-chromium(III) complexes prepared

Amino acid	Solid reaction			Solution reaction
	MeOH	EtOH	H_2O	
Alanine	no	no	(+)	(+)
Aminobutyric acid	+	no	no	(+)
Norvaline	+	−	−	−
Norleucine	(+)	−	−	−
Valine	no	no	no	+
Isoleucine	no	no	+	+
Leucine	+	−	no	mixture

no: No tris-complex was obtained.
( ): The CD spectrum was not measured due to the low solubility.

The interesting relation between the formation of optical isomers and the solvent in which the reaction product was dissolved, which is shown in Table 5, together with that for complexes prepared by the solution method. These data suggest that the preponderance of the type of optical isomers is changed depending upon the kind of solvent used, specifically, when reaction products were dissolved in methanol, (+) isomers were obtained, while (−) isomer were obtained in ethanol. The reason may be due to the difference in the solubilities of the diastereoisomers, although this is still not clear from the present work. When water was used as the solvent, the complex with alanine was obtained as a (+) isomer, but those with norvaline and norleucine in which the length of carbon chain is longer than that of aminobutyric acid are obtained as (−) isomers. On the other hand, the complexes with L-amino acids which have a side chain have no clear tendency, since the complex with L-isoleucine are obtained as a (+) isomer, while the other complexes obtained are not in tris form.

When the differences between the racemic and L-amino acids in the complexation were compared, L-amino acids which have no side chains were similar to the racemic acid, except for norleucine. The complexes with L-amino acids which have a side chain were obtained as bis- (val), tris-, bis- and dimer-(isoleu), and tris- and dimer-structures (leu), while the complexes with the corresponding racemic amino acids were obtained only as dimer-type structures. No circular dichroism for tris-type structures with racemic amino acids was observed, while the complexes with L-amino acids were found to be optically active.

ii) *Solution State Reaction.* The chromium(III) complexes with L-amino acids were all prepared as tris-type structures. All complexes of dimer-structure were prepared, except for alanine and leucine. By changing the amount of water in which the mixture was dissolved, tris- or dimer-complexes were selectively obtained. The optical isomer obtained by the solution method is similar to that resulting from the solid reaction which was dissolved in water, except for L-α-aminobutyric acid, L-valine and L-leucine which were not prepared as tris-type complexes in solid state.

When the differences between racemic and L-amino acids in complexation were compared, no significant difference was observed for the solution method, except that the complexes with L-amino acids were obtained as optically-active complexes. However, a different result was obtained for the complex with valine, since *dl*-valine gave only a dimer-type complex, while L-valine gave tris-, bis- and dimer-structures.

The author wishes to thank Professor Muraji Shibata and his corworkers of Kanazawa University for the CD measurements. The author also wishes to thank Professor Ryokichi Tsuchiya of Kanazawa University for valuable discussions and suggestions. This work was finally supported by a grant-in-aid from the Ministry of Education.

References

1) H. Oki and K. Otsuka, *Bull. Chem. Soc. Jpn.*, **49**, 1841 (1976).
2) R. D. Gillard and N. C. Payne, *J. Chem. Soc., Dalton Trans.*, **1969**, 1197; R. G. Denning and S. Piper, *Inorg. Chem.*, **5**, 1057 (1966).
3) A. J. McCaffery, S. F. Mason, and R. E. Ballard, *J. Chem. Soc., Dalton Trans.*, **1965**, 2883.
4) J. H. Dunlop and R. D. Gillard, *J. Inorg. Nucl. Chem.*, **27**, 361 (1965).
5) R. D. Gillard, S. H. Laurie, D. C. Price, D. A. Phopps and C. F. Weick, *J. Chem. Soc., Dalton Trans.*, **1974**, 1385.
6) B. E. Douglas and S. Yamada, *Inorg. Chem.*, **4**, 1561 (1965).

The Absolute Configuration of the (+)$_{546}$-β-Oxalato[(6*R*,8*S*)-dimethyl-2,5,9,12-tetraazatridecane]cobalt(III) Ion, (+)$_{546}$-β-[Co(ox)(*N*,*N'*-Me$_2$-*R*,*S*-2,3'',2-tet)]$^+$

Shigenobu YANO, Keizo FURUHASHI, and Sadao YOSHIKAWA

Department of Synthetic Chemistry, Faculty of Engineering, The University of Tokyo, Tokyo 113

(Received October 29, 1976)

The crystal and molecular structure of (+)$_{546}$-β-[Co(ox)(*N*,*N'*-Me$_2$-*R*,*S*-2,3'',2-tet)]$^+$ has been determined from three-dimensional intensity data collected by counter methods. The structure has been refined by least-squares techniques to an *R* factor of 5.9% for 838 reflections above the background. The red violet crystals are orthorhombic, with a space group of $P2_12_12_1$, with $Z=4$ ($D_m=1.501$, $D_c=1.505$ g/cm^3), and with cell constants of $a=14.175(5)$, $b=18.591(2)$ and $c=7.747(4)$ Å. The complex ion has the Δ absolute configuration, which was determined by the Bijvoet method. The quadridentate ligand, *N*,*N'*-Me$_2$-*R*,*S*-2,3'',2-tet, is coordinated to the Co *via* 4 N atoms in the *cis*-β configuration, yielding two terminal 5-membered chelate rings with the λ conformation and a central 6-membered ring with a chair conformation (both C–CH$_3$ groups are equatorial). The secondary N atoms have *R* chirality except for one terminal N atom, the absolute configuration of which is *S*. The N(*S*)–CH$_3$ group in the "out-of-plane" 5-membered ring is equatorial, whereas the N(*R*)–CH$_3$ group in the other ring has an axial disposition.

In recent years, metal complexes containing six-membered β-diamine with *C*-methyl groups have been under investigation.[1] However, only two complexes have been structurally elucidated by X-ray analysis. Kobayashi *et al.*, reported that each 2,4-pentanediamine chelate ring in the {Co[(*R*,*R*)-2,4-pentanediamine]$_3$}$^{3+}$ ion takes a skew-boat conformation, with both methyl groups in an equatorial position.[2] On the other hand, in the (+)$_{470}$-β-[Co(NO$_2$)$_2$(4-methyl-3,7-diazanonane-1,9-diamine)]$^+$ ion, the central six-membered chelate ring of the tetramine adopts a chair conformation, with an equatorial methyl group.[3] Thus, there are two probable conformations for the central 2,4-pentanediamine moiety of the tetramine in the [Co(ox)(*N*,*N'*-Me$_2$-*R*,*S*-2,3'',2-tet)]$^+$ ion, where *N*,*N'*-Me$_2$-*R*,*S*-2,3'',2-tet is (6*R*,8*S*)-6,8-dimethyl-2,5,9,12-tetraazatridecane.

Our present ligand, *N*,*N'*-Me$_2$-*R*,*S*-2,3'',2-tet, has two *N*-methyl groups, it is of interest in elucidating the stereochemistry of this system.

The crystal structure of (+)$_{546}$-[Co(ox)(*N*,*N'*-Me$_2$-*R*,*S*-2,3'',2-tet)]ClO$_4$, isolated by Dr. Fujio Mizukami,[4] has been determined by X-ray structure analysis in oder to establish the stereochemical configuration of the complex ion.

Experimental

The crystals of (+)$_{546}$-β-[Co(ox)(*N*,*N'*-Me$_2$-*R*,*S*-2,3'',2-tet)]ClO$_4$ were kindly supplied by Dr. Fujio Mizukami of the National Chemical Laboratory for Industry. The systematic absences observed on Weissenberg photographs are *h*00 for *h* odd, 0*k*0 for *k* odd, and 00*l* for *l* odd, all consistent with the $P2_12_12_1$ space group. The precise lattice conatsnts were obtained by the least-squares analysis of the 2θ angles of the reflections carefully measured on a Rigaku-Denki four-circle automatic X-ray diffractometer by the use of Mo*K*α radiation ($\lambda=0.7107$ Å). The values are $a=14.175(5)$, $b=18.591(2)$, and $c=7.747(4)$Å. The calculated density of 1.505 g/cm^3 for the four formula units in the unit cell agrees well with the density of 1.501 g/cm^3 measured by the floatation method in a mixture of carbon tetrachloride and dibromoethane. The crystal used in the data collection was an irregularly shaped plate with the approximate dimensions of 0.4×0.25×0.3 mm. The crystal was mounted with the c axis approximately parallel to the instrument axis. The intensity data ($2\theta\leqq60°$) were collected by the ω-2θ scan technique, using Mo*K*α radiation monochromated by a LiF crystal. The scan speed was 2°/min in 2θ, and the stationary-crystal, stationary-counter background counts of 10 s were taken at each end of the scan. As a general check on the electronic and crystal stability, the intensities of four standard reflections were monitored every 50 reflections during the collection of the intensity data, no significant variation was noted. A total of 838 indepent reflctions larger than 3σ were used for the structure determination, where σ is given by $|F|/2I_0[I_P+(B_1+B_2)(T_P/2T_B)^2]^{1/2}$ (I_P and I_0 are the total intensity and the net intensity respectively; B_1 and B_2 are the background counts, T_P and T_B are the times required for the measurements of the peak and background intensities).

Determination and Refinement of the Structure

In order to obtain a trial structure, a three-dimentional Patterson function was calculated. The coordinates of the cobalt and chlorine atoms were determined from the prominent peaks in the Patterson function. The remaining non-hydrogen atoms were located from a Fourier map phased by the heavy atoms. The conventional *R* value ($\sum||F_o|-|F_c||/\sum|F_o|$) was 0.561 at this stage. The atomic scattering factors were taken from the International Tables for X-ray Crystallography.[5] Refinement was carried out with a block-diagonal least-squares method in the isotropic mode. A weighting scheme, $\omega=1$ if $F_o\geq10.0$ and otherwise $\omega=0.2$, was employed. After several cycles of the refinement, the *R* value was reduced to 0.175 ($R'=(\sum\omega(|F_o|-|F_c|)^2/\sum\omega F_o^2)^{1/2}=0.196$). When the least-squares calculations were continued with anisotropic thermal parameters, the *R* and *R'* values reached 0.076 and 0.082 respectively. Differential synthesis showed no abnormal features except for the ambiguity in the positions of the hydrogen atoms. At this stage, the idealized positions of the hydrogen atoms were calculated using a C–H distance of 1.08 Å and H–C–H angles of 109°28'. These hydrogen atoms were included in the subsequent

TABLE. 1. OBSERVED AND CALCULATED STRUCTURE FACTORS ($\times 2$)

K	FO	FC	K	FO	FC	K	FO	FC	K	FO	FC	K	FO	FC	K	FO	FC	K	FO	FC	K	FO	FC
H=L= 0 0			3	84	83	15	54	56	8	49	47	8	24	17	15	43	47	4	73	72	4	83	87	H=L= 12 6		
6	215	211	4	26	27	18	33	33	9	77	72	11	45	48	H=L= 8 3			5	51	51	5	50	48	3	39	41
10	47	46	5	41	45	19	25	26	11	102	105	13	27	26	1	111	108	8	56	58	7	52	53	H=L= 14 6		
H=L= 1 0			11	26	20	H=L= 6 1			12	57	54	15	42	36	2	72	82	9	60	62	8	75	70	3	36	28
4	91	92	H=L= 12 0			0	52	40	14	61	58	H=L= 10 2			3	78	82	H=L= 9 4			H=L= 8 5			H=L= 0 7		
7	79	77	0	41	40	2	80	89	15	33	38	1	64	59	4	45	40	1	43	47	2	59	63	3	81	81
8	93	96	3	46	45	5	115	122	16	29	22	2	86	86	5	76	84	3	34	36	4	53	38	7	74	73
9	69	66	5	30	31	6	62	63	19	26	25	3	57	58	6	80	78	6	68	64	14	44	48	H=L= 1 7		
13	20	20	11	32	28	7	47	51	H=L= 2 2			6	39	34	7	90	88	10	62	62	H=L= 9 5			1	51	47
14	103	103	13	32	32	10	53	55	1	74	75	7	66	75	H=L= 9 3			12	32	21	0	71	72	2	47	47
15	46	47	19	32	27	11	25	27	2	65	58	9	59	63	1	81	89	H=L= 10 4			2	42	37	4	38	29
18	45	49	H=L= 13 0			12	54	57	3	123	118	10	38	41	3	56	54	0	45	41	4	80	86	9	30	27
22	39	42	1	84	77	15	27	25	5	125	123	12	24	24	4	64	66	1	43	46	5	47	41	11	29	30
H=L= 2 0			3	55	58	16	40	36	7	60	66	15	30	27	7	76	78	2	78	80	8	57	63	H=L= 2 7		
7	152	154	5	49	55	18	33	29	9	76	79	H=L= 11 2			9	45	48	4	67	70	9	36	36	1	60	57
12	42	48	6	29	26	H=L= 7 1			11	83	79	0	87	85	13	35	31	5	32	29	H=L= 10 5			3	67	65
14	43	41	8	22	22	1	29	29	12	22	16	1	47	53	H=L= 10 3			7	38	37	2	71	72	7	66	66
16	31	24	H=L= 14 0			3	39	33	13	68	69	2	26	36	0	70	75	9	42	35	6	51	53	8	48	44
17	51	52	1	37	37	6	47	48	14	65	63	3	28	28	2	52	53	10	31	27	H=L= 11 5			11	45	45
H=L= 3 0			5	35	32	8	85	81	17	30	34	5	29	28	5	84	92	12	46	41	0	65	67	H=L= 3 7		
1	66	67	9	36	33	9	80	73	18	28	32	6	21	16	6	57	63	H=L= 11 4			1	44	47	2	74	75
3	30	42	17	25	21	10	47	48	19	23	20	7	25	35	8	37	33	0	62	63	3	47	52	6	75	74
4	241	245	H=L= 15 0			11	36	35	21	24	23	8	66	68	9	63	57	2	32	36	4	46	43	14	45	45
6	96	98	1	35	33	12	46	50	H=L= 3 2			9	29	33	H=L= 11 3			3	27	25	H=L= 12 5			H=L= 4 7		
7	29	27	2	59	52	13	51	56	0	146	145	12	44	37	10	63	57	8	55	50	3	54	56	0	73	74
8	256	260	3	32	27	16	28	27	4	205	201	H=L= 12 2			13	39	33	11	45	37	9	24	24	4	78	83
9	153	150	5	42	37	H=L= 8 1			7	109	96	2	69	70	H=L= 12 3			H=L= 12 4			H=L= 13 5			8	76	82
10	124	119	H=L= 16 0			1	27	19	8	108	102	6	74	74	0	46	49	1	45	46	1	53	48	H=L= 5 7		
11	32	31	0	40	39	3	35	40	9	42	48	10	51	52	8	64	66	2	60	63	5	44	38	1	48	41
12	36	33	7	28	20	4	30	20	10	38	40	13	32	29	H=L= 13 3			6	58	52	H=L= 14 5			2	65	62
13	40	46	12	28	21	5	75	75	11	48	44	14	50	44	10	45	42	H=L= 13 4			3	40	37	3	43	50
14	66	67	H=L= 17 0			6	109	113	12	70	75	H=L= 13 2			H=L= 0 4			0	47	45	5	23	24	6	78	86
15	67	64	2	42	35	7	52	55	13	33	25	0	40	37	1	38	32	H=L= 14 4			H=L= 15 5			10	61	61
17	44	47	6	37	33	9	44	51	14	44	45	4	40	42	8	109	106	3	32	28	0	24	24	H=L= 6 7		
18	27	30	H=L= 19 0			10	80	80	15	23	28	8	53	56	11	119	119	6	45	43	H=L= 0 6			0	50	56
21	31	36	6	31	36	11	47	39	16	29	31	12	41	47	12	101	102	H=L= 17 4			0	243	244	2	41	39
H=L= 4 0			H=L= 0 1			14	37	36	20	37	32	H=L= 14 2			H=L= 1 4			0	32	28	1	135	130	4	62	66
3	75	79	6	89	91	15	31	26	H=L= 4 2			2	51	46	1	87	83	H=L= 18 4			3	104	107	5	53	61
8	99	98	7	37	31	H=L= 9 1			0	39	46	6	47	53	4	78	80	3	25	17	5	70	70	8	47	45
11	81	81	9	86	85	0	40	54	1	87	89	H=L= 16 2			5	50	44	H=L= 0 5			8	57	57	9	43	36
12	26	25	10	70	66	1	39	51	2	79	74	3	29	24	6	68	62	1	69	76	9	59	58	H=L= 7 7		
14	23	27	11	50	55	2	56	37	3	86	94	5	39	31	8	31	28	2	167	166	13	31	23	3	48	52
H=L= 5 0			12	89	88	3	59	55	4	29	24	H=L= 0 3			9	82	79	9	35	30	H=L= 1 6			7	48	50
2	24	22	13	63	60	4	144	144	5	62	61	3	32	35	10	96	94	10	82	82	1	103	96	H=L= 8 7		
7	131	129	14	34	36	5	34	28	6	143	151	7	65	59	11	40	36	13	38	34	2	151	151	3	53	61
8	117	120	16	28	27	7	53	46	7	112	106	10	82	77	13	41	41	14	53	56	3	36	33	5	53	54
12	51	46	H=L= 1 1			8	63	66	8	27	29	13	94	96	H=L= 2 4			H=L= 1 5			4	45	44	11	44	37
13	106	102	4	235	227	12	65	68	10	69	69	15	71	70	0	79	71	0	200	201	6	61	61	H=L= 9 7		
17	60	66	5	124	125	13	40	36	13	19	18	H=L= 1 3			1	40	49	1	78	75	8	32	29	1	49	50
H=L= 6 0			6	67	70	16	24	20	14	63	65	1	75	73	7	48	50	2	64	56	9	61	53	5	50	50
0	233	229	7	67	62	H=L= 10 1			18	48	48	3	88	88	8	74	74	3	39	43	H=L= 2 6			H=L= 10 7		
5	90	82	8	61	60	0	38	40	H=L= 5 2			7	42	42	11	76	81	4	78	77	0	93	97	1	47	48
7	54	55	9	38	41	1	48	44	1	65	69	8	35	35	12	58	60	5	62	64	1	138	141	H=L= 0 8		
8	52	46	10	45	39	2	106	106	2	57	59	9	103	107	13	33	37	8	71	74	2	45	42	1	56	55
9	58	61	11	49	51	3	43	42	3	58	54	10	96	96	H=L= 3 4			12	49	56	3	93	88	2	38	28
11	95	96	13	42	38	4	31	21	5	62	59	11	92	98	0	98	95	19	19	13	4	55	56	3	56	61
12	61	58	14	35	33	6	55	57	7	52	52	12	42	48	2	90	80	H=L= 2 5			5	58	58	9	51	51
15	52	50	16	88	88	8	49	50	8	92	91	13	102	97	3	139	134	1	80	80	6	47	47	11	43	44
16	31	34	20	36	32	10	44	41	9	49	54	H=L= 2 3			4	122	120	2	88	87	7	70	71	13	61	69
H=L= 7 0			H=L= 2 1			11	46	50	10	21	20	1	30	35	5	63	69	3	80	84	8	65	65	H=L= 1 8		
1	46	43	0	110	113	13	55	51	11	41	45	5	24	22	6	55	50	4	49	44	14	22	22	1	52	50
2	45	48	1	76	73	15	27	19	12	48	51	6	93	87	7	41	45	5	52	47	H=L= 3 6			H=L= 2 8		
5	47	52	4	147	143	H=L= 11 1			13	36	40	7	90	91	8	36	30	6	67	68	0	58	58	1	68	67
7	57	50	5	76	69	0	55	54	14	31	32	9	49	51	9	95	92	8	32	33	1	72	69	5	65	62
8	63	55	6	105	107	1	70	64	16	49	47	10	64	68	13	48	46	9	45	51	2	39	40	6	57	56
9	30	30	9	112	115	2	24	29	H=L= 6 2			11	94	97	H=L= 4 4			10	66	70	3	41	41	10	50	57
10	111	109	10	62	61	3	70	67	0	24	29	12	91	91	3	45	51	11	26	21	4	63	58	H=L= 3 8		
11	64	67	13	36	37	4	61	69	1	75	72	13	48	43	4	48	57	14	46	46	5	71	77	3	54	53
12	28	23	14	27	27	5	33	37	2	115	120	14	40	38	5	61	64	15	42	40	6	46	51	4	69	70
13	49	52	15	57	50	10	30	31	3	99	101	15	39	39	6	36	40	H=L= 3 5			8	66	69	8	70	66
14	42	47	H=L= 3 1			11	43	45	4	23	22	H=L= 3 3			7	89	82	1	94	87	9	68	64	12	46	46
15	43	38	0	200	199	12	32	34	5	65	61	2	244	237	9	53	51	2	56	56	10	52	54	H=L= 4 8		
16	33	31	1	66	54	H=L= 12 1			6	72	68	3	109	104	10	48	42	3	61	67	12	38	40	2	83	78
17	46	43	2	151	144	0	65	58	7	65	67	4	73	60	15	41	39	4	59	59	15	32	34	H=L= 5 8		
18	36	32	6	100	109	1	38	41	8	21	27	5	171	168	17	29	23	5	85	79	19	23	19	0	86	83
H=L= 8 0			7	149	145	2	45	47	9	42	47	6	171	176	H=L= 5 4			7	78	80	H=L= 4 6			4	64	64
1	26	25	8	24	26	4	32	33	10	50	53	9	42	39	1	120	125	8	52	45	1	49	47	H=L= 6 8		
3	38	25	9	71	75	7	24	19	11	22	22	10	87	91	2	28	25	9	41	41	2	76	77	2	73	77
4	86	91	10	57	56	8	39	40	14	28	36	H=L= 4 3			3	44	47	11	59	58	3	51	49	H=L= 7 8		
7	54	56	11	44	43	9	31	28	17	25	30	1	54	55	4	59	49	13	30	34	4	43	39	4	43	38
8	88	91	12	36	35	11	34	39	18	36	35	4	136	137	5	130	128	17	23	26	5	75	79	H=L= 8 8		
9	51	51	14	29	33	H=L= 13 1			H=L= 7 2			5	53	55	7	51	47	H=L= 4 5			6	67	76	0	47	43
12	105	105	15	56	56	1	56	53	0	147	141	8	81	79	8	43	44	1	54	59	7	67	68	H=L= 9 8		
20	30	27	18	23	25	3	46	50	4	78	75	10	26	19	10	46	43	3	56	59	9	46	43	0	A6	41
H=L= 9 0			20	33	22	5	35	34	6	76	78	12	60	65	13	50	55	5	68	70	11	36	37	H=L= 11 8		
2	64	68	H=L= 4 1			7	53	48	7	97	93	16	59	55	H=L= 6 4			7	81	76	H=L= 5 6			0	51	47
3	37	41	0	43	46	11	31	35	8	50	52	H=L= 5 3			1	37	31	9	70	69	0	40	38	H=L= 1 9		
6	101	102	2	61	63	H=L= 14 1			9	52	54	0	23	25	3	37	42	11	47	48	3	49	48	0	39	38
7	49	47	3	61	58	4	26	33	10	49	46	2	222	227	4	81	79	H=L= 5 5			4	74	77	1	40	33
8	45	45	4	180	181	7	29	31	11	57	60	3	142	138	7	44	47	1	39	48	5	53	57	4	60	68
9	27	26	5	146	139	8	29	24	15	46	48	4	70	72	8	36	39	2	35	32	7	71	71	8	47	48
10	73	74	6	38	28	9	29	26	19	33	27	6	139	136	9	69	70	3	96	91	8	52	53	H=L= 3 9		
14	56	53	8	94	101	H=L= 15 1			H=L= 8 2			7	76	83	10	39	33	5	74	66	16	28	29	1	43	42
15	29	31	9	110	110	3	44	43	0	23	17	H=L= 6 3			13	47	40	7	91	97	H=L= 6 6			4	34	31
H=L= 10 0			10	33	33	H=L= 17 1			1	114	117	0	134	134	H=L= 7 4			9	57	59	2	45	48	5	44	43
0	117	115	11	40	39	0	48	47	2	37	38	2	33	32	1	54	56	11	63	70	4	43	46	H=L= 4 9		
3	32	33	12	84	88	8	35	39	3	68	72	6	52	50	2	78	86	H=L= 6 5			H=L= 7 6			0	48	49
5	71	67	13	34	36	H=L= 0 2			4	36	47	7	73	78	3	44	42	2	52	57	6	58	61	H=L= 5 9		
6	82	82	16	34	39	4	72	73	5	98	100	8	65	60	4	52	58	3	42	39	10	47	43	3	46	45
7	75	79	17	23	20	5	28	25	7	79	73	11	35	35	5	72	78	5	67	66	11	46	45	5	43	38
9	69	70	H=L= 5 1			8	61	53	9	65	65	12	36	44	6	100	97	6	77	83	H=L= 9 6			H=L= 4 10		
10	30	33	0	44	49	9	77	72	15	42	33	H=L= 7 3			7	51	50	7	49	43	6	50	51	5	39	33
11	36	38	2	50	53	10	43	46	H=L= 9 2			0	67	67	9	39	34	9	51	54	10	48	35	H=L= 6 10		
12	31	35	4	118	119	11	159	164	0	34	38	1	133	133	10	76	77	10	41	39	11	49	52	0	43	43
13	32	28	8	46	47	14	43	45	2	58	49	2	135	140	H=L= 8 4			13	45	47	H=L= 10 6			1	35	31
16	23	22	10	54	68	15	28	35	3	80	79	3	114	118	0	69	72	H=L= 7 5			4	53	54	H=L= 7 10		
H=L= 11 0			11	30	31	17	50	50	5	70	68	6	72	75	1	68	72	0	45	37	10	22	13	3	30	23
1	69	74	13	48	42	H=L= 1 2			6	37	38	7	81	83	2	26	22	2	29	33	H=L= 11 6			H=L= 0 0		
2	75	78	14	47	47	6	31	32	7	81	80	10	39	42	3	37	40	3	40	37	0	23	22			

TABLE 2. FINAL ATOMIC PARAMETERS

(a) Final positional parameters ($\times 10^4$) and their estimated standard devations (in parentheses).

Atom	x	y	z
Co	5578(1)	3774(1)	1491(2)
N(1)	6363(7)	4236(6)	3320(15)
N(2)	4795(9)	4632(6)	1719(16)
N(3)	4750(7)	3221(7)	3117(12)
N(4)	6431(9)	2885(7)	1382(19)
O(1)	4831(7)	3466(6)	−498(15)
O(2)	6368(7)	4244(6)	−182(13)
O(3)	4853(8)	3549(8)	−3324(16)
O(4)	6576(9)	4283(8)	−3028(13)
C(1)	6179(10)	4977(10)	3247(27)
C(2)	5077(10)	5059(9)	3166(21)
C(3)	3721(8)	4575(8)	1683(21)
C(4)	3395(11)	3965(12)	3043(27)
C(5)	3695(11)	3235(11)	2724(21)
C(6)	5091(13)	2435(11)	2989(25)
C(7)	6079(17)	2481(7)	2942(30)
C(N1)	7412(10)	4107(8)	3324(24)
C(N4)	6418(16)	2425(11)	−146(29)
C(C3)	3224(13)	5296(11)	1799(27)
C(C5)	3252(11)	2623(14)	4062(25)
C(8)	5175(10)	3702(9)	−1911(15)
C(9)	6151(12)	4078(8)	−1743(20)
Cl	5268(3)	945(2)	7146(7)
O(5)	4708(10)	1132(8)	8666(18)
O(6)	4636(9)	956(9)	5565(23)
O(7)	5962(11)	1482(8)	6812(23)
O(8)	5623(14)	279(10)	7313(24)

(b) Final thermal parameters ($\times 10^4$) and their estimated standard deviations (in parentheses) in the form:
$\exp[-(\beta_{11}h^2+\beta_{22}k^2+\beta_{33}l^2+\beta_{12}hk+\beta_{13}hl+\beta_{23}kl)]$.

	β_{11}	β_{22}	β_{33}	β_{12}	β_{13}	β_{23}
Co	34(0)	24(0)	31(1)	−2(0)	0(1)	−3(1)
N(1)	37(6)	20(4)	36(19)	8(4)	0(10)	−18(8)
N(2)	48(6)	25(4)	62(21)	16(4)	−13(11)	−20(9)
N(3)	35(5)	36(4)	47(17)	13(4)	−17(8)	−1(7)
N(4)	33(8)	32(5)	37(21)	2(5)	0(13)	4(11)
O(1)	51(6)	33(4)	92(19)	−8(4)	21(10)	0(7)
O(2)	40(6)	37(4)	42(16)	−24(4)	15(8)	0(7)
O(3)	63(7)	78(7)	83(20)	−18(6)	−65(11)	7(11)
O(4)	68(8)	66(6)	31(18)	−4(6)	8(10)	10(9)
C(1)	21(7)	43(7)	185(41)	−13(6)	−16(17)	15(17)
C(2)	31(8)	40(6)	97(30)	16(6)	−19(13)	−20(13)
C(3)	11(5)	34(5)	81(28)	−1(4)	−16(13)	15(12)
C(4)	28(8)	61(9)	213(48)	3(7)	15(17)	0(19)
C(5)	17(8)	50(8)	113(29)	0(6)	10(14)	0(14)
C(6)	43(10)	52(8)	152(38)	14(7)	77(16)	22(15)
C(7)	75(17)	23(4)	198(54)	13(6)	−35(25)	6(12)
C(N1)	40(8)	30(5)	130(32)	5(6)	0(17)	−13(13)
C(N4)	93(16)	36(7)	145(40)	26(9)	11(22)	−10(15)
C(C3)	46(9)	53(8)	155(43)	7(8)	−20(18)	2(17)
C(C5)	46(8)	74(15)	63(42)	−49(10)	13(15)	−23(20)
C(8)	27(7)	42(6)	105(21)	6(7)	−10(10)	1(12)
C(9)	66(10)	17(4)	68(29)	10(6)	−19(15)	−8(10)
Cl	65(3)	34(1)	248(11)	−4(1)	14(5)	14(3)
O(5)	113(11)	60(6)	146(23)	44(7)	43(15)	−4(13)
O(6)	56(8)	68(7)	343(41)	0(6)	−58(17)	27(14)
O(7)	87(9)	63(7)	236(36)	1(6)	−15(16)	−6(13)
O(8)	117(14)	82(9)	313(42)	48(10)	6(25)	10(16)

TABLE 3. REFLEXIONS USED TO DETERMINE THE ABSOLUTE CONFIGURATION (Δ) ($\times 10$)

h	k	l	$\lvert F_c(hkl)\rvert$	$\lvert F_c(h\bar{k}l)\rvert$	Observed relationship
1	3	1	570	466	>
1	8	1	304	241	>
2	1	1	376	287	>
3	1	1	194	316	<
3	2	1	706	710	<
3	3	1	555	440	>
4	2	1	333	280	>
4	3	1	138	201	<
4	4	1	975	865	>
4	5	1	737	609	>
5	6	1	506	544	<
6	1	1	525	463	>
6	3	1	247	285	<
10	2	1	513	493	>

refinement, but their positional and isotropic thermal parameters (given the value of $B=3.5$) were not refined. The final refinement converged at the R value of 0.059 ($R'=0.064$). The observed and calculated structure factors all listed in Table 1. Table 2 summarizes the final values of the positional and thermal parameters. The absolute configuration of the complex was determined by using the absorption-edge technique.[6] An equi-inclination Weissenberg photograph of the 1st-layer about c axis was taken with Cu$K\alpha$ radiation. Some Bijvoet pairs, hkl and $h\bar{k}l$, were found to show appreciable differences in intensity. These pairs and the observed inequality relationships are listed in Table 3, in which the structure amplitudes calculated on the basis of the Δ configuration of the complex are also given.

Description and Discussion of the Structure

There are four complex and four perchlorate ions per unit cell. Figure 1 gives a stereoscopic pair of view of the contents of a unit cell of this structure. The absolute configuration of the complex ion is represented by a perspective drawing in Fig. 2. The cobalt atom is situated at the center of a slightly distorted octahedron. The tetramine ligand, $(H_3C)NH$-$(CH_2)_2$-NH-$CH(CH_3)$-CH_2-$CH(CH_3)$-NH-$(CH_2)_2$-$NH(CH_3)$, is coordinated to the cobalt atom in the Δ-*cis*-β geometry. Each conformation of the three chelate rings for the tetramine is present in Fig. 3. The central -HN(2)-C(3)H(CH_3)-C(4)H_2-C(5)H(CH_3)-N(3)H- atoms and the cobalt atom form a six-membered chelate ring with a chair conformation, both of the C-CH_3 groups being equatorial. The H_3C(N1)-N(1)H-C(1)H_2-C(2)H_2-

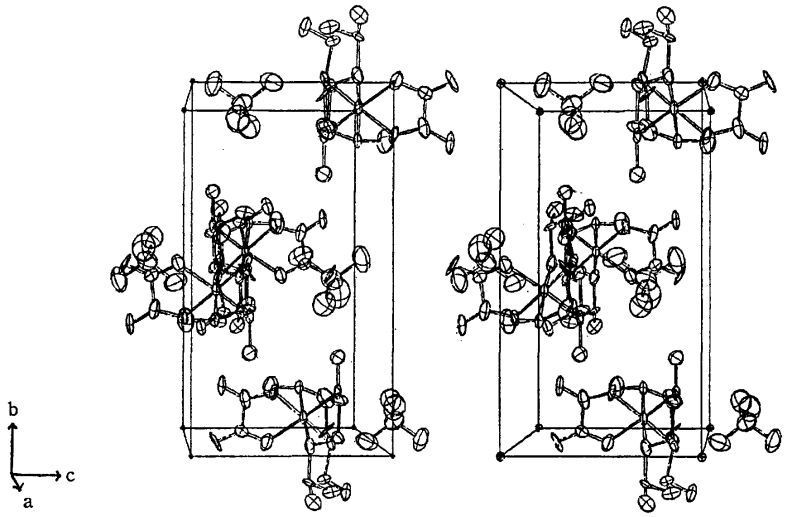

Fig. 1. Stereoscopic view of the unit cell contents.

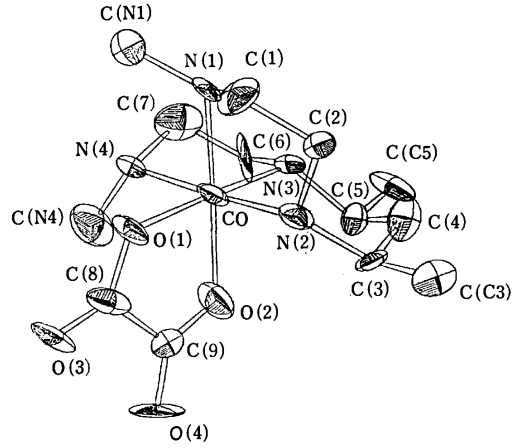

Fig. 2. A perspective drawing of the complex ion showing 50% probability ellipsoids of thermal motion.

TABLE 4. INTERATOMIC NON-BONDED DISTANCES WITHIN THE MOLECULAR AND THEIR STANDARD DEVIATIONS (IN PARENTHESES) LESS THEN 3.5 Å

C(N1)-Co	3.03(2) Å	C(N4)-Co	3.05(2) Å
C(N1)-C(1)	2.38(3)	C(N4)-C(6)	3.07(3)
C(N1)-N(4)	3.06(2)	C(N4)-C(9)	3.33(3)
C(N1)-O(2)	3.10(2)	C(N4)-O(1)	2.98(3)
		C(N4)-O(2)	3.38(3)

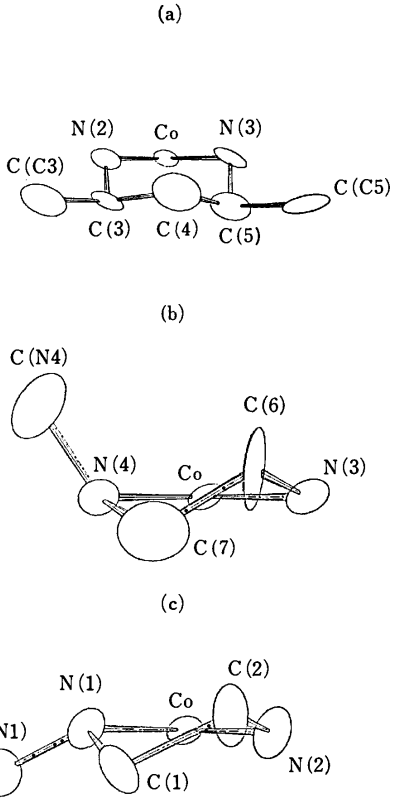

Fig. 3. A perspective drawing of the chelate rings; (a) central six-membered ring, (b) in-plane five-membered ring, and (c) out-of-plane five-membered ring.

N(2)H- fragment participates in the five-membered chelate ring with a λ gauche conformation, and the methyl group is equatorial. The other five-membered ring is composed of the -HN(3)-C(6)H_2-C(7)H_2-N(4)-H-C(N2)H_3 fragment with a metal atom and also has a λ conformation, but the methyl group is axial with respect to the chelate ring. Among the secondary nitrogen atoms, N(1)—N(4), the N(1) has *S* chirality, while the absolute configurations of the remainder are *R*. The two outer chelate rings have similar gauche conformations. The ring carbon atoms, C(1) and C(2), lie at −0.53 and 0.21 Å respectively from the plane formed by N(1), Co, and N(2). The corresponding deviations of C(7) and C(6) from the plane of N(4), Co, and N(3) are −0.41 and 0.33 Å. Close contacts between the *N*-methyl carbon atoms and other atoms in the complex (less than 3.5 Å) are listed in Table 4. These are similar values between the two *N*-methyl groups.

Four isomers can exist with respect to the orientation of the two *N*-methyl groups in relation to the *Δ-cis-β*

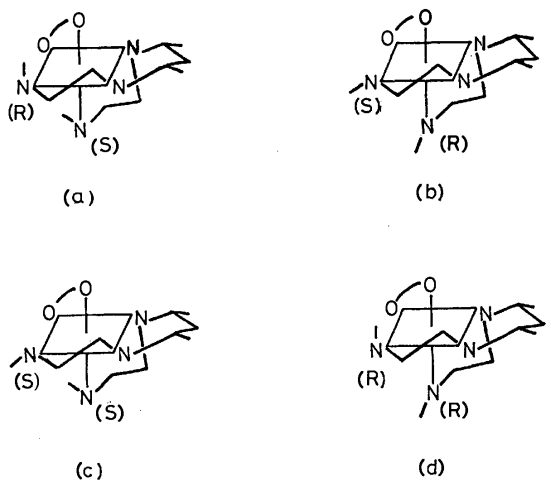

Fig. 4. Possible isomers of *Δ*-*β*-[Co(ox)(*N*,*N*′-Me$_2$-*R*,*S*-2,3″,2-tet)]$^+$.
(a) (N1(*S*), N4(*R*)), (b) (N1(*R*), N4(*S*)), (c) (N1(*S*), N4(*S*)), (d) N1(*R*), N4(*R*)).

form. They are (N1(*S*), N4(*R*)), (N1(*R*), N4(*S*)), (N1(*S*), N4(*S*)), and (N1(*R*), N4(*R*)), as shown in Fig. 4. The (N1(*S*), N4(*R*)) isomer to involve a smaller interaction than the other three forms, according to the molecular model study. This structural feature was supported by the present X-ray analysis. It is noteworthy that one *N*-methyl group has an axial orientation with that the equatorial orientation of the *N*-methyl group is preferable to the axial situation. This stereochemical feature can be attributed to severe steric interactions on the metal ion.

All the N–Co–N angles in five-membered chelate rings are less than 90°, and they have an average value of 86.0°. The N–Co–N angle in the central six-membered chelate ring is 91.7°. The bond distances and angles are given in Tables 5 and 6 respectively. The four Co–N distances are not significantly different from one another, and the average value (2.01 Å) is quite usual.

Absolute Configuration and Circular Dichroism. The stereochemical features which can contribute to the circular dichroism (CD) of a dissymmetric metal complex have been classified as follows: (1) a distribution of chelate rings about the metal ion (configurational effect), (2) the puckered dissymmetric conformation of individual chelate rings (conformational effect), and (3) the presence of asymmetric groups on the ligands, such as asymmetric carbon or asymmetric nitrogen atoms (vicinal effect). The latter two effects are considered to make minor contributions as compared with the configurational effect.

The CD spectrum of *Δ*-*β*-[Co(ox)(*N*,*N*′-Me$_2$-*R*,*S*-2,3″,2-tet)]$^+$ is shown in Fig. 5. The above results suggest the following conclusion: when the oxalato cobalt(III) complexes of 3,7-diaza-1,9-nonanediamine (2,3,2-tet) and its derivatives give two circular dichroism bands with opposed signs in the first absorption region,

Table 5. Bond distances and their standard deviations (in parentheses)

Co –N(1)	2.00(2) Å	O(2)–C(9)	1.29(3) Å
Co –N(2)	1.95(2)	O(3)–C(8)	1.22(4)
Co –N(3)	2.01(2)	O(4)–C(9)	1.22(4)
Co –N(4)	2.05(2)	C(1)–C(2)	1.57(4)
Co –O(1)	1.96(2)	C(3)–C(4)	1.62(4)
Co –O(2)	1.92(2)	C(3)–C(C3)	1.52(4)
N(1)–C(1)	1.40(4)	C(4)–C(5)	1.44(5)
N(1)–C(N1)	1.51(4)	C(5)–C(C5)	1.66(5)
N(2)–C(2)	1.43(4)	C(6)–C(7)	1.40(5)
N(2)–C(3)	1.53(3)	C(8)–C(9)	1.56(4)
N(3)–C(5)	1.53(4)	Cl –O(5)	1.46(3)
N(3)–C(6)	1.54(4)	Cl –O(6)	1.52(3)
N(4)–C(7)	1.51(4)	Cl –O(7)	1.43(3)
N(4)–C(N4)	1.46(5)	Cl –O(8)	1.34(4)
O(1)–C(8)	1.28(3)		

Table 6. Bond angles and their standard deviations (in parentheses)

N(1)–Co–N(2)	84.3(9)°
N(1)–Co–N(3)	95.8(9)
N(1)–Co–N(4)	92.7(9)
N(1)–Co–O(1)	170.9(10)
N(1)–Co–O(2)	87.6(8)
N(2)–Co–N(3)	91.7(9)
N(2)–Co–N(4)	176.8(11)
N(2)–Co–O(1)	90.2(9)
N(2)–Co–O(2)	91.2(9)
N(3)–Co–N(4)	87.6(9)
N(3)–Co–O(1)	91.6(9)
N(3)–Co–O(2)	175.7(10)
N(4)–Co–O(1)	92.9(10)
N(4)–Co–O(2)	89.7(10)
O(1)–Co–O(2)	85.2(8)
C(1)–N(1)–C(N1)	110(2)
C(2)–N(2)–C(3)	109(2)
C(5)–N(3)–C(6)	108(2)
C(7)–N(4)–C(N4)	111(3)
N(1)–C(1)–C(2)	106(2)
N(2)–C(2)–C(1)	105(2)
N(2)–C(3)–C(4)	109(2)
N(2)–C(3)–C(C3)	114(2)
C(4)–C(3)–C(C3)	117(2)
C(3)–C(4)–C(5)	118(2)
N(3)–C(5)–C(4)	106(2)
N(3)–C(5)–C(C5)	104(2)
C(4)–C(5)–C(C5)	115(3)
N(3)–C(6)–C(7)	105(2)
N(4)–C(7)–C(6)	112(2)
O(1)–C(8)–O(3)	123(2)
O(1)–C(8)–C(9)	115(2)
O(3)–C(8)–C(9)	121(2)
O(2)–C(9)–O(4)	125(2)
O(2)–C(9)–C(8)	114(2)
O(4)–C(9)–C(8)	121(2)
O(5)–Cl –O(6)	109(2)
O(5)–Cl –O(7)	111(2)
O(5)–Cl –O(8)	110(2)
O(6)–Cl –O(7)	105(2)
O(6)–Cl –O(8)	108(2)
O(7)–Cl –O(8)	114(2)

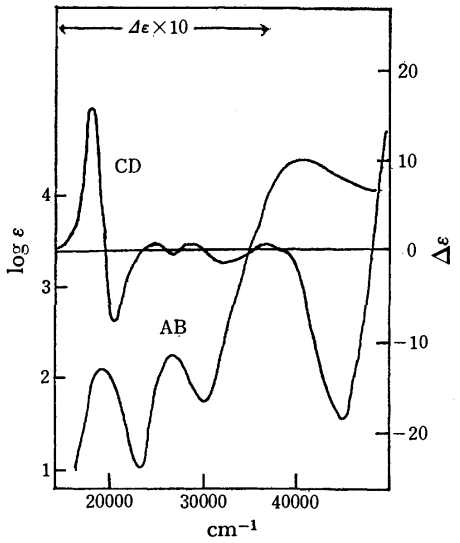

Fig. 5. Absorption (AB) and CD spectra of Δ-β-[Co(ox)(N,N'-Me_2-R,S-2,3″,2-tet)]$^+$.

an enantiomer which has a lawer-energy negative Cotton effect and a higher-energy positive one should be assigned the Δ configuration.

The calculation of the lattice constants, the Fourier synthesis the least-squares analysis, and drawings of the crystal or molecular structures were carried out on a HITAC 8700/8800 computer at the Computer Center of this University, using the RSCL3, ANSFR-2, HBLS-4, and ORTEP[7] programs of the UNICS system respectively.

The authors are grateful for Dr. Fujio Mizukami for providing crystals of $(+)_{546}$-β-[Co(ox)(N,N'-Me_2-R,S-2,3″,2-tet)]ClO_4. They also wish to thank Dr. T. Kodama for the operation of the diffractometer. This work was partially supported by a Grant-in-aid for Scientific Research from the Ministry of Education, Japan (No. 911502).

References

1) T. G. Appleton and J. R. Hall, *Inorg. Chem.*, **10**, 1717 (1971); F. Mizukami, H. Ito, J. Fujita, and K. Saito, *Bull. Chem. Soc. Jpn.*, **44**, 3051 (1971); *ibid.*, **45**, 2129 (1972); *ibid.*, **46**, 2410 (1972).

2) A. Kobayashi, F. Marumo, and Y. Saito, *Inorg. Nucl. Chem. Lett.*, **7**, 777 (1971).

3) P. W. R. Corfield, J. C. Dabrowiak, and E. S. Gore, *Inorg. Chem.*, **12**, 1734 (1973).

4) F. Mizukami, *Bull. Chem. Soc. Jpn.*, **48**, 472 (1975).

5) International Tables for X-Ray Crystallography (1962), Vol. III, Birmingham: Kynoch Press.

6) J. M. Bijvoet, A. F. Peerdeman, and A. J. van Bommel, *Nature*, **168**, 271 (1951).

7) C. K. Johnson, ORTEP Report No. ORNL-3794, Oak Ridge National Laboratory, Oak Ridge, Tennessee.

Polymer-supported Trichlorotitanium(III) Complexes and Their Dioxygen Adducts*

Yasuo CHIMURA, Masazo BEPPU, Satohiro YOSHIDA, and Kimio TARAMA

Department of Hydrocarbon Chemistry, Faculty of Engineering, Kyoto University, Sakyo-ku, Kyoto 606

(Received September 22, 1976)

Various polymer-supported trichlorotitanium(III) ($TiCl_3$) complexes were prepared in pyridine or THF from $TiCl_3$ and copolymers composed of 4-vinylpyridine (10, 20, and 65 mol%), divinylbenzene (0 and 20 mol%), and styrene. The ESR technique was employed for structural studies of titanium(III) species and their dioxygen adducts contained in the supported complexes. The supported complexes contained, as titanium(III) species, mainly (>88%) mixtures of $TiCl_3(pyr)_nL_{3-n}$ ($n=1$, 2, and 3), where pyr is a pyridyl group of the supports and L is a molecule of the solvents used in preparation. The relative amounts of the species having smaller n values increased with cross-linking, with a decrease in the content of pyridyl groups, and with pretreatment with tetrachlorotitanium(IV) ($TiCl_4$). On exposure to oxygen the supported complexes gave two or three kinds of dioxygen adducts (Ti(IV)-O_2^-) characterized by g_1, the principal g value along the axis of O–O bond. The g_1 values of three dioxygen adducts α, β, and γ were 2.027—2.028, 2.022—2.024, and 2.017—2.018, respectively. The probable structures of α, β, and γ, when L is THF, are $[TiCl_2(pyr)_3(O_2)]Cl$, $TiCl_3(pyr)_2(O_2)$, and $TiCl_3(pyr)L(O_2)$, respectively, their precursors being the titanium(III) species having the n values of 3, 2, and 1, respectively.

Many reports have appeared on dioxygen adducts of divalent cobalt and of lower valent transition metals of the group VIII.[1] Typical examples are $Co\{C_6H_5C(O^-)=CHC(CH_3)=NCH_2-\}_2(O_2)py$, $Ir(O_2)Cl(CO)\{P(C_6H_5)_3\}_2$, $Pt(O_2)\{P(C_6H_5)_3\}_2$, and $Ni(O_2)\{CNC(CH_3)_3\}_2$.

Dioxygen adducts of other metals are scarcely known. The main reason is that they react rapidly in solution with their original complexes (step b in the following scheme), even though they were once formed.

$$M + O_2 \underset{a}{\rightleftharpoons} M\text{-}O_2 \xrightarrow[b]{+M} \cdots \longrightarrow M\text{-}O\text{-}M \text{ or } M{=}O$$

Two devices have been developed to suppress step b: (1) dioxygen adducts are sterically protected by ligands with bulky substituents from reacting with their orginal complexes;[2] (2) metal complexes are attached to organic or inorganic polymers with coordinating groups so that no two metal complexes can approach each other. Misono *et al.*[3] reported that several cobalt(II) Shiff base complexes attached to poly-4-vinylpyridine gave 1:1 dioxygen adducts. Wang[4] reported the spectral evidence that oxygen was bound reversibly to the diethyl ester of heme embedded in a matrix of polystyrene and 1-phenethylimidazole. Leal *et al.*[5] showed recently that an iron(II) porphyrin attached to a modified silica gel adsorbed oxygen reversibly and was not oxidized to a μ-oxo dimer even at room temperature.

The ESR signals observed during the course of reaction of $TiCl_3$ with hydrogen peroxide in a flow system were ascribed to peroxy radical species of titanium.[6] No dioxygen adduct of titanium formed from a titanium(III) complex and molecular oxygen, however, has been observed in solution. We could detect a dioxygen adduct of $TiCl_3$, by binding $TiCl_3$ to a copolymer containing pyridyl groups and exposing it to oxygen.[7] The aim of the present work is to clarify the structures of titanium(III) species and of their dioxygen adducts contained in the supported $TiCl_3$ complexes.

* A part of this report was presented at the 35th Meeting of the Catalysis Society of Japan, Sendai, October 1974.

Experimental

Materials. All solvents were refluxed over sodium metal or calcium hydride, then distilled, and stored under nitrogen. Monomers 4-vinylpyridine, styrene, and divinylbenzene were distilled under reduced pressure immediately before use. The divinylbenzene contained about 45% ethylvinylbenzene and was employed when cross-linked polymers were desired. Trichlorotitanium(III) was used as a 0.1 M acetonitrile solution. Commercial oxygen and nitrogen gases were used without further purification.

Polymer Supports: The monomers (total 50 mmol) were copolymerized by the use of 2,2′-azobisisobutyronitrile (0.25 mmole) in benzene or ethanol (50 cm^3) under nitrogen at refluxing temperature for 5 h. The resulting polymers were either precipitated by addition of ethyl ether when they were linear and soluble or washed with benzene and methanol when cross-linked and insoluble. They were then dried *in vacuo* at 120°C and ground to powders of 100—300 mesh. The yields were 60—80%. The degree of cross-linking was assumed to be equal to the molar ratio of charged divinylbenzene to total monomers. The content of pyridyl groups (mol%) was calculated from nitrogen microanalysis.

Polymer-supported $TiCl_3$ Complexes: The acetonitrile solutions of $TiCl_3$ (0.072—0.146 mmol) were stirred with the polymer supports (0.180 g, 0.145—1.15 mequiv. N) dissolved or swelled in pyridine or THF (30 cm^3) under nitrogen at room temperature for 5 h. The solvents were then evaporated *in vacuo* when the supported complexes were prepared from cross-linked supports in pyridine or from soluble, linear ones in either of the solvents, while the solvent was decanted when prepared from cross-linked ones in THF. The resulting solids were then dried *in vacuo* at room temperature. The amounts of charged $TiCl_3$ were controlled to yield supported complexes containing about 5% of $TiCl_3$ based on the total aromatic rings of the supports. Thus, in order to prepare supported complexes with 20% cross-linking and 10, 20, and 65% pyridyl group in THF, 0.146, 0.100, and 0.080 mmol of $TiCl_3$, respectively, were charged. The amounts of $TiCl_3$ corresponding to 5% of the total aromatic rings of the supports were introduced when supported complexes were prepared in pyridine.

A support with 20% cross-linking and 65% pyridyl group (0.180 g, 1.02 mequiv. N) was stirred with $TiCl_4$ (0.29 mmol) in THF (30 cm^3) for 5 h, subsequently mixed with $TiCl_3$ (0.10 mmol) and worked up as described above.

Analysis of Titanium. The amounts of attached $TiCl_3$ were determined only in the case of supported complexes with cross-linking prepared in THF. The method was to titrate chelatometrically titanium ions not attached and dissolved in a supernatant liquid, and to subtract the titre from the amount of charged $TiCl_3$. A titanium(IV) ion is so apt to be hydrolyzed in water that a 50% aqueous ethanol solvent was employed, and EDTA added in excess was back-titrated at pH 5.5 with a 0.05 M zinc(II) solution by the use of xylenol orange as an indicator.

ESR Measurements. Fine solids of the supported complexes were transferred under nitrogen to ESR sample tubes equipped with three-way stopcocks. Their spectra were recorded under nitrogen at room temperature and 77 K with a JEOL-JES-3BS-X (X-band) spectrometer before and after contact with oxygen. The g values were calculated on the basis of that of manganese(II) ions doped into magnesium oxide, which was calibrated with an aqueous solution of peroxylamine disulfonate. The relative amounts of paramagnetic species were determined by the integration of their ESR spectra with a JEOL-JES-ID-2 integrator.

Results and Discussion

Polymer-supported $TiCl_3$ Complexes. The colors of polymer-supported $TiCl_3$ complexes depend upon the composition of supports and the solvents used in preparation (Table 1). Supported complexes without cross-linking are dark brown regardless of solvent. Those with 20% cross-linking change their colors from brown to light brown and from brown to light yellow with a decrease in the content of pyridyl groups, when they are prepared in pyridine and THF, respectively.

All the supported complexes gave two types (A and B) of ESR signals of titanium(III). Type A with g value of 1.96** was easily detected at room temperature and 77 K. Type B was very weak and broad at room temperature. On cooling down to 77 K it became strong showing g values of 1.87—1.91, but was much broader than type A. ESR spectra of a supported complex with 20% cross-linking and 65% pyridyl group prepared in pyridine recorded at room temperature and 77 K are shown in Fig. 1 as a typical example. Supported complexes without cross-linking showed, in addition to A and B signals, weak signals at $g \approx 4$ attributable to $\Delta M = \pm 2$ transitions of the triplet-state of a $TiCl_3$ dimer.[8,9]

The g values and relative amounts of the two types of signals are summarized in Table 1. Type A signals have almost constant g values throughout all the supported complexes. Their amounts are much smaller than those of type B signals, diminishing with cross-linking, a decrease in the content of pyridyl groups, the change of solvents from pyridine to THF, and pretreatment with $TiCl_4$. The g values of type B signals are greatly influenced by the solvents used in preparation, the composition of the supports, and pretreatment with $TiCl_4$. Supported complexes prepared in pyridine have larger g values than those prepared in THF except for those without cross-linking. Among supported complexes prepared in THF the g values decrease with a decrease in the content of pyridyl groups, while supported complexes prepared in pyridine have constant g values. Cross-linking makes the g value small when prepared in THF, while cross-linking has little effect when prepared in pyridine. Tetrachlorotitanium(IV) introduced prior to addition of $TiCl_3$ makes a small g value.

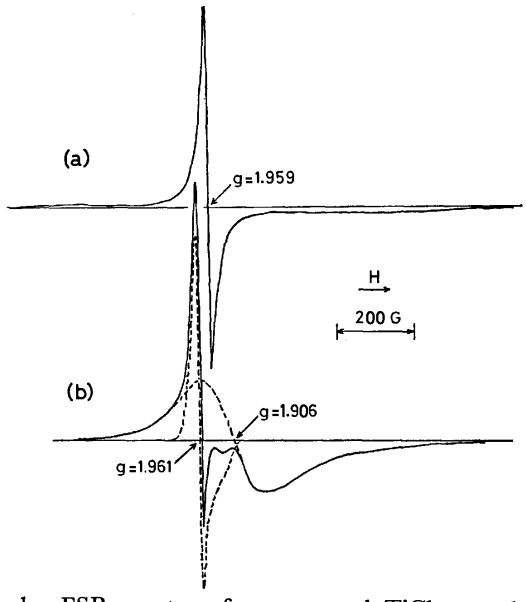

Fig. 1. ESR spectra of a supported $TiCl_3$ complex with 20% cross-linking and 65% pyridyl group prepared in pyridine, recorded under nitrogen at room temperature (a) and at 77 K (b).

When $TiCl_3$ is dissolved into pyridine, a sharp intense singlet signal at $g=1.96$[8] or 1.957[9] has been observed at room temperature along with a triplet-state spectrum of a $TiCl_3$ dimer. This signal has been ascribed to a $TiCl_3$ monomer whose structure, however, is unknown. The titanium(III) species giving type A signals has an analogous structure because of the similarity of g values and line widths between type A signals and the above signal in the pyridine solution. The titanium(III) species responsible for type A signals is coordinated only by the pyridyl groups of supports, since the g values of the signals depend neither upon the solvents used in preparation nor the composition of supports, the amounts of the signals decreasing with a decrease in chelating nature of the pyridyl groups.

Trichlorotitanium(III) forms hexacoordinated complexes of the type $TiCl_3L_3$, where L is a polar molecule such as acetonitrile, pyridine, acetone, or THF.[10] Further, $TiCl_3$ forms also hexacoordinated complexes of the type $TiCl_3L_2L'$ with two different non-halide ligands, where L and L' are acetonitrile, dioxane, THF, and 2-propanol.[11] Thus the following hexacoordinated titanium(III) species seem to be present in the supported complexes: $TiCl_3(pyr)_nL_{3-n}$ ($n=1$, 2, and 3), where pyr is a pyridyl group of the supports and L is a molecule of the solvents used in preparation.

In frozen solution at 77 K, $TiCl_3L_3$, where L is acetonitrile, pyridine, or THF, gave an ESR signal with $g_{//}=1.883$, $g_{\perp}=1.921$, $g_{av}=1.908$;[11] $g_1=1.86$, $g_2=$

** Each g value of the two types of signals was calculated at the center of each ESR signal, since the signal was a single line without peaks giving principal g values.

Table 1. *g* Values, relative amounts of two types of signals, and colors of polymer-supported $TiCl_3$ complexes

Expt. No.	Solvent used for preparation	Cross-linking %	Content of pyridyl groups %	*g* Value[a] type A	*g* Value[a] type B	Relative amount[a,b] type A/type B %	Color
1	pyridine	0	65	1.962	1.909	14	dark brown
2	pyridine	20	65	1.961	1.906	2	brown
3	pyridine	20	10	1.961	1.906	1	light brown
4	THF	0	65	1.959	1.908	10	dark brown
5	THF	20	65	1.960	1.901	2	brown
6	THF	20	20	1.959	1.883	1	light brown
7	THF	20	10	1.959	1.870	1>	light yellow
8[c]	THF	20	65	1.960	1.873	1>	yellow

a) Measured under nitrogen at 77 K. b) Ratio of the areas under both types of integrated signals.
c) Pretreated with $TiCl_4$.

1.89, $g_3=1.95$, $g_{av}=1.90$;[8] or $g_{//}=1.849$, $g_{\perp}=1.894$, $g_{av}=1.879$,[11] respectively, while it gave a very broad signal at room temperature.[12] Since the *g* values and the line widths of type B signals at room temperature and 77 K are similar to those of the above $TiCl_3L_3$ complexes, type B signals are ascribed to the $TiCl_3(pyr)_nL_{3-n}$ species.

In hexacoordinated titanium(III) complexes their *g* values increase with the increasing number of their ligands at higher order in the spectrochemical series.[11,13] The *g* values of the above $TiCl_3L_3$ complexes increase with the following order of L: THF<pyridine<acetonitrile. This is the same order of L in the spectrochemical series.[14]

The fact that supported complexes prepared in pyridine have larger *g* values than those prepared in THF indicates the presence of the $TiCl_3$ species having solvent molecules, *i.e.*, $TiCl_3(pyr)_nL_{3-n}$ ($n=1$ and 2), in the supported complexes. The decrease in the *g* values of supported complexes prepared in THF with a decrease in the content of pyridyl groups indicates the increase in the number of the $TiCl_3$ species having more solvent ligands, THF, with a decrease in the content of pyridyl groups. The decrease in the *g* values with cross-linking of the supports or with pretreatment with $TiCl_4$ indicates also the increase in the $TiCl_3$ species which have more solvent ligands, THF, with these changes in the conditions of preparation. Supported complexes prepared in pyridine would contain the $TiCl_3(pyr)_nL_{3-n}$ species having various values of *n*, as those prepared in THF contain, in spite of the small change of the *g* values with the change of the composition of the supports. The small change is ascribed to the similar effects of a pyridyl group (4-alkylpyridine) and pyridine upon the *g* value of a titanium(III) ion.

In conclusion, there are several $TiCl_3$ species with different environments (titanium(III) species responsible for type A signals and $TiCl_3(pyr)_nL_{3-n}$ ($n=1$, 2, and 3)) in polymer-supported $TiCl_3$ complexes, and the relative amounts of these titanium(III) species depend upon the composition of the polymer-supports (the content of pyridyl groups and the degree of cross-linking) and upon pretreatment with $TiCl_4$. In supported complexes with a high content of pyridyl groups, the pyridyl groups coordinate as chelate ligands to $TiCl_3$, and the number of the $TiCl_3$ species with two or three chelate pyridyl groups, *i.e.*, $TiCl_3(pyr)_nL_{3-n}$ ($n=2$ and 3), is large. On the other hand, such chelation is difficult in supported complexes with a low content of pyridyl groups and thus the $TiCl_3$ species with one pyridyl group, *i.e.*, $TiCl_3(pyr)L_2$, increase. Cross-linking makes supports rigid and their chelating nature weak. On addition of $TiCl_4$, the pyridyl groups coordinate as chelate ligands to $TiCl_4$ forming $TiCl_4(pyr)_2$, and thus the number of the pyridyl groups which can coordinate as chelates decreases and $TiCl_3$ added subsequently forms mainly $TiCl_3(pyr)L_2$.

Dioxygen Adducts of Polymer-supported $TiCl_3$ Complexes. By introduction of 1 atm of oxygen upon polymer-supported $TiCl_3$ complexes at room temperature, the intensities of both types of ESR signals became less than half of their original ones within a few minutes except for supported complexes without cross-linking. The colors of the supported complexes turned from brown or yellow to orange or yellowish orange at the same time. The decrease in intensities of both types of ESR signals and the change of color were very slow (half-life, *ca.* 2 h) in the case of supported complexes without cross-linking. This difference may be mainly caused by the difference in surface areas. Supported complexes with cross-linking are fine powders and may have greater surface areas than those without cross-linking which are fine pieces of films.

New sharp signals appeared at about $g=2.01$ as soon as the signals of titanium(III) diminished. The shapes of the new signals at 77 K were the same as those at room temperature. The new signals of two different supported complexes are given in Fig. 2. Each spectrum consists of two or three signals, each having three principal *g* values, *viz.*, $g_1=2.028$, $g_1'=2.023$, $g_2=g_2'=2.011$, $g_3=g_3'=2.004$ (Fig. 2a); $g_1=2.028$, $g_1'=2.022$, $g_1''=2.017$, $g_2=g_2'=g_2''=2.011$, $g_3=g_3'=g_3''=2.004$ (Fig. 2b). The new signals of all the supported complexes we examined had the following principal *g* values: $g_1=2.017$—2.028, $g_2=2.010$—2.011, and $g_3=2.003$—2.004 (Table 2). These values are nearly the same as those of O_2^- radicals on titanium dioxide.[15] Thus the new signals are ascribed to dioxygen adducts of support-

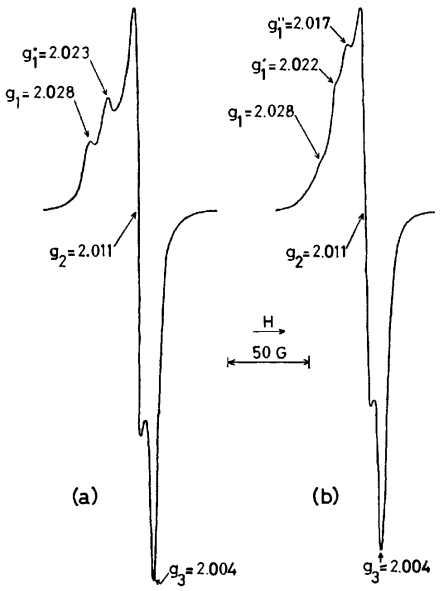

Fig. 2. New ESR signals of supported $TiCl_3$ complexes with 20% cross-linking and 65% (a) and 10% (b) pyridyl group prepared in THF, recorded under nitrogen at room temperature after contact with oxygen.

ed $TiCl_3$ complexes, whose electronic structure should be formally decribed as $Ti(IV)-O_2^-$.

The three principal g values of the dioxygen adducts of the supported complexes prepared from different supports in different solvents are given in Table 2. We denote principal g value along the axis of O–O bond by g_1. The g_1 values are greatly influenced by the conditions of preparation, whereas the g_2 and g_3 values remain nearly constant. The g_1 values can be classified into three groups: 2.027—2.028, 2.022—2.024, and 2.017—2.018. They correspond to three different $Ti(IV)-O_2^-$ species α, β, and γ, respectively, whose g_2 values as well as g_3 values are identical with each other. The g_1 peak of α is enhanced in supported complexes with a high content of pyridyl groups prepared in either of the solvents, becoming a shoulder in those with a low content of pyridyl groups. The g_1 peak of β behaves like that of α, but remains as a stronger peak than that of α when supported complexes are prepared from supports with a low content of pyridyl groups. The g_1 peak of γ appears only in supported complexes with a low content of pyridyl groups prepared in THF or pretreated with $TiCl_4$, being the strongest of the three peaks.

A few different O_2^- species have also been found on the surface of titanium dioxide. Naccache *et al.*[16] reported that two different O_2^- species were found on both anatase and rutile: $g_1=2.024$, $g_1'=2.020$, $g_2=g_2'=2.009$, $g_3=g_3'=2.003$ for anatase; $g_1=2.030$, $g_2=2.008$, $g_3=2.004$, $g_1'=2.020$, $g_2'=2.009$, $g_3'=2.003$ for rutile. Davydov *et al.*[17] found five different O_2^- species on anatase: $g_1^1=2.0330$, $g_1^2=2.0278$, $g_1^3=2.0254$, $g_1^4=2.0233$, and $g_1^5=2.0213$, the g_2 values as well as the g_3 values of which coincided with each other. However, the structures of the dioxygen adducts corresponding to these different g_1 values have not been described.

The structures of the dioxygen adducts α, β, and γ should be considered. These dioxygen adducts do not come mainly from the titanium(III) species responsible for type A signals, since the amounts of type A signals were small. There was no remarkable difference in the relative amounts of these dioxygen adducts of a supported complex with 0% cross-linking and 65% pyridyl group and that with 20% cross-linking and 65% pyridyl group, where the relative amounts of type A signals to type B signals were 14% and 2%, respectively. Adducts α and β were observed in supported complexes prepared in pyridine. They have no THF ligand though they appeared also in supported complexes prepared in THF. The relative amounts of the titanium(III) species $TiCl_3(pyr)_3$, $TiCl_3(pyr)_2L$, and $TiCl_3(pyr)L_2$ in supported complexes prepared in THF increased in this order with a decrease in the content of pyridyl groups. The relative amounts of α, β, and γ increased also in this order with a decrease in the content of pyridyl groups. Thus $TiCl_3(pyr)_3$, $TiCl_3(pyr)_2L$, and $TiCl_3(pyr)L_2$ might be the precursors of α, β, and γ, respectively.

The order of the g_1 values of α, β, and γ gives information on the structures of the dioxygen adducts. It has been shown both experimentally and theoretically that the g_1 value of a O_2^- radical coordinating to a cation approaches g_e (2.0023) more closely as the charge of the cation becomes more positive.[15] The g_1 values decreased in the order $\alpha>\beta>\gamma$, the negativity of titanium ions of the dioxygen adducts decreasing in the same order. Since a pyridyl group is more basic than THF or a chloride anion, a titanium ion which has more pyridyl

Table 2. Principal g values of dioxygen adducts of polymer-supported $TiCl_3$ complexes[a]

Expt. No.	Solvent used for preparation	Cross-linking %	Content of pyridyl groups %	g_1	g_1'	g_1''	g_2	g_3
1	pyridine	0	65	2.028	2.022	—	2.010	2.004
2	pyridine	20	65	2.028	2.023	—	2.010	2.003
3	pyridine	20	10	2.028 sh[b]	2.022	—	2.011	2.004
4	THF	0	65	2.028	2.024	—	2.010	2.004
5	THF	20	65	2.028	2.023	—	2.011	2.004
6	THF	20	20	2.027 sh	2.022 sh	2.017	2.010	2.004
7	THF	20	10	2.028 sh	2.022 sh	2.017	2.011	2.004
8[c]	THF	20	65	2.028 sh	2.022 sh	2.018	2.010	2.004

a) Measured under nitrogen at room temperature after contact with oxygen. b) Abbreviation: sh, shoulder.
c) Pretreated with $TiCl_4$.

groups becomes more negative. Thus the number of pyridyl groups coordinating to the titanium ions of the dioxygen adducts increases in the order $\gamma<\beta<\alpha$.

The tentative structures of α, β, and γ which agree with the above conclusions are shown in the following scheme along with their precursors. It is assumed that an oxygen molecule behaves as a unidentate ligand and a titanium ion is hexacoordinated.

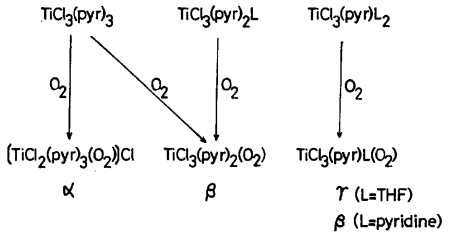

Scheme.

These dioxygen adducts were very stable at 77 K, but decomposed slowly at room temperature under either nitrogen or oxygen. Among the dioxygen adducts γ was the most unstable, half-life of which was about 1 h under oxygen at room temperature.

The total yields of the dioxygen adducts after a five minute contact with 1 atm of oxygen at room temperature were measured at 77 K under nitrogen and found to be a few percent based on the titanium(III) species reacted with oxygen.

The oxygenation of supported $TiCl_3$ complexes was almost irreversible, since the decomposition of their dioxygen adducts was very slow in a vacuum or under nitrogen as compared with their rapid formation. The decomposition would imply not only the liberation of oxygen to yield the original titanium(III) species but also irreversible oxidation to titanium(IV) species.

The authors wish to express their thanks to Dr. Toshimitsu Suzuki of this department for the supply of $TiCl_3$.

References

1) J. S. Valentine, *Chem. Rev.*, **73**, 235 (1973).
2) J. E. Baldwin and J. Huff, *J. Am. Chem. Soc.*, **95**, 5757 (1973); J. P. Collman, R. R. Gagne, C. A. Reed, T. R. Halbert, G. Lang, and W. T. Robinson, *ibid.*, **97**, 1427 (1975); J. Almog, J. E. Baldwin, and J. Huff, *ibid.*, **97**, 227 (1975).
3) A. Misono, S. Koda, and Y. Uchida, *Bull. Chem. Soc. Jpn.*, **42**, 3470 (1969).
4) J. H. Wang, *J. Am. Chem. Soc.*, **80**, 3168 (1958).
5) O. Leal, D. L. Anderson, R. G. Bowman, F. Basolo, and R. L. Burwell, Jr., *J. Am. Chem. Soc.*, **97**, 5125 (1975).
6) H. Fischer, *Ber. Bunsenges. Phys. Chem.*, **71**, 685 (1967).
7) Y. Chimura, *Chem. Lett.*, **1974**, 393.
8) S. G. Carr and T. D. Smith, *J. Chem. Soc., Dalton Trans.*, **1972**, 1887.
9) C. D. Schmulbach, C. C. Hinckley, C. Kolich, T. A. Ballintine, and P. J. Nassiff, *Inorg. Chem.*, **13**, 2026 (1974),
10) R. S. P. Coutts and P. C. Wailes, *Adv. Organomet. Chem.*, **9**, 136 (1970).
11) G. R. Hoff and C. H. Brubaker, Jr., *Inorg. Chem.*, **10**, 2063 (1971).
12) H. K. Ostendorf, *Recl. Trav. Chim. Pays-Bas*, **91**, 809 (1972).
13) W. Giggenbach and C. H. Brubaker, Jr., *Inorg. Chem.*, **8**, 1131 (1969).
14) R. J. H. Clark, J. Lewis, D. J. Machin, and R. S. Nyholm, *J. Chem. Soc.*, **1963**, 379; G. W. A. Fowles and R. A. Hoodless, *ibid.*, **1963**, 33.
15) J. H. Lunsford, *Catal. Rev.*, **8**,135 (1973).
16) C. Naccache, P. Meriaudeau, M. Che, and A. J. Tench, *Trans. Faraday Soc.*, **67**, 506 (1971).
17) A. A. Davydov, M. P. Komarova, V. F. Anufrienko, and N. G. Maksimov, *Kinet. Katal.*, **14**, 1519 (1973).

The Liquid-phase Oxidation of Acetaldehyde with Metal Polyphthalocyanines. Solvent Effect

Yasukazu OHKATSU, Takao HARA, and Tetsuo OSA

Department of Synthetic Chemistry, Faculty of Engineering, University of Tokyo, Hongo, Bunkyo-ku, Tokyo 113

(Received October 1, 1975)

Acetaldehyde was oxidized using metal polyphthalocyanines as catalysts. Metal polyphthalocyanines, especially Fe,Cu-polyphthalocyanine, were found to be useful oxidation catalysts for the selective formation of peracetic acid from acetaldehyde. The rate of oxidation was much affected by the nature of the solvents. The solvent is considered to take part in the initiation oxidation reaction in two ways: one is based on the prevention of the oxygen molecule from coordination with a metal polyphthalocyanine and subsequent activation, and the other is due to the solvation with the activated oxygen molecules on the catalyst. Preferable solvents were ethyl acetate, bromobenzene, benzene, and acetone.

Since metal phthalocyanines were discovered to carry oxygen molecules, they have been used as catalysts in the autoxidation of many organic compounds, the mechanism of their action on the oxidation reaction has also been investigated.[1-4] Kropf *et al.* reported that an active species, an oxygen complex derived from a metal pathalocyanine and molecular oxygen in the presence of a base such as pyridine, could abstract the hydrogen atom from a substrate to generate free radicals, resulting in the initiation of autoxidation.[5-7] Other investigators[8,9] proposed another mechanism for the action of metal phthalocyanines, especially the ability to decompose hydroperoxide homolytically to initiate autoxidation. Contrary to the oxidations using metal phthalocyanines, there are only a few papers available concerning the metal polyphthalocyanine-catalyzed autoxidation.[10-13] But studies of the metal polyphthalocyanine in comparison with its monomeric analogue are expected to throw some light on the elucidation to the chemical behavior of metal polyphthalocyanine as one of the macromolecular catalysts complexed with metal ions, the structure of which possesses a close similarity to hemoglobin. In our papers, various metal polyphthalocyanines were synthesized and shown to be effective catalysts for the autoxidation of cumene[11] and acrolein.[12,13]

In this paper, the liquid-phase oxidation of acetaldehyde was tried using various metal polyphthalocyanines as catalyst. The action of the catalyst and the effect of solvents on the oxidation are discussed in detail.

Experimental

Materials: Metal polyphthalocyanines were synthesized and purified according to the method descrided in an earlier paper.[13] The metal contents in Fe,Cu-polyphthalocyanine were analyzed by a spectrophotometric method; the ratio of iron to copper ions was 1.52. The metal polyphthalocyanine was sufficiently pulverized with a mortar before use. The oxidation rate with micro-crystals of metal polyphthalocyanine was, however, found to be essentially the same as that with the pulverized metal. Acetaldehyde was carefully distilled under nitrogen atmosphere to insure the complete removal of the oxidized materisls; solvents were used after conventional purification with careful drying.

Procedure and Analysis: The oxidation apparatus and oxidation process were described in the literature.[14]

Peroxide products were analyzed by an iodometric titration method determining individual concentrations of hydrogen peroxide, peracetic acid, and other peroxides such as acetoyl peroxide.[15] Other oxidation products were quantitatively determined by gas liquid chromatography.

Results and Discussion

Outline of Autoxidation: Purified samples of metal polyphthalocyanines have been shown to lack the ability to decompose a hydroperoxide, though they catalyzed the liquid-phase oxidation of organic compounds such as cumene and acrolein. The oxidation of acetaldehyde with a metal polyphthalocyanine also gave peracetic acid quantitatively in such solvents as benzene, ethyl acetate, and acetone (Table 1). This fact may be emphasized as one of the characteristic actions of metal polyphthalocyanines, because metal phthalocyanines and other catalysts such as metal acetylacetonates and naphthenates are known to decompose peracetic acid formed during the oxidation of acetaldehyde through a homogeneous mechanism.[16,17] The selectivity of peracetic acid in benzene and ethyl acetate as solvents was inclined to decrease with the reaction time. This may be ascribed to the formation of acetaldehyde monoperacetate in these solvents, followed by its heterogeneous decomposition. In acetone, the rate of oxidation was slower than in ethyl acetate, but the selectivity remained about 93% even after three hours. This suggests that metal polyphthalocyanines can be made use of as catalysts for the selective formation of peracetic acid, and shows that they have no ability to decompose peracetic acid, resulting in the initiation of autoxidation.

The rate of oxygen absorption, as shown in Table 2, was much affected by the nature of the solvent. The dielectric constants of the solvents are also listed in Table 2. The oxidation reaction seems to proceed much faster in a solvent which has an adequate polarity, such as ethyl acetate. There is, however, no linear relationship between the rate and the dielectric constant.

The role of solvents in an autoxidation reaction catalyzed by an organometallic complex can be considered in general in terms of the following two ways. First, the solvent may take part in the chain-propagating step to interrupt autoxidation:

$$CH_3COOO\cdot + RH \longrightarrow CH_3COOOH + R\cdot \quad (A)$$

in which RH denotes a solvent. Secondly, it may

Table 1. The oxidation products in the oxidation of acetaldehyde catalyzed by metal polyphthalocyanines

		Catalyst (solvent)		
		Fe, Cu (Benzene)	Fe, Cu (Ethyl acetate)	Fe (Acetone)
Acetaldehyde charged ($\times 10^3$M)		45.0	45.2	46.3
Peracetic acid formed ($\times 10^3$M)	a*	12.8	23.4	19.7
	b*	20.3	28.0	27.6
	c*	21.1	26.6	28.6
Peroxide formed ($\times 10^3$M)	a	0.57	0.39	0.49
	b	1.34	0.95	0.59
	c	1.29	1.10	0.82
Peracetic acid formed / Acetaldehyde charged (%)	a	28.4	51.7	42.5
	b	45.4	61.9	59.6
	c	47.0	58.8	61.4
Oxygen absorbed / Acetaldehyde charged (%)	a	29.5	57.4	44.2
	b	58.3	73.1	59.7
	c	60.5	79.5	66.1
Peracetic acid formed / Oxygen absorbed (%)	a	96.4	90.2	102
	b	77.8	84.7	99.9
	c	77.2	73.7	92.8

Reaction conditions: (catalyst), 4.82×10^{-3}M; temperature, 10 °C.
*a, b, and c represent one, two, and three hours of reaction time, respectively.

Table 2. The rate of oxygen absorption in the oxidation of acetaldehyde by two metal polyphthalocyanines in various solvents

Me-poly-Pc	Solvent	Dielectric constant	$-d(O_2)/dt$ $\times 10^5$M s^{-1}
Fe, Cu	*p*-Xylene	2.27	0.0
	Benzene	2.28	8.51
	Bromobenzene	5.40	10.6
	Ethyl acetate	6.02	13.7
	Acetone	20.7	8.44
	Benzonitrile	25.2	0.22
	Methanol	32.7	0.0
Fe	Chlorobenzene	5.62	7.64
	Acetone	20.7	7.62
	Nitrobenzene	34.8	0.61

Reaction conditions: (CH_3CHO), 4.52×10^{-1}M; (catalyst), 4.8×10^{-3}M; temperature, 10 °C.

Table 3. The rate of oxygen absorption with and without catalyst in carboxylate solvents

Solvent	$-d(O_2)/dt, \times 10^5$ M s^{-1} (a) Uncatalyzed	(b) Catalyzed	Ratio of (b) to (a)
Ethyl acetate	0.89	13.7	15.4
Isopropyl acetate	0.89	5.84	6.6
Ethyl chloroacetate	0.1	2.45	28.0

Reaction conditions: temperature, 10 °C; catalyst, Fe,Cu-poly-Pc, 4.81×10^{-3}M; acetaldehyde, 4.52×10^{-1}M.

interact with the complexes as a catalyst to change their activity. Imamura found that the oxidation rate of acetaldehyde catalyzed by cobalt naphthenate depended substantially on the kind of solvents and concluded that the oxidation was probably governed by a reaction according to Eq. A in the case of the presence of a hydrocarbon solvent.[17]

If the solvent effect is observed only on the propagation and termination steps of a general autoxidation mechanism as discussed below, though ester solvents were mostly used in this paper, the relative rates of the oxidation in the presence of the catalyst to that in the absence of the catalyst must be same regardless of the kind of solvents. The ratio in Table 3 does not show any solvent effect on such chain steps. This fact also proposes that the solvent effect is operative in the initiation step rather than the chain steps in the present oxidation reaction using a metal polyphthalocyanine as catalyst.

Solvent Effect: The effect of solvents on the rate of oxidation was investigated in detail using various esters, such as acetates (CH_3COOR) and ethyl carboxylates ($R'COOC_2H_5$), as solvents. The oxidation rate in the presence of a metal polyphthalocyanine was considerably dependent on the kind of substituent groups R and R' (Table 4). It was found that there was a certain relation between the oxidation rates and the electronic properties of the substituents (R and R') in terms of their polar substituent constants σ^* for Taft's equation.

In the case of acetates (Fig. 1), the logarithm of the rates increased linearly with increase of σ^* of R in the range of $\sigma^* < -0.10$. The constants ρ^* can be calculated as 6.7 and -0.3 over the ranges of σ^* below and above -0.10, respectively, except for methyl acetate, which is very difficult to purify and constains a small amount of methanol which makes the metal polyphthalocyanine inactive (Table 2). A similar result was also obtained for the ethyl carboxylates, as illustrated in Fig. 1b;

Table 4. Solvent effect of various acetates and ethyl carboxylates on the oxidation rates

Solvent	Substituents R–	Substituents R'–	$-d(O_2)/dt \times 10^5$ M s^{-1}
Acetates			
methyl acetate	CH_3–		2.33
butyl acetate	$CH_3(CH_2)_3$–		17.2
isopropyl acetate	$(CH_3)_2CH$–		5.84
benzyl acetate	$(C_6H_5)CH_2$–		2.58
ethyl acetate	C_2H_5–	CH_3–	13.7
Ethyl carboxylates			
ethyl propionate		C_2H_5–	6.10
ethyl chloroacetate		CH_2Cl–	2.45
ethyl isobutyrate		$(CH_3)_2CH$–	3.14
ethyl dichloroacetate		$CHCl_2$–	0.18

Reaction conditions: (acetaldehyde), 4.52×10^{-1}M; (Fe,Cu-poly-Pc), 4.8×10^{-3}M; temperature, 10 °C.

values of ρ^* were calculated as 4.4 and −1.0 for the straight lines of the left and right sides of ethyl acetate, respectively. For simplicity, a series of solvents having positive ρ^* value are hereafter called M, while the series having negative ρ^* are called N. Considering the absolute values of ρ^* for solvent series M and N, the values for the series M are much larger than those for series N. The ρ^*'s also have different signs for the two series of solvents. These facts imply that the mechanisms of solvent effects are different in these series. The rather large values of ρ^* for series M may suggest that such solvents take part as more polarized species in the initiation reaction.

Table 5. The constant k_1K_1 of the initiation reaction of acetaldehyde by various metal polyphthalocyanines

Metals	$-d(O_2)/dt \times 10^5$ M s	$k_1K_1 \times 10^2$ M^{-2} s^{-1}
Fe,Cu	21.6	7.2
Fe,Mo	12.1	2.0
Fe	8.6	1.1
Fe,Co	8.5	1.1
Cu,Co	1.1	0.0017

Reaction conditions: (CH_3CHO), 0.45M; (catalyst), 4.82×10^{-3}M; solvent, ethyl acetate; temperature, 10 °C.

A Possible Reaction Mechanism: In order to explain the results mentioned above and to explain the oxidation mechanism, especially the initiation reaction, in more detail, the oxidation reaction was investigated kinetically under reaction conditions including those shown in Figs. 1(a) and 1(b). The reactions were confirmed not to proceed under diffusion control of oxygen in the reaction system. The dependence of the rates of oxygen absorption on concentrations of acetaldehyde and the catalyst and on oxygen pressure was determined in three kinds of solvents, isopropyl acetate belonging to series M and ethyl acetate and ethyl monochloroacetate belonging to series N (Figs. 2a, 2b, and 2c).

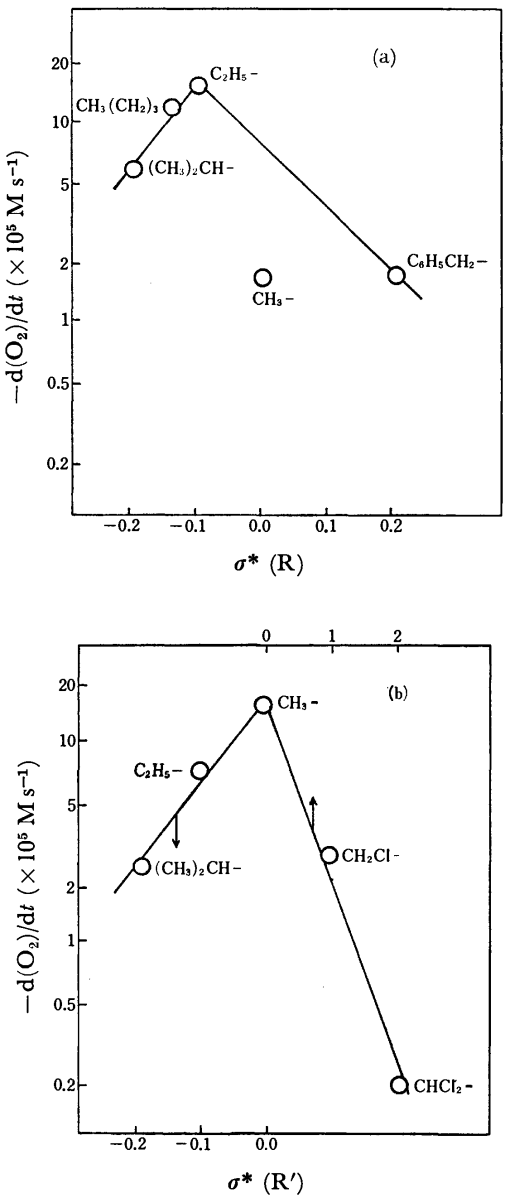

Fig. 1. The effects of the substituents R and R' of esters (R'COOR) as solvents on the rate of oxidation.

The rate equations, except for that obtained with a lower pressure of oxygen in isopropyl acetate, were equal and could be written as Eq. I:

$$-\frac{d(O_2)}{dt} = k(CH_3CHO)^{3/2}(\text{catalyst})^{1/2}(O_2)^{1/2} \quad \text{(I)}$$

in which k means a rate constant. This equation can be compared with the rate equation (II)

$$-\frac{d(O_2)}{dt} = k_p/(2k_t)^{1/2}(CH_3CHO)\cdot R_i^{1/2} \quad \text{(II)}$$

derived from the general elementary steps of autoxidation under no diffusion control of oxygen as follows;

initiation: $CH_3CHO \longrightarrow CH_3\dot{C}O$: R_i (1)

chain propagation:

$CH_3\dot{C}O + O_2 \longrightarrow CH_3COOO\cdot$ (2)

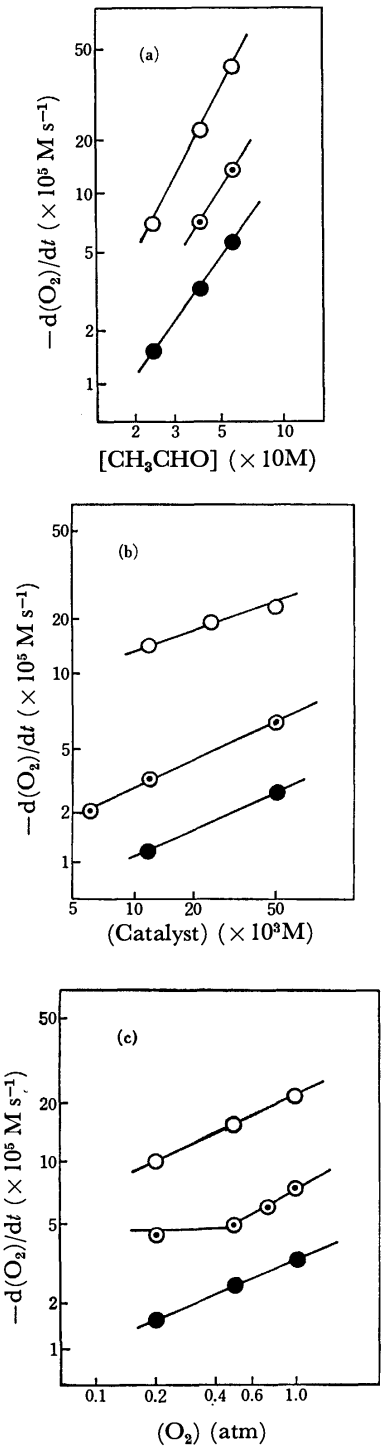

Fig. 2. Effects of concentrations of acetaldehyde, Fe, Cu-polyphthalocyanine, and oxygen on the oxidation rates.
Reaction conditions: (CH_3CHO), 0.45 M; (Fe,Cu-poly-Pc), 4.82×10^{-3} M; and O_2 pressure, 1 atm were used as standard. Temperature was 10°C.
○: Ethyl acetate, ⊙: isopropyl acetate, ●: ethyl chloroacetate.

$$CH_3COOO\cdot + CH_3CHO \xrightarrow{k_p} CH_3COOOH + CH_3\dot{C}O \quad (3)$$

$$\text{termination: } 2CH_3COOO\cdot \xrightarrow{k_t} \text{non-radical} \quad (4)$$

in which R_i represents the rate of initiation, and k_p and k_t represent the rate constants of Steps 3 and 4. Consequently the rate of initiation is obtained as

$$R_i = \{k/k_p/(2k_t)^{1/2}\}^2(CH_3CHO)(\text{catalyst})(O_2) \quad \text{(III)}$$

It is possible, therefore, to discuss the initiation mechanism as follows:

$$\text{Me-polyPc} + O_2 \rightleftarrows \text{Me}^+\text{-polyPc-}O_2^- \quad \text{(1-a)}$$

$$\text{Me}^+\text{-polyPc-}O_2^- + CH_3CHO \longrightarrow (\text{Me-polyPc-}O_2H) + CH_3\dot{C}O \quad \text{(1-b)}$$

When the equilibrium constant of Scheme 1-a and the rate constant of Scheme 1-b are assumed to be K_1 and k_1 respectively, the rate equation of initiation is

$$R_i = k_1K_1(CH_3CHO)(\text{catalyst})(O_2) \quad \text{(IV)}$$

at the stationary state. This equation is equal to Eq. III.

It is well known that such substrates as acetic acid and methanol are easily coordinated with a metal ion in the conjugated system of a metal phthalocyanine through the electron pair on the oxygen atom. In the above initiation mechanism, the solvents in series M are considered to have considerably stronger electron-donating substituents corresponding to the lower values of σ^*, resulting in the stronger coordination through their carbonyl oxygen. In other words, the degree of the electron density on the oxygen atom of the carbonyl group increases with the increase of the electron-donating ability of the substituents R and R′. The reaction 1-a is, therefore, considered to be competitive with the reaction between a metal polyphthalocyanine and a solvent as follows:

$$\text{Me-polyPc} \xrightarrow{O_2} \text{Me}^+\text{-polyPc-}O_2^- \quad \text{(1-a)}$$

$$\text{Me-polyPc} \xrightarrow{\text{RCOOR}'} \text{Me-polyPc-O=C}\begin{matrix}\text{OR}'\\ \text{R}\end{matrix} \quad \text{(1-a')}$$

As the σ^* values of the solvents become smaller, the equilibrium 1-a′ is much more shifted to the right side. The stronger interaction of a solvent with a metal ion will leave fewer chances for the O_2 molecule to be activated by coordination. This interaction can be explained by the higher values (6.7 and 4.4) of ρ^* in series M, which are considered to be based on the interaction of solvents with the polarized species as mentioned before.

Negative values of the reaction constant ρ^* were obtained in the solvents of series N. As the absolute values of ρ^* are smaller compared with those in series M, these solvents are considered to have a weaker interaction with the initiation reaction. According to the explanation with respect to solvents of series M, the larger value of σ^* has to facilitate the activation of the molecular oxygen by a metal ion. But in the case of the electron-attracting ability of the substituent becoming too large, the electron density on the oxygen atom decreases to a certain extent, and consequently the metal polyphthalocyanine-O_2 complex is not apt to react with acetaldehyde, because these kinds of solvents may solvate with such an activated oxygen complex, resulting in the prevention of the hydrogen-abstracting reaction from acetaldehyde (1-b). No

evidence to support this explanation is yet available, but this will be discussed in detail in our next paper.[18] A possible reaction mechanism is

$$\mathrm{Me^+\text{-}polyPc\text{-}O_2^-} \xrightarrow{CH_3CHO} \mathrm{Me^+\text{-}polyPc\text{-}O_2^-\text{-}CH_3CHO} \quad (1\text{-b})$$

$$\mathrm{Me^+\text{-}polyPc\text{-}O_2^-} \xrightarrow{solvent} \mathrm{Me^+\text{-}polyPc\text{-}O_2^-\text{-}solvent} \quad (1\text{-b}')$$

In this case, the lower absolute value of ρ^* may be explained by the above-mentioned Schemes 1-b and 1-b'.

It is concluded, as the sum of these two effects of solvents on the initiation mechanism, that such a solvent as ethyl acetate or ethyl propionate is an optimum one whose substituent shows an adequate degree of the electron-donating and -attracting abilities for the carbonyl group.

In the oxidation of acetaldehyde in isopropyl acetate, the partial pressure of oxygen had no influence on the rate of oxygen absorption in the range of the oxygen pressure below 400 Torr. This means that the activation of oxygen does not occur because of low concentration of oxygen dissolved and/or the more preferable conditions for the reaction 1-a' than 1-a, and suggests that Fe,Cu-polyphthalocyanine directly abstracts the hydrogen atom from aldehyde, as is well known.[19]

The constants k_1K_1 of Eq. IV are compared for various metal polyphthalocyanines. The rate equation can be written as when the R_i of Eq. IV is put into Eq. II.

$$-\frac{d(O_2)}{dt} = (k_1K_1)^{1/2}k_p/(2k_t)^{1/2}(CH_3CHO)^{3/2} \times (\text{catalyst})^{1/2}(O_2)^{1/2} \quad (V)$$

The rate constant k_p at 0 °C is reported to be 2.7×10^3 M^{-1} s^{-1} and the activation energy of k_p is assumed to be 4.2 kcal/mol, which is determined in the oxidation of decanal.[20] Then the approximate value of k_p at 10 °C is calculated to be 3.6×10^3 M^{-1} s^{-1}. On the other hand, the rate constant $2k_t$ at 0 °C is reported to be 1.04×10^8 M^{-1} s^{-1}. As $2k_t$ is considered not to be so influenced by the temperature, $k_p/(2k_t)^{1/2}$ can be obtained as 3.6×10^{-1} $M^{-1/2}$ $s^{-1/2}$ at 10 °C. The concentration of oxygen dissolved in ethyl acetate at 10 °C is reported to be 1.15×10^{-2} M.[21] Table 5 summarizes the calculated k_1K_1 values. The metal polyphthalocyanines are effective to activate the oxygen molecule in the order of Fe,Cu–≫Fe,Mo–>Fe–>Fe,Co–≫Cu, Co–polyphthalocyanines. Iron seems to be essential to such activation.

The authors would like to express their thanks to Prof. Teiji Tsuruta for giving fruitful advice on finishing this work.

References

1) C. Pacquout, *C. R. Acad. Sci.*, **209**, 171 (1939).
2) C. Pacquout, *Bull. Soc. Chim. Fr.*, **8**, 695 (1941).
3) J. A. Elvidge and A. B. P. Lever, *Proc. Chem. Soc.*, **1959**, 195.
4) A. Yamamoto, L. K. Philips, and M. Calvin, *Inorg. Chem.*, **7**, 847 (1968).
5) H. Hock and H. Kropf, *J. Parkt. Chem.*, **9**, 173 (1959).
6) H. Kropf, *Tetrahedron Lett.*, **1962**, 577.
7) H. Kropf and H. Hoffman, *Tetrahedron Lett.*, **1967**, 659.
8) Y. Kamiya, *Tetrahedron Lett.*, **1968**, 4965.
9) A. I. Minkov, *Kinet. Katal.*, **8**, 160 (1967).
10) H. Inoue, Y. Kida, and E. Imoto, *Bull. Chem. Soc. Jpn.*, **41**, 648, 692 (1968).
11) T. Hara, Y. Ohkatsu, and T. Osa, *Chem. Lett.*, **1973**, 103.
12) T. Hara, Y. Ohkatsu, and T. Osa, *Chem. Lett.*, **1973**, 953.
13) T. Hara, Y. Ohkatsu, and T. Osa, *Bull. Chem. Soc. Jpn.*, **48**, 85 (1975).
14) A. Misono, T. Osa, Y. Ohkatsu, and M. Takeda, *Kogyo Kagaku Zasshi*, **61**, 2129 (1966).
15) F. P. Greenspan, *Anal. Chem.*, **20**, 1061 (1948).
16) Y. Ohkatsu and T. Osa, unpublished.
17) J. Imamura, *Nippon Kagaku Kaishi*, **1975**, 1377.
18) Y. Ohkatsu, O. Sekiguchi, and T. Osa, *Bull. Chem. Soc. Jpn.*, **50**, 701 (1970).
19) C. H. E. Bawn and J. A. Sharp, *J. Chem. Soc.*, **1957**, 1854, 1866.
20) D. B. Sharp, *J. Am. Chem. Soc.*, **74**, 1802 (1952).
21) See "Kagaku Binran," ed by Chem. Soc. of Japan.

The Liquid-phase Oxidation of Aldehydes with Fe,Cu-Polyphthalocyanine and Cobalt Tetra-*p*-tolylporphyrin

Yasukazu OHKATSU, Osamu SEKIGUCHI, and Tetsuo OSA

Department of Synthetic Chemistry, Faculty of Engineering, University of Tokyo, Hongo, Bunkyo-ku, Tokyo 113

(Received October 1, 1975)

The effect of chemical species in a reaction system on the oxidation reaction of aldehydes was studied using Fe,Cu-polyphthalocyanine and cobalt tetra-*p*-tolylporphyrin as catalysts. Both catalysts activated the oxygen molecule on their central metals and then abstracted the hydrogen atom from aldehydes to initiate autoxidation. In this initiation step, every chemical species present in the reaction system, such as the solvent, the aldehyde, the oxygen molecule and the catalyst, is found to have an effect, one after another, either to accelerate or to retard the rate of initiation. The correlation of the nature of chemical species with such mutual interaction was discussed in detail.

There are only a few papers[1,2] about liquid-phase oxidations using metal polyphthalocyanines and porphyrins as catalysts. Imoto *et al.*[3] utilized polyphthalocyanines containing two kinds of transition metals in the oxidation of acetaldehyde ethylene acetal. Such polyphthalocyanines have been reported to show no activities except for polyphthalocyanines including both iron and manganese, or both manganese and another metal. The oxidation rates has a good correlation with the activated energies (ΔE) calculated from the dependence of the electroconductivity of the catalyst on the temperature. In other words, the oxidation activity of a polyphthalocyanine increased with the decrease in ΔE, namely, the enlargement of the π-electron conjugated system. They concluded that the central metal of a polyphthalocyanine was the active site, which contributed to the activation of oxygen and the decomposition of a hydroperoxide. We also investigated the effects of the kinds of transition metals on the oxidation rate, and found that iron was one of the essential metals and that Fe,Cu-polyphthalocyanine was most effective in the oxidation of acetaldehyde.[4]

In the oxidations of cumene,[5] acrylaldehyde,[6,7] and acetaldehyde,[4] the activity of a metal polyphthalocyanine was also found to be much affected by the nature of the solvents with respect to the activation of oxygen and the catalytic performance. The effect of solvents in the liquid-phase oxidation of acetaldehyde with a metal polyphthalocyanine complex was elucidated in terms of the interaction between the central metal ion of the complex and a solvent, or the interaction of the aldehyde and/or the solvent with the oxygen molecule activated on the complex:

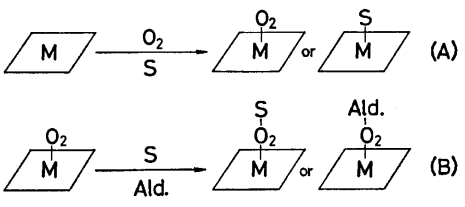

In the above schemes, M means the transition metals, S means the solvent, and Ald. means acetaldehyde. This paper will described some of the evidence for the vaguuness of the proposed schemes, especially Scheme B, using several kinds of aldehydes. Cobalt tetra-*p*-tolylporphyrin was utilized as a catalyst in comparison with Fe,Cu-polyphthalocyanine.

Experimental

Materials. The Fe,Cu-polyphthalocyanine used as a catalyst was synthesized and purified according to the conventional method.[8] Cobalt tetra-*p*-tolylporphyrin was prepared by the use of pyrrole, *p*-tolualdehyde, and cobalt(II) acetate.[9] Solvents such as ethyl carboxylates and aldehydes, such as acetaldehyde, propionaldehyde, butyraldehyde, isobutyraldehyde, acryldehyde, cinnamaldehyde, and benzaldehyde, were purified by conventinal methods. The aldehydes were carefully purified just before use in order to remove the pre-oxidation products.

Procedure. The liquid-phase oxidation of aldehydes was carried out using an atmosphere-tight and oxygen-circulating reaction apparatus reported before.[10] The reaction was started by the first charge of a solvent and the purge of the system with oxygen, subsequently we added a catalyst and an aldehyde.

In some cases, oxygen was bubbled and circulated into a reaction solution containing a solvent and a catalyst thirty minutes before the start of oxidation, so that the oxygen complex was formed previously, and then an aldehyde was added.

The amount of oxygen absorbed was followed by means of a gas burett, sometimes a portion of the reaction solution was sampled out to detemined its content of a percarboxylic acid by an iodine method.[11]

Results and Discussion

The oxidation of an aldehyde is widely accepted to proceed through the following steps:

$$\mathrm{RCHO} \longrightarrow \mathrm{R\dot{C}O} \text{ (initiation rate, } R_i\text{)} \quad (1)$$

$$\mathrm{R\dot{C}O} + \mathrm{O_2} \xrightarrow{k_2} \mathrm{RCOO_2\cdot} \quad (2)$$

$$\mathrm{RCOO_2\cdot} + \mathrm{RCHO} \xrightarrow{k_p} \mathrm{RCOO_2H} + \mathrm{R\dot{C}O} \quad (3)$$

$$2\mathrm{R\dot{C}O} \xrightarrow{k_4} \quad (4)$$

$$\mathrm{R\dot{C}O} + \mathrm{RCOO_2\cdot} \xrightarrow{k_5} \text{inert products} \quad (5)$$

$$2\mathrm{RCOO_2\cdot} \xrightarrow{k_6} \quad (6)$$

In the autoxidation of saturated aldehydes and benzaldehyde using Fe,Cu-polyphthalocyanine or cobalt tetra-*p*-tolylporphyrin as a catalyst, the rate of oxidation was obtained as follows (see, Tables 1 and 2):

Table 1. Oxidation of isobutyraldehyde using Fe,Cu-polyphthalocyanine in ethyl acetate

Isobutyraldehyde (M)	Fe,Cu-polyphthalocyanine $\times 10^4$(M)	Oxygen pressure (Torr)	$-d(O_2)/dt$ $\times 10^4$(M s^{-1})	$\frac{-d(O_2)/dt}{(RCHO)^{3/2}(cat)^{1/2}(O_2)^{1/2}}$ $\times 10^3$(M^{-1} s^{-1} $Torr^{-1/2}$)
0.5	1.0	760	0.93	0.95
0.5	5.0	760	2.24	1.0
0.5	10	760	3.39	1.1
0.5	20	760	4.32	0.99
0.5	5.0	500	1.73	0.98
0.5	5.0	400	1.42	0.90
0.5	5.0	160	0.80	0.80
0.1	5.0	760	0.10	0.98
0.3	5.0	760	1.03	1.0
0.7	5.0	760	3.39	1.1
1.0	5.0	760	7.39	1.2

Reaction condition: temperature, 10 °C.

Table 2. Oxidation of benzaldehyde using cobalt tetra-*p*-tolylporphyrin in ethyl isobutyrate

Benzaldehyde (M)	Cobalt tetra-*p*-tolylporphyrin $\times 10^4$(M)	Oxygen pressure (Torr)	$-d(O_2)/dt$ $\times 10^4$(M s^{-1})	$\frac{-d(O_2)/dt}{(RCHO)^{3/2}(cat)^{1/2}(O_2)^{1/2}}$ $\times 10^3$(M^{-1} s^{-1} $Torr^{-1/2}$)
0.5	2.0	760	1.15	0.83
0.5	3.0	760	1.61	0.95
0.5	5.0	760	2.16	0.99
0.5	8.0	760	2.70	0.98
0.5	5.0	500	1.56	0.88
0.5	5.0	400	1.34	0.85
0.1	5.0	760	0.16	0.83
0.3	5.0	760	0.97	0.96
0.8	5.0	760	4.41	1.0
1.0	5.0	760	6.47	1.1

Reaction condition: temperature, 10 °C.

$$-\frac{d(O_2)}{dt} = k(RCHO)^{3/2}(catalyst)^{1/2}(O_2)^{1/2} \quad (I)$$

It was ascertained that enough oxygen was present in a reaction system for Step 2 by other experiments using azobisisobutylonitrile under the radiation of UV as initiator.

These results give the rate of initiation:

$$R_i = K(RCHO)(catalyst)(O_2) \quad (II)$$

in which $K = \left\{\frac{k(2k_t)^{1/22}}{k_p}\right\}$

by the same treatment as that described in a previous paper.[4] This establishes that the initiation reaction consists of a reaction among an aldehyde, a catalyst, and oxygen.

Seven kinds of aldehydes were oxidized. Table 3 shows the rates of the oxidation of the aldehydes in combination with esters as solvents. Zaikov *et al.*[12] studied the oxidation of acetaldehyde, heptanal, octanal, pivaldehyde, and benzaldehyde in chlorobenzene at 0 °C. They concluded that the reason why these aldehydes were oxidized at similar rates under similar conditions was due to compensating changes in the rate constants for chain propagation (k_p) and chain termination ($2k_t$), that is to say, the values of $k_p/(2k_t)^{1/2}$ were almost constant, regardless of the kind of aldehydes.

The oxidation rates in Table 3, therefore, are estimated to parallel the initiation rates using Fe,Cu-polyphthalocyanine and tetra-*p*-polyporphyrin. The oxidation rates of some aldehydes are plotted in logarithm against Taft's σ^* values of alkyl groups of ethyl carboxylate (Fig. 1). Every aldehyde shows a similar type of figure; their slopes are calculated to be as is shown in Table 4.

The aldehyde with a conjugated double bond to the formyl group, such as acrylaldehyde and cinnamaldehyde, showed higher ρ^* values on the left-hand side of graph. This may be ascribed to the fact that the oxidation-rate equation cannot be written as Eq. I. In the autoxidation of acrylaldehyde,[13] for example, the equation is obtained as:

$$-\frac{d(O_2)}{dt} = \frac{R_i^{1/2}k_2k_p(acrylaldehyde)(O_2)}{k_p(2k_4)^{1/2}(acrylaldehyde)+k_2(2k_t)^{1/2}(O_2)} \quad (IV)$$

in which $k_p(2k_t)^{-1/2}=5.5\times10^{-2}$ $M^{-1/2}$ $s^{-1/2}$, and $k_2(2k_4)^{-1/2}=3.7\times10$ $M^{-1/2}$ $s^{-1/2}$ at 40 °C. This suggests that the reaction of the acyl radical of acrylaldehyde with oxygen is one of the rate-determining steps because of the stabilization of the acyl radical *via* the conjugated double bond:

Table 3. Rates of oxidation of aldehydes

Aldehydes	Rate of oxidation ($\times 10^5$ M s^{-1}) in solvent of						
	Ethyl isobutyrate	Ethyl butyrate	Ethyl propionate	Ethyl acetate	Ethyl acetyl-acetate	Ethyl chloro-acetate	Ethyl dichloro-acetate
Isobutyradehyde	20.1	26.5	25.5	22.4		11.3	
Butyraldehyde	15.3	20.0	23.2	21.2		8.50	5.95
Propionaldehyde	3.40	4.92	6.73	14.6		5.42	2.87
Acetaldehyde	3.14	4.58	6.10	13.7	4.75	2.45	6.79
Acrylaldehyde	0.38	1.57	2.07			1.50	0.015
Cinnamaldehyde	0.77	1.80	2.45			0.089	
Benzaldehyde	5.55	6.80 7.24	9.21 9.55	24.5		3.60	1.56
Acetaldehyde[a)]	14.1		12.3	11.8	3.05		
Benzaldehyde[a)]	21.6			15.4		7.03	

Reaction conditions: Fe,Cu-polyphthalocyanine, 5×10^{-4} M; aldehyde, 0.5 M; and 10 °C.
a) An equimolecular amount of cobalt tetra(*p*-methylphenyl)porphyrin was used in place of the polyphthalocyanine.

Table 4. Reaction constants, ρ^*, for solvents in the oxidation of aldehydes[a)]

Aldehydes	Left side		Right side	
	ρ^*	Relative value	ρ^*	Relative value
Isobutyraldehyde	3.23	0.74	−0.30	0.39
Butyraldehyde	3.01	0.69	−0.35	0.45
Propionaldehyde	3.70	0.85	−0.41	0.53
Acetaldehyde[b)]	4.35	1.00	−0.77	1.00
Acrylaldehyde	6.67		−1.10	
Cinnamaldehyde	5.50		−1.16	
Benzaldehyde[b)]	3.85		−0.66	

a) Reaction conditions: Fe,Cu-polyphthalocyanine, 5×10^{-4}M; aldehyde, 0.5M, and temperature, 10°C.
b) An equimolecular amount of cobalt tetra-*p*-tolylporphyrin was also used in place of the polyphthalocyanine. ρ^* values obtained: −0.77 for acetaldehyde and −1.11 for benzaldehyde.

$$CH_2=CH-\dot{C}=O \longleftrightarrow \dot{C}H_2-CH=C=O$$

Therefore, these aldehydes do not belong to the substrates, to which the correspondence of the oxidation rates to the initiation rates mentioned above can be applied.[13,14)]

According to the explanation presented in a previous paper,[4)] the reaction constant, ρ^*, of oxidation in ester solvents (R'COOR) with substituents (R and R') of lower σ^* values are most likely to be independent of the kind of aldehydes (see Scheme A). In such solvents as the reported as "left-side" in Table 4, almost constant values of ρ^* were obtained for all aldehydes except for acrylaldehyde and cinnamaldehyde, compared with those of the oxidation in solvents referred to as "right-side." This supports Scheme A, though it cannot positively be said to be true because of the incomplete constancy of ρ^* values: the small difference in the ρ^* values will be discussed hereafter.

On the other hand, a considerable difference among values of ρ^* was observed in solvents with higher σ^* values. This means some participation of solvent in the initiation reaction and suggests the effect of such solvents on the interaction with activated oxygen molecules on catalysts (Scheme B).

Table 5. Rates of oxygen absorbed in the oxidation of benzaldehyde with or without the pre-bubbling of oxygen

Solvents	Rates of oxygen absorbed $\times 10^5$ M s^{-1}	
	With pre-bubbling	Without pre-bubbling
Ethyl isobutyrate	7.66	5.55
Ethyl butyrate	10.3	7.24
Ethyl chloroacetate	3.83	3.60

Reaction conditions: Fe,Cu-polyphthalocyanine, 5×10^4M; benzaldehyde, 0.5 M, and temperature, 10 °C.

Other experimental data are shown in Table 5. In ethyl isobutyrate and ethyl butyrate, the oxidation rate corresponding to the initiation rate was higher when oxygen was bubbled into the reaction solution thirty minutes before the start of oxidation by the addition of an aldehyde, than when all of the reactants were charged at once to commence oxidation. This fact means not only that there occurs the competitive coordination of a solvent and an oxygen molecule with the complex, but also that an aldehyde has some interaction with such a coordination reaction. Ethyl chloroacetate belonging to a solvent as the "right side" did not show enough difference in the oxidation rate to be discussed. This supports the explanation mentioned above that the solvent is not considered to participate in the activation of the oxygen molecule, but to interact with the activated oxygen according to Scheme B. The coordination of carbonyl compounds such as an aldehyde and an ester with a metal complex is explained by the fact well known in the chemistry of the reaction of an alkyl metal complex with a carbonyl compound: an aldehyde is more reactive with the complex than an ester.[15)] The coordination of acrylaldehyde with cobaltous acetylacetonate through its carbonyl group has also been reported.[16)] It is not surprizing, therefore, that the formation of the oxygen complex is accelerated by the absence of the aldehyde, which will behave competitively as a ligand like an ester solvent. This pheno-

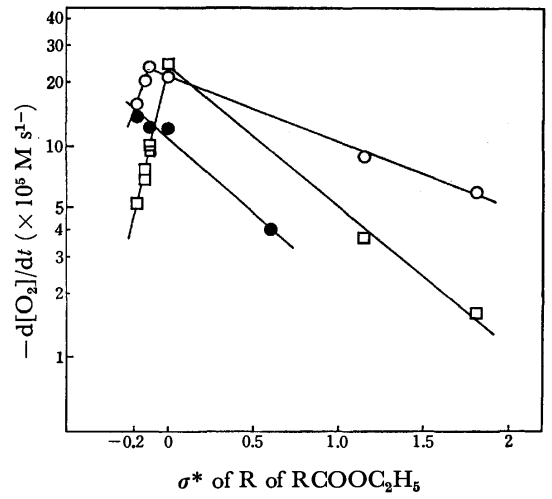

Fig. 1. Arrangement of rate of oxidation against σ^* value of R of $RCOOC_2H_5$ solvents.
Reaction consitions: aldehyde, 0.5 M; catalyst, 5×10^{-4} M; and temperature, 10°C.
○: Fe,Cu-polyphthalocyanine, butyraldenyde,
□: Fe,Cu-polyphthalocyanine, benzaldehyde,
●: cobalt tetra-*p*-tolylporphyrin, acetaldehyde.

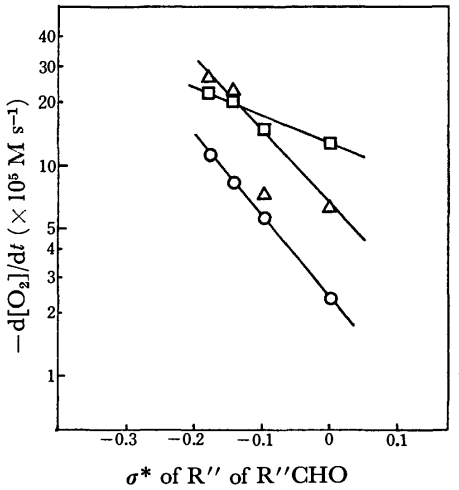

Fig. 2. Arrangement of rate of oxidation against σ* value of R″ of R″CHO.
Reaction conditions: aldehyde, 0.5 M; Fe,Cu-polyphthalocyanine, 5×10^{-4} M; and temperature, 10°C.
□: Ethyl acetate, △: ethyl propionate, ○: ethyl chloroacetate.

menon is not fully understood, but it may be related to the fact that the maximum points of the rate of oxidation seem to shift against the σ^* values of alkyl groups of esters, depending on the kind of aldehydes (see Fig. 1). The oxidation rates of all aliphatic aldehydes except for unsaturated ones are arranged against the σ^* values of the aliphatic residues as in Fig. 2. The lower the σ^* value was the higher the oxidation rate was. If an aldehyde is taken account of as a part of a solvent, this result seems to be the reverse of that shown in Fig. 1 with respect to the σ^* values of alkyl substituents of aldehydes. This may be explained as follows, not by the steric hindrance of aldehyde, but by the electron-donating property of aldehyde.

The value of σ^* of the alkyl residue has, in general, some relation with the steric hindrance factor (E_s). The E_s is considered to show the possibility for an aldehyde occupying the coordination site of oxygen sterically to prevent it from access to the site. However, this explanation is the just reverse of the inclination against σ^*, as is shown in Fig. 2.

In previous papers[5,7] we have reported that a strong electron-donating additive such as pyridine could accelerate the rate of oxidation if it is present in a catalytic amount. This was well interpreted by the idea that the additive could activate the oxygen molecule at the axial position through electron donation. The complexes used in this oxidation have vacant axial positions, which are probably solvated by a solvent in solution. The aldehyde with a stronger electron-donating power compared with an ester solvent may substitute the solvating ester or may occupy the coordination site in preference over the solvent molecule. Consequently, an aldehyde such as isobutyraldehyde is considered to assist the activation of oxygen, as does pyridine. The first coordination of an aldehyde with an electron-rich carbonyl group, that is, with an alkyl residue with a lower σ^* value makes its second coordination difficult because of the repulsion of electrons between the central metal of the complex given by the first aldehyde and of the carbonyl group of the second aldehyde approaching from the axial trans position. Thus, the electrophilic coordination and activation of the oxygen molecule at the second site is accomplished more easily, and the oxidation of isobutyraldehyde, for example, is initiated more easily and faster.

The difference as a catalyst between Fe,Cu-polyphthalocyanine and cobalt tetra-*p*-tolylporphyrin was also observed (Table 4 and Fig. 1). Though it is difficult to compare the two catalysts simply because of their probable different behavior in response to peracids, the latter catalyst, unlike the former, did not give mountain-shaped lines, but lost its oxygen-activating performance in the limited number of solvents used as the σ^* values of the ester solvents increase. This may be ascribed to the concept that cobalt tetra-*p*-tolylporphyrin is probably affected only with difficulty by solvents with electron-donating ability, compared with a metal polyphthalocyanine as may be seen in the comparable data of the effects of additives such as pyridine on the rate of oxidation.[2,7]

From the above-mentioned results and discussion, the behavior of chemical species present in the reaction system may be deduced in terms such scheme as shown on the next page. In the scheme, ------ indicates a weak coordination; ——, medium coordination; ——, strong coordination; S_1—S_3, an ester solvent and/or an aldehyde; S_4, the solvent, and Ald., an aldehyde. Fe,Cu-polyphthalocyanine and cobalt tetra-*p*-tolylpophyrin can initially activate an oxygen molecule to abstract the hydrogen atom from a substrate to be oxidized, and then initiate the autoxidation. The presence of a chemical species (S_1) which has a week interaction with the catalyst facilitates the coordination and activation of oxygen by substitution

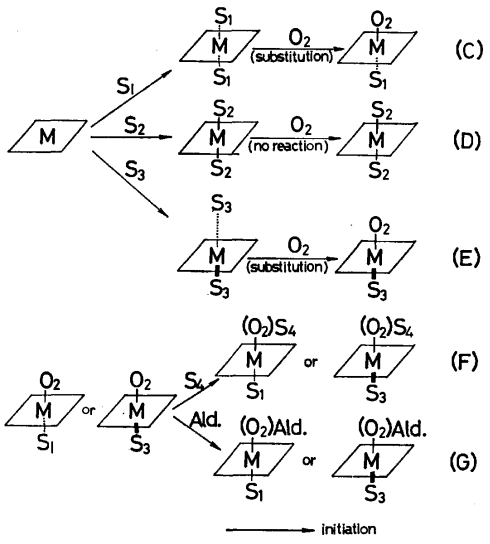

(Scheme C), whereas a chemical species (S_2) with a medium interaction obstracts the coordination of oxygen by its occupation of both trans-positioned sites, depending on the capacity of electron donation (Scheme D). However, a chemical species (S_3) including an aldehyde to be oxidized with a suitable capacity can activate oxygen more easily than in the absence of such a species because of the delivery of an electron to the trans-position through the central metal of the catalyst Subsequently, the chemical species (S_4) solvating strongly to the coordinated oxygen inhibits the approach of an aldehyde to be oxidized, resulting in a decrease in the rate of oxidation (Scheme F). When an aldehyde can react with the activated oxygen, the autoxidation is initiated (Scheme G).

To utilize polyphthalocyanines and porphyrins as oxidation catalysts, we must carefully select the reaction conditions, especially the circumstances of the oxidation reaction.

We should like to express our thanks to Professor Teiji Tsuruta for his fruitful discussions and suggestion throughout our work of this paper.

Rerences

1) R. V. Norton, Am. Chem. Soc. Chicago Meeting, Sept., 1970, Session of Petrochem., B 18.
2) Y. Ohkatsu and T. Osa, *Bull. Chem. Soc. Jpn.*, submitted for publication.
3) H. Inoue, Y. Ikeda, and E. Imoto, *Bull. Chem. Soc. Jpn.*, **41**, 684, 692 (1968)
4) Y. Ohkatsu, T. Hara, and T. Osa, *Bull. Chem. Soc. Jpn.*, **50**, 696 (1977).
5) T. Hara, Y. Ohkatsu, and T. Osa, *Chem. Lett.*, **1973**, 103.
6) T. Hara, Y. Ohkatsu, and T. Osa, *Chem. Lett.*, **1973**, 953.
7) T. Hara, Y. Ohkatsu, and T. Osa, *Bull. Chem. Soc. Jpn.*, **48**, 85 (1975).
8) J. E. Falk, "Porphyrins and Metalloporphyrins," Elsvier, Amsterdam (1964).
9) P. Rothemund and A. R. Menotti, *J. Am. Chem. Soc.*, **70**, 1808 ((1948).
10) A. Misono, T. Osa, Y. Ohkatsu, and M. Takeda, *Kogyo Kagaku Zasshi*, **69**, 2129 (1966).
11) F. P. Greenspan, *Anal. Chem.*, **20**, 1061 (1948).
12) G. E. Zaikov, J. A. Howard, and K. U. Ingold, *Can. J. Chem.*, **47**, 3017 (1969).
13) T. Hara, Y. Ohkatsu, and T. Osa, *Bull. Chem. Soc. Jpn.*, **47**, 156 (1974).
14) Y. Ohkatsu and T. Osa, to be contributed.
15) Japan Chem. Soc., "Zikken Kagaku Koza," **18**, 357, Maruzen, Tokyo (1958).
16) Y. Ohkatsu, T. Osa, and A. Misono, *Bull. Chem. Soc. Jpn.*, **40**, 2111 (1967).

The *O*-Alkylation of Phenols by Esters. II. The Steric Hindrance and Electronic Effect in the *O*-Alkylation of Phenol by Esters[1]

Taketoshi KITO, Kazumune YAMAMOTO, and Ichiro HIRAO

Laboratory of Industrial Chemistry, Department of Chemical Engineering, Kyushu Institute of Technology, Tobata-ku, Kitakyushu-shi, Fukuoka 804

(Received Junuary 27, 1976)

The steric hindrance in the *O*-alkylation of PhOK by alkyl acetate (PhOK+AcOR→PhOR+AcOK) was examined by means of competitive reactions. As a result, the following sequence of the reactivities of alkyl acetates was obtained: $CH_3 \gg C_2H_5 > n\text{-}C_3H_7 \gtrsim n\text{-}C_4H_9 > s\text{-}C_4H_9 > i\text{-}C_3H_7 \gtrsim i\text{-}C_4H_9 > t\text{-}C_4H_9$ and $n\text{-}C_4H_9 > n\text{-}C_5H_{11} > i\text{-}C_5H_{11}$. The electronic effect in the *O*-alkylation was also examined by means of the competitive reaction of *p*-substituted (CH_3 or CH_3O) methyl benzoate and methyl benzoate with PhOK. The reactivity decreases in the following order: $C_6H_5COOMe > p\text{-}CH_3C_6H_4COOMe > p\text{-}CH_3OC_6H_4COOMe$. Therefore, it was concluded that the rate-determining step is the attack of the phenoxide anion on the carbon atom of the methyl group.

There have been few reports on the *O*-alkylation of phenols by alkyl alkanoates except by alkyl oxalate and methyl trichloroacetate.[2,3] On the other hand, dialkyl sulfates and *p*-toluenesulfonic esters, which are the esters of strong acids, are known as powerful *O*-alkylating agents of phenols. The present authors have previously reported[1] that alkali phenoxides react with alkyl alkanoates at high temperatures to give alkyl phenyl ether. For example, alkali salts of phenols (RC_6H_4OH; where R is H, *o*-CH_3, *m*-CH_3, *p*-CH_3, *o*-Cl, or *p*-Cl) react with the methyl ester of acetic acid, acrylic acid, or methacrylic acid to give the corresponding anisoles ($RC_6H_4OCH_3$). The runs using alkali phenoxides with ortho-substituent or those with electron-attracting substituents gave the corresponding anisoles in lower yields. In this paper, the effects of the alkyl and the acyl components in alkyl alkanoates on the *O*-alkylation were examined from the standpoint of the steric hindrance and the electronic effect.

Results and Discussion

Steric Hindrance. The reactions of potassium phenoxide with nine alkyl acetates were carried out. The results are summarized in Table 1.

TABLE 1. YIELDS OF ALKYL PHENYL ETHERS[a]

R	Yield of ROPh (%)	
	200 °C[b]	250 °C[b]
CH_3	75.3	78.7
C_2H_5	42.1	56.6
n-C_3H_7	—	55.0
i-C_3H_7	4.8	35.6
n-C_4H_9	33.5	56.1
i-C_4H_9	3.3	18.9
s-C_4H_9	13.9	20.0
t-C_4H_9[c]	—	12.3
n-C_5H_{11}	17.1	37.9
i-C_5H_{11}	11.8	39.2

a) The reaction was carried out by using an excess of alkyl acetate (AcOR 0.5 mol and PhOK 0.05 mol). b) Reaction temp (Reaction time, 2 h). c) Many by-products were detected in the reaction mixture by gas chromatography.

In these esters, ethyl, propyl, and butyl acetates gave alkyl phenyl ethers in nearly equal yields. Branched alkyl acetates gave the ethers in lower yields.

In the previous paper,[1] the mechanism shown in Scheme 1 was suggested for the *O*-alkylation of alkali phenoxide by ester. According to this mechanism, not only the bulky alkyl component, but also the long-chain alkyl component, in alkyl acetate would hinder the attack of the phenoxide anion. However, we observed no great difference in yields when ethyl, propyl, and butyl acetates were used.

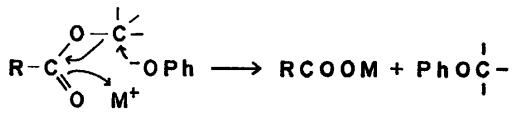

Scheme 1.

One method of evaluating the reactivity of each acetate towards potassium phenoxide is to compare the reaction rate constant in each reaction. However, there are few solvents which have high boiling points and which dissolve potassium phenoxide. Although potassium phenoxide is soluble in some aprotic polar solvents, such as *N*,*N*-dimethylformamide (DMF), dimethyl sulfoxide (DMSO), and hexamethyl phosphoric triamide (HMPA), the rate of the disappearance of the ester (methyl benzoate) in the initial period was abnormally great when the reaction was carried out at high temperatures in these solvents. This phenomenon must result from the side reactions: that is, the hydrolysis of the ester by the water contained in the solvents (it is difficult to remove the water completely from such solvents) and the decomposition of DMF into carbon monoxide and dimethylamine in the presence of the base (PhOK).[4] The latter product further reacts with the ester to produce undesirable products.

Competitive reactions were used to compare the reactivity of each acetate to potassium phenoxide. The merit of this method is that we can carry out the reactions of several kinds of alkyl acetates with potassium phenoxide under the same conditions.

The competitive reactions were carried out by heating potassium phenoxide with a mixture of three alkyl acetates, and then the three alkyl phenyl ethers formed were determined by gas chromatography. The results are shown in Table 2. As has already been mentioned,

Table 2. Competitive reactions of alkyl acetates with potassium phenoxide[a]

Components of the mixture of esters[b] AcOR, R=	i-C_3H_7OAc+ n-C_4H_9OAc+ s-C_4H_9OAc	C_2H_5OAc+ n-C_4H_9OAc+ i-C_4H_9OAc	C_2H_5OAc+ n-C_3H_7OAc+ n-C_4H_9OAc	C_2H_5OAc+ i-C_3H_7OAc+ n-C_4H_9OAc	CH_3OAc+ n-C_3H_7OAc+ n-C_4H_9OAc
	Yields of alkyl phenyl ethers (ROPh), (%)				
CH_3	—	—	—	—	60.4
C_2H_5	—	53.0	28.1	38.3	—
n-C_3H_7	—	—	12.3	—	4.9
i-C_3H_7	1.7	—	—	7.4	—
n-C_4H_9	43.3	15.1	11.7	13.3	3.4
i-C_4H_9	—	2.6	—	—	—
s-C_4H_9	5.9	—	—	—	—
Total yields (%)	50.9	70.7	52.1	59.0	68.7

a) PhOK, 0.05 mol; reaction temp, 250 °C; reaction time, 2 h. b) Every mixture contains 0.15 mol portions of three esters.

the phenoxide anion would attack the less hindered carbon atom adjacent to the ether oxygen. Therefore, the ester with a longer-chain alkoxyl group will give an alkyl phenyl ether in a lower yield. Thus, the reactivities of the esters may be supposed to decrease in the following order: $CH_3OAc > C_2H_5OAc > n$-C_3H_7-$OAc > n$-C_4H_9OAc. The branched alkyl acetate will give the alkyl phenyl ether in a yield lower than the normal alkyl acetate. From Table 2, the following sequence of the reactivities was obtained for the series of acetates: n-$C_4H_9 \gg s$-$C_4H_9 > i$-C_3H_7; $C_2H_5 > n$-$C_4H_9 > i$-C_3H_7; $C_2H_5 > n$-$C_4H_9 \gg i$-C_4H_9; $CH_3 \gg n$-$C_3H_7 > n$-C_4H_9; $C_2H_5 > n$-$C_3H_7 > n$-C_4H_9. It is preferable to use a mixture containing all the alkyl acetates in the competitive reaction, but it was difficult to determine each alkyl phenyl ether in the mixture by gas chromatography. The ratio of the yields in the same reaction will not be exactly equal to the ratio of the reactivities because the reaction rate is also dependent on the concentration of the ester. Under the present experimental conditions, the variation in the concentration of the ester can not be neglected when the yield of the alkyl phenyl ether is appreciably high. If a mixture containing excess amounts of esters is used to avoid the variation in the concentration during the reaction, the accurate determination of the products will become difficult. On the basis of the data shown in Tables 1 and 2, though, a reasonable order of the reactivities of alkyl acetates may be as follows: $CH_3 \gg C_2H_5 > n$-$C_3H_7 \gtrsim n$-$C_4H_9 > s$-$C_4H_9 \gtrsim i$-$C_3H_7 \gtrsim i$-$C_4H_9 > t$-C_4H_9 and n-$C_4H_9 > n$-$C_5H_{11} > i$-C_5H_{11}. Although the electronic effect, of course, influences the reactivity of the alkyl group, the reactivity might be controlled mainly by the steric hindrance.

It was reported previously[1] that ortho-substituted alkali phenoxides gave the corresponding ethers in lower yields. For example, potassium p- and m-methylphenoxide react with methyl methacrylate at 200 °C to afford anisole in 84.5 and 74.8% yields respectively. On the contrary, potassium o-methylphenoxide gave o-methylanisole in a 29.4% yield under the same conditions. Similarly, potassium o-chorophenoxide gave o-chloroanisole in a 13.9% yield, although potassium p-chlorophenoxide gave p-chloroanisole in a 48.9% yield. In Table 2, there are no examples of reactions using ortho-substituted phenoxide. The steric hindrance may also be caused by the interaction between the hydrogen atom on the ortho position of phenoxide and that of the alkoxyl group. In methyl acetate this interaction may be small, but the interaction will become important in ethyl and higher alkyl acetates. In fact, there was a great difference in the reactivity between methyl acetate and ethyl acetate, as is shown in Tables 1 and 2.

The steric hindrance of the acyl group was also examined; the results are summarized in Table 3. At a low temperature (150 °C), methyl pivalate and methyl decanoate gave anisole in lower yields than did the other esters. The decrease in the yield is attributable in part to the steric hindrance of the bulky group and the long chain.

Table 3. Relationship between the yield of anisole and the acid component of the methyl ester[a]

Ester RCOOMe	pK_a of RCOOH (25 °C)[a]	Yields of anisole (%) 150 °C	200 °C	250 °C[c]
$(CH_3)_3CCOOMe$	5.03[d]	13.4	—	—
$CH_3(CH_2)_8COOMe$	4.89	4.0	73.4[e]	—
CH_3CH_2COOMe	4.87	—	88.0	—
CH_3COOMe	4.76	54.5	79.2	—
$PhCH_2COOMe$	4.31	83.2	91.4	—
PhCOOMe	4.20	83.8	—	99.6

a) PhOK, 0.05 mol; ester/PhOK (mol/mol) = 10. b) "Kagaku Binran, Kisohen II," Maruzen (1966); "Handbook of Tables for Organic Compound Identification," The Chemical Rubber Co. (1967). c) Reaction temp (reaction time, 5 h). d) At 18 °C. e) Ester/PhOK = 8.8.

The Electronic Effect of the Acyl Group on the Reactivity. The electronic effect of the acyl group in alkyl alkanoate was also examined; the results are shown in Table 3. However, it is difficult to isolate only the electronic effect from the results shown in Table 3.

King reported[5] that methyl benzoate is a good O-alkylating agents (see also Table 3). Therefore, the electronic effect was investigated by using methyl p-substituted benzoate. A mixture of methyl p-substituted benzoate, methyl benzoate, potassium phenoxide, and cyclohexane (a heat medium) was heated in an autoclave, and the residual methyl p-substituted benzoate and methyl benzoate and the anisole formed from this

TABLE 4. COMPETITIVE REACTIONS OF *p*-SUBSTITUTED METHYL BENZOATE AND METHYL BENZOATE WITH POTASSIUM PHENOXIDE[a)]

Components of the mixture $xC_6H_5OK+yC_6H_5COOMe+zp\text{-}RC_6H_4COOMe$		Reaction time (h)	Yields of anisole (%)			Ratio
R;	$x:y:z$		from C_6H_5COOMe (I)	from $p\text{-}RC_6H_4COOMe$ (II)	Total yield	(I)/((I)+(II))
CH_3[b)]	1 : 2.95 : 2.95	6	52.6	38.9	91.5	0.575
CH_3	1 : 1.01 : 1.01	9	51.7	48.2	99.9	0.518
CH_3	1 : 1.00 : 1.00	1	47.8	39.6	87.4	0.547
CH_3O[c)]	1 : 3.38 : 3.35	6	66.9	17.4	84.3	0.794
CH_3O	1 : 0.99 : 0.99	0.5	41.4	24.3	65.7	0.630

a) C_6H_5OK, 0.1 mol; reaction temp, 250 °C. b) $\sigma_p=-0.17$. c) $\sigma_p=-0.27$.

reaction were determined by gas chromatography. The results are shown in Table 4. As the steric hindrance of the *p*-substituents can be disregarded, the inductive effect and the resonance effect of these groups must become important in this reaction. Benzoic acid is the strongest acid, and *p*-anisic acid is the weakest one, of the three (the pK_a values of the acids at 25 °C are as follows: benzoic acid, 4.21; toluic acid, 4.37; *p*-anisic acid, 4.49[6)]). The electron-donating group on the para-position may increase both the electron densities on the oxygen atom of the carbonyl group (>C=O) and on the carbon atom of the methyl group (-$COOCH_3$). If the rate-determining step of this reaction is the nucleophilic attack of the phenoxide anion on the carbon atom of the methyl group, the electron-donating group may retard the attack of the phenoxide anion. On the contrary, if the rate-determining step is the activation of the phenoxide anion (although the oxygen atom of potassium phenoxide has an anionic character, it is neutralized by the potassium cation), the electron-donating group is advantageous for the *O*-alkylating reaction because the potassium cation may be neutralized to a greater extent by the oxygen atom of the carbonyl group and a more active phenoxide anion may be formed.

The molar ratios (potassium phenoxide: methyl benzoate: methyl *p*-substituted benzoate) and the reaction time were varied, and the yields of anisole from methyl benzoate and methyl *p*-substituted benzoate and its ratio were calculated. From the results listed in Table 4, the following facts became clear. The reactivities of both methyl toluate and anisate are lower than that of methyl benzoate, and the reactivity of methyl anisate is lower than that of methyl toluate. Therefore, the results lead to the conclusion that the attack of the phenoxide anion on the carbon atom adjacent to the ether linkage is more important than the formation of the active phenoxide anion.

The competitive reaction of methyl *p*-nitrobenzoate and methyl benzoate with potassium phenoxide was also carried out at 200 °C for 5 h and at 170 °C for 9 h. Under the former conditions, the yield of anisole was 15.2 and 83.6% of the methyl benzoate was recovered. On the contrary, only 8.6% of the methyl *p*-nitrobenzoate was recovered, while 91.4% of the methyl *p*-nitrobenzoate was consumed to produce unidentified by-products. In this case, a side reaction, which has no relation with the *O*-alkylation, most likely occurred.

Experimental

Competitive Reactions of Alkyl Acetates with Potassium Phenoxide. Because the experiments of other competitive reactions were carried out similarly, only one example will be given in detail.

An equimolar mixture (0.15 mol each) of methyl acetate, propyl acetate, and butyl acetate, and 0.05 mol of potassium phenoxide was placed in a 300-ml autoclave equipped with an electromagnetic stirrer. The reaction mixture was then heated at 250 °C for 2 h. It takes about 20 min to raise the temperature to 250 °C. After cooling, the reaction mixture was poured into water and the alkyl phenyl ether was extracted with ether (about 100 ml). To the ethereal solution, 0.05 mol of *N,N*-dimethylaniline (6.060 g) was then added as an internal standard compound and the anisole, propyl phenyl ether, and butyl phenyl ether were determined by gas chromatography (internal standard method; column, PEG 20M; temp, 200 °C).

Competitive Reactions of p-*Substitued Methyl Benzoate and Methyl Benzoate with Potassium Phenoxide.* To an equimolar mixture of methyl benzoate and methyl *p*-substituted benzoate, potassium phenoxide was added, after which the mixture was heated at 250 °C. After cooling, the anisole and the benzoates were extracted with ether (100 ml) and the molar ratios of anisole/methyl benzoate and methyl *p*-substituted benzoate/methyl benzoate were obtained by gas chromatography (column, PEG 20M; temp, 200 °C). The mole number of the anisole formed in this reaction must be equal to the sum of the mole numbers of the methyl benzoate and methyl *p*-substituted benzoate consumed in this reaction, because no product other than anisole was detected in the gas chromatogram. On the basis of this fact, the yields of anisole from methyl benzoate and from methyl *p*-substituted benzoate were calculated.

Identification of Alkyl Phenyl Ethers. Authentic alkyl phenyl ethers were prepared by Williamson ether synthesis,[7)] but *t*-butyl phenyl ether was prepared according to the directions described in "Organic Syntheses" (Vol. 45, p. 89). These ethers were identified by elementary analysis, NMR, and gas chromatography. The retention times of the alkyl phenyl ethers formed in this reaction were compared with those of authentic ethers. The two retention times were agreed within 2 s (the retention times of these ethers were from 124 s, CH_3OPh, to 333 s, *i*-$C_5H_{11}OPh$; column, PEG 20M, 30%; temp, 200 °C). Four ethers obtained from the reactions of potassium phenoxide and alkyl acetates (propyl, butyl, isobutyl, and *s*-butyl acetates) were isolated by gas chromatography and were identified by NMR (solvent, CCl_4).

References

1) Part I of this series: T. Kito, N. Yanai, and I. Hirao, *Bull. Chem. Soc. Jpn.*, **45**, 3490 (1972).

2) T. Matsuura and Y. Sakakibara, *Nippon Kagaku Zasshi*, **73**, 367 (1952); Y. Sakakibara, *Nippon Kagaku Zasshi*, **81**, 495 (1960).
3) A. C. Pierce and M. M. Joullié, *J. Org. Chem.*, **27**, 3968 (1962).
4) The Society of Synthetic Organic Chemistry Japan, "Solvents Pocket Book," Ohm Book Company (1967).
5) H. King and E. V. Wright, *J. Chem. Soc.*, **1939**, 1168.
6) "Lange's Handbook of Chemistry," 11th ed, McGraw-Hill.
7) T. Kito, H. Minami, and I. Hirao, *Kogyo Kagaku Zasshi*, **74**, 2313 (1971).

Tautomerism of 4-Pyridones

Hiromichi Besso, Kimiaki Imafuku, and Hisashi Matsumura

Department of Chemistry, Faculty of Science, Kumamoto University, Kurokami, Kumamoto 860

(Received June 18, 1976)

The tautomeric constants, K_t, of several 4-pyridones were determined by measurement of pK_a values. For 2-substituted 5-methoxy-4-pyridones, the K_t values were correlated to the substituent constants σ, the equation $\log K_t = 2.98 + 2.93\sigma_m - 6.18\sigma_o$ being obtained.

The tautomerism of simple 4-pyridones having chlorine atom[1] or methoxycarbonyl group[2] in an α-position to nitrogen atom has been investigated in detail. Gordon *et al.* showed that the tautomeric equilibrium of 4-pyridones is displaced in favour of 4-hydroxypyridine form by electron-withdrawing groups of α-position.

We report the tautomerism of several 2-substituted 5-methoxy-4-pyridones and discuss the substituent effects by the Hammett equation. Little is known about the application of the Hammett equation to 4-pyridones.

Results and Discussion

Dissociation Constants. The dissociation constants of 4-pyridones (I), *N*-methyl-4-pyridones (II), and 4-methoxypyridines (III) were determined spectrophotometrically in water at 20 °C. The results are summarized in Table 1, where pK_1 and pK_2 represent respectively the first and second dissociation constants for 4-pyridones (I), and pK_{NCH_3} and pK_{OCH_3} correspond to the dissociation constants for *N*-methyl-4-pyridones (II) and 4-methoxypyridines (III), respectively.

Table 1. Dissociation constants

Substituent	(I) pK_1	(I) pK_2	(II) pK_{NCH_3}	(III) pK_{OCH_3}
CH_3	3.42	11.29	3.39	7.10
H	3.04	11.08		
CH_2OH	3.06	10.48	3.06	5.89
CH_2OCH_3	2.99	10.23	2.88	5.42
CHO				4.25
$COOCH_3$	2.17	8.23	2.18	3.16

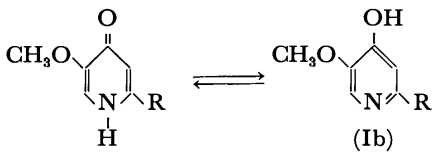

(Ia) (Ib)

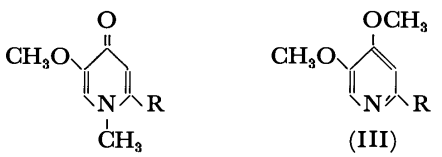

(II) (III)

Since activity coefficients were not introduced into the calculation, the dissociation constants do not represent thermodynamic terms, giving only a relative measure of base strength.

The pK_a values of 4-pyridones and 4-methoxypyridines decrease by electron-withdrawing groups attached to 2-position, the degree of decrease for 4-methoxypyridines being the greatest of all. It is concluded that these changes are related to the distance between the substituent and the reaction site.

Tautomeric Ratio. The tautomeric constants K_t which represent the ratio of NH-form (Ia) to OH-form (Ib), are given by the following equation[3] (Table 2).

$$\log K_t = pK_{OCH_3} - pK_{NCH_3} \quad (1)$$

Table 2. Tautomeric constants

Substituent	$\log K_t$
CH_3	3.7
CH_2OH	2.8
CH_2OCH_3	2.5
$COOCH_3$	1.0

The K_t values for 4-pyridones are affected by the substituents in the 2-position, decreasing by electron-withdrawing groups.

UV Spectra. The UV spectra of neutral species of 5-methoxy-4-pyridones (I) having methyl, hydroxymethyl, and methoxymethyl groups in the 2-position are similar to those of their *N*-methyl derivatives (II), but differ a great deal from those of their *O*-methyl derivatives (III). That is to say, these 4-pyridones exist essentially in the NH-form (Ia). However, 5-methoxy-2-methoxycarbonyl-4-pyridone exists in both NH-form (Ia) and OH-form (Ib) in water (Fig. 1).

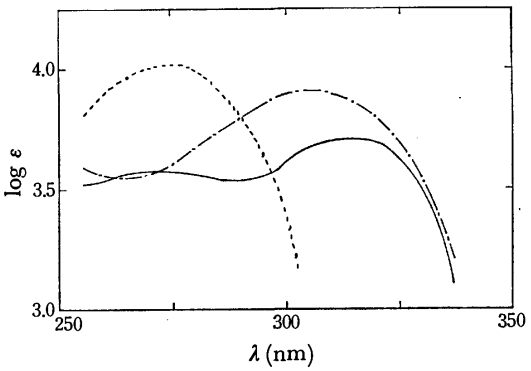

Fig. 1. The UV spectra of the neutral species of 5-methoxy-2-methoxycarbonyl-4-pyridone series.
——: 5-Methoxy-2-methoxycarbonyl-4-pyridone,
- - - -: 5-methoxy-2-methoxycarbonyl-1-methyl-4-pyridone,
……: 4,5-dimethoxy-2-methoxycarbonylpyridine.

Substituent Effects. The substituent constants σ_o for ortho-substituted pyridines were obtained from their dissociation constants by Clark and Perrin.[4] However, the σ_o values for hydroxymethyl and methoxymethyl groups are unknown. We obtained them by the following method. When the pK_a values of 2-substituted 4,5-dimethoxypyridines, 4-methoxypyridine (pK_a=6.62),[5] and 2-chloro-4-methoxypyridine (pK_a=1.93)[1] are plotted against the apparent substituent constants σ_o[4] for the 2-position and the substituent constants σ_m[6] for the 5-position, the plot gives a straight line, the following equation for 2,5-disubstituted 4-methoxypyridines being obtained by the least square methods.

$$pK_{OCH_3} = 6.75 - 6.07(\sigma_o+\sigma_m) \quad (r=0.992) \quad (2)$$

The regression of Eq. 1 gives the σ_o values which are 0.02 and 0.10 for hydroxymethyl and methoxymethyl groups, respectively.

The following Eqs. 3 and 4 are obtained for the proton gain and proton loss, respectively, of 2-substituted 5-methoxy-4-pyridones (I).[6,7]

$$pK_1 = 3.11 - 3.01\sigma_m \quad (r=0.989) \quad (3)$$

$$pK_2 = 10.77 - 4.94\sigma_o \quad (r=0.989) \quad (4)$$

Equations 5 and 6 are obtained for the proton gain of 2-substituted 5-methoxy-1-methyl-4-pyridones (II) and the proton loss of 2-substituted 4,5-dimethoxypyridines (III), respectively.

$$pK_{NCH_3} = 3.09 - 2.93\sigma_m \quad (r=0.978) \quad (5)$$

$$pK_{OCH_3} = 6.07 - 6.18\sigma_o \quad (r=0.985) \quad (6)$$

In Eq. 5, the value 0.01 obtained from the regression of Eq. 3 was assigned to the substituent constants σ_m for the hydroxymethyl group.

When Eqs. 4 and 5 are substituted into Eq. 1, the following equation is derived.

$$\log K_t = 2.98 + 2.93\sigma_m - 6.18\sigma_o \quad (7)$$

The electron-withdrawing groups in the 2-position stabilize the keto form for the carbonyl group and the hydroxy form for the nitrogen atom in the ring. In Eq. 7, the K_t values are defined as [NH]/[OH]. The ρ-value −6.18 for the substituent constants σ_o shows that the ratio of (Ib) increases with electron-withdrawing groups in the 2-position. In contrast, the ρ-value +2.93 for the substituent constants σ_m indicates the decrease of (Ib) owing to the stabilization of the carbonyl group by electron-withdrawing groups in the 2-position. Thus, Eq. 7 shows to what extent the substituents in the 2-position participate in the two reaction sites relating to the tautomerism of 4-pyridones. For 2-substituted 5-methoxy-4-pyridones, the electron-withdrawing substituents in the 2-position increase the ratio of the hydroxy form (Ib). Gordon *et al.*[2] showed that the K_t values are little affected by the substituents in β-position as compared with α-position, supporting our results.

It is concluded that most of the factors for the tautomerism of 4-pyridones are due to the electronic effect (including steric effect) of the substituents in the 2-position.

Experimental

All the melting points were measured on a Yanagimoto micro-melting point apparatus and are uncorrected. The IR spectra were taken on a JASCO IRA-1 spectrophotometer, and the NMR spectra on a Hitachi-Perkin-Elmer R-24 spectrometer (60 MHz).

The pK_a values of 4-pyridones, *N*-methyl-4-pyridones, and 4-methoxypyridines were measured specrophotometrically in water at 20 °C by the method of Albert and Serjeant.[8] The absorption spectra were taken on a Hitachi EPS-3T spectrophotometer, while the pH values were measured by a Hitachi-Horiba F-7 pH meter.

Materials. All the known compounds were prepared according to the methods described in references: 3-methoxy-4-pyridone, mp 170—172 °C (lit,[9] 173 °C); 5-methoxy-2-methyl-4-pyridone, mp 104—105 °C (lit,[10] 102—103 °C); 5-methoxy-1,2-dimethyl-4-pyridone, mp 145—147 °C (lit,[11] 150 °C); 4,5-dimethoxy-2-methylpyridine, bp 76—80 °C/1 Torr (lit,[10] 78—80 °C/1 Torr); 5-methoxy-2-hydroxymethyl-4-pyridone, mp 170—171°C (lit,[11] 172 °C); 5-methoxy-2-hydroxymethyl-1-methyl-4-pyridone, mp 203—205 °C (lit,[11] 203—205 °C); 4,5-dimethoxy-2-hydroxymethylpyridine, mp 117—118 °C (lit,[12] 117—118 °C); 5-methoxy-2-methoxymethyl-4-pyridone, bp 200—204 °C/1 Torr (lit,[13] 200 °C/1 Torr); 5-methoxy-2-methoxymethyl-1-methyl-4-pyridone, mp 58—59 °C (lit,[14] 59°C).

4,5-Dimethoxy-2-methoxymethylpyridine was obtained by methylation of 5-methoxy-2-methoxymethyl-4-pyridone[13] with diazomethane: Yield, 22%; mp 49—50 °C (from petroleum ether); IR ($CHCl_3$) 1590 cm^{-1} (C=C); NMR ($CDCl_3$) δ: 3.45 (s,3H), 3.95 (s,6H), 4.50 (s,2H), 6.97 (s,1H), 8.19 (s,1H). Found: C, 58.88; H, 7.13; N, 7.71%. Calcd for $C_9H_{13}NO_3$: C, 59.00; H, 7.15; N, 7.65%.

4,5-Dimethoxy-2-formylpyridine was obtained by manganese dioxide oxidation of 4,5-dimethoxy-2-hydroxymethylpyridine[12]: Yield, 59%; mp 136—137°C (from petroleum ether); IR ($CHCl_3$) 1730(C=O), 1580(C=C) cm^{-1}; NMR ($CDCl_3$) δ: 3.98(s,3H), 4.05(s,3H), 7.47(s,1H), 8.27(s,1H), 9.91(s,1H). Found: C, 57.57; H, 5.50; N, 8.41%. Calcd for $C_8H_9NO_3$: C, 57.48; H, 5.43; N, 8.38%.

5-Methoxy-2-methoxycarbonyl-4-pyridone was obtained by esterification of 5-methoxy-2-carboxy-4-pyridone[11] with methanol in the presence of dry hydrogen chloride: Yield, 15%; mp 174—177 °C (from ethyl acetate); IR ($CHCl_3$) 1730(C=O), 1615(C=O) cm^{-1}; NMR ($CDCl_3$) δ: 3.95(s,3H), 3.97(s,3H), 7.55(s,1H), 7.95(s,1H). Found: C, 52.17; H, 4.87; N, 7.71%. Calcd for $C_8H_9NO_4$: C, 52.46; H, 4.95; N, 7.65%.

5-Methoxy-2-methoxycarbonyl-1-methyl-4-pyridone was obtained from 5-methoxy-2-carboxy-4-pyrone[15] by *N*-methylation with methylamine and by esterification with methanol in the presence of hydrogen chloride: Yield, 21%; mp 147—149 °C (from benzene); IR ($CHCl_3$) 1750(C=O), 1620(C=O) cm^{-1}; NMR ($CDCl_3$) δ: 3.82(s,3H), 3.88(s,3H), 3.91(s,3H), 7.02(s,2H). Found: C, 54.65; H, 5.60; N, 7.11%. Calcd for $C_9H_{11}NO_4$: C, 54.82; H, 5.62; N, 7.10%.

4,5-Dimethoxy-2-methoxycarbonylpyridine was obtained by methylation of 5-methoxy-2-carboxy-4-pyridone[11] with a large excess of diazomethane: Yield, 29%; mp 125—126 °C (from ethyl ether); IR ($CHCl_3$) 1735(C=O,) 1580(C=C) cm^{-1}; NMR ($CDCl_3$) δ: 3.99(s,6H), 4.01(s,3H), 7.68(s,1H), 8.21 (s,1H). Found: C, 54.96; H, 5.69; N, 7.19%. Calcd for $C_9H_{11}NO_4$: C, 54.82; H, 5.62; N, 7.10%.

References

1) A. R. Katritzky, J. D. Rowe, and S. K. Roy, *J. Chem. Soc., B*, **1967**, 758.

2) A. Gordon, A. R. Katritzky, and S. K. Roy, *J. Chem. Soc., B*, **1968**, 556.

3) S. F. Mason, *J. Chem. Soc.*, **1958**, 674.
4) J. Clark and D. D. Perrin, *Quart. Rev.*, **18**, 295 (1964).
5) A. Albert and J. N. Phillips, *J. Chem. Soc.*, **1956**, 1294.
6) H. H. Jaffé, *Chem. Rev.*, **53**, 191 (1953).
7) O. Exner, *Coll. Czech. Chem. Comm.*, **31**, 65 (1966).
8) A. Albert and E. P. Serjeant,"Ionization Constants of Acids and Bases," 1st ed, Methuen & Co., Ltd., London (1962), Chap. 4.
9) A. Peratoner and A. Tamburello, *Gazz. Chim. Ital.*, **36** I, 53 (1905).
10) K. N. Campbell, J. F. Ackerman, and B. K. Campbell, *J. Org. Chem.*, **15**, 221 (1950).
11) J. W. Armit and T. J. Nolan, *J. Chem. Soc.*, **1931**, 3023.
12) M. Ishizaka, M. Sc. Thesis, Kumamoto Univ. (1970), p. 50.
13) T. Yabuta, *Tokyo Kagaku Kaishi*, **37**, 1185 (1916).
14) K. Heyns and G. Vogelsang, *Chem. Ber.*, **87**, 1377 (1954).
15) K. Heyns and G. Vogelsang, *Chem. Ber.*, **87**, 13 (1954).

The Reaction of 4-Thiazoline-2-thione with Methyl Iodide. Solvent Effects and Pressure Effects

Yasuhiko KONDO, Masayuki SHINZAWA, and Niichiro TOKURA

Department of Applied Chemistry, Faculty of Engineering, Osaka University, Suita, Osaka 565

(Received June 21, 1976)

Rate constants for the reaction of 3-isopropyl-4-methyl-4-thiazoline-2-thione with methyl iodide have been determined in several solvents at 1 atm. In acetonitrile and propylene carbonate, the reaction was studied at pressures up to 1500 atm by a conductivity method. A comparison of the activation volume and overall volume change of reaction, obtained from density measurements, suggests that the charge development at the transition state is only fractional. The results of CNDO/2 calculations support the argument.

In a previous paper[1] we called attention to the correlation of the solvent effect on reaction rates and activation volumes for a series of Menschutkin reactions. In particular, it was shown that the reaction in which the rate has a larger sensitivity to solvent characteristics exhibits a greater solvent effect on the activation volumes.

With the aim of determining the range of applicability of such correlations on reactions of the same charge type, we examined the solvent and pressure effects on the reaction of 3-isopropyl-4-methyl-4-thiazoline-2-thione (TT) with methyl iodide, since it is of the same charge type as the Menschutkin reaction[2] but with a different nucleophilic center. The results are given in this report.

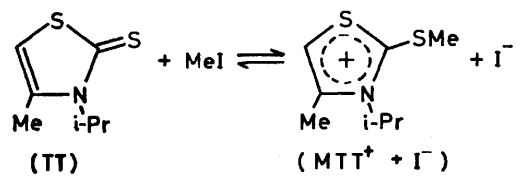

Experimental

Materials. Propylene carbonate (Wako EP grade) was dried over freshly activated molecular sieves and distilled three times under reduced pressure. The other solvents (Wako guaranteed grade) were purified.[1,3] 3-Isopropyl-4-methyl-4-thiazoline-2-thione (TT)[2,4,5] was recrystallized three times from aqueous ethanol and dried *in vacuo* at 65 °C before use. [Found: H, 6.39; C, 48.29; N, 8.09%. Calcd for $C_7H_{11}NS_2$: C, 48.51; H, 6.40; N, 8.08%]

2-Methylthio-3-isopropyl-4-methylthiazolium iodide ($MTT^+ I^-$), prepared by refluxing TT and methyl iodide, was recrystallized three times from *N,N*-dimethylacetamide–ether mixture and dried *in vacuo* at 65 °C before use. [Found; I, 40.14%, Calcd for $C_8H_{14}INS_2$: I, 40.26%] *N*-Methylpyridinium iodide, prepared from pyridine and methyl iodide, was recrystallized three times from *N,N*-dimethylacetamide–ether mixture and dried *in vacuo* at 65 °C before use. [Found; I, 57.06%, Calcd for C_6H_8IN: I, 57.41%]

Kinetic Measurements. Equal volumes of a halide solution and a TT solution (*ca.* 0.01 M), or pyridine solution (*ca.* 0.01 M) were mixed rapidly in a stoppered flask, aliquots of the reaction mixture being withdrawn at intervals and titrated potentiometrically with a siver nitrate solution.[1] In acetonitrile and propylene carbonate, the rates were determined conductimetrically in glass cells immersed in the pressure vessel. The conductivity cell, capacity *ca.* 15 ml, was equipped with platinum electrodes (1 cm × 1 cm, 1 cm apart). Since no direct proportionality between conductance and ion concentration was observed in these solvents, the dependence of conductance on concentration, not corrected for solvent compression, was dermined for methylpyridinium iodide and MTT^+I^- solutions in both solvents under pressure (1, 300, 600, 900, 1200 and 1500 kg cm^{-2}) at 30 °C. Calculation of the rate constant was carried out after transforming the measured resistance into the concentration at atmospheric pressure. The activation volumes thus calculated should be taken as expressed in mole fraction unit. A few runs at atmospheric pressure were followed by titration of halide ion. The rate constants determined by these methods agreed within experimental error. The errors were estimated to be less than ±2% from duplicate or triplicate runs.

Density Measurements. The densities of the solution were measured in a glass dilatometer calibrated with doubly distilled water, having a bulb of *ca.* 40 ml capacity and two graduated stems. The apparent molal volumes were calculated by the equation

$$\phi_v = \frac{1000(d_0-d)}{cd_0} + \frac{M_2}{d_0} \qquad (1)$$

where the quantities have their usual meaning. The concentration of the solute was 0.01—0.02 M except for methyl iodide and pyridine for which it was 0.1—0.2 M. The errors were estimated to be less than ±0.4 cm^3 mol^{-1} from duplicate or triplicate runs.

Results and Discussion

Rate Law. A characteristic feature of the reaction of TT with methyl iodide is that the rate law changes according to the polarity of the solvent, since in low or medium dielectric solvents the reverse process has an effect on the observed rate.

In dipolar solvents such as acetonitrile (AN), propylene carbonate (PC), methanol, *N,N*-dimethylacetamide, and nitrobenzene, the rate law followed second order kinetics as expected, *i.e.*, first order in TT and in methyl iodide.

In cyclohexanone and bromobenzene the rate behavior was rather complicated, probably because of ion-pair and various kinds of higher aggregates formed in these solvents.[6,7]

For a comprehensive treatment of these two cases the following reaction schemes were postulated.

$$\underset{a-x}{TT} + \underset{b-x}{MeI} \underset{k_r}{\overset{k_f}{\rightleftarrows}} \underset{x_{fi}}{MTT^+} + \underset{x_{fi}}{I^-} \rightleftarrows \underset{x_{ip}}{MTT^+ I^-}$$

$$2\underset{x_{ip}}{MTT^+ I^-} \rightleftarrows \underset{x_q}{(MTT^+ I^-)_2}$$

$$\frac{dx}{dt} = k_f(a-x)(b-x) - k_r x_{fi}^2 \quad (2)$$

$$K = (k_f/k_r) \quad (3)$$

$$K_{ip} = x_{ip}/(x_{fi})^2 \quad (4)$$

$$K_q = x_q/(x_{ip})^2 \quad (5)$$

$$x = x_{fi} + x_{ip} + 2x_q$$
$$= x_{fi} + K_{ip}x_{fi}^2 + 2K_qK_{ip}^2x_{fi}^4 \quad (6)$$

At equilibrium the following equation holds,

$$k_f(a-x_e)(b-x_e) = k_r x_{fi,e}^2 \quad (7)$$

where the suffix, e, denotes the concentration at equilibrium.

In cyclohexanone the observed equilibrium constant, K_{obsd}, is defined by the equation

$$K_{obsd} = x_e^2/\{(a-x_e)(b-x_e)\}. \quad (8)$$

This is transformed into the following equation by combining Eqs. 3, 6, 7, and 8:

$$K_{obsd} = K(x_e^2/x_{fi,e}^2)$$
$$= K(1+K_{ip}x_{fi,e}+2K_qK_{ip}^2x_{fi,e}^3)^2 \quad (9)$$

By rearranging we have,

$$(K_{obsd}/K)^{1/2} = 1 + K_{ip}(Kx_e^2/K_{obsd})^{1/2} + 2K_qK_{ip}^2(Kx_e^2/K_{obsd})^{3/2} \quad (10)$$

The values of K_{obsd}, determined analytically after keeping the reaction mixtures at 30 °C for a sufficiently long time (usually for a week), and the corresponding values of x_e were substituted into Eq. 10. Several such equations were solved simultaneously to give $K=1.08\times10^{-2}$, $K_{ip}=1.11\times10^3$ M^{-1}, and $K_q=3.35$ M^{-1}.

The calculated values of K_{obsd} (on the basis of the above set of equilibrium constants) as a function of x_e are compared with the experimental values (Fig. 1).

The values of K_{ip} thus determined (1.11×10^3) seem to be in the correct order of magnitude, since the association constants of quaternary ammonium halides in methyl ethyl ketone which has a dielectric constant comparable with that of cyclohexanone, are in the range 400—1000 M^{-1}.[8]

The values of x_{fi} at a given time were obtained by solving the biquadratic equation 6 with respect to x_{fi} by the Newton-Raphson method for the measured values of x.

The integration of Eq. 11 was carried out after expanding the integrand into a power series of x as given by Eq. 12.

$$\int_0^x \frac{dx}{(a-x)(b-x)-x_{fi}^2/K} = \int_0^t k_f dt \quad (11)$$

$$\frac{1}{(a-x)(b-x)-x_{fi}^2/K} = \frac{1}{ab} + Bx + Cx^2 + Dx^3 \quad (12)$$

The forward rate constants thus obtained showed no systematic deviation from the average value over three fold changes of initial concentration of the reactants.

In bromobenzene, the assumption $x_q \gg x_{fi}$ and x_{ip} seems plausible, and leads to a simplified rate law.

$$x \approx 2x_q = 2K_qK_{ip}^2x_{fi}^4 \quad (13)$$

$$\therefore\ x_{fi} = (x/2K_qK_{ip}^2)^{1/4} \quad (14)$$

If we denote the observed equilibrium constant by K_{obsd}, we have the following relation from a combination of Eqs. 3, 7, and 14.

$$K_{obsd} = k_e^{1/2}/\{(a-x_e)(b-x_e)\}$$
$$= K(2K_qK_{ip}^2)^{1/2} \quad (15)$$

Under these conditions Eq. 2 is reduced to

$$\frac{dx}{dt} = x_f\{(a-x)(b-x) - K_{obsd}^{-1}x^{1/2}\}. \quad (16)$$

$$\int_0^x \frac{dx}{(a-x)(b-x)-K_{obsd}^{-1}x^{1/2}} = \int_0^t k_f dt \quad (17)$$

On the basis of Simposon's rule, graphical integrations were repeated for the assumed values of k_f and K_{obsd}, until the calculated set of x *vs.* t data agreed with the experimental values. The best sets for K_{obsd} and k_f were 47.5 M$^{-1/2}$, and 2.97×10^{-4} M^{-1} s^{-1}, respectively.

The equilibrium constant determined kinetically (47.5

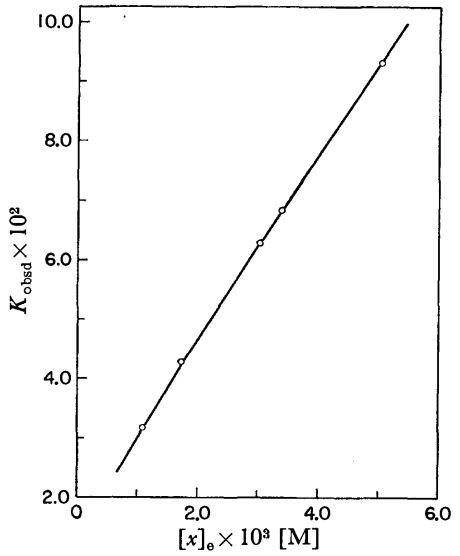

Fig. 1. Plots of K_{obsd} *vs.* $(x)_e$ at 30 °C.
○; Experimental, —; calculated with $K=1.08\times10^{-2}$, $K_{ip}=1.11\times10^3$(M^{-1}), $K_q=3.35$(M^{-1}).

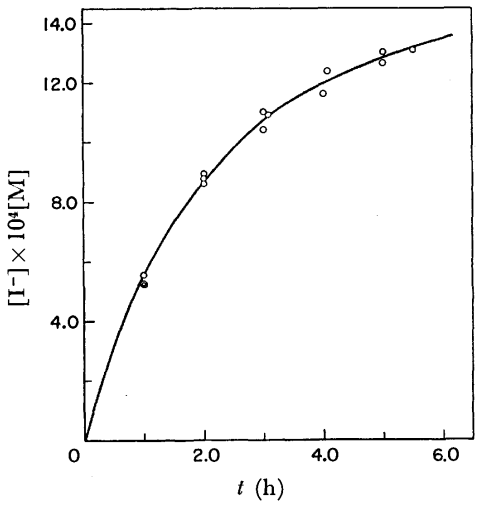

Fig. 2. Plots of (I^-) *vs.* t at 30 °C.
○; Experimental, —; calculated with $K_{obsd}=47.5$ (M$^{-1/2}$), $k_f=2.97\times10^{-4}$ (l mol^{-1} s^{-1}), $a=b=3.00\times10^{-2}$ (M).

$M^{-1/2}$) was in good agreement with the value determined analytically (46.5 $M^{-1/2}$). A comparison of the calculated values of x with the experimental ones is shown in Figure 2.

The values of k_f and K_{obsd} were also determined by direct differentiation of x with respect to t after expanding x into a power series of t as in $x=at+bt^2+ct^3$, followed by calculation of the value of K_{obsd} which gave a constant value of k_f throughout the run. The values determined by the two methods were in good agreement.

Solvent Effects on the Rate Constant, k_f. The rate constants, k_f, are summarized in Table 1, where k_x denotes the rate constant expressed in mole fraction unit as calculated from the rate constant, k_f, and the molar volume of the solvent, V_s, (expressed in liter) by the equation, $k_x=k_fV_s^{-1}$.

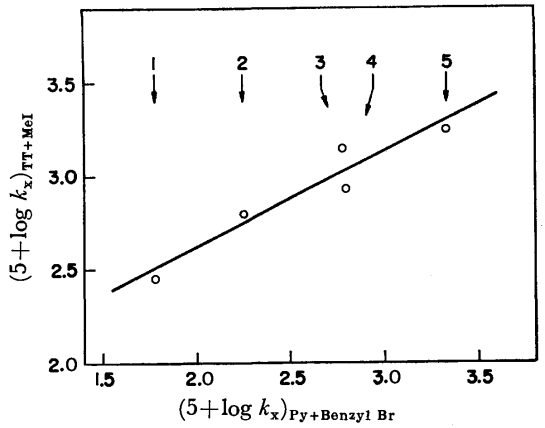

Fig. 3. Empirical correlations for the rate constants. Ordinate; present system, abscissa; pyridine+benzyl bromide, 1: bromobenzene, 2, cyclohexanone, 3; nitrobenzene, 4; methanol, 5; acetonitrile.

An empirical correlation exists[1] among log k_x values in spite of the different nucleophilic centers in the reactants (Fig. 3). The slope of the plots, which gives a relative sensitivity of the reaction to varying solvent characteristics, is smallest for the present reaction. This indicates that the charge development at the transition state is fairly small as compared with the quaternization reaction, or alternatively that charge delocalization in the thiazoline ring reduces the charge density on each atom, thus causing the reaction to be less sensitive to the solvent change.

The observation that the reverse rate process is also liable to solvent effects makes the first suggestion more plausible.

Table 1. Comparison of rate constants, k_f (30 °C)

Solvent	$k_f\times10^4$	$k_x\times10^2$
Propylene carbonate	20.5	2.40
Nitrobenzene	14.8	1.43
N,N-Dimethylacetamide	12.3	1.32
Acetonitrile	9.50	1.78
Methanol	3.48	0.849
Cyclohexanone	6.40	0.611
Bromobenzene	2.97	0.280

k_f; 1 mol^{-1} s^{-1}, k_x; s^{-1}.

Table 2. Comparison of the slopes

Reaction	$\Delta\log k/(\Delta\log k)_{Benzyl\ Br+Pyr}$
Benzyl bromide+Pyridine	1.0[1]
Methyl iodide+Pyridine	0.82[1]
ω-Bromoacetophenone+α-Picoline	0.68[1]
Methyl Iodide+TT	0.51

Pressure Effects and the Volume Change of Reaction. Activation volumes and pressure derivatives were determined by the least squares method after expanding the rate constants into power series of pressure as given by equations 18—20 and are summarized in Table 3.

$$\ln k_p = \ln k_0 + Bp + Cp^2 \quad (18)$$

$$\Delta V_0^* = (-1)BRT \quad (19)$$

$$(\partial\Delta V^*/\partial p)_0 = (-2)CRT \quad (20)$$

Table 3. Activation volumes and the pressure derivatives (30 °C)

Reaction	Solvent	ΔV_0^* (cm^3 mol^{-1})	$(\partial\Delta V^*/\partial p)_0$ (cm^5 mol^{-1} kg^{-1})
MeI+Pyr	AN	−25.8	0.0106
MeI+Pyr	PC	−19.7	0.00941
MeI+TT	AN	−24.9	0.00909
MeI+TT	PC	−16.1	0.00395

The apparent molal volumes of the solute, ϕ_v and the overall volume change in the reaction, $\Delta\phi_v$, are summarized in Table 4. In acetonitrile and propylene carbonate, the values of $\Delta\phi_v$ in the table would approximately be equal to the volume change of the reaction, $\Delta\bar{V}°$, since the association constants of the quaternary ammonium salts are usually small in these solvents.[9,10]

We see that the molal volumes of electrolytes are fairly small in acetonitrile as compared to those in propylene carbonate and that there is a near parallelism between the values of ΔV_0^* and of $\Delta\phi_v$, resulting in a nearly constant value of $(\Delta V_0^*/\Delta\phi_v)$.

ΔV_0^* is generally considered as the sum of two terms, Δ_1V^*, Δ_2V^*. The first term arises from changes in the molal volume of the reactant molecules as they form a transition state, while the latter is attributed to the volume change in the surrounding solvents due to electrostriction. A similar dissection of $\Delta\bar{V}°$ in terms of $\Delta_1\bar{V}°$ and $\Delta_2\bar{V}°$ is valuable for the following discussions.

Stewart and Weale[11] concluded that $\Delta_1\bar{V}°\approx0$, by combining the calculated values of Δ_1V^* for the forward and reverse Menschutkin reactions on the basis of a cylinder model. An alternative estimation of $\Delta_1\bar{V}°$ is possible by the substitution of the molal volume of methylpyridinium iodide by the molar volumes of neutral model compounds, *i.e.*, by the molar volume of toluene as a model compound for methylpyridinium ion, 107.4 cm^3 mol^{-1},[3] and of liquid xenon, 37.3 cm^3 mol^{-1} (−109 °C),[12] (or a little larger than this because of volume expansion due to temperature rise from −109 to 30 °C), as a model compound for iodide, thus leading to $\Delta_1\bar{V}°\approx107.4+37.3-(81.6+67.1)=-4$ to 0 (cm^3 mol^{-1}). Both estimates suggest that the major part

TABLE 4. APPARENT MOLALVOLUMES AND ACTIVATION VOLUMES (30 °C)

Reaction	Solvents	ϕ_v (cm_3 mol^{-1})			$\Delta\phi_v$	ΔV_0^*	$(\Delta V_0^*/\Delta\phi_v)$
		Pyr.	MeI	MePyr+I^{-1}			
MeI+Pyr.	AN	81.6	67.1	98.9	−49.8	−25.8	0.52
MeI+Pyr.	PC	81.3	65.1	116.3	−30.1	−19.7	0.65

Reaction	Solvents	ϕ_v (cm^3 mol^{-1})			$\Delta\phi_v$	ΔV_0^*	$(\Delta V_0^*/\Delta\phi_v)$
		TT	MeI	MTT+I^-			
MeI+TT	AN	145.2	67.1	166.9	−45.4	−24.9	0.55
MeI+TT	PC	151.8	65.1	191.3	−25.6	−16.1	0.63

of the observed values of $\Delta\phi_v$ comes from the term, $\Delta_2\bar{V}°$.

The observed molal volume of a solute V_M is usually larger than the calculated van der Waals volume, V_W, and the ratio (V_M/V_W) is known to range from 1.3 to 2.2 because of the existence of empty space in the liquid.[13] Calculation of van der Waals volumes as proposed by Edward[13] gives the factor (V_M/V_W) of 1.8 and 2.0 for pyridine and methyl iodide in acetonitrile.

Stewart and Weale[11] estimated $\Delta_1V^* = -6.5$ cm^3 mol^{-1} for the forward Menschutkin reaction on the basis of the cylinder model. A combination of the value −6.5 and the above factor of 1.8 gives $\Delta_1V^* = -11.7$ cm^3 mol^{-1}, which is in reasonable agreement with the estimated value of −10.7 cm^3 mol^{-1} obtained by a completely different method.[14]

The values of $\Delta_2V^*/\Delta_2\bar{V}°$ would serve as indices of the degree of charge development at the transition state throughout the series of reactions of the same volume profile along the reaction coordinate, *i.e.*, a slightly modified version of the proposals.[15,16] Making use of the value of $\Delta_1V^* = -11.7$ cm^3 mol^{-1} and the above conclusion that $\Delta\phi_v \approx \Delta_2\bar{V}°$, we find that the value $(\Delta_2V^*/\Delta_2\bar{V}°)$ becomes nearly constant at 0.26—0.29 for both reactions. An exception is the reaction of TT with methyl iodide in propylene carbonate for which a rather large uncertainty should be included in the value of Δ_2V^* obtained above. Abraham estimated the above indices as 0.4—0.41 from a comparison of the transfer free energy of the activated complex with that of the product ion-pair.[17] Our value of 0.26—0.27 is intermediate between the value 0.2 as estimated previously[1] and the value given by Abraham.[17]

The relative sensitivity difference to change of solvent observed in the case of the reaction rate constants is manifested neither on the activation volumes nor on the values of $(\Delta V_0^*/\Delta\phi_v)$.

Thus, the desirability of acquiring reliable values of Δ_1V^* and $\Delta_1\bar{V}°$ is obvious.

CNDO/2 Calculation. CNDO/2 calculations[18] were carried out for estimated structures of the transition state using model compounds.[19–21] In order to save time it was assumed that the reaction proceeds through a transition state which has a structure closely resembling a product, *i.e.*, ∠N-C-I=180° for pyridine and methyl chloride, and ∠C(ring)-S-C(methyl)=101° for TT with methyl chloride. Thus only two bond distances r_{N-C} and r_{C-Cl} change during the course of reaction, the others remaining unchanged. The central CH_3 group was assumed to lie in a plane. Calculations were repeated until a minimum total energy was reached, by changing the value of Δr according to $r_{N-C}=1.47+\Delta r$ (or $r_{S-C}=1.80+\Delta r$) and $r_{C-Cl}=1.78+\Delta r$, where the numerals indicate normal bond distances of a model compound.[19–21]

Charge densities for the minimized structures as given in Figs. 4 and 5 suggest that electronic charges are more developed at the transition state for the reaction of pyridine with methyl iodide, which corresponds to the arguments put forward on the basis of the rate studies.

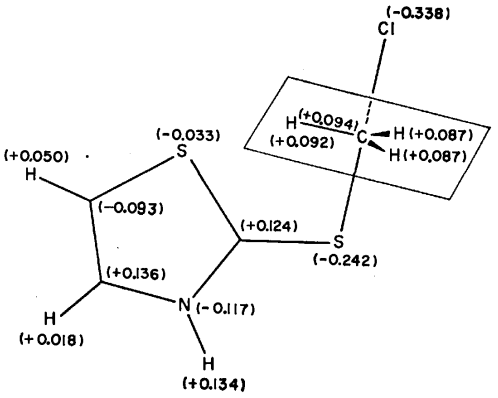

Fig. 4. Charge distribution for minized structure. $r_{C-S}=1.83$ Å, $r_{C-Cl}=1.81$ Å, $\mu=6.74$ D.

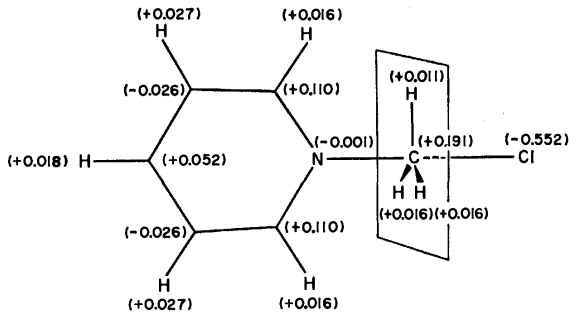

Fig. 5. Charge distribution for minimized structure. $r_{N-C}=1.59$ Å, $r_{C-Cl}=1.90$ Å, $\mu=10.7$ D.

Heydtman *et al.*[22] estimated the dipole moment of the activated complex to be 7.8 D by applying the Kirkwood approach[23] to the reaction of ω-bromoacetophenone with α-picoline. Eckert *et al.* derived a value of 5.9 D for the reaction of pyridine and methyl iodide by the same approach.[24] For the reaction of pyridine with

methyl iodide, the slope of the plots of $RT \ln k$ *vs.* $(D-1/2\ D+1)$ corresponds to 14.3 kcal mol^{-1}. This leads to the value 6.3 D for the dipole moment of the activated complex, when allowance is made for the empty space as mentioned above, *i.e.*, the factor of 1.8, and when radii are calculated from the molal volumes in Table 4 assuming a spherical molecule. A different application of the Kirkwood approach leads to a different dipole moment as described by Eckert.[25] Thus, the model CNDO/2 calculation provides an alternative way of estimating the dipole moment.

We are grateful to Dr. Michael H. Abraham, University of Surrey, England for helpful criticisms of the original version of this manuscript.

References

1) Kondo, M. Ohnishi, and N. Tokura, *Bull. Chem. Soc. Jpn.*, **45**, 3579 (1972).
2) C. Roussel, R. Gallo, M. Chanon, and J. Metzger, *J. Chem. Soc., Perkin Trans. 2*, **1974**, 1304.
3) J. A. Riddick and W. B. Bunger, "Organic Solvents," 3rd ed, Wiley-Interscience, N. Y. (1970).
4) C. M. Roussel, A. Babadjamian, M. Chanon, and J. Metzger, *Bull. Soc. Chim. Fr.*, **1971**, 1087.
5) C. M. Roussel, R. Gallo, M. Chanon, and J. Metzger, *Bull. Soc. Chim. Fr.*, **1971**, 1902.
6) L. E. Strong and C. A. Klaus, *J. Am. Chem. Soc.*, **72**, 166 (1950).
7) R. M. Fuoss and C. A. Klaus, *J. Am. Chem. Soc.*, **55**, 3614 (1933).
8) S. R. C. Hughes and D. H. Price, *J. Chem. Soc., A*, **1967**, 1093.
9) D. F. Evans, C. Zawoyski, and R. L. Kay, *J. Phys. Chem.*, **69**, 3878 (1965).
10) M. L. Jansen and H. L. Yeager, *J. Phys. Chem.*, **77**, 3089 (1973).
11) J. M. Stewart and K. E. Weale, *J. Chem. Soc.*, **1965**, 2854.
12) C. D. Hodgmann, "Handbook of Chemistry and Physics," 50 th ed, Chemical Rubber Publishing Co., Cleveland (1969).
13) J. T. Edward, *J. Chem. Educ.*, **47**, 261 (1970).
14) Y. Kondo, M. Uchida, and N. Tokura, *Bull. Chem. Soc. Jpn.*, **41**, 992 (1968).
15) K. Seguchi, A. Sera, and K. Maruyama, *Bull. Chem. Soc. Jpn.*, **47**, 2242 (1974).
16) W. J. le Noble and T. Asano, *J. Am. Chem. Soc.*, **97**, 1778 (1975).
17) M. H. Abraham, *J. Chem. Soc., Perkin Trans. 2*, **1972**, 1343.
18) J. A. Pople and D. L. Beveridge, "Approximate Molecular Orbital Theory," McGraw-Hill, N. Y. (1970).
19) L. E. Sutton, "Tables of Interatomic Distances and Configuration in Molecules and Ions," The Chem. Soc. Special Publication, No. 11, London (1958).
20) B. Bak, L. Hansen, and J. R. Andersen, *J. Chem. Phys.*, **22**, 2013 (1954).
21) P. J. Wheatley, *J. Chem. Soc.*, **1961**, 4379.
22) H. Heydtmann, A. P. Schmidt, and H. Hartmann, *Ber. Bunsenges. Phys. Chem.*, **70**, 444 (1966).
23) J. G. Kirkwood, *J. Chem. Phys.*, **2**, 351 (1934).
24) J. R. McCabe, R. A. Grieger, and C. A. Eckert, *Ind. Eng. Chem., Fundam.*, **9**, 156 (1970).
25) J. R. McCabe and C. A. Eckert, *Ind. Eng. Chem., Fundam.*, **13**, 168 (1974).

Peptides. VI. Some Oxime Carbonates as Novel *t*-Butoxycarbonylating Reagents[1)]

Masumi Itoh, Daijiro Hagiwara, and Takashi Kamiya,
Research Laboratories, Fujisawa Pharmaceutical Co., Ltd., Kashima-cho, Yodogawa-ku, Osaka 532
(Received July 15, 1976)

Several *t*-butoxycarbonyl derivatives of oximes were prepared through the corresponding oxime chloroformates. Of these, diethyl (*t*-butoxycarbonyloxyimino)malonate and 2-(*t*-butoxycarbonyloxyimino)-2-phenylacetonitrile were utilized for the preparation of *t*-butoxycarbonylamino acids under various conditions. The results are summarized in a table.

The *t*-butoxycarbonyl (Boc) group is one of the most important amino-protecting groups in peptide synthesis, and there have been many reagents proposed for its introduction.[2-18)] The most popular and still widely utilized one is *t*-butyl azidoformate (**1**),[2)] though it is toxic and relatively less reactive and should be prepared just before use. Most of the substitutes for **1** are, with a few exceptions, less attractive because of disadvantages such as difficult access or insufficient reactivity of the reagents, or cumbersome elimination of by-products from Boc-amino acids. The present authors wish to propose a new promising reagent, 2-(*t*-butoxycarbonyloxyimino)-2-phenylacetonitrile (**3c**), which is an easy-to-prepare, stable, and highly reactive crystalline material and affords contaminant-free Boc-amino acids in high yields by following a conventional procedure.

In the course of studies on the application of *N*-hydroxy compounds to peptide synthesis in our laboratory, it was noticed that some oximes could be suitable as the activator and carrier of Boc groups. Oximes are usually regarded as unstable compounds which are easily hydrolyzed or rearranged. However, certain ketoximes which possess electron-withdrawing substituents and have no hydrogen atoms on the α-carbon atoms are relatively stable and can be converted into their Boc derivatives through the corresponding chloroformates.

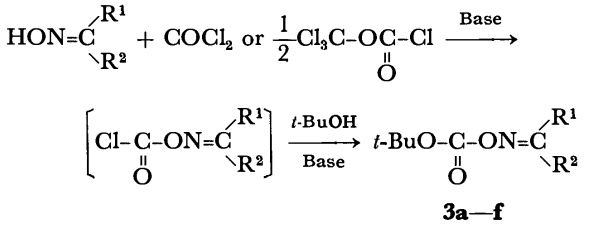

Scheme 1.

In practice those oximes were allowed to react first with phosgene or trichloromethyl chloroformate in the presence of *N,N*-dimethylaniline or pyridine in inert solvents, and the resultant chloroformates were treated *in situ* with *t*-butyl alcohol and pyridine to give Boc-oximes. Some of the derivatives prepared are listed in Table 1. Of these, diethyl (*t*-butoxycarbonyloxyimino)malonate (**3a**) was the most reactive one; it readily introduced the Boc group to amino acids within 1 to 3 h. Compound **3c** was a stable crystalline material and moderately reactive among the compounds listed in Table 1; it completed the reaction within 4 to 5 h. The other cardonates were so unstable that mainly **3a** and **3c** were subjected to further studies.

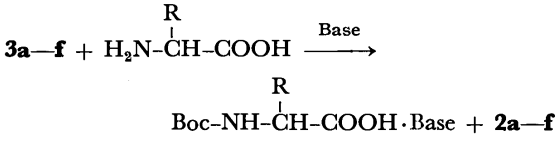

Scheme 2.

An advantage of **3c** over **3a** is the easy removal of 2-(hydroxyimino)-2-phenylacetonitrile (**2c**) from the reaction mixture. When **3a** is used it requires critical pH adjustment to 7.0 for the removal of diethyl (hydroxyimino)malonate (**2a**) from the reaction mixture. To simulate extraction conditions for the removal of **2a** and **2c**, their ethyl acetate solutions were shaken with water in the presence of sodium hydroxide, sodium hydrogencarbonate, or triethylamine. The oxime **2c** transferred only with sodium hydroxide but not with the others, suggesting an easy way for complete removal of **2c** from the reaction mixture. Both **3a** and **3c** were quite stable to competitive hydrolysis by sodium hydroxide or triethylamine in dioxane–water at room

Table 1. *t*-Butoxycarbonylated oximes

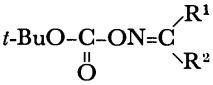

	R^1	R^2	Yield (%)	Mp (°C)	Recrystd. from
3a	COOEt	COOEt	77.2	oil	—
3b	$COCH_3$	COOEt	57.0	oil	—
3c	CN	C_6H_5	65.0	84—86	methanol
3d	CN	C_6H_4-Cl(*p*)	6.7	91—92	methanol
3e	CN	1-naphthyl	31.1	90—92	methanol
3f	C_6H_5	C_6H_5	70.6	131—133	toluene–pet. ether

Table 2. Yields of Boc-amino acids and reaction conditions employed[a]

Boc-Amino Acid	Reagent	Base (equiv)		Solvent[b]	Reaction time (h)	Oxime extraction	Yield (%)	Mp (°C)	Ref.
Boc-Ala-OH	**3a**	TEA	1.2	A*	1	ether	84.1	82—84	19
-Ala-OH	**3c**	TEA	1.5	B*	4	ether	80.3	82—84	
-Arg(NO_2)-OH	**3a**	$NaHCO_3$	1.5	A[c]	3	EtOAc	70.0	115—116(dec)[d]	31
-Arg(NO_2)-OH	**3c**	TEA	1.5	B*	1[e]	ether	80.0	123—125	19
-Asn-OH	**3c**	TEA	1.5	C	20	EtOAc	85.8	173(dec)	18
-CyS(Bzl)-OH	**3c**	TEA	1.5	C	3	EtOAc	94.0	65—67	19
-Glu$(OH)_2$	**3c**	TEA	1.5	C	3	EtOAc	78.4	103—105(dec)	18
-Gly-OH	**3c**	TEA	1.5	C	2	EtOAc	86.9	86—88	18
-Gly-OH	**3c**	TEA	1.5	C*	40 min[f]	EtOAc	81.4	86—88	
-Ile-OH·DCHA	**3c**	NaOH	1.0	A*	3	ether	89.2	123—125	9
-Leu-OH·1/2H_2O	**3c**	TEA	1.5	C*	3	EtOAc	72.0	78—84	19
-Leu-OH·1/2H_2O	**3c**	TEA	1.5	C	3	ether	99.1	78—82	
-Met-OH·DCHA	**3c**	TEA	1.5	C*,[g]	3	EtOAc	82.1	137—139	19
-Phe-OH	**3b**	TEA	1.0	A	2	EtOAc	54.0	84—86	19
-Phe-OH·DCHA	**3c**	TEA	1.5	C[h]	2	C_6H_6	65.5	222—223	20
-Phe-OH·DCHA	**3c**	TEA	1.5	C	5	ether	98.2	221—223	
-Phg-OH	**3a**	TEA	1.5	D*	3	EtOAc	86.0	87—89.5	21
-Pro-OH	**3c**[i]	TEA	1.5	E*	1.5	C_6H_6	87.8	132—133	19
-Pro-OH	**3f**	TEA	1.5	F*	24	EtOAc	13.0	132—133	
-Thr-OH·DCHA	**3c**	FEA	1.5	C	3	EtOAc	99.7	151—153	19
-Trp-OH	**3c**	TEA	1.5	C	3	EtOAc	98.6	137—138(dec)	19
-Tyr-OH·DCHA	**3c**	NaOH TEA	2.0[j] 1.0	C	4	EtOAc	81.8	212(dec)	9

a) The amino acids used, with the exceptions of glycine and D-phenylglycine, are of L-configuration. The reactions were carried out in 10 mmol scale with 1.1 equiv of the reagents at 20 to 25 °C unless stated otherwise. All products were purified following descriptions in the literatures, and optical rotations observed were within the limit of error in comparison with reported values. b) Five to 10 ml of organic solvents and water per 10 mmol amino acid were used unless cited below. Those with asterisks were removed *in vacuo* before the extraction of oximes; A: *t*-butyl alcohol/water, B: acetone/water, C: dioxane/water, D: methanol/water (70/70 ml), E: methanol/dioxane/water (15/5/10 ml), and F: dioxane/chloroform/water (20/10/10 ml). c) 40/100 ml. d) The difference of the melting points of the two N^{α}-Boc-N^{G}-nitro-L-arginine preparations will be due to polymorphism. e) Warmed for a while at 50 °C. f) At 40 °C. g) 14/20 ml. h) 30/20 ml. i) An equiv of **3c** was used. j) Sodium hydroxide was neutralized before the extraction.

temperature. Compound **3c** dissolves only partly in a solvent–water mixture at an initial stage of the reaction, but the mixture usually becomes homogeneous within 1 h. Yields of Boc-amino acids and conditions employed for each reaction are summarized in Table 2. In the case of L-tyrosine, two equivalents of sodium hydroxide and an equivalent of triethylamine were employed to obtain a clear solution, and a small amount of a side-product, *N,O*-bis-Boc-L-tyrosine, was detected on a thin layer chromatogram. However, the side-product could be eliminated effectively from *N*-Boc-L-tyrosine through salt formation with dicyclohexylamine. To secure a high yield and the purity of the products, other solvents than dioxane should be removed before the extraction of **2a** or **2c** from the reaction mixture. Omission of the removal of dioxane did not cause any trouble unless a large excess of it was used. The selection of a suitable solvent for the removal of **2a** or **2c** may be important

Table 3. Oxime carbonates prepared for the introduction of other amino protective groups

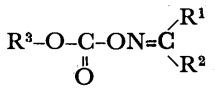

	R^3	R^1	R^2	Yield (%)	Mp (°C)	Recrystd. from
3g	C_6H_5-CH_2-	CN	C_6H_5	61.9[a]	73—75	EtOAc/Hex.[c]
3h	*p*-MeO-C_6H_4-CH_2-	CN	C_6H_5	35.5[b]	112—113	EtOAc/Hex.
3i	Cl_3C-CH_2-	CN	C_6H_5	87.2[a]	82—84	MeOH
3j	*c*-C_3H_5-CH(Me)-	CN	C_6H_5	18.1[b]	65—67	MeOH
3k	*p*-MeO-C_6H_4-CH_2-	COOEt	COOEt	80.0[a] 78.4[d]	syrup	—

a) Prepared from the corresponding alkyl or aralkyl chloroformates with the oximes by following the conventional procedure.[28] b) Prepared by following a similar procedure to that described for **3c**. c) Hexane. d) Prepared by following the procedure for **3a**.

for the Boc-amino acids with lipophilic side chains. For example, in the preparation of Boc-L-phenylalanine with **3c**, the use of ethyl acetate or benzene lowered the yield, whereas the use of ether gave a satisfactory result. Possible contaminants, **2a** and **2c**, were detected on fluorescent indicator-impregnated silica gel plates.

In comparison with **1** and 2-(*t*-butoxycarbonylthio)-4,6-dimethylpyrimidine (**4**),[18] **3c** showed a much higher reactivity. In the preparation of Boc-glycine, for example, **3c** completed the reaction within 2 h at room temperature,[1] whereas both **1** and **4** required more than 20 h at 40 °C and room temperature, respectively. Furthermore, **3c** is less toxic (LD_{50} orally in mice: 8000 mg/kg) and the by-product **2c** is easily recovered and recycled.

This procedure is wholly applicable to the preparation of other *N*-protected amino acids, and the reagents prepared for such purposes are listed in Table 3. Examples of *N*-protected amino acids, prepared by similar procedures to those described in the experimental section, are *N*-benzyloxycarbonyl-L-serine[32] (87.8%), *N*-(*p*-methoxybenzyloxycarbonyl)-L-phenylalanine[33] (64.6%), *N*-(2,2,2-trichloroethoxycarbonyl)-D-phenylglycine (mp 141—143 °C, 92.1%),[34] and *N*-(1-cyclopropylethoxycarbonyl)-D-phenylglycine (mp 94—96 °C, 88.5%).[34] The 1-cyclopropylethoxycarbonyl group was easily removed under the conditions required for the Boc group.

Experimental

The capillary melting points were observed on a Hoover "Uni-Melt" apparatus and are uncorrected. Precoated silica gel 60 F_{254} plates (Merck) were used for thin layer chromatography (TLC).

Materials. Trichloromethyl chloroformate was obtained from Hodogaya Chemical Co., Ltd., Tokyo. Diethyl (hydroxyimino)malonate (**2a**),[22] ethyl 2-(hydroxyimino)acetoacetate (**2b**),[23] 2-(hydroxyimino)-2-(*p*-chlorophenyl)acetonitrile (**2d**),[24] benzophenone oxime (**2f**),[25] 1-cyclopropylethanol,[29] and *p*-methoxybenzyl chloroformate[30] were prepared according to the literature.

2-(Hydroxyimino)-2-phenylacetonitrile (2c). Into an ice-cooled solution of benzyl cyanide (117 g, 1 mol) and sodium hydroxide (40 g, 1 mol) in methanol (300 ml) was introduced gaseous methyl nitrite[26] which was generated from a suspension of sodium nitrite (83 g) in a mixture of methanol (53 ml) and water (50 ml) by dropwise addition of a mixture of concentrated sulfuric acid (32 ml) and water (65 ml). The mixture was stirred for 2 h at room temperature and concentrated to dryness. The residue was dissolved in water and washed with toluene twice. The aqueous layer was acidified with concentrated hydrochloric acid to precipitate **2c**: 120 g (82%); mp 119—124 °C (lit,[27] mp 126—128 °C); TLC, R_f=0.50 (chloroform–methanol (9: 1)). This was used in the next step without further purification.

2-(Hydroxyimino)-2-(1-naphthyl)acetonitrile (2e). This was prepared from 2-(1-naphthyl)acetonitrile by the procedure described above. The syrupy product obtained in 36.2 % yield was used in the next step without purification.

Diethyl (t-Butoxycarbonyloxyimino)malonate (3a). To a well-stirred solution of phosgene (151 g, 1.53 mol) in benzene (800 ml) was added dropwise a solution of **2a** (289 g, 1.53 mol) and *N*,*N*-dimethylaniline (DMA) (186 g, 1.53 mol) in benzene(800 ml) at 5—6 °C over the period of 2.5 h under nitrogen atmosphere. The mixture was stirred for 2 h at 5—6 °C, and for 18 h at room temperature. To the resultant mixture was added dropwise a mixture of *t*-butyl alcohol (225 g, 3.06 mol) and pyridine (Pyr) (486 ml, 6.12 mol) at 5—6 °C over the period of 1.5 h under nitrogen. Stirring was continued for 18 h at room temperature. After filtration of precipitates the filtrate was washed with cold 1M hydrochloric acid (1 l×6) and cold water (1 l×3), and stirred with sodium hydrogencarbonate solution (70 g in 1 l) for 3 h at room temperature. The organic phase was washed with 5% sodium carbonate solution (100 ml×2), water (200 ml×2) and saturated sodium chloride solution (100 ml), and dried over magnesium sulfate with 15 g of charcoal. Evaporation gave 341 g (77.2%) of **3a**. IR (neat, cm^{-1}) 1800, 1750; nuclear magnetic resonance (NMR) (in CCl_4, δ(ppm)) 1.39 (3H, triplet, J=6.5 Hz), 1.41 (3H, triplet, J=6.5 Hz), 1.59 (9H, singlet), 4.34 (4H, quartet, J=6.5 Hz).

Ethyl 2-(t-Butoxycarbonyloxyimino)acetoacetate (3b). This was prepared from **2b** by a procedure similar to that described in the preparation of **3a**, except for the use of Pyr in the place of DMA. IR (neat, cm^{-1}) 1780, 1730, 1690; NMR (in CCl_4, δ(ppm)) 1.37 (3H, triplet, J=7 Hz), 1.57 (9H, singlet), 2.48 (3H, singlet), 4.34 (2H, quartet, J=7 Hz).

2-t-Butoxycarbonyloxyimino-2-phenylacetonitrile (3c). To a stirred solution of trichloromethyl chloroformate (6.7 ml, 0.055 mol) or an equivalent of phosgene (0.11 mol) in benzene (30 ml) was added dropwise a solution of **2c** (14.6 g, 0.1 mol), DMA (12.0 g), and dioxane (5 ml) in benzene (100 ml) at 3—5 °C. The mixture was stirred for 6 h at room temperature and allowed to stand overnight. To the resultant mixture was added a solution of *t*-butyl alcohol (11.1 g) and Pyr (16.0 ml) in benzene (20 ml) at 5—10 °C. The mixture was allowed to react for 3 h at the same temperature, then for 4 h at room temperature, and to stand overnight. The mixture was then washed with water, 1 M hydrochloric acid, water, 5% sodium hydrogencarbonate solution, and water again, and dried over magnesium sulfate. After evaporation of the solvent, the residue was triturated with 20 ml of 90% aqueous methanol, filtered, washed with 30 ml of the same solvent, and dried to give 17.0 g of **3c**: mp 84—86 °C; TLC, R_f=0.74 (chloroform–methanol (9: 1)).

Found: C, 63.69; H, 5.71; N, 11.20%. Calcd for $C_{13}H_{14}O_3N_2$: C, 63.40; H, 5.73; N, 11.38%. IR (Nujol, cm^{-1}) 1785; NMR (in $CDCl_3$, δ(ppm)) 1.62 (9H, singlet), 7.2—8.2 (5H, multiplet).

2-(t-Butoxycarbonyloxyimino)-2-(p-chlorophenyl)acetonitrile (3d). This was prepared from **2d** (37.5 mmol) by a procedure similar to that described above except that chloroformylation was done by the use of DMA in a mixture of dioxane (10 ml), tetrahydrofuran (10 ml), and dichloromethane (70 ml). (See Table 1).

Found: C, 55.80; H, 4.65; N, 10.07; Cl, 12.62%. Calcd for $C_{13}H_{13}O_3N_2Cl$: C, 55.62; H, 4.67; N, 9.98; Cl, 12.63%. IR (Nujol, cm^{-1}) 1790; NMR (in $CDCl_3$, δ(ppm)), 1.63 (9H, (singlet), 7.50 and 7.90 (2H, each, AB Quartet, J=4.5 Hz).

2-(t-Butoxycarbonyloxyimino)-2-(1-naphthyl)acetonitrile (3e). A similar procedure to that described above was followed in toluene. IR (Nujol, cm^{-1}) 1790.

Found: C, 68.85; H, 5.38; N, 9.40%. Calcd for $C_{17}H_{16}O_3N_2$: C, 68.90; H, 5.44; H, 9.46%.

(t-Butoxycarbonyloxyimino)diphenylmethane (3f). A similar procedure to that described above was employed. IR (Nujol, cm^{-1}) 1770; NMR (in $CDCl_3$, δ(ppm)), 1.48 (9H, singlet), 7.17—7.65 (10H, multiplet).

General Procedures for the Introduction of t-Butoxycarbonyl Group. a) By the Use of 3a: To a solution of L-alanine (0.89 g, 10 mmol) and triethylamine (TEA) (1.68 ml, 1.2 mmol) in a mixture of water (5 ml) and *t*-butyl alcohol (5 ml) was added

3a (3.2 g, 11 mmol). The mixture was stirred for 1 h at room temperature. After evaporation of *t*-butyl alcohol and addition of ether and 5% sodium hydrogencarbonate solution, the mixture was adjusted to pH 7.0 precisely with a citric acid solution. The aqueous layer was separated, overlaid with ether, and adjusted to pH 7.0 again. The aqueous layer separated was acidified with citric acid solution and extracted with ethyl acetate (EtOAc). The extract was treated in the usual manner to give *N*-*t*-butoxycarbonyl-L-alanine: 1.59 g (84.1%); mp 82—84 °C. Conditions employed in the other examples are presented in Table 2.

b) By the Use of ***3c***: To a solution of L-tryptophan (2.05 g, 10 mmol) and TEA (2.10 ml, 15 mmol) in water (6 ml) was added dioxane (6 ml) and crystalline **3c** (2.71 g, 11 mmol) at room temperature. The mixture became homogeneous within 1 h and stirring was continued for two more hours. After addition of water (15 ml) and EtOAc (20 ml), the aqueous layer was separated, washed with EtOAc (20 ml), acidified with 5% citric acid solution, and extracted with EtOAc. The extract was treated in the usual manner to give *N*-*t*-butoxycarbonyl-L-tryptophan: 3.00 g (98.6%); mp 137—138 °C (decomp). Other amino acids were allowed to react by the same procedure, unless stated otherwise in Table 2. Dicyclohexylammonium salts were crystallized by the addition of dicyclohexylamine (1.8 g per 10 mmol amino acid) to an ether solution of *t*-butoxycarbonylamino acids.

References

1) Part of this work was reported as a communication: M. Itoh, D. Hagiwara, and T. Kamiya, *Tetrahedron Lett.*, **1975**, 4393.

2) R. Schwyzer, P. Sieber, and H. Kappeler, *Helv. Chim. Acta.*, **42**, 2622 (1959).

3) G. W. Anderson and A. C. McGregor, *J. Am. Chem. Soc.*, **79**, 6180 (1957).

4) W. Klee and M. Brenner, *Helv. Chim. Acta.*, **44**, 2151 (1961).

5) L. A. Carpino, *J. Org. Chem.*, **29**, 2820 (1960).

6) R. B. Woodward, K. Heusler, J. Gosteli, P. Naegeli, W. Oppolzer, R. Ramage, S. Ranganathan, and H. Vorbruggen, *J. Am. Chem. Soc.*, **88**, 852 (1966).

7) J. H. Jones and G. T. Young, *Chem. & Ind.*, **1966**, 1722.

8) M. Frankel, L. Ladkany, C. Gilon, and Y. Wolman, *Tetrahedron Lett.*, **1966**, 4765.

9) W. Broadbent, W. J. Morley, and B. E. Stone, *J. Chem. Soc.*, **1967**, 2632.

10) H. Gross and L. Bilk, *Angew. Chem. Intern. Ed. Engl.*, **6**, 570 (1967).

11) M. Fujino and C. Hatanaka, *Chem. Pharm. Bull.*, **15**, 2015 (1967).

12) E. Schnabel, H. Herzog, P. Hoffmann, E. Klanke, and I. Ugi, *Justus Liebigs Ann. Chem.*, **716**, 175 (1968).

13) B. Rzeszotarska and S. Wiejak, *Justus Liebigs Ann. Chem.*, **716**, 216 (1968).

14) E. Guibé-Jampel, G. Bram, and M. Vilkas, *Tetrahedron Lett.*, **1969**, 3541.

15) E. Guibé-Jampel and M. Wakselman, *Chem. Commun.*, **1971**, 267.

16) U. Ragnarsson, S. M. Karlsson, and B. E. Sandberg, *Acta Chem. Scand.*, **26**, 2550 (1972).

17) G. Bram, *Tetrahedron Lett.*, **1973**, 467.

18) T. Nagasawa, K. Kuroiwa, K. Narita, and Y. Isowa, *Bull. Chem. Soc. Jpn.*, **46**, 1269 (1973).

19) E. Schnabel, *Justus Liebigs Ann. Chem.*, **702**, 188 (1967).

20) H. Otsuka and K. Inouye, *Bull. Chem. Soc. Jpn.*, **37**, 1465 (1964).

21) D. N. McGregor, U. S. Pat. 3579514; *Chem. Abstr.*, **75**, P63805k (1971).

22) V. Cerchez, *Bull. Soc. Chim. Fr.*, **47**, 1279 (1930); *Chem. Abstr.*, **25**, 919 (1931).

23) M. Z. Jovtchitch, *Chem. Ber.*, **35**, 151 (1902).

24) E. J. Poziomek and A. R. Melvin, *J. Org. Chem.*, **26**, 3769 (1961).

25) A. Lachman, *J. Am. Chem. Soc.*, **47**, 260 (1925).

26) W. H. Hartung and F. Crossley, *Org. Synth.*, Coll. Vol. II, 363 (1943).

27) M. Murakami, R. Kawai, and K. Suzaki, *Nippon Kagaku Zasshi*, **84**, 669 (1963); *Chem. Abstr.*, **60**, 4053d (1964).

28) M. Itoh, *Bull. Chem. Soc. Jpn.*, **47**, 471 (1974).

29) M. Lj. Mihailovic and Z. Cekovic, *Helv. Chim. Acta*, **52**, 1146 (1969).

30) S. Sakakibara, I. Honda, N. Naruse, and M. Kanaoka, *Experientia*, **25**, 576 (1969).

31) K. Hofmann, W. Haas, M. J. Smithers, R. D. Wells, Y. Wolman, N. Yanaihara, and G. Zanetti, *J. Am. Chem. Soc.*, **87**, 620 (1965).

32) E. Baer and J. Maurukas, *J. Biol. Chem.*, **212**, 25 (1955).

33) F. Weygand and K. Hunger, *Chem. Ber.*, **95**, 1 (1962).

34) Recrystallized from ethyl acetate–petroleum ether.

The Reactions of Carbonimidoyl Dichlorides with Metal Thioacetates, Acetates, Thiocyanates, and Selenocyanate

Sakuya TANAKA, Sakae UEMURA, and Masaya OKANO*
Institute for Chemical Research, Kyoto University, Uji, Kyoto 611
(Received August 6, 1976)

The reactions of carbonimidoyl dichlorides with potassium thioacetate and thiocyanate in tetrahydrofuran afford the corresponding isothiocyanates. Similarly, the reaction with potassium selenocyanate gives isoselenocyanates. Thallium(I) acetate reacts with phenylcarbonimidoyl dichloride with greater facility than potassium acetate to give a mixture of phenyl isocyanate and acetanilide in which the latter is predominant. A displacement of one chlorine atom in the carbonimidoyl dichlorides by a SAc, OAc, SCN, or SeCN group, followed by elimination of AcCl or CNCl, has been proposed as a reasonable reaction path.

The carbonimidoyl dichlorides can be used as starting materials for the preparation of many types of organic substances.[1] As one of a series of studies on carbonimidoyl dichlorides[2] and isocyanides,[3] we now report the results of the reactions of phenyl- and cyclohexylcarbonimidoyl dichlorides (hereinafter abbreviated as PCD and CCD respectively) with various metal thioacetates, acetates, and thiocyanates, as well as with potassium selenocyanate. Although the substitution reactions of imidoyl chlorides and their derivatives with metal acetates,[4] thioacetates,[4] and thiocyanates[5] have been reported, information about similar reactions on carbonimidoyl dichlorides is rare.

Results and Discussion

Reactions with Metal Thioacetates and Acetates (Table 1). The heterogeneous reaction of PCD or CCD with two equivalents of KSAc in tetrahydrofuran (THF) proceeded smoothly at room temperature to give the corresponding isothiocyanate in a fair yield without affoding any other organic products except for acetic thioanhydride (runs 3 and 4). In the case of 1 : 1 molar ratio, nearly 50% of the dichloride (PCD) or more was recovered, though the yield based on the consumed dichloride was nearly quantitative (runs 1 and 2). Thus the reaction appeared to occur in accord with the stoichiometry shown in Scheme 1 (Z=S):

$$\underset{\text{PCD (R=Ph)}\quad \text{CCD (R=}\textit{cyclo}\text{-}C_6H_{11})}{R\text{-}N{=}CCl_2} + 2CH_3COZM \longrightarrow R\text{-}N{=}C{=}Z + (CH_3CO)_2Z + 2MCl \quad (1)$$
(Z=S or O)

With TlSAc, probably less ionized than KSAc, the reaction was sluggish and was brought to completion by heating (run 5).

In a similar way, PCD reacted with two equivalents of metal acetates in boiling THF to give a mixture of phenyl isocyanate and acetanilide in which the latter was predominant; the combined yield was nearly quantitative (based on the consumed dichloride), but no acetic anhydride could be found in the reaction products. In order to examine whether acetanilide is formed by the reaction of phenyl isocyanate with acetic anhydride under the reaction conditions, some controlled

TABLE 1. REACTIONS OF $RN{=}CCl_2$ WITH METAL THIOACETATES AND ACETATES[a]

Run	Metal salt	(mmol)	Temp (°C)	Time (h)	Products and yield (%)[b]		
					$RN{=}CCl_2$	$RN{=}C{=}Z$	$PhNHCOCH_3$
1	KSAc	5	20	3	61	39[c]	—
2	KSAc	5	20	22	48	52[c]	—
3	KSAc	10	20	3	0	92[c]	—
4[d]	KSAc	10	20	24	29[d]	65[c,d]	—
5	TlSAc	10	68	3	27	70[c]	—
6	KOAc	10	68	3	73	trace[c]	13[f]
7	KOAc	2[g]	68	3	0	9[e]	75[f]
8	TlOAc	5	68	3	49	4[e]	45
9	TlOAc	10	68	3	18	4[e]	75
10	TlOAc	2[g]	68	3	0	0	95
11	AgOAc	10	68	3	90	0	10
12	AgOAc	2[g]	68	3	49	trace[e]	51
13	HgOAc	10	68	3	76	trace[e]	19

a) $RN{=}CCl_2$ (5 mmol; R=Ph) and THF (10 ml) were used unless otherwise stated. b) Determined by GLC; Based on $RN{=}CCl_2$. c) Z=S. d) R=*cyclo*-C_6H_{11}. e) Z=O. f) Other products; two unidentified compounds (*ca.* 3% each). g) $PhN{=}CCl_2$ 1 mmol; dicyclohexyl-18-crown-6 (2 mmol) was added.

* To whom correspondence should be addressed.

experiments were carried out. When either phenyl isocyanate or acetic anhydride was heated in THF (at 68 °C for 3 h), no appreciable change (including their hydrolysis) occurred in either case. However, when an equimolar mixture of these two compounds (5 mmol each) was similarly treated in the same solvent (10 ml), 14% of acetoanilide was produced; this was probably formed by the participation of external moisture (originated from the solvent, the acetate, and/or the atmosphere) in the reaction between two components. In this case considerable amounts of phenyl isocyanate and acetic anhydride remained unreacted, as opposed to the case of the dichloride-acetate reaction in which only 4% of the isocyanate and no acetic anhydride were found (see run 9). Though the reason for this disagreement is not clear at present, it may be possible that some acidic impurities formed during the course of the reaction accelerate the above acetanilide formation.

Further, it was found unexpectedly that in the reaction with metal acetates TlOAc (less ionized[6]) reacts more easily than KOAc (more ionized) (runs 9 *vs.* 6). In the case of other monovalent heavy-metal acetates such as Ag(I) and Hg(I), however, no such striking results were observed (runs 11 and 13). Since crown ethers have been known to increase the concentrations of "naked" anions by complexing with counter-cations, we also examined the reaction with metal acetates in the coexistence of dicyclohexyl-18-crown-6.[7] Considerable improvements in the yields were achieved in all cases, but it was insufficient in the case of AgOAc (runs 7, 10, and 12).

Next, we will briefly consider a probable reaction path for the above two reactions. It is known that the 1 : 1 molar reactions of carbonimidoyl dichlorides with alkoxide ions and amines afford the corresponding monosubstituted products in good yields.[1] In the present reactions, however, no detectable amounts of such products (**1**) were found in the reaction mixtures. This may suggest their rapid disappearance owing to some subsequent reaction. In connection with the present reactions, it has been reported that PCD reacts with acetic acid to afford phenyl isocyanate and acetyl chloride with generation of HCl.[8] It has also been reported that the reaction of PCD with ethanol affords *N*-phenylethylurethane with the liberation of HCl and ethyl chloride, suggesting the intermediacy of ethyl *N*-phenylchloroformimidate.[9] Based on these facts and the stoichiometry of the reactions, the following pathway would be highly probable:

$$R\text{-}N{=}CCl_2 \xrightarrow[-Cl^-]{CH_3COZ^-} \underset{\mathbf{1}}{\left[R\text{-}N{=}C\begin{matrix}\diagup Cl\\ \diagdown ZCOCH_3\end{matrix}\right]} \xrightarrow[-CH_3COCl]{} R\text{-}N{=}C{=}Z \quad (2)$$

$$CH_3COCl + CH_3COZ^- \longrightarrow (CH_3CO)_2Z + Cl^- \quad (Z{=}S \text{ or } O)$$

There may be another route for RNCZ which involes further displacement of the intermediate **1** by CH_3COZ^- to give $R\text{-}N{=}C(ZCOCH_3)_2$ (**2**), followed by elimination of $(CH_3CO)_2Z$, especially in the thioacetate reaction, since AcS^- is known to be a stronger nucleophile than AcO^-.

We must add a short comment on the facile reaction with TlOAc in the absence of crown ether. We roughly compared the solubility of this salt in boiling THF with those of other acetates, but it appeared that no significant differences were present (*i.e.*, 0.012 mol/l for TlOAc, 0.016 mol/l for AgOAc, and 0.002 mol/l for KOAc). Besides, no variations in the yields were observed within the experimental error by changing the amount of the solvent by half or five times in the reactions with TlOAc or KOAc respectively. Thus it is clear that the rate of dissolution of metal acetates is not the dominant factor in affecting the reaction rate. Since the considerably covalent character of the Tl-O bonds of similar compounds has been recognized,[6] most of the dissolved TlOAc is expected to exist in un-ionized form. Thus, the contribution of a four-center-type reaction between un-ionized TlOAc and carbonimidoyl dichlorides affording **1** may be possible, though no direct evidence is available at present. Needless to say, when the crown ether is added to the reaction system, the attack of the "naked" OAc^- which is in equilibrium with the un-ionized species becomes predominant.

Reactions with Potassium Thiocyanate, Selenocyanate, and Cyanate (Table 2). When PCD was treated with two equivalents of KSCN in boiling THF, phenyl isothiocyanate was obtained (run 15). The yield was rather poor, and the reaction was accompanied with the formation of an unidentified yellow solid of which the

Table 2. Reactions of $RN{=}CCl_2$ with potassium thiocyanate and selenocyanate [KZCN(Z=S or Se)]

Run	$RN{=}CCl_2$ (mmol) R	KZCN (mmol) Z	Solvent (ml)	Temp (°C)	Time (h)	Products and Yield (%)[a] $RN\text{-}CCl_2$	Products and Yield (%)[a] $RN\text{-}C\text{-}Z$
14	Ph 5	S 5	THF 10	68	3	45	20[b]
15	Ph 5	S 10	THF 10	68	3	3	37[b]
16	Ph 10	S 10	EtOH 20	25	3	0	44[b]
17	Ph 5	S 10	EtOH 10	25	3	0	40[b]
18	Ph 5	Se 5	THF 10	68	3	45	32
19	Ph 5	Se 10	THF 10	68	3	8	58
20	*cyclo*-C_6H_{11} 5	Se 10	THF 10	68	3	34	37
21	*cyclo*-C_6H_{11} 5	Se 10	THF 10	68	9	10	44

a) Determined by GLC; based on $RN\text{-}CCl_2$. b) An unidentified yellow solid was also obtained.

IR spectrum did not show any absorptions due to -N=C=S or -S-C≡N groups.[10] Neither the improvement of the yield and the depression of the by-product formation could be achieved by changing molar ratios or solvents (*e.g.*, diglyme, acetone, ethanol, and *N,N*-dimethylformamide). In the case of ethanol solvent, phenyl isothiocyanate was obtained in a similar yield, but a larger amount of yellow solid was formed (runs 16 and 17, see also Experimental section). Since the displacement of one Cl atom in carbonimidoyl dichlorides by CN is known to be achieved by using CuCN, we examined the reaction between PCD and CuSCN in diglyme (at 162 °C for 1 h). The reaction with the Ag(I) or Hg(I) salts was also examined under similar conditions. However, the yield of phenyl isothiocyanate was quite poor (17—28%) in all cases.

The reaction of PCD or CCD with KSeCN, in which $SeCN^-$ is isoelectronic to SCN^-, gave the corresponding isoselenocyanate in a good yield, together with small amounts of an unidentified by-product (runs 19 and 21). The reaction with KOCN did not occur to any extent under similar conditions.

In view of the facts that the stoichiometry of the reaction with KSCN (runs 14 and 15) or KSeCN (runs 18 and 19) was the same as that of the reaction with KSAc or KOAc, a reaction path quite similar to Scheme 2 may be postulated in this case:

$$R\text{-}N{=}CCl_2 \xrightarrow[-Cl^-]{ZCN^-} \underset{\mathbf{3}}{\left[R\text{-}N{=}C(Cl)(ZCN)\right]} \xrightarrow{-ClCN} R\text{-}N{=}C{=}Z \qquad (3)$$

$$ClCN + ZCN^- \longrightarrow (CN)_2Z + Cl^- \quad (Z{=}S \text{ or } Se)$$

In connection with this, the following result is worth noting. In an attempt to prepare the compound **3** (Z=S) by the reaction of phenyl isocyanide with ClSCN (formed *in situ* from a mixture of $Pb(SCN)_2$ and $SbCl_5$[11]), phenyl isothiocyanate rather than **3** was obtained in 8.5% yield, in addition to a slight amount of PCD (1.4%) and considerable amounts of a tarry compound (mostly a polymer of the isocyanide). Here, it was confirmed that the isothiocyanate was not formed by the reaction of PCD or the isocyanide with $Pb(SCN)_2$.

Experimental

The IR and NMR spectra were recorded with a Hitachi EPI-S2 and a Varian EM-360 apparatus respectively. GLC analyses were carried out on a Shimadzu 5APTF apparatus, using Apiezon-L (30%)-Celite (1m) and EGSS-X (30%)-Chromosorb-W (1m) columns (N_2 as the carrier gas, iodobenzene as an internal standard).

Materials. Two carbonimidoyl dichlorides ($R\text{-}N{=}CCl_2$) were prepared by the method of Kühle *et al.*:[12] R=*cyclo*-C_6H_{11} (CCD), bp 88—91 °C/23 Torr (lit,[12] bp 79—82 °C/13 Torr); R=Ph (PCD), bp 79—80 °C/8 Torr (lit,[12] bp 83—85 °C/11 Torr). KSAc was prepared by the method of Barnish *et al.*[13] TlSAc was prepared from thioacetic S-acid and $Tl(OAc)_3$.[14] Other organic materials and solvents were purified before use by distillation. Commercial inorganic materials, except KSCN, were used without further purification. KSCN was used after drying at *ca.* 70 °C under reduced pressure.

Reaction of PCD with KSAc. To a stirred suspension of KSAc (1.14 g, 10 mmol) in THF (10 ml) was slowly added PCD (0.87 g, 5 mmol) at room temperature. The mixture was stirred for 3 h at 20 °C and then the precipitated inorganic salt was filtered off. GLC analysis of the filtrate showed the presence of 4.58 mmol (92% yield based on PCD) of phenyl isothiocyanate as a product. The distillation gave 0.52 g of phenyl isothiocyanate: the IR spectrum [2120 cm^{-1} ($\nu_{N=C=S}$)] and the retention time in GLC were identical with those of an authentic sample. The formation of acetic thioanhydride was also confirmed by the IR spectrum of the distillate.

Reaction of PCD with TlSAc. To a stirred suspension of TlSAc (2.79 g, 10 mmol) in THF (10 ml) was slowly added PCD (0.87 g, 5 mmol) at room temperature. The mixture was stirred for 3 h under reflux. After being cooled down to room temperature the precipitated inorganic salt was filtered off. GLC analysis of the filtrate showed the presence of 3.50 mmol (70% yield based on PCD) of phenyl isothiocyanate and unreacted PCD (1.36 mmol, 27%).

Reaction of CCD with KSAc. A mixture of CCD (0.90 g, 5 mmol) and KSAc (1.14 g, 10 mmol) was stirred in THF (10 ml) at 20°C for 24 h. GLC analysis of the filtrate showed the presence of cyclohexyl isothiocyanate (3.23 mmol, 65%) and unreacted CCD (1.47 mmol, 29%).

Reaction of PCD with KOAc. A mixture of PCD (0.87 g, 5 mmol) and KOAc (0.98 g, 10 mmol) was stirred in THF (10 ml) under reflux for 3 h. GLC analysis of the filtrate showed the presence of acetanilide(0.64 mmol, 13%), unreacted PCD (3.63 mmol, 73%), and small amounts of two unidentified compounds (*ca.* 3% each, as calculated from peak area in GLC).

Reaction of PCD with KOAc in the Presence of Crown Ether. A mixture of PCD (0.174 g, 1 mmol), KOAc (0.196 g, 2 mmol) and dicyclohexyl-18-crown-6 (0.745 g, 2 mmol) was stirred in THF (10 ml) under reflux for 3 h. GLC analysis of the filtrate showed the presence of phenyl isocyanate (0.09 mmol, 9%) and acetanilide (0.75 mmol, 75%).

Reaction of PCD with TlOAc. A mixture of PCD (0.87g, 5 mmol) and TlOAc (2.63 g, 10 mmol) in THF (10 ml) was stirred under reflux for 3 h. GLC analysis of the filtrate showed the presence of phenyl isocyanate (0.21 mmol, 4.2%), acetanilide (3.74 mmol, 75%), and unreacted PCD (0.9 mmol, 18%). The presence of phenyl isocyanate was also confirmed by the IR spectrum ($\nu_{N=C=O}$, 2250 cm^{-1}) of the residue after evaporation of the solvent from the filtrate. The distillation of the residue gave 0.32 g of crude acetanilide, which was recrystallized from aqueous ethanol: the IR and NMR spectra were identical with those of an authentic sample.

Reaction of PCD with KSCN. A mixture of PCD (0.87 g, 5 mmol) and KSCN (0.97 g, 10 mmol) in THF (10 ml) was stirred under reflux for 3 h. GLC analysis of the filtrate showed the presence of phenyl isothiocyanate (1.85 mmol, 37%) and unreacted PCD (0.15 mmol, 3%). Similar treatment of PCD (10 mmol) with KSCN (10 mmol) in EtOH (20 ml) at 0—5 °C for 5 h, followed by extraction with $CHCl_3$, evaporation of the solvent, and addition of hexane to the residue, gave 0.84 g of yellow solid besides 17% yield of phenyl isothiocyanate. The solid was purified by repeated reprecipitation from DMF (DMF dissolves this solid) and water: mp 215—243 °C; IR, broad absorptions, with distinct ones due to phenyl group, and no absorptions due to -S-C≡N or -N=C=S groups; Found: C, 47.98; H, 3.36; N, 18.54; S, 18.08; Cl, 1.81%.

Reaction of PCD with KSeCN. A mixture of PCD (0.87 g, 5 mmol) and KSeCN (1.44 g, 10 mmol) in THF (10 ml) was stirred under reflux for 3 h. GLC analysis of the filtrate showed the presence of phenyl isoselenocyanate (2.91 mmol, 58%) and unreacted PCD (0.38 mmol, 8%). The distillation gave 0.38 g of phenyl isoselenocyanate: bp 81—83 °C/5 Torr (lit,[15] bp 82 °C/7 Torr); IR, 2130 and 2060 cm^{-1} ($\nu_{N=C=Se}$).

The IR and NMR spectra and the retention time in GLC were identical with those of an authentic sample.[15]

Reaction of Phenyl Isocyanide with ClSCN. A mixture of $SbCl_5$ (2.99 g, 10 mmol) and $Pb(SCN)_2$ (3.23 g, 10 mmol) in CCl_4 (10 ml) was heated to 60 °C under stirring. To this mixture was slowly added a CCl_4 (10 ml) solution of phenyl isocyanide (1.03 g, 10 mmol), keeping the temperature at 60—70 °C. The resulting mixture was then stirred for 1 h. After being cooled down to room temperature the precipitated inorganic salt and tarry compounds were filtered off. The organic layer was washed with water and dried over Na_2SO_4. GLC analysis of the organic layer showed the presence of phenyl isothiocyanate (0.85 mmol, 8.5%), PCD (0.14 mmol, 1.4%), unreacted phenyl isocyanide (*ca.* 20%), and two unidentified compounds (*ca.* 8—10% each, as calculated from peak area in GLC) which did not show any absorptions due to –S–C≡N in the IR spectrum.

References

1) E. Kühle, *Angew. Chem. Intern. Ed. Engl.*, **8**, 20 (1969).

2) S. Tanaka, M. Okano, and S. Tanimoto. *Bull. Chem. Soc. Jpn.*, **48**, 1862 (1975).

3) S. Tanaka, H. Kido, S. Uemura, and M. Okano, *Bull. Chem. Soc. Jpn.*, **48**, 3415 (1975).

4) R. Bonnett, "The Chemistry of the Carbon-Nitrogen Double Bond," ed by S. Patai, John Wiley & Sons, London (1970), pp. 635, 637.

5) a) J. Goerdeler and D. Weber, *Tetrahedron Lett.*, **1964**, 799; b) J. Goerdeler and D. Weber, *Chem. Ber.*, **101**, 3475 (1968); c) J. Goerdeler, F. M. Panshiri, and W. Vollrath, *Chem. Ber.*, **108**, 3071 (1975). d) W. Ried and W. Merkel, *Justus Liebigs Ann. Chem.*, **1973**, 122.

6) A. G. Lee, *J. Chem. Soc., A*, **1971**, 2007.

7) A similar displacement reaction of simple alkyl halide by OAc^- in the presence of 18-crown-6 in acetonitrile or benzene has been reported [C. L. Liotta, H. P. Harris, M. McDermott, T. Gonzalez, and K. Smith, *Tetrahedron Lett.*, **1974**, 2417].

8) E. Sell and G. Zierold, *Ber.*, **7**, 1228 (1874).

9) F. Lengfeld and J. Stieglitz, *Am. Chem. J.*, **16**, 70 (1894).

10) Since the formation of a polymeric substnace by the reaction between ClCN and AgNCO is known [E. Mayer and K. Kleboth, *Angew. Chem. Intern. Ed. Engl.*, **8**, 444 (1969)], it may happen that ClCN and/or $(CN)_2S$ copolymerized with RNCS.

11) S. Uemura, A. Onoe, H. Okazaki, and M. Okano, *Bull. Chem. Soc. Jpn.*, **48**, 619 (1975).

12) E. Kühle, B. Anders, and G. Zumach, *Angew. Chem. Intern. Ed. Engl.*, **6**, 649 (1967).

13) I. T. Barnish and M. S. Gibson, *J. Chem. Soc., C*, **1970**, 854.

14) S. Uemura, S. Tanaka, and M. Okano, *Bull. Chem. Soc. Jpnern.*, **50**, 220 (1977).

15) E. Bulka, K. -D. Ahlers, and E. Tuček, *Chem. Ber.*, **100**, 1367 (1967).

Investingation of the Reaction of Metal-Nitrosyl Complexes. I. New Nitrosolysis Reaction of Cycloalkanones Using Sodium Pentacyanonitrosylferrate(II)†

Akira Ishigaki, Masatoshi Ōue, Yoshikazu Matsushita,*
Isao Masuda,*,** and Toshiyuki Shono*

Department of Chemical Engineering, Nara Technical College, Yata, Yamato-Kōriyama, Nara 639-11
**Department of Applied Chemistry, Faculty of Engineering, Osaka University, Suita-shi, Osaka 565*

(Received August 30, 1976)

Cycloalkanones reacted with sodium pentacyanonitrosylferrate(II) (NP) to give red-brown or red-violet colored complexes under an alkaline condition. The solvolysis of the complexes gave ω-(hydroxyimino)alkanoic acids under a hot alkaline condition and gave ω-cyanoalkanoic acids or their esters in an acidic condition in good yields. These Products correspond to nitrosolysis products of cycloalkanones. The reaction mechanism was invesigated by use of ^{15}N labeled NP. The complex was formed initially by an electrophilic attack of the nitrosyl ligand of NP to the active methylene of the cycloalkanone. Then a C-C bond cleavage of the resulting ligand, 2-(hydroxyimino)cycloalkanone, occurred by an action of the solvent species under the influence of the central ferrate ion. The solvolysis of the ligand occurred through Beckmann fission by an action of the acid in the coordination sphere.

There have been a number of investigations of the nitrosation of aliphatic and alicyclic ketones by use of alkyl nitrite. While the nitrosation of aliphatic open chain ketones gave mononitrosation products,[1] cyclopentanone, cyclohexanone, and cycloheptanone gave the corresponding α,α′-bis(hydroxyimino) cyclic ketones.[1,2] A reaction of another type, the nitrosolysis reaction: a carbon–carbon bond cleavage through solvolytic nitrosation, was reported for the nitrosation of cycloalkanones by use of nitrosyl chloride.

Kataoka and Ohno[3] found that the nitrosolysis of cyclohexanone under the following conditions gave 5-cyanovaleric acid in 60% yield. The reaction was carried out by use of an ethereal solution of nitrosyl chloride in the presence of sulfuric acid and *N,N*-dimethylformamide under a chilled condition (−30 °C). Recently, Rogic *et al.*[4] reported a novel single step nitrosolysis of cyclopentanone, cyclohexanone, alkylcyclohexanone, cyclododecanone, and cyclotridecanone. The reaction was carried out in liquid sulfur dioxide by use of nitrosyl chloride in the presence of an alcohol. The nitrosolysis of the cycloalkanones under the above conditions gave corresponding ω-(hydroxyimino)alkanoic esters in max 95% yield.

We have been investigating the nitrosation of ketones by using sodium pentacyanonitrosylferrate(II), (sodium nitroprusside) NP, as a nitrosation reagent. In an earlier work[5] prior to these reports, we reported a similar nitrosolysis reaction which occurred in the alkaline hydrolysis of cycloalkanone–NP complexes.

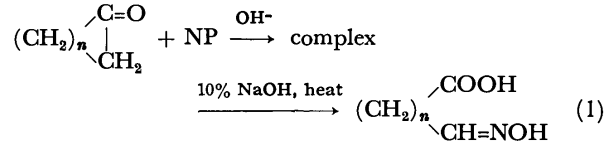

(1)

The complexes reacted in a hot alkaline medium to give ω-(hydroxyimino)alkanoic acids in good yield (Eq. 1).

The present paper deals with the other nitrosolysis reaction of the cycloalkanone–NP complexes under acid-catalyzed conditions: the complexes reacted with solvent species to give ω-cyanoalkanoic acids and their esters also in good yields (Eq. 2).

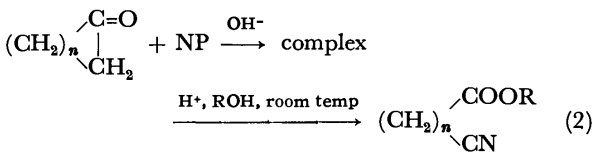

(2)

The role of nitrosyl ligand of NP in the reaction is discussed in the following section, based on the experimental results using ^{15}N labeled NP. The structure of the intermediate complex is also discussed, based on the information about the structural investigation of an isolated cyclododecanone–NP complex.

Results and Discussion

The Alkaline Hydrolysis Products of the Cycloalkanone–NP Complex. The red-violet or brown colored complexes prepared from NP and cycloalkanones were treated with aqueous alkali at the boiling point. The alkaline hydrolysis products of the cycloalkanone–NP complexes are shown in Table 1. These products were ω-(hydroxyimino)alkanoic acids; however, no 2-(hydroxyimino)-cycloalkanones were found in the hydrolysates. The detailed experimental results have already been described in the previous paper.[5]

The Acid Hydrolysis Products of Cycloalkanone–NP Complex. After the aqueous methanolic solutions of cycloalkanone–NP complexes had been allowed to stand under an acidic condition, other products were found in the solution. These products were ω-cyanoalkanoic acid and their methyl esters (Table 2), which revealed an IR absorption band characteristic of aliphatic nitriles at 2245 cm^{-1}. The NMR data and C, H, N, contents of *p*-bromophenacyl esters derived

† Preliminary reports of this work were presented at the 32nd and 33rd Annual Meetings of the Chemical Society of Japan, 1975.

** Present address: Department of Chemistry, Faculty of Science, Fukuoka University, Nanakuma, Nishi-ku, Fukuoka 814.

Table 1. Alkaline hydrolysis products of cycloalkanone-NP complexes

Cycloalkanone	Reaction product	Yield (%)	Mp[a] (°C)	Recovery of ketone (%)
Cyclopentanone	$HON{=}CH(CH_2)_3COOH$	38	105—107	60.0
Cyclohexanone	$HON{=}CH(CH_2)_4COOH$	50	112—113	47.5
Cycloheptanone	$HON{=}CH(CH_2)_5COOH$	25	80—83	70.2
4-Methylcyclohexanone	$HON{=}CHCH_2CH(CH_3)(CH_2)_2COOH$	40	68—70	58.0

a) Recrystallized from methyl acetate.

Table 2. Acid hydrolysis products of cycloalkanone-NP complexes

Cycloalkanone	Reaction products	Yield[a] (%)	Bp (3 Torr) (°C)	Mp (°C)
Cyclopentanone	$NC(CH_2)_3COOCH_3$	23.6	66—70	—
	$NC(CH_2)_3COOH$	5.0	110—115	—
	glutarimide	8.9	120—135	149.8
Cyclohexanone	$NC(CH_2)_4COOCH_3$	17.8	88—93	—
	$NC(CH_2)_4COOH$	27.8	133—137	<5
Cycloheptanone	$NC(CH_2)_5COOCH_3$	0.7	95—98	—
	$NC(CH_2)_5COOH$	25.6	140—145	<20
Cyclooctanone	$NC(CH_2)_6COOCH_3$	trace	120	—
	$NC(CH_2)_6COOH$	45.2	146—151	35.5
Cyclododecanone	$NC(CH_2)_{10}COOH$	37.9	185—190	53.5

a) About 40% cycloalkanones were recovered in each experiment.

Table 3. NMR spectral data of some products (δ ppm)

Product	CH_2	$COOCH_3$	Solvent
$NC(CH_2)_3COOCH_3$	1.94 (2H, m), 2.42 (4H, t)	3.62 (3H, s)	CCl_4
Glutarimide	2.00 (2H, m), 2.60 (4H, t)	—	$CDCl_3$
$NC(CH_2)_4COOCH_3$	1.65 (4H, m), 2.37 (4H, t)	3.69 (3H, s)	$CDCl_3$
$NC(CH_2)_4COOH$	1.65 (4H, m), 2.40 (4H, t)	—	$CDCl_3$
$NC(CH_2)_5COOCH_3$	1.60 (6H, m), 2.30 (4H, t)	3.60 (3H, s)	CCl_4
$NC(CH_2)_5COOH$	1.65 (6H, m), 2.34 (4H, t)	—	CCl_4
$NC(CH_2)COOH$	1.6—1.7 (8H, m), 2.35 (4H, t)	—	CCl_4

Table 4. C, H, N contents of *p*-bromophenacyl esters of the products

p-Bromophenacyl ester	Mp (°C)	Formula	Found			Calcd		
			C%	H%	N%	C%	H%	N%
4-Cyanobutyrate	70.5	$C_{13}H_{12}NBrO_3$	50.31	3.87	4.40	50.34	3.90	4.51
5-Cyanovalerate	78.6	$C_{14}H_{14}NBrO_3$	51.66	4.34	4.22	51.87	4.35	4.32
6-Cyanohexanoate	95.4	$C_{15}H_{16}NBrO_3$	53.19	4.61	3.98	53.27	4.77	4.13
7-Cyanoheptanoate	68.3	$C_{16}H_{18}NBrO_3$	54.28	5.21	4.00	54.56	5.15	3.98
11-Cyanoundecanoate	68.2	$C_{20}H_{26}NBrO_3$	58.20	6.49	3.12	58.85	6.42	3.43

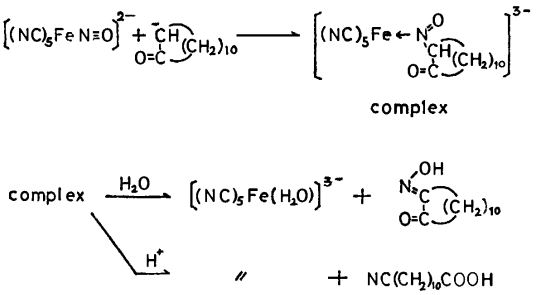

Fig. 1. A possible structure of the cyclododecanone-NP complex and reaction products from it.

from the acids are shown in Tables 3 and 4. No components other than these products were found, except for the products from cyclopentanone-NP complex: this complex gave a by-product, glutarimide.

Structural Investigation on the Cyclododecanone-NP Complex. Hydrolysis of cyclododecanone-NP complex normally gave 12-(hydroxyimino)dodecanoic acid under the alkaline conditions, and gave 11-cyanoundecanoic acid under the acidic conditions. However, after the aqueous solution of the complex had been allowed to stand under a weakly alkaline condition, another crystalline product, 2-(hydroxyimino)cyclododecanone,

was formed. These facts suggest the possible reaction routes which are illustrated in Fig. 1.

To investigate the structure of the intermediate complex shown in Fig. 1, we tried to isolate the cyclododecanone–NP complex in a pure form. The spectral data of the isolated complex supported the predicted structure of the complex illustrated in Fig. 1. As we would expect, hydrolysis of the isolated complex gave under the weakly alkaline conditions 2-(hydroxyimino)-cyclododecanone, and also gave 11-cyanoundecanoic acid under the acidic conditions.

*Investigation of the Reaction Products Prepared from Cyclohexanone and ^{15}N Labeled NP(N*P).* In the hydrolysis of the cycloalkanone–NP complexes, we assumed that the nitrogen atom in the hydroxyimino or cyano group of the reaction products must be introduced from the nitrosyl ligand of NP. To confirm the assumption we have investigated the reaction products prepared from cyclohexanone and N*P, which contained ^{15}N labeled nitrosyl ligands.

Three kinds of N*P (N*P-0, N*P-5 and N*P-30) were prepared from sodium hexacyanoferrate(II) and ^{15}N labeled sodium nitrites. These sodium nitrites contained ^{15}N of natural abundance, 5%, and 30%. The IR spectra of the prepared N*P revealed the characteristic bands at 2150 cm^{-1} (ν CN), 1945 cm^{-1} (ν ^{14}NO), and 1915 cm^{-1} (ν ^{15}NO, calcd 1911 cm^{-1}). The intensity of the last band increased with an increase in the ^{15}N content of N*P, as shown in Fig. 2.

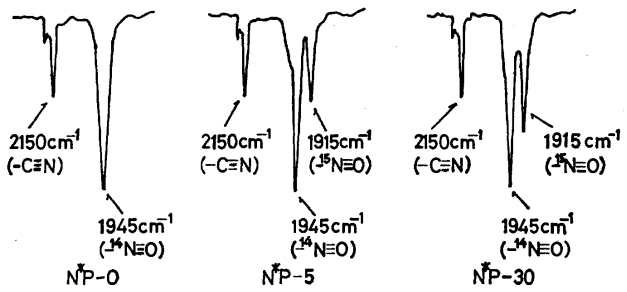

Fig. 2. IR spectra of N*P.

After having been prepared from cyclohexanone and N*P under the hot alkaline condition (Eq. 1), 6-(hydroxyimino)valeric acid was checked for the presence of the hydroxyimino-^{15}N group. Although the hydroxyimino-^{15}N group was difficult to characterize by IR spectral analysis, the presence of ^{15}N labeled fragment ion peaks (*m/e* 73, 128, and other values) in the mass spectra indicated the presence of the hydroxyimino-^{15}N group, as shown in Eq. 3. The relative abundance of the labeled ion peaks increased with an increase in the ^{15}N content of N*P, as shown in Table 5.

$$\begin{array}{l}[HO\text{-}^{15}N{=}CH(CH_2)_4COOH]^{\ddagger} \longrightarrow M^{\ddagger}\text{-}H_2O \quad m/e\ 128 \\ \quad M^+\ m/e\ 146 \qquad\qquad \searrow\ CH_2\text{-}CH_2 \\ \qquad\qquad\qquad\qquad\quad HO\text{-}{}^{15}\overset{|}{N}{}^{+}{=}\overset{|}{C}H \quad m/e\ 73\end{array} \tag{3}$$

A more reliable method for detecting the hydroxyimino-^{15}N group was performed by means of the following procedure. Methyl 5-cyanovalerate prepared from the 6-(hydroxyimino)valeric-^{15}N acid by an ordinary method (Eq. 4) was checked for the presence of the cyano-^{15}N group.

Table 5. Ratios of relative abundance of the fragment ions(I)

N*P	*m/e*73/*m/e*72	*m/e*128/*m/e*127
N*P-0	47%	25%
N*P-5	49	27
N*P-30	78	65

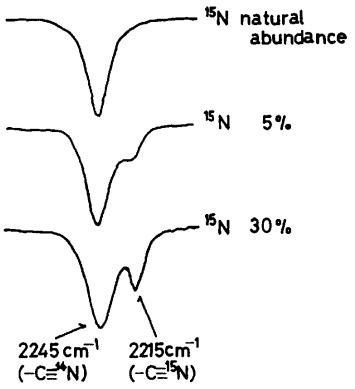

Fig. 3. IR spectra of the methyl 5-cyanovalerates-^{15}N prepared from cyclohexanone and N*P.

$$HO\text{-}{}^{15}N{=}CH(CH_2)_4COOH \xrightarrow{Ac_2O} {}^{15}NC(CH_2)_4COOH \xrightarrow{CH_3OH,\ H^+} {}^{15}NC(CH_2)_4COOCH_3 \tag{4}$$

The IR spectrum of the methyl 5-cyanovalerate-^{15}N revealed the characteristic bands at 2245 cm^{-1} (ν ^{14}NC) and 2215 cm^{-1} ($\nu^{15}NC$, calcd 2210 cm^{-1}). The intensity of the latter absorption band definitely increased with an increase in the ^{15}N content of N*P used for the preparation of 6-(hydroxyimino)valeric-^{15}N acid, as shown in Fig. 3.

The mass spectrum of the methyl 5-cyanovalerate-^{15}N of course revealed ^{15}N labeled fragment ion peaks at *m/e* 83, 111, and other values.

$$\begin{array}{l}[{}^{15}NC(CH_2)_4COOCH_3]^{\ddagger} \longrightarrow {}^{15}NC(CH_2)_4C{=}O^+ \quad m/e\ 111 \\ \quad m/e\ 142 \qquad\qquad \downarrow \\ \qquad\qquad\qquad\qquad {}^{15}NC(CH_2)_4{}^+ \quad m/e\ 83\end{array} \tag{5}$$

The relative abundance of the labeled ion peaks also increased with an increase in the ^{15}N content of N*P used. The ratios of the relative abundance of the labeled and the corresponding unlabeled ion peaks were in fair agreement with the calculated values, as shown in Table 6.

The methyl 5-cyanovalerate-^{15}N were directly prepar-

Table 6. Ratios of relative abundance of the fragment ions(II)

N*P	*m/e* 83/*m/e* 82		*m/e* 111/*m/e* 110	
	Found	Calcd[a)]	Found	Calcd[a)]
N*P-0	8.8%	5.9%	8.3%	7.0%
N*P-5	14.1	10.8	16.1	11.9
N*P-30	51.6	48.8	52.4	49.9

a) Calculated on the assumption that the ratios of ^{15}N and ^{14}N in the nitriles are nearly equal to the corresponding N*P.

ed from the cyclohexanone-N*P complexes according to the procedure described above (Eq. 2). The IR and mass spectra of these products were in fair agreement with those of the products which had been derived from the 6-(hydroxyimino)valeric-^{15}N acid (Eq. 4).

These facts indicate that the nitrogen atom in the functional group, *i.e.*, hydroxyimino or cyano group, is definitely introduced from the nitrosyl ligand of NP through the nitrosolysis of cyclohexanone under either the alkaline or the acidic condition.

Discussion on the Nitrosolysis of Cycloalkanones by Use of NP. There were a number of compounds which form colored complexes with NP. Ketones and aldehydes containing active methylene group showed a red, orange or violet color in an alkaline medium. These colors turned to bluish when the solution was made acidic.[6] For example, a deep coloration occurred when aqueous alkaline solution containing acetone or acetophenone was mixed with aqueous NP solution. The color gradually faded untill the final solution was yellow, producing pentacyanoaquoferrate(II) ion and α-hydroxyimino derivatives of the corresponding ketones, as shown in Eq. 6.[7-9] The colored complex should be formed by an electrophilic attack of the nitrosyl ligand to the active methylene. Therefore, NP acted like a nitrosation reagent, such as alkyl nitrites, in the reaction.

$$CH_3CO\text{-}Y \xrightarrow{NP,\ OH^-} \text{colored complex} \longrightarrow [Fe(CN)_5H_2O]^{4-} + HON{=}CHCO\text{-}Y \quad (6)$$
$$(Y = CH_3\text{-},\ C_6H_5\text{-})$$

For example, when an aqueous solution of the colored acetophenone-NP complex was made acidic, very soon a flocculent precipitate of α-(hydroxyimino)-acetophenone separated out, but no nitrosolysis products were formed under this condition. However, cycloalkanone-NP complexes reacted in a similar manner to give ω-cyanoalkanoic acids under the acidic conditions, in general. The ω-cyanoalkanoic acid could result from fission of a carbon-carbon bond of the corresponding 2-(hydroxyimino)cycloalkanone present as a ligand of the colored cycloalkanone-NP complex, a prusso complex, as shown in Fig. 4.

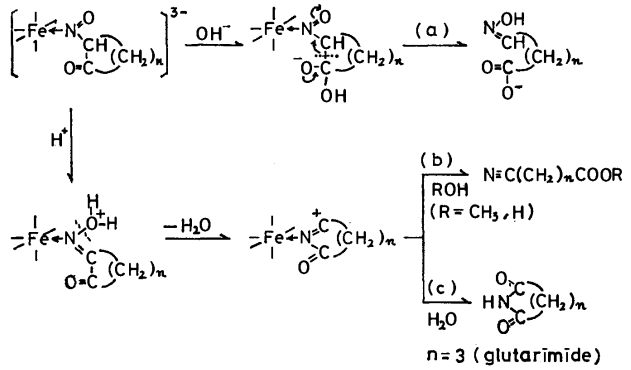

Fig. 4. A possible nitrosolysis reaction route of cycloalkanones using NP.

These facts indicate that the 2-(hydroxyimino)-cycloalkanone present as the ligand of the prusso complex should be in a labile state. The lability would be caused by a ring tension or an electron deficiency of the nitrogen atom under the influence of the electron-withdrawing effect of the central metal ion. In this way the carbon-carbon bond cleavage of the ligand occurred by hydrolysis even under the alkaline condition and gave ω-(hydroxyimino)alkanoic acids in a good yield (see Fig. 4a). Under the acidic condition another solvolytic carbon-carbon bond cleavage of the ligand occurred by Beckmann fission, a Beckmann rearrangement of an abnormal type[10] in the coordination sphere, and gave ω-cyanoalkanoic acids and their esters (see Fig. 4b). The Beckmann rearrangement of the normal type also occurred in a special case by use of cyclopentanone-NP complex. The ligand of this complex, 2-(hydroxyimino)cyclopentanone, was rearranged by acid into the more stable six-membered cyclic imide, *i.e.*, glutarimide (see Fig. 4c).

Experimental

All melting points were uncorrected. The IR spectra were obtained on a Hitatchi EPI S-2 infracord. The NMR spectra were obtained on a Nippon Denshi JNM-PS-100. The mass spectra were obtained on a Hitatchi RMU-6E spectrometer.

Reagent grade sodium pentacyanonitrosylferrate(II) hydrate (NP) and cycloalkanones were used without purification, while cyclohexanone was purified just before use by distillation under reduced pressure. Sodium nitrites-^{15}N (^{15}N contents: 5% and 30%) were obtained from The British Oxygen Co.,

Preparation of Cycloalkanone-NP Complexes. Cycloalkanone (0.05 mol) and sodium hydroxide(0.10 mol) were dissolved in 100 ml methanol. After having been cooled in an ice bath, the solution was poured into a solution of NP (0.05 mol) in 300 ml methanol and then the mixture was stirred for one hour at 0°C. The red-violet or red-brown colored complex was produced during the reaction. After the reaction had been completed, the solvent was removed under vacuum at room temperature to obtain a wet residue: crude cycloalkanone-NP complex.

The Alkaline Hydrolysis of the Cycloalkanone-NP Complex. The alkaline hydrolysis (Eq. 1) was performed by means of the following procedure. After the crude complex had been treated with 10% aqueous sodium hydroxide solution for one hour under reflux, the hydrolysate was filtered. After the filtrate had been extracted with ether to remove the unchanged ketone, the aqueous layer made acidic and was extracted with ether to separate the reaction product: ω-(hydroxyimino)-alkanoic acid was precipitated as colorless needles upon recrystallization from methyl acetate.

The Acid Hydrolysis of the Cycloalkanone-NP Complex. The acid hydrolysis (Eq. 2) was performed by means of the following procedure. After having been made acidic to pH 3 with an appropriate acid, such as phosphoric acid or others, the aqueous solution of the crude complex stood for 24 h at room temperature, and was then extracted with ether. The reaction products and the unchanged ketone were separated from the ethereal extract by fractional distillation under reduced pressure. The products, ω-cyanoalkanoic acid and its methyl ester, were derived into the corresponding crystalline *p*-bromophenacyl ester and were identified.

The by-product, glutarimide, produced from cyclopentanone-NP complex was confirmed by direct comparison with an authentic sample prepared from glutaric anhydride.

Preparation of 2-(Hydroxyimino)cyclododecanone from the Complex. After the crude cyclododecanone-NP complex, which was

prepared by the method described above, had been dissolved in water, the solution(pH 12) was extracted with ether. 2-(Hydroxyimino)cyclododecanone was separated from the ethereal extract; yield 0.2 g (from 0.05 mol cyclododecanone), mp 71—72 °C. Found: C, 68.15; H, 10.39; N, 6.65%. The IR, NMR, and mass spectral data corresponded to the authentic sample prepared by the other method by use of nitrosyl chloride.[3] After having been made acid to pH 3.5 with 6 M hydrochloric acid, the residual aqueous layer was extracted with ether. 11-Cyanoundecanoic acid was separated from the extract; yield 0.4 g, mp 52—54 °C.

Isolation of the Cyclododecanone–NP Complex. Three grams of cyclododecanone was dissolved in a sodium methylate solution prepared from sodium(0.5 g) and anhydrous methanol (35 ml). To the solution 5.0 g of NP in 65 ml of anhydrous methanol was added slowly and stirred for one hour. After the reaction had been completed, the mixture was concentrated to 35 ml under reduced pressure and was poured into 200 ml of anhydrous ethanol to precipitate the complex. The precipitate was separated by means of centrifugation, washed, and dried under reduced pressure. The pure complex was a reddish violet powder; IR: 3400(broad, νOH), 2850 and 2920 (νCH), 2040(sharp, νC≡N, bonded to Fe), 1660(weak, νC=O), 1610 and 1560 cm^{-1}; NMR: δ 1.35, 2.2(q) and 7.24(t) ppm (DMSO-d_6).

Hydrolysis of the Cyclododecanone–NP Complex. The purified cyclododecanone–NP complex(7.2 g, 14 mmol) was dissolved in 100 ml of water, and the solution was extracted with ether. 2-(Hydroxyimino)cyclododecanone was separated from the ethereal extract; yield 1.7 g(8 mmol). After having been made acid to pH 3.0 with 3M sulfuric acid, the residual aqueous layer was extracted with ether. 11-Cyanoundecanoic acid was separated from the extract; yield 1.0 g(4 mmol).

*Preparation of ^{15}N Labeled NP (N*P).* The general method of preparation of the N*P is as follows. Sodium nitrite containing an appropriate amount of ^{15}N was dissolved in an aqueous solution of sodium hexacyanoferrate(II). After an aqueous solution of barium chloride had been added to the solution, carbon dioxide was bubbed into the solution with stirring at 100 °C, and then the solution was filtered to remove barium carbonate. The appropriate amount of ethanol was added to the filtrate to precipitate sodium chloride. The red crystalline N*P was separated from the supernatant liquor by concentration.

The present work was partially supported by a Grant-in-Aid for Developmental Scientific Research from the Ministry of Education.

References

1) O. Touster, *Org. React.*, Vol. VII, 327 (1953).
2) A. F. Ferris, G. S. Johnson, and F. E. Gould, *J. Org. Chem.*, **25**, 496 (1960).
3) M. Kataoka and M. Ohno, *Bull. Chem. Soc. Jpn.*, **46**, 3474 (1973).
4) M. M. Rogić, J. Vitrone, and M. D. Swerdloff, *J. Am. Chem. Soc.*, **97**, 3848 (1975).
5) T. Shono, H. Nii, and K. Shinra, *Kogyo Kagaku Zasshi*, **72**, 1669 (1969).
6) F. Feigle, "Qualitative Analyse Tüpfelreaktionen," (1938), p. 396.
7) K. W. Lauch and T. A. Turney, *J. Inorg. Nucl. Chem.*, **18**, 179 (1961).
8) J. H. Sweinhart and W. G. Schmidt, *Inorg. Chem.*, **6**, 232 (1967).
9) S. K. Wolfe and J. H. Sweinhart, *Inorg. Chem.*, **7**, 1855 (1968).
10) A. F. Ferris, *J. Org. Chem.*, **25**, 12 (1960).

Odor and Volatile Compounds in Liquid Swine Manure. I. Carboxylic Acids and Phenols

Akio YASUHARA and Kei-ichiro FUWA

Division of Chemistry and Physics, National Institute for Environmental Studies, Yatabe, Tsukuba-gun, Ibaraki 300-21

(Received October 16, 1976)

Seventeen carboxylic acids and four phenol compounds were isolated from liquid swine manure by steam distillation and identified by gas chromatography-mass spectrometry. The major components are butyric, isovaleric, benzoic, phenylacetic acids, and *p*-cresol. The only carboxylic acid fraction has the same odor as liquid acidic swine manure. The odor of the phenols is rather pleasant and sweetish. The butyric, isovaleric, and phenylacetic acids have a very strong malodor, while the odor of phenylacetic acid is identical with that of liquid acidic swine manure.

The large quantities of manure produced by modern confinement swine buildings evolve a very strong and offensive odor by means of anaerobical microbial decomposition. The odor which is discharged into the atmosphere of the adjacent residential area is nuisance and polluting.

Little is known about the chemical nature of the odor of swine manure. Information on the nature of the odor would, however, be valuable for odor control and deodorization in confinement swine buildings.

The identification of some components in swine manure has been carried out by several research workers. Amines,[1] alcohols,[2] aldehydes,[2] acids,[2] ketones,[3] and other substances[4] which contain hydrogen sulfide, methane, *etc.* have been detected in the atmosphere of confinement swine buildings. However, in those studies only highly volatile components were caught because of the use of the head-space method. There is a possibility, therefore, that swine manure contains some other odorous components, because odor does not always result from major components. Another method is, then, required in order to isolate minor components possessing malodors.[5] Steam distillation is another useful method for isolating odorous compounds.[6,7]

An intolerable odor results from the acidification of swine manure. The acidic volatile compounds reported in poultry liquid manure[8] are acetic, propionic, isobutyric, butyric, isovaleric, and valeric acids, while in swine manure formic, acetic, propionic, and butyric acids have been reported.[2] However, none of these compounds explains the odor of acidic swine manure.

This paper will deal with the separation of odorous components by steam distillation and with the results of the application of gas chromatography-mass spectrometric and organoleptic techniques to the determination of the important compounds responsible for the malodor of liquid swine manure.

Experimental

Gas Chromatography. A Model Shimadzu GC-5A gas chromatograph was equipped with dual-flame ionization detectors, dual-thermoconductivity detectors, a matrix temperature programmer, a dual-pen recorder, and a Takeda Riken -*tr*-2215A degital integrator. The flame detectors were operated using a hydrogen-flow rate of 50 ml/min and an air-flow rate of 0.5 l/min. Thermoconductivity detectors were used for the organoleptic tests.

The gas-chromatographic conditions were as follows on the carboxylic acid fraction: injector and detector temperatures, 250 °C; column temperatures, 50 °C for 3 min, followed by an increase to 180 °C at a rate of 8 °C/min, and then held at 180 °C until the completion of the analysis; carrier-gas (nitrogen) flow rate, 20 ml/min at 6 kg/cm^2.

On the phenol fraction the gas-chromatographic conditions were as follows: injector and detector temperatures, 200 °C; column temperature, 160 °C; carrier-gas (nitrogen) flow rate, 20 ml/min at 6 kg/cm^2.

A 3m×3mm i.d. glass column packed with 2% DEGS+0.5% H_3PO_4 on 60- to 80-mesh, acid-washed, DMCS-treated Chromosorb-W was used for the analysis of the carboxylic acids and phenols.

Mass Spectrometry. A Model JEOL JMS-D 100 mass spectrometer was connected with a JEOL JGC-20K gas chromatograph. The gas-chromatographic conditions were the same as above. The mass-spectrometric conditions were as follows on both carboxylic acid and phenol fractions: ion-source temperature, 140°C; ionizing current, 3×10^{-4} A; ionizing voltage, 75 eV; accelerating voltage, 3 kV; scan speed, 5 sec from *m/e* 0 to 800.

Sampling Procedure and Fractionation. The experiments reported here were performed using accumulating liquid swine manure collected from pits under confinement swine buildings. Liquid manure (36 l) was acidified with concd hydrochloric acid in order to move its pH below 1.0 and was then shaken two times with dichloromethane (4.8 l). The resultive slurry was separated and steam-distilled. The distillate was saturated with sodium chloride and extracted two times with dichloromethane. The extract was evaporated by means of a Kvrderna-Danish concentrator under atmospheric pressure. The concentrated residue was dissolved in ether (50 ml) and fractionated as will be described below.

(a) Phenol Fraction. The ether solution was washed several times with a potassium hydroxide aquous solution. The organic layer was used for the neutral fraction. Sodium hydrogencarbonate was added to the aquous layer until saturation, and then carbon dioxide gas was passed into it. Then, the separate phenol compounds were extracted with ether (50 ml). The extract was washed, dried, and concentrated.

(b) Carboxylic Acid Fraction. After the extraction of the phenol compounds, the aquous layer was acidified with concd hydrochloric acid until it showed a pH below 1.0; then it was extracted with ether (50 ml). After washing and drying, the extract was evaporated to a small volume and then injected into the gas chromatgraph and the gas chromatograph-mass spectrometer without any protection of the carboxyl group.

(c) Neutral Fraction. The organic layer obtained in

Operation *(a)* was washed, dried, and concentrated.

Organoleptic Test for Odor. This test was carried out by means of smelling the odor of compounds progressively eluted from the outlet of the gas chromatograph.

Results and Discussion

The steam distillate has the same odor as acidic swine manure. In this case, steam distillation has been proved to be a useful method of obtaining odorous compounds.

Separation and Identification of Volatile Carboxylic Acids. From several microlitres of the prepared sample solution injected into the gas chromatograph, seventeen peaks were obtained on the DEGS+H_3PO_4 column. Figure 1 shows the gas chromatogram, while the table shows the results of the identification, which was performed by a comparison of the measured mass spectra with the standard mass spectral data and by a comparison of the retention times with those of authentic samples.

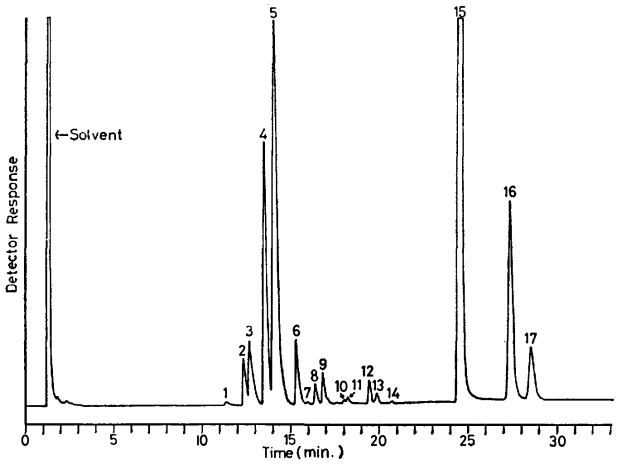

Fig. 1. Gas chromatogram of volatile carboxylic acids in swine manure.

TABLE 1. RESULTS OF IDENTIFICATION OF VOLATILE CARBOXYLIC ACIDS

Peak number	Name of compound	Content ratio (%)
1	Acetic acid	0.2
2	Propionic acid	1.6
3	Isobutyric acid	2.8
4	Butyric acid	10.1
5	Isovaleric acid	20.6
6	Valeric acid	2.2
7	2-Methylbutyric acid	0.1
8	2,2-Dimethylpropionic acid	0.6
9	Hexanoic acid	1.1
10	4-Methylhexanoic acid	0.1
11	Heptanoic acid	0.2
12	Octanoic acid	0.7
13	$C_8H_{16}O_2$	0.4
14	Nonanoic acid	0.1
15	Benzoic acid	45.8
16	Phenylacetic acid	9.9
17	3-Phenylpropionic acid	3.1

The main components are butyric, isovaleric, benzoic, and phenylacetic acids. The compound with the peak number of 13 was not identified, but it was confirmed to have the molecular formula of $C_8H_{16}O_2$, according to its mass spectrum, which is as follows: *m/e* (rel. intensity), 144 (2), 128 (35), 110 (15), 101 (17), 99 (29), 83 (44), 73 (100), 68 (32), 55 (54), 43 (29), 41 (34).

The organoleptic test shows that butyric, isovaleric, and phenylacetic acids have very strong malodors. The odor of phenylacetic acid is the most offensive among them; it is the same as that of acidic swine manure. Although butyric and isovaleric acids are recently considered as malodorous air pollutants, phenylacetic acid must be taken into consideration. Phenylacetic acid plays a very significant role in the malodor of liquid swine manure, although neutral or alkaline swine manure has a different order.

The origin of the carboxylic acids is considered to be proteinaceous material.[2)]

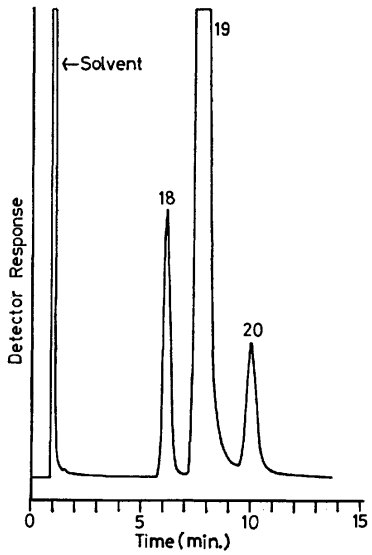

Fig. 2. Gas chromatogram of volatile phenols in phenol fraction of swine manure. (18): Phenol, (19): *m*- and *p*-cresols, (20): *p*-ethylphenol.

Separation and Identification of Volatile Phenols. Three peaks were obtained from the phenol fraction by gas chromatography using a DEGS+H_3PO_4 column. Identification was carried out by gas chromatograph-mass spectrometry. Figure 2 shows the gas chromatogram. It was confirmed by the use of a Golay R column (45 m×0.25 mm i.d.) that *p*-cresol was the major component, *m*-cresol was the minor component, and *o*-cresol was not present. Furthermore, another phenol compound was observed in the neutral fraction. It is 2,6-di-*t*-butyl-*p*-cresol, which is a well-known synthetic antioxidant. 2,6-Di-*t*-butyl-*p*-cresol is absent in the phenol fraction because of an obstruction of the dissociation of the hydroxyl group by the steric hindrance of the two tertiary butyl groups and the hydroxyl group.

Most of the phenols come from the disinfectant used in the confined swine buildings.

Organoleptically, phenols have a rather pleasant and sweetish odor. Although they evidently do not contribute

any offensive notes to the odor of swine manure, they most certainly contribute to the total odor.

References

1) J. R. Miner and T. E. Hazen, *Trans. Am. Soc. Agri. Eng.*, **12**, 772 (1969).
2) J. A. Merkel, T. E. Hazen, and J. R. Miner, *Trans. Am. Soc. Agri. Eng.*, **12**, 310 (1969).
3) L. D. Hartung, E. G. Hammond, and J. R. Miner, *Am. Soc. Agri. Eng. Publication Proc-271*, **1971**, 105.
4) D. L. Day, E. L. Hansen, and S. Anderson, *Trans. Am. Soc. Agri. Eng.*, **8**, 118 (1965).
5) J. Ronald Miner, "Odors from Confined Livestock Production," Office of Research and Development, U. S. Environmental Protection Agency, Washington, D. C., 1974.
6) R. L. Morris, J. D. Daugherty, and G. W. Ronald, *J. Am. Water Works Assoc.*, **55**, 1380 (1963).
7) J. D. Daugherty, R. D. Campbell, and R. L. Morris, *Science*, **152**, 1372 (1966).
8) W. E. Burnett, *Environ. Sci. Technol.*, **3**, 744 (1969).

Thermochemistry of Bis(tropolonato)copper(II)

Manuel A. V. RIBEIRO DA SILVA and Roger J. IRVING*

Chemistry Department, Faculty of Sciences, University of Oporto, Portugal

**Thermochemistry Laboratory, Chemistry Department, University of Surrey, Guildford GU2 5XH, England*

(Received May 10, 1976)

The standard enthalpy of formation of crystalline bis(tropolonato)copper(II) has been determined at 298.15 K by solution calorimetry: $\Delta H_f^\circ[Cu(trop)_2]\ (c) = -102.47 \pm 0.42$ kcal mol^{-1}. Enthalpy changes at 298.15 K for the following hypothetical gaseous reactions have been subsequently derived:

$$Cu(g) + 2\,trop^{\cdot}(g) = [Cu(trop)_2](c) \qquad \Delta H = -150.4 \pm 14.1 \text{ kcal mol}^{-1}$$

$$Cu^{2+}(g) + 2\,trop^{-}(g) = [Cu(trop)_2](c) \qquad \Delta H = -731.4 \pm 11.4 \text{ kcal mol}^{-1}$$

The corresponding homolytic (E) and heterolytic(E') copper(II)-oxygen bond energy parameters were calculated as

$$E_{Cu-O} = 38 \pm 4 \text{ kcal mol}^{-1} \text{ and } E'_{Cu-O} = 183 \pm 3 \text{ kcal mol}^{-1}$$

respectively.

The emphasis on the study of metal-complex compounds has been largely on questions of stereochemistry and reactivity, but much work has also been done on the stability of particular species in aqueous solutions. In marked contrast, however, direct information on the strength of metal-ligand bonds is scarce. The determination of the heat of formation of a coordination compound is not particulary difficult, but, using this result to calculate the metal-ligand bond strength, often needs auxiliary data which are inaccurate, and difficult, or even impossidle to determine at the present stage of the development of chemical knowledge.

In this paper we report the heat of formation of the copper(II) complex of tropolone and consider the problem of deriving the copper(II)-oxygen bond energies from it. Tropolone** forms complexes with metal ions analogous to β-diketones.[1] Many of the metal-tropolonates are crystalline, non-ionic solids, and volatile enough to sublime under reduced pressure. Stability constant studies[2] and the general behaviour of the tropolonates suggest that they are more stable than the corresponding acetylacetonates. Both complexes decompose into the metal cation and the protonated ligand in the presence of acid. We make use of this reaction to determine the enthalpy of formation of the crystalline complex bis-(tropolonato) copper(II) and the corresponding Cu–O bond energies.

Experimental

The Solution Calorimeter. The LKB 8700 reaction and solution precision calorimeter was used for all the reactions. This particular calorimeter has an 18 carat gold stirrer plated with pure gold, which was not attacked by acids, and a calibrating resistance (R_h) of 50.183 Ω measured at the leads midway between the calorimeter and its jacket; thermistor resistance at 25 °C is 2000 Ω.

The molar enthalpy of reaction was calculated from the relation $\Delta H = \varepsilon \Delta R_r / n R_{mr}$, where $\Delta R_r = R_i - R_f$, $R_{mr} = (R_i + R_f)/2$, n=number of moles of reactant, and R_i and R_f are the initial and final thermistor resistances in ohms as determined by the Dickinson treatment.[3] The energy constant, ε, of the calorimetric system is given by $\varepsilon = Q_c R_{mc} / \Delta R_c$, where Q_c is an accurately defined quantity of heat supplied electrically *via* the built-in heater, $Q_c = R_h I^2 t / 4.1840$ cal (R_h is the resistance of the calibrating heater in ohms, I the calibration current in amps, and t the heating time in seconds), and R_{mc} and ΔR_c have the same significance in a calibration experiment as R_{mr} and ΔR_r have in a reaction. The ratio $\Delta R_r / R_{mr}$ is directly proportional to the temperature change.

Thermochemical functions are expressed in terms of "the thermochemical calorie" (1 thermochemical calorie=4.184 J) and refer to the isothermal process at 298.15 K and the true mass, calculated with the atomic weights of 1966 based on the isotope ^{12}C. The uncertainty interval is twice the standard deviation of the mean. A check on the accuracy of the colorimeter was carried out by determining the heat of dissolution of *N,N',N''*-tris(hydroxymethyl)methane triamine (tham) in dilute hydrochloric acid. The result, -7.118 ± 0.006 kcal mol^{-1} is in agreement with previous results[4] (-7.120 ± 0.007 kcal mol^{-1}).

Materials. *Tropolone*, Htrop, was prepared by a modification of the method of Stevens *et al.*,[5] recrystallised from light petroleum (40—60 °C), sublimed, and recrystallised again from light petroleum, mp=51—52 °C (lit, 50—51 °C).

Found: C, 68.7; H, 4.95%. Calcd for $C_7H_6O_2$: C, 68.8; H, 4.95%.

Bis(tropolonato)copper(II). [Cu(trop)$_2$]—A solution of "AnalaR" copper(II) sulfate pentahydrate (2.0 g) in water (30 cm^3) was slowly added to a solution of tropolone (2.5 g) in ethanol (100 cm^3). The complex was filtered off, washed with cold ethanol, dried and recrystallised from benzene. Mp=298 °C (dec) (lit, 300 °C[6]).

Found: C, 54.93; H, 3.30; Cu, 20.78%. Calcd for $C_{14}H_{10}O_4Cu$: C, 54.99; H, 3.30; Cu, 20.78%.

Copper(II) Sulfate Pentahydrate: "AnalaR" grade copper(II) sulfate pentahydrate was powdered and dried in a desiccator, over sillica gel, for 48 h. Its composition was determined by means of copper analyses and was found to be $CuSO_4 \cdot 5H_2O$.

Sulfuric Acid. Concentrated "AnalaR" grade sulfuric acid was diluted with distilled water, and its concentration was determined by acid-base titration against $Na_2B_4O_7 \cdot 10H_2O$, after convenient dilution, and found to be 2.1567 ± 0.0003 M〈〉$H_2SO_4 \cdot 23.69\,H_2O$.[7]

Calorimetric Solvent. A molar solution of "AnalaR" grade sulfuric acid was made up, by using a "B. D. H." concentrated volumetric solution. The concentration of the prepared solution was checked by acid-base titration against $Na_2B_4O_7 \cdot 10H_2O$. A series of six determinations gave the

** Tropolone(Htrop) = 2-hydroxy-2,4,6-cycloheptatrien-1-one.

result 1.0000±0.0005 M, which corresponds to the composition $H_2SO_4 \cdot 53.5391 H_2O$.[7]

Analyses. All carbon and hydrogen analyses were carried out in the Microanalytical Service, University of Surrey; copper was analysed by a complexometric titration with ethylenediaminetetraacetic acid (H_4edta) and Pyrocatechol Violet as indicator.[8] Since bis(tropolonato)copper(II) is insoluble in water, it was necessary to decompose the complex by treating samples with successive small amounts of concentrated nitric acid, followed by gentle evaporation to dryness. The residures were dissolved in the minimum possible amount of 1 M sulfuric acid, transferred to volumetric flasks and diluted with distilled water.

Calculation. The standard enthalpy of formation of the bis(tropolonato)copper(II) complex can be determined from known standard enthalpies of formation and the enthalpy change for the reaction:

$$2\text{Htrop(c)} + CuSO_4 \cdot 5H_2O \xrightarrow{\Delta H_R} H_2SO_4 \cdot 5H_2O\text{(aq)} + [Cu(trop)_2]\text{(c)} \quad (1)$$

The difference between the enthalpies of solution of the products and reactants in the same stoichiometric ratio gives the required enthalpy of formation, provided equilibrium is reached from either side within the period of the experiment.

To 100.0 cm^3 of calorimetric solvent, ampoules of bis(tropolonato)copper(II) were added consecutively, and ΔH_2 was measured. To a second portion of the same solvent (100.0 cm^3) were added consecutively ampoules of tropolone and copper(II) sulfate pentahydrate, and ΔH_4 and ΔH_5 were measured. The thermochemical cycle and the general procedure used are given in the following scheme. The values of ΔH_1 and ΔH_3 were calculated from literature data,[9] and they were found to be $\Delta H_1 = +0.001 \pm 0.001$ kcal mol^{-1} and $\Delta H_3 = 0.000 \pm 0.001$ kcal mol^{-1}. In order to maintain the necessary stoichiometry of the reaction, the appropriate amounts of sulfuric acid and water were added to the calorimetric solvents by means of a calibrated microsyringe.

$$CuSO_4 \cdot 5.00\,H_2O\text{(c)} + 2\text{Htrop(c)} + 18.69\,H_2O(l) \xrightarrow{\Delta H_R}$$

$$\downarrow \Delta H_5 \qquad \downarrow \Delta H_4 \qquad \downarrow \Delta H_3$$

Calorimetric solvent ($H_2SO_4 \cdot 53.5391\ H_2O$)

Solution A_3

$$[Cu(trop)_2]\text{(c)} + H_2SO_4 \cdot 23.69\,H_2O(l)$$

$$\downarrow \Delta H_2 \qquad \downarrow \Delta H_1$$

Calorimetric solvent ($H_2SO_4 \cdot 53.5391\ H_2O$)

Solution B_2

Solution $A_3 \xrightarrow{\Delta H_6 = 0}$ Solution B_2

Solvent + $H_2SO_4 \cdot 23.69\,H_2O \xrightarrow{\Delta H_1}$ Solution B_1

Solution B_1 + $[Cu(trop)_2] \xrightarrow{\Delta H_2}$ Solution B_2

Solvent + $H_2O \xrightarrow{\Delta H_3}$ Solution A_1

Solution A_1 + Htrop $\xrightarrow{\Delta H_4}$ Solution A_2

Solution A_2 + $CuSO_4 \cdot 5.00\,H_2O \xrightarrow{\Delta H_5}$ Solution A_3

$$\Delta H_R = 18.69\Delta H_3 + 2\Delta H_4 + \Delta H_5 - \Delta H_1 - \Delta H_2 + \Delta H_6$$

Scheme.

The quantities of reactants in a particular series of experiments were determined by the amount of bis(tropolonato)copper(II) in the particular ampoule; strict control of stoicheiometry was maintained throughout each series.

When this procedure is used, the value calculated for ΔH_R refers to the reaction indicated in the first line of the scheme, provided that solutions A_3 and B_2 are identical, and that the value of ΔH_6 is zero. As a check on the validity of this assumption, ampoules of solution B_2 were broken into A_3 in the calorimeter; no detectable heat change occured.

Results and Discussion

The experimental data are given in Table 1, leading to the value $\Delta H_R = +6.88 \pm 0.06$ kcal mol^{-1}.

The following values were taken from the literature: $\Delta H_f^\circ[CuSO_4 \cdot 5.00\ H_2O\ (c)] = -544.85$ kcal mol^{-1},[10] $\Delta H_f^\circ[\text{Htrop(c)}] = -57.18 \pm 0.21$ kcal mol^{-1} [11,12] and $\Delta H_f^\circ[H_2SO_4 \cdot 5.00\ H_2O\ (aq)] = -549.863 \pm 0.001$ kcal mol^{-1}.[9] The standard enthalpy of formation of crystalline bis(tropolonato)copper(II), at 25 °C, was calculated from relationship (1) to be $\Delta H_f^\circ[Cu(trop)_2]\text{(c)} = -102.47 \pm 0.42$ kcal mol^{-1}.

Enthalpies of sublimation of few coordination compounds have been accurately measured, but from con-

Table 1. Calorimetric study of $[Cu(trop)_2]$

(a) Addition of $[Cu(trop)_2]$ to Solution B_1.

$[Cu(trop)_2]$ (10^4amount/mol)	$10^3(\Delta R/R_m)$	ε	ΔH_2/kcal mol^{-1}
5.0013	1.4018	2586.1	+7.249
5.0033	1.4099	2583.5	+7.280
4.9892	1.3992	2584.3	+7.248
5.0213	1.3967	2580.1	+7.177
5.0033	1.4276	2572.8	+7.341
4.9882	1.4046	2584.0	+7.276

Mean: $\Delta H_2 = +7.26 \pm 0.04$ kcal mol^{-1}

(b) Addition of Htrop to Solution A_1.

Htrop (10^4amount/mol)	$10^3(\Delta R/R_m)$	ε	ΔH_4/kcal mol^{-1}
10.0266	1.7224	2585.0	+4.441
10.0373	1.7189	2588.3	+4.433
10.0234	1.7153	2582.5	+4.420
10.1241	1.7332	2584.7	+4.425
10.0266	1.6952	2580.8	+4.364
9.9972	1.7134	2585.5	+4.431

Mean: $\Delta H_4 = +4.42 \pm 0.02$ kcal mol^{-1}

(c) Addition of $CuSO_4 \cdot 5.00\ H_2O$ to Solution A_2.

$CuSO_4 \cdot 5.00\ H_2O$ (10^4amount/mol)	$10^3(\Delta R/R_m)$	ε	ΔH_5/kcal mol^{-1}
4.9962	1.0114	2588.9	+5.240
5.0043	1.0266	2578.3	+5.289
4.9958	1.0266	2577.4	+5.296
5.0010	1.0343	2582.5	+5.332
5.0039	1.0297	2574.1	+5.297
4.9938	1.0237	2593.1	+5.316

Mean: $\Delta H_5 = +5.30 \pm 0.03$ kcal mol^{-1}

sideration of the existing data it is possible to make a reasonable estimate for the bis(tropolonato)copper(II) complex;[13] the uncertainty must be of the order of 10 kcal mol^{-1}, but this only produces an uncertainty of *ca.* 2.5 kcal in the bond energy. Accordingy, if we take $\Delta H^{\circ}_{sub}[Cu(trop)_2](c) = +35.0 \pm 10.0$ kcal mol^{-1}, the standard heat of formation of the geseous complex is $\Delta H^{\circ}_f[Cu(trop)_2](g) = -67.5 \pm 10.0$ kcal mol^{-1}.

The metal-oxygen bond strengh can be related to the energy needed to break the molecule into metal and ligands, and all referred to the gaseous state (Eq. 2), in order to remove the condensed state effects

$$[Cu(trop)_2](g) \xrightarrow{\Delta H_f(r)} Cu(g) + 2\,trop^{\cdot}(g) \qquad (2)$$

Since the oxygens in β-diketonates are known to be equivalent,[14] which is supported by the crystal structure of this particular complex,[15] the copper(II)-oxygen homolytic bond strengh E(Cu-O), is $\Delta H^{\circ}_f(r)/4$.

Calculating the heat of formation of the tropolone radical itself presupposes a knowledge of the dissociation energy of the tropolone, that is, the heat of reaction of process (3)

$$Htrop(g) \longrightarrow H^{\cdot}(g) + trop^{\cdot}(g) \qquad (3)$$

For acetylacetone (2,4-pentanedione),[16] trifluoroacetylacetone (1,1,1-trifluoro-2,4-pentanedione)[17] and dipivaloylmethane (2,2,6,6-tetramethyl-2,4-pentanedione)[17] we assumed a value of 100 ± 5 kcal mol^{-1}, but, because of the resonating tropolone ring, there is reason to suggest that a value closer to phenol (85 kcal mol^{-1} [18]) is more appropriate,[19] Accordingly we take 90 ± 5 kcal mol^{-1} [20] for the dissociation eneregy of Htrop. In this way, from the literature values of ΔH°_f[H trop] (c) $= -57.18 \pm 0.21$ kcal mol^{-1} [11,12] and ΔH°_{sub}[H trop](c) $= +20.1 \pm 0.1$ kcal mol^{-1},[21] we calculate ΔH°_f[H trop](g) $= -37.08 \pm 0.23$ kcal mol^{-1} and, using the value ΔH°_f H$^{\cdot}$(g) $= 52.095$ kcal mol^{-1},[9] we calculate $\Delta H^{\circ}_f[trop^{\cdot}](g) = 1 \pm 5$ kcal mol^{-1},[20]

As ΔH°_f[Cu(g)] $= 80.86$ kcal mol^{-1},[10] the value of $\Delta H_f(r) = 150.4 \pm 14.1$ kcal mol^{-1} and, hence, the copper(II)-oxygen homolytic bond energy E(Cu-O) $= 38 \pm 4$ kcal mol^{-1} was calculated.

It is sometimes convenient to consider the bond energy in terms of the ions, as defined by equation(4)

$$[Cu(trop)_2](g) \xrightarrow{\Delta H_f(i)} Cu^{2+}(g) + 2trop^{-}(g) \qquad (4)$$

Estimating the electron affinity of the ligands to be approximately equal to that of the oxygen atom, $E_L = 33.8$ kcal mol^{-1},[22] the enthalpy of formation of the gaseous tropolone ion was calculated to be -33 ± 5 kcal mol^{-1} [20] and using the literature value of $\Delta H^{\circ}_f[Cu^{2+}](g) = 729.93$ kcal mol^{-1} [10] the value of ΔH_f(i) for the ionic gas reaction (4) was calculated to be $\Delta H_f(i) = 731.4 \pm 11.2$ kcal mol^{-1} and, thence, the so-called heterolytic copper(II)-oxygen bond energy E'(Cu-O) $= \Delta H_f(i)/4$ is calculated as E'(Cu-O) $= 183 \pm 3$ kcal mol^{-1}.

In the present work, careful and precise measurements of molar enthalpies of solution led to a new value of the standard enthalpy of formation of the crystalline complex of bis(tropolonato)copper(II), with an accuracy better than 0.4%.

In attempting a rigorous determination of bond energies of complexes of tropolone, estimations of some enthalpies of sublimation have had to be made and, in addition, it has also been necessary to estimate the dissociation energy of the enolic hydrogen from tropolone. The resulting bond energies, therefore, have a large uncertainty attached to them.

Table 2. (all values in kcal mol^{-1})

Complex	ΔH_f(r)	E(M-O)	ΔH_f(i)	E'(M-O)
$[Be(trop)_2]$[23]	263 ± 11	66 ± 3	833 ± 11	208 ± 3
$[Al(trop)_3]$[20]	368 ± 15	61 ± 3	1468 ± 15	250 ± 3
$[Al(4\text{-}Metrop)_3]$[20]	357 ± 15	60 ± 3	1487 ± 15	248 ± 3
$[Cu(trop)_2]$	150 ± 14	38 ± 4	731 ± 11	183 ± 3

However, as is summarized in Table 2, the beryllium-oxygen bond is stronger than the aluminium-oxygen bond as one would expect from a simple electrostatic model. The copper(II) complex has been studied because it contains the metal in a planar environment of ligands. In spite of all the assumptions that were required to obtain the metal-oxygen bond parameters, it seems to provide a clear evidence that the copper(II) complex has considerably weaker bonds than the aluminium and beryllium complexes.

The value we obtained for the copper(II)-oxygen bond energy of the tropolonato complex (38 ± 4 kcal mol^{-1}) is very close to the value found by Jones and co-workers[24] for the copper complex of acetylacetone (2,4-pentanedione): 42 kcal mol^{-1}. One would expect to find a higher value for the tropolonato complex as a direct result of the interaction of the bulky seven membered ring of the ligand and the chelate rings. However, it must be pointed out that the value of Jones *et al.* has been derived from the measured heat of combustion of the metal complex. This method has two major disadvantages for coordination compounds with organic ligands: (a) a very large heat of combustion of the organic ligand, which tends to swamp the metal-ligand bond energy; (b) the difficulty of deciding the exact thermodynamic state of the combustion products at the reference temperature. Neither of these is encountered in solution calorimetry where the formation reaction $M + mL \rightarrow ML_m$ is directly involved.

As the conclusion of the above discussion we might think that a further investigation with other copper(II) complexes will be needed before more reliable information about this bond energy can be obtained.

We thank the Calouste Gulbenkian Foundation, Lisbon, for the award of a research scholarship (to M. A.V.R.S.) and the Chemistry Department of the Faculty of Sciences, Oporto University, and "Instituto de Alta Cultura," Portugal, for leave of absence (to M.A.V.R.S.).

References

1) P. L. Pauson, *Chem. Rev.*, **55**, 9 (1955).
2) B. E. Bryant and W. C. Fernelius, *J. Am. Chem. Soc.*, **76**, 3783 (1954).
3) H. C. Dickinson, *Bull. Nat. Bur. Stand.*, **11**, 189 (1915).

4) E. J. Prosen and M. V. Kilday, *J. Res. Nat. Bur. Stand.*, **A77** (5), 581 (1973).
5) H. C. Stevens, D. A. Reich, D. R. Brandt, K. R. Fountain, and E. G. Gaughan, *J. Am. Chem. Soc.*, **87**, 5257 (1965).
6) B. E. Bryant, W. C. Fernelius, and B. E. Douglas, *Nature*, **170**, 247 (1952).
7) R. C. Weast, Ed., "Handbook of Chemistry and Physics," 51 st ed, the Chemical Rubber Co., Cleveland, Ohio (1971).
8) A. I. Vogel, "Quantitative Inorganic Analysis," 3 rd ed, Longmans, London (1964).
9) D. D. Wagman *et al.*, "Selected Values of Chemical Thermodynamic Properties," Technical Note 270—3, U. S. Nat. Bur. Stand., Washington, D. C. (1968).
10) D. D. Wagman *et al.*, "Selected Values of Chemical Thermodynamic Properties," Technical Note 270—4, U. S. Nat. Bur. Stand., Washington, D. C. (1969).
11) J. D. Cox and G. Pilcher, "Thermochemistry of Organic and Organometallic Compounds," Academic Press, London (1970).
12) W. N. Hubbard, C. Katz, G. B. Guthrie, Jr., and G. Waddington, *J. Am. Chem. Soc.*, **74**, 4456 (1952).
13) M. A. V. Ribeiro da Silva, Ph. D. Thesis, University of Surrey, 1973.
14) E. C. Lingafelter and R. L. Braun, *J. Am. Chem. Soc.*, **88**, 2951 (1966).
15) W. M. Macintyre, J. M. Robertson and R. F. Zaharobsky, *Proc. R. Soc. London, Ser. A*, **289**, 161 (1966).
16) J. O. Hill and R. J. Irving, *J. Chem. Soc., A*, **1966**, 971.
17) R. J. Irving and M. A. V. Ribeiro da Silva, *J. Chem. Soc., Dalton Trans.*, **1976**, 1940.
18) S. W. Benson, *J. Chem. Educ.*, **42**, 502 (1965).
19) C. A. Coulson, personal communication (1973).
20) R. J. Irving and M. A. V. Ribeiro da Silva, *J. Chem. Soc., Dalton Trans.*, **1975**, 1257.
21) W. Jackson, T. S. Hung, and H. P. Hopkins Jr., *J. Chem. Thermodyn.*, **3**, 347 (1971).
22) L. M. Branscomb, D. S. Burch, S. Geltman, and S. J. Smith, *Phys. Rev.*, **111**, 504 (1955).
23) R. J. Irving and M. A. V. Ribeiro da Silva, *J. Chem. Soc. Dalton Trans.*, in press.
24) M. M. Jones, B. J. Yow and W. R. May, *Inorg. Chem.*, **1**, 166 (1962).

Extractive Spectrophotometric Determination of Mercury with Thiobenzoylacetone; Analysis of Waste Water

M. V. R. Murti and S. M. Khopkar

Department of Chemistry, Indian Institute of Technology, Bombay 400076, India

(Received June 14, 1976)

Thiobenzoylacetone was used for the extraction and spectrophotometric determination of mercury(II). The complex quantitatively extracted at pH 4.0 with 10 ml of 0.001 M reagent in benzene. After removing the excess of the reagent with the buffer solution of pH 12.0, the complex was measured at 345 nm against reagent blank prepared similarly. The system adhered to Beer's law in the concentration range of 0.6 to 12.1 μg of mercury per ml. The molar extinction coefficient was 1.7×10^4 and the sensitivity was 0.011 μg/cm². The complex was stable for 48 h. The extraction was quantitative within 10 min of equilibbrium. It was possible to determine mercury in the presence of a large number of ions (1 : 1000). The method was found to be applicable to the analysis of waste water from chloro-alkali industries.

Many investigations have been made on the extractive photometric determination of mercury(II) with chelating ligands. 1-(2-Pyridylazo)-2-naphthol[1] was used for such purpose but the pH range of extraction was very narrow. The extraction involving dithizone[2] has been considered unsatisfactory because of its extreme sensitivity to variations in the laboratory conditions, while Bindschedler's Green[3] was used with some advantage but the dissolved chlorine in water showed a strong interference in such determinations. Brilliant Green[4] is not a good extractant as gold, and thallium interfered seriously. The extraction with Crystal Violet[5] was feasible within a narrow pH range of 1.3—1.6. In the Rhodamine-B[6] extraction, heavy metals showed strong interferences, and the colour has to be stabilised by the addition of potassium bromide.

Amongst β-diketones, extraction with acetylacetone and benzoylacetone[7] were not quantitative. The extractions with dibenzoylmethane[7] needed a long period of equilibration. Although thiothenoyltrifluoroacetone[8–10] was a good extractant, it was necessary to remove the excess of the reagent in order to improve sensitivity. With di(thiobenzoyl)methane[11] (II) as an extractant the absorbance was measured in the ultraviolet region. In this paper a simple, selective and sensitive method is described for solvent extraction and spectrophotometric determination of mercury(II) with thiobenzoylacetone. The method has been further extended to the determination of mercury from waste water.

Experimental

Apparatus and Reagent. A Spektromom 204 spectrophotometer with matched 10 mm quartz cuvettes, and a Cambridge pH meter with glass and calomel electrodes were used.

Thiobenzoylacetone (SBA) was synthesised from benzoylacetone (Fluka, A. G.) by the procedure described earlier.[12] About 0.001 M reagent was used in benzene. The reagent was preferably preserved in a refrigerator.

A stock solution of mercury was prepared by dissolving 1.356 g of mercury(II) chloride (B. D. H. AnalaR) in 1 litre of distilled water. The solution was standardised gravimetrically as thionalide.[13] It contained 3.872 mg of mercury per ml. The solutions of lower concentrations were prepared by volumetric dilution of the stock solution.

Buffer solution of pH 4.0 was prepared by dissolving 14.0 g of sodium acetate in 500 ml of distilled water and acidified with 0.2 M acetic acid.

Buffer solution of pH 12.0 was prepared by mixing 100 ml of 0.05 M Borax and 126.5 ml of a 0.1 M sodium hydroxide solution.

General Procedure. An aliquot of mercury(II) chloride solution containing about 48.4 μg of mercury was taken. Then 10 ml of buffer solution of pH 4.0 was added, and the total volume of the aqueous phase was made to 25 ml. The solution was then introduced into a separatory funnel, and shaken with 10 ml of 0.001 M SBA in benzene for 10 min. The layers were allowed to settle and separate. After separating out the aqueous phase, the organic phase was washed twice to remove excess of the free reagent with the buffer solution of pH 12.0. The organic phase was carefully withdrawn into a 10 ml volumetric flask. It was measured spectrophotometrically at 345 nm against a reagent blank prepared similarly. The amount of mercury was then calculated from the calibration curve.

Results and Discussion

Absorption Spectra. The absorption spectrum of the Hg(II)-SBA complex extracted at pH 4.0 against the reagent blank as a reference solution is shown

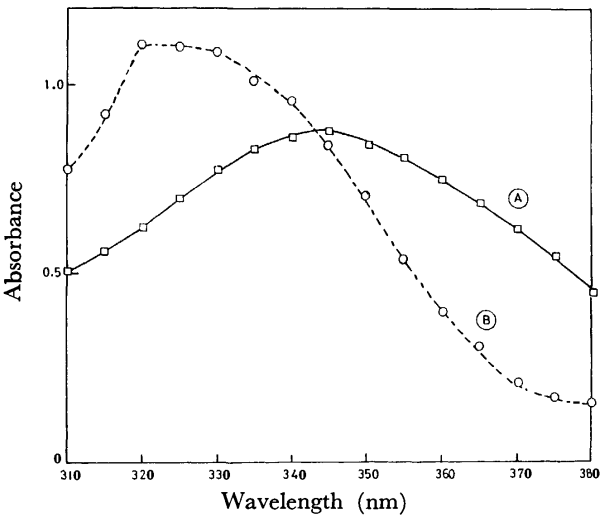

Fig. 1. Absorption of (A) mercury(II)-thiobenzoylacetone complex *vs.* reagent blank, and (B) reagent blank, and (B) reagent blank *vs.* benzene.
[Hg] = 4.84×10^{-5} M, SBA = 1.0×10^{-3} M, pH 4.0.

in Fig. 1. The spectrum of the reagent blank *vs.* benzene is also given. The difference in absorbance between the Hg(II)-SBA complex and the reagent blank appears to be maximum around 345 nm ; All absorbance measurements were therefore carried out at 345 nm. The molar extinction coefficient of the complex at 345 nm was 1.7×10^4 when the concentration of mercury was 48.4 μg/10 ml and the effective cell width was 10 mm. The sensitivity as per Sandell's definition was 0.011 μg/cm^2.

Extraction as the Function of pH. The exraction of mercury was studied as a function of pH(Fig. 2) from 1.0 to 11.0. Figure 2 shows that the extraction was quantitative between pH 0.2 to 9.0 ; the extraction started decreasing at pH 9.5 and at 11.0, it was 60.9%. Hence for all practical purposes pH 4.0 was employed for the purpose of extractions.

Adherence to Beer's Law. Different amounts of mercury(II) were taken and extracted at pH 4.0 and measured at various wavelengths, such as 335, 345 and 355 nm (Fig. 3). The Hg-SBA system conformed to Beer's law over the concentration range of 0.6 to 12.1 of mercury per ml at 345 nm only. Furthermore, at this wavelength there is a maximum slope for the absorbance-concentration plot. Hence all absorbance measurements were carried out at 345 nm.

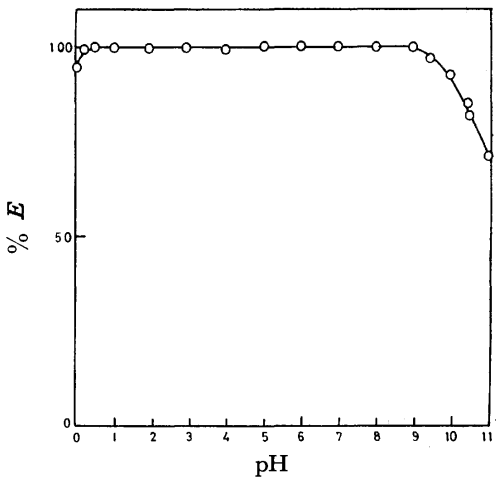

Fig. 2. Extraction of mercury as a function of pH.

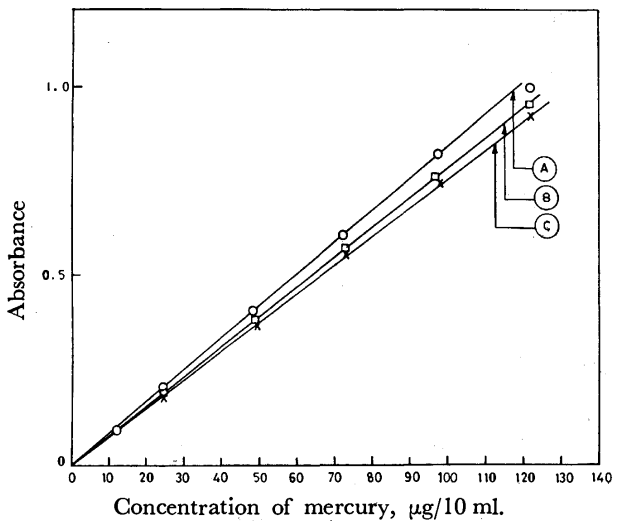

Fig. 3. Calibration curve at (A) 345 nm, (B) 335 nm, and (C) 355 nm.

Stability of the Colour of the Complex. As per the general procedure, the absorbance of the Hg(II) complex was measured at elapsed intervals of 0, 8, 16, 24, 48, 72, and 118 h. The absorbance of the complex was constant for 48 h. Hence the complex should be measured within 48 h of complexation.

Effect of Reagent Concentration. The extraction of mercury was carried out with varying concentration and varying volume of the reagent (Table 1). The result showed that a single extraction with 10 ml of 0.001 M reagent was adequate for quantitative extraction. There was insignificant enhancement in the extraction of mercury with greater concentration of reagent, and with dilute solutions the extraction was incomplete.

Table 1. Effect of reagent concentration
48.4 μg of Hg(II); 0.001 M SBA in benzene

SBA concentration $M\times10^{-4}$	SBA added, ml	Absorbance at 345 nm
2.0	10	0.165
4.0	10	0.280
5.0	10	0.380
6.0	10	0.410
8.0	10	0.410
10.0	10	0.410
	2.5[a)]	0.210
	5.0[a)]	0.380
	7.5[a)]	0.410
	15.0	0.290
15.0	10	0.410
20.0	10	0.415

a) Volume is made to 10 ml.

Effect of Salting-Out Agents. The chlorides of ammonium, lithium, sodium and calcium (1 to 3 M) were used as salting-out agents to study their effects on the extraction of mercury with 0.001 M SBA at pH 4.0 and 340 nm. The results showed that none of them had significant effects on extraction.

Period of Equilibration. The period of equilibration was varied from 2—30 min. It was observed that the extraction was quantitative after 7 min of equilibration. Hence for all purposes, 10 min equilibration period was employed.

Effect of Diverse Ions. The results in Table 2 show the effect of various ions the process of extraction. The tolerance limit was set at the amount of foreign ions required to cause a ±2% error in the mercury recovery. Alkali and alkaline earth metals, chloride, nitrite, nitrate, sulphate, acetate, perrhenate are tolerated in the ratio of 1 to 1000, whereas ions such as thallium(I), cadmium, antimony(V), bismuth(III), osmium(VI), platinum(IV), aluminium, thorium, cerium(IV), manganese(II), beryllium, sulphte, phosphate, fluoride and anions of organic dicarboxylic acids were tolerated in the ratio of 1 to 500. Other ions were tolerated in lesser ratios. Silver, lead, copper, pal-

Table 2. Effect of diverse ions
Hg(II)=48.4 μg; pH=4.0; 10^{-3} M reagent

Forign ion	Added as	Tolerance limit, μg	Forign ion	Added as	Tolerance limit, μg
Ag^+	$AgNO_3$	Interferes	K^+	KCl	100000
Pb^{2+}	$Pb(NO_3)_2$	500[a]	Rb^+	RbCl	100000
Tl^+	Tl_2SO_4	10000	Cs^+	CsCl	100000
Cd^{2+}	$Cd(NO_3)_2 \cdot 5H_2O$	10000	NH_4^+	NH_4NO_3	100000
Sb^{3+}	$Sb_2(SO_4)_3$	10000	Cl^-	NaCl	50000
Bi^{3+}	$Bi(NO_3)_3 \cdot 5H_2O$	10000	Br^-	NH_4Br	100
Os^{6+}	Na_2OsO_4	13000	I^-	KI	100
Pt^{4+}	$H_2PtCl_6 \cdot 4H_2O$	10000	NO_3^-	KNO_3	50000
Ir^{3+}	$IrCl_3$	500	NO_2^-	KNO_2	50000
Cu^{2+}	$CuSO_4 \cdot 5H_2O$	1000[b]	SO_3^{2-}	$Na_2SO_3 \cdot 7H_2O$	25000
Pd^{2+}	$PdCl_2 \cdot 2H_2O$	1200[c]	SO_4^{2-}	$Na_2SO_4 \cdot 10H_2O$	50000
Ru^{3+}	$RuCl_3$	200	PO_4^{3-}	$Na_2HPO_4 \cdot 12H_2O$	25000
Rh^{3+}	$RhCl_3$	2000	$S_2O_3^{2-}$	$Na_2S_2O_3 \cdot 5H_2O$	100
Au^{3+}	$HAuCl_4 \cdot xH_2O$	50	SCN^-	KSCN	1000
Fe^{3+}	$Fe_2(SO_4)_3 \cdot 6H_2O$	6000	CN^-	KCN	Interferes
Cr^{3+}	$CrCl_3 \cdot 6H_2O$	6000	F^-	NaF	20000
Al^{3+}	$Al(NO_3)_3 \cdot 9H_2O$	15000	$tart^{3-}$	tartaric acid	20000
Th^{4+}	$Th(NO_3)_4$	18000	cit^{3-}	citric acid	15000
U^{6+}	$UO_2(NO_3)_2 \cdot 6H_2O$	5000	$oxal^{2-}$	oxalic acid	20000
Ce^{4+}	$Ce(SO_4)_2 \cdot (NH_4)_2SO_4 \cdot 6H_2O$	15000	$ascorabate^-$	ascorbic acid	100
Zr^{4+}	$Zr(NO_3)_4$	1000	$malonate^{2-}$	malonic acid	20000
Be^{2+}	$Be(NO_3)_2$	20000	$EDTA^{4-}$	disodium salt of EDTA	5000
Zn^{2+}	$ZnSO_4 \cdot 7H_2O$	50000	$acetate^-$	sodium acetate	50000
Mn^{2+}	$MnSO_4 \cdot 7H_2O$	40000	$thiourea^-$	thiourea	10000
Co^{2+}	$CoSO_4 \cdot 6H_2O$	800	ClO_4^-	$HClO_4$	25000
Ni^{2+}	$Ni(NO_3)_2 \cdot 6H_2O$	1000	WO_4^{2-}	$Na_2WO_4 \cdot 2H_2O$	20000
Ca^{2+}	$Ca(NO_3)_2 \cdot 6H_2O$	50000	$Mo_7O_{24}^{6-}$	$(NH_4)_6Mo_7O_{24} \cdot 4H_2O$	25000
Ba^{2+}	$Ba(NO_3)_2 \cdot 4H_2O$	50000	AsO_3^{3-}	Na_2AsO_3	20000
Sr^{2+}	$SrCl_2 \cdot 2H_2O$	50000	ReO_4^-	$KReO_4$	50000
Mg^{2+}	$MgSO_4 \cdot 7H_2O$	50000	CrO_4^{2-}	K_2CrO_4	10000
Li^+	Li_2SO_4	100000	VO_3^-	$NaVO_3$	25000
Na^+	Na_2SO_4	100000			

a) Selectively extracted with 0.25 M TTA in benzene at pH 4.0.[2] b) Selectively extracted with 0.15 M TTA in benzene.[2] c) Selectively extracted with 1% dimethylglyoxime in methanol into chloroform.

Table 3. Determination of mercury from waste water with thiobenzoylacetone (SBA) and Bindschedler's Green (BG)[3]

Volume taken (in ml)	Absorbance		Amount found		Total amount of mercury present in 150 ml of waste water	
	SBA	BG	SBA	BG	SBA method in μg	BG method
2	0.065	0.240	8.24	8.24	1020.0	1031.0
4	0.135	0.470	16.30	16.40	1018.7	1025.0
6	0.205	0.700	24.30	24.50	1012.5	1020.0
10	0.340	—	40.4	—	1010.0	—

ladium and cyanide ions showed strong interference, but the interference of some of the ions was eliminated by selective extraction with 2-thenoyltrifluoroacetone[2] for copper and lead, and dimethylglyoxime[2] for palladium.

Analysis of Mercury in Waste Water. The method was applied on waste water containing ethyl mercury which was collected from chloro-alkali industry. About 150 ml of waste water was treated with 10 ml of concentrated sulfuric acid and 30 ml of 30% hydrogen peroxide. It was gently heated over a waterbath until the foaming ceased. The solution was allowed to cool and it was diluted to 250 ml.

A known volume of an aliquot of the solution was taken. Then 10 ml of buffer solution of pH 4.0 was added to it. The solution was extracted with 10 ml

of 0.001 M SBA in benzene. The absorbance of mercury–thiobenzoylacetone complex was measured spectrophotometrically at 345 nm. For the purpose of comparison and testing the reproducibility the mercury in waste water was also determined by the extraction with Bindschedler's Green.[3] The results obtained are summarised in Table 3. It was seen that the proposed method compares favourably with existing methods for the separation and determination of mercury.

From ten determinations with 48.4 μg of Hg, the absorbance was found to be 0.410±0.010. The total operation requires about 45 min. The standard deviation was ±1.54%.

References

1) S. Shibata, *Anal. Chim. Acta*, **25**, 348 (1961).
2) A. K. De, S. M. Khopkar, and R. A. Chalmers, "Solvent Extraction of Metals," Van Nostrand Reinhold, London (1970).
3) M. Tseubonchi, *Anal. Chem.*, **42**, 1087 (1970).
4) V. M. Tarayan, E. N. Ovsepyan, and N. S. Karimyan, *Dokl. Akad. Nauk Arm. SSR*, **49**, 242 (1969).
5) V. M. Tarayan, E. N. Ovsepyan, and S. P. Lebedeva, *Arm. Khim. Zh.*, **23**, 1085 (1970).
6) H. Imai, *J. Chem. Soc. Jpn.*, **90**, 275 (1969).
7) J. Stary and E. Hladky, *Anal. Chim. Acta*, **28**, 227 (1963).
8) H. Hashitani and K. Katsuyama, *Bunseki Kagaku*, **19**, 355 (1970).
9) K. R. Solanke and S. M. Khopkar, *Indian J. Chem.*, **11**, 1087 (1973).
10) K. Itsuki and H. Komuro, *Bunseki Kagaku*, **19**, 1214 (1970).
11) E. Uhleman and B. Schuknecht, *Anal. Chim. Acta*, **69**, 79 (1974).
12) M. V. R. Murti and S. M. Khopkar, *Indian J. Chem.* **14A**, 455 (1976)..
13) A. I. Vogel, "A Text Book of Quantitative Inorganic Analysis," 3 rd ed, Longman and Green, London (1961), p. 487.

Benzoyl-β-alaninato Nickel(II) Complexes. The Amino Effect on the Amino Acid Coordination around the Nickel Ion

Giuseppe MARCOTRIGIANO, Ledi MENABUE,* and Gian Carlo PELLACANI*

Cattedra di Chimica, Facoltà di Medicina-Veterinaria, University of Bari, 70126 Bari, Italy

** Istituto di Chimica Generale e Inorganica, University of Modena, 41100 Modena, Italy*

(Received July 27, 1976)

A compound of the type $Ni(Bz\text{-}\beta\text{-}ala)_2\cdot 2H_2O$ (Bz-β-ala=benzoyl-β-alaninate anion) and its amine adducts of the type $Ni(Bz\text{-}\beta\text{-}ala)_2B_n\cdot xH_2O$ ($n=1$; B=piperazine (pipz), 1,10-phenanthroline (*o*-phen) and $x=2$; $n=1$, B=2,2′-bipyridine (2,2′-bpy) and 4,4′-bipyridine (4,4′-bpy) and $x=4$; $n=2$, B=*N*-methylpiperazine (CH_3-pipz), morpholine (morph), pyridine (py), 3-methylpyridine (3-pic) and 4-methylpyridine (4-pic) and $x=2$; $n=3$, B=en, and $x=0$) were prepared. Each complex was characterized by elemental analysis, solid spectroscopy and magnetic moment. All the complexes are six-coordinated and the presence of NiO_6 and NiN_6 chromophores for $Ni(Bz\text{-}\beta\text{-}ala)_2\cdot 2H_2O$ and $Ni(en)_3(Bz\text{-}\beta\text{-}ala)_2$ complexes respectively and of NiO_4N_2 chromophores for the amine adducts is suggested. In all the complexes the amino acid appears to act as a bidentate ligand toward the carboxyl group. A ligand field strength in the aromatic heterocyclic amine adducts was found greater than in the aliphatic heterocyclic amine adducts. The amine adducts complexes appear to dissociate in solution with a change of the donor site, without changing in the stereochemistry, around the nickel ion.

In the framework of a systematic investigation we have examined the interaction of small peptides, as *N*-acetyl-[1-3] and *N*-benzoylglycine[4,5] with some transition metal ions. A recent study deals with the interaction of the copper ion with the benzoyl-β-alanine and the effect of the amines on the coordination properties of the amino acid and on the geometry around the copper ion.[6]

This work treats the nickel complexes of the benzoyl-β-alanine and their amine adducts. The nickel(II) peptide complexes may be of great help in understanding the reactions and stereochemistries of the peptide complexes of other metals, and thus the coordination behavior of peptides in general. Further interest may be derived by the fact that nickel may also have a biological role in animals, as it is recently suggested.[7]

Experimental

Preparation of the Compounds. The $Ni(Bz\text{-}\beta\text{-}ala)_2\cdot 2H_2O$ complex was prepared by mixing a potassium benzoyl-β-alaninate (2×10^{-2} mmol) solution in methanol with a nickel(II) perchlorate hexahydrate (1×10^{-2} mmol) in ethanol at room temperature. After cooling at 5 °C for one hour and filtering the potassium perchlorate precipitated, the solution was slowly evaporated until an oil was obtained. The oil was dissolved in acetone, treated with diethyl ether and cooled at 5 °C. After some days a microcrystalline pale-green compound separated from the solution. This nickel(II) salt was used as starting materials for the adduct preparation.

$Ni(Bz\text{-}\beta\text{-}ala)_2B_2\cdot 2H_2O$ (B=py and morph). The compounds were obtained by dissolving the nickel salt (1 mmol) in 3—4 cm^3 of the amines, adding acetone (5 cm^3) and diethyl ether (5 cm^3) and cooling at 5 °C.

$Ni(Bz\text{-}\beta\text{-}ala)_2B_2\cdot 2H_2O$ (B=3-pic, 4-pic and CH_3-pipz). The salts were prepared by dissolving the nickel salt (1 mmol) in the amines (5 cm^3), adding diethyl ether until an incipient precipitation was obtained and by cooling at 5 °C.

$Ni(Bz\text{-}\beta\text{-}ala)_2B\cdot xH_2O$ (B=pipz and o-phen and x=2; B=4,4′-bpy and x=4). The complexes were prepared by treating an ethanolic solution (5 cm^3) of the nickel salt (1 mmol) with an ethanolic solution (5 cm^3) of the amines (1.5 mmol), adding diethyl ether and cooling at 5 °C.

$Ni(en)_3(Bz\text{-}\beta\text{-}ala)_2$. Complex was prepared by suspending the nickel salt in ethanol (5 cm^3), adding en (1 cm^3) and warming the solution at 50—60 °C until a clear solution was obtained. By adding diethyl ether and cooling at 5 °C a crystalline compound precipitated.

Physical Measurments. Infrared spectra were recorded with a Perkin-Elmer 521 spectrophotometer in KBr pellets (4000—250 cm^{-1}) and in Nujol mull (600—250 cm^{-1}). The electronic spectra of the compounds were recorded with a Beckman DK 1A spectrophotometeter. Solid samples were prepared by grinding the complexes on a filter paper as support. The room-temperature magnetic moments were measured with Gouy method by using $Ni(en)_3S_2O_3$ as calibrant and correcting for diamagnetism with the appropriate Pascal constants.

Analyses. Nitrogen, carbon and hydrogen were analyzed by Mr. Giuseppe Pistoni using a Perkin-Elmer 240 Elemental Analyser.

Results and Discussion

The prepared compounds and their colors, analyses and magnetic moments are reported in Table 1. All the complexes are stable in air and soluble in chloroform or methanol. From these solvents the compounds cannot be recrystallized, as the ligand precipitated by evaporation of the solutions.

Electronic and Magnetic Properties of the Complexes in the Solid State. The coordination geometry of the complexes reported in this paper is studied and discussed in the light of their electronic and magnetic properties.

The magnetic moments (Table 1) of all the complexes, which do not show significant change, passing from the (benzoyl-β-alaninato) nickel(II) dihydrate to its adducts with bases, indicate a high spin configuration, corresponding to a possible cubic or tetragonal symmetry.[8]

The electronic spectra of all the nickel complexes (Table 2) are typical of hexacoordinated nickel(II). The three absorption peaks in each spectrum indicate a rather symmetric octahedral field.[9] The low energy band is broad, but all the others are quite symmetrical.

TABLE 1. ANALYTICAL AND MAGNETIC DATA

		C%		H%		H%		μ_{eff}
		Calcd	Found	Calcd	Found	Calcd	Found	
$Ni(Bz\text{-}\beta\text{-}ala)_2\cdot 2H_2O$	pale green	50.11	49.44	5.05	5.04	5.86	5.86	3.47
$Ni(Bz\text{-}\beta\text{-}ala)_2(pipz)\cdot 2H_2O$	pale green	50.97	50.47	6.07	6.50	9.92	10.11	3.43
$Ni(Bz\text{-}\beta\text{-}ala)_2(CH_3\text{-}pipz)_2\cdot 2H_2O$	pale green	53.01	53.40	7.12	7.62	12.38	12.27	3.19
$Ni(Bz\text{-}\beta\text{-}ala)_2(morph)_2\cdot 2H_2O$	pale green	51.44	51.80	6.48	6.82	8.58	8.37	3.22
$Ni(Bz\text{-}\beta\text{-}ala)_2(py)_2\cdot 2H_2O$	light blue	56.51	56.23	5.38	5.46	8.80	9.09	3.31
$Ni(Bz\text{-}\beta\text{-}ala)_2(3\text{-}pic)_2\cdot 2H_2O$	light blue	57.74	56.98	5.76	5.93	8.43	8.36	3.28
$Ni(Bz\text{-}\beta\text{-}ala)_2(4\text{-}pic)_2\cdot 2H_2O$	light blue	57.74	57.69	5.76	5.89	8.43	8.62	3.22
$Ni(Bz\text{-}\beta\text{-}ala)_2(2,2'\text{-}bpy)\cdot 4H_2O$	pale green	53.65	52.96	5.41	5.45	8.35	9.10	3.28
$Ni(Bz\text{-}\beta\text{-}ala)_2(4,4'\text{-}bpy)\cdot 4H_2O$	light blue	53.65	54.27	5.41	5.39	8.35	8.24	3.47
$Ni(Bz\text{-}\beta\text{-}ala)_2(o\text{-}phen)\cdot 2H_2O$	pale green	58.27	57.82	4.89	4.87	8.50	8.73	3.25
$Ni(Bz\text{-}\beta\text{-}ala)_2(en)_3$	lilac	50.07	50.01	7.11	7.64	17.98	16.99	3.06

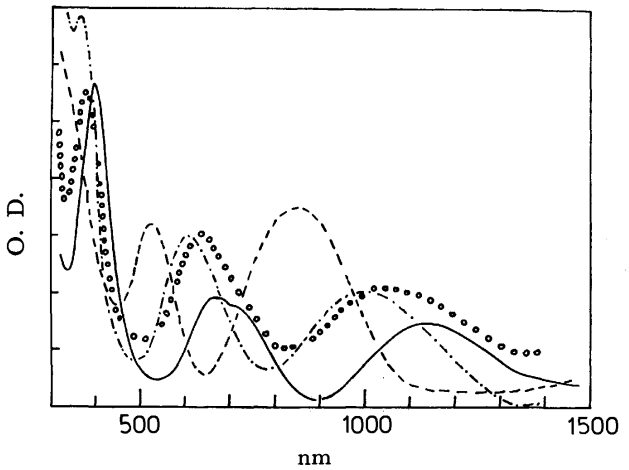

Fig. 1. Electronic spectra of the solid $Ni(Bz\text{-}\beta\text{-}ala)_2\cdot 2H_2O$ (——); $Ni(Bz\text{-}\beta\text{-}ala)_2(morph)_2\cdot 2H_2O$ (∘∘∘∘); $Ni(Bz\text{-}\beta\text{-}ala)_2(py)_2\cdot 2H_2O$ (-·-·-) and $Ni(en)_3(Bz\text{-}\beta\text{-}ala)_2$ (- - -) complexes.

The band maxima of the absorption spectra in Table 2 are listed in order of increasing energy. The energy represents the eletronic transition from the $^3A_{2g}$ ground state to the successively higher excited states, $^3T_{2g}(\nu_1)$, $^1E_g(\nu_2)$, $^3T_{1g}(F)(\nu_3)$, and $^3T_{1g}(P)(\nu_4)$.

The dihydrate bis(benzoyl-β-alaninato)nickel(II) complex shows an electronic spectrum similar to that of the hexaaqua nickel(II) cation[10,11] indicating no difference in ligand field strength between the oxygens of the water and of the benzoyl-β-alanine.

On the other hand the tris(ethylenediamine)nickel-(II) dibenzoyl-β-alaninato complex shows the typical spectrum of the tris(ethylenediamine)nickel(II) cation[11,12] suggesting the presence of the amino acids in the ionic form.

When the effect of additional binding of amine ligands on the electronic spectrum of the bis(benzoyl-β-alaninato)nickel(II) dihydrate (NiO_6 chromophore) was investigated, it was found that the d-d bands shift linearly to a shorter wavelength toward the position of the d-d bands found for the tris(ethylenediamine)-nickel(II) di-benzoyl-β-alaninato complex (NiN_6 chromophore). This may indicate that the adduct complexes have chromophore groups containing both the oxygen and nitrogen atoms, confirming the amine coordination. Spectra exemplifying this situation are reported in Fig. 1.

As the energy of the first band represents the average ligand field strength,[9] we found a greater ligand field effect in the aromatic heterocyclic amine adducts than in the aliphatic heterocyclic amine adducts.

Table 3 gives the wave numbers of the first band maximum of a series of nickel(II) and copper(II) complexes. The ratio between the observed wave numbers ν_{Cu}/ν_{Ni} gives a relative measure for the tetragonality of the copper complex and it was found that ν_{Cu}/ν_{Ni} varies from 1.1, in cases where the copper complexes approximate to cubic symmetry, to 1.7 in the cases of strong tetragonality.[13] The ν_{Cu}/ν_{Ni} values found for our adducts confirm that the copper adducts possess a strongly tetragonal distorted or square planar coordination as previously suggested.[6]

Infrared Spectra of the Complexes in the Solid State (Table 2). The assignment of the antisymmetric and symmetric carboxy stretching frequencies and of the CO ketonic and NH stretching frequencies of the benzoyl-β-alanine, which are considered very important in the assignment of the coordination sites on the amino acid, are made, as previously described,[6] by comparing the amino acid, its potassium salt and their deuterated analogues.

The peptide group is uncoordinated in all the complexes reported in this work, as in the case of the copper complexes,[6] as the shift to higher energies of the NH and CO ketonic stretching bands with respect to the free ligands suggests. These groups are however differently involved in some inter or intramolecular hydrogen bondings varying their position from 1640—1642 cm^{-1} $\nu(CO)_{ket}$ and 3400 cm^{-1} $\nu(NH)$ in the py, 3-pic and 4-pic adducts to 1618—1632 cm^{-1} $\nu(CO)_{ket}$ and 3400 cm^{-1} $\nu(NH)$ in the other complexes. This indicates lower hydrogen bonding interactions in the former complexes than in the latter.

IR-active $\nu(OCO)$ vibrations, associated with carboxylate ligands, RCO_2^-, give rise to bands in the region 1300—1700 cm^{-1}. Values of $\nu(OCO)_{asym}$ and $\nu(OCO)_{sym}$ for uni- or bi-dentate carboxylate ligands, RCO_2^-, are dependent upon the eletronic nature of the group R, the properties of the central metal ion, and

Table 2. Electronic and infrared spectra (cm^{-1}) on the complexes in the solid state[a)]

	ν_1	ν_2	ν_3	ν_4	ν(NH)	ν(NH)[B]	$\nu(CO)_{ket}$	$\nu(OCO)_a$	$\nu(OCO)_s$	$\Delta\nu$
$Ni(Bz\text{-}\beta\text{-}ala)_2\cdot 2H_2O$	8810(17)	13510 sh(16)	14930(21)	25970(62)	3330 vsb		1625 vs	1562 vs	1404 vs	158
$Ni(Bz\text{-}\beta\text{-}ala)_2\cdot pipz\cdot 2H_2O$	9430(12)		15630(39)	26320(114)	3347 m 3300 sh	3222 m 3180 sh	1625 vs	1560 vs	1400 s	160
$Ni(Bz\text{-}\beta\text{-}ala)_2(CH_3\text{-}pipz)_2\cdot 2H_2O$	9850(10)		16260(14)	27400(45)	3358 s	3232 s	1618 vs	1523 vs	1398 vs	125
$Ni(Bz\text{-}\beta\text{-}ala)_2(morph)_2\cdot 2H_2O$	9710(15)		15870(24)	26880(53)	3340 sb	3260 m 3200 vs	1632 vs	1530 vs	1390 vs	140
$Ni(Bz\text{-}\beta\text{-}ala)_2(py)_2\cdot 2H_2O$	10000(20)		16260(30)	28170(68)	3402 m		1642 vs	1512 vs	1393 vs	119
$Ni(Bz\text{-}\beta\text{-}ala)_2(3\text{-}pic)_2\cdot 2H_2O$	10100(15)		16530(25)	27770(48)	3404 m		1640 vs	1510 vs	1390 vs	120
$Ni(Bz\text{-}\beta\text{-}ala)_2(4\text{-}pic)_2\cdot 2H_2O$	9950(12)		16260(18)	27400(42)	3408 m		1642 vs	1507 vs	1388 vs	119
$Ni(Bz\text{-}\beta\text{-}ala)_2(2,2'\text{-}bpy)\cdot 4H_2O$	10310(29)		16130(35)	26320 sh(68)	3390 mb		1625 vs	1558 vs	1412 s	146
$Ni(Bz\text{-}\beta\text{-}ala)_2(4,4'\text{-}bpy)\cdot 4H_2O$	9900(21)		16340(46)	27030 sh(150)	3320 sb		1630 s	1588 vs	1402 sb	186
$Ni(Bz\text{-}\beta\text{-}ala)_2(o\text{-}phen)\cdot 2H_2O$	10200(19)		16130(24)	27400 sh(150)	3390 mb		1625 vs	1558 vs	1412 s	146
$Ni(en)_3(Bz\text{-}\beta\text{-}ala)_2$	11760(37)		18350(35)	28570 sh(135)	3300 s	3275 sh 3230 sh 3135 m	1625 vs	1550 vs	1382 vs	168

a) Optical density in arbitrary scale are reported in parenthesis.

Table 3. First absorption band (cm^{-1}) of several nickel(II) and copper(II) complexes

The ratio ν_{Cu}/ν_{Ni} gives a measure of the tetragonality effects.

Complex	ν_{Ni}	ν_{Cu}	ν_{Cu}/ν_{Ni}	Complex	ν_{Ni}	ν_{Cu}	ν_{Cu}/ν_{Ni}
$(Bz\text{-}\beta\text{-}ala)_2(pipz)$	9430	16950	1.80	$(Bz\text{-}\beta\text{-}ala)_2(4\text{-}pic)_2$	9950	16130	1.62
$(Bz\text{-}\beta\text{-}ala)_2(CH_3\text{-}pipz)_2$	9850	15630	1.59	$(Bz\text{-}\beta\text{-}ala)_2(2,2'\text{-}bpy)$	10310	15870	1.54
$(Bz\text{-}\beta\text{-}ala)_2(morph)_2$	9710	16000	1.65	$(Bz\text{-}\beta\text{-}ala)_2(4,4'\text{-}bpy)$	9900	16000	1.62
$(Bz\text{-}\beta\text{-}ala)_2(py)_2$	10000	16130	1.61	$(Bz\text{-}\beta\text{-}ala)_2(o\text{-}phen)$	10200	10530 13510	1.03

Table 4. Electronic and infrared spectra (cm^{-1} and ε/l mol^{-1} cm^{-1} (in parentheses)) of the complexes in solution[a)]

		ν_1	ν_2	ν_3	ν_4	ν(NH)	ν(NH)[B]	$\nu(CO)_{ket}$	$\nu(OCO)_a$	$\nu(OCO)_s$	$\Delta\nu$
$Ni(Bz\text{-}\beta\text{-}ala)_2\cdot 2H_2O$	MeOH	8930(6)	13700 sh(4)	15270(4)	25640(10)						
$Ni(en)_3(Bz\text{-}\beta\text{-}ala)_2$	MeOH	11560(7)		18690(7)	29850(19)						
$Ni(Bz\text{-}\beta\text{-}ala)_2(CH_3\text{-}pipz)_2\cdot 2H_2O$	$CHCl_3$	8700(7)	13510 sh(5)	15150(7)	25640(19)	3400 sh	3310 mb		1632 vs	1410 s	222
	$CHCl_3+CH_3$-pipz			15630(9)	26320(24)	3410 sh	3318 s		1638 vs	1410 sh	228
$Ni(Bz\text{-}\beta\text{-}ala)_2(morph)_2\cdot 2H_2O$	$CHCl_3$	8700(7)	13510 sh(5)	15130(7)	25640(17)	3400 sh	3300 mb		1630 vs	1410 vsb	220
	$CHCl_3+$morph		13330 sh(5)	15380(9)	25840(24)	3415 sh	3315 s		1638 vs	1410 sh	228
$Ni(Bz\text{-}\beta\text{-}ala)_2(py)_2\cdot 2H_2O$	$CHCl_3$	9260(8)	13610 sh(4)	16000(9)	26670(17)	3350 mb		1635 s	1592 vs	1408 vs	184
	$CHCl_3+$py	9430(8)	13610 sh(4)	16070(9)	26880(17)	3400 sh 3330 ms		1635 s	1590 vs	1403 s	187
$Ni(Bz\text{-}\beta\text{-}ala)_2(3\text{-}pic)_2\cdot 2H_2O$	$CHCl_3$	9170(8)	13510 sh(5)	15870(9)	26320(18)	3400 sh 3325 m		1638 s	1590 vs	1412 vs	178
	$CHCl_3+3$-pic	9480(8)	13420 sh(4)	16000(10)	25640(19)	3380 sh 3325 m		1638 s	1588 vs	1408 vs	180
$Ni(Bz\text{-}\beta\text{-}ala)_2(4\text{-}pic)_2\cdot 2H_2O$	$CHCl_3$	9170(8)	13510 sh(4)	15920(9)	26320(18)	3365, 3325 m		1638 s	1592 vs	1415 s	177
	$CHCl_3+4$-pic	9520(9)	13510 sh(4)	16130(11)	26880(22)	3400 sh 3322 s		1638 s	1600 vs	1409 s	191

a) The solution electronic and infrared spectra have identical concentration: $(2.10—3.20)\times 10^{-2}$ M.

possibly the identity of the *trans*-ligands present.[14]

The values of $\nu(OCO)_{asym}$ and the $\Delta\nu$ separation ($\nu(OCO)_{asym}-\nu(OCO)_{sym}$) afford the most sensitive indication of the mode of carboxylate coordination. Bidentate carboxylate has values of $\nu(OCO)_{asym}$ and $\nu(OCO)_{sym}$ close to those found in the corresponding free ion whereas unidentate carboxylate has $\nu(OCO)_{asym}$ at substantially higher frequencies and thus give larger values of $\Delta\nu$.[14,15] Our assignment of uni- or bi-dentate carboxylate group is based on these criteria.

The reported values of $\Delta\nu$ for the $Ni(en)_3(Bz\text{-}\beta\text{-}ala)_2$ complex of 168 cm^{-1} are assumed to typify ionic benzoyl-β-alaninate spectra, for which the values of $\Delta\nu$, found in all the complexes lower than 168 cm^{-1}, may indicate the presence of bidentate carboxyl groups. In the py, 3-pic and 4-pic and CH_3-pipz adducts in which the $\Delta\nu$(119—125 cm^{-1}) is strongly reduced compared with the ionic values, it may suggest that both benzoyl-β-alaninato ions act as symmetrical chelates.[16]

The highest values of $\Delta\nu$ are found for the pipz (160 cm^{-1}) and 4,4′-bpy (186 cm^{-1}) adducts. These ligands which cannot be bidentate, but have two donor sites, must therefore bind with different nickel ions giving rise to polymeric complexes. This is supported by their insolubility, by the similar behavior exhibited in other amino acid adducts.[6] The coordination of the amines is confirmed by the shift to lower frequencies of the $\nu(NH)^B$ (Table 2) in the aliphatic heterocyclic amine adducts and by the shift of the bands in the 800—500 cm^{-1} region in the aromatic heterocyclic amine adducts by respect to the free amines.[6] In the en complex the position of the $\nu(NH)^B$ bands is consistent with a bidentate coordination of the ethylenediamine.[17]

Since the amino acid acts as chelating agent and the amines turn out to be clearly coordinated to the metal ion, we may exclude the presence of coordinated water in all the amine adducts.

These results and the position of the d-d bands in all the amine adducts are consistent with the presence of N_2O_4 donor sets.

Electronic and Infrared Spectra of the Complexes in Solution (Table 4). The electronic spectra of all the complexes in solution moreover suggest the presence of hexacoordinated nickel(II). While the solution eletronic spectra of the $Ni(Bz\text{-}\beta\text{-}ala)_2\cdot 2H_2O$ and $Ni(en)_3(Bz\text{-}\beta\text{-}ala)_2$ complexes in methanol resemble those of the solid complexes, those of the other adducts show a red shift of the d-d bands compared with those of the corresponding solid compounds greater in chloroform in presence of an amine excess. The band at 3310 and 3300 cm^{-1} in the $Ni(Bz\text{-}\beta\text{-}ala)_2\cdot B_2\cdot 2H_2O$ (B=CH_3-pipz and morph), respectively, which is enhanced in intensity in presence of amine excess, may indicate the presence of uncoordinated amine. The $\nu(OCO)_{asym}$ position (1630—38 cm^{-1}) and the $\Delta\nu$ separation (220—228 cm^{-1}) in these complexes are similar to those found for the benzoyl-β-alaninato copper complexes and other copper complexes having dimeric carboxylate structure.[6] This may suggest that the carboxylate group acts as dimeric bidentate or bridging unidentate ligand. The hypothesis of a copper acetate monohydrate type coordination cannot be supported by magnetic measurements in solution, these complexes being insufficiently soluble.

Instead, an essentially unidentate coordination of the amino acid may be proposed for the aromatic heterocyclic amine adducts in chloroform solution from the $\nu(OCO)_{asym}$ position (1588—1600 cm^{-1}) and from the $\Delta\nu$ separation (177—191 cm^{-1}). Their electronic spectra are still consistent with a NiO_4N_2 chromophore, suggesting that the two coordination positions lost from the carboxylate groups may be replaced by water molecules.

The authors are grateful to Prof. Giorgio Peyronel of the Istituto di Chimica Generale ed Inorganica of the University of Modena for making the instruments available to us.

References

1) G. Marcotrigiano and G. C. Pellacani, *Inorg. Nucl. Chem. Lett.*, **11**, 643 (1975).
2) G. Marcotrigiano and G. C. Pellacani, *Can. J. Chem.*, **52**, 3607 (1974).
3) G. Marcotrigiano and G. C. Pellacani, *Z. Anorg. Allg. Chem.*, **415**, 268 (1975).
4) G. Marcotrigiano and G. C. Pellacani, *Z. Anorg. Allg. Chem.*, **413**, 171 (1975).
5) G. Marcotrigiano, L. Menabue, and G. C. Pellacani, *J. Inorg. Nucl. Chem.*, **37**, 2344 (1975).
6) G. Marcotrigiano, L. Menabue, and G. C. Pellacani, *Inorg. Chim. Acta*, **19**, 133 (1976).
7) N. E. Dixon, C Gazzola, R. L. Blakeley, and B. Zerner, *J. Am. Chem. Soc.*, **97**, 4131 (1975).
8) A. B. P. Lever, *Inorg. Chem.*, **4**, 763 (1965).
9) R. S. Drago "Physical Methods in Inorganic Chemistry," Reinhold, New York, N. Y. (1965), Chap. 6.
10) L. Sacconi, *Trans. Metal. Chem.*, **4**, 199 (1968).
11) A. B. P. Lever "Inorganic Electronic Spectroscopy," Elsevier, New York (1968), p. 334.
12) S. F. Pavkovic and D. W. Meek, *Inorg. Chem.*, **4**, 20 (1965).
13) C. K. Jørgensen, *Acta Chem. Scand.*, **9**, 1362 (1955).
14) K. Nakamoto, "Infrared Spectra of Inorganic and Coordination Compounds," J. Wiley, New York (1963) and references cited therein.
15) S. D. Robinson and M. F. Uttley, *J. Chem. Soc., Dalton Trans.*, **1973**, 1912, and references cited therein.
16) N. W. Curtis, *J. Chem. Soc., A*, **1968**, 1579.
17) W. Berg and K. Rasmussen, *Spectrochim. Acta*, **29A**, 319 (1973).

Photochemical Study of the Alkylammonium Molybdates. III. Preparation and Properties

Toshihiro YAMASE and Tsuneo IKAWA
Research Laboratory of Resources Utilization, Tokyo Institute of Technology, Ookayama, Meguro-ku, Tokyo 152
(Received April 30, 1976)

Six alkylammonium molybdates which we have prepared were examined for photochemical and photochromic properties in a solid and in an aqueous solution. The white crystals were reddish brown or violet when irradiated with UV light. Five compounds of the six were photochromic under aerobic conditions. The thermal return to the white color was slow, taking several hours at room temperature. The irradiation of the aqueous solution (pH 4.3—6.5) by UV light caused a blue coloration; the quantum yield increased with an increase in the molybdate concentration. A UV-induced coloration in both solid and solution was ascribable to the photoreduction of Mo(VI) to Mo(V). The blue form in the aqueous solution possesses several unique characteristics, including: (1) $g=1.926$ and $a=52$ G in its ESR spectrum; (2) the oxidation of Mo(V) to Mo(VI) upon exposure to oxygen, with an accompanying bleaching, and (3) thermochromism (blue form$\leftrightarrows$greenish yellow form) with $\Delta H_r \approx 15$ kcal/mol.

In previous papers we reported the photochromism of bis(dimethylammonium) trimolybdate monohydrate and bis(isopropylammonium) dimolybdate dihydrate.[1,2] When the polycrystalline material was irradiated with UV light, the white crystals became reddish brown or violet because of the formation of Mo(V). A return to the original white color was observed in the dark in the presence of oxygen. This color change could be repeated many times. Recently, Arnaud-Neu and Schwing-Weill reported, on the basis of photochromism tests of the various molybdates of different amines, that only secondary amines yield photochromic molybdates.[3] However, their conclusion is doubtful, since some of the primary aliphatic amines yield photochromic molybdates. This report will present several generalizations regarding the photochemical behavior of the 6 alkylammonium molybdates in a solid and an aqueous solution; these generalizations should provide a better understanding of this behavior.

Experimental

Preparation of Alkylammonium Molybdates. All the chemicals were of a G. R. or reagent grade of the Tokyo Kasei Co. and were used without further purification.

Bis(isopropylammonium) dimolybdate dihydrate (IPAM),—Isopropylamine (52 ml) was added to a solution of $(NH_4)_6Mo_7O_{24}\cdot 4H_2O$ (80 g) in water (50 ml). After stirring about 6 h, the solution was concentrated under reduced pressure to form a white solid, which was then filtered off and dried. One recrystallization of the crude product from water yielded colorless solids. Found: C, 13.96; H, 4.78; N, 5.96; Mo, 40.0%. Calcd for $(C_3H_{10}N)_2\ Mo_2O_7\cdot 2H_2O$: C, 15.65; H, 5.22; N, 6.09; Mo, 41.7%.

Hexakis(isopropylammonium) Octamolybdate Dihydrate (6IPA8M2),[4]—This compound was crystallized from an aqueous solution (10 ml) containing 5 g of bis(isopropylammonium) dimolybdate dihydrate at room temperature when the solution was kept in the dark for two weeks. Found: C, 13.09; H, 4.21; N, 5.40; Mo, 47.2%. Calcd for $(C_3H_{10}N)_6H_2Mo_8O_{28}\cdot 2H_2O$: C, 13.39; H, 4.09; N, 5.21; Mo, 47.6%.

Bis(dimethylammonium) Trimolybdate Monohydrate (DMAM),—$(NH_4)_6Mo_7O_{24}\cdot 4H_2O$ (300 g) was added to a solution of dimethylamine (40%) in 500 ml of water. After stirring about 4 h, the solution was concentrated under reduced pressure, and the resultant white solid was allowed to crystallize. The white solid then dissolved in 1500 ml of water. This solution was warmed 50—60 °C while stirred for 2—3 h to form white precipitates. The precipitated product was filtered off, washed with cold water, and dried under a vacuum. Found: C, 8.68; H, 3.25; N, 5.12; Mo, 53.4%. Calcd for $(C_2H_8N)_2Mo_3O_{10}\cdot H_2O$: C, 8.59; H, 3.26; N, 5.01; Mo, 51.6%. DMAN could be otained by another method, too: The dioxobis(dimethyldithiocarbamato) molybdenum (VI) complex, $MoO_2[(CH_3)_2NCS_2]_2$, was made by Moore and Larson's method[5] and a nearly saturated solution of 1 g of $MoO_2[(CH_3)_2NCS_2]_2$ in 1000 ml of chloroform was refluxed for 1—2 h. After cooling, a white product was allowed to crystallize.

Bis(diethylammonium) Trimolybdate Monohydrate (DEAM),—DEAM was obtained by a modification of the above DMAM-preparation procedure using an aqueous solution of $(NH_4)_6Mo_7O_{24}\cdot 4H_2O$ (10 g) in 20 ml of diethylamine (40%). Found: C, 15.11; H, 4.24; N, 4.45; Mo, 47.1%. Calcd for $(C_4H_{12}N)_2Mo_3O_{10}\cdot H_2O$: C, 15.64; H, 4.23; N, 4.56; Mo, 46.9%.

Bis(propylammonium) Dimolybdate Dihydrate (PAM),—PAM was obtained by a modification of the above IPAM-preparation procedure using an aqueous solution of $(NH_4)_6Mo_7O_{24}\cdot 4H_2O$ (50 g) in 100 ml of propylamine (30%). Found: C, 14.24; H, 4.68; N, 5.81; Mo, 42.1%. Calcd for $(C_3H_{10}N)_2Mo_2O_7\cdot 2H_2O$: C, 15.65; H, 5.22; N, 6.09; Mo, 41.7%.

Bis(methylammonium) Dimolybdate Dihydrate (MAM),—MAM was obtained by a modification of the above IPAM-preparation procedure using an aqueous solution of $(NH_4)_6Mo_7O_{24}\cdot 4H_2O$ (350 g) in 450 ml of methylamine (30%). Found: C, 6.12; H, 3.93; N, 7.35; Mo, 46.2%. Calcd for $(CH_6N)_2Mo_2O_7\cdot 2H_2O$: C, 5.94; H, 3.96; N, 6.93; Mo, 47.5%.

Procedures. The sample was irradiated using a 500-W super-high-pressure Hg lamp. The following filters were used for the different wavelength regions: $\geq$313 nm, a liquid filter (1 cm thick) consisting of an aqueous solution of 0.5 g of potassium hydrogen phthalate/100 ml; 313 nm, conjunction with a liquid filter (3 cm thick) consisting of an aqueous solution of 46 g of $NiSO_4\cdot 6H_2O$ + 14 g of $CoSO_4\cdot 7H_2O$/100 ml and a filter (1 cm thick) of a potassium hydrogen phthalate solution; 365 nm, Toshiba UV-DI + UV-35 filters. The light intensities were measured by means of potassium ferrioxalate actinometry. The UV-induced coloration of the aerobic solution to blue was followed by the conjuction with a He-Ne laser and a photodiode.[6] The oxygen concentration was measured with a kyusuikagaku Kenkyusho D.O. Meter-TP. Thermochromism studies were done in a homemade Dewar vessel. The tempera-

ture was measured by means of a copper-constantan thermocouple kept in contact with the sample cell (1 cm internal pathlength). The evacuation of solutions was carried out by several freeze-pump-thaw cycles on 10^{-4} Torr. Molybdenum analyses were done by means of a Varian Techtron Model 1000 atomic absorption spectrophotometer. Differential scanning calorimetry showed that each of the alkylammonium molybdates was stable below 100 °C. The IR (KBr discs) and Raman spectra were recorded on Shimadzu-IR-27G and JEOL laser Raman spectrophotometers respectively. The UV and visible absorption or reflectance spectra were taken with a Hitachi 624 spectrophotometer. The ESR spectra were obtained with a Varian E-12 spectrometer.

Photometry of Mo(V) in the Aqueous Solution. On the basis of the fact that the colored IPAM powder gave a blue color when dissolved in deaerated water, the photometric determination of Mo(V) in deaerated water was carried out, assuming that all of the Mo(V) in the colored powder was converted into the blue species in water. The number of spins due to Mo(V) in the UV-irradiated IPAM powder was obtained by comparing the sum of the intensities of the Mo(V) ESR signals with the intesity of a DPPH standard (1.44×10^{15} spin in the sample powder of 230 mg). When the sample powder was dissolved in the deaerated water, DPPH had no observable effect on the blue coloration, at least not during the experimental procedure. The numerical double integration of the Mo(V) signals showed that the Mo(V) exhibiting the blue color obeys Beer's law below 4×10^{-4} M ($\varepsilon_{730}=2.3\times10^{3}$ M^{-1} cm^{-1} at 20 °C).

Results and Discussion

Photosensitive Properties in the Solid. In Fig. 1 alkylammonium molybdates are divided into two categories according to the similarity among the IR spectra of the compounds in the Mo-O vibrational region (400—1000 cm^{-1}). The IR spectra of Group (1) compounds (IPAM, 6IPA8M2, PAM, and MAM) were very similar to those of $(NH_4)_6Mo_7O_{24}\cdot4H_2O$. The IR spectra of Group (2) compounds (DMAM and DEAM) showed characteristic strong bands at ≈500 and ≈640 cm^{-1}. Table 1 lists the solubility in water, the absorption maximum (λ_{max}) which is observed after irradiation with UV light, and the approximate speeds of the coloration and return reactions. Under irradiation with UV (313 or 365 nm) light, the white crystals were

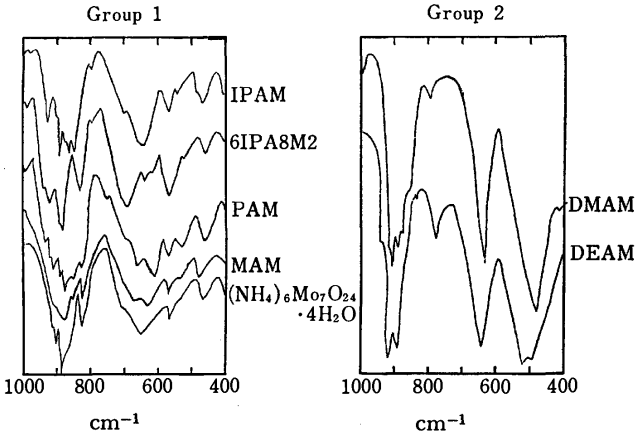

Fig. 1. IR spectra (KBr discs) of alkylammonium molybdates.

Table 1. Photosensitive alkylammonium molybdates

Group	Alkylammonium molybdate		λ_{max}, nm	Approx. coloration time, min[b]	Approx. return time, h[c]
(1)	IPAM	(108)[a]	510	5—7	7—10
	6IAP8M2	(11)	480	≈3	15—20
	PAM	(90)	490	5—7	4—5
	MAM	(330)	480	1—2	—
(2)	DMAM	(1.4)	470	<1	2—3
	DEAM	(1.0)	475	<1	2—3

a) Numbers in parentheses are solubilities in water (100 ml) at 20 °C. b) Numbers indicate the irradiation time required to obtain the reflectance of ≈50% at λ_{max} when the white briquetted powder is exposed to UV (≥313 nm) light at a distance of 30 cm from the light source. c) Numbers indicate the half-life period of the colored species at room temperature under aerobic conditions.

reddish brown or violet. No significant changes in the IR spectra and X-ray diffraction powder patterns after irradiation were observed. The effect of oxygen on the coloration seemed to be negligible. The apparent coloration decreased in this order: DMAM, DEAM> MAM>6IPA8M2>IPAM, PAM. For DMAM, DEAM, 6IPA8M2, IPAM, and PAM, a return to the original white color was observed in the dark under aerobic conditions. Although the entire bleaching did not obey the simple first-order law, the half-life period of the colored species was several hours at room temperature and increased in this order: DMAM, DEAM< PAM<IPAM<6IPA8M2. The return reaction was the thermal process which was catalyzed by oxygen, since irradiation with visible light or the deaerated system brought about no observable bleaching. Therefore, the stronger bleaching effect was obtained by thermal treatment in oxygen. For example, ≈1 atm of oxygen at 50 °C changed the return half-life of DMAM from 2—3 h under aerobic conditions at room temperature to less than 10 min. MAM was UV-sensitive, but did not return to the white color in the dark. It should be noted that Group (2) compounds exhibit lower solubilities in water, higher UV sensitivities, and faster return rates than Group (1) compounds. All of the colored polycrystallines exhibited an ESR signal due to Mo(V), while the white crystallines exhibited no significant ESR signal of Mo(V).[1,2] The colored samples in Group (1) turned blue (λ_{max} 730 nm, λ_{sh} 620 nm), when dissolved in deaerated water. The resulting solution gave rise to a single intense line ($g=$ 1.926), with six weak satelite lines, three on each side and equally spaced ($a=52$ G), in its ESR spectrum, as was previously reported for IPAM.[2] This equal spacing of the six weak lines indicated a hyperfine structure (hfs) due to isotopes with a nuclear spin of 5/2. The line-width was too great to allow the resolution of separate lines from ^{95}Mo and ^{97}Mo. This is not surprising, since the nuclear magnetic moments differ by only 2%.[7] The exposure of the blue solution to oxygen brought about the oxidation of Mo(V) to Mo(VI), with an accompanying bleaching, resulting in no observable ESR signal of Mo(V). The colored samples in Group (2) gave no detectable amount of Mo(V) in their

homogeneous deaerated solution, although the solution obtained was slightly blue. This seemed to be ascribable to the fact that each compound in Group (2) was much less soluble in water than these in Group (1). The difference in photosensitivity, reversibility, or the return rate among the 6 molybdates in the solid state may be strongly connected with their crystal structures. However, we have not made a crystal structure determination of any compounds except for 6IPA8M2.

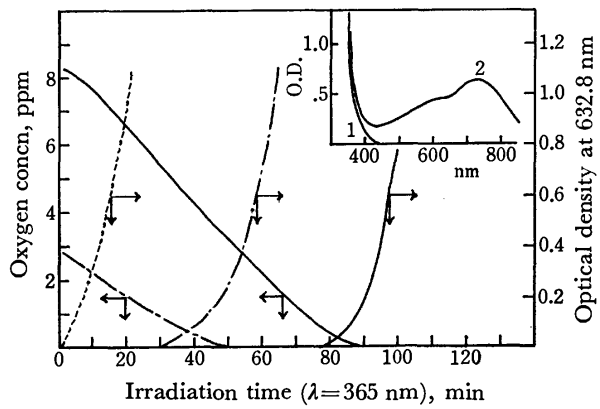

Fig. 2. Effect of oxygen on the UV-induced coloration of the aqueous solution containing 4% IPAM at 20 °C: $[O_2]_{ini}$=8.3 ppm (———), $[O_2]_{ini}$=3.0 ppm (—·—), N_2-bubbled (·····). Incident light intensity is 3.0×10^{-5} E/l min. Optical path length of the solution is 45 mm. Small figure shows spectral changes of a deaerated solution with 1 cm of its thickness: (1) before irradiation, (2) after 5 min of 365 nm irradiation with incident intensity of 2.4×10^{-4} E/l min.

Photosensitive Properties in the Aqueous Solution. Each of the fresh aqueous solutions exhibited pH levels of 4.3—6.5. Under the irradiation of a deaerated solution with UV light, the color changed from colorless to blue, as is shown in Fig. 2. Oxygen inhibited the UV-induced blue coloration of the solution: For the 4% solution of IPAM with initial oxygen levels of 8.3 3.0, and ≈0 ppm, UV irradiation caused the consumption of oxygen in the course of the induction period, and coloration at the steady state was observed when the oxygen level reached about 1 ppm (Fig. 2). The inhibiting effect of oxygen on the coloration may be explained in terms of the rapid oxidation process of Mo(V) to Mo(VI), judging from the fact that the blue form was oxidized by oxygen to yield the colorless form. The blue form was considered to be essentially the same as the blue form on the dissolution (in water) of a colored polycrystalline sample, judging from the similarity between their ESR spectra, giving g=1.926 and a=52 G. The blue forms in the deaerated solution exhibited thermochromism (blue⇄greenish yellow) over the temperature range from 0 to 70 °C.[8] Analysis of the temperature-dependent spectral changes in the IPAM solution revealed a single isosbestic point at 480 nm between the blue and greenish yellow forms, as is shown in Fig. 3(a). With OD_h and OD_l referring to the optical densities at 730 nm at the highest and the lowest temperatures respectively, a plot of (ODh—OD)

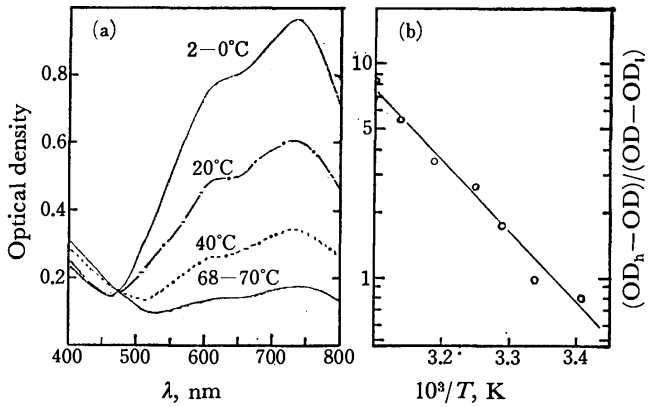

Fig. 3. Thermochromism of the blue form in the deaerated aqueous solution containing 4.3% IPAM: Mo(V)=2.6×10^{-4} M.

/(OD–OD_l) corresponding to the ratio of the concentration of the blue form to that of the greenish yellow form against the reciprocal absolute temperature was approximately linear, giving≈15 kcal as the value of the heat of reaction (ΔH_r) on the equilibrium of the blue form⇄ the greenish yellow form, as is shown in Fig. 3(b). The same value of ΔH_r was obtained for the MAM solution, supporting the idea that the chemical structure of the blue form is independent of the molybdates. The Mo(V) formation quantum yields (η) of the deaerated solution at 20 °C are summarized in Table 2. A comparison of these data shows that the blue form is photochemically produced at pH=4.3—6.5 without any significant difference in η between irradiations with 313 nm and 365 nm light and that η increases with an increase in the molybdate concentration. There have been no reports of the formation of blue species in an aqueous solution containing molybdates at pH 4.3—6.5. In aqueous solutions containing Na_2MoO_4 or $(NH_4)_6Mo_7O_{24}$, $Mo_7O_{24}^{6-}$, which is the predominant species at pH 4.8—6.8, is not reducible, although more acidic solutions (pH≤1.2) are easily reduced to a blue species, which is written as $H_2Mo_2^{V}Mo_4^{VI}O_{19}^{2-}$.[9,10] These

Table 2. Quantum yield of the deaerated aqueous solutions for the Mo(V) formation

Alkylammonium molybdate	Initial concn, wt%	Fresh solution pH	Quantum yield[a] η_{313}	Quantum yield[a] η_{365}
IPAM	4.3	5.3	0.48	0.48
	2.8		0.32	—
	1.2		0.30	—
	0.4		0.03	—
6IPA8M2	2.8	6.2—6.5	0.38	0.30
MAM	4.8	5.6	0.05	0.04
DMAM	1.4	4.3	0.04	—
$(NH_4)_6Mo_7O_{24}\cdot4H_2O$	4.0	5.3	0	—

a) η_{313} and η_{365} indicate the quantum yields obtained by using the exciting light of 313 nm and 365 nm respectively. The incident light intensities at 313 nm and 365 nm are $4—5\times10^{-5}$ E/l min and 2.3—2.4×10^{-4} E/l min respectively.

conclusions are also supported by these of our experimental results: bands in the Raman spectra of the molybdate solution appeared at 925, 890, 350, and 220 cm^{-1} and were close to those of the solid $(NH_4)_6Mo_7O_{24}\cdot 4H_2O$. Furthermore, the solution of $(NH_4)_6Mo_7O_{24}\cdot 4H_2O$ at pH 5.3 gave no blue species photochemically (Table 2). The tendency for η to increase with an increase in the molybdate concentration suggests that the primarily-formed photoproduct reacts with the ground-state molybdate to yield the mixed-valence blues containing molybdenum cluster groups. The possibility of a molybdenum cluster containing more than two atoms of Mo(V) (for example, $H_2Mo_2^{V}Mo_4^{VI}O_{19}^{2-}$ which may be produced when $pH \leq 1.2$), may be excluded, since Mo(V) should not obey Beer's law if this possibility is operative. In order to understand the reaction mechanism of the blue coloration, the structure of the blue form must be revealed at least. However, further speculation is inappropriate, since the true formula of the blue species is not known at present.

References

1) T. Yamase, T. Ikawa, H. Kokado, and E. Inoue, *Chem. Lett.*, **1973**, 615.
2) T. Yamase, H. Hayashi, and T. Ikawa, *Chem. Lett.*, **1974**, 1055.
3) F. Arnaud-Neu and M. J. Schwing-Weill, *Bull. Soc. Chim. Fr.*, **1973**, 3225, 3233, 3239.
4) The results of a single-crystal X-ray analysis led to the confirmation of the formula of $(C_3H_{10}N)_6H_2Mo_8O_{28}\cdot 2H_2O$ (M. Isobe, T. Yamase, T. Ikawa, and F. Marumo, in preparation).
5) F. W. Moore and M. L. Larson, *Inorg. Chem.*, **6**, 988 (1967).
6) T. Yamase and T. Ikawa, *Bull. Chem. Soc. Jpn.*, **48**, 3738 (1975).
7) W. G. Proctor and F. C. Yu, *Phys. Rev.*, **81**, 20 (1951).
8) The ESR spectra of the greenish yellow solution showed no observable change in *g* and *a* values.
9) W. P. Griffith and P. J. B. Lesniak, *J. Chem. Soc., A*, **1969**, 1066.
10) M. T. Pope, *Inorg. Chem.*, **11**, 1973 (1972).

NOTES

BULLETIN OF THE CHEMICAL SOCIETY OF JAPAN, VOL. 50, (3) 750 (1977)

The Reaction of Phenolic Compounds with Isoprenoids. VIII.[1] The *o*-Isoprenylation of Phenols in the Presence of Metallic Sodium

Shigetoshi YAMADA, Futara ONO, Takao KATAGIRI,* and Juntaro TANAKA*

Department of Industrial Chemistry, Junior College of Technology, Shizuoka University, Hamamatsu 432

**Department of Synthetic Chemistry, Faculty of Engineering, Shizuoka University, Hamamatsu 432*

(Received June 23, 1976)

Synopsis. Phenols (phenol, hydroquinone, resorcinol, and *o*-cresol) reacted with prenyl halides (3-methyl-2-buteny chloride and geranyl chloride) in the presence of an alkali metal (Na) in ether. In these reactions, phenols with the corresponding prenyl group at the ortho position were obtained selectively.

Claisen *et al.* have reported that, in general, the amount of C-alkylation can be greatly increased by the alkylation of sodium phenolates in benzene.[2] In a previous paper, we ourselves reported that phenol reacted with 3-methyl-2-butenyl chloride in the presence of metallic sodium in ether and that *o*-(3-methyl-2-butenyl)phenol (**1**) was thus isolated selectively (98%). In this paper, the studies of this reaction will be reported in detail.

In the reaction of phenol with geranyl chloride, *o*-geranylphenol (**2**) was also obtained in a high yield (90%) in a reaction similar to that in the case of 3-methyl-2-butenyl chloride. *o*-Cresol reacted with 3-methyl-2-butenyl chloride in the same manner, and 2-methyl-6-(3-methyl-2-butenyl)phenol (**3**) was obtained in a 76% yield. A similar reaction of hydroquinone with 3-methyl-2-butenyl chloride afforded 4-hydroxy-2-(3-methyl-2-butenyl)phenol (**4**) in a 66% yield. In the case of resorcinol, 3-hydroxy-4-(3-methyl-2-butenyl)-phenol (**5**) and 3-hydroxy-2-(3-methyl-2-butenyl)phenol (**6**) were obtained in 16 and 27% yields respectively. In this case, though the structures were not determined, the di- and tri-isoprenylated compounds were confirmed by GC-MS (GLC peaks showing molecular ion peaks at *m/e* 246 and 414 were observed).

From these results, metallic sodium in an aprotic solvent was found to be useful in obtaining selectively phenols with an acyclic isoprenyl group at the ortho position, while the Friedel-Crafts alkylation did not give such phenols mainly.[3]

Experimental

The Reaction of Phenols with Allylic Chloride. To an ethereal solution (50 ml) of phenol (0.05 mol), metallic sodium (0.2 mol) was added. After the mixture had been stirred for 0.5—1.5 h, an allylic chloride (0.05 mol) was added slowly; then the mixture was refluxed for 10 h. After the unreacted metallic sodium had been taken out, the solution was acidified with 0.1M aq HCl (20 ml) and extracted with ether. The ethereal solution was treated with 5% aq NaOH to remove the unreacted phenol, and then washed with water and dried over anhydrous sodium sulfate. After the removal of the solvent by distillation under reduced pressure, the products were obtained. The structures of the products were identified by means of the IR, NMR, and mass spectra. These IR and NMR spectral data agreed with the previously reported data.

2-Geranylphenol (2).[4] IR (cm^{-1}): 3400, 1925, 1890, 1780, 1210, 840, 750. NMR (δ, CCl_4): 1.57(s, 3,-CH_3), 1.65 (s, 3, -CH_3), 1.69 (s, 3, -CH_3), 2.00 (m, 4), 3.25 (d, 2, J=7.0 Hz, -CH_2-), 5.10 (s, 1, -OH), 5.25 (t, 2, J=7.0 Hz, =CH-), 6.50—7.10 (m, 4, aromatic protons). Mass (*m/e*): 230 (M^+).

2-Methyl-6-(3-methyl-2-butenyl)phenol (3.[5]*)* IR (cm^{-1}): 3500, 1910, 1780, 845, 760, 740. NMR (δ,CCl_4): 1.72 (s, 6, =C(CH_3)$_2$), 2.10 (s, 3, -CH_3), 2.00 (m, 4), 3.25 (d, 2, J= 7.0 Hz, -CH_2-), 5.10 (s, 1, -OH), 5.25 (t, 2, J=7.0 Hz, =CH-), 6.50—7.10 (m, 4, aromatic protons). Mass (*m/e*): 176 (M^+), 161 (M^+—15), 121 (M^+—55).

4-Hydroxy-2-(3-methyl-2-butenyl)phenol (4). mp 99—100 °C (colorless plates, lit,[6] mp 102°C). IR (cm^{-1}): 3500, 1895, 1815 1780, 840, 810. NMR (δ, CD_3OD): 1.67 (s, 6, =C(CH_3)$_2$), 3.15 (d, 2, J=7.0 Hz, -CH_2-), 5.10 (t, 1, J=7.0 Hz, =CH-), 6.25—6.70 (m, 3, aromatic protons). MS (*m/e*): 178 (M^+), 123 (M^+), 123 (M^+ —55).

3-Hydroxy-2-(3-methyl-2-butenyl)phenol (5).[7] IR (cm^{-1}): 3500, 1655, 1200, 840, 800. NMR (δ, CCl_4): 1.74 (s, 3, -CH_3), 1.79 (s, 3, -CH_3), 3.32 (d, 2, J=7.0 Hz, -CH_2-), 5.20(m, 3), 6.10—6.60 (m, 3, aromatic protons). MS (*m/e*): 178 (M^+), 163 (M^+ —15), 123 (M^+ —55).

3-Hydroxy-2-(3-methyl-2-butenyl)phenol (6).[7] IR (cm^{-1}): 3400, 1645, 1220, 835, 785, 775. NMR (δ, CCl_4): 1.66 (s, 3, -CH_3), 1.72 (s, 3, -CH_3), 3.09 (d, 2, J=7.0 Hz, -CH_2-), 4.85 (s, 2, -OH), 5.13 (t, 1, J=7.0 Hz, =CH-), 6.15—6.80 (m, 3, aromatic protons). MS (*m/e*): 178 (M^+), 163 (M^+—15), 123 (M^+—55).

References

1) Part VII of this series: S. Yamada, F. Ono, T. Katagiri, and J. Tanaka, *Synth. Commun.*, **5**, 181 (1975).

2) L. Claisen, F. Kremers, F. Roth, and E. Tietze, *Justus Liebigs Ann. Chem.*, **442**, 210 (1925).

3) J. Tanaka, T. Katagiri, and S. Yamada, *Yuki Gosei Kagaku Kyokai Shi*, **27**, 841 (1969).

4) S. Yamada, T. Katagiri, and J. Tanaka, *Yuki Gosei Kagaku Kyokai Shi*, **29**, 81 (1971).

5) G. Casnat, A. Guareschi, and A. Pochini, *Tetrahedron Lett.*, **1971**, 3737.

6) L. Jurd, K. Stevens, and G. Manners, *Tetrahedron Lett.*, **1971**, 2275.

7) S. Yamada, F. Ono, T. Katagiri, and J. Tanaka, *Nippon Kagaku Kaishi*, **1972**, 1987.

BULLETIN OF THE CHEMICAL SOCIETY OF JAPAN, VOL. 50 (3), 751—752 (1977)

The Effect of Urea on the First and Second CMC's of Aqueous Solutions of Sodium and Lithium Dodecyl Sulfates

Michiko KODAMA,* Ryukei BOKU, Toshio ISHIDA, and Masaji MIURA

Department of Chemistry, Faculty of Science, Hiroshima University, Higashisenda-machi, Hiroshima 730

**Department of Chemistry, Kansei Gakuin University, Uegahara, Nishinomiya 662*

(Received September 30, 1976)

Synopsis. The effect of urea on the 1st and 2nd CMC's of aqueous solutions of sodium and lithium dodecyl sulfates was investigated by the measuments of electric conductivity. The results were discussed in terms of the breaking effect of urea on the water structure not only around the hydrocarbon chains, but also around the counter ions of these surfactants.

In our previous papers, the micelle structure in the aqueous solutions of sodium dodecyl sulfate (NaDS) was investigated mainly in the concentration region above the 1st critical micelle concentration (CMC) through systematic studies including measurements of the electric conductivity,[1] density, viscosity,[2] light-scattering,[3] and depolarization of fluorescence.[4] It was revealed by these studies that there exists a 2nd CMC, where a change in the micelle structure takes place. Furthermore, in order to investigate the effect of the counter ions on the 2nd CMC, conductivity measurements were carried out in solutions of potassium (KDS) and lithium (LiDS) dodecyl sulfates in addition to NaDS.[5] It was revealed that, at the 2nd CMC, there occurs an increased counter-ion binding with the micelle.

It is well known that urea disrupts the water structure.[6] Several workers have used dissolved urea as a probe for investigating the contribution of structural changes in water to micelle formation.[7-9] In this study, conductivity measurements were carried out over a wide concentration range of NaDS and LiDS solutions in the presence of urea. The results were discussed by taking into account the effect of urea on the water structure, not only around the hydrocarbon chains, but also around the counter ions of these surfactants.

Experimental

The NaDS and LiDS used in this study were the same as those described in our previous paper.[5] Urea obtained from the Wako Pure Chemical Co. was recrystallized from 65 vol% aqueous etanol below 40°C.[10] The conductivity was measured in the manner described in a previous work.[1]

Results and Discussion

The results of the conductivity measurements in the neighborhood of the 1st CMC are shown in Fig. 1, where the specific conductivity (κ) is plotted againt the concentration of NaDS solutions containing various amounts of urea. The 1st CMC of a NaDS solution rises with an increase in the concentration of urea, as has been observed by other workers.[7-9] In recent investigations, the micelle formation has been discussed in terms of a change in the water structure according to Frank and Evan's theory;[11] the formation of the so-called iceberg structure around the hydrocarbon chains of surfactant molecules brings about a loss of entropy at their dissolution. The increase in CMC values in the presence of urea may be ascribed to a drop in the standard chemical potential of the surfactant in the monomeric state due to the breaking effect of urea on the iceberg structure, without any corresponding large change in the micellar state.

The ratio of the CMC in the presence of urea to the CMC in the absence of urea, CMC/CMC(0), is plotted against the concentration of urea in Fig. 2, where the results for the NaDS solution are compared with those for the LiDS solution. These results agree fairly well with those obtained by Schick,[9] who gives no explanation for the difference in CMC/CMC(0) between the NaDS solution and the LiDS solution. The effect of urea on the two hydrated counter ions, Li^+ and Na^+, needs to be discussed.

Bower and Robinson[12] revealed, by means of the isopiestic vapor pressure method, that the activity coefficient of NaCl is decreased by the addition of urea. The Na^+ ion is a structure-former, as is well known, and has a structural-orienting influence on neighboring water molecules.[11,13] The decrease in the activity coefficient of NaCl by urea may result from an increased electrostatic interaction between Na^+ and Cl^- due to a diminished hydration of Na^+. That is, urea disrupts the water structure in the vicinity of Na^+. This effect of urea may facilitate the adsorption of Na^+ as a counter ion on the micelle surface. The results shown in Fig. 2 may include the effect of urea on the counter ion, which lowers the 1st CMC, in addition to that on the hydrocarbon chain, which raises the 1st CMC. The Li^+ ion, which is more strongly hydrated in the absence of urea (than Na^+), may be more effective on the lowering of the 1st CMC in the presence of urea than Na^+. Thus, the increment in CMC/CMC(0) for LiDS solutions is less than that for NaDS solutions, as is shown in Fig. 2.

The conductivity measurements over a wide concentration range of NaDS solutions are shown in Fig. 3, where the results in the presence of urea are compared with those in the absence of urea. There occurs a break point corresponding to the 2nd CMC, in addition to that at the 1st CMC, as revealed by the conductivity measurements in our previous papers.[1,5] Moreover, the specific conductivity *vs.* concentration curve bends toward the concentration axis at the 2nd CMC in the presence of urea, while it breaks upward in the absence of urea, as was also observed in our previous work.[1,5] The conductivity behavior of the NaDS solutions at the 2nd CMC can be made clear in Fig. 4(a),which shows the deviation of the specific conductivity from the extrapolation of the linear plot of the specific conduc-

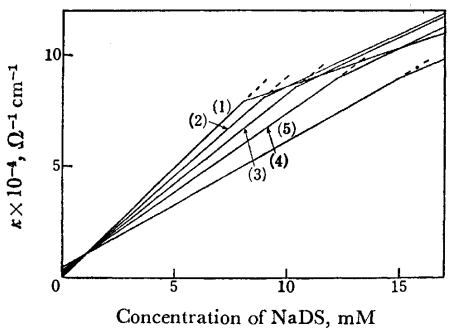

Fig. 1. Specific conductivities of NaDS solutions in the presence of urea in the neighborhood of the 1st CMC; concentration of urea: (1) 0 M, (2) 2 M, (3) 4 M, (4) 6 M, (5) 8 M.

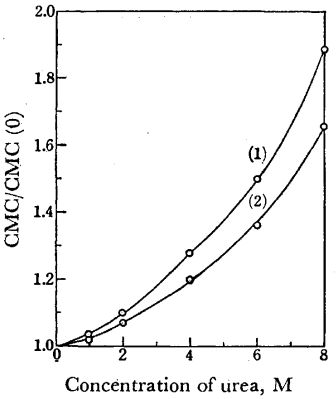

Fig. 2. CMC/CMC (0) of surfactant solutions; (1) NaDS, (2) LiDS.

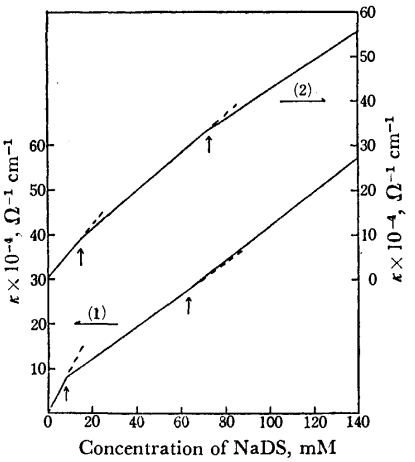

Fig. 3. Specific conductivities of NaDS solutions; (1) no additive, (2) 8 M urea. The arrows in the figure indicate the 1st and 2nd CMC's.

tivity *vs.* concentration below the 2nd CMC in Fig. 3 to a higher concentration, $\Delta\kappa$; $\Delta\kappa$ is negative, at least in the concentration range of urea studied. Furthermore, $\Delta\kappa$ increases and, at the same time, the 2nd CMC as well as the 1st CMC rises, with an increase in the concentration of urea. The effect of urea on the conductivity behavior above the 2nd CMC of LiDS solutions is similar to that in NaDS solutions, as is shown in Fig. 4(b).

It was suggested in our previous studies[1-5] that a change in the micelle structure at the 2nd CMC leads to an increase in the counter-ion binding with the micelle to compensate for the increment in the electrostatic energy resulting from the closer aggregation of hydrophilic parts of the amphipathic ions, of which the micelle is composed, above the 2nd CMC than below the 2nd CMC. As has been mentioned above, the disruption of the water structure by urea brings about a diminished hydration of the alkali metal counter ions of dodecyl sulfate. Under these circumstances, some counter ions in the bulk may be adsorbed additionally on the micelle surface at the 2nd CMC. As can be seen in Figs. 4 (a) and 4 (b), the lowering of the slopes of the straight lines above the 2nd CMC may be ascribed at least partly to a decrease in the counter-ion concentration in the bulk. Furthermore, the increase in the 2nd CMC with the concentration of urea (see Figs. 4 (a) and 4 (b)) may be caused primarily by the change in the standard chemical potentials of the surfactant in the monomeric state, as well as in the micellar state between 1st and 2nd CMC, relative to the corresponding change in the micellar state above the 2nd CMC.

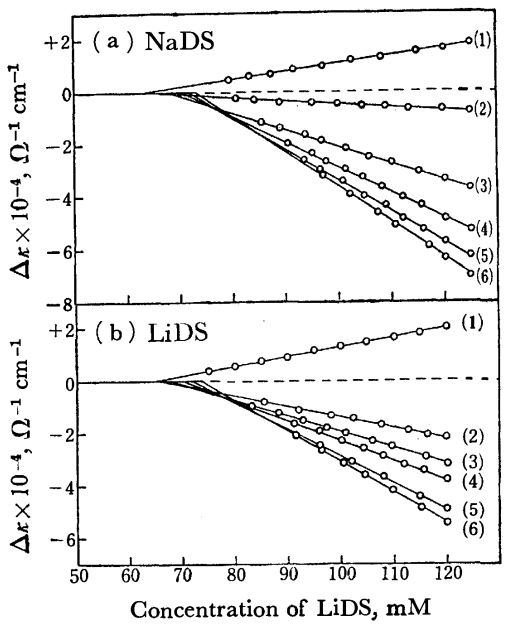

Fig. 4. $\Delta\kappa$ of NaDS (a) and LiDS (b) solutions; concentration of urea: (1) 0 M, (2) 1 M, (3) 2 M, (4) 4 M, (5) 6 M, (6) 8 M.

References

1) M. Miura and M. Kodama, *Bull. Chem. Soc. Jpn.*, **45**, 428 (1972).
2) M. Kodama and M. Miura, *Bull. Chem. Soc. Jpn.*, **45**, 2265 (1972).
3) M. Kodama, U. Kubota, and M. Miura, *Bull. Chem. Soc. Jpn.*, **45**, 2953 (1972).
4) Y. Kubota, M. Kodama, and M. Miura, *Bull. Chem. Soc. Jpn.*, **46**, 100 (1973).
5) M. Kodama, *J. Sci. Hiroshima Univ.*, Ser. A, **37**, 53 (1973).
6) J. A. Rupley, *J. Phys. Chem.*, **68**, 2002 (1964).
7) P. Mukerjee and A. Ray, *J. Phys. Chem.*, **67**,190 (1963).
8) W. Bruning and A. Holtzer, *J. Am. Chem. Soc.*, **83**, 4865 (1961).
9) M. J. Schick, *J. Phys. Chem.*, **68**, 3585 (1964).
10) M. Miura and A. Murakami, *J. Sci. Hiroshima Univ., Ser. A*, **18**, 403 (1955).
11) H. S. Frank and M. W. Evans, *J. Chem. Phys.*, **13**, 507 (1945).
12) V. E. Bower and R. A. Robinson, *J. Phys. Chem.*, **67**, 1524 (1963).
13) H. S. Frank and W. Y. Wen, *Discuss. Faraday Soc.*, **24**, 133 (1957).

BULLETIN OF THE CHEMICAL SOCIETY OF JAPAN, VOL. 50 (3), 753—754 (1977)

An Effect of Heat-treatment on the Activity of Titanium Dioxide Film Electrodes for Photo-sensitized Oxidation of Water

Hideo TAMURA, Hiroshi YONEYAMA, Chiaki IWAKURA, and Takaaki MURAI

Department of Applied Chemistry, Faculty of Enginnering, Osaka University, Yamadakami, Suita, Osaka 565

(Received July 21, 1976)

Synopsis. When an anodic oxide film of titanium and a pyrolytically prepared TiO_2 film were subjected to a heat-treatment in an argon atmosphere, their activities for photo-sensitized oxidation of water were improved.

The photo-sensitized oxidation of water on an illuminated rutile electrode[1] has been studied recently by many investigators with a special interest in photo-emf cells.[2,3] The electrochemical properties of TiO_2 film electrodes prepared by a variety of methods, such as chemical vapor deposition,[4,5] anodic oxidation,[5-7] thermal oxidation,[6,8,9] pyrolysis of titanium salts,[10] and spraying by a plasma jet,[8] as well as of single crystal rutile, have been investigated in connection with the photo-sensitized oxidation. The following points can be noticed in these investigations: (1) the anodic oxide film shows far less activity than that of single crystal rutile; (2) the films prepared by the thermal oxidation do not always have the same properties, but have some possibility of giving the same activity as that of single crystal rutile if a suitable preparation condition is chosen; and (3) the activities of the pyrolytically prepared film for oxygen adsorption and for photo-sensitized oxidation of chloride ions are influenced by the preparation temperature of the film.

It is suggested by the above information that the heat-treatment has a great influence on the activity of a TiO_2 film electrode for the photo-sensitized oxidation of water. The present study was conducted, therefore, to elucidate the effect of the heat-treatment on the activity of TiO_2 films. Anodically formed and pyrolytically prepared films were chosen for the TiO_2 films.

Experimental

A rectangular titanium sheet ($20 \times 10 \times 0.5$ mm) was anodically oxidized in ethylene glycol containing 100 g/l sodium borate.[11] Sodium borate was purified by recrystallization from distilled water twice, and ethylene glycol was distilled twice. When the titanium electrode was oxidized with a constant current of 0.5 mA/cm^2, its potenial increased with the oxidation time until it reached around 20 V *vs.* S.C.E., after which no further potential rise occurred. After the polarization under this condition for 20 min, the current density was changed to 1 mA/cm^2 and maintained at that value until the potential reached a desired value. The heat-treatment was conducted under an argon atmosphere at a desired temperature for 1 h. Pyrolytic TiO_2 films were prepared by the same procedure as that described previously,[12] except that a solution of 0.1 mol·dm^{-3} $TiCl_3$–20% HCl containing a few drops of 30% H_2O_2 was subjected to the pyrolysis. A 500 W xenon arc lamp was used as a light source and monochromatic light was obtained by using the grating of a spectrophotometer (Shimadzu, QB-50).

Results and Discussion

The activity of an anodically formed oxide film for the photo-sensitized oxidation of water was poor, as expected. When the film was heat-treated at 700 °C, however, it became almost as active as single crystal rutile. Figure 1 shows the polarization curves of an electrode formed at 50 V. In the measurement of each polarization curve, the photo-intensity was maintained at the same value. Trials of the heat-treatment at 800 °C were failures due to the fact that the film flaked off in some patches from the substrate. The polarization curves in 0.5 mol·dm^{-3} Na_2SO_4 and 1 mol·dm^{-3} NaOH were almost the same as those in Fig. 1, except that they shifted cathodically depending on the pH values of the electrolytes.

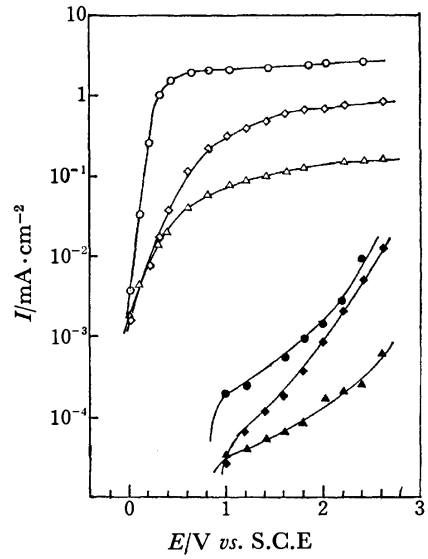

Fig. 1. Influence of heat-treatment on current-potential curves of anodic oxide films on titanium. Temperature of heat-treatment; -○-, -●-: 700°C, -◇-, -◆-: 600 °C, -△-, -▲-: non-heat-treatment, open symbol: under illumination, closed symbol: in the dark.

X-Ray diffraction patterns of the oxide film showed that the initial film formed by the anodization was amorphous and changed into rutile modification by the heat-treatment, as expected from the transformation of anatase to rutile by the heat-treatment.[13,14] It was also observed that the crystallization of the film was promoted with an increase of the temperature of the heat-treatment. Hence, one of the reasons for the increase of the activity is this crystallization. Another effect of the heat-treatment is to bring about an increase of the electrical conductivity of the film, as is usually

observed in single crystal rutile, although the determination of the carrier concentration of the film by Mott-Schottky plots before and after the heat-treatment was unsuccessuful, because the film thickness was so thin that the length of the space charge layer exceeded the film thickness by anodic polarization beyond a fairly low anodic potential.[4] As for the film thickness, it increases at a rate of 20—30 Å/V in the anodization.[11,15] Thus, the oxide film thickness formed at 50 V amounts only to 1000—1500 Å. By the heat-treatment, there is a possibility that the titanium substrate extracts oxygen from the oxide film,[16] by which a decrease in the film thickness would be expected. It was theoretically predicted that there is an optimum carrier concentration for a semiconductor electrode to attain a high quantum yield of a photo-sensitized reaction,[17] and the experimentally found optimum concentration was in the order of as high as 10^{18} carriers/cm^3.[18]

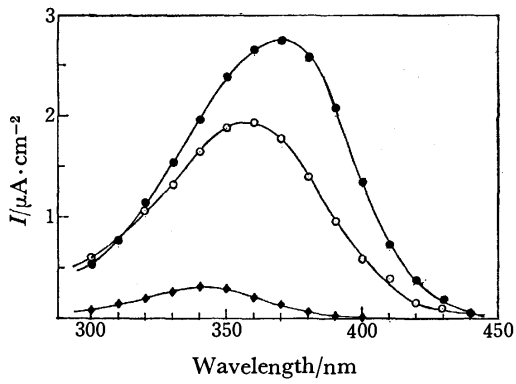

Fig. 2. Photo-current spectra of anodic oxide films on titanium.
-●- Heat-treated at 700 °C, -○- heat-treated at 600 °C, -◆- non-heat-treated.

Figure 2 gives the anodic current spectra of the film with and without the heat-treatment. By the heat-treatment, the photo-current at 2.0 V distinctly increased and its maximum occurred at a longer wavelength. Since the electrode was illuminated through the electrolyte, excitation of hole-electron pairs must be most predominant in a layer near the film/electrolyte interface. The results shown in Fig. 2, therefore, suggest that the probability of carrier recombination in the process in which electrons move from the excited sites to the substrate was decreased by the heat-treatment.

The above mentioned effects of the heat-treatment were also observed on a pyrolytic oxide film. The pyrolytic oxide film had a history of high temperature (450 °C) preparation. Nevertheless, the as-prepared film showed a poor activity.

When the activated TiO_2 film electrode was used as the electrode for the photo-sensitized oxidation of water in 0.5 mol·dm^{-3} H_2SO_4, a gradual deterioration of the activity was noticeable due to the oxidation of the electrode surface, as was already reported for a single crystal electrode.[3,19] From the above results, however, it is suggested that a TiO_2 film will be as effective as single crystal rutile as a semiconductor electrode if the film consists of highly crystalline TiO_2 with an appropriate conductivity.

References

1) A. Fujishima, K. Honda, and S. Kikuchi, *Kogyo Kagaku Zasshi.*, **72**, 108 (1969).
2) A. Fujishima and K. Honda, *Bull. Chem. Soc. Jpn.*, **44**, 1148 (1971); *Nature*, **238**, 37 (1972).
3) H. Yoneyama, H. Sakamoto, and H. Tamura, *Electrochim Acta*, **20**, 341 (1975).
4) F. Möllers, H. J. Tolle, and R. Memming, *J. Electrochem. Soc.*, **112**, 1160 (1974)
5) K. L. Hardee and A. J. Bard, *J. Electrochem. Soc.*, **122**, 739 (1975).
6) A. Fujishima, K. Kobayakawa, and K. Honda, *J. Electrochem. Soc.*, **122**, 1487 (1975).
7) J. Kenny, D. H. Weinstein, and G. M. Hass, *Nature*, **253**, 719 (1975).
8) W. Gissler, P. L. Lensi, and S. Pizzini, *J. Appl. Electrochem.*, **6**, 9 (1976).
9) J. G. Mavroides, D. I. Tchernev, J. A. Kafalas, and D. F. Kolesar, *Mat. Res. Bull.*, **10**, 1023 (1975).
10) D. M. Shub, A. A. Remnew, and V. I. Vaseloskii, *Élektrokhimiya*, **11**, 616 (1975); D. M. Shub, A. A. Remnev, and V. I. Vaselovskii, *ibid.*, **11**, 1100 (1975).
11) W. Mizushima, *J. Electrochem. Soc.*, **108**, 825 (1961).
12) C. Iwakura, K. Fukuda, and H. Tamura, *Electrochim. Acta*, **21**, 501 (1976).
13) R. O. Shannon and J. A. Pask, *J. Am. Ceram. Soc.*, **48**, 391 (1965).
14) R. D. Iyenger, M. Codell, H. Gisser, and J. Weisberg, *Z. Phys. Chem., N. F.*, **89**, 325 (1974).
15) P. F. Schmidt, H. Huber, and R. F. Schwartz, *J. Phys. Chem. Solid*, **15**, 270 (1960); M. Ogawa, *Rikagaku Kenkyusho Hokoku*, **39**, 21 (1963).
16) D. M. Smith, G. A. Shirn, and T. B. Tripp, *J. Electrochem. Soc.*, **110**, 1264 (1963); G. P. Klein, *ibid.*, **119**, 1551 (1972).
17) H. Gerischer, *J. Electroanal. Chem.*, **58**, 263 (1975).
18) H. Tamura, H. Yoneyama, C. Iwakura, H. Sakamoto, and S. Murakami, to be published in *J. Electroanal. Chem.*
19) L. A. Harris and R. H. Wilson, *J. Electrochem. Soc.*, **123** 1010 (1976).

BULLETIN OF THE CHEMICAL SOCIETY OF JAPAN, VOL. 50 (3), 755—756 (1977)

Flux Growth of Rare-earth Niobates with Fergusonite Structure

Yoshinori SUGITANI

Department of Chemistry, The University of Tsukuba, Sakuramura, Niihari-gun, Ibaraki 300-31

(Received November 1, 1976)

Synopsis. Single crystals of rare-earth niobates $RNbO_4$ (R denotes a rare-earth element) were grown from a melt of PbF_2–PbO flux. They are monoclinic and isostructural with natural and synthetic fergusonites. These crystals, except those containing Pr, Nd, Sm, and Ho were found to emit luminescent colors under UV irradiation.

Yttrium niobate $YNbO_4$, a member of mineral fergusonite (Y, Er, U) (Nb, Ta, Ti,···)O_4, belongs to a monoclinic system having a pseudo-sheelite type structure.[1] Natural fergusonite occurs mostly in metamict form due to the inclusion of radioactive elements such as uranium and thorium, so that its original structure had long been believed to be tetragonal from studies on samples recrystallized by heating to over 400 °C.[2] Studies of refractory materials such as $YNbO_4$ have been made mainly on powder samples prepared by the sintering or arc fusion method.[3]

Recently, Sugitani and Nagashima have grown crystals of $YNbO_4$ of macroscopic size by the flux method,[4] and have found that the monoclinic form of $YNbO_4$ is also supported by optical observations in addition to X-ray studies. In this note, the preparation of rare-earth niobate crystals which have monoclinic forms are reported. It was found that most of these crystals produce luminescent emission of various colors which is considered to be rare for "pure type" oxide phosphors.

As a typical case, the method of growing yttrium niobate is given here. Other rare-earth niobates can be grown, in general, in a manner similar to that for $YNbO_4$, with some minor changes in the growing conditions, such as the cooling rate, solute-flux ratio, *etc.* Equimolar Nb_2O_5 (purity 3N) and Y_2O_3 (purity 4N) were mixed in a platinum crucible together with the flux material PbF_2–PbO (purity 3N, the flux ratio PbF_2: PbO=80: 20) of an amount several times the molar ratio. All of the rare-earth oxides used as starting materials were sesquioxides R_2O_3, except for Pr_6O_{11} and Tb_4O_7. The crucible was tightly covered by a lid and was placed in an alumina-box filled with alumina powder. This system was placed in an electric furnace maintained at 1300 °C. After about two hours at that temperature, it was cooled down to 1100 °C at the rate of 1.2 °C/h by a programmed controller. At the final temperature the system was removed from the furnace and was allowed to cool down to room temperature. The products in the crucible were removed and washed with hot 6M–HNO_3 for several hours. The crystals thus obtained were confirmed to have the desired $RNbO_4$ composition by chemical analysis and/or by X-ray analysis. They are mostly in the shape of slightly elongated octahedra, and their sizes range from 0.2 to 3 mm for their largest dimension.

Table 1 shows a list of the rare-earth niobates prepared, together with their colors, cell parameters, and luminescent colors under UV irradiation. The values of the cell parameters were calculated from the $\bar{1}21$, 031, 121, 040, 200, 002, 112, and 240 reflections.

It was found that Bi_2O_3–V_2O_5 flux (the flux ratio

TABLE 1. CELL PARAMETERS AND LUMINESCENT COLORS OF SYNTHETIC RARE-EARTH NIOBATES

	Color	a (Å)	b (Å)	c (Å)	β (deg.)	Luminescent color (3650 Å irradiation)		Luminescent color (2537 Å irradiation)	
						at room temperature	at 77 K	at room temperature	at 77 K
$YNbO_4$	colorless	5.30	10.96	5.07	94.60	dark orange w	yellowish orange m	bluish white m	white w
	yellow[a]					greenish brown w	—	greenish brown w	—
$LaNbO_4$	pale yellow	5.57	11.55	5.21	94.07	brown w	orange w	green m	yellowish green w
$PrNbO_4$	green	5.51	11.35	5.17	94.52	—	—	—	—
$NdNbO_4$	violet	5.48	11.31	5.16	94.75	—	—	—	—
$SmNbO_4$	yellow	5.42	11.18	5.12	94.48	—	—	—	—
$EuNbO_4$	colorless	5.39	11.13	5.12	94.68	light red s	red s	dark red m	red m
$GdNbO_4$	pale brown	5.37	11.10	5.11	94.45	yellow w	yellow w	yellow w	yellow w
$TbNbO_4$	orange	5.33	11.07	5.10	94.03	greenish brown w	—	brown w	—
$DyNbO_4$	yellow	5.31	11.02	5.10	94.01	green w	—	green w	—
$HoNbO_4$	colorless	5.31	10.97	5.08	94.62	—	—	—	—
$ErNbO_4$	pink	5.21	10.95	5.07	94.81	—	yellow w	—	greenish yellow w

s: strong, m: medium, w: weak. —: not observed. a) Bi_2O_3–V_2O_5 flux.

Bi_2O_3: V_2O_5=120: 8) was also useful in growing these niobates, though the sizes of the crystals obtained were usually smaller than those obtained using PbF_2–PbO flux, for the same growing conditions. The color of $YNbO_4$ grown in PbF_2–PbO flux is pale yellow with a tint of brown, while that grown in Bi_2O_3–V_2O_5 flux is yellow (Table 1). This is considered to be due to contamination by the flux material, but details remain unknown.

Crystals which were obtained as by-products during the growing runs are CeO_2, $Pb_2Nb_2O_7$, $Pb_3Nb_2O_8$, PbO and other unidentified crystals.

Brixner[5] has reported the emission colors of sintered pellets of several niobates of $RNbO_4$ composition. His results are considered to agree with the present results within a small discrepancy in color description. Suemune[6] has reported coloring and bleaching of several $RNbO_4$ materials which had been exposed to UV light for 5 min at 25 °C and maintained at 100 °C for 24 h after the exposure. From the present experiments, it is apparent that the coloring for UV irradiation does not remain but the samples immediately return to their original colors when the irradiation ceases.

Spectroscopic studies as well as other studies, are needed to understand the luminescence and photochromism of fergusonite-type niobates. Such studies are now in progress.

The author is grateful to Professor Kozo Nagashima for his kind support of this work, and to the late Mr. Toshio Nakamura for his help in the early stages of this work.

References

1) A. I. Komkov, *Sov. Phys. Crystallogr.*, **4**, 796 (1959); A. I. Komkov, *Dokl. Akad. Nauk SSSR*, **126**, 853 (1959).
2) J. D. and E. S. Dana, "The System of Mineralogy," 7 th ed, John Wiley and Sons, Inc. London (1952).
3) C. Keller, *Z. Anorg. Allg. Chem.*, **318**, 89 (1962); H. P. Rooksby and E. A. D. White, *Acta Crystallogr.*, **16**, 888 (1963); G. M. Wolten and A. B. Chase, *Am. Miner.*, **52**, 1536 (1967).
4) Y. Sugitani and K. Nagashima, *Miner. J.*, **8**, 66 (1975).
5) L. H. Brixner, *J. Electrochem. Soc.*, **111**, 690 (1964).
6) Y. Suemune, *Jpn. J. Appl. Phys.*, **12**, 467 (1973).
7) A. Wachtel, *J. Electrochem. Soc.* **111**, 534 (1964); G. Blasse and A. Bril, *Z. Phys. Chem. (N. F.)*, **57**, 187 (1968).

BULLETIN OF THE CHEMICAL SOCIETY OF JAPAN, VOL. 50 (3), 757—758 (1977)

Transfer-free Energy Aspect on the Keto-enol Tautomerization Rate of Benzoylacetone in Water-Dimethyl Sulfoxide Mixtures

Hitoshi WATARAI and Nobuo SUZUKI*

Department of Chemistry, Faculty of Science, Tohoku University, Sendai 980

(Received September 24, 1976)

Synopsis. The transfer-free energies of the keto form, the enol form, and the transition state of benzoylacetone from water to water–dimethyl sulfoxide (DMSO) mixtures have been evaluated on the basis of kinetic and partition experiments at 25 °C. The results were compared with those of acetylacetone, and the substituent effects of methyl and phenyl groups on the transfer-free energies have been discussed in terms of the group transfer-free energy.

The study of solvent effect on the kinetic behavior of β-diketone is necessary in order to elucidate the formation reaction of metal chelates with β-diketone and the solvent extraction mechanisms of these compounds. In the course of our study of the solvent effect on the keto-enol tautomerization rate of acetylacetone, we pointed out the usefulness of the partition coefficient in interpreting the kinetic solvent effect.[1] When the extent of solvent effect on a reactant is measured as a function of the change in the partition coefficient, the solvent effect on a transition state can be conveniently evaluated by simultaneous knowledge of the rate constant and the partition coefficient of the reactant. In this study, the solvent effect on the keto-enol tautomerization rate of benzoylacetone (BA) in a water–DMSO mixture will be described in terms of the transfer-free energy and the estimated free energies will be compared with those of acetylacetone (AA) in order to examine the substituent effects of methyl and phenyl groups.

Experimental

Chemicals. Benzoylacetone (Wako Junyaku Co., G. R.) was purified by recrystallization from diethyl ether. Heptane and DMSO were purified by a method described previously.[1] All the mixed solvents were prepared from the purified DMSO and the doubly distilled water by weight.

Kinetic Measurements. The tautomerization reaction was initiated by injecting a minute amount of a dioxane solution of BA into the mixed solvent in an optical cell thermostated at 25±0.1 °C. Since BA exists solely as the enol form in dioxane, the decreasing absorbance of the enol form is observed at 310 nm immediately after the injection. From the decrease in the absorbance recorded on a spectrophotometer, a first-order rate constant (k_{obsd}) was obtained. The concentration of BA was below 10^{-4} M in all measurements.

Equilibrium Measurements. The enol fractions (f) of BA in the mixed solvents were estimated from the apparent molar absorptivity at 310 nm. The molar absorptivity of the enol form of BA in water has been determined to be 1.62×10^4 at 310 nm by means of a stopped-flow technique.[2] The apparent partition coefficients (P_{obsd}) of BA between heptane and the mixed solvents were determined photometrically at 25±0.05 °C by the same method as was used for AA.[1] All the photometric measurements were carried out by means of a Hitachi 356 spectrophotometer.

* To whom correspondence should be addressed.

Results and Discussion

The kinetic and equilibrium results are shown in Fig. 1. Both k_{obsd} and P_{obsd} decrease rapidly with an increase in the DMSO, while the enol fraction f increases moderately.

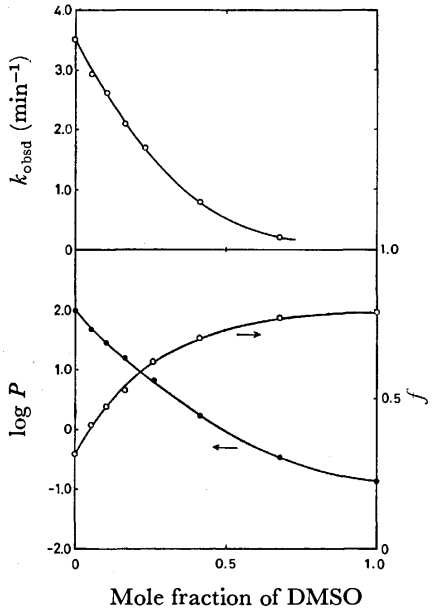

Fig. 1. Observed rate constant (k_{obsd}), enol fraction (f) and partition coefficient (P) of BA as a function of the mole fraction of DMSO.

From the equilibrium data, the transfer-free energies of the keto form ($\delta\Delta G_{s,K}$) and the enol form ($\delta\Delta G_{s,E}$) from water to the mixed solvents can be evaluated by means of Eqs. 1 and 2 respectively:

$$\delta\Delta G_{s,K} = RT\ln\frac{(1-f^\circ)}{(1-f)}\cdot\frac{P}{P^\circ} \quad (1)$$

$$\delta\Delta G_{s,E} = RT\ln\frac{f^\circ}{f}\cdot\frac{P}{P^\circ} \quad (2)$$

where the superscript $^\circ$ denotes the values in water, chosen as the reference solvent. Moreover, the transfer-free energies of the transition state can be estimated by means of the following equation:

$$\delta\Delta G^{\ddagger} = RT\ln\left(\frac{P}{P^\circ}\cdot\frac{1-f^\circ}{1-f}\cdot\frac{f^\circ}{f}\cdot\frac{k^\circ_{obsd}}{k_{obsd}}\right) \quad (3)$$

By using the partition coefficient on the mole fraction scale which is calculated from P_{obsd} and the density data of the mixed solvent in the literature,[3] we can obtain the transfer-free energies, $\delta\Delta G_{s,K}$, $\delta\Delta G_{s,E}$, and

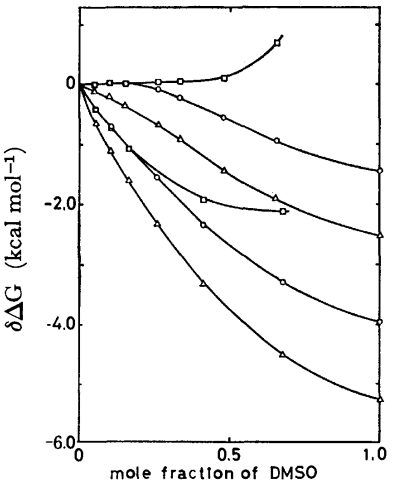

Fig. 2. Estimated transfer-free energies of AA (the upper three plots) and BA (the lower three plots) as a function of the mole fraction of DMSO. □: $\delta\Delta G^t$, ○: $\delta\Delta G_{s,K}$, △: $\delta\Delta G_{s,E}$.

$\delta\Delta G^t$, expressed as on the mole fraction scale. The estimated values, together with those for AA, are shown in Fig. 2 as a function of the DMSO mole fraction.

Figure 2 points to the following: (i) all the transfer-energy values of BA are smaller than those of AA; (ii) the $\delta\Delta G_{s,K}$ of AA is nearly zero in the composition region of $X_S<0.2$, whereas that of BA decreases with the increase in DMSO in the same region; (iii) the $\delta\Delta G^t$ of AA is zero or a positive value, whereas that of BA is negative. These differences are considered to be mainly due to the destabilization of BA in water, which is caused by the substitution of the phenyl group for one methyl group of AA.

The substituent effect on the transfer-free energy should be discussed in terms of the group transfer-free energy. The $\delta\Delta G_{s,K}$ values, for example, of AA and BA may be divided into the corresponding free energies of the groups as follows:

$$\delta\Delta G^A_{s,K} = \delta\Delta G^A_s(\text{-COCH}_2\text{CO-}) + 2\delta\Delta G^A_s(\text{CH}_3\text{-}) \quad (4)$$

$$\delta\Delta G^B_{s,K} = \delta\Delta G^B_s(\text{-COCH}_2\text{CO-}) + \delta\Delta G^B_s(\text{CH}_3\text{-}) + \delta\Delta G^B_s(\text{C}_6\text{H}_5\text{-}) \quad (5)$$

where the superscripts A and B denote AA and BA respectively. If the next assumption is valid:

$$\delta\Delta G^A_s(\text{-COCH}_2\text{CO-}) = \delta\Delta G^B_s(\text{-COCH}_2\text{CO-})$$
$$\delta\Delta G^A_s(\text{CH}_3\text{-}) = \delta\Delta G^B_s(\text{CH}_3\text{-}) \quad (6)$$

the difference between Eqs. 4 and 5 becomes:

$$\delta\Delta G^A_{s,K} - \delta\Delta G^B_{s,K} = \delta\Delta G^B_s(\text{CH}_3\text{-}) - \delta\Delta G^B_s(\text{C}_6\text{H}_5\text{-}) \quad (7)$$

Similar treatments of $\delta\Delta G_{s,E}$ and $\delta\Delta G^t$ lead to Eq. 8:

$$\delta\Delta G^A_{s,K} - \delta\Delta G^B_{s,K} = \delta\Delta G^{tA} - \delta\Delta G^{tB} = \delta\Delta G^A_{s,E} - \delta\Delta G^B_{s,E} . \quad (8)$$

This equation shows that the transfer-free energy differences between the corresponding states of the two diketones are independent of the solvent composition and equal each other. However, the experimentally estimated values of the differences do not show an equality as in Eq. 8. The estimated values are as follows:

$$\delta\Delta G^A_{s,K} - \delta\Delta G^B_{s,K} : \delta\Delta G^{tA} - \delta\Delta G^{tB} : \delta\Delta G^A_{s,E} - \delta\Delta G^B_{s,E} = 1 : 1.6 : 1.7 \quad (9)$$

The discrepancy between these data and the prediction in Eq. 8 may be due to a difference in the charge delocalization of the keto forms, the enol forms, and the transition states of the two diketones, which is caused by substituting the phenyl group for one methyl group of AA. The result of Eq. 9 suggest that the charge distribution in the transition state is closer to that for the enol form than to that for the keto form.

The reaction indices for the enolization and the ketonization, α_e and α_k,[1] which are defined as:

$$\alpha_e = \frac{\delta\Delta G^t}{\delta\Delta G_{s,K}}, \quad \alpha_k = \frac{\delta\Delta G^t}{\delta\Delta G_{s,E}} \quad (10)$$

respectively, were estimated in the low-mole-fraction region of DMSO as follows: $\alpha_e=-0.17$ and $\alpha_k=-0.05$ in AA and $\alpha_e=1.07$ and $\alpha_k=0.69$ in BA. The signs of α in the two diketones are opposite, according to the sign of $\delta\Delta G^t$.

From the above results, it seems that the effect of the mixed solvent on the transfer-free energies is more striking in AA than in BA. Recently, Symons[4] has investigated the hydrogen-gas solubility in the water–DMSO mixed solvent at 25 °C and has observed a distinct minimum of the solubility expressed on the molar scale in the region of 25—35 mol % DMSO. In a previous study of the liquid-liquid partition of AA between heptane and the mixed solvent, a distinct maximum in the partition coefficient of the keto form has been observed at $X_S=0.2$.[1] However in the case of BA no such phenomenon is observed at all. Although the hydrogen-gas solubility has been interpreted in terms of a changing entropy and energy of "hole" formation in the solvent with the composition,[4] the transfer-free energy of β-diketone is not likely to be solely interpreted by this factor. In the case of β-diketone, a solute-solvent interaction energy including a size contribution of solute and solvent[5] seems to be a possible factor governing the transfer-free energy, in addition to the "hole" formation energy which may be related to such a property as an internal pressure of the solvent.[6,7]

References

1) H. Watarai and N. Suzuki, *J. Inorg. Nucl. Chem.*, **38**, 1683 (1976).
2) N. Suzuki, K. Baba, and H. Watarai, unpublished results.
3) J. M. G. Cowie and P. M. Toporowski, *Can. J. Chem.*, **39**, 2240 (1961).
4) E. A. Symons, *Can. J. Chem.*, **49**, 3940 (1971).
5) M. Lucas and R. Bury, *J. Phys. Chem.*, **80**, 999 (1976).
6) D. D. Macdonald and J. B. Hyne, *Can. J. Chem.*, **49**, 611 (1971).
7) M. R. J. Dack, *Chem. Soc. Rev.*, **14**, 211 (1975).

BULLETIN OF THE CHEMICAL SOCIETY OF JAPAN, VOL. 50 (3), 759—760 (1977)

ESR and Optical Spectra of Low-spin Square Planar Cobalt(II) Complexes with Some Quadridentate Schiff Bases of the N_2S_2 Type[1)]

Yuzo NISHIDA, Akira SUMITA, and Sigeo KIDA

Department of Chemistry, Faculty of Science, Kyushu University, Fukuoka 812

(Received October 29, 1976)

Synopsis. ESR and electronic spectra of low-spin cobalt(II) complexes with some quadridentate Schiff bases of the N_2S_2 type were measured. Analysis of ESR parameters led to the conclusion that an unpaired electron is in the d_{yz} orbital of the cobalt atom. On this basis the absorption at 10×10^3 cm^{-1} was attributed to the $d_{x'-y'}\rightarrow d_{yz}$ transition.

The relative energies of d-orbitals in low-spin square-planar cobalt(II) complexes have been subjects of many investigations and still in controversies. Recently, we have reinvestigated the electronic structures of square planar cobalt(II) complexes with the quadridentate Schiff bases, **1-a**, **1-b**, and **1-c**, as shown in Fig. 1.[2)] As the results, it was concluded that an unpaired electron lies in the d_{yz} orbital and the separations among d_{yz}, $d_{x'-y'}$, d_{xz}, and $d_{z'}$ orbitals are small in these complexes.[2)] In this study the ESR and electronic spectra of cobalt(II) complexes with some quadridentate Schiff bases, **1-d**, were investigated in order to compare the ligand field effect of **1-d** with those of other quadridentate Schiff bases such as **1-a**, **1-b**, and **1-c**.

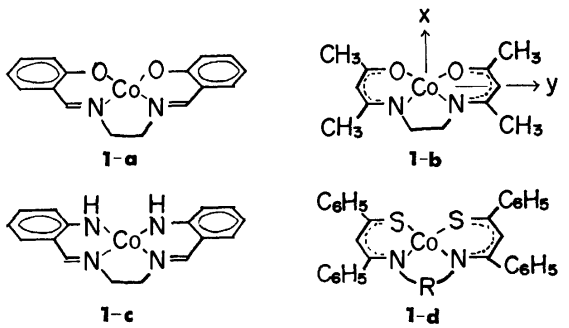

Fig. 1. Some quadridentate ligands cited in this paper. In **1-d**, R represents $-CH_2CH_2-$, $-CH_2CH_2CH_2-$, and $-CH(CH_3)CH_2-$ for H_2(nsen), H_2(nstn) and H_2(nspn), respectively. x and y axes are shown in **1-b**, z axis being perpendicular to the plane.

Experimental

The ligands, *N,N'*-bis(1-phenyl-2-thiobenzoylvinyl)ethylenediamine, *N,N'*-bis(1-phenyl-2-thiobenzoylvinyl)trimethylenediamine and *N,N'*-bis(1-phenyl-2-thiobenzoylvinyl)propylene diamine, abbreviated as H_2(nsen), H_2(nstn) and H_2(nspn), respectively, were prepared according to the modified methods of Uhlemann[3)] and Tang *et al.*[4)] The cobalt(II) complexes were obtained by mixing a methanol solution of cobalt(II) acetate tetrahydrate and a chloroform solution of the ligand under a nitrogen atmosphere. The nickel(II) complexes were also obtained according to the same method as described for cobalt(II) complexes.

ESR spectra were obtained with a JEOL ESR-apparatus model JES-ME-3X using an X-band. DPPH was used as a standad marker. Magnetic susceptibilities were measured by the Faraday method at room temperature, Pascal's constants being used for diamagnetic correction. $HgCo(NCS)_4$ was employed as a standard for magnetic susceptibility. Reflectance spectra were measured with a Shimadzu Multipurpose Spectrophotometer, MPS-5000 at room temperature.

Results and Discussion

The magnetic moments of cobalt(II) complexes with H_2(nsen), H_2(nstn) and H_2(nspn) were found to be in the range 2.2—2.3 BM at room temperature, indicating that all the complexes are of the low-spin type. Figure 2 shows the ESR spectrum of [Co(nstn)], diluted in [Ni(nstn)]. From the spectrum, it was found that $g_1=3.29$, $|A_1|=164\times10^{-4}$ cm^{-1}, and g_2, $g_3\approx2.0$. The other complexes, [Co(nsen)] and [Co(nspn)], showed ESR patterns similar to that of [Co(nstn)]. It should be noted that the ESR patterns of *cis*-[CoN_2S_2] type complexes obtained here are very similar to those of *cis*-[CoN_2O_2] type complexes with Schiff bases such as **1-a** and **1-b**,[5,6)] for which the $(yz)^1$ ground state* was assumed in our recent investigation.**,[2)] Therefore, it is reasonable to assume that an unpaired electron is localized in the d_{yz} orbital of the cobalt atom in the complexes with quadridentate Schiff bases of the *cis*-[CoN_2S_2] type.

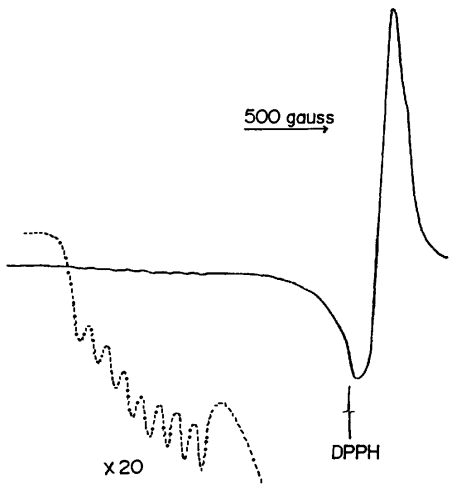

Fig. 2. ESR spectrum of [Co(nstn)] diluted in [Ni(nstn)] obtained at 123 K by an X-band.

* $(yz)^1$ represents electronic configuration $(d_{x'-y'})^2(d_{xz})^2(d_{z'})^2(d_{yz})^1$.

** Throughout this paper, x, y, and z axes were adopted as shown in Fig. 1.

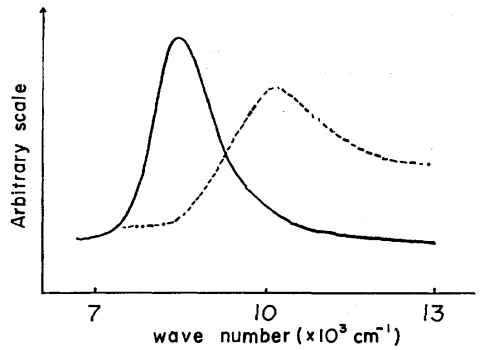

Fig. 3. Reflectance spectra of [Co(nspn)] (------) and [Co(sals)] (——).

The reflectance spectrum of [Co(nspn)] is shown in Fig. 3, together with that of [Co(sals)], which is one of the *cis*-$[CoN_2O_2]$ type complexes, and where H_2(sals) represents *N*,*N*′-disalicylidene-1,2-diphenylethylenediamine. A broad band was observed at 10×10^3 cm^{-1} for [Co(nspn)], whereas a similar band was observed at 8.4×10^3 cm^{-1} for the *cis*-$[CoN_2O_2]$ type complexes with quadridentate Schiff bases.[7] It is reasonable to assume that both bands are attributed to the same origin, to which the $d_{x^2-y^2} \rightarrow d_{yz}$ transition was assigned for the *cis*-$[CoN_2O_2]$ type complexes with Schiff bases.[2] The blue shift of the band upon substitution of the N_2S_2 ligand for the N_2O_2 ligand suggests that the energy separation between $d_{x^2-y^2}$ and d_{yz} orbitals is larger in the $[CoN_2S_2]$ complexes than those in the $[CoN_2O_2]$ complexes. From the above discussion, it can be concluded that the order of the d-orbitals in the cobalt(II) complexes with Schiff bases, **1-d** is the same as those in the complexes with **1-b** and **1-c**.

References

1) Part VII of the series, "Investigation on Low-spin Cobalt(II) Complexes."
2) Y. Nishida and S. Kida, *Inorg. Chem.*, to be submitted.
3) E. Uhlemann, *Z. Naturforsch.*, **B21**, 592 (1966).
4) S. C. Tang, S. Koch, G. N. Weinstein, R. W. Lene, and R. H. Holm, *Inorg. Chem.*, **12**, 2589 (1973).
5) Y. Nishida and S. Kida, *Chem. Lett.*, **1973**, 57.
6) C. Busetto, F. Cariati, A. Fusi, M. Gullotti, F. Morazzoni, A. Pasini, and R. Ugo, *J. Chem. Soc., Dalton Trans.*, **1973**, 754.
7) H. Nishikawa and S. Yamada, *Bull. Chem. Soc. Jpn.*, **37**, 8 (1964).

BULLETIN OF THE CHEMICAL SOCIETY OF JAPAN, VOL. 50 (3), 761—762 (1977)

Organic Photochemical Reactions. XXV. The Photoaddition of 1-Phenyl-1,2-propanedione to Olefins[1]

Kensuke SHIMA, Shigeki TAKEO, Ken-ichi YOKOYAMA, and Hideaki YAMAGUCHI
Department of Industrial Chemistry, Faculty of Engineering, Miyazaki University, Miyazaki 880

(Received September 1, 1976)

Synopsis. The irradiation of 1-phenyl-1,2-propanedione and olefins, such as 2,3-dimethyl-2-butene and α-methylstyrene, in benzene gives mainly oxetanes, in sharp contrast to the results obtained from the photoaddition of biacetyl to these olefins. The differences between these results are discussed in terms of the reactivity of the 1,4-biradical intermediates.

In a previous publication,[2] it was suggested that biacetyl adds to methyl-substituted olefins, such as 2,3-dimethyl-2-butene, 2-methyl-2-butene, α-methylstyrene and 2-ethoxypropene, to give unsaturated ethers (I),[3] which are the products expected from the disproportionation of 1,4-biradical intermediates (II). In order to investigate the scope and limitations of these photoaddition reactions, the photoaddition of 1-phenyl-1,2-propanedione (IIIa) and 1-(*p*-tolyl)-1,2-propanedione (IIIb) to 2,3-dimethyl-2-butene and α-methylstyrene was studied.

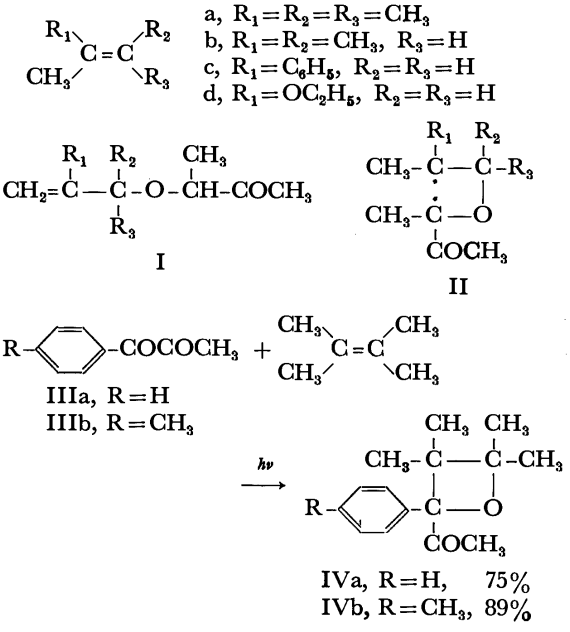

The irradiation of a benzene solution of IIIa and 2,3-dimethyl-2-butene using a 300-W high-pressure mercury lamp through a filter solution of naphthalene in hexane gave an oxetane (IVa) as the main product (75%).[4] IVa was isolated by column chromatography on silica gel and characterized by spectroscopic methods. The IR spectra of IVa showed absorption by an acetyl carbonyl at 1715 cm^{-1} and its NMR spectra showed an acetyl proton at δ 2.09. From these results, the structure of the oxetane was assigned to 1,1,2,2-tetramethyl-3-acetyl-3-phenyloxetane (IVa). Similarly, the addition of IIIb to 2,3-dimethyl-2-butene gave 1,1,2,2-tetramethyl-3-acetyl-3-(*p*-tolyl)oxetane (IVb) in an 89% yield. On the other hand, the photoaddition of IIIa (or IIIb) to α-methylstyrene gave three isolated products: Va, Vb, and Vc (or VIa, VIb, and VIc).[5] In these cases, addition products for acetyl carbonyl to α-methylstyrene were also observed. The stereochemistry of Vb and Vc can be deduced from a comparison of the NMR spectra of their methyl protons: the *trans* isomer (Vc) shows methyl absorption at a field higher than that of the *cis* isomer (Vb) due to the ring current of the phenyl group. The stereochemistry of Va was deduced using the same reasoning.

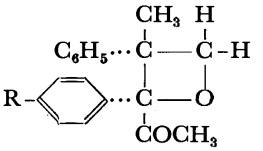

Vb (R=H), 40%
VIb (R=CH_3), 55.3%

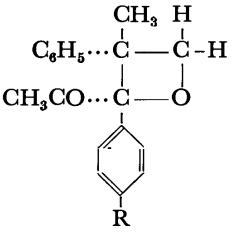

Vc (R=H), 36%
VIc (R=CH_3), 11.1%

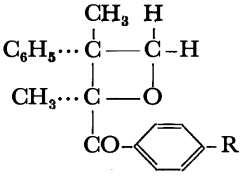

Va (R=H), 24%
VIa (R=CH_3), 33.4%

In the present experiment, unsaturated ethers, whose formation was a predominant process in the case of biacetyl and 2,3-dimethyl-2-butene, could not be detected. This sharp contrast can be explained by the

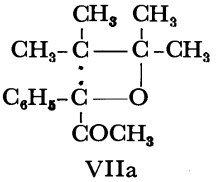

VIIa

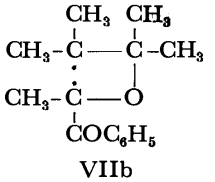

VIIb

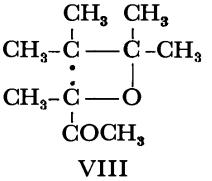

VIII

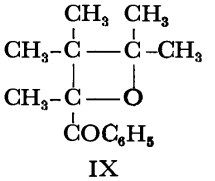

IX

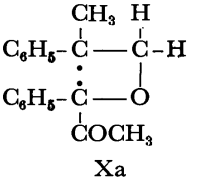

Xa

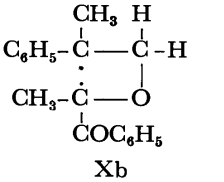

Xb

smaller hydrogen abstraction ability of 1,4-biradical VIIa compared with VIII. In addition, the absence of product IX could be a reflection of a difference in

the stability of 1,4-biradicals VIIa and VIIb. In the case of the reaction of IIIa with α-methylstyrene, the product expected from the addition of an acetyl carbonyl in IIIa to α-methylstyrene was obtained, though as a minor product. Probably the difference in the stability of 1,4-biradicals Xa and Xb is not as large as that of VIIa and VIIb. Finally, the absence of the stereoisomer of Va (or VIa) may be a reflection of a steric requirement in 1,4-biradicals: bulkier phenyl and aroyl groups may be far apart.

Experimental

General. NMR spectra were obtained with a JEOL JNM-MH 100 instrument for solutions in CCl_4 containing tetramethylsilane as the internal standard, IR spectra with a JASCO IRA-1 spectrophotometer, mass spectra with a Hitachi Perkin-Elmer RMU-60 spectrometer, and VPC with a Shimadzu GC-3BF apparatus using a column of Ucon Oil LB-550X (20% on Celite 545, 2 m) at 200 °C.

The following materials were prepared by previously reported procedures: 1-phenyl-1,2-propanedione (IIIa),[6,7] 1-(*p*-tolyl)-1,2-propanedione (IIIb),[6-8] and 2,3-dimethyl-2-butene.[9]

Irradiation of 1-Phenyl-1,2-propanedione (IIIa) and 2,3-Dimethyl-2-butene. A solution of IIIa (22.2 g, 0.15 mol) and 2,3-dimethyl-2-butene (17.7 g, 0.21 mol) in benzene (60 ml) was irradiated for 5 days using a 300-W high-pressure mercury arc filtered through a hexane solution of naphthalene in nitrogen at room temperature. After the removal of the low-boiling materials, the remaining liquid was distilled under reduced pressure to give a liquid (11 g, bp 82—107 °C/3 mmHg), leaving a viscous liquid (1 g). VPC of the distillate showed an oxetane (IVa, 75%), benzoic acid (14%), and a small amount of an unidentified product (11%). IVa was isolated by chromatography on silica gel: bp 59 °C/5.5 mmHg;[10] *m/e* 189(M^+-COCH_3), 105(base, $C_6H_5CO^+$), and 77($C_6H_5^+$); IR 1715 and 970 cm^{-1}; NMR δ 0.80(3H, s), 1.25 (3H, s), 1.26(3H, s), 1.37(3H, s), 2.09(3H, s), 7.27(3H, m), and 7.53(2H, m). Found: C, 77.43; H, 8.59%. Calcd for $C_{15}H_{20}O_2$: C, 77.55; H, 8.68%.

Irradiation of 1-(p-Tolyl)-1,2-propanedione (IIIb) and 2,3-Dimethyl-2-butene. A mixture of IIIb (8.1 g, 0.05 mol) and 2,3-dimethyl-2-butene (5.9 g, 0.07 mol) in benzene (20 ml) was irradiated for 5 days. After the removal of the unreacted materials, a fraction boiling at 92—119 °C/5 mmHg (4.7 g) was collected; residues, 1 g. VPC analysis showed three products with a relative ratio of peak areas of 89: 9.7: 1.3. The major product (IVb) was isolated by chromatography on silica gel: bp 94 °C/2 mmHg;[11] *m/e* 203, 119(base), and 91; IR 1715 and 980 cm^{-1}; NMR δ 0.78(3H, s), 1.23(3H, s), 1.26(3H, s), 1.37(3H, s), 2.07(3H, s), 2.35(3H, s), 7.12(2H, m), and 7.41(2H, m). Found: C, 78.26; H, 9.02%. Calcd for $C_{16}H_{22}O_2$: C, 78.01; H, 9.00%.

Irradiation of 1-Phenyl-1,2-propanedione (IIIa) and α-Methylstyrene. A solution of IIIa (10.4 g, 0.07 mol) and α-methylstyrene (11.8 g, 0.1 mol) in benzene (60 ml) was irradiated for 10 days. After the removal of the unreacted materials, a fraction boiling at 80—140 °C/3 mmHg(3.9 g)[12] was collected; residues, 4.8 g. The distillate was chromatographed on silica gel in hexane using 4% acetone as the eluent, giving three isolated products. The first eluted product was 1,*t*-2-dimethyl-1-benzoyl-2-phenyloxetane (Va, 24%): mp 85 °C; *m/e* 266(M^+), 118(base), 105, and 77; IR 1680 and 995 cm^{-1}; NMR δ 1.41(3H, s), 1.52(3H, s), 4.09(1H, d, J=5.7 Hz), 4.94(1H, d, J=5.7 Hz), 7.09(8H, m), and 7.95(2H, M). Found: C, 81.12; H, 6.67%. Calcd for $C_{18}H_{18}O_2$: C, 81.17; H, 6.81%. The second eluted product was 1,*c*-2-diphenyl-1-acetyl-2-methyloxetane (Vb, 40%): bp 145 °C/5 mmHg; *m/e* 266, 118, 105, and 77; IR 1715 and 990 cm^{-1}; NMR δ 1.77 (3H, s), 2.12(3H, s), 4.19(1H, d, J=5.7 Hz), 5.10(1H, d, J=5.7 Hz), 6.99(8H, m), and 7.23(2H, m). Found: C, 81.42; H, 6.84%. Calcd for $C_{18}H_{18}O_2$: C, 81.17; H, 6.81%. The third eluted product was 1,*t*-2-diphenyl-1-acetyl-2-methyloxetane (Vc, 36%): mp 71 °C; *m/e* 266, 118, 105, and 77; IR 1720 and 990 cm^{-1}; NMR δ 1.21(3H, s), 1.90(3H, s), 4.30(1H, d, J=5.7 Hz), 4.92(1H, d, J=5.7 Hz), 7.13(8H, m), and 7.47 (2H, m). Found: C, 81.21; H, 6.77%. Calcd for $C_{18}H_{18}O_2$: C, 81.17; H, 6.81%.

Irradiation of 1-(p-Tolyl)-1,2-propanedione (IIIb) and α-Methylstyrene. After 10 days of irradiation of a mixture of IIIb (8.1 g, 0.05 mol) and α-methylstyrene (8.4 g, 0.07 mol) in benzene (20 ml), a fraction boiling at 105—130 °C/4 mmHg (1.8 g)[13] was obtained; residues, 2 g. The distillate was chromatographed on silica gel. The first eluted product was VIa (33.4%): *m/e* 280(M^+), 119(base), 118, 91, and 43; IR 1675 and 990 cm^{-1}; NMR δ 1.42(3H, s), 1.53(3H, s), 2.41(3H, s), 4.16(1H, d, J=5.7 Hz), 5.06(1H, d, J=5.7 Hz), 7.24(7H, m), and 8.01(2H, m). The second eluted product was VIb(55.5%): *m/e* 280, 119(base), 118, and 91; IR 1715 and 990 cm^{-1}; NMR δ 1.74(3H, s), 2.07(3H, s), 2.12(3H, s), 4.14(1H, d, J=5.7 Hz), 5.07(1H, d, J=5.7 Hz), and 6.95(9H, m). The third eluted product was VIc(11.1%): *m/e* 119, 118, and 91; IR 1720 and 995 cm^{-1}; NMR δ 1.23(3H, s), 1.95(3H, s), 2.35(3H, s), 4.44 (1H, d, J=5.7 Hz), 5.05(1H, d, J=5.7 Hz), and 7.40(9H, m).

The authors wish to thank Dr. C. Pac of Osaka University, for helpful discussions. The present work was partially supported by a Grant-in-Aid for Scientific Research from the Ministry of Education (No. 747020).

References

1) Part XXIV, K. Shima, T. Kubota, and H. Sakurai, *Bull. Chem. Soc. Jpn.*, **49**, 2567 (1967).

2) H.-S. Ryang, K. Shima, and H. Sakurai, *Tetrahedron Lett.*, **1970**, 1094; *J. Am. Chem. Soc.*, **93**, 5270 (1971); *J. Org. Chem.*, **38**, 2860 (1973).

3) In the photoaddition of biacetyl to α-methylstyrene and 2-ethoxypropene, the major products are oxetanes. The ratio of oxetanes to unsaturated ethers are *ca.* 2.[2]

4) Unsaturated ethers were not detected in this photoreaction.

5) No other by-products are produced in this photoreaction. Also, no oxetanes such as XI were detected in these reactions.

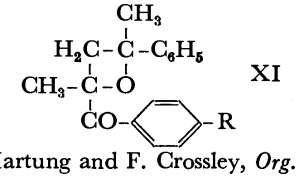

XI

6) W. H. Hartung and F. Crossley, *Org. Synth.*, Coll. Vol. II, 363 (1943).

7) W. W. Hartman and L. J. Roll, *Org. Synth.*, Coll. Vol. III, 20 (1955).

8) R. Adams, *J. Am. Chem. Soc.*, **46**, 1889 (1924).

9) I. Shurman and C. E. Boord, *J. Am. Chem. Soc.*, **55**, 4930 (1933).

10) Yield of IVa based on the IIIa used: 23.7 mol%.

11) Yield of IVb based on the IIIb used: 34 mol%.

12) Yield of products based on the IIIa used: total 20.9 mol%; Va, 5.0 mol%; Vb, 8.4 mol%; Vc, 7.5 mol%.

13) Yield of products based on the IIIb used: total 12.9 mol%; VIa, 4.3 mol%; VIb, 7.2 mol%; VIc, 1.4 mol%.

BULLETIN OF THE CHEMICAL SOCIETY OF JAPAN, VOL. 50 (3), 763—764 (1977)

Hydrogen-Deuterium Exchange Reaction *via* β-Sulfinyl Carbanion. Neighboring Sulfur Participation in Carbanion Formation

Tohru KOYANAGI, Jun-ichi HAYAMI, and Aritsune KAJI
Department of Chemistry, Faculty of Science, Kyoto University, Kyoto 606

(Received September 8, 1976)

Synopsis. The rate of base-catalyzed H-D exchange reaction of substituted cyclopropanes and cyclohexanes containing sulfur atom at the β-position of reaction center was investigated. Neighboring sulfur participation in stabilization of the carbanion was suggested in the case of ethyl *trans*-2-(phenylthio)cyclopropanecarboxylate.

Participation of neighboring sulfur, and sulfur located at a remote site has widely been known in reactions where carbenium ion takes part as an intermediate.[1] However, no similar participation has been reported for carbanions having sulfur-containing substituents at the β or more remote positions.[2] This is quite a contrast with the fact that the considerable experimental evidence has accumulated which indicates that carbanions are stabilized by the adjacent sulfur atom.[3]

We tried to reveal the effect of the participation of sulfur atom located at the β-position to carbanion. The reactions studied were base-catalyzed hydrogen-deuterium exchange of alicyclic compounds.

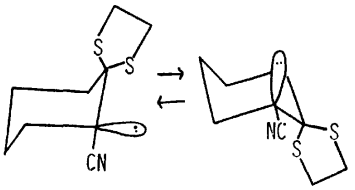

[A] [B]

Fig. 1. [A] Both of the sulfur atoms can participate in the carbanion lobe. [B] One of the sulfur atoms can participate in the carbanion lobe.

TABLE 1. SECOND-ORDER RATE CONSTANTS AND PARAMETERS OF ACTIVATION FOR THE H-D EXCHANGE REACTION OF CYCLOHEXANE CARBONITRILES

Substrate	$10^6\ k^{a,b)}$ ($M^{-1}\ s^{-1}$)	Rel. k	$\Delta H^{\neq}$ (kcal/mol)	$\Delta S^{\neq\ a)}$ (e.u.)
1	5.35	1.97	19.3±0.5	−27.0±2
2	2.72	1	21.9±0.5	−24.0±2

a) At 72 °C. b) [pyridine]$=9.90\times10^{-1}$ M.

The initial investigation was carried out with 1,1-ethylenedithio-2-cyanocyclohexane (**1**). In our study with cyclohexyl derivatives, though the ring inversion may be operative in **1**, at least one of the sulfur atoms should be able to interact with the carbanion lobe (Fig. 1). In Table 1, second-order rate constants and parameters of activation on pyridine-catalyzed deuterium exchange reaction of **1** are shown with those of cyclohexanecarbonitrile (**2**). Thus, in ethanol-*d*, **1** underwent the H-D exchange reaction about twice as fast as **2**, and **1** showed smaller enthalpy of activation than that of **2**. But it is too imprudent to discuss the presence of neighboring sulfur participation, since the separation of the potential effect of participation and inductive effect, both played by dithiacyclopentyl group, cannot be performed with certainty.

In the next trial, to make a clear distinction between these two effects, stereoisomers of cyclopropyl compounds were selected for the model compounds. Compounds used were ethyl *trans*-2-(phenylthio)cyclopropanecarboxylate (*trans*-**3**) and ethyl *cis*-2-(phenylthio)cyclopropanecarboxylate (*cis*-**3**), with ethyl *trans*-2-phenylcyclopropanecarboxylate (**4**) as the reference compound.

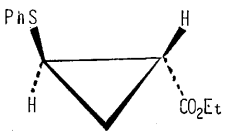

(*trans*-**3**)

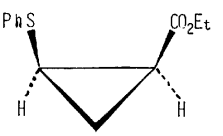

(*cis*-**3**)

Cyclopropyl derivatives should be suitable for our study, since they have acidic hydrogens, and in many cases the rate of the racemization of carbanion is much smaller than that of deuterium exchange owing to the strain of cyclopropane ring.[4] In fact no isomerization between *trans*-**3** and *cis*-**3** was observed during the deuterium exchange in the present study. Second-order rate constants and relative rate ratios of these compounds are listed in Table 2. More pronounced electron-withdrawing ability of phenylthio group than that of phenyl group makes *trans*-**3** and *cis*-**3** more reactive than **4**.[5] *Trans*-**3** exchanges faster than *cis*-**3**, thus in *trans*-ester the operation of neighboring sulfur participation may be suggested.

TABLE 2. SECOND-ORDER RATE CONSTANTS FOR THE H-D EXCHANGE REACTION OF CYCLOPROPANE CARBOXYLATE ESTERS

Substrate	$10^6\ k^{a,b)}$ ($M^{-1}\ s^{-1}$)	Rel. k
trans-**3**	45.7	18.4
cis-**3**	20.0	8.0
4	2.49	1.0

a) At 70 °C. b) [pyridine]$=2.48\times10^{-1}$ M.

TABLE 3. PARAMETERS OF ACTIVATION FOR THE H-D EXCHANGE OF *trans*-**3** AND *cis*-**3**

Substrate	$\Delta H^{\neq}$ (kcal/mol)	$\Delta S^{\neq\ a)}$ (e.u.)
trans-**3**	16.0±0.5	−34.0±2
cis-**3**	19.7±0.5	−27.7±2

a) At 70 °C.

Parameters of activation were evaluated for *trans*-**3** and *cis*-**3**, and are shown in Table 3. Large negative values of entropy of activation (ΔS^*) indicate that the rate-determining step of this reaction is the removal of the acidic proton by the base (pyridine) to form a hydrogen-bonded carbanion.[4] In *trans*-**3** the attack of pyridine is sterically more hindered than in *cis*-**3**, since both the phenylthio group and the hydrogen being attacked reside on the same side of the cyclopropane ring. Although the contribution of this steric hindrance can hardly be evaluated, such a hindrance can cause an increase in enthalpy of activation (ΔH^*) for *trans*-**3**, partly compensating a decrease in ΔH^* that results from the presence of the sulfur participation.

Thus the difference in ΔH^* between *trans*-**3** and *cis*-**3** should be appreciated to show apparently the neighboring sulfur participation for the former compound in stabilizing the transition state and the resulting carbanion.

Table 4. IR and UV absorptions of *trans*-**3** and *cis*-**3**

Substrate	cm^{-1} a)	λ_{max} b) (MeOH)	($\log \varepsilon$)
trans-**3**	1040	250.0	(4.1)
cis-**3**	1028	252.5	(4.1)

a) Skeletal vibration of cyclopropane ring in IR spectrum.
b) N→V transition of the three-membered ring.

Furthermore, IR and UV spectroscopic data, summarized in Table 4, suggest that *cis*-**3** is less stable than *trans*-**3** at the ground state due to the steric strain. In IR spectrum, frequencies of skeletal vibration for cyclopropane ring is lower in *cis*-**3**, which indicates the increase of molecular strain in *cis*-**3**.[6] In UV spectrum, the absorption maximum of *cis*-**3** appears at 252.5 nm (N→V transition of the three-membered ring), 2.5 nm longer than that of *trans*-**3**, reflecting the difference in the ground state strain perturbation.[7] Thus one can estimate that *cis*-**3** exists at about 1 kcal/mol higher in energy than *trans*-**3** does at the ground state.[8]

Therefore, taking into account the increase of ΔH^* by steric hindrance for the approach of base, and the difference in ground state energy, the stabilization should be more pronounced for *trans*-**3** than that inferred from the difference in observed ΔH^*.[8] Consequently it is quite probable that a neighboring sulfur atom participates in stabilizing the carbanion of *trans*-**3**.

Experimental

The IR spectra were obtained using a Perkin-Elmer 521 spectrophotometer. The NMR spectra were recorded on a JEOL PS-100 spectrometer. The UV spectra were measured with a Hitachi 200-10 spectrophotometer. All compounds gave satisfactory results on spectroscopic analysis (IR, NMR), and on elemental analysis.

Materials. *1,1-Ethylenedithio-2-cyanocyclohexane* (***1***): Dry HCl gas was bubbled into a benzene solution (30 ml) of 2-cyanocyclohexanone[9] (7.5 g) and 1,2-ethanedithiol (15 g) for 1 h at room temperature. After usual work-up and recrystallization from benzene, 2.0 g (13 %) of **1** was obtained; white needles, mp 61 °C.

Cyclohexanecarbonitrile (***2***): A benzene solution (10 ml) of cyclohexanecarboxamide (8.7 g) and thionyl chloride (17.8 g) was heated under reflux for 6 h. After cooling, the solution was poured in ice–water, and the organic layer was extracted with ether. After usual work-up, distillation of the residual oil gave 5.8 g (78 %) of **2**; bp 75 °C/18 mmHg.

Ethyl trans- *and* cis-*2-(Phenylthio)cyclopropanecarboxylate* (trans-***3***), (cis-***3***): Ethyl diazoacetate (12 g) was added dropwise to the refluxing xylene solution (50 ml) of phenyl vinyl sulfide (10 g) in 1 h. The solution was heated under reflux for additional 1 h, and then xylene was distilled off, leaving brown residual oil (18 g), which was fractionated by preparative GLC (Shimadzu GC-5A) to give *trans*-**3** and *cis*-**3**.

Ethyl trans-*2-phenylcyclopropanecarboxylate* (***4***): Ethyl diazoacetate (12 g) was added dropwise to refluxing xylene solution (30 ml) of styrene (20 g) and hydroquinone (0.5 g) in 1 h. After the same procedure for *trans*-**3** and *cis*-**3**, **4** was obtained.

Kinetics. The stock solutions were prepared in volumetric flask by adding the stock base solutions (pyridine in ethanol-*d*) to a weighed amount of the substrate. With a syringe each 0.5 ml portion was transferred to glass ampoules, which were then flame sealed. The tubes were placed in a thermostat at an appropriate temperature. After predetermined time, tubes were withdrawn and were quenched in a Dry Ice–acetone bath. After removing ethanol and pyridine *in vacuo*, the remaining substrate was transferred with CCl_4 to an NMR tube. Rate constants were evaluated by comparing the intensity of the specified peak with that of standard one in their NMR spectra.

References

1) H. Böhme and K. Sell, *Chem. Ber.*, **81**, 123 (1948).
2) The participation of the β-sulfur atom to the developing doule bond was suggested in the E2 reaction of 1-bromo-3-(phenylthio)propane. Y. Yano and S. Oae, *Tetrahedron*, **26**, 67 (1970).
3) D. J. Cram, "Fundamentals of Carbanion Chemistry," Academic Press, New York, N. Y. (1965).
4) H. M. Walborsky and J. M. Motes, *J. Am. Chem. Soc.*, **92**, 2445 (1970).
5) S. Oae, "Yuki Iou Kagobutsu No Kagaku," Kagakudojin, Kyoto (1968).
6) M. Ōki, "Sekigaisen Supekutoru," Tokyo University Press, Tokyo (1967).
7) R. C. Hahn, P. H. Howard, Sum-Man Kong, G. A. Lorenzo, and N. L. Miller, *J. Am. Chem. Soc.*, **91**, 3558 (1969).
8) A. Ohno and Y. Ohnishi, *Tetrahedron Lett.*, **1972**, 339.
9) M. E. Kuehne, *J. Am. Chem. Soc.*, **81**, 5400 (1959).

BULLETIN OF THE CHEMICAL SOCIETY OF JAPAN, VOL. 50 (3), 765—766 (1977)

The Action of Malononitrile and Ethyl Cyanoacetate on Diphenylcyclopropenone

Israel AGRANAT, Gerhard V. BOYD,* and Mark A. WIRT*

Department of Organic Chemistry, The Hebrew University of Jerusalem, Jerusalem, Israel

** Department of Chemistry, Chelsea College, London SW3 6LX, England*

(Received May 4, 1976)

Synopsis. Diphenylcyclopropenone reacts with malononitrile in the presence of ethanolic sodium methoxide to yield, after acidification, (*E*)-1,1-dicyano-2-hydroxy-3,4-diphenyl-1,3-butadiene (**1a**); an analogous product, ethyl (2*Z*, 4*E*)-2-cyano-3-hydroxy-4,5-diphenyl-2,4-pentadienoate (**1b**), is formed from ethyl cyanoacetate.

In the young chemistry of cyclopropenones, a leading role has been played by diphenylcyclopropenone (DCP).[1] The synthesis of DCP is considered 'a milestone in theoretical organic chemistry'[2] The 'state of the art' of the cyclopropenones has recently been reviewed.[3,4] The general picture that emerges is the *erratic* behaviour of these microcyclic ketones, particularly in addition reactions.[3] This trend, in which the unpredictable predominates, may be illustrated by the action of malononitrile and ethyl cyanoacetate on DCP.

The reactions of cyclopropenones with malononitrile have previously been employed as a synthetic route to triafulvenes. DCP reacted with malononitrile in boiling acetate anhydride solution to give 4,4-dicyano-1,2-diphenyltriafulvene;[5] aliphatic cyclopropenones condensed analogously.[6-8] The use of β-alanine[9] or boron trifluoride[10] as a catalyst resulted in increased yields.

Likewise, condensation of DCP and ethyl cyanoacetate gave the corresponding triafulvene.[9] In general, basic condensation agents which could cleave the three-membered ring were avoided. An improved procedure employed an active form of DCP. Thus, treatment of 3-ethoxy-1,2-diphenylcyclopropenium tetrafluoroborate and malononitrile with one mole of *N,N*-diethylisopropylamine in dichloromethane solution afforded the dicyanotriafulvene in 85% yield.[11] 3,3-Dichloro-1,2-diphenylcyclopropene reacted directly with malononitrile at 100—120° C without solvent to give the triafulvene in 10% yield.[12] It has been claimed that in the reaction of DCP with malononitrile in pyridine solution seven products were obtained, one of which was tentatively assingned the structure of 3-amino-2-cyano-4,4-diphenyl-2,4-cyclopentadien-1-one (or its 2-amino-3-cyano isomer).[13]

In the present investigation, the reactions of DCP with malononitrile and with ethyl cyanoacetate were studied under basic conditions in protic solutions. We had thought that a Michael addition of the nucleophile (*e.g.*, $\bar{C}H(CN)_2$) to the activated carbon-carbon double bond of the cyclopropenone ring might occur, followed perhaps by a ring enlargement process, leading eventually to a pyridinone derivative. Various nucleophilic addition reactions at the carbon-carbon double bond of cyclopropenones have been effected.[3,4] However, in this case the reactions followed a different course. Treatment of DCP with an ethanolic solution of malononitrile in the presence of sodium methoxide, followed by acidification, gave a high yield of a pale yellow acidic solid, whose analysis and mass spectrum corresponded to that of a 1:1 adduct. The NMR spectrum showed only a multiplet in the aromatic region, but the IR spectrum was more revealing, containing broad OH absorption and strong bands at 2214 and 2209 cm^{-1}, indicative of two α,β-unsaturated cyanide groups. We therefore considered that the product was the enolic dinitrile (**1a**) and this structure, together with the *cis*-configuration of the phenyl groups, was readily confirmed by an unambiguous synthesis of the compound from the sodium salt of malonoitrile and (*E*)-2,3-dipheylpropenoyl chloride.[14] The reaction of DCP with ethyl cyanoacetate under the same conditions yielded a colourless adduct, which was insoluble in aqueous alkali; however, the virtual identity of its UV spectrum with that of the previous compound, a positive $FeCl_3$ reaction, and the appearance of intense CN absorption and a sigle carbonyl band at 1655 cm^{-1} (chelated ester) in its IR spectrum suggested that it was the analogue (**1b**), and, indeed, it was also formed by condensation of ethyl sodio-cyanoacetate with the foregoing acid chloride.

The formation of **1a** and **1b** closely resembles the hydrolyses of cyclopropenones with sodium or potassium hydroxide, in which salts of α,β-unsaturated acids are produced.[3] The present reaction presumably involves the addition of the anion of malononitrile (and of ethyl cyanoacetate) to the carbonyl group of DCP, followed by collapse of the intermediate open chain carbanion species (Scheme 1). Protonation

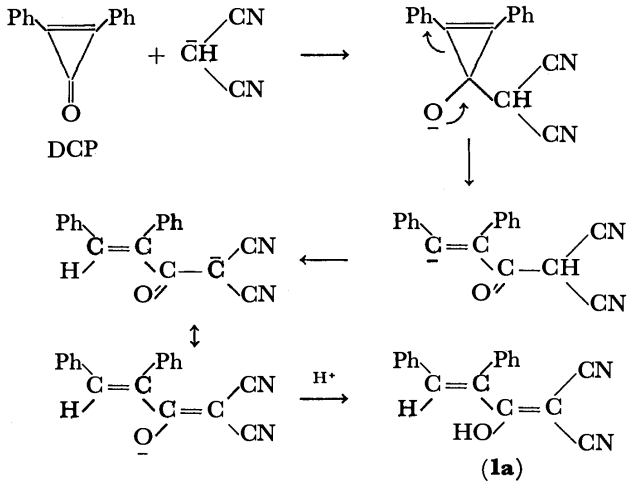

Scheme 1.

would then complete the process. It is interesting to note that the *cis*-configuration of phenyl groups in the substrate (DCP) is retained in the product, in analogy with various basic hydrolyses of cyclopropenones. It may be an indication of the high rate of protonation of the carbanion intermediate. The course of the nucleophilic addition to DCP contrasts with the reaction of malononitrile and 3-ethoxy-1,2-diphenylcyclopropenium tetrafluoroborate in the presence of *two* moles of *N,N*-diisopropylethylamine.[15] In the latter reaction, an addition of the nucleophile to the carbon-carbon doble bond is preferred, and the product is 1,3-diphenyl-3-ethoxy-4,4-dicyano-1,3-butadiene. The reduced cyclopropenium contribution in DCP might have been the determining factor which directed the addition of the nucleophile to the carbonyl rather than to the carbon-carbon double bond. Thermodynamic effects are probably responsible for the ultimate transformation to the conjugated dienols **1a** and **1b**.

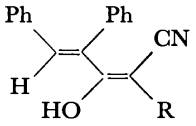

1 **a**; R=CN, **b**; R=CO_2Et

Experimental

Melting points were taken on a "Unimelt" Thomas-Hoover capillary melting point apparatus and are uncorrected. Infrared spectra were recorded on Perkin-Elmer 457 and 257 spectrophotometers for Nujol mulls. Ultraviolet spectra were determined with Unicam Model SP 800 and Perkin-Elmer 402 spectrophotometers and NMR spectra with a Perkin-Elmer R 32 instrument at 90 MHz and are reported in ppm relative to Me_4Si as internal standard. The mass spectra of the new compounds, obtained with a Varian Mat-311 spectrometer, contained the appropriate signals representing the molecular ions.

*(E)-1,1-Dicyano-2-hydroxy-3,4-diphenyl-1,3-butadiene (**1a**).* *(a)*: A magnetically stirred solution of sodium methoxide (0.60 g, 11 mmol) in absolute ethanol (100 ml) was treated under anhydrous conditions at room temperature first with malononitrile (0.86 g, 13 mmol) and then with DCP[16] (2.27 g, 11 mmol), whereupon the solution became yellow. After 12 h at room temperature most of the solvent was removed under reduced pressure, concentrated hydrochloric acid and water were added successively to the residue, and the remainder of the ethanol was distilled off. The resulting yellow solid was collected, washed with water, and recrystallised from aqueous ethanol or xylene to give **1a** (2.70 g, 90%) as pale yellow needles, mp 182 °C (decomp); IR 3170 (broad), 2214, 2209, and 1608 cm^{-1}; UV_{max} (CH_3CN) 259 (log ε 4.12) and 325 nm (4.06); UV_{max} (cyclohexane) 234, 258, and 338 nm; NMR (DMSO) δ=7.08—7.42 (m).

Found: C, 79.58; H, 4.22; N, 10.57%. Calcd for $C_{18}H_{12}N_2O$: C, 79.40; H, 4.44; N, 10.29%.

(b): A stirred solution of malononitrile (0.61 g, 9.2 mmol) in ethanolic sodium ethoxide, prepared from sodium (0.14 g, 6.1 mmol) and ethanol (50 ml), was slowly treated with (*E*)-2,3-diphenylpropenoyl chloride[14] (1.5 g, 6.1 mmol). After 12 h the solvent was removed under reduced pressure and the residue was stirred with 1 M hydrochloric acid (54 ml); the resulting oil was separated by decantation, washed with water, and dissolved in a small amount of aqueous 5% sodium carbonate. The solution was washed with ether (2×50 ml) and then acidified with 2 M hydrochloric acid; the resulting precipitate was recrystallised from xylene, giving **1a** (0.81 g, 48%), identical (IR spectrum, mp and mixed mp) with the previous product.

*Ethyl (2Z, 4E)-2-Cyano-3-hydroxy-4,5-diphenyl-2,4-pentadienoate (**1b**).* *(a)*: This compound was prepared analogously from ethyl cyanoacetate (1.774 g, 15.7 mmol), DCP (2.55 g, 12.4 mmol), sodium methoxide (0.756 g, 14 mmol), and ethanol (60 ml). After most of the solvent had been removed, dilute hydrochloric acid was added and the resulting oil was separated and crystallised from ethanol or cyclohexane to give **1b** (2.88 g, 73%) as colourless needless, mp 130 °C. IR 2210, 1655, and 1585 cm^{-1}; UV_{max} (CH_3CN) 265 (log ε 4.00) and 331 nm (4.18); UV_{max} (cyclohexane) 234 (4.07), 258 (3.96), and 338 nm (4.19); NMR ($CDCl_3$) δ=1.37 (t, *J*=7 Hz, 3H), 4.36 (q, *J*=7 Hz, 2H), 7.04—7.27 (m, 6H), 7.30—7.45 (m, 5H), and 7.57 (s, 1H).

Found: C, 75.28; H, 5.33; N, 4.64; OEt, 13.7%. Calcd for $C_{20}H_{17}NO_3$: C, 75.22; H, 5.37; N, 4.39; OEt, 14.1%.

(b): Diphenylpropenoyl chloride (1.5 g, 6.1 mmol) was condensed with ethyl cyanoacetate (1.5 g, 13.2 mmol), as described in (*b*) above, and the solvent was removed after 12 h. The residue was treated with 1 M hydrochloric acid and the resulting oil was washed with water (3×30 ml) and crystallised from ethanol to yield **1b** (0.55 g, 27%), identified by its IR spectrum, mp, and mixed mp.

References

1) R. Breslow, T. Eicher, A. Krebs, R. A. Peterson, and J. Posner, *J. Am. Chem. Soc.*, **87**, 1320 (1965).
2) W. D. Emmons, *Org. Synth.*, **47**, p. VIII (1967).
3) K. T. Potts and J. S. Baum, *Chem. Rev.*, **74**, 189 (1974).
4) T. Eicher and J. L. Weber, *Top. Curr. Chem.*, **57**, 1 (1975).
5) E. D. Bergmann and I. Agranat, *J. Am. Chem. Soc.*, **86**, 3587 (1964).
6) A. S. Kende and P. T. Izzo, *J. Am. Chem. Soc.*, **86**, 3587 (1964).
7) J. Ciabattoni and E. C. Nathan, III, *J. Am. Chem. Soc.*, **91**, 4766 (1969).
8) I. Belsky, *Israel J. Chem.*, **8**, 769 (1970).
9) S. Andreades, *J. Am. Chem. Soc.*, **87**, 3941 (1965).
10) Y. Kitahara and M. Funamizu, *Bull. Chem. Soc. Jpn.*, **37**, 1897 (1964).
11) T. Eicher, T. Pfister and N. Krüger, *Org. Prep. Proc. Int.*, **6**, 63 (1974).
12) I. Agranat and R. M. J. Loewenstein, unpublished results.
13) L. G. Wolgemuth, Ph. D. Thesis, University of Michigan, 1964; *Diss. Abstr.*, **25**, 3278 (1964).
14) R. Riemschneider and H. Kampfer, *Monatsh.*, **90**, 518 (1959).
15) T. Eicher and A. Hansen, *Chem. Ber.*, **102**, 319 (1969).
16) R. Breslow and J. Posner, *Org. Synth.*, **47**, 62 (1967).

BULLETIN OF THE CHEMICAL SOCIETY OF JAPAN, VOL. 50 (3), 767—768 (1977)

Further Studies on the Decarboxylation of Cinnamylidenemalonic Acid in Resorcinol and Catechol

M. A. HALEEM and M. A. HAKEEM
College of Engineering, University of Riyadh, Riyadh, Saudi Arabia

(Received March 17, 1976)

Synopsis. Kinetic data are reported for the decarboxylation of cinnamylidenemalonic acid in resorcinol and catechol. The activation parameters are culculated and compared with those previously reported for the decarboxylation of unsubstituted and substituted malonic acids.

The kinetics for decarboxylation of the derivatives of malonic acid[1] have been reported in our earlier investigations in resorcinol and catechol solvents. Bernoulli and Jakubowicz[2] studied the decarboxylation of malonic acid derivatives in aqueous solution in the range of 76—110 °C, including disubstituted malonic acids. Muus[3] reported the kinetic data of dibromomalonic acid in water at 45 °C. Clark[4] studied the decarboxylation of cinnamylidenemalonic and malonic acids in phenol, *m*-cresol, *p*-cresol and several aromatic amines. In the transition state of decarboxylation, it is considered that the carbonyl carbon atom of the reactant coordinates with a pair of unshared electrons on the nucleophilic atom of the solvent molecule and that these interactions between the reagents lower the enthalpy of activation ($\Delta H^{\neq}$) of the reaction. This principle has been tested on a number of compounds and it was thought to be worth-while to carry out the decarboxylation of cinnamylidenemalonic acid to see whether or not any exception could be found. For this purpose a kinetics study of the decarboxylation of cinnamylidenemalonic acid was carried out in resorcinol and catechol.

Experimental

Reagents. The cinnamylidenemalonic acid was prepared by Riaz Ahmed and Das Gupta in Sirohi College by condensation of cinnamaldehyde with malonic acid and purified several times with ethanol, mp 201 °C. Resorcinol and catechol were of analar reagent grade.

Apparatus and Technique. The reaction was usually followed by measuring the volume of carbon dioxide evolved. The apparatus and technique are similar to those described in previous articles.[5-7] About 20 g of resorcinol were separately taken in each run and 0.394 g of cinnamylidenemalonic acid weighed in a sample tube was placed on the movable probe inside the reactor. The set-up was then placed in a constant temperature oil-bath (±0.05 °C) and, when thermal equilibrium was established, the reaction was started by dropping the acid in the solvent. The evolved CO_2 was determined with a measuring burette filled with water saturated with carbon dioxide.

Results and Discussion

Plots of $\log(V_\infty - V_t)$ *vs.* t (where V_∞ is the volume of CO_2 after completion of the reaction and V_t is the volume at time t) showed straight lines, indicating a first order reaction. The rate constant at each temperature was calculated from the slope of the line and these values are tabulated in Table 1. The activation parameters calculated are tabulated in Table 2, along with the results of Clark in other solvents.

TABLE 1. APPARENT FIRST-ORDER RATE CONSTANTS FOR THE DECARBOXYLATION OF CINNAMYLIDENEMALONIC ACID IN RESORCINOL AND CATECHOL

Temp (°C)	No. of data pairs	$k_1 \times 10^5$ (s^{-1}) Catechol	Av. dev.	$k_1 \times 10^5$ (s^{-1}) Resorcinol	Av. dev.
140	5	3.63	±0.02	5.13	±0.01
145	3	5.37	±0.03	8.13	±0.02
150	2	7.76	±0.04	10.96	±0.02
155	3	12.02	±0.02	15.85	±0.02
160	4	16.60	±0.03	21.88	±0.03

In the same solvent, the $\Delta H^{\neq}$ was less for the decarboxylation of cinnamylidenemalonic acid that for malonic acid (see Table 2). Hall[8] found that the mono-anion and the free acid of malonic acid have different rates of decarboxylation in aqueous solution. In non-aqueous solvents the mono-ions may be few and a change is not expected to increase the rate of the process. However, carbon isotope effect studies on hydrogen malonate ions suggest that CO_2 originates from the COOH group and not from the COO^- group, in the decarboxylation in quinoline[9] or dioxane.[10]

As seen in Table 2 (lines 4 and 5) the entropy of activation ($\Delta S^{\neq}$) for the decarboxylation of cinnamylidenemalonic acid in catechol is more negative than in resorcinol, indicating that the activated complex is more stable in catechol than in resorcinol; this result is similar to that in 2,4-dihydroxybenzoic acid, xalic acid,[12] benzoic acid,[13] substituted benzoic acids,[14] oxanilic acid,[15] picolinic acid,[16] and hexylmalinic acid.[1] This proves that the adjacent hydroxyl groups of catechol are mainly responsible for forming the hydrogen bonding and for stabilizing the complex. The methyl and hydroxyl groups in *o*-cresol are adjacent and the entropy of activation is expected to be somewhat more negetive than in *p* and *m*-cresols. Unfortunately, no data is available. However, the comparative entropy of activation of malonic acid and butylmalonic acid[17] (Table 2, line 1) is in support of our conclusion. The decrease in entropy of activation in catechol is an indication of greater interaction towards the acid that in resorcinol. On the contrary, the malonic acid has almost the same enthalpy of activation, probaly due to a super-molecule cluster as proposed by Clark.[18] Substituted malonic acids gave less enthalpy of activation than malonic acid in most of the solvents.

Table 2. Comparative thermodynamic parameters

Solvents	Malonic acid		Cinnamylidenemalonic acid		Butylmalonic acid	
	$\Delta H^{\neq}$ a)	$\Delta S^{\neq}$ b)	$\Delta H^{\neq}$ a)	$\Delta S^{\neq}$ b)	$\Delta H^{\neq}$ a)	$\Delta S^{\neq}$ b)
o-Cresol[17]	24.2	−16.5	—	—	21.3	−22.8
m-Cresol[17]	32.3	+ 3.2	22.0	−25.2	29.7	− 2.3
p-Cresol[17]	29.8	− 2.4	27.1	−14.2	24.0	−15.8
Resorcinol	32.3	+ 1.95	27.08	−11.4	—	—
Catechol	32.2	+ 1.82	22.09	24.2	—	—

a) kcal/mol. b) kcal/mol K.

A plot of $\Delta H^{\neq}$ *vs.* $\Delta S^{\neq}$ for cinnamylidenemalonic acid is approximately linear. Such a linear relationship is evidence that the reaction mechanism in different phenolic solvents is almost the same.

The authors thank Dr. H. Siddiqui for helpful discussions and Dr. C. Balasubramanium for his valuable suggestions. We further thank Mr. Khalid Sayyid for reading this manuscript. Financial support from the Ministry of Education is acknowledged with gratitude.

References

1) M. A. Haleem and M. A. Hakeem, *J. U. A. R. Chem.*, in press.
2) A. L. Bernoulli and H. Jakubowicz, *Helv. Chim. Acta*, **4**, 1018 (1921).
3) J. Muus, *J. Phys. Chem.*, **40**, 121 (1936).
4) L. W. Clark, *J. Phys. Chem.*, **67**, 1481 (1963).
5) M. A. Haleem, M. Nabi, and M. A. Hakeem, *Collect. Czech. Chem. Commun.*, **35**, 1607 (1970).
6) M. A. Haleem, *Collect. Czech. Chem. Commun.*, **35**, 2856 (1970).
7) M. A. Haleem, *Bull. Coll. Sci., Univ. of Baghdad*, **11**, 73 (1969).
8) G. A. Hall, *J. Am. Chem. Soc.*, **71**, 2691 (1949).
9) P. E. Yankwich and H. S. Weber, *J. Am. Chem. Soc.*, **77**, 4513 (1955).
10) P. E. Yankwich and H. S. Weber, *J. Am. Chem. Soc.*, **78**, 564 (1956).
11) M. A. Haleem and M. A. Hakeem, *Aust. J. Chem.*, **29**, 443 (1976).
12) M. A. Haleem and M. Azeem, *Pak. J. Sci. Ind. Res.*, **16**, 1 (1973).
13) M. A. Haleem, *J. U. A. R. Chem*, **13**, 505 (1970).
14) M. A. Haleem and S. S. Ahmed, *Pak. J. Sci. Ind. Res.*, **17**, 6 (1974).
15) M. A. Haleem, M. A. Hakeem, and J. Salamah, *J. Indian Chem. Soc.*, **11**, 645 (1974).
16) M. A. Haleem and M. A. Hakeem, *J. Indian Chem. Soc.*, **52**, 1175 (1975).
17) L. W. Clark, *J. Phys. Chem.*, **70**, 627 (1966).
18) L. W. Clark, *J. Phys. Chem.*, **67**, 526 (1963).

BULLETIN OF THE CHEMICAL SOCIETY OF JAPAN, VOL. 50 (3), 769—770 (1977)

A Study of the Asymmetric Reaction of Methyloxirane with Acetic Acid Catalyzed by an Optically-Active Cobalt Complex

Michihiro ISHIMORI, Haruhiko AOI, Yasuyuki TEZUKA, and Teiji TSURUTA

Department of Synthetic Chemistry, Faculty of Engineering, University of Tokyo, Bunkyo-ku, Tokyo 113

(Received July 14, 1976)

Synopsis. A novel asymmetric reaction of methyloxirane with acetic acid catalyzed by an optically-active Co(salen)-type complex was explored. The products were identified to be propylene diacetate, 2-hydroxypropyl acetate, and 2-hydroxy-1-methylethyl acetate. The mechanistic features of this resolution-type reaction were characterized by the optical activities of the products and of the unchanged methyloxirane.

It has been reported that *N,N'*-disalicylidene-(1*R*,-2*R*)- 1,2-cyclohexanediaminatocobalt(II), $Co^{II}(sal)_2$(*R*-CHXDA), is a low-spin square-planar complex with a λ-conformation of the central chelate ring. Highly asymmetric selectivity was observed in a kinetic resolution of DL-methyloxirane using the $Co^{II}(sal)_2$(*R*-CHXDA)/$LiAlH_4$ system,[1] however, the isomerization of the selected methyloxirane to acetone was observed to occur by hydride shift involving electron transfer from the oxygen to the cobalt atom.[2]

It would be of interest and preparatively useful to explore a reaction in which an asymmetric center is maintained throughout the reaction. In the present series of our studies, the $Co^{II}(sal)_2$(*R*-CHXDA)/butyllithium/methyloxirane/acetic acid system has been found to give optically-active products. In this paper we would like to report the identification of the products and the mechanistic features of the reaction system.

Results and Discussion

Optically-active products I, II, and III, were found to be formed when a reaction was carried out at a mole ratio for Co^{II}: BuLi: methyloxirane: CH_3COOH of 1: 1: 150: 40 at 20 °C (the reaction conditions were as described in Table 1). The optical purity of the reacted methyloxirane calculated from the optical rotation of the unchanged methyloxirane, (L—D/L+D)rm, was 31% (conv. 11.8%). When $MgEt_2$, $ZnEt_2$, $LiAlH_4$, and $AlEt_3$ were used instead of BuLi, the (L—D/L+D)rm values were observed to be 18 (conv. 27.6%), 14 (2.9%), 8 (6.8%), and 0% (27.6%), respectively.

Products I, II, and III were isolated and respectively determined to be propylene diacetate, 2-hydroxypropyl acetate, and 2-hydroxy-1-methylethyl acetate, by mass spectral, elemental, and NMR analyses. Further confirmation of the products was obtained by comparison with authentic samples (see Experimental).

In order to clarify the features of the Co^{II}/BuLi/methyloxirane/CH_3COOH system, was carried out a series of experiments given in Tables 1 and 2. The ratio of the amount of product II $CH_3COOCH_2CH(CH_3)CH_2OH$ to the amounts of products II and III $CH_3COOCH(CH_3)CH_2OH$ was found to be 68—78% in the systems in Tables 1 and 2, indicating that the ring openings take place by acid-catalyzed reactions.[3] In accord with this observation, the systems involving little or no free acetic acid (Nos. 6 and 7 in Table 1) exhibit little or low reactivity for the ring opening reactions. The reaction of acetic acid with methyloxirane was catalyzed by the Co-complex, and presumably also by lithium acetate (formed by a rapid reaction of the Li moiety with CH_3COOH) as shown in Nos. 4, 5, and 9.

In Table 2, products I, II, and III were combined and hydrolyzed to 1,2-propanediol, their optical purities (L—D/L+D)mp* being about 11%. Assuming that III was formed by a complete inversion mechanism (CH–O opening),[3,5] the expected optical purity of 1,2-propanediol (L—D/L+D)cp was calculated from that of reacted methyloxirane (L—D/L+D)rm and the product ratio of III to II (see Table 2). Concerning the data at 25 °C (No. 2-1), the measured optical purity (L—D/L+D)mp is higher than the calculated value (L—D/L+D)cp, suggesting that another type of reaction such as oligomerization involving non-asymmetric selection [see the equations in d) of Table 1 and in e) of Table 2] may take place in parallel with the product(I/II/III)-forming reaction, a suggestion of which is supported by low material balance, (I+II+III)/reacted methyloxirane=78%. On the other hand, in Exp No. 2-2 of high material balance (98%) at 18 °C, the measured value (L—D/L+D)mp is lower than the calculated value; racemization is considered to take place to some extent during hydrolyzing of the products to 1,2-propanediol. The optical activity of pure D(+)-methyloxirane(neat) was assumed to be 15°, which, however, may be a higher value estimated to be 18.3°, using the highest $[\alpha]_{589}^{25}$ value (in $CHCl_3$) so far reported [14.05 (neat)×8.9 ($CHCl_3$)/7.0 ($CHCl_3$)];[6,7] the value of (L—D/L+D) cp (No. 2-2) would be 12.6% if this [α] value were used for [α_0].

It would be of interest to discuss some plausible mechanism for this asymmetric reaction, the mechanism of which is much different from the Co^{I}-catalyzed process observed for the systems $Co^{II}/LiAlH_4$/methyloxirane (L-selectivity, max. ee. 90%)[1] and Co^{II}/BuLi/methyloxirane (D-selectivity, 10%)[8] in dioxane/benzene solvents, where CH_2–O opening predominantly takes place, giving acetone by isomerization.

Comparing the data of No. 5 in Table 1 with those of Nos. 1, 2, 3, and 2-1, the chiral structure of the active species is suggested to be established by the Co^{II} species and acetic acid. In the reaction systems of Nos. 1, 2, 2-1, and 2-2 (addition order: Co^{II}/BuLi/methyloxirane/CH_3COOH), and of No. 3 (Co^{II}/BuLi/CH_3COOH/methyloxirane), there should be Co^{II} species produced

* (L—D/L+D)mp, (L—D/L+D)cp and (L—D/L+D)rm: optical purities measured for 1,2-propanediol, calculated for 1,2-propanediol, and measured for the reacted methyloxirane.

Table 1. Asymmetric reactions in the $Co^{II}(sal)_2$(*R*-CHXDA)/BuLi/methyloxirane(MO)/acetic acid system and related systems

Exp No.	Li Compd	Co^{II}	Li[a]	Conv (%)	$[\alpha]_{365}^{25}$[c] (°)	$\left(\frac{L-D}{L+D}\right)_{rm}$[d] (%)	I	II	III
							(rel. mol %)		
1	*n*-BuLi	1	1	29.8	+0.856	13.4	6	68	26
2	*n*-BuLi	1	1	27.0	+0.872	15.7	—	—	—
3	*n*-BuLi	1	1[b]	12.5	+0.406	18.9	4	72	24
4	*n*-BuLi	0	1	5.5	—	—		trace	
5	—	1	0	8.1	+0.176	13.3	1	74	25
6	*n*-BuLi	1	40	0.0	+0.001	—		nil	
7	CH_3COOLi	1	40	4.0	+0.011	1.7		nil	
8	$LiAlH_4$	1	1	13.0	+0.015	0.6		trace	
9	—	0	0	0.0	0.000	—	—	—	1.5

a) Moles relative to Co^{II} (0.35 mmol). AcOH/Co^{II}=40, but for No. 7 (AcOH, not added). Addition order, Co^{II}/Li/MO/AcOH, [MO 70 mmol, benzene (10 ml)/dioxane (5 ml), 25 °C, 8 days]. b) Addition order, Co^{II}/Li/AcOH/MO. c) [α] (neat) for non-reacted MO recovered, error ±0.005°. d) Optical purity of the reacted MO, evaluated by Eq. $[\alpha]/[\alpha_0]\times\{100-(\text{conv})\}/(\text{conv})$, where $[\alpha]/[\alpha_0]$ is the optical purity of the non-reacted MO. $[\alpha_0]_{365}^{25}=+15°$ for pure (*R*)-(*D*)-(+)-MO (Ref. 4).

Table 2. Asymmetric reactions in the $Co^{II}(sal)_2$(*R*-CHXDA)/BuLi/methyloxirane(MO)/acetic acid system[a]

Exp No.	Temp (°C)	Conv (%)	$[\alpha]_{365}^{25}$[b] (°)	$\left(\frac{L-D}{L+D}\right)_{rm}$[b] (%)	I	II	III	1,2-Propanediol $[\alpha]_{365}^{25}$[c] (°)	1,2-Propanediol $\left(\frac{L-D}{L+D}\right)_{mp}$[d] (%)	1,2-Propanediol $\left(\frac{L-D}{L+D}\right)_{ep}$[e] (%)
					(rel. mol %)					
2—1	25	23.0	+0.724	16.2	5	71	24	+1.60	10.8	8.0
2—2	18	9.5	+0.451	28.7	5	73	22	+1.61	10.8	15.4

a) Co^{II}/BuLi/AcOH=1/1/100 (mole ratio). Co^{II} 0.70 mmol, MO 140 mmol, benzene (20 ml)/dioxane (10 ml), 7 days. b) Described as in Table 1. c) [α] (neat) for 1,2-propanediol obtained by hydrolysis of I, II, and III. d) Measured optical purity. $[\alpha_0]_{mp}^{25}=15.9°$ for pure (*S*)-(*L*)-(+)-1,2-propanediol (Ref. 4). e) Expected optical purity calcd from $(L-D/L+D)rm\times[(II-III)/(II+III)]$.

by radical decompositions of the CH_3COOCo^{III}-[8,9] and HCo^{I}-complexes formed,[10] respectively. However, the (L−D/L+D)rm value of run No. 5, in spite of the low conversion, is similar to those of Nos. 1, 2, and 2—1, which suggests that a Li compound may also play an important role in this asymmetric reaction, since (L−D/L+D)rm usually decreases with conversion in kinetic resolution.

As to the reaction of cobalt complexes with acetic acid, Clifford and Waters have reported the following equilibrium:[9,11]

$$RCOOH + Co^{III}(H_2O)_6 \rightleftharpoons RCOO\text{-}Co^{III}(OH_2)_5 + H_3O^+$$

It seems reasonable to consider the enhancement of acidity of the acetic acid interacting with the $Co^{II}(sal)_2$-(*R*-CHXDA) complex in the present study using an aprotic solvent, $[Co^{II}\cdots RCOO\overset{\delta-}{-}\overset{\delta+}{H}]$. The selective ring opening of L(−)-methyloxirane with the acetic acid interacting with the chiral Co^{II}-complex leads to the resolution of DL-methyloxirane and formation of the optically-active products in this Co^{II}/BuLi/methyloxirane/acetic acid system.

Experimental

Measurements. The NMR spectra were taken on a JEOL PS-100 spectrometer. The mass spectra were measured by electron impact method using a Hitachi RMU-6E instrument and by the chemical ionization method with a Jasco/Finnigan 3100 instrument. Optical rotations were observed by means of a Perkin-Elmer model 241 polarimeter.

Reagents. The Co^{II}-complex, BuLi, and other reagents were prepared and/or purified by the usual methods described elsewhere.[1,8]

Procedure. To a benzene/dioxane solution of Co^{II}-$(sal)_2$(*R*-CHXDA) and BuLi, methyloxirane and acetic acid were added. The mixture was sealed in an ampule under dry nitrogen and reacted with stirring at an appropriate temperature. After a given reaction time, the non-reacted methyloxirane and products were analyzed by GLC. The methyloxirane was recovered by distillation and the products were isolated using the preparative GLC technique. The NMR analyses for the products were satisfactory; $-CH(CH_3)CH_2-$ parts: $ABMX_3$(I), A_2BX_3(II), and A_2MX_3(III) spin systems.

Authentic Samples. Propylene diacetate(I) was prepared by the reaction between 1,2-propanediol (60 ml) and acetic anhydride (300 ml) with a few drops of sulfuric acid at 170—180 °C for 4.5 h,[12] bp 81 °C/14 mmHg; n_D^{20} 1.4110; MW 160 (mass). Found: C, 52.41; H, 7.47%. Calcd for $C_7H_{12}O_4$: C, 52.49; H, 7.55%. 2-Hydroxypropyl acetate(II) and 2-hydroxy-1-methylethyl acetate(III) were prepared by the reaction of methyloxirane (8 ml) with acetic acid (80 ml) at 35 °C for 8 days.[13] The products (II and III) were isolated as a mixture from the distillate at 86—88 °C/16 mmHg, by preparative GLC. MW 118 (mass). Found: C, 50.85; H, 8.55%. Calcd for $C_5H_{10}O_3$: C, 50.84; H, 8.53%.

Hydrolysis. Products I, II, and III (in Table 2) were combined and hydrolyzed with a 5-M KOH aq solution to give 1,2-propanediol, which was extracted with ethyl acetate.

The authors are grateful to Prof. M. Tsuchiya of the University of Tokyo for the mass spectral measurements and analysis and to Dr. N. Akimori of Hitachi Ltd. (Naka) for his technical advice on GLC analysis. We also thank Mr. T. Takeichi for performing some of the experiments and other assistance.

References

1) H. Aoi, M. Ishimori, S. Yoshikawa, and T. Tsuruta, *J. Organometal. Chem.*, **85**, 241 (1975).
2) G. N. Schrauzer and J. W. Sibert, *J. Am. Chem. Soc.*, **92**, 1022 (1970).
3) R. E. Parker and N. S. Isaacs, *Chem. Rev.*, **59**, 737 (1959).
4) C. C. Price and M. Osgan, *J. Am. Chem. Soc.*, **78**, 4787 (1956).
5) M. Ishimori, K. Tsukigawa, and T. Tsuruta, *Makromol. Chem.*, **177**, 1221 (1976).
6) B. Franzus and J. H. Surridge, *J. Org. Chem.*, **31**, 4286 (1966).
7) N. Shieh and C. C. Price, *J. Org. Chem.*, **24**, 1169 (1959).
8) H. Aoi, M. Ishimori, and T. Tsuruta, *Bull. Chem. Soc. Jpn.*, **48**, 1897 (1975).
9) A. A. Clifford and W. A. Waters, *J. Chem. Soc.*, **1965**, 2796.
10) G. Costa, G. Mestroni, and G. Pellizer, *J. Organometal. Chem.*, **11**, 333 (1968).
11) T. A. Cooper, A. A. Clifford, D. J. Mills, and W. A. Waters, *J. Chem. Soc., B*, **1966**, 793.
12) S. Olsen, *Z. Naturforsch.*, **1**, 676 (1946).
13) N. S. Isaacs and K. Neelakantan, *Can. J. Chem.*, **46**, 1043 (1968).

COMMENTS

BULLETIN OF THE CHEMICAL SOCIETY OF JAPAN, VOL. 50 (3), 771 (1977)

On the Lowest Triplet State of the Pyridazine Crystal

Charles J. MARZZACCO

Department of Physical Science, Rhode Island College, Providence, R. I. 02908, U. S. A.

(Received June 22, 1976)

Synopsis. The lowest singlet-triplet transition recently observed at 440 nm by Yamamoto, Takemura, and Baba for pyridazine in EPA is shown to correlate with the 410 nm transition observed by Hochstrasser and Marzzacco. This correlation is contrary to that of Yamamoto *et al.*

In a recent article in this journal, Yamamoto, Takemura, and Baba[1] reported on the singlet-triplet absorption of pyridazine measured by means of sensitized-phosphorescence excitation in EPA rigid-glass solution at 77 K. They observed weak broad intensity in the 370—440 nm spectral region and assigned it to two singlet-triplet absorption transitions. The main basis for the two transition assignment is that there are two absorption regions, a weaker one at 440—410 nm and a stronger one at 410—370 nm. These authors correlate the long wavelength system with the 445 nm singlet-triplet absorption observed by Innes *et al.*[2] for pyridazine vapor and the short wavelength system to the 410 nm singlet-triplet absorption observed by Hochstrasser and Marzzacco[3] in the pyridazine neat crystal. This assignment of the 410 nm crystal absorption to the $S_0 \rightarrow T_2$ transition is contrary to Hochstrasser and Marzzacco's analysis and would imply that they missed the observation of a lower energy singlet-triplet system, $S_0 \rightarrow T_1$. In correlating their spectral data for pyradazine in EPA with spectral data of pyridazine in two different phases, Yamamoto, Takemura, and Baba do not take into account the large blue shifts in the $n \rightarrow \pi^*$ transitions upon going from the vapor to the solid phase of pyridazine. In the pyridazine vapor, the origin of the $S_0 \rightarrow S_1$ ($^1B_1(n\pi^*)$) transition lies at 26649 cm^{-1} [2] whereas it is found at 28351 cm^{-1} in the crystal.[3,4] This huge blue shift of 1702 cm^{-1} may be due in part to the large dipole moment change accompanying the transition. The origin of the triplet system observed by Innes *et al.*[2] appears at 22487 cm^{-1} in the vapor and that in the crystal appears at 24251 cm^{-1}.[3] The similarity of this 1764 cm^{-1} shift observed in the triplet system to the 1702 cm^{-1} shift in the singlet system is strong evidence that the 440 nm vapor and the 410 nm crystal absorptions are both due to the same singlet-triplet transition namely $S_0 \rightarrow T_1$. This transition correlates with the 440 nm absorption observed by Yamamoto *et al.* In the phosphorescence excitation of pyridazine in EPA. It should also be noted that the singlet-triplet gap is about 4000 cm^{-1} in all three environments consistent with the lowest triplet being of the same character as the lowest singlet excited state namely $B_1(n\pi^*)$.

These comments are in no way meant to refute the suggestion of Yamamoto *et al.* that a second singlet-triplet transition occurs at 410 nm for pyridazine in EPA. Since transitions to other than the lowest excited state of a given multiplicity are often very broad,[5] such a transition would not have been observed under the high resolution spectrographs used by Innes *et al.* for the vapor work or by Hochstrasser and Marzzacco for the low temperature crystal work.

References

1) K. Yamamoto, T. Takemura, and H. Baba, *Bull. Chem. Soc. Jpn.*, **48**, 2599 (1975).

2) K. K. Innes, W. C. Tincher, and E. F. Pearson, *J. Mol. Spectrosc.*, **36**, 114 (1970).

3) R. M. Hochstrasser and C. Marzzacco, *J. Chem. Phys.*, **46**, 4155 (1967).

4) C. Marzzacco, Ph. D. Thesis, University of Pennsylvania, Philadelphia, Pa., 1968.

5) R. M. Hochstrasser and C. Marzzacco, *J. Chem. Phys.* **49**, 971 (1968).

Polarography of α-Keto Acids in Aqueous and Nonaqueous Solutions

Mitsuaki OHMORI* and Masanosuke TAKAGI

Laboratory of Biophysical Chemistry, College of Agriculture, University of Osaka Prefecture, Sakai 591
**Osaka City Institute of Public Health and Environmental Sciences, Tennoji-ku, Osaka 543*

(Received March 22, 1976)

Phenylglyoxylic acid (I), phenylpyruvic acid (II), and pyruvic acid (III) were polarographically studied in buffer solutions and in DMF. Their reduction waves were reinvestigated in a wider pH range. Cyclic voltammetry showed that most electrode reactions of these acids in acidic pH are irreversible. pH-Dependence of $E_{1/2}$ and limiting current was studied. The observed decrease of the limiting currents of II and III in the strongly alkaline region was attributed to the dissociation of their corresponding enol forms. The *i-E* curves of these acids in DMF showed successive poorly-defined reduction waves, while those of the corresponding tetraethylammonium salts (TEA salts) were found to be much simpler in shape. A small oxidation wave was also observed with TEA salts of II and III, suggesting the presence of the enol form in DMF. The reduction products of I and its salt in DMF were studied by means of controlled potential electrolysis and NMR-spectroscopy. The electrode reaction mechanism of α-keto acids in nonaqueous solution is discussed, emphasizing the role of the free acid form as a proton-donor and the formation of a radical anion followed by a disproportionation reaction.

In polarographic investigations of biologically important α-keto acids, the first systematic study on the reduction of pyruvic acid was reported by Müller and Baumberger in 1939.[1] They found that the limiting currents of the two successive reduction waves change with pH, taking the form of an acid dissociation curve, the total current of the two waves being constant in the pH range studied. They attributed this phenomenon to the keto and enol forms of the acid in equilibrium in the buffer solutions.

It was pointed out by Brdička and Wiesner[2,3] that the two waves of pyruvic acid should be ascribed to the free acid and anion of the keto form and not to the enol form of the compound. The rate constants of the dissociation and recombination reactions of α-keto acids were determined by the polarographic method on the basis of the theory of kinetic current.[2-4] Because of this successful application of polarography, pyruvic acid has been considered to be representative of organic compounds whose rates of reaction in acid dissociation and recombination can thus be readily determined.

Later, participation of the hydrate form of α-keto acids in their polarographic behavior was suggested.[5-8] In 1961, Ono, Takagi, and Wasa[8] showed that the pH dependence of the limiting current of various α-keto acids could not be interpreted unless hydration and even enolization of the keto form when possible, in addition to the dissociation and recombination of the acid, were considered as factors in their equilibria in solution. The presented equilibria between an electroactive free keto form and various electroinactive ones should be considered in most cases even for the first reduction wave of α-keto acid.

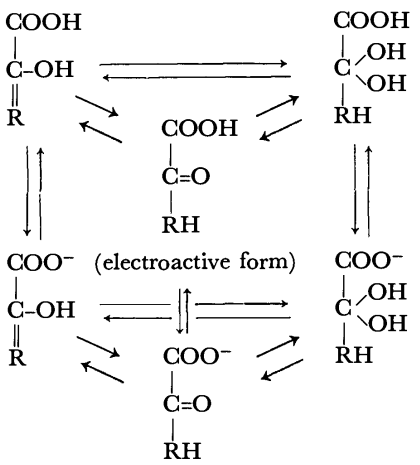

We took up the polarography of α-keto acids from our interest in electro-reduction of biologically-important conjugated carbonyl compounds such as dehydro-L-ascorbic acid.[9-11] We chose three α-keto acids: phenylglyoxylic acid (I), with no possibility of enolization; phenylpyruvic acid (II), which definitely includes enol forms in aqueous equilibria; pyruvic acid (III), in which enolization is possible but occurs in aqueous solution in a restricted concentration range (<2%).[12]

Experimental

Chemicals. Phenylglyoxylic acid (I) was prepared according to the method previously described.[13] For phenylpyruvic acid (II), since the instability of the free acid even as crystal is undesirable for quantitative experiments, α-acetoamidocinnamic acid was prepared and stored.[14] It was converted into α-hydroxycinnamic acid (the enol form of II) before each experiment, by hydrolysis in a dilute hydrochloric acid solution.[15] The specimen recrystallized from distilled water was dissolved in 0.1 M (mol dm^{-3}) HCl containing 10% ethanol. This was used as the stock solution for polarography in aqueous solutions. Pyruvic acid (III) (analytical grade, Wako Pure Chemicals Co., Ltd., Osaka) was used without further purification.

Tetraethylammonium hydroxide for neutralizing α-keto acids to the corresponding tetraethylammonium salts was of reagent grade (10% aqueous solution, Wako Pure Chemicals Co.)

Tetraethylammonium perchlorate (TEAP) was prepared according to Fujinaga *et al.*[16]

Nonaqueous Solvents. *N,N*-Dimethylformamide (DMF) and acetonitrile (AN) were purified and dried as prescribed by Mann.[17]

As buffer solutions, McIlvaine buffer and other buffers were employed. The ionic strength of the aqueous electrolytic solutions was not always controlled to a definite value. For the sake of confirmation, it was adjusted to 0.5 by adding the requisite amount of KCl in certain experiments.

Apparatus. A Yanagimoto Polarograph Type PA-202

combined with a Yanagimoto *iR*-drop compensator was used for most polarographic measurements. An aqueous saturated calomel electrode (SCE) was used as a reference electrode. The characteristics of the capillaries used were $m=2.40$ mg/s, $t=3.75$ s in pH 6.12 McIlvaine buffer when the Hg level was 60 cm and -1.0 V was applied, and $m=1.16$ mg/s, $t=3.77$ s in DMF at -1.5 V and 50 cm mercury head. All the polarographic experiments were carried out at (25 ± 0.1)°C.

For controlled potential electrolysis, a Yanagimoto Controlled Potential Electrolyzer was employed. NMR Spectra of the electro-reduction products were recorded on a JEOL MH-60 Spectrometer.

For cyclic voltammetry, a Yanagimoto Polarovision PA-20 was combined with a function generator of NF Circuit Design Block Co., Ltd., Osaka, Model FG-121A. The working electrode was a hanging mercury drop of appropriate size.

Experimental Procedures. Polarographic measurements in aqueous solutions were carried out by conventional methods. However, when the α-keto acids were not stable in the given pH, the buffer solution in an electrolytic cell was previously deoxygenated by bubbling nitrogen gas. To this oxygen-free buffer solution, the required volume of the stock solution was added and the polarogram was taken immediately.

For nonaqueous solvents, a salt bridge to connect with the SCE was constructed of three gel layers, modifying the bridge devised by Takaoka.[18] The layers were 3% aqueous agar gel saturated with KCl, 3% agar gel containing 70% DMF, 30% H_2O, and 0.5 M TEAP, and 3% methylcellulose gel in DMF or in a DMF–AN mixture containing 0.5 M TEAP.

For the experiments with tetraethylammonium salts of α-keto acids, aqueous solutions of each α-keto acid were carefully neutralized to pH 7 by adding 10% aqueous solution of tetraethylammonium hydroxide. The neutralized solution was lyophyllized and stored in a refrigerator as a tetraethylammonium salt of the given α-keto acid.

Results and Discussion

Behavior of α-Keto Acids in Aqueous Buffer Solutions. In previous papers[8,19] the pH range was restricted to 0—8. Since additional data for enol forms of α-keto acids were expected in the alkaline range, this range was examined most carefully.

Change of Limiting Currents with pH. As shown in Figs. 1 and 2, each of the α-keto acids showed two reduction waves whose limiting currents change with pH.

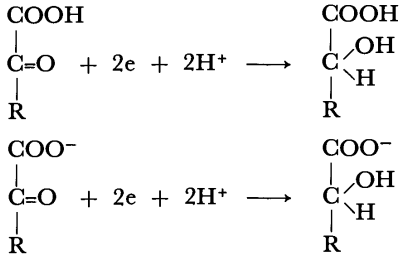

We see that the first wave corresponds to the reduction of the free α-keto acid and the second to that of its anion form, involving the kinetic current due to the recombination of the anion form with hydrogen ion.[2-8]

In the reduction of I, with no possibility of enolization, the small decrease of the limiting current of the

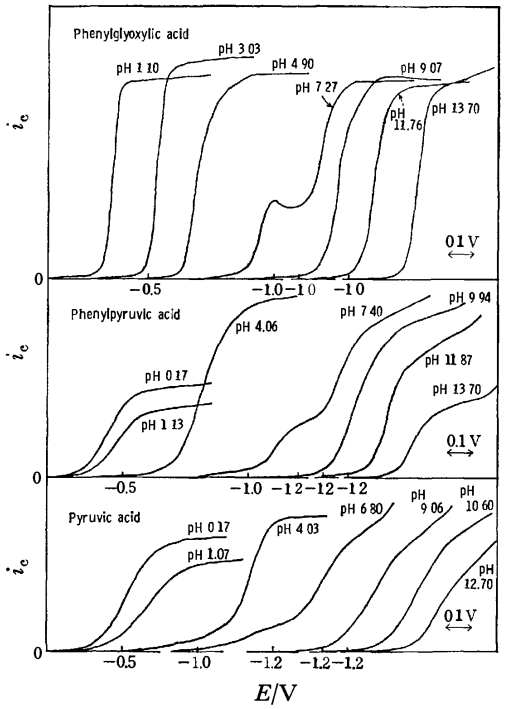

Fig. 1. Polarograms of α-keto acids in various pH.

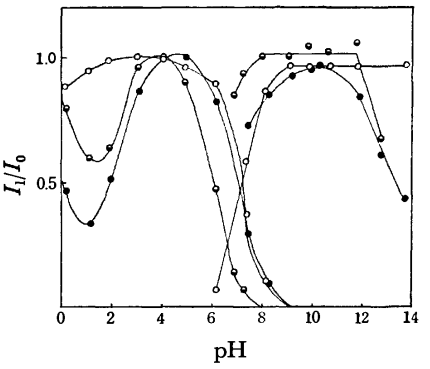

Fig. 2. pH Dependence of the reduction waves of α-keto acids.
Concn of keto acid 5×10^{-4}M, 25°C.
○: Phenylglyoxylic acid, ●: phenylpyruvic acid, ◒: pyruvic acid. I_0: the largest limiting current of each keto acid in acidic pH range was taken as I_0 for the corresponding acid.

first wave with decreasing pH in the acidic range may be attributed to the effect of hydration of the free acid.[8,19] The changes of the limiting current in the pH range above 4 can be interpreted by the kinetics of acid dissociation.[2-4]

However, for II, in which enolization was observed by UV spectroscopy,[8] a pronounced minimum in the limiting current-pH curve of the first wave near pH 1 was observed. A decrease of the limiting current of the second wave with pH could be seen in the pH range above 12. The decrease in the acidic range is due to the inactivation of the keto form by hydration and enolization, but that in the alkaline range may be explained by the inactivation of the anion by dissociation of the enol form and the increase of the enolate form with pH:

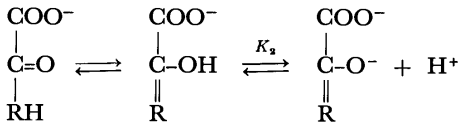

For III, decrease of the limiting current similar to that of II could be observed in both acidic and alkaline regions. The apparent pK_2 value of II and III is estimated to be *ca.* 13, provided that no kinetic current due to acid recombination is involved in such a high pH region. It is interesting that this pK_2 value is in good accordance with pK_3 value obtained by Bamann and Sethi for oxalacetic acid.[20]

Even in strongly alkaline pH, no decrease of the limiting current such as those of II and III was observed in I, in which enolization is not possible.

However, it is not clear whether the enolization of the free acid form would participate in the decrease of the limiting current of III in acidic region.

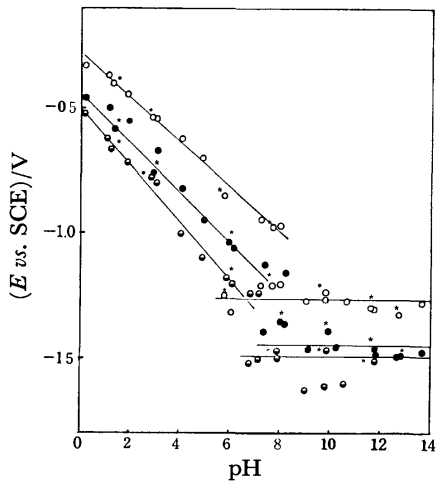

Fig. 3. Relation between the half-wave potentials of α-keto acids with pH.
The experimental conditions were the same as for Fig. 2.
* Ionic strength was adjusted to be 0.5.

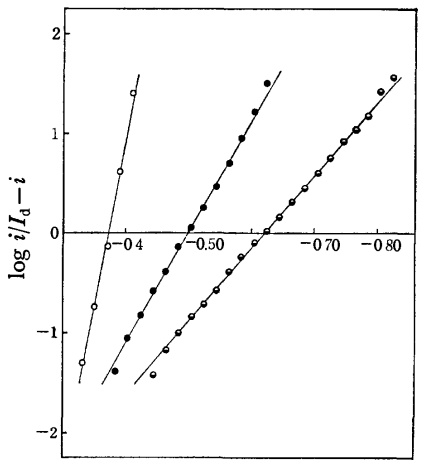

Fig. 4. Logarithmic analysis of the first wave of α-keto acids.
○: Phenylglyoxylic acid, ●: phenylpyruvic acid, ◒: pyruvic acid.

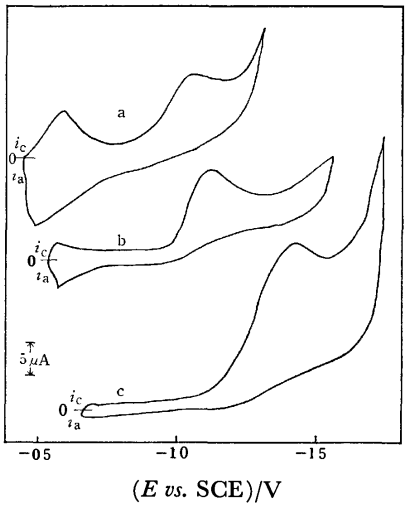

Fig. 5. Cyclic voltammetry of phenylglyoxylic acid in buffer solutions.
a: pH 1.13, b: pH 1.87, c: pH 4.95. Potential sweep: 2 V/s.

Relation between Half-wave Potentials of α-Keto Acids and pH. We see from Fig. 3 that each first wave of I, II, and III shows a linear relation of the $E_{1/2}$ with pH, the slopes being 84, 100, and 112 mV/pH, respectively, whereas the half-wave potentials of the second wave are almost unchanged with pH.

Reversibility of the Electrode Reaction. Since the presence of acid dissociation, enolization and hydration equilibria for three acids in the wide pH range makes analysis of the electrode reaction difficult, an acidic pH range was chosen in which the effects of acid recombination kinetics and dehydration kinetics, at least, can be minimized (pH near 1.1). In pH range below 1.1, increase of the limiting current with decreasing pH observed for II and III may be explained by the acid-catalyzed dehydration reaction of the hydrated free acid form.[8] The conventional logarithmic analysis

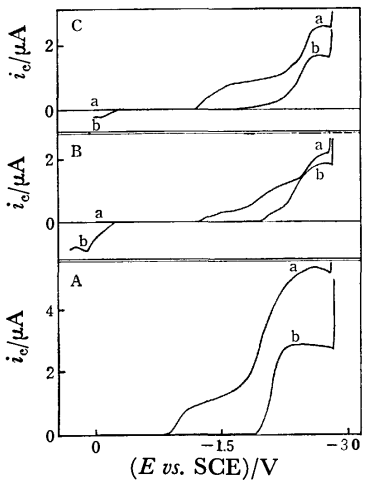

Fig. 6. Polarograms of α-keto acids and their tetraethylammonium salts in DMF.
A (a) Phenylglyoxylic acid (b) TEA salt
B (a) Phenylpyruvic acid (b) TEA salt
C (a) Pyruvic acid (b) TEA salt
Concn of the depolarizer around 5×10^{-4}M.

of the current-potential curve was applied. Each acid exhibited a linear relation with a slope of 31, 89, and 140 mV for I, II, and III, respectively (Fig. 4), suggesting the largest reversibility of the electrode reaction for I and the smallest for III. However, the results of cyclic voltammetry indicate no ideally reversible character of the electrode reaction, even for I, as seen in Fig. 5.

Behavior of α-Keto Acid in Nonaqueous Solvents. Polarograms of the Free α-Keto Acids: Polarograms of each α-keto acid examined, given in Fig. 6, show two or three poorly-defined reduction waves in DMF containing 0.1 M TEAP (curve a). Almost the same of results were obtained in AN. Of the three α-keto acids, the total wave height of I greatly exceeds that of II and III. The phenomena may be partly due to the presence of intramolecular proton donors, probably those of carboxylic groups. In order to eliminate the proton-donating effect of the carboxylic group, the acids were neutralized with tetraethylammonium hydroxide having the same cation as that of the supporting electrolyte. The results obtained with these tetraethylammonium salts of α-keto acids show much simpler reduction waves (curve b, Fig. 6). The limiting currents indicate a certain intermedial number of transferred electrons between 1 and 2 as compared with the 2-electron transferred current in aqueous solution, considering effects of viscosity on the limiting current in nonaqueous solvents.[21]

A small oxidation wave was observed for II and III, when the polarogram was taken with tetraethylammonium salt. The wave, which is absent in I, may be attributed to the oxidation of the enol form, but no further discussion is possible on this.

In order to examine the mechanism of electrode reactions of α-keto acids in nonaqueous solvents, electro-reduction products were studied with free acid and tetraethylammonium salt by applying controlled potential electrolysis. In preliminary experiments carried out with the three keto acids, only I gave reproducible results. This might be due to the instability of the reduction products. The experiment carried out with I is given in the following.

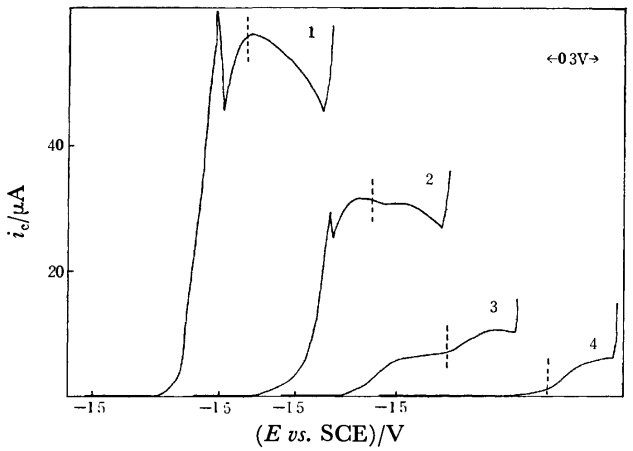

Fig. 7. Change of polarograms of phenylglyoxylic acid TEA salt by the controlled potential electrolysis in DMF.
Concn of the depolarizer *ca.* 1×10^{-2}M. Applied potential −2.4 V *vs.* SCE, 1: Before electrolysis, 2: 1 h, 3: 3 h, 4: 5 h.

Controlled potential electrolysis was carried out with the salt of I exhibiting a relatively simple current-potential curve. When started with a relatively high concentration of the depolarizer, the polarogram of the initial stage showed a pronounced maximum which had not been seen with dilute solutions of the same specimen (Fig. 7). The electrolysis was carried out at −2.4 V, using a mercury pool as the working electrode. After completion of the electrolysis at the applied potential, a small reduction wave appeared at a more negative potential, for which we have no explanation.

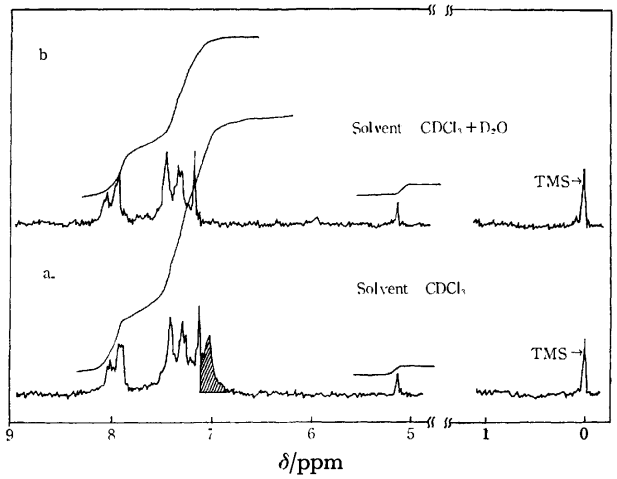

Fig. 8. NMR Spectra of the reduction products of phenylglyoxylic acid TEA salt in DMF at 60 MHz in $CDCl_3$.

The electrolyte solution after electrolysis was evaporated under reduced pressure, and the residue was acidified by addition of excess 0.5 M H_2SO_4 solution. The acid solution was then extracted with ethyl ether. The residue from the ether extract after evaporation was used for NMR measurement. The results are given in Fig. 8. In comparison with the spectrum of DL-mandelic acid,[22] a small signal at 5.13 ppm (a) can be attributed to the proton bound directly to the α-carbon of mandelic acid, while the proton of the alcoholic OH at the α-position seems to exhibit a signal near 7 ppm. It is not, however, a well-defined singlet, but a somewhat broad signal indicating the overlap with that of the carboxylic proton. The addition of D_2O to the electro-reduction product (Fig. 8-b) causes the disappearance of the hatched portion of Fig. 8-a. The change in the integrated absorption intensity caused by the addition of D_2O seems to correspond roughly to two protons, *i.e.*, carboxylic and hydroxyl, if we assume that the unchanged part is the total contribution of 5 phenyl protons. Consequently, the small signal at 5.13 ppm may indicate the formation of mandelic acid after the electrolysis, the yield of which may be 1/4 mol per 1 mol of the starting I. The remainder of the electrolytic product can therefore be attributed to the formation of the dimer.

The results suggest that the electrolytic product of I under these conditions is a mixture of DL-mandelic acid

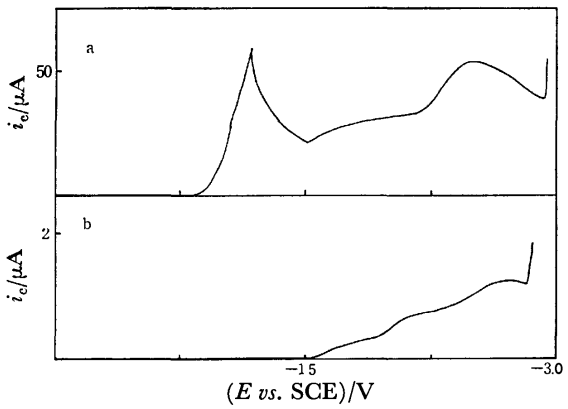

Fig. 9. Change of polarograms of phenyglyoxylic acid by controlled potential electrolysis in DMF.
Applied potential −1.2 V *vs.* SCE, a: before electrolysis (Concn of the depolarizer *ca.* 1.7×10^{-2}M), b: after the completion of the electrolysis (Concn of the depolarizer 6.6×10^{-4}M).

and the dimer due to the binding of two radicals from I

Electrolytic reduction was applied to the free acid form of I. The behavior of I in free acid form in relatively high concentrations differs a great deal from that in dilute concentrations (Fig. 9-a). −1. 2 V was chosen for the applied potential. The polarogram after electrolysis still shows poorly-defined reduction waves (Fig. 9-b).

The electro-reduction product was extracted in the same manner as in the treatment of the neutralized I. The products were confirmed to be a mixture of DL-mandelic acid and the dimer but in a different ratio from that in the above case, more mandelic acid formation being detected with the free acid form than with the neutralized specimen of I.

Proposed Scheme of the Electrode Reaction. From the results, the following schemes are proposed for the principal process of the electrolytic reduction of I in DMF.

For the neutralized specimen of I:

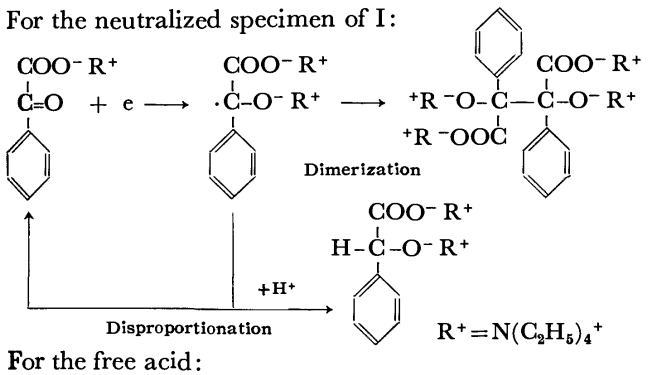

For the free acid:

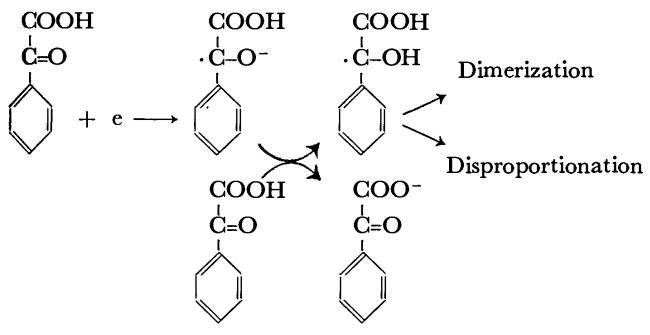

For the salt of I, one-electron reduction can produce the radical, most of which may be converted into the dimer. The remainder then exhibits a disproportionation reaction yielding the salts of I and mandelic acid, as is sometimes seen in the polarography of carbonyl groups in nonaqueous solvents,[23] provided that protons can be supplied from either DMF or TEAP.

The possibility of the involvement of two-electron reduction to form dianions is not completely excluded. However, since no well-defined stepwise reduction waves were observed, it is preferable to represent the simplified schemes using disproportionation only in the production of mandelic acid.

Electrolysis of the free acid would be more complicated than that of the salt. The effect of proton-donors should be considered. The radical anion formed in the first step of one-electron reduction might react with an unreacted molecule, and the protonated radical might perform the same kind of dimerization and disproportionation as in the case of the salt. The anion produced by the reaction of a radical with an unreacted free acid molecule would be reduced at a more negative potential than in the case of the original free acid.

Besides the electro-reduction of the carbonyl group, the discharge of protons liberated from carboxylic groups might be considered in the polarograms of the free acid. Since various chemical species having carboxylic groups can be produced as a result of the first electrode reaction, these acids with slightly different pK values may cause successive and poorly-defined, more negative waves.[24]

References

1) O. H. Müller and J. P. Baumberger, *J. Am. Chem. Soc.*, **61**, 590 (1939).
2) R. Brdička and K. Wiesner, *Collect. Czech. Chem. Commun.*, **12**, 39 (1947).
3) R. Brdička, *Collect. Czech. Chem. Commun.*, **12**, 212 (1947).
4) J. Koutecký and R. Brdička, *Collect. Czech. Chem. Commun.*, **12**, 337 (1947).
5) J. Kůta, *Collect. Czech. Chem. Commun.*, **24**, 2532 (1959).
6) M. Becker and H. Strehlow, *Z. Elektrochem.*, **64**, 42 (1960).
7) H. Strehlow, *Z. Elektrochem.*, **64**, 45 (1960).
8) S. Ono, M. Takagi, and T. Wasa, *Collect. Czech. Chem. Commun.*, **26**, 141 (1961).
9) S. Ono, M. Takagi, and T. Wasa, *J. Am. Chem. Soc.*, **75**, 4369 (1953).
10) S. Ono, M. Takagi, and T. Wasa, *Bull. Chem. Soc. Jpn.*, **31**, 356 (1958).
11) S. Ono, M. Takagi, and T. Wasa, *Bull. Chem. Soc. Jpn.*, **31**, 264 (1958).
12) M. Becker, *Ber. Bunsenges. Phys. Chem.*, **68**, 669 (1964).
13) B. B. Corson, R. A. Dodge, S. A. Harris, and R. K. Hanzen, *Org. Synth.*, Coll. Vol. I, 241 (1943).
14) R. M. Herbst and D. Shemin, *Org. Synth.*, Coll. Vol. II, 1 (1943).
15) R. M. Herbst and D. Shemin, *Org. Synth.*, Coll. Vol. II, 591 (1943).
16) T. Fujinaga, K. Izutsu, K. Umemoto, T. Arai, and K. Takaoka, *Nippon Kagaku Zasshi*, **89**, 105 (1968).
17) C. K. Mann, *Electroanal. Chem.*, **3**, 57 (1969).
18) K. Takaoka, *Rev. Polarog. Jpn.*, **14**, 63 (1966).

19) M. Takagi, S. Ono, and T. Wasa, *Rev. Polarog. Jpn.*, **11**, 210 (1963).
20) E. Bamann and V. S. Sethi, *Arch. Pharm.*, **301**, 12 (1968).
21) M. Suzuki and S. Sawada, *Rev. Polarog. Jpn.*, **17**, 69 (1971).
22) See for example "Varian NMR Spectra Catalog compiled by N. S. Bhacca *et al.*," Vol. 2, spectrum No. 499 (1963).
23) See for example F. Ammar, C. P. Andrieux, and J. M. Savéant, *J. Electroanal. Chem.*, **53**, 407 (1974).
24) L. Y. Kheifets, N. M. Przhiyalogvskaya, and L. I. Dmitrievskaya, *Zh. Obshch. Khim.*, **41**, 510 (1971).

The Correlation of Steric Effects and Equilibrium Constants Evaluated from Lanthanoid-induced ^{1}H Shifts in Aniline Derivative-Eu(fod)$_3$ Systems

Masatoshi HIRAYAMA and Norio ISHIDA

Department of Chemistry, Ibaraki University, Bunkyo, Mito 310

(Received June 7, 1976)

The equilibrium constants, K_1 and K_2, between a series of *o*- and *N*-substituted anilines and Eu(fod)$_3$ in CCl_4 were evaluated using a four-parameter analysis of lanthanoid-induced shifts. It was found that the order of magnitudes of the values of K corrected for the effect of the pK_a-value well corresponds to the accessibility of the nitrogen lone-pair to the Eu ion on the complexation.

Ernst *et al.*[1] have found that in a series of *p*-substituted anilines, the Eu(dpm)$_3$-induced ^{1}H-NMR shifts (the so-called *S*-values) can be linearly correlated to its basicity, and furthermore, that no such relation exists in comparisons of amines with a different steric accessibility of the N-lone pair. However, one may consider that the use of pure intrinsic shifts[2-5] should lead to a more precise discussion of the correlation between shift and basicity. The intrinsic shifts should be related to the tightness of the interaction between the N-lone pair and the Eu ion, while the equilibrium between an Eu-chelate and amine depends on the frequency of occurrence of the interaction between these in solution. Therefore, it may be reasonable to consider that the magnitudes of the equilibrium constants should be dependent on both the basicity of amine and the steric accessibility of the N-lone pair to the Eu ion, as would be expected from the amounts of the lanthanoid-induced intrinsic shifts.

The present paper describes the correspondence between the equilibrium constants obtained from a least-squares analysis of the experimental Eu(fod)$_3$-induced shifts for a series of *o*- and *N*-substituted anilines and the predicted steric hindrance on complexing to Eu(fod)$_3$.

Experimental

All the liquid aniline derivatives used were distilled *in vacuo* and dried over molecular sieves, and 2-aminobiphenyl, recrystallized from ethanol. CCl_4 (spectro grade) dried over molecular sieves was used as the solvent without further purification. Eu(fod)$_3$ obtained commercially was used after drying over P_2O_5 in a vacuum desiccator.[6] In order to prepare the observed lanthanoid-induced shifts (LIS) *vs.* [Eu(fod)$_3$]/[Aniline] (ρ) plots, an original complex solution with the largest value of ρ was first prepared in a ^{1}H-NMR tube. This solution was then diluted step by step with an amine solution of concentration [S_0], while the NMR spectrum was measured. The total amine concentration [S_0] was 0.19 to 0.25 M, the largest ρ value 2.1 to 3.4, and the number of data points 19 to 22.

The NMR spectra were recorded on a Hitachi R-20A spectrometer at a probe temperature of 34 °C at 60 MHz in the frequency-swept mode using TMS as an internal standard.

All computations for the fitting analysis were carried out on HITAC-8800/8700 computers at the Computer Center of the University of Tokyo, except for some of which were performed on the HITAC-8250 computer at the Computer Center of Ibaraki University. The program used was LISA2 which was prepared by Shapiro *et al.* and partially modified in this laboratory.

Results and Discussion

Several *o*- and *N*-substituted anilines were chosen, because various degrees of steric hindrance may be expected with these amines upon complexing to Eu(fod)$_3$ in solution, and moreover, because the basicities (given in terms of pK_a-values) of these amines do not vary widely in magnitude.

The fitting analysis of the LIS *vs.* ρ plot was made by postulating an equilibrium system in which a self-association effect of Eu(fod)$_3$ was added to the two-step mechanism for the complexation of amine to Eu(fod)$_3$, that is, L+S$\leftrightarrows$LS (K_1), LS+S$\leftrightarrows$LS$_2$ (K_2) and L+L$\leftrightarrows$L$_2$ (K_L).[2,7] These examinations using K_L-values up to 100 led to a monotonic increase or decrease in the standard deviation (σ) with increasing K_L-value for most proton resonances, although in a few cases a minimum value of σ was reached within this range of K_L. Therefore, the inclusion of this effect may be unfavorable. All the systems studied were therefore analyzed assuming K_L to be zero. Table 1 shows the intrinsic shifts (δ_1 and δ_2) and the σ-values obtained by the least-squares analysis. It can be said that these σ-values are adequately small. Representative examples are shown in Figs. 1 and 2. Table 2 shows the pK_a-values[8] and the averages of the K-values, for which the K-values were weighted according to the δ_1-value of each resonance in the molecule. The variation of K-values obtained from the various resonance lines in the molecule was fairly large (with a standard deviation of 18 to 50%). However, the averaged K-value changed considerably with the kind, position and number of substituents on aniline, as seen from Table 2. Therefore, these values may be useful for a qualitative discussion of the steric effect.

Table 2 shows that the large variation of K-values does not correspond to the small change in pK_a-values. This clearly indicates that the pK_a-value does not play a major role in the equilibria and suggests that steric hindrance may predominantly affect the complexation. *o*-Toluidine, *o*-ethylaniline and 2,3- and 2,4-, and 2,5-xylidines have much smaller equilibrium constants (both K_1 and K_2) than does aniline, in spite of the fact that their pK_a-values are similar in magnitude to that of aniline. Of these five compounds, *o*-ethylaniline has extraordinarily small values of K_1 and K_2. Consequently, the four remaining derivatives may be regarded as a

TABLE 1. THE INTRINSIC SHIFTS, δ_1 AND δ_2,[a] AND THE STANDARD DEVIATIONS, σ[h]

Compound		2H	3H	4H	5H	6H	Ethyl CH_2	Ethyl CH_3
o-Toluidine	δ_1	−7.16[b]	−2.14	−3.07	−3.22	−10.52		
	δ_2	−5.12[b]	−1.27	−2.03	−2.27	−6.66		
	σ	0.032	0.019	0.020	0.021	0.100		
o-Ethylaniline	δ_1		−3.51	−3.29	−2.41	−11.74	−8.82	−3.73
	δ_2		−2.08	−1.87	−2.41	−6.51	−5.47	−2.54
	σ		0.013	0.012	0.010	0.032	0.040	0.012
2,3-Xylidine	δ_1	−9.24[b]	−2.85[b]	−3.99	−2.74	−13.45		
	δ_2	−6.66[b]	−2.08[b]	−2.86	−1.42	−7.63		
	σ	0.047	0.014	0.015	0.013	0.040		
2,4-Xylidine	δ_1	−8.38[b]	−3.72	−0.73[b]	−2.59	−12.93		
	δ_2	−5.81[b]	−2.41	−0.29[b]	−1.38	−7.24		
	σ	0.044	0.018	0.005	0.011	0.048		
2,5-Xylidine	δ_1	−8.06[b]	−3.71	−3.61	−1.53[b]	−12.05		
	δ_2	−5.23[b]	−2.35	−2.21	−0.90[b]	−6.67		
	σ	0.032	0.015	0.028	0.007	0.066		
2,6-Xylidine	δ_1	−7.04[b]	−3.47	−4.10	−3.47	−7.04[b]		
	δ_2	−4.49[b]	−1.97	−2.56	−1.97	−4.49[b]		
	σ	0.030	0.019	0.019	0.019	0.030		
N-Methyl-*m*-toluidine	δ_1	−12.52	−1.37[b]	−2.99	−2.97	−13.33		−14.94[c]
	δ_2	−8.45	−1.94[b]	−3.37	−2.50	−14.26		−15.86[c]
	σ	0.072	0.008	0.022	0.018	0.076		0.083
N-Ethyl-*m*-toluidine	δ_1	−13.40	−1.85[b]	−3.00	−3.55	−13.84	−17.77[d]	−7.83[d]
	δ_2	−4.45	−0.57[b]	−1.21	−1.11	−4.45	−6.85[d]	−2.97[d]
	σ	0.041	0.010	0.014	0.011	0.048	0.056	0.022
2-Aminobiphenyl[e]	δ_1	−6.68[f]	−4.26	−4.23[g]		−12.76		
	δ_2	−7.49[f]	−1.81	−3.02[g]		−11.90		
	σ	0.044	0.021	0.016		0.028		

a) Measured in ppm. b) Values for methyl protons. c) Values for *N*-methyl protons. d) Values for *N*-ethyl protons. e) Only four curves were thoroughly analyzed. f) This resonance line was assigned to the 2′ proton in the neighboring ring. This assignment is probably correct from the amount of shift and the coupling pattern of this line. g) It cannot be determined whether this signal should be assigned to 4H or 5H. h) $\left[\sum_{i=1}^{N}(\delta_{\mathrm{obsd},i}-\delta_{\mathrm{calcd},i})^2/(N-1)\right]^{1/2}$ measured in ppm, where δ_{obsd} and δ_{calcd} are the observed and calculated LIS, respectively and N is the number of data points.

group having K-values larger than those of *o*-ethylaniline, in view of the accuracy of the present estimates for the K. *N*-Methyl, *N*-ethyl, and *N,N*-dimethyl derivatives have particularly small values of K_1 and K_2, in contrast to their relatively large pK_a-values, especially those which are much smaller for the latter derivative. However, it cannot be clearly decided which K-values, those for the *N*-methyl or *N*-ethyl derivatives, are the larger. Thus, the order of magnitudes of K_1 and K_2, after correction for the effect of basicity, is as follows:

aniline > *o*-methyl > *o*-ethyl > *N*-methyl, *N*-ethyl > *N,N*-dimethyl.

2,6-Xylidine and 2-aminobiphenyl have comparatively small pK_a-values. It may be said that the K_1 for 2,6-xylidine is located between those for *o*-ethylaniline and the *N*-monoalkyl-derivatives, but that the K_2 is similar in magnitude to that for the *N*-monoalkyl-derivatives, and that the K_1 and K_2 for 2-aminobiphenyl are similar in magnitude to those for the *N*-monoalkyl-derivatives having larger pK_a-values. Thus, the order, corrected for the effect of the pK_a-values, is

o,o-dimethyl > *o*-phenyl > *N*-methyl, *N*-ethyl,

which holds for both K_1 and K_2. From the trend in the variation of K_1 relative to that of pK_a for the four *o*-methyl derivatives, it is difficult to consider that the equilibrium constant for *o*-ethylaniline, which is about six times that for 2,6-xylidine (for both K_1 and K_2), can be ascribed to the difference in the pK_a-values, which is about 0.5 (see Table 2). Consequently, the overall order of the K-values corrected for the effect of the pK_a-values, is[9]

aniline > *o*-methyl > *o*-ethyl > *o,o*-dimethyl > *o*-phenyl > *N*-methyl, *N*-ethyl > *N,N*-dimethyl.

On the other hand, one may assume that the aniline adduct of $Eu(fod)_3$ has a geometry similar to those of $Eu(dpm)_3Py_2$[10] and $Ho(dpm)_3(4\text{-picoline})_2$,[11] although correct information about the present adduct is not known. Then, on the basis of this assumption, the degrees of steric hindrance for these aniline derivatives

Table 2. The equilibrium constants, K_1 and K_2,[a] and pK_a[b]

Compound	K_1	K_2	pK_a
o-Toluidine	1188	109	4.39
o-Ethylaniline	282	65	4.37
2,3-Xylidine	1081	95	4.72
2,4-Xylidine	1101	128	4.89
2,5-Xylidine	740	105	4.53
2,6-Xylidine	48.8	9.3	3.95
N-Methyl-*m*-toluidine	11.3	1.6	5.00
N-Ethyl-*m*-toluidine	9.2	9.0	5.12[c]
2-Aminobiphenyl[d]	9.5	5.5	3.83
N,*N*-dimethylaniline[e]	<0.1	—	5.07
N,*N*-Diethylaniline[f]	—	—	5.11
Aniline[g]	5230	582	4.62

a) These are average values in which the values of K are weighted according to the value of δ_1 for each resonance. When convergence of a K-value was unobtainable in the fitting analysis or one K-value was extremely different in magnitude from the other K-values for the resonances of the molecule, this value was excluded from the estimate of the averages. b) These values were taken from Ref. 8. c) Since the pK_a-value of *N*-ethyl-*m*-toluidine could not be found in the literature, that of *N*-ethylaniline is listed. This value is situated between 4.96 (*N*-ethyl-*o*-toluidine) and 5.72 (*N*-ethyl-*p*-toluidine) and appears to be plausible in analogy with the pK_a-values of aniline and toluidines: 4.62 (aniline), 4.39 (*o*-toluidine), 4.69 (*m*-toluidine), and 5.12 (*p*-toluidine). d) The averages of the K-values for only three resonances. e) All the values of K_2, δ_1 and δ_2 are very unreliable because the observed shifts are too small. However, the K_1-value is consistently less than 0.1 for all the protons. f)Analysis is almost impossible due to further small shift values. g) Listed for comparison with the present compounds, as a representative which may be considered to have no particular effect due to the steric hindrance.

have been discussed using the Eu-N distance, 2.65 Å,[10,12] and the angle (θ) between the Eu-N and N-C bonds, 120—140°.[12] Such a comparison of steric hindrance was made qualitatively based mainly on the access of substituent groups to several oxygen atoms of the β-diketonato ligands in both the 1:1 and 1:2 adducts. One may recognize that the order is unaffected by a slight variation of the geometry, and thus

$$\text{aniline} < o\text{-methyl} < o\text{-ethyl} < o\text{-phenyl}$$

holds for steric hindrance. For *o*-derivatives, in order to decrease the steric effect, the N-C bond can be slightly twisted so as to increase the distances between the *o*-substituent group and several oxygen atoms, at a small expense of the π-overlap in the N-C bond. However, no such possibility can be expected for the complexation of 2,6-xylidine.[13] Thus, it seems reasonable to consider that the steric effect for 2,6-xylidine is more rigorous than that for *o*-ethylaniline, because the methyl group in the ethyl group can be oriented in the direction away from the oxygen atoms. In *o*-aminobiphenyl, the two rings are considerably twisted with respect to each other and the neighboring ring may be fairly close to the *t*-butyl or heptafluoropropyl group. These must cause a fairly large hindrance, although whether 2,6-xylidine

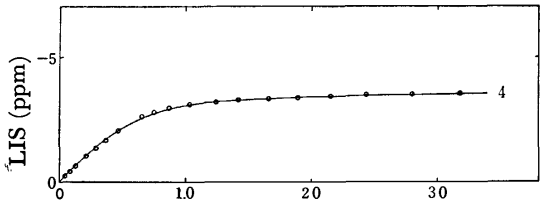

Fig. 1 (a)

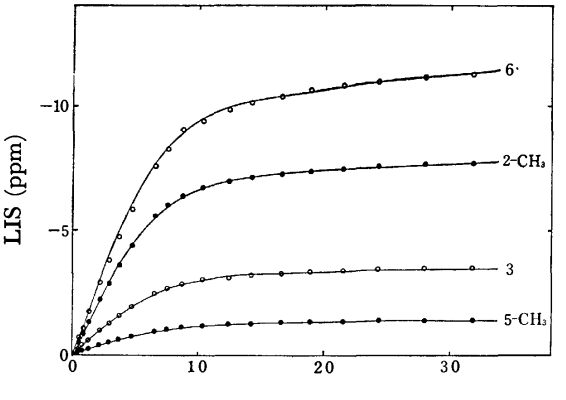

Fig. 1 (a)

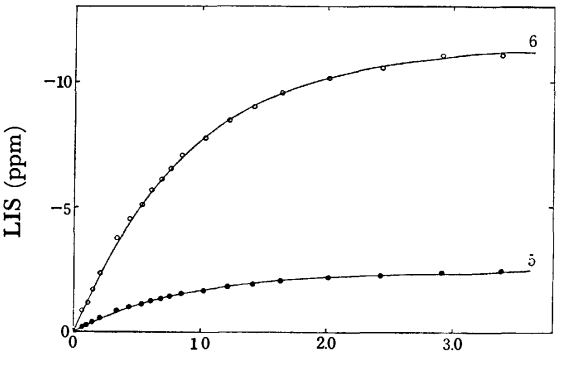

Fig. 1 (b)

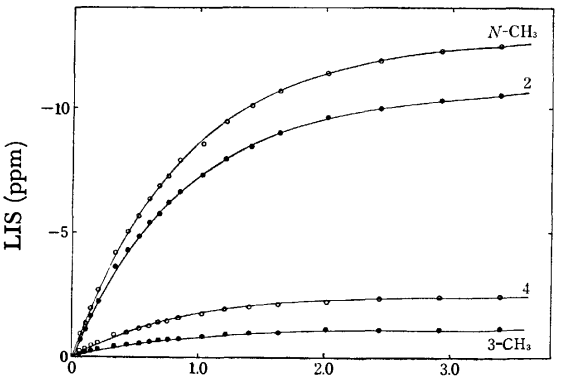

Fig. 1 (b)

Fig. 1. Results of theoretical fits of the two step mechanism, L+S⇄LS, LS+S⇄LS$_2$, to the observed Eu(fod)$_3$-induced data for (a) 2,5-xylidine at $[S_0]=0.25$ M and (b) *N*-methyl-*m*-toluidine at $[S_0]=0.19$ M. The numbers indicate the positions.
○, ●: The observed data.

or *o*-aminobiphenyl has the larger steric effect cannot be determined. In *N*-methyl, *N*-ethyl, and *N,N*-dimethyl derivatives, the *N*-methyl and *N*-methylene groups generally become much closer to some of the oxygen atoms than the ring-substituents in the other compounds, even though the degree of proximity is appreciably sensitive to a slight variation of θ. Such a situation allows us to consider that these *N*-derivatives are expected to have a steric effect that is considerably larger than those for the other amines mentioned above. *N,N*-Dimethylaniline should be less accessible to the Eu ion than the *N*-methyl or *N*-ethyl aniline, for the same reason as in the case of 2,6-xylidine.

Thus, it was found that the K_1- and K_2-values obtained from the present investigation in the aniline derivative–$Eu(fod)_3$ systems correspond well to the predicted steric accessibility of the *N*-lone pair to $Eu(fod)_3$, without any large discrepancy.

A quantitative correlation of the intrinsic shifts with the steric hindrance in the present systems is difficult to elucidate for the following reasons: (1) the steric effect possibly alters the geometry of the adduct, and consequently, the intramolecular distribution of the dipolar shifts may be changed, and (2) the variation of the extent of the steric effect may lead to a change in the cs-contribution to the LIS.

The authors would like to express their grateful appreciation to Professor B. L. Shapiro for providing them with the LISA2 program.

References

1) L. Ernst and A. Mannschreck, *Tetrahedron Lett.*, **1971**, 3023.

2) M. D. Johnston, Jr., B. L. Shapiro, M. J. Shapiro, T. W. Proulx, A. D. Godwin, and H. L. Pearce, *J. Am. Chem. Soc.*, **97**, 542 (1975).

3) B. L. Shapiro and M. D. Johnston, Jr., *J. Am. Chem. Soc.*, **94**, 8185 (1972).

4) F. Inagaki, M. Tasumi, and T. Miyazawa, *Bull. Chem. Soc. Jpn.*, **48**, 1427 (1975).

5) F. Inagaki, S. Takahashi, M. Tasumi, and T. Miyazawa, *Bull. Chem. Soc. Jpn.*, **48**, 853 (1975).

6) Since the use of $Eu(fod)_3$ in a few samples after purification by sublimation did not result in so much variation of the LIS as *K*-values are significantly affected, $Eu(fod)_3$ was used after only drying over P_2O_5 *in vacuo*.

7) The parameters derived from this sort of curve fitting have physical significance only when the number of data points is far larger than that of the parameters to be fit. Such a requirement is adequately satisfied for the present data.

8) D. D. Perrin, "Dissociation Constants of Organic Bases in Aqueous Solutions," Butterworths, London (1965).

9) There are two other possible values representative of the equilibrium constants, the simple average of the *K*-values obtained from all the separate determinations performed on the molecule and the *K*-value found for the proton with the largest δ_1.[2] However, it was confirmed that the choice of either of these two values for *K* does not influence the order of *K*-values estimated here.

10) R. E. Cramer and K. Seff, *Chem. Commun.*, **1972**, 400.

11) W. D. Horrocks, Jr., J. P. Sipe, III, and J.R. Luber, *J. Am. Chem. Soc.*, **93**, 5258 (1971).

12) M. Hirayama, M. Sato, M. Takeuchi, and M. Saito, *Bull. Chem. Soc. Jpn.*, **48**, 2690 (1975).

13) It is anticipated, from the molecular model, that a severe restriction on rotation about the Eu–N bond arises due to the potential barrier formed between the benzene ring or the substituent groups and the *t*-butyl or heptafluoropropyl group.

Photoelectrochemical Behavior of n-Type TiO_2 and Other Semiconductor Electrodes in Acetonitrile Solutions Containing Various Aromatic Amines

Kenji NAKATANI and Hiroshi TSUBOMURA

Department of Chemistry, Faculty of Engineering Science, Osaka University, Toyonaka, Osaka 560

(Received November 18, 1976)

The electrode behavior of n-type TiO_2 in acetonitrile solutions containing one of a variety of aromatic amines under illumination has been investigated. The onset potential of the anodic photocurrent leading to the oxidation of the amines changed from the most negative −0.51 V *vs.* SCE for *N,N,N′,N′*-tetramethyl-*p*-phenylenediamine to the least negative −0.27 V for aniline. These values parallel the change of the flat band potential by the amine and become more negative as the ionization potential of the amine decreases. The influence of the amine on the flat band potentials of ZnO, CdS, and GaP was also studied and found to be much less than in the case of TiO_2. From these results, the reason for the change of the flat band potential in the case of TiO_2 is attributed to a specific charge transfer interaction between the semiconductor and the amine.

The electro-photochemical behavior of semiconductor electrodes in aqueous solutions has been extensively studied for various semiconductors such as GaP,[2] ZnO,[3,4] CdS,[5,6] TiO_2,[7-9] and others.[13] The photocurrents observed for the n-type semiconductors such as GaP, ZnO and CdS under illumination are attributed to the anodic dissolution of the electrodes. Honda and Fujishima found that the n-type TiO_2 electrode is electrochemically stable and the electrode reaction under illumination is the decomposition of water.[7,8] A similar photoeffect may also play a role in organic electrosynthesis using sunlight as an energy source. However, very few studies have been made on the electrode behavior of semiconductors in non-aqueous solutions,[14] although it seems important for the elucidation of semiconductor properties as well as for use in organic synthesis.

We have now carried out studies in this relatively unexplored area and, in this paper, report the results on the n-type TiO_2 electrodes under illumination in acetonitrile solutions.

Experimental

Single crystals of TiO_2 in the form of a wafer with optically flat (001) surfaces were obtained from Nakazumi Crystals Corp. The electrodes were constructed in a way similar to those used in our previous work.[9] Figure 1 shows the experimental setup. High purity nitrogen gas was bubbled through the solution in order to remove oxygen. A saturated calomel electrode (SCE) was used as the reference electrode. Acetonitrile was purified according to the literature.[10] In order to prevent contamination by water, the SCE was placed in a vessel connected with a tube to the electrochemical cell. Both the vessel and the tube were filled with the same solution as that in the cell. Lithium perchlorate, dried at 180 °C for 6 h *in vacuo*, was used as a supporting electrolyte at the concentration of 0.1 M (mol dm^{-3}). Aromatic amines were purified from reagent grade materials by recrystallization or sublimation *in vacuo*. A 250 W super high pressure mercury lamp was used as the light source. The light was passed through a Toshiba UV-35 filter. A Hokutodenko HA 101 potentiostat and a Shimadzu VM 101 voltammeter were used for measurements of the voltage and current of the photo-cells. Differential capacitance measurements were made by use of a Yokogawa Hewlet-Packard 4265B Universal Bridge.

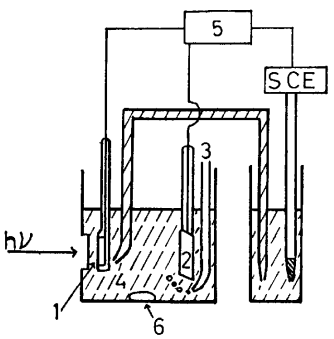

Fig. 1. Schematic diagram of the electrochemical cell. 1: TiO_2 electrode, 2: Pt electrode, 3: N_2 gas inlet, 4: CH_3CN solution containing 0.1 M $LiClO_4$, 5: potentiostat, 6: magnetic stirrer.

Results

Figure 2 shows typical current-voltage curves. In the dark, no anodic current was observed. From curves 1 and 2, we can see that the photocurrent for the acetonitrile solution shows no change in the onset potential, but an increase in the saturation current by addition of 0.8 M water. This result shows that the anodic photocurrent observed in the range 0 to +1 V, in the

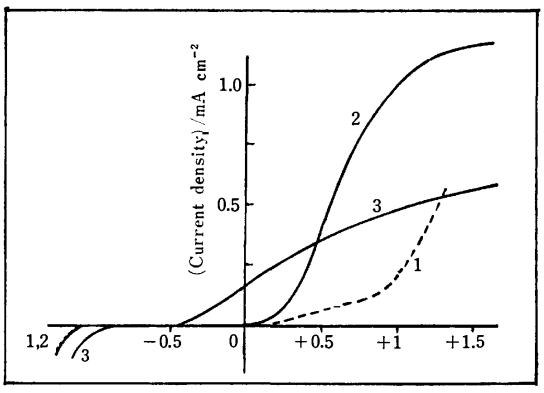

(Potential)/V *vs.* SCE

Fig. 2. Photocurrent density-potential curves for the TiO_2 electrode in acetonitrile solutions (0.1 M $LiClO_4$). 1: CH_3CN solution, 2: CH_3CN solution containing 0.8 M H_2O, 3: CH_3CN solution containing 10^{-3} M *p*-PD.

absence of amine, is not due to the oxidation of the solvent but to the decomposition of water dissolved in a trace amount. On the other hand, the anodic photocurrent of the solution containing 10^{-3} M *p*-phenylenediamine (*p*-PD) appeared at around −0.4 V, showing that the onset potential of the photocurrent shifted to the cathodic side by *ca.* 0.4 V by the addition of the amine. The onset potentials of the photocurrents for the other amines, *N,N,N',N'*-tetramethyl-*p*-phenylenediamine (TMPD), *N,N*-dimethyl-*p*-phenylenediamine (DMPD), *N,N*-dimethylaniline (DMA), *p*-toluidine (PTD) and aniline (AN), differed from each other as shown in Fig. 3.

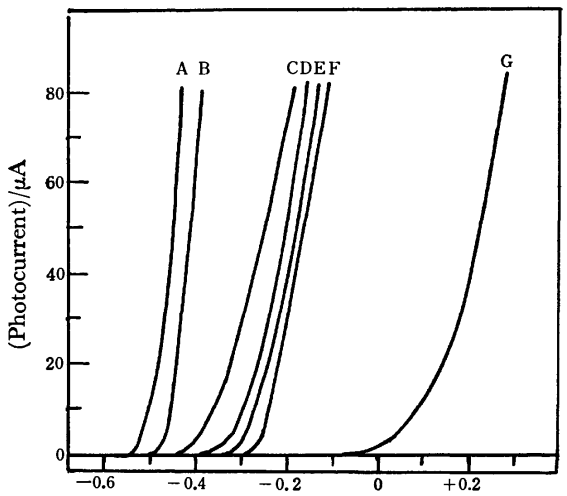

Fig. 3. Photocurrent-potential curves for the TiO_2 electrode in acetonitrile solutions containing 10^{-3} M amines.
A: TMPD, B: DMPD, C: *p*-PD, D: DMA, E: *p*-TD, F: AN, G: 0.8 M H_2O.

Although the onset potential is usually regarded to be approximatly equal to the flat-band potential (V_{fb}), more exact information about V_{fb} can be obtained from the differential capacitance measurements. A plot of $1/C^2$ against the electrode potential, V, according to the Schottky-Mott equation[1]

$$1/C^2 = (2/\varepsilon\varepsilon_0 eN_D)(V - V_{fb} - kT/e) \quad (1)$$

gives the flat band potential and the donor density (N_D), where C represents the space charge capacitance, e the electronic charge, ε the dielectric constant of the TiO_2, and ε_0 the permittivity of vacuum. Some typical results of the measurements are shown in Fig. 4. The

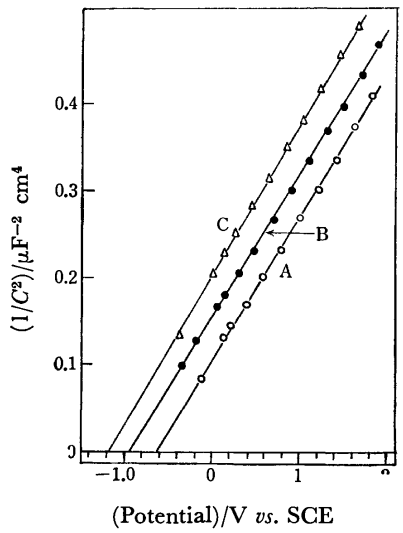

Fig. 4. Schottky-Mott plots of the capacitance *vs.* electrode potential for the TiO_2 in acetonitrile solutions.
A: 0.1 M CH_3CN solution of $LiClO_4$, B: CH_3CN solution containing 2×10^{-3} M DMA, C: CH_3CN solution containing 2×10^{-3} M TMPD.

donor concentration determined from these plots by assuming ε for TiO_2 to be 120[12] is about 8×10^{18} cm^{-3}. Though the V_{fb} for the TiO_2 in acetonitrile obtained from the Schottky-Mott plot varied with specimen between −0.64 V and −1.1 V (the value most frequently obtained being *ca.* −1.0 V), a constant shift of V_{fb} to the cathodic direction was obtained by adding an amine into the solution as shown by ΔV_{fb} in Table 1. An almost constant value was obtained for the V_{fb} for the aqueous solution of 0.1 M $LiClO_4$ to be −0.80 V. The onset potentials of the photocurrents, V_0, given in Table 1 are more positive than the V_{fb} in each of the

Table 1. Onset potentials of the photocurrent of the TiO_2 electrode for various acetonitrile solutions containing 10^{-3} M amines and the related quantities

	E_0[a] (V *vs.* SCE)	I_p^v(eV)[b]	V_0[c] (V *vs.* SCE)	ΔV_{fb}(V)[h]
N,N,N',N'-Tetramethyl-*p*-phenylenediamine		6.75[d]	−0.51	−0.50
N,N-Dimethyl-*p*-phenylenediamine		6.97[d]	−0.46	−0.44
p-Phenylenediamine	0.20	7.4[e]	−0.41	−0.40
N,N-Dimethylaniline		7.51[f]	−0.33	−0.30
p-Toluidine	0.73	7.78[f]	−0.30	−0.24
Aniline	0.87	8.04[f]	−0.25	−0.20
Water		12.61[g]	−0.05	

a) Oxidation potential of amine on Pt in CH_3CN solution. K. Sakaki, A. Kitani, and M. Tsuboi, *Nippon Kagaku Kaishi*, **1973**, 2269. b) Vertical ionization potential in gas phase. c) Onset potential of the photocurrent in acetonitrile solution. d) Y. Nakato, M. Ozaki, and H. Tsubomura, *Chem. Phys. Lett.*, **9**, 615 (1971). e) T. Tani, *Denki Kagaku*, **41**, 683 (1973). f) A. D. Baker, D. P. May, and B. W. Turner, *J. Chem. Soc., B*, **1968**, 22. g) W. C. Price, *J. Chem. Phys.*, **4**, 147, 539 (1936). h) Shift of V_{fb} caused by addition of amine.

Table 2. Flat band potentials of TiO_2, ZnO, CdS, and GaP in acetonitrile solutions (V *vs.* SCE)

	TiO_2	ZnO	CdS	GaP
in CH_3CN	−1.05	−0.20	−0.80	−1.24
p-PD(2×10^{-3} M/l)	−1.45	−0.25	−0.84	−1.54

corresponding solutions. However, the onset potentials for various amines parallel the corresponding ΔV_{fb} values. This change in V_{fb} by the addition of the amine does not occur in water but only in the acetonitrile solutions. The sequence of the V_{fb}'s for various amines did not change even when the supporting electrolyte concentration was increased from 0.1 to 0.4 M or the donor concentration of the TiO_2 was altered. Table 2 gives the V_{fb} values for other semiconductors, CdS, GaP, and ZnO in acetonitrile solutions with and without 2×10^{-3} M *p*-PD.

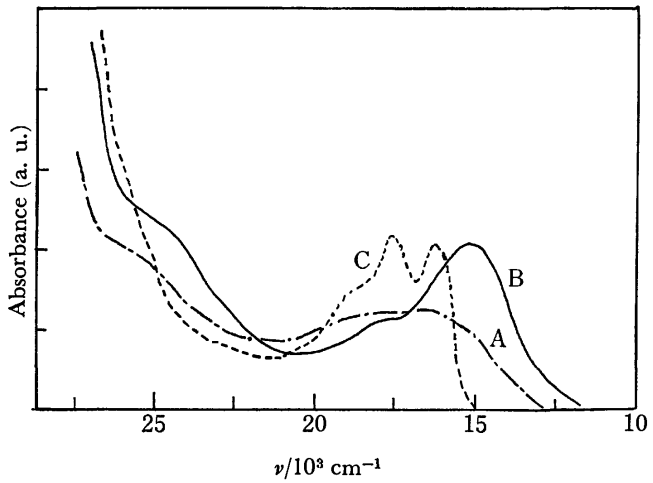

Fig. 5. The absorption spectra of acetonitrile solutions of 0.1 M $LiClO_4$ and 10^{-3} M amine after photo-anodic reactions A: *p*-PD, B: DMPD, C: TMPD.

The absorption spectra of the acetonitrile solutions were measured after letting the anodic photocurrent flow in the cell in order to identify the reaction products formed from the amines (Fig. 5). The spectra for the case of *p*-PD and DMPD resemble those of the Bandrowski's bases

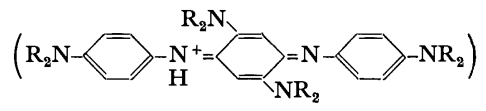

formed by the oxidation of the respective amine.[16] As it has been established that these Bandrowski's bases are formed by the reactions between the radical cations *p*-PD$^+$ or TMPD$^+$ and the neutral amines, the detection of the Bandrowski's bases shows that the primary products of the photo-anodic reactions at the electrodes are the cation radicals of the amines. The absorption spectrum, in the case of TMPD, resembles that of TMPD$^+$.[17] On the other hand, for aniline and dimethylaniline, the solutions remained colorless, a black solid substance being formed on the Pt surface, presumably the condensation reaction products formed from oxidized amines.

Discussion

On excitation of the TiO_2 electrode at the wavelength corresponding to the band gap (3.0 eV),[7] electrons are promoted from the valence band to the conduction band and driven inward by the electric field existing in the space charge layer, while the holes created in the valence band move onto the surface and presumably oxidize the molecules having oxidation potentials lower than the higher limit of the valence band (E_v) at the surface. The ionization potentials in acetonitrile, I_p(sol), of the amines used in this experiment are calculated to be 5.8 eV for TMPD and 6.3 eV for AN by the use of Born's equation,

$$I_p(\text{sol}) = I_p(\text{g}) - (e^2/2r)(1-1/n^2)$$

where I_p(g) represents the gas phase ionization potential of the amine, r the radius of the amine molecule, and n the refractive index of acetonitrile.[20]

The lower limit of the conduction band of TiO_2 (E_c) is calculated to be 3.7 eV by use of the flat band potential −1.0 V (*vs.* SCE) and the absolute energy level of SCE, *ca.* 4.7 eV.[21] Then, the higher limit of the valence band of the TiO_2 (E_v) is obtained to be *ca.* 6.7 eV using the band gap energy 3.0 eV of TiO_2.[7] Therefore, it is reasonable to assume that the amines are oxidized by the photoexcited TiO_2 electrode. The oxidation of the amine was experimentally verified from the absorption spectra of the solutions after illumination at the closed circuit condition, which showed the spectra of the oxidation products.

As described earlier, the onset potentials of the photocurrents and the flat band potentials are changed by adding amines to the solution. The magnitudes of the changes of these two types of potentials are parallel to each other and both become more negative, as the ionization potential of the amine is lowered. The flat band potential, V_{fb}, of the TiO_2 electrode has been reported to shift to the more negative direction with increasing pH of the electrolyte solution.[11] This shift of V_{fb} is explained by taking account of the increase of the negative charge at the surface of the TiO_2, which is produced by the following proton dissociation equilibrium.

It was also reported that the V_{fb}'s of ZnO[15] and GaP[19] have the similar pH dependence as that of the TiO_2, while CdS does not.[11]

It might be concluded therefore that the shift of V_{fb} of TiO_2 is caused by the enhanced proton dissociation by the amine. In order to verify this, we studied the V_{fb} of TiO_2 by changing the concentration of *p*-toluidine, whose basicity is relatively weak, from 10^{-6} to 5×10^{-2} M in the acetonitrile solution. The V_{fb} changed from −0.64 to −0.9 V as the amine concentration increased from 10^{-6} to 10^{-5} M and then remained almost constant up to the amine concentration of 5×10^{-2} M. This result shows that if the proton dissociation were to occur by the addition of the amine, it comes to equilibrium at a very small concentration

of amine. Therefore, it is clear that the difference of the ΔV_{fb} given in Table 1, which are for solutions containing 2×10^{-3} M amine, is not explained by the proton dissociation equilibrium.

As shown in Table 2, the change of V_{fb} for TiO_2 by the addition of *p*-PD is indeed large. But the change for GaP is much less and there is hardly any change for ZnO and for CdS. These results for GaP and especially for ZnO show also that the change in V_{fb} for these semiconductors cannot be explained by the proton dissociation equilibrium.

It seems, therefore, that there is a specific interaction, which affects the V_{fb}, between the semiconductor and the amine on the interface. One possibility is a charge transfer interaction. If one assumes that the TiO_2 electrode has unoccupied intrinsic surface states, the charge transfer interaction (S···D) between the amine (D) and the surface state (S) might bring about a surface dipole on the semiconductor, and cause a potential drop at the interface. Consequently, the V_{fb} of the TiO_2 electrode will shift towards the negative direction. The degree of the shift at a given concentration of amine depends on the degree of charge transfer between the amine and the surface state. The stronger the charge transfer force is, the greater is the negative shift of V_{fb}. The degree of charge transfer, X, is expressed approximately as $\sqrt{X}=\beta/(I_p-W_s)$,[18] where $-W_s$ is the energy of the surface state, I_p the ionization potential of the amine, and β the interaction energy between the ground state (S···D) and the ionized state ($S^-\cdots D^+$). It can then be expected that the change of the onset potential for the anodic photocurrent and that of V_{fb} will be proportional to $\sqrt{X}$. As shown in Fig. 6,

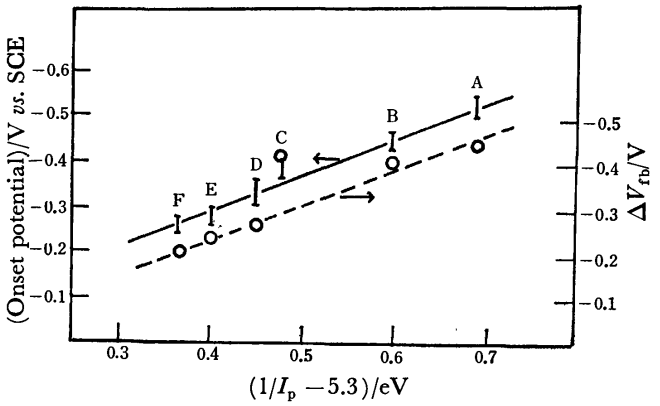

Fig. 6. Dependence of the onset potential of the photocurrent and that of V_{fb} on the ionization potential of amines.
A: TMPD, B: DMPD, C: *p*-PD, D: DMA, E: *p*-TD, F: AN.

straight lines are obtained for the plots of V_0 and ΔV_{fb} *vs.* $\sqrt{X}$ by assuming W_s to be 5.3 eV, which seems to be of a fairly reasonable magnitude (Fig. 6). These results seem to support our present interpretation by use of the specific charge transfer interaction of the surface state with the amine.

As stated in the Results, the V_{fb} of the TiO_2 electrode in aqueous solution does not change by addition of the amine. This is explained by taking account of the

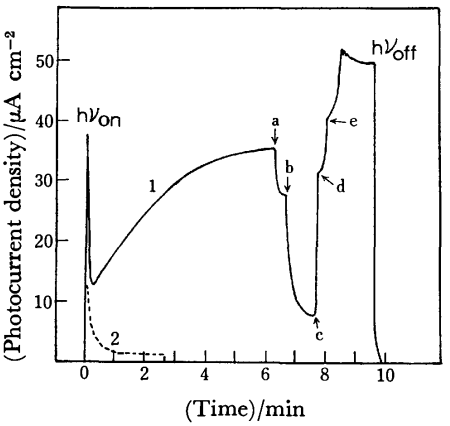

Fig. 7. Change of the photocurrent density of acetonitrile solution containing TMPD with time.
1: 0.1 M CH_3CN solution of $LiClO_4$, 2: the same solution containing 10^{-3} M TMPD.
a: Stirring stopped, b: N_2 gas bubbling stopped, c: N_2 gas started, d: stirring started, e: strong N_2 gas bubbling.

hydrogen bonding of water, or protonation, with amine, which decreases or prevents the charge transfer interaction of the amine with TiO_2.

Performance of the Photoelectric Cell. The performance of the system $<TiO_2|CH_3CN-amine|\ Pt>$ as a photocell has been examined with TMPD used as the amine. The photocurrent for 10^{-3} M acetonitrile solution of TMPD changes with time as shown in Fig. 7. It shows a spike just after illumination, which might be attributable to the charging on the surface of the Pt electrode because there is initially no cathode active species in the solution. With continued illumination, the generation of $TMPD^+$ is observed by the development of blue color in the solution, and the photocurrent increases gradually until saturation. When the nitrogen gas bubbling was stopped, the photocurrent decreased immediately, reappearing on stirring. These results suggest that the photocurrent depends on the diffusion rate of the charge carrier, the amine cation, in the solution. The photocurrent for the acetonitrile solution containing 5×10^{-4} M TMPD became constant after 6 min, began to decrease gradually after 20 min, and became one half

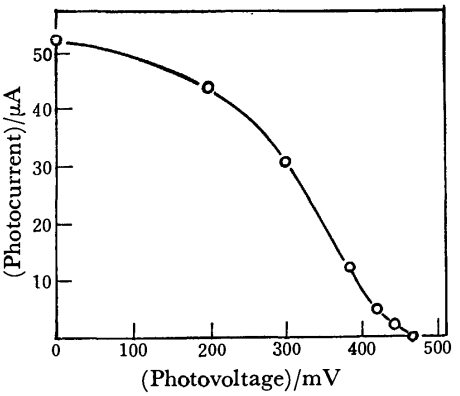

Fig. 8. The photocurrent-photovoltage curve for a cell $<TiO_2\ |CH_3CN(TMPD)|\ Pt>$. Illumination intensity was 4×10^{-3} W/cm².
The concentration of TMPD is 10^{-3} M.

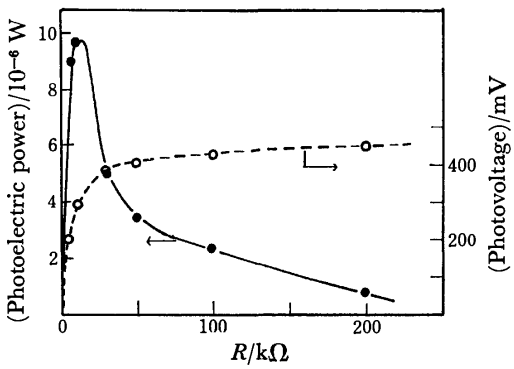

Fig. 9. The photoelectric power and photovoltages *vs.* outer resistance for same cell at the same working conditions as that of Fig. 8.

after about 3 h. This decrease of the photocurrent was proportional to the decrease of the absorbance of $TMPD^+$. These results indicate that $TMPD^+$ undergoes further reaction to form an electrochemically inactive colorless product.

Figure 8 shows a photocurrent-photovoltage curve obtained by illuminating the TiO_2 electrode in the cell $<TiO_2|CH_3CN\text{–}TMPD|Pt>$ with the electrodes connected by a variable resistance (R). Figure 9 shows the corresponding relation between photogenerated power output ($i \times V$) and the resistance, R. The maximum power was obtained to be 9.6×10^{-6} W/cm^2 at $R=10$ kΩ. The power efficiency with respect to the light intensity (4×10^{-3} W/cm^2) was 2.4×10^{-3}.

It was found that the CdS electrode which has a smaller band gap (2.4 eV) than TiO_2 can also be used in a similar photocell. In this case, the oxidation reaction of TMPD occured in competition with the dissolution reaction of the CdS electrode.

The present work partially supported by a Grant-in-Aid for Scientific Research from the Ministry of Education (No. 911504).

References

1) H. Gerischer, "Advances in Electrochemistry and Electrochemical Engineering," Vol. 1, ed by P. Delahay and C. Tobias, Interscience, New York (1961).
2) R. Memming and G. Schwandt, *Electrochim. Acta*, **13**, 1299 (1968).
3) F. Lohmann, *Ber. Bunsenges. Phys. Chem.*, **70**, 87 (1966).
4) H. Gerischer, *J. Electrochem. Soc.*, **113**, 1174 (1966).
5) D. M. Kolb and H. Gerischer, *Electrochim. Acta*, **18**, 987 (1973).
6) R. Williams, *J. Chem. Phys.*, **32**, 1505 (1960).
7) A. Fujishima, K. Honda, and C. Kikuchi, *Nippon Kagaku Zasshi*, **72**, 108 (1969).
8) A. Fujishima and K. Honda, *Nature*, **238**, 37 (1972).
9) T. Ohnishi, Y. Nakato, and H. Tsubomura, *Ber. Bunsenges. Phys. Chem.*, **79**, 523 (1975).
10) C. K. Mann, "Electroanalytical Chemistry," Vol. 3, ed by A. J. Bard, Marcel Dekker (1969).
11) T. Watanabe, A. Fujishima and K. Honda, *Chem. Lett.*, **1974**, 897.
12) F. Mollers, H. J. Tolle, and R. Memming, *J. Electrochem. Soc.*, **121**, 1160 (1974).
13) H. Gerischer, *Ber. Bunsenges. Phys. Chem.*, **69**, 578 (1965).
14) S. N. Frank and A. J. Bard, *J. Am. Chem. Soc.*, **97**, 7427 (1975).
15) F. Lohmann, *Ber. Bunsenges. Phys. Chem.*, **70**, 428 (1966).
16) Private communication from T. Sakata, Institute for Molecular Science.
17) Y. Nakato, N. Yamamoto, and H. Tsubomura, *Bull. Chem. Soc. Jpn.*, **40**, 2480 (1967).
18) R. S. Mulliken, *J. Am. Chem. Soc.*, **74**, 811 (1952).
19) R. Memming, *J. Electrochem. Soc.*, **116**, 785 (1969).
20) Y. Nakato, T. Chiyoda, and H. Tsubomura, *Bull. Chem. Soc. Jpn.*, **47**, 3001 (1974).
21) F. Lohmann, *Z. Naturforsch.*, **229**, 843 (1967).

Performance of Thermal Separation Column with Vertical Barriers

Kazuo SASAKI, Yoshio HIRANO, and Seiji TAO
Department of Applied Chemistry, Hiroshima University, Hiroshima 730
(Received August 6, 1976)

The relative performance of a new type thermal separation column has been reinvestigated. It was concluded that a column having a couple of vertical barriers is superior to an ordinary open column working under the same temperature gradient.

In previous papers[1,2] reports were given on the performance of a new type thermal separation column in which a couple of vertical screens are installed as flow barriers. The discussion given therewith was found to contain some defects.[3] The column consisted of a couple of cylindrical screens suspended coaxially between double cylinders each of which served as a hot and cold plate. Two different views can be considered in evaluating the performance of this type of column.

(1) The screens are merely inserted in a column space of width $2w$.

(2) Two additional spaces are produced outside the pair of screens.

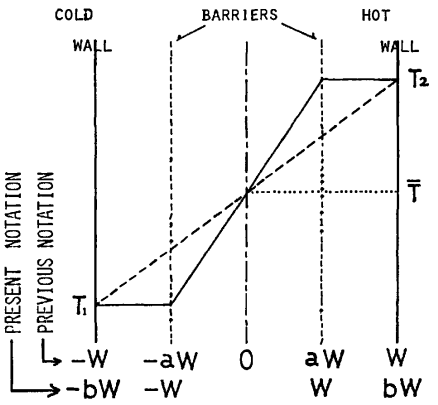

Fig. 1. Basic model of the column with vertical barriers. T_1; Temperature at cold wall, T_2; temperature at hot wall, T; mean temperature.

The reason for the confusing concept is closely related to the assumption as regards mathematical treatment, the underlying assumption being that the temperature gradient is located only over the space between the two screens and the spaces outside the screens are isothermal (Fig. 1). If the mathematical model is realized in an actual column, a larger temperature gradient will be obtained (solid line, Fig. 1) in the space between the two screens as compared with the case in which the same temperature difference is applied over the whole apparatus (dotted line). This will lead to an enhanced separation. The question arises: Is the better performance observed with the barrier-column simply caused by the enhanced temperature gradient? Comparison should be made under the same temperature gradient but not the temperature difference.

If the temperature gradient developed in the column is not much influenced by the installation of vertical barriers view (1) should be adopted. We thus need to use two reference columns for discussing the relative performance of the barrier-column. In order to fulfill the requirement of the same temperature gradient, one of the references should be an open column having two walls located at positions where screens are located in the barrier-column (narrower reference column). The other is an open column having the same geometry as that of the barrier-column (wider reference column). The previous discussion was developed only with the latter reference for the reason that the actual temperature gradient in the barrier-column might differ from that of the mathematical model, and that the externally applied temperature difference might be divided over each sub-column. It is also difficult to compare the performance when we take the narrower reference column with a different geometry as a standard.

Experimental

In order to confirm the reliability of the theory we have constructed an open column (narrower reference). Dimensions and characteristic constants of the two reference columns together with those for the barrier-columns are given in Table 1, and a schematic diagram of the reference columns in Fig. 2. The structure of the barrier-column and details of the experiments were reported.[2]

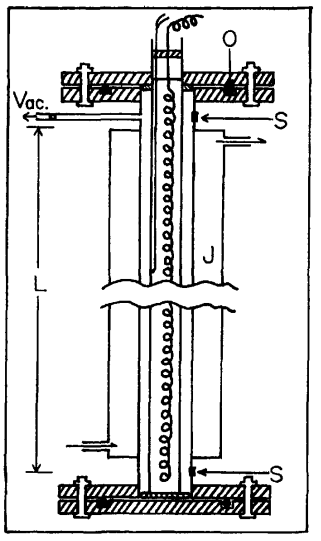

Fig. 2. Schematic view of double cylinder type thermal separation column.
S; Sampling port, O; O-ring, J; water jacket.

Table 1. Geometry and characteristics of columns

(A) Geometry of columns.

Column	Outer tube i.d. r_1 (cm)	Inner tube o.d. r_2 (cm)	r_1/r_2	Half width w (cm)	Mean circumference B (cm)
A (wider reference)	5.27	2.17	2.43	0.775	11.68
B (narrower reference)	4.50	2.95	1.53	0.388	11.70
C (barriered column)	5.27	2.17	2.43	0.775	11.68

(B) Temperature difference applied and characteristic constants.

Column	T (°C)	H (g/s)	K_c (g cm/s)	K_d (g cm/s)	$(2AL)$[a] calcd	$(2AL)$ exptl	t_r (exptl)[b] (min)
A	78	3.49×10^{-3}	13.69	6.88×10^{-3}	0.0305	0.033	0.35
B	78	4.23×10^{-4}	0.104	3.45×10^{-3}	0.500	0.394	3.53
C	78	1.27×10^{-3}	1.77	6.90×10^{-3}	0.086	0.0955	0.78

a) Corrected for cylindricity. b) Relaxation time.

Results and Discussion

If we take view (2) the narrower reference column should be taken as the standard. A slight modification of the theory is advantageous. It is convenient to use the reciprocal $b(=1/a)$ of design parameter a, which indicates the relative location of barriers against the hot and cold walls.

The basic coefficients of transport are then expressed as follows in terms of b:

$$H' = \{2(b-1)^3+1\}H \quad (1)$$

$$K_c' = \{4(b+1)(b-1)^6+4(b-1)^3+1\}K_c \quad (2)$$

$$K_d' = b\cdot K_d \quad (3)$$

where symbols with primes are for the barriered column and those without ones are for the reference column. The quality factor (Eq. 24, Ref. 1) thus becomes

$$\frac{A'}{A} = \frac{H'/2K_c'}{H/2K_c} = \frac{2(b-1)^3+1}{4(b+1)(b-1)^6+4(b-1)^3+1}, \quad (4)$$

A(or A') defined, respectively, by

$$A = H/2(K_c+K_d) \quad (5)$$

is a parameter appearing in the definition of equilibrium separation factor

$$q_e = e^{2AL}. \quad (6)$$

In the derivation of Eq. 4, the contribution of K_d (and K_d') was ignored. Equation 4 is graphically represented in Fig. 3 against parameter b. Experimental value of A'/A referred to the narrower reference was found to be 0.242, *ca.* 40% greater than the theoretical one, 0.175, at $b=2.0$ (*i.e.*, $a=1/2$). A 40% deviation is acceptable if local inhomogeneity in both the column structure and temperature distribution is taken into consideration. The result is in line with the theory. We see that the quality factor A'/A decreases with increasing b. This was expected, since gases in the additional spaces will have a diluting effect to reduce the separation.

Monotonous decrease in A'/A with increasing b (Fig. 3) does not mean that the performance of the barrier-column is inferior. The performance of a given column should be evaluated by taking into account the factors such as product yield per unit time, per unit volume of

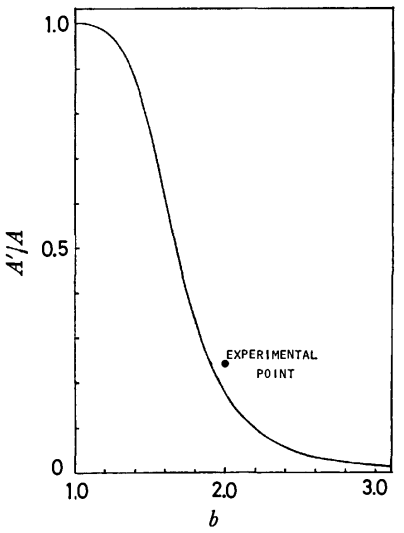

Fig. 3. Change in quality factor A'/A with b according to Eq. 4.
Experimental point is the ratio of columns C and B.

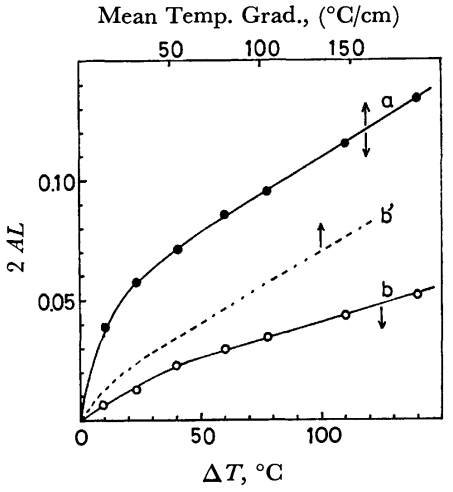

Fig. 4. Comparison of performance of barriered column (curve a) with that of the wider reference (b and b'). Curves b and b' are drawn on the base of applied temperature difference and temperature gradient, respectively.[3] Curve a can refer to both the two scales at upper and lower marginals.

apparatus, per unit energy consumed, *etc.* besides the degree of equilibrium separation. A comparison of any given two columns is complicated. We have no reliable means to compare the overall performances of two columns of different size. If, however, we take the wider reference as the standard, both total capacity of the column and energy consumed per unit time can be assumed almost to be common. This is clearly an advantage.

There still remains a question concerning the temperature gradient, which should be higher in the barrier-column than in the wider reference under the same temperature difference applied. The barrier-column was constructed to fulfill the design parameter a to be 0.5 ($b=2$). Thus the temperature gradient should be twice as high as the wider reference if applied temperature difference is equal. The performance for the barrier-column observed at a given ΔT should be compared with that for the wider reference column observed at a twice greater value of the given ΔT.

In Fig. 4, a part of which was reproduced from Ref. 2, the scale of abscissa is expressed as applied temperature difference and also as mean temperature gradient. Curve a, which stands for the barrier-column, refers to both the two scales, while b is drawn on the base of applied ΔT. Curve b′ was drawn by shifting[4] curve b in order to compare the performances at the same temperature gradient. It is clearly indicated that the performance of the barrier-column is much better than that of the wider reference column operating under a twice greater temperature difference.

References

1) K. Sasaki, T. Yoshitomi, and N. Miura, *Bull. Chem. Soc. Jpn.*, **49**, 363 (1976).
2) K. Sasaki, N. Miura, and T. Yoshitomi, *Bull. Chem. Soc. Jpn.*, **49**, 367 (1976).
3) *Cf.* Ref. 1, footnote 17.
4) This is equivalent to reducing the temperature scale to one-half for curve b.

Molar Excess Enthalpies of α,ω-Alkanediol Monoalkyl Ether+Heptane Systems at 298 K

Fumio KIMURA, Sachio MURAKAMI, Ryoichi FUJISHIRO, and Yoshio TOSHIYASU*

Department of Chemistry, Faculty of Science, Osaka City University, Sumiyoshi-ku, Osaka 558

**Science Education Institute of Osaka Prefecture, Sumiyoshi-ku, Osaka 558*

(Received August 23, 1976)

Enthalpies of mixing of some α,ω-alkanediol monoalkyl ether(ADAE)+heptane systems were measured at 298 K, and limiting partial molar excess enthalpies of ADAE at infinite dilution, $\lim_{x\to 0} H^E/x(1-x)$, were estimated. The ADAE used were $CH_3O(CH_2)_nOH$ (n=2, 3, 4), $C_2H_5O(CH_2)_nOH$ (n=2, 3), $C_3H_7O(CH_2)_nOH$ (n=2, 3), and $C_4H_9O(CH_2)_2OH$. The values of $\lim_{x\to 0} H^E/x(1-x)$ obtained were compared with those of normal alcohols, and discussed in the light of the intramolecular hydrogen bond contained in ADAE. The enthalpic contribution due to the intramolecular hydrogen bond in ADAE is estimated to be about 10 kJ mol^{-1}.

The solution behavior of α,ω-alkanediol monoalkyl ethers (ADAE), $C_mH_{2m+1}O(CH_2)_nOH$, in various solvents is of interest since the ADAE molecule contains both an etheric oxygen and a hydroxyl group, and hence can form hydrogen bonds in several different ways. Not only are intramolecular hydrogen bonds possible between the hydroxyl hydrogen and the etheric oxygen on the same molecule, but also intermolecular hydrogen bonds between the hydroxyl hydrogen on one molecule and either the etheric oxygen or the hydroxyl oxygen on another molecule can be formed. While, in general, investigations for the intramolecular hydrogen bond have been carried out by the use of infrared spectra,[1-5] NMR[6] or dielectric constant measurements,[7,8] it is worthwhile to obtain thermodynamic information about ADAE solutions, because few thermodynamic properties of these solutions have been investigated. In this paper, measurements of enthalpies of mixing for ADAE+heptane at 298 K are described and the results are discussed in view of the several kinds of hydrogen bonds forming in ADAE solutions.

Experimental

The α,ω-alkanediol monoalkyl ethers used were prepared by alkylation of the corresponding α,ω-alkanediols, and purified by fractional distillation in a nitrogen atmosphere. The middle fraction from each distillation was collected and analyzed by an analytical gas-liquid chromatograph (Shimadzu, Model GC-3BT) with a column packed 15% PEG6000 on Teflon; their purities were more than 99.5% for $C_mH_{2m+1}O(CH_2)_2OH$(m=1,2,3,4). As for $C_mH_{2m+1}(CH_2)_nOH$(n=3,4), peaks which seemed to show the existence of isomers were observed; their contents were estimated to be at the greatest 1 and 3% respectively. The heptane from Wako Pure Chemicals Co., Ltd. was purified using the conventional method. The purified heptane was also checked with the gas-liquid chromatograph. The result showed no impurity peaks.

Enthalpies of mixing for ADAE+heptane systems were determined by a successive dilution technique at 298 K using the isothermal displacement calorimeter described previously.[9] The precision is estimated to be ±0.5 per cent in a molar excess enthalpy of 100 J mol^{-1} for a equimolar mixture. In order to determine the limiting partial molar excess enthalpies of ADAE at infinite dilution, precise measurements of H^E at very low mole fractions of ADAE were especially needed. The concentration range covered by our calorimeter, where considerable precision can be expected, is within about 1/60–60/1 as volume fraction of components. So, the enthalpies of mixing in the dilute region were determined as follows. A previously prepared solution of a known mole fraction x_0 was diluted by the solvent, *i.e.* heptane, successively, and the enthalpy of dilution H_d^E per one mole of solution was measured at each step. The enthalpy of mixing H_0^E of the solution at a given concentration x_0 was estimated from the separately determined H^E *vs.* x curve for the pure component system with the least squares method, using the following polynomial:

$$H^E/x(1-x) = \sum_{i=0}^{n} h_i(x)^{i/2}$$

where x indicates the mole fraction of ADAE in the mixture. In this case, the enthalpies of mixing at each step in the dilute region are obtained as

$$H^E = (H_0^E/x_0)x + H_d^E$$

For each system measured, the process described above was repeated twice to evaluate H^E values in the dilute region. For the $CH_3O(CH_2)_2OH$ system, H^E changes linearly with composition from about 0.15 to 0.9 mole fraction of ADAE, because phase separation occurs in this region.[10] Hence, the enthalpy of mixing for this system was measured below the mole fraction of about 0.15.

Results and Discussion

Limiting Partial Molar Excess Enthalpy. For each system, the results were fitted by the method of least squares to the polynomial

$$H^E = x(1-x)\sum_{i=0}^{n} h_i(x)^{i/2} \quad (1)$$

Values of the coefficients h_i and the standard deviations σ for each system are collected in Table 1. In the dilute region of these systems, the remarkably unsymmetrical character of the excess enthalpies, such as seen in alcohol+nonpolar solvent systems, was observed.[11] Because of this asymmetrical dependence of H^E on x, the experimental results could not be fit by either polynomial (1) or $H^E = x(1-x)\sum_{i=0}^{n} h_i'(1-2x)^i$ in the dilute region of ADAE. So, the coefficients in Table 1 were obtained from the experimental H^E values in range of x=0.05 to 1.0. Hence, limiting partial molar excess enthalpies, $\lim_{x\to 0} H^E/x(1-x)$, could not be obtained by the use of the coefficients listed in Table 1. Even though, in order to obtain limiting partial molar excess enthalpies, several kinds of polynomials which represent the $H^E/x(1-x)$ *vs.* x relation were adopted to

TABLE 1. COEFFICIENTS AND STANDARD DEVIATIONS FOR EQ. 1

	$CH_3O(CH_2)_2OH$ +heptane	$CH_3O(CH_2)_3OH$ +heptane	$CH_3O(CH_2)_4OH$ +heptane	$C_2H_5O(CH_2)_2OH$ +heptane
h_0	1.8462×10^4	2.6287×10^4	2.6581×10^4	1.9827×10^4
h_1	-8.0817×10^3	-1.2626×10^5	-1.4181×10^5	-6.4466×10^4
h_2	-3.4681×10^5	3.1505×10^5	3.8227×10^5	1.0809×10^5
h_3	1.3389×10^6	-4.3079×10^5	-5.5075×10^5	-9.0194×10^4
h_4	-1.5824×10^6	3.0772×10^5	4.0981×10^5	3.2338×10^4
h_5		-8.6433×10^4	-1.2173×10^5	
$\frac{\sigma}{\text{J mol}^{-1}}$	2.99	2.21	2.35	3.88

	$C_3H_7O(CH_2)_2OH$ +heptane	$C_4H_9O(CH_2)_2OH$ +heptane	$C_2H_5O(CH_2)_3OH$ +heptane	$C_3H_7O(CH_2)_3OH$ +heptane
h_0	1.9589×10^4	1.7371×10^4	2.5139×10^4	2.5996×10^4
h_1	-6.3408×10^4	-5.0451×10^4	-1.2214×10^5	-1.2760×10^5
h_2	1.0088×10^5	6.8248×10^4	2.9963×10^5	3.2186×10^5
h_3	-7.7523×10^4	-4.0556×10^4	-3.9506×10^5	-4.4065×10^5
h_4	2.4451×10^4	8.5129×10^3	2.6970×10^5	3.1562×10^5
h_5			-7.4262×10^4	-9.1306×10^4
$\frac{\sigma}{\text{J mol}^{-1}}$	2.60	4.18	1.65	3.34

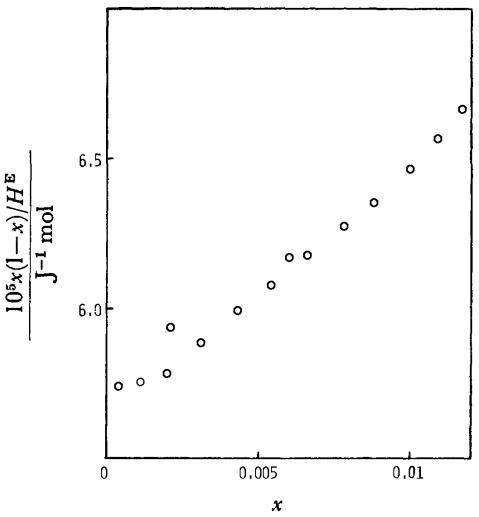

Fig. 1. Plot of $x(1-x)/H^E$ against x in dilute region for $C_3H_7O(CH_2)_3OH$-heptane system.

TABLE 2. LIMITING PARTIAL MOLAR EXCESS ENTHALPIES OF ADAE AT INFINITE DILUTION AND THE ENTHALPIC CONTRIBUTION DUE TO THE INTRAMOLECULAR HYDROGEN BOND IN THE ADAE MOLECULES

	$\lim_{x\to0} H^E/x(1-x)$ / kJ mol^{-1}	H_i / kJ mol^{-1}
$CH_3O(CH_2)_2OH$+heptane	17.6	−10
$CH_3O(CH_2)_3OH$+heptane	18.1	−9
$CH_3O(CH_2)_4OH$+heptane	21.2	−6
$C_2H_5O(CH_2)_2OH$+heptane	15.5	−12
$C_3H_7O(CH_2)_2OH$+heptane	15.5	−12
$C_4H_9O(CH_2)_2OH$+heptane	14.4	−13
$C_2H_5O(CH_2)_3OH$+heptane	17.3	−10
$C_3H_7O(CH_2)_3OH$+heptane	17.5	−10

our results, these curves were too steep in the dilute region of ADAE; an adequate form has not yet been found. So, the reciprocals of $H^E/x(1-x)$ were plotted against x, and the limiting partial molar excess enthalpies for all systems were estimated by extrapolation to infinite dilution "by eye." For an example, the observed points for the $C_3H_7O(CH_2)_3OH$ system are shown in Fig. 1. Values of limiting partial molar excess enthalpies determined by extrapolation to infinite dilution are listed in Table 2. The errors included in these values were estimated to be less than 5%.

Intramolecular Hydrogen Bond in ADAE. When liquids forming hydrogen bonds in the pure liquid state, such as alcohols, are diluted with nonpolar solvents, the hydrogen bonds are broken by the addition of the solvent molecules, and hence this process corresponds to an extremely large positive value of H^E. In general, the shapes of the $H^E/x(1-x)$ *vs.* x curves of such systems become very steep in the dilute region of solute. Although in the present systems the $H^E/x(1-x)$ *vs.* x curves show an appreciable rise in the dilute region, the slope is not so steep as that of normal alcohol+nonpolar solvent systems, and the difference of the limiting partial molar excess enthalpies between the two series is about several kJ mol^{-1}. This seems to mean that, in the dilute region ADAE molecules become free through the destruction of the intermolecular hydrogen bonds by the addition of solvent molecules, and each ADAE molecule forms an intramolecular hydrogen bond between the hydroxyl hydrogen and the etheric oxygen on the same molecule, and thus stabilizes itself.

To discuss the intramolecular hydrogen bond in the ADAE molecule, it will be useful to compare ADAE with normal alcohol. In a normal alcohol+nonpolar solvent system, alcohol molecules form intermolecular hydrogen bonds between hydroxyl groups in the pure

alcohol state. On the other hand, at infinite dilution of alcohol in a nonpolar solvent, the intermolecular hydrogen bonds are broken and each alcohol molecule is surrounded by solvent molecules. Therefore, the value of the limiting partial molar excess enthalpy of alcohol at infinite dilution is assumed to represent the energy sufficient to break the intermolecular hydrogen bond in pure alcohol.

While many investigations have been carried out for excess enthalpies of alcohol+nonpolar solvent systems so far,[12-15] available data for limiting partial molar excess enthalpies have not been provided because of the steep rise of $H^E/x(1-x)$ *vs.* x curves in the dilute region. However, values of limiting partial molar excess enthalpies reported so far are distributed in the neighborhood of 23 to 24 kJ mol^{-1} for normal alcohol systems.[12] This figure seems to be independent of nonpolar solvents, and constant within the experimental error.[11] Brown *et al.* suggest that, for normal alcohols larger than ethanol, the strength of the intermolecular hydrogen bond hardly depends on the carbon chain length in the molecule.[16] Further, for 1,3-butanediol which has two terminal hydroxyl groups in its molecule, it was suggested previously by Murakami *et al.* that almost all the molecules form intermolecular hydrogen bonds between the hydroxyl hydrogen on one molecule and the hydroxyl oxygen on another molecule in the pure liquid state, and the amount of the intramolecular form is negligibly small.[17] It can hence be presumed that ADAE molecules also hardly form intramolecular hydrogen bonds in the pure liquid state, and it will be reasonable to assume that the relation between the strength of the hydrogen bond and the carbon chain length of ADAE is also similar to that of normal alcohols. Therefore, the difference in the values of limiting partial molar excess enthalpies for various ADAE seems to be attributed mainly to the difference in the enthalpic contribution due to formation of the intramolecular hydrogen bond between the hydroxyl hydrogen and the etheric oxygen on the same molecule.

Evaluation of the Enthalpic Contribution due to the Intramolecular Hydrogen Bond in ADAE. On the basis of the consideration in the previous section, the enthalpic contribution due to the intramolecular hydrogen bond in the ADAE molecule, H_i, can be estimated. In this

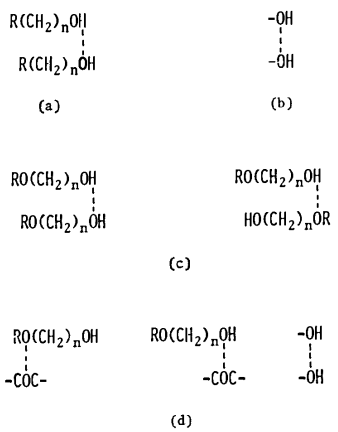

Fig. 2. Schematic diagram of main intermolecular interactions in pure liquid state of alcohol and ADAE.

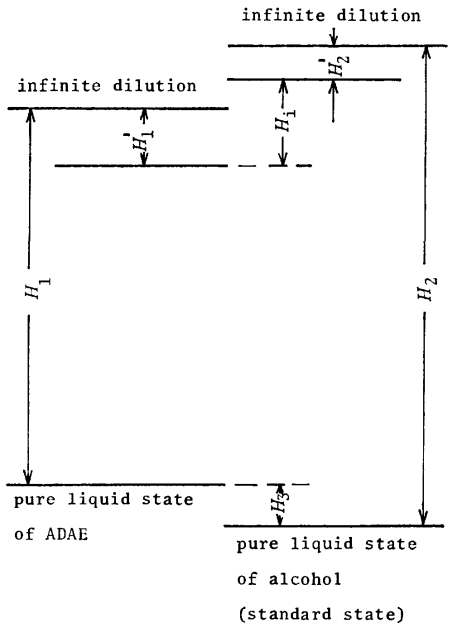

Fig. 3. Energy level diagram of ADAE and alcohol.

estimation, the pure liquid state of normal alcohol is taken as a standard state. As the main intermolecular interactions in this state, those shown in Fig. 2(a) and (b) are considered: (a) contribution due to the intermolecular hydrogen bond and (b) contribution due to the van der Waals force including the dipolar interaction. On the other hand, in the pure liquid state of ADAE, the intermolecular interactions shown in Fig. 2(c) and (d) are also considered: (c) contribution due to two types of intermolecular hydrogen bonds and (d) contribution due to three types of van der Waals forces. The process used to evaluate H_i is given in a form of an energy level diagram in Fig. 3. In this figure, H_2 represents the limiting partial molar excess enthalpy of normal alcohol in a nonpolar solvent. H_2 includes an enthalpic contribution arising from the interruption of the van der Waals interaction among alcohol molecules shown in Fig. 2(b) through dilution with the nonpolar solvent. This contribution is represented by H_2' in Fig. 3, and then the net contribution due to the hydrogen bond becomes H_2-H_2'. H_1 represents the limiting partial molar excess enthalpy of ADAE in a nonpolar solvent. H_1 also includes an enthalpic contribution arising from the interruption of the van der Waals interactions among ADAE molecules shown in Fig. 2(d) through dilution with the nonpolar solvent. H_1' represents this contribution; then the net contribution due to hydrogen bonds (including the intramolecular hydrogen bond) becomes H_1-H_1'. As shown in Fig. 2(c), two types of intermolecular hydrogen bonds may exist in the pure liquid state of ADAE, and the energy level of this state is considered to be different from that of the pure liquid state of alcohol which is taken as the standard state. This difference between the levels is designated as H_3. With these notations, the enthalpic contribution due to the intramolecular hydrogen bond in the ADAE molecule, H_i, can be evaluated as

$$H_i = (H_1-H_1'+H_3) - (H_2-H_2') \qquad (2)$$

Values of H_1', H_2', and H_3 are evaluated as follows. If the difference in nature of the oxygen atoms contained in the ADAE molecule and the alcohol molecule is assumed to be negligible, H_1' and H_2' can be replaced by limiting partial molar excess enthalpies of ethers, $RO(CH_2)_nOR$ and ROR, where R represents an alkyl group, in nonpolar solvent, which are unable to form hydrogen bonds. One mole of ADAE is assumed to consist of one mole of alcoholic hydroxyl groups and one mole of etheric oxygen atoms, and then the pure liquid state of ADAE will be approximated by one mole of alcohol plus one mole of ether. Hence, $H_3/2$ is replaced by the enthalpy of mixing of the alcohol+ether system at equimolar fraction, $H^E(x=0.5)$. According to these assumptions, H_1', H_2', and H_3 are estimated to be 5.8 kJ mol^{-1},[18] 0.4 kJ mol^{-1},[19] and 1.5 kJ mol^{-1},[19] respectively. As for H_2, the latest value of 23.2 kJ mol^{-1} for the ethanol+hexane system[11] is used, which was measured in a sufficiently dilute region. For H_1, the values listed in Table 2 are used. Using these values and Eq. 2, H_i values for various ADAE are found and are also listed in Table 2. These results are distributed in the neighborhood of 10 kJ mol^{-1}, and it seems that the values of H_i for ADAE depend on the length of the internal methylene group in the ADAE molecule, but hardly depend on the chain length of the terminal alkyl group in the ADAE molecule. The values of H_i for ADAE having the same terminal alkyl group are in the order of $RO(CH_2)_2OH>RO(CH_2)_3OH>RO(CH_2)_4OH$. On the other hand, the values of H_i for α,ω-alkanediols ($HO(CH_2)_nOH$, $n=3$, 4) were estimated from the infrared spectra[20] and dielectric measurements,[21] and are comparable with those in the present systems. However, the dependence of H_i values on the length of the internal methylene group seems to be the reverse of that of ADAE. At present, we have no satisfactory explanation of this fact.

In conclusion, the present results suggest that the enthalpic contribution due to the intramolecular hydrogen bond contained in the ADAE molecule is smaller than that due to the normal intermolecular hydrogen bond between hydroxyl groups, and in general can be estimated to be about 10 kJ mol^{-1}.

The present work was partially supported by a grant from the Ministry of Education.

References

1) L. P. Kuhn, *J. Am. Chem. Soc.*, **74**, 2492 (1952).
2) L. P. Kuhn, P. von R. Schleyer, W. F. Baitinger, and L. Eberson, *J. Am. Chem. Soc.*, **86**, 650 (1964).
3) A. B. Foster, A. H. Haines, and M. Stacey, *Tetrahedron*, **16**, 177 (1961).
4) P. J. Kruger and H. D. Mettee, *J. Mol. Spectrosc.*, **18**, 131 (1965).
5) N. Mori, E. Nakamura, and Y. Tsuzuki, *Bull. Chem. Soc. Jpn.*, **40**, 2191 (1967).
6) T. Yonezawa, H. Saito, S. Matsuoka, and K. Fukui, *Bull. Chem. Soc. Jpn.*, **38**, 1431 (1965).
7) Y. Toshiyasu, K. Kimura, and R. Fujishiro, *Bull. Chem. Soc. Jpn.*, **43**, 2676 (1970).
8) Y. Toshiyasu and R. Fujishiro, *Nippon Kagaku Kaishi*, **94**, 429 (1973).
9) R. Tanaka, S. Murakami, and R. Fujishiro, *Bull. Chem. Soc. Jpn.*, **45**, 2107 (1972).
10) R. Tanaka, S. Murakami, and R. Fujishiro, unpublished data.
11) R. H. Stokes and C. Burfitt, *J. Chem. Themodyn.*, **5**, 623 (1973).
12) C. G. Savini, D. R. Winterhalter, and H. C. Van Ness, *J. Chem. Eng. Data*, **10**, 168 (1965).
13) H. C. Van Ness, C. A. Soczek, G. L. Peloquin, and R. L. Machado, *J. Chem. Eng. Data*, **12**, 217 (1967).
14) H. C. Van Ness, C. A. Soczek, and N. K. Kochar, *J. Chem. Eng. Data*, **12**, 346 (1967).
15) I. Brown, W. Fock, and F. Smith, *Aust. J. Chem.*, **17**, 1106 (1964).
16) I. Brown, W. Fock, and F. Smith, *J. Chem. Thermodyn.*, **1**, 273 (1969).
17) M. Takami, S, Murakami, and R. Fujishiro, *Bull. Chem. Soc. Jpn.*, **38**, 291 (1965).
18) H. V. Kehiaian, K. Sosnkowska-Kehiaian, and R. Hryniewicz, *J. Phys. Chem.*, **68**, 922 (1971).
19) S. Murakami and R. Fujishiro, *Bull. Chem. Soc. Jpn.*, **39**, 720 (1966).
20) L. P. Kuhn and R. A. Wires, *J. Am. Chem. Soc.*, **86**, 2161 (1964).
21) Y. Toshiyasu, Ph. D. Thesis, Osaka City University, Osaka, 1973.

The Dimerization of 2-Methylpropene Induced by γ-Radiation at High Temperatures and Pressures

Teruyuki NAITO

National Chemical Laboratory for Industry, Meguro Division, Mita, Meguro-ku, Tokyo 153

(Received August 26, 1976)

The dimerization of 2-methylpropene by γ-irradiation occurred at a temperature of 300 °C and a 2-methylpropene density of 0.1 g/cm^3, giving rise to the formation of 1,1,3-trimethylcyclopentane. The G value of this dimer was 50 at an absorbed dose rate of 4.3×10^{18} eV/g h and a total absorbed dose of 2.2×10^{19} eV/g. The G value of this dimer was inversely proportional to about 0.47 the power of the absorbed dose rate and was proportional to the 2-methylpropene density. The formation of this dimer was suppressed by the addition of oxygen or nitrogen monoxide. These facts led to the conclusion that the dimer was formed *via* chain reactions with the participation of the 2-methylallyl radical.

The radiation chemistry of 2-methylpropene has been studied by several investigators. Collin and Herman[1] examined the products of the radiolysis of gaseous 2-methylpropene, and they proposed some mechanisms leading to the formation of several low boiling-point products.

Many studies of the low-temperature radiation-induced polymerization of 2-methylpropene, both in the gas phase and in the liquid phase, have shown that the chain propagation was not the free-radical mode but the ionic one and that the most likely initiating species was the *t*-butyl cation, *t*-$C_4H_9^+$. For instance, Okamoto *et al.*[2] studied the gas-phase radiation-induced polymerization of 2-methylpropene and established the *t*-butyl cation mechanism. This cation was considered to be produced from the 2-methylpropene parent ion, *i*-$C_4H_8^+$, *via* an ion-molecule reaction:

$$i\text{-}C_4H_8 \rightsquigarrow i\text{-}C_4H_8^+ + e$$
$$i\text{-}C_4H_8^+ + i\text{-}C_4H_8 \longrightarrow t\text{-}C_4H_9^+ + C_4H_7\cdot \qquad (1)$$

From their mass spectrometric observations, Tal'rose and Lyubimova[3] showed that Reaction 1 did indeed occur, and Koyano[4] showed that this reaction had a very large cross section.

Collinson *et al.*[5] suggested that Reaction 1 also occurred in the radiolysis of liquid 2-methylpropene and that the $C_4H_7\cdot$ produced together with the *t*-butyl cation was most likely a methyl allyl radical.

On the other hand, McKinley *et al.*[6] studied the thermal polymerization of 2-methylpropene at 370—460 °C, at maximum pressures of from 37 to 370 atm, and at times of from one half hour to four hours. Under these conditions a cyclic dimer, 1,1,3-trimethylcyclopentane (**1**), was the main reaction product.

The present work showed that dimer **1** is not formed at 300 °C and a 2-methylpropene density of 0.1 g/cm^3 for five hours, but by γ-irradiation under the same conditions **1** is formed as a major dimer product, while, 2,4,4-trimethyl-2-pentene (**2**) is formed as a minor one. It will then be concluded that the dimerization of 2-methylpropene induced by γ-radiation proceeds mainly by means of a radical chain reaction whose chain carrier is $C_4H_7\cdot$ and that the contribution of the *t*-butyl cation to the dimerization is not greater than that of $C_4H_7\cdot$.

Experimental

Research-grade 2-methylpropene and all the other gaseous meterials except oxygen were degassed by repeating the freezing-pumping-thawing cycle several times.

The reaction vessel was a stainless steel autoclave (2 cm in inner diameter and with a volume of about 20 cm^3) which was surrounded by a mantle heater. The temperature was controlled at 300±3 °C.

The samples were irradiated with γ-rays from ^{60}Co, and in most cases, the absorbed dose rate was 4.3×10^{18} eV/g h and the total absorbed dose was 2.2×10^{19} eV/g. The G values were calculated from the energy absorbed by the sample, where it was assumed that the absorbed energy was proportional to the electron density of the sample. The absolute energy absorption was determined by means of Fricke dosimetry, taking $G(Fe^{+3})=15.5$.

All the irradiations were carried out at a temperature of 300 °C and a 2-methylpropene density of 0.1 g/cm^3 except where otherwise specified.

After irradiation, the liquid products in the reaction vessel were collected in a trap immersed in liquid nitrogen by vaporizing and pumping them. In order to differentiate between the saturated compounds and the unsaturated compounds in the collected products, the products were hydrogenated in ethanol over Raney's nickel. Gas-liquid-phase chromatography and gas chromatograph-mass spectrography were applied to both the original and hydrogenated products for the identification and determination of the two dimers, **1** and **2**.

Results and Discussion

The yields of the liquid product from γ-irradiated 2-methylpropene were determined at temperatures between 30 and 300 °C. In the lower-temperature range, many kinds of products were formed, but their yields were poor. However, the yields increased with an increase in the temperature; moreover, the proportion of the **1** dimer in the product increased. It was expected that the dimerization proceeded by means of some chain mechanisms above 200 °C.

At 300 °C and a 2-methylpropene density of 0.1 g/cm^3, various scavengers were used in order to see whether the dimerization takes place by means of an ionic or radical mechanism. The experimental results are shown in Table 1.

The addition of ammonia, whose concentration range

TABLE 1. EFFECT OF SCAVENGERS ON THE γ-RADIATION-INDUCED DIMERIZATION OF 2-METHYLPROPENE AT A TEMPERATURE OF 300 °C AND A 2-METHYLPROPENE DENSITY OF 0.1 g/cm^3

Scavenger	Concn (mol %)	G value of dimer	
		1	**2**
None		50	5
NH_3	1.0	48	2
	3.0	51	1
	5.0	52	1
O_2	0.05	30	4
	0.15	14	4
NO	0.5	41	5
	1.0	30	4
	5.0	15	5

The absorbed dose rate is 4.3×10^{18} eV/g h, and the total absorbed dose is 2.2×10^{19} eV/g.

was 0.5—5.0% in the molar fraction, suppressed the formation of **2**, but had little influence on the formation of **1**. This implied at least that the precursor of **1** was not a cation, while **2** was formed by the participation of some cations.

Oxygen and nitrogen monoxides of various concentrations were used as the radical scavengers. It was observed that the addition of small amounts of them sup ressed the formation of **1**. On the other hand, the yield of **2** did not change upon the addition of the radical scavengers. Consequently, these observations were in marked contrast to those of ammonia addition.

It is well-known that the intermediary species formed during the γ-irradiation of 2-methylpropene are varieties of ions, radicals, and excited molecules. Among these species, the *t*-butyl cation and the $C_4H_7\cdot$ formed through Reaction 1 seem to be the most reasonable precursors of the 2-methylpropene dimers. Assuming this, it may be considered that, after the formation of the *t*-butyl cation and $C_4H_7\cdot$, they can bring about the subsequent reactions in the following ways:

$$t\text{-}C_4H_9^+ + i\text{-}C_4H_8 \longrightarrow C_8H_{17}^+ \longrightarrow \text{dimer} \longrightarrow \text{polymer} \quad (2)$$

$$C_4H_7\cdot + i\text{-}C_4H_8 \longrightarrow C_8H_{15}\cdot \quad (3)$$

$$C_8H_{15}\cdot + i\text{-}C_4H_8 \longrightarrow C_8H_{16} + C_4H_7\cdot \quad (4)$$

It has been found that the *t*-butyl cation reacts predominantly with the terminal carbon in 2-methylpropene both in the gas phase[7] and in the liquid phase[8] to give $C_8H_{17}^+$, the 2,2,4-trimethylpentyl cation, and that this cation then produces mainly **2** by means of a proton-transfer reaction with 2-methylpropene. In the present work also, **2** is probably formed by means of the ionic reaction mentioned above. This speculation seems reasonable because of the observation that the formation of **2** was suppressed by the addition of ammonia. Ammonia is a well-known scavenger of the *t*-butyl cation[9]:

$$t\text{-}C_4H_9^+ + NH_3 \longrightarrow i\text{-}C_4H_8 + NH_4^+ \quad (5)$$

On the other hand, it may be considered that $C_4H_7\cdot$ is a 2-methylallyl radical (structural formula (**3**)).[5] If so, **3** will readily react with 2-methylpropene to form a 1,3,3-trimethylcyclopentyl radical, (**5**), *via* an intermediary adduct, (**4**), and the radical **5** will subsequently abstract a hydrogen atom from 2-methylpropene; then, as a result of the abstraction, **1** and $C_4H_7\cdot$ (probably, the 2-methylallyl radical) will be formed. That is to say, the reformed $C_4H_7\cdot$ will serve as a chain carrier to repeat the above cyclic reaction and to cause a chain reaction:

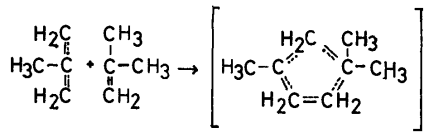

3 4

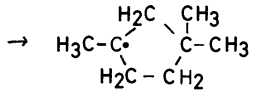

5

In this case, it is assumed that the primary $C_4H_7\cdot$ is formed only by way of Reaction 1, not by other ways such as the decomposition of the excited 2-methylpropene molecule:

$$i\text{-}C_4H_8 \rightsquigarrow i\text{-}C_4H_8^* \longrightarrow C_4H_7\cdot + H\cdot \quad (6)$$

No hydrogen or compounds formed by the participation of the hydrogen atom could be detected.

It is assumed that the termination reaction can be expressed as follows:

$$C_4H_7\cdot(\text{or } C_8H_{15}\cdot) + R \longrightarrow \text{Products} \quad (7)$$

where R denotes the $C_4H_7\cdot$ radical, the $C_8H_{15}\cdot$ radical, or other radicals in this system, for instance, the fragment radicals such as $CH_3\cdot$ or $C_3H_5\cdot$ from the radiolysis of 2-methylpropene. Unfortunately, in this work, the termination reactions could not be defined because it was not possible to determine accurately each product derived from the respective termination reactions because of the uncertainty of the gas-chromatographic analysis. However, it may be considered that $C_4H_7\cdot$ and $C_8H_{15}\cdot$ are the most important radicals and that the other radicals are negligible. Therefore, it is assumed that the overall velocity of the termination reaction is $k_t[C_4H_7\cdot][C_8H_{15}\cdot]$, where k_t is the rate constant.

In the reaction sequence mentioned above, provided a stationary state holds for the radicals of both $C_4H_7\cdot$ and $C_8H_{15}\cdot$, **1** can form only *via* Reactions 3 and 4; further, the rate of the formation of primary $C_4H_7\cdot$ (Reaction 1) is proportional to the absorbed dose rate, and the G value of **1** is inversely proportional to one-half the power of the absorbed dose rate and is proportional to the 2-methylpropene density:

$$G(\mathbf{1}) = k_4(k/k_t)^{1/2}I^{-1/2}[i\text{-}C_4H_8]$$

where k and k_4 are the rate constants of Reactions 1 and 4 respectively, and where I is the absorbed dose rate.

The variations in the G value of **1** with the absorbed dose rate and the 2-methylpropene density are shown in Figs. 1 and 2 respectively. The G value of **1** was

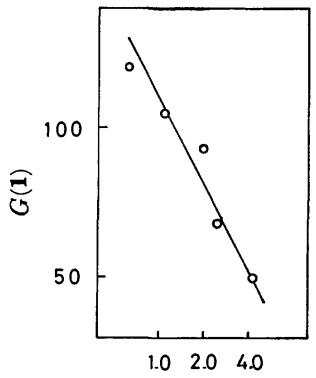

Absorbed dose rate (10^{18} eV/g h)

Fig. 1. A plot of G value of **1** *vs.* absorbed dose rate. The absorbed dose, about 2.2×10^{19} eV/g.

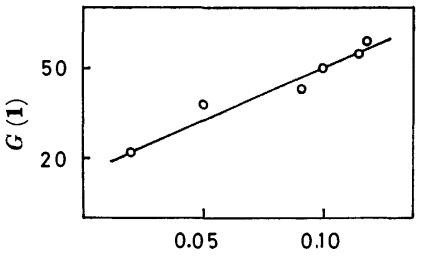

2-Methylpropene density (g/cm^3)

Fig. 2. A plot of G value of **1** *vs.* 2-methylpropene density. The absorbed dose rate, 4.3×10^{18} eV/g h and the total absorbed dose, 2.2×10^{19} eV/g

inversely proportional to about the 0.47 power of the absorbed dose rate and was proportional to the 2-methylpropene density. These experimental results were consistent with the schematic consideration. Therefore, it seems reasonable to conclude that, on γ-irradiation, 2-methylpropene dimerizes to form the cyclic dimer, **1**, by means of a radical chain mechanism where the chain carriers are both $C_4H_7\cdot$ and $C_8H_{15}\cdot$.

Lampe[10] showed a $G(C_4H_7\cdot)$ of 4.2 and $G(t\text{-}C_4H_9^+)=G(C_4H_7\cdot)$ in the liquid-phase polymerization of 2-methylpropene, where the *t*-butyl cation formed *via* Reaction 1 was a polymerization initiator. If it can be assumed that a $G(C_4H_7\cdot)$ of 4.2 is little affected by the phase of 2-methylpropene and the irradiation conditions, this value is equal to the initial G values of Reaction 1, that is, to the initial G values of $C_4H_7\cdot$ or the *t*-butyl cation under the conditions of this work. Therefore, the chain dimerizations concerned in the formation of **1** have chain-lengths of about 12, as evaluated by $G(\mathbf{1})/G(C_4H_7\cdot)=50/4.2$.

References

1) G. J. Collin and J. A. Herman, *Can. J. Chem.*, **45**, 3097 (1967); J. A. Herman and G. J. Collin, *ibid.*, **47**, 3837 (1969); J. A. Herman, *ibid.*, **48**, 3446 (1970).
2) K. Okamoto, K. Fueki, and Z. Kuri, *J. Phys. Chem.*, **71**, 3222 (1967).
3) V. L. Tal'rose and A. K. Lyubimova, *Dokl. Akad. Nauk, SSSR*, **86**, 909 (1952).
4) I. Koyano, *J. Chem. Phys.*, **45**, 706 (1966).
5) E. Collinson, F. S. Daiton, and H. A. Gillis, *J. Phys. Chem.*, **63**, 909 (1959).
6) J. B. McKinley, D. R. Stevens, and W. E. Baldwin, *J. Am. Chem. Soc.*, **67**, 1455 (1945).
7) G. R. Collin, *Can. J. Chem.*, **52**, 2341 (1974).
8) N. S. Viswanathan and L. Kevan, *J. Am. Chem. Soc.*, **89**, 2482 (1967).
9) T. Miyazaki and S. Shida, *Bull. Chem. Soc. Jpn.*, **39**, 2344 (1966).
10) F. W. Lampe, *J. Phys. Chem.*, **63**, 1986 (1959).

The Electronic States of $(SN)_x$ and $(SCH)_x$ Polymers

Tokio YAMABE, Kazuyoshi TANAKA, Akira IMAMURA,* Hiroshi KATO**, and Kenichi FUKUI

Department of Hydrocarbon Chemistry, Faculty of Engineering, Kyoto University, Sakyo-ku, Kyoto 606

**Shiga University of Medical Science, Seta, Otsu 520-21*

***College of General Education, Nagoya University, Chikusa-ku, Nagoya 464*

(Received October 12, 1976)

One-dimensional $(SN)_x$ and its isoelectronic system $(SCH)_x$ polymers are treated on the basis of the SCF-tight-binding MO theory. The Pennsylvania structure of $(SN)_x$ has been shown energetically favorable comparing the Lyon structure. Judging from the state density at the Fermi level of $(SCH)_x$, it may be expected to be a metallic conductor under some favorable condition.

There have been considerable experimental and theoretical interests in low-dimensional metallic conductors such as tetracyanoquinodimethane (TCNQ) charge-transfer salts and $K_2[Pt(CN)_4]Br_{0.3}\cdot 3H_2O$ mixed valence complex.[1] Recently, the third member, polymeric sulfur nitride, $(SN)_x$, has been revealed as a low-dimensional metallic polymer,[2] which does not show the Peierls transition like the above two, and even becomes a superconductor at $\approx$0.3 K.[3]

The theoretical band structure calculations of $(SN)_x$ have been performed with the OPW method[4] and several non SCF-tight-binding techniques such as the extended Hückel method.[5] In these tight-binding MO calculations, however, the electron-electron interaction potential is not taken into account explicitly, and hence these methods would be only reliable on the non-polar polymers such as polyethylene.[6] Since the sulfur-nitrogen bond in $(SN)_x$ has been estimated experimentally to be of rather polar character,[7] it would be suitable to calculate the MO including the electron repulsion integrals for this polymer. The SCF-tight-binding MO calculation including these repulsion integrals has been carried out only by Zunger and by Merkel and Ladik[8] for the one-dimensional structure of $(SN)_x$ in the crystal structure proposed by Boudeulle and Michel (Lyon structure)[9] based on the electron-diffraction analysis as shown in Fig. 1(A). The band structures obtained by them clearly show the metallic nature of $(SN)_x$, and the possibility of the occurrence of the Peierls transition has been denied by the former.

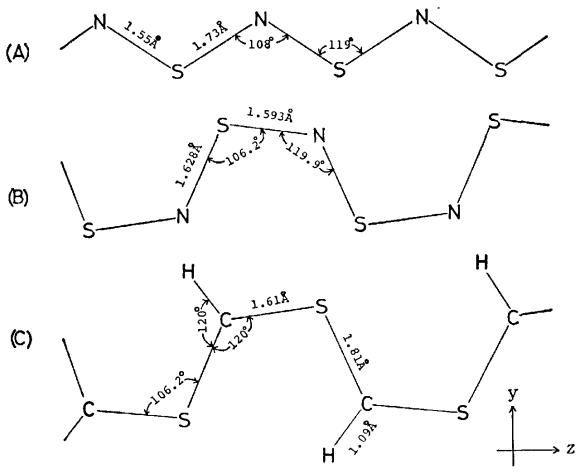

Fig. 1. The structures of $(SN)_x$ and $(SCH)_x$; (A) the Lyon structure (Ref. 9), (B) the Pennsylvania structure (Ref. 10), and (C) an assumed structure for the calculation here (see text).

More recently, however, the more reliable structure of $(SN)_x$ has been proposed by MacDiarmid *et al.* (Pennsylvania structure)[10] based on the X-ray diffraction analysis as shown in Fig. 1(B). In this paper, we present the result of electronic states of the one-dimensional Pennsylvania structure of $(SN)_x$ by the SCF-tight-binding MO calculation including the electron repulsion, and, furthermore, the calculation for an assumed structure of $(SCH)_x$ polymer has been made so as to study an isoelectronic system with the $(SN)_x$ polymer.

Method of Calculation

In order to avoid the complicated calculations of the all matrix elements by *ab initio* methods, we employ the CNDO/2 approximation by Pople and Segal[11] as Zunger did. The SCF iteration process is accelerated by the density matrix method previously introduced by Imamura and Fujita to calculate biopolymers.[12] The formalism of the calculation has been described thoroughly in their article, so we will not mention the details here again. All valence AOs and 3d orbitals for sulfur atoms were considered since it has been pointed out that the contribution from 3d orbitals is not negligible for $(SN)_x$.[8] For the parametrizations were adopted those of spd set by Santry and Segal,[13] and the number of representative wave vector K was chosen as 21 at regular intervals ($\pi/10a$; a is the length of the unit cell) in the Brillouin zone.

We assumed the structure of $(SCH)_x$ to be analogous to that of the Pennsylvania structure of $(SN)_x$, as shown in Fig. 1(C). The angle at sulfur was chosen as 106.2° after that in $(SN)_x$, and that at carbon as 120° after ordinary sp^2 hybridization. The two kinds of S–C bond distance, 1.81 and 1.61 Å, are employed from the data for dimethyl disulfide[14] and thioformaldehyde,[15] respectively. The C–H bond distance, 1.09 Å, also from the latter. Each of SN and SCH units consists of 11 valence electrons and, hence, an open-shell structure. Since the $(SN)_x$ crystal, however, does not show paramagnetism,[10] the system could be treated as a closed-shell system. We employed $(SN)_2$ as a unit cell in the MO calculation of the $(SN)_x$ polymer. We also assumed $(SCH)_2$ as a unit cell in the $(SCH)_x$ polymer. Since the polymer chains possess a two-fold screw rotation as a symmetry operation, all pairs of bands stick together at the edges of the Brillouin zone,[16] and in this case, the HOMO(π) and the LUMO(π^*) bands

TABLE 1. AO DENSITIES, ATOMIC NET CHARGES, AND THE TOTAL ENERGIES OF $(SN)_x$ AND $(SCH)_x$

		$(SN)_x$: Pennsylvania structure		$(SN)_x$: Lyon structure[a]		$(SCH)_x$		
		S	N	S	N	S	C	H
AO	s	1.810	1.550	1.824	1.549	1.768	1.114	0.912
	p_x	1.407	1.218	0.714	1.163	1.478	1.135	
	p_y	0.822	1.235	0.784	1.315	0.923	0.962	
	p_z	0.728	1.228	1.497	1.153	0.929	0.964	
	d_{xz}	0.242		0.308		0.296		
	d_{xy}	0.133		0.219		0.091		
	d_{yz}	0.290		0.044		0.202		
	$d_{x^2-y^2}$	0.087		0.326		0.065		
	d_{z^2}	0.250		0.098		0.160		
π Electron densities		1.782	1.218	1.947	1.153	1.865	1.135	
Atomic net charges		+0.231	−0.231	+0.186	−0.186	+0.087	−0.175	+0.088
Total energies per unit cell (in eV)		−1230.056		−1228.562[d]		−1018.057		
		(−1218.220)[b]				(−1005.877)[b]		
		(−1227.731)[c]						

a) Ref. 8. For this structure, p_z, d_{xz}, d_{yz} and d_{z^2} AOs are the components of π orbitals. b) The total energy of $(SN)_2$ or $(SCH)_2$ molecule with the same configuration of the unit cell in $(SN)_x$ or $(SCH)_x$, respectively. c) The total energy of the most stable configuration (square form) of $(SN)_2$ molecule (Ref. 10). d) The value calculated by us on the same basis for the Pennsylvania structure.

also degenerate there. At such points, it is in principle unreasonable to describe the system with a single Slater determinant. Thus we extrapolated the density matrix elements at $K=\pm 9\pi/10a$ and $\pm\pi/10a$ to obtain those at $K=\pm\pi/a$ and 0, respectively. The values of overlap integrals between the central unit cell and the N-th nearest neighboring cell rapidly decrease to 0 where $N=3$—4 (9—13.5 Å from the central unit cell). But as those of electron repulsion (Coulomb) integrals slowly decrease, we consider them as far as the 7-th nearest neighbors (≈31 Å from the central unit cell).

Results and Discussion

The calculated results of AO densities, atomic net charges and the total energies per unit cell are shown in Table 1 along those of the Lyon structure of $(SN)_x$. As we set the direction of the polymer chain along the z-axis and the polymer plane perpendicular to the x-axis, the π orbitals are of $2p_x$, $3p_x$, $3d_{xy}$, and $3d_{xz}$ AOs. Both of $(SN)_2$ and $(SCH)_2$ units have six π electrons, supplied two π electrons from the sulfur atom and one from the nitrogen or the carbon atom. In $(SN)_x$ calculated here, the densities of $3p_x$ and $2p_x$ AOs on S and N are 1.407 and 1.218, respectively, and the contribution from $3d_{xy}$ and $3d_{xz}$ AOs is totally 0.375, the magnitude of which is not negligible. The atomic net charge on S is +0.231, and it is somewhat larger than that estimated for the Lyon structure, +0.186,[8] but somewhat less than that estimated by XPS method, +0.30—0.42.[7] In $(SCH)_x$, although the π electron densities on S and C are not so different from those on S and N in $(SN)_x$, the atomic net charge on S is +0.087 which is by far less than that in $(SN)_x$. This would be direct reflection of the electronegativity of each atom, namely S<C<N in order. It is also interesting that the atomic net charge on H is very close to that on S. It is clearly shown, from the difference in the total energies of a unit cell and isolated $(SN)_2$ molecules, that the polymeric state is more stable than the isolated molecules. Moreover, the comparison of the total energies per unit cell of the two structures of $(SN)_x$ definitely shows that the Pennsylvania structure is favorable. For $(SCH)_x$, it is similarly predicted that the polymeric state is stable in comparison with the isolated $(SCH)_2$ molecule.

The energy bands and the state densities of the polymers are shown in Figs. 2(A) and (B). The curves of the state densities are obtained with the Brust's method[17] summing over 300 points sampled in the Brillouin zone for each energy band. The valence bands consist of three π bands and eight σ bands, and the HOMO and the LUMO bands are of π MOs mainly composed of the sulfur $3p_x$ AO in both $(SN)_x$ and $(SCH)_x$. These energy bands of $(SN)_x$ and $(SCH)_x$ are seen to be of rather similar shape and the Fermi energies (E_F) are obtained as −4.996 and −4.340 eV, respectively. E_F of the Lyon structure of $(SN)_x$ has been reported to be −5.714 eV.[8] The shape of the state density of $(SN)_x$ agrees qualitatively with those obtained previously by ESCA spectroscopy.[7,18] The state density at E_F ($D(E_F)$) is small but finite for $(SN)_x$, namely, 0.04 states/eV spin-molecule, which shows the metallic nature of $(SN)_x$. Experimental value of $D(E_F)$ is 0.12—0.18 states/eV spin-molecule[18,19] which agrees quantitatively with our result but is somewhat larger, showing perhaps the reflection of the actual three-dimensional structure of $(SN)_x$ crystal. For $(SCH)_x$, the shape of the state density again resembles that of $(SN)_x$ but the peaks are more sharpened than in $(SN)_x$, and $D(E_F)$ is 0.06 states/eV spin-molecule. This value encourages us that $(SCH)_x$ may become also a metallic conductor if it should be successfully synthesized, and unless any interference such as Peierls transition

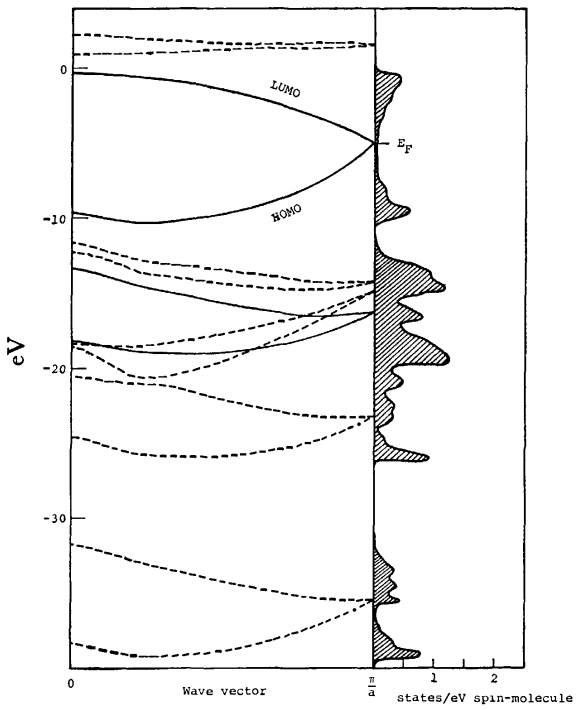

Fig. 2. The band structures and the state densities of (A) $(SN)_x$ and (B) $(SCH)_x$. Dotted lines and solid ones indicate σ bands and π bands, respectively. The upper several vacant MO bands and the state densities of those which are upper than the LUMO bands are not essential and omitted here.

should occur to break down the metallic state of $(SCH)_x$.

The E_{AB} analyses in the scheme of the CNDO/2 method are shown in Fig. 3 for $(SN)_x$ and $(SCH)_x$. It is shown that N_1–S_4 in $(SN)_x$ and S_1–C_6 in $(SCH)_x$

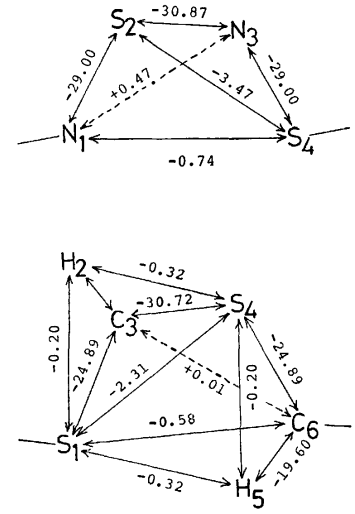

Fig. 3. The E_{AB} analyses for the representative unit cells of $(SN)_x$ and $(SCH)_x$. The energies are shown in eV. Dotted lines and solid ones indicate the repulsive and attractive interactions, respectively.

are both attractive. Moreover, it should be noticed that, both in $(SN)_x$ and in $(SCH)_x$, S_2–S_4 and S_1–S_4 are considerably attractive, while N_1–N_3 and C_3–C_6 are weakly repulsive, and hence the skeleton of each unit cell is held rather tightly. This would cause interesting effects to the force constant of the lattice displacement and to the Debye frequency of the system.

It is also noticed that much attention should be paid to the description of the system at $K=\pm\pi/a$, since there occurs a degeneracy of the HOMO and the LUMO bands. In order to overcome such a situation, some appropriate linear combination of the Slater determinants (Configuration Interaction) should be adopted.

The possibility of the interaction between two $(SN)_x$ chains or the highly anisotropic two- or three-dimensionality of $(SN)_x$ crystal has also been pointed out from some experimental aspects.[10,20] The SCF-tight-binding calculation including two chains is desirable.

We are grateful to the Data Processing Center of Kyoto University for its generous permission to use the FACOM 230-75 Computer. This work was supported by a Grant-in-Aid for Scientific Research from the Ministry of Education of Japan (No. 065101).

References

1) For example, see H. J. Keller, "Low-Dimensional Cooperative Phenomena," Plenum Press, New York (1975).
2) V. V. Walatka, Jr., M. M. Labes, and J. H. Perlstein, *Phys. Rev. Lett.*, **31**, 1139 (1973); C. Hsu and M. M. Labes, *J. Chem. Phys.*, **61**, 4640 (1974); C. K. Chiang, M. J. Cohen, A. F. Garito, A. J. Heeger, C. M. Mikulski, and A. G. MacDiarmid, *Solid State Commun.*, **18**, 1451 (1976).
3) R. L. Greene, G. B. Street, and L. J. Suter, *Phys. Rev. Lett.*, **34**, 577 (1975).
4) W. E. Rudge and P. M. Grant, *Phys. Rev. Lett.*, **35**, 1799 (1975).
5) D. E. Parry and J. M. Thomas, *J. Phys.*, *C*, **8**, L45(1975);

W. I. Friesen, A. J. Berlinsky, B. Bergersen, L. Weiler, and T. M. Rice, *J. Phys., C*, **8**, 3549 (1975); V. T. Rajan and L. M. Falicov, *Phys. Rev., B*, **12**, 1240 (1975); H. Kamimura, A. M. Glazer, A. J. Grant, Y. Natsume, M. Schreiber, and A. D. Yoffe, *J. Phys., C*, **9**, 291 (1976); A. A. Bright and P. Soven, *Solid State Commun.*, **18**, 317 (1976).

6) H. Fujita and A. Imamura, *J. Chem. Phys.*, **53**, 4555 (1970).

7) P. Mengel, P. M. Grant, W. E. Rudge, B. H. Schechtman, and D. W. Rice, *Phys. Rev. Lett.*, **35**, 1803 (1975).

8) A. Zunger, *J. Chem. Phys.*, **63**, 4854 (1975); C. Merkel and J. Ladik, *Phys. Lett., A*, **56**, 395 (1976).

9) M. Boudeulle and P. Michel, *Acta Crystallogr., Sect. A*, **28**, S199 (1972).

10) A. G. MacDiarmid, C. M. Mikulski, P. J. Russo, M. S. Saran, A. F. Garito, and A. J. Heeger, *J. Chem. Soc., Chem. Commun.*, **1975**, 476; C. M. Mikulski, P. J. Russo, M. S. Saran, A. G. MacDiarmid, A. F. Garito, and A. J. Heeger, *J. Am. Chem. Soc.*, **97**, 6358 (1975).

11) J. A. Pople and G. A. Segal, *J. Chem. Phys.*, **44**, 3289 (1966).

12) A. Imamura and H. Fujita, *J. Chem. Phys.*, **61**, 115 (1974).

13) D. P. Santry and G. A. Segal, *J. Chem. Phys.*, **47**, 158 (1967).

14) D. Sutter, H. Dreizler, and H. D. Rudolph, *Z. Naturforsch., Teil A*, **20**, 1676 (1965).

15) D. R. Johnson, F. X. Powell, and W. H. Kirchoff, *J. Mol. Spectrosc.*, **39**, 136 (1971).

16) For example, see V. Heine, "Group Theory in Quantum Mechanics," Pergamon Press, London (1960), p. 265.

17) J. Brust, "Methods of Computational Physics," Academic Press, New York (1968), Chap. 8.

18) L. Ley, *Phys, Rev. Lett.*, **35**, 1796 (1975)

19) R. L. Greene, P. M. Grant, and G. B. Street, *Phys. Rev. Lett.*, **34**, 89 (1975).

20) A. A. Bright, M. J. Cohen, A. F. Garito, A. J. Heeger, C. M. Mikulski, P. J. Russo, and A. G. MacDiarmid, *Phys. Rev. Lett.*, **34**, 206 (1975); H. Kamimura, A. J. Grant, F. Levy, A. D. Yoffe, and G. D. Pitt, *Solid State Commun.*, **17**, 49 (1975); L. Pintschovius, H. P. Geserich, and W. Möller, *ibid.*, **17**, 477 (1975).

Calorimetric Study of the Glassy State. XI. Plural Glass Transition Phenomena of Cyclohexene

Osamu HAIDA, Hiroshi SUGA, and Syûzô SEKI

Department of Chemistry, Faculty of Science, Osaka University, Toyonaka, Osaka 560

(Received October 14, 1976)

Two kinds of glassy crystalline phases (I and III) of cyclohexene were realized by different thermal treatments. The heat capacities of the glassy and the supercooled crystal-I and -III, as well as the stable crystalline phases were measured by an adiabatic calorimeter in the temperature range 12—300 K. The glass transition temperature T_g, the heat capacity jump at T_g and the residual entropy were found to be 81 K, 11.4 JK^{-1} mol^{-1} and 11.7 JK^{-1} mol^{-1} for crystal-I and 83 K, 3.6 JK^{-1} mol^{-1} and 2.6 JK^{-1} mol^{-1} for crystal-III, respectively. The glassy liquid state of cyclohexene was realized by vapor condensation technique, its T_g being 78 K as determined by DTA method. The results provide the first example of plural glass transition phenomena in one and the same low-molecular-weight compound.

The heat capacity of liquid contains a contribution from a potential energy variation caused by structural change with temperature. This degree of freedom is usually known as "configurational freedom" and has been used in many theoretical works for describing the thermal behavior of glass-forming liquid in a transfigured fashion such as free volume,[1] trans-gauche conformation[2] and bond-lattice model.[3] These treatments have been successful to a certain extent to explain thermodynamic and kinetic aspects of the glass transition in spite of their simplified models.

Discovery of glassy crystals[4] brought about an extension of the concept of glass from the originally defined non-equilibrium frozen state of liquid to that of a system including some kind of disorder. In addition it offers a new possibility for studying the glassy state. The site randomness will be eliminated from the configurational freedom in the case of glassy crystals since they have three-dimensional positional periodicity. Even in this favorable situation, however, the "configuration" is of a complex mixture of orientational and internal freedom of molecule, as pointed out by Adachi *et al.*[4] The realization of more than one kind of glassy state of a compound is therefore expected to give a clue in resolving the entanglement between these freedoms.

The calorimetric study by Huffman *et al.*[5] revealed the fact that cyclohexene has two crystalline phases, I and II. Adachi *et al.*[6] realized the glassy state of high temperature crystalline phase I based on the results of DTA experiment. We have found a new crystalline phase (crystal-III) and its glassy crystalline state. The glassy liquid state of cyclohexene was also realized by the vapor condensation method. A brief account of these findings was reported in a short communication.[7]

Experimental

Material. Commercial "Standard Material" of cyclohexene (Tokyo Kagaku Seiki Co., Ltd.) was deaerated and then distilled twice in a vacuun. The final purity of the sample was determined to be 99.98% by gas chromatography (Shimadzu Gas Chromatogram G.C./C. column; Apiezon grease on serite, column temperature; 70 °C) and 99.96% by calorimetric study.

Apparatus. The heat capacity was measured with an adiabatic calorimeter.[8] The purified sample was introduced into the calorimeter cell by vacuum distillation through a copper tubing attached to the top of the cell. When the procedure was over, the cell was pinched off at the copper tubing and sealed with a soft solder. The weight of the sample used for the heat capacity measurement was 23.154 g.

The DTA apparatus used in the preparation of the glassy liquid has also been reported.[9]

Experimental Results

DTA. The thermal behavior of cyclohexene at low temperature was examined by use of DTA, the results being given in Fig. 1. Run 1 shows the cooling curve with a rate of −2 K min^{-1}, and Run 2 the subsequent heating curve. Run 3 shows the heating curve of rapidly cooled sample at a rate greater than 7 K min^{-1} from high temperature crystal-I or liquid. The result of Run 3 coincides with that reported previously[6] except for a difference in anomalies at 120 and 140 K. The endothermic peaks at 140 K in Run 3 and 170 K in Runs 2 and 3 correspond to the processes crystal-I→crystal-II and crystal-II→liquid, respectively. When the liquid is cooled slowly as in Run 1, it crystallizes into crystal-I at around 130 K with successive two exothermic effects, and then the crystal-I transforms into a newly found crystal-III reversibly at about 115 K. The successive peaks at 130 K in Run 1 were separated

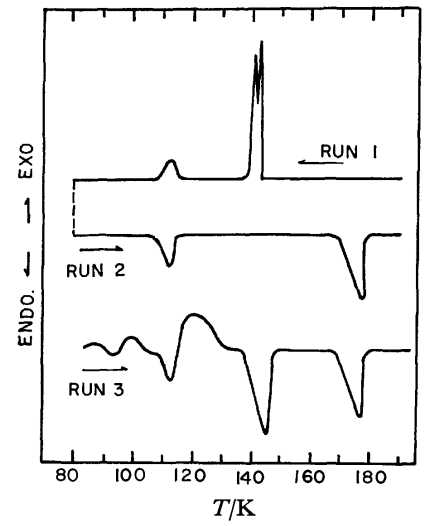

Fig. 1. DTA curves of cyclohexene.

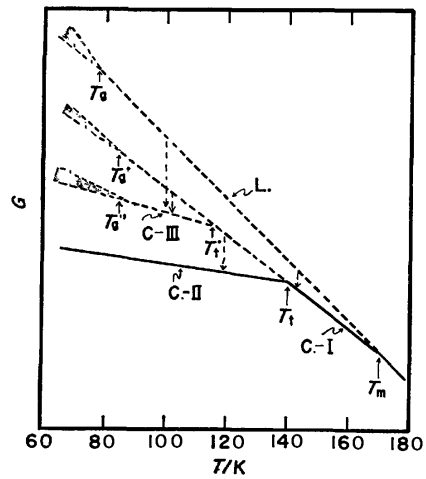

Fig. 2. Schematic diagram for Gibbs energy relationship of cyclohexene.

by chance and might be attributed to the appearance of a metastable phase on the way from liquid into crystal-I.

The thermogram Run 3 is interpreted as follows. When crystal-I is chilled through the transition temperature (115 K) at a rate greater than -7 K min^{-1}, the glassy crystal-I can be prepared. During the course of subsequent heating, the glassy crystal-I recrystallizes into crystal-III at *ca.* 100 K after the glass transition at 92 K is over, and then successive transformations of crystal-III→crystal-I→crystal-II→crystal-I→liquid take place at 115, 120, 140, and 160 K, respectively. This interpretation was confirmed by calorimetric studies. Among the transitions in Run 3 the rate of irreversible transition from crystal-I to crystal-II at 120 K was found to be sensitive to the purity and thermal history of the specimen. Thus a different thermal behavior in the temperature range 120—140 K is seen in the results of Runs 2 and 3 (Fig. 1), Runs 2, 3, and 4 (Fig. 6) and those reported by Adachi *et al.*[6] The phase relations represented by Gibbs energy are schematically illustrated in Fig. 2. Glassy state of liquid (glassy liquid) was obtained by vapor condensation method, but not by rapid cooling method. This can be seen from the fact that the samples quenched from liquid and crystal-I gave the same thermogram Run 3.

Measurement of Heat Capacity. Glassy crystal-I was prepared by rapid chilling of the liquid sample by introducing liquid nitrogen directly into the calorimeter can. The average cooling rate in the temperature interval 220—80 K was *ca.* -40 K min^{-1}, which is much greater than the limit -7 K min^{-1} to obtain the thermogram Run 3 (Fig. 1). Concerning the crystal-III, series of measurement were performed with different samples. Thermal treatments adopted to obtain these samples were as follows. For series-I, crystal-III was prepared by cooling crystal-I at the cooling rate of *ca.* -1 K min^{-1}; for series-2 crystal-III (obtained by the same procedure as series-I) was annealed at 78 K for *ca.* 36 h; for series-3, it was made through the phase transformation from crystal-I (on which the heat capacity measurement up to 100 K was carried out) and subsequent annealing at 80—100 K for about 2 days. Crystal-II was prepared by cooling the crystal-I to 78 K and subsequent annealing at *ca.* 120 K. Complete transformation of crystal-I into crystal-II was confirmed by observing the cessation of the heat evolution accompanied by irreversible phase transition.

The molar heat capacities are given in Table 1 and plotted in Fig. 3. Besides the big heat capacity jump due to the glass transition phenomenon of crystal-I, a small heat capacity jump for crystal-III at *ca.* 80 K can also be seen. In the measurement for crystal-I and -III, heat evolution was observed in the temperature range

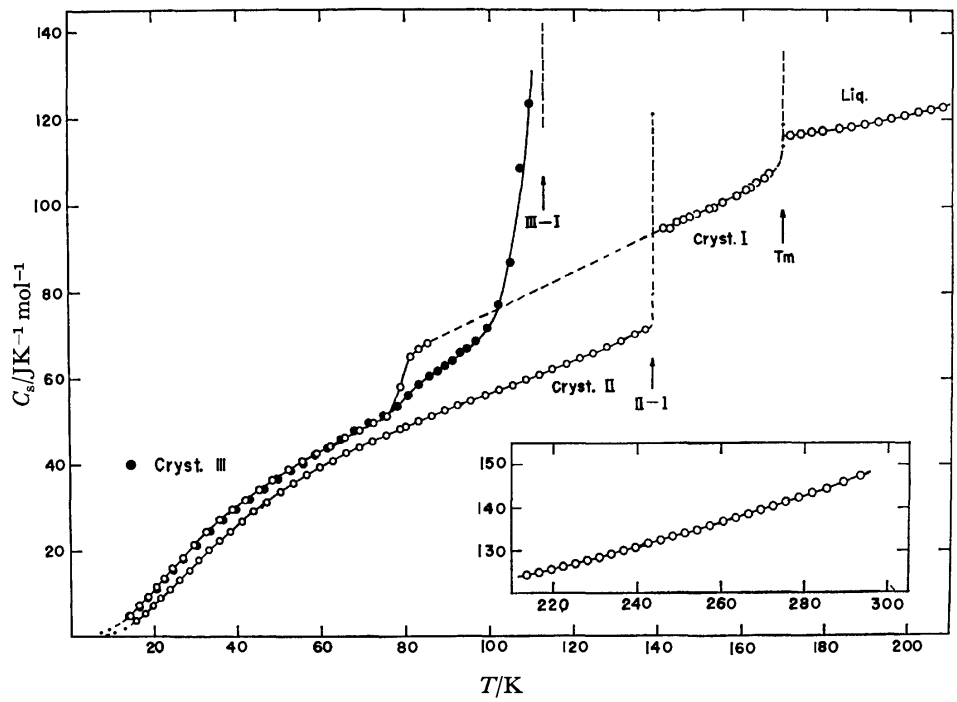

Fig. 3. Heat capacity curves of cyclohexene.

TABLE 1. MOLAR HEAT CAPACITY OF CYCLOHEXENE
mol wt=82.147 0 °C=273.15K

T_{av}/K	$\Delta H/\Delta T$/JK^{-1} mol^{-1}	ΔT/K
	Crystal-II	
15.63	3.580	2.372
17.86	5.294	2.081
19.87	7.057	1.918
21.78	8.792	1.884
23.76	10.86	2.064
26.03	13.06	2.456
28.41	15.48	2.314
30.77	17.83	2.414
33.22	20.20	2.485
35.74	22.47	2.542
38.35	24.59	2.694
41.09	26.86	2.774
43.89	29.28	2.839
46.94	31.38	3.252
50.16	33.74	3.184
53.32	35.70	3.149
56.46	37.54	3.129
59.61	39.32	3.164
62.71	40.86	3.037
65.83	42.71	3.203
68.98	44.04	3.101
72.17	45.45	3.277
75.44	46.89	3.265
78.68	48.32	3.217
79.92	48.81	2.920
82.98	50.14	3.208
86.15	51.48	3.128
89.24	52.70	3.063
92.28	53.81	3.005
95.46	54.93	3.354
98.78	56.13	3.290
102.04	57.33	3.244
105.25	58.48	3.176
108.40	59.65	3.123
111.52	60.78	3.091
114.72	62.00	3.313
118.01	63.25	3.254
121.23	64.50	3.202
124.40	65.74	3.124
127.66	67.13	3.402
131.03	68.55	3.345
134.35	70.06	3.290
136.81	71.27	1.623
	Glassy and supercooled crystal-I	
14.25	4.744	2.127
16.41	7.170	2.200
18.40	9.086	1.898
20.53	11.44	2.048
22.38	13.45	1.660
24.33	15.77	2.246
26.79	18.47	2.676
29.63	21.47	2.992
32.68	24.50	3.113
35.83	27.33	3.194
38.87	29.58	2.879
41.98	31.83	3.332
45.19	34.18	3.092
48.40	36.40	3.317
52.15	38.78	3.092
55.46	40.73	3.514
58.89	42.53	3.348
62.17	44.36	3.204
65.55	46.25	3.531
69.02	47.95	3.399
72.37	49.62	3.282
75.61	51.30	3.179
78.65	58.04	2.909
81.00	65.01	1.791
82.99	66.77	2.183
85.15	68.15	2.143
	Crystal-I (series 1)	
140.94	94.84	3.269
144.19	96.08	3.234
147.40	97.44	3.196
150.57	99.17	3.151
153.72	99.66	3.135
	(series 2)	
142.68	94.81	3.161
145.82	96.75	3.112
148.91	98.09	3.077
151.97	99.44	3.041
155.17	100.86	3.344
158.49	102.40	3.302
161.77	104.22	3.256
165.00	106.35	3.206
	Glassy crystal-III and crystal-III	
14.29	4.747	2.178
16.50	6.858	2.257
18.50	8.877	1.742
20.50	10.95	2.244
22.57	13.21	1.952
24.58	15.39	2.127
27.08	18.10	2.872
30.29	21.19	3.548
33.58	24.55	3.031
36.74	27.23	3.284
39.87	29.58	2.983
43.00	31.95	3.267
46.32	36.37	3.385
49.60	36.57	3.167
52.70	38.59	2.985
58.40	42.10	2.722
61.35	43.79	3.160
64.45	45.81	3.023
67.75	47.83	3.577
71.27	49.68	3.445
74.66	51.46	3.327
77.93	53.64	3.207
80.55	56.07	2.061
83.05	58.70	2.987
85.50	60.45	1.926
87.43	61.72	1.920

Table 1. (Continued)

T_{av}/K	$\Delta H/\Delta T$/JK^{-1} mol^{-1}	ΔT/K
89.27	62.96	1.757
91.01	64.09	1.723
92.75	65.99	1.661
94.47	66.84	1.874
96.66	68.54	2.394
99.25	71.71	2.819
101.99	77.19	2.657
104.73	87.09	2.421
107.13	108.65	2.771
109.29	123.41	1.543
	(series 2)	
81.51	57.26	2.906
84.37	59.61	2.812
87.14	61.43	2.730
89.84	62.99	2.676
	(series 3)	
79.07	55.44	2.275
80.99	57.40	1.570
82.68	58.62	1.799
84.46	59.80	1.770
86.22	60.89	1.742
87.95	62.08	1.715
	Liquid	
171.17	116.1	2.574
173.74	116.5	2.565
176.31	116.9	2.557
177.38	116.9	2.756
178.97	117.1	2.757
180.14	117.3	2.746
182.88	117.8	2.734
185.87	118.2	3.237
189.09	118.8	3.223
192.30	119.4	3.205
195.45	120.0	3.190
198.68	120.6	3.175
201.85	121.2	3.161
204.83	121.9	2.968
207.79	122.5	2.953
210.73	123.2	2.937
213.66	123.8	2.923
216.58	124.5	2.909
219.48	125.2	2.897
222.37	125.8	2.883
225.24	126.6	2.870
228.11	127.3	2.856
230.96	128.0	2.842
233.82	128.8	2.911
236.73	129.6	2.895
239.66	130.3	2.967
242.61	131.2	2.949
245.56	132.1	2.934
248.48	132.9	2.922
251.40	133.6	2.904
257.37	135.4	3.304
260.53	136.4	3.031
263.55	137.2	3.016
266.56	138.0	3.000
269.53	139.1	2.979
272.50	139.9	2.967
275.54	140.9	3.127
278.66	141.9	3.108
281.76	142.9	3.089
285.35	143.9	4.096
289.42	145.4	4.061
293.43	146.8	4.030

53—78 K. The effect of this heat evolution due to stabilization was removed from heat capacity values by correcting the temperature drift. At temperatures near 80 K, the temperature drift was followed for half an hour after the energy input was over. The last temperature observed was used as the final temperature for the calculation of heat capacity. Thus, these values correspond to the heat capacities for the time scale of 1/2 h. The heat capacity we obtained was compared with the data of Huffman *et al.*[5] Their data are 0.3—0.5% greater for liquid and 0.2—0.8% greater for crystal-I. For crystal-II, they are about 0.5% greater at temperatures near the melting point.

Studies on Phase Transitions. *a) Crystal-II→Crystal-I Phase Transition*: This phase transition is of a sluggish nature.[5] In order to determine the transition temperature, the electric energy for the completion of transition was added to the sample in eight separate stages, the temperature drift being followed each time for 2 h or more after the energy input was over. The temperature drift did not cease even after 2 h. The temperature after 2 h was observed to decrease in the first three stages. The temperature drift for 3rd and 4th energy inputs was analyzed by means of exponential function and the equilibrium temperature was estimated. Since the value coincides within 25/10000 K, we adopt it as the transition temperature. Heat of transition was measured twice, the results being given in Table 2 together with those of Huffman *et al.*

b) Fusion: The equilibrium temperature during the course of fusion was measured as a function of fraction melted. Assuming no solid solution formation, the

Table 2. Molar heat of transition
(Crystal-II → Crystal-I)

T_t=138.63±0.003 K	
	$\Delta_t H$/kJ mol^{-1}
Experiment 1	4.228
Experiment 2	4.235
mean	4.231±0.003
$\Delta_t S$=30.53±0.03 JK^{-1} mol^{-1}	
Huffman *et al.*	
T_t=138.7±0.2 K	$\Delta_t H$=4.251±0.004 kJ mol^{-1}

Table 3. Molar heat of fusion

$T_{t.p.}=169.66\pm0.01$ K	$\Delta_m H$/kJ mol^{-1}
Experiment 1	3.282
Experiment 2	3.286
mean	3.284±0.002
$\Delta_m S=19.36\pm0.01$ JK^{-1} mol^{-1}	
Huffman *et al.*	
$T_{t.p.}=169.67\pm0.05$ K	$\Delta_m H=3.293\pm0.002$ kJ mol^{-1}

purity of the specimen was determined to be 99.96%. The heat of fusion was measured twice (Table 3).

c) Crystal-III→Crystal-I Phase Transition: Since a rather long time (an hour or more) was necessary to obtain one heat capacity data, an irreversible phase transition from the newly formed crystal-I into crystal-II inevitably began during the measurement of crystal-III →crystal-I transition. The transition temperature and the molar heat of transition ($\Delta_{III-I}H$) were determined as follows: Crystal-III was heated by electric energy from T_i to a temperature at which the crystal-III was transformed almost completely into crystal-I. The spontaneous temperature rise due to the irreversible phase transition from crystal-I to crystal-II was then followed. When the transition was almost completed, the electric energy was further supplied to the sample in order to bring it into crystal-I, the final temperature being T_f. This last procedure was necessary because the final stage of the transition (metastable crystal-I→ crystal-II) was so sluggish that it caused a large error due to the heat leak during the time consuming observation for detecting the end point of transition. The value $\Delta_{III-I}H$ can be calculated by means of the following relations.

$$\Delta_{III-I}H = H^{I}_{T_t} - H^{III}_{T_t} \quad (1)$$

$$H^{I}_{T_t} = H^{I}_{T_m} - \int_{T_t}^{T_m} C_p^{I} dT \quad (2)$$

$$H^{III}_{T_t} = H^{I}_{T_i} + \int_{T_i}^{T_t} C_p^{III} dT - E \quad (3)$$

where T_t is the transition point of crystal-III→crystal-I, T_m the melting point, C_p^{I}, C_p^{III} the extrapolated values of heat capacity of crystals I and III, respectively, and E the total energy input. In Eqs. 1, 2 and 3 the terms for the empty cell are omitted for the sake of simplicity. The approximation that the whole of $\Delta_{I-III}H$ is absorbed at $T=T_t$ is also involved implicity. The data and equations used for calculating $\Delta_{III-I}H$ are summarized in Table 4. Because of the spontaneous recrystallization, the heat capacity measurement for crystal-I was intervened between 85 and 139 K. The heat capacities in this range were estimated by means of the equation given in Table 4, calculated by extrapolating the measured heat capacities between 140 and 152 K and bringing the result to fit smoothly the data around 85 K.

Table 4. Transition (Crystal-III→Crystal-I) data summary

$T_t=112.3\pm0.1$ K
$\Delta_t H=1.483\pm0.054$ kJ mol^{-1}
$\Delta_m S=13.72\pm0.45$ JK^{-1} mol^{-1}
$C_p^{I}=32.19+0.4437\ T$
$C_p^{III}=3.60+0.6650\ T$
$T_i=99.9117$ K
$T_f=141.5663$ K
$E=1830.84$ J

On the other hand, the transition temperature was determined by the dynamical method. Electric energy was put into the crystal-III at a constant rate and the time variation of temperature was followed. Transition temperature was determined to be the temperature where dT/dt (T; temperature, t; time) attained minimum value. The temperature difference between temperature during the energy input and that corresponding to the equilibrium state was corrected by measuring the difference at lower temperatures at which no phase transition effect takes place.

Residual Entropy of Glassy Crystalline States. Beckett *et al.*[10] calculated the entropy and heat capacity of ideal gas state of cyclohexene on the basis of spectroscopic data. Although spectroscopic entropy coincided with the experimental one within their error limits, there was a significant difference between the calculated and the observed heat capacity data. They explained the difference by assuming the existence of an energy-rich conformer having a larger strain energy (11.3 kJ mol^{-1}) than that of the ordinary half-chair conformer. Since the discrepancy for entropy (0.16 JK^{-1} mol^{-1}) is within experimental error, it might be that the crystal-II has

Table 5. Third law entropy of Crystal-I at 138.63 K

T/K		ΔS/JK^{-1}mol^{-1}
Via II-I transition		
0—14.0	Debye extrapolation ($\theta_D=157.4$ K, 6 freedom)	0.91
14.0—138.63	$\int C_p(II)/T\,dT$ (graphical)	71.12
138.63	II-I transition 4231/138.63	30.53
		102.56±0.17
Via Glassy Crystal-I		
0—14.0	Debye extrapolation ($\theta_D=129.4$ K, 6 freedom)	1.62
14.0—86.0	$\int C_p(I)/T\,dT$ (graphical)	50.53
86.0—138.63	$\int C_p(I)^{a)}/T\,dT$	38.74
		90.89±0.63
Via Glassy Crystal-III		
0—14.0	Debye extrapolation ($\theta_D=131.1$ K, 6 freedom)	1.55
14.0—90.0	$\int C_p(III)/T\,dT$	51.94
90.0—112.3	$\int C_p(III)/T\,dT$	15.63
	III-I transition	13.72
112.3—138.63	$\int C_p\,(I)/T\,dT$	17.11
		99.95±0.20
$S_0°(I)=102.56-90.89=11.67\pm0.70$ JK^{-1} mol^{-1}		
$S_0°(III)=102.56-99.95=2.61\pm0.37$ JK^{-1} mol^{-1}		

a) Estimated heat capacity given in Table 4.

Table 6. Thermodynamic functions of cyclohexene

T / K	$C_s°$ / JK^{-1} mol^{-1}	$S_s°$ / JK^{-1} mol^{-1}	$(H°-H_0°(\mathrm{I}))/T$ / JK^{-1} mol^{-1}	$-(G°-H_0°(\mathrm{I}))/T$ / JK^{-1} mol^{-1}
		(Crystal-II)		
10	(1.05)	(0.332)	(0.249)	(0.083)
20	7.14	2.552	1.897	0.655
30	17.03	7.291	5.272	2.019
40	26.09	13.47	9.376	4.091
50	33.52	20.12	13.49	6.631
60	39.55	26.78	17.35	9.435
70	44.58	33.27	20.89	12.38
80	48.92	39.51	24.13	15.38
90	52.98	45.51	27.11	18.40
100	56.60	51.28	29.88	21.40
110	60.23	56.84	32.47	24.37
120	64.00	62.24	34.94	27.30
130	68.14	67.52	37.33	30.19
138.63		Transition		
		(Crystal-I)		
140	94.29	103.48	70.14	33.35
150	98.59	110.13	71.88	38.25
160	103.22	117.83	74.28	43.55
169.66		Fusion		
		(Liquid)		
170	115.08	142.46	95.51	46.95
180	117.23	149.13	96.68	52.45
190	118.92	155.51	97.05	58.46
200	120.89	161.66	98.91	62.75
210	123.00	167.61	100.01	67.60
220	125.32	173.38	101.10	72.28
230	127.73	179.01	102.21	76.80
240	130.49	184.50	103.33	81.17
250	133.30	189.89	104.47	85.41
260	136.18	195.17	105.64	89.54
270	139.13	200.37	106.82	93.54
280	142.31	205.48	108.03	97.45
290	145.57	210.53	109.27	101.26
300	148.98	215.52	110.54	104.99
		(Glassy and Supercooled Crystal-I)		
10	(1.75)	(12.27)	(275.58)	(−263.31)
20	10.90	15.96	140.71	−124.75
30	21.84	22.48	99.29	−76.81
40	30.43	30.02	81.07	−51.05
50	37.43	37.57	71.65	−34.08
60	43.20	44.92	66.44	−21.52
70	48.46	51.61	63.50	−11.89
80	61.34	58.98	62.51	−3.54
		(Crystal-III)		
10	(1.65)	(3.18)	(131.68)	(−128.50)
20	10.38	6.73	68.40	−61.67
30	21.08	13.01	50.89	−37.89
40	29.83	20.33	44.60	−24.27
50	36.82	27.75	42.36	−14.61
60	43.03	35.03	41.97	−6.94
70	49.00	42.13	46.42	−4.29
80	55.48	49.05	47.03	1.94
90	63.45	56.09	48.53	7.57
100	72.91	63.19	50.42	12.77

no residual entropy at 0 K. Taking this into consideration, the residual entropies of glassy crystal-I and glassy crystal-III were calculated. Contribution below 14 K was calculated by means of extrapolated heat capacities with a Debye model. The contribution from 85—140 K for crystal-I was calculated by the equations given in

Table 4. Details of the calculation are given in Table 5. The residual entropies of glassy crystal-I and glassy crystal-III were found to be (11.67±0.70) and (2.61±0.37) JK^{-1} mol^{-1}, respectively.

Thermodynamic Functions. Smoothed values of heat capacity at rounded temperatures along with values of other derived thermodynamic functions are given in Table 6. For all the phases, $H_0°$ refers to the zero point enthalpy of crystal-II. The entropy values for all phases are also referred to the entropy of crystal-II at 0 K, which is considered to be zero.

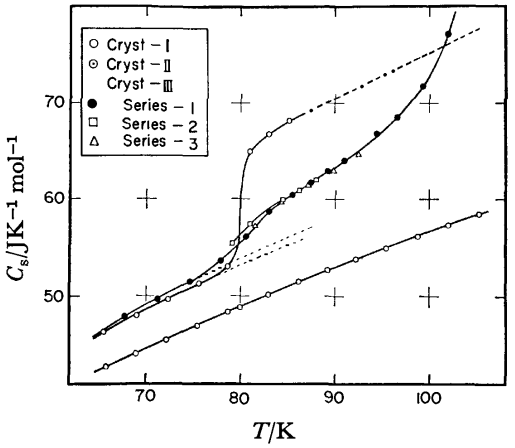

Fig. 4. Heat capacities of glassy crystal-I, -III and crystal-II around glass transition temperature.

Purity of the Crystal-III Phase. Heat capacity curves for crystal-I, -II, and -III around glass transition region are shown in Fig. 4. The temperatures at which the heat capacity jump occurs are very close for crystal-I and -III. Thus the possibility that the heat capacity jump for crystal-III is caused by crystal-I contained in crystal-III as an impurity might be considered. However, this possibility was discarded for the following reasons. (1) The results for series-1 and -3 agree in spite of the difference in the method of preparation of crystal-III. It is very improbable that different samples contain almost the same amount of impurity. (2) The ratios $S_0°$ (III)/$S_0°$ (I) (=0.22) and ΔC_p (III)/ΔC_p (I) (=0.32) differ from each other beyond the estimated error (ΔC_p is the heat capacity jump at around 80 K). (3) The activation enthalpies of the relaxation phenomena around glass transition region differ for crystal-I and crystal-III. (4) The heat capacity of crystal-III is greater in the temperature region 62—80 K. Our view that the heat capacity jump of crystal-III at around 80 K is an intrinsic property of this phase is thus supported.

Relaxation Around Glass Transition Region For both the glassy crystal-I and -III, heat evolution due to the enthalpy relaxation was observed to start at *ca.* 50 K, the temperature rising linearly with time (Fig. 5). If we assume an exponential type for the enthalpy relaxation, the following equation holds.

$$\frac{d\Delta H(t)}{dt} = -\frac{1}{\tau}\Delta H(t), \qquad (4)$$

where $\Delta H(t)$ is the enthalpy difference of the glassy state at time t and equilibrium state and τ the relaxation time. For small t ($t \ll \tau$), $\Delta H(t)$ is nearly equal to $\Delta H(0)$.

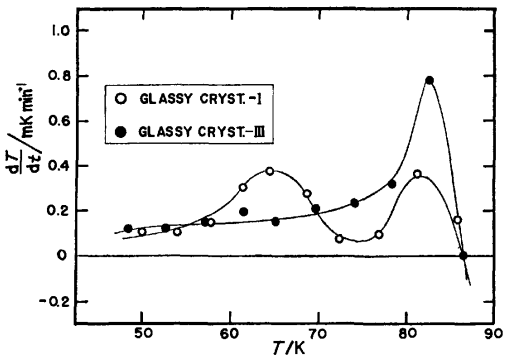

Fig. 5. Rate of the temperature rise at temperatures below T_g.

Thus, $d\Delta H(t)/dt$ is nearly constant, or the temperature of the sample rises linearly with time, the slope being proportional to $\Delta H(0)/\tau$. If a simple relaxation mechanism of the type of Eq. 4 is assumed, the behavior of the glassy crystal-III, in which one peak appears in dT/dt *vs.* T curve, seems to be normal. No interpretation can be given for the origin of the second peak in the dT/dt *vs.* T curve for glassy crystal-I. At temperatures above 78 K, the sign of the $\Delta H(0)$ changed, a negative temperature drift being observed. Relaxation times at various temperatures were determined by analysis of the drift by means of Eq. 4. From the Arrhenius plot of the relaxation time, the activation enthalpy of the relaxation was found to be 18 and 7 kJ mol^{-1} for glassy crystals -I and -III, respectively. The temperature at which the relaxation time for glassy crystal-I becomes one minute is found to be 92 K from this plot. The difference in the T_g values determined by the DTA method and heat capacity measurement might be explained by the difference in the time scale of the observation.

Preparation of Glassy Liquid by Vapor Condensation Method. DTA curves obtained with a vapor condensation type DTA apparatus are reproduced in Fig. 6. Run 1 is the heating curve of the sample condensed from vapor directly onto the sample holder maintained at 68 K. Runs 2 and 3 show the heating curves after the tempera-

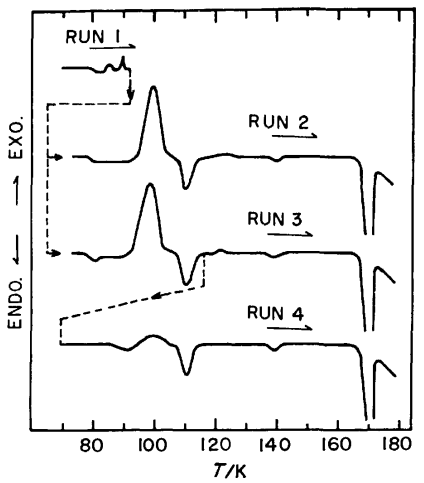

Fig. 6. DTA curves for the samples condensed from vapor.

ture cycling between 68 and 92 K. For Run 3 the sample was annealed for an hour at 77 K prior to the measurement. Run 4 shows the heating curve after the temperature cycling between 68 and 118 K and corresponds to Run 3 in Fig. 1. Although some exothermic anomalies in Run 1 cannot be assigned yet, there are evidences for concluding that each baseline shift to endothermic direction in these runs (Runs 1, 2, and 3) at 78 K is the manifestation of glass transition of liquid: (1) Annealing effect characteristic of the glass transition in Run 3. (2) Rough agreement of the liquid→crystal-III crystallization enthalpy (=4.3 kJ mol^{-1}) estimated from its peak area referring to the peak areas of crystal-III→crystal-I and melting of crystal-I with its value (4.8 kJ mol^{-1}) calculated from calorimetric data. It is tacitly assumed that the peaks in Run 1 do not represent the inherent property of a large part of the vapor condensed phase but that of the unstable crystalline phase formed as complex phase during the course of vapor condensation. Another interpretation that the peaks were caused by the transition occurring in all parts of the sample is also possible. If this is the case, the base line shift to endothermic direction in Run 1 corresponds to the glass transition of liquid but that in Runs 2 or 3 correspond to the glass transition of unstable new crystalline phase. We can conclude that the glassy liquid was prepared by the vapor condensation method, its glass transition temperature being 78 K.

Discussion

Molecular motions in crystalline state of cyclohexene were studied by Saffar *et al.*[11] by means of NMR. In their study on the temperature dependence of the second moment as well as of the spin lattice relaxation time, they found a phase transition at 128.5 K where we found no thermal anomaly. The lack of detailed description of the thermal treatment of their sample and the inconsistency between their assignment on the crystalline phases and ours make it difficult for us to discuss our results in reference to their work. A tentative interpretation is as follows.

Cyclohexene molecule has two half-chair conformations. The existence of another conformation (boat conformation) can be neglected in the low temperature region because of its high strain energy (11.3 kJ mol^{-1} by Beckett *et al.*[10] and 18.0 kJ mol^{-1} by Anet[12]). Saffar *et al.*[11] reported that the ring inversion motion appears at 115 K in crystal-I (our nomenclature). Above this temperature the Arrhenius plot of the correlation time obtained from their T_1 experiment gave 10 kJ mol^{-1} for the activation energy which we obtained from the plot in Fig. 4 of their paper. Similarity of the value with the activation enthalpy of the relaxation phenomenon in crystal-III (7 kJ mol^{-1}) suggests that the ring inversion mode dominates the relaxation phenomenon of crystal-III near the glass transition region. It is plausible that this mode will survive down to a lower temperature than the life of molecular rotation because the energy difference giving rise to the ordering of the mode of such a ring inversion will be created with the settling down of the rotational motion. The energy difference between the two conformers also depends upon the packing density and symmetry of the crystal; higher density or the lower symmetry will give larger energy difference. It is likely that the energy difference in crystal-II, which seems to have higher density and lower symmetry, is so large that the order is attained at the transition temperature. On the other hand, the energy difference for crystal-III may be of the order of thermal energy, so the relaxation phenomenon of the ring inversion was observed calorimetrically. Complete disorder of the ring inversion mode should contribute to the entropy by $R\ln 2$ (=5.8 JK^{-1} mol^{-1}). Thus the partial order is already attained at T_g in crystal-III since the residual entropy of the glassy crystal-III (2.7 JK^{-1} mol^{-1}) is less than the value for complete disorder.

Since the residual entropy of glassy crystal-I is larger than $R\ln 2$, there must be some other type of disorder such as orientational randomness around the axis (z axis) normal to the molecular plane. The rotation about the axis was suggested by Saffar for crystal-I. The energy difference between the two conformers in crystal-I at T_g may be smaller than that of crystal-III at T_g' because of the more disordered orientational freedom, lower density, and presumably of the higher crystal symmetry of crystal-I. Mode of ring inversion in crystal-I seems to contribute to the residual entropy by the amount corresponding to nearly complete disorder.

Glassy crystals of cyclohexene seem to provide an interesting example for the simplification of the configurational mode. It is likely that the configurational freedom may be the rotation about z axis+ring inversion and simply ring inversion in crystal-I and crystal-III, respectively. If this is the case, the glass transition of crystal-III corresponds simply to the mode of ring inversion and successive simplification of the configurational freedom is achieved in the order of glassy liquid→glassy crystal-I→glassy crystal-III.

References

1) D. Turnbull and M. H. Cohen, *J. Chem. Phys.*, **31**, 1164 (1959); *ibid.*, **34**, 120 (1961).
2) J. H. Gibbs and E. A. DiMarzio, *J. Chem. Phys.*, **28**, 373 (1958).
3) C. A. Angell, *J. Phys. Chem.*, **75**, 3698 (1971).
4) K. Adachi, H. Suga, and S. Seki, *Bull. Chem. Soc. Jpn.*, **41**, 1078 (1968); **43**, 1916 (1970); **44**, 77 (1971); **45**, 1960 (1972).
5) H. M. Huffman, M. Eaton, and G. D. Oliver, *J. Am. Chem. Soc.*, **70**, 2911 (1948).
6) K. Adachi, H. Suga, and S. Seki, *Bull. Chem. Soc. Jpn.*, **43**, 1916 (1970).
7) O. Haida, H. Suga, and S. Seki, *Chem. Lett.*, **1973**, 79.
8) H. Suga and S. Seki, *Bull. Chem. Soc. Jpn.*, **38**, 1000 (1965).
9) O. Haida, H. Suga, and S. Seki, *Thermochimica Acta*, **3**, 177 (1972).
10) C. W. Beckett, N. K. Freeman, and K. S. Pitzer, *J. Am. Chem. Soc.*, **70**, 4227 (1948).
11) Z. M. Saffar, R. G. Eades, and J. P. Llewelly, *J. Chem. Phys.*, **50**, 3462 (1969).
12) F. A. L. Anet and M. Z. Hag, *J. Am. Chem. Soc.*, **87**, 3147 (1965).

Heat Capacity of Potassium *p*-Chloranil Anion Radical Salt between 13 and 330 K*

Akio Kosaki,† Michio Sorai, Hiroshi Suga, and Syûzô Seki
Department of Chemistry, Faculty of Science, Osaka University, Toyonaka, Osaka 560
(Received October 18, 1976)

The heat capacity measurement for an organic free-radical salt, potassium *p*-chloranil, revealed a first-order phase transition at T_c=260.01 K. In spite of a first-order nature, the pre- and the post-transitional effects are remarkable. The enthalpy and the entropy of transition were determined to be ΔH=2796 J mol^{-1} and ΔS=11.06 JK^{-1} mol^{-1}, respectively. The magnetic contribution to ΔS is only 2.23 JK^{-1} mol^{-1} when a dimeric configuration with a singlet-triplet spin equilibrium is assumed in the low temperature phase and a monomeric behavior of radicals with spin doublet is assumed above T_c. The present phase transition bears a close resemblance to a spin-Peierls transition in a linear chain system. The infrared spectrum at 120 K indicates a possible formation of dimers in the low temperature phase of this salt. A phenomenological model for the present phase transition is presented.

Among a number of stable organic free radicals, the compounds which exhibit a cooperative phase transition due to unpaired electrons are very scarce. Moreover, these phase transitions are quite unique in that the spin and electronic state and the structural change are inseparably related to one another and that the mechanism of phase transition is different from radical to radical.

In this paper we report the heat capacity of potassium *p*-chloranil crystal [abbreviated hereafter as K$^+$(*p*-chloranil)$^-$ or more simply as K$^+$(CA)$^-$]. This is one of the typical anion radical salts together with the TCNQ salts. The magnetic susceptibility and the electron paramagnetic resonance (EPR) measured by Andre *et al.*[1] revealed a first-order phase transition at T_c=260 K on raising and at T_c=210 K on lowering temperature. The magnetic susceptibility above T_c follows well the Curie-Weiss law while the magnetic behavior below T_c is described by the energy scheme of a singlet-triplet equilibrium. This result suggests that the *p*-chloranil anion radicals exist as monomers in the K$^+$-(CA)$^-$ salt above T_c and as dimers below T_c. EPR,[1,2] electronic absorption spectra,[3-6] and X-ray diffraction analysis[7] of this salt support the monomeric behavior of the *p*-chloranil anion radicals in the high temperature phase. On the other hand, Hiroma and Kuroda[8] investigated the temperature dependence of the electronic absorption spectra of the K$^+$(CA)$^-$ salt and found that an abrupt increase of intensity occurs in the charge-transfer band at the phase transition point when the specimen is cooled. This fact suggests that the low temperature phase has a crystal structure of a dimeric arrangement of the *p*-chloranil anions. Although an X-ray diffraction analysis of the low temperature phase has not been made, this suggestion seems to be quite reasonable in comparison with the electronic absorption spectra of K$^+$(CA)$^-$ in solution,[5,6,9,10] where the monomer-dimer equilibrium is established.

In spite of a useful method which provides important information concerning the energetic aspects, the number of works in which heat capacity measurements are applied to organic free-radical salts are scarce.[11-21] The present paper clearly reveals a first-order phase transition at 260.01 K. As is in the case of other radicals, the magnetic contribution to the transition entropy is not dominant. Although a quantitative explanation for the phase transition is not given, a phenomenological model is described here.

Infrared spectroscopy also serves as a useful tool to elucidate the local symmetry of the constituent entity. But the infrared spectra hitherto reported are room temperature data.[22-24] We also report here the infrared spectra of the K$^+$(CA)$^-$ salt between 4000 and 30 cm^{-1} in both the high and the low temperature phases.

Experimental

Material. The starting materials, potassium iodide and *p*-chloranil, were recrystallized twice from water and benzene, respectively. The solvent, acetone, was purified by the method of Scheibe *et al.*[25] The K$^+$(CA)$^-$ salt was prepared according to the method of Torrey and Hunter.[26] The reaction temperature was 263±2 K. The product was washed with chilled acetone and dried *in vacuo* for three days. Found: C, 25.26; Cl, 49.37%. Calcd for $C_6Cl_4O_2K$: C, 25.29; Cl, 49.76%.

It has been reported[7,8,10] that the preparation method by Torrey and Hunter does not yield one and the same modification of the K$^+$(CA)$^-$ crystal. We prepared the K$^+$(CA)$^-$ salt at two different temperatures (263 and 273 K) and examined their thermal properties by using a differential scanning calorimeter (DSC). The salt prepared at 263 K exhibited a sharp endothermic peak due to the phase transition at 260 K while the salt precipitated above 273 K gave a broad peak. This fact implies the contamination of some impurities in the salt prepared above 273 K. On the other hand, it is possible that the salt prepared at 263 K would be a mixture of the high and the low temperature modifications as the synthesis temperature is close to the phase transition point (T_c=260.01 K) and thus the free energies of both phases are virtually the same magnitude in this temperature region. In fact the DSC curve showed the trace of a small amount of the low temperature modification. Therefore, whenever the infrared and the Raman spectra were recorded at roon temperature, the specimen was once cooled down to about 100 K and warmed up to a room temperature.

Heat Capacity Measurement. The heat capacity was measured with an adiabatic calorimeter[27] in the temperature

* Presented before the Symposium on the Magnetochemistry, Nagoya (1970).

† Deceased on July 16, 1974.

region from 13 to 330 K. The sample of 8.0239 g (=0.028156 mol) was sealed into the calorimeter cell together with a small amount of helium gas as the heat exchanger.

Infrared and Raman Spectra. The infrared spectra at a room temperature and 120 K were recorded on a Grating-type Infrared Spectrophotometer Model DS-402G (Japan Spectroscopic Co., Ltd.) in the wave number region from 4000 to 400 cm^{-1} and on a Spectrophotometer Model FIS-001 (Hitachi Ltd.) in the range from 400 to 30 cm^{-1}. Nujol mull method was employed for the preparation of samples.

The Raman spectra of $K^+(CA)^-$ salt were recorded on a laser Raman Spectrophotometer Model R-750 with the argon laser (514.5 nm) in the range from 0 to 4000 cm^{-1} at a room temperature. It was difficult to obtain a good Raman spectrum of this salt because of its continuous absorption band in the corresponding wave number region and the instability of this radical salt against the strong argon laser exposure.

Results

Heat Capacity of $K^+(CA)^-$ Salt. Prior to the heat capacity measurement, we performed the DSC measurement for the $K^+(CA)^-$ salt. An exothermic peak was observed at 220 K on cooling and an endothermic peak appeared at 260 K in a heating run. A large hysteresis effect with a temperature interval of 40 K indicates a typical first-order nature of the phase transition.

The measured values for the heat capacity are plotted in Fig. 1 and the numerical values are given in Table 1. The standard thermodynamic functions for the $K^+(CA)^-$ salt are shown in Table 2. A sharp heat capacity anomaly is found around 260 K. The phase transition

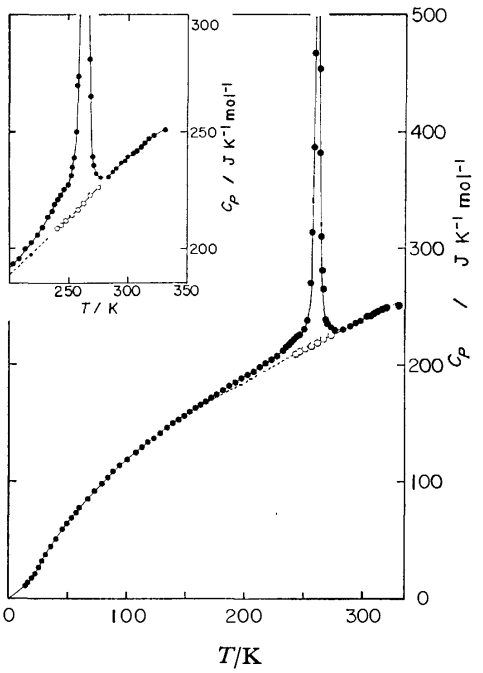

Fig. 1. The molar heat capacity of the $K^+(p$-chloranil)$^-$ anion radical salt. Open circles indicate the heat capacities of the supercooled high temperature phase. Broken line is the extrapolated curve of the supercooled high temperature phase and serves as a "normal" heat capacity for the estimation of the transition enthalpy and entropy.

Table 1. Heat capacity of $K^+(p$-chloranil)$^-$

T / K	C_p / JK^{-1} mol^{-1}	T / K	C_p / JK^{-1} mol^{-1}	T / K	C_p / JK^{-1} mol^{-1}	T / K	C_p / JK^{-1} mol^{-1}	T / K	C_p / JK^{-1} mol^{-1}
13.81	11.57	90.68	111.76	175.92	171.89	247.13	229.28	281.45	229.36
14.81	12.63	93.66	114.73	178.66	177.67	248.94	231.29	282.75	230.13
16.06	14.24	96.59	117.41	181.32	179.35	250.15	232.25	282.90	230.96
17.41	15.80	99.92	120.15	183.92	180.86	250.65	233.08	283.24	230.76
18.80	17.91	103.66	123.43	186.56	183.18	252.54	237.31	283.89	230.85
20.21	19.80	106.87	125.90	189.19	183.83	253.73	240.85	285.16	232.05
21.63	21.43	109.58	128.43	191.81	186.24	254.91	251.65	285.88	233.36
23.06	24.27	112.25	130.39	194.43	188.11	255.31	272.02	286.70	234.25
24.53	27.24	114.89	132.50	197.03	189.72	256.07	273.53	287.11	233.68
25.98	29.94	117.50	134.98	199.61	191.19	256.98	315.92	288.22	235.25
27.46	32.72	120.08	137.48	202.18	192.85	257.17	341.36	289.78	234.28
29.00	35.31	122.63	138.31	204.74	194.43	258.30	389.02	290.32	233.69
30.83	38.30	125.16	140.79	207.29	195.54	258.79	469.58	290.67	234.91
32.96	41.58	127.66	143.41	209.83	197.58	259.25	528.99	291.73	235.13
35.10	45.13	130.15	144.72	212.36	199.52	259.80	621.16	292.47	236.98
37.22	48.72	133.80	147.41	214.88	200.69	260.53	639.39	292.72	235.16
39.46	51.51	136.23	149.40	217.39	202.37	261.37	548.82	294.00	236.58
42.05	54.67	138.65	151.13	219.89	204.76	262.28	455.88	296.27	238.51
45.05	59.16	141.05	152.89	222.40	205.90	263.26	383.63	297.58	238.85
48.73	64.17	143.43	154.18	224.91	207.65	264.30	311.74	298.55	239.43
52.76	69.67	145.83	155.57	227.38	209.01	265.40	281.97	300.83	239.94
56.45	73.80	148.19	157.83	227.92	211.76	266.52	265.68	302.70	242.17
59.88	78.09	150.54	159.16	230.79	213.59	270.30	234.60	303.11	239.10
63.11	82.37	152.86	160.94	233.64	216.22	272.52	232.11	305.39	241.23
66.18	85.75	155.17	162.46	234.73	216.53	273.39	228.46	306.12	244.50
69.12	88.97	157.47	164.23	237.15	219.09	276.27	230.05	307.67	242.14
72.16	92.70	159.75	165.22	239.29	221.63	276.30	229.44	309.95	244.61
75.32	95.86	162.02	166.82	239.57	221.64	276.59	229.94	312.59	247.19
78.37	99.55	164.27	169.08	241.98	224.10	277.09	230.74	316.36	248.35
81.18	102.31	166.52	169.80	242.10	224.28	279.61	230.53	320.12	249.12
83.48	104.64	168.75	171.40	244.38	226.51	280.17	231.52	328.54	248.60
85.41	106.43	170.98	173.06	244.71	225.69	281.05	231.54	330.79	251.31
87.77	108.95	173.19	174.51	246.76	228.63	281.19	229.14		
			Supercooled Phase						
242.91	210.89	255.36	216.44	261.78	220.37	266.82	223.71	270.88	225.22
246.55	212.85	256.72	217.33	264.58	221.93	267.95	223.25	273.33	227.00
251.62	215.29	260.34	219.03						

Table 2. Standard thermodynamic functions of $K^+(p\text{-chloranil})^-$

T	$C_p°$	$S°$	$(H_T°-H_0°)/T$	$-(G_T°-H_0°)/T$
K	J K^{-1} mol^{-1}	J K^{-1} mol^{-1}	J K^{-1} mol^{-1}	J K^{-1} mol^{-1}
20	19.47	9.841	6.948	2.893
30	36.99	20.977	13.991	6.986
40	52.24	33.766	21.700	12.067
50	65.90	46.903	29.185	17.718
60	78.39	60.027	36.349	23.678
70	90.04	73.000	43.200	29.799
80	101.04	85.752	49.753	35.999
90	111.22	98.249	56.026	42.224
100	120.37	110.45	62.010	48.439
110	128.72	122.32	67.698	54.619
120	136.73	133.86	73.116	60.743
130	144.49	144.00	77.202	66.802
140	151.90	156.10	83.306	72.790
150	158.92	166.82	88.114	78.702
160	165.66	177.29	92.752	84.538
170	172.20	187.53	97.233	90.296
180	178.70	197.56	101.58	95.977
190	185.13	207.39	105.81	101.58
200	191.56	217.05	109.93	107.12
210	197.70	226.55	113.97	112.58
220	204.10	235.89	117.92	117.97
230	211.70	245.12	121.82	123.30
240	221.94	254.35	125.78	128.57
250	232.43	263.61	129.83	133.78
260	683.60	275.88	136.90	138.99
270	235.50	289.35	145.01	144.34
280	230.19	297.76	148.09	149.67
290	234.93	305.92	151.00	154.92
300	239.67	313.97	153.88	160.09
310	244.45	321.90	156.72	165.18

temperature T_c is determined to be 260.01 K. We succeeded in measuring the heat capacities for the supercooled high temperature phase between 240 and 270 K. These values are represented in Fig. 1 by open circles.

In order to determine the enthalpy and the entropy associated with the phase transition, it is necessary to separate the "excess" heat capacity from the total one by estimating a plausible "normal" heat capacity. In the present case, the normal heat capacity is rather easily determined by extrapolating the experimental values for the supercooled high temperature phase to the low temperature side. The broken line shown in Fig. 1 represents the normal heat capacity. In spite of the first-order nature of the present phase transition the excess heat capacity has its long tail down to about 150 K. This fact suggests a higher-order nature of the initial stage of the present phase transition. The enthalpy and the entropy of transition are determined to be $\Delta H=2796$ J mol^{-1} and $\Delta S=11.06$ J K^{-1} mol^{-1}, respectively. The transition entropy corresponds to R ln 3.78 and this value is too large to be accounted for solely in terms of the magnetic contribution.

According to the structural analysis by Konno *et al.*,[7] the $K^+(CA)^-$ salt has several polymorphs and two dominant modifications are denoted as the α-form (orthorhombic, space group $P2_12_12_1$ and molar volume $V_m=139.3$ cm^3 mol^{-1}) and the β-form (orthorhombic, $P22_12$ and $V_m=136.9$ cm^3 mol^{-1}). Hiroma and Kuroda[8] found that the amount ratio of the α- to the β-form is about 10: 1. As was described in the previous section, we found that when the synthesis temperature is higher than 273 K, the salt contains some impurities and when the salt is prepared at 263 K, the contamination of impurities is considerably reduced but a small amount of the crystals having the low temperature modification is mixed. In addition to this observation, the fact that the β-form has the slightly smaller molar volume than that of the α-form suggests that the β-form is the low temperature modification of the $K^+(CA)^-$ salt.

Temperature Dependence of Infrared Spectra. Figure 2 shows the infrared spectra of the $K^+(CA)^-$ salt at 295 and 120 K in the wave number region from 1800 to

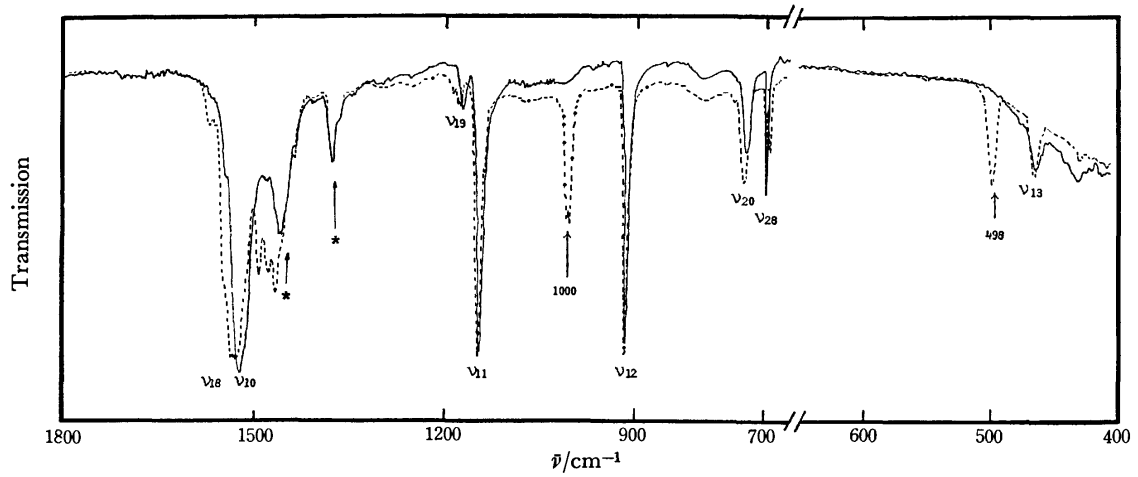

Fig. 2. Infrared spectra of the $K^+(CA)^-$ salt at 295 K (——) and at 120 K (——). The bands marked with an asterisk are the absorption bands due to Nujol. In this and in Fig. 3, the fundamentals already assigned by Girlando *et al.*[24] are indicated by their symmetry species.

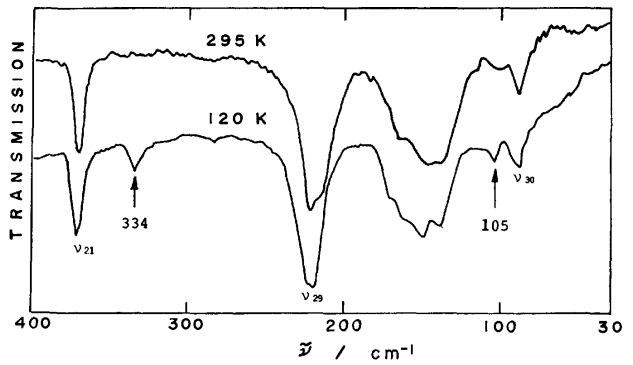

Fig. 3. Far infrared spectra of the $K^+(CA)^-$ salt at 295 and 120 K.

400 cm^{-1}. The far infrared spectra between 400 and 30 cm^{-1} are reproduced in Fig. 3. The spectra recorded at 295 K coincide well with the data previously reported.[23,24] The infrared spectra are markedly influenced by the effect of the phase transition. In the low temperature phase at 120 K, new absorption bands appear at 105, 334, 498, 1000 (doublet) and around 1450 cm^{-1} (doublet). Furthermore the band assigned as $b_{3u}\nu_{28}$ splits into a doublet.

Since the *p*-chloranil anion radical belongs to D_{2h} point group at least in the high temperature phase, it has a center of symmetry and a twofold axis. Under this symmetry the rule of mutual exclusion can be applied to the spectroscopic data. The gerade normal modes for the symmetry operation are infrared inactive and Raman active while the ungerade normal modes are infrared active and Raman inactive. The new bands at 1000, 498, and 334 cm^{-1} appeared in the low temperature phase seem to belong to the gerade normal modes in the high temperature phase because the Raman spectrum of this salt recorded at 295 K has the bands corresponding to the same wave numbers. Therefore, it is concluded that the D_{2h} symmetry of the *p*-chloranil anion radical in the high temperature phase is lowered in the low temperature phase through the intermolecular interaction characterized by the dimerization and/or by the variation of the crystalline field due to a possible structural change at the phase transition temperature. In this situation, some of the infrared inactive gerade modes are changed into the infrared active modes below the phase transition temperature.

Owing to the lower symmetry than D_{2h} of *p*-chloranil anion radical in the low temperature phase, there exist in general no multi-degenerate normal modes. Accordingly, the appearance of the doublets at 1000 and 698 cm^{-1} (the ν_{28} mode) should be attributed to two inequivalent anion radicals in the crystal lattice of the low temperature phase. Unfortunately the structural data on the low temperature phase of the $K^+(CA)^-$ radical salt, which confirms the present prediction, has not been reported. The *p*-chloranil anion radicals are known to behave as monomer in the high temperature phase and as dimer in the low temperature phase characterized by a siglet-triplet spin equilibrium.[8] This suggests a strong intermolecular interaction between adjacent radicals below the transition temperature. The selection rule of the infrared spectra in the low temperature phase is governed by the total symmetry of the dimeric entity. Two identical normal modes, which originally belong to two individual radicals forming a dimer, couple with each other and the absorption occurs at slightly different wave numbers. The origin of the seeming doublets at 1000 and 698 cm^{-1} can be interpreted in this way.

Hiroma and Kuroda[10] reported that the $K^+(CA)^-$ radical salt has a tendency to take water molecules into the crystal lattice when the crystal is exposed to a humid air. The hydrate is characterized by three infrared absorption bands at 3400 cm^{-1} (the O-H stretching), 1630 cm^{-1} (the H-O-H bending vibration) and 1000 cm^{-1} (the librational motion of water molecule). The present infrared spectra at 295 K show no bands at these wave number region, which indicates that the present salt is anhydrous.

Relationship between Magnetic Behavior and Phase Transition

Andre *et al.*[1] measured the magnetic susceptibility, χ, of the $K^+(CA)^-$ anion radical salt and concluded that the magnetic spins behave as in the singlet-triplet equilibrium below T_c while the magnetic behavior above T_c is accounted for in terms of spin doublet due to the monomeric radical. This prediction has been supported by various kinds of experiments such as EPR[1,2] electronic absorption spectra,[3-6,8] and the structural analysis.[7] However, the logic of Andre *et al.* leading to their conclusion is not correct in the meaning that they have drawn their conclusion based on their incorrect estimation of the asymptotic value of χT at infinite temperature for the singlet-triplet energy scheme. They obtained the value of $(\chi T)_\infty$ to be 1/4 and 3/8 for the singlet-triplet scheme (abbreviated as the ST-scheme) and the doublet scheme (the D-scheme), respectively. But in the present case, the value of $(\chi T)_\infty$ should be identical to each other.

The magnetic susceptibility for the ST-scheme is represented by

$$\chi = \left(\frac{N_A}{2}\right)\frac{S(S+1)g^2m_B^2}{3kT}\left\{1+\frac{1}{3}\exp(J/kT)\right\}^{-1} \quad (S=1), \quad (1)$$

where N_A is the Avogadro constant, g the electron g-factor (=2.0), m_B the Bohr magneton, S the spin quantum number, and J the triplet excitation energy corresponding to the energy separation between the singlet and the triplet states. If the triplet density is defined by

$$\rho_T \equiv \left\{1+\frac{1}{3}\exp(J/kT)\right\}^{-1}, \quad (2)$$

we obtain the following relation:

$$\chi T = \frac{1}{2}\rho_T. \quad (3)$$

Because of $0 \leqq \rho_T \leqq 3/4$, the range of χT becomes

$$0\,(T=0) \leqq \chi T \leqq \frac{3}{8}\,(T=\infty). \quad (4)$$

On the other hand, the susceptibility for the D-scheme is given by the Curie law,

$$\chi = \frac{Ng^2m_B^2}{3kT}S(S+1) \quad \left(S=\frac{1}{2}\right), \tag{5}$$

where N is the number of spins having $S=1/2$. Since the doublet density is defined by

$$\rho_D \equiv \frac{N_A}{N} \quad (0 \leqq \rho_D \leqq 1), \tag{6}$$

we obtain the following relations:

$$\chi T = \frac{3}{8}\rho_D \tag{7}$$

and

$$0(T=0) \leqq \chi T \leqq \frac{3}{8}(T=\infty). \tag{8}$$

We estimated the triplet excitation energy J and the doublet density ρ_D by applying respectively the ST- and the D-schemes to the magnetic susceptibility data obtained by Andre *et al.*[1] The results are shown in Fig. 4 in terms of J/k and ρ_D against T. It should be remarked here that the triplet excitation energy shows a constant value ($J/k=660$ K) below T_c. This fact supports the validity of the ST-scheme below T_c.

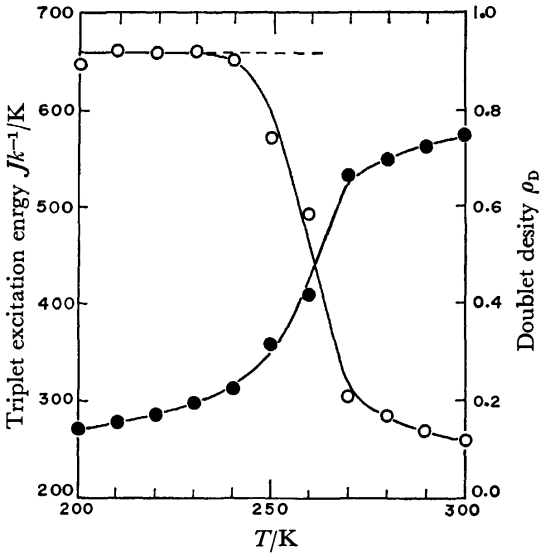

Fig. 4. The triplet excitation energy J/k(○) and the doublet density ρ_D(●) against temperature($T_c=260.01$ K) for the $K^+(CA)^-$ salt. These quantities are estimated from the magnetic susceptibility obtained by Andre *et al.*[1]

On the other hand, in the high temperature phase the magnetic feature is more complicated. If the doublet scheme is applied to the present system, the doublet density amounts to 0.75 at 300 K and shows a tendency to approach 1.00 with further increasing temperature. In case of the singlet-triplet scheme, the triplet excitation energy is considerably reduced to $J/k=250$ K at a room temperature. Although solely from the present result we cannot explicitly give an answer to the question of which scheme is established in the high temperature phase of the $K^+(CA)^-$ salt, it is very likely that most of the *p*-chloranil radicals behave as monomers with $S=1/2$ but the remaining minor fraction exists in the singlet-triplet equilibrium. With increasing temperature, the ST-scheme is transferred into the D-scheme. At any rate, the present phase transition is essentially characterized by the transition between dimer and monomer in a magnetic linear chain. This situation bears a close resemblance to a spin-Peierls transition in a Heisenberg linear chain system,[28] where an instability of magnetic linear chain at low temperatures is overcome by a structural phase transition coupled with the spin system.[29]

The entropy of the magnetic system with the triplet density ρ_T is represented by

$$S = \frac{1}{2}R\{\rho_T \ln 3 - \rho_T \ln \rho_T - (1-\rho_T)\ln(1-\rho_T)\}, \tag{9}$$

while the magnetic entropy due to the doublet density ρ_D is given by

$$S = R\rho_D \ln 2, \tag{10}$$

where R is the gas constant. We estimated the magnetic contribution to the transition entropy for the following three cases: (i) the ST-scheme below T_c and the D-scheme above T_c, (ii) the ST-scheme below and above T_c, and (iii) the D-scheme below and above T_c. As the pre- and the post-transitional effects are rather large in the heat capacity curve shown in Fig. 1, the estimation of the magnetic entropy has been made for the temperature interval between 200 and 285 K. In the case of (i), the change in spin state from the ST-scheme ($J/k=660$ K, $\rho_T=0.10$) to the D-scheme ($\rho_D=0.70$) yields the magnetic entropy of $\Delta S_{mag}=2.23$ J K^{-1} mol^{-1}. As to the case (ii), $\Delta S_{mag}=S(J/k=280\text{ K}, \rho_T=0.53)-S(J/k=660\text{ K}, \rho_T=0.10)=3.49$ J K^{-1} mol^{-1}. The case (iii) gives the magnetic entropy of $\Delta S_{mag}=S(\rho_D=0.70)-S(\rho_D=0.14)=3.23$ J K^{-1} mol^{-1}. Since the total entropy arising from the phase transition is $\Delta S=11.06$ J K^{-1} mol^{-1}, the magnetic contribution corresponds merely to 20% for the case (i) and 30% for (ii) and (iii). The remaining entropy results from the phonon system. On the other hand, the total magnetic entropy for the $K^+(CA)^-$ salt is at most $R\ln 2$ (=5.76 J K^{-1} mol^{-1}) independently of the spin scheme (see Eqs. 9 and 10), and the cooperative fraction of the magnetic entropy is 39, 61, and 56% for the cases (i), (ii), and (iii), respectively.

Phenomenological Model for Phase Transition

The phase transition found for the $K^+(CA)^-$ salt is of a first order in nature but the pre- and the post-transitional effects spread over a wide temperature region suggest easy fluctuations of the heterophases in this temperature region. We apply here a phenomenological model, which is virtually the same with the Frenkel theory of heterophase fluctuation in liquid,[30] to the present phase transition.

We shall assume that one phase contains "embryos" of a second phase in the transition region and that each embryo consists of a uniform size. We consider a system consisting of N cells each of which contains n molecules. The product of N and n is equated to Avogadro's constant N_A. The interaction energy between the adjacent cells belonging to the low and the high temperature phases is denoted by J_{LH}. As the surface area

of a cell changes with its dimension, the interaction energy is multiplied by $N^{1/3}$. The Gibbs energy of the system can be written as

$$G = G_L x + G_H(1-x) + N^{1/3}J_{LH}x(1-x) + NkT\{x\ln x + (1-x)\ln(1-x)\}, \quad (11)$$

where G_L and G_H are the Gibbs energies of the low and the high temperature phases, respectively, and x is the fraction of the cells belonging to the low temperature phase. The equilibrium value of x may be found by minimizing G with respect to x: $\partial G/\partial x=0$. The solution to this is given by those values of x which satisfy

$$\frac{1}{x} = 1 + \exp[\{G_L - G_H + N^{1/3}J_{LH}(1-2x)\}/NkT]. \quad (12)$$

The heat capacity of the system, C_p, is represented as follows:

$$C_p = xC_{pL} + (1-x)C_{pH} + \left(\frac{\partial x}{\partial T}\right)\{H_L - H_H + N^{1/3}J_{LH}(1-2x)\}, \quad (13)$$

here

$$\left(\frac{\partial x}{\partial T}\right)\frac{N^{2/3}x(1-x)}{N^{2/3}kT - 2J_{LH}x(1-x)}\left(\frac{S_H - S_L}{N} + k\ln\frac{x}{1-x}\right) \quad (14)$$

where H and S mean the enthalpy and the entropy of the system. When the denominator of Eq. 14 becomes zero, the heat capacity (Eq. 13) diverges infinitely at T_c. According to its definition, the J_{LH} is positive. Therefore, the condition under which a phase transition occurs is given by

$$J_{LH}/N^{2/3} \geqq 2kT_c. \quad (15)$$

When $(J_{LH}/N^{2/3})$ is equal to $2kT_c$, the phase transition is of a second order while in case of $(J_{LH}/N^{2/3})>2kT_c$ a first-order phase transition takes place. If we define f as a fraction of the transition enthalpy corresponding to the first-order phase transition, namely the latent heat, the following relationship is obtained:

$$f^2 = 1 - 2kT_cN^{2/3}/J_{LH}. \quad (16)$$

The fraction of the latent heat increases with increasing the value of $(J_{LH}/N^{2/3})$. On the other hand, when J_{LH} is constant, the anomalous heat capacity due to the phase transition becomes broad with increasing N.

In order to apply this model to the actual system, the hypothetical Gibbs energies of both the low and the high temperature phases are necessary. We estimated these energies by extrapolating the heat capacity curve of the K+(CA)$^{\tau}$ salt above and below T_c. Figure 5 demonstrates temperature dependences of the fraction of the low temperature phase, x, for four different values of N_A/N under a condition of $(J_{LH}/N^{2/3})=2.2\,kT_c$. A discontinuity of x at T_c is apparent.

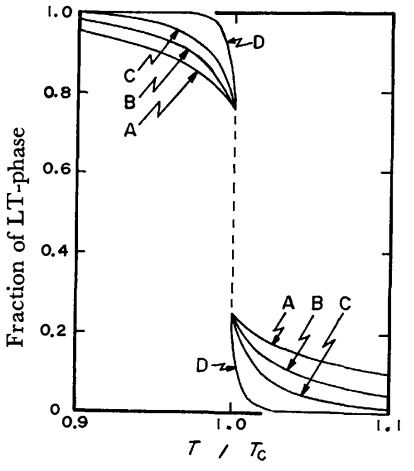

Fig. 5. Temperature dependence of the fraction of the low temperature phase, x, under a condition of $(J_{LH}/N^{2/3})=2.2kT_c$. $N_A/N=5$(A), 10(B), 20(C), and 100 (D).

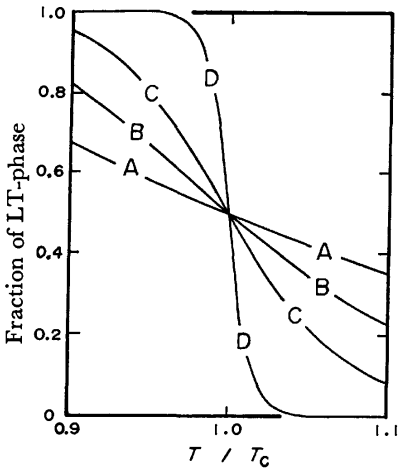

Fig. 6. Temperature dependence of the fraction of the low temperature phase, x, under a condition of $(J_{LH}/N^{2/3})=0$.
$N_A/N=5$(A), 10(B), 20(C), and 100(D).

When $(J_{LH}/N^{2/3})$ is smaller than $2kT_c$, the present model gives rise to neither a first- nor a second-order phase transition. This situation is illustrated in Fig. 6. The gradient of x at T_c increases with decreasing N.

The "best" fit of the calculated values to the experimental one is shown in Fig. 7. Here, the experimental value of x has been determined as $x=\Delta H(T)/\Delta H$. Although the phase transition of the K+(CA)$^{\tau}$ salt is of a typical first order, the "best" fit between the

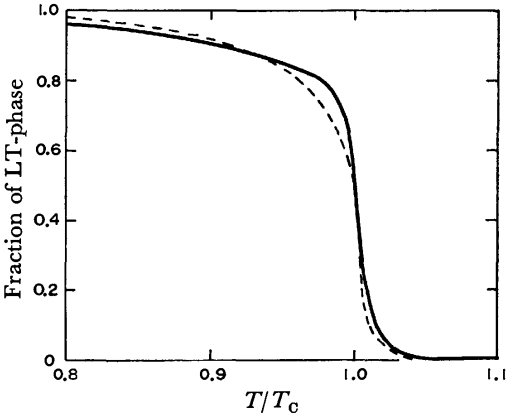

Fig. 7. Comparison of the fraction of the low temperature phase, x, between the experiment and the theory.
Solid line: the experimental curve.
Broken line: $(J_{LH}/N^{2/3})=1.8kT_c$, $N_A/N=5(T<T_c)$ and $200(T>T_c)$.

experiment and the present model is obtained under a condition of $(J_{LH}/N^{2/3})=1.8\,kT_c$. This fact indicates a complexity of the phase transition found for organic free radical salts as well as an incompleteness of the present model. However, it is interesting to note that the number of radicals included in a cell varies from $N_A/N=5$ in the low temperature phase to 200 in the high temperature phase. This suggests a considerably different correlation between radicals below and above T_c.

References

1) J. J. Andre, J. Clementz, R. Jesser, and G. Weill, *C. R. Acad. Sci., Ser. B*, **266**, 1057 (1968).
2) R. J. Faber and M. P. Faber, *J. Chem. Phys.*, **39**, 3541 (1963).
3) J. J. Andre and G. Weill, *C. R. Acad. Sci., Ser. B*, **269**, 499 (1969).
4) Y. Iida, *Bull. Chem. Soc. Jpn.*, **43**, 2772 (1970).
5) N. Sakai, I. Shirotani, and S. Minomura, *Bull. Chem. Soc. Jpn.*, **44**, 675 (1971).
6) J. J. Andre and G. Weill, *Chem. Phys. Lett.*, **9**, 27 (1971).
7) M. Konno, H. Kobayashi, F. Marumo, and Y. Saito, *Bull. Chem. Soc. Jpn.*, **46**, 1987 (1973).
8) S. Hiroma and H. Kuroda, *Bull. Chem. Soc. Jpn.*, **46**, 3645 (1973).
9) J. J. Andre and G. Weill, *Mol. Phys.*, **15**, 97 (1968).
10) S. Hiroma and H. Kuroda, *Bull. Chem. Soc. Jpn.*, **47**, 3014 (1974).
11) J. P. Goldsborough, M. Mandel, and G. E. Pake, "Proceedings of the VII-th International Conference on Low Temperature Physics," ed by G. M. Graham and A. C. H. Hallett, University of Toronto Press, Toronto (1961), p. 702.
12) W. O. Hamilton and G. E. Pake, *J. Chem. Phys.*, **39**, 2694 (1963).
13) H. Chihara, M. Nakamura, and S. Seki, *Bull. Chem. Soc. Jpn.*, **38**, 1776 (1965).
14) H. Lemaire, P. Rey, A. Rassat, A. Combarieu, and J. C. Michel, *Mol. Phys.*, **14**, 201 (1968).
15) A. Kosaki, H. Suga, S. Seki, K. Mukai, and Y. Deguchi, *Bull. Chem. Soc. Jpn.*, **42**, 1525 (1969).
16) W. Duffy, Jr., D. L. Strandburg, and J. F. Deck, *Phys., Rev.*, **183**, 567 (1969).
17) A. Kosaki, Y. Iida, M. Sorai, H. Suga, and S. Seki, *Bull. Chem. Soc. Jpn.*, **43**, 2280 (1970).
18) W. Duffy, Jr., J. F. Dubach, P. A. Pianetta, J. F. Deck, D. L. Strandburg, and A. R. Miedema, *J. Chem. Phys.*, **56**, 2555 (1972).
19) J. Yamauchi, K. Adachi, and Y. Deguchi, *Chem. Lett.*, **1972**, 733.
20) J. G. Vegter, T. Himba, and J. Kommandeur, *Chem. Phys. Lett.*, **3**, 427 (1969); J. G. Vegter and J. Kommandeur, *Mol. Cryst. Liq. Cryst.*, **30**, 11 (1975). These papers deal with the transition enthalpies of alkali-metal TCNQ salts by means of a differential scanning calorimeter.
21) A. Kosaki, M. Sorai, H. Suga, and S. Seki, *Bull. Chem. Soc. Jpn.*, **50**, 817 (1977).
22) Y. Matsunaga, *Can. J. Chem.*, **38**, 1172 (1960).
23) Y. Iida, *Bull. Chem. Soc. Jpn.*, **43**, 345 (1970).
24) A. Girlando, L. Morelli, and C. Pecile, *Chem. Phys. Lett.*, **22**, 553 (1973).
25) G. Scheibe, F. May, and H. Fischer, *Ber.*, **57**, 1330 (1924).
26) H. A. Torrey and W. H. Hunter, *J. Am. Chem. Soc.*, **34**, 702 (1912).
27) H. Suga and S. Seki, *Bull. Chem. Soc. Jpn.*, **38**, 1000 (1965).
28) J. W. Bray, H. R. Hart, Jr., L. V. Interrante, I. S. Jacobs, J. S. Kasper, G. D. Watkins, S. H. Wee, and J. S. Bonner, *Phys. Rev. Lett.*, **35**, 744 (1975).
29) E. Pytte, *Phys. Rev., B*, **10**, 4637 (1974).
30) J. Frenkel, "Kinetic Theory of Liquids," Oxford University Press, London (1947), Chap. VII.

Thermodynamic Properties and Phase Transitions of Methyltriphenylphosphonium and Methyltriphenylarsonium Bis(7,7,8,8-tetracyanoquinodimethanide)s and Their Solid Solutions*

Akio KOSAKI,† Michio SORAI, Hiroshi SUGA, and Syûzô SEKI

Department of Chemistry, Faculty of Science, Osaka University, Toyonaka, Osaka 560

(Received October 18, 1976)

The heat capacities of stable organic free-radical salts $[(C_6H_5)_3PCH_3]_{1-x}^+[(C_6H_5)_3AsCH_3]_x^+(TCNQ)_2^-$ (x=0, 0.159, 0.250, 0.449, and 1, and TCNQ=7,7,8,8-tetracyanoquinodimethane) have been measured with an adiabatic calorimeter in the temperature range between 12 and 370 K. The phase transitions are found for the former four cases at 315.65, 325.80, 333.05, and 357.92 K, respectively. The enthalpy and the entropy due to the phase transitions are determined. The transition temperature is raised by diluting the phosphonium salt with the arsonium one. This tendency is quite contrary to that found for usual solid solutions. The magnitude and the composition dependence of the transition entropy indicate that the phase transition of the solid solutions may be attributable to the changes in both the crystal structure and the magnetic spin state at the transition point. A plausible explanation for the present unusual tendency for the composition dependence is presented.

Organic anion radical salts based on 7,7,8,8-tetracyanoquinodimethane(TCNQ) have been found to exhibit very high electric conductivity and unusual magnetic properties.[1] The unpaired electron of a TCNQ anion radical is not necessarily lacalized on a particular atom but distributed over a whole TCNQ radical to a considerable extent.[2] The rather easy flip-flop motion of the unpaired electrons between adjacent radicals forming a column in a crystal brings about high electric conductivity. Because of the unique interaction of the spins associated with the unpaired electrons, the ground spin manifold is not a doublet but a singlet with a thermally accessible triplet state. Owing to these situations neither the localized spin model nor the continuous band model due to the collective motion of conduction electrons can describe satisfactorily the magnetic properties of anion radical salts. These peculiar behavior is of course expected to be reflected on their thermal properties.

In a previous publication[3] we reported briefly the heat capacity of methyltriphenylphosphonium bis(7,7,-8,8-tetracyanoquinodimethanide)[abbreviated hereafter as $[(C_6H_5)_3PCH_3]^+(TCNQ)_2^-$ or more simply as the P-salt] and pointed out that the phase transition observed at T_c=315.65 K cannot be described solely by the spin contribution. Based on the analysis of the transition entropy, it was predicted that the phase transition may be accompanied by a crystallographic change. The precise structural analyses by X-ray diffraction[4,5] demonstrated really the existence of a structural change at T_c. In the present paper we report thermodynamic properties and phase transitions of the P-salt and the methyltriphenylarsonium homolog[abbreviated as $[(C_6H_5)_3AsCH_3]^+(TCNQ)_2^-$ or more simply as the As-salt] as well as their solid solutions $[(C_6H_5)_3PCH_3]_{1-x}^+[(C_6H_5)_3AsCH_3]_x^+(TCNQ)_2^-$ (x=0.159, 0.250 and 0.449).

Since the first synthesis of these radical salts,[6] extensive studies have been made by means of electron paramagnetic resonance (EPR),[7–13] electric conductivity,[14–18] magnetic susceptibility[19] and of high-pressure experiment[20,21] and also by theoretical treatment.[22–25] As to the mechanism of phase transition, two simple phenomenological models have been reported.[20,23] On the one hand, Chesnut[23] tried to interpret the transition mechanism of the P-salt by assuming that the spin state exists in a singlet-triplet equilibrium with the attractive interaction between triplets. His model accounts for the occurrence of phase transition when adequate values be assigned to the triplet excitation energy and to the exciton-exciton interaction energy. On the other hand, Merkl *et al.*[20] observed the pressure-induced phase transition for the P- and the As-salts and explained the p-T phase diagram for the As-salt in terms of an elementary theory of non-interacting triplet excitons. These two models succeeded in accounting for the gross aspects of the phase transition but failed to explain the transition entropy.

Kepler[19] measured the magnetic susceptibilities of the solid solutions $[(C_6H_5)_3PCH_3]_{1-x}^+[(C_6H_5)_3AsCH_3]_x^+(TCNQ)_2^-$ with seven different values of x in the range from 100 to 450 K and found a discontinuity at each transition point for all the materials except for the pure As-salt. The interesting feature is that the transition temperature T_c was raised with increasing x. Iida[26] examined also this relationship between x and T_c by use of a differential scanning calorimeter (DSC). He confirmed the same result and found that the entropy of transition decreases in proportion to x. As will be seen below, the present investigation leads to a quite different conclusion as to the x-dependence of the transition entropy.

Experimental

Materials. The P-salt was prepared according to the method of Melby *et al.*[27] The purified starting materials, methyltriphenylphosphonium iodide and TCNQ, were dissolved respectively into purified acetonitrile. Then these two solutions were mixed at about 70 °C with vigorous stirring under nitrogen atmosphere. After the reaction was over, the solution was kept quietly standing for 24 hours at a cool and dark place to give blackish prism crystals. The As-salt was

* Presented before the 5th Annual Meeting of the Society of Calorimetry and Thermal Analysis, Japan, Osaka (1969) and the 26th Annual Meeting of the Chemical Society of Japan, Tokyo (1972).

† Deceased on July 16, 1974.

prepared from purified methyltriphenylarsonium iodide and TCNQ by the same method with that of the P-salt. Three kinds of solid solutions $[(C_6H_5)_3PCH_3]_{1-x}^+[(C_6H_5)_3AsCH_3]_x^+(TCNQ)_2^-$ (x=0.159, 0.250, and 0.449) were obtained by the following procedures: Methyltriphenylphosphonium and methyltriphenylarsonium iodides were dissolved into pure acetonitrile in the ratio of $(1-x)$ to x. To this solution the acetonitrile solution containing the stoichiometric amount of TCNQ was added with vigorous stirring under nitrogen atmosphere at 70 °C.

Table 1. Weight of the sample used for heat capacity measurements and the results of elementary analyses[a] for $[(C_6H_5)_3PCH_3]_{1-x}^+[(C_6H_5)_3AsCH_3]_x^+(TCNQ)_2^-$

x	Weight/g	C/%	H/%	N/%	P/%
0.000	9.3395	75.43 (75.76)	3.81 (3.84)	16.44 (16.44)	4.82 (4.52)
0.159	11.5078	74.06 (74.56)	3.72 (3.78)	17.45 (16.18)	—
0.250	4.8597	74.36 (74.13)	3.63 (3.76)	16.62 (16.08)	3.68 (3.33)
0.449	11.0887	72.77 (73.21)	3.50 (3.72)	16.76 (15.88)	—
1.000	12.1251	70.96 (70.78)	3.37 (3.59)	15.45 (15.36)	—

a) The figures in parentheses are the values expected from the initial composition of the starting materials.

The results of elementary analyses for the five kinds of specimens are given in Table 1. The arsonium concentration x in each specimen was simply estimated from the amounts of the starting materials. The estimated values seem to approximate well to the true ones because Table 1 indicates that the composition of each specimen is simply proportional to the initial composition of the starting materials.

Measurements of Heat Capacities and Infrared Spectra. Heat capacity measurements of these radical salts were made with adiabatic calorimeters[28,29] in the temperature region from 12 to 370 K. The sample was sealed into the calorimeter cell with a small quantity of helium gas as a heat exchanger. The amounts of the samples used for the measurements are given in Table 1.

Infrared absorption spectra were recorded on a Grating-type Infrared Spectrophotometer Model DS-402G(Japan Spectroscopic Co., Ltd.) in the wave number region from 400 to 4000 cm^{-1}. Nujol mull and KBr-disk methods were employed for the preparation of samples. Far infrared absorption spectra of these radical salts were obtained by using a Spectrophotometer Model FIS-001 (Hitachi Ltd.) in the range from 30 to 400 cm^{-1}. Nujol mull method could not be used at high temperatures, so the sample was mixed with a small amount of polyethylene having low melting point.

Results

Heat Capacities. Heat capacity measurements were made for five kinds of solid solutions $[(C_6H_5)_3PCH_3]_{1-x}^+[(C_6H_5)_3AsCH_3]_x^+(TCNQ)_2^-$($x$=0, 0.159, 0.250, 0.449, and 1) in the temperature range from 12 to 370 K. The observed heat capacities for the salts with x=0.159, 0.250, 0.449, and 1 are plotted in Fig. 1, while the heat capacity of the pure P-salt (x=0) has been given in a previous paper.[3] The numerical values of the heat capacities for the P- and the As-salts are summarized in Table 2 and their standard thermodynamic quantities are given in Table 3.

The P-salt and the solid solutions exhibited the phase transition phenomenon at T_c=315.65 K (x=0), 325.80 K (x=0.159), 333.05 K (x=0.250), and 357.92 K (x=0.449). In the case of the pure As-salt, however, any heat capacity anomaly due to a phase transition was not observed in the temperature region investigated. The phase transition temperature T_c was regularly raised with increasing x and the heat capacity anomaly concerning the phase transition of the solid solution was very sharp as that of the pure P-salt. From these two facts we can imagine that random mixing of the phosphonium and the arsonium cations is established and that the present specimens can be regarded as complete solid solutions.

The enthalpy and the entropy of transition were estimated by subtracting plausible normal heat capacities from the overall ones. In each case the normal heat capacity extrapolated from the high temperature phase was smaller than that of the low temperature phase at the transition point. The values of transition enthalpy ΔH and entropy ΔS thus obtained and also the jump of normal heat capacity ΔC_p detected at T_c are given in Table 4.

The heat capacities in the temperature region far below the transition points have a tendency to increase with increasing fraction x of the As-salt.

Infrared Absorption Spectra. In order to examine the influence of the phase transition we measured the infrared spectra of the P-salt both of the low and the high temperature phases. The spectra of both phases resembled closely each other except for minor changes in position and intensity of the absorption peaks. Figure 2 illustrates the far infrared spectra for the P-salt at 15 °C ($=T_c-27.5$ K), 40 °C ($=T_c-2.5$ K), and 80 °C ($=T_c+37.5$ K). In this wave number region only appreciable changes were observed at 320, 220, and 40 cm^{-1}. The band at 320 cm^{-1} vanished above T_c while a new band appeared at 40 cm^{-1}. The intensity of the band at 220 cm^{-1} was diminished above T_c. As a whole, it may be concluded that the phase transition phenomenon scarcely affected the infrared active modes of normal vibrations. This fact coincides well with the X-ray structural analyses,[4,5] which demonstrate that crystal structures of both the low and the high temperature modifications of the P-salt are triclinic system with the space group $P\bar{1}$.

Figure 3 represents the composition dependence of the infrared spectra for five kinds of materials in the wave number region from 1100 to 600 cm^{-1} at room temperature. The absorption bands at 710 and 900 cm^{-1} can safely be assigned to the phosphonium species since the intensities are proportional to the phosphonium concentration $(1-x)$. The band at 884 cm^{-1} is characteristic of the arsonium species because its intensity changes in proportion to the arsonium concentration x. Similar band arising from the arsonium species was observed in the far infrared region at 347 cm^{-1}. On the other hand, a new absorption peak was observed at

TABLE 2. HEAT CAPACITIES OF $[(C_6H_5)_3PCH_3]^+(TCNQ)_2^-$ AND $[(C_6H_5)_3AsCH_3]^+(TCNQ)_2^-$

T/K	C_p/J K^{-1} mol^{-1}	T/K	C_p/J K^{-1} mol^{-1}	T/K	C_p/J K^{-1} mol^{-1}	T/K	C_p/J K^{-1} mol^{-1}	T/K	C_p/J K^{-1} mol^{-1}
				The P-SALT					
12.22	17.90	61.14	233.22	148.85	474.53	259.06	755.99	314.37	1243.8
13.33	22.62	64.32	245.16	153.43	486.16	263.53	767.58	315.38	1590.0
14.44	26.15	67.53	255.86	158.49	499.61	268.09	776.85	315.76	1619.9
15.70	30.16	71.44	267.48	164.00	513.65	272.77	789.34	316.03	1516.3
17.02	36.85	75.96	279.70	169.43	527.06	277.38	800.90	316.25	1506.0
18.46	43.83	80.28	292.21	174.77	540.68	279.63	806.58	316.61	1231.3
19.97	51.31	84.44	305.24	180.03	552.73	281.91	811.58	317.23	1102.3
21.43	57.96	88.62	317.40	184.22	567.07	285.84	821.92	318.02	978.17
22.91	64.69	92.82	328.79	197.49	593.43	291.94	838.36	318.84	927.10
24.80	73.78	96.92	339.72	200.05	599.46	297.09	850.68	319.68	914.83
27.01	85.07	100.96	349.90	204.63	611.96	298.00	855.25	321.36	912.46
29.20	95.92	102.83	354.72	209.64	624.40	301.76	863.95	322.41	910.70
31.40	107.03	106.08	363.66	214.58	637.23	303.06	868.11	324.08	911.10
33.65	118.38	109.90	373.65	219.44	650.44	305.54	874.33	326.72	911.02
36.29	131.21	114.25	385.41	224.26	662.14	306.82	880.40	330.38	913.88
39.28	145.09	119.12	400.41	229.00	675.46	308.88	909.41	334.89	926.86
42.27	158.46	122.12	405.92	230.88	680.00	310.08	942.85	340.03	939.94
45.32	171.33	125.06	413.90	235.73	698.14	310.84	955.23	345.37	948.94
48.45	184.19	129.86	426.34	240.52	708.49	311.52	962.34	350.67	965.47
51.61	197.08	134.76	438.49	245.24	722.86	312.12	962.80		
54.77	209.40	139.54	451.39	249.91	734.29	312.72	997.19		
57.95	221.36	144.23	463.12	254.51	745.40	313.30	1061.8		
				The As-SALT					
14.06	24.81	54.59	224.78	108.21	398.73	168.34	561.66	251.57	764.71
15.22	30.01	57.29	235.17	111.17	406.62	173.10	573.89	256.42	777.52
16.33	35.53	60.47	247.30	114.08	414.99	177.80	585.78	262.01	790.57
17.69	42.79	60.81	248.90	116.95	423.06	182.46	598.04	267.11	806.07
19.26	51.18	64.09	260.82	120.13	431.60	187.08	608.87	268.34	807.21
20.82	59.29	67.53	273.60	123.60	440.17	191.80	622.57	270.99	812.55
22.33	67.31	70.80	284.93	127.03	450.17	196.66	634.73	275.60	823.12
23.83	75.27	73.95	295.27	130.41	459.23	201.46	647.23	280.21	829.71
25.59	84.58	76.99	305.39	130.74	459.53	206.21	658.92	284.77	842.78
27.59	95.10	79.93	314.98	133.43	468.26	210.91	671.37	289.32	849.35
29.48	105.42	82.61	322.93	136.53	475.97	215.56	686.01	294.04	864.55
31.28	114.99	82.79	323.97	139.93	485.07	216.98	679.36	298.88	878.67
33.17	125.20	85.58	332.23	143.29	493.63	219.91	691.96	304.51	890.86
35.46	137.00	85.72	332.72	146.93	503.60	221.91	691.55	310.99	908.64
38.00	149.47	89.18	343.20	150.95	514.40	222.88	694.30	317.52	922.44
40.65	161.72	92.54	353.56	155.00	524.50	226.88	724.30	324.00	938.35
43.45	175.68	95.82	363.00	159.01	532.79	231.79	714.59	330.46	956.78
46.23	188.91	99.01	372.78	160.48	540.69	236.76	726.80	336.88	974.17
49.00	200.84	102.14	380.95	162.98	545.74	241.75	740.80	343.29	998.48
51.78	212.57	105.21	390.15	163.77	550.45	246.68	752.30	349.73	1016.4

TABLE 3. STANDARD THERMODYNAMIC FUNCTIONS OF $[(C_6H_5)_3PCH_3]^+(TCNQ)_2^-$ AND $[(C_6H_5)_3AsCH_3]^+(TCNQ)_2^-$

T/K	$C_p°$/J K^{-1} mol^{-1}	$S°$/J K^{-1} mol^{-1}	$(H°-H_0°)/T$/J K^{-1} mol^{-1}	$C_p°$/J K^{-1} mol^{-1}	$S°$/J K^{-1} mol^{-1}	$(H°-H_0°)/T$/J K^{-1} mol^{-1}
		the P-salt			the As-salt	
20	50.48	22.358	16.012	55.24	23.146	16.731
30	100.00	52.031	35.634	108.46	55.478	38.333
40	148.22	87.586	57.915	159.34	93.778	62.338
50	190.64	125.30	80.291	205.26	134.36	86.418
60	228.86	163.49	101.92	245.62	175.40	109.63
70	263.34	201.48	122.63	282.02	216.08	131.73
80	292.05	238.49	141.99	314.76	255.92	152.61
90	321.17	274.60	160.30	345.88	294.81	172.38
100	347.42	309.79	177.70	375.44	332.80	191.22
120	400.74	377.85	210.43	431.28	406.24	226.63
140	452.34	443.48	241.29	485.34	476.77	259.71
160	503.29	507.19	270.84	538.83	545.05	291.24
180	552.74	569.38	299.47	591.63	611.60	321.72
200	599.83	630.01	327.11	643.42	676.60	351.29
220	651.42	689.59	354.23	692.22	740.20	380.05
240	706.80	748.57	381.23	734.92	802.13	407.71
260	758.26	807.29	408.36	785.72	862.98	434.86
280	807.32	865.25	435.08	833.68	922.97	461.64
300	859.26	922.69	461.60	879.74	982.05	487.97
320	915.30	984.36	492.55	929.76	1040.4	514.01
340	939.70	1040.1	517.67	983.60	1098.4	540.02
360	989.00	1095.2	542.48	1039.7	1156.2	566.22
370	1013.5	1122.6	554.88	1067.7	1185.0	579.39

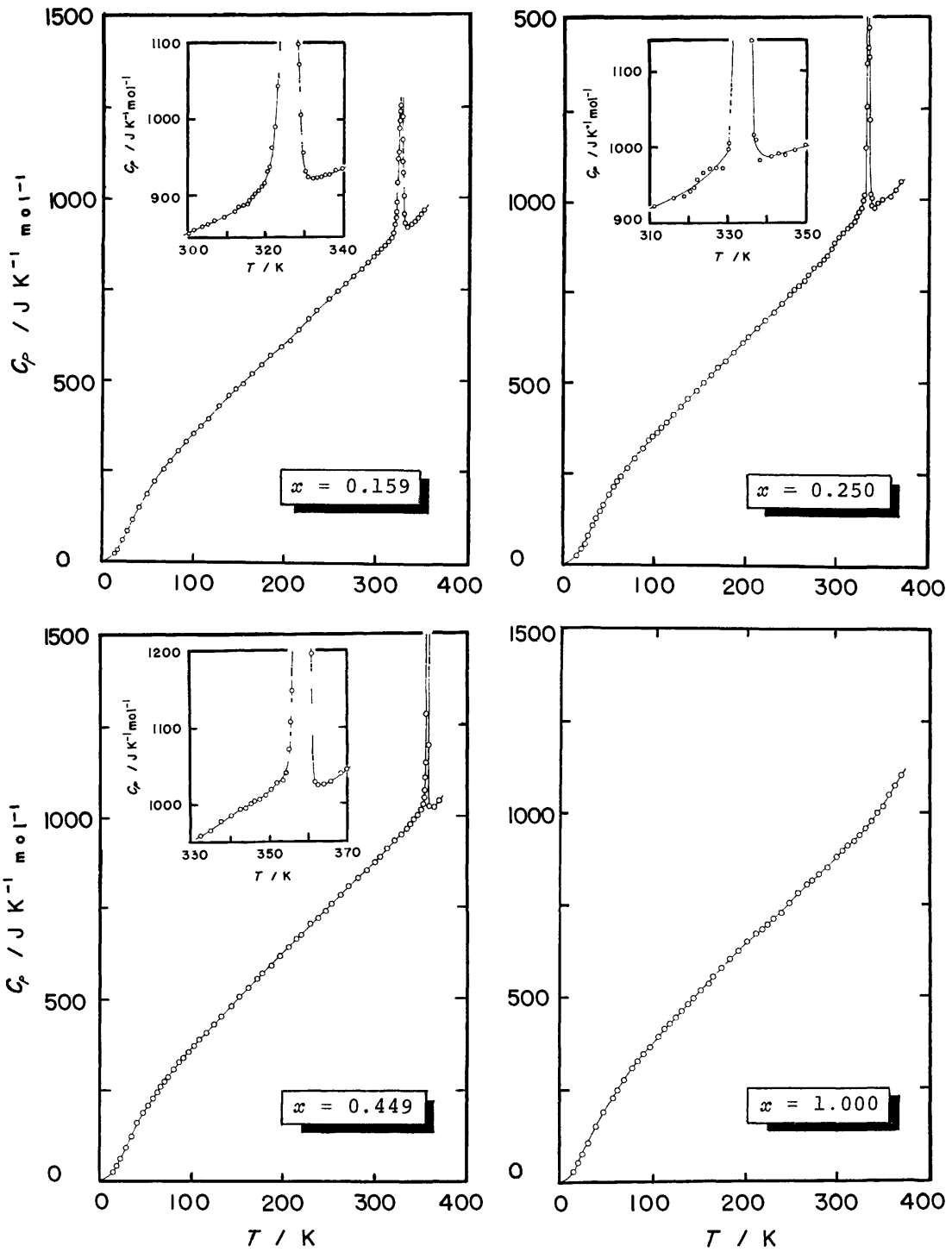

Fig. 1. Molar heat capacity of $[(C_6H_5)_3PCH_3]_{1-x}^{+}[(C_6H_5)_3AsCH_3]_x^{+}(TCNQ)_2^{-}$ (x=0.159, 0.250, 0.449, and 1.000).

Table 4. Thermodynamic quantities related to the phase transition of the solid solutions $[(C_6H_5)_3PCH_3]_{1-x}^{+}[(C_6H_5)_3AsCH_3]_x^{+}(TCNQ)_2^{-}$

x	T_c / K	ΔC_p / J K^{-1} mol^{-1}	ΔH / J mol^{-1}	ΔS / J K^{-1} mol^{-1}
0.000	315.65	−15.8	2030	6.431
0.159	325.80	−11.7	2028	6.224
0.250	333.05	−6.3	1967	5.905
0.449	357.92	−8.0	1927	5.383

860 cm^{-1} only when the specimen formed the solid solution. As the crystal structures of the P- and the As-salts are isomorphous at room temperature,[4] this new band may correspond to the boundary mode between the phosphonium and the arsonium cations.

Phase Transition of the P-salt

As was described in a previous section, the normal heat capacity of the high temperature phase was 15.75

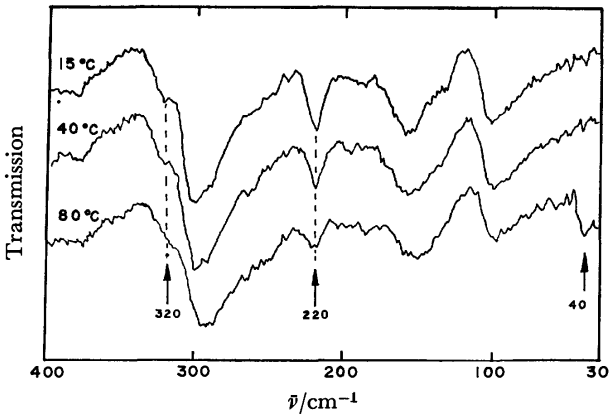

Fig. 2. Far infrared spectra of $[(C_6H_5)_3PCH_3]^+$-$(TCNQ)_2^-$ in the wave number region from 400 to 30 cm^{-1} at three different temperatures (T_C=42.50 °C).

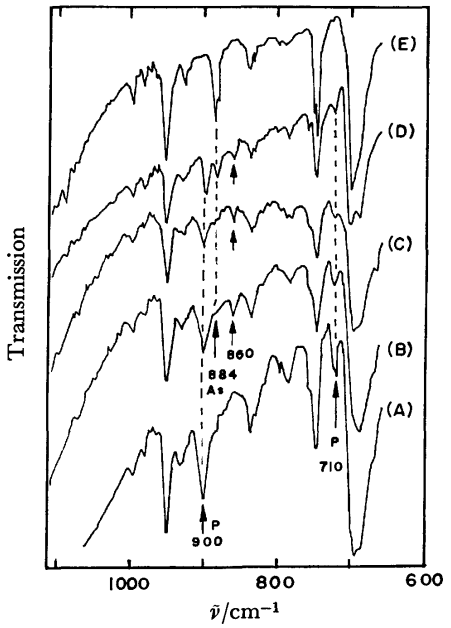

Fig. 3. Infrared spectra of $[(C_6H_5)_3PCH_3]_{1-x}^+[(C_6H_5)_3$-$AsCH_3]_x^+(TCNQ)_2^-$ in the wave number region from 1100 to 600 cm^{-1} at a room temperature. (A) x=0.000, (B) x=0.159, (C) x=0.250, (D) x=0.449, and (E) x=1.000.

J K^{-1} mol^{-1} smaller than that of the low temperature phase at T_c. This fact implies that the excitation of phonons is easier in the low- than in the high-temperature phase at least in the vicinity of T_c. This situation seems to be related with the contraction of crystal volume[5,20] at T_c.

The enthalpy and the entropy of transition were determined to be 2030 J mol^{-1} and 6.431 J K^{-1} mol^{-1}, respectively. The entropy corresponds to R ln 2.12. This value cannot be explained solely by the contribution from the elctronic spin freedom. We discuss below a problem what kinds of freedoms contribute to the phenomenon of the phase transition.

(1) Contribution of Magnetic Spin Freedom. The magnetic spin in this radical salt is known to behave just like being in the singlet-triplet equilibrium.[7,8,22] The contribution of the magnetic spin system to the entropy of transition can be estimated from the triplet density defined by

$$\rho \equiv \left\{1+\frac{1}{3}\exp(J/kT)\right\}^{-1}, \quad (1)$$

where J is the energy difference between a singlet ground state and an excited triplet state. The temperature dependence of ρ is obtained from the magnetic susceptibility measurements[19] as the paramagnetic contribution to the susceptibility can be fitted approximately to the expression

$$\chi = \frac{NS(S+1)g^2m_B^2}{3kT}\left\{1+\frac{1}{3}\exp(J/kT)\right\}^{-1}, \quad (2)$$

where g is the electronic g-factor, m_B the Bohr magneton, S the spin quantum number and N the number of quasimolecules. By assuming g=2.0, S=1 and $N=N_A/2$ (N_A is the Avogadro constant), we obtain the relation

$$\chi T = 0.5002\rho. \quad (3)$$

The entropy arising from the spin system corresponds to

$$S = \frac{1}{2}R\{\rho \ln 3 - \rho \ln \rho - (1-\rho)\ln(1-\rho)\}. \quad (4)$$

Since the triplet density is zero at 0 K and 3/4 at infinite temperature, the total spin entropy amounts to R ln 2(=5.763 J K^{-1} mol^{-1}). However, the observable magnetic entropy as the transition entropy is limited to only a small part of R ln 2 and the remaining part is smeared over a wide temperature region as the Schottky-type anomaly, because the present phase transition is characterized by a small jump of the magnetic susceptibility[19] and thus a small change in ρ. By using Kepler's data,[19] the contribution of the spin entropy to the phase transition was estimated to be 1.93 J K^{-1} mol^{-1}. Since the anomalous heat capacity has its skirt below T_c, the calculation is made based on the change in ρ over the temperature range corresponding to the heat capacity anomaly.[30] At any rate, the estimated magnetic entropy merely corresponds to thirty percent of the total entropy of transition. Therefore, the remaining entropy of transition due to other origins amounts to 4.50 J K^{-1} mol^{-1}. On the other hand, if the system be allowed to include a considerable fraction of doublet as well as the singlet-triplet equilibrium, the transition entropy due to the magnetic origin would become larger than 1.93 J K^{-1} mol^{-1}. The experimental evidence,[19] however, is not favorable to the existence of such a large amount of doublet in the temperature region investigated here.

(2) Contribution of Conduction Electrons. The electric conductivity of this radical salt[10] is abruptly increased at T_c. Increase in the number of conduction electrons will cause an increase in the entropy of the system. The energy gap between the conduction and the filled bands has been estimated to be 0.4 eV below T_c and 0.3 eV above it.[26] This difference leads to an increase in the excitation of conduction electrons in the high temperature phase. The energy gap, however, is about ten times larger than the thermal energy kT in the neighborhood of T_c. Accordingly the number of electrons which can be excited to the conduction band by the thermal energy is negligibly small and the

entropy gain due to such electrons is the order of magnitude of the present experimental error. Thus the freedom of conduction electrons cannot practically contribute to the entropy of transition.[31]

(3) Contribution of the Change in Lattice Structure. According to the recent structural analyses by Konno and Saito,[5] the conformations of the phosphonium cations are quite different each other in both the low- and the high-temperature phases, whereas the crystal structure and the space group are not changed by the phase transition. In the high temperature phase two of the three phenyl groups belonging to a phosphonium cation are rotated drastically by about 56 and 45° from the positions observed in the low temperature forms, and the interplanar distances in the TCNQ column are altered. These changes in the conformation and the packing geometry modify the distribution function of the lattice vibration to some extent. Accordingly, a part of the excess transition entropy other than the magnetic contribution may be attributable to this origin. The quantitative estimation of this effect is, however, not easy.

The interesting but peculiar feature concerning the high temperature phase is the existence of about ten percent of the phosphonium cations having the different configuration.[5] If it were the case, the entropy due to their mixing amounts to 2.70 J K^{-1} mol^{-1}. This corresponds to sixty percent of the remaining entropy other than the spin contribution.

Phase Transitions of Solid Solutions

In order to demonstrate clearly the composition dependence of heat capacities of the solid solutions, the heat capacity curves around T_c of the five samples are shown in Fig. 4. One of the interesting features is that the transition temperature was shifted toward the high temperature side with increasing fraction of the As-salt. If the solid solution is simply regarded as the P-salt being diluted with the As-salt, the composition dependence of the transition temperature seems to be quite curious. In general the effect of dilution would make the existing interaction weaker and thus would lead to a system having a lower transition temperature. In view of the fact, however, that it is not the cations but the $(TCNQ)_2^-$ anion radicals which are responsible for the magnetic spin system, the existence of the P-salt fraction should be regarded only as a trigger for the phase transition.

The transition enthalpy ΔH and the entropy ΔS

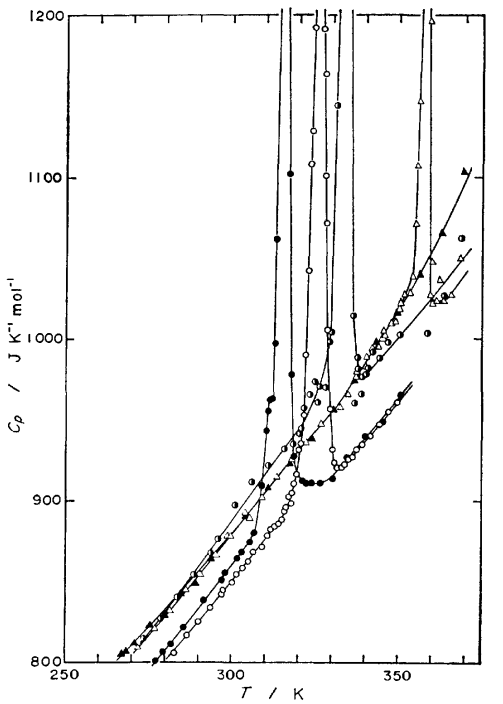

Fig. 4. Heat capacities of $[(C_6H_5)_3PCH_3]_{1-x}^+[(C_6H_5)_3AsCH_3]_x^+(TCNQ)_2^-$ in the vicinity of T_C. (●) x=0.000, (○) x=0.159, (◑) x=0.250, (△) x=0.449, and (▲) x=1.000.

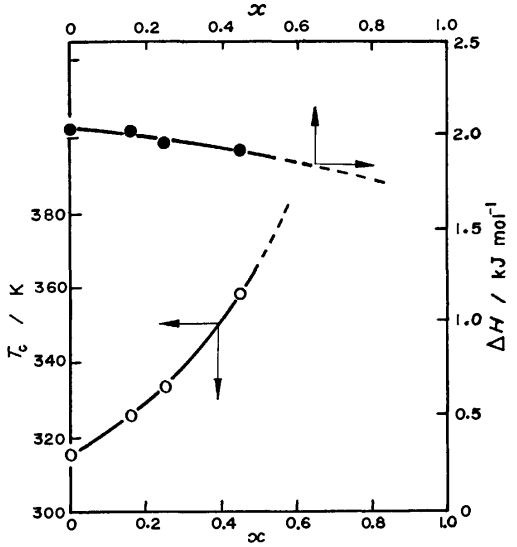

Fig. 5. Composition dependence of the transition temperature T_C(○) and the transition enthalpy ΔH(●) for $[(C_6H_5)_3PCH_3]_{1-x}^+[(C_6H_5)_3AsCH_3]_x^+(TCNQ)_2^-$.

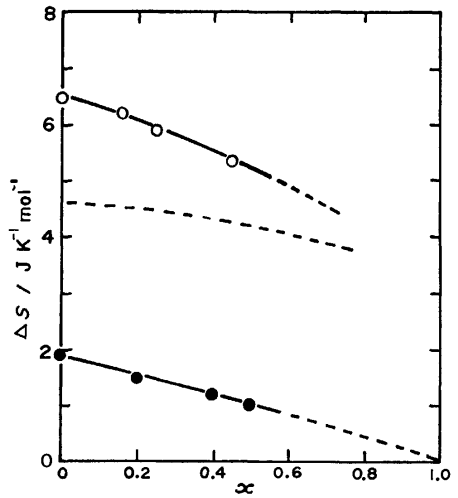

Fig. 6. Composition dependence of the transition entropy for $[(C_6H_5)_3PCH_3]_{1-x}^+[(C_6H_5)_3AsCH_3]_x^+(TCNQ)_2^-$; (○) the observed transition entropy, (●) the entropy due to the magnetic contribution estimated from the magnetic susceptibility data[19] and (----) the remaining entropy other than the magnetic contribution.

determined from the heat capacity anomalies are plotted in Figs. 5 and 6, respectively, as a function of the As-salt fraction. Also shown in Fig. 5 is the composition dependence of the transition temperature. A remarkable feature is that the enthalpy and the entropy of transition do not seem to converge to zero when the As-salt fraction x approaches to unity. These results are quite different from the previous ones by Iida[26] obtained with a differential scanning calorimeter(DSC). His results indicate that the ΔH and the ΔS are decreased linearly with x and finally vanished at $x=1$. The heat capacity anomaly due to the present phase transition becomes broader with increasing fraction of the As-salt and the contribution from the skirt of the heat capacity anomaly was increased. A shortcoming inherent in a thermal analysis by use of DSC is to fail in detecting a moderate thermal change and to truncate a heat capacity peak. Therefore, a simple thermal analysis has a risk to underestimate the enthalpy and the entropy of transition. The discrepancy between his results and ours may be due to these situations.

The entropy due to the magnetic contribution was estimated in a scheme of the singlet-triplet equilibrium. For this purpose, the magnetic susceptibilities of the solid solutions measured by Kepler[19] were used to obtain the value of triplet density below and above the transition point. The results are shown in Fig. 6. As is in the case of the P-salt, the contribution from the magnetic spin system amounts to only twenty or thirty percent of the total entropy of transition. A remarkable feature found here is that the entropy other than the magnetic contribution is nearly independent of the composition of the solid solution. This fact suggests that the solid solution may undergo almost the same structural or geometrical change with that of the pure P-salt independently of the arsonium fraction. A favorable evidence for the structural change is the discontinuity of the normal heat capacity found at T_c (see Table 4).

According to the high-pressure experiment by Merkl *et al.*[20] the transition temperatures of both the P- and the As-salts are lowered with increasing the external pressure although the As-salt does not show the corresponding phase transition at an atmospheric pressure because of its thermal decomposition. If the p-T diagram for the P-salt is extrapolated into the negative pressure region, the occurrence of a hypothetical phase transition would be possible at a temperature higher than 315.65 K where the P-salt undergoes the phase transition at 1 atm. The volume of the unit cell at negative pressure is considered to be slightly larger than that at 1 atm. According to the X-ray analyses for the P- and the As-salts at room temperature[4,5] the lattice volume of the As-salt is slightly larger than that of the P-salt. Therefore it is plausible that the increase of the As-salt fraction in the solid solution will bring about the increase in the lattice volume. This effect just corresponds to the lattice expansion of the P-salt or in other words the negative pressure in the p-T diagram. This is one of the most probable reasons why the transition temperature is raised with the increase of the arsonium salt fraction.

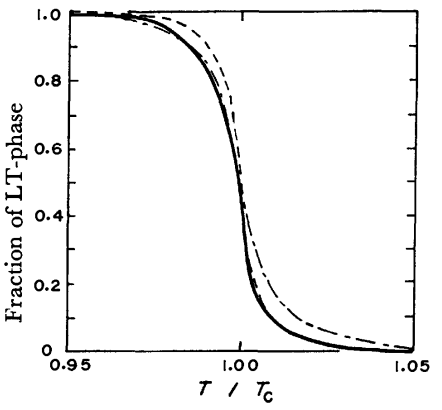

Fig. 7. Comparison of the low temperature fraction of the P-salt between the experiment and the theory (T_C= 315.65 K).
(——): The experimental value, (- - -): the calculated value for $(J_{LH}/N^{2/3}) = 1.5\,kT_C$ and $(N_A/N) = 100$, (----): the calculated value for $(J_{LH}/N^{2/3}) = 1.5\,kT_C$ and $(N_A/N) = 167$.

Table 5. The parameters determined by the "best" fit of the present model to the experimental values for $[(C_6H_5)_3PCH_3]_{1-x}^+[(C_6H_5)_3AsCH_3]_x^+(TCNQ)_2^-$

x	0.000	0.159	0.250	0.449
$J_{LH}/(N^{2/3}kT_C)$	1.5	1.1	1.0	0.5
$N_A/N\,(T<T_C)$	100	125	200	100
$N_A/N\,(T>T_C)$	167	217	500	1430

In a previous paper,[33] we presented a phenomenological model for the phase transition of potassium p-chloranil anion radical salt. The principle is virtually the same with the Frenkel theory of heterophase fluctuation in liquid.[34] The parameters characteristic of this model are the number of cells or embryos, N, and the interaction energy between adjacent cells belonging to the low and the high temperature phases, J_{LH}. If the Avogadro constant is denoted as N_A, the ratio, (N_A/N), corresponds to the number of molecules included in a cell. The phase transition becomes a first order when $(J_{LH}/N^{2/3})>2kT_c$, while the phase transition is of a higher order when $(J_{LH}/N^{2/3})$ is equal to $2kT_c$. Figure 7 illustrates the "best" fit of this model to the experimental value for the P-salt. The "best" fit below T_c is obtained under the condition of $(J_{LH}/N^{2/3})=1.5\,kT_c$ and $(N_A/N)=100$ but above T_c it is necessary to adopt a large value of $(N_A/N)=167$ for the "best" fit. This tendency is found for all the phase transitions observed for the solid solutions (see Table 5). This suggests that the intermolecular correlation is different below and above T_c. It should be remarked here that as shown in Table 5, the "best" fit value of $J_{LH}/(N^{2/3}kT_c)$ becomes small with increasing the arsonium fraction x while the value of (N_A/N) increases with x. These results indicate that the cooperativeness of the phase transition becomes weak with increasing x and that the more the P-salt is diluted with the As-salt, the larger number of molecules is included in a correlation region in which the

transition from the low to the high temperature modification takes place simultaneously.

References

1) P. L. Nordio, Z. G. Soos, and H. M. McConnell, *Ann. Rev. Phys. Chem.*, **17**, 237 (1966).
2) R. M. Metzger, *J. Chem. Phys.*, **57**, 1876 (1972).
3) A. Kosaki, Y. Iida, M. Sorai, H. Suga, and S. Seki, *Bull. Chem. Soc. Jpn.*, **43**, 2280 (1970).
4) A. T. McPhail, G. M. Semeniuk, and D. B. Chesnut, *J. Chem. Soc., A*, **1971**, 2174.
5) M. Konno and Y. Saito, *Acta Crystallogr., Sect. B*, **29**, 2815 (1973).
6) D. S. Acker, R. J. Harder, W. R. Hertler, W. Mahler, L. R. Melby, R. E. Benson, and W. E. Mochel, *J. Am. Chem. Soc.*, **82**, 6408 (1960).
7) D. B. Chesnut and W. D. Phillips, *J. Chem. Phys.*, **35**, 1002 (1961).
8) H. M. McConnell, H. O. Griffith, and D. Pooley, *J. Chem. Phys.*, **36**, 2518 (1962).
9) M. T. Jones and D. B. Chesnut, *J. Chem. Phys.*, **38**, 1311 (1963).
10) Y. Iida, M. Kinoshita, M. Sano, and H. Akamatu, *Bull. Chem. Soc. Jpn.*, **37**, 428 (1964).
11) D. D. Thomas, A. W. Merkl, A. F. Hildebrandt, and H. M. McConnell, *J. Chem. Phys.*, **40**, 2588 (1964).
12) T. D. Buckman, H. O. Griffith, and H. M. McConnell, *J. Chem. Phys.*, **43**, 2907 (1965).
13) I. M. Brown and M. T. Jones, *J. Chem. Phys.*, **51**, 4687 (1969).
14) W. J. Siemons, P. E. Bierstedt, and R. G. Kepler, *J. Chem. Phys.*, **39**, 3523 (1963).
15) Y. Iida, *J. Phys. Soc. Jpn.*, **30**, 583 (1971).
16) D. Zosel, H. Ritschel, and H. Hänsel, *Z. Phys. Chem. (Leipzig)*, **250**, 367 (1972).
17) E. Müller, H. Ritschel, and H. Hänsel, *Z. Phys. Chem. (Leipzig)*, **251**, 152, 163 (1972).
18) H. Ritschel and H. Eichler, *Z. Phys. Chem. (Leipzig)*, **255**, 629 (1974).
19) R. G. Kepler, *J. Chem. Phys.*, **39**, 3528 (1963).
20) A. W. Merkl, R. C. Hughes, L. J. Berliner, and H. M. McConnell, *J. Chem. Phys.*, **43**, 953 (1965).
21) R. J. Goll and W. D. Phillips, *J. Chem. Phys.*, **43**, 1076 (1965).
22) H. M. McConnell and R. Lynden-Bell, *J. Chem. Phys.*, **36**, 2393 (1962); *ibid.*, **37**, 794 (1962).
23) D. B. Chesnut, *J. Chem. Phys.*, **40**, 405 (1964).
24) H. M. McConnell and Z. Soos, *J. Chem. Phys.*, **40**, 586 (1964).
25) D. B. Chesnut, *J. Chem. Phys.*, **41**, 472 (1964).
26) Y. Iida, *Bull. Chem. Soc. Jpn.*, **43**, 578, 3685 (1970); *ibid.*, **44**, 3344 (1971).
27) L. R. Melby, R. J. Harder, W. R. Herlter, W. Mahler, R. E. Benson, and W. E. Mochel, *J. Am. Chem. Soc.*, **84**, 3374 (1962).
28) H. Suga and S. Seki, *Bull. Chem. Soc. Jpn.*, **38**, 1000 (1965).
29) T. Matsuo, H. Suga, and S. Seki, *J. Phys. Soc. Jpn.*, **30**, 785 (1971).
30) Iida[26] has reported the spin entropy of 0.55 J K^{-1} mol^{-1}. But this is underestimated because he has used only the first term of the right-hand side of Eq. 4.
31) It is interesting to note here that there still exists an example in which the conduction electrons considerably contribute to the entropy of a system. According to Epstein *et al.*[32] the Fermi temperature of *N*-methylphenazinium tetracyanoquinodimethanide is low enough to give an appreciable contribution of the conduction electrons to the entropy of the system even at a room temperature.
32) A. J. Epstein, S. Etemand, A. F. Garito, and A. J. Heeger, *Phys. Rev., B*, **5**, 952 (1972).
33) A. Kosaki, M. Sorai, H. Suga, and S. Seki, *Bull. Chem. Soc. Jpn.*, **50**, 810 (1977).
34) J. Frenkel, "Kinetic Theory of Liquids," Oxford University Press, London (1947), Chap. VII.

Calorimetric Study of the Glassy State. XIII.* Thermodynamic Properties of Normal and Deuterated Orthoboric Acid Crystals

Masaharu OGUNI, Takasuke MATSUO, Hiroshi SUGA, and Syûzô SEKI
Department of Chemistry, Faculty of Science, Osaka University, Toyonaka, Osaka 560
(Received November 18, 1976)

Thermal properties of normal and deuterated orthoboric acids were studied through the measurements of heat capacity in the temperature range from 13 to 370 K by using an adiabatic calorimeter and differential thermal analysis curves above room temperature. For both crystals, the heat capacity anomaly was found around 290 K in the heat capacity values dependent upon the thermal history of the specimen; *i.e.*, the endothermic or exothermic enthalpy relaxation was observed in this temperature range. This behavior is of characteristic to the glass transition and is considered to be ascribed to the freezing-in phenomenon of the motion of rearrangement of the protons in hydrogen bondings. The enthalpy relaxation curves were analyzed with the exponential law and the characteristic time constant toward the equilibrium state was longer for enthalpy-excessive side than for enthalpy-deficient side. The glass transition temperature at which the endothermic relaxation time becomes 1 ks is 296.6 K for normal orthoboric acid and 298.2 K for deuterated orthoboric acid, respectively. The activation enthalpies were estimated to be 88 ± 5 and 91 ± 5 kJ mol^{-1} for the endothermic processes of normal and deuterated orthoboric acid, respectively. The melting points of normal and deuterated orthoboric acids were determined from the differential thermal analysis curves to be 169.9 and 167.4 °C, respectively.

Orthoboric acid crystal is a typical example of the hydrogen-bonded systems with two-dimensional structure being essentially a molecular arrangement of planar $B(OH)_3$ (see Fig. 10). Each hydroxyl group is linked by hydrogen bonds to two others belonging to different molecules and forms a six-membered hydrogen bonded ring. The hydrogen atom is situated on the O–O line, occupying the ordered position at room temperature.[1] The ring is arranged in a pattern of triangular lattice in two dimension and the crystal is built up by the superposition of these layers. There have been discussions about the position of the hydrogen atoms since the first determination of B and O positions by Zachariasen[2] in an early X-ray study. Electron diffraction study of the thin crystal by Cowley[3] showed that the hydrogen was displaced off the O–O bonds and that the hydrogen positions are disordered. The nonlinear O–H···O hydrogen model was also favored by Kume and Kakiuchi[4] in their NMR study, which was criticized in a subsequent recalculation by Ibers and Holm.[5] In the reinvestigation of the structure by X-ray method, Zachariasen[6] found the hydrogen atom situated on the O–O line. The neutron diffraction experiment,[1] designed specifically for the determination of the hydrogen position, seemed to have settled the discussion conclusively. In both X-ray and neutron diffraction studies it was also found that the layers are not strictly planar, but some tilts occur between the individually coplanar molecules.

However, two questions remain still open about the behavior of the hydrogen atom in the crystal. First, is the hydrogen position completely ordered at room temperature? The hydrogen bond length in orthoric acid is comparable with that in ice I_h for which existence of the hydrogen-positional disorder is well-established. Therefore, one may expect *partial* disordering of the hydrogen position in a double minimum potential of the hydrogen bonding in the present crystal, although complete disordering is ruled out by the neutron diffraction study.[1] If such a disorder was actually observed, one would find a very typical order-disorder transition in two dimensional system. Another question is how rapid would be the change of the hydrogen position in such an order-disorder system. Our experience with ice I_h,[7] heavy ice I_h,[8] $SnCl_2\cdot2H_2O$[9] and $SnCl_2\cdot2D_2O$[9] showed that the positional change of hydrogen atoms can be extremely slow in spite of the small mass of the atom at low temperature. Its relaxation time can be of the order of one minute or one hour, or for that matter, may be one year or one century. In such cases, we can observe the relaxation process calorimetrically as a glass transition phenomenon at some appropriate temperature.

In view of the current interest in the molecular relaxational phenomena in relatively simple substances, we have investigated orthoboric acid and its deuterated analog by low temperature heat capacity measurements, and in fact found heat capacity anomalies that possess every characteristic of a glass transition. Based on this observation of a glass transition, which implied the existence of partial disordering of hydrogen position, we performed differential thermal analysis (DTA) of the substance in the temperature region higher than the glass transition, for the purpose of investigating the behavior due to development of the hydrogen atom disordering with increasing temperature. This paper reports the experimental facts and their interpretation briefly.

Experimental

Preparation of the Material and the Heat Capacity Measurement. The heat capacity of normal (undeuterated) orthoboric acid crystal was measured for two different samples. The first sample, "Suprapur" reagent from Merck Co., was vacuum-dried for an hour at 20 °C in order to remove excess water if

* A part of this paper was presented on The Fourth International Conference of Chemical Thermodynamics, Montpéllier, 1975.

For part XII, see O. Haida, H. Suga, and S. Seki, *J. Chem. Thermodyn.*, in press.

any, and its heat capacity was measured in the temperature region between 13 and 315 K. The second was obtained by recrystallizing the extrapure grade reagent, purchased from Wako Pure Chemical Co., from the aqueous solution, and was investigated in the temperature region from 250 to 370 K. The deuterated orthoboric acid sample was obtained by recrystallization of B_2O_3 from heavy water solution (99.75%). The B_2O_3 crystals were prepared by complete dehydration of the normal orthoboric acid (purchased from Yamanaka Chemical Co.) by heating *in vacuo* to 200 °C for three days. The deuterium exchange ratio of the obtained crystals was analysed to be 99.5% by NMR method. The sample weight was 40.472, 48.586, and 53.495 g for the first and second samples of normal orthoboric acid and the deuterated orthoboric acid sample, respectively.

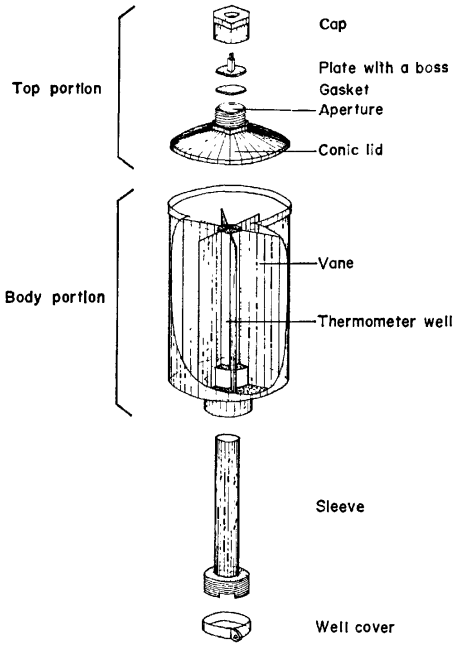

Fig. 1. A sectional drawing of the new calorimeter cell.

Calorimetric Apparatus. The calorimetric apparatus which was described before,[10] was so modified as to be capable of measurement up to 140 °C. Namely, the bronze adiabatic shields were replaced by those made of copper. This improved the temperature uniformity of the shields and hence the adiabatic regulation. The calorimeter cell, formerly sealed with low-melting solder, was replaced by a new cell of the Trowbridge and Westrum-type (marked with W-22) construction.[11] A sectional drawing of the cell pieces is given in Fig. 1. The body portion with a well and six vanes and the sleeve for a platinum thermometer were made of copper for achievement of rapid thermal equilibration, while the top portion, consisting of the cap, plate, and conic lid with an aperture, of stainless steel. The sleeve was settled on the body by being screwed in the well. High-melting solder was used for the seal between the lid and the body. The vacuum-tight closure was achieved by an annealed gold gasket forced against a circular knife edge of aperture. Plate with a boss served for preventing the gasket from turning in the closure by holding the boss. The typical equilibration time of the cell after turning off the calorimeter heater was around 13 min at room temperature. The second sample of the normal orthoboric acid and the deuterated orthoboric acid sample were measured with the improved apparatus. The inaccuracy of the measurement is estimated to be 1% at liquid hydrogen temperature and smaller than 0.2% above 40 K.

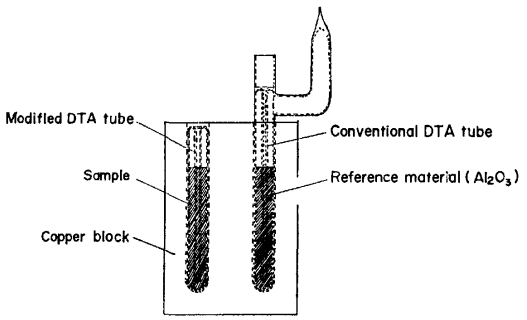

Fig. 2. Conventional and modified DTA tubes.

Differential Thermal Analysis. DTA studies of normal and deuterated orthoboric acids were carried out in the temperature region above the glass transition point. DTA apparatus previously reported[12] was modified for coping with the decomposition of the sample to metaboric acid and water vapor. For this purpose the sample tube as shown in Fig. 2 was used. The modified sample tube is smaller than the previous one. This modification decreased the dead volume in the tube and enabled the whole body of the sealed tube to be entirely embedded in the well of the copper block of the DTA apparatus. Thus any cold spot that might have caused trouble with the original sample tube was successfully avoided.

Results and Discussion

Melting. Melting of normal orthoboric acid has been reported by several authors. Carnelley[13] reported the melting at 184—186 °C from the heat capacity measurement and visual observation, and Stackelberg *et al.*[14] at 170 °C by visual observation under 4 atm pressure. Kracek *et al.*[15] obtained 170.9±0.2 °C from the solubility measurement. Benrath,[16] on the other hand, obtained 181 °C using the similar method. We performed the first observation for the melting of deuterated orthoboric acid, in addition to that of normal orthoboric acid. Figures 3 and 4 show melting curves in DTA for the normal and deuterated samples, respectively, obtained in the present study. The melting points were 169.9 and 167.4 °C for the respective substances, and the crystallization took place practically at the same temperature as the melting. These curves were reproduced repeatedly without significant changes.

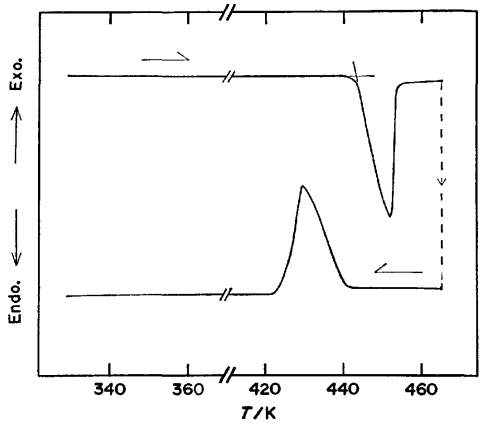

Fig. 3. DTA curves of normal orthoboric acid.

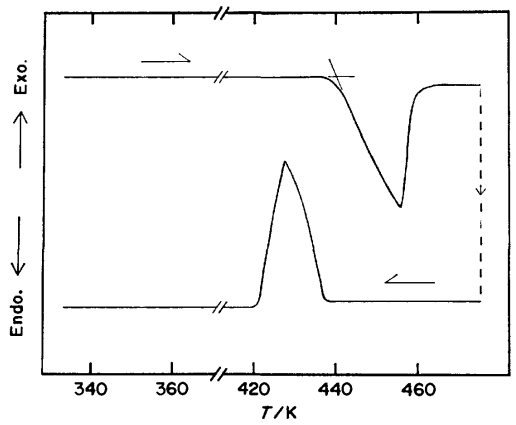

Fig. 4. DTA curves of deuterated orthoboric acid.

The melting points for normal orthoboric acid determined by Stackelberg *et al.* and Kracek *et al.* are in fairly good agreement with the present data, though their determination was performed through visual observation. The melting point of deuterated orthoboric acid is lower by 2.5 K than that of normal acid.

Heat Capacity. The heat capacity values are tabulated in Tables 1 and 2 for normal and deuterated orthoboric acid crystals, respectively. They are also shown in Fig. 5 as a function of temperature together with data (△) of Johnston and Kerr.[17] Johnston and Kerr's values are smaller than ours, the discrepancy increasing with the increasing temperature. This tendency may be attributed to a partial dehydration of their sample which might have happened during drying over a period of three days at 70 °C *in vacuo* in their

Table 1. Experimental molar heat capacity of normal orthoboric acid

T_{av}/K	C_p/J K^{-1} mol^{-1}	T_{av}/K	C_p/J K^{-1} mol^{-1}	T_{av}/K	C_p/J K^{-1} mol^{-1}	T_{av}/K	C_p/J K^{-1} mol^{-1}	T_{av}/K	C_p/J K^{-1} mol^{-1}
		58.29	22.35	165.44	51.47	300.69	86.73	291.95	80.76
First		59.37	22.82	167.71	51.96	302.72	87.69	294.17	82.84
measurement		60.48	23.31	170.03	52.48	304.72	88.23	296.27	84.79
		61.59	23.79	172.33	52.98	306.96	88.64	298.34	86.52
11.86	0.866	62.74	24.27	174.62	53.52	309.37	89.20	300.38	87.29
12.60	1.030	63.93	24.75	176.88	54.04	311.99	89.82	304.41	87.59
13.53	1.250	65.17	25.25	179.13	54.50			306.43	88.63
14.33	1.431	66.44	25.72	181.45	55.07	(annealed)		308.43	89.40
15.16	1.672	67.71	26.19	183.67	55.58			310.42	89.52
16.01	1.922	68.98	26.66	185.99	56.03	259.60	73.32	312.40	90.30
16.80	2.165	70.25	27.11	188.34	56.60	262.38	74.06		
17.60	2.432	71.52	27.57	190.82	57.20	264.94	74.59	(annealed)	
18.38	2.724	72.80	28.01	193.40	57.77	267.48	75.14		
19.16	3.018	74.09	28.45	195.96	58.38	270.01	75.78	262.13	73.95
19.93	3.318	75.36	28.90	198.50	58.97	272.52	76.33	264.46	74.50
20.70	3.646	76.63	29.32	201.02	59.53	275.01	77.05	266.78	75.05
21.50	3.993	77.91	29.76	203.60	60.12	277.58	77.65	269.11	75.57
22.32	4.346	79.16	30.18	206.24	60.79	280.19	79.04	271.41	76.09
23.13	4.746	80.43	30.59	208.86	61.40	282.74	80.24	273.70	76.73
20.86	3.741	75.10	28.79	211.45	61.98	285.21	81.71	276.02	77.27
21.71	4.091	77.62	29.64	214.08	62.57	287.64	83.36	278.32	77.94
22.67	4.546	79.79	30.37	216.69	63.18	290.05	84.88	280.57	78.81
23.73	4.997	81.90	31.07	219.23	63.75	292.43	86.10	282.94	80.31
24.72	5.487	83.97	31.73	221.83	64.39	294.79	86.86	285.42	81.95
25.65	5.923	85.99	32.37	224.50	65.02	297.13	87.10	287.81	83.57
26.55	6.393	88.08	33.00	227.14	65.66	299.46	87.41	290.13	84.94
27.47	6.833	90.22	33.58	229.76	66.29	301.80	87.46	292.41	86.08
28.35	7.281	92.33	34.15	232.37	66.93	304.12	87.97	294.69	86.54
29.19	7.727	94.51	34.73	235.00	67.53	306.43	88.38	296.97	86.86
30.00	8.179	96.76	35.31	237.65	68.18	308.74	88.96	299.24	87.26
30.81	8.595	98.98	35.89	240.29	68.85	311.03	89.60	301.57	87.44
31.66	9.069	101.16	36.43	243.86	69.53			303.95	87.98
32.53	9.520	103.32	36.93	246.44	70.18	Second		306.30	88.39
33.38	9.998	105.44	37.58	249.00	70.77	measurement		308.65	89.06
34.19	10.43	107.55	37.91	250.87	71.27			312.89	90.09
35.02	10.88	109.66	38.54	253.70	71.89	(quenched)		315.44	90.78
35.88	11.35	111.84	39.07	256.32	72.54			318.21	91.50
36.76	11.83	114.11	39.62	259.02	73.19	241.09	68.99	320.96	92.41
37.65	12.32	116.34	40.15			243.50	69.45	323.69	92.95
38.56	12.77	118.55	40.69	(quenched)		245.90	70.05	326.40	93.76
39.47	13.25	120.73	41.21			248.29	70.62	329.10	94.50
40.38	13.72	122.98	41.73	260.38	73.45	250.67	71.14	331.78	95.25
41.27	14.19	125.22	42.23	262.96	74.02	253.02	71.72	334.44	96.07
42.12	14.60	127.43	42.78	265.30	74.59	255.36	72.28	337.09	96.60
42.95	15.05	129.62	43.28	267.43	74.97	257.68	72.84	339.72	97.40
43.76	15.46	131.79	43.78	269.54	75.61	258.04	72.86	342.42	98.20
44.54	15.84	133.94	44.29	271.65	76.14	260.34	73.47	345.21	98.95
45.37	16.26	136.12	44.78	273.76	76.66	262.64	74.02	347.97	99.72
46.28	16.73	138.34	45.28	275.86	77.15	264.93	74.60	350.82	100.55
47.26	17.15	140.53	45.78	277.96	77.60	267.21	75.09	353.74	101.26
48.09	17.62	142.77	46.28	280.06	78.03	269.48	75.65	356.64	102.07
49.07	18.12	145.05	46.81	282.15	78.50	271.74	76.54	359.53	102.86
50.08	18.59	147.30	47.31	284.26	78.94	274.00	76.76	362.40	103.69
51.10	19.08	149.53	47.88	286.37	79.50	276.27	77.13	365.25	104.40
52.12	19.56	151.81	48.33	288.47	79.91	278.53	77.67	368.07	105.15
53.14	20.02	154.13	48.87	290.56	80.41	280.79	78.35	370.88	105.89
54.14	20.49	156.40	49.38	292.62	80.89	283.05	78.71	373.68	106.68
55.16	20.95	158.71	49.91	294.66	81.78	285.31	79.33		
56.20	20.41	160.97	50.43	296.64	83.25	287.55	79.78		
57.24	21.88	163.21	50.89	298.65	85.29	289.76	80.47		

TABLE 2. EXPERIMENTAL MOLAR HEAT CAPACITY OF DEUTERATED ORTHOBORIC ACID

T_{av}/K	C_p/J K^{-1} mol^{-1}	T_{av}/K	C_p/J K^{-1} mol^{-1}	T_{av}/K	C_p/J K^{-1} mol^{-1}	T_{av}/K	C_p/J K^{-1} mol^{-1}	T_{av}/K	C_p/J K^{-1} mol^{-1}
12.66	1.044	82.35	31.93	178.62	60.02	325.87	103.95	304.15	98.26
15.48	1.828	84.30	32.60	180.95	60.68	328.62	104.76	306.44	98.84
17.10	2.366	86.20	33.19	183.26	61.49	331.44	105.63	308.73	99.25
18.54	2.900	88.16	33.82	185.55	62.19	334.25	106.36	311.02	99.52
19.89	3.445	90.18	34.42	187.83	62.52	337.03	107.13	313.30	100.27
21.15	3.976	92.17	35.04	190.10	63.30	339.79	108.11	315.57	100.98
22.25	4.494	94.11	35.63	192.33	64.11	342.54	108.66		
23.42	5.032	96.03	36.20	194.54	64.66	345.27	109.48	(annealed)	
24.67	5.643	97.97	36.79	182.89	61.39	347.98	110.34		
25.87	6.246	99.96	37.41	185.09	61.80	350.67	110.99	251.56	80.69
27.15	6.902	101.94	37.97	187.16	62.53	353.33	111.86	253.79	81.25
28.56	7.636	103.95	38.52	189.32	63.15	356.06	112.55	256.01	81.77
30.07	8.453	106.08	39.17	191.56	63.82	358.87	113.42	258.21	82.44
31.55	9.252	108.27	39.79	193.78	64.44	361.67	114.13	260.40	83.02
32.96	10.03	110.46	40.42	195.98	65.07	364.45	114.92	262.58	83.72
34.34	10.80	112.66	41.04	198.20	65.72	367.20	115.56	264.84	84.11
35.67	11.53	114.84	41.67	200.40	66.35	369.95	116.38	267.11	84.79
36.97	12.25	116.99	42.29	202.64	67.01	372.68	117.19	269.38	85.40
38.29	12.96	119.13	42.85	204.96	67.67			271.73	85.90
39.65	13.69	121.35	43.52	207.27	68.26	(quenched)		274.07	86.63
41.01	14.41	122.17	43.75	209.60	69.00			276.39	87.18
42.38	15.15	124.34	44.33	211.96	69.72	251.24	80.53	278.70	88.13
43.76	15.87	126.49	45.01	214.30	70.29	253.56	81.27	281.00	88.41
45.13	16.56	128.74	45.61	216.61	70.94	255.84	81.80	283.26	89.76
46.49	17.27	131.08	46.31	218.91	71.64	258.07	82.46	285.35	91.72
47.85	17.96	133.40	46.93	221.18	72.25	260.28	82.99	287.31	92.92
49.27	18.67	135.69	47.61	223.45	72.90	262.47	83.59	289.27	94.28
50.71	19.37	137.93	48.27	225.68	73.53	264.67	84.11	291.23	95.12
52.41	20.19	140.16	48.85	227.90	74.14	266.86	84.75	293.18	96.03
54.37	21.11	142.38	49.51	230.11	74.78	269.03	85.32	295.12	96.40
56.23	21.96	144.56	50.16	232.36	75.50	271.20	85.94	297.05	96.64
58.04	22.78	146.72	50.77	234.63	76.09	273.37	86.46	298.97	97.06
59.80	23.56	148.97	51.42	236.89	76.70	275.52	87.16	300.90	97.05
61.58	24.31	151.32	52.10	239.16	77.23	277.67	88.22	302.83	97.49
63.39	25.04	153.64	52.81	241.41	77.90	279.83	87.59	304.75	98.10
65.18	25.78	155.92	53.45	243.71	78.60	281.98	88.49	307.28	98.71
66.96	26.45	158.19	54.11	246.10	79.22	284.14	89.15	309.24	99.18
68.74	27.17	160.48	54.76	248.47	79.78	286.29	89.66	311.34	99.82
70.51	27.80	162.79	55.46	250.85	80.53	288.43	90.36	313.61	100.40
72.28	28.47	165.08	56.12			290.56	90.79		
74.06	29.11	167.35	56.76	313.43	100.19	292.66	91.40		
75.88	29.72	169.60	57.39	315.61	100.97	294.72	91.81		
77.72	30.37	171.82	58.07	317.92	101.56	296.94	93.83		
79.61	31.02	173.98	58.69	320.50	102.45	299.38	96.11		
80.37	31.29	176.25	59.25	323.20	103.24	301.79	97.42		

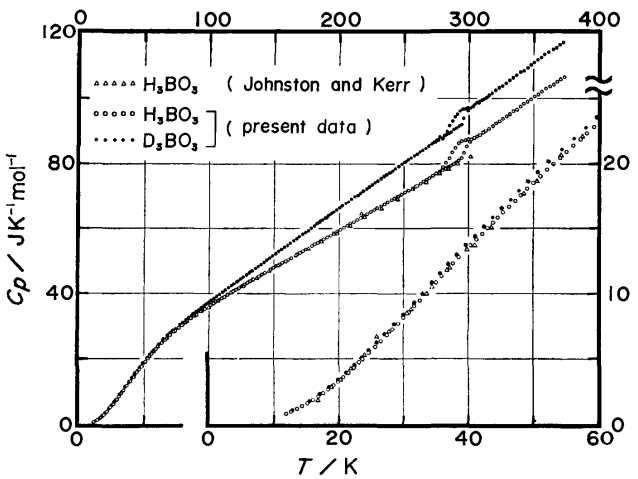

Fig. 5. Heat capacity of normal and deuterated orthoboric acids.

sample preparation. Johnston and Kerr stated that the heat capacity curve exhibits a double inflection at about 40 K. The anomaly is, however, scattering of their data. The present data, being more precise, preclude presence of any anomaly in this temperature region. Johnston and Kerr also mentioned the appearance of a spread-out hump, from about 20 to 150 K, which they interpreted as an indication of development of the hydrogen position disorder. However, this interpretation is not supported by recent evidence because the hydrogen atoms occupy almost completely their ordered positions even at room temperature, as was evidenced in a neutron diffraction study. It is likely that an unusual temperature dependence of the curve, resembling a spread-out hump, has the lattice-vibrational origin indicative of the two-dimensional feature of the crystal structure. Temperature dependence of the heat capacity of the deuterated orthoboric acid is similar to that of the normal acid, except that the deuterated compound has the larger heat capacity in the whole temperature range studied. Such an isotope effect is expected in terms of the increased mass by deuteration.

In contrast to the tolerably good agreement between the present data and those by Johnston and Kerr at the lower temperatures, there is a remarkable difference around 290 K. The present data exhibit occurrence of a step-like anomaly amounting to 3—4% of the total heat capacity. A similar anomaly is observed for the deuterat-

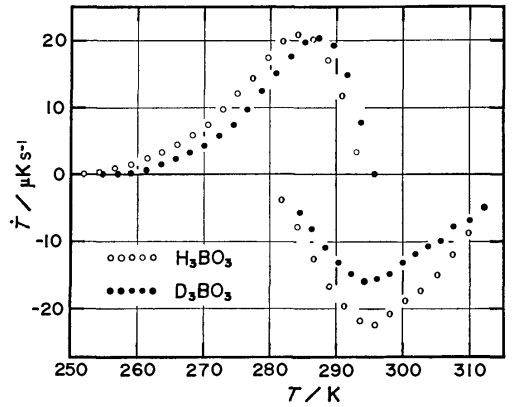

Fig. 6. Spontaneous temperature drift rate of the calorimeter cell for two different thermal treatments.

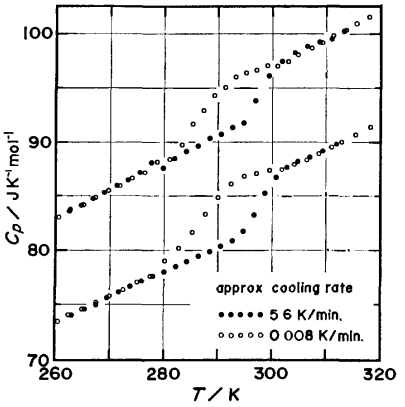

Fig. 7. Dependence of the heat capacity on the cooling rate around 290 K.

ed compound. A hysteretic behavior was also noted for both compounds at the same temperature. Thermal equilibration of the calorimeter was very sluggish in the temperature region between 260 and 310 K and an exothermic or endothermic effect was observed depending on the cooling rate and the thermal history of the sample. The heat capacity measurement was therefore performed in the following procedure. Prior to each measurement, the sample was first equilibrated at 315 K (at which temperature the thermal equilibrium was attained rapidly) and then cooled below 250 K at a respective cooling rate indicated in Fig. 7. A series of measurements was started at 250 K at which the temperature drift of the cell was normal within our experimental error. The temperature drift was then followed step by step up to 320 K. Each step of the measurement consisted of first heating the calorimeter by 2 K and then following its temperature drift. The energy input took 15 min and the drift measurement 40—60 min. Figure 6 illustrates the temperature drift rate of the calorimeter at 25 min after the calorimeter heater was switched off. If cooled rapidly the sample gave out heat in earlier stage of the subsequent warming, and then tended to absorb heat as indicated by the negative temperature drift at the higher temperature, whereas, if cooled slowly, it exhibited only negative temperature drift in the subsequent heat capacity measurement. The temperature drift approached normal behavior gradually above 300 K. This thermal behavior means that the anomaly in this region may be ascribed to a glass transition.[18] The heat capacity value was determined by employing the same method as used for $SnCl_2 \cdot 2H_2O$ and $SnCl_2 \cdot 2D_2O$.[9] The operational definition of the heat capacity involves an arbitrariness as to how the contribution from the strongly temperature-dependent relaxational degree of freedom is taken into account. The initial or final temperatures taken in the case of the exothermic drifts were calculated by extrapolating them to the mid-point of the heating period and consequently the contribution is excluded from the heat capacity, while in the endothermic case the temperatures at 40 min after the heating-off were employed as the temperatures for the heat capacity determination and therefore the heat capacities calculated involve the contribution deficiently or excessively compared with those in the equilibrium states. The heat capacity curve is illustrated in Fig. 7 in the temperature region from 260 to 320 K. The curve exhibits a clearly different behavior in the region depending on the cooling rate of the sample, *i.e.* the heat capacity is larger for the annealed sample than for the quenched one. This behavior can be also regarded as a general characteristic of a glass transition. The step-like increase around the transition point discloses the amount of configurational contribution to the heat capacity. The jump, ΔC_p, at 290 K was estimated by extrapolation to be 3.58 J K^{-1} mol^{-1} and 2.96 J K^{-1} mol^{-1} for the normal and deuterated orthoboric acids, respectively. It should be added that the behavior in the transition region was the same for the first and the second samples of normal orthoboric acid. This confirms that the glass transition is an intrinsic property of the substance.

Tables 3 and 4 give the thermodynamic functions derived from the smoothed heat capacity on the assumption that it jumps stepwise at 290 K. The heat capacity between 290 and 310 K where the annealing effect is prominent was estimated by extrapolation from above 310 K.

Kinetic Property of the Glass Transition. The exothermic and endothermic temperature drifts described above were analysed on the assumption that the

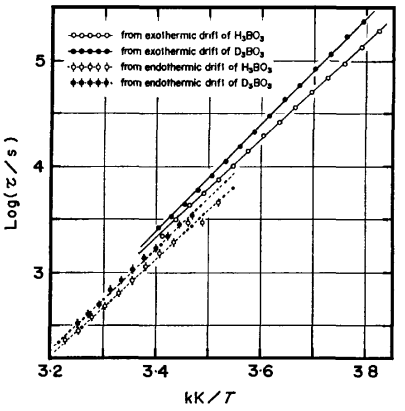

Fig. 8. Arrhenius plots of the characteristic times of exothermic and endothermic enthalpy relaxation drifts for normal and deuterated orthoboric acids.

Table 3. Thermodynamic functions of normal orthoboric acid

T/K	$C_p°$/J K^{-1} mol^{-1}	$S°-S_0°$[a)]/J K^{-1} mol^{-1}	$[H°-H_0°]/T$/J K^{-1} mol^{-1}
10	(0.54)	(0.185)	(0.138)
20	3.35	1.274	0.933
30	8.16	3.492	2.498
40	13.53	6.573	4.583
50	18.55	10.14	6.881
60	23.08	13.93	9.210
70	27.01	17.79	11.48
80	30.43	21.63	13.64
90	33.50	25.39	15.68
100	36.17	29.06	17.60
110	38.60	32.63	19.40
120	41.01	36.09	21.10
130	43.37	39.46	22.72
140	45.66	42.76	24.28
150	47.93	45.99	25.78
160	50.19	49.16	27.24
170	52.44	52.27	28.65
180	54.71	55.33	30.04
190	57.01	58.35	31.40
200	59.30	61.33	32.73
210	61.64	64.28	34.05
220	63.96	67.20	35.36
230	66.33	70.10	36.66
240	68.70	72.97	37.94
250	71.02	75.82	39.22
260	73.36	78.65	40.49
270	75.73	81.46	41.75
280	78.00	84.26	43.00
290	80.24	87.04	44.25
290	83.82	87.04	44.25
300	86.56	89.92	45.61
310	89.30	92.81	46.98
320	92.01	95.69	48.34
330	94.73	98.56	49.71
340	97.48	101.4	51.07
350	100.3	104.3	52.44
360	103.0	107.2	53.81
370	105.7	110.0	55.17
273.15	76.47	82.34	42.14
298.15	86.06	89.39	45.36
373.15	106.5	110.9	55.60

These thermodynamic functions were derived by assuming that the heat capacity jumps stepwise at 290 K. a) $S_0°$ is estimated to be 0.56 J K^{-1} mol^{-1} from molecular field approximation using heat capacity jump at 290 K.

Table 4. Thermodynamic functions of deuterated orthoboric acid

T/K	$C_p°$/J K^{-1} mol^{-1}	$S°-S_0°$[a)]/J K^{-1} mol^{-1}	$[H°-H_0°]/T$/J K^{-1} mol^{-1}
10	(0.54)	(0.184)	(0.138)
20	3.49	1.311	0.964
30	8.43	3.617	2.593
40	13.88	6.794	4.738
50	19.06	10.46	7.092
60	23.65	14.35	9.476
70	27.60	18.29	11.79
80	31.16	22.22	13.99
90	34.39	26.08	16.08
100	37.42	29.86	18.07
110	40.31	33.56	19.96
120	43.14	37.19	21.77
130	46.00	40.75	23.52
140	48.85	44.27	25.23
150	51.71	47.74	26.90
160	54.65	51.17	28.55
170	57.52	54.57	30.17
180	60.45	57.94	31.77
190	63.37	61.28	33.35
200	66.26	64.61	34.93
210	69.13	67.91	36.49
220	71.95	71.19	38.03
230	74.76	74.45	39.57
240	77.56	77.69	41.10
250	80.29	80.92	42.61
260	82.92	84.12	44.11
270	85.60	87.30	45.60
280	88.19	90.46	47.07
290	90.71	93.59	48.53
290	93.67	93.59	48.53
300	96.46	96.82	50.08
310	99.34	100.0	51.62
320	102.3	103.2	53.16
330	105.2	106.4	54.69
340	108.1	109.6	56.22
350	110.9	112.8	57.74
360	113.7	115.9	59.26
370	116.4	119.1	60.77
273.15	86.41	88.29	46.06
298.15	95.92	96.65	49.80
373.15	117.3	120.1	61.24

These thermodynamic functions were derived by assuming that the heat capacity jumps stepwise at 290 K. a) $S_0°$ is estimated to be 0.41 J K^{-1} mol^{-1} from molecular field approximation using heat capacity jump at 290 K.

enthalpy relaxation toward the equilibrium state follows an exponential law with a single relaxation time τ and they (*i.e.* exothermic and endothermic effects) were treated separately. The characteristic time for the former (*i.e.* exothermic) case was obtained by employing the evaluation method already explained in detail in the case of $SnCl_2 \cdot 2H_2O$ and $SnCl_2 \cdot 2D_2O$.[9] For the latter (*i.e.* endothermic) drift curves the exponential function fitted the experimental data within the imprecision of the temperature measurement, suggesting the validity of above assumption. The exothermic and endothermic effects resulted in two different straight lines as shown in Fig. 8, where the solid and dotted lines represent respectively the least square fits of the relaxation times derived from the exothermic and endothermic drifts. The difference means that the approach to the thermal equilibrium is governed by different characteristic times depending upon whether the equilibrium state is approached from the enthalpy-excessive side or from the enthalpy-deficient side. A similar behavior of the relaxation time was observed in $SnCl_2 \cdot 2H_2O$ and $SnCl_2 \cdot 2D_2O$. The Arrhenius plot of the relaxation

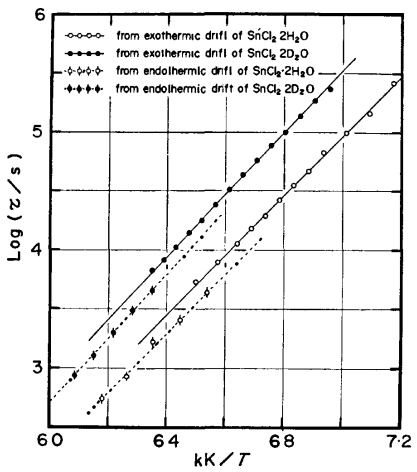

Fig. 9. Arrhenius plots of the characteristic times of exothermic and endothermic enthalpy relaxation drifts for $SnCl_2 \cdot 2H_2O$ and $SnCl_2 \cdot 2D_2O$.

time is shown in Fig. 9 for these compounds, where the relaxation times for the heat-absorption and heat-evolution processes follow different straight lines.

It should be noted that the characteristic time at a fixed temperature is longer for the exothermic process (*i.e.* on the enthalpy-excessive side) than for the endothermic process (*i.e.* on the enthalpy-deficient side) in these hydrogen-bonded systems. It should be added that the relaxation time was derived under the adiabatic condition. Thus, the temperature of the crystal changed as the relaxation proceeded. This means that the run of the adiabatic drift measurement corresponds to a small but finite temperature interval on the Arrhenius plot. This also means that the apparent final temperature to which the proton configuration tends is not constant but depends on the extent to which the relaxation has proceeded. These two aspects of the non-isothermal character of the drift measurement were not considered in the analysis of the relaxation effects in $SnCl_2 \cdot 2H_2O$ and $SnCl_2 \cdot 2D_2O$. Correction for these effects was found to decrease and increase the derived relaxation time typically by 0.5% for the exothermic and endothermic runs, respectively, and thus safely neglected. A relevant observation was reported by Davies and Jones[19] for glass transition in super-cooled liquids. They followed both the isothermal volume-relaxational change of glucose and the enthalpy-relaxational change of glycerol in the respective transition regions. According to their report, the characteristic time was longer on the volume-deficient (or enthalpy-deficient) side than on the volume-excessive (or enthalpy-excessive) side of the equilibrium state, and there occurred significant departure from the exponential form of the relaxation curve when the displacement from the equilibrium state was large. Thus the relaxational property of the present substance deviates from the idealized behavior, *i.e.* recovery of the equilibrium with a constant relaxation time independent of the sense and amount of the departure from the equilibrium. Furthermore, the deviation from the ideal relaxational behavior is in the direction opposite to Davies and Jones' observation on the super-cooled liquids. They explained their observation by arguing that the structure of the substance is looser in the volume-excessive state than in the volume-deficient state. Consequently the molecules are expected to be more mobile in the former non-equilibrium state, resulting in a smaller relaxation time. This is certainly a plausible explanation for the glassy liquids. In contrast, our present observation is difficult to understand in this intuitively agreeable argument. There exists, however, a peculiar character of the present hydrogen-boned system that might explain the difference qualitatively. In the glassy state of boric acid the hydrogen position has the long-range order, which means that if one particular site is occupied by a hydrogen atom an equivalent site in a distant unit cell has also non-zero probability of occupation by another hydrogen atom. When a disordered hydrogen atom tries to settle into a low energy site in the exothermic relaxation, it has a very limited choice as to the site it can occupy because the low energy site is dictated by the long-range order. In contrast, a molecule in a super-cooled liquid can find a local low energy conformation determined by its neighboring molecules. Thus, there is a formal probabilistic difference in addition to the structural and chemical differences between the long-ranged glassy state (glassy crystals) and the ordinary glassy state (glassy liquid). At present, however, we cannot find a convincing argument that relates the above mentioned peculiar features of the orthoboric acid with its observed relaxational property.

Table 5. Calorimetric quantities characterising the glass transition in H_3BO_3 and D_3BO_3 crystals

	T_g [a] / K	ΔC_p [b] / J K^{-1} mol^{-1}	σ [c]	$(H_a)_{exo}$ / kJ mol^{-1}	$(H_a)_{endo}$ / kJ mol^{-1}
H_3BO_3	296.6	3.58	0.94	89±5	88±5
D_3BO_3	298.2	2.96	0.96	97±5	91±5

a) The temperature at which the endothermic relaxation time becomes 1 ks. b) The heat capacity jump at 290 K in the transition region. c) The order parameter at 290 K estimated from the molecular field approximation.

The activation enthalpies estimated from the respective Arrhenius plots (Fig. 8) are given in Table 5 together with the glass transition points, the heat capacity jumps at 290 K, and the order parameters at 290 K calculated by a mean field approximation method. The values seem to be slighly larger for deuterated orthoboric acid than that for normal acid.

Interpretation of the Frozen-in Freedom. The glass transition in the present substance can be interpreted as the phenomenon originated from the disordered-frozen-in configuration of hydrogen-bonded system. Craven and Sabine[1] assigned uniquely all the atomic positions at room temperature. However the ordering of the atoms, in particular the hydrogen or deuterium atoms, is *not* completely attained in our interpretation. The six-membered oxygen ring, which is assumed to be the individual ordering unit of the hydrogen-bond network, has two permissible arrangements, *i.e.* clockwise and counterclockwise under the extended Bernal-Fowler condition, as is shown in Fig. 10. The interaction

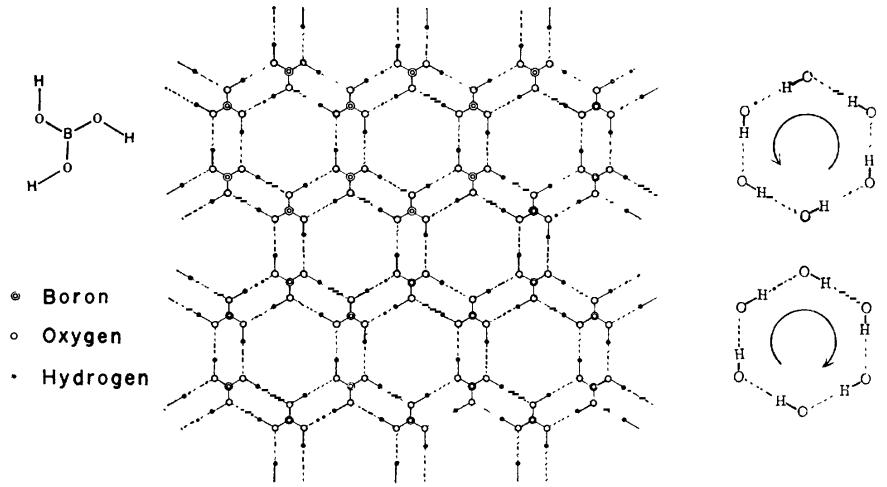

Fig. 10. The schematic atomic arrangement of a single layer in crystalline orthoboric acid and the two arrangements of the hydrogen atoms satisfying the local electric neutrality in the six-membered oxygen ring.

energy among the hydrogen-bonded hexagonal rings stabilizes the ferro-state where all of the hexagonal ring is the same (either all in the clockwise or all in the counterclockwise) arrangement. The entropy of this model is $(R/2)$ ln 2 at the completely disordered state. A mean field approximation can be applied, to a fairly good approximation, at the glass transition in such a system, since the hydrogen position is *almost* completely ordered at room temperature in the transition region. Then the order parameter σ is determined by the following equation at 290 K at which the configurational contribution to heat capacity is estimated:

$$C = \frac{\sigma R\left\{\ln\left(\frac{1+\sigma}{1-\sigma}\right)\right\}^2}{2\left\{\frac{2\sigma}{1-\sigma^2}-\ln\left(\frac{1+\sigma}{1-\sigma}\right)\right\}},$$

where the order parameter σ is given by $\sigma=(2n-N)/N$, n, the number of rearrangement units in the preferred arrangement, N, the number of total arrangement unit. The order parameter estimated at 290 K was *ca.* 0.94 and *ca.* 0.96 for normal and deuterated orthoboric acids, respectively. This degree of estimated ordering is consistent with Craven and Sabine's result[1] on account of the R factor in the neutron diffraction study. This interpretation of the "transition" as a relaxational effect of the hydrogen redistribution process in the crystal is also supported by comparison between the obtained activation energy and the hydrogen bond energy. The activation enthalpy of *ca.* 90 kJ mol^{-1} corresponds to the energy required for simultaneous activation of six hydrogen atoms, and therefore the activation enthalpy per atom amounts to *ca.* 15 kJ mol^{-1}, while the hydrogen bond energy between O-O in medium to long hydrogen bond systems such as ice is known to be 15—25 kJ mol^{-1}. These two values are in good agreement with each other, and thus the above interpretation of the transition would be reasonable provided that the activation process corresponds to the breaking of hydrogen bond.

There are alternative possibilities for the actual motion of the hydrogen atoms in the rearrangement. It is either an O-H librational mode around B-O axis or an O-H stretching-vibrational mode on an O-O bond. Recent NMR studies of inorganic hydrates have shown that a 180° flipping is a typical motion of water in the crystals.[20] If we adopted the former as the relevant mode, the activation enthalpy obtained above should be compared with the potential barrier (of the O-H librational mode) estimated by Durig *et al.*[21] They reported that the infrared absorption band at 808 cm^{-1} was assigned to this mode of vibration and estimated the potential barrier to be 96 kJ mol^{-1}. There is a large difference between this barrier height and the activation enthaply per hydrogen atom. The estimation of the hindering barrier rests entirely upon the assumption of a cosine-type potential function, which is not always a good approximation. In view of the hydrogen bond breaking of the mode discussed above, we may have to consider that the potential curve around the top of the barrier may be flatter than that given by the simple trigonometric function due to the interaction with the adjacent layer. A more reliable and direct estimation would be obtained by proton magnetic relaxation measurements. The relation between these two values will be a subject in the future work.

Deuterium Isotope Effect on a Glass Transition Temperature. In Table 6, the glass transition temperatures are collected for three hydrogen-bonded glassy crystals

Table 6. Glass transition temperature and its deuterium isotope effect for three hydrogen-bonded glassy crystals

	T_g (H) / K	T_g (D) / K	T_g (D) − T_g (H) / K
$H_2(D_2)O$	107.6	126.1	18.5
$SnCl_2 \cdot 2H_2(D_2)O$	159.1	163.7	4.6
$H_3(D_3)BO_3$	296.6	298.2	1.6

The glass transition temperature is defined for ice as temperature at which the exothermic relaxation time becomes an hour, and for $SnCl_2 \cdot 2H_2O$ and H_3BO_3 as the temperature at which the endothermic relaxation time becomes 1 ks.

together with the corresponding data for the respective deuterium compounds. Here the glass transition temperature is defined as the temperature described below the table. Evidently, the isotope effect is larger in the substance with the lower glass transition temperature.

Further Discussion on the Absence of the Phase Transition. The hydrogen-bonding model illustrated in Fig. 10, and the interpretation of the glass transition deduced thereby, have a definite implication on the thermodynamics of the order-disorder system; the molar configurational entropy at infinite temperature is $(R/2)\ln 2$ and the heat capacity is equal to the jump in the observed heat capacity at the glass transition. These two quantities enable us to determine exactly the hypothetical transition temperature of the present hydrogen-bonded system by a statistical triangular Ising model;[22] 378 K for H_3BO_3 and 404 K for D_3BO_3. No phase transition is observed at these temperatures. The estimated transition temperature should be a lower limit because the lattice statistics involved is solved in two-dimensions. On the other hand, the upper limit is given by the molecular field approximation. The transition temperatures predicted by this approximation are 536 K and 587 K for the ordinary and the deuterated orthoboric acids, respectively. These temperatures are higher than the respective melting temperatures. We may conclude that we should have observed the transition if it was not interrupted by the melting. This may also imply that the interaction among the hexagonal rings is three-dimensional in spite of the structural two-dimensionality, because the absence of the phase transition below the fusion means that the hypothesized transition temperature lies much higher than the two-dimensional limit.

References

1) B. M. Craven and T. M. Sabine, *Acta Crystallogr.*, **20**, 214 (1966).
2) W. H. Zachariasen, *Z. Krist.*, **88**, 150 (1934).
3) J. M. Cowley, *Acta Crystallogr.*, **6**, 522 (1953).
4) K. Kume and Y. Kakiuchi, *J. Phys. Soc. Jpn.*, **15**, 1277 (1960).
5) J. A. Ibers and C. H. Holm, *J. Phys. Soc. Jpn.*, **16**, 839 (1961).
6) W. H. Zachariasen, *Acta Crystallogr.*, **7**, 305 (1954).
7) O. Haida, T. Matsuo, H. Suga, and S. Seki, *Proc. Jpn. Acad.*, **48**, 489 (1972); *J. Chem. Thermodyn.*, **6**, 815 (1974).
8) O. Haida, H. Suga, and S. Seki, *Proc. Jpn. Acad.*, **49**, 191 (1973).
9) T. Matsuo, M. Oguni, H. Suga, and S. Seki, *Proc. Jpn. Acad.*, **48**, 237 (1972); T. Matsuo, M. Oguni, H. Suga, S. Seki, and J. F. Nagle, *Bull. Chem. Soc. Jpn.*, **47**, 57 (1974).
10) T. Matsuo, H. Suga, and S. Seki, *J. Phys. Soc. Jpn.*, **30**, 785 (1971).
11) J. C. Trowbridge and E. F. Westrum, Jr., *J. Phys. Chem.*, **67**, 2381 (1963).
12) H. Suga, H. Chihara, and S. Seki, *Nippon Kagaku Zasshi*, **82**, 24 (1961).
13) T. Carnelley, *J. Chem. Soc.*, **18**, 273 (1878).
14) M. V. Stackelberg, F. Quantram, and J. Dressel, *Z. Elektroch.*, **43**, 14 (1937).
15) F. C. Kracek, G. W. Morey, and H. E. Merwin, *Am. J. Sci.*, **A35**, 143 (1938).
16) Von A. Benrath, *Z. Anorg. Chem.*, **249**, 245 (1942).
17) H. L. Johnston and E. C. Kerr, *J. Am. Chem. Soc.*, **72**, 4733 (1950).
18) H. Suga and S. Seki, *J. Non-Cryst. Solids*, **16**, 171 (1974).
19) R. O. Davies and G. O. Jones, *Adv. in Phys.*, **2**, 370 (1953).
20) H. Kiriyama, *Nippon Kessho Gakkai Shi*, **16**, 255 (1974).
21) J. R. Durig, W. H. Green, and A. L. Marton, *J. Mol. Struct.*, **2**, 19 (1968).
22) Private communication from Professor J. F. Nagle of the Carnegie-Mellon University to one (H. S.) of the present authors.

The Microwave Spectrum of *anti*-Acetaldehyde Oxime-*d*

Osamu Ohashi, Hisao Hara, Keiko Noji, Takeshi Sakaizumi,
Masao Onda, and Ichiro Yamaguchi

Department of Chemistry, Faculty of Science and Technology, Sophia University, Chiyoda-ku, Tokyo 102

(Received October 22, 1976)

The microwave spectrum of *anti*-acetaldehyde oxime-*d* was investigated in the frequency region from 9 to 36 GHz. The rotational transition lines widely split into the A and E species due to the tunneling of the methyl group through the low potential barrier hindering the internal rotation. The transition lines belonging to the A species were fitted to the rigid rotor Hamiltonian, and the following effective rotational constants in MHz were obtained: $A_A=17250$, $B_A=6284.33$, and $C_A=4704.96$. All the observed transition frequencies were fitted to the Hamiltonian containing perturbation terms to the fourth order in order to obtain the internal-rotation parameters using the principal axis method. The potential barrier, V_3, hindering the internal rotation was determined to be 373 cal mol^{-1}. The dipole moment was determined to be 0.828 D from the Stark effect of the transitions belonging to the A species.

Rogowski and Schwendeman[1] studied the microwave spectrum of acetaldehyde oxime and revealed that the potential barrier hindering the internal rotation of the methyl group in the *anti* form is much lower than that in the *syn* form. The microwave spectrum of the deuterated species (CH_3CH=NOD) of *syn*-acetaldehyde oxime was investigated, and the orientation of the OH bond in the molecule was determined to be at the *trans* position to the CN bond.[2]

We have examined the microwave spectrum of *anti*-acetaldehyde oxime-*d* and determined the effective rotational constants, internal-rotation parameters, dipole moment, and r_s coordinates of the hydroxyl hydrogen atom.

Experimental

The sample of acetaldehyde oxime was commercially obtained from the Tokyo Kasei Kogyo Co., Ltd., and purified by trap-to-trap distillation *in vacuo*.

Acetaldehyde oxime in the *anti* form is solid at room temperature (melting point 46.5 °C).[3] We obtained the white solid sample of the *anti* form by gradual cooling in the course of distillation.

The deuterated species was prepared by the method used for *syn*-acetaldehyde oxime-*d*.[2]

The spectrometer used was a conventional 100 kHz sinusoial and square-wave Stark-modulation type with a phase-sensitive detector. The rotational spectrum was observed at 0— −10 °C in order to prevent the decomposition of the sample. The sample gas was renewed about every half hour.

Results and Discussion

Observed Spectrum and Assignment. There are two possible orientations of the OH bond in *anti*-acetaldehyde oxime when the molecule is assumed to have a plane of symmetry. Figure 1 shows the projections of the molecule on its plane of symmetry. In the present analysis, we assumed that the molecule is in the *trans* form (Fig. 1(a)) and predicted the transition frequencies from the structural parameters in Table 1.

From the results for *anti*-acetaldehyde oxime,[1] the following predictions were made: The transition lines of the deuterated species split widely into the A and E

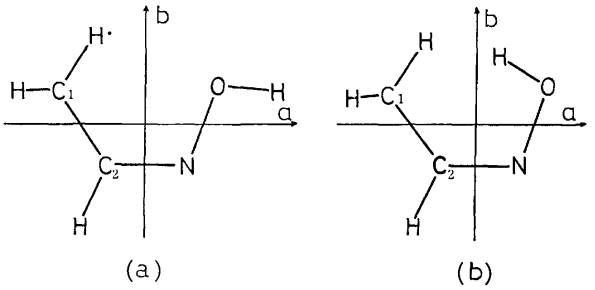

Fig. 1. Projection of *anti*-acetaldehyde oxime in its plane of symmetry.

Table 1. Structural parameters assumed for *anti*-acetaldehyde oxime-*d*

$r(C_2=N)$	1.276Å	∠NOD	102.68°
r(N–O)	1.408	$\angle C_2$=N–O	110.20°
r(O–D)	0.956	∠H–C_2=N	115.6°
$r(C_2-H)$	1.085	∠H–C_1–H	107.6°
$r(C_1-H)$	1.090	∠C_1–C_2=N	126.4°
$r(C_1-C_2)$	1.504		

C_1=methyl carbon.

members due to the internal rotation of methyl group; the transitions belonging to the A member have little effect on the internal rotation and show the usual second-order Stark effect.

In the first place, according to the predictions, the transition lines belonging to the A member were identified and were fitted to the rigid rotor Hamiltonian in order to obtain the effective rotational constants. The results, given in Table 2, show large differences between the observed and calculated frequencies of the 2_{02}-3_{03}, 2_{11}-3_{12}, 2_{21}-3_{22}, and 3_{13}-3_{12} transitions.

If the molecule has a plane of symmetry, only two hydrogen atoms of the methyl group are out of the symmetry plane. Consequently, the inertia defect, $\Delta(=I_\alpha+I_c-I_a-I_b)$, should be zero for the rigid-rotor model, where I_α is the moment of inertia of the methyl top about its rotational axis and where I_a, I_b, and I_c are the moments of inertia about the principal axes. The value of Δ was calculated to be 0.798 amu Å^2 from the effective rotational constants in Table 2, using the assumed value of $I_\alpha=3.1$ amu Å^2. This Δ value deviates greatly from zero. The facts mentioned above indicate

Table 2. Observed transitions for *anti*-acetaldehyde oxime-*d* (A species)

Transition	ν_{obsd}(MHz)	$\Delta\nu$[a](MHz)
$0_{00}\rightarrow 1_{01}$[b]	10989.39	0.10
$1_{11}\rightarrow 2_{12}$[b]	20399.17	−0.04
$1_{01}\rightarrow 2_{02}$[b]	21819.95	−0.02
$1_{10}\rightarrow 2_{11}$[b]	23557.88	−0.07
$2_{12}\rightarrow 3_{13}$	30503.80	−0.41
$2_{02}\rightarrow 3_{03}$	32342.09	−1.70
$2_{11}\rightarrow 3_{12}$	35231.37	−0.93
$2_{21}\rightarrow 3_{22}$	32965.49	−2.39
$2_{20}\rightarrow 3_{21}$	33592.07	0.10
$3_{13}\rightarrow 3_{12}$	9464.96	−1.24

a) $\Delta\nu=\nu_{obsd}-\nu_{calcd}$, ν_{calcd} obtained using these effective rotational constants; A_A= 17250 MHz, B_A=6284.33 MHz, C_A= 4704.96 MHz. b) Used to determine the effective rotational constants.

that the rotational transitions of *anti*-acetaldehyde oxime-*d* are affected by some kind of rotation-vibration interaction.

Using the method described by Rogowski and Schwendeman,[1] we estimated the barrier height, V_3, hindering the internal rotation of the methyl group, and then predicted the transition frequencies belonging to the E symmetry species. In the vicinity of the predicted transition frequencies, we observed lines which could be attributed to the E member. The lines belonging to the E member exhibited a characteristic first-order Stark effect. The assignment of the transitions was made by observing the Stark effect.

Table 3. Comparison of observed and calculated transition frequencies for *anti*-acetaldehyde oxime-*d*

Transition	ν_{obsd}(MHz)	$\Delta\nu$(MHz)[a]	
		I[b]	II[c]
	A Species		
$0_{00}\rightarrow 1_{01}$	10989.39	−0.99	−0.11
$1_{11}\rightarrow 2_{12}$	20399.17	−1.87	−0.29
$1_{01}\rightarrow 2_{02}$	21819.95	−0.63	0.11
$1_{10}\rightarrow 2_{11}$	23557.88	−1.57	0.13
$2_{12}\rightarrow 3_{13}$	30503.80	−2.32	−0.52
$2_{02}\rightarrow 3_{03}$	32342.09	1.04	−0.26
$2_{11}\rightarrow 3_{12}$	35231.37	−1.89	−0.10
$2_{21}\rightarrow 3_{22}$	32965.49	−2.74	−0.81
$2_{20}\rightarrow 3_{21}$	33592.07	−5.84	−0.04
$3_{13}\rightarrow 3_{12}$	9464.96	0.15	0.32
	E Species		
$0_{00}\rightarrow 1_{01}$	10864.60	−5.37	−0.45
$1_{11}\rightarrow 2_{12}$	20960.22	3.15	−1.40
$1_{01}\rightarrow 2_{02}$	21622.52	−5.85	−0.03
$1_{10}\rightarrow 2_{11}$	22880.04	6.19	2.15
$2_{12}\rightarrow 3_{13}$	30732.36	5.19	2.50
$2_{02}\rightarrow 3_{03}$	32140.50	−0.84	0.43
$2_{11}\rightarrow 3_{12}$	34748.08	3.55	−1.36
$2_{21}\rightarrow 3_{22}$	33199.51	0.66	0.95
$2_{20}\rightarrow 3_{21}$	33132.06	5.74	−1.06

a) $\Delta\nu=\nu_{obsd}-\nu_{calcd}$. b) ν_{calcd} obtained using the parameters with I_α=3.1 amu Å^2 in Table 4. c) ν_{calcd} obtained using the parameters with I_α =2.80 amu Å^2 in Table 4.

Table 4. Internal-rotation parameters for *anti*-acetaldehyde oxime-*d*

I[a]	II[b]
I_α=3.1 amu Å^2 (assumed)	I_α=2.80±0.02 amu Å^2
A_0=17000±42 MHz	A_0=17088±14 MHz
B_0=6254.59±0.44 MHz	B_0=6255.42±0.14 MHz
C_0=4704.43±0.40 MHz	C_0=4704.22±0.12 MHz
λ_a=cos (52.4±0.3°)	λ_a=cos (53.4±0.1°)
s =9.607±0.026	s =9.453±0.014
V_3=359 cal mol^{-1}	V_3=387 cal mol^{-1}
F =173959 MHz	F =190956 MHz

a) Parameters obtained from the least-squares fit, with I_α fixed at 3.1 amu Å^2. b) Parameters obtained from the least-squares fit with I_α varied. The uncertainties are standard deviations.

The hyperfine structure of the absorption lines due to the ^{14}N nuclear quadrupole moment could not be observed.

Barrier to Internal Rotation. All the observed transition frequencies are listed in Table 3. These frequencies were fitted to the internal-rotation parameters, by using the Hamiltonian described by Rogowski *et al.*[1] except for the denominator correction term, whose matrix elements were given by Stelman.[4] The internal-rotation parameters obtained are listed in Table 4. The parameters are defined as follows: A_0, B_0, and C_0 are the rotational constants in the absence of internal rotation; λ_g is the cosine of the angle between the axis of the internal top and the principal g axis; s is the dimensionless parameter, the reduced barrier height, and the $s=(4/9)(V_3/F)$ relation holds for a threefold barrier; F is defined by the expression $\hbar^2/(2rI_\alpha)$, where r is equal to the quantity of $1-\sum_g\lambda^2{}_g(I_\alpha/I_g)$.

In Table 4, Set I is obtained assuming I_α=3.1 amu·Å^2, while Set II is obtained with I_α as the fitting parameter. The value of 2.804 amu Å^2 for I_α in Set II is far from the value of 3.0—3.2 amu Å^2 usually found for the methyl top in various molecules. Therefore, the I_α parameter was fixed at 3.1 amu Å^2 in another fitting (Set I). The results of the two fittings are compared in Table 3. The deviations of the calculated frequencies from the observed ones, and the small value of I_α obtained by the least-squares fit in the present work, are comparable with those reported for normal species.[1] These deviations and the small value of I_α may be ascribed to the facts that the perturbation terms higher than the fourth order for the internal rotation were neglected and that no other rotation-vibration interaction except the methyl torsion was considered.

Although the uncertainty to the value of I_α remains, there is not much difference in the values of V_3 between Set I and Set II, as Table 4 shows. Therefore, it is likely that the value of V_3 for deuterated species is not much different from the values in Table 4. Consequently, the value of V_3 for deuterated species may safely be concluded to be 373±30 cal mol^{-1}. This value is comparable to that of 375 cal mol^{-1} for normal species.[1]

Dipole Moment. The A species transitions exhibited the usual second-order Stark effect. The dipole moment

was determined from measurements of the Stark shifts of the transitions, $J=0\rightarrow1$, $1\rightarrow2$, and $2\rightarrow3$, belonging to the A species. The electric field inside the absorption cell was calibrated by measurements of the Stark shifts of the $J=0\rightarrow1$ and $1\rightarrow2$ transitions of OCS with the dipole moment of 0.71521 D.[5]

Table 5. Stark effect of *anti*-acetaldehyde oxime-*d*

Transition	|M|	$(\partial\nu/\partial E^2)$[a] MHz $(V\,cm^{-1})^{-2}$ Obsd	Calcd I	Calcd II
$0_{00}\rightarrow1_{01}$	0	7.635×10^{-6}	7.242×10^{-6}	7.240×10^{-6}
$1_{01}\rightarrow2_{02}$	0	−1.889	−1.720	−1.712
	1	2.072	2.251	2.247
$1_{11}\rightarrow2_{12}$	0	1.751	1.648	1.647
	1	22.891	23.313	23.314
$1_{10}\rightarrow2_{11}$	0	1.668	1.617	1.617
	1	−21.464	−21.312	−21.311
$2_{02}\rightarrow3_{03}$	0	−0.410	−0.380	−0.380
	2	1.053	1.113	1.110
$2_{12}\rightarrow3_{13}$	1	0.881	0.763	0.764
	2	3.846	3.590	3.592
$2_{11}\rightarrow3_{12}$	1	−0.601	−0.565	−0.566
	2	−2.889	−2.708	−2.709
$3_{13}\rightarrow3_{12}$	3	2.441	2.456	2.465
		μ_a	0.753±0.004 D	0.753±0.004 D
		μ_b	0.34 ±0.02 D	0.34 ±0.03 D
		μ_c	0.02 ±0.02 D	0 (assumed) D
		μ_{total}	0.828±0.011 D	0.828±0.013 D

a) Based on μ(OCS)=0.71521 D.

The results obtained by the least-squares fit given in Table 5 show good agreements between the observed and calculated Stark coefficients. The fifth column of Table 5 shows the results obtained with the assumed value of $\mu_c=0$. The results given in the fourth column were obtained by the least-squares fit, using all three components, μ_a, μ_b, and μ_c, as parameters. The value of 0.02 D obtained for μ_c is comparable to the uncertainty in this work. Consequently, the value of μ_c is thought to be nearly equal to zero. The values of μ_a and μ_b determined in the fitting (Calcd I) are consistent with those obtained in the other fitting (Calcd II). From the above results, the molecule may reasonably be concluded to have a plane of symmetry.

Orientation of the OH Bond. The rotational constants, A_0, B_0, and C_0, in Table 4 are what the effective rotational constants A_A, B_A, and C_A, would be in the absence of internal rotation.[1] Consequently, from these rotational constants and the corresponding ones for the normal species,[1] the r_s coordinates of the hydroxyl hydrogen atom can be calculated using Kraitchman's expressions.[6] In Table 6, the first column

Table 6. Coordinates of the hydrogen atom of the hydroxyl group

	Obsd-I[a]	Obsd-II[b]	Calcd-I[c]	Calcd-II[d]
a	2.128± 0.031Å	2.129± 0.009Å	2.132Å	0.354Å
b	0.49± 0.13	0.48± 0.04	0.507	1.152
c	—	0.14± 0.19	0 (assumed)	0 (assumed)

a) Using the rotational constants with $I_\alpha=3.1$ amu·Å². b) Using the rotational constants with $I_\alpha=2.80$ amu Å. c) Obtained from the assumed structure shown in Fig. 1(a). d) Obtained from the assumed structure shown in Fig. 1(b).

shows the coordinates calculated from the rotational constants with $I_\alpha=3.1$ amu Å², while the second column refers to those obtained from the constants with $I_\alpha=2.80$ amu Å². The above two sets of results are consistent within the limits of accuracy of the present work. The third and fourth columns show the coordinates of the hydroxyl hydrogen atom calculated from the assumed structures given in Fig. 1(a) and Fig. 1(b) respectively. The coordinates determined experimentally are in good agreement with those calculated from the structure shown in Fig. 1(a). Consequently, it may clearly be concluded that the orientation of the OH bond in the *anti*-acetaldehyde oxime molecule is at the position *trans* to the C–N bond, as is shown in Fig. 1(a). This result is consistent with the orientation of the OH bond in formaldehyde oxime[7] and *syn*-acetaldehyde oxime.[2]

References

1) R. S. Rogowski and R. H. Schwendeman, *J. Chem. Phys.*, **50**, 397 (1969).
2) O. Ohashi, R. Ishihara, K. Murakami, T. Sakaizumi, M. Onda, and I. Yamaguchi, *Bull. Chem. Soc. Jpn.*, **49**, 891 (1976).
3) W. R. Dunstan and T. S. Dymond, *J. Chem. Soc.*, **61**, 470 (1892).
4) D. Stelman, *J. Chem. Phys.*, **41**, 2111 (1964).
5) J. S. Muenter, *J. Chem. Phys.*, **48**, 4544 (1968).
6) J. Kraitchman, *Am. J. Phys.*, **21**, 17 (1953).
7) I. N. Levine, *J. Chem. Phys.*, **38**, 2326 (1963).

Electrical Properties and Constitution of the Phenothiazine–Iodine and Related Complexes[1)]

Susumu Doi,* Tamotsu Inabe, and Yoshio Matsunaga**
Department of Chemistry, Faculty of Science, Hokkaido University, Sapporo 060
(Received November 4, 1976)

The electrical properties of the phenothiazine–iodine complex were examined in detail as a function of the composition. A shoulder in the resistivity-composition isotherm, a decrease in the activation energy for semiconduction by a factor of two, and a change in the sign of the Seebeck coefficient from negative to positive were observed at a composition of two molecules of phenothiazine to five atoms of iodine. These observations and the spectral behavior reported earlier indicate the formation of a complex cation radical salt, $(\text{phenothiazine})_2^+I_5^-$, which exhibits a resistivity of about 800 ohm cm at room temperature. By the incorporation of a half mole of iodine into this salt, the resistivity reaches a minimum of about 20 ohm cm at room temperature. Similar singularities in the resistivity-composition isotherms were observed with the complexes of the benzo[*a*]-, benzo[*c*]-, and *N*-methyl-derivatives.

Since Akamatu, Inokuchi, and Matsunaga reported anomalously low electrical resistivities exhibited by some polycyclic aromatic hydrocarbon–halogen complexes,[2,3)] a large number of halogen complexes, mostly iodine complexes, have been studied by various workers. For example, the organic component compounds so far examined include such hydrocarbons as pyrene,[4)] perylene,[2,4,5)] and violanthrene,[3,6)] such diamines as *p*-phenylenediamine,[7)] benzidine,[8)] and their derivatives,[9,10)] carotene,[11)] pyridazine,[12)] phenothiazine,[13–16)] its *N*-methyl derivative,[13,17–19)] and phenoselenazine.[16)] However, only relatively few works have been published on the nature of low-resistivity halogen complexes.

The vibrational spectrum of the phenothiazine–iodine complex of a mole ratio of 2: 3 has been shown to be clearly different from that of the parent organic compound, but nearly identical with that of the cation radical bromide.[13)] Later, we found two patterns rather similar to each other for the latter,[20)] and demonstrated that one of them can be ascribed to the simple cation radical bromide, and the other, to the complex cation radical bromide of the 2: 1 type.[21)] The spectrum identical to that of the iodine complex is the latter. Thus, this iodine complex appears to be a kind of the complex cation radical salt; however, six atoms of iodine per two molecules of phenothiazine do not fit to the composition of any polyiodide. Labes *et al.* have found that the vibrational spectrum of the perylene–bromine complex with a mole ratio of 2: 7 is quite different from that of either the parent hydrocarbon or the reaction product, 3,9-dibromoperylene, indicating a significant decrease in symmetry.[22)] They have suggested the formation of a σ-type complex.

Undoubtedly, the analysis of the crystal and molecular structure is a powerful tool in solving the problem. However, the task becomes more and more difficult with an increase in the heavy halogen content. There are only a few works on low-resistivity complexes with relatively low iodine contents. Both of the following compounds have been reported to contain cation radicals: [4,4′-bis(dimethylamino)diphenylamine] I and [*N*,*N*′-diphenyl-*p*-phenylenediamine]$_5$I$_{12}$. The former salt, with a resistivity of the order of 10^5 ohm cm, is a simple iodide.[23)] The halogen atoms in the latter are arranged in columns in the form of triiodide ions.[24)] As the number of the diamine molecules exceeds that of the triiodide ions, the salt contains both the cations and formally neutral molecules. This complex cation radical salt is known to exhibit a resistivity of about 3 ohm cm.[10)] More recently, the structure of highly conducting tetrathiafulvalene (TTF) halides with a deviation from the 1: 1 composition has been clarified.[25–27)] The halogen atoms are in the form of simple halide ions, and the stack of organic molecules consists of neutral and fully charged molecules or fractionally charged molecules. All the available results agree on the points that the low-resistivity halogen complexes are actually cation radical salts and that the resistivities are particularly low when the compositions are complex.

Until now, resistivity-composition isotherms have been prepared for the following systems: violanthrene–iodine,[3)] phenothiazine–iodine,[14)] and phenothiazine bromide–iodine.[20)] In these works, the resistivity minimum has been assumed to correspond to the composition of a distinct compound. This simple assumption is, however, good only for the systems in which two coexisting phases are stoichiometric and mechanically mixed without interaction. If the incorporation of a marked stoichiometric imbalance is conceivable, the electrical behavior should depend quite differently upon the composition. As conduction electrons or holes are introduced by incorporating an excess of one of the components to a pure, accurately stoichiometric compound, the composition must be indicated by a maximum or a shoulder in the resistivity-composition isotherm. On the other hand, the minimum, if any, may be indicative of the limit of the deviation from stoichiometry. Furthermore, we may expect a change in the sign of the Seebeck coefficient at the composition of this stoichiometric compound. No such singularity has been noted in the published isotherms; however, the Seebeck coefficient in the phenothiazine–iodine complex has been reported to change its sign somewhere between two and six iodine atoms per thiazine molecule.[15)] Thus, the careful examination of

* Present address: Central Research Laboratory, Showa Denko K. K., Tamagawa, Tokyo.
** To whom inquiries may be addressed.

the electrical properties as functions of the composition seemed to be a tool more powerful than has been supposed for elucidating the constitution of semiconducting organic compound-iodine complexes. Accordingly, we decided to initiate the present series of works with the four thiazine-iodine complexes.

Experimental

Materials. Samples were prepared by the following three methods, and the iodine contents were determined by microanalysis.

a) Thiazine-iodine complexes with a mole ratio of 2: 3 were precipitated by mixing the organic component and iodine separately dissolved in hot benzene or ether.[13,16,17] The preparation of samples of other mole ratios was carried out by the careful grinding of the weighed complex and the thiazine or iodine in the presence of a small amount of the solvent.

b) An equimolar mixture of the thiazine and its *S*-oxide was thoroughly ground in an agate mortar. The fine powder was spread in a beaker and moistened with concentrated hydroiodic acid. The reaction mixture was then dried in a vacuum desiccator containing potassium hydroxide pellets.[28] The "iodide" thus prepared was mixed with the thiazine or iodine in order to adjust the composition.

c) The weighed thiazine and iodine were directly ground in an agate mortar in the presence of a small amount of benzene or ether.

Measurements. The electrical resistivities and Seebeck coefficients of compactions were recorded as functions of the temperature by the procedures described in the paper by Kan and Matsunaga.[17]

Results and Discussion

Phenothiazine–Iodine In Fig. 1, the electrical resistivity values at 20 °C are plotted against the number of iodine atoms per phenothiazine molecule, *n*. The samples made by Method a are indicated by shaded circles, while those made by Method b are indicated by open circles. The "iodide" gave the following analytical results: C, 38.61; H, 2.77; I, 46.09%. Calcd for $C_{12}H_9NSI_{1.35}$: C, 38.81; H, 2.43; I, 46.33%. A shoulder appears at $n=2.5$ in the resistivity-composition isotherm, the value at this composition being about 800 ohm cm. Then the resistivity reaches a minimum of about 20 ohm cm at $n=3$. The latter is the composition of the iodine complex deposited from the solution. The temperature dependence of the resistivity, ρ, follows the typical semiconductor behavior: $\rho=\rho_0\exp(E/kT)$. As is shown in Fig. 2, the activation energy for semiconduction, E, is about 0.3 eV up to $n=2.5$; it then suddenly decreases to about 0.15 eV. For the above-mentioned reason, one may postulate that a distinct compound is formed at a composition of $n=2.5$. In conjunction with our earlier observation that the vibrational spectrum of the complex agrees well with that of the complex cation radical bromide of the 2: 1 type,[21] the compound may be identified as $(C_{12}H_9NS)_2^+I_5^-$. The two thiazine molecules are equivalent in the time scale of infrared spectroscopy. A deviation of as much as a half mole of iodine is allowed in this formula. This iodine plays a crucial role in the significant decrease in the activation energy. Thus, the very sharp decrease in the electrical resistivity arises undoubtedly from a drastic increase in the charge-carrier concentration. Above $n=3$, the resistivity increases as the iodine content becomes higher. As the vibrational spectrum of phenothiazine mixed with a large amount of iodine resembles that of the simple cation radical bromide, the increase may be attributed to the coexistence of a high-resistivity simple salt rather than free iodine. The rapid increase in the activation energy in this composition range appears to be consistent with the observed high resistivity. Although a resistivity minimum is located at $n=3$ in the isotherm reported by Gutmann and Keyzer, their value, 350 ohm cm, is considerably higher than ours.[14] Moreover, the change observed by them in the composition range from $n=1$ to 4 is merely about one order of magnitude.

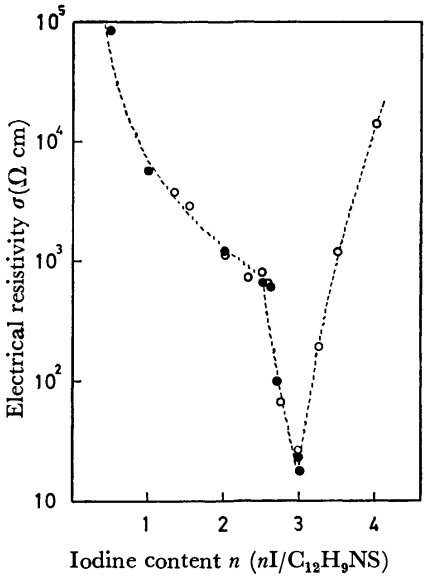

Fig. 1. Electrical resistivity at 20 °C plotted against the iodine content (*n* iodine atoms/thiazine molecule) in the phenothiazine–iodine system.

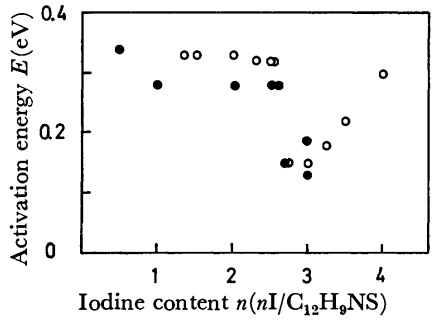

Fig. 2. Activation energy for semiconduction plotted against the iodine content in the phenothiazine–iodine system.

In Fig. 3, the variation in the Seebeck coefficient with the temperature for some representative samples made by Method b is presented. The coefficient depends remarkably upon the composition. Up to $n=2.5$, a linear relationship with the reciprocal temperature is observed near room temperature. Such a range is wider when the composition becomes closer to $n=2.5$. This behavior implies that the compound expressed by the

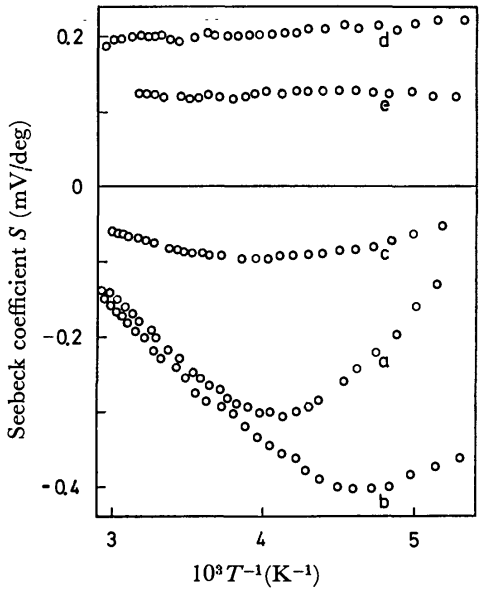

Fig. 3. Seebeck coefficient of the phenothiazine-iodine complexes; a) $n=1.35$, b) 2.50, c) 2.55, d) 2.75, and e) 4.00.

$(C_{12}H_9NS)_2^+I_5^-$ formula exists in these samples. In other words, the solubility of phenothiazine into the compound is rather small and the samples examined in this composition range are not homogeneous. The shape of the resistivity-composition isotherm does seem to be in accord with this view. The linear part appears to fit in with the expression for the thermoelectric motive force of an intrinsic semiconductor; therefore, we attempted to estimate the ratio of the electron mobility, μ_e, to the hole mobility, μ_h, tentatively assuming the applicability of the band model to the present compound. It is given by:

$$b = \mu_e/\mu_h = \left[\frac{E_G}{2} - \frac{\Delta S}{\Delta(10^3/T)}\right]\left[\frac{E_G}{2} + \frac{\Delta S}{\Delta(10^3/T)}\right]^{-1},$$

provided that S is measured in mV/deg.[29] E_G is the width of the forbidden band and is assumed to be twice the observed activation energy for semiconduction. With samples of $n=2.00$, 2.30, and 2.50, the above ratio is found within 4 and 6. Then, the conductivity, σ, is given by:

$$\sigma = \frac{1}{\rho} = e\mu_e\left(\frac{b+1}{b}\right)N\exp(-E/kT),$$

where N is taken to be equal to the number of phenothiazine molecules per cm³ of the compaction; that is, $(2.6—2.9)\times10^{21}$. Employing the resistivity and the activation energy presented in Figs. 1 and 2, the electron mobility is estimated to be 0.6—0.9 cm²/Vs. This value is a little smaller than those estimated similarly for the *N*-methylphenothiazine complex, 2.3 cm²/Vs,[17] and for the phenoselenazine complex, 2.6 cm²/Vs.[16,30]

Above $n=2.5$, the Seebeck coefficient becomes less negative (see Curve c), and finally it changes its sign (see Curve d). A maximum value of about 0.2 mV/deg is observed near $n=3$. In Fig. 4, the coefficient at 20 °C is plotted against the iodine content. This physical quantity is apparently more sensitive to the preparation methods than the electrical resistivity. The values

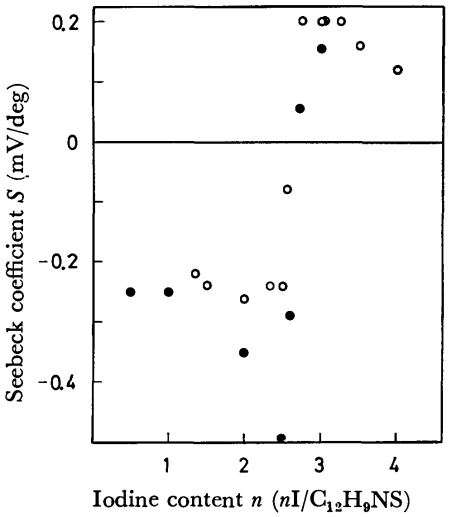

Fig. 4. Seebeck coefficient at 20°C plotted against the iodine content in the phenothiazine–iodine system.

observed with samples made by Method a are appreciably more negative than those made by Method b in the composition range from $n=2$ to 2.5. Regardless of such disagreement, though, the formation of the $(C_{12}H_9NS)_2^+I_5^-$ compound is strongly supported by the sudden change in the sign near this composition. The behavior above $n=2.5$ suggests that the electrical conduction is extrinsic and that the major charge carriers are holes.

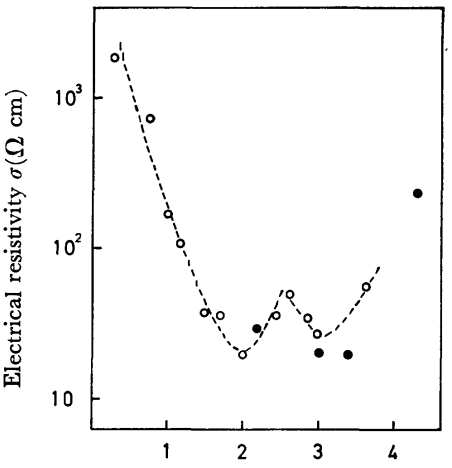

Fig. 5. Electrical resistivity at 20°C plotted against the iodine content in the benzo[*a*]phenothiazine–iodine system.

Benzo[a]*phenothiazine-Iodine.* The complex deposited from a benzene solution has a mole ratio of 2: 3 and exhibits a resistivity of about 20 ohm cm at room temperature.[13,16] For the present work, the samples were prepared by Methods a and c. The resistivity-composition isotherm at 20 °C is presented in Fig. 5. The shaded circles denote samples prepared from the 2: 3 complex, and the open circles those prepared by mixing the components. The maximum of about 50 ohm cm clearly observed near $n=2.5$ and the minima near $n=2$ and 3 make the formation of a complex cation radical salt, $(C_{16}H_{11}NS)_2^+I_5^-$, very plausible. The

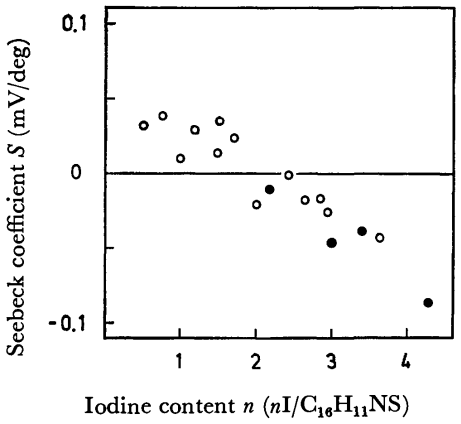

Fig. 6. Seebeck coefficient at 20 °C plotted against the iodine content in the benzo[*a*]phenothiazine–iodine system.

presence of two resistivity minima suggests that the solubilities of both iodine and the thiazine into this salt are appreciable. In other words, the salt is highly nonstoichiometric. It must be noted that the resistivity of this salt is lowered by only a factor of two by the deviation. The values of the activation energy for semiconduction near room temperature are mostly in the range from 0.11 to 0.15 eV. Higher values, 0.18—0.20 eV, were obtained at $n=0.27$, 3.63, and 4.29. Contrary to the phenothiazine–iodine system, no abrupt change could be detected at the composition of the resistivity maximum. The Seebeck coefficient of this system depends only slightly upon the temperature and seems to be dominated by some impurities. The values are rather small and scattered (see Fig. 6). Nevertheless, they are consistently positive at low iodine contents and negative at high iodine contents. The composition at which $S=0$ appears to be $n\simeq 2.2$. Although the values at higher temperatures are more positive or less negative in all the samples, the shift of this composition by the temperature is inconsiderable. The impurities mentioned above may be the components present in excess; however, the change in the sign here is in the direction opposite to that found with unsubstituted phenothiazine. We earlier noted the similarity in the vibrational patterns of the 2:3 iodine complex and the cation radical bromide.[16] Now this observation suggests the difficulty in drawing a distinction on the basis of the vibrational spectrum between the simple benzophenothiazine cation radical salt and the complex one. Furthermore, the electronic spectrum of the "iodide" was found to be quite different from those of the other simple cation radical salts, but to resemble that of the low-resistivity iodine complex.[28] In view of the present work, the "iodide" prepared earlier is probably a kind of complex cation radical salt. Even in the case of the bromide, the simple salt was found to convert easily into the complex salt at room temperature.[21] As iodine is less electronegative than bromine, the simple thiazine cation radical "monoiodide" may be unstable or may not exist at all.

Benzo[c]*phenothiazine–Iodine.* A shoulder with a resistivity of about 20 ohm cm is observed at $n=2.5$ and a minimum is located near $n=2$ in the isotherm presented in Fig. 7. Here, the samples prepared by Method a are indicated by shaded circles. The rest were prepared starting from the "iodide" which had the following composition: C, 46.36; H, 2.74; N, 3.07; I 38.63%. Calcd for $C_{16}H_{11}NSI_{1.27}$: C, 46.82; H, 2.68; N, 3.41; I, 39.27%. No singularity is seen at $n=3$, which is the composition of the complex deposited from a benzene solution.[13,16] Thus, the effect of excess thiazine is much larger than that of excess iodine on the electrical resistivity in this system. The activation energy for semiconduction increases gradually up to $n=2.5$ and sharply above this composition. The values at $n=0.5$, 2.5, and 4.0 are 0.09, 0.12, and 0.21 eV respectively. The thermoelectric behavior is similar to that of the isomeric thiazine–iodine system. As is illustrated in Fig. 8, the Seebeck coefficient at room temperature decreases nearly linearly with n and changes its sign near $n=2.3$. Even though the evidence is not so complete as in the case of the phenothiazine complex, one may conclude that the stoichiometric compound formed in this system has a composition of $(C_{16}H_{11}NS)_2{}^+I_5{}^-$.

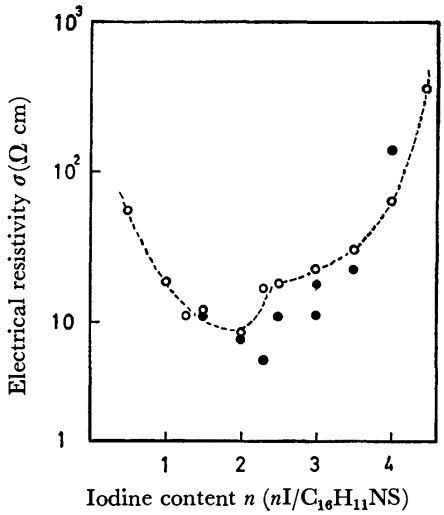

Fig. 7. Electrical resistivity at 20 °C plotted against the iodine content in the benzo[*c*]phenothiazine–iodine system.

N-*Methylphenothiazine–Iodine.* The complex deposited from ether has a mole ratio of 2:3 and is

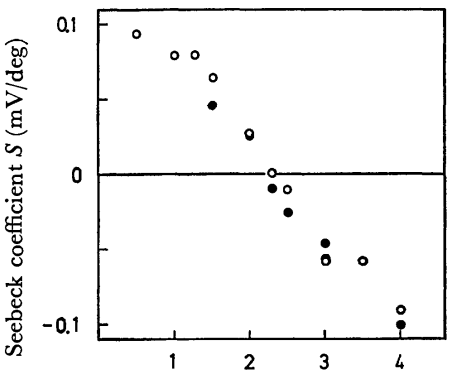

Fig. 8. Seebeck coefficient at 20 °C plotted against the iodine content in the benzo[*c*]phenothiazine–iodine system.

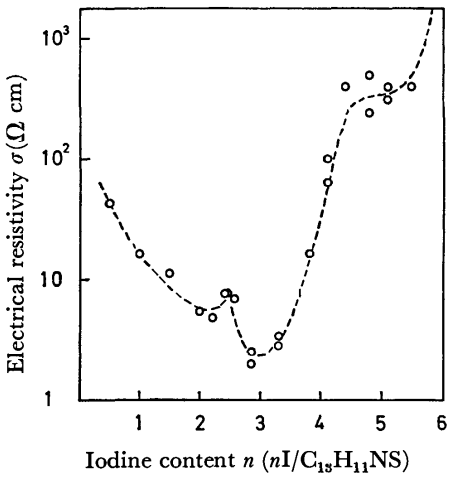

Fig. 9. Electrical resistivity at 20 °C plotted against the iodine content in the *N*-methylphenothiazine-iodine system.

more conductive by an order of magnitude than the unsubstituted phenothiazine complex.[13,17] The single crystal is known to be highly anisotropic. The principal conductivities at 23 °C, as measured by Dix, are as follows: 95, 0.96, and 0.022 ohm^{-1} cm^{-1}.[19] In addition to this complex, Dix has isolated two more, the 2: 5 and 2: 7 complexes. The resistivity-composition isotherm reported in Fig. 9 was derived from measurements of samples prepared by Method c. Clearly, the isotherm possesses a maximum of about 8 ohm cm at $n=2.5$, minima near $n=2$ and 3, and a shoulder around $n=4.5$. By analogy to the phenothiazine-iodine system, one may suggest the formation of the complex cation radical salt, $(C_{13}H_{11}NS)_2^+I_5^-$. The 2: 3 complex corresponds to a minimum at $n=3$. The low resistivity is, to some extent, due to the incorporation of a half mole of iodine into the above-mentioned salt. Because of the instability, the temperature-dependence is rather complicated and no obvious manifestation of the formation of the salt is apparent in the activation energy. The Seebeck coefficient of the 2: 3 complex depends markedly upon the temperature, as has been reported by Sano *et al.* and also by Kan and Matsunaga.[17,31] It is surprising to see that this feature is hardly modified by the composition change over the entire range examined here. The vibrational spectra of the samples with $n>4.5$ consist of sharp bands and are very different from both that of the parent compound and that of the 2: 3 complex. Therefore, the formation of a simple cation radical salt, $(C_{13}H_{11}NS)^+I_5^-$, seems to be likely. This composition agrees with the 2: 5 complex reported by Dix.

In conclusion, all the 2: 3 thiazine-iodine complexes studied may be expressed by $(thiazine)_2^+I_5^- + 1/2I_2$. Their low electrical resistivities are more or less attributable to the charge carriers generated by the incorporation of extra iodine into the complex cation radical pentaiodide. Some years ago, Wakayama determined the lattice constants of the *N*-methylphenothiazine complex.[32] This complex is orthorhombic with $a=11.4$, $b=21.4$, and $c=21.1$ Å. The unit cell is so large that six formally neutral thiazine molecules, six positively charged thiazine radicals, six pentaiodide anions, and three iodine molecules are accommodated. The exact form of the last constituent remains to be clarified, however. It may exist as the molecule, the triiodide ion, or a part of polyiodide ion(s). No matter which is the exact form, all the species derived from iodine are diamagnetic.

References

1) A part of the present work was presented at the Japan-U. S. Seminar "Energy and Charge Transfer in Organic Semiconductors," Osaka, 1973.
2) H. Akamatu, H. Inokuchi, and Y. Matsunaga, *Nature*, **173**, 168 (1954).
3) H. Akamatu, H. Inokuchi, and Y. Matsunaga, *Bull. Chem. Soc. Jpn.*, **29**, 213 (1956).
4) J. Kommandeur and F. R. Hall, *J. Chem. Phys.*, **34**, 129 (1961).
5) T. Uchida and H. Akamatu, *Bull. Chem. Soc. Jpn.*, **34**, 1015 (1961).
6) T. Uchida and H. Akamatu, *Bull. Chem. Soc. Jpn.*, **35**, 981 (1962).
7) S. Nishizaki and H. Kusakawa, *Bull. Chem. Soc. Jpn.*, **36**, 1681 (1963).
8) H. Kusakawa and S. Nishizaki, *Bull. Chem. Soc. Jpn.*, **38**, 313 (1965).
9) J. Honzl, K. Ulbert, V. Hadek, and M. Tlustakova, *Chem. Commun.*, **1965**, 440.
10) V. Hadek, *J. Chem. Phys.*, **49**, 5202 (1968).
11) C. M. Huggins and O. H. LeBalnc, *Nature*, **186**, 552 (1960).
12) R. J. Hoare and J. M. Pratt, *J. Chem. Soc., Chem. Commun.*, **1969**, 1320.
13) Y. Matsunaga, *Helv. Phys. Acta*, **36**, 800 (1963).
14) F. Gutmann and H. Keyzer, *J. Chem. Phys.*, **46**, 1969 (1967).
15) S. N. Bhat and C. N. R. Rao, *Can. J. Chem.*, **47**, 3899 (1969).
16) Y. Matsunaga and Y. Suzuki, *Bull. Chem. Soc. Jpn.*, **45**, 3375 (1972).
17) K. Kan and Y. Matsunaga, *Bull. Chem. Soc. Jpn.*, **45**, 2096 (1972).
18) A. Kehr, *Phys. Status Solidi A*, **9**, 267 (1972).
19) G. Dix, *Phys. Status Solidi A*, **24**, 139 (1974).
20) Y. Matsunaga and K. Shono, *Bull. Chem. Soc. Jpn.*, **43**, 2007 (1970).
21) S. Doi and Y. Matsunaga, *Bull. Chem. Soc. Jpn.*, **48**, 3747 (1975).
22) M. M. Labes, H. W. Blakeslee, and J. E. Bloor, *J. Am. Chem. Soc.*, **87**, 4251 (1965).
23) K. Toman and D. Ocenaskova, *Acta Crystallogr.*, **20**, 514 (1966).
24) K. Huml, *Acta Crystallogr.*, **22**, 29 (1967).
25) D. J. Dahm, G. R. Johnson, F. L. May, M. G. Miles, and J. D. Wilson, *Cryst. Struct. Commun.*, **4**, 673 (1975).
26) S. J. LaPlaca, P. W. R. Corfield, R. Thomas, and B. A. Scott, *Solid State Commun.*, **17**, 635 (1975).
27) J. J. Daly and F. Sanz, *Acta Crystallogr.*, **B31**, 620 (1975).
28) Y. Matsunaga and Y. Suzuki, *Bull. Chem. Soc. Jpn.*, **46**, 719 (1973).
29) G. Busch and U. Winkler, *Ergeb. Exakt. Naturw.*, **29**, 145 (1956).
30) The mobilities given in Refs. 16 and 17 should be multiplied by a factor of ten.
31) M. Sano, K. Ohno, and H. Akamatu, *Bull. Chem. Soc. Jpn.*, **44**, 3269 (1971).
32) N. I. Wakayama, personal communication.

Catalytic Activity of Silver and Gold Metals Doped with Alkali Metals

Shigenobu HAYASHI, Mitsuyuki SOMA, Tamotsu KONDOW, Takaharu ONISHI, and Kenzi TAMARU

Department of Chemistry, Faculty of Science, The University of Tokyo, Hongo, Bunkyo-ku, Tokyo 113

(Received November 4, 1976)

When alkali metals are brought into contact with silver or gold, catalytic activity for hydrogen activation reactions results which is higher than that for each of the constituent metals. The order of the activity per mole of alkali metal for the H_2-D_2 exchange reaction is Ag–Cs>Ag–K>Au–Cs>Ag–Na. The Ag–Cs and Ag–K systems absorb considerable amounts of hydrogen. The nature of the active sites and the contact effect of the IB metal with the alkali metal are discussed.

It has been reported that the addition of alkali metals to various materials results in marked changes in their catalytic properties.[1-3] The compounds formed between alkali metals and various aromatic compounds or graphite are of special interest because they exhibit marked catalytic activity for the activation of hydrogen molecules, although individually both constituents are of low activity in activating hydrogen molecules. Ichikawa *et al.* reported in a preliminary communication[4] that considerable catalytic activity was created when alkali metals were brought into contact with silver film, while the effect was not so large in the case of gold film. Since both silver and gold are regarded as inactive with respect to hydrogen activation, the study of the effect of the addition of alkali metals on the catalytic activity and selectivity may give clues to understanding the nature of catalysis for hydrogen activation. In this study the activation of molecular hydrogen on silver- and gold-alkali metal catalysts, as well as on each of the constituent elements, was examined in detail.

Experimental

Preparation of Catalysts. *Ag–Alkali Metal*: Silver powder was obtained by reducing silver oxide (Wako Pure Chemical Industries, 99.0%) with hydrogen at *ca.* 100 °C. Sodium (Merck) and potassium (Wako) metals were purified by repeated distillation under vacuum. Cesium metal was prepared *in vacuo* by a reaction between cesium chloride and calcium metal at 600 °C[5] and purified by repeated distillation. The alkali metals thus obtained were evaporated onto the silver powder in an evacuated glass vessel, and the resulting catalysts were subjected to heat treatments at various temperatures between 100 and 200 °C under vacuum. The surface areas of the catalysts were 0.1—0.5 m^2/g, which were determined by the BET method. The composition of the catalysts was determined by titration of the alkali metals. The sodium-doped silver catalyst (Ag–Na) weighed 9.39 g, which consisted of 9.38 g of Ag and 0.01 g of Na (0.10 wt%, 5×10^{-4} mol), (Ag–K) 9.8 g (Ag 9.1 g, K 0.7 g (7 wt%, 2×10^{-2} mol)) and (Ag–Cs) 9.5 g (Ag 8.7 g, Cs 0.8 g (8.3 wt%, 6×10^{-3} mol)).

Au–Cs: Gold powder was obtained by reducing chloroauric acid (Wako) with hydroquinone.[6] Cesium was introduced onto the gold powder sealed in a Pyrex glass tube, as shown in Fig. 1, by the "dual furnace" method[7] under vacuum. The gold powder was charged in A of the figure, and the cesium metal in B. A and B were heated

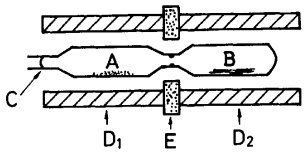

Fig. 1. Schematic diagram of "Dual Furnace" method. A: IB metal, B: alkali metal, C: breakable seal, D_1, D_2: furnaces; each furnace can be operated independently. E: insulating ring.

for 35 days at 146 and 140 °C, respectively. The catalyst weighed 1.1 g (Au 0.9 g, Cs 0.2 g (19 wt%, 2×10^{-3} mol)) and was dark-blue-violet.

Alkali Metals: The alkali metals, purified as above, were evaporated *in vacuo* onto the inside wall of a Pyrex glass tube which had been baked out beforehand at temperatures between 200 and 300 °C. The sodium film (Na) weighed 1.2×10^{-4} g, the potassium film 1 g, and the cesium film 1.2 g and the total geometrical surface areas were 50—90 cm^2.

Reactants. Commercial reactant gases were purified as follows. Hydrogen was passed through a DEOXO catalyst (Engelhard Industries, Ltd.) at room temperature and then through a 5A molecular-sieve column cooled to 77 K. Deuterium was passed through a 5A molecular-sieve column and then an activated charcoal column at 77 K. Ethylene was frozen at 77 K, evacuated, and then was passed through a dry ice–methanol trap. Propylene was purified by repeated freeze, evacuation and thaw cycles.

Apparatus and Procedures. The apparatus employed for the reactions was a closed circulating system whose dead volume was about 300 cm^3. The total pressures of the reactant gases were ordinarily between 13 and 27 kPa. The pressure change during the course of the reaction was followed using a mercury manometer. The reacting gas mixtures were analyzed by gas chromatography,[8] infrared spectroscopy, mass spectrometry, and microwave spectroscopy. The activity of the catalysts remained unchanged upon repeated runs and each run was normally carried out without pretreatment.

Results

Absorption of Hydrogen and the H_2-D_2 Exchange Reaction. When hydrogen was introduced into various catalyst systems, the absorption of hydrogen took place at various extents, as given in Table 1. The absorption of hydrogen by Ag–Cs, for example, is shown in Fig. 2. A negligible amount of thermal desorption of the

Table 1. Catalytic activity of the catalysts

Catalyst	Alkali metals			IB metal	Binary system 1[a]		Binary system 2[a]	
	Na	K	Cs	Ag	Ag–K	Ag–Cs	Ag–Na	Au–Cs
H_2 absorption[b] /cm³ STP (t/°C)					3×10^3 (46)	3×10^4 (23)	≈0 (120)	≈0 (22)
Ea/kJ mol^{-1} [c] (t/°C)	109±8 (150—250)	49±4 (35—120)	34±4 (25—100)	46±8 (90—220)	32.8±0.4 (−65—50)	26±1 (T[d]—55)	76±8 (50—100)	50±4 (110—140)
						<10.1 (−80—T[d])		15.5±0.4 (0—110)
k_1[e]/h^{-1} g^{-1} (0°C)	$<2\times10^{-5}$	2×10^{-4}	3×10^{-2}	3×10^{-6}	1.5	1.7	1×10^{-4}	1×10^{-1}
k_1[f]/h^{-1} (0°C)	$<5\times10^{-4}$	8×10^{-3}	4	—	8×10^2	3×10^3	2	7×10
log(A[g]/h^{-1} g^{-1})	<14±1	5.7±0.3	5.1±0.4	3.7±0.5	6.3±0.1	4.2±0.3	10.5±1.0	4.8±0.2
log(A[h]/h^{-1})	<15±1	7.3±0.3	7.2±0.4	—	9.0±0.1	7.4±0.3	14±1	7.6±0.2
k_1'[i]/h^{-1} g^{-1} (t/°C)	—	—	1×10^{-1} (100)	—	1×10^{-2} (94)	4×10^{-1} (100)	—	2×10^{-2} (140)
Site					A[j] and B[k]		A	

a) Binary system 2 forms metallic compounds, whereas binary system 1 does not. b) The amount of saturated absorption of hydrogen per mole of alkali metal in the catalyst. c) Apparent activation energy for the H_2-D_2 exchange reaction. d) $-40\,°C<T<-23\,°C$. e) Rate constant for the H_2-D_2 exchange reaction per gram of the catalyst. f) Rate constant for the H_2-D_2 exchange reaction per mole of alkali metal in the catalyst. g) Frequency factors for the H_2-D_2 exchange reaction per gram of the catalyst. h) Frequency factors for the H_2-D_2 exchange reaction per mole of alkali metal in the catalyst. i) Rate constants for ethylene hydrogenation. j), k) See text.

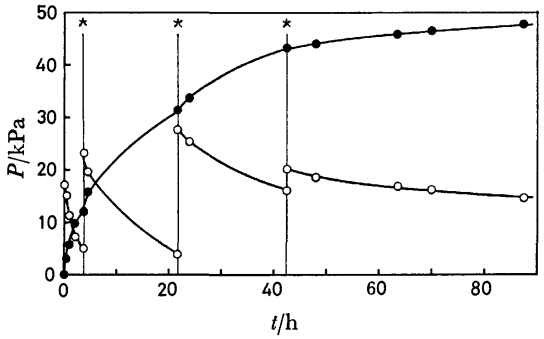

Fig. 2. Absorption of hydrogen on Ag–Cs at 23 °C. ○: pressure of hydrogen gas, ●: total decrease in pressure, *i.e.*, amount of absorbed hydrogen (The pressure decrease of 1 kPa corresponds to the absorption of 0.35 cm³ STP/g-catalyst.). At the point denoted by * hydrogen was added into gas phase.

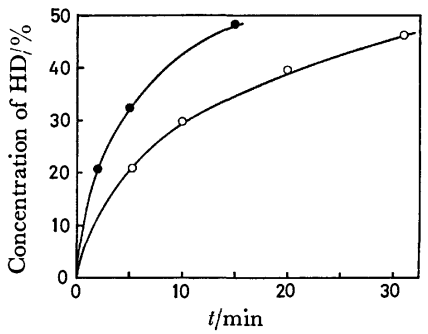

Fig. 3. The H_2-D_2 exchange reaction over Ag–Cs. The total pressure of reacting gas was 8 kPa. The equimolar mixture of H_2 and D_2 was introduced over the catalyst with preabsorbed hydrogen of 170 cm³ STP per 9.5 g catalyst. Reaction temperature; ○: 0 °C, ●: 23 °C.

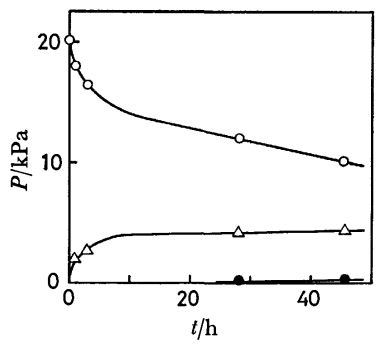

Fig. 4. The exchange reaction between gaseous deuterium and the absorbed hydrogen on Ag–Cs at 23 °C. The total amount of hydrogen preabsorbed at 23 °C was 150 cm³ STP per 9.5 g catalyst. ○: D_2, ●: H_2, △: HD.

absorbed hydrogen took place *in vacuo* below 170 °C, the amounts of saturated absorption remaining unchanged. No appreciable hydrogen absorption was detected on the alkali metals in the absence of silver under the same conditions. At higher temperatures, however, alkali metals reacted with hydrogen, forming hydrides.

When an equimolar mixture of H_2 and D_2 was introduced over Ag–K and Ag–Cs systems, the H_2-D_2 exchange reaction took place at a rather high rate at room temperature, as shown in Fig. 3. When deuterium was introduced over the Ag–K and Ag–Cs catalysts, which contained preabsorbed hydrogen, at a temperature above 100 °C and at room temperature, respectively, at first HD quickly appeared in the gas phase but soon slowed down, as shown in Fig. 4. The rate of HD formation after the initial surge was 10^2 or 10^3 times slower than that in the H_2-D_2 exchange reaction under similar reaction conditions. The deuterium preabsorbed over Ag–Cs participated in the hydrogenation of ethylene and propylene at 100 °C, whereas the deuterium in the alkali metal hydrides, in the absence of silver, did not.

The H_2-D_2 exchange reaction was of first order with respect to the total pressure. The dependence of the reaction rate with pressure for Ag–K at 0 °C is shown

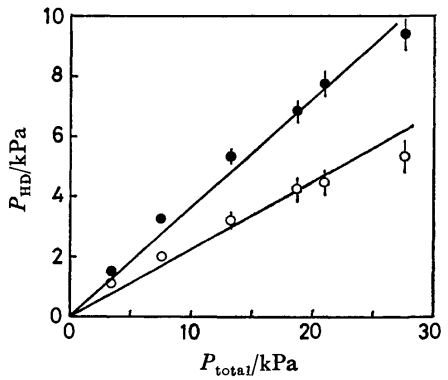

Fig. 5. Pressure dependence of the rate of the H_2-D_2 exchange reaction over Ag-K at 0 °C, with the initial amount of H_2 equal to that of D_2. Reaction time; ○: 2 min, ●: 6 min.

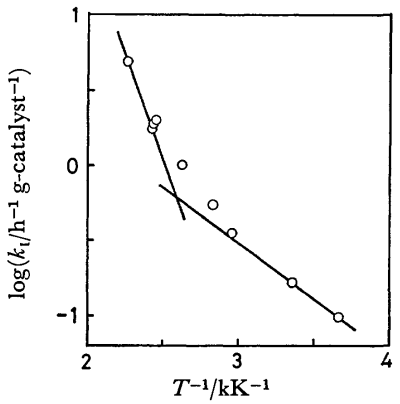

Fig. 6. Temperature dependence of the rate constants of the H_2-D_2 exchange reaction over Au-Cs.

in Fig. 5. The rate constant k_1 was calculated using the equation,

$$k_1 = -\frac{1}{t} \ln \frac{[HD_\infty]-[HD_t]}{[HD_\infty]},$$

where $[HD_t]$ and $[HD_\infty]$ are the concentrations of HD at time t and that at equilibrium, respectively. The temperature dependence of k_1 over Au-Cs is shown in Fig. 6. The apparent activation energies for the reaction over various catalysts are listed in Table 1. The activation energies were not affected by the heat treatments, although the rate of the exchange reaction was changed. The catalytic activity of each of the Ag-alkali metal catalysts was increased by repeated heat treatments and approached a saturated value at a given temperature between 100 and 200 °C under vacuum. The activity decreased, however, when the temperature of the heat treatment was higher than 200 °C. In the case of Au-Cs, the catalytic activity remained constant for heat treatments up to a temperature of 260 °C *in vacuo*. In the case of Ag-K and Ag-Cs catalysts, the rate of the H_2-D_2 exchange reaction was neither affected by the preabsorbed hydrogen nor by the presence of ethylene. The activity of Au-Cs was markedly enhanced (more than ten times) when fresh cesium metal was additionally evaporated onto the catalyst, but decreased and finally reached the original value after repeated heat treatments. The first order rate constants for the exchange reaction on each catalyst are listed in Table 1. In some systems, the measurements were carried out at temperatures above 0 °C, and the values of the rate constant k_1 at 0 °C were then estimated from their temperature dependences. The results given in Table 1 lead to the following conclusions.

(1) The catalytic activity of silver for the H_2-D_2 exchange reaction is increased by contact with alkali metals as follows:
3×10 for Ag-Na/Ag, 5×10^5 for Ag-K/Ag, and 6×10^5 for Ag-Cs/Ag.

(2) The increase in the activity per mole of the alkali metals by contact with IB metals are as follows: 5×10^3 for Ag-Na/Na, 1×10^5 for Ag-K/K, 7×10^2 for Ag-Cs/Cs and 2×10 for Au-Cs/Cs.

(3) The activity per mole of the alkali metal was in the following increasing orders:
Na<K<Cs and Ag-Na<Au-Cs<Ag-K<Ag-Cs.

The frequency factors for the exchange reaction are listed in Table 1.

Hydrogenation of Ethylene and Propylene. When ethylene or propylene was brought into contact with Ag-Cs which contained preabsorbed hydrogen (or deuterium) at 100 °C, olefin adsorption took place and simultaneously ethane or propane (with deuterium) appeared in the gas phase. Cs metal adsorbed the olefins at 100 °C and the alkanes were formed concurrently through self-hydrogenation of the olefins. When hydrogen was introduced after ethylene had been preadsorbed on Ag-Cs and Cs, 10—20% of the preadsorbed ethylene reacted to form ethane with a small amount of 2-butenes. On the other hand, most of the propylene adsorbed on Ag-Cs was desorbed into the gas phase upon the introduction of hydrogen with only a small amount of propane, followed by slow hydrogenation. Ag-K containing preabsorbed hydrogen adsorbed little ethylene at 20—50 °C, as hydrogen is adsorbed more strongly than ethylene.

The hydrogenation of ethylene with molecular hydrogen to form ethane took place on Ag-Cs, Ag-K, Au-Cs, and Cs, and the pressure dependence of this process was first order with respect to the amount of ethylene and zeroth order with respect to the amount of hydrogen, as shown in Fig. 7. The reaction rate can accordingly be expressed by the equation,

$$\text{rate} = k_1'[C_2H_4],$$

where k_1' is the rate constant and $[C_2H_4]$ is the partial pressure of ethylene. The k_1' for each catalyst is given in Table 1.

The initial rate of ethylene hydrogenation over Ag-Cs between hydrogen gas and ethylene was more than fifty times as fast as that between ethylene and preabsorbed hydrogen in the absence of gaseous hydrogen at 100 °C.

It was also demonstrated that hydrogen in the gas phase at higher pressures inhibits the production of propane over Ag-Cs and Cs at 100 °C, as is shown in Fig. 8.

The hydrogen exchange reaction between propylene and deuterium was approximately 100 times faster than the hydrogenation of propylene on Au-Cs at 215 °C. The isotopic distribution of the deuterated propylenes

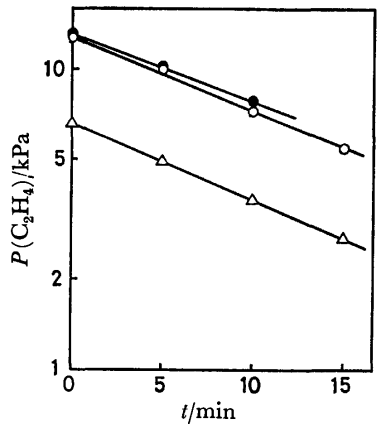

Fig. 7. The hydrogenation of ethylene in the presence of gaseous hydrogen over Ag–Cs with preabsorbed hydrogen at 0 °C. Total amount of the preabsorbed hydrogen was 170 cm³ STP per 9.5 g catalyst. The initial composition of the gaseous mixture; ○: C_2H_4 12.9 kPa, H_2 14.0 kPa, △: C_2H_4 6.6 kPa, H_2 13.4 kPa, ●: C_2H_4 13.2 kPa, H_2 6.6 kPa.

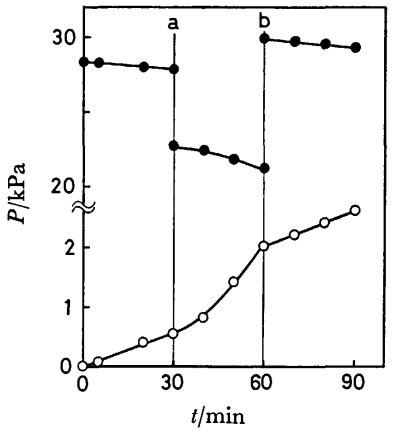

Fig. 8. The hydrogenation of propylene over Ag–Cs with preabsorbed hydrogen at 104 °C. The total amount of absorbed hydrogen was 170 cm³ STP per 9.5 g catalyst. The initial gas was composed of 15.0 kPa of propylene and 13.3 kPa of hydrogen. a) Hydrogen gas was partially removed. b) Hydrogen gas was added. ●: Total pressure of gas phase. ○: Propane pressure. Hydrogen absorption was saturated and the partial pressure of C_3 species in the gas phase was not changed in the course of reaction, and, consequently, the decrease in pressure during the reaction corresponds to the production of propane.

determined by their microwave spectra[9] indicated that no hydrogen exchange takes place at the 2-carbon positions and only the hydrogen at both end carbons participates in the exchange.

Discussion

It is, thus, demonstrated that alkali metal-doped IB metal catalysts have higher catalytic activities for hydrogen activation reactions per mole of each constituent than each of the IB metals or alkali metals, as given in Table 1. The activation energies for the H_2-D_2 exchange reaction were also changed by the doping. This behavior is similar to that of other alkali metal-doped catalysts, such as potassium-condensed aromatic hydrocarbons.[2] Thus, when they are brought into contact, the electron donor (alkali metals) and acceptor (IB metals) exhibit new catalytic activity, higher than each of the constituents.

The H_2-D_2 exchange reaction was of first order with respect to the total pressure, and the hydrogenation of ethylene was of first order with respect to the amount of ethylene and of zeroth order with respect to that of hydrogen. In addition to the kinetic expression, the H_2-D_2 exchange reaction was not retarded by the presence of ethylene, which strongly suggests that hydrogen is more strongly adsorbed than olefins.

It has been reported that the Ag–Na and the Au–alkali metal systems form metallic compounds, whereas no such compounds are formed in the Ag–K and Ag–Cs systems.[10] The latter group is more active in activating molecular hydrogen. The activity of these doped catalysts also depends upon the electropositivity of the alkali metals, which is in the following increasing order, Na<K<Cs. A higher electropositivity generally results in a higher catalytic activity.

The behavior of the IB metal–alkali metal catalysts suggests the following scheme for the active sites relevant to hydrogen activation. The IB metal–alkali metal catalysts appear to possess at least two kinds of active sites for hydrogen activation and absorption, site (A) and site (B). The H_2-D_2 exchange reaction proceeds mainly *via* adsorbed hydrogen (or deuterium) on site (A), while the absorption of hydrogen takes place on site (B), most of the hydrogen thus absorbed hardly participating in the exchange reaction.

Site (A) is apparently much more active when no metallic compounds are formed between the constituents or if the alkali metals are more electropositive. The heat treatment under vacuum changes only the number of sites, the apparent activation energy remaining unchanged. Site (A) may be considered to be located at the doped alkali metal which is in contact with the IB metal because of the similarity in the reaction kinetics over site (A) with those over alkali metals; *i.e.*, the similarity of the pressure dependences in the H_2-D_2 exchange reaction and in ethylene hydrogenation. The contact with IB metals reduces the activation energies for the reaction on the alkali metal.

In the case of Au–Cs, further addition of cesium by evaporation produced higher activity, but subsequent heat treatments reduced the enhanced activity to its original magnitude. Two different activation energies for the H_2-D_2 exchange reaction were observed over the reaction-temperature range, as shown in Fig. 6.

Hydrogen is strongly absorbed on site (B) such that the absorbed hydrogen is not desorbed by mild heat treatments *in vacuo*. Site (B) is less active than site (A) for the H_2-D_2 exchange reaction and the hydrogenation of ethylene. In the case of hydrogenation of propylene, higher hydrogen pressures even retard the rate of hydrogenation, as shown in Fig. 8.

Since the atomic ratio of the total amount of absorbed hydrogen to cesium was more than two on Ag–Cs, as

given in Table 1, the formation of alkali metal hydride cannot account for all of the absorbed hydrogen, while silver metal alone absorbs no hydrogen. It is thus revealed that the contact of cesium with silver exhibits new activity not only for hydrogen activation reactions, such as the H_2-D_2 exchange and hydrogenation reactions, but also for hydrogen uptake. Although the reason why such new activity appears is a matter of conjecture, electron donation from the alkali metal to the IB metal is most probably associated with this phenomenon.

Conclusion

High catalytic activity for hydrogen activation reactions was produced by the contact of alkali metals with IB metals. The addition of alkali metals activates the silver surface for the chemisorption of hydrogen. The enhanced activity of alkali metals upon contact with IB metals is due to the decrease in the activation energy.

The new catalytic activity is considered to be caused by electron donation from the alkali metal to the IB metal and not by the formation of metallic compounds.

The authors thank Dr. T. Kondo of the Sagami Chemical Research Center for undertaking the mass and microwave spectroscopic analyses.

References

1) M. A. M. Boersma, *Catal. Rev.*, **10**, 243 (1975).
2) M. Ichikawa, M. Soma, T. Onishi, and K. Tamaru, *J. Catal.*, **9**, 418 (1967); *Trans. Faraday Soc.*, **63**, 1215, 2015, 2528 (1967).
3) M. Ishizuka and A. Ozaki, *J. Catal.*, **35**, 320 (1974).
4) M. Ichikawa, M. Soma, T. Onishi, and K. Tamaru, *Z. Phys. Chem. N. F.*, **68**, 327 (1969).
5) G. Brauer, Ed., "Handbook of Preparative Inorganic Chemistry," 2nd ed, Vol. 1, Academic Press, New York, London (1963), p. 961.
6) J. C. Bailar, Jr., Ed., "Inorganic Syntheses," McGraw-Hill, Vol. 4 (1953), p. 15.
7) A. Herold, *Bull. Soc. Chim. Fr.*, **1955**, 999.
8) H. Inokuchi, N. Wakayama, T. Kondow, and Y. Mori, *J. Chem. Phys.*, **46**, 837 (1967).
9) T. Kondo, S. Saito, and K. Tamaru, *J. Am. Chem. Soc.*, **96**, 6857 (1974).
10) V. G. Kienast and J. Verma, *Z. Anorg. Allg. Chem.*, **310**, 143 (1961).

The Absorption Spectra of Disubstituted Benzenes. Interpretation by Means of Configuration Analysis

Tsuneo Fujii, Satoshi Suzuki, and Michiyuki Fujishima*

Department of Industrial Chemistry, Faculty of Engineering, Shinshu University, Wakasato, Nagano 380

(Received November 4, 1976)

The method of configuration analysis has been applied to the interpretation of the ground and the excited states of disubstituted benzenes with two electron-donating groups, *o*-, *m*-, and *p*-benzenediols and *o*-, *m*-, and *p*-phenylenediamines, with particular attention paid to the dependence of the spectra on the positions of substitution and on the molecular symmetry. The wave functions calculated by the Pariser-Parr-Pople method are analyzed in terms of locally-excited states and intramolecular charge-transfer states. The characteristic changes in the location of the L_b, L_a, and B_b bands caused by substitution are adequately explained by the analysis. The intensification of the L_b band caused by the introduction of the substituents is interpreted as due to the mixing between the L_b, B_b, and B_a bands for the *o*- and *m*-substituted benzenes and between the L_b and B_b bands for the *p*-disubstituted benzenes. It was found empirically that the magnitudes of the spectral shift from benzene to the derivatives are determined primarily by the extent of charge-transfer contributions.

Although the effects of substitution on the electronic spectra have been extensively investigated for monosubstituted benzenes,[1-7] the electronic spectra of disubstituted benzenes have received little attention.[8-14] Kiss and Szöke have calculated many disubstituted benzenes, including fluoro, chloro, hydroxyl, amino, formyl, carboxyl, and nitro groups, and have discussed the singlet transition energies as well as the ground-state charge densities and bond orders.

The present paper will report on the results of the configuration analysis (CA) of six disubstituted benzenes: *o*-, *m*-, and *p*-benzenediols (*o*-, *m*-, and *p*-$(OH)_2$) and *o*-, *m*-, and *p*-phenylenediamines (*o*-, *m*-, and *p*-$(NH_2)_2$). The *o*- and *m*-disubstituted benzenes both have the C_{2v} symmetry, but the former have the symmetry axis along the b-axis of the benzene ring, while the latter have the symmetry axis along the a-axis of the benzene ring. The *p*-disubstituted benzenes have the D_{2h} symmetry and have the symmetry axis along the b-axis of the benzene ring.

Calculation

The method of calculation, the procedure, the parameters, and the molecular geometry are the same as have previously been described except for one added substitution.[6,7] The geometry of the compounds studied in this paper are shown in Fig. 1. The SCF MO's are numbered in the order of increasing energy. In the CI calculation of all the compounds, the following 10 singly-excited configurations are included: 5→6, 7, 8; 4→6, 7, 8; 3→6, 7; 2→6, 7.

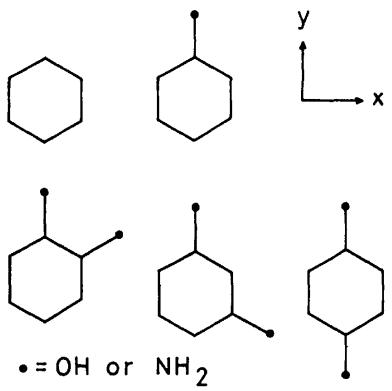

Fig. 1. The molecular geometry of the compounds.

Experimental

o-Benzenediol and phenylenediamines were purified by repeated crystallizations and subsequent sublimation *in vacuo* prior to use. Isooctane (2,2,4-trimethylpentane) was fractionally distilled and then passed through a column of silica gel. The absorption spectra were recorded on a Hitachi EPS-3 recording spectrophotometer.

Results

The calculated energies, the oscillator strengths, and the directions of the transition moments, which are the angles from the x-axis, for the lower singlet states of the six compounds are presented in Table 1, together with the available experimental data. The symbols used in the present paper for denoting the electronic states and absorption bands have the same meaning as the corresponding symbols in previous papers,[6,7] unless otherwise noted.

The results of the CA of the six compounds are given in Tables 3—8. The reference MO's employed in the analysis are the SCF MO's of benzene $\phi_1^\circ, \cdots, \phi_6^\circ$, and the 2 MO's of the substituents, ϕ_{X+}° and ϕ_{X-}°, which are the linear combination of the AO's, χ_1 and χ_2, of the substituents:

$$\phi_{X+}^\circ = \frac{1}{\sqrt{2}}(\chi_1+\chi_2),$$

$$\phi_{X-}^\circ = \frac{1}{\sqrt{2}}(\chi_1-\chi_2).$$

The reference states taken into account in the analysis are as follows: the ground and 4 locally-excited states of benzene, Ψ_G°, $\Psi_1^\circ, \cdots, \Psi_4^\circ$: 4 intramolecular charge-transfer reference states, Ψ_{CT4+}°, Ψ_{CT4-}°, Ψ_{CT5+}°, and Ψ_{CT5-}°. The Ψ_{CT4+}° corresponds to a one-electron excitation from ϕ_{X+}° to ϕ_4°, *etc.* The total weight means the sum of the weights of all 9 reference states described above.

* Present address: Waste Water Treatment Section, Matsushita Pollution Control Co., Ltd., 3-1-1 Inazu, Toyonaka, Osaka.

Table 1. Excited states of disubstituted benzenes

Compound	State function	Energy (eV) Calcd	Energy (eV) Obsd	Oscillator strength Calcd	Oscillator strength Obsd	Band assignment	Polarization (deg)
o-Benzenediol(catechol)							
	Ψ_G	0					
	Ψ_1	4.60	4.48	0.048	0.060	I	60
	Ψ_2	5.43	5.78	0.108	0.163	II	−30
	Ψ_3	6.40	6.24	0.848		III	−30
	Ψ_4	6.51		1.183		IV	60
	Ψ_5	7.77		0.008			−30
m-Benzenediol(resorcinol)							
	Ψ_G	0					
	Ψ_1	4.66	4.50[a]	0.030	0.052[a]	I	−60
	Ψ_2	5.56	5.69[a]	0.052	0.163[a]	II	30
	Ψ_3	6.37		0.845		III	30
	Ψ_4	6.49		1.291		IV	−60
	Ψ_5	7.65		0.027			−60
p-Benzenediol(hydroquinone)							
	Ψ_G	0					
	Ψ_1	4.47	4.26[a]	0.105	0.070[a]	I	0
	Ψ_2	5.50	5.54[a]	0.233	0.106[a]	II	90
	Ψ_3	6.69		0.838		III	0
	Ψ_4	6.73		1.215		IV	90
	Ψ_5	7.32		0.000			
o-Phenylenediamine							
	Ψ_G	0					
	Ψ_1	4.30	4.22	0.069	0.038	I	60
	Ψ_2	4.85	5.23	0.163	0.107	II	−30
	Ψ_3	5.84	6.02	0.364	0.662	III	−30
	Ψ_4	5.96		0.885		IV	60
	Ψ_5	7.06		0.032			−30
m-Phenylenediamine							
	Ψ_G	0					
	Ψ_1	4.40	4.19	0.035	0.021	I	−60
	Ψ_2	5.07	5.17	0.091	0.083	II	30
	Ψ_3	5.69	5.79	0.387	0.502	III	−60
	Ψ_4	5.70		0.867		IV	−60
	Ψ_5	6.91		0.228			−60
p-Phenylenediamine							
	Ψ_G	0					
	Ψ_1	4.13	3.89	0.108	0.031	I	0
	Ψ_2	4.90	5.10	0.440	0.180	II	−90
	Ψ_3	5.98		0.000			
	Ψ_4	6.16		0.000			
	Ψ_5	6.41	6.23	0.462	0.559	III	0
	Ψ_6	6.62		0.983		IV	−90
	Ψ_7	7.62		0.000			

a) Ref. 8.

The band assignments are given in Tables 3—8. When a single reference state has a weight higher than 50%, the state notation of the state is indicated in the column of the band assignments.

Discussion

The calculated band shifts in the transition energies caused by the introduction of hydroxyl and amino groups are compared with the observed band shifts including phenol and aniline in Table 2. There are 4 electronic absorption bands in the ultraviolet region. Although the same parameters are used irrespective of the positions of substitution, the calculated and observed band shifts agree very well except for Band II of the *o*-disubstituted benzenes. The effect of *o*-substitution may perhaps appear in Band II of *o*-disubstituted benzenes. The order of the observed band shifts, ΔE, of the individual absorption band are: $\Delta E(p\text{-}) > \Delta E(m\text{-}) \approx \Delta E(o\text{-})$ for Band I; $\Delta E(p\text{-}) > \Delta E(m\text{-}) > \Delta E(o\text{-})$ for

Table 2. Comparison of the calculated and observed band shifts caused by the introduction of the substituent into benzene (eV)

Compound		Band I	II	III	IV
Phenol	Calcd[a]	−0.24	−0.34	−0.26	−0.17
	Obsd[b]	−0.30	−0.35	−0.28	−0.05
Aniline	Calcd[c]	−0.47	−0.74	−0.65	−0.29
	Obsd[b]	−0.49	−0.78	−0.58	−0.10
o-$(OH)_2$	Calcd	−0.41	−0.64	−0.50	−0.39
	Obsd	−0.40	−0.40		
m-$(OH)_2$	Calcd	−0.35	−0.51	−0.53	−0.41
	Obsd	−0.39	−0.48		
p-$(OH)_2$	Calcd	−0.54	−0.57	−0.21	−0.17
	Obsd	−0.63	−0.63		
o-$(NH_2)_2$	Calcd	−0.71	−1.22	−1.06	−0.94
	Obsd	−0.68	−0.94	−0.96	
m-$(NH_2)_2$	Calcd	−0.61	−1.00	−1.21	−1.20
	Obsd	−0.70	−1.00	−1.19	
p-$(NH_2)_2$	Calcd	−0.88	−1.17	−0.50	−0.28
	Obsd	−1.00	−1.07	−0.75	

a) Ref. 6. b) K. Kimura, H. Tsubomura, and S. Nagakura, *Bull. Chem. Soc. Jpn.*, **37**, 1336 (1964); K. Kimura and S. Nagakura, *Mol. Phys.*, **9**, 117 (1965); S. Nagakura and K. Kimura, *Nippon Kagaku Zasshi*, **86**, 1 (1965). c) Ref. 7.

Band II; $\Delta E(m\text{-})>\Delta E(o\text{-})>\Delta E(p\text{-})$ for Band III.

Band Assignment. Tables 3—5 show the results of the CA of the benzenediols. The first and the second bands of *o*-, *m*-, and *p*-$(OH)_2$ can reasonably be assigned to the L_b and L_a respectively. Since a strong mixing is found to occur between the B_b and B_a reference states in the Ψ_3 and Ψ_4 excited states, one can hardly identify the B_b and B_a bands in the cases of *o*- and *m*-$(OH)_2$. On the other hand, Band III and IV, which may be found in the higher energy side of Band II, of *p*-$(OH)_2$ are assigned to the B_b and B_a respectively. The main charge-transfer reference states to each state are as follows: Ψ°_{CT4-} (Band I), Ψ°_{CT5+} (Band II), Ψ°_{CT4+} (Band III), and Ψ°_{CT4-} (Band IV) in *o*-$(OH)_2$, Ψ°_{CT4+} (Band I), Ψ°_{CT5-} (Band II), Ψ°_{CT4-} (Band III), and Ψ°_{CT5+} (Band IV) in *m*-$(OH)_2$, and Ψ°_{CT4+} (Band I), Ψ°_{CT5-} (Band II), Ψ°_{CT4+} (Band III), and Ψ°_{CT5-} (Band IV) in *p*-$(OH)_2$.

Table 3. Configuration analysis for *o*-benzenediol (weight in percent)

Reference state: Wave function[a]	State notation	Absorption band (upper) and state function (lower): Ψ_G	I Ψ_1	II Ψ_2	III Ψ_3	IV Ψ_4
Ψ_G°		82.2	0.2			3.5
Ψ_1°	L_b	0.0	66.2			7.3
Ψ_2°	L_a			56.2	8.7	
Ψ_3°	B_b	0.0	0.3	2.1	42.3	13.8
Ψ_4°	B_a	0.1	1.0	0.7	14.1	41.5
Ψ°_{CT4+}		2.2	0.7	1.7	8.6	0.9
Ψ°_{CT4-}		2.7	11.1	5.9	2.1	8.5
Ψ°_{CT5+}		0.9	3.7	17.8	6.2	2.8
Ψ°_{CT5-}		6.7	2.0	0.6	2.9	2.7
Total weight[a]		94.8	85.1	85.1	84.9	81.0
Assignment[a]		[G]	[L_b]	[L_a]		

a) See text for definition.

Table 4. Configuration analysis for *m*-benzenediol (weight in percent)

Reference state: Wave function[a]	State notation	Absorption band (upper) and state function (lower): Ψ_G	I Ψ_1	II Ψ_2	III Ψ_3	IV Ψ_4
Ψ_G°		80.0		6.3	0.1	
Ψ_1°	L_b		69.1			2.1
Ψ_2°	L_a	0.6		60.5	0.7	
Ψ_3°	B_b	0.0	0.3	0.7	43.1	13.8
Ψ_4°	B_a	0.0	1.0	0.2	14.4	41.5
Ψ°_{CT4+}		2.5	8.2	2.2	2.1	7.1
Ψ°_{CT4-}		2.6	0.8	2.7	12.0	4.0
Ψ°_{CT5+}		0.9	2.4	0.9	4.0	12.0
Ψ°_{CT5-}		7.5	2.7	6.5	6.2	2.4
Total weight[a]		94.1	84.5	80.0	82.5	82.9
Assignment[a]		[G]	[L_b]	[L_a]		

a) See text for definition.

Table 5. Configuration analysis for *p*-benzenediol (weight in percent)

Reference state: Wave function[a]	State notation	Absorption band (upper) and state function (lower): Ψ_G	I Ψ_1	II Ψ_2	III Ψ_3	IV Ψ_4
Ψ_G°		81.5				
Ψ_1°	L_b		61.0		16.1	
Ψ_2°	L_a			60.3		3.4
Ψ_3°	B_b		4.7		62.4	
Ψ_4°	B_a			4.9		66.2
Ψ°_{CT4+}			17.8		8.5	
Ψ°_{CT4-}						
Ψ°_{CT5+}		12.6				
Ψ°_{CT5-}				22.4		5.4
Total weight[a]		94.0	83.4	87.6	86.9	82.9
Assignment[a]		[G]	[L_b]	[L_a]	[B_b]	[B_a]

a) See text for definition.

Since the amino group is known to be a strong electron donor, charge-transfer configurations are mixed effectively with locally-excited states of benzene of a lower energy, as is seen in Tables 6—8. Accordingly, the amino-substitution has a greater influence on the electronic structure of benzene than does the hydroxy-substitution.

The most important reference states in the excited states of phenylenediamines are the charge-transfer reference states. Indeed, Ψ°_{CT4+} in the Ψ_3 of *o*-$(NH_2)_2$ and in the Ψ_1 of *p*-$(NH_2)_2$, Ψ°_{CT4-} in the Ψ_3 of *m*-$(NH_2)_2$, Ψ°_{CT5+} in the Ψ_2 of *o*-$(NH_2)_2$ and in the Ψ_4 of *m*-$(NH_2)_2$, and Ψ°_{CT5-} in the Ψ_2 of *p*-$(NH_2)_2$ are the most important reference states in the states of phenylenediamines.

The L_b reference state does not interact with the L_a reference state, but interacts with the B_b and B_a for the *o*- and *m*-$(OH)_2$ and the B_b for the *p*-$(OH)_2$, from which the intensity of Band I is derived.

Table 6. Configuration analysis for *o*-phenylenediamine (weight in percent)

Reference state		Absorption band (upper) and state function (lower)				
Wave function[a]	State notation	Ψ_G	I Ψ_1	II Ψ_2	III Ψ_3	IV Ψ_4
Ψ_G°		78.9	0.5			9.8
Ψ_1°	L_b	0.0	48.8			11.3
Ψ_2°	L_a			30.4	8.5	
Ψ_3°	B_b	0.0	0.4	2.2	18.5	5.4
Ψ_4°	B_a	0.1	1.1	0.7	6.2	16.2
Ψ_{CT4+}°		2.7	1.2	2.6	32.6	3.5
Ψ_{CT4-}°		3.2	20.2	11.3	2.1	12.1
Ψ_{CT5+}°		1.1	6.7	33.8	6.4	4.1
Ψ_{CT5-}°		8.0	3.5	0.9	10.9	10.6
Total weight[a]		94.0	82.3	81.9	85.1	74.7
Assignment[a]		[G]				

a) See text for definition.

Table 7. Configuration analysis for *m*-phenylenediamine (weight in percent)

Reference state		Absorption band (upper) and state function (lower)				
Wave function[a]	State notation	Ψ_G	I Ψ_1	II Ψ_2	III Ψ_3	IV Ψ_4
Ψ_G°		76.3		12.9	0.0	
Ψ_1°	L_b		54.0			0.6
Ψ_2°	L_a	0.7		35.3	0.0	
Ψ_3°	B_b	0.0	0.3	0.6	17.9	4.0
Ψ_4°	B_a	0.0	0.9	0.2	6.1	11.5
Ψ_{CT4+}°		3.0	16.0	3.8	4.0	11.3
Ψ_{CT4-}°		3.2	1.5	6.4	30.5	11.2
Ψ_{CT5+}°		1.1	4.4	2.2	9.8	34.7
Ψ_{CT5-}°		9.0	5.4	11.6	12.1	3.6
Total weight[a]		93.1	82.4	73.0	80.6	77.0
Assignment[a]		[G]	[L_b]			

a) See text for definition.

Table 8. Configuration analysis for *p*-phenylenediamine (weight in percent)

Reference state		Absorption band (upper) and state function (lower)				
Wave function[a]	State notation	Ψ_G	I Ψ_1	II Ψ_2	III Ψ_5	IV Ψ_6
Ψ_G°		78.1				
Ψ_1°	L_b		42.9		33.2	
Ψ_2°	L_a			32.8		28.8
Ψ_3°	B_b		4.3		33.7	
Ψ_4°	B_a			4.9		42.9
Ψ_{CT4+}°			33.1		17.7	
Ψ_{CT4-}°						
Ψ_{CT5+}°		15.1				
Ψ_{CT5-}°				46.5		6.5
Total weight[a]		93.3	80.3	84.2	84.6	78.2
Assignment[a]		[G]				

a) See text for definition.

Band Shift. The contributions of charge-transfer configurations to the individual excited states of substituted benzenes are expected to be the principal source of the spectral changes.[15] In order to ascertain the dependence of the spectral shifts on the contribution of charge-transfer states of substituted benzenes, the calculated state energies, E_{calcd}, for Bands I, II, III, and IV are plotted against the total charge-transfer weights, W_{CT}, including the corresponding values of phenol and aniline. The calculated state energies of benzene are also plotted on the axis of the ordinate in Fig. 2.

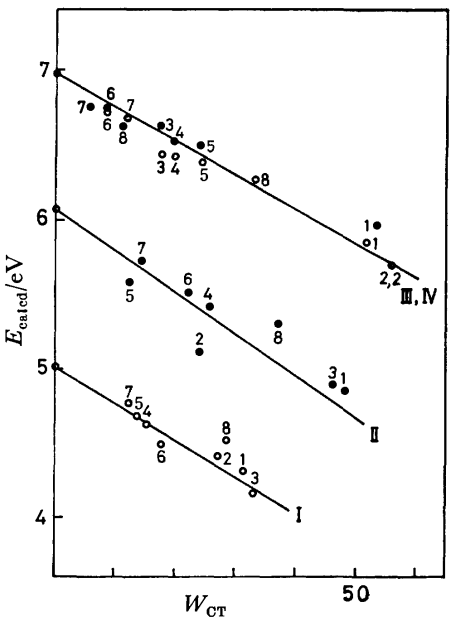

Fig. 2. The plots of E_{calcd} against W_{CT}. 1: *o*-Diaminobenzene, 2: *m*-diaminobenzene, 3: *p*-diaminobenzene, 4: *o*-dihydroxybenzene, 5: *m*-dihydroxybenzene, 6: *p*-dihydroxybenzene, 7: phenol, 8: aniline. The calculated state energies of benzene are plotted on the axis of ordinate. Band I: ○; Band II: ●; Band III: ○; Band IV: ●. Band III and IV lie on the same line.

It may be seen from Fig. 2 that approximately linear relationships exist between E_{calcd} and W_{CT} for individual bands of benzene derivatives including phenol and aniline. The plots of E_{calcd} against W_{CT} for Band I intersect the ordinate axis at the point corresponding to the L_b-state energy of benzene. The plot for Band II may be approximated by a straight line, and the point of intersection of the ordinate for Band II is the point representing the L_a-state energy of benzene. The plots for Bands III and IV also have an approximately linear relation and lie on the same straight line. It is to be noted that the gradients for the individual bands have approximately the same values. It is concluded that the plots of E_{calcd} against W_{CT} are approximately linear and that the extrapolations of the plots for each band to zero total weight give the corresponding state energies of benzene.

The plots for the observed state energies, E_{obsd}, against the total charge-transfer weights, W_{CT}, are presented in Fig. 3. Although the observed data are

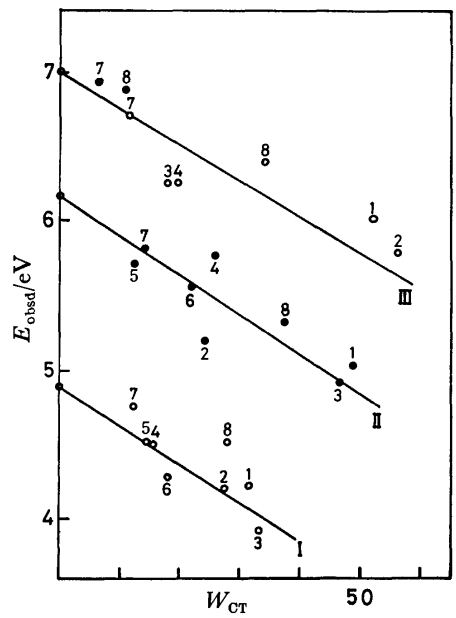

Fig. 3. The plots of E_{obsd} against W_{CT}. The numberings are the same as in Fig. 2. The observed state energies of benzene are plotted on the axis of ordinate.

not so many, approximately linear relationships also exist between E_{obsd} and W_{CT}. As is the case of E_{calcd} *vs.* W_{CT}, the gradients of the individual bands have nearly the same values.

Although the contribution of the charge-transfer configurations to individual bands is expected to increase with the decrease in molecular size, the total weight of the charge-transfer configurations is closely correlated with the spectral shifts on going from benzene to its derivatives, as in the case of naphthalene derivatives.[15] This shows that the total charge-transfer contributions determine the spectral shifts on going from parent compounds to their derivatives.

References

1) H. H. Jaffé and M. Orchin, "Theory and Applications of Ultraviolet Spectroscopy," Wiley, New York (1962).
2) J. N. Murrell, "The Theory of the Electronic Spectra of Organic Molecules," Methuen, London (1963).
3) J. R. Platt *et al.*, "Systematics of the Electronic Spectra of Conjugated Molecules," Wiley, New York (1964).
4) F. A. Matsen, R. S. Becker, and D. R. Scott, "Interpretation of Electronic Absorption Spectra," in "Chemical Application of Spectroscopy," Interscience, New York (1968).
5) C. J. Seliskar, O. S. Khalil, and S. P. McGlynn, "Luminescence Characteristics of Polar Aromatic Molecules," in "Excited States," Vol. 1, Academic Press, New York (1974).
6) H. Baba, S. Suzuki, and T. Takemura, *J. Chem. Phys.*, **50**, 2078 (1969).
7) S. Suzuki and T. Fujii, *Bull. Chem. Soc. Jpn.*, **48**, 835 (1975).
8) A. I. Kiss and J. Szöke, *Chem. Phys. Lett.*, **18**, 195 (1973).
9) A. I. Kiss and J. Szöke, *J. Mol. Struct.*, **18**, 457 (1973).
10) A. I. Kiss and J. Szöke, *Acta Chim. Acad. Sci. Hung.*, **74**, 59 (1972).
11) A. I. Kiss and J. Szöke, KFKI Report 72—58.
12) A. I. Kiss and J. Szöke, KFKI Report 72—72.
13) J. C. Dearden and W. F. Forbes, *Can. J. Chem.*, **37**, 1294 (1959).
14) W. F. Forbes, *Can. J. Chem.*, **37**, 1977 (1959).
15) S. Suzuki and T. Fujii, *J. Mol. Spectrosc.*, **61**, 350 (1976).

Relaxation Studies of the Adsorption-Desorption Equilibrium of Surfactants on the Gas-Liquid Interface. I. Theoretical Studies

Minoru SASAKI, Tatsuya YASUNAGA, and Nobuhide TATSUMOTO

Department of Chemistry, Faculty of Science, Hiroshima University, Higashisenda-machi, Hiroshima 730

(Received November 9, 1976)

A general theory for the propagation characteristics of the capillary wave on the gas-liquid interface, where the physicochemical equilibrium exists, is proposed. The theory is developed on the basis of the two-dimensional relaxation theory and the surface thermodynamics. The relaxation parameters in the equations are closely related to the dynamic behavior of the equilibrium. As an example, the theory was applied to the surfactant solution, taking account of the adsorption-desorption and diffusion processes of the surfactant. The derived equations revealed that the adsorption-desorption process plays an important role in the surfactant transfer between the surface and the bulk phase in a concentrated surfactant solution, while the diffusion process plays such a role in a dilute solution.

The measurements of the propagation characteristics of the capillary wave, *e.g.*, the propagation velocity and the damping coefficient, are effective for the study of the dynamic properties of materials existing on the gas-liquid interface. The theoretical studies for the insoluble monolayers have been performed by Dorrestein,[1] Mayer and Eliassen,[2] and Mann and Du,[3] while those for the soluble monolayer have been performed by van den Tempel and van de Riet,[4] Hansen and Mann,[5] and Lucassen and Hansen.[6] The former has developed their theories taking account of the surface rheologies, and the latter with the assumption that the rate-determining step of surfactant transfer between the surface and the bulk phase is the diffusion process.

Provided that the physicochemical equilibrium on the interface, *e.g.*, the conformational change and the monomer-dimer reaction, is perturbed by the propagation of the wave, the relaxation effect concerned with the equilibrium may be expected. Though studies of such phenomena are valuable for the clarification of the dynamic properties of the equilibrium, theoretical studies have never been performed, while experimentally Davies and Vose[7] have observed the relaxation effect on the surfactant solution.

In the present investigation, a general theory on a surface involving the physicochemical equilibrium is developed on the basis of the relaxation theory[11] and the surface thermodynamics.[12,13]

General Equation

Let us consider a plane wave moving on a liquid surface in the x direction. Here, the motion of an incompressible liquid must satisfy the Navier-Stokes equations:[8]

$$\frac{\partial u}{\partial t} = -\frac{1}{\rho}\frac{\partial p}{\partial x} + \nu\Delta u,$$

$$\frac{\partial v}{\partial t} = -\frac{1}{\rho}\frac{\partial p}{\partial y} + \nu\Delta v - g, \qquad (1)$$

with

$$\frac{\partial u}{\partial x} + \frac{\partial v}{\partial y} = 0,$$

where u and v are the velocity components in the x and y directions respectively; p is the hydrostatic pressure; ν, the kinematic viscosity, and g, the gravitational acceleration. u and v can be written by means of the stream function, Φ, and the potential function, Ψ:

$$u = -\frac{\partial \Phi}{\partial x} - \frac{\partial \Psi}{\partial y},$$

$$v = -\frac{\partial \Phi}{\partial y} + \frac{\partial \Psi}{\partial x}. \qquad (2)$$

In order to solve Eq. 1, one must impose a boundary condition that the liquid motion becomes zero as $y \to -\infty$. Under the condition that the liquid motion satisfies the requirement of simple periodic movement, Φ and Ψ are given by the following equations:

$$\Phi = E_1 \exp(ky) \exp\{i(rt+kx)\},$$

$$\Psi = E_2 \exp(my) \exp\{i(rt+kx)\}, \qquad (3)$$

with

$$m^2 = k^2 + \frac{ir}{\nu},$$

where E_1 and E_2 are the complex constants associated with the amplitudes of Φ and Ψ respectively; k is the wave number; m, the complex constant associated with the decay of liquid motion, and r, the complex angular frequency. From Eqs. 1—3, the equations for the velocities are obtained:

$$u = \{-ikE_1 \exp(ky) - mE_2 \exp(my)\} \exp\{i(rt+kx)\},$$

$$v = \{-kE_1 \exp(ky) + ikE_2 \exp(my)\} \exp\{i(rt+kx)\}. \qquad (4)$$

The liquid motion at the surface is described by the elevation of the surface, ϕ:

$$\frac{\partial \phi}{\partial t} = v_s, \qquad (5)$$

where the subscript s indicates the surface.

The boundary conditions for the normal and tangential stresses[4,6] are given as follows:

$$p - 2\eta\frac{\partial v}{\partial y} + \gamma\frac{\partial^2 \phi}{\partial x^2} = 0,$$

$$\eta\left(\frac{\partial v_s}{\partial x} + \frac{\partial u_s}{\partial y}\right) - \frac{\partial \gamma}{\partial x} - \eta_s\frac{\partial^2 u_s}{\partial x^2} = 0. \qquad (6)$$

The $\left(\frac{\partial \gamma}{\partial x}\right)$ term is expressed as

$$\frac{\partial}{\partial t}\left(\frac{\partial \gamma}{\partial x}\right) = C_s^{-1}\frac{\partial^2 u_s}{\partial x^2}, \qquad (7)$$

with

$$C_s^{-1} = \left(\frac{\partial\gamma}{\partial s}\right), \tag{8}$$

where C_S is the surface compressibility, and s, the surface area per unit area. As C_S reflects the dynamic behavior of the physicochemical equilibrium on the surface, the dynamic surface compressibility has to be introduced. It is derived by applying the relaxation theory to the perturbed equilibrium system.

The following one-step equilibrium existing on a surface is considered:

$$\nu_i R_1 + \cdots + \nu_i R_i \rightleftarrows \nu_1' P_1 + \cdots + \nu_j' P_j,$$

where ν_i and ν_j' are the stoichiometric coefficients, and R_i and P_j, the species. When the wave propagates on the surface, the accompanying liquid motion causes the periodic variation in the surface area, which acts as the external driving force for the disturbance of the equilibrium. Consenquently, the extensive variables such as the concentration or ordering parameter of species, are perturbed periodically, and so behind the external driving force. The relaxation process of the perturbed system is described by the ordering coefficient, ξ, as follows:[11]

$$\xi = LA, \tag{9}$$

with

$$\xi = \bar{\xi} + \Delta\xi \exp(i\omega' t),$$

$$d\xi = \Delta\xi \exp(i\omega' t) = \frac{dN_i}{\nu_i} = \frac{dN_j'}{\nu_j'},$$

where A denotes the chemical affinity; L, the constant; the bar, the equilibrium state; $\omega'(=2\omega)$, the angular frequency associated with the perturbation of the surface area (see Appendix I), and N_i and N_j', the numbers of moles of the R_i and P_j species respectively. A and γ are expanded in terms of the changes in s and ξ in the vicinity of the surface:[12,13]

$$A(\xi, s, S) = \left(\frac{\partial A}{\partial \xi}\right)_{s,S} d\xi + \left(\frac{\partial A}{\partial s}\right)_{\xi,S} ds,$$

$$d\gamma = \left(\frac{\partial \gamma}{\partial \xi}\right)_{s,S} d\xi + \left(\frac{\partial \gamma}{\partial s}\right)_{\xi,S} ds, \tag{10}$$

where S is the entropy. Here, the adiabatic approximation is reasonably applied (see Appendix II). If ds is zero, Eq. 10 becomes:

$$\dot{\xi} = L\left(\frac{\partial A}{\partial \xi}\right)_{s,S} d\xi = -\frac{d\xi}{\tau_{s,S}}. \tag{11}$$

$\tau_{s,S}$ denotes the relaxation time of the local fluctuation of equilibrium. The similarly obtained $\tau_{r,S}$ is related to $\tau_{s,S}$ by the ollowing relation

$$\frac{\tau_{r,S}}{\tau_{s,S}} = \frac{(C_S^{-1})_{\xi,S}}{(C_S^{-1})_{A,S}}. \tag{12}$$

The combination of Eqs. 9 and 10 gives the relationship between $d\gamma$ and ds:

$$d\gamma = \frac{\left(\frac{\partial\gamma}{\partial s}\right)_{A,S} + i\omega'\tau_{s,S}\left(\frac{\partial\gamma}{\partial s}\right)_{\xi,S}}{1+i\omega'\tau_{s,S}} ds. \tag{13}$$

From Eqs. 8 and 13, we obtain the dynamic surface compressibility, C_S^*:

$$(C_S^*)_S^{-1} = (C_S^{-1})_{A,S}\frac{1+i\omega'\tau(\delta+1)}{1+i\omega'\tau}, \tag{14}$$

with

$$\tau_{s,S} = \tau, \quad \delta = \frac{(C_S^{-1})_{\xi,S}}{(C_S^{-1})_{A,S}} - 1,$$

were δ is the relaxation strength.

The combination of Eqs. 2—7 and 14 gives two homogeneous equations for E_1 and E_2:

$$\{E_1(ir^2 - i\sigma^2 + 2\nu k^2 r) - E_2(\sigma^2 + 2i\nu k m r)\} \times \exp\{i(\omega t + kx)\} = 0,$$

$$\{E_1(2i\nu k^2 r + \chi^*\sigma^2) + E_2(ir^2 + 2\nu k^2 r - i\chi^*\sigma^2 m k^{-1})\} \times \exp\{i(\omega t + kx)\} = 0, \tag{15}$$

with

$$\sigma^2 = gk + \frac{\gamma k^3}{\rho}, \tag{16}$$

$$\chi^* = \frac{k^3}{\rho\sigma^2}\left\{(C_S^{-1})_{A,S} + i\eta_S r + (C_S^{-1})_{A,S}\frac{i\omega\tau\delta}{1+i\omega'\tau}\right\}, \tag{17}$$

χ^* consisting of two terms, χ_{ela} and χ_r. The former is attributed to the surface viscoelasticity, and the latter, to the relaxation:

$$\chi_{ela} = \frac{k^3}{\rho\sigma^2}\{(C_S^{-1})_{A,S} + i\eta_S r\}, \tag{18}$$

$$\chi_r = \frac{k^3}{\rho\sigma^2}(C_S^{-1})_{A,S}\left(\frac{\omega'^2\tau^2\delta}{1+\omega'^2\tau^2} + \frac{i\omega'\tau\delta}{1+\omega'^2\tau^2}\right).$$

The available solution of Eq. 15 is given by the following determinant:

$$\begin{vmatrix} ir^2 - i\sigma^2 + 2\nu k^2 r & -\sigma^2 - 2i\nu k m r \\ 2i\nu k^2 r + \chi^*\sigma^2 & ir^2 + 2\nu k^2 r - i\chi^*\sigma^2 m k^{-1} \end{vmatrix} = 0. \tag{19}$$

The propagation velocity, c, and the damping coefficient, α, are defined by the following equations:

$$c = \frac{r_{re}}{k}, \tag{20}$$

$$\alpha = \frac{r_{im}}{V}, \tag{21}$$

where the re and im subscripts indicate the real and imaginary parts respectively, and where $V(=3c/2)$ is the group velocity. In the case of $\chi^* \neq 0$, the complex angular frequency, r, exhibits the frequency dispersion. Then, the dispersion terms, ε_{ela} and ε_r, are introduced as follows.

$$r = \sigma(1 + \varepsilon_{ela} + \varepsilon_r). \tag{22}$$

ε_{ela} and ε_r are concerned with the surface viscoelasticity and the relaxation respectively. From Eqs. 18, 19 and 22, ε_{ela} and ε_r are obtained as:

$$\varepsilon_{ela} = \frac{\frac{2\nu k^2}{\sigma} i + \frac{1}{2}\chi_{ela}}{1 - (1+i)\chi_{ela}\left(\frac{2\nu k^2}{\sigma}\right)^{1/2}}. \tag{23}$$

and

$$\varepsilon_r = \frac{\chi_r}{2}.$$

Therefore, c and α are given by Eqs. 16 and 20—23:

$$c^2 = \left(\frac{g}{k} + \frac{\gamma k}{\rho}\right)(1 + 2\varepsilon_{ela,re} + 2\varepsilon_{r,re}), \tag{24}$$

$$\alpha = \frac{\sigma}{V}(\varepsilon_{ela,im} + \varepsilon_{r,im}). \tag{25}$$

These are the general equations for the propagation

characteristics of the capillary wave, taking account of the relaxation process.

Propagation Characteristics of Wave on the Surface of a Surfactant Solution

The surfactant transfer between the surface and the bulk phase is expressed by the following scheme, taking account of two processes; the adsorption-desorption process between the surface and the subsurface, and the diffusion process between the subsurface and the bulk phase, as is shown schematically in Fig. 1:

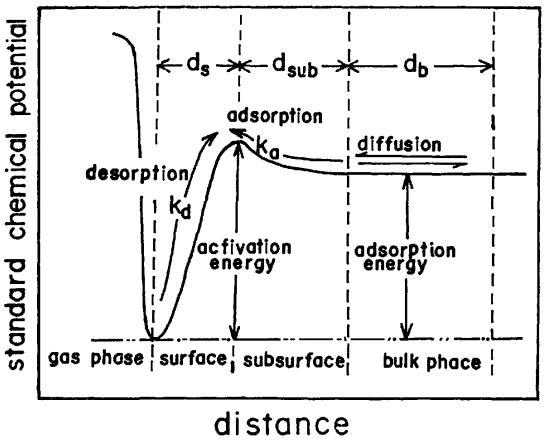

Fig. 1. Diagrammatic representation of the surfactants in the vicinity of surface. k_a and k_d are the adsorption and desorption rate constants, and d_s, d_{sub}, and d_b the thicknesses of the surface, subsurface, and bulk phase layers, respectively.

$$S_s \underset{\text{(adsorption)}}{\overset{k_d\ \text{(desorption)}}{\rightleftharpoons}} S_{sub} \rightleftharpoons S_b, \quad \text{(diffusion)}$$

where S_b, S_{sub}, and S_s are the surfactants in the bulk phase, the subsurface, and the surface, and where k_a and k_d are the adsorption and desorption rate constants, respectively. The adsorption-desorption process is governed by the activation energy of the adsorption and desorption processes and is represented by a Langmuir-type rate equation.[10,14] On the other hand, the diffusion process is expressed by the diffusion theory. Thus, the following equations are given for the adsorption-desorption mechanism:

$$\frac{dc_s}{dt} = k_a(1-\theta)c_{sub} - k_d c_s \quad (-d_{sub} \leq y \leq 0), \tag{26}$$

$$\frac{dc_b}{dt} = D\left(\frac{\partial^2 c_b}{\partial x^2} + \frac{\partial^2 c_b}{\partial y^2}\right) \quad (y < -d_{sub}), \tag{27}$$

where c_s, c_{sub}, and c_b are the molar concentrations of S_s, S_{sub}, and S_b respectively; θ is the fraction of sites occupied by S_s; d_{sub}, the thickness of the subsurface layer, and D, the diffusion coefficient. c_s and θ in Eq. 26 are related by

$$c_s = \frac{10^3 \Gamma_{max}\theta}{d_s}, \tag{28}$$

where Γ_{max} is the maximum value of the surface excess, and d_s, the thickness of the surface layer. When the equilibrium is perturbed, θ, c_{sub}, and c_b are expressed in these forms:

$$\begin{aligned} \theta &= \bar{\theta} + \Delta\theta \exp\{i(\omega' t + \kappa x)\}, \\ c_{sub} &= \bar{c}_{sub} + \Delta c_{sub} \exp\{i(\omega' t + \kappa x)\}, \\ c_b &= \bar{c}_b + \Delta c_b \exp\{i(\omega' t + \kappa x)\}, \end{aligned} \tag{29}$$

where $\kappa(=2k)$ is the wave number of perturbed variables (see Appendix I). Using Eqs. 28 and 29, Eq. 26 is rewritten as

$$i\omega'\Delta\theta = -(k_{a,\theta}\bar{c}_{sub} + k_d)\Delta\theta + k_{a,\theta}(1-\bar{\theta})\Delta c_{sub}, \tag{30}$$

with

$$k_{a,\theta} = \frac{d_s}{10^3 \Gamma_{max}} k_a.$$

The solution of Eq. 27 is

$$\Delta c_b = E_b \exp(ny), \tag{31}$$

with

$$n = d_b^{-1}, \quad n^2 = \kappa^2 + \frac{i\omega'}{D},$$

where E_b is the constant, and d_b, the thickness of the bulk phase concerned with the diffusion process. From Eq. 31, Δc_{sub} becomes (see Appendix III):

$$\Delta c_{sub} = -n d_s \Delta c_s. \tag{32}$$

c_{sub} is expressed by the theory of an electric double layer[8] with the electric potential, ψ_{sub}, at $y=-d_{sub}$:

$$c_{sub} = c_0 \exp\left(-\frac{Ze\psi_{sub}}{k_B T}\right), \tag{33}$$

where c_0 is the initial concentration; Z, the valency; e, the elementary charge; k_B, the Boltzmann constant, and T, the temperature. Combining Eqs. 30, 32 and 33, the relaxation time is derived:

$$\tau^{-1} = \frac{k_{a,\theta}c_0 \exp\left(-\frac{Ze\psi_{sub}}{k_B T}\right) + k_d + k_a n_{re} d_s (1-\bar{\theta})}{1 + k_a n_{im} d_s (1-\bar{\theta})}, \tag{34}$$

with

$$n = n_{re} + i\omega' n_{im}.$$

The relaxation strength δ is derived from Eq. 10 as (see Appendix IV)

$$\delta = -\frac{\left(\frac{\partial\gamma}{\partial\xi}\right)_{s,S}\left(\frac{\partial A}{\partial s}\right)_{\xi,S}}{\left(\frac{\partial\gamma}{\partial s}\right)_{A,S}\left(\frac{\partial A}{\partial\xi}\right)_{s,S}}. \tag{35}$$

This equation is then rewritten by means of the Maxwell relationship:[11]

$$\delta = -\frac{(\Delta\gamma)^2}{(C_s^{-1})_{A,S}\left(\frac{\partial A}{\partial\xi}\right)_{s,S}}, \tag{36}$$

with

$$\Delta\gamma = \left(\frac{\partial\gamma}{\partial\xi}\right)_{s,S},$$

where $\Delta\gamma$ denotes the standard surface tension change. Meanwhile, the chemical affinity, A, is expressed by the chemical potential as follows:

$$A = -\mu_{sub} + \mu_s, \tag{37}$$

with

$$\begin{aligned} \mu_{sub} &= \mu_{sub}^{\ominus} + RT\ln c_{sub}, \\ \mu_s &= \mu_s^{\ominus} + RT\ln\Gamma, \end{aligned}$$

where μ_{sub} and μ_s are the chemical potentials of S_{sub} and S_s respectively; primsol indicates the standard

state, and Γ, the surface excess. The $(\partial A/\partial\xi)_{s,S}$ term in Eq. 35 is rewritten as follows:

$$\left(\frac{\partial A}{\partial \xi}\right)_{s,S}=\left(\frac{\partial A}{\partial \mu_s}\right)_{s,S}\left(\frac{\partial \mu_s}{\partial \Gamma}\right)_{s,S}\left(\frac{\partial \Gamma}{\partial \xi}\right)_{s,S} + \left(\frac{\partial A}{\partial \mu_{sub}}\right)_{s,S}\left(\frac{\partial \mu_{sub}}{\partial c_{sub}}\right)_{s,S}\left(\frac{\partial c_{sub}}{\partial \xi}\right)_{s,S}, \quad (38)$$

$d\xi$ being

$$d\xi = dn_{sub} = -d\Gamma, \quad (39)$$

where n_{sub} is the number of moles of S_{sub} per unit area. Meanwhile, c_{sub} and n_{sub} are related by the following relation:

$$Nn_{sub} = \left(\frac{c_{sub}N}{10^3}\right)^{2/3}, \quad (40)$$

The combination of Eq. 36—40 gives

$$\delta = \frac{(\Delta\gamma)^2}{RT(C_s^{-1})_{A,S}}\left\{\frac{3}{2}\times 10^2 N^{1/3}c_0^{-2/3}\exp\left(\frac{2Ze\psi_{sub}}{3k_BT}\right)+\Gamma^{-1}\right\}^{-1}. \quad (41)$$

$(C_s^{-1})_{A,S}$ in Eqs. 18 and 41 is obtained on the assumption that the adsorption-desorption process is in equilibrium; this is the same as the assumption that the molecular transfer between the surface and the bulk phase is governed by only the diffusion process.[4-6] Thus, the following equation is obtained:

$$(C_s^{-1})_{A,S} = \left(-\frac{\partial\gamma}{\partial \ln\Gamma}\right)\frac{1}{1-\frac{inD}{\omega'}\left(\frac{\partial c_0}{\partial\Gamma}\right)}. \quad (42)$$

According to this equation, Eq. 41 becomes

$$\delta = \frac{(\Delta\gamma)^2}{RT\left(-\frac{\partial\gamma}{\partial\ln\Gamma}\right)}\left\{\frac{3}{2}\times 10^2 N^{1/3}c_0^{-2/3} \times \exp\left(\frac{2Ze\psi_{sub}}{3k_BT}\right)+\Gamma^{-1}\right\}^{-1}. \quad (43)$$

On combining Eqs. 34, 43, and 18, ε_{ela} and ε_r are obtained. Therefore, the equations for the propagation characteristics of the wave for surfactant solutions are finally given as follows:

$$c^2 = \left(\frac{g}{k}+\frac{\gamma k}{\rho}\right)(1+2\varepsilon_{ela,re}+2\varepsilon_{r,re}), \quad (24)$$

$$\alpha = \frac{\sigma}{V}(\varepsilon_{ela,im}+\varepsilon_{r,im}), \quad (25)$$

with

$$\varepsilon_{ela} = \frac{\frac{2\nu k^2}{\rho}i+\frac{k^3}{2\rho\sigma^2}\left[\left(-\frac{\partial\gamma}{\partial\ln\Gamma}\right)\left\{1-\frac{inD}{\omega'}\left(\frac{\partial c_0}{\partial\Gamma}\right)\right\}^{-1}+i\eta_s\sigma\right]}{1-\frac{k^3(1+i)}{\rho\sigma^2}\left[\left(-\frac{\partial\gamma}{\partial\ln\Gamma}\right)\left\{1-\frac{inD}{\omega'}\left(\frac{\partial c_0}{\partial\Gamma}\right)\right\}^{-1}+i\eta_s\sigma\right]\left(\frac{2\nu k^2}{\sigma}\right)^{1/2}}, \quad (44)$$

and

$$\varepsilon_r = \frac{k^3}{2\rho\sigma^2}\left(-\frac{\partial\gamma}{\partial\ln\Gamma}\right)\left\{1-\frac{inD}{\omega'}\left(\frac{\partial c_0}{\partial\Gamma}\right)\right\}^{-1}\left(\frac{\omega'^2\tau^2\delta}{1+\omega'^2\tau^2}+\frac{i\omega'\tau\delta}{1+\omega'^2\tau^2}\right). \quad (45)$$

The relaxation parameters in these equations are given by Eqs. 34 and 43.

Discussion

This theory is applicable to the two-dimensional relaxation phenomena on the surface of a surfactant solution and the monolayer. The derived equations can be simplified easily by evaluating the magnitudes of the parameters.

For the surfactant solutions, the two cases of approximations are given as follows.

Relaxation Effect (or χ_r) is Negligibly Small. This is satisfied at $\omega'\tau\ll 1$. Equations 24 and 25 are simplified to

$$c^2 = \left(\frac{g}{k}+\frac{\gamma k}{\rho}\right)(1+2\varepsilon_{ela,re}), \quad (46)$$

$$\alpha = \frac{\sigma\varepsilon_{ela,im}}{V} \equiv \alpha_d. \quad (47)$$

ε_{ela} in these equations is given by Eq. 44. These equations result in those based on only the diffusion process.[4,6]

Relaxation Effect (or χ_r) is Relatively Large. In a dilute solution, c and α are given by Eqs. 24, 25, 34, 43, and 45. Since the relaxation time depends on the frequency, however, the application of the equations is troublesome. In case of the concentrated solution, the following equations are obtained (see Appendix V):

$$c^2 = \left(\frac{g}{k}+\frac{\gamma k}{\rho}\right)\left(1+2\varepsilon_{ela,re}+\frac{\gamma k}{\rho c^2}\frac{\omega'^2\tau^2\delta'}{1+\omega'^2\tau^2}\right), \quad (48)$$

$$\alpha = \alpha_d + \frac{\gamma k}{2V\rho c}\cdot\frac{\omega'\tau\delta'}{1+\omega'^2\tau^2}, \quad (49)$$

with

$$\tau^{-1} = k_{a,\theta}c_0\exp\left(-\frac{Ze\psi_{sub}}{k_BT}\right)+k_d,$$

and

$$\delta' = \frac{(C_s^{-1})_{A,S}}{\gamma}\delta = \frac{3(\Delta\gamma)^2c_0\exp\left(-\frac{2Ze\psi_{sub}}{3k_BT}\right)}{2\times 10^2 RT\gamma N^{1/3}},$$

where δ' is the apparent relaxation strength.

For an insoluble monolayer, the following two kinds of approximations are given.

Relaxation Effect (or χ_r) is Negligibly Small. Since the solubility of molecules is negligibly small, Eq. 44 is simplified:

$$\varepsilon_{ela} = \frac{\frac{2\nu k^2}{\sigma}i+\frac{k^3}{2\rho\sigma^2}\{(C_s^{-1})_{mo}+i\eta_s\sigma\}}{1-\frac{k^3(1+i)}{\rho\sigma^2}\{(C_s^{-1})_{mo}+i\eta_s\sigma\}\left(\frac{2\nu k^2}{\sigma}\right)^{1/2}}, \quad (50)$$

where $(C_s^{-1})_{mo}$ is obtained from the (surface pressure)-(molecular surface area) curve. Inserting Eq. 50 into Eqs. 46 and 47, Dorrestein's equations[1] can be obtained.

Relaxation Effect (or χ_r) is Relatively Large. The relaxation time in χ_r is derived by solving the rate equation related to the equilibrium on monolayer. The relaxation strength is also derived in the same manner as in the treatment for a surfactant solution. Then, ε_r is expressed by the concentration of species and the kinetic parameters connected with the equilibrium. Consequently, from Eq. 50 and the equation for ε_r, Eqs. 24 and 25 are represented in a concrete form.

In conclusion, the derived equations can be extensively applied, particularly to concentrated surfactant solutions, and can be expected to give kinetic parameters associated with the adsorption-desorption process of the surfactant. The experimental results of the propagation

characteristics of the wave on the surface of various surfactant solutions and the applicability of the equations obtained in the present study will be reported in a subsequent paper.

Appendix

I. The relative change in the surface area, β, is expressed by the following equation, in which the wave is represented by $a=a_0\sin(\omega t+kx)$:

$$\beta = \left(\frac{a_0 k}{2}\right)^2[1+\cos\{2(\omega t+kx)\}]$$
$$= \left(\frac{a_0 k}{2}\right)^2\{1+\cos(\omega' t+\kappa x)\},$$

where a_0 is the amplitude, and ω, the frequency of the wave. As is seen from this equation, the surface tends to expand at the nodes.

II. The thermal diffusion coefficient, D_T, in water is 1.4×10^{-3} cm^2 s^{-1}, while that in gas is of the order of 10^{-4} cm^2 s^{-1}. Under the present experimental conditions, the wavelength is about 9.8 mm at the lowest frequency (25 Hz) and 0.4 mm at the highest frequency (2 kHz).[9] Therefore, the $2\pi/kD_T \gg k/\omega$ condition is always satisfied; *i. e.*, the adiabatic approximation can be applied.

III. The thickness of the subsurface layer, d_{sub}, is much thinner than $d_b(=n^{-1})$. From Eq, 29, therefore, Δc_{sub} is approximated as

$$\Delta c_{sub} = E_b \exp(-nd_{sub}) \simeq E_b.$$

Moreover, the law of mass conservation is given as

$$d_s\Delta c_s = \int_{-d_{sub}}^{-\infty} E_b \exp(ny)\,dy \simeq -\frac{E_b}{n}.$$

The above equations lead to the relation between Δc_{sub} and Δc_s:

$$\Delta c_{sub} = -nd_s\Delta c_s.$$

IV. By eliminating $d\xi$ from Eqs. 9 and 10, $d\gamma$ becomes:

$$d\gamma = \left\{\left(\frac{\partial\gamma}{\partial s}\right)_{\xi,S} - \left(\frac{\partial\gamma}{\partial\xi}\right)_{s,S}\left(\frac{\partial A}{\partial s}\right)_{\xi,S}\left(\frac{\partial A}{\partial\xi}\right)_{s,S}^{-1}\right\}ds + \left(\frac{\partial\gamma}{\partial\xi}\right)_{s,S}\left(\frac{\partial A}{\partial\xi}\right)_{s,S}^{-1} dA.$$

Therefore

$$\left(\frac{\partial\gamma}{\partial s}\right)_{A,S} = \left(\frac{\partial\gamma}{\partial s}\right)_{\xi,S} - \left(\frac{\partial\gamma}{\partial\xi}\right)_{s,S}\left(\frac{\partial A}{\partial s}\right)_{\xi,S}\left(\frac{\partial A}{\partial\xi}\right)_{s,S}^{-1}.$$

δ is obtained from the above equation and Eq. 14:

$$\delta = -\frac{\left(\frac{\partial\gamma}{\partial\xi}\right)_{s,S}\left(\frac{\partial A}{\partial s}\right)_{\xi,S}}{\left(\frac{\partial\gamma}{\partial s}\right)_{A,S}\left(\frac{\partial A}{\partial s}\right)_{s,S}}.$$

V. If $c_0 > 10^{-3}$ mol dm^{-3}, $k_a < 10^6$ s^{-1}, $\theta > 0.95$, and $\phi_{sub} \approx 0$, Eq. 34 is simplified, with $\omega' \approx 10^3$ s^{-1}, $D \approx 10^{-6}$ cm^2 s^{-1}, $d_s \approx 10^{-7}$ cm and $\Gamma_{max} \approx 5\times 10^{-10}$ mol cm^{-2}:

$$\tau^{-1} = k_{a,\theta}c_0 \exp\left(-\frac{Ze\phi_{sub}}{k_B T}\right) + k_d.$$

The second term in the bracket in Eq. 43 is neglected compared with the first term:

$$\delta = \frac{3(\Delta\gamma)^2 c_0 \exp\left(-\frac{2Ze\phi_{sub}}{3k_B T}\right)}{2\times 10^2 RT(C_s^{-1})_{A,S}N^{1/3}}.$$

Notations

A;	chemical affinity.
a, a_0;	displacement and amplitude of wave respectively.
C_s;	surface compressibility (10^{-5} N/cm).
C_s*;	dynamic surface compressibility.
$(C_s^{-1})_{mo}$;	reciprocal surface compressibility for an insoluble monolayer.
c;	propagation velocity of the capillary wave.
c_b;	concentration of the surfactant solution in the bulk phase.
c_0;	initial concentration.
c_s, c_{sub};	concentrations of S_s and S_{sub} respectively.
D;	diffusion coefficient.
D_T;	thermal diffusion coefficient.
d_b;	thickness of the bulk phase concerned with the diffusion process.
d_s, d_{sub};	thicknesses of the surface and the subsurface layers respectively.
E_1, E_2;	complex constants associated with the amplitudes of Φ and Ψ respectively.
E_b;	amplitude of perturbed concentration in the bulk phase.
e;	elementary charge.
g;	gravitational acceleration.
k;	wave number.
k_a, k_d;	adsorption rate constant (s^{-1}) and desorption rate constant (s^{-1}) respectively.
$k_{a,\theta}$;	converted adsorption rate constant (mol^{-1} dm^3 s^{-1}).
k_B;	Boltzmann constant.
L;	proportional constant in the relaxation equation.
m;	complex constant.
N;	Avogadro number.
N_i, N_j';	numbers of moles of R_i and P_j species respectively.
n;	reciprocal of the thickness of the bulk phase concerned with the diffusion process.
n_{sub};	number of moles of S_{sub} per unit surface area.
p;	hydrostatic pressure.
P_j, R_i;	species in equilibrium.
R;	gas constant.
r;	complex angular frequency.
S;	surface entropy.
S_s, S_{sub}, S_b;	surfactants on surface, subsurface, and bulk phase respectively.
s;	surface area per unit area.
T;	temperature.
t;	time.
u, v;	horizontal and vertical components of liquid velocity respectively.
V;	$(3/2)c$, group velocity.
x, y;	Cartesian coordinate.
Z;	valency of surfactant.
α;	damping coefficient (cm^{-1}).
β;	relative change in the surface area.
Γ;	surface excess.
γ;	sulface tension (10^{-5} N cm^{-1}).
$\Delta\gamma$;	standard surface tension change.
δ;	relaxation strength.
ε_{ela}, ε_r;	dispersion terms of the angular frequency.
η;	viscosity (10^{-5} N s cm^{-2}).
η_s;	surface viscosity (10^{-5} N s cm^{-1}).
θ;	fraction of sites occupied by S_s.
κ;	$2k$, wave number.

μ_s, μ_{sub}; chemical potentials of S_s and S_{sub} respectively.
ν; η/ρ kinematic viscosity.
ν_i, ν_j' stoichiometric coefficients of R_i and R_j respectively.
ξ; ordering coefficient.
ρ; density.
σ; $(g/k+\gamma k^3/\rho)^{1/2}$, angular frequency of the wave.
$\tau_{s,s}$, $\tau_{r,s}$; relaxation times.
Φ, Ψ; stream and potential functions respectively.
ϕ; elevation of the surface.
χ^*; dimensionless parameter associated with the dynamic surface compressibility and the surface viscosity.
ψ_{sub}; electric potential at $y=-d_{sub}$.
ω, $\omega'(=2\omega)$; angular frequencies of the wave and the external driving force respectively.

References

1) R. Dorrestein, *Proc. Acad. Sci.*, **B54**, 260 (1950).
2) E. Mayer and J. D. Eliassen, *J. Colloid Interface Sci.*, **37**, 228 (1971).
3) J. A. Mann and G. Du, *J. Colloid Interface Sci.*, **37**, 2 (1971).
4) M. van den Tempel and R. P. van de Riet, *J. Chem. Phys.*, **42**, 2769 (1965).
5) R. S. Hansen and J. A. Mann, *J. Appl. Phys.*, **35**, 152 (1964).
6) J. Lucassen and R. S. Hansen, *J. Colloid Interface Sci.*, **22**, 32 (1966).
7) J. T. Davies and R. W. Vose, *Proc. R. Soc. London, Ser. A*, **286**, 218 (1965).
8) H. Lamb, "Hydrodynamics," 6th ed, Dover, New York (1932).
9) J. A. Mann and R. S. Hansen, *J. Colloid Interface Sci.*, **18**, 757 (1963).
10) J. T. Davies and E. K. Rideal, "Interfacial Phenomena," Academic Press, New York and London (1961).
11) W. P. Mason, "Physical Acoustics," Vol. 2, Academic Press, New York (1965).
12) D. H. Everett, "An Introduction to the Study of Chemical Thermodynamics," Longmans Green (1959).
13) J. G. Kirkwood and I. Oppenheim, "Chemical Thermodynamics," Chap. 10, McGraw-Hill, New York (1962).
14) J. Rassing, P. J. Sams, and E. Wyn-Jones, *J. Chem. Soc., Faraday Trans. 2*, **10**, 1247 (1974).

Relaxation Studies of the Adsorption-Desorption Equilibrium of Surfactants on the Gas-Liquid Interface. II. Experimental Studies

Minoru SASAKI, Tatsuya YASUNAGA, and Nobuhide TATSUMOTO

Department of Chemistry, Faculty of Science, Hiroshima University, Higashisenda-machi, Hiroshima 730

(Received November 9, 1976)

The propagation characteristics of the capillary wave were studied in aqueous solutions of sodium dodecyl sulfate, octylamine hydrochloride, and dodecylamine hydrochloride. In most of the solutions, relaxation was observed both in the propagation velocity and the damping coefficient; it could be well interpreted by means of the theory for the propagation characteristics derived in Part I.[1] The obtained relaxation parameters reveal the dynamic behavior of the adsorption-desorption of surfactants on the gas-liquid interface.

The dynamic physicochemical properties of the gas-liquid interface have been studied by many investigators[2-5] by means of the capillary wave method. Davies and Vose[2] have found relaxation on the surface of the surfactant solutions and have attributed it to the adsorption-desorption process of surfactants on the surface. However, questions still remain concerning the definition of the relaxation frequency and the rate equation.[6]

The purpose of the present investigation is to explore the validity of the theory[1] which supports to solve the above problems. Since the experimental values of the damping coefficient reported by Davies and Vose[2] were not precise enough to apply the theoretical equations, the experimental studies were newly carried out in the surfactant solutions.

Experimental

The apparatus used was a modification of that described by Davies and Vose;[2] the schematic diagram is shown in Fig. 1. The capillary wave was generated by a vibrator attached to a drive-unit of the trumpet speaker. The vibrator was made of Teflon, which has a weak affinity to all solutions. The flash of the stroboscope was synchronized with the signal of the oscillator, and the stationary image of focus was observed with a microscope. The propagation velocity and the damping coefficient were obtained as has been described in Brown's paper.[7] The frequency range of the apparatus was from 25 Hz to 4 kHz.

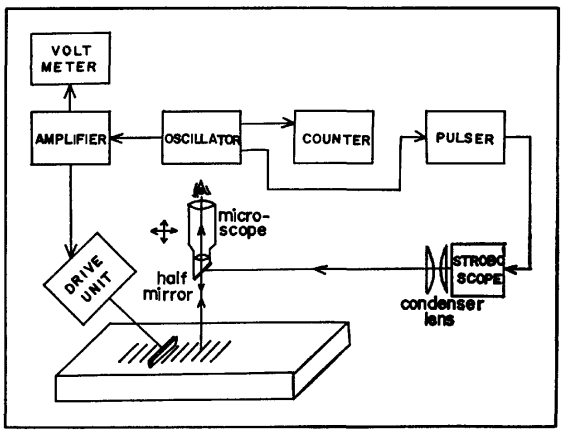

Fig. 1. Schematic diagram of the apparatus for measurements of the propagation characteristics of the capillary wave.

Sodium dodecyl sulfate (SDS) was prepared from Tokyo Kasei reagent-grade dodecyl alcohol (purity; 99.5%) according to the procedure of Dreger *et al.*[8] Octylamine hydrochloride (OAC) and dodecylamine hydrochloride (DAC) were prepared as follows. Octylamine and dodecylamine (Tokyo Kasei reagent-grade; Purities; 97.7 and 99.7% respectively) were neutralized by HCl in benzene solutions and were then recrystallized three times from benzene solutions and finally washed with petroleum ether. The values of the CMC were determined to be 8.3, 15.8, and 175 mM* for the SDS, DAC, and OAC solutions respectively by the electric conductivity method at 25 °C.

Results and Discussion

The propagation velocity, c, and the damping coefficient, α, of water were measured at various frequencies; they are shown in Figs. 2 and 3. The theoretical values

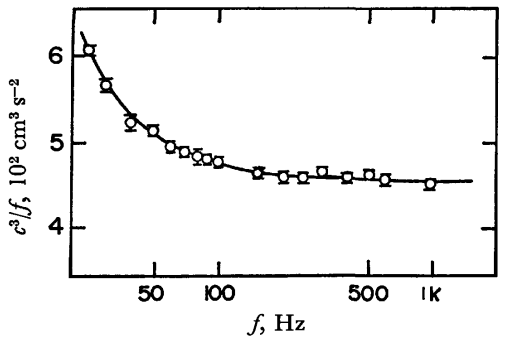

Fig. 2. The plots of c^3/f *vs.* f in water. The solid line shows the theoretical curve of c^3/f calculated by Eq. 1.

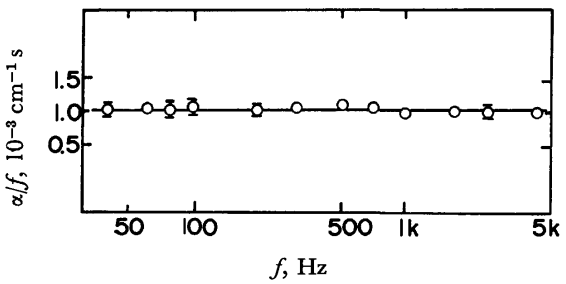

Fig. 3. The plots of α/f *vs.* f in water. The solid line shows the theoretical curve of α/f calculated by Eq. 2.

* Throughout this paper 1 M = 1 mol dm^{-3}.

of c and α were calculated by means of the following equations for a clean (fully mobile) surface,[2] using the literature values of ρ, ν, and γ:[9]

$$\frac{c^3}{f} = \frac{g\lambda^2}{2\pi} + \frac{2\pi\gamma}{\rho}, \tag{1}$$

$$\frac{\alpha}{f} = \frac{8\pi\rho\nu}{3\gamma}, \tag{2}$$

where f is the frequency, and λ, the wavenumber. The observed values of c^3/f and α/f fell on those curves within ± 0.7 and $\pm 4\%$ respectively in the frequency range studied. These facts confirm that the present apparatus can be applied to the measurements of c and α in the frequency range from 25 Hz to 4 kHz.

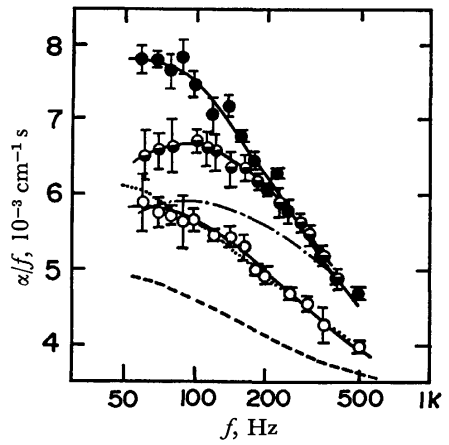

Fig. 4. The plots of α/f *vs.* f in SDS, DAC, and OAC solutions.
The theoretical curves of α_d/f are shown; ----: 8 mM SDS, ·····: 15 mM DAC, —·—: 121 mM OAC.
○: 8 mM SDS, ●: 15 mM DAC, ◒: 121 mM OAC.

The measurements were carried out on the surfaces of the SDS, DAC, and OAC solutions; the frequency depences of α/f are shown in Fig. 4. As seen from this figure, the experimental values of α/f are greater than the theoretical ones of α_d/f, where α_d refers to the damping coefficient based on only the diffusion process between the surface and the bulk phase. According to the theory presented in the previous paper,[1] the equations for the frequency dependences of c and α on the surface of relatively concentrated surfactant solutions are given by

$$c^2 = \left(\frac{g}{k} + \frac{\gamma k}{\rho}\right)\left(1 + 2\varepsilon_{\text{ela.re}} + \frac{\gamma k}{\rho c^2}\,\frac{\omega'^2\tau^2\delta'}{1+\omega'^2\tau^2}\right), \tag{3}$$

$$\frac{\alpha}{f} = \frac{\alpha_d}{f} + \frac{2\pi\gamma k}{3\rho c^3}\,\frac{\omega'\tau\delta'}{1+\omega'^2\tau^2}. \tag{4}$$

Equation 4 is, then, rearranged as follows:

$$\frac{3\rho c^3}{2\pi\gamma k}\left(\frac{\alpha}{f} - \frac{\alpha_d}{f}\right) = \frac{\omega'\tau\delta'}{1+\omega'^2\tau^2}. \tag{5}$$

The frequency dependences of the l. h. s. of this equation are shown in Fig. 5. This figure shows that the excess damping can be expressed by a single relaxation equation. The relaxation phenomena were also observed in all the other solutions except the 60 mM OAC solution, where the apparent relaxation strength was

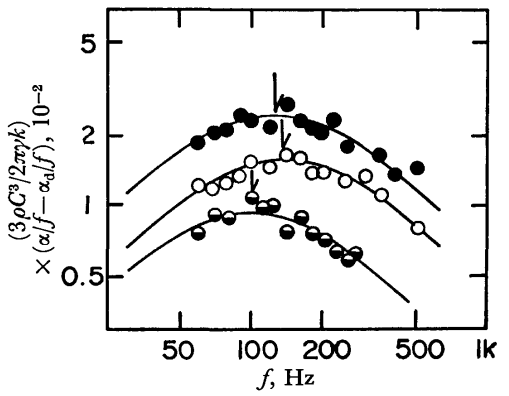

Fig. 5. The plots of $(3\rho c^3/2\pi\gamma k)\cdot(\alpha/f - \alpha_d/f)$ *vs.* f in SDS, DAC, and OAC solutions. The solid lines show the theoretical curves calculated by r. h. s. of Eq. 5 with the relaxation parameters listed in Table 1. The arrows show the relaxation frequency $f_r = (4\pi\tau)^{-1}$.
○: 8 mM SDS, ●: 15 mM DAC, ◒: 121 mM OAC.

negligibly small. Nonlinear least-squares routines employing a computer were used to calculate the relaxation parameters; the values of τ and δ' obtained are listed in Table 1.

Table 1. Relaxation parameters in SDS, DAC, and OAC solutions at 25 °C

	CMC (mM)	c_0 (mM)	τ^{-1} (10^3 s^{-1})	δ' (10^{-2})
SDS	8.3	4	1.3±0.2	2.2±0.5
		6	1.6±0.2	2.7±0.3
		8	1.7±0.2	3.0±0.4
		10	1.8±0.2	2.2±0.3
DAC	15.8	5	1.0±0.2	1.0±0.6
		8	1.4±0.4	1.2±0.3
		10	1.6±0.3	2.2±0.2
		12	1.4±0.2	3.4±0.3
		15	1.6±0.3	5.0±0.4
		20	1.9±0.2	4.3±0.3
OAC	175	60	—	0
		80	0.8±0.2	1.5±0.4
		100	1.0±0.3	1.4±0.4
		121	1.3±0.1	1.8±0.5

The relaxation parameters can also be obtained from the frequency dispersion of c, which was expressed by the following equation with the assumption that $\gamma k/\rho \gg g/k$:

$$\frac{c^3}{f} - \frac{g\lambda^2}{2\pi} = \frac{2\pi\gamma}{\rho}\left(1 + 2\varepsilon_{\text{ela.re}} + \frac{\gamma k}{\rho c^2}\,\frac{\omega'^2\tau^2\delta'}{1+\omega'^2\tau^2}\right). \tag{6}$$

The theoretical curves in Fig. 6 were calculated by means of this equation, using the values of the relaxation parameters in Table 1. Unfortunately, the apparent relaxation strength was so small that the experimental results of the propagation velocity were not precise enough to give the relaxation parameters, only to refine the validity of those obtained from the damping coefficient.

If the observed relaxation phenomena are based on the adsorption-desorption process of the surfactants, the concentration dependence of the relaxation time is

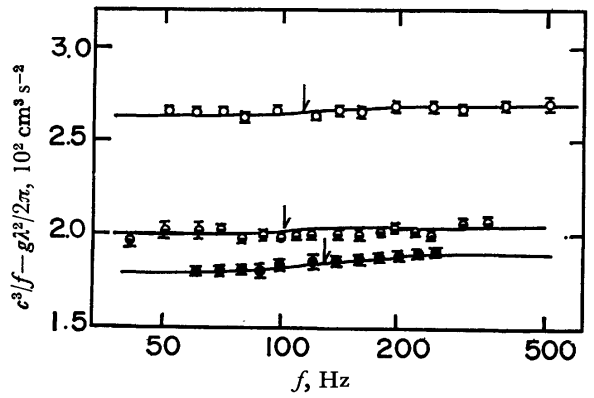

Fig. 6. The frequency dispersion of $(c^3/f-g\lambda^2/2\pi)$ in SDS, DAC, and OAC solutions. The solid lines show the theoretical curves calculated by Eq. 6 with the relaxation parameters listed in Table 1. The arrows show the relaxation frequency obtained from the experimental results of the damping coefficient.

expressed by[1]

$$\tau^{-1} = \frac{d_s k_a c_m \exp\left(-\frac{Ze\psi_{sub}}{k_B T}\right)}{10^3 \Gamma_{max}} + k_d, \qquad (7)$$

where c_m is the monomer concentration of the surfactants. In the concentrated surface concentration of ionic surfactants, most of the adsorbed surfactants are neutralized by the counter ions and the Stern layer is formed at the surface. Then, ψ_{sub} may be much smaller than k_BT/e. Under this condition, Eq. 7 is simplified to

$$\tau^{-1} = \frac{d_s k_a}{10^3 \Gamma_{max}} c_m + k_d = k_{a,\theta} c_m + k_d. \qquad (8)$$

The plots of τ^{-1} *vs.* c_m are on the straight lines, as is shown in Fig. 7. The linearity of these plots suggests that the relaxation phenomena are based on the adsorption-desorption process of the surfactants. The values of $k_{a,\theta}$ and k_d were calculated from the straight lines in Fig. 7; they are listed in Table 2. The values of k_a were calculated from $k_{a,\theta}$ with the literature values of d_s[10] and Γ_{max};[11] they are also listed in Table 2.

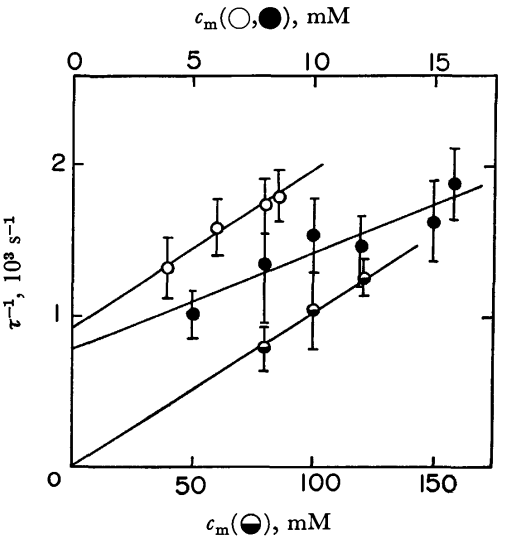

Fig. 7. The plots of τ^{-1} *vs.* c_m in SDS (○), DAC (●), and OAC (◒) solutions.

Table 2. KINETIC PARAMETERS IN SDS, DAC, AND OAC SOLUTIONS AT 25 °C

	$k_{a,\theta}$ (10^5 M^{-1} s^{-1})	k_a (10^5 s^{-1})	k_d (10^2 s^{-1})	ΔG ($-RT$)		$\Delta\gamma$ (10^{10} dyn·cm mol^{-1})[c]	
SDS	1.1±0.5	4±2	9±1	6.1[a]	6.8	10[b]	6
DAC	0.6±0.3	3±1	8±2	5.9[a]	6.3	8[b]	7
OAC	0.1±0.03	0.6±0.2	—	—		3[b]	7

a) The values were calculated by means of Szyszkowski's equation. b) The values were calculated by means of $\Delta\gamma \approx (\gamma_{water}-\gamma_{CMC})/\Gamma_{max}$. c) 1 dyn=$10^{-5}$ N.

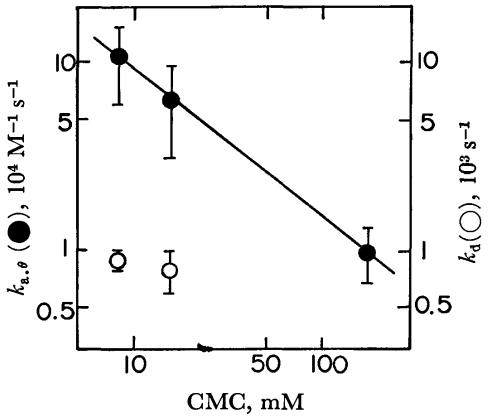

Fig. 8. The plots of $k_{a,\theta}$ (closed circles) and k_d (open circles) *vs.* CMC.

Among the values in Table 2, $k_{a,\theta}$ is fairly dependent on the CMC, but k_d is appreciably independent of the CMC, as is seen from Fig. 8. As a result, the following relation was obtained:

$$\log k_{a,\theta} = (3.4\pm0.3) - (0.8\pm0.3)\log \mathrm{CMC}. \qquad (9)$$

On the other hand, the values of k_d were evaluated as follows. Since the state of surfactants on an adsorbed layer is similar to that in a micelle in a surfactant solution, the desorption rate constant can be reasonably compared with the dissociation rate constant of the monomer from the micelle. In an SDS solution, the value of the former falls in the same order of magnitude as that of the latter, 7.5×10^2 s^{-1}, obtained by means of the pressure-jump method.[12] These facts support the idea that the adsorption-desorption mechanism proposed is reasonable.

The adsorption-desorption energies, ΔG, were calculated by means of k_a and k_d; $\Delta G=-RT\ln(k_a/k_d)$. They are listed in Table 2. The obtained values, however, cannot be referred to the literature ones by the static methods,[6] since the surface excess near the CMC increases appreciably with c_m. Then, the effective adsorption-desorption energy near the CMC was computed by means of Szyszkowski's equation; it is listed in Table 2. The values of ΔG obtained are in good agreement with the calculated ones. This also suggests that the proposed mechanism is reasonable.

The concentration dependences of the apparent relaxation strength obtained must also be interpreted by means of the following equation:[1]

$$\delta' = \frac{2(\Delta\gamma)^2 N^{-1/3} c_m^{2/3}}{3\times10^2 RT\gamma}. \qquad (10)$$

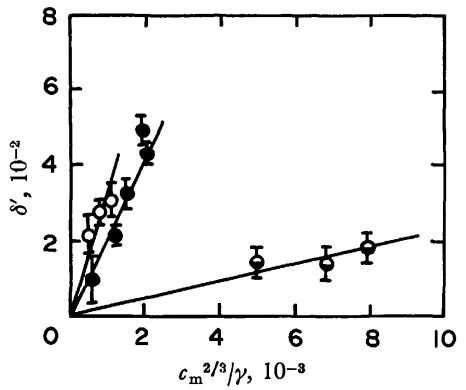

Fig. 9. The plots of δ' *vs.* $c_m^{2/3}/\gamma$ in SDS (○), DAC (●). and OAC (◒) solutions.

The plots of δ' *vs.* $c_m^{2/3}/\gamma$ are on the straight lines, as is shown in Fig. 9. The values of $\Delta\gamma$ calculated from the slopes of these straight lines are in good agreement with those of $\delta\gamma/\delta\Gamma \approx (\gamma_{water}-\gamma_{CMC})/\Gamma_{max}$ listed in Table 2, where γ_{water} and γ_{CMC} are the surface tensions in water and the surfactant solution at the CMC respectively.

A preliminary kinetic investigation of the adsorption-desorption on the surfaces of other surfactant solutions by means of the capillary-wave method has shown that similar relaxation phenomena exist in these systems. Further studies of these systems will lead to a quantitative clarification of the adsorption-desorption phenomena.

References

1) M. Sasaki, T. Yasunaga, and N. Tatsumoto, *Bull. Chem. Soc. Jpn.*, **50**, 852, (1977).
2) J. T. Davies and R. W. Vose, *Proc. R. Soc. London, Ser. A*, **286**, 218 (1965).
3) J. A. Mann and R. S. Hansen, *J. Colloid Sci.*, **18**, 805 (1963).
4) J. Lucassen and R. S. Hansen, *J. Colloid Interface Sci.*, **22**, 32 (1966).
5) J. Lucassen and R. S. Hansen, *J. Colloid Interface Sci.*, **23**, 319 (1967).
6) J. T. Davies and E. K. Rideal, "Interfacial Phenomena," Academic Press, New York and London (1961).
7) R. C. Brown, *Proc. Phys. Soc. Lond.*, **48**, 312 (1936).
8) E. E. Dreger, G. I. Keim, and G. D. Miles, *Ind. Eng. Chem.*, **36**, 610 (1944).
9) R. C. Weast, "Handbook of Chemistry and Physics," 47th ed, Academic Press, New York and London (1961).
10) W. D. Harkins and R. W. Motton, *J. Colloid Sci.*, **1**, 106 (1946).
11) M. Muramatsu, K. Tajima, and T. Sasaki, *Bull. Chem. Soc. Jpn.*, **41**, 1279 (1968).
12) K. Takeda, *J. Sci. Hiroshima Univ. Ser. A*, **40**, 69 (1976).

Crystal Field Levels of Neodymium and Erbium Ethylsulfate Nonahydrates

Yoshifumi KATO, Toshiyuki NAGAI, and Apollo SAIKA*

Department of Chemistry, Faculty of Science, Kobe University, Nada-ku, Kobe 657

**Department of Chemistry, Faculty of Science, Kyoto University, Sakyo-ku, Kyoto 606*

(Received December 8, 1976)

The energy levels of the Nd^{3+} ion in $Nd(C_2H_5SO_4)_3 \cdot 9H_2O$ and of the Er^{3+} ion in $Er(C_2H_5SO_4)_3 \cdot 9H_2O$ are calculated within the $4f^N$ configuration by the tensor operator method. The Hamiltonian containing a configuration interaction is diagonalized for the free ion levels and complete J-mixing is performed for the crystal field levels. The experimental "free-ion" energy levels of Nd^{3+} and Er^{3+} are fitted with a mean deviation of 70.8 cm^{-1} for 19 terms and 78.2 cm^{-1} for 22 terms, respectively. The crystal field parameters obtained for $Nd(C_2H_5SO_4)_3 \cdot 9H_2O$ and $Er(C_2H_5SO_4)_3 \cdot 9H_2O$ yield a mean deviation of 3.6 cm^{-1} for 43 levels and 3.6 cm^{-1} for 50 levels, respectively. The calculated Zeeman splitting factors (g values) in the direction along the crystal principal axis are in fair agreement with the experimental values.

It is well known that the crystal field theory provides a powerful tool for the energy level calculation of crystals containing rare earths, because the spin-orbit interaction of rare earths is not negligible as compared with the Coulomb or other interactions and f electrons in a crystal are generally well localized in an electrostatic field of the proper symmetry. On the reduction of the matrix elements of the Hamiltonian for rare earth crystals, the tensor operator method has been widely used instead of the early operator equivalent method, since the mathematical quantities necessary to apply the former method are now readily accessible in the form tabulated by Nielson and Koster.[1] Furthermore, the configuration interaction (CI) has a sizable effect on the energy levels of rare earths, and Rajnak[2] showed in the energy level calculation of trivalent neodymium and erbium ions that a least-squares fit by use of 4 or 5 parameters for CI reproduces the experimental "free-ion" levels with a deviation of about 50 cm^{-1}, which is less than half the deviation without CI.

Recently Crosswhite and Crosswhite[3] have carried out a crystal field calculation of Nd^{3+} doped in $LaCl_3$ by using as fully developed a Hamiltonian as appears feasible at the present time and by simultaneously diagonalizing the ion and crystal field parts of the Hamiltonian matrix. In their calculation, the experimental 101 crystal field levels have been fitted with a mean error of 8.1 cm^{-1} by using 24 adjustable parameters. Successively Carnall *et al.*[4] have made an energy level calculation of Pm^{3+} in the $LaCl_3$ host with similar accuracy to that by Crosswhite and Crosswhite.[3] In order to make such an extensive calculation, unambiguous experimental data must be available and the rare earths doped in $LaCl_3$ are probably the most adequate crystals among all the known salts. For these crystals, the absorption bands are sharp, there is very little evidence of superimposed crystal vibrations and furthermore strong fluorescences are observed in contrast with hydrated crystals.

For rare earth crystals which have been widely investigated, CI is expected to play a very important role in their electronic properties. However, previous energy level calculations for rare earth ethylsulfate crystals employ only partial J-mixing and no CI. In this paper crystal field level calculations of the neodymium and erbium ethylsulfate nonahydrates (Nd(ES) and Er(ES)) are carried out by simultaneously diagonalizing both the ion and crystal field parts of the Hamiltonian matrix with CI for the ion levels and complete J-mixing for the crystal field levels. Furthermore, the spectroscopic splitting factors (g factors) are evaluated from the wavefunctions obtained, and compared with the experimental values.

Calculational Procedure

Theoretical. The theoretical treatment for $4f^N$ configurations by use of the tensor operator method first introduced by Racah[5] and extended by Judd[6] is given in detail elsewhere.[7,8] Here the general procedure of calculations will be briefly outlined.

The $4f^N$ electronic states can be described satisfactorily in terms of intermediate coupling. Thus we may expand the wavefunction of a rare earth ion in crystals according to the Russell-Saunders coupling scheme to give

$$|\Psi\rangle = \sum_i a_i \psi_i |f^N, q, S, L, J, M\rangle, \quad (1)$$

where q is an additional quantum number introduced to distinguish the electronic states. The Hamiltonian for an ion placed in a crystal field may be written as

$$H = H_{coul} + H_{so} + H_{cry} + H', \quad (2)$$

where H_{coul}, H_{so}, and H_{cry} denote the Coulomb interaction between a pair of 4f electrons, the spin-orbit interaction and the potential due to the crystal field, respectively. The energy shift that gives the same contribution to all the levels belonging to a given configuration is neglected in the following treatment, because it does not affect the electronic structure of the configuration. The last term H' in Eq. 2 stands for an additional CI and may be taken as

$$\langle \Psi | H' | \Psi' \rangle = \delta(\Psi, \Psi')[\alpha L(L+1) + \beta G(G_2) + \gamma G(R_7)], \quad (3)$$

where α, β, and γ are linear combinations of radial integrals discussed by other authors[9,10] and are treated as parameters. Further minor CI parameters are not included in Eq. 3.

The matrix elements of the Hamiltonian in Eq. 2 can be reduced by the tensor operator method. Then the matrix element of the electrostatic interactions within the $4f^N$ configuration can be written as a linear combina-

tion of the Slater radial integrals F_n,

$$\langle f^N qSLJM|\sum_{i>j} e^2/r_{ij}|f^N q'SLJM\rangle = \sum_n p_n F_n(4f, 4f),$$
$$(n=2,\ 4,\ \text{and}\ 6), \quad (4)$$

where the coefficient p_n represents the angular part of the interaction. Similarly the matrix element of the spin-orbit interactions can be reduced to

$$\langle f^N qSLJM|\zeta_{4f}\sum_i (s_i\cdot l_i)|f^N q'S'L'J'M'\rangle$$
$$= \delta(J,J')\delta(M,M')2\sqrt{21}\zeta_{4f}(-1)^{J+L+S'} \times \begin{Bmatrix} L & L' & 1 \\ S' & S & J \end{Bmatrix} \langle f^N qSL\|V^{(11)}\|f^N q'S'L'\rangle, \quad (5)$$

where ζ_{4f} is the spin-orbit radial integral with respect to a 4f electron and $V^{(11)}$ is the double tensor defined by Racah.[5] The matrix elements of electrostatic interactions and those of spin-orbit interactions of the $4f^3$ configuration are already tabulated by Nielson and Koster,[1] and Judd and Loudon,[11] respectively. We need only to evaluate the matrix elements of the crystal field potential. This may also be expanded by the irreducible tensor operator $C_q^{(k)}$ as

$$H_{cry} = \sum_i \sum_{k,q} B_q^k (C_q^{(k)})_i, \quad (6)$$

in which the summation over i is for all the electrons and the coefficient B_q^k is the crystal field parameter. Then the matrix element of H_{cry} will be reduced to

$$\langle f^N qSLJM|H_{cry}|f^N q'S'L'J'M'\rangle$$
$$= \delta(S,S')\sum_{k,q} 7B_q^k(-1)^{2J+S+L'+k-M-1} \times [(2J+1)(2J'+1)]^{1/2} \begin{pmatrix} 3 & k & 3 \\ 0 & 0 & 0 \end{pmatrix} \times \begin{pmatrix} J & k & J' \\ -M & q & M' \end{pmatrix} \begin{Bmatrix} J & J' & k \\ L' & L & S \end{Bmatrix} \times \langle f^N qSL\|U^{(k)}\|f^N q'SL'\rangle, \quad (7)$$

in which the doubly reduced matrix elements of the unit tensor operator $U^{(k)}$ are given in the table of Nielson and Koster.[1]

Once the eigenvectors are determined by diagonalizing the Hamiltonian, we can obtain the z component of the g value as

$$g_z = \langle \Psi|\mu_z|\Psi\rangle = \sum_i a_i^2 M g_i(qSLJ), \quad (8)$$

where μ_z is the component of the magnetic dipole operator along the principal axis of a crystal and $g_i(qSLJ)$ denotes the Lande g factor for an ion level.

Application. The Nd^{3+} and Er^{3+} ions in ethylsulfates have $4f^3$ and $4f^{11}$ configurations, respectively. Since these two configurations are complementary to one another, the Er^{3+} ion has the same number and kind of states as the Nd^{3+} ion, for which there are 41 different $|JM\rangle$ states. According to the crystal structure of rare earth ethylsulfates determined by X-ray diffraction,[12] the space group is $P6_3/m$ (C_{6h}^2) and the local symmetry about a rare earth ion is D_{3h} as far as only the nearest-neighbor oxygen atoms of 9 crystalline waters are concerned.[13] The crystal field of the D_{3h} symmetry is expanded as

$$H_{cry} = B_0^2 C_0^{(2)} + B_0^4 C_0^{(4)} + B_0^6 C_0^{(6)} + B_6^6(C_6^{(6)} + C_{-6}^{(6)}). \quad (9)$$

Following Hellwege,[14] each ion level under this symmetry may be classified in three irreducible representations specified by the crystal quantum number η. As a result, the secular determinant for crystal levels can be reduced to two 60×60 matrices for $\eta=\pm 1/2$ and $\pm 5/2$ and one 62×62 matrix for $\eta=\pm 3/2$ by the usual group-theoretical procedure. Each crystal level has, of course, a twofold degenerate Kramers' pair.

After the subprograms for the 3-j and 6-j symbols were checked to agree with the tables already published,[15] the eigenvalue problem was solved by machine. With the parameters determined by Eisenstein[16] for the energy calculation of Nd^{3+} in $LaCl_3$ as a test run, our results reproduced those of Eisenstein with an accuracy of five significant figures. The actual determination of the parameters was made in the following manner. First, the Hamiltonian without H_{cry} in Eq. 2 was diagonalized to determine the intermediate coupling parameters (F_2, F_4, F_6, and ζ_{4f}) and the CI parameters (α, β, and γ) by fitting the calculated values to the centers of gravity of the experimental levels by an iterative procedure. Secondly, the diagonalization of the entire Hamiltonian with all the J-mixing was performed iteratively by adjusting the crystal field parameters (B_0^2, B_0^4, B_0^6, and B_6^6). Finally, a minor adjustment of all the parameters was made by a least-squares method. All the calculations were performed by the use of a FACOM 230-75 computer at Kyoto University.

Results and Discussion

The parameters used in the final calculation and the standard deviations are given in Tables 1 and 2 for Nd(ES) and Er(ES), respectively together with those obtained by others. Here, the root mean square (rms) deviation is defined as

$$\sigma = [\sum_i \Delta_i^2/N]^{1/2}, \quad (10)$$

in which Δ_i is the difference between the observed and

Table 1. Parameters used in the final calculation and root mean square deviation in $Nd(C_2H_5SO_4)_3\cdot 9H_2O$[a]

Parameter	Present	Gruber & Satten
F_2	329.3	331.33
F_4	49.90	47.956
F_6	5.338	5.313
ζ_{4f}	873.5	880.11
α	1.40±0.20	—
β	−200.0±30.0	—
γ	0.0	—
B_0^2	142.8	116.8
B_0^4	−587.4	−545.6
B_0^6	−757.1	−683.2
B_6^6	601.5	626.4
rms deviation		
For center of gravity	70.8(19)	104.7(19)[b]
For crystal level	2.9(28) 3.6(43)	7.7(37)[b]

a) Units in cm^{-1}. The number of energy levels fitted are given in parentheses. b) See Ref. 21.

TABLE 2. PARAMETERS USED IN THE FINAL CALCULATION AND ROOT MEAN SQUARE DEVIATION IN $Er(C_2H_5SO_4)_3 \cdot 9H_2O$[a]

Parameter	Present	Erath	Rajnak	Wheeler & Hill
F_2	445.5	433.64	446.16	
F_4	69.30	67.522	69.131	
F_6	7.715	7.090	7.7010	
ζ_{4f}	2355.0	2471.0	2353.4	
α	17.50	—	17.49	
β	−690.3	—	−690.3	
γ	0.0	—	$Y(22:1)=-4560.$	
B_0^2	228.7	251.60		237.6
B_0^4	−631.2	−649.52		−591.2
B_0^6	−515.3	−496.92		−486.4
B_6^6	412.0	407.60		395.7
rms deviation				
For center of gravity	78.2(22)	285.1(10)	50.0(22)	
For crystal level	3.6(50)	3.4(46)		

a) See the footnote (a) in Table 1.

calculated values of the ith level and N is the number of levels. The calculated numerical results are presented in Tables 3 and 4 for Nd(ES) and Er(ES), respectively.

Nd(ES). Among the experimental energy levels of Nd(ES) reported by several authors,[17–19] we use the 19 electronic terms proposed by Gruber and Satten.[19] For the definitely assigned 9 electronic terms, the centers of gravity by Gruber and Satten differ within 6 cm^{-1} from those proposed by others. The discrepancy is smaller than the final rms deviation and should not have any significant effect on the final results. Since the calculated terms are not so sensitive to the variation of CI parameters, both α and β contain a considerable amount of error; especially γ is not determined because the electronic term (100)(10) ^2F affected strongly by γ has not been observed in Nd(ES). As can be seen in Table 1, while there exist only small differences between the intermediate coupling parameters by ours and those by Gruber and Satten, the rms deviation is considerably improved by the inclusion of the CI parameters α and β. A further improvement should be expected by introducing other higher-order interactions for CI and the increasing the number of levels available. For several crystal levels, both the assignments and splittings by Gruber and Satten[19] differ slightly from those by Dieke.[20] In the present calculation the 28 reliable crystal field levels for 9 electronic terms by Dieke[20] could be fitted with an rms deviation of 2.9 cm^{-1}, and the 43 levels containing ambiguous ones fitted with 3.6 cm^{-1}. The calculation by Gruber and Satten yielded an rms deviation of 7.7 cm^{-1} for 37 levels by first-order perturbation treatment with only partial J-mixing for the ground multiplet.[21] The crystal field parameters thus obtained are somewhat different from those of Gruber and Satten; especially for the B_0^2 parameter the difference exceeds 20 percent. This is due to their use of only the ground state multiplet levels for fitting.

From the eigenfunctions obtained, it became clear that through spin-orbit interactions $^2P_{3/2}$, $^2G_{7/2}$, and $^2G_{9/2}$ couple strongly with $^2D_{3/2}$, $^4G_{7/2}$, and $^4G_{9/2}$, respectively, whereas the strong coupling through J-mixing, in particular, occurs between the terms with $\Delta J=1$ and 6. Comparison of the calculated g values with the

TABLE 3. EXPERIMENTAL AND CALCULATED VALUES OF THE ENERGY LEVELS AND g VALUES FOR $Nd(C_2H_5SO_4)_3 \cdot 9H_2O$[a]

Term	Center of gravity			Crystal level relative to center				$\lvert g \rvert$	
	Exptl	Calcd	Diff	2η	Exptl	Calcd	Diff	Exptl[b]	Calcd
$^4I_{9/2}$	0	0	0	5	−178.7	−179.5	0.8	1.75	1.96
				3	−29.2	−25.1	−4.1		1.44
				1	−24.7	−24.4	−0.3		0.35
				5	100.3	97.3	3.0		1.21
				3	132.3	131.7	0.6		0.79
$^4I_{11/2}$		1860.8		3		−61.6			3.75
				1		−13.1			1.74
				5		−11.5			2.26
				3		26.5			0.86
				5		26.5			1.30
				1		33.2			3.10
$^4I_{13/2}$		3834.8		1		−88.0			4.97
				3		−51.5			3.29
				5		−12.5			0.82
				1		−6.6			0.89
				3		36.9			0.03
				1		44.2			5.75
				5		77.5			0.28
$^4I_{15/2}$		5894.5		1		−222.7			3.41
				1		−139.2			0.15
				3		−99.5			0.91

TABLE 3. (Continued)

Term	Center of gravity			Crystal level relative to center				$\|g\|$	
	Exptl	Calcd	Diff	2η	Exptl	Calcd	Diff	Exptl[b]	Calcd
				5		−45.0			0.18
				1		29.2			1.46
				3		107.7			6.76
				3		150.8			0.44
				5		218.7			1.01
$^4F_{3/2}$	11368.0	11443.9	−75.9	1	−9.6	−9.0	−0.6	0.26	0.22
				3	9.6	9.0	0.6		0.64
$^4F_{5/2}$	12404.0	12472.8	−68.8	1	−23.2	−18.1	−5.1		0.52
				5	3.0	−0.5	2.5		2.55
				3	20.2	18.6	1.6		1.50
$^4H_{9/2}$	12525.0	12617.9	−92.9	5		−82.6			1.58
				3		−72.7			0.36
				3	(26.2)	27.9	(−1.7)		2.60
				1	(33.8)	31.3	(2.5)		0.50
				5		96.1			2.57
$^4F_{7/2}$	13367.0	13457.2	−90.2	5	−51.9	−50.4	−1.5		0.55
				1	−41.7	−43.8	2.1		0.61
				3	38.4	42.1	−3.7		1.81
				5	55.2	52.3	2.9		1.75
$^2S_{3/2}$	13454.0	13387.1	66.9	1	−1.7	−1.4	−0.3		0.98
				3	1.7	1.4	0.3	2.53[c]	2.94
$^4F_{9/2}$	14640.0	14719.1	−79.1	5	(−31.2)	−29.4	(1.8)		2.52
				5	−25.5	−24.9	−0.6		1.30
				3	−0.3	−0.2	−0.1		1.83
				1	16.5	13.4	3.1		0.62
				3	40.5	41.1	−0.6		5.52
$^4H_{11/2}$	15842.0	15867.4	−25.4	3		−25.1			3.42
				1		−18.1			0.48
				5		−15.1			1.30
				3		10.5			0.15
				1	(13.0)	14.5	(−1.5)		5.95
				5	(34.3)	33.3	(1.0)		0.22
$^4G_{5/2}$	17118.0	17046.7	71.3	1	(−58.6)	−47.8	(−10.8)	0.72[c]	0.30
				5		−20.1			1.01
				3	(77.1)	67.9	(9.2)		0.88
$^2G_{7/2}$	17239.0	17222.0	17.0	3		−35.6			1.36
				5	(−17.8)	−22.4	(4.6)		0.45
				1	(19.4)	21.5	(−2.1)		0.44
				5	(37.6)	36.5	(1.1)		0.10
$^2K_{13/2}$		18892.5		5		−75.9			3.13
				3		−55.9			3.44
				1		−41.7			4.99
				5		−35.5			2.07
				1		2.0			6.02
				3		101.9			1.38
				1		105.1			0.48
$^4G_{7/2}$	18996.0	18965.9	30.1	3	(−82.2)	−88.6	(6.4)		0.65
				1	(−22.4)	−26.5	(4.1)		0.38
				5	(13.9)	19.7	(5.8)		2.15
				5		95.4			1.29
$^4G_{9/2}$	19408.0	19391.9	16.1	3	(−17.6)	−16.6	(1.0)		3.92
				1		−4.6			0.56
				5		−2.3			3.71
				3	(11.9)	10.3	(1.6)		0.51
				5		13.2			2.62

TABLE 3. (Continued)

Term	Center of gravity			Crystal level relative to center				$\|g\|$	
	Exptl	Calcd	Diff	2η	Exptl	Calcd	Diff	Exptl[b]	Calcd
$^2K_{15/2}$		20842.7		1		−43.3			6.72
				3		−37.0			4.53
				1		−28.6			5.63
				5		−14.7			3.47
				3		−0.9			6.85
				5		25.9			2.39
				3		46.9			1.62
				1		51.7			0.47
$^2G_{9/2}$	20982.0	21019.1	−37.1	1	(−59.8)	−57.7	(−2.1)		0.43
				3	(−20.8)	−20.1	(−0.7)		1.64
				3		11.3			4.74
				5		19.8			0.04
				5		46.7			1.13
$^2D_{3/2}$	21116.0	21232.7	−116.7	1	−8.1	−12.6	4.5		0.55
				3	8.1	12.6	−4.5		2.00
$^4G_{11/2}$	21438.0	21404.1	33.9	1		−109.3			0.92
				3		−57.3			1.20
				1		−38.8			5.20
				3		39.9			2.41
				5		46.4			1.05
				5		119.1			2.27
$^2P_{1/2}$	23180.0	23045.7	134.3	1				0.37	0.31
$^2D_{5/2}$	23730.0	23745.0	−15.0	1	−19.5	−26.8	6.3	0.59	0.60
				3	−1.2	5.8	7.0		1.80
				5		21.0			2.99
$^2P_{3/2}$	26102.0	26113.4	−11:4	1	−12.4	−14.8	2.4	0.54	0.55
				3	12.4	14.8	−2.4		1.61
$^4D_{3/2}$	28049.0	28174.2	125.2	1	−3.4	−2.3	−1.1		0.56
				3	3.4	2.3	1.1		1.73
$^4D_{5/2}$		28391.7		3		−58.8			1.99
				5		−7.3			3.33
				1		66.1			1.07
$^2I_{11/2}$		28555.6		1		−135.6			3.32
				1		−19.7			0.35
				3		−4.5			1.13
				3		40.2			3.97
				5		44.6			2.22
				5		75.0			3.18
$^4D_{1/2}$		28754.0		1					0.01
$^2L_{15/2}$		29179.3		3		−102.6			6.97
				5		−83.7			1.73
				3		−75.7			3.63
				1		−17.6			3.62
				1		−5.1			4.72
				5		47.6			0.80
				3		96.1			0.91
				1		141.0			0.32
$^2I_{13/2}$		29883.1		1		−118.3			6.68
				5		−11.4			0.80
				1		−5.9			0.65
				3		−5.1			0.75
				5		40.6			1.87
				1		42.0			4.43
				3		58.1			3.96
$^4D_{7/2}$		30426.9		5		−65.3			4.98

TABLE 3. (Continued)

Term	Center of gravity			Crystal level relative to center				$\|g\|$	
	Exptl	Calcd	Diff	2η	Exptl	Calcd	Diff	Exptl[b]	Calcd
				1		12.9			0.71
				3		26.2			2.15
				5		26.2			3.65
$^2L_{17/2}$		30658.9		5		−123.9			8.83
				3		−48.1			3.81
				5		−38.1			1.93
				1		−28.8			5.24
				3		−23.0			7.32
				1		7.3			6.23
				5		57.5			0.93
				3		86.6			1.22
				1		110.5			0.59
$^2H_{9/2}$		32523.4		3		−63.8			2.68
				5		−50.8			1.31
				3		8.1			0.04
				1		36.8			0.46
				5		69.7			2.22
$^2D_{3/2}$		33329.4		3		−5.3			1.28
				1		5.3			0.39
$^2H_{11/2}$		33838.4		5		−132.9			0.19
				1		−65.1			5.30
				3		−31.0			0.46
				5		36.4			1.25
				1		78.4			0.06
				3		114.2			3.56
$^2D_{5/2}$		34546.9		3		−19.8			1.69
				5		−13.7			2.96
				1		33.5			0.53
$^2F_{5/2}$		39466.3		5		−20.2			2.25
				3		−9.8			1.36
				1		30.0			0.45
$^2F_{7/2}$		40870.4		5		−47.9			1.38
				5		10.5			2.51
				1		12.4			0.57
				3		25.0			1.71
$^2G_{9/2}$		47622.7		5		−53.9			2.91
				3		−37.9			4.29
				1		−7.6			0.56
				3		42.5			0.97
				5		56.9			1.81
$^2G_{7/2}$		48509.1		5		−74.5			1.44
				1		−11.5			0.45
				5		22.5			0.55
				3		63.5			1.33
$^2F_{7/2}$		68447.2		5		−108.8			3.77
				3		16.6			1.71
				1		25.8			0.57
				3		66.4			2.63
$^2F_{5/2}$		69531.2		5		−78.7			2.14
				1		12.0			0.43
				3		66.7			1.29

a) Energy units in cm^{-1}. Diff=Exptl−Calcd. When the location of the center of a term is not known experimentally, the position which yields the best agreement with the calculation is taken as the center assumed in column 2. Values in parentheses are less reliable. b) The values from the Zeeman effect (Ref. 17). Here, $s_1=2|g|$. c) The values are increased by 9% according to the footnote in Table 3 of Ref. 17.

TABLE 4. EXPERIMENTAL AND CALCULATED VALUES OF THE ENERGY LEVELS AND g VALUES FOR $Er(C_2H_5SO_4)_3 \cdot 9H_2O$[a)]

Term	Center of gravity			Crystal level relative to center				$\|g\|$	
	Exptl	Calcd	Diff	2η	Exptl	Calcd	Diff	Exptl[b)]	Calcd
$^4I_{15/2}$	0	0	0	5	−147.1	−148.9	1.8	0.76	0.71
				3	−103.1	−105.3	2.2	1.00	2.07
				3	−72.4	−74.5	2.1	6.60	5.20
				1	−36.9	−32.7	−4.2		0.49
				5	25.5	25.9	−0.4		0.49
				3	68.7	62.8	5.9		1.89
				1	108.9	112.8	−3.9		2.94
				1	156.9	159.9	−3.0		5.22
$^4I_{13/2}$		6424.4		5		−52.0			0.48
				3		−37.2			0.89
				1		−35.9			3.83
				1		−14.3			3.59
				5		12.3			1.58
				3		50.0			4.20
				1		77.1			5.76
$^4I_{11/2}$	10113.0	10040.6	72.4	1	−13.9	−20.2	6.3		0.23
				3	−13.0	−19.5	6.5		1.24
				5	−12.0	−13.8	1.8		1.88
				1	−10.3	2.9	−13.2		4.71
				5	12.4	13.4	−1.0		2.87
				3	37.1	37.6	−0.5		4.20
$^4I_{9/2}$	12366.7	12279.5	87.2	3	−87.6	−91.0	3.4		1.10
				5	−73.9	−76.4	2.5		1.35
				3	11.2	10.2	1.0		1.58
				1	26.4	23.9	2.5		0.44
				5	123.9	132.9	−9.0		2.26
$^4F_{9/2}$	15207.4	15196.5	10.9	3	−48.5	−48.0	−0.5	2.42	2.95
				1	−15.1	−17.3	2.2	0.58	0.57
				5	−6.0	−8.7	2.7		2.87
				3	22.7	22.4	0.3	0.78	0.52
				5	44.7	51.6	−5.6		1.74
$^4S_{3/2}$	18327.0	18571.1	−244.1	3	−13.0	−13.2	0.2	2.47	2.53
				1	13.0	13.2	−0.2		0.85
$^2H_{11/2}$	19087.3	19157.4	−70.1	5	−65.1	−59.7	−5.4		0.53
				5	−17.3	−10.8	−6.5		0.59
				3	−7.7	−9.7	2.0		1.43
				1	11.3	11.0	0.3		5.36
				3	24.0	24.5	−0.5		1.95
				1	54.9	44.1	10.8		0.30
$^4F_{7/2}$	20457.6	20400.6	57.0	5	−48.3	−49.0	0.7		2.13
				3	−16.6	−20.6	4.0	1.85	1.80
				5	18.4	23.3	−4.9		0.92
				1	46.4	46.3	0.1		0.60
$^4F_{5/2}$	22121.8	22056.7	121.5	3	−13.1	−10.0	−3.1	1.56	1.57
				5	1.8	−3.5	5.3		2.62
				1	11.2	13.5	2.3		0.52
$^4F_{3/2}$	22461.1	22425.1	36.0	3	−23.4	−17.5	−5.9	1.05	1.13
				1	23.4	17.5	5.9		0.37
$^2G_{9/2}$	24515.6	24412.2	103.4	3	−80.8	−76.1	−4.7	1.83	2.27
				5	−58.6	−61.6	3.0	1.60	1.56
				3	1.6	4.6	−3.0	1.50	0.96
				1	24.4	28.6	−4.2	0.15	0.54
				5	116.6	104.5	12.1		2.64
$^4G_{11/2}$	26348.5	26361.7	−13.2	5	−59.1	−61.6	2.5		2.35
				3	−23.2	−22.1	−1.1		3.93

TABLE 4. (Continued)

Term	Center of gravity			Crystal level relative to center				$\|g\|$	
	Exptl	Calcd	Diff	2η	Exptl	Calcd	Diff	Exptl[b]	Calcd
				5	−13.9	−19.5	5.6		1.15
				3	16.9	20.6	3.7		0.34
				1	22.3	26.3	−4.0		4.82
				1	57.5	56.5	1.0		1.17
$^4G_{9/2}$		27313.8		5		−23.0			2.73
				3		2.3			0.86
				1		3.0			0.55
				5		3.3			1.64
				3		14.4			4.18
$^2K_{15/2}$		27697.6		1		−133.5			0.52
				3		−103.4			1.55
				5		−45.5			2.38
				3		1.9			7.94
				5		34.3			3.43
				1		62.3			6.80
				3		85.4			4.71
				1		98.1			5.71
$^2G_{7/2}$		27942.6		5		−14.7			2.44
				1		−4.3			0.47
				5		6.2			1.48
				3		12.8			1.41
$^2P_{3/2}$		31642.8		3		−22.2			1.57
				1		22.2			0.54
$^2K_{13/2}$		32944.8		1		−95.1			0.50
				3		−72.1			1.40
				5		−40.4			2.16
				1		2.4			6.06
				5		25.1			3.12
				3		84.3			4.23
				1		95.8			5.16
$^4G_{5/2}$		33247.0		3		−53.1			0.88
				5		15.4			1.49
				1		37.7			0.29
$^2P_{1/2}$		33506.2		1					0.32
$^4G_{7/2}$		33865.5		5		−48.1			1.17
				5		1.1			2.11
				1		21.7			0.47
				3		25.3			1.42
$^2D_{5/2}$		34778.0		5		−20.1			2.99
				1		−1.8			0.60
				3		21.9			1.80
$^2H_{9/2}$		36369.6		5		−110.7			2.68
				3		−26.7			3.04
				1		−14.5			0.51
				3		74.4			0.05
				5		77.5			1.66
$^4D_{5/2}$		38517.2		1		−13.2			0.63
				5		−9.4			3.16
				3		22.6			1.89
$^4D_{7/2}$		39104.6		1		−38.8			0.71
				3		−34.6			2.12
				5		−20.0			3.49
				5		93.4			4.90
$^2I_{11/2}$		41036.9		3		−76.2			2.84
				1		−60.3			0.24

TABLE 4. (Continued)

Term	Center of gravity			Crystal level relative to center				$\|g\|$	
	Exptl	Calcd	Diff	2η	Exptl	Calcd	Diff	Exptl[b]	Calcd
				5		−27.2			1.04
				3		17.9			0.09
				1		63.6			5.15
				5		82.2			0.06
$^2L_{17/2}$		41567.7		1		−129.5			0.48
				3		−108.2			1.32
				5		−78.9			1.30
				5		−4.9			2.35
				3		20.2			4.45
				1		34.9			4.77
				1		38.2			5.88
				3		69.4			7.89
				5		158.8			8.99
$^4D_{3/2}$		42136.8		3		−10.4			1.58
				1		10.4			0.53
$^2D_{3/2}$		42893.5		1		−13.7			0.55
				3		13.7			1.64
$^2I_{13/2}$		43680.9		3		−74.0			3.42
				1		−60.9			4.11
				5		−57.4			1.25
				1		−0.5			1.16
				3		11·7			0.23
				5		22.3			0.18
				1		158.8			6.86
$^4D_{1/2}$		46853.8		1					0.03
$^2L_{15/2}$		47696.1		3		−87.4			0.73
				1		−81.3			0.29
				5		−54.4			2.56
				3		−42.9			1.37
				5		−30.7			1.92
				1		−18.3			0.13
				1		86.2			0.38
				3		228.6			4.11
$^2H_{9/2}$		47857.4		3		−61.3			2.83
				5		−47.5			2.92
				5		−39.1			1.71
				1		55.6			1.34
				3		92.3			3.32
$^2D_{5/2}$		48971.2		1		−69.6			0.61
				5		31.0			3.03
				3		38.6			1.81
$^2H_{11/2}$		50948.6		5		−65.1			3.33
				5		−44.9			2.29
				3		−22.7			4.56
				3		−5.9			1.45
				1		22.4			0.52
				1		116.2			5.70
$^2D_{3/2}$		55009.5		1		−24.5			0.44
				3		24.5			1.34
$^2F_{7/2}$		55788.5		3		−21.8			1.72
				5		−3.2			1.48
				1		−1.6			0.57
				5		26.7			2.79
$^2F_{5/2}$		63402.3		1		−15.0			0.45
				3		1.4			1.35

TABLE 4. (Continued)

Term	Center of gravity			Crystal level relative to center				$\|g\|$	
	Exptl	Calcd	Diff	2η	Exptl	Calcd	Diff	Exptl[b]	Calcd
				5		13.6			2.25
$^2G_{7/2}$		65426.8		1		−38.4			0.45
				3		−21.6			1.34
				5		22.4			0.51
				5		37.6			1.40
$^2G_{9/2}$		69535.0		3		−39.1			1.62
				1		−30.7			0.55
				5		−27.7			2.42
				5		32.4			3.53
				3		65.1			4.93
$^2F_{5/2}$		95149.8		3		−78.4			1.29
				1		−32.0			0.43
				5		110.4			2.14
$^2F_{7/2}$		98542.6		3		−77.4			1.71
				5		−64.0			2.85
				1		−32.7			0.57
				5		174.1			3.99

a) Energy units in cm^{-1}. Diff=Exptl−Calcd. b) The values from the Zeeman effect (Ref. 24).

experimental ones is possible only for a few levels as can be seen in the last two columns of Table 3. The agreement is fairly good except the $^4G_{5/2}$ ($\eta=\pm 1/2$) level, in which the experimental value is over twice as large as the calculated one. The resolution of this point must await further studies. Eisenstein[16] compared the g values of Nd^{3+} in $LaCl_3$ calculated by complete J-mixing with the experimental ones, and found the calculated values in good agreement with the experimental ones for all but 3 of 33 levels. Thus the g values in the present calculation should be fairly reliable and can be taken as a reference when the experimental values are not available.[22,23]

Er(ES). The spectrum of Er(ES) has been reported by several authors.[24-27] Wheeler and Hill[27] observed directly in the far infra-red the crystal field splitting of the $^4I_{15/2}$ ground multiplet and determined the crystal field parameters. Erath[25] calculated the crystal field parameters by a first-order perturbation on the ground multiplet in Er(ES) using the electrostatic and spin-orbit interaction parameters obtained by Wong.[28] He computed the splitting of excited levels due to the crystal field using these crystal parameters. Rajnak[2] made a CI calculation for the ion levels of Er^{3+} in Er(ES) by use of both the linear parameters, α, β, and γ, and the nonlinear parameter $Y(kk': l')$. The latter parameter results from the interactions of a configuration with the configurations differing from f^N in the quantum numbers of only one electron.[9]

As seen in Table 2, the inclusion of CI parameters reduces the rms deviation for the ion levels to less than one third of that without CI. Furthermore an improvement of about 30 cm^{-1} is achieved by including only one nonlinear parameter $Y(22: 1)$. This fact shows that CI effects are highly important for the ion levels. There are several differences between the present assignment of some electronic terms and those by previous authors, especially for the levels with $J=9/2$, of which the eigenvectors are given in Table 5. The present assignment of terms for higher levels over 30000 cm^{-1} is markedly different from that by Erath[25] in some cases; for example, the present $^2P_{3/2}$, $^4G_{5/2}$, and $^2P_{1/2}$ terms are assigned to the $^3D_{3/2}$, $^2P_{1/2}$, and $^4G_{5/2}$ terms by Erath, respectively. For the crystal field splitting, the present result including complete J-mixing does not show any improvement over Erath's result in contrast with Nd(ES). On the other hand, the centers of gravity of multiplets with complete J-mixing shift within 10 cm^{-1} from the ion levels without J-mixing among all the terms except the higher two terms, $^2L_{15/2}$ and $^2H_{9/2}$,

TABLE 5. EIGENVECTORS OF THE TERMS WITH $J=9/2$ IN $Er(C_2H_5SO_4)_3 \cdot 9H_2O$

Energy (cm^{-1})	Eigenvector							Assignment[b]			
	$\|^4F\rangle$	$\|^2G(1)\rangle$	$\|^2G(2)\rangle$	$\|^4G\rangle$	$\|^2H(1)\rangle$	$\|^2H(2)\rangle$	$\|^4I\rangle$	(A)	(B)	(C)	(D)
12366.7	0.3509	0.2737	−0.2206	0.0109	0.1940	−0.4162	−0.7364	^4I	^4I	^4I	^4F
15207.4	0.7736	0.2932	−0.2224	0.0905	0.0014	0.0780	0.5019	^4F	^4F	^4F	^4I
24515.6	−0.4915	0.4349	−0.3929	0.2484	0.2642	−0.4040	0.3467	^2G	^2H	^2H	^2G
27313.2[a]	−0.0200	0.0108	−0.0526	0.8906	−0.0998	0.3818	−0.2186	^4G	^2G	^4G	^4G
36366.8[a]	−0.1891	0.4872	−0.3970	−0.3561	−0.2918	0.5661	−0.1921	^2H	—	^2H	—

a) The calculated values. b) (A), the present results; (B), Dieke (Ref. 20); (C), Rajnak (Ref. 2); (D) Erath (Ref. 25).

with a shift of about 50 cm^{-1}. This means that J-mixing for Er(ES) is not so significant as for Nd(ES). Since the magnitude of the spin-orbit coupling of Er^{3+} ($\approx$2350 cm^{-1}) is considerably larger than that of Nd^{3+} ($\approx$870 cm^{-1}) and then the ion levels of Er^{3+} are more separated than those of Nd^{3+}, the mixing among the ion levels with different J due to a crystal field becomes smaller for Er(ES) than for Nd(ES). Thus it will generally be the case that the effect of J-mixing for crystal levels is not so important for electron holes with large spin-orbit interaction. In Table 4, good agreement between the calculated g values and those by the Zeeman experiment is found except for a few cases as in the case of Nd(ES).

In conclusion, it will be stated that: (1) CI for the ion levels of both Nd(ES) and Er(ES) makes a remarkable improvement. (2) Inclusion of complete J-mixing for the crystal field levels yields some improvement for Nd(ES) but not so for Er(ES). This originates exclusively from the fact that the ion levels of Er(ES) with large spin-orbit coupling are substantially well separated, and mixing among different J levels is small due to weak perturbation by a crystal field. (3) The g values obtained by the present procedure may be fairly reliable and of practical usage in some cases.

References

1) C. W. Nielson and G. F. Koster, "Spectroscopic Coefficients for the p^n, d^n, and f^n Configurations," M. I. T. Press, Cambridge, Mass. (1963).
2) K. Rajnak, *J. Chem. Phys.*, **43**, 847 (1965).
3) H. Crosswhite and H. M. Crosswhite, *J. Chem. Phys.*, **64**, 1981 (1976).
4) W. T. Carnall, H. Crosswhite, H. M. Crosswhite, and J. G. Conway, *J. Chem. Phys.*, **64**, 3682 (1976).
5) G. Racah, *Phys. Rev.*, **62**, 438 (1942); **63**, 367 (1943); **76**, 1352 (1949).
6) (a) B. R. Judd, *Proc. Phys. Soc. (London)*, **74**, 330 (1959); (b) B. R. Judd, "Operator Techniques in Atomic Spectroscopy," McGraw-Hill Book Co., New York (1963).
7) J. P. Elliott, B. R. Judd, and W. A. Runciman, *Proc. R. Soc. London, Ser. A*, **240**, 509 (1957).
8) B. G. Wybourne, "Spectroscopic Properties of Rare Earths," Interscience Publ., New York (1965).
9) K. Rajnak and B. G. Wybourne, *Phys. Rev.*, **129**, 2643 (1963); **134**, A 596 (1964).
10) K. Rajnak, *J. Opt. Soc. Am.*, **55**, 126 (1965).
11) B. R. Judd and R. Loudon, *Proc. R. Soc. London, Ser. A*, **251**, 127 (1959).
12) D. R. Fitzwater and R. E. Rundle, *Z. Kristallogr.*, **112**, 362 (1959).
13) B. Judd, *Proc. R. Soc. London, Ser. A*, **232**, 552 (1955); J. S. Margolis, *J. Chem. Phys.*, **35**, 1367 (1961). The adequacy of this assumption is discussed in Margolis' paper.
14) K. H. Hellwege, *Ann. Physik*, **4**, 95 (1949).
15) (a) M. Rotenberg, R. Bivins, N. Metropolis, and J. K. Wooten Jr., "The 3-*j* and 6-*j* Symbols," Technology Press, M. I. T., Cambrige Mass. (1959); (b) T. Inoue, "Table of the Clebsch-Gordan Coefficients," Tokyo Tosho Co., Tokyo (1966).
16) J. C. Eisenstein, *J. Chem. Phys.*, **39**, 2134 (1963).
17) G. H. Dieke and L. Heroux, *Phy. Rev.*, **103**, 1227 (1956).
18) S. Hüfner, *Z. Phys.*, **169**, 417 (1962).
19) J. B. Gruber and R. A. Satten, *J. Chem. Phys.*, **39**, 1455 (1963).
20) G. H. Dieke, "Spectra and Energy Levels of Rare Earth Ions in Crystals," Interscience Publ., New York (1968).
21) Gruber and Satten (Ref. 19) reported that the average deviations of the ion levels and the crystal field levels for Er(ES) were 72 and 4 cm^{-1}, respectively. However, according to the rms deviation given in Eq. 10, these values become 104.7 and 7.7 cm^{-1}, respectively.
22) Y. Kato, T. Nagai, and T. Nakaya, *Chem. Phys. Lett.*, **39**, 183 (1976).
23) Y. Kato, T. Nakaya, and T. Nagai, *Bull. Chem. Soc. Jpn.*, **50**, 589 (1977).
24) K. H. Hellwege, S. Hüfner, and H. G. Kahle, *Z. Phys.*, **160**, 146 (1960).
25) E. H. Erath, *J. Chem. Phys.*, **34**, 1985 (1961); **38**, 1787 (1963).
26) E. Y. Wong, *J. Chem. Phys.*, **39**, 2781 (1963).
27) R. G. Wheeler and J. C. Hill, *Phys. Lett.*, **20**, 496 (1966).
28) E. W. Wong, unpublished data.

The Theory of the Adsorption Monolayer with Lateral Intermolecular Interaction and Its Application to Aqueous Alcohol Solutions

Masayuki NAKAGAKI and Mihoko YAMAMOTO

Faculty of Pharmaceutical Sciences, Kyoto University, Sakyo-ku, Kyoto 606

(Received September 3, 1976)

A theoretical relation between the fractional adsorption amount, θ, and the concentration, C, taking account of the lateral interaction between the adsorbed molecules is used to integrate the Gibbs equation, and the relation between the surface pressure, F, and the molecular area, A, is derived. Since the equation does not contain the parameter, k_0, related to the strength of adsorption, it is concluded that there is no substantial difference between the adsorption monolayers and the insoluble monolayers. The relation between F and C is also derived and compared with the experimental data for normal alcohols. The standard affinity of adsorption, $-\Delta\mu^0$, and the energy of lateral interaction, ε, increased linearly with the number of carbon atoms of the alcohols, n. Finally, it has been shown that the experimental data can be explained well with the theoretical equation presented here, but not with Szyszkowski's, the latter being derived for negligible lateral interaction.

The energy or free energy of adsorption from a solution to its surface has been discussed for many years in connection with the surface activity of various substances, but not much attention has been paid to the lateral interaction between solute molecules in the adsorption monolayers. This interaction, however, seems to be important because the adsorption monolayers seem to fairly compact in ordinary concentration ranges.

The behavior of the adsorption monolayer could not be discussed hitherto in enough detail so that the effect of the lateral interaction could be detected. This is because some ambiguity is introduced when the experimental relation between the surface tension of a solution and the concentration of the surface-active solute is differentiated, graphically or numerically, in order to use the Gibbs differential equation in the determination of the adsorption amount or the molecular area in the adsorption monolayer.

In the present paper, theoretical equations will be derived for the adsorption monolayer with lateral intermolecular interaction. A method will be proposed to determine the values of the parameters which are used in the equations. Finally, the method will be applied to aqueous normal alcohol solutions and the parameter values thus obtained will be discussed.

Theoretical

Adsorption Equation of Interacting Molecules. Adsorption isotherms of surface active substances at the surfaces of their own solutions are often expressed by the Langmuir equation. This is in accord with the well-known fact that the surface tension of such a solution as a function of the concentration is expressed by the empirical Szyszkowski equation, because the latter equation can be derived theoretically when the Gibbs adsorption equation is integrated with the Langmuir equation if the solute is a nonelectrolyte at a dilute concentration, so the activity coefficient is assumed to be independent of the concentration.[1)]

The Langmuir equation takes the size of the adsorbed molecules, or the repulsion by steric hindrance, into account, but it does not take the lateral cohension between adsorbed molecules into account, since the equation was originally derived from the idea of site adsorption. If the lateral interaction is taken into consideration, the chemical potential of the solute in such an adsorption monolayer, μ, is taken to be different from that of the Langmuir monolayer, μ_L, by $\Delta\mu_{int}$:

$$\mu = \mu_L + \Delta\mu_{int}. \tag{1}$$

Since the probability of a molecule existing next to a given molecule may be assumed to be equal to the fractional adsorption amount, θ, the interaction energy in the monolayer is proportional to θn; therefore,

$$\Delta\mu_{int} = \frac{\partial}{\partial n}\left(-\frac{\varepsilon}{2}\theta n\right) = -\varepsilon\theta, \tag{2}$$

where ε is the energy of lateral interaction and

$$\theta = n/n_0 = \Gamma/\Gamma_0 = A_0/A. \tag{3}$$

Here, n is the moles of the adsorbed solute, Γ is the adsorption amount per unit area, A is the area occupied by one molecule, and the values with the 0 subscript are for the saturated adsorption.

At the adsorption equilibrium, μ is equal to the chemical potential of the solute in the solution, μ_S, which is given by the following equation if the activity coefficient is assumed to be independent of the concentration, C:

$$\mu_S = \mu_S^0 + RT\ln C, \tag{4}$$

where μ_S^0 is the standard chemical potential, R is the gas constant, and T is the absolute temperature. Together with the following equation for μ_L

$$\mu_L = \mu_L^0 + RT\ln[\theta/(1-\theta)], \tag{5}$$

the final result is obtained as

$$\theta/(1-\theta) = (k_0 e^{2K\theta})\cdot C, \tag{6}$$

which is the same equation as that used by Levine *et al.*[2)] for the adsorption of methanol from an aqueous solution by a plain solid surface. Here,

$$k_0 = \exp[-(\mu_L^0 - \mu_S^0)/RT], \tag{7}$$

and

$$K = \varepsilon/2RT. \tag{8}$$

The k_0 parameter is related to the strength of the adsorption from the solution to the adsorption monolayer, while K is related to the lateral interaction in the monolayer. The latter is so defined that $K<0$ for intermolecular repulsion, $K=0$ for the Langmuir

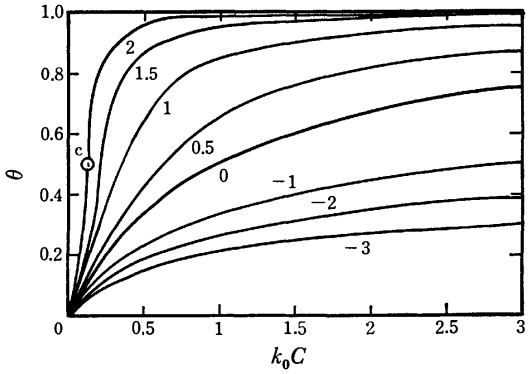

Fig. 1. Theoretical adsorption isotherms shown as the dependence of the fractional adsorption amount θ on k_0C, the parameter being K. The point C is the critical point where the phase separation in the adsorption monolayer starts.

case, and $K>0$ for intermolecular attraction. If $K>2$, phase separation occurs in the adsorption monolayer.[3] According to Eq. 6, the theoretical relations between θ and k_0C for various values of K are shown in Fig. 1. The C point, located at $\theta=0.5$, $k_0C=0.13534$ for $K=2$ in Fig. 1, shows the critical point at which the phase separation starts.

Equation of State of the Adsorption Monolayer. In the studies of the adsorption at the interface of a solution, the quantity measured experimentally is the surface tension, γ, of the solution, while the surface pressure, F, of the adsorption monolayer is defined by

$$F = \gamma_0 - \gamma, \tag{9}$$

where γ_0 is the surface tension of the solvent.

Theoretical equations for F can be derived by integrating the Gibbs equation:

$$F = \Gamma_0 RT\int_0^{\theta}\theta\left(\frac{\mathrm{d}\ln C}{\mathrm{d}\theta}\right)\mathrm{d}\theta. \tag{10}$$

By introducing Eq. 6 into Eq. 10,

$$(A_0/k_BT)F = -\ln(1-\theta) - K\theta^2 \tag{11}$$

is obtained, because $\Gamma_0 RT=k_BT/A_0$, where k_B is the Boltzmann constant. In the case of $K=0$, Eq. 11 is reduced, by using Eq. 6, to the Szyszkowski equation:

$$(A_0/k_BT)F = \ln(1+k_0C). \tag{12}$$

The equation of the state of the adsorption monolayer is derived from Eq. 11 by using Eq. 3:

$$(A_0/k_BT)F = \ln\left(\frac{A}{A-A_0}\right) - K\left(\frac{A_0}{A}\right)^2. \tag{13}$$

According to this equation, theoretical curves for various values of K are drawn in Fig. 2, where the relation between two dimensionless quatities, $(A_0/k_BT)F$ and (A/A_0) is shown instead of the F-A relation which is usually studied experimentally. It may be seen from Fig. 2 how a monolayer is expanded by the intermolecular repulsion ($K<0$) and is contracted by the intermolecular attraction ($K>0$).

The contraction of a monolayer by two-dimensional condensation is often examined by drawing the FA-A relation. Figure 3 shows the corresponding relation between the dimensionless quantities, FA/k_BT and $(A_0/k_BT)F$. Each theoretical curve has a minimum

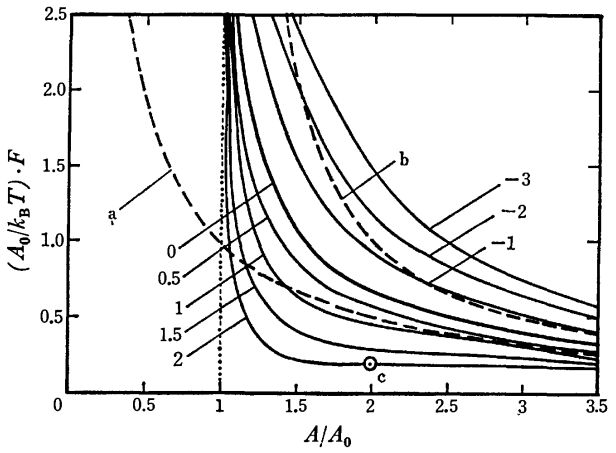

Fig. 2. Theoretical pressure-area curves of adsorption monolayers with various K values as indicated. The broken curve a is for $FA=k_BT$ and b for $F(A-A_0)=k_BT$.

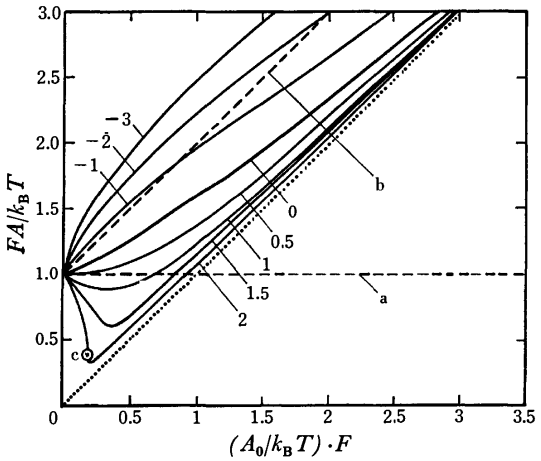

Fig. 3. Theoretical FA-A curves for various K values as indicated. The dotted line is for $A=A_0$. The broken straight line a is for $FA=k_BT$ and b for $F(A-A_0)=k_BT$.

point if $K>0.5$ and approaches to the asymptote, $A=A_0$, when F increases. If $K>2$, the entire curve is very close to the asymptote in the region where F is higher than that for the critical point, c, of the phase separation.

It may be emphasized here that the F-A relation, and also, therefore, the FA-A relation, of the adsorption monolayer are independent of the strength of the adsorption, because the equation of state, Eq. 13, does not contain the k_0 parameter. This conclusion is important both theoretically and experimentally. This means theoretically that there is no substantial difference between the adsorption monolayer and the insoluble monolayer. Experimentally, it is expected that the F-A relation or FA-A relation must be adequate for examining the intermolecular interaction in an adsorption monolayer, because the value of the K parameter may be determined on the basis of Fig. 2 or Fig. 3 without bothering to estimate the k_0 value. This expectation, however, was not realized because of the ambiguity brought in when the experimental γ-ln$C$ curve was differentiated graphically in order to obtain the value of Γ or A according to the Gibbs adsorption equation.

Therefore, a direct comparison between the experimental and theoretical γ-C relations is desirable in order to estimate the value of the K parameter.

Relation between the Surface Pressure and Concentration. The surface tension, γ, or the surface pressure, F, is given explicitly as a function of the concentration, C, if $K=0$, as has been shown in Eq. 12. If, however, $K\neq 0$, an explicit expression cannot be obtained; instead, the numerical relations between F and C for various values of K must be calculated by using Eqs. 6 and 11 simultaneously. This means that the following simultaneous equations must be solved numerically, taking θ as the parameter:

$$\left.\begin{aligned}(A_0/k_BT)F &= -2.303\log(1-\theta) - K\theta^2\\ \log(k_0C) &= \log\theta - \log(1-\theta) - 0.8686K\theta\end{aligned}\right\}. \quad (14)$$

The results are shown in Fig. 4, where dimensionless quantities, $(A_0/k_BT)F$ and k_0C, are used in place of F and C respectively.

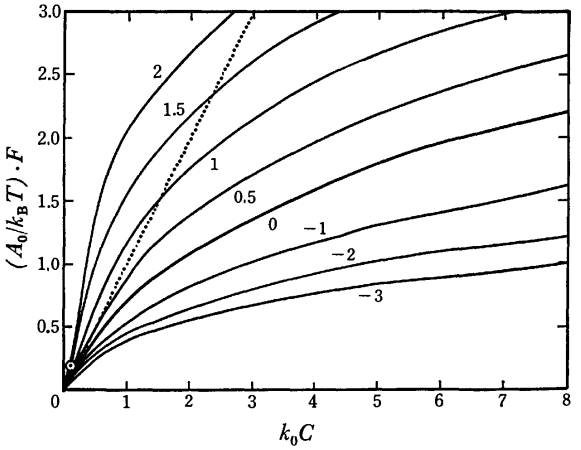

Fig. 4. Theoretical relations between the surface pressure F and concentration C, for various K values as indicated. The dotted line is the initial slope.

It might seem strange at first glance that the value of F, or the decrease of γ, is larger when the lateral intermolecular attraction is larger and when the value of K is larger for any given k_0 and (A_0/k_BT). This, however, does not mean that the adsorption monolayer of the larger lateral attraction shows a larger surface pressure at a given amount of adsorption; it does mean that the amount of adsorption is larger when the lateral attraction in the monolayer is larger, as has already been shown in Fig. 1.

To estimate the parameter values experimentally, two methods are commonly used, one in low-concentration, and the other in high-concentration, regions.

In the low concentration region ($\theta\rightarrow 0$), the expansion of $(A_0/k_BT)F$ in a power series of k_0C is performed by using the simultaneous equations 14; the following result is thus obtained:

$$(A_0/k_BT)F = k_0C + \left(K-\frac{1}{2}\right)(k_0C)^2 + \cdots. \quad (15)$$

According to this equation, it may be said that F is proportional to C if $k_0C\ll 1$ and that the proportionality coefficient is equal to $(k_0/A_0)k_BT$. This proportionality is considered to be helpful for the experimental determination of the parameter values. However, the theoretical curves in the low-concentration range, as shown in Fig. 5, start curving at an unexpectedly low concentration, except in the particular case of $K=0.5$, where the F-C relation is linear up to fairly large values of C because the coefficient of the C^2 term in Eq. 15 is zero. It may be seen from Fig. 5 that the concentration range where the F-C relation is not affected by the value of K and where the proportionality between F and C holds is as low as $(A_0/k_3T)F<0.03$. This means that the proportionality coefficient must be determined in the region where $F<0.4\times 10^{-3}$ N m^{-1} if $A_0=30\times 10^{-2}$ nm^2·molecule^{-1} at 25 °C. Experimentally, this is not always easy.

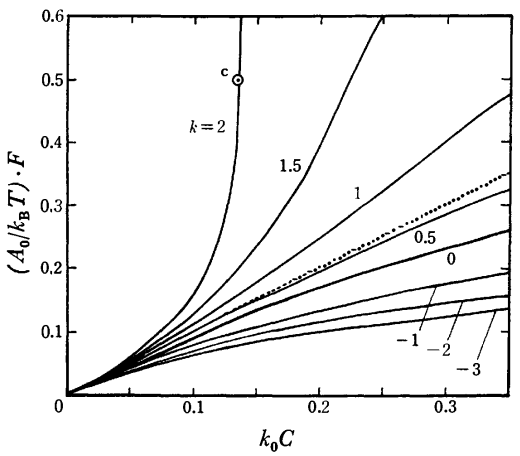

Fig. 5. Theoretical relations between F and C at a low concentration range. The dotted line is the initial slope, which is common to all curves and corresponds to the equation $F=(k_0/A_0)\,k_BTC$.

In the high-concentration region ($\theta\rightarrow 1$), the F-log C curve approaches an asymptotic straight line. The equation of this asymptote is obtained from Eq. 14:

$$(A_0/k_BT)F_{asymp} = K + \ln(k_0C) \quad (\theta\rightarrow 1). \quad (16)$$

Some of the theoretical curves obtained from Eq. 14 are shown in Fig. 6, together with the asymptotes of Eq. 16. It can be understood from Eq. 16 that the inclination of the asymptote of an F-log$C$ curve is equal to $(2.303\,k_BT/A_0)$, but it is clear from Fig. 6 that A_0 values thus estimated are acceptable only when K has a large positive value. If, for example, $K=0$, it may be seen from Fig. 6 that a correct value of the inclination may be obtained by using only the experimental data for $(A_0/k_BT)F>3.0$; this means that $F>41\times 10^{-3}$ N m^{-1} if $A_0=30\times 10^{-2}$ nm^2 molecule^{-1} at 25 °C. This condition is, however, not easy to realize experimentally, and it is impossible to fulfill when the monolayer collapses at this high surface pressure or when the concentration of the solution cannot be high enough because the solubility of the solute is not high enough. The method is, therefore, not applicable except for long-chain derivatives such as surfactants in which the K value may be supposed to be large.

As the conclusion of these considerations, it may be said that a method is needed which makes the estimation of the A_0, k_0, and K parameters possible by using the experimental data obtained in the intermediate

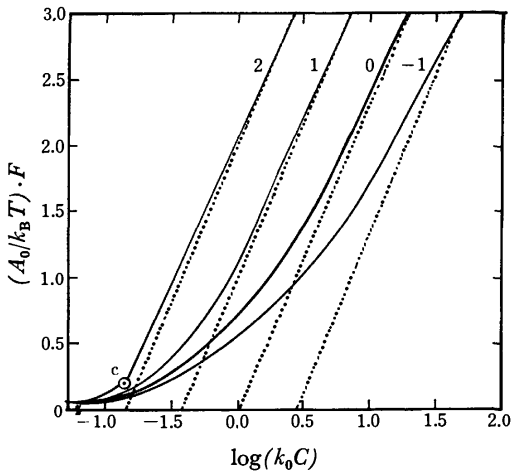

Fig. 6. Theoretical relations between F and log C for various K values as indicated. The dotted lines are the asymptotes.

concentration range.

Proposed Method to Determine Parameter Values. It has been found, after several trials, that the use of the relation between log (F/k_BTC) and log C is the most convenient for determining the values of A_0, k_0, and K. The theoretical curves of log $(F/k_BTC)+\log(A_0/k_0)$ against log $C+\log k_0$ are calculated by using Eq. 14 and are shown in Fig. 7 for the K values from 0 to 2 at regular intervals of 0.2. For $K>0.5$, each curve has a maximum point which corresponds to the θ_{max} given by the following equation:

$$\theta_{max} + \ln(1-\theta_{max}) + K\theta_{max}^2 = 0. \quad (17)$$

On the other hand, the experimental data are plotted, taking log (F/k_BTC) and log C on the ordinate and abscissa respectively, on the same scales as those of the theoretical plot in Fig. 7 and are superimposed on the latter so that the experimental data fit one of the theoretical curves. The shape of the theoretical curve for the best fit will give the K-value. Then, the k_0-value is obtained from the value of log C for log $C+\log k_0=0$, and the A_0-value, from the value of log (F/k_BTC) for log $(F/k_BTC)+\log(A_0/k_0)=0$.

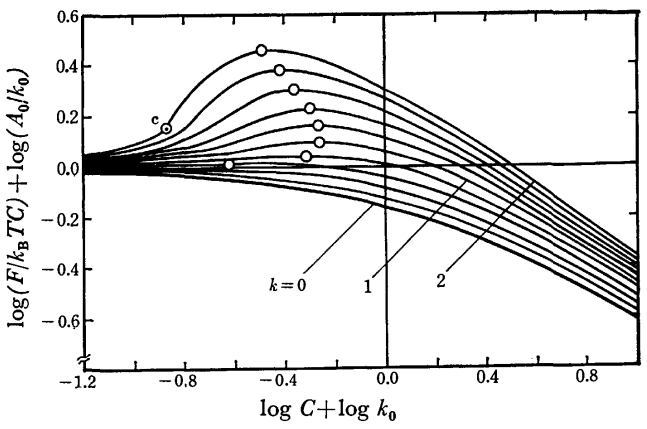

Fig. 7. Theoretical log (F/k_BTC)-log C curves for $K=$ 0(0.2)2. Open circles show the maximum points. The point c is the critical point of phase separation.

Comparison with Experimental Data

Parameter Values of Normal Alcohols. The experimental values of Posner *et al.*[4] were used to test the method proposed above. For example, the case of 25 °C is shown in Fig. 8, where the circles are experimental and the curves are theoretical. The parameter values thus obtained are given in Table 1, together with those obtained for other temperature values.

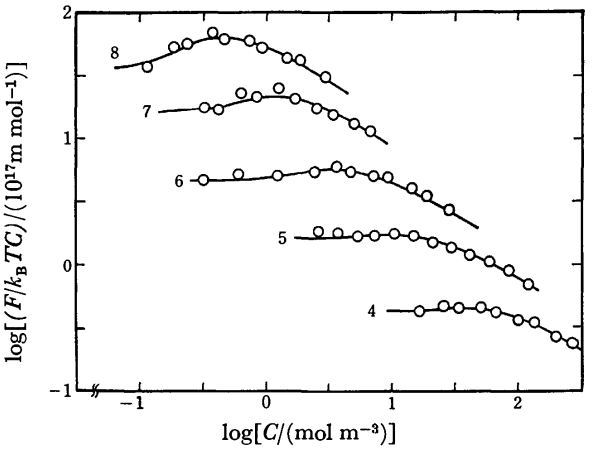

Fig. 8. Comparison between experimental values[4] (open circles) and theoretical curves for normal alcohols, which have the carbon numbers n as indicated, at 25 °C.

TABLE 1. PARAMETER VALUES OF NORMAL ALCOHOLS

Alcohol	Temp (°C)	K	$k_0\times10^3$ ($m^3\,mol^{-1}$)	$A_0\times10^2$ ($nm^2\cdot molecule^{-1}$)
Butyl	12	0.75	20.9	35.5
	25	0.75	14.8	34.7
	39	0.75	12.6	30.2
Pentyl	25	0.75	49.0	30.9
	39	0.75	37.2	30.9
Hexyl	12	1.00	251	38.9
	25	1.00	138	30.9
	39	1.00	123	33.9
Heptyl	12	1.25	525	30.9
	25	1.1	468	30.2
	39	1.1	302	29.5
Octyl	12	1.5	1700	33.1
	25	1.5	1000	29.5
	39	1.4	708	26.9

The k_0 parameter is essentially the equilibrium constant between solute molecules adsorbed on the surface and dissolved in the solution, and it is related to the change in the standard chemical potential due to the adsorption according to Eq. 7. Before the standard affinity of adsorption $(-\Delta\mu^0)$ is calculated, however, the experimental parameter value, k_0, in $m^3\,mol^{-1}$ based on the molar concentration, C, must be recalculated to the dimensionless "unitary" quantity,[5] k_x, based on the mole fraction, x,

$$k_x = (C/x)k_0 \simeq (d_1/M_1)k_0$$
$$= 55.34(k_0\times10^3)/(m^3\,mol^{-1}), \quad (18)$$

for aqueous solutions at 25 °C, where d_1 and M_1 are

Table 2. Affinity of the adsorption and energy of lateral interaction

Alcohol	Temp (°C)	$-\Delta\mu^0$ (kcal mol^{-1})		ε (kcal mol^{-1})	
Butyl	12	4.00	(4.02)	0.85	(0.89)
	25	3.98		0.89	
	39	4.07		0.93	
Pentyl	25	4.69	(4.72)	0.89	(0.91)
	39	4.74		0.93	
Hexyl	12	5.41	(5.40)	1.13	(1.19)
	25	5.30		1.19	
	39	5.48		1.24	
Heptyl	12	5.83	(5.97)	1.42	(1.36)
	25	6.03		1.30	
	39	6.04		1.37	
Octyl	12	6.49	(6.51)	1.70	(1.74)
	25	6.48		1.78	
	39	6.57		1.74	

( ): Averages.

the density and the molecular weight of water respectively.

The values of the standard affinity of adsorption obtained by the following equation from the k_0-values of Table 1 are shown in Table 2 (1 cal=4.184 J):

$$-\Delta\mu^0 = RT\ln k_x. \tag{19}$$

From these tables it may be seen that $(-\Delta\mu^0)$ does not depend much on the temperature, although k_0 and, therefore, k_x decrease with increase in the temperature. The energy of lateral interaction, ε, calculated by Eq. 8 from the K values given in Table 1 is shown in Table 2 as well. Since the temperature dependences of $-\Delta\mu^0$ and ε are not large, the average values (shown in parentheses in Table 2) are plotted against the number of carbon atoms of alcohols, n, in Fig. 9. It may be seen that the value of ε is about 1/4 of $-\Delta\mu^0$ for each alcohol in this region of n.

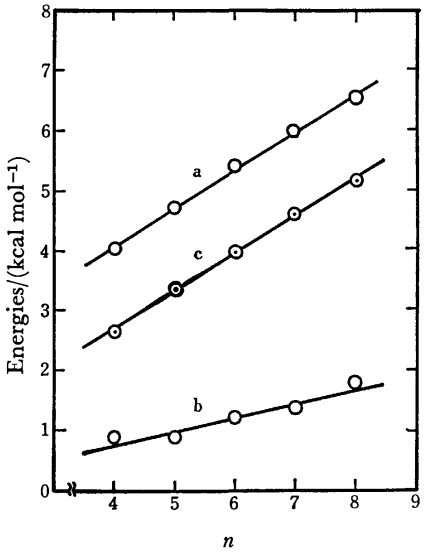

Fig. 9. Dependence, on the carbon number n, of (a) the standard affinity $-\Delta\mu^0$ of Eq. 19, (b) the energy of lateral interaction ε of Eq. 8 and (c) the standard free energy of adsorption $-\Delta G^0$ of Eq. 25.

The relations of $-\Delta\mu^0$ and of ε against n in Fig. 9 are linear and give the following empirical equations:

$$-\Delta\mu^0/(\text{kcal mol}^{-1}) = 1.60 + 0.62n \tag{20}$$

and

$$\varepsilon/(\text{kcal mol}^{-1}) = -0.16 + 0.23n. \tag{21}$$

Equation 20 means that the affinity of adsorption is 620 cal mol^{-1} per methylene group and 1600 cal mol^{-1} per hydroxyl group. The latter value, however, depends on the selection of the standard states. The former value, 620 cal mol^{-1}, is not much different from Traube's value,[6] 650 cal mol^{-1}. The former value obtained for n=4—8 is, however, a little smaller than the value, 682 cal mol^{-1}, for n=12—16 obtained for disodium monoalkyl phosphates,[7] probably because of the difference in the range of n. Equation 21 means that the energy of lateral attraction per methylene group is 230 cal mol^{-1}, while the energy of lateral repulsion per hydroxyl group is 160 cal mol^{-1}.

On the other hand, Ward and Tordai[8] and also Posner *et al.*[4] calculated the standard free energy of adsorption by means of

$$\Delta G^0 = -RT\ln(\alpha/k_BT\delta), \tag{22}$$

where δ is the thickness of the adsorption monolayer and α is the Traube constant defined at an infinite dilution by:

$$\alpha = \lim_{C\to 0}(F/CN_A), \tag{23}$$

where N_A is the Avogadro number.

According to our Eq. 15,

$$\alpha = k_BT(k_0/A_0N_A), \tag{24}$$

therefore, we have

$$-\Delta G^0 = RT\ln(k_0/A_0\delta N_A). \tag{25}$$

As for the parameter values to be used in this equation, the values of k_0 and A_0 have been shown in Table 1; the values of δ given by Posner *et al.*[4] are cited in Table 3. The values of $-\Delta G^0$ thus calculated are given in the same table, together with the values reported by Posner *et al.*,[4] the latter being indicated by $-\Delta G_p{}^0$. It may be seen that these values are in good agreement with each other. This is because, at an infinite dilution,

Table 3. Standard free energy of adsorption as calculated by means of Eq. 25

Alcohol	$\delta\times 10$ (nm)[4]	Temp (°C)	$-\Delta G^\circ$ (kcal mol^{-1})		$-\Delta G_p{}^\circ$ (kcal mol^{-1})[4]
Butyl	8.8_9	12	2.26	(2.65)	2.66
		25	2.59		
		39	2.70		
Pentyl	9.5_3	25	3.32	(3.32)	3.36
		39	3.31		
Hexyl	9.9_2	12	3.96	(3.95)	4.05
		25	3.92		
		39	3.97		
Heptyl	10.1_2	12	4.49	(4.58)	4.72
		25	4.64		
		39	4.60		
Octyl	10.2_4	12	5.11	(5.13)	5.42
		25	5.10		
		39	5.18		

( ): Averages.

the lateral interaction between the adsorbed molecules becomes negligible and the $k_0\exp(2K\theta)$ term in Eq. 6 approaches k_0.

Since the temperature dependence of $-\Delta G^0$ is negligible, the average values are plotted in Fig. 9. The linear relation in the figure gives the empirical relation

$$-\Delta G^0 = 0.17 + 0.63n. \quad (26)$$

The free energy of adsorption per methylene group is, therefore, 630 cal mol^{-1}, which is almost the same as the value of Eq. 20. This can be understood directly from Fig. 9 in view of the fact that the straight lines for $-\Delta\mu^0$ and $-\Delta G^0$ are parallel with each other.

By comparing Eqs. 19 and 25, it can be understood that the parallel relation means that the molar volume of the adsorption monolyer, $V_m = A_0\delta N_A$, obtainable from our value of the molecular area, A_0, is independent of the number of carbon atoms, n, of the alcohols. The value of V_m at 25 °C is actually almost constant and is 181.7×10^{-6} m^3 mol^{-1} on the average from butyl to octyl alcohols, while the molar volume of the liquid, V_l, increases from 91.6×10^{-6} m^3 mol^{-1} in butyl alcohol to 157.8×10^{-6} m^3 mol^{-1} in octyl alcohol, according to the increase in the molecular weight, because the density does not increase so much. This seems to be an interesting point.

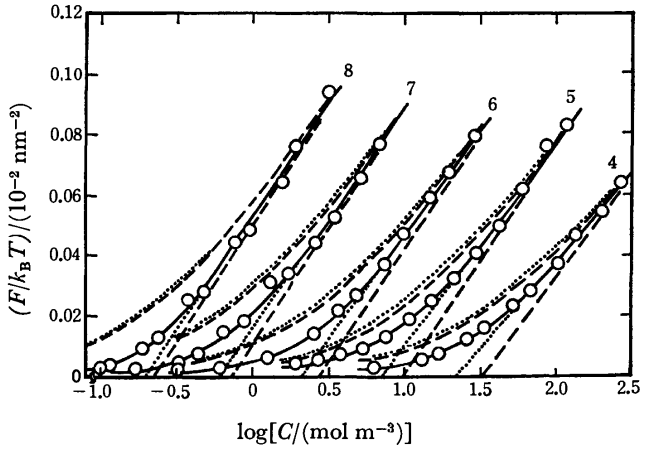

Fig. 10. Comparison between experimental values (open circles)[4] and theoretical solid curves drawn by Eq. 14 at 25 °C for normal alcohols whose carbon numbers are as indicated. Broken straight lines are calculated by Eq. 16, and broken curves are the Szyszkowski curves corresponding to them. Dotted straight lines are empirical and dotted curves are the corresponding Szyszkowski's.

Relation between F *and log* C. It is shown in Fig. 10 that the agreement is good between the experimental data by Posner *et al.*[4] at 25 °C (open circles) and the theoretical curves (solid lines) drawn according to Eq. 14 by using the parameter values given in Table 1. In Fig. 10 the asymptotes, too, are shown by broken straight lines according to Eq. 16, using the same parameter values.

Table 4. Comparison of parameter values of Eq. 27 at 25 °C

Alcohol	$A_0'\times10^2$ (nm^2 · molecule^{-1})	$k_0'\times10^3$ (m^3 mol^{-1})	A_0'/A_0	$k_0'/(k_0e^K)$
Butyl	39.6	44.7	1.14	1.43
Pentyl	34.6	142	1.12	1.37
Hexyl	34.1	490	1.10	1.31
Heptyl	32.2	1700	1.07	1.21
Octyl	31.1	5130	1.05	1.14

Experimentally, however, one might draw asymptotes like those shown by dotted straight lines in Fig. 10. For these asymptotes, if one used the following equation,

$$A_0'F_{asymp}/k_BT = \ln k_0' + \ln C \quad (27)$$

which can be derived from Szyszkowski's Eq. 12, the parameter values, A_0' and k_0', given in Table 4 may be obtained. By using these values for A_0 and k_0 of Eq. 12, Szyszkowski's theoretical curves are drawn in Fig. 10 by dotted curves; those curves are not, however, in agreement with the experimental values.

This discrepancy is partly due to the overestimation of the parameter values shown in Table 4 in that A_0'/A_0 and $k_0'/(k_0e^K)$ are larger than 1.0. Here, k_0' is compared to k_0e^K, because the latter is the value obtained from the broken straight lines, as can be understood by comparing Eq. 27 with Eq. 16. Even if the values of A_0 and k_0e^K are inserted into A_0 and k_0 of Eq. 12, however, the Szyszkowski curves shown by broken curves in Fig. 10 are still distant from the experimental values. The discrepancy is, therefore, mainly the result of the use of the Szyszkowski equation. It can be concluded that the use of Eq. 14, which takes the lateral interaction between the adsorbed molecules into account, is indispensable in explaining the experimental results over the entire concentration range.

References

1) M. Nakagaki, *Bull. Chem. Soc. Jpn.*, **24**, 269 (1951).
2) S. Levine, A. L. Smith, and E. Matijević, *J. Colloid Interface Sci.*, **31**, 409 (1969).
3) M. Nakagaki, T. Handa, and S. Shimabayashi, *J. Colloid Interface Sci.*, **43**, 521 (1973).
4) A. M. Posner, J. R. Anderson, and A. E. Alexander, *J. Colloid Sci.*, **7**, 623 (1952).
5) R. W. Gurney, "Ionic Processes in Solutions," Dover Publications, New York (1962), p. 104.
6) J. Traube, *Ann.*, **265**, 27 (1891).
7) M. Nakagaki and T. Handa, *Bull. Chem. Soc. Jpn.*, **48**, 630 (1975).
8) A. F. H. Ward and L. Tordai, *Trans. Faraday Soc.*, **42**, 413 (1946).

Intersystem Crossing Processes of Acridine

Koichi KIKUCHI, Koji UJI-IE, Yoshikatsu MIYASHITA, and Hiroshi KOKUBUN

Department of Chemistry, Faculty of Science, Tohoku University, Aoba, Aramaki, Sendai 980

(Received June 11, 1976)

The $T_1(\pi, \pi^*) \rightarrow T_3(\pi, \pi^*)$ absorption of acridine has first been observed at about 985 nm in ethanol. Temperature dependences of the fluorescence lifetime and the triplet yield of acridine were investigated in poly(vinyl alcohol) film, and it was found that the intersystem crossing from the first excited singlet state $S_1(\pi, \pi^*)$ to $T_1(\pi, \pi^*)$ occurs through both temperature dependent and independent processes. The activation energy of the temperature dependent process corresponds substantially to the energy difference between $T_3(\pi, \pi^*)$ and $S_1(\pi, \pi^*)$. The intersystem crossing from $S_1(\pi, \pi^*)$ to $T_2(n, \pi^*)$ followed by the internal conversion to $T_1(\pi, \pi^*)$ was assigned to the temperature independent process.

Photoreduction of acridine has been studied in various solvents,[1-5] particularly in alcohols in which acridine is fluorescent,[6] and it was suggested that there are two reactive states in alcohols; the first excited singlet state, S_1, and the second excited triplet state, $T_2(n, \pi^*)$.[7-9] However, it is still uncertain whether the reactive singlet state is of π, π^* character or of n, π^*,[10-12] because the energy levels of the $^1(\pi, \pi^*)$ and $^1(n, \pi^*)$ states are close together.[11-13]

The mechanism of the intersystem crossing of acridine from the first excited singlet state to $T_1(\pi, \pi^*)$ has been unknown because of the uncertainty of the energy levels responsible for the intersystem crossing. Recently, Hirata and Tanaka investigated the rise-up of the transient absorption of acridine in ethanol by a picosecond laser technique, and suggested that the intersystem crossing is essentially $S_1(\pi, \pi^*) \rightarrow T_2(n, \pi^*)$ transition followed by $T_2(n, \pi^*) \rightarrow T_1(\pi, \pi^*)$ transition.[14] It was suggested that all of $T_1(\pi,\pi^*)$ is produced through $T_2(n, \pi^*)$ in alcohols.[15]

The energy level of $T_1(\pi,\pi^*)$ was determined experimentally by Evans as 15840 cm^{-1} [16] and that of $T_2(n,\pi^*)$ was calculated by Goodman and Harrell as 21400 or 23500 cm^{-1},[17] while those of the $^1(\pi, \pi^*)$ and $^1(n, \pi^*)$ states are about 26600 cm^{-1} in hydrocarbon solvent.[17] Since the energy difference between the lowest excited singlet state and $T_1(\pi, \pi^*)$ is considerably large, it seems that the intersystem crossing occurs to $T_2(n, \pi^*)$ more easily than to $T_1(\pi, \pi^*)$, particularly if the S_1 state is of π, π^* character.[18]

Bowen *et al.* found that the fluorescence yield decreases with increasing temperature in the ethanol-water mixture.[6] The triplet yield of 9-methylacridine increases with increasing temperature in ethanol.[11] These earlier observations suggest that acridine is subject to temperature dependent intersystem crossing similar to the 9,10-disubstituted anthracenes.[19-22]

In order to clarify the mechanism of the intersystem crossing of acridine, we have measured the T-T absorption spectrum in the near infrared region and studied the temperature dependences of the fluorescence lifetime and the yield of $T_1(\pi, \pi^*)$ in poly(vinyl alcohol) film (PVA), where the photoreduction is negligible and the S_1 state seems to be a $^1(\pi, \pi^*)$ state.

Experimental

Materials. Acridine (C. P. grade, Tokyo Kasei) was recrystallized from the ethanol-water mixture after pretreatment with activated charcoal in ethanol. Ethanol (G. R. grade, Wako Jun-Yaku) and poly(vinyl alcohol) (the degree of polymerization 1400, Koso Kagaku) were used without further purification.

Apparatus and Procedure. The absorption spectrum was measured with a Hitachi EPS-3T spectrophotometer, and the fluorescence spectrum with a modified Hitachi EPU spectrophotometer. Lifetime measurement was made with a phase-fluorometer modulated at 10.7 MHz. Relative yields of the triplet acridine and the T-T absorption spectra in the visible region were measured with an ordinary flash apparatus. The T-T absorption spectrum in the near infrared region was measured by the use of the combination of a HTV R-406 photomultiplier and an Ushio JC-12-130 L halogen lamp as a monitoring light source. Absolute yield of the triplet acridine was determined by the use of a flash irradiation apparatus as shown in Fig. 1.

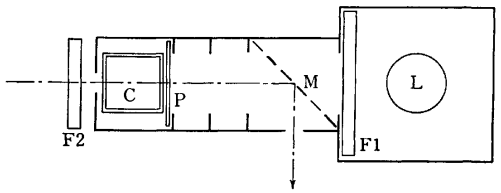

Fig. 1. The flash irradiation apparatus used to determine the intersystem crossing probability of acridine in PVA.
L: Xenon flash lamp, F_1: Hoya U 2 band path filter, M: half mirror, P: PVA film, C: actinometer cell, F_2: Toshiba V-Y 43 cut off filter.

Results and Discussion

The absorption and fluorescence spectra of acridine in PVA are shown in Fig. 2, from which the energy level of $S_1(\pi, \pi^*)$ is estimated to be 25450 cm^{-1} as an average of the absorption maximum in the ^1L_a band at 25900 cm^{-1} and the fluorescence maximum at 25000 cm^{-1}.[23] Figure 3 shows the T-T absorption spectra of acridine in PVA and ethanol. The absorption maxima in the near infrared region lie at 10150, 11500, and 12850 cm^{-1} in ethanol. Since no transient absorption was observed below 9800 cm^{-1}, the absorption at 10150 cm^{-1} was assigned to the 0-0 band of the $T_1(\pi,\pi^*) \rightarrow T_3(\pi, \pi^*)$ transition. Hence the energy level of $T_3(\pi, \pi^*)$ is estimated to be 25990 cm^{-1}.

The fluorescence lifetime in PVA is 8.2$_6$ ns at 13 °C. Since the rate constant of the fluorescence emission, k_f, is estimated to be 3.6×10^7 s^{-1} from the known values of

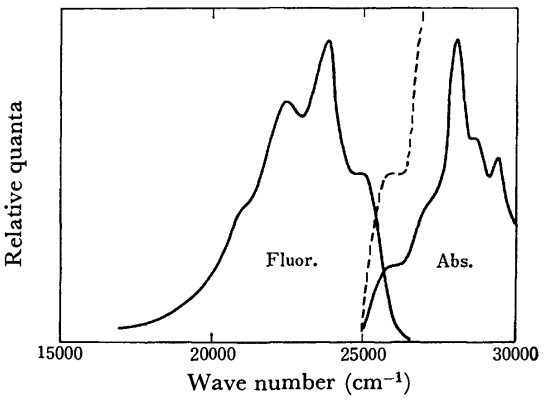

Fig. 2. The absorption and fluorescene spectra of acridine in PVA.

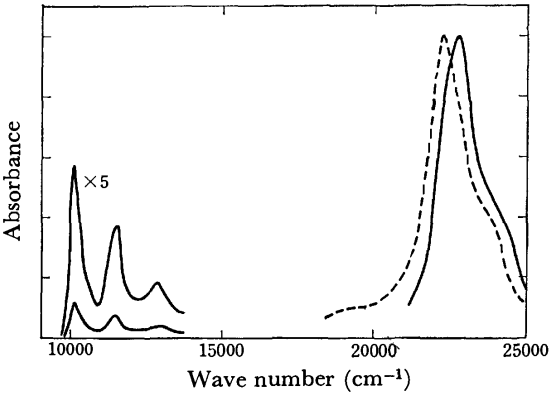

Fig. 3. The T-T absorption spectra of acridine in PVA (----) and in ethanol (——).

the fluorescence yield ($\phi_f=0.37$)[6] and the lifetime (10.3 ns)[24] in water, the fluorescence yield in PVA is evaluated as 0.30 at 13 °C. The large yield and the long lifetime imply that the S_1 state is a $^1(\pi, \pi^*)$ state in PVA.

According to a method similar to that in a previous paper,[15] the intersystem crossing probability of acridine from $S_1(\pi, \pi^*)$ to $T_1(\pi, \pi^*)$ was determined to be 0.56 in PVA at 23 °C by the use of the molar extinction coefficient of the T-T absorption maximum in ethanol, $\varepsilon_T=18500\ M^{-1}\ cm^{-1}$ at 440 nm.[25]

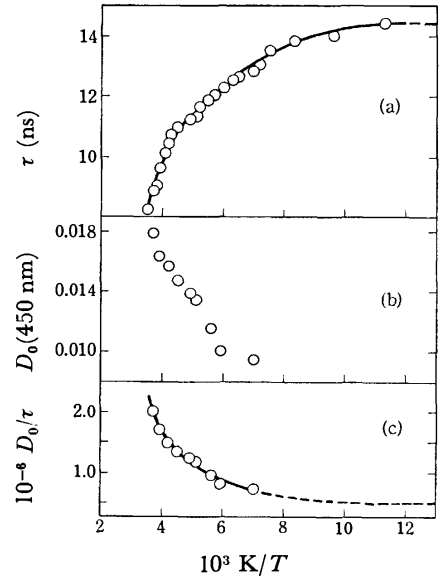

Fig. 4. The temperature dependencies of the fluorescence lifetime (a), the absorbance of the T-T absorption immediately after flashing (b), and their ratio (c).

Figure 4 shows the temperature dependences of the fluorescence lifetime (τ), the absorbance (D_0) of the T-T absorption immediately after flashing, and the ratio (D_0/τ). The lifetime increases with decreasing temperature and approaches to about 14 ns at low temperature. On the other hand, D_0/τ which is associated with the rate of intersystem crossing, decreases with decreasing temperature. It is obvious that both the decay of the singlet excited state and the intersystem crossing occur through temperature dependent and independent processes. When the extrapolated values of $1/\tau$ and D_0/τ at lower temperature are subtracted from their original values, the resulting Arrhenius plots are linear as shown in Fig. 5, and their slopes are nearly the same; the apparent activation energy is estimated to be 420 cm^{-1}. Therefore, we can safely conclude that both the deactivation of $S_1(\pi, \pi^*)$ and the production of $T_1(\pi, \pi^*)$ occur through two kinds of processes; one is temperature dependent and the other is temperature independent.

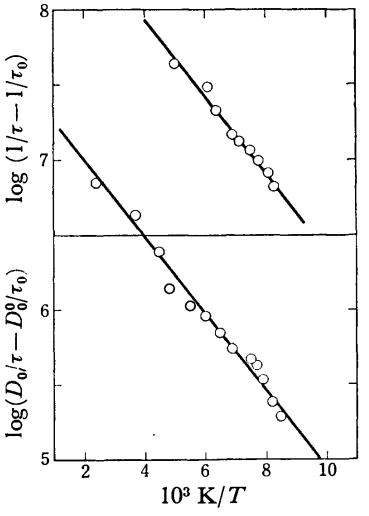

Fig. 5. The Arrhenius plots of $(1/\tau-1/\tau_0)$ and $(D_0/\tau-D_0^0/\tau_0)$ *vs.* temperature.

The energy difference between $S_1(\pi, \pi^*)$ and $T_3(\pi, \pi^*)$ is nearly equal to the activation energy, so that the temperature dependent process seems to be the intersystem crossing from $S_1(\pi, \pi^*)$ to $T_3(\pi, \pi^*)$. In the case of acridine, there are two low-lying triplet states, $T_1(\pi, \pi^*)$ and $T_2(n, \pi^*)$. According to the spin-orbit coupling selection rule of El-Sayed[18] and the energy gap law,[26] the $S_1(\pi, \pi^*)\rightarrow T_2(n, \pi^*)$ transition would be much easier than the $S_1(\pi, \pi^*)\rightarrow T_1(\pi, \pi^*)$ transition. This view coincides with the suggestions that $T_1(\pi, \pi^*)$ is mainly produced through $T_2(n, \pi^*)$ in alcohols,[15] and that the first step of the intersystem crossing is $S_1(\pi, \pi^*)\rightarrow T_2(n, \pi^*)$ transition in ethanol.[14]

On the basis of the above informations, we propose a Jablonski diagram as shown in Fig. 6, where k_d is the rate constant of non-radiative transitions other than intersystem crossing. According to the diagram, the

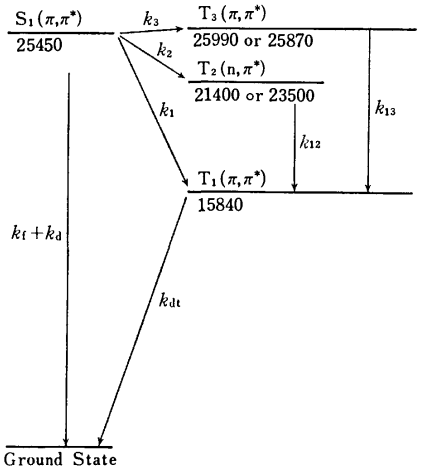

Fig. 6. The Jablonski diagram of acridine in PVA.

fluorescence lifetime and the yield of $T_1(\pi, \pi^*)$ are expressed as follows;

$$\tau = 1/(k_f+k_d+k_1+k_2+k_3), \quad (1)$$

$$\phi_{ST} = (k_1+k_2+k_3)\tau. \quad (2)$$

D_0 is related to the light absorbed during flashing, I_{ab}, as follows;

$$D_0 = \varepsilon_T[T]_0 d = \varepsilon_T d \cdot \phi_{ST} I_{ab}, \quad (3)$$

where $[T]_0$ is the triplet concentration immediately after flashing and d is the thickness of PVA. At sufficiently low temperature, following relations hold;

$$\tau_0 = 1/(k_f+k_d+k_1+k_2), \quad (4)$$

$$\phi^0_{ST} = (k_1+k_2)\tau_0, \quad (5)$$

$$D^0_0 = \varepsilon_T d \cdot \phi^0_{ST} I_{ab}. \quad (6)$$

Putting $k_3=k\exp(-\Delta E/RT)$, we obtain the following equations from Eqs. 1—6;

$$\frac{D_0}{\tau} - \frac{D^0_0}{\tau_0} = \varepsilon_T d I_{ab} k \exp\left(-\frac{\Delta E}{RT}\right), \quad (7)$$

$$\frac{1}{\tau} - \frac{1}{\tau_0} = k \exp\left(-\frac{\Delta E}{RT}\right). \quad (8)$$

These equations can analyze the results shown in Fig. 5, and the following values are obtained;

$$\frac{1}{\tau_0} = 7\times10^7\ s^{-1},$$

$$k = 3.7\times10^8\ s^{-1},$$

$$\Delta E = 420\ cm^{-1},$$

$$\varepsilon_T(450) d I_{ab} k = 1.3\times10^7\ s^{-1},$$

$$\frac{D^0_0}{\tau_0} = \varepsilon_T(450) d I_{ab} \cdot (k_1+k_2) = 5\times10^5\ s^{-1}.$$

From the last two relations, the rate constant of the intersystem crossing to the two lower triplet states, k_1+k_2, was calculated to be $1.4\times10^7\ s^{-1}$.

All of the rate constants involved in the Jablonski diagram were summarized in Table 1. The yield of $T_1(\pi, \pi^*)$ in PVA at any temperature can be calculated by the following relation derived from the above results;

$$\phi_{ST} = (k_1+k_2+k_3)\tau = \frac{0.20+5.3\times\exp(-604/T)}{1.0+5.3\times\exp(-604/T)}. \quad (9)$$

Table 1. Rate constants of the deactivation of excited acridine

$k_f=3.6\times10^7\ s^{-1}$	
$k_d=2.0\times10^7\ s^{-1}$	
$k_3=3.7\times10^8\times\exp\left(-\frac{\Delta E}{RT}\right)$	$\Delta E=420\ cm^{-1}$
$k_1+k_2=1.4\times10^7\ s^{-1}$	$k_1 \ll k_2$
$k_{dt}=4.2\times10\ s^{-1}$	

From Eq. 9, we get $\phi_{ST}=0.53$ at 23 °C, which agrees satisfactorily with the experimental value 0.56. Such agreement between the calculated and observed values supports strongly the validity of both the deactivation pathways shown in Fig. 6 and their rate constants cited in Table 1. The fluorescence and intersystem crossing yields at sufficiently low temperature are calculated to be 0.51 and 0.20, respectively.

In the above discussion, the contribution of the $^1(n, \pi^*)$ state to the deactivation of $S_1(\pi, \pi^*)$ has been ignored. The value of k obtained is the same order of magnitude for the frequency factor of a intersystem crossing process in aromatic hydrocarbons;[27] there seems to be no enhancement of the intersystem crossing due to the spin-orbit coupling between the $^1(n, \pi^*)$ state and $T_3(\pi, \pi^*)$. Therefore, it is probable that the energy level of the $^1(n, \pi^*)$ state is too high to play an important role in the intersystem crossing.

In this study, it has first been confirmed that there are two kinds of processes in the intersystem crossing of acridine from $S_1(\pi, \pi^*)$ to $T_1(\pi, \pi^*)$ in PVA; the temperature dependent process through $T_3(\pi, \pi^*)$ whose energy level is about 420 cm^{-1} higher than that of $S_1(\pi, \pi^*)$ and the temperature independent processes in which the path through $T_2(n, \pi^*)$ seems to be most important.

As regards k_d, the internal conversion is unreasonable because of the large energy gap between $S_1(\pi, \pi^*)$ and the ground state. Although the quantum yield of photoreduction of acridine by steady light illumination is very small in PVA, the weak transient absorption other than the T-T absorption was observed at about 560 nm where acridine radicals have the absorption.[28] Therefore, the non-radiative process may be due to the transient reaction in $S_1(\pi, \pi^*)$.

References

1) V. Zanker and P. Schmidt, *Z. Phys. Chem. N. F.*, **17**, 11 (1958).
2) A. Kellmann, *J. Chem. Phys.*, **57**, 1 (1960).
3) M. Koizumi, Y. Ikeda, and H. Yamashita, *Bull. Chem. Soc. Jpn.*, **41**, 1056 (1968).
4) Y. Miyashita, S. Niizuma, H. Kokubun, and M. Koizumi, *Bull. Chem. Soc. Jpn.*, **43**, 3435 (1970).
5) M. Hoshino, S. Niizuma, and M. Koizumi, *Bull. Chem. Soc. Jpn.*, **45**, 2988 (1972).
6) E. J. Bowen, N. J. Holder, G. B. Woodger, *J. Phys. Chem.*, **66**, 2491 (1962).
7) A. Kellmann and J. T. Dubois, *J. Chem. Phys.*, **42**, 2518 (1965).
8) E. V. Donckt and G. Porter, *J. Chem. Phys.*, **46**, 1173 (1967).
9) M. Koizumi, Y. Ikeda, and T. Iwaoka *J. Chem. Phys.*,

48, 1869 (1968).
10) F. Wilkinson and J. T. Dubois, *J. Chem. Phys.*, **48**, 2651 (1968).
11) V. Zanker and G. Prell, *Ber. Bunsenges. Physik. Chem.*, **73**, 791 (1969).
12) D. G. Whitten and Y. J. Lee, *J. Am. Chem. Soc.*, **93**, 961 (1971).
13) S. T. Lander and R. S. Becker, *J. Phys. Chem.*, **67**, 2481 (1963).
14) Y. Hirata and I. Tanaka, *Chem. Phys. Lett.*, **41**, 336 (1976).
15) K. Tokumura, K. Kikuchi, and M. Koizumi, *Bull. Chem. Soc. Jpn.*, **46**, 2279 (1973).
16) D. F. Evans, *J. Chem. Soc.*, **257**, 1351 (1957).
17) L. Goodman and R. W. Harrell, *J. Chem. Phys.*, **30**, 1131 (1959).
18) M. A. El-Sayed, *J. Chem. Phys.*, **38**, 2834 (1963).
19) W. R. Ware and B. A. Baldwin, *J. Chem. Phys.*, **43**, 1194 (1965).
20) E. C. Lim, J. D. Laposa, and J. M. H. Yu, *J. Mol. Spectrosc.*, **19**, 412 (1966).
21) A. Kearvell and F. Wilkinson, Transition Non-Radiatives dans les Molecules, Paris, 1969; *J. Chim. Phys.*, **1970**, 125.
22) R. E. Kellogg, *J. Chem. Phys.*, **44**, 411 (1966).
23) V. Zanker, *Z. Phys. Chem. (Frankfurt)*, **2**, 52 (1954).
24) H. Kokubun, *Bull. Chem. Soc. Jpn.*, **42**, 919 (1969).
25) K. Kikuchi, H. Kokubun, and M. Koizumi, *Bull. Chem. Soc. Jpn.*, **44**, 1527 (1971).
26) R. Englman and J. Jortner, *Mol. Phys.*, **18**, 145 (1970).
27) J. B. Birks, "Organic Molecular Photophysics," Vol. 1, ed by J. B. Birks, John Wiley & Sons, London (1973), p. 41.
28) A. Kira and M. Koizumi, *Bull. Chem. Soc. Jpn.*, **42**, 625 (1969).

Derivatographic Studies on Transition Metal Complexes. XVIII.[1] Thermal Isomerization of *cis*-$[CrCl_2tn_2]Cl \cdot 0.5H_2O$ in Solid Phase[2]

Tadatsugu YOSHIKUNI, Ryokichi TSUCHIYA, Akira UEHARA, and Eishin KYUNO*

Department of Chemistry, Faculty of Science, Kanazawa University, Kanazawa 920

**Department of Pharmaceutical Science, School of Pharmacy, Hokuriku University, Kanazawa 920*

(Received July 14, 1976)

The thermal *cis*-to-*trans* isomerization of *cis*-$[CrCl_2tn_2]Cl \cdot 0.5H_2O$ in a solid phase was studied by means of derivatographic and isothermal measurements. It was found that *cis*-$[CrCl_2tn_2]Cl \cdot 0.5H_2O$ in which trimethylenediamine(tn) forms six-membered chelate ring with chromium undergoes isomerization to the *trans*-complex in contrast with the isomerization of *trans*-$[MX_2(diam)_2]X \cdot HX \cdot nH_2O$ (M=Co or Cr, X=halogen) to the *cis*-one in which the diamine (diam) forms five-membered chelate ring with metal M. The isomerization proceeded in anhydrous state. The activation energy of the isomerization of the complex was found to be 163 kJ mol^{-1} from the isothermal measurements, which is fairly greater than that of the *trans*-$[CoCl_2pn_2](H_5O_2)Cl_2$ and *cis*-$[CoCl_2tn_2]Cl \cdot H_2O$. The difference was explained by whether or not water molecule involved as a lattice water contributes to the isomerization.

The thermal *trans*-to-*cis* isomerization of the transition metal complexes in a solid phase was reported for the dihalogenobis(diamine) series, *trans*-$[CoCl_2pn_2](H_5O_2)Cl_2$,[3,4] *trans*-$[CoBr_2pn_2](H_5O_2)Br_2$,[5] *trans*-$[CrCl_2en_2]Cl$[6], and *trans*-$[CrBr_2pn_2]Br \cdot H_2O$.[7] In these complexes of the type $[MX_2(diam)_2]X \cdot HX \cdot nH_2O$, the modes of isomerization are influenced more or less by the kind of metal ion, M, halide ion, X, and diamine (diam). In the complex, *trans*-$[CoCl_2pn_2](H_5O_2)Cl_2$, most part of the isomerization was reported to proceed simultaneously with dehydration and dehalogenation, the process being considered to follow an "aquation-anation" mechanism.[4] However, in the complex where the chloride ion is replaced by the bromide ion, *trans*-$[CoBr_2pn_2](H_5O_2)Br_2$, the ratio of isomerization was 55% at the most, no isomerization proceeding after the dehydration was complete.[5]

On the other hand, in the case of the corresponding chromium(III) complex, *trans*-$[CrBr_2pn_2]Br \cdot H_2O$, dehydration was complete rapidly, isomerization successively proceeding even after complete dehydration.[7]

So far as the three complexes are concerned, isomerization occurred in the presence of water molecules involved in the cobalt(III) complexes, whereas it took place mainly in anhydrous state in the chromium(III) complexes. Although the cobalt(III) and chromium(III) complexes containing propylenediamine which forms a five-membered chelate ring with metal undergoes the *trans*-to-*cis* isomerization, it might be of interest to study type of isomerization appearing in the complexes containing trimethylenediamine which forms a six-membered chelate ring.

The present work was undertaken to investigate the kinetics of the isomerization of *cis*-$[CrCl_2tn_2]Cl \cdot 0.5H_2O$, with the purpose of comparing its mode of isomerization with the modes of the corresponding cobalt(III) and propylenediamine complexes.

Experimental

Preparation of Complexes. Dichlorobis(trimethylenediamine)chromium(III) chlorides, *cis*-$[CrCl_2tn_2]Cl \cdot 0.5H_2O$, and *trans*$[CrCl_2tn_2]Cl$, were prepared by a modification of the methods reported.[8] The chemical formulas of these compounds were confirmed by elemental analysis and spectrophotometric measurement.

Found: C, 22.82; H, 6.81; N, 17.76%. Calcd for *cis*-$[CrCl_2tn_2]Cl \cdot 0.5H_2O$: C, 22.84; H, 6.71; N, 17.76%. Found: C, 23.73; H, 6.68; N, 18.28%. Calcd for *trans*-$[CrCl_2tn_2]Cl$: C, 23.51; H, 6.58; N, 18.28%.

Derivatography. The derivatogram for the complex *cis*-$[CrCl_2tn_2]Cl \cdot 0.5H_2O$ was obtained with a MOM Typ-OD-102 Derivatograph. 0.5 g of the sample was used in each run under a constant flow of nitrogen with a heating rate of 1 °C min^{-1}. The activation energy was estimated by analysis of the DTA peak in a manner similar to that reported.[9]

Isothermal Measurements. The rate of dehydration of *cis*-$[CrCl_2tn_2]Cl \cdot 0.5H_2O$ was measured at 129, 136, 144, and 155 °C with a CHO 100L thermobalance. 0.3 g of the sample in each run was heated at the desired temperature. The rate of dehydration was determined from the loss in mass of each sample in a constant time interval at each temperature, and the activation energy was calculated by means of the Arrhenius plots.

The rates of isomerization at 160, 170, 181, 190, 199, and 209 °C were followed by measuring the changes in absorbancy on the basis of the following equations similar to those report-

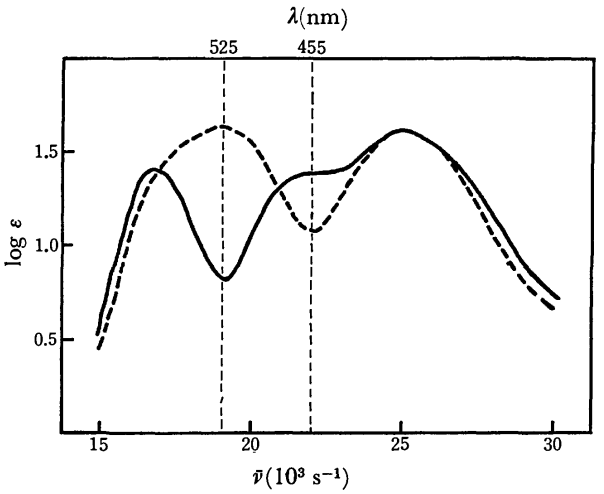

Fig. 1. Electronic spectra of *cis*-$[CrCl_2tn_2]Cl \cdot 0.5H_2O$ (——) and the corresponding *trans*-form complex (----).

ed.[7]

$$5.87X + 46.10Y = D_{525}$$
$$23.98X + 12.00Y = D_{455},$$

where 5.87 and 23.98 are the molar extinction coefficients of the *cis*-complex, and 46.10 and 12.00 are those of the corresponding *trans* complex at 525 and 455 nm, respectively. The electronic spectra of the *cis* and *trans* complexes are shown in Fig. 1.

Results and Discussion

Derivatography. The derivatogram of *cis*-$[CrCl_2tn_2]Cl \cdot 0.5H_2O$ is given in Fig. 2. The TG curve shows that the mass loss corresponding to the liberation of a half mole of water appears at 160 °C, followed by the presence of a plateau from 160 to 220 °C, the decomposition of complex then taking place rapidly.

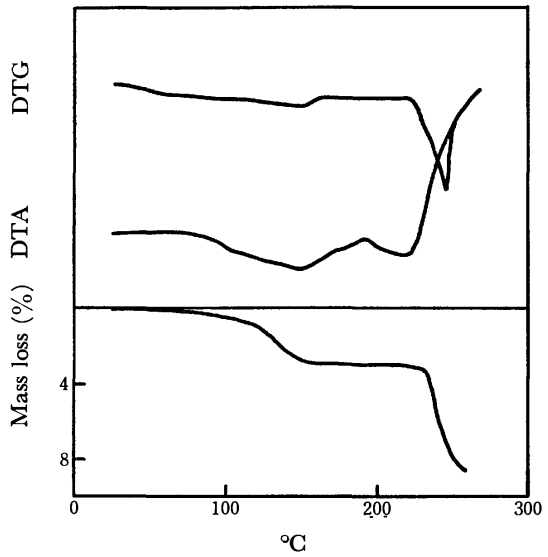

Fig. 2. Derivatogram of *cis*-$[CrCl_2tn_2]Cl \cdot 0.5H_2O$.

The DTA curve shows that an endothermic peak corresponding to the dehydration appears in the range 70—190 °C, one more endothermic peak due to the isomerization appearing at 200—225 °C before an exothermic decomposition reaction begins. The isomerization from *cis*- to *trans*-form could be detected to occur at the second endothermic peak by the color change of the sample from violet to green.

The results indicate that the isomerization of the complex proceeds after the dehydration is complete. Such a tendency was also observed in *trans*-$[CrBr_2pn_2]Br \cdot H_2O$. In contrast to those chromium(III) complexes, the isomerization of the cobalt(III) complexes such as *trans*-$[CoCl_2pn_2](H_5O_2)Cl_2$ and *trans*-$[CoBr_2pn_2](H_5O_2)Br_2$ is always accompanied by dehydration.[4,5] This conspicuous difference in the thermal reaction might

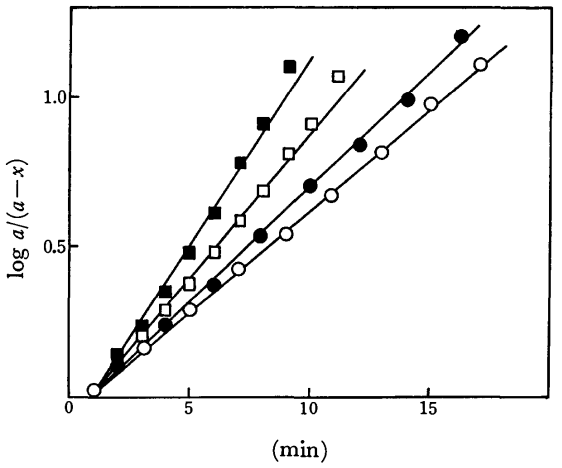

Fig. 3. Relation of log $a/(a-x)$ *vs.* time for the dehydration.
○129°C, ●136°C, □144°C, ■155°C.

arise from the difference in mechanism of the isomerization.

The enthalpy change, ΔH, of the dehydration was obtained by analysis of the endothermic curve in the derivatogram to be 25 kJ mol^{-1}. The value is twice to that for *trans*-$[CrBr_2pn_2]Br \cdot H_2O$, 12.6 kJ mol^{-1}.

Rate of Dehydration. If the rate of dehydration at each temperature follows the first order law, the following equation holds:

$$2.303 \log \frac{a}{(a-x)} = k_d t,$$

where a and x are the initial amount of the starting complex and the amount of an anhydrous complex formed during time t, respectively, and k_d is the rate constant of dehydration. Approximately linear relationships were obtained (Fig. 3) when the values of $\log a/(a-x)$ were plotted *versus* t for each temperature. The rate constants at each temperature were obtained from the slopes of the respective lines. Their values are given in Table 1, together with those of isomerization (*vide post*). From the Arrhenius plots the activation energy of dehydration, E_d, was found to be 42 kJ mol^{-1}. This value is almost equal to the heat of evaporation of water. It is presumed, therefore, that the lattice water molecule in *cis*-$[CrCl_2tn_2]Cl \cdot 0.5H_2O$ is bound loosely like liquid water.

Rate of Isomerization. If the rate of isomerization obeys the first order law, it could be expressed by the equation,

$$2.303 \log b/(b-y) = k_i t,$$

where b is the initial amount of the starting complex, *cis*-$[CrCl_2tn_2]Cl \cdot 0.5H_2O$, y is the amount of *trans* complex produced during time t and k_i is the rate constant of isomerization.

Table 1. Rate constants of dehydration and isomerization

t °C	129	136	144	155	160	170	181	190	199	209
$k_d \times 10^{-3}$ s^{-1}	2.46	2.79	3.69	4.98						
$k_i \times 10^{-5}$ s^{-1}					1.40	3.56	10.44	22.52	59.11	126.0

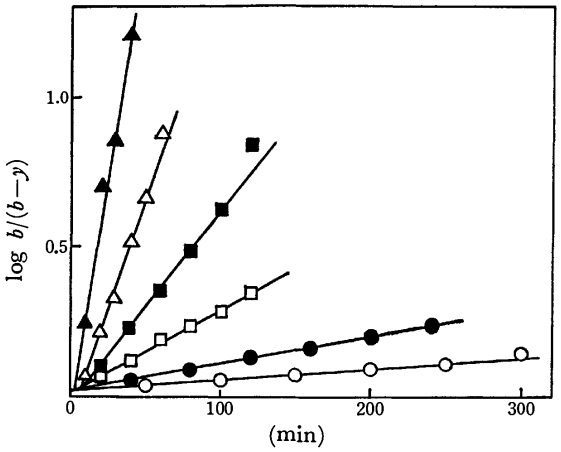

Fig. 4. Relation of log $b/(b-y)$ *vs.* time for the isomerization.
○ 160°C, ● 170°C, □ 181°C, ■ 190°C, △ 199°C, ▲ 209°C.

When the values of log $b/(b-y)$ were plotted *versus* t at each temperature, approximately linear relationships were also obtained (Fig. 4). The rate constants obtained from the slope of the respective lines are given in Table 1, together with those for dehydration. We see that the dehydration occurs at a relatively lower temperature, while most part of the isomerization proceeds in the higher temperature region.

From the Arrhenius plots of the rate constants, the activation energy, E_i, for the isomerization was calculated to be 163 kJ mol^{-1}. This value is slightly lower than 179.7 kJ mol^{-1} for the isomerization of *trans*-$[CrBr_2pn_2]Br \cdot H_2O$, but fairly greater than 96.1 kJ mol^{-1} for that of *trans*-$[CoCl_2pn_2](H_5O_2)Cl_2$ and 117.0 kJ mol^{-1} for that of *trans*-$[CoBr_2pn_2](H_5O_2)Br_2$.

As far as these complexes are concerned, the chromium(III) complexes give higher values of activation energy than the corresponding cobalt(III) complexes. This seems to be due to the fact that cobalt(III) complexes easily undergo isomerization with the aid of the lattice water through aqration-anation mechanism, whereas the chromium(III) complexes require excess energy for the structural change owing to the intramolecular rearrangement such as twisting or bond rupture in order to isomerize in anhydrous state. It should be noted that the coexistence of the lattice water noticeably causes the difference in the modes of isomerization between cobalt(III) and chromium(III) complexes.

It was found that the *trans*-to-*cis* isomerization occurs in the complexes $[MX_2pn_2]X \cdot HX \cdot nH_2O$ (M=Co or Cr; X=Cl or Br), where diamine forms a five-membered chelate ring, whereas the *cis*-to-*trans* isomerization takes place in the complex $[CrCl_2tn_2]Cl \cdot 0.5H_2O$, in which the diamine forms a six-membered chelate ring, as also observed in the complexes $[CoCl_2tn_2]X \cdot H_2O$ (X=Cl, ClO_4) and $[CoBr_2tn_2]X \cdot H_2O$ (X=Br, ClO_4).

Thermochemical Reaction Scheme. The thermochemical reaction scheme for the path-way of the *cis*-to-*trans* isomerization of $[CrCl_2tn_2]Cl \cdot 0.5H_2O$ can be expressed as follows.

cis-$[CrCl_2tn_2]Cl \cdot 0.5H_2O$

$-\frac{1}{2}H_2O$

$\Delta H = 9.2$ kJ mol^{-1}
(from analysis of the derivatogram)
129—155 °C
$E_d = 42$ kJ mol^{-1}

cis-$[CrCl_2tn_2]Cl \longrightarrow$ *trans*-$[CrCl_2tn_2]Cl$
160—209 °C
$E_i = 163$ kJ mol^{-1}

The scheme for the dehydration and isomerization of *cis*-$[CrCl_2tn_2]Cl \cdot 0.5H_2O$ is similar, except for the direction of isomerization, to that for *trans*-$[CrBr_2pn_2]Br \cdot H_2O$ in that isomerization occurs in an anhydrous state, but is quite different from that of the cobalt(III) complexes, *trans*-$[CoCl_2pn_2](H_5O_2)Cl_2$ and *trans*-$[CoBr_2pn_2](H_5O_2)Br_2$, in which isomerization takes place simultaneously with dehydration.

References

1) Part XVII: R. Tsuchiya, M. Omote, A. Uehara, and E. Kyuno, *Bull. Chem. Soc. Jpn.*, **49**, 1027 (1976).
2) Presented at the 11th Symposium on Calorimetry and Thermal Analysis, Fukuoka, November, 1975.
3) H. E. LeMay, Jr., *Inorg. Chem.*, **7**, 2531 (1968).
4) R. Tsuchiya, K. Murai, A. Uehara, and E. Kyuno, *Bull. Chem. Soc. Jpn.*, **43**, 1383 (1970).
5) R. Tsuchiya, Y. Natsume, A. Uehara, and E. Kyuno, *Thermochim. Acta*, **12**, 147 (1975).
6) C. Sato and S. Hatakeyama, *Bull. Chem. Soc. Jpn.*, **45**, 646 (1972).
7) R. Tsuchiya, T. Ohki, A. Uehara, and E. Kyuno, *Thermochim. Acta*, **12**, 413 (1975).
8) a) E. Pedersen, *Acta Chem. Scand.*, **24**, 3362 (1970); b) D. A. House, *Inorg. Nucl. Chem. Lett.*, **6**, 741 (1970).
9) R. Tsuchiya, Y. Kaji, A. Uehara, and E. Kyuno, *Bull. Chem. Soc. Jpn.*, **42**, 1881 (1969).

Quantitative Analysis of Hydrogen in Titanium with an Ion Microanalyzer

Yoshiaki OKAJIMA, Yukiyoshi AIZAWA, Katsumi SUZUKI, and Yasushi SUGAWARA

Hitachi Research Laboratory, Hitachi Ltd., Kuzi-machi, Hitachi-shi, Ibaraki 319-12

(Received July 31, 1976)

Quantitative analysis of hydrogen in titanium was investigated with an ion microanalyzer. Argon ions as primaries were accelerated at a voltage of 10 kV. The diameter and the current of the beam were 1 mm and 2 μA, respectively. A mass spectrum was measured at 2×10^{-7} Torr. It was found that the intensity ratio of $m/e=49(^{48}TiH^+)$ and $46(^{46}Ti^+)$ can be used for the determination of hydrogen in titanium. A linear relation was obtained between the intensity ratio and hydrogen concentration determined by the standard vacuum fusion method. The present method was applied to determine the hydrogen concentration in the surface layer of a sample treated by cathodic polarization. It was observed that hydrogen concentrations in the surface layer were much higher than those in the bulk of the sample.

It is well known that titanium is embrittled by the presence of small amounts of hydrogen. Phillips *et al.* investigated the kinetics of embrittlement by observing a sample cross section with an optical microscope, determining the hydrogen concentration by the vaccum fusion method.[1] In order to investigate the mechanism of embrittlement, it is necessary to determine hydrogen concentrations on a microscopic scale. The vacuum fusion method, however, cannot be applied to determination of hydrogen concentration in a microscopically thin layer.

An ion microanalyser (IMA) enables us to carry out analyses of the impurities contained in a small selected volume and in very thin layers. Gray[2] and Someno *et al.*[3] reported on the application of IMA to the determination of hydrogen in titanium. Gray used the intensity ratio of titanium ($m/e=48$) to hydrogen ($m/e=1$). However, Gray's method cannot be applied with sufficient reproducibility, due to a trace amount of contaminants containing hydrogen compounds in the sample chamber. Someno *et al.* used deuterium instead of hydrogen.

The present paper describes an IMA method which can be applied to the determination of hydrogen in titanium with good reproducibility.

Experimental

Materials. The titanium specimens used were 1 mm thick and 5×5 mm in size. Table 1 gives the composition obtained by chemical analysis. In order to obtain specimens with high concentrations of hydrogen, hydrogen was diffused in the specimen by cathodic polarization. Specimens were ultrasonically cleaned in acetone and methyl alcohol. The hydrogen concentration was analyzed by the standard vacuum fusion method.

Argon gas, used as a source of primary ions, was purified by passing through CuO particles heated to 500 °C, $Mg(ClO_4)_2$ particles and a liquid oxygen trap.

TABLE 1. CHEMICAL ANALYSIS OF TITANIUM SPECIMEN

Specimen	Concentration (%)				
	N	O	H	Fe	C
1	0.003	0.059	0.0012	—	—
2	0.008	0.057	0.0020	0.002	0.005
3	0.009	0.070	0.0020	0.030	0.007

Experimental Procedure. A Hitachi type IMA-2 ion microanalyzer was used. Argon ionized by a duoplasmatron was accelerated from 6 to 15 kV and struck the sample mounted with silver paste on a holder. The beam diameter was focused to about 1 mm. The primary ion current at the sample was 0.5 to 5 μA. The pressure in the sample chamber was 4×10^{-6}—8×10^{-8} Torr. Secondary ions sputtering from the sample surface were accelerated at a voltage of 3 kV and analyzed with a mass spectrometer.

Results

Principle of Quantitative Analysis. The secondary ion current I_x of an element X with one isotope only is given by

$$I_X = I_p S_X^+ C_X \eta_X, \quad (1)$$

where I_p is primary ion current, S_x^+ the yield of ions of element X, C_x the concentration of element X, and η_x the transmission of the instrument between sample and collector. Thus the ratio of the secondary ion current of an element X to a reference element (matrix) R is given by[4]

$$I_X/I_R = S(\mathrm{rel})^+ C_X/C_R, \quad (2)$$

where I_R is the secondary ion current of a reference element R, C_R the concentration of a reference element R, and $S(\mathrm{rel})^+$ the ratio of the yield of ions of an element X to a reference element R. When the analysis is carried out by means of Eq. 2, it is necessary to select the peak of the element to be analyzed and that of a reference element.

Selection of Peak. Figure 1 shows the mass spectra of samples of different hydrogen concentrations. The hydrogen concentrations of samples A and B analyzed by the vacuum fusion method are 12 and 3800 ppm, respectively. The heights of the peaks of hydrogen ($m/e=1$) do not show any appreciable difference. On the other hand, the peak height difference of $m/e=49$ between A and B is very large. The peak at $m/e=49$ contains both $^{49}Ti^+$ and $^{48}TiH^+$ ions. Hydrogen sources of the ion TiH^+ seem to be the hydrogen in the titanium sample and impurities such as water and hydrocarbons in the sample chamber. In order to determine the hydrogen in titanium using the peak at $m/e=49$, the impurities in the system should be minimized.

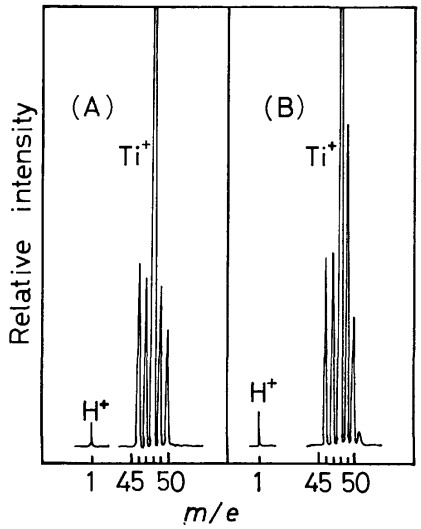

Fig. 1. Mass spectra of titanium before and after hydrogen absorption.
(A): Before absorption(12 ppm H), (B): after absorption (3800 ppm H).

In the present work, argon gas was purified by passing through CuO particles heated to 500 °C, $Mg(ClO_4)_2$ particles and a liquid oxygen trap. The impurities in the sample chamber were minimized by cooling with liquid nitrogen. Since the impurities adsorbed on the sample surface also give a TiH^+, they should be separated from other secondary ions using a high accelerating voltage.

Table 2. Peak height ratio for titanium

m/e	Peak height ratios (%)				
	46	47	48	49	50
Sample A	8.06	7.20	73.94	5.83	4.97
Sample B	6.94	7.82	66.67	13.47	5.10

Isotopic ratio of m/e=46, 47, 48, 49, and 50 is 7.93, 7.20, 73.94, 5.51, and 5.34, respectively.

Table 2 gives the peak height ratios for samples A and B, as compared to the isotopic ratio of titanium. The values at m/e=49 are greater than the isotopic ratio. The high value at m/e=49 for sample B indicates a high concentration of hydrogen. Thus the peak at m/e=49 can be used for the determination of the concentration of hydrogen.

It is preferable to select the peak at m/e=46 as a reference, since titanium of m/e=45 is not detected and the TiH^+ gives no signal at m/e=46. Since the intensities at m/e=46 and 49 are comparable, errors can be minimized.

Effect of Primary Ion Current on I_{49}/I_{46}. The temperature of the sample surface and the sputtering rate[5] are influenced by the primary ion corrent. When the sample is heated by primary ions, the absorbed hydrogen in titanium might be released. Figure 2 shows the relation between the intensity ratio of m/e=49 to 46(I_{49}/I_{46}) and to the primary ion current. I_{49}/I_{46} is constant in the range 0.5—5 μA. The results show that no thermal release of hydrogen occurs by the present method.

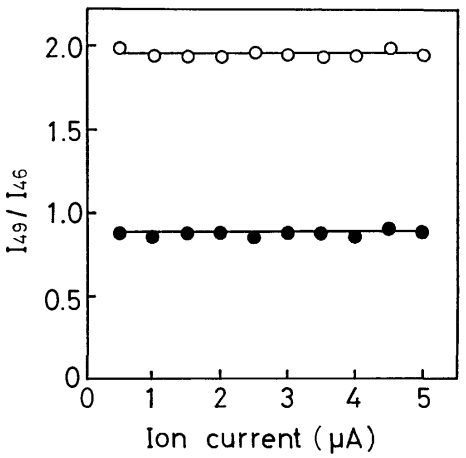

Fig. 2. Relation between I_{49}/I_{46} and primary ion current.
●: Before absorption (12 ppm H), ○: after absorption (3800 ppm H). Primary ion accelerating voltage :10kV.

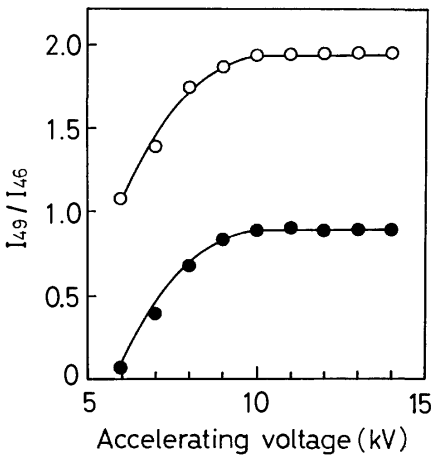

Fig. 3. Relation between I_{49}/I_{46} and primary ion accelerating voltage.
●: Before absorption(12 ppm H), ○: after absorption (3800 ppm H). Primary ion current: 2 μA.

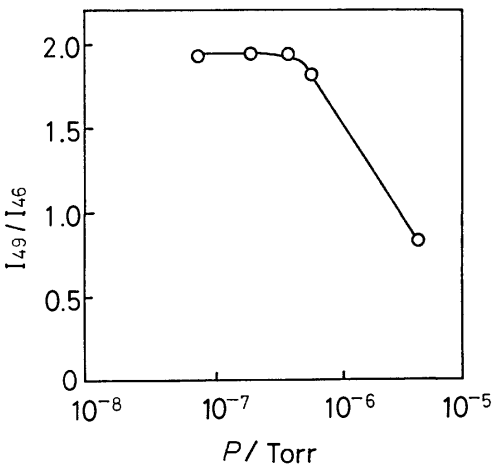

Fig. 4. Relation between I_{49}/I_{46} and pressure in sample chamber at primary ion current of 2 μA and primary ion accelerating voltage of 10 kV.

Effect of Primary Ion Accelerating Voltage on I_{49}/I_{46}. The measurements were carried out at a primary ion current of 2 μA. Figure 3 shows the relation between I_{49}/I_{46} and the primary ion accelerating voltage. I_{49}/I_{46} increases with the accelerating voltage and becomes constant at voltages above 10 kV.

Effect of Pressure in Sample Chamber on I_{49}/I_{46}. Figure 4 shows the relation between I_{49}/I_{46} and pressure. I_{49}/I_{46} decreases at pressure above 4×10^{-7} Torr. Decrease in I_{49}/I_{46} with pressure seems to be due to the increase of oxygen present in the sample chamber.[6]

Effect of Surface Layer on I_{49}/I_{46}. The sample surface is contaminated with impurities such as oxygen, water and hydrocarbons which generate secondary ions, making the quantitative analysis of hydrogen difficult. Surface sputtering is effective in removing the impurities on the surface. In the early stages of bombardment, the peak intensity changes widely. However, a stable signal can be obtained after bombardment for *ca.* 10 min. It was confirmed by surface roughness measurement that 2 μm or less had been sputtered by 10 min bombardment.

TABLE 3. WORKING CONDITIONS FOR QUANTITATIVE ANALYSIS

Ionic species	Argon(Ar^+)
Primary ion accelerating voltage	10 kV
Primary ion current	2 μA
Primary ion beam diameter	1 mm
Pressure in sample chamber	2×10^{-7} Torr
Preliminary sputtering time	10 min
Secondary ion accelerating voltage	3 kV

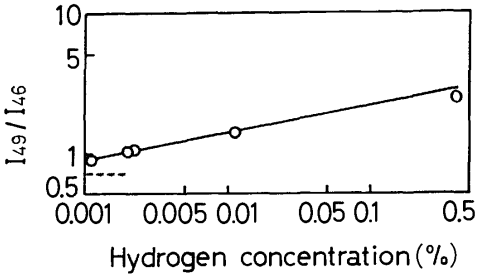

Fig. 5. Calibration curve.
----: Isotopic ratio($^{49}Ti/^{46}Ti$).

Calibration Curve. The working conditions for the IMA method are summarized in Table 3. Under these conditions, I_{49}/I_{46} was plotted as a function of hydrogen concentrations, which were determined by the vacuum fusion method. A linear relation was obtained between I_{49}/I_{46} and hydrogen concentration as shown in Fig. 5.

Hydrogen Concentration in Surface Layer. The present method has been applied to determine hydrogen concentration in the surface layer of a sample treated by cathodic polarization. The hydrogen concentration decreases with increase in depth (Fig. 6).

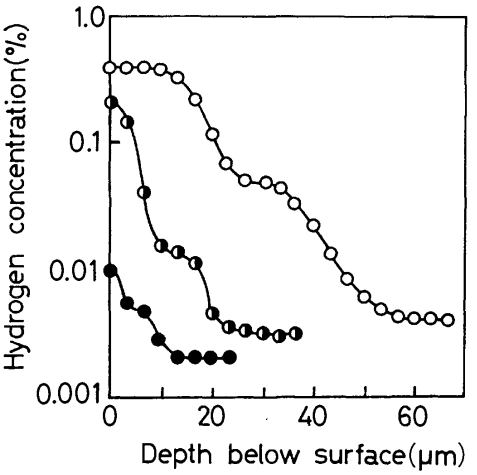

Fig. 6. In depth concentration profiles for titanium treated by cathodic polarization.
○: −5 V *vs.* SCE, 10 h, ◑: −1.5 V *vs.* SCE, 4940 h,
●: −0.5 V *vs.* SCE, 4940 h.

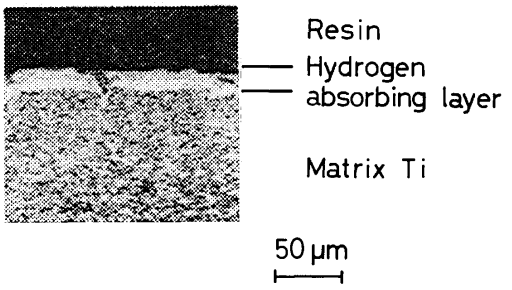

Fig. 7. Cross section of titanium treated by cathodic polarization at a potential of −5 V *vs.* SCE for 10 h.

Figure 7 shows a cross section of the sample treated for 10 h at a potential of −5 V *vs.* SCE. The 20 μm layer in the photograph corresponds to the layer in which the hydrogen concentration is higher than 0.05%.

References

1) I. I. Phillips, P. Poole, and L. L. Shreir, *Corros. Sci.*, **14**, 533 (1974).
2) H. R. Gray, *Corrosion-NACE*, **28**, 47 (1972).
3) M. Someno, H. Saito, and M. Kobayashi, *Trans. Jpn. Inst. Met.*, **16**, 305 (1975).
4) H. Tamura, T. Kondo, K. Nakamura, and T. Hirano, *Hyomen*, **11**, 233 (1973).
5) O. Almen and G. Bruce, *Nucl. Instrum. Methods*, **11**, 257 (1961).
6) H. Nishimura and J. Okano, *Mass. Spect.*, **23**, 9 (1975).

Phase Equilibria in Sm_2O_3-V_2O_3-V_2O_5 System at 1200 °C

Kenzo KITAYAMA and Takashi KATSURA

Department of Chemistry, Faculty of Science, Tokyo Institute of Technology, Ookayama, Meguro-ku, Tokyo 152

(Received September 1, 1976)

The phase equilibria in the Sm_2O_3-V_2O_3-V_2O_5 system was established at 1200 °C. In this system, Sm_2O_3, $Sm_{10}V_2O_{20}$, $SmVO_3$, $SmVO_4$, V_2O_3, V_3O_5, V_4O_7, V_5O_9, V_6O_{11}, and VO_2 were stable and $Sm_{10}V_2O_{20}$, $SmVO_4$, V_2O_3, and VO_2 had the non-stoichiometry. On the basis of the phase equilibria, the Gibbs free energy for the reactions, $SmVO_3+1/2O_2=SmVO_4$ and $4\,Sm_2O_3+2\,SmVO_3+O_2=Sm_{10}V_2O_{20}$, were determined to be -30.4 ± 0.1 and -76.8 ± 0.1 kcal, respectively. Also, standard Gibbs free energies of oxidation of various vanadium oxides were calculated.

$LnVO_4$ has been prepared and its crystallographic,[1,2] fluorescent,[3] and magnetic[4] properties have been investigated. $LnVO_4$ has a tetragonal structure, except for $LaVO_4$. On the other hand, $LnVO_3$ has the crystallographic form of orthorhombic, except for $LaVO_3$ and $CeVO_3$.[5]

Although $LnVO_4$ and $LnVO_3$ had been prepared and their various physical properties studied, as described above, the phase equilibria in the system Ln-V-O had not been determined at high temperature in low oxygen partial pressures.

Many studies have been carried out on the system V-O. Among early studies, Andersson[6] investigated the system VO-V_2O_5 at temperatures between 650—1000 °C, and found a series of vanadium oxides which could be represented with the general formula, V_nO_{2n-1}, changing the n's from 2 to 8.

Kosuge *et al.*[7] also investigated the system V_2O_3-V_2O_5 at 800 °C, and recognized the phases V_nO_{2n-1} of $n=2$—7.

Recently, thermochemical studies and phase equilibria in the system V_2O_3-VO_2 at 1600 K,[8] in the system V_2O_3-V_4O_7 at temperatures from 1400 to 1700 K,[9] in the system V_2O_3-VO_2 at 1307 K,[10] in the system V_nO_{2n-1} at temperatures from 1000 to 1200 °C,[11] and in the system V_2O_3-VO_2 at temperatures from 1173 to 1423 K[12] were investigated by means of the quenching and thermogravimetric methods under a controlled oxygen partial pressure by equilibration with CO_2 and H_2 or CO and CO_2. They reported the phases of vanadium oxide and standard free energies of oxidation,[8-12] standard enthalpy,[9,10,12] and entropy change.[9,10,12]

The precise phase equilibria in the system Sm_2O_3-V_2O_3 have not been reported. But the existence of stable phase of $SmVO_3$ is well known, as described above. Recently the phase equilibria in the system Sm_2O_3-V_2O_5 was studied by Brusset *et al.*[13] and Remizov *et al.*[14]

In the report, Brusset *et al.* showed the existence of compounds of $4Sm_2O_3\cdot V_2O_5$ and $5Sm_2O_3\cdot V_2O_5$. On the other hand Remizov *et al.* showed the existence of compounds of $Sm_2O_3\cdot 2V_2O_5$ and $3Sm_2O_3\cdot V_2O_5$. There are sharp differences in the results regarding to the composition.

The objectives of the present study are to establish the detailed phase equilibria in the system Sm_2O_3-V_2O_3-V_2O_5 at 1200 °C by changing the oxygen partial pressures, to calculate the thermochemical values based upon the phase equilibria, and to ascertain, upon completion of the studies of the Ln-V-O system, whether the trend of the linearity of the Gibbs free energy of reaction with rare-earth ionic radii in the system Ln-Fe-O[15] will be observed or not when the iron is changed to vanadium.

Experimental

Analytical grade of Sm_2O_3 (99.9%) and V_2O_5 which was made from the guaranteed grade of NH_4VO_3 by heating at 500 °C in air for 24 h have been employed as starting materials. The desired ratios of Sm_2O_3/V_2O_5 were obtained by mixing throughly in an agate mortar with ethyl alcohol. The mixed samples were heated at 600 °C for 24 h at an oxygen partial pressure of $10^{-10.0}$ atm to reduce V_2O_5 to V_2O_3. The temperature of the furnace was increased to 1200 °C in the same P_{O_2} to solidify the samples. After 6 h, the samples were quenched. Samples thus prepared were crushed to obtain small size pieces (about $2\times3\times3$ mm^3), as described previously.[16]

Mixed gases of CO_2 and H_2 were used to obtain low oxygen partial pressures in the present experiment. The actual oxygen partial pressure of the gas phases was measured by means of a solid electrolytic cell composed of $(ZrO_2)_{0.85}(CaO)_{0.15}$.[8] Phases in quenched samples were identified by the powder X-ray diffraction method with (Ni-filtered) Cu$K\alpha$ radiation.

Details of the apparatus, procedures for maintaing constant temperature, methods of thermogravimetry and quenching, and the criterion for equilibrium establishment were the same as those described in previous papers.[8,16,17]

Lattice constants were determined by the powder X-ray diffraction method with Ni-filtered Cu$K\alpha$ radiation and with a slow scanning speed of 0.5° per minute. Instrumental errors were calibrated by measuring the diffraction angles of a standard specimen of silicon.

It was found that the V_2O_3 phase was stable: that is, its composition remains constant over a wide range of oxygen partial pressures.[8] During the preliminary work in the present experiments on the V-O system and mixed samples, this fact was ascertained (Fig. 1). On the basis of these preliminary results, an oxygen partial pressure of $10^{-12.00}$ atm was chosen as the reference weight standard. Vanadium contents in the starting materials and quenched samples are determined volumetrically by adopting the zinc-amalgam method[18] in order to check the thermogravimetric results. Samarium contents in the samples are determined by precipitating as samarium oxalate and igniting of the precipitate to samarium sesquioxide.

The results of duplicated wet chemical analysis and the

TABLE 1. SOME COMPARISONS WITH RESULTS OBTAINED FROM THERMOGRAVIMETRY AND BY WET CHEMICAL ANALYSIS OF THE QUENCHED SAMPLES

	$-\log P_{O_2}$	V_t	V_a	Sm_t	Sm_a
$V_2O_{5.000}$[a)]	0.68	56.02	56.0		
$VO_{1.998}$	4.50	61.54	61.5		
$V_2O_{3.065}$	7.90	67.51	67.5		
$V_2O_{3.000}$	11.00	67.98	68.0		
$SmVO_{4.000}$	0.68	19.20	19.1	56.68	56.6
$SmVO_{3.980}$	9.00	19.22	19.2	56.75	56.7
$SmVO_{3.000}$	11.00	20.43	20.4	60.32	60.2

a) Starting material.

results of the thermogravimetric determination are shown in Table 1. Molecular formulas in the first column in Table 1 imply the compositions obtained from the thermogravimetry at each oxygen partial pressure in the second column. V_t and Sm_t are the weight % of the vanadium and samarium calculated from the compositions in the first coumn, whereas V_a and Sm_a are the weight % of the vanadium and samarium of the quenched samples obtained by wet chemical analysis.

Results and Discussion

Phase Equilibrium. Eight samples with Sm_2O_3/V_2O_5 compositions of 0.1111, 0.2500, 0.4286, 1.000, 1.500, 2.333, 5.000, and 5.667 were prepared. In Fig. 1, the relationship between oxygen partial pressures and compositions, VO_x or $W_{O_2}/W_T \times 100$, are shown, where W_{O_2} is the weight gain from the standard state and W_T the total weight gain of the mixed sample as if the reaction, $V_2O_3+O_2=V_2O_5$, were to be completed. Based upon the experimental results of the thermogravimetry and identifications of the sample phases (Table 2), a phase diagram can be depicted. The results of the phase equilibria are illustrated in Fig. 2. The following phases were stable under the present experimental conditions: Sm_2O_3(R), $Sm_{10}V_2O_{20}$(A), $SmVO_4$(B), $SmVO_3$(C), V_2O_3(D), V_3O_5(E), V_4O_7(F), V_5O_9(G), V_6O_{11}(H), V_7O_{13}(I), and VO_2(J). Letters in parentheses are the abbreviations of the compounds. Other Magnèli phases of V-O system could not definitely be detected as a single phase under the experimental

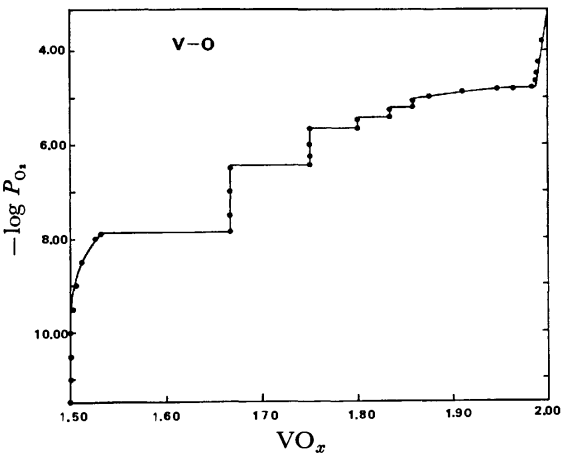

Fig. 1-1. The relationship between $-\log P_{O_2}$ and VO_x at 1200 °C.

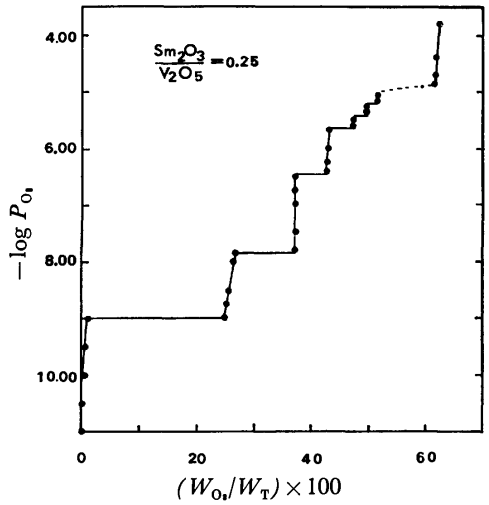

Fig. 1-2. The relationship between $-\log P_{O_2}$ and weight gains of the sample, $Sm_2O_3/V_2O_5=0.25$, at 1200 °C.

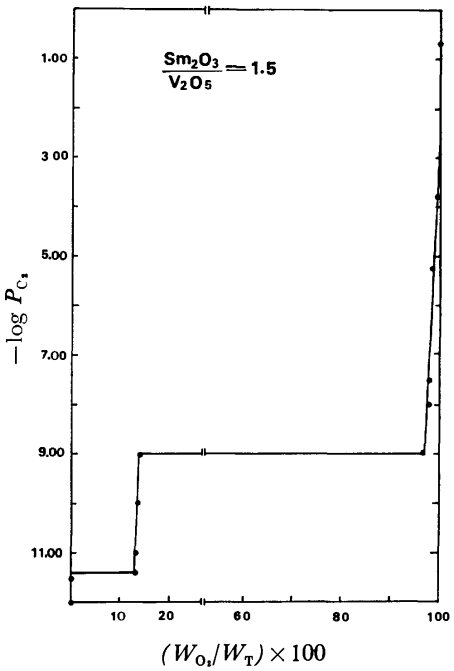

Fig. 1-3. The relationship between $-\log P_{O_2}$ and weight gains of the sample, $Sm_2O_3/V_2O_5=1.5$ at 1200 °C.

conditions.

Also the compounds of $3Sm_2O_3 \cdot V_2O_5$ and $4Sm_2O_3 \cdot V_2O_5$ did not appear under the experimental conditions.

Sm_2O_3 was stable in this experimental condition as already described.[19] $Sm_{10}V_2O_{20}$, $SmVO_4$, V_2O_3, and VO_2 have apparent deviations from the stoichiometric composition, judging by the results of thermogravimetry. As for V_2O_3, many investigators have already pointed out the same phenomena.[6-8] Deviations from the stoichiometry of VO_2 were recognized by Hoschek and Klemm.[20] They stated that the VO_2 phase was homogeneous between $VO_{1.8}$ and $VO_{2.0}$. But Andersson pointed out that the homogeneity range of this phase might be very low, arguing from his experimental

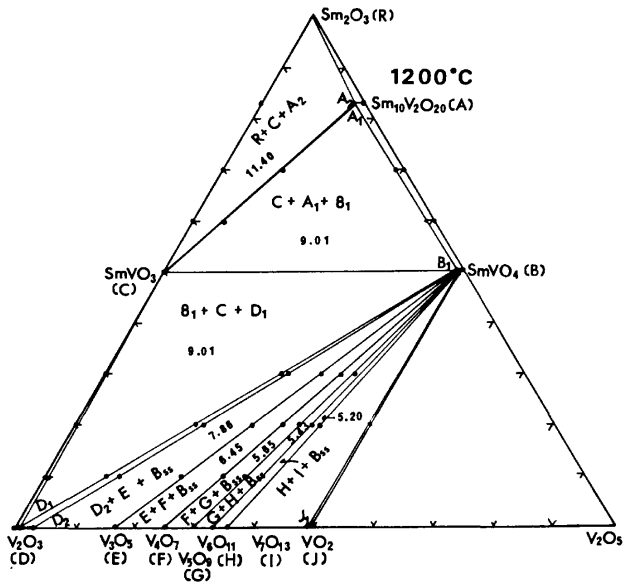

Fig. 2. Phase equilibria in the system Sm_2O_3–V_2O_3–V_2O_5 at 1200 °C. Numerical values in the three solid phases regions are the oxygen partial pressures in $-\log P_{O_2}$ in equilibrium. Abbreviations are the same as those in Table 4.

results of no displacement of the powder lines. The present results showed that the solid solution range is from $VO_{1.988}$ at $\log P_{O_2}=-4.71$ to $VO_{1.995}$ at $\log P_{O_2}=-3.79$ (in CO_2 at 1200 °C).

The deviation from the stoichiometric composition of $Sm_{10}V_2O_{20}$ extended up to $Sm_{10}V_2O_{19.78}$ at $\log P_{O_2}=-11.40$ atm, that of $SmVO_4$ up to $SmVO_{3.980}$ at $\log P_{O_2}=-9.01$, and that of V_2O_3 up to $V_2O_{3.065}$ at $\log P_{O_2}=-7.86$.

The lattice constants of the phases which appear in this system are given in Table 3, together with the data of other authors.[8,21,22,24] The crystal system of $Sm_{10}V_2O_{20}$ could not be determined. Although the relative intensities and *d*-values of $Er_{10}V_2O_{20}$,[26] $Gd_{10}V_2O_{20}$,[26] and $Y_{10}V_2O_{20}$[27] had been reported, their crystal systems have also not yet been determined. *d*-Values and relative intensities of $Sm_{10}V_2O_{20}$ obtained by the powder X-ray method are shown in Table 4. As shown in Table 3, the crystal data of the present samples are in very good agreement with those of the previous authors. Lattice constants of V_2O_3 were determined on the basis of the hexagonal type, and rhombohedral values recalculated from the hexagonal values are shown in parentheses. The lattice constants of $SmVO_4$ and VO_2 solid solutions are constant irrespective of the compositional variations, but those of V_2O_3 decrease with the increasing of the oxygen partial pressures. These phenomena seem to be reflected in the narrow solid solution range of $SmVO_4$ and VO_2, and in the more wide solid solution range of V_2O_3 and in the increasing of the smaller quadrivalent vanadium content.

Calculations of Standard Gibbs Free Energies of Ternary Compounds. On the basis of the phase equilibria, the standard Gibbs free energies of reaction of the $Sm_{10}V_2O_{20}$ and $SmVO_4$ compounds can be calculated

Table 2. Identification of phases

Starting Materials (mol%)		$-\log P_{O_2}$ (atm)	Time (h)	Phases
Sm_2O_3	V_2O_5			
85	15	0.68	48	$Sm_{10}V_2O_{20}+Sm_2O_3$
		8.00	23	$Sm_{10}V_2O_{20}+Sm_2O_3$
		10.00	23	$Sm_{10}V_2O_{20}+Sm_2O_3$
		12.00	23	$SmVO_3+Sm_2O_3$
70	30	0.68	48	$Sm_{10}V_2O_{20}+SmVO_4$
		8.00	23	$Sm_{10}V_2O_{20}+SmVO_4$
		10.00	23	$Sm_{10}V_2O_{20}+SmVO_3$
		12.00	23	$SmVO_3+Sm_2O_3$
50	50	0.68	38	$SmVO_4$
		9.00	32	$SmVO_4$
		11.00	24	$SmVO_3$
30	70	4.50	96	VO_2+SmVO_4
		5.10	60	$V_7O_{13}+SmVO_4$
		5.30	51	$V_6O_{11}+SmVO_4$
		5.50	56	$V_5O_9+SmVO_4$
		5.75	51	$V_4O_7+SmVO_4$
		7.60	48	$V_3O_5+SmVO_4$
		8.00	41	$V_2O_3+SmVO_4$
		10.00	26	$V_2O_3+SmVO_3$
		12.00	23	$V_2O_3+SmVO_3$
10	90	4.50	96	VO_2+SmVO_4
		5.10	60	$V_7O_{13}+SmVO_4$
		5.30	51	$V_6O_{11}+SmVO_4$
		5.50	56	$V_5O_9+SmVO_4$
		5.75	51	$V_4O_7+SmVO_4$
		7.60	48	$V_3O_5+SmVO_4$
		8.00	41	$V_2O_3+SmVO_4$
		10.00	26	$V_2O_3+SmVO_3$
		12.00	23	$V_2O_3+SmVO_3$
0	100	4.00	96	VO_2
		5.10	48	V_7O_{13}
		5.30	48	V_6O_{11}
		5.45	48	V_5O_9
		5.75	48	V_4O_7
		7.00	42	V_3O_5
		7.85	48	V_2O_3
		9.00	30	V_2O_3
		11.00	24	V_2O_3

by referring to the following equations:

$$SmVO_3 + 1/2O_2 = SmVO_4 \quad (1)$$

$$4Sm_2O_3 + 2SmVO_3 + O_2 = Sm_{10}V_2O_{20} \quad (2)$$

The standard Gibbs free energies of both reactions may be calculated directly by adopting the equilibrium oxygen partial pressures corresponding to the Eqs. 1 and 2. Here, the activity of each component, $SmVO_4$ and $Sm_{10}V_2O_{20}$, in each solid solution was set equal to one, the composition $SmVO_{3.980}$ (B_1 in Fig. 2) was in equilibrium with $SmVO_3$, and $Sm_{10}V_2O_{19.78}$ (A_2 in Fig. 2) was in equilibrium with $SmVO_3$ and Sm_2O_3. The standard Gibbs free energies of the reactions (1) and (2) may be determined from the equation: $\Delta G^\circ=-RT\ln K$, where R is the gas constant, T the absolute temperature, and K the equilibrium constant. The values, -30.4 ± 0.1 and -76.8 ± 0.1 kcal, are obtained by referring to reactions

TABLE 3. UNIT CELL DIMENSIONS OF THE COMPOUNDS

Compd.	$-\log P_{O_2}$	a(Å)	b(Å)	c(Å)	α	β	γ	V(Å^3)
$SmVO_4$	0.68	7.263±0.001		6.387±0.001				336.9±0.1
	9.00	7.261±0.001		6.387±0.001				336.7±0.1
		7.2625[21]		6.3894				
$SmVO_3$	11.00	5.398±0.002	5.591±0.002	7.677±0.002				231.7±0.2
		5.393[22]	5.588	7.672				
V_2O_3	11.00	4.950±0.001		13.990±0.002				296.8±0.1
		(5.469)			(53.8)			
	7.88	4.940±0.001		13.964±0.003				295.1±0.1
		(5.459)			(53.8)			
		5.472[8]			53.80			
V_3O_5	7.00	10.00 ±0.04	5.032±0.005	9.86 ±0.04		138.8±0.2		327 ±2
		9.993[8]	5.063	9.872		138.62		
V_4O_7	5.75	5.500±0.004	6.988±0.005	12.242±0.005	95.2±0.1	95.1±0.1	109.2±0.1	439.0±0.4
		5.51[24]	7.01	12.92	96.2	95.2	109.2	
V_5O_9	5.50	5.467±0.006	7.002±0.007	8.71 ±0.01	97.3±0.1	112.4±0.1	109.2±0.1	278.5±0.4
		5.47[24]	6.99	8.72	97.5	112.4	109.0	
V_6O_{11}	5.30	5.439±0.003	6.991±0.002	23.65 ±0.01	98.5±0.1	120.9±0.1	108.9±0.1	674.6±0.5
		5.44[24]	6.99	23.66	98.5	120.9	108.9	
V_7O_{13}	5.10	5.425±0.009	6.991±0.006	15.15 ±0.02	98.9±0.1	125.6±0.1	108.8±0.1	396.4±0.7
		5.43[24]	7.00	15.16	98.9	125.5	108.9	
VO_2	4.00	5.745±0.004	4.519±0.002	5.377±0.004		122.6±0.1		117.6±0.1
	4.60	5.748±0.009	4.519±0.004	5.369±0.008		122.5±0.1		117.6±0.2
		5.744[8]	4.526	5.375		122.55		

TABLE 4. d-VALUES AND RELATIVE INTENSITIES OF $Sm_{10}V_2O_{20}$

d(Å)	I/I_0	d(Å)	I/I_0
8.89	13	1.783	11
3.22	14	1.695	6
3.198	11	1.646	34
3.152	100	1.6186	7
3.009	10	1.5761	13
2.972	17	1.4935	6
2.730	41	1.4402	8
2.611	10	1.3649	6
2.162	11	1.2528	11
1.930	45	1.2208	8
1.886	9	1.2093	6
1.867	6	1.1145	8
1.810	7		

(1) and (2) respectively.

The activities of the $Sm_{10}V_2O_{20}$ and $SmVO_4$ components in stoichiometric composition, that is, A and B in Fig. 2, were readily calculated by means of the Gibbs-Duhem equation on the basis of the experimental results. The relationships, $\log P_{O_2}$ - N_O/N_{SmVO_4} and $\log P_{O_2}$ - $N_{O_2}/N_{Sm_{10}V_2O_{20}}$, are determined to be $N_O/N_{SmVO_4}= 3.77\times10^{-3} \log P_{O_2}+0.01377$ and $N_O/N_{Sm_{10}V_2O_{20}}=0.0227 \log P_{O_2}+0.0388$ from the thermogravimetric results. Here N_{O_2}/N_{SmVO_4} and $N_O/N_{Sm_{10}V_2O_{20}}$ are the fraction rations of oxygen to $SmVO_4$, and to $Sm_{10}V_2O_{20}$, indicating the deviation from the stoichiometry. A detailed calculation method has been described in the paper of Kimizuka and Katsura.[28] The calculated activity values and stability ranges of the oxygen partial pressures of the compounds which appeared are summarized in Table 5.

TABLE 5. COMPOSITIONS, STABILITY RANGES IN OXYGEN PARTIAL PRESSURES, AND ACTIVITIES IN SOLID SOLUTIONS

Component	Composition	Symbol	$-\log P_{O_2}$ (atm)	$\log a_i$
$Sm_{10}V_2O_{20}$	$Sm_{10}V_2O_{20.00}$	A	0.68[a] — 1.59[b]	0.533
	$Sm_{10}V_2O_{19.81}$	A_1	9.01	0.231
	$Sm_{10}V_2O_{19.78}$	A_2	11.40	0.0
$SmVO_4$	$SmVO_{4.000}$	B	0.68[a] — 3.70[b]	0.0264
	$SmVO_{3.980}$	B_1	9.01	0.0
$SmVO_3$	$SmVO_{3.000}$	C	9.01 —12.00[c]	0.0
V_2O_3	$V_2O_{3.000}$	D	9.98 —12.00[c]	
	$V_2O_{3.012}$	D_1	9.01	
	$V_2O_{3.065}$	D_2	7.86	
V_3O_5	$V_3O_{5.000}$	E	6.45 — 7.86	
V_4O_7	$V_4O_{7.000}$	F	5.65 — 6.45	
V_5O_9	$V_5O_{9.000}$	G	5.43 — 5.65	
V_6O_{11}	$V_6O_{11.00}$	H	5.20 — 5.43	
V_7O_{13}	$V_7O_{13.00}$	I	5.05 — 5.20	
VO_2	$VO_{2.000}$	J	3.07[b]	0.0046
	$VO_{1.988}$	J_1	4.71	0.0

a) Stability range in log P_{O_2} may be higher than −0.68. b) These values were obtained by extrapolations by using the experimental values. c) Stability range in log P_{O_2} may be lower than −12.00.

The Standard Gibbs Free Energies of Oxidation of Vanadium Oxides. On the basis of the phase equilibria of the V–O system, the standard Gibbs free energies of oxidation of vanadium oxides which appeared in the present experimental conditions can be calculated. Although the details of the method were already described by Katsura and Hasegawa[8] at 1600 K and by Smiltens,[29] we will briefly describe them below.

In the cases of the following reactions:

$$VO_{5/3} + 1/24O_2 = VO_{7/4}, \quad (3)$$

$$VO_{7/4} + 1/40O_2 = VO_{9/5}, \quad (4)$$

$$VO_{9/5} + 1/16O_2 = VO_{11/6}, \quad (5)$$

$$VO_{11/6} + 1/84O_2 = VO_{13/7}, \quad (6)$$

which are concerned with the stoichiometric compounds in equilibrium states at fixed oxygen partial pressures, the standard Gibbs free energies of the oxidations can be readily calculated. For example, in the case of reaction (3), $\Delta G^\circ = -RT \ln K = 1/24\ RT \ln P_{O_2}(eq)$ is applicable, where $P_{O_2}(eq)$ is the equilibrium oxygen partial pressure at which two solid phases are in equilibrium.

In the case of the following reactions, which involve solid solutions:

$$VO_{3/2} + 1/12O_2 = VO_{5/3}, \quad (7)$$

$$VO_{13/7} + 1/14O_2 = VO_2, \quad (8)$$

the method of the calculation of the standard Gibbs free energy of oxidation is more complicated. We assume from the results of the phase diagram that $VO_{13/7}$ has a solid solution, although the phase diagram between $VO_{13/7}$ and VO_2 is not so exactly determined because of the slow reaction rate.

On the basis of Smiltens's method, the standard free energies referring to reactions (7) and (8) may be given as follows:

$$\Delta G^\circ_{1473}(7) = RT/12 \ln P_{O_2}(eq) + RT/2\int_{0.000}^{0.0320} \ln [P_{O_2}/P_{O_2}(eq)]dx_1,$$

$$\Delta G^\circ_{1473}(8) = RT/14 \ln P_{O_2}(eq) + RT/2\int_{0.000}^{0.1301} \ln [P_{O_2}/P_{O_2}(eq)]dx_2,$$

where x_1 and x_2 are defined as $VO_{3/2}+x_1/2O_2=VO_{3/2+x1}$ and $VO_{13/7}+x_2/2O_2=VO_{13/7+x2}$, respectively.

The second term of the right side of the above equations is named by Smiltens as the correction term. We obtained the values by adopting the graphical integration method. The relationships, $\log [P_{O_2}/P_{O_2}(eq)]$ - x_1 and $\log [P_{O_2}/P_{O_2}(eq)]$ - x_2, are shown in Fig. 3-1 and 3-2. The results of the standard Gibbs free energies of the oxidation of vanadium oxides are summarized in Table 6 together with the values calculated from equations presented by Okinaka *et al.*[11] The present values are in good agreement with those of Okinaka *et al.*

The standard Gibbs free energy of the reaction,

$$VO_{3/2} + 1/4O_2 = VO_2 \quad (9)$$

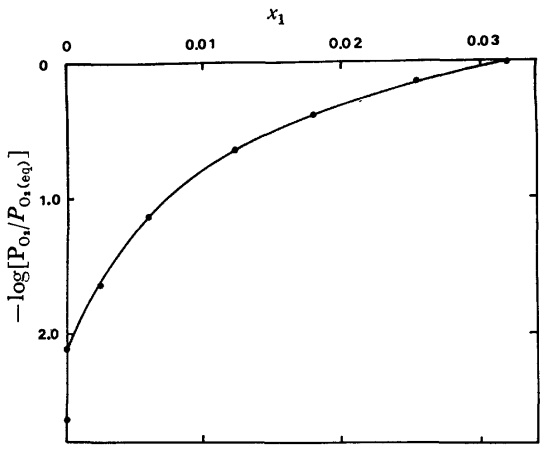

Fig. 3-1. The log $[P_{O_2}/P_{O_2}(eq)]$ *versus* x_1 curve for V_2O_3 solid solution at 1200 °C.

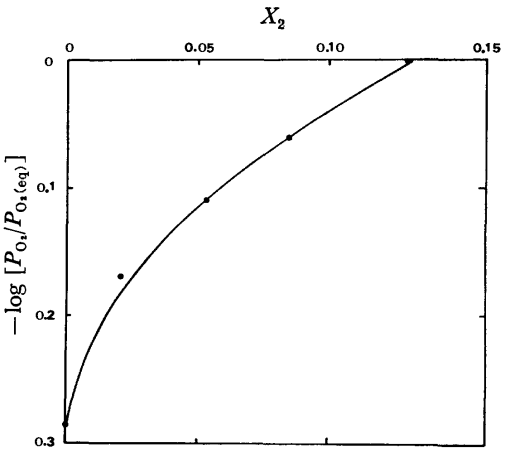

Fig. 3-2. The log $[P_{O_2}/P_{O_2}(eq)]$ *versus* x_2 curve for V_7O_{13} solid solution at 1200 °C.

can be calculated as the summation of the values of the respective reactions, and is also shown in Table 6.

Allen *et al.*[30] obtained the free energy equation, $\Delta G^\circ = 102800 - 33.5\ T$ (calcd, 1020—1180 K, ±5 kcal), for the reaction $4VO_2=2V_2O_3+O_2$ and Anderson *et al.*[12] −26.9 at 1173, −24.77 at 1273, and −21.24 kcal at 1473 K for the reaction $V_2O_3+1/2O_2=2\ VO_2$. Althoguh this equation and values are not adequate for 1200 °C, we obtained the values −13360 and −10070 cal for reaction (9) at 1200 °C by extrapolation.

According to Coughlin,[31] Mah and Kelly,[32] and Okinaka *et al.*,[11] the standard free energy of the reaction $V_2O_3+1/2O_2=2VO_2$ was given as $\Delta G^\circ = -43650+$

Table 6. Standrad free energies of oxidation at 1200 °C

Oxidation Reaction	$-\log P_{O_2}(eq)$ (atm)	Correction term (cal)	$-\Delta G^\circ$ (calcd)	
			Present	Okinaka *et al.*
$VO_{3/2}+1/12\ O_2=VO_{5/3}$	7.86	−70	4490±100	4370
$VO_{5/3}+1/24\ O_2=VO_{7/4}$	6.45	0	1810± 50	1710
$VO_{7/4}+1/40\ O_2=VO_{9/5}$	5.65	0	950± 50	910
$VO_{9/5}+1/60\ O_2=VO_{11/6}$	5.43	0	610± 50	550
$VO_{11/6}+1/84\ O_2=VO_{13/7}$	5.20	0	420± 50	390
$VO_{13/7}+1/14\ O_2=VO_2$	4.71	−40	2310±100	2400
$VO_{3/2}+1/4\ O_2=VO_2$			10590±400	10330

16.75 T (calcd, 500—1800 K, ±2000 cal), $\Delta G^\circ = -42200 + 13.0\ T$ (calcd, 800—1600 K, ±400 cal), and $\Delta G^\circ = -48860 + 19.14\ T$ (calcd, above 1120 K, ±200 cal), respectively. Values calculated by using these equations at 1200 °C are −9490, −11530, and −10330 cal, respectively. The present value (−10590 cal) is in good agreement with the value of Okinaka *et al.*

The relationship between N_O/N_{VO_2} and log P_{O_2} in the VO_2 solid solution is obtained to be $N_O/N_{VO_2} = 6.85 \times 10^{-3} \log P_{O_2} + 0.0210$. The activity of the stoichiometric VO_2 was also determined and is shown in Table 6.

References

1) W. O. Milligan and L. W. Vernon, *J. Phys. Chem.*, **56**, 145 (1952).
2) H. Schwarz, *Z. Anorg. Allgem. Chem.*, **323**, 44 (1963).
3) L. H. Brixner and E. Abramson, *J. Electrochem. Soc.*, **112**, 70 (1965).
4) G. W. Bazuev, I. I. Matveenko, and G. P. Shveikin, *Fiz. Tverd. Tela*, **16**, 240 (1974).
5) G. J. McCarthy, C. A. Sipe, and K. E. McIlvried, *Mat. Res. Bull.*, **9**, 1279 (1974).
6) G. Andersson, *Acta Chem. Scand.*, **8**, 1599 (1954).
7) K. Kosuge, T. Takada, and Y. Kachi, *Nippon Kagaku Zasshi*, **83**, 1243 (1962).
8) T. Katsura and H. Hasegawa, *Bull. Chem. Soc. Jpn.*, **40**, 561 (1967).
9) M. Wakihara and T. Katsura, *Met. Trans.*, **1**, 368 (1970).
10) H. Endo, M. Wakihara, M. Taniguchi, and T. Katsura, *Bull. Chem. Soc. Jpn.*, **46**, 2087 (1973).
11) H. Okinaka, K. Kosuge, and S. Kachi, *Trans. JIM.*, **12** 44 (1970).
12) J. S. Anderson and A. S. Khan, *J. Less-Common Metals*, **22**, 209 (1970).
13) H. Brusset, F. Madaule-Aubry, B. Blanck, J. P.Glaziou, and J. P. Laude, *Can. J. Chem.*, **49**, 3700 (1971).
14) V. G. Remizov, A. K. Molodkin, V. M. Skorikov, Yu. E. Bogatov, *Zh. Neorg. Khim.*, **21**, 1323 (1976).
15) T. Katsura, K. Kitayama, T. Sugihara, and N. Kimizuka, *Bull. Chem. Soc. Jpn.*, **48**, 1809 (1975).
16) N. Kimizuka and T. Katsura, *J. Solid State Chem.*, **13**, 176 (1975).
17) T. Katsura and A. Muan, *Trans. AIME*, **230**, 77 (1964).
18) I. Iwasaki, T. Katsura, M. Yoshida, and T. Tarutani, *Bunseki Kagaku*, **6**, 211 (1957).
19) K. Kitayama and T. Katsura, *Bull. Chem. Soc. Jpn.*, **49**, 998 (1976).
20) E. Hoschek and W. Klemm, *Z. Anorg. Allgem. Chem.*, **242**, 63 (1939).
21) X-Ray powder data, Card 17-260, A. S. T. M.
22) B. Reuter, Colloque International du C. N. R. S., 1053 (1965).
23) X-Ray powder data, Card 1-1293, A. S. T. M.
24) S. Andersson and L. Jahnberg, *Arkiv. Kemi.*, **21**, 413 (1963).
25) H. Brusset, R. Mahe, and A. Deboichet, *C. R. Acad. Sci.*, **274**, 1293 (1972).
26) H. Brusset, F. Madaule-Aubry, B. Blanck, and A. Deboichet, *Bull. Soc. Chim. Fr.*, **1969**, 15.
27) E. M. Levin, *J. Am. Ceram. Soc.*, **50**, 381 (1967).
28) N. Kimizuka and T. Katsura, *J. Solid State Chem.*, **15**, 151 (1975).
29) J. Smiltens, *J. Am. Chem. Soc.*, **79**, 4877 (1957).
30) N. P. Allen, O. Kubaschewski, and O. von Goldbeck, *J. Electrochem. Soc.*, **98**, 417 (1951).
31) J. P. Coughlin, *U. S. Bur. Mines. Bull.*, **1954**, 542.
32) A. D. Mah and K. K. Kelley, *U. S. Bur. Mines rept. Invest.*, **1961**, 5858.

Nickel(II) Complexes of *N,N'*-Polymethylenebis(*o*-mercaptobenzylamine)

Hiroyuki KOYAMA and Ichiro MURASE

Laboratory of Chemistry, College of General Education, Kyushu University, Ropponmatsu, Chuo-ku, Fukuoka 810

(Received October 15, 1976)

N,N'-Polymethylenebis(*o*-mercaptobenzylamine) ligands (polymethylene=ethylene, 1,2-cyclohexylene, trimethylene, and tetramethylene) have been synthesized by the reduction of the corresponding amides, which were prepared by the condensation of 2,2'-dithiodibenzoyl chloride and polymethylenediamines, and then their nickel(II) complexes have been prepared and characterized. The elemental analyses and the magnetic and spectroscopic data indicate that all of the complexes are monomeric with metal-ligand ratio of 1 : 1, and their geometries are essentially square-planar. When the bridging carbon chain was replaced from ethylene up to tetramethylene, the electronic spectra of the complexes exhibited pronounced change in the d-d bands.

As a typical N_2O_2 type quadridentate ligand, *N,N'*-ethylenebis(salicylideneimine)(salen) is well known to form square-planar complexes with nickel(II) ions as well as other transition metal ions.[1] A sulfur analogue of salen, *i.e.*, *N,N'*-ethylenebis(*o*-mercaptobenzylideneimine)(tib-en), has been synthesized and it acts as a N_2S_2 type quadridentate ligand and also forms a square-planar nickel(II) complex.[2] Both nickel(II) complexes are monomeric in solution, and no significant difference has been observed in their electronic spectra showing only one absorption band due to d-d transition at 18300 cm^{-1} for salen[3] and near 15000 cm^{-1} for tib-en.[2]

O'Connor and West[4] investigated a nickel(II) complex with the hydrogenated ligand of salen, *i.e.*, *N,N'*-ethylenebis(*o*-hydroxybenzylamine), and suggested a polymeric structure in which the donor atoms displayed a distorted octahedral arrangement around the nickel ion.

This was evidenced by the paramagnetic property and the spectroscopic observation. In this connection it is worthwhile to investigate the hydrogenated ligand of tib-en, *i.e.*, *N,N'*-ethylenebis(*o*-mercaptobenzylamine) (H_2enmba), for complex formation with nickel(II) ions.

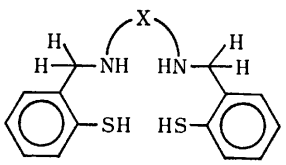

H_2Xmba

X=$-(CH_2)_2-$ (en)
= (ch)
$=-(CH_2)_3-$ (tri)
$=-(CH_2)_4-$ (tet)

This paper deals with the synthesis of H_2enmba as well as its polymethylene analogues such as *N,N'*-1,2-cyclohexylenebis(*o*-mercaptobenzylamine)(H_2chmba), *N,N'*-trimethylenebis(*o*-mercaptobenzylamine) (H_2-trimba), and *N,N'*-tetramethylenebis(*o*-mercaptobenzylamine)(H_2tetmba).

Their nickel(II) complexes have also been investigated in terms of the electronic spectra and the magnetic properties.

Experimental

Synthesis of the Ligands. To a solution of 2,2'-dithiodibenzoyl chloride (0.01 mol) in 60 ml of dry dioxane was added dropwise a mixture of polymethylenediamine (0.01 mol) and triethylamine (0.02 mol) in dry dioxane (10 ml). The mixture was stirred in an ice-cold water bath for one hour and the resulting precipitate was filtered and quickly washed with cold water. The product was crushed with a glass rod in a large amount of 1% acetic acid until it became nonsticky powder, and filtered, washed with water repeatedly, and dried at 60 °C.

Under a nitrogen stream the powdered polyamide (3 g) was added little by little to a stirred suspension of lithium aluminium hydride (3 g) in 120 ml of dry tetrahydrofuran at room temperature.

After the addition, the stirring was continued for 7 h and 10 ml of cold water carefully added to the mixture with cooling in an ice-bath and then 150 ml of 3 M hydrochloric acid was added. After stirring overnight, the tetrahydrofuran was removed under reduced pressure. The residual solution was allowed to stand in a refrigerator to separate the desired compound as a hydrochloride; it was filtered and washed with a small amount of cold water and acetone. These compounds were pure enough without recrystallization, and the analyses are listed in Table 1 together with the yields and the melting points.

Synthesis of the Nickel(II) Complexes. All of the nickel(II) complexes were prepared in a similar manner. The synthesis of Ni(tetmba) is given as an example: In a warm solution of 15 ml of 65% aqueous ethanol containing sodium hydroxide (0.004 mol), *N,N'*-tetramethylenebis(*o*-mercaptobenzylamine) dihydrochloride (0.001 mol) was dissolved. To this was added nickel(II) acetate tetrahydrate (0.001 mol) in 10 ml of water. Formation of a reddish-violet precipitate completed in a few minutes; it was collected by filtration and washed with water. The crude complex was dissolved in DMSO and recrystallized by adding water to give reddish-violet crystals.

Other complexes were purified in the following manner: Ni(enmba) was dissolved in a mixture of chloroform-DMSO (5: 8 V/V) and the solution was permitted to stand at room temperature until chloroform had evaporated spontaneously and dark reddish-violet prisms separated. Ni(chmba) and Ni(trimba) were recrystallized from DMF and from a mixture of chloroform-ethanol (2: 1 V/V) to give dark reddish-violet needles and blue-violet crystals respectively.

The elemental analyses are listed in Table 2.

Measurements. The molecular weights were determined on a Hitachi Osmometer Type-115 using DMF as a solvent. Electronic spectra were recorded in DMF with a Hitachi EPS-3T spectrophotometer.

A reflectance attachment was used for the measurement of the solid samples. Magnetic susceptibilities were measured by the Gouy method at room temperature and the susceptibilities of the ligand molecules were calculated using Pascal's constants.

Results and Discussion

The ligands may be prepared by the catalytic hydrogenation of corresponding Schiff bases of *o*-mercaptobenzaldehyde with polymethylenediamine, but sulfur poisoning of the catalyst may cause a poor yield of the products. In this case, reduction of a corresponding amide will be more preferable and we found that the following synthetic route gave a fairly good yield to obtain a series of *o*-mercaptobenzylamine bridged by a polymethylene chain.

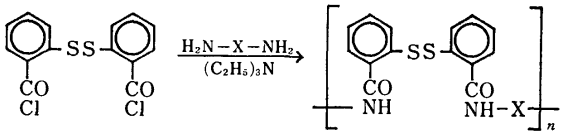

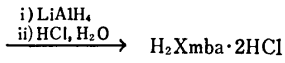

$H_2Xmba \cdot 2HCl$

The condensation of 2,2′-dithiodibenzoyl chloride with polymethylenediamine afforded polymeric amides. The elemental analyses of the amides were in agreement with the unit molecular formulas within an error of 1.9 for carbon, 0.3 for hydrogen, and 0.9 for nitrogen percentages. The amide carbonyl and the disulfide bond underwent reduction simultaneously with lithium aluminium hydride and the desired mercaptobenzylamine derivatives were finally isolated as hydrochlorides.

The infrared spectra of these compounds may exhibit absorptions due to a SH stretching vibration in the vicinity of 2550 cm^{-1}. However, these bands were not detected probably due to overlapping with the strong ammonium absorption which appeared in the same region. The nickel(II) complexes are insoluble in water, slightly soluble in most organic solvents, and moderately soluble in *N*,*N*′-dimethylformamide (DMF). Data for the elemental analyses and the molecular weight determination in DMF are listed in Table 2. They indicate that all complexes are monomeric and the ligands act as N_2S_2 type quadridentate dianions.

The electronic spectra of the complexes in DMF exhibit three bands in visible and near-ultraviolet regions as seen in Fig. 1.

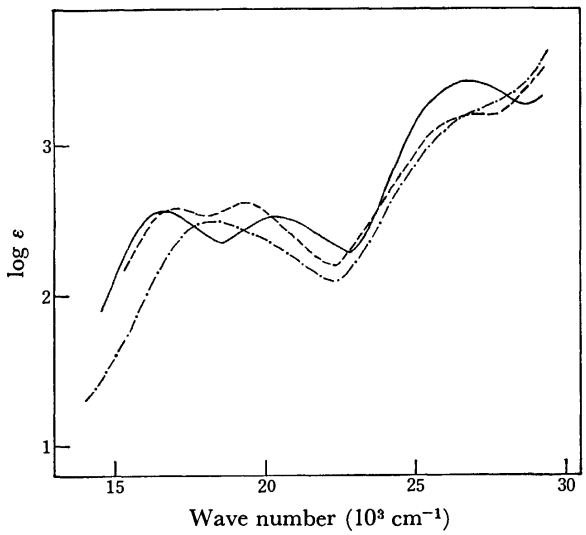

Fig. 1. Absorption spectra of Ni(enmba), ——; Ni(trimba), ——; Ni(tetmba), – · –.

The absorption maxima in 10^3 cm^{-1} are: Ni(enmba), 16.7(ε 362), 20.2(ε 319), 26.8(ε 2380); Ni(chmba), 16.8(ε 248), 20.6(ε 301), 27.0(ε 1654); Ni(trimba), 17.0(ε 374), 19.2(ε 405), 27.0(ε 1542); Ni(tetmba), 18.1(ε 309), 19.6sh(ε 258), 27.8sh(ε 1974).

The first and the second low energy bands having a moderate molar extinctions are attributed to d–d transitions, and the third bands in the near-ultraviolet region will be due to charge transfer considering from their high molar extinctions. These spectral patterns are different from that of the nickel(II) complex of tib-en[2] which exhibits only one band near 15000 cm^{-1} in the visible region, but similar to those of square-planar nickel(II) complexes of bis(*N*-substituted 2-aminoethanethiol) which consist of three bands around 16000 cm^{-1} and 20000 cm^{-1} in the visible and 27000—30000 cm^{-1} in the near-ultraviolet regions.[5]

The magnetic susceptibilities of the complexes are very low with magnetic moments of 0.18 B.M. for

Table 1. Analyses, yields, and melting points of the ligands

Ligand	Found (%)			Calcd (%)			Yield (%)	Mp (°C)
	C	H	N	C	H	N		
H_2enmba·2HCl	50.81	6.09	7.38	50.92	5.88	7.42	83	233
H_2chmba·2HCl	55.89	6.49	6.40	55.67	6.54	6.49	34	218—219
H_2trimba·2HCl·$2H_2O$	48.16	6.46	6.50	47.77	6.60	6.55	41	172—177
H_2tetmba·2HCl	53.18	6.44	6.73	53.32	6.46	6.91	40	221—224

Table 2. Analyses and molecular weight data of the complexes

Complex	Found (%)			Calcd (%)			Molecular weight Found(Calcd)
	C	H	N	C	H	N	
Ni(enmba)	53.31	5.05	7.61	53.21	5.02	7.76	422(361)
Ni(chmba)	57.61	5.85	6.73	57.85	5.83	6.75	
Ni(trimba)	53.84	5.33	7.28	54.42	5.37	7.47	406(375)
Ni(tetmba)	55.38	5.80	6.92	55.54	5.70	7.20	358(389)

Ni(enmba), 0.47 B.M. for Ni(chmba), 0.64 B.M. for Ni(trimba), and 0.41 B.M. for Ni(tetmba) at room temperature. These values are often observed for spin-paired ions,[6] and for the d^8 electron configuration of nickel(II), diamagnetism commonly means that the metal ion is coordinated with four strong donor atoms in a square-planar structure or with five donor atoms of phosphorus, arsenic, or sulfur in a trigonal bipyramidal or square-pyramidal structure.

Judging from the spectral similarity with known square-planar nickel(II) complexes with similar N_2S_2 type ligands which consist of a thiol sulfur and a secondary amine nitrogen, five-coordinate structure can be ruled out, and it is concluded that these nickel(II) complexes are essentially square-planar.

It should be noted as pointed out by Gerlach and Holm[7] that substitution of two or more oxygen atoms by sulfur without any other stereochemically significant alternations in ligand composition causes depolymerization of metal complexes. The present case is a typical example which is in conformity with this criterion, namely the nickel(II) complex of *N,N'*-ethylenebis(*o*-hydroxybenzylamine) is polymeric, whereas its mercapto analogues are monomeric.

As for the effect of increasing length of the bridging carbon chain in the diamine moiety, a significant change of the d-d transition bands has been observed in their electronic spectra. When the bridging ethylene was replaced by the trimethylene, the first band moved to a higher frequency, whereas the second one shifted to a lower frequency. In the case of the tetramethylene analogue, two bands almost overlapped at 18000 cm^{-1}.

From the steric consideration, increasing length of the bridging carbon chain will cause the weakening of the ligand field strength and distortion from planarity. Thus in the nickel(II) complexes of *N,N'*-polymethylenebis(salicylideneimine), red shift of the d-d bands with increasing chain length of the polymethylene bridge has been observed.[8] In the present case, the lowest energy bands undergo blue shift with increasing the number of bridged carbon atoms. The source of this phenomenon is not clear at present.

The reflectance spectrum of each complex is essentially similar to the corresponding spectrum in solution, except that a very weak band can be observed around 8000—11000 cm^{-1} in every complex in the solid state. Similar weak absorptions have been observed in the electronic spectra of dithiocarbazatonickel(II) and dithiocarbamatonickel(II) in the solid state and in concentrated solutions, and tentatively assigned to the spin-forbidden $^1A_{1g} \rightarrow {}^3B_{2g}(D_{4h})$ transition.[9] Nevertheless, the possibility of the presence of a small amount of high-spin species together with the predominant low-spin species could not be ruled out.

For the definite assignment, further investigations should be awaited.

The authors wish to thank Prof. K. Hirakawa and Dr. Y. Nishida, Kyushu University, for the magnetic measurements.

References

1) R. H. Holm, G. W. Everett, Jr., and A. Chakravorty, *Prog. Inorg. Chem.*, **7**, 83 (1966).
2) I. Bertini, L. Sacconi, and G. P. Speroni, *Inorg. Chem.*, **11**, 1323 (1972).
3) G. M. Mockler, G. W. Chaffey, E. Sinn, and H. Wong, *Inorg. Chem.*, **11**, 1308 (1972).
4) M. J. O'Connor and B. O. West, *Aust. J. Chem.*, **20**, 2077 (1967).
5) C. A. Root and D. H. Busch, *Inorg. Chem.*, **7**, 789 (1968).
6) C. J. Ballhausen, "Introduction to Ligand Field Theory," McGraw-Hill Book Co., Inc., New York (1962), p. 147.
7) D. H. Gerlach and R. H. Holm, *J. Am. Chem. Soc.*, **91**, 3457 (1969).
8) R. H. Holm, *J. Am. Chem. Soc.*, **82**, 5632 (1960).
9) C. Battistoni, G. Mattogno, A. Monaci, and F. Tarli, *J. Inorg. Nucl. Chem.*, **33**, 3815 (1971).

Circular Dichroism Studies of a Series of (Ammine)[(*RR*)-2,4-pentanediamine]cobalt(III) Complexes

Masaaki KOJIMA, Miho FUJITA,* and Junnosuke FUJITA

Department of Chemistry, Faculty of Science, Nagoya University, Chikusa, Nagoya 464
**Department of Chemistry, Nagoya City University, Mizuho, Nagoya 467*

(Received November 6, 1976)

The circular dichroism spectra of a series of complexes of the type $[Co(NH_3)_{2n}(RR\text{-ptn})_{3-n}]^{3+}$($n$=0, 1, 2), where the *RR*-ptn is (*RR*)-2,4-pentanediamine, were recorded in aqueous solutions with and without the addition of electrolytes such as chloride or sulfate, and in DMSO solutions. The circular dichroism spectra in the region of the first absorption band of Δ-$[Co(RR\text{-ptn})_3]^{3+}$ and *cis*-Δ-$[Co(NH_3)_2(RR\text{-ptn})_2]^{3+}$ were extremely sensitive to the environment of the complexes and showed a remarkable variation, while those of the corresponding diastereomers, Λ-$[Co(RR\text{-ptn})_3]^{3+}$ and *cis*-Λ-$[Co(NH_3)_2(RR\text{-ptn})_2]^{3+}$ were little affected by the given environment. The other complexes, *trans*-$[Co(NH_3)_2(RR\text{-ptn})_2]^{3+}$ and $[Co(NH_3)_4(RR\text{-ptn})]^{3+}$ exhibited small variations in the circular dichroism spectra. These variations seem to be accounted for by the conformational change of the flexible six-membered chelate ring brought about by ion-pair formation between the complex cations and anions.

In a previous paper,[1] we have reported that the solution CD spectra of $\Delta(lel_3)$-$[Co(RR\text{-ptn})_3]^{3+}$(*RR*-ptn=(*RR*)-2,4-pentanediamine) in the region of the first absorption band are seriously affected by its counter ions which comprise the complex salts; the chloride salt in water (2.7 mM) gives two CD bands, a strong negative and a weak positive band, while the perchlorate salt a single negative band in the same solvent. Such influences of counter ions have generally been reckoned to be negligibly small for the corresponding tris-chelated complexes formed with 1,2-diamines.

The *RR*-ptn chelate rings in the crystals of $\Delta(lel_3)$-[2] and $\Lambda(ob_3)$-$[Co(RR\text{-ptn})_3]Cl_3\cdot nH_2O$[3] have been shown by X-ray analyses to have the λ-*skew*(*twist*) conformation with two equatorially orientated methyl groups. However, PMR studies suggest that the *RR*(or *SS*)-ptn chelate ring is conformationally labile in solution at room temperature; in planar complexes such as $[Pt(RR\text{-(or }SS\text{)-ptn})_2]^{2+}$ [4,5] where no appreciable interaction is expected between the ligands, the chelate rings prefer to take the *chair* form with one axial methyl group rather than the *skew* form, while in octahedral complexes such as $[PtCl_2(NH_3)_2(RR\text{(or }SS\text{)-ptn})]^{2+}$ [5] and $[Ni(H_2O)_4(RR\text{(or }SS\text{)-ptn})]^{2+}$ [6] the stability of the *skew* form increases to reduce interactions between an apical ligand and the axial methyl group of the *RR*(or *SS*)-ptn in the *chair* form. Thus the stable conformation of *RR*(or *SS*)-ptn chelate ring in a complex seems to depend primarily on the magnitude of intramolecular interactions with other ligands. The conformation in solution may also be affected by various other factors such as the kind of solvent, the presence of excessive electrolyte, and temperature. That the CD spectrum of Δ-$[Co(RR\text{-ptn})_3]^{3+}$ in water is very sensitive to the kind of counter ion seems to be correlated with such a conformational behavior of the chiral six-membered *RR*-ptn chelate ring. In order to investigate this correlation, we have prepared a series of complexes of the type $[Co(NH_3)_{2n}(RR\text{-ptn})_{3-n}]^{3+}$ and measured their CD spectra in various matrices.

Very recently Boucher and Bosnich[7] reported the CD spectra of a number of complexes of the type, $[CoX_2(RR\text{-ptn})_2]^{n+}$, involving three isomers of the diammine complex, and found some unusual features in the CD spectra of the diammine complexes.

Experimental

Ligand. (*RR*)-2,4-pentanediamine was prepared by the method of Bosnich *et al.*,[8] and its hydrochloride (*RR*-ptn·2HCl) was used to prepare the complexes.

(−)$_{546}$-Δ-tris[(RR)-2,4-pentanediamine]cobalt(III) Complex. Mizukami *et al.*[9] prepared this complex from *trans*-$[CoCl_2(RR\text{-ptn})_2]ClO_4$ and *RR*-ptn. However, the following method gives pure Δ-isomer stereoselectively in a high yield.

RR-ptn·2HCl (2.7 g, 15.4 mmol) was dissolved in water (3 cm^3), and the pH of the solution was adjusted to 9 with NaOH. To this solution were added $[CoBr(NH_3)_5]Br_2$ (1.8 g, 4.6 mmol) and active charcoal (0.5 g). The mixture was stirred for 10 h at 50 °C, filtered off in hot to remove the charcoal, and the residue was washed with hot water. The resulting orange filtrate was then diluted with 1 dm^3 of water and poured on SP-Sephadex. The complex adsorbed on SP-Sephadex was found to be pure Δ-$[Co(RR\text{-ptn})_3]^{3+}$ by an SP-Sephadex column chromatography using a 0.2 M aqueous Na_2SO_4 solution as the eluent. The complex was isolated as various salts by the following methods.

(−)$_{546}$-Δ-[Co(RR-ptn)$_3$](ClO$_4$)$_3\cdot 3H_2O$. The complex adsorbed on SP-Sephadex was eluted with a 1.0 M $NaClO_4$ solution. The effluent was concentrated at 40 °C under reduced pressure to give orange needle crystals. They were filtered off, and recrystallized from water.

(−)$_{546}$-Δ-[Co(RR-ptn)$_3$]Cl$_3\cdot 2.5H_2O$. The complex was eluted similarly with 0.5 M HCl. Orange needle crystals were obtained by evaporating the effluent to almost dryness in a vacuum desiccator over NaOH and P_2O_5. They were recrystallized from a small amount of water by the addition of concd HCl.

(−)$_{546}$-Δ-[Co(RR-ptn)$_3$]Br$_3\cdot 2H_2O$. This complex was obtained by converting the perchlorate into bromide with the anion exchanger, Dowex 1×8, in the bromide form and recrystallized from water.

(−)$_{546}$-Δ-[Co(RR-ptn)$_3$]I$_3$. This complex was obtained by adding a NaI solution to an aqueous solution of the perchlorate. Orange crystals were filtered off, washed with cold water and recrystallized from ethanol.

(+)$_{546}$-Λ-tris[(RR)-2,4-pentanediamine)]cobalt(III) Complex. The preparative method reported by Mizukami *et al.*[9] was modified as follows. A suspension of *RR*-ptn·2HCl (0.256 g, 1.46 mmol) and sodium methoxide (0.158 g, 2.92 mmol) in methanol (5 cm^3) was added to a solution of *trans*-$[CoCl_2(RR\text{-ptn})_2]Cl$[9] (0.54 g, 1.46 mmol) in DMSO (20 cm^3). The reaction took place immediately to give a brown solution.

It was then diluted with about 1 dm^3 of water and passed through an SP-Sephadex column (ϕ 2.7×5 cm). A small portion of the Sephadex saturated with the product was poured on the top of an SP-Sephadex column (ϕ 2.7×120 cm), and the adsorbed complexes were eluted with a 0.2 M aqueous solution of Na_2SO_4. Two separate bands were obtained. The first and the second were *Δ*- and *Λ*-[Co(*RR*-ptn)$_3$]$^{3+}$, respectively. The formation ratio of the former to the latter was 10: 1. The effluent containing the *Λ*-isomer was poured again on an SP-Sephadex column (ϕ 1.5×3 cm) after dilution with water and the adsorbed complex was eluted by the following method.

*(+)$_{546}$-Λ-[Co(*RR*-ptn)$_3$](ClO$_4$)$_3$.* This complex was obtained from the SP-Sephadex adsorbed the *Λ*-isomer in a similar way to that for *Δ*-[Co(*RR*-ptn)$_3$](ClO$_4$)$_3$·3H$_2$O.

*(+)$_{546}$-Λ-[Co(*RR*-ptn)$_3$]Cl$_3$·3H$_2$O.* An aqueous solution of the complex perchlorate was passed through a column containing the anion exchanger, Dowex 1×8, in the chloride form to convert into the chloride. Needle crystals were obtained by evaporating the effluent to almost dryness in a vacuum desiccator over P_2O_5.

trans, *(+)$_{470}$*-cis-*Δ*-, *and (−)$_{470}$*-cis-*Λ*-*diamminebis[(RR)-2,4-pentanediamine]cobalt(III) Complexes.* To a solution of sodium methoxide (0.227 g, 4.2 mmol) in methanol (3 cm^3) was added *RR*-ptn·2HCl (0.45 g, 2.6 mmol) with stirring, and the mixture was filtered to remove NaCl. The filtrate was added to a solution of [Co(H$_2$O)(NH$_3$)$_5$](ClO$_4$)$_3$ (1 g, 2.2 mmol) in DMSO (20 cm^3). The solution was stirred for 25 min at 85 °C, diluted with 1 dm^3 of water and acidified (pH≈3) with HCl. This was poured on SP-Sephadex, and the adsorbed complexes were chromatographed by a method similar to that for [Co(*RR*-ptn)$_3$]$^{3+}$ with a 0.2 M aqueous Na_2SO_4 solution. The column gave three separate bands, I, II, and III in the order of elution, which were [Co(NH$_3$)$_6$]$^{3+}$, [Co(NH$_3$)$_4$(*RR*-ptn)]$^{3+}$, and a mixture of three isomers of [Co(NH$_3$)$_2$ (*RR*-ptn)$_2$]$^{3+}$, respectively. The effluent of the band III was reloaded on an SP-Sephadex column after dilution with water, and the adsorbed band was eluted with a 0.18 M sodium (+)$_{589}$-tartratoantimonate(III) solution. Two separate bands, III$_A$ and III$_B$ were eluted in this order. The band III$_B$ was (+)$_{470}$-*cis*-*Δ*-[Co(NH$_3$)$_2$(*RR*-ptn)$_2$]$^{3+}$, but the band III$_A$ was still a mixture of *trans*- and (−)$_{470}$-*cis*-*Λ*-[Co(NH$_3$)$_2$(*RR*-ptn)$_2$]$^{3+}$. However, these two isomers were successfully separated by a repeated SP-Sephadex column chromatography using a 0.2 M Na_2SO_4 solution as the eluent. The *trans*-isomer(III$_A$-1) moved faster than did the (−)$_{470}$-*cis*-*Λ*-isomer(III$_A$-2). The formation ratio, *trans*: *cis*-*Λ*: *cis*-*Δ* was about 1: 1: 20.

trans-[*Co(NH$_3$)$_2$(RR-ptn)$_2$](ClO$_4$)$_3$·H$_2$O*, *(+)$_{470}$*-cis-*Δ*- *and (−)$_{470}$*-cis-*Λ*-[*Co(NH$_3$)$_2$(RR-ptn)$_2$](ClO$_4$)$_3$*. These complexes were obtained from each separated eluate described above by a method similar to that for *Δ*-[Co(*RR*-ptn)$_3$](ClO$_4$)$_3$·3H$_2$O using 1.0 M HClO$_4$ as the eluent. The effluent was concentrated to a small volume with a rotary evaporator under a reduced pressure. Orange crystals which formed were filtered off and washed with ethanol.

(+)$_{470}$-cis-*Δ*-[*Co(NH$_3$)$_2$(RR-ptn)$_2$]Cl$_3$·1.5H$_2$O.* This complex was obtained by a method similar to that for *Δ*-[Co(*RR*-ptn)$_3$]Cl$_3$·2.5H$_2$O.

[*Co(NH$_3$)$_4$(RR-ptn)]Cl$_3$ and [Co(NH$_3$)$_4$(RR-ptn)](ClO$_4$)$_3$·H$_2$O.* These complexes were isolated from the reaction product of [Co(H$_2$O)(NH$_3$)$_5$](ClO$_4$)$_3$ and *RR*-ptn in DMSO described before and crystallized by methods similar to those for the chloride and the perchlorate salts of *Λ*-[Co(*RR*-ptn)$_3$]$^{3+}$.

(−)$_{589}$-Λ-Tris(trimethylenediamine)cobalt(III) Perchlorate The racemic complex was prepared by the method of Bailar and Works[10] and resolved by the method of Fujita *et al.*[11] The *Λ*-isomer was isolated as the perchlorate salt by a method similar to that for *Δ*-[Co(*RR*-ptn)$_3$] (ClO$_4$)$_3$·3H$_2$O.

Table 1 shows the results of chemical analyses of all the complexes obtained.

Measurements. Absorption spectra were obtained on a Hitachi 323 and a Carl Zeiss PMQ-II spectrophotometer, and CD spectra on a JASCO model J-20 spectropolarimeter. CD spectra in Nujol mulls were measured by a method simliar to that used for IR measurement with two quartz plates. PMR spectra were recorded in D_2O at 60 MHz on a JEOL PMX-60 spectrometer taking HOD signal as the internal reference. FT ^{13}C NMR spectra were obtained in D_2O at 15.04 MHz on a JEOL FX-60 spectrometer using dioxane as the internal reference, the chemical shift of which is at 67.69 ppm downfield from TMS sealed in an external capillary.

Results and Discussion

Preparation and Characterization of the Complexes. Mizukami *et al.*[9] prepared first a pair of diastereomers, (+)$_{546}$- and (−)$_{546}$-[Co(*RR*-ptn)$_3$]$^{3+}$ by the reactions of *trans*-[CoCl$_2$(*RR*-ptn)$_2$]$^+$ with *RR*-ptn in 50% aqueous methanol in the absence of active charcoal, and in water in the presence of active charcoal, respectively. In the

Table 1. Analytical data of the complexes

Complex	H/%		C/%		N/%	
	Found	Calcd	Found	Calcd	Found	Calcd
Δ-[Co(*RR*-ptn)$_3$]Cl$_3$·2.5H$_2$O	9.38	9.16	35.10	34.86	16.27	16.26
Δ-[Co(*RR*-ptn)$_3$]Br$_3$·2H$_2$O	7.45	7.23	27.97	28.10	13.14	13.11
Δ-[Co(*RR*-ptn)$_3$]I$_3$	6.00	5.67	24.63	24.15	10.62	11.26
Δ-[Co(*RR*-ptn)$_3$](ClO$_4$)$_3$·3H$_2$O	6.28	6.74	25.13	25.10	11.73	11.71
Λ-[Co(*RR*-ptn)$_3$](ClO$_4$)$_3$	6.37	6.38	27.23	27.14	12.65	12.66
Λ-[Co(*RR*-ptn)$_3$]Cl$_3$·3H$_2$O	8.74	9.20	34.11	34.26	16.10	15.98
[Co(NH$_3$)$_4$(*RR*-ptn)]Cl$_3$	7.76	7.81	17.77	17.90	24.74	25.04
[Co(NH$_3$)$_4$(*RR*-ptn)](ClO$_4$)$_3$·H$_2$O	4.88	5.17	11.05	11.01	15.46	15.40
trans-[Co(NH$_3$)$_2$(*RR*-ptn)$_2$]Cl$_3$·1.5H$_2$O	8.71	8.66	27.79	27.89	19.82	19.51
trans-[Co(NH$_3$)$_2$(*RR*-ptn)$_2$](ClO$_4$)$_3$·H$_2$O	5.55	5.91	19.77	19.57	13.59	13.69
cis-*Δ*-[Co(NH$_3$)$_2$(*RR*-ptn)$_2$]Cl$_3$·1.5H$_2$O	8.32	8.66	27.81	27.89	19.93	19.51
cis-*Δ*-[Co(NH$_3$)$_2$(*RR*-ptn)$_2$](ClO$_4$)$_3$	5.98	5.75	20.05	20.16	13.91	14.11
cis-*Λ*-[Co(NH$_3$)$_2$(*RR*-ptn)$_2$](ClO$_4$)$_3$	5.66	5.75	20.02	20.16	13.96	14.11

present study, these two isomers are formed by the same reaction in DMSO without the addition of active charcoal at room temperature, and separated by SP-Sephadex column-chromatography with a 0.2 M Na_2SO_4 solution as the eluent. On the other hand, the reaction of $[CoBr(NH_3)_5]Br_2$ with *RR*-ptn in water in the presence of active charcoal gives only the $(-)_{546}$-isomer. It is known that the $(+)_{546}$- and the $(-)_{546}$-isomers have $\Lambda(ob_3)$[3] and $\Delta(lel_3)$[2] configurations, respectively, all the *RR*-ptn chelate rings taking *λ-skew-(twist)* conformation. Niketic and Woldbye[12] showed by the conformational analysis that the $(+)_{546}$-$\Lambda(ob_3)$ isomer is about 18.8 kJ·mol^{-1} less stable than the $(-)_{546}$-$\Delta(lel_3)$ isomer. This value implies that the complexes formed under an equilibrium condition are almost all (>99.9%) the $\Delta(lel_3)$ isomer. The fact that only the $\Delta(lel_3)$ isomer is formed stereoselectively in the presence of active charcoal agrees well with this implication. The formation of the $(+)_{546}$-$\Lambda(ob_3)$ isomer in the absence of active charcoal may be related with a kinetic route to form $[Co(RR\text{-ptn})_3]^{3+}$ in the reaction between *trans*-$[CoCl_2(RR\text{-ptn})_2]^+$ and *RR*-ptn.

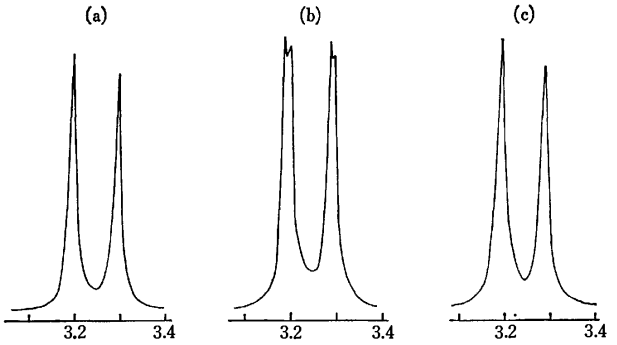

Fig. 1. PMR spectra of methyl signals of the isomers (a) III_A-1(*trans*), (b) III_A-2(*cis*)-Λ, and (c) III_B(*cis*-Λ) in D_2O.
Chemical shifts in ppm from HOD signal.

The complex, $[Co(NH_3)_2(RR\text{-ptn})_2]^{3+}$ exists in three isomers, *trans*, *cis*-Δ, and *cis*-Λ configurations, all of which have been obtained. Figure 1 shows the PMR spectra of these three isomers in D_2O at 60 MHz. The *trans*(D_2 symmetry) and the *cis*(C_2 symmetry) isomers are expected to show one and two kinds of doublet signal due to the methyl protons, respectively. The III_A-2 isomer exhibits two kinds of doublet in the methyl signal region and is assigned safely to the *cis* configuration. However, each isomer of the other two(III_A-1 and III_B) gives only one doublet methyl signal. To distinguish them ^{13}C-NMR spectroscopy has been utilized. As Fig. 2 shows, the III_A-1 isomer gives only one kind of signal for each resonance of the methyl, the methylene, and the methine carbons, while the III_B isomer two, one, and two signals for the corresponding carbons, respectively. The III_A-2 isomer exhibits the same spectral pattern as that of the isomer III_B. Thus, all of the NMR data lead to the conclusion that the III_A-1, the III_A-2, and the III_B isomers are *trans*, *cis*, and *cis* configurations, respectively. For the two *cis* III_A-2 and III_B isomers, the $\Lambda(ob_2)$ and $\Delta(lel_2)$ configurations are assigned, respectively on the basis of their CD patterns in the region of the first absorption band, as shown in Figs. 3 and 4. These assignments will be supported by the fact that the formation ratio of the $\Lambda(ob_2)$ to the $\Delta(lel_2)$ isomer is 1: 20 as described in the Experimental part, since the yield of one diastereomer

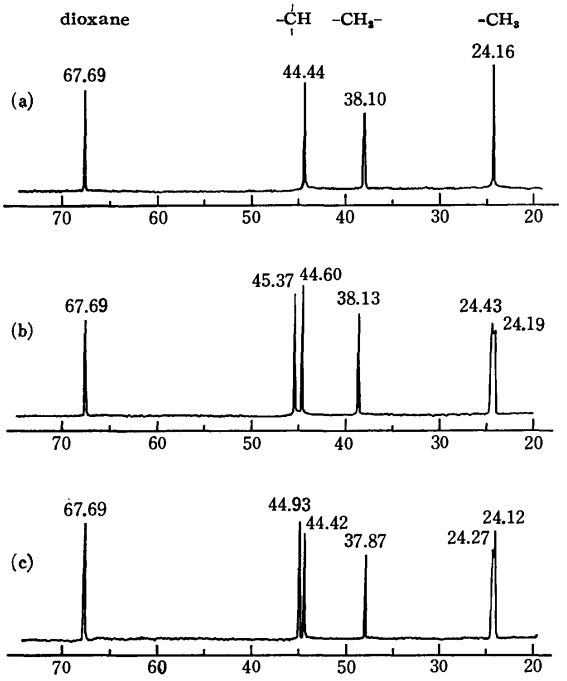

Fig. 2. Proton-decoupled 15.04 MHz ^{13}C-NMR spectra of the isomers (a)III_A-1(*trans*), (b)III_A-2(*cis*-Λ), and (c)III_B(*cis*-Δ) in D_2O.
Tantaive assignments for the signals are also given.

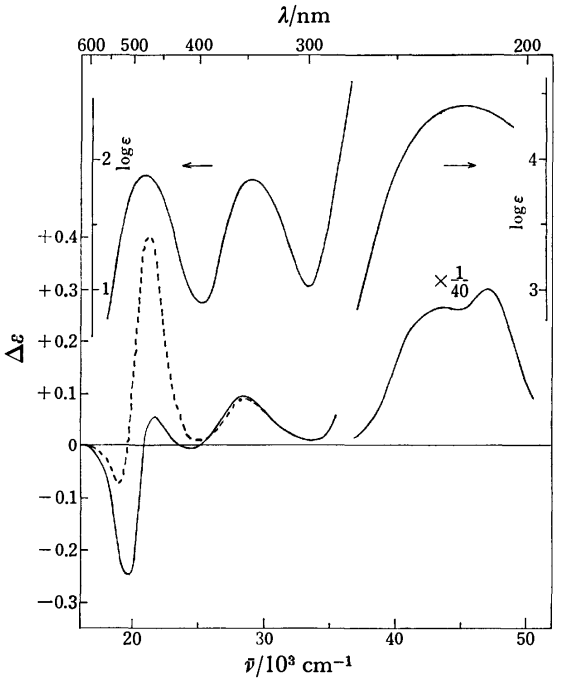

Fig. 3. Absorption and CD spectra of III_B: $(+)_{470}$-*cis*-Δ-$[Co(NH_3)_2(RR\text{-ptn})_2](ClO_4)_3$($3.31\times10^{-3}$ M in visible region and 1.32×10^{-4} M in UV region) in water(——) and in 0.2 M Na_2SO_4(----).

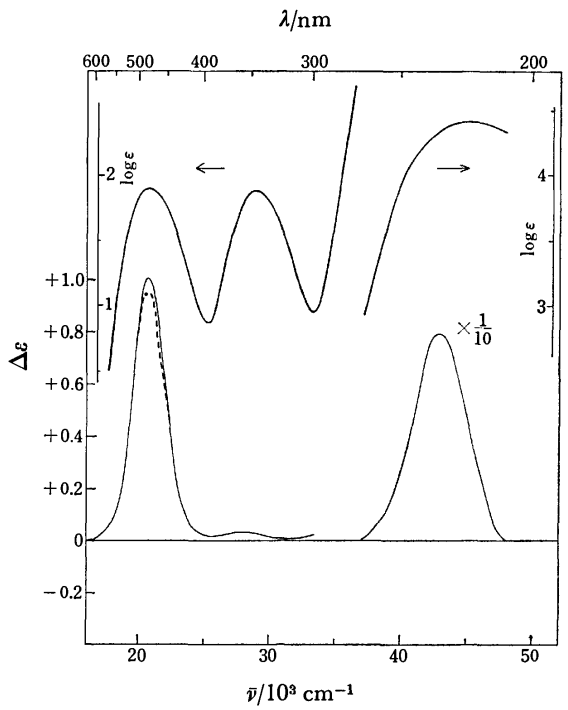

Fig. 4. Absorption and CD spectra of III_A-2: (—)$_{470}$-*cis*-*Λ*-[Co(NH_3)$_2$(*RR*-ptn)$_2$](ClO_4)$_3$(3.30×10^{-3} M in visible region and 1.32×10^{-4} M in UV region) in water(——) and in 0.2 M Na_2SO_4 (----).

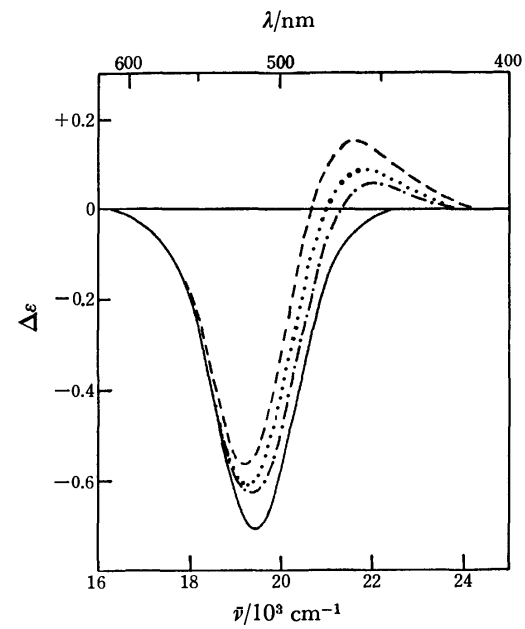

Fig. 5. CD spectra of *Λ*-[Co(*RR*-ptn)$_3$](ClO_4)$_3$·$3H_2O$ (——, 3.45×10^{-3} M), *Λ*-[Co(*RR*-ptn)$_3$]I_3(-·--·-, 3.51×10^{-3} M), *Λ*-[Co(*RR*-ptn)$_3$]Br_3·$2H_2O$(·····, 1.75×10^{-3} M), and *Λ*-[Co(*RR*-ptn)$_3$]Cl_3·$2.5H_2O$(----, 3.90×10^{-3} M) in water.

involving more steric interactions is expected to be lower than that of the other.[13] Molecular models indicate that the *Λ*(*ob*$_2$) structure involves such interactions to a greater extent than the *Δ*(*lel*$_2$) structure. The assignments for these three isomers of the diammine complex agree with those made by Boucher and Bosnich.[7]

The *cis*-*Λ*(*ob*$_2$) isomer gives the first absorption band at a longer wavelength (482 nm) than does the *cis*-*Δ*(*lel*$_2$) isomer (480 nm). These results agree with the observations reported by Mizukami *et al.*[9] that in a pair of diastereomers, the d-d absorption bands of the one involving more steric interactions lie at a longer wavelength than those of the other. For [Co(*RR*-ptn)$_3$]$^{3+}$, the first absorption band of the *Λ*(*ob*$_3$) isomer is at a longer wavelength side by 6 nm than that of the *Δ*(*lel*$_3$) isomer, as shown in Table 2.

Circular Dichroism Spectra. As stated previously, the solution CD spectra of *Λ*-[Co(*RR*-ptn)$_3$]$^{3+}$ in the region of the first absorption band are seriously affected by its counter ion. Figure 5 and Table 2 show the CD data of various salts of this complex ion in water. The positive CD component at a shorter wavelength side of the first absorption band, which has been assigned to the $^1A_2\leftarrow{}^1A_1$ transition (D_3 symmetry) based on the analysis of the solid state CD spectrum of the chloride,[14] increases the magnitude in the order of perchlorate< iodide<bromide<chloride. The absorption spectra are all nearly identical with one another in this region. Since all the anions have uni-negative charge and the sizes of ions decrease in this order, such CD changes are suggested to be correlated with ion-pair formation between the complex cation and anions. Figure 6 shows dependence of the CD spectra of *Λ*-[Co(*RR*-

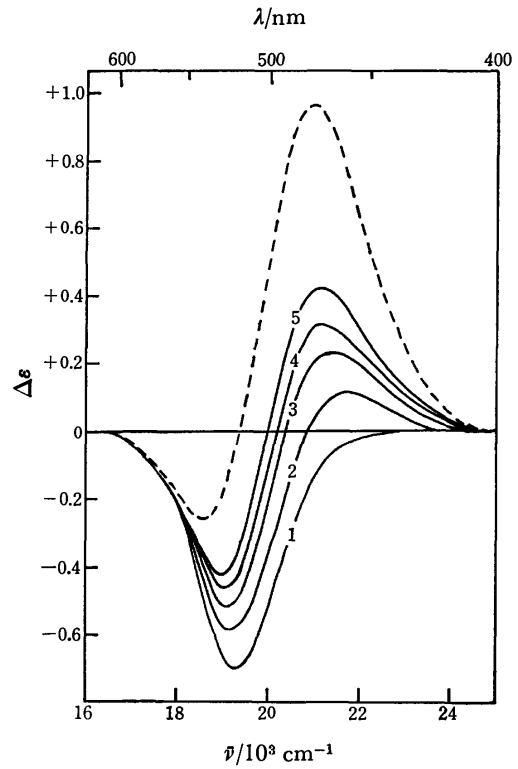

Fig. 6. Dependence of CD of *Λ*-[Co(*RR*-ptn)$_3$](ClO_4)$_3$·$3H_2O$(2.80×10^{-3} M) on the concentration of chloride ion at 25 °C and I=0.091($NaClO_4$).
1. [Cl^-]=0, 2. [Cl^-]=1.66×10^{-2} M, 3. [Cl^-]=3.33×10^{-2} M, 4. [Cl^-]=4.99×10^{-2} M, and 5. [Cl^-]=7.49×10^{-2} M.
Calculated CD curve of the ion-paired species, *Λ*-[Co(*RR*-ptn)$_3$]$^{3+}$·Cl^-(——).

Table 2. Absorption and CD spectral data

Complex	Absorption $\log\varepsilon$ ($\bar{\nu}_{max}/cm^{-1}$)	CD $\Delta\varepsilon$ $\bar{\nu}/cm^{-1}$	Concentration C/M
Δ-[Co(*RR*-ptn)$_3$](ClO$_4$)$_3$·3H$_2$O	1.90 (20750)	−0.704 (19340)	3.45×10^{-3}
	1.89 (28800)	+0.058 (28600)	
	4.49 (43500)	+18 (42200)	3.81×10^{-4}
Δ-[Co(*RR*-ptn)$_3$]Cl$_3$·2.5H$_2$O	1.90 (20750)	−0.565 (19190)	3.90×10^{-3}
		+0.154 (21550)	
	1.88 (28800)	+0.051 (28600)	
	4.47 (43500)	+18 (42200)	4.20×10^{-4}
Δ-[Co(*RR*-ptn)$_3$]Br$_3$·2H$_2$O	1.88 (20750)	−0.613 (19310)	1.75×10^{-3}
		+0.086 (21790)	
	1.84 (28800)	+0.061 (28300)	
	4.46 (43500)	+18 (42200)	4.01×10^{-4}
Δ-[Co(*RR*-ptn)$_3$]I$_3$	1.88 (20750)	−0.628 (19460)	3.51×10^{-3}
		+0.059 (21980)	
		+0.047 (28200)	
Λ-[Co(*RR*-ptn)$_3$](ClO$_4$)$_3$	1.98 (20500)	+3.22 (20750)	2.88×10^{-3}
	1.95 (28600)	−0.31 (28400)	
	4.46 (43100)	+5.9 (42000)	1.15×10^{-4}
		−4.1 (48800)	
Λ-[Co(*RR*-ptn)$_3$]Cl$_3$·3H$_2$O	1.98 (20500)	+3.18 (20790)	3.03×10^{-3}
	1.96 (28600)	−0.33 (28600)	
	4.52 (43100)	+6.5 (42000)	1.21×10^{-4}
		−4.5 (48800)	
[Co(NH$_3$)$_4$(*RR*-ptn)](ClO$_4$)$_3$·H$_2$O	1.85 (20920)	+0.104 (20410)	7.77×10^{-3}
		−0.012 (23370)	
	1.79 (29200)	+0.075 (28700)	
	4.38 (48300)	+5.8 (46500)	7.06×10^{-4}
[Co(NH$_3$)$_4$(*RR*-ptn)]Cl$_3$	1.82 (20920)	+0.103 (20410)	6.91×10^{-3}
		−0.011 (23470)	
	1.78 (29200)	+0.070 (28700)	6.28×10^{-4}
	4.34 (48300)	+5.5 (46500)	
trans-[Co(NH$_3$)$_2$(*RR*-ptn)$_2$](ClO$_4$)$_3$·H$_2$O	1.92 (20920)	+0.271 (19530)	3.12×10^{-3}
		−0.266 (21980)	
	1.92 (28900)	+0.234 (28800)	
	4.39 (43700)	+14 (43100)	1.25×10^{-4}
cis-Δ-[Co(NH$_3$)$_2$(*RR*-ptn)$_2$](ClO$_4$)$_3$	1.88 (20830)	−0.245 (19380)	3.31×10^{-3}
		+0.055 (21550)	
	1.85 (28900)	+0.098 (28500)	
	4.41 (45000)	+10sh (43500)	1.32×10^{-4}
		+12 (47400)	
cis-Δ-[Co(NH$_3$)$_2$(*RR*-ptn)$_2$]Cl$_3$·1.5H$_2$O	1.89 (20830)	−0.220 (19340)	3.78×10^{-3}
		+0.088 (21510)	
	1.86 (28900)	+0.093 (28400)	
	4.41 (45000)	+6.9sh (42600)	1.51×10^{-4}
		+11 (47400)	
cis-Λ-[Co(NH$_3$)$_2$(*RR*-ptn)$_2$](ClO$_4$)$_3$	1.90 (20750)	+1.01 (20750)	3.30×10^{-3}
	1.87 (28900)	+0.031 (27600)	
	4.42 (45000)	+7.9 (43100)	1.32×10^{-4}
Λ-[Co(tn)$_3$](ClO$_4$)$_3$	1.88 (20450)	+0.081 (18800)	5.68×10^{-3}
		−0.117 (21050)	
	1.88 (28500)	−0.018 (28400)	
	4.37 (43300)	−13 (40000)	2.27×10^{-4}
		+12 (45300)	
		−9.1 (50500)	

ptn)$_3$]$^{3+}$ on the concentration of chloride ion. The measurements were carried out at 25 °C, and at the ionic strength of 0.091 adjusted with $NaClO_4$, and using a 2.8 mM aqueous solution of the complex perchlorate. The CD spectrum of this perchlorate was little affected by the addition of $NaClO_4$ up to its 0.5 M concentration. From the change of CD strengths at 475 nm, association constant, K=13.8 was obtained by the method of Tanaka *et al.*[15] for the following equilibrium; Δ-[Co(*RR*-ptn)$_3$]$^{3+}$ + Cl$^-$ $\rightleftarrows$ Δ-[Co(*RR*-ptn)$_3$]$^{3+}$·Cl$^-$. On the other

hand, the constant K determined from the absorbancies[15] at 290 nm was 12.6 for the same equilibrium system. That the two K values obtained by both the CD and the UV methods are nearly the same strongly suggests that the CD variation of Δ-[Co(*RR*-ptn)$_3$]$^{3+}$ in the region of the first absorption band is brought about by ion-pair formation between the complex ion and counter ions. A further evidence to support this suggestion is that the CD spectra of the complex chloride in aqueous solutions depend clearly on its concentration as shown in Fig. 7. Figure 6 includes the calculated CD curve of the ion-paired species, Δ-[Co(*RR*-ptn)$_3$]$^{3+}\cdot$Cl$^-$ (K=13.8). The A_2 component is considerably enhanced and the sign of the so-called main CD band is reversed.

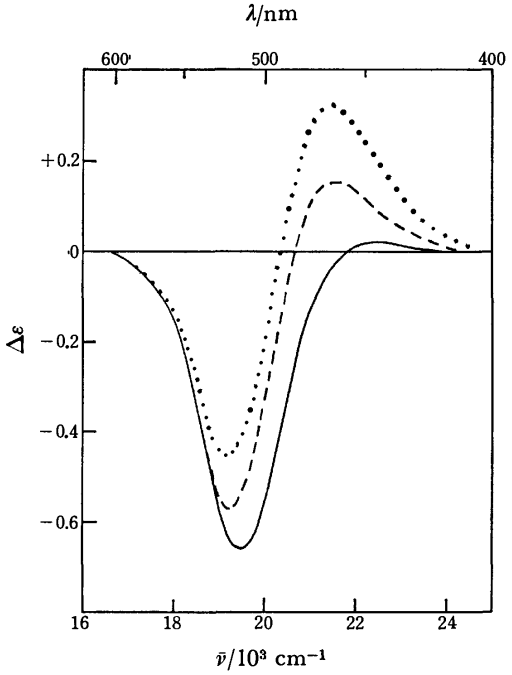

Fig. 7. Dependence of CD of Δ-[Co(*RR*-ptn)$_3$]Cl$_3\cdot$2.5 H$_2$O on its concentration in water; 1.76×10^{-4}M (——), 3.90×10^{-3} M(——), and 1.71×10^{-2} (·····).

The effect of sulfate ion on the CD spectrum of Δ-[Co(*RR*-ptn)$_3$]$^{3+}$ is very similar to that of chloride ion and the CD curve of the ion-paired species, Δ-[Co(*RR*-ptn)$_3$]$^{3+}\cdot$SO$_4^{2-}$ closely resembles that of the Δ-[Co(*RR*-ptn)$_3$]$^{3+}\cdot$Cl$^-$ (Fig. 8). The association constant K of the complex ion with a sulfate ion was determined to be 61.7 by the CD method under the same condition as that measured for chloride ion. This value and 13.8 (or 12.6) in the case of chloride ion may be reasonable for the constants of ion-pair formation in the systems of ions of a tripositive-dinegative and a tripositive-uninegative, respectively.[15,16] Thus, the CD pattern of Δ-[Co(*RR*-ptn)$_3$]$^{3+}$ in the region of the first absorption band seems to be affected in a similar manner by ion-pair formation with counter anions irrespective of their kinds.

The ion-pair formation should be facilitated in an organic solvent to a greater extent than in an aqueous solution. Figure 9 shows the CD spectra of Δ-[Co(*RR*-ptn)$_3$]Br$_3\cdot$2H$_2$O in DMSO at various concentrations. The spectra give strong A_2 components without the addition of excessive bromide ion and depend clearly

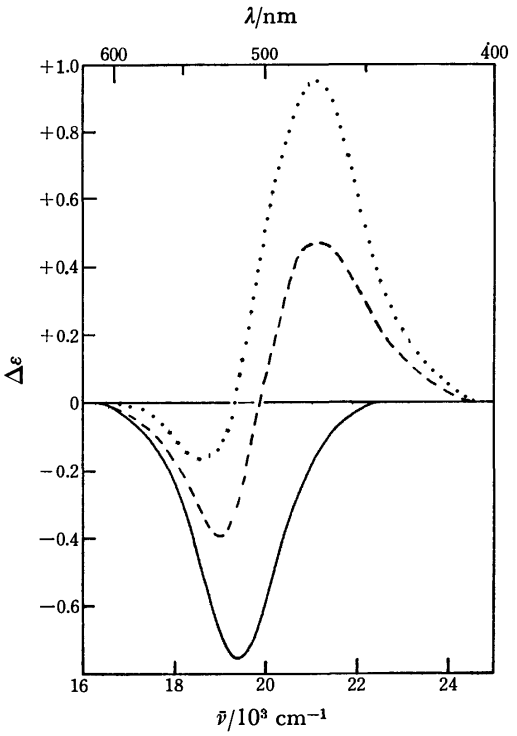

Fig. 8. CD spectra of Δ-[Co(*RR*-ptn)$_3$](ClO$_4$)$_3\cdot$3H$_2$O(3.45 $\times10^{-3}$ M) in water(——) and in 0.1 M Na$_2$SO$_4$(——). Calculated CD curve of the ion-paired species, Δ-[Co(*RR*-ptn)$_3$]$^{3+}\cdot$SO$_4^{2-}$(·····).

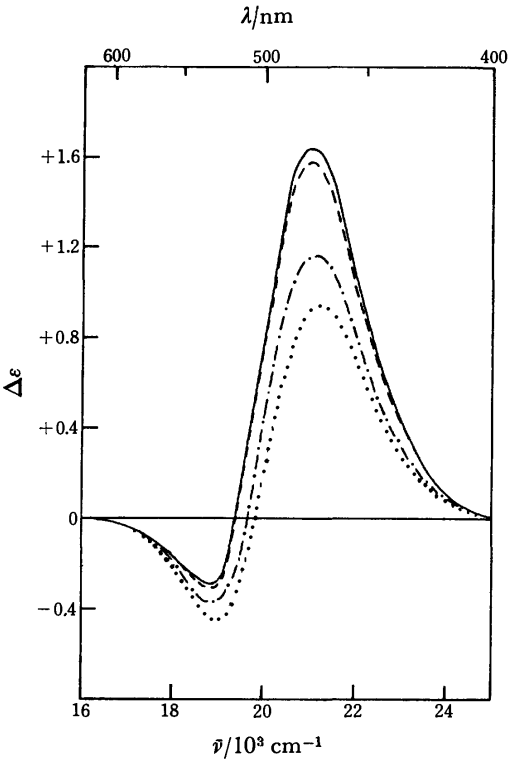

Fig. 9. CD spectra of Δ-[Co(*RR*-ptn)$_3$]Br$_3\cdot$2H$_2$O in DMSO; 4.52×10^{-5} M (·····), 2.09×10^{-4} M(-·-·-), 1.93×10^{-3} M(----), and 9.33×10^{-3} M(——).

on the concentration of the complex. The complex chloride in DMSO gives a CD pattern very similar to that of the ion-paired species shown in Fig. 6 even at a very dilute solution (6.13×10^{-5} M). With increase in the concentration of the complex chloride, both CD components, the A_2 and the E, increase their strengths. Since the association constant between the complex cation and a chloride ion is expected to be larger than that between the complex ion and a bromide ion, this might be attributed to the formation of higher ion-paired species, 1 : 2 or 1 : 3 than 1 : 1. The complex perchlorate in DMSO exhibits a marked A_2 component which is never observed in an aqueous solution, but shows no dependence on the concentration of the complex in the range between 9.75×10^{-3} and 7.05×10^{-5} M. The reason for this is not clear at present, but it is clear that a perchlorate ion is weak in ability to form an ion-pair with the complex ion in DMSO.

In marked contrast to the large variety of solution CD spectra of $\Delta(lel_3)$-[Co(*RR*-ptn)$_3$]$^{3+}$, the CD spectra of $\Lambda(ob_3)$-[Co(*RR*-ptn)$_3$]$^{3+}$ show little solvent dependence in the region of the first absorption band. As Fig. 10 shows, the CD patterns of the latter isomer are nearly the same in water, 0.2 M Na_2SO_4, and DMSO solutions, although the spectrum in the last solution gives a small negative CD band at a longer wavelength side.

It is known that the polarizable oxoanions such as phosphate and selenite have a marked effect on the CD spectra of some tris(diamine)cobalt(III) complexes. The CD spectrum of Δ(or Λ)-[Co(tn)$_3$]$^{3+}$(tn: trimethylenediamine) is particularly sensitive to the excessive presence of these oxoanions.[17,18] Figure 11 shows that a chloride ion affects also the CD of Λ-[Co(tn)$_3$]$^{3+}$ in a similar way, giving rise to the increase in the major negative CD band(A_2) at the expense of the minor positive CD band(E). Beddoe and Mason[17,19] found that the CD spectra of Δ-[Co(tn)$_3$]$^{3+}$ in the presence of phosphate or selenite resemble that of the solid Δ-[Co(tn)$_3$]$Br_3\cdot H_2O$ in a KBr disk. Since all the tn chelates in the crystals adopt the chair conformation,[20] they suggested that on the addition of oxoanions, [Co(tn)$_3$]$^{3+}$ in an aqueous solution is stabilized to have the tris-*chair* conformation by ion-pair formation (Fig. 12). However, CD spectra in KBr disks should be viewed with some caution for such conformationally labile complexes as [Co(tn)$_3$]$^{3+}$, because these spectra depend often on the condition such as pressure and its duration time employed for the preparation of KBr disk. In fact, Λ-[Co(tn)$_3$]$Br_3\cdot H_2O$ in Nujol mull exhibits no detectable CD in the region of the first absorption band, indicating that the tris-*chair* form has substantially very small CD. Furthermore, molecular models indicate that either the tris-*chair* or the ob_3 conformation ($\Delta(\delta\delta\delta)$ and $\Lambda(\lambda\lambda\lambda)$) of [Co(tn)$_3$]$^{3+}$ has no set of N-H bonds parallel to the C_3 axis of the complex ion to form an ion-pair most effectively with the oxoanion through

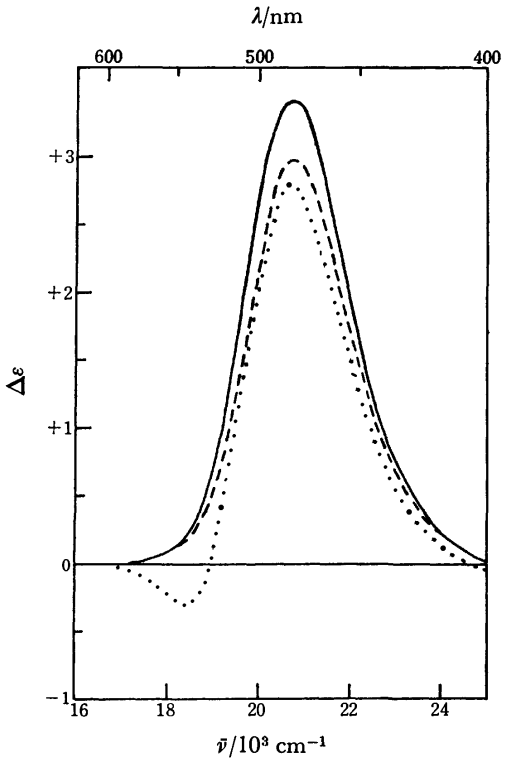

Fig. 10. CD spectra of Λ-[Co(*RR*-ptn)$_3$](ClO$_4$)$_3$; 2.88×10^{-3} M in water (——), 2.88×10^{-3} M in 0.2 M Na_2SO_4 (——), and 1.81×10^{-3} M in DMSO(·····).

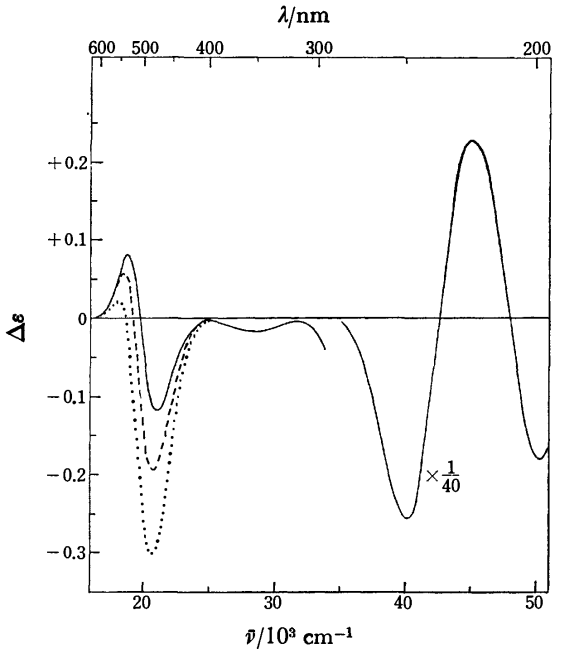

Fig. 11. CD spectra of Λ-[Co(tn)$_3$](ClO$_4$)$_3$(5.68×10^{-3} M in visible region and 2.27×10^{-4} M in UV region) in water(——), in 1 M NaCl(——), and in 0.2 M Na_2SO_4 (·····).

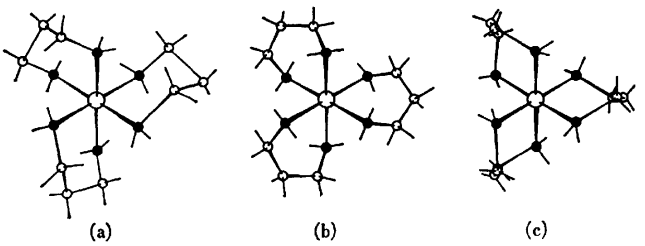

Fig. 12. Schematic structures of tris(trimethylenediamine)cobalt(III) complexes; (a) $\Lambda(chair_3)$, (b) $\Lambda(ob_3, \lambda\lambda\lambda)$, and (c) $\Lambda(lel_3,\delta\delta\delta)$.

hydrogen bonding, while that only the lel_3 conformation ($\Delta(\lambda\lambda\lambda)$ and $\Lambda(\delta\delta\delta)$) has a set of three N–H bonds suitable for forming such hydrogen bonds with the oxoanion.[21] This suggests that the conformer stabilized by ion-pair formation is not the tris-*chair* proposed by Beddoe *et al.*,[19] but the lel_3 conformation. Then, the increase in the magnitude of the negative CD band of Λ-$[Co(tn)_3]^{3+}$ in the presence of excessive anions can be attributed to the contribution of the vicinal effect of the *δ-skew* chelate rings in the lel_3-$\Lambda(\delta\delta\delta)$ conformer stabilized by ion-pair formation (Fig. 11). It is known that the vicinal effect due to a chiral chelate ring in *δ* form gives negative CD in the region of the first absorption band and that the vicinal and the configurational effect contribute additively to the CD in this region.[22] The addition of other anions such as a chloride ion than the oxoanions may result in a similar stabilization of the lel_3 form, since the effect of chloride ion on the CD spectrum of $[Co(tn)_3]^{3+}$ quite resembles that of sulfate ion. Thus the CD variation of $[Co(tn)_3]^{3+}$ on the addition of anions can resonably be explained by the stabilization of the lel_3 conformer due to ion-pair formation and by the contribution of the vicinal effect due to the chiral, skew tn chelate rings in this conformer. The interconversion between the tris-*chair* and the lel_3 conformation seems to occur easily in solution, since the energy difference between them has been calculated to be very small.[23] The ob_3 conformation has been shown to have a substantially higher energy.[23]

A similar discussion can be made on the CD variation of $[Co(RR\text{-ptn})_3]^{3+}$ in solution. As stated previously, the *RR*-ptn chelate ring has been shown to prefer to take the *chair* conformation with one axial methyl group rather than the *skew* conformation in solution, although those in the crystals of $\Delta(lel_3)$-[2] and $\Lambda(ob_3)$-$[Co(RR\text{-ptn})_3]Cl_3\cdot nH_2O$[3] are all in the *λ-skew* conformation with two equatorial methyl groups. As molecular models (Fig. 12) show, $\Delta(lel_3)[Co(RR\text{-ptn})_3]^{3+}$ has much less crowded structure than $\Lambda(ob_3)[Co(RR\text{-ptn})_3]^{3+}$ and the chelate rings in the former seem to be able to convert their conformations without difficulty into others, the *chair* or some intermediate conformations between the *λ-skew* and the *chair*. On the other hand, the more crowded $\Lambda(ob_3)$-isomer seems to have too rigid a structure to change the conformation.

If it is assumed that the conformations of Δ-$[Co(RR\text{-ptn})_3]^{3+}$ in an aqueous solution are in an equilibrium among the tris-*skew* and some others involving the *chair* conformation, the CD variation on the addition of anions can be explained by the same ion-pair effect as that described for $[Co(tn)_3]^{3+}$; on the addition of anions the $\Delta(lel_3, \lambda\lambda\lambda)$ conformer is stabilized by ion-pair formation and the positive CD component in the region of the first absorption band is strengthened by the contribution of the vicinal effect due to the increasing amount of the *λ-skew* chelate ring (Figs. 6 and 8). This explanation will be supported by the fact that the CD spectrum of $\Delta(lel_3, \lambda\lambda\lambda)$-$[Co(RR\text{-ptn})_3]Cl_3\cdot 2.5H_2O$ in Nujol mull shows a pattern very similar to that of the ion-paired species.

The small CD variation of $\Lambda(ob_3)$-$[Co(RR\text{-ptn})_3]^{3+}$ on the addition of anions may be due to the conformational rigidity resulted from the crowded and strained structure. Although this isomer will be thermodynamically much unstable than the $\Delta(lel_3)$-isomer[12] as stated previously, the $\Lambda(ob_3)$-isomer seems to be stable from the viewpoint of conformational lability.

The same difference in the CD variation on the addition of anions is seen between *cis*-$\Delta(lel_2)$- and *cis*-$\Lambda(ob_2)$-$[Co(NH_3)_2(RR\text{-ptn})_2]^{3+}$. As Figs. 3 and 4 show, the positive CD band of the *cis*-$\Delta(lel_2)$ isomer in the region of the first absorption band gives rise to a pronounced increase in the presence of sulfate ion, while the CD change of the *cis*-$\Lambda(ob_2)$ isomer is negligible under the same condition. The CD spectrum of the chloride of *cis*-$\Delta(lel_2)$ isomer in the region of the first absorption band also differs from that of the perchlorate in an aqueous solution, as shown in Table 2. The structures of *cis*-$\Delta(lel_2)$- and $\Lambda(ob_2)$-$[Co(NH_3)_2(RR\text{-ptn})_2]^{3+}$ may be compared to those of $\Delta(lel_3)$- and $\Lambda(ob_3)$-$[Co(RR\text{-ptn})_3]^{3+}$, respectively, and the *RR*-ptn chelate rings in the *cis*-$\Delta(lel_2)$ isomer are expected to be more conformationally flexible than those in the more crowded *cis*-$\Lambda(ob_2)$ isomer. Thus, on the addition of sulfate ion the $\Delta(lel_2)$ isomer is stabilized by forming an ion-pair in a mechanism similar to that described for $\Delta(lel_3)$-$[Co(RR\text{-ptn})_3]^{3+}$. A set of three N–H bonds suitable for hydrogen bonding may be provided by two *RR*-ptn and one ammonia ligands in the complex. The $\Lambda(ob_2)$ isomer which is insensitive to the ion-pair effect seems to have a rigid structure similar to that of $\Lambda(ob_3)$-$[Co(RR\text{-ptn})_3]^{3+}$, although the crowded structure of $\Lambda(ob_2)$ isomer might be reduced to some extent by coordinating two ammonia molecules in place of a bulky bidentate *RR*-ptn.

The CD spectra of *trans*-$[Co(NH_3)_2(RR\text{-ptn})_2]^{3+}$ in water, 0.2 M Na_2SO_4, and DMSO solutions show small variations in the region of the first absorption band, giving rise to an increase and a decrease in the magnitudes of the positive and the negative CD bands, respectively in the latter two solutions (Fig. 13). The $[Co(NH_3)_4(RR\text{-ptn})]^{3+}$ ion exhibits similar small variations, as shown in Fig. 14. Thus, the observed CD variations are rather small, although the tendency to increase the magnitude of the positive CD band in 0.2 M Na_2SO_4 and DMSO solutions is consistent with that observed for Δ-$[Co(RR\text{-ptn})_3]^{3+}$ and *cis*-Δ-$[Co(NH_3)_2(RR\text{-ptn})_2]^{3+}$. The *RR*-ptn chelate rings in *trans*-$[Co(NH_3)_2(RR\text{-ptn})_2]^{3+}$ and $[Co(NH_3)_4(RR\text{-ptn})]^{3+}$ seem to be more flexible than those in the more crowded *tris*- and *cis*-bis(*RR*-ptn) complexes. Furthermore, the ability to form ion-pairs between the present series of complexes, $[Co(NH_3)_{2n}(RR\text{-ptn})_{3-n}]^{3+}$ and sulfate ions will not differ greatly from one another.[15] However, molecular models seem to indicate that *trans*-$[Co(NH_3)_2(RR\text{-ptn})_2]^{3+}$ can not provide a set of three N–H bonds to form effective hydrogen bonds with a sulfate ion without distorting the *λ-skew* conformation of the *RR*-ptn chelate ring. On the other hand, $[Co(NH_3)_4(RR\text{-ptn})]^{3+}$ can have such a set of N–H bonds provided by two ammonia molecules and one *RR*-ptn chelate in the *λ-skew* conformation, but similar two sets of three N–H bonds can also be formed by the three ammonia ligands in the facial positions without the participation of the *RR*-ptn. An ion-pair may also be formed by hydrogen

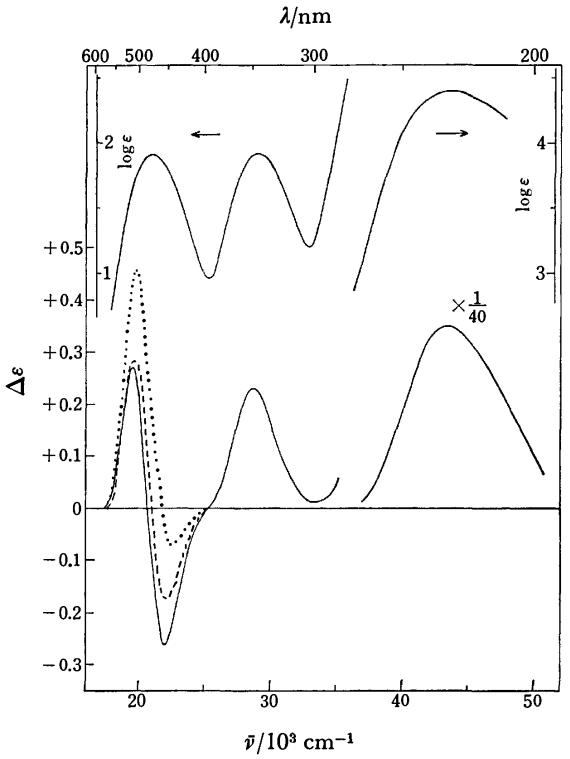

Fig. 13. Absorption and CD spectra of *trans*-$[Co(NH_3)_2(RR\text{-ptn})_2](ClO_4)_3 \cdot H_2O$; 3.12×10^{-3}M in visible region and 1.25×10^{-4} M in UV region in water (——), 3.12×10^{-3} M in 0.2 M Na_2SO_4(----), and 2.59×10^{-3} M in DMSO(·····).

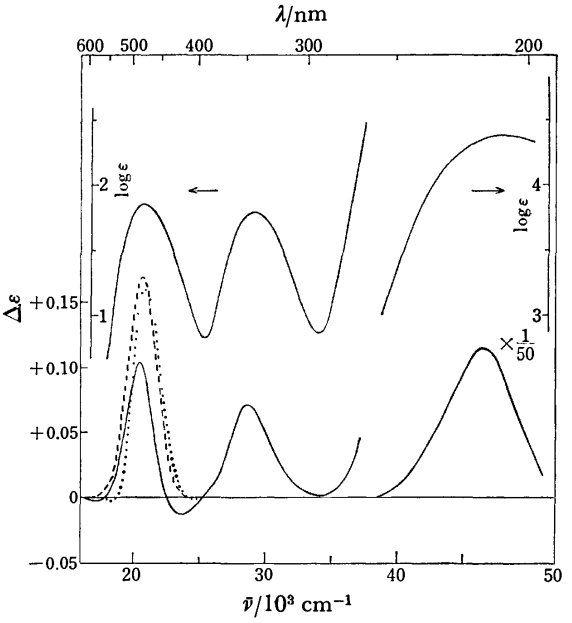

Fig. 14. Absorption and CD spectra of $[Co(NH_3)_4(RR\text{-ptn})](ClO_4)_3 \cdot H_2O$; 7.77×10^{-3} M in 0.1 M in visible region and 7.06×10^{-4} M in UV region in water(——), 7.77×10^{-3} M in 0.1 M Na_2SO_4(----), and 4.59×10^{-3} M in DMSO(·····).

bonding between such N–H bonds provided by three ammonia ligands and a sulfate ion. In this case, the *λ-skew* conformation of the *RR*-ptn chelate ring will not be stabilized by the ion-pair formation.

Other proposals[24,25] have been put forth in an attempt to rationalize the effect of electrolyte on the CD spectra in the region of the first absorption band of tris(diamine)-cobalt(III) complexes. However, so far as complexes containing puckerd six-membered chelate rings are concerned, a conformational change of the chelate ring seems to play the most important role in determining a pattern of CD bands in the region of the first absorption band. Such a conformational change may also account for the lack of the additivity of the vicinal (conformational) and the configurational contributions to the CD of these six-membered chelate complexes.[7,9]

The authors wish to thank Dr. Yuzo Yoshikawa of Nagoya University for measuring ^{13}C-NMR spectra.

References

1) R. Kuroda, J. Fujita, and Y. Saito, *Chem. Lett.*, **1975**, 225.
2) A. Kobayashi, F. Marumo, and Y. Saito, *Acta Crystallogr., Sect. B*, **29**, 2443 (1973).
3) A. Kobayashi, F. Marumo, and Y. Saito, *Acta Crystallogr., Sect. B*, **28**, 3591 (1972).
4) T. G. Appleton and J. R. Hall, *Inorg. Chem.*, **9**, 1807 (1970).
5) T. G. Appleton and J. R. Hall, *Inorg. Chem.*, **10**, 1717 (1971).
6) J. E. Sarneski and C. N. Reilley, *Inorg. Chem.*, **13**, 977 (1974).
7) H. Boucher and B. Bosnich, *Inorg. Chem.*, **15**, 1471 (1976).
8) B. Bosnich and J. MacB. Harrowfield, *J. Am. Chem. Soc.*, **94**, 3426 (1972).
9) F. Mizukami, H. Ito, J. Fujita, and K. Saito, *Bull. Chem. Soc. Jpn.*, **45**, 2129 (1972).
10) J. C. Bailar, Jr. and J. Works, *J. Am. Chem. Soc.*, **68**, 234 (1946).
11) M. Fujita, Y. Yoshikawa, and H. Yamatera, *J. Chem. Soc., Chem. Commun.*, **1975**, 941.
12) S. R. Niketic and F. Woldbye, *Acta Chem. Scand.*, **27**, 621 (1973).
13) F. Mizukami, H. Ito, J. Fujita, and K. Saito, *Bull. Chem. Soc. Jpn.*, **46**, 2410 (1973).
14) R. Kuroda and Y. Saito, *Bull. Chem. Soc. Jpn.*, **49**, 433 (1976).
15) N. Tanaka, Y. Kobayashi, and M. Kamada, *Bull. Chem. Soc. Jpn.*, **40**, 2839 (1967).
16) K. Ogino, *Bull. Chem. Soc. Jpn.*, **42**, 447 (1969).
17) P. G. Beddoe and S. F. Mason, *Inorg. Nucl. Chem. Lett.*, **4**, 433 (1968).
18) J. R. Gollogly and C. J. Hawkins, *Chem. Commun.*, **1968**, 689.
19) P. G. Beddoe, M. J. Harding, S. F. Mason, and B. J. Peart, *J. Chem. Soc., Chem. Commun.*, **1971**, 1283.
20) T. Nomura, F. Marumo, and Y. Saito, *Bull. Chem. Soc. Jpn.*, **42**, 1016 (1969).
21) S. F. Mason and B. J. Norman, *Proc. Chem. Soc. London*, **1964**, 339.
22) K. Ogino, K. Murano, and J. Fujita, *Inorg. Nucl. Chem. Lett.*, **4**, 351 (1968).
23) L. J. DeHayes and D. H. Busch, *Inorg. Chem.*, **12**, 1505 (1973).
24) J. E. Sarneski and F. L. Urbach, *J. Am. Chem. Soc.*, **93**, 884 (1971).
25) A. M. Sargeson, *Transition Metal Chem.*, **3**, 303 (1966).

Palladium(II) Complexes of 2,2,6,6-Tetramethylpiperidine *N*-Oxyl Radical

Masaaki OKUNAKA, Gen-etsu MATSUBAYASHI, and Toshio TANAKA

Department of Applied Chemistry, Faculty of Engineering, Osaka University, Yamada-kami, Suita, Osaka 565

(Received November 9, 1976)

2,2,6,6-Tetramethylpiperidine *N*-oxyl radical $(CH_3)_4C_5H_6NO\cdot$ (TMPNO·) reacts with palladium dichloride to give complexes of both anionic and cationic TMPNO; $[PdCl(TMPNO)]_2$ (I) and $[TMPNO^+]_2[Pd_2Cl_6]^{2-}$ (II). I further reacts with dimethylsulfonium phenacylide or triphenylphosphine (L) to afford a mononuclear complex of the PdCl(TMPNO)(L) type. II undergoes a facile reaction with acetone to yield bis(*N*-acetonyl-*N*-hydroxy-2,2,6,6-tetramethylpiperidinium)hexachlorodipalladate, $[(CH_3)_4C_5H_6\overset{+}{N}(OH)CH_2COCH_3]_2[Pd_2Cl_6]^{2-}$. Configurations of these complexes are described.

Di-*t*-butyl nitroxide radical (DTBNO·) reacts with palladium dichloride to give a diamagnetic dipalladium complex, $[PdCl(DTBNO)]_2$, involving the $DTBNO^-$ anion.[1] This is in contrast with other metal complexes of DTBNO·, in which the nitroxide coordinates to the metal as a neutral radical through the oxygen atom.[2-7] 2,2,6,6-Tetramethylpiperidine *N*-oxyl radical (TMPNO·) is also known to coordinate to several metal ions through the oxygen atom.[4-7] In addition, this radical reacts with tin(IV) halides to afford stable hexahalogenostannate(IV) complexes containing the $TMPNO^+$ cation.[8] Marked stabilities of the TMPNO· radical and its cation have been demonstrated by the electrochemical study.[9] Thus, no metal complex containing the $TMPNO^-$ anion has been isolated so far. This paper reports the isolation and configuration of some palladium(II) complexes of the $TMPNO^-$ anion as well as the $TMPNO^+$ cation; $[PdCl(TMPNO)]_2$, PdCl(TMPNO)(L) (L=dimethylsulfonium phenacylide, triphenylphosphine), and $[TMPNO^+]_2[Pd_2Cl_6]^{2-}$. It is also described that the latter compound easily reacts with acetone, giving bis(*N*-acetonyl-*N*-hydroxy-2,2,6,6-tetramethylpiperidinium) hexachlorodipalladate, $[(CH_3)_4C_5H_6\overset{+}{N}(OH)CH_2COCH_3]_2[Pd_2Cl_6]^{2-}$.

Experimental

Materials. The TMPNO·radical,[8] $(CH_3)_4C_5H_6NO\cdot$, and dimethylsulfonium phenacylide,[10] $Me_2\overset{+}{S}\overset{-}{C}HCOPh$, were prepared as described in the literatures.

Isolation of $[PdCl(TMPNO)]_2$ (I), $[TMPNO^+]_2[Pd_2Cl_6]^{2-}\cdot 2CH_3CN$ (II), and $[(CH_3)_4C_5H_6\overset{+}{N}(OH)CH_2COCH_3]_2[Pd_2Cl_6]^{2-}$ (III). A suspension of $PdCl_2$ (1.77 g, 10.0 mmol) in a dichloromethane solution (2 ml) of TMPNO· (2.34 g, 15.0 mmol) was stirred for 72 h at room temperature, followed by evaporation to dryness under reduced pressure. The resulting product was washed with diethyl ether several times to remove the unreacted radical. The solid (3.01 g) thus obtained was dissolved in dichloromethane (100 ml) in order to separate a soluble product from an insoluble one (1.44 g). To the dichloromethane solution was added ethanol (20 ml). The mixture was evaporated to about one-fifth volume under reduced pressure to give reddish brown crystals (0.31 g), mp 160—162 °C, whose elemental analysis agreed well with the composition of PdCl (TMPNO)·0.1$PdCl_2$, although this compound has not been further studied. Further evaporation of the residual solution to about a half volume yielded dark red crystals of I (0.14 g, 0.23 mmol, 9% yield), mp 151—154 °C. Found: C, 36.28; H, 6.25; N, 4.77%; mol wt, 622. Calcd for $C_9H_{18}NOClPd$: C, 36.26; H, 6.09; N, 4.70%; mol wt, 298.

The insoluble product in dichloromethane was recrystallized from a mixture of acetonitrile and diethyl ether to give brown crystals of II (1.12 g, 1.36 mmol, 55% yield), mp 94—96 °C. Found: C, 32.06; H, 5.25; N, 6.71%. Calcd for $C_9H_{18}NOCl_3Pd\cdot CH_3CN$: C, 32.21; H, 5.16; N, 6.83%. II (1.00 g, 1.22 mmol) was dissolved in acetone (20 ml), followed by the addition of diethyl ether (10 ml) to develop dark red crystals of III (0.58 g, 0.68 mmol, 56% yield), mp 164—166 °C. Found: C, 33.56; H, 5.90; N, 3.31%. Calcd for $C_{12}H_{24}NO_2Cl_3Pd$: C, 33.74; H, 5.66; N, 3.28%.

Isolation of PdCl(TMPNO)(L) (L=$Me_2\overset{+}{S}\overset{-}{C}HCOPh$ (IV) and PPh_3 (V)). To a dichloromethane (5 ml) solution of I (0.15 g, 0.5 mmol) was added dimethylsulfonium phenacylide (0.09 g, 0.5 mmol) in dichloromethane (5 ml). The mixture was stirred for 10 min at room temperature, and evaporated to dryness under reduced pressure. The resulting product was recrystallized from benzene–petroleum ether to give orange crystals of IV (0.14 g, 0.29 mmol, 59% yield), mp>145 °C (dec). Found: C, 46.99; H, 6.14; N, 2.60%; mol wt, 466. Calcd for $C_{19}H_{30}NO_2SClPd$: C, 47.70; H, 6.32; N, 2.93%; mol wt, 478. Orange crystals of V were similarly prepared by the reaction of I with triphenylphosphine, and recrystallized from benzene–petroleum ether (65% yield), mp >150 °C (dec). Found: C, 58.18; H, 5.97; N, 2.36%; mol wt, 553. Calcd for $C_{27}H_{33}NOPClPd$: C, 57.87; H, 5.93; N, 2.50%; mol wt, 560.

Physical measurements. Infrared and ^1H NMR spectra were recorded as described previously.[8,11] Molecular weight determinations were carried out in dichlomethane using a vapor pressure osmometer. Electric conductivities were measured at 25 °C as described elsewhere.[12]

Results and Discussion

Molecular weight determinations indicate that both IV and V are essentially monomeric in dichloromethane. The infrared spectrum of I shows the ν(Pd–Cl) band at 270 cm^{-1}, which is close to the ν(Pd–Cl) frequency of the corresponding DTBNO complex (303 cm^{-1}),[11] while this band of IV is obscured by ylide vibrations. The ^1H NMR spectrum of IV shows only one methine signal (Table). In addition, no exchange is observed between the coordinating ylide and free ylide added into the solution of the complex. These results suggest the presence of only one species of IV in solution. In the infrared spectrum, the ν(C=O) band of the ylide shifts to high frequency upon complexation (complexed ylide: 1605 cm^{-1}, free ylide: 1508 cm^{-1}), indicating, as

Table. Chemical shifts of the TMPNO complexes in chloroform-d_1 at 24 °C[a)]

Complex	CH_3	$-CH_2-$	Other protons
$[PdCl(TMPNO)]_2$	1.45(s), 2.33(s)	1.60(m)	—
$PdCl(TMPNO)(PPh_3)$	1.38(s), 1.97(s)	1.62(m), 1.77(m)	7.41(m), 7.57(m)(PPh_3)
$PdCl(TMPNO)(Me_2\overset{+}{S}\overset{-}{C}HCOPh)$	1.12(s), 1.25(s) 1.54(s), 1.93(s)	1.61(m)	2.87(s), 3.15(s)(SMe); 2.54(s) (CH); 7.42(m), 8.21(m) (Ph)

a) s: singlet, m: multiplet.

discussed previously,[13)] the coordination through the ylide-carbon atom. Thus, the coordinating ylide-carbon is an asymmetric center. This is also supported from the occurrence of two *S*-methyl proton signals with an identical intensity (Table), while free ylide exhibits only one *S*-methyl signal.

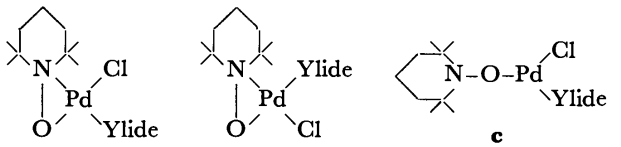

a **b** **c**

There are three possible configurations for IV, **a**—**c**, of which **a** and **b** are geometrical isomers. In spite of the presence of the chiral ylide-carbon, four methyl groups of TMPNO in the configuration **c** may be magnetically equivalent, because the inversion at the nitrogen atom would be very fast.[14)] On the other hand, both **a** and **b** involve a quadrivalent nitrogen atom, which predicts no inversion at the nitrogen. In fact, this kind of inversion is restricted in the *N*-hydroxyl-2,2,6,6-tetramethylpiperidinium cation (**d**), as confirmed by the ^1H NMR spectrum in dichloromethane at room temperature, which shows two separated methyl signals at δ 1.39 and 1.65 ppm.[15)] Thus, both configurations

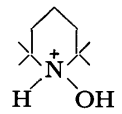

d

a and **b** predict the occurrence of the axial and equatorial methyl proton signals with an equal intensity. Furthermore, each signal should be split into two owing to the presence of the chiral ylide-carbon. This is compatible with the occurrence of two doublet signals due to the methyl protons (Table). Stereochemical considerations support the preference of **a** to **b**, since in **b** the piperidine ring is placed near to the bulky ylide.

The complex V involving no chiral atom exhibits two methyl proton signals with an equal intensity. This does not contradict with the assumption that the complex exists as only one species in solution and the inversion at the nitrogen atom of TMPNO is restricted. The bulkiness of triphenylphosphine suggests the configuration similar to **a**.

The conductivity measurement and molecular weight determination indicate that I is a non-electrolyte (0.02 $ohm^{-1}\,cm^2\,mol^{-1}$ at 1.51×10^{-3} M) and dimeric in dichloromethane. By analogy with $[PdCl(DTBNO)]_2$,[1)] I is considered to adopt chloride-bridged configurations (**e**) and/or (**f**). This is compatible with the occurrence

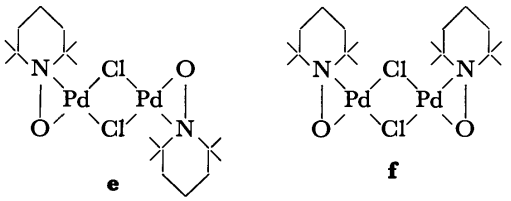

e **f**

of the ν(Pd-Cl) band at 270 cm^{-1}. The ^1H NMR spectrum shows two methyl signals with an identical intensity, suggesting the presence of either **e** or **f** with the restriction of inversion at the nitrogen atom.

Ionic structures of II and III are confirmed by conductivity measurements; Λ_M=256 and 121 $ohm^{-1}\,cm^2\,mol^{-1}$ (1.35×10^{-3} M in acetonitrile), respectively. Infrared spectra of both compounds show the ν(Pd-Cl) bands at 343 (very strong) and 303 (medium) cm^{-1}, which are characteristic of the hexachlorodipalladate anion.[16)] In addition, II exhibits a strong band at 1605 cm^{-1}, which is assigned to $\nu(\overset{+}{N}=O)$.[8)] The ^1H NMR spectrum of II in liquid sulfur dioxide shows somewhat broad methyl and methylene signals at δ 1.88 and 2.72 ppm, respectively; there is no separation of the methyl signal. These observations are consistent with the ionic formulation having the piperidineoxoammonium cation (**g**). On the other hand, III exhibits the ν(C=O) band at 1730 cm^{-1}, but no $\nu(\overset{+}{N}=O)$. The ^1H NMR spectrum shows again two methyl signals with an equal intensity, suggesting the presence of a quadrivalent nitrogen atom. These results and the following proton signals observed can well explain the formulation of **h**; δ 1.60 [singlet, 6 (relative intensity)] and 1.78 [s, 6] for the ring methyl; 1.96 [multiplet, 6] for the ring methylene; 2.36 [s, 3] for CH_3-C(O)-; 5.37 [s, 2] for $-CH_2$-C(O); 9.03 [broad, 1] for OH.

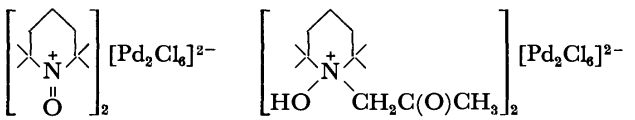

g **h**

References

1) W. Beck and K. Schmidtner, *Chem. Ber.*, **100**, 3363 (1967).
2) W. Beck, K. Schmidtner, and H. J. Keller, *Chem. Ber.*, **100**, 503 (1967).
3) R. A. Zelonka and M. C. Baird, *J. Am. Chem. Soc.*, **93**, 6066 (1971).
4) T. B. Eames and B. M. Hoffman, *J. Am. Chem. Soc.*, **93**, 3141 (1971).
5) Y. Y. Lim and R. S. Drago, *Inorg. Chem.*, **11**, 1334 (1972).
6) N. M. Karayannis, C. M. Paleos, C. M. Kikulski, L. L.

Pytlewski, H. Blum, and M. M. Labes, *Inorg. Chim. Acta*, **7**, 74 (1973).
7) A. H. Cohen and B. M. Hoffman, *Inorg. Chem.*, **13**, 1484 (1974).
8) Y. Takaya, G. Matsubayashi, and T. Tanaka, *Inorg. Chim. Acta*, **6**, 339 (1972).
9) M. Tsunaga, C. Iwakura, and H. Tamura, *Electrochim. Acta*, **18**, 241 (1973).
10) K. W. Ratts and A. N. Yao, *J. Org. Chem.*, **31**, 1185 (1966).
11) M. Okunaka, G. Matsubayashi, and T. Tanaka, *Bull. Chem. Soc. Jpn.*, **48**, 1826 (1975).
12) G. Matsubayashi, K. Wakatsuki, and T. Tanaka, *Org. Magn. Reson.*, **3**, 703 (1971).
13) H. Koezuka, G. Matsubayashi, and T. Tanaka, *Inorg. Chem.*, **15**, 417 (1976).
14) D. L. Griffith, B. L. Olson, and J. D. Roberts, *J. Am. Chem. Soc.*, **93**, 1648 (1971).
15) M. Okunaka, G. Matsubayashi, and T. Tanaka, unpublished.
16) D. M. Adams, P. J. Chandler, and R. G. Churchill, *J. Chem. Soc., A*, **1967**, 1272.

The Reaction of Aromatic Nitrile *N*-Oxides with Tetrahalo-*p*-benzoquinones

Shinsaku SHIRAISHI, Satoru IKEUCHI, Manabu SENŌ, and Teruzo ASAHARA
Institute of Industrial Science, University of Tokyo, Roppongi, Minato-ku, Tokyo 104
(Received May 21, 1976)

Cycloaddition reaction of aromatic nitrile *N*-oxides, such as benzonitrile *N*-oxide, 2,4,6-trimethylbenzonitrile *N*-oxide, and 2,3,5,6-tetramethylbenzonitrile *N*-oxide, with tetrahalo-*p*-benzoquinones was studied. The reaction gave 1: 1- and/or 2: 1-adducts of a nitrile *N*-oxide and a tetrahalobenzoquinone according to the conditions, especially the mole ratios of each reactant. The 2: 1-adducts are formed *via* 1: 1-adducts, each having two stereoisomers. The structures of these adducts were determined to be dioxazole derivatives formed by the addition of nitrile *N*-oxides to the carbonyl bonds of the tetrahalobenzoquinones.

Nitrile *N*-oxide is known to be a typical 1,3-dipole and to react with many unsaturated bonds to form heterocycles.[1] In general, nitrile *N*-oxides, like other 1,3-dipoles, react with C=C double bond much faster than with C=O bond. Benzonitrile *N*-oxide reacts with styrene by 180 times faster than with its isoelectronic compound, benzaldehyde.[2] *p*-Benzoquinone and alkenyl ketones each have two different dipolarophilic functions, C=C and C=O bonds in the molecules. They give C=C addition products in the reactions with various nitrile oxides.[3] In very rare cases, however, preference for C=O addition has been reported. Some *o*-quinones gave C=O addition products. As an example, benzonitrile *N*-oxide reacts with *o*-naphthoquinone to give two isomeric 1: 1-C=O adducts, followed by the addition of nitrile *N*-oxide to the C=C and/or C=O bonds according to the first addition site.[4] Cyclobutene diones have been found to react with mesitonitrile *N*-oxide at the C=O bonds.[5] α-Azidovinyl ketones react with nitrile *N*-oxides at both C=C and C=O bonds.[6]

We have studied the reaction of aromatic nitrile *N*-oxides with tetrahalo-*p*-benzoquinones (*p*-haloanils) and found that the reaction gives dioxazole derivatives unlike the reaction with unsubstituted *p*-benzoquinone, which gives isoxazoline derivatives.[3]

Results and Discussion

Aromatic nitrile *N*-oxides, such as benzonitrile N-oxide (BNO), 2,4,6-trimethylbenzonitrile *N*-oxide (MNO), and 2,3,5,6-tetramethylbenzonitrile *N*-oxide (DNO), were allowed to react with tetrahalo-*p*-benzoquinones, such as fluoranil (FA), chloranil (CA), bromanil (BA), and iodanil (IA), in chloroform at room temperature or at elevated temperatures. Completion of the reaction was confirmed by complete comsumption of the nitrile *N*-oxide in the reaction mixture by thin layer chromatography (TLC). An equimolar reaction of MNO with CA gave a 1: 1-adduct in 93% yield and a small amount of a 2: 1-adduct in 7% yield based on MNO, the reaction in 2: 1 mole ratio giving a 2: 1-adduct. When the reaction was interrupted at an earlier stage, the 1: 1-adduct was obtained as the sole isolable product with unreacted reactants. Irrespective of solvent and temperature, 1: 1- and/or 2: 1-adducts were obtained according to the mole ratio of the reactants in more than 90% yield on the completion of the reaction. The dependence of the product composition on the reaction conditions is shown in Table 1 for the reaction of MNO with CA. When haloanil was added very slowly to a refluxing solution of a nitrile *N*-oxide, the corresponding 2: 1-adduct was obtained quantitatively without contamination of 1: 1-adduct. The condition was fulfilled by using a Soxhlet extraction apparatus. The solubility of haloanils in chloroform is sufficiently small for this procedure. The result shows that the addition reaction proceeds stepwise and irreversibly, the second addition step being much slower than the first.

The 2: 1-adduct from MNO and CA has two isomers, which differ in solubility and thermal behavior. Their elementary analyses gave the same results, the IR spectra differing slightly in finger print region. One isomer (**6a**) is almost insoluble in hexane and the other (**6b**) fairly soluble. The product mixture could be separated into **6a** and **6b** by the difference in solubility. Their ratio was always 50: 50 as shown in Table 1. This indicates that the orientation of the second addition reaction is not influenced by the mode of the first, the addition reaction occurring such a mode that only two isomers are possible for the 2: 1-adduct.

TABLE 1. DEPENDENCE OF THE PRODUCTS COMPOSITION ON THE REACTION CONDITIONS FOR THE REACTION OF MNO WITH CA

Reactants (mole ratio)	Solvent	Temp °C	Time h	Products (yield, %)	2:1-Adduct isomer ratio **6b**:**6a**
MNO/CA (1/1)	$CHCl_3$	r.t.	15	1:1-adduct(93)[a] 2:1-adduct(7)[a]	
(1.5/1)	$CHCl_3$	r.t.	18	1:1-adduct(49) 2:1-adduct(46)	
(2/1)	$CHCl_3$	r.t.	18	2:1-adduct(98)	46:54
	$CHCl_3$	reflux	11	2:1-adduct(94)	53:47
	C_6H_6	r.t.	30	2:1-adduct(93)	52:48
(2.5/1)	$CHCl_3$	r.t.	18	2:1-adduct(96)	
MNO/1:1-adduct(1/1)	$CHCl_3$	r.t.	18	2:1-adduct(86)	54:46

a) The values are calculated based on the nitrile *N*-oxide.

The IR spectra of **6a** and **6b** have very strong absorption bands in the ν_{C-O-C} region 1100—1300 cm^{-1}, but no absorption in the $\nu_{C=O}$ region 1650—1750 cm^{-1}. The mass spectra of the 1: 1-adduct (**5**) and the 2: 1-adducts (**6a** and **6b**) have molecular ion peak (M^+)

Table 2. The reaction products from nitrile *N*-oxides and haloanils

Products[a]	Compd No.	Reactants mole ratio	React. time, h	Yield, %	Mp, °C	Found (Calcd) C	H	N	IR, $\nu_{C=O}$ cm^{-1}	MS, *m/e*
FA·MNO	**1**	1/1	9	94	102—104	56.53 (56.31	3.49 3.25	4.34 4.10)	1700	341(M^+),180, 161
FA·MNO_2	**2**	1/2	10	95	186—190	62.39 (62.15	4.48 4.41	5.41 5.58)	—	
CA·BNO	**3**	See exp. section			162—164	42.89 (42.78	1.59 1.38	3.97 3.84)	1690	
CA·BNO_2	**4**	do.			218—221	49.43 (49.62	2.27 2.08	5.92 5.79)	—	486, 484, 482(M^+), 363, 244, 119
CA·MNO	**5**	See Table 1.			128.5—129.5	47.30 (47.21	2.65 2.72	3.43 3.44)	1715	409, 407, 405(M^+), 244, 161
CA·MNO_2	**6a**[b]				190—194(d)	55.18	3.78	4.83	—	570, 568, 566(M^+), 405, 244, 161
	6b	do.			[e]	54.72 (54.95	3.86 3.90	4.93 4.93)	—	
CA·DNO	**7**	1/1		93	181—183	48.27 (48.40	3.10 3.11	3.36 3.33)	1705	423, 421, 419(M^+), 244, 175
CA·DNO_2	**8**	1/2		96	168—171	56.10 (56.40	4.29 4.39	4.72 4.70)	—	
BA·MNO	**9**	1/1	15	87	140(d)	32.65 (32.86	1.70 1.90	2.12 2.39)	1695	
BA·MNO_2	**10**	1/2	19	93	140(d)	41.55 (41.86	3.28 2.97	3.95 3.75)	—	750, 748, 746, 744, 742(M^+), 581, 420
BA·DNO	**11**	1/1	15	90	140(d)	33.95 (34.09	1.96 2.19	2.13 2.34)	1695	
BA·DNO_2	**12**	1/2	19	92	140(d)	43.27 (43.44	3.38 3.39	3.74 3.62)	—	
JA·MNO[c]	**13**	1/1	39	48[d]	102—104	24.63 (24.86	1.79 1.43	2.00 1.81)	1670	
JA·MNO_2[c]	**14**	1/2	40	71	186—190	33.59 (33.43	2.36 2.37	3.20 3.00)	—	

a) All the compounds were recrystallized from hexane unless otherwise stated. b) Recrystallized from chloroform. c) Recrystallized from a mixture of hexane and chloroform. d) Compound **14** was also obtained in 32% yield based on MNO. e) No apparent change was observed except for very gradual discoloration at above 160 °C, but a small endotherm was observed at 154 °C in its differential thermogram as shown in Fig. 1-(c).

at the *m/e* corresponding to their molecular weights with the peaks at $M^+ + 2$ and $M^+ + 4$ with the intensities characteristic to tetra-chlorinated compounds. They are also the composite of the fragmentation patterns of mesityl isocyanate and chloranil, except for their molecular ion peaks and the fragment ion peaks corresponding to the 1: 1-adduct for the spectra of **6a** and **6b**, which gave the same fragmentation patterns. All the other addition products obtained from the reactions of the nitrile *N*-oxides and haloanils show similar spectroscopic results. Characterization data of these reaction products are summarized in Table 2. Separation of the isomers of the 2: 1-adducts other than those from MNO and CA was not successful. The melting points might be those of isomer mixtures, showing fluctuation.

The results indicate that the structure of the addition products is not isoxazoline but dioxazole formed by the addition of nitrile *N*-oxides to the carbonyl bonds of haloanils as shown in the scheme.

The addition products, **5**, **6a**, and **6b**, decomposed into mesityl isocyanate and CA on heating. The isocyanate might be derived by the thermal rearrangement of MNO generated by thermal retro-addition reaction or by pyrolytic rearrangement of the dioxazoles. The precise mechanism of the decomposition should be

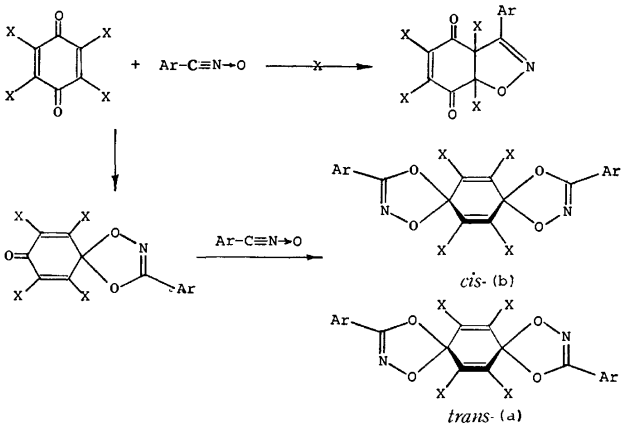

1:1-Adducts
X=F, Ar=Ms, **1**.
X=Cl, Ar=Ph, **3**; Ms, **5**; Du, **7**.
X=Br, Ar=Ms, **9**; Du, **11**.
X=I, Ar=Ms, **13**.

2:1-Adducts
X=F, Ar=Ms, **2**.
X=Cl, Ar=Ph, **4**; Ms, **6a** and **b**; Du, **8**.
X=Br, Ar=Ms, **10**; Du, **12**.
X=I, Ar=Ms, **14**.

where, Ph=C_6H_5, Ms=2,4,6-$(CH_3)_3C_6H_2$, and Du=2,3,5,6-$(CH_3)_4C_6H$.

Scheme.

determined by isotope labeling experiment. The

decomposition temperature differed among the products (Fig. 1). The differential thermal analysis (DTA) of **6b** gives a complicated thermogram with a small endothermic peak at 154 °C and exothermic ones at 163 and 173 °C, while **6a** shows no endotherm but only an exotherm at 192 °C. Thermogravimetric analysis (TGA) of the compounds shows rapid weight decrease at the temperature at which an exotherm was observed in DTA, followed by subsequent slow decrease. The first weight loss corresponds to the weight of nitrile oxide moiety, which volatiled as isocyanate rapidly with nitrogen stream. The second slow decrease might be due to the sublimation of chloranil.

The reaction of a nitrile *N*-oxide with a C=C double bond of a haloanil would give 2-isoxazoline derivative, pyrolysis of which might result in aromatization to afford isoxazole derivative rather than degradation to a quinone and an isocyanate. The angular C–Cl bond is thought to be cleaved more easily. Thus, the result of the pyrolysis of **5** also supports the dioxazole structure of the adducts.

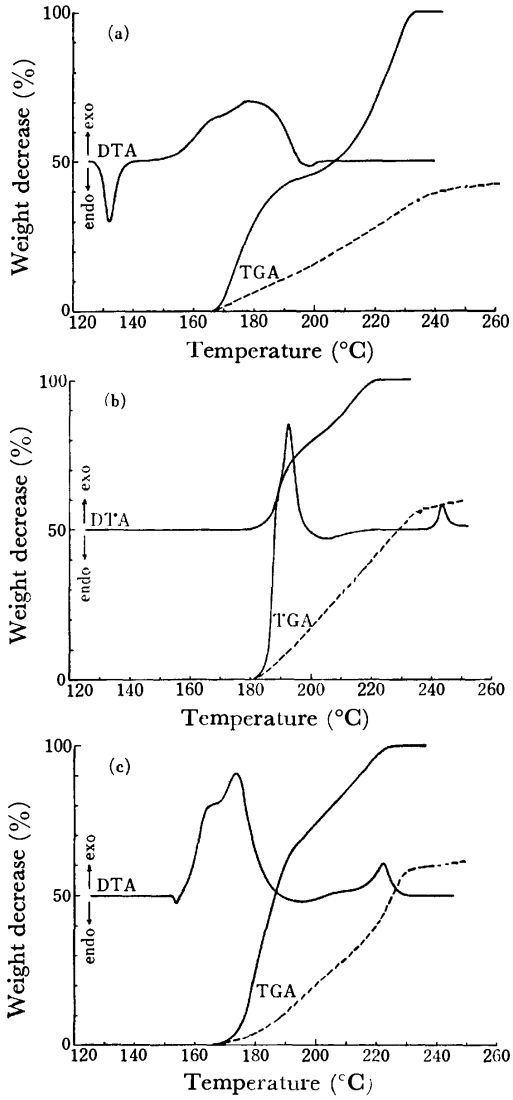

Fig. 1. Thermal analyses of the addition products of MNO with CA, (a): **5**, (b): **6a**, and (c): **6b**, under nitrogen stream (——) and under air (– – –). Heating rate: 5°C/min.

The fact that **6a** has higher melting point and is more thermally stable and less soluble in solvents than **6b** indicates that **6a** has a more symmetrical *trans* structure of the two stereoisomers.

FA, BA, and JA also reacted with MNO to give similar results, but the rate difference between the first addition and the second one differs among them. The rate difference for the reaction of MNO with IA was rather small, and thus the equimolar reaction of them gave 1: 1-(**13**) and 2: 1-adducts (**14**) in 48 and 32% yields based on MNO, respectively.

BNO and DNO also underwent similar cycloaddition with haloanils at the carbonyl sites (Table 2). In the reaction of BNO with haloanils, however, the usual *in situ* reaction process using triethylamine as an acid acceptor was not applicable because of faster reaction of the amine with haloanils. The cycloaddition was performed effectively with a solution of free BNO prepared prior to the reaction, or by heating a solution of benzhydroxamoyl chloride and a haloanil in toluene to reflux.

The PMR spectral data for the 1: 1-adducts from MNO are summarized in Table 3. The signals due to 2- and 6-methyl substituents on the mesityl radical move to down field with the change of the quinone substituents in the order of the atomic radii of halogen atoms, FA<CA<BA<JA, while the other signals due to 4-methyl and 3- and 5-hydrogens have almost the same chemical shifts. Considering the thru-space interaction of 2- and 6-methyl groups with halogens, this may also support the spiro-dioxazole structure of the adducts.

TABLE 3. PMR SPECTRAL DATA of 1:1-ADDUCTS OF MNO AND HALOANILS, 6,7,9,10-TETRAHALO-3-MESITYL-2-AZA-1,4-DIOXASPIRO[4,5]DECA-2,6,9-TRIEN-8-ONES, δ (ppm) IN $CDCl_3$

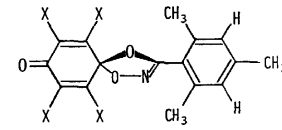

	MNO	X= F (**1**)	Cl (**5**)	Br (**9**)	I (**13**)
2- and 6-CH_3	2.40	2.36	2.47	2.53	2.60
4-CH_3	2.28	2.31	2.30	2.31	2.29
3- and 5-H	6.87	6.96	6.92	6.94	6.93

Addition of nitrile *N*-oxides to the carbonyl of the compounds having two potential dipolarophilic functions, C=C and C=O in the molecules is very rare. Preferential carbonyl addition in the reaction of nitrile *N*-oxides with haloanils is considered to be due to the halogen substituents on the quinones, which deactivate the reactivity of the C=C by steric hindrance and activate that of the C=O by inductive effect. This type of C=O addition is known in the reaction of diazomethane which also has a 1,3-dipole.[7] Diazomethane adds to a carbonyl group in quinones with all of the hydrogens replaced by electronegative groups. Many similarities in the modes of reaction feature were observed in 1,3-dipolar cycloaddition and Diels-Alder reactions. How-

ever, we see a distinct difference in the reactions with substituted quinones, where Diels-Alder reaction gave C=C addition products even with chloranil.[8] The reaction of diazomethane with tetramethyl-*p*-benzoquinone, however, occurs at the C=C bonds,[9] and 1,4-diphenyl-2,6-piperazinedione adds also to the C=C bond of chloranil *via* an azomethine ylide intermediacy.[10] The reactions with quinones might give clues for the elucidation of reaction mechanisms.

Experimental

All the melting points cited are uncorrected. Characterization data for the addition products from nitrile *N*-oxides and haloanils are given in Table 2.

Materials. 2,4,6-Trimethylbenzonitrile *N*-oxide and 2,3,5,6-tetramethylbenzonitrile *N*-oxide were prepared by Grundmann's procedure.[11] Commercial chloranil was purified by recrystallization from gracial acetic acid. Bromanil was prepared by the method of Jackson and Bolton[12] and recrystallized from gracial acetic acid. Iodanil was prepared from bromanil according to the procedure of Torrey and Hunder.[13]

Reaction of MNO with CA. 6,7,9,10-Tetrachloro-3-mesityl-2-aza-1,4-dioxaspiro[4, 5]deca-2,6,9-trien-8-one (5): A solution of 1.23 g (5.0 mmol) of CA and 0.18 g (5.0 mmol) of MNO in 300 ml of chloroform was stirred for 15 h at room temperature. After confirming the completion of the reaction by TLC on silica gel plate with benzene, the solvent was evaporated under vacuum. The residual solid was extracted with hot hexane to give 1.90 g (93%) of the title product as the extract, which was recrystallized from hexane.

*6, 7, 13, 14-Tetrachloro-3, 11-dimesityl-2, 10-diaza-1, 4, 9, 12-tetraoxadispiro[4,2,4,2]tetradeca-2,6,10,13-tetraene (**6a** and **6b**)*: A solution of 0.61 g (2.5 mmol) of CA and 0.81 g (5.0 mmol) of MNO in 200 ml of chloroform was heated to reflux for 11 h. The solvent was removed by evaporation under vacuum and the residue was extracted with hexane for 4 h using a Soxhlet extractor and then with chloroform for 6 h. The hexane extract (**6b**, 0.70 g, 50%) was recrystallized from hexane and 0.62 g (44%) of the chloroform extract (**6a**) from chloroform.

The same compounds were obtained by the reaction of **5** with MNO. A solution of 1.0 g (2.5 mmol) of **5** and 0.40 g (2.5 mmol) of MNO in 200 ml of chloroform was stirred for 18 h at room temperature. The reaction mixture was treated in the same manner as mentioned above to give 0.65 g (46%) of **6b** and 0.55 g (40%) of **6a**.

Reaction of BNO with CA. 6,7,9,10-Tetrachloro-3-phenyl-2-aza-1,4-dioxaspiro[4, 5]deca-2,6,9-trien-8-one (3): A solution of 0.55 g (5.0 mmol) of triethylamine in 100 ml of tetrahydrofuran (THF) was added dropwise into a solution of 0.85 g (5.0 mmol) of benzhydroxamoyl chloride in 300 ml of THF with vigorous stirring at room temperature. The mixture was stirred for 5 min, and then filtered into a solution of 1.23 g (5.0 mmol) of CA in 200 ml of THF. The solution was stirred for 10 h at room temperature. The solvent was evaporated to give tan yellow residue, which was worked up with column chromatography on silica gel (Wakogel C-100) with benzene as an eluent. The mixture was eluted in the order of diphenylfuroxan, the title compound, and chloranil. The title compound (0.88 g, 48%) was recrystallized from hexane.

The compound was also prepared by the following procedure. A solution of 1.23 g (5.0 mmol) of CA and 0.86 g (5.5 mmol) of benzhydroxamoyl chloride in 300 ml of toluene was heated to reflux for 12 h. Evolution of hydrogen chloride was observed during the course of reaction. The solvent was removed by evaporation under vacuum to give viscous tan yellow oil, which was treated in the same manner as described above to give 0.85 g (47%) of **3**.

6, 7, 13, 14-Tetrachloro-3, 11-diphenyl-2, 10-diaza-1,4,9, 12-tetraoxadispiro[4,2,4,2]tetradeca-2,6,10,13-tetraene (4): A solution of BNO prepared from 1.14 g (7.3 mmol) of benzhydroxamoyl chloride by treating with triethylamine was added into a solution of 0.82 g (3.3 mmol) of CA in THF and the mixture was stirred for 10 h. The mixture was treated in the same manner as mentioned above. Diphenylfuroxan, **3**, **4**, and CA were eluted in this order. The reaction gave 0.40 g (33%) of **3** and 0.22 g (14%) of the title compound **4**, which was recrystallized from hexane.

The compound was also prepared by the reaction of 0.82 g (3.3 mmol) of CA with 1.14 g (7.3 mmol) of benzhydroxamoyl chloride in 300 ml of toluene at refluxing temperature. The work-up of the product with column chromatography on silica gel with benzene gave 0.42 g (34%) of **3** and 0.30 g (19%) of **4**.

The Reaction of Other Haloanils with Nitrile N-*Oxides.* The reaction of other haloanils with MNO or DNO were ciarred out almost in the same manner as described in the preceding section. The results are given in Table 2.

Thermolysis of 5. Compound **5**, 2.0 g (4.9 mmol), was placed in a sublimer and heated up to 190 °C under reduced pressure (*ca.* 1 Torr). Colorless crystals and yellow ones deposited on the condenser. The colorless part weighed 0.38 g (38%) and melted at 44—46 °C. It was shown to be mesityl isocyanate from its IR spectrum and elementary analysis (Found: C, 74.27; H, 6.77; N, 8.43%. Calcd for $C_{10}H_{11}NO$: C, 74.51; H, 6.88; N, 8.69%). The yellow one weighed 0.56 g (46%) and was shown to be chloranil from its melting point and IR spectrum.

References

1) a) R. Huisgen, *Angew. Chem.*, **75**, 604 (1963); b) Ch. Grundmann, Nitrile Oxides, in "The Chemistry of the Cyano Group," ed by Z. Rappoport, Interscience Publishers, London (1970); c) Ch. Grundmann and P. Gruenanger, *The Nitrile Oxides*, Springer-Verlag, Berlin (1971); d) S. Shiraishi, *Yuki Gosei Kagaku Kyokai Shi*, **32**, 362 (1974).

2) Calculated from the data in the reference 1c, p. 93.

3) A. Quilico, C. Stagno, and D'Alcontres, *Gazz. Chim. Ital.*, **80**, 140 (1950); T. Sasaki and T. Yoshida, *Bull. Chem. Soc. Jpn.*, **41**, 2206 (1968).

4) S. Morrocchi, A. Ricca, A. Selva, and A. Zanarotti, *Gazz. Chim. Ital.*, **99**, 565 (1969).

5) N. G. Argyropoulos, N. E. Alexandron, and D. N. Nicolaides, *Tetrahedron Lett.*, **1976**, 83.

6) G. L'abbé and G. Mathys, *J. Org. Chem.*, **39**, 1221 (1974).

7) B. Eistert, H. Fink, K. Pfleger, and G. Kaeffner, *Justus Liebigs Ann. Chem.*, **735**, 145 (1970); B. Eistert, H. Fink, and A. Mueller, *Chem. Ber.*, **95**, 2403 (1962).

8) W. Rubin and A. Wassermann, *J. Chem. Soc.*, **1950**, 2205.

9) W. C. Howell, M. Ktenas, and J. M. MacDonald, *Tetrahedron Lett.*, **1964**, 1719.

10) T. Tanaka, *Chem. Lett.*, **1976**, 161.

11) Ch. Grundmann and J. M. Dean, *J. Org. Chem.*, **30**, 2809 (1965); *Angew. Chem.*, **76**, 682 (1964).

12) C. L. Jackson and E. K. Bolton, *J. Am. Chem. Soc.*, **67**, 1034 (1945).

13) H. A. Torrey and W. H. Hunter, *J. Am. Chem. Soc.*, **34**. 702 (1912).

Cyanamide Derivatives. Part 106.* The Preparation of ^{15}N-Labeled Cyanoguanidines

Akira OMURA,** Tsutomu NONAKA, Toshio FUCHIGAMI, Eiichi ICHIKAWA, and Keijiro ODO

Department of Electronic Chemistry, The Graduate School, Tokyo Institute of Technology, Ookayama, Meguro-ku, Tokyo 152

(Received July 12, 1976)

Methods for labeling the chemically non-equivalent nitrogen atoms of cyanoguanidine with ^{15}N were established. 1-Cyanoguanidine-1-^{15}N and 1-cyano-^{15}N-guanidine were prepared, and their labeled positions were also confirmed by mass spectroscopic analysis. ^{15}N FT-NMR spectra of cyanoguanidine enriched with ^{15}N were measured.

Cyanoguanidine (**1**), also called dicyandiamide, is one of the useful starting compounds for the synthesis of C–N alternating compounds. However, no reliable mechanisms of many reactions of **1** and its related compounds have been established because of the ambiguity in the correlation between the arrangement of nitrogen atoms in a product molecule and that in a reactant. Such a problem would be solved by using a ^{15}N tracer. The authors had already prepared a labeled **1**, 1-cyanoguanidine-2,3-$^{15}N_2$, and put it to use for clarification of the mechanism of cathodic crossed hydrocoupling of acetone with **1**.[1]

$$\underset{\displaystyle N^{2(a)}H_2}{\overset{\displaystyle H_2N^{3(a)}-C=N^{1(b)}-C\equiv N^{(c)}}{|}}$$

1

In this work, methods for labeling the non-equivalent nitrogen atoms (N^b and N^c) other than N^a and for enriching all nitrogen atoms with ^{15}N were developed. It is required in preparation of a labeled compound that its formation mechanism has been established, at least reliably. And also, the labeled position should be reconfirmed in some way. Such requirements were satisfied in this work.

Results and Discussion

A procedure for labeling the N^b was newly designed because there was no earlier literature which could be used for the preparation of 1-cyanoguanidine-1-^{15}N. At the first stage, 2-imino-1,3-dithiolane-^{15}N (**2**) was synthesized in a 98% yield from 1,2-ethanedithiol and cyanogen bromide-^{15}N.[2] Cyanogen bromide-^{15}N was prepared by the bromination of potassium cyanide-^{15}N (^{15}N abundance, 2.7 atom %).[3]

$$KC\equiv{}^{15}N + Br_2 \longrightarrow Br-C\equiv{}^{15}N + KBr$$

$$\begin{matrix}CH_2-SH\\|\\CH_2-SH\end{matrix} + Br-C\equiv{}^{15}N \longrightarrow \begin{matrix}CH_2-S\\|\quad\quad C={}^{15}NH\\CH_2-S\end{matrix} + HBr$$

2

And then the free base of **2** was also treated with ordinary cyanogen bromide in acetone so as to be converted into 2-[(cyano)imino-^{15}N]-1,3-dithiolane (**3**) in an 80% yield. The compound, **3**, was identified with an independently synthesized authentic sample by an IR spectrum and a mixed melting test.[4] The hydrobromide, which was inevitably produced, of **2** could be repeatedly used.

$$2\,\mathbf{2} + Br-C\equiv N \longrightarrow \begin{matrix}CH_2-S\\|\quad\quad C={}^{15}N-C\equiv N\\CH_2-S\end{matrix} + \mathbf{2}\cdot HBr$$

3

An attempt to obtain directly 1-cyanoguanidine-1-^{15}N by the ammonolysis of **3** was unsuccessful. The ammonolysis in the presence of silver nitrate afforded the ammonium salt of dicyanoamine-^{15}N (**4**) in a 47% yield. The compound, **4**, was converted into the potassium salt[5] and identified with an authentic sample by an IR spectrum. The by-product seemed to be mainly a compound, **5**. But **5** could not be purely isolated from the coprecipitated silver salt of 1,2-ethanedithiol.

$$\mathbf{3} + 4NH_3 + 2AgNO_3 \longrightarrow$$

$$N\equiv C-{}^{15}NH-C\equiv N\cdot NH_3 + \begin{matrix}CH_2-SAg\\|\\CH_2-SAg\end{matrix} + 2NH_4NO_3$$

4

$$AgS-CH_2-CH_2-S-\underset{\displaystyle NH_2}{\overset{\displaystyle C={}^{15}N-C\equiv N}{|}}$$

5

The compound, **4**, was converted into 1-cyanoguanidine-1-^{15}N in a 49% yield by reflux in 1-butanol.[6]

$$\mathbf{4} \longrightarrow H_2N-\underset{\displaystyle NH_2}{\overset{\displaystyle C={}^{15}N-C\equiv N}{|}}$$

1-Cyano-^{15}N-guanidine labeled at the N^c was prepared in an 84% yield from guanidine and cyanogen bromide-^{15}N (^{15}N abundance, 5.0 atom %) in DMF.

$$2H_2N-\underset{\displaystyle NH_2}{\overset{\displaystyle C=NH}{|}} + Br-C\equiv{}^{15}N \longrightarrow$$

$$H_2N-\underset{\displaystyle NH_2}{\overset{\displaystyle C=N-C\equiv{}^{15}N}{|}} + H_2N-\underset{\displaystyle NH_2}{\overset{\displaystyle C=NH\cdot HBr}{|}}$$

Also, **1** enriched at all the nitrogen atoms with ^{15}N was prepared in order to supply a sample to ^{15}N FT-NMR spectroscopy. After cyanamide-^{15}N prepared from cyanogen bromide and ammonia-^{15}N (^{15}N abundance, 10.3 atom %) was dissolved in dilute hydrochloric acid to disperse completely ^{15}N to the two nitrogen atoms by the formation of a carbodiimido form,[7] it was dimerized in an alkaline solution.[8] Yields of cyanamide and cyanoguanidine were 100 and 85%, respectively.

* Part 105: T. Fuchigami and K. Odo, *Bull. Chem. Soc, Jpn.*, **49**, 3607 (1976).

** Present address: Nippon (Japan) Carbide Industries Inc., Uozu, Toyama.

$$Br\text{-}C{\equiv}N + 2{}^{15}NH_3 \longrightarrow H_2{}^{15}N\text{-}C{\equiv}N + {}^{15}NH_4Br$$

$$H_2{}^{15}N\text{-}C{\equiv}N \xrightarrow{H^+} [H_2{}^{15}N^+{=}C{=}NH \longleftrightarrow H^{15}N{=}C{=}\overset{+}{N}H_2] \xrightarrow{-H^+} H_2{}^{15}N\text{-}C{\equiv}{}^{15}N$$

$$2H_2{}^{15}N\text{-}C{\equiv}{}^{15}N \longrightarrow H_2{}^{15}N\text{-}C(=\,{}^{15}NH_2){=}{}^{15}N\text{-}C{\equiv}{}^{15}N$$

The labeled position was confirmed by the measurement of ^{15}N abundance of ammonia generated in the hydrolytic decomposition of 2,4-diimino-5,5-dimethyl-1,3-oxazolidine (**6**), which was formed by the electrolytic reduction of a mixture of labeled cyanoguanidine and acetone.[1,9]

$$H_2N^a\text{-}C(=N^b\text{-}C{\equiv}N^c)(N^aH_2) + (CH_3)_2C{=}O + 2e + 2H^+ \longrightarrow \mathbf{6} + N^aH_3$$

$$\mathbf{6} \xrightarrow[-N^cH_3]{H_2O} \xrightarrow[-N^aH_3]{H_2O} \xrightarrow{H_2O} N^bH_3$$

The labeled position in 1-cyano-^{15}N-guanidine was further confirmed by the following procedure. Cyanoguanidine was converted into carbamoylguanidine (**7**) by reflux in dilute hydrochloric acid and then **7** was hydrolyzed to give guanidine and ammonia (yield, 93%) in a hot aqueous sodium hydroxide solution.[10] The guanidine was also decomposed quantitatively to ammonia by the Kjeldahl method.

$$H_2N\text{-}C(=N\text{-}C{\equiv}{}^{15}N)(NH_2) + H_2O \longrightarrow H_2N\text{-}C(=N\text{-}C(=O)\text{-}{}^{15}NH_2)(NH_2)$$

7

$$\mathbf{7} + H_2O \longrightarrow H_2N\text{-}C(=NH)(NH_2) + {}^{15}NH_3 + CO_2$$

As shown in Table 1, ^{15}N abundances in the samples of ammonia agreed with the calculated values.

^{15}N FT-NMR spectra of the enriched cyanoguanidine were measured in DMF to obtain some preliminary data. These exhibited three resonance peaks under the condition of proton decoupling at a long pulse interval (180 s). The peak at a lower magnetic field split into a triplet set in non-decoupling, while the peaks at a higher magnetic field did not split. In the measurement using a shorter pulse interval (1 s), no signal was observed at such a higher magnetic field even when accumulated ten thousand times. The peak at the lower magnetic field was also assigned to N^a by a spectrum of 1-cyanoguanidine-2,3-$^{15}N_2$.[1] These facts suggest that the two N^a nitrogen atoms are also magnetically equivalent to each other. The singlet peaks at the higher magnetic field would be assigned to N^b and N^c with no hydrogen atom. Some ambiguities in the assignment might be taken away by measuring spectra of labeled cyanoguanidines other than 1-cyanoguanidine-2,3-$^{15}N_2$, but those were not measured in this work because an extremely long time would be required for measurement. Some spectra are schematically shown in Fig. 1.

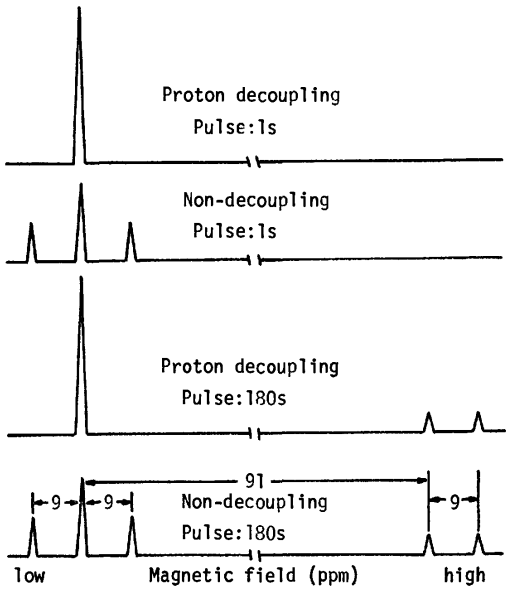

Fig. 1. Schematic ^{15}N FT-NMR spectra of enriched cyanoguanidine.

Experimental

Heavy Nitrogen Reagents. Ammonium chloride-^{15}N(^{15}N abundance, 10.3 atom %) and potassium cyanide-^{15}N(^{15}N abundance, 98.0 atom %) were supplied from the Japan Iso-

Table 1. Confirmation of labeled position

Method	^{15}N Abundance, atom %								
	1-Cyanoguanidine-1-^{15}N			1-Cyano(-^{15}N)guanidine			Enriched cyanoguanidine		
	N^a	N^b	N^c	N^a	N^b	N^c	N^a	N^b	N^c
Calculation[1]	0.7	2.7	0.7	0.7	0.7	5.0	5.5	5.5	5.5
Measurement[2]	0.8	2.5	0.8	0.7	0.7	5.0	5.6	5.5	5.7
Measurement[3]	—	—	—	0.9[4]		4.7	5.3[4]		5.4

[1]: 0.7 atom % of the natural abundance of ^{15}N is counted in.
[2]: The decomposition of 2,4-diimino-5,5-dimethyloxazolidine (**6**).
[3]: The direct decomposition of cyanoguanidine.
[4]: A mixture of N^aH_3 and N^bH_3.

tope Association.

Preparation of Labeled Cyanoguanidines. *1-Cyanoguanidine-1-^{15}N*: A solution of potassium cyanide-^{15}N (^{15}N abundance, 2.7 atom %, 11 g, 0.17 mol) in water (24 ml) was slowly added to an ice-cooled mixture of 27 g (0.17 mol) of bromine and 27 ml of water. Wet cyanogen bromide-^{15}N was first distilled from the reaction mixture, then redistilled after being dried with anhydrous calcium chloride: bp 60—62 °C; yield, 72%.

Into 21 ml of toluene containing small amounts of ethanol and hydrogen chloride as catalysts was dissolved 10.4 g (0.11 mol) of 1,2-ethanedithiol, and 10.9 g (0.10 mol) of cyanogen bromide-^{15}N in 50 ml of toluene was added dropwise into the solution. After three hours, 20.5 g of the hydrobromide of 2-imino-1,3-dithiolane-^{15}N (**2**) were crystallized out of the reaction mixture: mp 183—187 °C, dec.; yield, 98%. The hydrobromide was converted into the free base by sodium hydrogencarbonate in a mixture of ether and water as a suspension: yield, 86%; mp 64—65 °C (lit[2] 63.8—64.8 °C); and *m/e* 119 (M^+).

To an acetone solution containing 5.0 g (0.047 mol) of ordinary cyanogen bromide was added a solution of **2** (10.3 g, 0.087 mol) in acetone, dropwise. The hydrobromide of **2** was filtered off, then the solvent was evaporated to leave 4.5 g (yield, 80%) of 2-[(cyano)imino-^{15}N]-1,3-dithiolane (**3**) as a residue: mp 79—81 °C (an authentic sample,[4] 79—81 °C).

Concentrated ammonia water containing 3.5 g (0.024 mol) of **3** and 8.2 g (0.048 mol) of silver nitrate was heated in a sealed tube at 100 °C for 3 h. After cooling, the resultant precipitate was filtered off and the mother liquor was concentrated to dryness. Extraction of the solids with acetone gave 0.95 g of the ammonium salt of dicyanoamine-^{15}N (**4**): yield, 47%.

The ammonium salt was then heated in 1-butanol under reflux for 20 h. The solvent was evaporated to dryness and the residue was extracted with warm ethanol. Concentration of the extract afforded 0.49 g (yield, 49%) of 1-cyanoguanidine-1-^{15}N.

1-Cyano-^{15}N-guanidine: A mixture of 12.5 g (0.21 mol) of guanidine and 11.2 g (0.11 mol) of cyanogen bromide-^{15}N (^{15}N abundance, 5.0 atom %) in 50 ml of DMF was stirred at 5 °C for 2 h. After evaporation of the solvent under reduced pressure and treatment of the residue with a small amount of water, 3.5 g of the titled compound were left as an insoluble part: yield, 84%.

Enriched Cyanoguanidine: Ammonia generated from 13.9 g (0.26 mol) of ammonium chloride-^{15}N (^{15}N abundance, 10.3 atom %) was introduced into an ethereal solution of 14.2 g (0.13 mol) of cyanogen bromide with a nitrogen stream. Ammonium bromide was filtered off and ether was evaporated to dryness. Cyanamide-^{15}N (4.1 g) was left as a residue in 76% yield.

The above cyanamide was dissolved in 30 ml of water containing several drops of concentrated hydrochloric acid, and then the pH of the solution was adjusted to 8.5 with sodium hydroxide. After a few days, the solution was concentrated to 10 ml and 3.5 g (yield, 85%) of the titled compound was collected on a filter paper.

Confirmation of Labeled Position. Procedures for the preparation of **6**, its hydrolysis, and the determination of ^{15}N abundance were similar to those reported in the previous works.[1,9]

Decomposition of 1-Cyano-^{15}N-guanidine: A mixture of 0.42 g (0.005 mol) of cyanoguanidine in 6.7 ml of 1.5 M hydrochloric acid was heated at 100 °C for 2 h, then 6.7 ml of 1.5 M sodium hydroxide was added to the solution. The ammonia thus generated was introduced into dilute hydrochloric acid with a nitrogen stream, giving 0.25 g of ammonium chloride in 93% yield. On the other hand, the above solution was acidified with hydrochloric acid again, then the solvent was evaporated to dryness. Extraction of the residue with ethanol gave 0.47 g of guanidine hydrochloride (yield, 98%). The guanidine was strongly heated with sulfuric acid and potassium and copper(II) sulfates in a Kjeldahl flask to decompose completely to ammonia.

The authors wish to thank Dr. M. Itagaki, JEOL Ltd., for the measurement of the ^{15}N FT-NMR spectra and also for his many helpful discussions on the spectra.

References

1) T. Nonaka, A. Omura, T. Fuchigami, and K. Odo, *Denki Kagaku*, **45**, 111 (1977).
2) R. W. Addor, *J. Org. Chem.*, **24**, 738 (1964).
3) W. W. Hartman and E. E. Dreger, *Org. Synth.*, Coll. Vol. II, 150 (1943).
4) R. J. Timmons and L. S. Wittenbrook, *J. Org. Chem.*, **32**, 1566 (1967).
5) K. Kubo, T. Nonaka, and K. Odo, *Bull. Chem. Soc. Jpn.*, **49**, 1339 (1976).
6) F. E. King, R. M. Acheson, and P. C. Spensly, *J. Chem. Soc.*, **1948**, 1336.
7) K. Bloch and R. Schoeneimer, *J. Biol. Chem.*, **138**, 167 (1941); and A. Bendich, J. F. Tinker, and G. B. Brown, *J. Am. Chem. Soc.*, **70**, 3109 (1948).
8) J. L. Osborn, U. S. Pat., 2416542 (1947); *Chem. Abstr.*, **41**, 3120 (1947).
9) T. Nonaka and K. Odo, *Denki Kagaku*, **40**, 66 (1972).
10) K. Sugino and M. Yamashita, *Kogyo Kagaku Zasshi*, **45**, 1 (1942).

Studies on Hydroxy Amino Acids. VI. Formation of the Oxazoline Derivatives from *N*-Acyl-β-hydroxy Amino Acid Peptides[1]

Kiichiro NAKAJIMA, Haruki KAWAI, Michihiro TAKAI, and Kenji OKAWA
Department of Chemistry, Faculty of Science, Kwansei Gakuin University, Nishinomiya 662
(Received July 22, 1976)

Oxazoline derivatives were mainly obtained from the *O*-tosyl-*N*-acyl-β-hydroxy amino acid peptides by β-elimination reaction. Dehydroalanine or hydantoin derivatives were isolated when the urethane type acyl groups were used.

It was found in a study on the β-elimination reaction of the β-hydroxy amino acid derivatives that only oxazoline derivative (**3**) was obtained from *N*-(benzyloxycarbonyl)-glycyl-(or phenylalanyl-)-L-threonylglycine benzyl ester, *via* the corresponding *O*-tosylated intermediate.[2]

We have carried out further application of the β-elimination reaction to the *N*-acylseryl- or *N*-acylthreonyl peptide (Scheme 1).

Several acyl groups, benzoyl, phenylacetyl, benzyloxycarbonyl, *t*-butoxycarbonyl, *N*-(benzyloxycarbonyl)-glycyl, and *N*-(benzyloxycarbonyl)-D-phenylglycyl, were used as the *N*-acyl group of the β-hydroxy amino acid or peptide derivatives.

O-tosyl derivatives (**2**) were prepared by treatment of the *N*-acyl-β-hydroxy amino acid derivatives (**1**) and tosyl chloride in a pyridine solution at 0 °C. The yield and analytical data of *N*-acyl-β-hydroxy amino acid peptides (**1**) and *O*-tosylated peptides (**2**) are summarized in Tables 1 and 2, respectively.

The detosylation reaction was carried out in a solution of tetrahydrofuran with triethylamine at 70 °C. The results are summarized in Tables 3 and 4. The structure of the products was confirmed by NMR spectra.

From the results of β-elimination reaction *O*-tosyl-*N*-acyl-β-hydroxy amino acid derivatives (**2**), we see that the resulting main products are oxazoline derivatives (**3**) but not dehydroalanine (**4**) or aziridine derivatives.

Table 1. Analytical data and yield of *N*-acyl-β-hydroxy amino acid derivatives (**1**)

Compd **1**	R_1	R_2CO	R_3	Yield(%)	Mp (°C)	$[\alpha]_D^{23}$ (*c* 1.0, DMF)	Found (Calcd) C%	H%	N%
a	CH_3	C_6H_5CO	Gly-OEt	95.1	128—130	+27.4	58.30 (58.43	6.67 6.54	9.11 9.09)
b	CH_3	$C_6H_5CH_2CO$	Gly-OEt	80.0	151—151.5	+7.8	59.85 (59.61	6.91 6.88	8.79 8.69)
c	CH_3	$C_6H_5CH_2CO$	Gly-OBzl	78.0	154—156	+8.5	65.74 (65.61	6.62 6.29	7.49 7.29)
d	CH_3	Z-D-Phg	OEt	87.1	141.5—142.5	−69.0	63.90 (63.75	6.28 6.32	6.93 6.76)
e	CH_3	Z-D-Phg	NH_2	77.1	223—224	−24.2	62.66 (62.32	5.95 6.02	10.82 10.90)
f	CH_3	Z-D-Phg	$NHCH_3$	66.0	224—225	−28.2	63.26 (63.14	6.38 6.31	10.17 10.52)
g	CH_3	Z-D-Phg	Gly-OBzl	70.5	175—177	−25.1	65.04 (65.28	5.75 5.86	7.78 7.88)
h	H	Z-D-Phg	OMe	81.6	171—172	−41.3	62.42 (62.16	5.87 5.74	7.32 7.25)
i	H	Z-D-Phg	NH_2	68.7	191—193	−10.8	61.34 (61.44	6.02 5.70	11.55 11.32)
j	H	Z-D-Phg	$NHCH_3$	61.7	212.5—213	−35.9	62.58 (62.32	5.87 6.02	10.64 10.90)
k	H	Z-D-Phe	OMe	88.0	146—147	+15.1	63.12 (62.99	6.13 6.04	6.98 7.00)
l	H	Z-D-Phe	$NHCH_3$	82.8	187—188	+15.0	63.37 (63.14	6.28 6.31	10.36 10.52)
m	CH_3	Z	Gly-OEt	76.8	110—111	+12.6	56.63 (56.79	6.32 6.55	8.41 8.28)
n	CH_3	Boc	Gly-OEt	81.3	86—87	−0.8	51.19 (51.30	7.99 7.95	9.42 9.21)
o	H	Z	Gly-OEt	92.5	97—98	+2.7	55.62 (55.55	6.37 6.22	8.59 8.64)
p	H	Boc	Gly-OBzl	89.0	81—82	−4.0	57.99 (57.94	6.81 6.87	7.90 7.95)

Z: benzyloxycarbonyl, Boc: *t*-butoxycarbonyl, Gly: glycine, Phg: phenylglycine, Me: methyl, Et: ethyl, Bzl: benzyl.

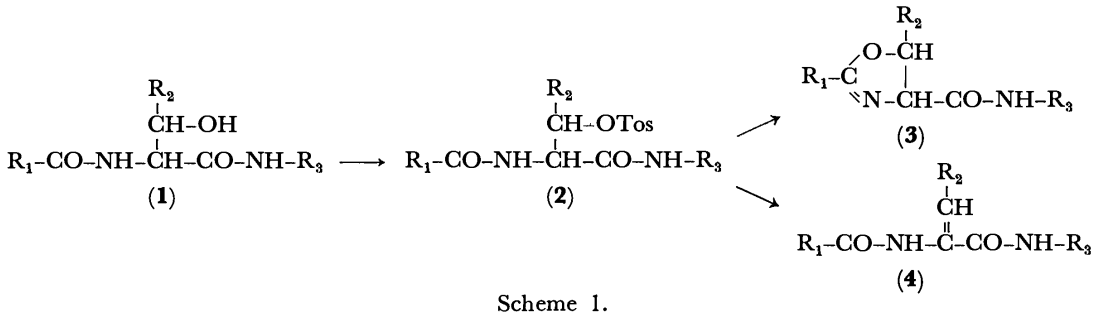

Scheme 1.

TABLE 2. ANALYTICAL DATA AND YIELD OF *O*-TOSYL-*N*-ACYL-*β*-HYDROXY AMINO ACID DERIVATIVES (**2**)

Compd **2**	Yield (%)	Mp (°C)	$[\alpha]_D^{23}$ (*c* 1.0, DMF)	Found (Calcd) C%	H%	N%	S%
a	94.0	105—106	+27.1	56.64 (57.13	5.62 5.67	5.92 6.06	6.55 6.93)
b	89.4	107—107.5	+18.9[a]	57.43 (57.97	5.95 5.92	5.84 5.88	6.71 6.73)
c	77.8	118.5—119.0	+23.7	62.43 (62.44	5.45 5.61	5.13 5.20	5.91 5.95)
e	39.4	135—136	+1.3	60.03 (60.10	5.22 5.42	7.91 7.79	5.96 5.94)
f	69.9	151—152	+0.7	60.49 (60.74	5.74 5.64	7.80 7.59	5.83 5.79)
g	90.0	96—97.5	+8.1	62.83 (62.87	5.40 5.42	6.12 6.11	4.48 4.66)
i	75.2	124—125	+1.6	59.27 (59.41	5.36 5.18	8.05 8.00	6.31 6.10)
j	80.0	139—139.5	+0.1	60.29 (60.10	5.44 5.42	7.80 7.79	6.02 5.94)
l	87.8	115—116	−71.6	60.63 (60.74	5.72 5.64	7.58 7.59	5.91 5.79)
m	90.0	93.5—94.0	+26.5	56.03 (56.08	5.73 5.73	5.69 5.69	6.30 6.51)
n	83.1	b)	+16.4[c]	52.32 (52.39	6.51 6.60	6.02 6.11	6.98 6.99)
o	77.8	97—98	+4.0	55.13 (55.22	5.62 5.48	5.90 5.85	6.83 6.70)
p	84.6	96—97[d]	+1.0	56.97 (56.90	5.91 5.97	5.65 5.53	6.45 6.33)

a) *c* 0.2, MeOH. b) Oil. c) *c* 1.2, DMF. d) Decomposition.

TABLE 3. REACTION PRODUCTS BY THE *β*-ELIMINATION REACTION OF THE *O*-TOSYLATED HYDROXY AMINO ACID DERIVATIVES (**2**)

Exp. No.	R_1	R_2	R_3	Yield (%) **3**	**4**	**5**
1	Ph–	$-CH_3$	$-CH_2-COOEt$	79.6	8.1	—
2	Ph–CH_2–	$-CH_3$	$-CH_2-COOEt$	80.3[a]	—	—
3	Ph–CH_2–	$-CH_3$	$-CH_2-COOBzl$	82.0[a]	—	—
4	Z–NH–CH_2–	$-CH_3$	$-CH_2-COOBzl$	80.0	—	—
5	Z–NH–CH(Ph)–	$-CH_3$	–H	70.7	—	—
6	Z–NH–CH(Ph)–	$-CH_3$	$-CH_3$	38.6	—	—
7	Z–NH–CH(Ph)–	$-CH_3$	$-CH_2-COOBzl$	70.4	26.7	—
8	Z–NH–CH(Ph)–	–H	–H	43.7	—	—
9	Z–NH–CH(Ph)–	–H	$-CH_3$	63.8	—	—
10	Z–NH–CH(CH_2–Ph)–	–H	$-CH_3$	65.4	—	—
11	Ph–CH_2–O–	$-CH_3$	$-CH_2-COOEt$	—	48.0	50.5
12	*t*-Bu–O–	$-CH_3$	$-CH_2-COOEt$	—	80.0	b)
13	Ph–CH_2–O–	–H	$-CH_2-COOEt$	—	52.0	38.6[c]
14	*t*-Bu–O–	–H	$-CH_2-COOBzl$	—	73.2	—

Ph: phenyl; Z: benzyloxycarbonyl; *t*-Bu: *t*-butyl; Et: ethyl; Bzl: benzyl. a) Small amounts of D-threonine derivative isolated. b) Trace amounts of **5**-11 isolated. c) **5**-13[4] not isolated by Photaki.

Table 4. Analytical data of the β-elimination reaction products (**3**, **4**, **5**)

Products	Mp(°C)	$[\alpha]_D^{23}$ (*c* 1.0, DMF)	Found (Calcd) C%	H%	N%
3-1	100—102	−20.6	61.78 (62.05	6.19 6.25	9.56 9.65)
3-2	88.5—89.0	−8.0[a]	63.41 (63.14	6.63 6.62	9.22 9.21)
3-3	94—94.5	−16.2[b]	68.87 (68.83	6.03 6.05	7.60 7.65)
3-5	144—145	+22.4	65.43 (65.38	5.68 5.76	11.28 11.44)
3-6	129—130	+25.5	65.87 (66.12	6.13 6.08	11.26 11.02)
3-7	c)	+3.0	67.43 (67.56	5.70 5.67	8.11 8.15)
3-8	157—158	+26.9	64.24 (64.58	5.47 5.42	11.89 11.89)
3-9	140—141	+67.7	65.45 (65.38	5.84 5.76	11.48 11.44)
3-10	114—115	+82.6	66.21 (66.12	6.06 6.08	11.02 11.02)
4-1	147—149	—	61.62 (62.05	6.23 6.25	9.60 9.65)
4-7	77—80	−21.7	67.12 (67.56	5.64 5.67	8.09 8.15)
4-11	109—110	—	59.65 (59.99	6.24 6.29	8.70 8.75)
4-12	93—93.5	—	54.69 (54.53	7.84 7.75	9.99 9.78)
4-13	81—82	—	58.69 (58.81	5.88 5.92	9.07 9.15)
4-14	103.5—104.5	—	61.11 (61.06	6.59 6.63	8.37 8.38)
5-11	155—155.5	—	50.86 (50.94	5.63 5.70	13.17 13.20)
5-13	104—105	—	48.39 (48.48	4.92 5.09	14.12 14.14)

a) *c* 0.2, MeOH. b) *c* 0.7, AcOEt. c) Oily product.

Z-Gly-Ser-Gly-OEt is an exceptional example to produce the dehydroalanine derivative (**4**) as the main product.[2]

In the case of urethane type acyl derivatives, however, both dehydroalanine (**4**) and hydantoin derivatives (**5**) were isolated from the *N*-benzyloxycarbonyl peptide derivatives, only the former being obtained from the *t*-butoxycarbonyl peptide derivatives (Scheme 2).

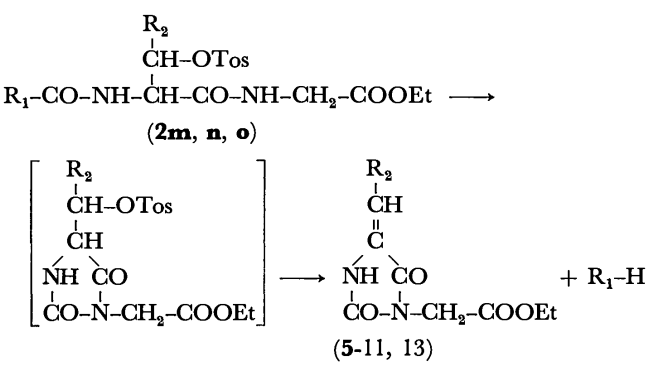

(**2m**, **n**, **o**)

(**5**-11, 13)

R_1: $C_6H_5CH_2O$- or $(CH_3)_3C$-O-, R_2: CH_3- or H-

Scheme 2.

Concerning the hydantoin formation, Dekker *et al.* reported[3] that compound (**5**) is produced when the *N*-[α-(benzyloxycarbonylamino)acyl]glycine ester is treated with methanolic ammonia at room temperature. However, we detected no aziridine derivatives.

Experimental

All the melting points are uncorrected. The NMR spectra were obtained with a Hitachi R-20 B High Resolution NMR Spectrometer, the chemical shifts being given from TMS as the internal reference. The purity of the compounds was confirmed by thin layer chromatography on silica gel. Hydroxy amino acid peptides were prepared by use of *N*,*N*′-dicyclohexylcarbodiimide (DCC). *N*-hydroxybenzotriazole (HOBt) or *N*-hydroxysuccinimide was employed in order to avoid the racemization of *N*-acyl-β-hydroxy amino acid during the course of coupling.

Synthesis of N-*Acyl-β-hydroxy Amino Acid Peptide Derivatives* (**1**). *Phenylacetyl*-L-*Thr*-*Gly*-*OEt* (**1b**): All the dipeptide derivatives were synthesized as follows. Phenylacetyl-L-Thr-OH (23.7 g, 0.1 mol) was treated with DCC (22.7 g, 0.11 mol), H-Gly-OEt (from the hydrochloride 15.3 g, 0.11 mol), HOBt (16.2 g, 0.12 mol) in DMF (100 ml) and dichloromethane (100 ml) at −10 °C. After the reaction mixture had been allowed to stand overnight in a refrigerator, acetic acid (2 ml) was added and the mixture was stirred for 15 min. The *N*,*N*′-dicyclohexylurea produced was filtered off, and the filtrate was washed successively with 1 M sodium hydrogencarbonate, 1 M hydrochloric acid and water, dried over anhydrous sodium sulfate, and concentrated under reduced pressure. **1b** was obtained from ethyl acetate–ether–hexane as crystals. The results are summarized in Table 1.

Z-D-*Phg*-L-*Thr*-*NHCH*$_3$ (**1f**): Methylamidation was carried out as follows. A solution of 30% methylamine (45 ml) in methanol was added to a solution of **1d** (4.5 g, 11.5 mmol) in methanol with stirring at 0 °C. After the reaction mixture had been allowed to stand at room temperature, the crystals (**1f**) produced were filtered off. Recrystallization was carried out from methanol–ether. The results are summarized in Table 1.

Z-D-*Phg*-L-*Ser*-*NH*$_2$ (**1i**): Amidation was carried out as follows. Dry ammonia gas was bubbled into a solution of **1h** (5 g, 12.9 mmol) in methanol at 0 °C until saturation. After the mixture had been allowed to stand at room temperature, the crystals (**1i**) produced were filtered off. Recrystallization was carried out from methanol–ether. The results are summarized in Table 1.

Z-D-*Phg*-L-*Thr*-*Gly*-*OBzl* (**1g**): Dry hydrogen chloride gas was bubbled for 30 min at 0 °C into a solution of Boc-Thr-Gly-OBzl[1] (2.02 g, 6 mmol) in ethyl acetate (20 ml) containing anisole (1 ml). The reaction mixture was allowed to stand at room temperature for 30 min. After the reaction mixture had been concentrated under reduced pressure, anhydrous ether was added to the residual products. Crystals were obtained in theoretical yield. The hydrochloride, Z-D-Phg-OH(1.71 g, 6 mmol), Et_3N (0.83 ml, 6 mmol) was treated with DCC (1.24 g, 6 mmol) in THF at −10 °C for 4 h. After the reaction mixture had been allowed to stand overnight in a refrigerator, acetic acid (1 ml) was added. The *N*,*N*′-dicyclohexylurea produced was filtered off, and the filtrate was concentrated under reduced pressure. The residual oil was dissolved in ethyl acetate and the solution was washed successively with 1 M sodium hydrogencarbonate, 1 M hydrochloric acid, and water, dried over anhydrous sodium sulfate, and concentrated under reduced pressure. The

oily products were crystallized from ethyl acetate–ether–hexane. **1g** was obtained 70.5% yield from Boc-Thr-Gly-OBzl.

Synthesis of O-Tosyl-N-acyl-β-hydroxy Amino Acid Peptide Derivatives (2). *Phenylacetyl-L-Thr(Tos)-Gly-OBzl(2c)*: *O*-tosylation was carried out as follows. A solution of tosyl chloride (3.73 g, 30 mmol) in dry pyridine (10 ml) was added drop by drop with stirring at −10 °C to a solution of **1c** (3.84 g, 10 mmol) in dry pyridine (30 ml). When the addition was over, the reaction mixture was allowed to stand at −10 °C for 3 days. It was then concentrated under reduced pressure, and the residual products were dissolved in ethyl acetate. The solution was washed with water and dried over anhydrous sodium sulfate, and concentrated under reduced pressure. The crystals (**2c**) produced were recrystallized from ethyl acetate–ether–hexane. The results are recrystallized from ethyl acetate–ether–hexane. The results are summarized in Table 2.

Detosylation of O-Tosyl Peptide Derivatives (2). *2-[α-(Benzyloxycarbonylamino)benzyl]-4-methylcarbamoyl-2-oxazoline (3-9)*: Detosylation was carried out as follows. A solution of **2j** (3.5 g, 6.5 mmol) and Et_3N (1.86 ml, 13 mmol) was refluxed at 70 °C for 3 days. After the solvent had been evaporated under reduced pressure, the oily product was dissolved in ethyl acetate. The solution was washed with water, dried over anhydrous sodium sulfate, and concentrated under reduced pressure. The residual product (**3**-9) was crystallized from ethyl acetate–ether. The results are summarized in Tables 3 and 4. NMR ($CDCl_3$): δ; 2.62 ppm (3H d, 4.9 Hz, -NHC$\underline{H}_3$); 4.35, 4.39, 4.53 ppm (3H 3q, 6.0, 12 Hz, 4.5, 12 Hz, 4.5, 6.0 Hz, -C$\underline{H}_2$-C$\underline{H}$-); 5.06 ppm (2H s, C_6H_5-C$\underline{H}_2$-); 5.43 ppm (1H d, 8.5 Hz, C_6H_5C$\underline{H}$=).

2-Benzyl-4-[(ethoxycarbonyl)methylcarbamoyl]-5-methyl-2-oxazoline (3-2): **2b** (8.19 g, 17.6 mmol) and Et_3N (4.9 ml, 35.2 mmol) were treated in THF as in the synthesis of **3**-9. The crude product was crystallized from ethyl acetate–ether. A small amount of crystals appeared were collected by filtration. The crystals were identified as Phenylacetyl-D-Thr-Gly-OEt [mp 147—148 °C, $[\alpha]_D^{23}$ −6.5° (*c* 1.0, DMF)]. **3**-2 was isolated from the mother liquor by the addition of hexane (Table 3). **3**-2 NMR ($CDCl_3$): δ; 1.11 ppm (3H d, 5.5 Hz, C$\underline{H}_3$-CH=); 1.15 ppm (3H t, 7.0 Hz, C$\underline{H}_3$-C$\underline{H}_2$-); 3.60 ppm (2H s, C_6H_5C$\underline{H}_2$-); 3.84 ppm (2H d, 6.2 Hz, -NH-C$\underline{H}_2$-CO-); 4.07 ppm (2H q, 7.0 Hz, CH_3-C$\underline{H}_2$-); 4.80 ppm (2H m, CH_3-C$\underline{H}$-C$\underline{H}$-); 7.28 ppm (5H s, $C_6\underline{H}_5$-CH_2-).

2c also gave a trace amounts of Phenylacetyl-D-Thr-Gly-OBzl [mp 165—166 °C, $[\alpha]_D^{23}$ −10.6° (*c* 1.0, DMF)].

N-[α-(Benzyloxycarbonylamino)crotonylglycine Ethyl Ester (4-11) and Ethyl 5-Ethylidenehydantoin-3-acetate (5-11): **2m** (2.1 g, 4.26 mmol) and Et_3N (1.78 ml, 12.8 mmol) was treated in THF by the above detosylation procedure. The crude product having two components was subjected to silica gel chromatography developed by the mixed solvent, $CHCl_3$–ethyl acetate (2:1 v/v). The product of R_f 0.85[5] was **4**-11 and R_f 0.65[5] was **5**-11: **4**-11 NMR (DMSO-d_6): δ; 1.17 ppm (3H t, 7.0 Hz, C$\underline{H}_3$-C$\underline{H}_2$-); 1.63 ppm (3H d, 7.0 Hz, C$\underline{H}_3$-CH=); 3.81 ppm (2H d, 6.0 Hz, -NH-C$\underline{H}_2$-); 4.08 ppm (2H q, 7.0 Hz, CH_3-C$\underline{H}_2$-); 5.04 ppm (2H s, C_6H_5C$\underline{H}_2$-); 6.30 ppm (1H q, 7.0 Hz, CH_3-C$\underline{H}$=); 7.35 ppm (5H s, $C_6\underline{H}_5CH_2$-); 8.18 ppm (1H t, 6.0 Hz, -N$\underline{H}$-CH_2-); 8.52 ppm (1H s, -N$\underline{H}$-C(=O)-), **5**-11 NMR ($CDCl_3$): δ; 1.26 ppm (3H t, 7.0 Hz, C$\underline{H}_3$-C$\underline{H}_2$-); 1.83 ppm (3H d, 7.8 Hz, C$\underline{H}_3$-CH=); 4.23 ppm (2H q, 7.0 Hz, CH_3-C$\underline{H}_2$-); 4.29 ppm (2H s, =N-C$\underline{H}_2$-); 5.99 ppm (1H q, 7.8 Hz, CH_3-C$\underline{H}$=); 9.01 ppm (1H s, -N$\underline{H}$-CO-).

N-[α-(t-Butoxycarbonylamino)crotonyl]glycine Ethyl Ester (4-12) and 5-11: **2n** (2.1 g, 4.26 mmol) and Et_3N (1.78 ml, 12.8 mmol) was subjected to the above detosylation procedure. The crude product having two components was subjected to silica gel chromatography with use of the mixed solvent, $CHCl_3$–ethyl acetate (2:1 v/v). The product of R_f 0.85[5] was **4**-12 and that of R_f 0.64[5] was **5**-11: **4**-12 NMR (DMSO-d_6): δ; 1.18 ppm (3H t, 7.0 Hz, C$\underline{H}_3$-C$\underline{H}_2$-); 1.39 ppm (9H s, (C$\underline{H}_3$)$_3$-C); 1.62 ppm (3H d, 7.0 Hz, C$\underline{H}_3$-CH=); 3.82 ppm (2H d, 6.0 Hz, -NH-C$\underline{H}_2$-CO-); 4.08 ppm (2H q, 7.0 Hz, CH_3-C$\underline{H}_2$-); 6.20 ppm (1H q, 7.0 Hz, CH_3-C$\underline{H}$=). Formation of a small amounts of **5**-11 was detected by thin layer chromatography, no isolation being carried out.

N-(Benzyloxycarbonyldehydroalanyl)glycine Ethyl Ester (4-13) and Ethyl 5-Methylenehydantoin-3-acetate (5-13): **2o** (1.9 g, 4 mmol) and Et_3N (1.1 ml, 8 mmol) were subjected to the above detosylation procedure in THF. The crude product having two components was subjected to silica gel chromatography with use of the mixed solvent, $CHCl_3$–ethyl acetate (1:1 v/v). The product of R_f 0.78[6] was **4**-13 and R_f 0.60[6] was **5**-13: **4**-13 NMR ($CDCl_3$): δ; 1.24 ppm (3H t, 7.1 Hz, C$\underline{H}_3$-C$\underline{H}_2$-); 4.02 ppm (2H d, 5.5 Hz, -NH-C$\underline{H}_2$-CO-); 4.19 ppm (2H q, 7.1 Hz, CH_3-C$\underline{H}_2$-); 5.12 ppm (2H s, C_6H_5C$\underline{H}_2$-); 5.21, 6.08 ppm (1H m, 1H d, 2.0 Hz, C$\underline{H}_2$=C<); 7.33 ppm (5H s, $C_6\underline{H}_5CH_2$-), **5**-13 NMR ($CDCl_3$): δ; 1.25 ppm (3H t, 6.5 Hz, C$\underline{H}_3$-C$\underline{H}_2$-); 4.22 ppm (2H q, 6.5 Hz, CH_3-C$\underline{H}_2$-); 4.28 ppm (1H s, =N-C$\underline{H}_2$-); 4.90 ppm (2H m, C$\underline{H}_2$=C<); 8.42 ppm (1H s, -N$\underline{H}$-CO-).

N-(t-Butoxycarbonyldehydroalanyl)glycine Benzyl Ester (4-14): **2p** (1.45 g, 3 mmol) and Et_3N (0.83 ml, 6 mmol) were subjected to the above detosylation procedure in THF. The crude product was purified by means of silica gel chromatography with use of the mixed solvent, $CHCl_3$–ethyl acetate (1:1 v/v). **4**-14 NMR ($CDCl_3$): δ; 1.45 ppm (9H s, (C$\underline{H}_3$)$_3$-C); 4.12 ppm (2H d, 5.0 Hz, -NH-C$\underline{H}_2$-CO-); 5.10 ppm, 6.02 ppm (1H m, 1H d, 2 Hz, C$\underline{H}_2$=C<); 5.19 ppm (2H s, C_6H_5C$\underline{H}_2$-); 7.34 ppm (5H s, $C_6\underline{H}_5CH_2$-).

References

1) Part V; K. Okawa, K. Nakajima, T. Tanaka, and Y. Kawana, *Chem. Lett.*, **1975**, 591.

2) Y. Nakagawa, T. Tsuno, K. Nakajima, M. Iwai, H. Kawai, and K. Okawa, *Bull. Chem. Soc. Jpn.*, **45**, 1162 (1972).

3) C. A. Dekker, S. P. Taylor, Jr., and J. S. Fruton, *J. Biol. Chem.*, **180**, 155 (1945).

4) I. Photaki, *J. Am. Chem. Soc.*, **85**, 1123 (1963).

5) Thin layer chromatography solvent system. $CHCl_3$–AcOEt (2:1 v/v).

6) Thin layer chromatography solvent system. $CHCl_3$–AcOEt (1:1 v/v).

Mechanism of Photochemical Reaction of Friedelin with Diethyl Ether and with Acetone[1)]

Hidekazu SHIRASAKI, Takahiko TSUYUKI, Takeyoshi TAKAHASHI, and Robert STEVENSON*

Department of Chemistry, Faculty of Science, The University of Tokyo, Hongo, Bunkyo-ku, Tokyo 113

**Department of Chemistry, Brandeis University, Waltham, Massachusetts, 02154 U.S.A.*

(Received July 24, 1976)

Photo-irradiation of friedelin (**1**) in diethyl ether gave a keto ether (**2**), a hydroxy ether (**3**), and an alcohol (**4**). A hydroxy ketone (**5**) was formed by the photo-irradiation reaction of **1** in diethyl ether containing acetone. In the latter case, labeled experiments showed that the photo-produced ketene (**12**) reacted with 1-hydroxy-1-methylethyl radical derived from acetone to give **5**. The formation of **2** could be explained by an attack of an α-radical derived from diethyl ether to **12**. Both **3** and **4** were shown to be derived from a norseco-aldehyde (**11**) which was produced from the ketene (**12**).

The photochemical reaction of friedelin (**1**) in various organic solvents has been reported.[2)] In the present communication, the formation of a keto ether (**2**), a hydroxy ether (**3**), and an alcohol (**4**) by photo-irradiation of **1** in diethyl ether is described. The isolation of a hydroxy ketone (**5**) from the photolysate of **1** in diethyl ether containing acetone is also reported.

Friedelin (**1**) was irradiated in anhydrous diethyl ether under nitrogen* with a high pressure mercury lamp (100 W) for 7 h at room temperature. After the usual work-up, the reaction product proved to be a complex mixture which showed on a thin layer chromatogram (silica gel) three major spots (A, B, and C) and three minor spots in addition to those attributable to known hydrocarbons,[2a,d)] aldehydes,[2f,g,i)] friedelin, and 4-epifriedelin.[2c)] The fraction A gave a keto ether component (**2**). Three diastereomers of hydroxy ether (**3a**—**c**) were obtained from the fractions A, B, and C. From the fraction C, an alcohol (**4**) was obtained.

The keto ether component (**2**) had a molecular formula $C_{31}H_{60}O_2$, which corresponds to a 1 : 1 addition product of friedelin (**1**) and diethyl ether. The IR spectrum showed a carbonyl absorption. In the PMR spectrum, the presence of an α′-methylene group and an α-methine group to an ether oxygen atom was detected. The presence of the ether-moiety was further substantiated by a peak at *m/e* 427 due to a fragmentation $(M-CH_3CH_2OCHCH_3)^+$.

Although the keto ether component (**2**) is considered to consist of a mixture of diastereomers, no information on this point was obtained from its spectral data and a separation of diastereomers by thin layer chromatography using various developing solvents was unsuccessful.

The proposed structure was supported by the following chemical transformations. The reduction of the keto ether (**2**) with lithium aluminium hydride afforded a mixture of hydroxy ethers (**6**). The ether linkage of **6** was cleaved by treatment with boron trichloride[3)] to give a mixture of diols (**7**), which on oxidation with lead tetraacetate afforded an aldehyde (**8**). This aldehyde was found to be identical with the seco-aldehyde (**8**) prepared by oxidation of the known seco-alcohol (**9**)[2d)] (Scheme 1). From these observations, the keto ether (**2**) was formulated as 10β-(4-ethoxy-3-oxopentyl)-5α-ethyl-des-A-friedelane.

Three stereoisomeric hydroxy ethers (**3a**—**c**) from the fractions A, B, and C gave similar spectral data. The IR spectrum and mass spectrum (a peak at *m/e* 414 due to a fragment ion $(M-CH_3CH_2OCH_2CH_3)^+$) of each hydroxy ether (**3a**—**c**) showed the presence of a hydroxyl group and an ether-moiety. The high resolution mass spectrum showed a formula $C_{33}H_{60}O_2$ for **3**. In the PMR spectrum of **3b**, an α′-methylene and α-methine to the ether oxygen atom resonated as quartet, respectively. These results suggest that these hydroxy ethers (**3**) should be formulated as 10β-(3-ethoxy-2-hydroxybutyl)-5α-ethyl-des-A-friedelane.

These hydroxy ethers (**3a**—**c**) were combined and were treated with boron trichloride[3)] to afford a mixture of diols (**10**), which was then oxidized with lead tetraacetate to give a known norseco-aldehyde (**11**)[2f,g,j)] (Scheme 1). The structure of **3** thus determined has two additional asymmetric carbon atoms in addition to those present in 3,4-seco-friedelane skeleton. Although four diastereomers should be obtained theoretically, only three isomers could be isolated from the photolysate. A question, however, whether one of them consists of a mixture of two diastereomers remains to be proved. Configurations have not been assigned to these diastereomers.

The alcohol (**4**) was identical with 5α-ethyl-10β-(2-hydroxyethyl)-des-A-friedelane[2j)] obtained by reduction of the known norseco-aldehyde (**11**).[2f,g,j)]

The oxidation state of the isolated norseco-products, corresponding to an overall reduction, was rather unexpected and requires an explanation. Since the norseco-alcohol (**4**) obtained from irradiation of friedelin-^{18}O (**1**-^{18}O; isotopic abundance, *ca.* 17%)[2g,j)] was shown to contain no ^{18}O atom, the oxygen atom in **4** is not derived from the oxygen atom of the friedelin carbonyl group. The experimental data is shown in Table 1.

We have previously shown[2g,j)] that the ketene (**12**), formed by irradiation of friedelin (**1**) *via* an acyl-alkyl biradical (**13**), is autoxidized with oxygen during the product isolation to afford the norseco-aldehyde (**11**). Two mechanisms have now been considered for the formation of **4**: (i) a mechanism involving a carbene (**14**)[4)] and (ii) a mechanism *via* the norseco-aldehyde (**11**).

In terms of mechanism (i), the ketene (**12**) might

* The commercial nitrogen was used without purification.

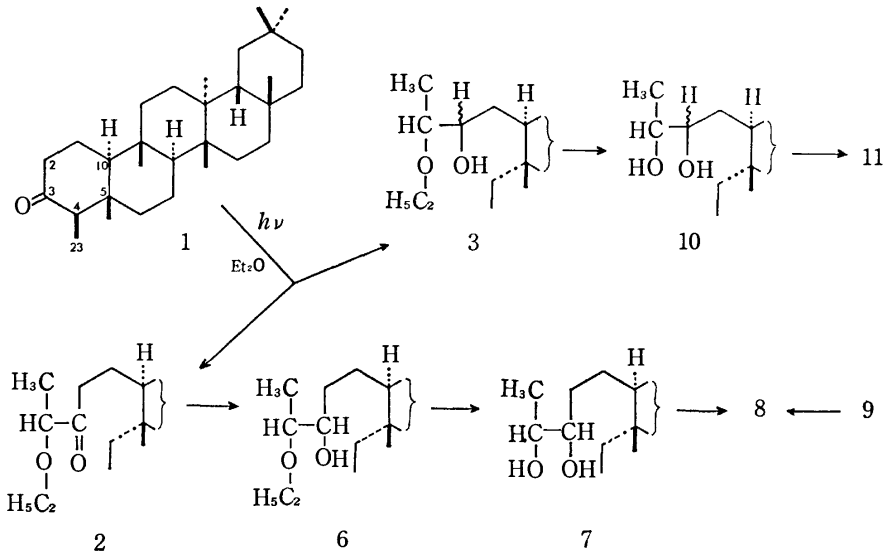

Scheme 1.

TABLE 1. ^{18}O-ISOTOPIC ABUNDANCE[a] IN **4** (FROM **1**-^{18}O) AND RELATED COMPOUNDS

	m/e 426	*m/e* 427	*m/e* 428
1 (M^+, *m/e* 426)	100	34.6	6.4
1-^{18}O	100	33.7	23.7
	m/e 416	*m/e* 417	*m/e* 418
4 (M^+, *m/e* 416)	100	32.3	5.8
4 (from **1**-^{18}O)	100	32.5	6.6

a) Relative intensities in %.

undergo decarbonylation on irradiation affording a carbene (**14**), which could react with water to give the norseco-alcohol (**4**) (Scheme 2).

To test this hypothesis, friedelin (**1**) was irradiated in water-free ether saturated with deuterium oxide (99.75% D_2O) and the norseco-alcohol (**4**) was isolated. If the reaction had proceeded through the carbene (**14**), the product would have been the dideuterio alcohol (**4**-d_2), which would give a monodeuterio alcohol (**4**-d_1) by usual aqueous work-up. Therefore, the reaction product should contain *one* deuterium atom at C-2 as shown in **4**-d_1.

The mass spectrometric examination of the product showed, however, that the incorporation of a deuterium atom had not occurred (Table 2) and that the mechanism (i) can consequently be excluded.

Directing attention to the second mechanism, the photo-produced ketene (**12**) could be autoxidized by oxygen[2g,j,5,6] which may be present in the reaction system to afford the norseco-aldehyde (**11**). The aldehyde (**11**) would then undergo photochemical reduction[7] in ether to give the norseco-alcohol (**4**).

TABLE 2. D-ISOTOPIC ABUNDANCE[a] IN **4**

	m/e 416	*m/e* 417	*m/e* 418
4 (authentic; M^+, *m/e* 416)	100	32.3	5.4
4 (photoproduct)	100	32.3	6.7
4 (photoproduct obtained by irradiation with D_2O)	100	32.1	5.7

a) Relative intensities in %.

The involvement of oxygen in the formation of **4** was demonstrated as follows. Friedelin (**1**) was irradiated in anhydrous diethyl ether under oxygen-free argon purified by passing over copper at 500 °C. The hydrocarbons, aldehydes, friedelin, 4-epifriedelin, and the keto ether (**2**) were obtained, while neither the hydroxy ether (**3**) nor the norseco-alcohol (**4**) was detected by thin layer chromatography. Since the irradiation of friedelin (**1**) under commercial nitrogen gave **3** and **4**, oxygen present in the commercial nitrogen is implicated in the formation of these products. Following this conclusion, the intermediacy of the ketene (**12**) and norseco-aldehyde (**11**) in the photo-reaction was examined.

Irradiation of 2α,2β,4α-trideuteriofriedelin (**1**-d_3)[2g,i] in ether afforded a deuteriated alcohol (**4**-d_3), which gave a molecular ion peak at *m/e* 419. The methylene group at C-2 in **4** resonated as a triplet with an integrated intensity due to two protons, while the integrated intensity of a triplet in **4**-d_3 corresponded to one proton. On addition of $Eu(dpm)_3$ as a shift reagent, the C-4 methyl protons were readily assignable with the triplet signal for nonlabeled alcohol (**4**) appearing as a singlet in **4**-d_3. These observations indicate that the methylene group at C-4 of **4**-d_3 was labeled with two deuterium atoms and the methylene group at C-2 with one deuterium atom, in accordance with formation of **4**-d_3 *via* the ketene (**12**-d_3).

The norseco-aldehyde (**11**)[2f,j] was irradiated in ether, and from the reaction products, the norseco-alcohol (**4**) and the hydroxy ether (**3**) were isolated.

These experimental results show that the ketene (**12**) formed by irradiation is autoxidized with oxygen in the reaction system to give the norseco-aldehyde (**11**), which is subsequently reduced photochemically to yield **3** and **4**. The final photoreduction step[7] is outlined in Scheme 3.

The formation of the keto ether (**2**) is likely to suggest a novel reaction between a photochemically produced ketene and an α-radical derived from diethyl ether.

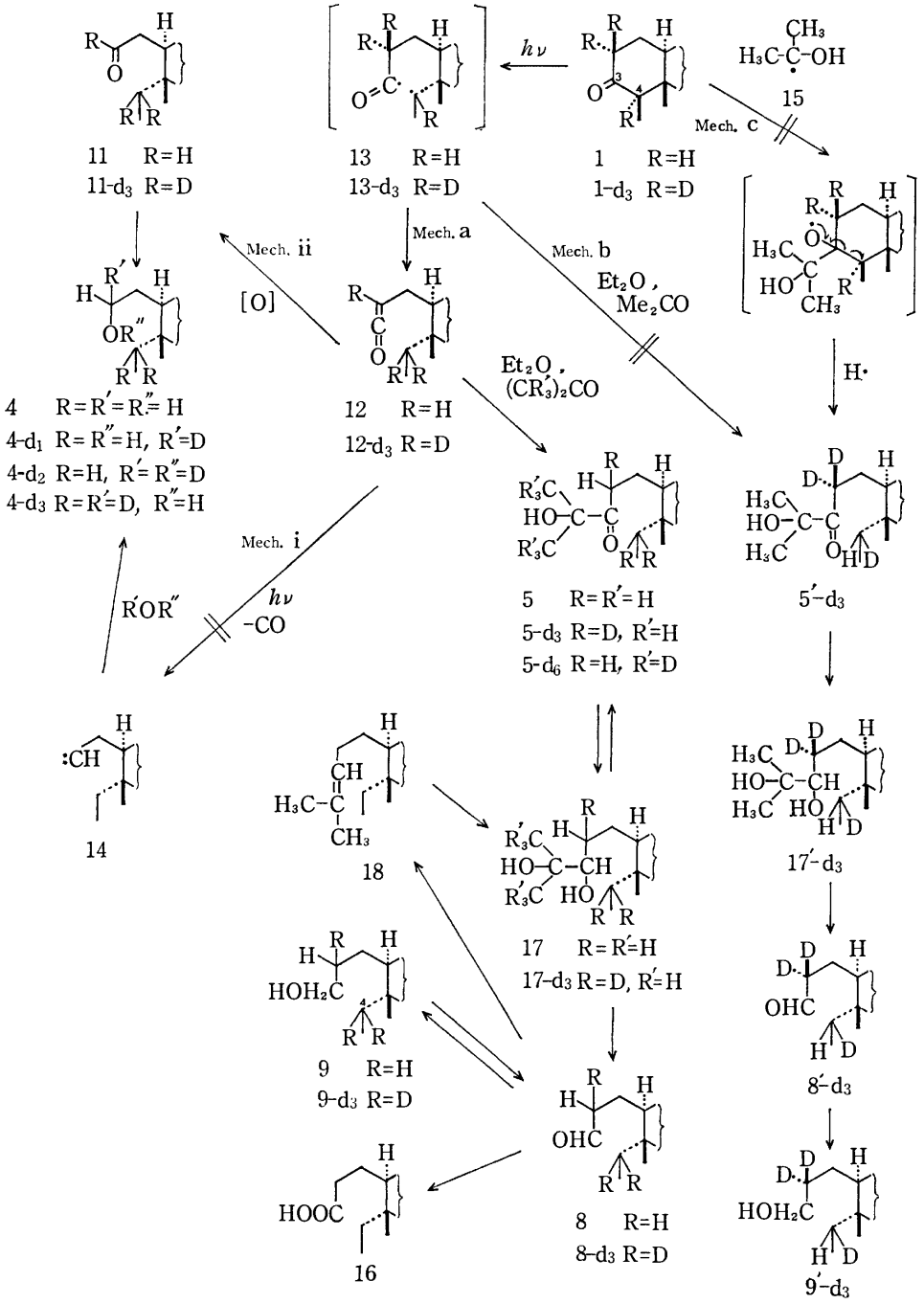

Scheme 2.

Friedelin (**1**) in ether containing acetone was irradiated in a quartz vessel under the usual conditions. The irradiation products were separated by column and thin layer chromatography to give a hydroxy ketone (**5**), whose PMR spectrum showed the presence of $(CH_3)_2C$-(OH)- group and whose molecular formula $C_{33}H_{58}O_2$ showed an increment of C_3H_8O in comparison with that of friedelin. On acetylation, the hydroxy ketone (**5**) gave an acetoxy ketone.

The structure of the hydroxy ketone (**5**) was confirmed by conversion to the known 10β-(2-carboxyethyl)-5α-ethyl-des-A-friedelane (**16**).[2b] It was subjected to consecutive reduction with lithium aluminium hydride, oxidation with lead tetraacetate and with silver oxide to afford a seco-acid (**16**) (Scheme 2).

A partial synthesis of **5** confirmed the proposed structure. The aldehyde (**8**) was treated with isopropyltriphenylphosphonium bromide.[8,9] The resulting isopropylidene derivative (**18**)[10] was oxidized with osmium tetraoxide[11] to give a mixture of diols (**17**), which on oxidation with chromium trioxide[12] yielded the hydroxy ketone (**5**), identical with the photo-irradiation product (Scheme 2).

A solution of **1** in ether and acetone-d_6 was irradiated for 5 h, and the resulting hydroxy ketone (**5**-d_6) was isolated and examined. The molecular ion peak was observed at *m/e* 492, *i.e.* 6 mass units higher than that of the non-labeled **5**. In the PMR spectrum, a singlet

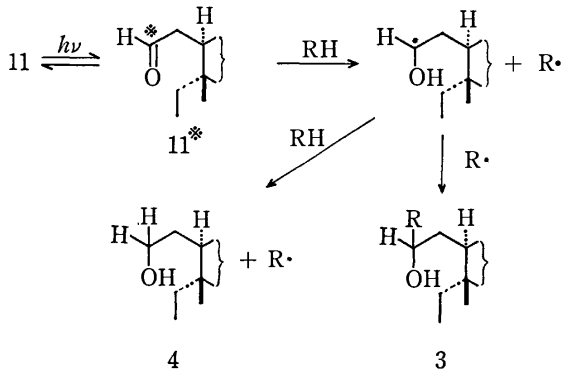

$$R = -\underset{\underset{CH_3}{|}}{CH}OC_2H_5$$

(An asterisk refers to an activated state.)

Scheme 3.

signal (δ 1.37) due to two tertiary methyl group in **5** was not observed in **5**-d_6. The presence of pinacol in the photolysate was demonstrated by gas chromatographic examination further supporting the involvement of 1-hydroxy-1-methylethyl radical (**15**) in the photolysis of friedelin (**1**) in ether containing acetone.

Three mechanisms (outlined in Scheme 2 as "a", "b", and "c") were considered for the formation of the hydroxy ketone (**5**). a) The attack of the radical (**15**) at the carbonyl carbon atom of the ketene (**12**), followed by addition of a hydrogen atom to C-2. b) The addition of the radical (**15**) to the acyl radical (C-3) of the biradical (**13**), followed by addition of a hydrogen atom to the alkyl radical (original C-4 of friedelin). c) The attack of the radical (**15**) to the carbonyl carbon atom (C-3) of friedelin (**1**), followed by β-scission between C-3 and C-4, and then by addition of a hydrogen atom to the carbon atom at C-4.

In order to distinguish among these hypotheses, 2α,2β,4α-trideuteriofriedelin (**1**-d_3) was irradiated in ether containing acetone. A trideuteriated hydroxy ketone (**5**-d_3) was obtained showing the molecular ion peak at *m/e* 489. The trideuteriated hydroxy ketone (**5**-d_3) was degradated to give **8**-d_3 and **9**-d_3 by the previously described procedures. In the PMR of the trideuteriated seco-aldehyde (**8**-d_3), the aldehydic proton was observed as a doublet. Furthermore, a triplet signal due to the methyl group (proton on C-23) attached to the C-4 atom of non-labeled alcohol (**9**) appeared as a singlet in the case of the trideuteriated seco-alcohol (**9**-d_3).

These observations lead to the conclusion that 1-hydroxy-1-methylethyl radical (**15**) attacked the carbonyl carbon atom of the ketene (**12**) to form a C-2 radical, which abstracts a hydrogen atom from the solvent (mechanism "a"). The alternative mechanisms "b" and "c" are excluded by the same experiment, since the degradation of the photo-product (**5'**-d_3) would lead to the aldehyde (**8'**-d_3) and then to the alcohol (**9'**-d_3). The aldehydic proton of **8'**-d_3 and the methyl protons at C-4 of **9'**-d_3 should resonate as a singlet and a doublet, respectively, in the PMR spectra. The formation of the keto ether (**2**), obtained by the photo-irradiation of friedelin (**1**) in ether, may also best be interpreted by a pathway analogous to the mechanism "a".

Experimental

Instruments and general procedures are described in previous papers.[1,2k] Gas-liquid phase chromatographic (GLC) analyses were determined on a Shimadzu gas chromatograph model GC-6A. Analytical and preparative thin layer chromatographies (TLC) were carried out on Kieselgel G nach Stahl (E. Merck) and Silica gel PF_{254} (E. Merck), respectively. Column chromatography was carried out on Wakogel C-200 (Wako). Diethyl ether (Wako) was washed with dilute sulfuric acid and water and dried over calcium chloride. The ether was distilled from lithium aluminium hydride. Acetone (Wako) was dried over potassium carbonate and distilled.

Photochemical Reaction of Friedelin (1) in Diethyl Ether. Nitrogen (Suzuki-shokan Co.) was bubbled through a refluxing solution of friedelin (**1**: 455 mg) in diethyl ether (300 ml) for 30 min, then the solution cooled to room temperature was irradiated with a high pressure mercury lamp for 7 h under nitrogen. The solvent was evaporated under reduced pressure, the residue dissolved in benzene and passed through a column of silica gel (50 g), and eluted with benzene (each fraction 50 ml). In fractions 1—3, hydrocarbons and aldehydes were eluted and from fractions 4—13 a residue (131 mg) was obtained. Subjection of the residue to preparative TLC using benzene–chloroform (1: 1) afforded fractions A, B, and C. Each fraction was further separated by preparative TLC developed with benzene–ether (10: 1).

The keto ether (**2**; 24 mg) was isolated from the fraction A but could not be separated into each diastereomer by TLC using various eluents. A few milli grams of a stereoisomer of the hydroxy ether (**3a**; IR (Nujol) 3580, 3470, and 1100 cm^{-1}; MS *m/e* 488) was also obtained from the fraction A.

The fraction B gave a diastereomer of the hydroxy ether (**3b**; about 40 mg) by the second preparative TLC, IR (Nujol) 3580, 3470, and 1100 cm^{-1}; MS *m/e* 488; the PMR and high resolution mass spectra (*vide infra*).

From the fraction C, the third isomer of the hydroxy ether (**3c**; a few mg; IR (Nujol) 3580, 3470, and 1100 cm^{-1}; MS *m/e* 488) and the norseco-alcohol (**4**; 9 mg) were isolated.

10β-(4-Ethoxy-3-oxopentyl)-5α-ethyl-des-A-friedelane (2). The keto ether (**2**) was obtained as an oil, IR (Nujol) 1705, 1110, 1000, 910, 850, and 800 cm^{-1}; PMR δ ≈0.80 (6H, s and t overlapped, 2×CH_3), 0.89, 0.97, 1.20, 1.25 (each 3H, s, *t*-CH_3), 1.00—1.05 (12H, br. s, 4×CH_3), 2.58 (2H, t, J=8 Hz, $C_{(2)}$-H), 3.49 (2H, q, J=7 Hz, $CH_3C\underline{H}_2O$), and 3.79 (1H, q, J=7 Hz, $CH_3\underline{C}H$–O); MS *m/e* 500 (M^+, 18%), 485, 471, 455, 427, 371, 333, 312, 301, 273 (100%), 259, 245, 231, 218, and 205; Found: C, 81.24; H, 11.93%. Calcd for $C_{34}H_{60}O_2$: C, 81.53; H, 12.08%.

10β-(3-Ethoxy-2-hydroxybutyl)-5α-ethyl-des-A-friedelane (3). Three diastereomers (**3a**—**c**) were obtained as oil and gave similar spectral data (*vide supra*). The hydroxy ether (**3b**), obtained from fraction B, provided the following data; IR (Nujol) 3580, 3470, 1100, 1000, 850, and 800 cm^{-1}; PMR δ ≈0.80 (6H, s and t overlapped, 2×CH_3), 0.90, 0.96 (each 3H, s, *t*-CH_3), 1.01 (12H, br. s, 4×CH_3), 1.19 (6H, s, 2×CH_3), 3.48 (2H, q, J=7 Hz, $CH_3C\underline{H}_2O$), 3.52 (1H, q, J=7 Hz, $CH_3\underline{C}H$–O), and 3.3—3.8 (1H, br. s, $C_{(2)}$–H); MS *m/e* 488 (M^+, 22%), 473, 459, 432, 411, 402, 387, 385, 301, 273 (100%), 218, and 205; MW 488.4636 (by high resolution mass spectrometry). Calcd for $C_{33}H_{60}O_2$: 488.4591.

5α-Ethyl-10β-(2-hydroxyethyl)-des-A-friedelane (4). Crystallization from ether gave colorless crystals, mp 155—156 °C; IR (Nujol) 3300, 1050, and 800 cm^{-1}; PMR δ ≈0.80

(6H, s, and t overlapped, $2\times CH_3$), 0.89, 0.97, 1.19 (each 3H, s, t-CH_3), 1.01 (9H, s, $3\times t$-CH_3), and 3.53 (2H, t, J=8 Hz, $C_{(2)}$-H); MS *m/e* 416 (M^+, 33%), 401, 387, 381, 360, 301, 273 (100%), 249, 218, and 205. This was identical with an authentic 5α-ethyl-10β-(2-hydroxyethyl)-des-A-friedelane (**4**).

Degradation of 10β-(4-Ethoxy-3-oxopentyl)-5α-ethyl-des-A-friedelane (2). The keto ether (**2**; 38 mg) in ether (30 ml) and lithium aluminium hydride (150 mg) were heated under reflux for 3 h. The usual work-up and separation on preparative TLC using benzene–ether (10: 1) gave 10β-(4-ethoxy-3-hydroxypentyl)-5α-ethyl-des-A-friedelane (**6**; 32 mg) as a mixture of diastereomers; an amorphous solid, IR (Nujol) 3550, 3450, 1100, 1000, 840, and 800 cm^{-1}; PMR $\delta \approx 0.79$ (6H, s and t overlapped, $2\times CH_3$), 0.89, 0.95 (each 3H, s, t-CH_3), 1.00 (12H, br. s, $4\times CH_3$), and 3.15—3.85 (4H, m, CH–O–); MS *m/e* 502 (M^+, 10%), 487, 473, 446, 430, 415, 401, 335, 323, 301, 273 (100%), 218, and 205.

A solution of **6** (26 mg) in dry methylene dichloride (1 ml) was kept at −78 °C, and a solution of boron trichloride (3 ml) in methylene dichloride (2 ml) was added. The resulting solution was stirred at −78 °C for 2 h and then allowed to stand overnight at room temperature. The solvent was removed under reduced pressure and aqueous methanol was added. Methanol was removed under reduced pressure and the residue was extracted with ether (100 ml). Usual work-up and purification by preparative TLC developed with benzene–ether (10: 1) afforded diastereomers of 10β-(3,4-dihydroxypentyl)-5α-ethyl-des-A-friedelane (**7**; 9 mg) as an oil; IR (Nujol) 3400 and 1080 cm^{-1}; PMR $\delta \approx 0.80$ (6H, s and t overlapped, $2\times CH_3$), 0.89, 0.95, 1.19 (each 3H, s, t-CH_3), 1.00 (12H, br. s, $4\times CH_3$), and 3.25—3.95 (2H, m); MS *m/e* 474 (M^+, 12%), 459, 457, 445, 441, 425, 418, 413, 380, 307, 301, 273 (100%), 218, and 205.

To a solution of the diastereomeric diols (**7**; 8.4 mg) in benzene (5 ml), a saturated solution of lead tetraacetate in acetic acid (10 ml) was added and the mixture was stirred at room temperature for 2 h. A saturated aqueous sodium hydrogencarbonate solution was added and the mixture was extracted with ether. The reaction products were separated by preparative TLC using benzene to afford 5α-ethyl-10β-(2-formylethyl)-des-A-friedelane (**8**; 5.4 mg). This was identical with an authentic seco-aldehyde (**8**).

Degradation of 10β-(3-Ethoxy-2-hydroxybutyl)-5α-ethyl-des-A-friedelane (3). Due to a paucity of the hydroxy ethers (**3a**—**c**), these compounds were combined and subjected to the following degradation.

A solution of the hydroxy ethers (**3a**—**c**; 41 mg) in methylene dichloride (1 ml) was kept at −78 °C and a solution of boron trichloride (3 ml) in methylene dichloride (2 ml) was added. The resulting solution was stirred at 0 °C for 1.5 h and then at room temperature for 5 h. The solvent was removed under reduced pressure and aqueous methanol (1 ml) was added. Methanol was removed under reduced pressure and the residue was extracted with ether (100 ml). After usual work-up, the reaction mixture was separated by preparative TLC using benzene–ether (10: 1) to give diastereomers of 10β-(2,3-dihydroxybutyl)-5α-ethyl-des-A-friedelane (**10**; 18 mg) as an oil; IR (Nujol) 3400, 1050, 980, 860, and 800 cm^{-1}; PMR $\delta \approx 0.83$ (6H, s and t overlapped, $2\times CH_3$), 0.90, 0.95, 1.19 (each 3H, s, t-CH_3), 1.10 (12H, br. s, $4\times CH_3$), and 3.20—3.38 (2H, m); MS *m/e* 460 (M^+, 31%), 445, 431, 427, 404, 380, 301, 293, 273 (100%), 218, and 205.

To a solution of the diols (**10**; 18 mg) in benzene (5 ml), a saturated solution of lead tetraacetate in acetic acid (10 ml) was added. The solution was treated according to the same procedure as in the case of the diols (**7**). 5α-Ethyl-10β-formylmethyl-des-A-friedelane (**11**; 10 mg) was obtained, mp 182 °C (crystallized from ether); IR (Nujol) 2710 and 1705 cm^{-1}; PMR $\delta \approx 0.80$ (6H, s and t overlapped, $2\times CH_3$), 0.90, 0.96, 1.20 (each 3H, s, t-CH_3), 1.01 (9H, s, $3\times CH_3$), and 9.78 (1H, t, J=2.5 Hz, -CHO); MS *m/e* 414 (M^+, 27%), 399, 301, 290, 273, 218, and 205 (100%). This was identical with an authentic norseco-aldehyde (**11**).[2f,g,j]

Photochemical Reaction of Friedelin-^{18}O (1-^{18}O) in Ether. Irradiation of friedelin-^{18}O (**1**-^{18}O; 180.7 mg) in ether (200 ml) in a quartz vessel under a nitrogen atmosphere for 10 h, followed by solvent removal under reduced pressure yielded a residue, which was chromatographed on silica gel (20 g). A norseco-alcohol fraction was further subjected to preparative TLC to give 5.2 mg of **4**. The ^{18}O-isotopic abundance in the starting material (**1**-^{18}O) and the product (**4**) was examined by the mass spectrometry (Table 1).

Photochemical Reaction of Friedelin (1) in Ether Containing Deuterium Oxide. Friedelin (**1**; 322 mg) was dissolved in ether (200 ml) which was freshly distilled from lithium aluminium hydride and was saturated with deuterium oxide (D_2O 99.75%, Showa-denko Co.). The solution was irradiated for 8 h as before. The same work-up and separation procedure gave the norseco-alcohol (**4**; 9.1 mg). The deuterium isotopic abundance of the product (**4**) was examined by mass spectrometry (*Cf.* Table 2).

Photochemical Reaction of 2α,2β,4α-Trideuteriofriedelin (1-d_3) in Ether. Trideuteriofriedelin** (**1**-d_3; 292 mg) in ether (200 ml) was irradiated under the same conditions for 10 h and worked up as before to afford a trideuterio norseco-alcohol (**4**-d_3; 7.3 mg), PMR $\delta \approx 0.80$ (6H, s, $2\times CH_3$), 0.89, 0.95, 1.19 (each 3H, s, t-CH_3), 1.00 (9H, s, $3\times t$-CH_3), and 3.53 (1H, t, J=8 Hz, $C_{(2)}$-H); MS *m/e* 419 (M^+, 19%), 404, 388, 301, 273, 218, and 205 (100%). When $Eu(dpm)_3$ was added to a 1% (w/v) solution of **4**-d_3 in $CDCl_3$ [$Eu(dpm)_3$/**4**-d_3=1.1 (in molar ratio)], $C_{(4)}$-CH_3 signal appeared at δ 2.35 as a singlet. Under the same conditions, $C_{(4)}$-CH_3 of non-labeled alcohol (**4**) resonated at δ 2.35 as a triplet (J=7 Hz).

Photochemical Reaction of Friedelin (1) in Ether Under Oxygen-free Argon. Friedelin (**1**; 1.07 g) in ether (700 ml) was heated under reflux for 30 min with bubbling of oxygen-free argon*** in a quartz irradiation vessel. The solution, after cooling, was irradiated for 24 h under the oxygen-free argon at room temperature. The solvent was removed under reduced pressure to give a residue, which was examined by TLC and shown to contain neither **3** nor **4**. The residue was dissolved in benzene, passed through a column of silica gel (100 g), and eluted with benzene (each fraction 100 ml). Fractions 5 and 6 were combined and further subjected to preparative TLC developed with benzene–petroleum ether–methylene dichloride (4: 3: 2) to give keto ether component (**2**; 78 mg).

Photochemical Reaction of 5α-Ethyl-10β-formylmethyl-des-A-friedelane (11). A solution of the norseco-aldehyde (**11**; 178 mg, prepared from norfriedelin[2j]) in ether (700 ml) was irradiated in a Pyrex vessel for 62 h under a nitrogen atmosphere at room temperature. After usual treatment, preparative TLC using benzene–chloroform (1: 1) gave the three diastereomers of hydroxy ether (**3a**—**c**; total weight 49 mg) and the norseco-alcohol (**4**; 11 mg).

Photochemical Reaction of Friedelin (1) in Ether Under an Oxygen Atmosphere. Friedelin (**1**; 1.01 g) in ether (800 ml)

** Mass spectrometry showed that the deuteriated friedelin (**1**-d_3) consisted of -d_3 (80%), -d_2 (20%), -d_1 (0%), and -d_0 (0%).

*** Argon was purified by passing over copper (pretreated with a flow of hydrogen at 200 °C) placed in a quartz tube and heated at 500 °C.

was irradiated in a Pyrex vessel with a high pressure mercury lamp for 48 h under an oxygen atmosphere at room temperature.[2h] The solvent was removed to afford a residue. The TLC examination showed the presence of friedelin (recovered unchanged, a major spot), the seco-carboxylic acid (**16**), a norseco-carboxylic acid[2e,j] and putranjivic acid,[2h,13] while the presence of the hydroxy ether (**3**) and the norseco-alcohol (**4**) could not be demonstrated.

Photochemical Reaction of Friedelin (1) in Ether Containing Acetone. Friedelin (**1**; 86 mg) was dissolved in ether (30 ml) containing acetone (0.5 ml) in a quartz vessel and heated under reflux for 30 h with bubbling of nitrogen. The solution was cooled and irradiated with a high pressure mercury lamp for 2 h at room temperature. A small quantity of the solution was taken out and subjected to GLC examination, which showed the formation of pinacol (R_t 7.7 min (Carbowax C-20 M, 100 °C) and 11.7 min (DGS, 100 °C)). The reaction mixture, after evaporation of the solvent under reduced pressure, was separated by preparative TLC with benzene as eluent. 5α-Ethyl-10β-(4-hydroxy-4-methyl-3-oxopentyl)-des-A-friedelane (**5**; 12 mg) was obtained after recrystallization from light petroleum, mp 180.5—181.5 °C; IR (Nujol) 3500, 1705, and 1140 cm^{-1}; PMR δ ≈0.80 (6H, s and t overlapped), 0.89, 0.95, 1.03, 1.18 (each 3H, s, *t*-CH_3), 1.00 (6H, s, 2×*t*-CH_3), 1.37 (6H, s, $(C\underline{H}_3)_2C(OH)$-), 2.40—2.75 (2H, m, -$C\underline{H}_2$-C=O), and 3.77 (1H, s, -C̈-OH; disappeared on addition of D_2O); (CD_3COCD_3) δ≈4.18 (1H, s, -C̈-OH; disappeared on addition of D_2O); MS *m/e* 486 (M^+, 10%), 471, 457, 453, 443, 430, 428, 413, 319, 307, 275, 274, 273, and 205 (100%); Found: C, 81.57; H, 12.07%. Calcd for $C_{33}H_{58}O_2$: C, 81.42; H, 12.01%.

Acetate of 5α-Ethyl-10β-(4-hydroxy-4-methyl-3-oxopentyl)-des-A-friedelane (5). A mixture of the hydroxy ketone (**5**; 32 mg), pyridine, and acetic anhydride was heated on stream bath for 10.5 h. The reaction mixture was treated as usual and the product crystallized from methanol twice to afford the acetate (21 mg), mp 159—160 °C; IR (Nujol) 1724 and 1247 cm^{-1}; PMR δ≈0.79 (6H, s and t overlapped, 2×CH_3), 0.86, 0.94, 1.01, 1.17 (each 3H, s, *t*-CH_3), 0.99 (6H, s, 2×*t*-CH_3), 1.44 (6H, s, $(C\underline{H}_3)_2C(OAc)$-), and 2.25—2.60 (2H, m, -CH_2C=O); MS *m/e* 528 (M^+).

Degradation of 5α-Ethyl-10β-(4-hydroxy-4-methyl-3-oxopentyl)-des-A-friedelane (5). To the hydroxy ketone (**5**; 12 mg) in ether (5 ml), lithium aluminium hydride (17 mg) in ether (5 ml) was added and the mixture was heated under reflux for 2 h. After decomposition of the excess reagent by addition of wet ether, the mixture was treated as usual. Column chromatography of the residue on silica gel (50 g) afforded a mixture of the diastereomeric diols (**17**; 9 mg), mp 188—189 °C; IR (Nujol) 3400, 1170, 1080, and 960 cm^{-1}; PMR δ ≈0.80 (6H, s and t overlapped, 2×CH_3), 0.90, 0.96, 1.03, 1.16, 1.19, 1.21 (each 3H, s, *t*-CH_3), 1.01 (6H, s, 2×*t*-CH_3), and 4.62 (1H, s, -C̈-OH; disappeared on addition of D_2O); MS *m/e* 488 (M^+, 15%), 473, 470, 459, 455, 441, 432, 430, 415, 321, 309, 301, 273 (100%), 218, and 205; Found: C, 79.80; H, 12.51%. Calcd for $C_{33}H_{60}O_2 \cdot 1/2\,H_2O$: C, 79.62; H, 12.35%.

A saturated solution of lead tetraacetate in acetic acid (10 ml) was added to the diols (**17**; 2.8 mg) in benzene (5 ml) and the mixture was stirred for 1 h. The excess lead tetraacetate was decomposed by addition of saturated sodium hydrogencarbonate solution until the solution became alkaline and the solution was extracted with ether (500 ml). After usual work-up, the residue was chromatographed on silica gel using benzene to give an aldehyde (**8**; 2.5 mg). This was identical with an authentic seco-aldehyde (**8**).

A mixture of silver nitrate (41 mg) in water (1 ml) and 0.05 M sodium hydroxide solution (5 ml) was added to the seco-aldehyde (**8**; 1.8 mg) in ethanol (5 ml) with stirring, which was continued for 2 h. The solvents were evaporated under reduced pressure to give a residue, to which ether (100 ml) was added. The resulting solution was acidified with 1 M hydrochloric acid and extracted with ether. After usual work-up, purification of the residue by preparative TLC afforded 10β-(2-carboxyethyl)-5α-ethyl-des-A-friedelane (**16**; 1.1 mg); IR (Nujol) 1705, 1290, and 1220 cm^{-1}; MS *m/e* 444 (M^+, 16%), 429, 405, 401, 388, 369, 368, 320, 301, 291, 273, 218 (100%), and 205. This was identical with an authentic seco-carboxylic acid (**16**).[2b]

Synthesis of 5α-Ethyl-10β-(4-hydroxy-4-methyl-3-oxopentyl)-des-A-friedelane (5) from 5α-Ethyl-10β-(3-hydroxypropyl)-des-A-friedelane (9). 5α-Ethyl-10β-(3-hydroxypropyl)-des-A-friedelane (**9**; 694 mg) was dissolved in a minimum volume of methylene dichloride and a mixture of chromium trioxide (1.34 g), pyridine (840 mg), and methylene dichloride (23 ml) was added to the solution. After stirring for 15 min, the methylene dichloride solution was separated by decantation and the precipitate was washed with methylene dichloride (150 ml). The supernatant and the washings were combined and washed with 5% sodium hydrogencarbonate solution (100 ml), 5% hydrochloric acid (100 ml), and then with 5% sodium hydrogencarbonate solution (100 ml). Usual work-up gave a residue, which was recrystallized from ether to afforded the seco-aldehyde (**8**; 657 mg); mp 147—148 °C; IR (Nujol) 2720, 1720, and 1005 cm^{-1}; PMR δ ≈0.81 (6H, s and t overlapped, 2×CH_3), 0.90, 0.96, 1.19 (each 3H, s, *t*-CH_3), 1.01 (9H, s, 3×*t*-CH_3), 2.20—2.60 (2H, m, -$C\underline{H}_2$-CHO), and 9.73 (1H, t, *J*=2 Hz, -CHO); MS *m/e* 428 (M^+, 9%), 413, 400, 399, 385, 372, 362, 319, 304, 279, 273, 265 (100%), 218, and 205; Found: C, 84.26; H, 12.44%. Calcd for $C_{30}H_{52}O$: C, 84.04; H, 12.23%.

To a suspension of isopropyltriphenylphosphonium bromide (960 mg) in ether, 15% butyllithium solution in hexane (2.1 ml) was added with stirring under nitrogen. A deep red solution was obtained, to which a solution of the seco-aldehyde (**8**; 206 mg) in ether (10 ml) was added. The reaction mixture was stirred for 3 h and then tetrahydrofuran (50 ml) was added. The ether was removed and the remaining solution was heated under reflux for 2 h. After cooling, water (100 ml) was added to the solution and the mixture was extracted with ether (200 ml). The ethereal extract was washed with saturated aqueous sodium chloride solution, 1 M hydrochloric acid (100 ml) and then with aqueous sodium chloride solution. Usual work-up gave a residue, which was purified by column chromatography on silica gel (30 g) using petroleum ether. Recrystallization from petroleum ether gave the isopropylidene derivative (**18**; 130 mg), mp 147.5—148 °C; IR (Nujol) 1050, 1000, and 990 cm^{-1}; PMR δ≈1.50 (3H, br., C=C-CH_3), 1.68 (3H, br., C=C-CH_3), and 5.10 (1H, t, *J*=7 Hz, C=C$\underline{H}$-CH_2-); MS *m/e* 454 (M^+, 17%) and 205 (100%); Found: C, 87.38; H, 12.90%. Calcd for $C_{33}H_{58}$: C, 87.14; H, 12.86%.

To a solution of the isopropylidene derivative (**18**; 68 mg) in ether (5 ml), osmium tetraoxide (55 mg) in pyridine (1 ml) was added and the reaction mixture was stirred for 6 h. The solvents were evaporated and ethanol (3 ml), sodium sulfite (406 mg), and water (1 ml) were added to the residue. The reaction mixture was heated under reflux for 2 h and, after cooling, filtered. The precipitate was washed with ethanol. The filtrate and the washings were combined and evaporated under reduced pressure, and the residue purified by column chromatography on silica gel (20 g). Elution with benzene–ether (5: 3) afforded a mixture of the diastereomeric diols (**17**; 27 mg), mp 188—189 °C (crystallized from ether); IR (Nujol) 3400, 1170, 1090, and 960 cm^{-1}; PMR δ ≈0.80 (6H,

s and t overlapped, $2\times CH_3$), 0.90, 0.96, 1.03, 1.16, 1.19, 1.21 (each 3H, s, *t*-CH_3), 1.01 (6H, s, $2\times$*t*-CH_3), and 4.62 (1H, s, -C̲-OH; disappeared on addition of D_2O); MS *m/e* 488 (M^+, 31%) and 273 (100%).

To a solution of chromium trioxide (60 mg) in pyridine (52 mg) and methylene dichloride (50 ml), the diols (**17**; 22 mg) in methylene dichloride (5 ml) was added and the reaction mixture was stirred for 15 min. The methylene dichloride solution was separated by decantation and the precipitate was washed with methylene dichloride (100 ml). The supernatant and washings were combined and washed with 5% sodium hydrogencarbonate solution. After usual work-up, the residue was subjected to column chromatographic separation to afford the seco-aldehyde (**8**; 12 mg) and the hydroxy ketone (**5**; 3 mg). The former was identical with the seco-aldehyde (**8**). The latter was completely identical with the photoproduced hydroxy ketone (**5**).

Photochemical Reaction of Friedelin (1) in Ether Containing Acetone-d_6. Friedelin (**1**; 317 mg) was dissolved in ether (150 ml) containing acetone-d_6 (1 ml; 99.8%, Showa-denko Co.) in a quartz vessel, The solution was irradiated for 5 h under the same conditions and then treated as before. The residue was chromatographed on silica gel (50 g), eluted with benzene and fractions containing the keto ether were collected and purified by preparative TLC to give 5α-ethyl-10β-(5,5,5-trideuterio-4-hydroxy-4-trideuteriomethyl-3-oxopentyl)-des-A-friedelane (**5**-d_6; 45 mg); IR (Nujol) 3500, 2220, 1705, and 1130 cm^{-1}; PMR δ ≈0.80 (6H, s and t overlapped), 0.89, 0.95, 1.03, 1.18 (each 3H, s, *t*-CH_3), 1.00 (6H, s, $2\times$*t*-CH_3), 2.40—2.75 (2H, m, -C̲H_2-C̲=O), and 3.75 (1H, s, -OH); MS *m/e* 492 (M^+, 15%), 477, 463, 446, 443, 428, 413, 325, 313, 301, 273, 218, and 205 (100%).

Photochemical Reaction of 2α,2β,4α-Trideuteriofriedelin (1-d_3*) in Ether Containing Acetone.* 2α,2β,4α-Trideuteriofriedelin (**1**-d_3; 514 mg) was dissolved in ether (450 ml) containing acetone (2 ml) and the solution was irradiated for 5 h. The reaction mixture was treated as usual and separated by column chromatography on silica gel (50 g) and subsequently preparative TLC to afford 5α-(1,1-dideuterioethyl)-10β-(2-deuterio-4-hydroxy-4-methyl-3-oxopentyl)-des-A-friedelane (**5**-d_3; 55 mg); IR (Nujol) 3500, 2160, 2100, 1705, 1130, and 980 cm^{-1}; PMR δ ≈0.80 (6H, s and t overlapped, $2\times CH_3$), 0.89, 0.95, 1.02, 1.08 (each 3H, s, *t*-CH_3), 1.00 (6H, s, $2\times$*t*-CH_3), 1.37 (6H, s, $(C\underline{H}_3)_2C(OH)$-), 2.30 (1H, m, -CHD-C=O), and 3.76 (1H, br., -OH); MS *m/e* 489 (M^+, 9%) and 205 (100%).

Degradation of Trideuterio-5α-ethyl-10β-(4-hydroxy-4-methyl-3-oxopentyl)-des-A-friedelane (5-d_3*).* The hydroxy ketone-d_3 (**5**-d_3; 48 mg) in ether (10 ml) was heated under reflux with lithium aluminium hydride (47 mg) and usual treatment and separation gave the diols-d_3 (**17**-d_3; 20 mg); MS *m/e* 419 (M^+, 24%), 476, 458, 324, 301, 273 (100%), 218, and 205.

To the diols-d_3 (**17**-d_3; 18 mg) in benzene (10 ml), was added lead tetraacetate (45 mg) in acetic acid (15 ml) and the reaction mixture was stirred for 3 h. Usual treatment and purification afforded the aldehyde-d_3 (**8**-d_3; 16 mg); PMR δ ≈0.80 (6H, s and t overlapped, $2\times CH_3$), 0.90, 0.97, 1.19 (each 3H, s, *t*-CH_3), 1.00 (9H, s, $3\times$*t*-CH_3), 2.20—2.60 (1H, m, -C̲HD-CHO), and 9.73 (1H, d, J=2 Hz, -CHD-C̲HO); MS *m/e* 431 (M^+, 19%), 416, 301, 273, 218 (100%), and 205.

A mixture of the trideuterio-seco-aldehyde (**8**-d_3; 15 mg) in ether (10 ml) and lithium aluminium hydride (70 mg) was heated under reflux for 3 h. After usual work-up, separation afforded 2,4,4-trideuterio-5α-ethyl-10β-(3-hydroxypropyl)-des-A-friedelane (**9**-d_3; 12 mg); IR (Nujol) 3600, 3450, 2160, 1280, and 1050 cm^{-1}; PMR δ ≈0.79 (6H, s and t overlapped, $2\times CH_3$), 0.88, 0.96, 1.19 (each 3H, s, *t*-CH_3), 1.00 (9H, s, $3\times$*t*-CH_3), 3.95 (2H, d, J=6 Hz, -CHD-C̲H_2OH); MS *m/e* 433 (M^+, 31%), 428, 402, 301, 279, 273 (100%), 265, 218, and 205. When $Eu(dpm)_3$ was added to a 1.6% (w/v) solution of **9**-d_3 in $CDCl_3$ [$Eu(dpm)_3$/**9**-d_3=1.1 (in molar ratio)], $C_{(4)}$-CH_3 signal appeared at δ 2.12 as a singlet. Under the same conditions, $C_{(4)}$-CH_3 of non-labeled alcohol (**9**) resonated at δ 2.12 as a triplet (J=7 Hz).

Photochemical Reaction of Friedelin (1) in Acetone. Friedelin (**1**; 705 mg) in acetone (88 ml) in a Pyrex vessel was photolyzed. The rate of the photolysis was very slow and the photolysate after 27 h-irradiation was found to consist of recovered friedelin (**1**; 545 mg), the hydroxy ketone (**5**; 12 mg), and an unknown hydroxy dicarbonyl compound (32 mg).

The authors wish to thank Dr. Hidehiro Ishizuka for PMR (100 MHz) measurements, and Dr. Kazuyuki Aizawa for the measurements of the high resolution mass spectrum.

References

1) A part of this work was reported in a preliminary form: H. Shirasaki, T. Tsuyuki, T. Takahashi, and R. Stevenson, *Tetrahedron Lett.*, **1975**, 2271.

2) a) F. Kohen and R. Stevenson, *Chem. Ind. (London)*, **1966**, 1844; b) T. Tsuyuki, S. Yamada, and T. Takahashi, *Bull. Chem. Soc. Jpn.*, **41**, 511 (1968); c) T. Tsuyuki, R. Aoyagi, S. Yamada, and T. Takahashi, *Tetrahedron Lett.*, **1968**, 5263; d) F. Kohen, A. S. Samson, S. J., and R. Stevenson, *J. Org. Chem.*, **34**, 1355 (1969); e) M. Takai, R. Aoyagi, S. Yamada, T. Tsuyuki, and T. Takahashi, *Bull. Chem. Soc. Jpn.*, **43**, 972 (1970); f) R. Stevenson, T. Tsuyuki, R. Aoyagi, and T. Takahashi, *ibid.*, **44**, 2567 (1971); g) R. Aoyagi, T. Tsuyuki, T. Takahashi, and R. Stevenson, *Tetrahedron Lett.*, **1972**, 3397; h) R. Aoyagi, T. Tsuyuki, and T. Takahashi, *Bull. Chem. Soc. Jpn.*, **46**, 692 (1973); i) R. Aoyagi, S. Yamada, T. Tsuyuki, and T. Takahashi, *ibid.*, **46**, 959 (1973); j) R. Aoyagi, T. Tsuyuki, M. Takai, T. Takahashi, F. Kohen, and R. Stevenson, *Tetrahedron.*, **29**, 4331 (1973); k) H. Shirasaki, R. Aoyagi, T. Tsuyuki, T. Takahashi, and R. Stevenson, *Bull. Chem. Soc. Jpn.*, **48**, 1073 (1975).

3) T. Murae, A. Sugie, T. Tsuyuki, S. Masuda, and T. Takahashi, *Tetrahedron*, **29**, 1515 (1973).

4) M. Jones, Jr. and R. A. Moss Ed., "Carbenes," Vol. I, John Wiley & Sons, New York (1973), p. 4.

5) H. Staudinger, *Ber.*, **58B**, 1075, 1079 (1925).

6) P. D. Bartlett and L. B. Gortler, *J. Am. Chem. Soc.*, **85**, 1868 (1963).

7) R. O. Kan, "Organic Photochemistry," McGraw-Hill, New York (1966), p. 222.

8) C. F. Hauser, T. W. Brooks, M. L. Miles, M. A. Raymond, and G. B. Butler, *J. Org. Chem.*, **28**, 372 (1963).

9) U. H. M. Fagerlund and D. R. Idler, *J. Am. Chem. Soc.*, **79**, 6473 (1957).

10) F. Sondheimer and R. Mechoulam, *J. Am. Chem. Soc.*, **79**, 5029 (1957).

11) C. Djerassi and C. R. Scholz, *J. Am. Chem. Soc.*, **71**, 3962 (1949).

12) R. Ratcliffe and R. Rodehorst, *J. Org. Chem.*, **35**, 4000 (1970).

13) a) G. R. Chopra, A. C. Jain, and T. R. Seshadri, *Curr. Sci.*, **37**, 301 (1968); *Chem. Abstr.*, **69**, 93685q (1968); b) G. R. Chopra, A. C. Jain, T. R. Seshadri, and G. R. Sood, *Indian J. Chem.*, **8**, 776 (1970); *Chem. Abstr.*, **74**, 1024a (1971); c) G. R. Chopra, A. C. Jain, and T. R. Seshadri, *Indian J. Chem.*, **7**, 1179 (1969); *Chem. Abstr.*, **72**, 67139g (1970); d) P. Sengupta and A. K. Dey, *Tetrahedron*, **28**, 1307 (1972).

A Facile Synthesis of Anomeric Methyl DL-Tolyposaminides, Methyl DL-Forosaminides, and Related Substances[1)]

Eisuke KAJI, Haruo KOHNO, and Shonosuke ZEN

School of Pharmaceutical Sciences, Kitasato University, Shirokane, Minato-ku, Tokyo 108

(Received August 7, 1976)

The reaction of β-nitro alcohols (2-nitroethanol, 1-nitro-2-propanol, and 1-nitro-2-butanol) with acrylaldehyde in the presence of diethylamine–formic acid gave anomeric mixture of 4-nitro-DL-pento-, hexo-, and heptopyranoses (**5**) in reasonable yields. **5** were converted to the corresponding methyl 4-amino-DL-pento-, hexo-, and heptopyranosides (**8**) by *O*-methylation followed by reduction. Anomeric methyl DL-tolyposaminides and DL-forosaminides were synthesized in a good yield from anomeric methyl 4-nitro-2,3,4,6-tetradeoxy-DL-*erythro*-hexopyranosides (**6b**$_1$ and **6b**$_2$). The configuration of methyl 4-nitro-DL-hexo-, and heptopyranosides (**6b** and **6c**) and methyl 4-acetamido-DL-hexo- and heptopyranosides (**8b** and **8c**) was established on the basis of PMR data.

As a part of the investigation on the exploration of newer synthetic reactions for aliphatic nitro compounds, we had been interested in a facile route to some nitropyranose derivatives, which are potentially useful as substrates for versatile syntheses of amino sugars, especially in the syntheses of amino-polydeoxy sugars contained in several antibiotics, *e.g.*, tolyposamine[2)] and forosamine.[3)] Recently several synthetic routes to these amino-polydeoxy sugars starting from carbohydrate[4)] or non-carbohydrate[5)] precursors have been reported. In this paper we describe a facile synthesis of 4-amino-polydeoxy sugars (**7**) *via* the respective 4-nitro derivatives (**5**) which were obtained by one-step cyclization reaction of β-nitro alcohols with acrylaldehyde using diethylamine–formic acid.[6)]

The reaction of excess nitro alcohols: 2-nitroethanol (**1a**), 1-nitro-2-propanol (**1b**), or 1-nitro-2-butanol (**1c**) with acrylaldehyde in the presence of a catalytic amount of diethylamine–formic acid (1 : 1.75 mol) at 60±5 °C for about 20 h gave anomeric mixtures of 4-nitro-DL-pento-, hexo-, and heptopyranoses (**5a**—**5c**) in a reasonable yield (Table 1). In the case of **5b**, optimum reaction conditions were examined and **5b** was obtained in a 52% yield by equimolar reaction of **1b** with acrylaldehyde at reflux temperature in benzene for 20 h. **5c** was separated into two diastereomers (**5c**$_1$ and **5c**$_2$)

Table 1. 4-Nitro-DL-pento-, hexo-, and heptopyranoses (**5**)

Compound No.	R	Mp (°C)	Yield (%)	α:β[a)]	Formula	Found (%) C	H	N	Calcd (%) C	H	N	IR (KBr) ν_{max} cm^{-1}		
5a	H	81.5—84	39	b)	$C_5H_9NO_4$	41.17	6.04	9.73	40.81	6.17	9.52	3350,	1550,	1380
5b	CH_3	64.5—68.5	52	4:3	$C_6H_{11}NO_4$	44.96	6.93	8.91	44.72	6.83	8.69	3360,	1550,	1350
5c$_1$[c)]	C_2H_5	126.5—128[d)]	66	1:1	$C_{14}H_{16}N_2O_7$[d)]	52.13	5.00	8.77	51.85	4.97	8.64	3400,	1550,	1380[e)]
5c$_2$[c)]	C_2H_5	113.5—116.5[d)]	22	1:1		51.66	4.99	8.60				3400,	1550,	1380[e)]

a) Anomeric composition was determined from signal intensity of anomeric protons in PMR spectra. b) Anomeric composition could not be determined because of overlapping with another signals. c) A diastereomer of **5c**. d) Melting points and analytical data were of *p*-nitrobenzoyl derivatives of **5c**. e) Measured in NaCl for liquid film.

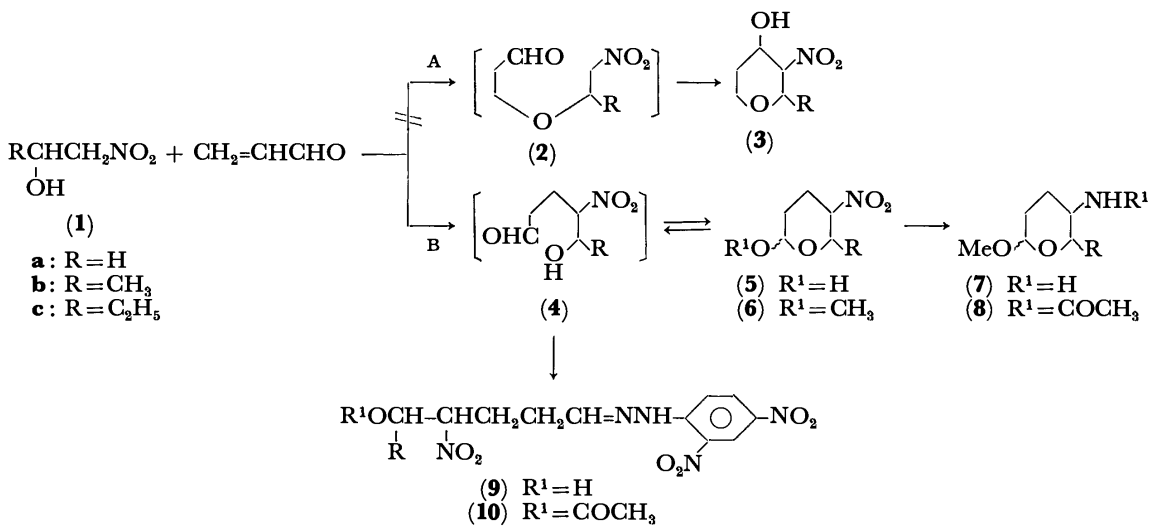

Fig. 1.

Table 2. δ-Hydroxy-γ-nitroaldehyde 2,4-dinitrophenylhydrazones (**9**)

Compound No.	R	Mp (°C)	Yield (%)	Formula	Found (%)			Calcd (%)		
					C	H	N	C	H	N
9a	H	126.5—127.5	79	$C_{11}H_{13}N_5O_7$	40.49	3.98	21.41	40.37	4.00	21.40
9b	CH_3	138—140	6	$C_{12}H_{15}N_5O_7$	41.95	4.37	20.29	42.23	4.43	20.52
9c$_1$[a]	C_2H_5	86—90	5	$C_{13}H_{17}N_5O_7$	43.92	4.98	19.47	43.94	4.82	19.71
9c$_2$[a]	C_2H_5	115—117	34		43.88	4.87	19.43			

a) A diastereomer of **9c**.

Table 3. Methyl 4-nitro-DL-pento-, hexo-, and heptopyranosides (**6**)

Compound No.	Bp°C/Torr (Mp °C)	n_D^{20}	Yield (%)	Formula	Found (%)			Calcd (%)			IR (film) ν_{max} cm^{-1}
					C	H	N	C	H	N	
6a	40—45[a]/0.05	1.4600	84	$C_6H_{11}NO_4$	44.34	6.73	8.98	44.71	6.88	8.69	1550, 1370
6b$_1$	33—35/0.02	1.4520	55	$C_7H_{13}NO_4$	48.12	7.54	7.61	47.99	7.48	8.00	1550, 1375
6b$_2$	39—41/0.02[b]	1.4562	20		47.89	7.52	7.83				1550, 1345
6c$_1$	49—51/0.04	1.4532	41		51.19	8.16	7.00				1550, 1375
6c$_2$	58—60/0.03	1.4540	20	$C_8H_{15}NO_4$	51.03	8.06	6.99	50.78	7.99	7.40	1550, 1390
6c$_3$	(36.5—37)[c]	—	37		50.52	8.09	7.24				1550, 1370[e]
6c$_4$	(44—45)[d]	—	13		51.08	8.16	7.30				1550, 1370[e]

a) Bath temperature. b) Mp 31.5—32°C recrystallized from ethanol-water. c) Recrystallized from ethanol-water. d) Recrystallized from hexane. e) Measured in KBr disk.

through column chromatography on silica gel.

We attempted an alternative route (path A) for cyclization, where 2-substituted 4-hydroxy-3-nitrotetrahydropyran (**3**) is formed *via* initial ether formation[7] followed by intramolecular condensation[8] as shown in Fig. 1. However, the formation of **3** could not be detected on TLC analysis and column chromatographic purification.

The main structure of **5** was deduced from the following experimental data: (i) The formation of 2,4-dinitrophenylhydrazone (**9**) of δ-hydroxy-γ-nitroaldehyde (**4**), as well as its acetate (**10a**). (ii) Treatment of **5b** with hydrochloric acid in methanol gave α- and β-anomers of methyl hexopyranosides (**6b**$_1$ and **6b**$_2$) which were separated by silica gel column chromatography with benzene as eluant. Analogous methylation of **5c**$_1$ gave anomeric methyl heptopyranosides (**6c**$_1$ and **6c**$_2$). **5c**$_2$ was also methylated to give **6c**$_3$ and **6c**$_4$. Ordinary methylation[9] of **5** using methyl iodide and silver oxide also gave the same **6**. On the other hand, methylation of **5a** under above conditions gave only α-anomer of **6a**. These results are shown in Table 3.

The assignment of configuration of **6** was based on its PMR spectral data. The chemical shifts and coupling constants were assigned as shown in Table 4 with the aid of double resonance method. The anomeric configuration of **6** was readily deduced from the first-order analysis of its spectrum. In the spectrum of **6a**, **6b**$_1$, **6c**$_1$, and **6c**$_3$ a relatively low-field signal (δ 4.65—4.87) of a methine proton exhibits a singlet with fine splitting ($J_{1,2}<5$ Hz), which is assigned to the equatorial hydrogen of C-1. Hence the anomeric configuration is α. On the other hand, in **6b**$_2$ and **6c**$_2$, the anomeric proton exhibits a pair of doublet ($J_{1,2a}=9$ Hz, and $J_{1,2e}<3$ Hz), which is deduced to be the axial hydrogen of the β-anomers. The methoxyl group of α-anomers appeared at higher field (δ 3.40—3.43) in comparison with that of β-anomers (δ 3.52—3.53) as shown in Table 4.

The orientation of C-3 and C-4 positions was established by spin decoupling studies. In the PMR spectrum of **6b**$_1$, irradiation of C-6 methyl protons (δ 1.25) collapsed C-5 methin proton (δ 4.28, multiplet) to a doublet ($J_{4,5}=9$ Hz). Reasonably assuming that **6** has chair conformation, a relatively large H-4, H-5 coupling

Table 4. PMR data of methyl 4-nitro-DL-pento-, hexo-, and heptopyranosides (**6**)

Compound No.	Chemical shift (δ in $CDCl_3$)[a]								Coupling Constant (Hz)				Configuration
	H-1	H-2	H-3	H-4	H-5	H-6	H-7	OCH_3	$J_{1,2a}$	$J_{1,2e}$	$J_{4,5}$	$J_{5,6}$	
6a	4.65	2.3	1.8	4.10	4.3	—	—	3.43	5.0	3.0	b)	—	α
6b$_1$	4.70	2.2	1.9	4.2	4.28	1.25	—	3.42	3.5	2.0	9.0	6.0	*α-erythro*
6b$_2$	4.47	2.3	1.9	4.1	3.94	1.32	—	3.52	9.0	3.0	9.0	6.0	*β-erythro*
6c$_1$	4.72	1.7—2.7		4.40	3.99	1.58	1.00	3.40	3.0	3.0	9.8	5.0	*α-erythro*
6c$_2$	4.46	1.7—2.5		4.18	3.75	1.53	1.02	3.53	9.0	2.5	9.5	6.0	*β-erythro*
6c$_3$	4.87	1.8—2.6		4.57	3.90	1.53	1.05	3.40	3.0	3.0	2.8	7.0	*α-threo*
6c$_4$	4.5	1.9—2.6		4.5	3.61	1.69	1.06	3.53	b)	b)	2.5	6.5	*β-threo*

a) Chemical shifts are in δ scale from TMS as internal standard at 100 MHz. b) Could not be observed from the spectrum by overlapping with another signals.

6b$_1$: R=CH_3, R^1=NO_2 **6b$_2$**: R=CH_3, R^1=NO_2 **6c$_3$**: R=C_2H_5, R^1=NO_2 **6c$_4$**: R=C_2H_5, R^1=NO_2
6c$_1$: R=C_2H_5, R^1=NO_2 **6c$_2$**: R=C_2H_5, R^1=NO_2
8b$_1$: R=CH_3, R^1=NHAc **8b$_2$**: R=CH_3, R^1=NHAc Ac: $COCH_3$, Bz: COC_6H_5
8c$_1$: R=C_2H_5, R^1=NHAc **8c$_2$**: R=C_2H_5, R^1=NHAc
11: R=CH_3, R^1=NHBz **12**: R=CH_3, R^1=NHBz
13: R=CH_3, R^1=NMe_2 **14**: R=CH_3, R^1=NMe_2

Fig. 2. Only the formulae for D-compounds are given.

constant (9 Hz) could be taken as an indication of 4,5-diaxial arrangement of protons.[2] From the above data, **6b$_1$** was concluded to be a methyl 4-nitro-2,3,4,6-tetradeoxy-α-DL-*erythro*-hexopyranoside, and **6c$_1$** was analogously assigned to α-*erythro* configuration. Accordingly **6b$_2$** and **6c$_2$** (anomer of **6b$_1$** and **6c$_1$**) were deduced to have a β-*erythro* configuration. In the spectrum of **6c$_3$**, irradiation of H-6 (δ 1.53) changed the H-5 signal (δ 3.90) into a doublet which has a relatively small coupling constant ($J_{4,5}$=2.8 Hz). Moreover, irradiation of H-5 collapsed the H-4 signal (δ 4.57) to a singlet with fine splitting ($J_{3a,4}$ and $J_{3e,4}$<3 Hz), indicating the equatorial orientation of C-4 hydrogen. Hence, we ascribed it to α-*threo* configuration. Alternatively, β-*threo* configuration was assigned to the minor product (**6c$_4$**), corroborated by $J_{4,5}$ (2.5 Hz) and the chemical shift of the methoxyl group (δ 3.53). This deduction is supported by the fact that **6c$_1$** and **6c$_3$** gave the same PMR spectrum in the presence of NaOD in D_2O in which they would be converted to the same aci-nitro type compound. It should be noted that stereoselectivity of this cyclization reaction depends on the kind of nitro alcohols. The reaction of acrylaldehyde with 1-nitro-2-propanol gave only the anomeric *erythro* isomers, whereas that with 1-nitro-2-butanol gave all the possible isomers.

The reduction of **6a**, **6b$_1$**, **6b$_2$**, **6c$_1$**, and **6c$_2$** over Raney nickel catalyst afforded the corresponding methyl 4-aminopyranosides, which were subsequently acetylated in the usual manner giving methyl 4-acetamido-DL-pento-, hexo-, and heptopyranosides (**8a**, **8b$_1$**, **8b$_2$**, **8c$_1$**, and **8c$_2$**) in reasonable yields (Table 5). However the yield of **8a** remained rather low under the same reaction condition. The structure of **8** was established by its PMR spectra (Table 6) as described above for compound **6**. The large coupling constants between H-4 and H-5 ($J_{4,5}$=9.5—10.0 Hz) strongly suggest that **8b$_1$**, **8b$_2$**, **8c$_1$**, and **8c$_2$** have *erythro* configuration as well as their corresponding nitropyranosides (**6**). Another evidence was provided by a correlation of reference compounds **11** and **12**. The configuration of **8a** was not deduced except anomeric configuration (see Table 6) because the spectrum was rather complicated.

The anomeric methyl *N*-benzoyl-DL-tolyposaminides (methyl 4-benzamido-2,3,4,6-tetradeoxy-α- and β-DL-*erythro*-hexopyranoside (**11** and **12**) were synthesized respectively from the corresponding methyl 4-nitro-DL-*erythro*-hexopyranosides (**6b$_1$** and **6b$_2$**) by hydrogenation followed by benzoylation in a good yield. **11** and **12** were identical with the authentic samples[10] by the

Table 5. Methyl 4-acetamido-DL-pento-, hexo-, and heptopyranosides (**8**)

Compound No.	Mp °C	Yield[a] (%)	Formula	Found (%) C	H	N	Calcd (%) C	H	N	IR (KBr) ν_{max} cm^{-1}			
8a	viscous oil	31	$C_8H_{15}NO_3$	55.09	8.46	7.72	55.47	8.73	8.09	3300,	1650,	1550,	1280[d]
8b$_1$	87.5—90[b]	86	$C_9H_{17}NO_3$	57.61	9.04	7.65	57.73	9.15	7.48	3290,	1635,	1550,	1275
8b$_2$	149.5—150.5[c]	73		57.44	9.07	7.27				3270,	1635,	1560,	1270
8c$_1$	101.5—102.5[b]	91	$C_{10}H_{19}NO_3$	59.70	9.56	6.72	59.67	9.52	6.96	3220,	1640,	1570,	1280
8c$_2$	134—135.5	73		59.60	9.44	6.80				3240,	1630,	1550,	1290

a) Based on methyl 4-aminopyranosides (**7**). b) Recrystallized from petroleum ether. c) Recrystallized from ligroin. d) Measured in NaCl for liquid film.

Table 6. PMR data of methyl 4-acetamido-DL-pento-, hexo-, and heptopyranosides (**8**)

Compound No.	Chemical shift (δ in $CDCl_3$) H-1	H-2	H-3	H-4	H-5	H-6	H-7	OCH_3	NAc	Coupling constant (Hz) $J_{1,2a}$	$J_{1,2e}$	$J_{4,5}$	Configuration
8a	4.58	1.3—2.2		3.57	4.0	—	—	3.43	2.02	3.5	2.0	a)	α
8b$_1$	4.63	1.6—2.2		*ca.* 3.6	3.52	1.18	—	3.33	1.99	3.0	3.0	10.0	α-*erythro*
8b$_2$	4.35	1.4—2.3		*ca.* 3.6	3.33	1.27	—	3.50	1.99	8.0	3.0	9.5	β-*erythro*
8c$_1$	4.70	1.6—2.2		*ca.* 3.8	3.32	1.5	0.97	3.35	1.98	3.0	3.0	9.5	α-*erythro*
8c$_2$	4.33	1.6—2.3		*ca.* 3.7	3.06	1.45	0.98	3.50	1.98	9.0	2.5	9.5	β-*erythro*

a) Could not be obtained because of covering by OMe protons signal.

mixed melting point determination, and IR and PMR spectra.

The reductive dimethylation of **6b**$_1$ and **6b**$_2$ over Raney nickel in the presence of formaldehyde led to methyl 2,3,4,6-tetradeoxy-4-dimethylamino-α-DL-*erythro*-hexopyranoside (methyl α-DL-forosaminide, **13**) and its β-anomer (**14**), respectively. The IR and PMR spectra of these compounds were in good agreement with those of the reported data.[4b]

Experimental

All boiling and melting points are uncorrected. TLC was carried out on Kiesel gel G (Merck), and spots were detected with iodine vapor or 10% sulfuric acid on hot plate. Kanto Kagaku silica gel (up to 100 mesh) was used for column chromatography. PMR spectra were recorded with a 60 MHz Varian T-60 spectrometer and a 100 MHz JEOL PS-100 spectrometer with a spin decoupler. Chemical shifts are given in δ value. IR spectra were measured for either liquid films or potassium bromide disks with a JASCO Model IRA-1 spectrometer.

*Typical Procedure for the Cyclization: 4-Nitro-2,3,4,6-tetradeoxy-*DL-*hexopyranose (5b).* A mixture of 3 g (53.6 mmol) of acrylaldehyde and 5.61 g (53.6 mmol) of 1-nitro-2-propanol[11] was refluxed in 30 ml of benzene for about 20 h in the presence of diethylamine and formic acid (1: 1.75 mol; employed 0.5 wt % of total reagent). After removal of the solvent *in vacuo*, the oily product was chromatographed on silica gel using di-isopropyl ether–hexane (2: 1) as eluant. 4.5 g of anomeric mixture (α: β=4: 3 by PMR signal intensity) of **5b** was thus obtained in 52% yield. In the case of **5a** and **5c**, excess nitro alcohols (4 equivalent to acrylaldehyde) were employed. **5c** was separated into two diastereomers (**5c**$_1$ and **5c**$_2$) through the column on silica gel with ethyl acetate–chloroform (1: 2) as eluant. Yields, physical constants and elemental analyses of **5a**—**5c** were summarized in Table 1.

Typical Procedure of Hydrazone Formation: 5-Hydroxy-4-nitropentanal 2,4-Dinitrophenylhydrazone (9a). To a solution of 0.6 g (4.1 mmol) of **5a** in 6 ml of methanol, 0.81 g (4.1 mmol) of 2,4-dinitrophenylhydrazine–hydrochloric acid (0.5 ml) in methanol (40 ml) was added and the solution was heated to boiling for 2 min. The reaction mixture was allowed to stand overnight at room temperature. The precipitated yellow crystals were collected and recrystallized from ethanol to give 1.05 g of **9a** in 79% yield; mp 126.5—127.5 °C, IR (KBr): 3480 (OH), 3280 (NH), 1610 (C=N), 1550, 1515, and 1330 cm^{-1} (C–NO$_2$). In the case of **9b** and **9c**, 2,4-dinitrophenylhydrazine–phosphoric acid reagent[12] was employed. The results are summarized in Table 2.

5-Acetoxy-4-nitropentanal 2,4-dinitrophenylhydrazone (10a). Trifluoroacetic anhydride (1.9 ml) was added to a solution of 190 mg (0.58 mmol) of **9a** in 0.8 ml of acetic acid. The mixture was heated at 55—60 °C for 15 min. After cooling to room temperature aqueous sodium hydrogencarbonate was added to the solution and it was extracted with chloroform. The extracts were dried over anhydrous sodium sulfate and the solvent was evaporated. The red-brownish residue was crystallized with ethyl acetate–hexane (1: 1) mixture and recrystallized from methanol to give 17 mg (3%) of **10a**, mp. 129—130 °C, IR (KBr): 3280 (NH), 1740 (acetyl C=O), 1620 (C=N), 1550, 1515, and 1330 cm^{-1} (C–NO$_2$). Found: C, 42.41; H, 4.22; N, 18.98%. Calcd for $C_{13}H_{15}N_5O_8$: C, 42.28; H, 4.09; N, 18.97%.

*Typical Procedure of O-Methylation of 5: Methyl 4-Nitro-2,3,4,6-tetradeoxy-α- and β-*DL-erythro-*Hexopyranosides (6b$_1$ and 6b$_2$).* i) Hydrochloric acid (0.03 ml) in 3 ml of methanol was added to 300 mg (1.86 mmol) of **5b** and the solution was heated at 50 °C for 0.5 h to give two products, α and β anomer of methyl hexopyranoside (**6b**$_1$ and **6b**$_2$), which were separated by silica gel column chromatography with benzene as developer. The first moving isomer was collected and distilled to give 180 mg of α-anomer (**6b**$_1$) in 55% yield; bp 33—35 °C/0.02 Torr, IR (liq. film): 1550 and 1375 cm^{-1} (C–NO$_2$). The second moving isomer was also collected and recrystallized from ethanol–water to give 65 mg of β-anomer (**6b**$_2$), 20% yield, mp 31.5—32 °C, IR (KBr): 1550 and 1345 cm^{-1} (C–NO$_2$). ii) A mixture of **5b**, excess methyl iodide, and silver oxide was stirred for 2.5 h at room temperature. Insoluble salts were filtered off and the filtrate was evaporated to give also an anomeric mixture of methyl hexopyranosides (**6b**) in analogous yield as above i). **6a**, **6c**$_1$, **6c**$_2$, **6c**$_3$, and **6c**$_4$ were also obtained from corresponding **5a** and diastereomeric **5c** in analogous way.

*Typical Procedure of Reduction and Acetylation of 6: 4-Acetamido-2,3,4,6-tetradeoxy-α-*DL-erythro-*hexopyranoside (8b$_1$).* To a suspension of Raney nickel T1 catalyst[13] (5 ml) in 50 ml of methanol was added 500 mg (2.86 mmol) of **6b**$_1$. The mixture was hydrogenated under 3.5 kg/cm^2 of hydrogen (initial) for 2 h at room temperature. The catalyst was filtered off and the solvent was evaporated to yield 250 mg of **7b**$_1$ as light yellow oil in 61% yield. Without further purification **7b**$_1$ was acetylated with 2.5 ml of pyridine and 4 ml of acetic anhydride under stirring for 1 h at room temperature. After removal of the solvent the residue was chromatographed on silica gel to give 277 mg of **8b**$_1$ as colorless crystals in 86% yield based on **7b**$_1$; mp 87.5—90 °C (from petroleum ether). **8a**, **8b**$_2$, **8c**$_1$, and **8c**$_2$ were also obtained in a similar procedure. The results are shown in Table 5.

Methyl N-*Benzoyl-α-*DL-*tolyposaminide (11).* **7b**$_1$ obtained by the reduction of 450 mg (2.57 mmol) of **6b**$_1$ described as above, was subsequently benzoylated with 580 mg of benzoic anhydride in methanol for 0.5 h at room temperature. The reaction mixture was poured into 20 ml of aqueous sodium hydrogencarbonate and extracted with chloroform (3×40 ml). The combined extracts were dried over anhydrous sodium sulfate and evaporated to give 505 mg (79% based on **6b**$_1$) of **11** as colorless crystals. Recrystallization from ethyl acetate–petroleum ether gave analytically pure sample; mp 148—149 °C (Reported[10] mp 148—149 °C), mixed mp 148—149 °C, IR and PMR spectra were identical with those of the authentic sample.[10] IR (KBr): 3220 (NH), 1625 (amide I), 1560 (amide II), 1275 cm^{-1} (amide III), PMR (CDCl$_3$ at 100 MHz): δ 1.25 (3H, d, H-6 $J_{5,6}$=6 Hz), 1.7—2.0 (4H, m, H-2,3), 3.35 (3H, s, OCH$_3$), 3.70 (1H, d-d, H-5, $J_{4,5}$=9 Hz, $J_{5,6}$=6 Hz), 3.6—4.1 (1H, m, H-4), 4.68 (1H, s with fine splitting, H-1, $J_{1,2a}$ and $J_{1,2e}$<3 Hz), 6.05 (1H, d, NH), 7.4 and 7.75 (5H, m, C$_6$H$_5$). Found: C, 67.52; H, 7.74; N, 5.51%. Calcd for $C_{14}H_{19}NO_3$: C, 67.44; H, 7.68; N, 5.62%.

Methyl N-*Benzoyl-β-*DL-*tolyposaminide (12).* Reduction and benzoylation of **6b**$_2$, carried out according to the procedure described above, gave **12** in 84% yield; mp 171.5—172.5 °C (from ethyl acetate–petroleum ether) (Reported[10] mp 169—171 °C). No depression was observed on mixed melting point. IR and PMR spectra were identical with those of the authentic sample.[10] IR (KBr): 3210 (NH), 1630 (amide I), 1570 (amide II), 1275 cm^{-1} (amide III). PMR (CDCl$_3$ at 100 MHz): δ 1.31 (3H, d, H-6, $J_{5,6}$=6 Hz), 1.5—2.3 (4H, m, H-2,3), 3.48 (3H, s, OCH$_3$), 3.47 (1H, d-d, H-5, $J_{4,5}$=9 Hz, $J_{5,6}$=6 Hz), 3.7—4.0 (1H, m, H-4), 4.37 (1H, d-d, H-1, $J_{1,2a}$=8 Hz, $J_{1,2e}$=3 Hz), 6.20 (1H, d, NH), 7.4 and 7.75 (5H, m, C$_6$H$_5$). Found: C, 67.78; H, 7.66; N, 5.91%.

Calcd for $C_{14}H_{19}NO_3$: C, 67.44; H, 7.68; N, 5.62%.

Methyl α-DL-Forosaminide (13). To a solution of 520 mg (2.97 mmol) of **6b**$_1$ in 80 ml of ethanol, was added 1 ml of aqueous formaldehyde (*ca.* 40%), 70 mg of sodium acetate, and Raney nickel T1 catalyst (3 ml of ethanolic slurry). The mixture was hydrogenated under 3.5 kg/cm^2 of hydrogen (initial) for 4 h at room temperature. After removal of the catalyst, the solvent was evaporated and the residue was dissolved with 50 ml of 2.5% aqueous ammonia. The solution was extracted with chloroform (3×15 ml), dried over anhydrous sodium sulfate and evaporated. The residual oil was distilled to give 255 mg of **13** as colorless oil in 49% yield; bp 57—59 °C/2.5 Torr (Reported[4b] bp 30—35 °C (bath)/0.5 Torr for D-isomer) n_D^{20} 1.4458. The PMR spectrum was identical with that reported data[4b] for D-isomer. IR (liq. film): 2820 and 2780 cm^{-1} (NMe_2), PMR ($CDCl_3$ at 100 MHz): δ 1.22 (3H, d, H-6, $J_{5,6}$=6.5 Hz), 1.5—2.0 (4H, m, H-2,3), 2.23 (6H, s, NMe_2), *ca.* 2.3 (1H, m, H-4), 3.33 (3H, s, OMe), 3.77 (1H, q, H-5, $J_{4,5}$=10 Hz, $J_{5,6}$=6.5 Hz), 4.59 (1H, s with fine splitting, H-1, $J_{1,2a}$ and $J_{1,2e}$<3 Hz).

Methyl β-DL-forosaminide (14). Reductive dimethylation of **6b**$_2$ as described above for **13**, gave **14** in 57% yield; bp 60—65 °C (bath)/2.5 Torr, n_D^{20} 1.4477. IR (liq. film): 2820 and 2770 cm^{-1} (NMe_2), PMR ($CDCl_3$ at 100 MHz): δ 1.33 (3H, d, H-6, $J_{5,6}$=6 Hz), 1.5—2.1 (4H, m, H-2,3), 2.28 (6H, s, NMe_2), *ca.* 2.3 (1H, m, H-4), 3.50 (3H, s, OMe), 3.35—3.6 (1H, m, H-5), 4.30 (1H, m, H-1).

Deep thanks are due to Dr. Y. Suhara (Institute of Microbial Chemistry) for providing the authentic samples of methyl *N*-benzoyltolyposaminides.

References

1) The Synthetic Reactions of Aliphatic Nitro Compounds. Part XII; Part XI of this series: E. Kaji, A. Igarashi, and S. Zen, *Bull. Chem. Soc. Jpn.*, **49**, 3181 (1976).

2) T. Kishi, M. Asai, M. Muroi, S. Harada, S. Terao, T. Miki, and K. Mizuno, *Tetrahedron Lett.*, **1969**, 91, 97.

3) R. Paul and S. Tchelitcheff, *Bull. Soc. Chim. Fr.*, **1957**, 443, 734, *ibid.*, **1965**, 1059.

4) a) J. S. Brimacombe, L. W. Doner, A. J. Rollins, and A. K. Al-Radhi, *Tetrahedron Lett.*, **1973**, 87; *J. Chem. Soc., Perkin Trans. 1*, **1973**, 1295; b) E. L. Albano and D. Horton, *Carbohydr. Res.*, **11**, 485 (1969); c) C. L. Stevens, G. Gutowski, K. G. Taylor, and C. P. Bryant, *Tetrahedron Lett.*, **1966**, 5717.

5) K. Koga, S. Yamada, M. Yoh, and T. Mizoguchi, The 94th Annual Meeting of the Pharmaceutical Society of Japan, Sendai, April, 1974; Abstracts, II, p. 90.

6) Preliminary communication, S. Zen, E. Kaji, and H. Kohno, *Chem. Lett.*, **1974**, 1029.

7) L. W. McTeer, U. S. Patent 2694732; 2694733 (1954).

8) H. Shechter, D. E. Ley, and J. Zeldin, *J. Am. Chem. Soc.*, **74**, 3664 (1952).

9) A. C. Ferguson and A. H. Haines, *J. Chem. Soc., C*, **1969**, 2372.

10) These compounds have been synthesized as the key intermediate for the total synthesis of kasugamycin by another procedure different from the present work; Y. Suhara, F. Sasaki, G. Koyama, K. Maeda, H. Umezawa, and M. Ohno, *J. Am. Chem. Soc.*, **94**, 6501 (1972).

11) L. Henry, *Bull. Soc. Chim. Fr.*, **13**, 999 (1895).

12) G. D. Johnson, *J. Am. Chem. Soc.*, **73**, 5883 (1951).

13) X. A. Dominguez, I. C. Lopez, and R. Franco, *J. Org. Chem.*, **26**, 1625 (1961).

The Synthesis of Benzannelated Annulenes. Tribenzo[*a,g,m*]-15,17-bisdehydro[18]annulene, and Bis[dibenzo[1,2:9,10]-11,13-bisdehydro[14]annuleno][5,6-*a*:5′,6′-*d*]benzene[1]

Jūro Ojima,* Michiko Enkaku, and Chikako Uwai
Faculty of Literature and Science, Toyama University, Gofuku, Toyama 930
(Received August 10, 1976)

The Wittig reaction between *o*-ethynylcinnamaldehyde (II) and α,α′-bis(triphenylphosphonio)-*o*-xylene dibromide (III) gave the corresponding acyclic compound (IV and V) in a good yield, while that between *o*-ethynylbenzaldehyde (VII) and α,α′,α″,α‴-tetrakis(triphenylphosphonio)durene tetrabromide (VIII) similarly afforded an acyclic compound (IX) in a moderate yield. The title compounds, VI and X, were obtained by the oxidative coupling of V (or, IV and V) and IX, respectively. The examination of the NMR spectra indicated that VI and tribenzo-fused, fourteen-membered periphery on the sides of the benzene nucleus of X are atropic.

The Wittig reaction has been used to synthesize many unsaturated cyclic compounds.[2]

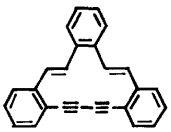

I

In the previous work, we reported the preparation of the tribenzo[*a,e,i*]-11,13-bisdehydro[14]annulene (I) from the *o*-ethynylbenzaldehyde (VII) by the Wittig reaction with α,α′-bis(triphenylphosphonio)-*o*-xylene dibromide (III) followed by the oxidative coupling.[3] In connection with our works on benzo-fused annulenes,[4] the present paper deals with syntheses of a higher vinylogue of I, *i.e.*, tribenzo[*a,g,m*]-15,17-bisdehydro[18]annulene (VI), and bis[dibenzo[1,2:9,10]-11,13-bisdehydro[14]annuleno][5,6-*a*:5′,6′-*d*]benzene (X), formally derived from I by the fusion of the second benzannelated fourteen-membered ring system on the opposite side of one benzene nucleus.

The preparation of VI and X was carried out according to the same procedure as used in that of I.

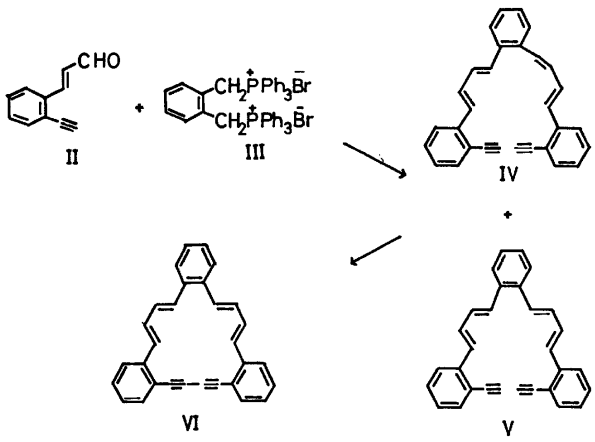

The double Wittig reaction of 2 molar equivalents of *o*-ethynylcinnamaldehyde (II)[5] and 1 molar equivalent of α,α′-bis(triphenylphosphonio)-*o*-xylene dibromide (III)[6] in *N,N*-dimethylformamide with ethanolic lithium ethoxide at 80 °C afforded an acyclic stereoisomeric mixture in a 53% yield, which, upon chromatography on alumina, yielded the *cis-trans* isomer (IV) and the *trans-trans* isomer (V) in a ratio of *ca.* 1 : 1. The structure of IV was assigned to the compound based on the following evidence. The two signals due to acetylenic protons were observed in the NMR spectrum of IV, whereas only one signal was observed in that of V (Table 1). In addition, the longest wavelength maximum of IV in the electronic spectrum appeared at a lower wave length than that of V (Experimental). Furthermore, the IR spectrum of IV exhibited a band at 660 cm^{-1} which is characteristic of *cis*-ethylene linkage. The oxidation with copper(II) acetate in pyridine[7] gave the desired VI in a 34% yield. The Dreiding molecular model of VI suggested that VI should be an almost strainless molecule.

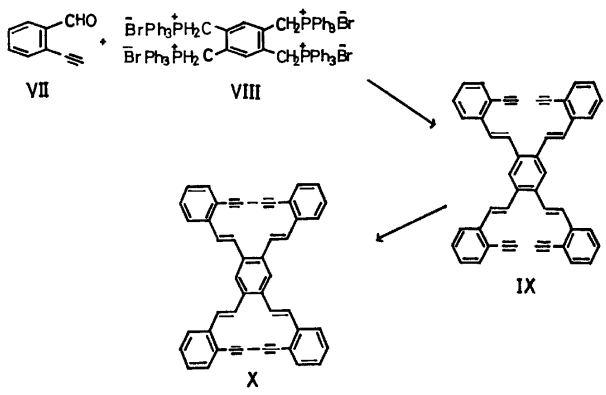

The Wittig reaction of α,α′,α″,α‴-tetrakis(triphenylphosphonio)durene tetrabromide (VIII)[8] and four equivalents of *o*-ethynylbenzaldehyde (VII),[2] under the same conditions as indicated for the reaction of II and III, yielded the acyclic compound (IX) in a moderate yield. The configuration of ethylenic bonds of IX was confirmed to be *trans*, since the IR spectrum exhibits a band at 960 cm^{-1} which is characteristic of *trans*-ethylenic linkage. Oxidation of IX with copper(II) acetate in pyridine[7] gave X in a 16% yield, together with an unidentified substance. Under the oxidation conditions employed, it seems likely that the IX also provides the alternative product, XI, arising from the coupling of 2-(*o*-ethynylphenyl)vinyl moieties at 1

* Author to whom correspondence should be addressed.

and 3 positions of the central benzene nucleus of IX. However, inspection by the use of the molecular model revealed that this possibility is presumably precluded, since the molecular model corresponding to the structure of X can be constructed more readily, as compared with that for XI, which can be done only with difficulty. Thus, the structure of X rather than XI was assigned to the oxidation product from IX, although the available spectral properties, such as NMR, UV, and IR, did not give a sufficient reason for such an assignment.

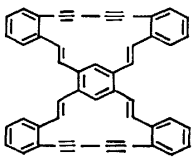

XI

Table 1. ^{1}H-NMR data of IV—VI and IX—X in $CDCl_3$ at 100 MHz
(τ-values, TMS as an internal standard)

	IV	V	VI[a)]	IX	X
Olefinic and Phenyl H	2.25—3.42	2.20—3.05	2.31—3.29	2.10—2.84	2.14—3.76
-C≡CH	6.65 6.67	6.64		6.73	

a) The NMR spectra of VI were found to be essentially temperature independent over the range from −60 to 25 °C.

The chemical shifts on the protons of the obtained compounds IV—VI and IX—X are given in Table 1. The signals due to olefinic protons could not be located precisely, because the signals due to phenyl protons were also observed in almost the same region as those of olefinic protons. Consequently, it is difficult to compare the chemical shifts between each proton of the acyclic compound (IV and V) and the corresponding proton of the cyclic one (VI). The same is true for the comparison of the NMR spectra between IX and X. However, the chemical shifts of all protons of VI and X are in the normal region. Therefore, it appears from this result that VI and tribenzo-fused, fourteen-membered periphery on both sides of the central benzene nucleus of X are atropic.

Experimental

All the melting points are uncorrected. Brockmann alumina (Act. II—III) was used for column chromatography. The IR and UV spectra were taken on a Hitachi EPI-S2 and a Hitachi 124 spectrophotometer respectively. Shoulders in the UV spectra are indicated by sh. The NMR spectra were recorded on a Varian XL-100 spectrometer. The mass spectra were measured using a JEOL-JMS-OI-SG-2 spectrometer operating at 75 eV.

The Isomeric o-*Bis[4-(*o-*ethynylphenyl)-1,3-butadienyl] benzene (IV) and (V).* Lithium ethoxide prepared from lithium (224 mg, 0.032 gatm) in ethanol (84 ml) was added drop by drop with stirring under a nitrogen atmosphere at 80—85°C over a period of 1 h to *o*-ethynylcinnamaldehyde (II, 5.0 g, 0.032 mol)[5] and α,α′-bis(triphenylphosphonio)-*o*-xylene dibromide (III, 12.9 g, 0.0165 mol)[6] in dry *N,N*-dimethylformamide (320 ml). After completion of the addition, the reaction mixture was stirred under a nitrogen atmosphere at the same temperature for 2 more hours; then it was poured into water (1000 ml) and extracted with ether (300 ml×3). The ethereal extracts were washed successively with dilute hydrochloric acid, sodium hydrogencarbonate, and saturated sodium chloride solutions, and dried over sodium sulfate. After the solvent had been evaporated, the residual dark red liquid obtained was chromatographed on alumina (100 g) with light petroleum-ether (92: 8—96: 4) to give a mixture of acyclic isomers as a partly crystallized liquid (3.2 g, 53%). The mixture was dissolved in ether and absorbed on alumina (75 g). Careful elution with solvents with increasing polarity resulted in the separation of stereoisomers. Fractions eluted with light petroleum-ether (97: 3) yielded *cis-trans* isomer, IV. Recrystallization from hexane-benzene gave pure IV as pale yellow cubes: mp 149.5—150.5 °C; IR (KBr disk): 3250 (-C≡CH), 2100 (-C≡C-), 990, 970, 950 (*trans* C=C), 660 cm^{-1} (*cis* C=C); UV: λ_{max}^{THF} 250 (28000), 260 sh (27200), 268 (23200), 287 sh (26100), 310 sh (38600), 325 (44000), 354 nm (53600); Mass: *m/e* 382 (M^+, 10), 253 (100); mol wt, 382.5; NMR: see Table 1.

Found: C, 93.93; H, 5.77%. Calcd for $C_{30}H_{22}$: C, 94.20; H, 5.80%.

The following fractions eluted with light petroleum-ether (96: 4—95: 5) gave *trans-trans* isomer, V. Recrystallization from hexane-benzene afforded pure V as yellow cubes: mp 185 °C (dec); IR (KBr disk): 3280 (-C≡CH), 2100 (-C≡C-), 975 cm^{-1} (*trans* C=C); UV; λ_{max}^{THF} 260 (28700), 269 sh (25300), 314 sh (51500), 325 (56000), 364 nm (54100); Mass: *m/e* (M^+, 25), 253 (100); mol wt, 382.5; NMR: see Table 1.

Found: C, 94.03; H, 6.06%. Calcd for $C_{30}H_{20}$: C, 94.20; H, 5.80%.

Tribenzo[a,g,m]-*15,17-bisdehydro*[*18*]*annulene (VI).* A solution of V (0.6 g, 0.0016 mol) dissolved in pyridine (13 ml) was added dropwise to a vigorously stirred solution of copper-(II) acetate monohydrate (4.9 g) in pyridine (16 ml) for 45 min at 50 °C, and the reaction mixture was stirred for an additional 2 h at 60—65 °C. The mixture, after had been chilled to room temperature and diluted with benzene (300 ml), was filtered through Hyflo Super-Cel,[9] and the resulting precipitate was further washed with benzene (100 ml×2). Then the filtrate was washed with 5% hydrochloric acid until it was acid to litmus, and then with a saturated sodium chloride solution, and dried over sodium sulfate. The dark red liquid obtained after evaporation of the solvent was chromatographed on alumina (130 g) with light petroleum-ether (8: 2) to give VI (0.2 g, 34%). Recrystallization from hexane-benzene afforded pure VI as yellow needles: mp 248 °C (dec); IR (KBr disk): 980 cm^{-1} (*trans* C=C); UV: λ_{max}^{THF} 275 sh (29700), 292 (42600), 328 (64100), 378 sh nm (14100); Mass *m/e* 380 (M^+, 100); mol wt, 380.5; NMR: see Table 1.

The elemental analyses of VI always afforded low values of carbon, but the spectral properties clearly support the structure of VI.

In a run performed under similar conditions using a mixture of IV and V, VI was obtained in a 23% yield.

1,2,4,5-Tetra[trans-*2-(*o-*ethynylphenyl)vinyl*]*benzene (IX).* Lithium ethoxide prepared from lithium (441 mg, 0.063 gatm) in ethanol (160 ml) was added dropwise, with stirring under a nitrogen atmosphere at 82—85 °C for 2 h, to *o*-ethynylbenzaldehyde (VII, 8.0 g, 0.062 mol) and α,α′,α″,α‴-tetrakis(triphenylphosphonio)durene tetrabromide (VIII, 19.4 g, 0.013 mol) in dry *N,N*-dimethylformamide (634 ml).

After completion of the addition, the reaction mixture was stirred maintaining the same temperature under a nitrogen atmosphere for an additional 2 h; then it was poured into water (1000 ml) and extracted with ether (500 ml×3). The ethereal extracts were worked up in the usual manner to give a dark red liquid. The liquid was chromatographed on alumina (150 g) with light petroleum–ether (8: 2) to give IX (1.3 g, 17%) as a partly crystallized liquid. Recrystallization from hexane–benzene afforded pure IX as yellow needles: mp 186 °C (dec); Mass: m/e 583 (M^+, 5), 149 (100); mol wt, 582.7; IR (KBr disk): 3300 (–C≡CH), 2100 (–C≡C–), 1600 (C=C), 960 cm^{-1} (*trans* C=C); UV: λ_{max}^{THF} 221 (56800), 240 sh (45000), 254 sh (41000), 344 (60400), 376 sh nm (48700); NMR: see Table 1.

Found: C, 94.29; H, 5.07%. Calcd for $C_{46}H_{30}$: C, 94.81; H, 5.19%.

*Bis[dibenzo[1,2:9,10]-11,13-bisdehydro[14]annuleno][5,6-a:5′,6′-*d*]benzene (X).* A solution of IX (1.82 g, 0.0031 mol) in pyridine (52 ml) was added dropwise to a stirred solution of copper(II) acetate monohydrate (18.0 g) in pyridine (37 ml) for 25 min at 55 °C, and the reaction mixture was stirred for an additional 3 h at 60—65 °C. Then the mixture was chilled, diluted with benzene (200 ml), and filtered through a Hyflo Super-Cel. The precipitate formed was washed with benzene (100 ml×3). Then the filtrate was washed with 5% hydrochloric acid until it was acid to litmus, and with saturated sodium chloride solution, and dried over sodium sulfate. The dark red liquid obtained after evaporation of the solvent was chromatographed on alumina (200 g). The fractions eluted with light petroleum–ether (7: 3—6: 4) gave X (0.29 g, 16%) as a partly crystallized liquid. Recrystallization from benzene afforded pure X as yellow cubes: mp 216 °C (dec). Although a satisfactory elemental analysis is not obtained, the Mass (*m/e* 579 (M^+, 57), 576 (100); mol. wt., 578.7), the IR (KBr disk) (2200 (–C≡C–), 965, 950 cm^{-1} (*trans* C=C)), the UV (λ_{max}^{THF} 224 (60200), 260 sh (32000), 307 (48400), 324 sh (38300), 352 sh (17200), 393 sh (6150)), and the NMR (see Table 1) were found to be consistent with the assigned structure.

The following fractions with the same solvents afforded crystals (0.15 g) which, on recrystallization from benzene, yielded yellow cubes, mp 206 °C (dec). The structure of the material is not established. Its spectral properties are as follows: Mass: *m/e* 280 (70), 254 (100); IR (KBr disk): 2200, 1635, 1620, 975 cm^{-1}; UV (THF): λ_{max} 228, 281, 296, 354, 376, sh nm; NMR ($CDCl_3$): 1.54[a] (d, J=16), 2.44—2.82[b] (m), 3.21[c] (d, J=16); The integral ratio of each signal (a, b, and c) is 1: 5: 1.

The authors wish to thank Dr. S. Akiyama and Prof. M. Nakagawa, Osaka University, for measuring the NMR spectra at 100 MHz. This work was financially supported by a Grant-in-Aid (054103, 1975) for Scientific Research from the Ministry of Education, which is gratefully acknowledged.

References

1) IUPAC nomenclature: Bis[dibenzo[1,2:7.8]cyclotetradeca-9,13-diene-3,5-diyno][11,12-*a*:11′,12′-*d*]benzene.

2) For a recent review, see K. P. C. Vollhardt, *Synthesis*, **1975**, 765.

3) J. Ojima, T. Yokomachi, and A. Kimura, *Bull. Chem. Soc. Jpn.*, **49**, 2840 (1976).

4) J. Ojima, A. Kimura, and M. Ikeguchi, *Bull. Chem. Soc. Jpn.*, **49**, 3709 (1976).

5) J. Ojima, A. Kimura, Y. Yokoyama, and T. Yokoyama, *Bull. Chem. Soc. Jpn.*, **48**, 367 (1975).

6) C. E. Griffin, K. R. Martin, and B. E. Douglas, *J. Org. Chem.*, **27**, 1627 (1962); C. E. Griffin and J. A. Peters, *ibid.*, **28**, 1715 (1963).

7) G. Eglinton and A. R. Galbraith, *Chem. Ind.*, **1956**, 737; *J. Chem. Soc.*, **1959**, 889.

8) C. A. Dornfeld and L. E. Thielen, U. S. Pat. 2865964; *Chem. Abstr.*, **53**, 8073 (1959).

9) Hyflo Super-Cel was obtained from Wako Pure Chemicals Co., Ltd.

A New Method for the Synthesis of 1-Cycloalkenyl Alkyl Sulfides

Fuminori AKIYAMA

Chemical Research Institute of Non-Aqueous Solutions, Tohoku University, Sendai 980

(Received August 23, 1976)

2-Isopropyl-5-methyl-1-cyclohexenyl alkyl sulfides were obtained in about a 60% yield by the reaction of 2-isopropyl-5-methylcyclohexanone with thioacetals or thiols in the presence of aluminum chloride. 1-Cycloalkenyl ethyl sulfides, $\overline{\text{-(CH}_2)_n\text{-C(R)=C-SEt}}$ (n=4, 5, or 6, R=H or alkyl) were obtained in good yields by the reaction of cycloalkanones with ethanethiol in the presence of diphosphorus pentaoxide. However, an attempt to apply this method to acyclic vinyl sulfides was unsuccessful.

Vinyl sulfides have been synthesized by the nucleophilic addition of thiols to acetylenic hydrocarbons[1-3] and by the reaction of α-halogenoalkenes with sodium ethanethiolate,[4] of cyclohexanethione with alkyl halides,[5] and of chloroalkyl sulfides with a base.[6,7]

Although the reaction of ketones with thiols in the presence of acids or metal salts have been reported to give bis(alkylthio)alkanes,[8-11] Mukaiyama *et al.* reported the synthesis of vinyl sulfides by the reaction of carbonyl compounds with thiols in the presence of titanium tetrachloride and triethylamine.[12] In our previous paper[13] the synthesis of substituted 1-cyclohexenyl alkyl sulfides by the reaction of substituted cyclohexanones with thiols or thioacetals in the presence of aluminum chloride was reported. In the present report a more convenient method for the synthesis of 1-cycloalkenyl ethyl sulfides by the reaction of cycloalkanones with ethanethiol in the presence of diphosphrus pentaoxide will be reported.

Results and Discussion

Reactions of Substituted Cyclohexanones with Thioacetals or Thiols in the Presence of Aluminum Chloride. The heating of a mixture of a thioacetal (0.02 mol), a substituted cyclohexanone (0.02 mol), and benzene (20 ml) under reflux for 15 min in the presence of a 1 mol equiv. $AlCl_3$ gave substituted 1-cyclohexenyl alkyl sulfide, as is shown in Table 1. The reaction using thiol instead of the thioacetal for 1 min gave the same product, but heating for 15 min caused the sulfide to disappear giving a resinous material. The different behaviors between the reaction using a thiol and that using a thioacetal are illustrated in Fig. 1.

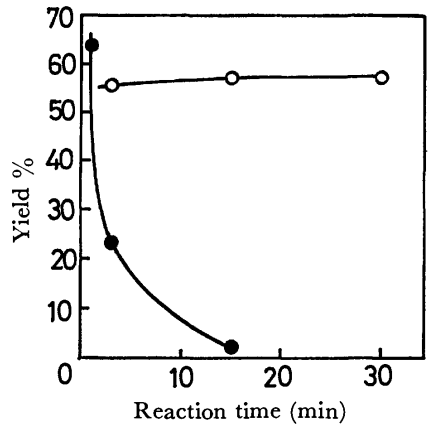

Fig. 1. Dependence of the yield of 2-isopropyl-5-methyl-1-cyclohexenyl propyl sulfide on the reaction time.
○: Reaction of menthone with $CH_3CH(SPr)_2$, ●: reaction of menthone with PrSH.

TABLE 1. YIELD OF SUBSTITUTED 1-CYCLOHEXENYL ALKYL SULFIDES

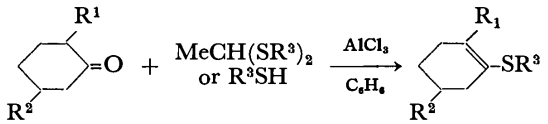

I: $R^1=CH_3$, $R^2=H$, $R^3=Et$
II: $R^1=CH_3$, $R^2=H$, $R^3=n$-Pr
III: $R^1=i$-Pr, $R^2=CH_3$, $R^3=Et$
IV: $R^1=i$-Pr, $R^2=CH_3$, $R^3=n$-Pr

ketone	$R^3=SH$[a]	$MeCH(SR^3)_2$[b]	Remaining ketone (%)	Product	(%)
$R^1=CH_3$, $R^2=H$	$R^3=Et$		Trace	I	35
	$R^3=n$-Pr		4	II	29
		$R^3=Et$	7	I	25
		$R^3=n$-Pr	12	II	19
$R^1=i$-Pr, $R^2=CH_3$	$R^3=Et$		17	III	48
	$R^3=n$-Pr		13	IV	64
		$R^3=Et$	27	III	46
		$R^3=n$-Pr	29	IV	57

a) Reaction time: 1 min. b) Reaction time: 15 min.

In a similar reaction of cyclohexanone with thioacetals or thiols, a quick disappearance of 1-cyclohexenyl alkyl sulfide and the formation of a resinous material were observed. Thus, reactions using aluminum chloride are useful only for the synthesis of such sterically hindered vinyl sulfides as 2-isopropyl-5-methyl-1-cyclohexenyl alkyl sulfides. This limitation appears to be attributable to the stability of the product in the presence of aluminum chloride. The reaction of acyclic ketones with thiol or thioacetal in the presence of aluminum chloride gave a resinous material and unidentified oily products.

Reactions of Cycloalkanones with Ethanethiol in the Presence of Diphosphorus Pentaoxide. The heating of a mixture of ethanethiol (0.02 mol), a cycloalkanone (0.02 ml), and benzene (20 ml) under reflux for one hour in the presence of a 1 mol equiv. of diphosphorus pentaoxide gave 1-cycloalkenyl ethyl sulfide, as is shown in Table 2. Although the reaction of thiols carried out in the presence of aluminum chloride showed a rapid disappearance of the products (see Fig. 1), the reactions

Table 2. Yield of 1-cycloalkenyl ethyl sulfides[a)]

Starting ketone	Product	Remaining ketone (%)	Yield (%) of product
	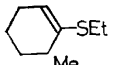	5	43
	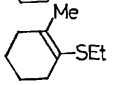	8	75
	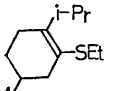	36	42
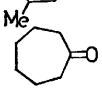	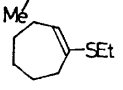	18	60
	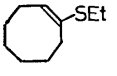	12	81

a) Reaction time: one hour.

carried out in the presence of diphosphorus pentaoxide showed only a slight decrease in 1-cycloalkenyl ethyl sulfide on prolonged heating.

1-Cyclopentenyl ethyl sulfide was obtained in a low yield (less than 20%) by the reaction of cyclopentanone with ethanethiol in the presence of diphosphorus pentaoxide. Similar reactions of acyclic ketones gave bis(alkylthio)alkanes.

As is shown in Table 2, the yields of 1-cycloalkenyl ethyl sulfides are in the order: 1-cyclooctenyl>1-cycloheptenyl>1-cyclohexenyl. This reaction appears to be useful for the synthesis of large-membered 1-cycloalkenyl alkyl sulfides, $\overline{\text{-(CH}_2)_n\text{-C(R')=C-SR}}$ ($n \geqq 4$, R'=H or alkyl). Although the application of the method using diphosphorus pentaoxide has thus far been restricted to the synthesis of 1-cycloalkenyl alkyl sulfides, it appears to be more convenient than that using $TiCl_4$ and triethylamine.[12)]

Experimental

Materials. Commercially available cycloalkanones and thiols were used. 1,1-bis(ethylthio)ethane or 1,1-bis(propylthio)ethane was obtained by the reaction of acetaldehyde with ethanethiol or 1-propanethiol respectively in the presence of calcium chloride.

General Procedure. A mixture of thiol (or thioacetal) (0.02 mol), cycloalkanone (0.02 mol), an internal standard (hexamethylbenzene), and benzene (20 ml) was heated under reflux in the presence of aluminum chloride or diphosphorus pentaoxide (0.02 mol). At an appropriate time a small portion of the solution was sampled and washed with water, and then this solution was analyzed by GLC using an ethylene glycol adipate polyester, 20% on a chromosorb W column at 150 °C. The reaction times shown in Table 1 or 2 are nearly optimum ones.

For the purpose of the isolation of 1-cycloalkenyl sulfides, a mixture of 0.06 mol of each material in benzene (30 ml) was heated under reflux. At an appropriate time, which is shown in Table 1 or 2, the benzene solution was cooled and washed several times and then distilled under reduced pressure. Redistillation and separation by GLC each gave pure 1-cycloalkenyl alkyl sulfide.

Identification of 1-Cycloalkenyl Alkyl Sulfides. The structures of the 1-cycloalkenyl sulfides were established on the basis of the following data.

2-Methyl-1-cyclohexenyl Ethyl Sulfide. NMR (in CCl_4): δ 2.56 (2H, q, J=7 Hz; -SC$\underline{H}_2$CH$_3$), 1.85 (3H, s, CH$_3$-C=C), 1.96—2.4 and 1.5—1.76 (8H, m, ring protons), 1.2 (3H, t, J=7 Hz, -SCH$_2$C$\underline{H}_3$). IR (neat): 1620 cm^{-1} (very weak, C=C). Elementary analyses: Found: C, 68.89; H, 10.01; S, 20.61%. Calcd for $C_9H_{16}S$: C, 69.17; H, 10.32; S, 20.50%.

2-Methyl-1-cyclohexenyl Propyl Sulfide. NMR (in CCl_4): δ 2.51 (2H, t, J=7 Hz, -SC$\underline{H}_2$CH$_2$CH$_3$), 1.84 (3H, s, CH$_3$-C=C), 1.90—2.30 and 1.3—1.74 (10H, m, ring protons and -SCH$_2$C$\underline{H}_2$CH$_3$), 1.0 (3H, t, J=7 Hz, -SCH$_2$CH$_2$C$\underline{H}_3$). IR (neat): 1600 cm^{-1} (weak, C=C). Elementary analyses: Found: C, 70.38; H, 10.57; S, 18.61%. Calcd for $C_{10}H_{18}S$: C, 70.52; H, 10.65; S, 18.82%.

2-Isopropyl-5-methyl-1-cyclohexenyl Ethyl Sulfide. NMR (in CCl_4): δ 3.45 (1H, seven, J=7 Hz, (CH$_3$)$_2$C$\underline{H}$-C=C), 2.57 (2H, q, J=7 Hz, -SC$\underline{H}_2$CH$_3$), 1.55—2.40 (7H, m, ring protons), 1.2 (3H, t, J=7 Hz, -SCH$_2$C$\underline{H}_3$), 0.88—1.04 (9H, m; CH$_3$ attached to ring and (C$\underline{H}_3$)$_2$CH). IR (neat): 1618 cm^{-1} (very weak, C=C). Elementary analyses: Found: C, 72.45; H, 11.06; S, 16.34%. Calcd for $C_{12}H_{22}S$: C, 72.65; H, 11.17; S, 16.16%.

2-Isopropyl-5-methyl-1-cyclohexenyl Propyl Sulfide. NMR (in CCl_4): δ 3.48 (1H, seven, J=7 Hz, (CH$_3$)$_2$C$\underline{H}$-C=C), 2.50 (2H, q, J=7 Hz, -SC$\underline{H}_2$CH$_3$), 1.40—2.3 (9H, m, ring protons and -SCH$_2$C$\underline{H}_2$CH$_3$), 0.88—1.08 (12H, m, CH$_3$ attached to ring (C$\underline{H}_3$)$_2$CH, and -SCH$_2$CH$_2$C$\underline{H}_3$). IR (neat): 1600 cm^{-1} (weak, C=C). Elementary analyses: Found: C, 73.63; H, 11.69; S, 15.43%. Calcd for $C_{13}H_{24}S$: C, 73.51; H, 11.39; S, 15.10%.

1-Cyclohexenyl Ethyl Sulfide. NMR (in CCl_4): δ 5.5 (1H, m, >C=C$\underline{H}$-), 2.62 (2H, q, J=7 Hz, -SC$\underline{H}_2$CH$_3$), 1.90—2.30 and 1.47—1.85 (8H, m, ring protons), 1.23 (3H, t, J=7 Hz, -SCH$_2$C$\underline{H}_3$). IR (neat): 1630 cm^{-1}. Elementary analyses: C, 67.40; H, 9.85; S, 22.26%. Calcd for $C_8H_{14}S$: C, 67.54; H, 9.92; S, 22.54%.

1-Cycloheptenyl Ethyl Sulfide. NMR (in CCl_4): δ 5.5 (1H, t, J=7 Hz, olefinic), 2.58 (2H, q, J=7 Hz, -SC$\underline{H}_2$CH$_3$), 2.04—2.30 and 1.36—1.90 (10H, m, ring protons), 1.28 (3H, t, J=7 Hz, -SCH$_2$C$\underline{H}_3$). IR (neat): 1632 cm^{-1}. Elementary analyses: Found: C, 69.10; H, 10.44; S, 20.84%. Calcd for $C_9H_{16}S$: C, 69.17; H, 10.32; S, 20.52%.

1-Cyclooctenyl Ethyl Sulfide. NMR (in CCl_4): δ 5.38 (1H, t, J=8 Hz, olefinic), 2.64 (2H, q, J=7 Hz; -SC$\underline{H}_2$CH$_3$), 2.04—2.40 and 1.40—1.90 (12H, m, ring protons), 1.28 (3H, t, J=7 Hz, -SCH$_2$C$\underline{H}_3$). IR (neat): 1619 cm^{-1}. Elementary analyses: Found: C, 70.36; H, 10.80; S, 19.08%. Cacld for $C_{10}H_{18}S$: C, 70.52; H, 10.65; S, 18.82%.

References

1) J. W. Copenhaver and M. H. Bigelow, "Acetylene and Carbon Monoxide Chemistry," Reinhold Publishing Corp., New York (1949), p. 33.

2) J. A. Nieuland and R. R. Vogt, "The Chemistry of Acetylene," Reinhold Publishing Corp., New York (1945), p. 129.

3) R. A. Raphael, "Acetylenic Compounds in Organic Synthesis," Academic Press, New York (1955), p. 43.

4) J. Loevenich, J. Losen, and A. Dierichs, *Ber.*, **60**, 950 (1927).

5) J. Morgenstern and R. Mayer, *J. Prakt. Chem.*, **34**, 116 (1966).

6) R. Brown and R. C. G. Moggridge, *J. Chem. Soc.*, **1946**, 816.

7) S. H. Bales and S. A. Nickelson, *J. Chem. Soc.*, **1922**, 2137.
8) E. Fromm, *Justus Liebigs Ann. Chem.*, **253**, 135 (1889).
9) T. Posner, *Ber.*, **33**, 3165 (1900).
10) E. Fromm, *Ber.*, **60**, 2090 (1927).
11) A. Recsei, *Ber.*, **60**, 1420 (1927).
12) T. Mukaiyama, K. Saigo, K. Narasaka, and M. Numata, Jpn. Patent, 100012 (1974).
13) F. Akiyama, *J. Chem. Soc., Chem. Commun.*, **1976**, 208.

Synthesis and Spectral Characteristics of 4*H*-1-Benzothiopyran-4-ones

Hiroyuki NAKAZUMI and Teijiro KITAO

Department of Applied Chemistry, College of Engineering, University of Osaka Prefecture, Sakai-shi 591

(Received August 26, 1976)

The physical properties of 4*H*-1-benzothiopyran-4-ones (thiochromones) and related compounds were characterized by means of mass, NMR, and UV spectra in order to distinguish thiochromones from 2*H*-1-benzothiopyran-2-ones (thiocoumarins). In the mass spectra, the fragmentation due to the retro-Diels-Alder reaction directly from the molecular ion is the most useful for differentiation. In the NMR spectra, thiochromones show the characteristic deshielding effect of benzenoid proton in 5-position and in the UV spectra a very strong absorption band in the region 250—270 nm. It was found that in the reaction of *S*-phenyl 3-oxobutanethioates with PPA, most of these compounds afford thiochromones through rearrangement giving an intermediate (IVa). The effect of the substituent of the *S*-phenyl 3-oxobutanethioate on the formation of the thiocoumarin was also discussed.

4*H*-1-Benzothiopyran-4-ones (thiochromones) and 2*H*-1-benzothiopyran-2-ones (thiocoumarins) are well known as a structural isomer. The thermal conversion of the thiochromone into the thiocoumarin is also known.[1] A new synthesis of thiocoumarin derivatives was reported by Konishi *et al.*,[2] but some structural formulas of these compounds are doubtful. We therefore carried out an extensive study of the chemical structure of the related compounds by means of mass and NMR spectra. We found that some thiocoumarins are in line with the structural formulas of thiochromone derivatives. In this paper, we wish to report on a) the characteristic physical properties of thiochromone derivatives in order to distinguish them from thiocoumarins by means of their mass, NMR, IR, and UV spectra, and b) the effect of the substituent of the *S*-phenyl 3-oxobutanethioate on the formation of the thiocoumarin by the reaction with polyphosphoric acid (PPA).

Results and Discussion

Most of the thiochromones and thiocoumarins were prepared from *S*-phenyl 3-oxobutanethioate derivatives obtained by the reaction of substituted thiophenols with diketene. The IR, NMR, UV, and mass spectra of these compounds are summarized in Tables 1 and 2.

Identification of Thiochromone and Thiocoumarin Derivatives. It is very difficult to distinguish thiochromones from thiocoumarins. Lozac'h and Pfister-Guillouzo[3] reported a comparative method to distinguish them by means of their IR spectra. However, sufficient and systematic data necessary for identification are still lacking. In the case of compound **2**, the mass spectra showed the fragmentation of retro-Diels-Alder reaction characteristic of chromone derivatives[4] and we deduced the compound to be 2-methyl(thiochromone). This is also supported by the following experimental results: When compound **2** was hydrolyzed with NaOH, isolated products were bis(*o*-acetylphenyl) disulfide and bis(*o*-carboxyphenyl) disulfide. Compound **2** was also obtained by the authentic method.[5]

Thus, 4-methyl(thiocoumarin) reported[2] should be 2-methyl(thiochromone). 2-Methyl-7-methoxy(thiochromone) (**3**), the isomer of thiocoumarin **12**, was prepared by the well known method[6] for thiochromone derivatives. Compounds **4**—**9** were also identified as thiochromone derivatives by means of their mass and NMR spectra. The structure of compound **11** was determined to be thiochromone derivative by the following preparative method and chemical reactivity. The same product was obtained by the reaction of 2,5-dimethoxybenzenethiol with ethyl acetoacetate in PPA. A bluish thianaphthalenium salt (λ_{max} 590 nm (in acetone)) was obtained by the *O*-alkylation of compound **11** with dimethyl sulfate and 60% $HClO_4$. A similar alkylation afforded a yellow thianaphthalenium salt[7] (λ_{max} 386 nm) in the case of compound **12** and a bluish thianaphthalenium salt (λ_{max} 590 and 596 nm) in the case of compounds **2** and **3**, respectively.

Spectral Characteristics. *1) NMR Spectra*: Methyl(thiochromone) derivatives showed the characteristic deshielding effect of benzenoid proton in 5-position by contribution of the carbonyl group in peri-position as indicated in the case of some thiochromones.[8,9] The proton showed the chemical shift in the range 8.30—8.50 ppm. The values are unusually greater than those of the aromatic protons (*ca.* 1 ppm). The abnormally strong deshielding effect might be due to the even closer proximity of the proton on the annelated benzene in compound **8**, which was observed at 10.10 ppm. In the case of thiocoumarin derivatives, no such unusual deshielding effect was observed because of the lack of carbonyl group affecting the benzenoid proton. This difference may be utilized to distinguish them.

2) Mass Spectra: Thiochromone derivatives were characterized by an abundant molecular ion as the base peak. The major fragmentation pathway for these compounds was the elimination of $CH{\equiv}C{-}CH_3$ by the retro-Diels-Alder reaction, followed by the loss of

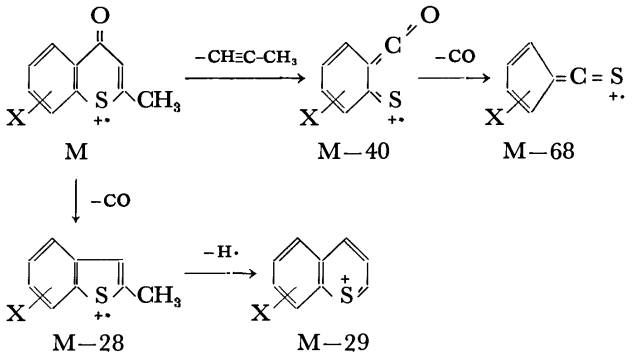

Scheme 1.

TABLE 1. SPECTRAL DATA OF THIOCHROMONE AND THIOCOUMARIN DERIVATIVES

No.	Compound		IR in KBr ν_{CO} (cm^{-1})	NMR in $CDCl_3$ δ (ppm)	UV in EtOH λ_{max} (nm)	UV in EtOH ε ($\times 10^{-4}$)
2		X=2-CH_3 Y=H	1620	2.40 (3H)s 6.75 (1H)s 7.37—7.50 (3H)m 8.40 (1H)m	224 247 335	1.8 2.4 1.1
3		X=2-CH_3 Y=7-OCH_3	1630	2.40 (3H)s 3.89 (3H)s 6.71 (1H)s 6.80—7.10 (2H)m 8.34 (1H)d	235 261 268 328	1.6 3.0 2.6 1.1
4		X=2-CH_3 Y=6-OCH_3	1625	2.45 (3H)s 3.90 (3H)s 6.80 (1H)s 7.15 (1H)d 7.45 (1H)d 7.90 (1H)d	224 254 260 357	1.6 2.4 2.4 0.88
5		X=2-CH_3 Y=7-CH_3	1610	2.41 (3H)s 2.43 (3H)s 6.75 (1H)s 7.15—7.30 (2H)m 8.30 (1H)d	228 254 337	1.6 2.4 1.1
6	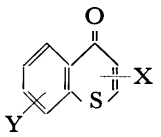	X=2-CH_3 Y=6-CH_3	1620	2.40 (3H)s 2.45 (3H)s 6.80 (1H)s 7.40 (2H)m 8.30 (1H)s	225 249 345	1.4 2.7 1.1
7		X=2-CH_3 Y=7-Cl	1635	2.40 (3H)s 6.75 (1H)s 7.30—7.45 (2H)m 8.35 (1H)d	229 255 261 338	1.7 3.0 2.7 1.1
8		X=2-CH_3 Y=5,6-Benzo	1620	2.44 (3H)s 6.97 (1H)s 7.37—8.00 (5H)m 10.10 (1H)m	216 278 326 340 356	5.3 2.2 0.89 0.84 0.53
9		X=2-CH_3 Y=7,8-Benzo	1605	2.48 (3H)s 6.90 (1H)s 7.48—7.95 (4H)m 8.15 (1H)m 8.42 (1H)d	217 277 314 342 360	3.8 2.8 0.81 0.73 0.75
10		X=3-CH_3 Y=H	1610	2.20 (3H)s 7.35—7.65 (4H)m 8.50 (1H)m	223 250 341	1.2 1.9 1.1
11		X=2-CH_3 Y=5,8-Dimethoxy	1620	2.35 (3H)s 3.88 (3H)s 3.90 (3H)s 6.70 (1H)s 6.90 (1H)s 6.93 (1H)s	241 293 363	2.2 1.2 0.71
12	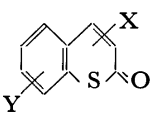	X=4-CH_3 Y=7-OCH_3	1645	2.50 (3H)s 3.92 (3H)s 6.48 (1H)s 6.95—7.15 (2H)m 7.80 (1H)d	224 273 343	4.2 0.64 1.0
13		X=4-OH Y=H	1620	6.24 (1H)s 7.50—7.84 (3H)m 8.28 (1H)m	232 320	4.0 1.4

Table 2. Mass spectra of thiochromone and thiocoumarin derivatives

Compound No.	Major fragment ion (*m/e*) [relative abundance (%)]
2	176[M, 100], 148[M−28,64], 147[M−29,62], 136[M−40,58], 115[10], 108[M−68,44]
3	206[M,100], 178[M−28,57], 177[M−29,7], 166[M−40,52], 163[64], 138[M−68,7], 136[8], 135[17], 134[9], 123[22]
4	206[M,100], 205[65], 191[M−15,10], 177[M−29,26], 176[41], 166[M−40,7], 163[15], 147[10], 138[M−68,7], 135[29], 134[9], 123[25]
5	190[M,100], 162[M−28,76], 161[M−29,57], 150[M−40,57], 147[27], 121[46]
6	190[M,100], 162[M−28,65], 161[M−29,51], 150[M−40,62], 147[22], 121[42]
7	212[38], 210[M,100], 184[29], 183[28], 182[M−28,82], 181[M−29,56], 172[24], 170[M−40,63], 147[30], 144[13], 142[M−68,32]
8	226[M,100], 225[43], 198[M−28,47], 197[M−29,41], 186[M−40,17], 165[12], 158[M−68,27]
9	226[M,100], 198[M−28,39], 197[M−29,37], 186[M−40,15], 165[9], 158[M−68,24]
10	176[M,100], 148[M−28,15], 147[M−29,34], 143[40], 136[M−40,63], 115[19], 108[M−68,36]
11	236[M,96], 221[100], 207[26], 203[36], 193[61], 192[37], 191[17], 178[12], 165[34], 164[15], 163[13], 150[13]
12	206[M,43], 178[M−28,100], 177[M−29,9], 163[82], 147[6], 135[51], 134[19], 102[10]
13	178[M,37], 150[M−28,100], 136[M−42,82], 121[56], 108[80], 105[16]

carbon monoxide (M→[M−40]→[M−68]). The other important fragmentation was initial loss of carbon monoxide from the molecular ion, followed by the loss of a hydrogen atom leading to the formation of the ring-expanded thianaphthalenium ion (M→[M−28]→[M−29]) (Scheme 1). The results are given together with relative abundance in Table 2. In the case of compounds **3** and **4**, the subsequent fragmentation of M-28 is modified by the methoxy substituent, *viz.*, the loss of methyl radical from M−28 giving an intensive fragment ion peak at *m/e* 163. However, in the case of 5,8-dimethoxy derivative **11**, fragmentation due to the retro-Diels-Alder reaction was not observed as in the case of some methoxyfuranochromones.[10]

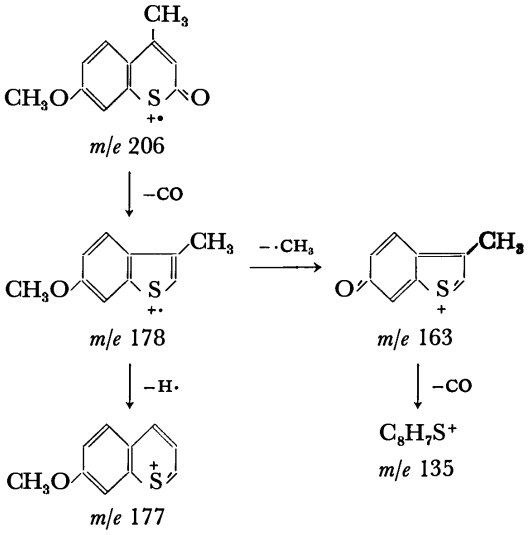

Scheme 2.

On the other hand, the base peak of thiocoumarin derivatives was due to M−28. The main fragmentation of thiocoumarin **12** involved the ejection of carbon monoxide followed by the loss of methyl radical and carbon monoxide. The sequence may be rationalized as in Scheme 2.

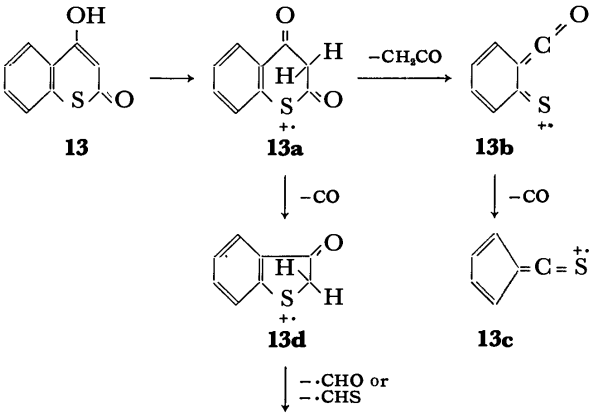

Scheme 3.

The mass spectra of 4-hydroxy(thiocoumarin) **13** showed the fragmentation of the retro-Diels-Alder reaction in spite of thiocoumarin derivatives. If the molecular ion exists in the tautomeric form **13a**, the spectra can be easily rationalized. There are two fragmentation pathways. One which differs a great deal from that of other thiocoumarins is the loss of a neutral ketene by the retro-Diels-Alder reaction, followed by the loss of carbon monoxide (**13a**→**13b**→**13c**). The other is the loss of carbon monoxide from the molecular ion, which gives **13d** as the base peak of the spectrum (**13a**→**13d**→*m/e* 121 and 105).

The fragmentations were formulated by analogy of coumarin derivatives[4] and by following the fragmention containing a chlorine atom in the fragmentation of compound **7**. The retro-Diels-Alder reaction of the molecular ion of thiochromones might be the most useful for mass spectrometric differentiation between isomeric thiocoumarin and thiochromone, except for hydroxy(thiocoumarin) and dimethoxy(thiochromone) derivatives.

3) UV Spectra: Monosubstituted methyl(thiochromone) derivatives showed three complicated strong absorption bands due to the substituent in the benzene ring. On the other hand, the spectra of thiocoumarins showed two strong absorption bands, very weak in the region 250—270 nm.

4) IR Spectra: The carbonyl bands of methyl(thiochromone) derivatives were found in the region 1605—1630 cm^{-1}, which is considerably lower than that of a general ketone. Legrand and Lozac'h[1] reported that carbonyl bands of thiochromone are lower by 10—20 cm^{-1} than those of thiocoumarins. However, the difference can not be used reliably to distinguish them, since the region of thiocoumarins overlapped considera-

Table 3. The NMR and IR spectra of *S*-phenyl 3-oxobutanethioate derivatives

Compound No.	X	IR in KBr ν_{CO} (cm^{-1})	NMR in $CDCl_3$ δ (ppm)			
1a	H	1670	2.38 (3H)s	5.20 (1H)s	7.51 (5H)s	8.28 (1H)b
1b	*m*-OCH_3	1675	1.90 (3H)s	3.80 (3H)s	5.90 (1H)s	7.00—7.30 (4H)m[a]
1c	*p*-OCH_3	1665	2.38 (3H)s 7.38 (2H)d	3.80 (3H)s 9.25 (1H)b	5.15 (1H)s	6.90 (2H)d
1d	*m*-CH_3	1670	2.30 (3H)s	2.35 (3H)s	5.15 (1H)s	7.35 (4H)m[b]
1e	*p*-CH_3	1665	2.30 (3H)s	2.35 (3H)s	5.10 (1H)s	7.35 (4H)m[b]
1f	*m*-Cl	1670 (s 1680)	2.43 (3H)s	5.25 (1H)s	7.38—7.48 (4H)m	9.0 (1H)b
1g	2,3-Benzo	1670	2.40 (3H)s	4.85 (1H)s	7.60—8.20 (7H)m[b]	
1h	3,4-Benzo	1670	2.40 (3H)s	5.15 (1H)s	7.55—8.20 (7H)m[b]	
1i	2,5-Dimethoxy	1675	1.90 (3H)s 6.90—7.10 (3H)m[a]	3.78 (3H)s	3.83 (3H)s	5.90 (1H)s

a) No enol proton was observed. b) The NMR spectra were measured in DMSO-d_6, no enol proton being observed.

bly with that of thiochromones as shown in compound **13** and 3-methyl(thiocoumarin) (1620 cm^{-1}).

Synthesis of Thiochromone Derivatives from S-*Phenyl 3-Oxobutanethioates.* It was shown by spectral data that all *S*-phenyl 3-oxobutanethioates retain the enol form; ν_{OH} was observed at 2500—3000 cm^{-1} in IR and a vinyl proton was observed at 5.15—5.90 ppm as shown in Table 3. When these *S*-phenyl 3-oxobutanethioates were cyclodehydrated with PPA, only *m*-methoxy derivative (compound **1b**) gave a thiocoumarin **12**. However, the other *S*-phenyl 3-oxobutanethioates with substituents such as chlorine and methyl group in the meta-position gave thiochromones (compounds **5** and **7**) as the isomeric product of thiocoumarins. Two annelated derivatives **1g** and **1h** gave the corresponding thiochromones.

Thus, the meta-position of methoxyl group on *S*-phenyl 3-oxobutanethioate seems to be important for the preparation of thiocoumarin derivatives. In the case of compounds **1c** and **1i** where one or two methoxyl group(s) are introduced in the other position, thiochromone derivatives **4** and **11**, respectively, were obtained as isomeric products.

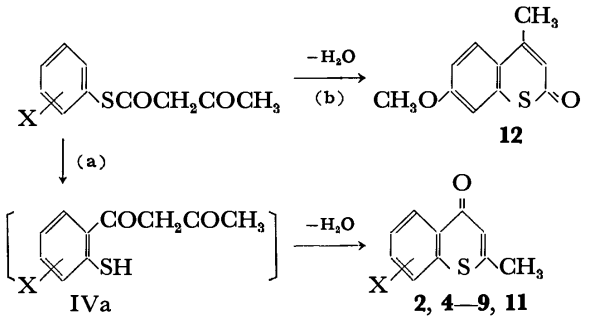

Scheme 4.

Cyclodehydration of *S*-phenyl 3-oxobutanethioate with 100% H_2SO_4 instead of PPA also afforded 2-methyl(thiochromone). The reaction with 100% H_2SO_4 in ether solution or concd H_2SO_4 gave diphenyl disulfide in a high yield (81%). The rearrangement of *S*-phenyl 3-oxobutanethioates giving an intermediate [IVa] (path a) predominantly occurs rather than the direct dehydration (path b) as shown in Scheme 4. The synthesis of thiocoumarins by the Pechmann reaction[11] is very difficult even from *S*-phenyl 3-oxobutanethioate.

Experimental

All the melting points are uncorrected. Infrared spectra were recorded on a Hitachi ESI-S2 spectrophotometer using KBr pellets. Ultraviolet spectra were recorded on a Hitachi EPS-3T spectrophotometer. H-NMR spectra were taken on a Hitachi Perkin-Elmer Model R-20 spectrometer, unless otherwise stated in $CDCl_3$ solution with tetramethylsilane as an internal standard. Mass spectra were recorded on a Hitachi RMU-6E mass spectrometer operating at 80 eV. Elemental analyses were recorded on a Yanaco CHN corder MT-2.

S-*Phenyl 3-Oxobutanethioate (**1a**).* Compound **1a** was obtained by the reaction of thiophenol with diketene.[2]

S-(m-*Methoxyphenyl) 3-Oxobutanethioate (**1b**).* Compound **1b** was prepared by the method reported[2] and isolated from the isomer mixture by repeated recrystallization from EtOH. The mixture contained an unidentified compound with the following data. NMR: δ 2.40 (3H) s, 3.80 (3H) s, 5.25 (1H) s, 6.90—7.30 (4H) m, 8.35 (1H) b; Found, C, 59.29; H, 5.52%. From the results, the compound was assigned as the structural isomer of compound **1b**.

S-(p-*Methoxyphenyl) 3-Oxobutanethioate (**1c**).* Concd H_2SO_4 (9.2 g) was added dropwise at 30 °C to a stirred Et_2O (50 ml) solution of *p*-methoxybenzenethiol (6.3 g, 0.045 mol).[12] Diketene (4.5 g, 0.054 mol) was then added to this reaction mixture at 25 °C. After 2.5 h, the ether was removed by rotary evaporation *in vacuo* at 20 °C and the residue was poured into an ice-water solution. White solid separated from the solution was collected by filtration and was recrystallized from EtOH to give 0.5 g of **1c**. Compounds **1d**, **1e**, **1g**, and **1h** were prepared by a similar method.

Recrystallization of compound **1g** from EtOH was repeated until the melting point became constant (mp 161—163 °C[2]).

S-(m-*Chlorophenyl) 3-Oxobutanethioate (**1f**).* *m*-Chlorobenzenethiol was obtained as a pale yellow oily material from *m*-chloroaniline by the Leukart reaction[12] in 60% yield; bp 76—78 °C (7 Torr), NMR (CCl_4); δ 2.30 (1H) s, 7.05 (3H) m, 7.20 (1H) m. Compound **1f** was prepared by the same method as for **1c** from *m*-chlorobenzenethiol.

S-(2,5-*Dimethoxyphenyl) 3-Oxobutanethioate (**1i**).* 2,5-Dimethoxybenzenethiol was obtained from 2,5-dimethoxyaniline by the Leukart reaction[12] in 64% yield; bp 104—106 °C (4 Torr), NMR (CCl_4); δ 3.70 (3H) s, 3.80 (3H) s, 3.75

Table 4. Physical properties of *S*-phenyl 3-oxobutanethioate derivatives

Compd	Mp (°C)	Yield (%)	Formula (MW)	Analysis (%) Calcd (Found) C	H
1b	170—171	trace	$C_{11}H_{12}O_3S$ (224)	58.93 (58.79	5.36 5.47)
1c	172—175	5	$C_{11}H_{12}O_3S$ (224)	58.93 (58.23	5.36 5.39)
1d	165—166	65[75][a]	$C_{11}H_{12}O_2S$ (208)	63.46 (62.91	5.77 5.81)
1e	204—207	60[65][a]	$C_{11}H_{12}O_2S$ (208)	63.46 (63.56	5.77 5.89)
1f	154—155	29[44][a]	$C_{10}H_9O_2SCl$ (228.5)	52.52 (53.04	3.94 4.14)
1g	194—196	10	$C_{14}H_{12}O_2S$ (244)	68.85 (67.92	4.92 4.89)
1i	169—171	22	$C_{12}H_{14}O_4S$ (254)	56.69 (57.07	5.51 5.66)

a) Yield (%) of the crude product.

(1H) b, 6.55—6.70 (3H) m. Concd H_2SO_4 (6.1 g, 0.060 mol) was added dropwise to a stirred solution of 2,5-dimethoxybenzenethiol (5 g, 0.029 mol) in ether (30 ml) at 5 °C. Diketene (3 g, 0.036 mol) was then added to this reaction mixture at the same temperature. After 5 h at 5—10 °C, a white solid was separated from the solution by filtration. Recrystallization from EtOH afforded 1.4 g (22%) of **1i**.

The results of elemental analysis, yield and mp are given in Table 4.

2-Methyl-4H-1-benzothiopyran-4-one (2). Method A). Compound **2** was obtained from condensation of thiophenol (10 ml, 0.1 mol) and ethyl acetoacetate (11 ml, 0.1 mol) in polyphosphoric acid (PPA).[5] Method B). *S*-Phenyl 3-oxobutanethioate **1a** (3 g, 0.015 mol) was added to 60 g of PPA at 60 °C. The solution was heated for 1 h at the same temperature. After cooling, the reaction mixture was poured into an ice-water solution and neutralized with NaOH. Crude product (2.3 g) was collected by filtration and washed with water. Recrystallization from a methanol-water mixture (3: 1) afforded 1.8 g (66%) of **2**.

7-Methoxy-2-methyl-4H-1-benzothiopyran-4-one (3). A solution of 14 g (0.1 mol) of *m*-methoxybenzenethiol and 28 g (0.2 mol) of ethyl acetoacetate was added to 300 g of PPA at 80 °C. The reaction mixture was heated at 90 °C for 2 h. After cooling, it was poured into an ice-water solution and collected by filtration and washed with water. Recrystallization from EtOH–water afforded 4 g (20%) of compound **3** as a pale yellow material; mp 118—119.5 °C, Found: C, 63.76; H, 4.85%; Calcd for $C_{11}H_{10}O_2S$: C, 64.08; H, 4.85%; mol wt 206.

Compounds **4**—**9** were prepared by a method silimar to method B for compound **2**. Reaction time in the case of compounds **8** and **9** was 2 h and 3 h, respectively. The yield, mp and elemental analysis are given in Table 5.

3-Methyl-4H-1-benzothiopyran-4-one (10). Compound **10** was prepared by the method of Martin *et al.*,[8] mp 103—104.5 °C (lit, 105 °C), Found: C, 67.42; H, 4.54%; Calcd for $C_{10}H_8OS$: C, 68.18; H, 4.54%; mol wt 176.

5,8-Dimethoxy-2-methyl-4H-1-benzothiopyran-4-one (11). Compound **11** was prepared by method B for compound **2** (36% yield) or by the method for compound **3** (31%).

7-Methoxy-4-methyl-2H-1-benzothiopyran-2-one (12) and 4-Hydroxy-2H-1-benzothiopyran-2-one (13). Compounds **12** and **13** were prepared by method B for compound **2** (reaction time 2 h) and by the method of Ruwet *et al.*[13] (mp 212—213.5; lit, 215 °C), repsectively.

Table 5. reaction of *S*-phenyl 3-oxobutanethioate derivatives with PPA

Compd	Yield (%)	Mp (°C)	Formula (MW)	Analysis (%) Calcd (Found) C	H
2	66[85][a]	103—104	$C_{10}H_8OS$ (176)	68.18 (68.20	4.54 4.78)
12	27	158—160	$C_{11}H_{10}O_2S$ (206)	64.08 (64.28	4.85 5.08)
4	87[90][a]	102—103	$C_{11}H_{10}O_2S$ (206)	64.08 (64.24	4.85 4.93)
5	38[44][a]	98—100	$C_{11}H_{10}OS$ (190)	69.47 (68.78	5.26 5.20)
6[b]	59	121 (lit,[5] 122)	$C_{11}H_{10}OS$ (190)	69.47 (69.74	5.26 5.37)
7	59[74][a]	163—165	$C_{10}H_7OSCl$ (210.5)	57.01 (57.26	3.33 3.45)
8	60[65][a]	126—128	$C_{14}H_{10}OS$ (226)	74.34 (74.28	4.42 4.42)
9[c]	44	192—194	$C_{14}H_{10}OS$ (226)	74.34 (75.88	4.42 4.45)
11	36[59][a]	146—148	$C_{12}H_{12}O_3S$ (236)	61.02 (61.58	5.08 5.23)

a) Yield (%) of the crude product. b) (**1e**) recovered (18% Yield). c) (**1g**) recovered (24% yield).

Hydrolysis of Compound 2. Compound **2** (5 g) was added to a solution of MeOH (100 ml) and NaOH (40 g). The reaction mixture was heated under reflux for 4.5 h. After cooling, the solution was neutralized to pH 5—6 with HCl and filtered. The residue was washed with water and extracted with ether. The extract was evaporated and the residue recrystallized from EtOH to give 0.6 g (7% yield) of bis(*o*-acetylphenyl) disulfide; mp 162—164 °C (lit,[14] 167 °C), γ_{CO} 1650 cm^{-1}, NMR; δ 2.65 (6H) s, 7.20—7.80 (8H) m. The first filtrate was, after concentration by evaporation, was extracted with MeOH. The extract was recrystallized from MeOH to give 0.5 g (6% yield) of bis(*o*-carboxyphenyl) disulfide; mp 287—288 °C (lit,[15] 288.5); γ_{CO} 1680 cm^{-1}, γ_{OH} 2500—3000 cm^{-1}.

References

1) L. Legrand and N. Lozac'h, *Bull. Soc. Chim. Fr.*, **1958**, 953.

2) K. Konishi, H. Umemoto, M. Yamamoto, and T. Kitao, *Nippon Kagaku Kaishi*, **1973**, 118.

3) G. Pfister-Guillouzo, and N. Lozac'h, *Bull. Soc. Chim. Fr.*, **1962**, 1624.

4) Q. N. Porter and T. Baldas, "Mass Spectrometry of Heterocyclic Compound," John-Wiley & Sons, New York (1971), p. 147.

5) F. Bossert and H. Henecka, Ger. 1089773 (1960).

6) F. Bossert, *Ann. Chem.*, **680**, 40 (1964).

7) H. Nakazumi, T. Yoshida, S. Sawada, and T. Kitao, *Nippon Kagaku Kaishi*, **1976**, 849.

8) R. H. Martin, N. Defay, F. Geerts-Evrard, P. H. Given, J. R. Jones, and R. W. Wedel, *Tetrahedron*, **21**, 1833 (1965).

9) E. Campaigne and S. W. Schneller, *J. Heterocycl. Chem.*, **9**, 115 (1972).

10) M. M. Badami, M. B. E. Fayes, T. A. Brice, and R. I. Reed, *Chem. Ind. (London)*, **1966**, 498.
11) R. C. Elderfield, "Heterocyclic Compounds," Vol. 2, John-Wiley & Sons, New York (1951), p. 542.
12) C. M. Suter and H. L. Hansen, *J. Am. Chem. Soc.*, **54**, 4100 (1932).
13) A. Ruwet, C. Draguet, and M. Renson, *Bull. Soc. Chem. Belg.*, **79**, 639 (1970).
14) Ruhemann, *Ber.*, **46**, 3394 (1913).
15) S. Smiles and E. W. McClelland, *J. Chem. Soc.*, **121**, 90 (1922).

Synthesis of Optically Active Bis(1-mesitylethyl) Ethers

Munehiro NAKATANI, Tadao KAMIKAWA,* Tsunao HASE, and Takashi KUBOTA**

Department of Chemistry, Faculty of Science, Kagoshima University, Kagoshima 890
**Department of Chemistry, Faculty of Science, Osaka City University, Sumiyoshi, Osaka 558*
***Department of Chemistry, Faculty of Medical Science, Kinki University, Kawachinagano, Osaka 586*

(Received September 6, 1976)

The racemic and meso bis(1-mesitylethyl) ethers were synthesized. The optical resolution of the dicarboxylic acid derivative showed that the high-melting compounds were racemic in form and the low-melting isomers meso in form.

In a previous paper,[1] we reported that 1-(4-substituted 2,6-dimethylphenyl)-1-ethanol gave meso and racemic bis[1-(4-substituted 2,6-dimethylphenyl)ethyl] ethers in the presence of a Lewis acid such as *p*-toluenesulfonic acid.

This paper will describe a synthesis of optically active and meso bis(1-mesitylethyl) ethers from mesitylene. This experiment clarified unambiguously that the high-melting isomer, **1B** (mp 119—120 °C), was racemic and the low-melting one, **1A** (mp 98.5—99.5 °C), was meso in form.

Results

Optically active bis(1-mesitylethyl) ethers (+)-**1B** and (−)-**1B** were synthesized from 2,4,6-trimethylbenzaldehyde by the following method. 2,4,6-Trimethylbenzaldehyde was treated with hydrogen cyanide in the presence of calcium oxide to give a cyanohydrin, **2**, in a 90% yield. When **2** was heated under reflux in absolute benzene in the presence of a catalytic amount of *p*-toluenesulfonic acid, a dibenzyl ether, **3**, was obtained in a 60% yield. Though, in the IR spectrum of **3**, the absorption for nitrile groups was not observed, an elemental analysis and the NMR spectrum supported the structure. The separation of meso and racemic isomers was unsuccessful (on TLC showed only a single spot), and in the NMR spectrum the presence of a hindered rotation was not observed. The treatment of **3** with hydrogen chloride in absolute ethanol gave a carboxamide, **4**. Again, the separation of isomers was unsuccessful (by either recrystallization or column chromatography). The hydrolysis of **4**, followed by methylation, gave a dimethyl ester. Careful chromatography over silica gel of the crude products and elution with acetone–$CHCl_3$ (3: 97) gave the dimethyl ester samples with a mp of 114—116 °C, **6A**, and a mp of 167—168 °C, **6B**, in a ratio of 1: 2. In the NMR spectra of these esters, the aromatic methyls at C_2 and C_6 appeared as singlets at 2.10 and 2.20 ppm respectively. Upon hydrolysis, dicarboxylic acids (**5A**, mp 199—199.5 °C (dec) and **5B**, mp 230—231 °C (dec) respectively) were obtained. On the other hand, the treatment of the carboxamide, **7**, which was obtained directly from the cyanohydrin, **2**, and of the methyl ester, **8**, with *p*-toluenesulfonic acid in benzene did not give the corresponding esters, **4** and **6**.

The treatment of the dicarboxylic acid **5B** with cinchonine and cinchonidine in methanol and the recrystallization of each salt gave optical active salts **I**; $[\alpha]_D^{20}+1°$ ($c=1$, MeOH) and **II**; $[\alpha]_D^{20}-29°$ ($c=1$, MeOH). The subsequent acid hydrolysis of these salts gave a (+)-dicarboxylic acid, (+)-**5B**, $[\alpha]_D^{20}+223.5°$ ($c=1$, MeOH) and a (−)-dicarboxylic acid, (−)-**5B**, $[\alpha]_D^{20}-235°$ ($c=1$, MeOH), respectively. The carboxylic acids gave the (+)-**6B** and (−)-**6B** esters. The reduction of the **6A**, (+)-**6B**, and (−)-**6B** esters with lithium aluminum hydride gave **9A**, (+)-**9B**, and (−)-**9B** respectively. The NMR spectra of these alcohols indicated the presence of a hindered rotation of the benzene rings. The meso isomer **9A** showed a broad singlet ($W_{1/2}=12$ Hz) at 2.15 ppm for two aromatic methyl resonances at C_2 and C_6 at room temperature; this singlet changed to two signals at a lower temperature, whereas the racemic **9B** showed two broad lines at 1.50 and 2.50 ppm at room temperature, while at a higher temperature, they changed to one sharp signal.

The treatment of the **9A**, (+)-**9B**, and (−)-**9B** alcohols with tosyl chloride in pyridine at room temperature gave only monotosylates, but at 80 °C it gave the **10A**, (+)-**10B**, and (−)-**10B** ditosylates respectively. The reduction of these ditosylates with lithium aluminum hydride failed to give the desired methyl derivatives, but it did give the starting alcohols. Then **10A** was converted into an iodide with sodium iodide in acetone in a sealed tube at 100 °C.[2] The iodide was treated with activated zinc in acetic acid to give 1-ethyl-2,4,6-trimethylbenzene, presumably formed by the cleavage of the ether linkage with hydrogen iodide formed *in situ*.

The conversion of the carboxyl group into the methyl one was finally achieved by the following routes. The **9A** alcohol was converted into a meso mesylate, **11A**, which was reduced by lithium aluminum hydride to give the **1A** ether (a low-melting isomer) in a 4% yield. The **1A** ether was identical with the specimen obtained by a different route[1] (IR and mixed mp). However, the corresponding optically active mesylates (+)-**11B** and (−)-**11B** gave only the starting alcohols on reduction with lithium aluminum hydride. Optically active **1B**'s were obtained from the ditosylates (+)-**10B** and (−)-**10B** by treatment with phenylmethanethiol, followed by desulfurization with Raney Ni, according to the method of Hussey *et al.*[3] (+)-**1B**; $[\alpha]_D^{20}+214°$ ($c=0.11$, MeOH), (−)-**1B**; $[\alpha]_D^{20}-212°$ ($c=0.175$, MeOH). A similar treatment of **10A** gave **1A** in an 8% yield. These isomers also indicated the presence of a hindered rotation of the benzene rings in their NMR spectra. The aromatic methyl resonances at C_2 and C_6 of **1A** and **1B** showed a singlet ($W_{1/2}=4.4$ Hz) at 2.20 ppm and a broad signal at 1.5—2.5 ppm at room temperature respectively; each

of them changed to two signals at lower temperatures and to one sharp signal at higher temperatures.

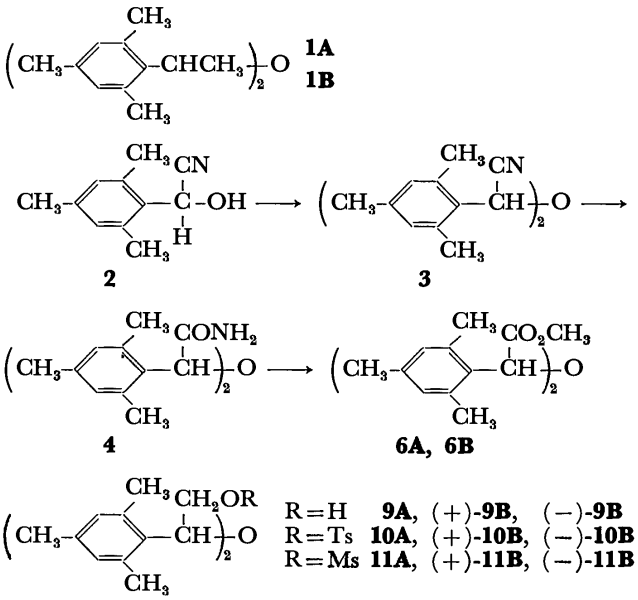

Experimental

All the melting points are uncorrected. The IR spectra were recorded with a Shimadzu IR-27C spectrophotometer. The NMR spectra were measured with a JEOL JNM 60 apparatus at room temperature and at different temperatures with a JEOL JNM 100 apparatus (with TMS as the internal standard). The optical rotations were measured with a Shimadzu photoelectropolarometer, TA-20.

Cyanohydrin 2 of 2,4,6-Trimethylbenzaldehyde. A mixture of 2,4,6-trimethylbenzaldehyde (2 g) and anhydrous HCN (2 ml) was kept with CaO (400 mg) in a sealed tube at 50 °C for 3 h. After the removal of the unchanged HCN and CaO, the crude product gave 2.1 g (90%) of a cyanohydrin, **2**, as plates from petroleum ether; mp 112 °C. Found: C, 75.64; H, 7.50; N, 7.96%. Calcd for $C_{11}H_{13}NO$: C, 75.40; H, 7.48; N, 7.99%. NMR ($CDCl_3$): δ 2.33 (3H, s, Ar-C$\underline{H}_3$), 2.41 (6H, s, Ar-C$\underline{H}_3$), 3.12 (1H, d, J=4 Hz, -O$\underline{H}$), 5.80 (1H, d, J=4 Hz, -C$\underline{H}$-OH), 6.84 (2H, s, Ar-$\underline{H}$) ppm.

Bis(α-cyano-2,4,6-trimethylbenzyl) Ether, 3. The cyanohydrin, **2**, (3 g) was refluxed with a catalytic amount of TsOH in dry benzene for 6 h. The crude product gave 1.7 g (61%) of **3** as prisms from EtOH; mp 150—151 °C. Found: C, 79.64; H, 7.32; N, 8.33%. Calcd for $C_{22}H_{24}N_2O$: C, 79.48; H, 7.28; N, 8.43%. NMR ($CDCl_3$): δ 2.28 (6H, s, Ar-C$\underline{H}_3$), 2.48 (12H, s, Ar-C$\underline{H}_3$), 5.82 (2H, s, Ar-C$\underline{H}$-O), 6.94 (4H, s, Ar-$\underline{H}$) ppm.

Bis(α-carbamoyl-2,4,6-trimethylbenzyl) Ether, 4. Into a solution of the ether **3** (250 mg) in abs EtOH, dry HCl gas was passed for 5 h at 45—50 °C. The subsequent crystallization of the crude product from acetone gave 237 mg (85%) of **4**; mp 261—295 °C. Found: C, 71.85; H, 7.77; N, 7.48%. Calcd for $C_{22}H_{28}N_2O_3$: C, 71.71; H, 7.60; N, 7.60%.

Bis(α-carboxy-2,4,6-trimethylbenzyl) Ether, 5. The **4** ether (300 mg) was hydrolyzed with 30% aq KOH in ethylene glycol to give 227 mg(75%) of **5** as prisms from ether-petroleum ether. Found: C, 70.84; H, 7.14%. Calcd for $C_{22}H_{26}O_5$: C, 71.33; H, 7.08%.

Bis(α-methoxycarbonyl-2,4,6-trimethylbenzyl) Ethers, 6A and 6B. The **5** acid was methylated with diazomethane, and the crude product was chromatographed over silica gel. Elution with $CHCl_3$ containing acetone (3% v/v) gave **6A** (32%) as needles from EtOH; mp 114—116 °C. Found: C, 72.44; H, 7.69%. Calcd for $C_{24}H_{30}O_5$: C, 72.33; H, 7.59%. IR (CCl_4): 1760, 1740, 1200, 1185 (sh), 1150, 1105 cm^{-1}. NMR (CCl_4): δ 2.10 (12H, s, Ar-C$\underline{H}_3$), 2.23 (6H, s, Ar-C$\underline{H}_3$), 3.65 (6H, s, $CO_2C\underline{H}_3$), 5.35 (2H, s, Ar-C$\underline{H}$-O), 6.73 (4H, s, Ar-$\underline{H}$) ppm. Further elution with the same solvent gave the second isomer, **6B** (61%), as prisms from EtOH; mp 167—168 °C. Found: C, 72.25; H, 7.83%. IR (CCl_4): 1740, 1210, 1195, 1180 (sh), 1145, 1100 cm^{-1}. NMR (CCl_4): δ 2.20 (12H, s, Ar-C$\underline{H}_3$), 2.23 (6H, s, Ar-C$\underline{H}_3$), 3.64 (6H, s, $CO_2C\underline{H}_3$), 5.35 (2H, s, Ar-C$\underline{H}$-O), 6.77 (4H, s, Ar-$\underline{H}$) ppm.

Mesitylglycolamide, 7. In a manner similar to that described for **3**, the **2** cyanohydrin gave **7** (78%) as plates from benzene; mp 145.5—146 °C. Found: C, 68.49; H, 7.91; N, 7.29%. Calcd for $C_{11}H_{15}NO_2$: C, 68.37; H, 7.82; N, 7.25%.

Methyl Mesitylglycolate, 8. The **7** amide was hydrolyzed with 30% aq KOH and methylated with diazomethane to give **8** (66%) as prisms from hexane-acetone; mp 149—150 °C. Found: C, 68.02; H, 7.27%. Calcd for $C_{12}H_{16}O_3$: C, 67.64; H, 7.38%.

Bis(α-carboxy-2,4,6-trimethylbenzyl) Ethers, 5A and 5B. The **6A** and **6B** esters were hydrolyzed to give **5A** (mp 199—199.5 °C (dec)) and **5B** (mp 230—231 °C (dec)) respectively.

Optical Resolution of Bis(α-carboxy-2,4,6-trimethylbenzyl) Ether, 5B. (1) The high-melting carboxylic acid **5B** (170 mg) was dissolved with cinchonidine (307 mg) in MeOH, after which the solution was allowed to stand overnight at room temperature. The residue, after removal of the MeOH, was crystallized from MeOH–AcOEt six times to give one optically active salt, **I** (110 mg) as prisms; $[\alpha]_D^{20}$ +1° (MeOH); mp 189—190 °C. Found: C, 73.41; H, 7.63; N, 5.62%. Calcd for $C_{60}H_{70}N_4O_7$+AcOEt: C, 73.39; H, 7.51; N, 5.35%. Into a solution of **I** in MeOH we stirred concd HCl to give (+)-**5B**; $[\alpha]_D^{20}$ +223.5° (MeOH); mp 219°C (dec). (2) **5B** (470 mg) was treated with cinchonine (250 mg) in MeOH, and the product was recrystallized from acetone–AcOEt five times to give another optically active salt, **II** (136 mg); $[\alpha]_D^{20}$ −29° (MeOH); mp 151—152 °C. Found: C, 70.07; H, 7.49; N, 3.71%. Calcd for $C_{41}H_{48}N_2O_6$ +2AcOEt: C, 69.97; H, 7.67; N, 3.33%. (−)-**5B** was afforded from **II**; $[\alpha]_D^{18}$ −235° (MeOH).

Optically Active Bis(α-methoxycarbonyl-2,4,6-trimethylbenzyl) Ethers, (+)-6B and (−)-6B. (+)-**5B** and (−)-**5B** were methylated with diazomethane to give (+)-**6B** ($[\alpha]_D^{20}$ +148° (MeOH); mp 157—157.5 °C) and (−)-**6B** ($[\alpha]_D^{20}$ −147° (MeOH)) respectively.

Bis[α-(hydroxymethyl)-2,4,6-trimethylbenzyl] Ethers, meso-9A, (+)-9B, and (−)-9B. The **6A**, (+)-**6B**, and (−)-**6B** esters were reduced with $LiAlH_4$ in ether to give **9A**, (+)-**9B**, and (−)-**9B** respectively as needles from acetone. **9A**; mp 147—147.5 °C. Found: C, 77.26; H, 8.83%. Calcd for $C_{22}H_{30}O_3$: C, 77.15; H, 8.83%. NMR ($CDCl_3$): δ 2.20 (18H, s, Ar-C$\underline{H}_3$), 3.15 (2H, dd, J=4.3 and 11.7 Hz, Ar-$\underline{\text{C}}\underline{\text{H}}$-$\underline{\text{C}}$(H)-OH), 4.20 (2H, dd, J=9.0 and 11.7 Hz, Ar-$\underline{\text{C}}\underline{\text{H}}$-$\underline{\text{C}}$(H)-OH), 5.15 (2H,dd,$J$=4.3 and 9.0 Hz, Ar-C$\underline{H}$-$CH_2$-), 6.75 (4H, s, Ar-H) ppm. (+)-**9B**; $[\alpha]_D^{23}$ +153° (MeOH); mp 172—173 °C. Found: C, 77.13; H, 8.87%. NMR ($CDCl_3$): δ 1.50 (6H, broad s, Ar-C$\underline{H}_3$), 2.20 (6H, s, Ar-C$\underline{H}_3$), 2.52 (6H, broad s, Ar-CH_3), 3.55 (2H, dd, J=4.5 and 10.5 Hz, Ar-$\underline{\text{C}}\underline{\text{H}}$-$\underline{\text{C}}$(H)-OH), 4.10 (2H, dd, J=8.5 and 10.5 Hz, Ar-

H
CH–C–OH), 4.80 (2H, dd, J=4.5 and 8.5 Hz, Ar–CH–CH_2–),
H
6.8 (4H, s, Ar–H) ppm. (−)-**9B**; $[\alpha]_D^{22}$ −154° (MeOH).

*Bis[α-(tosyloxymethyl)-2,4,6-trimethylbenzyl] Ethers, meso-**10A**, (+)-**10B**, and (−)-**10B**.* The **9A**, (+)-**9B**, and (−)-**9B** alcohols were tosylated with tosyl chloride in pyridine at 80 °C to give **10A** (78%), (+)-**10B** (73%), and (−)-**10B** (74%) respectively. **10A**; mp 163 °C. Found: C, 66.65; H, 6.62%. Calcd for $C_{36}H_{42}O_7S_2$: C, 66.45; H, 6.51%. (+)-**10B**; $[\alpha]_D^{22}$ +125° ($CHCl_3$); mp 140—141 °C. Found: C, 66.48; H, 6.63%. (−)-**10B**; $[\alpha]_D^{22}$ −125° ($CHCl_3$). Found: C, 66.52; H, 6.56%.

*Reaction of the **10A** Tosylate with Sodium Iodide.* The **10A** tosylate (250 mg) was reacted with sodium iodide (300 mg) in acetone in a sealed tube at 100 °C for 24 h. The reaction product (128 mg) was then treated with activated zinc (300 mg) in acetic acid under reflux for 3 h to give 63 mg of 1-ethyl-2,4,6-trimethylbenzene; bp 209—211 °C.

*Reactions of the **10A**, (+)-**10B**, and (−)-**10B** Tosylates with LAH.* The treatments of **10A**, (+)-**10B**, and (−)-**10B** with $LiAlH_4$ gave the **9A**, (+)-**9B**, and (−)-**9B** alcohols respectively in high yields.

*Bis[α-(mesyloxymethyl)-2,4,6-trimethylbenzyl] Ethers, meso-**11A**, (+)-**11B**, and (−)-**11B**.* The mesylations of the **9A**, (+)-**9B**, and (−)-**9B** alcohols with mesyl chloride in pyridine at 80 °C for 2 h gave **11A** (63%), (+)-**11B** (72%), and (−)-**11B** (68%) respectively. **11A**; mp 127—127.5 °C. Found: C, 58.02, H, 6.95%. Calcd for $C_{24}H_{34}O_7S_2$: C, 57.81; H, 6.87%. (+)-**11B**; $[\alpha]_D^{20}$ +41° (MeOH); mp 134 °C. Found: C, 58.01; H, 6.94%. (−)-**11B**; $[\alpha]_D^{20}$ −42° (MeOH). Found: C, 57.95; H, 6.92%.

meso-*Bis(1-mesitylethyl) Ether, **1A**.* (1) The treatment of the **11A** mesylate (200 mg) with $LiAlH_4$ (531 mg) in ether under reflux for 2 h gave 6 mg (4%) of **1A** (mp 98—99 °C) as plates from EtOH. IR (CCl_4): 1615, 1160, 1095, 1075, 945, 855 cm^{-1}. (2) The **10A** tosylate (440 mg) was reacted with phenylmethanethiol (330 mg) and Na (80 mg) in diethylene glycol monoethyl ether (8 ml) under reflux for 4 h. The reaction mixture was then poured into ice water, and the unreacted thiol was removed by steam distillation after acidification with dil HCl. An ether extract of the reaction product was treated with Raney Ni(w-2) in EtOH under reflux for 8 h to give 23 mg (11%) of **1A**.

*Reaction of the (+)-**11B** Mesylate with LAH.* The treatment of (+)-**11B** with $LiAlH_4$ in ether under reflux gave the (+)-**9B** alcohol (83%).

*Optically Active Bis(1-mesitylethyl) Ethers, (+)-**1B** and (−)-**1B**.* The optically active tosylates, (+)-**10B** and (−)-**10B**, were transformed into dibenzyl sulfides in a manner similar to that described for **10A**. These crude sulfides were then treated with Raney Ni(w-2) to give (+)-**1B** (8%) and (−)-**1B** (12%) respectively. (+)-**1B**; $[\alpha]_D^{20}$ +214° (MeOH); mp 132.5—133 °C. (−)-**1B**; $[\alpha]_D^{20}$ −212° (MeOH). IR (CCl_4): 1615, 1160, 1095, 1075, 945, 885 cm^{-1}. These compounds were identical in IR spectrum with, but differ in mp from, the high-melting isomer, **1B**, obtained by another route.[1]

We wish to express our sincere gratitude to Professor T. Tokoroyama of Osaka City University for his many helpful discussions.

References

1) T. Kamikawa, M. Nakatani, and T. Kubota, *Tetrahedron*, **24**, 2091 (1968).
2) L. Vargha and T. Puskas, *Ber.*, **76**, 859 (1943).
3) A. S. Hussey, H. P. Liaos, and R. H. Baker, *J. Am. Chem. Soc.*, **75**, 4727 (1953); G. Stork, E. E. Van Tamelen, L. J. Friedman, and A. W. Burgstahler, *ibid.*, **75**, 384 (1953); W. G. Dauben, R. C. Tweit, and R. L. Maclean, *ibid.*, **77**, 48 (1955); A. S. Dreiding and A. J. Tomasewski, *ibid.*, **77**, 168 (1955).

Reactions of Aromatic Compounds in Molten Salts. I. Dimerization of Aromatic Amines in a Molten Mixture of $AlCl_3$-NaCl-KCl

Hiroshi IMAIZUMI, Shizen SEKIGUCHI, and Kohji MATSUI

Faculty of Engineering, Gunma University, Kiryu, Gunma 376

(Received September 6, 1976)

Aromatic amines underwent dimerization in a molten salt consisting of a mixture of $AlCl_3$-NaCl-KCl. The reaction is an oxidative cationic polymerization but, in contrast with the reactions of the ordinary aromatic compounds which gave the corresponding polyaryls, in the cases of aromatic amines the reaction was regiospecific and stopped at the stage of biaryl to yield benzidine derivatives.

The coupling of aromatic nuclei using Lewis or protonic acids as a catalyst is called a Scholl reaction,[1] and is applicable to the preparation of derivatives of polyaryl;[2-4] however, this reaction is not useful for the synthesis of ordinary biaryl derivatives because of their low yields.

When aromatic amines were heated in a molten salt consisting of a mixture of $AlCl_3$-NaCl-KCl, derivatives of *p,p'*-diaminobiaryl were found to be obtained as a major product. This paper reports the reactions of aromatic amines in molten salts to give benzidine derivatives.

Experimental

All the melting points are uncorrected. NMR spectra were recorded on a Varian A-60D spectrometer. Mass spectra were recorded on a JEOL-JMS-07 mass spectrometer. Elemental analyses were performed in the Micro-analytical Center of Gunma University. The structural assignments of the reaction products were done by means of their NMR, MS spectra, and elemental analyses and by a mixed-melting-point test with an authentic sample.

Materials. $AlCl_3$, NaCl, KCl, and other inorganic materials used were of reagent grade. The aromatic amines employed were purified by distillation or recrystallization and their purities were checked by TLC before use.

Table 1. Benzidine derivatives

No.	Compound	Mp (°C) (Lit,)	Solvent for recrystalization	Anal. (%), Found (Calcd) C	H	N	Cl
1	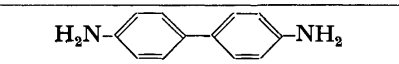	123—125 (125—126)[a]	C_6H_6	—	—	—	—
2	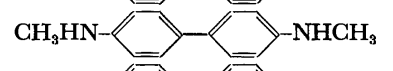	92—93 (74—76)[b]	EtOH-H_2O	—	—	—	—
3	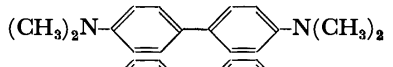	192—193 (193.5)[c]	EtOH	—	—	—	—
4	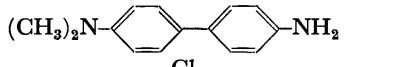	144—145	EtOH	78.67 (79.21	7.60 7.60	13.35 13.20)	—
5	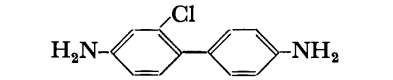	102—103	C_6H_{12}	66.04 (65.91	5.15 5.07	12.87 12.81	16.2 16.21)
6	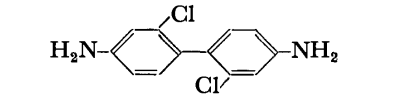	162—163 (163)[d]	C_6H_{12}	—	—	—	—
7	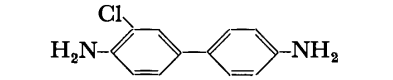	105—107	C_6H_{12}	66.23 (65.91	5.08 5.07	12.94 12.81	16.3 16.21)
8	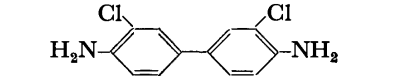	131—132 (132—133)[e]	CCl_4	—	—	—	—
9	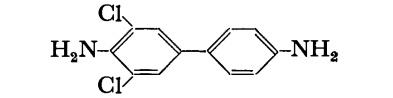	109—110	C_6H_{12}	56.52 (56.94	4.03 3.98	10.88 11.07	27.5 28.01)
10	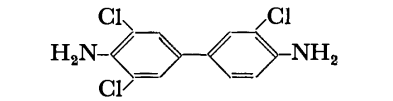	168—169	C_6H_{12}	50.41 (50.12	3.17 3.15	9.69 9.74	37.0 36.98)

a) R. J. W. Le Fèvre and E. E. Turner, *Chem. Zentr.*, **98, II,** 818 (1927). b) R. Willstätter and L. Kalb, *Ber.*, **37,** 3773 (1904). c) R. Willstätter and L. Kalb, *Ber.*, **37,** 3766 (1904). d) G. Schultz, *Ber.*, **17,** 465 (1884). e) P. Cohn, *Ber.*, **33,** 3552 (1900).

A typical example of the reaction is shown below: 5 ml of aniline (0.0549 mol) was added into a molten mixture of $AlCl_3$–NaCl–KCl (0.60: 0.20: 0.20 mol) under stirring and then the reaction mixture was stirred under blowing of O_2 (or N_2) (20—30 ml/min). The mixture was then poured into a mixture of 500 ml of 0.1M HCl and 100 g of ice. After a small amount of the insoluble matter had been filtered off, the filtrate was made alkaline and the unreacted aniline was removed by steam distillation. The reaction products which remained in the residue were extracted with benzene, separated by column chromatography [silica gel, benzene–acetone (10: 1 v/v)], and recrystallized (Table 1).

Results and Discussion

Formation of Benzidines. When aniline and some *N*-alkylanilines were heated at 150 °C in a mixture of $AlCl_3$–NaCl–KCl (0.6: 0.2: 0.2 mol), the corresponding benzidine derivatives were obtained as the major products. Table 1 lists the benzidine derivatives thus obtained in this work. The yields increased very much in the presence of O_2, but above 250 °C dealkylation of *N*-alkylanilines occurred. Table 2 lists the yields of benzidine derivatives in the presence of O_2. When a mixture of two kinds of amines (in a molar ratio 1: 1) was heated in the molten salt, the unsymmetric derivative of *p,p'*-diaminobiaryl was obtained along with the symmetric ones.

Effects of Lewis Acid. The dimerization of aromatic amines was affected very much by the Lewis acids used: in the reaction of aniline, $AlBr_3$ was found to be as effective as $AlCl_3$, but in the case of $ZnCl_2$, no benzidine derivative was found in the reaction mixture. On the other hand, $SnCl_4$ was ineffective at 100 °C; most of the starting material was recovered even after heating for a long time.

Table 2. Yields of benzidine derivatives in the reaction of anilines in molten salts ($AlCl_3$:NaCl:KCl=3:1:1)[a] at 150 °C in the presence of O_2

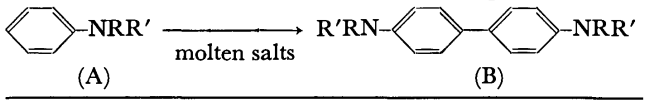

(A) (B)

(A) R	(A) R'	Condition: Atmosph.	Time (h)	Conv. (%)	(B) Yield (%)
R	H[b]	O_2	10	46	78
H	CH_3[c]	O_2	10	67	67
CH_3	CH_3[d]	O_2	10	57	65

a) $AlCl_3$:0.60 mol, NaCl:0.20 mol, and KCl:0.20 mol were used. b) 0.0549 mol, c) 0.0462 mol, d) 0.0394 mol of amines were used, respectively.

Table 3. Formation of benzidine derivatives in the reaction of amine mixture ($AlCl_3$: NaCl:KCl=3:1:1) at 150 °C[a]

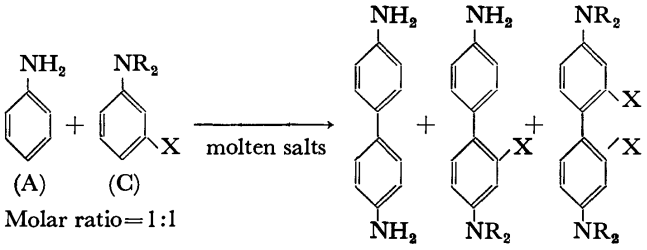

(A) (C) Molar ratio=1:1

(D-1) (D-2) (D-3)

	(C) R	(C) X	Condition: Atmosph.	Time (h)	products (%): (D-1)	(D-2)	(D-3)
(C-1)	CH_3	H	O_2	10	26	28	5
(C-2)	H	Cl	O_2	10	28	8	2

a) 5 ml (0.0549 mol) of aniline was used. $AlCl_3$: 0.60 mol, NaCl: 0.20 mol, and KCl: 0.20 mol were used.

Table 4. Effect of molten salt composition on product yields in the reaction of aniline[a]

Composition (mol)	Condition: Atmosph.	Temp (°C)	Time (h)	Product: Conv. (%)	Yield (%)	Coke (g)
$AlCl_3$:NaCl:KCl (0.6:0.2:0.2)	O_2	200	5	66	79	—
$AlBr_3$:NaCl:KCl (0.6:0.2:0.2)	O_2	150	5	62	78	—
$ZnCl_2$:NaCl:KCl (0.6:0.2:0.2)	O_2	200	100	30	trace	0.9
	O_2	240	40	100	—	5.2
$SnCl_4$[b] (0.5)	O_2	100	20	≃0	—	—

a) Substrate: aniline, 0.0549 mol. b) This system is not a molten salt, but cited here for comparison. In this case, anilinium salt was insoluble in $SnCl_4$ at 100 °C.

These Lewis acids are known to form complexes with aromatic amines. In our experiment, the complexation was much more exothermic in the mixture of $AlBr_3$–NaCl–KCl (0.6: 0.2: 0.2 mol) or of $AlCl_3$–NaCl–KCl (0.6: 0.2: 0.2 mol) than in the mixture of $ZnCl_2$–NaCl–KCl (0.6: 0.2: 0.2 mol).[5] Table 4 clearly shows that the above-described heat of complexation is parallel to the yields for the dimerization, and also comparable to the relative acid-strengths of $AlBr_3$, $AlCl_3$, and $ZnCl_2$ toward 2-methyl-4-nitroaniline in diethyl ether *ca.* 2: 1: *ca.* 0.01.[6] These results suggest that the complexation ability of the Lewis acids with amines plays an important role in the dimerization.

Formation of Chlorinated Benzidines. When aromatic amines were heated in the molten salts in the presence

Table 5. Effect of atmosphere on the yields of chlorinated benzidines in the reaction of benzidine hydrochloride in molten salt ($AlCl_3$: NaCl:KCl=3:1:1) at 150 °C[a]

Condition		
Atmosph.	N_2	O_2
Temp (°C)	150	150
Time (h)	10	10
% Conv.	≃0	60
Yield (%)		
3-Chlorobenzidine	trace	72
3,3'-Dichlorobenzidine	—	16
3,5-Dichlorobenzidine	—	4
3,3',5-Trichlorobenzidine	—	trace

a) $AlCl_3$: 0.60 mol, NaCl: 0.20 mol, and KCl: 0.20 mol were used. 0.0182 mol of benzidine hydrochloride was used.

of O_2, a small amount of chlorinated benzidines was obtained; their amounts increased with the reaction time. However, the formation of chlorinated benzidines was not observed in the absence of O_2; in the presence of O_2, the gas mixture evolved in the reaction vessel turned KI-starch test paper into blue, indicating the presence of Cl_2 which would react with amines to yield the chlorinated benzidines. Thus, when benzidine hydrochloride was heated in the molten salt, various chlorinated benzidines were obtained (Table 5). In the presence of aniline hydrochloride, chlorinated products were formed more rapidly and in high yields; thus, the formation of chlorinated products is assumed to proceed by the sequence shown in Scheme 1.

Table 6. Effect of hydrogen chloride on the formation of chlorinated benzidine in molten salt ($AlCl_3$:NaCl:KCl=3:1:1) at 150 °C[a]

Substrate	Aniline[b]	Aniline hydrochloride[c]
Condition		
Atmosph.	O_2	O_2
Temp (°C)	150	150
Time (h)	10	20
% Conv.	85	95
Yield (%)		
Benzidine	87	38
3-Chlorobenzidine	trace	37
3,3'-Dichlorobenzidine	—	10
3,5-Dichlorobenzidine	—	4
3,3',5-Trichlorobenzidine	—	trace

a) $AlCl_3$: 0.60 mol, NaCl: 0.20 mol, and KCl: 0.20 mol were used. b) 0.0549 mol. c) 0.0182 mol.

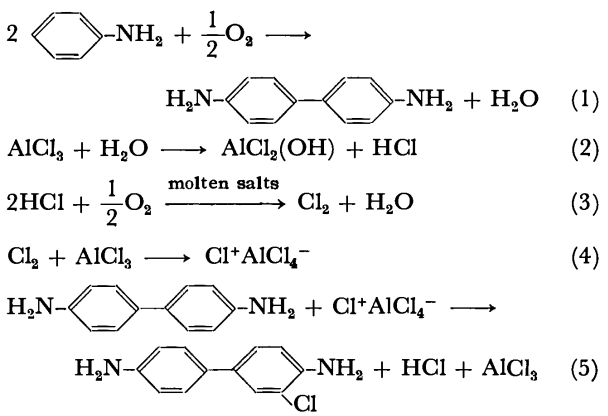

Scheme 1. Process for the formation of chlorinated benzidines.

Effects of Composition of Molten Salt. Although $AlCl_3$ is known to form the 1:1 complex with NaCl or KCl in a molten salt and only the remaining $AlCl_3$ has any catalytic activity,[7] benzidine was also formed even in the molten salt of a molar ratio [$AlCl_3$/(NaCl+KCl)] less than unity, suggesting that aniline took $AlCl_3$ away from the complex. When the molar ratio of aniline to free $AlCl_3$ was 1:4 or 1:2 in the molten salt of $AlCl_3$: NaCl: KCl (0.6: 0.2: 0.2 mol) at 200 °C in a stream of N_2, the reaction mixture remained completely clear. On the other hand, as the molar ratio became 1:1 or larger, the

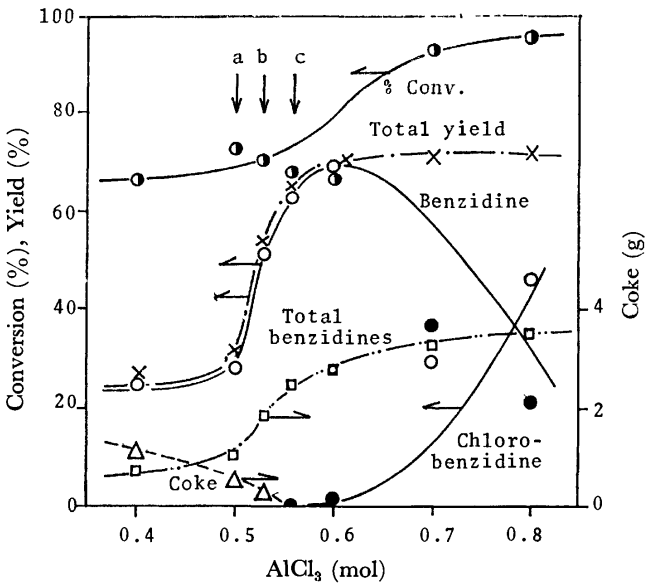

Fig. 1. Effect of molten salt composition on the product yields (reaction temp 200 °C, reaction time 5 h, substrate; aniline 0.0549 mol).
a) Aniline: free $AlCl_3$=1:0.
b) Aniline: free $AlCl_3$=1:1.
c) Aniline: free $AlCl_3$=1:2.
◑: Conversion(%). ×: Total yield(%).
○: Benzidine(%). □: Total Benzidines(g).
△: Coke(g). ●: Chlorobenzidine(%).

mixture increasingly became more turbid. These facts indicate that the $AlCl_3$-aniline, $AlCl_3$-NaCl, and $AlCl_3$-KCl complexes are practically soluble in a molten salt and that the free NaCl and KCl, formed when aniline takes $AlCl_3$ from the $AlCl_3$-NaCl or $AlCl_3$-KCl complex, are insoluble in a molten salt,[8-10] supporting the above-

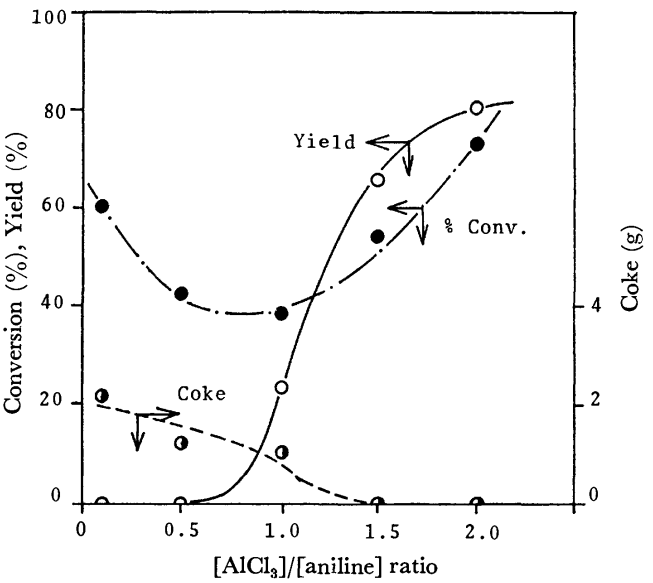

Fig. 2. Effect of [$AlCl_3$]/[aniline] ratio on the product yields (reaction temp 150 °C, reaction time 20 h, substrate; aniline 0.0549 mol).
—○—: yield (%).
-·-●-·-: Conversion (%).
---◑---: Coke (g).

described suggestion. Of course, the yield of benzidine increased with an increase in the ratio of $AlCl_3/(NaCl+KCl)$; in the region of ratio between 1—2 the increase in yield was most remarkable.

Reactions of Aniline with $AlCl_3$ in the Absence of NaCl and KCl. In the reaction of aniline with $AlCl_3$ in the absence of KCl and NaCl, a large amount of black tarry matter was obtained, and the yield of benzidine increased with an increase in the amount of $AlCl_3$. These results suggest that $AlCl_3$ complexed aniline at the site of amino group preferentially, arguing from a consideration of the similar spectral change on addition of $AlCl_3$ or HCl to aniline, and that more than one equivalent amount of $AlCl_3$ is necessary for the dimerization of aniline.

When aniline was heated with aniline hydrochloride in the absence of $AlCl_3$, no benzidine was formed, and no corresponding derivative of benzidine was similarly observed when dimethylaniline was heated with *N,N*-dimethyl-*N*-ethylanilinium iodide. Therefore, it may be obvious that the activation by quaternization of an amino group is not sufficient to dimerize an aromatic amine, in spite of the strong electron-withdrawing power of the $-\overset{+}{N}R_3$ group.[11]

From these results, a probable process for the formation of benzidine from aniline in the molten salt is shown in Scheme 2:

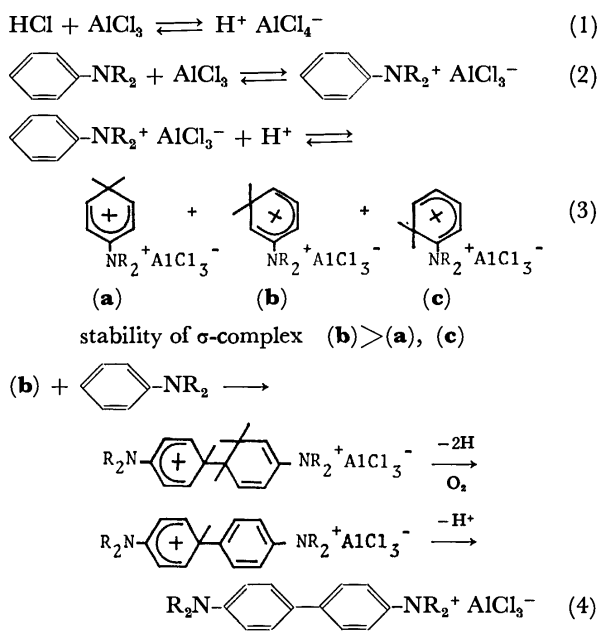

Scheme 2. A probable process for the formation of benzidine in molten salts.

1) Formation of $H^+AlCl_4^-$ from $AlCl_3$ and HCl, which would be formed from $AlCl_3$ and trace amounts of water in the molten salt.

2) Formation of a complex from aniline and $AlCl_3$. Although an equilibrium of the complex formation should lie far to the right, a slight amount of free aniline would be present in the reaction mixture, judging from the fact that all the chlorinated benzidine derivatives obtained in the reactions should be derived from free amines; all of them have halogen atoms at *ortho* or/and *para* positions to the amino group.

3) Formation of a σ-complex by the reaction of the aniline–$AlCl_3$ complex with $H^+AlCl_4^-$. In this reaction, the formation of three kinds of σ-complexes may be possible and from the adjacent charge rule the complex (**b**) should be the most stable and probable one among them; a similar σ-complex was observed by Olah *et al.*[11] However, the σ-complex formation would take place only with difficulty because of the positive character of the aniline–$AlCl_3$ complex. Thus, even though the concentration of the complex (**b**) is very low, **b** would be very electrophilic and a true reactive species in this reaction.

4) Formation of protonated dihydrobenzidine by a combination of the complex (**b**) with aniline, which would be present in a slight amount in the reaction mixture; this combination of two aromatic nuclei would be the key step in the benzidine formation from aniline in the molten salt.

5) Formation of a complex consisting of benzidine and $AlCl_3$ from protonated dihydrobenzidine by dehydrogenation and deprotonation. Monosubstituted benzenes such as halo-[3] and alkyl-benzenes[4] reacted with Lewis acids to give the derivatives of polyphenylene. However, the reaction of aromatic amines was very regiospecific and stopped at the stage of dimerization to yield *p,p'*-diaminobiaryls. The difference in the reaction between amine and other aromatic compounds would be attributed to the amino group which complexes $AlCl_3$ preferentially. Then the coordinated amine would react with $H^+AlCl_4^-$ to give the σ-complex of *meta* type (**b**), which would attack a free amine at the *ortho* or *para* position to the amino group, with the *para* attack predominating because of the steric hindrance in the *ortho* attack.

As to the reaction site of the free amine component, it may be reasonable to consider as follows: in the ordinary electrophilic substitution of aromatic compounds having an *o*- and *p*-directive group, the *para* attack proceeds more readily than the *ortho* attack even in the absence of steric hindrance. The positive charge of the reagent (**b**) spreads over three *o*- and *p*-positions to the sp^3 carbon in the ring, and consequently the electrophilic reactivities of *para* and *ortho* carbon atoms would be very low. Therefore, this reaction should be very selective, as in the cases of azo-coupling reactions of diazonium salts with aromatic amines; thus, in the present cases, the reactions took place almost exclusively at the *o*-position to the sp^3 carbon.

It may also be possible to form a similar benzidine–$AlCl_3$ complex (of the molar ratio of 1 : 1 or 1 : 2) to that from aniline. However, protonation of the 1 : 2 complex to yield a reactive species (**d**), corresponding to **b** in structure, would be much harder by two $-\overset{+}{N}\lessgtr$ groups than in the case of an aniline complex.[11] The concentration of a 1 : 1 complex should be very low in the presence of an excess of $AlCl_3$. Moreover, protonation would occur at the free amino group to give a complex similar to the 1 : 2 complex. After all, protonation is considered to be very difficult in the case of the benzidine–$AlCl_3$ complex (1 : 1 or 1 : 2), and, therefore, there is little possibility that a corresponding reactive

species to **b** reacts with aniline to produce a trimer.

On the other hand, the concentration of free benzidine would be very low in the presence of an excess of $AlCl_3$ compared with the case of aniline, and, moreover, the attack of **b** on the *ortho* position to the amino group of benzidine is considered to be very difficult because of the steric hindrance. Thus, **b** should react with aniline preferentially even in the presence of benzidine. Therefore, the possibilities of giving a trimer [reaction product of **b** with benzidine or reaction product of **d** with aniline] or tetramer [reaction product of **d** with benzidine] should be very low. This interpretation is consistent with the fact that the reaction of aromatic amines stopped at the stage of dimerization.

These speculations may be supported by the fact that *m*-phenylenediamine did not undergo dimerization and most of it was recovered in the molten salt; in the presence of an excess of $AlCl_3$, *m*-phenylenediamine would complex 2 mol of $AlCl_3$ to form a 1 : 2 complex, whose protonation to yield a σ-complex would occur with great difficulty. Even if a σ-complex is formed, little biphenyl would be formed, because *m*-phenylenediamine would not be present as a free base in the presence of an excess of $AlCl_3$.

References

1) A. T. Balaban and C. D. Nanitzescu, "Friedel-Crafts and Related Reactions," Vol. II, ed by G. A. Olah, Interscience Publishers, Inc., New York, N. Y. (1964), pp. 979—1047.

2) P. Kovacic and A. Kryiakis, *J. Am. Chem. Soc.*, **85**, 454 (1963).

3) P. Kovacic, J. J. Uchic, and L. Hse, *J. Polym. Sci., A-1*, **5**, 945 (1967).

4) P. Kovacic and J. S. Ramsey, *J. Polym. Sci., A-1*, **7**, 111 (1969).

5) On the addition of 5 ml (0.0549 mol) of aniline into the stirred molten mixtures of $AlBr_3$–NaCl–KCl (0.6: 0.2: 0.2 mol, 150 °C), $AlCl_3$–NaCl–KCl (0.6: 0.2: 0.2 mol, 150 °C), and $ZnCl_2$–NaCl–KCl (0.6: 0.2: 0.2 mol, 200 °C), the temperature of the reaction mixture rose by 30—35, 20—25, and 5—7 °C, respectively.

6) a) D. P. N. Satchell and R. S. Satchell, *Chem. Rev.*, **69**, 251 (1969); b) D. P. N. Satchell and J. L. Wardell, *J. Chem. Soc.*, **1964**, 4296; c) A. Mohammad and D. P. N. Satchell, *ibid., B*, **1968**, 331 d) *ibid., B*, **1967**, 331; e) *ibid., B*, **1966**, 527.

7) S. Kikkawa, T. Hayashi, T. Miura, and T. Tani, Reprint for 22nd Annual Meeting of the Chemical Society of Japan, Tokyo, April, 1969, Abstract IV, 2428.

8) U. I. Shvartsman, *J. Phys. Chem. (USSR)*, **14**, 254 (1940).

9) J. Kendall, E. D. Crittenden, and H. K. Miller, *J. Am. Chem. Soc.*, **45**, 976 (1923).

10) R. Midorikawa, *J. Electrochem. Soc. Jpn.*, **23[2]**, 74 (1955).

11) G. A. Olah, K. Dunne, D. P. Kelly, and Y. K. Mo, *J. Am. Chem. Soc.*, **94**, 7438 (1972).

Amidrazones and Related Compounds. IV.[1] The Cyclization of Hydrazidines to 2,3,4,5-Tetrahydro-1,2,4,5-tetrazine and 4-Amino-1,2,4-triazole Derivatives

Masahiko TAKAHASHI, Hideya TAN, Kunio FUKUSHIMA, and Hiroaki YAMAZAKI

Department of Industrial Chemistry, Faculty of Engineering, Ibaraki University, Hitachi, Ibaraki 316

(Received September 16, 1976)

Three methods of cyclization of hydrazidines are described. The reaction of N^4-arylhydrazidines (**2**) with dimethyl acetylenedicarboxylate in refluxing tetrahydrofuran afforded 6-alkyl and aryl-2-aryl-3-methoxycarbonyl-3-methoxycarbonylmethyl-2,3,4,5-tetrahydro-1,2,4,5-tetrazines (**3**). Oxidation of N^4-aryl-N^2-arylmethylenehydrazidines (**6**) with mercuric oxide in refluxing ethanol gave 3-alkyl and aryl-5-aryl-4-arylamino-1,2,4-triazoles (**7**). 3-Alkyl and aryl-4-arylamino-1,2,4-triazoles (**7f, g**) were obtained upon the heating of (**2a, e**) in formic acid.

In contrast to amidrazones[2] the use of hydrazidines, nitrogen analogues of amidrazone, as starting materials for the preparation of nitrogen heterocycles has not been extensively studied.

The reaction of N^4-arylhydrazidines with nitrous acid has been reported to give 2,6-diarylpentazines,[3] which were later corrected to be 1-arylamino-5-aryltetrazoles.[4] Methylthiohydrazonium salts have been noted[5] to cyclize in the presence of hydrazines to give 2,5-diphenyltetrazoles through intermediary hydrazidines. The synthesis of 3,5-disubstituted 4-arylamino-1,2,4-triazoles from acylhydrazidines has been investigated by Buzykin and coworkers.[6a,b] Recently, Neunhoeffer *et al.* have prepared some *N*-unsubstituted hydrazidines,[7] and pyrrolo[1,2-*b*][1,2,4,5]tetrazines.[8]

In this paper, the methods of cyclization of hydrazidines to some heterocycles by use of dimethyl acetylenedicarboxylate, mercuric oxide, and formic acid are reported.

Results and Discussion

Hydrazidines (**2**) are available by the reaction of hydrazonyl bromide (**1**) and hydrazine hydrate in alcohol.[9] Although the presence of the tautomerism **2A**⇌**2B** of hydrazidine appears possible, no study of it has been reported. However, the formation of 4-amino-1,2,4-triazoles[6,7] and 1-aminotetrazoles[4] supports the tautomerism. All the reported cyclization occured at the N^2 and N^3 positions. However, when **2** were treated with dimethyl acetylenedicarboxylate, compounds cyclized at the N^2 and N^4 positions were formed.

Thus, when N^4-(2-bromo-4-nitrophenyl)benzohydrazide hydrazone (**2a**) was allowed to react with dimethyl acetylenedicarboxylate in refluxing tetrahydrofuran, an orange product was obtained. This compound was proved to be a 1:1 adduct on the basis of elemental analysis and its mass spectrum (*m/e* 491, M^+). The IR spectrum showed NH, C=N, and ester absorptions at 3260, 1625, and 1705 cm^{-1}, respectively. The presence of two methyl and one methylene groups was ascertained by resonance at δ 3.65 (s, 3H), 3.75 (s, 3H), and 3.90 (s, 2H) in the NMR spectrum. However, these data do not distinguish between the tetrahydrotetrazine (**3a**) and dihydrotriazole (**5a**). Therefore, to determine the structure, some reactions were attempted and an oxidized product was obtained upon treatment of the adduct with nitric acid, which was previously used for the oxidation of dihydrotetrazine to tetrazine.[10] The oxidized product showed no NH absorption, but two ester absorptions at 1736 and 1725 cm^{-1}. In the NMR spectrum, the absorptions at δ 3.64, 3.74, and 3.31 were assigned to two methyl and one methylene groups, respectively. The mass spectrum (*m/e* 489, M^+) and elemental analysis suggest one molar dehydrogenation from the 1:1 adduct. From these data, it is concluded that the structure of the adduct is **3a**, 2,3,4,5-tetrahydro-1,2,4,5-tetrazine and the oxidized product is 2,3-dihydro-1,2,4,5-tetrazine (**4**).The physical properties and the spectral data of other tetrazine derivatives are listed in Table 1.

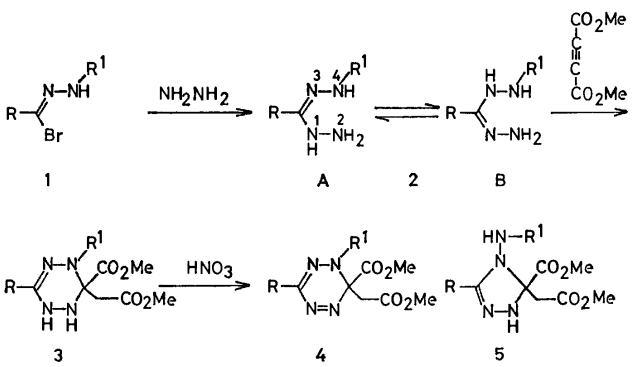

1, 2, 3, 4, 5,	R	R^1
a	C_6H_5	2-Br-4-$NO_2C_6H_3$
b	4-ClC_6H_4	2-Br-4-$NO_2C_6H_3$
c	C_6H_5	4-$NO_2C_6H_4$
d	1-MePr	2, 4-$(NO_2)_2C_6H_3$
e	Me	2, 4-$(NO_2)_2C_6H_3$
f	4-*i*-PrC_6H_4	2-Br-4-$NO_2C_6H_3$

Scheme 1.

The synthesis of nitrogen heterocycles from hydrazidines has also been attempted. Spasov *et al.*[11] have described the oxidation of arylmethylene derivatives of amidrazones with mercuric oxide to yield 3,4,5-triaryl-substituted 1,2,4-triazoles. Then this method was applied to hydrazidines. A mixture of N^2-benzylidene-N^4-(2-bromo-4-nitrophenyl)benzohydrazide hydrazone (**6a**) and mercuric oxide in ethanol was refluxed for 24 h. The elemental analysis, mass spectrum (*m/e*

TABLE 1. PHYSICAL PROPERTIES AND SPECTRAL DATA OF **3**

Compound	Yield (%)	Mp (°C) (Solvent)	Molecular formula	Found (Calcd) C%	Found (Calcd) H%	IR (KBr) (cm^{-1})	UV (MeOH) (nm, (log ε))
3a	77	184—187 (C_6H_5)	$C_{19}H_{18}O_6N_5Br$	46.35 (46.36)	3.80 (3.68)	3260, 1705, 1625, 1582, 1530	253 (4.21), 423 (4.32)
3b	86	191—193 (THF-MeOH)	$C_{19}H_{17}O_6N_5BrCl$	43.58 (43.32)	3.31 (3.25)	3260, 1728, 1702, 1636, 1582	238 sh (4.30), 256 sh (4.23), 300 sh (3.99), 403 (4.44)
3c	80	184—186 (C_6H_6)	$C_{19}H_{18}O_6N_5$	55.08 (55.34)	4.51 (4.40)	3190, 1735, 1705, 1625, 1590	227 (4.36), 286 sh (3.96), 405 (4.46)
3d	88	149—151 (MeOH)	$C_{17}H_{22}O_8N_6$	46.36 (46.57)	5.04 (5.06)	3250, 2960, 1715, 1655, 1620	234 (4.31), 262 (4.19), 398 (4.35)
3e	87	158—160 ($CHCl_3$-MeOH)	$C_{14}H_{16}O_8N_6$	42.21 (42.43)	3.93 (4.07)	3300, 3070, 2960, 1712, 1705, 1647	228 (4.23), 263 (4.19), 393 (4.28)

TABLE 2. PHYSICAL PROPERTIES AND SPECTRAL DATA OF **7**

Compound	Yield (%)	Mp (°C) (Solvent)	Molecular formula	Found (Calcd) C%	Found (Calcd) H%	IR (KBr) (cm^{-1})	UV (MeOH) (nm, (log ε))
7a	48	265—267 a)	$C_{20}H_{14}O_2N_5Br$	55.11 (55.00)	3.14 (3.20)	3140, 3060, 1589, 1500, 1475	253 (4.36), 326 (4.05)
7b	28	228—231 a)	$C_{22}H_{19}O_2N_6Br$	55.30 (55.12)	4.44 (4.00)	3130, 3060, 2900, 1610, 1580	220 sh (4.36), 230 sh (4.27), 317 (4.53)
7c	55	244—246 a)	$C_{20}H_{13}O_2N_5BrCl$	51.35 (51.03)	3.28 (2.78)	3160, 3080, 1590, 1500, 1473	260 (4.41), 324 (4.07)
7d[b]	29	213—214 (C_6H_6)	$C_{18}H_{18}O_4N_6$	56.32 (56.54)	4.83 (4.75)	3200, 3100, 2960, 1618, 1600, 1520	242 (4.36), 316 (4.06), 380 sh (3.76)
7e	75	244—245 a)	$C_{26}H_{26}O_2N_5Br$	59.72 (60.00)	5.09 (5.04)	3170, 2960, 1593, 1500, 1488	264 (4.45), 330 (4.09), 450 sh (2.68)
7f	56	222—224 (MeOH)	$C_{14}H_{10}O_2N_5Br$	46.92 (46.68)	3.09 (2.78)	3080, 1580, 1500, 1475, 1445	240 (4.29), 326 (4.10), 498 (2.97)
7g	69	260—261 (MeOH)	$C_9H_8O_4N_6$	40.97 (40.91)	3.05 (3.05)	3120, 1620, 1600, 1503, 1415	220 (4.10), 259 (4.04), 314 (4.11), 445 sh (2.84)

a) C_6H_6-petroleum ether. b) Column chromatographed on silica gel with $CHCl_3$.

435, M^+), and IR spectrum (NH absorption at 3140 cm^{-1}) of the product indicate it to be 4-amino-1,2,4-triazole (**7a**) or 2,5-dihydro-1,2,4,5-tetrazine (**9a**). The NMR measurement of a product, whose substituents R and R^2 are the same, would reveal the structure to be symmetric (**7**) or asymmetric (**9**). In the NMR spectrum of products **7e** and **9e** obtained from **6e**, four methyl and two methylidyne groups of the two isopropyl groups on R and R^2 were observed at δ 1.15 (12H, d, J=7.0 Hz) and 2.80 (2H, m, J=7.0 Hz), respectively, and the aromatic protons on R and R^2 were observed at δ 7.01 (4H, d, J=8.2 Hz) and 7.55 (4H, d, J=8.2 Hz). These results show that the product apparently is not asymmetric **9e**, but is symmetric **7e**. The confirmation of the structure of **7** has been further conducted according to reported method,[7] that is, the dehydration of N^2-acyl-N^4-substituted hydrazidines (**8**) to **7**. **8a** prepared from **1a** was heated in acetic acid and the product was identical with **7a**. The physical and spectral data for product **7** from **6a—e** are listed in Table 2.

When **2a** was heated in formic acid, a product was obtained. The analytical and mass spectral results suggest **7f** or **9f** to be possible structures. But **7f** is prefered on the basis of the NMR spectrum, which is as follows: six aromatic protons and one NH proton at δ 7.4—7.95 (m) and 9.04 (s), respectively, besides protons due to the 2-bromo-4-nitrophenyl group, which were clearly assigned (see Experimental). The reaction presumably proceeded *via* formylated hydrazidine (**8f**) to **7f**. However, this cyclization method was sometimes

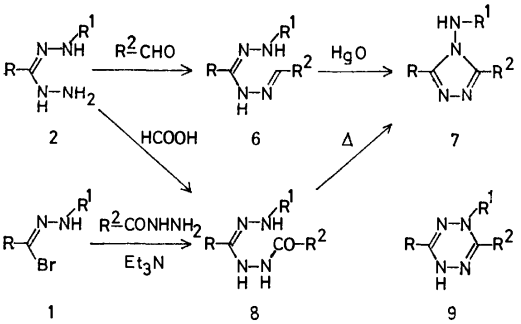

6, 7, 8, 9,	R	R^1	R^2
a	C_6H_5	2-Br-4-$NO_2C_6H_3$	C_6H_5
b	C_6H_5	2-Br-4-$NO_2C_6H_3$	4-$Me_2NC_6H_4$
c	4-ClC_6H_4	2-Br-4-$NO_2C_6H_3$	C_6H_5
d	1-MePr	2, 4-$(NO_2)_2C_6H_3$	C_6H_5
e	4-*i*-PrC_6H_4	2-Br-4-$NO_2C_6H_3$	4-*i*-PrC_6H_4
f	C_6H_5	2-Br-4-$NO_2C_6H_3$	H
g	Me	2, 4-$(NO_2)_2C_6H_3$	H

Scheme 2.

accompanied by by-products and only **7f** and **7g** were obtained in pure forms.

Experimental

All the melting points are uncorrected. The IR, UV, and NMR spectra were measured using a JASCO Model IRA-2 spectrometer, a Shimadzu Model MPS-501 spectrometer, and a Hitachi Model R-20 spectrometer, respectively. A Shimadzu Model UM-3B apparatus was used for the elemental analysis.

Materials. Compounds **1a**,[12] **1b**[12] **1c**,[12] **1d**,[13] **1e**,[13] and **1f**[12] were prepared using reported methods. The hydrazines (**2a—f**) were prepared by the method of Hegarty *et al.*[9] The arylmethylene hydrazidines **6a**,[9] **6c**,[9] and **6d**[13] were prepared by known methods. **6b** was prepared by refluxing the EtOH solution of **2a** and *p*-dimethylaminobenzaldehyde for 30 min. Recrystallization from benzene afforded red plates; mp 184—186 °C. Found: C, 55.02; H, 4.11%. Calcd for $C_{22}H_{21}O_2N_6Br$: C, 54.89; H, 4.40%. **6e** was prepared as follows: a mixture of **2f** (1.24 g, 3.2 mmol), *p*-isopropylbenzaldehyde (950 mg, 6.4 mmol), and triethylamine (320 mg, 3.2 mmol) in EtOH (64 ml) was refluxed for 2 h. After cooling, the precipitates were filtered to give **6e** (658 mg, 39% yield). Recrystallization from THF–MeOH gave brown needles; mp 193—195 °C. Found: C, 59.49; H, 5.25%. Calcd for $C_{26}H_{28}O_2N_5Br$: C, 59.77; H, 5.40%.

2-(2-Bromo-4-nitrophenyl)-3-methoxycarbonyl-3-methoxycarbonylmethyl-6-phenyl-2,3,4,5-tetrahydro-1,2,4,5-tetrazine (3a). A mixture of **2a** (1.0 g, 2.9 mmol) and dimethyl acetylenedicarboxylate (490 mg, 3.4 mmol) in THF (40 ml) was refluxed for 4 h. After evaporation of the solvent under reduced pressure, the residue was washed with a small amount of MeOH and filtered to give **3a** (1.1 g, 77% yield). Recrystallization from benzene afforded orange crystals; mp 184—187 °C. NMR (DMSO-d_6): δ 3.65 (3H, s, $-CH_3$), 3.75 (3H, s, $-CH_3$), 3.90 (2H, s, $-CH_2-$), 7.4—8.3 (8H, m, aromatic H), 10.85 (1H, s, NH), 11.30 (1H, s, NH). MS *m/e* (%): 493 (M^++2, 51), 491 (M^+, 53), 434 (54), 432 (54), 334 (13), 332 (15), 245 (33), 216 (38), 214 (40), 104 (82), 103 (100).

The tetrazines (**3b—3e**) were prepared in a manner similar to that described above by refluxing the reaction mixture for 2.5—4 h.

2-(2-Bromo-4-nitrophenyl)-3-methoxycarbonyl-3-methoxycarbonylmethyl-6-phenyl-2,3-dihydro-1,2,4,5-tetrazine (4). To a suspension of **3a** (500 mg, 1.0 mmol) in AcOH (20 ml) was added nitric acid (0.43 ml) dropwise with cooling and stirring. After the color of the reaction mixture became red, crushed ice was added and the solution was made alkaline with aq sodium carbonate. The resulting precipitates were filtered to give **4** (390 mg, 79% yield). Quick recrystallization from MeOH afforded orange plates; mp 133—136 °C. Found: C, 46.35; H, 3.30%. Calcd for $C_{19}H_{16}O_6N_5Br$: C, 46.54; H, 3.29%. IR (KBr): 3090, 2950, 1736, 1725, 1584 cm^{-1}. UV (MeOH) nm (log ε): 218 (4.46), 231 sh (4.32), 256 sh (4.00), 278 (3.87), 360 (4.32). NMR ($CDCl_3$): δ 3.31 (2H, s, $-CH_2-$), 3.64 (3H, s, $-CH_3$), 3.74 (3H, s, $-CH_3$), 7.3—8.6 (8H, m, aromatic H). MS *m/e* (%): 491 (M^++2, 0.4), 489 (M^+, 0.4), 463 (7.8), 461 (8.0), 404 (5.8), 402 (5.8), 360 (11), 358 (12), 332 (13), 330 (14), 301 (43), 299 (45), 279 (39), 269 (39), 267 (21), 258 (19), 256 (19), 233 (24), 116 (23), 103 (100).

4-(2-Bromo-4-nitroanilino)-3,6-diphenyl-1,2,4-triazole (7a). A mixture of **6a** (200 mg, 0.41 mmol) and yellow mercuric oxide (260 mg, 1.2 mmol) in EtOH (120 ml) was refluxed for 24 h. After the inorganic materials were filtered off, the filtrate was concentrated under reduced pressure and the resulting precipitates were filtered to give **7a** (138 mg, 48% yield). Recrystallization from benzene–petroleum ether afforded a pale yellow powder; mp 265—267 °C. MS *m/e* (%): 437 (M^++2, 41), 435 (M^+, 43), 221 (43), 192 (51), 118 (36), 103 (58), 89 (100). The triazoles (**7b—e**) were prepared in a manner similar to that described above by refluxing the reaction mixture for 15—28 h. The NMR spectrum of **7e** ($CDCl_3$): δ 1.15 (12H, d, J=7.0 Hz, $-CH_3$ on isopropyl), 2.80 (2H, m, J=7.0 Hz, CH on isopropyl), 5.98 (1H, d, J=9.0 Hz, 6-H on R^1), 7.01 (4H, d, J=8.2 Hz, *o*- or *m*-H on R and R_2), 7.55 (4H, d, J=8.2 Hz, *o*- or *m*-H on R and R^2), 7.73 (1H, dd, J=9.0 and 2.2 Hz, 5-H on R^1), 8.21 (1H, d, J=2.2 Hz, 3-H on R^1), 8.80 (1H, s, NH).

N^4-(2-Bromo-4-nitrophenyl)-N^2-benzoylbenzohydrazide hydrazone (8a). To a solution of **1a** (600 mg, 1.5 mmol) and benzoylhydrazine (245 mg, 1.8 mmol) in THF (10 ml) was added a solution of triethylamine (300 mg, 3.0 mmol) in THF (3 ml) dropwise with stirring at room temperature. After stirring for an additional 2 h, the resulting precipitates were removed by filtration and the filtrate was evaporated under reduced pressure giving an oily residue. To the residue was added a small amount of MeOH to lead to solidification. The solids were collected by filtration and recrystallized once from MeOH–THF to give **8a** (303 mg, 44% yield). An additional recrystallization afforded orange needles; mp 196—198 °C. Found: C, 53.16; H, 3.39%. Calcd for $C_{20}H_{16}O_3N_5Br$: C, 52.87; H, 3.55%. IR (KBr): 3440, 3280, 1653, 1588, 1508, 1488 cm^{-1}.

Cyclization of 8a to 7a. A solution of **8a** (100 mg, 0.22 mmol) in AcOH (3.0 ml) was refluxed for 30 min. After removal of the solvent under reduced pressure, the residual solid was washed with a small amount of MeOH and collected by filtration. One recrystallization from MeOH afforded white needles; mp 265—267 °C (60 mg, 62% yield). The mp and IR spectrum were identical to those of **7a**.

4-(2-Bromo-4-nitroanilino)-3-phenyl-1,2,4-triazole (7f). A solution of **2a** (200 mg, 0.57 mmol) in formic acid (1.0 ml) was refluxed for 2 h. After cooling, a small amount of MeOH was added to the reaction mixture to give crystalline precipitates, which were collected by filtration and recrystallized once from MeOH to give **7f** (116 mg, 56% yield). MS *m/e* (%): 361 (M^++2, 84), 359 (M^+, 86), 145 (36), 104 (100). NMR (DMSO-d_6): δ 6.28 (1H, d, J=9.0 Hz, 6-H on R^1), 7.4—7.95 (6H, m, aromatic H on R and the triazole ring), 8.08 (1H, dd, J=9.0 and 2.2 Hz, 5-H on R^1), 8.45 (1H, d, J=2.2 Hz, 3-H on R^1), 9.04 (1H, s, NH).

4-(2,4-Dinitroanilino)-3-methyl-1,2,4-triazole (7g). A solution of **2e** (300 mg, 1.2 mmol) in formic acid (3.0 ml) was refluxed for 1 h. Water was added to the reaction mixture and the solution was allowed to stand overnight. The resulting precipitates were collected by filtration to give **7a** (216 mg, 69% yield).

The authors wish to express their thanks to Dr. Masatoshi Hirayama and Mr. Mamoru Sekine for the NMR measurements and to the Sankyo Co., Ltd., for the mass spectral measurements.

References

1) Previous papers in this series; a) M. Takahashi and N. Sugawara, *Nippon Kagaku Kaishi*, **1975**, 334; b) M. Takahashi, S. Onizawa, and T. Satoh, *Bull. Chem. Soc. Jpn.*, **47**, 2724 (1974); c) M. Takahashi, S. Shirahashi, and N. Sugawara, *Nippon Kagaku Kaishi*, **1973**, 1519.

2) D. G. Neilson, R. Roger, J. W. M. Heatlie, and L. R. Newlands, *Chem. Rev.*, **70**, 151 (1970).

3) F. D. Chattaway and G. D. Parkes, *J. Chem. Soc.*, **1926** 113.
4) J. M. Burgess and M. S. Gibson, *Tetrahedron*, **18**, 1001 (1962).
5) R. Grashey, M. Baumann, and H. Bauer, *Chem. -Ztg.*, **96**, 225 (1972): *Chem. Abstr.*, **77**, 34427z (1972).
6) a) B. I. Buzykin, L. P. Sysoeva, and Yu. P. Kitaev, *Zh. Org. Khim.*, **11**, 173 (1975); b) L. P. Sysoeva, B. I. Buzykin, and Yu. P. Kitaev, *ibid.*, **11**, 348 (1975).
7) H. Neunhoeffer, H. -J. Degen, and J. J. Köhler, *Justus Liebigs Ann. Chem.*, **1975**, 1120.
8) H. Neunhoeffer and H.-J. Degen, *Chem. Ber.*, **108**, 3509, (1975).
9) A. F. Hegarty, J. B. Aylward, and F. L. Scott, *J. Chem. Soc., C*, **1967**, 2587.
10) F. Dallacker, *Monatsh. Chem.*, **91**, 294 (1960).
11) A. Spasov, E. Golovinskii, and G. Rusev, *Chem. Ber.*, **96**, 2996 (1963).
12) J. B. Aylward and F. L. Scott, *J. Chem. Soc., B*, **1969**, 1080.
13) A. F. Hegarty and F. L. Scott, *J. Org. Chem.*, **33**, 753 (1968).

Amidrazones and Related Compounds. V.[1] The Formation of Pyrazole, 1*H*-1,2,4-Triazepine, and 4*H*,11*H*-[1,5]Diazocino-[2,3-*e*: 6,7-*e'*]di[1*H*-1,2,4]triazepine Derivatives

Masahiko TAKAHASHI, Noriyuki SUGAWARA, and Kaoru YOSHIMURA

Department of Industrial Chemistry, Faculty of Engineering, Ibaraki University, Hitachi, Ibaraki 316

(Received September 30, 1976)

Amidrazones $RC(NH_2)=NNH_2$ (**1a**, **b**) (R=2-pyridyl, phenyl) reacted with $EtOCH=CR^1R^2$ (**2a—d**) (R^1,R^2=CN, $CO_2C_2H_5$, $COCO_2C_2H_5$) to give $RC(NH_2)=NNHCH=CR^1R^2$ (**3a—g**). 3,4-Disubstituted pyrazoles (**4a**, **b**) were obtained on the heating of **3a**, **b**, **e**, and **f** (R=2-pyridyl, phenyl, R^1=CN, R^2=CN, $CO_2C_2H_5$) in toluene. However, the heating of **3c** (R=2-pyridyl, $R^1=R^2=CO_2C_2H_5$) gave a dimer, the 2,3,7,9,10-pentaazadodeca-1,4,8,11-tetraene derivative (**9**), instead of **4**. 5-Amino-6-ethoxycarbonyl-3-(2-pyridyl)-1*H*-1,2,4-triazepine (**10**) was obtained by the reaction of **3a** (R=2-pyridyl, R^1=CN, $R^2=CO_2C_2H_5$) with ethanolic hydrogen chloride. The treatment of **10** with alkaline gave 2,9-di-2-pyridyl-6,7,13,14-tetrahydro-4*H*,11*H*-[1,5]diazocino-[2,3-*e*: 6,7-*e'*]di[1*H*-1,2,4]triazepine-6,13-dione (**11**). Triazepine (**10**) reacted with hydrazines to give 5-hydrazino-1*H*-1,2,4-triazepine derivatives (**13a**, **b**).

Amidrazones[2] show a strong nucleophilicity similar to hydrazine and are known as versatile reagents in the synthesis of some nitrogen heterocycles. However, the synthesis of monocyclic 1,2,4-triazepine derivatives by the use of amidrazone has not been reported. The fully or partially saturated monocyclic 1,2,4-triazepine derivatives have been synthesized by the reactions of thiosemicarbazides with malonyl dichloride,[3a,b] β-keto esters,[4,5] β-diketo compounds,[4] and 1,1,3,3-tetraethoxypropane.[6] On the other hand, the synthesis of fully unsaturated monocyclic 1,2,4-triazepine derivatives has been reported recently; 2*H*-1,2,4-triazepines were prepared by the cycloaddition reaction of 1,2,4,5-tetrazines with 1-azirines,[7a-d] and 4*H*-1,2,4-triazepines were formed photochemically from 3,4,7-triaza-2,4-norcaradienes.[8]

In the present paper we wish to report the results of the attempted synthesis of the 1*H*-1,2,4-triazepine derivative from amidrazones and ethoxymethylenic compounds.

Results and Discussion

When picolinamidrazone (**1a**) was treated with ethoxymethylenic compounds (**2a—d**) in EtOH at 0 °C, the products isolated were *N*-(2,2-disubstituted vinyl)-picolinamidrazones (**3a—d**). Similarly, the treatment of benzamidrazone (**1b**), which was generated *in situ* by the reaction of ethyl benzimidate with hydrazine hydrate, with **2a—c** gave **3e—g**. The physical properties and spectral data, shown in Table 1, are consistent with the assigned structure.

Next, the thermal and acid- or base-catalyzed cyclizations of **3** to 1,2,4-triazepine derivatives were attempted. When a toluene solution of **3a** was heated for 4 h, a product was obtained in an 87% yield as white needles. Its mp and IR spectrum were consistent with those of ethyl 3-amino-4-pyrazolecarboxylate (**4a**).[9] Similarly, the heating of a toluene solution of **3b** gave a white crystalline product (91% yield) which was identical with 3-amino-4-cyanopyrazole (**4b**).[10] In a similar manner, **4a** and **4b** were obtained from **3e** and **3f** respectively. It can be assumed that the formation of **4a** and **4b** has occurred by mean of the intramolecular nucleophilic attack of the N′ atom on the cyano group,

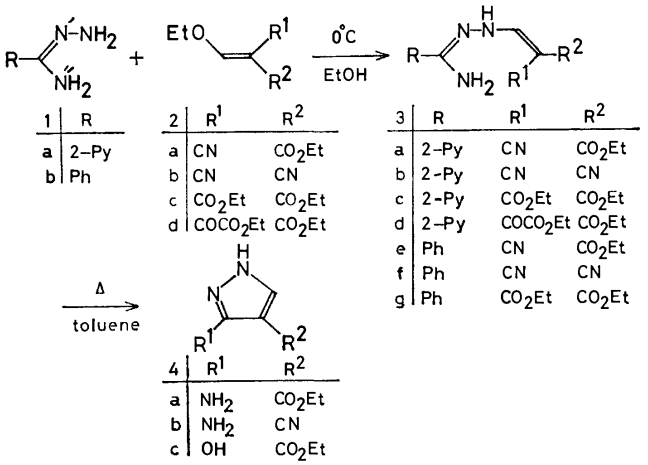

Scheme 1.

followed by the elimination of arylnitrile, as is shown in Scheme 2. In fact, when a toluene solution of *N*-(2,2-dicyanovinyl)-*N*″-phenylbenzamidrazone (**6**) was heated for 24 h, the pyrazole derivative was not obtained as expected, and the starting material was recovered.

However, on the treatment of **3c** in a similar manner, the pyrazole derivative was not obtained, rather yellow needles were obtained in a 45% yield. The IR spectrum showed the absorption band of the amide NH at 3440

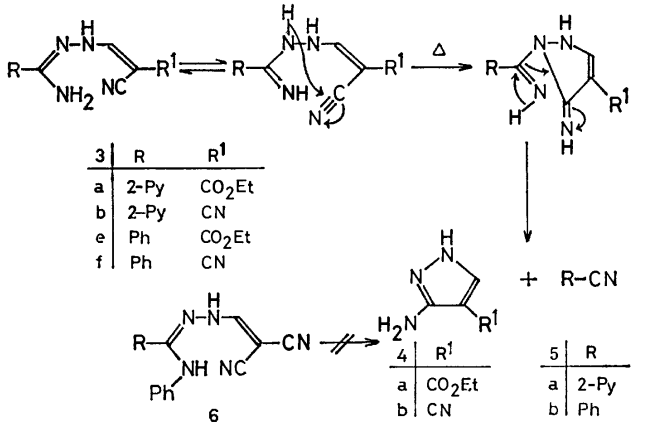

Scheme 2.

Table 1. The physical properties and the spectral data of **3**

Compd	Yield (%)	Mp (°C) (Solvent)	Molecular formula	Found (Calcd) C%	Found (Calcd) H%	IR (KBr) cm^{-1}	NMR δ, ppm
3a[a]	92	126—129 (MeOH)	$C_{12}H_{13}N_5O_2$	55.84 (55.59	5.08 5.05)	3300, 3200, 2200, 1685	10.85 (s, =NH), 7.63 (s, =CH–), 7.88—8.60 (m, aromatic H), 7.03 (s, $-NH_2$), 4.14 (q, J= 6.8 Hz, $-CH_2-$), 1.20 (t, J=6.8 Hz, $-CH_3$)
3b[b]	97	129—132 (MeOH)	$C_{10}H_8N_6$	56.81 (56.59	4.05 3.80)	3390, 3310, 2200	10.10 (s, =NH), 7.56 (s,=CH–), 7.59—8.71 (m, aromatic H), 6.99 (s, $-NH_2$)
3c[b]	71	131—132 (MeOH)	$C_{14}H_{18}N_4O_4$	55.06 (55.38	5.84 5.65)	3480, 3340, 3200, 1680	11.58 (d, J=11.4 Hz, =NH), 8.47 (d, J= 11.4 Hz,=CH–), 7.29—8.52 (m, aromatic H), 5.80 (s, $-NH_2$), 4.26 (q, J=6.8 Hz, $-CH_2-$), 4.20 (q, J=6.8 Hz, $-CH_2-$), 1.36 (t, J=6.8 Hz, $-CH_3$), 1.30 (t, J=6.8 Hz, $-CH_3$)
3d[b]	80	123—125 (MeOH)	$C_{15}H_{18}N_4O_5$	54.08 (53.88	5.43 5.43)	3440, 3340, 1720, 1695	8.51 (d, J=11.4 Hz, =CH–), 7.36—8.58 (m, aromatic H), 6.21 (s, $-NH_2$), 4.23 (q, J=6.8 Hz, $-CH_2-$), 4.33 (q, J=6.8 Hz, $-CH_2-$), 1.34 (t, J=6.8 Hz, $-CH_3$), 1.27 (t, J=6.8 Hz, $-CH_3$)
3e[a]	61	129—131 (EtOH)	$C_{13}H_{14}N_4O_2$	60.16 (60.45	5.37 5.46)	3340, 3240, 2200, 1675	10.48 (s, =NH), 7.58 (s, =CH–), 7.19—8.07 (m, aromatic H), 6.90 (s, $-NH_2$), 4.20 (q, J=6.8 Hz, $-CH_2-$), 1.25 (t, J=6.8 Hz, $-CH_3$)
3f	94	150—155 (benzene-MeOH)	$C_{11}H_9N_5$	62.48 (62.55	4.30 4.30)	3400, 3280, 2200	
3g[a]	78	140—142 (EtOH)	$C_{15}H_{19}N_3O_4$	58.69 (59.00	6.12 6.27)	3310, 3220, 1674, 1653	11.28 (d, J=10.8 Hz, =NH), 8.26 (d, J= 10.8 Hz, =CH–), 7.35—8.15 (m, aromatic H), 6.81 (s, $-NH_2$), 4.08 (q, J=6.8 Hz, $-CH_2-$), 1.22 (t, J=6.8 Hz, $-CH_3$)

a) The NMR spectrum was measured in DMSO-d_6. b) The NMR spectrum was measured in $CDCl_3$.

cm^{-1} and those of the carbonyl groups at 1645—1695 cm^{-1}. The mass spectrum showed the parent peak at *m/e* 566. From the above data and the results of the elemental analysis, the product was confirmed to be a dimer, triethyl 1-amino-6-oxo-1,8-di-2-pyridyl-2,3,7,9,10-pentaazadodeca-1,4,8,11-tetraene-5,12,12-tricarboxylate (**9**). The treatment of **3c** in EtOH in the presence of sodium ethoxide gave **4c**[11] and 1,2-bis(2-pyridylcarbonimidoyl)hydrazine (**7a**).[12a,b] Similarly, **4c** was obtained from **3g** in the same manner, but the method failed to isolate the corresponding product (**7b**). On the heating of an ethanol solution of **3d**, an orange product was obtained and revealed to be 1,2-dihydro-3,6-di-2-pyridyl-1,2,4,5-tetrazine (**8**).[13a,b]

When **3a** was treated with an ethanolic hydrogen chloride, followed by neutrallization with sodium hydrogen carbonate, a product was obtained in a 57% yield as white needles. The IR spectrum indicated the presence of ester (1700 cm^{-1}) and amino (3320—3110 cm^{-1}) groups, but it did not show the absorption band of the cyano group at *ca.* 2200 cm^{-1}. The ester group was confirmed by the signals at δ 3.96 and δ 1.15 ppm due to the ethyl group. Considering the above data and the parent peak at *m/e* 259, the structure of the product can clearly be assigned to the desired compound, 5-amino-6-ethoxycarbonyl-3-(2-pyridyl)-1*H*-1,2,-4-triazepine (**10**). However, all attempts at the cyclization of **3b**—**g** to 1*H*-1,2,4-triazepine derivatives were unsuccessful. Then the reactivity of **10** was studied. When an aqueous sodium hydroxide solution of **10** was

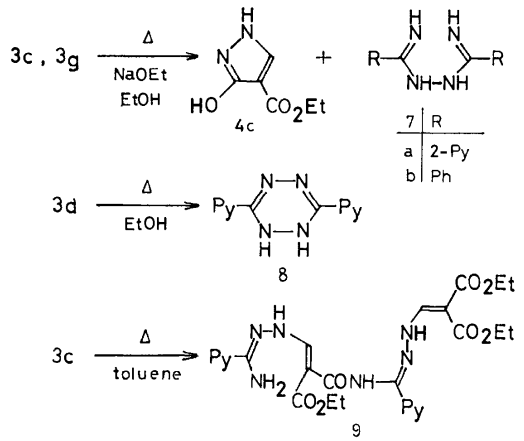

Scheme 3.

heated, a product was obtained in a 74% yield as white powder. According to the emperical formula, $C_{10}H_7N_5O$, and the mass spectral parent peak at *m/e* 213, the product seems to be [2,3-*e*][1*H*-1,2,4]triazepine (**12**). However, the carbonyl absorption observed at the comparably low frequency (1680 cm^{-1}) is in conflict with the strained β-lactam structure, **12**. Consequently, the only possible structure which satisfies both the analytical and mass spectral results is the dimeric and symmetric one, 2,9-di-2-pyridyl-6,7,13,14-tetrahydro-4*H*,11*H*-[1,5]diazocino[2,3-*e*: 6,7-*e'*]di[1*H*-1,2,4]triazepine-6,13-dione (**11a**), which belongs to a new ring system. A similar condensation, followed by a dimeriza-

tion reaction, that is the conversion of 4-amino-5-ethoxycarbonyl-pyrimidine to 5,6,11,12-tetrahydro[1,5]-diazocino[2,3-*d*: 6,7-*d'*]dipyrimidine-5,11-dione, has been reported by Bredreck *et al.*[14] Additional support for the structure of **11a** was provided by its methylation with methyl iodide. The IR spectrum of the product showed the absorption band of the carbonyl at 1705 cm^{-1} and none of the imino group in the NH region. The NMR spectrum showed the two singlet signals at δ 4.20 and δ 3.82 ppm due to two pairs of four methyl groups, although the mass spectrum showed the parent peak at *m/e* 241 corresponding to half the molecular weight. These data show the structure to be a tetramethyl derivative (**11a**).

The treatment of **10** with phenylhydrazine gave a substituted product, 6-ethoxycarbonyl-5-(2-phenylhydrazino)-3-(2-pyridyl)-1*H*-1,2,4-triazepine (**13a**), whose structure was clarified on the basis of the spectral and analytical measurements. Similarly, the treatment of **10** with hydrazine hydrate gave corresponding product (**13b**).

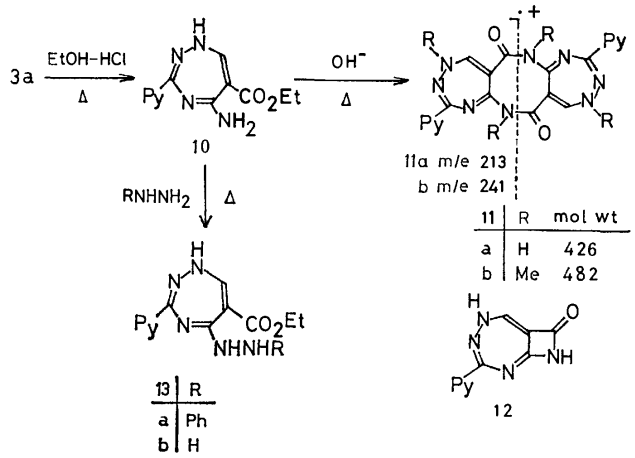

Scheme 4.

Experimental

All the melting points are uncorrected. The IR, UV, and NMR spectra were measured with a JASCO Model IRA-2 spectrometer, a Shimadzu Model MPS-501 spectrometer, and a Hitachi Model R-20 spectrometer respectively. A Shimadzu Model UM-3B apparatus was used for the elemental analysis.

Materials. The compounds **1a**,[15] **2a**,[16] **2b**,[16] and **2d**[17] were prepared by the reported methods. The **2c** was commercially available.

N-(2-Cyano-2-ethoxycarbonylvinyl)picolinamidrazone (3a). To a stirred solution of **2a** (1.01 g, 6.0 mmol) in EtOH (15 ml), was added **1a** (0.82 g, 6.0 mmol) at 0 °C. After the stirring had continued for 30 min, the resulting precipitates were filtered and dried to give **3a** (1.43 g, 92%). Recrystallization from MeOH afforded yellow plates; mp 126—129 °C. **3b—d** were prepared by the same procedure.

N-(2-Cyano-2-ethoxycarbonylvinyl)benzamidrazone (3e). Ethyl benzimidate hydrochloride[18] (1.91 g, 10.2 mmol) was added to an aq solution (10 ml) containing potassium hydroxide (10.2 mmol). The resulting oil was extracted twice with ethyl acetate (10 ml), and the organic phase was concentrated *in vacuo*. The oily residue was dissolved into EtOH (10 ml), and hydrazine hydrate (532 mg, 10.5 mmol) was stirred into this solution in portions at 0 °C. After the stirring had continued for 2 h, at 0 °C, **2a** (1.74 g, 10.3 mmol) was added to the EtOH solution with stirring at 0 °C. After the stirring had continued for 30 min, the precipitates were filtered and dried to give **3e** (1.63 g, 61% based on the hydrochloride). Recrystallization from EtOH afforded yellow needles; mp 129—131 °C. **3e** and **g** were prepared by the same procedure.

Ethyl 3-Amino-4-pyrazolecarboxylate (4a). A toluene solution (20 ml) of **3a** (520 mg, 2.0 mmol) was refluxed for 4 h. After cooling at 0 °C, the precipitates were filtered and dried to give **4a** (270 mg, 87%). Recrystallization from benzene afforded white needles; mp 100—101 °C. Its mp, TLC, and IR spectrum were identical with those of the authentic sample.[9] **4a** was also obtained from **3e** by the same procedure (84%).

3-Amino-4-cyanopyrazole (4b). A toluene solution (10 ml) of **3b** (420 mg, 2.0 mmol) was refluxed for 8 h. After cooling, the precipitates were filtered and dried to give **4b** (200 mg, 91%). Recrystallization from benzene–THF afforded white needles; mp 171—174 °C. Its mp TLC, and IR spectrum were identical with those of the authentic sample.[10] **4b** was also obtained from **3f** by the same procedure (71%).

N-(2,2-Dicyanovinyl)-N''-phenylbenzamidrazone (6). To a stirred solution of **2b** (122 mg, 1.0 mmol) in EtOH (5 ml) was added *N''*-phenylbenzamidrazone[19] (211 mg, 1.0 mmol) at room temperature. After 30 min, the resulting precipitates were filtered and dried to give **6** (159 mg, 55%). Recrystallization from EtOH afforded white needles; mp 223—226 °C. Found: C, 71.26; H, 4.47%. Calcd for $C_{17}H_{13}N_5$: C, 71.06; H, 4.56%. IR (KBr): 3360, 3250, 2200, 1640, 1618, 1550 cm^{-1}.

Ethyl 3-Hydroxy-4-pyrazolecarboxylate (4c) and 1,2-Bis(2-pyridylcarbonimidoyl)hydrazine (7a). To a solution of sodium ethoxide (3.0 mmol) in EtOH (10 ml) was added **3c** (569 mg, 1.9 mmol), after which the solution was refluxed for 2 h. The resulting sodium salts were filtered, dissolved in water (10 ml), and neutralized with dil hydrochloric acid. After cooling, white crystals were filtered out and dried to give **4c** (86 mg, 30%). Recrystallization from MeOH–H_2O afforded white needles; mp 182—183 °C. Its mp, TLC, and IR spectrum were identical with those of the authentic sample.[11] Then the filtrate was concentrated *in vacuo*, and a small amount of water was added to the residue. The resulting yellow crystals were filtered and dried to give **7a** (15 mg, 8%). Recrystallization from MeOH afforded yellow needles; mp 208—210 °C. Its mp, TLC, and IR spectrum were identical with those of the authentic sample.[12a,b] **4c** was also obtained from **3g** by the same procedure (30%).

1,2-Dihydro-3,6-di-2-pyridyl-1,2,4,5-tetrazine (8). An EtOH solution (10 ml) of **3d** (337 mg, 1.0 mmol) was refluxed for 24 h. After cooling, the precipitates were filtered and dried to give **8** (23 mg, 29%). Recrystallization from EtOH afforded orange needles; mp 198—202 °C. Its mp, TLC, and IR spectrum were identical with those of the authentic sample.[13a,b]

Triethyl 1-Amino-6-oxo-1,8-di-2-pyridyl-2,3,7,9,10-pentaaza-1,4,8,11-tetraene-5,12,12-tricarboxylate (9). A toluene solution (15 ml) of **3c** (461 mg, 1.5 mmol) was refluxed for 9 h. After cooling, the toluene was evaporated *in vacuo*, and a small amount of MeOH was added to the residue. Crystallization was induced by scratching the flask, and the resulting precipitates were filtered and dried to give **9** (194 mg, 45%). Recrystallization from MeOH–benzene afforded yellow needles; mp 196—198 °C. Found: C, 55.50; H, 5.35%. Calcd for $C_{26}H_{30}N_8O_7$: C, 55.12; H, 5.30%. IR (KBr):

3440, 3140, 2960, 1695, 1670, 1645, 1615, 1500 cm^{-1}. MS *m/e* (%): 566 (M^+, 0.4), 359 (3), 332 (5), 260 (7), 162 (10), 147 (40), 110 (20), 105 (100), 79 (26), 78 (30). UV (MeOH, nm (log ε)): 223 (4.50), 328 (sh, 4.70), 341 (4.80), 370 (sh, 4.40).

5-Amino-6-ethoxycarbonyl-3-(2-pyridyl)-1H-1,2,4-triazepine (10). A solution of **3a** (1.58 g, 6.1 mmol) in ethanolic hydrogen chloride (0.2 M, 46 ml) was refluxed for 1 h. The solvent was then evaporated *in vacuo*, and the water (10 ml) was added to the residue. The acidic solution was neutrallized with sodium hydrogen carbonate. After cooling, the resulting precipitates were filtered and dried to give **10** (901 mg, 57%). Recrystallization from MeOH–DMF afforded white needles; mp 200 °C (dec). Found: C, 55.63; H, 5.12%. Calcd for $C_{12}H_{13}N_5O_2$: C, 55.59; H, 5.05%. IR (KBr): 3320, 3250, 3110, 1700 cm^{-1}. NMR of **10**·HCl (D_2O): δ 7.97 (s, 1H, =CH–), 7.45—8.38 (m, 4H, aromatic H), 3.96 (q, J= 6.8 Hz, 2H, $-CH_2-$), 1.15 (t, J=6.8 Hz, 3H, $-CH_3$). MS *m/e* (%): 259 (M^+, 69), 214 (14), 186 (100), 155 (95), 109 (86), 105 (53), 78 (44). UV (MeOH, nm, (log ε)): 221 (4.29), 278 (3.96), 300 (3.98).

2,9-Di-2-pyridyl-6,7,13,14-tetrahydro-4H,11H-[1,5]diazocino[2,3-e:6,7-e']di[1H-1,2,4]triazepine-6,13-dione (11a). A solution of **10** (266 mg, 1.0 mmol) in aq NaOH (0.2 M, 10 ml) was refluxed for 1 h. After cooling, the solution was neutrallized with dil hydrochloric acid, and the resulting precipitates were filtered and dried to give **11a** (162 mg, 74%). Recrystallization from DMF–MeOH afforded white powder; mp>300 °C. Found: C, 56.17; H, 3.43%. Calcd for $C_{20}H_{14}N_{10}O_2$: C, 56.33; H, 3.31%. IR (KBr): 3200, 1680, 1550 cm^{-1}. NMR (CF_3COOH): δ 8.20—9.20 (m, 10H, aromatic H and =CH–). MS *m/e* (%): 213 (93), 157 (3), 135 (9), 109 (100), 105 (20), 89 (14), 88 (24), 78 (5). UV (MeOH, nm (log ε)): 228 (4.61), 301 (4.43).

2,9-Di-2-pyridyl-4,7,11,14-tetramethyl-6,7,13,14-tetrahydro-4H,11H-[1,5]diazocino[2,3-e:6,7-e']di[1H-1,2,4]triazepine-6,13-dione (11b). To a suspension of NaH (41 mg, about 50% in oil, 0.85 mmol) in *N,N*-dimethylacetamide (5 ml) added **11a** (113 mg, 0.27 mmol) in portions. After the evolution of hydrogen had ceased, methyl iodide (0.5 ml) was added, and the mixture was stirred at room temperature for 1 day. The reaction mixture was poured into water (20 ml), the resulting precipitates were filtered off, and then the filtrate was extracted three times with ethyl acetate (20 ml). The organic phase was evaporated *in vacuo*, and a small amount of ether was added to the residue. The resulting precipitates were filtered and dried to give **11b** (60 mg, 46%). Recrystallization from MeOH afforded white needles; mp 266—227 °C. Found: C, 59.71; H, 4.62%. Calcd for $C_{24}H_{22}N_{10}O_2$: C, 59.74; H, 4.60%. IR (KBr): 3100, 2960, 1705, 1560, 1550 cm^{-1}. NMR (CF_3COOH): δ 8.25—9.30 (m, 10H, aromatic H and =CH–), 4.20 (s, 6H, $-CH_3$), 3.82 (s, 6H, $-CH_3$). MS *m/e* (%): 241 (100), 240 (72), 213 (6), 212 (13), 171 (7), 105 (4), 82 (16), 79 (24). UV (MeOH, nm (log ε)): 213 (4.66), 261 (sh, 4.18), 282 (4.23).

6-Ethoxycarbonyl-5-(2-phenylhydrazino)-3-(2-pyridyl)-1H-1,2,4-triazepine (13a). A mixture of **10** (132 mg, 0.5 mmol) and phenylhydrazine (117 mg, 1.1 mmol) in EtOH (10 ml) was refluxed. After 3 h, additional phenylhydrazine (113 mg, 1.0 mmol) was added to the reactoin mixture and it was refluxed for 4 h again. After cooling, the precipitates were filtered off and the filtrate was concentated *in vacuo*. A small amount of ether was added to the residue, and crystallization was induced by scratching the flask. The resulting precipitates were filtered and dried to give **13a** (77 mg, 44%). Recrystallization from MeOH–H_2O afforded yellow plates; mp 181—183° °C. Found: C, 61.69; H, 5.11%. Calcd for $C_{18}H_{18}N_6O_2$: C, 61.70; H, 5.18%. IR (KBr): 3320, 3240, 3020, 2980, 1670, 1570, 1550 cm^{-1}. NMR (DMSO-d_6): δ 9.72 (br, 1H, =NH), 8.12 (s, 1H, =CH–), 7.60—8.58 (m, 4H, aromatic H), 7.03—7.55 (m, 5H, aromatic H), 6.75 (br, 1H, =NH), 4.34 (q, J=7.0 Hz, 2H, $-CH_2-$), 1.40 (t, J= 7.0 Hz, 3H, $-CH_3$).

6-Ethoxycarbonyl-5-hydrazino-3-(2-pyridyl)-1H-1,2,4-triazepine (13b). A mixture of **10** (529 mg, 2.0 mmol) and 100% hydrazine hydrate (213 mg, 4.0 mmol) was refluxed, with stirring, for 1 h, After cooling, the resulting precipitates were filtered and dried to give **13b** (161 mg, 29%). Recrystallization from benzene–THF afforded pale yellow particles; mp 163—166 °C. Found: C, 52.50; H, 5.18%. Calcd for $C_{12}H_{14}N_6O_2$: C, 52.54; H, 5.15%. IR (KBr): 3380, 3120, 1700, 1580, 1535 cm^{-1}.

The authors wish to express their thanks to Professor Masaki Ohta for his encouragement, to Dr. Masatoshi Hirayama and Mr. Mamoru Sekine for the NMR measurements, and to Sankyo Co., Ltd., for the mass measurements.

References

1) Part IV: M. Takahashi, H. Tan, K. Fukushima, and H. Yamazaki, *Bull. Chem. Soc. Jpn.*, **50**, 953 (1977).
2) D. G. Neilson, R. Roger, J. W. M. Heatlie, and L. R. Newland, *Chem. Rev.*, **70**, 151 (1970).
3) a) G. Losse and H. Uhlig, *Chem. Ber.*, **90**, 257 (1957); b) G. Losse, E. Wottgen, and H. Just, *J. Prakt. Chem.*, **7**, 28, (1958).
4) G. Losse, W. Hessler, and A. Barth, *Chem. Ber.*, **91**, 150, (1958).
5) G. Losse and W. Farr, *J. Prakt. Chem.*, **8**, 298 (1959).
6) B. Stanovnik and M. Tisler, *Naturwissenschaften*, **52**, 207 (1965).
7) a) G. C. Johnson and R. H. Levin, *Tetrahedron Lett.*, **1974**, 2303; b) D. J. Anderson and A. Hassner, *J. Chem. Soc., Chem. Commun.*, **1974**, 45; c) M. Takahashi, N. Suzuki, and Y. Igari, *Bull. Chem. Soc. Jpn.*, **48**, 2605 (1975); d) V. Nair, *J. Heterocycl. Chem.*, **12**, 183 (1975).
8) I. Saito, A. Yazaki, and T. Matsuura, *Tetrahedron Lett.*, **1976**, 2459.
9) R. K. Howe and S. C. Bolluyt, *J. Org. Chem.*, **34**, 1713 (1969).
10) R. K. Robins, *J. Am. Chem. Soc.*, **78**, 784 (1956).
11) T. Ishimaru, *Yakugaku Zasshi*, **77**, 796 (1957).
12) a) W. Ried and P. Schomann, *Justus Liebigs Ann. Chem.*, **714**, 122 (1968); b) S. Kubota, O. Kirino, Y. Koida, and K. Miyake, *Yakugaku Zasshi*, **92**, 275 (1972).
13) a) F. Dallacker, *Monatsh. Chem.*, **91**, 294 (1960); b) J. F. Geldard and F. Lions, *J. Org. Chem.*, **30**, 318 (1965).
14) H. Bredereck, F. Effenberger, E. Henseleit, and E. H. Shweizer, *Chem. Ber.*, **96**, 1868 (1963).
15) F. H. Case, *J. Org. Chem.*, **30**, 931 (1965).
16) R. G. Jones, *J. Am. Chem. Soc.*, **74**, 4889 (1952).
17) R. G. Jones, *J. Am. Chem. Soc.*, **73**, 3684 (1951).
18) A. Pinner, *Ber.*, **16**, 1654 (1883).
19) A. Spasov, E. Golovinski, and G. Demirov, *Chem. Ber.*, **98**, 932 (1965).

Synthetic Proof for the Structures of Maturinone and Cacalol

Yoshinobu INOUYE, Yuji UCHIDA, and Hiroshi KAKISAWA
Department of Chemistry, Tokyo Kyoiku University, Bunkyo-ku, Tokyo 112
(Received September 17, 1976)

By unambiguous syntheses, the structures of maturinone and cacalol were shown to be 3,5-dimethylnaphtho-[2,3-*b*]furan-4,9-dione (**1**) and 5,6,7,8-tetrahydro-3,4,5-trimethylnaphtho[2,3-*b*]furan-9-ol (**2**), respectively. 3,8-Dimethylnaphtho[2,3-*b*]furan-4,9-dione (**1a**), an isomer of maturione, was also synthesized.

In 1964, Romo and Joseph-Nathan[1] isolated several components, now known as a rearranged eremophilanoid sesquiterpene, from the root of *Cacalia decomposita* A. Gray, a compositae widely distributed in the northern part of Mexico. Maturinone (**1**), cacalol (**2**), and cacalone are the major components. They were initially erroneously assigned as **1a**, **2a**, and **3a**, respectively, using their chemical and spectroscopic data.[2,3] The relations among these three compounds were shown as follows:

maturinone $\xleftarrow[\text{ii) } CrO_3]{\text{i) DDQ}}$ cacalol $\xleftarrow{LiAlH_4}$ cacalone

The alternative possibility of **1**, **2**, and **3** was abandoned chiefly because the characteristic absorption for the 8-hydroxy-1-tetralone moiety (see **3**) in the IR and NMR spectra of cacalone[1] was not recognized.

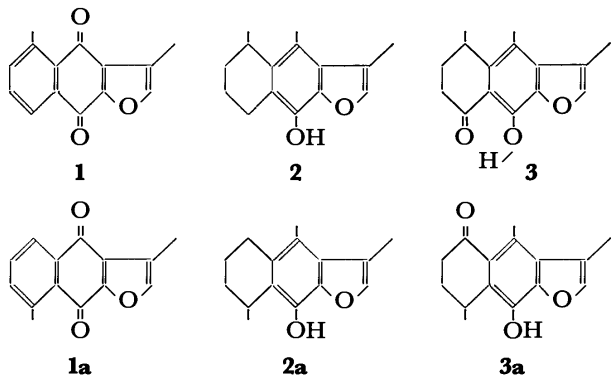

1 **2** **3**

1a **2a** **3a**

In 1969, however, we synthesized both quinones, **1** and **1a**, and established the identity of **1** with maturinone.[4] At the same time, two other groups[5,6] reached the same conclusion by independent syntheses of the quinone **1**. These results required the structures of cacalol and cacalone to be revised as **2** and **3**, respectively, although the latter was pointed out[5] to be inconsistent with the reported spectroscopic data for cacalone. Joseph-Nathan referred to the structure of cacalone and explained the anomalous data by considering the presence of an inherently dissymmetric chromophore (ORD study).[7]

Since then, several Japanese workers[8-10] have reported the isolation of new compounds which belong to this class of sesquiterpene, from various *Cacalia* species. Although we, in collaboration with Romo, reported[4] the relation of cacalol with the known 6-epidecompostin derivative,[11] a recent synthesis of **2**[12] has finally established the structure of cacalol.

The present paper deals with the details of our synthetic works on maturinone (**1**) and cacalol (**2**).

Synthesis of 3,8-Dimethylnaphtho[2,3-b]furan-4,9-dione (1a). In the course of our study on the Diels-Alder reaction of unsymmetrically substituted benzoquinones and dienes, both methoxybenzoquinone and 3-methylbenzofuran-4,7-dione (**4**) were found to exhibit high specificity to 6,6-dimethyl-1-vinylcyclohexene;[13] the orientation phenomena of both quinones were the same, with respect to the oxygen moiety, and were rationalized by considering the radical stabilities of the formal "biradical intermediates."[4,13] Based on the evidence that 1,3-pentadiene (**5**) reacted with methoxybenzoquinone to give mainly **6**,[14] we anticipated that the chief product in the Diels-Alder reaction of **4** and **5** would be **7**; the skeleton initially assumed was for maturinone.

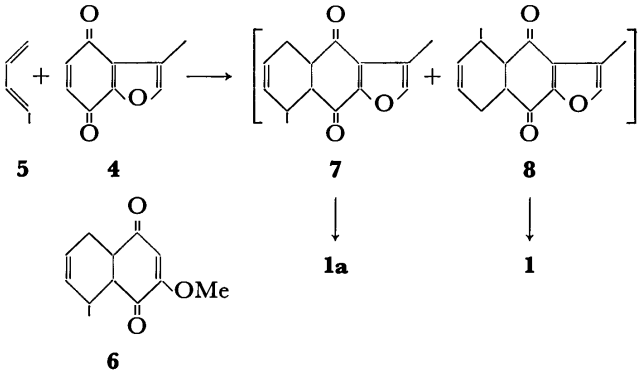

5 **4** **7** **8** **1a** **1** **6**

The reaction between **4** and **5** proceeded smoothly at room temperature and the *mixture* was oxidized by air in the presence of potassium hydroxide[15] to give the quinones **1a** and **1** (**1a**/**1**=7: 1) in 77% yield. Repeated recrystallization afforded the pure **1a**, mp 189—190 °C; its spectroscopic properties were very similar to those of maturinone, but distinct differences in the IR spectra were observed in the region of 1200—900 cm^{-1}.

Synthesis of 3,5-Dimethylnaphtho[2,3-b]furan-4,9-dione (1, Maturinone). Treatment[16] of 2-acetoxy-5-methyl-1,4-naphthoquinone (**10**), prepared from **9**[17] by acetylation with acetic anhydride and zinc chloride, with 1-morpholino-1-propene (**11**)[18] in the presence of a small amount of ethanol gave a quinone **1**, mp 164—166 °C, in 12% yield in a one-step reaction. The quinone **1** and maturinone were identical in every aspect.

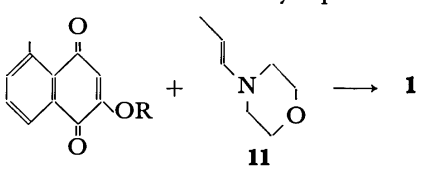

9 R=H
10 R=Ac
11

Synthesis of 5,6,7,8-Tetrahydro-3,4,5-trimethylnaphtho[2,3-b]furan-9-ol (2, Cacalol). The Friedel-Crafts reaction of 3,4-dimethoxytoluene (**12**) with γ-valerolactone in the presence of aluminium chloride gave a mixture **13** of two carboxylic acids, which without separation into each component was successively treated with diazomethane and dimethyl sulfate to afford a single ester **14** in 84% yield.

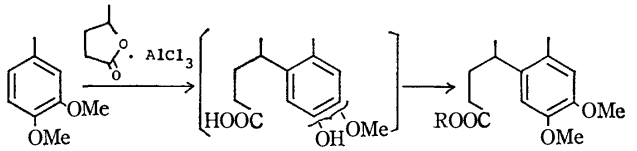

12 **13** **14** R=Me
15 R=H

The position of the new alkyl group was decided from the following facts. The two singlets which appear at 6.50 and 6.57 ppm in the NMR spectrum of **14** require the two hydrogens on the aromatic nucleus to be positioned para to each other and the pseudocontact shift with Eu-(fod)$_3$ clearly showed that the H_B proton present in **12** disappeared in **14** (Fig. 1). Furthermore, the corresponding acid **15** was converted into the 8-hydroxy-1-tetralone derivative **16**, as shown below.

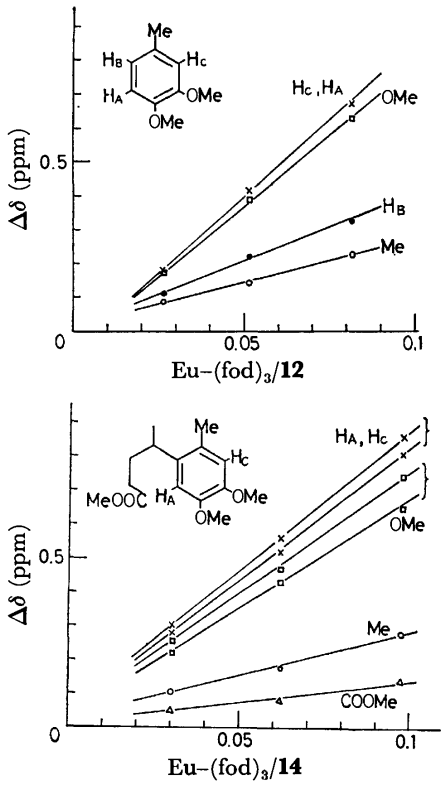

Fig. 1. Pseudocontact shifts of **12** (upper) and **14** (bottom) with Eu-(fod)$_3$ in CCl_4.

The acid **15** was cyclized with polyphosphoric acid at 160 °C to give 4,5-dimethyl-8-hydroxy-7-methoxy-1-tetralone (**16**); the carbonyl absorption at 1630 cm^{-1} in the IR spectrum and a singlet at 12.94 ppm in the NMR spectrum showed that the structure **16** has an 8-hydroxy-1-tetralone moiety. When diphosphorus pentoxide-methanesulfonic acid[19] was used, 7,8-dimethoxy-4,5-dimethyl-1-tetralone (**17**), $\nu_{C=O}$ at 1673 cm^{-1}, was obtained in 87% yield. Both tetralone **16** and **17** were convertible with each other. Catalytic hydrogenolysis of **17** over Pd-C in the presence of perchloric acid resulted in the removal of the carbonyl functional group to give 7,8-dimethoxy-4,5-dimethyltetraline (**18**).

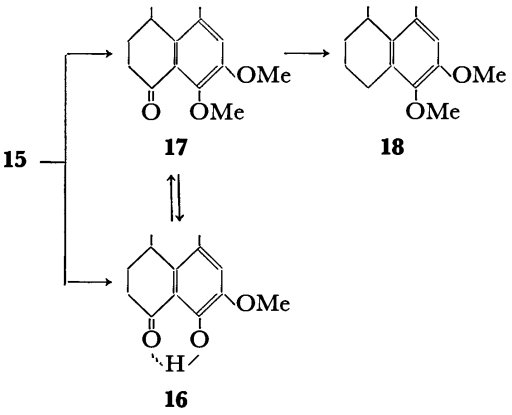

The next step is the introduction of the acetyl group at the remaining position on the aromatic nucleus. Friedel-Crafts acylations using two catalysts were investigated and the results are shown in Table 1.

Table 1. Friedel-Crafts acylation of **18**

Molar ratio **18**: Catalyst: AcCl			Temp (°C)	Time (h)	Yield (isolated %)		
					18	**19**	**21**
	$AlCl_3$						
1	2	6	70—75	4		58	22
	$ZnCl_2$						
1	5	10	0—2	41	20	16[b]	55[a]
1	5	10	30	4	15	22[b]	51
1	5	10	70	1/4	11	43[b]	30

a) After methylation with dimethyl sulfate. b) After hydrolysis to **22**.

In the case of aluminium chloride, a complex mixture resulted, and by chromatographic separation the acetate **19** was obtained as the main product, in 58% yield. The residue contained a mixture of acetophenone derivatives **20** and **23**, and after methylation with dimethyl sulfate, the dimethoxyacetophenone **21** was isolated in 22% yield. No aromatic proton was observed in the NMR spectrum of **21**, but the new acetyl protons appeared at 2.07 ppm.

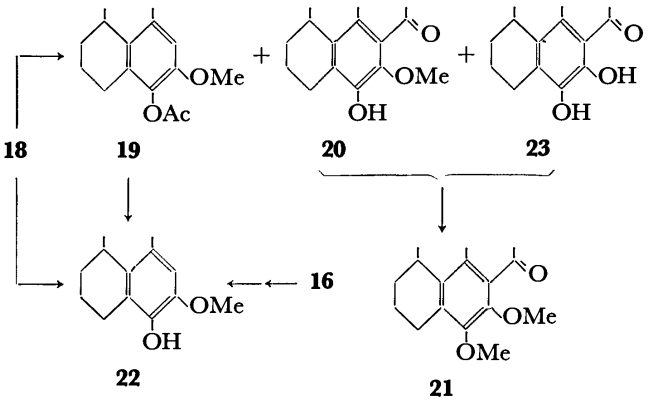

When the reaction was carried out without acetyl

chloride, only a monodemethylated compound **22** was obtained easily. **22** was also derived from the acetate **19** by lithium aluminium hydride reduction.

The position of the hydroxyl group in **22** was proved by deriving it from **16** with sodium borohydride reduction, followed by hydrogenolysis over Pd-C. The facile hydrolysis of the 8-methoxyl group in **18** would be explainable as due to a steric factor.[20]

On the other hand, the yield of **21** increased up to 55% when the reaction was done with zinc chloride, a fairly mild catalyst, at 0—2 °C. From Table 1, two points are worthy of notice in the case of zinc chloride. At low temperatures, introduction of the acetyl group on the aromatic nucleus was preferential but, at elevated temperatures, the hydrolysis increased drastically. Secondly, the reaction with zinc chloride differed from that with aluminium chloride in recovering some of the starting material in every case. These indicate that a complex reaction, including an equilibrium[21] between **18** and **21**, is involved in these conditions, but no further studies on these points were made in the present work.

The final step is the conversion of **21** into a furan derivative. As the ajacent methoxyl to the acetyl group was less reactive than the other to aluminium chloride or boron tribromide (see experimental), both methoxyl groups were cleaved with boron tribromide at room temperature to afford a dihydroxy compound **23**, which was subsequently converted into bis(methoxycarbonylmethyl) ether **24**, $\nu_{C=O}$ at 1760, 1740, and 1695 cm^{-1}. The corresponding carboxylic acid **25** was converted under the known process[22] into 5,6,7,8-tetrahydro-3,4,5-trimethylnaphtho[2,3-*b*]furan-9-yl carboxymethyl ether **26** in good yield. The structure assignment was based on the presence of two signals coupled to each other at 2.38 (br. s, 3H) and 7.27 ppm (m, 1H) in the NMR spectrum, which correspond to the adjacent β-methyl and α-proton groups on a furan nucleus.

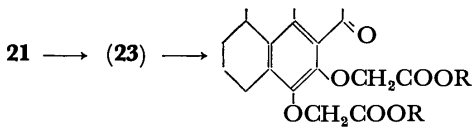

24 R=Me
25 R=H

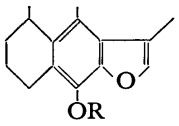

26 R=CH_2COOH
27 R=CH_2CH_2OH
28 R=CH_2CH_2OTs
29 R=CH_2CH_2Br
30 R=Ac

After reduction of **26** with lithium aluminium hydride, removal of the hydroxyethyl group in **27** was achieved[23] by successive treatment with tosyl chloride in pyridine, sodium bromide in dimethyl sulfoxide, and butyllithium in ether to get 5,6,7,8-tetrahydro-3,4,5-trimethylnaphtho[2,3-*b*]furan-9-ol (**2**). The alcohol **2**, however, decomposed[24] gradually on storage and failed to crystallize even after purification by chromatography.

When the crude **2** was acetylated, the acetate **30** was obtained as a crystal, mp 119—120 °C, in 71% yield from **27**. The IR and NMR spectra of both **30** and cacalol acetate in carbon tetrachloride were identical in all respects.

On the Structure of Cacalone. Confirmation of the structures of maturinone (**1**) and cacalol (**2**) by unambiguous syntheses requires a reexamination of the structure of cacalone. The structure **3**[4] was only based on the report that cacalone was converted into cacalol (**2**) by lithium aluminium hydride.[1] Its spectroscopic properties, however, are inconsistent with the structure **3**, although Joseph-Nathan explained these anomalies by means of the presence of an inherently dissymmetric chromophore.[7]

The tetralone **16** prepared in the present work is one of the model compounds for the structure **3**; the lack of the furan ring would cause little effect on the stereochemistry of cacalone. As shown before, the compound **16** showed normal spectroscopic properties for an 8-hydroxy-1-tetralone moiety: a strong chelation between the carbonyl and hydroxyl groups was observed in both IR and NMR spectra. Moreover, when **16** was subjected to react under the Romo's condition (lithium aluminium hydride reduction and subsequent acetylation),[1] no detectable amount of **19** was recognized, but two diacetates **31** and **32** were isolated in 88% yield (the ratio of **31**/**32** was *ca.* 2: 1; see experimental).

From these results, we can safely concluded that cacalone is neither **3** nor **3a** and abandon the former

Table 2. Pseudocontact shift on the mixture of **31** and **32**

		δ (ppm) in CCl_4		
		31+**32**	Adn of 0.1 mol eq of Eu-(fod)$_3$	$\Delta\delta$
31	C_4-Me	1.26	1.45[a]	0.19
	C_1-OAc	1.99	3.03	1.04
	C_8-OAc	2.16	2.62	0.46
	C_5-Me	2.40	2.42	0.02
	C_7-OMe	3.83	3.90	0.07
	C_1-H	6.02(m)	7.56(m)	1.54
	C_6-H	6.69	6.88	0.19
32	C_4-Me	1.13	1.25[a]	0.12
	C_1-OAc	1.91	2.96	1.05
	C_8-OAc	2.16	2.56	0.40
	C_5-Me	2.40	2.42	0.02
	C_7-OMe	3.83	3.90	0.07
	C_1-H	6.02(m)	7.56(m)	1.54
	C_6-H	6.69	6.88	0.19

a) The relative intensities of these two signals are 2:1 (**31**:**32**).

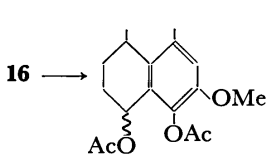

31 cis
32 trans

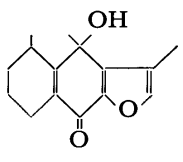

33

proposal[4] for its structure. Recently, the *p*-quinol structure **33** was presented for the structure of cacalone.

Experimental

All melting points were uncorrected. IR and UV spectra were recorded on a Hitachi 215 grating spectrophotometer and a Hitachi EPS-3T spectrophotometer, respectively, and NMR spectra were obtained on a Hitachi H-60 spectrophotometer using TMS as an internal standard. Microanalyses were carried out at the Institute for Physical and Chemical Research.

*Diels-Alder Reaction of 3-Methylbenzofuran-4,7-dione (**4**) and 1,3-Pentadiene (**5**).* A mixture of 260 mg of 3-methylbenzofuran-4,7-dione (**4**)[13] and 350 mg of 1,3-pentadiene (**5**) in 4 ml of ethanol was left overnight. After evaporating the ethanol, the residue was oxidized in ethanol containing potassium hydroxide by bubbling air through the solution.[15] The ether extract, when evaporated, gave yellow solids (314 mg), form which 207 mg of 3,8-dimethylnaphtho[2,3-*b*]-furan-4,9-dione (**1a**) was obtained by recrystallization from chloroform–ethanol.

1a: mp 189—190 °C; IR (KBr): 1670, 1190, 1170, 1100, 1040, 995, and 950 cm^{-1}; UV (EtOH): 251 (log ε=4.34), 267 sh (3.91), 294 (3.56), and 357 nm (3.55); NMR ($CDCl_3$): 2.33 (d, 3H, J=1.5 Hz), 2.79 (s, 3H), 7.4—7.7 (m, 3H), 8.03 ppm (dd, 1H, J=3.5 and 6 Hz); NMR (C_6H_6): 2.03 (br. s, 3H) and 2.68 (s, 3H). Found: C, 74.61; H, 4.40%. Calcd for $C_{14}H_{10}O_3$: C, 74.33; H, 4.46%.

From the mother liquor, 73 mg more (total yield: 77%) of dimethylnaphtho[2,3-*b*]furan-4,9-diones, **1a** and **1**, were obtained; IR (KBr): 1670, 1190, 1170, 1150, 1100, 1040, 1030, 995, 965, and 950 cm^{-1}; NMR (C_6H_6): 2.03 (br. s, 3H), 2.63 (s, 1.5 H, **1**), and 2.68 ppm (s, 1.5 H, **1a**).

*2-Acetoxy-5-methyl-1,4-naphthoquinone (**10**).* A solution of 770 mg of 2-hydroxy-5-methyl-1,4-naphthoquinone (**9**),[17] mp 152—154 °C (dec), and a small amount of zinc chloride in 5 ml of acetic anhydride was left for 30 min at room temperature. The cloudy mixture was heated for several min until the solution became clear and then cooled to room temperature. After pouring the solution into ice–water, the precipitates which formed were collected on a filter paper to give 899 mg (96%) of 2-acetoxy-5-methyl-1,4-naphthoquinone (**10**). Recrystallization from ethanol afforded a pure **10**: mp 119—120 °C. Found: C, 68.09; H, 4.40%. Calcd for $C_{13}H_{10}O_4$: C, 67.82; H, 4.38%.

*3,5-Dimethylnaphtho[2,3-b]furan-4,9-dione (**1**).* A mixture of 100 mg of **10**, 72 mg of 1-morpholino-1-propene (**11**),[18] and 0.05 ml of ethanol was left overnight at room temperature.[16] The whole was chromatographed directly on silicic acid (10 g) and 12 mg (12%) of 3,5-dimethylnaphtho[2,3-*b*]-furan-4,9-dione (**1**) was obtained from the chloroform eluates. Recrystallization from ethanol gave a pure **1**: mp 164—166 °C; IR (KBr): 1670, 1170, 1150, 1110, 1090, 1030, 995, and 965 cm^{-1}; UV (EtOH): 251 (log ε=4.40), 267 sh (4.00), 294 (3.67), and 352 nm (3.67); NMR ($CDCl_3$): 2.35 (d, 3H, J=1.5 Hz), 2.77 (s, 3H), 7.4—7.7 (m, 3H), and 8.10 ppm (dd, 1H, J=3 and 5.5 Hz); NMR (C_6H_6): 2.01 (d, 3H, J=1.5 Hz) and 2.63 ppm (s, 3H). Found: C, 74.22; H, 4.35%. Calcd for $C_{14}H_{10}O_3$: C, 74.33; H, 4.46%.

The quinone **1** was identical with maturinone in every aspect and melted at 163—165 °C when mixed with maturinone.

From later fractions, 45 mg of orange crystals, mp 178—180 °C (ethanol), were obtained but no characterization was tried.

*Friedel-Crafts Reaction of 3,4-Dimethoxytoluene (**12**) with γ-Valerolactone.* To a cold solution of 15 g of 3,4-dimethoxytoluene (**12**) and 4.92 g of γ-valerolactone in 15 ml of tetrachloroethane (TCE), there was added in portions 26.4 g of freshly powdered aluminium chloride. After the addition was complete, the mixture was stirred mechanically at 70 °C for 4 h; 5 ml more of TCE was added and stirring was continued for another 4 h. After standing overnight, the whole was poured into 75 ml of concd hydrochloric acid and 200 g of ice, and was extracted with ether (140 ml×3). A mixture **13** of acidic materials was treated with an excess of ethereal diazomethane followed by dimethyl sulfate to obtain a red oil. Fractional distillation gave 11.03 g (84%) of the ester **14**: bp 157—159 °C/2 Torr; IR (CCl_4): 1730, 1250, 1200, and 1155 cm^{-1}; NMR (CCl_4): 1.17 (d, 3H, J=7 Hz), 2.19 (s, 3H), 3.53 (s, 3H), 3.74 (s with a shoulder at 3.72, 6H), 6.50 (s, 1H), and 6.57 ppm (s, 1H). Found: C, 67.73; H, 8.39%. Calcd for $C_{15}H_{22}O_4$: C, 67.64; H, 8.33%.

*Cyclization of the Acid **15** with Polyphosphoric Acid.* The ester **14** was hydrolyzed under refluxing in 1 M sodium hydroxide–methanol to give an acid, **15**.

The acid **15** (824 mg) was heated with polyphosphoric acid (prepared from 4 g of diphosphorus pentaoxide and 3.3 ml of phosphoric acid) at 160 °C for 20 min and the mixture was poured into ice–water. Products were taken in ether and the ether layer was washed with water and dried over Na_2SO_4. After removal of the ether, the residual oil was purified through a silica gel column and distilled to give 203 mg (28%) of a yellow 4,5-dimethyl-8-hydroxy-7-methoxy-1-tetralone (**16**): bp 134—136 °C/0.15 Torr. When left in a refrigerator, **16** crystallized and melted at 62—63 °C (pentane); IR ($CHCl_3$): 3540 w, 3320—2600 br, 1630, 1345, and 1265 cm^{-1}; NMR ($CDCl_3$): 1.26 (d, 3H, J=7 Hz), 2.29 (s, 3H), 3.86 (s, 3H), 6.87 (s, 1H), and 12.94 ppm (s, 1H). Found: C, 70.90; H, 7.33%. Calcd for $C_{13}H_{16}O_3$: C, 70.89; H, 7.32%.

*Cyclization of the Acid **15** with Diphosphorus Pentaoxide–Methanesulfonic Acid.* The acid **15** (1.5 g) was heated at 50—55 °C for 6 h with 25 g of diphosphorus pentaoxide–methanesulfonic acid (1 : 10).[19] After cooling, the mixture was poured into ice–water and extracted with ether. The ether layer was washed with water, dil alkaline solution, water, and saline, and dried over Na_2SO_4. Evaporating the solvent gave 2.0 g (87%) of 7,8-dimethoxy-4,5-dimethyl-1-tetralone (**17**): mp 100—103 °C (methanol); IR (KBr): 1673 and 1585 cm^{-1}; NMR ($CDCl_3$): 1.21 (d, 3H, J=7 Hz), 2.33 (s, 3H), 3.85 (s, 3H), and 6.89 ppm (s, 1H). Found: C, 71.62; H, 7.81%. Calcd for $C_{14}H_{18}O_3$: C, 71.77; H, 7.74%.

*Methylation of **16**.* A solution of 60 mg of **16** in 2 ml of acetone was refluxed for 5 h with 480 mg of anhydrous potassium carbonate and 240 mg of dimethyl sulfate. The mixture was poured into water and was extracted with ether. The ether layer was washed with dil sodium hydroxide solution, water, and saline, and was dried over Na_2SO_4. Evaporating off the ether and purifying through a silica gel column gave 47 mg (74%) of **17**.

*Action of Aluminium Chloride on **17**.* To a solution of 500 mg of **17** in 5 ml of dry benzene, 570 mg of aluminium chloride was added at 0 °C and the mixture was stirred for for 3 h at room temperature. The whole was poured into ice–water, 4 ml of 6 M hydrochloric acid was added, and products were taken in ether. The ethereal extract was concentrated, purified through a silica gel column, and recrystallized from pentane to give 355 mg (76%) of **16**.

*7,8-Dimethoxy-4,5-dimethyltetralin (**18**).* The tetralone **17** (2.00 g) in 40 ml of acetic acid was hydrogenated over 280 mg of 10% Pd–C in the presence of 0.3 ml of 60% perchloric acid. After 8 h (468 ml of hydrogen consumed), 1 g of anhydrous potassium acetate was added and the catalyst

was removed by filtration. The filtrate was concentrated *in vacuo*, and the residue was dissolved in ether, which was washed with water, dil sodium hydroxide, water, and saline, and dried over Na_2SO_4. Evaporating off the solvent and fractional distillation gave 1.65 g (87%) of **18**; bp 145—146 °C/6 Torr; IR ($CHCl_3$): 1590, 1310, and 1120 cm^{-1}; NMR ($CDCl_3$): 1.11 (d, 3H, J=7 Hz), 2.20 (s, 3H), 3.66 (s, 3H), 3.73 (s, 3H), and 6.42 ppm (s, 1H). Found: C, 76.40; H, 9.14%. Calcd for $C_{14}H_{20}O_2$: C, 76.32; H, 9.15%.

Friedel-Crafts Acylation of ***18****.* *A) With Aluminium Chloride*: To a cooled (below −5 °C) solution of 962 mg of **18** and 2.06 g (6 eq) of acetyl chloride in 7 ml of TCE, there was added 1.16 g (2 eq) of aluminium chloride in portions, the mixture was stirred for one hour at room temperature, followed by heating at 70—75 °C for 4 h. The cooled mixture was poured into 200 ml of 6 M hydrochloric acid and 100 g of ice, and products were taken in ether. The ether layer was extracted with 1M sodium hydroxide to obtain acidic materials (mainly of **20** and **23**) and the neutral residue was chromatographed on silica acid. From the benzene eluates, 631 mg (58%) of **19** was obtained. Recrystallization from methanol gave a pure **19**: mp 68—69 °C; IR ($CHCl_3$): 1750, 1600, 1305, and 1115 cm^{-1}; NMR (CCl_4): 1.15 (d, 3H, J=7 Hz), 2.22 (s, 3H), 2.28 (s, 3H), 3.73 (s, 3H), and 6.53 ppm (s, 1H). Found: C, 72.56; H, 8.08%. Calcd for $C_{15}H_{20}O_3$: C, 72.55; H, 8.12%.

The acidic materials were refluxed in 30 ml of acetone with 0.5 ml of dimethyl sulfate in the presence of anhydrous potassium carbonate for 3 h. The mixture was poured into dil ammonia and a product was extracted with ether to give an oil. The oil was chromatographed on alumina (10 g) and 237 mg (22%) of **21** was collected from pentane to 10% benzene–pentane fractions: bp 100—115 °C (bath temp)/2 Torr; IR (CCl_4): 1700, 1320, and 1055 cm^{-1}; NMR (CCl_4): 1.15 (d, 3H, J=7 Hz), 2.07 (s, 3H), 2.38 (s, 3H), 3.75 (s, 3H), and 3.78 ppm (s, 3H). Found: C, 73.00; H, 8.13%. Calcd for $C_{16}H_{22}O_3$: C, 73.25; H, 8.45%.

When the acidic materials were directly subjected to chromatography (silicic acid, benzene–ethyl acetate (5: 1)), a monohydroxy compound **20** was obtained in 12% yield: mp 153—154 °C (ether–pentane); IR ($CHCl_3$): 3520, 1690, and 1620 cm^{-1}; NMR (CCl_4): 1.13 (d, 3H, J=7 Hz), 2.24 (s, 3H), 2.50 (s, 3H), 3.74 (s, 3H), and 8.24 ppm (s, 1H, exchangeable with D_2O). Found: C, 72.10; H, 8.08%. Calcd for $C_{15}H_{20}O_3$: C, 72.55; H, 8.12%.

B) With Zinc Chloride. To a cold solution of 220 mg (1 mmol) of **18** and 0.7 ml (10 mmol) of acetyl chloride in 2 ml of TCE, there was added 680 mg (5 mmol) of zinc chloride and the mixture was stirred at 0—2 °C for 41 h. The whole was treated with 4 ml of 6 M hydrochloric acid and was extracted with ether. The ether layer was washed with water, 1 M sodium hydroxide, water, and saline, and was dried over Na_2SO_4. Evaporating the solvent gave an oil, which was chromatographed on silicic acid (5 g). From 20% benzene–hexane eluates, 44 mg (20%) of **18** was recovered; from benzene to chloroform eluates, 193 mg of a mixture of **19** and **21** was obtained. The mixture was refluxed in 2 ml of methanol and 2 ml of 1 M sodium hydroxide for 30 min; 32 mg (16%) of **22** and 141 mg (54%) of **21** were separated from each other by a column chromatography on silicic acid (20% benzene–hexane).

By the same procedure, except for the temperature and time, several reaction were carried out; the results are shown in Table 1. In all cases, the optimal condition was not pursued.

*4,5-Dimethyl-8-hydroxy-7-methoxytetralin (****22****).* A) *From the Tetralone* ***16****.* To a solution of 86 mg of **16** in 2 ml of methanol, sodium borohydride was added until the yellow color disappeared. Dil hydrochloric acid was added, the solvent was evaporated, and the ether extract gave a colorless oil. The oil was hydrogenated under the same condition as **17** (9.5 ml of hydrogen consumed). By a chromatographic separation (silicic acid, benzene), 27 mg (33%) of **22** was obtained as a crystalline form. Recrystallization from pentane afforded a pure **22**: mp 46—48 °C; IR (CCl_4): 3540, 1610, 1480, 1295, and 1120 cm^{-1}; NMR (CCl_4): 1.14 (d, 3H, J=7 Hz), 2.22 (s, 3H), 3.80 (s, 3H), 5.32 (s, 1H, exchangeable with D_2O), and 6.42 ppm (s, 1H). Found: C, 75.58; H, 8.72%. Calcd for $C_{13}H_{18}O_2$: C, 75.69; H, 8.80%.

B) From the Acetate ***19****:* The acetate **19** was reduced with lithium aluminium hydride under refluxing in dry ether to give **22** quantitatively.

C) From the Tetralin ***18****:* A mixture of 104 mg of **18** and 136 mg (2 eq) of aluminium chloride in 1 ml of TCE was heated at 66 °C for 2 h. About half of **18** was found to have been converted into **22** by VPC analysis (1.5% SE-30, 2.9 m, 170 °C).

Demethylation of ***21*** *and Preparation of the Bis(methoxycarbonylmethyl) Ether* ***24****.* To a solution of 230 mg of **21** in 10 ml of dichloromethane, *ca.* 800 mg of boron tribromide in 2 ml of dichloromethane was dropwise added at −70 °C and the mixture was stirred at room temperature for 2 h. The whole was poured into ether then the ether solution was washed with water and dried over Na_2SO_4. Evaporating the solvent afforded 197 mg of an oil, from which 157 mg (77%) of **23** was obtained by chromatography on silicic acid (15 g) with benzene. **23**; IR (CCl_4): 3540, 1625, and 1295 cm^{-1}; NMR ($CDCl_3$): 1.17 (d, 3H, J=7 Hz), 2.44 (s, 3H), 2.65 (s, 3H), 5.80 (s, 1H, exchangeable with D_2O), and 11.50 ppm (s, 1H, exchangeable with D_2O). This material was used directly in the subsequent reaction without further purification.

When the reaction was carried out with one equivalent of boron tribromide at room temperature for 50 min or with one equivalent of aluminium chloride at room temperature for several hours, the main product was recognized as the monodemethylated compound **20** by IR spectra.

A mixture of 125 mg of **23**, 400 mg of anhydrous-potassium carbonate, and 1 ml of methyl bromoacetate in 6 ml of acetone was refluxed for 2.5 h. Potassium carbonate was removed by filtration, and the filtrate was evaporated. The residue was chromatographed on silicic acid (5 g). From 20% chroform–benzene fractions, 130 mg (65%) of **24** was obtained; mp 89—90 °C (methanol); IR (CCl_4): 1760, 1740, 1695, 1200, and 1075 cm^{-1}; NMR ($CDCl_3$): 1.16 (d, 3H, J=7 Hz), 2.16 (s, 3H), 2.55 (s, 3H), 3.77 (s, 3H), 3.80 (s, 3H), 4.55 (s, 2H), and 4.63 ppm (s, 2H). Found: C, 63.38; H, 6.97%. Calcd for $C_{20}H_{26}O_7$: C, 63.48; H, 6.93%.

*5,6,7,8-Tetrahydro-3, 4, 5-trimethylnaphtho[2,3-b]furan-9-yl Carboxymethyl Ether (****26****).* A solution of 132 mg of **24** in 3 ml of methanol and 3 ml of 1 M sodium hydroxide was refluxed under nitrogen for one hour. The whole was acidified with dil hydrochlocic acid and was extracted with ether. After evaporating the ether, crystals (**25**: IR (CCl_4): 3300—2500 br, 1740, 1725, and 1700 cm^{-1}) were dried in a dessicator over diphosphorus pentaoxide and were heated under reflux with 300 mg of sodium acetate and 3 ml of acetic anhydride for 2 h.[22] The mixture was poured into ice–water and products were taken in ether. Evaporating the solvent gave a solid **26** (100 mg); the compound was difficult to recrystallize. **26**: mp 168—169 °C (acetone–hexane); NMR ($CDCl_3$): 1.18 (d, 3H, J=7 Hz), 2.38 (br. s, 3H), 2.54 (s, 3H), 4.96 (br. s, 2H), 7.27 (m, 1H), and 9.45 (br. s, 1H). Found: C, 70.28; H, 7.04%. Calcd for $C_{17}H_{20}O_4$: C, 70.81; H, 6.99%.

5, 6, 7, 8-Tetrahydro-3, 4, 5-trimethylnaphtho[2, 3-b]furan-9-yl 2-Hydroxyethyl Ether (27). A solution of 110 mg of the acid **26** in 15 ml of dry ether was refluxed with lithium aluminium hydride for one hour. The excess lithium aluminium hydride was decomposed with the addition of ethyl acetate and the mixture was poured into dil hydrochloric acid. The ether extract was evaporated to give 105 mg of a crude alcohol, **27**. Recrystallization from pentane afforded a pure **27**: mp 78—79 °C; IR (CCl_4): 3580, 1335, and 1110 cm^{-1}; NMR (CCl_4): 1.16 (d, 3H, J=7 Hz), 2.18 (s, 1H, -OH), 2.38 (d, 3H, J=1.5 Hz), 2.52 (s, 3H), 3.80 (m, 2H), 4.30 (m, 2H), and 7.20 ppm (m, 1H). Found: C, 74.35; H, 8.17%. Calcd for $C_{17}H_{22}O_3$: C, 74.42; H, 8.08%.

5, 6, 7, 8-Tetrahydro-3, 4, 5-trimethylnaphtho[2, 3-b]furan-9-yl Acetate (30). To a solution of 50 mg of **27** in 0.3 ml of pyridine, there was added 50 mg of tosyl chloride in 0.3 ml of pyridine at 0 °C; the mixture was left at −6 °C for 17 h. According to Johnson's procedure,[23b] a crude tosylate **28** was isolated as an oil (72 mg). Without purification, **28** was stirred for 94 h with 300 mg of sodium bromide in 2 ml of dimethyl sulfoxide. The product was taken in ether and 45 mg of a bromide **29** was obtained as an oil by chromatography on silicic acid (3 g). **29**: IR (CCl_4): 1605, 1333, and 1110 cm^{-1}; NMR (CCl_4): 1.16 (d, 3H, J=7 Hz), 2.38 (d, 3H, J=1.5 Hz), 2.51 (s, 3H), 3.58 (t, 2H, J=7 Hz), 4.56 (t, 2H, J=7 Hz), and 7.20 ppm (m, 1H).

To a cooled solution of 45 mg of **29** in 2 ml of dry ether, 0.6 ml of 15% butyllithium–hexane solution was added dropwise and the mixture was stirred at room temperature for 10 min.[23a] Aqueous ammonium chloride was added and the ether extract, when evaporated, gave an oily **2** (39 mg) which showed one spot on TLC.

The oily **2** was left overnight with 0.6 ml of acetic anhydride and 1 ml of pyridine. Working up as usual afforded crystals (36 mg, 71% from **27**). Recrystallization from acetone–hexane gave the acetate **30**: mp 119—120 °C; IR (CCl_4): 1760, 1200, 1190, and 1110 cm^{-1}; NMR (CCl_4): 1.18 (d, 3H, J=7 Hz), 2.30 (s, 3H), 2.35 (d, 3H, J=1.5 Hz), 2.53 (s, 3H), and 7.15 ppm (m, 1H). Found: C, 74.79; H, 7.40%. Calcd for $C_{17}H_{20}O_3$: C, 74.97; H, 7.40%.

Lithium Aluminium Hydride Reduction of the Tetralone 16. According to the Romo's condition,[1] a solution of 53 mg of **16** in 5 ml of dry ether was treated with excess lithium aluminium hydride under reflux for one hour. Working up as usual gave an oil, which was acetylated with acetic anhydride in pyridine to give an oily mixture. The NMR spectrum of the mixture showed no detectable amount of **19** being formed. By a chromatographic separation on silicic acid (3 g), 65 mg (88%) of a mixture of *cis*-1,8-diacetoxy-4,5-dimethyl-7-methoxytetralin (**31**) and *trans*-1,8-diacetoxy-4,5-dimethyl-7-methoxytetralin (**32**) was obtained. The stereochemistry of both acetates was based on the pseudocontact shift with Eu-$(fod)_3$ (see Table 2). The ratio of **31**/**32** was *ca.* 2: 1.

We are deeply indebted to Dr. J. Romo for a gift of samples of maturinone and cacalol acetate.

References

1) J. Romo and P. Joseph-Nathan, *Tetrahedron*, **20**, 2331 (1964).
2) P. Joseph-Nathan, J. J. Morales, and J. Romo, *Tetrahedron.*, **22**, 301 (1966).
3) J. Correa and J. Romo, *Tetrahedron.*, **22**, 685 (1966).
4) H. Kakisawa, Y. Inouye, and J. Romo, *Tetrahedron Lett.*, **1969**, 1929.
5) P. M. Brown and R. H. Thomson, *J. Chem. Soc., C*, **1969**, 1184.
6) R. M. Ruiz, J. Correa, and L. A. Maldonado, *Bull. Soc. Chim. Fr.*, **1969**, 3612.
7) P. Joseph-Nathan and Ma. P. González, *Can. J. Chem.*, **47**, 2465 (1969).
8) K. Hayashi, H. Nakamura, and H. Mitsuhashi, *Phytochemistry*, **12**, 2931 (1973).
9) T. Takemoto, G. Kusano, K. Aota, M. Kaneshima, and N. A. El. Emary, *Yakugaku Zasshi*, **94**, 1593 (1974).
10) K. Naya, Y. Miyoshi, H. Mōri, K. Takai, and M. Nakanishi, *Chem. Lett.*, **1976**, 73.
11) Z. Samek, J. Harmatha, L. Novotný, and F. Sǒrm, *Collect. Czech. Chem. Commun.*, **34**, 2792 (1969).
12) Y. Inouye, Y. Uchida, and H. Kakisawa, *Chem. Lett.*, **1975**, 1317.
13) Y. Inouye and H. Kakisawa, *Bull. Chem. Soc. Jpn.*, **42**, 3318 (1969).
14) Y. Inouye, R. Yamakoshi, K. Sakamoto, and H. Kakisawa, Abstr. No. 16217, 22 nd Annual Meeting of the Chemical Society of Japan, Tokyo, April 1969.
15) C. F. H. Allen and A. Bell, *Org. Synth.*, Coll. Vol. III, 310 (1955).
16) H. Kakisawa and M. Tateishi, *Bull. Chem. Soc. Jpn.*, **43**, 824 (1970).
17) R. G. Cooke, H. Dowd, and W. Segal, *Aust. J. Chem.*, **6**, 38 (1953).
18) *Cf.* C. Mannich and H. Davidsen, *Ber.*, **69**, 2106 (1936).
19) P. E. Eaton, G. R. Carlson, and J. T. Lee, *J. Org. Chem.*, **38**, 4071 (1973).
20) C. F. Wilcox, Jr., and M. A. Seager, *J. Org. Chem.*, **34**, 2319 (1969) and references cited therein.
21) I. Agranat, Y. -S. Shih, and Y. Bentor, *J. Am. Chem. Soc.*, **96**, 1295 (1974) and references cited therein.
22) W. B. Whalley, *J. Chem. Soc.*, **1951**, 3229.
23) a) U. Schöllkopf, J. Paust, and M. R. Patsh, *Org. Synth.*, Coll. Vol. V, 859 (1973). b) A. van der Gen, K. Wiedhaup, J. J. Swoboda, H. C. Dunathan, and W. S. Johnson, *J. Am. Chem. Soc.*, **95**, 2656 (1973).
24) According to Dr. Romo's private communication, natural cacalol also decomposes even in a crystalline form on standing for a few weeks.
25) A. Casares and L. A. Maldonado, *Tetrahedron Lett.*, **1976**, 2485. They also referred to the fact that the authentic **3** was not identical with cacalone.

Thermal Analysis and NMR Observation of 66-Nylon

Masayoshi Ito, Tetsuo Kanamoto, and Koji Tanaka

Department of Chemistry, Faculty of Science, Science University of Tokyo, Kagurazaka, Shinjuku-ku, Tokyo 162

(Received October 1, 1976)

The effects of morphology on γ-relaxation in 66-Nylon is investigated. The morphology of the samples was characterized mainly by thermal analysis. Information about the molecular motion of 66-Nylon is obtained from the temperature dependence of the spin-lattice relaxation times (T_1). In order to compare the relaxation behavior of 66-Nylon with that of other semicrystalline polymers, the T_1 of polyoxymethylene (POM) was also measured as a function of temperature. It was found that in 66-Nylon, both solution-grown crystals and bulk samples are composed of folded chain lamellae with fairly large amounts of less perfect crystalline regions. Both the magnitude and the temperature of the T_1 minimum at about 30 °C (γ-region) for 66-Nylon are not sensitive to the sample history, in contrast to those for POM. In addition, the T_1-temperature curve in the γ-region for 66-Nylon is much broader than that for POM. These NMR results for 66-Nylon are interpreted in terms of a rather wide variety of structural heterogeneities from the usual amorphous regions to fairly restricted regions, such as the less-perfect crystalline regions at the lamellar surface.

It is well known that 66-Nylon has three principal relaxations α, β, and γ, in the decreasing order of the temperatures at which they occur.[1] The α-relaxation corresponds to the glass transition[1] and the β-relaxation is related to the motions of polar groups.[2] For the γ-relaxation, different results and explanations have been presented,[3-5] and a complete understanding of this relaxation is still lacking. Bell and Murayama[3] have reported that for 66-Nylon, melt-quenched sample exhibits mechanical γ-dispersion, while slowly-cooled and cold-drawn samples do not show this dispersion. These samples can be characterized from their melting behavior: the former has folded chain crystals and the latter two have less-perfect bundle crystals.[6] Olf and Peterlin[4] have proposed, on the basis of NMR data of drawn fibers of 66-Nylon, that the origin of the γ-relaxation is related to the motions of strained tie molecules. These suggest that 66-Nylon exhibits complex γ-relaxation related to various morphological origins. Hence, the morphological characterization of the sample is very important for understanding the γ-relaxation of 66-Nylon. In this study, thermal analysis, infrared spectroscopy, and density measurements were employed to make a detailed characterization of the morphology of the samples.

Information about the molecular motion of 66-Nylon for a variety of morphologies is obtained from the temperature dependence of the spin-lattice relaxation times (T_1). The relaxation behavior of 66-Nylon is compared with that of polyoxymethylene for which the relaxation mechanisms are well defined.[7,8] Marked differences between them are observed for γ-relaxation and are discussed in light of a morphological interpretation of 66-Nylon.

Experimental

Samples. Commercial 66-Nylon (Toray Co., Ltd.) was dissolved in formic acid and precipitated in an excess of methanol in order to remove impurities. After repeated washing with methanol, the polymer was dried *in vacuo* at 100 °C for one week. Morphological varieties of the samples were prepared by the following procedures.

Solution-crystallized 66-Nylon: *(1) Rapidly-cooled solution grown (SGQ) sample*: One gram of 66-Nylon was dissolved in one liter of glycerin at 220 °C for 40 min, and then the solution was cooled to room temperature at a rate of 30 °C/h. The precipitated crystals were washed with methanol several times and then dried *in vacuo* at 80 °C for one week. *(2) Isothermal solution grown (SGI) sample*: 0.5 g of 66-Nylon was dissolved in one liter of 1,4-butanediol at 180 °C for 15 min, and then the crystals were precipitated at 114 °C for 42 h. The washing and drying procedures for the crystals were identical with those for the SGQ sample.

Observation by electron microscopy indicated that these crystals consist of multilayer single crystals and two dimensional open spherulites.

Bulk-crystallized 66-Nylon: Various bulk-crystallized 66-Nylon specimens were prepared by the treatment similar to those described by Bell and Dumbleton.[6] The polymer samples, sealed in glass tube *in vacuo*, were heat-treated, melt-quenched (MQ) sample, annealed after melt quenching (MQA) sample, slowly-cooled (SC) sample, and annealed after slow cooling (SCA) sample. The thermal history of the bulk crystallized samples is summarized in Fig. 1.

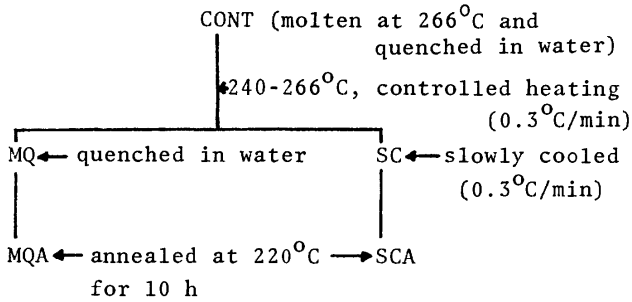

Fig. 1. Shematic representation of the procedures for heat treatment.

Solvent-cast films held in polytetrafluoroethylene sheets and powdered 66-Nylon were heat treated. The melting behavior and densities of the solvent-cast films were substantially identical to those powder samples in regard to the effects of thermal history.

Drawn 66-Nylon Fibers: Drawn fibers were prepared by stretching melt-spun fibers having no orientation to an elongation of about 400% at room temperature.

Polyoxymethylene: Delrin 500 (Du. Pont Co.) was crystallized at several crystallization temperatures. Another sample consisted of extended chain crystals obtained by solid-state

polymerization of trioxane, which was kindly supplied by the Japan Atomic Energy Research Institute, at Takasaki.

Measurements. The melting behavior was observed using a Perkin-Elmer differential scanning calorimeter (DSC-1B), in a nitrogen atmosphere. Sample weights of the order of 1—7 mg were required. The temperature and heat of fusion were calibrated against lead. The melting peak temperature was reproducible for the same sample to within ±0.5 °C.

Pulsed NMR experiments were carried out with a JEOL pulsed NMR (JSE-5) spectrometer, operating at a frequency of 60 MHz. The dead time was 10—12 μs following a 2-μs pulse. 90-τ-90° pulse sequences were used to obtain the proton spin-lattice relaxation times (T_1) to within a precision of ±6% or better. Samples were packed in a sample tube *in vacuo*. Fibers were placed randomly in the sample tube. The sample temperature was regulated to ±0.5 °C by a gas-flow thermostat.

IR spectra were recorded on a JASCO infrared photometer (DS-403G) at room temperature. Spectra of the bulk samples were obtained on films and those of the solution-grown crystals were obtained using samples of about 2 mg in KBr disks.

Densities were determined using a density gradient column at 30 °C in carbon tetrachloride and toluene for 66-Nylon, and in xylene and tetrachloroethylene for polyoxymethlene. The amorphous fraction was calculated using a two-phase model with a crystal density.[9] $\rho_c = 1.24$ g/cm³, and an amorphous density,[9] $\rho_a = 1.09$ g/cm³, for 66-Nylon, and ρ_c[10] = 1.492 g/cm³, ρ_a[11] = 1.25 g/cm³ for polyoxymethylene.

Results and Discussion

Regular Fold Content. Koenig *et al.*[12] have reported that infrared spectroscopy (IR) is a useful method for estimating the regular fold content of 66-Nylon. The regular fold content indexes (the ratio of the absorbances at 1329 and at 936 cm^{-1}) calculated using their method are given in Table 1. All the samples, except the drawn fibers clearly show the regular fold band at 1329 cm^{-1}. It should be noted that the regular fold content indexes for SC and SCA samples, which were previously assumed to be due to a bundle-like crystal structure,[6] have values similar to that for solution-grown crystals (SGI).

Table 1. Characterization data of the samples

Sample	Fold content 1329/936 (IR)	Density g/cm³	Amorphous fraction from density
MQ	0.053	1.162	0.491
MQA	0.059	1.164	0.474
SC	0.074	1.167	0.452
SCA	0.077	1.169	0.440
SGI	0.079	1.190	0.305
SGQ	0.088	1.198	0.250

Thermal Analysis. DSC thermograms for the solution-grown crystals and the heat-treated samples obtained for a heating rate 16 °C/min, are shown in Fig. 2. The MQ and SC samples exhibited a single endothermic peak. On annealing the MQ and SC samples at 220 °C, the former (MQA) produced a new additional peak at a low-temperature side of the original peak, while the latter (SCA) showed no such peak. In solution-grown crystals, the isothermally crystallized SGI sample had double melting peaks, while, the rapidly-cooled SGQ sample gave a single peak.

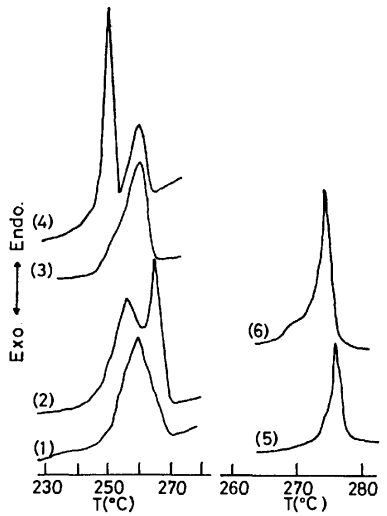

Fig. 2. DSC thermograms of the samples; (1) SGQ, (2) SGI, (3) MQ, (4) MQA, (5) SC, (6) SCA; heating rate was 16 °C/min.

The effect of the heating rate on the melting peaks for the samples are shown in Table 2. When the heating rate was increased, the melting temperature of the SC, SCA, and SGQ samples increased, while that of the MQ and the high-temperature side of the MQA and SGI samples tended to decrease. Such melting behavior of the heat-treated samples agrees well with that of samples used in the dynamic mechanical study by Bell and Murayama.[3]

Table 2. Effect of heating rate on the apparent melting temperature

Heating rate °C/min	Melting temperature, °C							
	MQ	MQA		SC	SCA	SGI		SGQ
2				274	272			
4	263	250	262			255	266	262
8	260	250	261	274	274	256	266	261
16	260	251	260	276	275	257	265	262
32	260			278				266

It has been suggested that extended chain crystals tend to superheat, whereas folded chain crystals do not.[13]

In addition to reorganization during the DSC scan, the thermal diffusivity or temperature gradient in the sample may sometimes affect the melting-peak temperature observed for rapid heating. Indeed, it was found in the present study that even the melting temperature of thin solution-grown crystals (SGQ) (*ca.* 60 Å thick) with typical chain foldings increased with increased heating rate. Furthermore, the samples (SC, SCA) which exhibited apparent superheating showed regular fold bands in their IR spectra. Hence, it was not possible to distinguish between folded chain crystals and extended chain crystals only on the basis of heating-rate dependence of the apparent melting temperature determined by DSC.

In order to reveal the melting behavior inherent in the morphology of the samples, the solution-grown crystals and heat-treated samples were methoxymethylated following the method proposed by Cairns *et al.*[14] This chemical treatment has been found by Arakawa *et al.*[15] to suppress the reorganization of Nylon-6 during thermal analysis, although this has not been applied to 66-Nylon of various morphologies.

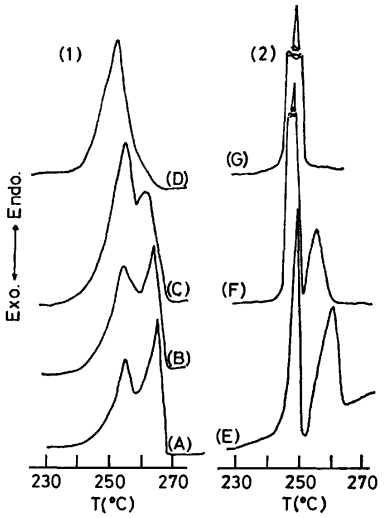

Fig. 3. Changes of melting behavior with methoxymethylation time for (1) MQA, (2) SGI; reaction time was (A) 0 h, (B) 0.7 h, (C) 2 h, (D) 3 h, (E) 0 h, (F) 4 h, (G) 6 h, heating rate was 8 °C/min.

Figure 3 shows the effects of the methoxymethylation time on the thermograms of the MQA and SGI samples obtained for a heating rate of 8 °C/min. The area under the higher melting peak decreased in both samples with increasing reaction time. In the SGI sample, a single melting peak was obtained after a reaction period of 3 h, while the MQA sample exhibited a sharp single peak after 6 h of treatment.

These facts clearly show that the double melting of untreated samples is not associated with the two different lamellar structures, as has been previously deduced from the heating-rate dependence of the melting temperature,[6] but is related to reorganization during the DSC scan

The reaction-time dependence of the melting temperature and the heat of fusion for the solution-grown crystals (SGI) and bulk samples (MQ and SC) are shown in Fig. 4. In all the samples, both the melting temperature and the heat of fusion decreased with increasing reaction time and approached nearly constant values for prolonged reaction times. Such changes were most prominent in the MQ sample. The reduction of the heat of fusion for the MQ, SC, and SGI samples was about 27, 13, and 6%, respectively. The fact that, with the chemical treatment, the heat of fusion decreased initially and reached a nearly constant value for prolonged reaction times indicates that some of the less-perfect crystalline regions or small crystallites were destroyed as a consequence of this treatment. Hence, the observed reduction in the heat of fusion is directly related to the amount of less-perfect crystalline regions

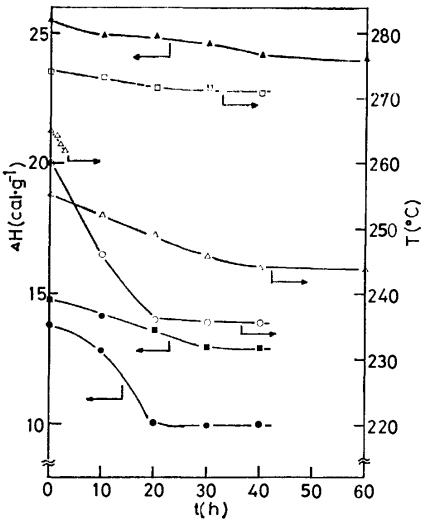

Fig. 4. Changes in the melting temperature with methoxymethylation time for △ SGI, □ SC, ○ MQ; heating rate was 8 °C/min, and changes in the heat of fusion with methoxymethylation time for ▲ SGI, ■ SC, ● MQ.

accessible to the chemical reaction. Although the lowering of the melting points in these samples might be caused primarily by the suppression of the reorganization during the DSC scan, the large decrease in the heat of fusion for the MQ sample suggests that the melting point was also affected by the partial breakdown of the less-perfect regions in the crystallites. In summary, for 66-Nylon, the heat-treated and solution-grown samples were composed of folded chain crystals with different amounts of fold content and of less-perfect crystalline regions depending on the sample history.

NMR Data. The temperature dependence of the spin-lattice relaxation times (T_1) of protons for samples with various morphologies are shown in Figs. 5 and 6. A broad T_1 minimum is present around 30 °C in all the samples studied. In addition to this minimum, the MQ, SC, and SGQ samples showed a small T_1 minimum at 70—80 °C. According to the relaxation map of 66-Nylon,[1,16] the T_1 minima observed here at about 30 and 80 °C at 60 MHz, correspond to the γ- and β-relaxations, respectively, which are usually observed at

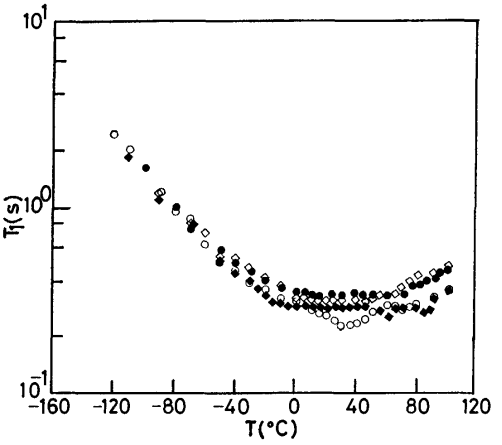

Fig. 5. Temperature dependence of T_1 for ○MQ, ●MQA, ◆SC, ◇SCA.

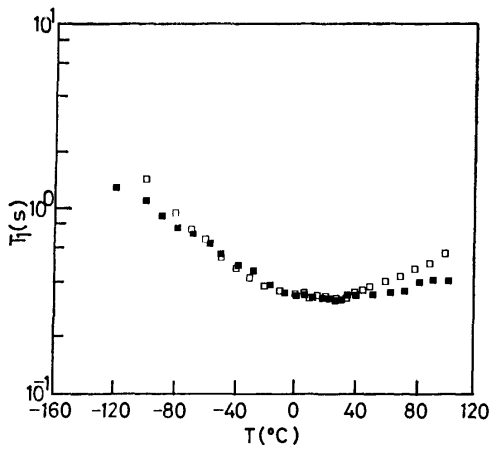

Fig. 6. Temperature dependence of T_1 for ■SGQ, □Drawn Fibers.

around −120 and −40 °C for low-frequency measurement. β-relaxation was found in the MQ, SC, and SGQ samples, but this is not discussed in detail in the present paper.

It should be noted that γ-relaxation in 66-Nylon was found for the SC, SCA, and drawn fibers samples for which other authors[3] failed to detect any mechanical γ-dispersion.

Although the SC, SCA, and drawn fibers samples have been previously considered to be composed of less-perfect bundle crystals,[6] it was confirmed in these measurements using IR and thermal analysis that the SC and SCA samples are composed of the usual folded chain crystals having different amounts of fold content. Furthermore, a large difference in morphology such as in the fold content, might be expected between drawn fibers and solution-grown crystals, these samples have similar spectra for molecular motion in the γ-region. Hence, it is not possible to explain the γ-relaxation in 66-Nylon in terms of only the molecular motions of folded chains at the lamellar surface, as proposed by Bell and Murayama.[3]

In the limit of rapid spin diffusion to the reorienting segments, if the simple two-phase (crystalline-amorphous) model is applicable, the observed maximum relaxation rate $(1/T_1)_{max}$ at the minimum is given by[17]

$$(1/T_1)_{max} = (1-X)/T_1^a, \quad (1)$$

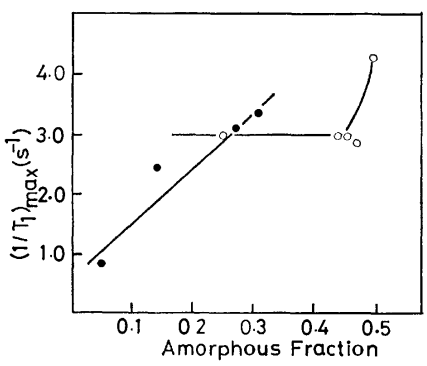

Fig. 7. Maximum relaxation rate at γ-relaxation as a function of the amorphous fraction for ○66-Nylon, ●POM.

where $(1-X)$ is the amorphous fraction and T_1^a is the relaxation time appropriate for the amorphous regions. In Fig. 7, the maximum relaxation rates for the γ-relaxation of 66-Nylon and polyoxymethylene (POM) are plotted against the amorphous fraction calculated from the density. The maximum relaxation rates for POM increased linearly with increasing amorphous fraction. A similar observation for polyethylene and POM has also been reported by Crist and Peterlin.[7,17] For 66-Nylon, on the other hand, all the samples except the MQ sample, exhibited similar relaxation rates despite the fairly large differences in the amorphous fraction.

It is well known that spin diffusion is sufficiently rapid in these γ-regions compared to the dipole-dipole relaxation rate. Therefore, the effects of the amorphous fraction on the maximum relaxation rates for 66-Nylon cannot be explained on the basis of Eq. 1. This means that the simple two-phase model cannot explain the γ-relaxation in 66-Nylon. This is unique to 66-Nylon in comparison with other well-known semicrystalline polymers such as POM[7] and PE,[17] and appears to be important to the understanding of the γ-relaxation in 66-Nylon.

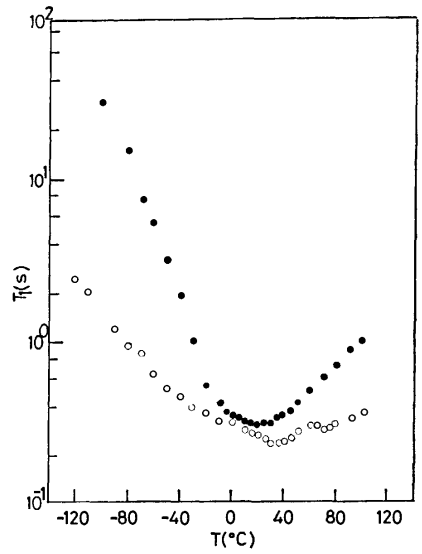

Fig. 8. Temperature dependence of T_1 for ○66-Nylon melt-quenched sample, ●POM melt-quenched sample.

In order to elucidate the characteristic relaxation behavior of 66-Nylon, the temperature dependence of T_1 for 66-Nylon was compared with that for POM for which the γ-relaxation has been explained on the basis of the simple two-phase model[7] in Fig. 8. It is clearly seen that the T_1-temperature curve in the γ-region for 66-Nylon is much broader than that for POM. The broadening of this curve in the higher temperature region could be caused by a coupling of the γ- and β-relaxations. However, this phenomenon in the lower temperature region cannot be caused by coupling with any other relaxation mechanism, because 66-Nylon is known to exhibit no noticeable relaxation below the γ-relaxation.[18] Thus, the broadening indicates that the local mode motions in 66-Nylon have a much wider distribution of correlation times.

Although no fundamental difference (chain folded or extended chain crystals) in the crystalline morphology was found in these bulk samples, they contained, depending on the sample history, different amounts of disordered crystalline regions which were accessible to the chemical reaction.

Atkins *et al.*[19] have carried out an X-ray diffraction analysis of the lamellar structure of 66-Nylon single crystals and found that sharp chain foldings occur at the lamellar surface but that half the lamellar thickness is composed of a less-perfect crystalline core; the chain packing becomes gradually looser in going from the lamellar interior to the fold surface. This type of crystalline disorder in 66-Nylon, which is not found in polyethylene and POM, is considered to occur as the result of a fairly long chemical repetition unit and the small number of such units contained within the lamellar thickness. The observed density defficiency of the SGI sample may be consistent with the lamellar structure revealed by the X-ray diffraction analysis. Hence, the small reduction in the heat of fusion of the solution-grown crystals (SGI) found as a consequence of the chemical treatment indicates that the fraction of the disordered crystalline regions accessible to the chemical reaction was very small. As the bulk samples are thought to be complex aggregates of amorphous materials and crystalline lamellae, it is postulated that both bulk samples and solution-grown crystals contain disordered crystalline regions varying in the degree of perfection from those accessible to the chemical reaction to those revealed by X-ray diffraction.

On considering the above discussions concerning morphology, the structure of the disordered regions of 66-Nylon appears to be very complex compared with those of POM which has a rather short chemical repetition unit and these disordered regions in 66-Nylon appear to consist of a rather wide variety of structural heterogeneity varying from the usual amorphous regions between lamellae or spherulites to fairly restricted regions including those of less-perfect crystalline regions at the lamellar surface. Therefore, it is postulated that the molecular motions in these disordered regions exhibit a wider distribution of correlation times corresponding to the degree of restriction.

Thus, the T_1-temperature curve in the γ-region for 66-Nylon becomes much broader than that for POM.

In summary, γ-relaxation in 66-Nylon cannot be explained by only the motions of the folds or in terms of the simple two-phase model. This relaxation appears to be associated with the motions of segments in the disordered region, which are much more complex than those of POM.

The difference between the dynamic mechanical results previously reported[3] and the present NMR results might be due to the different type and degree of perturbation imposed upon the samples during the measurements. In the NMR experiment, perturbation of the sample system is negligible, but in the dynamic mechanical test, the sample is subjected to a stress and the overall strain on the sample in a complex composition of deformation of the crystalline core and the disordered regions. Indeed, the magnitude of mechanical dispersion has been interpreted in relation to the fine structure of the crystalline polymers using series and parallel models of crystalline and amorphous regions.[20]

The authors wish to express their thanks to Professor Masatami Takeda for continuing interest and encouragement during this investigation.

References

1) N. G. McCrum, B. E. Read, and G. W. Williams, "Anelestic Dielectric Effects in Polymeric Solids," Wiley, London (1967), p. 478.
2) K. H. Illers and H. Jacobs, *Makromol. Chem.*, **39**, 234 (1960).
3) J. P. Bell and T. Murayama, *J. Polym. Sci., A-2*, **7**, 1059 (1969).
4) H. G. Olf and A. Peterlin, *J. Polym. Sci., A-2*, **9**, 1449 (1971).
5) K. H. Illers, *Colloid Polym. Sci.*, **253**, 329 (1975).
6) J. P. Bell and J. H. Dumbleton, *J. Polym. Sci., A-2*, **7**, 1033 (1969).
7) B. Crist and A. Peterlin, *J. Polym. Sci., A-2*, **9**, 557 (1971).
8) A. Tanaka, S. Uemura, and Y. Ishida, *J. Polym. Sci., A-2*, **8**, 1585 (1970).
9) J. B. Nichols, *J. Appl. Phys.*, **25**, 840 (1954).
10) G. Carazzolo, *J. Polym. Sci., A*, **1**, 1573 (1963).
11) C. F. Hammer, T. A. Koch, and J. F. Whitney, *J. Appl. Polym. Sci.*, **1**, 169 (1959).
12) J. L. Koenig and M. C. Agboatwalla, *J. Macromol. Sci., (B)*, **2**, 391 (1968).
13) E. Hellmuth and B. Wunderlich, *J. Appl. Phys.*, **36**, 3039 (1965).
14) T. L. Cairns, H. D. Foster, A. W. Larchar, A. K. Schneider, and R. S. Schreider, *J. Am. Chem. Soc.*, **71**, 651 (1949).
15) T. Arakawa, F. Nagatoshi, and N. Arai, *J. Polym. Sci., A-2*, **7**, 1461 (1969).
16) D. W. McCall and E. W. Anderson, *Polymer.* **4**, 93 (1963).
17) B. Crist and A. Peterlin, *J. Polym. Sci., A-2*, **7**, 1165 (1969).
18) J. M. Crissman, J. A. Sauer, and A. E. Woodward, *J. Polym. Sci., A*, **2**, 5075 (1964).
19) E. D. T. Atkins, A. Keller, D. M. Sadler, and H. H. Wills, *J. Polym. Sci., A-2*, **10**, 863 (1972).
20) M. Takayanagi, M. Yoshino, and K. Hoashi, *Zairyo Shiken*, **10**, 418 (1961).

Improved Syntheses of 3′-Deoxybutirosin A and B

Isamu WATANABE, Tsutomu TSUCHIYA, and Sumio UMEZAWA
Institute of Bioorganic Chemistry, 1614, Ida, Nakahara-ku, Kawasaki 211

(Received September 9, 1976)

3′-Deoxybutirosin B and A (**16**, **17**) were synthesized *via* condensation of 3,2′-bis-*N*-benzyloxycarbonyl-4′,6′-*O*-cyclohexylidene-3′-deoxyparomamine 1,6-carbamate (**2**) with tris-*O*-(*p*-nitrobenzoyl)-D-ribofuranosyl and -D-xylofuranosyl bromide, respectively, followed by 6′-*O*-tosylation of the decyclohexylidene derivative (**8** and **9**), cyclic 1,6-carbamate opening and amidation with (*S*)-4-benzyloxycarbonylamino-2-hydroxybutyric acid at the free C-1 amino group.

In a previous paper,[1] we described a synthesis of 3′-deoxybutirosin B starting from 3′-deoxyparomamine. Here we describe another synthesis of 3′-deoxybutirosin B as well as A by an alternative route. In the previous synthesis[1] there have been found the following disadvantages: 1) regioselective 6′-*O*-tosylation and 4′-*O*-α-naphthoylation gave unsatisfactory yields owing to the presence of other similarly reactive hydroxyl groups, 2) low solubilities of the 6′-*O*-tosyl and other related derivatives (compound **2**, **3**, **4**, and **5** in the previous paper[1]) in organic solvents render the column-chromatographical purification difficult, 3) the 4′-*O*-naphthoyl group unexpectedly resisted to the basic hydrolysis, and the removal of this group was forced to be incomplete in order to prevent the removal of the *N*-benzyloxycarbonyl groups. One device to overcome this disadvantage was the use of sodium *p*-methoxybenzylate, a stronger base.[1]

The condensing partner adopted in this paper is 4′,6′-*O*-cyclohexylidene-1,6-carbamate (**2**), prepared

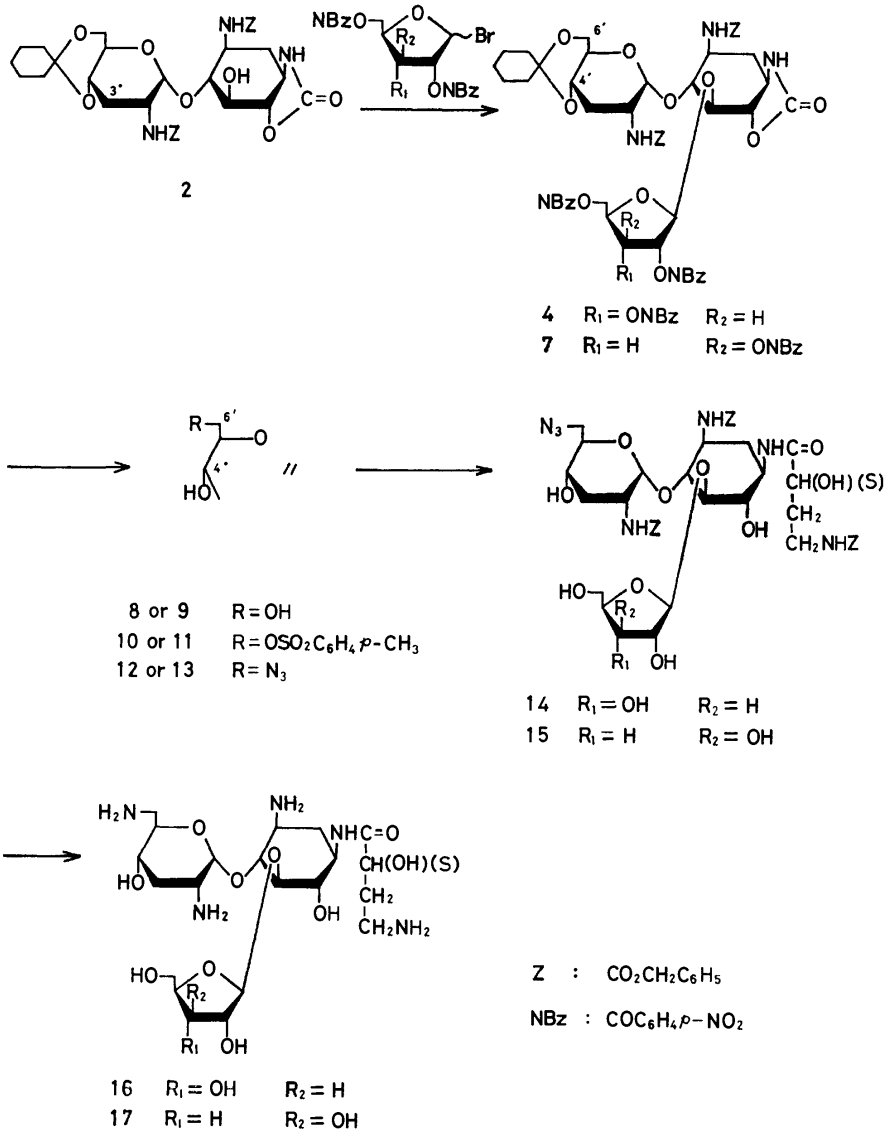

from tris-*N*-benzyloxycarbonyl-3′-deoxyparomamine[1] (**1**). The compound **2** has a free hydroxyl group only at C-5 and suitable solubilities in organic solvents. The condensation of **2** with tris-*O*-(*p*-nitrobenzoyl)-α,β-D-ribofuranosyl bromide[1] (**3**) or α,β-D-xylofuranosyl bromide[2] was successfully carried out to give **4** or **7**. The latter bromide was prepared from 1,2-*O*-isopropylidene-3,5-bis-*O*-(*p*-nitrobenzoyl)-α-D-xylofuranose (**5**) *via* methyl 2,3,5-tris-*O*-(*p*-nitrobenzoyl)-α,β-D-xylofuranoside[2] (**6**). The cyclohexylidene group of the condensation product (**4** or **7**) was then selectively hydrolyzed and the 6′-hydroxyl group of the resulting diol derivative (**8** or **9**) was tosylated to give **10** or **11**.

Treatment of **10** or **11** with sodium azide gave a 6′-azido derivative (**12** or **13**). Treatment with aqueous barium hydroxide cleaved their ester groups as well as cyclic carbamate smoothly in comparison to the *O*-α-naphthoyl group described in the previous paper.[1] Introduction of (*S*)-4-benzyloxycarbonylamino-2-hydroxybutyryl group to the amino group at C-1 gave **14** or **15** and catalytic hydrogenolysis of the *N*-benzyloxycarbonyl and azido groups gave 3′-deoxybutirosin B (**16**) or A (**17**). By taking this synthetic route, the aforementioned disadvantages were substantially avoided and the overall yields based on **1** were 10—15%.

Experimental

General procedures were the same as described in a previous paper.[1]

*3,2′-Bis-*N*-benzyloxycarbonyl-4′,6′-*O*-cyclohexylidene-3′-deoxyparomamine 1,6-Carbamate (2).* To an ice-cold solution of tris-*N*-benzyloxycarbonyl-3′-deoxyparomamine[1] (**1**) (9.60 g) in DMF (190 ml), 50% oily sodium hydride (1.92 g) was added and the mixture was vigorously stirred for 2 h in the cold. Acetic acid (5 ml) was added and the mixture was poured into ice–water (3 l). Precipitates were collected by filtration and dried. To a solution of the solid (7.53 g) in dry DMF (150 ml), 1,1-dimethoxycyclohexane (15 ml) and anhydrous *p*-toluenesulfonic acid (430 mg) were added and the solution was stirred for 2.5 h at 30 °C under reduced pressure (≈15 Torr). The solution was poured into aqueous acetic acid–sodium acetate buffer (0.2 M, pH 4.5, 2 l) and the precipitates were collected by filtration and thoroughly washed with hexane and then with water to give a solid, 8.1 g (89%). It was reprecipitated from dioxane–acetone–hexane, mp 264—265 °C, $[\alpha]_D^{20}$ +52° (*c* 1, C_5H_5N); IR (KBr): 2930, 1775, 1700 cm^{-1}.

Found: C, 61.47; H, 6.38; N, 5.97%. Calcd for $C_{35}H_{43}N_3O_{11}$: C, 61.66; H, 6.36; N, 6.16%.

*3,2′-Bis-*N*-benzyloxycarbonyl-4′,6′-*O*-cyclohexylidene-3′-deoxy-5-*O*-[2,3,5-tris-*O*-(p-nitrobenzoyl)-β-D-ribofuranosyl]paromamine 1,6-Carbamate (4).* A mixture of **2** (5.0 g), **3**[1] (20.5 g), mercuric cyanide (9 g), and calcium sulfate (Drierite, 18 g) in dichloromethane (115 ml) was vigorously stirred at room temperature overnight. After addition of methanol (20 ml) and pyridine (10 ml) followed by agitation for a while, the mixture was filtered and the solid was washed with dichloromethane (≈50 ml). The filtrate and the washings combined were washed with aqueous sodium hydrogencarbonate and water, dried (Na_2SO_4), and concentrated. The resulting solid was chromatographed over silica gel with chloroform–ethanol–triethylamine (30: 1: 0.1) to give a solid of **4**, 5.8 g, $[\alpha]_D^{23}$ +10° (*c* 1, $CHCl_3$); Though the solid still contained 1—2% ash, it was used without purification to the next step.

*1,2-*O*-Isopropylidene-3,5-bis-*O*-(p-nitrobenzoyl)-α-D-xylofuranose (5).* 1,2-*O*-Isopropylidene-α-D-xylofuranose[4] was treated with *p*-nitrobenzoyl chloride in pyridine in a usual manner to give a solid of **5**, which was recrystallized from ethyl acetate–hexane to give needles in a yield of 76%, mp 149—150 °C, $[\alpha]_D^{23}$ −70° (*c* 1, $CHCl_3$).

Found: C, 53.84; H, 4.11; N, 5.53%. Calcd for $C_{22}H_{20}N_2O_{11}$: C, 54.10; H, 4.13; N, 5.74%.

*Methyl 2,3,5-Tris-*O*-(p-nitrobenzoyl)-α,β-D-xylofuranoside (6).* To a solution of **5** (2.5 g) in dichloromethane (40 ml), 0.5 M methanolic hydrogen chloride (45 ml) was added and the solution was kept at room temperature for 60 h. Pyridine (10 ml) and toluene (20 ml) were added and the solution was concentrated. The residue was dissolved in pyridine (50 ml) and the solution was treated with *p*-nitrobenzoyl chloride in a usual manner to give a syrup of **6**, 3.1 g; PMR ($CDCl_3$) δ: 5.20 (≈0.6H s, β-H-1); the peaks corresponding to α-H-1 could not be discerned by overlapping with other signals. The syrup was used without purification to bromination followed by glycosylation (The crystalline β-anomer of **6** was described by El Khadem *et al.*[2]).

*3,2′-Bis-*N*-benzyloxycarbonyl-4′,6′-*O*-cyclohexylidene-3′-deoxy-5-*O*-[2,3,5-tris-O-(p-nitrobenzoyl)-β-D-xylofuranosyl]paromamine 1,6-Carbamate (7).* To a cold (≈10 °C) solution of **6** (2.02 g) in dry dichloromethane (40 ml), hydrogen bromide was introduced until saturation and the solution was kept at 0 °C overnight. Removal of the solvent and the excess hydrogen bromide by coevaporation with toluene gave a syrup, which was dissolved in dichloromethane (21 ml). To the solution, **2** (750 mg), mercuric cyanide (1.0 g), and calcium sulfate (Drierite, 2.0 g) were added and the mixture was vigorously stirred at room temperature overnight. The reaction mixture was then treated similarly as described for **4** to give a solid of **7**, 583 mg (42%), $[\alpha]_D^{23}$ +53° (*c* 1, $CHCl_3$).

Found: C, 57.66; H, 4.82; N, 6.51%. Calcd for $C_{61}H_{60}N_6O_{24}$: C, 58.09; H, 4.80; N, 6.66%.

*3,2′-Bis-*N*-benzyloxycarbonyl-3′-deoxy-5-*O*-[2,3,5-tris-O-(p-nitrobenzoyl)-β-D-ribo- and -β-D-xylofuranosyl]paromamine 1,6-Carbamates (8 and 9).* To a solution of crude **4** (350 mg) in acetone (3.5 ml), acetic acid (7 ml) and water (3.5 ml) were added and the mixture was heated at 60 °C for 6 h. The solution was concentrated and the residue was dissolved in chloroform. The solution was washed with aqueous hydrogencarbonate and water, dried (Na_2SO_4), and concentrated to give a solid of **8**, 230 mg (≈70%). Since the solid contained slight impurities, it was further purified by chroma tography over silica gel with chloroform–ethanol (20: 1) (30: 1, in the case of **9**), $[\alpha]_D^{22}$ +10° (*c* 1, $CHCl_3$); IR (KBr): 1775, 1720, 1525 cm^{-1}.

Found: C, 55.68; H, 4.51; N, 6.85%. Calcd for $C_{55}H_{52}N_6O_{24}$: C, 55.93; H, 4.44; N, 7.12%.

Compound **9**: Compound **7** (440 mg) was treated similarly as described for **8** to give a solid of **9**, 237 mg (57.5%); $[\alpha]_D^{23}$ +57° (*c* 1, $CHCl_3$); IR (KBr); 1780, 1725, 1530 cm^{-1};

Found: C, 55.71; H, 4.44; N, 6.92%.

*3,2′-Bis-*N*-benzyloxycarbonyl-3′-deoxy-5-*O*-[2,3,5-tris-O-(p-nitrobenzoyl)-β-D-ribo- and -β-D-xylofuranosyl]-6′-O-tosylparomamine 1,6-Carbamates (10 and 11).* To a solution of **8** (360 mg) in pyridine (10 ml), *p*-toluenesulfonyl chloride (230 mg) was added and the solution was kept at −10 °C for 40 h. Water (0.1 ml) was added and the solution was concentrated. A solution of the residue in chloroform was washed with aqueous potassium hydrogensulfate. aqueous sodium hydrogencarbonate and water, dried (Na_2SO_4), and concentrated to give a solid, which was chromatographed over silica gel with chloroform–ethanol (40: 1), giving a solid of **10**, 320 mg (79%), $[\alpha]_D^{22}$ +4° (*c* 0.4, $CHCl_3$); IR (KBr):

1770, 1725, 1525, 1175 cm^{-1} (Ts); PMR ($CDCl_3$) δ: 2.37 (3H, s, CH_3 (Ts)).

Found: C, 55.85; H, 4.54; N, 6.28; S, 2.35%. Calcd for $C_{62}H_{58}N_6O_{26}S$: C, 55.77; H, 4.38; N, 6.29; S, 2.40%.

Compound ***11***: Compound **9** (335 mg) was treated similarly as described for **10** to give a solid of **11**, 298 mg (79%); $[\alpha]_D^{23}$ +70° (*c* 0.6, $CHCl_3$); IR (KBr): 1775, 1725, 1530, 1180 cm^{-1} (Ts); PMR ($CDCl_3$ δ: 2.35 (3H, s, CH_3 (Ts)).

Found: C, 55.48; H, 4.48; N, 5.99; S, 2.36%.

*6'-Azido-3,2'-bis-*N*-benzyloxycarbonyl-3',6'-dideoxy-5-*O*-[2,3,5-tris-*O*-(*p*-nitrobenzoyl)-β-*D*-ribo- and -β-*D*-xylofuranosyl]paromamine 1,6-Carbamates (**12** and **13**).* To a solution of **10** (160 mg) in DMF (3.2 ml), sodium azide (80 mg) was added and the mixture was stirred at 60 °C for 4 h. Chloroform (30 ml) was added and the reaction mixture was washed with saturated sodium chloride solution (30 ml × 3) and then with water (30 ml). The solution was concentrated and the residue was washed with water to remove trace of DMF accompanied, and dried to give a solid of **12**, 142 mg (96%), $[\alpha]_D^{22}$ +6.5° (*c* 0.8, $CHCl_3$); IR (KBr): 2100 (N_3), 1775, 1720, 1525 cm^{-1}.

Found: C, 54.57; H, 4.34; N, 10.52%. Calcd for $C_{55}H_{51}N_9O_{23}$: C, 54.77; H, 4.26; N, 10.45%.

Compound ***13***: Compound **11** (130 mg) was treated similarly as described for **12** to give a solid of **13**, 115 mg (98%); $[\alpha]_D^{23}$ +54° (*c* 1, $CHCl_3$); IR (KBr): 2100 (N_3), 1775, 1720, 1525 cm^{-1}.

Found: C, 54.44; H, 4.36; N, 10.30%.

*6'-Azido-3,2'-bis-*N*-benzyloxycarbonyl-1-*N*-[(*S*)-4-benzyloxycarbonylamino-2-hydroxybutyryl]-3',6'-dideoxy-5-*O*-(β-*D*-ribo- and -β-*D*-xylofuranosyl)paromamines (**14** and **15**).* To a solution of **13** (260 mg) in dioxane (13 ml), 0.05 M aqueous barium hydroxide (5.8 ml) was added and the mixture was stirred at 60 °C for 30 min. To the resulting neutral solution, additional aliquots of the barium hydroxide solution (5.0 and 2.1 ml) were added at intervals and the mixture was treated as stated above. Carbon dioxide was introduced, and, after filtration, the solution was concentrated to give a residue, which was again dissolved in dioxane. After filtration, the solution was concentrated to give a solid.

To a solution of the solid in THF (2.7 ml), *N*-hydroxysuccinimide ester[3] (115 mg) of (*S*)-4-benzyloxycarbonylamino-2-hydroxybutyric acid and triethylamine (0.1 ml) were added and the solution was stirred at 0 °C for 1 h and then kept at room temperature overnight. The solution was concentrated and the residue was chromatographed over silica gel with chloroform–ethanol (7: 1) to give a solid of **15**, 142 mg (68%), mp 86—90 °C, $[\alpha]_D^{23}$ +23° (*c* 1, CH_3OH); IR (KBr): 2100, 1700, 1530 cm^{-1}.

Found: C, 55.47; H, 5.83; N, 9.77%. Calcd for $C_{45}H_{57}N_7O_{17}$: C, 55.84; H, 5.94; N, 10.13%.

Compound ***14***: Compound **12** (95 mg) was treated similarly as described for **15** to give a solid of **14**, 50 mg (66%); mp 94—96 °C, $[\alpha]_D^{22}$ +20° (*c*, 1 $CHCl_3$) (lit,[1] +19°); IR (KBr): 2100 (N_3), 1695, 1525 cm^{-1}.

Found: C, 55.67; H, 6.07; N, 9.87%.

*3'-Deoxybutirosin B (**16**).* Compound **14** (115 mg) was catalytically hydrogenated as described in the foregoing paper[1] to give a solid of **16**, 55 mg (77%), $[\alpha]_D^{22}$ +32° (*c* 1, H_2O) (lit,[1] +29°).

Found: C, 44.08; H, 7.37; N, 11.57%. Calcd for $C_{21}H_{41}N_5O_{11}\cdot H_2CO_3$: C, 43.92; H, 7.20; N, 11.64%.

*3'-Deoxybutirosin A (**17**).* Compound **15** (126 mg) was catalytically hydrogenated as described for the preparation of 3'-deoxybutirosin B in the foregoing paper[1] to give a solid of **17**, 55 mg (74%), $[\alpha]_D^{23}$ +23° (*c* 1, H_2O).

Found: C, 45.33; H, 7.49; N, 12.29%. Calcd for $C_{21}H_{41}N_5O_{11}\cdot 1/2H_2CO_3$: C, 45.26; H, 7.42; N, 12.27%.

The authors are grateful to Professor Hamao Umezawa, Director of Institute of Microbial Chemistry, for his support and encouragement.

References

1) I. Watanabe, A. Ejima, T. Tsuchiya, D. Ikeda, and S. Umezawa, *Bull. Chem. Soc. Jpn.*, **50**, 487 (1977).

2) H. S. El Kkadem, T. D. Audichya, D. A. Niemeyer, and J. Kloss, *Carbohydr. Res.*, **47**, 233 (1976).

3) H. Kawaguchi, T. Naito, S. Nakagawa, and K. Fujisawa, *J. Antibiot.*, **25**, 695 (1972).

4) W. N. Haworth and C. R. Porter, *J. Chem. Soc.*, **1928**, 611.

Synthesis of a Masked Derivative of 3′-Deoxydihydrostreptobiosamine, a Precursor for the Synthesis of 3″-Deoxydihydrostreptomycin

Hiroshi SANO, Tsutomu TSUCHIYA, Shigeru KOBAYASHI,*
Hamao UMEZAWA, and Sumio UMEZAWA
Institute of Bioorganic Chemistry, 1614 Ida, Nakahara-ku, Kawasaki 211
**Department of Applied Chemistry, Faculty of Engineering, Keio University, Hiyoshi, Yokohama 223*
(Received October 8, 1976)

2′-*N*-Acetyl-4′,6′-di-*O*-acetyl-3,3a-*O*-carbonyl-3′-deoxydihydrostreptobiosamine (**15**), a precursor in the synthesis of 3″-deoxydihydrostreptomycin, was prepared from benzyl α-dihydrostreptobiosaminide. The synthesis involves formation of L-allo compound (**5**) with inversion of the 3′-hydroxyl group of L-gluco derivative (**2**) in order to facilitate 3′-chlorination, dechlorination, of the 3′-chloro-L-gluco derivative (**7** or **11**) with tributyltin hydride, and utilization of cyclic 3,3a-*O*-carbonyl group instead of 3,3a-*O*-isopropylidene group which was unstable in the later reactions.

Recent studies have clarified that streptomycin is inactivated by resistant bacteria carrying R factor and resistant *Pseudomonas* producing enzymes which adenylylate[1] or phosphorylate[2] the 3″-hydroxyl group of the antibiotic. Removal of the 3″-hydroxyl group from dihydrostreptomycin is expected, therefore, to afford a dihydrostreptomycin derivative active against the resistant organisms. In this paper the synthesis of a key intermediate for the synthesis of 3″-deoxydihydrostreptomycin, namely, 4′,6′-di-*O*-acetyl-3′-deoxy-3,3a-*O*-carbonyldihydrostreptobiosamine** (**15**) starting from benzyl α-dihydrostreptobiosaminide is reported. The glycosyl chloride of **15** was successfully condensed with di-*N*-acetyl-di-*N*-benzyloxycarbonyl-4,5(5,6)-*O*-cyclohexylidenestreptidine[3] to give a condensation product which was led to 3″-deoxydihydrostreptomycin.[4]

Benzyl α-dihydrostreptobiosaminide[10] was treated with benzyl chloroformate to give the *N*-benzyloxycarbonyl derivative (**1**), which was converted to the di-*O*-isopropylidene derivative (**2**) by treatment with 2,2-dimethoxypropane in the presence of acidic catalyst. Thereafter, the free hydroxyl group at C-3′ of **2** was mesylated. Treatment of the 3′-*O*-mesyl derivative (**3**) with sodium iodide in *N*,*N*-dimethylformamide (DMF) afforded the *N*,*O*-carbonyl-L-allo derivative (**4**). It should be noted that, in the synthesis[5] of tobramycin, similar treatment of a structurally related compound having a 2,6-bis(ethoxycarbonylamino)-2,6-dideoxy-3-*O*-tosyl-α-D-glucopyranosyl moiety with sodium iodide in DMF gave a 3′-iodo derivative as a major product possibly with participation of the neighbouring ethoxycarbonyl group. It was further found that the derivative (**4**) was more easily obtained by alkaline treatment of **3** (86% yield). The L-allo structure of **4** was confirmed by the PMR spectra of **4** and **5** in which the $J_{2',3'}$ and $J_{3',4'}$ had suitable values (3—6 Hz) for *1C* L-allopyranoside.

Hydrolysis of the carbamate (**4**) with barium hydroxide gave **5**, which was acetylated to give **6**. It should also be noted that treatment of the 3′-*O*-mesyl derivative of **5** with sodium iodide in DMF gave no definite product. This result is unusual because, in a separate experiment,[6] we found that a 3-*O*-mesyl-D-allo compound, namely benzyl 4,6-*O*-benzylidene-2-benzyloxycarbonylamino-2-deoxy-3-*O*-mesyl-2-*N*-methyl-α-D-allopyranoside gave the corresponding 3-iodo derivative on treatment with 50% sodium iodide in DMF (100 °C, 48 h) in good yield.

Treatment of **6** with sulfuryl chloride successfully gave 3′-chloro-L-gluco derivative (**7**) with inversion of the configuration at C-3′. The L-gluco configuration of **7** was confirmed by its PMR spectrum, in which the $J_{2',3'}$, gave 11.5 Hz, an indication that the 3′-chlorine is equatorial. At this stage, we have to mention that treatment of **2** with sulfuryl chloride gave no 3′-chloro derivative.

Catalytic hydrogenolysis of **7** with platinum oxide only recovered the starting material. Hydrogenolysis of **7** with palladium black gave a debenzylated product, while treatment with Raney nickel with addition of potassium hydroxide or triethylamine gave a dechlorodebenzylated product, both products being useless for the present synthesis. Reduction with tributyltin hydride[7] in the presence of α,α′-azobisisobutyronitrile successfully gave the 3′-deoxy compound (**8**) quantitatively. Its structure was confirmed by its PMR spectrum.

The deoxy derivative was modified to a derivative suitable for glycosylation. In the first place the 4′,6′-*O*-isopropylidene group of **8** was selectively removed to give **9**, which was then acetylated to give 4′,6′-di-*O*-acetyl derivative (**12**). This requirement originated from our experience in the synthesis of dihydrostreptomycin,[3,8,9] in which similar replacement of an isopropylidene group by two acyl groups gave a successful result. Alternatively, compound **12** was prepared from **7** by acid hydrolysis of **7** (which selectively removed the isopropylidene group at C-4′ and 6′ to give **10**) followed by acetylation to give **11** and dechlorination with tributyltin hydride.

The 3,3a-*O*-isopropylidene group of **12** was unstable for later treatment with thionyl chloride to prepare a glycosyl chloride; transketalization[8] was expected to occur in the dihydrostreptose moiety. The 3,3a-*O*-isopropylidene group of **12** was therefore removed by treatment with 75% acetic acid and the resulting diol

** In this paper, the dihydrostreptose moiety is taken as a parent monosaccharide and numbers of the carbon atoms of the 2-deoxy-2-methylamino-L-glucose moiety, the second monosaccharide, are primed and the hydroxymethyl carbon of dihydrostreptose moiety is numbered 3a.

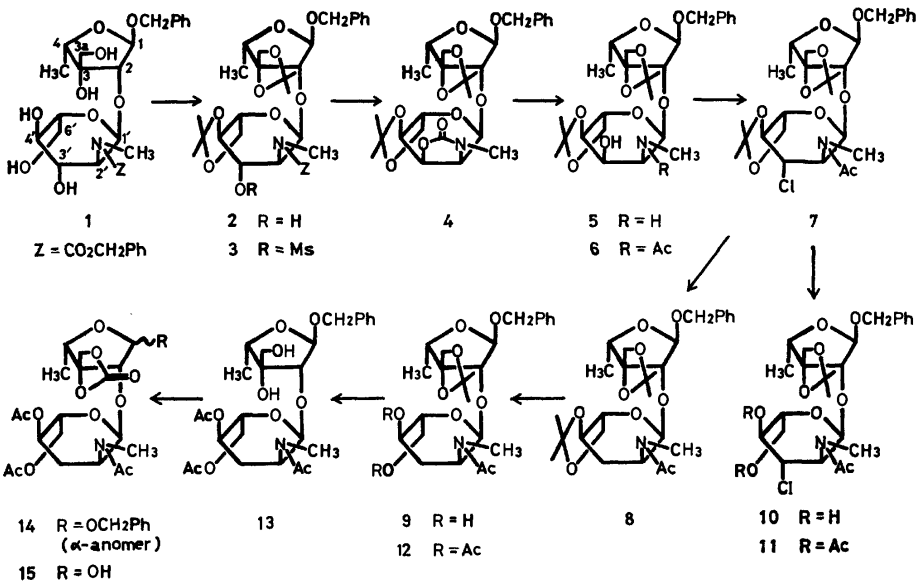

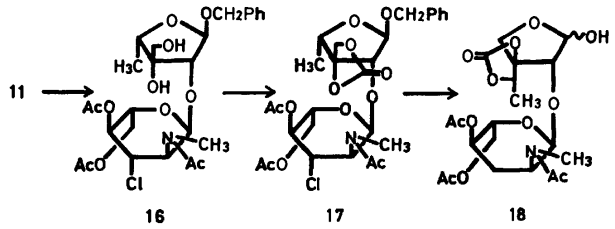

(**13**) was treated with *p*-nitrophenyl chloroformate by a procedure previously described[8] to give the 3,3a-carbonate derivative (**14**). The presence of the cyclic carbonate group was confirmed by the absorption peak at 1810 cm^{-1} in the IR spectrum. Catalytic hydrogenolysis of the benzyl group with palladium black gave a masked derivative (**15**) of 3'-deoxydihydrostreptobiosamine. As separately reported,[4] the C-1 chloride of **15** was prepared and coupled[4] with a protected derivative[3] of streptidine and the condensation product was successfully led to 3"-deoxydihydrostreptomycin.[4]

In an alternative approach to **15** from **11**, deisopropylidenation of **11** gave the corresponding diol (**16**), which was converted into a 3,3a-carbonate (**17**). An attempt to prepare **15** from **17** by simultaneous removal of the 3'-chloro and 1-*O*-benzyl groups by catalytic hydrogenolysis, however, gave an unusual result. Treatment of **17** with Raney nickel and hydrogen gave **18**, an isomer of **15**. Its structure was confirmed by PMR spectroscopy. The methine proton signal at C-4 appeared as a quartet at a low field (δ 5.16), indicating that 4-hydroxyl group is acylated. This observation is another example which shows that the dihydrostreptose moiety is labile and tends to undergo ring-isomerization.

Experimental

General. Infrared spectra were recorded for potassium bromide pellets with a Hitachi Model 285 grating infrared spectrophotometer. PMR spectra were recorded at 60 and 100 MHz with Hitachi R-24A and Varian XL-100 spectrometers. Thin layer chromatography (TLC) was performed on Wakogel B-5 with sulfuric acid spray for detection. For column chromatography, silica gel (Wakogel C-200) was used.

Benzyl 2'-N-Benzyloxycarbonyl-α-dihydrostreptobiosaminide (1). To a mixture of benzyl α-dihydrostreptobiosaminide hydrochloride[10] (6.81 g) and sodium carbonate (3.23 g) in aqueous acetone (1: 1, 180 ml), benzyl chloroformate (4.6 ml) was added and the mixture was stirred at 0 °C for 5 h. The mixture was filtered and the filtrate was concentrated. The residue, after washing with ether, was dissolved in chloroform. Filtration followed by concentration gave a residue. Recrystallization from chloroform–ether gave needles, 5.56 g (67%), mp 152—152.5 °C, $[\alpha]_D^{24}$ −140° (*c* 1, $CHCl_3$).

Found: C, 59.57; H, 6.57; N, 2.54%. Calcd for $C_{28}H_{37}NO_{11}$: C, 59.67; H, 6.62; N, 2.49%.

Benzyl 2'-N-Benzyloxycarbonyl-3,3a: 4',6'-di-O-isopropylidene-α-dihydrostreptobiosaminide (2). To a solution of **1** (6.72 g) in DMF (120 ml), anhydrous *p*-toluenesulfonic acid (960 mg) and 2,2-dimethoxypropane (19.2 ml) were added and the solution was heated at 50 °C for 3 h. The solution was poured into a mixture of aqueous 5% sodium hydrogencarbonate solution (850 ml) and chloroform (850 ml) with vigorous stirring and the organic layer separated was concentrated to a syrup. The chloroform solution of the syrup was washed with water, dried (Na_2SO_4), and concentrated to give a syrup, which was chromatographed over silica gel (benzene–methyl ethyl ketone 9: 1) to give a thick syrup of **2**, 7.28 g (94%), $[\alpha]_D^{24}$ −117° (*c* 1, $CHCl_3$); PMR ($CDCl_3$) δ: 1.25 (3H d, CCH_3); 1.23, 1.3, 1.42, and 1.48 (each 3H s, $2C(CH_3)_2$); 3.06 (3H s, NCH_3), 4.56 (2H q, OCH_2Ph) 4.9—5.15 (4H, H-1,1' and CO_2CH_2Ph).

Found: C, 63.14; H, 6.94; N, 1.94%. Calcd for $C_{34}H_{45}NO_{11}$: C, 63.34; H, 7.19; N, 2.17%.

Benzyl 2'-N-Benzyloxycarbonyl-3,3a: 4',6'-di-O-isopropylidene-3'-O-mesyl-α-dihydrostreptobiosaminide (3). Compound **2** was treated with methanesulfonyl chloride in pyridine in a usual manner to give a thick syrup of **3**, 99%, $[\alpha]_D^{24}$ −95° (*c* 1, $CHCl_3$); PMR ($CDCl_3$) δ: 3.07 and 3.10 (each 3H s, NCH_3 and SO_2CH_3).

Found: C, 58.03; H, 6.50; N, 1.99; S, 4.66%. Calcd for $C_{35}H_{47}NO_{13}S$: C, 58.24; H, 6.56; N, 1.94; S, 4.44%.

Benzyl 2-O-(2,3-N,O-Carbonyl-2-deoxy-4,6-O-isopropylidene-2-methylamino-α-L-allopyranosyl)-3,3a-O-isopropylidene-α-dihydrostreptoside (4). A solution of **3** (8.14 g) and sodium

acetate trihydrate (8.14 g) in 2-methoxyethanol (160 ml) was refluxed for 65 h. Evaporation of the solvent gave a solid, which was dissolved in chloroform. The solution was washed with water, dried (Na_2SO_4), and concentrated to give a solid. Recrystallization from ethanol gave prisms, 5.17 g (86%), mp 170.5—172 °C, $[\alpha]_D^{24}$ −171° (*c* 1, $CHCl_3$); IR: 1760 cm^{-1} (cyclic carbamate); PMR ($CDCl_3$) δ: 1.29 (3H, d J=6.5 Hz, CCH_3; collapsed to a singlet on irradiation at 4.05); 1.40 (6H), 1.45 (3H) and 1.50 (3H) (each s, $2C(CH_3)_2$); 3.00 (3H s, NCH_3), 3.5—3.9 (6H), 4.05 (1H q, J=6.5 Hz, H-4; collapsed to a singlet on irradiation at δ 1.29); 2H AB q centered at δ 4.07 (J=9 Hz, H-3a); 4.54 (1H q, J=3 and 6 Hz, H-3′; collapsed to a singlet on irradiation at δ ≈3.84 (H-2′,4′)); 2H AB q centered at δ 4.54 (OCH_2Ph); 5.04 (1H d, J≈1 Hz, H-1), 5.12 (1H d, J=5 Hz, H-1′), 7.27 (5H s, Ph). The doublets of H-1 and H-1′ were collapsed to singlets, respectively, on irradiation at δ ≈3.84, therefore, the signals at δ ≈3.84 were assigned to H-2, 2′,4′.

Found: C, 60.37; H, 6.87; N, 2.45%. Calcd for $C_{27}H_{37}NO_{10}$: C, 60.55; H, 6.96; N, 2.62%.

Benzyl 2-O-(2-Deoxy-4,6-O-isopropylidene-2-methylamino-α-L-allopyranosyl)-3,3a-O-isopropylidene-α-dihydrostreptoside (5). To a solution of **4** (4.74 g) in methanol (120 ml), 5.5% aqueous barium hydroxide (120 ml) was added and the mixture was stirred at 50 °C for 110 h. Filtration followed by evaporation of the filtrate gave a residue, which was extracted with chloroform. The solution was washed with water, dried (Na_2SO_4), and concentrated to give a thick syrup, which was crystallized from ether to give needles, 3.39 g (75%), mp 110—111 °C, $[\alpha]_D^{24}$ −131° (*c* 1, $CHCl_3$); PMR ($CDCl_3$) δ: 1.28 (3H d, CCH_3); 1.42 (3H) and 1.47 (9H) (each s, $2C(CH_3)_2$); 2.46 (3H s, NCH_3), 5.03 (1H d, J=4 Hz, H-1′), 5.05 (1H s, H-1). When measured in $CDCl_3$–D_2O, an 1H triplet ($J_{1',2'}=J_{2',3'}$ ≈3.5 Hz, H-2′) appeared at δ 2.65 and it was collapsed to a doublet on irradiation at δ 5.03.

Found: C, 61.31; H, 7.73; N, 2.66%. Calcd for $C_{26}H_{39}NO_9$: C, 61.28; H, 7.71; N, 2.75%.

Benzyl 2-O-(2-Acetamido-2-deoxy-4,6-O-isopropylidene-2-N-methyl-α-L-allopyranosyl)-3,3a-O-isopropylidene-α-dihydrostreptoside (6). To a solution of **5** (652 mg) in methanol (17.5 ml), acetic anhydride (0.28 ml) was added and the solution was kept at room temperature overnight. Concentration of the solution gave a syrup, which was dissolved in chloroform. The solution was washed with water, dried (Na_2SO_4), and evaporated to give a thick syrup, 659 mg (93%), $[\alpha]_D^{23}$ −132° (*c* 1.3, $CHCl_3$); IR: 1650 cm^{-1}; PMR ($CDCl_3$) δ: 2.12 (3H s, Ac), 3.38 (3H s, NCH_3).

Found: C, 60.75; H, 7.32; N, 2.35%. Calcd for $C_{28}H_{41}NO_{10}$: C, 60.96; H, 7.49; N, 2.54%.

Benzyl 2′-N-Acetyl-3′-chloro-3′-deoxy-3,3a: 4′,6′-di-O-isopropylidene-α-dihydrostereptobiosaminide (7). To a cold solution (−5 °C) of **6** (487 mg) in dichloromethane (5.3 ml), pyridine (0.9 ml) and sulfuryl chloride (0.35 ml) were added and the solution was kept in the cold for 18 h and then at 5 °C for 25 h. The solution was poured into a mixture of chloroform (90 ml) and saturated sodium hydrogencarbonate solution (90 ml) with vigorous stirring and the organic layer separated was dried (Na_2SO_4). Concentration gave a reddish-brown syrup, which was chromatographed over silica gel (benzene–methyl ethyl ketone 9: 1) and the fractions containing **7** were concentrated to give a reddish syrup (334 mg). Recrystallization from ether gave colorless prisms, 284 mg (56%), mp 170—171.5 °C, $[\alpha]_D^{24}$ −129° (*c* 1, $CHCl_3$). PMR ($CDCl_3$) δ: 1.26 (3H d, J=6.5 Hz, CCH_3); 1.36, 1.38, 1.47, and 1.51 (each 3H s, $2C(CH_3)_2$); 2.13 (3H s, Ac), 3.06 (3H s, NCH_3), 3.80 (1H d, J≈1 Hz, H-2; collapsed to a singlet on irradiation at δ 4.98 (H-1)); 3.83, 3.93, 4.14, and 4.23 (2H, AB q, H-3a); 4.38, 4.50, 4.65, and 4.77 (2H AB q, OCH_2Ph); 4.90 (1H q, J=3.5 and 11.5 Hz, H-2′; collapsed to a doublet (J=3.5 Hz) on irradiation at δ 4.15 (H-3′)), 4.98 (1H s, H-1; on irradiation at δ 3.80 (H-2), the signal sharpened), 5.08 (1H d, J=3.5 Hz, H-1′), 7.30 (5H s, Ph).

Found: C, 58.87; H, 7.00; N, 2.33; Cl, 6.38%. Calcd for $C_{28}H_{40}NO_9Cl$: C, 58.99; H, 7.07; N, 2.46; Cl, 6.22%.

Benzyl 2′-N-Acetyl-3′-deoxy-3,3a: 4′,6′-di-O-isopropylidene-α-dihydrostreptobisaminide (8). To a solution of **7** (1.01 g) in dry toluene (21 ml), tributyltin hydride (1.0 ml) and α,α′-azobisisobutyronitrile (10 mg) were added under the atmosphere of nitrogen and the solution was heated at 80 °C for 2 h. Concentration of the solution gave a syrup, which was chromatographed over silica gel (benzene–methyl ethyl ketone 4: 1). The fraction containing **8** were concentrated to give a thick syrup, 935 mg (99%), $[\alpha]_D^{25}$ −100° (*c* 1, $CHCl_3$); PMR ($CDCl_3$) δ: 1.27 (3H d, J=6.5 Hz, CCH_3); 1.36, 1.38, 1.42, and 1.50 (each 3H s, $2C(CH_3)_2$; 1.80 (1H double t, J≈4, ≈4, and 11 Hz, H-3′$_{eq}$; on irradiation at δ 3.8, the sextet collapsed to a quartet (J≈4 and 11 Hz (J_{gem})), 2.09 (3H s, Ac), 3.01 (3H s, NCH_3).

Found: C, 62.47; H, 7.46; N, 2.46%. Calcd for $C_{28}H_{41}NO_9$: C, 62.79; H, 7.72; N, 2.62%.

Benzyl 2′-N-Acetyl-3′-deoxy-3,3a-O-isopropylidene-α-dihydrostreptobiosaminide (9). A solution of **8** (932 mg) in 25% acetic acid in methanol (34 ml) was refluxed for 50 min. Concentration of the solution gave a syrup, which was chromatographed over silica gel (benzene–ethanol 9: 1) to give a thick syrup of **9**, 821 mg (95%), $[\alpha]_D^{25}$ −161° (*c* 1, $CHCl_3$).

Found: C, 60.36; H, 7.31; N, 2.75%. Calcd for $C_{25}H_{37}NO_9$: C, 60.59; H, 7.53; N, 2.83%.

Benzyl 2′-N-Acetyl-3′-chloro-3′-deoxy-3,3a-O-isopropylidene-α-dihydrostreptobiosaminide (10). A solution of **7** (284 mg) in 25% acetic acid in methanol (10 ml) was refluxed for 3 h. Concentration of the solution *in vacuo* gave a syrup. It showed, on TLC (benzene–ethanol 9: 1), spots of R_f 0.15 (very slight), 0.3 (**10**), and 0.45 (very slight, **7**). The syrup was chromatographed over silica gel (benzene–ethanol 12: 1) to give a colorless thick syrup, 253 mg (96%), $[\alpha]_D^{24}$ −148° (*c* 1, $CHCl_3$).

Found: C, 56.36; H, 6.92; N, 2.34; Cl, 6.92%. Calcd for $C_{25}H_{36}NO_9Cl$: C, 56.65; H, 6.85; N, 2.64; Cl, 6.69%.

Benzyl 2′-N-Acetyl-4′,6′-di-O-acetyl-3′-chloro-3′-deoxy-3,3a-O-isopropylidene-α-dihydrostreptobiosaminide (11). To a solution of **10** (215 mg) in pyridine (6 ml), acetic anhydride (0.13 ml) was added and the solution was kept at room temperature overnight. Water (0.1 ml) was added and the solution was concentrated. The chloroform solution of the residual syrup was successively washed with aqueous sodium hydrogencarbonate solution, aqueous potassium hydrogensulfate solution, and water, dried (Na_2SO_4), and concentrated to give a syrup of **11**, 236 mg (94%), $[\alpha]_D^{25}$ −84° (*c* 2, $CHCl_3$); PMR ($CDCl_3$) δ: 1.36 (6H s, $C(CH_3)_2$), 2.03 (3H s, Ac), 2.11 (6H s, Ac), 3.00 (3H s, NCH_3).

Found: C, 56.46; H, 6.49; N, 2.16; Cl, 5.86%. Calcd for $C_{29}H_{40}NO_{11}Cl$: C, 56.72; H, 6.57; N, 2.28; Cl, 5.77%.

Benzyl 2′-N-Acetyl-4′,6′-di-O-acetyl-3′-deoxy-3,3a-O-isopropylidene-α-dihydrostreptobisaminide (12). *From 11*: To a solution of **11** (2.04 g) in dry toluene (39 ml), tributyltin hydride (1.9 ml) and α,α′-azobisisobutyronitrile (19 mg) were added and the solution was treated similarly as described for **8**. Column chromatography over silica gel (benzene–methyl ethyl ketone 6: 1) gave an amorphous solid of **12**, 1.81 g (94%), $[\alpha]_D^{25}$ −140° (*c* 1, $CHCl_3$); PMR ($CDCl_3$) δ: 1.29 (3H d, CCH_3), 1.40 (6H s, $C(CH_3)_2$), 2.09 (6H s, Ac), 2.11 (3H s, Ac), 3.00 (3H s, NCH_3).

Found: C, 60.27; H, 7.16; N, 2.38%. Calcd for $C_{29}H_{41}$-

NO_{11}: C, 60.09; H, 7.13; N, 2.42%.

From ***9***: Compound **9** was treated with acetic anhydride in pyridine to give **12** in a 98% yield.

*Benzyl 2'-*N*-Acetyl-4',6'-di-*O*-acetyl-3'-deoxy-α-dihydrostreptobiosaminide (**13**).* A solution of **12** (1.73 g) in 75% acetic acid (43 ml) was heated at 80 °C for 3 h. Concentration of the solution gave a syrup, which was chromatographed over silica gel (benzene–ethanol 9: 1) to give **12** (470 mg, 27%) and **13**. The latter was recrystallized from ether to give needles, 811 mg (51%), mp 157—159 °C, $[\alpha]_D^{25}$ −169° (*c* 1, $CHCl_3$); PMR ($CDCl_3$) δ: 2.00, 2.06, and 2.09 (each 3H s, Ac).

Found: C, 57.82; H, 6.87; N, 2.51%. Calcd for $C_{26}H_{37}NO_{11}$: C, 57.87; H, 6.91; N, 2.60%.

*Benzyl 2'-*N*-Acetyl-4',6'-di-*O*-acetyl-3,3a-*O*-carbonyl-3'-deoxy-α-dihydrostreptobiosaminide (**14**).* To a solution of **13** (251 mg) in pyridine (7.5 ml), *p*-nitrophenyl chloroformate (115 mg) was added and the mixture was stirred at room temperature. Triethylamine (0.16 ml × 3) and the chloride (230 mg × 3) were added alternately in every 5 h. After 35 h, chloroform (80 ml) was added and the solution was washed with aqueous sodium hydrogencarbonate solution and water throughly, dried (Na_2SO_4), and concentrated to give a yellow syrup. Column chromatography over silica gel (benzene–methyl ethyl ketone 3: 1) gave a thick syrup of **14**, 225 mg (85%), R_f 0.35 (TLC, benzene–ethanol 9: 1), $[\alpha]_D^{25}$ −144° (*c* 1, $CHCl_3$). IR: 1810 (carbonate), 1740 (ester), 1640 (amide) cm^{-1}. PMR ($CDCl_3$) δ: 1.34 (3H d, CCH_3); 2.02, 2.07, 2.12 (each 3H s, Ac), 2.94 (3H s, NCH_3), 4.96 (1H d, J=3 Hz, H-1 or 1'), 5.19 (1H d, J=3 Hz, H-1' or 1; on irradiation at δ 4.24, the doublet collapsed to a singlet).

Found: C, 57.47; H, 6.21; N, 2.29%. Calcd for $C_{27}H_{35}NO_{12}$: C, 57.34; H, 6.24; N, 2.48%.

*2'-*N*-Acetyl-4',6'-di-*O*-acetyl-3,3a-*O*-carbonyl-3'-deoxydihydrostreptobiosamine (**15**).* Compound **14** was hydrogenated with palladium black in a usual manner to give **14** as a syrup in a yield of 96%, $[\alpha]_D^{25}$ −141°→−127° (*c* 1, $CHCl_3$). IR: 1820, 1740, 1640 cm^{-1}. PMR ($CDCl_3$) δ: 1.30 and 1.40 (totally 3H d in the ratio of ≈3: 1, J=6 Hz, CCH_3), 2.06 (6H s, OAc), 2.13 (3H s, NAc (?)), 2.95 (3H s, NCH_3), 5.39 (≈1H d, J=4 Hz, H-1 (?)).

Found: C, 49.67; H, 6.27; N, 2.51%. Calcd for $C_{20}H_{29}NO_{12}\cdot 0.5H_2O$: C, 49.58; H, 6.24; N, 2.89%.

*Benzyl 2'-*N*-Acetyl-4',6'-di-*O*-acetyl-3'-chloro-3'-deoxy-α-dihydrostreptobiosaminide (**16**).* Prepared from **11** in a similarn manner as described for **13** to give a thick syrup of **16** in a 77% yield, $[\alpha]_D^{23}$ −144° (*c* 2, $CHCl_3$).

Found: C, 54.34; H, 6.14; N, 2.24; Cl, 6.32%. Calcd for $C_{26}H_{36}NO_{11}Cl$: C, 54.40; H, 6.32; N, 2.44; Cl, 6.18%.

*Benzyl 2'-*N*-Acetyl-4',6'-di-*O*-acetyl-3,3a-*O*-carbonyl-3'-chloro-3'-deoxy-α-dihydrostreptobiosaminide (**17**).* Prepared from **16** in a similar manner as described for **14** to give a thick syrup of **17** in a 87% yield, $[\alpha]_D^{24}$ −126° (*c* 1, $CHCl_3$).

Found: C, 54.21; H, 5.72; N, 2.16; Cl, 6.00%. Calcd for $C_{27}H_{34}NO_{12}Cl$: C, 54.05; H, 5.71; N, 2.33; Cl, 5.91%.

*Hydrogenolysis of **17** with Raney Nickel to **18**.* A solution of **17** (28 mg) in aqueous dioxane (1: 10, 1 ml) was hydrogenated under pressure (50 lb/in²) with Raney nickel at room temperature for 26 h. Filtration followed by concentration of the filtrate gave colorless needles, which was filtered with aid of benzene to give **18**, 17 mg (66%), mp 188—190 °C, $[\alpha]_D^{25}$ −78° (final value, *c* 0.5, $CHCl_3$); IR: 1810, 1770 (sh), 1740, 1620 cm^{-1}. PMR ($CDCl_3$+CD_3OD) δ: 1.52 (3H d, J=7 Hz, $CHCH_3$); 2.09, 2.10, and 2.13 (each 3H s, Ac); 2.98 (3H s, NCH_3), 5.01 (1H d, J=3.5 Hz, H-1'; it collapsed to a singlet on irradiation at δ 4.61), 5.16 (1H q, J=7 Hz, $CHCH_3$; it collapsed to a singlet on irradiation at δ 1.52).

Found: C, 49.52; H, 6.52; N, 2.89%. Calcd for $C_{20}H_{29}NO_{12}\cdot 0.5H_2O$: C, 49.58; H, 6.24; N, 2.89%.

References

1) H. Umezawa, S. Takasawa, M. Okanishi, and R. Utahara, *J. Antibiot.*, **21**, 81 (1968); S. Takasawa, R. Utahara, M. Okanishi, K. Maeda, and H. Umezawa, *ibid.*, **21**, 477 (1968).

2) H. Kawabe, F. Kobayashi, M. Yamagichi, R. Utahara, and S. Mitsuhashi, *J. Antibiot.*, **24**, 651 (1971).

3) S. Umezawa, Y. Takahashi, and T. Tsuchiya, *Bull. Chem. Soc. Jpn.*, **48**, 560 (1975).

4) H. Sano, T. Tsuchiya, S. Kobayashi, M. Hamada, S. Umezawa, and H. Umezawa, *J. Antibiot.*, **29**, 978 (1976).

5) Y. Takagi, T. Miyake, T. Tsuchiya, S. Umezawa, and H. Umezawa, *J. Antibiot.*, **26**, 403 (1973).

6) Unpublished results.

7) G. J. M. Van Der Kerk, J. G. Noltes, and J. G. A. Luijten, *J. Appl. Chem.*, **7**, 366 (1957); H. Arita and Y. Matsushima, *J. Biochem.*, **70**, 795 (1971); H. Arita, N. Ueda, and Y. Matsushima, *Bull. Chem. Soc. Jpn.*, **45**, 567, 3614 (1972).

8) S. Umezawa, T. Tsuchiya, T. Yamasaki, H. Sano, and Y. Takahashi, *J. Am. Chem. Soc.*, **96**, 920 (1974); S. Umezawa, T. Yamasaki, Y. Kubota, and T. Tsuchiya, *Bull. Chem. Soc. Jpn.*, **48**, 563 (1975).

9) S. Umezawa, H. Sano, and T. Tsuchiya, *Bull. Chem. Soc. Jpn.*, **48**, 556 (1975).

10) G. K. J. Ferguson, I. J. McGilveray, and J. B. Stenlake, *J. Pharm. Pharmacol.*, **17**, Suppl., 68S (1965).

A Semi-empirical Calculation of the Substituent Effects on the ^1H Chemical Shifts of 1-Substituted Naphthalenes[1,2]

Jun NIWA

College of General Education, Nagoya University, Chikusa, Nagoya 464

(Received October 13, 1976)

A semi-empirical equation for predicting the ^1H chemical shift induced by substituents in an aromatic system (J. Niwa, *Bull. Chem. Soc. Jpn.*, **48**, 118, 1637 (1975)) has been applied to the ring protons of 1-substituted naphthalenes. The predictions of the equation are tested against the available experimental data for six representative substituents and are also compared with those of the electric-field model.

The ^1H chemical shifts of a number of 1-substituted naphthalenes have been examined by Emsley, Lindon, Salman, and Clark[3] in the light of some simple theories of the origins of substituent-induced chemical shifts (SCS). They have separately assessed the following models as the main factors governing the SCS values: (i) the local diamagnetic term of the relevant hydrogen atom; (ii) the magnetic anisotropy of the substituent group, calculated by using the expression developed by Pople for the paramagnetic part of the magnetic anisotropic tensor;[4] (iii) the empirically established correlation between the SCS values and changes in the π or total electron density on the attached carbon atom;[5] (iv) the modified equation of the correlation between the SCS values and changes in the π electron density, where the π electron densities on the attached and the next neighbor carbon atoms are considered,[6] and (v) the electric-field model derived by Buckingham.[7] It has been indicated by them that, although no one simple model can predict the SCS values of all the protons of 1-substituted naphthalenes, it is possible to predict some of the larger effects and to relate them to the structure, and that the electric-field model gives the best overall agreement with the observed SCS values.

In our preceding papers,[1,2] we derived a semi-empirical equation (Eq. 2) for obtaining the SCS values of protons in substituted aromatic side-chains[1] and monosubstituted benzenes[2] by considering the ring-current effect ($\sigma^{A,ring}$) in addition to the diamagnetic term of the hydrogen atom, A (σ^{AA}_{dia}), in the C–H bond in question and that from its bonded carbon atom, B (σ^{AB}_{dia}):

$$\delta_{calcd}(\equiv\Delta\sigma^A) = \Delta\sigma^{AA}_{dia} + \Delta\sigma^{AB}_{dia} + \Delta\sigma^{A,ring} \quad (1)$$

$$= a\Delta q^A + b\Delta q^B - 0.4f(\rho, z)|\sigma_\pi| \quad (2)$$

where the Δq's are the increments in electron densities on specified atoms, where a and b are, respectively, the constants particular to the hydrogen atom and the C–H bond, and where the third term is the modified Johnson and Bovey ring-current shift.[8] We showed that Eq. 2 could reasonably reproduce the observed SCS values of protons in the aromatic side-chains and the benzenes.

The aim of the present paper is to demonstrate the validity of the predictions by Eq. 2 for a variety of substituents in the series of 1-substituted naphthalenes, to examine the range of applicability of this approach, and to determine its limitations. The advantage of the naphthalenes in examining the success of Eq. 2 is that they have seven protons situated in different magnetic environments. Second, we will discuss which approach, Eq. 2 or the electric-field model, is more appropriate for understanding and predicting the SCS values in 1-substituted naphthalenes.

Results and Discussion

The local diamagnetic term, σ^{AA}_{dia}, of the hydrogen atom of naphthalene has been calculated by using the expression given by Kajimoto and Fueno.[9] The calculated values of σ^{AA}_{dia}, relative to the unsubstituted compound, are linearly correlated with the increments in electron densities on the hydrogen atoms:

$$\Delta\sigma^{AA}_{dia} = 16.1\Delta q^A. \quad (3)$$

The diamagnetic contribution from the bonded carbon (σ^{AB}_{dia}) in the case of naphthalene can be calculated in the same way as in the cases of olefinic compounds[1] and benzenes,[2] because the C–H bond length is taken to be 1.08 Å and the ring proton also bonds to the sp^2-hybridized carbon atom. Thus, the σ^{AB}_{dia} term, relative to the unsubstituted compound, becomes:

$$\Delta\sigma^{AB}_{dia} = 8.70\Delta q^B. \quad (4)$$

The paramagnetic term, σ^{AB}_{para}, of the B atom has been calculated according to Pople's expression.[4] It remains almost constant for the series of 1-substituted naphthalenes so long as we assume the same average excitation energy and the same value of the integral $\langle r_{AB}^{-3}\rangle$. Accordingly, we can ignore the contribution of the paramagnetic term to the SCS.

In order to estimate the contribution of the ring-current effect ($\sigma^{A,ring}$) to the ring proton of naphthalenes, we have used the ring-current model presented by Pople,[10] as Fig. 1 illustrates. The contribution of the "quinonoid" structure due to the introduction of a substituent into the A ring causes the decrease in the

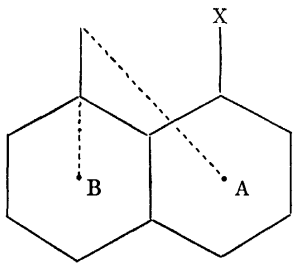

Fig. 1. The ring-current model for 1-substituted naphthalenes.

ring-current on the A ring. This contribution can be expressed by Eq. 5, which was derived for the ^1H chemical shifts in aromatic side-chains:[1,11]

$$\Delta\sigma^{A\text{-}ring} = -0.4f(\rho, z)|\sigma_\pi| \quad (5)$$

where $f(\rho, z)$ is the Johnson and Bovey ring-current shift in ppm, which is expressed as a function of the geometric factors for the proton located at the cylindrical co-ordinates, ρ and z, and where σ_π is the Yukawa-Tsuno parameter for measuring the resonance ability of the substituent. The "quinonoid" structure of the A ring may secondarily induce the localization of the π-electron system of the B ring. We may assume that the change in the ring-current induced on the B ring can be ignored, because the secondary effect may be considered to be very small compared with the contribution of the "quinonoid" structure of the A ring to the SCS value. Then, the ring-current effect due to the B ring cancels out the other in the calculation of the relative contribution of the ring-current effects in 1-substituted naphthalenes. Therefore, Eq. 5 can be applied, just as it is, to all the protons of the naphthalenes.

By combining Eqs. 3, 4 and 5, we obtain the following equation for the SCS of 1-substituted naphthalenes:

$$\delta_{calcd} = 16.1\Delta q^A + 8.70\Delta q^B - 0.4f(\rho, z)|\sigma_\pi|. \quad (6)$$

The value of $f(\rho, z)$ for each proton of the naphthalenes has been graphically estimated by utilizing the table of the Johnson and Bovey ring-current shift.[8] The values of $f(\rho, z)$ obtained are -1.50 ppm for the 2-, 3- and 4-protons, -0.60 ppm for the 5- and 8-protons, and -0.23 ppm for the 6- and 7-protons.

The geometry of naphthalene used in the calculation and that of the substituent group are taken from the standard compilations.[12] The molecules of 1-nitronaphthalene, 1-naphthylamine, 1-naphthol, and 1-naphthaldehyde are assumed to be planar. The stable conformation of 1-naphthaldehyde may be I or II, or some equilibrium between the two. The calculation of the chemical shifts has been performed for both the I and II forms.

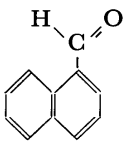

I

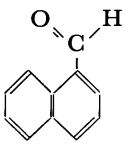

II

The 1-naphthol molecule may exist as an equilibrium between the two conformers, III and IV. These two conformers, however, give virtually identical predicted chemical shifts.

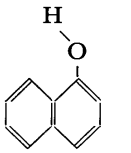

III

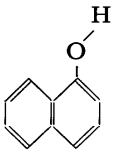

IV

In evaluating the first and second terms of Eq. 1, we have used the CNDO/2 formalism. In Table 1, the SCS values calculated by Eq. 6 are compared with the observed values. In Fig. 2, plots of the observed SCS

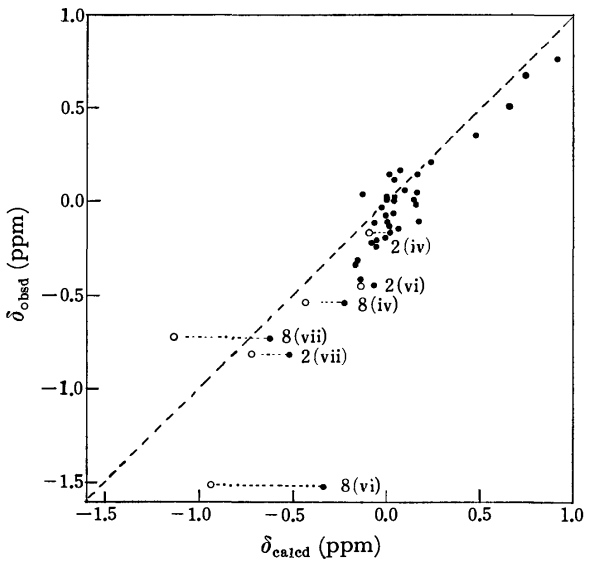

Fig. 2. Plots of δ_{obsd} against δ_{calcd} for ring protons of 1-substituted naphthalenes.
Numbered points correspond to entries in Table 1. Open circles are plotted against the chemical shifts corrected for the anisotropy effects of the substituent groups.

values are shown against the calculated shifts. As may clearly be seen from Fig. 2, the calculated chemical shifts can reasonably reproduce the overall aspect of the SCS. However, Fig. 2 shows that Eq. 6 can not sufficiently reproduce such major features of the SCS as the large negative values for the 8-proton of 1-naphthaldehyde. In deriving Eq. 6, the long-range shielding effect of the substituent group has not been taken into consideration. Therefore, the magnetic anisotropy effect should also be considered for the 2- and 8-protons in the neighborhood of a substituent group which has a large magnetic anisotropy, as in the cases of 1-chloronaphthalene, 1-naphthaldehyde, and 1-nitronaphthalene.*

Unfortunately, no theoretical and empirical estimations of the magnetic anisotropy effects of these substituent groups are yet completely settled. The point magnetic dipole approximation[13] is quantitatively not always reliable for the proton in the nearest neighborhood of the substituent group. Nevertheless, it may provide a qualitative basis for the discussion of the long-range shielding.

In the cases of 1-chloronaphthalene and 1-naphthaldehyde, we have attempted to estimate the magnetic

* On the whole, Eq. 6 correctly reproduces the SCS value of the 4-proton for the electron-donating substituent better than that for the electron-withdrawing substituent. A similar trend has also been obtained in the case of benzene.[2] The insufficiency of Eq. 6 for the 3-proton may be mainly attributed to ignoring the magnetic contributions from carbon atoms neighboring the B atom, but that for the electron-withdrawing substituent may not be attributed to ignoring the magnetic anisotropy of the substituent group, because the anisotropy effect on the 3- and 4-protons is too small to correct the calculated SCS to the observed SCS. Accordingly, this shortcoming of Eq. 6 may show an inherent limitation of the present calculation.

TABLE 1. CALCULATED AND OBSERVED CHEMIAL SHIFTS OF RING PROTONS IN 1-SUBSTITUTED NAPHTHALENES[a]

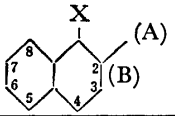

Proton	q^{A} [b]	q^{B} [b]	$\Delta\sigma^{AA}_{dia}$	$\Delta\sigma^{AB}_{dia}$	$\Delta\sigma^{A,\,ring}$	δ_{calcd}	δ_{obsd} [c]	$\Delta\sigma_{E}$ [c]
			(i) 1-Naphthylamine					
2	1.0074	4.0730	−0.054	0.715	0.252	0.91	0.766	0.45
3	1.0143	3.9634	0.056	−0.238	0.252	0.07	0.167	0.01
4	1.0080	4.0486	0.038	0.362	0.252	0.65	0.507	0.28
5	1.0050	4.0144	−0.010	0.064	0.101	0.16	0.052	0.11
6	1.0118	3.9839	0.016	−0.060	0.039	0.00	0.018	0.03
7	1.0117	4.0005	0.014	0.084	0.039	0.14	0.009	0.04
8	1.0114	3.9952	0.093	−0.103	0.101	0.09	0.060	−0.14
			(ii) 1-Naphthol					
2	1.0013	4.0705	−0.152	−0.693	0.204	0.74	0.676	0.40
3	1.0117	3.9672	0.014	−0.205	0.204	0.01	0.146	−0.01
4	1.0053	4.0378	−0.005	0.268	0.204	0.47	0.357	0.23
5	1.0042	4.0136	−0.022	0.057	0.031	0.07	−0.012	0.06
6	1.0108	3.9832	0.000	−0.066	0.031	−0.03	−0.031	0.04
7	1.0100	3.9994	−0.013	0.075	0.082	0.14	−0.064	0.00
8	0.9996	3.9924	−0.096	−0.127	0.082	−0.14	−0.410	−0.33
			(iii) 1-Methylnaphthalene					
2	1.0117	4.0098	0.014	0.165	0.047	0.23	0.211	0.13
3	1.0120	3.9864	0.019	−0.038	0.047	0.03	0.124	0.02
4	1.0065	4.0164	0.014	0.082	0.047	0.14	0.155	0.11
5	1.0058	4.0084	0.003	0.012	0.019	0.03	0.021	0.03
6	1.0111	3.9893	0.005	−0.013	0.007	0.00	0.028	0.00
7	1.0112	3.9923	0.006	0.013	0.007	0.03	0.006	0.02
8	1.0044	4.0074	−0.019	0.003	0.019	0.00	−0.110	0.00
			(iv) 1-Chloronaphthalene					
2	0.9927	4.0201	−0.290	0.255	0.042	0.01	−0.174	—
3	1.0057	3.9801	−0.082	−0.093	0.042	−0.13	0.035	—
4	1.0015	4.0155	−0.066	0.074	0.042	0.05	0.016	—
5	1.0029	4.0085	−0.043	0.130	0.017	−0.01	−0.071	—
6	1.0086	3.9856	−0.035	−0.045	0.006	−0.07	−0.115	—
7	1.0075	3.9917	−0.053	0.008	0.006	−0.05	−0.168	—
8	0.9947	3.9991	−0.174	−0.069	0.017	−0.23	−0.544	—
			(v) 1-Naphthaldehyde (I)					
2	0.9996	3.9654	−0.179	−0.221	0.138	−0.26	−0.443	−0.63
3	1.0060	4.0007	−0.077	0.009	0.138	0.15	−0.102	0.15
4	1.0023	3.9911	−0.053	−0.138	0.138	−0.05	−0.218	−0.27
5	1.0040	4.0032	−0.026	−0.033	0.055	0.00	−0.060	0.08
6	1.0082	3.9916	−0.042	0.007	0.021	−0.01	−0.147	0.16
7	1.0081	3.9844	−0.043	−0.056	0.021	−0.08	−0.237	0.17
8	0.9988	4.0151	−0.109	0.071	0.055	0.02	−1.525	−0.006
			(vi) 1-Naphtaldehyde (II)					
2	1.0085	3.9696	−0.037	−0.184	0.138	−0.08	−0.443	−1.72
3	1.0070	4.0018	−0.061	0.096	0.138	0.17	−0.102	−0.24
4	1.0025	3.9895	−0.050	−0.152	0.138	−0.06	−0.218	−0.52
5	1.0054	4.0047	−0.003	−0.020	0.055	0.03	−0.060	−0.14
6	1.0097	3.9910	−0.018	0.002	0.021	0.01	−0.147	0.15
7	1.0093	3.9847	−0.024	−0.053	0.021	−0.06	−0.237	0.21
8	0.9717	4.0241	−0.542	0.148	0.055	−0.34	−1.525	−0.65
			(vii) 1-Nitronaphthalene					
2	0.9790	3.9965	−0.509	−0.211	0.204	−0.52	−0.807	−0.62
3	0.9973	3.9988	−0.216	0.070	0.204	0.06	−0.146	−0.05
4	0.9955	3.9830	−0.162	−0.209	0.204	−0.17	−0.335	−0.20
5	1.0090	4.0035	−0.075	−0.030	0.082	−0.02	−0.195	−0.06
6	1.0055	3.9874	−0.085	−0.030	0.031	−0.08	−0.218	−0.14
7	1.0041	3.9806	−0.107	−0.089	0.031	−0.16	−0.322	−0.14
8	0.9502	4.0274	−0.886	0.177	0.082	−0.63	−0.725	−0.58

a) All the values are relative to the unsubstituted compound. b) All the electron densities are calculated by the CNDO/2 method. The electron densies of naphthalene are: q^{A} (the 1-proton)=1.0056, q^{A} (the 2-proton)=1.0108; q^{B} (the 1-carbon)=4.0070, q^{B} (the 2-carbon)=3.9908 c) Cited from Ref. 3. The chemical shifts were measured in 5 mol% in CCl_4.

TABLE 2. THE MAGNETIC ANISOTROPY EFFECTS OF FORMYL, NITRO, AND CHLORO GROUPS ON THE 2- AND 8-PROTONS

Substituent	χ_x ($\times 10^{-30}$ cm^3 esu)	χ_y	χ_z	2-proton (ppm)	8-proton (ppm)
CHO(form I)[14]	28.8	34.6	18.0	−0.45	−0.08
CHO(form II)[14]	28.8	34.6	18.0	−0.04	−0.59
NO_2[16]	−18	−3.3	−23	−0.16	−0.54
		$\Delta\chi$			
Cl[12]		−7.5		−0.09	−0.16

a) x is in the direction of the C=O bond for the formyl group and in that of the C–N bond for the nitro group, and y and z are in- and out-of-plane respectively.

anisotropy effect on the 2- and 8-protons by using the values of the magnetic susceptibilities given by McConnell for the chlorine atom[12] and those given by Pople for the carbonyl group.[14] The respective values of the anisotropy effects obtained on the 2- and 8-protons are listed in Table 2. When these anisotropy effects are taken into account, the predicted SCS values in 1-naphthaldehyde become, respectively, −0.8 and −0.1 ppm for the 2- and 8-protons of Form I, while those of Form II become, respectively, −0.1 and −0.9 ppm. This result predicts that Form I may cause the considerable low-field shift in the 2-proton, whereas Form II causes that in the 8-proton. The present approach favors Form II over Form I for the aldehyde on the basis of the predicted SCS values for the 2- and 8-protons. Recently Hatano has indicated, on the basis of NMR measurements with the paramagnetic reagent technique, that Form II may be the stable conformer.[15] The present result corresponds with his indication.

With respect to the magnetic anisotropy of the nitro group, no theoretical estimation has been presented. Therefore, we have attempted to estimate the anisotropy effect by utilizing the values of the magnetic susceptibilities empirically obtained by Yamaguchi, who investigated the magnetic anisotropy effect of the nitro group on ortho methyl groups in nitrobenzene derivatives.[16] The values obtained for the 2- and 8-protons are shown in Table 2.

Emsley *et al.* have indicated that, among the simple models which they have assessed, the electric-field model (Eq. 7) gives the best overall agreement with the observed SCS values.[3] The electric-field model given by Buckingham[7] is:

$$\sigma_E = -AE_z, \tag{7}$$

where A is calculated to be about 2×10^{-12} esu. E_z arises from point charges located on atoms; then E_z is given classically by Eq. 8, where q_B is the atomic charge:

$$E_z = \sum_{A\neq B} q_B \cos\theta_{AB}/r_{AB}^2. \tag{8}$$

The θ_{AB} angle is that between the C–H and r_{AB}. In deriving Eq. 7, the rough approximation is originally used. Moreover, Emsley *et al.* introduced some assumption in applying Eq. 8 to the naphthalenes; they rather arbitrarily restricted the summation in Eq. 8 to charges which neighbor the proton, because of the difficulty of knowing how electric fields are transmitted within

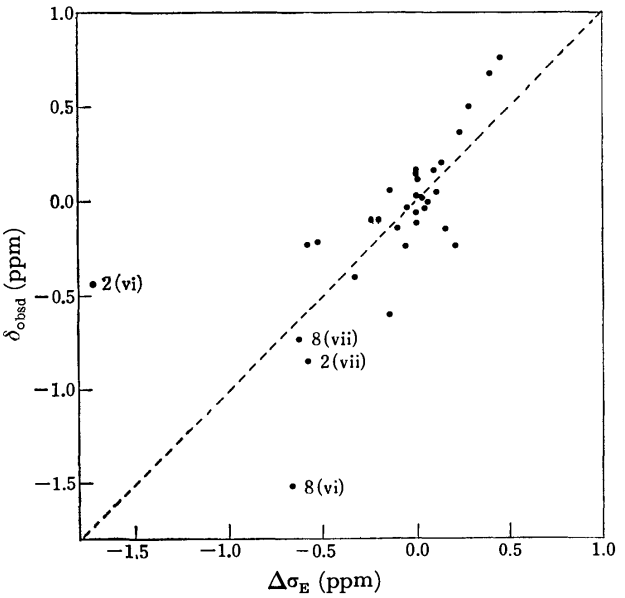

Fig. 3. Plots of δ_{obsd} against $\Delta\sigma_E$ calculated by Emsley *et al.*[3]
Numbered points correspond to entries in Table 1.

molecules.[3] The SCS values, $\Delta\sigma_E$, calculated by them are cited in Table 1. The correlation between the observed and the calculated SCS values is shown in Fig. 3. A comparison of Fig. 2 with Fig. 3 clearly shows that Eq. 6 can more correctly reproduce the observed SCS values than the electric-field model, even though Eq. 6 can not sufficiently reproduce the chemical shift of the 8-proton of 1-naphthaldehyde.

When the anisotropy effects are taken into consideration for the substituent groups, Cl, CHO, and NO_2, the shortcoming of Eq. 6 for the 2-protons of 1-chloronaphthalene, 1-naphthaldehyde, and 1-nitronaphthalene seems to be reasonably improved. However, the corrected chemical shift of the 8-proton of 1-nitronaphthalene seems to be overestimated, while that of 1-naphthaldehyde can not still sufficiently reproduce the observed SCS value. The improvement of Eq. 6 for the 8-protons of the two compounds remains a subject of future research, along with the exact estimation of the magnetic anisotropy effects of the substituent groups.

The CNDO/2 calculations were carried out on a FACOM-230 60 computer at the Nagoya University Computation Center.

References

1) J. Niwa, *Bull. Chem. Soc. Jpn.*, **48**, 118 (1975).
2) J. Niwa, *Bull. Chem. Soc. Jpn.*, **48**, 1637 (1975).
3) J. W. Emsley, J. C. Lindon, S. R. Salman, and D. T. Clark, *J. Chem. Soc., Perkin Trans. 2*, **1973**, 611.
4) J. A. Pople, *J. Chem. Phys.*, **37**, 53 (1962).
5) T. B. Cobb and J. D. Memory, *J. Chem. Phys.*, **50**, 4262 (1969); G. Frankel, R. E. Carter, A. McLachlan, and J. H. Richards, *J. Am. Chem. Soc.*, **82**, 5846 (1960); P. L. Corio and B. P. Dailey, *ibid.*, **78**, 3043 (1956).
6) J. C. Shug and J. C. Deck, *J. Chem. Phys.*, **37**, 2618 (1962).
7) A. D. Buckingham, *Can. J. Chem.*, **38**, 300 (1960).

8) J. S. Waugh and R. W. Fessenden, *J. Am. Chem. Soc.*, **79**, 846 (1957); G. E. Johnson and F. A. Bovey, *J. Chem. Phys.*, **29**, 1012 (1958); J. W. Emsley, J. Feeney, and L. H. Sutcliffe, "High Resolution Nuclear Magnetic Resonance Spectroscopy," Vol. 1, Pergamon Press, Oxford (1965), p. 595.
9) O. Kajimoto and T. Fueno, *Chem. Lett.*, **1972**, 103.
10) J. A. Pople, W. G. Schneider, and H. J. Bernstein, "High-resolution Nuclear Magnetic Resonance," McGraw-Hill, New York (1959), p. 251.
11) H. Yamada, Y. Tsuno, and Y. Yukawa, *Bull. Chem. Soc. Jpn.*, **43**, 1459 (1970).
12) "Tables of Interatomic Distance and Configuration in Molecules and Ions," Chem. Soc., London, Spec. Publ., No. 11 (1958).
13) a) P. T. Narasimhan and M. T. Rogers, *J. Phys. Chem.*, **63**, 1388 (1959); b) H. M. McConnell, *J. Chem. Phys.*, **27**, 226 (1957).
14) J. A. Pople, *J. Chem. Phys.*, **37**, 60 (1962).
15) A. Hatano, *Nippon Kagaku Kaishi*, **1975**, 1917.
16) I. Yamaguchi, *Mol. Phys.*, **6**, 105 (1963).

Reaction of Carbon Dioxide with Tetraphenylporphinatoaluminium Ethyl in Visible Light

Shohei INOUE and Norikazu TAKEDA

Department of Synthetic Chemistry, Faculty of Engineering, The University of Tokyo, Hongo, Bunkyo-ku, Tokyo 113

(Received October 12, 1976)

Tetraphenylporphinatoaluminium ethyl reacts with carbon dioxide in the presence of 1-methylimidazole to produce tetraphenylporphinatoaluminium propionate in the presence of visible light but not in the dark.

In the photosynthesis of green plants, carbon dioxide is fixed and reduced by species activated by the energy of light in visible region of the spectrum which is absorbed by and transferred from chlorophylls——a dihydroporphyrin system. In this connection, the reaction of carbon dioxide with species activated by visible light is very interesting.

In the course of the present study on the reaction of carbon dioxide with organometallic compounds and related systems,[1-3] it was found that the reaction of $\alpha,\beta,\gamma,\delta$-tetraphenylporphinatoaluminium ethyl with carbon dioxide was induced by visible light in the presence of 1-methylimidazole.

Experimental

Materials. $\alpha,\beta,\gamma,\delta$-Tetraphenylporphine ($TPPH_2$) was synthesized from pyrrole and benzaldehyde in propionic acid.[4] Contaminated $\alpha,\beta,\gamma,\delta$-tetraphenylchlorin was transformed into $TPPH_2$ using 2,3-dichloro-5,6-dicyanobenzoquinone in boiling methylene chloride.[5]

1-Methylimidazole was prepared by the alkylation of imidazole with methyl iodide in liquid ammonia.[6]

Carbon dioxide was purified upon passage through a series of columns packed with cupric sulfate, potassium bicarbonate, reduced copper, phosphorous pentoxide and activated cupric oxide.

Methylene chloride was washed with sulfuric acid followed by water, dried over calcium chloride and then calcium hydride, and distilled over calcium hydride in a nitrogen atmosphere. Benzene was washed with sulfuric acid and then with water, dried over calcium chloride, and distilled in the presence of sodium wire in a nitrogen atmosphere.

Triethylaluminium was purified by distillation under reduced pressure (111 °C/24 Torr).

Procedure. Formation of Tetraphenylporphinatoaluminium Ethyl (TPPAlEt) by the Reaction of Tetraphenylporphine ($TPPH_2$) with Triethylaluminium: The reaction of $TPPH_2$ and triethylaluminium was carried out in a quartz cell having four flat faces (2.5×2.5×4.0 cm) fitted with a three-way cock. The cell containing $TPPH_2$ (0.92 g, 1.5 mmol) was purged with nitrogen and a solvent (20 ml) was added to dissolve the $TPPH_2$. Triethylaluminium (0.21 ml, 1.5 mmol) was added slowly to the solution using a syringe from the three-way cock in a nitrogen stream at room temperature. The reaction of $TPPH_2$ with triethylaluminium was completed within a few minutes under the evolution of two equivalent amounts of ethane (Fig. 1) which was identified by gas chromatography and measured volumetrically by a mercury-sealed gas burette. By adding an excess of hydrochloric acid to this reaction mixture, a stoichiometric amount of ethane to aluminium was evolved, indicating the existence of one ethyl-aluminium bond.

In the ^1H NMR spectra of the reaction mixture, the ratio of phenyl protons (δ=8.22 ppm (ortho) and δ=7.85 ppm (meta and para)) to β-protons on the pyrrole ring (δ=9.05 ppm) of the porphine was found to be 5:2, excluding the possibility of the reaction of triethylaluminium with the C–H protons of the porphine ring. Methylene (-aluminium) and methyl signals are found at δ=−6.35 ppm (quartet) and δ=−3.40 ppm (triplet), respectively, which occur for a much higher magnetic field compared with the methylene (δ=0.46 ppm) and methyl (δ=1.26 ppm) signals of triethylaluminium. This fact clearly indicates that the ethyl group is attached to the aluminium atom as an axial ligand and is affected by the ring current of the porphine ring.

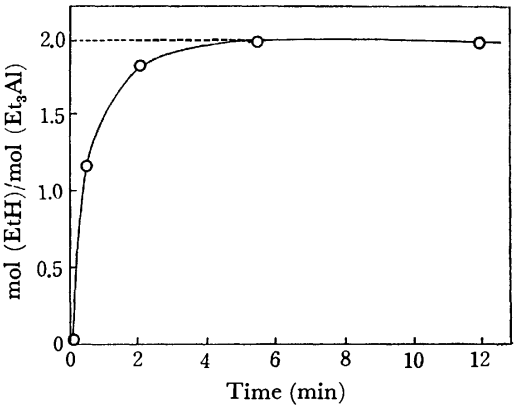

Fig. 1. Reaction of tetraphenylporphine($TPPH_2$) and triethylaluminium(Et_3Al), $TPPH_2$; 1.8 mmol, Et_3Al; 1.8 mmol, CH_2Cl_2; 30 ml, temp; 30 °C.

From these results, $TPPH_2$ and triethylaluminium are considered to react to form tetraphenylporphinatoaluminium ethyl (TPPAlEt):

$$TPPH_2 + Et_3Al \longrightarrow TPPAlEt + 2EtH$$

A similar reaction for triethylaluminium with octaethylporphyrin has been reported,[7] though a detailed examination of the reaction was not presented.

Reaction of Carbon Dioxide with TPPAlEt: Reactions of tetraphenylporphinatoaluminium ethyl (TPPAlEt) with carbon dioxide were carried out in the quartz cell which was placed in a glass water bath at 25 °C. Several hours after the formation of TPPAlEt, 1-methylimidazole (0.13 ml, 1.5 mmol) was added, followed by carbon dioxide bubbling for 5 min, and the mixture was irradiated for a given period of time by visible light (450—750 nm) obtained from a 500-W xenon lamp placed at a distance of 10 cm outside the water bath. Light of higher and lower wavelength was eliminated using appropriate filters.

Separation of the Reaction Product: In order to obtain the reaction product in an amount sufficient to conduct further examinations, carbon dioxide was bubbled for 10 min at room temperature in a 300 ml two-necked Pyrex flask which

contained $TPPH_2$ (6.14 g, 10 mmol), Et_3Al (1.37 ml, 10 mmol) and 1-methylimidazole (1.00 ml, 10 mmol). After an appropriate period of time, hydrogen chloride gas was bubbled through the above reaction mixture, and the solvent and excess hydrogen chloride were removed under reduced pressure at room temperature giving a solid residue, which was further treated in accordance with the following two procedures: 1) 1-Butanol (5 ml), concd sulfuric acid (1 ml) and sodium sulfate (5 g) were added to the residue, and the mixture was heated at 130 °C for 20 min. The reaction mixture was concentrated and extracted with hexane, then fractionated into several parts employing column chromatography on silica gel using hexane as the eluent. Some fractions which were found to contain butyl propionate by gas chromatography were collected and purified by passage through a column of silica gel using a mixture of hexane and methylene chloride as the eluent, then through another silica gel column using methylene chloride as the eluent. After removing the solvent from the fractions, a liquid was obtained, and its IR spectrum agreed with that of authentic butyl propionate.
2) An ether solution of diazomethane (in great excess with respect to TPPAlEt) was added to the residue at room temperature, and after one day the reaction mixture was concentrated to remove the solvent by evaporation and subjected to gas chromatography.

Measurement. Infrared spectra were measured in a fixed cell (0.1 mm) using a Hitachi EPI-G3 spectrophotometer. Ultraviolet and visible spectra were obtained with the sample in a quartz cell (of length 0.1 cm) using a Shimadzu RSP-7B spectrophotometer. ^1H NMR spectra were measured using a JEOL 4H-A type spectrometer. Gas chromatographic analysis was carried out using a Yanagimoto Model G80 gas chromatograph with the column (of 1—1.5 m) packed with dioctyl phthalate, silica gel, polyethylene glycol, and with hydrogen as the carrier gas.

Results

Reaction of Tetraphenylporphinatoaluminium Ethyl with Carbon Dioxide. When carbon dioxide was bubbled in a solution of TPPAlEt in methylene chloride in the presence of from one to three equivalent amounts of 1-methylimidazole and irradiated by visible light, a new carbonyl absorption band appeared at 1642 cm^{-1} in the infrared spectrum (Figs. 2 and 3). The figures show that the absorption increased with time fairly rapidly but substantially ceased after about 40 h. On the other hand, absorption due to carbon dioxide at 2340 cm^{-1} decreased as the band at 1642 cm^{-1} increased. In the dark, however, absorption at this frequency was very slight even after 48 h. The temperature in the irradiated case was the same as that for the measurements in the dark. The same effect was also observed when benzene was used as the solvent.

In the absence of 1-methylimidazole, no absorption at 1642 cm^{-1} was present even when the system was irradiated by visible light. Thus, TPPAlEt reacts with carbon dioxide only when irradiated by visible light in the presence of 1-methylimidazole.

Reaction Products. In the reaction of carbon dioxide and TPPAlEt in methylene chloride for 20 h, treatment of the reaction mixture with hydrogen chloride gas followed by 1-butanol gave butyl propionate in a 4% yield based on the amount of porphinatoaluminium ethyl.

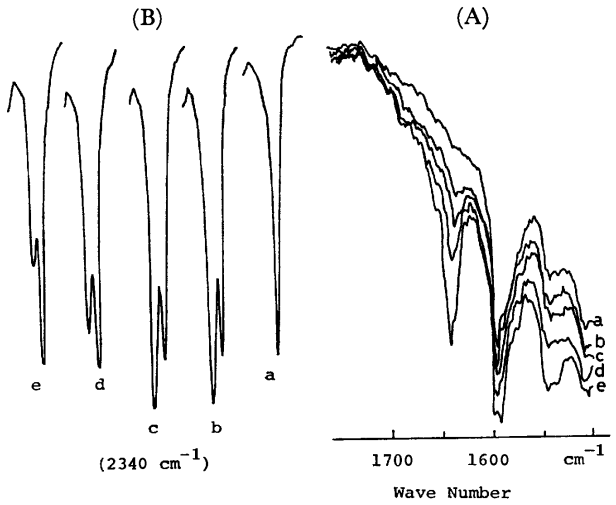

Fig. 2. Infrared spectra of the reaction mixture of tetraphenylporphinatoaluminium ethyl(TPPAlEt) with carbon dioxide(CO_2, bubbling for 5 min) in the presence of 1-methylimidazole.
TPPAlEt; 3mmol, 1-methylimidazole; 3mmol, CH_2Cl_2; 50ml, temp; 25 °C; (A) a; before bubbling of CO_2, b; 20 min, c; 40 min, d, 60 min, e; 14 h; (B) Absorption due to CO_2.

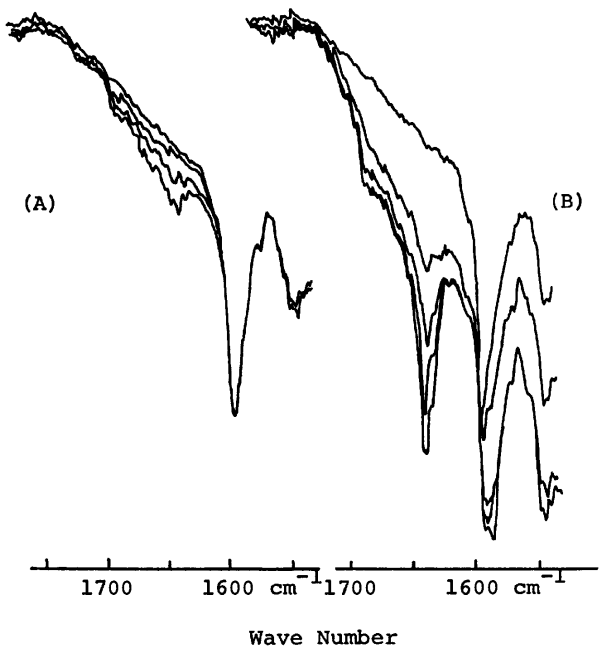

Fig. 3. Infrared spectra of the reaction mixture of tetraphenylporphinatoaluminium ethyl(TPPAlEt) with carbon dioxide(CO_2) in dark(A) and under radiation of visible light(B); TPPAlEt; 1.5mmol, 1-methylimidazole; 1.5mmol, CO_2 bubbling for 5 min.

In another reaction, treatment with diazomethane gave methyl propionate in a 12% yield based on the amount of porphinatoaluminium ethyl. Thus, carbon dioxide was inserted into aluminium-ethyl bond of TPPAlEt to form aluminium propionate.

$$\text{TPPAlEt} \xrightarrow{CO_2} \text{TPPAl-O-C(=O)-Et} \xrightarrow{HCl} \begin{cases} \xrightarrow{BuOH} \text{EtCOOBu} \\ \xrightarrow{CH_2N_2} \text{EtCOOMe} \end{cases} \text{EtCOOH}$$

Other expected products, such as 3-ethyl-3-pentanol, 3-pentanol and ethyl formate were not detected in the reaction mixture after treatment with hydrogen chloride.

Attempted direct esterification of the reaction mixture with methyl iodide and ethyl iodide at 130 °C were unsuccessful.

Discussion

As described above, irradiation by visible light in the presence of 1-methylimidazole is necessary for the reaction of TPPAlEt and carbon dioxide. Figure 4 shows the visible spectra of the TPPAlEt and TPPAlEt–1-methylimidazole (1 : 1) system in methylene chloride at room temperature. The absorption maximum of the TPPAlEt spectrum shifted from 548 to 568 nm in the presence of 1-methylimidazole. By changing the ratio of the amount of 1-methylimidazole to that of TPPAlEt, an isosbestic point was observed at 557 nm, and the strength of the absorption maximum at 568 nm remained almost the same when a more than equimolar amount of 1-methylimidazole was added. Therefore, 1-methylimidazole is considered to form an equimolar coordination compound with TPPAlEt in methylene chloride. Such coordination of 1-methylimidazole possibly to the aluminium is considered to increase the nucleophilicity of the ethyl group.

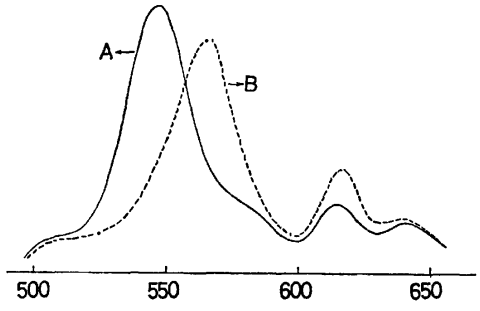

Fig. 4. Visible spectra of tetraphenylporphinatoaluminium ethyl(A) and tetraphenylporphinatoaluminium ethyl–1-methylimidazole(1:1) system(B) in methylene chloride, TPPAlEt; 7.0×10^{-3} mmol, CH_2Cl_2; 20ml, 1-methylimidazole; 7.0×10^{-3} mmol.

However, irradiation by visible light is essential for the reaction. Since neither 1-methylimidazole nor the aluminium-ethyl bond have absorptions in the visible region, it is reasonable to consider that the aluminium-ethyl bond of the TPPAlEt–1-methylimidazole complex was indirectly activated by visible light excitation of the porphine ring.

Such an activation effect by visible light on the reaction of carbon dioxide is very interesting in relation to the electron transfer in photosynthesis.

References

1) S. Inoue and Y. Yokoo, *J. Organomet. Chem.*, **39**, 11 (1972).
2) S. Inoue and Y. Yokoo, *Bull. Chem. Soc. Jpn.*, **45**, 3651 (1972).
3) S. Inoue, "Progress in Polymer Science Japan," Vol. 8, Kodansha, Tokyo (1975), p. 1.
4) A. D. Adler, *J. Org. Chem.*, **32**, 476 (1967).
5) G. H. Barnett and M. F. Hudson, *J. Chem. Soc., Perkin Trans. 1*, **1975**, 1401.
6) A. M. Roe, *J. Chem. Soc.*, **1963**, 2195.
7) J. W. Bucher and L. Ruppe, *Justus Liebigs Ann. Chem.*, **749**, 134 (1971).

Notes on the Formations of Oxaziridines by the Irradiation and Benzoylation of (22*S*, 25*S*)-*N*-Acetyl-11a-aza-c-homo-5*α*-veratra-11a,13(17)-diene-3*β*,11*β*,23*β*-triol 11a-Oxide, a Fused 6-Membered-ring Nitrone[1]

Hiroshi SUGINOME, Terutoshi MIZUGUCHI, and Tadashi MASAMUNE
Department of Chemistry, Faculty of Science, Hokkaido University, Sapporo, 060
(Received October 15, 1976)

The irradiation of the title nitrone (**5**) with monochromatic light afforded a single isomeric oxaziridine (**6**), which reverted to the original nitrone (**5**) thermally at room temperature. The title nitrone was also converted into another oxaziridine (**8**) by treatment with benzoic anhydride.

In our previous paper,[1] we proposed a pathway for the formation of the title nitrone (**5**) *via* the photorearrangement of a (22*S*, 25*S*)-veratr-13(17)-enine-11*β*-yl nitrite (**2**) on the basis of several pieces of experimental evidence.

We wish to report here on the transformations of the nitrone (**5**) into a single isomeric oxaziridine (**6**) by irradiation with monochromatic light (285 nm) and on a reaction toward acylating reagents which led to a product (**8**) with an oxaziridine ring.

Results

Photochemical Oxaziridine Formation.[2] The photochemical behavior of the nitrone (**5**) in ethanol toward Pyrex-filtered light was parallel to the nitrone we previously reported.[3] Thus, thenitrone (**5**) in ethanol was transformed into a single, less polar substance on 3 h irradiation with the Pyrex-filtered light generated by 100-W high-pressure Hg arc lamp. The less polar substance should be an oxaziridine (**6**), since it reverted to the starting nitrone when refluxed in acetone for *ca.* 1 h and it oxidized the iodide ion to iodine. The configuration of the oxaziridine ring could not be assigned since it was thermally unstable, even at room temperature. However, the α-configuration is more probable on the basis of the concideration of the relative stalility.

The quantitative transformation of the nitrone (**5**) into the corresponding oxaziridine (**6**) with monochromatic light and the quantitative thermal regeneration of the nitrone (**5**) from the oxaziridine (**6**) at room temperature were confirmed spectroscopically. Thus, a methanolic solution of the nitrone (**5**) (5.8×10^{-5} M) was irradiated with monochromatic light (285 nm) at room temperature. The nitrone (**5**) was completely transformed into the oxaziridine (**6**) by irradiation for 2 min, as was indicated by the vanishing of the absorption maximum at 285 nm of the nitrone (**5**) (Fig. 1). When the irradiated solution was set aside at room temperature in the dark, the oxaziridine gradually reverted to the nitrone, and after 18 h the oxaziridine (**6**) was quantitatively transformed into the nitrone (**5**)[2] as was indicated by the gradual appearance of the absorption maximum at 285 nm in the solution (Fig. 2).

The quantum yields of the oxaziridine formation in methanol and in isopropyl alcohol with monochromatic light (285 nm) were found to be 0.17 and 0.10 respectively. The formation of the oxaziridine was also observed in ethanol, *t*-butyl alcohol, dioxane, tetrahydrofuran, and cyclohexane. The nitrone (**5**) was equally transformed into the oxaziridine in methanol containing triplet quenchers, piperylene, or oxygen. The quantum yields of the oxaziridine formation were found to be 0.16 and 0.19 respectively. These facts indicated that the oxaziridine was formed from the singlet-excited nitrone.[4]

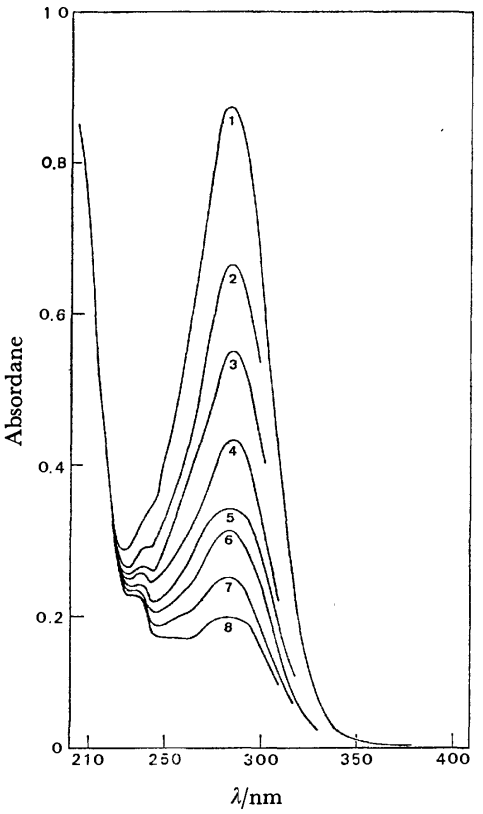

Fig. 1. Decline in the UV spectrum of **5** on irradiation with 285 nm light in 5.8×10^{-5} M methanol.
1: before irradiation, 2: 5 s irradiation, 3: 10 s, 4: 15 s, 5: 20 s, 6: 25 s, 7: 30 s, 8: 35 s.

The Reaction of the Nitrone (5) with Acylating Reagent. The treatment of this nitrone (**5**) with benzoic anhydride and pyridine at room temperature afforded a mixture of products from which only the major product, **8** (mp 194—195 °C) was obtained in a pure form. The results of the elemental analysis and the mass spectrum were consistent with a molecular formula of $C_{40}H_{54}O_8$-

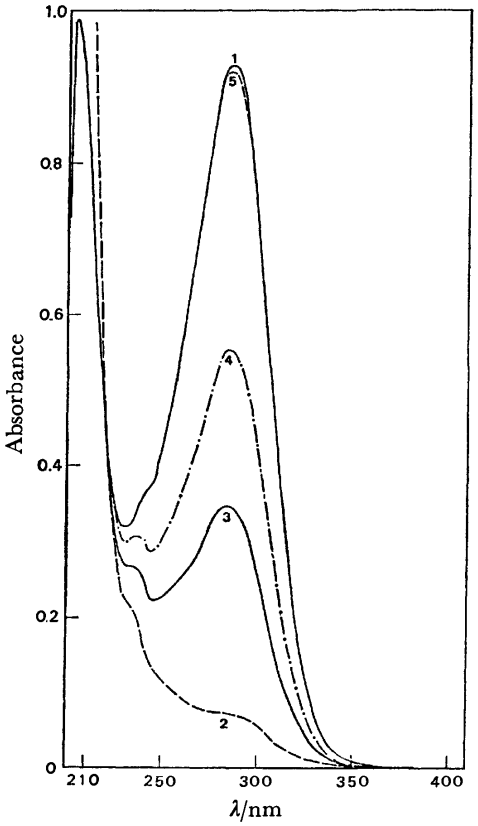

Fig. 2. Increase in the absorption maximum at 285 nm of the solution of **6** in 6.5×10^{-5} M methanol at room temperature.
1: the UV spectrum of **5** before irradiation, 2: after 2 min irradiation, 3: the UV spectrum of the solution when the solution irradiated for 2 min (the solution A) was set aside for 30 min in the dark at room temperature, 4: the UV spectrum of the solution A after 80 min in the dark, 5: the solution A after 18 h in the dark at room temperature.

N_2. The oxaziridine structure was assigned to this compound on the basis of the IR and NMR spectra in a manner entirely analogous to the product in the benzoylation of the nitrone we previously reported.[3] The assignments of the NMR signals are described in the table. As in the previous case,[2] the N-Ac protons were considerably shielded and appeared near the signal due to the 19-H. The signal due to the N-Ac was further confirmed by a comparison of ^{1}H NMR spectra between the product **8** and the deuterium-labeled compound **9**.

The partial $[^2H]_3$ acetylation of (22*S*,25*S*)-5α-veratr-13(17)-enine-3β,11β,23β-triol (**1**) afforded a deuterium-labeled derivative (**3**). Its subsequent nitrosation afforded (22*S*,25*S*)-*N*-$[^2H]_3$acetyl-5α-veratr-13(17)-enne-3β,11β,23β-triol 3,23-di-$[^2H]_3$ acetate 11-nitrite (**4**). The nitrite (**4**) in carbon tetrachloride was photolyzed by a procedure analogous to that used in the case of the **2** nitrite to afford the nitrone(**7**)in a 28% yield. The treatment of it with benzoic anhydride and pyridine under the same conditions as were used for the **5** nitrone afforded a mixture of products. Its recrystallization from ether afforded an oxaziridine (**9**). The ^{1}H NMR spectrum of compound **9** indicated the presence of all the signals found in the spectrum of compound **8** with the exceptions of two sharp signals at τ 8.02 and at τ 8.86 due to the OAc and NAc of the product (**8**).

Therefore, the singlet at τ 8.86 in the spectrum of the product (**8**) was assigned to that of NAc. This considerable shielding of NAc protons, found in the spectrum of the product (**8**), was attributable to an anisotropy by the newly introduced phenyl ring. The assignments of the rest of the signals of the product (**8**) are shown in the table. There was a clear doublet at τ 3.32 (J= 9.6) ascribable to the 11β-H on the newly formed oxaziridine ring. An inspection of the Dreiding model of compound **8** in conjunction with the considerable shielding of the *N*-acetyl protons by the benzene ring in the ^{1}H NMR spectrum suggested that the configura-

TABLE. CHEMICAL SHIFTS (τ values) AND COUPLING CONSTANTS (Hz)

Compound	Chemical shifts											
	3-αH	11-αH	12-αH	18-H	19-H	20β-H	21-H	22-βH	23-αH	26-H	27-H	N-Ac, OAc
4	5.35 br	5.85 (q)	7.35 (s)	8.27 (s)	9.03 (s)	6.85 (q)	8.86 (d)	5.21 (d)	4.89 (bs)	8.86 (d)		—
7	*ca.* 5.34	*ca.* 5.34	—	7.09 (s)	9.09 (s)	6.84 (q)	8.87 (q)	5.22 (d)	4.97 (bs)	8.87 (d)	6.64 (bs)	—
8	5.34 br	3.32 (d) (11-βH)	—	8.13 (s)	9.08 (s)	a	8.89 or 9.01 (d)	5.22 (d)	4.98 (bs)	8.89 or 9.01 (d)		8.86 (s) (NAc) 8.02 (s) (OAc)
9	5.34 br	3.32 (d) (11-βH)	—	8.14 (s)	9.09 (s)	a	8.89 or 9.01 (d)	5.22 (d)	4.98 (bs)	8.89 or 9.01 (d)		—

Compound	Coupling constants							
	11-αH, 12-αH	11-αH, (11-βH) 9-αH	12-αH, 14-αH	20-αH, 21-H	20-βH, 22-βH	22-βH, 23-βH	25-αH, 26-H	Other signals and the coupling constants
4	5.3	2.7	9.8	6.6	10.5	1.5	6.6	
7	—	a	—	6.6	10.5	1.5	6.6	
8	—	11-βH, 9-αH 9.6	—	6.6 or 6.0	10.5	1.5	6.6 or 6.0	1.8—2.7 (m) benzoyl H
9	—	11-βH, 9-αH 9.6	—	6.6 or 6.0	10.5	1.5	6.6 or 6.0	1.8—2.7 (m) benzoyl H

a) Unassignable.

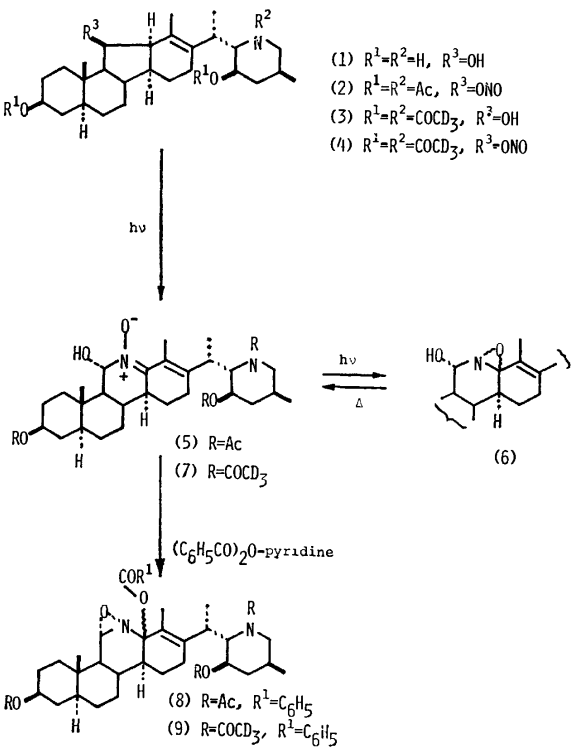

Scheme 1.

tion of compound **8** at the C-13 position was β. However, this assignment is not conclusive.

Although we obtained the oxaziridine(**8**)as the major product, we were unsuccessful in isolating a compound with a pyridine nucleus corresponding to the compound which was isolated previously.[2] This probably shows that the compound with the pyridine nucleus was formed only in a poor yield in this benzoylation. This difference from the previous case demonstrate that a balance of two competitive processes leading to oxaziridine and to a compound with a pyridine nucleus depends upon a rather slight modification of the substrate structure.

Experimental

For the instruments used and the general procedures, see Part 30.[5]

The Formation of the Oxaziridine (6) on the Irradiation of the Nitrone (5) in Ethanol and the Thermal Treatment of the Oxaziridine (6). The nitrone (**5**) (53 mg) in ethanol (73 ml) was irradiated through Pyrex with a 100-W high-pressure Hg arc lamp under nitrogen. The progress of the reaction was monitored by TLC (Solvent: acetone/chloroform 1/3). After 3.5 h, the nitrone disappeared and was transformed into a less polar substance which appeared as a single spot on the TLC. After the removal of the solvent at 22 °C, the residue developed a yellow color on the addition of a KI–acetic acid solution. This residue was dissolved in 10 ml of acetone and they refluxed for 1 h 10 min. An examination by TLC of this solution showed that nearly all the oxaziridine had reverted to the starting nitrone. The acetone was then evaporated and the residue was recrystallized from isopropyl ether to yield crystals (29 mg) which were identical with the starting nitrone.

The Transformation of the Nitrone (5) into the Oxaziridine (6) in Methanol on Irradiation with 285 nm Light. Quantum-yield Measurements: Solutions of the nitrone (**5**) containing 1,3-pentadiene or oxygen were prepared by dissolving 0.16 mg of the nitrone in 5 ml of methanol containing *ca.* 0.2 g of 1,3-pentadiene and 0.21 mg of the nitrone in 5 ml of methanol saturated with oxygen.

The solutions for the quantum-yield measurements were prepared by dissolving 0.17 mg of the nitrone (**5**) in 5 ml of methanol and 0.19 mg of **5** in 5 ml of isopropyl alcohol. Each 4 ml portion of the solutions in silica cells ($10\times10\times45$ mm) was placed in a chamber of the Jasco CRM-FA grating spectro-irradiator. The solutions were then irradiated with a 285 nm light. Figure 1 shows the decline in the intensity of the absorption maximum of compound **5** at 285 nm in methanol.

The quantum yields of the transformation of the nitrone (**5**) into the oxaziridine (**6**) were measured as in the case of the disappearance of the nitrite.[1] The decreases in the absorbance at 285 nm of the UV spectrum of the solutions upon the irradiation for 5 s in the case of methanol and for 20 s in the case of isopropyl alcohol were found to be 0.2 and 0.47.

Since the molar absorptivity at 285 nm in the UV spectrum of the **5** nitrone was known to be 15800, and since the output of the Xe arc lamp at 285 nm was 0.6×10^5 erg/cm², s, the quantum yield of the decomposition of the nitrone in methanol was calculated to be 0.18.

In the same manner, the quantum yield of the decomposition of the nitrone in isopropyl alcohol was calculated to be 0.10.

(22S,25S)-N-[H^2]$_3$Acetyl-veratr-13(17)-enine-3β,11β,23β-triol 3,23-di-[^2H]$_3$-acetate (3). The triol (**1**) (620 ml) and acetic anhydride-d_6 (2.5 ml) in pyridine (6.2 ml) were stirred for 22 h at room temperature. After the addition of methanol (10 ml), the solvent was removed with added benzene under reduced pressure. The residue was dissolved in chloroform and the chloroform solution was washed with 2M-hydrochloric acid, a 5% aqueous sodium hydrogencarbonate solution, and water successively. After the removal of the chloroform, the amorphous residue (955 mg) was submitted to column chromatography (Mallinckrodt silicic acid; 100 mesh: eluent, benzene) to yield 462 mg of colorless crystals of the tri-[^{2}H]$_3$ acetyl derivative (**3**). The analytical specimen was obtained by recrystallization from ether. Mp 196—197°C. Found: C, 69.84, H and D, 10.80, N, 2.36%. Calcd for $C_{33}H_{42}D_9O_6N$: C, 69.92; H and D, 10.67; N, 2.47%. ν_{max} 1736 cm^{-1} ($OCOCD_3$), 1632 cm^{-1} ($NCOCD_3$), 3468 (OH), 1244, 1079 cm^{-1}. NMR; see Table. MS, *m/e* 568 (M+2, 0.2%), *m/e* 361 (0.5%), *m/e* 204 (54%), *m/e* 160 (100%), *m/e* 116 (16%).

Nitrosation of the 11β-ol (3). To a solution of the 11β-ol (**3**) (430 mg) in acetic acid (6 ml) at 60°C, there was added sodium nitrate (200 mg) within a period of 30 s. To the reaction mixture there was then added water (40 ml). The resultant precipitates of the nitrite were collected by filtration, washed with a 10% aqueous sodium hydrogencarbonate solution, washed with water, and dried *in vacuo*. Yield, 435 mg. NMR; see Table.

Photolysis of the Nitrite (4). The above nitrite (435 mg) in carbon tetrachloride (20 ml) was irradiated through Pyrex with a 100-W high-pressure Hg arc for 8.5 h under argon. A small amount of a solid which appeared on the wall of the vessel was dissolved in chloroform. The photolyzed solution and the chloroform solution were combined, and the solvent was removed. The residue was submitted to preparative TLC (solvent: acetone/benzene 1/5). The amorphous crude nitrone was recrystallized from ether to afford 120 mg of the nitrone (**7**). Mp 126—127 °C. Found: C, 66.30; H and D, 10.20; N, 4.52%. Calcd for $C_{33}H_{41}D_9O_7N_2$: C, 66.50; H and

D, 9.98; N, 4.73%. NMR; see Table.

Benzoylation of the Nitrone (5). The nitrone (**5**) (79 mg) and benzoic anhydride (100 mg) in pyridine (3.5 ml) were stirred for 24 h at room temperature. The reaction mixture was then poured into a mixture of ice and water (80 ml). The mixture was extracted with chloroform (20 ml×2). The chloroform solution was washed successively with 2M-hydrochloric acid (20 ml), a 5% aqueous sodium hydrogencarbonate solution (20 ml), and water, and then dried (Na_2SO_4). The removal of the solvent afforded a residue (310 mg). This was submitted to preparative TLC (acetone/chloroform 1: 3). Four fractions-A (142 mg), B (44 mg), C (17 mg), and D (17 mg) were obtained in the order of increasing polarity. The least polar fraction, A, was recovered benzoic anhydride. The B fraction was recrystallized from ether to yield 11 mg of the oxaziridine (**8**). Mp 194—195 °C. Found: C, 69.40, H, 7.55; H, 4.30%. Calcd for $C_{40}H_{54}O_8N_2$: C, 69.54; H, 7.88; N, 4.06%. UV λ_{max}^{EtOH} 231 nm (ε; 11000). ν_{max} ($CHCl_3$) 1720 cm^{-1} (OAc and $OCOC_6H_5$), 1629 cm^{-1} (NAc). NMR; see text.

Benzoylation of the Nitrone (7). The above nitrone (**7**) (90 mg) and benzoic anhydride (110 mg) in pyridine (3.5 ml) were stirred for 3 h. After the addition of 2 M hydrochloric acid (500 ml), the reaction mixture was extracted with chloroform (50 ml+40 ml+20 ml). The chloroform solution was washed successively with a 5% aqueous sodium hydrogencarbonate solution and water and then dried (Na_2SO_4). After the removal of the solvent, the residue was recrystallized from ether to yield 28 mg of the pure oxaziridine (**9**). Mp 243—244 °C (from acetone). Found: C, 68.40; H and D, 8.90; N, 3.80%. Calcd for $C_{40}H_{45}D_9O_8N$: C, 68.64; H and D, 9.07; N, 4.00%. NMR see Table.

The authors wish to thank the Application Laboratory, Japan Spectroscopic Co., Ltd., where the experiments with monochromatic light were undertaken. We also wish to thank Mrs. Satoko Araki and Mrs. Tomoko Okayama for their measurements of the 100 MHz NMR spectra.

References

1) Photoinduced Transformations. Part 34. Part 33: H. Suginome, T. Mizuguchi, S. Honda, and T. Masamune, *J. Chem. Soc., Perkin Trans. 1*, in press.

2) M. J. Kamlet and L. A. Kaplan, *J. Org. Chem.*, **22**, 576 (1957); J. S. Splitter and M. Calvin, *ibid.*, **23**, 651 (1958), **30**, 3427 (1965); R. Bonnett, V. M. Clark, and A. R. Todd, *J. Chem. Soc.*, **1959**, 2102; J. B. Bapat and D. St. C. Black, *J. Chem. Soc., Chem. Commun.*, **1976**, 73; J. S. Splitter, T. Su, H. Ono, and M. Calvin, *J. Am. Chem. Soc.*, **93**, 4075 (1971).

3) H. Suginome, N. Sato, and T. Masamune, *Tetrahedron*, **27**, 4863 (1971).

4) H. Shinzawa and I. Tanaka, *J. Phys. Chem.*, **68**, 1205 (1964).

5) H. Suginome, N. Tsuneno, N. Sato, N. Maeda, T. Masamune, H. Shimanouchi, Y. Tsuchida, and Y. Sasada, *J. Chem. Soc., Perkin Trans. 1*, **1976**, 1297.

Chemical Synthesis of Antigenic Determinants in Hen Egg-White Lysozyme. I. Heneicosapeptide Corresponding to Positions 34—54 in the Primary Structure

Takayuki MITAKI and Yasutsugu SHIMONISHI

Institute for Protein Research, Osaka University, Yamada-kami, Suita, Osaka 565

(Received October 18, 1976)

For elucidating one of the antigenic determinants of hen egg-white lysozyme close to its catalytic site, heneicosapeptide was synthesized by a conventional method. This peptide, phenylalanylglutamylserylasparaginylphenylalanylasparaginylthreonylglutaminylalanylthreonylasparaginylarginylasparaginylthreonylaspartylglycylserylthreonylaspartyltyrosylglycine, corresponds to positions 34—54 of the amino acid sequence of hen egg-white lysozyme.

Two methods have been used in studies on the antigenic structures of hen egg-white lysozyme (HEL). One is screening of proteolytic digests of HEL for immunologically active peptides;[1-7] characterization of these peptides then provides various informations about the structures of the antigenic determinants. This method has the disadvantages that fractions of digests may be contaminated with small quantities of immunologically active materials and that it cannot be used to study the minimal structures of antigenic determinants for activity and the functions of the individual amino acid residue. The second method is chemical synthesis of antigenic structures of HEL.[8-10] This method does not have the disadvantages of the other method, because it can give pure substance with natural structure and also various artificial analogs, whereas it cannot be used alone for determining the antigenic determinants.

Sakato *et al.*[4] found that certain peptides isolated from thermolytic digests of HEL, *i.e.*, P_{Ib} [sequence[11,12] Val^{29} to Gly^{54} and Val^{109} to Trp^{123} linked by a single disulfide (Cys^{30} and Cys^{115}) bond], P_{Ba-1} (sequence Phe^{34} to Gly^{54}) and P_{Ba-2} (sequence Phe^{38} to Gln^{57}), are immunologically active, and described that the antigenic determinant of HEL included in these peptides is in the sequence Phe^{38} to $Gly.^{54}$ It seemed interesting to characterize this determinant, because these immunoreactive peptides are close to a catalytic site of HEL and because antibody populations directed to them also neutralize the enzymatic activity of HEL.[4] The second method described above seemed most suitable for examining this antigenic determinant of HEL, because various peptides related to this determinant could not be isolated from enzymatic digests of HEL. Studies on this have been carried out in collaboration[13] with Prof. T. Amano and his group of the Research Institute for Microbial Diseases, Osaka University. This paper reports the synthesis of a heneicosapeptide, phenylalanylglutamylserylasparaginylphenylalanylasparaginylthreonylglutaminylalanylthreonylasparaginylarginylasparaginylthreonylaspartylglycylserylthreonylaspartyltyrosylglycine corresponding to P_{Ba-1}, which includes two residues of the catalytic sites of HEL (Glu^{35} and Asp^{52}).[14]

This peptide was synthesized from appropriately protected smaller fragments by the azide coupling reaction. In planning the synthesis, easy ways of purifying peptide intermediates and the ultimate removal of protecting groups with liquid hydrogen fluoride[15] were considered. For the synthesis, heneicosapeptide (sequence Phe^{34} to Gly^{54}) was divided into four subfragments (P_1—P_4), as shown in Figs. 1—4. For synthesis of subfragment P_1, N^{α}-benzyloxycarbonyl-γ-*t*-butylglutamic acid *N*-hydroxysuccinimide ester[16] was condensed with serine methyl ester. Then N^{α}-benzyloxycarbonyl-γ-*t*-butylglutamylserine methyl ester (I) was hydrogenated catalytically and the resulting peptide ester was not isolated but coupled directly with benzyloxycarbonylphenylalanine[17] by dicyclohexylcarbodiimide to give benzyloxycarbonylphenylalanyl-γ-*t*-butylglutamylserine methyl ester (II). The protected tripeptide methyl ester was converted to the corresponding hydrazide (III). Benzyloxycarbonylphenylalanyl-γ-*t*-butylglutamylserine azide obtained from compound III

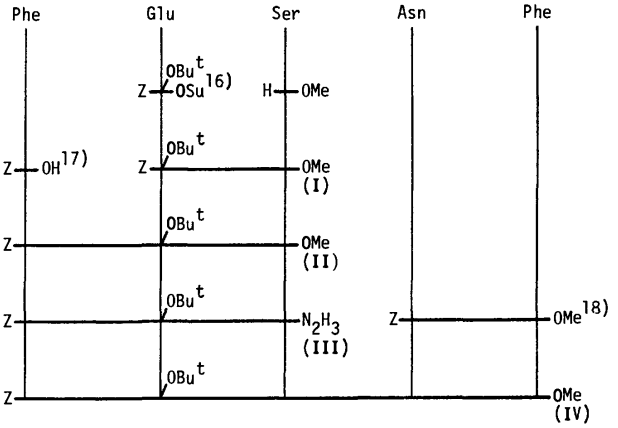

Fig. 1. Scheme for synthesis of subfragment P_1 (sequence 34—38)[28]

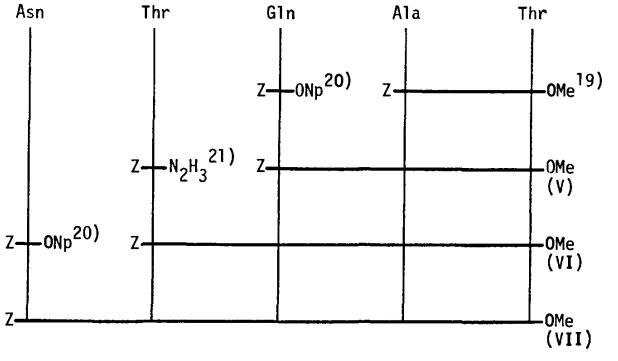

Fig. 2. Scheme for synthesis of subfragment P_2 (sequence 39—43).

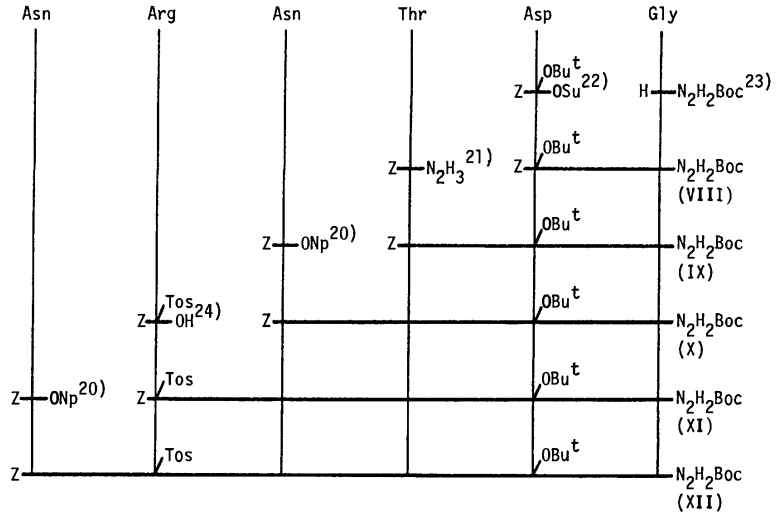

Fig. 3. Scheme for synthesis of subfragment P_3 (sequence 44—49).

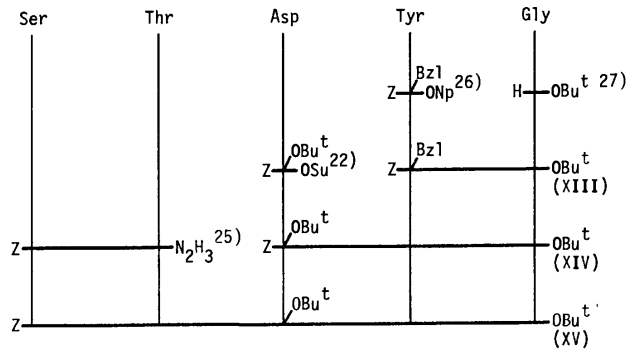

Fig. 4. Scheme for synthesis of subfragment P_4 (sequence 50—54).

was not isolated but allowed to react directly with asparaginylphenylalanine methyl ester, which was obtained by removal of the benzyloxycarbonyl group from the protected peptide[18] by catalytic hydrogenation. In this way benzyloxycarbonylphenylalanyl-γ-*t*-butylglutamylserylasparaginylphenylalanine methyl ester (IV) was obtained without difficulty.

Subfragment P_2 was synthesized using benzyloxycarbonylalanylthreonine methyl ester[19] as starting material by a stepwise elongation procedure. The benzyloxycarbonyl group was removed by catalytic hydrogenation and the resulting peptide ester was not isolated but coupled directly with benzyloxycarbonylglutamine *p*-nitrophenyl ester[20] to yield benzyloxycarbonylglutaminylalanylthreonine methyl ester (V). The protecting group was cleaved by catalytic hydrogenation and the tripeptide methyl ester was condensed with benzyloxycarbonylthreonine azide prepared from its corresponding hydrazide[21] to give benzyloxycarbonylthreonylglutaminylalanylthreonine methyl ester (VI). The benzyloxycarbonyl group was removed by catalytic hydrogenation and the tetrapeptide methyl ester thus obtained was coupled with benzyloxycarbonylasparagine *p*-nitrophenyl ester[20] to give benzyloxycarbonylasparaginylthreonylglutaminylalanylthreonine methyl ester (VII).

Subfragment P_3 was constructed using benzyloxycarbonyl-β-*t*-butylaspartylglycine *t*-butoxycarbonylhydrazide (VIII), which was prepared by coupling benzyloxycarbonyl-β-*t*-butylaspartic acid *N*-hydroxysuccinimide ester[22] with glycine *t*-butoxycarbonylhydrazide.[23] The benzyloxycarbonyl group of compound VIII was removed by catalytic hydrogenation and the resulting peptide *t*-butoxycarbonylhydrazide was coupled with benzyloxycarbonylthreonine azide to yield benzyloxycarbonylthreonyl-β-*t*-butylaspartylglycine *t*-butoxycarbonylhydrazide (IX). The protecting group for amino terminus was removed by catalytic hydrogenation and the chain elongated by further three single steps using benzyloxycarbonylasparagine *p*-nitrophenyl ester,[20] N^{α}-benzyloxycarbonyl-N^{ω}-tosylarginine[24] and dicyclohexylcarbodiimide in the presence of *N*-hydroxysuccinimide, and benzyloxycarbonylasparagine *p*-nitrophenyl ester[20] for acylation. Thus, benzyloxycarbonylasparaginyl-N^{ω}-tosylarginylasparaginylthreonyl-β-*t*-butylaspartylglycine *t*-butoxycarbonylhydrazide (XII) was obtained.

Subfragment P_4 (XV) was synthesized by coupling benzyloxycarbonylserylthreonine azide with β-*t*-butylaspartyltyrosylglycine *t*-butyl ester, which was obtained by removal of the benzyloxycarbonyl group from the protected tripeptide ester (XIV) by catalytic hydrogenation, without isolation. The tripeptide derivative (XIV) was prepared by condensation of benzyloxycarbonyl-β-*t*-butylaspartic acid *N*-hydroxysuccinimide ester[22] with tyrosylglycine *t*-butyl ester, which was prepared by removal of the protecting groups from benzyloxycarbonyl-*O*-benzyltyrosylglycine *t*-butyl ester (XIII) by catalytic hydrogenation. The dipeptide derivative (XIII) was obtained by condensation of benzyloxycarbonyl-*O*-benzyltyrosine *p*-nitrophenyl ester[26] with glycine *t*-butyl ester.[27]

The couplings of subfragment P_1 with P_2 and of subfragment P_3 with P_4 were carried out separately, as shown in Fig. 5. The hydrazide (XVI) of subfragment P_1 was converted to the corresponding azide and coupled with pentapeptide methyl ester, which was prepared by removal of the benzyloxycarbonyl group of subfragment P_2 by catalytic hydrogenation. The decapeptide

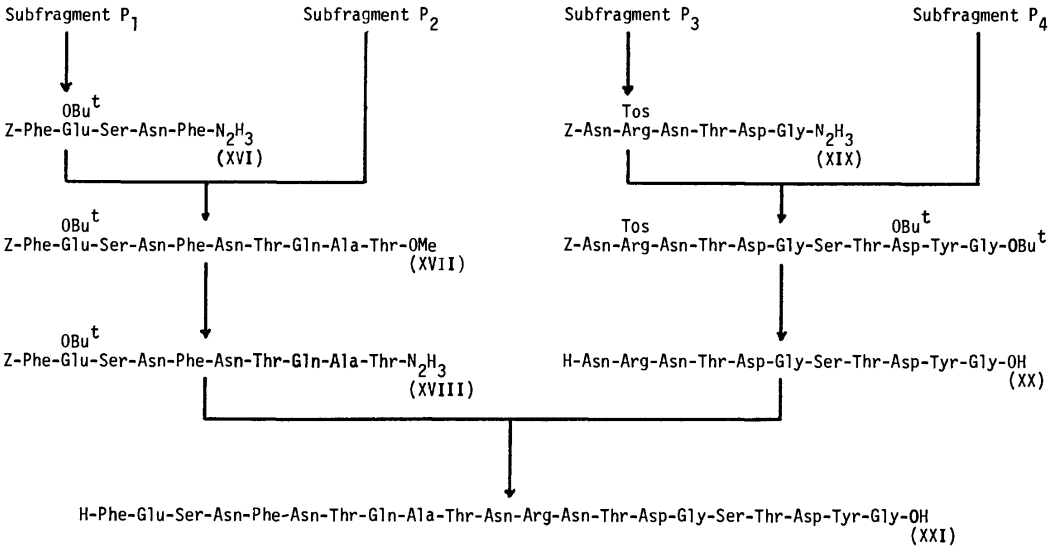

Fig. 5. Scheme for synthesis of the heneicosapeptide (sequence 34—54).

derivative (XVII) obtained was converted to its corresponding hydrazide (XVIII). On the other hand, subfragment P_3 was treated with trifluoracetic acid and the corresponding hydrazide (XIX) obtained was coupled with serylthreonyl-β-*t*-butylaspartyltyrosylglycine *t*-butyl ester prepared from subfragment P_4 by Rudinger's azide method[29] to give a protected undecapeptide. Without further purification the peptide was treated with liquid hydrogen fluoride in an HF-apparatus[15] to remove its protecting groups. The free undecapeptide (XX), asparaginylarginylasparaginylthreonylaspartylglycylserylthreonylaspartyltyrosylglycine, was purified on a column of diethylaminoethyl-cellulose. The azide, prepared from the hydrazide (XVIII) by Rudinger's method,[29] was further coupled *in situ* with free undecapeptide (XX) to give protected heneicosapeptide. The crude heneicosapeptide was not purified due to its low solubility but was directly treated with hydrogen fluoride[15] to remove its protecting groups. The resulting free peptide was fractionated on a column of Sephadex G-25, as shown in Fig. 6, and the main fraction collected was purified further on a column of carboxymethyl-cellulose, as shown in Fig. 7.

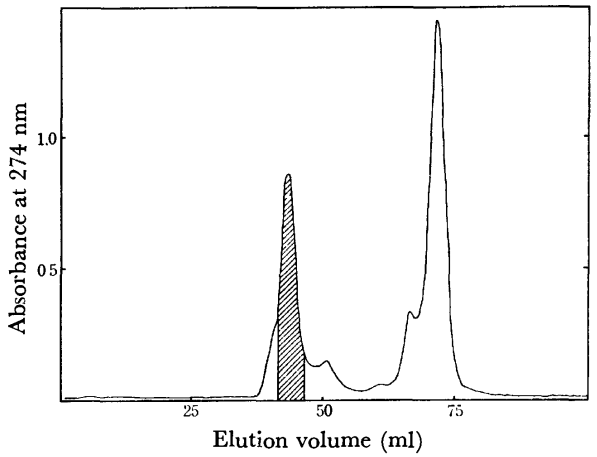

Fig. 6. Gel-filtration of crude heneicosapeptide (XXI) on Sephadex G-25 in 50% acetic acid.

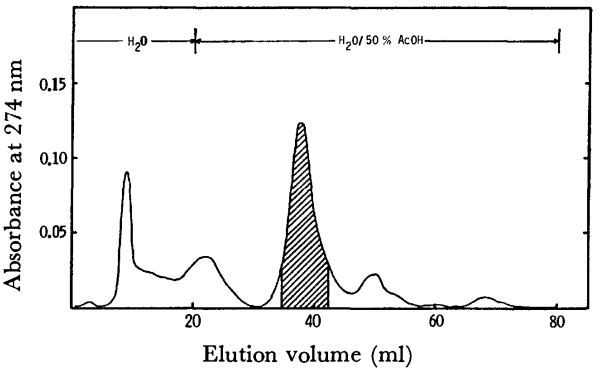

Fig. 7. Chromatogram of the main fraction shown in Fig. 6 on carboxymethyl-cellulose (H^+ cycle) using a linear gradient from water to 50% acetic acid.

The heneicosapeptide thus synthesized showed the same order of inhibitory activity in a precipitin reaction between ^{125}I-HEL and the purified *anti*-P_{Ib} antibody, as that reported elsewhere.[13] This confirms that one of the antigenic determinants of HEL is in the region from Phe^{34} to Gly^{54} of HEL. Chemical synthesis of the minimal structure necessary for inhibitory activity is now in progress.

Experimental

All chemicals were of reagent grade and they were used without further purification. The amino acids except glycine were of the L-configuration. Sephadex G-25 fine was purchased from Pharmacia Co. (Uppsala). Thin layer chromatography was performed on silica gel G (Merck) using the following solvent systems (volume ratios); chloroform: methanol: acetic acid (95: 5: 3), ethyl acetate: benzene (1: 1), 1-butanol: acetic acid: water (4: 1: 1), 1-butanol: acetic acid: pyridine: water (15: 3: 10: 12), phenol: water (3: 1) and chloroform: methanol: acetic acid: water (10: 10: 1: 10, lower phase). Paper electrophoresis was performed at pH 4.8 in 0.2 M pyridinium acetate buffer. Peptide derivatives were hydrolyzed in 6 M hydrochloric acid with phenol in sealed tubes for 24 h at 105 °C, and amino acids in the hydrolysates were examined in a Hitachi KLA-5

analyzer by the method of Moore *et al.*[30] Optical rotations were determined with a Perkin-Elmer Model 241 polarimeter. The purities of the peptide derivatives synthesized were confirmed by thin layer chromatography and paper electrophoresis and by the ratio of their constituent amino acids measured in acid hydrolysates by amino acid analysis. Melting points were measured by the capillary method and are given as uncorrected values.

N$^{\alpha}$-Benzyloxycarbonyl-γ-t-butylglutamylserine Methyl Ester (I). A solution of serine methyl ester hydrochloride (6.80 g, 44.0 mmol) in *N,N*-dimethylformamide (50 ml) was cooled to 0—5 °C. The chilled solution was mixed with triethylamine (6.2 ml) and then a solution of *N$^{\alpha}$*-benzyloxycarbonyl-γ-*t*-butylglutamic acid *N*-hydroxysuccinimide ester[16] (17.4 g, 40.1 mmol) in *N,N*-dimethylformamide (40 ml) and stirred for 2 h at room temperature. Then the mixture was concentrated *in vacuo*, and diluted with ethyl acetate. The diluted solution was washed successively with 0.1 M hydrochloric acid, 5% aqueous sodium hydrogencarbonate, and water, and dried over anhydrous sodium sulfate. The dried solution was concentrated *in vacuo* to a syrup, and the material was crystallized in a mixture of ethyl acetate and hexane; wt 15.7 g (89.2%). The crude product was recrystallized from ethyl acetate and hexane; wt 12.7 g (72.2%); mp 70—72 °C; $[\alpha]_D^{19}$ −5.3° (*c* 0.9, ethanol).

Found: C, 57.64; H, 6.91; N, 6.40%. Calcd for $C_{21}H_{30}O_8N_2$: C, 57.52; H, 6.90; N, 6.39%.

Benzyloxycarbonylphenylalanyl-γ-t-butylglutamylserine Methyl Ester (II). Compound I (12.7 g, 29.0 mmol) was dissolved in methanol (500 ml), and hydrogenated over a 5% palladium-charcoal catalyst for 1.5 h at atmospheric pressure. The catalyst was filtered off and washed with a small volume of methanol. The filtrate and washings were combined and concentrated to a syrupy residue *in vacuo*. The residue was dissolved with benzyloxycarbonylphenylalanine[17] (8.70 g, 29.1 mmol) in *N,N*-dimethylformamide (70 ml), and the solution was cooled to −10 °C. Then a solution of dicyclohexylcarbodiimide (6.00 g, 29.1 mmol) in *N,N*-dimethylformamide (20 ml) was added and the mixture was stirred for one hour at the same temperature and then overnight at room temperature. The precipitate formed was filtered off and washed with *N,N*-dimethylformamide. The filtrate and washings were combined, concentrated to a small volume *in vacuo*, and diluted with ethyl acetate. The diluted solution was washed successively with 0.1 M hydrochloric acid, 5% aqueous sodium hydrogencarbonate, and water, and dried over anhydrous sodium sulfate. The dried solution was concentrated to a syrup under reduced pressure, and crude material was crystallized from ethyl acetate and hexane; wt 12.6 g (74.1%). It was recrystallized from ethyl acetate and hexane; wt 11.7 g (68.8%); mp 87.5—89 °C; $[\alpha]_D^{19}$ −14.9° (*c* 1.1, ethanol).

Found: C, 61.67; H, 6.87; N, 7.30%. Calcd for $C_{33}H_{39}O_9N_3$: C, 61.52; H, 6.71; N, 7.18%.

Benzyloxycarbonylphenylalanyl-γ-t-butylglutamylserine Hydrazide (III). A solution of compound II (11.7 g, 20.0 mmol) in methanol (200 ml) was cooled to 0—5 °C, and then 90% hydrazine hydrate (7 g) was added. The mixture was kept for 24 h at room temperature, and the precipitate formed was filtered off and washed with methanol; wt 10.9 g (91.6%); mp 171—173 °C.

Found: C, 58.85; H, 6.70; N, 11.65%. Calcd for $C_{29}H_{39}O_8N_5 \cdot 0.5H_2O$: C, 58.57; H, 6.78; N, 11.78%.

Benzyloxycarbonylphenylalanyl-γ-t-butylglutamylserylasparaginylphenylalanine Methyl Ester (IV). Benzyloxycarbonylasparaginylphenylalanine methyl ester[18] (6.41 g, 15.0 mmol) was dissolved in methanol (1 liter) and hydrogenated over a 5% palladium-charcoal catalyst for 3.5 h at atmospheric pressure. The catalyst was filtered off and washed with methanol. The filtrate and washings were combined and concentrated to a solid residue *in vacuo*. The residue was dissolved in *N,N*-dimethylformamide (50 ml), and cooled to −10 °C. Compound III (8.78 g, 14.8 mmol) was suspended in *N,N*-dimethylformamide (40 ml), cooled to −20 °C and mixed with 3.90 M HCl in dioxane (11.5 ml). The clear solution was mixed with isopentyl nitrite (2.10 ml) at the same temperature. After 10 min a solution of *N*-methylmorpholine (4.55 g) in *N,N*-dimethylformamide (10 ml) and then a cooled solution of the amino component were added. The mixture was stirred for 40 h in a refrigerator (0 °C). Then a solution of *N*-methylmorpholine (0.98 g) in *N,N*-dimethylformamide (2.1 ml) was added and the mixture was stirred for 48 h at the same temperature. Then, the solution was poured into large volume of water. The precipitate formed was collected by filtration; wt 10.2 g (79.7%). The crude product was reprecipitated from *N,N*-dimethylformamide and ethyl acetate; wt 8.70 g (68.0%); mp 214—215 °C; $[\alpha]_D^{27}$ −3.8° (*c* 1.1, *N,N*-dimethylformamide). Amino acid ratio: Asp, 1.00 (1); Ser, 0.93 (1); Glu, 1.05 (1); Phe, 2.00 (2).

Found: C, 60.51; H, 6.45; N, 9.92%. Calcd for $C_{43}H_{54}O_{12}N_6 \cdot 0.5H_2O$: C, 60.33; H, 6.47; N, 9.82%.

Benzyloxycarbonylglutaminylalanylthreonine Methyl Ester (V). Benzyloxycarbonylalanylthreonine methyl ester[19] (3.38 g, 10.0 mmol) was dissolved in ethanol (120 ml) and hydrogenated over a 5% palladium-charcoal catalyst. The catalyst was filtered off and the filtrate was concentrated to a syrup *in vacuo*. The syrup was dissolved with benzyloxycarbonylglutamine *p*-nitrophenyl ester[20] (3.34 g, 8.33 mmol) in *N,N*-dimethylformamide (25 ml). The solution was stirred for an hour at room temperature, and then concentrated to a syrup *in vacuo*. The syrup was triturated in ethyl acetate. The solid thus formed was collected by filtration, and recrystallized from methanol; wt 2.64 g (68.0%); mp 190.5—191 °C; $[\alpha]_D^{10}$ −7.6° (*c* 0.94, *N,N*-dimethylformamide).

Found: C, 53.80; H, 6.47; N, 12.09%. Calcd for $C_{21}H_{30}O_8N_4$: C, 54.07; H, 6.48; N, 12.01%.

Benzyloxycarbonylthreonylglutaminylalanylthreonine Methyl Ester (VI). Compound V (11.7 g, 25.1 mmol) was suspended in methanol (900 ml) and hydrogenated over a 5% palladium-charcoal catalyst at atmospheric pressure for 1.5 h. The catalyst was filtered off and washed with methanol. The filtrate and washings were combined and evaporated to dryness under reduced pressure. The residue was dissolved in a mixture of *N,N*-dimethylformamide (100 ml) and dimethyl sulfoxide (40 ml), and then cooled in ice-water. Benzyloxycarbonylthreonine hydrazide[21] (6.70 g, 25.1 mmol) was suspended in *N,N*-dimethylformamide (50 ml) and cooled to −25 °C. The chilled suspension became clear on adding 3.55 M HCl in dioxane (21.1 ml). The solution was mixed with isopentyl nitrite (3.50 ml) and stirred for 15 min at the same temperature. Then it was carefully mixed with a solution of triethylamine (10.5 ml) in *N,N*-dimethylformamide (10 ml). The mixture was combined with the above cooled solution of the hydrogenated product of compound V, and stirred for 48 h at 0 °C. The mixture was concentrated to a solid residue *in vacuo*, and collected with water; wt 10.4 g (72.7%). The crude material was reprecipitated from *N,N*-dimethylformamide and water; wt 9.30 g (65.0%); mp 241—243 °C; $[\alpha]_D^{20}$ −7.6° (*c* 1.1, *N,N*-dimethylformamide).

Found: C, 52.82; H, 6.62; N, 12.34%. Calcd for $C_{25}H_{37}O_{10}N_5$: C, 52.90; H, 6.57; N, 12.34%.

Benzyloxycarbonylasparaginylthreonylglutaminylalanylthreonine Methyl Ester (VII). Compound VI (8.00 g, 14.1 mmol) was suspended in methanol (750 ml) and hydrogenated over a

5% palladium-charcoal catalyst at atmospheric pressure for 3 h. The catalyst was filtered off and the filtrate was evaporated to dryness *in vacuo*. The residue was dissolved in a mixture of *N,N*-dimethylformamide (40 ml) and dimethyl sulfoxide (20 ml), and mixed with benzyloxycarbonylasparagine *p*-nitrophenyl ester[20] (5.40 g, 14.0 mmol). The solution was stirred overnight at room temperature, and then poured into a large volume of ethyl acetate. The precipitate formed was collected by filtration; wt 9.20 g (94.0%). The crude material was dissolved in a boiling mixture of *N,N*-dimethylformamide (200 ml) and water (100 ml), and insoluble material was filtered off. The filtrate was mixed with ethyl acetate (250 ml), and allowed to stand overnight in a refrigerator. The precipitate formed was collected by filtration; wt 6.70 g (68.4%); mp 245—246 °C (decomp); $[\alpha]_D^{27}$ −21.0° (*c* 1.0, *N,N*-dimethylformamide). Amino acid ratio: Asp, 1.00 (1); Thr, 2.00 (2); Glu, 1.07 (1); Ala, 1.00 (1).

Found: C, 50.38; H, 6.39; N, 13.96%. Calcd for $C_{29}H_{43}O_{12}N_7 \cdot 0.5H_2O$: C, 50.43; H, 6.42; N, 14.20%.

N$^{\alpha}$-Benzyloxycarbonyl-β-t-butylaspartylglycine t-Butoxycarbonylhydrazide (VIII). A solution of glycine *t*-butoxycarbonylhydrazide[23] (14.5 g, 76.7 mmol) in *N,N*-dimethylformamide (150 ml) was mixed with benzyloxycarbonyl-β-*t*-butylaspartic acid *N*-hydroxysuccinimide ester[22] (32.2 g, 76.7 mmol). The solution was stirred for 50 min at room temperature and concentrated to a syrup *in vacuo*, and this was dissolved in ethyl acetate. The solution was washed successively with 0.1 M hydrochloric acid, 5% aqueous sodium hydrogencarbonate, and water, and then dried over anhydrous sodium sulfate. The dried solution was concentrated to an oily residue *in vacuo*, and this was treated with hexane to give an amorphous powder; wt 35.8 g (94.2%); mp 60—65 °C.

Benzyloxycarbonylthreonyl-β-t-butylaspartylglycine t-Butoxycarbonylhydrazide (IX). Compound VIII (35.3 g, 71.3 mmol) was dissolved in methanol (1 liter) and hydrogenated over a 5% palladium-charcoal catalyst at atmospheric pressure. The catalyst was filtered off and the filtrate was concentrated to a syrup *in vacuo*. This was dissolved in *N,N*-dimethylformamide (170 ml). On the other hand, benzyloxycarbonylthreonine hydrazide[21] (19.1 g, 71.5 mmol) was suspended in *N,N*-dimethylformamide (200 ml) and cooled to −30 °C. To the cooled suspension were added 3.90 M HCl in dioxane (55.0 ml) and then isopentyl nitrite (10.1 ml). After 15 min a solution of *N*-methylmorpholine (21.7 g) in *N,N*-dimethylformamide (20 ml) and then the solution obtained above were added. The mixture was stirred for 48 h at 0 °C, and then diluted with ethyl acetate. The diluted mixture was washed successively with 0.1 M hydrochloric acid, 5% aqueous sodium hydrogencarbonate, and water, and dried over anhydrous sodium sulfate. The dried solution was concentrated to a syrup *in vacuo*. The syrup was triturated in ethyl acetate and ether; wt 25.7 g (60.5%); mp 107—109 °C; $[\alpha]_D^{10}$ −19.3° (*c* 1.0, ethyl acetate).

Found: C, 54.53; H, 7.03; N, 11.69%. Calcd for $C_{27}H_{41}O_{10}N_5$: C, 54.44; H, 6.94; N, 11.76%.

Benzyloxycarbonylasparaginylthreonyl-β-t-butylaspartylglycine t-Butoxycarbonylhydrazide (X). Compound IX (10.7 g, 18.0 mmol) was dissolved in methanol (700 ml) and hydrogenated over a 5% palladium-charcoal catalyst at atmospheric pressure. The catalyst was filtered off and washed with methanol. The filtrate and washings were combined and concentrated to a syrup under reduced pressure, and the syrup was dissolved with benzyloxycarbonylasparagine *p*-nitrophenyl ester[20] (8.40 g, 21.7 mmol) in *N,N*-dimethylformamide (40 ml). The solution was stirred overnight at room temperature, and then concentrated to a residue under reduced pressure. The residue was triturated in ethyl acetate and ether; wt 11.3 g (85.0%). The powder obtained was reprecipitated from ethanol and water; wt 7.70 g (57.9%); mp 121—125 °C; $[\alpha]_D^{27}$ −22.1° (*c* 1.0, *N,N*-dimethylformamide).

Found: C, 50.33; H, 6.74; N, 13.02%. Calcd for $C_{31}H_{47}O_{12}N_7 \cdot 1.5H_2O$: C, 50.53; H, 6.84; N, 13.31%.

N$^{\alpha}$-Benzyloxycarbonyl-N$^{\omega}$-tosylarginylasparaginylthreonyl-β-t-butylaspartylglycine t-Butoxycarbonylhydrazide (XI). N$^{\alpha}$-Benzyloxycarbonyl-N$^{\omega}$-tosylarginine[24] (3.70 g, 7.99 mmol) and *N*-hydroxysuccinimide (0.92 g, 8.0 mmol) were dissolved in tetrahydrofuran (6 ml). The solution was cooled to −10 °C and then mixed with dicyclohexylcarbodiimide (1.70 g, 8.25 mmol). The solution was stirred for one hour at −10 °C and then for one hour at room temperature. The precipitate formed was filtered off and the filtrate was concentrated to a solid residue *in vacuo*. The residue was dissolved in *N,N*-dimethylformamide (10 ml) with the material which was obtained by hydrogenation of compound X (3.60 g, 4.89 mmol) over a 5% palladium-charcoal catalyst at atmospheric pressure. The solution was stirred for 4 h at room temperature and then concentrated to a small volume *in vacuo*. The residue was diluted with ethyl acetate and washed with 0.1 M hydrochloric acid, and water, and then dried over anhydrous sodium sulfate. The dried solution was concentrated to a gelatinous solid *in vacuo*, and this was collected by filtration; wt 4.50 g (89.3%). The crude material was reprecipitated from ethanol and water; wt 3.30 g (65.5%); mp 148—151 °C; $[\alpha]_D^{10}$ −19.2° (*c* 1.1, *N,N*-dimethylformamide). Amino acid ratio: Asp, 1.94 (2); Thr, 0.92 (1); Gly, 1.00 (1); Arg, 1.02 (1).

Found: C, 51.38; H, 6.59; N, 15.00; S, 3.09%. Calcd for $C_{44}H_{65}O_{15}N_{11}S \cdot 0.5H_2O$: C, 51.35; H, 6.46; N, 14.97; S, 3.12%.

Benzyloxycarbonylasparaginyl-N$^{\omega}$-tosylarginylasparaginylthreonyl-β-t-butylaspartylglycine t-Butoxycarbonylhydrazide (XII). Compound XI (3.25 g, 3.16 mmol) was dissolved in methanol (300 ml) and hydrogenated over a 5% palladium-charcoal catalyst at atmospheric pressure. The catalyst was filtered off and the filtrate was concentrated to a syrup under reduced pressure. The syrup was dissolved with benzyloxycarbonylasparagine *p*-nitrophenyl ester[20] (1.41 g, 3.64 mmol) in *N,N*-dimethylformamide (7 ml). The solution was stirred for 24 h at room temperature, and then concentrated to a residue *in vacuo*. The residue was collected with ethanol; wt 1.80 g (50.0%). The crude product was reprecipitated from *N,N*-dimethylformamide and ethanol; wt 1.60 g (44.4%); mp 190—191 °C; $[\alpha]_D^{23}$ −24.4° (*c* 1.0, *N,N*-dimethylformamide). Amino acid ratio: Asp, 3.09 (3); Thr, 1.02 (1); Gly, 1.00 (1); Arg, 0.96 (1).

Found: C, 50.35; H, 6.48; N, 16.03; S, 2.80%. Calcd for $C_{48}H_{71}O_{17}N_{13}S \cdot 0.5H_2O$: C, 50.45; H, 6.34; N, 15.93; S, 2.80%.

Benzyloxycarbonyl-O-benzyltyrosylglycine t-Butyl Ester (XIII). Glycine *t*-butyl ester, prepared by the hydrogenation of benzyloxycarbonylglycine *t*-butyl ester[27] (11.8 g, 44.5 mmol) over a 5% palladium-charcoal catalyst at atmospheric pressure, was dissolved with benzyloxycarbonyl-*O*-benzyltyrosine *p*-nitrophenyl ester[26] (19.0 g, 36.0 mmol) in *N,N*-dimethylformamide (60 ml). The solution was stirred overnight at room temperature, and then concentrated to a syrup *in vacuo*. The syrupy residue was dissolved in ethyl acetate, and washed successively with 0.1 M hydrochloric acid, 5% aqueous sodium hydrogencarbonate, and water, and then dried over anhydrous sodium sulfate. The dried solution was concentrated to a crystalline residue *in vacuo*; wt 15.8 g (84.5%); mp 120—121 °C; $[\alpha]_D^{13}$ −13.4° (*c* 1.0, ethanol).

Found: C, 69.33; H, 6.60; N, 5.35%. Calcd for $C_{30}H_{34}$-

O_6N_2: C, 69.48; H, 6.61; N, 5.40%.

N^{α}-Benzyloxycarbonyl-β-t-butylaspartyltyrosylglycine t-Butyl Ester (XIV). Compound XIII (14.3 g, 27.6 mmol) was dissolved in methanol (500 ml) and hydrogenated over a 5% palladium-charcoal catalyst at atmospheric pressure. The catalyst was filtered off and washed with methanol. The filtrate and washings were combined and concentrated to a syrup *in vacuo*. The syrup was dissolved with benzyloxycarbonyl-β-*t*-butylaspartic acid *N*-hydroxysuccinimide ester[22] (12.8 g, 30.5 mmol) in *N,N*-dimethylformamide (50 ml). The solution was stirred for 24 h at room temperature, and then diluted with ethyl acetate. The diluted solution was washed successively with 0.1 M hydrochloric acid, 5% aqueous sodium hydrogencarbonate, and water, and then dried over anhydrous sodium sulfate. The dried solution was concentrated to a syrup *in vacuo*. The syrup was washed with a mixture of ethyl acetate and hexane, and triturated in hexane. The crude material obtained was reprecipitated from ether and hexane; wt 11.2 g (67.5%); mp 97—99 °C; $[\alpha]_D^{14}$ −35.4° (*c* 1.0, ethanol).

Found: C, 62.19; H, 7.02; N, 6.86%. Calcd for $C_{31}H_{41}O_9N_3$: C, 62.09; H, 6.89; N, 7.01%.

Benzyloxycarbonylserylthreonyl-β-t-butylaspartyltyrosylglycine t-Butyl Ester (XV). Benzyloxycarbonylserylthreonine hydrazide[25] (4.61 g, 13.0 mmol) was suspended in *N,N*-dimethylformamide (40 ml) and cooled to −20 °C. Then 3.90 M HCl in dioxane (10 ml) was added. The resulting clear solution was mixed with isopentyl nitrite (1.82 ml) and stirred for 20 min at the same temperature. Then a solution of *N*-methylmorpholine (1.37 g) in *N,N*-dimethylformamide (5 ml) was added. The solution was mixed with a solution in *N,N*-dimethylformamide (30 ml) of the material obtained by hydrogenation of compound XIV (8.40 g, 14.0 mmol) over a 5% palladium-charcoal catalyst. The solution was stirred for 48 h at 0 °C, and then poured into cold water. The precipitate formed was collected by filtration; wt 6.70 g (64.4%). The crude product was reprecipitated from *N,N*-dimethylformamide and water; wt 6.00 g (57.5%); mp 174—176 °C; $[\alpha]_D^{24}$ −13.5° (*c* 1.0, *N,N*-dimethylformamide). Amino acid ratio: Asp, 1.11 (1); Thr, 1.05 (1); Ser, 1.02 (1); Gly, 1.00 (1); Tyr, 0.97 (1).

Found: C, 57.33; H, 6.85; N, 8.93%. Calcd for $C_{38}H_{53}O_{13}N_5 \cdot 0.5H_2O$: C, 57.27; H, 6.83; N, 8.79%.

Benzyloxycarbonylphenylalanyl-γ-t-butylglutamylserylasparaginyl-phenylalanine Hydrazide (XVI). A solution of compound IV (4.23 g, 4.90 mmol) in *N,N*-dimethylformamide (50 ml) was cooled to 0—5 °C in an ice-bath, and then 80% hydrazine hydrate (2 g) was added. The solution was stirred for 24 h at room temperature, and then the precipitate formed was collected by filtration and washed with ethanol. The product was boiled in hot ethanol, and then cooled and filtered; wt 4.15 g (100%); mp 238—240 °C (decomp).

Found: C, 59.61; H, 6.49; N, 13.29%. Calcd for $C_{42}H_{54}O_{11}N_8$: C, 59.56; H, 6.43; N, 13.23%.

Benzyloxycarbonylphenylalanyl-γ-t-butylglutamylserylasparaginyl-phenylalanylasparaginylthreonylglutaminylalanylthreonine Methyl Ester (XVII). Compound XVI (1.27 g, 1.50 mmol) was suspended in *N,N*-dimethylformamide (4 ml) and cooled to −20 °C. Then 3.90 M HCl in dioxane (1.15 ml) and isopentyl nitrite (0.212 ml) were added. The mixture was stirred for 80 min at the same temperature and insoluble material was filtered off. The filtrate was mixed with *N*-methylmorpholine (0.46 g) and then with a solution in a mixture of *N,N*-dimethylformamide (5 ml) and dimethyl sulfoxide (1 ml) of the material obtained by hydrogenation of compound VII (1.36 g, 1.97 mmol) over a 5% palladium-charcoal catalyst at atmospheric pressure. The mixture was stirred for 48 h at 0 °C, and then poured into cold water. The precipitate formed was filtered off and washed with 0.1 M hydrochloric acid and water; wt 1.60 g (77.3%). The crude material was reprecipitated repeatedly from *N,N*-dimethylformamide and water; wt 1.04 g (50.2%); mp 233 °C (sintered) and 248 °C (decomp); $[\alpha]_D^{18}$ −10.7° (*c* 0.42, dimethyl sulfoxide). Amino acid ratio: Asp, 1.98 (2); Thr, 1.93 (2); Ser, 0.89 (1); Glu, 2.02 (2); Ala, 0.97 (1); Phe, 2.00 (2).

Found: C, 54.65; H, 6.44; N, 13.08%. Calcd for $C_{63}H_{87}O_{21}N_{13} \cdot H_2O$: C, 54.81; H, 6.50; N, 13.19%.

Benzyloxycarbonylphenylalanyl-γ-t-butylglutamylserylasparaginyl-phenylalanylasparaginylthreonylglutaminylalanylthreonine Hydrazide (XVIII). Compound XVII (0.92 g, 0.67 mmol) was dissolved in a mixture of dimethyl sulfoxide (60 ml) and *N,N*-dimethylformamide (10 ml) and mixed with 80% hydrazine hydrate (5 g). The solution was stirred for 48 h at room temperature, concentrated to a small volume *in vacuo*, and mixed with ethanol. The precipitate formed was boiled in ethanol and collected by filtration; wt 0.87 g (94%); mp 240 °C (sintered) and 246—247 °C (decomp).

Found: C, 53.22; H, 6.55; N, 14.74%. Calcd for $C_{62}H_{87}O_{20}N_{15} \cdot 2H_2O$: C, 53.25; H, 6.56; N, 15.02%.

Benzyloxycarbonylasparaginyl-N^{ω}-tosylarginylasparaginylthreonyl-aspartylglycine Hydrazide Trifluoracetate (XIX). Compound XII (0.60 g, 0.53 mmol) was dissolved in cold trifluoracetic acid (8 ml). The solution was stirred for 40 min at room temperature, and then concentrated to a syrup *in vacuo*. The syrup was triturated in ether; wt 0.57 g (95.0%).

Asparaginylarginylasparaginylthreonylaspartylglycylserylthreonyl-aspartyltyrosylglycine (XX). Compound XIX (0.57 g, 0.52 mmol) was suspended in *N,N*-dimethylformamide (2 ml), cooled to −20 °C and mixed with 3.90 M HCl in dioxane (0.40 ml). The clear solution was mixed with isopentyl nitrite (0.074 ml) and stirred for 20 min at the same temperature. Then, the solution was mixed with *N*-methylmorpholine (0.32 g) and with a solution in *N,N*-dimethylformamide (1 ml) of the material (0.41 g, 0.63 mmol) prepared by hydrogenation of compound XV over a 5% palladium-charcoal catalyst. The solution was stirred for 48 h at 0 °C and poured into cold 0.1 M hydrochloric acid. The precipitate formed was collected by filtration; wt 0.64 g (77%). The crude product was reprecipitated from *N,N*-dimethylformamide and ethanol; wt 0.53 g (64%). Amino acid ratio: Asp, 4.35 (4); Thr, 2.05 (2); Ser, 0.99 (1); Gly, 2.00 (2); Tyr, 0.92 (1); Arg+Orn, 0.76 (1). The protected peptide (161.1 mg) was steeped in anisole (0.46 ml) and dissolved in cold trifluoracetic acid (10 ml). The solution was stirred for 60 min at room temperature, and then concentrated to a syrup *in vacuo*. The syrup was triturated in ether; 140.3 mg. The powder and anisole (0.5 ml) were put into the Daiflon cylinder of an HF-reaction apparatus.[15] Anhydrous hydrogen fluoride (5 ml) was distilled into the cylinder cooled to −78 °C in a Dry Ice and methanol bath. The contents of the cylinder were stirred for 60 min at −15 °C, and then the hydrogen fluoride was evaporated off *in vacuo*. The residue was dissolved in 1 M acetic acid and washed with ether. Then, the solution was applied to a column of Amberlite IR-45 (acetate cycle) and eluted with 1 M acetic acid. The eluate was lyophilized; wt 111.8 mg. The lyophilized material (35.0 mg) was dissolved in water (1 ml) and charged on a column of diethylaminoethylcellulose (OH^- cycle, 0.7×10 cm). The column was eluted with a linear gradient from water (150 ml) to 0.2 M ammonium acetate (150 ml). The fractions (from 33 ml to 58 ml) of the eluate with absorption at 274 nm were collected and lyophilized; wt 29.3 mg. Thin layer chromatography: R_f 0.18 in 1-butanol: acetic acid: pyridine: water (15: 3: 10: 12, by volume) and 0.08 in phenol: water (3: 1, by volume);

paper electrophoresis: $R_{f,ala}$ 1.7 (0.2 M acetic acid, 14 V/cm); $[\alpha]_D^{18}$ −33.5° (*c* 0.55, water). Amino acid ratio: Asp, 4.06 (4); Thr, 1.94 (2); Ser, 0.93 (1); Gly, 2.00 (2); Tyr, 0.89 (1); Arg, 1.03 (1).

Found: C, 43.35; H, 6.18; N, 17.63%. Calcd for $C_{46}H_{70}O_{22}N_{16}\cdot 4H_2O$: C, 43.39; H, 6.14; N, 17.43%.

Phenylalanylglutamylserylasparaginylphenylalanylasparaginylthreonylglutaminylalanylthreonylasparaginylarginylasparaginylthreonylaspartylglycylserylthreonylaspartyltyrosylglycine (XXI). Compound XVIII (0.82 g, 0.59 mmol) was suspended in a mixture of dimethyl sulfoxide (3.3 ml) and *N,N*-dimethylformamide (1 ml), cooled to −10 °C and mixed with 4.74 M HCl in dioxane (0.45 ml) and isopentyl nitrite (0.09 ml). The mixture was stirred for 60 min at −20 °C and then mixed with a solution of compound XX (0.53 g, 0.42 mmol) in dimethyl sulfoxide (2.1 ml) and *N,N*-dimethylformamide (0.5 ml), and then with a solution of *N*-methylmorpholine (0.26 g) in dimethyl sulfoxide (0.5 ml). The mixture was stirred for 3 days at 0 °C, and then poured into cold 0.1 M hydrochloric acid. The precipitate formed was collected by filtration and dried over P_2O_5; wt 0.84 g. The crude product (403.1 mg) and anisole (0.62 ml) were treated with hydrogen fluoride (5 ml) at −10 °C for 60 min in an HF-reaction apparatus.[15] Hydrogen fluoride was distilled off, and the residue was dissolved in aqueous formic acid and lyophilized; wt 411.8 mg. The freeze-dried powder was dissolved in 50% acetic acid, charged on a column of Sephadex G-25 (2×130 cm) and eluted using the same solvent. The fractions shaded in Fig. 6, with an absorption at 274 nm, were collected and lyophilized; wt 93.5 mg. The lyophilized powder (46.4 mg) was dissolved in water and charged on a column of carboxymethyl-cellulose (H^+ cycle, 15×170 mm). The column was eluted with a linear gradient from water (150 ml) to 50% acetic acid (150 ml). The portions shaded in Fig. 7 with an absorption at 274 nm were collected and lyophilized; wt 22.4 mg; R_f (TLC) 0.18 in 1-butanol: acetic acid: pyridine: water (15: 3: 10: 12, by volume); $R_{f,ala}$ (paper electrophoresis) 1.1 (0.2 M acetic acid, 14 V/cm). Amino acid ratio: Asp, 5.84 (6); Thr, 3.85 (4); Ser, 1.81 (2); Glu 2.08 (2); Ala, 1.00 (1); Gly, 1.92 (2); Tyr, 0.87 (1); Phe, 1.92 (2); Arg, 1.00 (1).

References

1) S. Shinka, M. Imanishi, N. Miyagawa, T. Amano, M. Inoue, and A. Tsugita, *Biken J.*, **10**, 89 (1967).

2) H. Fujio, M. Imanishi, K. Nishioka, and T. Amano, *Biken J.*, **11**, 207 (1968).

3) R. Arnon and M. Sela, *Proc. Natl. Acad. Sci. U. S. A.*, **62**, 163 (1969).

4) N. Sakato, H. Fujio, and T. Amano, *Biken. J.*, **15**, 135 (1972).

5) M. Z. Atassi, A. F. S. A. Habeeb, and K. Ando, *Biochim. Biophys. Acta*, **303**, 203 (1973).

6) H. Fujio, R. E. Martin, Y. -M. Ha, N. Sakato, and T. Amano, *Biken J.*, **17**, 73 (1974).

7) Y. -M. Ha, H. Fijio, N. Sakato, and T. Amano, *Biken J.*, **18**, 47 (1975).

8) R. Arnon, E. Maron, M. Sela, and C. B. Anfinsen, *Proc. Natl. Acad. Sci. U. S. A.*, **68**, 1450 (1971).

9) M. Z. Atassi, J. Koketsu, and A. F. S. A. Habeeb, *Biochim. Biophys. Acta*, **420**, 358 (1976).

10) M. Z. Atassi, C. -L. Lee, and R. -C. Pai, *Biochim. Biophys. Acta.*, **427**, 745 (1976).

11) I. Jauregui-Adell, J. Jolles, and P. Jolles, *Biochim. Biophys. Acta*, **107**, 97 (1965).

12) R. E. Canfield and A. K. Liu, *J. Biol. Chem.*, **240**, 1997 (1965).

13) H. Fujio, Y. Takagaki, Y. -M. Ha, T. Amano, T. Mitaki, and Y. Shimonishi, Proc. 6th Ann. Meeting of the Japanese Soc. Immunol. Abstracts: p. 388 (1976).

14) D. C. Phillips, *Scientific American*, **215**, 78 (1966).

15) S. Sakakibara, Y. Shimonishi, Y. Kishida, M. Okada, and H. Sugihara, *Bull. Chem. Soc. Jpn.*, **40**, 2164 (1967).

16) J. Beacham, G. Cupuis, F. M. Finn, H. T. Storey, C. Yanaihara, N. Yanaihara, and K. Hofmann, *J. Am. Chem. Soc.*, **93**, 5526 (1971).

17) W. Grassmann and E. Wünsch, *Chem. Ber.*, **91**, 462 (1958).

18) W. L. Haas, E. V. Krumkalns, and K. Gerzon, *J. Am. Chem. Soc.*, **88**, 1988 (1966).

19) Th. Wieland and R. Sarges, *Justus Liebigs Ann. Chem.*, **658**, 181 (1962).

20) M. Bodanszky and V. du Vigneaud, *J. Am. Chem. Soc.*, **81**, 2504 (1959).

21) E. Schröder and H. Gibian, *Justus Liebigs Ann. Chem.*, **655**, 211 (1962).

22) K. Hofmann, W. Haas, M. J. Smithers, and G. D. Zanetti, *J. Am. Chem. Soc.*, **87**, 631 (1965).

23) A. M. Felix and R. B. Merrifield, *J. Am. Chem. Soc.*, **92**, 1385 (1970).

24) J. Ramachandran and C. H. Li, *J. Org. Chem.*, **27**, 4006 (1962).

25) F. Marchiori, R. Rocchi, and E. Scoffone, *Gazz. Chim. Ital.*, **93**, 834 (1963).

26) M. Itoh, *Chem. Pharm. Bull.*, **18**, 784 (1970).

27) G. W. Anderson and F. M. Callahan, *J. Am. Chem. Soc.*, **82**, 3359 (1960).

28) The abbreviations used in this report are those recommended by IUPAC-IUB: *J. Biol. Chem.*, **247**, 977 (1972).

29) J. Honzl and J. Rudinger, *Collect. Czech. Chem. Commun.*, **26**, 2333 (1961).

30) S. Moore, D. H. Spackman, and W. Stein, *Anal. Chem.*, **30**, 1185 (1958).

Effects of Pressure on the Disproportionation of Olefins over MoO_3-Al_2O_3 and Re_2O_7-Al_2O_3 Catalysts

Toshiaki SODESAWA, Eisuke OGATA, and Yoshio KAMIYA

Department of Reaction Chemistry, Faculty of Engineering, University of Tokyo, Hongo, Bunkyo-ku, Tokyo 113

(Received October 28, 1976)

The disproportionation of propylene and 1-butene over MoO_3-Al_2O_3 and Re_2O_7-Al_2O_3 catalysts was carried out in order to investigate the effects of reaction pressure in the range from 1.0 to 130 kg/cm^2. The effects of the pressure on the reaction can be identified as two independent of the reaction phase; the catalytic activity increased with the reaction pressure, and the time needed to reach the maximum conversion (T_{max}) as well as the time when the conversion falls to half the maximum value ($\tau_{1/2}$) decreased with the increase in the reaction pressure. It can be concluded that the catalytic activity by the polymers formed over the catalyst falls off rapidly with the increase in the pressure. In both phases, the disproportionation of olefins over the Re_2O_7-Al_2O_3 catalyst exhibits the following features as compared with that over the MoO_3-Al_2O_3 catalyst: (1) a much higher activity at temperatures of 0—140 °C; (2) a much higher selectivity for disproportionation, and (3) a lower apparent activation energy.

The disproportionation of propylene over the MoO_3-Al_2O_3 catalyst shows a high selectivity, but the catalytic activity decreases markedly with the lapse of time.[1] Several methods to improve these defects have been studied— *e.g.*, the addition of third materials and solvents.[2-4] We reported in the previous papers[3,4] that the polymers produced under pressure on MoO_3-Al_2O_3 have high molecular weights.

Hardly studies of the disproportionation of olefins over the Re_2O_7-Al_2O_3 catalyst have been reported. Echigoya and his co-workers observed, however, that the metathesis of isobutene with 2-butene or propylene produces isoamylene in high yields, even at low temperatures.[5,6] In the case of disproportionation over the Re_2O_7-Al_2O_3 catalyst, it was found that the longest catalyst life is attained under the lowest pressure for liquefying the olefins.[7]

In this paper, the disproportionation of propylene or 1-butene was carried out in order to compare the effect of the reaction pressure on the catalytic activity of MoO_3-Al_2O_3 with that of Re_2O_7-Al_2O_3 in the pressure range from 1.0 to 130 kg/cm^2.

Experimental

The MoO_3-Al_2O_3 catalyst was prepared in the way reported in the previous papers.[2-4] The Re_2O_7-Al_2O_3 catalyst was obtained by impregnating the 20% Re content of $HReO_4$ with γ-Al_2O_3 and by then calcining it at 550 °C for 5 h. The atomic ratio of Re to Al was 1 : 25, the same as that of Mo to Al in the case of the MoO_3-Al_2O_3 catalyst. The pretreatment of catalysts before starting the reaction was carried out in a flow of oxygen or air for a few hours, and then in a flow of nitrogen for several hours at 600 °C.

A conventional flow system with a fixed catalyst bed was used as the experimental apparatus. The upper and lower sections of the catalyst bed were filled with γ-Al_2O_3. The reaction products were analyzed by gas chromatography, as has been reported in the previous papers.[2-4]

Results and Discussion

Effects of Pressure. The disproportionation of propylene over the MoO_3-Al_2O_3 catalyst in the pressure range from 1.0 to 130 kg/cm^2 is shown as Figs. 1 and 1′. The relationship of the maximum conversion (Max_{conv}), the time when the conversion attains to its maximum value(T_{max}), and the time when the conversion falls to half its maximum value ($\tau_{1/2}$) is shown in Fig. 2. In both the gas-phase reactions at various GHSV values and the liquid-phase reaction as the same LHSV, the maximum conversion increased with the increase in the pressure, while T_{max} and $\tau_{1/2}$ decreased. In the reaction at 1.05 kg/cm^2, the catalytic activity was markedly more elongated than that at higher pressures. This phenomenon is in good agreement with the following equation suggested by Milanovic and his co-workers:[9]

$$r = \text{Conversion} \times D/22400 \times 273/T \times P/760 \times 1/m$$

D: Total flow rate (ml/h)
T: Reactant temperature (K)
P: Reactant pressure (Torr)
m: Catalyst weight (g).

The molar ratio of butenes to ethylene was 1.03 at 1.05

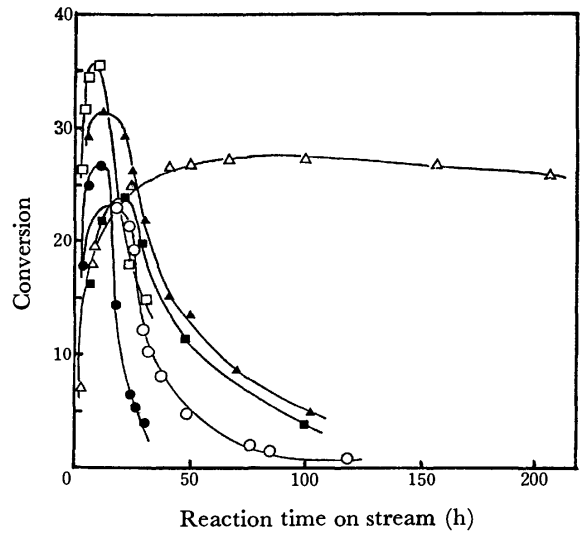

Fig. 1. Effect of pressure on the activity of MoO_3-Al_2O_3 catalyst in the disproportionation of propylene at 80 °C.
●: 130 kg/cm^2, LHSV=30, ○: 80 kg/cm^2, LHSV =30, ■: 50 kg/cm^2, LHSV=30, □: 30 kg/cm^2, GHSV =360, ▲: 15 kg/cm^2, GHSV=720, △: 1.05 kg/cm^2, GHSV=2520.

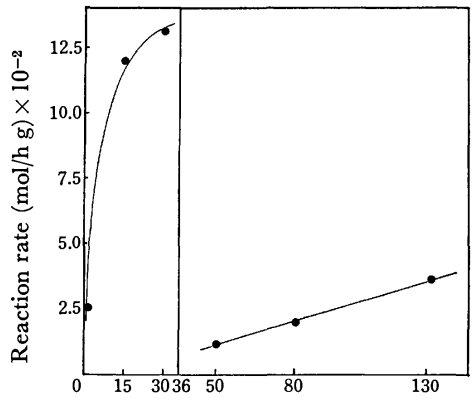

Fig. 1′. Effect of pressure on the activity of MoO_3–Al_2O_3 catalyst in the disproportionation of propylene at 80 °C (calculated from Milanovic's equation).

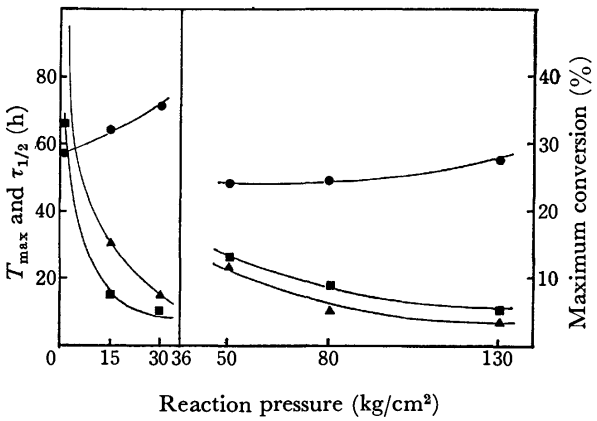

Fig. 2. Effect of pressure on the disproportionation of propylene at 80 °C.
▲: Reaction time when the conversion falls to half its maximum value ($\tau_{1/2}$), ■: reaction time when the conversion attains to maximum value (T_{max}), ●: maximum conversion.

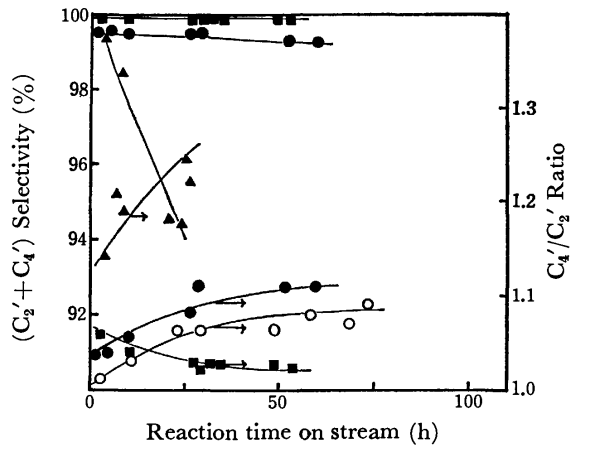

Fig. 3. Effect of pressure on the various values in the disproportionation of propylene over MoO_3–Al_2O_3 catalyst at 80 °C.
▲: 130 kg/cm², ●: 30 kg/cm², ○: 15 kg/cm², ■: 1.05 kg/cm².

kg/cm², but 1.24 at 130 kg/cm². On the other hand, the selectivity to ethylene and butenes under 130 kg/cm² was 94.5%, showing that the selectivity to ethylene and butenes decreases with an increase in the reaction pressure, as is shown in Fig. 3. The amount of the polymers formed over the MoO_3–Al_2O_3 catalyst increased with the reaction pressure. This suggests that the degradation of the catalytic activity results from the polymers formed over the catalyst.[3,4]

We reported in the previous papers[3,4] that the catalyst life of MoO_3–Al_2O_3 was elongated in the presence of solvents and that heptane was the most effective. This indicates that the surface of the MoO_3–Al_2O_3 catalyst is kept clean in the presence of solvents. In the presence of heptane, the effect of the pressure on the conversion of propylene is shown in Fig. 4. At every pressure, the catalyst life of MoO_3–Al_2O_3 was remarkably elongated by the addition of heptane.

The time when the conversion attains to its maximum values under 15 kg/cm² was about twice that under

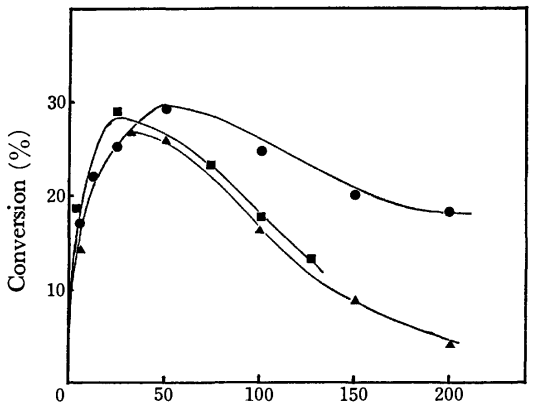

Fig. 4. Effect of pressure on the activity of MoO_3–Al_2O_3 catalyst in the disproportionation of propylene in the presence of heptane at 80 °C.
▲: 50 kg/cm², ■: 30 kg/cm², ●: 15 kg/cm².

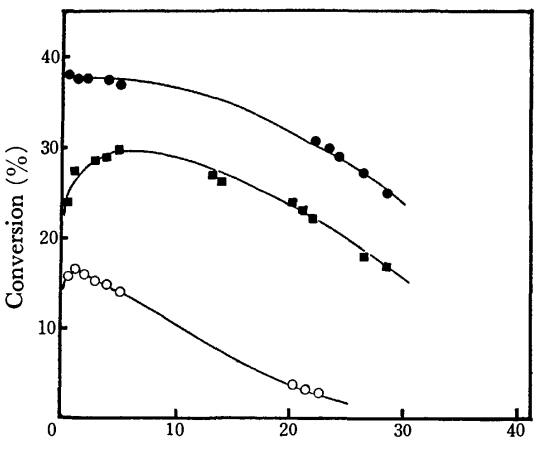

Fig. 5. Gas phase disproportionation of propylene at GHSV=350.
●: Re_2O_7–Al_2O_3, 40 °C, ■: Re_2O_7–Al_2O_3, 0 °C, ○: MoO_3–Al_2O_3, 40 °C.

50 kg/cm². However, it was not observed that the maximum conversion was greatly affected by the reaction pressure. The time when the conversion falls to half its maximum value under 15 kg/cm² was approximately 400 h, five times longer than that under 50 kg/cm².

Gas-phase Reaction of Propylene. In the disproportionation of propylene over the Re_2O_7–Al_2O_3 catalyst, the catalytic activity changed with the reaction time as is shown in Fig. 5. In the reaction at 80 °C the conversion showed approximately the equilibrium value of 44.0%. At the same GHSV of 350, the catalytic activity of the Re_2O_7–Al_2O_3 catalyst was twice the value of the MoO_3–Al_2O_3 catalyst and decreased rather slowly with the reaction time. Even at 0 °C, the Re_2O_7–Al_2O_3 was a considerably active catalyst.

The ratio of *trans*-2-butene to *cis*-2-butene showed a lower value than the equilibrium value at every temperature, indicating that the amount of *trans*-2-butene formed increases with the reaction temperature. The selectivity to ethylene and butenes was 99.5% at a steady state, and the molar ratio of butenes to ethylene was approximately 1.0. These facts show that the disproportionation over the Re_2O_7–Al_2O_3 catalyst is highly selective. The apparent activation energy of the Re_2O_7–Al_2O_3 catalyst obtained from the Arrhenius plots was 2.51 kcal/mol, lower than the 4.09 kcal/mol of the MoO_3–Al_2O_3 catalyst. The selectivity to ethylene and butenes or the ratio of butenes to ethylene was not much affected by the reaction temperature. The ratio of 1-butene in the butenes produced over Re_2O_7–Al_2O_3 was lower than that over MoO_3–Al_2O_3. This seems to show that the Re_2O_7–Al_2O_3 catalyst has fewer active sites for isomerization.

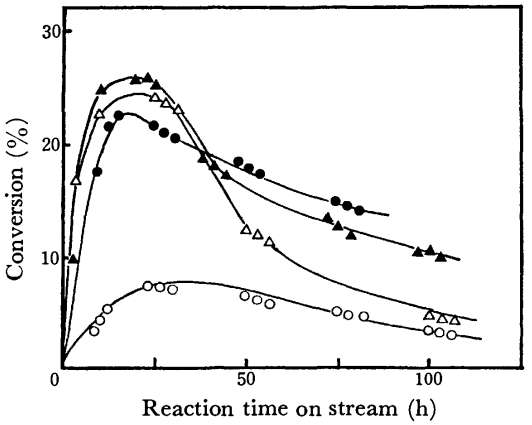

Fig. 6. Comparison of the activity of MoO_3–Al_2O_3 catalyst with that of Re_2O_7–Al_2O_3 catalyst.
△: MoO_3–Al_2O_3, 80 °C, ○: MoO_3–Al_2O_3, 40 °C,
▲: Re_2O_7–Al_2O_3, 80 °C, ●: Re_2O_7–Al_2O_3, 40 °C.

Liquid-phase Reaction of Propylene. In the reaction over Re_2O_7–Al_2O_3 and MoO_3–Al_2O_3 under 50 kg/cm², the catalytic activity changed as is shown in Fig. 6. The difference in catalytic activity between Re_2O_7–Al_2O_3 and MoO_3–Al_2O_3 at 80 °C seems not to be significant. However, in the reaction at 40 °C, the difference becomes larger, suggesting that the difference in apparent activation energy between Re_2O_7–Al_2O_3 and MoO_3–Al_2O_3 is larger than in the case of the gas-phase disproportionation. It can be assumed that Re_2O_7–Al_2O_3 offers a lower activation energy than MoO_3–Al_2O_3. The selectivity to ethylene and butenes in the disproportionation over Re_2O_7–Al_2O_3 at 40 °C was entirely 100%, with the ratio of butenes to ethylene nearly 1.0.

In the liquid-phase reaction, the selectivity to ethylene and butenes was lower than in the gas-phase reaction. This shows that polymerization of propylene or ethylene increases with the reaction pressure, the ratio of butenes to ethylene having a larger value than that in the gas phase. The ratio of *trans*-2-butene to *cis*-2-butene showed a little higher value. It seems that, in the liquid-phase disproportionation, the desorption from the surface of the catalyst does not proceed easily and that the steric hindrance in the reaction is larger than in the gas phase.[10]

As has been mentioned above, it was concluded that the pressure increase in the liquid-phase disproportionation enhances the reaction rate.*

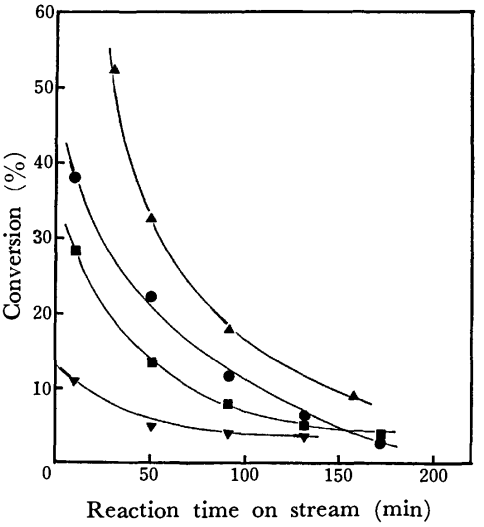

Fig. 7. Dispropornation of 1-butene in the gas phase over Re_2O_7–Al_2O_3 catalyst at GHSV=2000.
▲: 140 °C, ●: 80 °C, ■: 40 °C, ▼: 0 °C.

Gas-phase Reaction of 1-Butene. In the range from 0 to 140 °C, the catalytic activity of Re_2O_7–Al_2O_3 was the highest at 140 °C (Fig. 7); it decreased markedly with a decrease in the reaction temperature. At any temperature the catalytic activity of Re_2O_7–Al_2O_3 was higher than that of MoO_3–Al_2O_3. In the disproportionation of 1-butene, the reaction scheme can be written as follows:

* The relationship between the equilibrium constant K and the pressure P (molar concentration) can be written as follows:[8]

$$\frac{\partial RT\ln K}{\partial P} = -\Delta V.$$

ΔV will have a large negative value in a polymerization where the difference in molecular volume between the original system and the production system is quite high.

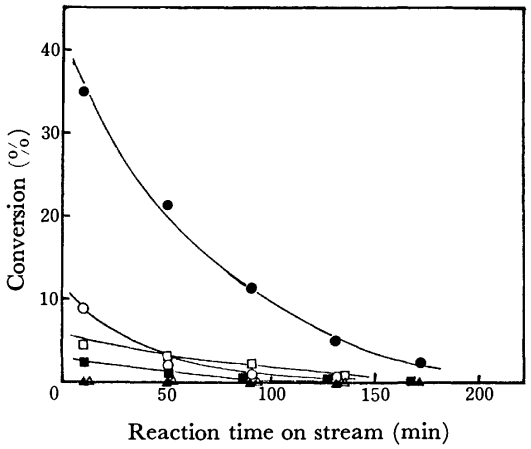

Fig. 8. Disproportionation of 1-butene in the gas phase at 80 °C and GHSV=2000.
Re_2O_7–Al_2O_3: ● Disproportionation, ■ isomerization, ▲ hydrogenation,
MoO_3–Al_2O_3 : ○ disproportionation, □ isomerization, △ hydrogenation.

$$2\ 1\text{-}C_4H_8 \xrightarrow{D_1} C_2H_4 + 3\text{-}C_6H_{12} \quad (D_1)$$

$$1\text{-}C_4H_8 \xrightarrow{I} 2\text{-}C_4H_8 \quad (I)$$

$$C_2H_4 + 2\text{-}C_4H_8 \xrightarrow{D_2} 2\ C_3H_6 \quad (D_2)$$

$$1\text{-}C_4H_8 + 2\text{-}C_4H_8 \xrightarrow{D_3} C_3H_6 + 2\text{-}C_5H_{10} \quad (D_3)$$

$$2\text{-}C_6H_{12} + 1\text{-}C_4H_8 \xrightarrow{D_4} C_3H_6 + C_7H_{14} \quad (D_4)$$

$$2\ C_3H_6 \xrightarrow{P_1} C_6H_{12} \quad (P_1)$$

$$C_2H_4 + C_3H_6 \xrightarrow{P_2} C_5H_{10} \quad (P_2)$$

$$1\text{-}C_4H_8 \xrightarrow{Deh} [C_4H_{8-x}] + x/2\ H_2 \quad (Deh)$$

$$1\text{-}C_4H_8 + H_2 \xrightarrow{Hyd} n\text{-}C_4H_{10} \quad (Hyd)$$

The disproportionation of 1-butene over MoO_3–Al_2O_3 and Re_2O_7–Al_2O_3 is shown in Fig. 8. The relative reactivities in the various reactions may be shown as follows:

Disproportionation ($C_2'+C_6'$)	MoO_3–$Al_2O_3 < Re_2O_7$–Al_2O_3
Isomerization (2-C_4')	$\gg$
Hydrogenation (C_4H_{10})	≈ 0

At a conversion of 13.0%, Re_2O_7–Al_2O_3 showed a higher selectivity to ethylene and hexenes than MoO_3–Al_2O_3, as is shown in Fig. 9. Moreover, the relationship between the yield of the disproportionation products and the yield of the isomerization products is shown in Fig. 10. These figures indicate that a more selective disproportionation occures over the Re_2O_7–Al_2O_3 catalyst than over MoO_3–Al_2O_3.

Liquid-phase Reaction of 1-Butene. The liquid-phase disproportionation of 1-butene over MoO_3–Al_2O_3 was very different from the reaction of propylene. That is to say, in the former case saturated hydrocarbons, such as butane, propane, and isobutane, were produced.[4] The hydrogen produced by dehydrogenation (Deh.) will result in the formation of saturated

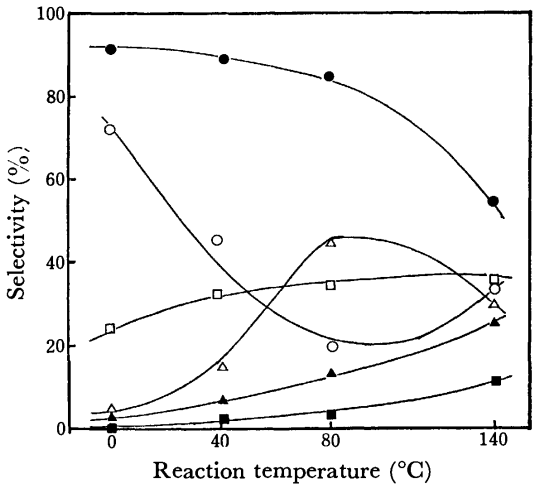

Fig. 9. Disproportionation of 1-butene in the gas phase at 13.0% of conversion.
Re_2O_7–Al_2O_3: ● $C_2'+C_6'$, ▲ $C_3'+C_5'$, ■ 2-C_4'
MoO_3–Al_2O_3: ○ $C_2'+C_6'$, △ $C_3'+C_5'$, □ 2-C_4'.

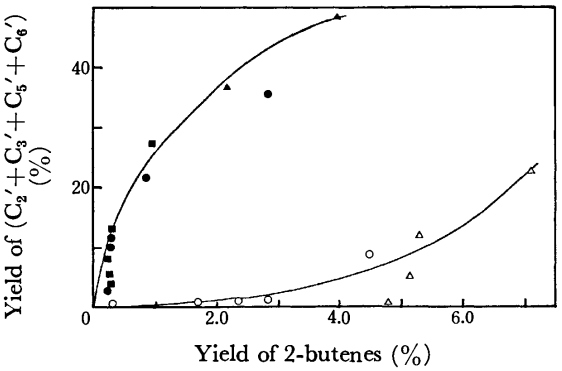

Fig. 10. Disproportionation of 1-butene in the gas phase over Re_2O_7–Al_2O_3 and MoO_3–Al_2O_3 catalyst.
Re_2O_7–Al_2O_3: ▲ 140 °C, ● 80 °C, ■ 40 °C,
MoO_3–Al_2O_3: △ 140 °C, ○ 80 °C.

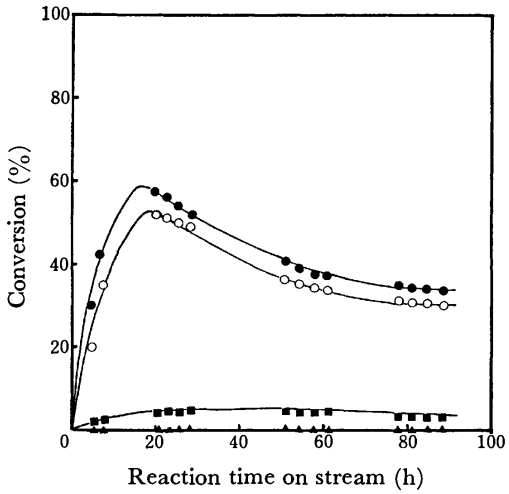

Fig. 11. Liquid phase disproportionation of 1-butene under 50 kg/cm² at 80 °C and LHSV=40.
Re_2O_7–Al_2O_3: ●Total conversion, ○disproportionation, ■isomerization, ▲hydrogenation.

hydrocarbons.[11] From the product distribution, it is estimated that the reaction of 1-butene proceeds not only by means of the D_1 reaction but also by means of the D_3 reaction.

On the other hand, the total conversion over Re_2O_7–Al_2O_3 has shown a maximum at 20 h, then it gradually decreased. Most of the reaction products over Re_2O_7–Al_2O_3 derived from the disproportionation. The difference between the two catalysts for isomerization (I) was not observed clearly, but the catalytic activity of Re_2O_7–Al_2O_3 for hydrogenation was markedly smaller.

From these facts, it seems that the Re_2O_7–Al_2O_3 catalyst is preferable to MoO_3–Al_2O_3 for the disproportionation of 1-butene.

References

1) R. L. Banks and G. C. Bailey, *Ind. Eng. Chem., Prod. Res. Dev.*, **3**, 1970 (1064).
2) T. Sodesawa, E. Ogata, and Y. Kamiya, *Nippon Kagaku Kaishi*, **1975**, 1046.
3) E. Ogata, T. Sodesawa, and Y. Kamiya, *Bull. Chem. Soc. Jpn.*, **49**, 1317 (1976).
4) T. Sodesawa, E. Ogata, and Y. Kamiya, *Bull. Jpn. Petrol. Inst.*, **18**, 162 (1976).
5) R. Nakamura and E. Echigoya, *Chem. Lett.*, **1972**, 273.
6) R. Nakamura, H. Iida, and E. Echigoya, *Nippon Kagaku Kaishi*, **1976**, 221.
7) Japanese Patent No. 42-36725.
8) Y. Kamiya, *Koatsugasu*, **9**, No. 3 (1972).
9) A. Ismayel-Milanovic, J. M. Basset, H. Praliaud, M. Dufaux, and L. De Mourgnnes, *J. Catal.*, **31**, 408 (1973).
10) E. S. Davie, D. A. Whan, and C. Kemball, 5 th International Congress on Catalysis, Preprint, **88**, August (1972).
11) M. Taniewski and M. Otremb, *Tetrahedron Lett.*, **1967**, 1983.

Reaction of Di-*t*-butyl Thioketone with Aryllithium. Effect of Temperature and Solvent

Atsuyoshi OHNO, Kaoru NAKAMURA, Yasumasa SHIZUME, and Sinzaburo OKA
Institute for Chemical Research, Kyoto University, Uji, Kyoto 611
(Received November 4, 1976)

Di-*t*-butyl thioketone reacts with phenyllithium affording both *C*-phenylated and *S*-phenylated products. The product distribution largely depends on the reaction temperature and solvent: the lower the temperature and the more solvated the counter cation, the larger the yield of the *S*-phenylated product. Steric effect is also important: 2,6-dimethylphenyllithium affords only *S*-arylated product. The result has been interpreted in terms of the charge-transfer-intermediate—radical-combination mechanism.

In contrast to carbonyl compounds, thiocarbonyl compounds have abnormal reactivity in the sense that thiocarbonyl-sulfur, in general, reacts with a nucleophile.[1-6]

$$\text{C=S} + \text{Nu}^- \xrightarrow{\text{H}^+} \text{CHSNu}$$

Although several prausible explanations have been proposed for the thiophilic attack of nucleophiles to thiocarbonyl compounds, none of them are satisfactory to explain the reactivity universally. In a previous paper we reported that the charge-transfer (CT)-intermediate —radical-combination mechanism is most prausible for the reaction of thiocarbonyl compounds with nucleophiles.[6] We now wish to report that the preference of the thiophilic attack over the carbophilic attack in the reaction of phenyllithium with di-*t*-butyl thioketone changes largely with the change of reaction temperature or the solvent and the result is consistent with the previously proposed CT-intermediate—radical-combination mechanism.

Results

The reaction of di-*t*-butyl thioketone with phenyllithium in ether afforded two products, 2,2,4,4-tetramethyl-3-phenylpentane-3-thiol (**1**) and di-*t*-butylmethyl phenyl sulfide (**2**).

$$\text{Bu}^t_2\text{C=S} + \text{PhLi} \xrightarrow{\text{ether}} \underset{\textbf{1}}{\text{Bu}^t_2\text{C}(\text{SH})(\text{Ph})} + \underset{\textbf{2}}{\text{Bu}^t_2\text{CHSPh}}$$

The yields depended largely on the reaction temperature: for example, **1** was isolated in 80% yield together with trace amount of **2** from the reaction mixture kept at 30 °C, whereas the reaction at −30 °C resulted in the formation of **2** in 80% yield with trace amount of **1**. It was reported that the reaction at 0 °C aforded **1** and **2** in 25 and 35% yields, respectively.[6,7] It has been confirmed that **2** does not rearrange into **1** under the reaction condition. That is, the reaction mixture at −30 °C was warmed to 30 °C before the addition of water and no difference in the yield was observed from that obtained by quenching the reaction mixture at −30 °C.

$$\text{Bu}^t_2\text{CSPh} \not\longrightarrow \text{Bu}^t_2\text{C}(\text{S}^-)(\text{Ph})$$

Table 1. Reaction of di-*t*-butyl thioketone with phenyllithium in various solvents at 20 °C

Solvent	Yield, %	
	Bu^t_2CH–SPh	Bu^t_2CPh–SH
Ether	trace	75
Tetrahydrofuran	80	trace
Ether–Hexane (1:1)	trace	70
Ether–THF (1:1)	94	
Ether–THF (9:1)	98	
Ether–THF[a]	43	31

a) Mole-equivalent to phenyllithium.

When the reaction at 20 °C was run in tetrahydrofuran (THF), the sole product isolated was **2**. As shown in Table 1, the effect of THF is striking and the presence of an equivalent-to-phenyllithium amount of THF results in the formation of **2** in 43% yield. On the other hand, the presence of nonpolar hexane in a reaction mixture did not affect the product distribution.

The reaction of di-*t*-butyl thioketone with 2,6-dimethylphenyllithium at 20 °C afforded 1,1-dimethyl-2-*t*-butylcyclopropane and 2,6-dimethylphenyl thiol in 40 and 70% yields, respectively. No product expected from the carbophilic attack of a 2,6-dimethylphenyl anion was detected.

Discussion

Since **1** and **2** are kinetically controlled products of the reaction of di-*t*-butyl thioketone with phenyllithium, the ratio of yields (Y_s/Y_c) may reflect the ratio of rate constants (k_s/k_c) for the formations of products, where

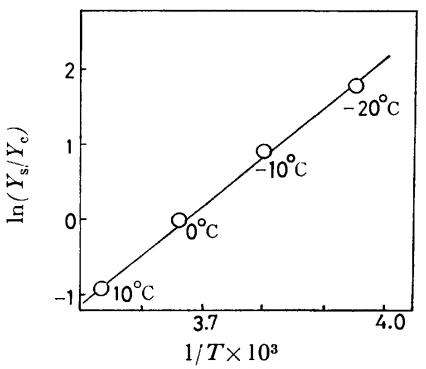

Fig. 1. Temperature-dependency of the ratio of yields of *S*-phenylated and *C*-phehnylated products.

subscripts s and c denote thiophilic and carbophilic attacks, respectively. A plot of $\ln(Y_s/Y_c)$, which is equivalent to $\ln(k_s/k_c)$, against $1/T$ shows a good linear relationship as illustrated in Fig. 1. From the slope and intercept of the line, the differences in apparent parameters of activation were calculated to be -11.2 kcal/mol and -48 e.u. for $\Delta H_s^{\ddagger}-\Delta H_c^{\ddagger}$ and $\Delta S_s^{\ddagger}-\Delta S_c^{\ddagger}$, respectively. Although the absolute values may not represent the real physical meaning, the values indicate, at least qualitatively, that the thiophilic attack is more favored in enthalpy but much less favored in entropy than the carbophilic attack. Since it is not the sulfur atom but the thiocarbonyl-carbon which has bulky substituents, the result may suggest that the transition state for the carbophilic attack resembles the reactant much more than that for the thiophilic attack. In other words, the electronic structure of the reactant may contribute more for the carbophilic attack than for the thiophilic attack. Together with the fact that a nucleophile which has an β-hydrogen reduces di-*t*-butyl thioketone into the corresponding thiol, the above result leads to the conclusion that **3a** is more important canonical form than **3b** for the anion radical of di-*t*-butyl thioketone as previously proposed.[6] That is, a phenyl radical is sterically prevented from the carbophilic attack by two *t*-butyl groups and radical combination takes place with the sulfur atom, although the spin density on this atom is smaller than that on the carbon atom.

$$\mathrm{Bu}^t_2\dot{\mathrm{C}}\text{-}\bar{\mathrm{S}} \longleftrightarrow \mathrm{Bu}^t_2\bar{\mathrm{C}}\text{-}\dot{\mathrm{S}}$$

3a **3b**

The steric inhibition for the carbophilic attack is also recognized in the reaction with 2,6-dimethylphenyllithium: products from the reaction with this reagent indicate that the reaction proceeds only with the thiophilic attack under the condition where phenyllithium attacks on the thiocarbonyl-carbon. Here, two methyl groups on a phenyl ring interfere further the carbophilic attack. However, since these methyl groups still cause steric crowd in the intermediate carbanion **4**,[8] it decomposes either to products or to starting materials.

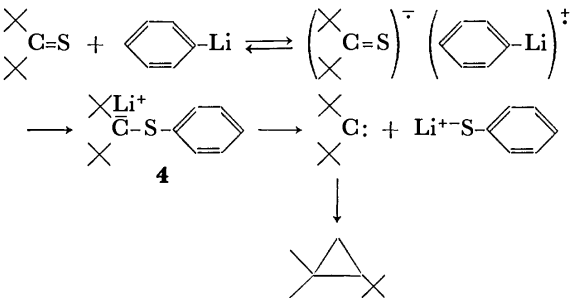

The effect of THF is also understandable with the idea of steric bulk of a nucleophile at the transition state for the carbophilic attack. The cation radical of phenyllithium, which is formed from phenyllithium after the transfer of an electron onto di-*t*-butyl thioketone, still remaines covalent bond character between the lithium and carbon atoms. Since THF has larger ability of solvation than ether, the net bulk of the nucleophile becomes larger in the presence of THF, **5**, than in its

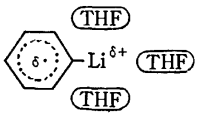

absence and the carbophilic attack is sterically more reduced under the former condition than the latter. The phenomenon is the reverse of that normally observed in nucleophilic attack of anions, where dipolar aprotic solvents make an anion free and reactive by the solvation onto a cation.[9] We believe that this is another support for the presence of a CT-intermediate in the reaction of di-*t*-butyl thioketone with a nucleophile.

Experimental

Reaction of Di-t-butyl Thioketone with Phenyllithium. The reaction was carried out in a thermostat kept at an appropriate temperature. The general procedure was described in a previous paper.[6] Products were analyzed on a VPC (Yanagimoto G-1800; Dexil, 1 m; 150 °C; N_2, 0.4 kg/cm^2).

Reaction of Di-t-butyl Thioketone with 2,6-Dimethylphenyllithium. Into 20 ml of ether solution containing 168 mg (1.5 mmol) of 2,6-dimethylphenyllithium, was added 148 mg (1.0 mmol) of di-*t*-butyl thioketone in 20 ml of ether over a period of 24 h under an atmosphere of nitrogen. After the color of the thioketone had disappeared, 30 ml of water was added to the mixture and organic materials were extracted with ether. The extract was subjected to preparative VPC(Varian 920; Dexil, 1 m; 80 °C) and 50 mg (40% yield) of 1,1-dimethyl-2-*t*-butylcyclopropane. NMR $\delta^{\mathrm{TMS}}_{\mathrm{CCl_4}}$ 0.07—0.9 (3H, m), 0.93 (9H, s), 1.00 (3H, s), and 1.44 (3H, s). Mass spectrum M$^+$: *m/e* 126. Found: C, 85.04; H, 14.43%. Calcd for C_9H_{18}: C, 85.63; H, 14.34%.

The aqueous layer was acidified with dil sulfuric acid and organic materials were extracted with ether. The extract was chromatographed on silica gel with hexane eluent to give 96 mg (70% yield) of 2,6-dimethylphenylthiol. NMR $\delta^{\mathrm{TMS}}_{\mathrm{CCl_4}}$ 2.30 (6H, s), 3.00 (1H, s), and 6.80—6.90 (3H, m).

Support of a part of this research by the Ministry of Education, Japanese Government, with a Scientific Research Grant is acknowledged.

References

1) P. Beak and J. W. Worley, *J. Am. Chem. Soc.*, **94**, 597 (1972) and references cited therein.

2) (a) M. Dagonneau and J. Vialle, *Tetrahedron*, **30**, 3119 (1974); (b) D. Paquer, *Bull. Soc. Chim. Fr.*, **1975**, 1435 and references cited therein.

3) S. Tamagaki, K. Sakai, and S. Oae, *Bull. Chem. Soc. Jpn.*, **46**, 2608 (1973).

4) D. Horton and C. G. Tindall, Jr., *J. Org. Chem.*, **35**, 3558 (1970).

5) J. C. Wesdorp, J. Meijer, P. Vermeer, H. J. T. Bos, L. Brandsma, and J. F. Arens, *Recl. Trav. Chim. Pays-Bas*, **93**, 184 (1974).

6) A. Ohno, K. Nakamura, M. Uohama, S. Oka, T. Yamabe, and S. Nagata, *Bull. Chem. Soc. Jpn.*, **48**, 3718 (1975).

7) A. Ohno, K. Nakamura, M. Uohama, and S. Oka, *Chem. Lett.*, **1975**, 983.

8) Inspection with a CPK model.

9) For example, see (a) H. D. Zook and T. J. Rass, *J. Am. Chem. Soc.*, **82**, 1258 (1960); (b) R. J. Kern, *J. Org. Chem.*, **31**, 1274 (1966); (c) J. C. Martin and D. R. Bloch, *J. Am. Chem. Soc.*, **93**, 451 (1971).

Generation of Ketocarbenoid by α-Elimination of ω,ω-Dibromoacetophenone with Copper, and Trapping by Cycloaddition to Olefins

Nariyoshi KAWABATA,* Tetsuya FUJII, Michiharu NAKA, and Shinzo YAMASHITA
Department of Chemistry, Kyoto Institute of Technology, Matsugasaki, Sakyo-ku, Kyoto 606
(Received December 17, 1976)

Ketocarbenoid was generated by the reaction of ω,ω-dibromoacetophenone with copper in aromatic hydrocarbon, and was trapped by cycloaddition to olefins. This is the first example of cyclopropanation of olefins by formally divalent carbon intermediate without use of diazoketones.

Thermal, photochemical, and catalytic decomposition of diazoketones have been the source of ketocarbenes and carbenoids.[1] The most useful reaction of carbene and carbenoid in synthesis is the cycloaddition to olefins to give the corresponding cyclopropane derivatives. However, in the reaction of the above ketocarbenes and carbenoids with olefins, the yields of acylcyclopropane derivatives are low due to Wolff rearrangement[2] and other side reactions.

On the other hand, α-elimination reaction provides a good route to most classes of carbenes and carbenoids.[1] The metal α-haloenolates of α-haloketones have served as intermediates in a number of synthetically useful reactions such as Darzens condensation and related reactions, but these enolates usually do not decompose to ketocarbenes.[3] Even the addition of copper(I) compounds does not promote their decomposition to ketocarbenes.[3] Charpentier-Morize and Sansoulet[4] reported the formation of 1,2,3-tripivaloylcyclopropane and 1,2,3,4,5,6-hexapivaloylcyclohexane by the reaction of dichloromethyl *t*-butyl ketone with zinc-copper couple in ether. Furukawa and coworkers[5] reported that the reaction of ω,ω-dibromoacetophenone with zerovalent transition metal complexes gave *trans*-1,2,3-tribenzoylcyclopropane, or *trans*-1,2-dibenzoylethylene. Ketocarbene or carbenoid seems to be included as an intermediate of these reactions, but it was not trapped by cycloaddition to olefins. Scott and Cotton[6] reported the formation of ketocarbenoid by α-elimination of α,α-dibromoketone with zinc dust or diethylzinc. The ketocarbenoid was trapped by an intramolecular carbon-hydrogen insertion reaction, but not by the cycloaddition to olefins. The reaction of the ketocarbenoid with olefin was reported to give a substituted dihydrofuran, which represents the product of formal 1,3-dipolar addition of the ketocarbenoid to olefin.[7]

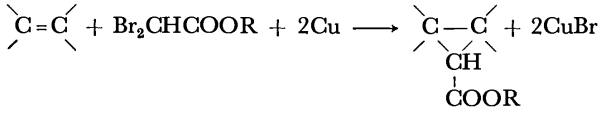

Recently, we found that the reaction of dibromoacetic esters with copper powder in the presence of olefins gave the corresponding alkoxycarbonylcyclopropane derivatives.[8] As an extension of this work, we have investigated the α-elimination of α,α-dihaloketones with copper powder, and found that ketocarbenoid was generated by the reaction and was trapped by cycloaddition to olefins. This is the first example of acylcyclopropanation of olefins by formally divalent carbon intermediate without use of diazoketones.

* To whom correspondence should be addressed.

Results and Discussion

The reaction of ω,ω-dibromoacetophenone with copper powder in toluene at 100 °C for 93 h was found to give acetophenone, benzoic acid, *cis*- and *trans*-1,2-dibenzoylethylene, and *trans*-1,2,3-tribenzoylcyclopropane. In addition, a large amount of unidentified tar was obtained. Most of ω,ω-dibromoacetophenone was consumed under the conditions. This result suggests that the reaction involves ketocarbene or carbenoid intermediate. In order to ascertain the nature of the intermediate, we attempted to trap it by the cycloaddition to olefins.

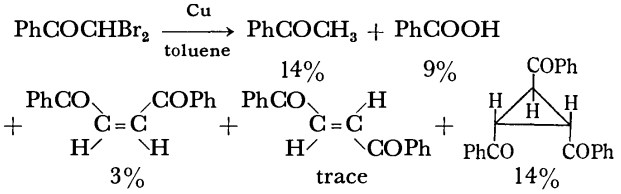

Treatment of *cis*-cyclooctene, ω,ω-dibromoacetophenone, and copper powder in toluene at 100 °C for 93 h gave *exo*-9-benzoyl-*cis*-bicyclo[6.1.0]nonane (**1**) together with ω-1-cycloocten-1-ylacetophenone (**2**) in 12 and 3% yields, respectively, based on the olefin.

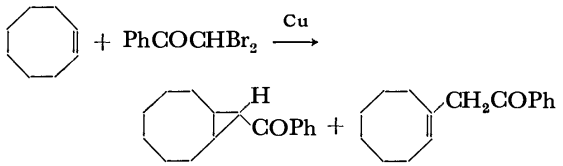

1 **2**

Assignment of the exo stereochemistry of **1** rests on NMR coupling constant arguments. That is, with the aid of a shift reagent, the absorption of the cyclopropane ring proton in the geminal position to the benzoyl group was shown to exhibit a triplet (J=3.5 Hz). The coupling constant is consistent with the exo structure. The *cis* and *trans* coupling constants of the cyclopropane ring protons were reported to be 4—9 and 3—5 Hz, respectively.[9] The coupling constant 3.5 Hz of **1** agrees well with the corresponding coupling constants in the structurely similar cyclopropane derivatives. The absorption of the ring proton in the geminal position to the methoxycarbonyl group of *exo*-9-methoxycarbonyl-*cis*-bicyclo-[6.1.0]nonane, *exo*-8-methoxycarbonylbicyclo[5.1.0]-octane, and *exo*-7-methoxycarbonylbicyclo[4.1.0]-heptane appeared as triplets with the coupling constants of 4.2, 3.9, and 4.2 Hz, respectively.[8] The coupling constants of the corresponding endo isomers were 8.6,

8.3, and 9.4 Hz, respectively.[8]

The endo isomer of **1** was not detected in the reaction mixture. Presumably the steric repulsion between the benzoyl group and the cyclooctane ring is significant.

Treatment of styrene, ω,ω-dibromoacetophenone, and copper powder in ethylbenzene at 100 °C for 120 h gave a 1: 1.6 mixture of *cis*- and *trans*-1-phenyl-2-benzoylcyclopropane in 2% yield based on the olefin. In this case, most of styrene polymerized during the course of the reaction.

Since organocopper intermediates rather than free carbenes are probable intermediates in the reaction of copper powder with diiodomethane, chlorodiiodomethane, and dibromoacetic esters,[8] reaction of ω,ω-dibromoacetophenone with copper powder would also proceed *via* organocopper intermediate (ketocarbenoid of copper) rather than free ketocarbene.

Experimental

Elementary analyses were performed at the Elementary Analysis Center of Kyoto University. IR spectra were recorded on a Hitachi Model 215 grating spectrometer or Japan Spectroscopic Co. Model 402G grating spectrometer. NMR spectra were obtained with a Varian T-60-A spectrometer using tetramethylsilane as an internal standard. Mass spectra were obtained on a Hitachi Model RMU-6 mass spectrometer. Gas chromatographic analysis was carried out on a Shimadzu GC-4A or GC-4B gas chromatograph.

Materials. ω,ω-Dibromoacetophenone was prepared according to the procedure of Taylor.[10] The ordinary commercial grade of copper powder provided by Nakarai Chemicals Ltd., Kyoto, was used without further purification. Olefins and solvents were purified by distillation.

Reaction of ω,ω-Dibromoacetophenone with Copper Powder. Copper powder (11.4 g, 180 mmol) was treated with 0.5 g (2 mmol) of iodine in 50 ml of toluene at room temperature with stirring. After the brown color of iodine disappeared, ω,ω-dibromoacetophenone (22.2 g, 80 mmol) was added, and the mixture was heated at 100 °C for 93 h. After the reaction, the inorganic materials were separated by filtration. Weight of the inorganic materials was 23.7 g after drying, suggesting that most of copper powder was converted to copper(I) bromide under the reaction condition. Solvent and other volatile materials were removed from the organic layer by heating under a reduced pressure, and the residue was dissolved in benzene. Addition of light petroleum ether to this benzene solution gave 1.29 g (14%) of *trans*-1,2,3-tribenzoylcyclopropane as a crystalline solid, which was purified by washing with carbon tetrachloride followed by recrystallization from benzene. It was identified by comparing its IR and NMR spectra with those of an authentic sample.[11] When solvents were removed from the filtrate, 7.26 g of unidentified tar was obtained.

In another run of experiment which was carried out under the same reaction condition, the organic layer was analyzed by gas chromatography. The analysis showed the formation of acetophenone and benzoic acid in 14 and 9% yields, respectively, which were identified by comparing spectral data with those of authentic samples, and the presence of only 1.3% of unchanged ω,ω-dibromoacetophenone in the reaction mixture. The analysis also showed the presence of two minor reaction products in 3% and trace yields, respectively. Spectral data of these products were identical with *cis*- and *trans*-1,2-dibenzoylethylene, respectively.

Reaction of ω,ω-Dibromoacetophenone with Copper Powder in the Presence of cis-*Cyclooctene.* Copper powder (1.14 g, 18.0 mmol), iodine (0.05 g, 0.2 mmol), ω,ω-dibromoacetophenone (2.22 g, 8.0 mmol), and *cis*-cyclooctene (0.44 g, 4.0 mmol) were treated in a similar manner in 3.0 ml of toluene at 100 °C for 93 h, and **1** and **2** were obtained in 12 and 3% yields, respectively, based on the olefin. The yields were determined by gas chromatographic analysis of the reaction mixture. A sample of **1** collected by gas chromatography was analyzed. $n_D^{30}=1.5546$; IR (neat) 1660 cm^{-1} ($\nu_{C=O}$); NMR (CCl_4) τ 2.1 (2H, m), 2.6 (3H, m), 8.0 (3H, m), 8.42 (12 H, m). With aid of a shift reagent, tris(dipivaloylmethanato)europium ($Eu(dpm)_3$), the absorption of the cyclopropane ring proton in the geminal position to the benzoyl group was shown to exhibit a triplet ($J=3.5$ Hz). Found: C, 84.31; H, 9.01%. Calcd for $C_{16}H_{20}O$: C, 84.16; H, 8.83%. A sample of **2** collected similarly from the reaction mixture was also analyzed. NMR (CCl_4) τ 2.1 (2H, m) 2.6 (3H, m), 4.5 (1H, m), 7.04 (2H, s), 7.9 (2H, m), 8.40 (10H, m); IR (neat) 1681 cm^{-1} ($\nu_{C=O}$); MS *m/e* (rel intensity) 228 (7, M^+), 120 (28), 108 (15), 105 (100), 77 (39), 67 (13), 44 (47), 40 (22).

Reaction of ω,ω-Dibromoacetophenone with Copper Powder in the Presence of Styrene. Copper powder (11.4 g, 180 mmol), iodine (0.5 g, 2 mmol), ω,ω-dibromoacetophenone (22.2 g, 80 mmol) and styrene (4.2 g, 40 mmol) were treated in a similar manner in 30 ml of ethylbenzene at 100 °C for 120 h. Gas chromatographic analysis of the reaction mixture showed the presence of two reaction products in a ratio of 1: 1.6 in 2% yield based on the olefin. Spectral data of these two products were consistent with *cis*- and *trans*-1-phenyl-2-benzoylcyclopropane, respectively. A sample of the cis isomer collected from the reaction mixture by gas chromatography was analyzed. NMR (CCl_4) τ 2.1 (2H, m), 2.6 (2H, m), 2.8 (1H, m), 2.91 (5H, narrow m), 7.2 (2H, m), 7.9 (1H, m), 8.7 (1H, m); IR (CCl_4) 1675 cm^{-1} ($\nu_{C=O}$). A sample of the trans isomer collected similarly was also analyzed. NMR (CCl_4) τ 2.1 (2H, m), 2.6 (2H, m), 2.8 (1H, m), 2.83 (5H, narrow m), 7.3 (2H, m), 7.8—9.2 (2H, m); IR (CCl_4) 1670 cm^{-1} ($\nu_{C=O}$).

References

1) W. Kirmse, "Carbene Chemistry," 2nd ed, Academic Press, New York, N. Y. (1971).
2) F. Weygand and H. J. Bestmann, *Angew. Chem.*, **72**, 535 (1960).
3) H. O. House, W. F. Fischer, M. Gall, T. E. McLaughlin, and N. P. Peet, *J. Org. Chem.*, **36**, 3429 (1971).
4) M. Charpentier-Morize and J. Sansoulet, *C. R. Acad. Sci.*, **267**, 1060 (1968).
5) J. Furukawa, A. Matsumura, Y. Matsuoka, and J. Kiji, *Bull. Chem. Soc. Jpn.*, **49**, 829 (1976).
6) L. T. Scott and W. D. Cotton, *J. Am. Chem. Soc.*, **95**, 2708 (1973).
7) L. T. Scott and W. D. Cotton, *J. Am. Chem. Soc.*, **95**, 5416 (1973).
8) N. Kawabata, M. Naka, and S. Yamashita, *J. Am. Chem. Soc.*, **98**, 2676 (1976).
9) H. Weitkamp and F. Korte, *Tetrahedron*, **20**, 2125 (1964).
10) W. Taylor, *J. Chem. Soc.*, **1937**, 304.
11) B. M. Trost, *J. Am. Chem. Soc.*, **88**, 1587 (1966).

NOTES

BULLETIN OF THE CHEMICAL SOCIETY OF JAPAN, VOL. 50 (4), 1007—1008 (1977)

Principal Axes of the EFG Tensors and Torsional Oscillations in Boron Triiodide

Tsutomu OKUDA, Hideta ISHIHARA, Koji YAMADA, and Hisao NEGITA
Department of Chemistry, Faculty of Science, Hiroshima University, Hiroshima 730
(Received October 14, 1976)

Synopsis. The Zeeman effect of ^{127}I NQR and the quadrupole effect of ^{11}B NMR on a single crystal of BI_3 were observed in order to investigate the principal axes of the EFG tensors. The frequencies of the torsional oscillations were determined from the temperature dependence of e^2Qq_{ii}/h.

From X-ray analysis, it is well known that the BI_3 molecule has a planar trigonal structure with D_{3h} symmetry.[1] From the molecular symmetry, it can be expected that the z principal axis of the ^{11}B EFG tensor is consistent with the 3-fold rotation axis of the molecule. Using a single crystal, the direction of the principal axes of the ^{127}I and ^{11}B atoms can be determined experimentally from the Zeeman effect of ^{127}I NQR and the quadrupole effect of ^{11}B NMR, respectively.

The infrared and Raman spectra of BI_3 have been observed and the frequencies of the lattice vibrations were estimated.[2] With regard to these results it appears worthwhile to examine the effect of torsional oscillations from the temperature dependence of e^2Qq_{ii}/h.

Experimental

The NQR spectrometer was a self-quenching, super-regenerative oscillator with frequency modulations; the absorption lines were displayed on an oscilloscope. The temperature dependence of the NQR frequencies was found for a sample which was immersed in petroleum ether cooled to a given temperature using liquid nitrogen. The Zeeman effect was examined by the zero-splitting cone method. A magnetic field of *ca.* 250 G was applied by means of a Helmholtz coil.

Using a broad line NMR spectrometer of Japan Electron Optics Lab. Co., Ltd., the measurement of the ^{11}B NMR was made at 13.00 MHz and the magnetic field was varied to observe the resonance.

Results and Discussion

^{127}I NQR. Two resonance lines for ^{127}I NQR were observed and were attributed to the ν_1 and ν_2 lines, corresponding to the $\pm1/2\leftrightarrow\pm3/2$ and $\pm3/2\leftrightarrow\pm5/2$ transitions, respectively.[3] Each of the resonance lines consisted of a doublet with an intensity ratio of *ca.* 2 to 5 and a frequency difference of *ca.* 25 to 30 kHz at room temperature. They were observed at temperatures ranging from −186 to 23 °C. The cause of the doublet has been attributed to the existence of ^{10}B and ^{11}B in BCl_3 and BBr_3.[4] This is true for BI_3 as well.

Figure 1 shows the zero-splitting pattern of the ν_1 line which was observed at room temperature. Since the derived asymmetry parameter η is 0.460 which is greater than the critical value of 0.412, the direction of the axis

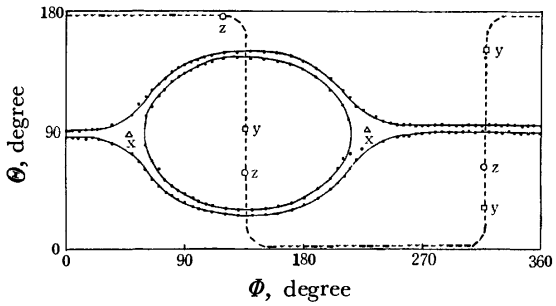

Fig. 1. Zero-splitting pattern of the Zeeman effect on the resonance line, ν_1. The molecular plane is indicated by the broken line.

of the zero-splitting cone is parallel to the y principal axis of the ^{127}I EFG tensor.[5] On the other hand, the direction of the x principal axis of the ^{127}I EFG tensor lies along the 3-fold rotation axis of the molecule. The direction of the z principal axis of the ^{127}I EFG tensor is considered to be parallel to the B–I bond, so that the angle <I–B–I can be obtained from the Zeeman effect, which gives a value of $120\pm0.6°$.

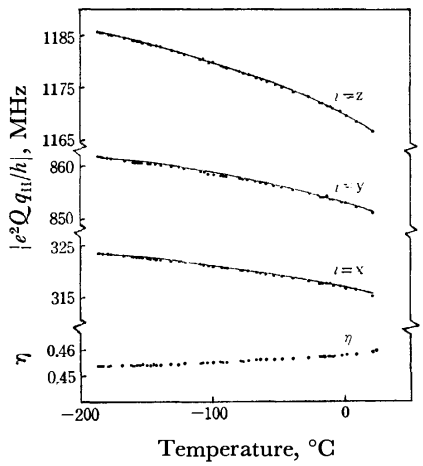

Fig. 2. Temperature dependences of the quadrupole coupling constants and the asymmetry parameter.

The temperature dependence of the quadrupole coupling constants, e^2Qq_{ii}/h (i=x, y, and z) and the asymmetry parameter, η, were derived from the temperature dependence of the ν_1 and ν_2 lines, as shown in Fig. 2. It was found that the absolute temperature coefficients of the quadrupole coupling constants are in the sequence $e^2Qq_{zz}/h>e^2Qq_{yy}/h>e^2Qq_{xx}/h$, and that η increases gradually with temperature. If the

amplitudes of the torsional oscillation about the x, y, and z principal axes of the ^{127}I EFG tensor are denoted by ϑ_x, ϑ_y, and ϑ_z, respectively, the averaged principal values of the EFG tensor can be expressed by the following equations,[6]

$$V_{xx} = eq_0[-(1-\eta_0)/2-\langle\vartheta_z^2\rangle\eta_0+\langle\vartheta_y^2\rangle(3-\eta_0)/2],$$
$$V_{yy} = eq_0[-(1+\eta_0)/2+\langle\vartheta_z^2\rangle\eta_0+\langle\vartheta_x^2\rangle(3+\eta_0)/2], \quad (1)$$
$$\text{and } V_{zz} = eq_0[1-\langle\vartheta_y^2\rangle(3-\eta_0)/2-\langle\vartheta_x^2\rangle(3+\eta_0)/2],$$

where q_0 and η_0 are the values in the static lattice, and the $\langle\vartheta_i^2\rangle$ (i=x, y, and z) indicate the mean square amplitudes of the oscillation about each i principal axis of the EFG tensor. If the torsional oscillations are approximated by harmonic oscillations, $\langle\vartheta_i^2\rangle$ is given by[7]

$$\langle\vartheta_i^2\rangle = h\coth(h\nu_i/2kT)/8\pi^2I_i\nu_i, \quad (2)$$

where the I_i are the moments of inertia about each i principal axis of the inertia tensor and the ν_i are the torsional frequencies. In order to reflect the effect of thermal expansion of the lattice, the ν_i are expressed empirically by

$$\nu_i = \nu_{i0}(1-\alpha_i T), \quad (3)$$

where the α_i are coefficients of expansion. In the case of BI_3, the principal axes of the ^{127}I EFG tensor coincide with the principal axes of the inertia tensor. Considering the molecular symmetry it can be assumed that $\langle\vartheta_y^2\rangle = \langle\vartheta_z^2\rangle$. Thus a best fit using the least-squares method was tried.[8] The following results were obtained: $e^2Qq_0/h = 1190.6\pm1.1$ MHz, $\eta_0 = 0.4518\pm0.0003$, $\nu_{x0} = 46.1\pm2.6$ cm^{-1}, $\nu_{y0}=\nu_{z0}=34.9\pm1.2$ cm^{-1}, $\alpha_x = 0.0012\pm0.0002$ deg^{-1}, and $\alpha_y=\alpha_z=0.0003\pm0.0004$ deg^{-1}. The curves reproduced using these values are shown as full lines in Fig. 2. The standard deviation is between 0.11 and 0.22 MHz. The frequencies of the torsional oscillations obtained above are comparable to those of the R_z and R_{xy} modes of the lattice vibrations.[2] Consequently, it is believed that the effective vibrations for the temperature dependence of the quadrupole coupling constants are in the lattice region.

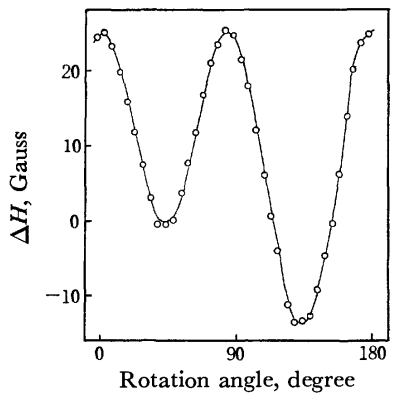

Fig. 3. The rotation pattern of ^{11}B central line.

^{11}B NMR. In ^{11}B NMR, only one central resonance line corresponding to the $m=+1/2\leftrightarrow m=-1/2$ transition was observed and was seen to be affected by the second-order quadrupole interaction. The rotation pattern of the central line was obtained by measuring its shift from the magnetic field corresponding to the Larmor frequency as a function of the rotation angle of the crystal, the results of which are shown in Fig. 3. A second-order frequency shift, $\Delta\nu$, can be represented in terms of the magnetic field by[9]

$$\Delta\nu = -\nu_L(\Delta H/H_L^2)(\Delta H+H_L), \quad (4)$$

where ν_L and H_L are the Larmor frequency of 13.00 MHz and the corresponding magnetic field, respectively. $\Delta H=H_R-H_L$, where H_R is the resonance magnetic field of ^{11}B shifted by the second-order quadrupole interaction. From the molecular symmetry it can be assumed that the asymmetry parameter for ^{11}B is zero. Accordingly, the frequency shifts of the central transition are given by the following equation for $\eta=0$[10]

$$\Delta\nu = -(\nu_Q^2/16\nu_L)(a-3/4)(1-\mu^2)(9\mu^2-1), \quad (5)$$

where $\nu_Q=3e^2Qq/2I(2I-1)h$, $a=I(I+1)$, $\mu=\cos\vartheta$, and ϑ is the angle between the direction of the z principal axis of the EFG tensor and that of the applied magnetic field. From this analysis it is found that the direction of the 3-fold rotation axis of the molecule which was determined by the Zeeman effect of the ^{127}I NQR is consistent with the direction of the z principal axis of the ^{11}B EFG tensor within an experimental error of $\pm0.6°$. The quadrupole coupling constant of the ^{11}B atom obtained was 2.32 ± 0.05 MHz at room temperature. This value differs slightly from 2.40 ± 0.04 MHz at -196 °C.[11] The ratio of e^2Qq_{zz} at -196 °C to that at room temperature is 1.03. This ratio can be explained by the torsional oscillations of the ^{11}B atom about the principal axes of the EFG tensor as follows: assuming $\eta_0=0$, the z component of the quadrupole coupling constant, which is averaged over the torsional oscillation, is given by

$$e^2Qq_{zz} = e^2Qq_0(1-\langle\vartheta_x^2\rangle3/2-\langle\vartheta_y^2\rangle3/2). \quad (6)$$

The x and y principal axes of the ^{11}B EFG tensor lie in the plane of the molecule and it can be assumed that $\langle\vartheta_x^2\rangle=\langle\vartheta_y^2\rangle$. The evaluation of $\langle\vartheta_x^2\rangle$ and $\langle\vartheta_y^2\rangle$ can be derived from the results of the temperature dependence of the ^{127}I NQR. The ratio e^2Qq_{zz} (-196 °C)/e^2Qq_{zz} (23 °C) is found to be 1.02 from Eq. 6.

References

1) M. A. Ring, J. D. H. Donnay, and W. S. Koski, *Inorg. Chem.*, **1**, 109 (1962).
2) O. S. Binbrek, N. Krishnamurthy, and A. Anderson, *J. Chem. Phys.*, **60**, 4400 (1974).
3) W. G. Laurita and W. S. Koski, *J. Am. Chem. Soc.*, **81**, 3179 (1959).
4) T. Chiba, *J. Phys. Soc. Jpn.*, **13**, 860 (1958).
5) K. Shimomura, *J. Phys. Soc. Jpn.*, **14**, 86 (1959).
6) B. L. Barton, *J. Chem. Phys.*, **46**, 1553 (1967).
7) K. R. Jefferey and R. L. Armstrong, *Phys. Rev.*, **174**, 359 (1968).
8) This estimate was tried using the "Least Square Estimation for Non-linear Functions (Powell's Method)" computer program originally written by Mr. Y. Koyanagi of the Tokyo University Computer Centre.
9) M. Kasahara and I. Tatsuzaki, *J. Phys. Soc. Jpn.*, **36**, 786 (1974).
10) M. H. Cohen and F. Reif, *Solid State Physics*, **5**, 321 (1957).
11) P. A. Casabella and T. Oja, *J. Chem. Phys.*, **50**, 4814 (1969).

BULLETIN OF THE CHEMICAL SOCIETY OF JAPAN, VOL. 50 (4), 1009—1010 (1977)

Mesomorphic Properties of 2-(4-*n*-Alkoxybenzylideneamino)anthracenes

Sakumitsu SAKAGAMI and Minoru NAKAMIZO

National Industrial Research Institute of Kyushu, Tosu, Saga 841

(Received October 26, 1976)

Synopsis. 2-(4-*n*-Alkoxybenzylideneamino)anthracenes were synthesized, and the phase transitions were determined using a differential scanning calorimeter and a polarizing microscope. Methoxy through propoxy derivatives exhibit the monotropic nematic state, whereas the higher members show the enantiotropic nematic state.

It is well recognized that the molecules which can form liquid crystalline phases generally possess common structural features. The four structural features that appear essential are; (1) the molecules will be rod-like in shape; (2) they must be rigid; (3) the simultaneous presence of permanent dipoles and easily polarizable groups within a molecule plays an important role, and (4) weak dipoles at the end groups of the molecule are of importance.[1-4] Indeed, the molecules of an unelongated and plate-like shape exhibit no mesomorphic properties. It has, however, been found that naphthalene,[5] fluorene,[6] and phenanthrene,[7] the molecular structures of which are not rod-like, can exhibit liquid crystalline states if one introduces appropriate substituents to them. In order to elucidate the relationship between the molecular structure and the mesomorphic properties, it is of much interest that a liquid crystalline compound can be obtained by introducing the end substituent to the compounds which exhibit potentially non-mesomorphic behavior. In this paper we wish to report first that anthracene, whose molecule is plate-like and is much wider than that of naphthalene or phenanthrene, can indeed exhibit a liquid crystal state if a 4-*n*-alkoxybenzylidene group is introduced at the 2-position.

Experimental

Materials. The 2-(4-*n*-alkoxybenzylideneamino)anthracenes studied here were synthesized from 4-*n*-alkoxybenzaldehyde and 2-aminoanthracene which were themselves commercially obtained by refluxing several hours in a mixed solution of benzene and methanol. The crude products were successively recrystallized from methanol, benzene, and hexane. They were thoroughly dried under a vacuum in order to remove the solvent and any moisture.

Measurements. The transition heat was determined by means of a Rigaku differential scanning calorimeter which was calibrated in terms of the temperature and the energy using potassium nitrate, indium, benzoic acid, and tin. All the samples were packed in closed aluminium sample pans. Each sample was heated and cooled under a flow of nitrogen gas to prevent the decomposition of the sample. The phase transition and the liquid crystal texture were observed by using a polarizing microscope and a Mettler FP 52 microfurnance for sample temperature control.

Results and Discussion

All the compounds studied exhibit the nematic liquid crystal state, except for 2-(benzylideneamino)-

TABLE 1. THERMODYNAMIC DATA FOR A SERIES OF 2-(4-*n*-ALKOXYBENZYLIDENEAMINO)ANTHRACENES

n-Alkoxy	Transition	Transition: Temperature (°C)	Transition: Heat (cal/mol)	Transition: Entropy (cal·K^{-1}·mol^{-1})
Methoxy-	solid-isotropic	202	9550	20.1
	isotropic-nematic	199	76	0.16
Ethoxy-	solid-isotropic	199	7670	16.2
	isotropic-nematic	201	105	0.22
Propoxy-	solid-isotropic	186	8410	18.3
	isotropic-nematic	179	74	0.16
Butoxy-	solid-nematic	177	9140	20.3
	nematic-isotropic	183	91	0.20
Pentyloxy-	solid II-solid I	137	587	1.43
	solid I-nematic	165	8730	19.9
	nematic-isotropic	173	71	0.16
Hexyloxy-	solid II-solid I	124	220	0.55
	solid I-nematic	162	8990	20.7
	nematic-isotropic	174	90	0.20
Heptyloxy-	solid II-solid I	129	1600	3.98
	solid I-nematic	157	8730	20.3
	nematic-isotropic	167	79	0.18
Octyloxy-	solid III-solid II	125	910	2.29
	solid II-solid I	136	530	1.30
	solid I-nematic	154	9450	22.1
	nematic-isotropic	167	102	0.23

1 cal=4.184 J

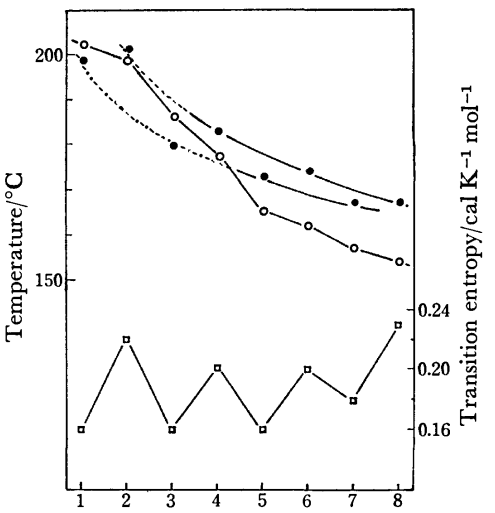

Fig. 1. Phase transition diagram and the transition entropy for 2-(4-*n*-alkoxybenzylideneamino)anthracene series.
○: Solid-nematic or isotropic; ●: nematic-isotropic; □: transition entropy for the nematic-isotropic transition. The dotted lines indicate the monotropic transitions.

anthracene, which gives no mesomorphic state. The phase-transition temperatures are summarized in Table 1, together with the calorimetric data. The first three members in this series show the monotropic nematic state, while the higher members, starting with 2-(4-*n*-butoxybenzylideneamino)anthracene, exhibit the enantiotropic nematic phase. Furthermore, the solid-solid transition is observed for the homologous series with longer alkoxy chains than pentyloxy. This is not surprising since the presence of two or more solid phases is very common with materials forming mesomorphic states.

Figure 1 shows the variation in the transition temperature with the increase in the length of the alkoxy chain. Both the solid-nematic and the nematic-isotropic liquid transition temperatures become lower as the alkoxyl group grows. In addition, an even-odd alternation of the nematic-isotropic liquid transition temperature is apparent. Such an even-odd effect for the nematic-isotropic liquid transition has frequently been found in most homologous series of liquid crystals.[1-4] In particular, for a homologous alkoxy series[1-4,8] each of the clearing points for both even and odd carbon-chain members falls on a smooth curve. In the homologous series of 2-(4-*n*-alkoxybenzylideneamino)-anthracenes studied here, two smooth curves can be drawn, as shown in Fig. 1, one connecting the even carbons and the other connecting the odd carbons. The curve for the even carbons lies above that for the odd carbons, as in other homologous alkoxy series. The even-odd alternation can be understood as a consequence of the even-odd effect in the chain-order parameter with respect to the molecular axis.[9] The entropies of transition for the nematic-isotropic liquid transition are also shown in Fig. 1. As is expected in view of the results mentioned above, the transition entropy shows the even-odd alternation more striking than the transition temperature.

References

1) G. W. Gray, "Molecular Structure and the Properties of Liquid Crystals," Academic Press, New York (1962).
2) G. H. Brown, J. W. Doane, and V. D. Neff, "A Review of the Structure and Physical Properties of Liquid Crystals," Chemical Rubber Co., Cleveland (1971).
3) G. W. Gray, "Liquid Crystals and Plastic Crystals," Vol. 1, ed by G. W. Gray and P. A. Winsor, Ellis Horwood, Chichester (1974), p. 103.
4) D. Demus, H. Demus, and H. Zaschke, "Fluessige Kristalle in Tabellen," Verlag, Leipzig (1974).
5) G. W. Gray and B. Jones, *J. Chem. Soc.*, **1954**, 683; Ch. Wiegand, *Z. Naturforsch.*, **9b**, 516 (1954).
6) G. W. Gray and A. Ibbotson, *J. Chem. Soc.*, **1957**, 393; G. W. Gray, J. B. Hartley, A. Ibbotson, and B. Jones, *ibid.*, **1955**, 4359.
7) G. W. Gray, *J. Chem. Soc.*, **1958**, 552.
8) H. Arnold, *Z. Phys. Chem.*, **226**, 146 (1964); A. J. Herbert, *Trans. Faraday Soc.*, **63**, 555 (1967); W. R. Yound, I. Haller, and A. Aviram, *Mol. Cryst. Liq. Cryst.*, **13**, 357 (1971).
9) D. P. Pink, *J. Chem. Phys.*, **63**, 2533 (1975); S. Marčelja, *ibid.*, **60**, 3599 (1974).

BULLETIN OF THE CHEMICAL SOCIETY OF JAPAN, VOL. 50 (4), 1011—1012 (1977)

The Analytical Application of Oleophilic Quaternary Ammonium Salts. X.[1-9] The Extraction of the Niobium-Pyrocatechol Violet-Tridodecylethylammonium Ternary Complex

Yoshio SHIJO

Department of Industrial Chemistry, Faculty of Engineering, University of Utsunomiya, Ishii-machi, Utsunomiya 321-31

(Received August 20, 1976)

Synopsis. The formation and extraction of the niobium–Pyrocatechol Violet–tridodecylethylammonium ternary complex have been examined. The optimal pH for the extraction is 4—5. The molar absorptivity of the complex is 4.4×10^4 $cm^{-1}\cdot mol^{-1}\cdot l$ at 553 nm. Its composition is estimated to be $Nb(PV)_2(R-\overset{R}{\underset{R}{N}}-R')_3$.

Pyrocatechol Violet (PV) reacts with niobium[10] to form a violet chelate which is suitable for photometric determination. The sensitivity of the color reaction increases upon the addition of a long-chain quaternary ammonium salt.[11] Many papers[12-15] have been published on the extraction of Pyrocatechol Violet chelate anions with large organic cations. The lack of information on the extraction of ionic associates in the case of the niobium–Pyrocatechol Violet chelate anion with large organic cations, however, led us to carry out the present investigation. Furthermore, the investigation of the extraction of the metal chelate anions with an oleophilic quaternary ammonium salt such as tridodecylethylammonium bromide (TDEA), its superior extraction efficiency with relation to many chelate anions has been demonstrated. On the extraction of the Pyrocatechol Violet chelate anion with TDEA, we have already reported the spectrophotometric study of copper,[2] tin,[4] aluminum,[5] and zirconium.[8] In this paper, the fundamental conditions for the extraction of niobium as a niobium–PV–TDEA ternary complex with carbon tetrachloride and the composition of the ternary complex will be discussed.

Experimental

Reagent. A 2.5×10^{-3} M niobium solution was prepared by the following procedure. A definite amount of diniobium pentoxide and a small amount of potassium disulfate were placed in a platinum crucible and melted. After cooling, a 104-ml portion of sulfuric acid was added and the solution was diluted to 250 ml with de-ionized water. A working standard solution was prepared as needed by the dilution of the 2.5×10^{-3} M solution with 7.5 M sulfuric acid to each desired concentration. A 5.0×10^{-4} M PV solution was prepared by dissolving the Dotite PV in de-ionized water without further purification. TDEA was prepared, by refluxing for 4 h, to an ethanolic solution of tridodecylamine and ethyl bromide. After the evaporation of the solvent, the salt was recrystallized two times from butyl acetate. The 10^{-3} M TDEA solution was prepared by dissolving the above TDEA in carbon tetrachloride. All the other chemicals used were of a guaranteed-reagent quality.

Apparatus. All the measurements of the absorbance were made with a Hitachi manual spectrophotometer, model Epu-2A. Matched 10-mm absorption cells were used. The pH measurements were made with a Hitachi-Horiba model M-5 glass electrode pH meter.

Standard Procedure. Up to 7 μg of niobium were placed in a 50-ml polyethylene beaker; 0.5 ml of 0.03% hydrogen peroxide, a definite amount of 1 M sulfuric acid, and 3 ml of a 5×10^{-4} M PV solution were then added. The pH of the solution was adjusted to 4.5 by the addition of 2 ml of a 2 M sodium acetate solution and a definite amount of ammonia buffer solution (pH 9). Then the solution was diluted to 25 ml with de-ionized water. The solution was transferred into a 35-ml test tube, and a 5-ml portion of 10^{-3}M TDEA in carbon tetrachloride was added. The extraction was carried out for 5 min by turing the test tube upside down two times per 5 s. After a complete phase separation, the organic layer was taken out and centrifuged for 3 min at 3000 rpm. The extract was transferred into an absorption cell, and the absorbance at 553 nm was measured against the reagent blank.

Results and Discussion

Absorption Spectra. The absorption spectra of the ternary complex extracted into carbon tetrachloride and of the niobium–PV chelate anion in an aqueous solution are given in Fig. 1, along with that of the reagent blank. The ternary complex and the niobium–PV chelate anion have absorption maximum at 553 nm and 562 nm respectively. The absorbance of the ternary complex increases about two times more than that of the niobium–PV chelate anion.

Effect of pH. The effect of the pH on the extraction of the ternary complex with 2×10^{-6} M niobium, 6×10^{-5} M PV in the aqueous phase, and 10^{-3} M TDEA

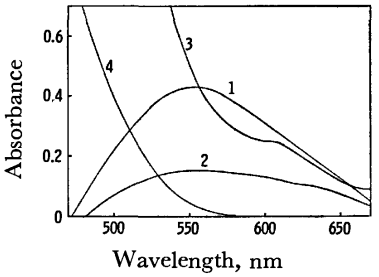

Fig. 1. Absorption spectra of the Nb–PV–TDEA in carbon tetrachloride and the Nb–PV in aqueous solution.
pH=4.5
(1): Nb–PV–TDEA in carbon tetrachloride $[Nb]_w=2\times10^{-6}$ M, (2): Nb–PV in aq soln $[Nb]_w=10^{-5}$ M, (3): PV–TDEA in carbon tetrachloride $[PV]_w=6\times10^{-5}$ M, (4): PV in aq soln $[PV]_w=6\times10^{-5}$ M.

in carbon tetrachloride was examined. The optimum pH range for the extraction is found to be 4—5. The pH dependence of the extraction may change with the change in the reagent concentration. The carbon tetrachloride extract is stable for at least 30 min. The absorbance of the reagent blank in the organic layer increases remarkably with an increase in the pH value.

Organic Solvents. The niobium–PV–TDEA ternary complex can be extracted into such substances as carbon tetrachloride, butyl acetate, carbon disulfide, benzene, and nitrobenzene, but not into 1-butanol, methyl isobutyl ketone, and chloroform.

The Effect of the PV Concentration. The effect of the PV concentration in the aqueous phase on the extraction of the ternary complex was also examined. The absorbance of the extract is constant when the initial aqueous phase is in the concentration range 4×10^{-5}—1×10^{-4} M. The absorbance of the extract gradually decreases, however, upon the further addition of PV.

The Effect of the TDEA Concentration. The effect of the concentration of TDEA in carbon tetrachloride on the extraction of the ternary complex was also examined. The constant and maximum absorbance of the extract is obtained when the organic phase is in the concentration range 5×10^{-4}—2×10^{-3} M.

The Effect of the Mixing Time. The extractability of the ternary complex with 10^{-3} M TDEA in carbon tetrachloride at pH 4.5 is given as a function of the mixing time. The absorbance of the extract is constant for the mixing times from 3 to 10 min.

Extractability and Molar Absorptivity. The extractability of the ternary complex under optimum conditions was examined by the spectrophotometric determination of niobium in the extract with Xylenol Orange after evaporating the organic layer. When a 250-ml portion of an aqueous layer containing 46.5 μg of niobium is mixed with 50 ml of a carbon tetrachloride solution of TDEA, 98.1% of the niobium is extracted by one extraction. The distribution ratio and the molar absorptivity are 2.58×10^{2} and 4.3×10^{4} $cm^{-1}\cdot mol^{-1}\cdot l$ respectively.

Calibration Curve. A calibration curve was made by extracting different amounts of niobium under optimum conditions. A good linear relationship is obtained over the concentration range from 0.58 to 7 μg of niobium per 5-ml portion of carbon tetrachloride. The variation coefficient of the absorbance is 1.3% for the 7 measurements. The effect of foreign ions was also examined. Copper, bismuth, and tin were masked with 2-mercaptoethanol, but uranium, thorium, molybdenum, tungsten, aluminum, iron, and vanadium interfered seriously. Of the anions tested, nitrate, iodide, thiocyanate, and perchlorate interfered considerably, giving a negative error.

The Composition of the Ternary Complex. The molar ratio of the components in the ternary complex was established by the continuous variation method. The results indicate that the molar ratios of niobium to PV to TDEA are 1 : 2 : 3, as is shown in Figs. 2 and 3. The same results were also obtained by the mole-ratio method. The application of the equilibrium-shift method to this system had not been successfully carried out because the complete formation of the ternary complex occurred in a small excess of reagents. Consequently, it may be assumed that the ternary complex is an ion-association system for $\{[Nb(PV)_2]^{3-}\}\cdot\left\{(R-\overset{R}{\overset{|}{N}}{}^{\pm}-R')_3\right\}$.

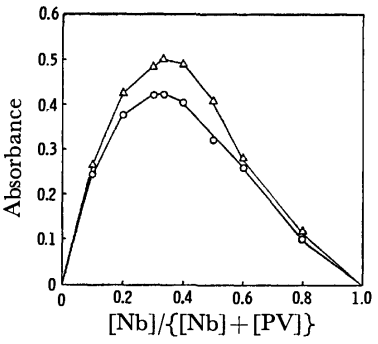

Fig. 2. Continuous variation method applied to the Nb–PV–TDEA system.
$[Nb]_w+[PV]_w=4\times10^{-5}$ M, pH=4.5, —○—: 553 nm, —△—: 590 nm.

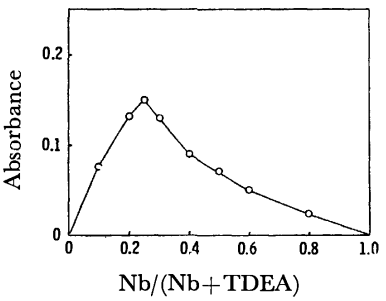

Fig. 3. Continuous variation method applied to the Nb–PV–TDEA system.
$Nb+TDEA=2.5\times10^{-7}$ mol, pH=4.5, 553 nm.

References

1) Part I: Y. Shijo, *Nippon Kagaku Kaishi*, **1974**, 889.
2) Part II: Y. Shijo, *Bull. Chem. Soc. Jpn.*, **47**, 1642 (1974).
3) Part III: Y. Shijo, *Bunseki Kagaku*, **23**, 884 (1974).
4) Part IV: Y. Shijo, *Nippon Kagaku Kaishi*, **1974**, 1658.
5) Part V: Y. Shijo, *Nippon Kagaku Kaishi*, **1974**, 1912.
6) Part VI: Y. Shijo, *Bull. Chem. Soc. Jpn.*, **48**, 1674 (1975).
7) Part VII: Y. Shijo, *Bull. Chem. Soc. Jpn.*, **48**, 2793 (1975).
8) Part VIII: Y. Shijo, *Bull. Chem. Soc. Jpn.*, **49**, 3029 (1976).
9) Part IX: Y. Shijo, *Bunseki Kagaku*, **25**, 680 (1976).
10) A. K. Babko and M. I. Shtokalo, *Ukr. Khim. Zh.*, (*Russ. Ed.*), **29**, 963 (1963); **30**, 220 (1964).
11) R. Nakashima, S. Sasaki, and S. Shibata, *Bunseki Kagaku*, **22**, 729 (1973).
12) H. Kohara, N. Ishibashi, and K. Abe, *Bunseki Kagaku*, **19**, 48 (1970).
13) T. Ishito and K. Tonosaki, *Bunseki Kagaku*, **20**, 689 (1971).
14) M. K. Akhmedli, E. L. Glushchenko, and Z. L. Gasanova, *Zh. Anal. Khim.*, **26**, 1947 (1971).
15) R. Jurevicius, I. Blazis, and C. Valiukevicius, *Zh. Anal. Khim.*, **30**, 708 (1975).

BULLETIN OF THE CHEMICAL SOCIETY OF JAPAN, VOL. 50 (4), 1013—1014 (1977)

The Analytical Application of Oleophilic Quaternary Ammonium Salts. XI.[1] The Extraction of the Iron(III)-Pyrocatechol Violet-Tridodecylethylammonium Ternary Complex

Yoshio SHIJO

Department of Industrial Chemistry, Faculty of Engineering, University of Utsunomiya, Ishii-machi, Utsunomiya 321-31

(Received August 30, 1976)

Synopsis. The ionic associate of the iron(III)–Pyrocatechol Violet chelate anion with tridodecylethylammonium bromide is extracted into methyl isobutyl ketone. The ternary complex has an absorption maximum at 623 nm. The optimum pH for the extraction is 5.7—6.4 The molar absorptivity of the complex is 7.76×10^4 $cm^{-1}\cdot mol^{-1}\cdot l$. Its composition is estimated to be $Fe(PV)_2(R\text{–}\overset{\overset{R}{|}}{N}\text{–}R')_2$.

Pyrocatechol Violet (PV) reacts with many metal ions to form water-soluble chelates. The utility of its extraction-photometric variant in ionic-association systems has been reported by many workers.[2–5] Ishito and Ichinohe[6] studied the formation of the iron(III)–PV chelate in an aqueous solution. The extraction of the iron(III)–PV chelate anion in the presence of diphenylguanidine was studied by Jurevicius and Valiukevicius.[7] The author has found that the iron(III)–PV chelate anion is extracted with tridodecylethylammonium bromide (TDEA) in methyl isobutyl ketone to form an ionic associate and that the molar absorptivity is greater than that of the iron(III)–PV–diphenylguanidine system. The sensitivity of the present method is higher than those of the bathophenanthroline, 4-(2-pyridylazo)-resorcinol, and chromazurol S methods. In this paper, the fundamental conditions for the extraction of iron(III) as the iron(III)–PV–TDEA ternary complex in methyl isobutyl ketone and the composition of the ternary complex will be discussed.

Experimental

Reagent. A 2.5×10^{-3} M iron(III) solution was prepared by dissolving a definite ammount of ferric ammonium sulfate in 0.5 M sulfuric acid. The iron(III) concentration in the solution was determined by EDTA titration. A working standard solution was prepared as needed by the dilution of the 2.5×10^{-3} M solution to the desired concentration with de-ionized water. A 5×10^{-4} M PV solution was prepared by dissolving the Dotite PV in de-ionized water without further purification. The TDEA was prepared by the refluxing of an ethanolic solution of tridodecylamine and ethyl bromide for 4 h. After the evaporation of the solvent, the salt was recrystallized two times from butyl acetate. A 10^{-3} M TDEA solution was prepared by dissolving the above TDEA in methyl isobutyl ketone. All the other chemicals used were of a guaranteed reagent quality.

Apparatus. All the measurements of the absorbance were made with a Hitachi mannual spectrophotometer, model Epu-2A. Matched 10-mm absorption cells were used. The pH measurements were made with a Hitachi-Horiba model M-5 glass electrode pH meter.

Standard Procedure. To 2 ml of the 2.5×10^{-5} M iron(III) solution in a 50-ml polyethylene beaker, a definite amount of 0.1 M sulfuric acid and 2 ml of the 5×10^{-4} M PV solution were added. The pH of the solution was then adjusted to 5.8 by the addition of 2 ml of the 2 M sodium acetate solution and diluted to 25 ml with de-ionized water. The solution was transferred into a 35-ml test tube, and a 5-ml portion of 10^{-3} M TDEA in methyl isobutyl ketone was added. The extraction was carried out for 5 min by turning the test tube upside down two times per 5 s. After the complete phase separation, the organic layer was taken out and centrifuged for 3 min at 3000 rpm. The extract was then transferred into an absorption cell, and the absorbance was measured at 623 nm against the reagent blank.

Results and Discussion

Absorption Spectra. The absorption spectra of an aqueous solution of the iron(III)–PV chelate and of a solution of the iron(III)–PV–TDEA ternary complex in methyl isobutyl ketone, and also the absorption spectra of the respective blanks, are shown in Fig. 1. The ternary complex and the iron(III)–PV chelate anion have their absorption maxima at 623 and 604 nm respectively. The absorption maxima of the ternary complex shifted toward wavelengths longer by 20 nm compared with that of the iron(III)–PV chelate.

Effect of pH. The effect of the pH of the aqueous phase on the extraction was also examined. The maximum extraction was obtained at pH values from 5.7 to 6.4. PV itself is readily extracted with TDEA in methyl isobutyl ketone.

Organic Solvents. Of the solvents examined,

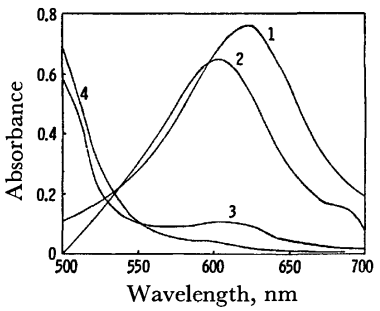

Fig. 1. Absorption spectra of the Fe–PV–TDEA in methyl isobutyl ketone and the Fe–PV in aqueous solution.
pH=5.8.
(1): Fe–PV–TDEA in MIBK, $[Fe]_w=2\times10^{-6}$ M, (2): Fe–PV in aq soln $[Fe]_w=10^{-5}$ M, (3): PV–TDEA in MIBK, $[PV]_w=4\times10^{-5}$ M, (4): PV in aq soln $[PV]_w=1\times10^{-4}$ M.

methyl isobutyl ketone, butyl acetate, carbon tetrachloride, carbon disulfide, and benzene were suitable for the quantitative extraction of the ternary complex. The organic layers separated out rapidly, and the molar absorptivity was maximal, when the methyl isobutyl ketone was used.

The Effect of the PV Concentration. With other factors kept constant, the PV concentration in the aqueous phase was varied from 2×10^{-6} to 10^{-4} M. The optimum concentration range of PV is from 2×10^{-5} to 6×10^{-5} M. The absorbance of the extract gradually decreases upon the further addition of PV.

The Effect of the TDEA Concentration. The concentration of TDEA in the organic phase was varied from 1×10^{-4} to 3×10^{-3} M. The optimum concentration range of TDEA is from 4×10^{-4} to 2×10^{-3} M.

The Effect of the Mixing Time. The mixing time was varied from 10 s to 15 min. The absorbance of the extract is constant for mixing times over 3 min.

The Extractability and Molar Absorptivity. 25 ml of an aqueous solution containing 2.8 μg of iron(III) and the reagents of an optimum concentration were mixed with 5 ml of 10^{-3} M TDEA in methyl isobutyl ketone. Extraction was repeated with 5 ml of an organic layer for the remaining aqueous phase, to which 0.2 ml of the 5×10^{-3} M PV solution was added afresh after the separation of the extract. It was found that 97.9% of the iron(III) was extracted by one extraction. The distribution ratio and the molar absorptivity were 2.33×10^{2} and 7.76×10^{4} $cm^{-1}\cdot mol^{-1}\cdot l$ respectively.

Calibration Curve. The plot of the absorbance of the extract *versus* the concentration of iron(III) in the aqueous phase gave a straight line from 2×10^{-7} to 3×10^{-6} M. The variation coefficient of the absorbance was 1.1% for the 8 measurements. The effects of foreign ions were also examined. Copper, bismuth, and tin were masked with 2-mercaptoethanol. Thorium, aluminum, and uranium, also, were masked with hydrogen peroxide and potassium fluoride. However, vanadium, molybdenum, tungsten, chromium, and zirconium interfered seriously. Of the anions tested, nitrate, iodide, thiocyanate, and perchlorate interfered considerably, giving a negative error.

The Composition of the Ternary Complex. The ratio of iron(III) to PV was found to be 1:2 by the continuous-variation method. To find the iron(III) to TDEA ratio, we attempted to apply the continuous-variation, molar-ratio, and equilibrium-shift methods. However, all these experiments were unsuccessful because the complexes precipitated on the aqueous-organic interface in a lower concentration of TDEA when the methyl isobutyl ketone was used as the solvent. When carbon tetrachloride was used as a solvent, no precipitates of the complex appeared on the interface, and the application of the continuous-variation method was successful. The results indicate that the

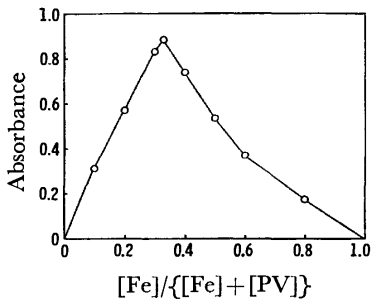

Fig. 2. Continuous variation method applied to the Fe–PV–TDEA system in carbon tetrachloride. $[Fe]_w+[PV]_w=1\times10^{-5}$ M, pH=5.8.

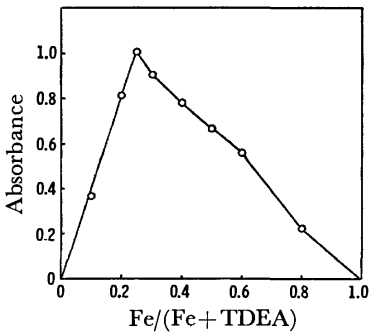

Fig. 3. Continuous variation method applied to the Fe–PV–TDEA system in carbon tetrachloride. Fe+TDEA=5×10^{-7} mol, pH=5.8.

ratio of iron(III) to PV to TDEA is 1:2:2, as is shown in Figs. 2 and 3. Consequently, it may be assumed that the ternary complex in carbon tetrachloride is an ion-association system for $\{[Fe(PV)_2]^{2-}\}\cdot\left\{\begin{matrix}R\\|\\(R-\overset{+}{N}-R')_2\\|\\R\end{matrix}\right\}$. The same composition may hold in the methyl isobutyl ketone.

References

1) Y. Shijo, *Bull. Chem. Soc. Jpn.*, **50**, 1011 (1977).
2) H. Kohara, N. Ishibashi, and K. Abe, *Bunseki Kagaku*, **19**, 48 (1970).
3) T. Ishito and K. Tonosaki, *Bunseki Kagaku*, **20**, 689 (1971).
4) M. K. Akhmedli, E. L. Gluschenko, and Z. L. Gasanova, *Zh. Anal. Khim.*, **26**, 1947 (1971).
5) R. Jurevicius, I. Blazis, and C. Valiukevicius, *Zh. Anal. Khim.*, **30**, 708 (1975).
6) T. Ishito and S. Ichinohe, *Bunseki Kagaku*, **21**, 1207 (1972).
7) R. Jurevicius and C. Valiukevicius, *Zh. Anal. Khim.*, **27**, 1125 (1972).

BULLETIN OF THE CHEMICAL SOCIETY OF JAPAN, VOL. 50 (4), 1015—1016 (1977)

Solvent Extraction Equilibria of Acids. V. The Extraction of Hydrobromic, Hydroiodic, and Thiocyanic Acids with Trioctylphosphine Oxide in Hexane

Masaru NIITSU and Tatsuya SEKINE*

Faculty of Pharmaceutical Sciences, Josai University, Sakado, Saitama 350-02
**Department of Chemistry, Science University of Tokyo, Kagurazaka, Shinjuku-ku, Tokyo 162*

(Received November 4, 1976)

Synopsis. The solvent extraction of hydrohalogenic acids and thiocyanic acid (HX) in 1 mol dm^{-3} electrolyte solutions with trioctylphosphine oxide (E) has been studied at 25 °C. The extraction constant, $K_{ex_1}=[HXE]_{org}[H^+]^{-1}[X^-]^{-1}[E]_{org}^{-1}$, for thiocyanic acid was found to be $10^{2.5}$, while $K_{ex_2}=[HXE_2]_{org}[H^+]^{-1}[X^-]^{-1}[E]_{org}^{-2}$ for hydrobromic and hydroiodic acids were found to be $10^{0.34}$ and $10^{1.78}$ respectively.

The solvent extraction of such metal ions as halides and thiocyanates has been employed for various purposes. In these systems, an extraction of the hydrohalogenic acids or thiocyanic acid in the aqueous phase should occur when the acidity of the aqueous phase is high. In the present study, the solvent extraction of hydrobromic, hydroiodic, and thiocyanic acids in 1 mol dm^{-3} aqueous electrolyte solutions with trioctylphosphine oxide (TOPO) in hexane has been studied at 25 °C. The extraction constants of these acids were compared with those for other strong inorganic acids under the same conditions.

Experimental and Statistical

All the experiments were carried out in a thermostatted room at 25 °C. A portion of an aqueous solution and the same volume of an organic solution were placed in a stoppered glass tube, the tube was vigorously agitated for one minute and then centrifuged. The acid in the two phases was titrated with a standard barium hydroxide solution, and the thiocyanate ions, with a standard silver nitrate solution.

In the present study, the acid and TOPO are denoted by HX and E respectively. The subscript "org" denotes a chemical species in the organic phase, while the lack of a subscript denotes one in the aqueous phase. It was assumed that only one species containing X^- was extracted and that the extracted species could be written as HXE_n where n was unity or two. After several trials, these assumptions were confirmed to be reasonable, as will be shown later; thus, the following equations were derived.

The equilibrium under the above assumptions can be written as:[1)]

$$H^+ + X^- + nE(org) \rightleftharpoons HXE_n(org)$$

$$K_{ex_n} = [HXE_n]_{org}[H^+]^{-1}[X^-]^{-1}[E]_{org}^{-n} \quad (1)$$

where n is unity or two.

Since the amount of TOPO in the aqueous phase is probably very small, the following equations can also be written under the above assumptions for the extraction of HX in the presence of Na^+, H^+, and ClO_4^-:[1)]

$$[E]_{org,initial} = [E]_{org} + 2[HClO_4E_2]_{org} + n[HXE_n]_{org} \quad (2)$$

$$[H^+]_{org} = [HClO_4E_2]_{org} + [HXE_n]_{org} \quad (3)$$

The concentration of these species containing HX can be determined by titration with silver nitrate and that of the hydrogen-ion by titration with barium hydroxide.

When the aqueous phase contains only the HX acid, the terms of perchloric acid in Eqs. 2 and 3 can be eliminated and the distribution ratio of HX may be defined as:

$$D(HX) = [HXE_n]_{org}[H^+]^{-1} \quad (4)$$

Results and Discussion

It was found that the oxidation of iodide to iodine occurred during the two-phase agitation if it was continued for a long time, and the two phases turned pale yellow. This caused an extraction of the HI_3E_n species and introduced positive errors. However, when the agitation continued for only one minute, no color appeared in the two phases and still the equilibrium was reached. No trouble of this kind was encountered in the extraction of other acids.

The distribution ratio of thiocyanic acid with 3.0×10^{-2} mol dm^{-3} TOPO in hexane from aqueous solutions containing 1.0×10^{-1} mol dm^{-3} thiocyanate ions, 9.0×10^{-1} mol dm^{-3} perchlorate ions, and hydrogen and sodium ions at various molar ratios was determined as a function of the hydrogen-ion concentration. Under these conditions, the extraction of thiocyanic acid was much better than that of perchloric acid. After several trials, only the solvation number of unity was found to give a reasonable extraction constant; the error of the constant obtained by assuming an extraction of other species such as $(HX)_2E_2$ was always larger than that of the constant obtained by assuming the extraction of the

TABLE 1. EXTRACTION DATA OF THIOCYANIC ACID

Aqueous phase initially containing 0.1 mol dm^{-3} of thiocyanate and 0.9 mol dm^{-3} of perchlorate. The organic phase initially contained 3.0×10^{-2} mol dm^{-3} TOPO in hexane. The concentration is given by mol dm^{-3}.

$[H^+]_{initial}$	$[H^+]_{org}$	$[SCN^-]_{org}$	log K_{ex_1}
0.24	2.34×10^{-2}	2.15×10^{-2}	2.43
0.20	2.21	2.03	2.37
0.16	2.13	1.92	2.41
0.12	2.01	1.75	2.46
0.10	1.85	1.62	2.41
0.09	1.86	1.57	2.49
0.07	1.72	1.41	2.51
0.06	1.61	1.31	2.50
0.05	1.52	1.20	2.53
0.04	1.39	1.06	2.55
0.03	1.17	8.97×10^{-3}	2.54
		Av	2.47

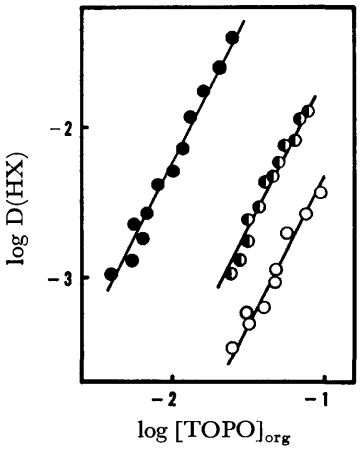

Fig. 1. Distribution ratio of hydrochloric (○) (taken from Ref. 1), hydrobromic (◐), and hydroiodic (●) acid between hexane containing various amounts of TOPO and aqueous 1 mol dm^{-3} of the acid as a function of the free TOPO concentration.

TABLE 2. SUMMARY OF EXTRACTION CONSTANTS AT 25°C

Org. phase: hexane containing TOPO (E).

Aq phase: 1 mol dm^{-3} (H, Na) (X, ClO_4) for HSCN and 1 mol dm^{-3} HX for others (for H_2SO_4, X^- is HSO_4^-).

$$Kex_n = [HXE_n]_{org}[H^+]^{-1}[X^-]^{-1}[E]_{org}^{-n}$$

HX	log Kex_1	log Kex_2
HSCN	2.5	—
HCl[a)]	—	−0.31
HBr	—	0.34
HI	—	1.78
HNO_3[a)]	0.86	—
$HClO_4$[a)]	—	3.20
H_2SO_4[a)]	—	−0.30

a) Data taken from Ref. 1.

HXE species. Table 1 shows the extraction data and the calculated extraction constants.

The extraction equilibria of hydrobromic and hydroiodic acids were studied when the initial aqueous phase contained 1 mol dm^{-3} of the acid and when the hexane phase contained TOPO at various concentrations. Figure 1 gives the results, together with those of hydrochloric acid, in Ref. 1. From the slope of the plot, the solvation number of these acids was concluded to be two and their extraction constants were determined to be as is listed in Table 2. The solid lines in the figure were drawn on the basis of Eqs. 1 and 4 and the constants in Table 2.

Khopkar and Narayanankutty[2)] reported the value of Kex_1 of thiocyanic acid extracted from 1 mol dm^{-3} ammonium thiocyanate solutions at pH 1.6 to 3 with TOPO in xylene to be $10^{2.43}$, which agrees well with the present value. There have also been some reports on the solvent extraction of thiocyanic acid with TOPO.[3,4)]

As may be seen from Table 2, the values of the extraction constant, Kex_2, increase in the order of: HCl<HBr<HI<$HClO_4$. This order agrees with the order of the molar volumes of the anion. The extraction constant of Kex_1 of thiocyanic acid is much greater than that of nitric acid. Thus, when a metal ion in an acid solution containing thiocyanate ions is extracted with a neutral extractant such as TOPO, the extraction of thiocyanic acid should be taken into account in the analysis of the data, because this thiocyanic acid extraction probably decreases the concentration of thiocyanate ions in the aqueous phase and also that of the free extractant in the organic phase.

References

1) M. Niitsu and T. Sekine, *J. Inorg. Nucl. Chem.*, **37**, 1056 (1975); **38**, 1053 (1976).

2) P. K. Khopkar and P. Narayanankutty, *J. Inorg. Nucl. Chem.*, **34**, 2617 (1972).

3) V. V. Trasov, G. A. Yagodin, and N. F. Kizim, *Dokl. Akad. Nauk SSSR*, **194**, 1385 (1970); *Chem. Abstr.*, **74**, 46166.

4) O. A. Sinegribova and G. A. Yagodin, *Zh. Neorg. Khim.*, **16**, 1148 (1971); *Chem. Abstr.*, **75**, 10981.

BULLETIN OF THE CHEMICAL SOCIETY OF JAPAN, VOL. 50 (4), 1017—1018 (1977)

Condensation Products of Benzanthrone Obtained Using Copper Powder and Fused Zinc Chloride

Junji AOKI, Minoru TAKEKAWA, Shoji FUJISAWA, and Satoshi IWASHIMA*

Department of Chemistry, Faculty of Science, Toho University, Miyama-cho, Funabashi-shi, Chiba 274

**Department of Chemistry, Faculty of Science and Technology, Meisei University, Hino-shi, Tokyo 191*

(Received June 28, 1976)

Synopsis. By heating benzanthrone (**3**) with copper powder, zinc chloride, and sodium chloride, violanthrene B (**8**) and isoviolanthrene B (**13**) were obtained in addition to the tetrabenzo[*a, cd, j, lm*]perylene (**4**) reported previously. This method may be considered to be a convenient method of synthesizing not only **4**, but also **13**.

Previously, Aoki reported[1] that 1-phenalenone (**1**) and benzanthrone (**3**) gave dibenzo[*cd, lm*]perylene (**2**) and tetrabenzo[*a,cd,j,lm*]perylene (**4**), respectively, upon heating with copper powder in a mixed flux of zinc chloride and sodium chloride. However, in the case of **3**, other compounds are possibly produced by coupling at positions other than the carbonyl carbon atom. In this paper, the results of a reinvestigation of work reported in Ref. 1 are reported.

By elution chromatography of the reaction products, a small amount of violanthrene B (**8**)[2,4] and a considerable amount of isoviolanthrene B (**13**)[3–5] were isolated along with **4**, and small amounts of unidentified materials.

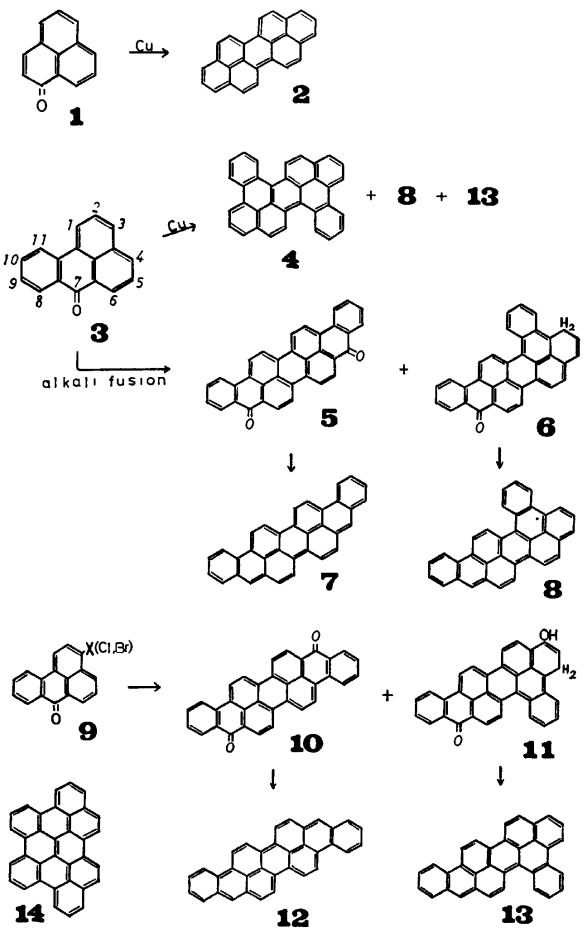

On the other hand, however, alkali fusion, the typial condensation method for ketones such as **3**, gives violanthrones[6] (**5**, **6**;[6b] **10**, **11**[6c]). Since the carbonyl group remains, the Clar reduction method[7] must be applied in order to obtain the hydrocarbons (**7**, **8**; **12**, **13**).[2,3] Futhermore, no reports have been published concerning the formation of products having a 4-type skeleton.

In the present work, the above unidentified materials were not obtained in a pure state, but they were considered to be present in a mixture with a few hydrocarbons.[8] Consequently, the present method produces hydrocarbons in a single step from **3**, but affords no A-type substances (**5**, **7**, **10**, **12**).[9] This method may be considered to be a convenient method for preparing not only **4**, but also **13**, since it more readily gives pure **13** in a higher yield than the method of reducing **11**.

Experimental

The UV spectra were recorded with a Shimadzu Model D 40 RW Multiconvertible Spectrophotometer.

Dibenzo[*a,cd*]naphtho[3,2,1-*lm*]perylene (**8**) (violanthrene B). The synthesis from **6** has already been reported.[2] Mp 344 °C (corr.), $\lambda_{max}^{benzene}$ nm (log ε): 482 (5.00), 451 (4.57), 424 (4.21), 400 (sh., 3.70), 363 (4.69), 345.5 (4.46), 318 (4.63), 305 (4.48).[10]

Dibenzo[*a,cd*]naphtho[1,2,3-*lm*]perylene (**13**) (isoviolanthrene B).[5] Using the Clar method,[3,7] 1.00 g of isoviolanthrone B (**11**) was reduced. The crude product (0.95 g) was sublimated at high vacuum (10^{-3}—10^{-4} Torr), and the yellowish-brown sublimates (0.35 g) were purified by means of recrystallization from benzene and then column chromatography on alumina with benzene, to give 0.05 g of brown-yellow, fine needles. Mp 307 °C (uncorr.), 319 °C (corr.), $\lambda_{max}^{benzene}$ nm (log ε): 471 (4.87), 441 (4.55), 415 (4.22), 390 (sh., 3.70), 357 (4.81), 340.5 (4.50), 325 (4.24), 308 (4.76), 294 (4.55).

Found: C, 95.61; H, 4.31%. Calcd for $C_{34}H_{18}$: C, 95.75; H, 4.25%.

Condensation. A mixture of 5.00 g of benzanthrone (**3**), 5.0 g of copper powder, 25 g of zinc chloride and 5 g of sodium chloride was maintained at 230 °C for 30 min, and treated, by a method similar to that reported previously.[1] The crude product (9.85 g) was refluxed with 600 g of xylene for 2 h, and the insoluble part was filtered off after cooling. The filtrate was chromatographed on alumina into several fractions (using xylene as the eluent). The product, obtained by evaporation of successive fractions, were purified by recrystallization and high vacuum sublimation, to give 616 mg of **4**, 56 mg of **8**, 308 mg of recovered **3**, 623 mg of **13**, and 85 mg of reddish-brown crystals. This last material has absorption peaks at about 420, 495, and 530 nm in benzene and appeared to be a mixture of unidentified hydrocarbons[8] not of the A-type (**7**, **12**),[9] however, further purification was

very difficult.

That part insoluble in xylene (7.0 g) was refluxed with 200 g of *o*-dichlorobenzene for 2 h, and the insoluble material (5.25 g) was removed by hot filtration. This filtrate was evaporated to dryness, and the residue was chromatographed on alumina with chlorobenzene, and worked up in a manner similar to that used for the xylene filtrate, giving various amounts of the same products described above.

The total amounts and yields of the products were:

tetrabenzo[*a*,*cd*,*j*,*lm*]perylene (**4**)	754 mg	18.1%,
violanthrene B (**8**)	90 mg	2.2%,
isoviolanthrene B (**13**)	833 mg	20.0%,
unidentified material	195 mg	4.7%,
recovered benzanthrone (**3**)	505 mg	10.1%.

References

1) J. Aoki, *Bull. Chem. Soc. Jpn.*, **37**, 1079 (1964).
2) J. Aoki, *Bull. Chem. Soc. Jpn.*, **34**, 1817 (1961).
3) J. Aoki, *Bull. Chem. Soc. Jpn.*, **34**, 1820 (1961).
4) The formulae were indicated as shown in the scheme for the X-ray analysis of the present samples; T. Maekawa, Disertation, The University of Tokyo (1968).
5) Further examination showed that the previous sample[3] was somewhat impure. Reliable results are reported in the present paper.
6) For example, a) A. Lüttringhaus and H. Neresheimer, *Ann.*, **473**, 259 (1929); b) T. Maki, *Kogyo Kagaku Zasshi*, **35**, 1441 (1932); c) T. Maki and Y. Nagai, *ibid.*, **37**, 493 (1934).
7) E. Clar, *Ber.*, **72**, 1648 (1939).
8) One may be **14**.[1]
9) The unidentified material is readily soluble even in benzene, whereas the A-type hydrocarbons (**7**, **12**) are sparingly soluble although their UV spectra show λ_{max} around 495 and 520 nm, respectively.
10) These spectral data are more plausible than those previously published.[3]

BULLETIN OF THE CHEMICAL SOCIETY OF JAPAN, VOL. 50 (4), 1019—1020 (1977)

The Electrochemical Behavior of Mononitrophenyltrimethylsilanes and 2,4-Dinitrophenyltrimethylsilane

Hamao WATANABE, Masafumi AOKI, Hideyuki MATSUMOTO, Yoichiro NAGAI, and Takeo SATO*

Department of Applied Chemistry, Faculty of Engineering Gunma University, Kiryu, Gunma 376
**Department of Chemistry, Faculty of Science, Tokyo Metropolitan University, Setagaya, Tokyo 158*

(Received October 1, 1976)

Synopsis. The CV data for *o*-, *m*-, and *p*-nitrophenyltrimethylsilanes and 2,4-dinitrophenyltrimethylsilane revealed that the former three show E_{pc} slightly more anodic than the corresponding nitrotoluenes; the latter shows a third peak (O_3) together with two successive reversible couples, while the methyl analogue exhibits no peak corresponding to O_3, but shows extremely weak O_1. The behavior of these silyl compounds are interpreted in terms of less electron-donating nature of trimethylsilyl group and (p-d)π bonding between the siliicon and benzene ring.

To date only a few reports have appeared on the study of the electrochemical behavior of organosilicon compounds by polarography,[1,2] and controlled potential electrolysis in non-aqueous solutions.[3,4] Recently, Allred and co-worker have reported on the electrochemical reduction of chloropermethylpolysilanes by means of cyclic voltammetry (CV) and discussed the effect of chain length of the polysilanes on the reduction potentials.[5] It is interesting to investigate by the CV technique the electrochemical behaviors for other types of silicon compounds which contain at least one of electroactive groups. The present study was undertaken to examine the substituent effect on reduction-oxidation potentials and electron transfer processes for *o*-, *m*-, and *p*-nitrophenyltrimethylsilanes and 2,4-dinitrophenyltrimethylsilane.

Results and Discussion

o-, m-, *and* p-*Nitrophenyltrimethylsilanes.* In Table 1, the CV data are listed to compare mononitrophenyltrimethylsilanes with nitrotoluenes. The peak potentials E_{pc}, E_{pa}, and $E_{p1/2}$, for the silyl compounds are both slightly more anodic than those of the corresponding toluene derivatives. This may be attributable to the polar effect of substituent attached to the nitrophenyl group, less electron-donating trimethylsilyl substituent compared with methyl group requires lower reduction potentials as shown by Hammett σ constants.[6]

TABLE 1. THE CV DATA OF NITROPHENYLTRIMETHYLSILANES AND NITROTOLUENES[a]

Compound	E_{pc} (V)	E_{pa} (V)	$E_{p1/2}$ (V)	i_{pa}/i_{pc}
o-$MeC_6H_4NO_2$	−1.66	−0.80	−1.23	1.0
o-$Me_3SiC_6H_4NO_2$	−1.62	−0.68	−1.14	0.9
m-$MeC_6H_4NO_2$	−1.52	−0.76	−1.13	1.0
m-$Me_3SiC_6H_4NO_2$	−1.50	−0.76	−1.11	1.0
p-$MeC_6H_4NO_2$	−1.29	−0.92	−1.11	0.9
p-$Me_3SiC_6H_4NO_2$	−1.26	−0.84	−1.05	1.0

a) Scan rate: 80 mV/s.

It is seen that from the values of the ratio of i_{pa} to i_{pc} all the compounds are chemically stable during the electron transfer over a wide range of scan rates. However, the features of the potentials for *para* silyl and tolyl compounds are distinctly different from those of *ortho* and *meta* compounds. Thus, the value of $|E_{pc}|-|E_{pa}|$ of the former is about one-half relative to the latter two. It could be interpreted in terms of the poor reversible electron-transfer process in the *ortho* and *meta* compounds, the peak separation of which increased at a higher scan rate. The E_{pc} values for the compounds became more cathodic by 400 mV on 10-fold increase in the scan rate (40 mV/s→400 mV/s). At 3 V/s scan the peak separation reached 1.6 V.

2,4-Dinitrophenyltrimethylsilane. Cyclic voltammograms of 2,4-dinitrophenyltrimethylsilane, 2,4-dinitrotoluene and *m*-dinitrobenzene are shown in Figs. 1a—c. Of the compounds tested in the range of 0——2.0 V, two cathodic peaks (R_1 and R_2) and the corresponding two anodic peaks (O_1 and O_2) appeared. When scanning was clipped at −1.20 V, the CV charts show that all the anion radicals, formed by one electron transfer (R_1), are chemically stable. However, in the scan range of 0——2.0 V, the CV behavior among these compounds

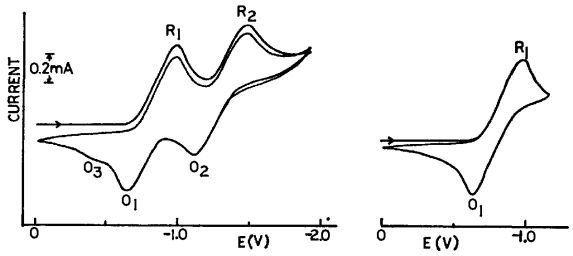

Fig. 1a. Cyclic voltammogram of 2,4-dinitrophenyltrimethylsilane. (First and second cyclic scan; scan rate: 80 mV/s.)

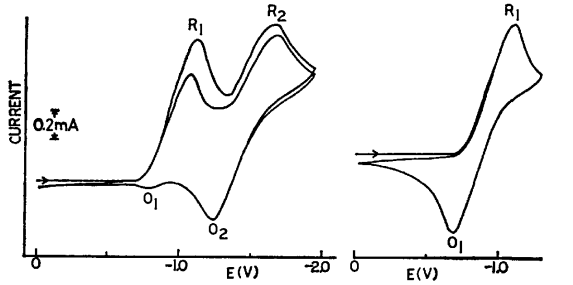

Fig. 1b. Cyclic voltammogram of 2,4-dinitrotoluene. (First and second cyclic scan; scan rate: 80 mV/s.)

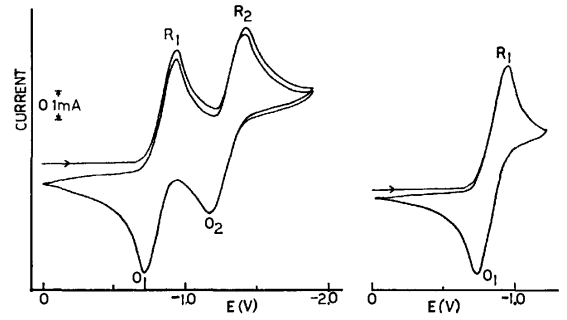

Fig. 1c. Cyclic voltammogram of *m*-dinitrobenzene. (First and second cyclic scan; scan rate: 80 mV/s.)

differed significantly. Thus, on potential reversal, 2,4-dinitrophenyltrimethylsilane exhibited a weak third anodic peak (O_3) at a low potential (Fig. 1a), which was absent when the potential was clipped at −1.20 V. This is presumably due to the reduction product which was derived from dianion. The explanation was supported by the fact that the addition of a proton donor such as methanol to the system causes an increase in peak O_3 and a decrease in peak O_1 and O_2, although the structure of the reduction product was not determined. On the other hand, the CV chart of 2,4-dinitrotoluene is very different from those of 2,4-dinitrophenyltrimethylsilane and *m*-dinitrobenzene. As Fig. 1b shows, the anodic peak of O_1 is extremely weak relative to the corresponding cathodic peak of R_1 when the scan was extended to −2.0 V. This fact indicates that the resulting anion radical is chemically unstable when it was allowed to stand until the second peak is swept and one electron removal from the anion radical to the starting compound is slow compared with chemical process.

The above observation might be expressed as following equations (1 and 2):

2,4-Dinitrophenyltrimethylsilane (DNS)

$$[\mathrm{DNS}] \underset{-e(O_1)}{\overset{+e(R_1)}{\rightleftharpoons}} [\mathrm{DNS}]^{-} \underset{-e(O_2)}{\overset{+e(R_2)}{\rightleftharpoons}} [\mathrm{DNS}]^{=} \quad (1)$$

2,4-Dinitrotoluene (DNT)

$$[\mathrm{DNT}] \underset{-e(O_1)}{\overset{+e(R_1)}{\rightleftharpoons}} [\mathrm{DNT}]^{-} \underset{-e(O_2)}{\overset{+e(R_2)}{\rightleftharpoons}} [\mathrm{DNT}]^{=} \quad (2)$$

From the values of peak separation of $|R|-|O|$ in Figs. 1a and 1b, that the silane compound has better reversibilities (Eq. 1) than the toluene in the electron transfer processes could be interpreted in terms of the substituent effect, in which the trimethylsilyl group contributes to stabilize the system *via* (p-d)π bonding between silicon and benzene ring, although the both dianions are considered to be highly reactive species. With respect to $[DNS]^{-}$ and $[DNS]^{=}$, many resonance structures are possible and the evidence for such a structure has been shown by ESR spectrum in the electrochemical reduction of *p*-nitrophenyltrimethylsilane.[7]

Experimental

Cyclic Voltammetry. All measurements were performed in purified anhydrous *N,N*-dimethylformamide (DMF) containing 0.1 M tetrabutylammonium perchlorate (TBAP) as supporting electrolyte using a divided cell. The working electrode is a platinum inlay electrode (Beckman 32273) and the counter electrode is a platinum wire. A saturated calomel electrode was used as a reference which was connected to the cell using two salt bridges, saturated KCl solution and DMF-TBAP solution. A Hokuto Denko Model HB-107A function generator and Hokuto Denko Model HA-101 potentiostat were used. Cyclic voltammetry performed at the scan rate of 40—400 mV/s was recorded using a Rikadenki X-Y recorder Model BW 133. For higher speed recording, two channel wave memory, NF Model WM-812A, was employed. All runs were made after a 15 min purge with purified nitrogen and within 30 min of preparing the solutions.

Materials. Nitrophenyltrimethylsilanes and 2,4-dinitrophenyltrimethylsilanes were obtained by the method reported elsewhere.[8] Mono- and di-nitrotoluenes and *m*-dinitrobenzene were commercially available (extra pure grade).

This work was supported by a Scientific Research Grant from the Ministry of Education (No. 080422).

References

1) R. E. Dessy, W. Kitching, and T. Chivers, *J. Am. Chem. Soc.*, **88**, 453 (1966).
2) H. Alt and H. Bock, *Tetrahedron*, **25**, 4825 (1969).
3) R. A. Benkeser and C. A. Tincher, *J. Organomet. Chem.*, **13**, 139 (1968).
4) C. Eaborn, R. A. Jackson, and R. Pearce, *J. Chem. Soc., Perkin 1*, **1974**, 2055.
5) W. G. Boberski and A. L. Allred, *J. Organomet. Chem.*, **88**, 73 (1975).
6) C. G. Swain and E. C. Lupton, Jr., *J. Am. Chem. Soc.*, **90**, 4328 (1968).
7) V. M. Kazakova, I. G. Makarov, M. E. Kurek, and E. A. Chernyshev, *Zh. Strukt. Khim.*, **9**(3), 525 (1968); *Chem. Abstr.*, **69**, 105703j (1968).
8) H. Matsumoto, K. Yoshihiro, M. Aoki, Y. Inokuchi, H. Watanabe, and Y. Nagai, *J. Organomet. Chem.*, (1976), in press.

BULLETIN OF THE CHEMICAL SOCIETY OF JAPAN, VOL. 50 (4), 1021—1022 (1977)

Palladium-catalyzed Reaction of Olefins and Acetylenes with Iodoferrocenes

Akira KASAHARA, Taeko IZUMI, and Mitsugi MAEMURA

Department of Applied Chemistry, Faculty of Engineering, Yamagata University, Yonezawa 992

(Received November 11, 1976)

Synopsis. Iodoferrocene (**1**) reacts readily with olefinic compounds in the presence of a catalytic amount of palladium(II) acetate to produce alkenylferrocene derivatives. In the presence of a copper(I) iodide and palladium complex, **1** also reacts with acetylene to afford diferrocenylacetylene.

Recently, the palladium-catalyzed reaction of olefin[1-5] with aryl and vinylic halides has received wide attention. Meanwhile, Sonogashira *et al.*[6] have reported the palladium-catalyzed substitution of acetylenic hydrogen with aryl iodide. We are, therefore, intrigued by the palladium-catalyzed reaction of olefins and acetylenes with iodoferrocene (FcI) (**1**) and 1,1′-diiodoferrocene (**2**) and wish to report herein the results of a study of these reactions.

In the presence of triethylamine and catalytic amounts of palladium(II) acetate and triphenylphosphine, **1** and **2** were allowed to react separately with various olefins at 100 °C; the substitution reaction on the double bond has been observed to lead to the formation of 1-alkenylferrocenes and 1,1′-dialkenylferrocenes. The reactions carried out are summarized in Table 1.

The reaction of **1** with simple olefins, such as styrene and ethyl acrylate, resulted in the formation of strylferrocene (**3**) and ethyl 3-ferrocenylacrylate (**4**) respectively in moderate yields. The mechanism of the

Table 1. A palladium-catalyzed ferrocenylation of olefins and acetylenes

Halide	Olefin or acetylene	Product, mp °C	Yield %[a]
1	Styrene	Styrylferrocene (**3**), 120—121[b]	59
1	Ethyl acrylate	Ethyl 3-ferrocenylacrylate (**4**), 74—75[c]	54
1	Methyl methacrylate	Methyl 3-ferrocenylmethacrylate (**5**), 62—63[d]	64
1	Acrylonitrile	3-Ferrocenylacrylonitrile (**6**), 80—81[d]	60
1	Methyl vinyl ketone	4-Ferrocenyl-3-buten-2-one (**7**), 84—85[e]	52
1	Phenyl vinyl ketone	3-Ferrocenyl-1-phenyl-2-porpen-1-one (**8**), 136—137[f]	70
1	Allyl alcohol	3-Ferrocenylpropanal (**9**), 48—51[g]	48
1	3-Buten-2-ol	4-Ferrocenyl-2-butanone (**10**), 45—46[h]	57
1	Vinyl acetate	1,2-Diferrocenylethylene (**11**), 270—272[i]	38
1	Isopropenyl acetate	1,2-Diferrocenyl-1-propene (**12**), 163—165[j]	32
1	Acetophenone enol acetate	Styrylferrocene (**3**), 120—121[b] 1-Acetoxy-1-phenyl-2-ferrocenylethylene (**13**), 153—154[k]	21 14
2	Styrene	1,1′-Distyrylferrocene (**14**), 166—167[l]	42
2	Ethyl acrylate	1,1′-Bis(2-ethoxycarbonylvinyl)ferrocene (**15**), 84—85[d]	62
2	Methyl vinyl ketone	1,1′-Bis(2-acetylvinyl)ferrocene (**16**), 112—113[d]	76
2	3-Buten-2-ol	1,1′-Bis(3-oxobutyl)ferrocene (**17**), 153—154[m]	53
1	Acetylene	Diferrocenylacetylene (**18**), 244—246[b]	78
1	Phenylacetylene	Ferrocenylphenylacetylene (**19**), 122—124[b]	85
2	Phenylacetylene	1,1′-Bis(phenylethynyl)ferrocene (**20**), 159—161[n]	46

a) The yields are based upon the iodoferrocene (**1**) or 1,1′-diiodoferrocene (**2**) used. b) P. L. Pauson and E. E. Watts, *J. Chem. Soc.*, **1963**, 2990. c) P. De Re and E. Sianesi, *Experientia*, **21**, 648 (1966). d) A. Kasahara, T. Izumi, G. Saito, M. Yodono, R. Saito, and Y. Goto, *Bull. Chem. Soc. Jpn.*, **45**, 895 (1972). e) J. M. Osgerby and P. L. Pauson, *J. Chem. Soc.*, **1961**, 4604. f) C. R. Hauser and J. Lindsay, *J. Org. Chem.*, **23**, 906 (1957). g) Compound **9** gave a correct elemental analysis. IR spectrum: 2750, 1725 (C=O), 1104, and 998 cm^{-1}. NMR spectrum (δ, ppm): 2.66 (4H, m, CH_2), 4.09 and 4.12 (9H, m, ferrocene ring protons), and 9.93 (1H, s, H–C=O). Mass spectrum: $M^+=242$. h) J. Decombe, J. P. Ravoux, and A. Dormond, *C. R. Acad. Sci.*, **258**, 2348 (1964). i) K. Schoegel and H. Egger, *Angew. Chem.*, **75**, 1123 (1963). j) Compound **12** gave a correct elemental analysis. IR spectrum: 1620, 1101, 998, and 810 cm^{-1}. NMR spectrum (δ, ppm): 2.13 (3H, d, CH_3–C=CH), 4.12 and 4.35 (18H, m, ferrocene ring protons), and 6.36 (1H, m, C=CH). Mass spectrum: $M^+=410$. k) Compound **13** gave a correct elemental analysis. IR spectrum: 1760 (O–C=O), 1650 (C=C), 1104, and 998 cm^{-1}. NMR spectrum (δ, ppm): 2.36 (3H, s, O–CO–CH_3), 4.15 and 4.38 (9H, m, ferrocene ring protons), 6.54 (1H, s, C=CH), and 7.32 (5H, m, benzene ring protons). Mass spectrum: $M^+=330$. l) K. Sonogashira and N. Hagihara, *Kogyo Kagaku Zasshi*, **66**, 1090 (1963). m) Compound **17** gave a correct elemental analysis. IR spectrum: 1718 cm^{-1} (C=O). NMR spectrum (δ, ppm): 2.09 (6H, s, CH_3C=O), 2.55 (4H, m, CH_2C=O), 2.64 (4H, m, FcCH_2–), 4.08 and 4.11 (8H, m, ferrocene ring protons). Mass spectrum: $M^+=310$. n) Compound **20** gave a correct elemental analysis. IR spectrum: 2210 cm^{-1} (C≡C). NMR spectrum (δ, ppm): 4.36 and 4.59 (8H, m, ferrocene ring protons) and 7.33 (10H, m, benzene ring protons). Mass spectrum: $M^+=386$.

reaction involves the formation of ferrocenylpalladium iodide by oxidative addition, followed by addition to the olefin and the elimination of [HPdI], as in the palladium-catalyzed reaction of olefins with aryl halide.[3a)]

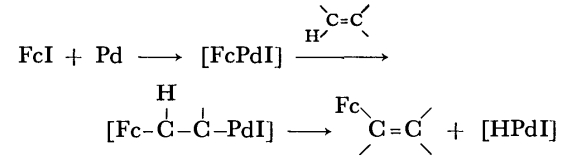

The ferrocenylation of allylic alcohols with **1** or **2** led to the formation of the 3-ferrocenyl-aldehyde or -ketone (**9**, **10**, or **17**) in a good yield; neither 2-ferrocenyl-isomer nor 3-ferrocenylated allyl alcohol was observed. The allylic alcohol ferrocenylation can account for the reaction mechanism, which is similar to the one proposed for the allylic alcohol arylation:[4)]

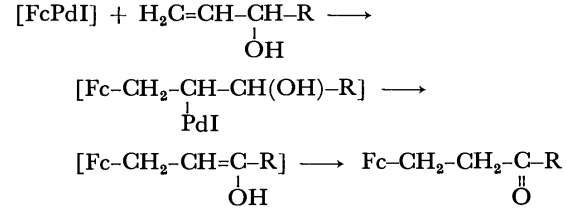

Vinyl acetate and isopropenyl acetate reacted with **1** to yield differrocenylethylene (**11**) and 1,2-diferrocenyl-1-propene (**12**) respectively. In addition, the reaction of acetophenone enol acetate with **1** afforded a mixture of **3** and 1-acetoxy-1-phenyl-2-ferrocenylethylene (**13**). The formation of **3** suggested that the addition of the ferrocenyl group occurs on the terminal carbon atom, followed by the elimination and a re-addition of palladium hydride in the reverse direction and another elimination of Pd(OAc)I.

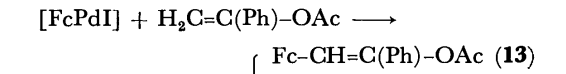

In the presence of copper(I) iodide and dichlorobis-(triphenylphosphine)palladium(II), **1** reacted with acetylene and phenylacetylene to yield diferrocenylacetylene (**14**) and ferrocenylphenylacetylene (**15**) respectively in good yields.

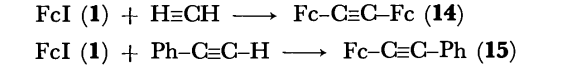

Experimental

Materials. All the melting points are uncorrected. Iodoferrocene (**1**) and 1,1′-diiodoferrocene (**2**) were prepared according to the method described by Fish and Rosenblum.[7)] All the olefinic compounds were commercial products and were purified by distillation before use.

General Procedure for the Ferrocenylation of Olefins. A mixture of 1.56 g (5 mmol) of **1**, 0.7 g (7 mmol) of triethylamine, 7 mmol of olefin, 0.026 g (0.1 mmol) of triphenylphosphine, 0.011 g (0.05 mmol) of palladium(II) acetate, and 10 ml of acetonitrile was heated under nitrogen in a sealed tube at 100 °C for 8 h. In the reaction with **2**, 1.08 g (2.5 mmol) of **2** was used. The cooled reaction mixture was diluted with ether and water. The ether phase was separated, washed with water, dried over anhydrous magnesium sulfate, filtered, and concentrated. The residue was then purified by column chromatography (Al_2O_3–benzene or chloroform), followed by recrystallization from ethanol or benzene. The structure of the products was confirmed by a mixed-melting-point determination with an authentic sample and by the observation of the IR and NMR spectra. The results are summarized in Table 1.

General Procedure for the Ferrocenylation of Acetylenes. A mixture of 1.56 g (5 mmol) of **1** (or 2.5 mmol of **2**), 0.61 g (6 mmol) of phenylacetylene, 0.095 g (0.05 mmol) of copper(I) iodide, 0.033 g (0.1 mmol) of dichlorobis(triphenylphosphine)-palladium(II), and 40 ml of diethylamine was heated under nitrogen in a sealed tube at 80 °C for 6 h. In the case of the reaction with acetylene, a slow current of acetylene was passed through the reaction mixture for 6 h at room temperature. After the removal of diethylamine under reduced pressure, ether and water were added to the residue. The ether phase was separated, washed with water, dried over anhydrous magnesium sulfate, filtered, and concentrated. The residue was purified by column chromatography (Al_2O_3–benzene or chloroform), followed by recrystallization from ethanol or benzene. The structure of the products was confirmed by a mixed-melting-point determination with an authentic sample and by the observation of the IR and NMR spectra. The results are summarized in Table 1.

References

1) T. Mizoroki, K. Mori, and A. Ozaki, *Bull. Chem. Soc. Jpn.*, **44**, 581 (1971); *ibid.*, **46**, 1505 (1973).
2) R. F. Heck and J. P. Nolley, Jr., *J. Org. Chem.*, **37**, 2320 (1972).
3) a) H. A. Diek and R. F. Heck, *J. Am. Chem. Soc.*, **96**, 1133 (1974); b) *J. Org, Chem.*, **40**, 1083 (1975).
4) J. B. Melpolder and R. F. Heck, *J. Org. Chem.*, **41**, 265 (1976).
5) A. J. Chalk and S. A. Magennis, *J. Org. Chem.*, **41**, 273, 1206 (1976).
6) K. Sonogashira, Y. Tohda, and N. Hagihara, *Tetrahedron Lett.*, **1975**, 4467.
7) R. E. Fish and M. Rosenblumn, *J. Org. Chem.*, **30**, 1253 (1965).

Synthesis and Electrical Conductivity of Phosphorus-Nitrogen Compounds. V. Synthesis and Electrical Resistivity of Poly[bis(amino)phosphazenes]

Takashi HAYASHI and Hajime SAITO

Department of Applied Chemistry, Faculty of Engineering, Nagoya University, Chikusa-ku, Nagoya 464

(Received August 26, 1976)

Three new poly[bis(amino)phosphazenes] of formulas $[NP(NHC_6H_{13})_2]_n$, $[NP(NHCH_2CHCH_2)_2]_n$, and $[NP(NHCH_2C_6H_5)_2]_n$ have been synthesized by direct aminolysis of $(NPCl_2)_n$. The electrical resistivity and thermal stability of a series of poly[bis(amino)phoshazenes], (NPR_2) (R: amino group), have been examined. Most polymers showed an increase in resistance with time to an equilibrium value, possibly due to space charge effects, allowance for this conductivity being ohmic up to 500(V/cm). The aliphatic amino derivatives have a lower resistivity and a lower ΔE value than the aromatic amino derivatives. The resistivity of the poly [bis(amino)-phosphazenes] was found to decrease in the order, R : $NHC_2H_5 > NHC_3H_7 > NHC_4H_9 > NHC_6H_{13} \gg N(CH_3)_2$. This seems to be predominantly due to the nature of an inductive electron supply of amino side groups. In some polymers the change of energy gap, ΔE, was observed in the range 70—90 °C. The ΔE value was usually lower in the low temperature region than in the high temperature region. All the polymers were found to decompose at about 200 °C, losing the amino side group.

Although the synthesis and chemistry of phosphazene compounds have been extensively investigated, very little[1,2] has been done to measure the electrical resistivity of these compounds. In previous papers[3,4] we reported on the electrical resistivity of the phosphonitrilic chloride, $(NPCl_2)_3$, and its derivatives.[3,4]

It was found that the resistivity of phosphazene compounds obeys an equation of the form : $\rho = \rho_0 \exp(E/kT)$, where ρ is the resistivity, E the activation energy, k Boltzmann constant, and T the absolute temperature. It has been suggested that the resistivity of $(NPR_2)_3$ was remarkably dependent upon side group R. It was found that the highest conductivities were obtained with side groups containing amino groups.

The purpose of this work is to synthesize poly[bis-(amino)phosphazenes] and to measure the resistivity of the polymers. The difference in side group R of (NPR_2) is expected to affect the electrical resistivity of the polymers.

Experimental

Preparation of Poly(dichlorophosphazene). Sublimed hexachlorocyclotriphosphazene (5.000 g) and benzoic acid (0.200 g) were weighed directly into a carefully cleaned Pyrex ampoule. The ampoule was evacuated to 10^{-1} Torr for 1 h and then sealed. The sealed ampoule was placed in a furnace and heated at 210±2 °C for 4 h. After polymerization, the ampoule was opened and the conetnts were extracted with dry benzene. The solvent was removed and the unreacted materials were separated from the residue by vacuum sublimation. Linear $(NPCl_2)_n$ was obtained.

Preparation of Poly[bis(amino)phosphazenes]. Aliphatic primary amines (ethylamine, propylamine, butylamine, hexylamine, allylamine, benzylamine), secondary amine (dimethylamines), and aromatic amine (aniline) were used. The amino-substituted polymers of the structure $[NP(NHR)_2]_n$ (NHR: NHEt, $NHPr^n$, $NHBu^n$, NHPh) and $[NP(NMe_2)_2]_n$ were synthesized and purified according to the procedure given by Allcock and Kugel.[5,6] The amino-substituted polymers of the structure $[NP(NHR)_2]_n$ (NHR: $NHhexyl^n$, $NHCH_2CHCH_2$, $NHCH_2Ph_5$) were prepared as follows.

Poly[bis(mono-hexylamino)phosphazene]; $[NP(NHC_6H_{13})_2]_n$: A solution of polydichlorophosphazene (3.68 g, 0.032 mol) in tetrahydrofuran (150 ml) was added slowly to a stirred solution of mono-hexylamine (25.0 g, 0.25 mol) and triethylamine (25.3 g, 0.25 mol) in tetrahydrofuran (100 ml). The reaction was allowed to proceed at 25 °C for 5 days and then allowed to proceed at 40 °C for 7 h.

The mixture of polymer and amine salts was filtered off, and the solvent was removed from the filtrate by distillation.

The residue obtained was dissolved in trifluoroethanol and the polymer was precipitated from the solution by addition of acetone. The procedure was repeated, and the polymer was dried in a vacuum over P_2O_5.

Poly[bis(allylamino)phosphazene]; $[NP(NHCH_2CH{=}CH_2)_2]_n$: This polymer was prepared by a modification of the method of Allcock *et al.*[7] A solution of polydichlorophosphazene (7.20 g, 0.062 mol) in benzene (80 ml) was added dropwise to a stirred solution of allylamine (56.50 g, 0.990 mol) and triethylamine (12.5 g, 0.124 mol) in benzene (60 ml).

The mixture was then boiled under reflux for 55 h and then allowed to stand at 25 °C for 2 days. The upper benzene layer was decanted from the amine salts and the oily bottom layer. The benzene solution was washed with water and dried over anhydrous magnesium sulfate. Filtration and evaporation of the filtrate at reduced pressure gave a white solid.

Poly[bis(benzylamino)phosphazene]; $[NP(NHCH_2C_6H_5)_2]_n$: A solution of polydichlorophosphazene (8.450 g, 0.073 mol) in benzene (70 ml) was added slowly to a stirred solution of benzylamine (46.8 g, 0.437 mol) and triethylamine (44.2 g, 0.437 mol) in tetrahydrofuran (70 ml). The reaction mixture was stirred at 25 °C for 50 h and then at 45 °C for 7 h. The mixture of polymer and amine salts was filtered off, solvent being removed from the filtrate by distillation. The residue was redissolved in acetone, and the polymer was then precipitated from the solution by addition of ehtanol and dried in a vacuum over P_2O_5.

Resistivity Measurement. All the polymers were powdered and molded pellets were used for resitivity measurements. Pellets (12 mm diameter and 1—2 mm thick) were molded at pressures up to 500 kg/cm^2). The pellets were provided with vacuumevaporated platinum–palladium alloy contacts. Among the contact materials platinum–palladium alloy seemed to give the best ohmic contacts.

The electrical resistivity was studied as a function of temperature in the range 20—180 °C. In order to get exact resistivity values, the current was measured as a function of the voltage in the range 0—90 V, with use of a guard electrode.

Physical Measurements. Molecular weights were measured by vapor pressure osmometry with a Hitachi Model-117 type osmometer using benzene as a solvent.

TABLE 1. CHEMICAL ANALYSIS OF THE PRODUCTS

Compound	Calcd(%) P	Calcd(%) N	Found(%) P	Found(%) N	Mol wt	Yield (%)	Appearance
$[NP(NH\text{-}monoC_6H_{13})_2]_n$	12.74	12.55	12.62	17.27	4.0×10^3	25	White powder
$[NP(NHCH_2CH{=}CH_2)_2]_n$	21.67	26.19	19.70	26.74	7.6×10^3	12	White powder Resinous material[a)]
$[NP(NHCH_2C_6H_5)_2]_n$	11.20	16.90	12.04	16.34	—	3	White powder

a) A small amount.

IR spectra were recorded on a Shimadzu Model-450 type spectrometer by means of the KBr disk technique.

Thermogravimetric analysis and differential thermal analysis were carried out with a Shimadzu Model DT 20-B under dry nitrogen (50 ml/min) at a heating rate of 15 °C/min.

Results and Discussion

Syntheses. In general, poly[bis(amino)phosphazenes] are synthesized by the reaction of poly(dichlorophosphazene) with a primary or secondary amine according to the following scheme.

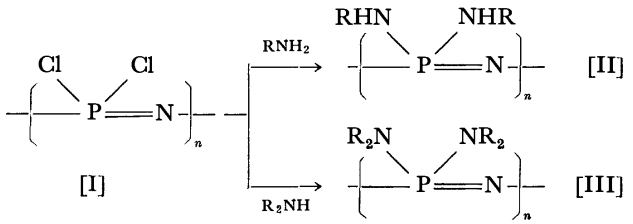

We have synthesized three new compounds: poly(mono-hexylaminophosphazene), poly(allylamino phosphazene), and poly(benzylaminophosphazene).

Excess amines and triethylamine were used as hydrohalide acceptors for the steric property of these bulky amines. The results of chemical analysis and molecular weights of the products are given in Table 1.

We see that the elemental compositions of the polymers correspond satisfactorily to the expected structures.

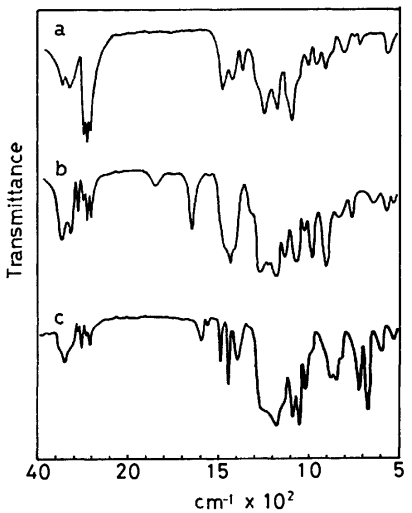

Fig. 1. IR spectrum of the products.
a: $[NP(NH\text{-}mono\text{-}C_6H_{13})_2]_n$,
b: $[NP(NHCH_2CH{=}CH_2)_2]_n$,
c: $[NP(NHCH_2C_6H_5)_2]_n$.

The IR spectra of the products obtained from the reaction of poly(dichlorophosphazene) with monohexylamine, allylamine, benzylamine are shown in Fig. 1. All the polymers exhibit a characteristic P=N stretching absorption in the region 1200—1260 cm^{-1}.

The assignments for the main peaks are as follows (frequncies in cm^{-1}): for $[NP(NHR_2]_n$ where R is mono-C_6H_{13}, 1260 (P–N), 1180, 1100 (C–N), 905 (P–N, C–N), 1467, 1370(–CH_3), 3360, 3250, (N–H), CH_2-CH=CH_2, 1260, 1230(P–N), 1190, 1080(C–N), 915, 995, 1420, 1640, 3080, (allyl), 3220(N–H), CH_2–C_6H_5, 1220, 1250(P–N), 1180(P–N, C–N), 1070, 1090(C–N), 1450, 1500, 1580, 1600(–C_6H_5), 2900, 2850(–CH_2), 3345(N–H). The results indicate that the monohexylamino, allylamino, and benzylamino derivatives are of open chain structure similar to that of the $(NPCl_2)_n$.

The complete replacement of chlorine atoms of poly(dichlorophosphazene) by monohexylamine or benzylamine required severer conditions than those reported for ethylamine, methylamine, propylamine, *etc.* This seems to be associated with steric hindrance of side group.

All the polymers are soluble in mineral acid, trifluoroethanol or benzene, but not in common organic solvents or water. The solubility of the polymers indicates that the meterials are not cross-linked. The polymers seem to have a linear structure. It was found from IR spectra, chemical analysis, and UV spectra that the five polymers prepared by the method of Allcock are consistent with the expected structure, $[NP(NHR)_2]_n$ (NHR: NHEt, $NHPr^n$, $NHBu^n$, NHPh) and $[NP(NMe_2)_2]_n$.

Thermal Stability. The thermal stability of the eight poly[bis(amino)phosphazenes] were examined by TGA and DTA. The results are given in Figs. 2 and 3. The polymers begin to decompose at about 200 °C, a remarkable weight loss being observed between 250 and 400 °C. On the other hand, in the ethylamino, propylamino, butylamino, mono- hexylamino, allylamino, and diethylamino derivatives, the broad endothermic peaks appear between 200 and 400 °C. In the phenylamino and benzylamino derivatives the endothermic peaks appear between 400 and 470 °C.

In the decomposition of all the polymers at 400 °C, the corresponding amines to side groups were detected by gas chromatography. Decomposition took place with elimination of appropriate amines. The endothermic peaks appearing above *ca.* 500 °C might be due to breakdown of phosphorus nitrogen bonds. In the ethylamino, propylamino, butylamino, and monohexylamino derivatives, exothermic peaks which seem

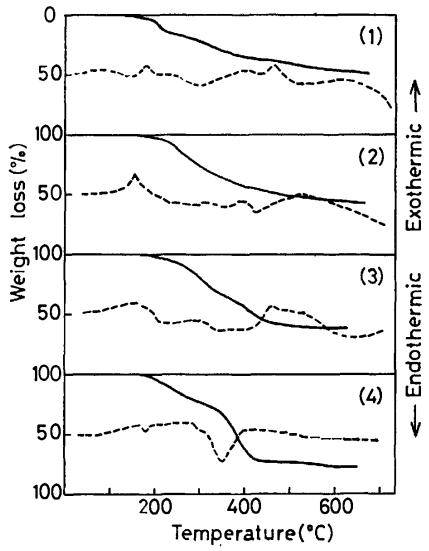

Fig. 2. TGA and DTA curves for poly[bis(amino)-phosphazenes], $[NPR_2]_n$.
(1): R=NHC_2H_5, (2): $NHC_3H_7{}^n$, (3): $NHC_4H_9{}^n$, (4): NH-mono-C_6H_{13}.
——: TGA, ----: DTA.

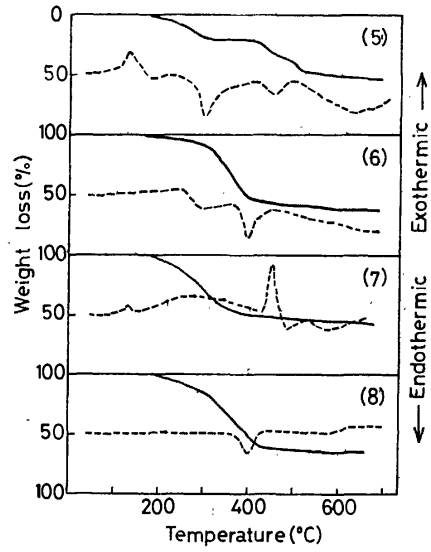

Fig. 3. TGA and DTA curves for poly[bis(amino)-phosphazenes], $[NPR_2]_n$.
(5): R=$NHCH_2CHCH_2$, (6): $N(CH_3)_2$, (7): NHC_6H_5, (8): $NHCH_2C_6H_5$.
——: TGA, ----: DTA.

to be oxidation of the alkyl groups appear between 150 and 175 °C. In the allylamino derivative, the sharp exothermic peak appears at 125 °C. This is probably due to the addition polymerization of the allylamino side group similar to that reported for $[NP(NHCH_2CH{=}CH_2)_2]_3$ and $[NP(NHCH_2CH{=}CH_2)_2]_4$ by Allcock *et al.*[7]

D. c. Resistivity. The results of initial measurements of all the samples were not reproducible.

Several thermal cycles for each sample were carried out in order to obtain reproducible results. A typical example is shown for dimethylamino derivative in Fig. 4.

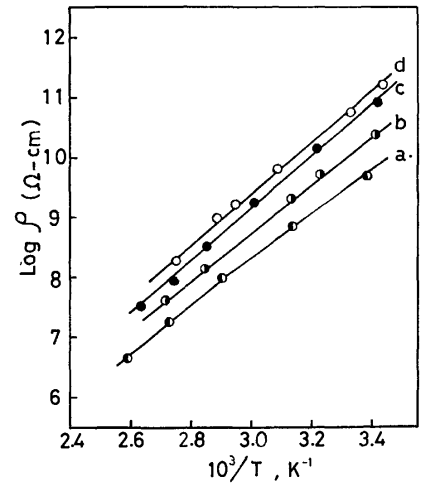

Fig. 4. Temperature dependence of resistivity of $[NP(N(CH_3)_2)_2]_n$.
a: Ascend first time, b: ascend second time, c: ascend third time, d: desend third time.

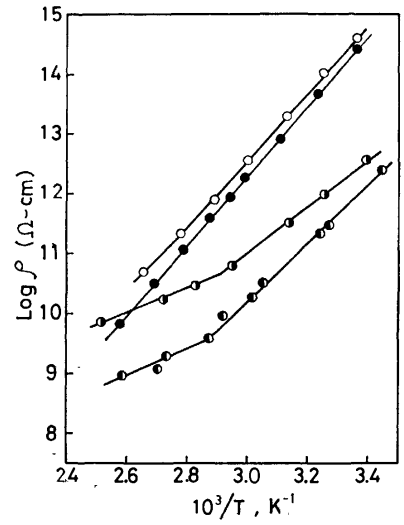

Fig. 5. Temperature dependence of resistivity of poly-[bis(amino)phosphazenes], $[NPR_2]_n$.
○: R=NHC_2H_5, ●: R=$NHC_3H_7{}^n$, ◑: R=$NHC_4H_9{}^n$, ◐: R=NH-mono-C_6H_{13}.

Lower resistivity was always observed in the initial runs.

Initial heating curves are usually of anomalous low ΔE and frequently curved, due to the evaporation of moisture or solvents. Reproducible results were obtained after several thermal cycles had been carried out.

The results are given in terms of log ρ *vs.* $1/T$ (Figs. 5 and 6).

The results can be expressed by the relationship $\rho=\rho_0 \exp(\Delta E/2RT)$. The calculated energy gaps ΔE and values of log ρ_0 are given in Table 2. Some curves show a break point in the range 70—90 °C. A break point was found by measurements on other polymers.[8] The break point is usually associated with thermal decomposition of the sample.

However, our investigations of thermal stability show-

TABLE 2. VALUES OF RESISTIVITY, ENERGY GAP, AND log ρ_0

Side group[a] R		Temp (°C)		Energy gap ΔE (eV)	log ρ_0 (Ω cm)	ρ (20 °C) (Ω cm)
(1)	NHC_2H_5	25	90	2.20	−4.1	8.1×10^{14}
(2)	$NHC_3H_7{}^n$	25	120	2.30	−5.3	6.3×10^{14}
(3)	$NHC_4H_9{}^n$	20	70	1.54	−0.7	4.5×10^{12}
		70	125	0.84	+4.5	
(4)	NH-monoC_6H_{13}	20	75	1.95	−4.5	1.8×10^{12}
		75	120	0.84	+3.5	
(5)	$NHCH_2CHCH_2$	20	43	1.69	−3.0	2.8×10^{11}
		43	75	0.53	+6.2	
(6)	$N(CH_3)_2$	20	90	1.75	−3.8	1.8×10^{11}
(7)	NHC_6H_5	70	90	1.46		1.6×10^{15} (75 °C)
		90	120	5.80	—	
(8)	$NHCH_2C_6H_5$	85	120	(1.85)	—	1.3×10^{15} (90 °C)

a) $[NPR_2]_n$.

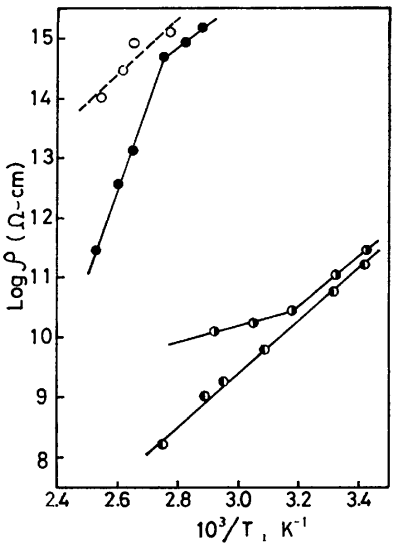

Fig. 6. Temperature dependence of resistivity of poly-[bis(amino)phosphazenes], $[NPR_2]_n$.
○: R=$NHCH_2CHCH_2$, ●: R=$N(CH_3)_2$,
◑: R=NHC_6H_5, ◐: R=$NHCH_2C_6H_5$.

ed no decomposition of the polymers in the range 70—90 °C. It was found that the resistivity of poly(aminophosphazenes), $[NP(NHR)_2]_n$, decreases in the order, NHR: $NHCH_2C_6H_5$, $NHC_6H_5 \gg NHC_2H_5 > NHC_3H_7 > NHC_4H_9 > NHC_6H_{13} \gg N(Me_3)_2$. Thus, the resistivity of polymers decreases with an increase in the number of C in side groups of aliphatic primary amino derivatives, and the resistivity of the secondary amino derivative, $[NP(NMe_2)_2]_n$, showed lower values than those of the primary amino derivatives. This is probably attributed to the nature of an inductive electron supply. Both the inductive electron supply from amino to phosphorus, and π effects involving donation of the nitrogen lone pair electrons into phosphorus d_{z^2} orbitals would raise the electron density at phosphorus,[9] raising electrical conductivity. However, it appears that P_π–d_π bonding cannot bring about enough π-orbital overlap to cause high electrical conduction. If the π bonds in the phosphazene chain were delocalized, as suggested for cyclic oligomers,[10] then the conductivity would be expected to be comparable to that of the carbon polyene polymers.

On the other hand, the values of resistivity of phenylamino and benzylamino derivatives are greater than 10^{-15} Ω cm at room temperature. The bulky side groups such as aromatic amino would be expected to reduce the interaction between molecules, as compared with aliphatic amines which possess a possible degree of rotation about the C–C single bonds. A similar behavior was reported for polyacethylenes.[11] In phenylamino derivatives, the break point was observed at 90 °C corresponding to the glass transition temperature reported by Allcock and Kugel.[5] The amino derivatives have low resistivity when compared to alkoxy or aryloxy derivatives.[12] Thus, it appears that the high side-group polarity of amine and increased opportunities for hydrogen bonding (when NHR groups are present) decrease the resistivity of the polymers. The conductivity observed for the poly(aminophosphazenes) is assumed to be associated primarily with the electrons of its conjugated double bond.

When an external field was applied, polarization, *i.e.*, an increase in resistance with time to a steady value, occurred for most samples, the resistivity reaching equilibrium values after 30 min—1h. Although similar results have been described,[13,14] it is assumed that

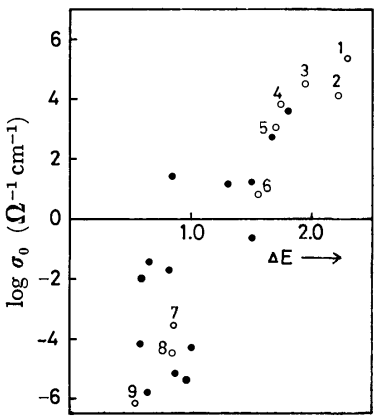

Fig. 7. Correlation of energy gap and log σ_0.
1: (2), 2: (1), 3: (4), 4: (6), 5: (5), 6: (3), 7: (4), 8: (3), 9: (6).
●: Previous data.

the effect arises from either space-charge build-up in the sample or barrier between electrode and sample.

The correlation of energy gap ΔE and preexponential factor $\log \sigma_0 (=1/\rho_0)$ is shown in Fig. 7. A straight line with a large amount of scatter is obtained, suggesting the relationship $\log \sigma_0 \approx \Delta E(\text{eV}) - 6$. The compensation law is valid for poly[bis(amino)phosphazenes]. However, it is difficult to give a physical meaning. An interpretation is given in terms of molecular motion as a condution mechanism such as presented by Gutmann and Lyons[13] and Cardew and Eley.[15] However, exprimental results are so few that a quantitative discussion of this type of conduction mechanism cannot be realized.

Most polymers showed ohm's law behavior up to *ca.* 500 (V/cm) or above.

The authors wish to express their appreciation to Mr. T. Yamamoto for his cooperation in the experiments.

References

1) D. D. Eley and M. R. Willis, *J. Chem. Soc.*, **1963**, 1534.
2) P. J. Reucroft, P. L. Kronick, H. Scott, and M. M. L. Labes, *Nature*, **201**, 609 (1964).
3) T. Hayashi and H. Saito, *Nippon Kagaku Kaishi*, **74**, 134 (1971).
4) T. Hayashi and H. Saito, *Nippon Kagaku Kaishi*, **1973**, 2191.
5) H. R. Allcock and R. L. Kugel, *Inorg. Chem.*, **5**, 1716 (1966).
6) H. R. Allcock and R. L. Kugel, *Inorg. Chem.*, **11**, 2584 (1972).
7) H. R. Allcock, P. S. Forgione, and K. J. Valan, *J. Org. Chem.*, **30**, 947 (1965).
8) D. M. Carlton, D. K. McCarthy, and R. H. Genz, *J. Phys. Chem.*, **68**, 2661 (1964).
9) H. R. Allcock, "Phosphorus-Nitrogen Compounds," Academic Press, New York (1972).
10) D. P. Craig and N. L. Paddock, *J. Chem. Soc.*, **1962**, 4118.
11) J. E. Katon, "Organic Semiconducting Polymers," Marce; Dekker, Inc., New York (1968), p. 87.
12) T. Hayashi and H. Saito, Unpublished data.
13) F. Gutmann and L. E. Lyons, "Organic Semiconductors," John Wiley & Sons, Inc., New York (1967), p. 428.
14) D. D. Eley and B. M. Pacini, *Polymer*, **1967**, 159.
15) M. H. Cardew and D. D. Eley, *Discuss. Faraday Soc.*, **27**, 115 (1959).

The Hindered Internal Rotation of Amide Groups of Polyacrylamide of Low Molecular Weights

Yoshiyuki HIRAI, Mitsuyoshi YUKAWA, and Yoshio IMAMURA

Department of Chemistry, Faculty of Science, Science University of Tokyo, Kagurazaka, Shinjuku-ku, Tokyo 162

(Received August 31, 1976)

Polyacrylamides of low molecular weights (average degrees of polymerization($\overline{DP}$): 7.2, 18.3, 21.3, and 45.4) were prepared by radical polymerization, and their PMR spectra were observed over the temperature range of 30—90 °C. From the temperature dependence of the PMR spectra, the values of the energy barrier to the internal rotation about C–N bonds were determined by means of a total line-shape analysis. The energy barriers for the polymers above $\overline{DP}$: 18.3 were 10.6 kcal/mol, while those for the polymer of $\overline{DP}$: 7.2 were 9.2 kcal/mol. These results were interpreted in terms of the local environment around the amide groups. The intramolecular hydrogen bonding was also investigated.

In a previous investigation,[1] we observed an anomalous broadening for the absorption of *ortho* protons of poly(*p*-chlorostyrene) of very low molecular weights (average degrees of polymerization($\overline{DP}$)$<$15). This phenomenon was elucidated by assuming the "permissible conformation" which is permitted only in very short chains, and was termed the "polymeric effect on molecular structure" of polymers in solutions. The present investigation will be concerned with the "polymeric effect on intramolecular motion" of polymers in solutions.

Recent studies by various authors[2-6] have shown that the NMR spin-lattice relaxation times (T_1) of polymers in solutions change appreciably with the chain length in the region of short chains, and that T_1 becomes less sensitive to the chain length as the chains become longer ($\overline{DP}$: 10—30). Similar phenomena were also observed in ESR studies of spin-labeled polymers.[7,8] These observations have been interpreted in terms of the "polymeric effect on relaxation process"[4] (in other words, the "polymeric effect on molecular motion" of polymer chains). However, the rigorous analysis of NMR T_1 or ESR line widths is not always easy; that is, the precise separation of motional modes is impossible at the present stage. Therefore, the observations were understood rather qualitatively in either case, and a discussion focused on a local motion in the molecular motions of polymer chains was desired.

If the rate constants or the energy barriers on the specific local motion of polymer chains are estimated precisely as functions of the molecular weights, the polymeric effect on molecular motion could be understood in more detail.

Polyacrylamide is one of the most favorable samples for such a purpose. The amide protons of polyacrylamide represent the characteristic patterns of PMR signals reflecting the internal rotation about C–N bonds in amide groups. They make it possible to evaluate precisely the rate constants or the energy barriers on the specific local motion by analyzing the spectra of amide protons.

The PMR spectra of amide protons of polyacrylamide of a high molecular weight were analyzed by Bovey and Tiers[9] by means of peak separation method.* In the present investigation, the PMR spectra for the polymers of low molecular weights($\overline{DP}$: 7.2—45.4) were analyzed by means of more exact procedures (the total line-shape analysis). The local environment around the amide groups was discussed on the basis of the obtained rotational barriers.

The intramolecular hydrogen bonding was also investigated in a conventional manner.

Experimental

The samples of polyacrylamide were prepared by the procedure of Bovey and Tiers.[9] In order to control the molecular weights, the amount of the chain-transfer agent (sodium mercaptoacetate) was changed over the range from 0.5 g to 3 g per 10 g of the monomer. The polymers were precipitated in a large amount of ethanol in order to free them from any residual monomer, and were then dried *in vacuo*. The number-average molecular weights of these polymers were determined by using "KUNAUAR's vapor-pressure osmometer" in aqueous solutions at 37 °C. The number-average degrees of polymerization ($\overline{DP}$) of the polymer samples were 7.2, 18.3, 21.3, and 45.4 (they will be denoted as 7-, 18-, 21-, and 45-polymer).

The infrared spectra of these polymer samples were nearly identical. They consist of the absorption bands which were assigned by Savitskaya and Kholodova.[11]

The polymer solutions for PMR spectral measurements were prepared by dissolving 0.08 g of the polymer in 1.0 ml of water, previously adjusted to the proper pH, in small vials. One per cent of 2,2-dimethyl-2-silapentane-5-sulfonate (DSS) was added to each solution to serve as the internal reference. The pH of the solutions was adjusted according to the directions of Bovey and Tiers.[9]

The polymer solutions were then transferred to 5 mm o.d. NMR tubes, which were sealed after the atmosphere had been replaced with nitrogen gas. The PMR spectra were observed by using a Japan Electric Laboratory "JNM PS-100 spectrometer" operated at 100 MHz. In the spectra, the peak-position values of each absorption were termed δ values to the methyl peak of DSS as the reference.

Results and Discussion

Hindered Internal Rotation of Amide Groups and Molecular Weight. Figure 1a shows the absorption of the amide protons (NH_2) of the 21-polymer in the aqueous solution of pH 4.5 at 40 °C. The absorption

* However, Allerhand *et al.*[10] estimated the errors introduced in various approximate methods; the errors involved in the peak-separation method reach 100% in some cases, and so approximations are undesirable.

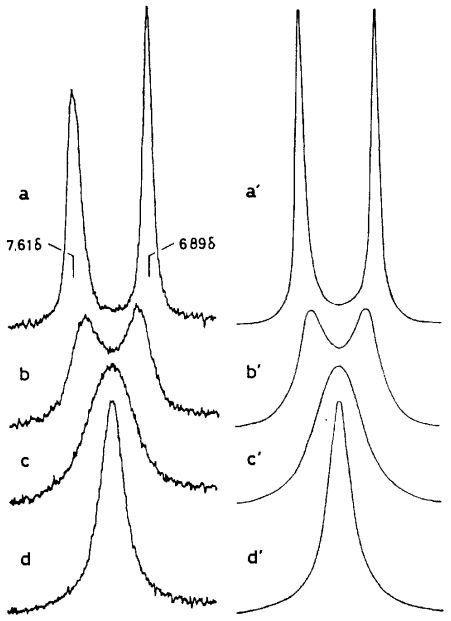

Fig. 1. Experimental PMR spectra (left) of amide protons of polyacrylamide ($\overline{DP}$: 21.3) in aqueous solutions of pH 4.5 (8 w/v%): (a) 40 °C; (b) 70 °C; (c) 80 °C; (d) 90 °C. The best-fit calculated spectra (right): the mean life time $\tau_{AB}(\tau_{BA})$ (a') 0.032 s; (b') 0.0090 s; (c') 0.0050 s; (d') 0.0030 s.

in the lower field is broader than that in the higher field; such spectra were also observed by Bovey and Tiers.[9] The broadening of the absorption may be attributed to the spin coupling with protons of the main chain.[12] In the line-shape analysis to be described below, the line-widths of the calculated spectra are arranged for the absorptions in the higher field. The absorption of water protons appeared to the right (4.62δ) of these amide peaks. Figures 1b, c, and d show the NH_2 absorptions at 70, 80, and 90 °C respectively.

The structure of amides is generally regarded as being approximately planar, and the two sites marked A and B are chemically nonequivalent. The C–N bond

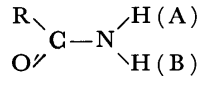

R: $-CH_2CH-$ in the present study

has a partial double-bond character, and the rotation about the bond can be described as a rate process which interchanges the two protons between two environments. The rate process is characterized by rate constants in the range of 10^{-1} to 10^5 s^{-1}; such a rate process causes profound changes in the shapes of the PMR signals. On the other hand, when water is used as the solvent, the amide protons undergo a hydrogen-exchange reaction with the hydrogen of water. This rate process is also characterized by similar rate constants. Therefore, the spectra shown in Fig. 1 should be analyzed by assuming the three-site exchange system represented in Fig. 2.[13a] A total line-shape analysis[13b] can be used for the exact analysis of the spectra reflecting such an exchange system.

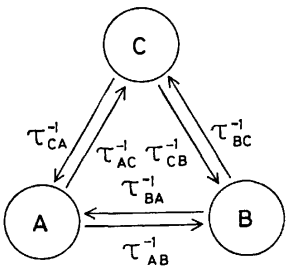

Fig. 2. Diagram for three-site exchange process. A: position A in amide group; B: position B in amide group; C: solvent(water). The arrows indicate the six possible transitions. τ_{ij}^{-1}(i, j=A, B, and C): the rate constants for jumps from site i to j.

Table 1. Parameters yielding the best-fit calculated curves

Temperature (°C)	$\overline{DP}$: 21.3 $\tau_{AB}(\tau_{BA})$ (s)	$\overline{DP}$: 7.2 $\tau_{AB}(\tau_{BA})$ (s)
30	0.060	0.050
40	0.032	0.026
50	0.022	0.016
60	0.016	0.012
70	0.0090	0.0080
80	0.0050	0.0050
90	0.0030	

$\tau_{AC}(\tau_{BC})$: 1.0×10^2 s, $\tau_{CA}(\tau_{CB})$: 9.8×10^3 s. Spin-spin relation times(T_2): 0.6 s for the proton at each site.

The analysis is accomplished by fitting a calculated curve to an experimental curve. Figures 1a'—d' show the best-fit calculated curves for the NH_2 spectra of the 21-polymer. The parameters which yield the best-fit curves are listed in Table 1. The values of T_2 were determined in the following way: we calculated the theoretical spectra for various T_2 values and chose 0.6 s as the most reasonable value of T_2; the line-width of the calculated spectra for 0.6 s does not exceed that of the observed spectra. The parameters, $\tau_{AC}(\tau_{BC})$ and $\tau_{CA}(\tau_{CB})$, did not depend on the temperature; the values of these parameters remained constant. The spectra of other polymer samples ($\overline{DP}$: 7.2, 18.3, and 45.4) were also analyzed in the same way. For example, the parameters for the NH_2 spectra of the 7-polymer are also given in Table 1. In these parameters, the parameters which characterize the rotation about C–N bonds are the mean life-times $\tau_{AB}(\tau_{BA})$. The rotational barriers about the C–N bonds can be calculated by means of the Arrhenius plots of those mean life-times.[13b] The energy barriers for each polymer sample were determined, and they are collected in Table 2. The energy bar-

Table 2. Degrees of polymerization and energy barriers for internal rotation about the C–N bond in polyacrylamide

$\overline{DP}$	7.2	18.3	21.3	45.4
E_a(kcal/mol)	9.2	10.6	10.6	10.6

riers for the 18-, 21-, and 45-polymer were 10.6 kcal/mol, while those for the 7-polymer were smaller by 1.4 kcal/mol.

In NMR or ESR studies of polymers, the molecular motion of polymer chains has mainly been discussed on the basis of NMR T_1 or ESR line-width measurements. The effective correlation times, reduced from the T_1 or line-widths, can be divided into two terms: (a) an overall rotation with rate (τ_o^{-1}), and (b) a segmental motion with rate (τ_s^{-1}). The polymeric effect on molecular motion cited in the beginning section has been understood in terms of τ_o and τ_s.[3,5-8] However, such an analysis provides only limited insight into the details of molecular motion because such a motional model is undoubtedly oversimplified for realistic models of the molecular motion of polymer chains. In these investigations, a detailed discussion of the motion of the local mode was not presented. Analyses of the detailed motion of polymer chains (the rigorous analyses of correlation times) have been devised by various investigators;[14-17] however, they are not yet useful.

On the other hand, the reciprocals of the mean life-times (τ_{AB}, τ_{BA}) obtained in this experiment are the rate constants for the rotation about C–N bonds of amide groups. The energy barriers(E_a) reflect the amount of hindrance to this internal rotation. Therefore, $\tau_{AB}(\tau_{BA})$ or E_a is well suited for a detailed discussion of the local motion. Tables 1 and 2 obviously show that the internal rotation in the 7-polymer is less hindered than that in the polymers above $\overline{DP}$:18. This observation may be termed the polymeric effect on local motion.

In the previous work,[1] we assumed the "permissible conformation" in order to elucidate the PMR spectra of poly(*p*-chlorostyrene) of low molecular weights. This conformation is permitted only in short chains: in short chains side groups are able to escape from each other, whereas in long chains such a conformation is limited by steric restrictions. The phenomenon called the "polymeric effect on molecular structure" was understood as the limitation of the permissible conformation.

Meanwhile, the limitation of the permissible conformation would result in a decrease in the distance between side groups in a polymer chain. This intramolecular packing of side groups causes an increse in the interaction between side groups, and may interfere with the local motion of polymer chains.

The permissible conformation can be assumed not only for poly(*p*-chlorostyrene), but also for polyacrylamide chains. Therefore, on the basis of the experimental fact and the consideration described above, we can draw a reasonable interpretation for the molecular-weight dependence of the energy barriers to the internal rotation about C–N bonds.

Although the 7-polymer could occupy the permissible conformations, in the polymers above $\overline{DP}$: 18 such conformations are forbidden. The intramolecular packing of side groups resulting from the limitation of the conformation increases the intraction between side groups in a polymer chain. The increase in this interaction inhibits the internal rotation about the C–N bonds of amide groups. As a result, the energy barriers (E_a) increase from 9.2 to 10.6 kcal/mol as the degrees of polymerization increase from 7.2 to 18.3.

This change in the local environment arising from the limitation of the conformation corresponds to the phenomenon called the "polymeric effect on molecular motion" cited in the beginning section.

Recently, Nomura and Miyahara[18] observed the molecular-weight dependence of the local motion (the tumbling motion of phenyl groups of polystyrene). Their observation may also be termed the polymeric effect on local motion.

Hydrogen Exchange and Intramolecular Hydrogen Bond. Polyacrylamide has NH groups and CO groups, which can form hydrogen bonds. For some polymer amides, intramolecular hydrogen bonds (NH···O=C) were observed.[19] If such intramolecular hydrogen bonds exist in polyacrylamide chains, a modification of the conclusion presented in the preceding section may be required. Therefore, in this section, the possibility of the existence of the intramolecular hydrogen bond in polyacrylamide will be discussed in a conventional manner(the investigation of the pH dependence of hydrogen exchange between amide groups and water).[20]

Figure 3 shows the NH_2 absorptions of the 45-polymer in solutions of various pH at 30 °C, and the best-fit calculated curves for these absorptions. The exchange rates, τ_{AC}^{-1}, which characterize the hydrogen-exchange reaction between amide groups and water are shown in Fig. 4 as a function of the pH. Figure 4 indicates that the hydrogen exchange is catalyzed by both H^+ and OH^- and that the rates of the reaction are minimum at near pH 4.5 and the rates (k_{min}) are 9×10^{-3} s^{-1}. The discussion of the intramolecular hydrogen bonds is carried out on the basis of this k_{min}.

Snyder and Klotz[19] investigated the k_{min} of poly(*N*-isopropylacrylamide) in the range of molecular

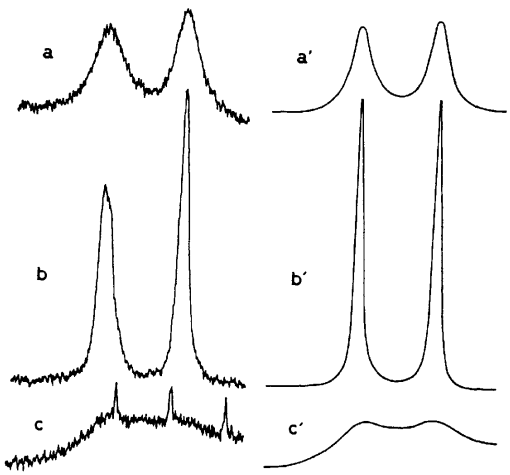

Fig. 3. Experimental PMR spectra (left) of amide protons of polyacrylamide ($\overline{DP}$: 45.4) in aqueous solutions of various pH (8 w/v%) at 30 °C: (a) pH 8.6; (b) pH 7.0; (c) pH 0.0. The spike peaks in (c) are side bands of absorptions of solvent. The best-fit calculated spectra (right): the mean life times τ_{AC} (τ_{BC}) (a') 0.020 s; (b') 0.90 s; (c') 0.0050 s.

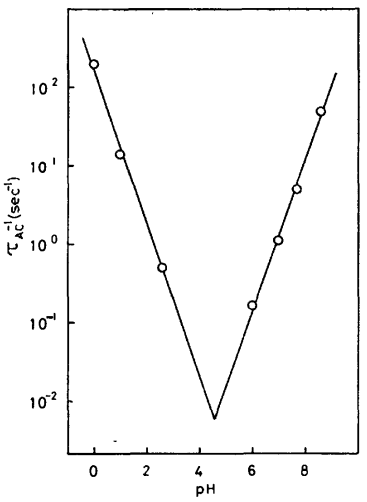

Fig. 4. Hydrogen exchange rates between amide groups and solvent (water) as a function of pH.

weights from 100 (monomer) to 2×10^5. They found that the k_{min} decreased abruptly from 1×10^{-2} to 8×10^{-5} s^{-1} when the amide was transferred from the monomer to the polymer of molecular weights 10^3 ($\overline{DP}\approx10$). The abrupt decrease in k_{min} was concluded to be due to the formation of intramolecular hydrogen bonds.

If the intramolecular hydrogen bonds are formed by NH and CO groups in polyacrylamide chains, the k_{min} must be of the order of 10^{-5}. However, the k_{min} values of the 45-polymer were quite large, and were of the same magnitude as the k_{min} values of small amides (poly(*N*-isopropylacrylamide)-monomer (k_{min}: 1×10^{-2} s^{-1})[19] or *N*-methylacetamide (k_{min}: 2×10^{-3} s^{-1}),[21] *etc.*). The k_{min} for the 21-polymer gave the same value as that for the 45-polymer.

These results mean that no intramolecular hydrogen bond exists in polyacrylamide chains, and indicate that the modification of the conclusion presented in the preceding section is not required.

References

1) Y. Hirai, Y. Nunomura, and Y. Imamura, *Bull. Chem. Soc. Jpn.*, **49**, 2200 (1976).
2) D. E. Woessner, *J. Chem. Phys.*, **41**, 84 (1964).
3) K. J. Liu and R. Ullman, *J. Chem. Phys.*, **48**, 1158 (1968).
4) K. J. Liu and J. E. Anderson, *J. Macromol. Sci.*, **C5**(**1**), 1 (1970).
5) A. Allerhand and R. K. Hailstone, *J. Chem. Phys.*, **56**, 3718 (1972).
6) J. E. Anderson, K. J. Liu, and R. Ullman, *Discuss. Faraday Soc.*, **49**, 257 (1970).
7) A. T. Bullock, G. G. Cameron, and P. M. Smith, *J. Phys. Chem.*, **77**, 1635 (1973).
8) A. T. Bullock, G. G. Cameron, and P. M. Smith, *J. Chem. Soc., Faraday Trans. 2*, **1974**, 1202.
9) F. A. Bovey and G. V. D. Tiers, *J. Poly. Sci., Part A*, **1**, 849 (1963).
10) A. Allerhand, H. S. Gutowsky, J. Jonas, and R. A. Mainzer, *J. Am. Chem. Soc.*, **88**, 3185 (1966).
11) M. N. Savitskaya and Yu. D. Kholodova, *Vysokomol. Soedin., Ser.*, **6**, 493 (1964).
12) H. Kamei, *Bull. Chem. Soc. Jpn.*, **38**, 1212 (1965).
13) a) H. M. McConnell and S. B. Berger, *J. Chem. Phys.*, **27**, 230 (1957); b) G. Binsch, "Topics in Stereochemistry," Vol. 3, ed. by E. L. Eliel and N. L. Allinger, Interscience Publishers, New York, N. Y. (1968), p. 97.
14) T. M. Connor, *Trans. Faraday Soc.*, **60**, 1579 (1963).
15) D. E. Woessner, *J. Chem. Phys.*, **37**, 647 (1962).
16) Y. K. Levine, P. Partington, and G. C. K. Roberts, *Mol. Phys.*, **25**, 497 (1973).
17) J. R. Lyerla, Jr., H. M. McIntyre, and D. A. Torchia, *Macromolecules*, **7**, 11 (1974).
18) H. Nomura and Y. Miyahara, *Polymer J.*, **8**, 30 (1976).
19) W. D. Snyder and I. M. Klotz, *J. Am. Chem. Soc.*, **97**, 4999 (1975).
20) I. M. Klotz, *J. Colloid Interface Sci.*, **27**, 804 (1968), and the references therein cited.
21) A. Berger, A. Loewenstein, and S. Meiboom, *J. Am. Chem. Soc.*, **81**, 62 (1959).

Statistical Mechanical Calculation of the Radial Distribution Function for a Water-like Fluid

Fumio HIRATA

Research Institute of Applied Electricity, Hokkaido University, Sapporo 060

(Received October 15, 1976)

The radial distribution function (RDF) for a *water-like system*, which has the fundamental characteristics of water, is calculated using the graph-theoretical technique developed by Andersen and Chandler. An interaction potential devised to simulate the hydrogen bond is regarded as a perturbation of the pair interaction between the two molecules of a reference system which consists of hard spheres each having a point dipole at each center. The effect of the hydrogen bond-like potential on the distribution of the molecules is shown explicitly. The results show a tetrahedral coordination similar to that in water. The resulting RDF has qualitatively reproduced the features observed in the experimental RDF curve for water.

Water possesses various anomalous physicochemical properties. It is believed that such properties are caused by an "ice-like" structure tetrahedrally-linked *via* hydrogen bonds.[1] The strongest evidence for the tetrahedral coordination is radial distribution function (RDF) obtained from X-ray diffraction and neutron scattering data.[2] The first peak in the RDF is narrow in comparison with that of simple fluids, and corresponds to the low local-density caused by the tetrahedral coordination of the molecules. Another feature in the RDF of water concerns the location of the second peak. The location is characteristic not of simple fluids but of ice. Molecular dynamics and Monte Carlo studies have reproduced the features of the RDF of water.[3]

If we confine ourselves to simple fluids, there are theoretical methods which satisfactorily reproduce the observed values without the aid of any assumptions concerning the arrangement of the molecules.[4] In the case of water, however, if we do not wish to use such assumptions, we are immediately faced with the trouble problem of how to treat strong orientational correlations between water molecules.

Ben-Naim has numerically solved the Percus-Yevick (PY) equation,[5] which has been generalized to involve angular coordinates, in order to obtain the RDF of water.[6a] They used a model potential that effectively accounts for some geometrical features of the hydrogen bond, favoring the tetrahedral orientation. This model potential has a Lennard-Jones (12,6) part and an angle-dependent part based on Bjerrum's four point-charge model of a water molecule. Ben-Naim has proposed another model for the effective pair potential of water. This is expressed by the superposition of the following three terms: a Lennard-Jones (12,6) potential, a dipole-dipole interaction, and a potential devised to act only along the four directions pointing to the vertices of a regular tetrahedron. The hydrogen bond is simulated by the third term. However, actual calculations were carried out only for the case of a two-dimensional system with no dipole-dipole interaction.[6b,7]

New graph-theoretical methods, which are based on the technique of topological reduction, have recently been developed,[4] and have been successfully applied to electrolyte solutions, and dipolar and molecular fluids.[8–14] On the basis of their previous work,[12] Chandler and Andersen have proposed computationally simple techniques for calculating the thermodynamic properties and pair distribution functions of molecular fluids in which the intermolecular interactions are highly angular dependent.[13] The technique is based on the idea that a molecule has several interaction sites, and that the total interaction between two molecules is the sum of the site-site interactions that depend only on the distances between the sites of the two molecules.

Here, an application of this technique to a model system, which we refer to as a "water-like system," is reported. The water-like system is the simplest model which maintains the fundamental features of water, and is distinguished from water by the simplifications described in the following section.

In section I, the model which was used throughout this study is described in detail. In section II, a brief summary is given of the theoretical methods employed and then the methods are extended to the model system. In section III, the procedure for applying the method described in section II to the model is given and the results of the calculation are shown. In the final section, some consideration is given to the results obtained.

I. Effective Pair Potential for a Water-like System

It is expected that the interaction energy between two real water molecules consists of several parts: (1)

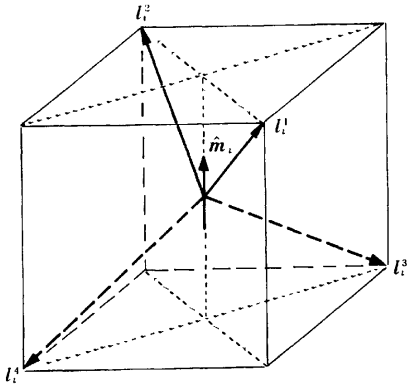

Fig. 1. Schematic representation of the water-like molecule. The molecule is a hard sphere which has a point dipole at its center and four interaction sites seated on the vertices of a regular tetrahedron. The positions of the four sites in a molecule are denoted by vectors starting from the center, $\boldsymbol{l}_i^1$, $\boldsymbol{l}_i^2$, $\boldsymbol{l}_i^3$, and $\boldsymbol{l}_i^4$. The sites at $\boldsymbol{l}_i^1$ and $\boldsymbol{l}_i^2$ correspond to hydrogen atoms of a water molecule and $\boldsymbol{l}_i^3$ and $\boldsymbol{l}_i^4$ to the lone pairs.

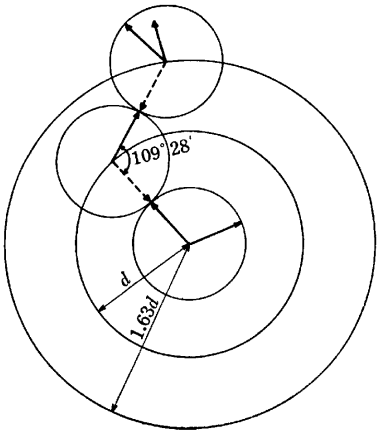

Fig. 2. A typical arrangement of a triplet of molecules in the crystal which consists of water-like molecules.

a steep repulsive part which plays a dominant role in the liquid state and a weak attraction at a short distance, (2) the dipole-dipole interaction at large distances, and (3) hydrogen bonding which is presumably of very short range and highly dependent on the orientation of the molecules. In place of a more realistic system, we consider a simplified model which maintains the fundamental characteristics of the real system. Imagine a hard sphere which has a point dipole at its center and four interaction sites situated on the surfaces of the sphere in the four tetrahedral directions from the center. Let unit vectors pointing to the four sites from the center of the i-th molecule be $\hat{\boldsymbol{l}}_i^\alpha$ (α; 1, 2, 3, 4). The vector giving a dipole orientation is denoted by $\hat{\boldsymbol{m}}_i$. The angles between $\hat{\boldsymbol{l}}_i$ and $\hat{\boldsymbol{m}}_i$ are denoted by χ_α, thus

$$\cos\chi_\alpha = (\hat{\boldsymbol{m}}_i\cdot\hat{\boldsymbol{l}}_i^\alpha), \qquad (\alpha = 1,\cdots,4) \tag{1-1}$$

It is assumed that

$$\begin{aligned}&\cos\chi_1 = \cos\chi_2 = \cos\chi,\\ \text{and}\quad&\\ &\cos\chi_3 = \cos\chi_4 = -\cos\chi.\end{aligned} \tag{1-2}$$

Figure 1 shows a schematic picture of such a model particle. The interaction energy between two such molecules may be expressed as the superposition ot three terms:

$$u(i,j) = u_{\rm d}(R) + u_{\rm DD}(i,j) + u_{\rm HB}(i,j), \tag{1-3}$$

where i and j denote the positions and the orientations of molecules i and j, respectively, and R is the distance between the centers of the two molecules. In particular, let i represent $\boldsymbol{R}_i$ (the position of the center of the i-th molecule) and $\boldsymbol{\Omega}_i$ (the Euler angle required to specify the orientation of the i-th molecule). The position of the α-site on the i-th molecule is denoted by $\boldsymbol{r}_i^\alpha = \boldsymbol{R}_i + \boldsymbol{l}_i^\alpha$. The molecules are assumed to be rigid. Thus, $\boldsymbol{l}_i^\alpha$ depends only on $\boldsymbol{\Omega}_i$. The magnitudes of all $\boldsymbol{l}_i^\alpha$ (α=1, 2,3,4) are identical and are represented by l. $u_{\rm d}(R)$ and $u_{\rm DD}(i,j)$ are defined as

$$\begin{aligned}u_{\rm d}(R) &= \infty, \qquad R<d,\\ &= 0, \qquad R>d,\end{aligned} \tag{1-4}$$

and

$$u_{\rm DD}(i,j) = (-m^2/R^3)D(i,j), \tag{1-5}$$

where

$$D(i,j) = 3(\hat{\boldsymbol{m}}_i\cdot\hat{\boldsymbol{R}})(\hat{\boldsymbol{m}}_j\cdot\hat{\boldsymbol{R}}) - (\hat{\boldsymbol{m}}_i\cdot\hat{\boldsymbol{m}}_j),$$

d is the hard-sphere diameter and $\hat{\boldsymbol{R}}$ the unit vector along the relative position $\boldsymbol{R}=\boldsymbol{R}_i-\boldsymbol{R}_j$. The $u_{\rm HB}(i,j)$ is a sum of site-site interactions of the two molecules, and thus the hydrogen bonding is simulated by

$$u_{\rm HB}(i,j) = \sum_\alpha^4\sum_\gamma^4 u_{\alpha\gamma}(|\boldsymbol{r}_i^\alpha-\boldsymbol{r}_j^\gamma|). \tag{1-6}$$

It is assumed that the site located at $\boldsymbol{l}_i^1$ is identical with that at $\boldsymbol{l}_i^2$ in kind and is different from those at $\boldsymbol{l}_i^3$ and $\boldsymbol{l}_i^4$, which are of the same kind. The sites at $\boldsymbol{l}_i^1$ and $\boldsymbol{l}_i^2$ correspond to the hydrogen atoms of a water molecule and those at $\boldsymbol{l}_i^3$ and $\boldsymbol{l}_i^4$ to lone pairs. A site on one molecule is assumed to interact with a site on another molecule only if the two sites differ in kind. A square-well potential is chosen as the interaction potential, such that

$$\begin{aligned}u_{\alpha\gamma}(|\boldsymbol{r}_i^\alpha-\boldsymbol{r}_j^\gamma|) &= -\varepsilon_{\rm H}, \qquad 0<|\boldsymbol{r}_i^\alpha-\boldsymbol{r}_j^\gamma|<b,\\ &= 0, \qquad b<|\boldsymbol{r}_i^\alpha-\boldsymbol{r}_j^\gamma|,\end{aligned} \tag{1-7}$$

where $\varepsilon_{\rm H}$ and b are parameters which represent the depth and the width of the hydrogen-bond potential. These circumstances correspond to the fact that the hydrogen bond in water occurs only if a hydrogen atom of one molecule encounters a lone pair of another molecule.

The model potential just described is similar to that of Ben-Naim but is apparently distinguishable from the latter in the details of the short-range and the hydrogen bond parts.[7]

II. Application of Graph-Theoretical Techniques to the Water-like System

Outline of the Andersen-Chandler Theory. In this section, the graph-theoretical technique of Andersen and Chandler is applied to the model described in the preceding section. The technique is outlined here.[12]

An interaction potential between two molecules is expressed as a superposition of two parts, a reference part $u_0(1,2)$ and a perturbation $u_1(1,2)$:

$$u(1,2) = u_0(1,2) + u_1(1,2). \tag{2-1}$$

Let $h_0(1,2)$ be the total correlation function[4] of the reference system which depends only upon $u_0(1,2)$. Functions $F_0(1,2)$ and $\Phi(1,2)$, which are referred to as the "*reference system hypervertex*"[8b,12] and the "*perturbation bond*,"[12] respectively, are defined as:

$$F_0(1,2) = \rho\delta(1,2) + \rho^2 h_0(1,2), \tag{2-2}$$

$$\Phi(1,2) = -\beta u_1(1,2), \tag{2-3}$$

where $\beta=1/kT$, k is the Boltzmann constant and $\delta(1,2)$ the Dirac delta function. The sum of an infinite series is defined by convolution integrals of functions F_0 and Φ, whose first few terms are represented with the aid of diagrams:

$$\begin{aligned}C(1,2) &= \sum_{n=1}^\infty C^{(n)}(1,2),\\ C^{(1)}(1,2) &= \int F_0(1,3)\Phi(3,4)F_0(4,2)\mathrm{d}(3)\mathrm{d}(4)\end{aligned} \tag{2-4}$$

$$= \quad ,$$

and

$$C^{(2)}(1,2) = \int F_0(1,3)\Phi(3,4)F_0(4,5)\Phi(5,6) \times F_0(6,2)\mathrm{d}(3)\mathrm{d}(4)\mathrm{d}(5)\mathrm{d}(6)$$

where the large circles with two small circles tangent to their circumferences represent F_0 and the lines with small circles at both ends denote Φ. $C^{(n)}(1,2)$ and $C(1,2)$ are called a "*generalized chain*" with n perturbation bonds and a "*renormalized potential*," respectively. Andersen and Chandler have shown that the pair distribution function is approximately expressed by the equation:[12]

$$\rho^2 g(1,2) = \rho^2 g_0(1,2)\exp C(1,2), \tag{2-5}$$

where $\rho^2 g_0(1,2)$ is the pair distribution function of the reference system and

$$g_0(1,2) = h_0(1,2) + 1. \tag{2-6}$$

Thus, our problem is reduced to the evaluation of the renormalized potential $C(1,2)$, if we know $h_0(1,2)$ in advance.

Application of Graph-Theoretical Techniques to the Water-like System. Here a representation for the pair distribution function of the water-like system is presented using the graph-theoretical technique above outlined. The procedure follows the method presented by Chandler and Andersen.[13]

The first two terms of Eq. 1-3 are regarded as the reference potential and the last term as the perturbation. Thus,

$$u_0(1,2) = u_{\mathrm{d}}(R) + u_{\mathrm{DD}}(1,2), \tag{2-7}$$

$$u_1(1,2) = u_{\mathrm{HB}}(1,2). \tag{2-8}$$

Many studies have been devoted to applying the graph-theoretical and integral equation techniques of the theory of classical fluids to the problem of the dielectric constant or the pair distribution function of a system possessing the pair interaction described by Eq. 2-7. Recent progress in such studies involves an analytical solution of the MSM equation[15] and treatments based on the γ-ordering technique.[8,10,11] These studies can be employed to postulate the form of the total correlation function of our reference system. It has been proven that the renormalized potential (Eq. 2-4) for such a system reduces to only the sum of convolution integrals of the perturbation bonds, $-\beta u_{\mathrm{DD}}(1,2)$.[16] The convolution intergrals can be evaluated to explicitly represent the renormalized potential:[10]

$$C_{\mathrm{DD}}(1,2) = \frac{\beta m^2}{(1+2y)(1-y)} \times \left\{\frac{1}{R^3}D(1,2) + \frac{8\pi y}{3}\delta(R)\boldsymbol{\Delta}(1,2)\right\} \tag{2-9}$$

where $y=4\pi\beta m^2\rho/9$ and $\boldsymbol{\Delta}(1,2)=(\hat{\boldsymbol{m}}_1\cdot\hat{\boldsymbol{m}}_2)$.

It is assumed that the total correlation function of the present reference system can be represented by the superposition of two terms,

$$h_0(1,2) = h_{\mathrm{d}}(R) + C_{\mathrm{DD}}(1,2), \tag{2-10}$$

where $h_{\mathrm{d}}(R)$ is the total correlation function of the hard-sphere fluid. The right-hand side of Eq. 2-10 coincides with the MSM approximation if the PY approximation is used for $h_{\mathrm{d}}(R)$[5,17] and $C_{\mathrm{DD}}(1,2)$ equals zero for $R<d$.[12,16] Using Eqs. 1-6, 2-3, 2-8, and 2-10 the perturbation bond and the reference system hypervertex for the water-like system are, respectively, defined as:

$$\Phi_{\alpha\gamma}(1,2) = -\beta u_{\alpha\gamma}(|\boldsymbol{r}_1^\alpha - \boldsymbol{r}_2^\gamma|), \tag{2-11}$$

and

$$F_0(1,2) = (\rho/\Omega)\delta(\boldsymbol{R}_1-\boldsymbol{R}_2)\delta(\boldsymbol{\Omega}_1-\boldsymbol{\Omega}_2) + (\rho/\Omega)^2 h_0(1,2). \tag{2-12}$$

The generalized chain with n perturbation bonds is given by

$$C_{\mathrm{WL}}^{(n)}(1,2) = (\rho/\Omega)^{-2}\int \mathrm{d}(3)\mathrm{d}(4)\cdots\mathrm{d}(2n+2) \times \sum_{\alpha,\gamma}\cdots\sum_{\eta,\nu} F_0(1,3)\Phi_{\alpha\gamma}(3,4)F_0(4,5)\cdots \times \Phi_{\eta\nu}(2n+1,2n+2)F_0(2n+2,2). \tag{2-13}$$

The simple case of $n=2$ is investigated in some detail.

$$C_{\mathrm{WL}}^{(2)}(1,2) = (\rho/\Omega)^{-2}\int \mathrm{d}(3)\cdots\mathrm{d}(6) \times \sum_{\alpha,\gamma}\sum_{\eta,\nu} F_0(1,3)\Phi_{\alpha\gamma}(3,4)F_0(4,5) \times \Phi_{\eta\nu}(5,6)F_0(6,2). \tag{2-14}$$

We assume that the Fourier transform of $\Phi_{\alpha\gamma}(1,2)$ is $\Phi_{\alpha\gamma}(k)$ and hence,

$$\Phi_{\alpha\gamma}(1,2) = (2\pi)^{-3}\int \mathrm{d}\boldsymbol{k}\tilde{\Phi}_{\alpha\gamma}(k)\exp[i\boldsymbol{k}\cdot(\boldsymbol{r}_1^\alpha - \boldsymbol{r}_2^\gamma)]. \tag{2-15}$$

By inserting Eq. 2-15 into Eq. 2-14, we obtain

$$C_{\mathrm{WL}}^{(2)}(1,2) = (\rho/\Omega)^{-2}(2\pi)^{-6}\int \mathrm{d}(3)\cdots\mathrm{d}(6)\int \mathrm{d}\boldsymbol{k}_1\mathrm{d}\boldsymbol{k}_2 \times \sum_{\alpha,\gamma}\sum_{\eta,\nu}\tilde{\Phi}_{\alpha\gamma}(k_1)\tilde{\Phi}_{\eta\nu}(k_2) \times F_0(1,3)F_0(4,5)F_0(6,2) \times \exp[i\boldsymbol{k}_1\cdot(\boldsymbol{r}_3^\alpha - \boldsymbol{r}_4^\gamma) + i\boldsymbol{k}_2\cdot(\boldsymbol{r}_5^\eta - \boldsymbol{r}_6^\nu)]. \tag{2-16}$$

Integrals over the configurations of molecules 4 and 5 are carried out, giving

$$(2\pi)^{-3}\int \mathrm{d}(4)\mathrm{d}(5)F_0(4,5)\exp[-i(\boldsymbol{k}\cdot\boldsymbol{r}_4^\alpha + \boldsymbol{k}'\cdot\boldsymbol{r}_5^\gamma)] = \delta(\boldsymbol{k}+\boldsymbol{k}')\Gamma_{\alpha\gamma}(k) \tag{2-17}$$

$\Gamma_{\alpha\gamma}(k)$ is the sum of two terms, $\Gamma^{\mathrm{h}}_{\alpha\gamma}(k)$ and $\Gamma^{\mathrm{c}}_{\alpha\gamma}(k)$ as follows,

$$\Gamma_{\alpha\gamma}(k) = \Gamma^{\mathrm{h}}_{\alpha\gamma}(k) + \Gamma^{\mathrm{c}}_{\alpha\gamma}(k). \tag{2-18}$$

$\Gamma^{\mathrm{h}}_{\alpha\gamma}(k)$ and $\Gamma^{\mathrm{c}}_{\alpha\gamma}(k)$ are given by

$$\Gamma^{\mathrm{h}}_{\alpha\gamma}(k) = \rho\omega_{\alpha\gamma}(k) + \rho^2 z_\alpha(k)z_\gamma(-k)\tilde{h}_{\mathrm{d}}(k) \tag{2-19}$$

and

$$\Gamma^{\mathrm{c}}_{\alpha\gamma}(k) = \frac{\beta m^2}{(1+2y)(1-y)}\left(\frac{\rho}{\Omega}\right)^2 \times \int \mathrm{d}\boldsymbol{\Omega}_i\mathrm{d}\boldsymbol{\Omega}_j\tilde{C}'_{\mathrm{DD}}(i,j)\exp[-i\boldsymbol{k}\cdot(\boldsymbol{l}_i^\alpha - \boldsymbol{l}_j^\gamma)], \tag{2-20}$$

where

$$\omega_{\alpha\gamma}(k) = \frac{\sin(k|\boldsymbol{l}_i^\alpha - \boldsymbol{l}_i^\gamma|)}{k|\boldsymbol{l}_i^\alpha - \boldsymbol{l}_i^\gamma|}, \tag{2-21}$$

$$z_\alpha(k) = \frac{\sin(kl^\alpha)}{kl^\alpha}, \tag{2-22}$$

$$\tilde{C}'_{DD}(i,j) = -\frac{4\pi}{3}\tilde{D}(i,j) + \frac{8}{3}\pi y\tilde{\Delta}(i,j), \quad (2\text{-}23)$$

$$\tilde{D}(i,j) = 3(\hat{m}_i\cdot\hat{k})(\hat{m}_j\cdot\hat{k}) - (\hat{m}_i\cdot\hat{m}_j), \quad (2\text{-}24)$$

$$\tilde{\Delta}(i,j) = (\hat{m}_i\cdot\hat{m}_j), \quad (2\text{-}25)$$

and $\hat{k}$ is the unit vector pointing in the direction of k. Substituting Eq. 2-17 into Eq. 2-16 and integrating over k', we have

$$C^{(2)}_{WL}(1,2) = (\rho/\Omega)^{-2}(2\pi)^{-3}\int d(3)d(6)\int dk \sum_{\alpha,\gamma}\sum_{\eta,\nu}\tilde{\Phi}_{\alpha\gamma}(k)\Gamma_{\gamma\eta}(k)\tilde{\Phi}_{\eta\nu}(k)F_0(1,3)F_0(6,2)\exp[ik\cdot(r_3^\alpha + r_6^\nu)]. \quad (2\text{-}26)$$

The integrals of Eq. 2-26 over the configurations of molecules 3 and 6 lead to

$$\begin{aligned} C^{(2)}_{WL}(1,2) = {} & (2\pi)^{-3}\int dk \sum_{\alpha,\gamma}\sum_{\eta,\nu}\tilde{\Phi}_{\alpha\gamma}(k)\Gamma_{\gamma\eta}(k)\tilde{\Phi}_{\eta\nu}(k)\exp[ik\cdot(r_1^\alpha - r_2^\nu)][1+\rho\{z_\alpha(k)\tilde{h}_d(k) \\ & + \Omega^{-1}\int d\Omega_3\tilde{C}_{DD}(1,3)\exp(ik\cdot l_3^\alpha)\}\exp(-ik\cdot l_1^\alpha)] \\ & \times [1+\rho\{z_\nu(-k)\tilde{h}_d(k) + \Omega^{-1}\int d\Omega_6 C_{DD}(6,2)\exp(-ik\cdot l_6^\nu)\}\exp(ik\cdot l_2^\nu)] \end{aligned} \quad (2\text{-}27)$$

The generalized chain with n perturbation bonds is analyzed in the same way. The result is

$$\begin{aligned} C^{(n)}_{WL}(1,2) = {} & (2\pi)^{-3}\int dk \sum_{\alpha,\nu}\{\tilde{\Phi}(k)[\Gamma(k)\tilde{\Phi}(k)]^{n-1}\}_{\alpha,\nu}\exp[ik\cdot(r_1^\alpha - r_2^\nu)] \\ & \times [1+\rho\{z_\alpha(k)\tilde{h}_d(k) + \Omega^{-1}\int d\Omega_3\tilde{C}_{DD}(1,3)\exp(ik\cdot l_3^\alpha)\}\exp(-ik\cdot l_1^\alpha)] \\ & \times [1+\rho\{z_\nu(-k)\tilde{h}_d(k) + \Omega^{-1}\int d\Omega_6\tilde{C}_{DD}(6,2)\exp(-ik\cdot l_6^\nu)\}\exp(ik\cdot l_2)], \end{aligned} \quad (2\text{-}28)$$

where $\Phi(k)$ and $\Gamma(k)$ are 4×4 matrices with elements $\tilde{\Phi}_{\alpha\gamma}(k)$ and $\Gamma_{\alpha\gamma}(k)$, respectively. The renormalized potential is given by the sum over the entire generalized chain ($n\geq1$):

$$\begin{aligned} C_{WL}(1,2) = \sum_{n=1}^{\infty} C^{(n)}_{WL}(1,2) = {} & \sum_{\alpha,\nu}(2\pi)^{-3}\int dk\{\tilde{\Phi}(k)[\mathbf{1}-\Gamma(k)\tilde{\Phi}(k)]^{-1}\}_{\alpha,\nu}\exp[ik\cdot(r_1^\alpha - r_2^\nu)] \\ & \times [1+\rho\{z_\alpha(k)\tilde{h}_d(k) + \Omega^{-1}\int d\Omega_3\tilde{C}_{DD}(1,3)\exp(ik\cdot l_3^\alpha)\}\exp(-ik\cdot l_1^\alpha)] \\ & \times [1+\rho\{z_\nu(-k)\tilde{h}_d(k) + \Omega^{-1}\int d\Omega_6\tilde{C}_{DD}(6,2)\exp(-ik\cdot l_6^\nu)\}\exp(ik\cdot l_2^\nu)], \end{aligned} \quad (2\text{-}29)$$

where $\mathbf{1}$ is the 4×4 identity matrix. Remembering Eq. 2-5, we have the representation for the pair distribution function of the water-like fluid, thus

$$g_{WL}(1,2) = g_0(1,2)\exp C_{WL}(1,2), \quad (2\text{-}30)$$

or in its linearized version,

$$g_{WL}(1,2) = g_0(1,2)\{1+C_{WL}(1,2)\}. \quad (2\text{-}31)$$

The radial distribution function is obtained by integrating Eq. 2-31 over the orientations of molecules 1 and 2. Remembering Eq. 2-10 and taking account of the fact that

$$\Omega^{-2}\int C_{DD}(1,2)d\Omega_1 d\Omega_2 = 0,$$

we get

$$\begin{aligned} g_{WL}(R) &= \Omega^{-2}\int g_{WL}(1,2)d\Omega_1 d\Omega_2 \\ &= \{1+C_{WL}(R)\}g_d(R) + C_{WL}{*}C_{DD}, \end{aligned} \quad (2\text{-}32)$$

where $g_d(R)$ is the RDF for the hard-sphere fluid and $C_{WL}(R)$ and $C_{WL}{*}C_{DD}$ are defined by

$$C_{WL}(R) = \Omega^{-2}\int C_{WL}(1,2)d\Omega_1 d\Omega_2 \quad (2\text{-}33)$$

and

$$C_{WL}{*}C_{DD} = \Omega^{-2}\int C_{WL}(1,2)C_{DD}(1,2)d\Omega_1 d\Omega_2. \quad (2\text{-}34)$$

III. Computational Procedures and Results

After some manipulation, we obtain a more tractable quation for $C_{WL}(R)$ from Eqs. 2-29 and 2-33:

$$\begin{aligned} C_{WL}(R) = {} & (2\pi)^{-2}\int_0^\infty dk\frac{2k\sin(kR)}{R}[z(k)(1+\rho\tilde{h}_d(k))]^2 \\ & \times \sum_{\alpha,\nu}\{\tilde{\Phi}(k)[\mathbf{1}-\Gamma(k)\tilde{\Phi}(k)]^{-1}\}_{\alpha,\nu}, \end{aligned} \quad (3\text{-}1)$$

where $z(k)=\sin(kl)/kl$. The integral in Eq. 2-20 must be carried out to obtain the elements of $\Gamma(k)$. It can be performed by a suitable choice of Euler angles to give

$$\Gamma^s_{\alpha\gamma}(R) = \frac{-6y\rho}{(1+2y)}\cos\chi_\alpha\cos\chi_\gamma\left\{\frac{\cos(kl)}{kl} - \frac{\sin(kl)}{(kl)^2}\right\}^2. \quad (3\text{-}2)$$

The details of calculations leading to Eq. 3-2 are given in the appendix. The equation for $C_{WL}{*}C_{DD}$ is obtained from Eqs. 2-9, 2-29, and 2-34 after some tedious calculations and the result is

$$\begin{aligned} C_{WL}{*}C_{DD} = {} & \frac{(2\pi)^{-2}\beta m^2}{(1+2y)^3(1-y)}\left\{\frac{2}{R^2} + \frac{8\pi y}{3}\delta(R)\right\} \\ & \times \int_0^\infty dk k^2\left\{\frac{\cos(kl)}{(kl)} - \frac{\cos(kl)}{(kl)^2}\right\}^2 \\ & \times \left\{\frac{2\sin(kR)}{kR} + \frac{4\cos(kR)}{(kR)^2} + \frac{4\sin(kR)}{(kR)^3}\right\} \\ & \times \sum_{\alpha,\nu}\cos\chi_\alpha\cos\chi_\nu\{\tilde{\Phi}(k)[\mathbf{1}-\Gamma(k)\tilde{\Phi}(k)]^{-1}\}_{\alpha,\nu}. \end{aligned} \quad (3\text{-}3)$$

It is necessary to obtain explicit forms of the summations in Eqs. 3-1 and 3-3. Combining Eqs. 2-18, 1-2, and 3-2, we obtain the explicit form of $\Gamma(k)$:

$$\Gamma(k) = \begin{pmatrix} \Gamma'_- & \Gamma_- & \Gamma_+ & \Gamma_+ \\ \Gamma_- & \Gamma'_- & \Gamma_+ & \Gamma_+ \\ \Gamma_+ & \Gamma_+ & \Gamma'_- & \Gamma_- \\ \Gamma_+ & \Gamma_+ & \Gamma_- & \Gamma'_- \end{pmatrix}, \tag{3-4}$$

where Γ_-, Γ'_- and Γ_+ are

$$\Gamma_- = \Gamma_h - \Gamma_c, \tag{3-5}$$

$$\Gamma'_- = \Gamma'_h - \Gamma_c, \tag{3-6}$$

and

$$\Gamma_+ = \Gamma_h + \Gamma_c, \tag{3-7}$$

and

$$\Gamma_h = \rho\omega(k) + \rho^2 z(k)^2 \tilde{h}_d(k), \tag{3-8}$$

$$\Gamma'_h = \rho + \rho^2 z(k)^2 \tilde{h}_d(k), \tag{3-9}$$

and

$$\Gamma_c = -\frac{6y\rho}{(1+2y)}\cos^2\chi\left\{\frac{\cos(kl)}{kl} - \frac{\sin(kl)}{(kl)^2}\right\}^2. \tag{3-10}$$

Taking into account the characteristics of the site-site interactions described in the section I, we have

$$\tilde{\Phi}(k) = \tilde{\Phi}(k)\begin{pmatrix} 0 & 0 & 1 & 1 \\ 0 & 0 & 1 & 1 \\ 1 & 1 & 0 & 0 \\ 1 & 1 & 0 & 0 \end{pmatrix}, \tag{3-11}$$

where $\tilde{\Phi}(k)$ is given by

$$\tilde{\Phi}(k) = -4\pi\beta\varepsilon_H\left\{\frac{b\cos(kb)}{k^2} - \frac{\sin(kb)}{k^3}\right\}. \tag{3-12}$$

The inverse matrix which appears in Eqs. 3-1 and 3-3 can easily be calculated thanks to the high symmetry of matrices $\Gamma(k)$ and $\tilde{\Phi}(k)$, and as a result we obtain

$$\sum_{\alpha,\nu}\{\tilde{\Phi}(k)[\mathbf{1}-\Gamma(k)\tilde{\Phi}(k)]^{-1}\}_{\alpha,\nu} = \frac{8\tilde{\Phi}(k)}{1-2\tilde{\Phi}(k)\{3\Gamma_h(k)+\Gamma'_h(k)\}}, \tag{3-13}$$

and

$$\sum_{\alpha,\nu}\cos\chi_\alpha\cos\chi_\nu\{\tilde{\Phi}(k)[\mathbf{1}-\Gamma(k)\tilde{\Phi}(k)]^{-1}\}_{\alpha,\nu} = \frac{-8\tilde{\Phi}(k)\cos^2\chi}{1-2\tilde{\Phi}(k)\{\Gamma_h(k)-\Gamma'_h(k)+4\Gamma_c(k)\}}. \tag{3-14}$$

The correlation function obtained on the basis of the PY approximation is used as the total correlation function of the hard-sphere system, h_d, and its Fourier transform is expressed as

$$\tilde{h}_d(k) = \frac{\tilde{C}_{PY}(k)}{1-\tilde{C}_{PY}(k)}, \tag{3-15}$$

where $\tilde{C}_{PY}(k)$ is the Fourier transform of the direct correlation function of the hard-sphere fluid, which is the Wertheim solution to the PY equation.[5,17] Although $h_d(R)$, and hence $g_d(R)$, are obtained from the Fourier transform of $\tilde{h}_d(k)$, the numerical calculation is performed in practice with the aid of a function,

$$\tilde{\gamma}(k) = \tilde{h}_d(k) - \tilde{C}_{PY}(k), \tag{3-16}$$

because $h_d(R)$ and its derivatives are discontinuous at $R=d$.[18] All the integrals over k are performed numerically on the basis of the Simpson rule. The accuracy

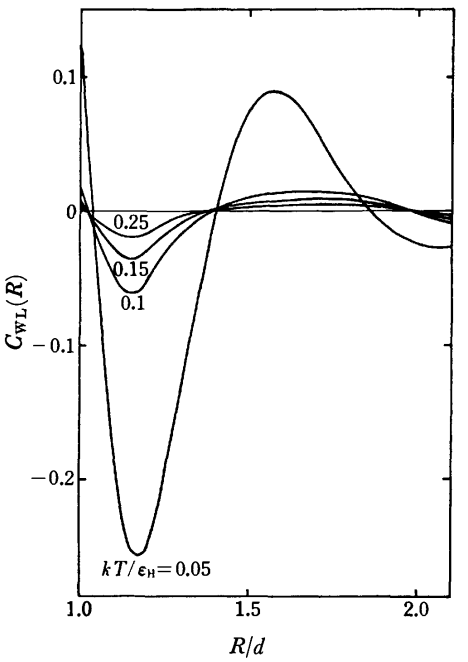

Fig. 3. The functions $C_{WL}(R)$ for $b=0.2d$, $\rho d^3=0.6$, $kT/\varepsilon_H=0.05$, 0.1, 0.15, and 0.25. It represents the effect of the hydrogen bonds.

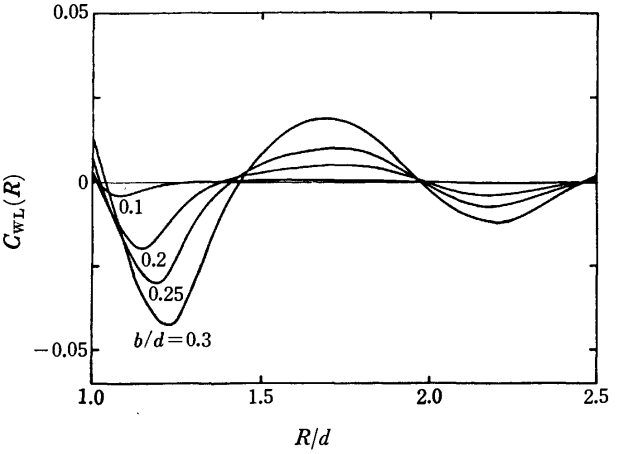

Fig. 4. The functions $C_{WL}(R)$ for $\rho d^3=0.6$, $kT/\varepsilon_H=0.25$, $b=0.3d$, $0.25d$, $0.2d$, and $0.1d$.

of the calculations has been checked against the exact values of $g_d(R)$ given by Throop and Bearman.[19] The results for $C_{WL}(R)$ are shown in Figs. 3—5 and those for $g_{WL}(R)$ in Figs. 6 and 7. $C_{WL}{}^*C_{DD}$ is not shown explicitly, since its contribution is very small compared with that of $C_{WL}(R)$. It should be noted that $C_{WL}(R)$ represents the effect of the hydrogen bonds on the molecular distribution.

IV. Discussion

We imagine a crystal consisting of water-like molecules, which has a tetrahedral structure similar to ice. A typical arrangement for a triplet of molecules in the crystal is depicted in Fig. 2. If the model potential described in section I favors such an arrangement, it is expected that the following two effects on the molec-

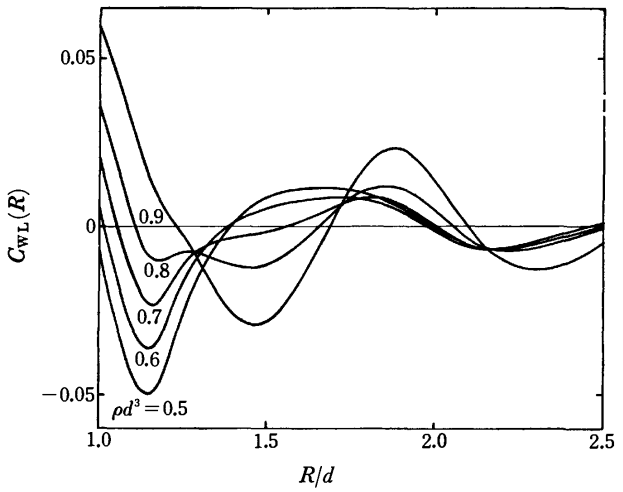

Fig. 5. The functions $C_{WL}(R)$ for $kT/\varepsilon_H=0.15$, $b=0.2d$, $\rho d^3=0.5$, 0.6, 0.7, 0.8, and 0.9.

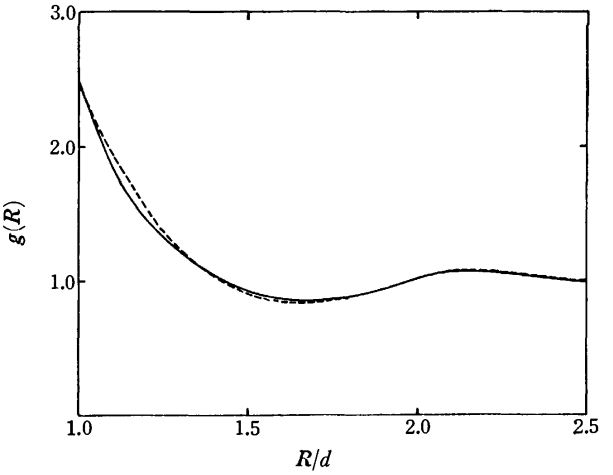

Fig. 6. The calculated RDF for the water-like fluid (solid line) at $\rho d^3=0.6$, $kT/\varepsilon_H=0.1$, and $b=0.2d$, compared with one for the hard-sphere fluid (dashed line).

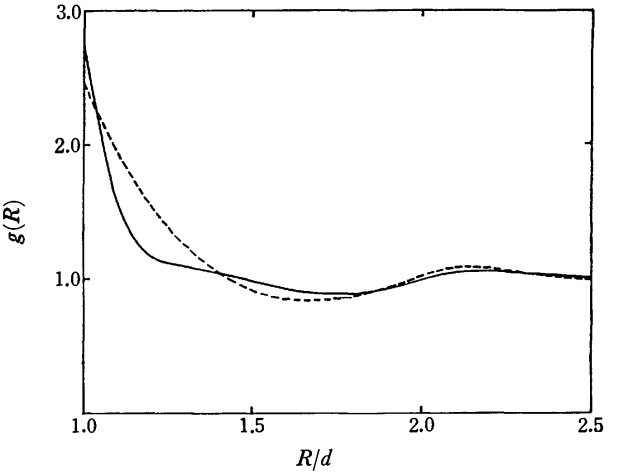

Fig. 7. The calculated RDF for the water-like fluid (solid line) at $\rho d^3=0.6$, $kT/\varepsilon_H=0.05$, and $b=0.2d$, compared with one for the hard-sphere fluid (dashed line).

ular distribution of the reference system are produced: a decrease in the density of the first coordination shell and an increase in the density in the neighborhood of a position $1.63d$ distant from the central molecule. The behavior of $C_{WL}(R)$ in Fig. 3 is consistent with this expectation. The negative value of $C_{WL}(R)$ at short distances is due to the former effect and the positive values in the neighborhood of $R=1.6d$ to the latter. It should be noted that there is a peak in the neighborhood of $R=1.6d$. It is also reasonable that the features become more prominent as the depth of the square-well potential, ε_H, increases. All the curves with various values of kT/ε_H given in Fig. 3 are observed to have a nearly common point of intersection with the abscissa. This is supposed to be primarily due to the maintenance of the magnitude of b as a constant through all the calculations. This is determined easily from Fig. 4, where several $C_{WL}(R)$ curves with different values of b are depicted. An evident shift in the location of the intersection is observed. The manner in which the $C_{WL}(R)$ curves change with density is shown in Fig. 5. Appreciable differences are observed between the curves for high and low densities. It appears that the trend of forming a tetrahedral geometry is dominant at low densities and that it weakens with increasing density. On the basis of rapid increase of the first peak, the behavior of $C_{WL}(R)$ at higher densities appears to indicate that the square-well potential serves as a central attractive force rather than as a non-central force leading to the tetrahedral geometry. The increase in density would have two results: an enhancement of the role of repulsive force in the determination of the molecular distribution and an increase in the probability of sites on one molecule encountering those on another molecule. The former effect prevents the hydrogen bonds from forming a tetrahedral geometry, and the latter produces a strong attraction between the two molecules.

The results for the RDF are shown in Figs. 6 and 7. A narrowing of the first peak similar to that observed for the RDF of water[2,7] is found, and this feature increases as the magnitude of ε_H increases. Although characteristics of the second peak for the RDF of water do not appear in the present calculation, this peak does appear to grow. This is noticeable in spite of the use of overestimated values of ε_H.

The coordination number is to be obtained from the first peak of the RDF curve using the equation,

$$n_{CN}=\rho\int_0^{R_m} g(R)4\pi R^2 dR. \qquad (4\text{-}1)$$

It should be noted that the values of n_{CN} depend on the choice of R_m. The most reasonable choice of R_m would be the location of the first minimum in the RDF. However, this choice cannot be adopted in the present case since no minimum corresponding to the first minimum in the RDF of water is found. Therefore, it is only possible to give the coordination number obtained for a rather arbitrary value of R_m. The coordination number is about 6.2 when R_m equals $1.4d$ which corresponds to the point of intersection of the $C_{WL}(R)$ curve with the abscissa.[20] It should be noted that a similar arbitrariness in the choice of R_m is also found

in the report of Ben-Naim.[6a]

It is hoped that the application of the method proposed here to water and ionic solutions will be reported in future publications. There are several possibilities for improving the model and the mathematical formalism. It is not too difficult to replace the hard-sphere potential with the Lennard-Jones (12,6) potential. Systematic ways of performing such a replacement have been given.[21] Moreover, the present rough representation of $h_0(1,2)$, Eq. 2-10, could be replaced by a more elaborate representation. More fundamental improvements concern the graph-theoretical treatment. A possible improvement could be achieved by taking account of the graphs ignored in this study. However, it would be rather promising to employ the optimization procedure proposed by Andersen and Chandler.[12]

It is interesting to apply this method to the problems of ion-water interactions. The orientational effect due to ion-dipole interactions is different in charater from that due to the hydrogen bonds. It is possible that the ion-dipole interaction exerts a torque on the molecule, which prevents the molecule from hydrogen-bonding. If this is true, the contribution of ion-dipole interactions to the molecular distribution should be opposite to the effect of the hydrogen bonds. It is expected, therefore, that the RDF for a water-like system under the influence of an electrostatic field due to ions approaches that for a simple fluid. This would provide an explanation of the so-called "*structure-breaking effect*" of ions.[22-24]

The author wishes to thank Assistant Professor Kiyoshi Arakawa for his kind supervision and continuous encouragement.

Appendix: the Derivation of Eq. 3-2

Let $\boldsymbol{k}$ be the z-axis, then Eq. 2-23 becomes:

$$\tilde{C}'_{DD}(i,j) = -\frac{4\pi}{3}\tilde{D}(i,j) + \frac{8\pi}{3}y\tilde{\Delta}(i,j)$$
$$= \frac{8}{3}\pi(y-1)\cos\theta_{ik}\cos\theta_{jk} + \frac{4}{3}\pi(1+2y)\cos(\phi_i-\phi_j), \quad \text{(A-1)}$$

where θ_{ik} and ϕ_i are the polar and the azimuthal angles of the unit vector $\hat{\boldsymbol{m}}_i$ of the i-th molecule, respectively, and θ_{jk} and ϕ_j are those of the j-th molecule. Eq. 2-20 can, therefore, be rewritten as

$$\Gamma^c_{\alpha\gamma}(k) = -\frac{8\pi\beta m^2\rho^2}{3(1+2y)}\frac{1}{\Omega^2}\int d\boldsymbol{\Omega}_i\cdot d\boldsymbol{\Omega}_j \times \exp[-i\boldsymbol{k}\cdot(\boldsymbol{l}^\alpha_i-\boldsymbol{l}^\gamma_j)]\cos\theta_{ik}\cos\theta_{jk} + \frac{4\pi\beta m^2\rho^2}{3(1-y)}\frac{1}{\Omega^2}\int d\boldsymbol{\Omega}_i\cdot d\boldsymbol{\Omega}_j \times \exp[-i\boldsymbol{k}\cdot(\boldsymbol{l}^\alpha_i-\boldsymbol{l}^\gamma_j)]\cos(\phi_i-\phi_j). \quad \text{(A-2)}$$

The integrals can be broken up into factors each of which is an integral over $\boldsymbol{\Omega}_i$ or $\boldsymbol{\Omega}_j$. As an example, we investigate in some detail the integral, involving the i-th molecule and the α site.

Let us first take the Cartesian-coordinate system, x'y'z', fixed to the i-th molecule, whose origin coincides with the center of the molecule and the z'-axis points in the direction of the α site of the molecule. The Cartesian coordinates of the unit vector of the dipole, $\hat{\boldsymbol{m}}_i$, in the coordinate system are denoted by $m_{x'}$, $m_{y'}$ and $m_{z'}$. Then, this coordinate system is rotated to a new coordinate system, xyz, whose z axis coincides with $\boldsymbol{k}$. The orientation of the xyz system relative to the x'y'z' system can be specified by the Euler angles θ, ϕ and ψ. Thus, the components of $\hat{\boldsymbol{m}}_i$ in the new xyz system are given by the linear transformation:[25]

$$\begin{bmatrix} m_x \\ m_y \\ m_z \end{bmatrix} = \begin{bmatrix} \cos\psi\cos\phi - \cos\theta\sin\phi\sin\psi & \cos\psi\sin\phi + \sin\theta\cos\phi\sin\psi & \sin\psi\sin\theta \\ -\sin\psi\cos\phi - \cos\theta\sin\phi\cos\psi & -\sin\psi\sin\phi + \cos\theta\cos\phi\sin\psi & \cos\psi\sin\theta \\ \sin\theta\sin\phi & -\sin\theta\cos\phi & \cos\theta \end{bmatrix} \begin{bmatrix} m_{x'} \\ m_{y'} \\ m_{z'} \end{bmatrix} \quad \text{(A-3)}$$

The components of $\hat{\boldsymbol{m}}_i$ are also represented by the polar coordinate system whose polar axis coincides with $\boldsymbol{k}$:

$$m_x = \sin\theta_{ik}\cos\phi_i, \quad m_y = \sin\theta_{ik}\sin\phi_i, \quad m_z = \cos\theta_{ik}. \quad \text{(A-4)}$$

From Eqs. A-3 and A-4, we obtain

$$\left.\begin{aligned} \cos\theta_{ik} &= m_{x'}\sin\theta\sin\phi - m_{y'}\sin\theta\cos\phi + m_{z'}\cos\theta, \\ \cos\phi_i &= \{m_{x'}(\cos\psi\cos\phi-\cos\theta\sin\phi\sin\psi) + m_{y'}(\cos\psi\sin\phi+\sin\theta\cos\phi\sin\psi) + m_{z'}\sin\psi\sin\theta\}/\sin\theta_{ik} \\ \sin\phi_i &= \{m_{x'}(-\sin\psi\cos\phi-\cos\theta\sin\phi\cos\psi) + m_{y'}(-\sin\psi\sin\phi+\cos\theta\cos\phi\cos\psi) + m_{z'}\cos\psi\sin\theta\}/\sin\theta_{ik}. \end{aligned}\right\} \quad \text{(A-5)}$$

Thus, the integral over $\boldsymbol{\Omega}_i$ can be performed using Eq. A-5.

$$\frac{1}{\Omega}\int d\boldsymbol{\Omega}_i\exp(-i\boldsymbol{k}\cdot\boldsymbol{l}^\alpha_i)\cos\theta_{ik} = \frac{1}{8\pi^2}\int_0^\pi d\theta\sin\theta\int_0^{2\pi}d\phi\int_0^{2\pi}d\psi\exp(-ikl\cos\theta)\{m_{x'}\sin\theta\sin\phi - m_{y'}\sin\theta\cos\phi + m_{z'}\cos\theta\}$$
$$= \frac{m_{z'}}{2}\int_0^\pi d\theta\sin\theta\cos\theta\exp(-ikl\cos\theta) = im_{z'}\left\{\frac{\cos(kl)}{kl} - \frac{\sin(kl)}{(kl)^2}\right\} = i\cos\chi_\alpha\left\{\frac{\cos(kl)}{kl} - \frac{\sin(kl)}{(kl)^2}\right\}. \quad \text{(A-6)}$$

The last equation results since the angle between vectors $\boldsymbol{l}^\alpha_i$ and $\hat{\boldsymbol{m}}_i$ is χ_α. By similar manipulations, we obtain

$$\frac{1}{\Omega}\int d\boldsymbol{\Omega}\exp(i\boldsymbol{k}\cdot\boldsymbol{l}^\gamma_j)\cos\theta_{jk} = \frac{\cos\chi_\gamma}{i}\left\{\frac{\cos(kl)}{kl} - \frac{\sin(kl)}{(kl)^2}\right\}. \quad \text{(A-7)}$$

Therefore, the first intergal in Eq. A-2 is

$$\frac{1}{\Omega^2}\int d\boldsymbol{\Omega}_i\cdot d\boldsymbol{\Omega}_j\exp[-i\boldsymbol{k}\cdot(\boldsymbol{l}^\alpha_i-\boldsymbol{l}^\gamma_j)]\cos\theta_{ik}\cos\theta_{jk} = \cos\chi_\alpha\cos\chi_\gamma\left\{\frac{\cos(kl)}{kl} - \frac{\sin(kl)}{(kl)^2}\right\}^2. \quad \text{(A-8)}$$

It may be proved in the same way that the second integral vanishes. Using the relation, $y=4\pi\beta m^2\rho/9$, one obtains

$$\Gamma^{c}_{\alpha\gamma}(k) = \frac{-6y\rho}{1+2y}\cos\chi_\alpha\cos\chi_\gamma\left\{\frac{\cos(kl)}{kl}-\frac{\sin(kl)}{(kl)^2}\right\}^2. \quad \text{(A-9)}$$

References

1) K. Arakawa, *Kagaku Sosetsu*, No. 11 (1976), p. 35.
2) (a) A. H. Narten, M. D. Danford and H. A. Levy, *Discuss. Faraday Soc.*, **43**, 97 (1967); (b) A. H. Narten, *J. Chem. Phys.*, **56**, 5681 (1972); (c) A. H. Narten, C. G. Venkatesh, and S. A. Rice, *J. Chem. Phys.*, **64**, 1106 (1976).
3) (a) A. Rahman and F. H. Stillinger, *J. Chem. Phys.*, **55**, 3336 (1971); (b) F. H. Stillinger and A. Rahman, *ibid.*, **60**, 1545 (1974); (c) G. C. Lie, E. Clementi, and M. Yoshimine *ibid.*, **64**, 2314 (1976).
4) (a) "The Equilibrium Theory of Classical Fluids," ed. by H. L. Frisch and J. L. Lebowitz, W. A. Benjamin Company, Inc. (1964). (b) K. Arakawa, *Kagaku Sosetsu*, No. 11 (1976), p. 13.
5) J. K. Percus and G. J. Yevick, *Phys. Rev.*, **110**, 1 (1958).
6) A. Ben-Naim, (a) *J. Chem. Phys.*, **52**, 5531 (1970); (b) *ibid.*, **54**, 3682 (1971).
7) A. Ben-Naim, "Water and Aqueous Solutions. (Introduction to a Molecular Theory)," Plenum Press, New York.
8) (a) P. C. Hemmer, *J. Math. Phys.*, **5**, 75 (1964); (b) J. L. Lebowitz, G. Stell and S. Baer, *ibid.*, **6**, 1282 (1965).
9) G. Stell and J. L. Lebowitz, *J. Chem. Phys.*, **49**, 3706 (1968).
10) J. S. Høye and G. Stell, *J. Chem. Phys.*, **61**, 562 (1974).
11) G. Nienhuis and J. M. Deutch, *J. Chem. Phys.*, **55**, 4213 (1971); *ibid.*, **56**, 235 (1972); *ibid.*, **56**, 1819 (1972).
12) H. C. Andersen and D. Chandler, *J. Chem. Phys.*, **57**, 1918 (1972).
13) D. Chandler and H. C. Andersen, *J. Chem. Phys.*, **57**, 1930 (1972).
14) H. C. Andersen D. Chandler, and J. D. Weeks, *J. Chem. Phys.*, **57**, 2626 (1972).
15) M. S. Wertheim, *J. Chem. Phys.*, **55**, 4291 (1971).
16) L. Verlet and J. J. Weis, *Mol. Phys.*, **28**, 665 (1974).
17) M. S. Wertheim, *J. Math. Phys.*, **5**, 643 (1964).
18) Y. Tago, private communication.
19) G. J. Throop and R. J. Bearman, *J. Chem. Phys.*, **42**, 2408 (1965).
20) As the value of R_m in the integration of Eq. 4-1, Ben-Naim adopted $1.25d$. This corresponds to the first minimum in the observed RDF curve. Our value of n_{CN} calculated for $R_m=1.25d$ becomes about 4.0, which is compared with Ben-Naim's value of 7.4.
21) J. D. Weeks, D. Chandler, and H. C. Andersen, *J. Chem. Phys.*, **54**, 5237 (1971).
22) H. S. Frank and W. Y. Wen, *Discuss. Faraday Soc.*, **24**, 133 (1957).
23) F. Hirata and K. Arakawa, *Bull. Chem. Soc. Jpn.*, **46**, 3367 (1973).
24) F. Hirata and K. Arakawa, *Bull. Chem. Soc. Jpn.*, **48**, 2139 (1975).
25) H. Goldstein, "Classical Mechanics," Addison-Wesley, Reading, Mass. (1950).

Isomerization of Butenes over Thorium Dioxide

Yuzo IMIZU, Tsutomu YAMAGUCHI, Hideshi HATTORI, and Kozo TANABE
Department of Chemistry, Faculty of Science, Hokkaido University, Sapporo 060
(Received November 1, 1976)

The isomerization of butenes has been studied over four kinds of ThO_2 catalysts which differ in starting materials or preparative procedures. The selective ThO_2 catalysts for the formation of 1-olefin in the dehydration of 2-alkanol, which were prepared from nitrate and oxalate, were active and gave high *cis*/*trans* ratios in the isomerization of 1-butene, whereas the non-selective ThO_2 catalyst, which was prepared from chloride, was completely inactive. The isomerization reaction was poisoned by both CO_2 and NH_3. The activity was enhanced by the treatment with hydrogen, but was reduced by the treatment with oxygen, the selectivity being unchanged with both treatments. The coisomerization of *cis*-2-butene and *cis*-2-butene-d_8 showed that the isomerization involved an intramolecular hydrogen transfer, and a large isotope effect, 6.0, for the formation of 1-butene and a small isotope effect, 1.5, for the formation of *trans*-2-butene were observed. With these results, the nature of active sites on thorium oxide, and the reaction mechanism were discussed.

Thorium dioxide has been used as a catalyst for dehydration of alcohols.[1,2] In recent years, it has been recognized to be a selective catalyst for the dehydration of 2-alkanol to form 1-alkene when it is properly prepared.[3,4]

Davis and Brey reported that the selectivity of thorium dioxide in dehydration and dehydrogenation of alcohols strongly depended upon the preparative procedures of the catalyst.[5] The thorium dioxide prepared from nitrate shows a high selectivity for the formation of 1-octene in the dehydration of 2-octanol, whereas the thorium dioxide prepared from thorium chloride gives a considerable amount of 2-octenes. Besides the preparative procedure, the pretreatment condition is another major factor for determining selectivity. Thorium dioxide pretreated with hydrogen is a dehydration catalyst, while thorium dioxide pretreated with oxygen is a dehydrogenation catalyst.[5]

The nature of active sites on thorium dioxide which determines the selectivity, however, has not yet extensively been investigated. Yamaguchi *et al.* reported in the dehydration of alcohol over alumina[6] and zirconium dioxide[7,8] that the selectivity of the catalysts can be determined by surface acidic and basic properties. The isomerization of butenes is known to be a reaction suitable for testing the correlation of acidic and basic properties of catalysts with the activity and selectivity.[9—13] In the present work, the isomerization of butenes was carried out over several thorium dioxides to investigate the nature of active sites.

Experimental

Catalysts and Reactants. Four kinds of thorium dioxide were prepared, which differ in starting materials or in preparative procedures. ThO_2(I) and ThO_2(II) were obtained from oxalate and nitrate, respectively, by thermal decomposition in air at 500 °C for 6—8 h. ThO_2(III) was prepared from nitrate by the precipitation method as shown by Brey *et al.*[14] To 5000 ml aqueous solution of thorium nitrate (0.145 M), 500 ml aqueous ammonia (28%) was added. Precipitate was filtered, followed by washing with 1500 ml distilled water. The resulting thorium hydroxide was dried for 2 days and finally calcined at 500 °C in air for 6 h. ThO_2(IV) was prepared from thorium chloride by precipitation as follows. Aqueous ammonia (28%, 50 ml) was added to 500 ml aqueous solution of 50 g thorium chloride. Precipitate was washed, dried, and calcined as in the case of ThO_2(III). Those thorium salts were supplied from Wako Pure Chemical Co. All catalysts were evacuated at 500 °C for 3 h before use for the reaction.

Butenes (Takachiho pure grade) were purified by passage through a column of molecular sieves 3A or 4A maintained at the temperature of dry ice–acetone. 2-Butanol was obtained from Wako Pure Chemical Co. and purified by passage through molecular sieves 3A at room temperature.

Apparatus and Procedure. Dehydration of *s*-butyl alcohol and isomerization of butenes were carried out in two recirculation reactors whose volumes were 3000 ml for dehydration and 410 ml for isomerization. For dehydration, the initial pressure of *s*-butyl alcohol was 6 Torr and about 300 mg of a catalyst was used. Reaction temperature was 300 °C. Products were analyzed by gas chromatography. A 1 m column packed with TCP 30% on Celite 545 was operated at 100 °C. For isomerization of butenes, 88 Torr of butene and 50—150 mg of catalyst were used. Reaction temperature was 80 °C. Products were analyzed by gas chromatography with a 5 m column containing VZ-7, operating at room temperature.

For poisoning experiment with carbon dioxide or ammonia, the catalyst that had been evacuated at 500 °C was cooled to 100 °C and was exposed to 88 Torr of carbon dioxide or ammonia for 1 h. After evacuation at certain temperatures (200—500 °C) for 1 h, the catalyst was served for a reaction.

For hydrogen or oxygen treatment, the catalyst that had been evacuated at 500 °C was exposed to hydrogen or oxygen (60 Torr) at 500 °C or 300 °C for 2 h, followed by evacuation at various temperatures for 1 h.

For the coisomerization of non-deuterated and perdeuterated *cis*-2-butenes,[10,15] a mixture containing about equal amount of *cis*-2-butene-d_0 and *cis*-2-butene-d_8 was reacted at 80 °C.

Results

Specific surface areas, the activities, and the selectivities for the dehydration of 2-butanol and the isomerization of butenes are listed in Table 1. The catalysts showed a high selectivity for the formation of 1-alkene in the dehydration except for ThO_2(IV), over which considerable amounts of 2-alkenes were produced.[5] For the isomerization of butenes, the ThO_2(IV) was completely inactive. This was true even for the catalyst evacuated at 900 °C. The other thorium dioxides were active and gave high *cis*/*trans* and 1-/*trans* ratios in the isomerization of 1-butene and

Table 1. Catalytic activity and selectivity of ThO_2 for isomerization of butenes and dehydration of *s*-butyl alcohol

Catalyst	Surface area (m^2/g)	1-Butene		2-Butanol			
		Activity[a]	Ratio of *cis* to *trans*	Activity[a]	composition of butenes[b]		
					1-butene	*trans*-2-butene	*cis*-butene
ThO_2(I)	59.1	29.8	3.4	1.87×10^{-1}	84.2	9.3	6.5
ThO_2(II)	62.3	22.9	3.1	2.36×10^{-1}	82.4	10.6	7.0
ThO_2(III)	41.7	10.8 (1.1)[c]	3.2 (3.3)[d]	0.74×10^{-1}	76.6	14.8	8.6
ThO_2(IV)	46.3	0.0	—	2.22×10^{-1}	39.8	26.8	33.4

a) Initial activity; $\%^{-1}\,min^{-1}$. b) Extrapolated to 0 conversion. c) Reactant; *cis*-2-butene. d) Ratio of 1- to *trans*-. Reaction temperature: 80 °C for isomerization; 300 °C for dehydration.

Table 2. Poisoning effects of CO_2 and NH_3 on the activity and selectivity for isomerization of 1-butene

Poison	Evacuation temp (°C)	k[a]	*cis*-/*trans*-
CO_2	300	0.02	4.1
CO_2	400	0.12	3.9
CO_2	450	0.28	3.5
CO_2	500	1.00	3.2
NH_3	200	0.35	3.8
NH_3	300	0.37	4.1
NH_3	350	0.73	3.5
NH_3	400	1.00	3.2

a) Ratio of the activity after poisoning to the original activity.

Table 3. Effect of oxygen or hydrogen treatment on the activity and selectivity for isomerization of 1-butene

Treatment gas	Treatment temp (°C)	Evacution temp (°C)	Relative activity[a]	Selectivity *cis*-/*trans*-
No treatment	—	—	1.00	3.2
Oxygen	500	200	0.48	3.4
Oxygen	300	300	0.74	3.5
Oxygen	80[b]	—	0.00	—
Hydrogen	500	500	3.52	3.3

a) Ratio of the activity after treatment to the original activity. b) Reaction was carried out in the presence of 5.6 Torr oxygen.

cis-2-butene, respectively.

Poisoning effects of carbon dioxide and ammonia are given in Table 2. Both carbon dioxide and ammonia poisoned the active sits for isomerization. The catalyst regained the original activity by evacuation at 400 °C for ammonia poisoned catalyst and by evacuation at 500 °C for carbon dioxide poisoned catalyst. Poisoning with ammonia and carbon dioxide did not result in appreciable change in selectivity.

In Table 3 are listed the effects of oxygen or hydrogen treatment on the activity and selectivity in the isomerization. While hydrogen treatment resulted in an increase in the activity, oxygen treatment reduced the activity. The selectivity was almost unchanged with these treatments.

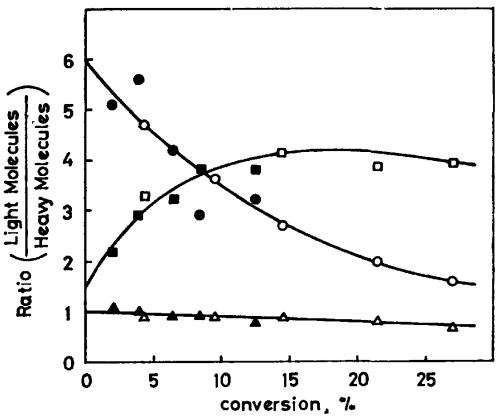

Fig. 1. The variations of the ratios of "*light molecules*" to "*heavy molecules*" with the conversion in the coisomerization of *cis*-2-butene d_0/d_8 over both untreated ThO_2 and hydrogen treated ThO_2. Reaction temperature; 80 °C, untreated ThO_2; (●) 1-butene, (■) *trans*-2-butene, (▲) *cis*-2-butene, treated ThO_2; (○) 1-butene, (□) *trans*-2-butene, (△) *cis*-2-butene.

Isotopic distribution of butene isomers in the coisomerization of *cis*-2-butene d_0/d_8 are listed in Table 4. Since the numbers of hydrogen (or deuterium) atoms exchanged per molecule (AEM value) are much smaller than 0.5, the value of which is expected if the reaction involves an intermolecular hydrogen transfer, the reaction is suggested to involve an intramolecular hydrogen transfer. The ratios of "*light molecule*" to "*heavy molecule*" are plotted against isomerization conversion in Fig. 1 for both untreated and hydrogen treated catalysts. The plots are on the same lines for both untreated and hydrogen treated catalysts. The intercepts of the plots show the isotope effect. A large isotope effect, 6.0, for the formation of 1-butene and a small isotope effect, 1.5, for the formation of *trans*-2-butene were observed.

Discussion

As suggested by Davis and Brey, catalytic properties of thorium dioxide vary with both preparative procedure and pretreatment.[5] There seem to be different types of active sites on the surface of thorium dioxide.

In the isomerization of butenes, the selectivities did

TABLE 4. ISOTOPIC DISTRIBUTIONS OF BUTENE ISOMERS IN COISOMERIZATION OF *cis*-2-BUTENE d_0/d_8

Catalyst	Product	% each product	% Isotopic species						Atoms exchanged/ molecule[a]	Ratio of *light molecule/ heavy molecule*[b]
			d_0	d_1	d_2—d_5	d_6	d_7	d_8		
ThO_2(III)	*cis*-		47.8	0.1	0	0.9	2.9	48.3		0.9
	1-	1.2	81.6	1.9	0	0	3.6	12.9	0.055	5.1
	trans-	0.9	66.5	2.3	0	0	2.7	28.5	0.050	2.2
	cis-	97.9	50.9	0.4	0	0	3.1	45.6	0.035	1.1
	1-	3.9	77.0	3.8	0	0	4.4	14.8	0.082	4.2
	trans-	1.6	72.2	3.7	0	0	3.0	21.1	0.067	3.2
	cis-	93.5	46.6	0.4	0	0.9	3.4	48.7	0.056	0.9
	1-	6.1	72.3	4.0	0	0	5.7	18.0	0.097	3.2
	trans-	6.5	73.9	5.4	0	0	3.5	17.2	0.089	3.8
	cis-	87.4	44.2	1.1	0	0	4.4	50.3	0.055	0.8
ThO_2(III) treated with hydrogen at 500 °C	1-	2.2	79.9	2.7	0	0	3.4	14.0	0.061	4.7
	trans-	2.1	76.0	0.0	0	0	3.2	20.8	0.032	3.2
	cis-	95.7	46.9	0.6	0	0.5	3.6	48.3	0.052	0.9
	1-	6.0	67.0	5.0	0	1.0	5.7	20.2	0.150	2.7
	trans-	8.6	75.2	5.5	0	0.0	3.6	15.7	0.091	4.2
	cis-	85.4	44.4	1.9	0	1.2	4.9	47.6	0.092	0.9
	1-	8.2	53.8	7.6	0	2.1	8.4	28.1	0.202	1.6
	trans-	19.9	69.4	10.3	0	0.9	5.3	14.1	0.174	3.9
	cis-	71.9	36.6	4.2	0	1.7	8.2	49.3	0.159	0.7

a) Calculated from $\sum_{i=0}^{4} i \cdot N_i + \sum_{i=5}^{8} (8-i) \cdot N_i$, N_i; formation of isotopic species containing i deuterium atoms.

b) Calculated from $(\sum_{i=0}^{3} N_i + N_4/2)/(\sum_{i=5}^{8} N_i + N_4/2)$.

not substantially change with either pretreatment or poisoning. It appears that only one type of active sites is operative for the isomerization of butenes. One type of active sites on ThO_2(IV) which is non-selective for dehydration, is not active for isomerization of butenes. Oxygen treatment of ThO_2(III) resulted in the elimination of the active sites for the isomerization. By referring to the report that oxygen treatment enhances the active sites for dehydrogenation,[5] the active sites for dehydrogenation are not considered to be active for the isomerization. On the other hand, hydrogen treatment was reported to produce the active sites for selective dehydration to 1-alkene. Since it actually increased the activity for the isomerization, it is suggested that the active sites for the isomerization are of a type of active sites which catalyze the selective dehydration.

The active sites for the isomerization were poisoned by both an acidic molecule, carbon dioxide, and a basic molecule, ammonia. It is plausible that the active site is an acid-base pair site. If either part of a pair site is blocked by a poison, the rest of the pair site may not show any activity. This interprets the observed selectivity which was unchanged by poisoning with both molecules.

Breysse has shown that the treatment of thorium dioxide with hydrogen or oxygen at 500 °C caused a slight deviation from stoichiometry.[16] It is suggested that hydrogen treatment removes surface oxygen ion and provides a surface with excess thorium ions. The coordinatively unsaturated thorium ion is expected to be more strongly acidic than saturated thorium ion.[17] There should be oxygen ions adjacent to the unsaturated thorium ion. These oxygen ions are expected to be more strongly basic than oxygen ion adjacent to saturated thorium ion.

Since the isomerization involves an intramolecular hydrogen transfer, the reaction may be initiated by the abstraction of a hydrogen atom (or ion) from a butene molecule. In the isomerization of 1-butene where a π-allyl carbanion is an intermediate, a preferential formation of *cis*-2-butene is generally observed[9,12,18,19] which is attributed to a greater stability of a π-allyl carbanion in *cis*-form than in *trans*-form. A rotation of a C^2–C^3 bond within a π-allyl carbanion may not easily occur because of a double bond character of the bond. Therefore, if the reaction proceeds *via* a π-allyl carbanion intermediate, high raios of *cis*-2-butene to *trans*-2-butene and 1-butene to *trans*-2-butene are expected. This is the case observed. The reaction is considered to be initiated by the abstraction of a proton from butene to form a π-allyl carbanion. Oxygen ion may abstract a proton. A π-allyl carbanion may be adsorbed on the coordinatively unsaturated thorium ion.

In the isomerization of *cis*-2-butene, the abstraction of a proton may be common for both the formation of 1-butene and the formation of *trans*-2-butene. If the slow step were the abstraction of a proton, a large isotope effect would be observed for formation of both compounds. A small isotope effect for the formation of *trans*-2-butene indicates that the abstraction of a proton is not a slow step. A rotation of the C^2–C^3 bond within a π-allyl carbanion may be the slow step for the formation of *trans*-2-butene. A large isotope effect observed only for the formation of 1-butene

suggests that a slow step is involved in a transfer of the adsorbed proton which had been abstracted from one of the terminal carbon atoms to the carbon atom 3 of a π-allyl carbanion.

The autors gratefully acknowledge the financial assistance provided by the Takeda Science Foundation.

References

1) M. E. Winfield, "Catalysis" Vol. VII, P. H. Emmett, Reinhold, New York, Chapman and Hall, London (1960), p. 93.
2) H. Knözinger, "The Chemistry of Functional Groups; The Chemistry of the Hydroxyl group," S. Patai, Interscience, London (1971), p. 641.
3) A. J. Lundeen and R. van Hoozer, *J. Am. Chem. Soc.*, **85**, 2180 (1963).
4) A. J. Lundeen and R. van Hoozer, *J. Org. Chem.*, **32**, 3386 (1967).
5) B. H. Davis and S. Brey, Jr., *J. Catal.*, **25**, 81 (1972).
6) T. Yamaguchi, T. Kobayashi, and K. Tanabe, *Nippon Kagaku Zasshi*, **92**, 1076 (1971).
7) T. Yamaguchi, H. Sasaki, and K. Tanabe, *Chem. Lett.*, **1973**, 1017.
8) T. Yamaguchi, Y. Nakano, T. Iizuka, and K. Tanabe, *Chem. Lett.*, **1976**, 677.
9) N. F. Foster and R. J. Cvetanović, *J. Am. Chem. Soc.*, **82**, 4274 (1960).
10) J. W. Hightower and W. K. Hall, *Chem. Eng. Prog.*, **63**, 122 (1967).
11) G. Perot, M. Guisnet, and R. Maurel, *J. Catal.*, **41**, 14 (1976).
12) C. C. Chang, W. C. Conner, and R. J. Kokes, *J. Phys. Chem.*, **77**, 1957 (1973).
13) Y. Sakai and H. Hattori, *J. Catal.*, **42**, 37 (1976).
14) W. S. Brey, Jr., B. H. Davis, P. G. Schmidt, and C. G. Moreland, *J. Catal.*, **3**, 303 (1964).
15) J. W. Hightower and W. K. Hall *J. Am. Chem. Soc.*, **89**, 778 (1967).
16) M. Breysse, *Ann. Chim.*, **2**, 367 (1967).
17) J. Hensel and H. Pines, *J. Catal.*, **24**, 1967 (1972).
18) S. Band, A. Schriesheim, and C. A. Rowe, Jr., *J. Am. Chem. Soc.*, **87**, 3244 (1965).
19) H. Hattori, N. Yoshii, and K. Tanabe, *Proc. 5th Intern. Congr. Catal.*, Miami Beach, Florida, J. W. Hightower 1972, **1**, 233 (1973).

Pyrolysis of Acetylene behind Shock Waves

Hiroo OGURA

Institute of Space and Aeronautical Science, The University of Tokyo, Komaba, Meguro-ku, Tokyo 153

(Received November 12, 1976)

The pyrolysis of acetylene was investigated behind the reflected shock waves in a single-pulse shock tube over the temperature range from 1000 to 1670 K. The major products were 1-buten-3-yne, 1,3-butadiyne, and hydrogen. The main primary C_4 product, however, changes from 1-buten-3-yne to 1,3-butadiyne with the increase of temperature. At the lower temperatures the formation of 1-buten-3-yne dominates the pyrolysis of acetylene. The rate of 1-buten-3-yne formation is second order with respect to acetylene concentration, and its second-order rate constant is expressed as follows:

$$k(\mathrm{cm^3\ mol^{-1}\ s^{-1}}) = 10^{14.39\pm0.26}\exp((-46400\pm1400)/RT)$$

The isotopic distribution of 1-buten-3-yne in the pyrolysis of the equimolar C_2H_2 and C_2D_2 mixture, proved that the pyrolysis proceeds *via* a free-radical mechanism. A free-radical chain mechanism initiated by the bimolecular reaction of acetylene, $2C_2H_2 \rightarrow C_4H_3+H$, was proposed.

The thermal decomposition of acetylene has been studied over a wide temperature range by various methods. At low and intermediate temperatures, static[1–6] and flow[7–16] systems were employed and the reaction rate of acetylene consumption, reaction order, products distribution, wall effects, and the effects of a variety of additives, for example, reaction products and radical scavengers such as nitrogen oxide, were extensively investigated.

There is substantial agreement on some aspects of the pyrolysis at low and intermediate temperatures. At the initial stage of the reaction, an induction period is observed and succeeded by a homogeneous reaction. The latter is second order with respect to acetylene with a low activation energy of 40—50 kcal*/mol. The reaction leads to the formation of high molecular weight compounds and is inhibited markedly by nitric oxide. The polymer produced at the early stage is solely 1-buten-3-yne(vinylacetylene), and benzene is an important secondary product. Palmer and Dormish[15] have shown that there is a transition as regards the primary C_4 product at about 1500 K, where 1,3-butadiyne (diacetylene) becomes predominant.

In high temperature region shock tube technique was used exclusively, because it is excellent to realize high temperature without worry about wall effects. The experimetal results obtained from the shock tube studies,[17–28] however, are somewhat confusing with regard to the reaction order and the main C_4 product, butenyne or butadiyne. These discrepancies may be ascribed to the difficulties to analyze the reaction products and to determine the reaction order by shock tube technique. It seems desirable to study the pyrolysis over a fairly wide temperature range, the lower of which overlaps the flow tube investigations.

The mechanism of the pyrolysis has not been well established. Many investigators favored a bimolecular reaction of acetylene to give an excited molecule of acetylene or butenyne in the triplet state or biradical. Recently several attempts have been made to interpret the pyrolysis of unsaturated hydrocarbons in terms of free-radical chain mechanisms initiated by the bimolecular reactions of unsaturated hydrocarbons,[29,30] and have attracted the attention of many investigators. In the shock tube experiments above 1700 K, Gay and coworkers,[25] and Bopp and Kern[28] detected C_4H_3 radical by use of a time of flight mass spectrometer.

In the present experiment, a wide temperature range from 1000 to 1670 K was covered. Complete analysis of the reaction products was performed as far as possible. Particular attention has been paid to determine the order of the reaction and the major products as a function of temperature. In the temperature range studied, it is difficult to find radicals in a direct manner,[12] but the deuterium content of the main primary product in the pyrolysis of the equimolar C_2H_2 and C_2D_2 mixture, may be expected to provide information for testing the mechanisms.

Experimental

Apparatus and Procedure. The pyrolysis was studied in a 4-cm i.d. single-pulse shock tube. The driven section was 277 cm long, the main portion of which was made of terex glass tubing. The driver section was steel tubing and its length was variable, but it was fixed at 157 cm in the present runs. A 80-l dump tank was connected to the driven section near the diaphragm. The driver section was seperated from the driven section by a "Lumirror" (polyethylene terephthalate) film of 0.05 mm thickness. The details of the shock tube was described by Tsuda and Kuratani,[31] but a slight modification was made.

Before each test run, the shock tube was evacuated to below 1×10^{-4} Torr by an oil diffusion pump. The ultimate vacuum was 8×10^{-5} Torr, and the leak plus outgassing rate was approximately 6×10^{-5} Torr/min.

In order to measure the incident shock velocity, the outputs of the three pressure gauges(barium titanate-lead zirconate) spaced at 23.1 cm intervals were fed into a home-built electronic counter(Hop Step Jump Counter),[32] having the accuracy of 0.1 μs. Reflected shock parameters were calculated from the incident shock velocity extrapolated to the end-plate, considering the attenuation of the shock wave. Ideal shock wave theory was used. The thermodynamical data were taken from the JANAF tables.[33] The pressure profiles at the downstream end were recorded on an oscilloscope, from which the reaction times were determined with the accuracy of ±5%. Helium was used as the driver gas throughout the experiment. The shocks were fired within five minutes after the two section were filled with the desired gases.

* 1 $\mathrm{cal_{th}}$=4.184 J.

Materials. The three kinds of mixtures, with the ratios of C_2H_2/Ar equal to 5/95 and 10/90; and with the ratio of C_2H_2/C_2D_2/Ar equal to 5/5/90, were prepared in a glass vessel of 5-l volume, and were allowed to stand at least one day before use.

Acetylene, from Matheson Company, was bubbled through concentrated sulfuric acid, passed through a sodalime tower and then collected in a liquid nitrogen trap. The condensate was purified by bulb-to-bulb vacuum distillation. Acetylene-d_2(99% D atom guaranteed) was obtained from Merck Sharp and Dohme of Canada. For the purification, it was condensed in a liquid nitrogen trap, and subjected to a brief pumping period. Argon(nominal purity of 99.9995%), from Nippon Sanso Co., was used without further purification and served as the diluent.

Butenyne and butadiyne were prepared from 1,3-dichloro-2-butene and 1,4-dichloro-2-butyne, respectively.[34,35] They were purified by distillation through a low temperature column. The purified gases were quickly diluted with a large amount of argon as the stabilizer, and stored. Gas chromatographic analysis showed that the butenyne and butadiyne contained allene, propyne, and butadiene as the impurities. The purity of the butenyne and butadiyne was found 82.0 and 91.4%, respectively.

Research Grade CH_4, C_2H_4, C_2H_6, allene, propyne, and 1,3-butadiene were obtained from Takachiho Shoji Co., and used as received. The reference gases for the gas chromatographic calibration were prepared barometrically with mercury and oil manometers. Argon was used as the diluent gas.

Analytical. As soon as the shock was fired, the test gas around the end-plate was quickly extracted into an evacuated bulb of 60-ml volume with the aid of a solenoid valve operated by compressed air. The hydrocarbons in the products were analyzed on Yanaco G-80 and Shimadzu GC-3AF gas chromatographs using flame ionization detectors. CH_4, C_2H_4, C_2H_6 were analyzed at 50 °C on a 3 mm× 2 m column packed with 80—100 mesh Porapak N. The higher molecular weight hydrocarbons were analyzed at 130 °C. The hydrogen was detected at a room temperature by a thermal conductivity cell, on a 4-m column packed with 40—50 mesh molecular sieve 5A with argon as the carrier gas. The concentration of each product was determined from the peak area relative to that of the reference gas.

The shock heated samples of the equimolar mixture of C_2H_2 and C_2D_2 in argon were analyzed by a Hitachi model RM-50 mass spectrometer to determine the isotopic distributions of acetylene and butenyne. The ionization potential was kept at 50 eV. The pattern coefficient of acetylene-d_1 was taken equal to the arithmetical mean of those acetylene-d_0 and acetylene-d_2. The fragmentation patterns of butenyne isomers were calculated statistically from that of butenyne-d_0 assuming the same fragmentation.

Results

The two mixtures with the ratios of C_2H_2/Ar equal to 5/95 and 10/90 were pyrolyzed over the temperature range from 1000 to 1670 K. The shock heated samples were analyzed by gas chromatography. Complete analysis was carried out for the hydrocarbons having carbon number from 1 to 4.

Major Products. Under the experimental conditions employed, the major products of the pyrolysis were butenyne, butadiyne, and hydrogen. Butenyne and butadiyne were identified by both gas chromatography and mass spectrometry. The analytical results are shown in Fig. 1. As shown in Fig. 1, at the lower temperatures the yield of butenyne increases with temperature. And it attains to its maximum at about 1500 K, and then with the increase of temperature, it becomes to decrease.

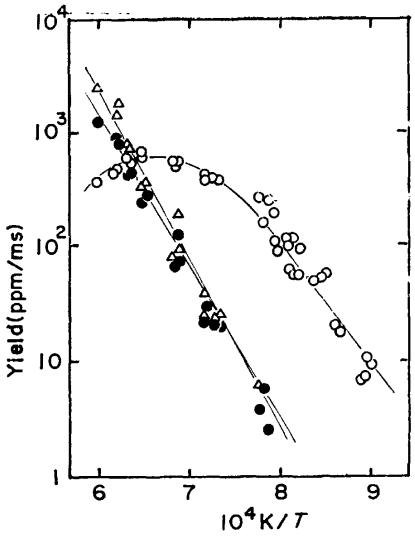

Fig. 1. Major products distribution as a function of temperature. (C_2H_2/Ar=5/95).
○: Butenyne, ●; butadiyne, △; hydrogen.

The yields of butadiyne and hydrogen increase linearly with increasing temperature in the temperature range studied. At the lower temperatures approximately equal amounts of butadiyne and hydrogen are produced, while at the higher temperatures above 1500 K the yield of hydrogen evidently goes beyond that of batadiyne. It is thus confirmed that at the lower temperatures butenyne is the main primary product, on the other hand, butadiyne and hydrogen become predominant at the higher temperatures.

Minor Products. CH_4, C_2H_4, allene, and propyne were found as the minor products. They are shown in Fig. 2 in the case of the mixture of C_2H_2/Ar=10/90. On the gas chromatograph a low and broad peak with a very long retention time (about 3 h) was observed, and identified as benzene. But the quantitative analysis was not carried out. In addition, trace amounts(less than 1 ppm) of C_2H_6 and 1,3-butadiene were detected. It is noteworthy that the hydrocarbons containing odd number of carbon atoms such as CH_4 and C_3H_4 were observed.

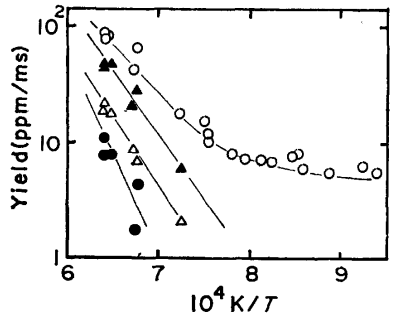

Fig. 2. Minor products distribution as a function of temperature. (C_2H_2/Ar=10/90)
○; Ehtylene, △; allene, ▲; propyne, ●; methane.

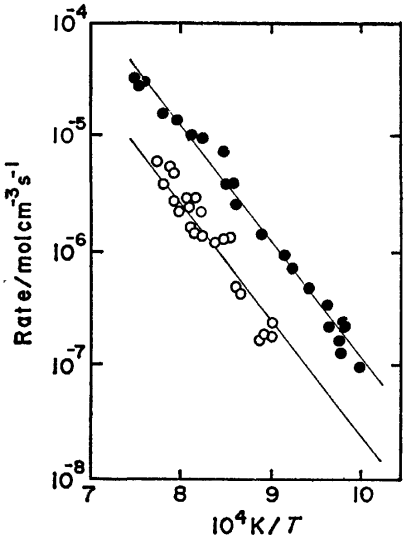

Fig. 3. Dependence of the rate of butenyne formation on acetylene concentration.
○; C_2H_2/Ar=5/95, ●; C_2H_2/Ar=10/90.

Formation Rate of Butenyne. The two kinds of mixtures stated above also served to determine an empirical reaction rate formula of butenyne formation. The total densities behind the reflected shock waves were $(2.35\pm0.11)\times10^{-5}$ mol/cm^3 throughout all runs. And the reaction times were limited within 1 ms to maintain the low conversions of acetylene. Since we are concerned with the early stage of the pyrolysis, where the yields of butadiyne and hydrogen are negligible compared with that of butenyne, only the data obtained below 1350 K are collected. The dependence of the rate of butenyne production on the acetylene concentration is shown in Fig. 3. The empirical power rate equation such as, $d[C_4H_4]/dt=A\exp(-E/RT)[C_2H_2]^n$, was assumed. Applying the method of least squares to A, E, and n;

$$d[C_4H_4]/dt = k_1[C_2H_2]^{2.35\pm0.15} \quad (1)$$

where

$$k_1 = 10^{16.74\pm1.05}\exp((-48000\pm1500)/RT) \quad (2)$$

was obtained in cm^3 mol^{-1} s^{-1} units. The errors denote the standard deviation of the least squares method.

In the literatures of the shock tube studies, first[19,24,26] or second[20-23,25] order rate with respect to acetylene was reported. And in the context of the first or second order reaction, the second-order reaction is supported from the present analysis. Therefore, when we take the view of the second-order reaction, the experimental data will be fitted by the following rate constant:

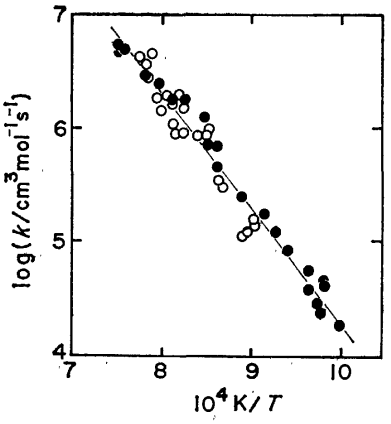

Fig. 4. Arrhenius plot of the second-order rate constants.
○; C_2H_2/Ar=5/95, ●; C_2H_2/Ar=10/90.

$$k_3(\text{cm}^3\,\text{mol}^{-1}\,\text{s}^{-1}) = 10^{14.39\pm0.26}\exp((-46400\pm1400)/RT) \quad (3)$$

The Arrhenius plot of the second-order rate constant is shown in Fig. 4.

Isotopic Distribution. The equimolar mixture of C_2H_2 and C_2D_2 in argon was shock heated below 1350 K, and the isotopic distributions of butenyne and acetylene were determined by mass spectrometry. In the temperature range up to 1350 K, the interference due to butadiyne on the mass spectra of butenyne isomers could be neglected, for the amount of butadiyne formed was negligibly small compared with that of butenyne. The results of the mass spectral analyses are given in Table 1. Evidently, considerable amounts of butenyne isomers containing odd number of hydrogen and deuterium atoms, C_4H_3D and C_4HD_3, are produced. This finding may be useful for testing the proposed mechanisms, which will be discussed in the following section.

Discussion

Comparison of the Second-order Rate. An exact analysis showed that at the early stage of the pyrolysis, butenyne is the main primary product, and the second-order rate with respect to acetylene is preferred for the formation of butenyne. It is noticed that the second-order rate constants for the consumption of acetylene

Table 1. Isotopic distribution of butenyne

T_5 [a] / K	C_4H_4 [b]	C_4H_3D	$C_4H_2D_2$	C_4HD_3	C_4D_4	C_2HD [b]	τ [c] / μs
1069	0.159	0.155	0.262	0.280	0.143	0.005	790
1180	0.161	0.167	0.304	0.261	0.107	0.011	860
1185	0.171	0.169	0.303	0.248	0.108	0.012	760
1201	0.152	0.176	0.306	0.256	0.110	0.013	700
1285	0.147	0.190	0.320	0.237	0.106	0.024	870
1325	0.148	0.189	0.324	0.249	0.090	0.075	880

a) T_5 is the temperature behind the reflected shock wave. b) The total amounts of butenyne and acetylene are taken equal to 1.000, respectively. c) τ is the dwell time.

obtained by many investigators, covering the temperature range 620—2450 K, apparently lie on a single Arrhenius expression:[25]

$$k_4(\mathrm{cm^3\,mol^{-1}\,s^{-1}}) = 10^{13.8}\exp(-41600/RT) \quad (4)$$

At the early stage of the pyrolysis, the relationship of $2\mathrm{d}[C_4H_4]/\mathrm{d}t = -\mathrm{d}[C_2H_2]/\mathrm{d}t$ holds well, since butenyne is the only reaction product and the other minor products may be neglected. In the temperature range 1000—1350 K the absolute values of $2k_3$ agree well with those of k_4.

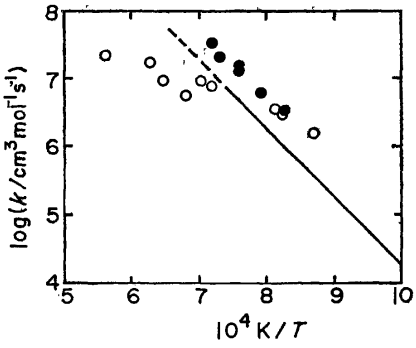

Fig. 5. Comparison of the second-order rate constant of butenyne formation with the literatures.
○; Skinner and Sokoloski, ●; Towell and Martin, ——; this work.

The second-order rate constants for butenyne formation were obtained by only two groups; by Towell and Martin in a flow tube study[14] and by Skinner and Sokoloski in a shock tube experiment.[20] A comparison with the literatures is made in Fig. 5. The absolute values of the present rate constant are about a factor of 0.5 lower than those obtained by them in the temperature range 1000—1350 K. But when the activation energy is compared, the present rate constant is in good agreement with that of Towell and Martin's rather than with that of Skinner and Sokoloski's. The rate constant derived by Towell and Martin is expressed as:

$$k_5(\mathrm{cm^3\,mol^{-1}\,s^{-1}}) = 10^{14.5}\exp(-45000/RT) \quad (5)$$

As shown in Fig. 1, the concentration of butenyne has a maximum value. Consequenly, in the neighborhood of the temperature where the yield of butenyne shows its maximum, the increase of butenyne concentration slows down with increasing temperature. It seems probable that under the conditions employed by Skinner and Sokoloski, the apparent lower activation energy may be obtained by the reason mentioned above.

As far as the second-order rate is concerned, the absolute values are fairly well consistent among many investigators, although there are significant dissents as to the main primary product of the pyrolysis.

The reaction products observed in the present analysis, are in good accordance with those detected in static and flow systems, for example, Cullis and Franklin[16] reported butenyne, butadiyne, CH_4, C_2H_4, C_2H_6, H_2, propyne, and benzene as the reaction products. Further, the nature and sequence of the formation of their products as a function of time have strong resemblance to those in the present shock tube experiment as a function of temperature. This may suggest that the same or similar mechanism is operative in the temperature range up to 1350 K, where the formation of butenyne is predominant.

Mechanism of Butenyne Formation. The strong inhibition by nitric oxide observed especially at low temperatures[2,3,5] cannot be accounted for by a simple bimolecular reaction of acetylene. The excited-state molecule mechanisms were proposed to be compatible with the low activation energy and the inhibition by radical scavengers. The following molecular chain mechanism involving excited-state molecules was presented as the most probable one to explain the fairly high frequency factor;[2,15]

$$C_2H_2 + C_2H_2 \rightarrow C_2H_2^* + C_2H_2 \quad \text{initiation}$$

$$C_2H_2^* + C_2H_2 \rightarrow C_4H_4^*$$
$$C_4H_4^* + C_2H_2 \rightarrow C_4H_4 + C_2H_2^* \quad \text{chain propagation}$$

where, $C_2H_2^*$ and $C_4H_4^*$ were supposed to be the excited molecules in the triplet state or biradicals.

In the pyrolysis of the equimolar mixture of C_2H_2 and C_2D_2, C_4H_3D and C_4HD_3 would be formed by the reaction of C_2HD molecule with C_2H_2 and C_2D_2 molecules, respectively. C_2HD molecule may result from the H–D exchange reaction between C_2H_2 and C_2D_2 molecules.

As can be seen from Table 1, the yields of C_4H_3D and C_4HD_3 are too large to be accounted for by the above mechanism, because the yield of C_2HD in the present experiment is less than 10% of the initial acetylene concentration.

The appearance of C_4H_3D and C_4HD_3 in significant quantities in the C_2H_2–C_2D_2 system may suggest that the pyrolysis of acetylene proceeds *via* a free-radical mechanism. The acitivation energy of 46.4 kcal/mol is too low to allow the initiation process of unimolecular scission of bonds, C≡C and C–H, in acetylene molecule. We have tried to interpret our data in terms of a free-radical chain mechanism initiated by a bimolecular reaction of acetylene. This attempt is basically an extention of that proposed by Back.[36] And in this study each reaction participated in the pyrolysis was examined in detail from the thermochemical point of view.

The heats of formation for the relevant C_4 molecules and radicals used in the following calculation are the same as those evaluated by Cowperwaite and Bauer,[37] and the heat of formation of 59.6 kcal/mol, the smallest value in the literatures, is adopted for C_2H_3 radical.[38] The other values are taken from the JANAF tables. The standard heats of the reactions, $\Delta H°$(kcal/mol), are given at 298 K.

The most probable free-radical chain mechanism is represented as follows:

$$2C_2H_2 \rightarrow C_4H_3 + H \qquad \Delta H° = 46.2 \quad (6)$$
$$H + C_2H_2 \rightarrow C_2H_3 \qquad \Delta H° = -46.7 \quad (7)$$
$$C_2H_3 + C_2H_2 \rightarrow C_4H_4 + H \qquad \Delta H° = 13.6 \quad (8)$$
$$C_4H_3 + C_2H_2 \rightarrow C_6H_5^{39)} \qquad \Delta H° \simeq -22.0 \quad (9)$$
$$C_6H_5 + C_2H_2 \rightarrow C_4H_4 + C_4H_3 \qquad \Delta H° \simeq -11.0 \quad (10)$$

Ethynylvinyl(C_4H_3) radical has two isomers, 1-ethynyl-

vinyl and 2-ethynylvinyl radicals. The heat of formation of the former radical is about 20 kcal/mol lower than that of the latter.[40] In our mechanism C_4H_3 is supposed to be 1-ethynylvinyl radical, since it is more advantageous than 2-ethynylvinyl radical in the view of the enthalpy change of Reaction 6.

In the above mechanism Reactions 8 and 10 are regarded as elementary reactions. In reality, however, the formation of C_4H_4 proceeds *via* relevant hot radical, for example, C_4H_5* in the case of Reaction 8. And when the energy present in the hot radical C_4H_5* is low enough, the hot radical may be stabilized by the collision with the third body to the C_4H_5 radical. Thus Reaction 8 should be divided into the following two reactios;

$$C_2H_3 + C_2H_2 \rightarrow C_4H_5 \qquad \Delta H^\circ = -33.4 \quad (11)$$

$$C_4H_5 \rightarrow C_4H_4 + H \qquad \Delta H^\circ = 47.0 \quad (12)$$

Reactions 11 and 12 show that C_4H_4 is formed by addition and subsequent decomposition reactions of the radicals. For simplicity the reactions of both types will be referred to addition-decomposition reactions hereafter.

The chain propagation processes to form butenyne are composed of addition reaction to acetylene and subsequent addition-decomposition reaction. Both radicals, C_4H_3 and H, generated by the initiation step can lead to the production of butenyne .

When the equimolar mixture of C_2H_2 and C_2D_2 in argon is pyrolyzed, appreciable amounts of C_4H_3D and C_4HD_3 among the butenyne isomers will be produced by the above mechanism. This prediction is consistent with the observed isotopic distribution of butenyne summarized in Table 1.

The isotopic distribution for the above mechanism was calculated in the case where H atom and C_2H_3 radical are predominant. If equal collision probability for C_2H_2 and C_2D_2 is assumed and the kinetic isotope effect is neglected, H and D atoms are produced by Reaction 6 in equal amounts, and the amounts of vinyl radical isomers, C_2H_3, C_2H_2D, C_2HD_2, and C_2D_3 formed by Reaction 7 are also equal. And then C_2H_2D radical, for instance, will react with C_2D_2 in the following process:

$$\begin{aligned} HDC{=}\dot{C}H + DC{\equiv}CD &\rightarrow HDC{=}CHCD{=}\dot{C}D \\ &\rightarrow HDC{=}CHC{\equiv}CD(C_4H_2D_2) + D \end{aligned} \quad (13)$$

By the similar reactions to Reaction 13, the equal amounts of H and D atoms will be generated again. The above estimation produces the ratios among the butenyne isomers, $C_4H_4/C_4H_3D/C_4H_2D_2/C_4HD_3/C_4D_4 = 1/2/2/2/1$. The agreement between the calculated and the observed values seems considerably good. The similar isotopic distribution of butenyne may be obatined when the chain propagation step of Reactions 9 and 10 is dominant.

In order to estimate the rate constant of the initiation step of Reaction 6, the enthalpy and entropy of C_4H_3 radical were calculated from the spectroscopic data of butenyne[41] following the evaluation method presented by O'Neal and Benson.[42] At 1300 K the enthalpy and entropy changes of Reaction 6 are 47.4 kcal/mol and 1.16 cal K^{-1} mol,$^{-1}$ respectively. The reverse rate constant of Reaction 6 is uncertain, but may be assumed to be the same as that of recombination reaction of atom with radical estimated by Benson and O'Neal:[43]

$$k_{-6}(\mathrm{cm^3\ mol^{-1}\ s^{-1}}) = 10^{13.3} \quad (14)$$

Then combining Eq. 14 with the equilibrium constant at 1300 K, the approximate forward reaction rate constant is given by:

$$k_6(\mathrm{cm^3\ mol^{-1}\ s^{-1}}) = 10^{13.55} \exp(-47400/RT) \quad (15)$$

An alternative initiation step was proposed by Back:[36]

$$2C_2H_2 \rightarrow C_2H + C_2H_3 \qquad \Delta H^\circ = 65.2 \quad (16)$$

And the estimated rate constant was given by:

$$k_{16}(\mathrm{cm^3\ mol^{-1}\ s^{-1}}) = 10^{15.7} \exp(-70000/RT) \quad (17)$$

The frequency factor of k_{16} seems abnormally high,[44] and k_6 is above ten times faster than k_{16} in the temperature range 1000—1350 K. Therefore, it may be concluded that Reaction 16 is not likely to occur as the initiation step for the formation of butenyne. Reaction 16, however, may be more important at higher temperatures than Reaction 6 in the view of the entropy change.[28]

In the above mechanism the termination occurs *via* the recombination or disproportionation reaction of the radicals involved. For the rate constants of the termination, the recombination rate constant of alkyl radical with radical[43] may be used as an alternative one;

$$k_t(\mathrm{cm^3\ mol^{-1}\ s^{-1}}) = 10^{12.3} \quad (18)$$

where, k_t is rate constant of the termination reaction.

Under the present shock tube experiment the reaction times are extremely short. This provides a serious problem in applying the steady-state assumption to the system stated above. As to the formation of butenyne, however, Silcocks,[2] and Cullis and Franklin[16] observed no appreciable induction period at lower temperatures. Accordingly the assumption of steady-state of the radicals may apply to some extent. Imposing the steady-state of the radicals on the above mechanism, the second-order rate of butenyne formation is expressed as;

$$\mathrm{d[C_4H_4]/dt(mol\ cm^{-3}\ s^{-1})} = k_{ad}(k_6/2k_t)^{1/2}[C_2H_2]^2 \quad (19)$$

where, k_{ad} is the rate constant of Reaction 8 or 10. By the comparison with the observed second-order rate constant k_3, k_{ad} in Eq. 19 is derived as follows:

$$k_{ad}(\mathrm{cm^3\ mol^{-1}\ s^{-1}}) = 10^{13.9} \exp(-22600/RT) \quad (20)$$

When compared with the rate constant $k_4/2$:

$$k_{ad}(\mathrm{cm^3\ mol^{-1}\ s^{-1}}) = 10^{13.0} \exp(-17900/RT) \quad (21)$$

The addition and addition-decomposition reactions may compete with each other. And the addition of the radicals to acetylene may proceed successively at the lower temperatures, since the addition reaction to acetylene has, in general, lower activation energy than that of the addition-decomposition reaction. Consequently butenyne may be produced by the subsequent addition-decomposition reaction. In the case of the competition between Reactions 8 and 11, butenyne

may be formed by the reaction of C_4H_5 radical with acetylene:

$$C_4H_5 + C_2H_2 \rightarrow C_4H_4 + C_2H_3 \quad \Delta H^\circ = 13.3 \quad (22)$$

Generally the bond dissociation energy of C–C is lower than that of C–H bond in the larger radicals, and low molecular weight molecules may be formed by the C–C bond scission rather than the C–H bond fission at the lower temperatures. In some experiments at the lower temperatures benzene is reported as the main primary product.[11,13] This might be interpreted in the similar way:

$$C_6H_5 + C_2H_2 \rightarrow C_8H_7 \quad (23)$$

$$C_8H_7 + C_2H_2 \rightarrow C_6H_6(\text{benzene}) + C_4H_3 \quad (24)$$

As mentioned above, the chain propagation steps consist of addition and addition-decomposition reactions, and both of which may be expected to show similar kinetic behavior regardless of different radicals involved. An Arrhenius plot linear within the error limits involved in the measurement of acetylene pyrolysis[25] is therefore consistent with our mechanism. Palmer and Dormish[15] pointed out that the Arrhenius plot of the data in the literatures shows a discontinuity in the neighborhood of 1000 K, and suggested a change of the mechanism of the pyrolysis. But on the basis of the similarities that exist between frequency factors and activation energies of homologous reactions, it seems more likely that from the kinetic data obtained at low temperatures where the formation of butenyne dominates, we can predict no change of the chain propagation step in the mechanism.

Furthermore, the chain propagation steps initiated by H atom and C_4H_3 radical, respectively, will show quite similar kinetic behavior. Thus in the present stage we could not determine the relative importance of H atom and C_4H_3 radical in the above mechanism. Further study as regards the relative importance of the two radicals, C_4H_3 and H, is in progress.

Formation of Butadiyne and Hydrogen. At the higher temperatures the formation of butadiyne and hydrogen becomes important, which may be interpreted in terms of a free-radical chain mechanism in the same way. The abstraction reaction of H atom from acetylene becomes faster than the addition of H atom to acetylene with increasing temperature. The following chain propagation may dominate:[28,34]

$$H + C_2H_2 \rightarrow H_2 + C_2H \quad \Delta H^\circ = 7.7 \quad (25)$$

$$C_2H + C_2H_2 \rightarrow C_4H_2 + H \quad \Delta H^\circ = -4.8 \quad (26)$$

The alternative scheme of Reaction 26 is as follows:

$$HC{\equiv}C\cdot + HC{\equiv}CH \rightarrow HC{\equiv}CCH{=}\dot{C}H \quad \Delta H^\circ = -44.8 \quad (27)$$

$$HC{\equiv}CCH{=}\dot{C}H \rightarrow HC{\equiv}C\text{-}C{\equiv}CH + H \quad \Delta H^\circ = 40.0 \quad (28)$$

As shown in Reaction 27, the stabilized C_4H_3 radical is 2-ethynylvinyl radical, which is different from that produced by Reaction 6.

At the higher temperatures covered in the present experiment the amount of hydrogen is greater than that of butadiyne. This implies that another path to yield hydrogen is operative, since by the above chain propagation nearly equal amounts of hydrogen and butadiyne may be formed. One of the possible paths is the decomposition of butenyne by the following reactions:

$$H + C_4H_4 \rightarrow H_2 + C_4H_3 \quad \Delta H^\circ = -24.9 \quad (29)$$

$$C_2H + C_4H_4 \rightarrow C_2H_2 + C_4H_3 \quad \Delta H^\circ = -32.6 \quad (30)$$

In the present experiment the sum of carbon atom over the whole products was less than that of hydrogen atom. There must have been some undetected hydrocarbons present, containing on the average less than one atom of hydrogen per atom of carbon. Thus C_6H_2 and C_8H_2[25,26] appear possible hydrocarbons undetected in the present analysis. As the pyrolysis continues the following reactions may be expected to occur;

$$H + C_4H_2 \rightarrow C_4H + H_2 \quad (31)$$

$$C_4H + C_2H_2 \rightarrow C_6H_2 + H \quad (32)$$

and succeeded by:

$$H + C_6H_2 \rightarrow C_6H + H_2 \quad (33)$$

$$C_6H + C_2H_2 \rightarrow C_8H_2 + H \quad (34)$$

The formation of carbon soot becomes very important with increasing temperature at high temperatures. But this problem is beyond our discussion. Under the experimental conditions studied, however, the formation of soot was insignificant.

As shown in Fig. 1, the activation energies of butadiyne and hydrogen formation are higher than that of butenyne. Assuming the second-order rates for butadiyne and hydrogen production, the activation energies of 69.5 and 77.6 kcal/mol were obtained, respectively. If the formation of butadiyne and hydrogen were the predominant reaction consuming acetylene, the low activation energy of 41.6 kcal/mol of k_4 would be difficult to be accounted for. Therefore, the secondary reactions which consume acetylene, with lower activation energies than those of the main reactions, or which reproduce acetylene might contribute to lowering the apparent activation energy of the over-all acetylene consumption reaction.

Secondary Products. As the minor products the hydrocarbons containing odd number of carbon atoms, CH_4 and C_3H_4, were produced. The formation of these products may be easily accounted for by the reaction of the radical involved in the mechanism stated above. For example, CH_3 radical may be formed by the isomerization and decomposition of C_6H_7 radical as follows;[36]

$$C_4H_5 + C_2H_2 \rightarrow H_2C{=}CH\text{-}CH{=}CH\text{-}CH{=}\dot{C}H \quad (35)$$

and then 1,5 hydrogen shift may occur:

$$\rightarrow H_3C\text{-}\dot{C}H\text{-}CH{=}CH\text{-}C{\equiv}CH \quad (36)$$

The terminal methyl group may split off to CH_3 radical. CH_3 radical will abstract a hydrogen atom from acetylene to form CH_4 molecule. C_3H_3 radical may be generated in the similar way, which will ultimately lead to the formation of allene and propyne. Benzene may also be produced from C_6H_7 radical:[45]

$$C_6H_7 \rightarrow C_6H_6(\text{benzene}) + H \quad (37)$$

The formation of benzene provides an evidence that the

chain of carbon atoms has extended to six within the reaction times in the present experiment. And the participation of C_6 radicals may be justified. Considerable amount of ethylene was obtained in the persent analysis. There are two possible paths to yield ethylene:

$$C_2H_3 + C_2H_2 \rightarrow C_2H_4 + C_2H \quad \Delta H^\circ = 12.7 \quad (38)$$

$$2C_2H_3 \rightarrow C_2H_4 + C_2H_2 \quad \Delta H^\circ = -52.5 \quad (39)$$

The trace amounts of ethane and 1,3-butadiene may result from the recombination reactions of two CH_3 and C_2H_3 radicals, respectively. The ratio of disproportionation reaction rate constant to that of recombination is uncertain, but it is more likely that ethylene is formed mainly by the reaction of C_2H_3 radical with acetylene.

The author would like to thank Professor Kenji Kuratani, The University of Tokyo, for his valuable discussions and suggestions throughout this investigation.

References

1) H. A. Taylor and A. Van Hook, *J. Phys. Chem.*, **39**, 811 (1935).
2) C. G. Silcocks, *Proc. R. Soc. London, Ser. A*, **242**, 411 (1957).
3) G. J. Minkoff, D. M. Newitt, and P. Rutledge, *J. Appl. Chem.*, **7**, 406 (1957).
4) G. J. Minkoff, *Can. J. Chem.*, **36**, 131 (1958).
5) C. F. Cullis, G. J. Minkoff, and M. A. Nettleton, *Trans. Faraday Soc.*, **58**, 1117 (1962).
6) C. F. Cullis and M. A. Nettleton, *Trans. Faraday Soc.*, **59**, 361 (1963).
7) R. N. Pease, *J. Am. Chem. Soc.*, **51**, 3470 (1929).
8) E. A. Westbrook, K. Hellwig, and R. C. Anderson, *Int. Symp. Combust.*, **5**, 631 (1955).
9) F. C. Stehling, J. D. Frazee, and R. C. Anderson, *Int. Symp. Combust.*, **6**, 247 (1957).
10) R. S. Slysh and C. R. Kinney, *J. Phys. Chem.*, **65**, 1044 (1961).
11) F. C. Stehling, J. D. Frazee, and R. C. Anderson, *Int. Symp. Combust.*, **8**, 775 (1962).
12) K. C. Hou and R. C. Anderson, *J. Phys. Chem.*, **67**, 1579 (1963).
13) M. S. B. Munson and R. C. Anderson, *J. Phys. Chem.*, **67**, 1582 (1963).
14) C. D. Towell and J. J. Martin, *AIChE J.*, **7**, 693 (1963).
15) H. B. Palmer and F. L. Dormish, *J. Phys. Chem.*, **68**, 1553 (1964).
16) C. F. Cullis and N. H. Franklin, *Proc. R. Soc. London, Ser. A*, **280**, 139 (1964).
17) C. F. Aten and E. F. Greene, *Discuss. Faraday Soc.*, **22**, 162 (1956).
18) E. F. Greene, R. L. Taylor, and W. L. Patterson Jr., *J. Phys. Chem.*, **62**, 238 (1958).
19) W. J. Hooker, *Int. Symp. Combust.*, **7**, 949 (1959).
20) G. B. Skinner and E. M. Sokoloski, *J. Phys. Chem.*, **64**, 1952 (1960).
21) C. F. Aten and E. F. Greene, *Combust. Flame*, **5**, 55 (1961).
22) T. Asaba, K. Yoneda, and T. Hikita, *Nippon Kogyo Kagaku Zasshi*, **64**, 47 (1961).
23) J. N. Bradley and G. B. Kistiakowsky, *J. Chem. Phys.*, **35**, 264 (1961).
24) G. I. Kozlov and V. G. Knorre, *Combust. Flame*, **6**, 253 (1962).
25) I. D. Gay, G. B. Kistiakowsky, J. V. Michael, and H. Niki, *J. Chem. Phys.*, **43**, 1720 (1965).
26) I. L. Mar'yasin and Z. A. Nabutovskii, *Kinet. Katal.*, **11**, 856 (1970).
27) W. H. Beck and J. C. Mackie, *J. Chem. Soc., Faraday Trans. 1*, **71**, 1363 (1975).
28) A. F. Bopp and R. D. Kern, *J. Phys. Chem.*, **79**, 2579 (1975).
29) A. S. Kalland, J. H. Purnell, and B. C. Shurlock, *Proc. R. Soc. London, Ser. A*, **300**, 120 (1967); M. C. Lin, *Can. J. Chem.*, **44**, 1237 (1968); M. L. Boyd, T. M. Wu, and M. H. Back, *ibid.*, **46**, 2415 (1968); G. B. Skinner, R. C. Sweet, and S. K. Davis, *J. Phys. Chem.*, **75**, 1 (1971); M. P. Schuchmann and K. J. Laidler, *Int. J. Chem. Kinet.*, **4**, 491 (1972).
30) S. W. Benson and G. R. Haugen, *J. Phys. Chem.*, **71**, 1735 (1967); *ibid.*, **71**, 4404 (1967).
31) M. Tsuda and K. Kuratani, *Bull. Chem. Soc. Jpn.*, **41**, 53 (1968).
32) M. Yamashita, Y. Sano, T. Tanaka, H. Ogura, and K. Kuratani, *Tokyo Daigaku Uchu Koku Kenkyusho Hokoku*, **11**, 545 (1975).
33) "JANAF Thermochemical Tables," 2nd ed, National Bureau of Standards NSRDS-NBS 37, U. S. Goverment Printing Office, Washington D. C., 1971.
34) M. Nakagawa and T. Inui, *Nippon Kagaku Zasshi*, **73**, 143 (1952).
35) G. F. Hennion, C. C. Price, and T. F. Mckeon, Jr., *J. Am. Chem. Soc.*, **76**, 5494 (1945).
36) M. H. Back, *Can. J. Chem.*, **49**, 2119 (1971).
37) M. Cowperwaite and S. H. Bauer, *J. Chem. Phys.*, **36**, 1743 (1962).
38) F. P. Lossing, *Can. J. Chem.*, **49**, 357 (1971).
39) The heat of formation of C_6H_5 radical was calculated as a rough approximation from that of C_6H_6 (straight chain) estimated by Westbrook *et al.*,[8] supposing the bond dissociation energy of the C–H bond in C_6H_6 is 104 kcal/mol.
40) The heat of formation of 2-ethynylvinyl radical is estimated to be 123.4 kcal/mol, when the bond dissociation energy of the C–H is taken equal to 40 kcal/mol.[36]
41) R. F. Stamm, F. Halverson, and J. J. Whalen, *J. Chem. Phys.*, **17**, 104 (1949).
42) H. E. O'Neal and S. W. Benson, *Int. J. Chem. Kinet.*, **1**, 221 (1969).
43) "Kinetic Data on Gas Phase Unimolecular Reactions," S. W. Benson and H. E. O'Neal, National Bureau of Standards NSRDS-NBS 21, U. S. Goverment Printing Office, Washington D. C., 1970, p. 26.
44) Taking the collision diameter of C_2H_2 molecule as 4.56 Å, the classical collision frequency is estimated as $10^{14.48}$ $cm^3\ mol^{-1}\ s^{-1}$, which is about one order of magnitude smaller than the frequency factor of k_{16}.
45) G. J. Mains, H. Niki, and M. H. Wijinen, *J. Phys. Chem.*, **67**, 111 (1963).

The Crystal and Molecular Structures of *trans*-Dichlorobis(dimethylneomenthylphosphine)nickel(II), an Asymmetric Hydrosilylation Catalyst of Olefin*

Kojiro KAN, Yasushi KAI, Noritake YASUOKA, and Nobutami KASAI**
Department of Applied Chemistry, Faculty of Engineering, Osaka University
Yamadakami, Suita, Osaka 565
(Received November 18, 1976)

The molecular structure of $[NiCl_2\{Me_2neoMen)P\}_2]$, an asymmetric hydrosilylation catalyst of olefin was determined by means of X-ray diffraction. This complex forms dark red monoclinic crystals; $a=9.527(1)$, $b=8.048(2)$, $c=19.461(3)$ Å, $\beta=99.12(1)°$, space group $P2_1$ with $Z=2$. The structure, determined by the heavy-atom method, has been refined anisotropically by a least-squares procedure to $R=0.099$ for 3023 non-zero reflections. The geometry around the nickel atom is *trans*-square planar [Ni–Cl 2.151(5) and 2.175(6) Å, Ni–P 2.239(5) and 2.230(5) Å]. Two neomenthyl groups are located above and below the co-ordination plane.

A variety of dihalodiphosphinenickel(II) complexes have been found to be effective catalysts for hydrosilylation of olefins and acetylene by Kumada and co-workers.[1–3] Dichlorobis(dimethylneomenthylphosphine)nickel(II) is a complex in which each phosphine has a chiral substituent, and is also a catalyst for the hydrosilylation of olefins.[4]

This paper describes the X-ray molecular structure of dichlorobis(dimethylneomenthylphosphine)nickel(II) $[NiCl_2\{Me_2neoMen)P\}_2]$.*** Interest in the correlation between molecular structure and the catalytic activity for asymmetric hydrosilylation of olefins promoted this study.

Experimental

The crystals of $[NiCl_2\{Me_2neoMen)P\}_2]$ used in this study were provided by Professor Kumada and co-workers of Kyoto University. They are dark red, long and prismatic and sublime gradually at room temperature. Preliminary oscillation and Weissenberg photographs taken with Cu$K\alpha$ radiation showed that the crystal belongs to the monoclinic system. The systematic absence of reflections ($0k0$ for $k=2n+1$) indicated the space group to be $P2_1$ or $P2_1/m$. The correct space group was determined to be $P2_1$ on the basis of the optical activity of this complex since the molecule contains asymmetric carbon atoms.

The unit-cell dimensions were determined by a least-squares fit from 2θ values of 20 high-angle reflections measured on a G. E. single-crystal orienter mounted on a Rigaku SG-2 goniometer.

Crystal Data: $C_{24}H_{50}Cl_2NiP_2$, FW 530.2, monoclinic, space group $P2_1$, $a=9.527(1)$, $b=8.048(2)$, $c=19.461(3)$Å, $\beta=99.12(1)°$, $U=1473.3(4)$Å^3, $Z=2$, $D_c=1.20$ g cm^{-3}, μ(Mo)$=9.5$ cm^{-1}.

The intensity data were collected using a Rigaku automated, four-circle diffractometer using zirconium-filtered Mo$K\alpha$ radiation. The $\theta-2\theta$ scan technique was employed. The integrated intensity of each reflection was determined by scanning over a peak at a rate of 4° min^{-1}, and subtracting the background obtained by averaging the two values measured for 5 s at both ends of the scan. The 2θ scan width was from $-1.0°$ for the $K\alpha_1$ peak to 1.0° for the $K\alpha_2$ peak. A total of 1508 reflections ($F(hkl)$'s, $\sin\theta/\lambda\leq0.482$) was measured at room temperature. At the same time an other set of data ($F(\bar{h}k\bar{l})$'s) was also collected in order to determine the absolute configuration of the molecule. The crystal used had the dimensions of $0.20\times0.18\times0.10$ mm and was coated with collodion. This crystal was too small, however, to give sufficient intensity for high-angle reflection measurements. Therefore, a second crystal of dimensions of $0.25\times0.20\times0.18$ mm was chosen, and the remaining 1802 reflections ($0.48\leq\sin\theta/\lambda\leq0.63$) were measured. The intensities of three standard reflections, 020, 003, and 400 were measured after every 50 reflections. The intensities of these reflections decreased almost uniformly with time due to the gradual decomposition of the crystal. A linear correction was applied to each set of data, and then the relative scaling between two sets of data was carried out by comparing the intensities of standard reflections in the two sets. A total of 3310 independent intensity values within a 2θ sphere of 53°($\sin\theta/\lambda\leq0.63$) was obtained. Lorentz and polarization corrections were made in the usual manner, while neither absorption nor extinction corrections were applied to the intensity data.

Solution and Refinement of the Structure

The structure was determined by the heavy-atom method. Approximate co-ordinates of the nickel, the two chlorine and the two phosphorus atoms were obtained from a three-dimentional Patterson function. The subsequent Fourier synthesis revealed positions of all the remaining non-hydrogen atoms.

The structure was refined by the block-diagonal least-squares procedure using the HBLS-V program.[5] The quantity minimized was $\Sigma(|F_o|-k|F_c|)^2$, where k is a scaling factor. The atomic scattering factors used were taken from those given by Hanson and co-workers.[6] Since the space group is $P2_1$, the y parameter of the nickel atom was fixed at 0.25 in order to define the origin of the unit-cell. The difference Fourier map did not clearly reveal any hydrogen atom positions. An attempt to find the positions of the hydrogen atoms by the technique of LaPlaca and Ibers[7] was also unsuccessful. Hydrogen atoms except for methyl hydrogen (20 out of the 50 hydrogen atoms) were then located assuming a C–H bond length of 1.08 Å and a tetrahedral angle for each carbon atom. In subsequent refinements, the contributions were included in the structure factor calculations, their parameters being fixed. The final R is 0.099 for 3023 non-zero reflections.

* Read at the 21st symposium on Organometallic Chemistry Japan, Sendai, Oct. 4 (1973).

** To whom correspondence should be addressed.

*** *neo*Men: neomenthyl group.

In order to determine the absolute configuration of the molecule, a refinement was also carried out of the structure obtained and its enantiomorph. The R factors converged to 0.0689 and 0.0702, respectively, for the sets of $F(hkl)$ and $F(\bar{h}\bar{k}\bar{l})$ data ($\sin\theta/\lambda=0.48$), whereas for the enantiomorphic structure it converged to the slightly higher R values, 0.0697 and 0.0710, respectively. The former structure was, therefore, chosen as the final result (Fig. 1). This result confirmed the absolute configurations of both neomenthyl groups.

TABLE 1. POSITIONAL AND THERMAL PARAMETERS OF ATOMS
(e.s.d.'s in parentheses)

(a) Fractional co-ordinates.

Atom	x	y	z	Atom	x	y	z
Ni	−0.01391(17)	0.25000	0.24917(8)	C(19)	0.1447(14)	−0.0607(26)	0.1683(8)
Cl(1)	0.0086(5)	0.4215(5)	0.1668(2)	C(20)	0.0975(17)	−0.0803(26)	0.0363(11)
Cl(2)	−0.0358(5)	0.0791(5)	0.3334(2)	C(3)	0.2526(16)	0.2558(23)	0.3920(8)
P(1)	−0.2060(4)	0.1292(4)	0.1882(2)	C(4)	0.3242(14)	0.3862(20)	0.2628(8)
P(2)	0.1726(4)	0.3737(5)	0.3125(2)	C(31)	−0.0740(17)	0.5348(21)	0.4034(7)
C(1)	−0.2874(15)	0.2292(18)	0.1088(7)	C(32)	−0.0359(13)	0.5984(16)	0.3354(6)
C(2)	−0.3553(17)	0.1376(27)	0.2379(9)	C(33)	0.1246(12)	0.5899(15)	0.3314(5)
C(11)	−0.4187(13)	−0.2038(20)	0.1042(7)	C(34)	0.2105(13)	0.6902(16)	0.3918(6)
C(12)	−0.3066(13)	−0.2116(17)	0.1703(6)	C(35)	0.1697(18)	0.6315(21)	0.4637(6)
C(13)	−0.1785(10)	−0.0975(14)	0.1706(6)	C(36)	0.0098(18)	0.6304(21)	0.4633(7)
C(14)	−0.1043(15)	−0.1337(19)	0.1054(6)	C(37)	−0.2365(17)	0.5454(29)	0.4039(10)
C(15)	−0.2156(15)	−0.1291(20)	0.0384(7)	C(38)	0.3716(13)	0.7054(18)	0.3902(8)
C(16)	−0.3441(15)	−0.2431(26)	0.0423(7)	C(39)	0.4009(15)	0.7924(26)	0.3235(9)
C(17)	−0.5389(15)	−0.3233(24)	0.1081(10)	C(40)	0.4497(16)	0.8019(24)	0.4558(9)
C(18)	0.0318(14)	−0.0319(17)	0.1014(7)				

(b) Anisotropic temperature factors ($\times 10^4$) expressed in the form $\exp\{-(\beta_{11}h^2+\beta_{22}k^2+\beta_{33}l^2+\beta_{12}hk+\beta_{13}hl+\beta_{23}kl)\}$.

Atom	β_{11}	β_{22}	β_{33}	β_{12}	β_{13}	β_{23}
Ni	139.6(18)	119.8(19)	18.6(3)	27.9(41)	7.0(12)	−0.1(14)
Cl(1)	245.3(65)	171.6(64)	24.1(9)	−44.4(109)	6.4(38)	18.4(40)
Cl(2)	283.5(74)	172.1(65)	22.7(8)	−68.9(117)	18.9(39)	30.8(41)
P(1)	124.2(40)	130.8(51)	27.7(9)	50.0(79)	−0.5(31)	−11.8(38)
P(2)	123.3(39)	139.9(54)	25.9(9)	71.0(80)	5.9(30)	16.6(38)
C(1)	184(20)	135(23)	46(5)	182(40)	−55(16)	8(19)
C(2)	157(21)	396(52)	55(6)	92(56)	104(20)	−76(31)
C(11)	104(15)	241(32)	38(4)	56(36)	−8(13)	1(20)
C(12)	146(17)	175(26)	29(4)	4(34)	14(12)	−39(16)
C(13)	81(12)	110(17)	28(3)	23(24)	7(10)	−12(13)
C(14)	170(19)	205(27)	20(3)	92(39)	17(12)	−25(16)
C(15)	182(21)	213(29)	29(4)	21(44)	−2(14)	−47(19)
C(16)	192(21)	297(37)	30(4)	52(60)	−35(14)	−55(24)
C(17)	133(19)	285(41)	64(7)	−86(48)	0(19)	−28(29)
C(18)	156(19)	138(22)	44(5)	52(35)	56(16)	−7(18)
C(19)	115(17)	340(45)	46(5)	44(48)	9(15)	−24(27)
C(20)	208(24)	331(44)	34(5)	−20(56)	89(17)	5(24)
C(3)	192(21)	221(30)	42(5)	−21(52)	−80(16)	50(24)
C(4)	136(18)	210(30)	58(8)	−37(40)	82(17)	−113(24)
C(31)	212(24)	219(30)	26(4)	−28(46)	35(15)	6(18)
C(32)	133(16)	140(21)	27(3)	34(31)	−8(11)	−24(15)
C(33)	123(14)	127(18)	17(3)	40(27)	6(9)	10(12)
C(34)	129(15)	143(21)	29(4)	58(30)	−14(12)	−21(15)
C(35)	258(27)	233(31)	17(3)	15(50)	−3(14)	−51(17)
C(36)	244(26)	234(33)	30(4)	49(51)	92(17)	−22(20)
C(37)	176(24)	369(51)	71(8)	−3(61)	153(24)	−16(36)
C(38)	113(16)	176(28)	56(6)	18(33)	−24(15)	−10(22)
C(39)	136(19)	338(48)	55(6)	0(50)	49(18)	65(30)
C(40)	159(21)	311(44)	56(7)	−17(48)	−9(18)	−154(29)

TABLE 1. (continued)

(c) Calculated co-ordinates and assigned isotropic temperature factors for hydrogen atoms.

Atom	x	y	z	B	Atom	x	y	z	B
H(11)	−0.464	−0.075	0.099	5.0	H(31)	−0.039	0.405	0.411	5.0
H(12A)	−0.269	−0.340	0.176	5.0	H(32A)	−0.071	0.727	0.329	5.0
H(12B)	−0.357	−0.183	0.215	5.0	H(32B)	−0.093	0.526	0.293	5.0
H(13)	−0.105	−0.127	0.218	5.0	H(33)	0.155	0.657	0·287	5.0
H(14)	−0.064	−0.262	0.110	5.0	H(34)	0.176	0.819	0.384	5.0
H(15A)	−0.167	−0.166	−0.006	5.0	H(35A)	0.223	0.707	0.506	5.0
H(15B)	−0.256	−0.004	0.031	5.0	H(35B)	0.208	0.502	0.474	5.0
H(16A)	−0.306	−0.372	0.047	5.0	H(36A)	−0.012	0.581	0.513	5.0
H(16B)	−0.418	−0.235	−0.006	5.0	H(36B)	−0.025	0.760	0.461	5.0
H(18)	−0.004	−0.098	0.098	5.0	H(38)	0.412	0.571	0.390	5.0

The positional and thermal parameters are given in Table 1.†

Results and Discussion

The molecular structure is illustrated in Fig. 1. A stereoscopic drawing of the molecule is given in Fig. 2. Bond lengths and bond angles are listed in Table 2.

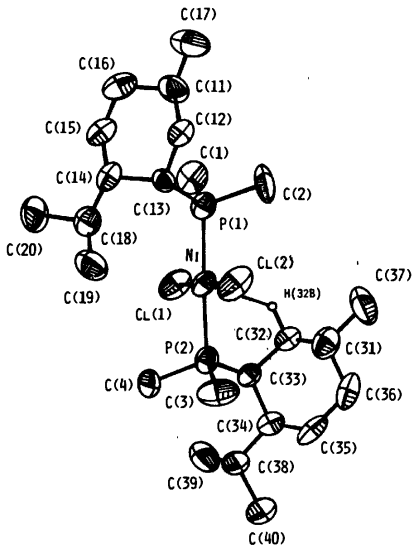

Fig. 1. An ORTEP drawing[19] of the molecule with the numbering of atoms.

The co-ordination geometry around the nickel atom is *trans*-square planar, the deviations of Ni, Cl(1), Cl(2), P(1), and P(2) atoms from the co-ordination plane being 0.018, 0.009, 0.009, −0.018, and −0.018 Å, respectively.

The Ni–Cl bond lengths, 2.151(5) and 2.175(6) (av 2.163) Å are in agreement with the value 2.166(1) Å reported for $[NiCl_2(C_8H_{14}PPh)_2]$,[8] and are comparable to those of 2.175(2) and 2.167(2) Å found in $[NiCl_2\{(MeO)_2C_5H_8PPh\}_2]$.[9] The Ni–P length are 2.239(5) and 2.230(5) (av 2.235) Å, which are equal to the values 2.227(1) and 2.232(3) Å reported for $[NiCl_2(C_8H_{14}PPh)_2]$ and $[NiBr_2\{(t\text{-}Bu)_2PF\}_2]$,[10] respectively. They are equal to or slightly shorter than the values 2.245(2) and 2.254(2) Å in $[NiCl_2\{(MeO)_2C_5H_8PPh_2\}]$. They are significantly shorter than those of 2.251(3) and 2.263(7) Å found in diamagnetic *trans*-square planar $[NiBr_2(Me_2PhP)_2]$[11] and $[NiBr_2(PhCH_2PPh_2)_2]$,[12] respectively, and are also shorter than those of 2.263(3) and 2.273(3) Å in distorted tetrahedral $[Ni(N_3)(NO)(PPh_3)_2]$.[13] However, they are slightly longer than the values 2.175(4) or 2.220(3) Å in *trans*-square planar $[Ni(PhC{\equiv}C)_2(Et_3P)_2]$[14,15] and 2.221(1) Å in distorted tetrahedral $[Ni(CO)_2(Ph_3P)_2]$.[16]

The conformation about P(1)–Ni–P(2) shown in Fig. 3 is approximately staggered. Two neomenthyl groups bonded to the P(1) and P(2) atoms are located above and below the co-ordination plane. The conformations about the P(1)–C(13) and P(2)–C(33) bonds

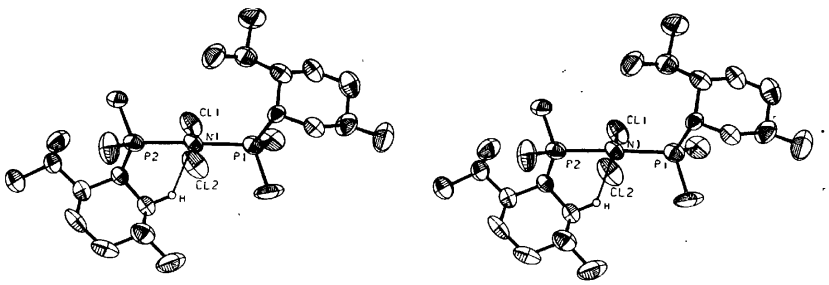

Fig. 2. A stereoscopic drawing[19] of the molecule.

† The table of observed and calculated structure factors is kept as Document No. 7705 at the Chemical Society of Japan.

TABLE 2. BOND LENGTHS AND BOND ANGLES (e.s.d.'s in parentheses)

(a) Bond lengths [l/Å]

Ni-Cl(1)	2.151(5)	Ni-Cl(2)	2.175(6)	C(14)-C(18)	1.546(21)	C(15)-C(16)	1.541(26)
Ni-P(1)	2.239(5)	Ni-P(2)	2.230(5)	C(18)-C(19)	1.569(25)	C(18)-C(20)	1.549(25)
P(1)-C(1)	1.805(15)	P(1)-C(2)	1.844(22)	C(31)-C(32)	1.516(21)	C(31)-C(36)	1.514(24)
P(1)-C(13)	1.883(12)	P(2)-C(3)	1.871(19)	C(31)-C(37)	1.551(29)	C(32)-C(33)	1.545(17)
P(2)-C(4)	1.864(17)	P(2)-C(33)	1.852(12)	C(33)-C(34)	1.549(19)	C(34)-C(35)	1.538(21)
C(11)-C(12)	1.537(21)	C(11)-C(16)	1.525(26)	C(34)-C(38)	1.544(20)	C(35)-C(36)	1.522(24)
C(11)-C(17)	1.507(25)	C(12)-C(13)	1.527(18)	C(38)-C(39)	1.538(26)	C(38)-C(40)	1.577(25)
C(13)-C(14)	1.573(19)	C(14)-C(15)	1.546(22)				

(b) Bond angles[φ/°]

Cl(1)-Ni-Cl(2)	179.2(2)	Cl(1)-Ni-P(1)	93.1(2)
Cl(1)-Ni-P(2)	87.7(2)	Cl(2)-Ni-P(1)	87.6(2)
Cl(2)-Ni-P(2)	91.7(2)	P(1)-Ni-P(2)	178.0(2)
Ni-P(1)-Cl(1)	117.7(5)	Ni-P(1)-C(13)	113.0(4)
Ni-P(2)-C(33)	109.2(4)	Ni-P(1)-C(2)	109.8(7)
Ni-P(2)-C(3)	110.6(5)	Ni-P(2)-C(3)	114.5(6)
C(13)-P(1)-C(2)	105.8(8)	C(13)-P(1)-Cl(1)	109.3(6)
C(33)-P(2)-C(3)	113.2(7)	C(11)-P(1)-C(2)	99.8(8)
C(3)-P(2)-C(4)	102.1(8)	C(33)-P(2)-C(3)	106.8(7)
C(12)-C(11)-C(17)	111.4(14)	C(12)-C(11)-C(16)	107.7(13)
C(11)-C(12)-C(13)	115.3(11)	C(16)-C(11)-C(17)	111.1(15)
C(12)-C(13)-C(14)	110.3(10)	P(1)-C(13)-C(12)	116.7(8)
C(13)-C(14)-C(15)	109.9(12)	P(1)-C(13)-C(14)	114.8(9)
C(15)-C(14)-C(18)	114.4(12)	C(13)-C(14)-C(18)	115.5(12)
C(15)-C(16)-C(11)	112.9(15)	C(14)-C(15)-C(16)	112.8(14)
C(14)-C(18)-C(20)	111.1(13)	C(14)-C(18)-C(19)	110.5(13)
C(32)-C(31)-C(36)	109.3(13)	C(19)-C(18)-C(20)	109.1(14)
C(36)-C(31)-C(37)	111.9(15)	C(32)-C(31)-C(37)	111.3(14)
C(32)-C(33)-C(34)	110.3(10)	C(31)-C(32)-C(33)	113.9(11)
C(34)-C(33)-C(35)	110.0(11)	P(2)-C(33)-C(32)	109.3(8)
C(33)-C(34)-C(38)	115.7(11)	P(2)-C(33)-C(34)	121.5(9)
C(34)-C(35)-C(36)	112.5(13)	C(35)-C(34)-C(38)	115.2(12)
C(34)-C(38)-C(39)	111.5(13)	C(35)-C(36)-C(31)	114.3(14)
C(39)-C(38)-C(40)	109.5(14)	C(34)-C(38)-C(40)	111.4(13)

(c) Short atomic contacts [l/Å] and angle [φ/°]

Ni···C(19)	3.431(21)	Ni···H(32B)[a]	2.54	P(2)-Ni-H(32B)[a]	71.1

a) Positional parameters of the H(32B) atom were calculated under the assumption that the C(sp^3)-H bond length is 1.08Å.

are intermediate between staggered and eclipsed conformations (Fig. 4). However, there is a significant difference in both conformations. The neomentyl group about the P(1)–C(13) bond is rotated by *ca.* 120° with respect to that about the P(2)–C(33) bond.

The steric hindrance between the neomenthyl and methyl groups on the phosphorus causes distortions of the P–C–C angles. The P(1)–C(13)–C(12), P(1)–C(13)–C(14), and P(2)–C(33)–C(34) angles, 116.7(8), 114.8(9), and 121.5(9)°, are considerably different from the normal value of 109.5°.

The C(19) and C(32) atoms are located in the vacant positions respectively above and below the nickel atom. An equatorial hydrogen atom, H(32B) attached to the C(32) atom has a short intramolecular atomic distance of 2.54 Å with the nickel atom. Although the position of this hydrogen atom is the calculated value, this short distance suggests the existence of a metal-hydrogen interaction in the present complex. Such short distances between metal and hydrogen atoms are also found in $[PdI_2\{(Me_2Ph)P\}_2]$ (Pd···H 2.84 and 2.85 Å (red isomer) and 3.28 Å (yellow isomer))[17] and $[PdI_2(Ph_3P)_2]$(Pd···H 3.18 Å).[18]

The bond lengths and bond angles of both the neomenthyl groups appear to be normal for the sp^3 carbon (C–C(av)=1.543 Å and C–C–C(av)=111.9°), except for the bond angles given above.

Figure 5 shows a stereoscopic drawing of the molecular packing along the b axis. No abnormally short intermolecular atomic distance is present.

The calculations were carried out on the NEAC 2200-500 computer at Osaka University.

This work was supported in part by a Grant-in-Aid for Scientific Research from the Ministry of Education (No. 843005), for which the authors express their grati-

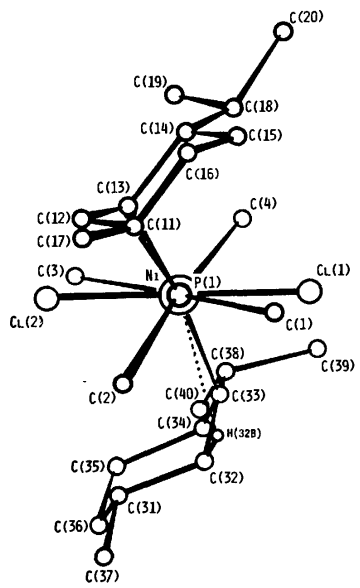

Fig. 3. The conformation about the P(1)–Ni–P(2) bond.

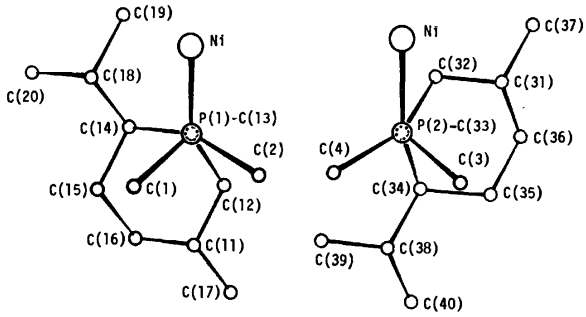

Fig. 4. The conformations about the P(1)–C(13) and P(2)–C(33) bonds.

tude. The authors express their deep thanks to Professor Makoto Kumada and his co-workers of Kyoto University for kindly providing the crystals and for many helpful discussions.

References

1) Y. Kiso, M. Kumada, K. Tamao, and M. Umeno, *J. Organomet. Chem.*, **50**, 297 (1973).
2) Y. Kiso, M. Kumada, K. Maeda, K. Sumitani, and K. Tamao, *J. Organomet. Chem.*, **50**, 311 (1973).
3) M. Kumada, K. Sumitani, Y. Kiso, and K. Tamao, *J. Organomet. Chem.*, **50**, 319 (1973).
4) Y. Kiso, K. Tamao, and M. Kumada, private communication.
5) T. Ashida, The Universal Crystallographic Computing System, Osaka. The Computation Center, Osaka University (1973), p. 55.
6) H. P. Hanson, F. Herman, J. D. Lea, and S. S. Skillman, *Acta Crystallogr.*, **17** 1040 (1964).
7) S. J. LaPlaca and J. A. Ibers, *Acta Crystallogr.*, **18**, 511 (1965).
8) A. E. Smith, *Inorg. Chem.*, **11**, 3017 (1972).
9) A. T. McPhail, J. C. H. Steele, Jr., and P. M. Gross, *J. Chem. Soc. Dalton*, **1972**, 2680.
10) W. S. Sheldrick and O. Stelzer, *J. Chem. Soc. Dalton*, **1972**, 926.
11) J. K. Stalick and J. A. Ibers, *Inorg. Chem.*, **9**, 453 (1970).
12) B. T. Kilbourn and H. M. Powell, *J. Chem. Soc., A*, **1970**, 1688.
13) J. H. Enemark, *Inorg. Chem.*, **10**, 1952 (1971).
14) G. R. Davis, R. H. B. Mais, and P. G. Owston, *J. Chem. Soc., A*, **1967**, 1750.
15) W. A. Safford, III, P. D. Carfagna, and E. L. Amma, *Inorg. Chem.*, **6**, 1553 (1967).
16) C. Krüger and Y. -H. Tsay, *Cryst. Struct. Commun.*, **3**, 455 (1974).
17) N. A. Bailey and R. Mason, *J. Chem. Soc., A*, **1968**, 2594.
18) T. Debaerdemaeker, A. Kutoglu, G. Schmid, and L. Weber, *Acta Crystallogr., Sect. B*, **29**, 1287 (1973).
19) C. K. Johnson, *ORTEP, Report ORNL-3794*, Oak Ridge National Laboratory, Tennesee, 1965.

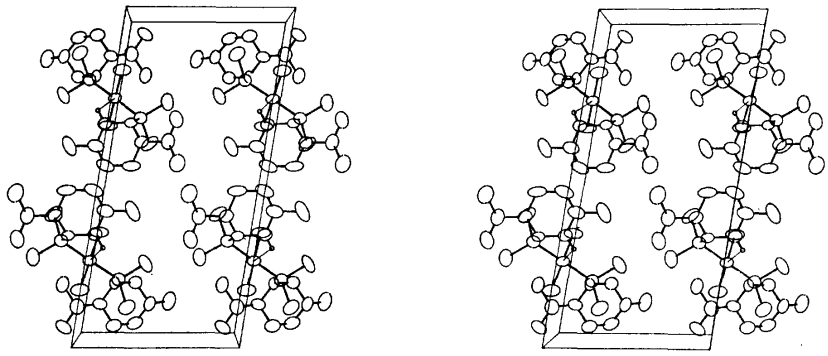

Fig. 5. A stereoscopic drawing[19] of the molecular packing viewed along the b axis.

Violet Emission Bands of the CN Radical Produced by Photodissociation of BrCN

Setsuko TATEMATSU, Tamotsu KONDOW, Toru NAKAGAWA, and Kozo KUCHITSU
Department of Chemistry, Faculty of Science, The University of Tokyo, Bunkyo-ku, Tokyo 113
(Received January 10, 1977)

The violet emission spectra of $CN(B^2\Sigma-X^2\Sigma)$, $\Delta v=0$, were observed by the photodissociation of BrCN by Lyman-α radiation (121.6 nm). The peak intensities for the vibrational levels $v'\geqq 1$ relative to $v'=0$ decreased with the BrCN pressure (up to 2 Torr), whereas at 0.1 Torr or lower the spectrum was essentially independent of the pressure. The relative vibrational populations ($v'=0$—10) and the effective rotational temperatures were estimated by a band-envelope analysis. The effective rotational temperature, estimated to be 2000±200 K for $v'=0$—4, was practically independent of the pressure. Within the low-pressure limit the distributions of the excess energy to vibration and rotation were estimated to be 0.50±0.08 and 0.17±0.02 eV, respectively.

The kinetic and internal energies contained in the fragments produced by dissociation of polyatomic molecules have been investigated by various methods. Wilson *et al.*[1,2] measured the translational energies of fragments by the time-of-flight technique applied to laser photodissociation of molecular beams. The internal excitation of fragments can be studied by emission spectroscopy. For instance, the rotational distribution of the $OH(A^2\Sigma)$ formed in the photodissociation of H_2O was measured by Carrington.[3]

The emission spectra of the $CN(B^2\Sigma)$ produced in the vacuum-ultraviolet photodissociation of cyanides were measured by Mele and Okabe,[4] by whom the vibrational and rotational distributions were reported. Their estimations could be only qualitative,[5] since their spectral resolution was only about 0.5 nm and since their light sources, mostly rare-gas resonance lines, were not monochromatic. Despite these limitations, they showed that the distributions of internal energies contained in $CN(B^2\Sigma)$ had a characteristic dependence on the cyanides from which they were formed. Their estimates of the energy distributions were often referred to as a basis for theoretical considerations on the dynamics of dissociative excitation.[6–8] Furthermore, the distributions appeared to be remarkably different from those of the $CN(B^2\Sigma)$ radicals formed from the same cyanides by impact of electrons[9] or metastable argon atoms[10,11] instead of photons. In order to supply more quantitative information in this regard, we have undertaken systematic measurements of the CN violet bands produced from various cyanides by Lyman-α radiation using higher resolution. The present report is concerned with the BrCN case measured at different sample pressures.

Experimental

The apparatus consists of a vacuum-ultraviolet source, a sample cell and a detection system (Fig. 1). The Lyman-α radiation was obtained by 2450 MHz microwave discharge in a 1:3 mixture of hydrogen and helium gases. This mixture, purified by a liquid-nitrogen trap filled with molecular sieve 13X, was introduced into a quartz discharge tubing (15 mm o.d.), and the light was admitted into the sample cell through a MgF_2 window of 1.0 mm thickness. The pyrex cell, o.d. about 40 mm and length 60 mm, was coated inside with graphite to reduce stray light. The sample gas was introduced through needle valves, the pressure being monitored during the observation with a Pirani gauge calibrated against a McLeod gauge.

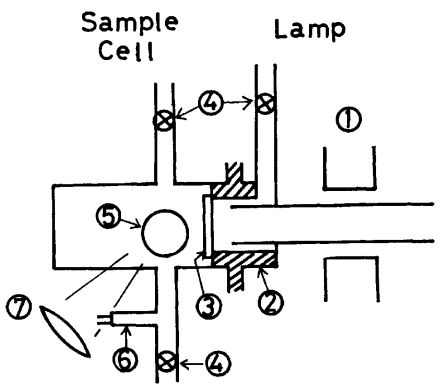

Fig. 1. A schematic design of the apparatus.
1) Microwave discharge, 2) water-jacket, 3) MgF_2 window, 4) needle valves, 5) quartz window, 6) Pirani gauge, 7) quartz lens.

Fluorescence from the emission region was detected in a direction perpendicular to the incoming photons. The emission was focussed through a Suprasil window (20 mm diameter) and a collimating lens into the entrance slit of Nikon P-250 grating monochromator (1200 Gr/mm). The slit width was adjusted in the range between 10—60 μm. The slit width of 50 μm corresponds to an energy resolution of 0.2 nm. The signal from a photomultiplier (HTV R585) was measured by a photon counting system. The relative intensity response of the spectrometer and the detection system was calibrated by a halogen standard lamp (JC 12V-50W of Ushio Electric Co.), the color temperature of which was determined at the Electrotechnical Laboratory.

A commercial sample of BrCN (Nakarai Chemical, Co.) was purified by vacuum distillation. The IR spectrum showed no evidence of impurities. The emission spectra were observed at BrCN pressures ranging from about 0.01 to 2 Torr.

The reproducibility of the observed spectra depends mainly on the stability of the light source and the sample pressure, which was kept constant by needle valves during the observation. Though the intensity of the lamp was not monitored during the spectral measurement, its stability was tested by recording the emission intensity at a fixed wavelength over the time interval needed for scanning the whole spectral region. Moreover, a check of reproducibility of the intensity signal was made immediately before and after each measurement. From these tests, the total error in the observed spectrum, including the random errors caused by the instability of the light source, the sample pressure and the detection system, was estimated to be less than 10% of the

highest peak.

Results and Analysis

Observed Spectra. The $\Delta v=0$ series of the CN violet band ($B^2\Sigma-X^2\Sigma$) observed around 388 nm (Fig. 2) was assigned according to the table prepared by Pearce and Gaydon.[12] Though the sequences of $\Delta v=0$ and $\Delta v=-1$ of the violet system were observed, the former was used in the analysis, because the intensity of the latter was not strong enough. The $v'=0$ peak is the strongest and the intensities of the $1\leqq v'\leqq 4$ peaks decrease with v'. Bands of the $5\leqq v'\leqq 10$ levels are overlapped by those of the lower levels, and the $v'\geqq 11$ bands, which should appear above 391 nm, are not detectable.

The observed dependence of the spectrum on the BrCN pressure is shown in Fig. 3. Below about 0.1 Torr the spectrum is nearly independent of the sample pressure, but at a higher pressure the peak intensities for $v'\geqq 1$ relative to $v'=0$ decrease with the pressure, until at about 2 Torr they are almost completely obscured by the R-branch tail of the (0,0) band. On the other hand, there is no observable effect of pressure on the band shapes, particularly as regards the peak (the P-branch head) of the (0,0) band.

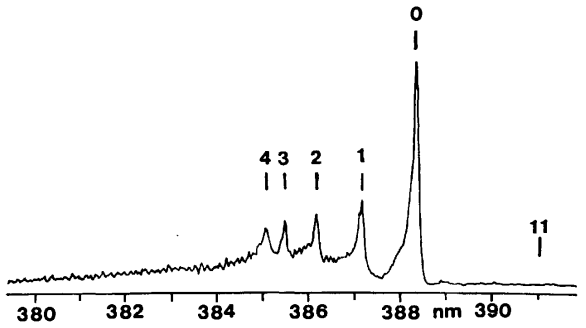

Fig. 2. Emission spectra of the CN($B^2\Sigma-X^2\Sigma$), $\Delta v=0$ band from BrCN taken with a slit width of 10 μm. The numbers indicate positions of the P-branch heads for the $v'=0$—4 and 11 bands.

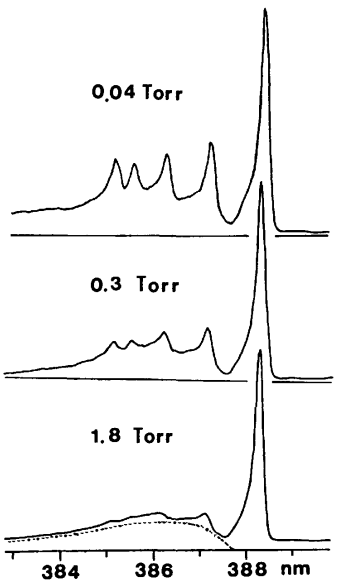

Fig. 3. Emission spectra of the CN($B^2\Sigma-X^2\Sigma$), $\Delta v=0$ band produced by the photodissociation of BrCN taken at different sample pressures with a slit width of 40 μm.
The broken line represents the background contribution from the R-branch contour of the (0, 0) band calculated at $T_r=2000$ K.

Band-Envelope Analysis. The relative vibrational populations were estimated by a band-envelope simulation using a MELCOM 7000 computer in the Educational Computer Center of the University of Tokyo.

The relative intensity (the number of photons) of a transition from the (v',N') level to the (v'',N'') level can be expressed[13] by

$$I(v',N'-v'',N'')\propto\frac{P_{v'}}{Q_{r,v'}}\cdot\nu^3\cdot q_{v',v''}\cdot S_{N',N''}\cdot R_{v'}(N') \quad (1)$$

where v and N are the vibrational and rotational quantum numbers, respectively, ν is the transition frequency, $P_{v'}$ is the population, $q_{v',v''}$ is the Franck-Condon factor, $S_{N',N''}$ is the rotational line strength, and $R_{v'}(N')$ is the rotational distribution function. The rotational state sum, $Q_{r,v'}$, is given by

$$Q_{r,v'}=\sum_{N'} g_{N'}R_{v'}(N') \quad (2)$$

where $g_{N'}$ represents degeneracy. If the rotational distribution is described by a Boltzmann function, then $R_{v'}(N')$ is given by

$$R_{v'}(N')=\exp\{-hcB_{v'}N'(N'+1)/kT_r(v')\} \quad (3)$$

where $T_r(v')$ is an effective rotational temperature for the vibrational state v'.

The band envelope was obtained from $I(v',N'-v'',N'')$ by use of the experimental parameters of the band origin ν_0,[14,15] $B_{v'}$,[14,15] and $q_{v',v''}$.[16] A Gaussian slit function, which was estimated from the observed shape of the Hg 404.7 nm line measured under similar experimental conditions, was taken into account. The

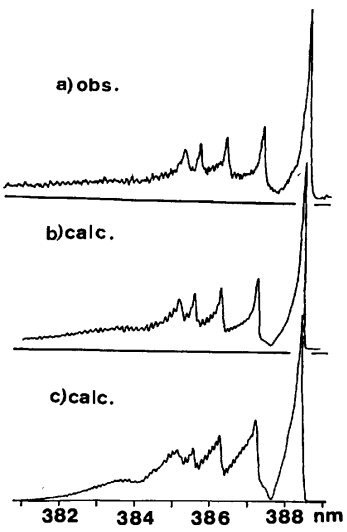

Fig. 4. Comparison of the calculated band envelopes of the CN violet $\Delta v=0$ bands with the observed spectrum produced by the photodissocation of BrCN.
a) Observed at 0.03 Torr, b) calculated with $T_r(v'=0$—$10)=2000$ K; best-fit, c) calculated with $T_r(v'=0$—$10)=1000$ K.

parameters, $N_{v'}$ and $T_r(v')$, were adjusted in such a way that the calculated band envelope fits the observed spectrum. A typical comparison of the observed and calculated band envelopes is shown in Fig. 4.

It was possible to estimate the effective rotational temperatures for $v'=0$—4 independently from their individual band shapes. The values turned out to be essentially equal, 2000±200 K. On the other hand, the band shapes were insensitive to the assumed values of $T_r(v')$ for $v'=5$—10. The effective temperatures were therefore assumed to be all equal, 2000 K.

The relative vibrational populations of CN($B^2\Sigma$) thus estimated are plotted in Fig. 5 for the different sample pressures. The population for $v'=11$ level, which has a negligible intensity, is assumed to be zero, and those for the levels $v'=5-10$ are estimated by a smooth interpolation. Since the vibrational populations estimated for pressures lower than 0.1 Torr are essentially unchanged, they are assumed to be the initial populations unaffected by collisional relaxation

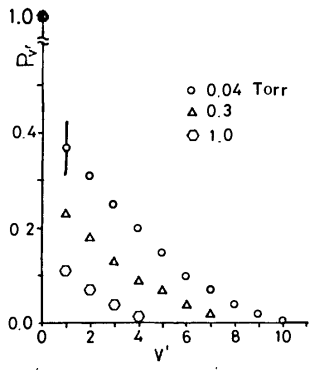

Fig. 5. Pressure dependence of the relative vibrational populations, $P_{v'}/P_0$, of CN($B^2\Sigma$) produced by the photodissociation of BrCN. Estimated from the analysis of the spectra at different sample pressures. A bar indicates estimated limit of uncertainties.

TABLE 1. RELATIVE VIBRATIONAL POPULATIONS ($P_{v'}/P_0$) AND THE EFFECTIVE ROTATIONAL TEMPERATURES OF CN($B^2\Sigma$) PRODUCED BY THE PHOTODISSOCIATION OF BrCN

v'	$P_{v'}/P_0$	$E_{v'}$/eV[a]	$T_r(v')$/K
0	1.00	0.0000	2000±200
1	0.37(6)[b]	0.2633	2000±200
2	0.31(6)	0.5216	2000±200
3	0.25(6)	0.7746	2000±200
4	0.20(6)	1.0221	2000±200
5	0.15[c]	1.2636	
6	0.10	1.4989	
7	0.07	1.7276	2000[c,d]
8	0.04	1.9492	
9	0.02	2.1634	
10	≦0.01	2.3699	

a) Vibrational energies taken from Ref. 17 (above zero-point energy). b) Uncertainties represent estimated limits of error in the last significant digits. c) The $P_{v'}/P_0$ and $T_r(v')$ values for $v'=5$—10 are only rough estimates. d) The effective rotational temperatures for $v'=5$—10 are assumed to be equal.

(see Discussion), as listed in Table 1.

The uncertainties in $P_{v'}$ and $T_r(v')$ estimated in Table 1 originate mainly from the limitation in recording the spectrum, the overlapping of bands, and the approximations made in the analysis. Since the $5\leqq v'\leqq 10$ bands are buried within those of the lower vibrational levels, the estimated values of $P_{v'}$ and $T_r(v')$ for $v'=5$—10 are less reliable than those for $v'=0$—4. In addition, a strong correlation is found between the vibrational population and the rotational temperature for each of the $v'\geqq 5$ bands. For these reasons, the above estimates of $P_{v'}$ and $T_r(v')$ for the $v'\geqq 5$ simply represent one of the most probable sets of the parameters for which calculated envelope agrees well with the observed spectrum. However, the values of $P_{v'}$ and $T_r(v')$ for the $v'=0$—4 bands can be estimated independently, since each of the $v'=0$—4 bands forms a distinct head peak.

Discussion

Internal Energy Distribution. The average energy distributed to the vibration of CN($B^2\Sigma$) is estimated as a sum of the vibrational energies[17] multiplied by the estimated populations to be 0.50±0.08 eV above the zero-point energy. Since the effective rotational temperature is estimated to be 2000±200 K, the average rotational energy is 0.17±0.02 eV. Therefore, the rotational excitation, about one third of the vibrational excitation, is much lower than that of OH($A^2\Sigma$) formed by the photodissociation of H_2O.[3]

Energetically possible processes producing CN($B^2\Sigma$) from BrCN by Lyman-α radiation (10.20 eV) are the following:

$$BrCN + h\nu \rightarrow Br(^2P_{3/2}) + CN(B^2\Sigma) \quad (v'\leqq 14) \quad (1)$$

$$\rightarrow Br(^2P_{1/2}) + CN(B^2\Sigma) \quad (v'\leqq 12) \quad (2)$$

The threshold of process (1) was estimated by Davis and Okabe[18] to be 6.97 eV. They reported that process (2) was insignificant, because they observed no apparent inflection in the excitation curve of CN($B^2\Sigma$) near the threshold of process (2), 7.43 eV. If the $Br(^2P_{3/2})$ atom is produced, then the available excess energy distributed to the fragments is 3.23 eV. Thus the average kinetic energy is estimeted to be *ca.* 2.56 eV. From the conservation of momenta, the CN radical has an average kinetic energy of *ca.* 1.9 eV.

Comparison with Other Experiments. The CN($B^2\Sigma$) states formed from cyanides exited by photons (10.2 eV), electrons (≈300 eV) and metastable argon atoms (11.5 and 11.7 eV) have distinctly different vibrational populations, as illustrated in Fig. 6. The intensity enhancements in higher vibrational levels ($v'\geqq 11$) observed in the case of metastable-atom impact[9] are interpreted as a result of the rotational perturbation between the A and B states. In the electron-impact case,[10,11] lower vibrational levels have larger relative populations than in the metastable-atom impact case. In contrast with either case, photodissociation gives a monotonically decreasing curve. Photodissociation by Lyman-α radiation can excite the CN($B^2\Sigma$) radical up to $v'=14$. However, only a small fraction of the available energy goes into vibrational excitation so that

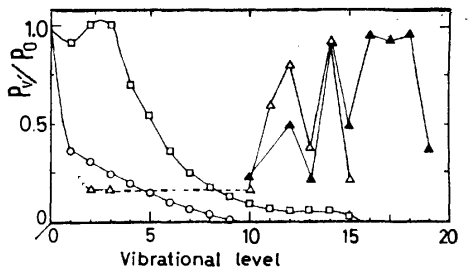

Fig. 6. Relative vibrational populations, $P_{v'}/P_0$, of the CN($B^2\Sigma$) radicals produced from BrCN by photodissociation (○), electron impact (□ for Ref. 9) and impact of metastable argon ($^3P_{0,2}$) atoms (▲ for Ref. 10 and △ for Ref. 11).

no detectable populations in the $v' \geqq 11$ levels are observed, and overall vibrational excitation is very much weaker than in the electron-impact case.

Effect of Collisions. From the following argument, the present estimates can be regarded as "initial" energy distributions since the values relate to a pressure region where any energy transfer processes induced by collision may be disregarded.

The spontaneous radiative lifetime of CN($B^2\Sigma$) is reported to be 60—85 ns by measurements of a decay curve[19,20] or phase shifts.[21,22] The cross section for electronic quenching was estimated by Luk and Bersohn[20] to be 19.4 Å^2 as a lower limit calculated from a measurement of the electronic quenching rate of BrCN. If one assumes that excited CN radicals have average translational energy of 1.9 eV, the mean time between collisions of CN($B^2\Sigma$) with BrCN is estimated to be about 60 ns when the sample pressure is about 0.7 Torr, which is comparable with the radiative lifetime of CN($B^2\Sigma$). This pressure is much higher than that used in the present study from which the energy distribution was determined. In other words, in the pressure region of the present measurements electronic quenching is probably negligible. Furthermore, the vibrational and rotational distributions have been estimated at a low-pressure limit, where no pressure-dependence was observed. Therefore, the distribution seems to be free from the effect of collisions.

Pressure Dependence. The relative vibrational populations depend strongly on the BrCN pressure when it is higher than 0.1 Torr. In particular, the emission spectrum is essentially that of the (0,0) band (Fig. 3) when the BrCN pressure is higher than about 0.8 Torr. Possible processes causing the vibrational relaxation are the following: 1) The vibrational energy of CN($B^2\Sigma$) is transmitted to the translational and/or vibrational energy (possibly the ν_3 mode) of BrCN. In the latter case, the deficiency of the energy ranging from 75 cm^{-1} (from $v'=1$ to $v'=0$) to 250 cm^{-1} (from $v'=5$ to $v'=4$) has to be supplied by the translational energy of the CN radical. 2) The rates of collision-induced transitions (B-X) for higher vibrational levels may be much larger than those for lower levels. However, no further experimental evidence for any of these processes has yet been provided.

On the other hand, the effective rotational temperature of the (0,0) band, *ca.* 2000 K, seems to be essentially independent of the sample pressure up to 2 Torr. Therefore, the pressure effect seems to appear only in the vibration and not in the rotation in the pressure region of the present study (from 0.01 to 2 Torr). However, such a trend has not been observed for any other cyanides studied so far,[23] namely, HCN, DCN, ICN and $(CN)_2$.

The authors are grateful to Professor Ikuzo Tanaka and the members of his laboratory of Tokyo Institute of Technology and to Dr. Hideo Okabe of U.S. National Bureau of Standards for their helpful advice.

References

1) K. R. Wilson, *Discuss. Faraday Soc.*, **44**, 234 (1967).
2) J. H. Ling and K. R. Wilson, *J. Chem. Phys.*, **63**, 101 (1975).
3) T. Carrington, *J. Chem. Phys.*, **41**, 2012 (1964).
4) A. Mele and H. Okabe, *J. Chem. Phys.*, **51**, 4798(1969).
5) H. Okabe, private communication, October 1976.
6) M. J. Berry, *Chem. Phys. Lett.*, **29**, 323, 329 (1974).
7) Y. B. Band and K. F. Freed, *J. Chem. Phys.*, **63**, 3382, 4479 (1975).
8) J. P. Simons and P. W. Tasker, *Mol. Phys.*, **27**, 1961 (1974).
9) I. Tokue, T. Urisu, and K. Kuchitsu, *J. Photochem.*, **3**, 273 (1974/75).
10) J. A. Coxon, D. W. Setser, and W. H. Duewer, *J. Chem. Phys.*, **58**, 2244 (1973).
11) T. Urisu and K. Kuchitsu, *J. Photochem.*, **2**, 409 (1973/74).
12) R. W. B. Pearce and A. G. Gaydon, "The Identification of Molecular Spectra," John Wiley & Sons, Inc., New York (1963).
13) G. Herzberg, "Molecular Spectra and Molecular Structure I. Spectra of Diatomic Molecules," Van Nostrand, Princeton (1950).
14) R. Engleman, Jr., *J. Mol. Spectrosc.*, **49**, 106 (1974).
15) L. Wallace, *Astrophys. J. Suppl.*, **7**, 165 (1962).
16) R. J. Spindler, *J. Quant. Spectrosc. Radiat. Transfer*, **5**, 165 (1965).
17) R. J. Fallon, J. T. Vanderslice, and R. D. Cloney, *J. Chem. Phys.*, **37**, 1097 (1962).
18) D. D. Davis and H. Okabe, *J. Chem. Phys.*, **49**, 5526 (1968).
19) R. G. Bennet and F. W. Dalby, *J. Chem. Phys.* **36**, 399 (1962).
20) C. K. Luk and R. Bersohn, *J. Chem. Phys.*, **58**, 2153 (1973).
21) J. H. Moore, Jr. and D. W. Robinson, *J. Chem. Phys.*, **48**, 4870 (1968).
22) H. S. Liszt and J. E. Hesser, *Astrophys. J.*, **159**, 1101 (1970).
23) S. Tatematsu and K. Kuchitsu, unpublished data.

2-Mercaptobenzothiazole Supported on Silica Gel for the Chromatographic Concentration of Cadmium, Copper, Lead, and Zinc in Natural Water Samples

Kikuo TERADA, Akihiko INOUE, Junko INAMURA, and Toshiyasu KIBA

Department of Chemistry, Faculty of Science, Kanazawa University, Kanazawa, Ishikawa 920

(Received August 2, 1976)

The preparation and characteristics of 2-mercaptobenzothiazole supported on silica gel (MBT–SG), and its application to the preconcentration and determination of cadmium, copper, lead, and zinc in natural water samples are described. The MBT–SG was prepared by impregnating silica gel with MBT in a dioxane–methyl acetate solvent mixture, drying, washing with deionized water, and finally drying. The chelating capacity of the material was 0.01 meq. Cu/g. Cadmium, copper, lead, and zinc were quantitatively retained on the MBT–SG at pH values of 4.8, 2.5, 4.8, and 6.5 for an aqueous solution, and at pH values of 4.8, 2.8, 4.8, and 6.5 for sea water. A column made of the material provided quantitative recovery of these metals from natural water samples at higher flow rates (2—5 l/h) than other chelating resins, *e. g.*, chelex 100. Cadmium was eluted with hydrochloric acid (1 : 99), copper and lead with acetone–hydrochloric acid mixture (9 : 1), and zinc with an acetate–hydrochloric acid buffer solution (pH 4.0). Then, the quantities of the four metals in their effluents were determined by atomic absorption spectrometry.

Because of their low concentration in natural water, including sea water, heavy metals often require preliminary concentration prior to the determination of their quantities. Recently, chelating resins have been conveniently used for this purpose by many investigators[1–3] in a manner originally described by Riley and Taylor.[1] Dingman *et al.*[4] prepared some new polyamine–polyurea resins and used them to concentrate several heavy metals from dilute solutions. They found that, among these resins, TEPA (tetraethylenepentamine polymerized with methylphenylene diisocyanate) is the most effective for this purpose when the resin is used in the column mode of operation with concentration factors as high as 1000. On the other hand, Mussarelli *et al.*[5–9] have used chitosan, a natural chelating polymer, to collect traces of transition metals from salt solutions and sea water using column chromatography. Since this natural polymer does not appreciably react with sodium and magnesium, it is useful for the separation of small amounts of transition metals from sodium and magnesium matrices. These methods are thought to be simpler and less time-consuming than solvent extraction[10] or the precipitation method. However, if a large volume of natural water must be treated, these resins cannot withstand the rapid flow of the sample water through the column.

Previously, Terada *et al.*[11] revealed the excellent ion-exchange properties of some inorganic exchangers supported on silica gel, *e.g.* KCFC–, NCFC–, and AMP–SiO_2, and applied them to the concentration of Cs-137 in natural water. Most inorganic exchangers appear to have been used preferentially for the concentration of alkali metals and some univalent metals such as silver and thallium *etc.*, but rarely for that of the transition metals.[12,13]

2-Mercaptobenzothiazole has been used as a precipitant for several metals, especially copper, gold, and lead to form sparingly soluble chelates in neutral solutions, and also as an extractant for solvent extraction of these metals. This reagent itself is insoluble in water, but soluble in ethanol, benzene, dioxane, and other organic solvents. This reagent will be used for the selective preconcentration of copper and some other transition metals in a large volume of natural water as previously described.[11]

The present paper describes a simple method for preparing such material, called 2-mercaptobenzothiazole–silica gel (MBT–SG), and its successful application to natural water concentration, especially for sea water, in the monitoring of the environmental pollution resulting from some heavy metals.

Experimental

Reagents. The 2-mercaptobenzothiazole, dioxane, methyl acetate, acetone, ethanol used were of analytical reagent grade.

A standard solution of metals was prepared as follows: copper metal was dissolved in nitric acid plus sulfuric acid, recrystallized lead nitrate was dissolved in nitric acid (1:100), zinc metal was dissolved in concd hydrochloric acid, nickel sulfate and cobalt sulfate were dissolved in deionized water, and chromium metal was dissolved in concd hydrochloric acid. Each stock solution was made up to contain the metal of interest at a concentration of 1000 ppm.

Silica gel of chromatographic grade (WAKOGEL C-100) was sieved in the range of 60—80 mesh and digested with a double volume of hydrochloric acid (1 : 1) for one day and then washed with deionized water until no chloride appeared in the washings. The cleaned silica gel was dried at 110 °C for one day.

Apparatus. A Perkin-Elmer 303-type atomic absorption spectrophotometer, Hitachi-Horiba M-5 type glass-electrode pH meter.

An Iwaki Model VS electric shaker.

A Toyo Type E-E SF200A fraction collector.

The chromatographic column was a glass tube of 9.8 and 20 mm inside diameters 140 mm in length with a coarse sintered-glass disc and a stop-cock at the bottom.

Preparation of 2-Mercaptobenzothiazole–Silica Gel (MBT–SG). About 70 g of silica gel (60—80 mesh) were put into a solution of 2-mercaptobenzothiazole in 100 ml of a dioxane–methyl acetate mixture (4 : 1 v/v) and stirred occasionally. After standing for about 20 h the supernatant was sucked out and the remaining silica gel impregnated with the reagent was then heated at about 80 °C at reduced pressure for about 20 h. The dried materials were washed repeatedly with deionized water to remove any nonadsorbed reagent until the washings appeared clear. Finally, the product was dried

at about 80 °C under reduced pressure for about 20 h. The product was sieved (60—80 mesh) using a nylon sieve and stored in a darkened bottle.

Procedure for Batch Experiments. Into a 50-ml centrifuge tube, 10 ml of a metal solution (5 ppm), 5 ml of a buffer solution and 0.5 g of MBT-SG were mixed together. The contents were then agitated with an electric shaker for 30 min at room temperature. The supernatant was filtered through a millipore filter into a 20-ml measuring flask and adjusted to the desired volume. The metal concentration was measured with an atomic absorption spectrophotometer and then the percent retention was calculated.

Chelating Column Preparation. The chromatographic tube (20 mm in diameter) was filled with 10 g of dried MBT-SG, and a piece of glass wool was placed on the top of the column so that the bed was not disturbed during sample passage. In this case, the bed length became about 7 cm.

Procedure for Column Method. A given volume of an aqueous sample containing individual metal ions was adjusted to a suitable pH, then percolated through the column at a flow rate of 2—5 l/h under the suction of an aspirator. The lower level of the sample solution was maintained about 1 cm above the surface of the column bed during sample passage. After washing the column with about 20 ml of deionized water, an eluting solution of definite composition was passed through at a flow rate of about 1 ml/min. The effluent was collected in a measuring flask, diluted to the desired volume, and the metal concentration was determined with an atomic absorption spectrophotometer.

Results and Discussion

Characteristics of the Chelating Material. The amount of 2-mercaptobenzothiazole on the silica gel was determined as follows. One gram of the dried material was put onto the column tube. Then about 20 ml of ethanol was passed through to completely remove the reagent from the column. The effluent was collected in a 50-ml measuring flask and diluted to the desired volume with ethanol. Two milliliters of the solution were pipetted out and put into another 50-ml measuring flask and diluted to the desired volume with ethanol. The absorbance of the solution was measured at a wavelength of 327 nm using ethanol as a reference. The absorption spectra of the effluent and the ethanol solution of the reagent are shown in Fig. 1. Both absorption curves have identical absorption peaks at 239 and 327 nm. This fact suggests that the reagent was retained without any loss. The amount of reagent supported on the silica gel was found using the conventional working curve method to be about 11±1 mg per g of the material.

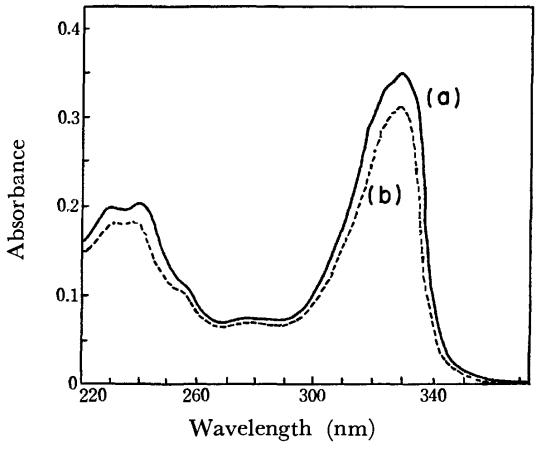

Fig. 1. Absorption spectra of 2-mercaptobenzothiazole.
(a) MBT dissolved in ethyl alcohol, (b) MBT in the effluent.

The chelating capacity for copper was measured by the batch method. Ten milliliters of the copper solution (50 ppm), 5 ml of a buffer solution (pH 4.0), and 0.5 g of MBT-SG were mixed together in a 50-ml centrifuge tube. The contents were then agitated for 30 min at room temperature. The copper concentration in the supernatant was measured with an atomic absorption spectrophotometer. The capacity was calculated to be about 0.01 meq. Cu(II)/g of MBT-SG. The chelating capacity of the material appeared to be large enough to collect copper from a large volume (*e. g.* 10 l) of sea water which is believed to contain as low as 1—20 μg copper per liter,[14] 10 g of the material has an operating capacity at least 32 times greater than the total amount of copper in 10 l of sea water (200 μg).

This solid chelating material also showed no change in its adsorbability after a storage period of about one month and was then dipped in a solution over the range from pH 1 to 10.

Recovery of Cadmium, Copper, Lead, and Zinc at Various pH Values. The recovery of each individual metal ion was examined by the batch method, using a 10 ml sample solution with a 5 ppm concentration of each metal and 0.5 g of MBT-SG, for a pure aqueous solution and for sea water of various pH values. The pH of the solution was adjusted using the following buffer solutions: sodium acetate plus hydrochloric acid for pH 1—5, potassium dihydrogen phosphate plus sodium hydroxide for pH 6—7, and boric acid plus potassium chloride and sodium hydroxide for pH 8—10. The results are illustrated in Fig. 2 along with those obtained using only silica gel. The pH value mentioned is that measured after equilibration. Copper was found to be retained quantitatively on the material at pH 2.5 for aqueous solutions and at pH 2.8 for sea water, but when untreated pure silica gel was put into an aqueous solution copper began to be adsorbed when the pH increased above 6. However, in the case of sea water only a recovery rate of 25% (the maximum value) was obtained at pH values of 7 or above. Cadmium and lead showed similar behavior on MBT-SG, and their quantitative retention values were obtained for pH 4.8—5.2 in both aqueous solutions and sea water. A remarkable difference in adsorbability was observed between MBT-SG and untreated silica gel. On the other hand, zinc ions showed similar adsorption rates for both MBT-SG and untreated silica gel and quantitative retention was obtained at pH 6.5 for both aqueous solutions and sea water. However, in column experiments, a reduction of about ten percent in the adsorption for zinc was observed when 5 l of an aqueous solution containing 2 ppb of zinc was passed through the untreated silica gel column at a flow rate of 4 l/h, although it was quantitative for the MBT-SG column.

From these results, the separation of copper from

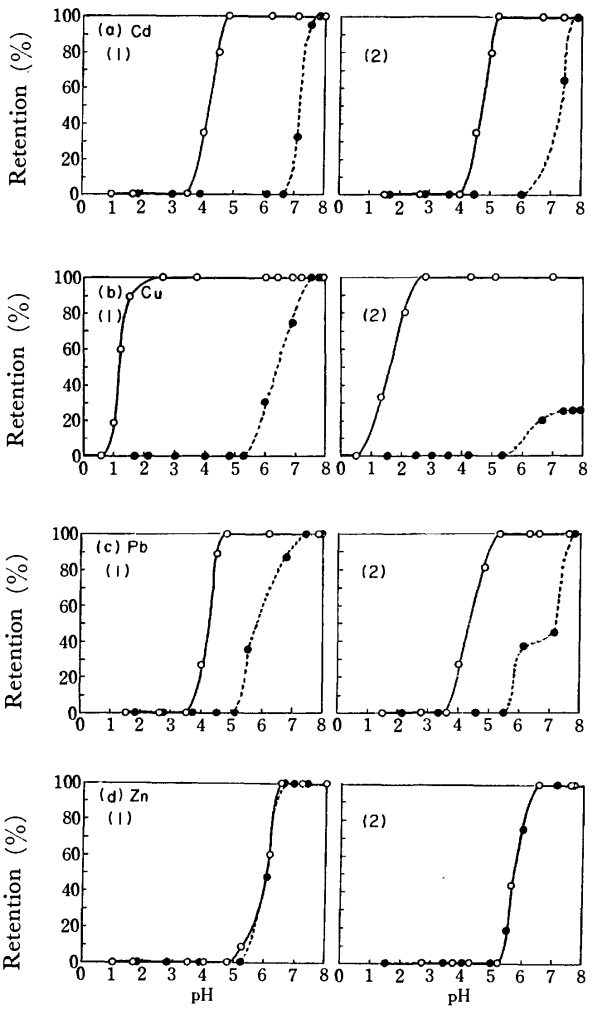

Fig. 2. Effect of pH on retention of (a) cadmium, (b) copper, (c) lead, and (d) zinc.
(1): Pure aqueous solution, (2): sea-water.
—○— MBT-SG, --●-- untreated silica gel.

lead and cadmium, and lead and cadmium from zinc will be possible with eluting solutions of different pH values with column operation.

Retention of Individual Ions on the Column. To examine quantitatively the retention of each metal ion on a column, several kinds of test solutions (an aqueous solution, a sodium chloride solution of ionic strength 0.63, and sea water) containing metals in various concentrations were passed through the column at different flow rates. In the experiment, copper(II) at pH 4.0, lead(II) at pH 5.0, and cadmium(II) and zinc(II) at pH 7.0 were individually fed onto a column (20 mm in dia. ×70 mm) of MBT-SG. After washing the column with about 20 ml of deionized water, cadmium was eluted with hydrochloric acid (1 : 99) and zinc with a buffer solution at pH 4.0 (sodium acetate–hydrochloric acid). Copper and lead adhered tightly to the column, and therefore, the following treatment was necessary to remove them quantitatively. Water held on the column had to be removed as much as possible by sucking under aspiration, then 20 ml of ethanol was run through to remove any untreated reagent, then copper and lead were eluted with 20 ml of a solvent mixture of acetone and hydrochloric acid (9 : 1 v/v). Each effluent was adjusted to be exactly 25 ml in a measuring flask and subjected to atomic absorption spectrometry for the determination of the quantities of the various metals.

Table 1. Recovery of metal ions using the column method

Ion	Vol. of sample (l)	Flow rate (l/h)	Concn of metal (ppb)	Recovery (%)
Cd(II)	1.0	2.3	100	100±2
	1.0	4.0	10	100±2
	5.0	4.2	1	100±2
	1.0	2.7	0.1	100±2
Cu(II)	1.0	3.7	100	100±2
	5.0	5.0	1	100±2
	5.0[a]	5.0	1	100±2
Cb(II)	1.0	3.0	100	100±2
	5.0	2.5	1	100±2
	5.0[a]	2.5	1	100±2
Zn(II)	1.0	3.0	100	100±2
	5.0	5.0	1	100±2
	5.0[b]	4.1	5	100±2

Pure aqueous solution at adjusted pH 4.0 (Cu), 5.0 (Pb) and 7.0 (Cd and Zn).
a) NaCl solution, μ=0.63. b) Sea water. MBT-SG: 10 g, column: 20 mm in dia.×70 mm.

The separation data in Table 1 show that quantitative retention was obtained for cadmium in the 0.1—100 ppb range, and for copper, lead, and zinc below in the range from 1—100 ppb at flow rates from 2.3 to 5.0 l/h. Thus, preconcentration of each metal from 5 l of sample water was attainable within 1 h.

Elution of Each Metal. Zinc(II) was found to be eluted from the column with 20—25 ml of a buffer solution which contained 20 ml of 1 M sodium acetate and 16 ml of 1 M hydrochloric acid per liter (pH 4.0), while lead and copper were not released from the column at all; consequently, separation of lead and copper from zinc was achieved. However, part of the cadmium was released by passing this buffer solution through the column. Both cadmium and zinc were completely eluted with nitric acid (1 : 99) or hydrochloric acid (1 : 99), with the latter eluting solution being more favorable for the subsequent atomic absorption spectrometric determination of the cadmium content. However, in this case, 30—38% of the retained amount of lead was also released using 25 ml of either of the above acids while no copper appeared in the eluate.

Effect of Various Ions and Substances on the Adsorption of Cadmium, Copper, Lead, and Zinc. The various metal ions thought to react with MBT, cobalt(II), iron(III), and nickel(II) were examined for their effects on this separating procedure. One liter of a test solution containing cadmium, copper, lead, and zinc in concentrations of 5 ppm, as well as one of other ions in the concentration range of 0.1—10 ppm was prepared. This solution was passed through a column containing 7 g of MBT-SG at flow rate of 2—5 l/h. At the same time, the mutual separation of the four ions of interest was also

Table 2. Effect of various ions on the recovery of metal ions

Ion	Concn (ppm)	Recovery (%)[a]			
		Cd(II)	Cu(II)	Pb(II)	Zn(II)
Cd(II)	10	—	93	34	3
	1	—	≈100	≈100	≈100
Co(II)	10	≈100	59	52	≈100
	1	≈100	≈100	93	≈100
Cu(II)	5	33	—	32	≈100
	1	≈100	—	≈100	≈100
Fe(III)	1	27	53	3	3
	0.1	≈100	93	≈100	97
Ni(II)	10	≈100	39	2	≈100
	1	≈100	91	91	≈100
Pb(II)	10	37	48	—	10
	1	≈100	≈100	—	≈100
Zn(II)	10	39	19	34	—
	1	≈100	72	≈100	—

a) Metal: 0.05 ppm, MBT-SG: 7 g, column: 20 mm in dia. × 50 mm.

Table 3. Effect of various substances on the recovery of metal ions

Substance	Concn (mol/l)	Recovery (%)			
		Cd(II)	Cu(II)	Pb(II)	Zn(II)
EDTA	10^{-5}	0	7	0	5
	10^{-6}	0	≈100	4	57
	10^{-7}	65	≈100	≈100	≈100
Citric acid	10^{-4}	89	53	46	6
	10^{-5}	≈100	≈100	100	92
Tartaric acid	10^{-4}	89	48	32	13
	10^{-5}	≈100	89	≈100	93
	10^{-6}	≈100	≈100	≈100	≈100

Metal: 0.05 ppm, MBT-SG: 7 g, column: 20 mm in dia. × 50 mm.

examined in varying concentrations. The results are given in Tables 2 and 3. At the 1 ppm level, iron(III) significantly reduced the recovery of the other four metal ions. Since iron(III) itself was found to be retained quantitatively on the both MBT-SG and on untreated silica gel at pH 7, it is not expected that iron competed with copper, cadmium, and lead on MBT. In fact, in the first solutions passed, which originally contained microgram amounts of each metal and 1 ppm of iron(III), no copper, cadmium, lead, and zinc at all were found. Therefore, iron appears to be adsorbed on the column as a hydroxide, retaining some of these metals with it and not liberating them on elution. Nickel(II) at the 1 ppm level produced a slight reduction in the recovery of copper and lead, and also zinc and cobalt at the same concentration produced the same effect for copper and lead, respectively. In general, 1 l of sea water contains about 0.3×10^{-3} meq. of heavy metal ions in all which is compatible with 0.03 g of MBT-SG. Therefore, the interference of heavy metal ions on the adsorption of these four metal ions from sea water may be practically neglected. On the other hand, some organic compounds, such as EDTA, citric acid, and tartaric acid, substantially hindered the adsorption of the metal ions. Particularly, EDTA considerably lowered adsorbability on MBT-SG of cadmium, lead, and zinc at a concentration of 10^{-6} mol EDTA/l. However, since in natural water, especially in sea water, these organic substances are never found in the concentrations shown in Table 3, the interference produced by these substances may be neglected.

Atomic Absorption Measurements for Copper and Lead. To determine the optimum conditions for atomic absorption measurements of copper and lead in an acetone–hydrochloric acid solvent mixture, the effects of acid and reagent concentrations and the mixing ratio of air and fuel were examined.

The effect of the hydrochloric acid concentration in acetone on the absorption of copper is shown in Fig. 3, from which it is seen that the smaller the absorbance, the higher the acid concentration. The solvent mixture used in the present experiments is considered to have no effect on the absorbance of copper. For lead, similar results were obtained. As shown in Fig. 4, the concentration of the MBT reagent in acetone had no significant effect on the absorption measurements under these conditions. Since the effluent became turbid when free MBT remained in it, excessive reagent was removed from the column by passing ethanol prior to the elution of the metal–MBT complexes with an acetone–hydrochloric acid solvent mixture. After several

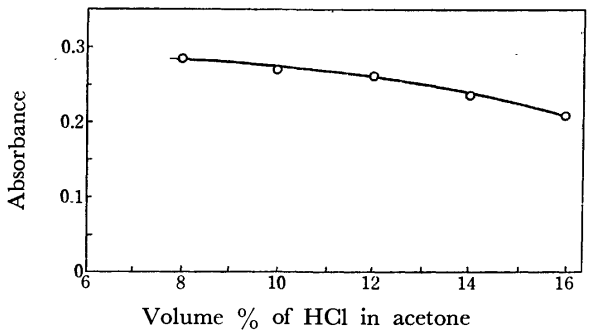

Fig. 3. Effect of concentration of hydrochloric acid in acetone on atomic absorption spectrometry for copper.

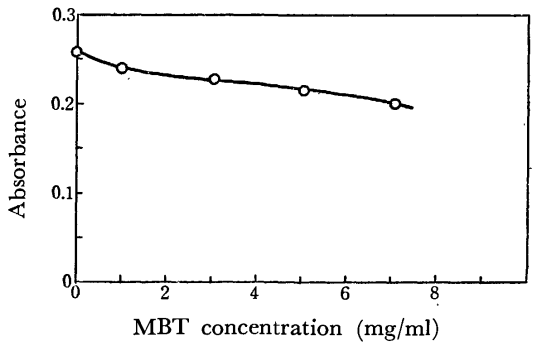

Fig. 4. Effect of concentration of 2-mercaptobenzothiazole in acetone on atomic absorption spectrometry for copper.

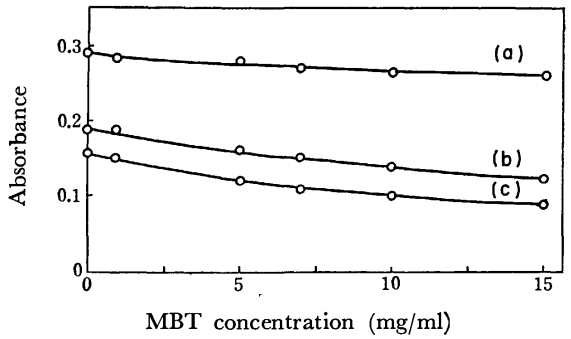

Fig. 5. Effect of mixing ratio of air and acetylene on atomic absorption spectrometry for copper in the presence of various concentration of MBT.
(a) Air : acetylene 4.7 : 2.7—5.0 : 3.0, (b) air : acetylene 9.0 : 7.0, (c) air : acetylene 9.0 : 9.0.

tests, it was found that the mixing ratio and the fuel flow rate had serious effects on the absorbance of copper and lead, and that maximum absorption was obtained at mixing ratios of air and acetylene of 4.7 : 2.7 to 5.0 : 3.0 for copper (Fig. 5) and 6.0 : 4.0 for lead.

Analytical Procedure Recommended. In general, the cadmium content of natural water is lower than the contents of the other three metals by a factor 10 to 100. Consequently, from these results, the copper, lead, and zinc contents should be determined in one sample after preconcentration using this method and the cadmium content should be measured in another smaller portion of the sample using flameless atomic absorption spectrometry.

Thus, the recommended procedure is as follows: two to five liters of the water sample adjusted to about pH 7, is passed through the MBT-SG column (20 mm in dia. ×70 mm) at a flow rate of 2—5 l/h. Even at a higher flow rate, if the sample solution is poured onto the column by aspiration, numerous minute air bubbles appear on all parts of the column which are of course, not filled with sample solution and rather quantitative retention of the metal ions can be maintained. This may result from closer contact between the sample solution film and the MBT-SG particles. Subsequently, the column is washed with about 20 ml of deionized water, and then 20 ml of an acetate–hydrochloric acid buffer solution (pH 4.0) is passed through at a flow rate of 1 ml/min. The effluent is diluted to the desired volume with deionized water in a 25-ml measuring flask and subjected to atomic absorption measurement for the zinc content. The absorbance is measured at a wavelength of 213.8 nm in a flame of air and acetylene (9 : 9). The column is washed again with 20 ml of deionized water and then with about 20 ml of ethanol, and finally 20 ml of a solvent mixture of acetone–hydrochloric acid in a volume ratio of 9 : 1 is passed through. The effluent is diluted to 25 ml with acetone and subjected to the atomic absorption measurement for copper and lead. The absorption is measured at wavelengths of 324.8 and 283.3 nm for copper and lead, respectively, in a flame of air and acetylene (5 : 3 for copper and 6 : 4 for lead).

Cadmium and zinc are detemined in another manner, as follows: two liters of the water sample adjusted to pH 7.0 is passed through the column. Then the column is washed with about 20 ml of deionized water, and 20 ml of hydrochloric acid (1 : 99) is passed at a flow rate of 1 ml/min. The effluent is diluted to 25 ml with deionized water and submitted to the atomic absorption measurement for cadmium and zinc. Cadmium is measured with flameless atomic absorption using a carbonrod atomizer at a wavelength of 228.8 nm and the absorption of zinc is measured as described above. From the remaining column material, copper can be eluted with an acetone–hydrochloric acid solvent mixture as indicated above.

Analysis of Tap, River and Sea Water. Using the recommended method, laboratory tap water, river water, and sea water were analyzed for cadmium, copper, lead, and zinc. The results are summerized in Table 4.

TABLE 4. CADMIUM, COPPER, LEAD AND ZINC CONTENTS OF VARIOUS WATER SAMPLES

Sample water	Cd(II) ppb	Cu(II) ppb	Pb(II) ppb	Zn(II) ppb
Pacific Ocean (10 m)	0.1_4[a)]	0.2_2	3.1	3.0[a)]
Pacific Ocean (7 m)	0.07[a)]	20.9	3.4	$13._1$[a)]
Tsukumo Bay (0 m)	—	0.2_7	—	2.9
Watarase River	—	55	6.7	74
Tap water (Marunouti)	0.03[a)]	0.5[a)]	—	8.3[a)]

MBT-SG: 10 g, column: 20 mm in dia. × 70 mm, flow rate: 5 l/h. a) MBT-SG: 7 g, column: 20 mm in dia. × 50 mm, flow rate: 2.3 l/h.

Two samples of Pacific Ocean water and a sample of Watarase River water were distributed to a number of laboratories in Japan for comparison of the analytical results and the results using the recommended method are in good agreement with those obtained by the other laboratories. The 7-m sample of Pacific Ocean water with remarkably high values for copper and zinc was collected with a pump equipped on a research vessel, the Hakuho Maru belonging to the University of Tokyo. This contamination may originated from the metal in the gun-metal parts of the pump used for the sampling.

Conclusion

2-Mercaptobenzothiazole–silica gel (MBT–SG) provides an easy means of preconcentrating cadmium, copper, lead, and zinc and of separating copper from cadmium, lead, and zinc, and lead and cadmium from zinc for subsequent atomic absorption measurements of the contents of each metal. The attractive features of this chelating material are the easiness of preparation, reproducibility, and fast adsorbability for several metal ions from water samples in spite of its relatively low chelating capacity. Because dissolution of the reagent from the column is too small to be measured, a large volume of sample water (5—10 l) can be treated with a relatively small column, and the preconcentrated metal ions can be eluted from the column with a small volume of eluant resulting in a high concentration factor.

The authors wish to thank the Ministry of Education, for a Grant-in-Aid (Special Project Reseach "Fundamental Reseach for the Preservation of Marine Environment" Project No. 111313).

References

1) J. P. Riley and D. Taylor, *Anal. Chim. Acta*, **40**, 479 (1968).
2) J. P. Riley and D. Taylor, *Anal. Chim. Acta*, **41**, 175 (1968).
3) B. Holynska, *Radiochem. Radioanal. Lett.*, **17**, 313(1974).
4) J. Dingman, Jr., S. Siggia, C. Barton, and K. B. Hiscock, *Anal. Chem.*, **44**, 1351 (1972).
5) R. A. A. Muzzarelli and O. Tubertini, *Talanta*, **16**, 1571 (1971).
6) R. A. A. Muzzarelli, G. Reith, and O. Tubertini, *J. Chromatogr.*, **47**, 414 (1970).
7) R. A. A. Muzzarelli, *Anal. Chim. Acta*, **54**, 133(1971).
8) R. A. A. Muzzarelli and L. Sipos, *Talanta*, **18**, 853 (1971).
9) R. A. A. Muzzarelli and R. Rochelli, *Anal. Chim. Acta*, **69**, 35 (1974).
10) R. R. Brooks, B. J. Presley, and I. R. Kaplan, *Talanta*, **14**, 809 (1967).
11) K. Terada, H. Hayakawa, K. Sawada, and T. Kiba, *Talanta*, **17**, 955 (1970).
12) V. Veselý and V. Pekárek, *Talanta*, **19**, 219 (1972).
13) V. Pekárek and V. Veselý, *Talanta*, **19**, 1245 (1972).
14) J. P. Riley, in J. P. Riley and G. Skirrow, Ed., "Chemical Oceanography," Vol. 2, Academic Press, New York (1965), p. 382.

Photoemission and Solvation Free Energies of Electrons in Polar Solvents

Kazuo YAMASHITA and Hideo IMAI

Faculty of Integrated Arts and Sciences, Hiroshima University, Hiroshima 730

(Received September 24, 1976)

The red limit potential of electron photoemission was measured in various polar solvents, and the apparent solvation free energies of the electrons were estimated. The energy state and transformation of photoemitted electrons in solution were discussed as regards the role of dry or damp electrons as an intermediate species. A proportionality between the intermediate solvation free energy and the energy quantum of the optical absorption band maximum of solvated electron in various polar solvents is pointed out.

In polar solvents the electrons produced by high energy radiation are localized or trapped by the surrounding solvent molecules in a delicate balance of short- and long-range interactions.[1] Such a solvated electron can also arise in photo-electrochemical processes, where the photoemission from a cathode under suitable conditions of illumination is measured as the cell current flowing due to the homogeneous electron capture process.[2] The dependence of the photocurrent on the square root of the scavenger concentration and rate constant of a scavenging reaction has been proved by the theory based on the semi-infinite diffusion equation.[3] The red limit potential or threshold potential, which can be estimated from the photoelectrochemical process, is related to the estimate of the work function of the electron from a metal into solution. The interaction of photoemitted electron with solvent molecules can be expressed in terms of the difference between the work function of the electron from a metal into vacuum and that from the metal into solution, when the Volta potential difference is taken into account. The values estimated for water from this relationship, however, show a fairly remarkable discrepancy from the hydration free energy of the electron obtained by radiation chemical studies.[4,5] Schiffrin[6] extensively discussed the difference, attributing it to the contribution of the solvent reorganization energy. On the other hand, Pleskov and his co-workers[7,8] interpreted the difference by assuming free or delocalized electrons.

In this paper precise data of the red limit potential in various polar solvents are presented. The physical meaning of the energy value estimated as an interaction energy of emitted electrons with solvent molecules prior to the electron capture reaction is discussed.

Experimental

The apparatus is shown in Fig. 1. A lock-in amplifier (Model LI-572B, NF Circuit Design Block Co.) with a light chopper, Model CH-352, was used at a *ca.* 20 Hz frequency. A three-electrode cell, equipped with a water jacket to control the temperature, was used. The potential of the working electrode (a mercury pool electrode renewed by spilling mercury in each run; illuminated area *ca.* 0.3 cm^2) was controlled with a potentiostat (Shimadzu Model PS-2). A 500 watt super high pressure mercury lamp (Ushio Type USH 500D) was used for illumination through a monochrometer or color filters. The wavelength of the incident light was 365 nm. When gas bubbles are evolved by a scavenging reaction, *e. g.* N_2 from N_2O or H_2 from H_3O^+, it is preferable to measure under a small current density. Since the current signal is very small, an electrode with wide illumination area gives more accurate measurements.

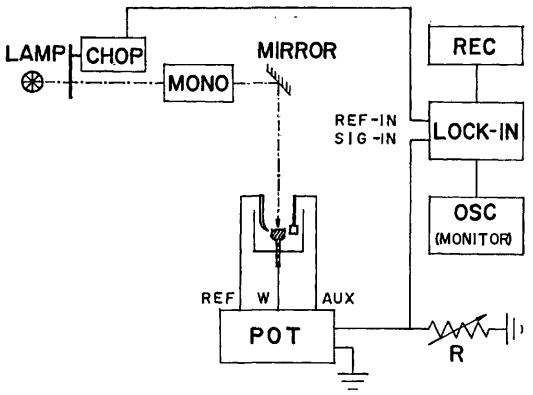

Fig. 1. Apparatus used for experimental measurements of photocurrents.
LAMP, super high pressure mercury lamp; CHOP, chopper; MONO, monochrometer; POT, potentiostat; REC, recorder; LOCK-IN, lock-in amplifier; OSC, oscilloscope; R, decade resistance.

All the solvents were purified by the usual methods.[9] Measurements were carried out at 25 °C.

Results and Discussion

Estimation of Intermediate Solvation Free Energy of Electron from Red Limit Potential. The dependence of photoemission current, I_e, on the quantum energy of incident light, $h\nu$, and the field strength or electrode potential, ϕ, under sufficiently high electrolyte concentration is given by[10]

$$I_e = A(h\nu - h\nu_0 - e\phi)^{5/2}, \quad (1)$$

where A is a constant depending upon the properties of the metal, h the Planck constant, and ν_0 the threshold frequency at the potential of zero charge, ϕ_{pzc}. All the potential values are referred to ϕ_{pzc}. The relationship known as the law of five halves, was derived as an approximate solution of a theoretical equation postulating the transmission of electrons through the energy barrier at the electrode-solution interface. The equation was verified experimentally to hold not only in aqueous solutions,[7,10] but also in non-aqueous solutions.[11] Figure 2 shows the linear relationship between $i_p^{0.4}$ and ϕ in hexamethylphosphoramide (HMPA) solution saturated with nitrous oxide, where i_p is the photocurrent measured in experiments. The extrapolation of $i_p^{0.4}$-ϕ straight line to $i_p=0$ gives the red limit potential of -0.42 V *vs.* Ag/0.01 M $AgClO_4$

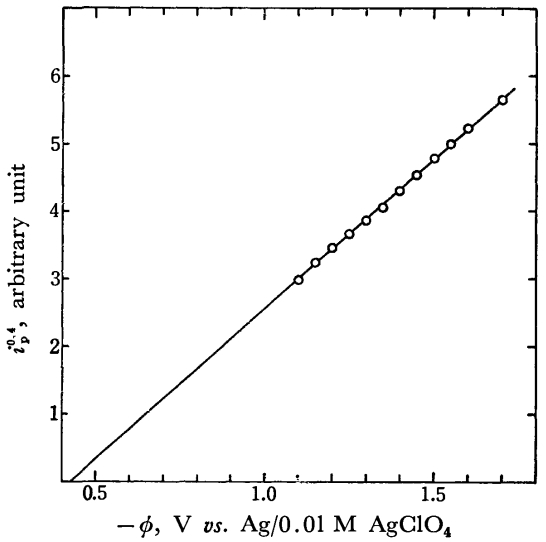

Fig. 2. Dependence of $i_p^{0.4}$ on ϕ for 0.2 M $NaClO_4$ HMPA solution saturated with N_2O.

electrode. According to the definition of the red limit potential, ϕ_0, Eq. 1 leads to

$$h\nu_0 = h\nu - e\phi_0 \tag{2}$$

The energy quantum, $h\nu_0$, can be replaced by the work function, W_{m-s}, of the electron emission from a metal into solution as given by

$$W_{m-s} = h\nu - e\phi_0. \tag{3}$$

A tentative energy cycle was proposed from a comparison of the electron photoemission in solution with that *in vacuo* (the work function; W_{m-v}).[12] However, there is a discrepancy between the data obtained by this method and those by radiation chemical studies. A modification of the energy cycle can be deduced by taking the discrepancy into consideration. The

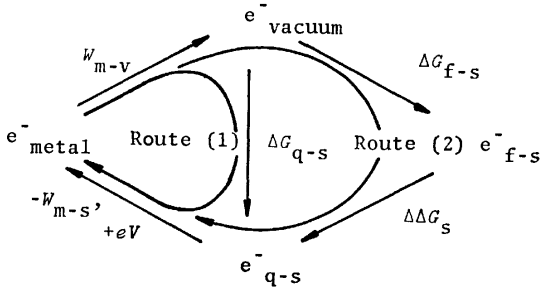

Fig. 3. Modified energy cycle of the electron.

modified energy cycle involves two stages of the electron-solvent interaction, namely an intermediate state[6] of solvation (a quasi-solvated state) and fully solvated state as shown in Fig. 3. The symbols, e^-_{q-s} and e^-_{f-s}, represent the quasi-solvated and fully solvated electrons, respectively, ΔG the free energy change for respective solvation process, and $\Delta\Delta G_s$ the difference between ΔG_{f-s} and ΔG_{q-s}. The energy balance in routes (1) and (2) lead to the following expressions.

$$-\Delta G_{q-s} = W_{m-v} - W_{m-s} + eV_{m-s}$$
$$= W_{m-v} - h\nu + e(\phi_0 + V_{m-s}) \tag{4}$$
$$-\Delta G_{f-s} = -\Delta G_{q-s} + \Delta\Delta G_s, \tag{5}$$

where V_{m-s} is the Volta potential difference between a metal and solution.

Taking $W_{Hg-vacuum}$=4.52 eV, $h\nu$=3.40 eV corresponding to λ=365 nm, $e\phi_0$=0.26 eV for saturated-N_2O aqueous solution containing 0.2 M KCl, and eV_{Hg-aq}=−0.26 eV, which is evaluated from the data obtained by Randles[13] and Grahame *et al.*,[14] we obtain $-\Delta G_{q-s}$=1.14 eV from Eq. 4. This value coincides with previous estimates,[3,6,7] the value of $-\Delta G_{f-s}$ estimated in radiation chemical studies being

Table 1. Values of threshold potentials, quasi-solvation free energies of electrons and transition energies for the optical absorption maxima of solvated electrons in various polar solvents

Solvent	ϕ_0/V	ϕ_{pzc}/V	V_{m-s}/V	$\Delta G_{q-s}+eV_{m-s}$/eV	ΔG_{q-s}/eV	λ_{max}/nm	$h\nu_{max}$/eV	ε
HMPA	-0.42_2	−0.30		−1.01		2250[d]	0.55	30
MeOH	-0.36_2	-0.78_6	−0.53[a]	−1.55	−1.02	630[e]	1.97	32.6
DMF	−0.54	−0.68	−0.63[b]	−1.27	−0.64	1680[f]	0.74	36.7
						650[g]	1.91	
MeCN	-0.46_8	−0.62		−1.28		690[h]	1.80	38
DMSO	-0.76_5	-0.59_4		−0.96				48.9
PC	−1.03	−1.24		−1.34				64.4
H_2O	-0.18_5	−0.44	−0.26[c]	−1.40	−1.14	720[i]	1.72	78.5

HMPA, hexamethylphosphoramide; MeOH, methanol; DMF, *N*,*N*-dimethylformamide; MeCN, acetonitrile; DMSO, dimethylsulfoxide; PC, propylene carbonate; Scavenger, N_2O; Supporting electrolyte, 0.2 M $NaClO_4$ (0.2 M KCl in the case of water); Reference electrode, Ag/0.01 M $AgClO_4$ (SCE in the case of water).

a) B. Case and R. Parson, *Trans. Faraday Soc.*, **63**, 1224 (1967). b) I. M. Ganzhina, B. B. Damaskin, R. I. Kaganovich, and R. V. Ivanova, *Elektrokhimiya*, **7**, 362 (1971). c) J. Randles, *Trans, Faraday Soc.*, **52**, 1573 (1956). d) J. M. Brooks and R. R. Dewald, *J. Phys. Chem.*, **72**, 2655 (1968). e) S. Arai and M. C. Sauer, Jr., *J. Chem. Phys.*, **44**, 2297 (1966). f) L. M. Dorfman and J. F. Cavlas in "Radiation Research, Biomedical, Chemical and Physical Properties," ed by O. F. Nygaard, H. Adler, and W. K. Sinclair, Academic Press, New York, San Francisco, London (1975), p. 326. g) N. Hayashi, E. Heyon, T. Ibata, N. N. Lichtin, and A. Matsumoto, *J. Phys. Chem.*, **75**, 2267 (1971). h) A. Singh, H. D. Gesser, and A. R. Scott, *Chem. Phys. Lett.*, **2**, 271 (1968). i) J. P. Keene, *Discuss. Faraday Soc.*, **36**, 304 (1963).

1.67[4] or 1.71[5] eV. Thus the value of $\Delta\Delta G_s$ is estimated to be 0.53—0.57 eV, *viz.*, the energy of the quasi-hydrated state is higher by 0.53—0.57 eV than that of the fully hydrated state.

The data of ΔG_{q-s} estimated similarly in various polar solvents and related values are summarized in Table 1.

Transformation of Emitted Electrons and the Succeeding Reaction. In the reaction sequence of the photo-emitted electrons in solution containing a scavenger, it seems that the emitted electrons are thermalized and solvated, and then the solvated electrons are captured by scavengers, resulting in the photocurrent. At low concentrations of electron acceptor the mechanism was supported by the coincidence with a theory[2,3] based on the semi-infinite diffusion coupled with the scavenging reaction. The solvent effect on the rate of scavenging process was also confirmed experimentally.[3] At low scavenger concentrations the participation of the fully solvated electron in the reaction pathway seems to be predominant. In the present case, however, the experiment was carried out at relatively high scavenger concentrations, so that the emitted electrons may have been captured by the scavenger prior to full solvation. Hunt and his co-workers[15–17] developed a picosecond stroboscopic pulse radiolysis technique. They found that there are precursors called dry or damp electrons, around which solvent molecules relax to form the fully solvated electrons. This intermediate species might be quasi-solvated and reacts with a scavenger prior to full solvation. The life of the intermediate species is shown to be within the order of picoseconds in aqueous solutions and much longer in alcoholic media.[18]

Taking these findings into consideration, the transformation of photoemitted electrons and the reaction sequence in solution can be expressed as shown in Fig. 4.

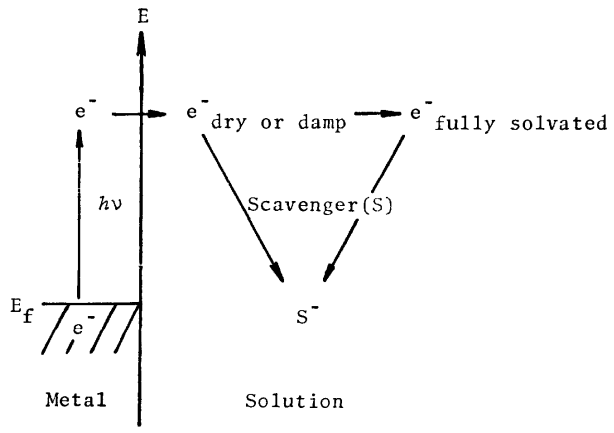

Fig. 4. Transformation of photoemitted electrons and the sequence of reactions.

Relationship between ΔG_{q-s} and $h\nu_{max}$ of Optical Absorption Band Maximum of Solvated Electron. A plot of ΔG_{q-s} *vs.* $h\nu_{max}$, the energy quantum of the optical absorption band maximum of solvated electrons, is shown in Fig. 5.

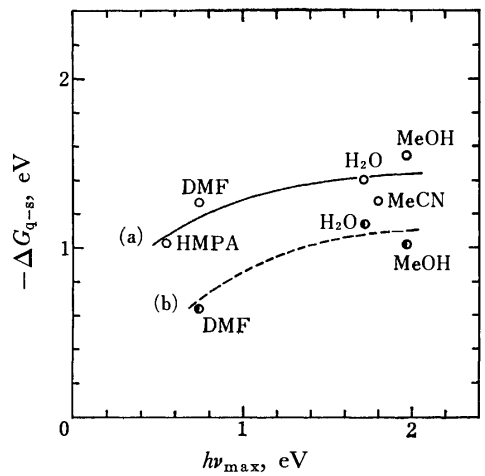

Fig. 5. Empirical correlation between quasi-solvation free energy of the electron and energy of optical absorption band maximum of the solvated electron.
(a) Values uncorrected for the Volta p. d.
(b) Values corrected for the Volta p. d.

The value of $-\Delta G_{q-s}$ increases with increase in $h\nu_{max}$. The solvents used have static dielectric constants ranging from 17 to 84 at room temperature. The optical absorption spectra[1] of the solvated electrons in hydroxy compounds including water are mostly in the visible or near-infrared region. The amides or amines are in the intermediate region 1400—2050 nm, and the ethers are in the infrared region 1800—2300 nm. Corresponding to this trend, it is expected that the free energy of fully solvated electrons decreases in the solvents in the order

hydroxy compounds>amides and amines>ethers,

since the transition energy, $h\nu_{max}$, for optical absorption maximum corresponds to the depth of the potential well of the solvated electron. It is noteworthy that the energy of quasi-solvated electrons also shows the same trend as shown in Fig. 5.

This investigation was supported by the Science Research Grant 054194 of the Ministry of Education.

References

1) M. S. Matheson, in "Physical Chemistry," ed by H. Eyring, Vol. 7, Academic Press, New York (1975), Chap. 10.
2) G. C. Barker, A. W. Gardner, and D. S. Sammon, *J. Electrochem. Soc.*, **113**, 1182 (1966).
3) K. Yamashita and H. Imai, *Bull. Chem. Soc. Jpn.*, **45**, 628 (1972).
4) J. Baxendale, *Radiat. Res. Suppl.*, **4**, 139 (1964).
5) J. Jortner and R. M. Noyes, *J. Phys. Chem.*, **70**, 770 (1966).
6) D. J. Schiffrin, *J. Electroanal. Chem.*, **63**, 283 (1975).
7) Yu. V. Pleskov and Z. A. Rotenberg, *J. Electroanal. Chem.*, **20**, 1 (1969).
8) R. R. Dogonadze, L. I. Krishtalik, and Yu. V. Pleskov, *Elektrokhimiya*, **10**, 507 (1974).
9) C. K. Mann, "Electroanalytical Chemistry," ed by A. J. Bard, Marcel Dekker, New York (1969), pp. 57—134.
10) A. M. Brodsky and Yu. Ya. Gurevich, *Electrochim. Acta*, **13**, 1245 (1968).

11) H. Imai and K. Yamashita, *Chem. Lett.*, **1972**, 423.
12) K. Yamashita and H. Imai, *Denki Kagaku*, **43**, 386 (1975).
13) J. Randles, *Trans. Faraday Soc.*, **52**, 1573 (1956).
14) D. C. Grahame, E. Coffin, J. Cummings, and M. A. Poth, *J. Am. Chem. Soc.*, **74**, 1207 (1952).
15) M. J. Bronskill, R. K. Wolf, and J. W. Hunt, *J. Chem. Phys.*, **53**, 4201 (1970).
16) R. K. Wolf, M. J. Bronskill, and J. W. Hunt, *J. Chem. Phys.*, **53**, 4211 (1970).
17) J. E. Aldrich, M. J. Bronskill, R. K. Wolf, and J. W. Hunt, *J. Chem. Phys.*, **55**, 530 (1971).
18) L. Gilles, J. E. Aldrich, and J. W. Hunt, *Nature (London)*, **243**, 70 (1973).

Preparations and Properties of Some Cationic Palladium(II) Complexes of the Di-*t*-butylnitroxide Radical

Masaaki Okunaka, Gen-etsu Matsubayashi, and Toshio Tanaka

Department of Applied Chemistry, Faculty of Engineering, Osaka University, Yamada-kami, Suita, Osaka 565

(Received October 27, 1976)

Cationic palladium(II) complexes of the di-*t*-butylnitroxide radical, $[Pd(Bu^t_2NO)(L\text{-}L)]X$ (L-L=2,2'-bipyridine, 1,10-phenanthroline, *N*-substituted 2-pyridylmethyleneamine and bis(triphenylphosphine); $X^-=ClO_4^-$ and/or BPh_4^-), were prepared. ^1H NMR spectra of the complexes indicate that the nitroxide forms a three-membered ring with the palladium atom. The *N*-methyl- and *N*-ethyl-2-pyridylmethyleneamine complexes exist as two geometrical isomers in solution, whose ratios are 1 : 1 and 1 : 0.2, respectively. In the *N*-butyl and *N*-*p*-tolyl analogs, however, only one of the isomers exists in solution. These results are interpreted in terms of steric repulsion between the *t*-butyl groups and *N*-substituents. The bipyridine complex reacts with dialkyl disulfides in the presence of catalytic amounts of bipyridine to give a sulfur-bridged dimeric complex, $[Pd(bipyridine)(SR)]_2(ClO_4)_2$(R=Me and Pr), and a free nitroxide radical.

Nitroxide radicals ($R_2NO\cdot$) usually coodinate to metal ions through the oxygen atom as a neutral ligand.[1-7] However, di-*t*-butylnitroxide has been reported to react with palladium dichloride to form a chloride-bridged diamagnetic complex **A**, in which the nitroxide was assumed to coordinate to the palladium atom as an

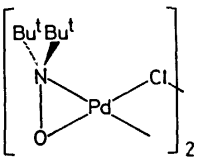

A

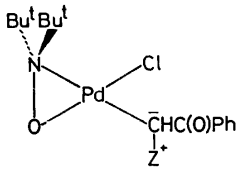

B

anionic ligand.[8] A recent ^1H NMR study by the present authors on the nitroxide-palladium(II) complexes **B** which involve prochiral phenacylides, $Z\overset{+}{C}H\overset{-}{C}(O)Ph$ (Z=PPh_2Me, PPh_3, $AsPh_3$, and SMe_2), has demonstrated that a three-membered ring exists in the complexes.[9] It was also found that **A** reacts with triphenylphosphine to give a mononuclear complex **C**, which undergoes a novel redox reaction of the nitroxide-palladium moiety by nucleophilic attack of excess triphenylphosphine yielding tetrakis(triphenylphosphine)palladium(0).[10]

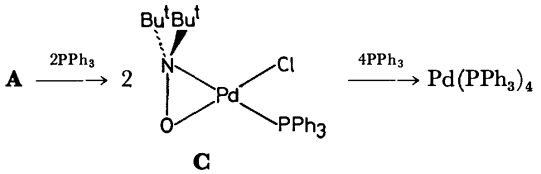

C

$$+\ PdCl_2(PPh_3)_2 + 2Bu^t_2NO\cdot$$

This reaction indicates a characteristic coordination property of the nitroxide toward palladium. However, few palladium complexes with nitroxides have so far been isolated. It is, therefore, of interest to extend the study of the nitroxide-palladium(II) complexes.

This paper reports the preparations and properties of cationic palladium(II) complexes having the chemical formula $[Pd(Bu^t_2NO)(L\text{-}L)]X$ (L-L=2,2'-bipyridine (bipy), 1,10-phenanthroline(phen), *N*-substituted 2-pyridylmethyleneamine(pyma-R) and bis(triphenylphosphine); $X^-=ClO_4^-$ and/or BPh_4^-), and the redox reactions using dialkyl disulfides as oxidizing reagents.

Experimental

Materials. The chloride-bridged dipalladium complex, $[PdCl(Bu^t_2NO)]_2$, and *N*-substituted 2-pyridylmethyleneamines, 2-C_5H_4N-CH=N-R (R=Me, Et, Bu, and *p*-tolyl), were prepared as described elsewhere.[8,11]

Preparation of $[Pd(Bu^t_2NO)(L\text{-}L)]X$ (L-L=bipy, phen, pyma-R and bis(triphenylphosphine); $X^-=ClO_4^-$ and/or BPh_4^-). Into a dichloromethane solution (10 ml) of $[PdCl(Bu^t_2NO)]_2$ (286 mg, 0.5 mmol) was poured an acetone solution (15 ml) containing bipy (156 mg, 1.0 mmol) and sodium perchlorate monohydrate (140 mg, 1.0 mmol) with vigorous stirring at room temperature. The original brown solution changed immediately to a yellow suspension, which was filtered to remove the sodium chloride produced. The filtrate was evaporated to dryness under reduced pressure. The resulting product was recrystallized from acetone/petroleum ether to afford yellow crystals of $[Pd(Bu^t_2NO)(bipy)]ClO_4\cdot 1/2Me_2CO$ (427 mg, 80% yield). Other yellow perchlorate complexes were prepared by the same method (50—80% yields), and yellow tetraphenylborate complexes were similarly obtained using sodium tetraphenylborate in place of sodium perchlorate monohydrate (70—85% yields). The results of elemental analysis, the melting points and the molar electric conductances of the complexes are summarized in Table 1.

Reaction of $[Pd(Bu^t_2NO)(bipy)]ClO_4$ with Dialkyl Disulfides in the Presence of bipy. Dimethyl disulfide (470 mg, 5.0 mmol) was mixed with an acetone solution (15 ml) of $[Pd(Bu^t_2NO)(bipy)]ClO_4$ (268 mg, 0.5 mmol) in an atmosphere of dry nitrogen, followed by the addition of bipy (15.6 mg, 0.1 mmol) in acetone (5 ml) with stirring at room temperature. The solution was further stirred for 40 h to give a precipitate, which was collected by filtration. Recrystallization from acetonitrile gave yellow crystals of $[Pd(bipy)(SMe)]_2(ClO_4)_2$-MeCN (160 mg, 82% yield). Found: C, 33.46; H, 2.89; N, 8.21%. Calcd for $C_{24}H_{25}N_5O_8S_2Cl_2Pd_2$: C, 33.54; H, 2.94; N, 8.20%. Λ_M=309 ohm^{-1} cm^2 mol^{-1} (1.0×10^{-3} M in acetonitrile). The propyl analog, $[Pd(bipy)(SPr)]_2(ClO_4)_2$, was prepared by the same method (75% yield). Found: C, 35.59; H, 3.42; N, 6.57%. Calcd for $C_{26}H_{30}N_4O_8S_2Cl_2Pd_2$: C, 35.71; H, 3.46; N, 6.41%. Λ_M=328 ohm^{-1} cm^2 mol^{-1} (1.0×10^{-3} M in acetonitrile).

Physical Measurements. ^1H NMR and ESR spectra were measured as described previously,[10] and the electric con-

TABLE 1. ELEMENTAL ANALYSIS RESULTS, MELTING POINTS AND MOLAR ELECTRIC CONDUCTANCES[a] OF THE COMPLEXES

No.	Complex[b]	Mp (°C)	Found (Calcd) % C	H	N	Λ_M ($ohm^{-1}\,cm^2\,mol^{-1}$)
1a	$[Pd(Bu^t_2NO)(bipy)]ClO_4\cdot 1/2Me_2CO$	—	43.72 (43.72)	5.49 (5.47)	7.81 (7.85)	148
1b	$[Pb(Bu^t_2NO)(bipy)]BPh_4$	169(d)	69.36 (69.47)	6.43 (6.40)	5.77 (5.79)	109
2	$[Pd(Bu^t_2NO)(phen)]BPh_4\cdot Me_2CO$	175(d)	70.53 (69.84)	6.77 (6.50)	5.22 (5.20)	110
3a	$[Pd(Bu^t_2NO)(pyma\text{-}Me)]ClO_4$	—	38.23 (38.33)	5.77 (5.59)	8.89 (8.95)	152
3b	$[Pd(Bu^t_2NO)(pyma\text{-}Et)]ClO_4$	—	39.11 (39.68)	5.66 (5.84)	8.71 (8.68)	168
3c	$[Pd(Bu^t_2NO)(pyma\text{-}Bu)]BPh_4$	138(d)	68.38 (68.90)	7.21 (7.17)	5.89 (5.74)	94
3d	$[Pd(Bu^t_2NO)(Pyma\text{-}p\text{-}tolyl)]BPh_4\cdot Me_2CO$	130(d)	69.93 (69.94)	6.89 (6.86)	5.22 (5.10)	98
4	$[Pd(Bu^t_2NO)(PPh_3)_2]ClO_4$	—	60.16 (60.41)	5.50 (5.54)	1.61 (1.60)	142

a) Measured in acetonitrile at 25 °C (1.65×10^{-3} M). b) pyma-R = *N*-substituted 2-pyridylmethyleneamine.

TABLE 2. ^1H NMR CHEMICAL SHIFTS (δ, ppm) OF $[Pd(Bu^t_2NO)(L\text{-}L)]X$ IN ACETONITRILE AT 24 °C[a]

Complex[b]	Configuration	Bu^t	H_{6a}	H_{6b}	N-CH_n-
1a	I	1.76	8.71(+0.09)	8.47(−0.15)	—
1b	I	1.75	8.68(+0.06)	8.45(−0.17)	—
2	I	1.82	9.05(−0.06)[e]	8.84(−0.27)[e]	—
3a	IIa	1.72	8.66(+0.06)	—	3.69(+0.18) [N-CH_3]
	IIb	1.72	—	8.46(−0.14)	3.82(+0.31) [N-CH_3]
3d[c]	IIa	1.72	8.66(+0.04)	—	3.78(+0.11) [N-CH_2-]
	IIb	1.72	—	8.42(−0.20)	3.96(+0.29) [N-CH_2-]
3c	IIa	1.69	8.61(+0.01)	—	3.66(+0.04) [N-CH_2-]
3d	IIa	1.77	8.70(0)	—	—
4[d]		1.46	—	—	—

a) The values in parentheses denote $\delta_{complexed}-\delta_{free}$. b) Refer to Table 1 for the number of complexes. c) Measured in acetonitrile-d_3. d) Measured in acetone. e) H_2 or H_9 signal.

ductance was determined at 25 °C using a universal bridge, as has also been described elsewhere.[12]

Results and Discussion

The complexes are stable in air in the solid state, however, they gradually decompose in solution. Electric conductance measurements appear to indicate that the complexes are 1 : 1 electrolytes in acetonitrile (Table 1). The assignment of the ^1H NMR spectra is easily carried out by refering to those of other metal complexes of bipy,[13] phen,[13] and 2-pyridylmethyleneamines,[11,14] as summarized in Table 2.

Configuration of the $[Pd(Bu^t_2NO)(L\text{-}L)]^+$. Figure 1 shows a comparison of the ^1H NMR spectra of the bipy complex and free bipy in the bipy proton region in acetonitrile. The H_4 and H_5 signals of bipy move down-field upon complex formation with the former being observed near the H_3 signal. It is to be noted that two distinct H_6 signals appear separately with equal intensities; one of the H_6 signals undergoes a little down-field shift, while the other H_6 signal occurs at a higher field than does bipy itself. This result

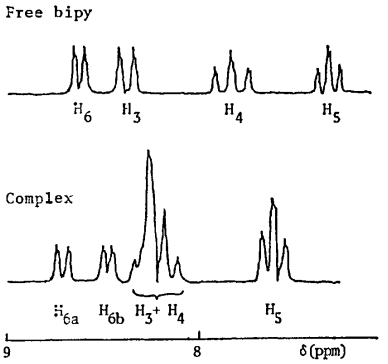

Fig. 1. ^1H NMR spectra of bipy and $[Pd(Bu^t_2NO)(bipy)]ClO_4$ in the bipy proton region, in acetonitrile at 24 °C.

indicates a three-membered ring formed by the nitroxide and the palladium atom in a square planar configuration, as shown in I. The small shifts of the H_6 signals are ascribed to the counteraction of two opposite effects: a down-field shift due to a decrease in the electron density on the pyridine ring and an

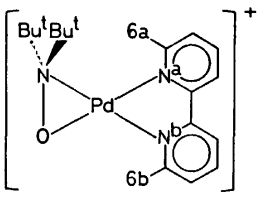

I

up-field shift due to a decrease in the original paramagnetic anisotropy of lone pair electrons of the bipy nitrogen upon coordination, as was suggested for the pyridine complexes of triethylaluminum.[12] Steric repulsion between the *t*-butyl groups and the pyridine ring can possibly weaken the Pd–N^a bond compared with the Pd–N^b bond. Therefore, the larger paramagnetic anisotropy effect of the lone pair electrons may dominate more in N^a than in N^b. As a result, the H_{6a} signal is considered to occur at a lower field than the H_{6b} signal. The phen complex also exhibits two separated H_2 and H_9 signals, which suggests that the configuration is similar to I.

The ^1H NMR spectrum of the *N*-methyl-2-pyridylmethyleneamine complex shows two sets of H_6, *N*-methyl and *t*-butyl signals, as shown in Fig. 2; the intensity ratio of each pair is 1 : 1. This is due to the presence of two equimolar geometrical isomers, IIa and IIb, in solution. In the *N*-ethyl-2-pyridylmethyleneamine complex, the intensity ratio of each pair of H_6 and *N*-ethyl signals is 1 : 0.2, whereas the *N*-butyl and *N*-*p*-tolyl analogs exhibit only one set of signals. In view of the steric repulsion between the *t*-butyl and *N*-alkyl or *N*-aryl groups, configuration IIa would be more probable than IIb. This is consistent with the X-ray crystallographic analysis of $PdCl(Bu^t_2NO)(Me_2\overset{+}{S}\overset{-}{C}HC(O)Ph)$, in which the bulky phenacylide is located in the position *trans* to the di-*t*-butyl nitrogen.[15] The preference of IIa over IIb is also supported by failure to isolate the nitroxide–palladium(II) complex of *N*,*N*′-di-*p*-tolyl-2,3-butanediimine, in which the *p*-tolyl group should be located in the position *cis* to the di-*t*-butyl nitrogen.

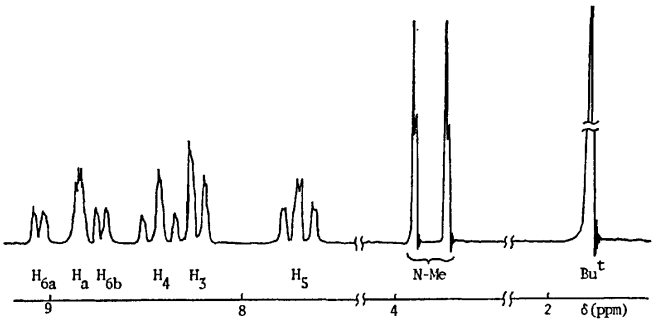

Fig. 2. The ^1H NMR spectrum of $[Pd(Bu^t_2NO)$-(pyma-Me)$]ClO_4$ in acetone at 24 °C; the solvent signals are omitted.

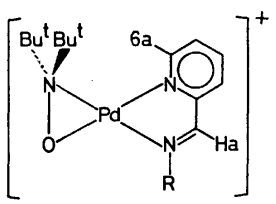

IIa

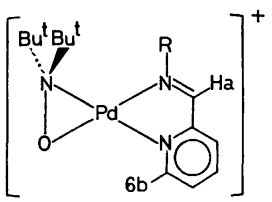

IIb

The bis(triphenylphosphine) complex is obtained in a high yield. On the other hand, the isolation of the corresponding 1,2-bis(diphenylphosphino)ethane complex was not successful possibly because the inflexibility of the bidentate ligand results in an unfavorable steric repulsion upon chelation.

Stability of the Complex to Nucleophiles. The ESR spectrum of $[Pd(Bu^t_2NO)(bipy)]ClO_4$ in degassed acetone shows a weak triplet signal due to a free di-*t*-butylnitroxide radical which may be produced by slight dissociation from the palladium atom. No appreciable enhancement of the ESR signal is observed upon the addition of bipy to a degassed acetone solution of the complex. These observations confirm that no reaction occurs between the complex and bipy. $[Pd(Bu^t_2NO)(PPh_3)_2]ClO_4$ does not react with excess PPh_3. This is in contrast to the facile reaction of $PdCl(Bu^t_2NO)(PPh_3)$ with PPh_3, generating a free nitroxide radical.[10]

Reaction of $[Pd(Bu^t_2NO)(bipy)]ClO_4$ *with Some Oxidizing Reagents.* When bipy is added to an acetone (not degassed) solution of $[Pd(Bu^t_2NO)(bipy)]ClO_4$ in air, an orange crystalline complex is obtained and a free nitroxide radical is generated as confirmed by the ESR spectrum of the reaction mixture. The ^1H NMR spectrum of the orange complex in DMSO-d_6 shows only the signals due to the coordinated bipy, but no signal for the di-*t*-butyl protons. The results of elemental analysis confirm the chemical formula, $[Pd(bipy)_2]$-$(ClO_4)_2 \cdot O_2$. Although details of the configuration are ambiguous, a redox reaction appears to occur between the $Bu^t_2NO^-$ moiety and dioxygen.

The redox reaction of $[Pd(Bu^t_2NO)(bipy)]ClO_4$ with dialkyl disulfides was further examined in the presence of catalytic amounts of bipy in an atmosphere of dry nitrogen. This reaction yields $[Pd(bipy)(SR)]_2$-$(ClO_4)_2$ (R=Me and Pr) (Reaction 1),

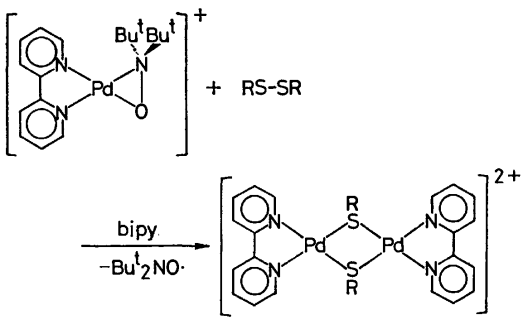

(1)

III
(R=Me and Pr)

where the anionic nitroxide is oxidized to a neutral radical and dialkyl disulfides are reduced. Analogous complexes $[Pd(ethylenediamine)(SPh)]_2X_2$ (X=Cl and Br) were prepared by Boschi *et al.*,[16] who proposed a configuration similar to III.

References

1) W. Beck, K. Schmidtner, and H. J. Keller, *Chem. Ber.*, **100**, 503 (1967).
2) D. L. Wilbur and R. Kreilick, *J. Chem. Phys.*, **52**, 1643 (1970).
3) T. B. Eames and R. Hoffman, *J. Am. Chem. Soc.*, **93**, 3140 (1971).
4) R. A. Zelonka and M. C. Baird, *J. Am. Chem. Soc.*, **93**, 6066 (1971).
5) Y. Y. Lim and R. S. Drago, *Inorg. Chem.*, **11**, 1334 (1972).
6) N. M. Karayannis, C. M. Paleos, C. M. Kikulski, L. L. Pytlewski, H. Blum, and M. M. Labes, *Inorg. Chim. Acta*, **7**, 74 (1973).
7) A. H. Cohen and B. M. Hoffmann, *Inorg. Chem.*, **13**, 1484 (1974).
8) W. Beck and K. Schmidtner, *Chem. Ber.*, **100**, 3363 (1967).
9) M. Okunaka, G. Matsubayashi, and T. Tanaka, *Inorg. Nucl. Chem. Lett.*, **12**, 813 (1976).
10) M. Okunaka, G. Matsubayashi, and T. Tanaka, *Bull. Chem. Soc. Jpn.*, **48**, 1826 (1975).
11) K. Kawakami, T. Ohara, G. Matsubayashi, and T. Tanaka, *Bull. Chem. Soc. Jpn.*, **48**, 1440 (1975).
12) G. Matsubayashi, K. Wakatsuki, and T. Tanaka, *Org. Magn. Reson.*, **3**, 703 (1971).
13) G. Matsubayashi and T. Tanaka, *J. Organomet. Chem.*, **120**, 347 (1976).
14) G. Matsubayashi, M. Okunaka, and T. Tanaka, *J. Organomet. Chem.*, **56**, 215 (1973).
15) N. Kasai and N. Yasuoka, private communication.
16) T. Boschi, B. Crociani, L. Toniolo, and U. Belluco, *Inorg. Chem.*, **9**, 532 (1970).

Studies on 5-8 Fused Ring Compounds. I. Halogenation of 4,4-Dimethylbicyclo[6.3.0]undecane-2,6-dione

Misao UMEHARA, Shinzaburo HISHIDA,* Kunimi FUJIEDA,* and Hirooki SASAKI

Department of Chemistry, Keio University, Hiyoshi-cho, Kohoku-ku, Yokohama 223

**Naka Works, Hitachi Ltd., Ichige, Katsuta, Ibaraki 312*

(Received July 12, 1976)

Bromination and chlorination of 4,4-dimethylbicyclo[6.3.0]undecane-2,6-dione (**2**) with pyridinium bromide perbromide and sulfuryl chloride gave several α-halo-diones. The substituted positions and the stereochemistry of the halogen atoms have been assigned on the basis of their dehydrohalogenation and spectral data. The chlorination of **2** also gave a tricyclic dione (**8**) containing a cyclopropane ring. The structure of **8** was determined by means of ^{13}C-NMR, as well as other types of spectroscopy. Dehydrochlorination of **7** gave a 5*H*-benzocycloheptene derivative (**18**).

Umehara *et al.* recently reported results concerning the photochemical cycloaddition of the enol acetate of dimedone to cyclopentene, and indicated that the photoadducts, 2-acetoxy-4,4-dimethyltricyclo[6.3.0.$0^{2,7}$]-undecan-6-one (**1a** and **1b**), undergo retro-aldol cleavage under acidic conditions to give 4,4-dimethylbicyclo-[6.3.0]undecane-2,6-dione (**2**).[1] Halogenation of the dione (**2**) was attempted to prepare intermediates for the synthesis of terpenes containing a medium-size ring, and several α-halo-diones were obtained. In the present paper, the dehydrohalogenation of the α-halo-diones and the substituted positions of the halogen atoms are reported.

It is interesting to study the chemical properties of compounds containing a 5-8 fused ring, since few investigations have been reported concerning them. Furthermore, such compounds constitute the partial skeleton of sesterterpenes (5-8-5 fused ring) and are of interest in this respect.

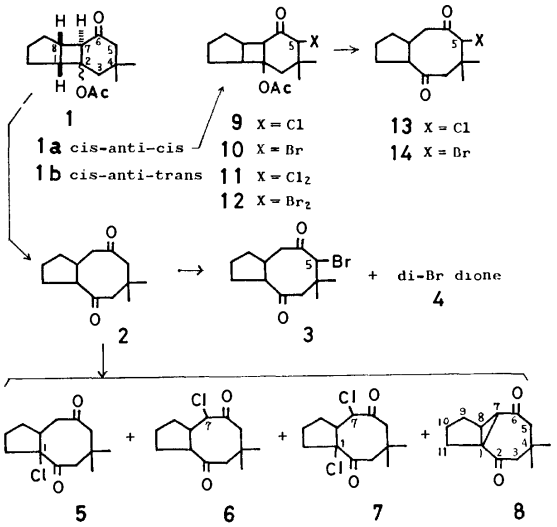

Scheme 1.

Results and Discussion

Bromination of the dione (**2**) with pyridinium bromide perbromide in ethanol yielded only a monobromo-dione (**3**), but, in acetic acid, **3** and a dibromo-dione (**4**) were obtained.

Chlorination of **2** with sulfuryl chloride in carbon tetrachloride yielded a mixture of two monochloro-dione (**5** and **6**), a dichloro-dione (**7**) and a compound (**8**) presumably formed as the result of the dehydrochlorination.

Other halogenated diones were also synthesized through the halogenation of the photoadduct **1a** (*cis-anti-cis*), followed by retro-aldol cleavage. The halogenation of **1a** with sulfuryl chloride and pyridinium bromide perbromide gave chloro derivatives (**9** and **11**), and bromo derivatives (**10** and **12**), respectively. Then retro-aldol cleavage of **9** and **10** under similar conditions,[1] used for the synthesis of **2** from **1a** and **1b**, gave monohalo-diones (**13** and **14**), respectively.

The monohalo-diones (**3**, **5**, **6**, **13**, and **14**) were subjected both to mass spectrometric analysis and to dehydrohalogenation with γ-collidine in order to determine the positions of halogen. The halogen atom can be substituted on the dione (**2**) at positions 1, 3, 5, or 7.

Compounds **3**, **13**, and **14** were found to remain unreacted upon treatment with γ-collidine, suggesting that the halogen atom is present at position 3 or 5 in any of these compounds because of the absence of a hydrogen atom at a neighboring position. The mass spectral data also support this. Scheme 2 shows the possible fragmentation patterns giving the fragment ions, $m/e=55+X$ (or $54+X$) (containing a *gem*-dimethyl group) and $m/e=67+X$ (containing a halogenated five-membered ring). Compounds **3**, **13**, and **14** showed a fragment peak corresponding to $m/e=55+X$ (or $54+X$) [where m/e is 133 for **3** (X=Br), 134 for **14** (X=Br), and 90 for **13** (X=Cl)], but none corresponding to $m/e=67+X$ indicating that the halogen atom is present at the 3 or the 5 positions of these compounds. The resemblance of the IR spectra of **13** and **14** indicates that a chlorine or bromine atom is substituted at the same position. Since **13** and **14** arose from **9** and **10**, respectively, the halogenation occurred at position 5 in **13** and **14**.

To identify the position of the bromine atom in **3**, compound **3** was reduced with $NaBH_4$ to a mixture of stereoisomers of diol (**15**), which was refluxed with zinc

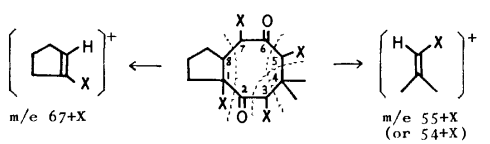

Scheme 2. (X=Cl or Br)

in acetic acid,[2] converted to **16** and then oxidized to enone **17** with chromic acid. The enone **17** was subjected to ^{13}C-NMR spectroscopy by proton noise decoupling and off-resonance decoupling and the multiplicity of the α-carbon atom in the carbonyl group was carefully observed. The ^{13}C-NMR spectroscopy of the enone revealed that the one α-carbon atom of the carbonyl group resonated at 62.6 ppm as a doublet while the other occured at 52.4 ppm as a triplet. This finding suggests that the enone has the same structure as **17** (4,4-dimethylbicyclo[6.3.0]undec-5-en-2-one) and it can be concluded that the bromine atom in **3** is not at position 3 but is at position 5. Therefore, **3** and **14** are epimers.

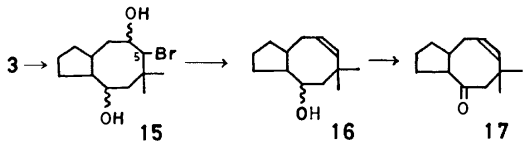

Scheme 3.

In α-halo ketones, the relationship between the IR[3] or UV[4] spectra and the orientations of the halogen atoms is known. The IR spectra of the dione (**2**) and the α-halo-diones (**3**, **5**, **6**, **13**, and **14**) were measured in carbon tetrachloride and the UV spectra in ethanol (Table 1). From these results, the C–X links in **6**, **13**, and **14** are nearly coplanar with the carbonyl group while the bromine atom in **3** is twisted away from the carbonyl oxygen atom. These results agree with the above-mentioned finding that **3** and **14** are epimers with respect to the bromine atom at position 5.

Table 1. The spectral data of monohalo-diones

Compound	UV (EtOH)			IR (CCl_4)	
	λ_{max}(nm)	ε	Δλ	ν(cm^{-1})	Δλ
2 (dione)	300	53	0	1700	0
3 (5-Br)	317	120	+17	1703	+3
14 (5-Br)	308	76	+8	1700 1720	+20
13 (5-Cl)	305	58	+5	1700 1723	+23
5 (1-Cl)	313	77	+13	1700 1710	+10
6 (7-Cl)	313	74	+13	1700 1720	+20

Both **5** and **6**, which were obtained by chlorination of **2**, undergo dehydrochlorination upon treatment with γ-collidine yielding **8**. The mass spectra of **5** and **6** show no fragment peak of m/e=55+Cl (or 54+Cl). On the other hand, **5** has a fragment peak at m/e=102 (67+Cl), which was not detected in **6**. Hence, it is inferred that the chlorine atom of **5** is at position 1 and the chlorine atom of **6** is at position 7.

In the mass spectrum of **8**, the parent peak is 206 (M^+). The IR spectrum of **8** shows a weak C–H stretching peak at 3040 cm^{-1}, and carbonyl absorption peaks appear at 1660 and 1675 cm^{-1} in Nujol, which are at frequencies lower than the 1695-cm^{-1} peak observed for **2**. In the UV spectrum of **8**, the end absorption at 210 nm has a higher intensity (ε=7100 in EtOH) compared with the value for **2** (ε=131, EtOH). Furthermore, the ^{1}H-NMR spectrum of **8** has no signal for any magnetic field lower than 3δ, and no signals appear in the ^{13}C-NMR spectrum over the range from 100—160 ppm. These experimental results can be explained more satisfactorily by the presence of a three-membered ring than by the presence of a double bond.

The structure of **8** was determined to be 4,4-dimethyltricyclo[6.3.0.$0^{1,7}$]undecane-2,6-dione with the aid of the multiplicity results of the ^{13}C-NMR spectra due to proton noise decoupling and off-resonance decoupling. In addition to the signals of two carbonyl carbon atoms (both at 206 ppm), two singlet peaks are present at 49.2 and 34.2 ppm. The peak at 34.2 ppm is assigned to C-4 carrying a *gem*-dimethyl group, and that at 49.2 ppm to C-1, since only C-1 can be converted into a quarternary carbon by dehydrohalogenation. Moreover, two doublet peaks at 40.9 and 37.6 ppm indicate the presence of two tertiary carbon atoms which are assigned to C-7 and C-8, respectively.

The cyclopropane ring of **8** is probably formed by intramolecular nucleophilic substitution involving an intermediate carbanion.[5] Compound **8** appears to be rather strained judging from a molecular model, but conjugation of the cyclopropane ring and two carbonyl groups is likely to stabilize the compound to such an extent as to readily permit its formation.

The dichloro compound (**7**) obtained by the chlorination of **2** yielded 7,7-dimethyl-6,7,8,9-tetrahydro-5*H*-benzocycloheptene-5,9-dione (**18**) containing a benzene ring when treated with γ-collidine. The structure of **18** was determined by ^{1}H-NMR spectroscopy. The signals centered at 7.71 δ, attributable to benzene ring protons, appear as a symmetrical multiplet. The signal for the *gem*-dimethyl protons appears as a singlet (6H) at 1.25 δ and that for the equivalent two methylene protons as a singlet (4H) at 2.75 δ.

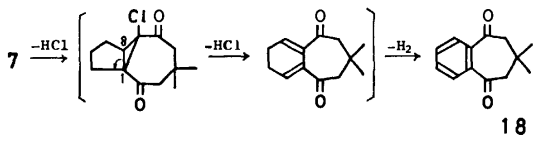

Scheme 4.

Experimental

The ^{13}C-NMR and the ^{1}H-NMR spectra were obtained on Hitachi R-26 and R-22 spectrometers in $CDCl_3$ with TMS as the internal standard. The mass spectra were measured with Hitachi RMU-6L and RMU-7M spectrometers. The IR and UV spectra were recorded using JASCO IR-G and Hitachi EPS-3 spectrophotometers, respectively. The VPC analysis was carried out on a 063 Hitachi gas chromatograph.

Bromination of Dione (2). A mixture of **2** (0.2 g) and pyridinium bromide perbromide (0.3 g) in ethanol (10 ml) was stirred at 40—50 °C. The reaction mixture was poured into water (150 ml) and the precipitated bromodione (**3**) (0.21 g) was collected. The product showed one spot on a TLC (silica gel). Recrystallization from ethanol gave pure **3** (0.15 g); mp 111—113 °C. IR and UV (see Table 1). Found: C, 54.67; H, 6.58%. Calcd for $C_{13}H_{19}O_2Br$: C,

54.37; H, 6.62%. MS: *m/e* 288 (M+2, 4%), 286 (M^+, 5), 273 (5), 271 (6), 232 (7), 230 (7), 220 (5), 218 (5), 207 (72), 191 (5), 189 (6), 179 (47), 163 (5), 161 (6), 151 (35), 135 (5), 133 (5), 123 (30), 109 (48), 95 (27), 83 (base, 100), 81 (62), 67 (27), 55 (62), and 41(62).

A similar reaction of **2** in acetic acid (10 ml) yielded a crude product (0.25 g) which was subjected to column chromatography on silica gel. Elution with ether–hexane (1 : 1) gave **4**. Crystallization (EtOH) gave pure **4**; mp 164—165 °C. IR (CCl_4) 1710 cm^{-1}. UV (EtOH) λ_{max} 324 nm (ε, 180). Found: C, 42.53; H, 4.86%. Calcd for $C_{13}H_{18}O_2Br_2$: C, 42.65; H, 4.92%. Further elution with ether–hexane (1 : 1) gave **3**. Mp 110—112 °C (EtOH), which was identified by IR spectroscopy.

Chlorination of Dione (2). Into a solution of **2** (0.4 g) in CCl_4 (15 ml), a solution of sulfuryl chloride (0.26 g) in CCl_4 (10 ml) was added dropwise with stirring. The mixture was allowed to stand at room temperature overnight. The resulting solution was washed successively with water and aqueous sodium hydrogencarbonate. After the organic solution had been dried over sodium sulfate, it was concentrated under reduced pressure. The residual oil was chromatographed on a silica gel column with ether–hexane (1 : 2). The amounts of the products isolated in the order of their elution were: 51 mg of dichloro-dione (**7**), 42 mg of monochloro-dione (**6**), 20 mg of monochloro-dione (**5**), 58 mg of dione (**2**), and 167 mg of 4,4-dimethyltricyclo[6.3.0.$0^{1,7}$]-undecane-2,6-dione (**8**). Recrystallization of chlorodiones **5**, **6**, and **7** from ethanol and of **8** from hexane–ether (5 : 1) gave pure products.

5: mp 108—110 °C. IR and UV (see Table 1). Found: C, 64.47; H, 7.68%. Calcd for $C_{13}H_{19}O_2Cl$: C, 64.33; H, 7.84%. MS: *m/e* 242 (M^+, 3%), 207 (3), 151 (3), 141 (80), 123 (5), 112 (36), 109 (2), 104 (2), 102 (6), 95 (7), 83 (base, 100), 81 (10), 67 (17), 55 (13), and 41 (18).

6: mp 126—127 °C. IR and UV (see Table 1). Found: C, 64.39; H, 7.52%. MS: *m/e* 242 (M^+, 2%), 207 (37), 179 (7), 151 (2), 123 (3), 122 (3), 111 (12), 109 (6), 95 (13), 83 (base, 100), 81 (17), 67 (12), 55 (16), and 41 (14).

7: mp 168—170 °C. IR and UV (see Table 1). Found: C, 56.47; H, 6.24%. Calcd for $C_{13}H_{18}O_2Cl_2$: C, 56.32; H, 6.50%. MS: *m/e* 276 (M^+, 0.5%), 261 (1.5), 243 (5), 242 (14), 227 (2), 213 (3), 207 (3), 205 (3), 178 (2), 176 (8), 174 (25), 163 (2), 161 (7), 159 (3), 157 (4), 153 (2), 150 (2), 149 (2), 143 (4), 141 (5), 123 (4), 115 (6), 111 (17), 108 (3), 107 (3), 102 (3), 95 (3), 83 (base, 100), 79 (13), 77 (12), 67 (12), 55 (19), and 41 (19). The mass spectrum of **7** shows a fragment peak at *m/e*=102 (67+Cl) and it is likely that one chlorine atom is present at the ring junction and the other at position 7.

8: mp 106—107 °C. IR: (CCl_4) 3040, 2950, and 2805 cm^{-1} (C–H), 1685 cm^{-1} (C=O); (Nujol) 1660 and 1675 cm^{-1} (C=O). UV (EtOH) λ_{max} 288 nm (ε, 69), ε at 210 nm (7100). ^{1}H-NMR ($CDCl_3$) 0.91 δ (s, 3H, CH_3) and 1.10 δ (s, 3H, CH_3). ^{13}C-NMR ($CDCl_3$) 206 ppm (s, C-2, C-6), 56.2 and 54.6 ppm (t, C-3, C-5), 49.2 ppm (s, C-1), 40.9 ppm (d, C-7), 37.6 ppm (d, C-8), 34.2 (s, C-4), 32.9 and 24.7 ppm (q, diCH_3), 29.0 and 27.7 ppm (t, C-9, C-11), and 19.5 ppm (t, C-10). Found: C, 75.45; H, 9.06%. Calcd for $C_{13}H_{18}O_2$: C, 75.73, H, 8.74%. MS: *m/e* 206 (M^+, $C_{13}H_{18}O_2$, 63%), 191 ($C_{12}H_{15}O_2$, 8), 188 ($C_{13}H_{16}O$, 5), 178 ($C_{12}H_{18}O$, 9), 163 ($C_{11}H_{15}O$, 11), 150 ($C_9H_{10}O_2$, 41), 135 ($C_8H_7O_2$, 11), 122 ($C_8H_{10}O$, 48), 108 (C_7H_8O, 80), 94 (C_6H_6O, C_7H_{10}, 14), 83 (C_5H_7O, 100), 79 (C_6H_7, 36), and 67 (C_5H_7, 8).

Chlorination of 1a. To a solution of **1a** (0.3 g) in CCl_4 (10 ml), sulfuryl chloride (0.1 ml) in CCl_4 (5 ml) was added dropwise with stirring at 60 °C. The resulting solution was stirred for 1 h and then washed with water, aqueous sodium hydrogencarbonate and aqueous sodium chloride. After the organic solution had been dried over (sodium sulfate) and concentrated under reduced pressure, a crude crystalline compound (0.35 g) was obtained. Recrystallization (EtOH) afforded pure **9** (0.22 g); mp 130—132 °C. IR (Nujol) 1703 cm^{-1} (C=O) and 1730 cm^{-1} ($OCOCH_3$). Found: C, 63.41; H, 7.10%. Calcd for $C_{15}H_{21}O_3Cl$: C, 63.27; H, 7.38%.

From the parent solution, **11** (25 mg) was obtained; mp 163—165 °C. IR (Nujol) 1708 cm^{-1} (C=O) and 1733 cm^{-1} ($OCOCH_3$). Found: C, 56.32; H, 6.03%. Calcd for $C_{15}H_{20}O_3Cl_2$: C, 56.43; H, 6.27%.

Bromination of 1a. A mixture of **1a** (0.3 g) and pyridinium bromide perbromide (0.5 g) in acetic acid (10 ml) was stirred at room temperature until the reagent was dissolved and the mixture had reacted. The reaction mixture was poured into ice water (150 ml) and the precipitate (0.42 g) was collected. Recrystallization (EtOH) gave **10** (0.25 g); mp 142—144 °C. IR (Nujol) 1690 cm^{-1} (C=O) and 1740 cm^{-1} ($OCOCH_3$). Found: C, 54.88; H, 6.61%. Calcd for $C_{15}H_{21}O_3Br$: C, 54.73; H, 6.38%.

From the parent solution, **12** (48 mg) was obtained; mp 164—166 °C. IR (Nujol) 1705 cm^{-1} (C=O) and 1730 cm^{-1} ($OCOCH_3$). Found: C, 43.96; H, 5.14%. Calcd for $C_{15}H_{20}O_3Br_2$: C, 44.14; H, 4.90%.

Chloro-dione (13) and Bromo-dione (14). A solution of 0.35 g of **9** (or **10**) in methanol (40 ml) containing sulfuric acid (2 ml) was left to stand at room temperature for two weeks. The reaction mixture was concentrated at reduced pressure and extracted with ether. The ethereal extract was neutralized with aqueous sodium hydrogencarbonate, washed with water, and then dried over sodium sulfate. After the removal of the ether, a crystalline residue was obtained. Recrystallization from methanol gave **13** (0.10 g) (or **14** (0.12 g)).

13: mp 90—92 °C. IR and UV (see Table 1). Found: C, 64.17; H, 7.96%. Calcd for $C_{13}H_{19}O_2Cl$: C, 64.33; H, 7.84%. MS: *m/e* 242 (M^+, 1%), 207 (1.5), 188 (2), 186 (4), 175 (11), 173 (18), 152 (17), 124 (56), 109 (10), 95 (73), 92 (5), 90 (12), 83 (base, 100), 81 (25), 67 (73), 55 (38), and 41 (58).

14: mp 115—116 °C. IR and UV (see Table 1). Found: C, 54.52; H, 6.40%. Calcd for $C_{13}H_{19}O_2Br$: C, 54.37; H, 6.62%. MS: *m/e* 288 (M+2, 2%), 286 (M^+, 2), 232 (4), 230 (4), 221 (11), 219 (14), 207 (64), 179 (4), 152 (42), 136 (7), 134 (7), 124 (72), 111 (10), 109 (10), 97 (23), 95 (70), 83 (base, 100), 81 (28), 67 (56), 55 (37), and 41 (50).

Dehydrochlorination of 5, 6, and 7. A mixture of **5** (20 mg) and γ-collidine (0.5 ml) was refluxed for 10 min in a nitrogen atmosphere. Rapidly, a precipitate of γ-collidine hydrochloride was produced. The resulting mixture was diluted with petroleum ether, filtered to separate of γ-collidine hydrochloride and then washed successively with 4% aqueous hydrochloric acid, aqueous sodium hydrogencarbonate, and water. The solvent was removed and the residue was crystallized from hexane, mp 100—103 °C (92% yield). The product was identical to **8** on the basis of a comparison of their IR spectra.

A similar reaction of **6** (20 mg) with refluxing for 2 h also gave **8** (85% yield).

Similarly, **7** (0.2 g) was refluxed with γ-collidine (1.5 ml) for 2 h and treated in the manner described above. The product was crystallized from hexane, mp 90—92 °C (58 mg). Recrystallization (hexane) afforded pure **18**; mp 97—99 °C. IR (Nujol) 1690 cm^{-1} (C=O) and 1590 cm^{-1} (C=C). UV

(EtOH) λ_{max} 221.5 nm (ε, 22700), 258 (7080), and 296 (2070). ^{1}H-NMR ($CDCl_3$) 1.25 δ (s, 6H, diCH_3), 2.75 δ (s, 4H, 2CH_2), and 7.56—7.87 δ (m, 4H, ArH). Found: C, 77.18; H, 7.06 %. Calcd for $C_{13}H_{14}O_2$: C, 77.23; H, 6.93%. MS: *m/e* 202 (M^+, 14%), 174 (3), 159 (3), 146 (base, 100), 129 (4), 104 (26), 90 (9), 76 (22), 50 (9), and 41 (9), The formation of **18** from **7** probably proceeds *via* an intermediate containing a cyclopropane ring similar to **8**, followed by the opening of the cyclopropane ring at C_1–C_8 and further dehydrogenation (Scheme 4).

*Reactions of **3**, **13**, and **14** with γ-Collidine.* In the manner described above, **3**, **13**, and **14** (20 mg) were refluxed with γ-collidine for 2 h. In each case, no precipitation of γ-collidine hydrochloride occured and the starting material was recovered in a 80—87% yield, and identified by IR spectroscopy.

*4,4-Dimethylbicyclo[6.3.0]undec-5-en-2-one (**17**).* In a solution of **3** (0.3 g) in ethanol (20 ml), $NaBH_4$ (0.15 g) in ethanol (20 ml) was added at 20 °C. The solution was left to stand at room temperature for 48 h, diluted with water and extracted with ether. The ethereal solution was dried and evaporated *in vacuo*. The glassy residue (**15**) was dissolved in acetic acid (30 ml) and refluxed with zinc dust (2 g) for 1.5 h. The reaction mixture was filtered and extracted with ether. The extract was processed by the usual method and gave an oily residue (**16**); Tetranitromethane test positive. To a solution of crude **16** in acetic acid (10 ml), chromic trioxide (0.3 g) in acetic acid (12 ml) was added dropwise with stirring at 25 °C and the solution was allowed to stand at room temperature overnight, diluted with water and extracted with ether. After the usual procedure, the extract gave an oily residue. Column chromatography (on silica gel) of the product using hexane elution gave **17** (62 mg) and a by-product (54 mg) which is probably acetate of **16** (ν 1730 cm^{-1}). Product **17** was further purified by column chromatography and preparative TLC (Silica Gel G) and obtained as a colorless oil which solidified in a refrigerator and showed one peak on a VPC; Beilsteine test negative and tetranitromethane test positive. Mp 26 °C. IR (neat) 3000, 2940, and 2850 cm^{-1} (C–H), 1695 cm^{-1} (C=O), 1640 cm^{-1} sh (C=C). ^{1}H-NMR ($CDCl_3$) 0.93 δ (s, 3H, CH_3), 1.12 δ (s, 3H, CH_3) and 5.56—5.80 δ (m, 2H, olefinic). ^{13}C-NMR ($CDCl_3$) 211.6 ppm (s, C-2), 134.8 and 128.8 ppm (d, C-5, C-6), 62.6 ppm (d, C-1), 52.4 ppm (t, C-3), 43.2 ppm (d, C-8), 39.6 and 34.2 ppm (t, C-7, C-11), 33.0 ppm (s, C-4), 29.0 and 29.4 ppm (q, diCH_3), 25.8 and 23.0 ppm (t, C-9, C-10). Found: C, 81.07; H, 10.51%. Calcd for $C_{13}H_{20}O$: C, 81.25; H, 10.42%. MS: *m/e* 192 (M^+, 6%), 177 (16), 159 (2), 149 (5), 136 (28), 121 (11), 108 (base, 100), 93 (47), 81 (17), 80 (18), 79 (15), 68 (15), and 67 (14). 2,4-DNP: mp 148—149 °C.

References

1) M. Umehara, T. Oda, Y. Ikebe, and S. Hishida, *Bull. Chem. Soc. Jpn.*, **49**, 1075 (1976).

2) L. F. Fieser and R. Ettorre, *J. Am. Chem. Soc.*, **75**, 1700 (1953); L. F. Fieser and X. A. Dominguez, *ibid.*, **75**, 1704 (1953).

3) R. N. Jones, D. A. Ramsay, F. Herling, and K. Dobriner, *J. Am. Chem. Soc.*, **74**, 2828 (1952); R. N. Jones, *ibid.*, **75**, 4839 (1953); E. J. Corey, *ibid.*, **75**, 2301 (1953); N. J. Leonard and F. H. Owens, *ibid.*, **80**, 6039 (1958).

4) R. C. Cookson, *J. Chem. Soc.*, **1954**, 282.

5) A. C. Knipe and C. J. M. Stirling, *J. Chem. Soc., B*, **1968**, 67; R. Bird and C. J. M. Stirling, *ibid.*, **1968**, 111.

The Transannular Cyclization and Hydrogen Shift in the Chlorination of 1,5-Cyclooctadiene and *cis*-Cyclooctene with Antimony(V) Chloride

Sakae UEMURA,* Akira ONOE, and Masaya OKANO
Institute for Chemical Research, Kyoto University, Uji, Kyoto 611

(Received September 18, 1976)

The slow addition of $SbCl_5$ to a CCl_4 solution of 1,5-cyclooctadiene or *cis*-cyclooctene gives an isomeric mixture of *endo*- and *exo*-2, *anti*-8-dichlorobicyclo[3.2.1]octanes (**1** and **2**) or an isomeric mixture of *trans*- and *cis*-1,4-dichlorocyclooctanes (**12** and **13**) respectively in a good yield. The former reaction involves the transannular cyclization, while the latter is accompanied by the transannular hydrogen shift. The addition of 1,5-cyclooctadiene to a CCl_4 solution of $SbCl_5$ (reverse addition) affords *endo*-2,6- and *endo*, *exo*-2,6-dichlorobicyclo[3.3.0]octanes (**6** and **7**) as additional products, besides **1** and **2**. In the case of *cis*-cyclooctene, however, a reverse addition produces only chlorocyclooctane. It has been revealed that a mixture of **6** and **7** is readily isomerized to a mixture of **1** and **2** by the interaction with $SbCl_5$. The 1,4-chlorination of *cis*-cyclooctene which gives **12** and **13** also occurs with VCl_4, $SeCl_4$, $PhICl_2$, and PCl_5, although the selectivity and the yield are low compared to the case of $SbCl_5$.

It has been reported that $SbCl_5$ is a good reagent for the *cis*-chlorination of simple olefins[1,2] and for the formation of *cis*-1,4-dichloro-2-butene from 1,3-butadiene.[2,3] Other features of $SbCl_5$ have recently been recognized in the favorable *cis*-chlorination of alkylphenylacetylenes[4] and in the facile isomerization of some dichloronorbornenes to other isomers.[5] As a part of the study of chlorination with $SbCl_5$, we now wish to report the unusual chlorinations of 1,5-cyclooctadiene (1,5-COD) and of *cis*-cyclooctene, both involving a transannular interaction.[6]

Results and Discussion

Chlorination of 1,5-COD (Table 1). When two equivalents of $SbCl_5$ in CCl_4 were slowly added to a CCl_4 solution of one equivalent of 1,5-COD at −20 °C, an isomeric mixture of *endo*- and *exo*-2, *anti*-8-dichlorobicyclo[3.2.1]octanes (**1** and **2**, respectively) was obtained in a 59% yield (**1** : **2**=67 : 33 by GLC). When equimolar amounts of $SbCl_5$ and 1,5-COD were used, the yields of **1** and **2** were increased, and the additional formation of small amounts of stereoisomeric dichlorobicyclo[3.3.0]octanes (**6** and **7**) was observed (Scheme 1). Almost identical results were obtained by the use of CH_2Cl_2 or $CHCl_3$ as the solvent. Some typical results are recorded in Table 1 (Runs 1—3).

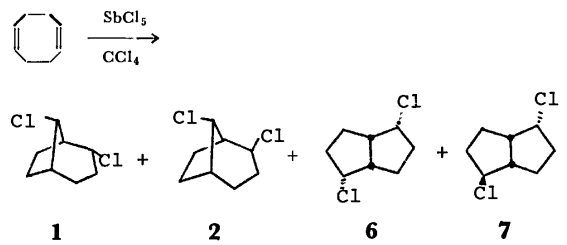

1 **2** **6** **7**

Scheme 1.

A mixture of **1** and **2** was analyzed as $C_8H_{12}Cl_2$, did not have any absorption due to olefinic protons in its IR and NMR spectra, did not decolorize bromine in CCl_4, and was monodehydrochlorinated to *anti*-8-chlorobicyclo[3.2.1]oct-2-ene (**3**) by treatment with *t*-BuOK in DMSO (Scheme 2).

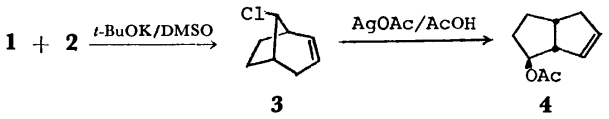

3 **4**

Scheme 2.

Here, it was observed that **2** was more readily dehydrochlorinated than **1**, as was expected from the E2 elimination.[7] In **2**, the chlorine, two carbons (C_2 and C_3), and the hydrogen on C_3 lie in a common plane. By this procedure **1** was separated from **2**. A sharp singlet at δ 3.85 in **1** and δ 4.23 in **3** could be assigned to a *syn*-hydrogen at C_8, the absorption being very similar to that of *anti*-8-chloro-*endo*-2-(methoxymethyl)bicyclo[3.2.1]octane[8] [δ 3.94, singlet] (See Experimental). Although the isolation of pure **2** was not achieved, a sharp singlet at δ 4.60 in the NMR spectrum of a mixture of **1** and **2** could be assigned to a *syn*-hydrogen at C_8 in **2**. This greater deshielding of the C_8-hydrogen in **2** than that in **1** may be due to the anisotropy of *exo*-chlorine at C_2. Additional proof for the structure of **3** was obtained by its reaction with silver acetate in acetic acid, which gave *exo-cis*-bicyclo[3.3.0]oct-7-en-2-yl acetate (**4**).[9] LeBel and Spurlock[10] have reported that **4** was formed by the acetolysis of the *p*-toluenesulfonate analogue of **3**.

It has been known that the transannular cyclization of 1,5-COD usually gives bicyclo[3.3.0]octane derivatives.[8] The formation of bicyclo[3.2.1]octane derivatives has been reported only in the case of the reaction with $MeOCH_2Y$ (Y=OAc, Cl, and OMe), and even in this case the main products were bicyclo[3.3.0]octane derivatives.[8] Considering that $SbCl_5$ is a very effective catalyst for isomerization between the isomeric dichloronorbornanes,[5] the most probable pathway for the formation of **1** and **2** seems to be that a mixture of *endo*-2,6- and *endo*, *exo*-2,6-dichlorobicyclo[3.3.0]octanes (**6** and **7**) is first formed through the **5** cation (*endo*-Cl) and then isomerized to a mixture of **1** and **2** by the $SbCl_5$ catalyst through the **8** cation (*exo*- and *endo*-Cl) (Scheme 3). In fact, when 1,5-COD was added all at once to a CCl_4 solution of equimolar $SbCl_5$ at −20 °C, instead of slow addition of $SbCl_5$ to a CCl_4 solution of 1,5-COD, the

* To whom correspondence should be addressed.

Table 1. Chlorination of 1,5-COD with $SbCl_5$

Run	1,5-COD (mmol)	$SbCl_5$ (mmol)	Solvent (ml)	Temp (°C)	Time (min)	Product Isomer distribution 1	2	6	7	Yield[a] (%)
1[b]	25	50	CCl_4 100	−20	30	67	33	<0.5	<0.5	59[c]
2[b]	25	25	CCl_4 100	−20	30	68	29	3	<0.5	72[c]
3[b]	25	25	CH_2Cl_2 100	−20	30	59	33	5	3	75
4[d]	50	25	CCl_4 100	40—50	1	35	14	35	16	83
5[d]	25	4.4	CCl_4 50	0	0.17	30	9	41	20	69
6[b]	50	25	CS_2 100	−20	30	44	17	30	9	76
7[d]	50	25	CS_2 100	40	1	29	11	40	20	71

a) Based on the amount of $SbCl_5$. Determined by GLC. b) A solution of $SbCl_5$ was slowly added. c) Based on the amount of 1,5-COD. d) A solution of 1,5-COD was added all at once.

Table 2. Chlorination of *cis*-cyclooctene

cis-Cyclooctene (mmol)	Chlorinating agent (mmol)	Solvent (ml)	Temp (°C)	Time (h)	Product Isomer distribution 10	11	12	13	Yield[a] (%)
50	$SbCl_5$ 25	CCl_4 100	−30	0.5	0	5	7	88	81[b]
20	VCl_4 2.4	CCl_4 50	25	15	20	9	56	15	63
20	VCl_4 2.5	CCl_4 50	76	2	35	22	26	17	22
10	$SeCl_4$ 3	CCl_4 50	76	5	43	0	11	46	12
50	PCl_5 25	CCl_4 50	76	3	75	19	3	3	87
50	PCl_5 25	CH_2Cl_2 50	25	10	97	<0.5	2	1	83
50	SO_2Cl_2 25	CCl_4 50	76	2	75	25	0	<0.5	81
50	$CuCl_2$ + LiCl 50 each	CH_3CN 50	82	12	55	45	0	0	24
5	$PhICl_2$ 2 (O_2)	$CHCl_3$ 10	61	0.5	55	1	9	35	80
5	$PhICl_2$ 2 (N_2)	$CHCl_3$ 10	61	0.5	74	25	0	1	89
50	$PbCl_4$ 10	CH_2Cl_2 50	−40	2	3	0	20	77	69[c]
50	$PbCl_4$ 10	CH_2Cl_2 50	−10	2	49	0	22	29	93

a) Based on the amount of chlorinating agent charged. Determined by GLC. b) Other product: chlorocyclooctane (2 mmol). c) Other product: chlorocyclooctane (7.7 mmol). In Ref. 13; **10**:**11**:**12**:**13**=9:0:20:70.

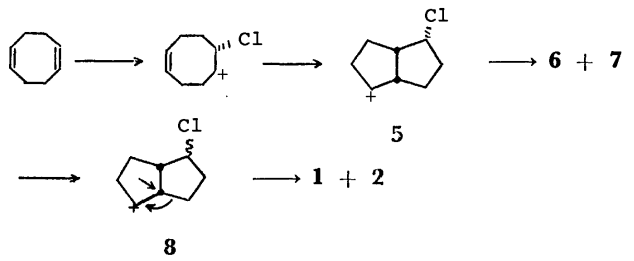

Scheme 3.

formation of considerable amounts of **6** and **7** besides **1** and **2** was observed (Table 1, Runs 4 and 5). Since **6** and **7** could not be isolated in a pure state, and since, also, several attempts at the preparation by different methods were unsuccessful, these structures were tentatively assigned by means of NMR spectra and the analytical data of the mixture (See Experimental). In separate experiments we observed that a mixture containing **1**, **2**, **6**, and **7** was readily converted to a mixture of **1** and **2** by treatment with $SbCl_5$. These results appear to show that the $SbCl_5$-catalyzed isomerization of a mixture of **6** and **7** to that of **1** and **2** considerably rapid and that their rates are sufficient to compete with that of the first step (producing **6** and **7**) of the chlorination. That is, in the case of the rapid addition of excess 1,5-COD, enough $SbCl_5$ did not remain to make the isomerization of **6** and **7** complete, because $SbCl_5$ turned to $SbCl_3$ as soon as chlorination took place. This finding parallels that in the chlorination of norbornene with $SbCl_5$.[5] Although we have not yet been successful in finding out the reaction conditions under which only **6** and **7** were formed, it may be worthwhile to refer to the facts that the isomerization is slower in the CS_2 solvent than in CCl_4 and that more **6** and **7** are obtained in this solvent (Table 1, Runs 6 and 7).

As has been described above, we proposed and partly confirmed that **1** and **2** could be formed through **6** and **7**. Apparently, another route for all the products may be considered when the attack of $SbCl_6^-$ on the nonclassical cation **9**, which is a stabilized form of **5**, is involved. However, the lesser stereospecificity in the bicyclo[3.2.1]octane ring formation and the complete absence of isomers of dichlorobicyclooctanes other than **1**, **2**, **6**, and **7** appear to imply that such a route is improbable.

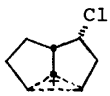

9

The chlorination of 1,5-COD with other chlorinatingi agents, such as Cl_2, $PhICl_2$, $CuCl_2$, $SeCl_4$, $MoCl_5$, and $PbCl_4$, gave a mixture of *cis*- and *trans*-5,6-dichlorocyclooctenes and no **1** or **2**.[11]

Chlorination of cis-*Cyclooctene (Table 2).* The application of the chlorination with $SbCl_5$ to *cis*-cyclooctene at −30 °C (the addition of $SbCl_5$ to olefin) resulted in the preferable formation of *cis*-1,4-dichlorocyclooctane (**13**, 71% yield), together with small amounts of the *trans*-1,4-isomer (**12**, 6%) and the *cis*-1,2-isomer (**11**, 4%). It was confirmed that no interconversion occurred between the 1,2- and 1,4-isomers or also between the *cis*- and *trans*-1,4-isomers under the present conditions. The reaction apparently involves a transannular 1,5-hydride shift, and the strikingly high selectivity for the formation of the *cis*-1,4-isomer **13** may be explained by assuming a hydrogen-bridged chlorocyclooctyl cation intermediate (Scheme 4), almost the same as that

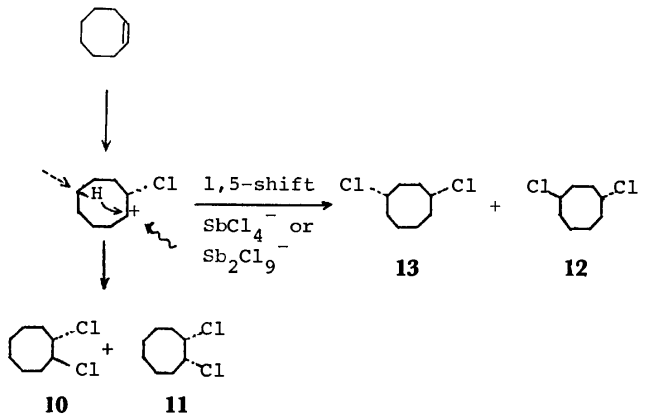

Scheme 4.

proposed in the formolysis of *cis*-cyclooctene oxide.[12] Both the total yields of the products (**10**—**13**) and the selectivities affording **13** were decreased when the reaction was carried out at 0 °C or at room temperature. A reverse addition, namely, the addition of *cis*-cyclooctene to $SbCl_5$, afforded only chlorocyclooctane at −20, 20, or 76 °C, irrespective of the speed of the addition. This may be explained by the rapid hydride abstraction by $SbCl_5$ from olefin, followed by the addition of the produced hydrogen chloride to olefin, because excess $SbCl_5$ is present in the solution when olefin has been added. Such hydride abstraction by $SbCl_5$ from alkane and alkene to form hydrogen chloride has previously been reported.[2] Although the 1,4-chlorination with $PbCl_4$ has been known,[14] $SbCl_5$ is superior to $PbCl_4$ in its yield and in its selectivity for the formation of the *cis*-1,4-isomer. This seems to be another feature of the chlorination of olefin with $SbCl_5$. As a part of our study of the chlorination of olefins with various chlorinating agents,[5,11,14] we have examined their behavior toward *cis*-cyclooctene and found that 1,4-chlorination also occurred with $PhICl_2$ (ionic condition), VCl_4, $SeCl_4$, and PCl_5, although the selectivities and the yields were low compared to those in the cases of $SbCl_5$ and $PbCl_4$. The chlorinations with $CuCl_2$, SO_2Cl_2 (radical condition), and $PhICl_2$ (radical condition) gave almost only the 1,2-somers, **10** and **11**.

Experimental

All the organic and inorganic materials were commercial products. The IR and NMR spectra were recorded with a Hitachi EPI-S2 and a Varian A-60 (CCl_4 as solvent) apparatus respectively. The GLC analyses were carried out on Shimadzu 4BMPF apparatus, using EGSS-X(15%)-Chromosorb-W (3 m), PEG 6000(25%)-Chromosorb-W (3 m), and Apiezon-L(30%)-Celite (1 m) columns (N_2 as carrier gas).

Chlorination of 1,5-COD with $SbCl_5$. To a CCl_4 (200 ml) solution of 1,5-COD (16.2 g), we slowly added a solution of $SbCl_5$ (45 g, 150 mmol) in CCl_4 (100 ml) at −20 °C under N_2 for 30 min. Aqueous NaOH was then added, and the organic layer was separated after the usual work-up. Distillation gave 13.2 g of a mixture of **1** and **2** (**1** : **2**=*ca.* 70 : 30), contaminated by a trace amount of **6**; bp 117—119 °C/22 Torr. Found: C, 53.30; H, 7.06; Cl, 39.75%. Calcd for $C_8H_{12}Cl_2$: C, 53.64; H, 6.76; Cl, 39.60%.

When 1,5-COD (5.4 g, 50 mmol) was added, all at once, to a CS_2 (100 ml) solution of $SbCl_5$ (7.5 g, 25 mmol) at a refluxing temperature, an isomeric mixture of four dichloroalkanes which contained **6** and **7** besides **1** and **2** was obtained (18 mmol, **1** : **2** : **6** : **7**=29 : 11 : 40 : 20 by GLC). Although it was not possible to isolate both **6** and **7** in a pure state by fractional distillation, two fractions (**A** and **B**) which contain mainly **6** and **7** respectively were obtained by the distillation of the combined reaction products of several runs. The NMR spectrum of Fraction **A** (bp 110—114 °C/21 Torr, **1** : **2** : **6** : **7**=7 : 4 : 14 : 75 by GLC) showed two multiplet peaks at δ 4.7—4.3 and δ 4.3—3.8 which could be assigned to *exo*- and *endo*-hydrogen in **7** respectively. Found: C, 53.37; H, 7.07%. Calcd for $C_8H_{12}Cl_2$: C, 53.64; H, 6.76%. The NMR spectrum of Fraction B (bp 118—122 °C/21 Torr, **1** : **2** : **6** : **7**=30 : 12 : 55 : 3 by GLC) showed a broad multiplet peak at δ 4.65—4.0 which could be assigned to two *exo*-hydrogen in **6**. Found: C, 52.93; H, 7.22%. Calcd for $C_8H_{12}Cl_2$: C, 53.64; H, 6.76%.

*Dehydrochlorination of **1** and **2**.* A mixture of **1** and **2** (25 g, 140 mmol) was added, drop by drop, to a DMSO (200 ml) solution of *t*-BuOK (50 g, 446 mmol) at room temperature, and then the mixture was heated to 60 °C for 10 h. The reaction mixtures were worked up by the following successive treatments: dilution with water, extraction with ether, and then the evaporation of the ether. After the fractional distillation of the residue, the monochloride (**3**; 2.8 g, 20 mmol, bp 78—81 °C/22 Torr) and the dichloride (**1**; 8.7 g, 49 mmol, bp 123—124 °C/25 Torr) were both purely isolated. **3**, NMR: δ 6.0—5.2 (m, 2H), 4.23 (s, 1H), 2.8—1.2 (m, 8H); mass: *m/e* 142 (M^+), 144 (M^++2). **1**, NMR: δ 4.1—3.85 (m, 1H), 3.85 (s, 1H), 2.7—1.2 (m, 10H); mass: *m/e* 178 (M^+), 180 (M^++2), 182 (M^++4). Found: C, 53.51; H, 7.01%. Calcd for $C_8H_{12}Cl_2$: C, 53.64; H, 6.76%. **2**, NMR: δ 4.60 (s, 1H); the other absorptions overlap those of **1** and have not been clarified.

*Acetolysis of **3**.* The reaction of **3** (2.9 g, 20.3 mmol) with AgOAc (4.0 g, 24.0 mmol) in acetic acid (40 ml) at a refluxing temperature for 10 h gave 2.1 g of **4**; bp 101—102 °C/18 Torr (lit,[9] 69—73 °C/5 Torr), *m/e* 166 (M^+). The NMR spectrum (in $CDCl_3$) of **4** was identical with that of *exo-cis*-bicyclo[3.3.0]oct-7-en-2-yl acetate reported by Fujita *et al.*;[9] δ 5.6 (s, 2H), 4.9—4.7 (m, 1H), 1.94 (s, 3H), 3.1—1.2 (m, 8H).

*Isomerization of a Mixture of **6** and **7** to a Mixture of **1** and **2** with $SbCl_5$.* A CCl_4 (10 ml) solution containing a

mixture of the dichlorides (0.14 g, 0.76 mmol; **1** : **2** : **6** : **7**= 29 : 11 : 40 : 20) and $SbCl_5$ (0.65 g, 2.2 mmol) was kept at 0 °C for 30 min. A GLC analysis of the CCl_4 layer after a usual work-up revealed the presence of a mixture of **1** (63%) and **2** (37%); yield of the mixture, 65%.

Chlorination of cis-*Cyclooctene with* $SbCl_5$. To a solution of *cis*-cyclooctene (5.5 g, 50 mmol) in CCl_4 (40 ml), we added $SbCl_5$ (7.5 g, 25 mmol) in CCl_4 (10 ml) at −30 °C under N_2 for 30 min; aqueous NaOH was then added to stop the reaction. After the usual work-up, the distillation of the organic layer afforded 2.3 g of **13** in an almost pure state; bp 115—118 °C/8 Torr (lit,[13] 116—119 °C/10 Torr). NMR: δ 4.5—3.9 (m, 2H), 2.4—1.8 (m, 12H). The NMR spectrum was identical with that of *cis*-1,4-dichlorocyclooctane reported by Havinga *et al.*[13]

When the reverse addition was carried out at 20—30 °C under N_2——namely, the addition of *cis*-cyclooctene (5.5 g, 50 mmol) to a solution of $SbCl_5$ (7.5 g, 25 mmol) in CCl_4 (100 ml), chlorocyclooctane (1.2 g, bp 98—104 °C/30 Torr, lit,[15] 82—90 °C/21 Torr) was the sole product; none of dichlorocyclooctane was formed.

The chlorinations with other metal salts were carried out by almost the same method as those previously reported.[5,11,14]

We wish to thank Dr. Kahee Fujita of Department of Pharmaceutical Sciences of Kyushu University for showing us the NMR spectrum of **4**.

References

1) S. Uemura, O. Sasaki, and M. Okano, *J. Chem. Soc., Chem. Commun.*, **1971**, 1064; F. Akiyama, T. Horie, and H. Matsuda, *Bull. Chem. Soc. Jpn.*, **46**, 1888 (1973).
2) S. Uemura, A. Onoe, and M. Okano, *Bull. Chem. Soc. Jpn.*, **47**, 692 (1974).
3) R. P. Vigners and J. Hamer, *J. Org. Chem.*, **39**, 849 (1974).
4) S. Uemura, A. Onoe, and M. Okano, *J. Chem. Soc., Chem. Commun.*, **1975**, 925.
5) S. Uemura, A. Onoe, and M. Okano, *Bull. Chem. Soc. Jpn.*, **48**, 3702 (1975).
6) Preliminary communication: S. Uemura, A. Onoe, and M. Okano, *J. Chem. Soc., Chem. Commun.*, **1975**, 210.
7) E. S. Gould, "Mechanism and Structure in Organic Chemistry," Holt, Rinehart, and Winston, New York (1959), p. 484.
8) I. Tabushi, K. Fujita, and R. Oda, *J. Org. Chem.*, **35**, 2376 (1970).
9) K. Fujita, K. Hata, R. Oda, and I. Tabushi, *J. Org. Chem.*, **38**, 2640 (1973).
10) N. A. LeBel and L. A. Spurlock, *Tetrahedron*, **20**, 215 (1964).
11) S. Uemura, A. Onoe, H. Okazaki, M. Okano, and K. Ichikawa, *Bull. Chem. Soc. Jpn.*, **49**, 1437 (1976).
12) Ref. 7, p. 600.
13) P. W. Henniger, L. J. Dukker, and E. Havinga, *Recl. Trav. Chim. Pays-Bas*, **85**, 1177 (1966).
14) A. Onoe, S. Uemura, and M. Okano, *Bull. Chem. Soc. Jpn.*, **49**, 345 (1976).
15) S. Uemura, O. Sasaki, and M. Okano, *Bull. Chem. Soc. Jpn.*, **45**, 1482 (1972).

Photochemical Valence Bond Isomerization of Some Benzo-C_9H_{10} Hydrocarbons*

Masahiko KATO, Takeji CHIKAMOTO, and Toshio MIWA

Faculty of Science, Osaka City University, Sugimoto-cho, Sumiyoshi-ku, Osaka 558

(Received September 18, 1976)

Studies have been carried out on the photochemical valence bond isomerization of some benzobicyclo-C_9H_{10} hydrocarbons, *i. e.*, benzo[8,9]bicyclo[5.2.0]nona-2,4,8-triene (**2**), benzo[2,3]bicyclo[6.1.0]nona-2,4,6-triene (**3**), *cis*-3*a*,9*b*-dihydro-1*H*-benz[*e*]indene (**6**), and benzo[6,7]bicyclo[3.2.2]nona-2,6,8-triene (**10**), with use of a low pressure mercury lamp. From a comparison of photolysis at low temperatures with that at room temperature, the stereochemical courses are discussed in terms of conformations of these compounds.

Interest has been taken in the thermal isomerization of benzo-C_9H_{10} hydrocarbons in connection with the valence bond isomerization of parent C_9H_{10}-hydrocarbons,[1] several studies[2] having been carried out. In the photochemical reaction of benzo[7,8]bicyclo-[4.2.1]nona-2,4,7-triene (**1**), Hahn and Johnson reported a difference in the product distribution between the direct and sensitized irradiation.[3] Their recent

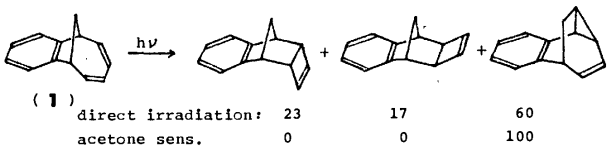

Scheme 1.

paper on photochemical rearrangements of benzo[2,3]-bicyclo[6.1.0]nona-2,4,6-triene (**3**) with use of a medium pressure mercury lamp (MPL)[4] has prompted us to report our independent study* on these reactions and those of other benzo-C_9H_{10} hydrocarbons photoinduced by a low pressure mercury lamp (LPL). Compound **3** was formed by thermal isomerization of **2**,[2a] both **2** and **3** being related to (*Z*,*Z*,*Z*,*Z*)-benzo[2,3]cyclonona-1,3,5,7-tetraene. Photochemical interconversion of these compounds is allowed in view of the orbital symmetry rule.

Results and Discussion

Photolysis of Benzo[2,3]bicyclo[6.1.0]nona-2,4,6-triene (3). Photolysis of **3** in tetrahydrofuran using an LPL at room temperature gave, along with some Skellysolve B insoluble polymeric material, a Skellysolve B soluble hydrocarbon mixture consisting of more than 70% *anti*-benzo[5,6]bicyclo[5.2.0.$0^{2,4}$]nona-5,8-diene (**4**) and less than 30% benzotetracyclononene (**5**).[5] The structure of **4** was deduced from its spectral data. The small coupling between H_1 and H_2 in the NMR spectrum is consistent only with the *anti*-structure. Compound **5** was also obtained by UV irradiation of *cis*-3*a*,9*b*-dihydro-1*H*-benz[*e*]indene (**6**) (*vide infra*). The latter compound is very likely to be an intermediate product in the formation of **5** from **3**. The production of **4** and **5** by photolysis of **3** with an MPL was reported by Hahn and Johnson, but their product ratio of **5** to **4** is larger than that we obtained using an LPL. Since it is reasonable to assume that the efficiency of a four pi-electrocyclic reaction is much grater with an LPL than that with an MPL, **4** was considered to be the main product in our experiment.

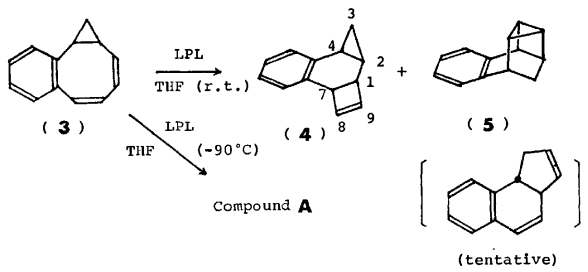

Scheme 2.

On the other hand, when **3** dissolved in THF-d_8 in a quartz NMR tube was irradiated at −90 °C using the same lamp, an unknown isomer **A**[6] (mass *m/e* 168 (M^+)) was obtained along with some polymeric material at the expense of **3**. Compound **4** was not detected.

The rigid extended conformation (**3a**) for **3** in its ground state very likely predominates at ambient temperature from the fact that thermal rearrangement occurs moderately only at elevated temperature, 150 °C, probably *via* inversion to the envelope conformer (**3b**), and that the NMR spectrum of **3** shows no temperature dependence in the range from room temperature to −90 °C. The following surmise on the photochemical behavior of **3** is possible from an examination of the molecular model. If the excitation occurs with 2537 Å light, one of the double bonds slightly conjugated to phenyl or another ethylenic group would change the conformation by turning its p-orbitals to nearly right angles to each other,[7] and the p-orbitals would enter into conjugation with either an aromatic or some other olefinic double bond as depicted in **3c** and **3d** with no additional strain. Since **3c** and **3d** are more flexible than **3a** or **3b** at room temperature, fast bonding between the nearest lobes of p-orbitals at C_4 and C_7 occurs in disrotatory motion to give **4**.[8]

On the other hand, **3** would be more firmly fixed in the extended conformation, **3a**, at −90 °C, rearrangement to **4** thus being suppressed and some other slow reaction becoming dominant. In sensitized irradiation at room temperature, **3** gives **6**[4] probably through inversion to **3b** from its triplet state followed by allowed

* Parts of this work (on the photolysis of Compounds **3** and **6**) were presented at the 30th Spring Meeting of the Japan Chemical Society, April 1—4, 1974 (Osaka). See the abstracts (1974), p. 1528.

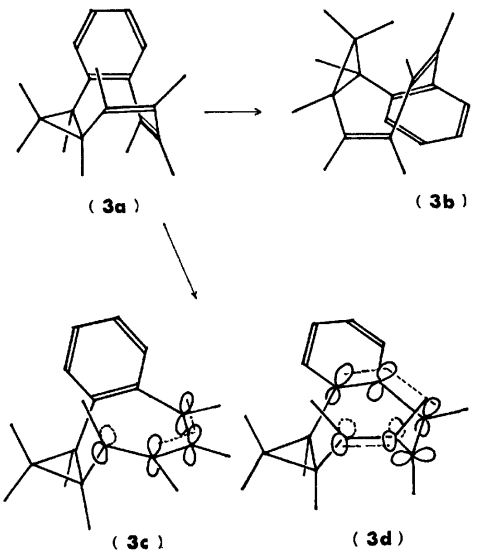

Scheme 3.

1,3-sigmatropic shift of 1-8 bond to 1-6.

Photolysis of Benzo[8,9]bicyclo[5.2.0]nona-2,4,8-triene (2). Irradiation of **2** in methanol with an LPL for 35 min gave three compounds; **6** (yield 9%), **7** (15%), and **8** (15%). They were separated by GLC, **7** and **8** being identified respectively as *anti*- and *syn*-benzo[3,4]-tricyclo[5.2.0.$0^{2,5}$]nona-3,8-diene in the following way. The UV spectra of the two compounds [**7** λ_{max}^{EtOH}: 262 (log ε, 3.16), 268 (3.34), 274 (3.31); **8** λ_{max}^{EtOH}; 265 sh (3.13), 270 (3.27), 276 (3.22)] showed a strong benzenoid band, suggesting the presence of benzocyclobutene moiety.[9] Their NMR spectra showed AB type proton signals characteristic of cyclobutene olefinic: δ 6.04 and 5.96 ppm (J=2.6 Hz) in **7** and δ 5.90 and 5.55 ppm (J=2.5 Hz) in **8**. Comparing the spectra with those of bicyclo[3.2.0]hept-6-ene derivatives,[10] and considering the splitting pattern of C_2 protons [**7** δ 3.76, d, $J_{2,5}$=4.0 Hz; $J_{1,2}$=quite small; **8** δ 3.94, d,d $J_{1,2}$= 9.0 Hz, $J_{2,5}$=5.0 Hz], we conclude that the structures of **7** and **8** are respectively of *anti* and *syn* conformation. Hahn and Johnson reported the formation of **3**, **6**, and **5** in addition to the main product (**7**) by photolysis of **2** with an MPL.[4] It is worth while to note that a new electrocyclic reaction product **8** was produced in an amount almost equal to that of **7** in the photolysis with an LPL. Neither **3** nor **4** was detected in the UV irradiation mixture of **2**. Even if compound **3** is formed, showing a high intensity absorption at 258 nm in UV spectrum, it would absorb light of the LPL to undergo change to **4** and others. The presence of **6** and the absence of **4** suggest a possible direct route from **2** to **6** under the present conditions.

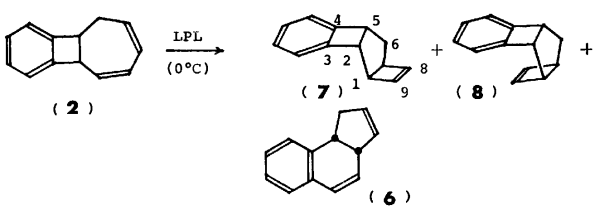

Scheme 4.

Photolysis of cis-*3a,9b-Dihydro-1H-benz*[e]*indene (6).* In the photochemical isomerization of the parent C_9H_{10}-hydrocarbons, it was reported that *cis*-8,9-dihydroindene and *cis*-bicyclo[6.1.0]nona-2,4,6-triene afford a similar photostationary mixture *via cis-trans* interconversion between (*E,Z,Z,Z*)- and (*Z,Z,Z,Z*)-cyclonona-1,3,5,7-tetraene.[1a] Taking this into consideration, we studied the photochemical behavior of **6**. Benzo[4,5]tetracyclo[4.3.0.$0^{2,9}$.$0^{3,8}$]non-4-ene(**5**) was formed readily, along with **4**, by irradiation of **6** with an LPL at room temperature. Compound **5** was separated by means of GLC and characterized by UV and NMR spectra. The unusually high field resonance of one of the methylene protons in the NMR spectrum was observed in the case of a similar compound (**9**).[1b] The formation of **3** from **6** has been proved by photolysis at low temperature, a condition which suppresses the conversion of **3** into **4**.

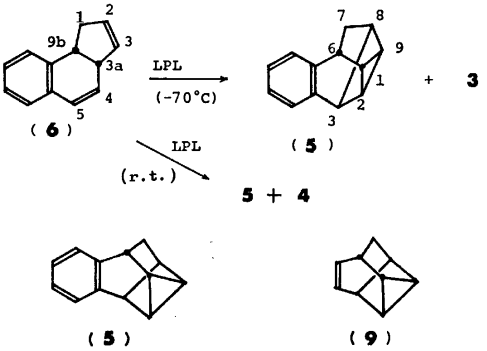

Scheme 5.

Thus compound **6** dissolved in THF in a quartz NMR tube was irradiated with an LPL at −65——70 °C and was partly transformed into **5** along with a small quantity of **3**. The acetophenone sensitized irradiation of **6** proceeded more distinctly, compound **5** being the only product detected.

Photolysis of Benzo[6,7]bicyclo[3.2.2]nona-2,6,8-triene (10). Photochemical isomerization of **10** has been studied, since 4-oxo derivative of **10** is photochemically related to 1-oxo derivative of **6**.[11] Sensitized photochemical isomerization of this sort of compound has been extensively studied and found to proceed in two directions through di-pi-methane mechanism.[12] In the case of the 9-*exo*-methylene analogue (**11**) of **10**, two products are formed, of which **13** is formed through stabilized biradical **12**

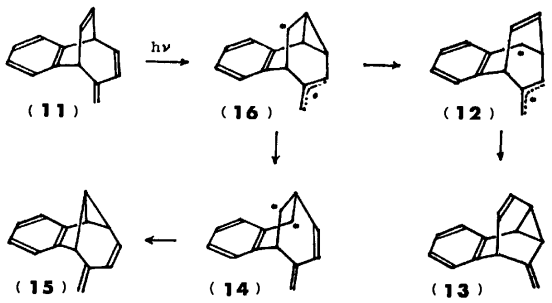

Scheme 6.

preferably to **15** produced through less stabilized biradical **14**.

In contrast, photolysis of **10** in acetone[13] using a high pressure mercury lamp (HPL) through a Pyrex filter gave rise to the formation of **17** and **18** in 52 and 9% yields, respectively, accompained by recovery of **10** (15%). If we assume that the initial bonding occurs between olefinic carbons as observed in the case of benzobicyclo[2.2.2]octatriene,[14] the reaction is governed by the comparative easiness of bond fission at *b* rather than *a* in the biradical intermediate (**19**). From an examination of the molecular model, the bond C_1–C_2 is seen to be more parallel to benzenoid pi-orbitals than the bond C_1–C_8. Thus the fission at *b* predominates over *a* to give **17** as the main product.

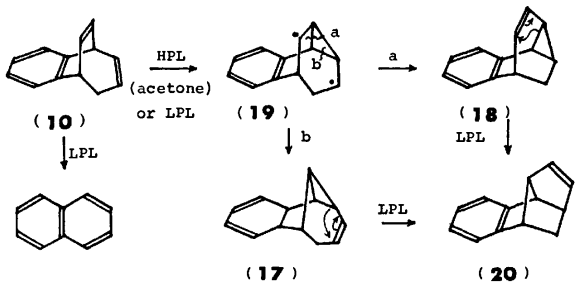

Scheme 7.

The difference in behavior of benzobicyclo[2.2.2]-octatriene in direct and sensitized irradiation[14] led us to study direct photolysis of **10**. When irradiation was carried out by use of an LPL at room temperature, **10** in ether was transformed into **17** (18%) and **18** (12%) accompanied by naphthalene (8%)[15] and a new compound (**20**)(11%). Both **17** and **18** isolated in pure form were independently transformed entirely into **20** by photolysis (LPL) in quartz NMR tubes in ether solution; *i.e.*, **17** gave **20** in 52% yield after 12 h irradiation, and **18**, **20** in 4% yield after 15 h irradiation. In acetone using a HPL, both **17** and **18** remained unchanged. Examination of Newman's projection formula of **17** and **18** revealed that in **17**, pi-electron at C_3 position is nearly parallel to the sigma bond at C_2 extended to C_9, while in **18**, the C_6–C_7 olefinic plane bisects the interior angle at C_8 of the three membered ring. It is reasonable to assume that the fission of C_2–C_9 in **17** is easier than that of C_2–C_8 in **18**, if we assume that the difference in ring strains between **17** and **18** is small. From the experiments, it is evident that, in contrast to benzobicyclo[2.2.2]-octatriene, **10** does not undergo the rearrangement involving aromatic-olefinic [$\pi 2+\pi 2$] intermediates such as **24** and **25**, **20** being a secondary product originating mainly from **17** and partly from **18** on irradiation of **10** using an LPL.

Characterization of ***17***, ***18***, *and* ***20***. Compound **17** was synthesized starting from benzo[7,8]bicyclo-[4.2.1]nona-2,4,7-trien-9-one (**21**)[16] as follows. Its hydrazone (**22**) was treated with potassium *t*-butoxide in DMSO giving its isomeric azo-compound (**23**), which was either pyrolyzed at 180 °C or photolyzed with a HPL (Pyrex filter) to give **17**, each in 70% yields. The compound was identical with a product obtained by photolysis of **10**.

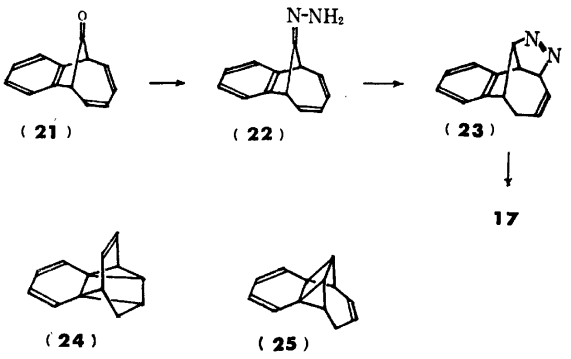

Scheme 8.

Benzobarbaralane (**18**) is one of the products obtained by the thermal rearrangement of **10**,[2b] the physical data being identical with those reported.

The structure of **20** was deduced mainly on the basis of its NMR spectrum and decoupling experiments. The UV spectrum [λ_{max}^{EtOH}: 262 (log ε, 3.14), 268 (3.16), 275 (3.13)] showed the presence of benzocycloalkene moiety of ring size less than 5.[17] Introduction of a methylene group and an ethylenic linkage without conjugation to aromatic ring, and its structural relationship to **17** and **18** make up the structure of **20**.

As expected, the proton coupling constants (Table 1) of **20** were similar to those of norbornane and norbornene,[18] strongly supporting the structure.

TABLE 1. THE PMR CHEMICAL SHIFTS AND THE COUPLING CONSTANTS OF COMPOUND **20** BY MEANS OF THE FIRST-ORDER ANALYSIS OF THE 100 MHz SPECTRA AND ITS DECOUPLING EXPERIMENTS

Chemical shifts (δ):

7.3—6.74 ppm	m	Ar-H	2.74—2.56	m	H_3
6.38	d, d	H_9	2.50—2.32	m	H_1
5.72	d, d, d	H_8	1.38	d, d	H_{2exo}
3.3—3.02	m	H_6, H_7	1.19	d, d	H_{2endo}

Coupling constants (J):

$J_{2exo,3}$=5.0 Hz — $J_{1,9}$=3.4 Hz

$J_{1,2endo}$=4.5 Hz — $J_{7,8}$=2.8 Hz

$J_{8,9}$=5.8 Hz — $J_{2exo,2endo}$=11.0 Hz

$J_{2endo,3}$, $J_{1,2exo}$, $J_{3,7}$; quite small

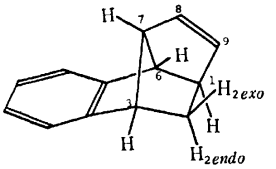

The photochemical relationship between compounds **2**—**8** is summarized in Scheme 9. We could not obtain evidence for the transient formation of **26** when **2**, **3** and **6** were photolysed. We consider that the formation of **5** on photolysis of **2** and **3** takes place *via* an intermediate **6** and not *via* a route involving **26** and **27**.

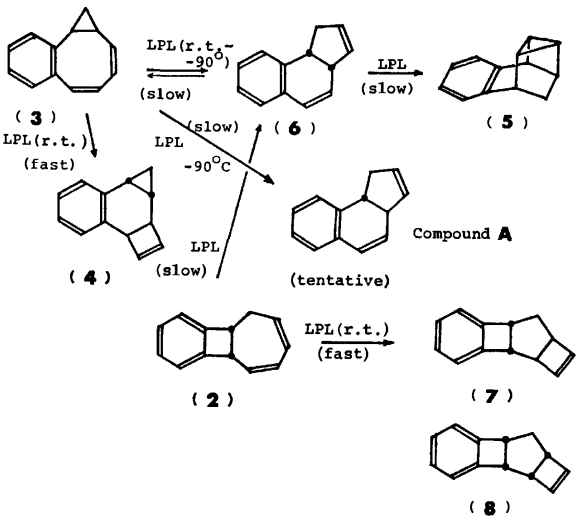

Scheme 9.

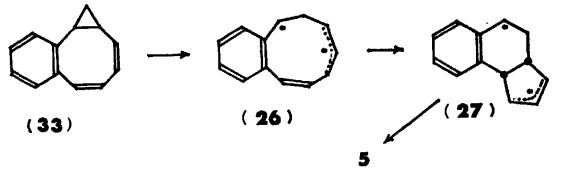

Scheme 10.

Experimental

The NMR spectra were obtained on a JEOL Model PS-100 spectrometer, with tetramethylsilane as the internal standard. The chemical shifts are expressed in ppm from TMS. The Mass spectra were measured on a Hitachi RMU-6 mass spectrometer by the indirect injection method at 180 °C. The IR were recorded on a JASCO Model IRE spectrometer, and the UV on a Hitachi Recording Spectrometer, Model EPS-2 or Model 323. VPC analysis was carried out on a Varian Aerograph Model-90P gas chromatograph under the quoted conditions. The NMR measurements at low temperatures were carried out at the University of Alberta by courtesy of Professor Satoru Masamune.

Photolysis of Benzo[2,3]bicyclo[6.1.0]nona-2,4,6-triene (3). Irradiation at Room Temperature: The triene **3** (14 mg), dissolved in anhydrous THF (1 ml) in a sealed quartz test tube, was externally irradiated with an LPL (200 Watts) for 30 min. The subsequent evaporation of the solvents gave a semi-solid, which was extracted with Skellysolve B. The Skellysolve B soluble oily material (10.5 mg) showed an NMR spectrum mainly composed of **4**, along with some **5**. The GLC separation of **4** was carried out using GLC [10% Apiezone L on Chromosorb WAW 1/4″×6 ft; He flow rate, 40 ml/min; column temperature, 150 °C; retention time, 20 min]. **4** UV, λ_{max}^{EtOH}; 258 (infl.), 270.5, 280. NMR (CCl_4) δ: 6.7—7.2 (4H, m), 6.20, 6.10 (H_8, H_9, AB-type, J=2.7 Hz), 3.70, 3.50 (H_1, H_7, AB-type, J=4.5 Hz), 1.86 (H_4, d, J=2.1, t, J=4.3 Hz), 1.43 (H_{3exo}, d, J=2.9, t, J=4.3 Hz), 1.06 (H_2, d, J=4.3, t, J=2.1 Hz), 0.22 (H_{3endo}, d, J=2.9, t, J=2.1 Hz). MS (80 eV), *m/e* (rel. intensity), 168(M^+,63), 167(100), 165(46), 153(73), 152(52), 141(39), 115(55), 83(27). Found: C, 92.88; H, 7.12%. Calcd for $C_{13}H_{12}$: C, 92.81; H, 7.19%.

Irradiation at −90 °C: Compound **3** (17 mg), dissolved in THF-d_8 (0.3 ml) containing 15% of TMS, was degassed and sealed in a quartz NMR tube. This was then irradiated at −90 °C for 6 h while the reaction was monitored by NMR measurements at −90 °C. The gradual appearance of a sharp singlet at 6.48 ppm in compensation for those of the starting material was noticed. After six hours' irradiation, the peak height at 6.48 ppm became almost the same intensity as the 2H signal at 5.74 ppm of the starting **3**. The NMR spectra of the mixture remained unaltered when taken at several elevated temperatures, *i.e.*, −60, −30, 0 °C, and room temperature. After the evaporation of the solvent, a Skellysolve B insoluble material (4 mg) was filtered out and the soluble part (13 mg) was separated by GLC [10% Apiezone L on Chromosorb WAW, 1/4″×5 ft; He, 38 ml/min; 138 °C]. The materials corresponding to Peak 1 [retention time, 17.9 min; 7.5 mg] and Peak 2 [r.t., 21.1min; 2.6 mg] were collected. The physical data of the former were consistent with those of **3**.[17] The latter was separated again using GLC[10% Carbowax 20M on Chromosorb WAW 1/8″×6ft; He, 40 ml/min; 160 °C] and gave two peaks in almost equal intensities [r.t., (*i*) 11.8 min; (*ii*) 12.9 min]. From the physical data, it was revealed that the compound corresponding to *i* was an unknown substance, A[6], while the one corresponding to *ii* was **6**.[17,18] The physical data of **3** and **6**: **3**; IR $\nu_{max}^{liq.\ film}$: 3050, 3000, 2910, 2840, 1497, 1455, 1448 sh, 1125, 1115, 1030, 985, 945, 895, 850, 830, 790, 782, 760, 724, 700 cm^{-1}. UV λ_{max}^{EtOH}: 259 (log ε; 3.69), 269(3.61). NMR (CCl_4) δ: 7.40—6.80 (4H, m), 6.53 (H_4, d, J=12 Hz), 5.99 (H_5, broad d, J=12 Hz), 5.71 (H_6, H_7 ,broad s), 2.01 (H_1, broad t, d, $J_{1,8}=J_{1,9exo}$=8.8 Hz, $J_{1,9endo}$=6.0 Hz), 1.57 (H_8, broad t, d, $J_{1,8}=J_{8,9exo}$=8.8 Hz, $J_{8,9endo}$=6.0 Hz), 1.06 (H_{9exo}, t, d, $J_{1,9exo}=J_{8,9exo}$= 8.8 Hz, $J_{9exo,9endo}$=4.0 Hz), 0.53 (H_{9endo}, t, d, $J_{1,9endo}=J_{8,9endo}$=6.0 Hz, $J_{9exo,9endo}$=4.0 Hz). MS (80 eV), *m/e* (rel. intensity), 168 (M^+, 84), 167(100), 166(22), 165(47), 153 (55), 152(41). Found: C, 92.52; H, 7.27%. Calcd for $C_{13}H_{12}$: C, 92.81; H, 7.19%. **6**; UV λ_{max}^{EtOH}: 225 sh (log ε; 4.32), 261(3.89), 269.5(3.90), 280 sh (3.66). NMR(CCl_4) δ: 7.08—6.81 (4H, m), 6.21 (H_5, d, d, $J_{4,5}$=9.6 Hz, $J_{5,3a}$=2.6 Hz), 5.93—5.70 (H_2, H_3, m), 5.46 (H_4, $J_{4.5}$= 9.6 Hz, $J_{4,3a}$=2.6 Hz), 3.71—3.29 (2H, m), 2.86—2.11 (2H, m). MS (80 eV), *m/e* (rel intensity), 168 (M^+, 100), 167(97), 166(26), 165(46), 153(53), 152(32). Found: C, 92.65; H, 7.17%. Calcd for $C_{13}H_{12}$: C, 92.81; H, 7.19%.

Photolysis of Benzo[8,9]bicyclo[5.2.0]nona-2,4,8-triene (2). Compound **2** (170 mg), dissolved in methanol (150 ml), was irradiated using an LPL (10 watts) for 35 min under nitrogen with external cooling. After the rough separation of the products by column chromatography on alumina, the hydrocarbon mixture was separated by GLC [10% Apiezone L on Chromosorb WAW 1/4″×5 ft; He 40 ml/min; 150 °C], yielding **7** (15%), **8** (15%), and **6** (9%). Physical data of **7** and **8**: **7**; NMR (CCl_4) δ: 7.25—6.76 (4H, m), 6.04 (1H, d, J=2.6 Hz), 5.96 (1H, d, J=2.6 Hz), 4.32 (H_5, m), 3.76 (H_2, d, J=4.0 Hz), 3.72—3.56 (H_7, m), 3.38 (H_1, d, J=3.5 Hz), 2.08—1.60 (H_6, m). **8**; NMR (CCl_4) δ: 7.15—6.60 (4H, m), 5.90 (1H, d, J=2.5 Hz), 5.55 (1H, d, J=2.5 Hz), 4.32—4.1 (H_5, m), 3.94 (H_2, d, d, J=9.0, 5.0 Hz), 3.72—3.48 (H_1, H_7, m), 1.80—1.52 (H_6, m).

Photolysis of Benzo[2,3]bicyclo[4.3.0]nona-2,4,7-triene (6). Compound **6** (50 mg), dissolved in THF (0.6 ml) in a quartz NMR tube, was degassed and sealed. The tube was then irradiated externally with an LPL (200 watts) while being cooled externally with dry ice–methanol in a quartz Dewar bottle with a quartz window. In the course of 7 hours' irradiation, a characteristic broad doublet at δ 0.61 ppm appeared, and gradually increased in the NMR spectrum. The separation of the products by column chromatography on silicic acid gave a colorless liquid (21 mg), which contained

6, **5**, and **3** in a ratio of *ca.* 6 : 3 : 1, as estimated by means of the NMR spectrum. The GLC separation of the liquid was carried out as follows: 10% Apiezone L on Chromosorb WAW 1/4″×6 ft; He, 40 ml/min; 147 °C: Retention times; **5**, 22 min; **3**, 24 min; **6**, 28 min. **5**; NMR (CCl_4) δ: 7.2—6.8 (4H, m), 3.44 (2H, m), 2.56 (1H, m), 2.88 (1H, m), 2.05—1.6 (3H, m), 0.62 (1H, d, J=10 Hz).

Similarly, **6** (20—70 mg), dissolved in THF (80 ml), was irradiated using an LPL (10 watts) at room temperature for 1 h under nitrogen; this resulted in **5** and **4**, instead of **5** and **3**. The NMR analysis of the products revealed that it contained **5** and **4** in a ratio of *ca.* 3 : 1.

*Photolysis of Benzo[6,7]bicyclo[3.2.2]nona-2,6,8-triene (**10**).*

Irradiation Using a HPL (Ushio High Pressure Mercury Lamp, UM-425, 450 Watts) in Acetone: Compound **10** (300 mg), dissolved in acetone (350 ml), was irradiated using a HPL through a Pyrex filter under nitrogen for 70 min. After a usual work up, the product was roughly chromatographed on silicic acid (hexane), giving a colorless liquid (228 mg). The GLC separation of the liquid, performed on 10% Apiezone L on Chromosorb WAW at 141 °C, gave three peaks, which led us to estimate the yields as follows; **10** (15%), **17** (52%), and **18** (9%). The tetracyclic compound, **17**, was identical with the sample synthetically obtained below. **18**; IR $\nu_{max}^{liq.\ film}$: 3020, 2916, 2840, 1629, 1495, 1462, 1040, 1025, 1000, 962, 945, 868, 835, 810, 781, 767, 740, 707 cm^{-1}. NMR (CCl_4) δ: 7.3—6.8 (4H, m), 5.88—5.4 (2H, finely-splitted m), 3.20 (1H, b), 2.52 (1H, t, J=8Hz), 2.3—1.9 (2H, m), 1.44 (1H, t, J=2Hz). MS (80 eV) *m/e* (rel intensity), 168(M^+, 100), 167(90), 165(29), 153(48), 152(27).

Irradiation Using an LPL at 0 °C: Compound **10** (188 mg), dissolved in ether (230 ml), was irradiated using an LPL (10 watts, immersion type) for 4.5 h under nitrogen while the reaction was monitored with TLC. After the evaporation of the solvent, the residue was chromatographed on silicic acid (hexane), and the hydrocarbon fractions were collected. The GLC analysis [5% Apiezone L, 1/4″×6 ft; He, 50 ml/min; 141 °C] revealed that it contained five species, estimated to be as follows: Retention times (yield); (a) 3.2 min (naphthalene, 8%), (b) 5.7 min (**20**, 11%), (c) 8.1 min (**10**, 18%), (d) 9.4 min (**17**, 18%), (e) 12 min (**18**, 12%). They were separated in pure forms and characterized. **20**; IR $\nu_{max}^{liq.\ film}$: 3060, 2970, 2865 1572, 1328, 1265, 958, 915, 866, 726, 729 cm^{-1}. NMR: Table 1. MS (80 eV), *m/e* (rel intensity); 168 (M^+, 88), 167 (100), 165 (28), 153 (38), 152 (23).

*The Direct Irradiation of **17** and **18** Using an LPL*: Compound **17**, (20 mg), dissolved in anhydrous ether (0.5 ml) in a quartz NMR tube, was irradiated using an LPL (10 Watts) for 12 h at 0—5 °C. The NMR and GLC analysis of the products showed that they were composed of **20** and **17** in a ratio of 48 : 52. The same experiment using **18** (20 mg) instead of **17** was also carried out (15 hs' irradiation). The products were **20** and **18** in a ratio of 4 : 96.

*Synthesis of **17**. Preparation of the Hydrazone (**22**)*: The **21** ketone (180 mg) and 100% hydrazine hydrate (0.4 ml), dissolved in absolute ether (7 ml), were stirred under reflux for 20 h. The solvent was then evaporated *in vacuo*, and the residual liquid, dissolved in benzene, was dried with anhydrous sodium sulfate. The subsequent evaporation of the solvent gave a crude hydrazone (220 mg). **22**; IR $\nu_{max}^{liq.\ film}$: 3360, 3200, 3020, 2940 cm^{-1}, (no νC=O). NMR ($CDCl_3$) δ: 7.22, 7.19 (4H, Ar-H), 6.4—5.5 (4H, m), 4.56 (1H, d, J=8 Hz), 4.08 (1H, d, J=8 Hz), 6.0—4.0 (very broad, N-H).

*9,10 - Diazabenzo [2,3] tricyclo [6.3.0.0^{4,11}] undeca - 2,6,9 - triene (**23**)*: To the hydrazone (**22**), dissolved in anhydrous DMSO (1.5 ml), was added, drop by drop, a solution of potassium *t*-butoxide (1.5 g) in DMSO (3.8 ml) over a period of 95 min. After the mixture had then been stirred further for 19 h at room temperature, it was poured into water and extracted with dichloromethane. The combined organic extracts were washed with water, dried (anhydrous Na_2SO_4), and concentrated to dryness. The residue was chromatographed on silicic acid, using hexane–ether (10 : 1 v/v) as the solvent. The crude crystalline product (138 mg) was purified by sublimation. **23**; 100 mg (52%), mp 80—81 °C. UV λ_{max}^{EtOH}: 261.5 (log ε, 2.90), 268.5 (3.08), 275.5 (3.09), 335(2.53). IR $\nu_{max}^{CCl_4}$: 3040, 2960, 1537, 1485, 1465 cm^{-1}. NMR (CCl_4) δ: 7.2—6.84 (4H, m), 5.58 (H_{11}, t, J=8Hz), 5.68—5.16 (H_6,H_7,H_8, m), 3.77—3.56 (H_4, m), 3.31 (H_1, bt, J=8Hz), 2.38—1.80 (H_5, 2H, m). Found: C, 79.71; H, 6.25; N, 13.81%. Calcd for $C_{13}H_{12}N_2$: C, 79.56; H, 6.16; N, 14.28%.

*Preparation of **17**: Photolysis of the Azo Compound (**23**).* The azo compound, **23** (12 mg), dissolved in anhydrous ether (1.5 ml), was irradiated for one hour with a HPL through a Pyrex filter at room temperature. Silicic acid chromatography of the products gave pure **17** (7 mg; 69%).

*Thermal Decomposition of **23**.* Compound **23** (30 mg), dissolved in diethylene glycol (1 ml), was heated at 180 °C for 4 h. The reaction mixture was then poured into water and extracted with ether. After being washed and dried, the combined organic layer was concentrated and chromatographed on silicic acid (hexane–ether 1: 1 v/v) to give **17** (18 mg; 70%), along with recovered **23** (7 mg). **17**; IR $\nu_{max}^{liq.\ film}$: 3025, 2910, 2840, 1483, 1462, 1182, 1142, 1027, 998, 943, 912, 880, 843, 808, 772, 745, 718 cm^{-1}. UV λ_{max}^{EtOH}: 266.5 sh (log ε, 2.95), 272(3.07), 279.5(3.03). NMR (CCl_4) δ: 7.2—6.7 (4H, m), 5.7—5.3 (H_3, H_4, m), 3.50 (H_6, d, t, $J_{1,6}$=6.0 Hz, $J_{6,5exo}$=$J_{6,5endo}$=3.2 Hz), 2.74—2.32 (H_{5exo}, m), 2.50 (H_9, d, d, $J_{1,9}$=6.0, $J_{2,9}$=7.5 Hz), 2.12 (H_1, q, $J_{1,9}$=$J_{1,6}$=6.0, $J_{1,2}$=7.5 Hz), 1.87 (H_{5endo}, d,d,d, $J_{5endo,5exo}$=16.5 Hz, $J_{4,5endo}$=5.5 Hz, $J_{6,5endo}$=2.7 Hz), 1.52 (H_2, broad t, $J_{2,9}$=$J_{1,2}$=7.5 Hz). MS (80 eV), *m/e* (rel. intensity), 168 (M^+, 91), 167(100), 165(49), 153(77), 152(66), 141(21), 115(47). Found: C, 92.81; H, 7.29%. Calcd for $C_{13}H_{12}$: C, 92.81; H, 7.19%.

The authors thank Professor Satoru Masamune, who kindly allowed one of them (M.K.) the use of his low temperature photochemical apparatus at the University of Alberta, for his helpful discussions. The authors are grateful to Mr. Jun-ichi Goda for the analytical data and to Dr. Yoshiko Hirose of the Institute of Food Chemistry for the mass spectral measurements.

References

1) (a) A. V. Kemp Jones and S. Masamune, "Topics in Nonbenzenoid Aromatic Chemistry", Vol. 1, ed by T. Nozoe, R. Breslow, K. Hafner, S. Ito, and I. Murata, Hirokawa Publishing Co., Tokyo, Japan (1973), p. 140; (b) H. Tsuruta, T. Kumagaya, and T. Mukai, *Chem. Lett.*, **1973**, 933; (c) A. G. Anastassiou and R. C. Griffith, *J. Am. Chem. Soc.*, **95**, 2379 (1973).

2) (a) M. Kato, T. Sawa, and T. Miwa, *Chem. Commun.*, **1971**, 1635; (b) T. Tsuji, H. Ishitobi, and H. Tanida, *Bull. Chem. Soc. Jpn.*, **44**, 2447 (1971); (c) A. G. Anastassiou, S. S. Libisch, and R. C. Griffith, *Tetrahedron Lett.*, **1973**, 3103; (d) A. G. Anastassiou and R. C. Griffith, *J. Am. Chem. Soc.*, **96**, 611 (1974); (e) L. Lombardo and D. Wege, *Tetrahedron*, **30**, 3945 (1974).

3) (a) R. C. Hahn and R. P. Johnson, *Tetrahedron Lett.*, **1973**, 2149; (b) *J. Am. Chem. Soc.*, **97**, 212 (1975).

4) R. C. Hahn and R. P. Johnson, *J. Am. Chem. Soc.*, **98**, 2600 (1976).

5) It has been reported that Compounds **4** and **5** were formed in a ratio of 1.0 : 1.2 when Compound **3** was irradiated using an MPL.[4]

6) Owing to its limiting amount, the structure of the unknown substance, **A**, has not yet been limited. This compound was thermally stable and showed a fragmentation pattern in its mass spectrum very similar to that of **6**. The UV spectrum of this compound exhibited strong absorptions at 247 and 255 nm. Its NMR spectrum showed a sharp aromatic proton peak at 7.01, olefinic at 6.38 and 5.96 ppm and aliphatic at 3.6—2.1 ppm in a ratio near 4 : 2 : 2 : 4. The catalytic hydrogenation of **A** gave 2,3-dihydro-1*H*-benz[*e*]indene and a substance whose UV spectrum was similar to that of *cis*- or *trans*-2,3,3*a*,4,5,9*b*-hexahydro-1*H*-benz[*e*]indene. Therefore we tentatively identified this compound, **A**, as *trans*-3*a*,9*b*-dihydro-1*H*-benz[*e*]indene.

7) When Compound **3** was irradiated with an LPL at room temperature in the presence of O_2, a mixture of dialdehydes was formed by the cleavage of one of the double bonds. The spectral data of the product: IR $\nu_{max}^{liq.\ film}$: 2840, 2750, 1700(vs), 1680(vs), 1620, 1600 cm^{-1}. UV λ_{max}^{EtOH}: 288. NMR (CCl_4) δ: 8.64 (d,d, J=2.5 Hz, 6 Hz), 9.72 (d, J=8 Hz).

Another explanation is possible involving the isomerization of one of the *cis* double bond to *trans*, followed by thermal conrotatory ring closure to a cyclobutene, as is often observed in medium-sized cyclic polyenes. However we consider this as an unlikely possibility because we could not detect in the NMR spectra either a *trans* compound isomeric to **3**, taken at −90 °C just after the irradiation of **3** at the same temperature, or **4**, taken at room temperature after the solution had been allowed to warm up.

8) J. Saltiel, J. D'Agostino, E. D. Megarity, L. Metts, K. R. Neuberger, M. Wrington, and O. C. Zafiriou, "Organic Photochemistry," Vol. 3, ed by O. L. Chapman, Mercel Dekker, New York (1973), p. 85.

9) M. P. Cava and D. R. Napier, *J. Am. Chem. Soc.*, **80**, 2255 (1958).

10) M. Kato, M. Kawamura, Y. Okamoto, and T. Miwa, *Tetrahedron Lett.*, **1972**, 1171.

11) A. S. Kende, Z. Goldschmidt, and P. T. Izzo, *J. Am. Chem. Soc.*, **91**, 6858 (1969).

12) (a) A. S. Kende and Z. Goldschmidt, *Tetrahedron Lett.*, **1970**, 783; (b) M. J. Goldstein and B. G. Odell, *J. Am. Chem. Soc.*, **89**, 6356 (1967); (c) Z. Goldschmidt and A. Worchel, *Tetrahedron Lett.*, **1973**, 3621, 3623; (d) Z. Goldschmidt and A. S. Kende, *Tetrahedron Lett.*, **1971**, 4625; (e) I. Murata and Y. Sugihara, *Chem. Lett.*, **1972**, 625.

13) When methanol was used as the solvent, Compound **10** remained unchanged under the same conditions.

14) H. E. Zimmerman, R. S. Givens, and P. M. Pagoni, *J. Am. Chem. Soc.*, **90**, 4194, 6090 (1968).

15) Naphthalene was not detected on the irradiation o **17**, **18**, and **20** using an LPL. This compound must be formed directly from **10**.

16) T. Miwa, M. Kato, and T. Tamano, *Tetrahedron Lett.*, **1969**, 1761.

17) H. Meier, J. Heiss, H. Suhr, and E. Müller, *Tetrahedron*, **24**, 2320 (1968).

18) L. M. Jackman and S. Sternnell, "Applications of Nuclear Magnetic Resonance Spectroscopy in Organic Chemistry," 2nd ed, Pergamon press, New York (1969), p. 289.

Studies of Unusual Amino Acids and Their Peptides. VII. The Syntheses and the Reactions of Iminopeptides[1]

Takashi YAMADA, Kazuko SUEGANE, Shigeru KUWATA, and Hiroshi WATANABE

Laboratory of Chemistry, Faculty of Science, Kōnan University, Okamoto, Higashinada-ku, Kobe 658

(Received September 20, 1976)

As a basic study for synthesis of bottromycin, the syntheses and the reactions of iminodipeptides were investigated. Nine *N*-benzyloxycarbonyl(Z) iminodipeptides were prepared by the condensation of ethyl Z-amino carboximidates with amino acids according to the method of Ried *et al.* All the imidates were prepared from the corresponding nitriles, and ethyl *N*-Z-2-pyrrolidinecarboximidate (IIIf) was also successfully obtained from Z-proline thioamide by the method of Suydam *et al.* Though Z-(iminoprolyl)glycine was easily deprotected or esterified, its *C*-terminal could not be elongated because it was likely to cyclize into an imidazolone ring. This side reaction could be avoided by locating a carboxyl group further apart from an imino group in a molecule; *i. e.*, the imidate (IIIf) could be coupled with methyl glycylphenylalaninate, thus affording the desired iminotripeptide, Z-ImPro-Gly-Phe-OMe, in a good yield.

Bottromycin, a family of peptide antibiotics produced by *Streptomyces bottropensis*[2] and analogous strains,[3] is an iminopeptide, *i.e.*, a peptide in which an oxo group in the peptide bond is replaced by an imino group. The structure shown in Fig. 1 was given by Umezawa and his co-workers.[4]

An iminopeptide bond is very rare in peptides, though an amidino group itself can be found in amidinomycin,[5] netropsin,[6] and so on.[7] This structural feature of bottromycin has been asserted to contribute to its biological activity to some extent.[8] The present paper will deal with a study of such iminopeptides.

Syntheses of amidines have been widely investigated, but there have been few studies of the syntheses of iminopeptides: Ried and his co-workers[9] synthesized some *N*-benzyloxycarbonyl(Z) iminodipeptides containing optically-active amino acids, and Vargha and Balàzs[10] synthesized *N*-phthalyl(iminoglycyl)-D-valine, along with some analogues. In both cases, however, nothing was reported about their optical properties.

As a basic study of the synthesis of bottromycin, we undertook to investigate the syntheses and the reactions of optically-active iminopeptides, especially those of (iminoprolyl)glycine,[11] which would be an important unit if bottromycin could be conveniently built up by the fragment condensation of three dipeptides (pivaloyl-*t*-leucylvaline,[12] (iminoprolyl)glycine, *β*-methylphenylalanyl-*β*-(2-thiazolyl)-*β*-alanine methyl ester[13]). In principle, we adopted the method of Ried *et al.* for the syntheses of iminopeptides. As an *N*-protecting group, the Z group was chosen because it can easily be removed by hydrogen bromide in anhydrous acetic acid, under which conditions an amidino group seems to be stable. A scheme of the synthesis is shown in Scheme 1.

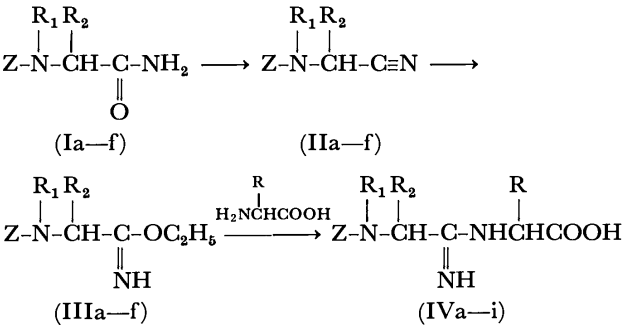

Scheme 1.

Z-Amino nitriles (II) were prepared by dehydrating the corresponding amides (I) with *p*-toluenesulfonyl chloride in pyridine according to the method of Hirotsu *et al.*[14] The reaction temperature was, however, kept at 50 °C instead of refluxing, and three equivalents of *p*-toluenesulfonyl chloride were used to cover the lowered reaction rate. The excess sulfonyl chloride could easily be removed by stirring the reaction mixture for a few hours with 10% aqueous pyridine at room temperature. Thus, the nitriles were obtained quantitatively in a purer state, hardly any by-products being observed. It is noteworthy that 2-(Z-amino)-3-methylvaleronitrile (IId), which has been reported to solidify only after distillation,[14] could be obtained in crystalline forms without further purification. The results are shown in Table 1.

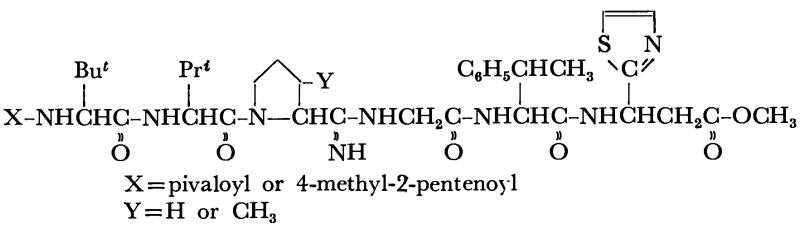

Fig. 1. The structure of bottromycin proposed by Umezawa *et al.*

Table 1. Physical properties of nitriles $\left(\begin{array}{l} R_1\ R_2 \\ |\ \ | \\ Z\text{-}N\text{-}CH\text{-}C{\equiv}N \end{array}\right)$ (IIa—f)

Compd	R_1	R_2	Starting amino acid	Yield (%)	Mp °C	$[\alpha]_D^{23}$ (ethanol)	Molecular formula	Analysis (%) Found (Calcd) C	H	N
IIa	H	H	Gly	99	61—62[a]					
IIb	H	CH_3	Ala	99	82—82.6	−68.9° (*c* 5.0)[b]				
IIc	H	$(CH_3)_2CH$	Val	100	55.5—56	−61.3° (*c* 4.5)[c]				
IId	H	$(CH_3)_2CHCH_2$	Leu	99	32—33.3	−53.1° (*c* 5.0)[d]				
IIe	H	$C_6H_5CH_2$	Phe	99	136—137	−62.4° (*c* 0.5)	$C_{17}H_{16}N_2O_2$	73.03 (72.84)	5.84 (5.75)	9.92 (9.99)
IIf	$-CH_2CH_2CH_2-$		Pro	99	oil	−87.9° (*c* 5.0)	$C_{13}H_{14}N_2O_2$	68.17 (67.81)	6.18 (6.13)	12.06 (12.17)

Lit[14]: a) Mp 61—62 °C. b) Mp 84—85.5 °C, $[\alpha]_D^{15}$ −69.1° (*c* 5.62, ethanol). c) Mp 55—56 °C, $[\alpha]_D^{12}$ −55.2° (*c* 4.48, ethanol). d) Mp 29.5—32.0 °C, $[\alpha]_D^{24}$ −51.0° (*c* 5.86, ethanol).

Table 2. Physical properties of *N*-benzyloxycarbonyl-iminodipeptides (IVa—i)

	Compound	Yield (%)	Mp (°C)	$[\alpha]_D$	Molecular formula	Analysis (%) Found (Calcd) C	H	N
IVa	Z-ImGly-Gly-OH	62	245—250 (dec)		$C_{12}H_{15}N_3O_4$	54.18 (54.33)	5.75 (5.70)	15.63 (15.84)
IVb	Z-ImGly-Ala-OH	55	198.5—199.5 (dec)	−27.4°[a]	$C_{13}H_{17}N_3O_4$	55.52 (55.90)	6.32 (6.14)	14.91 (15.05)
IVc	Z-ImGly-Leu-OH	59	178—179 (dec)	−45.7°[b]	$C_{16}H_{23}N_3O_4$	59.61 (59.79)	7.42 (7.21)	13.00 (13.08)
IVd	Z-ImGly-Phe-OH	72	195—196 (dec)	+42.2°[a]	$C_{19}H_{21}N_3O_4$	64.20 (64.21)	6.09 (5.96)	11.72 (11.83)
IVe	Z-ImGly-Pro-OH	73	147—149	−84.9°[b]	$C_{15}H_{19}N_3O_4$	58.57 (59.00)	6.41 (6.27)	13.55 (13.76)
IVf	Z-ImAla-Gly-OH	55	213—215 (dec)	− 2.8°[a]	$C_{13}H_{17}N_3O_4$	55.76 (55.90)	6.29 (6.14)	14.78 (15.05)
IVg	Z-ImLeu-Gly-OH	50	194—196 (dec)	−11.0°[c]	$C_{16}H_{23}N_3O_4 \cdot 1/2H_2O$	58.14 (58.16)	7.14 (7.32)	12.57 (12.72)
IVh	Z-ImPhe-Gly-OH	69	204—206 (dec)	+ 7.4°[a]	$C_{19}H_{21}N_3O_4 \cdot H_2O$	61.05 (61.11)	6.23 (6.21)	11.08 (11.25)
IVi	Z-ImPro-Gly-OH	81	200—201.5 (dec)	−64.4°[b] −65.8°[d]	$C_{15}H_{19}N_3O_4$	58.80 (59.00)	6.29 (6.27)	13.56 (13.76)

a) *c* 1 in acetic acid at 23 °C. b) *c* 1 in methanol at 20 °C. c) *c* 1 in methanol at 25 °C. d) *c* 1 in ethanol at 28 °C.

Ethyl Z-amino carboximidates (III) were prepared from the nitriles (II) by the method of Pinner.[14,15] Except from glycine and alanine, every free imidate was obtained as an oil and was used in the next reaction without any purification.

Two types of optically-active iminodipeptides (IV) (Z-ImGly-AA-OH and Z-ImAA-Gly-OH)[11] were successfully prepared by the reactions of the imidates (III) with free amino acids in anhydrous methanol under reflux. The results are summarized in Table 2.

Suydam and his co-workers[16] have reported another convenient method for preparing imidate directly from amide. They obtained a number of aliphatic imidates in fairly good yields by the reaction of the corresponding amides with ethyl chloroformate. Though their method could not be applied to Z-proline amide (If) itself, the corresponding thioamide (V) reacted smoothly with ethyl chloroformate at room temperature, giving an optically-active imidate (VI), which then, by reaction with glycine, afforded Z-(iminoprolyl)-glycine (VII). The optical rotation of this product

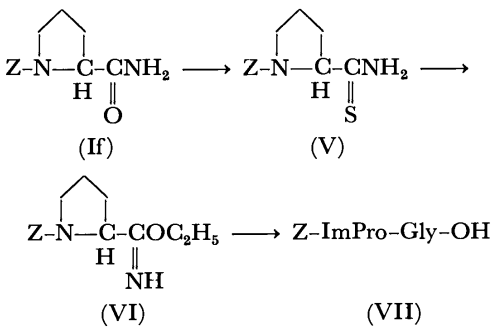

Scheme 2.

(VII) agreed well with that of the same compound (IVi) obtained through Pinner's method. (Scheme 2)

Some reactions of iminodipeptides were investigated by using Z-(iminoprolyl)glycine (IVi). When IVi was treated with saturated hydrogen chloride in methanol at room temperature in order to esterify it, the removal of the Z group rapidly occurred, followed by slow esterification, and (iminoprolyl)glycine methyl ester was

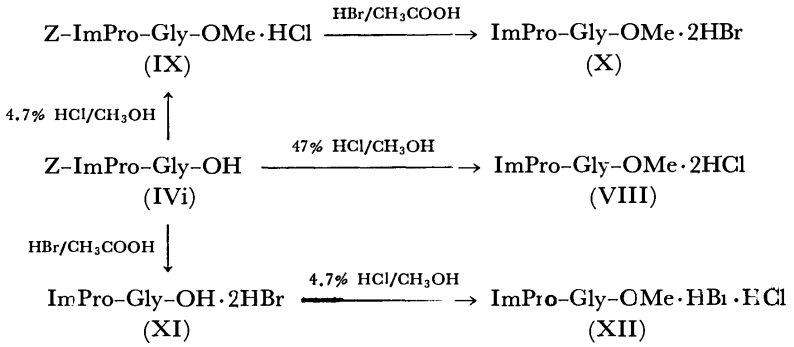

Scheme 3.

obtained as dihydrochloride (VIII). On the other hand, when IVi was treated with 4.7% hydrogen chloride in methanol, it could be quantitatively esterified without the removal of the protecting group and the resulting ester was isolated as monohydrochloride (IX), which was then further treated with hydrogen bromide in acetic acid to give (iminoprolyl)glycine methyl ester dihydrobromide (X). The same ester was also obtained by the esterification of (iminoprolyl)-glycine dihydrobromide (XI) with 4.7% hydrogen chloride in methanol, though the ester was isolated as a hydrochloride-hydrobromide salt (XII). The iminodipeptide (XI) was obtained as expected in the form of dihydrobromide on the treatment of IVi with hydrogen bromide in acetic acid. The correlation between these compounds is shown in Scheme 3.

In order to elongate the *C*-terminal of Z-iminodipeptides (IV), many attempts were made under various conditions, but the expected results were not obtained. One of the troubles is the low solubilities of these compounds in solvents; *e. g.*, Z-(iminoglycyl)glycine (IVa) dissolved neither in acetonitrile, tetrahydrofuran, *N,N*-dimethylformamide, nor dimethyl sulfoxide, though it is fairly soluble in such protic solvents as methanol and acetic acid, and in such basic solvents as pyridine it is soluble to some extent. On the other hand, even a more soluble compound, Z-(iminoprolyl)-glycine (IVi), was hardly soluble in polar aprotic solvents. The use of *N*-isobornyloxycarbonyl(IBOC) derivatives[17] was attempted with hopes founded on their high solubilities:[18] IBOC-proline amide (XIII) and the corresponding nitrile (XIV) were prepared successfully, but the conversion of the nitrile to IBOC-(iminoprolyl)glycine *via* an imidate did not occur smoothly.

We attempted to couple the iminopeptide (IVi) with methyl phenylalaninate in the presence of dicyclohexylcarbodiimide (DCC) in pyridine. The isolated main product, however, was not the desired iminotripeptide derivative, but probably an imidazolone derivative (XV),[19] which might have been produced by the intramolecular cyclization of the starting iminodipeptide, since the same compound was also obtained in a good yield instead of the free iminodipeptide ester (XVII) when the iminodipeptide ester hydrochloride (IX) was treated with triethylamine in methanol. Furthermore, when the imidate (IIIf) was coupled with methyl glycinate, the same compound (XV) was again produced as the main product. Compound XV was too unstable to purify; it was identified by its conversion to a more stable derivative, (*p*-methoxyphenylmethylene)imidazolone (XVI).[20] These facts provide evidence for the smooth cyclization reaction of the iminodipeptide ester (Scheme 4).

From the facts mentioned above, we could not but conclude that it is impossible to elongate the *C*-terminal of an iminodipeptide directly. If an imino group and a carboxyl group were situated further apart in a molecule, such an intramolecular cyclization might be avoided. In order to confirm this possibility, the imidate (IIIf) was coupled with glycylphenylalanine methyl ester hydrobromide in the presence

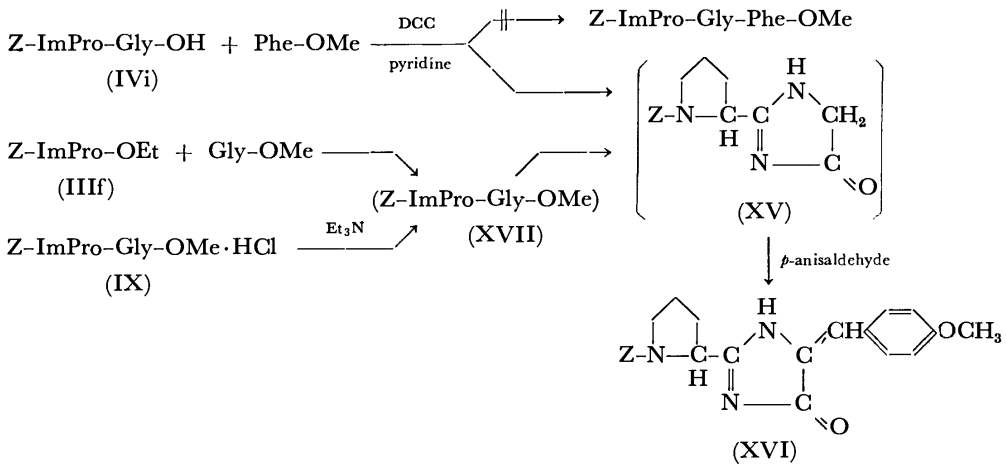

Scheme 4.

of triethylamine in methanol at room temperature for 2 days. The desired iminotripeptide derivative, *i.e.*, Z-(iminoprolyl)glycylphenylalanine methyl ester (XVIII), was thus successfully obtained in a 61.4% yield after purification by column chromatography. It is interesting that the iminotripeptide ester (XVIII) was isolated as a hydrobromide, though an equimolecular amount of triethylamine was added in order to remove hydrogen bromide.

Consequently, it was concluded that, for the syntheses of bottromycin and its analogues, the route through the fragment condensation of three dipeptides described above is not adequate, while the route through the condensation by the formation of an iminopeptide bond between two tripeptides may be better.

Experimental

All the melting points are uncorrected. The optical rotations were measured by means of a Yanagimoto polarimeter, OR-10. The ORD-curves were recorded on a JASCO ORD/UV-5 spectropolarimeter. The NMR spectra were recorded on a Varian A-60 spectrometer or a Hitachi R-20A spectrometer, using TMS or DSS as the internal standard. Thin-layer chromatographies (TLC) were carried out on Merck's Kieselgel GF_{254} (Type 60). The amino acids and their derivatives mentioned in this report are all of the L-configuration unless otherwise mentioned.

Benzyloxycarbonylamino Acid Amides (I). All the amides were prepared by the mixed anhydride method using ethyl chloroformate.[21] The ammonolysis of the mixed anhydride intermediates was successfully carried out with 28% aqueous ammonia instead of liquid ammonia.

α-Benzyloxycarbonylamino α-Substituted Acetonitriles (II). The nitriles were prepared by the dehydration of the corresponding amides with *p*-toluenesulfonyl chloride in pyridine in the usual way,[14,22] but with some modifications. A typical example was as follows: into a solution of Z-proline amide (12.4 g, 0.15 mol) in dry pyridine, *p*-toluenesulfonyl chloride (28.5 g, 0.15 mol) was stirred at room temperature, and thus the mixture was heated at 50 °C for 4 h. After pyridine had been removed under reduced pressure, the residue was treated with 10% aqueous pyridine (200 ml) with stirring for 2 h. The mixture was extracted with ethyl acetate. The organic layer was washed with 1M-HCl, 1M-$NaHCO_3$, and then water, and dried over $MgSO_4$. The solution was concentrated to afford a pale yellow oil; yield, 11.4 g (99%). The other nitriles, prepared in the same manner, are summarized in Table 1.

α-Benzyloxycarbonylamino Carboximidates (III). The imidates were prepared according to the method of Pinner.[14,15] A typical example was as follows: to a cold solution of *N*-Z-2-cyanopyrrolidine (IIf) (1.15 g, 5 mmol) in a mixture of absolute ethanol (0.3 g, 6.5 mmol) and dry ether (15 ml), dry hydrogen chloride was passed with stirring below −5 °C until the gas was saturated, and then at room temperature for 1 h. The reaction mixture was evaporated under reduced pressure to leave ethyl *N*-Z-2-pyrrolidinecarboximidate hydrochloride as a foamy solid. The imidate hydrochloride was immediately converted to a free imidate in the manner described by Hirotsu *et al.*;[14] a colorless oil of IIIf was thus obtained; yield, 1.375 g (99%); $[\alpha]_D^{21}$ −59° (*c* 1, methanol). All the imidates obtained were used for the next reaction without any purification.

N-Benzyloxycarbonyl Iminodipeptides (IV). General Procedure. A mixture of imidate (0.01 mol) and amino acid (0.012 mol) in dry methanol (50 ml) was refluxed for 3 h. After cooling, the unreacted amino acid was filtered off, and the filtrate was evaporated to dryness. The residual crude iminodipeptide was purified by recrystallization from methanol–ethyl acetate or by column chromatography (silica gel, methanol or methanol–ethyl acetate). The results are summarized in Table 2.

N-Benzyloxycarbonylproline Thioamide (V). This compound was prepared from the corresponding amide (2.48 g, 10 mmol) according to our previously described procedure.[23] The reaction was completed in 2.5 h at room temperature. The recrystallization of the crude product from benzene–petroleum ether gave colorless crystals; yield, 1.78 g (67%); mp 93—94 °C, $[\alpha]_D^{26}$ −49.4° (*c* 1, methanol). Found: C, 59.06; H, 6.24; N, 10.46%. Calcd for $C_{13}H_{16}N_2O_2S$: C, 59.07; H, 6.10; N, 10.60%.

N-Benzyloxycarbonyl(iminoprolyl)glycine (VII), via Imidate from N-Benzyloxycarbonylproline Thioamide (V). A mixture of thioamide (V) (529 mg, 2 mmol), ethyl chloroformate (260 mg, 2.4 mmol), and absolute ethanol (0.5 ml) was stirred at room temperature. The reaction proceeded with a smooth evolution of gas and was completed in 2 h. The reaction mixture was then diluted with dry ether to separate a yellow oil. The oil, imidate hydrochloride, was immediately converted to a free imidate, a slightly yellow oil, as described above; yield, 399 mg (65%); $[\alpha]_D^{28}$ −48.9° (*c* 4, methanol).

The imidate, without any purification, was coupled with glycine (150 mg, 2 mmol) in dry methanol under reflux for 3.5 h, giving Z-(iminoprolyl)glycine (222 mg, 56%). $[\alpha]_D^{28}$ −66.9° (*c* 1, ethanol).

(Iminoprolyl)glycine Methyl Ester Dihydrochloride (VIII). To saturated hydrogen chloride in methanol (47%) (1 ml) was added in portions Z-(iminoprolyl)glycine (IVi) (100 mg, 0.33 mmol), which immediately dissolved with the evolution of gas. The solution was allowed to stand at room temperature for 3 days, and then evaporated under reduced pressure to leave white crystals; yield, 80 mg (94.5%); mp 167—168 °C (dec) (methanol–ether), $[\alpha]_D^{20}$ −0.5° (*c* 3, methanol). ORD: $[\phi]_{260}$ +372°, $[\phi]_{300}$ +111°, $[\phi]_{400}$ +23° (*c* 3, methanol). NMR(D_2O): δ 1.9—2.8 (m, 4H, C_3–H and C_4–H in proline), 3.57 (t, J=7 Hz, 2H, C_5–H in proline), 3.81 (s, 3H, CH_3-OCO–), 4.36 (s, 2H, glycine-CH_2). Found: C, 37.05; H, 6.79; N, 16.28%. Calcd for $C_8H_{15}N_3O_2 \cdot 2HCl$: C, 37.22; H, 6.64; N, 16.28%.

N-Benzyloxycarbonyl(iminoprolyl)glycine Methyl Ester Hydrochloride (IX). A solution of IVi (100 mg, 0.33 mmol) in 4.7% hydrogen chloride in methanol (3 ml) was allowed to stand overnight at room temperature. After the solvent had then been removed under reduced pressure, the residue was dissolved in methanol–ethyl acetate and the solution was again evaporated to afford a colorless foamy solid; yield, 115 mg (98.5%); mp 83—87 °C, $[\alpha]_D^{20}$ −55.0° (*c* 0.5, methanol). TLC: R_f 0.18 (methanol–ethyl acetate (1 : 4)). UV: λ_{max}^{MeOH} (ε); 257 nm (197). NMR(D_2O): δ 1.6—2.5 (m, 4H, C_3–H and C_4–H in proline), 3.58 (t, J=7 Hz, 2H, C_5–H in proline), 3.76 (s, 3H, CH_3OCO–), 4.06 (s, 2H, glycine-CH_2), 5.18 (s, 2H, benzyl-CH_2), 7.43 (s, 5H, phenyl). Found: C, 51.34; H, 6.45; N, 11.21%. Calcd for $C_{16}H_{21}N_3O_4 \cdot HCl \cdot H_2O$: C, 51.41; H, 6.47; N, 11.24%.

(Iminoprolyl)glycine Methyl Ester Dihydrobromide (X). The treatment of IX (50 mg) with 25% hydrogen bromide in acetic acid (0.15 g) at room temperature for 45 min gave (iminoprolyl)glycine methyl ester dihydrobromide; yield, 41 mg (84%); mp 165—166 °C (dec) (methanol–ether), $[\alpha]_D^{17}$ −2.0° (*c* 1, methanol). ORD: $[\phi]_{250}$ +510°, $[\phi]_{300}$ +101°, $[\phi]_{400}$ +14° (*c* 1, methanol). Found: C, 27.44; H, 5.12;

N, 11.94%. Calcd for $C_8H_{15}N_3O_2 \cdot 2HBr$: C, 27.69; H, 4.94; N, 12.11%.

(Iminoprolyl)glycine Dihydrobromide (XI). This compound was obtained by the removal of the Z group from IVi (100 mg, 0.33 mmol) with 25% hydrogen bromide in acetic acid (340 mg) as usual; yield, 100 mg (92%); mp 161—162 °C (methanol-ether), $[\alpha]_D^{20}$ −9.2° (*c* 0.4, methanol). Found: C, 25.65; H, 4.67; N, 12.28%. Calcd for $C_7H_{13}N_3O_2 \cdot 2HBr$: C, 25.25; H, 4.54; N, 12.62%.

(Iminoprolyl)glycine Methyl Ester Hydrochloride-hydrobromide (XII). The treatment of XI (60 mg) with 4.7% hydrogen chloride in methanol (3 ml) at room temperature for 4 days gave white crystals; yield, 39 mg (84%); mp 164—165 °C (dec) (methanol-ether). Found: C, 31.41; H, 5.35; N, 14.65%. Calcd for $C_8H_{15}N_3O_2 \cdot HBr \cdot HCl$: C, 31.75; H, 5.66; N, 13.89%.

N-*Isobornyloxycarbonylproline.* This compound was prepared in the manner described by Fujino and his co-workers;[17] yield, 57%; mp 134—135 °C (lit,[17] mp 135.5—136 °C).

N-*Isobornyloxycarbonylproline Amide (XIII).* The mixed anhydride method described above for Z-amino acid amides gave the desired amide (65.4%), along with the recovered starting material (30.6%). The recrystallization of the amide from aqueous ethanol afforded white crystals; mp 175.5—176 °C, $[\alpha]_D^{28}$ −83.7° (*c* 1, ethanol). Found: C, 65.14; H, 9.26; N, 9.41%. Calcd for $C_{16}H_{26}N_2O_3$: C, 65.28; H, 8.90; N, 9.52%.

N-*Isobornyloxycarbonyl-2-cyanopyrrolidine (XIV).* IBOC-proline amide (XIII) (3.94 g, 0.01 mol) was dehydrated with *p*-toluenesulfonyl chloride (5.7 g, 0.03 mol) in pyridine (20 ml) in the manner described above for the Z series, giving colorless crystals; yield, 3.70 g (98.7%); mp 73—76 °C.

The analytical sample was obtained by recrystallization from petroleum ether; mp 78—79 °C, $[\alpha]_D^{28}$ −127.1° (*c* 1, ethanol). Found: C, 69.39; H, 9.00; N, 10.20%. Calcd for $C_{16}H_{24}N_2O_2$: C, 69.53; H, 8.75; N, 10.14%.

Formation of the Imidazolone Derivative (XV). a) By the Reaction of N-*Benzyloxycarbonyl(iminoprolyl)glycine (IVi) with Methyl Phenylalaninate in the Presence of Dicyclohexylcarbodiimide:* Into a solution of IVi (153 mg, 0.5 mmol), methyl phenylalaninate hydrochloride (113 mg, 0.5 mmol), and triethylamine (51 mg, 0.5 mmol) in pyridine (5 ml), DCC (103 mg, 0.5 mmol) was stirred at room temperature. After 1 day, the resulting white crystals were filtered off and the filtrate was concentrated under reduced pressure. The residue was chromatographed on a preparative thin layer with methanol–ethyl acetate (1 : 9) to afford an oil; yield, 18 mg (19%); TLC: R_f 0.37 (methanol–ethyl acetate (1 : 9)).

b) By the Treatment of N-*Benzyloxycarbonyl(iminoprolyl)glycine Methyl Ester Hydrochloride (IX) with Triethylamine:* A solution of the hydrochloride (IX) (100 mg) and triethylamine (60 mg) in methanol (3 ml) was allowed to stand at room temperature for 3 h. The solution was then evaporated under reduced pressure to give a brown-yellow oil, which was chromatographed on a preparative thin layer; yield, 62 mg (77%); TLC: R_f 0.37 (methanol–ethyl acetate (1 : 9)).

c) By the Reaction of Ethyl N-*Benzyloxycarbonyl-2-pyrrolidinecarboximidate (IIIf) with Methyl Glycinate:* A mixture of the imidate (IIIf) (2.36 g, 8.5 mmol), methyl glycinate hydrochloride (0.76 g, 8.5 mmol), and triethylamine (0.86 g, 8.5 mmol) in dry tetrahydrofuran (50 ml) was stirred at room temperature for 2 days. After a white precipitate had been filtered off, the filtrate was concentrated to give a reddish brown oil. The oil was chromatographed on a silica gel column with methanol–ethyl acetate (1 : 4), thus affording as the main product a yellow oil, which soon turned a reddish brown; yield, 0.82 g (29%); TLC: R_f 0.37 (methanol–ethyl acetate (1 : 9)).

*2-(*N-*Benzyloxycarbonyl-2-pyrrolidinyl)-5(or 4)-(*p-*methoxyphenylmethylene)-2-imidazolin-4(or 5)-one (XVI).* a) A solution of the crude compound (XV) (100 mg) and *p*-anisaldehyde (360 mg) in methanol (1 ml) was allowed to stand at room temperature for 2 days. The reaction mixture was then chromatographed on a preparative thin layer with benzene–ethyl acetate (3 : 2) to give two sorts of yellow crystals; major product; yield, 43 mg; TLC: R_f 0.62 (benzene–ethyl acetate (2 : 3)); minor product: yield, 11 mg; TLC: R_f 0.44. The analytical sample of the major product was obtained by recrystallization from ethyl acetate; mp 194—195 °C, $[\alpha]_D^{20}$ −53.1° (*c* 1, $CHCl_3$). UV: $\lambda_{max}^{CHCl_3}$ (ε); 368 nm (3.70×10^4). NMR ($CDCl_3$): δ 1.8—2.5 (m, 4H, C_3–H and C_4–H in pyrrolidine ring), 3.58 (t, J=6 Hz, 2H, C_5–H in pyrrolidine ring), 3.86 (s, 3H, OCH_3), 4.7—5.0 (m, 1H, C_2–H in pyrrolidine ring), 5.19 (s, 2H, benzyl-CH_2), 6.95 (d, J=9 Hz, 2H, *meta*-H of *p*-methoxyphenyl), 7.09 (s, 1H, C=C<u>H</u>), 7.35 (s, 5H, C_6H_5–), 8.13 (d, J=9 Hz, 2H, *ortho*-H of *p*-methoxyphenyl), 9.36 (s, 1H, NH). Found: C, 68.06; H, 5.72; N, 10.05%. Calcd for $C_{23}H_{23}N_3O_4$: C, 68.13; H, 5.72; N, 10.36%.

The minor product seemed to be an isomer since it gradually changed into the major product in methanol, but it was not investigated further.

b) A more convenient method to prepare XVI was as follows: a mixture of IX (608 mg), *p*-anisaldehyde (2.23 g), and triethylamine (331 mg) in methanol (2 ml) was allowed to stand at room temperature for 2 days. After the solvent had been removed under reduced pressure, the residue was taken up in ethyl acetate in order to remove triethylamine hydrochloride. The solution was then concentrated to give a yellow oil, which was chromatographed on a silica gel column with benzene–ethyl acetate (4 : 1—3 : 2), affording yellow crystals; yield, 507 mg (77%); mp 193—194 °C, TLC: R_f 0.62 (benzene–ethyl acetate (2 : 3)).

Glycylphenylalanine Methyl Ester Hydrobromide. This compound was prepared by the coupling of Z-glycine with methyl phenylalaninate using DCC, followed by the removal of the Z group with 25% hydrogen bromide in acetic acid, according to the method of Mazur and Schlatter;[24] yield, 94%; mp 166—168 °C (dec) (lit,[24] mp 167—170 °C). It was used for the next reaction without further purification.

N-*Benzyloxycarbonyl(iminoprolyl)glycylphenylalanine Methyl Ester (XVIII).* A solution of the imidate (IIIf) (665 mg, 2.4 mmol), glycylphenylalanine methyl ester hydrobromide (634 mg, 2.0 mmol), and triethylamine (220 mg, 2.0 mmol) in dry methanol (10 ml) was stirred at room temperature for 1 day. The solution was then evaporated under reduced pressure to leave a syrup with some crystals. The syrup was taken up in ethyl acetate, and any insoluble materials were filtered off. The filtrate was evaporated under reduced pressure, and the residue was chromatographed on a silica gel column with methanol–ethyl acetate (1 : 9), giving a foamy solid; yield, 683 mg (61.4%); mp 90—94 °C, $[\alpha]_D^{23}$ −23.6° (*c* 0.75, methanol). Found: C, 53.94; H, 5.84; N, 10.03%. Calcd for $C_{25}H_{30}N_4O_5 \cdot HBr \cdot 1/2H_2O$: C, 53.96; H, 5.80; N, 10.07%.

The present work was supported in part by a Grant-in-Aid for Scientific Research from Ministry of Education.

References

1) A part of this work was presented at the 32nd National Meeting of the Chemical Society of Japan, Tokyo, Preprint

III (1975), p. 1702.

2) J. M. Waisvisz, M. G. van der Hoeven, J. van Peppen, and W. C. M. Zwennis, *J. Am. Chem. Soc.*, **79**, 4520 (1957).

3) S. Nakamura, T. Chikaike, K. Karasawa, N. Tanaka, H. Yonehara, and H. Umezawa, *J. Antibiot.*, **18A**, 47 (1965); S. Omura, Y. C. Lin, T. Yajima, S. Nakamura, N. Tanaka, H. Umezawa, S. Yokoyama, Y. Homma, and M. Hamada, *J. Antibiot.*, **20A**, 241 (1967); W. J. Miller, L. Chaiet, G. Rasmussen, B. Christensen, J. Hannah, A. K. Miller, and F. J. Wolf, *J. Med. Chem.*, **11**, 746 (1968).

4) S. Nakamura, T. Chikaike, H. Yonehara, and H. Umezawa, *J. Antibiot.*, **18A**, 60 (1965); S. Nakamura, T. Chikaike, H. Yonehara, and H. Umezawa, *Chem. Pharm. Bull.*, **13**, 599 (1965); S. Nakamura, N. Tanaka, and H. Umezawa, *J. Antibiot.*, **19A**, 10 (1966); S. Nakamura and H. Umezawa, *Chem. Pharm. Bull.*, **14**, 981 (1966); S. Nakamura, T. Yajima, Y. C. Lin, and H. Umezawa, *J. Antibiot.*, **20A**, 1 (1967).

5) S. Nakamura, *Chem. Pharm. Bull.*, **9**, 641 (1961).

6) S. Nakamura, H. Yonehara, and H. Umezawa, *J. Antibiot.*, **17A**, 220 (1964).

7) These peptides should be classified as peptide amidines instead of as iminopeptides, since they contain an amidino group in the terminal of the molecule, not between amino acid residues in peptide.

8) S. Nakamura, S. Omura, T. Nishimura, N. Tanaka, and H. Umezawa, *J. Antibiot.*, **20A**, 162 (1967).

9) W. Ried, W. Stephan, and W. von der Emden, *Chem. Ber.*, **95**, 728 (1962); W. Ried and W. von der Emden, *Ann. Chem.*, **661**, 76 (1963); W. Ried and E. Schmidt, *Ann.*, **695**, 217 (1966).

10) E. Vargha and I. Balàzs, *Studia Univ. Babes-Bolyai, Ser. Chem.*, **11**, 85 (1966); *Chem. Abstr.*, **66**, 2757 m (1967).

11) The following nomenclatures and abbreviations are used for iminopeptides. An amino acid containing =NH instead of =O in the carboxyl group is called an imino amino acid and abbreviated as ImAA (AA=amino acid); *e.g.*, 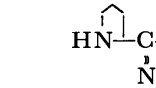 is called iminoproline (ImPro). Therefore, 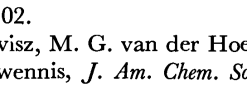 is called (iminoprolyl)glycine (ImPro-Gly), and ethyl Z-amino carboximidate (III) may be abbreviated as Z-ImAA-OEt.

12) E. Frauendolfer, W. Steglich, and F. Weygand, *Chem. Ber.*, **106**, 1019 (1973).

13) Y. Kataoka, Y. Seto, M. Yamamoto, T. Yamada, S. Kuwata, and H. Watanabe, *Bull. Chem. Soc. Jpn.*, **49**, 1081 (1976).

14) Y. Hirotsu, T. Shiba, and T. Kaneko, *Bull. Chem. Soc. Jpn.*, **40**, 2945 (1967).

15) R. Roger and D. G. Neilson, *Chem. Rev.*, **61**, 193 (1961); M. Mengelberg, *Chem. Ber.*, **89**, 1185 (1956); *ibid.*, **91**, 1961 (1958).

16) F. H. Suydam, W. E. Greth, and N. R. Langerman, *J. Org. Chem.*, **34**, 292 (1969).

17) M. Fujino, S. Shinagawa, O. Nishimura, and T. Fukuda, *Chem. Pharm. Bull.*, **20**, 1017 (1972).

18) M. Fujino and S. Shinagawa, *Chem. Pharm. Bull.*, **20**, 1021 (1972).

19) A. Kjaer, *Acta Chem. Scand.*, **7**, 1017, 1024, 1030 (1953).

20) H. Lehr, S. Karlan, and M. W. Goldberg, *J. Am. Chem. Soc.*, **75**, 3640 (1953); A. R. Kidwai and G. M. Devasia, *J. Org. Chem.*, **27**, 4527 (1962).

21) K. Sturm, R. Geiger, and W. Siedel, *Chem. Ber.*, **96**, 609 (1963); J. M. Davey, A. H. Laird, and J. S. Morley, *J. Chem. Soc., C*, **1966**, 555; C. Ressler, *J. Am. Chem. Soc.*, **82**, 1641 (1960).

22) M. Zaoral and J. Rudinger, *Coll. Czech. Chem. Commun.*, **24**, 1993 (1959); T. Itoh, *Bull. Chem. Soc. Jpn.*, **36**, 25 (1963).

23) Y. Seto, K. Torii, K. Bori, K. Inabata, S. Kuwata, and H. Watanabe, *Bull. Chem. Soc. Jpn.*, **47**, 151 (1974).

24) R. H. Mazur and J. M. Schlatter, *J. Org. Chem.*, **28**, 1025 (1963).

A Three-Component Reaction of Isocyanides with Halogens and Cyclic Ethers

Takeshi YAMAZAKI,* Yasuo WADA,* Shigeo TANIMOTO, and Masaya OKANO**

Institute for Chemical Research, Kyoto University, Uji, Kyoto 661

(Received October 8, 1976)

In the presence of a Lewis-acid catalyst, such as $HgCl_2$ or $ZnCl_2$, cyclohexyl isocyanide reacted with chlorine and tetrahydrofuran to give, after hydrolysis, 4-chlorobutyl cyclohexylcarbamate in a fair yield. When one of the reactants was replaced by another isocyanide, bromine, or another cyclic ether, the reactions proceeded similarly, but the corresponding carbamate yields were rather poor.

Isocyanides are known to undergo multi-component reactions[1] in which more than two reactants selectively combine to form a single product, as represented by the Passerini reaction. In an attempt to find a new example of triple addition reactions, reactions of isocyanides with halogens and 3- to 5-membered cyclic ethers were examined in the presence of Lewis-acid catalysts. The ω-haloalkyl carbamates, $RNHCOO(CH_2)_nX$ (n=2—4), which correspond to the hydrolysis products of the 1 : 1 : 1 adducts, were successfully obtained in various yields, by treatment of the reaction mixtures with water. The present paper deals with the new reaction:

$$R\text{-}N{\equiv}C + X_2 + (CH_2)_nO \xrightarrow{MX_n} R\text{-}N{=}C(X)O(CH_2)_nX \xrightarrow{H_2O} RNHCOO(CH_2)_nX \quad (1)$$

In connection with this, phenylcabonimidoyl dichloride has been known to undergo an insertion reaction of ethylene oxide into the C–Cl bond of the dichloride in the presence of triethylamine, the isolated product being not 2-chloroethyl *N*-phenylchloroformimidate, but the isomeric carbamoyl chloride resulting from a Chappmann rearrangement of the expected product (Eq. 2).[2]

$$Ph\text{-}N{=}CCl_2 + \underset{O}{CH_2\text{-}CH_2} \xrightarrow{Et_3N} [Ph\text{-}N{=}C(Cl)O(CH_2)_2Cl] \longrightarrow Ph\text{-}N(COCl)CH_2CH_2Cl \quad (2)$$

On the other hand, it has also been reported that the $ZnCl_2$- or $SnCl_4$-catalyzed cycloaddition of arylcarbonimidoyl dichlorides to aliphatic epoxides, followed by hydrolysis, gives 3-aryl-5-alkyl-2-oxazolidinones, although the yields are very low (Eq. 3).[3]

$$Ar\text{-}N{=}CCl_2 + \underset{O}{R\text{-}CH\text{-}CH_2} \xrightarrow{\text{Lewis acid}} \left[Ar\text{-}N\text{—}C(Cl_2)\text{—}O\text{—}R\right] \xrightarrow{H_2O} Ar\text{-}N(C{=}O)\text{—}O\text{—}R \quad (3)$$

* Koei Chemical Co., Ltd. Jôtô-ku, Osaka 536.

** To whom correspondence should be addressed.

Results and Discussion

When cyclohexyl isocyanide was treated with chlorine in tetrahydrofuran (hereinafter abbreviated as THF) at room temperature in the presence of $HgCl_2$ or $ZnCl_2$ and the reaction mixture was hydrolyzed before isolation, 4-chlorobutyl cyclohexylcarbamate was obtained in a good yield, along with small amounts of various by-products which will be described below. Some results are shown in Table 1.

Table 1. Reaction of cyclohexyl isocyanide with halogens and THF

Isocyanide 24 mmol: Halogens 72 mmol; THF 360 mmol. Reaction conditions: 5—10 °C, 1.5 h and 20—25 °C, 50 h.

X_2	Catalyst (mmol)	Yield (%) of cyclo-$C_6H_{11}NHCOO(CH_2)_4X$[c]
Cl_2	None	0[d]
Cl_2	$HgCl_2$, 3	2[e]
Cl_2	$HgCl_2$, 8[a]	0[f]
Cl_2	$HgCl_2$, 8	70
Cl_2	$HgCl_2$, 8[b]	80
Cl_2	$HgCl_2$, 24	67
Br_2	$HgBr_2$, 8	32
Cl_2	$ZnCl_2$, 8	59
Cl_2	$ZnCl_2$, 24	68

a) Reaction conditions: −15 °C, 1 h and −10—0 °C, 5 h. b) Reaction conditions: 55—60 °C, 6.5 h. c) Based on isocyanide (determined by GLC). d) cyclo-$C_6H_{11}N{=}CCl_2$, 90%. e) cyclo-$C_6H_{11}N{=}CCl_2$, 69%. f) cyclo-$C_6H_{11}N{=}CCl_2$, 87%.

When $AlCl_3$ or $FeCl_3$ was used as the catalyst, the reaction was considerably exothermic and afforded mainly a polymeric substance which consists mostly of oligomers of THF rather than the desired carbamate. Moreover, the reaction without the catalyst yielded only cyclohexylcarbonimidoyl dichloride and no amount of the carbamate could be found in the reaction mixture. In the case of a $HgCl_2$ catalyst, *ca.* 4 mol% (based on chlorine) was found to be insufficient to yield the carbamate predominantly, and the optimum amount was estimated to be *ca.* 10 mol%, although no accurate determination was made.

An increase in the yield of the carbamate was observed for a rise in the reaction temperature. However, the reaction below 0 °C, even in the presence of 11.5 mol% of $HgCl_2$, afforded only the carbonimidoyl dichloride as the reaction product.

When bromine and $HgBr_2$ were used in place of chlorine and $HgCl_2$, respectively, the reaction with cyclohexyl isocyanide proceeded similarly affording 4-bromobutyl cyclohexylcarbamate, but the yield was rather poor compared with the preparation of the corresponding chlorine compound. An analogous reaction with iodine and HgI_2, however, did not give the desired compound and yielded only a tarry product.

Data on the reaction of some aliphatic and aromatic isocyanides with chlorine in THF are shown in Table 2a. In the case of *t*-butyl isocyanide, the yield of carbamate was rather low. This is probably due to the decreased stability of the intermediate *t*-butylchloroimidoyl cation, which tends to decompose to *t*-butyl cation and ClCN rather easily.[4] Phenyl isocyanide afforded carbamate in a low yield, although the recorded yield was only the isolated yield in this case.

Table 2. Reaction of isocyanides with chlorine and cyclic ethers

(a) Variation of the isocyanide component.
Isocyanides 24 mmol; Cl_2 72 mmol; THF 360 mmol; $HgCl_2$ 8 mmol. Reaction conditions: 55—60 °C, 6.5 h.

Isocyanide	Yield (%) of $RNHCOO(CH_2)_4Cl$[a]	
n-BuNC	R=*n*-Bu,	67
cyclo-$C_6H_{11}NC$	R=cyclo-C_6H_{11},	80
t-BuNC	R=*t*-Bu,	49
PhNC	R=Ph,	44[b]

a) Based on isocyanide (determined by GLC).
b) Isolated yield.

(b) Variation of the cyclic ether component.
Cyclohexyl isocyanide 24 mmol; Cl_2 72 mmol; Cyclic ethers 360 mmol; $HgCl_2$ 8 mmol. Reaction conditions: 5—10 °C, 1.5 h and 20—25 °C, 50 h.

Cyclic ether	Yield (%) of cyclo-$C_6H_{11}NHCOOR$[a]	
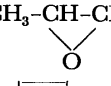	R=$CH_2CH(CH_3)Cl$,	12
	R=$(CH_2)_3Cl$,	37
	R=$(CH_2)_4Cl$,	68

a) Based on isocyanide (determined by GLC).

The $HgCl_2$-catalyzed reaction of cyclohexyl isocyanide with chlorine was also carried out in trimethylene oxide and propylene oxide, for comparison with that in THF. The results are shown in Table 2b. The yields of the corresponding carbamates decreased as the ring size changed from 5 to 3 *via* 4. This order is the same as that obtained for the case of Lewis acid-catalyzed ring-opening polymerization of cyclic ethers.[5]

In this reaction, the chloroimidoyl cation (**1**), formed by the electrophilic addition of Cl^+ to isocyanide, appears to act as a key intermediate. This reacts with THF, and with a complex halide anion successively to afford a chloroformimidate (**2**), which then forms 4-chlorobutyl carbamate (**3**) when hydrolyzed.

$$Cl_2 + HgCl_2 \rightleftharpoons Cl^+ + HgCl_3^- \quad (4)$$

$$R\text{-}N{\equiv}C \xrightarrow{Cl^+} R\text{-}N{=}C^+\text{-}Cl \xrightarrow{THF} \left[R\text{-}N{=}C\begin{matrix}Cl\\ O^+\end{matrix}\right]$$

1

$$\xrightarrow{HgCl_3^-} R\text{-}N{=}C\begin{matrix}Cl\\ O(CH_2)_4Cl\end{matrix} \quad (5)$$

2

$$\mathbf{2} \xrightarrow{H_2O} RNHCOO(CH_2)_4Cl \quad (6)$$

3

Here, the intermediate **1** may be formed by another route *via* carbonimidoyl dichloride. However, when cyclohexylcarbonimidoyl dichloride was treated with THF in the presence of $HgCl_2$ under the same reaction conditions (20—25 °C, 50 h), the expected carbamate was obtained in only a 6% yield and most of the unreacted dichloride was recovered. Therefore, such a possibility can be ruled out as the main course of the reaction.

Finally, a short comment on the by-products of the reaction must be added. From the reaction mixture of cyclohexyl isocyanide, chlorine, and THF, small amounts of 1,4-dichlorobutane, 4-chloro-1-butanol, bis(4-chlorobutyl) ether, and 2-(4-chlorobutoxy)-3-chlorotetrahydrofuran (**4**) were isolated, along with the carbamate and occasionally with the carbonimidoyl dichloride. It is obvious that all the minor products come from the reaction between THF and chlorine. It has been reported that the chlorination of THF at room temperature results only in 2,3-dichlorotetrahydrofuran (**5**) (Reaction 7).[6] In the presence of a $ZnCl_2$ catalyst, cleavage of THF by **5** is known to afford **4** (Reaction 8).[7] 4-Chloro-1-butanol is probably formed by the action of HCl on THF during the chlorination of THF. This compound would be a precursor of 1,4-dichlorobutane and bis(4-chlorobutyl) ether.

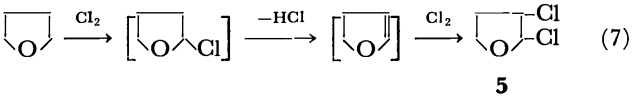

$$\xrightarrow{-HCl} \xrightarrow{Cl_2} \quad (7)$$

5

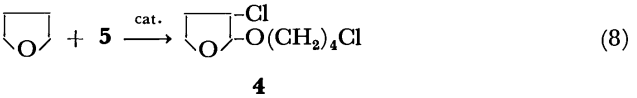

$$\xrightarrow{cat.} \quad (8)$$

4

Experimental

GLC analysis was carried out on a Shimadzu 5APTF apparatus using an EGSS-X(30%)-Chromosorb-W (1 m) column (with N_2 as the carrier gas). The IR spectrum was recorded with a Hitachi EPI-S2 apparatus.

Isocyanides (RNC) were prepared using the method of Ugi *et al.*:[8] R=C_6H_{11}, bp 67—69 °C/20 Torr (lit,[8] bp 67—72 °C/13 Torr); R=*n*-Bu, bp 48 °C/20 Torr (lit,[8] bp 40—42 °C/11 Torr); R=*t*-Bu, bp 48 °C/60 Torr (lit,[8] bp 92—93 °C/750 Torr); R=Ph, bp 61—62 °C/18 Torr (lit,[8] bp 50—51 °C/11 Torr). Trimethylene oxide was prepared from 3-chloropropyl acetate[9] (bp 47—49 °C, lit,[9] bp 47—48 °C). Commercial THF and propylene oxide were used after distillation, while the inorganic substances were used without further purification.

$HgCl_2$-Catalyzed Reaction of Isocyanides with Chlorine and THF. A typical example is given below. Into a stirred solution of $HgCl_2$ (2.2 g, 8 mmol) in THF (29 ml, 360 mmol) containing cyclohexyl isocyanide (2.6 g, 24 mmol), chlorine gas (5.1 g, 72 mmol) was bubbled over a period of 1.5 h, the temperature being maintained at 5—10 °C by cooling with ice water. After stirring for an additional 50 h at 20—25 °C, the reaction mixture was added to a suspension of $CaCO_3$ (5 g) in water (20 ml). The resulting heterogeneous mixture was stirred at 20—25 °C for 3 h. Then ether was added and inorganic precipitates were filtered off. The ether extract was separated from the aqueous layer. This was combined with a dichloromethane extract in the aqueous phase. The combined organic layer was washed with aqueous K_2CO_3 and aqueous NaCl, successively, dried over anhydrous $MgSO_4$, and most of the solvents were evaporated. GLC analysis of the residue using isopropylbenzene, *p*-methoxyacetophenone, and triphenylmethane as internal standards showed the presence of 1,4-dichlorobutane (**6**) (1.4 g, 10.9 mmol), 4-chloro-1-butanol (**7**) (3.5 g, 32.3 mmol), bis(4-chlorobutyl) ether (**8**) (0.6 g, 2.8 mmol), 2-(4-chlorobutoxy)-3-chlorotetrahydrofuran (**4**) (2.9 g, 13.6 mmol), and 4-chloro butyl cyclohexylcarbamate (**3**, R=cyclo-C_6H_{11}) (4.0 g, 17.3 mmol, 72% yield). Distillation afforded the following fractions: fraction A, bp 55—90 °C/25 Torr (3.4 g), fraction B, bp 90—100 °C/3 Torr (3.1 g), fraction C, bp 131—133 °C/3 Torr (4.5 g), and a black semi-solid residue D (1.7 g). The fractions A and B were shown by GLC to be a mixture of **6** and **7**, and of **7**, **8**, and **4**, respectively. The fraction C was revealed to contain **3** (89%) and **8** (11%), and redistillation gave the pure carbamate, bp 132 °C/3 Torr, mp 55—56 °C (from hexane) (lit,[10] mp 57—58 °C). The IR spectrum of residue D showed the characteristic absorptions due to carbamate [1710 cm^{-1} (CO), 1530, 3380 cm^{-1} (NH) and 1055 cm^{-1} (C–O–C)] and ether [1120 cm^{-1} (C–O–C)] groups, indicating the existence of oligomers of **3**, cyclo-$C_6H_{11}NHCO[O(CH_2)_4]_nCl$($n>1$), and of THF.

Reaction of Cyclohexyl Isocyanide with Chlorine in THF without the Catalyst. Chlorine gas (5.1 g, 72 mmol) was slowly bubbled into a stirred solution of cyclohexyl isocyanide (2.6 g, 24 mmol) in THF (29 ml, 360 mmol) at 5—10 °C, as described above. After being maintained for an additional 50 h at 20—25 °C with stirring, the mixture was poured into water. The resulting mixture was extracted with ether, and the extract was dried over anhydrous $MgSO_4$. Distillation gave cyclohexylcarbonimidoyl dichloride (3.9 g, 90% yield), bp 91—92 °C/20 Torr (lit,[11] 79—82 °C/13 Torr).

Authentic Samples for GLC Analysis. All ω-haloalkyl carbamates were prepared by the reaction of ω-halo-1-alkanols with isocyanates.[10,12] cyclo-$C_6H_{11}NHCOOR$: R=$(CH_2)_4Cl$, bp 132 °C/3 Torr; R=$(CH_2)_3Cl$, bp 126 °C/3 Torr (Found: C, 54.42; H, 8.52; N, 6.27%. Calcd for $C_{10}H_{18}NO_2Cl$: C, 54.67; H, 8.26; N, 6.38%); R=$CH_2CH(CH_3)Cl$, bp 107 °C/5 Torr (Found: C, 54.54; H, 8.22; N, 6.28%. Calcd for $C_{10}H_{18}NO_2Cl$: C, 54.67; H, 8.26; N, 6.38%); R=$(CH_2)_4Br$, bp 148 °C/2.8 Torr (Found: C, 47.73; H, 7.21; N, 5.17%. Calcd for $C_{11}H_{20}NO_2Br$: C, 47.49; H, 7.25; N, 5.04%). RNHCOO$(CH_2)_4Cl$: R=*n*-Bu, bp 115—118 °C/4 Torr (Found: C, 51.89; H, 9.03; N, 6.95%. Calcd for $C_9H_{18}NO_2Cl$: C, 52.05, H, 8.74; N, 6.74%); R=*t*-Bu, bp 92 °C/3 Torr (Found: C, 51.97; H, 9.03; N, 6.54%. Calcd for $C_9H_{18}NO_2Cl$: C, 52.05, H, 8.74; N, 6.74%); R=Ph, mp 54—55 °C (from hexane) (lit,[12] mp 54 °C).

References

1) I. Ugi, *et al.*, "Isonitrile Chemistry," Academic Press, New York, N. Y. (1971), Chaps. 7 and 8.
2) V. S. Etlis, A. P. Sinekov, and M. E. Sergeva, *Zh. Org. Khim.*, **2**, 1684 (1966); *Chem. Abstr.*, **66**, 65206 (1967).
3) R. Oda, T. Hamada, Y. Ito, and M. Okano, *Bull. Inst. Chem. Res. Kyoto Univ.*, **44**, 227 (1966).
4) For facile decomposition of *N-t*-butylimidoyl cations, see N. J. Leonard and E. W. Nommensen, *J. Am. Chem. Soc.*, **71**, 2808 (1949); T. Saegusa, N. Takaishi, and Y. Ito, *J. Org. Chem.*, **34**, 4040 (1969).
5) T. Saegusa in "Advances in Polymer Synthesis," ed by E. Imoto *et al.*, Kagaku-dojin, Kyoto (1964), p. 156.
6) G. Sosnovsky, "Free Radical Reactions in Preparative Organic Chemistry," Macmillan Co. New York, N. Y. (1964), p. 370.
7) N. B. Lorette, *J. Org. Chem.*, **23**, 1590 (1958).
8) I. Ugi, U. Fetzer, U. Eholzer, H. Knupfer, and K. Offermann, *Angew. Chem. Int. Ed. Engl.*, **4**, 472 (1965).
9) C. R. Noller, *Org. Synth.*, Coll. Vol, III, 835 (1955).
10) H. Paul, G. Manfred, and T. Hans, East German Patent, 73192; *Chem. Abstr.*, **74**, 124974 (1971).
11) E. Kühle, B. Anders, and G. Zumack, *Angew. Chem. Int. Ed. Engl.*, **6**, 649 (1967).
12) W. R. Kirner and G. H. Richter, *J. Am. Chem. Soc.*, **51**, 2503 (1929).

Reactivities of Stable Rotamers. II. Lithiation of 9-(2-Methyl-1-naphthyl)-fluorene and Related Compounds[1]

Mikio NAKAMURA, Nobuo NAKAMURA, and Michinori ŌKI

Department of Chemistry, Faculty of Science, The University of Tokyo, Tokyo 113

(Received October 26, 1976)

Studies were carried out on the rates of lithiation of 9-arylfluorenes, in which the aryls are hydrocarbons. The reactivities of these compounds are explained in terms of the effective blocking of the reaction site by the substituent. The steric effect of the substituent which is attached to the aryl group but is over the fluorene ring is found to play a role in the reactivities.

Abundant data on the reactivity of organic compounds have been obtained but they are usually weighted means of rotational isomers, except when the compound in question reacts at a site where no rotamer is possible. In the former case, the observed reaction rates may be expressed by the following equation if there are two possible rotamers:[2]

$$k_{obsd} = k_a N_a + k_b N_b, \quad (1)$$

where k and N denote the intrinsic reaction rates and molar fractions of each rotamer, respectively. When the reactivities of both rotamers are comparable, the reactivity of a less populated isomer can be neglected if the molar fraction is one-sided. However, it becomes significant if the reaction rate of a trace-populated rotamer is exceedingly high. Our recent finding on the difference in reactivities of rotamers[1] singles out the importance of this view.

In discussing the solvent effect on reactions, the consideration of rotamers becomes important because the solvation can stabilize the ground states of rotamers to a different degree, thus controlling the populations. The transition states derived from the different rotamers can also be affected by solvation in a different manner. Study of behavior of rotamer in various solvents thus is necessary for understanding the reactions which are affected by solvents.

We thought it would be worthwhile to launch a project on the reactivities of rotamers, since we could isolate various types of stable rotamers.[3] This is the first full paper of such a series giving a discussion on the lithiation of 9-arylfluorenes together with the origin of the difference in reactivities. The series of hydrocarbons was studied first, since it would not contain complexities such as ligation by oxygen atom in the case of 9-(2-methoxy-1-naphthyl)fluorene.[1] The numbering of arylfluorenes used throughout this text is given below.

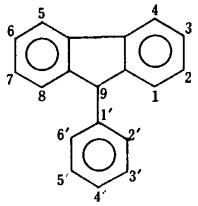

Experimental

NMR Measurement. ^1H NMR spectra were determined on a Hitachi R-20B spectrometer obtained at 60 MHz. The temperature was calibrated by the peak separation of ethylene glycol. The error in temperature reading was estimated to be ±1.0 °C. ^{13}C NMR spectra were measured on a JNM-FX 60 spectrometer operating at 15.04 MHz, ^{13}C–^1H coupling constants being obtained from all proton undecoupled spectra. The estimated error in the coupling constants was ±0.5 Hz.

Kinetic Measurement. A solution of 0.098 mmol of a 9-arylfluorene in 0.08 ml of benzene was mixed with 0.2 ml of butyllithium in hexane. The quantity of butyllithium was calculated to be *ca.* 1.0 mmol from the integration of methylene signals α to lithium. The rates of reaction were followed by integrating the proton signals due to 4-H and 5-H of the fluorene ring. The protons give signals at δ *ca.* 7.8 in the mother compounds whereas the lithio dervatives give signals at δ 8.0 or below.

9-(*p*-Tolyl)fluorene gave signals at δ *ca.* 8.0 due to 4 protons, two of which are unknown, on lithiation. Integration and calculation were carried out with this fact being taken into consideration. In the case of 9-(2-methyl-1-naphthyl)fluorene, the lithio derivative was hardly soluble in the solvent system and the integrated area of a signal due to 9-H of the mother compound had to be compared with that of a signal due to 9-H of 9-(2,6-xylyl)fluorene which did not react to a measurable extent.

In each case, plot of $\log(1-x/a)$ *vs.* time gave a straight line and the pseudo-first order rate constants were obtained in the usual way. The errors are given in Table 3. The rates of reaction of 9-(2,6-xylyl)- and 9-(2-*t*-butylphenyl)-fluorene were too small to measure in hexane–benzene solution whereas those of other compounds were too large to measure in ether.

Syntheses. Syntheses were carried out by the Grignard reaction of fluorenone with the corresponding arylmagnesium halide followed by reduction with hydriodic acid.[4]

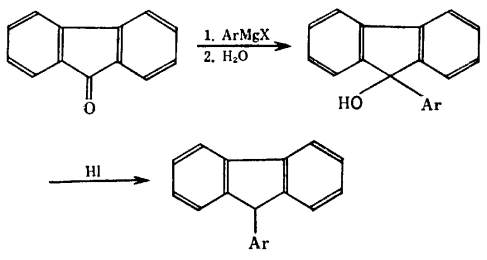

Some 9-aryl-9-fluorenols were not isolated but reduced directly. The overall yields were 50—70%.

9-Aryl-9-fluorenol. To a vigorously stirred solution of arylmagnesium halide prepared from 0.02 mol of aryl halide, 0.02 mol of magnesium and 40 ml of tetrahydrofuran, 0.02 mol of fluorenone was added at 0 °C. The mixture was stirred for 3 h at room temperature and then heated under reflux for 1 h. The cooled mixture was decomposed with dilute hydrochloric acid. The organic layer was separated and the aqueous layer was extracted with ether. The

combined organic layer was washed with aqueous sodium bicarbonate and dried over sodium sulfate. The following compounds were isolated by chromatography on silica gel.

9-(2-Isopropylphenyl)-9-fluorenol. Mp 147—148 °C. Yield 65%. ^{1}H NMR ($CDCl_3$, δ): 0.48 [$(CH_3)_2CH$], 2.18 [$(CH_3)_2CH$], 2.3(OH), 8.3(6'-H). Found: C, 88.11; H, 6.77%. Calcd for $C_{22}H_{20}O$: C, 87.96; H, 6.71%.

The compound exists in an ap form solely. The high chemical shift of the $(CH_3)_2CH$ signals and appearance of a signal due to 6'-H at a low field support the assignment.

9-(2-t-Butylphenyl)-9-fluorenol. Mp 156.5—158.0 °C. Yield 66%. ^{1}H NMR ($CDCl_3$, δ): 1.79 (*t*-Bu), 2.3 (OH), 6.42 (6'-H). Found: C, 88.16; H, 7.08%. Calcd for $C_{23}H_{22}O$: C, 87.86; H, 7.05%.

The compound is judged to exist in an sp form from the low field *t*-butyl signal and a high field 6'-H signal.

9-Arylfluorene. 9-Aryl-9-fluorenol (*ca.* 0.01 mol) was dissolved in 30—60 ml of acetic acid and heated with 10 ml of 57% hydriodic acid for 1 h at 80 °C. The mixture was washed with aqueous sodium bisulfite and then with sodium bicarbonate, and dried over sodium sulfate. After evaporation of the solvent the product was purified by either chromatography on alumina or thin layer chromatography on silica gel. The yield was 75—80%. Pertinent data are given in Tables 1 and 2.

TABLE 1. 9-ARYLFLUORENES

Aryl	Mp (°C)	Calcd %		Found %	
		C	H	C	H
p-$CH_3C_6H_4$	127.0—127.5[a]				
2,6-$(CH_3)_2C_6H_3$	84.5—85.0	93.29	6.71	93.08	6.69
o-$CH_3C_6H_4$	90.5—91.5[b]	93.71	6.29	93.99	6.27
o-$(CH_3)_2CHC_6H_4$	88.0—89.0	92.91	7.09	92.78	7.13
o-$(CH_3)_3CC_6H_4$	179.5—180.5	92.57	7.43	92.61	7.40
2-Methyl-1-naphthyl					
sp	118.0—119.0	94.08	5.92	93.81	5.74
ap	125.0—126.0	94.08	5.92	93.85	5.75

a) Reported melting point was 125 °C.[12]
b) Reported melting point was 129—130.5 °C.[13]

Results and Discussion

Assignment of the Conformation of 9-Arylfluorenes. Features of the conformation of the ap and sp forms of 9-arylfluorenes are characterized by the fact that the alkyl group is located over the fluorene ring in ap (sp in the case of 2-methyl-1-naphthyl derivative (**8**)) form, whereas it is almost within the plane of the fluorene ring in sp (ap in the case of **8**) form. The opposite situation exists for 6'-protons of the aryl group.

The spacial arrangement of the alkyl group is reflected in the chemical shift of the alkyl protons. 9-(2,6-Xylyl)fluorene (**2**) gives signals due to methyls at δ 1.12 and δ 2.70. The former should be due to a methyl over the ring and the latter to a methyl within the plane of the ring. Thus, if we can observe two forms in ^{1}H NMR spectra, the assignment is straightforward by comparison of the chemical shift.

The conformation of the *t*-butyl compound can also be assigned by taking advantage of the above facts, although it exists as a single form. The *t*-butyl signal is located in a lower field than that of *t*-butylbenzene (δ 1.32),[5] the chemical shift of the 6'-H signal being located at a high field close to the other known sp forms. Thus the conformation of 9-(2-*t*-butylphenyl)fluorene (**3**) should be sp, this being in line with the consideration of the steric effect.

Rates of Lithiation. The pseudo-first order rate constants of lithiation of 9-arylfluorenes are given in Table 3. For the sake of convenience we will start the discussion from the symmetric compounds.

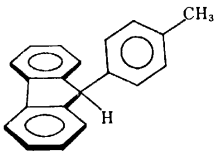

(**1**)

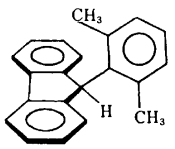

(**2**)

The internal rotation about the C_9–C_{ar} bond in 9-(*p*-tolyl)fluorene (**1**) should be fast at room temperature since analogous 9-(*m*-tolyl)fluorene is known to rotate fast even at −85 °C, whereas that in **2** is frozen.[6] The very low reactivity of **2** can be attributed to the steric blocking of the approach of the deprotonating reagent by the methyl group. Room for the approach of the reagent is made by rotation about the C_9–C_{ar} bond, the rotation itself requiring a fair amount of energy in com-

TABLE 2. NMR SPECTRAL DATA OF ROTAMERIC 9-ARYLFLUORENES IN $CDCl_3$ AT ROOM TEMPERATURE (δ from TMS)

Aryl		^{1}H NMR			^{13}C NMR			$J_{^{13}C-^1H}$ of 9-C
		CH_3	9-H	6'-H	CH_3	9-C	Other aliphatic C	
p-$CH_3C_6H_4$		2.27	4.99		22.73	53.93		128.8
2,6-$(CH_3)_2C_6H_3$		2.70 1.12	5.50		21.67 18.67	49.88		124.4
o-$CH_3C_6H_4$[a]	sp	2.63	5.30	6.38	20.33	49.79		127.6
	ap	1.13	4.90	>7.5	18.28	55.96		125.1
o-$(CH_3)_2CHC_6H_4$	sp	1.46	5.42	6.33	24.93	48.90	29.42	127.6
	ap	0.47	4.87	>7.5	23.13	56.33	28.04	122.7
o-$(CH_3)_3CC_6H_4$	sp	1.72	5.86	6.22	32.55	50.97	35.55	127.2
2-Methyl-1-naphthyl	sp	1.33	6.16	8.50[b]	19.48	48.50		122.7
	ap	2.83	5.78	6.43[b]	21.51	50.04		123.3

a) The ^{1}H NMR data were obtained at 0 °C.
b) These signals are due to 8'-H's of the naphthalene ring.

Table 3. Rates of lithiation of 9-arylfluorenes in hexane–benzene-d_6 at 42 °C

Aryl	Conformation	Pseudo-first order rate constant (k s^{-1})	k_{rel}
p-$CH_3C_6H_4$		$(1.2\pm0.1)\times10^{-4}$	23
2,6-$(CH_3)_2C_6H_3$[a]		0	0
o-$CH_3C_6H_4$	ap	$(4.1\pm0.2)\times10^{-5}$	8
o-$(CH_3)_2CHC_6H_4$	ap	$(1.9\pm0.4)\times10^{-5}$	4
o-$(CH_3)_3CC_6H_4$[a]	sp	0	0
2-Methyl-1-naphthyl	sp	$(3.6\pm0.6)\times10^{-5}$	7
	ap	$(5.2\pm0.6)\times10^{-6}$	1

a) These compounds were successfully lithiated in diethylether. The rate constants at 34 °C were $(5.4\pm0.4)\times10^{-4}$ s^{-1} and $(4.3\pm0.3)\times10^{-6}$ s^{-1} for the dimethyl and the t-butyl compounds, respectively.

pound **2**. The steric hindrance toward the reaction seems to be of major importance in this case.

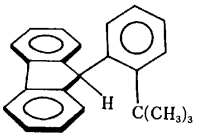

(**3**)

The importance of the steric hindrance is also demonstrated in **3**. Although the barrier to internal rotation about the C_9–C_{ar} bond is unknown, the compound exists as one form exclusively even at 180 °C, probably because the steric interference between the t-butyl group and the fluorene ring in an ap form is very severe. Compound $\mathbf{3}_{sp}$ failed to react with butyllithium in hexane–benzene-d_6 as did compound **2**. This should be attributed to the steric effect of the t-butyl group. Importance of the steric effect on lithiation of thiophene derivatives has been pointed out by Wiersema and Gronovitz.[7]

Both compounds **2** and **3** can be lithiated in ether, though they cannot be lithiated in hexane–C_6D_6. Ether would stabilize the transition state of proton abstraction where the polar nature of the C–H bond is developed to some extent. The pseudo-first order rate constants of **2** and **3** at 34 °C were 5.4×10^{-4} s^{-1} and 4.3×10^{-6} s^{-1}, respectively. The rates reflect the steric effect, compound **3** reacting much more slowly than compound **2**. The occurrence of the reaction of compound **3** in spite of the presence of the bulky substituent might be ascribed to rotation about the C_9–C_{ar} bond to some degree to open a path for the reagent approach.

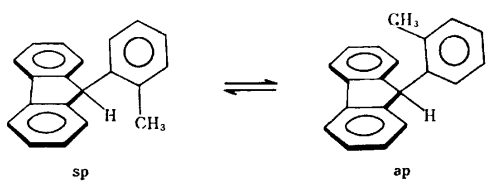

(**4**)

Rates of rotation about the C_9–C_{ar} bond of 9-(o-tolyl)-fluorene (**4**) are estimated to be 10^1-10^2 s^{-1} at ambient temperature from the reported barrier.[6] Thus the rates of rotation are much greater than those of lithiation by butyllithium, the factor being 10^5-10^6. Equilibration between the sp and ap forms is quick. The observed reaction rates can be expressed by the following equation, where the suffixes sp and ap stand for the respective rates and moleculr fractions of the rotamers:

$$k_{obsd} = k_{sp}N_{sp} + k_{ap}N_{ap}. \quad (2)$$

The circumstances of the reaction site of the sp and ap forms can be taken to be similar to those of compounds **2** and **1**, respectively, since o-tolyl, p-tolyl, and 2,6-xylyl groups should not differ much in giving the electronic effect. It is reasonable to assume that $\mathbf{4}_{sp}$ does not react with butyllithium, when the k_{sp} value is practically zero. Equation 2 can be rewritten as follows and k_{ap} can be obtained from the observed rates and the equilibrium constant K:

$$k_{ap} = \left(1+\frac{1}{K}\right)k_{obsd}. \quad (3)$$

The equilibrium constant was obtained in toluene-d_8 as 1/1.3* by integrating the two methyl signals. It was found to be independent of temperature. Putting the equilibrium constant and the observed rate constant, $k_{obsd}=(1.8\pm0.2)\times10^{-5}$ s^{-1}, into Eq. 3, we find k_{ap} at 42 °C to be $(4.1\pm0.2)\times10^{-5}$ s^{-1}.

So far discussion has been given on the rates of lithiation from the viewpoint of steric effect given by the group located closely to the hydrogen to be abstracted. Close examination of the data reveals, however, that the above treatment is only a first approximation; the rate of lithiation of $\mathbf{4}_{ap}$ is about 1/3 of that of **1**. We wish to attribute the fact to the steric effect of the methyl group anti to the 9-hydrogen for the following reasons.

Two possibilities can be considered. One is the bond-angle enlargement due to the substituent-fluorene interaction (see **5**). This will necessarily give additional steric hindrance to the approach of the reagent toward the 9-H and simultaneously cause the change in hybridization. From an examination of the NMR C–H coupling constants (Table 2), the larger substituent in 2′-position of the aryl group in the ap form causes a decrease in magnitude of the coupling constant: $^1J_{CH}$'s decrease from 128.8 to 125.1 Hz by going from **1** to $\mathbf{4}_{sp}$ and from 125.1 to 122.7 Hz by going from $\mathbf{4}_{ap}$ to $\mathbf{7}_{ap}$. The s-character and C–H coupling constants are correlated,[8] although the correlation is questionable in highly strained molecules.[9] The difference in the chemical shifts of 9-C's in ^{13}C NMR spectra increases as the size of the alkyl group increases, the results supporting the bond-angle deformation at 9-C. Thus the decrease in $^1J_{CH}$ and the change in chemical shifts are interpreted as an increase in p-character of the C–H bond orbital. However, this should result in easier deprotonation of $\mathbf{4}_{ap}$ relative to **1** from a kinetic viewpoint and is contrary to the observed trend. Thus the change in hybridization is of minor importance. The steric effect resulting from deformation may also be a minor one since the equilibrium constant is 1/1.3 for $\mathbf{4}_{sp}\rightleftharpoons\mathbf{4}_{ap}$. If it were a major effect, the population ratio should have been affected to a greater extent.

The other possibility is the steric effect caused by the substituent on rotation about the C_9–C_{ar} bond. The access of the deprotonating reagent to the 9-H would

* The equilibrium constant in $CDCl_3$ at 0 °C was reported to be 1/1.6.[6]

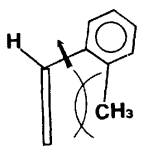

(5)

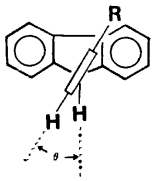

(6)

be facilitated by the rotation (see **6**) which forms room for the access at the expense of increasing steric interaction between the substituent and the fluorene ring. Thus higher energy is required for rotation about the bond to a same degree (θ) in compound $\mathbf{4}_{ap}$ than in compound **1**.

Although the second possibility can be tested in the case of 9-(2-*t*-butylphenyl)fluorene (**2**), the ap form is not detected because of its relative instability to the sp form. Thus 9-(2-isopropylphenyl)fluorene (**7**) was prepared and its reactivity was examined. The compound shows a barrier to rotation (ΔG_c^*) of 19 kcal/mol at 92 °C as determined from the coalescence temperature of the 9-H signals. The rate of rotation at 42 °C is of the order of 10^{-1} s^{-1}. The equilibrium constants for rotamers at 42 °C were 1/2.4 in $CDCl_3$, and 1/1.8 in hexane–C_6D_6.

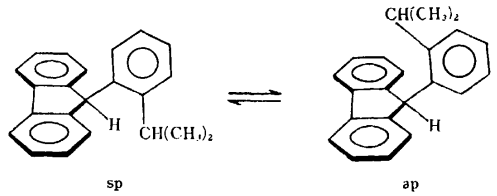

(7)

The results expected from the steric effect are as follows. The population of the sp form is greater than that of **4**, but the ap form is still detectable. The deformation of the bond angle for the ap form is detected by a decrease in C–H coupling constant from the sp form. If the angle deformation is a main factor which retards the reaction, the isopropyl compound ($\mathbf{7}_{ap}$) should react still more sluggishly than the methyl compound ($\mathbf{4}_{ap}$). On the other hand, if the steric effect on rotation to open room for access of the reagent is the main factor, $\mathbf{7}_{ap}$ is expected to show a little less reactivity than $\mathbf{4}_{ap}$, since the isopropyl group is known to be a little bulkier than the methyl group.[10]

The observed pseudo-first order rate constant was 6.9×10^{-6} s^{-1} for compound **7** at 42 °C. The value was treated in the same way as in the case of compound **4**, the value obtained for k_{ap} being 1.9×10^{-5} s^{-1}. The result is in line with the expectation, as in the change in $^1J_{CH}$ values. We conclude that the steric effect on the rotation is a main factor controlling the reactivities of these compounds of similar steric environment at the reaction site.

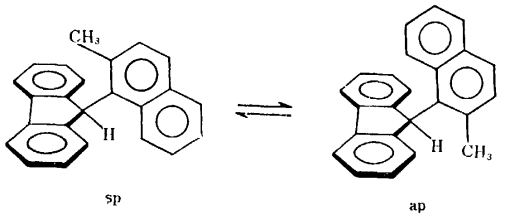

(8)

We thought it would be worthwhile to compare the reactivities of stable rotamers of 9-(2-methyl-1-naphthyl)-fluorene (**8**) as an extension of the above discussion. The compound was prepared by Siddall and Stewart, although the rotamers were concentrated but not completely isolated.[6] The equilibrium constant of the two forms was 1.0 and was not affected by temperature. The barrier (ΔG^*) to rotation about the C_9–C_{ar} bond was reported to be 29.2 kcal/mol at 116 °C. The rate of isomerization was 6.2×10^{-7} s^{-1} at 67 °C.

We were able to isolate these stable rotamers by repeated thin layer chromatography: sp, mp 121—122 °C; ap, mp 125—126 °C. The pseudo-first order rate constants for deprotonation obtained were 5.2×10^{-6} s^{-1} and 3.6×10^{-5} s^{-1} for $\mathbf{8}_{ap}$ and $\mathbf{8}_{sp}$, respectively, at 42 °C. Since the rotation about the C_9–C_{ar} bond is negligible at 42 °C, we observed the net reaction rates for the respective isomers. There is a difference in reactivities by a factor of **7**.

The results indicate that a methyl group is more effective than a benzo group in blocking the reaction. This is an unusual indication since the benzo is usually a larger group than the methyl in stereochemistry and 9-(1-naphthyl)fluorene is known to give a higher barrier to rotation than 9-(*o*-tolyl)fluorene by *ca.* 1 kcal/mol.[6] The apparent discrepancy can be understood by considering the geometry of the transition state for the proton abstraction. The main factor which rules the reaction rate is the easiness of rotation to open up room for access for the reagent. The methyl group is considered to be a rotating top and its van der Waals radius is 2.0 Å, whereas the benzo ring extends within a plane but has van der Waals thickness of only 1.85 Å. Thus room for the reagent would be made by a smaller displacement for the sp form than for the ap form. The higher reactivity of $\mathbf{8}_{ap}$ than **2** might be attributed to a similar cause. The methyl group over the fluorene ring would give larger steric hindrance than the benzo group when the same degree of rotation is required. It is also interesting to note that $\mathbf{8}_{sp}$ shows about the same reactivity as $\mathbf{4}_{ap}$. The same degree of rotation would be sufficient for the reaction to occur in these compounds.

Although both $\mathbf{8}_{ap}$ and $\mathbf{8}_{sp}$ give identical ^{1}H NMR spectra on lithiation, stereochemistry of the lithio derivatives is hard to study because of its poor solubility and the difficulty in detecting the difference in spectral characteristics. It might be a mixture of two forms which give resembling NMR peaks, or a single form, or a mixture which shows no signals of a minor constituent. Quenching an extremely dilute solution of the lithio derivative of **8** in hexane–benzene with water afforded the sp and the ap forms in an 8 : 1 ratio. If we can assume that quenching of the lithio derivative with a highly covalent C–Li bond proceeds with the retention of configuration, as is observed in other cases,[11] the stability of the lithio derivatives could be discussed.

References

1) Preceding paper: M. Nakamura and M. Ōki, *Chem. Lett.*, **1975**, 671.
2) E. L. Eliel, *J. Chem. Educ.*, **37**, 126 (1960).
3) M. Ōki, *Angew. Chem. Intern. Ed. Engl.*, **15**, 87 (1976): M. Nakamura and M. Ōki, *Chem. Lett.*, **1976**, 651.
4) R. Adams and J. Campbell, *J. Am. Chem. Soc.*, **72**, 153 (1950); see also Ref. 12.
5) L. M. Jackman and S. Sternhell, "Applications of Nucl. Magn. Resonance Spectros. in Org. Chem.," Pergamon Press (1969), p. 164.
6) T. H. Siddall, III and W. E. Stewart, *J. Org. Chem.*, **34**, 233 (1969).
7) A. Wiersema and S. Gronowitz, *Acta Chem. Scand.*, **25**, 1195 (1971).
8) a) J. H. Goldstein, V. S. Watts, and L. S. Rattet, *Progr. Nucl. Magn. Reson. Spectros.*, **8**, 103 (1971); b) T. L. Marshall, D. E. Miller, S. A. Conn, A. Seiwell, and A. M. Ihrig, *Acc. Chem. Res.*, **7**, 333 (1974).
9) L. S. Bartell and H. B. Bürgi, *J. Am. Chem. Soc.*, **94**, 5239 (1972); see also Ref. 8a.
10) J. A. Hirsch, "Table of Conformational Energies—1967," in "Topics in Stereochemistry," Vol. 1 ed by N. L. Allinger and E. L. Eliel, Interscienece Publishers, New York (1967), p. 199.
11) H. M. Walborsky, F. J. Impastato, and A. E. Young, *J. Am. Chem. Soc.*, **86**, 3283 (1964).
12) A. Mathieu, *Bull. Soc. Chim. Fr.*, 1526 (1971).
13) R. Weiss and E. Knapp, *Monatsch*, **61**, 61 (1932).

Preparation and Properties of Stable Alkylcopper(I) Complexes Containing Tertiary Phosphine Ligands

Akira MIYASHITA and Akio YAMAMOTO

Tokyo Institute of Technology, Research Laboratory of Resources Utilization
O-okayama, Meguro-ku, Tokyo 152

(Received November 12, 1976)

A variety of stable alkylcopper(I) complexes of composition $RCuL_n$ ($n=1-3$) containing various monodentate tertiary phosphine ligands (L), such as triphenylphosphine, diphenylmethylphosphine, dimethylphenylphosphine, tributylphosphine, triethylphosphine, and tricyclohexylphosphine have been prepared by the reactions of copper(II) acetylacetonate, dialkylaluminium monoethoxide, and the tertiary phosphines. Similar reactions employing 1,2-bis(diphenylphosphino)ethane(dpe) give $(RCu)_2(dpe)_3$. The complexes have been isolated and characterized by elemental analysis, determination of molecular weight, chemical reactions, IR and NMR spectroscopy. All the isolated complexes show considerable thermal stability compared with alkylcopper compounds without phosphine ligand indicating the marked contribution of these phosphine ligands to the stabilization of the copper-carbon bond. The dpe-coordinated alkylcopper complexes are thermally stable in the solid state but readily decompose in solution with hydrogen abstraction accompanied by scission of the C–P bond of dpe to give $Ph_2PCu(dpe)$, $Ph_2PCH{=}CH_2$, and alkane. These alkylcopper complexes initiate the polymerization of vinyl monomers such as acrylonitrile, methacrylonitrile, methyl acrylate, and methyl methacrylate. Alkyl halides and acyl halides react with the alkylcopper complexes to give cross-coupling products of alkyl groups and alkyl-acyl groups.

The chemistry of organocopper compounds is worthy of study in its own right as a branch of rapidly developing organotransition metal chemistry and also because of its relevance to various copper-catalyzed organic reactions in which organocopper compounds play an important role as reactive intermediates.[1] Many attempts have been made to prepare alkylcopper compounds since the first report by Buckton in 1859.[2] The preparation of methyl- and ethylcopper by the reaction of copper salts with methyllithium,[3a,b] methylmagnesium chloride,[3a] dimethylzinc[4] and tetramethyl- and tetraethyllead[5] has been reported, but most compounds have been prepared *in situ* and attempts to isolate them in the pure state, free from the alkylating agents and reaction by-products, have encountered great difficulties because of their extreme instability which often leads to violent explosions and of their insolubility in common organic solvents.[3-6] The instability of the simple alkylcopper compounds is in contrast to the stability of alkylcopper compounds having electronegative substituents such as fluoroalkylcopper[7] and cyanomethylcopper.[8] Some considerably stable arylcopper complexes are also known.[9]

Employment of ligands such as tertiary phosphines and 2,2′-bipyridine often contributes to the stabilization of alkyltransition metal compounds.[10] Concerning the unsubstituted alkylcopper compounds, however, failure to stabilize the copper-alkyl bond using triphenylphosphine,[11] 2,2′-bipyridine,[4] and *N,N*-dimethylformamide[4] has been claimed. Some alkylcopper complexes coordinated with trimethylphosphite and tributylphosphine have been prepared *in situ* at low temperatures but the complexes have not been isolated in analytically pure state.[3b,12]

We have been able to isolate alkylcopper(I) complexes containing triphenylphosphine[13] and tricyclohexylphosphine[6] by the reactions of bis(acetylacetonato)copper, dialkylaluminium monoethoxide, and the phosphine ligands. Extension of the study to the preparation of other phosphine-containing ligands has revealed the marked stabilizing effect of tertiary phosphine ligands in contrast to statements of some of previous papers and led to the isolation not only of the methylcopper complex but also of series of alkylcopper complexes containing longer alkyl chains which are usually regarded unstable because of their tendency to undergo β-elimination. We now describe the preparation and some properties of these alkylcopper complexes containing various tertiary phosphine ligands. The thermal stability of these complexes will be discussed subsequently.

Results and Discussion

Preparation of the Alkylcopper(I) Complexes Containing Various Monodentate Tertiary Phosphines. The methylcopper(I) complexes having various monodentate tertiary phosphine ligands such as triphenylphosphine (PPh_3), diphenylmethylphosphine(PPh_2Me), dimethylphenylphosphine($PPhMe_2$), tributylphosphine(PBu_3), triethylphosphine(PEt_3), and tricyclohexylphosphine (PCy_3), were prepared from copper bis(acetylacetonate), dimethylaluminium monoethoxide, and the appropriate tertiary phosphine (in a 1 : 4 : 3—4 mole ratio) in diethyl ether or toluene under nitrogen. They were isolated as yellow or light yellow crystals, free from aluminum compounds, after recrystallization from appropriate solvents such as tetrahydrofuran(THF), diethyl ether, toluene or mixture thereof.

$Cu(acac)_2$, $Al(CH_3)_2OEt$, Tertiary phosphine →

$CH_3Cu(PPh_3)_2(ether)_{0.5}$	**1a**
$CH_3Cu(PPh_3)_3(toluene)$	**1b**
$CH_3Cu(PPh_2Me)_3$	**3**
$CH_3CuPPhMe_2$	**4**
CH_3CuPEt_3	**5**
CH_3CuPBu_3	**6**

Methylcopper(I) complexes of triphenylphosphine contained toluene or ether as solvent of crystallization. White yellow prisms of $PPhMe_2$, PBu_3, and PEt_3 complexes contained 1—2 molar equivalent of ether or THF as solvent of crystallization which was eliminated by drying *in vacuo*.

Table 1. Analytical data for triphenylphosphine-alkylcopper(I) complexes

No.	Formula	Mp (dec) °C	R/Cu[a]	[P]/Cu[b]	Found (Calcd) C%	H%	Cu%
1a	$CH_3Cu(PPh_3)_2(ether)_{0.5}$	75—76	1.01	2.12	72.8 (73.2)	5.8 (6.0)	10.0 (9.9)
1b	$CH_3Cu(PPh_3)_3(toluene)$	70—75	1.02	2.86	77.0 (77.7)	5.8 (5.9)	6.6 (6.6)
1c	$C_2H_5Cu(PPh_3)_2$	56—58	0.97	2.02	72.8 (73.8)	5.5 (5.9)	10.3 (10.3)
1d	$C_2H_5Cu(PPh_3)$	55—58	0.83	0.85	68.1 (67.7)	5.9 (5.7)	19.0 (17.9)
1e	n-$C_3H_7Cu(PPh_3)_2$	61—62	0.98	2.14	74.0 (74.2)	5.8 (5.9)	9.9 (10.1)
1f	i-$C_4H_9Cu(PP_3)_2$	60—63	1.02	1.96	73.9 (74.4)	6.1 (6.0)	10.0 (9.9)

a) Alkyl groups were determined by measuring the amounts of gases evolved after reaction with concd sulfuric acid or decyl alcohol. b) See experimental section. [P] is the amount of coordinated phosphine in the complex.

Table 2. Analytical data for other tertiary phosphine-alkylcopper(I) complexes

No.	Formula	Mp (dec) °C	R/Cu[a]	[P]/Cu[b]	Found (Calcd) C%	H%	Cu%
3	$CH_3Cu(PPh_2Me)_3$	95—98	1.01	3.00	71.7 (70.9)	6.9 (6.2)	9.5 (9.4)
4	$CH_3CuPPhMe_2$[c]	50—51	1.09	0.93	—	—	30.5 (29.3)
5	CH_3CuPEt_3[c]	40—45	1.12	0.91	—	—	29.0 (29.9)
6	CH_3CuPBu_3[c]	57—60	1.07	1.14	—	—	23.8 (22.6)
7	i-$C_4H_9CuPCy_3$	100—102	0.98	1.00	65.7 (65.9)	10.2 (10.6)	15.6 (15.8)

a), b) See Table 1. c) Micro analyses were not feasible because of extreme air sensitivity.

The ethyl-, propyl-, isobutylbis(triphenylphosphine)-copper(I) complexes and isobutyl(tricyclohexylphosphine)copper(I) complex were prepared from diethylaluminum ethoxide, dipropylaluminum ethoxide and isobutylaluminum ethoxide, respectively, by a procedure similar to that used for the methyl analogs and were recrystallized from diethyl ether or THF–diethyl ether.

All the isolated complexes are diamagnetic, fairly stable at room temperature in an inert gas atmosphere or *in vacuo* but decomposed rapidly in air. Triphenylphosphine complexes are somewhat light-sensitive and decompose slowly, even at low temperature in sunlight or upon UV irradiation, releasing alkane. Micro analyses of the $PPhMe_2$, PBu_3, and PEt_3 complexes were not feasible because of their extreme instabilities to air. Tables 1 and 2 summarize the analytical data for the isolated alkyl copper complexes having various monodentate tertiary phosphines. Acidolysis or alcoholysis of each alkyl-copper complex released 1 mol equivalent of the corresponding alkane; deuteriolysis with D_2SO_4 liberated alkane-d_1, further supporting the presence of the alkyl-copper bond. These reactions are considered to proceed through stepwise exchange of the acetylacetonato ligands with the alkyl group of AlR_2OEt. Although the nickel[14] and iron[15] complexes with alkyl, acetylacetonato, and triphenylphosphine ligands were isolated respectively as intermediates in the alkylation of their acetylacetonates in the presence of triphenylphosphine to give unstable dialkyl complexes, our attempts to isolate alkylcupric complex containing the acetylacetonato ligand were unsuccessful. However, judging from the gas evolved during the reaction, we believe that the intermediate, unstable alkylCu(II) complex is reduced by splitting of the R–Cu bond yielding the alkylCu(I) complexes.

The alkylcopper(I) complexes having various tertiary phosphine ligands have been also prepared by ligand exchanges of triphenylphosphine complexes with more electron-releasing phosphines such as PPh_2Me, $PPhMe_2$, PBu_3, PEt_3, and PCy_3.

$$RCu(PPh_3)_2 + L \xrightarrow[\text{ether}]{} RCuL + 2PPh_3 \qquad (2)$$

$L = PPh_2Me$, $PPhMe$, PBu_3, PEt_3, PCy_3

In none of these reactions could alkylcopper complexes containing mixed ligands be obtained. Examination of the composition of the alkylcopper complexes in Tables 1 and 2 reveals that the 18 electron rule is fulfilled only for the methylcopper complexes with triphenylphosphine and diphenylmethylphosphine, the least basic ligands among the phosphines used. There seems to be a delicate balance in the number of ligands capable of coordination to copper. Replacement of the methyl group bonded to copper by the ethyl, propyl or isobutyl groups, which are more electron-releasing than methyl, led to alkylcopper complexes containing

two triphenylphosphine ligands even when three molar equivalents of phosphine were used. Furthermore, for ethylcopper, when *ca.* 1 mol equivalent of triphenylphosphine was used, a pale grey complex of approximate composition, $EtCu(PPh_3)$, was obtained, which on further addition of 1 mol equivalent of triphenylphosphine was converted into $EtCu(PPh_3)_2$. Replacement of PPh_2Me with the more basic ligand, $PPhMe_2$, caused a decrease in the number of coordinated phosphine ligands from 3 to 1, and coordination of more basic ligands such as PBu_3, PEt_3, and PCy_3 gave only the alkylcopper complex containing one phosphine ligand.

Since some organocopper compounds are known to be aggregated[16] and some of our complexes are coordinatively unsaturated, it was suspected that some might have polymeric structures. Cryoscopic determination of these complexes, however, revealed the complexes to be all monomeric in benzene as shown in Table 3. The molecular weight determination of $CH_3Cu(PPh_3)_2$-$(ether)_{0.5}$ and $CH_3Cu(PPh_3)_3(toluene)$ gave about the half of the calculated values for the compositions indicated, presumably owing to the dissociative removal of the solvents of crystallization and also, in part, of the three triphenylphosphine ligands in benzene solution.

The IR spectra of the alkylcopper complexes showed ν(C–H) bands assigned to the alkyl group bonded to copper at 2980—2750 cm^{-1} and the characteristic absorption bands of coordinated phosphine ligands. The IR spectra of the ν(C–H) bands in the methylcopper complexes appeared at rather low frequencies, (summarized in Table 4) compared with those of the saturated alkanes. A similar trend has been noted also in other methyl-transition metal complexes.[15,17] The medium intensity IR band observed in the methylcopper complexes in the region from 570 to 610 cm^{-1} which decreases on contact with air or upon pyrolysis was tentatively assigned to the ν(Cu–C) band.

The ^{1}H-NMR spectra of the methylcopper complexes showed a singlet due to the methyl group bonded to copper (Table 4). This band was observed as a somewhat broadened singlet but no splitting due to coupling with ^{31}P and ^{65}Cu or ^{63}Cu was observed at the temperature above −30 °C.

The NMR spectrum of the ethyl complex, **1c,** in toluene-d_8 at −20 °C showed a broad unresolved methyl peak at τ 8.90 and a methylene peak at 8.60. The propyl complex **1e** showed broad peaks due to the methyl and the copper-bonded methylene groups at τ 8.95 (5H) and a peak due to the central methylene at 8.60 (2H). In toluene-d_8 at 25 °C the spectrum of i-$C_4H_9Cu(PPh_3)_2$, **1f**, showed a doublet at τ 9.13 (2H, $C\underline{H}_2$–Cu, $^3J_{H-H}$ 7 Hz), a doublet at 8.68 (6H, $2C\underline{H}_3$, $^3J_{H-H}$ 6 Hz) and an unresolved multiplet at 8.00 (1H, C<u>H</u>). It is note-worthy that the protons attached to carbon bonded to copper appear at considerably higher field because of the shielding effect of copper in the complexes. It appears that peaks of methyl protons in copper complexes coordinated to rather basic ligands is slightly shifted to higher field, but the effect is not particulary conspicuous.

The ^{1}H-decoupled ^{31}P NMR spectrum of **3** in toluene at −80 °C showed a sharp singlet resonance at 6.1 ppm (up-field from the external PPh_3 reference in toluene) and a small signal of free PPh_2Me at 19.3 ppm whereas at −40 °C the singlet at 6.1 ppm broadened and shifted to higher field 8.4 ppm accompanied by disappearance of the free PPh_2Me signal. The spectrum of a toluene solution of **3** containing three mol equivalents of added PPh_2Me at −80 °C exhibited a somewhat broadened singlet at 9.2 ppm and a sharp singlet due to free PPh_2Me at 19.7 ppm. At −20 °C the two peaks collapsed to a broadened singlet centered at 16.8 ppm. These results indicate that at −80 °C the methylcopper complex with three PPh_2Me ligands is not extensively

TABLE 3. MOLECULAR WEIGHTS OF COPPER–ALKYL COMPLEXES

No.	Formula	Found	Required
1c	$C_2H_5Cu(PPh_3)_2$	633 (±10)	617
1e	n-$C_3H_7Cu(PPh_3)_2$	544	631
1f	i-$C_4H_9Cu(PPh_3)_2$	663	645
3	$CH_3Cu(PPh_2Me)_3$	676	679
7	i-$C_4H_9CuPCy_3$	395	401

Cryoscopic determination in benzene solution.

TABLE 4. IR[a] AND NMR[b] SPECTRA OF METHYLCOPPER(I) COMPLEXES

No.	Formula	IR ν(C–H) in alkyl group		IR ν(Cu–CH_3)	NMR[b] Methyl-Cu signal $\tau_{Cu\text{-}CH_3}$
1a	$CH_3Cu(PPh_3)_2(ether)_{0.5}$	2830 m	2790 s	612 m	10.3
1b	$CH_3Cu(PPh_3)_3(toluene)$	2830 m	2780 s	603 m	10.4
3	$CH_3Cu(PPh_2Me)_3$	2940 m	2770 s	590 m	10.5
4	$CH_3CuPPhMe_2$	2825 m	2775 s	560 w	10.1
5	CH_3CuPEt_3	2830 m	2770 m	575 m	10.3
6	CH_3CuPBu_3	2830 m	2770 m	575 m	10.5
2a	$(CH_3)_4CuAl_2(dpe)_2(OEt)_2$	2970 m, 2920 m, 2875 m 2820 s		615 m	9.84[c]
2b	$(CH_3Cu)_2(dpe)_3$	2820 m	2775 s	596 m, 615 m, 640 m	—
	CH_3CuPCy_3[d]	2820 m	2770 w	568 m	10.5

a) KBr disk; s, strong; m, medium; w, weak; frequencies in cm^{-1}. b) Toluene-d_8 10% solution, toluene-d_8 impurities as internal standard, at room temperature, all singlet signals. c) THF-d_8 15% solution, TMS internal standard. d) See Ref. 6.

dissociated but that upon raising the temperature the complex liberates part of the coordinated PPh_2Me ligands. In the presence of added PPh_2Me at −20 °C the exchange between the coordinated and added PPh_2Me ligands is considered to be taking place rapidly.

Preparation of the Alkylcopper(I) Complexes Containing a Bidentate Tertiary Phosphine. The alkylcopper complexes containing a coordinated bidentate ligand, dpe, present unique features quite different from those of the alkylcopper complexes containing monodentate ligands. Ethyl, propyl, and isobutylcopper complexes of composition $(RCu)_2(dpe)_3$ have been obtained by the reaction of bis(acetylacetonato)copper, dpe and dialkylalminium monoethoxides in diethyl ether or in toluene under nitrogen. Analytical data are given in Table 5.

$$\left.\begin{array}{l}Cu(acac)_2\\ Ph_2PCH_2CH_2PPh_2(dpe)\\ AlR_2(OEt)\end{array}\right\} \longrightarrow (RCu)_2(dpe)_3 \qquad (3)$$

2c, R=C_2H_5; **2d**, R=C_3H_7; **2e**, R=i-C_4H_9

The number of alkyl groups and dpe ligands attached to copper has been determined by elemental analysis, volumetry after acidolysis or alcoholysis, and spectroscopic determination of the released dpe ligands upon acidolysis. Copper complexes having dpe ligands in a Cu/P ratio of 2/3 are known for the arylcopper(I)[18] and copper(I) halide complexes[19] and the molecular structure,[20] in which dpe ligands are bonded with copper, one forming a chelate and the other bridging between copper atoms has been established. The present alkyl complexes with dpe ligands may well have a similar structure, but the instability of the complexes in solution (*vide infra*) has precluded further characterization.

The use of dimethylaluminium monoethoxide in the reaction with $Cu(acac)_2$ and dpe gave a binary complex which is thermally very stable and moderately insensitive to air. The complex contains both copper and aluminum in a ratio of 1 : 2 and four methyl groups per copper, one of which is probably bonded to copper since one mol equivalent of methane was liberated from the complex on thermolysis at 180 °C. On treatment with HCl in diethyl ether, a quantitative yield of ethyl alcohol was obtained. The overall complex composition is $CuAl_2(CH_3)_4(dpe)_2(OEt)_2$ **2a**. Similar binary addition products containing alkylaluminium components are known for manganese[21] and titanium.[22]

Recrystallization of this complex **2a** from relatively basic solvents such as tetrahydrofuran led to dissociation of the aluminium and copper components and gave a cream yellow complex $(CH_3Cu)_2(dpe)_3$, **2b**. Use of more basic solvents such as pyridine and *N,N*-dimethylformamide led to decomposition of the methylcopper complex liberating CH_4.

Intramolecular Reaction of Alkylcopper Complexes with dpe Ligands Involving the P–C Bond Cleavage of the dpe Ligand. Despite the fact that the dpe-coordinated complexes show substantially enhanced thermal stability in the solid state, dissolution of $(RCu)_2(dpe)_3$ type complexes **2b**—**2e** in THF, benzene, toluene, and pyridine, leads to a quite facile decomposition with the evolution of an almost quantitative amount of alkane as expressed by the following equation.

$$\underset{\textbf{(2b—2d)}}{(RCu)_2(dpe)_3} \xrightarrow[\text{solvent}]{} \underset{\textbf{(2f)}}{Ph_2PCu(dpe)} + Ph_2PCH{=}CH_2 + RH + [RCu(dpe)] \qquad (4)$$

R=CH_3, C_2H_5, n-C_3H_7, i-C_4H_9

The greenish yellow complex **2f** isolated from the reaction solution analyzed as $Ph_2PCu(dpe)$ (Table 5) and gas chromatographic analysis of the reaction products confirmed the formation of diphenylvinylphosphine and of alkanes. Complex **2f** was characterized by its reaction with dry hydrogen chloride yielding diphenylphosphine, PPh_2H, and with methyl iodide or ethyl iodide affording PPh_2Me or PPh_2Et.

The reaction may proceed as shown in the following Scheme 1.

Dissolution of the coordinatively saturated binuclear complex $(RCu)_2(dpe)_3$ may cause dissociation to RCu(dpe) and complex (A) containing one chelated dpe ligand and the other dpe ligand bonded to copper as a monodentate ligand having the other phosphine end free in solution. This situation may lead to the approach of one of the methylene groups in the partially dissociated dpe into the proximity of the alkyl group which then attacks the methylene and abstracts hydro-

Table 5. Analytical data for DPE-alkylcopper(I) complexes

No.	Formula	Decomp (mp)°C	R/Cu[a]	[P]/Cu[b]	Found (Calcd) C%	H%	Cu%
2a	$(CH_3)_4CuAl_2(dpe)_2(OEt)_2$	230	4.05	1.88	71.4 (71.4)	6.6 (7.0)	6.4 (6.3)
2b	$(CH_3Cu)_2(dpe)_3$	149—150	1.00	1.53	71.1 (71.0)	6.6 (5.8)	9.2 (9.4)
2c	$(C_2H_5Cu)_2(dpe)_3$	124—127	0.90	1.56	71.4 (71.3)	5.4 (5.9)	8.7 (9.1)
2d	$(n$-$C_3H_7Cu)_2(dpe)_3$	130—140	0.98	1.54	72.1 (71.7)	6.6 (6.3)	8.6 (9.0)
2e	$(i$-$C_4H_9Cu)_2(dpe)_3$	102—105	1.00	1.51	71.9 (71.9	7.2 (6.4)	9.0 (8.8)
2f	$CuPPh_2(dpe)$	115—116	/	/	70.6 (70.5)	5.6 (5.3)	9.5 (9.8)

a), b) See Table 1.

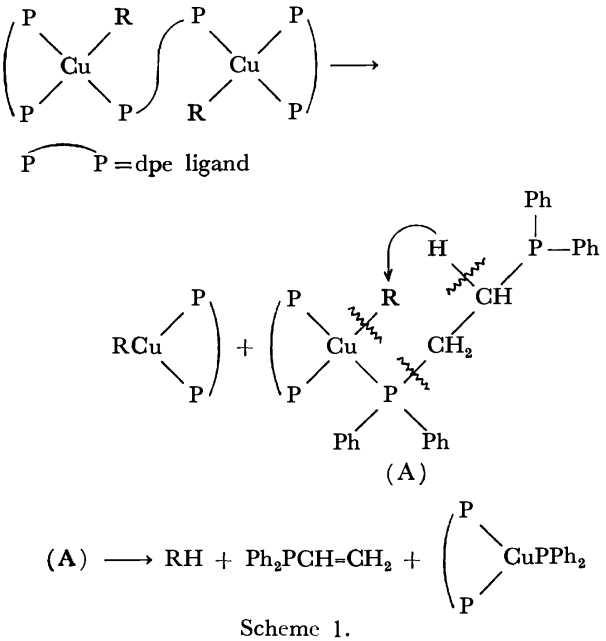

Scheme 1.

gen, at the same time causing scission of the P–C bond in dpe, thus yielding alkane, diphenylvinylphosphine, and $Ph_2PCu(dpe)$. Addition of one or more equivalent of dpe to the system promoted the reaction: all the alkyl groups were liberated as alkane more rapidly than in the absence of added dpe, and $(RCu)_2(dpe)_3$ was quantitatively converted into $Ph_2PCu(dpe)$, $Ph_2PCH=CH_2$, and the alkane. Presumably the addition of the extra dpe ligand enhances the formation of intermediate species (A) thus promoting decomposition. Addition of Lewis acids such as trimethylaluminium, aluminium trichloride, and boron trifluoride markedly promoted the decomposition even at low temperature. Similar promotion of decomposition of a stable arylcopper complex in the presence of dpe has been reported by van Koten and Noltes.[23]

Attempts to isolate RCu(dpe) using the dpe ligand and $Cu(acac)_2$ (1 : 1 ratio) led to the isolation of an extremely air-sensitive white powder, which could not be identified.

Properties of Alkylcopper Complexes. Polymerization: The isolated alkylcopper complexes exhibited polymerization activity toward vinyl monomers containing electron-withdrawing substituents. Acrylonitrile, methacrylonitrile, acrylaldehyde, methyl acrylate, methyl methacrylate, and 2-vinylpyridine were rapidly polymerized in the presence of alkylcopper complexes. As with other alkyltransition metal complexes polymerization mayproceed by a coordination mechanism.[24] Polymerization of vinyl compounds by organocopper complexes has also been reported.[25]

Among the alkylcopper complexes, the binary complex **2a** showed the highest polymerization activity. The polymerization of acrylonitrile, methacrylonitrile, and acrylaldehyde took place explosively, and methyl acrylate and methyl methacrylate also polymerized very rapidly with **2a**. Other dpe-coordinated complexes **2b** and **2c** were also very active, quantitatively converting acrylonitrile, methacrylonitrile, and methyl methacrylate, into their polymers below −10 °C within several minutes.

Reactions with Alkyl and Acyl Halides: Methylcopper complexes **1a**, **1b**, **2b**, and **3** reacted with methyl iodide to yield one mol equivalent of C_2H_6. Reactions with ethyl bromide gave mainly C_3H_8 and small amounts of CH_4, C_2H_4, and C_2H_6. The reactions of the ethylcopper complexes **1c**, **1d**, and **2c** with methyl iodide released only C_3H_8 and propylcopper complexes **1e** and **2d** with methyl iodide liberated only C_4H_{10}. The formation of the cross-coupling products as the main gaseous products and of small amounts of CH_4, C_2H_4, and C_2H_6 in the reaction of the methylcopper complexes with ethyl bromide suggests that an unstable Cu(III) intermediate might be formed by oxidative addition of the alkyl halide to the alkylcopper complexes. Cu(III) complexes have not been isolated, but the comparison of the behavior of the alkylcopper complexes with that of alkylgold complexes, the Au(III) state of which is well known,[26] makes the assumption of the intermediacy of Cu(III) complexes not too unreasonable.

$CH_3Cu(PPh_3)_2(ether)_{0.5}$ **1a** reacted also readily with acetyl chloride to give acetone and with benzoyl chloride to yield acetophenone.

Experimental

Materials and General Procedures. All preparations and recrystallizations were carried out under deoxgenated nitrogen, argon, or *in vacuo*. Solvents were dried by usual procedures, distilled, and stored under argon or nitrogen.

Copper bis(acetylacetonate) was prepared as described in the literature.[27] Found; C, 45.3; H, 5.49; Cu, 24.4%(Calcd for; C, 45.8; H, 5.39; Cu, 24.3%). Dialkylaluminium monoethoxide was prepared by the reaction of trialkylalminium with ethyl alcohol in hexane followed by vaccum distillation.

Triphenylphosphine was used as purchased, mp 80—81 °C. dpe,[28] tricyclohexylphosphine,[29] diphenylmethylphosphine,[30] dimethylphenylphosphine,[28] triethylphosphine,[30] and tributylphosphine[31] were prepared as described in the literature.

Analytical Methods. IR spectra were recorded on a Hitachi Model EPI-G3 using KBr discs prepared under nitrogen and proton NMR spectra were recorded on a Japan Electron Optics Lab. JNM-PS-100 spectrometer. Evolved gases were analyzed using a Hitachi RMU-5B mass-spectrometer and a Shimadzu GC-5B gas chromatograph. Microanalyses for carbon, hydrogen and nitrogen were performed by Mr. T. Saito of our laboratory with a Yanagimoto CHN Autocorder Type MT-2. Triphenylphosphine and dpe contents were determined spectroscopically after hydrolysis with dilute sulfuric acid or by weighing triphenylphosphine oxide. The tricyclohexylphosphine-content was also determined by weighing its oxide, as described above. The other phosphine contents were determined by NMR proton concentration measurements as compared with internal references in their NMR spectra. Molecular weights were determined in benzene solution by a cryoscopic method.

The copper-content was determined by iodometry after digesting the sample with concentrated sulfuric acid. The aluminium content was determined, after the removal of cupric hydroxide and phosphine, gravimetrically as the alminium oxime complex, $Al(C_9H_6ON)_3$.

Preparation of a Series of Alkylcopper Complexes with Triphenylphosphine. *$CH_3Cu(PPh_3)_2(ether)_{0.5}$, **1a***: To an ethereal suspension of copper bis(acetylacetonate) 2.6 g (10 mmol)

and 3 molar eqivalents of triphenylphosphine(7.8 g), 4 molar equivalents of dimethylalminium ethoxide(6.5 ml) was added slowly at −40 °C. The mixture was allowed to react initially at −40 °C and the temperature was subsequently raised gradually to −10 to 0 °C until yellow crystals precipitated from the yellow orange solution. The complex wihch was separated by filtration was dissolced in ether–THF below 0 °C. From the yellow orange solution, the yellow cristals which were obtained upon cooling, were filtered, repeatedly washed with dry ether, dried *in vacuo* at room temperature in the dark and characterized as $CH_3Cu(PPh_3)_2\cdot(ether)_{0.5}$; yield, 5.5 g (86%). Upon pyrolysis at 85 °C, **1a** gave one half molar equivalent of diethyl ether which was identified by mass spectrometry. The NMR spectrum of **1a** in THF had a singlet at τ 10.3 (3H, C$\underline{H}_3$–Cu), a quartet at 7.5 (2H, –C$\underline{H}_2$– in ether), a triplet at 8.8 (3H, C$\underline{H}_3$– in ether) and a multiplet at 2.5 (30H, C$_6\underline{H}_5$).

$CH_3Cu(PPh_3)_3$(toluene), ***1b***: Dimethylalminium ethoxide (5 ml, 30 mmol) was added slowly to an ethereal suspension of copper bis(acetylacetonate) (2.0 g, 7.6 mmol) and PPh_3 (7.3 g, 27 mmol) at −40 °C. The mixture was subsequently raised gradually to room temperature (6 h) to give a deep yellow solution. On cooling, the light yellow needles which precipitated were filtered off and recrystallized from toluene, washed with hexane, dried *in vacuo* and characterized as $CH_3Cu(PPh_3)_3$(toluene); yield, 3.6 g (50%). On pyrolysis at 160 °C, **1b** gave one molar equivalent of toluene. The NMR spectrum of **1b** in THF showed singlets at τ 10.4 (3H, C$\underline{H}_3$–Cu), 7.7 (3H, C$\underline{H}_3$–C$_6$H$_5$) and a multiplet at 2.7 (50H, C$_6\underline{H}_5$).

$C_2H_5Cu(PPh_3)_2$, ***1c***: $Cu(acac)_2$ (2.6 g, 10 mmol), PPh_3 (7.8 g, 30 mmol) and diethylalminium ethoxide 7 ml were mixed at −30 °C. The temperature was gradually raised to 0 °C, and a bright yellow complex slowly precipitated with dissolution of $Cu(acac)_2$ in ether. After 7 h stirring the reaction products were removed by filtration, recrystallized from ether–THF, dried *in vacuo* and characterized as C_2H_5-$Cu(PPh_3)_2$; yield, 4.4 g (71%).

$C_2H_5CuPPh_3$, ***1d***: Diethylaluminium monoethoxide (7.0 ml, 45.6 mmol) was added to the ethereal suspension containing $Cu(acac)_2$ (4.0 g, 15.2 mmol) and triphenylphosphine (4.5 g, 17.2 mmol) at −40 °C. From the dark yellow solution, obtained after the $Cu(acac)_2$ had completely dissolved in ether, a white gray complex gradually precipitated as the temperature was raised to 0 °C. After stirring for 3 h below 0 °C, the complex was filtered, washed repeatedly with ether and dried *in vacuo* at room temperature (yield, 60%).

n-*$C_3H_7Cu(PPh_3)_2$*, ***1e***: $Cu(acac)_2$ (2.6 g, 10 mmol), PPh_3 (7.8 g, 30 mmol) and dipropylalminium ethoxide(8 ml) were mixed at −30 °C. The temperature was gradually raised to 0 °C, and an orange yellow solution was obtained with dissolution of $Cu(acac)_2$ in ether. On cooling the solution after addition of a small amount of hexane, greenish yellow prisms precipitated, which were filtered, repeatedly washed with ether–hexane, and dried *in vacuo* at room temperature in the dark. The complex was characterized as n-$C_3H_7Cu(PPh_3)_2$; 3.0 g (48%).

i-*$C_4H_9Cu(PPh_3)_2$*, ***1f***: This compound was prepared by the procedure described above. The complex, obtained as primrose-yellow crystals, was characterized as i-C_4H_9Cu-$(PPh_3)_2$, (yield, 54%).

Preparation of Alkylcopper Complexes with 1,2-Bis(diphenyl phosphino)ethane. Methylcopper Complex Containing Alkylalminium Components, $CuAl_2(CH_3)_4(dpe)_2(OEt)_2$, ***2a***: Dimethylalminium ethoxide, 10 ml, was added slowly to an ethereal suspension containing copper bis(acetylacetonate) (4.5 g) and dpe (17.1 g) at −40 °C. When the mixture was subsequently raised gradually to room temperature, a cream yellow complex slowly precipitated with dissolution of copper bis(acetylacetonate) in ether. After about 10 h of stirring a light yellow precipitate formed was filtered, repeatedly washed with ether, dried *in vacuo*, and characterized as $CuAl_2(CH_3)_4(dpe)_2(OEt)_2$. The complex was diamagnetic and had the correct elemental analyses, (yield, 80—90%). Acidolysis with dry HCl in ether resulted in a quantitative yield of CH_4 together with ethyl alcohol.

$(CH_3Cu)_2(dpe)_3$, ***2b***: The alminium-containing complex **2a** was dissolved in THF and addition of ether to the resultant light orange solution gave white yellow prisms on cooling overnight. The crystals were filtered, washed repeatedly with ether, dried *in vacuo* and characterized as $(CH_3Cu)_2$-$(dpe)_3$, (yield, 20%).

$(C_2H_5Cu)_2(dpe)_3$, ***2c***: Copper bis(acetylacetonate) (2.6 g) and dpe (8.8 g) were suspended in 100 ml of ether and 6.5 ml of diethylalminium ethoxide was added at −40 °C. The mixture was allowed to react initially at this temperature which was then raised gradually to room temperature until the reagents completely dissolved in ether, and then a lemon yellow complex was gradually precipitated from the resulted yellow orange solution. After about 5 h of stirring at room temperature, the reaction product was filtered, repeatedly washed with ether, dried in vacuum, and characterized as $(C_2H_5Cu)_2(dpe)_3$, (yield, 85%). Attempts of recrystallization resulted in decomposition.

(n-$C_3H_7Cu)_2(dpe)_3$, ***2d*** *and (i-$C_4H_9Cu)_2(dpe)_3$*, ***2e***: These were prepared by the procedure described above but attempts of recrystallization resulted in decomposition, (yield, 80—90%).

$Ph_2PCu(dpe)$, ***2f***: The alkylcopper complexes of dpe, $(CuR)_2(dpe)_3$, were suspended in THF or toluene and then allowed to warm from room temperature until the complexes were completely dissolved in THF or toluene. After cooling the solution, greenish yellow prisms were obtained, which were recrystallized from THF or toluene, (yield, 45%).

Preparation of Alkylcopper(I) Complexes with Other Tertiary Phosphines. $CH_3Cu(PPh_2Me)_3$, ***3***: To an ethereal suspension of $Cu(acac)_2$, 4 molar equivalents of PPh_2Me was added at −45 °C and then 4 molar equiv of Me_2AlOEt was slowly added at the same temperature. Blue crystals of $Cu(acac)_2$ gradually dissolved in ether with evolution of CH_4 and C_2H_6 with temperature being raised gradually to room temperature. A white yellow complex precipitated from the orange yellow solution on stirring for 6 h. The complex which was separated by filtration was dissolved in ether–THF at the temperature below 0 °C. From the yellow solution, white yellow crystals were obtained on cooling, washed repeatedly with ether, dried *in vacuo* at room temperature in the dark and characterized as $CH_3Cu(PPh_2Me)_3$, (yield, 63%). The NMR spectrum of **3**, in toluene-d_8 at −20 °C, had a singlet at τ 10.50 (3H, C$\underline{H}_3$–Cu), a singlet at 8.60 (9H, C$\underline{H}_3$–P), a multiplet at 3.16—2.50 (30H, (C$_6\underline{H}_5$)$_2$–P).

$CH_3Cu(PPhMe_2)$, ***4***: At −45 °C, 3 molar equivalents of $PPhMe_2$ was added to an ethereal suspension of $Cu(acac)_2$ and then 4 molar equiv of Me_2AlOEt was slowly added. After the temperature was gradually raised to 0 °C with stirring, a light yellow solution was obtained. The solution was allowed to condense by evaporation under a reduced pressure and then a small amount of hexane was added to it. After cooling the solution at −78 °C, white yellow crystals slowly precipitated and were recrystallized from ether–hexane solvent mixture. The white yellow complex thus obtained was characterized as $CH_3CuPPhMe_2$, (yield, 35%).

CH_3CuPBu_3, ***6***: To an ethereal suspension of $Cu(acac)_2$, 3—4 molar equiv of PBu_3 was added at −40 °C and then 4 molar equiv of dimethylalminium ethoxide was slowly added at the same temperature. With a gradual raise of the temperature, $Cu(acac)_2$ dissolved in ether and CH_4 and C_2H_6 were released to give a yellow solution at room temperature. After condensation of the ether solution, the residue was extracted with hexane. White yellow prisms, isolated from the hexane solution upon cooling, were washed repeatedly with small amounts of hexane below 0 °C, dried *in vacuo* and characterized as CH_3CuPBu_3, **6**, (yield 65%).

CH_3CuPEt_3, ***5***: This was prepared by the procedure described above, and recrystallized from an ether–THF–hexane solvent mixture, (yield, 45%). Light yellow crystals.

Preparation of Butyl(tricyclohexylphosphine)copper, ***7***:

$Cu(acac)_2$ 4 g (15 mmol) and tricyclohexylphosphine 9 g (31.9 mmol) were suspended in 100 ml of ether, and 13 ml of diisobutylaluminium ethoxide was added to the suspension at −30 °C. After the temperature was raised gradually to room temperature with stirring, a pale yellow solution was obtained. After cooling the solution, cream yellow prisms deposited, which were filtered, washed repeatedly with ether and hexane, dried *in vacuo*, and characterized as *i*-$BuCuPCy_3$. The complex was recrystallized from ether, (yield, 60%).

Polymerization. Most of the polymerizations were carried out in a sealed ampoule or in a Schlenk type flask in which the alkylcopper complex (50—100 mg) and olefin (5—10 ml) were transferred in an atmosphere of nitrogen or by a trap-to-trap distillation *in vacuo*. After the polymerization was complete, the content in the flask was poured into acidic methanol. The precipitate was filtered, washed with methanol and dried. The polymers of acrylonitrile obtained with **Ia** and **Ic** had molecular weights of *ca.* 1.2×10^4, and poly(methyl methacrylate) 1.3—7.1×10^5 determined by a viscosity method.

References

1) (a) R. G. R. Bacon and H. O. Hill, *Quart. Rev.*, **19**, 95 (1965); (b) J. F. Normant, *Synthesis*, **1972**, 63; (c) T. Saegusa, T. Tsuda, and Y. Ito, *Kogyo Kagaku Zasshi*, **72**, 1627 (1969); (d) T. Saegusa and Y. Ito, *Kagaku no Ryoiki, Special Issue*, No. 89, 157 (1970); (e) T. Saegusa and Y. Ito, *Synthesis*, **1975**, 291.

2) G. Buckton, *Ann. Chem.*, **109**, 225 (1859).

3) (a) H. Gilman, R. G. Jones, and L. A. Woods, *J. Org. Chem.*, **17**, 1630 (1952); (b) H. O. House, W. L. Respess, and G. M. Whitesides, *J. Am. Chem. Soc.*, **31**, 3128 (1966).

4) K. H. Thiele and J. Kölher, *J. Organomet. Chem.*, **12**, 225 (1968).

5) (a) H. Gilman and L. A. Woods, *J. Am. Chem. Soc.*, **65**, 435 (1943); (b) G. Costa, G. De Alti, L. Stefani, and G. Boscarato, *Ann. Chim.*, **52**, 289 (1962); (c) C. E. H. Bawn and F. H. Whitby, *J. Chem. Soc.*, **1960**, 3926, 4162.

6) T. Ikariya and A. Yamamoto, *J. Organometal. Chem.*, **72**, 145 (1974).

7) (a) J. Burdon, P. L. Coe, C. R. Marsh, and J. C. Tatlow, *Chem. Commun.*, **1967**, 1259; (b) J. Burdon, P. L. Coe, C. R. Marsh, and J. C. Tatlow, *J. Chem. Soc., Perkin Trans. 1*, **5**, 639 (1972); (c) V. C. Macloughlin and J. Thrower, *Tetrahedron*, **25**, 592 (1969).

8) T. Tsuda, T. Nakatsuka, T. Hirayama, and T. Saegusa, *J. Chem. Soc., Chem. Commun.*, **1974**, 557.

9) (a) G. Costa, A. Camus, L. Gatti, and N. Marsich, *J. Organomet. Chem.*, **5**, 568 (1966); (b) G. Costa, A. Camus, N. Marsich, and L. Gatti, *J. Organomet. Chem.*, **8**, 339 (1967); (c) G. van Koten and J. G. Noltes, *J. Organomet. Chem.*, **84**, 117, 129, 419 (1975) and references cited therein.

10) For example, M. L. H. Green, "Organometallic Compounds," Vol. 2, Methuen, London (1968).

11) G. Costa, G. Pellizer, and F. Rubessa, *J. Inorg. Nucl. Chem.*, **26**, 961 (1964).

12) (a) H. O. House and W. F. Fischer, Jr., *J. Org. Chem.*, **33**, 949 (1968); (b) G. M. Whitesides, E. J. Panek, and E. R. Stedronsky, *J. Am. Chem. Soc.*, **94**, 232 (1972); (c) G. M. Whitesides, E. R. Stedronsky, C. P. Casey, and J. San Filippo, Jr., *J. Am. Chem. Soc.*, **92**, 1426 (1970).

13) A. Yamamoto, A. Miyashita, T. Yamamoto, and S. Ikeda, *Bull. Chem. Soc. Jpn.*, **45**, 1583 (1972).

14) (a) P. W. Jolly, K. Jonas, C. Krüger, and T. H. Tsay, *J. Organomet. Chem.*, **33**, 109 (1971); (b) A. Yamamoto, T. Yamamoto, T. Saruyama, and Y. Nakamura, *J. Am. Chem. Soc.*, **95**, 4073 (1973); T. Yamamoto, T. Saruyama, Y. Nakamura, and A. Yamamoto, *Bull. Chem. Soc. Jpn.*, **49**, 589 (1976).

15) Y. Kubo and A. Yamamoto, *J. Organomet. Chem.*, **46**, C50 (1972); *ibid.*, **84**, 369 (1975).

16) (a) A. Cairncross and W. A. Sheppard, *J. Am. Chem. Soc.*, **93**, 248 (1971); (b) M. R. Churchill, S. A. Bezman, J. A. Osborn, and J. Wormald, *Inorg. Chem.*, **11**, 1818 (1972); (c) G. van Koten and J. G. Noltes, *J. Chem. Commun.*, **1970**, 1107; (d) J. M. Guss, R. Mason, and K. M. Thomas, *J. Organomet. Chem.*, **40**, C79 (1972).

17) (a) L. Dahlenburg and R. Nast, *J. Organomet. Chem.*, **71**, C49 (1974); (b) D. M. Adams, *J. Chem. Soc.*, **1962**, 1220.

18) A. Camus and N. Marsich, *J. Organomet. Chem.*, **21**, 249 (1970).

19) N. Marsich, A. Camus, and E. Cebulec, *J. Inorg. Nucl. Chem.*, **34**, 933 (1972).

20) V. G. Albano, P. L. Bellon, and G. Ciano, *J. Chem. Soc., Dalton Trans.*, **1972**, 1938.

21) A. Yamamoto, K. Kato, and S. Ikeda, *J. Organomet. Chem.*, **60**, 139 (1973).

22) A. Yamamoto, T. Murai, E. Ooshima, and S. Ikeda, unpublished.

23) G. van Koten and J. G. Noltes, *J. Chem. Soc., Chem. Commun.*, **1972**, 452.
They have confirmed the dimeric structure for $Ph_2PCu(dpe)$, private communication.

24) (a) A. Yamamoto and S. Ikeda, Progress in Polymer Science Japan, Vol. 3, 49, ed by S. Okamura and M. Takayanagi, Kodansha, Tokyo (1972); (b) T. Yamamoto, A. Yamamoto, and S. Ikeda, *Bull. Chem. Soc. Jpn.*, **45**, 1111 (1972); (c) Y. Kubo, A. Yamamoto, and S. Ikeda, *ibid.*, **47**, 393 (1974); (d) S. Komiya, A. Yamamoto, and S. Ikeda, *ibid.*, **48**, 101 (1975); (e) A. Yamamoto, *Ann. N.Y. Acad. Sci.*, **239**, 60 (1974); A. Yamamoto and S. Ikeda, *J. Macromol. Sci. Chem.*, **A9**, 931 (1975).

25) T. Saegusa, S. Horiguchi, and T. Tsuda, *Macromolecules*, **8**, 112 (1975).

26) A. Tamaki and J. K. Kochi, *J. Organomet. Chem.*, **40**, C81 (1972).

27) M. M. Jones, *J. Am. Chem. Soc.*, **71**, 3188 (1959).

28) W. Hewertson and H. R. Watson, *J. Chem. Soc.*, **1962**, 1490.

29) W. H. Gruber and J. Ellermann, *Chem. Ber.*, **23**, 1307 (1968).

30) J. A. C. Allison and F. G. Mann, *J. Chem. Soc.*, **1949**, 2915.

31) M. J. Mays and S. M. Pearson, *J. Chem. Soc., A*, **1968**, 2281.

Thermal Stability of Alkylcopper(I) Complexes Coordinated with Tertiary Phosphines

Akira MIYASHITA, Takakazu YAMAMOTO, and Akio YAMAMOTO
Research Laboratory of Resourecs Utilization, Tokyo Institute of Technology, O-okayama, Meguro-ku, Tokyo 152
(Received November 12, 1976)

Thermolysis of isolated alkylcopper(I) complexes having tertiary phosphine ligand(s) $RCuL_n$ ($R=CH_3$, C_2H_5, n-C_3H_7, i-C_4H_9) in the solid state and in toluene has been studied in order to clarify the role of the tertiary phosphine ligand in stabilizing the alkylcopper(I) complexes. The distribution of the thermolysis products shows that the thermolysis of the alkylcopper complexes having ethyl or longer alkyl chain proceeds through a β-elimination mechanism. The rate of the thermolysis obeys the first order rate law, $-d[RCuL_n]/dt=k[RCuL_n]$. The activation parameters of the thermolysis were obtained from the temperature dependence of k and a compensation effect between ΔH^* and ΔS^* was demonstrated. The activation energy E_a of the thermolysis of $RCu(PPh_3)_2$ increases in the order of $R=C_2H_5<n$-$C_3H_7<i$-C_4H_9. Coordination of electron-donating tertiary phosphine decreases E_a and a linear relationship between $\nu(Cu-CH_3)$ frequencies and E_a for thermolysis of the methylcopper complexes was observed. Addition of PPh_3 into the toluene solutions of $CH_3Cu(PPh_3)_2$(diethyl ether)$_{0.5}$ and C_2H_5-$Cu(PPh_3)_2$ causes some retardation of the thermolysis. The major role of the tertiary phosphine ligand in stabilizing the alkylcopper complexes is proposed to strengthen the Cu–C bond by changing the electronic state of copper atom. An energetic consideration based on Chatt and Shaw's theory is given in order to account for the results concerning the stabilities of the alkylcopper complexes. Photolysis of the alkylcopper complexes takes a quite different decomposition pathway producing mainly RH from $RCuL_n$.

The problem of the stability of transition metal to carbon bond is of fundamental importance in organotransition metal chemistry. Information regarding the stability of trasition metal-carbon σ bond and how to stabilize or activate the σ bond is quite desirable for theoretical discussion of the nature of the metal-carbon σ bond as well as in accounting for the mechanisms of organic syntheses promoted by transition metal compounds.[1] However, because of the scarcity of the isolated alkyltransition metal compounds possessing considerable thermal stabilities, the discussions have remained empirical and often have been based on the relative ease for the preparation of an alkyltransition metal compound. Two lines of theories have been proposed concerning the factors determining the stability of a transition metal-carbon bond. The first one, originally proposed by Chatt and Shaw,[2] relates the stability with the energy gap required to promote an electron from predominantly non-bonding d-orbitals to antibonding metal-carbon orbitals (σ^*_{M-C}) or from bonding metal-carbon orbitals (σ_{M-C}) to vacant or half-filled d-orbitals, and the role of the stabilizing ligand was accounted for in terms of the increase in the energy gap. A partially modified scheme of this model was proposed by us to account for the stability of dialkyl(2,2′-bipyridine)nickel and activation of the Ni–C bonds in the presence of electronegative olefins.[3] The other theory stresses the importance of low energy decomposition pathway, particularly a β-elimination process[4,5] and accounts for the role of the "stabilizing ligand" mainly as blocking the site required for the β-elimination process to proceed. On the basis of the latter theory some "elimination stabilized alkyls" such as trimethylsilylmethyl have been successfully prepared.[4,5c,5d]

Although the number of isolated alkyltransition metal complexes is rapidly increasing in recent years, works reporting the kinetics of the decomposition process and dealing with the analysis of the decomposition products are relatively limited.[3,5,6,12,15] Thermolysis of alkylcopper complexes have been studied by Whitesides[5a,5e] and Kochi.[7] Unfortunately, however, the studies have been made on the complexes prepared *in situ* from copper salts and alkylating agents and the systems studied may well contain some impurities, albeit in small quantities. Since the presence of a Lewis acid is known to affect the stability and decomposition course of an alkyl- or hydridotransition metal complex,[8,9] results obtained in somewhat impure systems are not quite unequivocal.

We have isolated series of alkylcopper complexes containing various tertiary phosphines and observed the pronounced effect of the tertary phosphine ligands on stabilization of the alkylcopper compounds.[10] In contrast to the extremely unstable ligand-free methylcopper which decomposes violently at room temperature, the phosphine-stabilized alkylcopper complexes are considerably stable and provide a suitable probe for testing the validity of the existing theories. We report here the kinetic study of thermolysis of the alkylcopper complexes and analysis of the gaseous products generated in the thermolysis with a hope to provide pertinent data relevant to the discussion of the thermal stability of alkylcopper complexes.

Results and Discussion

Thermolysis of Alkylcopper Complexes in Solid State. Decomposition Temperature and Thermolysis Products: The isolated alkylcopper complexes containing tertiary phosphine ligands were thermolyzed in solid state in vacuum and the composition of the evolved gases was analyzed. Table 1 summarizes the decomposition points of various alkylcopper complexes with teriary phosphine ligands and the compositions of the evolved gases. Table 1 also includes the sum of the amounts of gaseous products generated per copper atom (ΣR).

The results in Table 1 indicate almost quantitative

Table 1. Decomposition points (dp) of alkylcopper complexes and their pyrolysis products

Compound[a]	Dp (°C)	Composition of the gas evolved[b]				ΣR(%)[j]
		H_2	R(−H)	RH	R-R	
$CH_3Cu(PPh_3)_2(ether)_{0.5}$	75—76	0	3[g]	7	90	108
$CH_3Cu(PPh_3)_3(toluene)$	70—75	0	0	25	75	98
$C_2H_5Cu(PPh_3)_2$	56—58	14	55	29	2	97
$C_2H_5CuPPh_3$	55—58	11	54	32	3	87
n-$C_3H_7Cu(PPh_3)_2$	61—62	22	60	18	0	96
i-$C_4H_9Cu(PPh_3)_2$	60—63	29	60[h]	11[i]	0	102
CH_3CuPCy_3	105—110	0	0	0	100	71
$C_2H_5CuPCy_3$	75—80	17	67	17	0	88
$C_3H_7CuPCy_3$	85—90	26	70	4	0	77
i-$C_4H_9CuPCy_3$	100—102	29	65[h]	7[i]	0	98
$(CH_3)_4CuAl_2(dpe)_2(OC_2H_5)_2$	230[c]	0	0	37	63	—
$(CH_3Cu)_2(dpe)_3$	149—150	0	9[g]	48	43	95
$(C_2H_5Cu)_2(dpe)_3$	124—127	2	53	45	0	81
$(n$-$C_3H_7Cu)_2(dpe)_3$	130—150	4	41	55	0	96
$(i$-$C_4H_9Cu)_2(dpe)_3$	102—105	5	45[h]	50[i]	0	95
$CH_3Cu(P(C_6H_5)_2(CH_3))_3$	95—98	0	0	2	98	100
$CH_3Cu(P(C_6H_5)(CH_3)_2)$	50—90[d]	0	0	62	38	110
$CH_3Cu(P(n$-$C_4H_9)_3)$	90—130[e]	0	0	61	39	112
$CH_3Cu(P(C_2H_5)_3)$	60—90[f]	0	0	85	15	93

a) PPh_3=triphenylphosphine, PCy_3=tricyclohexylphosphine, dpe=1,2-bis(diphenylphosphino)ethane, ether=diethyl ether. b) Mol%. c) At 136—139 °C it melted turning to black and decomposed at 230 °C. d) Mp, 50—51 °C. e) Mp, 57—60 °C. f) Mp, 40—45 °C. g) C_2H_4. h) 2-Methylpropene. i) 2-Methylpropane. j) The mol percent of the alkyl group decomposed was determined by measuring the volume of the gas evolved. The amount of R-R was doubled in calculation.

liberation of the alkyl groups as gaseous products on the thermolysis. Decomposition points in Table 1 refer to the temperature at which smooth evolution of gas started on heating the complexes in vacuum. Most complexes decompose with melting but some complexes evolve gas at much higher temperature than their melting points. The dpe-coordinated complexes (dpe=1,2-bis(diphenylphosphino)ethane) showed the highest decomposition points and particularly the methylcopper complex containing an aluminum component was so stable as it was not decomposed up to 230 °C. A similar enhancement of the thermal stability was observed in a manganese hydride complex containing an alkylaluminum component.[9] The decomposition points of the tricyclohexylphosphine (PCy_3) -coordinated complexes ranked next to the dpe-containing complexes to be followed by PPh_3-coordinated (PPh_3=triphenylphosphine) complexes. The dpe- and PCy_3-coordinated complexes showed some variation in decomposition points depending on the alkyl group bonded to copper, whereas the difference in decomposition points of the PPh_3-coordinated complexes was not so marked.

In the thermolysis of solid methylcopper complexes coordinated with $P(C_6H_5)(CH_3)_2$, $P(C_2H_5)_3$, and $P(C_4H_9)_3$ ligands, considerable amounts of methane were evolved in addition to ethane. Since the value of ΣR is about 100%, the source of hydrogen for methane formation should be the phosphine ligands and this fact together with the absence of ethylene in the thermolysis products excludes the possibility of α-elimination which was observed for thermolysis of $(CH_3)_2Fe(dpe)_2$[11] and $CH_3CrCl_2L_n$.[12] On the other hand, evolution of ethylene was observed in thermolysis of $CH_3Cu(PPh_3)_2$(diethyl ether)$_{0.5}$ and $(CH_3Cu)_2(dpe)_3$ which may partly decompose by the α-elimination.

In the thermolysis of the alkylcopper complex with ethyl or longer alkyl chain, both alkane and alkene are formed, the latter being more predominant, accompanied by evolution of molecular hydrogen. Examination of the distributions of alkanes, alkenes and H_2 evolved from PPh_3- and PCy_3-coordinated complexes revealed that the amounts of H_2 evolved correspond to about half of the difference between the amounts of alkanes and alkenes.

These observations suggest that the thermolysis of the alkylcopper complexes having ethyl or longer alkyl chain proceeds by the following scheme comprising β-elimination (Eq. 1), coupling of the alkyl and hydrido ligands (Eq. 2), and evolution of H_2 from the copper hydride (Eq. 3). The participation of all molecules of the copper hydride in either the reaction (2) or (3) was confirmed by the absence of hydrogen evolution on treatment of the thermolysis residue with H_2SO_4.

$$RCuL_n \rightarrow CuHL_n + R(-H) \quad (1)$$

$$HCuL_n + RCuL_n \rightarrow RH + 2CuL_n \quad (2)$$

$$HCuL_n \rightarrow 1/2H_2 + CuL_n \quad (3)$$

Whitesides and coworkers have proposed a similar mechanism for the thermolysis of butyl-1,1-d_2-(tributylphosphine)copper(I) prepared *in situ* by analyzing the composition of the gases evolved.[5a]

Kinetics of the Thermolysis of Solid Alkylcopper Complexes: The thermolysis of the alkylcopper complexes

Table 2. The first-order rate constants of pyrolysis of alkylcopper(I) complexes

Compound[a]	Rate constant[b]
$CH_3Cu(PPh_3)_2(ether)_{0.5}$	0.91(69.5), 3.56(74.6), 5.08(76.8), 9.28(79.0)
$CH_3Cu(PPh_3)_3(toluene)$	0.79(59.6), 1.60(62.6), 3.53(66.2), 8.45(71.8)
$C_2H_5Cu(PPh_3)$	1.23(34.0), 3.69(37.3), 12.0(41.2), 39.1(44.6)
$C_2H_5Cu(PPh_3)_2$	1.14(40.8), 2.45(45.2), 8.36(50.5), 20.8(53.0)
n-$C_3H_7Cu(PPh_3)_2$	0.65(40.6), 1.12(45.2), 5.61(48.0), 8.40(50.4), 20.3(53.2), 90.8(57.5)
i-$C_4H_9Cu(PPh_3)_2$	1.31(34.5), 2.30(39.0), 5.67(41.5), 12.8(43.3), 26.1(45.5)
$CH_3Cu(P(C_6H_5)_2(CH_3))_3$	1.23(87.5), 3.71(93.0), 16.4(102.5), 42.0(107.5)
CH_3CuPCy_3	3.82(76.5), 5.68(80.0), 6.49(82.6), 10.4(86.0), 14.6(89.2)
i-$C_4H_9CuPCy_3$	3.44(75.4), 8.52(80.0), 21.4(85.0), 41.9(89.0)
$(CH_3Cu)_2(dpe)_3$	2.04(120.0), 2.49(129.0), 12.2(134.5), 31.0(139.0)
$(i$-$C_4H_9Cu)_2(dpe)_3$	0.88(78.2), 3.24(84.2), 4.47(88.5), 13.3(94.5)

a) For abbreviations, see Table 1. b) $10^4\ k\ s^{-1}$. The numbers in the parentheses refer to the thermolysis temperatures in °C.

in solid state was followed by measuring the gas evolved at fixed temperatures.

Figure 1 shows the results of typical thermolysis experiments. The volume of gas evolved on heating a solid sample at certain temperature was measured and plotted *versus* time. Since the composition of the gas evolved during the course of thermolysis did not vary significantly, the value of $(V_\infty - V_t)$, where V_∞ and V_t refer to the gas volumes evolved at infinite time and time t, corresponds to the amount of the alkylcopper complex remaining undecomposed. Plots of $\log(V_\infty - V_t)$ *versus* time t give straight lines with some curvatures in the initial stages as shown in Fig. 2. In most cases the portion of the straight line covers a

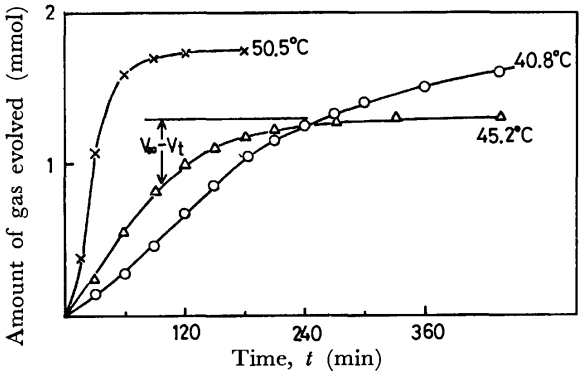

Fig 1. Time curves of the amount of gas evolved in the thermolyses of $C_2H_5Cu(PPh_3)_2$ at fixed temperatures. Amount of $C_2H_5Cu(PPh_3)_2$: 50.5 °C, 920 mg; 45.2 °C, 690 mg; 40.8 °C, 950 mg.

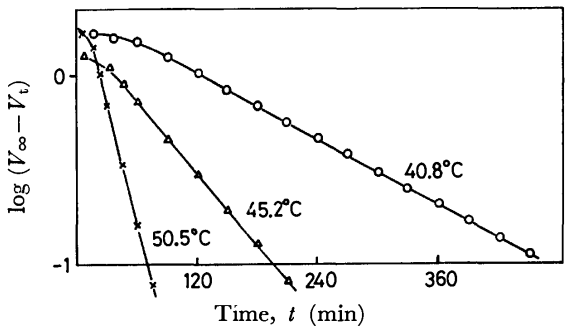

Fig. 2. The first-order plots of the data in Fig. 1.

range corresponding to decomposition of about 80% of the alkylcopper complex. In this paper we are concerned with the region where the linear relationship holds between $\log(V_\infty - V_t)$ and time. The rate constants in the first-order expression

$$-d[RCuL_n]/dt = k[RCuL_n]$$

are given in Table 2. From Arrhenius plots of the rate constants in Table 2 activation energies and kinetic parameters were computed and are summarized in Table 3.

That the first-order rate law holds in the thermolysis of the alkylcopper complexes having ethyl or longer alkyl chain indicates that the formation of the copper hydride by the β-elimination (Eq. 1) is rapidly followed by the process (2) or (3). This is consistent with Whitesides and coworker's observation[13] that the copper hydride prepared *in situ* decomposed even at −20 °C to evolve H_2 and in the presence of an alkylcopper(I) complex it underwent a facile coupling reaction to produce RH at −20 °C to −30 °C.

Furthermore, the first-order rate law for the thermolysis of the methylcopper complexes suggests that the methyl group ("CH_3") liberated from the methylcopper complex by a spontaneous unimolecular process

Table 3. Activation energies and kinetic parameters for thermolysis of alkylcopper compounds

Compound[a]	E_a (kcal·mol^{-1})	ΔH^* (kcal·mol^{-1})	ΔS^* (e.u.)	ΔF^* (kcal·mol^{-1})
$CH_3Cu(PPh_3)_3(toluene)$	50	50	72	26
$CH_3Cu(PPh_3)_2(ether)_{0.5}$	57	57	85	27
$C_2H_5Cu(PPh_3)$	62	61	123	22
$C_2H_5Cu(PPh_3)_2$	48	47	74	24
n-$C_3H_7Cu(PPh_3)_2$	63	63	119	25
i-$C_4H_9Cu(PPh_3)_2$	71	70	151	23
$CH_3Cu(P(C_6H_5)_2(CH_3))_3$	46	45	49	28
CH_3CuPCy_3	27	26	0.3	26
i-$C_4H_9CuPCy_3$	47	46	57	26
$(CH_3Cu)_2(dpe)_3$	50	50	50	30
$(i$-$C_4H_9Cu)_2(dpe)_3$	43	42	43	27

a) For abbreviations see Table 1.

(Eq. 4) will rapidly abstract hydrogen from the phosphine ligand (Eq. 5) or couple with the CH_3 group in another molecule of the methylcopper complex (Eq. 6) to evolve CH_4 and C_2H_6, respectively. Abstraction of hydrogen of CH_3 group in the methylcopper complex by "CH_3" to produce CH_4 and a carbenoid species (Eq. 7) may also take place,

$$CH_3CuL_n \rightarrow \text{"}CuL_n\text{"} + \text{"}CH_3\text{"} \quad (4)$$

$$\text{"}CuL_n\text{"} + \text{"}CH_3\text{"} \rightarrow CH_4 + CuL_{n-1}(L(-H)) \quad (5)$$

$$\text{"}CH_3\text{"} + CH_3CuL_n \rightarrow C_2H_6 + CuL_n \quad (6)$$

$$\text{"}CH_3\text{"} + CH_3CuL_n \rightarrow CH_4 + CH_2{=}CuL_n \quad (7)$$

$$CH_2{=}CuL_n \rightarrow 1/2C_2H_4 \quad (8)$$

where L(−H) represents a ligand from which a hydrogen atom was taken away by the methyl group.

The course of the thermolysis of $CH_3Cu(PPh_3)_2$ (diethyl ether)$_{0.5}$ consists of two stages. The gas evolved at the earlier stage was composed mainly of diethyl ether and scission of the Cu–CH_3 bond started after the quantitative evolution of diethyl ether. The rate constants in Table 2 and the activation energy in Table 3 are referred to the latter stage.

A Compensation Effect between the Enthalpy of Activation and the Entropy of Activation: Examination of the results in Tables 1, 2 and 3 reveals several interesting features of the thermolysis. Although it may be expected that a complex having higher activation energy for the thermolysis has a higher decomposition temperature, it is seen from the tables that there exists no correlation between the decomposition point of an alkylcopper complex and its activation energy for thermolysis. We consider that the activation energy for thermolysis more directly reflects the intrinsic strength of the Cu–C bond than the decomposition temperature. The present observation suggests that it is not always justified to discuss the strength of the alkyl-transition metal bond referring only to the decomposition points of the complexes, although they may be often used as practical criteria of the strength of the alkyl-transition metal bond.

A plot of the enthalpy of activation ΔH^* against the entropy of activation ΔS^* for the thermolysis of the alkylcopper complexes gave a straight line with a slope $\Delta H^*/\Delta S^* = 270$ deg (Fig. 3) which corresponds to a value of about one for $\Delta H^*/T\Delta S^*$ under the experimental conditions indicating that the increase in ΔH^* does not cause a direct increase in ΔF^* but is almost completely cancelled by the decrease in $-T\Delta S^*$.

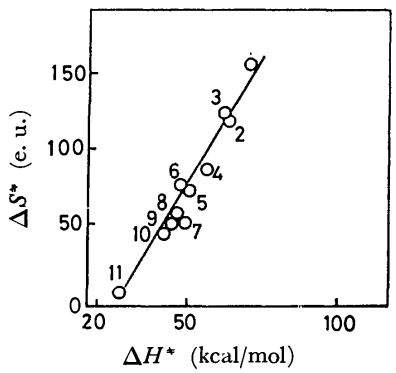

Fig. 3. The compensation effect between ΔH^* and ΔS^*. 1: i-$C_4H_9Cu(PPh_3)_2$, 2: n-$C_3H_7Cu(PPh_3)_2$, 3: $C_2H_5CuPPh_3$, 4: $CH_3Cu(PPh_3)_2$(diethyl ether)$_{0.5}$, 5: $CH_3Cu(PPh_3)_3$(toluene), 6: $C_2H_5Cu(PPh_3)_2$, 7: $(CH_3Cu)_2(dpe)_3$, 8: i-$C_4H_9CuPCy_3$, 9: $CH_3Cu(P(C_6H_5)_2CH_3)_3$, 10: $(i\text{-}C_4H_9Cu)_2(dpe)_3$, 11: $CH_3Cu(PCy_3)$.

These results explain the lack of correlation between the decomposition points of alkylcopper complexes and their activation energies for thermolysis. The compensation effect is particularly well demonstrated in a series of $RCu(PPh_3)_2$ complexes. In contrast to the steady and significant increase of the activation energy for thermolysis from the ethyl (47 kcal/mol) through the propyl (63) to the isobutyl (70) the decomposition points vary only slightly (Table 1).

We have observed a compensation effect between ΔH^* and ΔS^* for the splitting of nickel-alkyl bonds induced by olefin coordination.[14]

Thermolysis of Alkylcopper Complexes in Solution.

The alkylcopper complexes have lower stability in solution than in the solid state. The decomposition of the complexes in solution set in at the lower temperature by 40—50 °C than that in the solid state. One mol of $C_2H_5Cu(PPh_3)_2$ evolved 0.59 mol of ethylene, 0.33 mol of ethane and 0.15 mol of H_2 on the thermolysis in toluene at 10 °C. The distribution of the gases evolved in toluene is essentially the same as that of gases evolved in solid state. The results indicate that the thermolysis of the ethylcopper complex in toluene proceeds through the same processes as those proposed for the thermolysis in the solid state (Eqs. 1, 2 and 3). The thermolysis in toluene obeyed

Table 4. The first-order rate constants of the thermolysis of $C_2H_5Cu(PPh_3)_2$ and $CH_3Cu(PPh_3)_2$(diethyl ether)$_{0.5}$ in toluene

Compound[a]	[PPh_3 added]/[Cu complex]	Rate constant[b] (s^{-1})
$C_2H_5Cu(PPh_3)_2$	0	4.8(−2.1), 7.1(0.3), 18(4.7), 34(7.8)
$C_2H_5Cu(PPh_3)_2$	1.0	13(4.7)
$C_2H_5Cu(PPh_3)_2$	2.0	9.4(4.7)
$C_2H_5Cu(PPh_3)_2$	4.1	1.3(−3.3), 3.0(0.2), 8.9(4.7)
$CH_3Cu(PPh_3)_2(Et_2O)_{0.5}$	0	1.3(22.6), 3.4(27.1), 7.7(30.0)
$CH_3Cu(PPh_3)_2(Et_2O)_{0.5}$	1.9	3.0(27.0)
$CH_3Cu(PPh_3)_2(Et_2O)_{0.5}$	4.0	0.52(17.0), 1.2(21.6), 2.7(27.0), 7.1(30.3)

a) Et_2O=diethyl ether. b) 10^4 k. The numbers in the parentheses show the thermolysis temperatures in °C.

the first-order rate law and the first-order rate constants are listed in Table 4.

The activation energy for the thermolysis of $C_2H_5Cu(PPh_3)_2$ in toluene calculated from an Arrhenius polt of the rate constants was 32 kcal/mol, being considerably smaller than that in the solid state (48 kcal/mol) The heat of fusion of the ethylcopper complex required in the thermolysis in the solid phase accounts for a part of the difference between the two activation energies. However, in order to account for whole of such a great difference, it will be necessary to consider other unrevealed factors such as ease of intramolecular rearrangement of the copper complex in forming the so-called activated complex and the coordination of solvent.

On addition of PPh_3 into the toluene solution of $C_2H_5Cu(PPh_3)_2$ the first-order rate constant decreased approaching a limiting value. The effect of the addition of PPh_3 on the rate constant can be accounted for by assuming the formation of a stabler ethylcopper complex having three PPh_3 ligands $C_2H_5Cu(PPh_3)_3$. In fact the methyl analog of $C_2H_5Cu(PPh_3)_3$ is isolable from toluene containing sufficient amount of PPh_3.[10c] An alternative explanation that there exists a dissociation equilibrium in the solution to form a less stable complex $C_2H_5Cu(PPh_3)$ by an equilibrium, $C_2H_5Cu(PPh_3)_2 \rightleftharpoons C_2H_5Cu(PPh_3)+PPh_3$, and addition of PPh_3 suppresses the dissociation seems less probable, since the molecular weight determination of $C_2H_5Cu(PPh_3)_2$ in benzene showed a negligible dissociation of PPh_3 from the complex.[10c]

Thermolysis of $CH_3Cu(PPh_3)_2$(diethyl ether)$_{0.5}$ in toluene also obeyed the first-order rate law and the rate constants are included in Table 4. Addition of PPh_3 into the solution influences the rate of the thermolysis. However, this is not so marked as that observed in the thermolysis of $C_2H_5Cu(PPh_3)_2$ and the result suggests that the methylcopper complex having three PPh_3 ligands which is formed in solution on addition of PPh_3 is thermolyzed at almost the same rate as the methylcopper complex having two PPh_3 ligands.

Thermolysis of $CH_3Cu(P(n\text{-}C_4H_9)_3)_3$ in toluene did not obey the first-order rate law. $(RCu)_2(dpe)_3$ in solutions underwent a quite different reaction, a selective hydrogen abstraction reaction from the methylene group of the dpe ligand by the alkyl group.[10c]

Consideration of the Effect of the Tertiary Phosphine Ligands on the Thermal Stability of the Cu–R Bond.

The Role of the Tertiary Phosphine Ligands in Stabilizing the Alkylcopper Complexes: If addition of ligand L to the solution of an alkyltransition metal complex R_mML_n causes complete inhibition of the thermolysis of the alkyltransition metal complex as observed in the thermolysis of alkylplatinum,[5b] -iron[6d,15a] and -cobalt[15b] complexes in solutions, the major role of the ligand in stabilizing the alkyltransition metal complex may be the blocking the site to hinder the β-elimination to proceed.[4,5] However, this is not the case for the thermolysis of the present alkylcopper complexes, since addition of PPh_3 into a toluene solution of $C_2H_5Cu(PPh_3)_2$ did not cause complete inhibition of the thermolysis of the ethylcopper complex though it caused a change in the rate of the thermolysis which may be accounted for by assuming a change in the strength of the Cu–C bond by the coordination of the third PPh_3(see above). Furthermore, ^{31}P-NMR spectra of mixtures of the alkylcopper complex ($C_2H_5Cu(PPh_3)_2$ or $CH_3Cu(PPh_3)_2$(diethyl ether)$_{0.5}$) and PPh_3 in toluene showed that a rapid exchange between the coordinated PPh_3 and free PPh_3 occurs even at -60 °C. This observation is not compatible with the assumption that the dissociation of a ligand from copper constitutes the rate determining step in the thermolysis.

The following three observations also are not consistent with the assumption that the predominant role of the tertiary phosphines in stabilizing the Cu–R bond is the blocking of the site for β-elimination.

(1) Comparison of the activation energies of $C_2H_5Cu(PPh_3)$ and $C_2H_5Cu(PPh_3)_2$ (Table 3) reveals that the ethylcopper complex containing one triphenylphosphine ligand has a *higher* activation energy than the ethylcopper complex with two PPh_3 ligands. As far as one compares the stability of an alkylcopper complex in terms of the activation energy for the thermolysis, this is not compatible with the theory to explain the role of the stabilizing ligand as blocking the site to hinder the β-elimination.

(2) The alkylcopper complexes generally have a monomeric structure in benzene as revealed by the cryoscopic molecular weight measurements of the complexes in benzene.[10c] This indicates that the copper complexes, especially those having one or two tertiary phosphines are not fully coordinated and have vacant site(s) at least in benzene. Thereupon the dissociation of the tertiary phosphine ligand seems not to be required for the β-elimination to proceed.

(3) The presence of the compensation effect between ΔH^* and ΔS^* (Fig. 3) for both the methylcopper complexes and the other copper complexes having ethyl or longer alkyl chain implies that the same factor which control the thermal stability of the methylcopper complexes dominates the thermal stability of the copper complexes having ethyl or longer alkyl chains. Since the thermal stability of the methylcopper complexes seems to be controlled only by the strength of the Cu–C bond, the observation concerning the compensation effect implies that even the thermolysis of the copper complexes having ethyl or longer alkyl chain is controlled by the intrinsic strength of the Cu–C bond. We assume that the loosening of the Cu–C bond as shown below is necessary to allow the copper atom to approach the β-hydrogen and thus to allow the β-elimination to proceed. If the β-elimination does not require the loosening of the Cu–C bond, we may anticipate that the activation energy for the thermolysis of copper complexes having ethyl or longer chain is much smaller than that for the

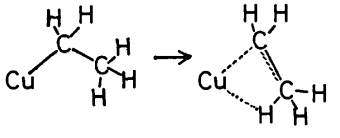

thermolysis of the methylcopper complexes. However, this is not the case in the thermolysis of the alkylcopper complexes.

From the above described reasons we conclude that the prime role of the tertiary phosphine ligand in stabilizing the present alkylcopper complexes is not simply to block the site but rather to strengthen the Cu–C bond by changing the electronic state of the complexes.

Effect of the Tertiary Phosphine Ligands on the Strength of the Cu–C Bond: Figure 4 shows a correlation between the activation energies for thermolysis and ν(Cu–CH_3) frequencies of the methylcopper complexes. The correlation supports our assumption that the activation energy for thermolysis corresponds to the energy required for loosening the Cu–C bond. Figure 5 shows the relationship between ν(Cu–CH_3) frequencies and pK_a of the conjugate acid of the tertiary phosphine ligand $[HPR'_3]^+$, and Fig. 6 shows the correlation between the activation energy and the pK_a value. It is seen that the complex with less basic ligands exibits the ν(Cu–CH_3) band at higher frequency and has a higher activation energy.

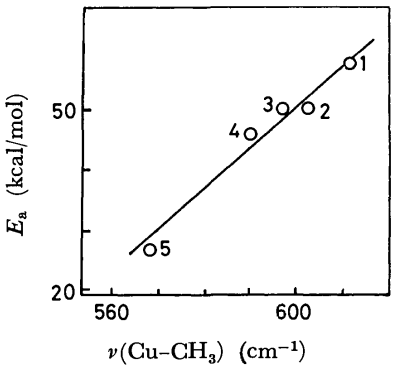

Fig. 4. Relationship between activation energy for thermolysis of methylcopper complexes and ν(Cu–CH_3). 1: $CH_3Cu(PPh_3)_2$(diethyl ether)$_{0.5}$, 2: $CH_3Cu(PPh_3)_3$(toluene), 3: $(CH_3Cu)_2$(dpe)$_3$, 4: $CH_3Cu(P(C_6H_5)_2CH_3)_3$, 5: $CH_3Cu(PCy_3)$.

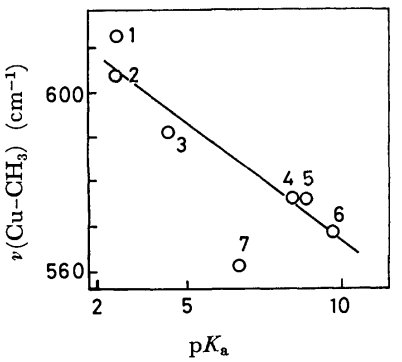

Fig. 5. Relationship between ν(Cu–CH_3) frequencies of methylcopper complexes and pK_a value of the conjugate acid of the tertiary phosphine ligand. 1: $CH_3Cu(PPh_3)_2$(diethyl ether)$_{0.5}$, 2. $CH_3Cu(PPh_3)_3$(toluene), 3: $CH_3Cu(P(C_6H_5)_2CH_3)_3$, 4: $CH_3Cu(P(n\text{-}C_4H_9)_3)$, 5: $CH_3Cu(P(C_2H_5)_3)$, 6: $CH_3Cu(PCy_3)$, 7: $CH_3Cu(P(C_6H_5)(CH_3)_2)$.

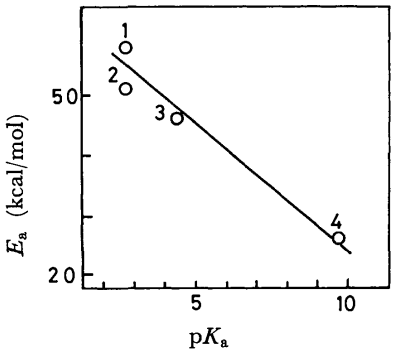

Fig. 6. Relationship between activation energy for thermolysis of methylcopper complexes and pK_a value of the conjugated acid of the tertiary phosphine ligand. 1: $CH_3Cu(PPh_3)_2$(diethyl ether)$_{0.5}$, 2: $CH_3Cu(PPh_3)_3$(toluene), 3: $CH_3Cu(P(C_6H_5)_2CH_3)_3$, 4: $CH_3Cu(PCy_3)$.

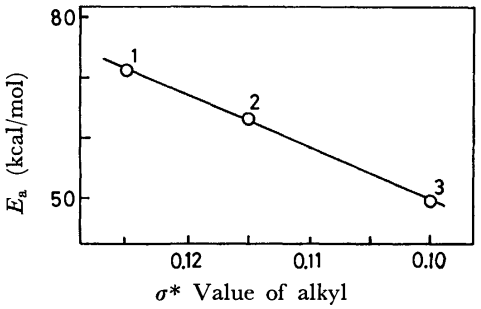

Fig. 7. Relationship between Taft's σ^* value of alkyl and activation energy for thermolysis of $RCu(PPh_3)_2$. 1: R=i-C_4H_9, 2: n-C_3H_7, 3: C_2H_5.

In order to see the effect of the alkyl group bonded to copper on the activation energy for thermolysis, the activation energies were plotted *versus* Taft's σ^* values[16] of the alkyl groups in Fig. 7.

The theory originally proposed by Chatt and Shaw,[2] upon some modification by Yamamoto and coworkers,[3] is consistent in accounting for the strength of the alkyl-copper bond which may be evaluated from the activation energy.

Since alkylcopper(I) complex has completely filled d-orbitals it is not necessary in terms of Chatt-shaw's theory[2] to consider the electronic promotion from bonding Cu–R orbital to vacant d-orbitals ($\sigma_{M-R}\rightarrow$d) and consideration of only the promotion from the filled d-orbital to anti-bonding Cu–R orbital (d$\rightarrow\sigma^*_{Cu-R}$) is required. If we assume that the order of energy of anti-bonding Cu–R orbitals (σ^*_{Cu-R}) is related to the order of electron affinities (E.A.) of alkyl radicals (E. A. in kcal/mol: CH_3, 32.2; C_2H_5, 21.6; C_3H_7, 15.9; C_4H_9, 15.0),[17] the anti-bonding Cu-methyl orbital ($\sigma^*_{Cu-CH_3}$) is expected to have the lowest energy and the energy level of σ^*_{Cu-R} is expected to increase in the order of R=CH_3<C_2H_5<n-C_3H_7<i-C_4H_9. The energy gap required for an electronic promotion from the metal d-orbitals to the σ^*_{Cu-R} orbital may be related to the activation energy for thermolysis of the alkyl-copper complex (Fig. 8). The agreement between the order of the increasing activation energy of the thermolysis of $RCu(PPh_3)_2$ by changing

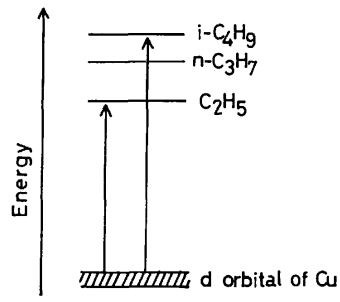

Fig. 8. Tentative energy level relation diagram in activation of Cu–R bond.

R,R=C_2H_5<*n*-C_3H_7<*i*-C_4H_9, and the order of the increasing energy gap in Fig. 8, R=C_2H_5<*n*-C_3H_7<*i*-C_4H_9, can be seen. The effect of the tertiary phosphine on the stability of the alkylcopper complexes can also be accounted for by assuming the scheme represented in Fig. 8. The fact that the methylcopper complex having phosphines with the larger Lewis basicity shows the smaller thermolysis activation energy may arise from raise in the energy of the d-orbital by coordination of phosphines with the larger Lewis basicity thus causing the decrease in the energy required for promotion. If this interpretation is valid the pronounced stabilizing effect of the tertiary phosphine ligand may be related with its ability of accepting d-electron by back-donation from the metal to phosphorus orbital, the consequence being the lowering of the energy of d-orbitals and higher stability for alkylcopper complexes with phosphine ligands having greater π-accepting ability.

One serious argument against this type of energetic consideration is that the concept of such a direct electronic exitation as depicted in Fig. 8 may not be related to thermolysis. We agree that in the thermolysis the simple electronic exitation may not be involved, but the energy gap for the excitation may still provide a measure for the stability to a first approximation. In lack of the knowledge about the potential energy curves for the bonding and anti-bonding orbitals a discussion based on energetic consideration admittedly remain speculative. However, the scheme depicted in Fig. 9 seems to be fairly consistent with the experimental facts obtained in this work. When an electron is directly promoted to the anti-bonding orbital shown as the upper curve in Fig. 9a, the splitting of Cu–C bond will take place. In the thermal reaction, if the potential curve of the anti-bonding orbital is crossed with that of d-orbital (Fig. 9a), on loosening of the Cu–C bonding to a certain extent a crossing over to the anti-bonding potential curve may take place, thus splitting of the Cu–C bond will result. The effects of the alkyl group and of the basicity of the tertiary phosphine ligands are explained similarly in this model as in Fig. 8. The crossing over to the anti-bonding orbital curve would take place at lower energy when the energy of the σ^*_{Cu-R} orbital lies lower (Fig. 9b), and the raise in the d-orbital by coordination of more electron-donating phosphines would lead to the crossing-over at smaller ΔE (Fig. 9c).

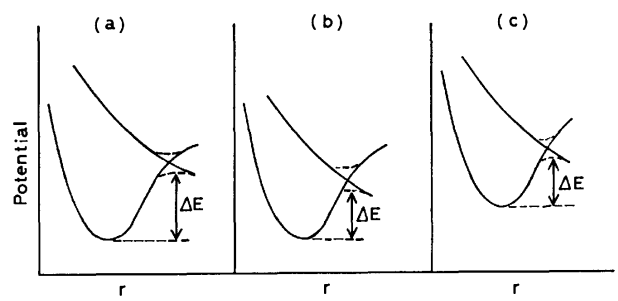

Fig. 9. Tentative potential energy curves for the splitting of Cu–R bond. Upper curve, σ^*_{Cu-R}; lower curve, d-orbital. For (a), (b), and (c) see the text. *r*=distance between Cu and C.

Previously Yamamoto *et al.* discussed the stability of alkylnickel[3] and alkylchromium[12b] complexes by taking into account similar energetic consideration. In contrast to the alkylcopper(I) complexes, these alkyltransition metal complexes have vacant d-orbital(s) and the stability of the transition metal-alkyl (M–R) bond in the series of the alkyltrasition metal complexes increased in a reverse order compared with the stability of the Cu–R bond, R=*n*-C_3H_7<C_2H_5<CH_3. Furthermore, the effect of the basicity of ligand in stabilizing the M–R bond in these alkyltransition metal complexes is reversed to that observed in the alkylcopper complexes; coordination of electron-donating ligand enhanced the stability of the M–R bond, whereas that acidic ligand destabilized the M–R bond. The stability of these alkyltransition metal complexses with vacant d-orbitals was explained by considering the electronic promotion from the low-lying bonding M–R orbital to the vacant d-orbital(s) ($\sigma_{M-R}\rightarrow$d) instead of that from the d-orbital to σ^*_{M-R} bond(d$\rightarrow\sigma^*_{M-R}$). Therefore, the postulate considered here is consistent with previously proposed scheme to explain the order of the stability in the series of the alkylnickel and alkylchromium complexes, although the order of the stability of these alkyltransition metal complexes is reversed to that of alkylcopper complexes.

We are concerned here with the loosening of the copper-alkyl bond in the thermolysis, but it should be stressed that we do not imply the formation of a free radical of any significant life time. The experimental results concerning the thermolysis do not indicate the formation of the free radicals. As described above the alkyl group will be subject to the further reaction, such as β-elimination reaction (Eq.1) at the instant when the copper-carbon bond in the alkylcopper complex become loose.

Photolysis of the Alkylcopper(I) Complexes. In order to get further information concerning the stability of the alkylcopper complexes we studied the photolysis of the alkylcopper complexes. The alkylcopper complexes are quite light-sensitive[10] and decompose even below −20 °C upon illumination by light. Comparison of the gaseous products in the thermolysis (Table 1) with those in the photolysis (Table 5) indicates a considerable difference in the decomposition pathways. In contrast to the thermolysis of $CH_3Cu(PPh_3)_3$(toluene) which gave ethane as the main product, the photolysis of the complex gave methane exclusively. Since the use of dueterated PPh_3 ligand and solvent did not

TABLE 5. PRODUCTS IN THE PHOTOLYSIS OF THE ALKYLCOPPER(I) COMPLEXES

Complex[a]	Solvent[a]	Temp (°C)	Time (h)	Products (Yield[b])			
				CH_4	CH_3D	C_2H_4	C_2H_6
$CH_3Cu(PPh_3)_3(C_7D_8)$	None	−30	48	31	0	0	0
$CH_3Cu(PPh_3)_3(C_7D_8)$	C_7D_8	−30	48	41	0	0	0
$CH_3Cu(PPh_3\text{-}d_6)_3(C_7D_8)$	None	−30	48	26	0	0	0
$CH_3Cu(PPh_3\text{-}d_3)_3(C_7D_8)$	None	80	5	21	2	6	31
$CH_3Cu(PPh_3\text{-}d_3)_3(C_7D_8)$	C_7D_8	−30	48	42	1	0	0
				H_2	C_2H_6	C_2H_4	C_4H_{10}
$C_2H_5Cu(PPh_3)_2$	None	−30	24	0	33	4	0
$C_2H_5Cu(PPh_3)_2$	C_7D_8	−30	24	0	55	37	0

a) C_7D_8=toluene-d_8, PPh_3-d_6=triphenylphosphine-2,6,2′,6′,2″,6″-d_6. b) Mol per 1 mol of the complexes.

cause the deuterium incorporation into methane, abstraction of a hydrogen of CH_3 group by another CH_3 group may consitute an important decomposition pathway in the photolysis of the methylcopper complex. Evolution of considerable amount of ethylene on irradiation of the methyl copper complex at 80 °C also suggest the hydrogen abstraction from the methyl group which will yield a carbenoid species. Formation of carbenoid species during thermolysis[11,12,18] and photolysis[19] of methyltrasition metal complexes has been proposed, and isolation of an alkylcarbene complex of tantalum has been reported.[20]

Photolysis of $C_2H_5Cu(PPh_3)_2$ produced ethane as the main gaseous product and ethylene as the minor product. This result is in contrast with thermolysis which generated ethylene as the major decomposition product.

Experimental

General Procedures and Preparation of Alkylcopper(I) Complexes. All experiments were carried out under deoxygenated argon or nitrogen atmosphere, or in vacuum. IR spectra were recorded on a Hitachi Model EPI-G3 spectrometer, and ^{31}P-NMR and ^1H-NMR spectra were recorded with a Japan Electron Optics Lab. JNM-PS-100 spectrometer. Evolved gas was analyzed with a Hitachi RMU-5B mass spectrometer and with a Shimadzu GC-5B gas chromatograph, using an active carbon column for C_1 and C_2 hydrocarbons, a VZ-7 column for C_1–C_4 hydrocarbons and a column with 20% TCP on 40/60 Uniport B for diethyl ether. A series of alkylcopper(I) complexes having various tertiary phosphines were prepared as previously reported.[10]

Preparation of $CH_3Cu(PPh_3\text{-}d_6)_3$(toluene-$d_8$). Triphenylphosphine-2,6,2′,6′,2″,6″-d_6 (PPh_3-d_6) was prepared by exchange reaction of PPh_3 with excess deuterium gas catalyzed by $RuH_2(PPh_3)_4$[21] and had 98.0% isotopic purity as determined by ^1H-NMR spectroscopy. To an etheral suspension of copper(II) acetylacetonate (2.0 g.) and PPh_3-d_6 (4.0 g.), 4 ml of dimethylaluminum monoethoxide was added slowly at −40 °C. The light yellow complex $CH_3Cu(PPh_3\text{-}d_6)_2$-(diethyl ether)$_{0.5}$ precipitated after sufficient reaction time at −10 °C was separated by filtation, washed with dry ether and then dried *in vacuo*. From toluene-d_8 (isotopic purity, 98.8%) solution containing $CH_3Cu(PPh_3\text{-}d_6)_2$(diethyl ether)$_{0.5}$ (3.0 g) and PPh_3-d_6 (1.0 g), yellow crystals of $CH_3Cu(PPh_3\text{-}d_6)_3$-(toluene-$d_8$) was isolated.

Kinetic Studies for the Thermal Decomposition of Alkylcopper(I) Complexes. A 20 ml Schlenk tube containing 0.10—0.20 g of the solid alkylcopper(I) complex or a toluene solution (3 ml) of the alkylcopper(I) complex (0.13—0.35 g) and PPh_3 (0—400 mg) was connected to a vacuum line equipped with a mercury manometer and the system was evacuated. The Schlenk tube was placed in a thermostatted bath controlled to ±0.5 °C. The rate constant for the thermal decomposition of the complex was obtained by measuring the volume of the gas evolved with time.

Photolysis of Alkylcopper(I) Complexes. A 10 ml quartz Schlenk tube containing 0.3 g of the alkylcopper(I) complex in the solid state or its solution in 2 ml of toluene-d_8 was irradiated by a 100-Watt Toshiba super high-pressure mercury lamp in a thermostatted aqueous ethylalcohol bath controlled to −30±0.5 °C. The sample tubes were positioned in the region of maximum luminosity. Evolved gas was collected with a Toepler pump and analyzed by mass spectrometry.

The sample in toluene-d_8 solution was immediately decomposed on irradiation turning to dark brown.

References

1) (a) M. C. Baird, *J. Organomet. Chem.*, **64**, 289 (1974), and references cited therein; (b) P. S. Braterman and R. J. Cross, *J. Chem. Soc., Dalton Trans.*, **1972**, 657; *Chem. Soc. Rev.*, **12**, 271 (1973); (c) R. R. Schrock and G. W. Parshall, *Chem. Rev.*, **76**, 243 (1976).

2) (a) J. Chatt and B. L. Shaw, *J. Chem. Soc.*, **1959**, 705; (b) *ibid.*, **1960**, 1718.

3) T. Yamamoto, A. Yamamoto, and S. Ikeda, *J. Am. Chem. Soc.*, **93**, 3350 (1971).

4) (a) W. Mowat, A. Shortland, G. Yagupsky, N. J. Hill, and G. Wilkinson, *J. Chem. Soc., Dalton Trans.*, **1972**, 533; (b) G. Yagupsky, C. K. Brown, and G. Wilkinson, *J. Chem. Soc., A*, **1970**, 1392; (c) G. Wilkinson, *Angew. Chem.*, **86**, 651 (1974).

5) (a) G. M. Whitesides, E. R. Stedronsky, C. P. Casey, and S. Filippo, Jr., *J. Am. Chem. Soc.*, **92**, 1426 (1970); (b) G. M. Whitesides, J. F. Gaasch, and E. R. Stedronsky, *ibid.*, **94**, 5258 (1972); (c) C. S. Cundy, B. M. Kingston, and M. F. Lappert, *Adv. Organomet. Chem.*, **37**, 317 (1972); (d) P. J. Davidson, M. F. Lappert, and R. Pearce, *Acc. Chem. Res.*, **7**, 209 (1974) and references cited therein; (e) G. M. Whitesides, E. J. Panek, and E. R. Stedronsky, *J. Am. Chem. Soc.*, **94**, 232 (1972).

6) (a) C. P. Boekel, J. H. Teuben, and H. J. de Liefde Meijer, *J. Organomet. Chem.*, **81**, 371 (1974); (b) C. P. Boekel, J. H. Teuben, and H. J. de Liefde Meijer, *ibid.*, **102**, 161 (1975); (c) J. A. Waters, V. V. Vickroy, and G. A. Mortimer, *ibid.*, **33**, 41 (1971); (d) D. L. Reger and E. C. Culbertson, *J. Am. Chem. Soc.*, **98**, 2789 (1976); (e) M. P. Brown, R. J. Puddephatt, and C. E. E. Upton, *J. Chem. Soc., Dalton Trans.*, **1974**, 2457; (f) T. J. Marks and W. A. Wachter,

J. Am. Chem. Soc., **98**, 703 (1976).
7) (a) M. Tamura and J. Kochi, *J. Am. Chem. Soc.*, **93**, 1485 (1971), *J. Organomet. Chem.*, **42**, 205 (1972); (b) K. Wada, M. Tamura, and J. Kochi, *J. Am. Chem. Soc.*, **92**, 6656 (1970).
8) T. Yamamoto and A. Yamamoto, *J. Organomet. Chem.*, **57**, 127 (1973).
9) A. Yamamoto, K. Kato, and S. Ikeda, *J. Organomet. Chem.*, **60**, 139 (1973).
10) (a) A. Yamamoto, A. Miyashita, T. Yamamoto, and S. Ikeda, *Bull. Chem. Soc. Jpn.*, **45**, 1583 (1972); (b) T. Ikariya and A. Yamamoto, *J. Organomet. Chem.*, **72**, 145 (1974); (c) A. Miyashita and A. Yamamoto, *Bull. Chem. Soc. Jpn.*, **50**, 1102 (1977).
11) T. Ikariya and A. Yamamoto, *J. Chem. Soc. Chem. Commun.*, **1974**, 720; T. Ikariya and A. Yamamoto, *J. Organomet. Chem.*, **118**, 65 (1976).
12) (a) K. Nishimura, H. Kuribayashi, A. Yamamoto, and S. Ikeda, *J. Organomet. Chem.*, **37**, 317 (1972); (b) A. Yamamoto, Y. Kano, and T. Yamamoto, *ibid.*, **102**, 57 (1975).
13) G. M. Whitesides, J. S. Filippo, Jr., E. R. Stredronsky, and C. P. Casey, *J. Am. Chem. Soc.*, **91**, 6542 (1969).
14) A. Yamamoto and T. Yamamoto, *Bull. Chem. Soc. Jpn.*, **49**, 1403 (1976).
15) (a) T. Yamamoto, A. Yamamoto, and S. Ikeda, *Bull. Chem. Soc. Jpn.*, **45**, 1104 (1972); (b) T. Ikariya and A. Yamamoto, *J. Organomet. Chem.*, **120**, 257 (1976).
16) R. W. Taft, Jr., *J. Am. Chem. Soc.*, **75**, 4231 (1953).
17) (a) F. M. Page, Symp. Combust. 8th. Pasadena, Calif. p. 160 (1960); (b) "Kagaku Binran," Basic II, p. 1132, Maruzen, Tokyo (1966).
18) H. Bürger and H. -J. Neese, *J. Organomet. Chem.*, **21**, 371 (1974).
19) H. De Vries, *Recl. Trav. Chim. Pays-Bas*, **80**, 866 (1961).
20) (a) R. R. Schrock, *J. Am. Chem. Soc.*, **96**, 6796 (1974); (b) *ibid.*, **97**, 6577 (1975); (c) L. J. Guggenberger and R. R. Schrock, *ibid.*, **97**, 6578 (1975).
21) S. Komiya and A. Yamamoto, *J. Organomet. Chem.*, **87**, 333 (1975).

Oxidative Addition of α-Bromo Esters to Tetrakis(isocyanide) Rhodium(I) Complexes. Evidence for a Chain Mechanism

Sei Otsuka and Kikuo Ataka

Department of Chemistry, Faculty of Engineering Science, Osaka University, Toyonaka, Osaka 560

(Received November 15, 1976)

The oxidative additions of chiral alkyl halides, (*S*)-(−)-ethyl α-bromopropionate $[\alpha]_D$ −18.9° (*c* 3.3, $CHCl_3$) and (*S*)-(+)-ethyl α-phenylbromoacetate $[\alpha]_D$ +56.4° (*c* 1.6, C_2H_5OH) to $[Rh(R'NC)_4]^+$ (R′=*t*-Bu, *p*-$CH_3C_6H_4$) produced the corresponding adducts, *trans*-$[RhBr(R)(R'NC)_4]^+$ (R=CH_3CHCO_2Et, $PhCHCO_2Et$), which were well characterized by elemental analysis, IR and ^1H NMR spectra. These adducts were found optically inactive, a fact which precludes a concerted mechanism. The reaction of $C_6H_5CHBrCO_2C_2H_5$ with $[Rh(t\text{-}BuNC)_4]^+$ commenced immediately in the absence of light. Taking this system as a typical example, the rate was studied by the stopped-flow method to find a rate equation, $R=k[Rh(I)]^2[RX]$. The relative rate of addition of *p*-$XC_6H_4CHBrCO_2C_2H_5$ to $[Rh(t\text{-}BuNC)_4]^+$ decreases in an order of Cl>H>CH_3 for X. The addition of $C_6H_5CHBrCO_2C_2H_5$ to $[Rh(p\text{-}CH_3C_6H_4NC)_4]^+$ in the dark proceeds only slowly, but rapidly under a low energy photo-irradiation (440 nm) with a large quantum yield (Φ 4.8). The addition of $CH_3CHBrCO_2C_2H_5$ requires photo-initiation. The optical activity of (*S*)-(−)-$CH_3CHBrCO_2C_2H_5$ was completely lost before the oxidative addition commenced. The rate of decrease in optical activity of the system (*S*)-(−)-$C_6H_5CHBrCO_2C_2H_5$ /$[Rh(t\text{-}BuNC)_4]^+$ exhibited approximate second order kinetic behavior, and quantitative racemization took place prior to the completion of the oxidative addition. A chain mechanism appears to be consistent with all these results. Alternate mechanisms are also discussed in the light of the present results.

So called oxidative additions have received widespread interest in recent years from the stand point of their novelty as a new class of transition metal reactions and of their significance in homogeneous catalytic reactions.[1] A number of papers have reported mechanistic studies on the alkyl halide addition reaction yielding divergent conclusions. Halpern's group[2] and others[3,4] proposed a linear dipolar transition state $M^+\cdots R\cdots X^-$ similar to that involved in the Menschutkin reaction. Ugo[5] *et al.* have invented a somewhat sophisticated version of a multi-center mechanism, *i.e.* a non-concerted polar three center S_N2 attack. In contrast to these views is the radical mechanism proposed by Osborn.[6–9] Lappert's[10] group has detected a radical in the system, MeI/*t*-BuNO/Pt(O). Recently Stille[11,12] *et al.* reported the stereospecific oxidative addition of chiral C_6H_5CHDCl to Pd(O) complexes. Kinetic studies on the addition of alkyl halides to Ir(I)[5,13,14] or Rh(I)[15–17] complexes gave a general impression in favor of the polar mechanism. Doubtless the mechanisms will depend on the electronic and steric characteristics of reactants involved and also on the nature of solvent.

The stereochemical course of addition should be related to the structure of the transition state and to the timing of bond-forming and bond-breaking processes. Our previous study[18] on the addition of an optically active *s*-alkyl bromide, $CH_3CHBrCO_2C_2H_5$ or $C_6H_5CHBrCO_2C_2H_5$, to a strong nucleophile, "$Pd(t\text{-}BuNC)_2$", indicates loss of the stereochemical integrity at the chiral carbon. Pearson *et al.*[19] reported that addition of $CH_3CHBrCO_2C_2H_5$ to Ir(I) was stereospecific, but Osborn[7] *et al.* reexamined this reaction to show that the adduct has no optical activity. We were able to isolate the oxidative adducts from the reaction of two chiral *s*-alkyl halides, (*S*)-(−)-$CH_3CHBrCO_2C_2H_5$ and (*S*)-(+)-$C_6H_5CHBrCO_2C_2H_5$ with $[Rh(R'NC)_4]^+$ (R′=*t*-Bu, *p*-$CH_3C_6H_4$). The adducts, however, showed no optical activity. Various other experimental facts were then collected to elucidate the reaction mechanism. The study has led to a discovery of a dramatic effect of low-energy photo-irradiation in the alkyl halide addition, a fact intelligible in terms of a chain reaction. In this paper we also describe a few other interesting observations consistent with the chain mechanism.

Experimental

IR spectra were measured with a Hitachi-Perkin Elmer 225, UV spectra with a Hitachi EPS-3T, ^1H NMR spectra with a Jeol JNM-4H-100 or JNM-C60-HL, ESR spectra with a JES-ME-2X and optical rotation with a JASCO DIP-SL equipped with an automatic recorder using a 0.5 dm, 5φ mm cell incorporating a three way stop cock allowing measurements to be carried out in an inert atmosphere. Solvents were dried and distilled under nitrogen. All reactions and manipulations were carried out under a pure nitrogen atmosphere.

Preparation of Starting Materials. "$Pd(t\text{-}BuNC)_2$",[20] $[Rh(t\text{-}BuNC)_4]BPh_4$[21] and $[Rh(p\text{-}CH_3C_6H_4NC)_4]BPh_4$[21] were prepared by known methods. (*S*)-(−)-Ethyl α-bromopropionate, $[\alpha]_D$ −18.9° (*c* 3.3; $CHCl_3$), was prepared from L-alanin according to the conventional method.[22] The optical purity was estimated to be about 38%. (*S*)-(+)-Ethyl phenylbromoacetate, $[\alpha]$ +56.4° (*c* 1.75; C_2H_5OH), was prepared from (−)-ethyl mandelate by bromination with PBr_3.[23] The rotation was about 70% of the highest literature value.[23] Methyl 1-bromo-2,2-diphenylcyclopropanecarboxylate was prepared by the reaction of methyl α-bromoacrylate with diazodiphenylmethane.[24] *d*-3-*endo*-Bromocamphor was a commercial product of which stereochemical purity was found by ^1H NMR to be 95%. *d*-3-*endo*-Iodocamphor was prepared by known method from *d*-3-*endo*-bromocamphor.[25]

Kinetic Experiments. The initial rates were measured in CH_2Cl_2 with a stopped-flow spectrophotometer (Union RA-1100) by following the intensity of the 440 nm absorption band (ε=358) of $[Rh(t\text{-}BuNC)_4]^+$ at 25±0.5 °C.

The initial concentration of $C_6H_5CHBrCO_2C_2H_5$ being kept at 0.16 M, the concentration of $[Rh(t\text{-}BuNC)_4]^+$ was varied over a range of $3.2—11\times10^{-3}$ M. Similarly, with an initial concentration of 0.16×10^{-2} M for $[Rh(t\text{-}BuNC)_4]^+$,

the concentration of $C_6H_5CHBrCO_2C_2H_5$ was varied from 7.8×10^{-2} M to 2.7×10^{-1} M. Generally a short induction period (3—20 s) was observed. It was found in case of the addition of $CH_3CHBrCO_2C_2H_5$ to $[Rh(t\text{-BuNC})_4]^+$ that the light (440 nm) used to monitor the reaction initiates the addition with some induction periods. After the commencement of the reaction, the spectrum showed a diffusion controlled process preventing determination of the kinetic orders (see Text).

The rates of decrease in optical rotation during slow addition of α-bromoesters were followed by the polarimetric measurement of the $[\alpha]_D$ values. A dichloromethane solution of a mixture of $[Rh(t\text{-BuNC})_4]^+$ and the α-bromoesters was prepared and an aliquot was immediately transferred to the cell. The rotation was measure at 20 °C using the following two solutions; one containing 1.9×10^{-2} M of $[Rh(t\text{-BuNC})_4]^+$ plus 2.0×10^{-2} M of $C_6H_5CHBrCO_2C_2H_5$ and other containing 0.10 M of $[Rh(t\text{-BuNC})_4]^+$ plus 0.98 M of $CH_3CHBrCO_2C_2H_5$. The initial rates could not be measured accurately because a few minutes were required to secure a stable response on the polarimeters.

Addition of (S)-(−)-*Ethyl α-Bromopropionate to* $[Rh(t\text{-}BuNC)_4]BPh_4$. (*S*)-(−)-Ethyl α-bromopropionate (44 mg, 0.22 mmol) was added to a solution of $[Rh(t\text{-BuNC})_4]BPh_4$ (150 mg, 0.2 mmol) in 2 ml of CH_2Cl_2 at room temperature. When the reaction mixture was stirred under diffused sun light, the yellow color rapidly (within a few min) faded yielding a colorless solution. After stirring was continued for 2 h, the mixture was concentrated. Treatment of the concentrate with a few ml of hexane allowed isolation of *trans*-$[RhBr(CH_3CHCO_2C_2H_5)(t\text{-BuNC})_4]BPh_4$ (**1**), as colorless powder (130 mg, 70%), which showed no optical activity in $CHCl_3$ at 24°. Recrystallization from methanol gave an analytically pure sample, mp 110—111° dec. The mother liquor from the above concentrate contains approximately equimolar amounts of ethyl acrylate and ethyl propionate as detected by GLC.

Addition of (S)-(+)-*Ethyl Bromophenylacetate to* $[Rh(t\text{-}BuNC)_4]BPh_4$. To a suspension of $[Rh(t\text{-BuNC})_4]BPh_4$ (160 mg, 0.21 mmol) in ethanol (5 ml) was added (*S*)-(+)-ethyl phenylbromoacetate (60 mg, 0.25 mmol) at room temperature. The reaction appears to occur immediately even in dark. After stirring for a few hours, the reaction mixture yielded the adduct, *trans*-$[RhBr(PhCHCO_2C_2H_5)(t\text{-BuNC})_4]BPh_4$ (**2**) as a pale yellow precipitate (190 mg, 90%) which was separated, washed with hexane, and dried *in vacuo*. The optical activity was totally lost. Recrystallization from methanol gave an analytically pure sample, mp 118—119° dec.

Addition of (S)-(−)-*Ethyl α-Bromopropionate to* $[Rh(p\text{-}CH_3C_6H_4NC)_4]BPh_4$. Similar to the above, reaction of $[Rh(p\text{-}CH_3C_6H_4NC)_4]BPh_4$ (251 mg, 0.28 mmol) with an excess of ethyl α-bromopropionate (0.21 ml, 1.6 mmol) was carried out under irradiation of tungsten lamp (500 W) in CH_2Cl_2 solution at room temperature for 2 h. The product obtained was optically inactive *trans*-$[RhBr(CH_3CHCO_2C_2H_5)(p\text{-}CH_3C_6H_4NC)_4]BPh_4$ (**3**), colorless crystals, recrystallized from a methanol-ethanol system, mp 140—145° dec (115 mg, 36% yield). The reaction does not take place in the absence of light.

Addition of (S)-(−)-*Ethyl Phenylbromoacetate to* $[Rh(p\text{-}CH_3C_6H_4NC)_4]BPh_4$. The reaction of $[Rh(p\text{-}CH_3C_6H_4NC)_4]BPh_4$ (144 mg, 0.16 mmol) with ethyl phenylbromoacetate (150 mg, 0.6 mmol) in CH_2Cl_2 occurs rapidly under irradiation with decoloration producing the adduct, *trans*-$[RhBr(C_6H_5CHCO_2C_2H_5)(p\text{-}CH_3C_6H_4NC)_4]BPh_4$. (**4**), as pale yellow crystals, recrystallized from ethanol (80 mg, 45% yield).

Reaction of d-*3*-endo-*Bromocamphor with "Pd*(t-*BuNC)*$_2$*"*. To a suspension of "$Pd(t\text{-BuNC})_2$" (530 mg, 1.9 mmol) in ether (40 ml) was added at −70 °C *d*-*3*-*endo*-bromocamphor (460 mg, 2 mmol). The temperature was allowed to rise to 0 °C and stirring was continued for 4 h at 0 °C to give a slurry. The slurry was filtered and the solid was washed with cold ether (50 ml). The combined ether solution was concentrated to give ,on cooling to −20°, an adduct as almost colorless crystals (520 mg, 53%), mp. 114° (dec). ^1H NMH ($CDCl_3$): a double doublet peak at τ 6.5 (M–CH).

Found: C, 46.6; H, 6.50; N, 5.64%. Calcd for $C_{20}H_{25}N_2OBrPd$: C, 47.7; H, 6.60; N, 5.56%.

Rection of d-*3*-endo-*Iodocamphor with* $[Rh(p\text{-}CH_3C_6H_4NC)_4]BPh_4$. A mixture of the Rh(I) compound (670 mg, 0.75 mmol) and iodocamphor (230 mg, 0.75 mmol) in ethanol–dichloromethane (2 : 1, 10 ml) was stirred overnight to give a yellow brown slurry. Filtration gave the adduct as pale yellow crystals (430 mg, 49%) mp 140—143° (dec).

Found: C, 67.7; H, 5.38; N, 4.71%. Calcd for $C_{66}H_{63}N_4BIORh$: C, 67.8; H, 5.43; N, 4.79%.

Quantum yield for the Reaction of $[Rh(p\text{-}CH_3C_6H_5NC)_4]BPh_4$ *with* $C_6H_5CHBrCO_2C_2H_5$. Noyes's method was essentially followed.[26] The photo-reaction was carried out using the following optical system; a 150 W Xenon lamp, a slit, a lens for paralleling the beam, a filter cutting off ultraviolet light shorter than 350 nm, and a square window of *ca.* 2 cm^2. Two 1 cm quartz cells, one for the reaction mixture and another for the actiometer, were placed so as to successively receive the incident light. A mixture of 40 ml of $K_3[Fe(C_2O_4)_3]$ (5.2×10^{-2} M) in 1/2 M sulfuric acid and 10 ml of a buffer solution containing acetic acid (1 M) and sodium acetate (1 M) was used as the actinometer solution.[27] The quantity of Fe^{2+} ion formed by irradiation was measured colorimetrically as the 1,10-phenanthroline complex (λ_{max} 510 nm). Irradiating the solution containing $[Rh(p\text{-}CH_3C_6H_4NC)_4]BPh_4$ (1.8×10^{-3} M) and $C_6H_5CHBrCO_2C_2H_5$ (1.1×10^{-2} M) in dichloromethane for 180 s, the concentration of the unreacted Rh(I) complex was determined by measuring the absorption at 462 nm. Correction was made by measuring the difference in concentration of the Rh(I) complex between the irradiated sample and the unirradiated one as the blank. The quantum yield (Φ) was calculated by the equation, $\Phi=A/I\cdot F$, where A is the number of the Rh(III) molecules formed by the photo-reaction, I the number of photons entering the reaction cell, and F the fraction of photons absorbed by the reaction mixture.[26]

Spin Trap Experiment. ESR samples, *e.g.*, a mixture of $[Rh(t\text{-BuNC})_4]BPh_4$, RBr (R=$C_6H_5CHCO_2C_2H_5$, $CH_3CHCO_2C_2H_5$) and *t*-BuNO in CH_2Cl_2, was prepared in a 50 ml flask in the dark under pure nitrogen. The solutions ($1.3—1.5\times10^{-3}$ M for each component) were transferred to the 2 mm ESR tubes by syringe, and the measurement was carried out for a temperature range 77—300 K.

ESR Measurement. A sample solution was prepared by mixing two dichloromethane solutions of $[Rh(p\text{-}CH_3C_6H_4NC)_4]BPh_4$ (1.1×10^{-2} M) and $C_6H_5CHBrCO_2C_2H_5$ (4.4×10^{-2} M) of equal volume at room temperature. After standing for a few minutes under diffuse sunlight, the mixture was chilled to 195 K. ESR measurements (X band) were carried out at 77, 200, 240 K, and room temperature. Signals were difficult to detect at 77 K. Broad signals of weak intensities centered at $g=2.14$ were observed above 200 K, the hyperfine structure being unresolved.

Results

Product Characterization. The reaction of the cationic square planar complexes $[Rh(R'NC)_4]^+$(R′=

Table 1. Properties and analytical data of $[RhBr(R)L_4]BPh_4$

	Compound	Color	Mp °C[a]	Found %				Calcd %			
				C	H	N	Br	C	H	N	Br
1	$[RhBr(CH_3CHCO_2C_2H_5)(t\text{-BuNC})_4]BPh_4$	colorless	110—111	62.60	7.01	6.08	8.32	62.89	7.00	5.99	8.31
2	$[RhBr(C_6H_5CHCO_2C_2H_5)(t\text{-BuNC})_4]BPh_4$	colorless	118—119	65.03	6.83	5.64	8.33	65.00	6.77	5.62	8.01
3	$[RhBr(CH_3CHCO_2C_2H_5)(p\text{-}CH_3C_6H_4NC)_4]BPh_4$[b]	pale yellow	140—145	66.85	5.31	5.11	—	66.20	5.24	5.02	—
4	$[RhBr(C_6H_5CHCO_2C_2H_5)(p\text{-}CH_3C_6H_4NC)_4]BPh_4$	pale yellow	120	70.25	5.16	5.00	7.65	69.91	5.24	4.94	7.05

a) All compounds decompose without melting at the temperature. b) Containing crystallization solvent (1/2 CH_2Cl_2).

Table 2. Spectral data of $[RhBr(R)L_4]BPh_4$

Compound	IR, cm^{-1} [a]		NMR, τ[b]				
	$\nu_{N\equiv C}$	$\nu_{C=O}$	*t*-Bu,	$CH_3C_6H_4$,	M-CH,	CH_3-CH	$^2J_{Rh-H}$, Hz
1	2240	1710	8.45(s)		5.7(m)	8.60(d)	c)
2	2210	1715	8.55(s)		5.68(d)		3.0
3	2220	1703		7.60(s)	5.90(q,d)	8.39(d)[d]	2.7
4	2220	1713		7.59(s)	5.05(d)		2.8

a) Measured in Nujol mull. b) Measured in $CDCl_3$. TMS as internal reference. Multiplicity is indicated in parentheses. c) Not fully resolved. d) This CH_3 peak appears as doublet-doublet pattern presumably due to $^3J_{Rh-H} \approx 1.5$ Hz.

t-Bu, *p*-$CH_3C_6H_4$) with $CH_3CHBrCO_2C_2H_5$ or C_6H_5-$CHBrCO_2C_2H_5$ in CH_2Cl_2 produces the corresponding thermally unstable adducts, *trans*-$[RhBr(CHR''CO_2C_2H_5)(R'NC)_4]^+$($R''=CH_3$, C_6H_5) as characterized by the elemental analysis, and IR and ^1H NMR spectra (Tables 1, 2). The *trans* geometry is deduced from the IR spectra which contain only one N≡C stretching absorption. Consistently the ^1H NMR spectra show one singlet signal for the *t*-butyl or *p*-methyl protons of the four isocyanide ligands. The NC stretching

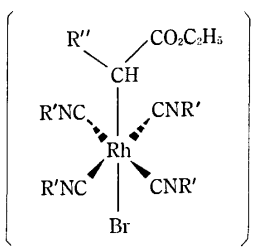

1 $R'=t$-Bu, $R''=CH_3$
2 $R'=t$-Bu, $R''=C_6H_5$
3 $R'=p$-$CH_3C_6H_4$, $R''=CH_3$
4 $R'=p$-$CH_3C_6H_4$, $R''=C_6H_5$

frequencies of the adducts **1**—**4** are higher than those of the corresponding starting complex $[Rh(t\text{-BuNC})_4]^+$ (2170 cm^{-1}) or $[Rh(p\text{-}CH_3C_6H_4NC)_4]^+$ (2190 cm^{-1}) reflecting the oxidation state, Rh(III). The CO stretching vibration of the carboxylate group in the adducts shifts to the lower frequency region compared to that of free ester (1740 cm^{-1} for $CH_3CHBrCO_2C_2H_5$ or 1750 cm^{-1} for $C_6H_5CHBrCO_2C_2H_5$). Thermal decomposition of **1** or **3** takes place at 80 °C during a few hours yielding ethyl propionate and ethyl acryate indicating *β*-hydrogen elimination. The optical rotation of adducts **1**—**4**, measured immediately after the solution make-up below 20 °C, was still zero.

Methyl 1-bromo-2, 2-diphenylcyclopropanecarboxylate does not react with $[Rh(t\text{-BuNC})_4]^+$ or with a stronger nucleophile, "$Pd(t\text{-BuNC})_2$". Other halocycloalkanes, *e. g.* 3-*endo*-halocamphor, react with the low valent metal complexes. Thus, *d*-3-*endo*-bromocamphor reacts with "$Pd(t\text{-BuNC})_2$" to give an adduct [PdBr-(η^1-3-camphor)(t-BuNC)$_2$] which retains the *endo* form. The conformation can be readily established by the ^1H NMR of the methine signal at the 3-position which shows a double doublet pattern ($^3J_{HH}=4$ Hz, $^4J_{HH}=1.3$ Hz). It has been established[28] that the *exo* proton at the 3-position couples with the methine proton at the 4-position and the *exo* proton at the 5-position, but the *endo* proton does not couple with the proton at the 4-position, because of the bond angle of nearly 90 °C. $[Rh(t\text{-BuNC})_4]^+$ reacts with 3-*endo*-iodocamphor at ambient temperature to give an adduct whose conformation could not be determined from the key ^1H NMR signal due to the complexity induced by the coupling with ^{103}Rh. Interestingly, it fails to react with 3-*endo*-bromocampher under diffused light. *erythro*-1-Bromo-3,3-dimethyl-1,2-didueteriobutane does not react with $[Rh(t\text{-BuNC})_4]^+$ or "$Pd(t\text{-BuNC})_2$".

Photochemical Effects. Unexpectedly, the addition reaction of $CH_3CHBrCO_2C_2H_5$ to $[Rh(RNC)_4]^+$ ($R'=$ *t*-Bu, *p*-$CH_3C_6H_4$) does not take place in the absence of light, as indicated by the IR NC stretching absorption which shows no change over a day or two at room temperature, reflecting the retention of the oxidation state Rh(I). There is, however, some indication in the ^1H NMR spectrum for complexation of the bromo ester as will be described later. On exposure to light the addition occurred with an induction period ranging from a few minutes to half an hour, depending on the intensity of light. Remarkably, this irradiation effect was observed even with a low-energy light beam

(440 nm) used for monitoring the concentration of the species $[Rh(t\text{-BuNC})_4]^+$. Generally, the induction period is followed by a very rapid addition reaction which prevents an accurate kinetic measurement and intelligible analysis. A photo-initiation was required for the reaction of $[Rh(p\text{-}CH_3C_6H_4NC)_4]BPh_4$ with both of the α-bromo esters; under irradiation with a 500 W tungsten lamp the reaction of $C_6H_5CHBrCO_2C_2H_5$ is complete within a few minutes and that of $CH_3CHBrCO_2C_2H_5$ within one hour. The quantum yield of the photo-reaction of the former system was estimated to be 4.8, implying a chain mechanism. Since the addition of $CH_3CHBrCO_2C_2H_5$ to $[Rh(R'\text{-}NC)_4]BPh_4$ ($R'=t$-Bu, p-$CH_3C_6H_4$) exhibits an induction period even under photo-irradiation, it was impossible to obtain the quantum yield.

Mechanistic Features. The reaction of $C_6H_5CHBrCO_2C_2H_5$ with $[Rh(t\text{-BuNC})_4]^+$ does not require photo-initiation. However, the oxidative addition shows an induction period ranging from a few seconds to half a minute depending on the concentration of substrates. The intensity of the absorption at 440 nm of the reaction mixture increased slightly during the induction period. After the induction period, the rate was found, by differential analysis, to be first order with respect to the alkyl halide, while it approximated an order of 1.5 with respect to Rh(I). Integral analyses of a few typical runs using a large excess of the alkyl halide (*e. g.* $[Rh(I)]=1.6\times10^{-2}$ M, $[RBr]=0.22$ M) revealed pseudo second-order dependence on [Rh(I)]. Thus the overall rate roughly follows the following rate equation:

$$R = k[Rh(I)]^2[RX].$$

Perhaps the accuracy of the differential analysis suffers from the occurrence of the induction period. Addition of 1—3 mol of free *t*-BuNC to system RX/$[Rh(t\text{-BuNC})_4]^+$ does not affect the rate appreciably.

The relative rate of addition of p-$XC_6H_4CHBrCO_2C_2H_5$ to $[Rh(t\text{-BuNC})_4]^+$ was measured at 20 °C. The rate decrease in a sequence of Cl>H>CH_3 for X, *i.e.*, t 1/2 (min) at 20 °C: Cl, 2.8; H, 6.0; CH_3, 9.6, a trend suggestive of nucleophilic character of the metal species. The relative rate, however, deviates from the Hammett plots. In contrast to $C_6H_5CHBrCO_2C_2H_5$ the oxidative addition of the corresponding chloride does not occur.

Attempting to study solvent effect, we found that the addition of $C_6H_5CHBrCO_2C_2H_5$ to $[Rh(t\text{-BuNC})_4]^+$ in acetone and CH_3CN also exhibits a complex kinetic feature thus preventing a reasonable analysis. Qualitatively the reaction rate does not vary appreciably among the solvents, acetone, CH_3CN, and CH_2Cl_2. A peculiar phenomenon was observed for the reaction in acetone; the time-conversion curve obtained by recording the intensity of the absorption at 440 nm on an ordinary spectrometer exhibited oscillations of small amplitudes suggesting a diffusion-controlled process. In addition to the 440 nm absorption the acetone solution shows two absorption maxima at 524 ($\varepsilon=692$) and 670 nm ($\varepsilon=365$) and the acetonitrile solution one maximum at 566 nm ($\varepsilon=1420$), indicating strong solvation in both solvents.

The rates of decrease in optical activity of the alkyl halide upon interaction with metal nucleophiles deserve investigation. The decrease in optical rotation of the system $C_6H_5CHBrCO_2C_2H_5/[Rh(t\text{-BuNC})_4]^+$ was fairly fast at 20 °C in CH_2Cl_2. Apart from the initial peroid (2—3 min), we were able to follow the polarimetric rate for a certain limited initial concentration (1.0×10^{-2}M), and found approximate second order kinetics with a rate constant, k_2, of 0.6 $M^{-1}s^{-1}$. As the addition of $CH_3CHBrCO_2C_2H_5$ to $[Rh(t\text{-BuNC})_4]^+$ takes place neither in the dark nor under irradiation of Na-D light beam (589 nm), the rate of optical loss can be followed by the polarimeter in the absence of concurrent oxidative addition. Surprisingly, the optical activity of a mixture of $CH_3CHBrCO_2C_2H_5$ (4.4×10^{-2} M) and $[Rh(t\text{-BuNC})_4]^+$ (0.92×10^{-2} M) decreases rapidly even in the dark. The initial rate could not be measured accurately because of the experimental difficulty due to the low $[\alpha]_D$ value of the bromo ester and to the strong color of $[Rh(t\text{-BuNC})_4]^+$, which prevents use of high concentrations. The rotation of a mixture containing 4.4×10^{-2} M of $CH_3CHBrCO_2C_2H_5$ and 0.92×10^{-2} M of $[Rh(t\text{-BuNC})_4]^+$ in CH_2Cl_2 kept at 20 °C decreased after 2 hr from a calculated value of 0.167 to 0.116° which corresponds to a value of a solution containing 3.4×10^{-2} M of the chiral propinate. Hence the amount (1.0×10^{-2} M) of the propionate which has lost the chirality is quite close to that (0.93×10^{-2} M) of $[Rh(t\text{-BuNC})_4]^+$ initially present in the system. Beyond this stoichiometric point, the rate of decrease in optical rotation became extremely slow. The starting complex, $[Rh(t\text{-BuNC})_4]^+$ was recovered almost completely from the sample solution upon precipitation by adding ethanol. The racemization of chiral $CH_3CHBrCO_2C_2H_5$ in the presence of $[Rh(t\text{-BuNC})_4]^+$ in methanol, which is faster than in CH_2Cl_2, was completed within a few hours at 80 °C. In the absence of the metal complex no racemization took place under the comparable conditions. The rate of decrease in optical rotation of the system $C_6H_5CHBrCO_2C_2H_5/[Rh(t\text{-BuNC})_4]^+$ was faster than the system $CH_3CHBrCO_2C_2H_5/[Rh(t\text{-BuNC})_4]^+$, and the rapid rate prevented accurate measurements.

Since the racemization suggests a possibility of complexation of the bromo esters to the metal, the IR and ^1H NMR spectra were examined. Electronic absorption spectroscopy cannot be employed here, as light of wavelength shorter than 440 nm initiates the addition reactions. An equimolar mixture of $CH_3CHBrCO_2C_2H_5$ and $[Rh(t\text{-BuNC})_4]^+$ in CH_2Cl_2 shows a slight bathochromic shift (10 cm^{-1}) in the IR CO stretching band as compared to the free bromoester. The sharp single absorption of NC stretching remains unchanged. The free bromo ester exhibits six peaks (1 : 2 : 4 : 5 : 4 : 2) for the methine and methylene protons derived from overlap of two quartet signals ($^3J_{HH}=6.2$ Hz). The equimolar mixture of the bromo ester and $[Rh(t\text{-BuNC})_4]^+$ in $CDCl_3$ gives a complex pattern for the protons, in which at least fourteen peaks are discernible. Although the complete assignment was impossible, these spectral data point to the presence of the complexed bromo ester. This is consistent with the slight intensity increase at 440 nm observed during

the induction period.

An ESR measurement was carried out during the oxidative addition of the bromo ester to $[Rh(t\text{-BuNC})_4]^+$, using *t*-BuNO as a spin trap as applied to a system of $CH_3I/Pt(PPh_3)_3$.[10] The ESR signals of a radical, *t*-Bu(R)NO·(R=$CH_3CHCO_2C_2H_5$, $C_6H_5CHCO_2C_2H_5$) were observed as three doublets with hyperfine coupling constants (Gauss): $A_0(N)=14.5$, $A_0(H)=3.0$ for R=$CH_3CHCO_2C_2H_5$; $A_0(N)=15.5$, $A_0(H)=4.5$ for R=$C_6H_5CHCO_2C_2H_5$. The ESR signals were more intense in the case of bromo phenylacetate than that of the bromo propionate. An irradiation of a few minutes duration of both systems with a low pressure mercury lamp does not cause any essential change in the ESR signals. The ESR signals was observed for system $[RhBr(C_6H_5CHCO_2C_2H_5)(t\text{-BuNC})_4]^+/t$-BuNO, but not for the alkyl halides/*t*-BuNO or $[Rh(t\text{-BuNC})_4]^+/t$-BuNO system.

A radical scavenger, duroquinone, was not effective in inhibiting the reaction. Because of the facile reaction of reactive radical scavengers like galvinoxyl with Rh(I) species itself, the use as a diagnostic probe was not attempted.

Discussion

Here we focus our discussion on the mechanism of the oxidative addition of *s*-alkyl halides, α-bromo esters, to $[Rh(R'NC)_4]^+$(R'=*t*-Bu, *p*-$CH_3C_6H_4$). Other alkyl halides were also studied as the substrate and "$Pd(t\text{-BuNC})_2$" was used as the acceptor to argue the above results. The oxidative addition of RX to $[Rh(t\text{-BuNC})_4]^+$, producing *trans*-octahedral Rh(III) complexes **1**—**4**, may be viewed as a substitution reaction at the saturated carbon atom. Any proposal on the mechanism must accommodate various experimental observation: (i) the *trans* geometry of the Rh(III) complexes formed, (ii) the absence of the dihalide complex, alkene, and alkane in the products, (iii) the effect of leaving group X, (iv) the electronic effect and structural effect of the alkyl moiety, (v) the racemization of the chiral bromoesters prior to the oxidative addition, (vi) the observed kinetic behaviors involving an induction period, (vii) the low-energy photoinitiation and the large quantum yield, and (viii) the results of spin-trap experiments. These results, *inter alia* vi and vii strongly suggest a chain mechanism. While non-radical chain mechanisms cannot be excluded conclusively we favor a radical chain as will be discussed later.

The following simple scheme is sufficient to describe the radical chain reaction ($[Rh(RNC)_4]^+$=M).

Scheme 1.

initiation:

$$M + RX \underset{k_{-1}}{\overset{k_1}{\rightleftharpoons}} M\cdots X\cdots R \quad (1)$$

$$M\cdots X\cdots R \underset{k_{-2}}{\overset{k_2}{\rightleftharpoons}} M\text{—}X + R\cdot \quad (2)$$

chain:

$$M^*\cdots X\cdots R + M\text{-}X \xrightarrow{k_3} M^*\text{-}X + RMX \quad (3)$$

termination:

$$M\text{-}X + R\cdot \xrightarrow{k_t} RMX \quad (4)$$

Note: Star was added to distinguish the metal identity in the product R-M-X from that involved the reagent M-X.

Step (1) is a reversible formation of an intermediate from RX and $[Rh(R'NC)_4]^+$. Although the instability prevents isolation and characterization, the existence in system $CH_3CHBrCO_2C_2H_5/[Rh(t\text{-BuNC})_4]^+$ is supported by the IR, ^1H NMR, and electronic spectra. Three possible modes may be distinguished for the interaction between the alkyl halide and the metal species; a) an essentially linear complex with a metal-carbon interaction, $(R'NC)_4Rh\cdots R\cdots X$, similar to a Menshutkin-type intermediate, b) a three-centered cyclic structure, and c) an essentially linear complex with a metal-halogen interaction, $(R'NC)_4Rh\cdots X\cdots R$.

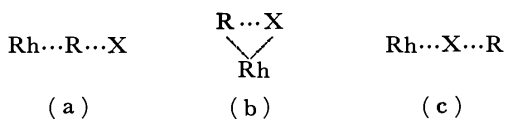

The former, (a), corresponds to a transition state of an S_N2 type attack of the metal species at the alkyl carbon. The *para*-substituent effect on the rate of oxidative addition of *p*-$XC_6H_4CHBrCO_2C_2H_5$ shows the feeble nucleophilic character of $[Rh(R'NC_4]^+$. If the interaction of type (a) leads to the final adduct, then the stereochemical course should be inversion. Although Stille[11,12,29] has observed the inversion of configuration the oxidative addition of PhCHDCl to $Pd(PPh_3)_4$, the racemization observed for the present system renders the transition state structure untenable. The addition of 3-*endo*-iodocamphor, to which an *exo*-attack by a bulky nucleophile is prohibited, would not occur through the S_N2 type complex.

A cyclic intermdieate (b) is evidently incompatible with the observed loss of stereochemical integrity at the carbon atom. Ugo *et al.*[5] proposed a polar asymmetric three center transition state in which the iridium-carbon interaction takes place prior to the carbon-halogen bond breaking. The mechanism alleged would still imply retention of the carbon atom configuration since the incipient metal-alkyl bond formation prohibits configurational change at the carbon atom. Both claims of retention[19] and inversion[30] for an oxidative addition of a chiral *s*-alkyl halide to Ir(I) complexes were found erroneous. The cyclic transition state would lead to stereospecific *cis*-addition of alkyl halides to the metal. The possibility of *cis*-addition in a kinetically-controlled process followed by a rapid isomerization to the *trans*-adduct is unlikely in the present case where even trace of the *cis*-product was not detected. This was confirmed by monitoring the IR NC stretching band region (2200 cm^{-1}) which showed no indication for appearance of absorptions other than the bands due to the starting materials and the *trans*-adduct.

The third intermediate (c) appears to be the most likely species whose incipient formation must be assumed in order to account for the racemization preceding

the addition. Complexation of the corresponding chloride is not detected spectroscopically for the system $C_6H_5CHClCO_2C_2H_5/[Rh(t\text{-}BuNC)_4]^+$, and the system shows neither racemization nor oxidative addition. Thus, the racemization of the chiral α-bromoesters may be associated with step (1) and/or (2). The racemization of (*S*)-(+)-$CH_3CHBrCO_2C_2H_5$ in CH_2Cl_2 became extremely slow after the amount of the racemate reached a stoichiometric amount, equivalent to that of the complex present, while it proceeds catalytically in methanol. Practically, no oxidative addition takes place during the racemization in both solvents. The result in CH_2Cl_2 can then be accounted for by the large formation constant, $K_1=(k_1/k_{-1})$, coupled with a small value of k_2. Thus, the reversible step (1) appears to be responsible for the racemization. This constitutes, in turn, strong evidence for complexation of the *s*-alkyl halides forming (c). The observation of an increase in absorption intensity around 440 nm delineates the formation of an intermediate complex. This intermediate complex, albeit not isolable, must be fairly substitution stable since the catalytic racemization occurs slowly.

A radical or an ionic character could emerge in the alkyl moiety in intermediate, $L_4Rh\cdots X\cdots R$. If the alkyl group is held in the vicinity of the metal through, *e. g.*, a weak interaction of the carbonyl group with metal, the intermediate resembles a radical pair or an ion pair. Some cage reactions of chiral radical pairs have been shown to lead to racemization before diffusing apart with a rate depending on solvents.[31] Thus the observed solvent effect for the racemization does not necessarily imply an ionic intermediate.

The step (2) is the formation of the chain carrier. The failure of $CH_3CHBrCO_2C_2H_5$ to initiate the reaction in the dark and the contrasting smooth initiation of $C_6H_5CHBrCO_2C_2H_5$ reflect the relative ease of the halide abstraction. The primary importance of the C–Br bond cleavage for the initiation is evident. The facile addition of $CH_3CHBrCO_2C_2H_5$ to "Pd-(*t*-Bu)$_2$" in the dark suggests that the nucleophilicity of the metal species affects the initiation. There is no indication for disproportionation or coupling of the radicals. The acrylate and propionate detected in small amounts during isolation of adduct $[Rh(CH_3CHCO_2C_2H_5)(R'NC)_4]^+$ are presumably produced due to the thermal decomposition of the adduct once formed. CIDNP was not observed. The system RX/PtL_3 ($L=P(C_2H_5)_3$) showed CIDNP due to the alkane or alkene derived from diffused encounter of the alkyl radical only when PtX_2L_2 was formed.[9] Consistently the present system does not produce $[RhX_2(RNC)_4]$.$^+$ Spin-trap experiments using *t*-BuNO showed formation of a radical *t*-BuN(R)O. This again does not prove the presence of a free alkyl radical in the reaction mixture, since *t*-BuNO could react with both the alkyl halide complex $(R'NC)_4Rh\cdots X\cdots R$ and the final product, $[(R'NC)_4RhX(R)]$.$^+$

$$(R'NC)_4Rh^+\cdots X\cdots R \text{ or } [(R'NC)_4RhX(R)]^+ + t\text{-BuNO} \longrightarrow [(R'NC)_4Rh^{II}X(R)]^+ + t\text{-BuN(R)O}\cdot \quad (5)$$

The ineffectiveness of radical scavengers, *e.g.* 1,2,4,5-tetramethyl-*p*-benzoquinone, was observed. These results, however, fail to exclude conclusively the formation of organic radicals (in fact, the formation in a small amount is implied in Eq. 2). A mechanism involving short lived radicals or caged radical pairs is perfectly consistent with the available data.

Both possibilities, radical and ionic chains, must then be examined for step (3) which is rate-determining. The relative rates of $[Rh(p\text{-}CH_3C_6H_4NC)_4]^+$ and $[Rh(t\text{-}BuNC)_4]^+$ suggest that the nucleophilicity of the metal species affects the rate-determining step too. Although this trend is in accord with the observed electronic effect for the addition of $p\text{-}XC_6H_4CHBrCO_2C_2H_5$, the chain cannot be described in terms of a simple S_N2 type scheme as is evident from the molecularity of the step and the deviation from the Hammett rule. Since a low-energy photo-exitation of a similar Ir(I) compound is known,[32] let us examine an ionic chain mechanism such as Scheme II, which assumes a dissociative process (Eq. 6) to be photochemically induceable.

Scheme 2.

$$RhL_3^+ \rightleftharpoons RhL_3^+ + L \quad (6)$$

$$RhL_3^+ + RX \longrightarrow \{RhL_3X + R^+\} \rightarrow RhL_3X(R)^+ \quad (7)$$

$$RhL_3X(R)^+ + RhL_4^+ \longrightarrow RhL_4S(R)^+ + RhL_3^+ \quad (8)$$

$$RhL_3X(R)^+ + L \longrightarrow RhL_4X(R)^+ \quad (9)$$

Irradiation effect for the addition or substitution reaction of $[Rh(t\text{-}BuNC)_4]^+$ with neutral ligand such as CO, PR_3 or RNC was examined to find no effect. Further, an addition of free *t*-BuNC (1—3 mol) caused practically no effect on the rate of oxidative addition of the bromo ester to $[Rh(t\text{-}BuNC)_4]^+$.
Thus the dissociative process (Eq. 6) appears not to be important.

Alternative mechanisms involving carbonium ions may be possible. However, participation of carbonium ions in the rate-determining step is incompatible with the observed relative rate, *i. e.*, $C_6H_5CHBrCO_2C_2H_5 > CH_3CHBrCO_2C_2H_5$. Therefore we favor Scheme 1. Experimental tools are not available to kinetically discern the photochemical effect for the addition of $C_6H_5CHBrCO_2C_2H_5$, which occurs rapidly without irradiation. The information, even if available, would not affect our conclusion.

The low-energy of light (440 nm) used for initiating the reaction of $CH_3CHBrCO_2C_2H_5$ is insufficient to cause fission of the RX bond. The photochemical effect can only be expected for the complexed RX, but not for the free RX. The possibility of an alkyl radical as the chain carrier is excluded on the basis of the quantum yield ($\Phi=4.8$ for $C_6H_5CHBrCO_2C_2H_5$). It is most unlikely for a reactive alkyl radical (or carbonium ion) in solution to achieve such a high quantum yield.[33] Tentatively RhL_4X^+ species is assigned as the carrier.

It is rather surprising to find the inability of 1-bromo-2,2-diphenyl-cyclopropanecarboxylate to undergo the oxidative addition to $[Rh(R'NC)_4]$.$^+$ At first sight, this seems to support an ionic, solvolysis mechanism, because the formation of an S_N2-type transition state would be hindered sterically. The steric hindrance,

however, could also be influential for the bimolecular reaction step (3). The observed addition of 3-*endo*-iodo campher to $[Rh(R'NC)_4]^+$ is apparently incompatible with an S_N2-type transition state. The failure of the bromocyclopropane toward the addition may then be accounted for by the high activation energy required for a substituted cyclopropane to form the cyclopropyl radical.[35] The inertness of a primary alkyl bromide, *erythro*-1-bromo-3,3-dimethyl-1,2-dideuteriobutane, to $[Rh(t\text{-}BuNC)_4]^+$ can be accounted for by the steric effect primarily operating in step (3). The steric congestion around the carbon atom carrying the bromine atom is apparently more enhanced in step (3) than in the preceding steps (1)—(2).

The reverse reaction of the initiation constitutes the terimination (4). A similar situation has been found for halogen radical chain reactions.[34] Another termination could be dimerization of the Rh(II) species[36] forming $[RhX(t\text{-}BuNC)_4]_2^{2+}$. The formation, however, could not be detected, a result expected from the high yield of the oxidative addition. The whole sequence may be depicted as shown.

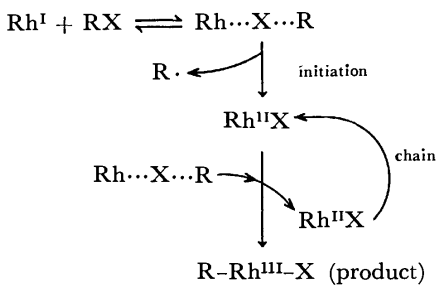

Although the addition of α-bromopropionate showed complicated kinetic features, it seems reasonable to assume a similar radical chain mechanism involving a rate-determining initiation. Once the initiation has started photochemically, the reaction apparently proceeds through the same sequence as for $C_6H_5CHBrCO_2C_2H_5$.

In summary, various facts described above appear to be mostly consistent with a radical chain mechanism. Osborn[9] has suggested such a mechanism for a similar addition reaction to a stronger metal nucleophile PtL_3 without direct experimental evidence. The present results clearly exclude an intermediacy of an alkylrhodium species[37] such as $[Rh^{III}(R)L_4]^{2+}$. We do not claim that this radical chain mechanism is valid for the addition of different types of alkyl halides to the metal system. However, a similar radical mechanism should be valid for the addition of these α-bromo esters to Pd(0) systems which also show complete loss of stereochemical integrity at the carbon atom.[18]

References

1) An extensive review may be found in A. J. Deeming, MTP International Review of Science. Inorganic Chemistry Series on Vol. 9, ed by M. L. Tobe, Butteroworths, London (1972), p. 117.

2) P. B. Chock and J. Halpern, *J. Am. Chem. Soc.*, **88**, 3511 (1966).

3) C. D. Cook and G. S. Jauhal, *Can. J. Chem.*, **45**, 301 (1967).

4) A. J. Deeming and B. L. Shaw, *J. Chem. Soc.*, **1969**, 1128.

5) R. Ugo, A. Pasini, A. Fusi, and S. Cenini, *J. Am. Chem. Soc.*, **94**, 7364 (1972).

6) J. S. Bradley, D. E. Connor, D. Dolphin, J. A. Labinger, and J. A. Osborn, *J. Am. Chem. Soc.*, **94**, 4043 (1972).

7) J. A. Labinger, A. V. Kramer and J. A. Osborn, *J. Am. Chem. Soc.*, **95**, 7098 (1973).

8) A. V. Kramer, J. A. Labinger, J. S. Bradley, and J. A. Osborn, *J. Am. Chem. Soc.*, **96**, 7146 (1974).

9) A. V. Kramer and J. A. Osborn, *J. Am. Chem. Soc.*, **96**, 7832 (1974).

10) M. F. Lappert and P. W. Lednor, *J. C. S. Chem. Commun.*, **1973** 948.

11) K. S. Y. Lau, P. K. Wong, and J. K. Stille, *J. Am. Chem. Soc.*, **98**, 5832 (1976).

12) P. K. Wong, K. S. Lau, and J. K. Stille, *J. Am. Chem. Soc.*, **96**, 5956 (1974).

13) W. Strohmeier and T. Onoda, *Z. Naturforsch*, **236**, 1527 (1968).

14) L. Vaska and M. F. Werneke, *Trans. N. Y. Acad. Sci.*, **33**, 70 (1971).

15) I. C. Douek and G. Wilkinson, *J. Chem. Soc., A*, **1969**, 2604.

16) A. J. H. Davis and W. A. G. Graham, *Inorg. Chem.*, **9**, 2658 (1970).

17) A. J. H. Davis and W. A. G. Graham, *Inorg. Chem.*, **10**, 1653 (1971).

18) S. Otsuka, A. Nakamura, T. Yoshida, M. Naruto, and K. Ataka, *J. Am. Chem. Soc.*, **95**, 3180 (1973).

19) R. G. Pearson and W. R. Muir, *J. Am. Chem. Soc.*, **92**, 5519 (1970).

20) S. Otsuka, A. Nakamura, and Y. Tatsuno, *J. Am. Chem. Soc.*, **91**, 6694 (1969).

21) J. W. Dart, M. K. Lloyd, J. A. McCleverty, and R. Mason, *Chem. Commun.*, **1971**, 1197.

22) O. Warburg, *Ann. Chem.*, **340**, 168 (1905); E. Fisher and K. Raske, *Chem. Ber.*, **39**, 3981 (1906); D. J. Prescott and J. L. Rabinowitz, *J. Biol. Chem.*, **243**, 1551 (1968).

23) W. Gerrad, *J. Chem. Soc.*, **1945**, 848.

24) H. M. Walborsky and F. J. Impastato, *J. Am. Chem. Soc.*, **81**, 5835 (1959).

25) J. W. Grühl, *Ber.*, **37**, 2163 (1904).

26) W. A. Noyes Jr., and V. Boekelheide, "Photochemical Reactions," in "Technique of Organic Chemistry," Vol II, Interscience (1948).

27) C. A. Parker, *Proc. R. Soc., London, Ser. A*, **220**, 104 (1953).

28) J. Meinwald, Y. C. Meinwald, and T. N. Baker, III, *J. Am. Chem. Soc.*, **85**, 2513 (1963).

29) J. K. Stille and K. S. Y. Lau, *J. Am. Chem. Soc.*, **98**, 5841 (1976).

30) J. A. Labinger, R. J. Brams, D. Dolphin, and J. A. Osborn, *J. Chem. Soc., D*, **1970**, 612. The claim has been withdrawn in Ref. 6).

31) J. F. Garst, *J. Am. Chem. Soc.*, **97**, 5062 (1975); references are therein.

32) a) W. M. Bedford and G. Rouschias, *J. Chem. Soc. Chem. Commun.*, **1972**, 1224; b) W. M. Bedford and G. Rouschias, *J. Chem. Soc., Dalton Trans.*, **1974**, 2531.

33) Kh. S. Bagdasaryan, "Theory of Radical-type Polymerization," Moscow, Izdatel. Akad. Nauk, S. S. S. R. (1959), p. 61.

34) M. L. Poutsma, "Free Radicals," Vol II, ed by J. K. Kochi, John Wiley & Sons, New York (1973), p. 159.

35) C. Walling and P. S. Fredrichs, *J. Am. Chem. Soc.*, **84**, 3326 (1962).

36) A. L. Balch, M. M. Olmstead, *J. Am. Chem. Soc.*, **98**, 2355 (1976).

37) P. R. Branson and M. Green, *J. Chem. Soc., Dalton Trans.*, **1972**, 1303.

Enzyme-like Reaction Catalyzed by NAD$^+$–Reduced Keratin Systems

Morio HIRANO and Fujio TAKAHASHI*

Research Laboratory of Resources Utilization, Tokyo Institute of Technology, Ookayama, Meguro-ku, Tokyo 152

**Faculty of Engineering, Utsunomiya University, Ishii-cho, Utsunomiya 321-31*

(Received November 24, 1976)

Reduced keratin, which was obtained by reductive cleavage of human hair, was found to form a 1 : 1 complex with nicotinamide adenine dinucleotide (NAD$^+$). The complex exhibited catalytic activity for the oxidation of glyceraldehyde to form glyceric acid. It was found from the results of pH titration, polarograms and NMR measurements that the NAD$^+$-reduced keratin complex binds to glyceraldehyde to form an intermediate, which is susceptible to oxidation by oxygen. It was concluded from kinetic studies that this catalytic reaction showed a homotropic effect.

In a previous paper, it was reported that reduced keratin (RK) was found to form a 1 : 1 complex with flavin adenine dinucleotide (FAD) and that the complex exhibits catalytic activity for dehydrogenation of succinic acid to form fumaric acid.[1] It was suggested that the FAD–RK complex is formed by the interaction between arginine residues of RK and an adenine moiety and the pyrophosphate linkage of FAD. From this conclusion, it is expected that NAD$^+$, which has a nicotinamide moiety in place of an isoalloxazine moiety of FAD, might form a complex with the RK and act as an enzyme-like catalyst.

It is well known that there are many dehydrogenases in which NAD$^+$ and mercapto group are located in the active center of an enzyme, such as alcohol dehydrogenase, aldehyde dehydrogenase, *etc.*

Since it is expected that the NAD$^+$–RK system possesses catalytic activity like that of an enzyme, various substrates such as ethanol, monosaccharide (glucose, mannose, xylose), methyl mandelate, glyceraldehyde 3-phosphate and glyceraldehyde were examined. The formation of NADH (the reduced form of NAD$^+$) was observed spectrophotometrically when glyceraldehyde was added as a substrate into a solution containing NAD$^+$ and RK. The results of kinetic studies of the catalytic reaction between glyceraldehyde and the NAD$^+$–RK complex will be presented in this paper.

Experimental

Materials. The RK used was prepared by the procedure described in a previous paper.[2] The molecular weight of the RK was 4500 (measured by viscometry). Mercapto group: 0.2 mgeq/g of protein. S content: 2.7%. The glyceraldehyde, NAD$^+$, dichlorophenolindophenol (DCIP), and other chemicals used were of reagent grade or the best commercially available.

Equipment and Measurements. The equilibrium constant and the maximum number of bonds in the NAD$^+$–RK system were determined by the dialysis-equilibrium method[3] as follows: Into a 50-ml Ehrenmyer flask containing 20 ml of 0.2—5.0$\times$10^{-3}M NAD$^+$ in a 0.1 M phosphate buffer (pH 8.0) (or 20 ml of a buffer solutoin as a reference solution without NAD$^+$), a cellulose tube containing 10 ml of 1.0$\times$10^{-4} M RK in a 0.1 M phosphate buffer (pH 8.0) was inserted. The cellulose tube used was made by the Visking Company. The flasks were allowed to stand at 35 °C for 24 h. The NAD$^+$ concentration in the flasks were determined spectrophotometrically after 24 h.

The UV absorption spectra were determined with a Shimadzu spectrophotometer UV-200. The anode polarograms were obtained using a Yanaco platinum rotating-electrode polarograph equipped with a Hokuto Denko LS-1D linear scanning unit, and PS-500B potentiostat and a Toa Electronics SXR-1A X-Y recorder. The NMR spectra were measured with a JEOL JNM-FX60.

Glyceric acid was identified using paper chromatography with a mixture of 1-propanol and concentrated aqueous ammonia (6 : 4) as the developer, and using NMR.

Results

The Formation of the NAD$^+$–RK Complex. The binding number, n, and the concentration of free NAD$^+$, [NAD$^+$], were determined using the method of Klotz *et al.* Plots of $1/n$ *vs.* $1/[\mathrm{NAD}^+]$ are shown in Fig. 1. A straight line was obtained. The values of the equilibrium constant, K, and the maximum number of bonds were calculated from the intercept and the slope of this line to be 1.2×10^3 M^{-1} and 1.3 (35 °C), respectively.

The Reaction Product. RK, NAD$^+$, and glyceraldehyde were dissolved into 100 ml of a 0.02 M phoshpate buffer (pH 8.0) to produce 1.0×10^{-4}, 1.0×10^{-3}, and 1.0×10^{-3} M solutions and the mixtures were allowed to stand at 35 °C. The absorption spectra of the mixtures were measured in the 230—400 nm region 0, 24, 48, and 68 h after perparation. The reference solution contained the same concentrations of RK and glyceraldehyde as the sample solution, except that no NAD$^+$ was present. The results are shown in Fig. 2. The absorption maximum at 340 nm, which was assigned to NADH, was found to increase with the lapse of time.

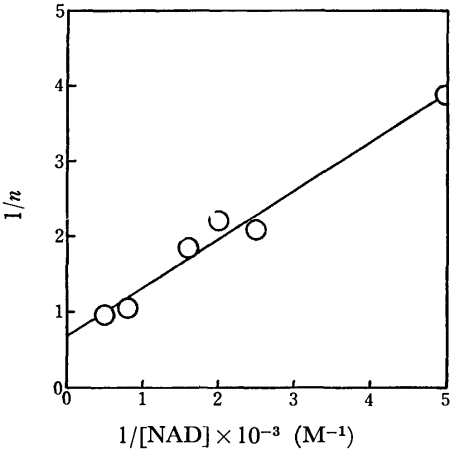

Fig. 1. The $1/n$ - $1/[\mathrm{NAD}]$ plots for the dialysis equilibrium.

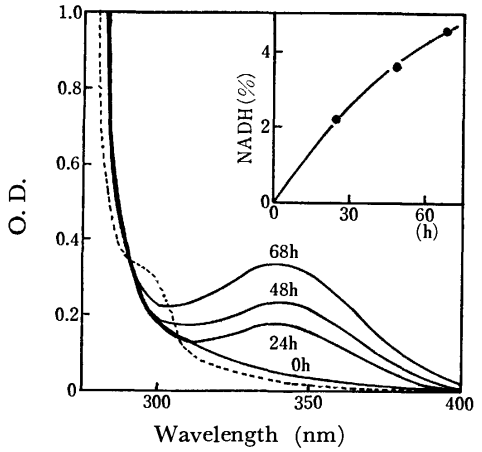

Fig. 2. Absorption spectra.
——: pH 8.0, ----: pH 7.0.

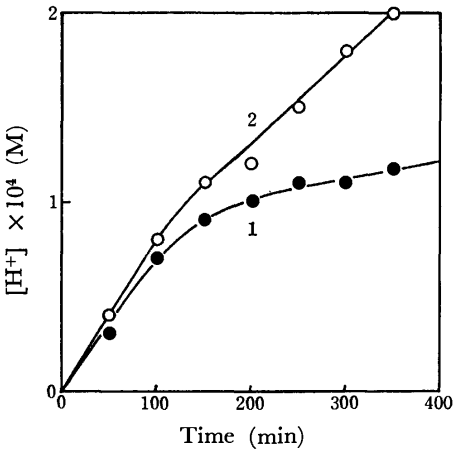

Fig. 3. The alkaline titration curves.
—○—: Oxygen bubbling,
—●—: nitrogen bubbling.

In the case of a pH 7.0 mixture, an absorption shoulder appeared at 290 nm and no absorption maximum was observed at 340 nm. On the paper chromatogram of the mixture 68 h after preparation, only one spot was observed at R_f=0.25, which is agreement with an authentic sample of glyceric acid (R_f=0.26).

Into 100 ml of distilled water, 1.0×10^{-4} M of RK, 1.0×10^{-4} M of NAD$^+$ and 1.0×10^{-3} M of glyceraldehyde were dissolved and adjusted to pH 8.0 by adding a sodium hydroxide solution. The mixture was bubbled with oxygen at 35 °C for 40 h, and the pH of the mixture was maintained at 8.0 by adding a sodium hydroxide solution. It was estimated from alkaline titration that 70% of the glyceraldehyde was converted to produce acid for a period of 40 h. The reaction mixture was dialyzed against distilled water, concentrated by evaporation, and then treated with an ion exchange resin (SE-sephadex-C50 H type) to remove any sodium ions. The solution was decolored by active charcoal and then evaporated resulting in a sticky syrup. The NMR spectrum of the syrup in deuterium oxide was found to be in agreement with that of glyceric acid (a multiplet at 3.68 (CH_2) and another at 4.32 (CH) ppm using the signal from tetramethylsilane as the external reference).

It is concluded from these results that glyceraldehyde was oxidized to form glyceric acid and NAD$^+$ was reduced to form NADH in the solution containing glyceraldehyde, NAD$^+$, and RK. The catalytic reaction could not proceed in either case because one component of the glyceraldehyde, NAD$^+$, and RK system had been omitted. Glyceraldehyde 3-phosphate, which is a compound similar to glyceraldehyde, was not oxidized by the NAD$^+$–RK system.

Reaction Rate. The rate of acid formation was determined by the alkaline titration method. A sample solution was prepared by dissolving glyceraldehyde, NAD$^+$ and RK into distilled water to produce 0.4—6.0×10^{-3}, 2.0×10^{-4}, and 1.0×10^{-4} M solutions and by adding a 0.1 M sodium hydroxide solution to adjust the mixture to pH 8.0. The reaction commenced immediately upon preparation of the sample solution at 35 °C. The alkaline titration was carried out manually to maintain the pH at 8.0. Typical results are shown in Fig. 3. Curves 1 and 2 in Fig. 3 show the results obtained by bubbling nitrogen and oxygen into the sample solution, respectively. The initial rate of acid formation did not appear to be influenced by the presence of oxygen. In the case of nitrogen bubbling, however, the rate of acid formation was found to decrease after the amount of acid produced in the reaction had reached the equivalent amount of RK.

The relation between the initial rate and the concentration of glyceraldehyde is shown by Lineweaver-Burk plots in Fig. 4. The plots are lines which gave two slopes about a turning point at 1.4×10^{-3} M of glyceraldehyde. It is speculated from this fact that same glyceraldehyde was tightly bound to the NAD$^+$–RK complex to be inactivated. The Lineweaver-Burk plot is a straight line in the case that 2.0×10^{-3} M glyceraldehyde 3-phosphate, which was not oxidized, was contained in the NAD$^+$–RK solution before adding glyceraldehyde. The values of the Michaelis constant and the maximum rate of the oxidation of glyceraldehyde were obtained from the intercept and the slope of the line to be 1.1×10^{-3} M and 3.6×10^{-6} M/min, respectively.

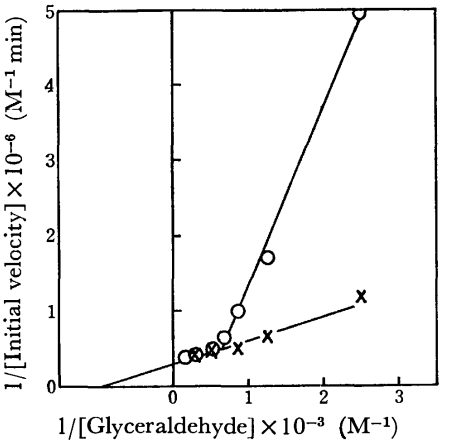

Fig. 4. Lineweaver-Burk plots.
—○—: Glyceraldehyde, —×—: glyceraldehyde with 2.0×10^{-3} M glyceraldehyde-3-phosphate.

Intermediates. This reaction should obey Michaelis-Menten kinetics. The glyceraldehyde–NAD+–RK complex appears to be an intermediate which was susceptible to oxidation by oxygen. In order to verify the existence of the intermediate, a polarographic study and DCIP oxidation were carried out.

The sample solution contained 2.0×10^{-4} M of glyceraldehyde, 2.0×10^{-4} M of NAD+, and 2.0×10^{-4} M of RK in a 0.1 M phosphate buffer (pH 8.0). Polarograms were measured (1) as fast as possible after preparation of the sample solution and (2) after 24 h at 35 °C. The sample solution was bubbled with nitrogen. The polarogam of NADH in the phosphate buffer was obtained and compared with that of the sample solution. The results are shown in Fig. 5. The oxidation wave of NADH was found to appear around +0.66 V *vs.* SCE. In the case of measurement immediately after preparation of the sample solution, no oxidation wave was observed in this region. Polarograms of the sample solutions after 24 h of preservation showed an oxidation wave at +0.19 V *vs.* SCE. It is plausible that this new oxidation wave can be assigned to the intermediates. No oxidation wave for NADH was observed.

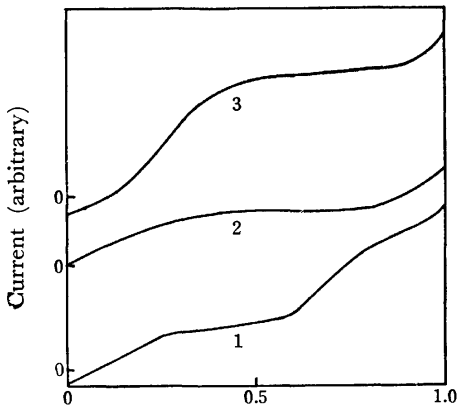

Fig. 5. Anode polarography.
1: NADH solution, 2: the NAD+–RK–glyceraldehyde system immediately after preparation, 3: the same system after 24 h.

DCIP oxidation was carried out by inserting the constituents as given in Table 1 into the Tunberg tube in which oxygen was removed by the passage of nitrogen gas. The conversion ratios of DCIP to reduced DCIP were determined spectrophotometrically at 600 nm after 30 min. DCIP was found to oxidize glyceraldehyde directly (Table 1). The conversion ratio decreased for a solution containing both NAD+ and RK. The DCIP oxidation was thought to be disturbed by the complexation of glyceraldehyde with the NAD+–RK complex.

It is assumed that the absorption shoulder at 290 nm in the pH 7.0 solution can be assigned to the intermediate, which is more stable in a pH 7.0 solution than in a pH 8.0 solution, because the absorption change at 290 nm is smaller than that at 340 nm. The NMR spectra at pH 7.0 were measured in order to better understand the struture of the intermediate. Proton signals (H4–6) of the nicotinamide moiety of NAD+ in the NAD+–RK solution were found to shift by 0.15—0.25 ppm to higher fields compared to that in NAD+ itself, as is indicated in Table 2. The RK signal may be located on the H4—6 side of the nicotinamide moiety, and that due to glyceraldehyde may be on the H2 side.

Table 1. DCIP oxidation of various systems

	Formation of $DCIPH_2$
NAD+–RK GCHO (1 : 1 : 10)	24.8 (%)
NAD+–RK (1 : 1)	0.0 (%)
NAD+–GCHO (1 : 10)	43.0 (%)
RK–GCHO (1 : 10)	18.2 (%)
NAD+	0.0 (%)
RK	0.0 (%)
GCHO	45.4 (%)

1.0×10^{-4} M NAD+, 1.0×10^{-4} M RK, 10×10^{-4} M GCHO, 1.0×10^{-4} M DCIP.
pH 8.0, 35 °C, 30 min, GCHO: glyceraldehyde.

Table 2. NMR of NAD+ in an NAD+–RK–GCHO solution

	NAD+	NAD+–RK	NAD+–RK–GCHO
H2	10.55	10.50	10.41
H4	9.67	9.52	9.50
H5	9.50	9.25(s)	9.23(d)
H6	10.05	9.87	9.85

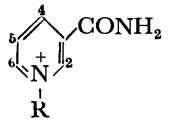

1.0×10^{-3} M NAD+, 1.0×10^{-3} M RK, 1.0×10^{-3} M GCHO in D_2O (pH 7.0), GCHO: glyceraldehyde.

Discussion

It can be speculated from the fact that in Fig. 4 the catalytic reaction of NAD+–RK complex is seen to proceed *via* a similar reaction mechanism, which is called a homotropic effect, as that for tryptophane pyrolase.[4] It is possible for an aldehyde group of glyceraldehyde to form a Schiff base linkage with an amino group of RK. Glyceraldehyde forming the Schiff base linkage may be only slightly oxidized because the active center of the NAD+–RK complex may be located in a position different from that of the Schiff base linkage. Therefore, the actual concentration of glyceraldehyde is reduced. It is surely possible that glyceraldehyde 3-phosphate can bind more easily to RK than to glyceraldehyde, because ionic bond formation of that phosphate group may facilitate the formation of the Schiff base linkage. In the mixture of glyceraldehyde 3-phosphate and glyceraldehyde, the former may preferentially form a Schiff base linkage, so that oxidation may be carried out by a Michaelis-Menten type reaction as follows:

$$\text{NAD+RK} + \text{GCHO} \rightleftharpoons \text{NAD+RK GCHO} \longrightarrow \text{X} + \text{H+}, \quad (1)$$

where X and GCHO indicate an intermediate and glyceraldehyde, respectively.

The rate of NADH formation shown in Fig. 2 was

very slow as compared with that of acid formation. Therefore, the conversion of the intermediate in the following reaction is thought to be the rate-determining step:

$$X + H_2O \xrightarrow{A} NADH + RK + GCOOH, \quad (2)$$

where GCOOH denotes glyceric acid.

The intermediate is susceptible to oxidation by oxygen and to an anodic reaction (Figs. 3, 5). Oxygen may participate in the second step in a subsequent reaction. The reaction can be expressed as follows:

$$X + 1/2O_2 \longrightarrow NAD^+RK + GCOO^-. \quad (3)$$

The DCIP oxidation suggests the existence of the ES complex in Fig. 1. Tagaki *et al.* have isolated *N*-benzyl-5-[hydroxy(1-pyridyl)methyl]nicotinamide, which exhibits an absorption maximum at 290 nm, by a reaction between aldehyde and a reduced nicotinamide derivative.[5] They explained that the product obtained may be one of the intermediates in the reaction. The absorption shoulder at 290 nm in Fig. 2 can thus be assigned to a similar intermediate.

Many authors have recently proposed that, at the active center of glyceraldehyde 3-phosphate dehydrogenase, a nicotinamide moiety in NAD^+ combines with an apoenzyme located near Cys-149 and that this center is activated by a mercapto group.[6-9] If the NAD^+–RK complex is assumed to catalyze the oxidation of glyceraldehyde in the same way as glyceraldehyde 3-phosphate dehydrogenase, a mercapto group on RK may play a similar role in the catalytic reaction. However, this assumption is still open to further investigation.

The authors express their sincere thanks to Professor Shuichi Suzuki of the Tokyo Institute of Technology for his encouragement.

References

1) F. Takahashi, T. Ogasa, M. Hirano, and S. Suzuki, *Bull. Chem. Soc. Jpn.*, **49**, 1130 (1976).
2) F. Takahashi, T. Ogasa, and S. Tanaka, *Nippon Kagaku Kaishi*, **1975**, 738.
3) I. M. Klotz, F. M. Walker, and R. B. Pivan, *J. Am. Chem. Soc.*, **68**, 1486 (1946).
4) Y. Ishimura and O. Hayashi, *J. Biol. Chem.*, **248**, 8610 (1973).
5) W. Takagi, H. Sasaki, Y. Yano, K. Ozaki, and Y. Shimizu, *Tetrahedron Lett.*, **1976**, 2541.
6) J. E. Bell and K. Dalziel, *Biochim. Biophys. Acta*, **391**, 249 (1975).
7) M. Buehner, G. C. Ford, D. Moras, K. W. Olsen, and M. G. Rossmann, *J. Mol. Biol.*, **90**, 25 (1974).
8) K. S. You, L. V. Benitez, W. A. McConachie, and W. S. Allison, *Biochim. Biophys. Acta*, **384**, 317 (1975).
9) H. D. Heilmann and G. Pfleiderer, *Biochim. Biophys. Acta*, **384**, 331 (1975).

Effect of Hydrogen Bonding on the Rotational Barriers of Partial Double Bonds. III. 2,6-Dihydroxyaryl Carbonyl Compounds

Minoru HIROTA, Toshio SUZUKI, and Kazuhisa ABE

Department of Applied Chemistry, Faculty of Engineering, Yokohama National University, Minami-ku, Yokohama 233

(Received December 20, 1976)

Activation parameters of internal rotation around C_{ar}–$C_{carbonyl}$ bonds are determined by means of DNMR spectroscopy for 2,6-dihydroxybezaldehyde and some 2,6-dihydroxybenzoates. The ΔG^* and ΔH^* of these compounds are *ca.* 10 kJ mol^{-1} higher than those for the reference compounds void of *ortho*-hydroxyl groups, and the excess stabilization is attributed to the contribution of the intramolecular hydrogen bonding. The intramolecular hydrogen bonding in these compounds were discussed on the basis of their infrared spectra in the ν_{OH} region.

The intramolecular hydrogen bond is formed when the hydrogen donating and the hydrogen accepting groups are located close enough to interact each other, and the whole molecule is stabilized at the sacrifice of the freedom of the intramolecular motion. Thus, the intramolecular hydrogen bonding in salicylaldehyde and salicylate esters fixes their molecules to the conformation I, and the rotational barrier around the C_{ar}–$C_{carbonyl}$ single bonds becomes considerably higher.

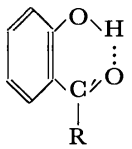

I : R=H or OCH_3

In other words, the coplanar conformation I of ortho-hydroxy derivatives are stabilized by the intramolecular hydrogen bonding in addition to the π-stabilization energy of conjugation common with the aryl carbonyl compounds void of the hydrogen bond, and the difference in the barrier heights between the aryl carbonyl compounds with and without *o*-hydroxyl group will reflect the energy of the intramolecular hydrogen bonding. In the previous report of the present authors, the hydrogen bond energy of *o*-hydroxybenzaldehyde was estimated in this way from the rotational barriers of 2,6-diformylphenols.[1,2] Rotational barriers of partial double bonds (C_{sp^2}–C_{sp^2} single bonds) can be best estimated by the techniques of dynamic nuclear magnetic resonance (DNMR) from the separations or from the widths of the NMR signals at various temperatures.[3-6]

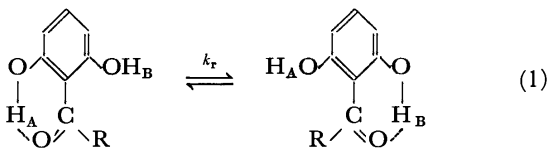

IIa $\qquad$ II_b $\qquad$ (1)

For this purpose, such protons should be chosen as the probe of the intramolecular rotation that they are equivalent in the condition of fast exchange but nonequivalent when the exchange is slow. Since two hydroxyl protons (H_A and H_B in II) of 2,6-dihydroxyaryl carbonyl compound are suitable for this purpose, the DNMR measurements were carried out on these compounds and their intramolecular hydrogen bonding was discussed in this paper.

Experimental

Preparation of Materials. 2,6-Dihydroxybenzaldehyde and 2,6-dihydroxyacetophenone were prepared from resorcinol by the methods in literatures.[7,8] 2,6-Dihydroxybenzoate esters were obtained by reacting the corresponding alkyl halides with silver 2,6-dihydroxybenzoates.[9] All materials and solvents employed in this investigation were purified either by distillation or by recrystalization.

Measurement of the Spectra. Infrared spectra were recorded on a Hitachi Model 225 infrared spectrometer. Nuclear magnetic resonance spectra were obtained on a JEOL JNM C-60H spectrometer. Chemical shifts are given as parts per million (ppm) downfield from TMS.

Evaluation of the Rotational Barriers from the Line Shapes Above Coalescence. Because of the relatively low coalescence temperature (T_c), the exchange rate of the two equivalent protons without the splitting caused by spin-spin coupling (H_A and H_B in II) was obtained from the half-widths W^* (in Hz) of the signal above T_c by the following equation.[3]

$$(\pi\delta\nu\tau)^{-1} = [(\delta\nu/W^*)^2 - (W^*/\delta\nu)^2 + 2]^{1/2}$$

where $\delta\nu$ refers to the chemical shift difference (in Hz) of the two protons H_A and H_B. As the measurements were carried out within the temperature range where the signals were considerably broader than usual, it is assumed that the exchange contribution W^* to the observed line width W is by far greater than that from the natural width (hence, $W=W^*$).

Results and Discussion

Kinetic studies of some alkyl 2,6-dihydroxybenzoates in chloroform-*d* and of 2,6-dihydroxybenzaldehyde in diethyl ether were carried out employing the techniques of DNMR spectroscpy. From Eq. 1, the rate constants (k_r in s^{-1}) of the intramolecular exchange process between H_A and H_B due to the rotational interconversion between II_a and II_b were calculated from the half widths (in Hz) observed at various temperatures, and given, together with the half widths, in Table 1.

In 2,6-dihydroxy-benzaldehyde and -acetophenone, H_A and H_B are the free and the intramolecularly hydrogen bonded hydroxyl protons, while, in alkyl 2,6-dihydroxybenzoates, they are the hydroxyl protons intramolecularly hydrogen bonded to the alkoxyl and to the carbonyl groups of the ester.

The Arrhenius plot (k_r *vs.* $1/T$ plot in Fig. 1) gives the enthalpy and the entropy of activation of the interconversion between the degenerate geometrical isomers II_a and II_b, and thus obtained activation parameters

TABLE 1. KINETIC DATA FOR THE INTERNAL ROTATION AROUND THE C_{ar}–$C_{carbonyl}$ BONDS OF SOME 2,6-DIHYDROXYARYL CARBONYL COMPOUNDS[a)]

	T/K	W/Hz	k_r/s^{-1}
2,6-Dihydroxybenzaldehyde **1** (Solvent: $C_2H_5OC_2H_5$)	251.5	5.55	7567
	248.3	6.45	6247
	243.6	10.05	3687
	238.1	18.40	1907
	233.6	24.30	1434
	231.3	29.50	1184
	229.0	33.45	1049
	223.4	55.50	669
	222.7	58.50	640
	221.2	74.30	531
	219.6	99.90	428
Methyl 2,6-dihydroxybenzoate **3** (Solvent: $CDCl_3$)	224.2	17.50	1983
	218.4	38.40	979
	215.1	64.80	625
	212.1	87.60	498
	211.8	105.00	437
Ethyl 2,6-dihydroxybenzoate **4** (Solvent: $CDCl_3$)	251.7	8.80	5212
	246.1	10.50	4175
	240.4	21.00	1893
	228.4	60.00	691
	227.9	67.00	631
	225.7	80.00	550
Propyl 2,6-dihydroxybenzoate **5** (Solvent: $CDCl_3$)	254.2	10.00	3625
	245.2	23.50	1579
	239.2	36.50	1029
	233.9	46.00	834
	230.5	94.00	474

a) The $\Delta\nu$ values given in Table 2 were used for the calculations of k_r values, and $W=W^*$ is assumed. (See text.)

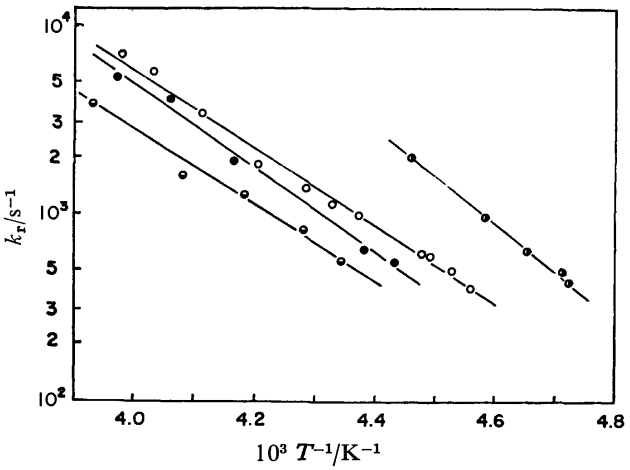

Fig. 1. Arrhenius plots for 2,6-dihydroxybenzaldehyde (—○—), methyl 2,6-dihydroxybenzoate (—◑—), ethyl 2,6-dihydroxybenzoate (—●—), and propyl 2,6-dihydroxybenzoate (—◒—).

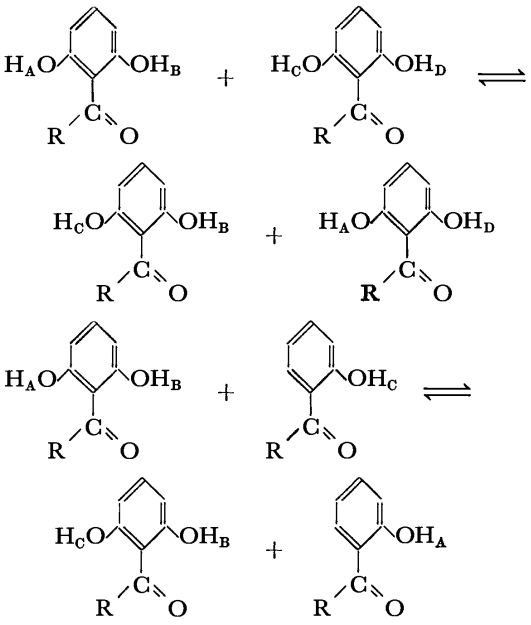

The OH proton signals of the two species appear separately and quite sharply in the spectra of the above ternary systems even at room temperature and when their chemical shift difference is only 5 Hz or so.[10)]

are shown in Table 2. The activation parameters of 2,6-dihydroxyacetophenone could not be determined owing to its very low coalescence temperature (≈195 K) which made difficult the determination of the exact resonance frequencies of the free and the hydrogen bonded hydroxyl protons.

Since the activation parameters are obtained only for the fastest process, any other process faster than the internal rotation will prevent the determination of the rotational barrier height. Thus, the effect of intermolecular exchange processes (rate constant k_e), such as Eq. 2, is checked by the measurement of the spectra on salicylaldehyde–methyl salicylate–chloroform-*d* and methyl 2,6-dihydroxybenzoate–salicylaldehyde–chloroform-*d* ternary systems.

TABLE 2. ACTIVATION PARAMETERS FOR THE INTERNAL ROTATION IN SOME 2,6-DIHYDROXYARYL CARBONYL COMPOUNDS AND RELATED SUBSTANCES

Compound	T_c/K	$\Delta\nu$/Hz	ΔG^*/kJ mol^{-1}	ΔH^*/kJ mol^{-1}	ΔS^*/J mol^{-1} K^{-1}
1	215.6	143.0	41.8	37.4	−21
2	≈195		≈33		
Benzaldehyde	150		33.1		
3	207.5	147.6	40.2	41.8	+8
4	222.1	150.0	43.1	41.1	−9
5	227.1	148.0	44.1	38.4	−25
6[a)]	<163		<34.7[b)]		

a) 3,4,5-Trimethoxybenzoic acid as the reference substance without intramolecular hydrogen bond. b) To calculate the upper limit of the ΔG^* value, $\Delta\nu$ is assmed to be 10 Hz, which corresponds to the chemical shift difference between H_3 and H_5 of 2,6-diformylphenol in the frozen state.

Thus, the intermolecular exchange processes are proven to be slower than the intramolecular process, *i.e.* $k_r \gg k_e$.

The ΔG^* and ΔH^* for 2,6-dihydroxybenzaldehyde (**1**) are 41.8 and 37.4 kJ mol^{-1}, respectively, and a little smaller than those of 2,6-diformylphenols (46.4 and 43.9 kJ mol^{-1}, respectively, for the *p*-methyl derivative in chloroform-*d*).[1] The measurement on **1** was carried out in diethyl ether instead of chloroform-*d*, and the lower energy barrier in **1** is at least partly due to the effect of the more polar solvent. While, the steric interaction between formyl hydrogen atom and the free hydroxyl group should be slightly repulsive, which may contribute additionally to the instabilization of the planar hydrogen bonded conformation. However, the stabilization due to the intramolecular hydrogen bond is remarkably more predominant, and the planar conformations of **1** are about 9 kJ mol^{-1} more stable than those of benzaldehyde. The activation parameters for 2,6-dihydroxyacetophenone (**2**) could not be determined exactly because of its lower T_c and of its poor solubilities in available solvents (chloroform, diethyl ether, vinyl chloride, *etc.*) under the experimental conditions. The remarkably lower rotational barrier of **2** must be caused by the increase in steric hindrance, since the C–H···OH interaction in **1** is replaced by much serious repulsive interaction between the methyl and the hydroxyl groups in this molecule. Judging from the Stuart molecular models, the most stable conformation of **2** is expected to become nonplanar, and its rotational barrier might be illustrated schematically by the broken line in Fig. 2. The nonplanar conformation is supported by the fact that the ν_{OH} absorption due to the chelated hydroxyl group is very weak in the infrared spectrum of **2** in dilute carbon tetrachloride solution.

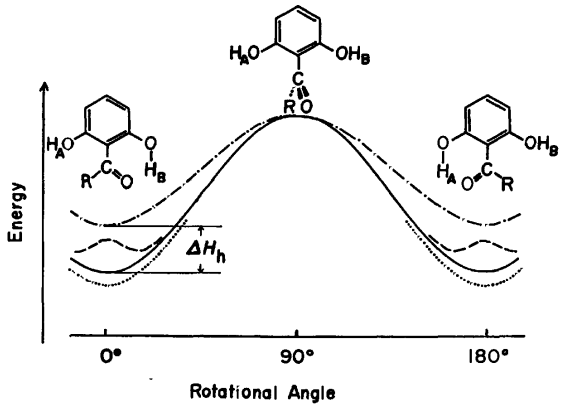

Fig. 2. Schematic diagrams for the potential energy barriers of 2,6-dihydroxybenzaldehyde (——), 2,6-dihydroxyacetophenone (----), and 2,6-dihydroxybenzoate esters (·····).
The potential barriers of benzaldehyde (—·—·) is also illustrated as reference.

Table 3. Infrared spectra of 2,6-dihydroxyaryl carbonyl compounds in the ν_{OH} region (3600—3000 cm^{-1})

Compound	c/mol l^{-1}	ν_{OH}/cm^{-1}	ε_{max}/l mol^{-1} cm^{-1}	Assignment[a]
1	0.013	3596.9 3140	137 27	f. h. c.
2	0.020	3593.2[b]	190	f.
3	0.010	3473.2 3202	149 70	h. a. h. c.
4	0.010	3461.0 3202	129 40	h. a. h. c.

a) f=free, h. c.=hydrogen-bonded to carbonyl oxygen atom, h. a.=hydrogen-bonded to alkoxyl oxygen atom. b) A broad absorption band centered at about 3150 cm^{-1} is observed, but its intensity is by far lower than that of **1**.

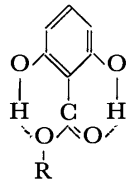

(III)

The infrared spectra of 2,6-dihydroxybenzoate esters (**3**,**4**) in Table 3 show the presence of two kinds of hydrogen bonded species. However, the absorption of the free species is not detected in any of their spectra. The fact is reasonably explained by assuming a planar conformation in which one hydroxyl group is chelated to the carbonyl oxygen atom and the other to the alkoxyl oxygen atom by forming intramolecular hydrogen bonds, as illustrated by III. Since the OH···O=C hydrogen bond is stronger than the OH···OR hydrogen bond,[11] the OH stretching absorption at the lower frequency is assigned to the hydroxyl group hydrogen bonded to the carbonyl, and the absorption at the higher ferquency to the hydroxyl group hydrogen bonded to the alkoxyl oxygen atom (as shown in Table 3).

The ΔG^* and ΔH^* values of the 2,6-hydroxybenzoates **3**, **4**, **5** are similar to those of **1** and a considerable stabilization due to the intramolecular hydrogen bond formation is suggested. In order to estimate the contribution of the hydrogen bonding to the stability of the planar conformation, DNMR measurement of methyl 3,4,5-trimethoxybenzoate **6**, as a reference, was also carried out. However, the aromatic proton signal of **6** was rather a sharp singlet even at 173 K, and no indication of splitting into an AB quartet was observed. The π-bond order of the C_{ar}–$C_{carbonyl}$ bond from MO calculation serves as a criterion for the potential barrier height.[12] The π-bond orders for benzoate ester and benzaldehyde are calculated to be 0.247 and 0.271, respectively, by PPP approximation, and the rotational barrier of **6** is expected to be lower than that of benzaldehyde. Anyhow, the rotational barrier is at least 10 kJ mol^{-1} higher than that of the reference compound, and the excess stabilization energy is again attributed to the contribution of the intramolecular hydrogen bonding. The OH···OR hydrogen bonding in the esters **3**—**5** must increase the stability of the planar conformation III, but its contribution cannot be determined quantitatively because of the uncertain activation parameters of the reference substance **6**.

The rotational barriers of the aryl carbonyl compunds are illustrated schematically in Fig. 2. In the transition state of the internal rotation het

aromatic nucleus is perpendicular to the plane of the carbonyl group, and both the hydrogen bonding and the steric hindrance do not affect its potential energy remarkably. Thence, the hydrogen bond energy can be estimated as the difference in ΔH^* (ΔH_h in Fig. 2) of the chelated and the reference substances. Hydrogen bond energies thus obtained are *ca.* 9 kJ mol^{-1} for 2,6-dihydroxybenzaldehyde and 8 kJ mol^{-1} for 2,6-dihydroxybenzoates. These values are considerably smaller than the hydrogen bond energies of the similar substances obtained by other methods.[13] The lower ΔH_h may be justified by the polar nature of the solvents used and the negative contribution of the steric hindrance in the planar conformation.

The authors are grateful to Mrs. Shigeko Yoshida and to Miss Hiroko Endo for their technical assistance in the measurement of NMR spectra.

References

1) M. Tabei, T. Tezuka, and M. Hirota, *Tetrahedron*, **27**, 301 (1971).
2) M. Hirota and K. Todokoro, *Chem. Lett.*, **1974**, 777.
3) A. Allerhand, H. S. Gutowsky, J. Jones, and R. A. Meinzer, *J. Am. Chem. Soc.*, **88**, 3185 (1966).
4) L. H. Piette and W. A. Anderson, *J. Chem. Phys.*, **30**, 899 (1959).
5) M. Takeda and E. O. Stejskal, *J. Am. Chem. Soc.*, **82**, 25 (1960).
6) L. M. Jackman and F. A. Cotton, "Dynamic Nuclear Magnetic Resonance Spectroscopy," Academic Press, New York (1975), pp. 45—78.
7) R. Adams, *J. Am. Chem. Soc.*, **70**, 2120 (1948). 2,6-Dimethoxybenzaldehyde was synthesized by the method described by J. W. Morton Jr., (*Org. React.*, **8**, 288 (1954)) and used for the preparation.
8) A. Russel and J. R. Frye, *Org. Synth.*, Col. Vol. III, 281 (1955).
9) K. Tomino, *Yakugaku Zasshi*, **78**, 1425 (1958).
10) For example, the OH proton signals of salicylaldehyde and methyl salycylate resonate at 10.79 and 10.72 ppm, respectively, in the above ternary system.
11) D. N. Shigorin, "Hydrogen Bonding," ed by D. Hadzi, Pergamon Press, London (1959), p. 191.
12) The linear relation between the barrier height and the bond order has been reported by several authors. For example, see: K. Spaargaren, P. K. Korver, P. J. van der Haak, and Th. J. de Boer, *Org. Magn. Reson.*, **3**, 615 (1971).
13) Hydrogen bond energies are listed in the following: G. C. Pimentel and A. L. McClellan, "The Hydrogen Bond," Freeman, San Francisco (1960), pp. 356—360. See also, E. Funk and R. Mecke, "Hydrogen Bonding," ed by D. Hadzi, Pergamon, London (1959), p. 433 and M. Davies, *ibid.*, p. 393.

A New Synthesis of Pyrocin and Related Compounds*

Akira TAKEDA, Takashi SAKAI, Shohei SHINOHARA, and Sadao TSUBOI

Department of Synthetics Chemistry, School of Engineering, Okayama University, Tsushima, Okayama 700

(Received January 5, 1977)

A new synthesis of pyrocin (**1**) and related compounds is described. The reaction of 2-benzoyl-4,4-dimethyl-2-buten-4-olide (**5b**) with 2-methyl-1-propenylmagnesium bromide (**6**) in the presence of CuCl gave α-benzoylpyrocin (**7b**) in 90% yield. The product of **7b** with a specific rotation of +2.43° was obtained when the reaction was carried out in the presence of (−)-sparteine. α-Acetylpyrocin (**7a**) was prepared in the similar manner in 63% yield. The treatment of **7a** and that of **7b** with ethanolic sodium ethoxide gave **1** in 65% and 81% yields, respectively. The reaction of **1** with large excess of $SOCl_2$ in absolute ethanol gave ethyl 3-(1-chloro-1-methylethyl)-5-methyl-4-hexenoate (**8**) in 82% yield. Similar treatment of **7** with $SOCl_2$ gave ethyl 2-substituted-4-(2-methyl-1-propenyl)-5,5-dimethyl-4,5-dihydrofuran-3-carboxylate (**12**). Compound **8** was transformed to ethyl *trans*-(±)-chrysanthemate (**2**) in 75% yield.

Several syntheses of pyrocin (**1**), found in the pyrolysate of pyrethrine and known to possess insecticidal activity,[1a–1d] have been reported.[2a–2k] Recently, we[3] have reported an efficient preparation of 2-acyl-4,4-dimethyl-2-buten-4-olide (**5**) by the thermal decomposition of 2-acyl-3-[benzoyl(ethoxycarbonyl)methyl]-4,4-dimethyl-4-butanolide (**4**), which is readily obtained by the reaction of 2-chloro-2-methylpropanal and ethyl acylacetate (**3**) in aqueous K_2CO_3. In this paper, we wish to report a new synthesis of **1** and ethyl (±)-*trans*-chrysanthemate (**2**) using **5** as a starting material. An attempted synthesis of optically active pyrocin using (−)-sparteine as a chirality-creating reagent also has been described.

The Michael addition of 2-methyl-1-propenylmagnesium bromide (**6**) to the butenolide **5b** in the presence of CuCl in THF medium afforded α-benzoylpyrocin (**7b**) in 90 % yield. The IR spectrum of **7b** showed strong bands at 1765 and 1685 cm^{-1} due to lactone carbonyl and benzoyl carbonyl, respectively. The NMR spectrum exhibited a multiple splitting doublet at δ 5.03 due to one olefinic proton. α-Acetylpyrocin (**7a**) was obtained similarly from **5a** and **6** in 63% yield.

Deacylation of **7a** and **7b** with ethanolic EtONa at reflux temperature afforded **1** in 65% and 81% yields, respectively. The NMR spectrum of this product was identical with that[5] of the authentic sample. Hirai, *et al.*,[6] have reported a synthesis of optically active pyrocin *via* the asymmetric, catalytic hydrogenation of optically active alcohol esters of 2,2,5,5-tetramethyltetrahydrofurylidene-3-acetic and 2,2,5,5-tetramethyldihydrofuryl-3-acetic acids. We now describe the preparation of optically active **1** by an asymmetric Michael addition of the Grignard reagent **6** to the butenolide **5b**.[7a,7b] The reaction, carried out in the presence of twice molar amount of (−)-sparteine as well as a catalytic amount of CuCl, gave a product of **7b** with $[\alpha]_D^{25}$ +2.43° (ethanol) in 47% synthetic yield. Debenzoylation of this product gave **1** with $[\alpha]_D^{25}$ +1.36° (ethanol), 2.0% optical yield.

Several procedures to transform **1** to the ester **2** have been reported.[1d,2k,8a,8b] They involve the base-catalyzed cyclization of the dichloro ester **9**, which is obtained from **1** by the treatment with $SOCl_2$ in benzene and the subsequent addition of ethanolic HCl. While the isomer **10** is usually produced as an undesirable by-product in these procedures, we are successful to prevent the formation of **10** by using ethyl 3-(1-chloro-1-methylethyl)-5-methyl-4-hexenoate (**8**)[8c] in place of **9** as a starting material. Successive treatments of **1** with large excess of $SOCl_2$ in ethanol, at room temperature for 1 h and then at 60 °C for additional 4 h, yielded the desired ester **8** in 82% yield. The NMR spectrum showed a multiple splitting doublet at δ 4.95 due to one olefinic proton. The treatment of **8** with lithium diisopropylamide in the presence of

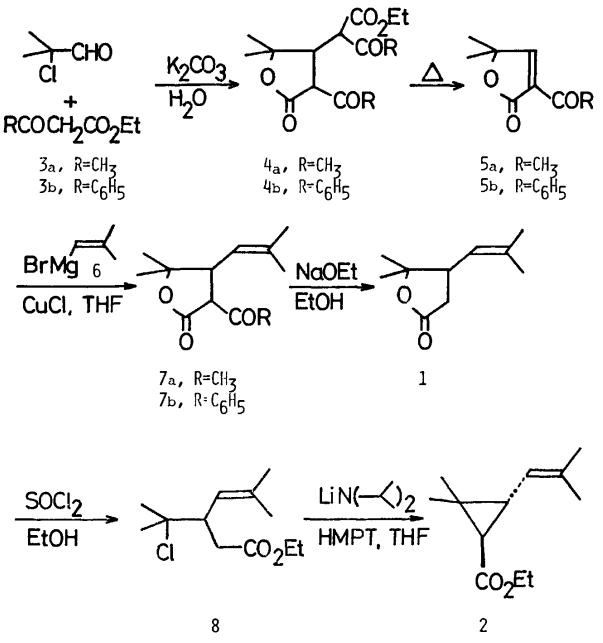

Scheme 1.

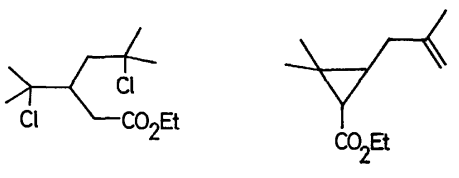

9 **10**

* Presented in part at the 32nd Annual Meeting of the Chemical Society of Japan, Tokyo, April 1975 and in part at the 5th International Congress of Heterocyclic Chemistry, Ljubljana, Yugoslavia, July 1975.

a catalytic amount of hexamethylphosphoric triamide (HMPT) in THF afforded **2** in 75% yield. Its spectral data (IR, NMR, and MS) were identical with those described in the literatures.[9a,9b] The reaction conducted in ethanolic EtONa gave rise to the cyclization of **8** to pyrocin.

Because of the facile formation of dihydrofuran ring, we failed to obtain the α-acyl derivatives of the chloro ester **8**. The reaction of **7** with $SOCl_2$, carried out in the same manner as **1**, gave only ethyl-2-substituted-4-(2-methyl-1-propenyl)-5,5-dimethyl-4,5-dihydrofuran-3-carboxylate (**12**) in good yields (>82%). Ethylene acetal of α-acetylpyrocin (**13**) also underwent the re-cyclization to produce **12**.

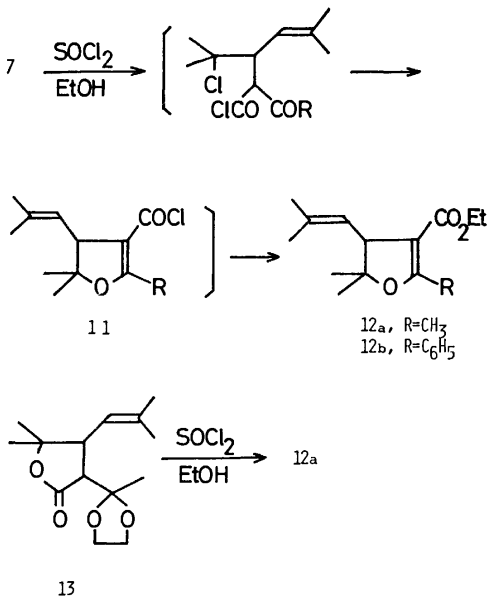

Scheme 2.

The present work was partially supported by a Grant-in-Aid for Scientific Research from the Ministry of Education (Grant No. 647079).

Experimental

Melting points and boiling points are uncorrected. Elemental analyses were carried out by Mr. Eiichiro Amano of our laboratory. Distillations were evaporative bulb-to-bulb distillations using a Büchi Kugelrohrofen at the pressure and oven temperature indicated. Analytical determination and preparative isolation by GLPC were performed on a Hitachi K-53 model gas chromatograph and a Yanagimoto G-80 model gas chromatograph respectively. IR spectra were determined on a Hitachi EPI-S2 model spectrometer. ^1H NMR spectra were taken at 60 MHz on a Hitachi R-24 model spectrometer using TMS as an internal standard. ^{13}C NMR spectra were taken at 25 MHz on a JEOL FX-100 model spectrometer equipped with FT facilities using TMS as an internal standard and $CDCl_3$ as solvent. The pulse width was 6 μs (45° tip) and the FIDs were compiled by using 8 K data points over a spectral width of 6000 Hz. MS spectra were obtained at 70 eV with a Hitachi RMS-4 model mass spectrometer. Optical rotation was measured with a Yanagimoto OR-50 model polarimeter and the cell path length was 0.1 dm. Analytical and preparative TLC were done on a silica gel PF_{254} (E. Merck AG., Darmst.) with layers of 0.25 mm and 1.0 mm thickness respectively. Column chromatography was done on a silica gel, Wakogel C-200 and C-300 (Wako Junyaku Kogyo Co., Ltd.).

Starting materials such as **5a**, **5b**[3] and 1-bromo-2-methyl-propene[10] were prepared by the procedure described in the literatures.

(±)-α-Benzoylpyrocin (7b). To a refluxing mixture of magnesium turnings (0.98 g, 0.04 g-atom), a few drops of ethyl bromide and trace of iodine in 20 ml of THF, was added isobutenyl bromide (5.40 g, 0.04 mol) dropwise. The mixture was refluxed until magnesium turnings were completely dissolved. After cooling to 0 °C and addition of copper(I) chloride (0.2 g, 0.02 mol), the mixture was stirred for 20 min. To the mixture was added the butenolide **5b** (4.32 g, 0.02 mol) in 20 ml of THF dropwise at 0 °C. After being stirred for 2 h at 0 °C, the mixture was allowed to warm to room temperature. To the resulting mixture was added 10 ml of saturated aqueous NH_4Cl and then it was acidified with 10% HCl. An organic layer was extracted with ether and dried over $MgSO_4$. After removal of the solvent, the residual brown oil was obtained and separated by column chromatograph on a silica gel (30 g of Wakogel C-200, hexane : acetone=10 : 1) to give 4.90 g (90% yield) of **7b**. The analytical sample was obtained by one recrystallization from the mixed solvent of benzene and petroleum ether (1 : 1 in v/v): mp 94—95 °C; IR (KBr) 1767 (lactone C=O), 1683 (benzoyl C=O), 1598, 1579 cm^{-1} (benzene C=C); NMR ($CDCl_3$) δ 1.37 (s, 3H, γ-CH_3), 1.49 (s, 3H, γ-CH_3), 1.70 (t, 6H, J=0.1 Hz, $=\langle^{CH_3}_{CH_3}$), 3.37 (dd, 1H, J=11 Hz and 10 Hz, β-H), 4.55 (d, 1H, J=11 Hz, α-H), 5.03 (md, 1H, J=10 Hz, >-H), 7.23—8.18 (m, 5H, C_6H_5); MS *m/e* (rel. intensity) 272 (M^+), 227 (8.0), 214 (4.0), 186 (6.3), 171 (100), 105 ($C_6H_5CO^+$, 97), 77 (C_6H_5, 62).

Found: C, 75.12; H, 7.41%. Calcd for $C_{17}H_{20}O_3$: C, 74.97, H, 7.40%.

The natural abundance ^{13}C NMR spectra of **5b** and **7b** are summarized in the following structure.

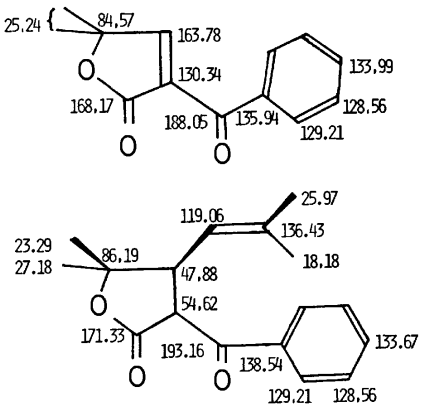

(±)-α-Acetylpyrocin (7a). The mixture of butenolide **5a** (3.08 g, 0.02 mol), 2-methyl-1-propenylmagnesium bromide (0.04 mol), and 0.02 g of copper(I) chloride in 40 ml of THF was reacted and worked up in the same manner as the foregoing experiment to give 2.62 g (63% yield) of **7a**: IR (neat) 1760 (lactone C=O), 1717 (acetyl C=O), 1645 cm^{-1} (C=C); NMR (CCl_4) δ 1.22 (s, 3H, γ-CH_3), 1.38 (s, 3H, γ-CH_3), 1.73 (sharp m, 6H, $=\langle^{CH_3}_{CH_3}$), 2.32 (s, 3H, $COCH_3$), 3.29 (d, 1H, J=16 Hz, α-H), 3.50 (dd, 1H, J=16 Hz and 11 Hz, β-H), 4.83 (m, 1H, >-H); MS *m/e* (rel. intensity) 210 (M^+), 195 ($M-CH_3$, 0.3), 177 (0.4), 167 ($M-COCH_3$), 152 (5), 137 (4), 124 (11), 108 (100).

Found: C, 68.66; H, 8.42%. Calcd for $C_{12}H_{18}O_3$: C, 68.55; H, 8.63%.

The natural abundance ^{13}C NMR spectra of **5a** and **7a** are summarized in the following structure. Off-resonance decoupling was used to support the assignments in each case.

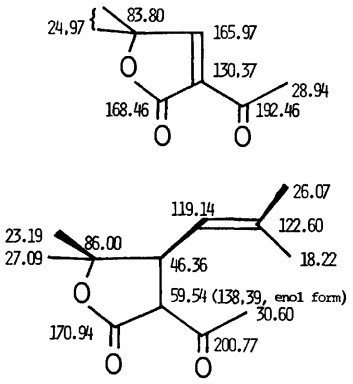

(±)-Pyrocin (1) (Debenzoylation of 7b). To a stirried mixture of EtONa (4.76 g, 0.07 mol) in 100 ml of ethanol was added **7b** (3.82 g, 0.014 mol) dissolved in 50 ml of ethanol. The resulting mixture was refluxed for 42 h. After evaporation of ethanol under reduced pressure, the residue was acidified with 10% HCl, and then extracted with ether. The ether extract was washed with aqueous $NaHCO_3$ to remove benzoic acid and dried over $MgSO_4$. After removal of the solvent 2.0 g of crude pyrocin was obtained. The purification by column chromatograph on a silica gel (15 g of Wakogel C-200, hexane : acetone=10 : 1) gave 1.90 g of pyrocin, 81% yield: mp 58—58.5 °C (lit,[4] 59—60 °C); IR (KBr) 1761 cm^{-1} (lactone C=O); NMR (CCl_4) δ 1.20 (s, 3H, γ-CH_3), 1.36 (s, 3H, γ-CH_3), 1.68 (d, 3H, J=0.2 Hz, $\gtrless$-CH_3), 1.75 (d, 3H, J=0.2 Hz, $\gtrless$-CH_3), 1.95—2.45 (m, 2H, α-H_2, ABX), 2.60—3.35 (m, 1H, β-H, ABX), 5.01 (md, 1H, J=10 Hz, $\gtrless$-H).[5]

The natural abundance ^{13}C NMR spectrum of **1** is summarized in the following structure. Off-resonance decoupling was used to support the assignment.

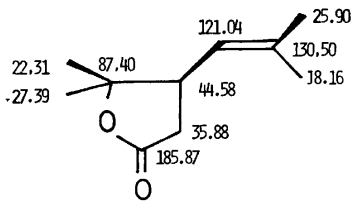

Deacetylation of **7a** (343 mg, 1.63 mmol) with EtONa gave 177 mg of **1**, 65% yield.

Optically Active α-Benzoylpyrocin and Pyrocin. To a stirred solution of 2-methyl-1-propenylmagnesium bromide (10.4 mmol) in 15 ml of THF prepared by the same procedure as **7b**, were added copper(I) chloride (100 mg, 1.0 mmol) and (−)-sparteine (5.0 g, 20.8 mmol) at 0 °C. The mixture was stirred for 1 h at 0 °C. To the mixture, a solution of **5b** (2.25 g, 10.4 mmol) in 15 ml of THF was added slowly. The stirring was continued for 7 h at 0 °C and for additional 12 h at room temperature. The resulting mixture was poured into a saturated aqueous solution of NH_4Cl. It was then acidified with 10% HCl. An organic layer was extracted with ether and dried over $MgSO_4$. After removal of the solvent, 2.77 g of brown oil was obtained. After separation by column chromatograph on a silica gel (40 g of Wakogel C-200, hexane : acetone=10 : 1), 0.98 g of **5b** and 1.36 g of (+)-α-benzoylpyrocin were obtained, 47% synthetic yield. An analytical sample was obtained after one recrystallization from the mixed solvent of benzene and petroleum ether (1 : 1 in v/v): mp 94—95 °C; $[\alpha]_D^{25}$ +2.43° (*c* 4.12 g, ethanol). Its NMR and IR spectra were completely identical with those of **7b**.

(+)-Pyrocin was obtained from this product of (+)-α-benzoylpyrocin in the same manner as described in the foregoing section: $[\alpha]_D^{25}$ +1.36° (*c* 1.21 g, ethanol), optical yield 2%. Its IR and NMR spectra were identical with those of authentic sample of **1**.

Ethyl 3-(1-chloro-1-methylethyl)-5-methyl-4-hexenoate (8). To a stirred solution of **1** (750 mg, 4.46 mmol) in 40 ml of ethanol was added thionyl chloride (3.8 ml, 44.6 mmol) with caution at room temperature. The stirring was continued for 1 h at room temperature and then for additional 4 h at 60 °C. After removal of the solvent and low boiling materials, 1.41 g of dark brown oil was obtained. It was separated by column chromatograph on a silica gel (30 g of Wakogel C-300, hexane) to afford 852 mg of **8**, 82% yield. The analytical sample was obtained by bulb-to-bulb distillation: bp 90 °C (0.06 Torr); IR (neat) 1734 cm^{-1} (C=O); NMR (CCl_4) δ 1.19 (t, 3H, J=7 Hz, ester CH_3), 1.44 (s, 3H, CH_3), 1.53 (s, 3H, CH_3), 1.65 (d, 3H, J=2 Hz, $\gtrless$-CH_3), 1.70 (d, 3H, J=2 Hz, $\gtrless$-CH_3), 1.8—3.2 (m, 3H, α-H_2 and β-H), 3.99 (q, 2H, J=7 Hz, ester CH_2), 4.95 (md, 1H, J=10 Hz, $\gtrless$-H); MS *m/e* (rel. intensity) 196 (M^+−HCl, 20), 181 (6), 155 (42), 109 (100), 123 (32), 77 (75).

Found. C, 62.10; H, 8.88%. Calcd for $C_{12}H_{21}O_2Cl$: C, 61.92; H, 9.10%.

Ethyl (±)-trans-Chrysanthemate (2). To a solution of diisopropylamine (0.39 ml, 3.0 mmol) in 3 ml of THF was added dropwise the solution of butyllithium (3.6 mmol) in 3 ml of ether at 0 °C. After the mixture was stirred for 30 min at 0 °C, 0.25 ml of HMPT was added dropwise. After being stirred for additional 30 min at 0 °C, was added the solution of the chloroester **8** (225 mg, 0.97 mmol) in 2 ml of THF. The mixture was stirred for 40 min at 0 °C and then allowed to react for overnight at room temperature. The resulting mixture was poured into a large exess of 10% HCl and extracted with ether, dried over $MgSO_4$. After removal of the solvent, an yellow oil was obtained. It was separated by column chromatograph on a silica gel (7 g of Wakogel C-200, hexane : acetone=10 : 1) to afford 114 mg of **2**, 75% yield. The analytical sample was obtained by preparative GLPC[11] and identified by comparison of its IR and NMR spectra with those of authentic sample.[9]

Ethyl 2-Methyl-4-(2-methyl-1-propenyl)-5,5-dimethyl-4,5-dihydrofuran-3-carboxylate (12a). To a stirred solution of lactone **7a** (331 mg, 1.58 mmol) in 15 ml of ethanol was added thionyl chloride (1.16 ml, 15.8 mmol) dropwise at room temperature. During the addition a vigorous exothermic reaction occurred. The resulting solution was stirred for 6 h at 70 °C. After removal of the solvent and low boiling materials under reduced pressure, there was obtained a residual dark brown oil. It was separated by column chromatograph on a silica gel (Wakogel C-200, hexane : acetone=10 : 1) to give 308 mg of crude **12a**, 82% yield. The analytical sample was obtained by preparative TLC on a silica gel (hexane : acetone=4 : 1) followed by bulb-to-bulb distillation: bp 110 °C (5 Torr); IR (neat) 1695 (conjugated ester C=O), 1648 cm^{-1} (C=C); NMR (CCl_4) δ 1.17 (t, 3H, J=7 Hz, ester CH_3), 1.17 (s, 3H, 5-CH_3), 1.28 (s, 3H, 5-CH_3), 1.64 (d, 3H, J=1 Hz, $\gtrless$-CH_3), 1.69 (d, 3H, J=1 Hz, $\gtrless$-CH_3), 2.08 (d, 3H, J=0.2 Hz, 2-CH_3), 3.45 (d, 1H, J=10 Hz, 4-H), 4.01 (q, 2H, J=7 Hz, ester CH_2), 4.91 (md, 1H, J=10 Hz, $\gtrless$-H); MS *m/e* (rel. intensity) 238 (M^+), 223 (M−CH_3), 183 (32), 177 (12), 149 (14), 119 (14), 1.0

(14), 107 (27), 91 (32), 79 (17), 67 (20), 43 (100).

Found: C, 70.77; H, 9.35%. Calcd for $C_{14}H_{20}O_3$: C, 70.56; H, 9.30%.

Ethyl 2-Phenyl-4-(2-methyl-1-propenyl)-5,5-dimethyl-4,5-dihydrofuran-3-carboxylate (**12b**). The reaction of α-benzoylpyrocin (971 mg, 3.57 mmol) with thionyl chloride (3.04 ml, 35.7 mmol) in 20 ml of ethanol was carried out in the same manner as the foregoing experiment to give 940 mg of **12b**, 87% yield. The analytical sample was obtained by preparative TLC on a silica gel (hexane : acetone=4 : 1): IR (neat) 1685—1690 (conjugated ester C=O), 1622 (C=C), 1597—1580 cm^{-1} (phenyl C=C); NMR (CCl_4) δ 1.17 (t, 3H, J=8 Hz, ester CH_3), 1.25 (s, 3H, 5-CH_3), 1.35 (s, 3H, 5-CH_3), 1.68 (d, 3H, J=1 Hz, $\gtrless$-CH_3), 1.70 (d, 3H, J=1 Hz, $\gtrless$-CH_3), 3.66 (d, 1H, J=10 Hz, 4-H), 3.97 (q, 2H, J=8 Hz, ester CH_2), 5.05 (md, 1H, J=10 Hz, $\gtrless$-H), 7.2—7.8 (m, 5H, C_6H_5); MS *m/e* 300 (M^+), 285 ($M-CH_3$), 227 ($M-CO_2Et$).

Found: C, 76.11; H, 8.16%. Calcd for $C_{19}H_{23}O_3$: C, 75.97; H, 8.05%.

The natural abundance ^{13}C NMR spectra of **12a** and **12b** are summarized in the following structures. Off-resonance decoupling was used to support the assignment of **12a**.

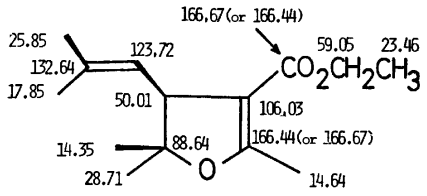

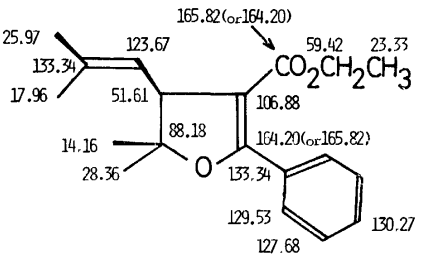

2-(1,1-Ethylenedioxyethyl)-3-(2-methyl-1-propenyl)-4,4-dimethyl-4-butanolide (**13**). A mixture of α-acetylpyrocin **7a** (840 mg, 4 mmol), ethylene glycol (248 mg, 4 mmol), and *p*-toluenesulfonic acid (3 mg, 0.02 mmol) in 5 ml of benzene was refluxed for 6.5 h with continuous removing of water as a benzene azeotrope. After cooling, the reaction mixture was washed with saturated aqueous $NaHCO_3$ and brine. An organic layer was separated and dried over $MgSO_4$. The removal of the solvent left 840 mg of the crude acetal **13**, 82% yield. The analytical sample was obtained as a clean oil by column chromatograph on a silica gel (7 g of Wakogel C-200, hexane : acetone=10 : 1): IR (neat) 1766 cm^{-1} (lactone C=O); NMR (CCl_4) δ 1.16 (s, 3H, γ-CH_3), 1.32 (s, 6H, γ-CH_3 and CH_3- ), 1.68 (d, 3H, J=0.1 Hz, $\gtrless$-CH_3), 1.74 (d, 3H, J=0.1 Hz, $\gtrless$-CH_3), 2.68 (d, 1H, J=11 Hz, α-H), 3.04 (dd, 1H, J=11 Hz and 9 Hz, β-H), 3.83 (m, 4H, O-CH_2CH_2-O), 5.06 (md, 1H, J=9 Hz, $\gtrless$-H).

Reaction of 2-(1,1-Ethylenedioxyethyl)-3-(2-methyl-1-propenyl)-4,4-dimethyl-4-butanolide with Thionyl Chloride in Ethanol. To a stirred solution of acetal **13** (372 mg, 1.47 mmol) in 15 ml of ethanol was added thionyl chloride (1.17 ml, 14.7 mmol) slowly at room temperature and allowed to react for additional 3 h at 60 °C. The removal of the solvent and low boiling materials left a dark brown oil. Filtration through a silica gel column (3 g of Wakogel C-200, hexane : acetone=10 : 1) helped to remove dark brown impurities. Evaporation of the solvent yielded 240 mg of an yellow oil. The GLPC analysis of the oil[12] showed two peaks at the retention times of 1.5 and 3.4 min in the ratio of 54 : 46. Each fraction was collected by preparative GLPC. The component with the retention time of 1.5 min was identified as dihydrofuran **12a** (20% yield estimated by GLPC) and the other as **7a**.

References

1) (a) M. Nagase and M. Matsui, *Nippon Nogei Kagaku Kaishi*, **20**, 249 (1942); (b) M. Matsui, *Botyu Kagaku*, **15**, 1 (1950); (c) L. Crombie, S. H. Harper, and R. A. Thompson, *J. Sci. Food Agric.*, **2**, 421 (1951); (d) M. Matsui and M. Uchiyama, *Agric. Biol. Chem.*, **26**, 532 (1962).

2) (a) M. Matsui, T. Ohno, S. Kitamura, and M. Toyao, *Bull. Chem. Soc. Jpn.*, **25**, 210 (1952); (b) M. Matsumoto and S. Suzuki, *J. Org. Chem.*, **25**, 1666 (1960); (c) M. Julia, S. Julia, C. Jeanmart, and M. Langlois, *C. R. Acad. Sci.*, **251**, 249 (1960); (d) M. Julia, S. Julia C. Jeanmart, and M. Langlois, *Bull. Soc. Chim. Fr.*, **1962**, 2243; (e) M. Matsui, H. Yoshioka, Y. Yamada, H. Sakamoto, and T. Kitahara, *Agric. Biol. Chem.*, **29**, 784 (1965); (f) M. Julia, Fr. Patent 1519895 (1968); *Chem. Abstr.*, **70**, 114638q (1968); (g) M. Julia, Fr. Patent Addn. 92123 (1968); *Chem. Abstr.*, **71**, 101395d (1968); (h) W. Sucroward and W. Richter, *Tetrahedron Lett.*, **1970**, 3675; (i) M. Matsui and K. Ueda, Jpn. Patent 7132175 (1971); *Chem. Abstr.*, **75**, 140668x (1971); (j) K. Kondo and F. Mori, *Chem. Lett.*, **1974**, 471; (k) H. Hirai, K. Ueda, and M. Matsui, *Agric. Biol. Chem.*, **40**, 153 (1976).

3) A. Takeda, S. Tsuboi, and T. Sakai, *J. Org. Chem.*, **39**, 2601 (1974).

4) L. Crombie and S. H. Harper, *J. Chem. Soc.*, **1954**, 470.

5) The courtesy of Dr. K. Kondo of Sagami Chemical Research Center, Sagamihara, and Dr. F. Mori of Kuraray Co., Ltd., Kurashiki.

6) H. Hirai and M. Matsui, *Agric. Biol. Chem.*, **40**, 161 (1976).

7) (a) R. A. Kretchmer, *J. Org. Chem.*, **37**, 2744 (1972); (b) J. S. Zweig, J. L. Luche, E. Rarreiro, and P. Crabbe, *Tetrahedron Lett.*, **1975**, 2355. These authors have found that (−)-sparteine causes asymmetric Michael addition of organometallic reagents to $\Delta^{\alpha,\beta}$-unsaturated carbonyl compounds. It has been suggested in these literatures that this chiral diamine acts as a bindetate ligand which creates a chiral environment around the metal atom, and this chirality is reflected in the stereochemistry of the addition product. It also has been suggested that the synthetic yield is reduced, due to the formation of bulky and hindered metal complex of **6** and (−)-sparteine.

8) (a) M. Julia, S. Julia, and M. Langlois, *C. R. Acad. Sci.*, **256**, 436 (1963); (b) M. Julia, S. Julia, and M. Langlois, *Bull. Soc. Chim. Fr.*, **1965**, 1014; (c) M. Julia, Fr. Patent 1269127 (1961); *Chem. Abstr.*, **57**, 2096g (1962). The synthetic method of **2** *via* the ester **8** has been patented by M. Julia. It involves the preparation of **8** by the treatment of **1** with $SOCl_2$ in $CHCl_3$ followed by the addition of ethanolic HCl. There has been given any scientific datum of **8** supporting its structure neither in the patent record nor in other publications.

9) (a) J. L. Pierre, R. Perraud, and P. Arnaud, *Bull. Soc. Chim. Fr.*, **1970**, 1540; (b) G. Pattenden, L. Crombie, and P. Hemesley, *Org. Mass Spectrom.*, **7**, 719 (1973).

10) E. A. Bauole and E. A. Evans, *J. Chem. Soc.*, **1955**, 3324.

11) 10% Apiezone Grease L on Chromosolb W; oven temperature 170 °C, N_2 1000 ml/min.

12) Carbo Wax 20 M on Celite 545; oven temperature 180 °C, N_2 1000 ml/min.

Substituent Effects on the Photo-ethoxycarbonylation of Monosubstituted Ferrocenes

Takeo AKIYAMA, Taro KITAMURA, Takao KATO, Haruo WATANABE, Toshio SERIZAWA, and Akira SUGIMORI

Department of Chemistry, Faculty of Science and Technology, Sophia University, Kioi-cho 7, Chiyoda-ku, Tokyo 102

(Received March 17, 1976)

The effect of the substituent in the ferrocene nucleus on the photo-ethoxycarbonylation of monosubstituted ferrocene in carbon tetrachloride–ethanol solution is described. The electron withdrawing substituents, such as chloro, bromo, iodo, cyano, and acetyl, retarded the photo-ethyoxycarbonylation, whereas the electron releasing substituents, such as ethyl accelerated the reaction. The electronic effects which affect the formation of the charge transfer complex and those which affect the reactivity of the cyclopentadienyl ring toward the attack of a trichloromethyl radical can be considered for the photo-ethoxycarbonylation.

In the previous paper,[1a] we reported the photochemical introduction of ethoxycarbonyl, formyl, and ethoxymethyl into the ferrocene nucleus in carbon tetrachloride–, chloroform–, and dichloromethane–ethanol solutions. In the photo-ethoxycarbonylation of ferrocene in the carbon tetrachloride–ethanol system, the excitation of the charge transfer complex of ferrocene with carbon tetrachloride plays an important role in the initial stage of the photo-substitution.[1b] This paper deals with the effect of the substituent in the ferrocene nucleus upon the photo-ethoxycarbonylation of monosubstituted ferrocene in carbon tetrachloride–ethanol solutions.

Experimental

Materials. Ethylferrocene[2] [bp 92 °C/1 Torr, (lit,[3] 93—94 °C/1 Torr)], acetylferrocene[4] [mp 85—86.5 °C(lit,[4] 85—86 °C)], iodoferrocene[5] [mp 48—49 °C (lit,[5] 43—45 °C)], chloroferrocene[6] [mp 59 °C(lit,[7] 59—60 °C)], bromoferrocene[6] [mp 36.1—36.2 °C(lit,[6] 30—31 °C)], cyanoferrocene[6] [mp 103.5 °C(lit,[8] 107—108 °C)], methoxyferrocene[7] [mp 41.5—41.8 °C(lit,[7] 38.5—40 °C)], and phenylferrocene[9] [mp 114 °C(lit,[9] 114—5 °C)] were prepared from ferrocene(Wako Junyaku Co., G. R. grade reagent) by the method given in the literatures. Carbon tetrachloride and ethanol were purified by the method described in the previous paper.[1a]

Irradiation Procedure. General procedure is similar to that described previously.[1a]

Separation of the Photoproducts (General Procedure). After irradiation, the reaction mixture was washed successively with water, aqueous sodium hydrogencarbonate solution and aqueous sodium thiosulfate solution, and then extracted with dichloromethane or ether. The extract was dried over anhydrous sodium sulfate, then the solvent was removed by a rotary evaporator below 30 °C. The residue was subjected to thin layer(Merck, GF-254) or column(Wako Junyaku Co., Wakogel C-200) chromatography in order to separate the photoproducts and the starting material, and then the ethoxycarbonylated compounds were isolated by the second thin layer chromatography(TLC).

Identification of the Photoproducts. The assignments of the chemical shifts of 2-, 3-, 4-, and 5-position were done based on the calculated chemical shifts of those positions. The calculated chemical shifts were obtained by summing the deshielding or the shielding effect of the substituent and the deshielding effect of ethoxycarbonyl to α- and β-positions.[10] The experimentally obtained chemical shifts agreed generally with the calculated ones.

Ethyl 2-Ethylferrocenecarboxylate: A dark red liquid substance. NMR(CCl_4), δ(ppm from TMS) 4.60(t), 1H(H_5); 4.26—4.09, 2H(H_3 and H_4); 4.20(q), 2H(–CH_2– of ester); 4.0(s), 5H(C_5H_5); 2.45—2.93(m), 2H(–CH_2– of ethyl[11,12]); 1.34(t), 3H(–CH_3 of ester); 1.13(t), 3H(–CH_3 of ethyl). IR (direct), 3100, 2960, 2920, 1100, 1000, 920 cm^{-1} (2-substituted ethylferrocene), 1705, 1290 cm^{-1} (ester). MS(70 eV), *m/e*, 286(M^+). Found: C, 62.13; H, 6.35%. Calcd for $C_{15}H_{18}O_2Fe$: C, 62.94; H, 6.29%, Mol wt, 286.

Ethyl 3-Ethylferrocenecarboxylate: A dark red oily substance. NMR(CCl_4), δ(ppm from TMS) 4.62(t), 2H(H_2 and H_5); 4.26—4.2(q and t), 3H(–CH_2– of ester and H_4); 4.05(s), 5H(C_5H_5); 2.35(q), 2H(–CH_2– of ethyl); 1.32(t), 3H(–CH_3 of ester); 1.19(t), 3H(–CH_3 of ethyl). IR(direct), 3100, 2960, 2920, 1100, 1000, 930, 910 cm^{-1} (3-substituted ethylferrocene), 1705, 1285 cm^{-1}(ester). MS(70 eV), *m/e*, 286(M^+). Found: C, 62.29; H, 6.45%. Calcd for $C_{15}H_{18}O_2Fe$: C, 62.94; H, 6.29%, Mol wt, 286.

Ethyl 1'-Ethylferrocenecarboxylate: A red oily substance. NMR(CCl_4), δ(ppm from TMS) 4.61(t), 2H(H_2 and H_5); 4.24—4.15, 4H(H_3 and H_4, and –CH_2– of ester); 3.98(s), 4H($H_{2'}$, $H_{3'}$, $H_{4'}$, $H_{5'}$); 2.30(q), 2H(–CH_2– of ethyl); 1.32(t), 3H(–CH_3 of ester); 1.12(t), 3H(–CH_3 of ethyl). IR(direct), 3080, 2960, 2920, 900, 890 cm^{-1} (the absence of absorption at 9 and 10 μ indicates 1,1'-disubstituted ferrocene), 1710, 1270 cm^{-1} (ester). MS(70 eV), *m/e*, 286(M^+). Found: C, 62.67; H, 6.60%. Calcd for $C_{15}H_{18}O_2Fe$: C, 62.94; H, 6.60%, Mol wt, 286.

Ethyl 3-Phenylferrocenecarboxylate: A yellow orange solid. NMR(CCl_4), δ(ppm from TMS) 7.50—7.05(m), 5H(–C_6H_5); 5.18(t), 1H(H_2); 4.83(t), 1H(H_5); 4.74(t), 1H(H_4); 4.24(q), 2H(–CH_2– of ester); 4.01(s,) 5H(C_5H_5); 1.36(t), 3H(–CH_3 of ester). IR(KBr), 3100, 3050, 1600, 1100, 1000, 925, 890 cm^{-1} (3-substituted phenylferrocene), 1705, 1240 cm^{-1} (ester). MS (70 eV), *m/e*, 334(M^+). Found: C, 68.27; H, 5.36%. Calcd for $C_{19}H_{18}O_2Fe$: C, 68.26; H, 5.39%, Mol wt, 334.

Ethyl 2-Phenylferrocenecarboxylate: A yellow oily substance. IR(KBr), 3100, 3050, 1600, 1105, 997, 950 cm^{-1} (2-substituted phenylferrocene), 1705, 1240 cm^{-1} (ester). MS(70 eV), *m/e*, 334(M^+). Found: C, 68.77; H, 5.44%. Calcd for $C_{19}H_{18}O_2Fe$: C, 68.26; H, 5.39%, Mol wt, 334.

Ethyl 1'-Phenylferrocenecarboxylate: A yellow orange solid. NMR(CCl_4), δ(ppm from TMS) 7.5—7.1(m), 5H(–C_6H_5); 4.55(t), 4H($H_{2'}$, $H_{5'}$ and H_2, H_5); 4.25(t), 2H(H_3 and H_4); 4.14(t), 2H($H_{3'}$ and $H_{4'}$); 4.01(q), 2H(–CH_2– of ester); 1.26 (t), 3H(–CH_3 of ester). IR(KBr), 3090, 3050, 1600, 920, 880 cm^{-1} (1'-substituted phenylferrocene), 1685, 1280 cm^{-1} (ester). MS(70 eV), *m/e*, 334(M^+). Found: C, 68.14; H, 5.38%. Calcd for $C_{19}H_{18}O_2Fe$: C, 68.26; H, 5.39%, Mol wt, 334.

Ethyl p-*Ferrocenylbenzoate*: A yellow orange solid substance. NMR(CCl_4), δ(ppm from TMS) 7.95—7.35(q), 4H (1,4-disubstituted benzene); 4.16(t), 2H(H_2 and H_5); 4.28(t), 2H(H_3 and H_4); 4.35(q), 2H(-CH_2- of ester); 3.96(s), 5H(C_5H_5); 1.38(t), 3H(-CH_3 of ester). IR(KBr), 3070, 3040, 1610, 1100, 1000 cm^{-1} (phenylferrocene), 1705, 1235 cm^{-1}(ester). Found: C, 68.00; H, 5.39%. Calcd for $C_{19}H_{18}O_2Fe$: C, 68.26; H, 5.39%.

Ethyl 3-Methoxyferrocenecarboxylate: A yellow liquid substance. NMR(CCl_4), δ(ppm from TMS) 4.58(t), 1H(H_2); 4.45(q), 1H(H_5); 4.23(q), 1H(H_4); 4.19(q), 2H(-CH_2- of ester); 4.10(s), 5H(C_5H_5); 3.60(s), 3H(-OCH_3); 1.32(t), 3H (-CH_3 of ester). IR(KBr), 3100, 2960, 2920, 2860, 1100, 1000(sh), 940, 920 cm^{-1} (3-substituted methoxyferrocene), 1700, 1300 cm^{-1} (ester). MS(70 eV), *m/e*, 288(M^+). Found: C, 57.71; H, 5.51%. Calcd for $C_{14}H_{16}O_3Fe$: C, 58.38; H, 5.55%, Mol wt, 288.

Ethyl 1'-Methoxyferrocenecarboxylate: A yellow oily substance. NMR(CCl_4), δ(ppm from TMS) 4.71(t), 2H(H_2 and H_5); 4.26(t), 2H(H_3 and H_4); 4.19(q), 2H(-CH_2- of ester); 3.97 (t), 2H(H_2' and H_5'); 3,74(t), 2H(H_3' and H_4'); 3.55 (s), 3H(-OCH_3), 1.33(t), 3H(-CH_3 of ester). IR(KBr), 3100, 2960, 2920, 2860, 1100, 920, 865 cm^{-1} (1'-substituted methoxyferrocene), 1710, 1280 cm^{-1} (ester). MS (70 eV), *m/e*, 288(M^+).

Ethyl 2-Chloroferrocenecarboxylate: A yellow oily substance. NMR(CCl_4), δ(ppm from TMS) 4.68(t), 1H(H_5); 4.32—4.16, 4H(H_3 and H_4, and -CH_2- of ester); 4.10(s), 5H(C_5H_5); 1.33(t), 3H(-CH_3 of ester). IR(KBr), 3100, 3020, 1100, 1000, 915 cm^{-1} (2-substituted chloroferrocene), 1710, 1280 cm^{-1} (ester). MS(70 eV), *m/e*, 292(M^+).

Ethyl 3-Chloroferrocenecarboxylate: A yellow oily substance. NMR(CCl_4), δ(ppm from TMS) 4.97(t), 1H(H_2); 4.65(t), 1H(H_5); 4.54(*t*), 1H(H_4); 4.21(q), 2H(-CH_2- of ester); 4.23(s), 5H(C_5H_5); 1.31(t), 3H(-CH_3 of ester). IR(KBr), 3100, 1100, 1000, 905, 900 cm^{-1} (3-substituted chloroferrocence), 1710, 1280 cm^{-1} (ester). MS(70 eV), *m/e*, 292(M^+).

Ethyl 1'-Chloroferrocenecarboxylate: A yellow oily substance. NMR(CCl_4), δ(ppm from TMS) 4.77(t), 2H(H_2 and H_5); 4.35(t), 4H(H_2', H_5', and H_3, H_4); 4.24(q), 2H(-CH_2- of ester); 4.03(t), 2H(H_3' and H_4'); 1.35(t), 3H(-CH_3 of ester). IR(KBr), 3120, 1090, 915, 880 cm^{-1} (1'-substituted chloroferrocene), 1710, 1280 cm^{-1}(ester). MS(70 eV), *m/e*, 292(M^+).

Ethyl 2-Bromoferrocenecarboxylate: A yellow oily substance. NMR(CCl_4), δ(ppm from TMS) 4.63(t), 1H(H_5); 4.30—4.15, 4H(H_3, H_4, and -CH_2- of ester); 4.11(s), 5H(C_5H_5); 1.32(t), 3H(-CH_3 of ester). IR(KBr), 3100, 1095, 1000, 905 cm^{-1} (2-substituted bromoferrocene), 1700, 1265 cm^{-1} (ester). MS(70 eV), *m/e*, 337(M^+).

Ethyl 3-Bromoferrocenecarboxylate: A yellow oily substance. NMR(CCl_4), δ(ppm from TMS) 4.97(t), 1H(H_2); 4.67(t), 1H(H_5); 4.53(t), 1H(H_4); 4.20(s), 5H(C_5H_5); 4.30—4.15(q), 2H(-CH_2- of ester); 1.31(t), 3H(-CH_3 of ester). IR(KBr), 3110, 1100, 1000, 875 cm^{-1} (3-substituted bromoferrocene), 1700, 1275 cm^{-1} (ester). MS(70 eV), *m/e*, 337(M^+).

Ethyl 1'-Bromoferrocenecarboxylate: A yellow oily substance. NMR(CCl_4), δ(ppm from TMS) 4.73(t), 2H(H_2 and H_5); 4.35(t), 4H(H_2', H_5', and H_3, H_4); 4.23(q), 2H(-CH_2- of ester); 4.07(t), 2H(H_3' and H_4'); 1.38(t), 3H(-CH_3 of ester). IR(KBr), 3100, 910, 865 cm^{-1} (1'-substituted bromoferrocene), 1705, 1270 cm^{-1} (ester). MS(70 eV), *m/e*, 337(M^+).

Ethyl 2-Iodoferrocenecarboxylate: An orange red oily substance. NMR(CCl_4), δ(ppm from TMS) 4.68(t), 2H(H_3 and H_5); 4.24(t), 1H(H_4); 4.23(q), 2H(-CH_2- of ester); 1.33(t), 3H(-CH_3 of ester). IR(KBr), 3060, 1100, 1000(sh), 960, 930(sh) cm^{-1} (2-substituted iodoferrocene), 1700, 1270 cm^{-1} (ester). MS(70 eV), *m/e*, 384(M^+).

Ethyl 3-Iodoferrocenecarboxylate: An orange red oily substance. NMR(CCl_4), δ(ppm from TMS) 4.98(t), 1H(H_2); 4.68 (t), 1H(H_5); 4.52(t), 1H(H_4); 4.19(q), 2H(-CH_2- of ester); 4.12(s), 5H(C_5H_5); 1.24(t), 3H(-CH_3 of ester). IR(KBr), 3080, 1100, 990, 915, 860 cm^{-1} (3-substituted iodoferrocene), 1710, 1265 cm^{-1} (ester). MS(70 eV), *m/e*, 384(M^+).

Ethyl 1'-Iodoferrocenecarboxylate: An orange red oliy substance. NMR(CCl_4), δ(ppm from TMS) 4.70(t), 2H(H_2 and H_5); 4.34(t), 2H(H_3 and H_4); 4.27(t), 2H(H_2' and H_5'); 4.22(q), 2H(-CH_2- of ester); 4.12(t), 2H(H_3' and H_4'); 1.31 (t), 3H(-CH_3 of ester). IR(KBr), 3100, 905, 860 cm^{-1} (1'-substituted iodoferrocene), 1700, 1270 cm^{-1} (ester). MS(70 eV), *m/e*, 384(M^+).

Quantitative Analysis: For the photoreaction of phenyl- and haloferrocenes, quantitative analyses were carried out with GLPC(carbowax 20 M, 2 m glass column, column temperature: 170 °C for phenylferrocene and 202—230 °C for haloferrocenes. Ethyl ferrocenecarboxylate was used as an internal standard). For other monosubstituted ferrocenes, quantitative analyses were carried out by gravimetry, after the isolation of the photoproducts by column or thin layer chromatography.

Measurements: UV-spectra were recorded on a Hitachi 124 UV-VS spectrophotometer. IR-spectra were recorded on a Hitachi 215 grating infrared spectrophotometer. NMR spectra were taken with a Hitachi R-22(90 MHz) spectrometer. Mass spectra were recorded on a Hitachi RMU-6 spectrometer. Gas chromatography were performed on a Yanagimoto 550F gas chromatograph equipped with glass column.

Results and Discussion

On the irradiation with 365 nm light, ethyl-, methoxy-, phenyl-, and bromoferrocene in carbon tetrachloride–ethanol (1 : 1, v/v) solutions afforded the corresponding ethoxycarbonylated products, whereas chloro- and iodoferrocene gave only a small amount of ethoxycarbonylated products. No ethoxycarbonylation occurred in the case of cyano- and acetylferrocene. The yields of ethoxycarbonylated products and the yields of isomers are listed in Tables 1 and 2.

Ethylferrocene was effectively ethoxycarbonylated on the irradiation with 365 nm light. Ethyl 2-ethylfer-

Table 1. Photo-ethoxycarbonylation of monosubstituted ferrocenes in carbon tetrachloride–ethanol (1 : 1, v/v) solutions[a)]

Fc-R[b)] R	(mmol)	Irradiation conditions: Wavelength (nm)	Irradiation conditions: Time (h)	Conversion (%)	Ethoxycarbonyl products (%)[c)]
R=-C_2H_5	(2.3)	365	42	20.2	88.0
R=-H	(1.5)	365	50	17.0	61.0
R=-OCH_3	(1.3)	365	42	56.0	32.1
R=-C_6H_5	(1.3)	365	42	29.6	42.7
R=-Cl	(1.3)	365	42	17.0	4.7
R=-Br	(1.3)	365	42	11.0	16.9
R=-I	(1.3)	365	42	9.0	7.3
R=-$COCH_3$	(0.5)	365	42	29.0	0.0
R=-CN	(1.3)	365	42	39.0	0.0

a) Each reaction was carried out at room temperature under nitrogen atmosphere. The volume of the sample solution is 40 ml. b) Fc- denotes (C_5H_5)Fe(C_5H_4-). c) Yields based on consumed monosubstituted ferrocene.

Table 2. Yields of the isomers of ethoxycarbonylated ferrocene derivatives[a)]

Fc-R[b)] R	(mmol)	Irradiation conditions: Wavelength (nm)	Time (h)	Products and yields[c)] (%) Disubstituted ferrocene: 1,2-	1,3-	1,1'-	Ethyl *p*-ferrocenylbenzoate
R=-C_2H_5	(2.3)	365	42	10.8	35.9	41.3	—
R=-H	(1.5)	365	50	(Ethyl ferrocenecarboxylate, 61.0)		—	—
R=-OCH_3	(1.3)	365	42	0.0	8.6	23.5	—
R=-C_6H_5	(1.3)	365	42	2.1	12.0	20.9	7.7
R=-Cl	(1.3)	365	42	0.2	0.9	3.6	—
R=-Br	(1.3)	365	42	4.0	2.9	11.0	—
R=-I	(1.3)	365	42	1.6	1.4	4.3	—
R=-$COCH_3$	(0.5)	365	42	0.0	0.0	0.0	—
R=-CN	(1.3)	365	42	0.0	0.0	0.0	—

a) Each reaction was carried out at room temperature under nitrogen atmosphere. b) Fc- denotes $(C_5H_5)Fe-(C_5H_4-)$. c) Yields were calculated based on consumed monosubstituted ferrocene.

rocenecarboxylate, ethyl 3-ethylferrocenecarboxylate, and ethyl 1'-ethylferrocenecarboxylate were obtained. In phenylferrocene, ethoxycarbonylation occurred not only on the ferrocene ring but also on the *para*-position of the benzene ring. In spite of the high conversion of methoxyferrocene, the yield of ethoxycarbonylated product is low. Among the haloferrocenes, bromoferrocene was most effectively ethoxycarbonylated on the irradiation with 365 nm light, and 1,2- and 1,3-isomer were obtained in addition to 1,1'-isomer. Although the yields were lower, both 1,2- and 1,3-isomer were obtained in the case of iodoferrocene. The 2-position of chloroferrocene was less effectively ethoxycarbonylated than the same position of other haloferrocenes. No ethoxycarbonylation occurred in acetyl- and cyanoferrocene on the irradiation with 365 nm light, and only decomposition of the starting materials was observed. The results listed in Table 1 indicate that the reactivities of the monosubstituted ferrocenes toward photo-ethoxycarbonylation seem to be determined primarily by the electronic character of the substituent. Based on the proposed mechanism of photo-ethoxycarbonylation of ferrocene,[1b)] the effects of the substituent on the photo-ethoxycarbonylation can be considered in the following two separate cases:

(1) The effect of the substituent on the formation of the charge transfer complex of monosubstituted ferrocene with carbon tetrachloride.

(2) The effect of the substituent on the reactivity

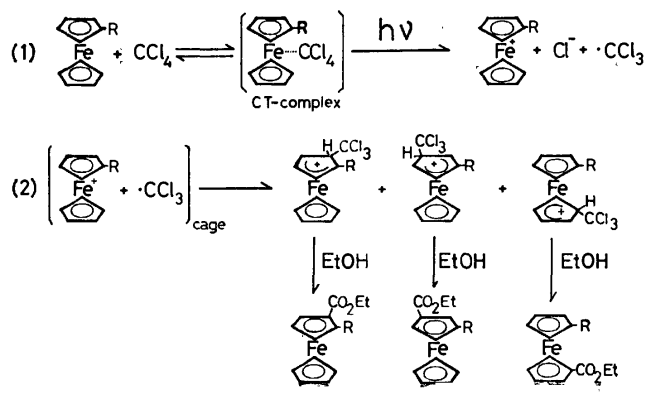

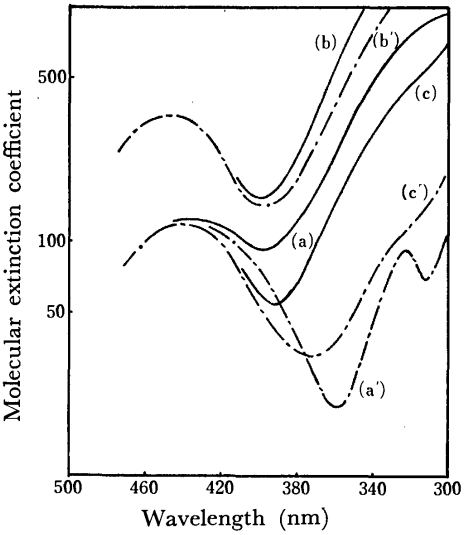

Fig. 1. UV-Spectra of ethylferrocene(2×10^{-3} mol l^{-1}), phenylferrocene(2×10^{-3} mol l^{-1}), and methoxyferrocene (2×10^{-3} mol l^{-1}) in ethanol and in carbon tetrachloride–ethanol(1 : 1, v/v) solutions. (a) Ethylferrocene in carbon tetrachloride–ethanol(1 : 1, v/v) solution. (a') Ethylferrocene in ethanol. (b) phenylferrocene in carbon tetrachloride–ethanol(1 : 1, v/v) solution. (b') Phenylferrocene in ethanol. (c) Methoxyferrocene in carbon tetrachloride–ethanol(1 : 1, v/v) solution. (c') Methoxyferrocene in ethanol.

of the cyclopentadienyl ring of ferrocene toward the attack of a trichloromethyl radical.

The contribution of the charge transfer complex to this photo-substitution was examined by the analyses of UV-spectra. The UV-spectra of monosubstituted ferrocenes in ethanol solutions and in carbon tetrachloride–ethanol(1 : 1, v/v) solutions are shown in Figs. 1, 2, and 3. The UV-spectra of methoxy-, ethyl-, phenyl-, chloro-, bromo-, and iodoferrocene in carbon tetrachloride–ethanol solutions show an increment of absorption compared with those in ethanol solutions in 300—360 nm region, whereas only slight enhancements of absorption were observed in the cases of acetyl- and cyanoferrocene. The increment of absorption in this region can be ascribed to the formation of a charge

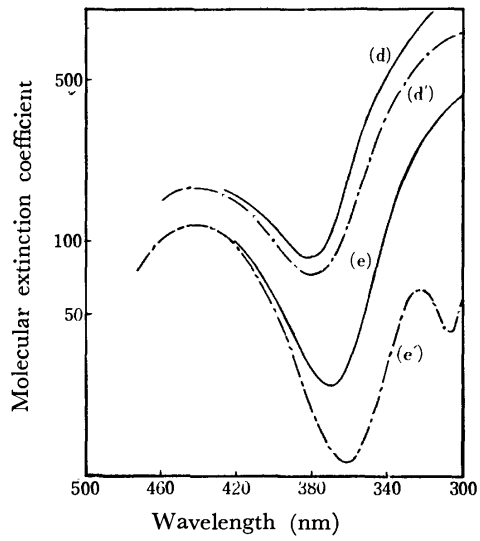

Fig. 2. UV-Spectra of iodoferrocene(2×10^{-3} mol l^{-1}), and chloroferrocene(2×10^{-3} mol l^{-1}) in ethanol and in carbon tetrachloride-ethanol(1 : 1, v/v) solutions. (d) Iodoferrocene in carbon tetrachloride-ethanol(1 : 1, v/v) solution. (d') Iodoferrocene in ethanol. (e) Chloroferrocene in carbon tetrachloride-ethanol(1 : 1, v/v) solution. (e') Chloroferrocene in ethanol.

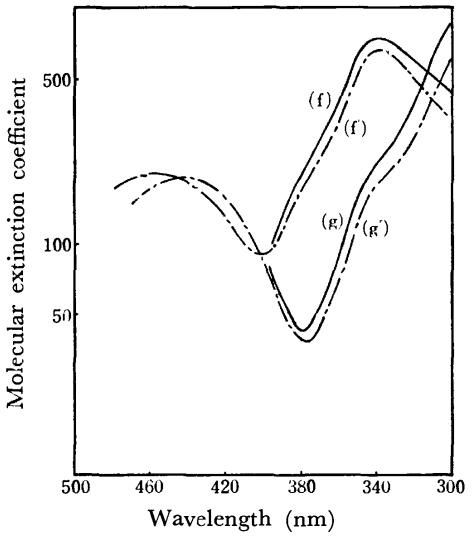

Fig. 3. UV-Spectra of acetylferrocene(2×10^{-3} mol l^{-1}) and cyanoferrocene(2×10^{-3} mol l^{-1}) in ethanol and in carbon tetrachloride-ethanol(1 : 1, v/v) solutions. (f) Acetylferrocene in carbon tetrachloride-ethanol(1 : 1, v/v) solution. (f') Acetylferrocene in ethanol. (g) Cyanoferrocene in carbon tetrachloride-ethanol (1 : 1, v/v)solution. (g') Cyanoferrocene in ethanol.

transfer complex between monosubstituted ferrocene and carbon tetrachloride. The increment of absorption, $\Delta\varepsilon$ (expressed in terms of the increase in apparent molar extinction coefficient, therefore, $\Delta\varepsilon=\varepsilon_{app.}-\varepsilon$) at 300 nm for monosubstituted ferrocenes, was used as a measure of the ability of charge transfer complex formation of monosubstituted ferrocene. Ferrocenes with an electron releasing substituent, such as ethyl and methoxyl, gave higher $\Delta\varepsilon_{300}$ values, whereas those with an electron withdrawing substituent gave lower values

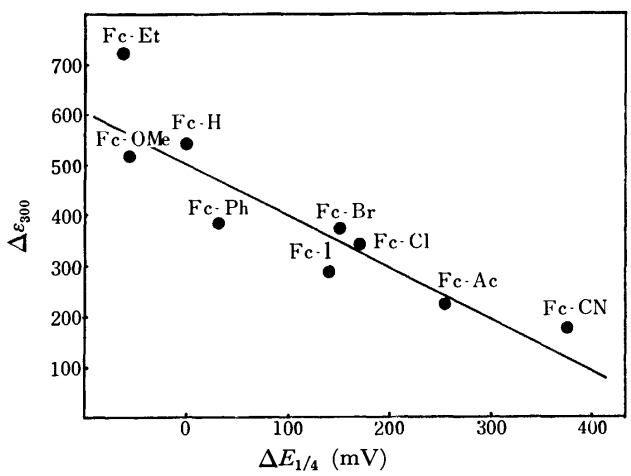

Fig. 4. Plot of the increment of UV-absorption at 300 nm against the oxidation potential, $\Delta E_{1/4}$.

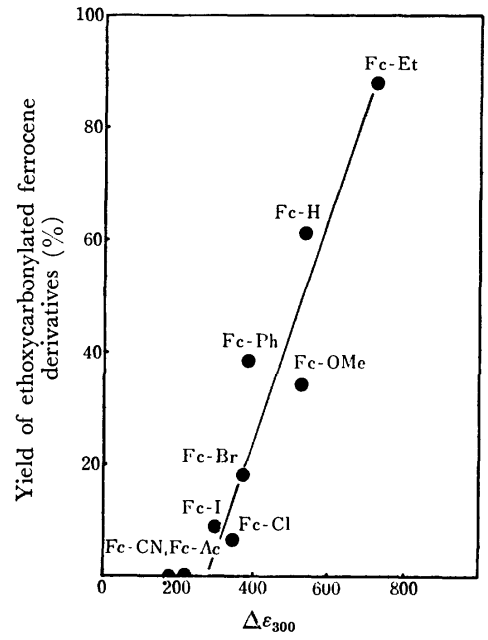

Fig. 5. Plot of the yield of ethoxycarbonylated ferrocene derivative against the increment of UV-absorption at 300 nm.

than ferrocene. These values and the oxidation potentials $\Delta E_{1/4}$(the difference of the chronopotentiometric quarter wave oxidation potentials of substituted ferrocene from that of ferrocene)[13] show a good correlation(Fig. 4). The yields of ethoxycarbonylated products of monosubstituted ferrocenes can also be correlated to $\Delta\varepsilon_{300}$(Fig. 5). These results indicate that the excitation of the charge transfer complex of monosubstituted ferrocene and carbon tetrachloride contribute greatly to the photo-ethoxycarbonylation, as in the case of ferrocene.[1b]

Because of the electrophillic nature of the trichloromethyl radical, the site reactivities of monosubstituted ferrocenes for photo-ethoxycarbonylation can be compared with those for Friedel Crafts' acetylation, which have been extensively investigated by many workers.[14] The site reactivities of monosubstituted ferrocenes for

Table 3. Site reactivities of monosubstituted ferrocenes for photo-ethoxycarbonylation and for acetylation[a)]

Fc-R[b)]	Position		
	2	3	1′
R=-C_2H_5	0.65	2.17	1.00
	(1.4)	(4.2)	(1.0)
R=-OCH_3	0.00	1.02	1.00
	(3.7)	(2.3)	(1.0)
R=-C_6H_5	0.25	1.44	1.00
	(0.7)	(0.4)	(1.0)
R=-Cl	0.02	0.65	1.00
	(0.0)	(0.0)	(1.0)
R=-Br	0.90	0.72	1.00
	(0.0)	(0.0)	(1.0)
R=-I	0.92	0.85	1.00
	(0.0)	(0.0)	(1.0)

a) The values in parentheses are the site reactivities for Friedel Crafts' acetylation taken from references.[14)] The reactivity of unsubstituted ring (1′-position) is taken as 1.00. b) Fc- denotes $(C_5H_5)Fe(C_5H_4-)$.

photo-ethoxycarbonylation and those for acetylation are shown in Table 3.

In the case of ethylferrocene, the reactivities of 2- and 3-position for photo-ethoxycarbonylation are lower than those for acetylation, but the relative reactivities of 2-position to 3-position are similar to that of acetylation. The lower reactivity of 2-position than those of 3- and 1′-position indicates that the steric effect is also important in the substitution. In the case of methoxyferrocene, an extremely low reactivity of 2-position can not be explained only by a steric effect, since this position is one and a half times more reactive than 3-position for the electrophillic substitution.[14a)] In the case of phenylferrocene, the reactivities of 2- and 3-position seem to be quite different from those for acetylation; although the higher reactivity of 3-position than 2-position for ethoxycarbonylation can be explained by a steric repulsion of a large phenyl group and a bulky trichloromethyl radical, the value 1.44 for 3-position is very high compared to 0.4 for 3-position in acetylation. In the cases of haloferrocenes, this tendency is more obvious; although the homoannular substitution is completely inhibited in acetylation even under drastic conditions,[15)] homoannular substitution occurred with nearly the same efficiency as heteroannular substitution in the photo-ethoxycarbonylation. These results indicate that the electrophilicity of the trichloromethyl radical is not so high as to be affected by the electronic nature of the substituents. Therefore, the low yields of ethoxycarbonylated products for haloferrocenes may be due mainly to the efficiency of the formation of the charge transfer complex between monosubstituted ferrocene and carbon tetrachloride.

The authors wish to express their thanks to Mr. Tatsuzo Ishigami of Aoyama Gakuin University for the measurement of mass spectra. The present work was partially supported by a Grant-in-Aid for Scientific Research from the Ministry of Education.

References

1) a) T. Akiyama, Y. Hoshi, S. Goto, and A. Sugimori, *Bull. Chem. Soc. Jpn.*, **46**, 1851 (1973); b) T. Akiyama, A. Sugimori, and H. Hermann, *Bull. Chem. Soc. Jpn.*, **46**, 1855 (1973).

2) K. Sakai, M. Ishige, H. Kono, I. Motoyama, K. Watanabe, and K. Hata, *Bull. Chem. Soc. Jpn.*, **41**, 1902 (1968).

3) A. N. Nesmeyanov, E. G. Perevalova, and L. S. Shilovtseva, *Izv. Akad. Nauk SSSR, Otdel. Khim. Nauk*, **1961**, 1982.

4) P. J. Graham, R. V. Lindsey, G. W. Parshall, M. L. Peterson, and G. M. Whitman, *J. Am. Chem. Soc.*, **79**, 3416 (1957).

5) H. Shechter and J. F. Helling, *J. Org. Chem.*, **26**, 1035 (1961).

6) M. Sato, T. Ito, I. Motoyama, K. Watanabe, and K. Hata, *Bull. Chem. Soc. Jpn.*, **42**, 1976 (1969).

7) A. N. Nesmeyanov, W. A. Sazonova, and V. N. Drozd, *Chem. Ber.*, **93**, 2717 (1960).

8) A. N. Nesmeyanov, E. G. Perevalova, and L. P. Yur'eva, *Chem. Ber.*, **93**, 2729 (1960).

9) M. Rosenblum, W. G. Howells, A. K. Banerjee, and C. Bennett, *J. Am. Chem. Soc.*, **84**, 2726 (1962).

10) D. W. Slocum and C. R. Ernst, "Advances in Organometallic Chemistry," Vol. 10, ed by F. G. A. Stone and R. West, Academic Press, New York, N. Y. (1972), p. 83.

11) R. Benkaser, Y. Nagai, J. Hooz, *Bull. Chem. Soc. Jpn.*, **36**, 482 (1963).

12) P. L. Pauson, M. A. Sandhu, W. E. Watts, R. C. Haley, and G. R. Knox, *J. Chem. Soc., C*, **1967**, 1851.

13) D. W. Hall and C. D. Russell, *J. Am. Chem. Soc.*, **89**, 2316 (1967), and Ref. 10, p. 98.

14) a) G. R. Knox, I. G. Morrison, P. L. Pauson, M. A. Sandhu, and W. E. Watts, *J. Chem. Soc., C*, **1967**, 1853; b) M. Rosenblum, "Chemistry of the Iron Group Metallocenes," Vol. 1, John Wiley (Interscience), New York, N. Y. (1965), p. 75.

15) D. W. Hall and J. H. Richards, *J. Org. Chem.*, **28**, 1549 (1963).

ESR Studies of Nitrogen-centered Free Radicals, *N*-Aryl-*N*-phenylthioaminyls[1)]

Yozo MIURA and Masayoshi KINOSHITA

Department of Applied Chemistry, Faculty of Engineering, Osaka City University, Sumiyoshi-ku, Osaka 558

(Received September 21, 1976)

A variety of substituted *N*-phenyl-*N*-phenylthioaminyls (**2**), Ar–N̈–S–Ar′, were generated by the photolysis of benzenesulfenanilides (**1**) in benzene in the presence of di-*t*-butyl peroxide or by the oxidation of **1** in benzene with lead dioxide. The ESR spectra of the radicals were completely analyzed by labeling some radicals with deuterium and with the aid of a computer simulation technique. The unpaired electron is distributed mainly on the nitrogen atom and the *N*-phenyl ring. The values of a_N were plotted against the σ or σ^- in the Hammett equation, and it was found that **2**, in terms of Walter's criteria, belong to class S.

A number of nitrogen-centered free radicals have been prepared, and extensive ESR spectroscopic studies have been undertaken.[2)] In the course of our studies of nitrogen-centered free radicals bearing sulfur atoms adjacent to the radical centers, *N*-aryl-*N*-phenylthioaminyls (**2**) have been found to be easily generated by hydrogen-abstraction from benzenesulfenanilides (**1**). The radicals possess a divalent sulfur atom adjacent to the radical center and have never been reported to be detected unambiguously.[3)] A few radicals relating to **2** have thus far been reported, but no systematic ESR spectroscopic investigation of the radicals has yet been undertaken.[4–7)] More recently, however, Ingold *et al.* have reported a detailed ESR spectroscopic investigation of radicals which are generated by radical additions to di-*t*-butyl sulfur diimide.[8)]

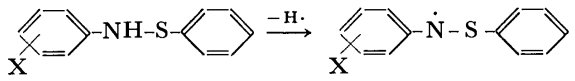

1 **2**

The present authors have now generated a variety of substituted *N*-aryl-*N*-phenylthioaminyls (**2**) and investigated them in detail by means of ESR spectroscopy. In the present report, the results will be described and discussed.

Results and Discussion

The generation of **2** was performed by two procedures: a) the photolysis of **1** in degassed benzene in the presence of di-*t*-butyl peroxide, and b) the oxidation of **1** in degassed benzene with lead dioxide and potassium carbonate. In the present studies, procedure a has been mainly employed, because that the procedure is more convenient and, although a low-power mercury lamp (100 W) was used as the source, the procedure generated **2** at a sufficient concentration for us to record well-resolved ESR spectra (10^{-5} mol/l except for **2a** and **2c**, the concentrations of which were lower). The radicals **2a** and **2c**, after irradiation for 10 min, immediately decayed on the turning out of the lamp. On the other hand, the radicals **2f** and **2m** could be detected over a period of more than 1 h, and the radicals **2d** and **2g** over a period of at least 2 h.

The radical **2a** presented a very complex ESR spectrum (Fig. 1). In order to facilitate the analysis of the spectrum and to avoid erroneous assignments, the

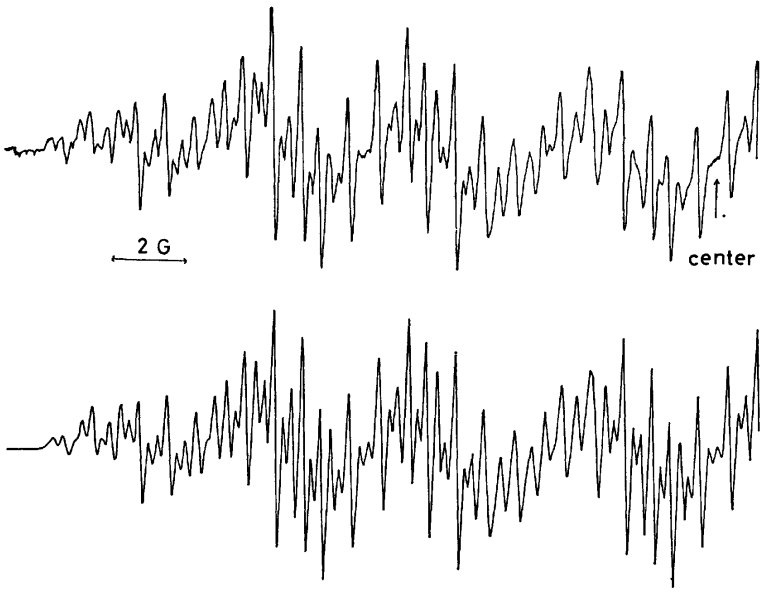

Fig. 1. Experimental ESR spectrum (low-field half) of *N*-phenyl-*N*-phenylthioaminyl (**2a**) in benzene (upper), and computer simulated, using Lorentzian line shapes and a line width of 0.20 G (lower).

radical was labeled with deuterium. The labeled radical, **2b**, gave a simple 1 : 1 : 1 triplet spectrum, which was obviously split by the interaction with the nitrogen nucleus. On the other hand, the spectrum of the other labeled radical, **2c**, was split into a 1 : 1 : 1 triplet due to the nitrogen nucleus, and each component of the triplet was split into 1 : 2 : 1 triplets of a 1 : 3 : 3 : 1 quartet due to the three equivalent *ortho*- and *para*-protons and the two *meta*-protons respectively. On the basis of these results, the spectrum of **2a** was analyzed.

Next, substituted *N*-phenyl-*N*-phenylthioaminyls were generated and the spectra were analyzed. The radicals **2f**—**h** each gave a relatively simple ESR spectrum (Fig. 2). On the other hand, the spectra of the other radicals were very complex (Figs. 3 and 4). Thus, some radicals were also labeled with deuterium, and the complex spectra were analyzed on the basis of the data from the labeled radicals. The ESR parameters for **2** are summarized in Table.

In general, it is well known that nitrogen-centered free radicals tend to convert into the corresonding ni-

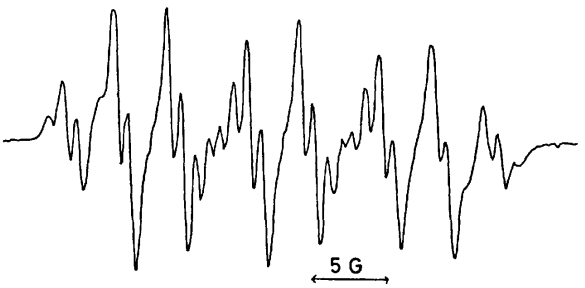

Fig. 2. Experimental ESR spectrum of *N*-3,5-dichlorophenyl-*N*-phenylthioaminyl (**2g**) in benzene.

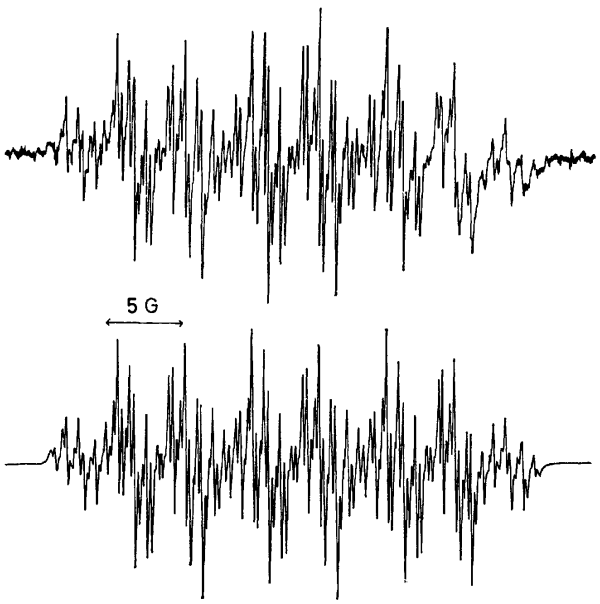

Fig. 3. Experimental ESR spectrum of *N*-3-acetylphenyl-*N*-phenylthioaminyl (**2k**) in benzene (upper), and compuer simulated, using Lorentzian line shapes and a line width of 0.19 G (lower).

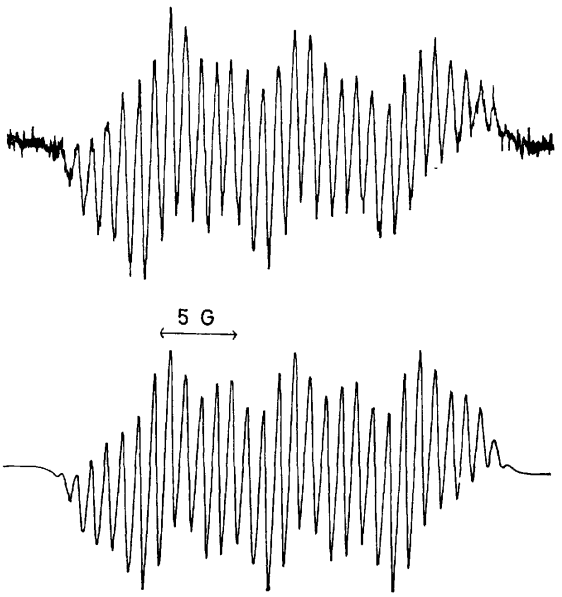

Fig. 4. Experimental ESR spectrum of *N*-4-nitrophenyl-*N*-phenylthioaminyl (**2m**) in benzene (upper), and computer simulated, using Lorentzian line shapes and a line width of 0.46 G (lower).

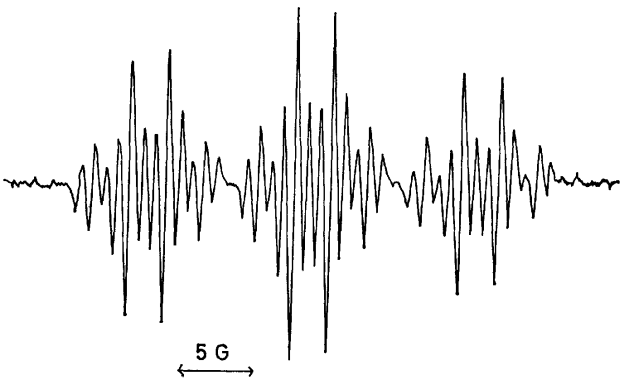

Fig. 5. Experimental ESR spectrum of the nitroxide radical **3** generated by photolysis of diphenyl disulfide in benzene in the presence of nitrosobenzene.

troxide radicals by reactions with oxidizing agents (*e. g.* atmospheric oxygen, *etc.*). In order to exclude this possibility, the corresponding nitroxide radical, **3**, was generated by the photolysis of diphenyl disulfide in benzene in the presence of nitrosobenzene (Fig. 5). The ESR parameters for **3** are 11.52 (a_N), 2.56 ($a_{o\text{-}H}$ and $a_{p\text{-}H}$), and 0.86 G ($a_{m\text{-}H}$).[9] From the results, it is clear that the radicals **2** are not nitroxide radicals.

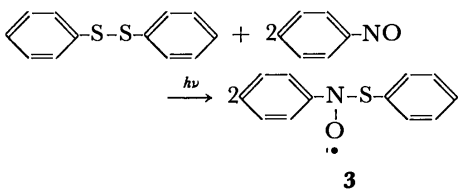

3

The radicals **2** can also be generated by the treatment of **1** with lead dioxide and potassium carbonate. For example, the sulfenamide **1d** in benzene, on contact

Table 1. The ESR parameters for *N*-aryl-*N*-phenylthioaminyls (**2**)[a]

Radical	Ar_1-$\dot{N}$-S-Ar_2		Coupling constant (G)								g-Value
				N-Phenyl			*S*-Phenyl				
	Ar_1	Ar_2	a_N	$a_{o\text{-H}}$	$a_{m\text{-H}}$	$a_{p\text{-H}}$	$a_{o\text{-H}}$	$a_{m\text{-H}}$	$a_{p\text{-H}}$	a_{other}	
2a[b]	C_6H_5	C_6H_5	9.59	3.70	1.26	4.18	0.78	0.27	0.84		2.0059
2b	C_6D_5	C_6H_5	9.56								2.0059
2c	C_6H_5	C_6D_5	9.59	3.78	1.23	3.78					2.0059
2d[b]	4-$CH_3C_6H_4$	C_6H_5	9.55	3.79	1.17	—	0.79	0.27	0.82	4.83(CH_3)	2.0059
2e[b]	4-$CH_3OC_6H_4$	C_6H_5	9.56	3.87	1.10	—	0.78		0.83	0.58(CH_3O)	2.0059
2f	4-ClC_6H_4	C_6H_5	9.48	3.79		—					2.0061
2g	3,5-$Cl_2C_6H_3$	C_6H_5	9.26	3.68	—	3.68	0.90		0.90		2.0061
2h	4-BrC_6H_4	C_6H_5	9.43	3.73		—					
2i[b]	4-$CH_3COC_6H_4$	C_6H_5	8.97	3.46	1.24	—	0.90		0.94		
2j	4-$CH_3COC_6H_4$	C_6D_5	8.97	3.43	1.24	—					2.0063
2k[b]	3-$CH_3COC_6H_4$	C_6H_5	9.45	3.59	1.22	3.92	0.83	0.25	0.87		
2l[b]	4-$NO_2C_6H_4$	C_6H_5	8.77	3.35	1.23	—	0.95		0.95	0.89(NO_2)	2.0065
2m[b]	4-$NO_2C_6H_4$	C_6D_5	8.75	3.37	1.22	—				0.88(NO_2)	2.0065
2n[b]	3-$NO_2C_6H_4$	C_6H_5	9.25	3.45	1.25	3.74	0.89	0.26	0.92	0.26(NO_2)	

a) In benzene at room temperature. b) The coupling constants were determined by means of the computer simulation technique.

with the oxidizing agents under degassed conditions, instantly turned dark blue. The color remained for *ca.* 10 s, after which, it slowly turned brown. The blue color seems to be responsible for **2d**,[10] while the brown color is probably attributable to decomposition products of **2d**. Similar blue solutions were also obtained in the cases of **1e**, **1f**, and **1m**. On the other hand, in **1j**, a greenish blue solution, and in **1g** and **1m**, green solutions were obtained. These colors immediately turned brown (except for **1g**, and in this case, the green color remained for *ca.* 20 min). From the brown solutions, however, only **2** was detected as a paramagnetic species by ESR spectroscopic measurements.

From the values of the coupling constants shown in the table, it may be concluded that, in **2**, the unpaired electron is distributed mainly on the nitrogen ($2p_z$ orbital) and the *N*-phenyl ring. On the other hand, it is of interest that couplings due to the *S*-phenyl ring protons are observed, indicating that the unpaired electron is also delocalized onto the *S*-phenyl ring across the divalent sulfur atom, though the degree of delocalization is small.

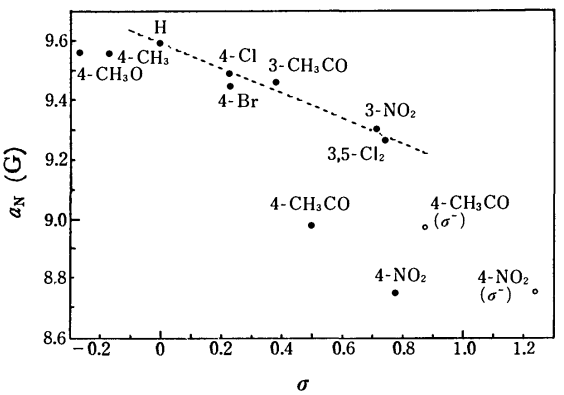

Fig. 6. Plot of nitrogen coupling constants (a_N) of *N*-aryl-*N*-phenylthioaminyls (**2**) *vs.* σ (and σ^-).

The values of a_N were plotted against the Hammett σ and σ^- parameters (Fig. 6).[11] In terms of Walter's criteria,[12] substituted aryl nitroxide radicals and nitrobenzene anion radicals[11] belong to class O, while *N*-alkyl-*N*-arylamino radicals have been reported to belong to class S.[13] As may be found in the figure, the values of a_N are correlated by neither σ nor σ^-,[14,15] indicating that **2** belong to class S. In the present radicals, the values of a_N seem to be decreased by two effects:[16] the delocalization of spin onto the substituents and the polar effect to be described below (Form B), as has been pointed out by Danen *at al.* in the case of *N*-alkoxy-*N*-arylamino radicals.[13]

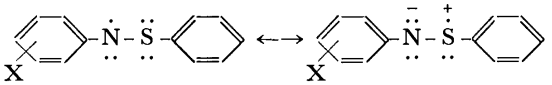

Form A Form B

About the polar effect, as more powerful electron-withdrawing substituents are introduced into the *N*-phenyl ring, the polar form B becomes more important. Therefore, the effect results in a decrease in the spin density on the nitrogen atom, while, on the contrary, that on the sulfur atom is increased. The degree of the effect may reflect the magnitude of coupling due to the *S*-phenyl ring protons. As can be seen in the table, the introduction of electron-withdrawing groups brings about an increase in the magnitude of the proton coupling constants. Although the difference in the magnitude of the coupling constants of the *para* protons in the *S*-phenyl ring is small, we attempted to plot the values against σ (and σ^-), the values being correlated by σ (and σ^-).

In the cases of non- and *meta*-substituted radicals (**2a**, **2g**, **2k**, and **2n**), only the polar effect is important because, as the spin density at the *meta* position is

considerably smaller than those at the *ortho* and *para* positions, the delocalization of the spin onto the substituents is negligibly small. About the four free radicals, the values of a_N are well correlated by σ, as may be found in the figure. In the cases of the other free radicals, on the other hand, the two effects are operative and the values of a_N are significantly decreased. Therefore, the values of a_N are correlated by neither σ nor σ^-.

Experimental

All the melting points are uncorrected. The IR spectra were run on a Jasco Model IR-G Spectrometer. The NMR spectra were recorded on a Hitachi-Perkin Elmer R-20 Spectrometer, using TMS as the internal standard. The elemental analyses were carried out with a Yanaco MT-2 CHN Corder.

Meterials. The benzene used for the ESR measurement was purified by the usual method.[1] Commercially available di-*t*-butyl peroxide was used without further purification, while nitrosobenzene was recrystallized once from ethanol just before use.

Benzenethiol-2,3,4,5,6-d_5. Aniline-2,3,4,5,6-d_5 (*D*-content; 99%, E. Merck, Darmstadt, Germany) was diazotized and treated with potassium xanthate.[17] The resulting xanthate ester was hydrolyzed with potassium hydroxide in ethanol, and then neutralized with sulfuric acid and water-distilled. The resulting oily product was extracted with ether and dried over anhydrous sodium sulfate. After filtration, ether was evaporated and the product was distilled (82—83 °C/55 Torr) to give the desired benzenethiol in a 53% yield. The *D*-content was determined to be 98% from the proton ratio in the NMR spectrum.

*General Procedure for the Preparation of Benzenesulfenanilides (**1**).* Benzenethiol was allowed to react with chlorine gas in dry chloroform at −5—0 °C. After the subsequent removal of chloroform, the resulting oily residue was distilled (56—57 °C/3 Torr) to give pure benzenesulfenyl chloride.[1] However, benzenesulfenyl chloride-d_5 was used for the following step without distillation.

Benzenesulfenyl chloride (0.025 mol) in dry ether (25 ml) was added, drop by drop, to aniline (0.055 mol) in dry ether (100—1000 ml) at −20——30 °C under stirring. After the completion of the addition, the reaction mixture was stirred for an additional 30 min and the reaction temperature was raised to room temperature. After the formed aniline hydrochloride had been filtered off, ether was evaporated to give crude **1**, which was treated with decoloring carbon and repeatedly recrystallized from the appropriate solvents.

Benzenesulfenanilide (**1a**): 54—56 °C (petroleum ether, lit,[18] 53—55 °C). 4'-Methylbenzenesulfenanilide (**1d**): 51—52 °C (petroleum ether, lit,[19] 52 °C). 4'-Methoxybenzenesulfenanilide (**1e**): 69—70 °C (hexane, lit,[19] 67 °C). 4'-Nitrobenzenesulfenanilide (**1l**): 109—110 °C (methanol-water, lit,[18] 108 °C).

Benzenesulfenanilide-2',3',4',5',6'-d_5 *(**1b**).* Mp 59—60 °C (petroleum ether). Yield 44%. IR (KBr): 3320 cm^{-1} (NH). NMR (CCl_4): δ 4.78 (s, NH) and 7.06 (s, C_6H_5). Found: C, 69.83; H, 5.53; N, 6.75%. Calcd for $C_{12}H_6D_5NS$: C, 69.85; H, 5.38; N, 6.79%.

Benzenesulfen-2,3,4,5,6-d_5*-anilide (**1c**).* Mp 57—58 °C (petroleum ether). Yield 69%. IR (KBr): 3350 cm^{-1} (NH). NMR (CCl_4): δ 5.10 (s, NH) and 6.70—7.25 (m, C_6H_5). Found: C, 69.57; H, 5.44; N, 6.69%. Calcd for $C_{12}H_6D_5NS$: C, 69.85, H, 5.38; N, 6.79%.

*4'-Chlorobenzenesulfenanilide (**1f**).* Mp 82—83 °C (hexane). Yield 75%. IR (KBr): 3340 cm^{-1} (NH). NMR ($CDCl_3$): δ 5.12 (s, NH) and 6.81—7.40 (m, C_6H_5 and C_6H_4). Found: C, 61.33; H, 4.35; N, 5.73%. Calcd for $C_{12}H_{10}ClNS$: C, 61.14; H, 4.28; N, 5.94%.

*4'-Bromobenzenesulfenanilide (**1h**).* Mp 94—95 °C (hexane). Yield 68%. IR (KBr); 3340 cm^{-1} (NH). NMR ($CDCl_3$): δ 5.10 (s, NH), and 6.74—7.43 (m, C_6H_5 and C_6H_4). Found: C, 51.45; H, 3.80; N, 4.93%. Calcd for $C_{12}H_{10}BrNS$: C, 51.43; H, 3.60; N, 5.00%.

*3',5'-Dichlorobenzenesulfenanilide (**1q**).* Mp 95—96 °C (hexane). Yield 75%. IR (KBr): 3340 cm^{-1} (NH). NMR ($CDCl_3$): δ 5.17 (NH), 6.82—6.93 (m, C_6H_3), and 7.24 (s, C_6H_5). Found: C, 53.37; H, 3.26; N, 5.10%. Calcd for $C_{12}H_9Cl_2NS$: C, 53.34; H, 3.36; N, 5.19%.

*4'-Acetylbenzenesulfenanilide (**1i**).* Mp 98—99 °C (methanol-water and then benzene-hexane). Yield 52%. IR (KBr): 3230 and 3270 cm^{-1} (NH). NMR ($CDCl_3$): δ 2.46 (s, CH_3), 5.82 (s, NH), 7.16 (s, C_6H_5), and 7.02 and 7.83 (d, J=9 Hz, C_6H_4). Found: C, 69.08; H, 5.28; N, 5.77 %. Calcd for $C_{14}H_{13}NOS$: C, 69.10; H, 5.38; N, 5.76%.

4'-Acetylbenzenesulfen-2,3,4,5,6-d_5*-anilide (**1j**).* Mp 103—104 °C (methanol-water and then benzene-hexane). Yield 40%. IR (KBr): 3250 cm^{-1} (NH). NMR ($CDCl_3$): δ 2.49 (s, CH_3), 5.80 (s, NH), and 7.02 and 7.83 (d, J=9 Hz, C_6H_4). Found: C, 67.49; H, 5.13; N, 5.59%. Calcd for $C_{14}H_8D_5NOS$: C, 67.70; H, 5.27; N, 5.64%.

*3'-Acetylbenzenesulfenanilide (**1k**).* Mp 84—85 °C (methanol-water and then benzene-hexane). Yield 61%. IR (KBr): 3290 cm^{-1} (NH). NMR ($CDCl_3$): δ 2.50 (s, CH_3), 5.57 (s, NH), and 7.05—7.65 (m, C_6H_5 and C_6H_4). Found: C, 69.22; H, 5.27; N, 5.73%. Calcd for $C_{14}H_{13}NOS$: C, 69.10; H, 5.38; N, 5.76%.

4'-Nitrobenzenesulfen-2,3,4,5,6-d_5*-anilide (**1m**).* Mp 105—106 °C (methanol-water). Yield 33%. IR (KBr): 3300 and 3330 cm^{-1} (NH). NMR ($CDCl_3$): δ 5.86 (s, NH) and 7.08 and 8.12 (d, J=9 Hz, C_6H_4). Found: C, 56.98; H, 3.92; N, 11.41%. Calcd for $C_{12}H_5D_5N_2O_2S$: C, 57.35; H, 4.01; N, 11.15%.

*3'-Nitrobenzenesulfenanilide (**1n**).* Mp 110—111 °C methanol-water). IR (KBr): 3300 cm^{-1} (NH). NMR ($CDCl_3$): δ 5.50 (s, NH) and 7.15—7.90 (m, C_6H_5 and C_6H_4). Found: C, 58.22; H, 4.13; N, 11.52%. Calcd for $C_{12}H_{10}N_2O_2S$: C, 58.51; H, 4.09; N, 11.38%.

Generation of N-*Aryl*-N-*phenylthioaminyls (**2**).* a) Benzenesulfenanilide (**1**, 5 mg), di-*t*-butyl peroxide (0.02 ml), and benzene (0.2 ml) were placed in an ESR tube. After the solution had been degassed by three freeze-and-thaw cycles, the tube was sealed off. An ESR spectrum of the solution was recorded while the solution was being UV-irradiated from a distance of 40 cm using a high-pressure mercury lamp (JES-UV-1, 100 W) at room temperature; b) in one arm of a two-armed glass tube which was attached to an ESR tube, **1** (0.1 g) and benzene (2 ml) were placed, while lead dioxide (0.5 g) and potassium carbonate (0.5 g) were placed in the second arm. After the contents had been degassed as has been described above and the tube had been sealed off, the benzene solution of **1** was poured into the second arm containing the oxidizing agents and the resulting mixture was shaken well. A part of the supernatant of the mixture was poured into the ESR tube, and the tube was sealed off.

*Generation of the Nitroxide Radical **3**.* Nitrosobenzene (4 mg), diphenyl disulfide (5 mg), and benzene (0.2 ml) were placed in an ESR tube and the solution was degassed as has been described above, the tube was then sealed off. An ESR spectrum of the solution was recorded under UV-irradiation as has been described above.

The ESR spectra were recorded on a JES-ME 3X Spectrometer equipped with 100 kHz field modulation. Computer simulations of the ESR spectra were carried out using a FACOM 270-30 Computer with a FACOM 6201B Plotter; they were fitted by means of a trial-and-error method.

References

1) Part III of this series; "ESR Studies of Nitrogen-centered Free Radicals." For Part II, see Y. Miura, N. Makita, and M. Kinoshita, *Bull. Chem. Soc. Jpn.*, in press.

2) For recent reviews, (a) A. R. Forrester, J. M. Hay, and R. H. Thomson, "Organic Chemistry of Stable Free Radicals," Academic Press, New York, N. Y. (1968); (b) S. F. Nelsen, "Free Radicals," Vol. II, ed by J. K. Kochi, John Wiley, New York, N. Y. (1973), p. 527; (c) W. C. Danen and F. A. Neugebauer, *Angew. Chem.*, **87**, 823 (1975).

3) It has recently been reported that a substituted *N*-phenyl-*N*-phenylthioaminyl may be generated in the reaction of 2,2-diphenyl-1-picrylhydrazyl with 2,4,6-tri-*t*-butylbenzenethiol; J. Flood and K. E. Russell, *Can. J. Chem.*, **53**, 1123 (1975).

4) U. Schmidt, K. H. Kabitzke, and K. Markau, *Angew. Chem.*, **76**, 376 (1964).

5) S. Oae, Y. Tsuchida, K. Tsujihara, and N. Furukawa, *Bull. Chem. Soc. Jpn.*, **45**, 2856 (1972).

6) D. H. Barton, I. A. Blair, P. D. Magnus, and R. K. Norris, *J. Chem. Soc., Perkin Trans. 1*, **1973**, 1031.

7) R. S. Atkinson, S. B. Awad, E. A. Smith, and M. C. R. Symons, *J. Chem. Soc., Chem. Commun.*, **1976**, 22.

8) G. Brunton, J. F. Taylor, and K. U. Ingold, *J. Am. Chem. Soc.*, **98**, 4879 (1976). This report was found after we had submitted the present article.

9) The proton couplings are due to the protons in the *N*-phenyl ring, as was confirmed from the ESR parameters ior the phenyl phenylthio-d_5 nitroxide radical.

10) Recently, the present authors have found that *N*-3,5-di-*t*-butylphenyl-*N*-4′-chlorophenylthioaminyl, which is considerably long-lived, gives a blue solution (602 nm in benzene).

11) E. G. Janzen, *Acc. Chem. Res.*, **2**, 279 (1969).

12) R. I. Walter, *J. Am. Chem. Soc.*, **88**, 1923 (1966).

13) W. C. Danen, C. T. West, and T. T. Kensler, *J. Am. Chem. Soc.*, **95**, 5716 (1973).

14) For the σ values, see D. H. McDaniel and H. C. Brown, *J. Org. Chem.*, **23**, 420 (1958).

15) For the σ^- values, see A. I. Biggs and R. A. Robinson, *J. Chem. Soc.*, **1961**, 388.

16) The results obtained could be explained without considering the electron-sharing conjugative effect (Ar–N=$\dot{S}$–Ar′).

17) D. S. Tarbell and D. K. Fukushima, *Org. Synth.*, Coll. Vol. III, 809 (1955).

18) H. Lecher, F. Holschneider, K. Köberberle, W. Speer, and P. Stöcklin, *Ber.*, **58**, 409 (1925).

19) J. Goerdeler and B. Redies, *Chem. Ber.*, **92**, 1 (1959).

The Formation of Amino Acids and Related Oligomers from Formaldehyde and Hydroxylamine in Modified Sea Mediums Related to Prebiotic Conditions*

Hiroshi HATANAKA and Fujio EGAMI

Mitsubishi-Kasei Institute of Life Sciences, 11 Minamiooya, Machida-shi, Tokyo 194

(Received September 22, 1976)

Amino acids and related oligomers were produced from formaldehyde and hydroxylamine in modified sea mediums at pH 5.5 and 105 °C. The modified sea mediums are characterized by a lower concentration of sodium chloride and a higher concentration of essential transition metal** ions (Zn^{2+}, Mo^{6+} as MoO_4^{2-}, Fe^{3+}, Cu^{2+}, Co^{2+}, and Mn^{2+}) than in sea water; generally small amounts of clays (kaolin and montmorillonite) were added. About 40 species of amino acids were detected in the automatic amino acid analyzer, and 20 of them were tentatively assigned. Glycine, alanine, and serine among the protein amino acids and β-alanine were further confirmed by thin-layer chromatography. Oligomers with molecular weights of about 200—1000 were produced which gave rise to an amino acid mixture by acid hydrolysis. From the ratio (maximum, about 5) of the content of the amino groups after to before hydrolysis and the molecular size, the oligomers were tentatively regarded as oligopeptides of an unknown nature, resistant to pronase digestion. The large-molecular fraction (M. W. about 700) had a phosphatase-like activity able to hydrolyze *p*-nitrophenyl phosphate.

Since the first experimental demonstration of the synthesis of amino acids under possible primeval conditions published by Miller,[1] a substantial number of investigations have been carried out in this field of research, most of which have been collected in two volumes.[2,3] For the further chemical evolution, that is, for the formation of primary organisms, the existence of an aqueous medium is absolutely required.[4] The dissolved substances in earth's primeval hydrosphere are regarded as the initial materials for the development of life.

Egami, one of the present authors,[5] has reported that a good correlation was found between the biological behaviour of minor elements, such as molybdenum and iron, and their concentrations in the present sea water. A hypothesis has been presented that the composition of the present sea water reflects that of the primeval sea water at the time of early evolution. In accordance with the above hypothesis, iron, molybdenum, and zinc, which are the most abundant transition elements in sea water, are found to be essential components of the enzymes in microorganisms, including *Clostridium*, which is regarded as the most primitive existing organism.[6] These transition elements presumably complexed with compounds accumulated in the primeval sea in the course of chemical evolution, thus forming compounds which subsequently evolved to form protoenzymes with a low activity and a broad specificity.

Taking into consideration the fact that essential transition metal ions had to contribute to chemical evolution in primeval sea water, and anticipating the concerted catalytic action of clays and metal ions, we have been investigating the formation of biomolecules in modified sea mediums, in which the concentration of sodium chloride is lower, and that of transition metal ions in higher, than in sea water. We suppose that the modified sea mediums are essentially similar to primeval sea conditions and are more effective for the formation of organic substances from simple materials.

The present paper will deal with the formation of amino acids and related oligomers from formaldehyde (as the C_1 compound) and hydroxylamine (as the N_1-compound) in the modified sea mediums, with special reference to the effects on their formation of essential transition elements, *i.e.*, iron, molybdenum, zinc, copper, cobalt and manganese, and of such clays as kaolin and montmorillonite. The starting materials, formaldehyde and hydroxylamine, were selected on the basis of the experiments of Oró *et al.*[7] Preliminary experiments under similar conditions by Ventilla and Egami[8] were reported elsewhere.

Materials and Methods

Materials. The formaldehyde was obtained from Wako Chemicals, and the hydroxylamine hydrochloride, from Nakarai Chemicals. They were of a reagent grade. All of the six transition elements, 0.1 M solutions in the chemical forms of $Fe(NO_3)_3$, Na_2MoO_4, $ZnCl_2$, $Cu(NO_3)_2$, $CoCl_2$, and $MnCl_2$, were kind gifts of Miss Kayoko Nakamura (Laboratory of Social Life Science, in our Institute). The kaolin was purchased from Kukita Chemicals and the montmorillonite, from Hohjun Yoko Co. All the other compounds used as the components in the modified sea mediums were of a reagent grade.

The Nuclepore (pore size of 0.4 μ, 47 mm disc) was obtained from the Nomura Micro Science Co. The Dowex 1 (2X, 100—200 mesh, OH form) and Dowex 50 (8X, 100—200 mesh, H^+ form)were purchased from the Muromachi Kagaku Co. The biogel P-2 (100—200 mesh) and P-10 (100—200 mesh) were obtained from Bio-Rad Chemicals. The fluorescamine (Fluram<Roche>) and disodium *p*-nitrophenyl phosphate were purchased from the Japan Roche Co. and Sigma Chemicals respectively. Six M HCl for acid hydrolysis was purified by distillation at a constant boiling temperature. The dioxane was used after distillation over solid NaOH. The other chemicals were reagent-grade.

Preparation of the Modified Sea Mediums for Large-scale Experiments. The original solution (250 ml), with a concentration of 0.6 M of formaldehyde and 0.1 M of hydroxylamine hydrochloride and of containing 0.02 M of magne-

* A part of this report was presented at the 67 th Annual Meeting of the American Society of Biological Chemists, San Francisco, June 7, 1976: *Fed. Proc., Fed. Am. Soc. Exp. Biol.*, 35, 1458 (1976)

** The term "transition element" is used here in its broader sense to include zinc and similar elements.

TABLE 1. COMPOSITIONS OF A MODIFIED SEA MEDIUM (500 ml)

Compositions	Concentration
HCHO	0.3 M
NH_2OH	0.05 M
HPO_4^{2-}, SO_4^{2-}, Mg^{2+}, Ca^{2+}	0.01 M each
Na^+	0.015 M
K^+	0.045 M
Cl^-	0.07 M
NO_3^-	0.0005 M
Zn^{2+}, Mo^{6+} as MoO_4^{2-}, Fe^{3+}, Cu^{2+}, Co^{2+}, Mn^{2+}	0.0001 M each
Kaolin, Montmorillonite	2% (wt/vol) each

sium sulfate, 0.02 M of calcium chloride, 0.02 M potassium phosphate (dibasic), and 0.0002 M each of the six transition elements, was adjusted to pH 5.5 by titration with an alkaline solution containing 0.7 M KOH and 0.3 M NaOH. The volume of the solution was diluted to 500 ml, and then 10 g each of kaolin and montmorillonite were added to the solution. The original pH value, 5.5, of the solution was not changed by the addition of clays. The final composition of the reaction mixture, in a total volume of 500 ml, is listed in Table 1. This reaction mixture (namely the modified sea medium) was glass-sealed *in vacuo* under a nitrogen atmospher and kept at 105 °C±5 °C for 35 days in a Dry-Block DB-3H (M ε S Instruments Co.). As the reaction proceeded, the reaction mixture turned yellow after about 2 weeks and reddish brown after about 3 weeks.

Extraction Procedure of the Products from Modified Sea Mediums after the Reaction. After a 35-day reaction at 105 °C, the sealed ampoule was cut off in an ice bath. After centrifugation at 10000 rpm for 30 min, the sediment was at once washed by 100 ml of distilled water. The resulting supernatants (590 ml) were combined and filtered off on a 0.4 μ pore size Nuclepore membrane. The washed sediment was then resuspended in 400 ml of 2 M aqueous ammonia, and the suspension was vigorously shaken at 37 °C for 1 day. After the centrifugation of the suspension, the supernatant (390 ml) was filtered off. Further extraction from the resulting sediment with 200 ml of 2 M aqueous ammonia was repeated twice. After the final extraction at 37 °C for 2 days, the resulting sediment was washed twice with 150 ml of distilled water.

All of the extracts (total volume of 1670 ml) were lyophilized by means of a Virtis-model 10—145 MR-BA freeze-mobile. The lyophilized dark brown powder was redissolved in distilled water and filtered off on a Nuclepore membrane. The color of the resulting extract (19 ml) was a deep reddish brown. It was designated "Golden Primordial Broth" from the color tone and the richness of the products.

Biogel P-2-column Chromatographic Separation of Products. Biogel P-2 column chromatography was used for the initial separation of oligomeric products with different molecular weights. An aliquot (15 ml) of concentrated "Golden Primordial Broth" was placed in the column beds under an overlying buffer layer. Biogel P-2 (100—200 mesh) was equilibrated with 0.1 M ammonium hydrogencarbonate (approximate pH value of 9.0) and then packed in a large column (2.65×130 cm=700 ml). The fraction (5.0 ml each) was eluted at 13 ml/h with a constant pressure head of 15 cm by means of 0.1 M ammonium hydrogencarbonate.

For the purpose of the further characterization of each fraction, for example, the determination of the primary amino groups before and after acid hydrolysis, and the measurement of the alkaline phosphatase activity, each fraction was lyophilized in order to remove the ammonium hydrogencarbonate and then, with distilled water, brought back to the original volume.

The molecular weight of each fraction was calibrated on the basis of the interpolation of semi-logarithmic plots (elution volume *versus* molecular weight) obtained from separate experiments with the following standard compounds; horse heart cytochrome *c*, oxidized and reduced glutathione, adenosine triphosphate, and sodium chloride.

Small-scale Experiments. In order to examine the reaction requirements of catalysts such as transition elements and clays, small-scale (total volume of 10 ml) experiments were carried out under essentially the same reaction conditions and using the same extraction procedures as those of the above large-scale experiments except for their experimental scale. After the reaction an aliquot of each extract was placed in a small Biogel P-2 column (1.25×49 cm=60 ml) equilibrated with 0.1 M ammonium hydrogencarbonate. Each fraction (5 ml) was lyophilized and then brought back to the original volume with distilled water.

The same small-scale experiments used to discover the time course of the formation of amino acids and related oligomers were carried out in the same way.

Determination of the Content of Primary Amino Groups. The fluorescamine reagent has been employed for the fluorometric determination of the content of primary amino groups. The advantages of the use of this reagent instead of ninhydrin are the high sensitivity of amino acid, the non-sensitivity of hydroxylamine, and the low sensitivity of ammonia. The manual determination procedure was undertaken according to Böhlen *et al.*[9] An aliquot of the sample (10—250 μl, 1—25 nmol of primary amino groups) was transferred into a 18×105 mm test tube, and then the volume was brought to 2.5 ml with a 0.05 M sodium phosphate buffer (pH 8.0). While the test tube was being vigorously shaken on a vortex-type mixer [a Thermomixer (Termonics Co.)], 0.5 ml of a fluorescamine solution in dioxane (30 mg/100 ml) was rapidly added to the buffer solution by means of a Finnpipette (Kemistien Oy). A reagent blank and a standard leucine solution in two different concentrations (5 and 10 nmol) were run routinely. The fluorescence was measured on a Shimadzu model RF-502 recording spectrofluorometer with the excitation wavelength at 390 nm and the emission at 470 nm with a slit width of 5 μm in each. Measurement was made with a regular quartz cuvette (1 cm light path).

As a more sensitive method, we also employed a one-fifth-scal-down procedure. Its sensitivity range for leucine was 0.1—10 nmol. The final volume was 0.6 ml. The quartz cuvette used had a 0.25 cm light path.

Acid Hydrolysis. An aliquot of the sample was transferred to a 15×105 mm test tube (made of Pyrex glass) and lyophilized to a powder; the volume was then brought up to about 1 ml of 6M HCl. This solution was glass-sealed *in vacuo* and kept at 110 °C for 20 h in a hydrolysis furnace (Mitamura Riken Co.). After hydrolysis, the HCl was removed *in vacuo* at 40 °C.

Amino Acid Analysis. Amino acid analyses were conducted using a JEOL model JLC-6AH automatic amino acid analyzer. Before the amino acid analysis, the sample was placed in a small Dowex 1 (OH^- form) anion-exchange column (1.2×5 cm=5.7 ml). The pass-through fraction (neutral) was discarded. After washing with distilled water, the amino acid fraction (acidic) was eluted with about 10 ml of 4 M acetic acid. The acetic acid solution was evaporated to dryness *in vacuo* at 40 °C. Then the sample was dissolved

in a 0.2 M sodium citrate–citric acid buffer (pH 2.2) and eluted from a long column (0.8×50 cm) with a pH gradient of 3.30 to 4.25 by a step-by-step procedure. The sample solution was eluted from a short column (0.8×15 cm) with a pH of 5.29. JEOL custom spherical resin LCR-2 (strong-acidic cation exchange resin) was used to pack the column.

Manual Handling of Amino Acid Analyzer for the Preparation of Individual Amino Acids. The acid hydrolysates of an aliquot of the concentrated "Golden Primordial Broth" were subjected to Dowex 1 (OH^- form)-column treatment. The resulting acidic fraction was evaporated and dissolved with a 0.2 M sodium citrate-citric acid buffer (pH 2.2). An aliquot (0.8 ml; 12.9 μmol of primary amino groups) was placed in a moderately long column (0.8×50 cm) of the amino acid analyzer. The elution was carried out by the step-by-step pH gradients of 3.30 and 4.25 at a constant elution speed of 0.84 ml/min. At the end of the buffer (pH 4.25) elution, the residual amino acids retained on the resin were eluted off with 0.2 M NaOH. The fractionation (0.5 ml for each fraction volume) was done by means of a LKB model 7000 Ultrolac fraction collector. An aliquot (10 μl) of each fraction was estimated for the primary amino groups with fluorescamine. The fractions—peak No. 9 shown in Fig. 1 (possibly containing serine), Peak No. 15 (possibly containing glycine), Peak No. 16 (possibly containing alanine), Peak No. 30 (possibly containing β-alanine) and the 0.2 M NaOH eluate (the basic amino acid fractions)—were pooled. The pooled fractions except for the 0.2 M NaOH eluates were then adjusted to pH 1.0 with HCl and placed in a Dowex 50 (H^+ form) resin column (1.2×5 cm=5.7 ml). After the drying of the 2 M aqueous ammonia eluate, they were subsequently placed in a Dowex 1 (OH^- form) resin column (1.2×2 cm=2.3 ml). The 4 M acetic acid eluate was evaporated to dryness and then dissolved with a small volume of distilled water. An aliquot of each desalted sample was placed on a thin-layer chromatogram coated with cellulose on a plastic roll (DC-Plastikrolle Cellulose; 20 cm height; Merick). The solvent system used was butyric acid : acetic acid : water (4 : 1 : 5, by volume).[10] After developing for 8 h, each spot was visualized by means of a spray of 0.2% ninhydrin butyric acid saturated in a water solution and heating at 95 °C for 10 min.

Spectrophotometric Analysis of the Oligomers. The oligomers used for analysis were concentrated pooled fractions (Fractions Number 51—58 in the Biogel P-2 column shown in Fig. 2) which contained 4.25 μmol of primary amino groups per ml. The ultraviolet spectrum was measured in a diluted aqueous solution (17.9 nmol of primary amino groups per ml) of the oligomer, using a Hitachi model 323 spectrophotometer. The infrared spectrum was recorded as potassium bromide disc on a JASCO model IRA-1 spectrophotometer.

Attempted Pronase-catalyzed Hydrolysis of the Oligomers. In order to remove the small-molecular weight peptides contaminating the commercially available pronase preparation (Pronase E from the Kaken Kagaku Co.), a 30-mg portion of Pronase E was placed in a small column (1.25×47 cm =58 ml) packed with Biogel P-10 equilibrated with a 0.02 M potassium phosphate buffer (pH 7.5). The main peak just behind the void peak of Biogel P-10 chromatography was collected and then used immediately for the following hydrolysis experiment. The oligomers used were the same preparation as the one above used for the spectrophotometric analysis. The reaction mixture for pronase-catalyzed hydrolysis, in a total volume of 0.5 ml, contained 0.904 μmol of the oligomers, as calculated from the content of the primary amino groups, 0.63 mg of Biogel P-10-treated pronase, and 20 μmol of a potassium phosphate buffer (pH 7.5). After incubation at 37 °C for 17 h, the mixture was placed in a Biogel P-10 column (1.25×47 cm=58 ml) equilibrated with a 0.02 M potassium phosphate buffer (pH 7.5). The fractions (1 ml each) were then collected by eluting at 2.5 ml/h with a pressure head of 15 cm. The effluents were monitored in terms of their absorbance at 280 nm, using a LKB Uvicord II absorption spectrophotometer, and by then measuring their content of primary amino groups by the use of fluorescamine.

Measurement of Alkaline Phosphatase Activity. The reaction rate of alkaline phosphatase activity in the oligomer fractions formed was determined by measuring the *p*-nitrophenol released from *p*-nitrophenyl phosphate according to the method of Oshima,[11] with slight modifications. The assay mixture, in a total volume of 0.9 ml, contained 90 μmol of the Tris-acetic acid buffer (pH 7.5), 9 μmol of $MgCl_2$, 0.9 μmol of $ZnCl_2$, 9 μmol of disodium *p*-nitrophenyl phosphate, 80 μl of the oligomer fraction, and 5 μl of toluene. The reaction was carried out at 37 °C in a 13×100 mm test tube (Corning Co.) with a tight cap, and the reaction rate was directly measured at 400 nm, using a Zeiss PMQ II spectrophotometer, at suitable time intervals (1—5 days).

Results and Discussion

Extraction of "Golden Primordial Broth" after the Reaction in Modified Sea Mediums Containing Formaldehyde and Hydroxylamine. After 35 days at 105±5 °C, the following four-step extractions from a sealed ampoule containing 500 ml of modified sea mediums were done:

Table 2. Extraction of the products from a modified sea medium (500 ml)

Steps of extraction	Volume	Content of primary amino groups		Ratio of (B) to (A)
		Before acid hydrolysis (A)	After acid hydrolysis (B)	
	ml	μmol		
H_2O extract	590	154	1214	7.88
1st 2 M NH_4OH extract	390	178	423	2.38
2nd 2 M NH_4OH extract	190	33.3	100	3.00
3rd 2 M NH_4OH extract	500	34.6	107	3.09
Summation	1670	400	1844	4.61
Concentrated "Golden Primordial Broth"	19	404	1519	3.76

The extraction procedures are described in the text.

extraction with distilled water, and 1st, 2nd, and 3rd extractions with 2 M aqueous ammonia. The extraction volumes and their contents of primary amino groups before and after the acid hydrolysis are listed in Table 2. As is shown in Table 2, the compounds with a high ratio of the content of the primary amino groups after acid hydrolysis to that before the procedure were extracted with distilled water. The extraction percent reached 65% of the total extraction. However, it appeared that even the third extraction with 2 M aqueous ammonia did not accomplish the complete extraction of the products. Although tightly bound compounds seem to be present in the clays, most of the products with primary amino groups might be recovered in the concentrated "Golden Primordial Broth." In order to eliminate the clays finely pulverized in 2 M aqueous ammonia, the concentrated solution was filtered through a Nuclepore membrane (pore size 0.4 μ). As can be seen in Table 2, though, this operation did not reduce the recovery of primary amino groups.

The yield of primary amino groups in the concentrated "Golden Primordial Broth" was calculated to be 6.06% from the amount of hydroxylamine used as the starting N_1 compound. The fraction eluted from a Dowex 1 (OH^- form) anion-exchange resin column by 4 M acetic acid contained 1311 μmol of primary amino groups (5.24% yield calculated from the hydroxylamine). That is, most (86.3%) of the compounds with primary amino groups in the hydrolyzate of the "Golden Primordial Broth" were acidic ones (probably with a carboxyl or sulfonate group). This amphoteric character strongly suggested that most of the hydrolyzates were amino acids.

Amino Acid Analysis of the Hydrolyzate Formed from "Golden Primordial Broth". After the treatment of the Dowex 1 (OH^- form), an aliquot of the hydrolyzate formed from the "Golden Primordial Broth" was examined by means of the automatic amino acid analyzer using cation-exchange resin. The resulting chart is shown in Fig. 1. As is shown in Fig. 1, the peaks of the ninhydrin-positive materials consisted of 40 species. The retention times of natural protein amino acids are presented in the same chart (shown in Fig. 1). In the separate experiments, the retention times of 16 non-protein amino acids (β-alanine, α-aminobutyric, α-aminoisobutyric, β-aminobutyric, β-aminoisobutyric, γ-aminobutyric and α,γ-diaminobutyric acids, homoserine, phosphoserine, taurine, norvaline, norleucine, alloisoleucine, sarcosine, citrulline, and ornithine) were also measured. The substances with the same retention times as these authentic amino acids are listed in Table 3. The identities with respect to the retention times on the amino acid analyzer were further confirmed by a mixed experiment using the samples and authentic amino acids. The individual peak area calculated on the basis of the response factor to the peak area of a known amount of glycine gave the content of the products as is shown in Table 3. The recovery (46.9%) introduced by the summation of the peak area was rather wrong. This might be due to the difference in sensitivity between the fluorescamine and ninhydrin detections. Another possibility was that the sample might contain high-basic compounds yet retained on the resin. To confirm the former possibility, the determination of the amino groups in the hydrolyzate by the ninhydrin method is required, but this is difficult because of the unavoidable contamination of the ammonia used in a large amount in the extraction procedure. However, the lesser sensitivity of β-amino groups compared with that of α-amino groups is well-known. It seems to explain the incomplete recovery in the amino acid analyzer with ninhydrin detection.

In a separate experiment, several individual peaks were obtained by means of the manual handling of the amino acid analyzer. The total recovery was about 70% by the use of fluorescamine. Especially, the amount of Peak No. 30 was 5.22 mol%. The difference between the yields determined by ninhydrin (2.40 mol%) and by fluorescamine seems to show, together with the fact of the same retention time, that this peak (Peak No. 30) was β-alanine. Furthermore, the fractions corresponding to Peaks No. 9, 15, 16, and 30, shown in Fig. 1, were analyzed by thin-layer chromatography coated with cellulose powder. The R_f values

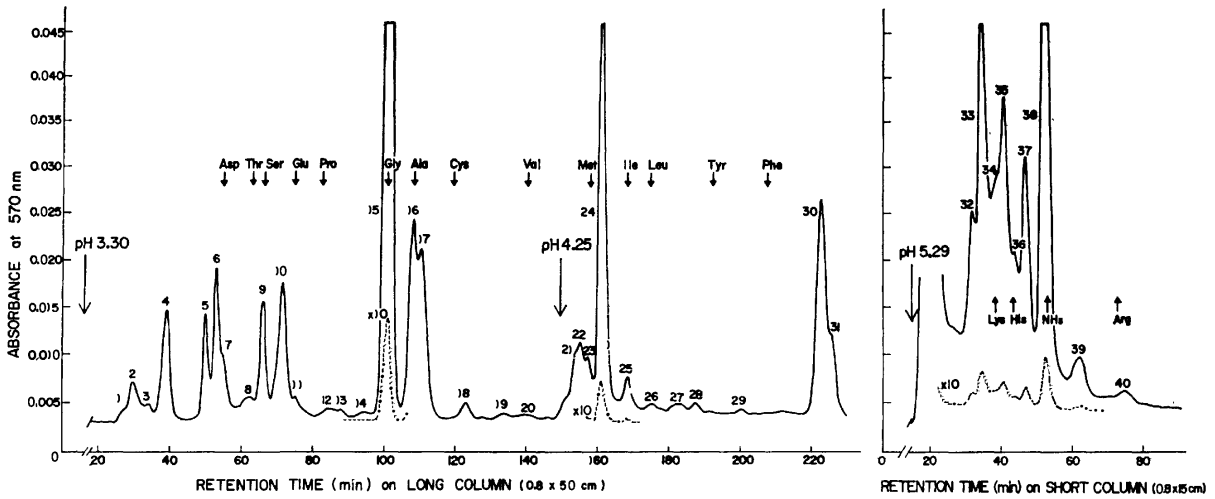

Fig. 1. Amino acid analysis of the acid hydrolyzate from the concentrated "Golden Primordial Broth." The experimental conditions were given in the text.

TABLE 3. AMINO ACID ANALYSIS OF THE HYDROLYSATE OF "GOLDEN PRIMORDIAL BROTH"

Peak No.	t_R	Amounts of amino acid residues		Authentic amino acids with the same t_R value
	min	μ mol	mol %	
1.	27.6	3.20	0.244	Phosphoserine
2.	29.8	6.08	0.466	
3.	34.1	2.06	0.157	Taurine
4.	39.1	13.55	1.03	
5.	49.9	9.36	0.714	
6.	52.9	15.44	1.18	
7.	55.0	3.43	0.262	Asp
8.	62.0	6.24	0.476	Thr
9.	66.0	11.68	0.891	Ser
10.	71.5	18.37	1.40	Homoserine
11.	75.0	4.72	0.360	Glu
12.	84.4	2.50	0.191	
13.	87.8	1.52	0.116	
14.	94.6	1.82	0.139	
15.	100.9	114.20	8.71	Gly
16.	108.0	25.95	1.98	Ala
17.	110.2	28.51	2.17	
18.	123.0	2.32	0.177	α-Aminobutyric acid
19.	133.6	1.14	0.087	
20.	140.0	0.95	0.072	Val
21.	153.4	7.40	0.564	
22.	154.8	8.55	0.652	
23.	157.0	4.98	0.380	Met
24.	161.0	42.59	3.25	Norvaline
25.	168.2	4.71	0.359	Ile
26.	175.0	1.71	0.130	Leu
27.	182.5	1.71	0.130	Norleucine
28.	187.4	1.46	0.112	
29.	200.0	0.40	0.031	
30.	222.6	31.46	2.40	β-Alanine
31.	225.2	12.52	0.955	
32.	32.0	33.85	2.58	
33.	34.8	72.02	5.49	
34.	39.0	3.53	0.269	Lys and γ-Aminobutyric acid
35.	41.0	59.87	4.57	
36.	44.0	1.37	0.104	His
37.	47.3	34.47	2.63	
38.	52.9			Ammonia
39.	62.6	12.08	0.921	
40.	75.0	6.75	0.515	Arg

The amounts of amino acid residues corresponding to the respective peaks shown in Fig. 1 were calculated on the basis of the response factor to the peak area of the known amount of glycine obtained from a separate experiment under the same operation conditions of the automatic amino acid analyzer.

in the butyric acid : acetic acid : water (4 : 1 : 5, by volume) solvent system were 0.13, 0.15, 0.22, and 0.23 respectively. These values agreed with those obtained with the authentic amino acids, serine, glycine, alanine, and β-alanine respectively. The purple colorations after the spray of ninhydrin except in the case of β-alanine were practically the same (the coloration for β-alanine was blue-violet). Since these compounds had the same retention times on the automatic amino acid analyzer as those of the respective authentic amino acids, these results indicate that the compounds eluted at the positions of Peaks No. 9, 15, 16, and 30, shown in Fig. 1, correspond to serine, glycine, alanine, and β-alanine respectively. The other compounds eluted on the automatic amino acid analyzer could not be analyzed by means of the thin-layer chromatography because of their small amounts.

Gel-filtration of Concentrated "Golden Primordial Broth" using Biogel P-2. Most (15 ml) of the concentrated "Golden Primordial Broth" was placed in a column packed with Biogel P-2 (fractionation range; MW 100—1800) equilibrated with 0.1 M ammonium hydrogencarbonate. The chromatographic patterns of the products containing, as expected, the high-molecular-weight

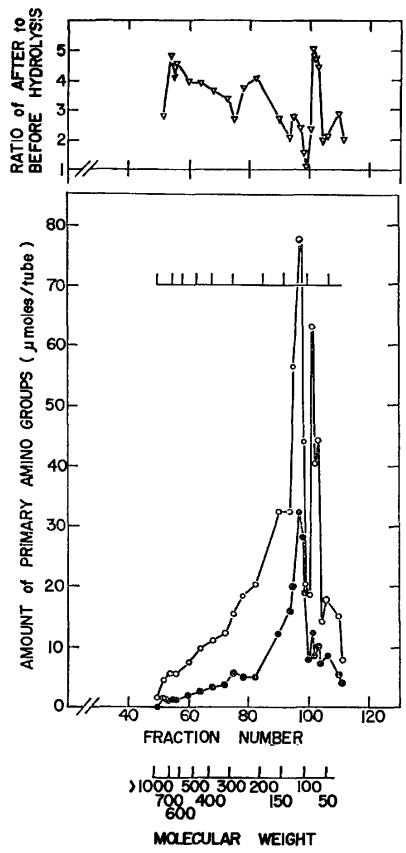

Fig. 2. Elution profiles of Biogel P-2 column chromatography of the concentrated "Golden Primordial Broth." The procedure of the column chromatography was given in the text. Closed and open circles represent the amount of primary amino groups determined by the usage of fluorescamine before and after acid hydrolysis, respectively. Reversed open triangles in the upper figure represent the ratio of the amount of primary amino groups after to before acid hydrolysis. The given scale of molecular weight was obtained from the separate experiment using the several authentic compounds listed in the text.

compounds are shown in Fig. 2. After the lyophilization of each fraction in order to remove the excess of ammonium hydrogencarbonate, the resulting powder was brought back to the original volume with distilled water. The amount of primary amino groups in each fraction before and after acid hydrolysis was measured by using fluorescamine, with leucine as the standard. As can be seen in Fig. 2, a considerable amount of the compounds with primary amino groups was found in the high-molecular-weight fractions. In addition, the ratio of the amount of primary amino groups after to before acid hydrolysis in the column effluents increased by about 5-fold, together with the molecular size. These results mean that the compounds present in the high-molecular-weight fractions possessed latent primary amino groups which appeared as primary amino groups upon 6 M HCl hydrolysis, and suggest that they were oligomers consisting of several amino acid residues.

The sharp peak having a rather high ratio of the amount of primary amino groups after to before acid hydrolysis but eluted in the small-molecular-weight region (corresponding to a molecular weight of about 100) might contain a cyclic dipeptide of glycine, 2,5-piperadinedione.

Three column effluents — *i. e.*, Fraction Number 55 (at the position with 700 daltons as the average molecular weight), Fraction Number 75 (at 300 daltons), and Fraction Number 95 (at 130 daltons) — were analyzed for amino acid composition using the automatic amino acid analyzer. The amount of 40 species of ninhydrin positive materials is shown in Table 4 in mol%. The difference between the composition in the high- and low-molecular-weight fractions was tended to be small under the present experimental conditions.

Some Characteristics of the Oligomer Fractions Eluted from the Biogel P-2 Column. The collected fractions from Fraction Numbers 51 to 58 (oligomer fractions) were subjected to the following spectrophotometric measurements. Figure 3 shows the ultraviolet and infrared absorption spectra of the oligomer fraction. A shoulder peak in the neighborhood at 280 nm was observed in the ultraviolet spectrum. A rather broad, low-resolution band in the region at 1500—1600 cm^{-1} was also detected in the infrared spectrum. These results were not in contradiction with the existence of oligopeptides in the oligomer fraction. However, this fraction certainly contains various compounds other than oligopeptides. In fact, a considerble amount of sugar derivatives was detected in a separate experiment. Thus, the above findings can not be regarded as evidence for the presence of oligopeptides or peptide bonds.

In a separate experiment, an enzymatic degradation of the oligomers was attempted using pronase, a bac-

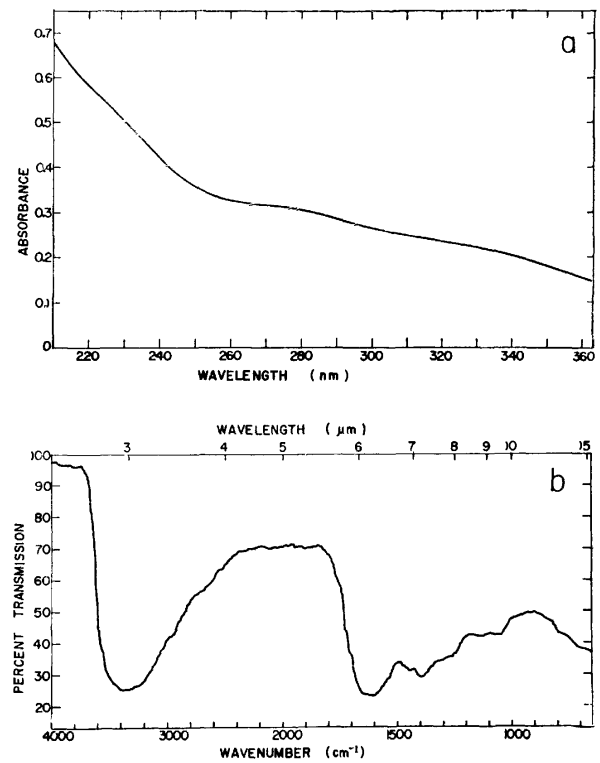

Fig. 3. Ultraviolet (a) and infrared (b) spectra of the oligomers. Experimental conditions were given in the text.

Table 4. Amino acid analysis of the hydrolysate of biogel *P*-2-column effluents

Peak No.	t_R	Amounts of amino acid residues in these fractions			Authentic amino acids with the same t_R value
		No. 55	No. 75	No. 95	
	min		mol %		
1.	27.6	0.090	0.0832	0.141	Phosphoserine
2.	29.8	0.489	0.670	0.441	
3.	34.1	0.206	0.254	0.220	Taurine
4.	39.1	1.23	1.66	0.679	
5.	49.9	0.504	0.832	1.21	
6.	52.9	0.0326	0.208	1.55	
7.	55.0	0.662	1.04	0.397	Asp
8.	62.0	0.348	0.208	0.727	Thr
9.	66.0	0.557	1.02	1.27	Ser
10.	71.5	0.472	0.924	2.22	Homoserine
11.	75.0	0.574	0.333	0.304	Glu
12.	84.4	0.0869	0.259	0.0529	
13.	87.8	0.0326	0.0555	0.264	
14.	94.6	0.104	0.222	0.0353	
15.	100.9	9.81	8.65	13.74	Gly
16.	108.0	1.33	1.47	3.31	Ala
17.	110.2	0.424	0.970	2.01	
18.	123.0	0.335	0.162	0.370	α-Aminobutyric acid
19.	133.6	0.209	0.0693	0.0441	
20.	140.0	0.313	0.0104	0.0441	Val
21.	153.4	0.804	0.243	0.645	
22.	154.8	0.804	1.22	0.705	
23.	157.0	1.09	0.635	0.487	Met
24.	161.0	1.46	2.51	2.38	Norvaline
25.	168.2	0.417	0.403	0.317	Ile
26.	175.0	0.209	0.0924	0.0661	Leu
27.	182.5	0.109	0.0693	0.0661	Norleucine
28.	187.4	0.304	0.243	0.0551	
29.	200.0	0.0326	0.0139	0.0220	
30.	222.6	1.44	4.46	1.78	
31.	225.2	0.526	0.776	0.446	β-Alanine
32.	32.0	0.522	1.39	4.17	
33.	34.8	4.90	9.98	7.29	
34.	39.0	0.261	3.70	3.53	Lys and γ-Aminobutyric acid
35.	41.0	4.07	3.70	6.08	
36.	44.0	3.00	0.693	4.26	His
37.	47.3	2.29	6.70	1.98	
38.	52.9				Ammonia
39.	62.6	1.28	0.834	1.96	
40.	75.0	0.176	0.231	0.848	Arg

terial non-specific protease. Contray to expectations, no amino acids and no newly-formed primary amino groups were detected — only the autolysis of pronase itself. A similar observation was reported by Ferris *et al.*,[12] who used the oligomers derived from HCN. They reported that no amino acids were released from the oligomers by pronase. Based on their results, they concluded that the oligomers did not contain peptide bonds.

In our case, however, taking into consideration the abundant formation of amino acids in the monomer fractions and the reasonable ratio of the primary amino group content after acid hydrolysis to before the procedure for the molecular size, the apparent non-susceptibility to pronase may be attributed, not to the absence of peptide bonds, but to the complex nature of the products with the predominant amount of unnatural peptide bonds due to D-amino acids, other nonprotein amino acids such as β-alanine, and those due to diamino or dicarboxylic amino acids.

Phosphate Ester Hydrolysis by the Oligomer Fractions Formed from Formaldehyde and Hydroxylamine. The oligomers formed in the modified sea mediums containing several transition elements were tested for the hydrolysis of the phosphate ester bond of *p*-nitrophenyl phosphate, as is shown in Fig. 4. Four column effluents, *i.e.*,

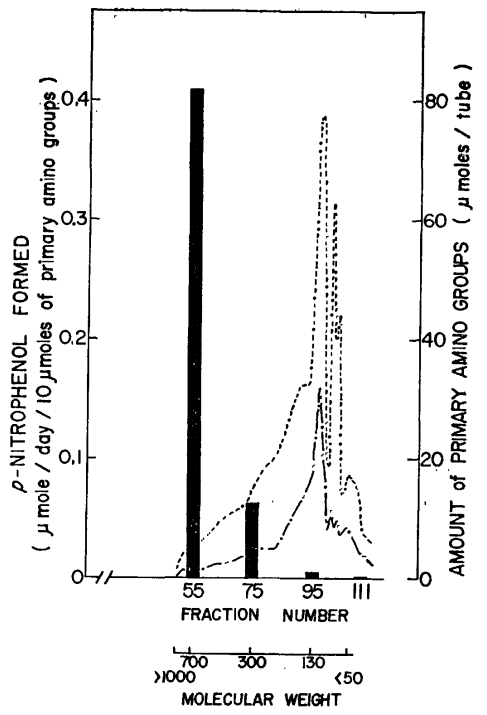

Fig. 4. Phosphate ester hydrolysis by the oligomer fractions. Closed bar represent the specific activity of alkaline phosphatase in the fractions obtained from the Biogel P-2 column chromatography shown in Fig. 2. Dotted and broken lines were the trace lines of the amount of primary amino groups before and after acid hydrolysis, respectively, obtained from the experiment shown in Fig. 2.

Fraction Numbers 55, 75, 95, and 111, were tested; only the high-molecular-weight fractions were found to show any hydrolytic activity for *p*-nitrophenyl phosphate. This catalytic activity was presented as μmol of *p*-nitrophenol formed per day per 10 μmol of primary amino groups in its hydrolyzate. This representation was regarded as μmol/day/mg oligopeptide, by assuming that each amino acid residue has 100 daltons as its molecular weight. Oshima[11] reported that proteinoid (molecular weight, 2500—4000), termally prepared polyamino acids containing 18 common amino acids, promotes the hydrolysis of the ester bond of *p*-nitrophenyl phosphate; its specific activity, 3 μmol/day/mg proteinoid at 30 °C. As can be seen in Fig. 4, the oligomers in Fraction Number 55 (average molecular weight, 700) had 0.409 μmol/day/mg oligopeptide at 37 °C. Its specific activity seems reasonable considering the different molecular weight. The possibility that the activity found was due to contamination by microorganisms or by phosphatases from them can be rejected on the basis of the following observations: toluene was added to hinder the growth of microorganisms; the time course of the reaction was linear, unlike the logarithmic growth curve occurring in the case of bacterial growth; only the high-molecular-weight fractions showed catalytic activities. Of course, another possibility — that this catalytic hydrolysis of *p*-nitrophenyl phosphate might be due to a high-molecular-weight metal complex of different constituents — cannot be excluded. At any rate, it is remarkable that a phosphatase-like activity appeared.

Dependency of the Production of Amino Acids and the Related Oligomers from Formaldehyde and Hydroxylamine on Transition Elements and Clays. The requirements for the production of amino acids and related oligomers from formaldehyde and hydroxylamine were investigated in small-scale (10 ml) experiments, as is shown in Table 5. The production of primary amino groups after acid hydrolysis in the complete system (Exp. a) was calculated as a 5.52% yield from hydroxylamine; this value is almost the same as that in the former large-scale experiment. However, the production of primary amino groups in the hydrolyzates in the minus experiments, such as minus transition elements (Exp. b) and minus clays (Exp. c), was considerably decreased, by 81.5% and 75.7% respectively. The composition of the amino acid residues was examined by using the automatic amino acid analyzer in separate experiments. The composition was almost the same as that in the former large-scale experiments. The no-reaction control (stocked at −20 °C instead of reacted at 105 °C) experiment (Exp. d) gave a small amount of the primary amino groups (0.67% yield). It was found to consist practically exclusively of glycine (41.3 mol%) by a separate experiment using the automatic amino acid

TABLE 5. REQUIREMENTS OF THE PRODUCTION OF AMINO ACIDS AND THE RELATED OLIGOMERS FROM FORMALDEHYDE AND HYDROXYLAMINE IN MODIFIED SEA MEDIUMS

Experiments	Amounts of primary amino groups		Ratio of (B) to (A)
	Before acid hydrolysis (A)	After acid hydrolysis (B)	
	μmol		
a. Complete	9.51	27.6	2.90
b. Minus transition elements (Mo^{6+}, Zn^{2+}, Cu^{2+}, Fe^{3+}, Co^{2+}, Mn^{2+})	7.18	22.5	3.13
c. Minus clays (kaolin, montmorillonite)	7.69	20.9	2.71
d. No-reaction control	1.95	3.34	1.71

The reaction in the complete system (Exp. a) with the reaction mixture listed in Table 1 was carried out in a glass-sealed ampoule at 105±5 °C for 35 days on a small scale (10 ml of total volume). The reaction in the minus system (Exp. b and c) was carried out in the same way except for the omission of transition elements and clays respectively. The no-reaction control (Exp. d) with the same reaction mixture as the complete system was stocked in a glass-sealed ampoul at −20 °C for 35 days. The extraction procedures and the determination of primary amino groups are described in the text.

analyzer. This result shows that most of the compounds with primary amino groups formed in the no-reaction control were not due to the contamination of the impurities in the starting materials such as clays or to the contamination during the experimental handling, and that the formation of glycine in modified sea mediums was so easy that such a detectable amount of glycine could be formed during storage at −20 °C and operation at room temperature. It should be pointed out that clays were not absolutely required for either the formation of amino acids or that of oligomers, as had been observed in preliminary experiments by Ventilla and Egami.[8] It remains unsolved, however, whether the formation of amino acids and oligomers in the case of minus transition elements was realized by the clays themselves or by transition elements contained in the clays.

An aliquot of each product formed from Exps. a, b, c, and d was placed in a small column packed with Biogel P-2 and equilibrated with 0.1 M ammonium hydrogencarbonate. The elution profile obtained by measuring the amount of primary amino groups before and after acid hydrolysis is shown in Fig. 5. All these elution patterns except for that of Exp. d (no-reaction control) were observed to be almost the same. However, the formation of primary amino groups in the high-molecular-weight fraction in Exp. b (minus transition elements) was considerably decreased compared with that in Exp. a (complete). The relatively low production suggests that these transition elements were required for the formation of oligomers in the modified sea mediums. In fact, a separate experiment using a higher concentration (0.001 M) of molybdenum was found to give about twice as much of the primary amino groups.

Effect of the Reaction Time on the Formation of Amino Acids and the Related Oligomers from Formaldehyde and Hydroxylamine in Modified Sea Mediums. The time-dependent formation of primary amino groups before and after acid hydrolysis was measured as is shown in Fig. 6. The formation of primary amino groups before acid hydrolysis was observed to reach its maximum in about 30 days. However, the formation of primary amino groups after acid hydrolysis seemed to progress over a reaction time of about 40 days. As a consequence, the ratio of the content of primary amino groups after to before acid hydrolysis was found to increase linearly for 30 days. This means that the formation of oligomers required rather a long reaction time at 105 °C. The products obtained in different reaction times were measured for their amino acid composition using the automatic amino acid analyzer in separate experiments. No amino acids required a specially long reaction time for the formation, but the formation of alanine, β-alanine, and especially glycine was found to reach the maximum at rather an early stage.

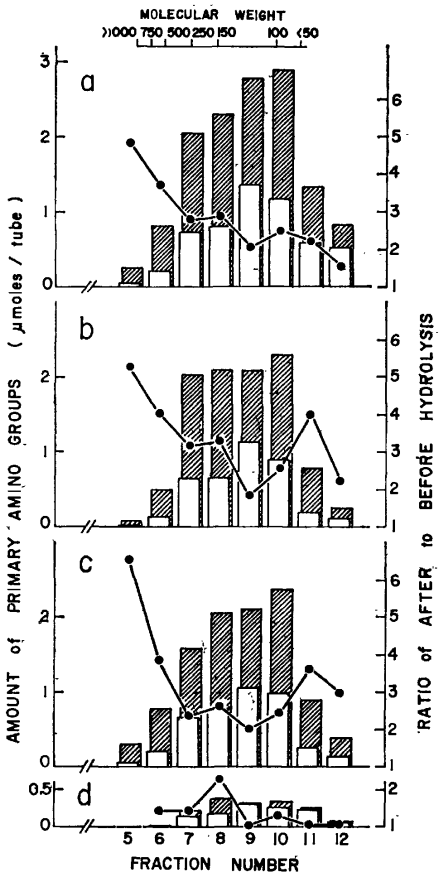

Fig. 5. Elution profiles of small-scale Biogel P-2 column chromatographies of the products obtained from the requirement experiments. Four column profiles; a, b, c, and d, represent that obtained from the Exp. a, b, c, and d, respectively, shown in Table 5. Open and shadowed bars represent the amount of primary amino groups before and after acid hydrolysis, respectively. Closed circles represent the ratio of the amount of primary amino groups after to before acid hydrolysis.

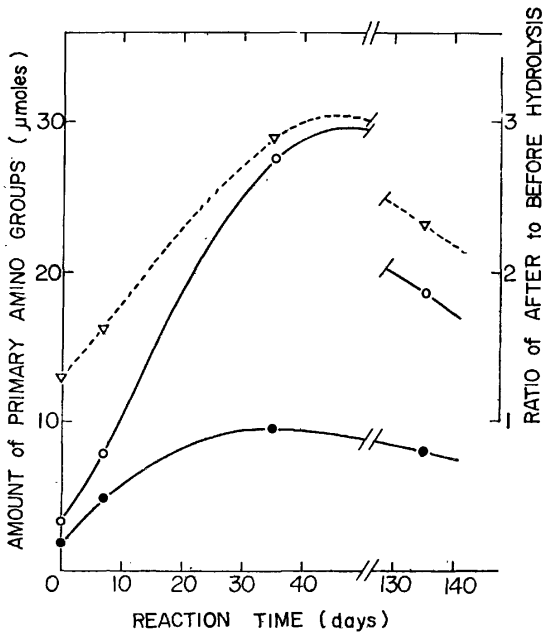

Fig. 6. Time course of the formation of amino acids and related oligomers from formaldehyde and hydroxylamine. Closed and open circles represent the amount of primary amino groups before and after acid hydrolysis, respectively. Reversed open triangles represent the ratio of the amount of primary amino groups after to before acid hydrolysis.

General Discussion. Amino acids were the first organic compounds of biological interest produced under simulated primitive earth conditions.[1] Reactions in one-step processes from simple compounds of carbon with simple nitrogen compounds have been accomplished by several investigators using highly activating forms of energy, such as electric discharges, ultraviolet light, and ionizing radiation [shown in the literature listed in the monograph[13]]. A common feature of all these experiments is the employment of highly activating forms of energy. In these experiments, part of the energy was found to be used to oxidize methane to formaldehyde, and in the reduction of nitrate. Thus, certain C_1 and N_1 compounds, such as formaldehyde and hydroxylamine respectively, of intermediate degrees of oxidation could be expected to produce amino acids even in the absence of electric discharges, ultraviolet, and ionization radiation. Based on the above consideration, Oró *et al.*[7] first reported that it is possible to synthesize appreciable amounts of glycine and certain amino acids by heating aqueous solutions of paraformaldehyde and hydroxylamine hydrochloride at a moderate temperature [Compare 14].

Egami's hypothesis that the composition of the present sea water reflects that of the primeval sea water at the time of early evolution suggests the possibility that the abundant transition elements in sea media, such as iron, molybdenum, and zinc, might play an important role in the prebiotic amino acid synthesis.[5] In addition, these transition elements would be expected to evolve to form protoenzymes.[6] In fact, as is reported in the present paper, the possible direct formation of amino acids and the related oligomers from formaldehyde and hydroxylamine, with six species of essential transition elements and clays, was realized in modified sea mediums. It was of especial interest to ascertain the phosphatase activity in the oligomeric products. The hydrolytic activity of the oligomers (with 700 daltons as the average molecular weight) was found to be 0.409 μmol/day/mg oligopeptide by regarding the oligomers as oligopeptides. This protoenzyme-like activity is in good correlation with the consideration by Egami[6] that the zinc complex in the early stage of evolution may be regarded as a precursor of hydrolytic and transferring enzymes, including enzymes participating in the metabolism of macromolecules and information transfer.

However, attempts to find positive evidence for the existence of peptide bonds in the oligomers formed from formaldehyde and hydroxylamine were unsuccessful. It must be considerably difficult to find the peptide linkage in the crude oligomers mixture, for the oligomers would consist of various compounds of different natures, but all highly microheterogeneous. We hope that it will be elucidated by future experiments.

In the former paper of Oró *et al.*,[7] they reported that the formation of amino acids from paraformaldehyde and hydroxylamine occurred under acidic as well as basic conditions, but no measurable formation of amino acids took place between pH 3 and 6.

Contrary to their finding, in our experiments with modified sea mediums amino acid formation took place at pH 5.5. We chose the pH expecting the accumulation of oligopeptides. As can be seen in Fig. 6, although a rather long time (approximately 40 days) was required for the maximum yield of primary amino groups in the acid hydrolysate, oligomers accumulated as expected. The total yield of primary amino groups was comparable with that reported by Oró *et al.*[7]

In course of the reaction the reaction mixture gradually colored and finally gave rise to the "Golden Primordial Broth." The nature of the colored substance has not been studied, but in view of the nature of the starting materials and intermediates, it might be regarded as a melanoidin-like polymer, the important role of which in chemical evolution has recently been suggested by Nissenbaum *et al.*[15]

It is generally accepted that the origin of life took place in the primeval sea of the earth and that most of the organic substances of general biological interest accumulated in the primeval sea. Our research may be regarded as an attempt to search for the synthesis of organic compounds in modified or improved primeval sea mediums. We hope that it will not only contribute to the elucidation of chemical evolution, but will also open a new way to organic synthesis in general.

The authors are indebted to the following persons (all in the Mitsubishi-Kasei Institute of Life Sciences) for their helpful discussions: Drs. Tairo Oshima, Tsuneko Uchida, Martha Ventilla, Hiroshi Yanagawa, and Nobuyuki Wakayama. The authors also wish to express their gratitude to Miss Yoko Ogawa for her technical assistance and to Mrs. Michiko Tanaka for her amino acid analysis.

References

1) S. L. Miller, *Science*, **117**, 528 (1953).
2) A. I. Oparin, ed, "The Origin of Life of the Earth," Pergamon Press, Oxford (1959).
3) S. W. Fox ed, "The Origins of Prebiological Systems and Their Molecular Matrices," Academic Press, New York (1965).
4) A. I. Oparin, in "Prebiotic and Biochemical Evolution," ed. by A. P. Kimball and J. Oró, North-Holland, Amsterdam (1971).
5) F. Egami, *J. Mol. Evol.*, **4**, 113 (1974).
6) F. Egami, *J. Biochem. (Tokyo)*, **77** 1165 (1975).
7) J. Oró, A. Kimball, R. Fritz, and F. Master, *Arch. Biochem. Biophys.*, **85**, 115 (1959).
8) M. Ventilla and F. Egami, *Proc. Jpn. Acad.*, **52**, 21 (1976).
9) P. Böhlen, S. Stein, W. Dairman, and S. Udenfriend, *Arch. Biochem. Biophys.*, **155**, 213 (1973).
10) A. L. Levy and D. Chung, *Anal. Chem.*, **25**, 396 (1953).
11) T. Oshima, *Arch. Biochem. Biophys.*, **126**, 478 (1968).
12) J. P. Ferris, D. B. Donner and A. P. Lobo, *J. Mol. Biol.*, **74**, 499 (1973).
13) S. L. Miller and L. E. Orgel, "The Origins of Life on the Earth," Prentice-Hall, New Jersey (1974).
14) J. Oró, in "The Origins of Prebiological Systems," ed. by S. W. Fox, Academic Press, New York (1965), pp. 137—162.
15) F. Nissenbaum, D. M. Kenyon, and J. Oró, *J. Mol. Evol.*, **6**, 253 (1975).

Synthesis of Ferrocene–Phenol Resins and Liberation of Iron Particles by Pyrolysis

Mamoru OMORI, Kazuo NAGASHIMA, and Seishi YAJIMA
The Oarai Branch, The Research Institute for Iron, Steel and Other Metals, Tohoku University, Oarai, Ibaraki 311-13
(Received October 15, 1976)

Ferrocene–phenol resin was synthesized from 1-ferrocenylethanol, phenol, and formaldehyde in the presence of an ammonia catalyst. The resin structure was elucidated by chemical and infrared analyses and then confirmed by micro Vickers hardness measurements. To liberate iron atoms from ferrocene skeletons, the resin was pyrolyzed *in vacuo* at 400 °C. The properties of the iron dispersed in a glasslike carbon matrix were investigated by magnetic susceptibility measurements, ESR, and Mössbauer spectroscopy. The iron atoms coagulated into ferromagnetic iron particles in the glasslike carbon matrix. This coagulation is discussed in connection with the resin structure.

In recent years considerable efforts have been made to prepare ultra-fine particles of metals and metal compounds. These ultra-fine particles have proven to be a powerful tool in the clarification of physical properties. Furthermore, various kinds of ultra-fine particles, from atoms to submicroscopic particles, provide important information about the mechanism of crystal growth. Several workers have reported methods for preparing the ultra-fine particles.[1–4] In previous papers[5,6] we reported an approach to the size control of ultra-fine iron particles dispersed in a glasslike carbon matrix prepared from acetylferrocene–furfural resins by heat treatment. However, it still remains obscure whether the formation of ultra-fine particles depends on the molecular structure of acetylferrocene–furfural resin or the dispersion of glasslike carbon.

This investigation has been undertaken to determine the relationship between the preparation of ultra-fine iron particles and the molecular structure of a resin. The acetylferrocene-furfural resin is synthesized from furfural and acetylferrocene. The ferrocene skeleton forms the main chain of this resin and is fixed in the resin structure.[7] On the other hand, the ferrocene skeleton of the side chain is not fixed in the resin structure. Such a resin (ferrocene–phenol resin) was synthesized from 1-ferrocenylethanol, phenol, and formaldehyde in the presence of an ammonia catalyst. The structure of ferrocene–phenol resin was elucidated by chemical analyses, infrared spectroscopic analyses, and micro Vickers hardness measurements. The ferrocene–phenol resin was pyrolyzed up to 400 °C *in vacuo* to liberate iron. The properties of iron particles dispersed in the glasslike carbon matrix were investigated by magnetic susceptibility measurements, ESR, and Mössbauer spectroscopy.

Experimental

Materials. Ferrocene was synthesized according to the method proposed by Hata *et al.*[8] Acetylferrocene[9] derived from ferrocene and acetic anhydride was reduced to 1-ferrocenylethanol using $LiAlH_4$.[10] The product was purified by recrystallization from hexane and sublimation *in vacuo*: mp 72—74 °C (Ref. 11, 73—75 °C). The other chemicals used were reagent grade.

Preparation of Resins. Ferrocene–phenol resin was synthesized in the presence of an alkali catalyst according to the method for the preparation of resole-type phenolic resin.[11] 30% aqueous ammonia was used as the alkali catalyst to avoid contamination with metal elements in the resin. 1-Ferrocenylethanol (0—1.0 mol), 1 mol of phenol, and 1.5 mol of formaldehyde (37% solution) were mixed in a three-necked separable flask. To this mixture was added aqueous ammonia amounting to 0.7 mol% of 1-ferrocenylethanol, phenol, and formaldehyde. The reaction mixture was vigorously stirred at 70 °C for 3 h, cooled to room temperature, and then neutralized with dilute hydrochloric acid. The water in the reaction product was removed to form oligomers under reduced pressure at 70 °C. Further, the oligomer was dried *in vacuo* at 70 °C for 24 h in order to remove the volatile materials. The yield of the oligomer was 70—80% The oligomer containing ferrocene was mixed with 10 wt % of hexamethylenetetramine and then heated in argon at 150 °C for 24 h. The yield of the ferrocene–phenol resin was 85—93%.

Pyrolysis. The ferrocene–phenol resin was pyrolyzed up to 400 °C *in vacuo*: 20—350 °C, 3h; 350—400 °C, 2.5 h. The heat-treated samples in the vacuum container were placed in a glovebox filled with argon gas. The following operations were carried out in the glovebox. The heat-treated resins were ground to a powder using an agate mortar and a pestle. The powdered sample for magnetic susceptibility measurements was put in the glass tube filled with anhydrous hexane, and then sealed with a rubber cap. For ESR spectral measurements, the powdered samples were put into a silica tube ($5\phi \times 200$ mm) and sealed with an epoxy resin. The powdered sample mixed with silicone grease was used for Mössbauer spectral measurements.

Elemental Analysis and Measurement of Properties. Iron determination was carried out with a Hitachi-207 atomic absorption spectrophotometer. IR spectra were measured with a Jasco IR-S grating spectrometer using potassium bromide disks. Micro Vickers hardness was measured with an Akashi model MVK type D instrument with a load of 200 g. The magnetic susceptibility was recorded on a Shimadzu MB-10A magnetic balance at temperatures of 77 to 293 K. Number-average molecular weights were determined by a Hitachi model-117 vapor pressure osmometer using dimethyl sulfoxide as a solvent. ESR spectra were taken on a Hitachi model 771-0061 spectrometer at 77 K. Mössbauer spectra were measured with an automechanical acceleration spectrometer at 4.2 K using a ^{57}Co-in-Cu source. All of the isomer shifts were obtained with respect to the centroid of iron metal at 293 K.

Results and Discussion

Polycondensation Reaction and Resin Structure. 1-Ferrocenylalkanols are polycondensed in the pre-

Table 1. Polycondensation reaction and elemental analysis of resins

Resin No.	Starting material[a]		Elemental analysis of resins (wt%)				
	1-Ferrocenylethanol (mol)	Fe (wt%)	C	H	Fe	N	O[b]
1	0.010	0.40	76.5	5.77	0.65	0.59	16.49
2	0.017	0.67	76.3	5.82	1.14	0.74	16.00
3	0.025	0.97	75.8	5.84	1.56	0.76	16.04
4	0.050	1.86	76.0	5.88	3.33	0.87	13.92
5	0.10	3.46	74.9	5.61	6.23	0.84	12.42
6	0.20	6.05	73.3	5.91	9.53	1.89	9.37
7	0.40	9.24	72.6	5.83	13.5	1.74	6.33
8	0.60	12.1	71.0	5.87	14.8	1.75	6.58
9	0.80	13.9	70.8	5.99	15.2	1.80	6.21
10	1.00	15.2	70.6	5.96	15.3	1.78	6.36
11	0	0	76.0	5.67	0	0.19	18.14

a) Phenol: 1 mol; formaldehyde: 1.5 mol. b) O=100−C−H−Fe−N.

sence of an acid and a Lewis acid. However, a base does not catalyze the polycondensation. The polycondensation reaction of aldehydes and cyclopentadienyl rings of ferrocene is catalyzed by a Lewis acid, but not by a base.[12] A resole-type oligomer is synthesized from 1 mol of phenol and 1.5 mol of formaldehyde in the presence of an alkali catalyst. Cured resole-type phenolic resins are obtained by the thermosetting of a resole-type oligomer.[11]

1-Ferrocenylethanol, phenol, and formaldehyde were polycondensed to make ferrocene–phenol oligomers, using aqueous ammonia as a catalyst. The curing of the ferrocene–phenol oligomer was not achieved in the absence of hexamethylenetetramine. The larger the amount of ferrocene skeletons in the oligomer was, the less the thermosetting reaction took place. The elemental analyses of the cured resins are shown in Table 1, together with the molar ratios of the starting materials. The nitrogen in the resin arose from hexamethylenetetramine, since no nitrogen is contained in any oligomer. The reactivities of 1-ferrocenylethanol and formaldehyde with phenol have not been investigated. Nevertheless, it is possible to estimate the reactivity and the structure of ferrocene–phenol resin from the data of elemental analyses. As shown in Table 1, the iron contents in the starting materials were less than those in resins 1 to 9. This relation was not valid for resin 10. The result of elemental analysis of resin 9 was identical with that of resin 10. Thus, the rate of reaction of 1-ferrocenylethanol and phenol was much faster than that of formaldehyde and phenol. The maximum quantity of 1-ferrocenylethanol allowed to react with phenol seemed to be restricted by a stoichiometric reaction. The stoichiometric reaction of 1-ferrocenylethanol, phenol, and formaldehyde should be an intermediate reaction between resins 8 and 9. From the elemental analysis of resins 9 and 10, the structural unit of the resin was calculated to be $C_{46}H_{47}O_3Fe_2N$. The number-average molecular weight of the oligomer of resin 9 was 650, which was close to the molecular weight of the structural unit of the resin. It was obvious that two ferrocene units ($C_{12}H_{13}Fe$) were contained in the structural unit. If three phenols (C_6H_6O) were bonded in it, four carbons and a nitrogen constituted the structure of the resins as the crosslinking unit. The above results suggest the resin structure shown in Fig. 1. The structure of the oligomer of resin 9 would be similar to this structure. On the initial step in the polycondensation reaction of the resin, 2 mol of phenol react with 2 mol of 1-ferrocenylethanol and the hydroxymethylation of phenol (1 mol) takes place. The ferrocenyl phenol (2 mol) reacts with 1 mol of the hydroxymethylated phenol to form the oligomer. The structure of the oligomer is classed as a novolac-type oligomer, because the cure reaction does not proceed sufficiently in the absence of hexamethylenetetramine.

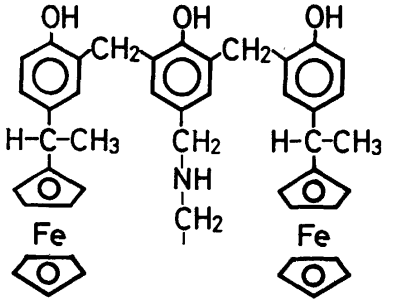

Fig. 1. The structure of ferrocene–phenol resin 9.

The amount of crosslinkage in a resin is related to its rigidity.[13] The micro Vickers hardness of resins, which is an indication of the rigidity, decreased rapidly with the increase in iron content, as shown in Fig. 2. The amount of crosslinkages in the resins decreased with an increase in the amount of ferrocene skeletons. This result indicated that the unsubstituted cyclopentadienyl ring does not take part in the formation of the main chain.

The IR spectra of ferrocene–phenol and resole-type phenolic resins are shown in Fig. 3. The absorption bands at 480, 818, 998, 1103, and 3080 cm^{-1} were assigned to ferrocene. The 480 cm^{-1} band was due to the ring metal stretching of ferrocene.[14] The

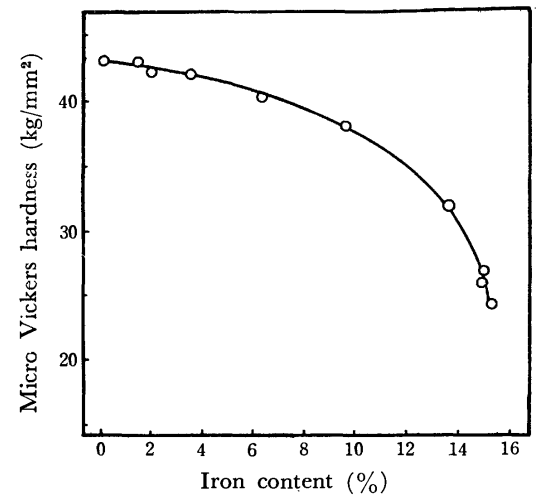

Fig. 2. Relation between micro Vickers hardness and iron contents of ferrocene-phenol resins.

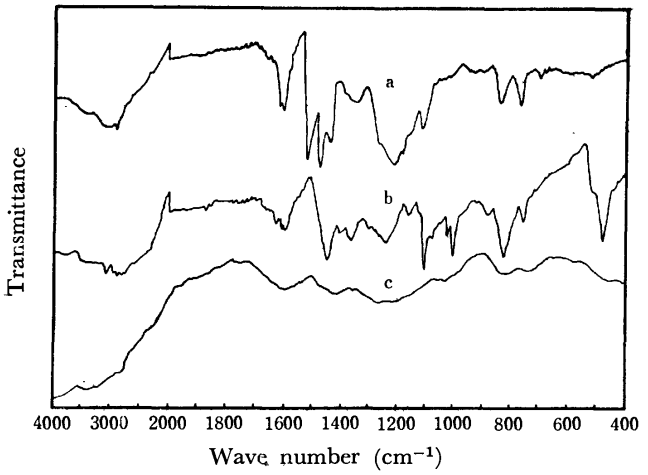

Fig. 3. IR spectra of phenolic resin and ferrocene-phenol resin, the heat-treated at 400 °C; (a) phenolic resin 11, (b) ferrocene-phenol resin 9, (c) ferrocene-phenol resin 9 heat-treated at 400 °C.

out-of-plane bending of ferrocene CH was manifested by the band at 818 cm^{-1}.[15] The presence of unsubstituted cyclopentadienyl rings was revealed by two bands at 998 and 1103 cm^{-1}.[16] The absorption band which appeared at 3080 cm^{-1} could be assigned to the stretching of ferrocenyl C–H.[14] In the IR spectrum of resole resin, the three bands at 1500—1650 cm^{-1} were assigned to the skeletal stretching mode of semi-unsaturated carbon-carbon bond. The band at 1220 cm,$^{-1}$ which was observed in both ferrocene–phenol and resole resins, corresponded to the absorption band of phenolic OH. In the IR spectrum of resole resin, two bands at 855 and 753 cm^{-1} were assigned to a 1,2,4,6-tetrasubstituted aromatic ring and a 1,2,4-trisubstituted aromatic ring, respectively. However, two bands at 753 and 874 cm^{-1} due to the 1,2,4-trisubstituted aromatic ring were strongly observed in the IR spectrum of ferrocene–phenol resin.[17] Results of IR spectral studies are in accord with the structure of ferrocene–phenol resin shown in Fig. 1.

Pyrolysis. The pyrolysis of resins was carried out by heat treatment up to 400 °C *in vacuo*. The IR spectrum of heat-treated ferrocene–phenol resin is shown in Fig. 3. All absorption bands due to ferrocene disappeared in the spectrum. This shows that the ferrocene skeleton in the ferrocene–phenol resin was destroyed, and iron was liberated by the heat treatment at 400 °C. Elemental analyses of heat-treated resins are shown in Table 2. The heat-treated resins contained carbon, hydrogen, iron, nitrogen, and oxygen. The nitrogen contents were less than those of the resins. The iron contents were 0.55—14.7%, which were close to that of acetylferrocene–furfural resin (1.00—13.2%).[5] It is well known that phenol and furan resins are converted into the hard and impervious carbon which does not contain open pores.[18] Especially, the impervious carbon prepared at 400 °C is in a completely glassy state.

TABLE 2. ELEMENTAL ANALYSIS OF RESINS HEAT-TREATED AT 400 °C

Resin No.	Elemental analysis (wt%)				
	Fe	C	H	N	O[a]
1	0.55	82.01	4.84	0.00	12.96
2	0.98	81.68	4.85	0.00	12.49
3	1.03	81.27	4.77	0.00	12.93
4	3.71	80.33	4.84	0.00	11.12
5	4.29	79.41	5.98	0.00	10.32
6	7.95	76.13	5.18	0.00	10.74
7	11.60	73.56	5.18	0.00	9.66
8	13.20	72.10	5.15	0.00	9.55
9	14.70	71.41	5.16	0.15	8.58
10	14.65	71.87	5.14	0.21	8.13
11	0.00	82.31	4.88	0.00	12.81

a) O=100−Fe−C−H−N.

Properties of Liberated Iron Particles. The measurement of magnetization is useful in determining whether the iron particles dispersed in the glasslike carbon matrix are superparamagnetic or not. Magnetic susceptibilities of heat-treated resins 1 to 10 indicated that the iron particles were ferromagnetic. The measurement of ESR spectra was carried out for all heat-treated resins. The ESR spectra of heat-treated resins

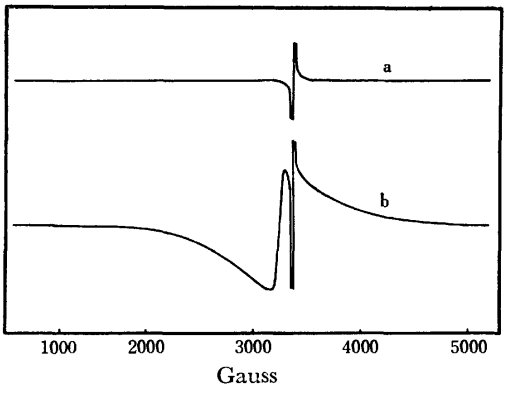

Fig. 4. ESR spectra of phenolic and ferrocene-phenol resins heat-treated at 400 °C; (a) phenolic resin 11, (b) ferrocene-phenol resin 1.

1 and 11 are shown in Fig. 4. The broad line near $g=2.09$ in resin 1 was due to the ferromagnetic resonance absorption of iron.[19] The ferromagnetic resonance absorption was common to the other heat-treated resins, 2 to 10. However, the peak intensity in the spectra increased with increase in iron contents. The sharp line at $g=2.002$, which was observed in the resins 1 and 11, corresponded to the resonance of free electrons on the carbon atom.[20] Further, the presence of ferromagnetic irons was confirmed in detail by their magnetic hyperfine splitting in the Mössbauer spectrum of the heat-treated resin 3, as shown in Fig. 5.[21] Because additional lines were not observed in the spectrum, only ferromagnetic iron was formed in the glasslike carbon matrix.

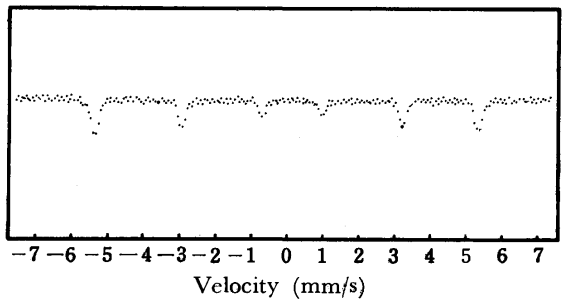

Fig. 5. Mössbauer spectrum of ferrocene–phenol resin 3 heat-treated at 400 °C.

The results of the present work lead to the following conclusions. Iron particles are formed in the glasslike carbon matrix by the heat treatment of ferrocene–phenol resins, in which the ferrocene skeleton is contained as a side chain. These iron particles are ferromagnetic and are different from the iron particles prepared from acetylferrocene–furfural resins in which the ferrocene skeleton forms the main chain of the resin. In the case of the side chain structure, the iron liberated from ferrocene skeletons is considered to coagulate to form the ferromagnetic iron because the spaces around the ferrocene skeleton are loosely surrounded by the resin structure. In this respect, it is necessary to take into account the differences between the properties of glasslike carbons prepared from ferrocene–phenol resin and acetylferrocene–furfural resin. However, these differences are considered to be small compared with the structural differences between these two resins; the details of these differences are now under investigation.

The authors would like to thank Dr. T. Shinjo, the Institute for Chemical Research, for performing the Mössbauer spectral measurements. Thanks are also due to Mr. T. Shoji and Mrs. H. Arai, Tohoku University, for their cooperation in the iron and CH analyses.

References

1) H. Micklitz and P. H. Barrett, *Phys. Rev. Lett.*, **28**, 1547 (1972).
2) D. W. Collins, L. N. Mulay, and W. F. Fisher, *Jpn. J. Appl. Phys.*, **6**, 1342 (1967).
3) C. S. Brooks and G. L. M. Christopher, *J. Catal.*, **10**, 211 (1968).
4) W. N. Delgass, R. L. Garten, and M. Boudart, *J. Phys. Chem.*, **73**, 2970 (1969).
5) S. Yajima and M. Omori, *Chem. Lett.*, **1972**, 843.
6) S. Yajima and M. Omori, *Chem. Lett.*, **1974**, 277.
7) M. Omori, M. Kurono, and S. Yajima, *Bull. Chem. Soc. Jpn.*, **48**, 1291 (1975).
8) K. Hata, I. Motoyama, and H. Watanabe, *Bull. Chem. Soc. Jpn.*, **38**, 853 (1965).
9) C. R. Hauser and J. K. Lindsay, *J. Org. Chem.*, **22**, 482 (1957).
10) F. S. Arimoto and A. C. Haven, *J. Am. Chem. Soc.*, **77**, 6295 (1955).
11) W. R. Sorenson and T. W. Campbell, "Preparative Methods of Polymer Chemistry," John Wiley and Sons Inc., New York (1961).
12) E. W. Neuse, "Advances in Macromolecular Chemistry," Vol. 1, ed by W. M. Pasika, Academic Press, London (1968), p. 1.
13) L. Holliday, *J. Appl. Polym. Sci.*, **12**, 333 (1968).
14) E. R. Lippincott and R. D. Nelson, *Spectrochim. Acta*, **10**, 307 (1958).
15) C. U. Pittman, Jr., *J. Polym. Sci., Part A-1*, **5**, 2027 (1967).
16) M. Rosenblum and R. B. Woodward, *J. Am. Chem. Soc.*, **80**, 5443 (1958).
17) P. J. Secrest, *Off. Digest.*, **37**, 187 (1965).
18) T. Ishikawa, *Tanso*, **7**, 13 (1959).
19) M. Bersohn and J. C. Baird, "An Introduction to Paramagnetic Resonance," W. A. Benjamin Inc., New York (1966).
20) F. H. Winslow, W. O. Baker, and W. A. Yager, *J. Am. Chem. Soc.*, **77**, 4751 (1955).
21) R. S. Preston, S. S. Hanna, and J. Heberle, *Phys. Rev.*, **128**, 2207 (1962).

A New Method for the Preparation of δ-Alkoxy-α,β-unsaturated Aldehydes and Polyenals

Akihiko ISHIDA* and Teruaki MUKAIYAMA

Department of Chemistry, Faculty of Science, The University of Tokyo, Hongo, Bunkyo-ku, Tokyo 113

(Received October 16, 1976)

Dienoxysilanes (**2**) react with acetals in the presence of $TiCl_4$ and also in the coexistence of $TiCl_4$ and $Ti(O^iPr)_4$ to give δ-alkoxy-α,β-unsaturated aldehydes (**3**—**5**) in good yields. In the presence of 1,8-diazabicyclo[5.4.0]undec-7-ene or 1,5-diazabicyclo[4.3.0]non-5-ene and molecular sieves 3A or 4A, the elimination reaction of δ-alkoxyl group of α,β-unsaturated aldehydes (**3**—**5**) proceeds smoothly to afford the corresponding polyenals in good yields.

In previous papers,[1,2] it was reported that the reaction of 1-trimethylsiloxy-1,3-butadiene (**2a**)[3] with various acetals (**1**) in the coexistence of $TiCl_4$ and $Ti(O^iPr)_4$ gives δ-alkoxy-α,β-unsaturated aldehydes (**3**), and that the aldehydes (**3**) are converted into polyenals by the elimination of δ-alkoxyl group with tertiary amines as 1,8-diazabicyclo[5.4.0]undec-7-ene (DUB) and 1,5-diazabicyclo[4.3.0]non-5-ene (DBN) in the presence of molecular sieves 3A and 4A. In the present paper, the preparation of δ-alkoxy-α,β-unsaturated aldehydes and polyenals is described in detail.

Results and Discussion

Preparation of δ-Alkoxy-α,β-unsaturated Aldehydes. Dienoxysilanes (**2**) reacted exclusively at their terminal sp^2 carbon atoms with acetals (**1**) activated by $TiCl_4$ to give the corresponding δ-alkoxy-α,β-unsaturated aldehydes (**3**—**5**) without the accompanying competitive products, β-alkoxy aldehydes[4] as shown in the following scheme 1.

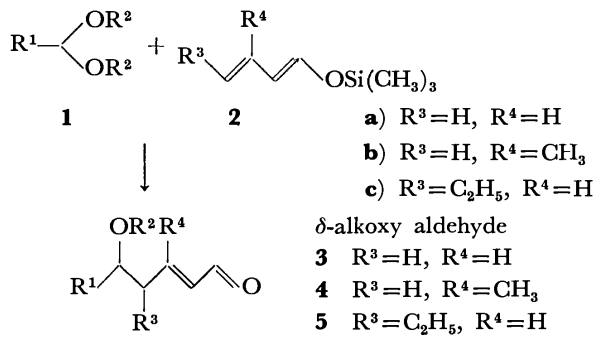

Scheme 1.

Dienoxysilanes (**2**) are very sensitive toward $TiCl_4$ readily undergoing polymerization. When the reaction was carried out in solvents inert to $TiCl_4$, such as dichloromethane and toluene, dienoxysilanes (**2**) instantaneously afforded polymeric substance instead of the desired δ-alkoxy-α,β-unsaturated aldehydes (**3**—**5**). The difficulty was overcome by diminishing the effect of $TiCl_4$ on dienoxysilanes (**2**) by a proper choice of solvents or addition of $Ti(O^iPr)_4$. Aldehydes (**3**—**5**) were prepared according to methods A, B, and C as follows.

Method A). $TiCl_4$-THF + **1** $\xrightarrow[-78\,°C\ THF]{2}$ **3**—**5**

Method B). **1** + $TiCl_4$ + $Ti(O^iPr)_4$ $\xrightarrow[-40\,°C\ CH_2Cl_2]{2}$ **3**—**5**

Method C). $TiCl_4$ + $Ti(O^iPr)_4$ $\xrightarrow[-40\,°C\ CH_2Cl_2]{1+2}$ **3**—**5**

Method A. $TiCl_4$ formed a yellow complex with tetrahydrofuran (THF). The complex still possessed sufficient ability to activate unsaturated acetals (**1d**—**f**), the reaction proceeding smoothly at −78 °C to give the desired aldehydes (**3**—**5**) in good yields. The saturated acetals (**1a** and **1c**), however, gave unsatifactory results. The results are summarized in Table 1.

Method B. In order to moderate the activity of $TiCl_4$, $Ti(O^iPr)_4$ was added to a mixture of $TiCl_4$ and acetals (**1**) in dichloromethane at −40 °C followed by the addition of dienoxysilane (**2**). Combined use of $TiCl_4$ and

TABLE 1. YIELDS OF δ-ALKOXY-α,β-UNSATURATED ALDEHYDES (METHOD A)

	Acetal (**1**)		Dienoxy-silane	Product		Isolated yield (%)
	R^1	R^2			R^2	
a	$C_6H_5CH_2CH_2$	CH_3	**2a**	**3a**	CH_3	trace
c	C_6H_5	CH_3	**2a**	**3c**	CH_3	16
d	$C_6H_5CH{=}CH$	CH_3	**2a**	**3d**	CH_3	88
d	$C_6H_5CH{=}CH$	C_2H_5	**2a**	**3d**	C_2H_5	82
d	$C_6H_5CH{=}CH$	$-CH_2-$	**2a**	**3d**	CH_2CH_2OH	60
d	$C_6H_5CH{=}CH$	CH_3	**2b**	**4d**	CH_3	85
d	$C_6H_5CH{=}CH$	CH_3	**2c**	**5d**	CH_3	69
e	$CH_3CH{=}CH$	CH_3	**2a**	**3e**	CH_3	86
f	n-$C_3H_7CH{=}CH$	CH_3	**2b**	**4f**	CH_3	70

* Present address: Organic Chemistry Res. Lab. Tanabe Seiyaku Co. Ltd., Toda, Saitama 335.

Table 2. Yields of δ-alkoxy-α,β-unsaturated aldehydes (Method B)

	Acetals (1)		Dienoxy-silane	Product	Isolated yield (%)	
	R^1	R^2			$R^2=CH(CH_3)_2$,	R^2
a	$C_6H_5CH_2CH_2$	CH_3	**2a**	**3a**	80	5
a	$C_6H_5CH_2CH_2$	C_2H_5	**2a**	**3a**	79	5
a	$C_6H_5CH_2CH_2$	CH_3	**2b**	**4a**	76	trace
b	n-C_5H_{11}	CH_3	**2a**	**3b**	75	5
c	C_6H_5	CH_3	**2a**	**3c**	83	3
d	$C_6H_5CH=CH$	CH_3	**2a**	**3d**	90	trace
g		CH_3	**2b**	**4g**	—	81
h		CH_3	**2a**	**3h**	—	69
		CH_3	**2b**	**4h**	—	68

$Ti(O^iPr)_4$ enabled us to use dichloromethane as a solvent. The saturated acetals (**1a**, **c**) also gave the corresponding δ-alkoxy-α,β-unsaturated aldehydes (**3**—**5**) in good yields (Table 2). However, the δ-alkoxyl group of most products prepared according to Method B was replaced by the isopropoxyl group originated from $Ti(O^iPr)_4$. In the case of sterically blocked α- and β-cyclocitral dimethyl acetal (**1g** and **1h**), no replacement of a methoxyl group of the parent acetal by an isopropoxyl group took place, and the normal δ-methoxy aldehydes could be obtained.

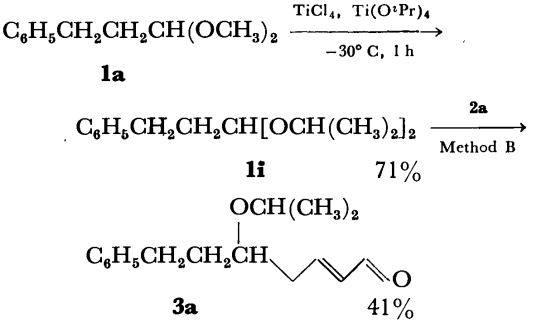

3-Phenylpropionaldehyde dimethyl acetal (**1a**) was readily converted into the diisopropyl acetal (**1i**)[5] in 71% yield by treatment with a mixture of $TiCl_4$ and $Ti(O^iPr)_4$ at −30 °C for 1 h under an argon atmosphere. When the diisopropyl acetal (**1i**) was treated with dienoxysilane (**2a**) under the conditions of Method B, 5-isopropoxy-7-phenyl-2-heptenal (**3a**) was isolated only in 41% yield. The lower yield of **3a** from **1i** might indicate that the reaction according to Method B proceeded through an intermediate, monoisopropyl acetal (**6**) rather than diisopropyl acetal (**1i**).

Method C. By changing the order of addition of the reagents, the replacement of the alkoxyl groups of starting acetals (**1**) with the isopropoxyl group of $Ti(O^iPr)_4$ could be easily prevented. A mixture of dienoxysilanes (**2**) and acetals (**1**) was added to a solution of $TiCl_4$ and $Ti(O^iPr)_4$ in dichloromethane at −40 °C. Various kinds of δ-alkoxy-α,β-unsaturated aldehydes (**3**—**5**) could be obtained in satisfactory yields without exchanging the alkoxyl groups of the parent acetals during the course of reaction (Table 3).

Table 3. Yields of δ-alkoxy-α,β-unsaturated aldehydes (Method C)

	Acetals(1)		Dienoxy-silane	Product	Isolated yields (%)
	R^1	R^2			
a	$C_6H_5CH_2CH_2$	CH_3	**2a**	**3a**	51
a	$C_6H_5CH_2CH_2$	C_2H_5	**2a**	**3a**	50
b	n-C_5H_{11}	CH_3	**2a**	**3b**	54
c	C_6H_5	CH_3	**2a**	**3c**	80
c	C_6H_5	C_2H_5	**2a**	**3c**	80
c	C_6H_5	CH_3	**2b**	**4c**	75
c	C_6H_5	CH_3	**2c**	**5c**	69
d	$C_6H_5CH=CH$	CH_3	**2a**	**3d**	85
d	$C_6H_5CH=CH$	C_2H_5	**2a**	**3d**	83
d	$C_6H_5CH=CH$	CH_3	**2b**	**4d**	76
d	$C_6H_5CH=CH$	CH_3	**2c**	**5d**	71
e	$CH_3CH=CH$	CH_3	**2a**	**3e**	80
f	n-$C_3H_7CH=CH$	CH_3	**2a**	**3f**	84
f	n-$C_3H_7CH=CH$	CH_3	**2b**	**4f**	74
g		CH_3	**2b**	**4g**	62
h		CH_3	**2a**	**3h**	80
		CH_3	**2b**	**4h**	80

The δ-alkoxy-α,β-unsaturated aldehydes (Tables 1, 2, and 3) can be classified into three groups: i) α,β-Unsaturated aldehydes, **3**(**a**—**f**, **h**); ii) 3-Methyl-α,β-unsaturated aldehydes, **4**(**a**, **c**, **d**, **f**, **g**); iii) 4-Ethyl-α, β-unsaturated aldehydes, **5**(**c**, **d**). The configuration of each aldehyde was determined mainly on the basis of NMR spectroscopy.

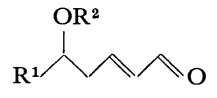

3 $J_{1,2}=8$Hz
$J_{2,3}=16$Hz

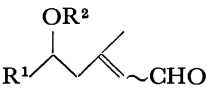

4 C_3-CH_3 group
2*E* δ 2.15—2.25
2*Z* δ 1.95—2.05

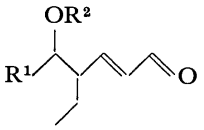

5 $J_{1,2}$=8Hz
$J_{2,3}$=16Hz

The aldehydes (**3**) of the first group were obtained as the sole product by this reaction, exhibiting peaks due to α,β-olefinic protons in the region of δ 5.00—6.10(C_2–H) and δ 6.75—6.80(C_3–H) with large coupling constants($J_{2,3}$=16 Hz), which supported the *trans* configuration of the double bonds in aldehydes (**3**).

On the other hand, the aldehydes (**4**) of the second group were mixtures of 2*E* and 2*Z* isomer(2*E* : 2*Z*=*ca.* 3—5 : 1). 3-Methyl group of 2*Z* isomers showed the signal in the region of δ 1.95—2.05 as a singlet or a doublet. In 2*E* isomers, the corresponding signal shifted to δ 2.15—2.25 as expected.[6]

The aldehydes (**5**) of the final group were found to be mixtures of *threo* and *erythro* isomers from their NMR spectra. No double bond isomer was detected. Without separation, these diasteromeric mixtures were subjected to the subsequent elimination reaction discussed later.

From the results, the reaction is assumed to proceed through a similar pathway proposed in the reaction of acetals with various nucleophiles,[7] *viz.*, the acetals (**1**) activated by $TiCl_4$ react with dienoxysilanes (**2**) to afford aldehydes (**3**—**5**) (path A of Scheme 2). The formation of δ-isopropoxy aldehydes by Method B could be explained by assuming an initial formation of monoisopropyl acetals (**6**) (path B).

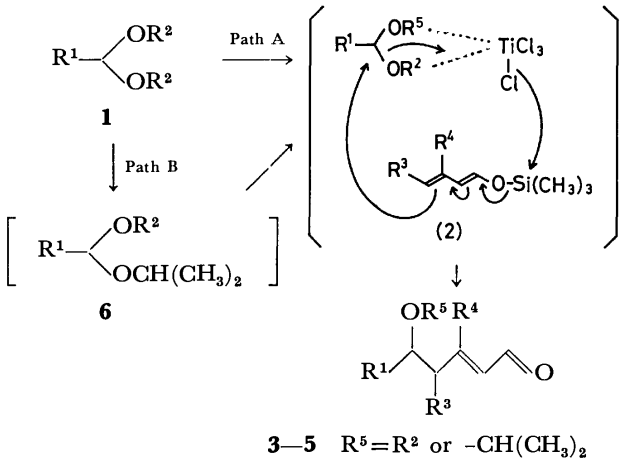

3—5 R^5=R^2 or $-CH(CH_3)_2$

Scheme 2.

Preparation of Polyenals: The conversion of δ-alkoxy-α,β-unsaturated aldehydes into polyenals was examined under acidic[8-11] and basic conditions.[12] The results obtained by use of 5-methoxy-7-phenyl-2,6-heptadienal (**3d**) as a substrate are summarized in Table 4. Besides low yields, disadvantage of the use of acids might be expected when the reaction is undertaken with 5-methoxy-5-(2,6,6-trimethyl-1-cyclohexen-1-yl)-2-pentenals (**3h**, **4h**), since a double bond of 2,6,6-trimethyl-1-cyclohexenyl group of these compounds is very labile to acids and the double bond migration takes place readily.[13]

Table 4. Yield of 7-phenyl-2,4,6-heptatrienal (**7c**)

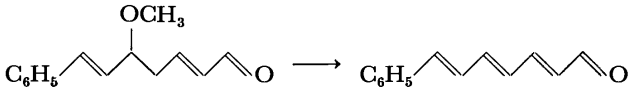

3d **7c**

	Acid or Base	Conditions	Yield (%)
1)	*p*-TsOH–C_6H_6	refl. 5 h	46
2)	CH_3CO_2Na-CH_3CO_2H	refl. 2 h	13
3)	$BF_3 \cdot O(C_2H_5)_2$-$(CH_3CO)_2O$	−10 °C 0.5 h	26(63)[a]
4)	$BF_3 \cdot O(C_2H_5)_2$-CH_2Cl_2	−10 °C 1 h	63
5)	*t*-BuOH–THF	−10 °C 1 h	59

a) 7-Phenyl-1,1,5-triacetoxy-2,6-heptadiene is obtained as a major product and converted into **7c** in 37% yield based on **3d**.

After several experiments on the elimination under basic conditions,[2] we found that 5-methoxy-7-phenyl-2,6-hetadienal (**3d**) gives the desired trienal (**7c**) in 92% yield by treatment with 2 molar amounts of DBU or DBN in the presence of molecular sieves 3A or 4A. There is no singificant difference either between the yields of DBU and DBN, or those of molecular sieves 3A and 4A. The longer reaction time was required when the reaction was carried out in the absence of molecular sieves.

In a similar manner, various δ-alkoxy-α,β-unsaturated aldehydes can be easily converted into corresponding polyenals (**7a**—**f**). **3h** also gave 5-(2,6,6-trimethyl-1-cyclohexen-1-yl)-2,4-pentadienal (**7f**) in 78% yield without the migration of double bond. The reactions usually proceed at room temperature in a short reaction time. The results are summarized in Table 5.

Although the method is applicable to the preparation of various polyenals from δ-alkoxy-α,β-unsaturated aldehydes, the results with 3-methyl-5-alkoxy-α,β-unsaturated aldehydes (**4**) (Table 6) were unsatisfactory even after prolonged refluxing. For conversion of **4** into polyenals (**8**, **9**), 4 molar amounts of DBU and addition of CH_3CN were required.

By this procedure, 5-methoxy-3-methyl-7-phenyl-2,6-heptadienal (**4d**) gave a mixture of (2*E*,4*E*,6*E*)-3-methyl-7-phenyl-2,4,6-heptatrienal (**8b**) and its (2*Z*,4*E*,6*E*)-isomer (**9b**). **8b** and **9b** were isolated by preparative TLC in 78% and 15% yields, respectively. Their configurations were easily determined by a comparison of the chemical shift of the 3-methyl group; 2*E* isomer (**8b**) has a signal due to 3-methyl protons at δ 2.30 and 2*Z* isomer (**9b**) has the corresponding signal at δ 2.10. The NMR data are consistent with the assigned configurations.

9b can be converted into thermodynamically stable **8b** in 67% yield by treating with a catalytic amount of iodine[12] in benzene–ether (1 : 1) at room temperature for 7 h. Oxidation of **8b** with silver oxide[14] afforded (2*E*,4*E*,6*E*)-3-methyl-7-phenyl-2,4,6-heptatrienoic acid (**10a**). The melting point of the acid (**10a**) and the NMR spectrum of its methyl ester (**10b**) coincide with those reported.[15,16]

Table 5. Elimination reaction of δ-alkoxy group of α,β-unsaturated aldehyde with DBU or DBN

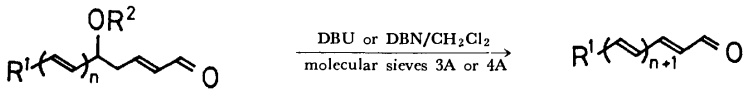

3 7

δ-Alkoxy aldehyde (3)			Conditions		Product	Yield of 7 (%)		
R^1	R^2	n	Temp	Time(h)		A[a]	B[b]	C[c]
n-C_3H_7	CH_3	1	r. t.	3.0	**7a**	81	82	80
C_6H_5	CH_3	0	r. t.	1.0	**7b**	82	80	80
C_6H_5	C_2H_5	0	r. t.	1.5	**7b**	79	79	—
C_6H_5	CH_3	1	r. t.	1.0	**7c**	92	92	89
C_6H_5	C_2H_5	1	r. t.	1.5	**7c**	92	—	—
C_6H_5	$CH(CH_3)_2$	1	refl.	2.0	**7c**	65	—	—
C_6H_5	CH_3	2	r. t.	1.0	**7d**	90	—	—
C_6H_5	CH_3	3	r. t.	1.0	**7e**	84	—	—
	CH_3	0	r. t.	4.0	**7f**	78	78	—

a) DBU–molecular sieves 3A. b) DBN–molecular sieves 3A. c) DBU–molecular sieves 4A.

Table 6. Yield of 3-methyl polyenal

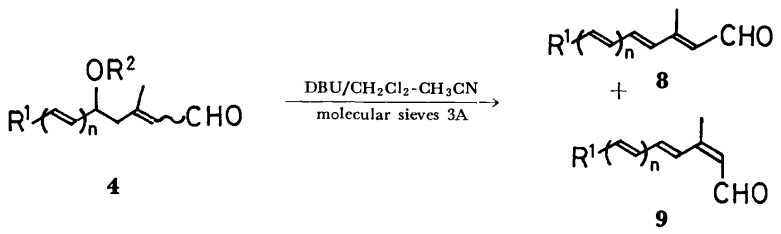

4

δ-Alkoxy aldehyde (4)		Conditions		Yield (%) of 8 and 9			
R^1	n	Temp	Time (h)	Product 2E		Product 2Z	
C_6H_5	0	refl.	4.0	**8a**	54	**9a**	10
C_6H_5	1	refl.	1.5	**8b**	78	**9b**	15
	0	refl.	5.0	**8c**	56	**9c**	19

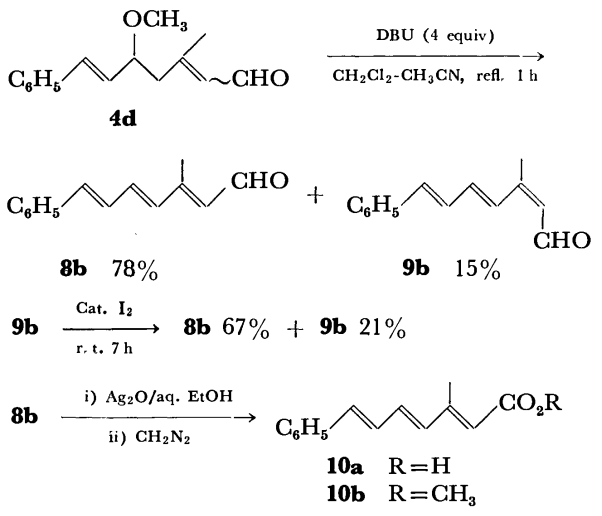

Similarly, 5-methoxy-3-methyl-5-phenyl-2-pentenal (**4c**) and 5-methoxy-3-methyl-5-(2,6,6-trimethyl-1-cyclohexen-1-yl)-2-pentenal (**4h**) were converted into the corresponding polyenals **8a** and **8c** (Table 6). The product **8c** is a useful intermediate for the syntheses of vitamin A and β-carotene.[17,18]

Elimination of a methoxyl group of 4-ethyl-5-methoxy-α,β-unsaturated aldehydes (**5**) proceeded smoothly under the conditions described for compounds **3a**—**f** in Table 5, as shown in the following Scheme 3.

4-Ethyl-5-methoxy-5-phenyl-2-pentenal (**5c**) gave (2E, 4E)-dienal (**11a**) and its (2E,4Z)-isomer (**11b**) in 44% and 12% yields, respectively. The configuration of **11a** and **11b** were deduced from their NMR data. The NMR spectrum of **11a** showed a doublet centered at δ7.25 (J=16 Hz) due to the C_3-vinyl proton and a quartet centered at δ 2.57 due to methylene protons of

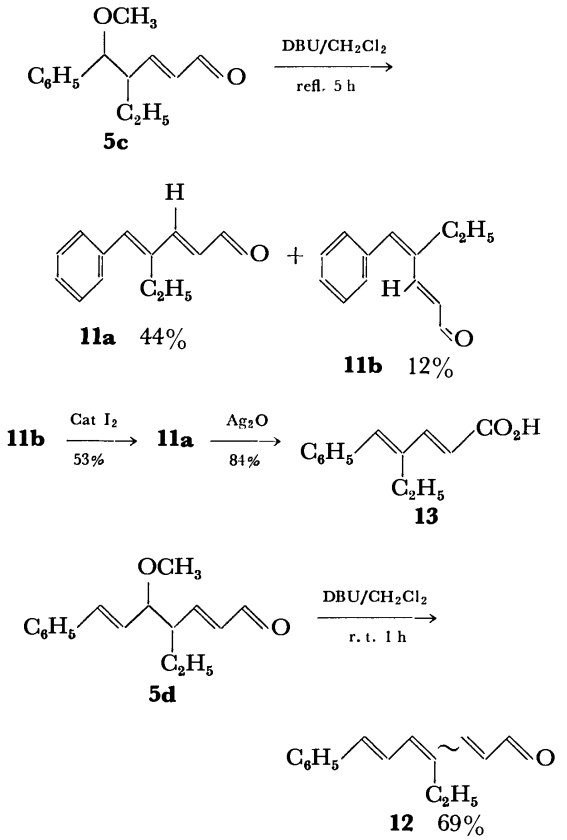

Scheme 3.

a 4-ethyl group, whereas the corresponding signals of **11b** appeared at δ 7.63(J=16 Hz) and δ 2.47. The differences in the chemical shifts of the corresponding signals could be produced from the anisotropic effect of the benzene ring at C-5. The data obtained are in line with the assigned stuctures.

Isomerization of **11b** by iodine also indicates that **11a** has a stable (2*E*,4*E*)-configuration. Further proof of the structure was provided by a comparision of the NMR spectrum of the dienoic acid (**13**) derived from **11a** with that of (2*E*,4*E*)-4-methyl-5-phenyl-2,4-pentadienoic acid.[19] Both spectra are almost the same except for the peaks due to 4-substituents.

Similarly, 4-ethyl-5-methoxy-7-phenyl-2,6-heptadienal (**5d**) was easily converted into the polyenal (**12**) in 69% yield at room temperature.

By a proper choice of conditions (Method A, B, or C) various δ-alkoxy-α,β-unsaturated aldehydes (**3**—**5**) can be easily synthesized in good yields by the reaction of dienoxysilanes (**2**) and acetals (**1**) activated by $TiCl_4$. Elimination of the resulting δ-alkoxy-α,β-unsaturated aldehydes was found to proceed in satiafsctory yields by the use of tertiary amines in the presence of molecular sieves 3A or 4A. The present work would provide a simple and useful route for the synthesis of polyenals.

Experimental[20]

Materials. Commercial $TiCl_4$ and $Ti(O^iPr)_4$ were distilled under an argon atmosphere before use.

*Perparation of 1-Trimethylsiloxy-1,3-butadiene (**2a**).*[3] To a solution of crotonaldehyde(8.4 g, 120 mmol) and triethylamine (12.6 g, 125 mmol) in anhydrous C_6H_6(15 ml) were added quickly anhydrous $ZnCl_2$ (120 mg), hydroquinone (200 mg), and trimethylchlorosilane(12.7 g, 125 mmol). The mixture was heated at 70 °C for 8 h in a sealed tube and quenched with aqueous $NaHCO_3$ solution at 0 °C. After filtration of undissolved substance filtrate was washed with 10% $KHSO_4$ solution and water, and dried over anhydrous Na_2SO_4. The solvent was removed and the residual oil was distilled. 1-Trimethylsiloxy-1,3-butadiene (**2a**) was obtained in 65% yield (10.4 g, bp 57—60 °C/50 Torr).

In a similar way, dienoxysilanes (**2b** and **2c**) were obtained in 70% and 65% yields, respectively. **2b**: bp 68—70 °C/40 Torr; **2c**: bp 80—83 °C/28 Torr.

*Reaction of Dienoxysilane (**2a**) with Cinnamaldehyde Dimethyl Acetal (**1d**) by Method A.* To a mixture of $TiCl_4$(3.0 mmol) and cinnamaldehyde dimethyl acetal(455 mg, 2.5 mmol) in 10 ml of dry THF was added a solution of dienoxysilane (**2a**) (426 mg, 3.0 mmol) in 4 ml of dry THF at −78 °C under an argon atmosphere. The mixture was stirred for 4 h at the same temperature and quenched with K_2CO_3 (3.0 g, in 10 ml of water). The resulting precipitate was filtered off and the filtrate was extracted with ether. The extract was washed with water, dried over anhydrous Na_2SO_4 and concentrated under reduced pressure. 5-Methoxy-7-phenyl-2,6-heptadienal (475 mg) was isolated in 88% yield by preparative TLC on silica gel developing with hexane–ethyl acetate (4 : 1). IR(neat): 1695, 1640, 1600 cm^{-1}; NMR(CCl_4): δ 9.45(1H, d, J=8 Hz, aldehyde H), 7.25(5H, s, aryl CH), 5.7—7.2(4H, m, olefinic H), 3.6—3.9(1H, br. q, C_5–H), 3.25 (3H, s, $-OCH_3$), 2.4—2.7(2H, br. t, $-CH_2-$); Found: C, 77.89; H, 7.41%. Calcd for $C_{14}H_{16}O_2$: C, 77.75; H, 7.46%.

The IR and NMR spectra of the other δ-alkoxy-α,β-unsaturated aldehydes (**3c—e**, **4d—f**, and **5d**) prepared by Method A are consistent with the assigned structures. **3c**(R^2=CH_3): bp 80 °C/0.05 Torr (bath temperature); IR(neat): 1690, 1640 cm^{-1}; NMR(CCl_4): δ 9.50(1H, d, J=8 Hz, aldehyde H), 7.30(5H, s, aryl CH), 6.80(1H, ddd, J=16, 8, 8 Hz, C_3–H), 6.05(1H, dd, J=8,16 Hz, C_2–H), 4.1—4.4(1H, br. t, C_5–H), 3.20(3H, s, $-OCH_3$), 2.45—2.80(2H, m, $-CH_2-$); Found: C, 75.91; H, 7.55%. Calcd for $C_{12}H_{14}O_2$: C, 75.76; H, 7.42%. **3d**(R^2=C_2H_5): IR(neat): 1690, 1640 cm^{-1}; NMR(CCl_4): δ 9.45(1H, d, J=8 Hz, aldehyde H), 7.30(5H, s, aryl CH), 5.8—7.5(4H, m, olefinic H), 3.7—4.1 (1H, q, C_5–H), 3.2—3.7(2H, br. q, $-OCH_2-$), 2.4—2.7(2H, br. t, $-CH_2-$), 1.20(3H, t, CH_3). **3d**(R^2=CH_2CH_2OH): IR (neat): 3430, 1690, 1640 cm^{-1}; NMR(CCl_4): δ 9.45(1H, d, J=8 Hz, aldehyde H), 7.30(5H, s, aryl CH), 5.6—7.1(4H, m, olefinic H), 3.8—4.1(1H, m, C_5–H), 3.0—3.8(5H, m, $-OCH_2CH_2OH$), 2.5—2.8(2H, $-CH_2-$). **3e**(R^2=CH_3): bp 70 °C/0.5 Torr(bath temperature); IR(neat): 1690, 1630 cm^{-1}; NMR(CCl_4): δ 9.55(1H, d, J=8 Hz, aldehyde H), 6.85(1H, ddd, J=16, 8, 8 Hz, C_3–H), 6.10(1H, dd, J=16,8 Hz, C_2–H), 5.2—5.8(2H, m, olefinic H), 3.4—3.8(1H, br. q, C_5–H), 3.20(3H, s, $-OCH_3$), 2.4—2.7(2H, t, $-CH_2-$), 1.75(3H, d, J=6 Hz, CH_3). **4d**(R^2=CH_3, a mixture of 2*E* and 2*Z* isomers): IR(neat): 1670, 1630 cm^{-1}; NMR(CCl_4): δ 10.00(1H, d, J=8 Hz, aldehyde H), 7.35(5H, s, aryl CH), 6.63(1H, d, C_7–H), 5.8—6.3(2H, br, C_6–H, C_2–H), 3.7—4.2 (1H, br. C_5–H), 3.30(3H, s, $-OCH_3$), 2.20(s, 2E, C_3-CH_3), 2.05(s, 2*Z*, C_3-CH_3), 2.35—2.5(2H, $-CH_2-$). **4f**(R^2=CH_3) 2*E* isomer: bp 80 °C/0.05 Torr (bath temperature): IR (neat): 1670, 1630 cm^{-1}; NMR(CCl_4): δ 9.95(1H, d, J= 8 Hz, aldehyde H), 5.65—5.95(1H, br, C_2–H), 5.00—5.65 (2H, m, olefinic H), 3.5—3.9(1H, m, C_5–H), 3.15(3H, s, $-OCH_3$), 2.15(3H, s, C_3-CH_3), 0.7—2.5(9H, aliphatic H); Found: C, 73.56; H, 9.98%. Calcd for $C_{12}H_{20}O_2$: C, 73.43; H, 10.27%. **4f**(R^2=CH_3) 2*Z* isomer: bp 80 °C/0.05 Torr(bath temperature); IR(neat): 1670, 1630 cm^{-1}; NMR

(CCl_4): δ 9.80(1H, d, J=8 Hz, aldehyde H), 5.70—5.95 (1H, br, C_2–H), 5.0—5.7(2H, m, olefinic H), 3.45—3.90(1H, m, C_5–H), 3.20(3H, s, $-OCH_3$), 1.95(3H, s, C_3–CH_3), 0.7—2.8(9H, aliphatic H), Found: C, 73.53; H, 10.05%. Calcd for $C_{12}H_{20}O_2$: C, 73.43; H, 10.27%. **5d**(R^2=CH_3, a mixture of *threo* and *eythro* isomers): IR(neat): 1690, 1640, 1600 cm^{-1}; NMR(CCl_4): δ 9.63(1H, d, J=8 Hz, aldehyde H), 7.40(5H, s, aryl CH), 5.8—7.7(4H, olefinic H), 3.6—3.9 (1H, C_5–H), 3.33(3H, s, $-OCH_3$), 1.2—2.7(3H, aliphatic H), 0.90(3H, t, CH_3); Found: C, 78.82; H, 8.33%. Calcd for $C_{16}H_{20}O_2$: C, 78.65; H, 8.25%.

*Reaction of Dienoxysilane (**2a**) with Cinnamaldehyde Dimethyl Acetal (**1d**) by Method B.* To a mixture of $Ti(O^iPr)_4$ (2.0 mmol) and 356 mg(2.0 mmol) of cinnamaldehyde dimetl yl acetal (**1d**) in 25 ml of CH_2Cl_2 was added $TiCl_4$ (2.3 mmol) in 1 ml of CH_2Cl_2 at -40 °C under an argon atmosphere. After stirring for a minute, dienoxysilane (**2a**, 355 mg, 2.5 mmol in 4 ml of CH_2Cl_2) was added to the mixture. The mixture was kept at -40 °C for 30 min, quenched with K_2CO_3 (2 g in 10 ml of H_2O) and worked up in the usual way. 5-Isopropoxy-7-phenyl-2,6-heptadienal(441 mg) was isolated in 90 % yield by preparative TLC on silica gel developing with hexane–ethyl acetate(4 : 1). IR(neat): 1690, 1640, 1600 cm^{-1}; NMR(CCl_4): δ 9.50(1H, d, J=8 Hz, aldehyde H), 7.30(5H, s, aryl CH), 5.8—7.2(4H, m, olefinic H), 3.4—4.3 (2H, m, $-OCH<$, C_5–H), 2.4—2.8(2H, m, $-CH_2-$), 1.15(6H, d, $2\times CH_3$).

The IR and NMR spectra of other δ-alkoxy-α,β-unsaturated aldehydes (**3a**—**h** and **4a**—**h**) prepared by Method B are consistent with the assigned structures. **3a** (R^2=*i*-pr): IR (neat): 1690, 1630, 1600 cm^{-1}; NMR(CCl_4): δ 9.50(1H, d, J=8 Hz, aldehyde H), 7.20(5H, s, aryl CH), 6.80(1H, ddd, J=16, 8, 8 Hz, C_3–H), 6.05(1H, dd, J=16, 8 Hz, C_2–H), 3.2 —3.8(2H, m, $2\times$–O–CH<), 2.2—2.8(4H, m, $-CH_2-$), 1.5—1.9(2H, m, $-CH_2-$), 1.10(6H, d, $2\times CH_3$). **3b**(R^2=*i*-pr): bp 140 °C/0.2 Torr (bath temperature); IR(neat); 1680, 1625 cm^{-1}; NMR(CCl_4); δ 9.55(1H, d, J=8 Hz, aldehyde H), 6.80 (1H, ddd, J=16, 8, 8 Hz, C_3–H), 6.05(1H, dd, J=16, 8 Hz, C_2–H), 3.2—3.8(2H, m, $2\times$–O–CH<), 2.3—2.7(2H, m, $-CH_2-$), 0.7—1.6(17H); Found: C, 73.23; H, 11.35%. Calcd for $C_{13}H_{24}O_2$: C, 73.53; H, 11.39%. **3c**(R^2=*i*-pr): IR(neat): 1695, 1640 cm^{-1}; NMR(CCl_4): δ 9.45(1H, d, J=8 Hz, aldehyde H), 7.30(5H, s, aryl CH), 6.80(1H, ddd, J=16, 8, 8 Hz, C_3–H), 6.00(1H, dd, J=16, 8 Hz, C_2–H), 4.2 —4.65 (1H, m, C_5–H), 3.3—3.7 (1H, m, $-OCH<$), 2.5—2.8 (2H, $-CH_2-$), 1.00—1.30(6H, $2\times CH_3$). **3h**(R^2=CH_3): IR (neat); 1690, 1635 cm^{-1}; NMR(CCl_4): δ 9.50(1H, d, J=8 Hz, aldehyde H), 6.85(1H, ddd, J=16, 8, 8 Hz, C_3–H), 6.05 (1H, dd, J=16, 8 Hz, C_5–H), 3.15(3H, s, $-OCH_3$), 1.75(3H, s, C=C–CH_3), 0.95—1.00(6H, 2s, $2\times CH_3$), 1.20—2.90(7H, aliphatic H), **4a**(R^2=*i*-pr, a mixture of 2*E* and 2*Z* isomers): IR(neat): 1680, 1630, 1600 cm^{-1}; NMR(CCl_4): δ 9.90(1H, d, J=8 Hz, aldehyde H), 7.15(5H, s, aryl CH), 5.7—6.0(1H, br. d, C_2–H), 3.25—3.8(2H, m, $2\times$–O–CH<), 1.5—3.0(5H, m, aliphatic H), 1.10(6H, d, $2\times CH_3$), 2.15(s, 2*E*, C_3–CH_3), 1.95(s, 2*Z*, C_3–CH_3). **4g**(R^2=CH_3): 2*E* isomer: IR(neat): 1680, 1625 cm^{-1}; NMR(CCl_4); δ 9.95(1H, d, J=8 Hz, aldehyde H), 5.6—5.9(1H, br. d, C_2–H), 5.2—5.9(1H, br, olefinic H), 3.0—3.3(1H, br, C_5–H), 3.25(3H, s, $-OCH_3$), 1.75 (3H, s, C=C–CH_3), 1.00, 0.85(6H, 2s, $2\times CH_3$), 0.5—2.5(7H, aliphatic H), 2.20(3H, s, C_3–CH_3). 2*Z* isomer: IR(neat): 1680, 1625 cm^{-1}; NMR(CCl_4): δ 9.90(1H, d, J=8 Hz, aldehyde H), 5.65—5.95(1H, br. d, C_2–H), 5.3—5.6(1H, br, olefinic H), 3.25(3H, s, $-OCH_3$), 2.00(3H, s, C_3–CH_3), 1.75 (3H, s, C=C–CH_3), 1.05, 0.90(6H, 2s, $2\times CH_3$).

*Reaction of Dienoxysilane(**1a**) with 3-Phenylpropionaldehyde Dimethyl Acetal (**1a**) by Method C.* To a stirred solution of $TiCl_4$(1.5 mmol) and $Ti(O^iPr)_4$ (1.5 mmol) in 10 ml of CH_2Cl_2 was added a solution of 3-phenylpropionaldehyde dimethyl acetal(180 mg, 1.0 mmol) and dienoxysilane (**2a** 170 mg, 1.2 mmol) in 5 ml of CH_2Cl_2 at -40 °C under an argon atmosphere. After being stirred for 30 min at the same temperature, the mixture was quenched with K_2CO_3 (1.5 g in 10 ml of H_2O), and the resulting precipitate was filtered off. The filtrate was extracted with ether and the resulting solution was dried over anhydrous Na_2SO_4. After removal of the solvent, the residual oil was chromatographed on silica gel developing with hexane–ethyl acetate(4 : 1) to give 5-methoxy-7-phenyl-2-heptenal (112 mg) in 51% yield. IR(neat): 1690, 1640, 1600 cm^{-1}; NMR(CCl_4): δ 9.55(1H, d, J=8 Hz, aldehyde H), 7.20(5H, s, aryl CH), 6.80(1H, ddd, J=16, 8, 8 Hz, C_3–H), 6.05(1H, dd, J=16, 8 Hz, C_2–H), 3.35(3H, s, $-OCH_3$), 3.0—3.4(1H, br, C_5–H), 2.3—2.9(4H, m, $-CH_2-$), 1.5—2.0(2H, m, $-CH_2-$).

2,4-Dinitrophenylhydrazone: mp 123—124 °C; Found: C, 60.29; H, 5.57; N, 14.06%. Calcd for $C_{20}H_{22}O_5N_4$: C, 60.06; H, 5.76; N, 13.96%.

The IR and NMR spectra of other δ-alkoxy-α,β-unsaturated aldehydes (**3a**—**h**, **4c**—**h** and **5c**—**d**), prepared by Method C are consistent with the assigned structures. **3a**(R^2=C_2H_5): IR (neat): 1685, 1630, 1600 cm^{-1}; NMR(CCl_4): δ 9.50(1H, d, J=8 Hz, aldehyde H), 7.20(5H, s, aryl CH), 6.75(1H, ddd, J=16, 8, 8 Hz, C_3–H), 6.00(1H, dd, J=16, 8 Hz, C_2–H), 3.2 —3.7(3H, m, $-OCH_2-$, C_5–H), 2.3—2.9(4H, m, $-CH_2-$), 1.5 —2.0(2H, m, $-CH_2-$), 1.20(3H, t, $-CH_3$). **3b**(R^2=CH_3): bp 125 °C/0.1 Torr(bath temperature); IR(neat): 1695, 1640 cm^{-1}; NMR(CCl_4): δ 9.50(1H, d, J=8 Hz, aldehyde H), 6.80(1H, ddd, J=16, 8, 8 Hz, C_3–H), 6.05(1H, dd, J=16, 8 Hz, C_2–H), 3.30(3H, s, $-OCH_3$), 3.1—3.5(1H, br, C_5–H), 2.4 —2.7(2H, m, $-CH_2-$), 0.7—1.6(11H); Found: C, 71.84; H, 11.18%. Calcd for $C_{11}H_{20}O_2$: C, 71.69; H, 10.94%. **3c** (R^2=C_2H_5): IR(neat): 1690, 1640 cm^{-1}; NMR(CCl_4): δ 9.40(1H, d, J=8 Hz, aldehyde H), 7.25(5H, s, aryl CH), 6.75(1H, ddd, J=16, 8, 8 Hz, C_3–H), 6.00(1H, dd, J=16, 8 Hz, C_2–H), 4.25(1H, t, C_5–H), 3.5(2H, q, $-OCH_2-$), 2.5—2.8(2H, br. t, $-CH_2-$), 1.15(3H, t, CH_3). **3d**(R^2=C_2H_5): IR(neat): 1690, 1640 cm^{-1}; NMR(CCl_4): δ 9.45(1H, d, J=8 Hz, aldehyde H), 7.30(5H, s, aryl CH), 5.8—7.5(4H, m, olefinic H), 3.7—4.1(1H, q, C_5–H), 3.2—3.7(2H, q, $-OCH_2-$), 2.4—2.7(2H, br. t, $-CH_2-$), 1.20(3H, t, CH_3). **3f**(R^2=CH_3): bp 85 °C/0.1 Torr (bath temperature); IR(neat): 1685, 1635 cm^{-1}; NMR(CCl_4): δ 9.45(1H, d, J=8 Hz, aldehyde H), 6.75(1H, ddd, J=16, 8, 8 Hz, C_3–H), 6.00(1H, dd, J=16, 8 Hz, C_2–H), 5.1—5.8(2H, m, olefinic H), 3.4—3.8(1H, m, C_5–H), 3.20(3H, s, $-OCH_3$), 0.7—2.7(9H, aliphatic H); Found: C, 72.29; H, 10.09%. Calcd for $C_{11}H_{18}O_2$: C, 72.49; H, 9.96%. **4c**(R^2=CH_3): 2*E* isomer; IR(neat): 1670, 1630 cm^{-1}; NMR(CCl_4): δ 10.00(1H, d, J=8 Hz, aldehyde H), 7.35(5H, s, aryl CH), 5.8—6.1(1H, br. d, C_2–H), 4.25—4.55(1H, C_5–H), 3.21(3H, s, $-OCH_3$), 2.5—2.8(2H, $-CH_2-$), 2.18(3H, d, J=1.2 Hz, C_3–CH_3). 2*Z* isomer: IR (neat): 1670, 1630 cm^{-1}; NMR(CCl_4): δ 9.80(1H, d, J=8 Hz, aldehyde H), 7.33(5H, s, aryl CH), 5.8—6.1(1H, br. d, C_2–H), 4.25—4.55(1H, C_5–H), 3.21(3H, s, $-OCH_3$), 2.8—3.3 (2H, $-CH_2-$), 1.96(3H, d, J=1.2 Hz, C_3–CH_3). **5c**(R^2=CH_3, a mixture of *threo* and *erythro* isomers): bp 85 °C/0.05 Torr(bath temperature); IR (neat): 1700, 1640 cm^{-1}; Found: C, 76.92; H, 8.37%. Calcd for $C_{14}H_{18}O_2$: C, 77.03; H, 8.31%. isomer A: NMR($CDCl_3$): δ 9.48(d, J=8 Hz, aldehyde H), 7.35(s, aryl CH), 6.85(dd, J=16, 8 Hz, C_3–H), 6.04(dd, J=16, 8 Hz, C_2–H), 4.18(d, C_5–H), 3.24(s, $-OCH_3$). Isomer B: NMR($CDCl_3$): δ 9.60(d, J=8 Hz, aldehyde H), 7.35(s, aryl CH), 6.65(dd, J=16, 8 Hz, C_3–H), 5.98(dd, J=16, 8 Hz, C_2–H), 4.18(d, C_5–H), 3.21(s, $-OCH_3$).

*Conversion of 3-Phenylpropionaldehyde Dimethyl Acetal (**1a**) into Diisopropyl Acetal (**1i**) in the Presence of $TiCl_4$ and $Ti(O^iPr)_4$*[4]. To a mixture of 3-phenylpropionaldehyde dimethyl acetal (360 mg, 2.0 mmol) and $Ti(O^iPr)_4$ (2.0 mmol) in 25 ml of CH_2Cl_2 was added a solution of $TiCl_4$(2.4 mmol) in 5 ml of CH_2Cl_2 at −30 °C under an argon atmosphere. The mixture was stirred for 1 h and quenched with K_2CO_3(2 g in 10 ml of water). The precipitate was filtered off and the filtrate was extracted with ether. The extract was washed with water and dried over anhydrous Na_2SO_4. After removal of the solvent, the resulting oil was distilled. 3-Phenyl propionaldehyde diisopropyl acetal(335 mg) was obtained in 71% yield. bp 135 °C/11 Torr; NMR(CCl_4): δ 7.25(5H, s, aryl CH), 4.6(1H, t, $-CH\langle^{O-}_{O-}\rangle$), 3.7—4.1(1H, m, 2×$-OCH\langle$), 2.6—2.9, 1.7—2.2(4H, m, $-CH_2-$), 1.12, 1.22(12H, 2d, 4×CH_3). The IR and NMR spectra of this diisopropyl acetal (**1i**) are identical with those of the sample prepared from 3-phenylpropionaldehyde and isopropyl alcohol according to the method of Roelofsen and Bekkum.[5]

*Conversion of 5-Methoxy-7-phenyl-2,6-heptadienal (**3d**) into 7-Phenyl-2,4,6-heptatrienal (**7c**) under Acidic and Basic Conditions.* p-*TsOH–C_6H_6*: A solution of **3d** (108 mg, 0.5 mmol) and *p*-toluensulfonic acid(5 mg) in 10 ml of abs. C_6H_6 was refluxed for 3 h under an agron atmosphere. The C_6H_6 solution was washed with 10% $NaHCO_3$ solution and water, dried over anhydrous Na_2SO_4 and concentrated under reduced pressure. The resulting solid was chromatographed on silica gel and eluted with hexane–ethyl acetate(4 : 1) to afford **7c**(42 mg) in 46% yield. IR(KBr): 1670, 1605, 1595 cm^{-1}; NMR (CCl_4): δ 9.55(1H, d, J=8 Hz, aldehyde H), 7.35(5H, s, aryl CH), 6.4—7.5(5H, m, olefinic H), 6.15(1H, dd, J=8,16 Hz, C_2–H).

AcONa–AcOH: A solution of **3d**(108 mg, 0.5 mmol) and sodium acetate(30 mg) in 1 ml of acetic acid was refluxed for 2 h under an argon atmosphere. The reaction mixture was poured into 10% $NaHCO_3$ solution at 0 °C and extracted with ether. After being worked up in the usual way, **7c**(12 mg) was obtained in 13% yield.

$BF_3\cdot O(C_2H_5)_2$–Ac_2O: To a solution of **3d**(216 mg, 1 mmol) in 1 ml of acetic anhydride was added one drop of $BF_3\cdot O(C_2H_5)_2$ at −10 °C under an argon atmosphere. The mixture was stirred for 0.5 h at −10 °C, poured into ice cold water and extracted with ether. The extract was washed with 10% $NaHCO_3$ solution and water, dried and worked up in the usual way. **7c**(48 mg) and 7-phenyl-1,1,5-triacetoxy-2,6-heptadiene(150 mg) were obtained in 26% and 43% yields, respectively. 7-Phenyl-1,1,5-triacetoxy-2,6-heptadiene: IR (neat), 1760, 1740, 1600, 1240, 1200 cm^{-1}; NMR(CCl_4): δ 7.20(5H, s, aryl CH), 5.2—7.5(6H), 2.3—2.6(2H, $-CH_2-$), 2.00(9H, s, 3×$-COCH_3$). A mixture of the above triacetate (150 mg) in 3 ml of CH_3OH and 20% KOH solution(0.5 ml) was stirred for 15 h at room temperature under an argon atmosphere. After removal of CH_3OH, the residual aqueous solution was neutralized with dil. HCl and extracted with ether. The ether layer was washed with water, dried over anhydrous Na_2SO_4 and concentrated under reduced pressure. Another crop of crystals, **7c**(68 mg), was obtained in 37% yield based on **3d**, the total yield of **7c** being 63%.

$BF_3\cdot O(C_2H_5)_2$–CH_2Cl_2: To a solution of **3d** (108 mg, 0.5 mmol) in 3 ml of CH_2Cl_2 was added a solution of $BF_3\cdot O(C_2H_5)_2$ (1 mmol) in 2 ml of CH_2Cl_2 at −10 °C under an argon atmosphere. The mixture was stirred for 1 h and quenched with 10% K_2CO_3 solution. After the usual work up, **7c** (58 mg) was isolated in 63% yield.

t-*BuOK–THF*: To a solution of *t*-BuOK (125 mg, 1.1 mmol) in 5 ml of dry THF was added a solution of **3d** (108 mg, 0.5 mmol) in 3 ml of dry THF at −10 °C under an argon atmosphere. The mixture was stirred for 1 h at −10 °C and poured into ice cold water containing hydrochloric acid. After being worked up in the usual way, **7c** (54 mg) was obtained in 59% yield.

*Conversion of 5-Methoxy-7-phenyl-2,6-heptadienal(**3d**) to 7-Phenyl-2,4,6-heptatrienal (**7c**) with DBU.* To a solution of 5-methoxy-7-phenyl-2,6-heptadienal(350 mg, 1.6 mmol) in 10 ml of CH_2Cl_2 were added a solution of DBU(492 mg, 3.2 mmol) in 5 ml of CH_2Cl_2 and molecular sieves 3A(500 mg) at room temperature under an argon atmosphere. The mixture was stirred for 1 h and poured into ice cold brine containing acetic acid. The organic layer was separated, washed with brine and dried over anhydrous Na_2SO_4. After removal of the solvent, the residual solid was chromatographed on silica gel and eluted with hexane–ethyl acetate(4 : 1) to afford 274 mg of 7-phenyl-2,4,6-heptatrienal(**7c**) in 92% yield. mp 114—115 °C, (lit,[21] mp 116 °C).

The IR, UV, and NMR spectra of polyenals(**7a**—**f**) are consistent with the assigned structures: **7a**: bp 70 °C/0.5 Torr(bath temperature), (lit,[22] bp 70 °C/0.7 Torr); IR(neat): 1680, 1610 cm^{-1}; NMR(CCl_4): δ 9.50(1H, d, J=8 Hz, aldehyde H), 5.8—7.3(6H, m, olefinic H), 2.0—2.5(2H, m, $-CH_2-$), 1.2—1.7(2H, m, $-CH_2-$), 0.8—1.2(3H). **7b**: mp 39—41 °C(lit,[23] mp 37—39 °C); IR(KBr): 1670, 1615 cm^{-1}; NMR(CCl_4): δ 9.60(1H, d, J=8 Hz, aldehyde H), 7.35(5H, s, aryl CH), 5.9—7.4(4H, m, olefinic H). **7d**: mp 141—142 °C(lit,[24] mp 139—141 °C); IR(Nujol): 1680, 1595, 1560 cm^{-1}; NMR(d_6-DMSO): δ 9.55(1H, d, J=8 Hz, aldehyde H), 7.35(5H, s, aryl CH), 6.4—7.4(7H, m, olefinic H), 6.10 (1H, dd, J=8,16 Hz, C_2–H); UV λ_{max}^{EtOH} 382 nm(ε 5.6×10⁴), 275 nm(ε 1.1×10⁴); Mass: *m/e* 210(M^+). **7e**: mp 185—186 °C(lit,[25] mp 183 °C); IR(KBr): 1660, 1600, 1560 cm^{-1}; UV λ_{max}^{EtOH} 406 nm(ε 7.49×10⁴), 295 nm(ε 1.49×10⁴); Mass: *m/e* 236 (M^+). **7f**: IR(neat): 1680, 1610 cm^{-1}; NMR (CCl_4): δ 9.55(1H, d, J=8 Hz, aldehyde H), 5.85—7.30 (4H, m, olefinic H), 1.75(3H, s, C=C–CH_3), 1.05(6H, s, 2×CH_3), 0.9—2.4(6H, aliphatic H).

*Conversion of 5-Methoxy-3-methyl-7-phenyl-2,6-heptadienal (**4d**) to 3-Methyl-7-phenyl-2,4,6-heptatrienal with DBU.* To a solution of 5-methoxy-3-methyl-7-phenyl-2,6-heptatrienal (450 mg, 1.96 mmol) in 8 ml of CH_2Cl_2 were added a solution of DBU(1.0 g) in 8 ml of CH_3CN and molecular sieves 3A (1.0 g) under an argon atmosphere. The mixture was refluxed for 1.5 h and poured into ice cold brine containing acetic acid, and worked up in the usual way. After separation by preparative TLC on silica gel [hexane–ethyl acetate(4 : 1)], (2*E*, 4*E*,6*E*)-3-methyl-7-phenyl-2,4,6-heptatrienal (**8b**) (303 mg) and (2*Z*,4*E*,6*E*)-isomer (**9b**) (58 mg) were obtained in 78% and 15% yields, respectively. **8b**: mp 76—77 °C; IR (Nujol) 1650, 1600, 1580 cm^{-1}; NMR($CDCl_3$): δ 10.15(1H, d, J= 8 Hz, aldehyde H), 6.4—7.7(9H, aryl CH, olefinic H), 6.00 (1H, d, C_2–H), 2.30(3H, s, CH_3); Found: C, 85.06; H, 7.19%. Calcd for $C_{14}H_{14}O$: C, 84.81; H, 7.12%. **9b**: IR(neat): 1650, 1600, 1580 cm^{-1}; NMR($CDCl_3$): δ 10.20 (1H, d, J=8 Hz, aldehyde H), 6.4—7.6(9H, aryl CH, olefinic H), 5.90(1H, d, C_2–H), 2.15(3H, s, CH_3).

The IR and NMR spectra of other 3-methyl polyenals (**8a**—**c** and **9a**—**c**) are consistent with the assigned structures. **8a**: IR(neat): 1660, 1615, 1590 cm^{-1}; NMR($CDCl_3$): δ 10.23(1H, d, J=8 Hz, aldehyde H), 6.99—7.80(7H, m, aryl CH, olefinic H), 6.11(1H, d, J=8 Hz, C_2–H), 2.37(3H, s, C_3–CH_3). **9a**: NMR($CDCl_3$): δ 10.33(1H, d, J=8 Hz, aldehyde H), 7.1—7.8(7H, m,) 5.98(1H, d, J=8 Hz, C_2–H), 2.21 (3H, s, C_3–CH_3). **8c**: IR(neat): 1660, 1600 cm^{-1}; NMR (CCl_4); δ 10.20(1H, d, J=8 Hz, aldehyde H), 6.10, 6.65 (2H, 2d, J=16 Hz, C_4–H, C_5–H), 5.85(1H, d, J=8 Hz, C_2–

H), 2.30(3H, s, C_3-CH_3), 1.70(3H, s, C=C-CH_3), 1.50—2.20 (6H, aliphatic CH_2), 1.05(6H, s, 2×CH_3). **9c**: IR(neat): 1670, 1610 cm^{-1}; NMR(CCl_4): δ 10.15(1H, d, J=8 Hz, aldehyde H), 6.50, 7.10(2H, 2d, J=16 Hz, C_4-H, C_5-H), 5.75(1H, d, J=8 Hz, C_2-H), 2.10(3H, s, C_3-CH_3), 1.75(3H, s, C=C-CH_3), 1.50—2.20(6H, aliphatic H), 1.05(6H, s, 2×CH_3).

*Conversion of 4-Ethyl-5-methoxy-5-phenyl-2-pentenal (**5c**) to 4-Ethyl-5-phenyl-2,4-pentadienal (**11**) with DBU.* To a solution of 4-ethyl-5-methoxy-5-phenyl-2-pentenal(218 mg, 1 mmol) in CH_2Cl_2 (5 ml) were added a solution of DBU (304 mg, 2 mmol) in CH_2Cl_2 (5 ml) and molecular sieves 3A (500 mg) under an argon atmosphere. The mixture was refluxed for 5 h and the solvent was removed at 20 °C under reduced pressure. The residual oil was chromatographed on silica gel using hexane–ethyl acetate(8 : 1) as an eluent. (2*E*,4*E*)-4-Ethyl-5-phenyl-2,4-pentadienal (**11a**) (82 mg) and (2*E*, 4*Z*) isomer (**11b**) (23 mg) were obtained in 44% and 12% yields, respectively. **11a**: IR(neat): 1680, 1600 cm^{-1}; NMR($CDCl_3$): δ 9.75(1H, d, J=8 Hz, aldehyde H), 7.24(5H, s, aryl CH), 7.25(1H, d, J=16 Hz, C_3-H), 6.93(1H, s, C_5-H), 6.38 (1H, dd, J=16, 8 Hz, C_2-H), 2.57(2H, q, -CH_2-), 1.21(3H, t, CH_3). **11b**: IR(neat): 1680, 1610 cm^{-1}; NMR($CDCl_3$): δ 9.76(1H, d, J=8 Hz, aldehyde H), 7.38(5H, s, aryl CH), 7.63(1H, d, J=16 Hz, C_3-H), 6.93(1H, s, C_5-H), 6.35(1H, dd, J=16,8 Hz, C_2-H), 2.47(2H, q, -CH_2-), 1.20(3H, t, CH_3).

4-Ethyl-5-methoxy-7-phenyl-2,6-heptadienal (**5d**) was convered into 4-ethyl-7-phenyl-2,4,6-heptatrienal (**12**) in 69% yield by treating with DBU(4 equiv) at room temperature for 1 h. **12**: mp 93—94 °C: IR(Nujol): 1660, 1600, 1580 cm^{-1}; NMR($CDCl_3$): δ 9.75(1H, d, J=8 Hz, aldehyde H), 5.5—7.7(9H, aryl CH, olefinic H), 6.25(1H, dd, J=8, 16 Hz, C_2-H), 2.52(2H, q, -CH_2-), 1.12(3H, t, CH_3). Found: C, 84.97; H, 7.65%. Calcd for $C_{15}H_{16}O$: C, 84.87; H, 7.60%.

*Isomerization of (2Z,4E,6E)-3-Methyl-7-phenyl-2,4,6-heptatrienal(**9b**) to (2E,4E,6E)-3-Methyl-7-pehnyl-2,4,6-heptatrienal (**8b**) with Iodine.* A solution of (2*E*,4*Z*,6*E*)-3-methyl-7-phenyl-2,4,6-heptatrienal (106 mg) in 10 ml of abs. C_6H_6–ether(1 : 1) was treated with a catalytic amount of iodine at room temperature under an argon atmosphere. After stirring for 7 h, the reaction mixture was washed with aqueous $Na_2S_2O_3$ solution and dried over anhydrous Na_2SO_4. The solvent was removed and the crystalline residue was chromatographed on silica gel and eluted with hexane–ethyl acetate (4 : 1) to afford 71 mg of **8b** and 21 mg of **9b** in 67% and 21% yields, respectively.

(2*E*,4*Z*)-4-Ethyl-5-phenyl-2,4-pentadienal (**11a**) and the recovered (2*E*,4*Z*)-isomer(**11b**) were obtained in 53% and 14% yields, respectively, by treating (2*E*,4*Z*)-isomer(**11b**) with iodine under similar conditions.

*Oxidation of (2E,4E,6E)-3-Methyl-7-phenyl-2,4,6-heptatrienal (**8b**) to (2E,4E,6E)-3-Methyl-7-phenyl-2,4,6-heptatrienoic Acid (**10a**).* To a solution of silver nitrate(123 mg, 0.72 mmol) in 1.5 ml of water were added a solution of (2*E*,4*E*,6*E*)-3-methyl-7-phenyl-2,4,6-heptatrienal(120 mg, *ca.* 0.6 mmol) in ethanol(2.5 ml) and NaOH(112 mg in 1.5 ml of water). The mixture was stirred for 15 h at room temperature in the dark and the precipitate was filtered off. Ethanol was removed under reduced pressure. The residual aqueous solution was acidified with dil. HCl and extracted with ethyl acetate. (2*E*,4*E*,6*E*)-3-Methyl-7-phenyl-2,4,6-heptatrienoic acid (**10a**) (116 mg) was obtained in 89% yield. mp 201—203 °C, (lit,[15] mp 203 °C); IR(Nujol): 1660, 1590 cm^{-1}; NMR($CDCl_3$): δ 6.27—7.6(10H), 5.88(1H, br. s, C_2-H), 2.35(3H, s, C_3-CH_3); UV λ_{max}^{EtOH} 329 nm(ε 6.0×10^4), 242 nm(ε 1.0×10^4).

Acid (**10a**) was converted into the corresponding methyl ester (**10b**) in 90% yield according to the method of Wiley *et al.*,[16] **10b**: mp 56—57 °C; IR(Nujol): 1700, 1600 cm^{-1}; NMR(CCl_4): δ 7.26(5H, br. s, aryl CH), 6.3—6.9(4H, olefinic H), 5.72(1H, br. s, C_2-H), 3.60(3H, s, -OCH_3), 2.29 (3H, s, C_3-CH_3); UV λ_{max}^{MeOH} 336 nm(ε 5.06×10^4), 245 nm(ε 9.66×10^3).

Similarly, (2*E*,4*E*)-4-ethyl-5-phenyl-2,4-pentadienoic acid (**13**) was obtained in 84% yield by treating with silver oxide in the dark. **13**: mp 98—99 °C; IR(KBr): 1670, 1600 cm^{-1}; UV λ_{max}^{hexane} 302 nm(ε 2.76×10^4), 225 nm(ε 6.65×10^3); NMR($CDCl_3$): δ 10.56(1H, br. -CO_2H), 7.56(1H, d, J= 16 Hz, C_3-H), 7.41(5H, s, aryl CH), 6.87(1H, s, C_5-H), 6.06 (1H, d, J=16 Hz, C_2-H), 2.55(2H, q, -CH_2-), 1.21(3H, t, CH_3); Found: C, 71.75; H, 6.37%. Calcd for $C_{13}H_{14}O_2$: C, 71.54; H, 6.47%.

References

1) T. Mukaiyama and A. Ishida, *Chem. Lett.*, **1975**, 319.
2) A. Ishida and T. Mukaiyama, *Chem. Lett.* **1975**, 1167.
3) P. Cazeau and E. Frainnet, *Bull. Soc. Chim. Fr.*, **1972**, 1958.
4) T. Mukaiyama and M. Hayashi, *Chem. Lett.*, **1974**, 15.
5) D. P. Roelofsen and H. van Bekkum, *Synthesis*, **1972**, 419.
6) D. J. Faulkner, *Synthesis*, **1971**, 175.
7) a) T. Mukaiyama and H. Ishikawa, *Chem. Lett.*, **1974**, 1077; b) T. Izawa and T. Mukaiyama, *ibid.*, **1974**, 1189; c) T. Mukaiyama, K. Watanabe, and M. Shiono, *ibid.*, **1974**, 1457.
8) J. W. Copenhaver, U. S. 2586305 (1953); *Chem. Abstr.*, **47**, 2212a (1953).
9) H.H. Inhoffen, F. Bohlmann, K. Iartram, G. Rummert, and H. Pommer, *Ann. Chem.*, **507**, 54 (1950).
10) C. R. Narayanan and K. N. Lyer, *J. Org. Chem.*, **30**, 1734 (1965).
11) a) I. N. Nazarov, S. N. Markin, and B. K. Kruptsov, *Zh. Obshch. Khim.*, **29**, 3683 (1959); *Chem. Abstr.*, **54**, 19462i (1960). b) I. N. Nazarov and Zh. A. Krasnaya, *Dokl. Akad, Nauk SSSR*, **121**, 1034 (1958); *Chem. Abstr.*, **53**, 1183i (1953). c) B. M. Mikhailov, L. S. Povarov, and G. S. Ter Sarkisya, *Dokl. Akad, Nauk Az. SSR*, **17**, 203 (1961); *Chem. Abstr.*, **58**, 444f (1963).
12) G. Cainell, G. Cardillo, M. Contento, P. Grasselli, and A. U. Ronchi, *Gazz. Chim. Ital.*, **103**, 117 (1973).
13) O. Isler and P. Schudel, "Advances in Organic Chemistry," Vol. **4**, ed by R. A. Raphael, E. C. Taylor, and H. Wynberg, Interscience Publishers, New York, N. Y. (1963), p. 115.
14) K. J. Clark, G. I. Fray, R. H. Jaeger, and Sir R. Robinson, *Tetrahedron*, **6**, 217 (1959).
15) J. D. Cawley and D. R. Nelan, *J. Am. Chem. Soc.*, **77**, 4130 (1955).
16) R. H. Wiley, P. E. G. Nau, and T. H. Crawford, *J. Org. Chem.*, **26**, 4285 (1961).
17) T. Mukaiyama and A. Ishida, *Chem. Lett.*, **1975**, 1201.
18) A. Ishida and T. Mukaiyama, *Chem. Lett.*, **1976**, 1127.
19) D. Molho and M. Giraud, *Bull. Soc. Chim. Fr.*, **1970**, 1143.
20) All melting and boiling points are not corrected.
21) B. M. Mikhailov and G. W. Ter Sarkisya, *Zh. Obshch. Khim.*, **29**, 2560 (1959); *Chem. Abstr.*, **54**, 10988g (1960).
22) F. Bohlmann and P. Hanel, *Chem. Ber.*, **102**, 3293 (1969).
23) D. Marshall and M. C. Whiting, *J. Chem. Soc.*, **1956**, 4083.
24) V. G. Wittig and P. Hornberger, *Ann. Chem.* **577**, 11 (1952).
25) J. Schmitt, *Ann. Chem.*, **547** 270 (1941).

Photochemical Reactions of 4-Flavanols in the Presence of Ketone Sensitizers

Morio SUZUKI, Jiro AMANO, Motonobu MORIOKA, Hideo MIZUNO, and Ryoka MATSUSHIMA*

Department of Industrial Chemistry, Faculty of Engineering, Shizuoka University, Hamamatsu 432

(Received October 18, 1976)

Irradiation of an oxygen-free benzene solution of *cis*-4-flavanol **1a** by a mercury lamp in the presence of benzophenone gave 4-flavanone (32%), benzopinacol (85%), *cis*- and *trans*-2-(diphenylhydroxymethyl)-4-flavanols (7.6%), and 2-(diphenylhydroxymethyl)-4-flavanone (7.7%), whereas photolysis of *cis*-4-acetoxyflavane under similar conditions gave *cis*-2-(diphenylhydroxymethyl)-4-acetoxyflavane(24%), 2,2′-bi-4-acetoxyflavane (6%), and benzopinacol. Photolysis of **1a** in acetone gave 4-flavanone (3.6%), *trans*-4-(1-hydroxy-1-methylethyl)-4-flavanols (9.9%). The *cis* isomers of the parent and substituted 4-flavanols showed higher reactivities than the corresponding *trans* isomers.

For epimeric cycloalkanols, significant structural effects on oxidation rates are known.[1,2] Significant rate ratios, *cis*/*trans*=3.3—12, have been reported for the oxidation of a series of *cis* and *trans* substituted 4-chromanols with chromic acid,[3] and the observed ratio has been attributed to the stereoelectronic effect[1] and the strain relaxation of the chromate esters of the substrates.

The present work was undertaken to determine the structural effects on the photoreactions of 4-flavanols with ketones. It has been assumed that the hydrogen atom at the 4-position on the dihydropyrane ring is quasi-axial for the *cis* isomer **1a** and quasi-equatorial for the *trans* isomer **1b**, while the hydrogen atom at the 2-position is axial for both isomers.[4,5] The rates of the photoreactions of these isomeric substrates with ketones are expected to depend on the respective structures. It was observed, however, that not only the rate, but also the course of the photoreaction, changed remarkably with changes in the structures of the 4-flavanols and ketones.

Results and Discussion

*Photoreactions of **1a** and **1b** with Benzophenone.*

A deaerated benzene solution of *cis*-4-flavanol **1a** (0.02 M) containing benzophenone (0.02 M) gave 4-flavanone **5**, 2-(diphenylhydroxymethyl)-flavanone **6**, benzopinacol **7**, and *cis*- and *trans*-2-(diphenylhydroxymethyl)-4-flavanols **8** and **9**, upon irradiation

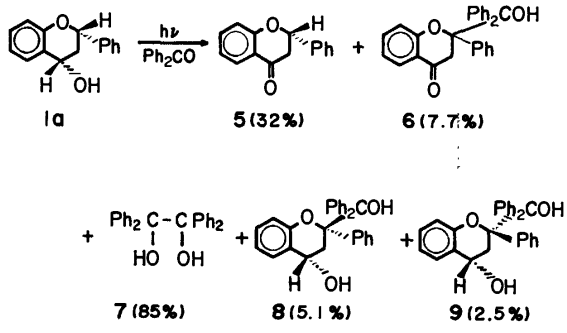

Scheme 1. Photolysis of **1a** with benzophenone.

* To whom correspondence should be addressed.

TABLE 1. MAIN PRODUCTS AND THEIR YIELDS IN THE PHOTOREACTIONS OF **1a** AND **1b** WITH BENZOPHENONE

Substrate	Product, %		Recovery, %	
	5	**7**	Substrate	Benzophenone
1a	32	85	40[a]	trace
1b	15	60	53[a]	20

a) No epimerization product (*via* inversion at the 4-position) was detected.

with a 100 W high-pressure mercury lamp for 100 min (Scheme 1). The NMR signal of the proton at the 3-position of **6** showed a singlet at δ=3.49 ppm. This suggests rapid inversion of the carbon at the 2-position of the dihydropyrane ring of **6**. Photolysis of *trans*-4-flavanol **1b** under similar conditions gave **5** and **7** as the main products, but the rate or the yields were significantly lower than those for **1a** (Table 1).

In the recovered 4-flavanol resulting from the irradiation of **1a** and benzophenone, no epimerized product, **1b**, was detected, nor was any pinacol-type dimer, 4,4′-bi-4-flavanol, **12**. The lack of the formation of **12** is not necessarily due to the steric hinderance of the coupling of the 4-(4-hydroxyflavanyl) radical, **A**, since **12** can be formed as the main product in the photoreaction of **1a** with acetone, as is shown below (Scheme 4). The lack of formation of **12** (4) and **1b** (5, 6), may imply that radical **A** rapidly reacts with ground state benzophenone to give benzophenone ketyl radical **B** (3), before coupling and disproportionation or reaction with **B** (4—6). The benzophenone ketyl radical, which is stabilized by two phenyl groups, is assumed to be more stable than radical **A**, which is stabilized by only one phenyl group. Hence, radical **A** could transfer a hydrogen atom from its oxygen atom to a ground-state benzophenone molecule, thus producing a benzophenone ketyl radical and a molecule of flavanone (3), as is proposed for the photochemical reduction of aliphatic alcohols with benzophenone. On the other hand, the formation of a small amount of the cross coupling products, **8** and **9**, may imply the intermediacy of the 2-(4-hydroxyflavanyl) radical, **C** (2). This radical would combine with **B** giving an epimeric mixture, **8** and **9** (8).

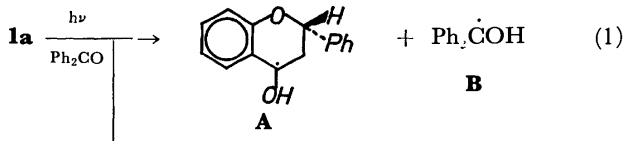

(1)

(2)

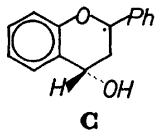

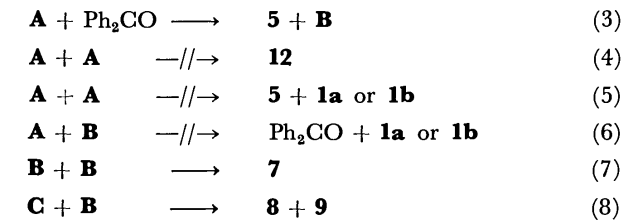

Scheme 2. Photolysis of **1a** and benzophenone.

Product **6** may be formed by further photoreaction of **5**, **8**, or **9**. However, it seems likely that the main source of **6** is **5**, since the yields of **8** and **9** are low and photolysis of **5** and benzophenone actually gave **6** under similar conditions.

*Photoreaction of **4a** with Benzophenone.* Photolysis of *cis*-4-acetoxyflavane **4a** and benzophenone under conditions similar to those for **1a** gave no **5**, but 2,2′-bi-4-acetoxyflavanes **11** and a cross coupling product, *cis*-2-(diphenylhydroxymethyl)-4-acetoxyflavane **10**, besides benzopinacol **7**, as shown in Scheme 3. Because of the insolubility of **11**, its NMR spectrum was not obtained. The NMR signal due to the proton of the 4-position of **10** showed a quartet at $\delta=5.42$ (1H, $J=11$ Hz), which implies that the diphenylhydroxymethyl group at the 2-position and the hydrogen atom at the 4-position are of *cis* conformation.[4]

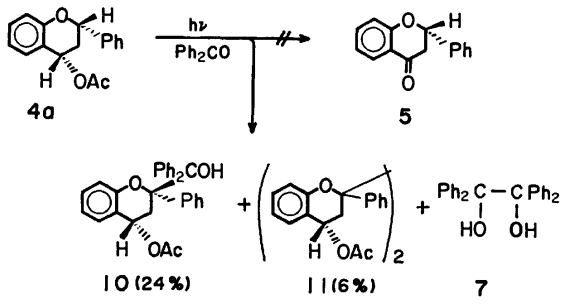

Scheme 3. Photolysis of **4a** with benzophenone.

In contrast to the results of **1a** (Scheme 1), high yields of products derived from the *cis*-2-(4-acetoxyflavanyl) radical and the lack of products derived from the *cis*-4-(4-acetoxyflavanyl) radical may be noted. The inefficiency of the abstraction of the hydrogen atom at the 4-position of **4a** may be due to the electron-withdrawing effect of the acetyl group[6] as well as steric hinderance.

Photolysis of a mixture of **4a** and the *trans* isomer **4b** in the presence of benzophenone gave the following ratio of the consumption rates, *cis*/*trans*=3.6.

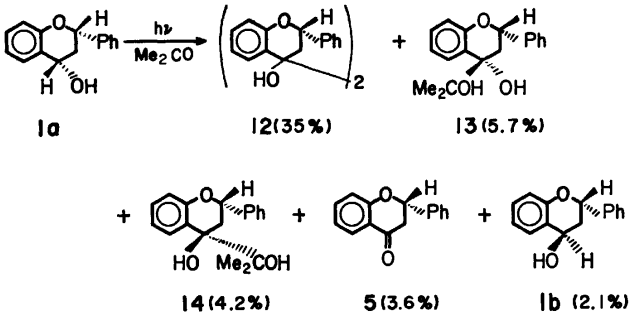

Scheme 4. Photolysis of **1a** with acetone.

*Photoreaction of **1a** with Acetone.* Photolysis of **1a** in acetone gave 4,4′-bi-4-flavanols, **12** (mixture of isomers), *cis*- and *trans*-4-(1-hydroxy-1-methylethyl)-4-flavanols, **13** and **14**, 4-flavanone, **5**, and **1b**, besides the recovered **1a** (40%), as shown in Scheme 4. The photochemical behavior of **1a** and acetone (acetone acts as a photosensitizer as well as the solvent) differs markedly from that with benzophenone in the following respects: a) neither 4-flavanone, **5**, nor acetone pinacol, **15**, was obtained, while **5** and **7** were the main products in the **1a**–benzophenone system, b) dimeric products, **12** were obtained in a significant yield, while they none were detected in the photolysis of **1a** and benzophenone, c) cross-coupling products, **13** and **14**, derived from radical **A** were obtained instead of the cross-coupling products analogous to **8** and **9** in Scheme 1, d) the formation of **1b**, *i.e.*, epimerization at the 4-position, was observed.

Radical **A**, which is stabilized due to its benzylic structure, is assumed to be more stable than ketyl radical **D**. Hence the latter should transfer a hydrogen atom from an oxygen atom to **1a**, to produce acetone and radical **A** (13), before collisional coupling with another **D** resulting in **15** (14). For similar reasons, the reaction of **A** with acetone giving **D** and **5** (12) is assumed to be unfavorable (an endothermic process) and hence racical **A** should either couple to give **12** (10) or disproportionate resulting in **5** and **1a** or **1b** (11). In the case of the **1a**–benzophenone system, however, radical **A** should rapidly undergo process (3) because of the higher stability of **B**, before the coupling and disproportionation processes (4)—(6) can occur.

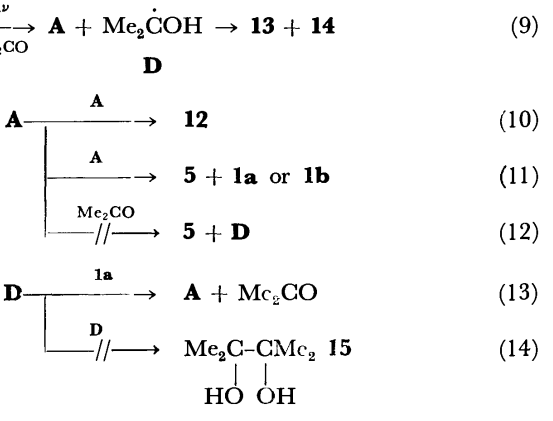

(9)

(10)

(11)

(12)

(13)

(14)

Scheme 5. Photolysis of **1a** with acetone.

Table 2. Relative reactivities of the *cis* and *trans* isomers of the substituted 4-flavanols with benzophenone

Substrate	Form	Rel. reactivity[a]
4-Chromanol		1.00
1a	*cis*	1.8
1b	*trans*	0.17
2a	*cis*	2.2
2b	*trans*	0.91
3a	*cis*	1.3
3b	*trans*	0.18

a) The relative reactivity is based on that of 4-chromanol.

In Scheme 5 process (9) represents the cross-coupling reaction within the solvent cage.

No suitable explanation is available as yet, as to why no cross-coupling products analogous to **8** and **9**, shown in Scheme 1, were formed in the photolysis of the **1a**–acetone system.

Relative Photoreactivities of cis- *and* trans-*4-Flavanols with Benzophenone.* Table 2 shows the relative consumption rates, as compared with the consumption rate of 4-chromanol, for the photolysis of **1a**, **1b**, *cis*-7-methoxy-4-flavanol **2a**, *trans*-7-methoxy-4-flavanol **2b**, *cis*-7-chloro-4-flavanol **3a**, and *trans*-7-chloro-4-flavanol **3b**.

It may be noted that a) the reactivities of the *cis* isomers (**1a**, **2a**, **3a**) are higher than the corresponding *trans* isomers (**1b**, **2b**, **3b**), and b) that the order of the reactivities is **2a**>**1a**>**3a**, **2b**>**1b**≒**3b**. Yamaguchi *et al.*[3] have explained the relative reactivities of the *cis*- and *trans*-substituted chroman-4-ols with chromic acid in terms of the stereoelectronic effect[1] and the strain relaxation of the chromate esters of the substrates. Also, in the present photoreaction system, the stereoelectronic effect may be assumed to be one of the factors controlling the relative reactivities of the isomers. In addition to these effects, abstraction of the hydrogen atoms from these substrates by triplet benzophenone is assumed to be significantly sterically hindered for effective encounter collisions. A reactivity ratio *cis*/*trans* of 3.6 was found for the photoreaction of isomeric 4-acetoxyflavanes **4a** and **4b**. The products resulting from the photolysis of **4a** or **4b** and benzophenone (Scheme 3) imply that the intermediate radical is not the radical at the 4-position but is that at the 2-position. The latter is not conjugated with the 5,6-fused benzene ring and is free from the stereoelectronic effect. Thus, the reactivity ratio of 3.6 for isomeric 4-acetoxyflavanols is assumed to be due to the steric hinderance for encounter collisions. The abstraction of hydrogen atoms would be sterically less favorable for the *trans* isomers than for the *cis* isomers, since for the *trans* isomers the phenyl group at the 2-position would interfer with the attack of the triplet benzophenone.

The order of the reactivities indicates that electron releasing substituents stabilize the intermediate radical, such as **A**, and accelerate the reaction rate.

Experimental

The light souce was a 100-W high pressure mercury lamp (Riko Kagaku) immersed in a 200-ml reaction vessel. Each solution was bubbled using a purified nitrogen stream before and during photolysis. The temperature was maintained at 20—25 °C. The melting points are uncorrected. NMR and IR spectra were obtained by using Hitachi IRA-1 and R-24 spectrometers, respectively.

Materials. *cis*-4-Flavanol **1a**,[7] *cis*-7-methoxy-4-flavanol **2a**, and *cis*-7-chloro-4-flavanol **3a** were prepared from 4-flavanone,[8] 7-methoxy-4-flavanone,[9] and 7-chloro-4-flavanone,[10] respectively, by reduction with sodium borohydride. *trans*-4-Flavanol **1b**,[11] *trans*-7-methoxy-4-flavanol **2b**, and *trans*-7-chloro-4-flavanol **3b** were prepared from **1a**, **2a**, and **3a**, respectively, by treatment with phosphorus tribromide in ether followed by hydrolysis in a *t*-butyl alcohol–water solution of potassium hydroxide. *cis*-4-Acetoxyflavane **4a** and *trans*-4-acetoxyflavane **4b**, were prepared from **1a** and **1b**, respectively, by acetylation in acetic anhydride–pyridine.

Table 3. Yields and physical constants of a series of 4-flavanols

Substrate	Yield, %	Mp (solvent)[a]	NMR ($CDCl_3$) δ, ppm	IR, cm^{-1}
1a	87	147—148 (M)	1.9—2.1 (M, 2H), 4.5 (d, 1H), 5.0 (q, 1H) 5.2 (q, 1H), 6.7—7.6 (m, 9H)	3410, 1580 1210
1b	61	117—118 (B)	2.0—2.2 (m, 2H), 2.4 (s, 1H), 4.7 (t, 1H) 5.2 (q, 1H), 6.7—7.5 (m, 9H)	3410, 1580 1210
2a	72	102—103 (M)	1.7—2.6 (m, 2H), 2.2 (s, 1H), 3.7 (s, 3H) 4.9 (q, 1H), 5.1 (q, 1H), 6.4—7.6 (m, 8H)	3230, 1605
2b	65	110—111 (B)	1.7—2.3 (m, 2H), 2.3 (s, 2H), 3.7 (s, 3H) 4.7 (t, 1H), 5.2 (q, 1H), 6.4—7.5 (m, 8H)	3220, 1600 1570
3a	69	103—104 (EW)	1.7—2.5 (m, 2H), 2.3 (s, 1H), 4.9 (q, 1H) 5.1 (q, 1H), 6.8—7.4 (m, 8H)	3330, 1590 1560, 1104
3b	45	49—51 (BH)	2.0—2.2 (m, 2H), 2.2 (s, 1H), 4.7 (t, 1H) 5.2 (q, 1H), 7.3—6.9 (m, 8H)	3400, 1600
4a		85—86 (E)	1.6—2.8 (m, 2H), 2.0 (s, 3H), 5.1 (q, 1H) 6.1 (q, 1H), 6.7—7.5 (m, 9H)	1700
4b		97—98 (E)	2.0 (s, 3H), 2.0—2.3 (m, 2H), 5.2 (q, 1H) 6.0 (t, 1H), 6.7—7.6 (m, 9H)	1700

a) Solvents for crystallization; M: methanol, E: ethanol, B: benzene, EW: ethanol–water, BH: benzene–hexane.

4-Chromanol was prepared by reduction of chromanone[12] with sodium borohydride. The yields and the phydical constants of these substrates are summarized in Table 3.

*Photolyses of **1a** and **1b** with Benzophenone.* A 200-ml benzene solution containing 0.025 M **1a** and 0.07 M benzophenone was irradiated for 100 min. Isolation by column chromatography on silica gel gave **7** (0.62 g), **5** (0.29 g), **6** (0.19 g), **8** (0.05 g), **9** (0.10 g), in addition to the recovered **1a** (0.13 g). The photolysis of **1b** and the analysis of the products were carried out under conditions similar to those for **1a**, but only the main products **5** and **7** were isolated. The acetylation of **8** and **9** in pyridine-acetic anhydride gave *cis*-2-(diphenylhydroxymethyl)-4-acetoxyflavane **8'** and *trans*-2-(diphenylhydroxymethyl)-4-acetoxyflavane **9**. Products **5** and **7** were identified by comparing their mp and IR and NMR spectra with authentic samples. **6**: colorless needles from ethanol; mp 182—183 °C; IR (KBr): 3440, 1680 cm^{-1}; NMR ($CDCl_3$): δ 2.95 (s,1H), 3.49 (s, 2H), 6.7—7.9 (m, 19H). Found: C, 82.32; H, 5.49%. Calcd for $C_{28}H_{22}O_3$: C, 82.73; H, 5.45%. **8**: colorless needles from ethanol; mp 222—223 °C; IR: 3570, 3335, 1590 cm^{-1}. **8'**: colorless prisms from ethanol; mp 207—212 °C; IR: 3445, 1700 cm^{-1}; NMR ($CDCl_3$): δ 1.98 (s, 3H), 2.30 (q, 1H), 2.90 (s, 1H), 3.31 (q, 1H), 5.42 (q, 1H), 6.8—7.9 (m, 19H). J_{3a-4}=11 Hz, J_{3a-3e}=13.4 Hz, J_{3e-4}=6.5 Hz. **9'**: colorless prisms from ethanol; mp 212—213 °C; IR: 3445, 1700 cm^{-1}; NMR ($CDCl_3$) : δ 1.50 (s,3H), 2.67 (q, 1H), 2.98 (s, 1H), 3.20 (q, 1H), 5.71 (q, 1H), 6.8—7.8 (m, 14H). J_{3a-3e}=16.0 Hz, J_{3a-4}=2.0 Hz. Found: C, 79.34; H, 5.81%. Calcd for $C_{30}H_{26}O_4$: C, 79.98; H, 5.82%.

*Photolysis of **4a** and Benzophenone.* A 200-ml benzene solution containing **4a** (0.025 M) and benzophenone (0.06 M) was irradiated for 10 h. Isolation of the products by column chromatography on silica gel gave **7** in an undetermined significant amount, **11** (0.08 g), and **10** (0.36 g), in addition to the recovered **4a** and benzophenone. **11**: colorless crystal from benzene-ethyl acetate; mp 275—280 °C; IR: 1720, 1220 cm.$^{-1}$ Found: C, 74.35; H, 5.68%. Calcd for $C_{34}H_{30}O_6$: C, 76.39; H, 5.66%. The NMR spectra of **11** was not obtained because of the low solubility in any suitable solvent.

*Photolysis of **1a** and Acetone.* A 150-ml acetone solution of **1a** (0.067 M) was irradiated for 60 h. Isolation by CC on silica gel, after acetylation with pyridine-acetic anhydride, gave **4a** (0.76 g), **4b** (0.05 g), **5** (0.08 g), bi-4-(acetoxyflavane) **12'** (0.79 g), and *cis*- and *trans*-4-(1-hydroxy-2-methylethyl)-4-flavanols **13** (0.16 g) and **14** (0.12 g). The TLC of **12** on silica gel with benzene gave four spots which were identified as isomeric mixtures by comparing their NMR spectra with those of authentic samples.[13] **13**: white crystals from CCl_4; mp 130—132 °C; IR: 3520, 3450 cm^{-1}; NMR ($CDCl_3$): δ 1.26 (s, 3H), 1.34 (s, 1H), 2.0—3.0 (m, 4H), 5.63 (q, 1H), 6.7—7.7 (m, 9H). **14**: colorless crystals from petroleum benzine; mp 125—130 °C; IR: 3400, 2900, 1600 cm^{-1}; NMR: δ 1.00 (s, 3H), 1.30 (s, 3H), 2.0—2.2 (m, 2H), 2.70 (s, 2H), 5.05 (q, 1H), 6.8—7.0 (m, 9H).

Relative Photoreactivities. A 100-ml benzene solution of each substrate (0.005 M) in the presence of 4-chromanol (0.005 M) and benzophenone (0.03 M) was irradiated for 20 min. After separation by PLC on silica gel with benzene, the NMR signal intensities for 4-chromanone at δ=4.39 and 4-flavanones at δ=5.34 ppm were measured. In the case of **4a** and **4b**, for which the photoreaction rates are slow compared to those of 4-chromanol, a 50-ml benzene solution containing **4a** (0.01 M), **4b** (0.01 M), and benzophenone (0.016 M) was irradiated for 3 h.

The authors wish to thank Miss S. Yamazaki for her help during this work.

References

1) H. Kwart and P. S. Francis, *J. Am. Chem. Soc.*, **81**, 2116 (1959).
2) J. C. Richer, L. P. Pilato, and E. L. Eliel, *Chem. Ind. (London)*, **1961**, 2007.
3) S. Yamaguchi, K. Kabuto, Y. Kikuchi, and N. Inoue, *Bull. Chem. Soc. Jpn.*, **44**, 3487 (1971).
4) J. W. C. Lewis, *Aust. J. Chem.*, **21**, 2059 (1968).
5) A. L. Tokes and R. Bognar, *Tetrahedron*, **29**, 909 (1973).
6) S. G. Cohen, *J. Am. Chem. Soc.*, **91**. 6824 (1969).
7) S. Mitsui and N. Kasahara, *Nippon Kagaku Zasshi*, **79**, 1382 (1958).
8) A. Lowenbein, *Ber.*, **57**, 1515 (1924).
9) J. Shinoda, *Yakugaku Zasshi*, **48**, 35 (1928).
10) F. C. Chen and C. T. Chang, *J. Chem. Soc.*, **1958**, 146.
11) H. Fletcher, D. Kehoe, E. M. Philbin, and T. S. Wheeler, *Tetrahedron*, **18**, 135 (1962).
12) W. E. Parham, *J. Am. Chem. Soc.*, **84**, 813 (1962).
13) R. Matsushima, T. Kishimoto, and M. Suzuki, *Chem. Lett.*, **1976**, 579.

Sequential Polypeptides. The Steric Hindrance of L-Valine Residues in the Polycondensation of Peptide Active Esters

Ryoichi KATAKAI

Department of Industrial Chemistry, College of Technology, University of Gunma, Tenjin-cho, Kiryu-shi 376

(Received October 23, 1976)

Five tripeptide *N*-hydroxysuccinimide esters with *N*-terminal L-valine, L-phenylalanine, and L-alanine were polymerized in *N,N*-dimethylformamide with a variety of concentration of the monomers. The yields and molecular weights of the resulting sequential polypeptides were then compared in order to demonstrate the presence of the steric hindrance of the L-valine residue in polycondensation. The results of the polycondensation and the conformational study of the resulting polypeptides suggest that the side chain of the L-valine residue at the *N*-terminal position of the monomers hinders the polycondensation of the monomers.

L-Valine is a very interesting amino acid in polypeptide chemistry from synthetic as well as conformational aspects. Poly(L-valine) takes predominantly the β-structure and does not form the α-helix, although the L-valine residues can be incorporated in the stable α-helical conformation in naturally occurring proteins[1] and synthetic sequential polypeptides.[2,3] These facts can be explained by the steric hindrance of the side chain of the amino acid.

In a previous study,[4] we reported on the synthesis and conformation of two sequential polypeptides, $(\text{L-Ala–L-Val–Gly})_n$ and $(\text{L-Val–L-Ala–Gly})_n$. In that study, we found that the HBr·H–L-Ala–L-Val–Gly–ONSu monomer polymerized to give a sequential polypeptide, $(\text{L-Ala–L-Val–Gly})_n$, with high molecular weights and in higher yields than the HBr·H–L-Val–L-Ala–Gly–ONSu monomer.[5] This fact was tentatively explained by the presence of the steric hindrance of the side chain of L-valine at the *N*-terminal position of the latter monomer. However, a question if the lowering of the yield and the molecular weight of $(\text{L-Val–L-Ala–Gly})_n$ results only from the steric hindrance of the L-valine residue remains unresolved, because there are many factors responsible for the yield and the molecular weight of the sequential polypeptides. Among them, the conformations of the growing polypeptide chains may greatly influence the results of polycondensation. The previous study compared the results of the polycondensation of different polypeptides which may take different conformations in the polymerization system.

We chose in this study monomers with the same composition, but with different sequences of amino acids, which give the same sequential polypeptide—for example, HCl·H–L-Val–L-Phe–L-Phe–ONSu and HCl·H–L-Phe–L-Val–L-Phe–ONSu, which give the same polymer $(\text{L-Val–L-Phe–L-Phe})_n$. In the polycondensation of these monomers, the conformational effect is removed and the sterical effect of the L-valine residue may be clearly demonstrated. We polymerized five monomers: the above two monomers, HCl·H–L-Val–L-Ala–L-Ala–ONSu, HCl·H–L-Ala–L-Val–L-Ala–ONSu, and HCl·H–L-Val–L-Val–Gly–ONSu. The results are discussed, together with a conformational study in the solid state.

Results and Discussion

Synthesis of Monomers. For such a study as this, in which the mechanism of the polycondensation of peptide active esters is deduced from the yields and the molecular weights of the resulting polypeptides, exact and reproducible values of the yield must be obtained in polycondensation. Thus, a large amount of the peptide active esters as a monomer for polycondensation must be prepared for repeated polycondensations. The peptide active esters are comparatively difficult to synthesize because many treatments are needed for their synthesis. An easy synthetic method giving a high yield must be adopted to prepare a large amount of the monomers.[6] In this study, the monomers were prepared by means of the *o*-nitrophenylthio *N*-carboxy α-amino acid anhydride (Nps-NCA) method,[7] which can rapidly produce in a high yicld a peptide derivative protected by the Nps group.[8] This method is especially useful for the synthsis of a large amount of peptides. The Nps-NCA method gives no by-products such as the *N,N'*-dicyclohexylurea in the dicyclohexylcarbodiimide method, and the resulting product is easily purified by simple recrystallization.

An amino acid ethyl ester was treated with an Nps-NCA to give the Nps-dipeptide ethyl ester in a yield above 85%. The subsequent removal of the Nps group of the dipeptide derivative by treatment with hydrochloric acid in dioxane gave, almost quantitatively, the dipeptide ethyl ester hydrochloride, which was then treated with another Nps-NCA to give the Nps-tripeptide ethyl ester in a yield above 82%. The Nps-tripeptide ester was saponified to lead to Nps-tripeptide free acid, which was active-esterified by treating it with *N*-hydroxysuccinimide and dicyclohexylcarbodiimide.[9] The resulting Nps-tripeptide ONSu ester was purified by recrystallization from tetrahydrofuran.

A series of treatments for the synthesis leading to Nps-tripeptide ONSu esters was started from the 0.2 mol scale of the amino acid ester. Though many reactants were used, every condensation with Nps-NCA produced in a yield above 82%, and all the products were easily purified by recrystallization. The results of the syntheses are shown in Table 1.

Polycondensation of the Monomers. All the polymerizations of the tripeptide ONSu esters were done in *N,N*-dimethylformamide for one day at room temperature.[4,6] Every polymerization system was treated with different procedures for the isolation of the resulting polypeptide. We supposed that the yield of polycondensation may vary with each isolation pro-

TABLE 1. RESULTS OF SYNTHESES OF Nps-TRIPEPTIDE ONSu ESTERS

N-Protected monomer	Yield[a] %	Mp °C	$[\alpha]_D$ (c 1.0, $HCONMe_2$)	Found, % / Calcd, % C	H	N
Nps-L-Phe-L-Val-L-Phe-ONSu	64.8	185—190 (dec)	+22.0	59.97 59.89	5.45 5.33	10.47 10.59
Nps-L-Val-L-Phe-L-Phe-ONSu	71.4	185—190 (dec)	−12.7	59.84 59.89	5.40 5.33	10.61 10.59
Nps-L-Ala-L-Val-L-Ala-ONSu	67.5	158—160 (dec)	−34.5	49.39 49.50	5.44 5.34	13.81 13.75
Nps-L-Val-L-Ala-L-Ala-ONSu	61.4	170—175 (dec)	−76.4	49.51 49.50	5.39 5.34	13.84 13.75
Nps-L-Val-L-Val-Gly-ONSu	58.2	185—190 (dec)	−23.7	50.53 50.47	5.64 5.58	13.29 13.38

a) The yields are the values from the starting amino acid ethyl ester hydrochloride.

TABLE 2. RESULTS OF POLYCONDENSATION OF HCl·H-L-Val-L-Phe-L-Phe-ONSu AND HCl·H-L-Phe-L-Val-L-Phe-ONSu

Monomer concn mol/l	(L-Val-L-Phe-L-Phe)$_n$ Yield[a] %	Yield[b] %	Yield[c] %	$\eta_{sp/c}$[d]	(L-Phe-L-Val-L Phe)$_n$ Yield[a] %	Yield[b] %	Yield[c] %	$\eta_{sp/c}$[d]
1.0	99	92	90	0.095	93	91	89	0.148
0.50	97	87	88	0.106	92	91	90	0.153
0.33					90	86	—	0.157
0.25	87	83	—	0.119	88	85	84	0.148
0.14					84	82	—	0.161
0.13	83	80	76	0.140	85	81	79	0.142

a) The yields are the values by the first isolation procedure. b) The yields are the values by the second isolation procedure. c) The yields are the values by the third isolation procedure. d) The viscosities are the values of the polypeptides isolated by the second isolation procedure.

cedure, because we have found that the solubility of peptides in solvents such as *N*,*N*-dimethylformamide differs greatly with the sequences of amino acids.[10] The results of the polycondensation of HCl·H-L-Val-L-Phe-L-Phe-ONSu and HCl·H-L-Phe-L-Val-L-Phe-ONSu are shown in Table 2. For the first isolation procedure, the polymerization system was diluted with diethyl ether. This treatment precipitates from the polymerization system the polymer, an oligomer with a very low molecular weight, and also triethylammonium chloride. The precipitate was collected by filtration and washed with methanol to remove the salt. The yields by the first procedure are shown by the values with the superscript a. The polymer isolated by the first procedure was suspended in *N*,*N*-dimethylformamide and reprecipitated by the addition of methanol. By this treatment, the oligomer with very low molecular weights and cyclic oligomers were removed from the polymer.[11] The yields by the second procedure are shown with the superscript b. In the third procedure the polymer was precipitated from the polymerization system by the addition of methanol. The yields by the third procedure are shown with the superscript c.

A comparison of the yields of the two polymers suggests an interesting feature of polycondensation. The HCl·H-L-Val-L-Phe-L-Phe-ONSu monomer with the *N*-terminal L-valine residue, gave, by the first isolation procedure, the (L-Val-L-Phe-L-Phe)$_n$ polymer in higher yields than did another HCl·H-L-Phe-L-Val-L-Phe-ONSu monomer with *N*-terminal L-phenylalanine. However, the yields of the (L-Val-L-Phe-L-Phe)$_n$ polymer decreased after the second treatment to become similar to the values of the yields of (L-Phe-L-Val-L-Phe)$_n$. These results suggest that the first procedure of isolation precipitated not only the polymer but also oligomers with very low molecular weights, which were then removed by the second isolation procedure. This is demonstrated by the fact that the second procedure gave the yields similar to those of the third isolation procedure, which does not precipitated the lower oligomers.

We should also discuss the results of the polycondensation in connection with the values of the yields obtained by the second and third procedures for the isolation of the polymer. Two polymers with the same sequence, (L-Val-L-Phe-L-Phe)$_n$ and (L-Phe-L-Val-L-Phe)$_n$, were isolated in similar yields. This is also true for other sequential polypeptides. The results of the polycondensation of another pair of monomers, HCl·H-L-Val-L-Ala-L-Ala-ONSu and HCl·H-L-Ala-L-Val-L-Ala-ONSu, are shown in Table 3. Table 3 also contains the yields of the polymers isolated by the third procedure. These sequential polypeptides, (L-Val-L-Ala-L-Ala)$_n$ and (L-Ala-L-Val-L-Ala)$_n$, were obtained in the same yields by three different isolation

Table 3. Results of polycondensation of HCl·H-L-Val-L-Ala-L-Ala-ONSu and HCl·H-L-Ala-L-Val-L-Ala-ONSu

Monomer concn	(L-Val-L-Ala-L-Ala)$_n$			(L-Ala-L-Val-L-Ala)$_n$		
	Yield %	$\eta_{sp/c}$	$\overline{DP}_n$	Yield %	$\eta_{sp/c}$ %	$\overline{DP}_n$
0.50	100	0.157	8	100	0.192	20
0.33	100	0.178	12	100	0.192	20
0.25	99	0.186	14	97	0.224	27
0.20	99	0.161	10	97	0.186	17
0.17	98	0.157	8	96	0.182	16
0.14	98	0.140	6			
0.13	98	0.152	8	94	0.178	15

procedures, in contrast to the results for the sequential polypeptides containing L-phenylalanine residues. The polymer containing L-alanine residues, therefore, may contain lower oligomers. This is consistent with the fact that the yields of the polypeptides containing L-alanine residues are higher than those containing L-phenylalanine residues. Another fact which is analogous for the polymers containing L-phenylalanine is that the polymers containing L-alanine residues were isolated in the same yields and no effect of the *N*-terminal amino acid residue appeared. It may be conclusively stated from the above results that the effect of the *N*-terminal amino acid of the monomer in polycondensation, if it is present, cannot detected by comparing the yields of the resulting sequential polypeptides.

Contrary to the above results for the yields, the viscosity of the resulting sequential polypeptides clearly shows the influence of the *N*-terminal amino acid of the monomers on the polycondensation. The sequential polypeptide, (L-Val-L-Phe-L-Phe)$_n$ obtained from a monomer with the *N*-terminal L-valine has lower viscosities than the polypeptide, (L-Phe-L-Val-L-Phe)$_n$, obtained from a monomer with *N*-terminal L-phenylalanine (Table 2). An analogous result was obtained by the polycondensation of another pair of monomers containing L-alanines (Table 3). The polymer with *N*-terminal L-valine (L-Val-L-Ala-L-Ala)$_n$ has lower viscosities than those of the polymer with *N*-terminal L-alanine (L-Ala-L-Val-L-Ala)$_n$. We determined the number-average degree of polymerization ($\overline{DP}$) of these polymers by measuring the NMR peak area of the *N*-terminal amino protons and the internal amide protons. These results are also shown in Table 3. The polymer with *N*-terminal L-alanine has $\overline{DP}$s from 15 to 27, about ten repeating units longer than those of the polymer with *N*-terminal L-valine, which has $\overline{DP}$s from 6 to 14. This finding is consistent with the results of the viscosity measurement.

As the pairs of the monomers studied in this study give the same polypeptides, the growing polymer chains may have similar conformations in the polycondensation system. Therefore, the most important factors responsible for the molecular weight of the resulting polymers is the *N*-terminal amino acid of the monomers. The above results can best be explained by the presence of the steric hindrance of the side chain of L-valine at the *N*-terminal position of the monomers. Though the detailed mechanism of polycondensation of peptide active esters has not yet been demonstrated because there are many complicated factors resulting from the use of the very concentrated polymerization system containing the salt, the monomer-active ester may polymerize in a manner similar to that of the monomers of conventional polycondensation; *i.e.*, the monomers are condensed to give dimers, which are then again condensed to give tetramers. The resulting oligomers with the *C*-terminal active ester is condensed with the amino group of another oligomer-active ester to give a higher oligomer. The reactivity of the terminal functional groups may not vary with the chain lengths, but the rate of polycondensation decreases greatly as the peptide chains become longer, because the molecular motion is prevented, especially in a solid state or in gelatinous systems. As the sterical effect of the L-valine residue may not be very large, the presence of L-valine at the *N*-terminal position does not influence the condensation of short peptide chains, but does hinder the condensation of larger peptides. Thus, the polycondensation of monomers with *N*-terminal L-valine was terminated at a lower peptide stage; the polymer thus obtained had lower molecular weight than those with *N*-terminal L-phenylalanine and L-alanine. This explanation points out the importance of stirring the polycondensation system containing the monomer with *N*-terminal L-valine. In fact, the sequential polypeptide, (L-Val-L-Phe-L-Phe)$_n$ with the highest viscosity was obtained in a polycondensation system with the lowest concentration of the monomer-active ester, which was a gelatinous liquid state which could be well stirred (Table 2). In a more gelatinous polycondensation system containing a higher concentration of the monomer, where effective stirring becomes difficult, the molecular motion and the reaction of the growing peptide chains may be prevented to form a lower-molecular-weight polymer. This is demonstrated by the conformational study in the solid state (see below).

In order to demonstrate further the presence of the steric hindrance of L-valine in polycondensation, we polymerized another monomer with L-valines, HCl·H-L-Val-L-Val-Gly-ONSu. The results are shown in Table 4. The (L-Val-L-Val-Gly)$_n$ polymer has $\overline{DP}$s of about 10 over the range of concentration of the monomer used in this study. These $\overline{DP}$s are

Table 4. Results of polycondensation of HCl·H-L-Val-L-Val-Gly-ONSu

Monomer concn mol/l	Yield %	$\eta_{sp/c}$	$\overline{DP}_n$
0.50	95	0.185	10
0.33	92	0.167	8
0.25	91	0.180	10
0.17	90	0.185	10
0.13	89	0.172	8

similar to those of (L-Val–L-Ala–L-Ala)$_n$ with the *N*-terminal L-valine and are lower than those of (L-Ala–L-Val–L-Ala)$_n$ with *N*-terminal L-alanine. This comparison may not be reasonable because these polymers are different compounds, and so many effects other than the steric hindrance of the *N*-terminal amino acid must be taken into consideration in discussing the results. However, the fact that the *N*-terminal L-valine decreases the molecular weight of the resulting polypeptides suggests the presence of the steric hindrance of the amino acid.

Conformations of the Polypeptides in the Solid State.

The conformations of the sequential polypeptides were studied by means of far-infrared spectroscopy. Itoh *et al.*[12] found some characteristic bands of amino acid residues with the α-helical and β-form structures, and showed that the far-infrared spectroscopy is very useful for elucidating the conformations of polypeptides in the solid state. We analyzed the far-infrared spectra of the sequential polypeptides according to the assignments established by Itoh *et al.* Figure 1 shows the far-infrared spectra of the sequential polypeptide (L-Ala–L-Val–L-Ala)$_n$. This polypeptide showed a strong band at 441 cm^{-1} characteristic of the L-alanine residue with the β-structure and weak bands at 540, 520, 409, and 375 cm^{-1} characteristic of the L-alanine and L-valine residues with the α-helix. The spectra suggest that the polypeptide takes predominantly the β-structure and contains a portion of the α-helix. Some polypeptides are known to transform their conformation from the β-structure to the α-helix upon treatment with dichloroacetic acid. The polypeptide (L-Ala–L-Val–L-Ala)$_n$ with $\overline{DP}$ 16, when treated with dichloroacetic acid, showed the infrared bands at 540, 524, 409, and 374 cm^{-1}, while the band at 441 cm^{-1} almost disappeared. This suggests that the polypeptide transformed the conformation to the α-helix upon treatment. Figure 2 shows the spectra of (L-Val–L-Ala–L-Ala)$_n$. The polypeptide isolated showed the band at 441 cm^{-1} characteristic

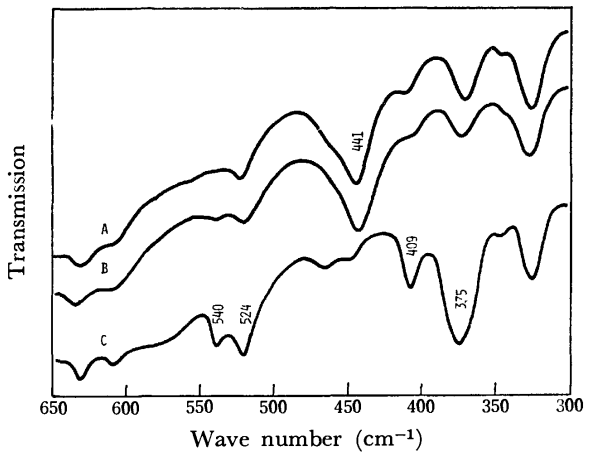

Fig. 1. Far-infrared spectra of the sequential polypeptide (L-Ala–L-Val–L-Ala)$_n$. A: The polypeptide with $\overline{DP}$ 27, B: The polypeptide with $\overline{DP}$ 16, C: The polypeptide with $\overline{DP}$ 16 after treatnemt with dichloroacetic acid.

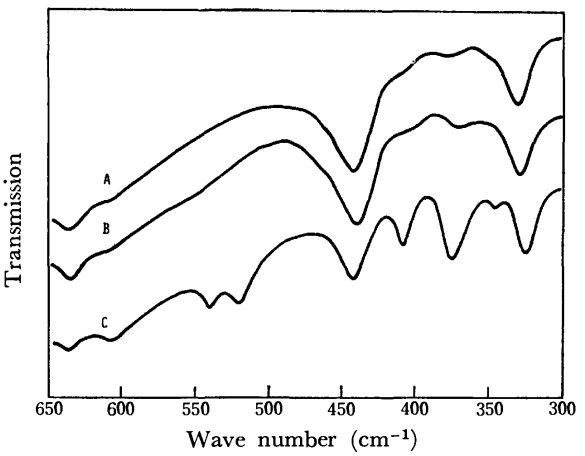

Fig. 2. Far-infrared spectra of the sequential polypeptide (L-Val–L-Ala–L-Ala)$_n$. A: The polypeptide with $\overline{DP}$ 8, B: The polypeptide with $\overline{DP}$ 14, C: The polypeptide with $\overline{DP}$ 14 after treatment with dichloroacetic acid.

of the β-structure, while the sample with $\overline{DP}$ 14 treated with dichloroacetic acid showed the bands at 540, 524, 409, and 375 cm^{-1} characteristic of the α-helix, and also that at 441 cm^{-1} characteristic of the β-structure. These results suggest that the polypeptide with *N*-terminal L-valine takes not only the α-helix but also the β-structure after the treatment. We suppose that the β-structure of the latter polypeptide may result from the presence of the oligomers with low molecular weights, perhaps five or lower repeating tripeptide units, because we have shown in another series of studies that some sequential tripeptide oligomers begin to take the α-helix at pentadecapeptides in the solid state.[13] Thus, the above results demonstrate that the sequential polypeptide with *N*-terminal L-valine (L-Val–L-Ala–L-Ala)$_n$ contains a fair portion of the lower oligomers, which cannot form the α-helical conformation. This is consistent with the results of polycondensation described above.

Some interesting results were obtained by the conformational study of the polypeptides, (L-Phe–L-Val–L-Phe)$_n$, (L-Val–L-Phe–L-Phe)$_n$, and (L-Val–L-Val–Gly)$_n$, though no evidence for elucidating the sterical

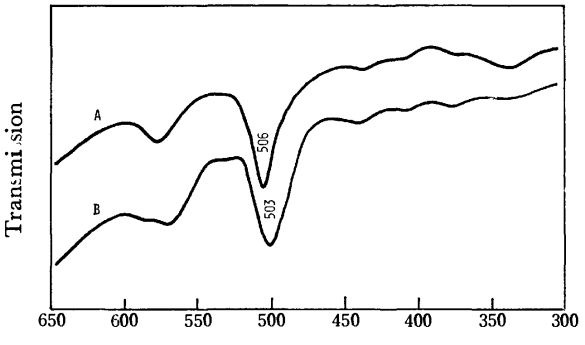

Fig. 3. Far-infrared spectra of the sequential polypeptide (L-Phe–L-Val–L-Phe)$_n$ with η_{sp}/c 0.161. A: Before treatment with dichloroacetic acid, B: After the treatment.

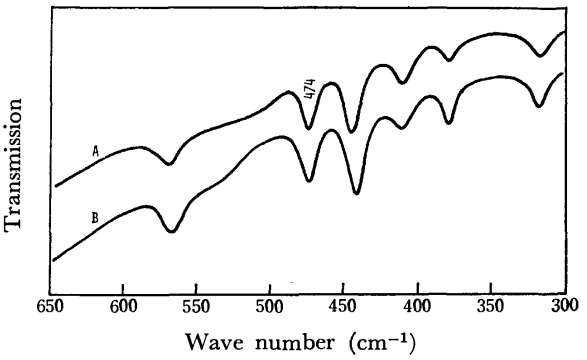

Fig. 4. Far-infrared spectra of the sequential polypeptide (L-Val-L-Val-Gly)$_n$. A: Before treatment with dichloroacetic acid, B: After the treatment.

effect of the *N*-terminal L-valine in polycondensation was obtained. Fig. 3 shows the far-infrared spectra of the polypeptide (L-Phe-L-Val-L-Phe)$_n$ before and after treatment with dichloroacetic acid. The spectrum of (L-Val-L-Phe-L-Phe)$_n$ was similar to those shown in Fig. 3. The spectra have the band near 505 cm^{-1} which has been assigned as characteristic of the L-phenylalanine residue with the β-structure. It is known that poly(L-phenylalanine) can take the α-helical conformation, but the stability of the α-helix is not so large as that for poly(L-alanine) and poly(L-leucine).[14] The β-structure of the sequential polypeptide in this study shows that it may not have an adequate molecular weight to form the α-helical conformation. Figure 4 shows the spectra of (L-Val-L-Val-Gly)$_n$ before and after the treatment. The polypeptide has already been studied by Itoh *et al.*[15] They found the band at 470 cm^{-1} characteristic of the poly(L-valine) structure, which differs from the β-structure.[3] Though the spectra of our sample have some new bands at 568, 412, and 380 cm^{-1} which were not found in the spectrum reported by Itoh, they have the characteristic band at 474 cm.$^{-1}$ This shows that the polypeptide takes the structure characteristic of poly(L-valine) before and after the treatment with dichloroacetic acid.

Experimental

Synthesis of Monomers. Nps-tripeptide ONSu esters were prepared by the stepwise synthesis of the Nps-tripeptide ethyl ester, the saponification of the tripeptide esters, and the active esterification of the tripeptide free acid. A typical synthesis of the monomers is illustrated by the following preparation of Nps-L-Phe-L-Val-L-Phe-ONSu.

Nps-L-Val-L-Phe-OEt. L-Phenylalanine ethyl ester hydrochloride (46.0 g (0.2 mol)) was suspended in 400 ml of tetrahydrofuran, and then 28 ml of triethylamine was added. The resulting crystals of the salt were removed by filtration. To the filtrate were added 59.2 g (0.2 mol) of Nps-L-valine NCA, after which the solution was stirred for 3 h at room temperature. The solvent was evaporated under reduced pressure. The residue was dissolved in 600 ml of ethyl acetate. The solution was washed with 5% citric acid, 5% sodium hydrogencarbonate, and water, and dried over sodium sulfate. The solution was concentrated under reduced pressure. To the residue hexane was added to crystallize the product, which was then recrystallized from warm ethyl acetate to give 81.1 g (91%) of a pure dipeptide; mp 149—150 °C, $[\alpha]_D$ −11.4 (*c* 1.0, *N,N*-dimethylformamide). Found: C, 59.25; H, 6.19; N, 9.40. Calcd for $C_{22}H_{27}N_3O_5S$: C, 59.31; H, 6.11; N, 9.43%.

Nps-L-Phe-L-Val-L-Phe-OEt. The above Nps-dipeptide ester (80.2 g (0.18 mol)) was dissolved in 180 ml of 2 M hydrochloric acid in ethanol. To the solution were added 500 ml of diethyl ether and 300 ml of hexane to precipitate the dipeptide ester hydrochloride. The precipitate was collected by filtration, washed with diethyl ether, and reprecipitated from methanol. The product was dissolved in 600 ml of tetrahydrofuran, and then 26 ml of triethylamine was added. The resulting crystals were removed. To the solution were added 63.7 g (0.18 mol) of Nps-L-phenylalanine NCA, after which the solution was stirred for 2 h at room temperature. The solution was treated analogously to the case of the dipeptide synthesis. The obtained Nps-tripeptide ester was recrystallized from tetrahydrofuran; 99.2 g (93%); mp 165—166 °C, $[\alpha]_D$ +41.9 (*c* 1.0, *N,N*-dimethylformamide). Found: C, 62.76; H, 6.21; N, 9.48. Calcd for $C_{31}H_{36}N_4O_6S$: C, 62.82; H, 6.12; N, 9.45%.

Nps-L-Phe-L-Val-L-Phe-OH. The Nps-triprptide ethyl ester (59.3 g (0.1 mol)) was dissolved in 200 ml of acetone, and then 100 ml of 1 M sodium hydroxide was added. The system was stirred for 1 h to give a clear solution, which was then concentrated under reduced pressure at 30 °C: the residual aqueous solution was diluted with 200 ml of water. The solution was extracted with 300 ml of diethyl ether and acidified with 15% citric acid. The system was extracted with ethyl acetate. The extract was washed with water and dried over sodium sulfate. The solution was concentrated under reduced pressure. Hexane was added to crystallize the product. The crude product was purified by recrystallization from tetrahydrofuran; 48.5 g (86%); mp 111—113 °C, $[\alpha]_D$ +50.5 (*c* 1.0, *N,N*-dimethylformamine). Found: C, 61.60; H, 5.82; N, 9.98%. Calcd for $C_{29}H_{32}N_4O_6S$: C, 61.68; H, 5.71; N, 9.93%.

Nps-L-Phe-L-Val-L-Phe-ONSu. The Nps-tripeptide free acid (56.5 g (0.1 mol)) was dissolved in 500 ml of tetrahydrofuran. To the solution were added 12.7 g (0.11 mol) of *N*-hydroxysuccinimide, after which the system was stirred for 10 min to give a clear solution. The solution was cooled at −10 °C, and 20.9 g (0.11 mol) of dicyclohexylcarbodiimide was added. The solution was then stirred for 5 h at −10 °C and allowed to stand for 20 h at 0 °C. The crystals of the urea were removed by filtration. A few drops of glacial acetic acid were added, and the solution was concentrated under reduced pressure at 10 °C. Hexane was added to the residue. The crystals were isolated and redissolved in tetrahydrofuran. The undissolved materials were removed, and the solution was concentrated. To the residue hexane was added to crystallize the product; 58.9 g (89%); mp 185—190 °C (dec). $[\alpha]_D$ +22.0 (*c* 1.0, *N,N*-dimethylformamide). Found: C, 59.97; H, 5.45; N, 10.46%. Calcd for $C_{33}H_{35}N_5O_8S$: C, 59.89; H, 5.33; N, 10.59%.

Polycondensation of Tripeptide ONSu Esters. Nps-tripeptide ONSu ester (0.03 mol) was dissolved in 30 ml of 2 M hydrochloric acid in dioxane, and 300 ml of diethyl ether were added. The resulting precipitate was isolated by filtration, washed with diethyl ether until the yellow color disappeared, and dried. The product was dissolved in a small amount of methanol. To the solution was added diethyl ether to precipitate the tripeptide ONSu ester hydrochloride. The hydrochloride (0.005 mol) was dissolved in *N,N*-dimethyl formamide at the concentrations listed in Table 2 to 4. To the solution was then added, with vigorous stirring, 0.84 ml of triethylamine. The system was stirred or allowed to

stand for 1 day at room temperature. After the polycondensation, the system was treated by the following three different procedures for the isolation of the polypeptide. First procedure: the polymerization system was diluted with 100 ml of diethyl ether. The precipitate was collected by filtration, washed with 200 ml of methanol and 50 ml of diethyl ether, and dried over P_2O_5. Second procedure: the product isolated by the first procedure was suspended with vigorous stirring in 30 ml of *N,N*-dimethylformamide for 6 h. The system was then diluted with 100 ml of methanol, and the resulting precipitate was isolated by filtration, washed with 50 ml of methanol and 50 ml of diethyl ether, and dried. Third procedure: the polymerization system was diluted with 100 ml of methanol. The resulting precipitate was treated in the same way as in the second procedure.

Measurements. The viscosity of the sequential polypeptides was measured at 25±0.1 °C with an Ostwald viscometer. The concentration of the polypeptide was adjusted to 0.5 g/100 ml of dichloroacetic acid. The NMR spectrum of the polypeptides was obtained with a JEOL JNM-PMX 60 NMR spectrometer at room temperature. The concentration of the polymer was adjusted to 10% in trifluoroacetic acid. The far-infrared spectrum was measured with a JASCO IR-F spectrophotometer. Nujol mulls were used.

References

1) H. C. Watson and J. C. Kendrew, *Nature*, **190**, 670 (1961).
2) R. Katakai, F. Toda, K. Uno, Y. Iwakura, and M. Oya, *Chem. Lett.*, **1973**, 763.
3) K. Itoh and H. Katabuchi, *Biopolymers*, **12**, 921 (1973).
4) R. Katakai, M. Oya, and Y. Iwakura, *Biopolymers*, **14**, 1315 (1975).
5) Abbreviations are those recommended by the IUPAC-IUB commission on Biochemical Nomenclature, *Biochemistry*, **11**, 1726 (1972).
6) R. Katakai, M. Oya, F. Toda, K. Uno, and Y. Iwakura, *Macromolecules*, **6**, 827 (1973).
7) R. Katakai and M. Oya, *Chem. Lett.*, **1974**, 1529; R. Katakai and M. Oya, *J. Polym. Sci., Polym. Lett. Ed.*, **12**, 719 (1974); R. Katakai, *J. Org. Chem.*, **40**, 2697 (1975); R. Katakai and M. Oya, *Biopolymers*, **14**, 2507 (1975).
8) R. Katakai and Y. Nakayama, *Biopolymers*, **15**, 747 (1976); *J. Chem. Soc., Perkin 1*, **1977**, 292.
9) G. W. Anderson, J. E. Zimmerman, and F. M. Callahan *J. Am. Chem. Soc.*, **86**, 1839 (1964).
10) R. Katakai, *Biopolymers*, **15**, 1815 (1976).
11) R. Schwyzer and P. Lieber, *Helv. Chem. Acta*, **41**, 2168 (1958).
12) K. Itoh, H. Katabuchi, and T. Shimanouchi, *Nature, New Biol.*, **239**, 42 (1972).
13) R. Katakai, *J. Am. Chem. Soc.*, **99**, 232 (1977).
14) G. D. Fasman, "Poly-α-Amino Acids," Marcel Dekker, New York (1967), p. 513.
15) K. Itoh H. Katabuchi, *Biopolymers*, **11**, 1593 (1972).

The Reactions of Aryldiazomethanes with Sulfur Dioxide in the Presence of Enamines

Toyoshige TANABE and Toshikazu NAGAI

Institute of Chemistry, College of General Education, Osaka University, Toyonaka, Osaka 560

(Received October 28, 1976)

The reactions of several arydiazomethanes with sulfur dioxide in the presence of 2-methyl-1-morpholinopropene gave cyclic sulfones, thietane 1,1-dioxides, indicating the existence of sulfene as a reaction intermediate. The stereoselectivity of the sulfene–enamine cycloaddition showed that the less thermodynamically stable *cis* orientation was generally preferred. On the other hand, the reactions in the presence of 1-morpholinocyclohexene, which has a labile proton β to the morpholino moiety, afforded acyclic or cyclic sulfones, depending on the substituents of diazomethanes. The mechanism of these reactions is discussed.

Recently sulfenes, generated by the action of amines on alkanesulfonyl chlorides, have received considerable attention.[1] Though the reactivities of sulfene towards enamines have been extensively investigated, the research on the stereochemistry of the products is meager and the mechanism for sulfene–enamine addition is still not determined.[2] Another useful method for generating sulfene is the reaction of diazoalkanes and sulfur dioxide,[3] but there are only a few publications[4] about this reaction, where episulfones and olefins are formed. In the present paper,[5] we deal with the stereoselecitve formations of thietane 1,1-dioxide in the reactions of aryldiazomethanes with sulfur dioxide in the presence of enamines and with the preference of non-cyclo to cycloaddition.

The mechanism of sulfene–enamine addition has already been discussed in the base-induced β-elimination reaction of alkanesulfonyl chlorides in the presence of enamines.[2] But in this system, the triethylamine used as the elimination reagent is liable to cause a slow post-isomerization[2b] of the cycloadduct, 3-aminothietane 1,1-dioxide. The present system, as compared with the amine–chloride system, could be more favorable for the mechanistic study of sulfene–enamine addition from the stereochemical point of view.

Results and Discussion

Reactions in the Presence of 2-Methyl-1-morpholinopropene (MMP). The reactions of mono- and di-arylsubstituted diazomethanes (**1**) with sulfur dioxide in the presence of MMP, which has no hydrogen atom β to the morpholino moiety, led to the cycloadducts, thietane 1,1-dioxide derivatives (**2**) (Scheme 1).

In the reactions of mono-arylsubstituted diazomethanes (**1c, 1d,** and **1e**) with sulfur dioxide in the presence of MMP, mixtures of *cis* and *trans* isomers were obtained. The less thermodynamically stable *cis* orientation of the morpholino and the aryl groups was preferred in the cycloadducts **2c** and **2d**; on the contrary, the *trans* orientation was preferred in the case of **2e** which has an electron-withdrawing group. The results are summarized in Table 1.

Table 1. The reaction of **1** with SO_2 in the presence of MMP

Diazomethane	R^1	R^2	Solvent	Yield of **2** mol%[a]	*cis* %[b]
1a	fluorenylidene		C_6H_6	99	—
1b	Ph	Ph	C_6H_6	95	—
1c	*p*-Me-Ph	H	C_6H_6	51	73
			THF	57	64
1d	Ph	H	C_6H_6	62	73
1e	*p*-NO_2-Ph	H	C_6H_6	82	29
			THF	82	22

a) Isolated yield calculated on the basis of **1** used.
b) The value shows the ratio of the *cis* isomer in the yield of **2**.

The product, **2d**, obtained from the reaction of **1d** was separated into its *cis* and *trans* isomers (*cis*-**2d** and *trans*-**2d**) by repeated fractional recrystallizations; the isolation of only the *trans* isomer had been made by Truce and Rach.[2b] The isolated isomers were identified on the basis of the NMR spectra. The signals of the phenyl protons appeared as a separate peak in *cis*-**2d** and as a single peak in *trans*-**2d**. The difference between the chemical shifts of the two methyl proton signals was 6 Hz in *cis*-**2d** and 1.8 Hz in *trans*-**2d**, showing an interaction between the phenyl ring and one methyl group in *cis*-**2d**. In the NMR spectra of *cis*-**2d** and *trans*-**2d**, both coupling constants for the two methylidyne protons in the thietane rings were the same and equal to 10 Hz. The large conpling coustant (10 Hz) suggests a dihedral angle between the two protons

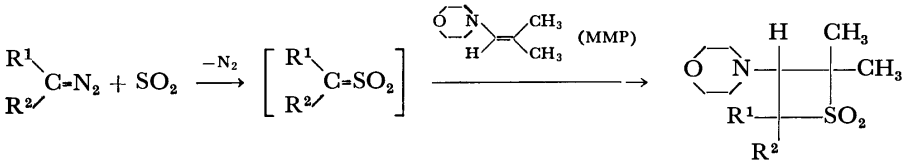

1 (**a**) R^1, R^2=fluorenylidene; (**b**) R^1=R^2=phenyl; (**c**) R^1=*p*-tolyl, R^2=H; (**d**) R^1=phenyl, R^2=H; (**e**) R^1=*p*-nitrophenyl, R^2=H. **2a, b, c, d, e**

Scheme 1.

of 0 or 180°.[6] The former angle can be attained only in a planar thietane ring by a *cis* orientation of the morpholino and aryl groups, while the 180° alignment can be achieved only by *trans* substituents in a puckered conformation, as shown in Scheme 2. The assigned stereochemistry was further supported by a study of epimerization: the *cis* isomer or the *cis–trans* mixutre of **2d** was isomerized to the pure *trans* isomer by stirring its methanol solution under the influence of a catalytic amount of sodium methoxide over a period of several days (Scheme 2).

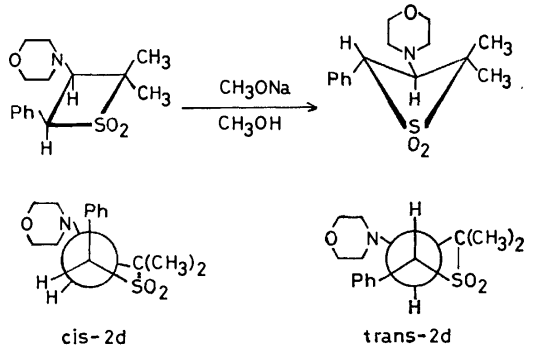

Scheme 2.

The assignment of each of the isomers of **2c** and **2e** was established with their respective NMR spectra, with reference to those of **2d**. And the findings in **2d**, described above, were also applicable to **2c** and **2e**. The *cis* percentages in the yields of **2** were determined by the intensity measurement of the methylidyne proton signals in the NMR spectra of the crude reaction products.

In order to examine the effect of solvent on the stereoselectivity, reactions of **1d** were carried out in various solvents. These results are presented in Table 2. An increasing tendency of the *trans* isomer, though not so drastic, was observed in the polar solvents. Such an effect was also observed in the case of the *para*-substituted phenylsulfene, as seen in Table 1: the reaction of **1c** or **1e** gave the increasing *trans* adduct in THF instead of benzene.

Reactions in the Presence of 1-Morpholinocyclohexene (MCH). A series of reactions of aryldiazomethanes (**1**) and MCH, which has a hydrogen atom β to the morpholino moiety,

TABLE 2. THE REACTION OF PHENYLDIAZOMETHANE (**1d**) WITH SO_2 IN THE PRESENCE OF MMP IN VARIOUS SOLVENTS

Solvent	Yield of **2d** mol%[a]	*cis* %[b]
cyc-C_6H_{12}	80	77
CCl_4	57	77
C_6H_6	62	73
CH_3CN	43	68
THF	50	63
DMF	77	64

a) Isolated yield calculated on the basis of **1** used. b) The value shows the ratio of the *cis* isomer in the yield of **2d**.

TABLE 3. THE REACTION OF **1** WITH SO_2 IN THE PRESENCE OF MCH

Diazomethane	R^1	R^2	Solvent	Yield(mol%)[a] cyclic (**5**)	acyclic (**3**)
1a	fluorenylidene		C_6H_6	—	84
1b	Ph	Ph	C_6H_6	—	87
1c	*p*-Me-Ph	H	C_6H_6	49	—
			THF	54	—
1d	Ph	H	C_6H_6	87	—
			THF	87	—
1e	*p*-NO_2-Ph	H	C_6H_6	—	89
			THF	—	93

a) Isolated yield calculated on the basis of **1** used.

was carried out in the same way. The reactions of 9-diazofluorene (**1a**), diphenyldiazomethane (**1b**), and *p*-nitrophenyldiazomethane (**1e**) were carried out and the spectra of IR and NMR for these reaction products could be explained satisfactorily by the structures of the acyclic sulfones (**3**) instead of the other acyclic sulfones (**4**)[7] or the expected cyclic sulfones (**5**). On the contrary, the reactions of *p*-tolyldiazomethane (**1c**) and phenyldiazomethane (**1d**) gave a *cis–trans* mixture of cyclic sulfone (**5**) (Scheme 3). Table 3 shows the results.

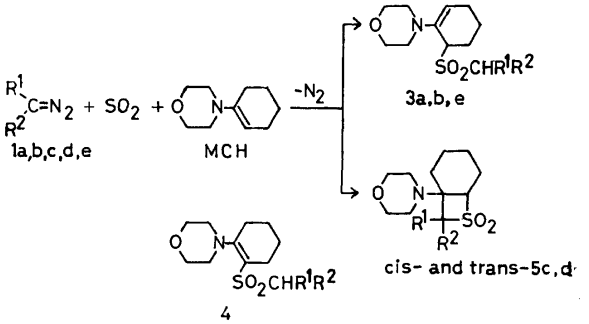

Scheme 3.

Three cyclic products (*cis*-**5c**, *cis*-**5d**, and *trans*-**5d**) were isolated respectively by careful recrystallizations from suitable solvents and their configurations were determined by NMR analysis using a shift reagent, Eu(dpm)$_3$.[8] The results of the complexation studies for *cis*-**5d** and *trans*-**5d** are shown in Fig. 1. The primary site of complexation with Eu(dpm)$_3$ is the oxygen of the morpholine ring, since the largest shifts were induced in the protons vicinal to oxygen. In Fig. 1a, the difference in chemical shifts of the two methylidyne protons H_6 and H_8 decreased whereas, in Fig. 1b, the difference remained essentially constant. Thus in *cis*-**5d**, H_8 is deshielded less than H_6, whereas in *trans*-**5d** both protons are deshielded to approximately the same extent. The observed difference in induced shifts must lie in the distance from the chelation site to the protons, establishing the fact that H_6 and H_8 are *trans* to each other in *cis*-**5d** and *cis* to each other in *trans*-**5d**. The induced shift spectra for *cis*-**5c** were similar to those of *cis*-**5d**.

The ratio of the two geometric isomers was deter-

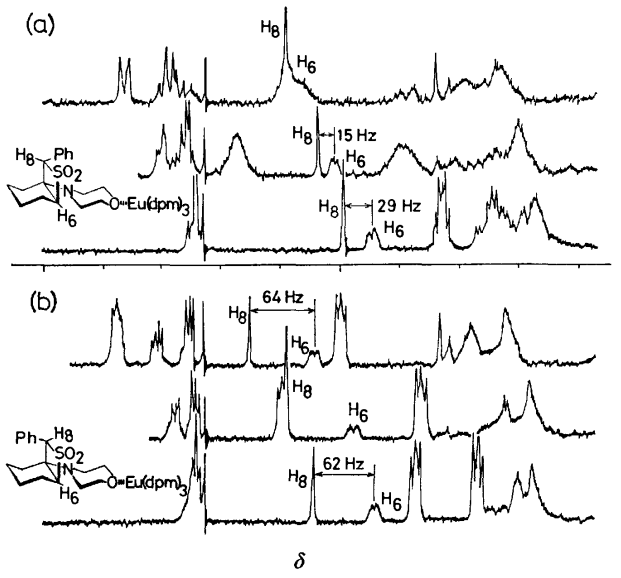

Fig. 1. Succesive scans displaying the effect of the addition of incremental amounts of $Eu(dpm)_3$ on the 60 MHz NMR spectra in $CDCl_3$; (a): for *cis*-**5d**, (b): for *trans*-**5d**.

mined by means of the intensity measurement of the H_8 proton signal in the NMR spectrum of the crude product. In the isomeric mixture of **5d**, the *cis* percentage was as high as 81% in benzene and was lowered to 70% in THF. In the case of **5c**, the predominant yield of the *cis* isomer was evident in the spectrum, though the *cis* percentage could not be determined because the peaks assigned to the *trans* isomer were weak and ambiguous. Interesting to say, the results suggest that the alternative of acyclic (**3**) or cyclic (**5**) is caused by the electronic character of the α-carbon atom in the sulfene.

Reaction Mechanism. On the basis of the frontier orbitals' interaction in the [2+2] cycloaddition,[2b,9] different mechanistic processes are possible (Scheme 4). A concerted $[{}_{\pi}2_a+{}_{\pi}2_s]$ process could conceivably account for the *cis* preference in the cyclic sulfones (**2** and **5**). In this concerted process, one unsaturated system must approach the other with an orthogonal orientation.[12] The most probable transition state is shown for the formation of *cis*-**2**, such as **6**. If the reaction indeed proceeds *via* this concerted process, it should be required that the acyclic sulfones (**3a**, **3b**, and **3e**) were formed through the cyclic sulfones. And so, from the consideration of a steric interaction between the morpholino and the aryl groups, the cyclic isomers of **3a**, **3b**, and **3e** like **5c** and **5d** should also be isolated even in the MCH system, as well as in the MMP system. Actually, however, in the current observation, only acyclic sulfones **3a**, **3b**, and **3e** were afforded without the cyclic isomers in the MCH system. And in the case of the formation of cyclic sulfone, the *cis* preference was lowered when polar solvents were employed.

As an alternative, a concerted $[{}_{\pi}2_s+{}_{\pi}2_s]$ process can be significantly preferred, as pointed out by Epiotis *et al.*,[13] if one addend is very electron rich and the other is very electron defficient. However, from the evidence of the preference of noncycloaddition when a zwitterionic intermediate (**7**) is stabilized, a stepwise process, which is a third alternative, is rather likely.

The formation of the less stable *cis* isomer of cyclic sulfone (**2** and **5**) can be well explained on the basis of an electrostatic interaction of cisoid 1,4-dipolar intermediate (**7**). In the addition of sulfene to MMP, which has no proton β to the morpholino moiety, the *cis* isomer of **2** was predominantly afforded. If the carbanion is stabilized and given a long lifetime by its substituting group(like *p*-NO_2–Ph) or by a solvation in the polar solvents, the amount of the more thermodynamically stable *trans* isomer of **2** may increase. The addition of sulfene to MCH, which has a labile proton β to the morpholino moiety, resulted in the formation of **5c** and **5d**, where the *cis* isomer was predominant. However, if the carbanion was stabilized or if the negative charge is dispersed and the effective electrostatic attraction is reduced to a great extent by its substituting group, *e. g.* fluorenylidene, diphenyl, or *para*-nitrophenyl group, the proton migration to the carbanion to afford **3** would be more favored than the cyclization of the zwitterion to give **5**.

Experimental

The NMR spectra were recorded on a Varian EM-360 (60 MHz) instrument in $CDCl_3$ with tetramethylsilane as the internal standard. The IR spectra were measured in KBr disks with Hitachi EP-S and 215 spectrophotometers.

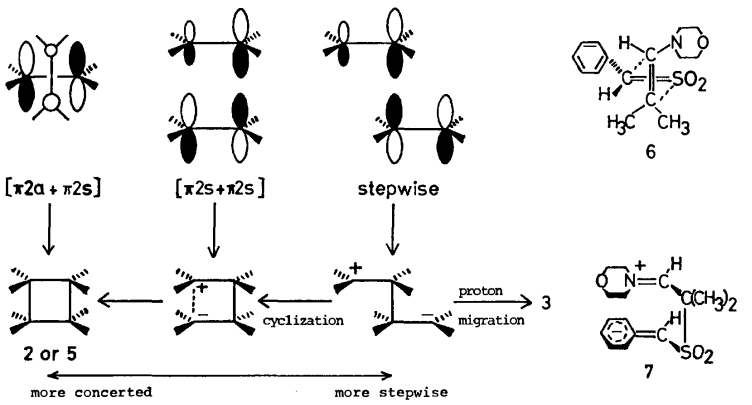

Scheme 4. Indicates acceptor(sulfene) LUMO[10]-donor(enamine) HOMO[11] interaction.

Materials. All the diazomethanes were prepared according to the procedures given in the literature: 9-diazofluorene (**1a**),[14] diphenyldiazomethane (**1b**),[15] *p*-tolyldiazomethane (**1c**),[16] phenyldiazomethane (**1d**),[17] and *p*-nitrophenyldiazomethane (**1e**).[18] The enamines were also prepared by the methods in the literature: 2-methyl-1-morpholinopropene(MMP)[19] and 1-morpholinocyclohexene (MCH).[20] Sulfur dioxide, obtained from a commercial source, was dried by passing it through $CaCl_2$ and P_2O_5 tubes. The solvents were purified according to the published directions,[21] stored over sodium wire or calcium hydride, and redistilled just before use.

General Procedure. In a 100 ml three-necked flask equipped with a magnetic stirrer, a dropping funnel, a thermometer, and a calcium chloride drying tube were placed 70 ml of a dry solvent containing 50 mmol of sulfur dioxide and 10 mmol of an enamine, and the flask was kept at 20 °C. To this solution, 30 ml of dry solvent containing 5 mmol of diazomethane was added dropwise over a period of 15 minutes with stirring. After the addition was complete, the mixed solution was stirred for an additional 45 minutes. Then the solvent and the excess sulfur dioxide were removed as quickly as possible *in vacuo* at room temperature. After an aliquot of the oily residue was dissolved in $CDCl_3$ and analyzed by NMR, the NMR solvent was removed at reduced pressure and the combined residue was crystallized from a suitable solvent. The NMR data for *cis* isomers were obtained from the mixtures except where noted. An analytically pure sample was obtained by recrystallization.

*2-Fluorenylidene-3-morpholino-4,4-dimethylthietane 1,1-Dioxide (**2a**).* The white powder was obtained in 99% yield by adding a small amount of cold petroleum ether to the oily residue. The recrystallization from methanol gave the colorless leaflets, mp 156—157 °C. IR(KBr): 1106 and 1315 cm^{-1} (SO_2). NMR($CDCl_3$): δ 1.55—2.33[4H, broad m, $(CH_2)_2N$], 1.84(3H, s, CH_3), 2.01(3H, s, CH_3), 3.43[5H, m, $(CH_2)_2O$ and methylidyne], and 7.3—8.1(8H, m, aromatic). Found: C, 68.12; H, 6.42; N, 3.89%. Calcd for $C_{21}H_{23}NO_3S$: C, 68.28; 6.28; N, 3.79%.

*2,2-Diphenyl-3-morpholino-4,4-dimethylthietane 1,1-Dioxide (**2b**).* The white powder was obtained in 95% yield in the same manner as described above. The recrystallization from benzene-ethanol(1 : 1) gave the colorless plates, mp 136—137 °C. IR(KBr): 1112 and 1305 cm^{-1} (SO_2). NMR($CDCl_3$): δ 1.64(3H, s, CH_3), 1.70(3H, s, CH_3), 2.37[4H, m, $(CH_2)_2N$], 3.64[4H, m, $(CH_2)_2O$], 3.77(1H, s, methylidyne), 7.15—7.65 (8H, m, C_6H_5 *trans* to morpholine ring and 3H of C_6H_5 *cis* to morpholine ring), and 7.8—8.2(2H, m, 2H of C_6H_5 *cis* to morpholine ring). Found: C, 68.01; H, 6.82; N, 3.85%. Calcd for $C_{21}H_{25}NO_3S$: C, 67.90; H, 6.78, N, 3.77%.

*3-Morpholino-2-*p*-tolyl-4,4-dimethylthietane 1,1-Dioxide (**2c**).* The *cis-trans* mixture was obtained in the yield of 51% in benzene and 57% in THF by adding a small amount of cold methanol to the oily residue. NMR($CDCl_3$) (*cis* isomer): δ 1.62 and 1.73(each 3H, s, *gem*-dimethyl), 2.28[4H, m, $(CH_2)_2N$], 2.32(3H, s, CH_3-Ph), 3.30(1H, d, J=10 Hz, CHN), 3.60[4H, m, $(CH_2)_2O$], 5.27(1H, d, J=10 Hz, $CHSO_2$), and 7.17 and 7.53(each 2H, d, J=7.8 Hz, phenyl). Repeated recrystallization of the crude product from methanol gave analytically pure *trans* isomer, colorless plates, mp 167—168 °C. IR(KBr): 1098, 1118, 1292, and 1304 cm^{-1} (SO_2). NMR ($CDCl_3$): δ 1.63 and 1.67(each 3H, s, *gem*-dimethyl), 2.29 [4H, m, $(CH_2)_2N$], 2.35(3H, s, CH_3-Ph), 3.08(1H, d, J= 10 Hz, CHN), 3.65[4H, m, $(CH_2)_2O$], 5.08(1H, d, J=10 Hz, $CHSO_2$), and 7.25(4H, broad s, phenyl). Found: C, 61.72; H, 7.37; N, 4.52%. Calcd for $C_{16}H_{23}NO_3S$: C, 62.12; H, 7,49; N, 4.53%.

*3-Morpholino-2-phenyl-4,4-dimethylthietane 1,1-Dioxide (**2d**).* The crude isomeric mixtures of the *cis* and *trans* cycloadducts were obtained in the yields of 43—80% according to the solvent used. The mixture was separated into the *cis* and *trans* isomers by repeated fractional recrystallization from a mixed solvent of petroleum ether and benzene. The *cis* isomer: colorless prisms, mp 128—129 °C. IR(KBr): 1089 and 1301 cm^{-1} (SO_2). NMR($CDCl_3$): δ 1.67 and 1.77(each 3H, s, *gem*-dimethyl), 2.33[4H, m, $(CH_2)_2N$], 3.35 (1H, d, J=10 Hz, CHN), 3.63[4H, m, $(CH_2)_2O$], 5.30(1H, d, J=10 Hz, $CHSO_2$), and 7.2—7.8(5H, m, phenyl). Found: C, 61.10; H, 7.23; N, 4.75%. Calcd for $C_{15}H_{21}NO_3S$: C, 61.00; H, 7.17; N, 4.74%. The *trans* isomer was also obtained by treating the *cis* isomer or the isomeric mixture in methanol containing a 0.02 part of sodium methoxide for about a week. The *trans* isomer: colorless plates, mp 179—180 °C(lit, 181—182 °C).[2b] IR(KBr): 1105 and 1298 cm^{-1} (SO_2). NMR ($CDCl_3$): δ 1.65 and 1.68(each 3H, s, *gem*-dimethyl), 2.26 [4H, m, $(CH_2)_2N$], 3.10(1H, d, J=10 Hz, CHN), 3.64[4H, m, $(CH_2)_2O$], 5.13(1H, d, J=10 Hz, $CHSO_2$), and 7.40(5H, s, phenyl). Found: C, 60.89; H, 7.25; N, 4.75%. Calcd for $C_{15}H_{21}NO_3S$: C, 61.00; H, 7.17; N, 4.74%.

*3-Morpholino-2-*p*-nitrophenyl-4,4-dimethylthietane 1,1-Dioxide (**2e**).* The NMR spectrum of the crude product showed the peaks derived from both *cis* and *trans* isomers. The yield of the product was 82% both in benzene and in THF. The *cis* isomer: NMR($CDCl_3$): δ 1.67 and 1.77(each 3H, s, *gem*-dimethyl), 2.25[4H, m, $(CH_2)_2N$], 3.41(1H, d, J=10 Hz, CHN), 3.63[4H, m, $(CH_2)_2O$], 5.40(1H, d, J=10 Hz, CH-SO_2), and 7.79 and 8.32(each 2H, d, J=9 Hz, phenyl). The pure *trans* isomer was obtained by recrystallization of the crude product from methanol: colorless plates, mp 193—194 °C. IR(KBr): 1115 and 1305 cm^{-1} (SO_2). NMR(CD-Cl_3): δ 1.67 and 1.69(each 3H, s, *gem*-dimethyl), 2.23[4H, m, $(CH_2)_2N$], 3.10(1H, d, J=10 Hz, CHN), 3.61[4H, m, $(CH_2)_2O$], 5.17(1H, d, J=10 Hz, $CHSO_2$), and 7.58 and 8.25(each 2H, d, J=9 Hz, phenyl). Found: C, 52.87; H, 5.97; N, 8.46%. Calcd for $C_{15}H_{20}N_2O_5S$: C, 52.93; H, 5.92; N, 8.46%.

*3-(9-Fluorenylsulfonyl)-2-morpholinocyclohexene (**3a**).* A white powder was afforded in 84% yield by adding a small amount of cold petroleum ether to the oily residue. An analytiacally pure sample was obtained by recrystallization from methanol: colorless plates, mp 142—143 °C. IR(KBr): 1120 and 1315 cm^{-1}(SO_2), 1653 cm^{-1}(C=C). NMR($CDCl_3$): δ 1.25—2.75(6H, broad m, cyclohexane ring), 2.58[4H, m, $(CH_2)_2N$], 3.48[5H, m, $(CH_2)_2O$ and $CHSO_2$], 5.28(1H, t, J=3 Hz, vinyl), 5.58(1H, s, SO_2CH-Ar), and 7.2—8.1(8H, m, aromatic). Found: C, 70.48; H, 6.40; N, 3.31%. Calcd for $C_{23}H_{25}NO_3S$: C, 69.85; H, 6.37; N, 3.54%.

*3-Diphenylmethylsufonyl-2-morpholinocyclohexene (**3b**).* A white powder was obtained in 87% yield by adding a small amount of cold petroleum ether to the oily residue and was recrystallized from ethanol, giving the colorless plates, mp 150.5—151.5 °C. IR(KBr): 1112 and 1305 cm^{-1} (SO_2), 1645 cm^{-1} (C=C). NMR($CDCl_3$): δ 1.3—3.2(6H, broad m, cyclohexane ring), 2.76[4H, m, $(CH_2)_2N$], 3.83[5H, m, $(CH_2)_2O$ and $CHSO_2$], 5.43(1H, t, J=4 Hz, vinyl), 6.02(1H, s, SO_2CH-Ar), and 7.3—8.0(10H, m, aromatic). Found: C, 69.41; H, 6.96; N, 3.65%. Calcd for $C_{23}H_{27}NO_3S$: C, 69.50; H, 6.85; N, 3.52%.

*3-*p*-Nitrobenzylsulfonyl-2-morpholinocyclohexene (**3e**).* The NMR spectrum of the residue showed that the reaction products consisted exclusively of acyclic isomer. The crude product was collected as white powder by adding cold methanol to the residue in the yield of 88.5% in benzene and 93% in THF. Recrystallization from methanol afforded analytically

pure **3e**: colorless needles, mp 181—182 °C. IR(KBr): 1128 and 1304 cm^{-1} (SO_2), 1639 cm^{-1} (C=C). NMR($CDCl_3$): δ 1.5—2.7(6H, broad m, cyclohexane ring), 2.48—3.35[4H, broad m, $(CH_2)_2N$], 3.83[4H, m, $(CH_2)_2O$], 3.87 (1H, m, methylidyne), 4.40 and 4.73 (each 1H, ABq, J= 12.5 Hz, SO_2CH_2-Ph), 5.40(1H, t, J=3.5 Hz, vinyl), and 7.53 and 8.22 (each 2H, d, J=8.5 Hz, phenyl). Found: C, 55.55; H, 6.02; N, 7.69%. Calcd for $C_{17}H_{22}N_2O_5S$: C, 55.72; H, 6.05; N, 7.65%.

*1-Morpholino-8-*p*-tolyl-7-thiabicyclo[4.2.0]octane 7,7-Dioxide (5c).* The crude product consisted exclusively of cyclic adduct; the peaks in the NMR spectrum which are derived from *trans*-**5c** were weak and ambiguous. After careful recrystallization from cold methanol, analytically pure *cis* isomer was isolated in the yield of 49% in benzene and 54% in THF; its structure was established by means of NMR, using $Eu(dpm)_3$. The *cis* isomer: colorless plates, mp 123—124 °C. IR(KBr): 1120 and 1320 cm^{-1} (SO_2). NMR($CDCl_3$): δ 1.3—2.8(8H, broad m, cyclohexane ring), 2.32(3H, s, CH_3), 2.47[4H, m, $(CH_2)_2N$], 3.30[4H, m, $(CH_2)_2O$], 4.42 (1H, m, H_6), 4.86(1H, s, H_8), and 7.24 and 7.36(each 2H, d, J=8.5 Hz, phenyl). Found: C, 65.06; H, 7.49; N, 4.16 %. Calcd for $C_{18}H_{25}NO_3S$: C, 64.46; H, 7.51; N, 4.18%.

1-Morpholino-8-phenyl-7-thiabicyclo[4.2.0]octane 7,7-Dioxide (5d).[22] The mixture of *cis* and *trans* cyclic adducts was obtained when **1d** was used. The NMR spectrum of the residue showed that the reaction product consisted exclusively of cyclic adduct. The yields were 87% both in benzene and THF. The *cis* and *trans* isomers were isolated by careful fractional recrystallization from methanol. The ratios of the *cis* isomer were 81% in benzene and 70% in THF. Each of the structures was confirmed by means of NMR using $Eu(dpm)_3$, as described before. The *cis* isomer: white crystalline, mp 103—104.5 °C. IR(KBr): 1150 and 1314 cm^{-1} (SO_2). NMR($CDCl_3$): δ 1.2—2.8(8H, broad m, cyclohexane ring), 2.50[4H, m, $(CH_2)_2N$], 3.30[4H, m, $(CH_2)_2O$], 4.44(1H, m, H_6), 4.92(1H, s, H_8), 7.37(5H, m, phenyl). Found: C, 64.04; H, 7.09; N, 4.87%. Calcd for $C_{17}H_{23}NO_3S$: C, 63.53; H, 7.21; N, 4.36%. The *trans* isomer; colorless prisms, mp 115—116 °C. IR(KBr):1140 and 1298 cm^{-1} (SO_2). NMR($CDCl_3$): δ 1.2—2.6(8H, broad m, cyclohexane ring), 2.63[4H, m, $(CH_2)_2N$], 3.80[4H, m, $(CH_2)_2O$], 4.37(1H, m, H_6), 5.40(1H, s, H_8), and 7.2—7.7(5H, m, phenyl). Found: C, 63.48; H, 7.22; N, 4.23%. Calcd for $C_{17}H_{23}NO_3S$: C, 63.53; H, 7.21; N, 4.36%.

References

1) For a review, see: a) G. Opitz, *Angew. Chem. Int. Ed. Engl.*, **6**, 107 (1967); b) T. Nagai and N. Tokura, *Int. J. Sulfur Chem.*, **7B**, 207 (1972); c) J. F. King, *Acc. Chem. Res.*, **8**, 10 (1975).

2) a) L. A. Paquette, J. P. Freeman, and S. Maiorana, *Tetrahedron*, **27**, 2599 (1971); b) W. E. Truce and J. F. Rach, *J. Org. Chem.*, **39**, 1109 (1974).

3) H. Staudinger and F. Pfenninger, *Ber.*, **49**, 1941 (1916).

4) a) G. Hesse and E. Reichold, *Chem. Ber.*, **90**, 2101 (1957); b) N. Tokura, T. Nagai, and S. Matsumura, *J. Org. Chem.*, **31**, 349 (1966); c) T. Nagai, H. Namikoshi, and N. Tokura, *Tetrahedron*, **24**, 3267 (1968); d) N. H. Fischer, *Synthesis*, **1970**, 393.

5) Part of this work was reported in a preliminary communication: T. Tanabe, T. Shingaki, and T. Nagai, *Chem. Lett.*, **1975**, 679.

6) M. Karplus, *J. Chem. Phys.*, **30**, 11 (1959); *J. Am. Chem. Soc.*, **85**, 2871 (1963).

7) In discussing the exclusive formation of the acyclic sulfone **3** instead of the isomeric sulfone **4** as shown in Scheme 3, the following consideration may be made: the sulfone **4** is destabilized by steric inhibition of the resonance involving the nitrogen lone pair and the double bond.

8) C. T. Goralski and T. E. Evans, *J. Org. Chem.*, **37**, 2080 (1972).

9) K. N. Houk, *Acc. Chem. Res.*, **8**, 361 (1975).

10) The MO of sulfene was calculated: a) J. P. Snyder, *J. Org. Chem.*, **38**, 3965 (1973); b) K. N. Houk, R. W. Strozier, and J. A. Hall, *Tetrahedron Lett.*, **1974**, 897.

11) In HOMO of enamine, the coefficient magnitude is $c_\beta > c_\alpha$: R. Huisgen, *J. Org. Chem.*, **41**, 403 (1976).

12) R. B. Woodward and R. Hoffman, "The Conservation of Orbital Symmetry," Academic Press, New York, N. Y. (1970), pp. 68—69.

13) N. D. Epiotis, R. L. Yates, D. Carlberg, and F. Bernardi, *J. Am. Chem. Soc.*, **98**, 453 (1976), and references therein.

14) H. Staudinger and O. Kupfer, *Ber.*, **44**, 2207 (1911).

15) L. I. Smith and K. L. Howard, *Org. Synth.*, Coll. Vol. III, 351 (1955).

16) W. R. Bamford and T. S. Stevens, *J. Chem. Soc.*, **1952**, 4775.

17) C. G. Overberger and J. P. Anselme, *J. Org. Chem.*, **28**, 592 (1963).

18) H. W. Davies and M. Schwarz, *J. Org. Chem.*, **30**, 1242 (1965).

19) E. Benzing, *Angew. Chem.*, **71**, 531 (1959).

20) S. Hünig, E. Lücke, and W. Brenninger, *Org. Synth.*, Coll. Vol. V, 808 (1973).

21) J. A. Riddick and W. B. Bunger, "Organic Solvents," 3rd ed, Wiley-Interscience, New York (1970).

22) A. M. Hamid and S. Trippett, *J. Chem. Soc., C*, **1968**, 1612, reported the formation of **5d** from the reaction of phenylmethanesulfonyl chloride and MCH in the presence of Et_3N, but the stereochemistry of the reaction was not discussed.

The Nucleophilic Displacement Reactions of 8-Chloro- and 2,8-Dichloro-3-phenyl-1-azaazulenes[1]

Kameji YAMANE,* Kunihide FUJIMORI,* Je-Kyun SIN,** and Tetsuo NOZOE***

Department of Chemistry, Faculty of Science, Tohoku University, Sendai 980

**Department of Chemistry, Faculty of Science, Shinsyu University, Matsumoto 390*

(Received November 5, 1976)

The reaction of 3-phenylpyrrolo[2,3-*b*]tropone (**7**) with phosphoryl chloride gave 8-chloro-3-phenyl-1-azaazulene (**5**). When **5** and **7** were treated with *N*-chlorosuccinimide, 2,8-dichloro-3-phenyl-1-azaazulene (**6**) and 2-chloro-3-phenylpyrrolo[2,3-*b*]tropone (**8**) were obtained respectively. **6** was also obtained from **8** by treatment with phosphoryl chloride. The reactions of **5** and **6** with nucleophilic reagents gave the corresponding substituted products (**14a—m** and **15a—m**). 8-Hydrazino-3-phenyl-1-azaazulene (**14m**) and 2-chloro-8-hydrazino-3-phenyl-1-azaazulene (**10**), which had been obtained by the reaction of **5** and **6** with hydrazine hydrate, were decomposed by treatment with copper(II) sulfate in acetic acid to give 3-phenyl-1-azaazulene (**2**) and 2-chloro-3-phenyl-1-azaazulene (**11**) respectively.

1-Azaazulene (**1**),[2] a seven-membered analog of indole, and its 3-phenyl derivative (**2**),[3] were synthesized a little more than twenty years ago by one of the present authors (T. N.) and his co-workers; the molecular diagram of this interesting compound (**1**) was calculated by Kon[4] (*cf.* Fig. 1). As the reactivity of the same

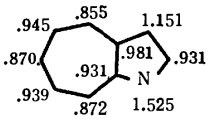

Fig. 1. Charge density of 1-azaazulene calculated by H. Kon.[4]

functional group should be different according to its position in such a nonbenzenoid nucleus, we first studied the nucleophilic substitution reaction of 2-chloro- (**3**)[2] and 2,6-dichloro-1-azaazulene (**4**).[5] Brief mention was

(**1**): R=H
(**2**): R=Ph

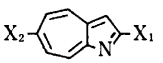

(**3**): X_1=Cl, X_2=H
(**4**): X_1=X_2=Cl

also made of the nucleophilic displacement reaction of 8-chloro-(**5**)[1,3] and 2,8-dichloro-3-phenyl-1-azaazulene (**6**),[1] the results of which have remained unpublished. We now wish to report on the nucleophilic substitution reaction of these two compounds (**5** and **6**).

Results and Discussion

The reaction of 3-phenylpyrrolo[2,3-*b*]tropone (3-phenylcyclohept[2,3-*b*]pyrrol-8-one) (**7**)[3] with phosphoryl chloride gives 8-chloro-3-phenyl-1-azaazulene (**5**) as reddish purple needles. When **5** and **7** are treated with *N*-chlorosuccinimide, dichloro- (**6**) and monochloro compound (**8**) are obtained respectively in good yields. The same compound (**6**) is also obtained by the treatment of **5** or **7** with thionyl chloride or sulfuryl chloride, but in poor yields. Compound **6** is also obtained from **8** by treatment with phosphoryl chloride. Compounds (**5** and **6**) afford **7** and **8** respectively on treatment with ethanolic alkali. Similarly, one of the two chlorine atoms in **6** is easily replaced by a hydrazino group on treatment with hydrazine hydrate to give **10**; the latter compound (**10**) reverts back to **6** upon treatment with concentrated hydrochloric acid and copper(I) chloride, while the monochloro compound (**11**) is obtained when **10** is decomposed by treatment with copper(II) sulfate in acetic acid.

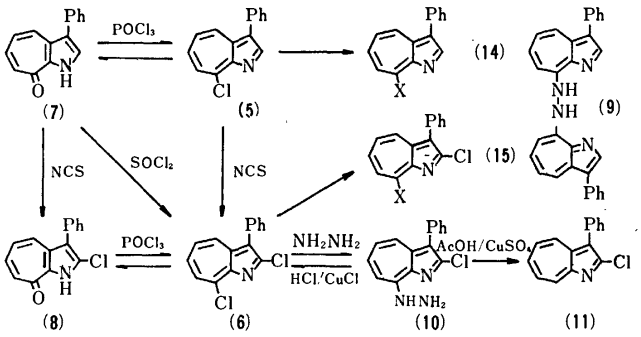

When **11** is treated with ethanolic alkali, 1,2-dihydro-3-phenyl-1-azaazulen-2-one (**12**) is formed as a saponification product. The structure of **12** was confirmed by a direct comparison with the sample obtained by the reaction of aminotropone with methyl phenylacetate.

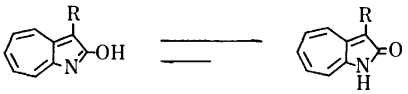

(**12**) : R=Ph
(**13**) : R=H

From the above-mentioned experimental evidence and the results of elemental analyses, **6** is identified as 2,8-dichloro-3-phenyl-1-azaazulene. The UV and NMR spectra of **5** and **6** also support the structure described above (Tables 4 and 5).

8-Hydroxy, 8-amino, and related derivatives of 1-azaazulene have two tautomeric forms, such as A and B. It seems that those substances exist mainly in their

** Present address: Faculty of Science, Korean University, 1-700, Ogawacho, Kodaira-shi, Tokyo 187.
*** Present address: No. 811, 2-5-1, Kamiyoga, Setagaya-ku, Tokyo 158.

Table 1. Nucleophilic substitution reaction products (**14**) from 8-chloro-3-phenyl-1-azaazulene (**5**)

Compound	X	Reagent/Solvent	React Temp	React Time	Yield (%)	Mp °C Appearance (Color, crystal form)	Formula	Found (Calcd) % C	H	N	S
14a	OCH_3 (Picrate)	$CH_3ONa/MeOH$	boiling	0.5 h	(97)	190—191 yellow micro needles[a]	$C_{22}H_{16}O_8N_4$	56.59 (56.90	3.43 3.47	12.16 12.07)	
14b	OCH_2CH_3 (Picrate)	C_2H_5ONa/C_2H_5OH	boiling	0.5 h	(98)	177—178 yellow micro needles[a]	$C_{23}H_{18}O_8N_4$	57.56 (57.74	3.48 3.70	11.44 11.71)	
14c	NH_2	$NH_3/MeOH$	room temp	3 days	65	200—201 yellow micro needles[b]	$C_{15}H_{12}N_2$	81.65 (81.79	5.24 5.49	12.63 12.72)	
14d	$NHCOCH_3$	$(CH_3CO)_2O$/—	100 °C	5 min	71	160—161 red needles[c]	$C_{17}H_{14}ON_2$	77.74 (77.84	5.69 5.38	11.10 10.68)	
14e	SH	a : $NaSH/C_2H_5OH$ b : NaSH/DMSO	boiling room temp	0.5 h 15 min	a : 17 b : 70	161—162 orange yellow prisms[c]	$C_{15}H_{11}NS$	76.04 (75.93	4.75 4.67	5.68 5.90)	
14f	$SC_6H_4CH_3$-*p*	*p*-$CH_3C_6H_4SH$/DMSO	room temp	10 min	70	177 (decomp) red plates[c]	$C_{22}H_{17}NS$	81.28 (80.71	5.20 5.24	4.25 4.28	10.17 9.78)
14g	NHC_6H_5	$C_6H_5NH_2/C_2H_5OH$	boiling	5 min	76	153—154 orange yellow prisms[c]	$C_{21}H_{16}N_2$	85.15 (85.11	5.32 5.44	9.33 9.45)	
14h	$NHCH(CH_3)_2$ (Picrate)	$(CH_3)_2CHNH_2/C_2H_5OH$	boiling	30 min	(93)	237—239 yellow needles[a]	$C_{24}H_{21}O_7N_5$	58.73 (58.65	4.32 4.31	14.32 14.25)	
14i	$NHC_6H_4CH_3$-*p*	*p*-$CH_3C_6H_4NH_2$/DMSO	room temp	10 min	93	145—146 yellow needles[d]	$C_{22}H_{18}N_2$	85.05 (85.13	5.83 5.85	8.94 9.03)	
14j	$NHC_6H_4N(CH_3)_2$	$(CH_3)_2C_6H_4NH_2$/DMSO	room temp	15 min	64	165—167 orange prisms[c]	$C_{23}H_{21}N_3$	81.11 (81.38	6.22 6.24	12.46 12.38)	
14k	$N(CH_3)_2$	a : $(CH_3)_2NH/C_2H_5OH$ b : $(CH_3)_2NH$/DMSO	boiling room temp	15 min 15 min	a : 42 b : 81	125—127 orang yellow prisms[c]	$C_{17}H_{16}N_2$	82.29 (82.22	6.49 6.50	11.29 11.28)	
14l	 (Picrate)	 /DMSO	room temp	15 min	(88)	200—202 yellow micro needles[a]	$C_{25}H_{21}O_8N_5$	57.92 (57.80	4.18 4.08	13.24 13.48)	
14m	$NHNH_2$	$NH_2NH_2 \cdot H_2O$/MeOH	room temp	2 h	40	139—140 orange needles[c]	$C_{15}H_{13}N_3$	76.67 (76.57	5.00 5.57	17.86 17.86)	
2	H (Picrate)	$CuSO_4/AcOH$-H_2O	100 °C	5 min	(60)	236 (decomp) orange needles[a]	$C_{21}H_{14}O_7N_4$	57.92 (58.07	3.44 3.25	12.52 12.90)	
	(Styphnate)					230 (decomp) red needles[a]	$C_{21}H_{14}O_8N_4$	56.48 (56.00	3.04 3.13	12.44 12.44)	

These solvents were used for the recrystallization: a) ethanol, b) benzene, c) cyclohexane, d) hexane. Compound **14d** was obtained by the acetylation of **14c**. Compound **2** was obtained from **14m**.

TABLE 2. NUCLEOPHILIC SUBSTITUTION REACTION PRODUCTS (15) FROM 2,8-DICHLORO-3-PHENYL-1-AZAAZULENE (6)

Compound	X	Reagent/Solvent	React Temp	React Time	Yield (%)	Mp °C Appearance (Color, crystal form)	Formula	Found (Calcd) % C	H	N	S
15a	OCH_3	$CH_3ONa/MeOH$	boiling	0.5 h	92	150—151 orange micro needles[e]	$C_{16}H_{12}ONCl$	71.64 (71.24	4.52 4.49	5.32 5.19)	
15b	OC_2H_5	C_2H_5ONa/C_2H_5OH	boiling	0.5 h	26	99—100 orange plates[f]	$C_{17}H_{14}ONCl$	72.07 (71.95	5.01 4.97	4.91 4.94)	
15c	NH_2	$NH_3/MeOH$	room temp	a week	67	185—186 yellow micro needles[b]	$C_{15}H_{11}N_2Cl$	70.81 (70.72	4.68 4.32	11.25 11.00)	
15d	$NHCOCH_3$	$(CH_3CO)_2O$/—	100 °C	5 min	77	171—172 orange needles[c]	$C_{17}H_{13}N_2OCl$	68.56 (68.80	4.59 4.41	9.52 9.44)	
15e	SH	a : $NaSH/C_2H_5OH$ b : NaSH/DMSO	boiling room temp	10 min 15 min	a : 53 b : 71	118 (decomp) reddish brown needles[c]	$C_{15}H_{10}NSCl$	66.46 (66.29	3.71 3.71	5.39 5.16)	
15f	$SC_6H_4CH_3$-*p*	*p*-$CH_3C_6H_4SH$/DMSO	room temp	15 min	69	216—217 orange plates[c]	$C_{22}H_{16}NSCl$	73.00 (73.01	4.50 4.46	3.90 3.87	8.90 8.86)
15g	NHC_6H_5	$C_6H_5NH_2/C_2H_5OH$	boiling	10 min	75	148—150 orange needles[g]	$C_{21}H_{15}N_2Cl$	76.11 (76.24	4.55 4.57	8.57 8.47)	
15h	$NHCH(CH_3)_2$	$(CH_3)_2CHNH_2/C_2H_5OH$	boiling	10 min	73	149—150 orange yellow needles[d]	$C_{18}H_{17}N_2Cl$	72.84 (72.76	5.77 5.77	9.44 9.52)	
15i	$NHC_6H_4CH_3$-*p*	*p*-$CH_3C_6H_4NH_2/C_2H_5OH$	boiling	10 min	85	143—144 orange prisms[d]	$C_{22}H_{17}N_2Cl$	77.13 (76.62	4.98 4.97	8.23 8.13)	
15j	$NHC_6H_4N(CH_3)_2$	$(CH_3)_2NC_6H_4NH_2/C_2H_5OH$	boiling	10 min	81	182—184 orange micro needles[c]	$C_{23}H_{20}N_3Cl$	74.09 (73.88	5.41 5.39	11.13 11.24)	
15k	$NH(CH_2)_3CH_3$ (Picrate)	$CH_3(CH_2)_3NH_2/C_2H_5OH$	boiling	3 h	(20)	169—170 yellow needles[a]	$C_{25}H_{22}N_5O_4Cl$	55.73 (55.61	4.11 4.11	12.55 12.97)	
15l	$N(CH_3)_2$	$(CH_3)_2NH_2/C_2H_5OH$	boiling	15 min	93	149—150 yellow plates[a]	$C_{17}H_{15}N_2Cl$	72.19 (72.20	5.28 5.35	9.89 9.91)	
15m		 NH/DMSO	room temp	15 min	68	131—132 orange prisms[d]	$C_{19}H_{17}ONCl$	69.69 (70.25	5.29 5.28	8.59 8.63)	
10	$NHNH_2$	$NH_2NH_2 \cdot H_2O$/MeOH	room temp	3 h	82	175—176 orange needles[b]	$C_{15}H_{12}N_3Cl$	66.72 (66.79	4.20 4.45	15.49 15.58)	
15n	Br	$CuSO_4$-HBr	100 °C	5 min	25	154—155 red plates[e]	$C_{15}H_9NClBr$	56.42 (56.54	2.85 2.85	4.40 4.40)	
11	H	$CuSO_4/AcOH$-H_2O	100 °C	15 min	61	100 °C/1 Torr (Bp) red oil	$C_{15}H_{10}NCl$	74.84 (75.16	4.33 4.21	5.79 5.84)	
	(Picrate)					199 (decomp) orange needles[a]	$C_{21}H_{13}O_7N_4Cl$	54.06 (53.79	2.54 2.77	11.89 11.95)	

These solvents were used for the recrystallization: a) ethanol, b) benzene, c) cyclohexane, d) hexane, e) benzene-cyclohexane, f) petroleum ether, g) hexane-cyclohexane. Compound **15d** was obtained by the acetylation of **15c**. Compounds **15n** and **11** were both obtained from **10**.

TABLE 3. UV, IR, AND NMR SPECTRA OF SUBSTITUTION REACTION PRODUCTS

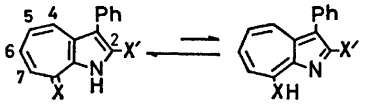

Compound	X	X′	UV λ_{max}, nm (log ε)	IR (KBr) cm^{-1}	NMR ppm in $CDCl_3$ (100 MHz)
7	O	H	228(4.51), 290(4.49) 345(3.68), 360(3.77) 380(3.78) (MeOH)	3183, 1619 1552, 1520	6.88(1H, ddd, J=10.5, 7.3, 2.0 Hz, H-5) 7.28—7.54(7H, m, H-6, 7 and phenyl) 7.59(1H, s, H-2) 7.86(1H, dm, J=10.5 Hz, H-4)
8	O	Cl	230(4.42), 287(4.38) 362(3.76), 373(3.65) (MeOH)	3080, 1621 1548, 1513	6.85(1H, ddd, J=10.5, 6.8, 2.8 Hz, H-5) 7.28—7.48(7H, m, H-6, 7 and phenyl) 7.58(1H, dm, J=10.5 Hz, H-4)
14c	NH	H	243(4.51), 316(4.52) 445(3.03) (MeOH)	3460, 3300 1610, 1595 1548	6.39(bs, NH) 6.88—7.61(8H, m, H-5, 6, 7 and phenyl) 8.19(1H, s, H-2) 8.28(1H, dm, J=10.5 Hz, H-4)
15c	NH	Cl	249(4.48), 312(4.62) 412(3.46) (MeOH)	3471, 3316 1614, 1601 1554	6.36(b, NH) 6.91—7.56(8H, m, H-5, 6, 7 and phenyl) 8.04(1H, dm, J=9.8 Hz, H-4)
14e	S	H	257(4.36), 308(4.00) 407(4.13) (cyclohexane)	3280, 1601 1496	7.06—7.52(7H, m, H-5, 6 and phenyl) 7.67(1H, d, J=2.7 Hz, H-2) 7.89(1H, dd, J=8.0, 2.4 Hz, H-7) 8.25(1H, dd, J=9.2, 2.4 Hz, H-4)
15e	S	Cl	256(4.34), 309(3.94) 413(4.13) (cyclohexane)	3248, 1602 1494	7.03—7.72(8H, m, H-5, 6, 7 and phenyl) 8.21(1H, dd, J=9.3, 2.0 Hz, H-4)
14k	$N(CH_3)_2$	H	252(4.41), 264(4.38) 329(4.56), 408(3.32) (cyclohexane)	1612, 1513	3.63(6H, s, $N(CH_3)_2$) 6.81(1H, ddd, J=10.0, 8.6, 1.0 Hz, H-5) 7.12(1H, dm, J=12.0 Hz, H-7) 7.30—7.62(7H, m, H-6 and phenyl) 8.28(1H, dm, J=10.0 Hz, H-4)
15l	$N(CH_3)_2$	Cl	253(4.38), 265(4.40) 331(4.54), 390(3.72) 412(3.70) (sh), 447 (3.52) (sh) (cyclohexane)	1613, 1518	3.60(6H, s, $N(CH_3)_2$) 6.83(1H, ddd, J=10.0, 8.4, 1.0 Hz, H-5) 7.09(1H, dm, J=11.6 Hz, H-7) 7.25—7.53 (7H, m, H-6 and phenyl) 7.94(1H, dm, J=10.0 Hz, H-4)

ketonic form (B) rather than in the enolic form (A), as in the case of 2-hydroxy derivatives of 1-azaazulene (**13**)[6] or its 3-substituted products (**12** or other compounds),[5] as is shown by their spectroscopic data, presented in Table 3.

(A) (B)

As for the 8-dimethylamino derivatives (**14k** and **15l**), the visible and PMR spectra indicate that there is a contribution of the zwitterion structure (D),[5] as will be described below. In the absorption spectra of **14k** and **15l**, the absorption maxima in the visible region were shifted to shorter wavelengths than those of **5** and **6** (Tables 3 and 4). The PMR spectra of **14k** and **15l** exhibited the signals for H-5 at *ca.* 6.8 PMR, and they were observed upfield from those of **5** and **6**, as in the case of the 8-hydroxy derivatives of 1-azaazulene (**7** and **8**) (Tables 3 and 5).

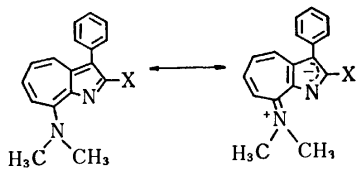

(C) (D)

The C_8-positions of Compounds **5** and **6** are easily replaced by the treatment of various nucleophilic reagents; the results are summarized in Tables 1 and 2. Only the chlorine atom at C_8 in the dichloro compound (**6**) is displaced by the nucleophilic reagent. However, a strong nucleophile such as *p*-thiocresol afforded a disubstituted product (**16**). This is quite understandable in view of Fig. 1 and the electron-releasing effect

TABLE 4. ULTRAVIOLET AND VISIBLE ABSORPTION MAXIMA OF SUBSTITUTED 1-AZAAZULENES

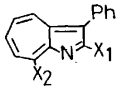

Compound	X_1	X_2	λ_{max}, nm (log ε)
2	H	H	227(4.81), 285(4.95), 358(4.14), 512(3.30) (MeOH)
5	H	Cl	237(4.59), 296(4.61), 528(2.82) (cyclohexane)
6	Cl	Cl	242(4.58), 298(4.65), 379(3.31), 500(2.89) (cyclohexane)
11	Cl	H	232(4.39), 288(4.53), 370(3.40), 500(2.87) (cyclohexane)

TABLE 5. NMR SPECTRA OF **5** AND **6**

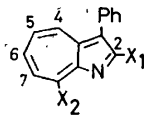

Compound	X_1	X_2	ppm in $CDCl_3$ (100 MHz)
5	H	Cl	7.37—7.65(6H, m, H-5 and phenyl) 7.77(1H, ddd, J=10.3, 9.0, 1.0 Hz, H-6) 8.01(1H, dd, J=10.3, 2.0 Hz, H-7) 8.68(1H, dd, J=9.0, 1.5 Hz, H-4) 8.89(1H, s, H-2)
6	Cl	Cl	7.42—7.86(7H, m, H-5, 6 and phenyl) 8.02(1H, dd, J=9.9, 2.0 Hz, H-7) 8.39(1H, dd, J=9.0, 2.4 Hz, H-4)

of the reaction products (**15**).

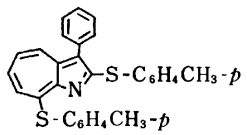

(**16**)

The reaction of **5** with hydrazine hydrate in methanol gave **9** besides **14m**.[3]

Experimental†

All the melting points are uncorrected.

Phenylacetaldehyde Troponylhydrazone. To a solution of 2-hydrazinotropone (16.7 g) in ethanol (200 ml), phenylacetaldehyde (16.1 g) was added, and the mixture was refluxed for 30 min. After cooling, the separated precipitates were collected and recrystallized from ethanol to give yellow needles (27.5 g, 94%); mp 127—128 °C. UV: λ_{max}^{MeOH} 252 (log ε=4.32), 350 (4.24), and 410 (4.29) nm. Found: C, 75.33; H, 6.20; N, 11.70%. Calcd for $C_{15}H_{14}ON_2$: C, 75.60; H, 5.92; N, 11.76%.

3-Phenylpyrrolo[2,3-b]tropone (7). A mixture of phenylacetaldehyde troponylhydrazone (23.5 g), water (650 ml), and concd sulfuric acid (32 ml) was refluxed at 110—120 °C for 3 h. After cooling, the reaction mixture was made slightly acid with 2 M sodium hydroxide and, then extracted with chloroform. The extract was dried over anhydrous sodium sulfate, and the solvent was removed. The residue was recrystallized from benzene to give pale yellow needles (15.2 g, 70%); mp 188—189 °C. Found: C, 81.21; H, 5.09; N, 6.24%. Calcd for $C_{15}H_{11}ON$: C, 81.43; H, 5.01; N, 6.33%.

8-Chloro-3-phenyl-1-azaazulene (5). A mixture of **7** (7.0 g) and phosphoryl chloride (28.0 g) was heated at 105 °C for 1 h. After cooling, the reaction mixture was poured onto ice water and the solution was made alkaline with a sodium hydrogencarbonate solution, followed by extraction with benzene. The extract was dried, the solvent was removed, and the residue was recrystallized from cyclohexane to give reddish purple needles (6.5 g, 85%); mp 106—107 °C. Found: C, 75.57; H, 4.29; N, 6.01%. Calcd for $C_{15}H_{10}NCl$: C, 75.17; H, 4.18; N, 5.84%.

Picrate: Orange micro needles (from ethanol); mp 189 °C (decomp). Found: C, 53.75; H, 2.84; N, 11.34%. Calcd for $C_{21}H_{13}O_7N_4Cl$: C, 53.79; H, 2.78; N, 11.95%.

Hydrolysis of 5. A solution of **5** (0.3 g) in ethanol (8 ml) containing 2 M sodium hydroxide (4 ml) was refluxed for 30 min. The solvent was then removed, the residue was made acid with dil hydrochloric acid, and the solution was extracted with chloroform. The dried extract was concentrated, and the residue was recrystallized from ethanol to give colorless needles (0.11 g, 60%); mp 187—188 °C. The IR spectrum was identical with that of **7**, and the mixed melting point with the sample was not depressed.

2,8-Dichloro-3-phenyl-1-azaazulene (6). *(a)* A mixture of **5** (0.3 g) in carbon tetrachloride (210 ml), *N*-chlorosuccinimide (2.6 g), and benzoyl peroxide (0.06 g) was refluxed for 3 h. The solvent was then removed, and the residue was washed with hot water several times and extracted with benzene. The dried extract was concentrated to about 30 ml and chromatographed on silica gel. From the bright red effluent, **6** was obtained as bright red plates (2.5 g, 73%); mp 160—161 °C. Found: C, 65.76; H, 3.48; N, 5.58%.

† The authors are grateful to the Sankyo Co., Ltd., for the elemental analyses.

Calcd for $C_{15}H_9NCl_2$: C, 65.69; H, 3.28; N, 5.11%.

(b) A mixture of **7** (6.0 g) in dry benzene (300 ml) and thionyl chloride (20.0 g) was refluxed for 15 h with stirring at 80—90 °C. The solvent was then removed, and the residue was treated with a saturated solution of sodium hydrogencarbonate and extracted with benzene. The extract was dried, concentrated, and chromatographed on alumina. The red effluent gave bright red needles (1.5 g, 20%), which were subsequently recrystallized from cyclohexane. The mixed melting point with the sample obtained by Method (a) was not depressed.

(c) A mixture of **5** (6.0 g) in carbon tetrachloride (150 ml) and sulfuryl chloride (3.4 g) was refluxed for 1 h. The solvent was then removed, and the residue was treated with a saturated of sodium hydrogencarbonate and extracted with benzene. The extract was concentrated and chromatographed on alumina. From the red effluent, **6** was obtained as bright red plates (1.2 g, 35%).

From the purple effluent, a purple powder was obtained; its structure can not be clarified yet. Mp 193—195 °C. UV: $\lambda_{max}^{CHCl_3}$ 256, 302, and 514 nm. Found: C, 58.50; H, 2.64; N, 4.73; Cl, 34.39%. Calcd for $C_{15}H_8NCl_3$: C, 58.38; H, 2.61; N, 4.54; Cl, 34.37%.

(d) A mixture of **8** (0.5 g) and phosphoryl chloride (2.6 g) was heated at 105 °C for 1 h. After cooling, the reaction mixture was poured into ice water, and the solution was treated with a saturated solution of sodium carbonate and extracted with benzene. The dried extract was concentrated, and the residue was recrystallized from cyclohexane to give red plates (0.37 g, 63%). The mixed melting point with the sample obtained by Method (a) was not depressed.

(e) A mixture of **7** (0.6 g) in dry benzene (30 ml) and thionyl chloride (3.0 g) was heated under reflux for 16 h at 90—100 °C. The reaction mixture was then worked up as above (Method b). A small amount of **6** was obtained, and most of the starting material (**7**) was recovered.

(f) A mixture of **10** (0.1 g), concd hydrochloric acid (2.5 ml), and 1 M copper(II) sulfate (3 ml) was heated for a few min on a water hath. After cooling, the reaction mixture was neutralized with a 5% sodium hydrogencarbonate solution and extracted with benzene. The dried extract was concentrated and passed through a silica gel column. From the red effluent, **6** was obtained as red plates (0.06 g, 54%); mp 160—161 °C.

2-Chloro-3-phenylcyclohept[2,3-b]pyrrol-8(1H)-one (8). A mixture of **7** (1.0 g) in carbon tetrachloride (60 ml), *N*-chlorosuccinimide (0.97 g), and benzoyl peroxide (0.06 g) was refluxed for 3 h. The solvent was then removed, and the residue was treated with hot water and extracted with chloroform. The extract was washed with water, dried, and concentrated, and the residue was recrystallized from benzene to give pale yellow needles (0.52 g, 47%); mp 223—224 °C. Found: C, 70.44; H, 4.11; N, 5.58%. Calcd for $C_{15}H_{10}ONCl$: C, 70.45; H, 3.91; N, 5.48%. The spectral data are shown in Table 3.

Hydrolysis of 6. A solution of **6** (0.2 g) in ethanol (8 ml) containing 2 M sodium hydroxide (5 ml) was refluxed for 1 h on a water bath. The solvent was then removed, and the residue was made acid with dil sulfuric acid and extracted with chloroform. The dried extract was evaporated, and the residue was recrystallized from benzene to give pale yellow needles (0.18 g, 94%); mp 224—225 °C. The IR spectrum was identical with that of **8**, and the mixed melting point was not depressed.

The Reaction of 8-Chloro- and 2,8-Dichloro-3-phenyl-1-azaazulenes (5 and 6) with Nucleophilic Reagents. The mixtures obtained by the reaction of chloroazaazulenes (**5** and **6**) with nucleophilic reagents were worked up in the usual manner, and the products were purified by chromatography and recrystallization. The conditions and results are given in Tables 1 and 2.

The Reaction of 8-Chloro-3-phenyl-1-azaazulene (5) with Hydrazine Hydrate.[3] A solution of 80% hydrazine hydrate (4.0 g) in methanol (100 ml) was added, drop by drop, to a solution of **5** (1.0 g) in methanol (100 ml), after which the solution was stirred at room temperature for 2 h. The reddish purple crystals which precipitated out were collected and recrystallized from cyclohexane–benzene to give *N,N'*-bis(3-phenyl-1-azaazulen-8-yl)hydrazine as reddish purple micro prisms (0.55 g); mp 277—278 °C.

On the other hand, the solvent was removed from the filtrate of the reaction mixture, water was added, and the solution was extracted with benzene. The extract was dried, the solvent was removed, and the residue was recrystallized from cyclohexane to afford 8-hydrazino-3-phenyl-1-azaazulene (**11**) (0.40 g).

3-Phenyl-1-azaazulene (2). A mixture of 8-hydrazino-3-phenyl-1-azaazulene (0.2 g), acetic acid (5 ml), water (5 ml), and a 10% copper(II) sulfate solution was heated for a few min on a water bath. After cooling, the reaction mixture was made slightly alkaline with 2 M sodium hydroxide and the solution was extracted with ether. The dried extract was concentrated to leave a reddish purple oil. The residual oil was purified by distillation under reduced pressure (bp 90 °C/0.01 Torr). *Picrate*: Orange needles, mp 236 °C (decomp.). The results are given in Table 1.

2-Chloro-3-phenyl-1-azaazulene (11). A mixture of **10** (0.7 g), acetic acid (28 ml), 1 M copper(II) sulfate (56 ml), and water (28 ml) was heated for 15 min on a water bath. After cooling, the reaction mixture was made slightly alkaline with 2 M sodium hydroxide and extracted with chloroform. The dried extract was concentrated and chromatographed on silica gel. From the red effluent, a red oil was obtained and subsequently distilled under reduced pressure (bp 100 °C/1 Torr) (0.37 g). The results are given in Table 2.

2-Chloro-8-bromo-3-phenyl-1-azaazulene (15n). A mixture of **10** (0.12 g), 48% hydrobromic acid (8 ml), and 1 M copper(II) sulfate (9.6 ml) was heated for a few min on a water bath. After cooling, the reaction mixture was treated with a 5% sodium hydrogencarbonate solution and extracted with chloroform. The dried extract was concentrated and chromatographed on silica gel. The product obtained from the red effluent was recrystallized from cyclohexane to give red plates (0.04 g). The results are given in Table 2.

1,2-Dihydro-3-phenyl-1-azaazulen-2-one (12). *(a)* A mixture of **11** (0.37 g) in ethanol (15 ml) and 2 M sodium hydroxide (30 ml) was refluxed for 5 h on a water bath. After cooling, the reaction mixture was made slightly acid with a dil sulfuric acid solution and extracted with benzene. The dried extract was then concentrated, and the residue was recrystallized from benzene to give micro prisms (0.04 g, 12%); mp 264—265 °C. IR(KBr): 1638 cm^{-1} (C=O). UV λ_{max}^{MeOH} 235(log ε=4.34), 283(4.41), 420(4.00)nm. Found: C, 81.33; H, 5.00; N, 6.13%. Calcd for $C_{15}H_{11}ON$: C, 81.43; H, 5.01; N, 6.33%.

(b) To a sodium ethoxide solution prepared from sodium metal (1.25 g) and absolute ethanol (30 ml), aminotropone (3.0 g) and methyl phenylacetate (7.4 g) were added, after which the mixture was heated in a sealed tube at 130 °C for 5 h. The reaction mixture was concentrated, made acid with 2 M hydrochloric acid, and then extracted with benzene. The benzene layer was dried over anhydrous sodium sulfate and the benzene was removed. From the residual oily product, a small amount of **12** (0.14 g, 3%) was obtained,

with the recovery of the starting material. The mixed melting point with the sample obtained by Method (a) was not depressed.

*2,8-Di(p-tolylthio)-3-phenyl-1-azaazulene (**16**).* *(a)* To a sodium methoxide solution prepared from sodium metal (0.37 g) and absolute methanol (7 ml), *p*-thiocresol (0.2 g) and **6** (0.2 g) were added, and then the mixture was heated under reflux for 15 min. The reaction mixture was concentrated under reduced pressure and extracted with benzene, and the benzene extracts were washed with water, dried over anhydrous sodium sulfate, and chromatographed on alumina. The product obtained from the benzene effluent was recrystallized from cyclohexane to give red prisms (0.12 g, 39%); mp 209—210 °C. Found: C, 77.46; H, 5.16; N, 3.12; S, 14.26%. Calcd for $C_{29}H_{23}NS_2$: C, 77.10; H, 5.19; N, 3.04; S, 13.97%.

(b) A mixture of **6** (0.2 g) and *p*-thiocresol (0.18 g) in dimethyl sulfoxide (10 ml) was stirred for 15 h at room temperature. The reaction mixture was diluted with water, made alkaline with aqueous sodium carbonate, and extracted with benzene. The benzene extracts were dried over anhydrous sodium sulfate and chromatographed on alumina. The product obtained from the benzene effluent was recrystallized from cyclohexane to give red prisms (0.13 g, 42%); mp 209—210 °C. The IR spectrum was identical with that of the sample obtained by Method (a), and the mixed melting point was not depressed.

This work was financially supported by grants from the Ministry of Education of Japan, to which the authors' thanks are due. One of the authors (Je-Kyun Sin) especially wishes to acknowledge the kind guidance of the late Professor Yoshio Kitahara of Tohoku University. We also wish to thank Dr. Masafumi Yasunami of Tohoku University for his helpful suggestions regarding the NMR spectra.

References

1) a) Presented at the 10th Annual Meeting of the Chemical Society of Japan, Tokyo, April, 1957; (b) J.-K. Sin, Doctoral Thesis, Tohoku University, Sendai, March, 1958; (c) Some of this work was reported in the following reviews: T. Nozoe, *Croat. Chim. Acta*, **29**, 207 (1957); T. Nozoe in "Non-benzenoid Aromatic Compounds," ed by D. Ginsburg, Interscience, New York, N. Y. (1959), p. 442.

2) T. Nozoe, S. Seto, S. Matsumura, and T. Terasawa, *Chem. Ind. (London)*, **1954**, 1357.

3) T. Nozoe, Y. Kitahara, and T. Arai, *Proc. Jpn. Acad.*, **30**, 478 (1954).

4) H. Kon, *Sci. Repts. Tohoku Univ., First Ser.* **38**, 67 (1954).

5) T. Toda, S. Seto, and T. Nozoe, *Bull. Chem. Soc. Jpn.*, **41**, 2102 (1968).

6) T. Nozoe, S. Seto, S. Matsumura, and T. Terasawa, *Chem. Ind. (London)*, **1954**, 1356.

Branched-chain Sugars. IX. Reaction of 3,6-Anhydro-1,2-*O*-isopropylidene-α-D-*ribo*-hexofuranos-3-ulose with Nitromethane or Hydrogen Cyanide[1]

Ken-ichi SATO, Juji YOSHIMURA, and Chung-gi SHIN*

Laboratory of Chemistry for Natural Products, Faculty of Science, Tokyo Institute of Technology, Meguro-ku, Tokyo 152

**Laboratory of Organic Chemistry, Faculty of Technology, Kanagawa University, Rokkakubashi, Kanagawa-ku, Yokohama 221*

(Received December 1, 1976)

3,6-Anhydro-1,2-*O*-isopropylidene-α-D-*ribo*-hexofuranos-3-ulose (**2**) was converted into 5,6-di-*O*-acetyl-1,2-*O*-isopropylidene-α-D-*ribo*-hexofuranos-3-ulose (**5**) by the protection of the carbonyl function with hydroxylamine, followed by acetylation and removal of the protecting group with chromium(II) acetate. Nitromethane condensation of **2** and **5** at room temperature gave the corresponding 3-nitromethyl derivatives having D-gluco- and D-*allo*-configuration, respectively. The difference in the stereoselectivity was explained by the easiness of isomerization of the initial product to thermodynamically stable epimer, because the reaction temperature was essential to control the selectivity in the same reaction of 1,2 : 5,6-di-*O*-isopropylidene-α-D-*ribo*-hexofuranos-3-ulose. Reaction of **2** with hydrogen cyanide in dry pyridine followed by acetylation gave the corresponding 3,5,6-tri-*O*-acetyl-3-cyano derivative of D-*allo*-type, whereas, the reaction in water gave instantly 3-(hydroxycarbonimidoyl)-1,2-*O*-isopropylidene-α-D-allofuranose 3',5-lactone, by the participation of the C_5-hydroxyl group.

Up to date, many works have been reported on the nucleophilic reaction of easily available 1,2 : 5,6-di-*O*-isopropylidene-α-D-*ribo*-hexofuranos-3-ulose (**1**),[2-4] and we also reported on the stereoselectivities of some reactions.[5] This compound decomposes often to 3,6-anhydro-1,2-*O*-isopropylidene-α-D-*ribo*-hexofuranos-3-ulose (**2**)[6] during the storage, unless kept at lower temperature in pure state. Although **2** is easily obtained by the partial hydrolysis of **1**,[7] it is unfavorably formed during the preparation of **1** by the dimethyl sulfoxide oxidation of 1,2 : 5,6-di-*O*-isopropylidene-α-D-glucofuranose, and easily separated from the chloroform solution of the products by extraction with water, sometimes in *ca.* 30% yield. Intramolecular hemiacetal structure of **2**[8] indicates a diminished reactivity of the carbonyl function, but the hydrogenation[6] and *p*-nitrophenylhydrazone formation[7] of **2** were described in literatures.

In order to find useful utilizations of **2** as a starting material for the branched-chain sugar synthesis, **2** was converted into 5,6-di-*O*-acetyl-1,2-*O*-isopropylidene-α-D-*ribo*-hexofuranos-3-ulose, and the addition of nitromethane and hydrogen cyanide to both compounds were carried out in this paper. A new evidence on the stereoselectivity of the former reaction and a participation of a neighboring hydroxyl group in the latter reaction are described.

Results and Discussion

Attempted acetonation of **2** into **1** and the Grignard reaction of **2** gave unsuccessful results, indicating that the intramolecular hemiacetal ring of **2** is fairly stable like that of 2-ketoses. Although much stronger nucleophiles such as nitromethanide anion and cyanide ion are deduced to be reactable with **2**, conversion of **2** into a more reactive 3-ulose derivative having the naked carbonyl group was tried at first. Condensation of **2** with hydroxylamine in aqueous ethanol gave the cor-

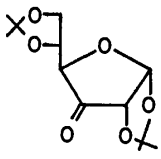

(**1**)

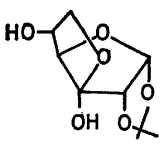

(**2**)

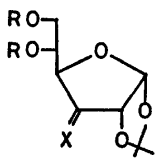

(**3**) R=H, X=NOH
(**4**) R=Ac, X=NOAc
(**5**) R=Ac, X=O

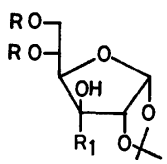

(**6**) R=H, R_1=CH_2NO_2
(**7**) R=Ac, R_1=CH_2NO_2
(**8**) R=H, R_1=CH_2NH_2
(**9**) R=Ac, R_1=CH_2NHAc

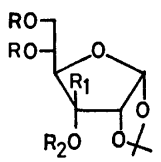

(**10**) R=Ac, R_2=H, R_1=CH_2NO_2
(**11**) R=R_2=H, R_1=CH_2NO_2
(**12**) R=R_2=Ac, R_1=CN
(**16**) R=R_2=H, R_1=COONa

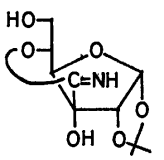

(**13**)

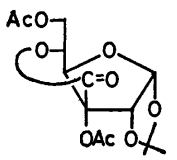

(**14**)

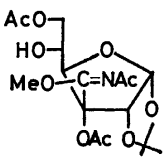

(**15**)

responding oxime derivative (**3**) in 74% yield, and then base-catalyzed acetylation of **3** gave the tri-*O*-acetate (**4**) quantitatively. The NMR spectrum of **4** indicated the presence of both *syn*- and *anti*-forms, but they were not assigned. Treatment of **4** with excess chromium-(II) acetate[9] in tetrahydrofuran–water (9 : 1) at room temperature for 12 h gave successfully the corresponding 3-ulose (**5**) in 85% yield. Tronchet *et al.* synthesized **5** from 3-*O*-benzyl-1,2;5,6-di-*O*-isopropylidene-α-D-glucose *via* four step conversions, and reported that **5** is unstable on TLC.[7]

Reaction of **2** with *aci*-nitro salt of nitromethane in ethanol does not proceeded at −70 °C; however, at room temperature for 30 min a condensation product (**6**) was obtained in 83% yield. The configuration of **6** was determined to be D-*gluco*-type by acetonation of **6** into well known 1,2 : 5,6-di-*O*-isopropylidene-3-(nitromethyl)-α-D-glucofuranose.[10] Base-catalyzed acetylation of **6** gave the corresponding 5,6-di-*O*-acetate (**7**) quantitatively. Hydrogenation of **6** in the presence of palladium–charcoal afforded the 3-*C*-aminomethyl derivative (**8**), which was then converted into the corresponding *N*,*O*-triacetate (**9**) in a good yield. Besides, the nitromethane condensation of **5** under the same conditions as used for **2** gave unexpectedly a different 3-*C*-nitromethyl derivative (**10**) from **7** in 71% yield. These compounds are considered to be 3-epimer to each other, however, there is also the possibility of the inversion at C-4 position[11] under the reaction conditions. Consequently, 1,2 : 5,6-di-*O*-isopropylidene-3-(nitromethyl)-α-D-allofuranose[5,10] was partially hydrolyzed to the corresponding 1,2-*O*-isopropylidene derivative (**11**) quantitatively, and then acetylated. The identity of the di-*O*-acetate obtained and **10** clearly established the 3-epimeric interrelation between **10** and **7**.

Table 1. The predominant epimer produced in the nitromethane condensation of **1** under various conditions[a]

Reaction conditions				Epimer ratio	
Temp (°C)	Time (min)	Solvent[b]	Base[c]	*gluco*	*allo*
−78	30	EtOH	NaOEt	0	1
−78	30	EtOH	Et_3N	0	1
−78	30	THF	Et_3N	0	1
−78	30	Dioxane	Et_3N	0	1
25	3	EtOH	NaOEt	0	1
25	30	EtOH	NaOEt	1	0
25	30	EtOH	Et_3N	1	0
25	30	THF	NaOFt	1	0
25	30	Dioxane	NaOEt	1	0
25	30	THF	Et_3N	1	0
25	30	CH_3NO_2	NaH	1	0
25	[24 h]	Glyme	NaH	0.8	0.2[d]
25	30	DMF	Et_3N	0.8	0.2
25	30	HMPA	HMPA	0	1
25	30	DMSO	Et_3N	0	1

a) The reaction mixture was extracted with chloroform, after neutralization with 60% acetic acid. The configuration and ratio of epimers were estimated from the intensity of H_1-proton signals in the NMR spectrum. b) THF=tetrahydrofuran, DMF=*N*,*N*-dimethylformamide, HMPA=hexamethylphosphoramide, DMSO =dimethyl sulfoxide, Glyme=1,2-dimethoxyethane. c) The amount of bases used are a slightly excess than the equivalent. d) Cited from the literature, A. Rosenthal, K.-S. Ong, and D. Baker, *Carbohyd. Res.*, **13**, 113 (1970).

In general, the nitromethane condensation of uloses give one epimer or mixture of epimers depending on the reaction conditions.[12] As is seen in Table 1, the reaction temperature is the most essential to control the stereoselectivity of the nitromethane condensation of **1**. This fact implies that the composition of the product is determined by the rate of isomerization of the initial product: kinetically controlled product, to the thermodynamically stable isomer. Thus, the difference of the configuration of the products in the reaction of **2** and **5** should be explained from the free energy difference between the epimers in each case. The kinetic studies will be reported elsewhere.

On the other hand, reaction of **2** with hydrogen cyanide in pyridine at 0 °C for 6 h and successive acetylation of the reaction mixture with acetic anhydride gave the corresponding 3-cyano-tri-*O*-acetate (**12**) in 54% yield. The configuration of **12** was confirmed to be D-*allo*-type by comparison of the NMR spectrum with that of the authentic sample, prepared from the corresponding 5,6-*O*-isopropylidene derivative.[13] Besides, the reaction of **2** with potassium cyanide in water in the presence of sodium hydrogencarbonate at 0 °C gave instantly a crystalline product (**13**) in 66% yield, which shows charateristic IR absorptions at 3300 (C=NH) and 1705 (–O–C=NH) cm^{-1}. From the elemental analysis and the following reactivities, **13** was deduced to be 3-(hydroxycarbonimidoyl)-1,2-*O*-isopropylidene-α-D-allofuranose 3′,5-lactone. On standing in water, **13** changed gradually into the corresponding lactone ($\nu_{C=O}$ 1785 cm^{-1}).[13] When **13** was acetylated with acetic anhydride in pyridine and then the reaction mixture poured into water, known 3,6-di-*O*-acetyl-3-carboxy-1,2-*O*-isopropylidene-α-D-allofuranose 3′,5-lactone (**14**)[13,14] was obtained in 61% yield, whereas treatment of the acetylated product with methanol gave 3,6-di-*O*-acetyl-1,2-*O*-isopropylidene-3-[(acetylimino)methoxymethyl]-α-D-allofuranose (**15**) in 65% yield. The structure of **15** was determined from the analytical values and the absence of the deshielding effect of acetyl group on H_5 proton in the NMR spectrum. Moreover, treatment of **13** with sodium hydrogencarbonate in methanol overnight at reflux temperature gave quantitatively the corresponding carboxylate (**16**) which can be converted into **14** by acetylation with acetic anhydride in a good yield.

Bourgeois reported on the isomerization of the initially formed 3-cyano-1,2 : 5,6-di-*O*-isopropylidene-α-D-allofuranose to the corresponding D-gluco-epimer in the reaction of **1** with hydrogen cyanide.[15] From the fact, it is considered that the kinetically controlled product **12** was simply formed in the same reaction of **2** in pyridine at 0 °C. However, the reaction in water gave **13**, whose formation is attributed to the further participation of a sterically favorable hydroxyl group in the same molecule. The reason for this difference is

ambiguous at present, but the similar participations are known in carbohydrate chemistry.[16,17]

Experimental

All the melting points are uncorrected. The solution were evaporated under diminished pressure at a bath temperature not exceeding 45 °C. Specific rotations were measured in a 0.5 dm tube, with a Carl Zeiss LEP-Al polarimeter. The IR spectra were recorded with a Hitachi Model EPI-G2 spectrometer. The NMR spectra were taken with a JEOL-4H-100 MHz spectrometer, using tetramethylsilane as an internal standard, in deuteriochloroform unless otherwise stated. Chemical shifts and coupling constants were recorded in δ and Hz units, and frequencies in cm^{-1}.

1,2-O-Isopropylidene-α-D-ribo-hexofuranos-3-ulose Oxime (3). To an aqueous ethanol solution (1 : 1, 100 ml) of hydroxylamine prepared from hydroxylamine hydrochloride (1.8 g, 25.9 mmol) and sodium hydroxide (1.10 g, 27.5 mmol) was added the hemiketal **2** (5 g, 22.9 mmol). After standing the reaction mixture at room temperature for 18 h, the solution was concentrated to a half volume, and then extracted with 1-butanol. Evaporation of the butanol solution gave crystals which were recrystallized from ethanol–hexane. Yield, 3.95 g (74%); mp 161—164 °C; $[\alpha]_D^{23}$ +97.2° (*c* 1.3, MeOH); IR: 3400, 3210, and 3125(OH).

Found: C, 46.30; H, 6.38; N, 5.83%. Calcd for $C_9H_{15}NO_6$: C, 46.35; H, 6.48; N, 6.01%.

3-Acetoxyimino-5,6-di-O-acetyl-1,2-O-isopropylidene-α-D-ribo-hexofuranose (4). Base-catalyzed acetylation of **3** with acetic anhydride in the usual manner gave a sirupy product quantitatively. NMR spectrum of the sirup showed the presence of two kind of isomers (*syn-* and *anti-*form) in the ratio of 1 : 1 (H_1 : 6.05 and 5.98). This sirup was used for the next conversion without further identification. IR; 1740 (OAc).

5,6-Di-O-acetyl-1,2-O-isopropylidene-α-D-ribo-hexofuranos-3-ulose (5). A suspension of the above sirup (200 mg, 0.56 mmol) and excess chromium(II) acetate (340 mg, 2 mmol) in tetrahydrofuran–water (9 : 1, 10 ml) was stirred at room temperature for 24 h until the starting material had disappeared on TLC. The reaction mixture was bubbled with air to oxidize excess chromous ion and most of tetrahydrofuran was evaporated. The remaining solution was diluted with water, and then extracted with ether. The ether extract was washed with water, and then evaporated to give a nearly pure sirupy ulose in 85% yield. The NMR spectrum was identical with that of authentic sample: 6.10 (H_1: d, $J_{1,2}$=4.4), 5.26 (H_5: m), 4.53 (H_4: dd, $J_{2,4}$= 1.2, $J_{4,5}$=3.4), 4.45—4.16 (H_2, H_6, $H_{6'}$: m), 2.08 and 2.01 (2×OAc), 1.47 and 1.42 (2×C-CH_3).

1,2-O-Isopropylidene-3-(nitromethyl)-α-D-glucofuranose (6). A solution of **2** (5.0 g, 22.9 mmol) in ethanol (15 ml) was added to a solution of nitromethane (20 ml) and sodium ethoxide (sodium 0.53 g, 23.0 mmol) in ethanol (50 ml) with stirring. The reaction mixture was kept at room temperature for 30 min, neutralized with 60% acetic acid, and then evaporated. A 1-butanol solution (100 ml) of the residue was washed with a small amount of water and then evaporated to give crystals which were recrystallized from ether. Yield, 5.2 g (81.4%), mp 104—105 °C, $[\alpha]_D^{23}$ +57.1° (*c* 0.99, MeOH). IR: 3430 and 3250 (OH), 1540 (NO_2).

Found: C, 43.11; H, 6.14; N, 4.90%. Calcd for $C_{10}H_{17}NO_8$: C, 43.01; H, 6.14; N, 5.02%.

The configuration of this compound was determined by conversion into 1,2 : 5,6-di-*O*-isopropylidene-3-(nitromethyl)-α-D-glucofuranose as follows: a suspension of **6** (1.0 g, 3.6 mmol) and anhydrous copper(II) sulfate (3.0 g) in dry acetone (50 ml) was stirred at 50 °C for 24 h, filtered through active carbon, and the filtrate was evaporated. A chloroform solution of the residue was washed with water and evaporated to give crystals which were recrystallized from ethanol. Yield, 0.82 g (71.4%), mp 139—140 °C, $[\alpha]_D^{23}$ +22.3° (*c* 1.0, $CHCl_3$) [lit,[10] mp 140—141 °C, $[\alpha]_D^{23}$ +22.8° ($CHCl_3$)]. This specimen showed no depression of mp by admixture with an authentic sample.

5,6-Di-O-acetyl-1,2-O-isopropylidene-3-(nitromethyl)-α-D-glucofuranose (7). Base-catalyzed acetylation of **6** with acetic anhydride in the usual manner gave the corresponding di-*O*-acetate quantitatively. Mp 163.5—164.5 °C, $[\alpha]_D^{23}$ +52.6° (*c* 0.5, $CHCl_3$). IR: 3430 (OH), 1745 (OAc), 1560 (NO_2); NMR: 5.97 (H_1: d, $J_{1,2}$=3.8), 5.25 (H_5; oct), 4.62 (H_2: d), 4.62 (H_6: q, $J_{5,6}$=2.5), 4.18 ($H_{6'}$: q, $J_{5,6'}$=5.3, $J_{6,6'}$=12.8), 4.87 and 4.60 (CH_2: ABq $J_{A,B}$=14.8), 4.05 (H_4: d, $J_{4,5}$=8.5), 3.76 (OH, s), 2.10 and 2.06 (2×OAc), 1.52 and 1.34 (2×C-CH_3).

Found: C, 46.28; H, 5.82; N, 3.87%. Calcd for $C_{14}H_{21}NO_{10}$: C, 46.28; H, 5.82; N, 3.86%.

3-(Aminomethyl)-1,2-O-isopropylidene-α-D-glucofuranose (8). A suspension of **6** (300 mg, 1.07 mmol) and palladium-charcoal (5%, 0.2 g) in water (20 ml) was hydrogenated under hydrogen atmosphere, filtered, and then the filtrate was evaporated. The ninhydrin-positive residue was crystallized from ethanol–ether. Yield, 168 mg (68.2%), mp 122—123 °C, $[\alpha]_D^{23}$ +41.5° (*c* 0.68, EtOH).

Found: C, 47.78; H, 7.68; N, 5.34%. Calcd for $C_{10}H_{19}NO_6$: C, 48.18; H, 7.68; N, 5.62%.

3-(Acetaminomethyl)-5,6-di-O-acetyl-1,2-O-isopropylidene-α-D-glucofuranose (9). To a solution of **8** (100 mg, 0.36 mmol) in pyridine (2 ml) was added acetic anhydride (1 ml), and the mixture was kept at room temperature for 5 h. The solution was treated in the usual procedure to give a sirup which was crystallized from ethanol. Yield, 128 mg (95%), mp 130.5–131 °C; $[\alpha]_D^{23}$ +82.9° (*c* 0.23, $CHCl_3$). IR: 3320 (OH and NH), 1740 (OAc); NMR: 6.40 (NH : t), 5.86 (H_1: d, $J_{1,2}$=3.4), 5.26 (H_5: sex), 4.59 (H_6: q, $J_{5,6}$=2.4), 4.34 (H_2: d), 4.24 ($H_{6'}$: q, $J_{5,6'}$=6.1, $J_{6,6'}$=13.0), 4.06 (H_4: d, $J_{4,5}$=6.4), 3.74 and 3.47 (CH_2: dABq, $J_{A,B}$= 13.0, $J_{NH,3'}$=6.4), 2.12, 2.08, and 2.06 (2×OAc, NAc), 1.51 and 1.32 (2×C-CH_3).

Found: C, 51.16; H, 6.72; N, 3.60%. Calcd for $C_{16}H_{25}NO_9$: C, 51.19; H, 6.71; N, 3.73%.

5,6-Di-O-acetyl-1,2-O-isopropylidene-3-(nitromethyl)-α-D-allofuranose (10). i) From **5**. A solution of **5** (200 mg, 0.6 mmol) in ethanol (5 ml) was added with stirring to a solution of nitromethane (1 ml) and sodium (100 mg, 4.3 mmol) in ethanol (5 ml) at room temperature. After standing the reaction mixture for 30 min, it was neutralized with 60% acetic acid, and then evaporated to give crystals which were recrystallized from ethanol–hexane. Yield, 154 mg (71%), mp 130—132 °C $[\alpha]_D^{23}$ +42.4° (*c* 0.9, $CHCl_3$). IR: 3420 (OH), 1740 (OAc), 1550 (NO_2); NMR: 5.79 (H_1: d, $J_{1,2}$=4.0), 5.22 (H_5: septet), 4.93 and 4.43 (CH_2: ABq, $J_{A,B}$=12.4), 4.77 (H_2: d), 4.40 (H_6: q, $J_{5,6}$=3.5), 4.17 ($H_{6'}$: q, $J_{5,6'}$=6.1, $J_{6,6'}$=12.5), 4.03 (H_4: d, $J_{4,5}$=8.2), 3.30 (OH), 2.10 and 2.06 (2×OAc), 1.58 and 1.37 (2×C-Me).

Found: C, 46.28; H, 5.85; N, 3.80%. Calcd for $C_{14}H_{21}NO_{10}$: C, 46.28; H, 5.83; N, 3.86%.

ii) From 1,2 : 5,6-di-*O*-isopropylidene-3-(nitromethyl)-α-D-allofuranose. A solution of the starting material (500 mg) in acetic acid (70%, 20 ml) was kept at room temperature for 24 h, and then evaporated to give a glassy solid [1,2-*O*-isopropylidene-3-(nitromethyl)-α-D-allofuranose (**11**)] quantitatively, which could not be crystallized. $[\alpha]_D^{23}$ +18.5° (*c*

0.7, MeOH), IR: 1560 (NO_2).

Found: C, 42.55; H, 6.12; N, 4.60%. Calcd for $C_{10}H_{17}NO_8$: C, 43.01; H, 6.14; N, 5.02%.

Acetylation of **11** (200 mg) with acetic anhydride (3 ml) in pyridine (3 ml) in the usual manner gave **10** quantitatively which was identical with the above mentioned sample.

3,5,6-Tri-O-acetyl-3-cyano-1,2-O-isopropylidene-α-D-allofuranose (12). To a solution of **2** (1 g, 4.6 mmol) and hydrogen cyanide (0.3 ml) in pyridine (10 ml) which was stirred at 0 °C for 6 h was added acetic anhydride (3 ml), the mixture was kept at room temperature for 15 h, and the excess hydrogen cyanide was evacuated under reduced pressure. The reaction mixture was poured into ice-water, and the resulting solution was extracted with methylene dichloride. The extracted solution was washed with water and evaporated to give a sirup which was crystallized and recrystallized from ethanol-hexane. Yield, 0.92 g, (54%), mp 140—142 °C, $[\alpha]_D^{23}$ +70.4° (*c* 0.47, $CHCl_3$) [lit,[13] mp 129.5—130.5 °C, $[\alpha]_D^{21}$ +72.8° (*c* 0.3, $CHCl_3$)]. IR and NMR spectra were also identical with those of theauthentic sample.

3-(Hydroxycarbonimidoyl)-1,2-O-isopropylidene-α-D-allofuranose 3',5-Lactone (13). An aqueous solution (2 ml) of potassium cyanide (325 mg, 5 mmol) was added to an aqueous solution (15 ml) of **2** (1.0 g, 4.6 mmol) and sodium hydrogencarbonate (630 mg, 5.1 mmol) with stirring at 0 °C. The crystals deposited immediately were filtered and recrystallized from methanol. Yield, 744 mg (66%), mp 166—168 °C, $[\alpha]_D^{23}$ +60.4° (*c* 0.4, H_2O). IR: 3450 (OH), 3300 (NH), 1705 (-O-C=NH).

Found: C, 48.81; H, 6.07; N, 5.23%. Calcd for $C_{10}H_{15}NO_6$: C, 48.97; H, 6.17; N, 5.71%.

3,6-Di-O-acetyl-3-carboxy-1,2-O-isopropylidene-α-D-allofuranose 3',5-Lactone (14). i) From **13**. To a suspension of **13** (245 mg, 1.0 mmol) in acetic anhydride (1.5 ml) was added pyridine (0.1 ml), and kept at room temperature for 12 h until the mixture became homogenous. The reaction mixture was poured into ice-water to give crystals which were recrystallized from ethanol-hexane. Yield, 201 mg (61%), mp 114—115 °C, $[\alpha]_D^{23}$ +5.2°, $[\alpha]_{365}^{23}$ −28.7° (*c* 0.9, $CHCl_3$), [lit,[14] mp 113—113.5 °C: $[\alpha]_D^{22}$ +6.2°, $[\alpha]_{365}^{22}$ −33.0° (*c* 1.7, $CHCl_3$)].

Found: C, 51.00; H, 5.52%. Calcd for $C_{14}H_{18}O_9$: C, 50.91; H, 5.49%.

IR and NMR spectra were also identical with those of authentic sample.[14]

ii) From **16**. Base-catalyzed acetylation of **16** with acetic anhydride in the usual manner gave **14** quantitatively.

3-[(Acetylimino)methoxymethyl]-3,6-di-O-acetyl-1,2-O-isopropylidene-α-D-allofuranose (15). To a homogeneous reaction mixture of the above experiment was added absolute methanol (4 ml) instead of pouring into ice-water, and then evaporated to give a sirup. The main component of the sirup composed of three components was isolated by TLC (benzene : methanol =8 : 1, and recrystallized form ethanol-hexane. Yield, 273 mg (65%), mp 145—147 °C, $[\alpha]_D^{23}$ +53.5° (*c* 0.6, $CHCl_3$). IR: 3450 (OH), 1765 (OAc), 1660 (C=NAc). NMR: 5.98 (OH : s), 5.85 (H_1 : d, $J_{1,2}$=3.6), 5.34 (H_2 : d), 4.73 (H_4 : d, $J_{4,5}$=1.8), 4.45—4.05 (H_5, H_6, $H_{6'}$: m), 3.30 (OMe), 2.07 and 1.98 (2×OAc, NAc), 1.49 and 1.34 (2×C-CH_3).

Found: C, 50.10; H, 6.19; N, 3.42%. Calcd for $C_{17}H_{25}NO_{10}$: C, 50.61; H, 6.25; N, 3.42%.

3-Carboxy-1,2-O-isopropylidene-α-D-allofuranose Sodium Salt (16). A solution of **13** (245 mg, 1.0 mmol) and sodium hydrogen carbonate (84 mg, 1.0 mmol) in methanol (5 ml) was refluxed for 12 h, evaporated, and the residue was crystallized from ethanol-hexane to give needles quantitatively. Mp 269—271 °C (decomp), $[\alpha]_D^{23}$ +46.6° (*c* 0.9, H_2O). IR: 3350 and 3250 (OH), 1610 (C=O).

Found: C, 41.91; H, 5.42%. Calcd for $C_{10}H_{15}O_8Na$: C, 41.96; H, 5.28%.

References

1) Part VIII: *Bull. Chem. Soc. Jpn.*, **49**, 1686 (1976).
2) J. S. Brimacombe, S. Mahmood, and J. Rollins, *Carbohyd. Res.*, **38**, C7 (1974).
3) H. Paulsen, V. Sinnwell, and P. Stadler, *Chem. Ber.*, **105**, 1978 (1972)
4) A. Rosenthal and M. Splinzl, *Can. J. Chem.*, **47**, 4478 (1969).
5) J. Yoshimura, K. Kobayashi, K. Sato, and M. Funabashi, *Bull. Chem. Soc. Jpn.*, **45**, 1806 (1972).
6) O. Theander, *Acta Chem. Scand.*, **17**, 1751 (1963).
7) J. M. J. Tronchet and J. M. Bourgeois, *Helv. Chim. Acta*, **54**, 1580 (1971).
8) O. Theander, *Acta Chem. Scand.*, **18**, 2209 (1964).
9) E. J. Corey and J. E. Richman, *J. Am. Chem. Soc.*, **92**, 5276 (1970).
10) H. P. Albrecht and J. G. Moffat, *Tetrahedron Lett.*, **1970**, 1063.
11) K. N. Slessor and A. S. Tracey, *Can. J. Chem.*, **47**, 3989 (1969).
12) S. W. Gunner, R. S. King, W. G. Overend, and N. R. Williams, *J. Chem. Soc., C*, **1970**, 1954.
13) J. M. Bourgeois, *Helv. Chim. Acta*, **58**, 368 (1975).
14) D. L. Baker, D. K. Brown, D. Horton, and R. G. Nickol, *Carbohyd. Res.*, **32**, 299 (1974).
15) J. M. Bourgeois, *Helv. Chim. Acta*, **56**, 2880 (1973).
16) R. Kuhn and W. Kirschenlohr, *Ann. Chem.*, **600**, 126 (1957); *cf.* R. Kuhn and D. Weiser, *ibid.*, **600**,144 (1957).
17) P. W. Austin, J. G. Buchanan, and E. M. Oakes, *Chem. Commun.*, **1965**, 374.

Spin Trapping of Aryl and Arylcyclohexadienyl Radicals by *N*-*t*-Butyl-α-phenylnitrone (*N*-Benzylidene-*t*-butylamine Oxide) and α,*N*-Diphenylnitrone (*N*-Benzylideneaniline Oxide)[1]

Mariko KAMIMORI, Hirochika SAKURAGI,* Tadashi SUEHIRO,**
Katsumi TOKUMARU, and Masayuki YOSHIDA*

Institute of Chemistry, The University of Tsukuba, Sakura-mura, Ibaraki 300-31
**Department of Chemistry, Faculty of Science, The University of Tokyo, Hongo, Bunkyo-ku, Tokyo 113*
***Faculty of Sciences, Gakushuin University, Mejiro, Toshima-ku, Tokyo 171*

(Received December, 22, 1976)

Monosubstituted phenyl radicals produce only aryl spin adducts in the reaction with nitrones described in the title, while polyhalo-substituted phenyl radicals add to solvent benzene, in competition with the formation of aryl spin adducts, to give arylcyclohexadienyl radicals, which in turn are trapped by the nitrones giving nitroxides incorporating the solvent benzene (Scheme 3).

The relative merits and applications of spin traps have been well discussed. Of various spin traps, comparison of the scavenging ability to some limited radicals was made.[2] For example, nitrones are shown to offer considerable advantages over nitroso compounds as a probe for alkoxyl radicals.[3] However, little is known about the relative reactivity of different radicals to a given spin trap. Previously we reported the decomposition of arylazotriphenylmethanes in benzene in the presence of nitrosodurene (2,3,5,6-tetramethylnitrosobenzene)[1] and showed that the aryl radicals carrying electron donating groups add to nitrosodurene to give arylduryl-nitroxides (*N*-aryl-2,3,5,6-tetramethylanilinyloxyls),[1] the aryl spin adducts, while those with electron withdrawing groups produce no such aryl spin adducts, but afford spin adducts incorporating the solvent benzene.[4] The relative reactivity of different aryl radicals to nitrosodurene and benzene changes according to the nature of substituents attached to the aryl radicals. We have undertaken a study on decomposition of arylazotriphenylmethanes in benzene in the presence of *N*-*t*-butyl-α-phenylnitrone (PBN) and *N*-pentadeuteriophenyl-α-phenylnitrone (DPN-d_5) in order to see whether aryl radicals behave in a similar manner to the nitrones or not, and the results are described in this paper.

Results and Discussion

Reaction of Monosubstituted Phenyl Radicals with Nitrones. The thermal decomposition of phenylazotriphenylmethane (PAT) at 80 °C in benzene or in carbon tetrachloride containing *N*-*t*-butyl-α-phenylnitrone (PBN) under an atmosphere of argon gave an ESR spectrum of a triphenylmethyl radical and a nitroxide (**1**; a_N=14.1 and $a_{\beta\text{-H}}$=2.1 G) with the same hyperfine splitting constants as obtained for the phenyl spin adduct.[5] However, the signals of the triphenylmethyl radicals disappeared on standing or on exposure to air, presumably due to the reaction with oxygen. Similarly, 2- or 4-substituted phenylazotriphenylmethanes (2- or 4-X-PAT) produced the corresponding aryl spin adducts of PBN in both benzene and carbon tetrachloride (Scheme 1). The structural assignment of the spin adducts is based on the consistency of the hfsc's within the series, which are recorded in Table 1.

When α,*N*-diphenylnitrone was used as a spin trap in the decomposition of PAT, an ESR spectrum consisting of complex sets identified as the phenyl spin adduct was observed.[6] By the use of *N*-pentadeuteriophenyl-α-phenylnitrone (DPN-d_5) as a spin trap the spectrum of the phenyl spin adduct was simplified to a signal composed of broad three doublets (**12**; a_N=10.4 and $a_{\beta\text{-H}}$=3.4 G) (Fig. 1). Similar spectra were obtained in the decomposition of 2- and 4-X-PAT's in

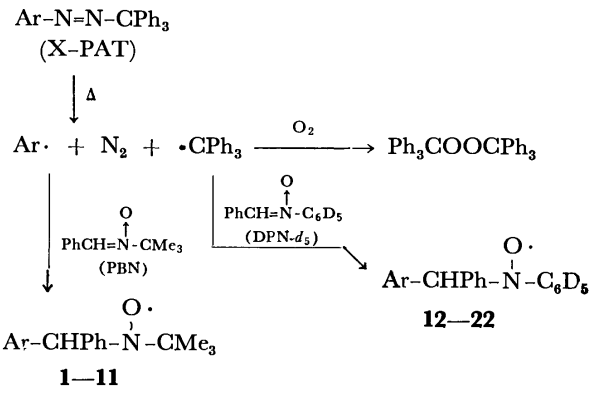

Scheme 1.

Table 1. Hyperfine splitting constants of aryl spin adducts of *N*-*t*-butyl-α-phenylnitrone[a]

Nitroxide	Ar in nitroxide	a_N	$a_{\beta\text{-H}}$
1	C_6H_5	14.1	2.1
2	4-CH_3-C_6H_4	14.0	2.2
3	4-CH_3O-C_6H_4	14.0	2.1
4	4-Cl-C_6H_4	14.0	2.1
5	4-Br-C_6H_4	14.0	2.1
6	4-NO_2-C_6H_4	13.9	2.1
7	2-CH_3-C_6H_4	14.0	3.2
8	2-CH_3O-C_6H_4	14.0	2.7
9	2-CH_3S-C_6H_4	14.0	2.8
10	2-Cl-C_6H_4	14.0	2.9
11	2-Br-C_6H_4	14.0	3.1

a) In G in benzene and carbon tetrachloride at room temperature.

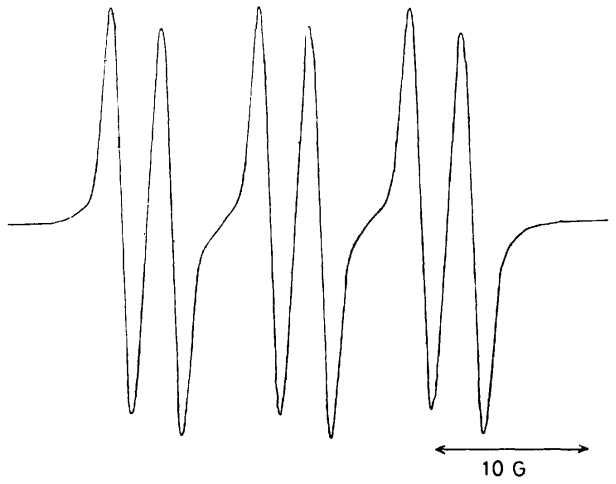

Fig. 1. The ESR spectrum of **12** obtained from the decomposition of PAT in benzene at 80 °C in the presence of DPN-d_5.

TABLE 2. HYPERFINE SPLITTING CONSTANTS OF ARYL SPIN ADDUCTS OF *N*-PENTADEUTERIOPHENYL-α-PHENYLNITRONE[a)]

Ar-CHPh-N(O·)-C_6D_5

Nitroxide	Ar in nitroxide	a_N	$a_{\beta\text{-H}}$
12	C_6H_5	10.4	3.4
13	4-CH_3-C_6H_4	10.1	3.5
14	4-CH_3O-C_6H_4	10.2	3.6
15	4-Cl-C_6H_4	10.2	3.4
16	4-Br-C_6H_4	10.2	3.4
17	4-NO_2-C_6H_4	10.2	3.4
18	2-CH_3-C_6H_4	10.1	4.5
19	2-CH_3O-C_6H_4	10.2	3.8
20	2-CH_3S-C_6H_4	10.1	4.2
21	2-Cl-C_6H_4	10.2	4.0
22	2-Br-C_6H_4	10.2	4.1

a) In G in benzene and carbon tetrachloride at room temperature.

both benzene and carbon tetrachloride and the ESR parameters are shown in Table 2.

We showed previously[4)] that the aryl radicals having an electron donating substituent, such as methyl and methoxy at the 4 position, are trapped directly by nitrosodurene (Du–NO) in benzene to produce the aryl spin adducts (**23**). On the contrary, the aryl radicals with an electron withdrawing group, like chloro, bromo, or nitro group, add exclusively to benzene to give arylcyclohexadienyl radicals (**24**), which are subsequently trapped by Du–NO to yield the nitroxides (**25** and **26**) incorporating the solvent benzene (Scheme 2). However, this is not the case for the nitrones, PBN and DPN-d_5. The aryl radicals carrying a substituent at the *ortho* or the *para* position produced only the aryl spin adducts of PBN (**1**—**11**) and DPN-d_5 (**12**—**22**).

Substituent effects on the ESR spectra of various nitroxides have been reported and the nitrogen hfsc's in nitroxides are known to be correlated with the Hammett σ constants.[7)] To illustrate this relationship further-

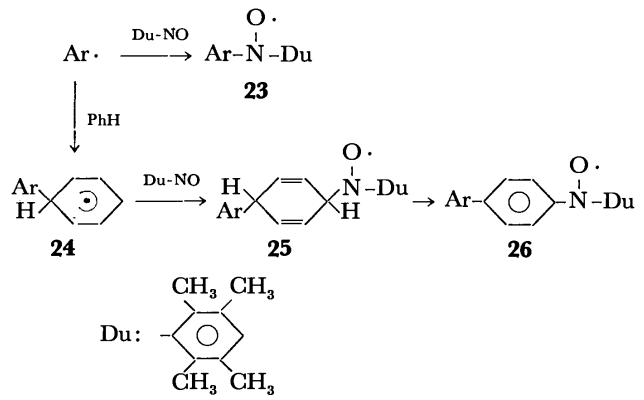

Scheme 2.

more, the N hfsc's of the 4-substituted phenyldurylnitroxides[4)] (**23**) are plotted against σ. The correlation is only approximate, but the ρ value ($\rho=-1.2$, correlation coefficient=0.93) is consistent with the value reported for 4-substituted anilinyloxyl (Ar–NHO·; $\rho=-1.2$).[8)]

In the aryl spin adducts of PBN (**1**—**11**) and DPN-d_5 (**12**—**22**), the substituents attached to the β-phenyl group might exert influence on the N hfsc's. The data listed in Tables 1 and 2, however, show that the N hfsc's are essentially the same irrespective of the substituents within each series (**1**—**11** and **12**—**22**). The β-aryl group is two bonds apart from the nitrogen atom in both species of the nitroxides (**1**—**22**) and thus, the effect of substituents does not extend as far as the nitrogen atom through the bonds.

Other features emerged from the data are that the β-H hfsc does not depend on the nature of the substituents, but on the position of the substituents in the respective nitroxides. The nitroxides having the *ortho*-substituents (**7**—**11** and **18**—**22**) and those with the *para*-ones (**2**—**6** and **13**—**17**) are distinguished definitely to different groups. Thus, operation of other factors such as steric effect is suspected and this problem will be further discussed in the latter part.

Reaction of Polysubstituted Phenyl Radicals with Nitrones. The decomposition of 2,4,6-tribromophenylazotriphenylmethane (Br_3–PAT) in carbon tetrachloride containing PBN (30 mM) at 80 °C gave a spectrum ascribable to a 2,4,6-tribromophenyl spin adduct (**28**; $a_N=14.0$ and $a_{\beta\text{-H}}=7.5$ G) (Fig. 2-A), while in benzene Br_3–PAT produced another nitroxide (**33**; $a_N=14.1$ and $a_{\beta\text{-H}}=2.1$ G) along with **28** and triphenylmethyl radicals (Fig. 2-B). Since **33** is only produced in benzene, the incorporation of the solvent benzene in **33** is inferred. The relative intensity of **28** to **33** in the ESR spectra was raised with increasing amounts of PBN (see Figs. 2-C and 2-D). These facts indicate that **28** is formed directly by the reaction of 2,4,6-tribromophenyl radicals with PBN, while **33** is not. From the analogy of the reaction of aryl radicals with Du–NO, it is suggested that 2,4,6-tribromophenyl radicals add benzene to form arylcyclohexadienyl radicals (**24**; Ar=2,4,6-$Br_3C_6H_2$) in competition to the reaction with PBN. The intermediate radicals (**24**) are further scavenged by PBN to give the spin adduct (**33**). Since triphenylmethyl radicals are observed in the spectra, the further

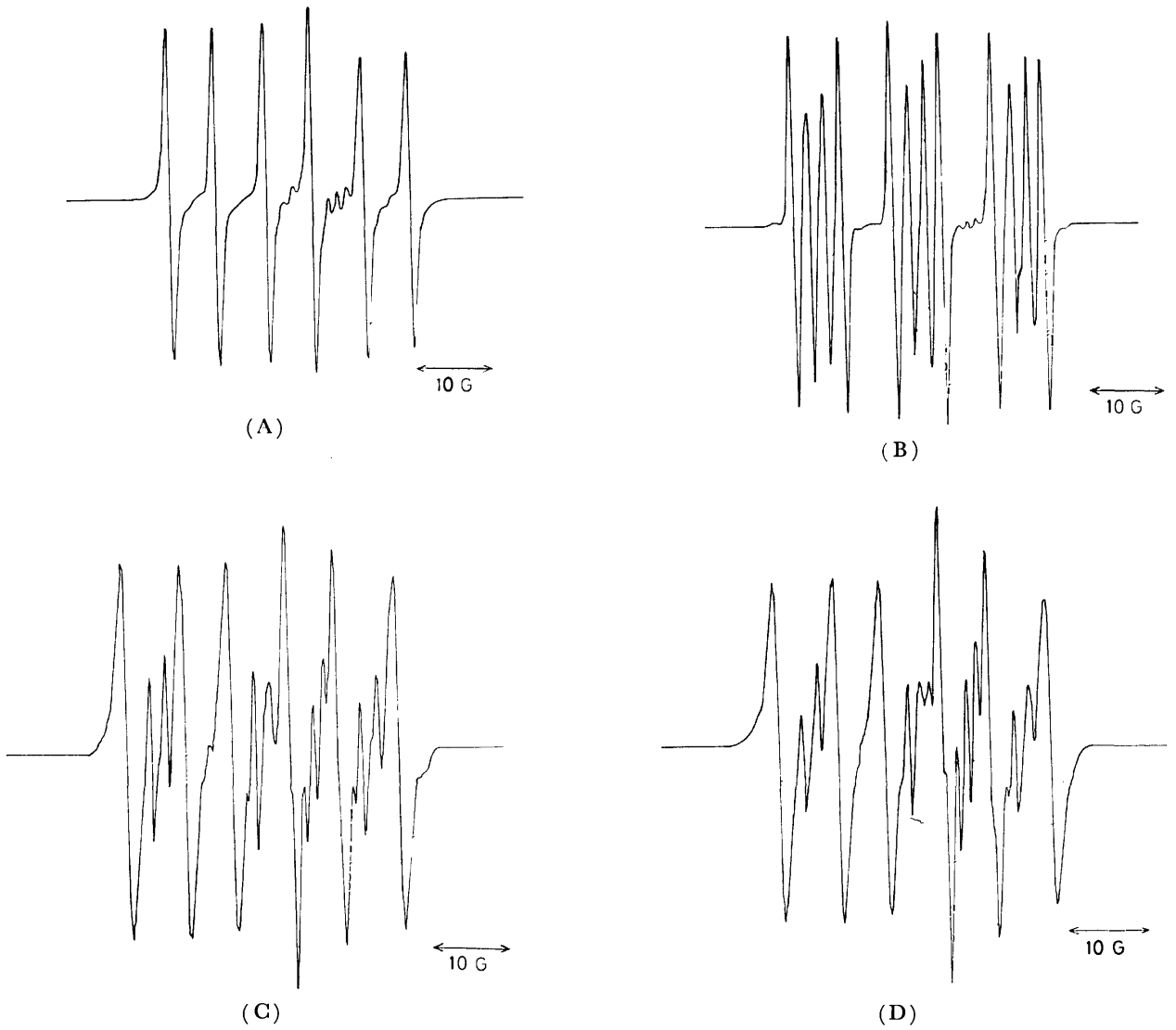

Fig. 2. (A) The ESR spectrum of **28** obtained from the decomposition of Br_3-PAT in carbon tetrachloride at 80 °C in the presence of PBN (30 mM). (B) The ESR spectrum obtained from the decomposition of Br_3-PAT in benzene at 80 °C in the presence of PBN (30 mM). The spectrum is due to both **28** and **33**. (C) The ESR spectrum of **28** and **33** obtained from the decomposition of Br_3-PAT in benzene at 80 °C in the presence of PBN (68 mM). (D) The ESR spectrum of **28** and **33** obtained from the decomposition of Br_3-PAT in benzene at 80 °C in the presence of PBN (135 mM). A small concentration of triphenylmethyl radicals is always present in all the cases.

Table 3. Hyperfine splitting constants of nitroxides obtained in the decomposition of polysubstituted phenylazotriphenylmethanes (X_n-PAT) in benzene containing PBN

X_n-PAT	Aryl radicals generated (Ar·)	Nitroxides[a]					
		Ar-CHPh-N(O·)-CMe_3[b]					
			a_N	$a_{,\text{-H}}$		a_N	$a_{\beta\text{-H}}$
Cl_3-PAT	2,4,6-$Cl_3C_6H_2$·	**27**	13.9	6.6	**32**	14.0	2.1
Br_3-PAT	2,4,6-$Br_3C_6H_2$·	**28**	14.0	7.5	**33**	14.1	2.1
F_5-PAT	C_6F_5·	**29**	14.0	4.4	**34**	13.8	2.1
Me_3-PAT	2,4,6-$Me_3C_6H_2$·	**30**[c]	14.5	8.8	**35**[d]	14.0	2.2

a) In G in benzene at room temperature. b) Unless otherwise noted, the same spectrum was obtained in CCl_4. c) A trichloromethyl spin adduct (**31**; a_N=13.6, $a_{\beta\text{-H}}$=1.6 G) was obtained concurrently in CCl_4. d) The structure was tentatively assigned to a 3,5-dimethylbenzyl spin adduct (**35a**).

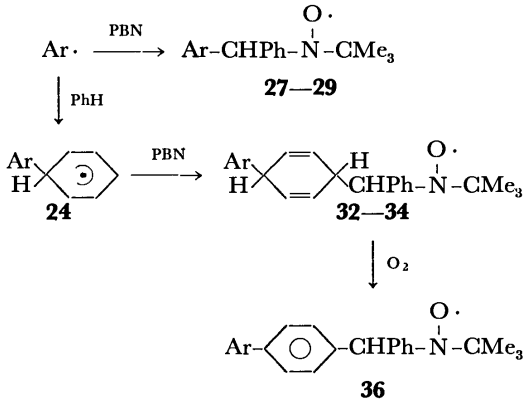

Ar: 2,4,6-$Cl_3C_6H_2$ (**27** and **32**), 2,4,6-$Br_3C_6H_2$ (**28** and **33**), and C_6F_5 (**29** and **34**).

Scheme 3.

oxidation of **33** to a nitroxide (**36**; Ar=2,4,6-$Br_3C_6H_2$) by molecular oxygen is highly improbable (Scheme 3).

Similar results were obtained with 2,4,6-trichloro- (Cl_3–PAT) and 2,3,4,5,6-pentafluoro-phenylazotriphenylmethane (F_5–PAT) in carbon tetrachloride and benzene. The hfsc's of the nitroxides obtained are recorded in Table 3.

Migita and his co-workers[9] reported recently that the relative rate of addition of 4-nitrophenyl radicals and phenyl radicals to benzene is 5.6 at 60 °C. Accordingly, electron withdrawing halogen substituents increase the rate of addition of the aryl radicals to benzene, but the effect is small. Thus, the formation of the benzene incorporated nitroxides (**32**—**34**) may be accounted for in view that the rate of addition of aryl radicals to PBN is much suppressed in the polyhalogenated phenyl radicals than in phenyl ones due to steric or electronic effects.

When 2,4,6-trimethylphenylazotriphenylmethane (Me_3–PAT) was decomposed in carbon tetrachloride in the presence of PBN, ESR spectra due to two nitroxides were observed (Fig. 3-A). One spectrum was attributed to a 2,4,6-trimethylphenyl spin adduct (**30**; a_N=14.5 and $a_{\beta\text{-H}}$=8.8 G) by analogy with the values obtained for the polyhalophenyl spin adducts (**27**—**29**). Further verification for the structural assignment of **30** was obtained in the decomposition of PAT with *N*-*t*-butyl-α-2,4,6-trimethylphenylnitrone [*N*-(2,4,6-trimethylbenzylidene)-*t*-butylamine oxide; Me_3–PBN] in benzene. The ESR spectrum obtained is completely the same as that observed above. The other spectrum was assigned as a trichloromethyl spin adduct (**31**; a_N= 13.6 and $a_{\beta\text{-H}}$=1.6 G), because the same spectrum was independently produced from the photolysis of di-*t*-butyl peroxide in chloroform in the presence of PBN (Scheme 4). Chlorine abstraction from carbon tetrachloride by 2,4,6-trimethylphenyl radicals may be facilitated by the electron donating substituents on the phenyl radicals[10] to afford trichloromethyl radicals, which were subsequently trapped by PBN.

In benzene, Me_3–PAT produced another nitroxide as well as **30** with PBN (Fig. 3-B). The newly formed nitroxide (**35**; a_N=14.0 and $a_{\beta\text{-H}}$=2.2 G) has almost the same N and β-H hfsc's as those of **33**. Thus, incorporation of the solvent benzene in the nitroxide (**35**)

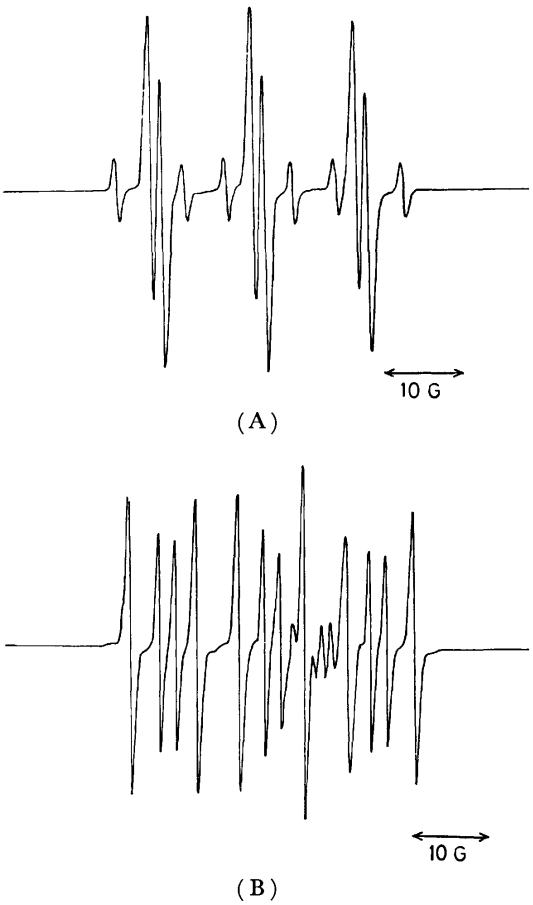

Fig. 3. (A) The ESR spectrum of **30** and **31** obtained from the decomposition of Me_3–PAT in carbon tetrachloride at 80 °C in the presence of PBN. (B) The ESR spectrum of **30** and **35a** obtained from the decomposition of Me_3–PAT in benzene at 80 °C in the presence of PBN. A small concentration of triphenylmethyl radicals is also present.

was suspected. Recently, it was found by the use of CIDNP technique that the rearrangement of 2-methylphenyl radicals to benzyl radicals occurs during the thermolysis of bis(2-methylbenzoyl) peroxide.[11] If such a rearrangement would take place for the 2,4,6-trimethylphenyl radicals, the resulting 3,5-dimethylbenzyl radicals would produce a spin adduct (**35a**) consistent with the observed spectrum. Since a benzyl spin adduct is known to have similar hfsc's (a_N=13.9 and $a_{\beta\text{-H}}$=2.4 G)[5] to those of **35**, assignment of **35a** is also consistent with the observation. Thus, the structure of the nitroxide (**35**) could be assigned as either the 3,5-dimethylbenzyl spin adduct (**35a**) or 2,4,6-trimethylphenylcyclohexadienyl spin adduct (**35b**). Judging from the known behavior of aryl radicals to benzene,[9] the reactivity of 2,4,6-trimethylphenyl radicals is supposed to be lowered, and the formation of the benzene incorporated nitroxide **35b** is implausible. Accordingly, the nitroxide is believed to be **35a** rather than **35b**.

With Me_3–PBN, Cl_3–PAT produced a trichlorophenyl spin adduct (**37**; a_N=14.1 and $a_{\beta\text{-H}}$=8.8 G) in carbon tetrachloride. The same spectrum was obtained in benzene, but none of signals due to a benzene in-

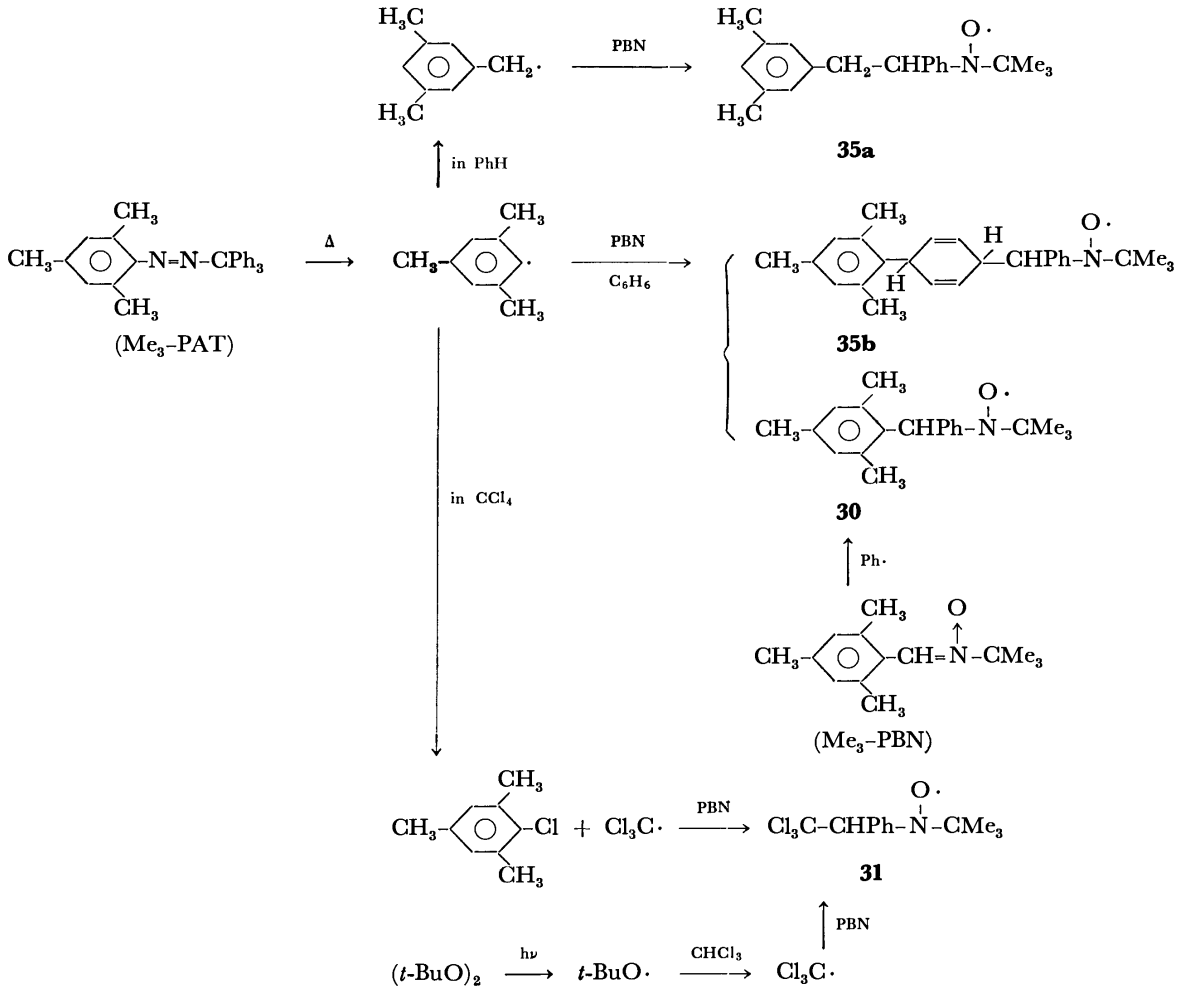

Scheme 4.

corporated nitroxide were observed. These findings show that Me_3–PBN is much more efficient than PBN in trapping of 2,4,6-trichlorophenyl radicals. In other words, the 2,4,6-trichlorophenyl radical is electrophilic and the transition state has some polar character with electron donation from Me_3–PBN. The view is borne out, because the rate of addition of the electrophilic benzoxyl radical to PBN is known to increase with electronegative substituents on PBN (Hammett ρ against $\sigma^+ = -0.47$).[12]

The decomposition of Cl_3–PAT, Br_3–PAT, and F_5–PAT in CCl_4 in the presence of DPN-d_5 gave the corresponding aryl spin adducts (**38**—**40**) (Table 4).

Table 4. Hyperfine splitting constants of aryl spin adducts of DPN-d_5[a]

Nitroxide	Ar in nitroxide	a_N	$a_{\beta\text{-H}}$
38[b]	2,4,6-$Cl_3C_6H_2$	9.8	6.5
39[b]	2,4,6-$Br_3C_6H_2$	9.8	6.5
40	C_6F_5	10.2	5.6

a) In G in carbon tetrachloride at room temperature. b) The same spectra were obtained in benzene.

In benzene containing DPN-d_5, Cl_3–PAT produced **38** and another nitroxide (**41**), but the spectra observed are not well resolved. Br_3–PAT produced definitely a similar mixture of **39** and **42**, while F_5–PAT gave only a benzene incorporated nitroxide (**43**; $a_N = 10.3$ and $a_{\beta\text{-H}} = 3.5$ G). The structure of **41** and **42** was believed to be the benzene incorporated nitroxides by the analogy with the behavior of polyhalogenated phenyl radicals to PBN.

Finally, it is of interest to discuss conformations of the nitroxides obtained. Since the $a_{\beta\text{-H}}$ value depends on the dihedral angle between the C–H bond and the p orbital on the nitrogen atom, the generally low $a_{\beta\text{-H}}$ values of the nitroxides listed in Tables 1 (**1**—**6**) and 2 (**12**—**17**) certainly indicate that the C–H bond lies close to the plane perpendicular to the p orbital on the nitrogen atom. The nitroxides should then be assigned as the *trans* conformer (**44**), in which the C–H bond is approximately *trans* with respect to the N–O bond, between two preferred conformers. The *cis* conformer should be disregarded because of large steric hindrance between the two aryl and *t*-butyl groups. Thus, we infer that, for the species with *ortho* substituents, the steric repulsion between the *ortho* group and the oxygen atom in the *trans* conformer (**44**) causes the twisting around the C–H bond, resulting in a decrease of the dihedral angle and in concomitant higher $a_{\beta\text{-H}}$ values (**45**).

TABLE 5. SUBSTITUTED PHENYLAZOTRIPHENYLMETHANES (X_n-PAT's)

Compd X_n in X_n-PAT	Mp (dec), °C	Elemental analysis, % Found C	Found H	Found N	Molecular formula	Calcd C	Calcd H	Calcd N
2,4,6-Me_3	101—102	86.29	6.71	6.89	$C_{28}H_{26}N_2$	86.29	6.71	7.17
2,4,6-Br_3	125—126	51.23	2.92	4.87	$C_{25}H_{17}N_2Br_3$	51.30	2.90	4.79
2,4,6-Cl_3	116.5—117.0	66.61	4.15	6.35	$C_{25}H_{17}N_2Cl_3$	66.44	3.76	6.20
2,3,4,5,6-F_5[a]	81.5—82.0	69.92	3.85	6.42	$C_{25}H_{15}N_2F_5$	68.49	3.42	6.39
2-SMe	127—127.5	78.99	5.72	7.17	$C_{26}H_{22}N_2S$	79.15	5.62	7.10

a) In spite of careful and repeated purification on recrystallization from benzene-ethanol, the results of C-H analysis are not satisfactory. The inconsistency with the calculated values may be ascribed to its instability.

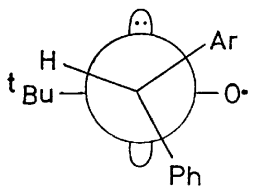

44

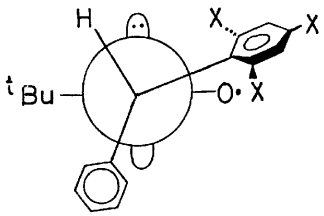

45

Experimental

Materials. *N-t*-Butyl-α-phenylnitrone[13] (PBN) and substituted phenylazotriphenylmethanes[14,15,16] (X_n-PAT's) were prepared according to published procedures. Newly prepared X_n-PAT's were listed in Table 5.

N-Pentadeuteriophenyl-α-phenylnitrone (DPN-d_5). DPN-d_5 was obtained in a method similar to the preparation of α,*N*-diphenylnitrone:[17] mp 106—107 °C (from ethanol); NMR ($CDCl_3$) δ 2.0(s, 1H, vinyl proton) and 7.5—8.5(m, 5H, phenyl protons). Found: C, 77.07; H, 8.80; N, 6.92%. Calcd for $C_{13}H_6D_5NO$: C, 77.19; H, 7.97; N, 6.92%.

N-t-Butyl-α-2,4,6-trimethylphenylnitrone (Me_3-PBN). To a mixture of 2,4,6-trimethylbenzaldehyde (3.5 g) and *t*-butylamine (8.0 g) in 10 ml of benzene was added dropwise a solution of $TiCl_4$ (2.3 g) in 20 ml of benzene at 0 °C with stirring. After the addition was completed, the mixture was allowed to warm at room temperature and left for 3 days. The precipitate was filtered off and the filtrate was concentrated on evaporation of the solvent under reduced pressure. Residual oil (1.9 g) was oxidized and isomerized in similar ways described in the literature:[13] mp 112—114 °C (from hexane); NMR($CDCl_3$) δ 2.2(s, 1H, vinyl proton), 1.6(s, 9H, *t*-butyl protons), 2.2(s, 9H, methyl protons), and 6.9—7.7(m, 2H, aromatic protons). Found: C, 76.67; H, 9.81; N, 6.22%. Calcd for $C_{14}H_{21}NO$: C, 76.66; H, 9.65; N, 6.39%.

Thermal Decomposition of Arylazotriphenylmethanes. A solution of arylazotriphenylmethanes (10 mM) in benzene or carbon tetrachloride containing *N-t*-butyl-α-phenylnitrone or *N*-pentadeutetriophenyl-α-phenylnitrone (30 mM) was purged with argon for 2 min in an ESR tube in order to remove dissolved oxygen, and was heated at 80 °C for 3 min. ESR signals were observed by use of a JEOL JES-ME-1X spectrometer.

References

1) In the present paper trivial names such as nitrones and nitroxides are used instead of systematic names, because these terms have found wide use in literatures. The systematic names are shown in parentheses.
2) E. G. Janzen, *Acc. Chem. Res.*, **4**, 31 (1971).
3) M. J. Perkins and B. P. Roberts, *J. Chem. Soc., Perkin Trans. 2*, **1974**, 297.
4) T. Suehiro, M. Kamimori, K. Tokumaru, and M. Yoshida, *Chem. Lett.*, **1976**, 531.
5) E. G. Janzen and B. J. Blackburn, *J. Am. Chem. Soc.*, **91**, 4481 (1969).
6) A. L. Bluhm and J. Weinstein, *J. Org. Chem.*, **37**, 1748 (1972).
7) E. G. Janzen, *Acc. Chem. Res.*, **2**, 279 (1969).
8) Th. A. J. W. Wajer, A. Mackor, and Th. J. de Boer, *Tetrahedron Lett.*, 1941 (1967).
9) T. Migita, M. Kosugi, K. Takayama, Y. Abe, and le Tho Vong, "The 21st Symposium on Organic Free Radicals," Tokyo, 1974, Abstracts, p 63.
10) K. Takayama, M. Kosugi, and T. Migita, *Chem. Lett.*, **1973**, 215.
11) B. C. Childress, A. C. Rice, and P. B. Shevlin, *J. Org. Chem.*, **39**, 3056 (1974).
12) E. G. Janzen, C. A. Evans, and Y. Nishi, *J. Am. Chem. Soc.*, **94**, 8236 (1972).
13) W. D. Emmons, *J. Am. Chem. Soc.*, **79**, 5739 (1957).
14) H. Wieland, E. Popper, and H. Seefried, *Ber.*, **55**, 1816 (1922).
15) S. G. Cohen and Chi Hua Wang, *J. Am. Chem. Soc.*, **75**, 5504 (1953).
16) T. Yamamoto, *Nippon Kagaku Zasshi*, **85**, 691 (1964).
17) O. H. Wheeler and P. H. Gore, *J. Am. Chem. Soc.*, **78**, 3363 (1956).

Rishitin I. The Isolation and Structure Elucidation[1)]

Tadashi MASAMUNE, Akio MURAI, Mitsuo TAKASUGI, Akira MATSUNAGA, Nobukatsu KATSUI, Norio SATO*, and Kohei TOMIYAMA*

Department of Chemistry, Faculty of Science, Hokkaido University, Sapporo 060

**Hokkaido National Agricultural Experiment Station, Sapporo 060-01*

(Received November 1, 1976)

A modification of the isolation procedure and the details of the structure elucidation of rishitin (**1**) are described.

One decade ago we reported in preliminary communications[2)] on the isolation and structure of rishitin, an antifungal norsesquiterpene qualified as "phytoalexin",[3)] from tuber tissues of white potatoes (*Solanum tuberlosum*×*S. demissum*) infected by an incompatible race of *Phytophthora infestans*. Since the isolation of rishitin, a number of sesquiterpenes have been isolated and characterized as antifungal stress metabolites from various plants of the Solanaceae in our and other laboratories.[4)] In this paper we describe our recently modified isolation procedure of rishitin from diseased potatoes, leading to separation of thermally unstable compounds, and the details of its structure determination.

Tuber slices of R_1 cultivar "Rishiri" (338 kg) were inoculated with a zoospore suspension of an incompatible race of *Phytophthora infestans* (Mont.) de Bary, race 0, and incubated at 18—20 °C for 2 days. The inoculated slices were stored in an ice-box (−30 °C) for a week, and then immersed in methanol at room temperature for a week. The methanol extracts were concentrated below 30 °C and extracted with chloroform. The chloroform extracts were treated with acetone and then with hexane to remove the respective solvent-insoluble meterials, and the resulting hexane-soluble fraction was evaporated to leave an oily residue (160 g), which was dissolved in ether. The ether solution, after removal of acidic and basic components, gave a neutral syrup (107 g), which contained many compounds as shown in Fig. 1. The neutral syrup was separated over silicic acid and celite, hexane, benzene, ether, acetone, and methanol being used successively as eluents. Fractions eluted with a 1 : 1 mixture of benzene and ether gave crude rishitin (**1**, *ca.* 8.0 g), which was further purified by rechromatography over silica gel to yield rishitin (**1**, 3.9 g), mp 65—67 °C and $[\alpha]_D$ −35.1°,[5)] in pure state.

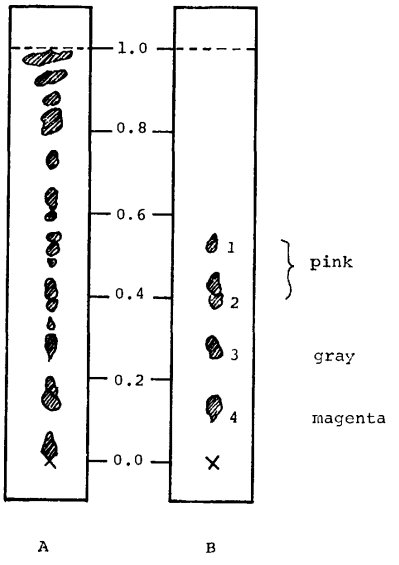

Fig. 1. TLC of the neutral syrup (silica gel, ether).
A, ceric sulfate and B, Ehrlich reagent.
1: Rishitinol, 2: lubimin, 3: rishitin, 4: oxylubimin.

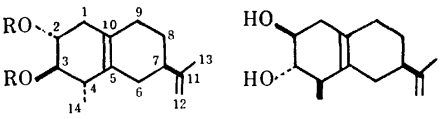

1 R=H **1'**
1a R=Ac
1b R=$COC_6H_3(NO_2)_2$

Rishitin (**1**) was analyzed for $C_{14}H_{22}O_2$ [*m/e* 222 (M^+)] and gave the diacetate (**1a**), mp 70—71 °C and $[\alpha]_D$ −14.1°,[5)] and also the bis(3,5-dinitrobenzoate) (**1b**), mp 172—173 °C and $[\alpha]_D$ −45°, which were reconverted into the starting alcohol (**1**) by saponification. When hydrogenated over platinum in ethyl acetate, compound **1** formed the dihydro derivative (**2**), $C_{14}H_{24}O_2$ [*m/e* 224 (M^+)], mp 64—66 °C and $[\alpha]_D$ −8.7°, which consumed *ca.* 1.2 mol of peroxybenzoic acid and showed an intense yellow color with tetranitromethane, and also gave the diacetate (**2a**), mp 79—81 °C and $[\alpha]_D$ +4.3°. Further hydrogenation of **2** over rhodium-platinum[6)] in ethanol produced tetrahydrorishitin (**3**), $C_{14}H_{26}O_2$ [*m/e* 226 (M^+)], mp 112—114 °C, which was negative to the tetranitromethane test. On the other hand, rishitin consumed 0.96 mol of periodic acid at room temperature for 20 h, and also was converted readily into the acetonide (**4**), mp 32—35 °C, when treated with acetone over silica gel (Wakogel Q-23). These chemical reactions and the UV, IR, and NMR spectral data of each compound indicated that rishitin contains the following structural units: a secondary methyl group [**1**, δ 1.12 (3H, d, J=6 Hz); **1a**, δ 1.06 (3H, d, J=6.5 Hz)]: an isopropenyl group [**1**, ν_{max} 3060, 1640 and 890 cm^{-1}, δ 1.70 (3H, s) and 4.64 (2H, br); **2**, ν_{max} 1386 and 1370 cm^{-1}, and no absorption near 1640 and 890 cm^{-1}; **2a**, δ 0.91 (6H, d, J= 6 Hz)]: a tetrasubstituted double bond [**1**, **2**, and **3**, only end absorptions (log ε 3.89, 3.74, and less than 2.8 at 205 nm, respectively, *cf.*, cholesterol and 5α-cholestanol, log ε 3.58 and 2.82 at 205 nm); **2**, no absorption below δ 5.0]: two vicinal secondary hydroxyl groups [**1**, ν_{max} 3320 cm^{-1}, δ 3.12 (1H, t, J=9 Hz), 3.55 (1H, br do d, J=9 and 7 Hz), and 4.18 (2H, br s, 2OH); **1a**, ν_{max} 1745 and 1250 cm,$^{-1}$

δ 2.00 and 2.04 (each 3H, s), 4.80 (2H, br), and no absorption near δ 3.5; **4**, ν_{max} 1378 and 1370 cm^{-1}; δ 3.18 (1H, t, J=9 Hz) and 3.59 (1H, do t, J=9, 9, and 7 Hz)].

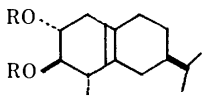

2 R=H
2a R=Ac

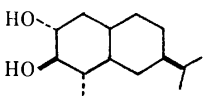

3

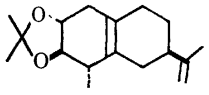

4

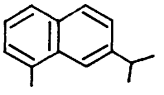

5

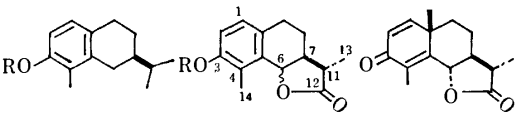

6 R=H
6a R=$COC_6H_3(NO_2)_2$

7 6βH, R=H
7b 6αH, R=Ac

8

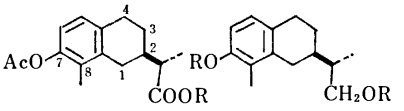

9 R=H
9a R=CH_3

10 R=H
10a R=Ts

Dehydrogenation of dihydrorishitin (**2**) with selenium proceeded smoothly to give eudalene (**5**) in a high (60%) yield, which formed the picrate, mp 92—93 °C, and the trinitrobenzene adduct, mp 113—114 °C.[7] This result, combined with the presence of the functional groups described above, led to proposal of the (planar) formula (**1**) for rishitin. The structure was supported by the ^{13}C NMR spectra of **1**, obtained with proton noise decoupling and also under off-resonance decoupled conditions; manely, the spectra indicated, together with chemical shift considerations,[8] that the skeleton of rishitin consisted of the following carbon units; three C(C=C)–C (δ 148.9, 129.0, and 124.9 for C_{11}, C_5, and C_{10}), one CH_2(=C)–C (109.0 for C_{12}), two C–CH(OH)–C (79.2 and 71.5 for C_3 and C_2), two C–CH(C)–C (41.6 and 40.4 for C_7 and C_4), four C–CH_2–C (38.3, 31.1, 29.7, and 26.5 for C_8, C_6, C_9, and C_1), and two CH_3–C (21.0 and 16.4 for C_{13} and C_{14}).[9]

Oxidation of dihydrorishitin (**2**) with the Jones reagent in a heterogeneous mixture of ether and water[10] followed by acid treatment produced a mixture of phenols, from which a 3,5-dinitrobenzoate (**6a**), $C_{21}H_{22}O_6N_2$ [*m/e* 398 (M^+)], mp 159—160 °C and $[\alpha]_D$ +56°, was isolated in a low (3%) yield after treatment with 3,5-dinitrobenzoyl chloride and subsequent purification by preparative TLC. On the other hand, "6-epi-1-desmethyldesmotroposantonin 3-acetate" (**7b**), prepared from (−)-α-santonin (**8**) *via* a known two-step process,[11] was submitted to hydrogenolysis over palladium–charcoal in acetic acid to yield a phenol acetate acid (**9**), oil, which was converted with diazomethane into the methyl ester (**9a**), oil, and then reduced with lithium aluminium hydride to give a phenol alcohol (**10**), mp 126—127 °C and $[\alpha]_D$ +76.7 °C, in an 86% yield from **7b**. The bis(*p*-toluenesulfonate) (**10a**), oil, obtained from **10**, gave on the hydride reduction a phenol (**6**), oil and $[\alpha]_D$ +85.7°, in a 65% yield from **10**. This phenol (**6**) was converted into its 3,5-dinitrobenzoate, mp 159.5—160 °C and $[\alpha]_D$ +60.1°, which was identical with the dinitrobenzoate (**6a**), derived from **2**, in all respects. This correlation confirms the structure **1** for rishitin and also elucidates the absolute configuration at C_7.

The configurations of a methyl at C_4 and two hydroxyl groups at C_2 and C_3 in rishitin (**1**) were deduced from the spectra of **1** and its dihydro-dibromo derivative (**11**), mp 129—130 °C, prepared in good yields by treatment of dihydrorishitin (**2**) with bromine or pyridinium bromide perbromide[12] in chloroform; δ 3.78 (1H, t, J=9 Hz, H at C_3) and 4.32 (1H, do t, J=9, 9, and 7 Hz, H at C_2) for **11**. Both the compounds (**1** and **11**) exhibited almost the same absorption patterns due to the protons at C_3 and C_2, indicating that the ring of **1** in question adopts a half-chair conformation and the three substituents are oriented equatorial, equatorial, and quasi-equatorial at C_2, C_3, and C_4, respectively. Rishitin is, therefore, represented either by the formula **1** or **1'**. Of these formulas, the former structure (**1**) seems to be more favorable on the basis of the following considerations. If rishitin is formulated as structure **1'** the bromination would possibly result in formation of two dibromides (**11'** and **11"**) with comparable instability due to severe 1,3-diaxial interaction(s), assuming the reaction in question proceeded in a kinetically controlled and *trans*-addition manner as observed usually. The situation becomes completely different with formula **1**, and the bromination is expected to produce only one dibromo compound (**11**) of two possible dibromides derivable from **2**. The observed fact that the relevant dibromodihydrorishitin was obtained stereoselectively in a high yield and was recovered unchanged on standing in a refrigerator for 6 months or after repeated recrystallizations, is in line with this expectation. Confirmatory evidence for structure **1** was later presented independently on the basis of the CD spectrum of a chelate complex of rishitin in a cuprammonium solution by Bukhari and Guthrie[13] as well as the CD spectrum of rishitin dibenzoate (the dibenzoate chirality rule) by Harada and Nakanishi.[14] Hence, rishitin is represented correctly by the formula **1**, which has completely been demonstrated by the synthesis (the succeeding paper).[15]

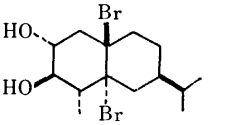

11

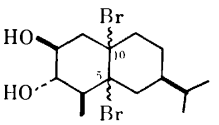

11' 5β-Br, 10α-Br
11" 5α-Br, 10β-Br

Experimental

All the melting points were uncorrected. The homogenity of each compound was always checked by TLC on silica gel (Wakogel B-5) with various solvent systems, and the spots were developed with ceric sulfate in dil sulfuric acid and/or iodine. The optical rotations, UV and IR spectra were measured in ethanol, ethanol and Nujol, respectively, unless otherwise stated. The NMR and ^{13}C NMR spectra were obtained in chloroform-*d* at 60 and/or 100 MHz, and the chemical shifts were given in δ-values, TMS being used as an internal reference. The abbreviations "s, d, t, m, br, and do" in the NMR spectra denote "singlet, doublet, triplet, multiplet, broad, and double", respectively.

*Isolation of Rishitin (**1**).* *(i) Materials.* Tubers of potato variety, Rishiri *(Solanum tuberosum×S. demissum)*, having the R_1 gene, were used for the experiments. Zoosporangia of an incompatible race of *Phytophthora infestans* (Mont.) de Bary, race 0, were obtained from mycerial mats growing on the cut surfaces of fresh potato tuber slices, Irish Cobbler, having no resistance gene. Zoospores were liberated by holding the sporangial suspensions at 11—12 °C for 2—3 h. Both sides of the tuber slices (338 kg) of 1.5—2.0 mm thickness were inoculated with the zoospore suspension (250000—500000 zoospores/ml), and the inoculated slices were incubated at 18—20 °C for 2 d. Tubers showing abundant brown spots were then stored at −30 °C for a week.

(ii) Extraction and Isolation. The frozen tuber slices were immersed in methanol (250 l) for a week, and the supernatant was separated by decantation. The tubers were re-extracted twice with methanol (2×150 l), and the methanol extracts were combined and concentrated to *ca.* 200 l by a film evaporator under reduced pressure (30—60 Torr) below 30 °C. The concentrate was extracted with an equal volume of chloroform under shaking, and the emulsion forming unavoidably was centrifuged to be separated into chloform and aqueous layers. The chloroform layer was evaporated to leave an oily residue. When the residue was treated with acetone (1.2 l), precipitates separated out and were removed by filtration. The filtrate was concentrated again to give an oily residue, which was treated with hexane (1.2 l). After removal of hexane-insoluble materials by decantation and filtration, the hexane solution was evaporated to give oily substances, which were dissolved in ether (5 l) and washed with 10% aq sodium carbonate and then with 0.1 M hydrochloric acid to remove acidic and basic components. The ether solution was washed with water, dried and evaporated to yield a neutral syrup (107 g), which was subjected to chromatographic purification over silicic acid (Mallinckrodt AR-100, 900 g) and celite (300 g), hexane, benzene, ether, acetone and methanol being used as eluents. Eluates with hexane, hexane–benzene (1 : 1) and benzene, on evaporation of the solvents, left oily (Fraction A, 2.1 g), semi-solid (B, 6.2 g), and solid residues(C, 42 g), respectively, the last fraction consisting mainly of higher fatty acids. Fractions D and E (2.5 g and 4.8 g) eluted with benzene–ether (3 : 1) and benzene–ether (3 : 2) contained rishitinol[16] and lubimin,[17] respectively. The following fraction (F), eluted with benzene–ether (1 : 1 and 1 : 2), afforded crude rishitin (8.0 g). Further eluates with benzene–ether (3 : 7) and ether gave an oil (G, 1.7 g) and those with ether–acetone (9 : 1) an oil (H, 2.4 g), the latter containing oxylubimin[17] and lubiminol.[17b] Subsequent fractions eluted with ether–acetone (1 : 1), acetone, acetone–methanol (1 : 1), and methanol were combined to give a resinous oil (I, 3.9 g). The crude rishitin, showing an almost single spot on TLC, was again purified by chromatography over silica gel (Merck 400 g) with ether, each fraction (60 ml) being checked by the NMR spectrum. Fractions (No. 11—40) were combined, crystallized on standing and amounted to 3.9 g.

*Rishitin (**1**), and Its Diacetate, Bis(3,5-dinitrobenzoate), and Acetonide (**1a**, **1b**, and **4**).* *(i)* Rishitin (**1**) had mp 65—67 °C and $[\alpha]_D$ −34.1°,[5] and showed the Mass, UV, IR, NMR, (CCl_4), and ^{13}C NMR spectra, in the text. Found: C, 75.58; H, 9.75%. Calcd for $C_{14}H_{22}O_2$: C, 75.63; H, 9.97%.

A soln of **1** (100 mg) was treated with acetic anhydride (Ac_2O, 0.5 ml) and pyridine (Py, 1 ml) at room temp for 19 h. The reaction mixture was poured into ice-water and extracted with ether. The ether soln was washed with 2 M hydrochloric acid, 5% aq sodium carbonate and water, dried, and evaporated to give **1a** (115 mg), mp 68—70 °C. This was recrystallized from hexane to yield an analytical sample (70 mg), mp 70—71 °C and $[\alpha]_D$ −14.1°;[5] MS, in the text; IR, ν_{max} 1745, 1250, 1645, and 885 cm^{-1}; NMR (CCl_4), δ 1.06 (3H, d, J=6.5 Hz, 14-C$\underline{H}_3$), 1.75, 2.00, and 2.04 (each s, 3H, 13-C$\underline{H}_3$ and 2OCOC$\underline{H}_3$), 4.70 (2H, br s, 12-C$\underline{H}_2$), and 4.80 (2H, br m, 2$\underline{H}$ at C_2 and C_3). Found: C, 70.74; H, 8.51%. Calcd for $C_{18}H_{26}O_4$: C, 70.56; H, 8.55%.

A soln of crude rishitin (*cf.*, the isolation of rishitin) (279 mg) in benzene (10 ml) and Py (3 ml) was stirred with 3,5-dinitrobenzoyl chloride (760 mg) in benzene (10 ml) at room temp for 15 h, and diluted with ether (30 ml). The soln was washed with 0.5 M hydrochloric acid, water, 1 M aq sodium hydroxide (30 ml) and water, dried and evaporated to leave a crystalline residue (580 mg), which on recrystallization from ethyl acetate gave **1b** (230 mg), mp 172—173 °C and $[\alpha]_D$ −45° ($CHCl_3$). Found: C, 55.14; H, 4.42; N, 9.40%. Calcd for $C_{28}H_{26}O_{12}N_4$: C, 55.08; H, 4.29; N, 9.18%.

(ii) A suspended mixture of **1b** (240 mg) in methanol (20 ml) containing potassium hydroxide (1 M) was refluxed for 1 h under nitrogen. After being cooled, the mixture was mixed with 3 M hydrochloric acid, when the pH value became *ca.* 9.0, and was concentrated and then shaken with water and ether. The ether soln, after being worked up as usual, gave oily rishitin (**1**, 100 mg), showing a single spot on TLC, which was distilled at 90—100 °C (bath temp) under less than 1 mmHg pressure and allowed to stand to give crystalline rishitin (**1**, 83 mg). Compound **1a** was also converted under the same conditions as **1b** to give crystalline rishitin (**1**).

(iii) A suspended mixture of silica gel (Wakogel Q-23, 5 g) in chlorcform was packed in a column, and washed with acetone and then hexane. Compound **1** (10 mg) was passed through the column, using 8% acetone in hexane to yield **4** (10 mg), oil, which was distilled at 100 °C (bath temp) (1 mmHg) to give its crystalline acetonide (**4**, 8.5 mg), mp 32—35 °C; MS, *m/e* 262 (M^+) and 131 (base); IR (liquid), ν_{max} 3080, 1643, 1378, 1370, 1229, 1100, 1083, 1042, and 888 cm^{-1}; NMR (CCl_4), δ 1.13 (3H, d, J=7 Hz, 14-C$\underline{H}_3$), 1.39 [6H, s, $(C\underline{H}_3)_2CO$], 1.74 (3H, s, 13-C$\underline{H}_3$), 3.18 (1$\underline{H}$, t, J=9 Hz, $\underline{H}$ at C_3), 3.59 (1H, do t, J=9,9, and 7 Hz, $\underline{H}$ at C_2), 4.59 and 4.68 (each 1H, s, 2$\underline{H}$ at C_{12}). Found: C, 77.70; H, 9.82%. Calcd for $C_{17}H_{26}O_2$: C, 77.82; H, 9.99%.

Attempted formation of **4** from **1** (14 mg) with *p*-toluenesulfonic acid (7 mg) in dry acetone (5 ml) under reflux or from **1** (10 mg) in acetone (4 ml) containing one drop of 60% aq perchloric acid led to recovery of the starting glycol (**1**). When treated with acetone over anhydrous copper sulfate at room temp for 90 h, compound **1** was converted into **4** only in 20—30% yields.

*11,12-Dihydrorishitin (**2**) and Its Diacetate (**2a**).* A soln of **1** (110 mg) in ethyl acetate (30 ml) was hydrogenated over

Adams platinum (100 mg as $PtO_2 \cdot H_2O$) at room temp for 30 min, when one equiv of hydrogen had been consumed. The reaction mixture was worked up as usual to leave a crystalline substance (118 mg), which was recrystallized from hexane to give **2** (95 mg), mp 64—66 °C and $[\alpha]_D$ −8.7°; MS and UV, in the text; IR (CCl_4), ν_{max} 3360, 1386, and 1370 cm^{-1}. Found: C, 74.52; H, 10.62%. Calcd for $C_{14}H_{24}O_2$: C, 74.95; H, 10.78%.

Compound **2** (44 mg) was treated with Ac_2O (0.4 ml) and Py (0.8 ml) at room temp for 15 h. The mixture was worked up as usual to give a crystalline substance (60 mg), which was recrystallized from hexane to yield **2a** (38 mg), mp 79—81 °C and $[\alpha]_D$ +4.3°; IR (CCl_4), ν_{max} 1751, 1385, 1369, 1245, 1228, and 1029 cm^{-1}; NMR, δ 0.91 (6H, d, J=6 Hz, 12- and 13-C$\underline{H}_3$), 1.05 (3H, d, J=7 Hz, 14-C$\underline{H}_3$), 2.04 and 2.08 (each 3H, s, 2OCOC$\underline{H}_3$), and 4.95 (2H, br m, 2$\underline{H}$ at C_2 and C_3). Found: C, 69.93; H, 8.95%. Calcd for $C_{18}H_{28}O_4$: C, 70.10; H, 9.15%.

*5,10,11,12-Tetrahydrorishitin (**3**).* A soln of **1** (100 mg) in a 1 : 9 mixture (40 ml) of acetic acid and ethanol was hydrogenated over rhodium-platinum catalyst[6] (60 mg as $Rh_2O_3 \cdot PtO_2 \cdot H_2O$) at room temp for 20 h with shaking. The mixture was worked up as usual to leave an oily residue (100 mg), showing two spots on TLC, which was separated into two fractions by preparative TLC over silica gel. A major, more polar fraction gave a crystalline substance, which on recrystallization from ether afforded **3** (50 mg), mp 112—114 °C; MS and UV, in the text; IR, ν_{max} 3380, 1385, and 1370 cm^{-1}; NMR, δ 0.86 and 0.97 (total 9H, each d, J=6 and 7 Hz, 12-, 13- and 14-C$\underline{H}_3$), and 3.42 (2H, br m, 2$\underline{H}$ at C_2 and C_3).

*5,10-Dibromo-11,12-dihydrorishitin (**11**).* To a soln of **2** (60 mg) in chloroform (1 ml) was added dropwise bromine in chloroform (1.6 ml) (278 mg of Br_2 in 10 ml of $CHCl_3$) with stirring, when crystalline substances precipitated and were collected by filtration and recrystallized from carbon tetrachloride to give **11** (85 mg), mp 129—130 °C. This compound (**11**, 13 mg) was also obtained from **2** (11.2 mg) with pyridinium bromide perbromide[12] (16 mg); $[\alpha]_D$ +30.9°; MS, *m/e* 222 (M^+−2HBr), 204 (M^+−2HBr−H_2O), 186 (M^+−2HBr−2H_2O), 161 (204−C_3H_7), and 143 (186−C_3H_7); IR, ν_{max} 3475, 3340 and 1040 cm^{-1}; NMR ($CDCl_3$), δ 0.92 (6H, d, J=6.5 Hz, 12- and 13-C$\underline{H}_3$), 1.22 (3H, d, J=6.5 Hz, 14-C$\underline{H}_3$), 2.44 (2H?, s, 2O$\underline{H}$), 3.78 (1H, t J=9 Hz, $\underline{H}$ at C_3), and 4.32 (1H, do t, J=9, 9, and 7 Hz, $\underline{H}$ at C_2); NMR (C_5D_5N), δ 0.87 (6H, d, J=7 Hz, 12- and 13-C$\underline{H}_3$), 1.54 (3H, d, J=6.5 Hz, 14-C$\underline{H}_3$), 4.31 (1H, t, J=9.5 Hz, $\underline{H}$ at C_3), 4.90 (1H, do t, J=9.5, 9.5, and 6 Hz, $\underline{H}$ at C_2) and 5.93 (2H, s, 2O$\underline{H}$).

*Dehydrogenation of **2** with Selenium.* A mixture of **2** (100 mg) and selenium (170 mg) was heated at 240 °C for 22 h and then at 300 °C for 6 h in a sealed tube, and cooled. The reaction mixture was extracted with ether, and the ether soln was washed with 1 M aq sodium hydroxide and water, dried and evaporated to leave a neutral oil (68 mg), which was distilled at 60—70 °C (bath temp) under reduced pressure (1 Torr) to give an oil (45 mg), showing a single spot on TLC. This was further purified by preparative TLC over silica gel to yield eudalene (**5**, 20 mg) in pure state, which formed the picrate, mp 92—93 °C, and the trinitrobenzene adduct, mp 113—114 °C; (lit,[7] 92.8 °C and 113 °C, respectively).

*Conversion of **2** into (2R)-2-Isopropyl-8-methyl-1,2,3,4-tetrahydronaphthalen-7-ol 3,5-Dinitrobenzoate (**6a**).* To a stirred mixture of **2** (90 mg) in ether (10 ml) and water (5 ml) was added dropwise the Jones reagent[9] (0.5 ml) at room temp,[10] and the whole mixture was further stirred for 1 h. The ether soln was worked up as usual to leave an oily residue (46 mg), which without further purification was refluxed with concd hydrochloric acid (2.5 ml) in methanol (5 ml) for 1 h under nitrogen. The resulting soln was mixed with water (10 ml) and extracted with ether repeatedly. The ether soln, after usual work-up, left an oily residue, showing two mian spots on TLC, which was purified by preparative TLC over silica gel with chloroform. One (less polar) of the two main fractions gave a colorless oil (6 mg), which was treated with 3,5-dinitrobenzoyl chloride (8 mg) in Py (0.5 ml) at room temp overnight and heated on a water bath for 1 h. The soln, after being worked up as usual, gave a crystalline substance, which on recrystallization from ethanol-acetone gave **6a** (3 mg), mp 159—160 °C and $[\alpha]_D$ +56° ($CHCl_3$). Compound **6a** was identical with an authentic sample obtained from (−)-α-santonin in all respects.

*6-Epi-1-desmethyldesmotroposantonin 3-Acetate (**7b**).* This compound (**7b**) was prepared by the procedure of Sharif and coworkers.[11] (−)-α-Santonin (20 g), mp 170—172 °C and $[\alpha]_D$ −172.4°, was stirred with activated zinc powder (200 g) under reflux in *N,N*-dimethylformamide (200 ml) and water (15 ml) for 30 min, and gave 1-desmethyldesmotroposantonin (**7a**, 4.1 g), mp 231—232 °C (acetone) (lit.,[11] 228—229 °C) and $[\alpha]_D$ +105.1° ($CHCl_3$) (lit,[11] +115°); MS, *m/e* 232 (M^+), 217, 204, 189, and 159; IR, ν_{max} 3400, 1764, 1605, 1588, and 812 cm^{-1}; NMR, δ 1.28 (3H, d, J=6.5 Hz, 13-C$\underline{H}_3$), 1.60 (1H, s, O$\underline{H}$), 2.35 (3H, s, 14-C$\underline{H}_3$), 2.93 (2H, br m, W_H=14Hz, 2$\underline{H}$ at C_9), 5.02 (1H, d, J=9 Hz, $\underline{H}$ at C_6), 6.66 and 6.83 (each 1H, ABq, J=8 Hz, 2$\underline{H}$ at C_2 and C_1).

A soln of **7a** (1.76 g) in Ac_2O (28 ml) containing 7 drops of concd sulfuric acid was heated on a water bath for 20 min, and gave **7b** (1.78 g), mp 157.5—158 °C (methanol) (lit,[11] 159.5—160.5 °C) and $[\alpha]_D$ −170.8° ($CHCl_3$) (lit,[11] −155.7°); Mass, *m/e* 274 (M^+), 232 (base, M^+−CH_2CO), 217, 188, 173, and 159; IR, ν_{max} 1769 and 1747 cm^{-1}; NMR, δ 1.40 (3H, d, J=7 Hz, 13-C$\underline{H}_3$), 2.25 and 2.34 (each 3H, s, 14-C$\underline{H}_3$ and OCOC$\underline{H}_3$ or *vice versa*), 5.59 (1H, d, J=5.5 Hz, $\underline{H}$ at C_6), and 6.98 (2H, s, 2$\underline{H}$ at C_1 and C_2). The overall yield amounted to 18.7% (lit,[11] 12.2%).

*2-(7-Acetoxy-8-methyl-1,2,3,4-tetrahydro-2-naphthyl)propanoic Acid (**9**) and Its Methyl Ester (**9a**).* A solnof **7b** (3.00 g) in acetic acid (50 ml) was hydrogenated over 5% palladium charcoal (Wako, 1.5 g) at room temp for 20 h, when 327 ml (1.24 equiv) of hydrogen had been consumed. The mixture was filtered to remove the catalyst, which was washed with chloroform. The filtrate and washings were combined and evaporated to leave a foamy residue (**9**, 3.33 g), showing a single spot on TLC, after azeotropization; IR ($CHCl_3$), ν_{max} 1750, 1702, 1601, and 1063 cm^{-1}; NMR, δ 1.30 (3H, d, J=6 Hz), 2.01 and 2.32 (each 3H, s), 6.76 and 6.95 (each 1H, ABq, J=8 Hz).

The residue (**9**), without further purification, was dissolved in ether (50 ml) and treated with diazomethane, prepared from nitrosomethylurea (10.5 g), in ether (80 ml) at room temp for 4 h. The soln was concentrated to dryness, leaving oily residue (3.66 g), which was purified by column chromatography over silica gel (60 g). Eluates with benzene-ether (5 : 1, 150 ml) gave **9a** (3.17 g), after being dried *in vacuo* for 2 d, oil and $[\alpha]_D$ +77.2° ($CHCl_3$); MS, *m/e* 290 (M^+), 248 (M^+−CH_2CO), 216, 203, 201, 189, 160 (base), and 145; IR ($CHCl_3$), ν_{max} 1762, 1736, and 1603 cm^{-1}; NMR, δ 1.23 (3H, d, J=7 Hz), 2.00 and 2.30 (each 3H, s), 3.69 (3H, s, COOC$\underline{H}_3$), 6.74 and 6.92 (each 1H, ABq, J=8 Hz). Found: C, 70.31; H, 7.44%. Calcd for $C_{17}H_{22}O_4$: C,

70.32; H, 7.64%.

*2-(7-Hydroxy-8-methyl-1,2,3,4-tetrahydro-2-naphthyl)-1-propanol (**10**) and Its Bis(*p*-toluenesulfonate) (**10a**).* To a suspended mixture of lithium aluminium hydride (LAH, 1.3 g) in tetrahydrofuran (THF, 100 ml) was added dropwise a soln of **9a** (2.67 g) in dry THF (35 ml) under cooling with ice. The mixture was stirred under reflux for 24 h, and cooled to 0 °C. After addition of ethyl acetate, methanol and water to decompose an excess of the reagent, the mixture was submitted to filtration to remove insoluble materials, which were washed with ethanol. The filtrate and washings were combined and evaporated to dryness, leaving an oily residue, which was shaken with ethyl acetate and 2 M hydrochloric acid. The acidic layer was washed twice with ethyl acetate. The ethyl acetate solns were combined, washed with 2 M hydrochloric acid, 5% aq sodium hydrogen carbonate and saturated brine, dried and evaporated to leave a crystalline residue (2.02 g), which on recrystallization from ethyl acetate–hexane yielded **10** (1.76 g), mp 126—127 °C and $[\alpha]_D$ +76.7°; MS, *m/e* 220 (M^+), 187, 173, 161, and 159 (base); IR, ν_{max} 3565, 3280, 1605, 1591, 1200, 1070, and 816 cm^{-1}; NMR, δ 1.00 (3H, d, J=7 Hz), 2.10 (3H, s), 3.67 (2H, m, W_H=11 Hz, $C\underline{H}_2OH$), 4.96 (1H, s, O$\underline{H}$), 6.53 and 6.76 (each 1H, ABq, J=8 Hz). Found: C, 76.33; H, 9.07%. Calcd for $C_{14}H_{20}O_2$: C, 76.32; H, 9.15%.

Compound **10** (223 mg) was treated with *p*-toluenesulfonyl chloride (446 mg) in Py (3 ml) at room temp for 40 h, and then poured into ether (100 ml). The whole soln was washed with 2 M hydrochloric acid (3×10 ml), 5% aq sodium hydrogencarbonate and saturated brine, dried and evaporated to leave an oily residue (523 mg), which was purified by column chromatography over silica gel (30 g). Eluates with benzene gave **10a** (438 mg) in pure state, oil and $[\alpha]_D$ +39.5° ($CHCl_3$); MS, *m/e* 528 (M^+), 356, 314, 313, 238, 201, 159 (base), and 157; IR ($CHCl_3$), ν_{max} 3030, 1600, 1175 (strong), 850, 832, and 815 cm^{-1}; NMR, δ 0.95 (3H, d, J=7 Hz), 1.90 (3H, s), 2.44 and 2.46 (each 3H, s, $2C\underline{H}_3C_6H_4SO_3$), 4.00 (2H, s, $C\underline{H}_2OSO_2C_6H_4CH_3$), 6.62 and 6.77 (each 1H, ABq, J=8 Hz), 7.20 and 7.72 (each 4H, m, $2CH_3C_6\underline{H}_4SO_3$).

*Conversion of **10a** into (2R)-2-Isopropyl-8-methyl-1,2,3,4-tetrahydronaphthalen-7-ol (**6**) and Its 3,5-Dinitrobenzoate (**6a**).* Compund **10a** (315 mg) in dry THF (20 ml) was treated with LAH (364 mg) under reflux for 24 h. The reaction mixture, after being cooled, was worked up as described above to leave an oily residue (131 mg), showing a single spot, which was purified by column chromatography over silica gel (6 g). Eluates with benzene yielded **6** (98 mg) in pure state, oil and $[\alpha]_D$ +85.7° ($CHCl_3$); MS, *m/e* 204 (base, M^+), 189, 161, 147, 146, 134, 122, and 121; IR (liquid), ν_{max} 3420, 1598, 1386, 1367, and 817 cm^{-1}; NMR, δ 0.98 [6H, d, J=6 Hz, $CH(C\underline{H}_3)_2$], 2.11 (3H, s, $C\underline{H}_3$ at C_8), 4.76 (1H, s, O$\underline{H}$), 6.51 and 6.75 (each 1H, ABq, J=8 Hz, 2$\underline{H}$ at C_6 and C_5).

Compound **6** (73.5 mg) was stirred with 3,5-dinitrobenzoyl chloride (112.5 mg) in dry Py (1 ml) at room temp for 16 h. The mixture was poured into ice-water (50 ml), when precipitates separated out and were collected by filtration, washed with water, 5% aq sodium carbonate and water, and dried to give a crystalline material (140 mg). This was recrystallized from acetone to give **6a** (106.5 mg), mp 159.5—160 °C and $[\alpha]_D$ +60.1° ($CHCl_3$); MS, *m/e* 398 (M^+), 368, 355, 204, 195, 186, 165 (base), 149, and 135; IR, ν_{max} 3095, 1740, 1629, 1599, 1545, 1343, 1163, 1073, 921, and 717 cm^{-1}; NMR, δ 1.01 [6H, d, J=6 Hz, $CH(C\underline{H}_3)_2$], 2.08 (3H, s, $C\underline{H}_3$ at C_8), 6.82 and 6.96 (each 1H, ABq, J=8 Hz, 2$\underline{H}$, at C_5 and C_6), and 9.24 [3H, m, $(NO_2)_2C_6\underline{H}_3COO$]. Found: C, 63.37; H, 5.55; N, 6.82%. Calcd for $C_{21}H_{22}O_6N_2$: C, 63.31; H, 5.57; N, 7.03%.

References

1) Part XIII of "Studies on the Phytoalexins," Part XII, N. Katsui, H. Kitahara, F. Yagihashi, A. Matsunaga, and T. Masamune, *Chem. Lett.*, **1976**, 861.

2) a) K. Tomiyama, T. Sakuma, N. Ishizaka, N. Sato, N. Katsui, M. Takasugi, and T. Masamune, *Phytopathology*, **58**, 115 (1968); b) N. Katsui, A. Murai, M. Takasugi, M. Imaizumi, T. Masamune, and K. Tomiyama, *Chem. Commun.*, **1968**, 43.

3) For recent reviews, see, J. L. Ingham, *Bot. Rev.*, **38**, 343 (1972); T. Tani, *Kagaku*, **31**, 446 (1976).

4) For a recent review, see, A. Stoessl, J. B. Stothers, and E. W. B. Ward, *Phytochemistry*, **15**, 855 (1976).

5) The optical rotations (−29 and −6.2°) of rishitin and its diacetate in ref. 2b should be revised to these values (−35.1 and −14.1°), respectively; *cf.*, Refs. 2a and 15.

6) S. Nishimura, *Bull. Chem. Soc. Jpn.*, **33**, 566 (1960).

7) R. P. Linstead, K. O. A. Michaelis, and L. S. Thomas, *J. Chem. Soc.*, **1940**, 1139.

8) G. C. Levy and G. L. Nelson, "Carbon-13 Nuclear Magnetic Resonance for Organic Chemists," Wiley-Interscience, New York (1972).

9) During the preparation of this manuscript, Stoessl and coworkers reported the ^{13}C NMR spectral data of rishitin; A. Stoessl, E. W. B. Ward, and J. B. Stothers, *Tetrahedron Lett.*, **1976**, 3271.

10) *Cf.*, A. E. Vanstone and J. S. Whitehurst, *J. Chem. Soc., C*, **1966**, 1973.

11) S. M. Sharif, S. Nozoe, K. Tsuda, and N. Ikekawa, *J. Org. Chem.*, **28**, 793 (1963).

12) *Cf.*, J. A. Marshall and N. H. Andersen, *Tetrahedron Lett.*, **1967**, 1611.

13) S. T. K. Bukhari and R. D. Guthrie, *J. Chem. Soc., C*, **1969**, 1073.

14) N. Harada and K. Nakanishi, *J. Am. Chem. Soc.*, **91**, 3989 (1969).

15) A. Murai, K. Nishizakura, N. Katsui, and T. Masamune *Tetrahedron Lett.*, **1975**, 4399; *Bull. Chem. Soc. Jpn.*, **50**, 1206 (1977).

16) N. Katsui, A. Matsunaga, K. Imaizumi, T. Masamune, and K. Tomiyama, *Tetrahedron Lett.*, **1971**, 83; *Bull. Chem. Soc. Jpn.*, **45**, 2871 (1972).

17) a) N. Katsui, A. Matsunaga, and T. Masamune, *Tetrahedron Lett.*, **1974**, 4483; b) N. Katsui, A. Matsunaga, F. Yagihashi, A. Murai, T. Masamune, and N. Sato, *Bull. Chem. Soc. Jpn*, **50**, 1217 (1977).

Rishitin. II. Synthesis[1]

Akio MURAI, Kouichi NISHIZAKURA, Nobukatsu KATSUI, and Tadashi MASAMUNE
Department of Chemistry, Faculty of Science, Hokkaido University, Sapporo 060
(Received November 1, 1976)

The regio- and stereo-selective synthesis of rishitin (**1**) from (−)-α-santonin (**2**) is described. The transformation involves twelve steps including two known processes, the overall yield amounting to 2.9% from the santonin (**2**).

In the preceding paper[2] a report was given on the details of isolation and structure elucidation of rishitin (**1**), a representative member of a group of sesquiterpenes qualified as "phytoalexin" from diseased potatoes. As a result of continuing studies on the phytoalexins, we reported[3] the regio- and stereo-selective synthesis of rishitin (**1**) from (−)-α-santonin[4] (**2**). Details of the transformation are given in this paper.

The structure and configuration of rishitin (**1**) are characterized by an eudesmane skeleton with a double bond intervening between the two rings as well as three asymmetric centers in the flexible A ring. After many attempts starting with (2*R*)-2-isopropenyl-7-methoxy-8-methyl-1,2,3,4-tetrahydronaphthalene (**3**), bp 89—91 °C (0.07 Torr), obtained from "desmethyl-6-epidesmotroposantonin"[5] (**4**) *via* several steps (see Experimental), we functionalized the rigid A ring of a compound with a *trans*-decalin system, derivable from santonin **2**, as stereoselectively as possible and then introduce a double bond between both the A and B rings.

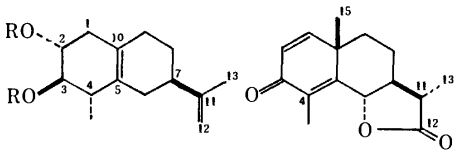

1 R=H
1a R=Ac

2

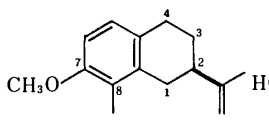

3

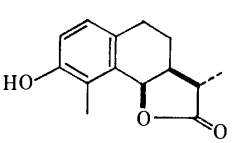

4

(−)-α-Santonin (**2**) was converted into (11*S*)-3-oxo-4β,5α-eudesman-6β,12-olide[6] (**5**) by the two-step procedure,[7] which on treatment with isopropenyl acetate in the presence of acid under reflux for 3 h[8] gave the corresponding Δ^2-3-ol acetate (**7**), mp 140—141 °C, in a 99% yield. The spectral data [*m/e* 292 (M^+) and 250 (M^+-CH_2CO);[9] ν_{max} 1773, 1755, and 1682 cm^{-1}; δ 2.17 (3H, s, $OCOC\underline{H}_3$) and 5.28 (1H, do t, *J*=5.5, 2.5, and 2.5 Hz)] were in good accord with the structure. Oxidation of enol acetate (**7**) with perbenzoic acid in chloroform at 0 °C for 24 h afforded 2α,3α-epoxy 3β-acetate (**8**), mp 156—156.5 °C, in a 91% yield, which was rearranged by heating at 170 °C for 10 min to 3-oxo 2β-acetate (**9**), mp 128—129 °C, and then epimerized with hydrobromic acid in acetic acid at room temperature[10] to give 3-oxo 2α-acetate (**10**), mp 204—205 °C, in a 72% yield from **8**. The oxo acetate (**10**) could be obtained in a 74% overall yield from **5**, when the afore-mentioned four-step reactions (**5**→**10**) were carried out without isolation of the intermediates (**7**, **8**, and **9**). The mass [*m/e* 308 (M^+) and 266] and IR (ν_{max} *ca.* 1780 and 1740 cm^{-1}) spectra of the oxo acetates (**9** and **10**) were consistent with the assigned structures. The spectral patterns due to the C_2-proton in the respective NMR spectra clearly determined the configurations of the 2-acetoxyl groups [H at C_2, δ 5.35 (1H, do d, *J*=9 and 6 Hz) for **9**, and δ 5.45 (1H, do d, *J*=13 and 7 Hz) for **10**], as compared with those of the corresponding protons of 2-acetoxycholestan-3-ones[11] [H at C_2, δ 5.12 (1H, do d, *J*=9.5 and 7.4 Hz) for 2β-acetate, and δ 5.07 (1H, do d, *J*=13.1 and 6.6 Hz) for 2α-acetate]. On the other hand, the 2α,3α-epoxy configuration of epoxide **8** was assigned on mechanistic considerations on transformation of **8** into unstable 3-oxo 2β-acetate (**9**).[10,11]

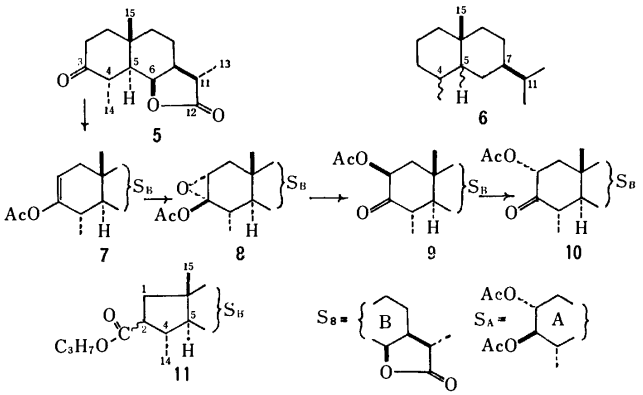

One-step oxidation of 3-ketone (**5**) to 3-oxo 2α-acetate (**10**) was carried out under various conditions. Treatment of **5** with lead tetraacetate in benzene containing boron trifluoride and 2-propanol at room temperature[12] produced a mixture, from which 3-oxo 2α-acetate(**10**), 3-oxo 2β-acetate (**9**), and a new compound (**11**), mp 112.5—113 °C, were isolated after chromatography in 41, 9, and 14% yields, respectively. Compound **11**, $C_{18}H_{28}O_4$, gave the following spectra: MS, *m/e* 308 (M^+), 249 ($M^+-C_3H_7O$) and 221 ($M^+-C_3H_7OCO$); IR, ν_{max} 1772, 1728, 1213, 1200, 1184, 1163, and 1111 cm^{-1}; NMR, δ 0.91 (3H, s, 15-$C\underline{H}_3$), 1.04 and 1.32 (each 3H, d, *J*=7 and 7.5 Hz, 14- and 13-$C\underline{H}_3$), 1.26 [6H, d, *J*=6 Hz, $(C\underline{H}_3)_2CHOCO$], 1.68 (2H, br d, *J*=8.5 Hz, 2H at C_1), 2.39 (1H, q, *J*=7.5 Hz, H at C_{11}), 2.51 (1H, m, H at C_4), 3.05 (1H, do t, *J*=10.5, 8.5, and 8.5 Hz, H at C_2), 4.68 (1H, t, *J*=4 Hz, H at C_6), and 5.01 [1H, sep, *J*=6 Hz, $(CH_3)_2C\underline{H}OCO$]. These spectra indicated that (i) the B ring, including

the γ-lactonic group, and one secondary methyl group in the original A ring remained unchanged, and (ii) an isopropoxycarbonyl group was newly formed. Assignment of formula **11** was made from these data together with those of spin decoupling studies. It is interesting that the ring contraction occurred in the presence of 2-propanol, in contrast to the corresponding reaction of 5α-cholestan-3-one.[12c]

Reduction of 3-oxo 2α-acetate (**10**) with sodium borohydride in methanol at 0 °C afforded a mixture of diastereoisomeric 3-alcohols, which was separated by preparative TLC to give 3β-alcohol (**12**), mp 251—252 °C, and 3α-alcohol (**13**), mp 191—192 °C, in 41 and 48% yields, respectively. Each of these alcohols, when oxidized with the Jones reagent, was reconverted into the original 3-ketone (**10**) in 85—90% yields, indicating the configurational retention during the course of reduction. The C_3 configuration in question in these alcohols is evident from the NMR spectra. The former (**12**) showed two one-proton signals (1H, t, J=9 Hz and 1H, do do d, J=11.5, 9, and 5 Hz) due to the protons at C_3 and C_2 at δ 3.13 and 4.93, respectively, and the latter (**13**) the corresponding signals (1H, br s, W_H=6.5 Hz, and 1H, do do d, J=11, 5.5, and 3 Hz) at δ 3.91 and 5.01. These hydroxy acetates (**12** and **13**) were converted into the diacetates (**12a** and **13a**), mp 189.5—190.5 °C and 150—151 °C, and were hydrolyzed quantitatively to the glycols (**12b** and **13b**), mp 184—185 °C and 94.5—95 °C, respectively. In line with the assigned configurations, *cis*-glycol (**13b**) readily formed the acetonide (**14**), mp 131—132 °C, on treatment with acetone over silica gel (Wakogel Q-23), whereas *trans*-glycol (**12b**) was recovered unchanged under the same conditions.

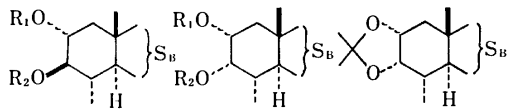

12 R_1=Ac, R_2=H **13** R_1=Ac, R_2=H
12a $R_1=R_2$=Ac **13a** $R_1=R_2$=Ac
12b $R_1=R_2$=H **13b** $R_1=R_2$=H

14

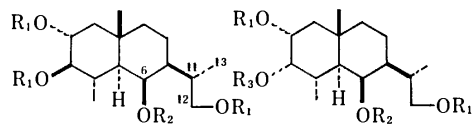

15 $R_1=R_2$=H **16** $R_1=R_2=R_3$=H
15a R_1=Ac, R_2=H **16a** $R_1=R_3$=Ac, R_2=H
17 R_1=Ac, R_2=NO **16b** R_1=Ac, $R_2=R_3$=H

Further reduction of 2α-acetoxy 3β-hydroxy γ-lactone (**12**) with lithium aluminium hydride under reflux gave tetraol (**15**), amorphous, which was isolated as the triacetate (**15a**), mp 96.5—98 °C, almost quantitatively after acetylation at room temperature. The triacetate (**15a**) showed a broad singlet (W_H=6.5 Hz) due to the C_6-proton at δ 4.08, and the steric interaction between 1,3-diaxial methyl and hydroxyl groups at C_{10} and C_6 evidently hindered acetylation of the hydroxyl group. By the same treatment the 3α-hydroxy epimer (**13**) gave the 3-epimeric tetraol (**16**), mp 174—174.5 °C, which was also converted into the triacetate (**16a**), mp 80—81 °C, showing a broad singlet (W_H=7 Hz) due to the C_6-proton at δ 4.00, in an 80% yield, along with the 2,12-diacetate (**16b**), oil (15%). The same hydride reduction of 3-oxo 2α-acetate (**10**) followed by acetylation produced a mixture of **15a** and **16a**, from which the desired 2α, 3β,12-triacetate (**15a**) could be isolated in an 80% yield with the epimer (**16a**) (9%). The triacetate (**15a**) was then transformed quantitatively into the 6-nitrite (**17**), mp 103.5—105.5 °C, by treatment with nitrosyl chloride in pyridine, whose NMR spectrum was in line with the structure; δ 4.72 (1H, t, J=10 Hz, H at C_3), 5.05 (1H, do do d, J=11.5, 10, and 5 Hz, H at C_2), and 5.94 (1H, br s, W_H=5 Hz, H at C_6).

Irradiation of the 6-nitrite (**17**) by a 200 watt high pressure Hanovia lamp in benzene at room temperature for 2 h followed by reflux in a 1 : 1 mixture of tetrahydrofuran and 2-propanol[13] resulted in functionalization at C_{15}, giving a three-component mixture, which was separated by chromatography over Florisil to yield 15-oxime (**18**), amorphous, as a major product (78%) with 6,15-oxolane and 6-ketone (**19** and **20**), mp 100—101 °C and 109.5—111 °C (5 and 7%). The 6-ketone (**20**) could readily be identified by oxidation of **15a** with the Jones reagent. The structure of oxime **18** was deduced from the following spectra. The mass spectrum indicated fragmentation peaks at *m/e* 410 (M^+—OH), 367 ($M^+-C_2H_4O_2$), and 350. The NMR spectrum revealed, instead of a singlet peak due to the 15-methyl protons, a doublet (J= 9 Hz) and two singlet peaks at δ 6.56, 7.18, and 10.45, which were ascribed to 6-hydroxy, hydroxyimino methylidene and oxime-hydroxy protons, respectively. The structure was further supported by oxidation of **18** with the Jones reagent to γ-lactone (**21**), mp 126—127 °C, in a 56% yield. The γ-lactone (**21**) was characterized by fragmentation peaks at *m/e* 382 (M^+—CO), 350 ($M^+-C_2H_4O_2$), and 322 (350—CO) as well as absorption maxima at 1780 and 1745 cm^{-1} and at δ 4.49 (1H, br s, W_H=2.5 Hz, H at C_6) in the mass, IR, and NMR spectra. Similarly, the structure of oxolane (**19**) was assigned as shown in the formula on the basis of the following spectral data: *m/e* 396 (M^+) and 336 ($M^+-C_2H_4O_2$); ν_{max} 1743, 1478, and 862 cm^{-1};[14]

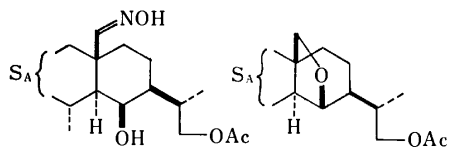

18 **19**

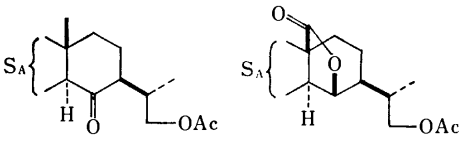

20 **21**

δ 3.62 and 3.86 (each 1H, ABq, J=8 Hz, 2H at C_{15}),[14] and 4.18 (1H, s, H at C_6). The oxolane (**19**) was also obtained by direct hypoiodite reaction[15] of **15a** in a 73% yield, confirming the structure for oxolane **19**. However, the oxolane resisted further oxidation to **21** and/or its analogues under various conditions, giving only multi-component intractable materials.

Treatment of 15-oxime (**18**) with acetic anhydride in pyridine at room temperature led to only dehydration of the hydroxyimino group to give 6β-hydroxy 10-nitrite (**22**), mp 175—176 °C in an 89% yield, whose functional groups were characterized by absorption maxima at 3530, 2230, 1739, and 1728 cm^{-1} in the IR spectrum. Compound **22**, when treated with methanesulfonyl chloride in pyridine at room temperature and then with collidine under reflux, underwent further dehydration to yield an oily mixture of olefins, from which Δ^5- and Δ^6-10-nitriles (**23** and **24**), mp 106—107 °C and 81—82 °C, were isolated after chromatography in 78 and 9% yields, respectively. Alternately, the hydroxy nitrile (**22**) was obtained by prolonged treatment of **18** with phosphoryl chloride at room temperature in 60—70% yields with a small amount of **23** (4%). However, attempted double dehydration of 15-oxime (**18**) with methanesulfonyl chloride under the afore-mentioned conditions resulted in formation of an intractable material, from which the desired nitrile (**23**) could be isolated only in a 15% yield.

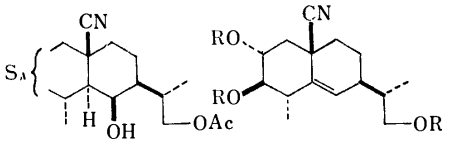

22

23 R=Ac
23a R=H
23b R=CH_2OCH_3

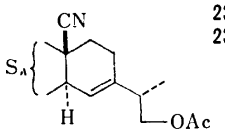

24

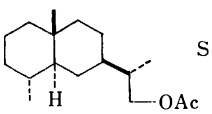

25

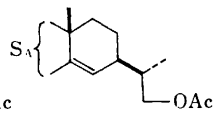

26

Both the olefins (**23** and **24**) exhibited almost the same mass [m/e 331 ($M^+-C_2H_4O_2$) and 211], IR (ν_{max} *ca.* 2230 and 1745 cm^{-1}), and NMR spectra [δ *ca.* 5.55 (1H, br s, W_H=5 Hz, olefinic H)], indicating that the olefins are isomers differing only in the double bond position (Δ^5 or Δ^6). The position was assigned on the basis of the following considerations. i) In the NMR spectra of normal[16] and modified steroids,[17] the shielding effects of various substituents on the chemical shift of 19-methyl protons are additive. The additivity is expected to hold for the present 4β,5α-eudesmanes, in which the A and B rings are regared as the A and B rings in normal steroids, and the 15-methyl protons as the 19-methyl protons. The chemical shifts of 15-methyl protons were then estimated, by assuming the relevant shift of 4β,5α-eudesman-12-ol acetate[6] (**25**), a hypothetical compound, to be δ 0.18 (reference chemical shift) and by using well-established contributions of functional groups in the A and B rings of normal steroids.[16] The calculated values were in good accord with the observed: δ_{calcd} (δ_{obsd}) 1.18 (1.18), 1.15 (1.15), 1.14 (1.13), and 0.90 (0.88) for **15a**, **16a**, **16b**, and **20**, respectively. Compound **15a**, a 10-methyl analogue of **22**, when treated with methanesulfonyl chloride under the above conditions, underwent dehydration to give an olefin (**26**), oil, in a 97% yield, as the only isolatable product, whose 15-methyl protons appeared as a singlet at δ 1.18 in the NMR spectrum. The chemical shift coincided with the calculated value, δ 1.18, only when the compound (**26**) was assigned Δ^5-triacetate formula (*cf.*, δ_{calcd} 0.92 for Δ^6-triacetate). The result indicates that dehydration of the 6β-hydroxyeudesmanes would proceed regioselectively to form the corresponding Δ^5-eudesmanes, and hence the major dehydration product (**23**) would be represented by Δ^5-10-nitrile structure rather than Δ^6-10-nitrile. (ii) Tori and co-workers[16b] discussed the chemical shifts of the A ring protons in normal steroids in terms of the effects of functional groups in the A and B rings. The discussion apparently applies to eudesmanes; *e.g.*, the axial 3α-proton (δ 4.60) of Δ^5-triacetate (**26**) was observed at a field 0.10 ppm higher than that (δ 4.70) of 6β-hydroxy triacetate (**15a**), as expected by their presumption. The 3α-proton of the relevant major olefin (**23**) appeared as a double doublet (J= 11 and 9.5 Hz) at 0.13 ppm higher field, δ 4.56, as compared with the corresponding proton of 6β-hydroxy-10-nitrile (**22**), δ 4.69, and that of the minor olefin (**24**) as a triplet (J=9.5 Hz) at 0.09 ppm lower field, δ 4.78.

Δ^5-10-Cyano triacetate (**23**) was saponified to the triol (**23a**), oil, which was converted into Δ^5-10-cyano tris(methoxymethyl ether) (**23b**), oil, in a 56% yield from **23**, showing absorption maxima at 2255 cm^{-1} and at δ 3.38, 3.41, 3.46 (each 3H, s, $3OCH_3$), and 5.57 (1H, br s, W_H=4 Hz, H at C_6) in the IR and NMR spectra. Hydrolysis of the cyano group of **23** followed by decarboxylation with concomitant migration of the 5,6-double bond was unsuccessful, giving a tarry material. However, treatment of Δ^5-10-nitrile (**23**) with sodium in toluene containing ethanol under reflux[18] effected reductive decyanation with concurrent migration of the double bond to give $\Delta^{5(10)}$-triol (**27**), oil, which was converted into the triacetate (**27a**), oil, showing no olefinic proton in the NMR spectrum, in a 71% yield from **23**. The structure of olefin **27a** was identified by comparison with an authentic sample obtained from natural rishitin (**1**) *via* a four-step process (formation of the acetonide, hydroboration, acid hydrolysis, and acetylation). On the other hand, $\Delta^{5(10)}$ 2,3,10-triol (**27**), when treated with acetone over silica gel (Wakogel Q-23), formed the 2,3-acetonide (**28**), oil, ν_{max} 3390, 1380, and 1371 cm^{-1} and δ 1.46 [6H, s, $(CH_3)_2CO$], in a 75% yield from **23**. The 2,3-acetonide (**28**) was treated successively with tosyl chloride in pyridine at room temperature and then

with sodium iodide in acetone under reflux to give the 12-iodide (**29**), semi-soild, *m/e* 390 (M^+) and ν_{max} 1380 and 1371 cm^{-1}, in a 92% yield. Further treatment of the 12-iodide (**29**) with potassium hydroxide in refluxing methanol led to formation of a mixture of two compounds, which were separated by chromatography to give the 12-methoxy derivative (**30**), oil, *m/e* 294 (M^+), ν_{max} 1105 and 1088 cm^{-1}, and δ 3.32 (3H, s, $OC\underline{H}_3$), and $\Delta^{5(10),11}$-2,3-diol acetonide (**31**), oil, in 14 and 70% yields, respectively. The latter (**31**) exhibited parent and fragmentation peaks at *m/e* 262 (M^+) and 131 (base) in the mass spectrum and absorption maxima at 3080, 1643, and 888 cm^{-1} and δ 1.72 (3H, s, 13-$C\underline{H}_3$), 4.63 and 4.74 (each 1H, br s, W_H=4 Hz, 2H at C_{12}) in the IR and NMR spectra, and was identical with an authentic specimen[2] derived from natural rishitin (**1**). Hydrolysis of the acetonide (**31**) with 0.5% phosphoric acid in ethanol under reflux afforded $\Delta^{5(10),11}$-2,3-diol, mp 58—60 °C and $[\alpha]_D$ −30.4°, in a 78% yield, which was converted into the diacetate, mp 66—68 °C and $[\alpha]_D$ −14.1°. The glycol and diacetate were identical with natural rishitin[2] (**1**) and the diacetate[2] (**1a**), respectively. The present transformation from (−)-α-santonin (**2**) into rishitin (**1**) completes the first and total[4] synthesis of rishitin. The overall yield of rishitin amounted to 12.0% from compound **5** and 2.9% from (−)-α-santonin.

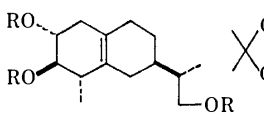

27 R=H
27a R=Ac

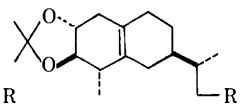

28 R=OH
28a R=OTs
29 R=I
30 R=OCH_3

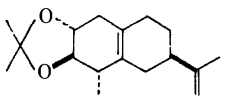

31

Experimental

All the melting points were uncorrected. The homogenity of each compound was checked by TLC on silica gel (Wakogel B-5) with various solvent systems, and the spots were developed with cerium(IV) sulfate in dil sulfuric acid. The optical rotations, ORD curves, IR, and NMR (100 MHz) spectra were measured in chloroform, methanol, Nujol, and chloroform-*d*, respectively, unless otherwise stated. Abbreviations "s, d, t, q, m, br, and do" in the NMR spectra denote "singlet, doublet, triplet, quartet, multiplet, broad, and double," respectively.

(2R)-2-Isopropenyl-7-methoxy-8-methyl-1,2,3,4-tetrahydronaphthalene (3). *(i)* A soln of 2-(7-acetoxy-8-methyl-1,2,3,4-tetrahydro-2-naphthyl)propanoic acid[2] (12.63 g) in dry tetrahydrofuran (THF, 200 ml) was stirred with lithium aluminium hydride (LAH, 3.15 g) under reflux for 17 h. After addition of water to decompose an excess of the reagent, the suspended mixture was mixed with chloroform and stirred vigorously. The insoluble substance was removed by filtration and washed with chloroform and water. The filtrate and all the chloroform and water washings were combined and evaporated to dryness to leave an oily residue, which was again dissloved in chloroform. The chloroform soln was washed with water, dried, and evaporated to leave a crystalline residue (1.50 g), which was collected and recrystallized from ethyl acetate–hexane to give 2-(7-hydroxy-8-methyl-1,2,3,4-tetrahydro-2-naphthyl)-1-propanol[2] (1.26 g), mp 125—126 °C. The water washings were acidified (pH<4.0) with 6 M hydrochloric acid and extracted with chloroform repeatedly. The extracts were washed with water, dried, and evaporated to leave an amorphous substance (7.35 g), showing a single spot, which was identified as the corresponding saponified product, 2-(7-hydroxy-8-methyl-1,2,3,4-tetrahydro-2-naphthyl)-propanoic acid on the basis of the spectral data: IR ($CHCl_3$), ν_{max} 3585, 1704, 1598, 1486, 1271, and 1063 cm^{-1}; NMR, δ 1.27 (3H, d, J=6.5 Hz), 2.09 (3H, s), 5.85 (2H, br, 2O$\underline{H}$), 6.59 and 6.81 (each 1H, d, J=8 Hz). The hydroxy acid was dissolved in ether (150 ml), without further purification, and treated with diazomethane, prepared from nitrosomethylurea (20.6 g), in ether (230 ml) at room temp for 22 h. The soln was concentrated to give the corresponding methyl ester (6.72 g), oil, showing a single spot on TLC, which was purified by distillation at 168—172 °C (bath temp) under reduced pressure (1 Torr) and crystallized on standing: mp 43—45 °C and $[\alpha]_D$ +92.5°; MS, *m/e* 248 (M^+); IR ($CHCl_3$), ν_{max} 3410, 1722, 1597, 1483, 1267, 1162, and 1060 cm^{-1}; NMR, δ 1.27 (3H, d, J=7 Hz), 2.11 (3H, s), 3.74 (3H, s), 6.57 and 6.80 (each 1H, d, J=8 Hz). Found: C, 72.26; H, 8.11%. Calcd for $C_{15}H_{20}O_3$: C, 72.55; H, 8.12%.

(ii) A soln of methyl 2-(7-hydroxy-8-methyl-1,2,3,4-tetrahydro-2-naphthyl)propanoate (6.61 g) in methanol (250 ml) was treated with diazomethane, prepared from nitrosomethylurea (20.6 g), in ether (220 ml) at room temp for 13 h. After addition of the same amount of diazomethane in ether (220 ml), the soln was allowed to stand at room temp for 66 h and then evaporated below 36 °C to leave an oily residue (7.34 g), which was purified by column chromatography over silica gel (70 g) and celite (30 g) followed by distillation to give methyl 2-(7-methoxy-8-methyl-1,2,3,4-tetrahydro-2-naphthyl)propanoate in pure state: bp 143—148 °C (bath temp) (1 Torr) and $[\alpha]_D$ +89.3°; MS, *m/e* 262 (M^+); IR ($CHCl_3$), ν_{max} 1727, 1599, 1483, 1262, 1163, and 1088 cm^{-1}; NMR, δ 1.26 (3H, d, J=7 Hz), 2.13 (3H, s), 3.75 and 3.83 (each 3H, s), 6.67 and 6.93 (each 1H, d, J=8.5 Hz). Found: C, 73.10; H, 8.35%. Calcd for $C_{16}H_{22}O_3$: C, 73.25; H, 8.45%.

(iii) A soln of the methoxy methyl ester (6.14 g) in THF (160 ml) was mixed with LAH (3 g) in THF (250 ml), and the whole mixture was stirred at room temp for 18 h. After careful addition of water (40 ml), the resulting suspension was submitted to filtration to remove insoluble materials, and the filtrate was evaporated to dryness to leave an oily residue, which was extracted in ether. The ether soln was washed with saturated brine, dried, and evaporated to give an oil (5.69 g), showing a single spot, which was identical with an authentic sample of 2-(7-methoxy-8-methyl-1,2,3,4-tetrahydro-2-naphthyl)-1-propanol prepared from the corresponding 7-hydroxy analogue as described in the following.

A soln of 2-(7-hydroxy-8-methyl-1,2,3,4-tetrahydro-2-naphthyl)propanol[2] (896 mg), mp 125—126 °C, in acetone (40 ml) was stirred with dimethyl sulfate (1.6 ml) and potassium carbonate (4.8 g) under reflux for 9 h, cooled and then filtered. The ppts were washed with chloroform, and the filtrate and washings were combined and evaporated to leave an oily

residue, which was again dissolved in chloroform. The chloroform soln was washed with water, dried, and evaporated to leave an oily substance (1.82 g), which was purified by chromatography over silica gel (Merck 30 g). Eluates with benzene–ether (3 : 1) (100 ml) afforded the methyl ether (800 mg), which was distilled for analysis: bp 97—102 °C (bath temp) (1 Torr) and $[\alpha]_D$ +70.9°; MS, *m/e* 234 (M^+), 216, 201, 186, 175, and 173 (base); IR (film), ν_{max} 3360, 1601, 1485, 1463, 1441, 1260, 1103, 1031, 812, and 794 cm^{-1}; NMR δ 1.00 (3H, d, J=7 Hz), 1.83 (1H, s, OH), 2.13 (3H, s), 3.69 (2H, m), 3.81 (3H, s), 6.69 and 6.93 (each 1H, d, J=8 Hz). Found: C, 76.69; H, 9.43%. Calcd for $C_{15}H_{22}O_2$: C, 76.88; H, 9.46%.

(iv) The methoxy-propanol (730 mg), described in *(iii)*, was treated with *p*-toluenesulfonyl chloroide (660 mg) in pyridine (Py, 8 ml) at room temp for 20 h, and then poured into ice-water (300 ml). The resulting ppts were collected by filtration, washed with water, dried in a desiccator, and triturated with isopropyl ether to yield a crystalline substance (980 mg). Recrystallization from isopropyl ether afforded 2-(7-methoxy-8-methyl-1,2,3,4-tetrahydro-2-naphthyl)-1-propanol tosylate, mp 86.5—87 °C and $[\alpha]_D$ +56.3°; MS, *m/e* 388 (M^+), 216, 201, and 174 (base); IR, ν_{max} 1598, 1485, 1355, 1261, 1188, 1180, 1171, 1106, 1096, 957, 929, 850, and 792 cm^{-1}; NMR, δ 0.97 (3H, d, J=6.5 Hz), 2.04, 2.45, and 3.78 (each 3H, s), 4.05 (2H, d, J=5 Hz), 6.65 and 6.87 (each 1H, d, J=8.5 Hz), 7.31 and 7.78 (each 2H, ABq, J=8 Hz). Found: C, 68.01; H, 7.23; S, 8.30%. Calcd for $C_{22}H_{28}O_4S$: C, 68.01; H, 7.26; S, 8.25%.

(v) The tosylate (650 mg) was stirred with sodium iodide (3 g) in acetone (30 ml) under reflux for 20 h. After removal of the insoluble substance by filtration, the mixture was evaporated to dryness and extracted with ether (50 ml). The extracts were washed with 5% aq sodium thiosulfate and saturated brine, dried, and evaporated to leave a crystalline substance (617 mg), which was recrystallized from hexane to give the corresponding iodide (570 mg), mp 73.5—75.5 °C. This was recrystallized from hexane for analysis: mp 75.5—77.5 °C and $[\alpha]_D$ +95°; MS, *m/e* 344 (M^+), 217, 175, and 161 (base); IR, ν_{max} 1599, 1587, 1479, 1258, 1105, and 801 cm^{-1}; NMR, δ 1.09 (3H, d, J=6.5 Hz), 2.14 (3H, s), 3.37 (2H, d, J=5 Hz, CH_2I), 3.82 (3H, s), 6.70 and 6.94 (each 1H, d, J=8 Hz). Found: C, 52.32; H, 6.20; I, 37.21%. Calcd for $C_{15}H_{21}OI$: C, 52.33; H, 6.15; I, 36.87%.

(vi) The iodide (4.97 g) was refluxed in methanol (300 ml) containing potassium hydroxide (17.6 g) under nitrogen for 2.5 h. The reaction mixture was concentrated below 40 °C under reduced pressure (90 Torr), and then shaken with water (150 ml), ether (100 ml), and sodium chloride (40 g). The aqueous layer was separated and washed with ether (4×50 ml). The ether layer and washings were combined, washed with saturated brine (2×50 ml), dried, and evaporated to leave an oily residue (3.19 g), which was purified by column chromatography over silica gel (Mallinckrodt, 21 g) and celite (9 g). Eluates with hexane (1.6 l), after distillation, afforded (2*R*)-2-isopropenyl-7-methoxy-8-methyl-1,2,3,4-tetrahydronaphthalene (**3**, 2.68 g), bp 89—91 °C (bath temp) (0.07 Torr) and $[\alpha]_D$ +76.6°; MS, *m/e* 216 (M^+), 201, and 173 (base); IR (CCl_4), ν_{max} 3080, 1645, 1601, 1484, 1260, 1114, 1090, and 890 cm^{-1}; NMR, δ 1.83, 2.13, and 3.79 (each 3H, s), 4.80 (2H, s, $=CH_2$), 6.69 and 6.94 (each 1H, d, J=8.5 Hz). Found: C, 83.52; H, 9.25%. Calcd for $C_{15}H_{20}O$: C, 83.28; H, 9.32%.

(11S)-3-Oxo-4β,5α-eudesman-6β,12-olide[6,7] *(**5**).* Compound **5** was prepared by a modification of the procedure of Cocker *et al.*[7b] A soln of "6-epi-(−)-α-santonin"[7,19] (3 g), mp 102—103 °C, in acetic acid (AcOH, 400 ml) was hydrogenated over 10% palladium charcoal (200 mg) at room temp for 2 h, when 590 ml of hydrogen had been absorbed. The reaction mixture was worked up as usual to leave neutral crystalline substances (1.64 g), showing two 1 : 1 overlapped spots on TLC. The mixture, dissolved in AcOH (150 ml) at 50 °C, was stirred with *p*-toluenesulfonic acid (PTS, 1.5 g) at room temp for 18 h, evaporated to dryness, and diluted with water (500 ml). The resulting ppts were separated, collected by filtration and washed with water. Recrystallization from aq ethanol gave **5** (1.16 g), mp 164—165 °C. This was recrystallized from ethanol for analysis: mp 164—165 °C and $[\alpha]_D$ −106.0° (lit,[7] mp 177—178° and $[\alpha]_D$ −91°); ORD, $[\Phi]_{304}^{peak}$ +800°, $[\Phi]_{265}^{trough}$ −4790°, a=+55.9°; IR, ν_{max} 1762, 1703, 1420, 1210, 1178, 1153, 975, and 937 cm^{-1}; NMR, δ 1.14 (3H, d, J=7 Hz, 14-CH_3), 1.22 (3H, s, 15-CH_3), 1.33 (3H, d, J=8 Hz, 13-CH_3), and 4.66 (1H, t, J=4 Hz, H at C_6). Found: C, 72.10; H, 9.07%. Calcd for $C_{15}H_{22}O_3$: C, 71.97; H, 8.86%.

*(11S)-3-Acetoxy-4β,5α-eudesm-2-en-6β,12-olide (**7**).* A soln of **5** (67.2 g) in isopropenyl acetate (250 ml) containing concd sulfuric acid (0.7 ml) was refluxed for 3 h with stirring in a stream of argon gas. The mixture was cooled, concentrated, mixed with water, and extracted with dichloromethane. The extracts were worked up as usual to leave a crystalline residue, which on trituration with a 2 : 1 mixture of acetone and water followed by filtration afforded **7** (63.4 g), mp 139—140 °C. The filtrate (15.2 g), still containing the unreacted ketone (**5**) (TLC), was again treated with isopropenyl acetate (62 ml) and concd sulfuric acid (10 drops) for 3 h under reflux. The resulting crystalline residue, subjected to the same treatment as above, yielded **7** (14.3 g), mp 139—140 °C. The samples (**7**) were recrystallized from aq acetone for analysis: mp 140—141 °C and $[\alpha]_D$ −74.3 °C; MS, *m/e* 292 (M^+), 250 (base), and 177; IR, ν_{max} 1773, 1755, 1682, 1214, 1207, 1063, and 1021 cm^{-1}; NMR, δ 1.07 (3H, s, 15-CH_3), 1.10 and 1.32 (each 3H, d, J=7 and 8 Hz, 14- and 13-CH_3), 2.17 (3H, s, $OCOCH_3$), 2.41 (1H, q, J=8 Hz, H at C_{11}), 2.74 (1H, br, W_H=24 Hz, H at C_4), 4.76 (1H, t, J=4 Hz, H at C_6), and 5.28 (1H, do t, J=5.5, 2.5, and 2.5 Hz, H at C_2). Found: C, 69.97; H, 8.47%. Calcd for $C_{17}H_{24}O_4$: C, 69.83; H, 8.27%.

*(11S)-3β-Acetoxy-2α,3α-epoxy-4β,5α-eudesman-6β,12-olide (**8**).* A soln of **7** (2.45 g) in chloroform (40 ml) was treated with peroxybenzoic acid (purity 99.3%, 2 g) at 0 °C for 24 h. The mixture was washed with 5% aq sodium thiosulfate, 5% aq sodium hydrogencarbonate and water, dried, and evaporated to leave a crystalline substance, which was collected with acetone to give **8** (2.34 g), mp 153—154 °C. This was recrystallized from acetone for analysis: mp 156—156.5 °C and $[\alpha]_D$ −58.7°; MS, *m/e* 308 (M^+), 266 (base), 248, and 193; IR, ν_{max} 1771, 1750, 1223, 1158, 1050, and 976 cm^{-1}; NMR, δ 1.20 (3H, s, 15-CH_3), 1.24 and 1.30 (each 3H, d, J=6.5 and 7.5 Hz, 14- and 13-CH_3), 2.10 (3H, s, $OCOCH_3$), 2.37 (1H, q, J=7.5 Hz, H at C_{11}), 2.67 (1H, do q, J=10.5, 6.5, 6.5, and 6.5 Hz, H at C_4), 3.45 (1H, d, J=5 Hz, H at C_2), and 4.67 (1H, t, J=4 Hz, H at C_6). Found: C, 66.15; H, 7.79%. Calcd for $C_{17}H_{24}O_5$: C, 66.21; H, 7.85%.

*(11S)-2β-Acetoxy-3-oxo-4β,5α-eudesman-6β,12-olide (**9**).* Compound **8** (1.27 g) was heated in an oil-bath maintained at 170 °C for 10 min. The mixture, when cooled, crystallized spontaneously and showed a single spot on TLC. This was recrystallized from acetone–isopropyl ether to give **9** (1.187 g), mp 127—129 °C. Further recrystallization from the same solvent mixture afforded an analytical sample: mp 128—129 °C and $[\alpha]_D$ −7.7°; ORD, $[\Phi]_{304}^{peak}$ +3040°, $[\Phi]_{270}^{trough}$ −3790°, a=+68.3°; MS, *m/e* 308 (M^+), 266 (base), 248, and

193; IR, ν_{max} 1782, 1737, and 1229 cm^{-1}; NMR, δ 1.06 (3H, s, 15-C$\underline{H}_3$), 1.26 and 1.33 (each 3H, d, J=7 and 8 Hz, 14- and 13-C$\underline{H}_3$), 2.14 (3H, s, OCOC$\underline{H}_3$), 2.43 (1H, q, J=8 Hz, $\underline{H}$ at C_{11}), 2.92 (1H, do q, J=12, 7, 7, and 7 Hz, $\underline{H}$ at C_4), 4.69 (1H, t, J=4 Hz, $\underline{H}$ at C_6), and 5.35 (1H, do d, J=9 and 6 Hz, $\underline{H}$ at C_2). Found: C, 65.91; H, 7.82%. Calcd for $C_{17}H_{24}O_5$: C, 66.21; H, 7.85%.

*(11S)-2α-Acetoxy-3-oxo-4β,5α-eudesman-6β,12-olide (**10**).* *(i)* A soln of **9** (1.76 g) in glacial AcOH (35 ml) containing 47% hydrobromic acid (0.25 ml) was allowed to stand at room temp for 41 h. The soln was concentrated, diluted with water, and extracted with chloroform. The chloroform soln was worked up as usual to leave an oily residue, which on trituration with acetone-isopropyl ether followed by filtration afforded slightly crude **10** (1.24 g), mp 191—193 °C. The filtrate (0.35 g) was purified by chromatography over silica gel (25 g) to give an another sample of **10** (0.1 g), mp 193—195 °C, from ether-benzene (1 : 4) eluates. Recrystallization of both samples repeated twice yielded an analytical sample of **10**: mp 204—205 °C and $[\alpha]_D$ −32.8°; ORD, $[\Phi]_{305}^{peak}$ +2570°, $[\Phi]_{269}^{trough}$ −5010°, a=+75.8°; MS, *m/e* 308 (M^+), 266 (base), 248, and 193; IR, ν_{max} 1779, 1747, 1718, and 1244 cm^{-1}; NMR, δ 1.19 (3H, d, J=7 Hz, 14-C$\underline{H}_3$), 1.32 (3H, s, 15-C$\underline{H}_3$), 1.34 (3H, d, J=8 Hz, 13-C$\underline{H}_3$), 2.17 (3H, s, OCOC$\underline{H}_3$), 2.45 (1H, q, J=8 Hz, $\underline{H}$ at C_{11}), 2.89 (1H, do q, J=12, 7, 7, and 7 Hz, $\underline{H}$ at C_4), 4.63 (1H, t, J=4 Hz, $\underline{H}$ at C_6), and 5.45 (1H, do d, J=13 and 7 Hz, $\underline{H}$ at C_2). Found: C, 65.98; H, 7.83%. Calcd for $C_{17}H_{24}O_5$: C, 66.21; H, 7.85%.

*Oxidation of Compound **5** with Lead Tetraacetate.* A soln of **5** (1.44 g, 5.8 mmol) and lead tetraacetate (3.2 g, *ca.* 6.4 mmol) in a mixture of benzene (154 ml, 1.73 mol) and 2-propanol (4 ml, 57 mmol) containing boron trifluoride etherate (BF_3 5 ml, 39.6 mmol) was stirred at 25 °C under argon gas for 3.5 h, when the starch-iodide test for lead tetraacetate showed negative, an appreciable amount of **5** remaining unreacted (TLC). After addition of fresh lead tetraacetate (1.6 g, *ca.* 3.2 mmol), the soln was further stirred for 20 h under the same conditions. The reaction mixture was washed with 1 M hydrochloric acid, 5% aq sodium hydrogencabonate and water, dried, and evaporated to leave a crystalline residue (1.79 g), which was separated into three fractions by chromatography over silica gel (60 g) with ether-benzene (1 : 5) as eluents. The most mobile fraction gave A-nor-ester (**11**, 0.25 g), mp 111—112 °C, on trituration with hexane-isopropyl ether. Recrystallization from the same solvent mixture yielded an analytical sample of **11**: mp 112.5—113 °C and $[\alpha]_D$ −116.8°; MS, *m/e* 308 (M^+), 293, 249, 221, and 193 (base); IR and NMR, in the text. Found: C, 69.77; H, 9.05%. Calcd for $C_{18}H_{28}O_4$: C, 70.10; H, 9.15%.

The middle and least mobile fractions were triturated with acetone-isopropyl ether to give **10** (0.73 g), mp 202—203 °C, and **9** (0.16 g), mp 127.5—128.5 °C, respectively, which were identical with the corresponding authentic specimens.

*(11S)-2α,3β- and (11S)-2α,3α-Dihydroxy-4β,5α-eudesman-6β,12-olides (**12b** and **13b**), their 2-acetates (**12** and **13**), and their 2,3-diacetates (**12a** and **13a**).* *(i)* A soln of **10** (200 mg) in methanol (6 ml) was stirred with sodium borohydride (14 mg) at 0 °C for 14 min. After addition of AcOH (0.2 ml), the mixture was worked up as usual to leave a crystalline residue, showing two spots on TLC, which was separated into two fractions by preparative TLC over silica gel (Wakogel B-5) with a 2 : 3 mixture of ether and benzene. The more mobile fraction (117 mg), when triturated with acetone-isopropyl ether, gave **13** (96 mg), mp 190—191 °C. This was recrystallized from the same solvent mixture for analysis: mp 191—192 °C and $[\alpha]_D$ −77.6°; MS, *m/e* 250 (base, $M^+-C_2H_4O_2$), 235, 232, 217, and 204; IR, ν_{max} 3440, 1755, 1741, 1243, 1214, 1025, and 1018 cm^{-1}; NMR, δ 1.03 (3H, s, 15-C$\underline{H}_3$), 1.13 and 1.29 (each 3H, d, J=6 and 7.5 Hz, 14- and 13-C$\underline{H}_3$), 1.93 (1H, br s, O$\underline{H}$), 2.07 (3H, s, OCOC$\underline{H}_3$), 2.35 (1H, q, J=7.5 Hz, $\underline{H}$ at C_{11}), 3.91 (1H, br s, W_H=6.5 Hz, $\underline{H}$ at C_3), 4.59 (1H, t, J=4 Hz, $\underline{H}$ at C_6), and 5.01 (1H, do do d, J=11, 5.5, and 3 Hz, $\underline{H}$ at C_2). Found: C, 65.59; H, 8.53%. Calcd for $C_{17}H_{26}O_5$: C, 65.87; H, 8.44%.

The less mobile fraction (94 mg) on trituration with acetone-isopropyl ether afforded **12** (82 mg), mp 249—249.5 °C. This was recrystallized from the same solvent mixture for analysis: mp 251—252 °C and $[\alpha]_D$ −88.2°; MS, *m/e* 250 (base, $M^+-C_2H_4O_2$), 235, 232, 217, and 204; IR, ν_{max} 3435, 1742, 1732, 1243, and 1055 cm^{-1}; NMR, δ 1.06 (3H, s, 15-C$\underline{H}_3$), 1.16 and 1.31 (each 3H, d, J=6 and 7.5 Hz, 14- and 13-C$\underline{H}_3$), 2.07 (3H, s, OCOC$\underline{H}_3$), 2.36 (1H, q, J=7.5 Hz, $\underline{H}$ at C_{11}), 2.45 (1H, br s, O$\underline{H}$), 3.13 [(1H, do t, J=9, 9, and 5 Hz, $\underline{H}$ at C_3) (1H, t, J=9 Hz, on addition of D_2O)], 4.65 (1H, t, J=4 Hz, $\underline{H}$ at C_6), and 4.93 (1H, do do d, J=11.5, 9, and 5 Hz, $\underline{H}$ at C_2). Found: C, 65.58; H, 8.46%. Calcd for $C_{17}H_{26}O_5$: C, 65.78; H, 8.44%.

(ii) A soln of **12** (40 mg) in methanol (1 ml) containing 5% potassium hydroxide was stirred at room temp for 1 h. The reaction mixture was worked up as usual to leave a crystalline substance (32 mg), which was recrystallized from acetone-isopropyl ether to yield **12b** (29 mg), mp 182—183 °C. This was recrystallized from the same solvent mixture for analysis: mp 184—185 °C and $[\alpha]_D$ −93 °C; MS, *m/e* 268 (M^+), 250, 235, 232, 224 (base), 217, 209, and 206; IR, ν_{max} 3380, 3220, 1764, 1204, 1164, 1047, and 968 cm^{-1}; NMR, δ 0.99 (3H, s, 15-C$\underline{H}_3$), 1.14 and 1.30 (each 3H, d, J=6 and 7.5 Hz, 14- and 13-C$\underline{H}_3$), 2.37 (1H, q, J=7.5 Hz, $\underline{H}$ at C_{11}), 2.93 (1H, do d, J=9.5 and 8.5 Hz, $\underline{H}$ at C_3), 3.03 (2H, br s, 2O$\underline{H}$), 3.73 (1H, do do d, J=11, 8.5, and 5 Hz, $\underline{H}$ at C_2), and 4.66 (1H, t, J=4 Hz, $\underline{H}$ at C_6). Found: C, 66.97; H, 8.95%. Calcd for $C_{15}H_{24}O_4$: C, 67.13; H, 9.02%.

Compound **13** (139 mg) was hydrolyzed in methanol (4 ml) in the same manner as described above, giving a crystalline glycol (141 mg), which on recrystallization from ethyl acetate-isopropyl ether afforded **13b** (101 mg), mp 90—92 °C. This was recrystallized from the solvent mixture for analysis: mp 94.5—95 °C and $[\alpha]_D$ −90.1°; MS, *m/e* 268 (M^+), 250, 235, 232, 224, 217, and 206; IR, ν_{max} 3480, 3440, 1763, 1213, 1177, 1063, 1036, 1013, 999, and 971 cm^{-1}; NMR, δ 0.96 (3H, s, 15-C$\underline{H}_3$), 1.13 and 1.29 (each 3H, d, J=6.5 and 7.5 Hz, 14- and 13-C$\underline{H}_3$), 2.35 (1H, q, J=7.5 Hz, $\underline{H}$ at C_{11}), 2.65 (2H, br s, 2O$\underline{H}$), 3.84 (1H, br s, W_H=7 Hz, $\underline{H}$ at C_3), 3.91 (1H, br, W_H=20 Hz, $\underline{H}$ at C_2), and 4.62 (1H, t, J=4 Hz, $\underline{H}$ at C_6). Found: C, 65.00; H, 9.09%. Calcd for $C_{15}H_{24}O_4 \cdot 1/2CH_3COOC_2H_5$: C, 65.36; H, 9.03%.

(iii) Compound **12** (41 mg) was treated with acetic anhydride (Ac_2O, 1 ml) and Py (1 ml) at room temp for 12 h. The mixture was worked up as usual to leave a crystalline substance (47 mg), which on recrystallization from acetone-isopropyl ether gave **12a** (33.5 mg), mp 189.5—190.5 °C and $[\alpha]_D$ −82.0°; MS, 292 ($M^+-C_2H_4O_2$), 250 (base), 235, 232, and 217; IR, ν_{max} 1769, 1750, 1245, 1219, 1043, and 1030 cm^{-1}; NMR, δ 0.99 (3H, d, J=6.5 Hz, 14-C$\underline{H}_3$), 1.07 (3H, s, 15-C$\underline{H}_3$), 1.31 (3H, d, J=7.5 Hz, 13-C$\underline{H}_3$), 1.99 and 2.08 (each 3H, s, 2OCOC$\underline{H}_3$), 2.39 (1H, q, J=7.5 Hz, $\underline{H}$ at C_{11}), 4.66 (1H, t, J=4 Hz, $\underline{H}$ at C_6), 4.70 (1H, t, J=10 Hz, $\underline{H}$ at C_3), and 5.12 (1H, do do d, J=11, 9.5, and 5 Hz, $\underline{H}$ at C_2). Found: C, 64.70; H, 8.00%. Calcd for $C_{19}H_{28}O_6$: C, 64.75; H, 8.01%. Compound **12b** (14.5 mg) was acetylated in the same manner as **12** to give **12a** (crude 18.7 mg, pure 13.5 mg), mp 189—189.5 °C.

Compound **13** (84 mg) was treated with Ac_2O (1 ml) and Py (1 ml) at room temp for 24 h. The mixture was worked up as usual to leave a crystalline substance (97 mg), which was recrystallized from acetone–isopropyl ether to give **13a** (87 mg), mp 149.5—150.5 °C. Recrystallization from the same solvent mixture afforded an analytical sample: mp 150—151 °C and $[\alpha]_D$ −59.9 °; MS, *m/e* 292 ($M^+-C_2H_4O_2$), 250 (base), 235, 232, and 217; IR, ν_{max} 1772, 1741, 1260, 1248, 1233, and 1030 cm^{-1}; NMR, δ 1.01 (3H, d, J=8 Hz, 14-C$\underline{H_3}$), 1.05 (3H, s, 15-C$\underline{H_3}$), 1.30 (3H, d, J=7.5 Hz, 13-C$\underline{H_3}$), 1.97 and 2.11 (each 3H, s, 2OCOC$\underline{H_3}$), 2.39 (1H, q, J=7.5 Hz, $\underline{H}$ at C_{11}), 4.60 (1H, t, J=4 Hz, $\underline{H}$ at C_6), 5.11 (1H, do do d, J=11, 6, and 3 Hz, $\underline{H}$ at C_2), and 5.33 (1H, br, W_H=6.5 Hz, $\underline{H}$ at C_3).

Found: C, 64.52; H, 7.97%. Calcd for $C_{19}H_{28}O_6$: C, 64.75; H, 8.01%. Compound **13b** (37.5 mg) was acetylated in the same manner as **13** to give **13a** (crude 48.5 mg, pure 31.8 mg), mp 150—151 °C.

(11S)-2α,3α-Dihydroxy-4β,5α-eudesman-6β,12-olide 2,3-acetonide (14). (*i*) Silica gel (Wakogel Q-23, 25 g) packed in a column was washed twice with methanol, thrice with acetone, and once with hexane. Compound **13b** (100 mg) dissolved in hexane–acetone (1 : 1) was adsorbed onto the column and eluted with hexane–acetone (92 : 8) to give a crystalline material (112 mg), which was collected with hexane–isopropyl ether to yield **14** (57 mg), mp 115—117 °C. Recrystallization from the same solvent mixture afforded an analytical sample: mp 131—132 °C and $[\alpha]_D$ −53.9°; MS, *m/e* 293 (M^+-CH_3), 251, 233, 187, and 159 (base); IR (CCl_4), ν_{max} 1782, 1380, 1368, 1240, 1213, 1171, 1151, 1051, 1030, 1010, and 977 cm^{-1}; NMR, δ 0.90 (3H, s, 15-C$\underline{H_3}$), 1.19 and 1.30 (each 3H, d, J=7 and 7.5 Hz, 14- and 13-C$\underline{H_3}$), 1.35 and 1.48 [each 3H, s, $(C\underline{H_3})_2CO$], 2.37 (1H, q, J=7.5 Hz, $\underline{H}$ at C_{11}), 4.23 (2H, br m, 2$\underline{H}$ at C_2 and C_3), and 4.70 (1H, t, J=4 Hz, $\underline{H}$ at C_6). Found: C, 70.09; H, 9.06%. Calcd for $C_{18}H_{28}O_4$: C, 70.10; H, 9.15%.

(*ii*) Compound **12b** (22.6 mg) was treated with silica gel (Wakogel Q-23, 25 g) and acetone in the same manner as **13b**. The crystalline eluate (22.8 mg) was triturated with acetone–isopropyl ether to give a crystalline material (13.7 mg), mp 170.5—172 °C, which was identical with the unreacted starting glycol (**12b**).

*Oxidation of Compounds **12** and **13** to **10**.* (*i*) A soln of **12** (25 mg) in acetone (3 ml) was stirred with the Jones reagent (0.3 ml) at 0 °C for 1 h. After addition of ethanol, the mixture was evaporated *in vacuo* below 40 °C, diluted with water, and extracted with chloroform. The chloroform soln was worked up as usual to leave a crystalline residue (27.4 mg), showing a single spot, which on recrystallization from acetone–isopropyl ether yielded **10** (22 mg), mp 203.5—204 °C, identical with an authentic sample.

(*ii*) Compound **13** (25 mg) was oxidized with the Jones reagent (0.3 ml) in the same manner as **12** to yield **10** (21 mg), mp 203—204 °C, on recrystallization from acetone–isopropyl ether.

(11S)-4β,5α-Eudesmane-2α,3β,6β,12-tetraol (15) and Its 2,3,12-Triacetate (15a). A soln of **12** (403 mg) in dry THF (40 ml) was stirred with LAH (400 mg) under reflux for 24 h and cooled. After successive addition of ethyl acetate, methanol and water, the mixture was filtered to remove insoluble materials, which were washed with hot ethanol. The filtrate and ethanol washings were combined, evaporated below 40 °C, diluted with water, and extracted with chloroform with a Soxhlet apparatus for 5 d. The chloroform soln was concentrated to dryness to leave an oily substance (**15**, 410 mg), showing a single spot, which was treated with Ac_2O (2.7 ml) in Py (4 ml) at room temp for 19 h. The reaction mixture was worked up as usual to leave an oily residue (654 mg), which on trituration with isopropyl ether gave **15a** (427 mg), mp 96.5—98 °C. This was recrystallized from isopropyl ether for analysis: mp 96.5—98 °C and $[\alpha]_D$ −7.6 °C; MS, *m/e* 338 ($M^+-C_2H_4O_2$), 279, 278, 236, 219 (base), and 218; IR, ν_{max} 3535, 1733, 1241, 1050, 1033, and 1027 cm^{-1}; NMR, δ 0.92 and 1.02 (each 3H, d, J= 6.5 and 7 Hz, 14- and 13-C$\underline{H_3}$), 1.18 (3H, s, 15-C$\underline{H_3}$), 1.99 and 2.08 (3H and 6H, each s, 3OCOC$\underline{H_3}$), 3.89 and 4.21 (each 1H, do d, J=11, 6 and 11, 5 Hz, 2$\underline{H}$ at C_{12}), 4.08 (1H, br s, W_H=6.5 Hz, $\underline{H}$ at C_6), 4.70 (1H, t, J=10 Hz, $\underline{H}$ at C_3), and 5.11 (1H, do do d, J=11.5, 10, and 5 Hz, $\underline{H}$ at C_2). Found: C, 63.21; H, 8.74%. Calcd for $C_{21}H_{34}O_7$: C, 63.29; H, 8.60%.

Compound **15a** (132 mg) was refluxed in methanol (5 ml) containing 5% potassium hydroxide under nitrogen for 1 h. The soln was worked up as usual to give **15** (84 mg), amorphous; $[\alpha]_D$ −3.2° (EtOH). Found: C, 64.00; H, 10.17%. Calcd for $C_{15}H_{28}O_4 \cdot 1/2H_2O$: C, 64.02; H, 10.39%.

(11S)-4β,5α-Eudesmane-2α,3α,6β,12-tetraol (16) and Its 2,3,12-Triacetate and 2,12-Diacetate (16a and 16b). A soln of **13** (211 mg) in dry THF (21 ml) was stirred with LAH (300 mg) under reflux for 24 h. The reaction mixture was worked up in almost the same manner as that for **12** to leave a crystalline substance (118 mg), showing a single spot, which was recrystallized from acetone–isopropyl ether to give **16** (76 mg), mp 170—171 °C. Recrystallization twice from the same solvent mixture afforded an analytical sample: mp 174—174.5 °C and $[\alpha]_D$ −14.6° (EtOH); IR, ν_{max} 3410, 3290, 1077, 1053, 1038, 1022, and 1000 cm^{-1}. Found: C, 66.16; H, 10.32%. Calcd for $C_{15}H_{28}O_4$: C, 66.14; H, 10.36%.

The tetraol (**16**, 133 mg) was treated with Ac_2O (1.3 ml) and Py (1.5 ml) at room temp for 17 h. The mixture was worked up as usual to leave an oily residue (231 mg), showing two spots, which was separated into two fractions by column chromatography over silica gel (20 g) with a 3 : 1 mixture of benzene and ether. The more mobile fraction (175 mg) was crystallized and recrystallized from hexane–isopropyl ether to give **16a** (127 mg), mp 78.5—80 °C. This was recrystallized from the same solvent mixture for analysis: mp 80—81 °C and $[\alpha]_D$ +7.2°; MS, *m/e* 338 ($M^+-C_2H_4O_2$), 296, 279, 278, 263, 260, 236, 219, 218, 203, 200, 176, 161, and 107 (base); IR, ν_{max} 3590, 1743, 1253, 1226, and 1024 cm^{-1}; NMR, δ 0.97 and 1.02 (each 3H, d, J= 7 Hz, 14- and 13-C$\underline{H_3}$), 1.15 (3H, s, 15-C$\underline{H_3}$), 1.97, 2.08, and 2.11 (each 3H, s, 3OCOC$\underline{H_3}$), 3.87 and 4.22 (each 1H, do d, J=11, 6 and 11, 5 Hz, 2$\underline{H}$ at C_{12}), 4.00 (1H, br s, W_H= 7 Hz, $\underline{H}$ at C_6), 5.10 (1H, do do d, J=11.5, 5.5, and 3 Hz $\underline{H}$ at C_2), and 5.33 (1H, t, J=3 Hz, $\underline{H}$ at C_3). Found: C, 63.42; H, 8.65%. Calcd for $C_{21}H_{34}O_7$: C, 63.29; H, 8.60%. The less mobile fraction afforded **16b** (29 mg), oil and $[\alpha]_D$ −1.2°; MS, *m/e* 338 (M^+-H_2O), 296 ($M^+-C_2H_4O_2$), 278, 254, 236, 221, 218, and 203; IR ($CHCl_3$), ν_{max} 3610, 3500, 1733, 1246, and 1023 cm^{-1}; NMR, δ 1.00 and 1.07 (each 3H, d, J=7 Hz, 14- and 13-C$\underline{H_3}$ or *vice versa*), 1.13 (3H, s, 15-C$\underline{H_3}$), 2.08 (6H, s, 2OCOC$\underline{H_3}$), 3.88 and 4.21 (each 1H, do d, J=11, 6 and 11, 5 Hz, 2$\underline{H}$ at C_{12}), 3.97 (2H, m, 2$\underline{H}$ at C_3 and C_6), and 5.06 (1H, do do d, J=11.5, 5, and 3 Hz, $\underline{H}$ at C_2).

*Reduction of **10** with LAH and Subsequent Acetylation to **15a**.* To a cold suspension of LAH (15 g) in dry THF (1000 ml) was added dropwise a soln of **10** (30 g) in THF (200 ml) at 0 °C during a period of 15 min with stirring. The mixture, after further addition of THF (200 ml), was stirred under reflux for 24 h and cooled. After successive addition of ethyl

acetate (100 ml), ethanol (200 ml), and water (100 ml), the resulting suspension was stirred overnight at room temp and then filtered to remove an insoluble substance, which was washed with ethanol. The filtrate and ethanol washings were combined and evaporated to dryness to leave an oily residue (40.9 g), which was treated with Ac_2O (170 ml) and Py (260 ml) at room temp for 13 h. After being worked up as usual, the mixture left oily substances (40 g), which on trituration with isopropyl ether gave **15a** (25.2 g), mp 95.5—96.5 °C, identical with the authentic sample described in the previous section. The mother liquors, obtained by removal of the pure sample of **15a**, were dissolved in methanol (150 ml), refluxed with 10% potassium hydroxide in methanol (150 ml) for 1 h under nitrogen and then allowed to stand overnight at room temp. The reaction mixture was concentrated at 50 °C, diluted with water (50 ml), neutralized with 6 M hydrochloric acid at 0 °C, and extracted with chloroform with a Soxhlet apparatus for 5 d. The chloroform extracts afforded a foamy residue (9.4 g), showing two spots, which was separated into two fractions by chromatography over silica gel (500 g) with ethyl acetate. The more mobile fraction (3.1 g) crystallized on trituration with acetone-isopropyl ether to yield **16** (2.6 g), mp 174—174.5 °C, identical with an authentic sample. The less mobile fraction (5.1 g), amorphous, was again treated with Ac_2O (36 ml) and Py (50.5 ml) at room temp for 17 h to give **15a** (5.8 g) on trituration with isopropyl ether.

*(11S)-2α,3β,12-Triacetoxy-4β,5α-eudesman-6-one (**20**).* A soln of **15a** (103 mg) in acetone (11 ml) was stirred with the Jones reagent (0.6 ml) at 0 °C for 1 h. After addition of ethanol, the mixture was concentrated, diluted with water, and extracted with chloroform. The chloroform extracts, after being worked up as usual, left a crystalline residue, which was recrystallized from isopropyl ether to give **20** (87.5 mg), mp 109—109.5 °C. Recrystallization from isopropyl ether afforded an analytical sample: mp 109.5—111 °C and $[\alpha]_D$ −44.7°; MS, *m/e* 396 (M^+), 336, 276, and 216 (base); IR, ν_{max} 1751, 1738, 1703, 1253, 1235, 1222, 1080, 1038, and 1025 cm^{-1}; NMR, δ 0.88 (3H, s, 15-C$\underline{H}_3$), 0.89 and 0.93 (each 3H, d, J=7 and 6.5 Hz, 14- and 13-C$\underline{H}_3$ or *vice versa*), 2.00, 2.05, and 2.06 (each 3H, s, 3OCOC$\underline{H}_3$), 3.96 (2H, d, J=5 Hz, 2$\underline{H}$ at C_{12}), 4.72 (1H, t, J=10 Hz, $\underline{H}$ at C_3), and 5.03 (1H, do do d, J=11, 10, and 4.5 Hz, $\underline{H}$ at C_2). Found: C, 63.72; H, 8.28%. Calcd for $C_{21}H_{32}O_7$: C, 63.61; H, 8.14%.

*Photolysis of (11S)-2α,3β,12-Triacetoxy-4β,5α-eudesman-6β-ol 6-Nitrite (**17**).* To a soln of **15a** (2.94 g) in Py (30 ml) cooled at −20——30 °C was added dropwise excess nitrosyl chloride in Py during a period of 20 min, the yellow color of nitrosyl chloride remaining unchanged and the starting alcohol (**15a**) disappearing on TLC. The mixture was poured into ice-water (800 ml), and the resulting crystalline ppt was collected by filtration, washed with water, and dried over phosphorus pentaoxide for 18 h in a vacuum desiccator to yield **17** (3.13 g), mp 103.5—105.5 °C; IR, ν_{max} 1748, 1653, 1643, 1253, 1050, and 768 cm^{-1}; NMR, δ 0.89 and 0.91 (each 3H, d, J=6.5 Hz, 14- and 13-C$\underline{H}_3$ or *vice versa*), 1.01 (3H, s, 15-C$\underline{H}_3$), 1.98, 2.04, and 2.06 (each 3H, s, 3OCOC$\underline{H}_3$), 3.99 (2H, d, J=5 Hz, 2$\underline{H}$ at C_{12}), 4.72 (1H, t, J=10 Hz, $\underline{H}$ at C_3), 5.05 (1H, do do d, J=11.5, 10, and 5 Hz, $\underline{H}$ at C_2), and 5.94 (1H, br s, W_H=5 Hz, $\underline{H}$ at C_6).

The 6β-nitrite (**17**, 3.00 g) in dry benzene (thiophene-free, 200 ml) in a Pyrex vessel, without further purification, was irradiated with a 200 watt Hanovia high pressure mercury arc lamp at room temp for 2 h under a stream of argon. The reaction mixture was evaporated to dryness to leave a foamy residue, which was dissolved in THF (50 ml) and 2-propanol (50 ml) and refluxed for 1 h to decompose the nitroso dimer. The soln was evaporated below 50 °C to leave an oily residue, which was purified by chromatography over Florisil (100 g). Elution with benzene (180 ml), benzene–dichloromethane (5 : 1, 300 ml), and dichloromethane (570 ml) afforded oily materials (884 mg), which were purified as described later. Further elution with dichloromethane (280 ml) and dichloromethane–methanol (4 : 1, 240 ml) gave 15-oxime (**18**, 2.22 g), amorphous, resisting crystallization: $[\alpha]_D$ +12.1°; MS, *m/e* 410 (M^+−OH), 395, 382, 367, 350 (base), 335, 322, and 308; IR ($CHCl_3$), ν_{max} 3235, 3135, 1739, 1250, 1048, and 1032 cm^{-1}; NMR, δ 0.98 and 0.99 (total 6H, each d, J=7 and 6 Hz, 14- and 13-C$\underline{H}_3$ or *vice versa*), 2.00 and 2.07 (3H and 6H, each s, 3OCOC$\underline{H}_3$), 4.04 (3H, m, 3$\underline{H}$ at C_6 and C_{12}), 4.77 (1H, do d, J=8.5 and 7.5 Hz, $\underline{H}$ at C_3), 4.85 (1H, br m, W_H=10 Hz, $\underline{H}$ at C_2), 6.56 (1$\underline{H}$, d, J=9 Hz, O$\underline{H}$), 7.18 (1H, s, C$\underline{H}$=N), and 10.45 (1H, s, N-O$\underline{H}$).

The oily material (884 mg) described above was separated by rechromatography over silica gel (30 g). Elution with ether–benzene (1 : 5, 50 ml) afforded a crystalline substance (186 mg), which was recrystallized from isopropyl ether to give **20** (70 mg), mp 109—109.5 °C, identical with an authentic sample. Further elution with ether–benzene (1 : 2, 75 ml) afforded an oily substance (131 mg), which crystallized on standing, giving 6,15-oxolane (**19**, 80 mg), mp 72.5—74 °C, on trituration with hexane–isopropyl ether. Recrystallization twice from the same solvent mixture yielded an analytical sample: mp 100—101 °C and $[\alpha]_D$ −8.9°; MS, *m/e* 396 (M^+), 336, 294 (base), 277, 276, 251, 234, and 216; IR, ν_{max} 1741, 1244, 1230, and 1032 cm^{-1}; IR (liquid), ν_{max} 1743, 1478, 1240, 1229, 1035, and 862 cm^{-1}; NMR, δ 0.96 (6H, d, J=6.5 Hz, 14- and 13-C$\underline{H}_3$), 2.00, 2.05, and 2.07 (each 3H, s, 3OCOC$\underline{H}_3$), 3.62 and 3.86 (each 1H, ABq, J=8 Hz, 2$\underline{H}$ at C_{15}), 4.04 (2H, d, J=5.5 Hz, 2$\underline{H}$ at C_{12}), 4.18 (1H, s, $\underline{H}$ at C_6), 4.76 (1H, t, J=10 Hz, $\underline{H}$ at C_3), and 5.01 (1H, do t, J=5, 10, and 10 Hz, $\underline{H}$ at C_2). Found: C, 63.65; H, 8.24%. Calcd for $C_{21}H_{32}O_7$: C, 63.61; H, 8.14%. Further elution with ether–benzene 1 : 2, 175 ml) gave 15-oxime (**18**, 125 mg), amorphous, identical with the afore-mentioned sample.

*Hypoiodite Reaction of **15a** to **19**.* A suspection of lead tetraacetate (7.1 g) and calcium carbonate (4 g), precipitated and dried, in benzene (100 ml) was stirred under reflux for 40 min. To the mixture were added iodine (1.95 g), freshly sublimed, and **15a** (1.22 g) in benzene (50 ml), and the whole mixture was refluxed for 1.3 h and then stirred at room temp for 1.5 h under nitrogen. This was filtered through celite to remove an insoluble substance and the filtrate was washed with 30% aq sodium thiosulfate (200 ml) and water, dried, and evaporated to leave an oily residue (1.43 g), showing a single spot on TLC, which was purified by chromatography over silica gel (30 g). Eluates with benzene–ether (5 : 1) afforded an oily substance (893 mg), which crystallized on standing. This was recrystallized from hexane–isopropyl ether to give 6,15-oxolane (**19**), mp 99—100 °C, identical with an authentic sample.

*(11S)-2α,3β,12-Triacetoxy-4β,5α-eudesman-6β,15-olide (**21**).* Compound **18** (100 mg) was stirred with the Jones reagent (0.25 ml) in acetone (2 ml) at 0 °C for 30 min. The reaction mixture was worked up as usual to leave an oily residue (112 mg), showing an almost single spot on TLC, which was purified by preparative TLC over silica gel (Wakogel B-5) with ether–benzene (1 : 2). Elution with methanol gave a crystalline substance (54 mg), which was recrystallized from acetone–isopropyl ether to yield **21** (36 mg), mp 125—126 °C. This was recrystallized from the same solvent

mixture for analysis: mp 126—127 °C and $[\alpha]_D$ −1.5°; MS, *m/e* 382 (M^+−CO), 350, 322, 308, 290, 280, 262, 248, 230, 202, and 186; IR, ν_{max} 1780, 1745, 1242, 1229, 1116, 1047, and 1028 cm^{-1}; NMR, δ 0.96 and 1.00 (each 3H, d, J=6.5 and 5.5 Hz, 14- and 13-$C\underline{H}_3$ or *vice versa*), 1.97, 2.03, and 2.04 (each 3H, s, 3OCO$C\underline{H}_3$), 2.42 (1H, do d, J=13 and 5 Hz, $\underline{H}$ at C_1), 3.92 and 4.10 (each 1H, do ABq, J=5 and 11 Hz, 2$\underline{H}$ at C_{12}), 4.49 (1H, br s, W_H= 2.5 Hz, $\underline{H}$ at C_6), 4.68 (1H, t, J=10 Hz, $\underline{H}$ at C_3), and 4.74 (1H, do t, J=5, 10, and 10 Hz, $\underline{H}$ at C_2). Found: C, 60.89; H, 7.38%. Calcd for $C_{21}H_{30}O_8$: C, 61.45; H, 7.37%.

*(11S)-4β,5α-Eudesm-5-ene-2α,3β,12-triol Triacetate (**26**).* Compound **15a** (855 mg) was treated with methanesulfonyl chloride (MsCl, 1.5 ml) in Py (4 ml) at room temp for 44 h. The mixture was poured into ice-water and extracted with chloroform. The chloroform soln, after being worked up as usual, left an oily residue (928 mg), showing a single spot on TLC. This was purified by column chromatography over silica gel (50 g) with benzene–ether (5 : 1) to yield **26** (801 mg), bp 121—123 °C (bath temp) (5 Torr) and $[\alpha]_D$ −35.1°; MS, *m/e* 380 (M^+), 320, 260, and 200; IR (liquid), ν_{max} 1743, 1651, 1240, and 1041 cm^{-1}; NMR, δ 0.86 and 1.02 (each 3H, d, J=7 and 6.5 Hz, 13- and 14-$C\underline{H}_3$), 1.18 (3H, s, 15-$C\underline{H}_3$), 2.00 and 2.06 (3H and 6H, each s, 3OCO$C\underline{H}_3$), 3.98 (2H, br d, J=7 Hz, 2$\underline{H}$ at C_{12}), 4.60 (1H, do d, J=11 and 9.5 Hz, $\underline{H}$ at C_3), 5.16 (1H, do do d, J=12, 9.5, and 5 Hz, $\underline{H}$ at C_2), and 5.27 (1H, br s, W_H= 5 Hz, $\underline{H}$ at C_6). Found: C, 65.75; H, 8.50%. Calcd for $C_{21}H_{32}O_6$: C, 66.30; H, 8.48%.

*Dehydration of (11S)-15-Hydroxyimino-4β,5α-eudesmane-2α,3β, 6β,12-tetraol 2,3,12-Triacetate (**18**).* (*i*) A soln of **18** (1.24 g) in Py (20 ml) was stirred with phosphoryl chloride (8.5 ml) at room temp for 70 h, cooled, poured into ice-water (1 l) and extracted with chloroform. The chloroform soln, after being worked up as usual, left a foamy residue (1.13 g), which was separated by chromatography over silica gel (36 g). Eluates with benzene–ether (2 : 1) afforded an oily substance, which was crystallized on trituration with isopropyl ether and collected to give Δ^5-10-nitrile (**23**, 44 mg), mp 101—103 °C. Recrystallization from the same solvent afforded an analytical sample: mp 106—107 °C and $[\alpha]_D$ −90.3°; MS, *m/e* 331 ($M^+-C_2H_4O_2$), 289, 271, 262, 244, 229, 211 (base), 202, and 184; IR, ν_{max} 2225, 1745, 1252, 1227, 1052, and 1038 cm^{-1}; NMR, δ 0.87 and 1.09 (each 3H, d, J=7 and 6.5 Hz, 14- and 13-$C\underline{H}_3$ or *vice versa*), 2.01, 2.06, and 2.08 (each 3H, s, 3OCO$C\underline{H}_3$), 3.98 (2H, br d, J=6.5 Hz, 2$\underline{H}$ at C_{12}), 4.56 (1H, do d, J=11 and 9.5 Hz, $\underline{H}$ at C_3), 5.21 (1H, do do d, J=11.5, 9.5, and 4.5 Hz, $\underline{H}$ at C_2), and 5.58 (1H, br s, W_H=5 Hz, $\underline{H}$ at C_6). Found: C, 64.30; H, 7.51; N, 3.53%. Calcd for $C_{21}H_{29}O_6N$: C, 64.43; H, 7.47; N, 3.58%.

Eluates with benzene–ether (1 : 1) afforded a crystalline substance (751 mg), which on recrystallization from acetone–isopropyl ether gave 6β-hydroxy-10-nitrile (**22**, 606 mg), mp 174.4—175.5 °C. This was recrystallized from the same solvent mixture for analysis: mp 175—176 °C and $[\alpha]_D$ +21.5°; MS, *m/e* 409 (M^+), 366, 350 (base), 308, and 248; IR, ν_{max} 3530, 2230, 1739, 1728 (shoulder), 1240, 1050, and 1030 cm^{-1}; NMR, δ 0.98 and 1.02 (each 3H, d, J= 6.5 Hz, 14- and 13-$C\underline{H}_3$ or *vice versa*), 1.79 (1H, s, O$\underline{H}$), 1.98, 2.04, and 2.06 (each 3H, s, 3OCO$C\underline{H}_3$), 4.00 (3H, br m, 3$\underline{H}$ at C_6 and C_{12}), 4.69 (1H, do d, J=10.5 and 9.5 Hz, $\underline{H}$ at C_3), and 5.11 (1H, do do d, J=11.5, 9.5, and 5 Hz, $\underline{H}$ at C_2). Found: C, 61.62; H, 7.65; N, 3.46%. Calcd for $C_{21}H_{31}O_7N$: C, 61.59; H, 7.63; N, 3.42%.

(*ii*) Compound **18** (566 mg) was treated with Ac_2O (6 ml) and Py (10 ml) at room temp for 26 h. The mixture was worked up as usual to leave a foamy residue, showing a single spot on TLC, which was purified by chromatography over silica gel (25 g). Elution with ether–benzene (1 : 2) afforded a crystalline substance (484 mg), which on recrystallization from acetone–isopropyl ether yielded 6β-hydroxy-10-nitrile (**22**, 331 mg), mp 171.5—173.5 °C, identical with an authentic sample.

(*iii*) A soln of **18** (308 mg) in Py (2 ml) was treated with MsCl (0.5 ml) at room temp for 47 h. The mixture was worked up as usual to leave an amorphous residue (321 mg), which was dissolved in collidine (6 ml) and refluxed in a silicon-bath kept at 190 °C for 3 h. The mixture was cooled and diluted with chloroform. The whole soln gave an amorphous substance after the usual work-up, showing at least seven spots on TLC, which were purified by chromatography on silica gel (15 g). Elution with benzene–ether (2 : 1, 50 ml) afforded Δ^5-10-nitrile (**23**, 42 mg), mp 104—105 °C, on recrystallization from isopropyl ether. The other fractions were not examined further.

*Dehydration of (11S)-2α,3β,12-Triacetoxy-6β-hyrdoxy-15-nor-4β,5α-eudesmane-10β-carbonitrile (**22**).* A soln of **22** (4.24 g) in Py (20 ml) was stirred with MsCl (6.5 ml) at room temp for 47 h. The mixture was worked up as usual to leave an amorphous residue (5.00 g), which was refluxed in collidine (60 ml) for 3 h. The mixture was worked up in the same manner as that for **18** to give an oily residue (4.90 g), which was separated by chromatography over silica gel (100 g). Eluates with benzene–ether (2 : 1, 240 ml) afforded an oily substance (4.18 g), which was crystallized and recrystallized from isopropyl ether to give Δ^5-10-nitrile (**23**, 2.19 g), mp 106—107 °C, identical with an authentic sample. The mother liquors, obtained on crystallization and recrystallization, were concentrated to dryness and rechromatographed over silica gel (80 g). Eluates with benzene–ether (5 : 1, 180 ml) gave a crystalline substance (0.97 g), which on recrystallization from isopropyl ether yielded **23** (0.84 g), mp 106—106.5 °C. Further elution with benzene–ether (5 : 1, 240 ml) afforded an oily substance (0.38 g), which was crystallized and recrystallized from isopropyl ether to give Δ^6-10-nitrile (**24**), mp 80.5—82 °C. Recrystallization from the solvent gave an analytical sample: mp 81—82 °C and $[\alpha]_D$ −18°; MS, *m/e* 391 (M^+), 349, 331, 289, 271, 262, 244, 229, 211 (base), 202, 196, and 184; IR, ν_{max} 2230, 1742, 1242, 1224, 1051, and 1033 cm^{-1}; NMR, δ 1.04 and 1.09 (each 3H, d, J=5.5 and 7 Hz, 14- and 13-$C\underline{H}_3$), 2.02, 2.05, and 2.10 (each 3H, s, 3OCO$C\underline{H}_3$), 3.92 and 4.16 (each 1H, do d, J=11, 6.5 and 11, 7.5 Hz, 2$\underline{H}$ at C_{12}), 4.78 (1H, t, J=9.5 Hz, $\underline{H}$ at C_3), 5.24 (1H, do do d, J=11.5, 9.5, and 5 Hz, $\underline{H}$ at C_2), and 5.51 (1H, br s, W_H= 5 Hz, $\underline{H}$ at C_6). Found: C, 64.31; H, 7.49; N, 3.47%. Calcd for $C_{21}H_{29}O_6N$: C, 64.43; H, 7.47; N, 3.58%.

*(11S)-2α,3β,12-Trihydroxy-15-nor-4β-eudesm-5-ene-10β-carbonitrile (**23a**) and Its 2,3,12-Trimethoxymethyl Ether (**23b**).* A soln of **23** (2.53 g) in methanol (60 ml) was stirred with 10% potassium hydroxide in methanol (60 ml) at room temp overnight. The mixture was concentrated below 40 °C, diluted with water (100 ml), salted out, and extracted with ethyl acetate (4×250 ml). The ethyl acetate soln was washed with saturated brine (4×50 ml), dried, and evaporated to leave an amorphous substance (**23a**, 1.79 g), showing a single spot on TLC; NMR, δ 0.87 and 1.23 (each 3H, d, J=7 Hz, 14- and 13-$C\underline{H}_3$), 2.94 (1H, do d, J=10 and 8 Hz, $\underline{H}$ at C_3), 3.58 (2H, br d, J=6.5 Hz, 2$\underline{H}$ at C_{12}), 3.72 (1H, br m, $\underline{H}$ at C_2), and 5.58 (1H, br s, W_H=4 Hz, $\underline{H}$ at C_6). Compound **23a** (32 mg) was treated with Ac_2O (0.5 ml) in Py (0.5 ml) at room temp overnight to give **23** (38 mg), mp 102—104 °C, identical with the starting triacetate.

To a stirred soln of **23a** (269 mg) in dry chloroform (10 ml) and dimethoxymethane (10 ml), cooled at 0 °C, was added in portions phosphorus pentaoxide (5.7 g) during a period of 20 min.[20] The mixture was poured into cold 10 % aq sodium carbonate (400 ml) and extracted with chloroform. The chloroform extracts were washed with water, dried, and evaporated to leave an oily residue (362 mg), showing two spots on TLC, which was separated into two fractions by chromatography over alumina (Merck, standard, activity II-III, 40 g). Elution with benzene (460 ml) afforded an oily substance (55 mg), which would be the 2,3-methylenedioxy-12-methoxymethyl ether but was not further examined: IR ($CHCl_3$), ν_{max} 2255, 1141, 1114, 1093 (shoulder), 1040, and 917 cm^{-1}; NMR, δ 0.87 and 1.20 (each 3H, d, J=7 and 6.5 Hz, 14- and 13-C$\underline{H}_3$), 2.94 (1H, do d, J=10 and 8 Hz, $\underline{H}$ at C_3), 3.37 (3H, s, OC$\underline{H}_3$), 3.45 (2H, br d, J=6.5 Hz, $\underline{2H}$ at C_{12}), 3.82 (1H, do do d, J=12, 8, and 4 Hz, $\underline{H}$ at C_2), and 5.59 (1H, br s, W_H=6 Hz, $\underline{H}$ at C_6).

Eluates with benzene–ether (2 : 1, 400 ml) gave **23b** (235 mg), oil; MS, *m/e* 304 (M^+-3OCH_3); IR ($CHCl_3$), ν_{max} 2255, 1150, 1105, 1039, 1030, and 915 cm^{-1}; NMR, δ 0.87 and 1.23 (each 3H, d, J=7 and 6 Hz, 14- and 13-C$\underline{H}_3$), 3.02 (1H, do d, J=11 and 9 Hz, $\underline{H}$ at C_3), 3.38, 3.41, and 3.46 (each 3H, s, 3OC$\underline{H}_3$), 3.42 ($\underline{2H}$, br d, J=6 Hz, $\underline{2H}$ at C_{12}), 3.89 (1H, do do d, J=12, 9, and 4 Hz, $\underline{H}$ at C_2), 4.81 (6H, br m, 3OC$\underline{H}_2$O), and 5.57 (1H, br s, W_H=4 Hz, $\underline{H}$ at C_6).

(11S)-15-Nor-4β-eudesm-5(10)-ene-2α,3β,12-triol (27), Its Triacetate (27a), and 2,3-Acetonide (28). (*i*) To a suspension of sodium metal (1 g) in refluxing dry toluene (15 ml) was added dropwise a soln of **23** (125 mg) in dry ethanol (1.5 ml) and dry toluene (1.5 ml) during a period of 2 min. After 2 min, dry ethanol (4 ml) was again added, and the mixture was refluxed for 10 min and cooled. After addition of ethanol to decompose an excess of the sodium, the mixture was concentrated below 50 °C, diluted with water, salted out, and extracted with ethyl acetate. The acetate extracts were worked up as usual to leave **27** (79 mg), showing a single spot on TLC: NMR ($CDCl_3$ at 50 °C), δ 0.94 and 1.14 (each 3H, d, J=7 Hz, 13- and 14-C$\underline{H}_3$), 3.21 (1H, do d, J=9.5 and 8 Hz, $\underline{H}$ at C_3), and 3.60 (4H, br m, $\underline{3H}$ at C_2 and C_{12}, and O$\underline{H}$). Compound **27** (79 mg), without further purification, was treated with Ac_2O (2 ml) in Py (2 ml) at room temp overnight. The mixture was worked up as usual to give an oily residue (106 mg), which was purified by chromatography over silica gel (5 g). Elution with benzene–ether (5 : 2) yielded **27a** (83 mg) in pure state, oil and $[\alpha]_D$ +1.7°; MS, *m/e* 306 ($M^+-C_2H_4O_2$), 264, 246, 204, 203, 186, 171, 157, 144 (base), and 143; IR (CCl_4), ν_{max} 1748, 1242, 1228, and 1031 cm^{-1}; NMR, δ 0.95 and 1.05 (each 3H, d, J=6.5 and 7 Hz, 13- and 14-C$\underline{H}_3$), 2.03 and 2.08 (3H and 6H, each s, 3OCOC$\underline{H}_3$), 3.91 and 4.11 (each 1H, do d, J=11, 6 and 11, 5.5 Hz, $\underline{2H}$ at C_{12}), and 4.98 (2H, br m, $\underline{2H}$ at C_2 and C_3). Found: C, 65.27; H, 8.41%. Calcd for $C_{20}H_{30}O_6$: C, 65.55; H, 8.25%.

(*ii*) To a suspension of sodium metal (16.1 g) in refluxing dry toluene (240 ml) was added dropwise a soln of **23** (1.99 g) in dry ethanol (24 ml) and dry toluene (24 ml) during a period of 7 min. After 5 min, dry ethanol (64 ml) was again added over a period of 8 min, and the whole mixture was stirred under reflux for 10 min. The reaction mixture was worked up in the same manner as described above to yield triol (**27**, 1.20 g), showing a single spot on TLC. A soln of the triol was immediately dissolved in a 1 : 1 mixture of acetone and hexane and passed through silica gel (Wakogel Q-23, 240 g), which had been packed in a column with chloroform and washed successively with methanol, acetone and hexane. Elution with acetone–hexane (1 : 3) afforded crude acetonide (**28**, 1.15 g), which was purified twice by chromatography over alumina (60 g). Eluates with ether–benzene (1 : 2) gave **28** (1.07 g) in pure state, oil and $[\alpha]_D$ −54.7°; MS, *m/e* 280 (M^+), 265, 222, 145, and 131 (base); IR (CCl_4), ν_{max} 3390, 1380, 1371, 1229, 1152, 1089, and 1034 cm^{-1}; NMR, δ 0.94 and 1.14 (each 3H, d, J=6.5 Hz, 13- and 14-C$\underline{H}_3$), 1.46 [6H, s, $(C\underline{H}_3)_2CO$], 3.20 (1H, t, J=9.5 Hz, $\underline{H}$ at C_3), and 3.57 (3H, br m, $\underline{3H}$ at C_2 and C_{12}).

(*iii*) To a soln of rishitin acetonide[2] (**31**, 388 mg), obtained from natural rishitin (**1**), in dry ether (40 ml) was bubbled at room temp excess diborane, generated by dropwise addition of boron trifluoride etherate (1.2 ml) in dry diglyme (10 ml) to a soln of sodium borohydride (450 mg) in dry diglyme (15 ml), with stirring over a period of 25 min. The soln was stirred at room temp for 2 h, while the generator flask of diborane was allowed to stand at room temp for 1 h and then heated at 70—80 °C for 1 h. After removal of the generator and subsequent careful addition of water to decompose an excess of the diborane, the whole mixture was treated with 30% aq hydrogen peroxide (2 ml) and 3 M aq sodium hydroxide (2 ml) at 30—50 °C for 1 h with stirring. The mixture was cooled and extracted with ether repeatedly. The ether extracts were worked up as usual to leave an oily residue (500 mg), which was, without further purification, refluxed with 10% aq phosphoric acid (5 ml) in ethanol (30 ml) for 1 h. The reaction mixture was concentrated and extracted with ethyl acetate. The acetate extracts were worked up as usual to leave an oily residue (320 mg), showing two spots on TLC. A part (230 mg) of the residue was treated with Ac_2O (3 ml) in Py (6 ml) at room temp for 8 h to give oily materials, showing two spots on TLC, which were separated into two fractions by chromatography over silica gel (15 g) with benzene–ether (5 : 1). The less polar fraction (140 mg) was found to be identical with the diacetylrishitin[2] by comparison with an authentic sample. The more polar fraction (83 mg), oil, was identical with the triacetate (**27a**), derived from **23**, described above (TLC, Mass, IR, and NMR).

(11S)-15-Nor-4β-eudesm-5(10)-ene-2α,3β,12-triol 2,3-Acetonide 12-Methyl Ether (30) and Rishitin Acetonide (31). (*i*) Compound **28** (1.00 g) was treated with *p*-toluenesulfonyl chloride (1.03 g) in Py (10 ml) at room temp for 20 h. The soln was poured into ice-water (400 ml), salted out, and extracted with ether (4×200 ml). The ether extracts were worked up as usual to leave 12-tosylate (**28a**, 1.52 g), oil and $[\alpha]_D$ −5.8°; IR (CCl_4), ν_{max} 1600, 1377, 1371, 1229, 1189, 1180, 1100, 1087, 1044, 1032, 970, 842, and 815 cm^{-1}; NMR, δ 0.91 and 1.06 (each 3H, d, J=6 and 6.5 Hz, 13- and 14-C$\underline{H}_3$), 1.45 [6H, s, $(C\underline{H}_3)_2CO$], 2.44 (3H, s, $C\underline{H}_3C_6H_4SO_2$), 3.18 (1H, t, J=9 Hz, $\underline{H}$ at C_3), 3.51 (1H, m, $\underline{H}$ at C_2), 3.89 and 3.97 (each 1H, do ABq, J=5 and 9.5 Hz, $\underline{2H}$ at C_{12}), 7.30 and 7.75 (each 2H, d, J=8 Hz, $CH_3C_6\underline{H}_4SO_2$).

(*ii*) A soln of 12-tosylate (**28a**, 1.49 g) in acetone (80 ml) was stirred with sodium iodide (8 g) under reflux for 22 h. The mixture was evaporated and extracted with ether (100 ml). The ether extracts were washed with 5% aq sodium thiosulfate (yellow color disappeared) and saturated brine, dried, and evaporated to leave 12-iodide (**29**, 1.26 g), showing a single spot, oil, which crystallized on cooling at −15 °C, and had mp 58—61 °C and $[\alpha]_D$ −28.5°; MS, *m/e* 390 (M^+), 375, 332, 315, 263, 262, 247, 205, 187, 163, 145, and 131; IR (CCl_4), ν_{max} 1380, 1371, 1230, and 1098 cm^{-1}; NMR, δ 0.99 and 1.15 (each 3H, d, J=6 and 6.5 Hz, 13- and 14-C$\underline{H}_3$), 1.45 [6H, s, $(C\underline{H}_3)_2CO$], 3.25 (3H, br m, $\underline{3H}$ at C_3 and C_{12}), and 3.59 (1H, do t, J=7, 9, and 9 Hz, $\underline{H}$ at C_2).

(*iii*) 12-Iodide (**29**, 1.21 g) was refluxed with 5% potassium hydroxide in methanol (100 ml) for 2.5 h under nitrogen.

The mixture was worked up as usual to leave an oily residue (0.82 g), showing two spots on TLC, which was separated into two fractions by chromatography over alumina (60 g). Elution with hexane–benzene (1 : 1, 50 ml) afforded **31** (0.57 g), oil and $[\alpha]_D$ −71.7° (EtOH); MS, *m/e* 262 (M^+), 247, 205, 204, 203, 187, and 131 (base); IR (liquid), ν_{max} 3080, 1643, 1378, 1370, 1229, 1100, 1083, 1042, and 888 cm^{-1}; NMR, δ 1.14 (3H, d, J=6.5 Hz, 14-C$\underline{H}_3$), 1.44 [6H, s, ($C\underline{H}_3$)$_2$CO], 1.72 (3H, s, 13-C$\underline{H}_3$), 3.20 (1H, t, J=9 Hz, $\underline{H}$ at C_3), 3.58 (1H, do t, J=7, 9, and 9 Hz, $\underline{H}$ at C_2), 4.63 and 4.74 (each 1H, br s, W_H=4 Hz, 2$\underline{H}$ at C_{12}). This was identical with an authentic sample derived from natural rishitin. Further elution with hexane–benzene (1 : 1, 100 ml) gave **30** (0.13 g), oil and $[\alpha]_D$ −43.1°; MS, *m/e* 294 (M^+), 279, 236, and 131 (base); IR (liquid), ν_{max} 1378, 1371, 1105, and 1088 cm^{-1}; NMR, δ 0.92 and 1.14 (each 3H, d, J=6 and 6.5 Hz, 13- and 14-C$\underline{H}_3$), 1.45 [6H, s, ($C\underline{H}_3$)$_2$CO], 3.32 (3H, s, OC$\underline{H}_3$), and 3.41 (4H, br m, 4$\underline{H}$ at C_2, C_3 and C_{12}).

*Rishitin (**1**) and Its Diacetate (**1a**).* A soln of **31** (96 mg) in ethanol (24 ml) was stirred with 10% aq phosphoric acid (1.2 ml) under reflux for 1 h. After being worked up as usual, the soln gave an oily residue (84 mg), which was purified by chromatography over silica gel (9 g). Eluates with ether afforded an oily substance (**1**, 63 mg), which was further purified by distillation at 100—115 °C (bath temp) under reduced pressure (1 Torr) to yield crystalline rishitin (**1**), mp 58—60 °C and $[\alpha]_D$ −30.4° (EtOH) (lit,[2] mp 65—67 °C and $[\alpha]_D$ −35.1°); MS, *m/e* 222 (M^+), 204, and 189; IR (CCl_4), ν_{max} 3370, 3080, 1642, 1075, 1039, 1017, and 890 cm^{-1}; NMR, δ 1.14 (3H, d, J=6.5 Hz, 14-C$\underline{H}_3$), 1.75 (3H, s, 13-C$\underline{H}_3$), 3.18 (1H, t, J=9 Hz, $\underline{H}$ at C_3), 3.63 (1H, br do d, J=9 and 7 Hz, $\underline{H}$ at C_2), 4.64 and 4.74 (each 1H, br s, W_H=4 Hz, 2$\underline{H}$ at C_{12}). The synthetic rishitin (33 mg) was treated with Ac_2O (1 ml) and Py (1 ml) at room temp overnight. The mixture, after being worked up as usual, gave an oily substance, which was crystallized and recrystallized from hexane to give the diacetate (**1a**, 15 mg), mp 66—68 °C and $[\alpha]_D$ −14.1° (EtOH) (lit,[2] mp 70—71 °C and $[\alpha]_D$ −14.1°); Mass, *m/e* 246 ($M^+-C_2H_4O_2$), 204, 186, and 171; IR (CCl_4), ν_{max} 3070, 1749, 1642, 1242, 1225, 1030, and 890 cm^{-1}; NMR, δ 1.06 (3H, d, J=6.5 Hz, 14-C$\underline{H}_3$), 1.75 (3H, s, 13-C$\underline{H}_3$), 2.03 and 2.08 (each 3H, 2OCOC$\underline{H}_3$), 4.64 and 4.74 (each 1H, br s, W_H=4 Hz, 2$\underline{H}$ at C_{12}), and 4.98 (2H, br m, 2$\underline{H}$ at C_2 and C_3). These synthetic rishitin and diacetylrishitin were identical with the corresponding authentic specimens of natural rishitin (**1**) and its diacetate (**1a**) in all respects, respectively.

References

1) Part III of "Synthetic Studies of Rishitin and Related Compounds;" Part II, Ref 3.

2) T. Masamune, A. Murai, M. Takasugi, A. Matsunaga, N. Katsui, N. Sato, and K. Tomiyama, *Bull. Chem. Soc. Jpn.*, **50**, 1201 (1977).

3) A. Murai, K. Nishizakura, N. Katsui, and T. Masamune, *Tetrahedron Lett.*, **1975**, 4399.

4) For the total synthesis of (−)-α-santonin, *cf.*, Y. Abe, T. Harukawa, H. Ishikawa, T. Miki, M. Sumi, and T. Toga, *J. Am. Chem. Soc.*, **78**, 1422 (1956).

5) S. M. Sharif, S. Nozoe, K. Tsuda, and N. Ikekawa, *J. Org. Chem.*, **28**, 793 (1963).

6) In this paper we define eudesmane as 4,10β-dimethyl-7β-isopropyldecahydronaphthalene (**6**) and use the same nomenclature as that for steroids; *J. Org. Chem.*, **34**, 1517 (1969).

7) a) E. Piers and K. F. Cheng, *Can. J. Chem.*, **46**, 377 (1968); H. Ishikawa, *J. Pharm. Soc. Jpn.*, **76**, 504 (1956). b) W. Cocker, H. Gobinsingh, T. B. H. McMurry, and M. A. Nisbet, *J. Chem. Soc.*, **1962**, 1432.

8) *Cf.*, K. Kato, Y. Hirata, and S. Yamamura, *Tetrahedron*, **27**, 5987 (1971).

9) For the mass spectra of santonin derivatives, *cf.*, N. Wasada, T. Tsuchiya, E. Yoshii, and E. Watanabe, *Tetrahedron*, **23**, 4623 (1967).

10) *Cf.*, K. L. Williams and W. S. Johnson, *J. Org. Chem.*, **26**, 4563 (1961).

11) K. L. Williams and W. S. Johnson, *J. Am. Chem. Soc.*, **83**, 4623 (1961).

12) a) H. B. Henbest, D. N. Jones, and G. P. Slater, *J. Chem. Soc.*, **1961**, 4472; b) J. D. Cocker, H. B. Henbest, G. H. Phillipps, G. P. Slater, and D. A. Thomas, *J. Chem. Soc.*, **1965**, 6; c) H. B. Henbest, D. N. Jones, and G. P. Slater, *J. Chem. Soc., C*, **1967**, 756.

13) *Cf.*, D. H. R. Barton, J. M. Beaton, L. E. Geller, and M. M. Pechet, *J. Am. Chem. Soc.*, **83**, 4076 (1961).

14) *Cf.*, J. F. Bagli, P. F. Marand, and R. Gaudry, *J. Org. Chem.*, **28**, 1207 (1965).

15) *Cf.*, R. M. Moriarity and T. D. J. D'Silva, *Tetrahedron*, **21**, 547 (1965).

16) a) N. S. Bhacca and D. H. Williams, "Application of NMR Spectroscopy in Organic Chemistry," Holden-Day, Inc., San Francisco (1964), p. 13; b) K. Tori and T. Komeno, *Terahedron*, **21**, 309 (1965); K. Tori and K. Ando, *Ann. Rept Shionogi Res. Lab.*, **14**, 136 (1964).

17) T. Masamune, A. Murai, K. Nishizakura, T. Orito, S. Numata, and H. Sasamori, *Bull. Chem. Soc. Jpn.*, **49**, 1622 (1976), and refs cited therein.

18) *Cf.*, R. Gardi, C. Pedrali, and A. Ercoli, *Gazz. Chim. Ital.*, **93**, 525 (1963).

19) M. Nakazaki and K. Naemura, *Bull. Chem. Soc. Jpn.*, **37**, 1842 (1964).

20) *Cf.*, K. Fuji, S. Nakano, and E. Fujita, *Synthesis*, **1975**, 276.

Lubimin and Oxylubimin. The Structure Elucidation[1]

Nobukatsu KATSUI, Akira MATSUNAGA, Haruo KITAHARA, Fujio YAGIHASHI, Akio MURAI, Tadashi MASAMUNE, and Norio SATO*

Department of Chemistry, Faculty of Science, Hokkaido University, Sapporo 060
**Hokkaido National Agricultural Experiment Station, Sapporo 060-01*

(Received November 1, 1976)

The isolation and structure elucidation of lubimin (**3**) and oxylubimin (**4**), stress metabolites from diseased white potato tubers, are described.

In continuing studies on phytoalexins produced by diseased potato tubers, we have isolated several new sesquiterpenes besides rishitin[2] (**1**) and rishitinol[3] (**2**) from white potato tubers (*Solanum tuberlosum* × *S. demissum*, "Rishiri") infected by an incompatible race of *Phytophthora infestans*. On the other hand, in 1971 Metlitskii and coworkers[4] reported the isolation of an antifungal metabolite, qualified as phytoalexin and designated as lubimin[4a] (**3**), along with rishitin (**1**) from white potato tubers (*S. tuberlosum*, "Lubimets") stressed with various pathogens. They presumed the metabolite to be sesquiterpene aldehyde and proposed formula **3'** on the basis of the spectral data.[4b] One of our new sesquiterpenes could immediately be identified as the Metlitskii lubimin, and one of the other sesquiterpenes was designated as oxylubimin (**4**). We recently reported in preliminary communications[5] that lubimin is represented more favorably by formula **3** rather than the proposed formula (**3'**),[4b] and oxylubimin correctly by formula **4**. The same structures and configurations for these stress metabolites have recently been reported independently by Stoessl and coworkers.[6]

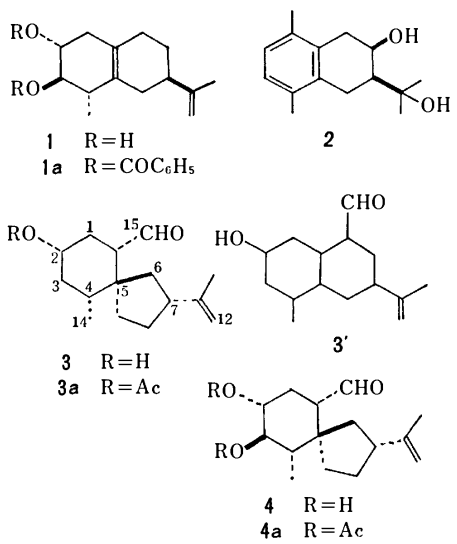

1 R=H
1a R=COC$_6$H$_5$

2

3 R=H
3a R=Ac

3'

4 R=H
4a R=Ac

Lubimin. Planar Structure. Lubimin (**3**), colorless oil and $[\alpha]_D$ +36°, had the molecular formula $C_{15}H_{24}O_2$ and gave the monoacetate (**3a**), oil and $[\alpha]_D$ +35°. These compounds exhibited the following spectra: **3**, MS, *m/e* 236 (M^+); IR, ν_{max} 3410, 3085, 2740, 1715, 1640, and 890 cm^{-1}; NMR, δ 0.94 (3H, d, J=7 Hz), 1.68 (3H, s), 3.65 (1H, m, W_H=25 Hz), 4.65 (2H, s), and 9.74 (1H, d, J=3 Hz): **3a**, MS, *m/e* 278 (M^+); IR, ν_{max} 2715, 1735, 1720, 1640, 1238, and 888 cm^{-1}; NMR, δ 1.69 (3H, s) and 4.70 (1H, m, W_H=25 Hz). These spectral data were indistinguishable from the corresponding data reported by Metlitskii and coworkers[4b] and indicated that the following structural units are involved in the molecule, as had been pointed out by them;[4b] –(CH$_3$)CH–, –C(CH$_3$)=CH$_2$, –CH(OH)–, and –CHO.

Reduction of lubimin (**3**) with sodium borohydride in ethanol afforded unsaturated glycol, dihydrolubimin[7] (**5**), mp 129—130 °C; *m/e* 238 (M^+); δ 3.28 (1H, t, J= 10 Hz) and 3.90 (1H, do d, J=10 and 2.5 Hz), which formed the diacetate (**5a**), oil; ν_{max} 1743 and 1238 cm^{-1}; δ 2.04 and 2.07 (each 3H, s) 3.83 and 4.36 (each 1H, do ABq, J=11, 8 and 11, 4 Hz), and 4.69 (1H, br m, W_H=25 Hz). Compound **5**, when hydrogenated over Adams platinum in ethanol, gave saturated glycol, tetrahydrolubimin (**6**), mp 145—147 °C; *m/e* 240; ν_{max} 1387 and 1372 cm^{-1}; δ 0.86 (9H, d, J=7 Hz). All these spectra confirmed the presence of the four groupings in bicyclic lubimin.

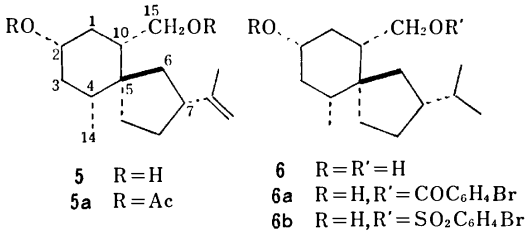

5 R=H
5a R=Ac

6 R=R'=H
6a R=H,R'=COC$_6$H$_4$Br
6b R=H,R'=SO$_2$C$_6$H$_4$Br

Treatment of tetrahydrolubimin (**6**) with *p*-bromobenzoyl chloride (one mole) and pyridine resulted in monobenzoylation, giving the mono-*p*-bromobenzoate (**6a**), mp 106—108 °C; IR, ν_{max} 3400, 1718, 1594, and 847 cm^{-1}; NMR, δ 3.64 (1H, br m, W_H=25 Hz), 3.99 and 4.46 (each 1H, do ABq, J=11, 10 and 11, 2 Hz). Likewise, compound **6**, when treated with *p*-bromobenzenesulfonyl chloride (2 mole) and pyridine, underwent monobrosylation to give the monobrosylate (**6b**), oil; IR, ν_{max} 3400, 1372, and 1183 cm^{-1}; NMR, δ 3.64 (1H, br m, W_H=25 Hz), 3.70 and 4.15 (each 1H, do ABq, J=11, 8 and 11, 4 Hz). The NMR spectra revealed that the primary hydroxyl group, formed by reduction of the formyl group, was acylated but the secondary hydroxyl remained unchanged in each of the compounds (**6a** and **6b**). Oxidation of the benzoate (**6a**) with chromium(VI) oxide produced oxo-benzoate (**7**), mp 71—73 °C; MS, *m/e* 220 (M^+–BrC$_6$H$_4$CO$_2$H) and 177; IR, ν_{max} 1720 and 1705 cm^{-1} (sh). Treatment of the ketone (**7**) with sodium deuteroxide in a mixture of dioxane and deuterium oxide effected deuteration of

two methylene groups adjacent to the carbonyl group with concomitant hydrolysis to yield the d_5-derivative (**8**), $C_{15}H_{21}D_5O_2$; MS, *m/e* 243; IR, ν_{max} 1705 cm^{-1}. This result elucidated that a moiety $-CH_2CH(OH)CH_2-$ would be included in a six- or seven-membered ring but not in a five-membered ring. On the other hand, the monobrosylate (**6b**), on treatment with potassium *t*-butoxide in *t*-butyl alcohol, was converted into oxolane (**9**), oil. In accordance with the assigned structure, compound **9** exhibited parent and fragmentation peaks at *m/e* 222 and 179 in the mass spectrum and absorption maxima at 1105 and 912 cm^{-1},[8] and at δ 0.87, 0.89, and 1.10 (each 3H, d, J=7—7.5 Hz), 3.49 and 3.78 (each 1H, do ABq, J=10, 4.5 and 10, 0 Hz), and 4.19 (1H, narrow m, W_H=10 Hz). These results revealed the presence of a moiety $-CH_2CH(OH)CH_2CH(CHO)-$ in lubimin (**3**), implying that the proposed structure (**3'**) should be revised.

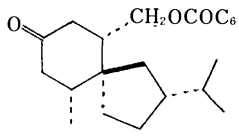

7

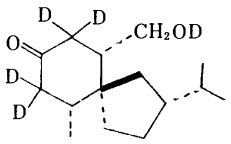

8

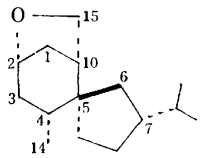

9

The ^{13}C NMR spectra of diacetyldihydrolubimin (**5a**) were then obtained at 25.2 MHz under proton noise decoupled and single-frequency off-resonance decoupled conditions, and each signal was assigned, as summarized in Table 1, on the basis of the multiplicity and chemical shift.[9] As shown in Table 1, compound **5a** contained a quaternary carbon at δ 46.7[10] besides those of the isopropenyl and two acetoxyl groups, again excluding the proposed structure (**3'**). It is noted that the carbon in question would evidently be of spiro type

Table 1. The ^{13}C NMR spectra of dihydrolubimin (**5**), its diacetate (**5a**), and triacetyldihydrooxylubimin (**11a**)

Compound	**5**	**5a**	**11a**
Carbon no.	Chemical shift (δ, $CDCl_3$, 100 MHz)		
1	48.3	40.5	41.1
2	69.6	72.1	73.7
3	40.4	36.8	75.5
4	40.7 or 40.9	40.9 or 44.8	45.8 or 47.3
5	46.4	46.7	48.0
6	32.6	32.6	31.4
7	47.1	47.3	47.3 or 45.8
8	36.6	33.0	32.9
9	25.3	25.2	26.1
10	40.9 or 40.7	44.8 or 40.9	45.8 or 47.3
11	147.5	147.9	147.4
12	107.8	108.8	109.2
13	21.2	21.0	21.0
14	16.1	16.6	11.4
15	63.9	66.3	65.7

Table 2. The NMR spectrum of lubimin (**3**) in the presence of the europium shift reagent $Eu(fod)_3$ (CCl_4, 100 MHz) and spin-decoupling results

Run	Mole ratio **3** : $Eu(fod)_3$	Irradiated proton (δ, Hz)	Observed proton (δ) Multiplicity change and decoupled splitting (Hz)
1	2 : 1	11.13 (H_a at C_{15})	4.24 (H_b) br t ⟶ t (2.5)
2a	2 : 1	4.24 (H_b at C_{10})	11.13 (H_a) d ⟶ s (2.5)
b			7.30 (H_c) br t ⟶ br s
3a	2 : 1	7.30 (H_c at C_1)	4.24 (H_b) br t ⟶ br s (8 and 8)
b			10.36 (H_d) m (W_H=25) ⟶ m (W_H=20)
4a	2 : 1	10.36 (H_d at C_2)	7.30 (H_c) br t ⟶ br d
b			6.05 (H_e) br t ⟶ br d
5a	2 : 1	6.05 (H_e at C_3)	10.36 (H_d) m (W_H=25) ⟶ m (W_H=20)
b			≈3.4 (H_f) ch?
6a	2 : 1	3.38 (H_f at C_4)	6.05 (H_e) br t ⟶ br s
b			1.90 (H_g) d ⟶ s (7)
7	2 : 1	1.90 (H_g at C_{14})	≈3.4 (H_f) ch?
8a	2 : 1	3.82 (H_h at C_6)	≈3.2 (H_i) ch
b			≈2.3 (H_j) ch
9a	2 : 1	3.20 (H_i at C_6)	3.82 (H_h) do d ⟶ d (13)
b			≈2.3 (H_i) ch
10a	2 : 1	2.30 (H_j at C_7)	3.82 (H_h) do d ⟶ d (7)
b			≈3.2 (H_i) ch
11	1 : 1	4.54 (H_f at C_4)	2.50 (H_g) d ⟶ s (7)
12	1 : 1	2.50 (H_g at C_{14})	4.54 (H_f) br m ⟶ br d (J=11) (7)

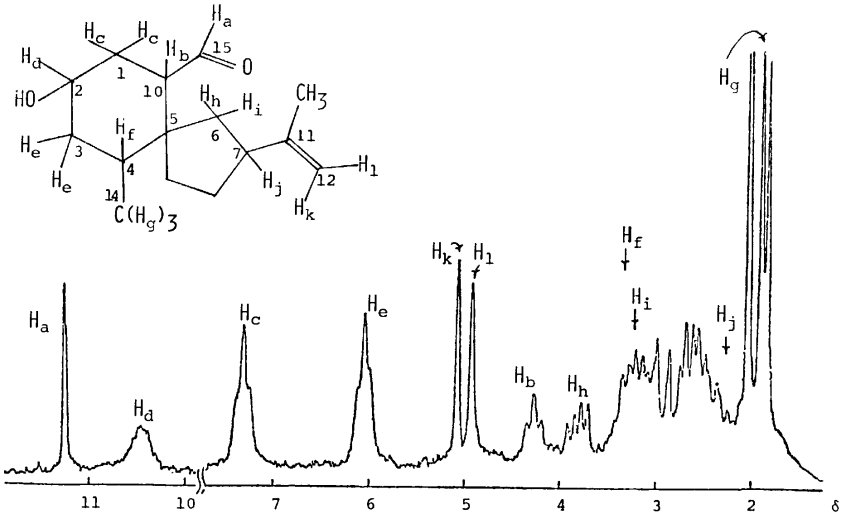

Fig. 1. The NMR spectrum of lubimin (**3**) in the presence of the shift reagent $Eu(fod)_3$ (CCl_4, 100 MHz, and the reagent: **3**=1 : 2).

owing to the absence of a methyl group attached to the quaternary carbon atom.

The whole structure of lubimin (**3**) was finally deduced from spin-decoupling studies of its NMR spectra of lubimin (**3**) in the presence of shift reagent $Eu(fod)_3$.[11] While the ring methylene and methine protons overlapped each other and appeared as a broad multiplet without the shift reagent, addition of 0.25—1.0 mole of $Eu(fod)_3$ per mole of the compound caused down-field shifts of all the signals. The down-field shifts were approximately linear with respect to concentration of the reagent and resulted in separation of most of the protons in question, as exemplified by Fig. 1. Decoupling studies were carried out on the europium-shifted spectra (the reagent : lubimin=1 : 2 and 1 : 1), the result being summarized in Table 2. In the spectrum (the reagent : lubimin=1 : 2, Fig. 1), signals centered at δ 11.13, 10.36, and 1.90 were readily assignable to the protons due to formyl, hydroxy-methine, and secondary methyl groups, respectively. Irradiation at δ 11.13 (C<u>H</u>O) collapsed a broad triplet at δ 4.24 [C<u>H</u>(CHO)] to a sharp triplet (run 1). Conversely, by irradiation at δ 4.24, the doublet (J=2.5 Hz) at δ 11.13 and a broad triplet at δ 7.30 [C<u>H</u>$_2$CH(CHO)] were simplified to a sharp singlet and a broad singlet, respectively (run 2). Further irradiation at δ 7.30 decoupled the broad triplet signal at δ 4.24 to a broad singlet and also narrowed a broad multiplet at δ 10.36 [C<u>H</u>(OH)CH$_2$CH-(CHO)] slightly but definitely (run 3). Similar change of the signal at δ 10.36 was also observed on irradiation at δ 6.05 [C<u>H</u>$_2$CH(OH)CH$_2$CH(CHO)], which simultaneously caused change of a signal pattern near δ 3.4 [C<u>H</u>CH$_2$CH(OH)CH$_2$CH(CHO)] (run 5). Inversely, irradiation at δ 3.38 collapsed the broad triplet at δ 6.05 to a broad singlet and also decoupled a doublet at δ 1.90 [CH(C<u>H</u>$_3$)] to a singlet (run 6), indicating the presence of a moiety -(CH$_3$)CHCH$_2$CH(OH)CH$_2$-CH(CHO)-. Fortunately, the methine protone (δ 3.38) adjacent to the methyl group appeared separately as a broad multiplet at δ 4.54 in the spectrum containing an equimolar shift reagent $Eu(fod)_3$. This multiplet signal was simplified to a broad doublet (J=11 Hz) by irradiation at δ 2.50, a center of a doublet due to the methyl protons (run 12). In view of the decoupling behaviors of the signals due to two relevant methine protons adjacent to the methyl and formyl groups (runs 12, 1, and 3a) as well as the presence of a quaternary carbon atom of spiro type, the quaternary carbon in question must be flanked by these two methine carbon atoms. Hence lubimin is represented either by (planar) formula **10a** or **10b**.

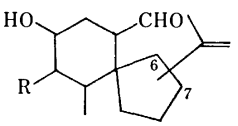

10a R=H, 6-isopropenyl
10b R=H, 7-isopropenyl
10c R=OH, 7-isopropenyl

In the NMR spectrum shown in Fig. 1, a clearly separated signal centered at δ 3.82 must be a methine or one of a methylene protons in a five-membered ring. The multiplicity (do d, J=13 and 7 Hz) revealed that the proton would probably be coupled to only two protons, one being a geminal proton and another a proton on the adjacent carbon atom. In fact, irradiation at δ 3.20 and 2.30 decoupled the signal to two doublets with coupling constants of 7 and 13 Hz, respectively. Thus the proton in question (δ 3.82) must be one of the methylene protons at C_6. The remarkable europium-induced down-field shift of this proton, as compared with the other five-membered ring protons, suggested that the proton would be disposed in the neighborhood of the formyl group. This result was not compatible with formula **10a** but only with formula **10b**. On the analogy of the structure and configuration of oxylubimin (**4**) described later, lubimin is represented most favorably by the stereostructure **3**, because the three substituents, formyl, hydroxyl, and methyl groups at C_{10}, C_2, and C_4 in the A ring would evidently be oriented

equatorial.

Oxylubimin. Planar Structure. The titled compound (**4**), mp 85—86 °C and $[\alpha]_D$ +27°, had the molecular formula $C_{15}H_{24}O_3$ and gave the diacetate (**4a**), oil and $[\alpha]_D$ +22°. Reduction of oxylubimin (**4**) with sodium borohydride afforded unsaturated triol, dihydrooxylubimin (**11**), mp 170—171 °C, which formed the triacetate (**11a**), oil, and, on hydrogenation over Adams platinum, yielded saturated triol, tetrahydrooxylubimin (**12**), mp 163—165 °C. Likewise, the diacetate (**4a**) was reduced with sodium borohydride to give diacetyldihydrooxylubimin (**11b**), oil, which was converted into the triacetate (**11a**). The IR and NMR spectra of these compounds indicated that oxylubimin (**4**) contained the following structural units: $-CH(CH_3)-$ [**4** and **11b**, δ 1.08 and 0.89 (each 3H, d, J=7 Hz)]: $-CH(CHO)-$ [**4**, ν_{max} 2715 and 1715 cm^{-1}, δ 2.38 (1H, do do d, J=10, 4, and 2.5 Hz) and 9.80 (1H, d, J=2.5 Hz); **11b**, ν_{max} 3460 cm^{-1}, δ 3.34 and 3.92 (each 1H, do ABq, J=11, 8 and 11, 3 Hz)]: $-CH(CH_3)=CH_2$ [**4**, ν_{max} 1645 and 895 cm^{-1}, δ 1.72 (3H, s) and 4.75 (2H, br s); **11b**, ν_{max} 1643 and 885 cm^{-1}, δ 1.73 (3H, s) and 4.68 (2H, br s); **12**, ν_{max} 1388 and 1372 cm^{-1}]: $-CH(OH)CH(OH)-$ [**4**, positive to the HIO_4 test,[12] ν_{max} 3560, 3300, and 3080 cm^{-1}, δ 3.01 (1H, t, J= 10 Hz), 3.48 (1H, br t, J=10 Hz, W_H=20 Hz), and 3.90 (2H, br s, disappeared on addition of D_2O); **11b**, ν_{max} 3460, 1745, and 1250 cm^{-1}, δ 2.00, 2.04 (each 3H, s), and 4.76 (2H, m).

These results and the spin-decoupling studies on the NMR spectra of oxylubimin (**4**) in the absence and also in the presence of the shift reagent Eu(fod)$_3$, the results being summarized in Table 3, elucidated the presence of a moiety ■(quaternary carbon)-$CH(CH_3)$-$CH(OH)$-$CH(OH)$-CH_2-$CH(CHO)$-■ and hence oxylubimin (**4**) could be regarded as a 3β-hydroxyl derivative of lubimin (**3**). In good accord with this presumption, triacetyldihydrooxylubimin (**11a**) exhibited the ^{13}C NMR spectra (Table 1) closely similar to that of diacetyldihydrolubimin (**5a**), apart from a signal due to the 3-carbon atom, in which a quaternary carbon of spiro type was observed as a singlet peak at δ 48.0. Moreover, oxidation of triacetate (**11a**) by the Lemieux-Johnson procedure[13] gave methyl ketone (**13**), oil, which displayed a three-proton singlet and a broad one-proton peak (W_H=25 Hz) due to the acetyl and acetyl-methine protons at δ 2.16 and 2.83 in the NMR spectrum. The wide half-width of the methine proton signal indicated that the acetyl group, derived from the isopropenyl group in oxylubimin (**4**), would not be located on the carbon atom adjacent to the spiro-carbon. Hence oxylubimin must be represented by (planar) formula **10c**.

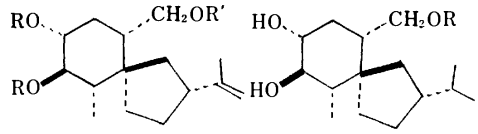

11 R=R'=H
11a R=R'=Ac
11b R=Ac, R'=H
11c R=COC_6H_5, R'=H

12 R=H
12a R=$SO_2C_6H_4Br$

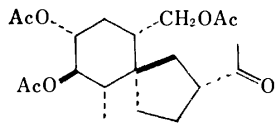

13

Stereochemistry. The four substituents in the A ring

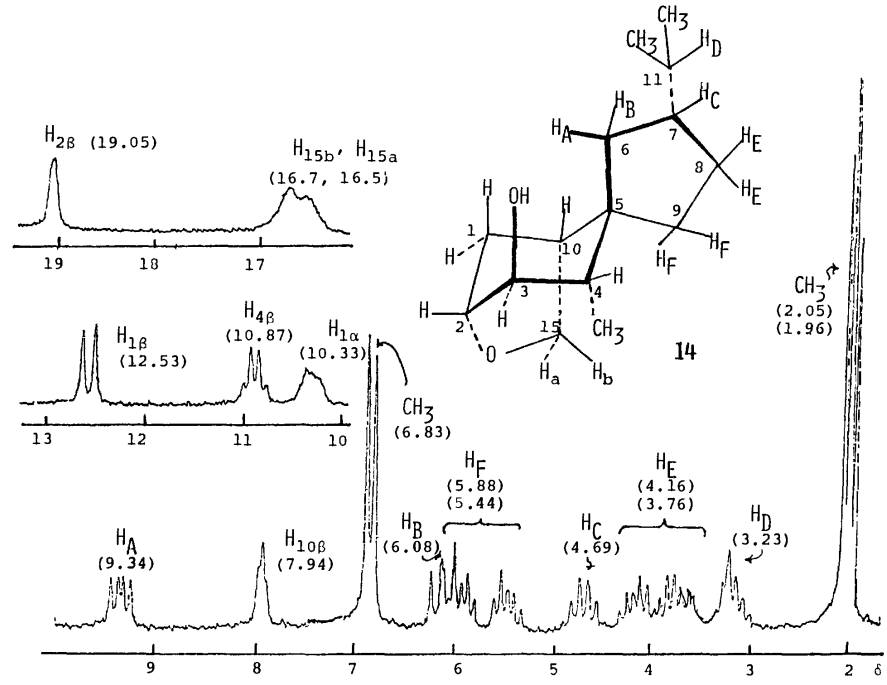

Fig. 2. The NMR spectrum of hydroxyoxolane (**14**) in the presence of the shift reagent Eu(dpm)$_3$ (CCl_4, 100 MHz, and the reagent: **14**=0.8 : 1).

Table 3. The NMR spectra of oxylubimin (**4**) in the absence [A] and in the presence of the shift reagent $Eu(fod)_3$ [B] and spin-decoupling results

Irradiated proton (δ, Hz)	Observed proton (δ) Multiplicity change and decoupled splitting (Hz)			
[A] (CCl_4, 100 MHz)				
9.80 (H_a) CH(CHO) (d, J=2.5)	2.38 (H_b)	do t	⟶	do d (2.5)
2.38 (H_b) CH(CHO) (do do d, J=10, 4, and 2.5)	9.80 (H_a)	d	⟶	s (2.5)
1.76 (H_c) H (ax) at C_1 (not clearly obsd)	2.38 (H_b)	do do d	⟶	br s (10)
	3.48 (H_e)	br t	⟶	br d (10)
2.08 (H_d) H (eq) at C_1 (not clearly obsd)	2.38 (H_b)	ch		
	3.48 (H_e)	br t	⟶	t (small)
3.48 (H_e) CH(OH) at C_2 (br t, J=10)	3.01 (H_f)	t	⟶	d (10)
3.01 (H_f) CH(OH) at C_3 (t, J=10)	3.48 (H_e)	br t	⟶	br d (10)
1.60 (H_g) CH(CH_3) (not clearly obsd)	3.01 (H_f)	t	⟶	d (10)
	1.08 (CH_3)	d	⟶	s (7)
[B] (CCl_4, 100 MHz; the shift reagent: **4**=1 : 1)				
8.86 (H_b) CH(CHO) (br d, J=10)	11.38 (H_c)	br q	⟶	do t (10)
	10.77 (H_d)	br d	⟶	do d (small)
11.38 (H_c) H (ax) at C_1 (br q, $J\approx$10)	8.86 (H_b)	br d	⟶	br s (10)
	10.77 (H_d)	br d	⟶	br s (12)
10.77 (H_d) H (eq) at C_1 (br d, J=12)	8.86 (H_b)	br d	⟶	d (small)
	11.38 (H_c)	ch		
11.20 (H_g) CH(CH_3) (br m)	5.68 (CH_3)	d	⟶	s (7)
5.68 (CH_3) (d, J=7)	11.20 (H_g)	br m	⟶	d (J=10) (7)

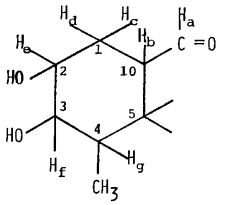

of oxylubimin (**4**) were presumed to be all equatorial on the basis of the magnitudes of the vicinal coupling constants for each of the methine, methylene, and hydroxy-methine protons ($J_{b,c}$, $J_{b,d}$, $J_{e,c}$, $J_{e,d}$, $J_{e,f}$, and $J_{f,g}$ =10, 4, 10, small, 10, and 10 Hz), estimated from the data in Table 3. Since the A ring would probably adopt a chair conformation, the relative configurations of the four substituents at C_{10}, C_2, C_3, and C_4 must be *cis*, *trans*, and *trans*, respectively. Moreover, the *trans*-diequatorial disposition between the C_3-hydroxyl and C_4-methyl groups was also deduced from the ^{13}C NMR specrum of triacetyldihydrooxylubimin (**11a**), in which the 14-methyl carbon atom was observed at a higher field (δ 11.4) as compared with the corresponding carbon (δ 16.6) in diacetyldihydrolubimin (**5a**). This high-field shift of the methyl carbon atom could be explained well as a neighboring effect due to the diequatorially-oriented acetoxyl group at C_3.[14] The absolute configrations of these substituents were decided by application of "exciton chirality method"[15] to dibenzoyldihydrooxylubimin (**11c**), mp 58—59 °C. This dibenzoate was obtained by benzoylation of oxylubimin followed by sodium borohydride reduction and exhibited a characteristic split curve in the CD spectrum (ethanol); $\Delta\varepsilon$ −19.2 (235 nm) and +5.9 (219) [*cf.*, rishitin dibenzoate, $\Delta\varepsilon$ −17.6 (235 nm) and +6.1 (218)].[16] The negative sign of the first splitting effect indicated a left-hand helix for the vicinal dibenzoate moiety, leading to assignment of α-, α-, β-, and α-configurations to the four substituents at C_{10}, C_2, C_3, and C_4 in the A ring.

Tetrahydrooxylubimin (**12**), when treated with *p*-bromobenzenesulfonyl chloride, underwent partial brosylation to give monobrosylate (**12a**), mp 98—100 °C, which on treatment with potassium *t*-butoxide in *t*-butyl alcohol at 0 °C for 30 min yielded hydroxyoxolane (**14**), oil. The mass [*m/e* 238 (M^+) and 220] and IR spectra (ν_{max} 3420, 1390, 1372, 1079, and 1010 cm^{-1}) were consistent with the assigned structure, and the NMR spectrum [δ 0.88 (6H, d, J=6.5 Hz, 12- and 13-CH_3), 1.06 (3H, d, J=8 Hz, 14-CH_3), 1.90 (1H, t, J=4.5 Hz, β-H at C_{10}), 2.36 (1H, d, J=12 Hz, β-H at C_1), 3.66 (1H, do d, J=8 and 4.5 Hz, a-H at C_{15}), 3.78 (1H, d, J=5 Hz, α-H at C_3), 3.87 (1H, d, J=8 Hz, b-H at C_{15}), and 4.18 (1H, t, J=5 Hz, β-H at C_2)], indicated the A ring to take a slightly deformed chair-form with the four substituents at C_{10}, C_2, C_3, and C_4 all axial; $J_{1\beta,1\alpha}$, $J_{1\beta,2\beta}$, $J_{1\alpha,2\beta}$, $J_{2\beta,3\alpha}$, $J_{3\alpha,4\beta}$, $J_{10\beta,1\beta}$, $J_{10\beta,1\alpha}$, $J_{10\beta,15a}$, $J_{10\beta,15b}$, and $J_{15a,14b}$=12, 0, 5, 5, 0, 0, 4.5, 4.5, 0, and 8 Hz, respectively (see formula **14**). Addition of 0.8 mol equiv of the shift reagent $Eu(dpm)_3$ effected complete separation of the NMR signals due to individual protons which were correlated to the respective signals by spin-decoupling studies (Fig. 2). As expected, most of the protons on the B ring were observed at higher fields (below δ 7.00) as compared with those on the A

Table 4. The NMR spectrum of hydroxyoxolane (**14**) in the presence of the shift reagent $Eu(dpm)_3$ (CCl_4, 100 MHz; the reagent; **14**=0.8 : 1) and spin-decoupling results

Irradiated proton (δ, Hz)	Observed proton (δ) Multiplicity change and decoupled splitting (Hz)
9.34 (H_A) (do d, J=13 and 8)	6.08 (H_B) do d ⟶ d (13); 4.69 (H_C) sex ⟶ qui (8)
6.08 (H_B) (do d, J=13 and 9)	9.34 (H_A) do d ⟶ d (13); 4.69 (H_C) sex ⟶ qui (9)
4.69 (H_C) (sex, $J\approx8$)	9.34 (H_A) do d ⟶ d (8); 6.08 (H_B) do d ⟶ d (9); 3.23 (H_D) ch
3.23 (H_D) (m)	4.69 (H_C) sex ⟶ qui (8); 2.05 and 1.96 (11- and 12-CH_3) each d ⟶ s (6.5)

ring. Only one exceptional signal at a low field, δ 9.34, was reasonably assigned to the β-proton at C_6 (H_A), because the 6-carbon atom was disposed 1,3-diaxial to the 3β-hydroxyl group.[17] Spin-decoupling studies (Table 4) confirmed that the relevant proton (H_A) and the isopropyl group were located on the vicinal carbon atoms, establishing the relative disposition of the isopropenyl group to the A ring in oxylubimin (**4**). Unfortunately, no assignments could be made to the configuration of the isopropyl group from the coupling constants ($J_{A,C}$ and $J_{B,C}$=8 and 9 Hz). However, in view of the absolute configuration (R) of the 7-carbon atom in naturally occurring vetispiranes,[18] oxylubimin must be represented correctly by formula **4**. Recently, Stoessl and coworkers[6b] completely defined the relative configruation of the whole molecule of oxylubimin on the basis of the X-ray crystallography. The present result leads to the same conclusion and also invloves decision of the absolute cofiguration.

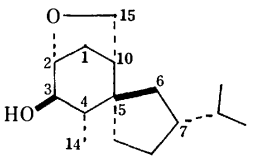

14

Experimental

All the melting points were uncorrected. The purity of each compound was always checked by TLC over silica gel (Wakogel B-5 or Merck GF-254) with various solvent systems, and the spots were developed with cerium(IV) sulfate in dil sulfuric acid, iodine, vanilin–sulfuric acid and/or the Ehrlich reagent. The vanilin–sulfuric reagent was prepared by dissolving vanilin (250 mg) in concd sulfuric acid (100 ml), and the Ehrlich reagent by dissolving *p*-dimethylaminobenzaldehyde (100 mg) in acetone (9 ml) and concd hydrochloric acid (1 ml). The optical rotations, UV, and IR spectra were measured in 95% ethanol, in 95% ethanol, and in liquid state (oil) or in Nujol (crystals), respectively, unless otherwise stated. The NMR spectra were obtained in chloroform-*d*, unless otherwise stated, at 100 MHz, tetramethylsilane being used as an internal reference. The abbreviations "s, d, t, q, qui, sex, m, br, do, ch, and sh" in the spectral data denote "singlet, doublet, triplet, quartet, quintet, sextet, multiplet, broad, double, changed, and shoulder," respectively. The preparative TLC was carried out over silica gel (Merck GF-254), and the column chromatography over silica gel (Mallinckrodt AR-100) or alumina (Merck Active I, neutral).

*Isolation of Lubimin (**3**), Oxylubimin (**4**), and Lubiminol[7] (**5**).* The fraction E (4.8 g), yellow oil, described in the section of "Isolation of rishitin,"[1] was dissolved again in ether and shaken with 10% aq sodium carbonate to remove acidic components. The ether soln was washed with 0.1 M hydrochloric acid and water, dried, and evaporated to leave neutral substances (3.8 g), which consisted of two main components and showed two pink spots with the Ehrlich reagent on TLC, the R_f values being 0.54 and 0.47 (benzene : ether= 2 : 1). These were separated into two fractions by chromatography over silicic acid with benzene–ether (3 : 1). The less polar fraction (0.75 g) with R_f 0.54, oil, was further purified by preparative TLC, showing two bands, detected by spraying a soln of iodine in hexane, on TLC with benzene–ether (1 : 2). The more polar fraction on TLC was extracted with ethyl acetate containing a small volume of methanol to give crude lubimin, which was purified by TLC to give lubimin (**3**, 400 mg), in pure state, oil and $[\alpha]_D$ +39°; MS, *m/e* 236 (M^+), 218, 203, 193, and 175; IR and NMR, in the text; GLC, Silicone SE-52 (Chromosorb W, DMCS, 80—100 mesh), injection temp 200 °C, carrier gas nitrogen, 45 ml/min, retention time 5.8 min. Found: C, 76.65; H, 10.19%. Calcd for $C_{15}H_{24}O_2$: C, 76.22; H, 10.24%.

The fraction H (2.42 g), oil,[1] was dissolved in ether and shaken with 10% aq sodium carbonate. The ether soln was washed with 0.1 M hydrochloric acid and water, dried, and evaporated to leave oily neutral substances (2.37 g), which were again dissolved in ether and separated roughly into two fractions by chromatography over silicic acid (130 g) with ether, ether–acetone, and acetone. Fractions, eluted later with ether and then with acetone, showed a magenta spot with the Ehrlich reagent on TLC and were combined and concentrated to leave oily residue (1.34 g), showing two spots on TLC with cerium(IV) sulfate. The residue was rechromatographed over silicic acid (120 g) with mixtures of ether–ethyl acetate. Early fractions eluted with ether–ethyl acetate (9 : 1, 400 ml) gave oily materials (378 mg). Subsequent fractions eluted with the same solvent mixture (220 ml) gave a crystalline material (670 mg), showing a single spot on TLC (R_f 0.50, ether). This was purified by recrystallization from isopropyl ether to give oxylubimin (**4**, 330 mg), needles, mp 85—86 °C and $[\alpha]_D$ +27°; MS, *m/e* 252 (M^+), 234, 209, and 191; IR and NMR, in the text. Found: C, 71.48; H, 9.59%. Calcd for $C_{15}H_{24}O_3$: C, 71.39; H, 9.59%. Further fractions eluted with ether–ethyl acetate (9 : 1, 80 ml and 4 : 1, 100 ml) afforded a crude crystalline material (122 mg), which was again purified by chromatography over silicic acid (1.2 g) with a 4 : 1 mixture of ether and ethyl acetate to give a crystalline substance (92 mg), showing a single spot on TLC. This was recrystallized from ether to give lubiminol[7] (**5**, 56 mg) in pure state, mp 129—130 °C and $[\alpha]_D$ +33°; MS, *m/e* 238 (M^+), 220, 202, 187, and 107 (base); IR, ν_{max} 3410, 3140, 1642, 1048, 1036, 1009, and 884 cm^{-1}; NMR, δ 0.89 (3H,

d, J=6.5 Hz, 14-C$\underline{H}_3$), 1.70 (3H, s, 13-C$\underline{H}_3$), 2.49 (2H, br s, 2O$\underline{H}$), 3.28 (1H, t, J=10 Hz, $\underline{H}$ at C_{15}), 3.60 (1H, br m, W_H=25 Hz, $\underline{H}$ at C_2), 3.90 (1H, do d, J=10 and 2.5 Hz, $\underline{H}$ at C_{15}), and 4.66 (2H, br s, 2$\underline{H}$ at C_{12}). Found: C, 75.77; H, 11.00%. Calcd for $C_{15}\underline{H}_{26}O_2$: C, 75.58; H, 11.00%.

*Acetyllubimin (**3a**), Diacetyloxylubimin (**4a**), and Diacetyloxylubiminol (**5a**).* (*i*) Lubimin (**3**, 39 mg) was treated with acetic anhydride (Ac_2O, 0.5 ml) and pyridine (Py, 0.5 ml) at room temp for 16 h. After addition of ethanol, the reaction mixture was worked up as usual to leave oily residue, which was purified by preparative TLC to give **3a** (23 mg), colorless oil and $[\alpha]_D$ +35°; MS, *m/e* 278 (M^+), 236, 218, 203, 191, 190, 189, and 175; IR, ν_{max} 3060, 2715, 1735, 1640, 1235, 1029, and 888 cm^{-1}; NMR, 0.95 (3H, d, J=7 Hz, 14-C$\underline{H}_3$), 1.69 (3H, s, 13-C$\underline{H}_3$), 4.65 (2H, s, 12-C$\underline{H}_2$), 4.70 (1H, m, W_H=25 Hz, $\underline{H}$ at C_2), and 9.76 (1H, d, J=3 Hz, C$\underline{H}$O).

(*ii*) Oxylubimin (**4**, 28 mg) was acetylated with Ac_2O (0.5 ml) and Py (0.5 ml) at room temp for 15 h to give **4a** (35 mg), colorless oil and $[\alpha]_D$+22°; MS, *m/e* 336 (M^+) and 276; IR, ν_{max} 3080, 2720, 1745, 1720, 1643, 1250, 1030, and 885 cm^{-1}; NMR, δ 0.90 (3H, d, J=7 Hz, 14-C$\underline{H}_3$), 1.69 (3H, s, 13-C$\underline{H}_3$), 1.96 and 1.99 (each 3H, s, 2OCOC$\underline{H}_3$), 2.35 (1H, m, $\underline{H}$ at C_{10}), 4.65 (2H, br s, 12-C$\underline{H}_2$), 4.65 (2H, m, 2$\underline{H}$ at C_2 and C_3), and 9.85 (1H, d, J=3 Hz, C$\underline{H}$O).

(*iii*) Lubiminol[7] (**5**, 30 mg) was treated with Ac_2O (0.2 ml) in Py (1.0 ml) at room temp for 23 h under stirring. The reaction mixture was worked up as usual to leave oily residue (39 mg), which was purified by chromatography over silica gel (3.0 g) with benzene–ether (30 : 1) to give **5a** (35 mg), oil and $[\alpha]_D$+43°; MS, *m/e* 262 ($M^+-C_2H_4O_2$) and 202; IR, ν_{max} 2970, 2890, 1743, 1642, 1465, 1432, 1365, 1238, 1027, and 886 cm^{-1}; NMR, 0.94 (3H, d, J=6.5 Hz, 14-C$\underline{H}_3$), 1.74 (3H, s, 13-C$\underline{H}_3$), 2.04 and 2.07 (each 3H, s, 2OCOC$\underline{H}_3$), 3.83 and 4.36 (each 1H, do ABq, J=11, 8, and 4 Hz, 2$\underline{H}$ at C_{15}), 4.69 (1H, br m, W_H=25 Hz, $\underline{H}$ at C_2), and 4.70 (2H, br s, 12-C$\underline{H}_2$).

*Dihydrolubimin (**5**) and Its Acetate (**5a**).* A soln of crude lubimin (**3**, 180 mg) in ethanol (3 ml) was treated with sodium borohydride (18 mg) at room temp for 1.5 h under stirring. The mixture was worked up as usual to leave amorphous residue (196 mg), which crystallized on trituration with isopropyl ether and was collected by filtration to give crude **5** (55 mg), mp 123—126 °C. The mother liquors were evaporated to leave oil, showing four spots on TLC, which was separated by preparative TLC over silica gel. A fraction with the smallest R_f value gave a crystalline substance (28 mg), which was recrystallized from isopropyl ether to give crude **5**, mp 124—127 °C. Both the samples **5** were combined and recrystallized from isopropyl ether to give **5** (75 mg) in pure state, mp 128—130 °C and $[\alpha]_D$ +28°. The mass, IR, and NMR spectra were identical with the corresponding spectra of lubiminol, isolated from the natural sources.

Compound **5** (83 mg), described above, was treated with Ac_2O (1 ml) and Py (1 ml) at room temp for 16 h. After being worked up as usual, the reaction mixture gave an oily product, which was purified by preparative TLC over silica gel to give **5a** (86 mg), oil and $[\alpha]_D$+35°. This sample was identical with that obtained from lubiminol in the mass, IR, and NMR spectra.

*Tetrahydrolubimin (**6**), Its 15-p-Bromobenzoate (**6a**), and Its 15-Brosylate (**6b**).* (*i*) Compound **5** (33 mg) was hydrogenated over Adams platinum (10 mg as $PtO_2 \cdot 2H_2O$) in ethanol (20 ml) at room temp for 3.5 h, when 2 mol of hydrogen had been consumed. After removal of the catalyst and solvent, the mixture gave a crystalline substance (33 mg), which was recrystallized from isopropyl ether to give **6** (27 mg), mp 145—147 °C and $[\alpha]_D$+35°; MS, *m/e* 240 (M^+), 222, 204, 197, 179, and 161; IR ($CHCl_3$), ν_{max} 3640 (sh), 3400, 1387, 1372, 1045 (sh), 1030, and 916 cm^{-1}; NMR, δ 0.86 (9H, d, J=7 Hz, 12-, 13-, and 14-C$\underline{H}_3$), 0.88 (2H, s, 2O$\underline{H}$), 3.32 and 3.90 (each 1H, do ABq, J=11, 8 and 11, 4 Hz, 2$\underline{H}$ at C_{15}), and 3.64 (1H, br m, W_H=25 Hz, $\underline{H}$ at C_2).

(*ii*) To a soln of **6** (17 mg, 7.8×10^{-5} mol) in Py (1 ml) was added dropwise a soln of *p*-bromobenzoyl chloride (14 mg, 6.3×10^{-5} mol) in Py (2.5 ml) at 0 °C under stirring. The mixture was stirred at room temp for 20 h, and then diluted with dichloromethane (25 ml) and poured slowly into 0.6 M sulfuric acid (40 ml) cooled with ice. The whole mixture was separated into two layers, and the aq layer was extracted with dichloromethane (2×30 ml). The combined organic soln was washed successively with 0.6 M sulfuric acid (2×30 ml), 10% aq sodium carbonate (2×30 ml) and water, dried, and evaporated to leave gummy solid, which was submitted to preparative TLC over silica gel with chloroform–ether (7 : 1). A fraction eluted with a low R_f value was extracted with ether containing methanol and gave a solid substance (14 mg), which was again purified by preparative TLC with benzene-ethyl acetate (5 : 1). Extraction of a band with a lower R_f value afforded a crystalline substance (11 mg), which was recrystallized from ethanol to give **6a** (10 mg), mp 106—108 °C; MS, *m/e* 424 (M^++2), 422 (M^+), 222, 204, 179, and 161; IR ($CHCl_3$), ν_{max} 3400, 1718, 1594, 1389, 1372, 1277, 1270, 1118, 1103, 1012, 963, and 847 cm^{-1}; NMR, δ 0.89 (9H, d, J=7 Hz, 12-, 13-, and 14-C$\underline{H}_3$), 3.64 (1H, br m, W_H=25 Hz, $\underline{H}$ at C_2), 3.99 and 4.46 (each 1H, do ABq, J=11, 10 and 11, 2 Hz, 2$\underline{H}$ at C_{15}), 7.73 and 7.81 (each 2H, ABq, J=8 Hz, $BrC_6\underline{H}_4CO$), and 1.60 (1H, br s, O$\underline{H}$). Extraction of a band with higher R_f value gave the 2,15-dibenzoate (8 mg), on trituration with hexane, mp 112—114 °C

(*iii*) A soln of **6** (33 mg, 1.4×10^{-4} mol) and *p*-benzenesulfonyl chloride (85 mg, 3.4×10^{-4} mol) in dry Py (1 ml) was allowed to stand at 0 °C for 10 h. The mixture was poured into ice-water and extracted with ether and then with chloroform. Both the solns were washed successively with 0.5 M hydrochloric acid (2×15 ml), 5% aq sodium hydrogencarbonate (2×15 ml), and saturated brine, combined, dried, and evaporated to leave colorless oil (45 mg), showing two spots with a UV lamp on TLC, which was separated into two fractions by preparative TLC over silica gel with benzene–ethyl acetate (9 : 1). A less polar fraction afforded colorless oil (19 mg), which showed a single spot on TLC and was presumed to be the dibrosylate; NMR, δ 0.86 (9H, d, J=7 Hz), 3.70 and 4.17 (each 1H, do ABq, J=11, 8 and 11, 4 Hz), 4.36 (1H, br m, W_H=25 Hz), and 7.67 (8H, s). A more polar fraction gave **6b** (23 mg), colorless oil, showing a single spot on TLC; MS, *m/e* 238 and 236 ($BrC_6H_4SO_3H^+$), 222 (M^+-236), 204, 189, and 161; IR ($CHCl_3$), ν_{max} 3400, 1580, 1393, 1372, 1183, 1095, 1070, 1012, 962, 945, and 820 cm^{-1}; NMR (CCl_4), δ 0.86 (9H, d, J=7 Hz, 12-, 13-, and 14-C$\underline{H}_3$), 3.64 (1H, br m, W_H=25 Hz, $\underline{H}$ at C_2), 3.70 and 4.15 (each 1H, do ABq, J=11, 8 and 11, 4 Hz, 2$\underline{H}$ at C_{15}), 7.62 and 7.73 (each 2H, ABq, J=8 Hz, $BrC_6\underline{H}_4SO_4$).

*Oxidation of **6a** into the 2-Dehydro Derivative (**7**) Followed by Deuteration.* (*i*) A soln of **6a** (7 mg) in Py (0.3 ml) was added to a slurry, prepared by adding chromium(VI) oxide (30 mg) to vigorously stirred Py (0.3 ml), under cooling with ice-bath during 15 min. The mixture was stirred at the temp for 1 h and then allowed to stand at room temp for 16 h. The reaction mixture was poured into water

(10 ml) and extracted with ether. The ether soln was worked up as usual to leave oil (6 mg), showing two spots, which was purified by preparative TLC over silica gel with benzene–ethyl acetate (10 : 1). A fraction with a higher R_f value gave **a** crystalline material, which on recrystallization from hexane yielded **7** (3 mg), mp 71—73 °C; MS, *m/e* 220 ($M^+ - BrC_6H_4CO_2H$), 205, 195, 193, and 177: IR, ν_{max} 1720, 1705, 1387, 1370, 1598, 1265, and 842 cm^{-1}; NMR, δ 0.90 (9H, d, J=7 Hz, 12-, 13-, and 14-C$\underline{H}_3$), 3.99 and 4.40 (each 1H, do ABq, J=11, 9 and 11, 3 Hz, 2$\underline{H}$ at C_{15}), 7.67 and 7.77 (each 2H, ABq, J=8 Hz, $BrC_6\underline{H}_4SO_2$).

(*ii*) A soln of **7** (5 mg) in a sodium deuteroxide soln, which had been prepared by adding sodium (50 mg) to a 2 : 1 mixture (3.2 ml) of dry dioxane and deuterium oxide, was heated at 70 °C for 15 min under a stream of nitrogen. After removal of the solvents *in vacuo*, the mixture was extracted with ether. The ether extracts, oil, were again treated in the same manner as described above. The resulting oil was dissolved in chloroform, and the chloroform soln, after being dried, and evaporated, afforded a mixture of deuterated ketones including the d_5-derivative (**8**). The mixture showed the following spectra: MS, *m/e* 243 (M^+ of **8**), 242, 241, 240, 239, 238, 225, 224, 223, 181, and 180; IR, ν_{max} 3450, 2230, 1705, 1388, and 1372 $cm.^{-1}$

*Conversion of **6b** into Oxolane (**9**).* A soln of **6b** (24 mg) in *t*-butyl alcohol (0.4 ml) was stirred with potassium *t*-butoxide in *t*-butyl alcohol (0.2 ml), which had been prepared by dissolving potassium (29.7 mg) into *t*-butyl alcohol (1 ml), at room temp for 150 min under nitrogen. The reaction mixture was poured into water and extracted with ether. The ether soln, after being worked up as usual, left oil, showing two spots, which was separated into two fractions by preparative TLC over silica gel with benzene–ethyl acetate (5 : 1). A less polar fraction gave **9** (9.5 mg), showing a single spot, oil; MS, *m/e* 222 (M^+), 207, 191, 179, 161, and 152; IR, ν_{max} 1388, 1372, 1205, 1170, 1105, 1072, 1052, 1000, 912, 895, 860, and 815 cm^{-1}; NMR, in the text.

*The Periodic Acid Test for Oxylubimin (**4**) and Its Derivatives.* To a soln of periodic acid (50 mg as H_5IO_6) in water (10 ml) were added a drop of concd nitric acid and then a soln of sample in dioxane, and the whole soln was kept at room temp for 10—15 s. To the resulting soln were added two drops of 5% aq silver nitrate: oxylubimin (**4**), dihydrooxylubimin (**11**), and rishitin (**1**) formed white ppts of silver iodate, but lubimin (**3**) and methyl palmitate formed no ppt with the reagent.

*Dihydrooxylubimin (**11**), Its 2,3,15-Triacetate (**11a**), 2,3-Diacetate (**11b**), and 2,3-Dibenzoate (**11c**).* (*i*) A soln of **4** (150 mg) in ethanol (7 ml) was treated with sodium borohydride (30 mg) at room temp for 5 h under stirring. The reaction mixture was worked up as usual to leave crystalline residue (160 mg), which was recrystallized from isopropyl ether containing methanol to give **11** (107 mg), mp 170—171 °C; MS, *m/e* 254 (M^+), 236, and 218; IR, ν_{max} 3340, 3080, 1645, 1090, 1072, 1033, 1002, and 890 cm^{-1}; NMR, δ 1.01 (3H, d, J=7 Hz, 14-C$\underline{H}_3$), 1.71 (3H, s, 13-C$\underline{H}_3$), and 4.66 (2H, br s, 12-C$\underline{H}_2$). Found: C, 70.59; H, 10.28%. Calcd for $C_{15}H_{26}O_3$: C, 70.83; H, 10.30%.

(*ii*) Compound **11** (120 mg) was stirred with Ac_2O (2.5 ml) and Py (2.5 ml) at room temp for 19 h. The mixture was worked up as usual to leave oily residue (187 mg), which was purified by preparative TLC over silica gel with benzene–ethyl acetate (9 : 1) to give **11a** (161 mg) in pure state, colorless oil and $[\alpha]_D$+21°; MS, *m/e* 380 (M^+), 320, 260, and 200; IR, ν_{max} 3080, 1750, 1650, and 895 cm^{-1}; NMR, δ 0.90 (3H, d, J=7 Hz, 14-C$\underline{H}_3$), 1.73 (3H, s, 13-C$\underline{H}_3$), 2.00 and 2.04 (3H and 6H, s, 3OCOC$\underline{H}_3$), 3.86 and 4.25 (each 1H, do ABq, J=11, 9 and 11, 4 Hz, 2$\underline{H}$ at C_{15}), 4.70 (2H, br s, 12-C$\underline{H}_2$), and 4.76 (2H, br m, W_H=30 Hz, 2$\underline{H}$ at C_2 and C_3).

(*iii*) A soln of **4a** (33 mg) in ethanol (1.5 ml) was stirred with sodium borohydride (4 mg) at room temp for 4 h. The reaction mixture was worked up as usual to give oil, which was purified by preparative TLC over silica gel to yield **11b** (18 mg) in pure state, colorless oil and $[\alpha]_D$+24°; MS, *m/e* 320 ($M^+ - H_2O$), 295, 278, 260, 218, 200, 187, and 159; IR and NMR, in the text.

(*iv*) A soln of **4** (10 mg) in chloroform (0.3 ml) and Py (0.2 ml) was stirred with benzoyl chloride (25 mg) at room temp for 3.5 h. The mixture was diluted with chloroform, washed with 0.5 M sulfuric acid, water, 5% aq sodium carbonate, and water, dried, and evaporated to leave amorphous residue, which was treated with sodium borohydride (15 mg) at room temp for 3 h. The reaction mixture was worked up as usual to leave oily residue, (19 mg), which was purified by preparative TLC over silica gel with benzene–ethyl acetate (5 : 2) to give **11c** (8.5 mg), mp 58—59 °C (from hexane): CD, $\Delta\varepsilon$ −19.2 at 235 nm and +5.9 at 219 nm (c 1.6×10^{-3} in ethanol, cell length 0.01 dm); MS, *m/e* 462 (M^+), 340 ($M^+ - C_7H_6O_2$), 322, 218, and 105 (base); IR ($CHCl_3$), ν_{max} 3480, 3080, 1720, 1643, 1607, 1452, 1315, 1280, 1175, 1115, 1024, 975, and 890 cm^{-1}; NMR, δ 0.99 (3H, d, J=7 Hz, 14-C$\underline{H}_3$), 1.75 (3H, s, 13-C$\underline{H}_3$), 3.45 and 3.99 (each 1H, do ABq, J=11, 8 and 11, 3 Hz, 2$\underline{H}$ at C_{15}), 5.15 (1H, t, J=10 Hz, $\underline{H}$ at C_3), 5.21 (1H, m, $\underline{H}$ at C_2), 7.47 and 7.93 (6H and 4H, m, $2COC_6\underline{H}_5$).

*Tetrahydrooxylubimin (**12**) and Its 15-Brosylate (**12a**).* (*i*) Compound **4** (40 mg) was hydrogenated over Adams platinum (50 mg) in ethanol (10 ml) at room temp for 3 h, when 2 mol of hydrogen had been absorbed. After being worked up as usual, the reaction mixture left amorphous residue (39 mg), which crystallized on trituration with isopropyl ether–methanol. This was recrystallized from the same solvent mixture to give **12** (18 mg), mp 163—165 °C; MS, *m/e* 256 (M^+), 238, 220, 195, and 177, IR, in the text. This compound was also obtained by hydrogenation of **11**.

(*ii*) Compound **12** (63 mg) was stirred with *p*-bromobenzenesulfonyl chloride (89 mg, 1.4 equiv) in Py (1.2 ml) at 5 °C for 22 h. The mixture was worked up as usual to leave oily residue (97 mg), which was purified by preparative TLC over silica gel with benzene–ethyl acetate (5 : 1) to give **12a** (51 mg), mp 97—100 °C. This was recrystallized from isopropyl ether for analysis: mp 98—100 °C; MS, *m/e* 458 (M^++2), 456 (M^+), 440, 438, and 236 ($M^+ - BrC_6H_4SO_3H$); IR ($CHCl_3$), ν_{max} 3360, 1583, 1373, and 1183 cm^{-1}; NMR, δ 0.84 and 0.99 (6H and 3H, each d, J=7 Hz, 12-, 13-, and 14-C$\underline{H}_3$), 2.93 (1H, do d, J=10 and 8 Hz, $\underline{H}$ at C_3), 3.41 (1H, br m, W_H=24 Hz), 3.41 and 4.27 (each 1H, do ABq, J=11, 8 and 11, 4 Hz, 2$\underline{H}$ at C_{15}), and 7.75 (4H, s, $BrC_6\underline{H}_4SO_4$).

*The Lemieux-Johnson Oxidation of **11a** to Methyl Ketone (**13**).* To a soln of **11a** (31 mg, 8.2×10^{-4} mol) in distilled dioxane (2ml) and water (0.6 ml) was added osmium tetraoxide (5 mg) at room temp under stirring. The soln became dark brown. To this soln was added sodium metaperiodate (60 mg, 2.8×10^{-3} mol) at 27 °C (bath temp) under stirring. After being kept for 2 h, the reaction mixture was diluted with water (10 ml), and the aq soln was extracted with ether (30 ml) and chloroform (20 ml). Both the solns were combined, washed with water, dried, and evaporated to leave oily residue (32 mg), which was purified by preparative TLC over silica gel with benzene–ethyl acetate (2 : 1). A main fraction gave **13** (27 mg), colorless oil and $[\alpha]$ +27 °; MS, *m/e* 382 (M^+), 367, 325, 322, 307, 280, 262, 220, 219, 160,

and 159; IR, ν_{max} 1745, 1713, 1435, 1370, 1230, 1053, and 1030 cm^{-1}; NMR δ 0.90 (3H, d, J=7 Hz, 14-C$\underline{H}_3$), 2.00 and 2.06 (3H and 6H, s, 3OCOC$\underline{H}_3$), 2.16 (3H, s, COC$\underline{H}_3$), 2.83 (1H, br m, W_H=25 Hz, $\underline{H}$ at C_7), 3.82 and 4.29 (each 1H, do ABq, J=11, 8 and 11, 3 Hz, 2$\underline{H}$ at C_{15}), 4.69 (1H, t, J=10 Hz, $\underline{H}$ at C_3), and 4.75 (1H, m, $\underline{H}$ at C_2).

Conversion of ***12a*** *into Hydroxyoxolane (****14****).* Compound **12a** (51 mg) in *t*-butyl alcohol (0.8 ml) was stirred with potassium *t*-butoxide (0.15 ml), which had been prepared by dissolving potassium (37.5 mg) into *t*-butyl alcohol (1 ml), at 0 °C for 30 min under nitrogen. The mixture was mixed with water (4 ml) and extracted with ether. The ether soln was washed with water, dried, and evaporated to leave **14** (26 mg), showing a single spot on TLC. This was purified by preparative TLC to give **14** in pure state, oil; MS, *m/e* 238 (M^+), 220, 195, 177, 151, 109, and 95 (base); IR and NMR, in the text.

References

1) Part XIV of "Studies on the Phytoalexins;" Part XIII, T. Masamune, A. Murai, M. Takasugi, A. Matsunaga, N. Katsui, N. Sato, and K. Tomiyama, *Bull. Chem. Soc. Jpn.*, **50**, 1201 (1977).

2) a) K. Tomiyama, T. Sakuma, N. Ishizaka, N. Sato, N. Katsui, M. Takasugi, and T. Masamune, *Phytopathology*, **58**, 115 (1968); b) N. Katsui, A. Murai, M. Takasugi, M. Imaizumi, T. Masamune, and K. Tomiyama, *J. Chem. Soc., Chem. Commun.*, **1968**, 43, and Ref 1; c) A. Murai, K. Nishizakura, N. Katsui, and T. Masamune, *Tetrahedron Lett.*, **1975**, 4399; *Bull. Chem. Soc. Jpn.*, **50**, 1206 (1977).

3) N. Katsui, A. Matsunaga, K. Imaizumi, T. Masamune, and K. Tomiyama, *Tetrahedron Lett.*, **1971**, 83; *Bull. Chem. Soc. Jpn.*, **45**, 2871 (1972).

4) a) L. V. Metlitskii, Yu. T. Dyakov, O. L. Ozeretskovskaya, L. A. Yurganova, L. I. Chalova, and N. I. Vasyukova, *Izv. Akad. Nauk SSSR, Ser. Biol.*, **1971**, 339; b) L. V. Metlitskii, O. L. Ozeretskovskaya, N. S. Vul'fson, and L. I. Chalova, *Mikol. Fitopatol.*, **5**, 439 (1971).

5) a) N. Katsui, A. Matsunaga, and T. Masamune, *Tetrahedron Lett.*, **1974**, 4483; b) N. Katsui, H. Kitahara, F. Yagihashi, A. Matsunaga, and T. Masamune, *Chem. Lett.*, **1976**, 861.

6) a) A. Stoessl, J. B. Stothers, and E. W. B. Ward, *J. Chem. Soc., Chem. Commun.*, **1974**, 709; b) A. Stoessl, J. B. Stothers, and E. W. B. Ward, *ibid.*, **1975**, 431; G. I. Birnbaum, C. P. Huber, M. L. Post, J. B. Stothers, J. R. Robinson, A. Stoessl, and E. B. Ward, *J. Chem. Soc., Chem. Commun.*, **1976**, 330; c) A. Stoessl, E. B. Ward, and J. B. Stothers, *Tetrahedron Lett.*, **1976**, 3271.

7) This compound was isolated from natural sources (see Experimental) and was designated as lubiminol. Both dihydrolubimin (**5**) and lubiminol were identical in all respects, *cf.*, Ref. 6c.

8) *Cf.*, G. M. Barrow and S. Searless, *J. Am. Chem. Soc.*, **75**, 1175 (1953).

9) G. C. Levy and G. L. Nelson, "Carbon-13 Nuclear Magnetic Resonance for Organic Chemists," Wiley-Interscience, New York (1972).

10) The δ value 47.6 in Ref. 5 should be revised to δ 46.7.

11) *Cf.*, R. E. Rondeau and R. E. Sievers, *J. Am. Chem. Soc.*, **93**, 1522 (1972).

12) R. L. Shriner, R. C. Fuson, and D. Y. Curtin, "The Systematic Identification of Organic Compounds," John Wiley and Sons, Inc., New York (1956), p. 129.

13) R. Pappo, D. S. Allen Jr., R. U. Lemieux, and W. S. Johnson, *J. Org. Chem.*, **21**, 478 (1956).

14) *Cf.*, G. I. Birnbaum, A. Stoessl, S. H. Grover, and J. B. Stothers, *Can. J. Chem.*, **52**, 993 (1974),

15) N. Harada and K. Nakanishi, *Acc. Chem. Res.*, **5**, 257 (1972).

16) N. Harada and K. Nakanishi, *J. Am. Chem. Soc.*, **91**, 3989 (1969).

17) *Cf.*, P. V. Demarco, T. K. Elzey, R. B. Lewis, and E. Wenkert, *J. Am. Chem. Soc.*, **92**, 5734, 5737 (1970).

18) *Cf.*, M. Deighton, C. R. Hughes, and R. Ramage, *J. Chem. Soc., Chem. Commun.*, **1975**, 662.

Intramolecular Cyclization of 3,4-Epoxy Alcohols; Oxetane Formation

Akio MURAI, Mitsunori ONO, and Tadashi MASAMUNE
Department of Chemistry, Faculty of Science, Hokkaido University, Sapporo 060
(Received November 26, 1976)

1-(2,3-Epoxypropyl)-1-cyclohexanol (**1**) and its methyl analogues (**2** and **3**), when treated with base in 75% aqueous dimethyl sulfoxide, gave the corresponding oxetanes (**9**—**11**) as the main products, while treatment of compound **1** under anhydrous conditions afforded the oxolane dimer (**17**) as the sole identified product.

Intramolecular cyclization of epoxy alcohols by ring cleavage usually leads to the formation of oxiranes, oxolanes, and/or oxanes.[1] In an effort to prepare β-hydroxyoxolanes by ring closure of 3,4-epoxy alcohols with bases, we found that the reactions under controlled conditions resulted in regiospecific attack of the alkoxide anion at the 3-carbon atom to give α-hydroxyalkyloxetanes. The results were recently reported in a preliminary communication[2] and the details are described in the present paper.

Three compounds, 1-(2,3-epoxypropyl)-1-cyclohexanol (**1**) and its methyl analogues (**2** and **3**[3]), were used for the reactions. These compounds (**1**—**3**), each oil, were prepared by epoxidation[4] of the corresponding olefins (**4**,[5] **5**, and **6**) as depicted in Scheme 1, and exhibited absorption signals near δ 2.7 due to the oxirane ring protons in the NMR spectra. Contrary to the expectation, an attempted epoxidation of 1-(3-methyl-2-butenyl)-1-cyclohexanol (**7**) with perbenzoic acid[4b] failed and, instead, produced an oxolane (**8**), oil, suggesting facile cyclization to a five-membered ring under the acidic conditions used.[6] Compound **8** and its monoacetate (**8a**), oil, displayed one-proton signals at δ 4.00 (1H, t, J=7 Hz, CHOH) and 5.00 (1H, do d, J=6 and 4 Hz, CHOAc) in the respective NMR spectra.

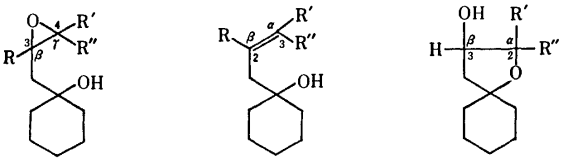

1 R=R′=R″=H
2 R=CH_3, R′=R″=H
3 R=R″=H, R′=CH_3

4 R=R′=R″=H
5 R=CH_3, R′=R″=H
6 R=R″=H, R′=CH_3
7 R=H, R′=R″=CH_3

8 R′=R″=CH_3
15 R′, R″=H or CH_3

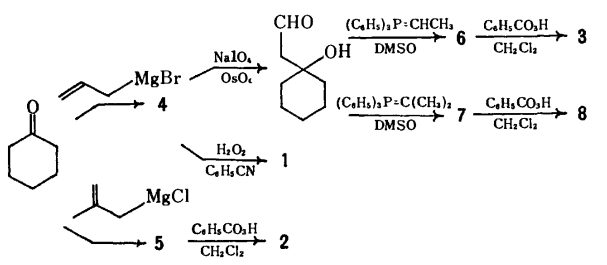

Scheme 1.

Treatment of monosubstituted oxirane (**1**) and its methyl analogues (**2** and **3**) with a base in 75% aqueous dimethyl sulfoxide[7] at 140—150 °C (bath temp) produced a mixture of the corresponding oxetanes (**9**—**11**), each oil, and the triols (**12**—**14**), each crystals, no oxolane (**15**) being detected (Table 1). Evidently, the oxetanes resulted from attack of the alkoxide anion at the 3-carbon atom, because triol **12** was not converted into oxetane **9** (recovered unchanged) under the same conditions.

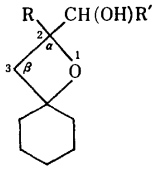

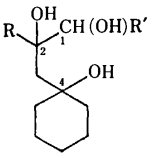

9 R=R′=H
10 R=CH_3, R′=H
11 R=H, R′=CH_3

12 R=R′=H
13 R=CH_3, R′=H
14 R=H, R′=CH_3

Table 1. Reactions of 3,4-epoxy alcohols with bases in aqueous solvents[a]

Compound	Base	Time (min)	Products (%)
1	KOH	90	**9** (49), **12** (32)
1	NaOH	45	**9** (49), **12** (32)
1	LiOH[b]	15	**9** (49), **12** (32)
2	KOH	60	**10** (67), **13** (14)
3	KOH	60	**11** (73), **14** (9)

a) The reactions were carried out by heating (bath temp, 140—150 °C) with 10 mol equiv of bases in 75% aqueous DMSO, and were ceased when the starting oxiranes were consumed. b) Slightly heterogeneous.

The structures of these products were elucidated on the basis of the chemical and spectral evidence, and one example is illustrated by oxetane **9**. The compound (**9**), $C_9H_{16}O_2$, readily formed its monoacetate (**9a**), an oil, $C_{11}H_{18}O_3$: *m/e*, **9**, 156 (M^+); **9a**, 198 (M^+). Each of these compounds (**9** and **9a**) exhibited NMR signals due to the three protons on the oxetane ring as well as that due to the hydroxy-methylene or acetoxy-methylene protons: δ, **9**, 2.22 (2H, d, J=8 Hz, 2H at C_β), 4.70 (1H, m, H at C_α), and 3.64 (2H, m, CH_2OH); **9a**, 2.08 and 2.34 (each 1H, do ABq, J=12, 5.5 and 12, 8 Hz, 2H at C_β), 4.76 (1H, m, H at C_α), and 4.18 (2H, m, CH_2OAc). Treatment of oxetane **9** with lithium aluminium hydride in a 4 : 1 mixture of dioxane and tetrahydrofuran under reflux effected cleavage of the oxetane ring[1c] to give a glycol (**16**), mp 53—54 °C, showing a triplet signal (2H, t, J=6 Hz) at δ 3.62 in the NMR spectrum. This glycol (**16**) was also obtained by hydroboration of 1-allylcyclohexanol (**4**) followed by oxida-

tion, confirming the structure of the glycol (**16**) and hence that of the oxetane (**9**).

Oxirane ring opening reactions were then examined by treatment of oxirane **1** with various bases under anhydrous conditions, the result being listed in Table 2. As shown in Table 2, the reactions effected formation of a five-membered ether and produced the oxolane dimer (**17**), oil, and oligomers (not completely identified); however, the monomer (**15**, R′=R″=H) or oxetane (**9**) could not be detected. The structure of oxolane **17** was deduced from the following evidence. The mass spectrum, *m/e* 312 (M^+), 294, and 276, indicated the compound to be a dimeric substance $C_{18}H_{32}O_4$, having two hydroxyl groups susceptible to dehydration. While the dimer (**17**), ν_{max} 3440 and 1128 cm^{-1}, was converted readily into its monoacetate (**17a**), ν_{max} 3440, 1750, and 1248 cm^{-1}, hydride reduction of oxolane **17** under the same or more severe conditions as that of oxetane **9** led to only recovery of the starting material. Moreover, these oxolanes (**17** and **17a**) revealed NMR signals due to the four alkoxyl-methylene and one alkoxy-methine protons and also that due to the hydroxy-methine or acetoxy-methine proton in the respective spectra, which were consistent with the assigned structures: δ, **17**, 3.42 (4H, m, 4H at C_α and $C_{\alpha'}$), 4.64 (1H, m, H at C_β), and 4.13 (1H, m, CHOH); **17a**, 3.54 (4H, m, 4H at C_α and $C_{\alpha'}$), 4.71 (1H, m, H at C_β), and 5.23 (1H, m, CHOAc).

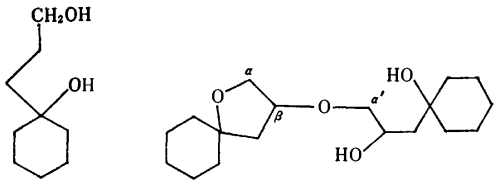

16 **17**

The results in Tables 1 and 2 are summarized as follows. Treatment of 3,4-epoxy alcohol (**1**) with base in aqueous dimethyl sulfoxide produced a *monomeric four-membered* ether ring (**9**), while the treatment under anhydrous conditions (in aprotic solvents) led to formation of a *dimeric five-membered* ether ring (**17**). Moreover, it is emphasized from Table 1 that (i) the oxetanes were formed preferentially under the hydrolysis conditions,[8] regardless of the relative degree of substitution of the oxirane ring,[9] (ii) the yields of the oxetanes increased with the number of substituents on the epoxy alcohols,[10] and (iii) the reaction of oxirane **1** with different bases gave the products (**9** and **12**) in the same ratio (49 : 32) with the reaction rate varying slightly but definitely depending on the nature of the base used. Here we add the fact that these major products, the oxetane (**9**) and the oxolane (**17**), were recovered unchanged, when the former (**9**) was treated under the anhydrous conditions (NaH in THF, reflux, 11 h) and the latter (**17**) under the hydrous conditions (KOH in 75% aq DMSO, 140—150 °C, 60 min), respectively.

Recently, Stork and coworkers[11] reported intramolecular cyclization of epoxy nitriles with bases, which involved results inconsistent with usual cyclization reactions proceeding through S_N2 type transition states.[12,13] They pointed out the necessity of a proper collinear arrangement in the transition state for displacement at the oxirane carbon atom and rationalized their result, specially the small (three- and four-membered) ring formation, in terms of the collinearity requirement and the relative degree of substitution of the oxirane ring. This collinearity requirement and the preference for diaxial opening were later accentuated in intramolecular cyclization of allyl 2,3-epoxyalkyl ether to a four-membered ring (oxetane).[14] Baldwin's "rules for ring closure"[15] appears to be based on these results for the cyclization to small rings. However, the collinearity requirement for the four-membered ring formation has recently been criticized by Lallemand and Onanga,[16] who observed preferential cyclization of (4*E*)-4,5-epoxy nitriles to five-membered rings (cyclopentane), indicating the importance of "statistical and geometrical factors." All these factors seem to be useful and necessary for interpretation of their results and also of our result.

Our result constitutes the first example indicating a pronounced solvent dependency in the intramolecular ether ring formation by the oxirane ring cleavage and is not readily explained on the basis of the current "S_N mechanisms." One plausible explanation, based on the recent works, assuming that the proposed factors controlling the reaction pathway in intramolecular attack of carbanions to oxirane rings are applicable to the corresponding reactions of alkoxide anions, follows as. The cyclization in aprotic solvents (anhydrous conditions) with *low* solvating power involves attack of anions with extremely *high* nucleophilicity,[17] which

Table 2. Reactions of 3,4-epoxy alcohol (**1**) with bases in anhydrous solvents

Base	Mol	Solvent	Temp (°C)	Time (h)	Products (%)
NaH	1.5	THF	reflux	9	**1** (95)
NaH	2.5	THF	reflux	11	**17** (60)
NaH	1.5	THF-HMPA	reflux	9	**1** (23), **17** (38)
NaH	1.5	THF-HMPA	reflux	19	**17** (31)[a]
NaH	1.5	DMSO	50—60	14.5	**17** (29)[a]
NaH	2.0	DME	reflux	25	**17** (32)[a]
NaH	1.5	THF-DMF	reflux	16	**1** (11), **17** (31)[a]
BuLi	1.2	THF	15—18	48	**1** (98)
LiN(*i*-Pr)$_2$	1.2	THF-HMPA	−70—0[b]	2[b]	**1** (97)

a) The remaining products were oxolane oligomers, not completely identified. b) 0.5 h at −70 °C and 1.5 h at 0 °C.

would not always require the collinearity in the transition state. Then, the reaction would proceed with displacement at the less substituted carbon of the oxirane ring, as had been illustrated by many base-catalyzed oxirane ring opening reactions,[9a] leading to formation of an oxolane ring with less steric constraint. On the other hand, the cyclization in aqueous dimethyl sulfoxide (hydrous conditions) would take place only when the collinearity is satisfied in the transition state, because of *lower* nucleophilicity of an attacking anion as well as *higher* solvating power of the solvent system as compared with those in aprotic solvents.[17,18] The observed enhanced rate in passing from potassium to lithium hydroxide would result from increasing coordinating power of the metal cation[19] to the oxirane oxygen in the relevant solution. The hypothesis undoubtedly requires evidence to be demonstrated and investigations in line with this are now in progress. In connection with this, we treated 1-(epoxylethyl)-1-cyclohexanol (**18**), prepared from 1-vinylcyclohexanol,[20] in aqueous dimethyl sulfoxide under the same conditions and isolated the corresponding oxirane (**19**) as a single product (78%). The result was consistent not only with well-known facile formation of a three-membered ring[1c,21] but also with the "collinearity" principle. Here we again emphasize that the present result offers intrinsic interest for the mechanistic studies and also constitutes a *new non-photochemical synthesis of oxetanes.*[22]

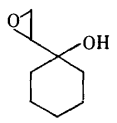

18

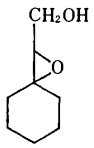

19

Experimental

All the melting and boiling points were uncorrected. The homogeneity of each compound was always checked by TLC over silica gel (Wakogel B-5) with various solvent systems, and the spots were developed with cerium(IV) sulfate in dil sulfuric acid and/or iodine. The IR and NMR (100 MHz) spectra were measured in liquid state and in chloroform-*d*, unless otherwise stated. The abbreviations "s, d, t, m, br, and do" in the NMR spectra denote "singlet, doublet, triplet, multiplet, broad, and double," respectively. The preparative TLC and column chromatography were carried out over silica gel (Wakogel B-5) and silicic acid (Kieselgel 60), respectively. All the solvents were distilled before use after being dried; ether, tetrahydrofuran (THF), and 1,2-dimethoxyethane (DME) from lithium aluminium hydride (LAH); dichloromethane and benzene from phosphorus pentaoxide; dimethyl sulfoxide (DMSO) and hexamethylphosphoramide (HMPA) from calcium hydride. The latter two solvents were stored over molecular sieves.

*1-Allylcyclohexanol (**4**), and Its Methyl Analogues (**5** and **6**).* *(i)* Compound **4** (7.14 g) was prepared by the Grignard reaction of cyclohexanone (6.5 g) in ether (50 ml) with allylmagnesium bromide, prepared from allyl bromide (12 g) and magnesium turnings (3.5 g) in ether (30 ml), at room temp for 3.5 h, and had bp 75—77 °C/15 Torr [lit,[5] 62—64 °C/3 Torr]; IR, ν_{max} 3400, 1605, 1000, 975, and 910 cm^{-1}; NMR, δ 2.22 (2H, d, J=7 Hz), 4.98 (1H, m), 5.20 (1H, br s, OH), and 5.93 (2H, br m).

(ii) A soln of cyclohexanone (30 g), freshly distilled, in ether (400 ml) was added to a cold suspension of 2-methylallylmagnesium chloride, prepared from 2-methylallyl chloride (90 g) and magnesium turnings (30 g) in ether (360 ml), during 2 h under stirring, and the whole mixture was stirred at room temp for 2 h. The reaction mixture was worked up as usual to leave a colorless oil (49.5 g), which was distilled to give **5** (45 g), in pure state, bp 80—85 °C/11 Torr; MS, *m/e* 154 (M^+) and 136; IR, ν_{max} 3460, 1640, and 885 cm^{-1}; NMR, δ 1.83 (3H, s), 2.16 (2H, s), 4.66 and 4.92 (each 1H, br s). Found: C, 77.71; H, 11.62%. Calcd for $C_{10}H_{18}O$: C, 77.86; H, 11.76%.

(iii) A soln of **4** (7.0 g) in a 1 : 4 mixture (150 ml) of dioxane and water was mixed with a 1 mM soln of osmium tetraoxide in dioxane (25 ml), and was stirred vigorously for 0.5 h. To the soln was added a soln of sodium periodate (25 g) in water (80 ml). The whole mixture was stirred at room temp for 2.5 h, and ppts formed were removed by filtration. The filtrate was evaporated *in vacuo* to remove dioxane and extracted with ethyl acetate repeatedly. The acetate soln was washed with water, dried, and evaporated to leave a pale brown oil, 2-cyclohexyl-2-hydroxyacetaldehyde (7.2 g); IR, ν_{max} 3440, 1743, and 1723 cm^{-1}; NMR, δ 2.59 (2H, d, J=2.5 Hz), 3.0 (1H, br, OH), and 9.82 (1H, t, J=2.5 Hz). This sample was used for the next reaction without further purification.

To a stirred soln of sodium methylsulfinylmethanide[23] in DMSO, prepared by addition of sodium hydride (NaH, 192 mg) into DMSO (4 ml) under nitrogen, was added a soln of ethyltriphenylphosphonium bromide (2.6 g) in DMSO (8 ml) under cooling in an ice-cooled bath, when the soln became deeply red, indicating formation of the ethylidenephosphorane. To the soln was added the afore-mentioned β-hydroxy aldehyde (710 mg) in DMSO (3 ml) at room temp during 15 min under stirring, and the whole mixture was further stirred at 50—60 °C for 24 h. The mixture was cooled, poured into ice-water, and extracted with ether repeatedly. The ether soln, after being washed with water and dried, was evaporated to leave an oily solid, which was separated by chromatography over silica gel to give **6** (149 mg) from benzene eluates, bp (bath temp) 90—94 °C/7 Torr; MS, *m/e* 154 (M^+) and 138; IR, ν_{max} 3420 and 1660 cm^{-1}; NMR, δ 1.66 (3H, d, J=6 Hz), 2.21 (2H, d, J=7 Hz), and 5.50 (2H, br m). Found: C, 77.88; H, 11.57%. Calcd for $C_{10}H_{18}O$: C, 77.86; H, 11.76%.

(iv) To a soln of sodium methylsulfinylmethanide in DMSO, prepared from NaH (172 mg) and DMSO (5 ml), was added a soln of isopropyltriphenylphosphonium bromide (2.8 g) in DMSO (5 ml), when the soln became deeply red. A soln of the β-hydroxy aldehyde (710 mg) in DMSO (3 ml) was added to the red soln. The whole mixture was stirred at 50—60 °C for 18 h and, after being worked up as usual, left an oily solid (330 mg), which was separated by chromatography over silicic acid to give **7** (71 mg), showing a single spot: MS, *m/e* 168 (M^+) and 150; IR, ν_{max} 3220 and 1680 cm^{-1}; NMR, δ 1.64 and 1.76 (each 3H, s), 2.14 (2H, d, J= 8 Hz), and 5.22 (2H, br m, OH and CH=).

*1-(2,3-Epoxypropyl)-1-cyclohexanol (**1**), and Its Methyl Analogues (**2** and **3**).* *(i)* A soln of **4** (6.05 g) in methanol (35 ml) and benzonitrile (4.20 g) was stirred with 30% aq hydrogen peroxide (8 ml) and potassium hydrogencarbonate (0.30 g) at room temp for 24 h and, after addition of 30% aq hydrogen peroxide (6 ml) and benzonitrile (4.0 g), was further stirred at the temp for 26 h.[4a] The reaction mixture, after being treated with 10% aq sodium thiosulfate to decompose excess of the hydrogen peroxide, was evaporated to

remove methanol and extracted with chloroform repeatedly. The chloroform extracts were washed with saturated aq sodium hydrogencarbonate, saturated brine and water, dried, and evaporated to leave an oil (**1**), which was distilled to give **1** (5.73 g) in pure state, bp 85—86 °C/2 Torr; MS, *m/e* 156 (M^+) and 138; IR, ν_{max} 3420, 980, and 965 cm^{-1}; NMR, δ 2.45 and 2.76 (each 1H, do ABq, J=5.5, 2.5 and 5.5, 4 Hz, 2H at C_γ), and 3.15 (1H, m, H at C_β). Found: C, 69.52; H, 10.49%. Calcd for $C_9H_{16}O_2$: C, 69.23; H, 10.26%.

(ii) A soln of **5** (1.5 g) in dichloromethane (50 ml) was stirred with perbenzoic acid (2.5 g, purity 97%) at room temp for 18 h.[4b] The mixture was washed with 5% aq sodium thiosulfate, 5% aq hydrogencarbonate and water, dried, and evaporated to leave a pale yellow oil, which was distilled to give **2** (1.3 g) in pure state, bp 140—143 °C/13 Torr; MS, *m/e* 170 (M^+) and 152; IR, ν_{max} 3360, 975, and 960 cm^{-1}; NMR, δ 1.44 (3H, s, CH_3), 2.66 and 2.72 (each 1H, ABq, J=5.5 Hz, 2H at C_γ). Found: C, 70.15; H, 10.23%. Calcd for $C_{10}H_{18}O_2$: C, 70.54; H, 10.66%.

(iii) Compound **6** (61 mg) in dichloromethane (3 ml) was oxidized with perbenzoic acid (86 mg) in a refrigerator (0 °C) for 24 h under stirring. The mixture was worked up as usual to leave an oil (83 mg), which was purified by distillation to yield **3** (54 mg), bp (bath temp) 130—134 °C/5 Torr; MS, *m/e* 170 (M^+) and 152; IR, ν_{max} 3420, 1250, 975, 960, and 855 cm^{-1}; NMR, δ 1.28 (3H, d, J=6 Hz, CH_3) and 3.14 (2H, m, 2H at C_β and C_γ). Found: C, 70.15; H, 10.23%. Calcd for $C_{10}H_{18}O_2$: C, 70.54; H, 10.66%.

2,2-Dimethyl-3-hydroxy-5,5-pentamethyleneoxolane (8), and Its Acetate (8a). A soln of **7** (50 mg) in dichloromethane (3 ml) was treated with perbenzoic acid (50 mg) in a refrigerator (0 °C) for 3 h. The reaction mixture was worked up as usual to leave an oil (51 mg), which was purified by passing through a short column packed with silicic acid to give **8** (45 mg); IR, ν_{max} 3460 and 1073 cm^{-1}; NMR, δ 1.22 and 1.24 (total 6H, each s, $2CH_3$), and 4.00 (1H, t, J=7 Hz, H at C_3).

Compound **8** (10 mg) was treated with acetic anhydride (Ac_2O, 50 mg) and pyridine (Py, 100 mg) at room temp for 15 h. The mixture was worked up as usual to give an oil (12 mg), which was purified by chromatography over silicic acid with benzene to yield **8a** (9 mg) in pure state; MS, *m/e* 226 (M^+), 167, 166, and 151; IR, ν_{max} 1746, 1235, 1079, and 1030 cm^{-1}; NMR, δ 1.18 and 1.23 (each 3H, s, $2CH_3$), 2.05 (3H, s, $OCOCH_3$), and 5.00 (1H, do d, J=6 and 4 Hz, H at C_3). Found: C, 68.69; H, 10.21%. Calcd for $C_{13}H_{22}O_3$: C, 68.99; H, 9.80%.

1-(Epoxyethyl)-1-cyclohexanol (18). 1-Vinylcyclohexanol (5.9 g) was prepared by the Grignard reaction of cyclohexanone (6.7 g) in THF (10 ml) with vinylmagnesium bromide, prepared from vinyl bromide (12.7 g) and magnesium turnings (3.1 g) in THF (10 ml), at room temp overnight under stirring, and had bp 68—70 °C/23 Torr [lit,[14] 66—68 °C/14 Torr]; IR, ν_{max} 3500, 1650, 965, and 920 cm^{-1}; NMR, δ 4.96 and 5.18 (each 1H, do ABq, J=17, 2 and 17, 12 Hz, 2H at C_β), and 5.92 (1H, do d, J=12 and 17 Hz, H at C_α).

The cyclohexanol (1.26 g) was treated with perbenzoic acid (2.76 g) in dichloromethane (90 ml) at room temp for 15 h under stirring. The mixture was worked up as usual to leave an oil (1.31 g), which was purified by distillation to give **18** (1.02 g) in pure state, bp 96—98 °C/12 Torr; MS, *m/e* 142 (M^+), 124, 99, and 98; IR, ν_{max} 3448, 975, and 965 cm^{-1}; NMR, δ 3.88 (3H, m, 3H at C_α and C_β). Found: C, 67.46; H, 9.94%. Calcd for $C_8H_{14}O_2$: C, 67.57; H, 9.93%.

Cleavage of Oxiranes (1—3, and 18) under Hydrous Conditions. The reaction conditions and results were summarized in Table 1 and two representative examples are described.

(i) A soln of oxirane **1** (156 mg, 1 mmol) in DMSO (30 ml) and water (10 ml) was stirred with potassium hydroxide (560 mg, 10 mmol) at 140—150 °C (bath temp) for 90 min under nitrogen, when the spot of **1** had disappeared on TLC. The mixture was cooled, poured into large excess of ice-water, and extracted with ethyl acetate repeatedly. The acetate extracts were washed with water, dried, and evaporated to leave an oil (142 mg), showing two spots on TLC, which was separated into two fractions by preparative TLC over silica gel with ethyl acetate–benzene (1 : 3). Each fraction was purified by distillation and/or recrystallization to give 2-(hydroxymethyl)-4,4-pentamethyleneoxetane (**9**, 76 mg) and 3-(1-hydroxycyclohexyl)-1,2-propanediol (**12**, 40 mg). Compound **9** had bp (bath temp) 97—99 °C/1 Torr; MS, *m/e* 156 (M^+), 138, 125, and 98; IR, ν_{max} 3400, 1017, 995, 965, 930, and 915 cm^{-1}; NMR, δ 2.22 (2H, d, J=8 Hz, 2H at C_3), 3.64 (2H, m, CH_2OH), and 4.70 (1H, m, H at C_2). Found: C, 69.54; H, 10.50%. Calcd for $C_9H_{16}O_2$: C, 69.23; H, 10.26%. Compound **12** had mp 65—66 °C (from ether); MS, *m/e* 174 (M^+), 156, 143, 125, and 107; IR, ν_{max} (Nujol) 3480 cm^{-1}; NMR, δ 3.48 (2H, m, CH_2OH), and 4.07 (1H, m, CHOH). Found: C, 62.25; H, 10.26%. Calcd for $C_9H_{18}O_3$: C, 62.07; H, 10.23%.

(ii) A soln of oxirane **18** (284 mg, 2 mmol) in DMSO (60 ml) and water (20 ml) containing potassium hydroxide (1.12 g, 20 mmol) was heated at 130—140 °C (bath temp) for 15 min under stirring. The mixture was worked up as described above to leave an oil (370 mg), showing a single spot, which still contained DMSO. The oily residue was purified by chromatography over silicic acid with ether–benzene (2 : 1) followed by distillation to give 2-(hydroxymethyl)-3,3-pentamethyleneoxirane (**19**, 225 mg) as a single product, bp (bath temp) 105—110 °C/5 Torr; MS, *m/e* 142 (M^+), 126, and 111; IR, ν_{max} 3394, 1241, 951, and 891 cm^{-1}; NMR, δ 2.96 (1H, do d, J=5 and 7 Hz, H at C_2), 3.62 and 3.84 (each 1H, do d, J=12, 5 and 12, 7 Hz, CH_2OH). Found: C, 67.62; H, 9.93%. Calcd for $C_8H_{14}O_2$: C, 67.57; H, 9.93%.

(iii) Oxetanes **10** and **11** and triols **13** and **14** had the following properties. Compound **10**, bp (bath temp) 105—108 °C/2 Torr; MS, *m/e* 170 (M^+), 139, and 99; IR, ν_{max} 3400, 1028, 1002, 952, 927, and 912 cm^{-1}; NMR, δ 1.38 (3H, s, CH_3), 1.96 and 2.36 (each 1H, ABq, J=11 Hz, 2H at C_3), and 3.42 (2H, s, CH_2OH). Found: C, 70.15; H, 10.58%. Calcd for $C_{10}H_{18}O_2$: C, 70.54; H, 10.66%.

Compound **11**, bp (bath temp) 108—112 °C/2 Torr; MS, *m/e* 170 (M^+), 125, and 98; IR, ν_{max} 3440, 1040, 996, 976, 935, and 920 cm^{-1}; NMR, δ 1.08 (3H, d, J=6 Hz, CH_3), 2.02 and 2.27 (each 1H, do ABq, J=11, 8 and 11, 7 Hz, 2H at C_3), 3.80 (1H, m, CHOH), and 4.36 (1H, m, H at C_2). Found: C, 70.47; H, 10.49%. Calcd for $C_{10}H_{18}O_2$: C, 70.54; H, 10.66%.

Compound **13**, mp 39—41 °C (from ether); MS, *m/e* 188 (M^+), 170, 157, 139, and 121; IR (Nujol), ν_{max} 3400 cm^{-1}; NMR, δ 1.40 (3H, s, CH_3), 3.34 and 3.50 (each 1H, ABq, J=11 Hz, CH_2OH). Found: C, 64.18; H, 10.60%. Calcd for $C_{10}H_{20}O_3$: C, 63.79; H, 10.71%.

Compound **14**, mp 39—41 °C (from ether); MS, *m/e* 188 (M^+), 170, 143, and 107; IR, (Nujol) ν_{max} 3400 cm^{-1}; NMR, δ 1.14 (3H, d, J=6 Hz, CH_3), and 3.64 (2H, m, 2CHOH). Found: C, 63.75; H, 10.98%. Calcd for $C_{10}H_{20}O_3$: C, 63.79; H, 10.71%.

(iv) Oxetanes **9**—**11** and oxirane **19** were converted almost quantitatively into the respective monoacetates (**9a**—

11a, and **19a**) by treatement with Ac_2O and Py at room temp, which had the following properties. Compound **9a**, bp (bath temp) 95—97 °C/2 Torr; MS, *m/e* 198 (M^+) and 138; IR, ν_{max} 1750, 1240, 1035, and 960 cm^{-1}; NMR, δ 2.11 (3H, s, $OCOC\underline{H}_3$), 2.08 and 2.34 (each 1H, do ABq, J=12, 5.5 and 12, 8 Hz, 2H at C_3), 4.18 (2H, m, $C\underline{H}_2OAc$), and 4.76 (1H, m, H at C_2).

Compound **10a**, bp (bath temp) 85—92 °C/2 Torr; MS, *m/e* 212 (M^+) and 152; IR, ν_{max} 1751, 1232, 1040, 963, and 938 cm^{-1}; NMR, δ 1.42 (3H, s, $C\underline{H}_3$), 2.10 (3H, s, $OCOC\underline{H}_3$), 2.14 and 2.26 (each 1H, ABq, J=11 Hz, 2H at C_3), and 4.00 (2H, s, $C\underline{H}_2OAc$).

Compound **11a**, bp (bath temp) 92—95 °C/2 Torr; MS, *m/e* 152 ($M^+-C_2H_4O_2$); IR, ν_{max} 1743, 1235, 1030, 1010, 970, 940, and 920 cm^{-1}; NMR, δ 1.14 (3H, d, J=6 Hz, $C\underline{H}_3$), 2.08 (3H, s, $OCOC\underline{H}_3$), 2.14 and 2.30 (each 1H, do ABq, each, J=12 and 7 Hz, 2H at C_3), 4.48 (1H, do t, J=11, 7, and 7 Hz, H at C_2), and 4.91 (1H, m, $C\underline{H}OAc$).

Compound **19a**, bp (bath temp) 95—103 °C/5 Torr; MS, *m/e* 184 (M^+); IR, ν_{max} 1751, 1230, 1033, 970, and 900 cm^{-1}; NMR, δ 2.12 (3H, s, $OCOC\underline{H}_3$), 2.98 (1H, do d, J=7 and 5 Hz, H at C_2), 4.02 and 4.32 (each 1H, do ABq, J=12, 7 and 12, 5 Hz, $C\underline{H}_2OAc$).

3-(1-Hydroxycyclohexyl)-1-propanol (**16**). *(i)* A soln of oxetane **9** (23 mg) in THF (1 ml) was added to a stirred suspension of LAH (100 mg) in a 4 : 1 mixture (10 ml) of dioxane and THF, and the mixture was refluxed for 20 h. After addition of a few drops of saturated aq ammonium chloride, the mixture was poured into ice-water, evaporated to remove most of the organic solvents, and extracted with ethyl acetate. The acetate extracts were washed with water, dried, and evaporated to leave an oil (27 mg), showing two spots on TLC, which was separated into two fractions by preparative TLC over silica gel to give **16** (10 mg) and **9** (11 mg), oil, the latter being was identified as starting oxetane. Compound **16** had mp 53—54 °C (from ether); MS, *m/e* 158 (M^+), 140, and 127; IR (Nujol), ν_{max} 3280 cm^{-1}; NMR, δ 3.62 (2H, t, J=6 Hz, $C\underline{H}_2OH$). Found: C, 68.36; H, 11.44%. Calcd for $C_9H_{18}O_2$: C, 68.35; H, 11.39%.

(ii) Into a stirred soln of olefin **4** (164 mg, 1.2 mmol) in THF (5 ml) was passed diborane, generated by addition of a soln of boron trifluoride etherate (0.75 ml, 6 mmol) in THF (3 ml) into a soln of sodium borohydride (170 mg) in THF (7.5 ml), at room temp for 10 min. The mixture was then heated at 50 °C (bath temp) for 3 h under stirring, cooled, and treated with water (1 ml) and then immediately with 30% aq hydrogen peroxide (7 ml) and 0.2 M aq sodium hydroxide (6 ml) at room temp for 48 h under stirring. After addition of 5% aq sodium thiosulfate to decompose excess of the peroxide, the reaction mixture was extracted with ether and then with ethyl acetate. The combined extracts were washed with water, dried, and evaporated to leave an oil (169 mg), which was separated by chromatography over silicic acid with benzene-ether (1 : 1) to give **16** (111 mg), mp 51—53 °C identical with the sample described above (MS, IR, NMR, and TLC).

Cleavage of Oxirane **1** *under Anhydrous Conditions.* The reaction conditions and results were summarized in Table 2, and two representative examples are described. *(i)* A soln of **1** (520 mg, 3.3 mmol) in THF (30 ml) was added dropwise to a stirred suspension of mineral oil-free sodium hydride (NaH, 200 mg, 8.3 mmol) in THF (30 ml). The mixture was refluxed gently for 11 h, cooled, and poured into ice-water, and extracted with ethyl acetate. The acetate extracts, after being worked up as usual, left a pale yellow oil (52 mg), which was separated by chromatography over silicic acid with benzene-ethyl acetate (4 : 1) to give an oxolane dimer (**17**, 311 mg) and unidentified polymers (102 mg) with smaller R_f value. The dimer had bp (bath temp) 169—172 °C/2 Torr; MS, IR, and NMR, in the text. Found: C, 69.18; H, 10.32%. Calcd for $C_{18}H_{32}O_4$: C, 68.77; H, 10.32 %.

The dimer gave its monoacetate (**17a**), bp (bath temp) 155—159 °C/2 Torr; MS, *m/e* 354 (M^+), 295, 294, and 276; IR and NMR, in the text.

(ii) A soln of lithium diisopropylamide (LDA, *ca.* 1.2 mmol), prepared by treatment of diisopropylamine (0.167 ml) with 10% butyllithium (BuLi) in hexane (0.768 ml) under cooling with Dry Ice-acetone (−78 °C), was added dropwise to a soln of **1** (156 mg, 1 mmol) and HMPA (179 mg, 1 mmol) in THF (1 ml) at −78 °C under nitrogen. The whole soln was stirred at the temp for 30 min and then at 0 °C for 2 h. The reaction mixture was worked up as usual to leave a colorless oil (171 mg), showing a single spot on TLC, which was purified by chromatography over silicic acid to give the starting oxirane (**1**, 152 mg).

References

1) a) M. F. Grundon and H. M. Okely, *J. Chem. Soc., Perkin 1*, **1975**, 150; M. C. Sacquet, B. Graffe, and P. Maitte, *Tetrahedron Lett.*, **1972**, 4453; H. Huerre, M. Mousseron-Canet, and C. Levallois, *Bull. Soc. Chim. France*, **1966**, 658; J. G. Buchanan and A. R. Edgar, *Carbohydr. Res.*, **10**, 295 (1969); b) T. Masamune, M. Takasugi, A. Murai, and K. Kobayashi, *J. Am. Chem. Soc.*, **89**, 4521 (1967); c) H. B. Henbest and B. Nicolls, *J. Chem. Soc.*, **1959**, 221; d) J. G. Buchanan and E. M. Oakes, *Carbohydr. Res.*, **1**, 242 (1965); e) G. B. Payne, *J. Org. Chem.*, **27**, 3819 (1962).

2) A. Murai, M. Ono, and T. Masamune, *J. Chem. Soc., Chem. Commun.*, **1976**, 864.

3) Compounds **3** and **6** were mixtures of stereoisomers, which showed a single spot on TLC and resisted further separation.

4) a) *Cf.*, R. G. Carlson and N. B. Behn, *J. Org. Chem.*, **32**, 1363 (1967); b) *cf.*, H. B. Henbest and J. J. McCullough, *Proc. Chem. Soc.*, **1962**, 74.

5) E. A. Braude and O. H. Wheeler, *J. Chem. Soc.*, **1955**, 320.

6) *Cf.*, J. A. Marshall and M. T. Pike, *J. Org. Chem.*, **33**, 435 (1968).

7) This solvent system was selected for carrying out the reactions in homogeneous state.

8) *Cf.*, G. Berti, B. Macchia, and F. Macchia, *Tetrahedron Lett.*, **1965**, 3421; *Tetrahedron*, **24**, 1755 (1968).

9) For oxirane ring opening accompanied by no cyclization under basic (a) and acidic (b) conditions, see: a) *e.g.*, C. L. Browne and R. E. Lutz, *J. Org. Chem.*, **17**, 1187 (1952); P. L. Nichlos, Jr. and J. D. Ingham, *J. Am. Chem. Soc.*, **77**, 6547 (1955); b) *E.g.*, A. Balsamo, P. Crotti, B. Macchia, and F. Macchia, *J. Org. Chem.*, **39**, 874 (1974), and refs cited therein.

10) *Cf.*, N. Nilson and L. Smith, *Z. Phys. Chem.*, **166a**, 136 (1936) (Thorpe-Ingold effect).

11) G. Stork, L. D. Cama, and D. R. Coulson, *J. Am. Chem. Soc.*, **96**, 5268 (1974); G. Stork and J. F. Cohen, *ibid.*, **96**, 5272 (1974).

12) a) *Cf.*, A. C. Knipe and C. J. M. Stirling, *J. Chem. Soc., B*, **1968**, 67; P. A. Cruickshank and M. Fishman, *J. Org. Chem.*, **34**, 4060 (1969). b) For cyclization to heterocycles by oxirane ring cleavage, see: R. Achini and W. Oppolzer, *Tetrahedron Lett.*, **1975**, 369; J. G. Buchanan and H. Z. Sable, "Selective Organic Transformations," ed by B.

S. Thyagarajan, John Wiley & Sons, Inc., Vol. 2, New York (1972), p. 53.

13) *E.g.*, R. R. Sauers, R. A. Parent, and S. B. Damle, *J. Am. Chem. Soc.*, **88**, 2257 (1966); R. B. Woodward, T. Fukunaga, and R. C. Kelly, *ibid.*, **86**, 3162 (1964); G. Büchi, D. Minster, and J. C. F. Young, *ibid.*, **93**, 4319 (1971); G. L. Hodgson, D. F. Macsweeney, and T. Money, *Tetrahedron Lett.*, **1972**, 3685.

14) W. C. Still, *Tetrahedron Lett.*, **1976**, 2115.

15) J. E. Baldwin, *J. Chem. Soc., Chem. Commun.*, **1976**, 734.

16) J. Y. Lallemand and M. Onanga, *Tetrahedron Lett.*, **1975**, 585.

17) R. Alexander, E. C. F. Ko, A. J. Parker, and T. J. Broxton, *J. Am. Chem. Soc.*, **90**, 5049 (1968).

18) *Cf.*, T. J. M. Pouw and P. Zuman, *J. Org. Chem.*, **41**, 1614 (1976).

19) K. Sugino, and T. Tanaka, *J. Org. Chem.*, **33**, 3354 (1968); W. I. O'Sullivan, F. W. Swamer, W. J. Humphlett, C. R. Hauser, *ibid.*, **26**, 2306 (1961).

20) P. A. Robins, *J. Chem. Soc.*, **1952**, 646.

21) *Cf.*, J. H. Babler and A. J. Tortorello, *J. Org. Chem.*, **41**, 885 (1976).

22) For preparative methods for oxetanes, see: J. P. Bates, J. Moulines, and J. C. Pommier, *Tetrahedron Lett.*, **1976**, 2249; J. Biggs, *ibid.*, **1975**, 4825; B. Delmond, J. C. Pommier, and J. Valende; *J. Organomet. Chem.*, **47**, 337 (1973); *Tetrahedron Lett.*, **1969**, 2089; F. Nerdal and P. Weyerstal, *Angew. Chem.*, **71**, 339 (1959); G. Büchi, G. G. Inman, and E. S. Lipinsky, *J. Am. Chem. Soc.*, **76**, 4327 (1954); L. F. Schmoyer and L. C. Case, *Nature*, **183**, 389 (1959); A. C. Farthing, *J. Chem. Soc.*, **1955**, 3648; S. Searles and M. J. Gortatowski, *J. Am. Chem. Soc.*, **75**, 3030 (1953).

23) R. Greenwald, M. Chaykovsky, and E. J. Corey, *J. Org. Chem.*, **28**, 1128 (1963).

Studies of the Isomerization of Unsaturated Carboxylic Acids. III.[1] Thermal Rearrangement of Dimethyl Methylenesuccinate to Dimethyl Mesaconate

Mutsuji SAKAI

Department of Fiber Chemistry, Faculty of Textile Science, Kyoto University of Industrial Arts and Textile Fibers, Matsugasaki, Sakyo-ku, Kyoto 606

(Received April 2, 1976)

Dimethyl methylenesuccinate (**1**) was found to equilibrate with dimethyl mesaconate (**3**) at elevated temperatures. Thermal rearrangements of **1** and **3** were studied kinetically and a plausible mechanism is proposed.

The rearrangement[2] and isomerization[2] of unsaturated esters in thermal[3-5] and photochemical[6-8] reactions have received much attention. In the preceding paper of this series, it was reported that some unsaturated dicarboxylic acids exhibited unique equilibrium composition during thermal reactions[2] and a plausible mechanism was proposed.[1]

On the other hand, it has been found that the corresponding unsaturated esters behave quite differently from the free acids. The present paper deals with the interconversion between dimethyl methylenesuccinate (**1**), dimethyl citraconate (**2**), and dimethyl mesaconate (**3**), and the mechanism for this interconversion will be discussed.

Experimental

All the boiling points are uncorrected.

Materials. Dimethyl methylenesuccinate (dimethyl methylenebutanedioate) (**1**), bp 105 °C/22 Torr, dimethyl citraconate (dimethyl (*Z*)-2-methyl-2-butenedioate) (**2**), bp 104 °C/25 Torr, and dimethyl mesaconate (dimethyl (*E*)-2-methyl-2-butenedioate) (**3**), bp 96 °C/20 Torr, were prepared according to the literature.[9] Organic solvents were purified by the standard methods. Other reagents were commercial materials and were used without further purification.

Procedure. A mixture of 0.30 g (1.9 mmol) of an unsaturated ester, 0.60 g of methanol, and a small amount of hydroquinone was sealed at atmospheric pressure in a glass tube, which was heated to an appropriate temperature in an autoclave filled with aqueous methanol. After cooling the autoclave, the tube was opened and the mixture was analyzed by GLC as described in a preceding paper.[1] When the reaction was carried out in the presence of iodine, the cooled reaction mixture was treated with aqueous sodium thiosulfate, and then the products were extracted with benzene. The benzene solution was subjected to GLC.

Reaction in Methanol-d. A mixture of 0.40 g of **1** and 1.30 g of methanol-*d* was sealed in a glass tube. After the reaction, the mixture of esters was recovered by distillation under reduced pressure. The distillate diluted with CCl_4 was subjected to NMR analysis. The deuterium content was calculated from the relative intensities of the NMR signals (in CCl_4, TMS) at δ 6.26 ($=CH_2$), 5.70 ($=CH_2$), and 3.28 ($-CH_2-$) for **1**, and 6.83 (=CH) and 2.24 ($-CH_3$) for **3**. The NMR spectra were recorded on a Varian T-60A spectrometer.

Kinetics. A mixture, consisting of 0.30 g of ester and 0.60 g of methanol, in a sealed tube was placed in an autoclave. The temperature was raised at a rate of 5 °C/min. After maintaining the mixture at an appropriate temperature for a desired period of time, the vessel was cooled immediately to room temperature. The cooled mixture was analyzed using GLC. Each run correctly followed first-order kinetics. The results at 250 °C were analyzed using equilibrium kinetics.[10]

Results

It was confirmed by GLC that the reaction mixture contained three isomers of the esters and no by-product was detected. The reaction was carried out in methanol, since thermal reaction without a solvent brought about the polymerization of **1** and the decomposition of the esters. In benzene, practically no reation occurred.

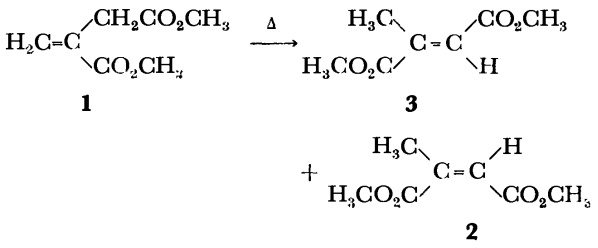

Equilibria. The reactions in methanol for **1**, **2**, and **3** were studied at 250 °C and the results are summarized in Table 1. The equilibrium composition in methanol at 250 °C were found to be 41% for **1**, 5% for **2**, and 54% for **3**. For the corresponding diethyl

Table 1. Equilibrium at 250 °C[a]

Starting ester	Time, h	Composition, %			Total yield, %
		1	**3**	**2**	
1	2	90.8	9.2	—	90.5
3	2	15.2	84.5	0.3	89.6
1	4	77.5	22.1	0.5	81.3
3	4	23.6	76.4	—	86.6
1	7	64.7	34.4	0.8	78.7
3	7	27.1	72.0	0.9	88.9
1	10	61.8	37.3	1.1	80.9
3	10	39.0	54.3	6.7	87.0
1	26	42.2	53.7	4.1	67.1
3	26	41.6	53.5	5.1	74.1
1	44	41.5	53.9	4.6	53.3
1:**3**=1:2	44	40.3	54.4	5.3	46.3
1:**3**=1:2	44	41.4	54.5	4.1	56.0
3	44	40.3	54.2	5.5	47.5
2	44	37.0	47.1	16.0	62.5

a) Ester, 0.3 g; methanol, 0.6 g.

Table 2. *cis-trans* Isomerization in the presence of I_2[a]

Starting ester	Temp, °C	Time, h	I_2, mmol	Composition, %			Total yield, %
				1	**3**	**2**	
2	200	6	0	0.2	0.4	99.4	86.6
2	200	6	0.76	0.4	90.1	9.5	83.7
3	200	6	0.76	0.4	90.6	9.6	83.0
1	200	6	0.76	98.8	1.2	—	53.7
1	250	2	0	99.4	0.6	—	84.8
1	250	2	0.19	78.5	15.7	6.0	48.8
3	250	2	0	0.2	99.8	—	97.7
3	250	2	0.19	7.3	82.5	10.2	64.8
2	250	2	0	0.6	0.4	99.0	100.0
2	250	2	0.19	7.3	82.0	10.7	65.9

a) Ester, 0.3 g; benzene, 0.6 g.

Table 3. NMR data for the reaction[a]

Starting ester	Solvent	Relative area[b]				
		H_a (δ 6.26)	H_b (5.70)	H_c (3.28)	H_d (6.83)	H_e (2.24)
1	Methanol	1.0	1.1	2.1	1.1	3.1
1	Methanol-*d*	1.0	1.1	0.98	0.30	1.5
3	Methanol	1.0	1.1	2.1	1.3	4.0
3	Methanol-*d*	1.0	1.1	1.1	0.61	2.1

a) Ester, 0.4 g; solvent, 1.3 g; temp, 250 °C; reaction time, 26 h. b) The relative area of terminal methylene of **1** (δ 6.26) is estimated to be 1.0.

(a) H, (c) $C{=}CCH_2CO_2CH_3$, (b) H, CO_2CH_3

(e) H_3C, CO_2CH_3, $C{=}C$, H_3CO_2C, H (d)

esters, the values were 27, 3, and 70%, respectively.

The addition of iodine to the reaction mixture dramatically accelerated the isomerization, whereas the rate of rearrangement remained unaffected. The results are shown in Table 2.

The results of the reactions of the esters in methanol-*d* are shown in Table 3. When **1** was heated in methanol-*d*, deuterium atoms were incorporated into the α-methylene group of **1** recovered and into the methyl group of **3** produced.

Kinetics. Kinetic studies were undertaken in the temperature range from 200 to 280 °C. In methanol, the esters were recovered in good yield even after prolonged heating. The reaction was unaffected by the presence of hydroquinone. The first-order rate constants for the disappearance of **1**, **2**, and **3** were measured at appropriate temperature. The results are listed in Table 4. It should be noted that the initial rate constants, k, obtained from an analysis using first-order kinetics (the sum of the rate constants for the forward and reverse reactions) do not differ markedly from the rate constants, k', obtained on the basis of equilibrium kinetics[10] (the rate constants for the forward reaction only). The linearity of $\ln[C]_0/[C]$ plotted against time was observed up to a conversion of about 30%. The Arrhenius plot for the rate of disappearance of **1** was correctly linear (r=0.995), from which ΔH^* and ΔS^* were calculated to be 77.8 kJ mol^{-1} and 184 J K^{-1} mol^{-1}, respectively.

Table 4. Temperature dependence of the rate constants for the disappearance of the esters[a]

Starting ester	Temp,[b] °C	Rate constant	
		$k \times 10^5$ s^{-1} [c]	$k' \times 10^5$ s^{-1} [d]
1	200	0.228	
1	230	0.984	
1	250	1.58	1.76
1	280	4.96	
3	250	1.50	1.35
2	250	1.14	1.15

a) Ester, 0.3 g; methanol, 0.6 g. b) ±1 °C. c) The error in k is expected to be in the range of 5—10%. d) First-order rate constants calculated for equilibrium systems.[10]

Discussion

The equilibrium composition of the esters is completely different from that of the corresponding acids, for which methylenesuccinic and mesaconic acids are the most and the least abundant materials, respectively.[1] This fact appears to indicate that the factor which governs the relative stability of the esters in equilibrium is different from that for free acids.

A free-radical mechanism may be disregarded in the rearrangement of the esters, because the addition of iodine as a radical source accelerated isomerization at

low temperature (200 °C), whereas little rearrangement occurred. In addition, it was found that hydroquinone affected neither the equilibrium composition nor the rate constants.

For thermal rearrangement of unsaturated esters, a mechanism has been proposed which involves enolization followed by the intramolecular rearrangement of the enol-proton to the terminal methylene group.[4] However, an inspection of the Dreiding model of enol-methylenesuccinate, a possible common intermediate of the rearrangement, reveals that the orbital of the terminal methylene is not arranged in a position suitable for accepting the enol-proton intramolecularly. In the reverse process, the intramolecular abstraction of a methyl-proton in **3** by the carbonyl-oxygen must produce a twisted enolate of **1**, in which conjugative stabilization of diene is hardly conceivable. Thus, from a consideration of the orbital arrangement, it is predicted that cyclic intramolecular process for the rearrangement is unfavorable.

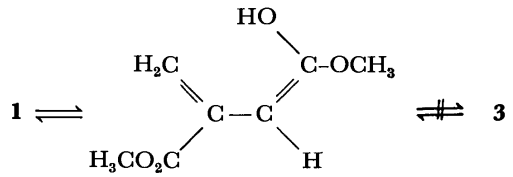

Consequently, another plausible mechanism is the intervention of a carbanion, which has been proposed for the corresponding free acids:[1]

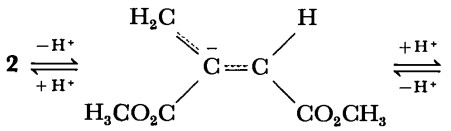

4

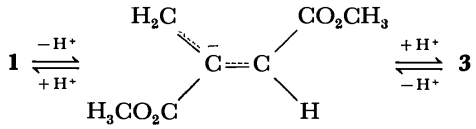

5

The rate-determining reaction for the formation of carbanions, **4** and **5**, under the general-base catalysis of methanol, is supported by the facile hydrogen-deuterium exchange at the position expected for these species and by first-order kinetics for the rearrangement of the esters. If the reaction proceeds for the carbonium ion under the general-acid catalysis of methanol, the protons of the terminal methylene group in **1** must be replaced by deuterium atoms faster than those of the α-methylene group, because protonation to **1** is expected to take place at the terminal methylene group. Similarly, for general-acid catalysis, the α-methylene protons in **1** formed should be replaced by deuteriums faster than the methyl protons in **3**. This is, however, is not the case. The general-base catalysis of methanol is also confirmed by preliminary results for triethylamine-catalyzed reactions of the esters.[11] Since it was observed that the addition of triethylamine accelerated both the rearrangements of **1** and **3**, the mechanism involving carbanion intermediates is the more reasonable for this reaction. Furthermore, the formation of **1** from **2** is not interpreted using the intramolecular mechanism. Once again the intramolecular mechanism appears doubtful.

The fact that the thermodynamically least-stable ester (**2**) has the smallest rate constant is compatible with the carbanion mechanism. The rate for the formation of **2** is slower than that of **3**, because carbanion **5** is more stable than **4**. It is interesting to note that **1** predominated over **3** at the initial stage of the rearrangement of **2**. Direct interconversion between carbanions, **4** and **5**, may be negligible, since the rate constant for the disappearance of **1** is larger than that of **3** and since **1** is less abundant than **3** at equilibrium. The above results show that it is unreasonable to expect facile direct isomerization between **2** and **3**.[12]

The difference between the compositions resulting from the rearrangement of the free acids and the rearrangement of the esters is accounted for as follows. Equilibrium between citraconic and methylenesuccinic acids is interpreted using the intermediate *cis*-carbanion, whose configuration is fixed by intramolecular hydrogen bonding.[1] However, the esters are free from intramolecular hydrogen bonding and the *trans*-carbanion favors the rearrangement of the esters. Consequently, **3** appears as the most abundant product.

The author wishes to thank Professor Emeritus Sango Kunichika of Kyoto University for his encouragement throughout this work. He is also grateful to Professors Shinzaburo Oka, Norito Uchino, Yasumasa Sakakibara, and Atsuyoshi Ohno for their continuous guidance and helpful discussions.

References

1) For the preceding article in this series, see M. Sakai, *Bull. Chem. Soc. Jpn.*, **49**, 219 (1976).

2) Rearrangement is defined as the migration of a double bond, whereas isomerization is used to mean *cis-trans* interconversion. A reaction is any transformation including both rearrangement and isomerization.

3) J. N. Butler and G. J. Small, *Can. J. Chem.*, **41**, 2492 (1963).

4) a) D. E. McGreer and N. W. K. Chiu, *Can. J, Chem.*, **46**, 2217, 2225 (1968); b) C. D. Weis and T. Winkler, *Helv. Chim. Acta*, **57**, 856 (1974).

5) E. S. Lewis, J. T. Hill, and E. R. Newman, *J. Am. Chem. Soc.*, **90**, 662 (1968).

6) R. R. Rand and W. von E. Doering, *J. Org. Chem.*, **33**, 1671 (1968).

7) M. Itoh, M. Tokuda, K. Seguchi, K. Taniguchi, and A. Suzuki, *Kogyo Kagaku Zasshi*, **72**, 219 (1969).

8) S. Majeti and T. W. Gibson, *Tetrahedron Lett.*, **49**, 4889 (1973).

9) R. L. Shriner, S. G. Ford, and L. J. Roll, *Org. Synth.*, Coll. Vol. II, 140, 368, 382 (1943).

10) K. J. Laidler, "Chemical Kinetics," McGraw-Hill Book Company, New York, N. Y. (1965), p. 19.

11) The rearrangement of the esters proceeds at 50 °C in the presence of triethylamine in dimethyl sulfoxide, whereas the equilibrium composition remains unaltered; M. Sakai, unpublished results (1976).

12) Y. Mialhe and R. Vessière, *Bull. Soc. Chim. Fr.*, **1968**, 4181.

ESR Study on the Photoreduction of *N*-Acetyldiphenylmethyleneamine in 2-Propanol

Naoki Toshima, Kyoji Aoki, and Hidefumi Hirai

Department of Industrial Chemistry, Faculty of Engineering, The University of Tokyo, Hongo, Bunkyo-ku, Tokyo 113

(Received November 27, 1976)

Photoreduction of *N*-Acetyldiphenylmethyleneamine (**1**) in 2-propanol was studied both by the ESR spectroscopy of irradiated imine **1** in a matrix solvent at −196 °C and by the deuteration analysis of acetone formed from 2-propanol-*d* in the photoreduction process. The ESR spectrum consists of a broad singlet and a quartet. The latter is assigned to the $CH_3\dot{C}H(OH)CH_2$ radical, which can be produced by β-hydrogen abstraction by the excited imine **1** from 2-propanol, but not by the excited benzophenone. Formation of acetone-*d* on irradiation of **1** in 2-propanol-*d* suggests that the imine **1** in the excited state has a hydrogen abstracting character.

When acyclic imino compounds are irradiated in 2-propanol, a C=N bond is reduced to a –CH–NH– group. This photoreduction has been studied on various derivatives as one of the fundamental photoreactions of a C=N chromophore.[1–5] Two reaction mechanisms are proposed for this photoreduction. One is the "chemical sensitization" mechanism.[3] According to this mechanism, the reaction proceeds *via* an aminoalkyl radical formed by thermal hydrogen transfer from a ketyl radical to the imine. The ketyl radical is derived from the excited triplet state of the corresponding ketone present in the starting imine as an impurity. The other is the mechanism where imine itself has a hydrogen abstracting character in the excited state.[4,5]

We have reported that the irradiation of *N*-acetyldiphenylmethyleneamine (**1**) in 2-propanol gives the amide derivative and that only the C=N bond is selectively reduced.[4]

$$Ph_2C{=}NCOCH_3 + (CH_3)_2CHOH \quad (\mathbf{1})$$
$$\xrightarrow{h\nu} Ph_2CHNHCOCH_3 + (CH_3)_2C{=}O$$

In order to decide which mechanism is reasonable in this reaction, it seems important to compare the photoreaction of the imine **1** with that of benzophenone. The reaction proceeds in a radical fashion, whichever mechanism is adopted. So we have investigated this reaction by an ESR technique to detect the intermediate radical of the reaction.

Experimental

Materials. 2-Propanol was refluxed on anhydrous barium oxide and distilled. Acetonitrile was used after distillation. 2-Propanol-*d* was obtained from E. Merck Japan Ltd. Benzophenone was recrystallized from ethanol. *N*-Acetyldiphenylmethyleneamine (**1**), bp 170—172 °C/3 Torr (lit,[6] bp 168—170 °C/1 Torr) and *N*-propionyldiphenylmethyleneamine (**2**), mp 79.3—79.9 °C (lit,[6] mp 78—79.5 °C), were prepared by the reaction of diphenylmethyleneamine with acetic anhydride and propionic anhydride, respectively, and purified before use.

ESR Measurement. A solution of imine (*ca.* 250 mg) in a solvent (1 ml) was poured into an ESR tube and was degassed in four successive freeze-thaw cycles. The sealed sample tube in a transparent qaurtz Dewar bottle filled with liquid nitrogen was set in a cavity. UV light was irradiated from outside and ESR spectra were measured by using a JEOL 3BS-X type spectrometer. All irradiations were carried out with an Ushio type 500D ultrahigh pressure mercury lamp through a glass filter transparent to wavelengths longer than 320 nm. The field modulation was 100 kHz, and modulation width was 5.3 gauss during ESR measurements. *g*-Factors and hyperfine coupling constants were corrected by using a Mn^{2+} marker.

*Photoreaction of the Imine in 2-Propanol-*d. One gram of imine **1** was dissolved in 5 ml of 2-propanol-*d* in a quartz tube. Irradiation was carried out at room temperature or at −196 °C for 20 h in a similar manner as described in ESR measurements. A 2-propanol-*d* (5 ml) solution of benzophenone (260 mg) was also irradiated for 5 h at room temperature. After irradiation, the solvent was separated by vacuum distillation and mass spectra of acetone produced were measured by a Hitachi M-52 type GC-MS analyzer. The deuteration degree of the acetone was calculated from the base peak of the mass spectrum.

Results

ESR Measurements. On irradiation of imine **1** in 2-propanol at −196 °C, stable five lines were observed in an ESR spectrum as shown in Fig. 1A. When the system was warmed up to −154 °C, a broad single line remained and other four lines disappeared (Fig. 1B). The absorption and the second derivative type spectra of Fig. 1A are shown in Fig. 2A and 2B, respectively. The former indicates the intensity ratio of four lines to be *ca.* 1 : 3 : 3 : 1, and the latter indicates that four lines have the same splitting constant of 23.2 G

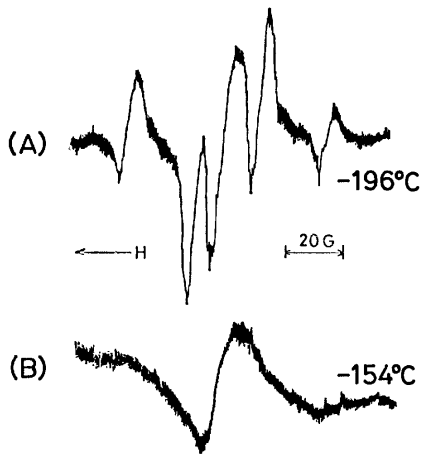

Fig. 1. ESR spectra (First Derivatives) of UV-irradiated *N*-acetyldiphenylmethyleneamine (**1**) in 2-propanol at (A) −196 °C and (B) −154 °C. Irradiations were carried out at −196 °C for 20 min.

Table 1. Parameters of observed ESR spectrum

Run	Imine	Solvent	Quartet		Singlet	
			a_H (G)	Intensity ratio	g	ΔH_{msl}[a] (G)
A	**1**	2-PrOH	23.2±0.4	*ca.* 1 : 3 : 3 : 1	2.002	10
B	**1**	2-PrOH/CH_3CN[b]	23.0±0.4	*ca.* 1 : 3 : 3 : 1	2.002	8
C	**2**	2-PrOH/CH_3CN[b]	22.5±0.4	*ca.* 1 : 3 : 3 : 1	2.003	9

a) The maximum slope distance. b) 1 : 1 by volume ratio.

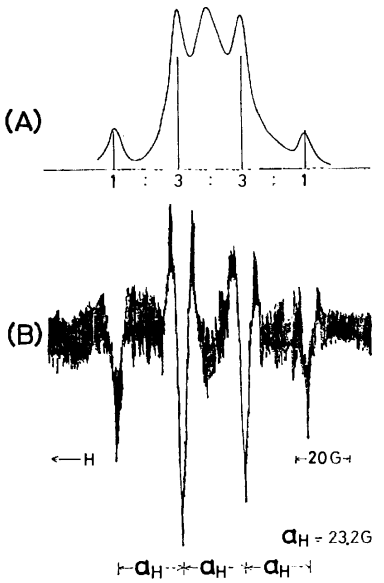

Fig. 2. Absorption (A) and 2nd derivative (B) of ESR spectra of UV-irradiated *N*-acetyldiphenylmethyleneamine (**1**) in 2-propanol at −196 °C.

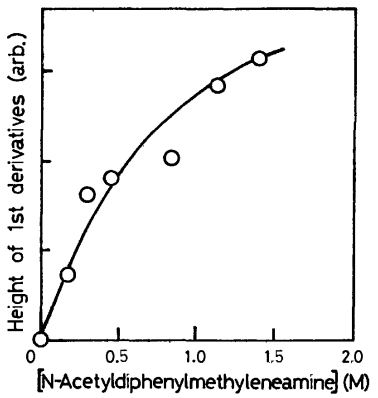

Fig. 3. Dependence of quartet intensity on the *N*-acetyldiphenylmethyleneamine (**1**) concentration. Samples of 2-propanol solution were UV-irradiated for 30 min at −196 °C with constant concentration of benzophenone (0.48 mol/l).

When *N*-propionyldiphenylmethyleneamine (**2**) was used instead of **1**, the ESR spectra of the solution gave the same signal.[7] A central singlet was broad in all cases and have no special relation to the quartet in intensity. The parameters of these ESR spectra are given in Table 1. The dependence of the intensities of a quartet upon the concentration of the imine **1** was investigated. The experiment was carried out with the constant concentration of benzophenone at each point. The heights of the outer lines of the quartet noticeably increased with the concentration of **1** as shown in Fig. 3.

*Photoreaction of Imine **1** in 2-Propanol*-d. In order to detect the position of hydrogens abstracted in 2-propanol, the deuteration degree of acetone was investigated. Acetone is formed from 2-propanol during the photoreaction of **1**. The results are shown in Table 2. The deuteration degree was small when benzophenone was used as a substrate, but relatively high when imine **1** was used .

Table 2. Deuteration degrees of acetone formed by the photoreductions in 2-propanol-*d*

Substrate	Temperature	Deuteration degree of acetone (%)
Benzophenone	Room temperature	≈ 5
Imine **1**	Room temperature	≈ 15
Imine **1**	−196 °C	≈ 21

Discussion

Assignment of ESR Signals. From the temperature dependence of signals as shown in Fig. 1, it is concluded that the five lines observed on irradiation at −196 °C consist of a broad singlet and a quartet. A quartet is not due to the radical from imine because both ESR spectra from imine **1** and imine **2** show the same patterns (*cf.* Table 1, Runs A and C). As an acetonitrile solution of imines gives no quartet, the quartet is not due to a radical from acetonitrile either. Furthermore, quite different signals were observed when other alcohols than 2-propanol were used as a solvent. From these experimental facts, the quartet is attributed to a radical from 2-propanol used as a solvent. As regards 2-propanol radicals, the ESR spectra of two radicals have been reported.[8] One is an α-hydroxy radical $(CH_3)_2\dot{C}OH$ which is formed by α-hydrogen abstraction from 2-propanol with Fenton's reagent, and shows a septet signal with intensity ratio of 1 : 6 : 15 : 20 : 15 : 6 : 1 and a_H of 19.5 G. The other is a β-hydroxy radical $CH_3\dot{C}H(OH)CH_2$ by β-hydrogen abstraction and this radical shows a quartet signal with intensity ratio 1 : 3 : 3 : 1 and a_H of 22.5 G. Comparison of the experimental values (Table 1) with these reported values clearly indicates that the quartet observed in the present experiment is due to the radical $CH_3\dot{C}H(OH)CH_2$.

As regards a broad singlet, it may be attributed to

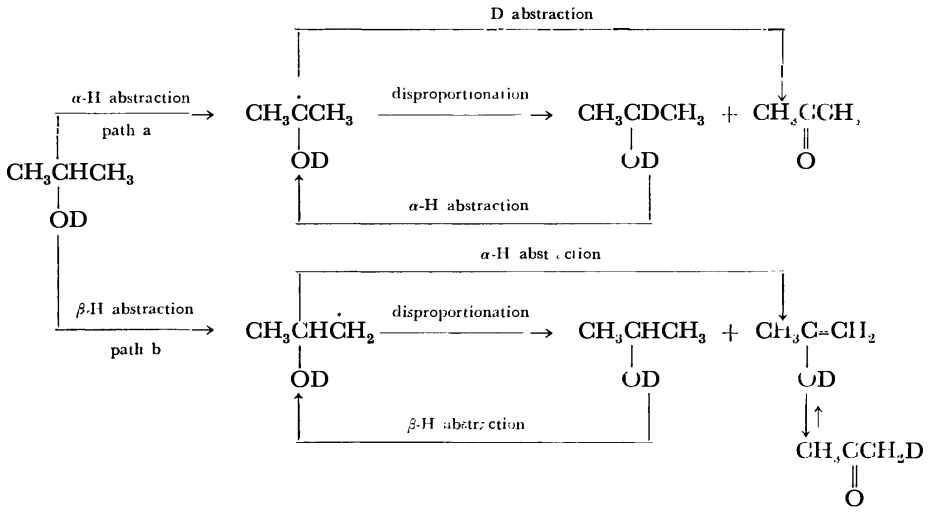

Scheme 1.

a mixed signal composed of $Ph_2\dot{C}NHCOCH_3$ from imine **1** and benzophenone ketyl radical from benzophenone as an impurity of **1**. Thus it is reported that the ESR spectra of both the ketyl radical[9] from benzophenone and the aminoalkyl radical $Ph_2\dot{C}NH_2$,[2] analogous to the radical $Ph_2\dot{C}NHCOCH_3$, were observed not to split by the coupling with the adjacent nitrogen atom and showed a broad singlet with the similar *g*-values on irradiation in a matrix solvent at a low temperature (ΔH_{msl} values of both radicals are 14 and 18 G, respectively). As the acetyl group of $Ph_2\dot{C}NHCOCH_3$ can be supposed not to effect also to the hyperfine structure of the radical in a rigid matrix, it is reasonable that $Ph_2\dot{C}NHCOCH_3$ shows a signal not so different from that of $Ph_2\dot{C}NH_2$. Therefore it is conceivable that the observed singlet is due to the mixed signal of radicals $Ph_2\dot{C}OH$ and $Ph_2\dot{C}NHCOCH_3$.

Reaction Processes. The ESR studies show the formation of the β-hydroxy radical $CH_3CH(OH)\dot{C}H_2$ on irradiation of imine **1** in 2-propanol in a rigid matrix at −196 °C. In the photoreduction of imine **1** in 2-propanol at low temperature, however, only acetone was produced from 2-propanol quantitatively, and no 2,5-hexanediol, a coupling product of the β-hydroxy radical, was detected. In order to satisfy the both facts, acetone must be formed from 2-propanol through the path b of Scheme 1. Contribution of both paths a and b to the reaction can be determined by product analysis when 2-propanol-*d* is used in the present photoreduction instead of 2-propanol.

The results show that the deuteration degree of acetone produced is low (5%) in the case of benzophenone which is recognized generally to abstract α-hydrogen of 2-propanol. In the case of the imine **1**, however, the deuteration degree is 15% when irradiation was carried out at room temperature, and 21% at −196 °C. As these values are apparently higher than that in the case of benzophenone, β-hydrogen abstraction from 2-propanol occurs more frequently in the photoreduction of the imine **1** in 2-propanol than that of benzophenone in 2-propanol.

As shown in Fig. 3, the quartet intensity of the β-hydroxy radical increased with the concentration of the imine **1**, and became zero when the concentration of the imine **1** was zero though benzophenone was exist in the solution. Since the concentration of benzophenone was equal at each point, it can be concluded that the $CH_3CH(OH)\dot{C}H_2$ radical is formed through the hydrogen abstraction from 2-propanol by the imine **1**. This conclusion is supported by the following experimental result. Thus, when the ESR spectrum of a 2-propanol solution of benzophenone was measured under irradiation in a matrix at −196 °C, the quartet due to $CH_3CH(OH)\dot{C}H_2$ was not observed, but weak outer bands of septet due to $(CH_3)_2\dot{C}OH$ and a strong broad singlet due to benzophenone ketyl radical were obtained. It is not clear why the imine **1** abstracts β-hydrogen from 2-propanol, but one of the reasons might be the specific interaction between the imine **1** and 2-propanol as a Fenton's reagent generally abstracts ω-hydrogen of alcohols.[8] It can be concluded that not the excited benzophenone, but the excited imine **1** abstracts β-hydrogen from 2-propanol especially in the photoreduction of imine **1** in 2-propanol. Namely the imine **1** in the excited state has a great deal to do with the photoreduction in contrast with the chemical sensitization mechanism.[3]

Partial financial supports of this work by the Grant-in-Aid for Scientific Research from the Ministry of Education, the Kawakami Foundation, and the Sakkokai Foundation (to N. T.) are gratefully acknowledged.

References

1) E. S. Huyser, R. H. S. Wang, and W. T. Short, *J. Org. Chem.*, **33**, 4323 (1968); B. Fraser-Reid, A. Mclean, and E. W. Usherwood, *Can. J. Chem.*, **47**, 4511 (1969); G. Balogh and F. C. De Schryver, *Tetrahedron Lett.*, **1969**, 1371; P. Beak and C. R. Payet, *J. Org. Chem.*, **35**, 3281 (1970); N. Toshima, S. Asao, K. Takada, and H. Hirai, *Tetrahedron Lett.*, **1970**, 5123; N. Toshima, M. Saeki, and H. Hirai, *Chem. Commun.*, **1971**, 1424; Y. Ogata and K. Takagi, *Tetrahedron*, **27**, 2785 (1971); N. Baumann, *Helv. Chim. Acta*, **56**, 2227 (1973); A.

Castellano, J. P. Catteau, A. Lablache-Combier, and B. Planckaert, *Tetrahedron Lett.*, **1973**, 4185; K. N. Mehrotra and T. Singh, *Indian J. Chem.*, **11**, 499 (1973).

2) N. Toshima, H. Hirai, and S. Makishima, *Kogyo Kagaku Zasshi*, **72**, 184 (1969).

3) M. Fischer, *Chem. Ber.*, **100**, 3599 (1967); A. Padwa, W. Bergmark, and D. Pashayan, *J. Am. Chem. Soc.*, **91**, 2653 (1969); A. Padwa and M. Dharan, *Tetrahedron Lett.*, **1972**, 1053.

4) T. Okada, M. Kawanisi, H. Nozaki, N. Toshima, and H. Hirai, *Tetrahedron Lett.*, **1969**, 927; T. Okada, K. Saeki, M. Kawanisi, and H. Nozaki, *Tetrahedron*, **26**, 3661 (1970).

5) N. Toshima, S. Asao, and H. Hirai, *Chem. Lett.*, **1975**, 451; M. Saeki, N. Toshima, and H. Hirai, *Bull. Chem. Soc. Jpn.*, **48**, 476 (1975); S. Asao, N. Toshima, and H. Hirai, *Bull. Chem. Soc. Jpn.*, **48**, 2068 (1975); **49**, 224 (1976).

6) J. E. Banfield, G. M. Brown, F. H. Davey, W. Davies, and T. H. Ramsay, *Aust. J. Sci. Res.*, **A1**, 330 (1948).

7) The solubility of imine **2** in 2-propancl was so low that the mixed solvent of 2-propanol and acetonitrile (1 : 1 v/v) was used in this experiment. In this mixed solvent imine **1** showed the same ESR signal as that in 2-propanol.

8) T. Shiga, *J. Phys. Chem.*, **69**, 3805 (1965).

9) Y. Iwakura, K. Takeda, T. Nakazawa, and O. Watarai, *J. Polymer Sci. Part B*, **6**, 115 (1968).

ESR Studies of the g- and D-Tensor Values of Stable *p*- and *m*-Phenylenebis(galvinoxyl) Biradicals

Kazuo MUKAI and Toshiko TAMAKI

Department of Chemistry, Faculty of Science, Ehime University, Matsuyama 790

(Received July 23, 1976)

The **g**- and **D**-tensor values of *p*- and *m*-phenylenebis(galvinoxyl) biradicals in several solvents have been determined from their asymmetric frozen ESR spectra. The spectra suggested that only one conformer out of two possible ones, "*propeller*" and "*anti-propeller*" structures, exists in each biradical. The **D**-tensor values were calculated for the two possible conformers, based on assumed molecular structures and spin distribution. The results indicate that the "*propeller*" structure with a 30° twist angle is preferable for the *m*-phenylenebis(galvinoxyl). In the case of the *p*-phenylenebis(galvinoxyl), a considerable accordance between the measured and calculated values for the two conformers with a 30° twist angle was obtained. Notable solvent effects in the **g**- and **D**-tensor values were observed for the *m*-phenylenebis(galvinoxyl), but not for the *p*-phenylenebis(galvinoxyl).

Recently, one of the present authors has reported the preparation of *p*- and *m*-phenylenebis(galvinoxyl) biradicals, (I) and (II), which are fairly stable phenoxyl biradicals; their structures are shown in Fig. 1.[1] The biradicals were produced by the PbO_2 oxidation of phenol precursors in 2-methyltetrahydrofuran (2-MTHF) under a vacuum. The fluid solution ESR spectra of the biradicals consist of nine lines due to eight equivalent meta-ring protons. Gierke *et al.* also obtained the biradicals from different phenol precursors by PbO_2 oxidation.[2] ESR zero-field splittings in rigid media at 77 K were observed, indicating the existence of the triplet state in the biradicals. However, no detailed analyses of the ESR spectra of the biradicals have been reported, although various types of information about the conformation, symmetry, and electronic state of triplet molecules have been obtained from the rigid matrix ESR spectra.[3-7]

In the present paper, the **g**- and **D**-tensor values of *p*- and *m*-phenylenebis(galvinoxyl) biradicals (I and II) in several solvents have been determined from their asymmetric frozen ESR spectra. The **D**-tensor values were calculated for two possible conformers in each biradical, based on the assumed molecular structures and spin distribution. On the basis of these data, the conformation and electronic structure of the biradicals and the solvent effect have been discussed. The hyperfine splittings of many stable hindered phenoxyl radicals, including several biradicals, have been studied by a number of investigators with the aid of the ESR spectra.[8] However, the **g**- and **D**-tensor values of these phenoxyl radicals have never been reported, as far as we know.

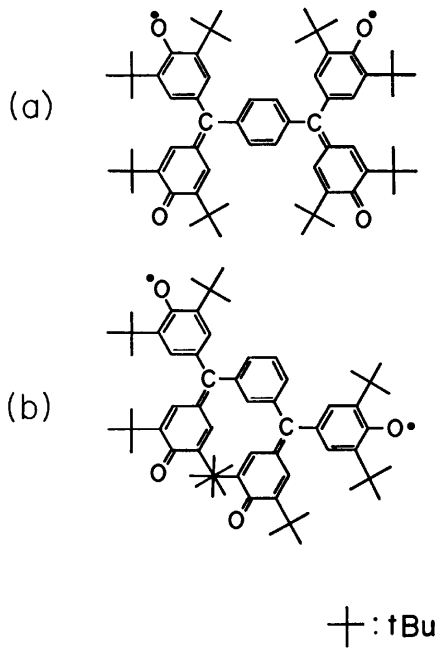

Fig. 1. Molecular structures of (a) *p*-phenylenebis(galvinoxyl) biradical (I) and (b) *m*-phenylenebis(galvinoxyl) biradical (II).

Experimental

The syntheses of *p*-bis[bis(3,5-di-*t*-butyl-4-hydroxyphenyl)-methyl]benzene (mp 290—292 °C) and *m*-bis[bis(3,5-di-*t*-butyl-4-hydroxyphenyl)methyl]benzene (mp 223—224 °C) were reported previously.[1] The *p*- and *m*-phenylenebis(galvinoxyl) biradicals (I and II) were prepared by the oxidation of the above phenol precursors with PbO_2 in the 2-MTHF solvent under a nitrogen atmosphere, with the temperature kept between 5 and 10 °C, following the method of Kharash and Joshi.[9]

All the ESR measurements were carried out using a JES-ME-3X spectrometer equipped with a Takeda-Riken microwave frequency counter. The ESR splittings were determined using $(KSO_3)_2NO$ ($a^N = 13.05 \pm 0.03$ G) as a standard. The *g*-values were measured relative to the value of Li-TCNQ powder, calibrated with $(KSO_3)_2NO$ ($g = 2.0054$).[10]

Results and Discussion

ESR Spectral Analyses. The 2-MTHF solution spectra of the *p*- and *m*-phenylenebis(galvinoxyl) radicals (I and II) show nine line hyperfine splittings due to the equivalent eight *meta*-ring protons in the two galvinoxyl rings, as has been reported previously.[1] The spectra were ascribed to a biradical whose exchange energy, J, is larger than the proton coupling constant, a_m^H ($J \gg a_m^H$; $a_m^H/2 = 0.69$ G for I and II). When the solution containing the I and II biradicals is frozen into a rigid glass (77 K), one can observe some dipolar splittings, as Figs. 2 and 3 show.

The biradical in a rigid glass can be treated as a two-spin system which forms a triplet and a singlet state. The usual spin Hamiltonian[3,6] for the triplet state is:

$$H = \beta \mathbf{H} \cdot \hat{\mathbf{g}} \cdot \mathbf{S} + \mathbf{S} \cdot \hat{\mathbf{D}} \cdot \mathbf{S}, \quad (1)$$

where $\hat{\mathbf{g}}$ is the **g** tensor, $\hat{\mathbf{D}}$ is the spin-spin dipolar interaction tensor, and the other symbols have the usual meanings. When the radical has the property of a triplet without axial symmetry, we usually observe three pairs of absorption lines, from whose separations the zero-field parameters (D and E) of the dipolar electron-electron interaction can be obtained.[3,6,7] The spectrum of the I biradical can be explained as two inner pairs of lines overlapping each other, because of the small distances between zero-field absorption lines compared with the line-width of each absorption line. In the spectrum, the high-field line of the inner pair of lines is broader than the other and has a shoulder, suggesting the overlapping of two lines. A central line at $g=2$ is attributable to the monoradical impurity. In fact, in the case of the II biradical, five out of six lines

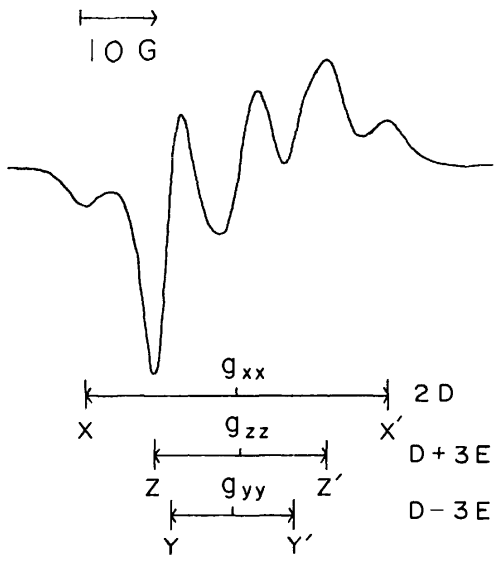

Fig. 2. ESR spectrum of the biradical (I) in 2-MTHF at 77 K.

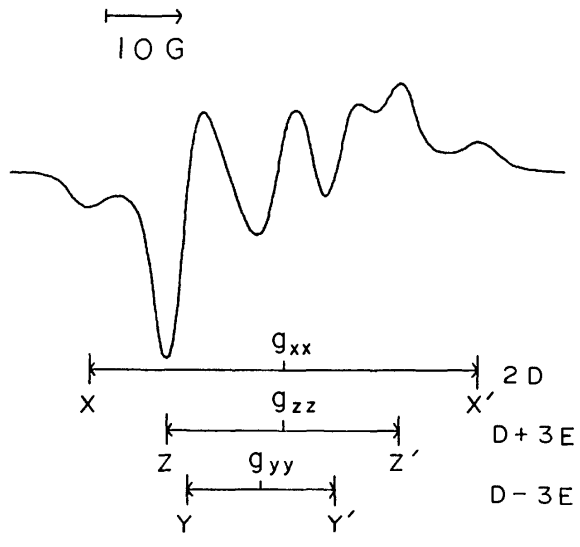

Fig. 3. ESR spectrum of the biradical (II) in 2-MTHF at 77 K.

theoretically expected for a non-axially symmetrical triplet are resolved, as is shown in Fig. 3.

In both the biradicals (I and II), the zero-field parameters (D and E) and the **g**-tensor values have been estimated from the positions of three pairs of turning points (XX', YY', and ZZ'), which are shown in Figs. 2 and 3, in the following way. The separation between the outer pair of lines (XX') in the spectrum of the I biradical is $2D=40.0\pm0.4$ G. Because of the localization of each unpaired electron on two galvinoxyl rings, as will be discussed later, the principal X axis of the **D** tensor, corresponding to the maximum value of $2D$, is probably parallel to the line connecting two carbon atoms bonded to the centered phenylene ring. Because of the symmetry of the biradical molecules, we can expect that the principal axes of the **D** and **g** tensors are coaxial. Consequently, the frequency center of these lines gives $g_{xx}=2.0045\pm0.0002$. The remaining pairs, ZZ' and YY', are separated by $(D+3E)=22.7\pm0.6$ G and $(D-3E)=16.0\pm0.6$ G respectively. Although, because of overlapping lines, this distance cannot be measured accurately, the value of $D=19.4\pm0.6$ G shows a considerable accordance with the value ($D=20.0\pm0.2$ G) from two external lines; thus, the E value was estimated to be $E=1.1\pm0.2$ G. The g-values from the frequency center of these two pairs of absorption lines are $g_1=2.0043\pm0.0002$ (ZZ') and $g_2=2.0049\pm0.0002$ (YY'). By comparing g_1 and g_2, the smaller, $g_1=2.0043$, was tentatively assigned to g_{zz}, and the larger, $g_2=2.0049$, to g_{yy}, as will be discussed later.* The isotropic g_{iso} value of the I biradical was measured in 2-MTHF at room temperature. The average g_{av} value of $(1/3)(g_{xx}+g_{yy}+g_{zz})=2.0045\pm0.0002$ is in agreement with the isotropic $g_{iso}=2.00441\pm0.00003$ value measured at room temperature, indicating that the **g**-tensor values obtained by the above analysis are reliable. All these values are summarized in Table 1. Similar analyses were performed for the frozen solution ESR spectrum of the II biradical in 2-MTHF. The **D**- and **g**-tensor values obtained are $D=26.1\pm0.2$ G, $E=1.9\pm0.2$ G, and $g_{xx}=2.0039\pm0.0002$, $g_{yy}=2.0056\pm0.0002$, $g_{zz}=2.0038\pm0.0002$, respectively. The average g_{av} value of $(1/3)(g_{xx}+g_{yy}+g_{zz})=2.0044\pm0.0002$ is in agreement with the isotropic $g_{iso}=2.00443\pm0.00003$ value measured in 2-MTHF at room temperature. The **D**- and **g**-tensor values obtained are listed in Table 2. Both the D and E values of the II biradical are larger than those of the I biradical.

The shift of the g value from that ($g_e=2.0023$) of the free electron is determined mainly by spin-orbit coupling, which may be large because of the presence of the nonbonding σ electrons of the oxygen atom. The energy due to the so-called n-π transitions may be low

* This assignment was also supported by the calculations of the dipolar splitting parameters, D and E, as will be described below. The values of the D and E parameters calculated for both the "*propeller*" and "*anti-propeller*" structures of *p*-phenylenebis(galvinoxyl) biradical are negative and positive respectively. Therefore, $D_{zz}>D_{yy}>0$, where D_{zz} and D_{yy} are the principal values of the **D**-tensor; thus, the smaller, $g_1=2.0043$, is attributable to g_{zz}.[3]

Table 1. **g**- and **D**-tensor values of the *p*-phenylenebis(galvinoxyl) biradical

Solvent	$\|D\|$[a] (G)	$\|E\|$[a] (G)	g_{xx}[b]	g_{yy}	g_{zz}	g_{av}[c]	g_{iso}[d]
2-MTHF	20.0	1.1	2.0045	2.0049	2.0043	2.0045	2.00441
Toluene	19.8	1.0	2.0044	2.0048	2.0042	2.0044	2.00443
Ethyl alcohol	19.9	1.2	2.0045	2.0049	2.0040	2.0045	2.00440
Diethyl ether	20.0	1.2	2.0045	2.0047	2.0039	2.0044	2.00441

a) The experimental errors in the values of $|D|$ and $|E|$ are ±0.2 G. b) The experimental errors in the values of g_{xx}, g_{yy}, g_{zz}, and g_{av} are ±0.0002. c) The average $g_{av}=(1/3)(g_{xx}+g_{yy}+g_{zz})$. d) The experimental errors in the values of g_{iso} are ±0.00003.

Table 2. **g**- and **D**-tensor values of the *m*-phenylenebis(galvinoxyl) biradical

Solvent	$\|D\|$[a] (G)	$\|E\|$[a] (G)	g_{xx}[b]	g_{yy}	g_{zz}	g_{av}[c]	g_{iso}[d]
2-MTHF	26.1	1.9	2.0039	2.0056	2.0038	2.0044	2.00443
Toluene	21.9	1.5	2.0043	2.0055	2.0039	2.0046	2.00441
Ethyl alcohol	26.0	1.9	2.0038	2.0054	2.0039	2.0044	2.00434
Diethyl ether	26.9	1.8	2.0039	2.0057	2.0041	2.0046	2.00441

a) The experimental errors in the values of $|D|$ and $|E|$ are ±0.2 G. b) The experimental errors in the values of g_{xx}, g_{yy}, g_{zz}, and g_{av} are ±0.0002. c) The average $g_{av}=(1/3)(g_{xx}+g_{yy}+g_{zz})$. d) The experimental errors in the values of g_{iso} are ±0.00003.

in these systems; therefore, these transitions contribute strongly to the shift in the g value.[11,12] However, in the planar aromatic radicals the contribution to the g_{zz} value (perpendicular to the molecular plane) from the n-π transitions vanishes. Therefore, the value of g_{zz} should be close to the free-spin value, while g_{xx} and g_{yy} are larger than g_e. In the *p*-phenylenebis(galvinoxyl) radical, the **g**-tensor values estimated from the frozen-solution spectrum are $g_{xx}=2.0045\pm0.0002$, $g_1=2.0043\pm0.0002$, and $g_2=2.0049\pm0.0002$. By comparing g_1 and g_2, the smaller g_1 was tentatively assigned to g_{zz}, and the larger g_2, to g_{yy}. Similarly, the **g**-tensor values of the *m*-phenylenebis(galvinoxyl) radical are $g_{xx}=2.0039\pm0.0002$, $g_{yy}=2.0056\pm0.0002$, and $g_{zz}=2.0038\pm0.0002$. The g_{zz} values of both biradicals show a large deviation from that of the free electron. This is mainly due to the nonplanar character of the I and II biradicals.

D-*Tensor Calculation with Spin Densities.* In order to clarify the molecular structures of the *p*- and *m*-phenylenebis(galvinoxyl) biradicals, and in order to determine the directions of the principal axes, X_d, Y_d, and Z_d, of the **D**-tensor in the molecules, the calculations of the dipolar splitting tensors were performed for two possible conformers in each biradical, based on the assumed molecular structures and spin distribution.

p- And *m*-phenylenebis(galvinoxyl)s (I and II) are thought to be weakly π-conjugated biradicals because of the small spin density on the central phenylene ring. The orbital containing the unpaired electron of phenylgalvinoxyl radical has, at least in the Hückel approximation, a node in the phenyl ring; in fact, a recent ENDOR study found a small hyperfine splitting ($a^H=0.207$ G) for phenyl-ring protons.[13] In such a case, the electronic structures of the two galvinoxyl rings in these biradicals must be similar to that of the phenylgalvinoxyl. The isotropic g_{iso} values also show an excellent agreement between the phenylgalvinoxyl ($g_{iso}=2.00440\pm0.00003$), the I biradical ($g_{iso}=2.00441\pm0.00003$), and the II biradical ($g_{iso}=2.00443\pm0.00003$), supporting the above anticipation. Therefore, the dipolar magnetic system of the I and II biradicals can be adequately described as an isolated two-spin system consisting of two galvinoxyl groups, each containing one unpaired electron.

The phenylgalvinoxyl radical may, on the other hand, be considered a triphenylmethyl derivative. A molecular model indicates that the main steric interaction in phenylgalvinoxyl works between the ring protons, although weak interactions can be seen between the substituted tertiary butyl groups. Thus, the radical probably adopts a propeller configuration, the twist angle of phenyl rings being estimated to be about 30° about the methyl bond.[14] The *p*-phenylenebis(galvinoxyl) radical will have a similar configuration. Because the steric interactions between the substituted tertiary butyl groups of the two galvinoxyl rings are considered to be weak (see Fig. 1), the twist angle of phenyl rings about the methyl bond will still be about 30°. Consequently, we can expect two possible conformations, (A) and (B), in *p*-phenylenebis(galvinoxyl), in which each monoradical half is considered to have a propeller configuration. In the (A) conformation, the two $2p_z$ orbitals of two triphenylmethyl carbon atoms twist by 60° each other, while in the (B) conformation, the two $2p_z$ orbitals are parallel to each other, having a 30° twist angle to the π-orbital of the centered phenylene ring. These two conformations, (A) and (B), are shown in Fig. 4 and are named as "*propeller*" and "*anti-propeller*" structures, considering the figure as a whole molecule. Similarly, two conformations can be expected in *m*-phenylenebis(galvinoxyl). However, the Stuart molecular model indicates that the "*anti-propeller*" structure is not probable in this radical because of the strong steric interaction between two galvinoxyl rings, especially through nearest-neighboring tertiary butyl groups (see Fig. 1(b)); thus, only the "*propeller*" structure is probable (see Fig. 5).

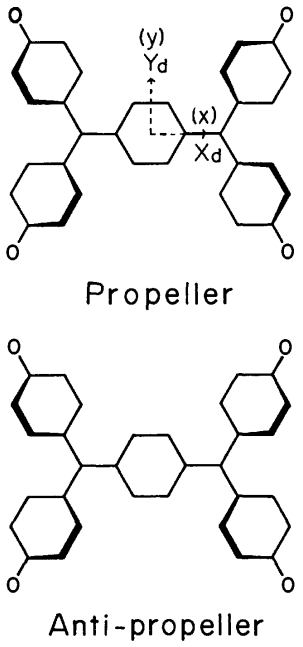

Fig. 4. "*Propeller*" and "*anti-propeller*" structures of *p*-phenylenebis(galvinoxyl) biradical, showing the molecular axes x, y, and z and the principal axes X_d, Y_d, and Z_d of the **D**-tensor.

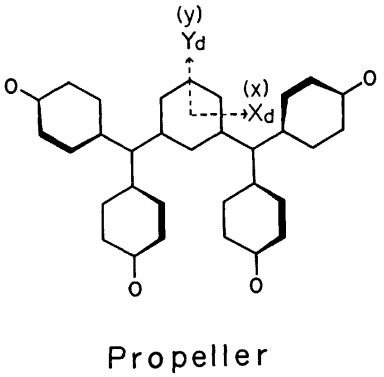

Fig. 5. "*Propeller*" structure of *m*-phenylenebis(galvinoxyl) biradical, showing the molecular axes x, y, and z and the principal axes X_d, Y_d, and Z_d of the **D**-tensor.

In the "*propeller*" structure of the I and II biradicals, to achieve symmetry, the molecular z axis is chosen perpendicular to the central phenylene ring, while the x axis parallels a line connecting the two carbon atoms bonded to the central phenylene ring. On the other hand, in the "*anti-propeller*" structure of the I biradical, while the x axis is chosen similarly, the z axis is chosen perpendicular to a plane containing four oxygen atoms. We assumed that the principal axes—X_d, Y_d, and Z_d of the **D**-tensor are parallel to the molecular axes—x, y, and z, because of the symmetry of the biradical molecules, as is shown in Figs. 4 and 5. This is a favorable situation for calculating the **D**-tensor values, because, in such a case, the matrix of the **D**-tensor can be diagonalized. Therefore, the D and E parameters of the dipolar splitting can be calculated with the aid of the following equations:[15-17]

$$D = \frac{3}{4} g_{iso}^2 \beta^2 \sum_{i,j} \frac{r_{ij}^2 - 3x_{ij}^2}{r_{ij}^5} \rho_i \rho_j \tag{2}$$

$$E = \frac{3}{4} g_{iso}^2 \beta^2 \sum_{i,j} \frac{y_{ij}^2 - z_{ij}^2}{r_{ij}^5} \rho_i \rho_j \tag{3}$$

where r_{ij} is the distance between the i and j atoms and where ρ_i and ρ_j are the π-spin densities on the i atom in one galvinoxyl group and on the j atom in the other galvinoxyl group in a molecule. Here we have chosen the following parameters: the twist angle of each phenyl ring to the $2p_z$ orbitals of the two triphenylmethyl carbon atoms is 30°, as has been described above; the C–O bond length is 1.27 Å, and the C–C bond length is 1.40 Å in the average, as obtained by an X-ray analysis of the galvinoxyl radical;[18] the McLachlan spin densities were taken from Ref. 13.

Using these parameters, the calculations of the D and E values were performed for two possible conformations, the "*propeller*" and "*anti-propeller*" structures, of the I biradical, and one possible conformation, the "*propeller*" structure, of the II biradical. The results are summarized in Table 3, together with those obtained experimentally in the 2-MTHF solvent. For the I biradical, the calculated D and E parameters are 18.0 and 0.6 G for the "*propeller*" structure, and 21.7 and 1.7 G for the "*anti-propeller*" structure, while the observed ones are 20.0 and 1.1 G in 2-MTHF respectively. For the II biradical, the calculated D and E values are 27.0 and 1.3 G for the "*propeller*" structure, while the observed ones are 26.1 and 1.9 G in 2-MTHF respectively. The *p*- and *m*-phenylenebis(galvinoxyl) biradicals (I and II) are thought to be weakly π-conjugated biradicals, with a twist angle of the phenyl rings of about 30°. Therefore, the calculations of the D and E parameters were performed by assuming that the I and II biradicals consist of isolated two galvinoxyl groups, each containing one unpaired electron, as has been described above. The considerable accordance between calculated and observed values indicates that the above assumptions for the electronic structure and the twist angle of the I and II biradicals are reliable. The results also suggest that the principal X_d axis of the **D** tensor, corresponding to the maximum $2D$ value, is parallel to the molecular x axis; this is consistent with our expectations.

TABLE 3. THE D AND E PARAMETERS (IN G) OF THE DIPOLAR SPLITTING CALCULATED FOR THE "*propeller*," "*anti-propeller*," AND "*planar*" STRUCTURES OF THE *p*- AND *m*-PHENYLENEBIS(GALVINOXYL) BIRADICALS (I AND II)

	I Biradical		II Biradical	
	$\|D\|$ (G)	$\|E\|$ (G)	$\|D\|$ (G)	$\|E\|$ (G)
Propeller	18.0	0.6	27.0	1.3
Anti-propeller	21.7	1.7	—	—
Planar	22.3	1.9	94.2	4.5
Experimental[a]	20.0	1.1	26.1	1.9

a) **D**-tensor values measured in 2-MTHF at 77 K.

The frozen-solution ESR spectrum of the I biradical in 2-MTHF (see Fig. 2) suggests that only one conformer exists in the biradical; if two conformers exist in the I biradical at the same time, we should, at least, observe a splitting in the X and/or X' absorption lines, as the results of the calculation of the D and E parameters indicate. Unfortunately, it is not possible to decide whether the I biradical molecule takes a "*propeller*" or an "*anti-propeller*" structure, because both the D and E values experimentally obtained are just the medium ones of those calculated for the two assumed conformers. By comparing the **g**-tensor values of the biradicals with those of the monoradicals, the conformations of some nitroxide biradicals have been determined recently.[5,6] The **g**-tensor values of phenoxyl monoradicals including galvinoxyl and the phenylgalvinoxyl radical have not been reported, though, as far as we know. Therefore, we can not utilize the observed **g**-tensor values of the I biradical in order to determine the conformation of the radical. The frozen-solution ESR spectrum of the II biradical in 2-MTHF (see Fig. 3) also indicates that only one conformer exists in this radical. The observed D and E parameters show a considerable accordance with those calculated for the expected "*propeller*" structure, as described above.

The discrepancy between the observed and the calculated parameters will depend mainly on the difference between the true and the presumed vector distances, that is, probably in this case, the twist angle. Therefore, calculations were also performed for the "*planar*" structure of both the biradicals for reference. In fact, in the case of the II biradical, the D and E parameters (D=94.2 and E=4.5 G) calculated for the "*planar*" structure show a large discrepancy from those (D=26.1, E=1.9 G) observed in 2-MTHF and from those (D=27.0, E=1.3 G) calculated for the "*propeller*" structure with a 30° twist angle. The results indicate that the dipolar splitting calculations are very sensitive to the twist angle, because, for instance, the nearest neighboring interatomic distances are 4.79 Å for the "*propeller*" structure and 2.42 Å for the "*planar*" structure. On the other hand, in the case of the I biradical, the dipolar splitting values are not sensitive to whether the radical molecule takes the "*planar*" or the "*non-planar*" structure, as is shown in Table 3. However, the "*planar*" structure shows the largest deviations of both the calculated D and E parameters from the experimental ones among the three structures.

Solvent Effect for the Structure of the Biradicals. Many investigations of the solvent effects of free radicals, including phenoxyl radicals, in solution have been reported.[19] The effects may be explained as a redistribution of the π-electron spin density in a radical molecule induced by the electrostatic interaction and/or the hydrogen-bond formation between radical and solvent molecules. In addition to the above effects, recent ENDOR studies of the phenylgalvinoxyl radicals in solution have provided evidence that solvent molecules may play an important role in fixing the conformation and, thus the unpaired electron distribution, of the radical molecules.[13] Based on the ENDOR data, interesting changes in conformation and symmetry for these radicals due to steric interactions and solvent effects have been discussed. Therefore, the effects of the solvent in the frozen-solution ESR spectra of the I and II biradicals have also been examined.

In the I biradical, identical spectra were obtained in frozen toluene, ethanol, and diethyl ether solutions. The observed values of the zero-field splittings, the **g** tensors, and the average g_{av} have been summarized in Table 1. The isotropic g_{iso} values of the I biradical were also measured in toluene, ethanol, and diethyl ether solvents at room temperature. In the I biradical, all these values are very close to the corresponding ones in 2-MTHF, within the limits of experimental error. This indicates that the effect of the solvent is too small to induce the change in the unpaired spin distribution and the molecular structure.

On the other hand, notable solvent dependences were observed in frozen-solution spectra of the II biradical; the results are summarized in Table 2. The observed D values are 26.1 G in 2-MTHF, 21.9 G in toluene, 26.0 G in ethanol, and 26.9±0.2 G in diethyl ether. The **g**-tensor values also appear to be slightly different from the corresponding ones in other solvents, whereas the respective average g_{av} values are close to the corresponding g_{iso} values. In addition, the g_{iso} values for the II biradical in 2-MTHF, toluene, ethanol, and diethyl ether at room temperature are 2.00443, 2.00441, 2.00434, and 2.00441±0.00003 respectively; *i. e.*, there are virtually the same, within the limits of experimental error, except for the small change in ethanol. From the values of D, the distances between the radical centers in the point-dipole approximation were estimated to be about 10.2 Å for the largest D-value in diethyl ether and 10.8 Å for the smallest D-value in toluene. These results may be explained by assuming that the twist angle between the $2p_z$ orbitals of the triphenylmethyl carbon atom and of the centered phenylene ring of the II biradical is larger in toluene than in diethyl ether.

We are very grateful to Professor Kazuhiko Ishizu and Professor Yasuo Deguchi for their kind advice and encouragement. We are also grateful to Miss Atsuko Shibayama for her kind help in the calculation of the zero-field splitting parameters.

References

1) K. Mukai, *Bull. Chem. Soc. Jpn.*, **48**, 2405 (1975).
2) W. Gierke, W. Harrer, H. Kurreck, and J. Reusch, *Tetrahedron Lett.*, **38**, 3681 (1973).
3) E. Wasserman, L. C. Snyder, and W. A. Yager, *J. Chem. Phys.*, **41**, 1763 (1964).
4) R. Breslow, H. W. Chang, R. Hill, and E. Wasserman, *J. Am. Chem. Soc.*, **89**, 1112 (1967).
5) R. M. Dupeyre, A. Rassat, and J. Ronzaud, *J. Am. Chem. Soc.*, **96**, 6559 (1974).
6) P. Michon and A. Rassat, *J. Am. Chem. Soc.*, **97**, 696 (1975).
7) K. Mukai, T. Mishina, and K. Ishizu, *J. Chem. Phys.*, **66**, 1680 (1977).
8) See, for example, A. R. Forrester, J. M. Hay, and R. H. Thomson, "Organic Chemistry of Stable Free Radicals," Academic Press, London and New York (1968), Chap. 7.
9) M. S. Kharasch and B. S. Joshi, *J. Org. Chem.*, **22**, 1435 (1975).
10) J. J. Windle and A. K. Wiersma, *J. Chem. Phys.*, **39**,

1139 (1963).
11) A. J. Stone, *Mol. Phys.*, **6**, 509 (1963).
12) T. Kawamura, S. Matsunami, T. Yonezawa, and K. Fukui, *Bull. Chem. Soc. Jpn.*, **38**, 1935 (1965).
13) K. Mukai, T. Kamata, T. Tamaki, and K. Ishizu, *Bull. Chem. Soc. Jpn.*, **49**, 3376 (1976).
14) P. Andersen and B. Klewe, *Acta Chem. Scand.*, **16**, 1817 (1962).
15) D. A. Wiersma and J. Kommandeur, *Mol. Phys.*, **13**, 241 (1967).
16) D. D. Thomas, H. Keller, and H. M. McConnell, *J. Chem. Phys.*, **39**, 2321 (1963).
17) N. Azuma, H. Ohya-Nishiguchi, J. Yamauchi, K. Mukai, and Y. Deguchi, *Bull. Chem. Soc. Jpn.*, **47**, 2369 (1974).
18) D. E. Williams, *Mol. Phys.*, **16**, 145 (1969).
19) K. Mukai, H. Nishiguchi, K. Ishizu, Y. Deguchi, and H. Takaki, *Bull. Chem. Soc. Jpn.*, **40**, 2731 (1967), other references therein.

Adsorption of Benzoic Acid on a Mercury Electrode

Isao TANIGUCHI, Koji MACHIDA, Norio SATO, and Taro SEKINE

Department of Electronic Chemistry, Graduate School at Nagatsuta, Tokyo Institute of Technology, Ookayama, Meguro-ku, Tokyo 152

(Received August 23, 1976)

The differential capacity and the surface tension at the electrode-electrolyte interface of a dropping-mercury electrode were measured in 0.5 M H_2SO_4 and 0.5 M Na_2SO_4 solutions for various concentrations of benzoic acid. On the basis of the Frumkin-Damaskin theory, the adsorption of benzoic acid on mercury was studied in the acid solution, and the parameters involved in the F-D theory were determined: $A=1.6$ μJ cm^{-2} ($\Gamma_m=6.5\times10^{-10}$ mol cm^{-2}), $B_0=597$ l mol^{-1}, $a=-0.35-2.5\,E$/V, and $C'=5.95$ μF cm^{-2}. The experimental values of the capacity and the surface tension are in good agreement with the theoretical values calculated by using the parameters obtained. The absence of an anodic maximum in the capacity-potential curve in the presence of benzoic acid was determined to be associated with a strong repulsive force between the adsorbed molecules. The value obtained for the maximum surface excess of benzoic acid is explained in terms of adsorption of the acid molecules for a vertical orientation on the electrode surface. This conclusion was supported by comparing the B_0 value for benzoic acid with those for phenol and aniline. The adsorption of benzoic acid in neutral solutions is also discussed.

The adsorption of organic substances on mercury electrodes has been reported by many workers.[1,2] At present, two theories developed by Frumkin and Damaskin (F-D theory)[1] and by Bockris, Devanathan, and Müller (B-D-M theory)[3] are applicable for describing the effect of an electric field on the adsorption of organic substances on the electrode surface. The adsorption of aliphatic amines,[4] alcohols,[4,5] carboxylic acids,[6,7] aromatic amines,[8,9] and phenol[10] has been investigated on the basis of the F-D theory, since this theory gives a quantitative description of the relationship between the surface tension or the differential capacity and the electrode potential in the presence of organic substances. Good agreement between the theoretical and experimental results has usually been obtained. In addition to the above compounds, the adsorption of aliphatic ketones[11,12] was studied using a modified F-D theory.[7] However, only a few reports have been made on the adsorption of aromatic carboxylic acids. Blomgren *et al.*[13] have carried out the measurement of electrocapillary curves on a mercury electrode in 0.1 M HCl solutions containing benzoic acid at concentrations less than 10 mM with the results treated on the basis of the Langmuir isotherm. Therefore, a precise experiment is required to further clarify the adsorption behavior and to elucidate the reduction mechanism of benzoic acid.[14]

Here, the adsorption of benzoic acid on a mercury electrode in aqueous sulfuric acid and sodium sulfate solutions investigated by measuring the differential capacity at the electrode-electolyte interface and the surface tension of a dropping-mercury electrode are reported. The results are discussed on the basis of the F-D theory.

Experimental

The differential capacity of the double layer was measured by means of an AC impedance bridge possessing a large capacity to prevent DC flow through the bridge and having a choke to prevent AC flow through the DC polarization circuit. The measurements were carried out on a dropping-mercury electrode with a droplife of 11—13 s (rate of mercury flow: 0.629 mg s^{-1}), and at various frequencies (0.2—10 kHz, V_{pp}: 5 mV). In the case of benzoic acid solutions of more than 1 mM, the frequency dispersion of the capacity was not observed at the bottom of the capacity curves. At the peak of the curves, the capacity depends slightly on the frequency of the applied AC signal. The capacity at equilibrium was obtained from an extrapolation of the peak capacity to zero frequency as a function of the square root of the frequency, as described by Hansen *et al.*[15] When the electrode has a long droplife, the influence of diffusion on the measured capacity is negligible. The capacity at equilibrium obtained by extrapolation is nearly equal to the capacities measured at 0.5 or 1 kHz, and the curves measured at 0.5 and 1 kHz are considered to be the equilibrium curves for solutions of more than 10 mM of benzoic acid without introducing any appreciable error.

The surface tension of the mercury electrode was measured by the drop-time method.[16] The surface tension at the electrocapillary maximum was evaluated from the measured surface tension.[17,18]

All measurements were repeated at least three times and the average of the measured values is adopted as the final value. The uncertainty is within ±3%.

Benzoic acid (analytical GR reagent grade) was recrystallized twice from water. The test solution was freshly prepared before the measurements. The concentration of benzoic acid was determined by means of UV absorption at 230 nm. The solution in the cell was deaerated by bubbling for more than one hour with purified nitrogen that had been passed through a washing bottle containing the same solution.

The physical meanings of all symbols appearing in this paper are summarized as follows:

(Roman letters)

A	Constant equal to $RT\Gamma_m$ (μJ cm^{-2})
a	Interaction constant of adsorbed molecules; a is a function of E
a_0	Value of a at zero charge potential in the solution without benzoic acid
B	Equilibrium adsorption constant at potential E (l mol^{-1})
B_0	Value of B at zero charge potential in the solution without benzoic acid (l mol^{-1})
C	Differential capacity (μF cm^{-2})
C_0	Differential capacity of the solution without benzoic acid (μF cm^{-2})
C'	Differential capacity for full coverage of electrode with benzoic acid (μF cm^{-2})
C^{min}	Minimum differential capacity of the capacity-potential curves in the presence of benzoic acid (μF cm^{-2})
C^{max}	Peak capacity (μF cm^{-2})

c Concentration of benzoic acid (mol l^{-1})
E Electrode potential with respect to zero charge potential in the solution without benzoic acid (V)
ΔE Width of the capacity peak (V)
E^{min} Potential corresponding to the minimum capacity (V)
E^{max} Potential corresponding to the maximum capacity (V)
E_N Potential difference between the respective zero charge potentials for zero and full coverage of the electrode with benzoic acid (V)
E_Z Shift of the zero charge potential for a given coverage (V)
K_0 Integral capacity in the solution without benzoic acid (μF cm^{-2})
q_0 Charge density of the electrode surface in the solution without benzoic acid (μC cm^{-2}); q_0 was determined by graphical integration of C_0
R Gas constant (J K^{-1} mol^{-1})
r Function of a for a given fraction of the peak height
T Absolute temperature (K)
y Relative concentration of benzoic acid, $c/c_{\theta=0.5}$
(Greek letters)
β Coefficient of the potential dependence of a (V^{-1})
Γ_m Maximum surface excess of benzoic acid (mol cm^{-2})
γ Interfacial tension of the solution with benzoic acid (10^{-5} N cm^{-1})
γ_0 Interfacial tension of the solution without benzoic acid (10^{-5} N cm^{-1})
θ Surface coverage
θ^{max} Value of θ at E^{min}
ν Frequency (kHz)

Results

In Acid Solution. Examples of typical capacity-potential curves for 0.5 M H_2SO_4 solutions of various concentrations of benzoic acid are shown in Fig. 1. The capacity curves exhibit no anodic maximum.

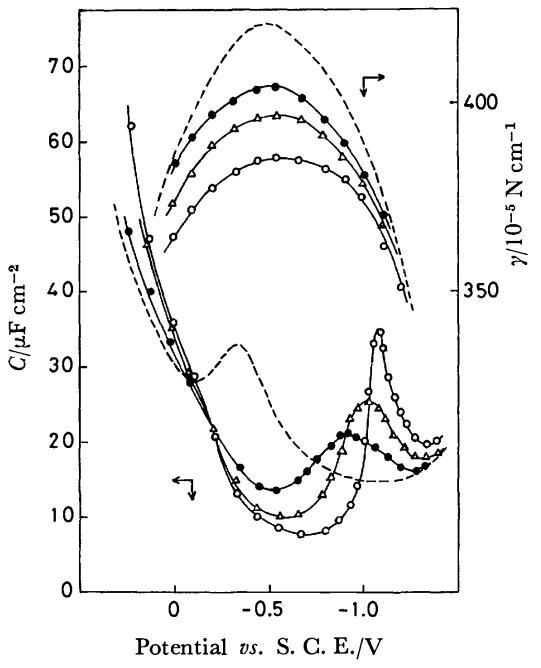

Fig. 1. Differential capacitance curves and electrocapillary curves at 1 kHz and 25 °C in solutions of 0.5 M H_2SO_4 at various concentrations of benzoic acid; ---: 0 mM, ●: 2.5 mM, △: 7.5 mM, ○: 15 mM.

At high negative potentials, the capacity-potential curves and the electrocapillary curves approach the curve obtained for a 0.5 M H_2SO_4 solution without benzoic acid, and this indicates the desorption of benzoic acid from the mercury surface.

To obtain the values of the constants characterizing the adsorption of benzoic acid on mercury, the results were treated on the basis of the Frumkin-Damaskin adsorption isotherm at the potentials corresponding to the maximum adsorption and the maximum capacity.

$$Bc = \frac{\theta}{1-\theta}\exp(-2a\theta). \quad (1)$$

The dependence of a on E was first evaluated as follows. Since the coverage is given in the potential region of maximum adsorption by

$$\theta = \frac{C_0 - C}{C_0 - C'}, \quad (2)$$

the attraction constant a was determined from the reduced adsorption isotherm[1,2]

$$y = \frac{c}{c_{\theta=0.5}} = \frac{\theta}{1-\theta}\exp[a(1-2\theta)]. \quad (3)$$

The value of C' was determined by extrapolating the plot of $1/C^{min}$ against $1/c$ to $1/c=0$.[19] The extrapolation was made by the least-squares method for the data obtained in benzoic acid solutions of more than 7.5 mM. The results are shown in Figs. 2 and 3.

The values of a at the peak potentials were calculated from ΔE using[1,2,19]

$$f(a) = \lg\frac{1-r}{1+r} - \frac{ar}{2.3} = \frac{\Delta E}{2}\left|\frac{\partial \lg c}{\partial E^{max}}\right|, \quad (4)$$

where r is a function of a for a given fraction of the peak height, that is,

$$r_{1/2} = \sqrt{\frac{2-a}{4-a}} \text{ and } r_{3/4} = \sqrt{\frac{2-a}{8-a}}, \quad (5)$$

with the subscripts indicating the function of a which should be used for r in Eq. 4 when ΔE is used either at one half or at three-quarters of the peak height. The values of a at the peak potentials were also determined from the slope of the curve of lg c *vs.* E^{max} using

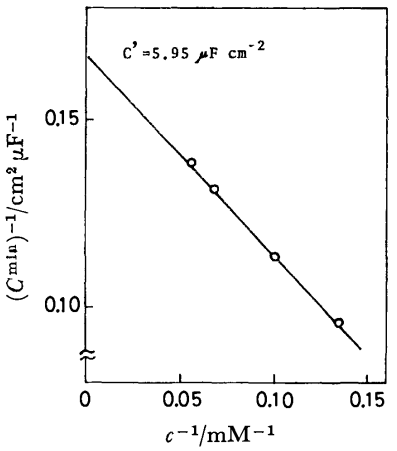

Fig. 2. The plot of the inverse of the minimum capacity against the inverse of the concentration of benzoic acid in 0.5 M H_2SO_4 solution.

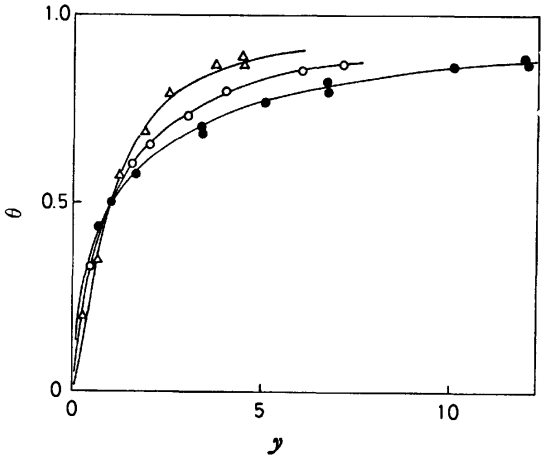

Fig. 3. Adsorption isotherm of benzoic acid in 0.5 M H_2SO_4 solution at −0.55 (●), −0.60 (○), and −0.66 (△) V *vs.* S. C. E. Solid lines are calculated from Eq. 3 with $a=-0.7$(at −0.55 V), −0.1(at −0.6 V), and 0.55(at −0.66 V).

$$\frac{\partial E^{max}}{\partial \lg c} = \frac{2.3(C_0-C')}{2-a}. \quad (6)$$

Since this treatment is applicable only to equilibrium capacity-potential curves, the data obtained at 0.5 and 1 kHz in benzoic acid solutions of concentration greater than 10 mM and those obtained by extrapolation to $\nu=0$ were used for the above calculation.

The values of a thus found are plotted against the electrode potentials in Fig. 4. When the values of a were assumed to be a linear function of E,

$$a = a_0 + \beta E, \quad (7)$$

thus (although some deviation was observed) the values of a_0 and β are found to be −0.35 and −2.5 V^{-1}, respectively.

Other parameters, such as E_N, A, and B_0, were evaluated using the following treatment. The value of E_N was determined from the electrocapillary curves[2,19] to be −0.05 V. The value of A was calculated from the following relation:[2]

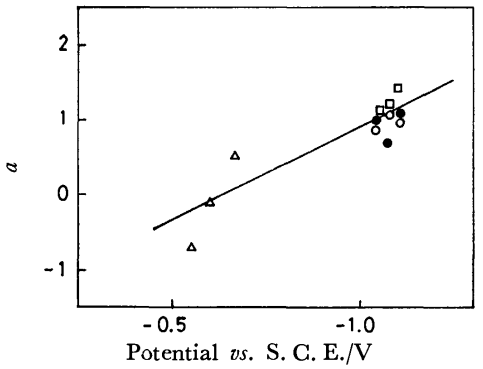

Fig. 4. Dependence of the attraction constant on potential in 0.5 M H_2SO_4 solution. The values of a were obtained from; △: the shape of the adsorption isotherm (Eq. 3), ○: the width of the capacitance peaks at half of their height (Eqs. 4 and 5), ●: the width of the capacitance peaks at three-quarters of their height (Eqs. 4 and 5), □: the slope of the curve of lg c *vs.* E^{max} (Eq. 6).

$$A = \frac{\gamma-\gamma_0}{\ln(1-\theta)+a\theta^2}. \quad (8)$$

The mean value of A was 1.60 μJ cm^{-2} in the 15 mM benzoic acid solution (Table 1). The value of B_0 was evaluated from[19]

$$\ln B_0 = -a_0 - \ln c + \frac{\int_0^{E^{max}} q_0 dE + C'E^{max}(E_N - E^{max}/2)}{A}. \quad (9)$$

The value of B_0 was also calculated by substituting the coverage θ and a into Eq. 1 for zero charge potential in the solution without benzoic acid (*i.e.*, −0.5 V *vs.* S.C.E.). The values of B_0 obtained by the different methods are in fairly good agreement with each other (Table 2).

Thus, the parameters were found to be $A=1.6$ μF cm^{-2}, $B_0=597$ l mol^{-1}, $C'=5.95$ μF cm^{-2}, $a_0=-0.35$, and $\beta=-2.5$ V^{-1}.

Table 1. Value of A calculated from Eq. 8 using the data for the 15 mM benzoic acid solution

E *vs.* SCE V	$\gamma-\gamma_0$ 10^{-5} N cm^{-1}	θ	a	A μJ cm^{-2}
−0.55	−34.0	0.865	−0.23	1.56
−0.60	−33.0	0.856	−0.10	1.64
−0.70	−30.0	0.861	0.15	1.61
			mean	1.60

Table 2. Estimate of the B_0 value

Benzoic acid concentration mM	B_0 l mol^{-1} From Eq. 9	From Eq. 1
15.0	596	598
17.8	578	617
	mean 597	

In Neutral Solution. The capacity-potential curves and electrocapillary curves in 0.5 M Na_2SO_4 solutions containing various amounts of benzoic acid are shown in Fig. 5 (The pH value of the solution was adjusted to 7.2 by adding an NaOH solution). Small peaks (or humps) were observed around −0.5 V (*vs.* S.C.E.) for the capacity-potential curves. A decrease in surface tension due to adsorption of benzoate anions was observed for a positively-charged surface, while for a negatively-charged surface the surface tension and the capacity approached the values obtained in a 0.5 M Na_2SO_4 solution without benzoic acid. Thus, the hump appearing in the capacity curve is regarded as the adsorption-desorption peak of the benzoate anion.

Discussion

The adsorption of benzoic acid in acid sulutions is now considered in detail. At negative potentials, an attractive force is observed between the adsorbed acid molecules. The attractive force changes to a repulsive force as the potential becomes positive (Fig. 4). A similar change in a with the potential has been

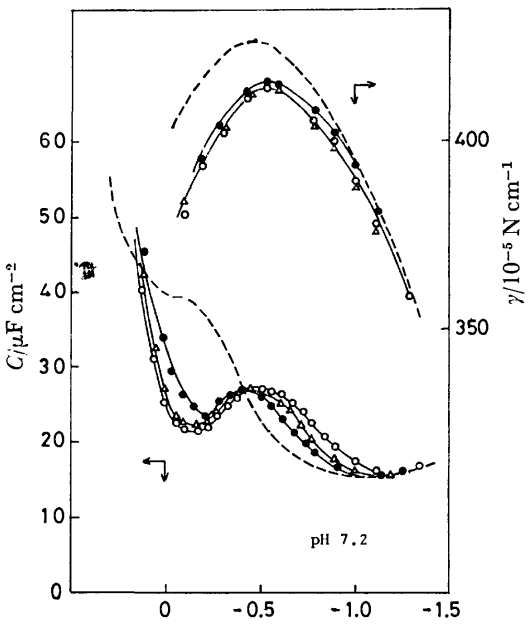

Fig. 5. Differential capacitance curves and electrocapillary curves at 1 kHz and 25 °C in solutions of 0.5 M Na_2SO_4 at various concentrations of benzoic acid; ---: 0 mM, ●: 5 mM, △: 15 mM, ○: 50 mM. The pH value of the solution was adjusted to 7.2 by adding an NaOH solution.

observed for pyridine ($\beta=-2.8\ V^{-1}$)[1,20] and phenol ($\beta=-2.05\ V^{-1}$).[10] When the value of a is considerably negative, no peak is observed in the capacity-potential curves.[19,21] It is also considered that the strong repulsion between the adsorbates observed for positive potentials causes appreciable desorption of the adsorbed benzoic acid in spite of the increase in the π-electron interaction between the adsorbed molecules and the positively-charged surface. These considerations are consistent with the experimental results for a positively-charged surface: no anodic maxima in the capacity-potential curves were observed and the degree of decrease of the surface tension became smaller with increasing potential, as is shown in Fig. 1. The potential E^{min} shifted to more negative potentials with increasing benzoic acid concentration (Fig. 1). The degree of this shift was explained using the negative β value ($-2.5\ V^{-1}$) obtained in this study according to the following relation[19] (Fig. 6)

$$\frac{\partial E^{min}}{\partial \theta^{max}} = \frac{2A\beta}{K_0 - C'}. \tag{10}$$

The experimental results were compared with the calculated capacity-potential curve and electrocapillary curve in order to examine whether or not the adsorption of benzoic acid follows the F-D theory over the entire potential region. The curves relating the capacity and the surface tension to the potential were calculated using

$$C = C_0(1-\theta) + C'\theta + \frac{[q_0 + C'(E_N - E) + \beta A(1-2\theta)]^2 h}{A}, \tag{11}$$

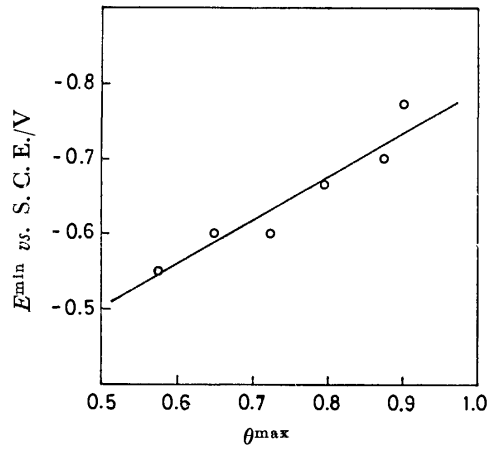

Fig. 6. Variation of the potential of minimum capacity with the coverage. Solid line indicates the theoretical dependence of E^{min} on θ^{max} calculated from Eq. 10 by assuming the value of K_0 of 20 $\mu F\ cm^{-2}$.

where

$$h = \frac{\theta(1-\theta)}{1-2a\theta(1-\theta)}, \tag{12}$$

and

$$\gamma = \gamma_0 + A[\ln(1-\theta) + a\theta^2]. \tag{13}$$

The value of θ appearing in Eqs. 11 and 13 was evaluated as follows.[2,19] The value of B was first determined using

$$B = B_0 \exp\left[-\frac{\int_0^E q_0 dE + C'E(E_N - E/2)}{A}\right]\exp(-\beta E), \tag{14}$$

for a given potential, and then θ was calculated from Eq. 1 for a given concentration of benzoic acid. As is shown in Fig. 7, good agreement is obtained between the calculated values and experimental results for the capacity and the surface tension over the potential region investigated. The discrepancy observed for positively-charged surfaces in the capacity-potential curves is probably due to the π-electron interaction. However the agreement between the experimental electrocapillary curve and the calculated curve shows that the interaction is probably rather small.

When benzoic acid molecules are adsorbed on the electrode in either the vertical or the flat orientations, the two-condensers-in-parallel model (F-D theory) may be applied. If benzoic acid molecules are adsorbed on the electrode for both orientations, the three-condensers-in-parallel model would be applicable.[2] Both the two- and three-condenser models were tested by plotting the shift of the zero charge potential, E_z, against the coverage. For the two-condenser model, E_z is a function of θ:[2]

$$E_z = \frac{E_N\theta}{(C_0/C')(1-\theta)+\theta}. \tag{15}$$

On the other hand, the relationship between E_z and θ derived for the three-condenser model is[2,22]

$$E_z = \frac{E_{N1}\theta[(E_{N2}/E_{N1})(1-\theta)+\theta]}{(C_0/C')(1-\theta)+\theta}, \tag{16}$$

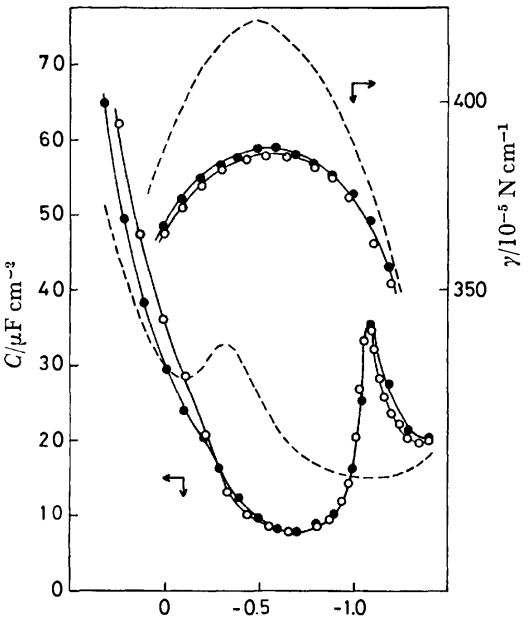

Fig. 7. Differential capacitance curves and electrocapillary curves in 0.5 M H_2SO_4 solution (broken line) containing 15 mM of benzoic acid. ○: experimental results at 1 kHz, ●: calculated from Eqs. 11 and 13.

where E_{N1} and E_{N2} are the shifts of the zero charge potential when the electrode is fully covered by adsorbed molecules in the vertical and flat orientations, respectively. E_{N2} was calculated to be −0.72 V from[2]

$$\beta = \frac{-C'(E_{N1}-E_{N2})}{A}, \qquad (17)$$

assuming $E_{N1}=E_N=-0.05$ V.

The experimental results for the relation between E_z and θ are shown in Fig. 8, together with the theoretical curves given by Eqs. 15 and 16. The two-condenser model is more successful in explaining the experimental results.

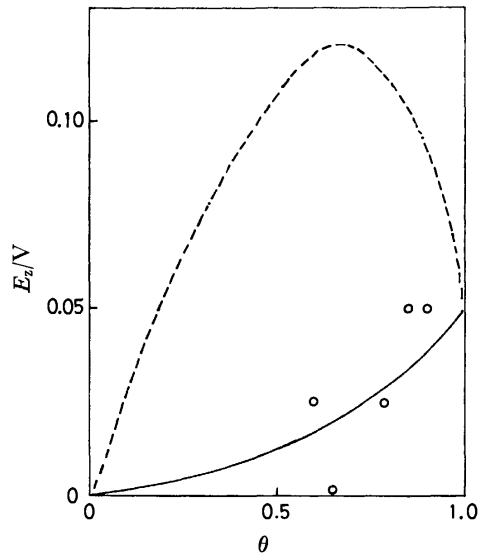

Fig. 8. Dependence of the point of zero charge on surface coverage with adsorbed benzoic acid in 0.5 M H_2SO_4 solution. Solid and broken lines are calculated from Eqs. 15 and 16.

From the above arguments, it is concluded that the adsorption of benzoic acid molecules follows the F-D theory of the two-condenser model and that the values of the parameters obtained are reasonable.

Orientation of Adsorbed Molecules. The orientation of the adsorbed benzoic acid molecules on the electrode surface can be discussed on the basis of the values of A, because A is related to the maximum surface excess. The experimental value of A corresponds to a maximum surface excess of 6.5×10^{-10} mol cm^{-2}. In the case of monolayer adsorption, the area occupied by one molecule of benzoic acid is calculated to be 26 Å^2 (1 Å=0.1 nm). According to the Fisher-Taylor-Hirschfelder model,[13] one molecule of benzoic acid occupies 56 Å^2 for flat orientation and 20 Å^2 for vertical orientation. The area estimated from the A value indicates that for adsorption, benzoic acid has a vertical orientation.

The vertical orientation of the adsorbed benzoic acid molecules is also supported by the value of B_0 as follows. The value of B_0 is related to the standard free energy of adsorption, $-\Delta G_A^\circ$, by[2]

$$-\Delta G_A^\circ = RT\ln(55.5\,B_0/1\ \text{mol}^{-1}). \qquad (18)$$

The calculated $-\Delta G_A^\circ$ value is 26 kJ mol^{-1} (6.2 kcal mol^{-1}). The value of B_0 (597 l mol^{-1}) obtained is less than that of phenol[10] (1640 l mol^{-1}) for the flat orientation and is larger than that of aniline[9] (191 l mol^{-1}) for the vertical orientation. The $-\Delta G_A^\circ$ and B_0 values decrease when the π-electron interaction between the adsorbate and the electrode decrease, and the specific interaction between functional groups and a mercury surface is considered to result in a change in orientation from flat to vertical. Taking into account the specific interaction of functional groups of aliphatic compounds with a mercury surface (the order of specific interaction has been reported to be -OH<-COOH<-NH_2),[7] the decrease of B_0 values in the order, phenol>benzoic acid>aniline, is explained reasonably well in terms of the change in orientation from flat to vertical. Since some phenol molecules can undergo adsorption in the vertical orientation,[15,22] benzoic acid is expected to be adsorbed in the vertical orientation. This is because benzoic acid has a greater possibility of existing in the vertical orientation than phenol, because of its smaller value of B_0 and the stronger interaction of a carboxyl group with a mercury surface than a hydroxyl group. This conclusion agrees with that derived from the evaluation of the maximum surface excess.

In the neutral solution (0.5 M Na_2SO_4, pH 7.2), the value $a<-4$ obtained from the shape of the hump indicates that there is a strong repulsive force between the adsorbates in the potential region of the hump. Since the pK_a of benzoic acid is 4.2,[23] the adsorbed species at pH 7.2 should be the benzoate anion. The repulsive force may be caused by the Coulombic interaction between adsorbed benzoate anions, because no strong repulsive force was observed in the acid solution. The low and broad humps in the capacity-potential curves due to desorption extend to −0.25 V

(*vs.* S.C.E.), and this fact indicates that desorption occurs even on a positively-charged surface because of the significantly large repulsive force between the adsorbed anions. The capacity-potential curves and electrocapillary curves are almost independent of the concentration of benzoate anion. These phenomena suggest that the adsorbed anions covered the electrode surface almost completely in the solution of a low concentration of benzoic acid.

References

1) A. N. Frumkin and B. B. Damaskin, "Modern Aspects of Electrochemistry," Vol. 3, ed by J. O'M. Bockris and B. E. Conway, Butterworths, London (1964), pp. 149—223.
2) B. B. Damaskin, O. A. Petrii, and V. V. Batrakov, "Adsorption of Organic Compounds on Electrodes," Plenum Press, New York (1971), Chaps. 2—4.
3) J. O'M. Bockris, M. A. V. Devanathan, and K. Müller, *Proc. R. Soc. London, Ser. A*, **274**, 55 (1963).
4) R. Lerkkh and B. B. Damaskin, *Russ. J. Phys. Chem.*, **38**, 631 (1964); *ibid.*, **39**, 112 (1965).
5) B. B. Damaskin, A. A. Survila, and L. E. Rybalka, *Elektrokhimiya*, **3**, 146, 927, 1138 (1967).
6) V. K. Venkatesyan, B. B. Damaskin, and N. V. Nikolaeva-Pedrovich, *Russ. J. Phys. Chem.*, **39**, 63 (1965).
7) B. B. Damaskin, A. N. Frumkin, and A. V. Cizov, *J. Electroanal. Chem.*, **28**, 93 (1970).
8) B. E. Conway and R. G. Barradas, *Electrochim. Acta*, **5**, 319, 349 (1961).
9) B. B. Damaskin, I. P. Mishutushkina, V. M. Gerovich, and R. I. Kaganovich, *Russ. J. Phys. Chem.*, **38**, 976 (1964).
10) B. B. Damaskin, V. M. Gerovich, I. P. Glakikh, and R. I. Kaganovich, *Russ. J. Phys. Chem.*, **38**, 1351 (1964).
11) O. Fischer, S. Standara, and J. Totusek, *Collect. Czech. Chem. Commun.*, **39**, 924 (1974).
12) O. Fischer and S. Standara, *Collect. Czech. Chem. Commun.*, **39**, 1965 (1974).
13) E. Blomgren, J. O'M. Bockris, and C. Jesch, *J. Phys. Chem.*, **65**, 2000 (1961).
14) I. Taniguchi, A. Yoshiyama, and T. Sekine, *Denki Kagaku*, in press.
15) R. S. Hansen, D. J. Kelsh, and D. H. Grantham, *J. Phys. Chem.*, **67**, 3216 (1963).
16) R. S. Perkins and T. N. Andersen, "Modern Aspects of Electrochemistry," Vol. 5, ed by J. O'M. Bockris and B. E. Conway, Plenum Press, New York (1969), p. 219.
17) L. I. Antropov and S. N. Banerjee, *J. Indian Chem. Soc.*, **35**, 531 (1958); *ibid.*, **36**, 451 (1959).
18) R. I. Kaganovich, V. M. Gerovich, and T. G. Osotova, *Dokl. Akad. Nauk SSSR*, **155**, 893 (1964).
19) B. B. Damaskin, *Russ. J. Phys. Chem.*, **37**, 1341 (1963).
20) L. D. Klyukina and B. B. Damaskin, *Izv. Akad. Nauk SSSR, Ser. Khim.*, **N6**, 1022 (1963); *Chem. Abstr.*, **59**, 7013h (1963).
21) B. B. Damaskin, *Dokl. Akad. Nauk SSSR*, **144**, 1073 (1962).
22) K. Niki, *Bull. Chem. Soc. Jpn.*, **48**, 997 (1975).
23) L. A. Flexser, L. P. Hammet, and A. Dingwall, *J. Am. Chem. Soc.*, **57**, 2103 (1935).

Production of ^{61}Cu by α and ^{3}He Bombardment on Cobalt Target

Yoshio HOMMA and Yukio MURAKAMI*

Kyoritsu College of Pharmacy, Shibakoen, Minato-ku, Tokyo 105

** Department of Chemistry, Faculty of Science, Tokyo Metropolitan University, Fukazawa, Setagaya-ku, Tokyo 158*

(Received September 28, 1976)

In order to determine the optimum irradiation conditions to produce the ^{61}Cu for nuclear medical use, excitation curves and thick-target yield curves were determined for the α reactions producing ^{61}Cu, ^{57}Co, and ^{58}Co, and ^{3}He reactions producing ^{61}Cu, ^{56}Co, ^{57}Co, and ^{58}Co, both from natural cobalt. The ^{59}Co(α, 2n) ^{61}Cu and the ^{59}Co(^{3}He, n) ^{61}Cu reactions give cross section peaks of 340 mb and 6 mb at 25 MeV and 35 MeV, respectively. The ^{61}Cu thick-target yields for these reactions at 40 MeV were 6 mCi/μAh and 110 μCi/μAh, respectively. A simple and reliable anion-exchange method was developed to provide carrier-free ^{61}Cu. The purity of ^{61}Cu was determined with a Ge(Li) spectrometer. Photopeak efficiencies have been calculated at principal γ-ray energies of ^{61}Cu, ^{64}Cu, and ^{67}Cu, for a 1/2 in. NaI scintillation camera. Alternative nuclear reactions and the methods for producing ^{61}Cu are compared.

^{61}Cu has better nuclear properties for use in nuclear medicine.[1] Its 3.32 h half-life and 284 keV γ-ray make it a particularly useful diagnostic scanning agent giving a much lower absorbed dose for a given count rate than the more readily available ^{64}Cu and ^{67}Cu. ^{61}Cu can be produced with a cyclotron by a ^{59}Co(α,2n) ^{61}Cu reaction: this reaction results in a maximum of 6 mCi/μAh for 40 MeV α bombardment.[1] Bombardment of cobalt has an additional advantage in that the inexpensive monoisotopic element cobalt can be used.

In producing a short-lived radionuclide for use in clinical diagnostic procedures, two factors of prime importance are the yield of the desired nuclide and the degree of contamination with other isotopes, particularly those which have relatively long half-lives and which cannot be separated chemically. To determine the optimum irradiation condition to maximize the yield of the desired nuclide and to minimize the yield of other by-product nuclides, the excitation curves for the reactions concerned must be known.

We have investigated the excitation curves and the thick-target yield curves of ^{61}Cu and by-product nuclides such as ^{56}Co, ^{57}Co, and ^{58}Co. Photopeak efficiencies have been calculated at γ-ray energies of these nuclides for sodium iodide crystals. This is of interest in the design of γ-ray taking devices such as a scintillation camera. The information would be of value to users of medical cyclotron interested in the production of ^{61}Cu.

Experimental

Target Preparation. A thin cobalt target (15—25 mg/cm^2) was electro-deposited from a cobalt sulfate solution ($CoSO_4 \cdot 7H_2O$ 500 g/l, NaCl 17 g/l, H_3BO_4 45 g/l) onto a disk of electrolytic copper foil (35 μ thick). The electro-deposition was performed at 20—28 °C in a 30 mm diam cell with a platinum wire anode at the current density of 50 mA/cm^2 for 170—380 min. After electro-deposition the cobalt foils were carfeully removed from the cathode, washed, dried, and weighed. About ten to fifteen foils were stacked on a brass target-holder with water cooled pipes.

Bombardment. The stacked target was attached to the beam duct of No. 2 of IPCR cyclotron and bombarded with 0.5—1 μA beam of 40 MeV α and ^{3}He particles. A collimater situated in front of the target reduced the spead in width of beam to *ca.* 1.5 × 1.5 cm^2. The beam current was measured with a beam current integrator. There was 8% excess in the reading owing to the secondary electrons in the slit edge, the target and of α and ^{3}He particles scattering at the slit edge[2]. The duration of bombardment was 30—60 min.

Measurement. After bombardment, γ-ray spectra of each foil were measured with a 15 cm^3 Ge(Li) detector, which had been accurately calibrated using IAEA γ-ray standard sources. The specific γ-rays and half-lives were sufficiently distinguished without chemical separation. The principal photopeaks of nuclide were followed in order to determine the half-life and confirm the identity of the nuclides. The dead time losses were always less than 10%. For the sake of obtaining better sensitivities the longer-lived nuclides (^{56}Co, ^{57}Co, and ^{58}Co) were analyzed after the decay of ^{61}Cu was complete. The yields of the nuclides produced in each target were calculated in terms of μCi/μAh at the end of bombardment. The data, foil thickness and the result of beam current measurement were used to calculate the reaction cross sections for all the nuclides observed in each foil. The energy and the intensity of the photopeaks: ^{61}Cu (284 keV, 12%), ^{56}Co (847 keV, 100%), ^{57}Co (122 keV, 87%), ^{58}Co (810 keV, 99%).

Results and Discussion

γ-Ray Spectra. A representative example of the γ-ray spectra is shown in Fig. 1. The upper curve was taken 3.3 h after the end of α bombardment. The median energy in this foil was 28.8 MeV. The lower curve was taken 6 days after the end of bombardment. γ-Rays from the decay of the longer-lived radionuclide ^{57}Co can be identified in addition to the 511 keV annihilation quanta from positron emitters such as ^{61}Cu and ^{58}Co. No peaks which seem to be due to impurities were observed. The spectra of γ-rays from a ^{3}He bombardment foil in which the median ^{3}He energy was 38.8 MeV are shown in Fig. 2. In addition to γ-rays from ^{61}Cu, ^{57}Co, and ^{58}Co, photopeaks from ^{56}Co can be identified. The Q values for the nuclear reaction concerned are given in Table 1.

Excitation Curves and Thick-target Yield Curves.

α Reactions: The yields of ^{61}Cu, ^{57}Co, and ^{58}Co in each target were calculated in terms of μCi/μAh at the end of bombardment. The reaction cross sections were then calculated by means of the relation:

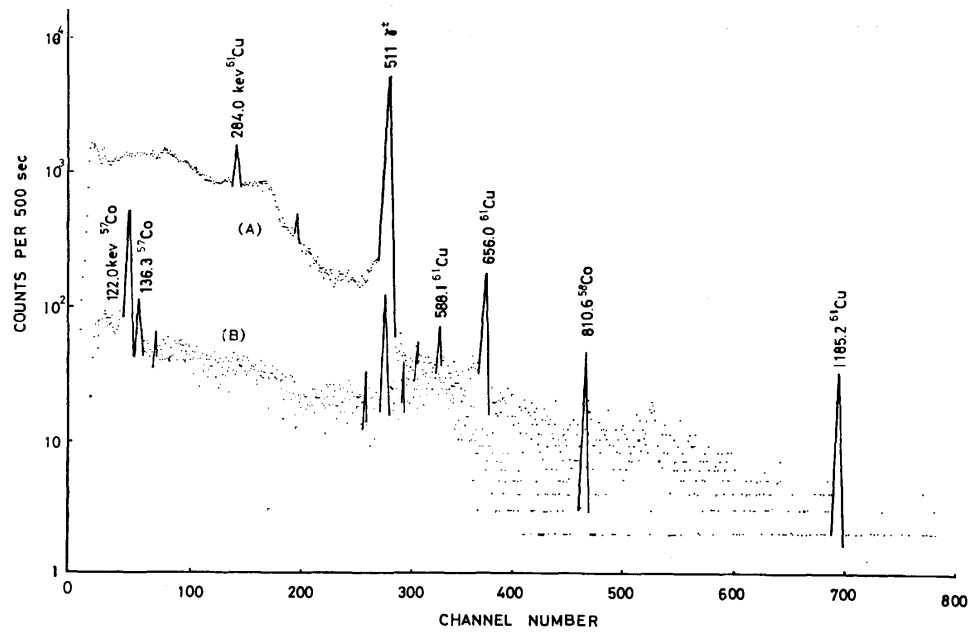

Fig. 1. γ-Ray spectra for α bombarded target of cobalt. A) taken 3.3 h after bombardment, B) taken 6 d after bombardment.

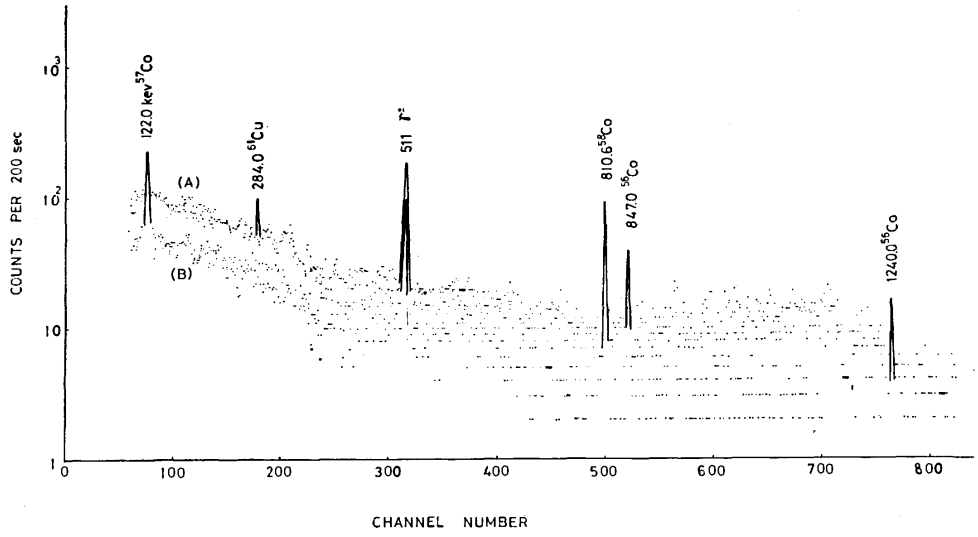

Fig. 2. γ-Ray spectra for ^{3}He bombarded target of cobalt. A) taken 3.3 h after bombardment, B) taken 3 d after bombardment.

$$\sigma_E = \frac{A_0}{(1-e^{-\lambda t})\cdot N\cdot\phi},$$

where

σ_E=the cross section for the reaction at energy E,
A_0=activity in dps at the end of bombardment,
N=number of target nuclei of cobalt target,
ϕ=particle flux,
λ=decay constant for the nuclide,
t=duration of bombardment.

The excitation curves for the production of ^{61}Cu by α bombardment on cobalt are shown in Fig. 3. The maximum cross section of 350 mb is shown at 25 MeV. Above 25 MeV the cross section for ^{61}Cu production decreases; probably because the ^{59}Co(α,αn)^{58}Co and ^{59}Co(α,α2n)^{57}Co reactions are more probable than the ^{59}Co(α,2n)^{61}Cu reaction in this energy region (Fig. 4).

The thick-target yield curves were obtained by integrating the thin-target yield *vs.* target depth curves. The thick-target yield curves of ^{61}Cu, ^{57}Co, and ^{58}Co for α bombardment of cobalt are given in Figs. 3 and 5.

^{3}He Reactions: The yields of ^{61}Cu, ^{56}Co, ^{57}Co, and ^{58}Co were calculated in terms of μCi/μAh and the reaction cross sections were calculated exactly in the same way as for the α particle bombardment described above. The excitation curves for these reactions are plotted in Figs. 6 and 7. The Coulomb barrier for the interaction of ^{3}He with ^{58}Co is about 9.72 MeV, whereas the Q values for the ^{59}Co(^{3}He,n)^{61}Cu, ^{59}Co-(^{3}He,α)^{58}Co, ^{59}Co(^{3}He,αn)^{57}Co, and ^{59}Co(^{3}He,α2n)^{56}Co

Table 1. α and ^{3}He reactions with cobalt target

α Reactions	Q Value (MeV)	^{3}He Reactions	Q Value (MeV)
^{59}Co(α, n)^{62}Cu	−5.4	^{59}Co(^{3}He, n)^{61}Cu	+6.6
(α, 2n)^{61}Cu	−14.0	(^{3}He, 2n)^{60}Cu	−5.1
(α, 3n)^{60}Cu	−25.6	(^{3}He, 3n)^{59}Cu	−15.2
(α, 4n)^{59}Cu	−37.7	(^{3}He, 4n)^{58}Cu	−27.9
(α, p)^{62}Ni	−0.4	(^{3}He, p)^{61}Ni	+9.6
(α, pn)^{61}Ni	−10.9	(^{3}He, pn)^{60}Ni	+1.8
(α, p2n)^{60}Ni	−18.7	(^{3}He, p2n)^{59}Ni	−9.6
(α, p3n)^{59}Ni	−30.1	(^{3}He, p3n)^{58}Ni	−18.6
(α, αn)^{58}Co	−10.4	(^{3}He, α)^{58}Co	+10.1
(α, α2n)^{57}Co	−19.0	(^{3}He, αn)^{57}Co	+1.5
(α, α3n)^{56}Co	−30.4	(^{3}He, α2n)^{56}Co	−9.4
		(^{3}He, α3n)^{55}Co	−19.9

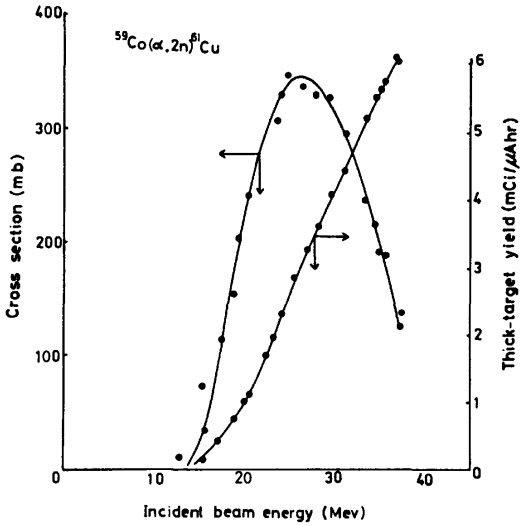

Fig. 3. Excitation curve and thick-target yield curve for α reaction on cobalt producing ^{61}Cu.

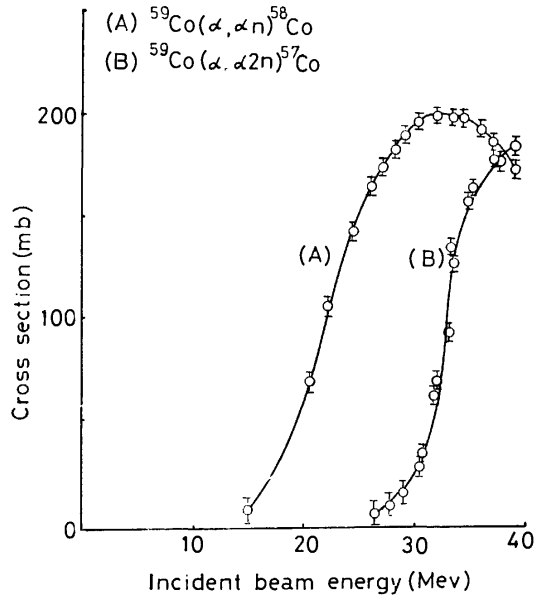

Fig. 4. Excitation curves for α reaction on cobalt producing ^{57}Co and ^{58}Co.

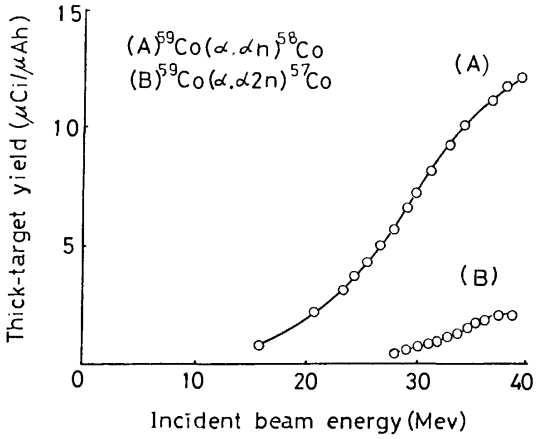

Fig. 5. Thick-target yield curves for α reactions on cobalt producing ^{57}Co and ^{58}Co.

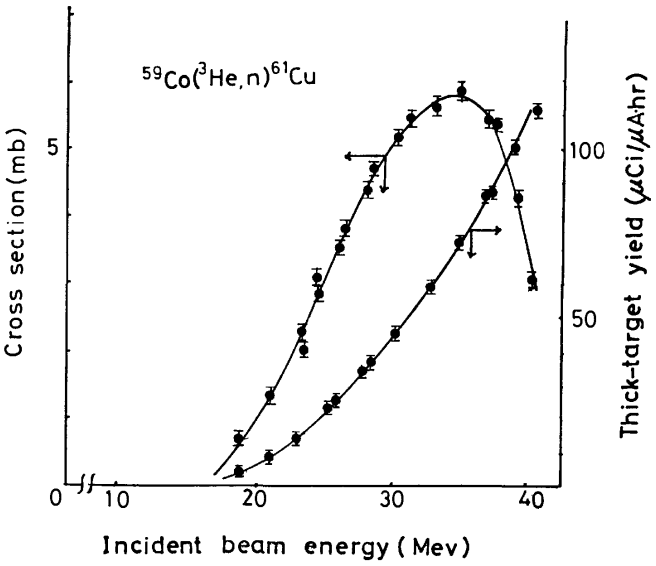

Fig. 6. Excitation curve and thick-target yield curve for ^{3}He reaction on cobalt producing ^{61}Cu.

reactions are +6.6, +10.1, +1.5, and −9.4 MeV, respectively (Table 1). This indicates that, for the ^{3}He particles with sufficient kinetic energy to cross the Coulomb barrier, the cross section for the first reaction is negligibly small.

The ^{59}Co(α,2n)^{61}Cu and the ^{59}Co(^{3}He,n)^{61}Cu reactions have cross section peaks of 340 and 6 mb at 25 and 35 MeV, respectively. The ^{61}Cu thick-target yields for these reactions were 6 mCi/μAh and 110 μCi/μAh, respectively. This shows that α bombardment is more advantageous than ^{3}He bombardment for the production of ^{61}Cu.

Chemical Separation and Radionuclidic Purity. In order to separate ^{61}Cu from ^{56}Co, ^{57}Co, ^{58}Co, and target material, we used the anion-exchange method.[1] The method has been simplified, with completely satisfactory results, and used for routine production as follows: After 4 h cooling period required to allow the short-lived nuclides such as ^{60}Cu(23.4 m) and ^{62}Cu(9.76 m) to decay almost completely, irradiated

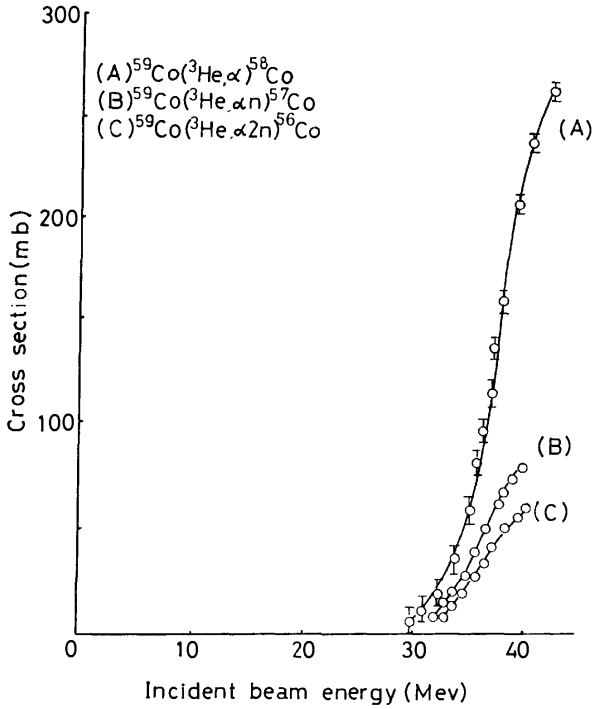

Fig. 7. Excitation curves for ^{3}He reactions on cobalt producing ^{56}Co, ^{57}Co, and ^{58}Co.

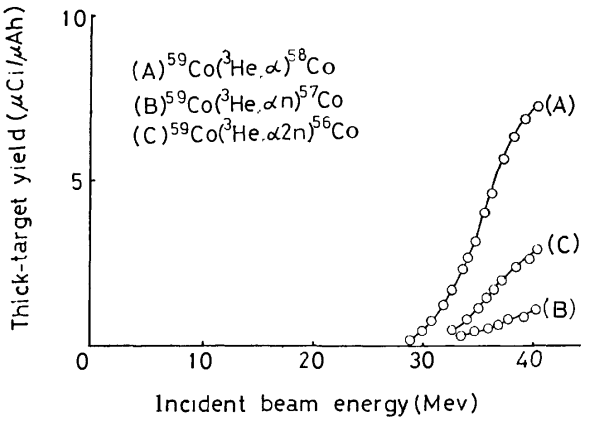

Fig. 8. Thick-target yield curves for ^{3}He reactions on cobalt producing ^{56}Co, ^{57}Co, and ^{58}Co.

cobalt target (150 mg) was dissolved in a mixture of 2 ml of 4M HNO_3 and a few ml of 6M HCl to which a drop of bromine had been added in order to oxidize copper ions. The solution was evaporated nearly to dryness in order to remove excess HNO_3 and Br_2. Twenty-five ml of 8M HCl was added to form chloride complexes of Cu^{2+} and Co^{2+}. The solution was then transferred into a 150 mm × 13 mm column of Dowex 1-X8 anion-exchanger resin,chloride form, 100—200 mesh. Under these conditions, Co^{2+} and Cu^{2+} are adsorbed on the resin but not Ni^{2+}.[1,4] Co^{2+} and Cu^{2+} can be eluted from the column with 25 ml of 4M HCl and 2M HCl, respectively. Carrier-free ^{61}Cu is recovered as a radionuclidically pure material in 25 ml of 2M HCl solution, which can be easily evaporated to dryness. This make it possible to convert the tracer into a suitable chemical form. The radiochemical yield was 95%. The procedure is simple, taking less than 150 min. The high radionuclidic purity of ^{61}Cu attained was determined by γ-ray spectrometry using a Ge(Li) detector. No radionuclides of longer-life could be detected.

Comparison of Nuclear Reactions for Producing ^{61}Cu.

Deuteron Bombardment of Natural Zinc Targets: The thick-target yield of ^{61}Cu from deuteron bombardment of natural zinc target was *ca.* 1.2 mCi/μAh at 15 MeV.[5] However, the purity of ^{61}Cu produced by the ^{64}Zn(d,αn)^{61}Cu is restricted by ^{64}Cu produced by the ^{66}Zn(d,α)^{64}Cu, ^{67}Zn(d,αn)^{64}Cu, and ^{64}Zn(d,2p)^{64}Cu reactions and ^{67}Cu produced by the ^{68}Zn(d,^{3}He)^{67}Cu and ^{67}Zn(d,2p)^{67}Cu reactions. At a bombardment energy of 15 MeV, the maximum levels of ^{64}Cu and ^{67}Cu contaminants were 45 and 30%, respectively.

^{3}He Bombardment of Natural Copper Targets: The maximum cross section for the ^{63}Cu(^{3}He,αn)^{61}Cu reaction is 88.2 mb at 19.6 MeV, whereas those for the ^{63}Cu(^{3}He,2p)^{64}Cu and the ^{63}Cu(^{3}He,α)^{62}Cu reactions are 126 mb at 21.7 MeV and 42.7 mb at 22.4 MeV, respectively.[6] The results indicate that the purity of ^{61}Cu produced by this method is not suitable for *in vivo* studies, even if other by-product nuclides such as ^{65}Ga, ^{66}Ga, ^{67}Ga, ^{62}Zn, ^{63}Zn, and ^{65}Zn are chemically separable.

Proton Bombardment of Natural Copper Targets: ^{61}Cu is also produced by the ^{63}Cu(p,p2n)^{61}Cu and the ^{65}Cu(p,p4n)^{61}Cu reactions. A limitation of the above nuclear reactions is that the required particle energies (*e.g.* 35—60 MeV protons) are not attainable with compact cyclotrons suitable for routine production. Only the cyclotron of the National Institute of Radiological Science can be used. The maximum cross sections for these reactions are approximately 3 times less than that for the ^{59}Co(α,2n)^{61}Cu reaction. The experimental data available show that the maximum cross sections for the ^{63}Cu(p,p2n)^{61}Cu and the ^{65}Cu(p,p4n)^{61}Cu reactions are 130 mb at 35 MeV and 100 mb at 60 MeV, respectively.[7] This indicates that the yield of these reactions are not practical for routine production.

α Bombardment of Enriched Nickel Targets: A relatively high cross section has been reported for the ^{58}Ni(α,p)^{61}Cu reaction which has a maximum value of 310 mb at particle energy 11 MeV.[8] However, the method is not practical, because of the use of a Van de Graaff accelerator and highly enriched nickel isotope (98.4%).

An alternative method was studied in order to obtain ^{61}Cu by the ^{3}He bombardment on natural nickel target. The results of preliminary studies are satisfactory and have advantages over the above mentioned ^{58}Ni(α,p)^{61}Cu, primarily because its thick-target yield is 4.9 mCi/μAh with ^{3}He particle bombardment energy of 40 MeV.[9]

Relative Detection Efficiency. The average absorbed dose delivered to the total body, spleen, kidneys, liver, heart, and brain by ^{61}Cu, ^{64}Cu, and ^{67}Cu has been calculated.[1] The results show that ^{61}Cu

Table 2. Percentage of usable γ-rays of ^{61}Cu, ^{64}Cu, and ^{67}Cu

Radionuclide	Decay mode	γ-Ray Energy (MeV)	γ-Ray Intensity (%)	Transmission (%)	Detection efficiency (%)	Usable γ-ray (%)
^{61}Cu(3.32 h)	β^+ 60%	0.284	12	62	58	4.3
	β^- 30%	0.511	120	63	35	26.5
		1.19	5	53	21	0.5
^{64}Cu(12.8 h)	β^+ 19%	0.511	38	63	35	8.3
	β^- 38%	1.34	0.5	53	19	0.05
	EC43%					
^{67}Cu(61.7 h)	β^-	0.092	23	53	99	12.1
		0.184	40	59	58	13.7

has the lowest absorbed dose to various organs and tissues. The relative photopeak efficiencies have been calculated at several γ-ray energies of ^{61}Cu, ^{64}Cu, and ^{67}Cu for a 1/2 in. NaI scintillation camera. The photopeak detection efficiencies for 1/2 in. NaI crystal,[10] intensity[3] and the tissue attenuation of γ-rays were used to calculate the relative usable γ-ray flux. The results of these calculations are given in Table 2. Usable γ-ray flux from ^{61}Cu was higher than that from an equal amount of ^{64}Cu. With the scintillation camera, the 284 keV γ-ray of ^{61}Cu provides 4.3% usable γ-ray, while the 1340 keV γ-ray of ^{64}Cu gives as small as 0.05% usable γ-ray. This indicates that the principal γ-ray of ^{61}Cu(284 keV) is more intense and in an energy range that is more advantageous for scinti-scanning than that of ^{64}Cu.

On the other hand, five millicuries of ^{67}Cu is produced by the reaction ^{68}Zn(γ,p)^{67}Cu for 48 h irradiation of natural zinc in the bremsstrahlung beam from a linear accelerator.[11] ^{67}Cu has the advantage that the relative detection efficiency for its intense 184 keV γ-ray (40%) is 13.7%. However, its absorbed dose is too high to be used *in vivo* clinical studies,[1] even if high specific activity ^{67}Cu, having a half-life of 61.7 h, is useful in particularly time consuming biochemical studies.

The 284 keV γ-ray of ^{61}Cu approaches an optimum energy that is low enough to be efficiently counted with thin NaI crystals allowing use of high resolution collimators, but high enough to obtain necessary tissue penetration. These characteristics make this nuclide highly desirable for nuclear medical application.

Conclusion

We found the bombardment of cobalt at 40 MeV to be the best method to produce ^{61}Cu in sufficient quantity for radiopharmaceutical studies. Advantages are the relatively high yield as compared with other methods, and the high radionuclidic purity of carrier-free ^{61}Cu. For routine production we have chosen the following bombardment conditions: energy of the incident particles 40 MeV, target thickness 250 mg/cm,^{2} beam current 5μA. The irradiation time varies according to the required quantity of ^{61}Cu from 1—2 h. Under these conditions, the yield of ^{61}Cu obtained at the end of 1 and 2 h of bombardment is *ca.* 13 and 26 mCi, respectively, corrected for losses during the course of recovery.

The authors wish to thank Dr. Tadashi Nozaki and members of the cyclotron group of the Institute of Physical and Chemical Research for their valuable discussions and cooperation.

References

1) Y. Homma and Y. Murakami, *Chem. Lett.*, **1976**, 397.
2) T. Nozaki, Private communication.
3) C. M. Lederer, J. M. Hollander, and I. Perlman, "Table of Isotopes," Wiley, New York (1967).
4) K. A. Kraus and G. E. Moore, *J. Am. Chem. Soc.*, **75**, 1460 (1953).
5) D. C. Williams and J. W. Irvine, Jr., *Phys. Rev.*, **130**, 265 (1963).
6) E. A. Bryant, D. R. F. Cochran, and J. D. Knight, *Phys. Rev.*, **130**, 1512 (1963).
7) I. R. Williams and C. B. Fulmer, *Phys. Rev.*, **162**, 1055 (1967).
8) F. K. McGowan, P. H. Stelson, and W. G. Smith, *Phys. Rev.*, **133**, B907 (1964).
9) E. Shirai, H. Nakahara, and Y. Murakami, Abstr, No. 2S02, National Meeting of the Chemical Society of Japan, Hiratsuka, April 1976.
10) H. O. Anger and D. H. Davis, *Rev. Sci. Instrum.*, **35**, 693 (1964).
11) N. Marceau, T. P. A. Kruck, D. B. McConnel, and N. Aspin, *Int. J. Appl. Radiat. Isot.*, **21**, 667 (1970).

Interaction between Aromatics and Zinc Chloride in the Molten State. The Formation of σ-Complexes and Radicals

Mikio MORITA, Kunio HIROSAWA, and Toshio SATO

Government Industrial Development Laboratory, Hokkaido, Higashitsukisamu, Toyohira-ku, Sapporo-shi, Hokkaido 061-61

(Received October 8, 1976)

The electronic absorption spectra of naphthalene, anthracene, and naphthacene in dried, molten zinc chloride were measured and found to be almost the same as those of aromatics–aluminum chloride complexes in the solid state. ESR measurements were also made; they confirmed the presence of radicals. From these results, it was concluded that the aromatics reacted with molten zinc chloride to form EDA-complexes, *i. e.*, σ-complexes and cation radicals.

It has been known that a massive quantity of zinc chloride used in the molten state is a superior catalyst for the hydrocracking of polycondensed aromatics into gasoline fractions, although partial hydrogenation is predominant when the amount of zinc chloride is relatively small; the activity of the catalyst has been considered to originate in a proton produced by the dissociation of water coordinated to the zinc chloride molecule.[1–4]

However, when aromatics come into contact with dried, molten zinc chloride under a vacuum, colored products are observed to be produced. This suggests that the products are complexes of the electron donor-acceptor type and might also play a role in the hydrocracking of aromatics as reaction intermediates, because we have already confirmed that, in the hydrocracking of aromatics with molten zinc chloride, the conversion is correlated with their ionization potentials.[2]

The measured electronic spectra of aromatics–zinc chloride complexes were almost the same as those of aromatics–aluminum chloride complexes in the solid state observed by Perkampus and Kranz[5] and by Sato and Aoyama.[6] Furthermore, the complexes gave strong ESR signals of the singlet type.

From these results, aromatics and zinc chloride in the molten state were found to form σ-complexes, radicals, and additional intermediates between the σ-complexes and the aromatics.

Experimental

Materials. Zinc chloride, naphthalene, anthracene, and naphthacene of the G. R. grade were used without purification.

Electronic Absorption Spectra. Zinc chloride, after having been introduced into the rectangular quartz cell shown in Fig. 1, was heated at 200±10 °C under a vacuum below 10^{-3} Torr in an electric furnace for 2—3 h. After the cell has then cooled to room temperature, an aromatic compound sample in a vacuum stopcock (*cf.* Fig. 1) was dropped into the cell. The cell was then evacuated again at about 10^{-3} Torr, and the upper neck of the cell was sealed off by fusion. The cell containing the sample was then heated in an electric furnace above 280 °C to melt it. When this molten zinc chloride was placed in sufficient contact with aromatics, colored products were observed to develop in the transparent molten zinc chloride. This sample cell was mounted in a specially constructed cell holder kept at 300±10 °C, and the absorption spectra were measured with a Hitachi 624-type spectrophotometer.

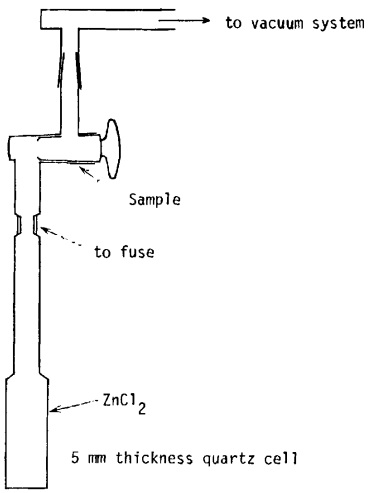

Fig. 1. Apparatus for the absorption spectroscopic study.

To confirm more exactly the formation of colored products of the σ-type, anhydrous zinc chloride was carefully prepared from silver chloride and metallic zinc powder in a vacuum according to a procedure similar to Wallace and Willard's for the preparation of anhydrous aluminum chloride;[7] it was then reacted with anthracene in a sealed glass tube.

ESR. Samples for the ESR measurements were prepared in ESR tubes in a way similar to that described above. The ESR signals were measured with a Jasco model ME-type spectrometer at room temperature, while the *g*-values were determined by the use of MnO as the reference substance.

Results and Discussion

Electronic Absorption Spectra. The absorption spectra of the colored products in molten zinc chloride for naphthalene, anthracene, and naphthacene are shown in Fig. 2 and are summarized in Table 1 for purposes of comparison.

The spectrum of molten zinc chloride only (Fig. 2-(1)) did not show any special absorption bands within the range in question. Upon reaction with molten zinc chloride, anthracene gave three absorption bands at 425, 620, and 725 nm (Fig. 2-(3)), naphthalene gave two weak absorption bands at 385 and 590 nm (Fig. 2-(2)), and naphthacene gave strong absorption bands at 360 and 460 nm (Fig. 2-(4)). After prolonged contact, a new band at 705 nm for naphthalene (Fig. 2-(2')) and one at 710 nm for naphthacene (Fig. 2-(4'))

Table 1. Comparison of the absorption bands of the σ-complexes, radicals, $HF-BF_3$, BF-1,2-dichloroethane, and Na- or K-THF systems

Species	System	Naphthalene	Anthracene	Naphthacene
σ-Complex	A	385	425	460
	B	380	420	468
	D		423	452
Proton-addition complex	C	390	408	435
Radical, monopositive ion, or negative ion	A	705	725	710
	B		735	355, 385, 395, 670, 769, 850
	E	366, 735, 813	369, 715	359, 403, 704
Dinegative ion or others	A	590	620	360
	B		665	
	E		333, 613	353, 398, 621
			(unit; nm)	

A; Molten zinc chloride. B; Aluminum chloride.[5,6] C; $HF-BF_3$.[10,11] D; BF_3-1,2-Dichloroethane.[9] E; Sodium- or Potassium-THF.[16,17]

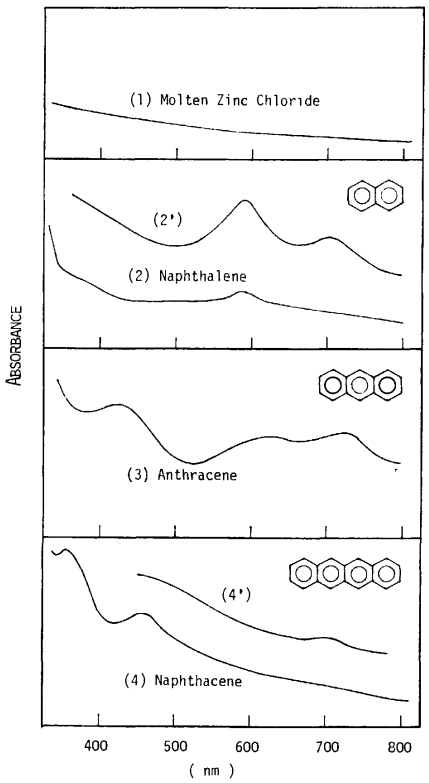

Fig. 2. Absorption spectra of aromatics in molten zinc chloride. Absorbance *vs.* wavelength (nm).
(1) Molten zinc chloride, (2)(2′) naphthalene, (3) anthracene, (4)(4′) naphthacene.

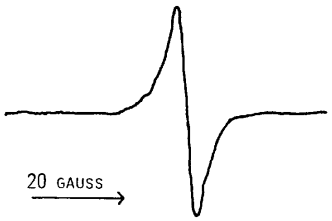

Fig. 3. ESR spectrum of naphthalene cation radical formed in molten zinc chloride.

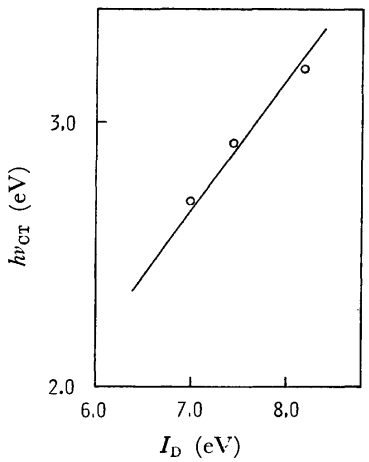

Fig. 4. Dependence of the position of CT bands on ionization potentials of donors.

were observed to develop.

ESR Signals. All the samples gave strong and broad singlets with the *g*-values of 2.0028, 2.0031, and 2.0030 for naphthalene, anthracene, and naphthacene respectively (*cf.* Fig. 3).

σ-Complex Formation. As may be seen in Table 1, the absorption bands at 385 nm for naphthalene, 425 nm for anthracene, and 460 nm for naphthacene in molten zinc chloride were found to be almost the same as those of the corresponding aromatics–aluminum chloride complexes in the solid state, the latter being confirmed as σ-complexes(π, v-complexes according to their notation) by Perkampus and Kranz.[5]

Figure 4 shows the linear correlation between their absorption energy, $h\nu_{CT}$, and the ionization potential, I_D, of the corresponding aromatics; this correlation suggests EDA-complex, *i.e.*, σ-complex formation, as in the case of aromatics–ethanol–zinc chloride–chloroform system investigated previously by the present authors.[8]

However, since the proton-addition complexes are quite similar to the σ-complexes in the position of the absorption band (Table 1),[9-11] we tried to eliminate the effect of the trace amount of water on the complex formation in the present system; it could be confirmed that a colored product was produced by the reaction of anthracene with anhydrous molten zinc chloride carefully prepared from zinc metal and silver chloride in a vacuum.

These results strongly suggest that aromatics directly react with molten zinc chloride to form EDA-complexes, *i.e.*, σ-complexes. Accordingly, the absorption bands at 385 nm for naphthalene, 425 nm for anthracene, and 460 nm for naphthacene can be attributed to the formation of aromatics–zinc chloride σ-complexes.

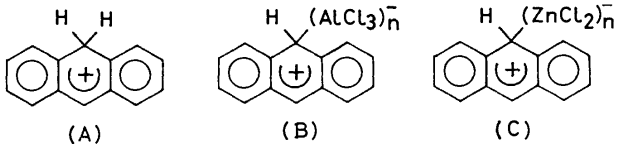

(A) (B) (C)

The structure of the proton-addition complexes of aromatics proposed by Gold and Tye[12] has been both experimentally and theoretically confirmed;[11,13,14] for example, the proton-addition complex of anthracene has been fomulated in the form of (A). Perkampus and Kranz proposed the (B) structure for the anthracene–aluminum chloride complex on the basis of the similarity in the absorption spectrum.[5] The (C) structure can also be proposed for the anthracene–zinc chloride complex on the basis of the similarity of the absorption spectrum of anthracene in molten zinc chloride with that in aluminum chloride in the solid state.

Ion or Radical Formation. Naphthalene in molten zinc chloride has a paramagnetic property and a characteristic color which gradually changes from purple to dark green.[15] It gave an absorption band at 705 nm quite different from the absorption band for sodium[16] or potassium[17] naphthalenide in the THF solution assigned as a free radical. However, this band is assumed to correspond to the naphthalene cation radical, because it is more difficult for naphthalene to form a radical than for the other two aromatics and because the band at 705 nm in the spectrum of Fig. 2-(2′) and the strong ESR signal appeared only when naphthalene was in sufficient contact with molten zinc chloride. The band at 590 nm in the spectrum of Fig. 2-(2) or (2′) has been attributed to the dipositive ion or an intermediate between naphthalene and the naphthalene–zinc chloride σ-complex, as Sato predicted,[6] but further investigation is necessary for a certain assignment.

Distler and Hohlneicher showed that the anthracene cation radical has absorption maximum at 735 nm, and the naphthacene radical, at 348, 397, 667, 752, and 833 nm.[18] The present work confirmed that anthracene, when in sufficient contact with molten zinc chloride, showed a characteristic deep green color[15] and was strongly paramagnetic. The absorption band at 725 nm can thus be attributed to the formation of the cation radical derived by the ionization of the σ-complex (C). The absorption band at 620 nm seemed to correspond to that observed on the silica–alumina surface[19] and that observed for the anthracene–aluminum chloride complex.[6] Hall[19] supposed that the 665 nm species might be a dipositive anthranium ion on the basis of Aalbersbers's work[20] and from the calculations of Balk *et al.*[21] Sato and Aoyama proposed that it might be a secondary σ- or π-complex produced by anthracene and the anthracene–aluminum chloride σ-complex. In the case of the anthracene–molten zinc chloride system, further investigation is necessary to assign the band at 620 nm.

In the case of naphthacene, the formation of the cation radical was also confirmed by the production of ESR signals and the characteristic blue color.[15] The absorption spectrum (Fig. 2-(4)) did not show any special band within the range between 500 and 800 nm, but a weak absorption band around 710 nm (Fig. 2-(4′)) grew with prolonged contact. This band may be attributed to one band of the naphthacene cation radical. The absorption band about 360 nm may be supposed to be overlapped with the absorption bands of naphthacene itself, the cation radical, and the dipositive ion.

References

1) C. W. Zielke, R. T. Struck, J. M. Evans, C. P. Costanza, and E. T. Gorin, *Ind. Eng. Chem., Process Des. Dev.*, **5**, 151 (1966).
2) M. Morita and K. Hirosawa, *Nippon Kagaku Kaishi*, **1975**, 1555.
3) M. Morita and K. Hirosawa, *Nippon Kagaku Kaishi*, **1976**, 1259.
4) A. Mitsutani, "Shokubai Kogaku Koza," Vol. 10, ed by Catalysis Society of Japan, Chijin Shokan, Tokyo (1967), p. 108.
5) H. H. Perkampus and T. Kranz, *Z. Phys. Chem., N. F.*, **34**, 213 (1962); *ibid.*, **38**, 295 (1963).
6) H. Sato and Y. Aoyama, *Bull. Chem. Soc. Jpn.*, **46**, 631 (1973).
7) C. H. Wallace and J. E. Willard, *J. Am. Chem. Soc.*, **72**, 5275 (1950).
8) M. Morita, K. Hirosawa, and Y. Hasegawa, Abstr. No. 13405, 23rd National Meeting of the Chemical Society of Japan, Tokyo, April 1970.
9) W. I. Aalbersberg, G. J. Hoijtink, E. L. Mackor, and W. P. Weijland, *J. Chem. Soc.*, **1959**, 3055.
10) A. A. Verrijn Stuart and E. L. Mackor, *J. Chem. Phys.*, **27**, 826 (1957).
11) C. Reid, *J. Am. Chem. Soc.*, **76**, 3264 (1954).
12) V. Gold and F. Tye, *J. Chem. Soc.*, **1952**, 2173, 2181.
13) G. Dallinga, E. L. Mackor, and A. A. Verrijn Stuart, *Mol. Phys.*, **1**, 123 (1958).
14) C. MacLean, J. H. van der Waals, and E. L. Mackor, *Mol. Phys.*, **1**, 247 (1958).
15) I. C. Lewis and L. S. Singer, *J. Chem. Phys.*, **43**, 2712 (1965).
16) D. E. Paul, D. Lipkin, and S. I. Weissman, *J. Am. Chem. Soc.*, **78**, 116 (1956).
17) K. K. Brandes and R. J. Gedes, *J. Phys. Chem.*, **71**, 508 (1967).
18) D. Dister and G. Hohlneicher, *Ber. Bunzenges. Phys. Chem.*, **74**, 960 (1970).
19) W. K. Hall, *J. Catal.*, **1**, 53 (1962).
20) W. I. Aalbersberg, G. J. Hoijtink, E. L. Mackor, and W. P. Weijland, *J. Chem. Soc.*, **1959**, 3005, 3049.
21) P. Balk, S. D. Bruijn, and G. J. Hoijtink, *Mol. Phys.*, **1**, 151 (1958).

The Structure of the Cyclodextrin Complex. IV. The Crystal Structure of *a*-Cyclodextrin–Sodium 1-Propanesulfonate Nonahydrate

Kazuaki HARATA

Research Institute for Polymers and Textiles, Sawatari-4, Kanagawa-ku, Yokohama 221

(Received October 20, 1976)

α-Cyclodextrin, which is a cyclic oligosaccharide consisting of six D-glucose residues, forms a 1 : 1 complex with sodium 1-propanesulfonate. The crystal structure was determined by the X-ray method. The crystal is orthorhombic, and the space group is $P2_12_12$ with cell dimensions of $a=21.608(2)$, $b=16.700(2)$, and $c=8.302(1)$ Å, and $Z=2$. The structure was solved on the basis of 2219 diffractometer data and refined by the block-diagonal least-squares method to the final R-value of 0.077. The α-cyclodextrin molecule is nearly hexagonal with diagonal distances of 8.40—8.59 Å between the glycosidic oxygen atoms. The framework of the crystal is built up of a stack of α-cyclodextrin rings along the c axis in head-to-tail arrangement, with channel-type structure. The adjacent α-cyclodextrin molecules along the channel are linked by six O(3)···O(6) hydrogen bonds. The guest 1-propanesulfonate anions are located in channels, having statistical disorder. The primary hydroxyl groups of α-cyclodextrin exhibit *gauche-trans* conformation, and they form hydrogen bonds with the sulfonato group resulting in oxygen-oxygen distances of 2.72—2.80 Å. The propyl group is in contact with the O(2), O(3) side of the α-cyclodextrin ring. The sodium ion is located outside the channel, and is surrounded by five oxygen atoms which form a distorted trigonal bipyramid.

α-Cyclodextrin (α-CDx) is a cyclic oligosaccharide consisting of six D-glucose residues. It has a cylindrical cavity with a diameter of about 5 Å and a height of 8 Å in the center of the molecule. At both ends of the cavity, the hydroxyl groups are located, while in the interior of the ring the twelve C–H groups are oriented to the center of the cavity. Therefore, the cavity is of relatively hydrophobic nature. α-CDx forms a number of inclusion complexes with a variety of guest molecules which range from polar ones, such as potassium acetate, to non-polar ones, such as the rare gases.[1–4] The complexing ability has been considered to be largely determined by the relative size of the guest molecule. Recent X-ray analyses have revealed that the guest molecules are situated in the interior of the cavity, and that the macro-cyclic conformation of the α-CDx ring changes with the dimension and the shape of the guest molecule.[5–16] The α-CDx ring in the 1-propanol complex[8] is nearly hexagonal, but remarkable deformation of the α-CDx ring is observed in the water complex.[6]

α-CDx has been used as an enzyme model,[3] since it exhibits catalytic properties for some chemical reactions. The interaction between α-CDx and the guest molecule is of interest in relation to the enzyme-substrate interaction. Saenger and his coworkers[6–9] have proposed the inclusion mechanism on the basis of the fact that the driving force for the complex formation is derived from the difference between the conformational energy of α-CDx for the "tense" state and that for the "relaxed" state. On the other hand, a theoretical calculation of the complex formation energy[15] has shown that the stability of the complex is mainly determined by the difference between the solvation energy for the complexed state and that for the uncomplexed state, and that the inclusion of the hydrophobic group gives a more stable complex than does the inclusion of the hydrophilic group. Sodium 1-propanesulfonate (PSNa) consists of a hydrophobic propyl group and a hydrophilic sulfonato group. An X-ray analysis of the α-CDx–PSNa complex was performed to investigate the conformation of α-CDx and the interaction between α-CDx and PSNa, in comparison with those of other α-CDx complexes.

Experimental

Crystals of the α-CDx–PSNa complex were obtained by cooling an aqueous solution containing α-CDx and PSNa with a 1 : 1 molar ratio. These are colorless and orthorhombic prisms elongated along the c axis. The density was measured by the flotation method in a mixture of chloroform and dioxane. The diffraction measurements were carried out with the crystal enclosed in a quartz capillary containing a small amount of water, since the crystal decomposes in air. The crystal data are given in Table 1. The intensity data were obtained on a Rigaku automatic four-circle diffractometer using graphite monochromatized Cu$K\alpha$ radiation and the θ-2θ scan technique. 2570 independent reflections were obtained up to 120° in 2θ, but 351 reflections with $|F_o|<3\sigma(F)$ were treated as unobserved, where $\sigma(F)$ is the standard deviation estimated from counting statistics. No correction was made for absorption and extinction.

TABLE 1. CRYSTAL DATA

$C_{36}H_{60}O_{30}\cdot C_3H_7SO_3Na\cdot 9H_2O$,		Orthorhombic
Molecular weight		1281.1
Cell dimensions	a	21.608(2) Å
	b	16.700(2)
	c	8.302(1)
Cell volume	V	2995.7 Å^3
Space group		$P2_12_12$
	Z	2
Density	D_m	1.42 g cm^{-3}
	D_x	1.42

Determination and Refinement of the Structure

The crystal structure of the α-CDx–PSNa complex was solved on the basis of the assumption that the location of the α-CDx molecule is same as that of the isomorphous crystal of the sodium benzenesulfonate (BSNa) complex[15]. The atomic parameters of α-CDx were refined by the block-diagonal least-squares method, starting from those of the BSNa complex. Then, a

Fourier map was calculated, and the PSNa and water molecules were found from it. The 1-propanesulfonate anion is statistically disordered on the two-fold axis. Unreasonably short intermolecular distances were found for Na···O(W6), O(W3)···O(W6), O(W5)···O(W7), and O(W6)···O(W7), indicating that the locations of these atoms are statistically disordered. An average population of 0.5 is assigned to the sodium ion, since there are only two PSNa molecules per unit cell in spite of the four equivalent positions. The population of O(W6) is also 0.5 since the O(W6) atom occupies the position when the sodium ion is absent. Then, the abnormally short distances for O(W3)···O(W6), O(W5)···O(W7), and O(W6)···O(W7) can be reasonably interpreted by assigning 0.5 to the respective occupancies of O(W3), O(W5), and O(W7). The 27 hydrogen atoms were found on the difference-Fourier map. A refinement of the atomic parameters was carried out by the block-diagonal least-squares method. The isotropic thermal factors of hydrogen atoms were taken to be equal to those of the carbon or oxygen atoms to which the hydrogen atoms are bonded, and were not refined. The final R-value is 0.077 for the 2219 reflections. The quantity minimized was $\Sigma w(|F_o|-|F_c|)^2$ with $w=1.0$ for all reflections used. The atomic scattering factors were taken from "International Tables for X-ray Crystallography."[17] The atomic parameters are shown in Tables 2 and 3. The observed and calculated structure factors are given in Table 4.*

TABLE 2. ATOMIC PARAMETERS ($\times 10^4$) FOR NON-HYDROGEN ATOMS

The anisotropic thermal factors are of the form: $\exp[-(B_{11}h^2+B_{22}k^2+B_{33}l^2+B_{12}hk+B_{23}kl+B_{31}lh)]$.

	x	y	z	B_{11}	B_{22}	B_{33}	B_{12}	B_{23}	B_{31}
C(1,G1)	1541(4)	2457(6)	3331(12)	12(2)	19(4)	66(15)	-5(5)	7(13)	-5(10)
C(2,G1)	1272(5)	2873(6)	4801(13)	14(3)	25(4)	78(16)	-2(6)	-7(15)	7(11)
C(3,G1)	586(4)	2620(7)	4986(13)	9(2)	32(5)	71(15)	-1(6)	-36(15)	5(10)
C(4,G1)	240(4)	2831(6)	3450(12)	13(2)	25(4)	62(14)	-2(5)	-2(15)	10(11)
C(5,G1)	556(4)	2412(6)	1986(12)	10(2)	25(4)	56(15)	-7(5)	-1(14)	11(10)
C(6,G1)	269(5)	2690(7)	409(12)	14(2)	37(5)	59(15)	-2(6)	21(16)	-12(10)
O(2,G1)	1619(3)	2675(4)	6208(9)	16(2)	30(3)	82(11)	7(4)	-15(11)	-22(8)
O(3,G1)	313(3)	3043(5)	6284(9)	16(2)	41(4)	61(11)	4(4)	-18(12)	7(8)
O(4,G1)	-362(3)	2473(4)	3632(8)	7(1)	23(3)	85(11)	-1(3)	15(10)	6(7)
O(5,G1)	1198(3)	2673(4)	1943(8)	11(2)	28(3)	64(11)	5(4)	9(10)	7(7)
O(6,G1)	518(4)	2235(5)	-905(9)	20(2)	47(4)	59(11)	-2(5)	-16(12)	1(8)
C(1,G2)	2469(5)	-504(7)	3323(13)	13(3)	29(5)	79(16)	7(6)	25(15)	12(12)
C(2,G2)	2614(5)	24(7)	4743(12)	12(2)	24(4)	81(16)	9(6)	5(17)	-6(11)
C(3,G2)	2116(5)	646(6)	4949(13)	10(2)	26(4)	67(15)	-2(5)	-5(15)	-8(11)
C(4,G2)	2058(4)	1139(6)	3384(13)	11(2)	28(4)	84(17)	-1(5)	24(16)	7(11)
C(5,G2)	1942(5)	589(7)	1953(14)	16(3)	28(5)	83(17)	14(6)	9(16)	10(12)
C(6,G2)	1974(6)	1024(7)	357(13)	30(4)	30(5)	42(15)	7(7)	-11(15)	2(13)
O(2,G2)	2685(4)	-451(4)	6175(9)	23(2)	27(3)	97(12)	-6(4)	32(12)	-22(10)
O(3,G2)	2263(3)	1200(4)	6228(9)	19(2)	30(3)	65(11)	2(4)	6(11)	-3(8)
O(4,G2)	1503(3)	1619(4)	3609(9)	9(1)	16(2)	92(11)	2(3)	17(10)	4(7)
O(5,G2)	2429(3)	-20(5)	1906(8)	16(2)	27(3)	72(10)	9(4)	-3(12)	30(8)
O(6,G2)	1817(5)	536(5)	-935(10)	46(3)	40(4)	87(13)	0(6)	15(13)	21(12)
C(1,G3)	888(5)	-2963(6)	3306(14)	13(2)	23(4)	89(17)	0(5)	14(15)	0(11)
C(2,G3)	1319(5)	-2885(6)	4769(12)	17(3)	26(4)	58(15)	4(6)	34(14)	-3(11)
C(3,G3)	1497(5)	-2002(6)	4977(12)	15(3)	22(4)	44(14)	-1(5)	0(13)	-12(10)
C(4,G3)	1797(4)	-1699(6)	3434(12)	11(2)	26(4)	53(15)	3(5)	11(14)	11(10)
C(5,G3)	1371(5)	-1831(6)	1963(12)	18(3)	19(4)	41(14)	1(5)	-1(13)	8(11)
C(6,G3)	1689(5)	-1651(7)	395(13)	21(3)	36(5)	57(16)	-3(7)	23(16)	6(12)
O(2,G3)	1014(3)	-3194(5)	6152(10)	16(2)	37(4)	108(13)	1(4)	58(13)	-1(9)
O(3,G3)	1939(3)	-1921(5)	6247(9)	15(2)	42(4)	52(10)	1(4)	29(11)	-13(8)
O(4,G3)	1874(3)	-586(4)	3646(8)	14(2)	15(2)	57(10)	0(3)	2(9)	19(8)
O(5,G3)	1200(3)	-2680(4)	1904(8)	11(2)	24(3)	63(10)	8(4)	-17(10)	0(7)
O(6,G3)	1271(4)	-1704(5)	-913(9)	26(2)	47(4)	72(12)	-6(5)	8(13)	-6(10)
Na	3521(5)	-95(7)	671(11)	33(3)	36(4)	108(14)	12(6)	13(16)	30(12)
S	0(-)	0(-)	-1164(6)	26(1)	33(2)	160(8)	5(3)	0(-)	0(-)
O(1,PS)	44(18)	-785(12)	-683(39)	113(15)	21(8)	477(78)	-88(20)	5(45)	-8(72)
O(2,PS)	530(12)	378(32)	-722(38)	28(7)	393(58)	359(70)	-196(37)	40(117)	5(40)
O(3,PS)	-501(19)	399(19)	713(40)	132(21)	119(22)	369(75)	205(37)	63(72)	82(70)
C(1,PS)	0(-)	0(-)	-3205(32)	119(21)	205(37)	94(38)	-14(52)	0(-)	0(-)
C(2,PS)	222(37)	-93(75)	-4268(45)	102(46)	214(54)	208(67)	150(94)	-29(176)	144(87)
C(3,PS)	148(12)	5(62)	-6157(33)	18(13)	128(22)	159(44)	32(54)	-21(103)	4(32)
O(W1)	3582(5)	1315(6)	887(12)	49(4)	40(4)	149(17)	-36(7)	-9(15)	-38(14)
O(W2)	3311(4)	-1572(6)	774(11)	32(3)	47(4)	124(15)	33(6)	-4(14)	18(11)
O(W3)	1229(10)	4898(11)	2170(23)	47(7)	31(8)	219(37)	15(13)	-19(31)	-189(29)
O(W4)	0(-)	5000(-)	3400(33)	157(17)	49(9)	471(64)	17(23)	0(-)	0(-)
O(W5)	4685(11)	-355(15)	3114(42)	39(7)	63(13)	558(88)	-41(16)	48(63)	-98(50)
O(W6)	3872(12)	-177(13)	647(43)	37(8)	37(11)	632(97)	25(16)	44(60)	80(52)
O(W7)	4135(9)	-297(12)	2994(33)	28(5)	52(10)	394(60)	-14(12)	85(44)	-51(34)

TABLE 3. FRACTIONAL COORDINATES ($\times 10^3$) AND ISOTROPIC THERMAL FACTORS OF HYDROGEN ATOMS

The thermal factors are equal to those of the adjacent carbon or oxygen atoms.

	x	y	z	B/Å^2
H(C1, G1)	196(5)	262(6)	300(15)	1.7
H(C2, G1)	129(5)	362(6)	462(13)	2.7
H(C3, G1)	53(5)	188(6)	521(14)	2.2
H(C4, G1)	17(4)	357(5)	343(12)	1.6
H(C5, G1)	55(4)	171(6)	217(12)	1.8
H(C6A, G1)	34(4)	345(6)	18(12)	1.9
H(C6B, G1)	−19(5)	262(7)	41(15)	1.9
H(O2, G1)	175(5)	222(7)	621(15)	2.7
H(O3, G1)	35(6)	287(8)	704(17)	2.5
H(C1, G2)	280(5)	−95(6)	302(14)	2.3
H(C2, G2)	313(6)	19(8)	457(15)	3.0
H(C3, G2)	159(5)	35(7)	530(14)	2.2
H(C4, G2)	247(4)	146(6)	304(12)	2.4
H(C5, G2)	144(5)	28(7)	205(14)	2.3
H(C6A, G2)	240(4)	126(6)	−3(13)	3.1
H(C6B, G2)	168(6)	142(7)	33(16)	3.1
H(O2, G2)	251(6)	−79(7)	623(16)	2.6
H(O3, G2)	222(6)	100(7)	726(16)	2.7
H(C1, G3)	77(6)	−370(7)	295(16)	3.3
H(C2, G3)	167(5)	−328(6)	450(13)	2.8
H(C3, G3)	108(5)	−157(6)	529(13)	2.4
H(C4, G3)	222(5)	−194(6)	319(14)	1.9
H(C5, G3)	98(5)	−137(7)	213(15)	1.5
H(C6A, G3)	204(4)	−201(6)	3(12)	2.0
H(C6B, G3)	182(5)	−111(7)	40(15)	2.0
H(O2, G3)	67(5)	−316(5)	613(14)	2.9
H(O3, G3)	178(6)	−186(7)	708(16)	2.4

Description and Discussion of the Structure

The structure and numbering scheme of the α-CDx–PSNa complex are shown in Fig. 1. The α-CDx molecule is nearly hexagonal. The 1-propanesulfonate anion is located in the channel which is formed by the stacking of the α-CDx rings (Fig. 2). Bond distances, angles, and conformation angles are given in Table 5. The geometrical data describing the macro-cyclic conformation of α-CDx ring are shown in Tables 6 and 7. The crystal structure and hydrogen-bonding scheme are shown in Figs. 4—7.

Bond Distances and Angles. The bond distances and angles for α-CDx in the present complex are not significantly different from those for the potassium acetate (ACK) complex,[13] the Methyl Orange complexes,[14] and the BSNa complex[15] which have channel-type structures. The average bond lengths for the three glucose residues are in good agreement with the average values for the α-D-glucose residues given by Arnott and Scott.[18] However, regarding bond angles, the average value for C(3)–C(4)–O(4) in α-CDx is 105.2°, which is smaller than the Arnott and Scott value of 110.4°. The C(1)–O(4′)–C(4′) angles of 117.5—119.0° are larger than those for the disaccharides.[18] These C(3)–C(4)–O(4) and C(1)–O(4′)–C(4′), however, are commonly observed in α-CDx complexes.

The abnormally short bond length and large angles are found in the 1-propanesulfonate anion (Fig. 3). This may be due to the disorder of the anion on the two-fold axis. The C(1, PS) atom is found to lie on the two-fold axis, but the thermal factor is relatively

* Table 4 is kept as a Document at the office of The Chemical Society of Japan. (Document No. 7706).

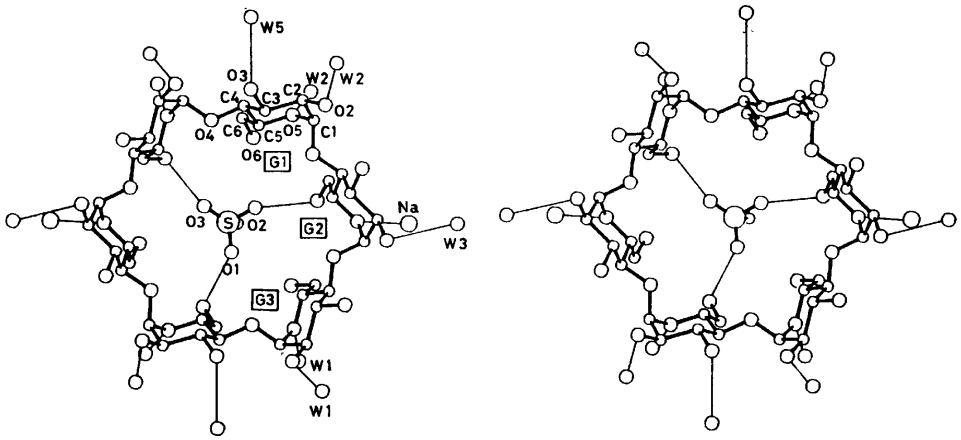

Fig. 1. A stereoview of the α-CDx–PSNa complex. Intermolecular O···O and O···Na contacts less than 3.0 Å are shown with thin lines. W1, W2, W3, and W5 denote oxygen atoms in water molecules.

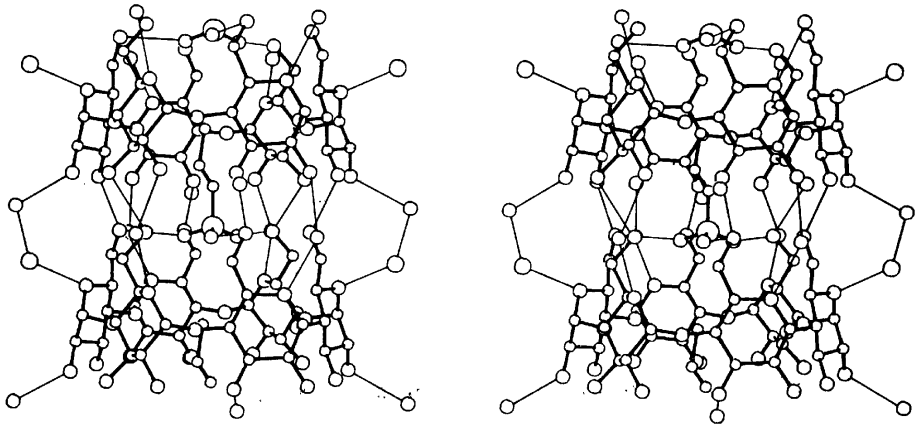

Fig. 2. A stereoview showing the stacking feature of α-CDx molecules. Intermolecular O···O and O···Na contacts less than 3.0 Å are shown with thin lines. Circles, in order of decreasing size, represent sulfur, sodium, oxygen, and carbon atoms.

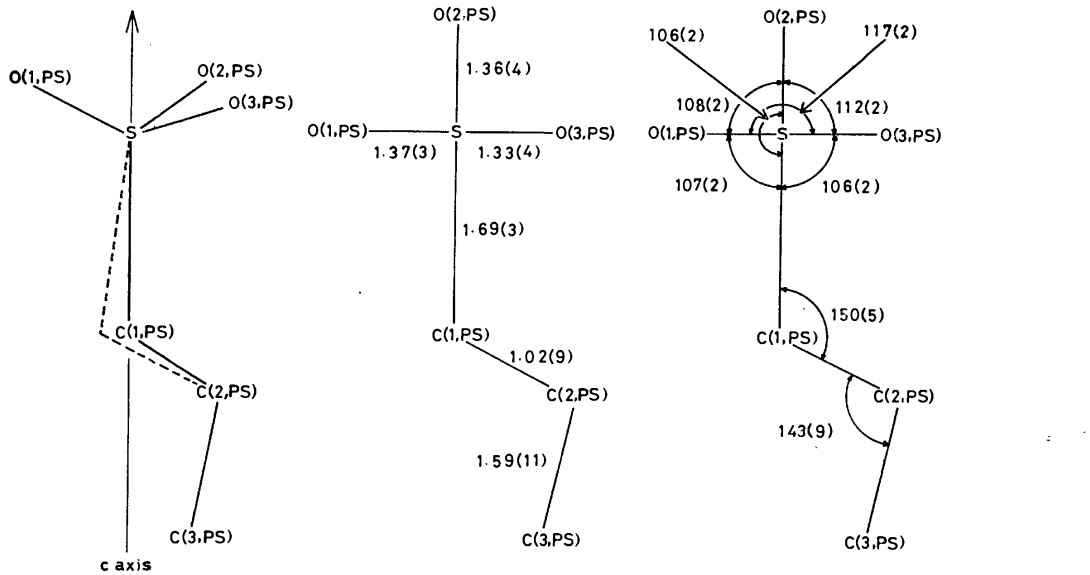

Fig. 3. Bond distances (l/Å) and angles (ϕ/°) in the 1-propanesulfonate anion. The short C(1,PS)–C(2,PS) distances and large valence angles of C(1,PS) and C(2,PS) are due to the small displacement of C(1,PS) from the c axis, as shown with the broken line.

TABLE 5. BOND DISTANCES (l/Å), ANGLES (ϕ/°), AND CONFORMATION ANGLES (ϕ/°) IN α-CYCLODEXTRIN

A prime (′) denotes the atom in the adjacent glucose residue.

	G1	G2	G3	AVERAGE
C(1)-C(2)	1.520(14)	1.505(15)	1.537(15)	1.521
C(1)-O(5)	1.418(12)	1.430(13)	1.425(12)	1.424
C(1)-O(4′)	1.420(12)	1.438(12)	1.426(12)	1.428
C(2)-C(3)	1.547(15)	1.506(15)	1.534(14)	1.529
C(2)-O(2)	1.427(13)	1.438(13)	1.420(13)	1.428
C(3)-C(4)	1.520(14)	1.543(15)	1.523(14)	1.529
C(3)-O(3)	1.418(13)	1.443(13)	1.429(12)	1.430
C(4)-C(5)	1.560(14)	1.522(15)	1.545(14)	1.542
C(4)-O(4)	1.439(12)	1.456(12)	1.428(12)	1.441
C(5)-C(6)	1.522(15)	1.512(16)	1.502(15)	1.512
C(5)-O(5)	1.453(12)	1.464(13)	1.467(12)	1.461
C(6)-O(6)	1.434(13)	1.389(15)	1.415(14)	1.413

	G1	G2	G3	AVERAGE
C(2)-C(1)-O(5)	109.6(8)	109.0(8)	109.3(8)	109.3
C(2)-C(1)-O(4′)	107.3(8)	106.3(8)	106.6(8)	106.7
O(5)-C(1)-O(4′)	110.6(8)	109.3(8)	110.0(8)	110.0
C(1)-C(2)-C(3)	108.8(8)	110.2(9)	108.8(8)	109.3
C(1)-C(2)-O(2)	110.5(8)	110.3(8)	109.1(8)	110.0
C(3)-C(2)-O(2)	111.0(8)	111.2(8)	112.0(8)	111.4
C(2)-C(3)-C(4)	108.9(8)	109.3(8)	109.4(8)	109.2
C(2)-C(3)-O(3)	109.8(8)	111.7(8)	110.0(8)	110.5
C(4)-C(3)-O(3)	108.5(8)	107.2(8)	107.8(8)	107.8
C(3)-C(4)-C(5)	109.5(8)	110.5(9)	111.3(8)	110.4
C(3)-C(4)-O(4)	105.1(8)	104.7(8)	105.9(8)	105.2
O(5)-C(4)-O(4)	106.9(8)	107.3(8)	107.9(8)	107.4
C(4)-C(5)-C(6)	110.8(8)	112.8(9)	112.5(9)	112.0
C(4)-C(5)-O(5)	107.6(8)	108.7(9)	108.3(8)	108.2
C(6)-C(5)-O(5)	106.1(8)	106.1(9)	106.2(8)	106.1
C(5)-C(6)-O(6)	109.8(8)	112.6(10)	111.1(9)	111.2
C(1)-O(5)-C(5)	113.8(7)	114.5(8)	114.3(7)	114.2
C(1)-O(4′)-C(4′)	118.3(7)	119.0(7)	117.5(7)	118.3

	G1	G2	G3	AVERAGE
C(1)-C(2)-C(3)-C(4)	-57.3	-57.3	-57.1	-57.2
C(2)-C(3)-C(4)-C(5)	57.3	55.4	55.6	56.1
C(3)-C(4)-C(5)-O(5)	-57.7	-54.2	-54.4	-55.4
C(4)-C(5)-O(5)-C(1)	61.8	59.0	59.1	60.0
C(5)-O(5)-C(1)-C(2)	-63.5	-61.4	-62.6	-62.5
O(5)-C(1)-C(2)-C(3)	59.0	59.4	59.7	59.4
O(4′)-C(1)-C(2)-O(2)	61.0	64.9	63.2	63.0
O(2)-C(2)-C(3)-O(3)	62.2	61.6	64.2	62.7
O(3)-C(3)-C(4)-O(4)	-68.8	-68.3	-67.8	-68.3
O(4)-C(4)-C(5)-C(6)	73.5	74.9	72.7	73.7
O(5)-C(5)-C(6)-O(6)	69.8	66.1	67.1	67.7
C(4)-C(5)-C(6)-O(6)	-173.7	-175.0	-174.5	-174.4
C(2)-C(1)-O(4′)-C(4′)	-129.1	-132.1	-128.9	-130.0
O(5)-C(1)-O(4′)-C(4′)	111.4	110.5	112.7	111.5
C(1)-O(4′)-C(4′)-C(3′)	129.0	130.0	131.2	130.1
C(1)-O(4′)-C(4′)-C(5′)	-113.6	-110.7	-112.5	-112.3

TABLE 6. LEAST-SQUARES PLANES AND DEVIATIONS OF ATOMS (d/Å)

An asterisk (*) indicates an atom related by the two-fold symmetry.

(1) The plane through six O(4) atoms

$0.0000X + 0.0000Y + 1.0000Z = 3.0127$

O (4, G1)	0.003	O (4, G1)*	0.003
O (4, G2)	−0.017	O (4, G2)*	−0.017
O (4, G3)	0.014	O (4, G3)*	0.014

(2) Planes through C(2), C(3), C(5), and O(5) atoms in glucose residues

(i) G1 residue

$-0.2915X + 0.9491Y - 0.1197Z = 3.2812$

C (2, G1)	−0.007	O (5, G1)	0.007
C (3, G1)	0.006	C (1, G1)	−0.689[a]
C (5, G1)	−0.007	C (4, G1)	0.712[a]

(ii) G2 residue

$0.6815X + 0.7194Y - 0.1342Z = 3.3449$

C (2, G2)	0.004	O (5, G2)	−0.005
C (3, G2)	−0.004	C (1, G2)	−0.686[a]
C (5, G2)	0.004	C (4, G2)	0.676[a]

(iii) G3 residue

$0.9613X - 0.2399Y - 0.1352Z = 3.3559$

C (2, G3)	0.004	O (5, G3)	−0.004
C (3, G3)	−0.004	C (1, G3)	−0.697[a]
C (5, G3)	0.004	C (4, G3)	0.672[a]

a) Atoms not included in the plane.

TABLE 7. GEOMETRICAL DATA FOR THE CONFORMATION OF α-CYCLODEXTRIN

Asterisks (*) and primes (′) indicate atoms related by two-fold symmetry and atoms in the adjacent glucose residues, respectively.

Guest	Residue	Torsion-angle index (°)	O(4)···O(4′) distances (Å)	O(4)···O(4*) distances (Å)	O(2)···O(3′) distances (Å)
ACK	G1	127.1	4.29	8.31	2.82
	G2	136.3	4.20	8.50	2.85
	G3	127.9	4.25	8.67	2.86
	Average	130.4	4.25	8.49	2.85
BSNa	G1	122.0	4.36	8.19	2.83
	G2	136.4	4.12	8.52	2.93
	G3	128.1	4.28	8.81	2.85
	Average	128.8	4.25	8.51	2.87
MONa[a]	G1	127.8	4.38	8.08	2.84
	G2	133.5	4.07	8.56	2.87
	G3	129.6	4.28	8.82	2.78
	Average	130.3	4.24	8.49	2.83
MOK[b]	G1	121.0	4.35	8.06	2.84
	G2	136.1	4.09	8.54	2.89
	G3	128.7	4.28	8.84	2.81
	Average	128.6	4.24	8.48	2.85
PSNa	G1	126.6	4.27	8.40	2.83
	G2	127.5	4.21	8.45	2.94
	G3	128.5	4.24	8.59	2.88
	Average	127.5	4.24	8.48	2.88

a) Methyl Orange sodium salt. b) Methyl Orange potassium salt.

large (the isotropic thermal factor is 13.2 Å^2). The short C(1, PS)–C(2, PS) distance and large angles for S–C(1, PS)–C(2, PS) and C(1, PS)–C(2, PS)–C(3, PS) are reasonably explained as being due to a slight deviation of the C(1, PS) atom from the fwo-fold axis, as shown in Fig. 3, although this was not resolved on the electron-density map.

Conformation of α-Cyclodextrin. Each glucose residue is in a C1 chair conformation, and is α-1,4-linked. The primary hydroxyl groups show a *gauche-trans* conformation. None of the conformation angles in the glucose residues deviates from the mean value of the three glucose residues by more than 2.3°. The conformation angles in the pyranose ring are in good agreement with the Arnott and Scott values.[18] The α-CDx ring in the PSNa complex is more symmetrical than those in the ACK,[13] Methyl Orange,[14] and BSNa[15] complexes. The diagonal distances between the glycosidic oxygen atoms are 8.40, 8.45, and 8.59 Å (Table 7). In the Methyl Orange complexes and the BSNa complex, the α-CDx rings are elliptical due to the inclusion of the planar group; the O(4, G3)···O(4*, G3) distances are longer than the O(4, G1)···O(4*, G1) distances by 0.6—0.8 Å. The conformation angles involving C(1)–O(4′)–C(4′) linkages are in good agreement with each other for complexes having a channel-type structure. Therefore, the distortion of the α-CDx ring is not described by the conformation angles involving the glycosidic linkages.

French and Murphy[19] have discussed the deformation of the pyranose ring of the α-D-glucose residue in terms of the O(1)···O(4) distance and the torsion-angle index; the torsion-angle index is defined by $|\phi(C(1)-C(2))|+|\phi(C(2)-C(3))|+|\phi(C(5)-O(5))|+|\phi(O(5)-C(1))|-|\phi(C(3)-C(4))|-|\phi(C(4)-C(5))|$ when the torsion-angle of C(1)–C(2)–C(3)–C(4) is expressed by $\phi(C(2)-C(3))$. They have also shown that the O(1)···O(4) distance is closely related to the torsion-angle index. The O(4)···O(4′) distances in the PSNa complex are 4.24±0.03 Å, and this value agrees with 4.25 Å predicted for the α-CDx having regular hexagonal symmetry.[20] In the Methyl Orange complexes and the BSNa complex, the O(4)···O(4′) distances in the G2 residues are shorter by 0.24—0.31 Å than those in the G1 residues, although the average values are close to 4.25 Å. The different conformations of the pyranose ring result in different torsion-angle indices. In the PSNa complex, the torsion-angle indices are 126.6—128.5°. In the Methyl Orange complexes and the BSNa complex, the torsion-angle indices of the G2 residues are greater by 4.7—15.1° than those of the G1 residues. Therefore, the elliptical structure of α-CDx in the Methyl Orange complexes and the BSNa complex is ascribed to a deformation of the pyranose rings, that is, a difference between the conformation angles in the pyranose rings. No significant difference was observed for the O(2)···O(3′) distances, indicating that the distortion of the α-CDx ring does not affect the intramolecular hydrogen bonds in complexes with channel-type structures.

Geometry of Inclusion. α-CDx molecules are stacked in a head-to-tail arrangement, and form endless channels along the c axis. The α-CDx molecule has two-fold symmetry, but the asymmetric 1-propanesulfonate anion is located in a channel with statistical disorder on the two-fold axis. The anion is in contact with two α-CDx molecules. The propyl group contacts with the O(2), O(3) side of the α-CDx ring (Fig. 2). The sulfonato group is hydrogen-bonded to three of the primary hydroxyl groups, O(6*, G1), O(6, G2), and O(6*, G3) with oxygen-oxygen distances of 2.72, 2.80, and 2.75 Å, respectively. A different hydrogen-bonding contact was observed in the BSNa complex.[15] The sulfonato group forms hydrogen bonds with four of the primary hydroxyl groups, O(6, G1), O(6, G3), O(6*, G1), and O(6*, G3), with the respective distances being 2.80, 2.86, 2.71, and 2.86 Å. The primary hydroxyl groups of the G2 residues in the BSNa complex do not form hydrogen bonds because of the elliptical structure of α-CDx. In the ACK complex and the Methyl Orange complexes, the primary hydroxyl groups are also hydrogen-bonded to the ionized group of the guest molecule. It is noted that the sulfonato group and the acetate ion are nearly trigonal. The trigonal group fits well into the O(6) side of the α-CDx ring, as is shown in Figs. 1 and 2.

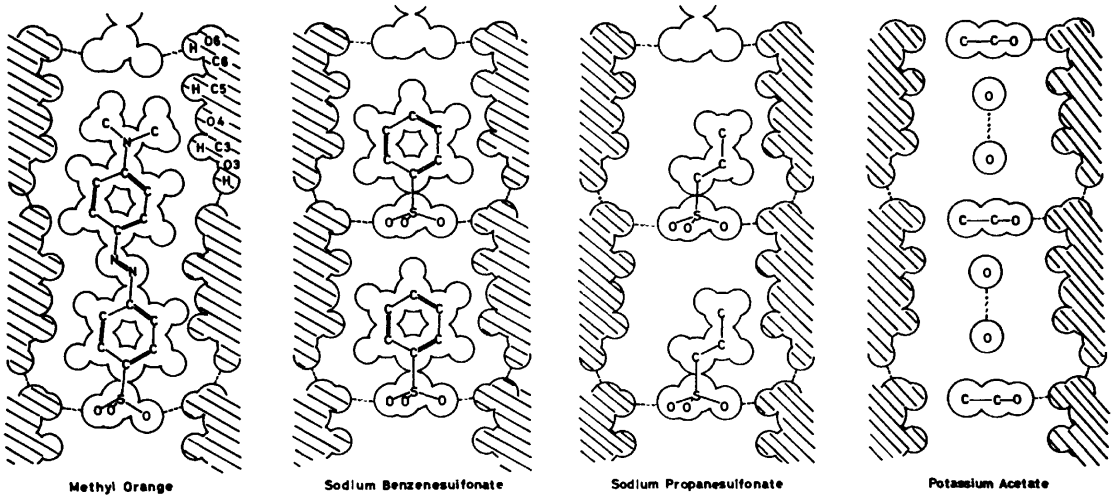

Fig. 4. A comparison of the arrangements of guest molecules in the channel. Broken lines denote hydrogen bonds.

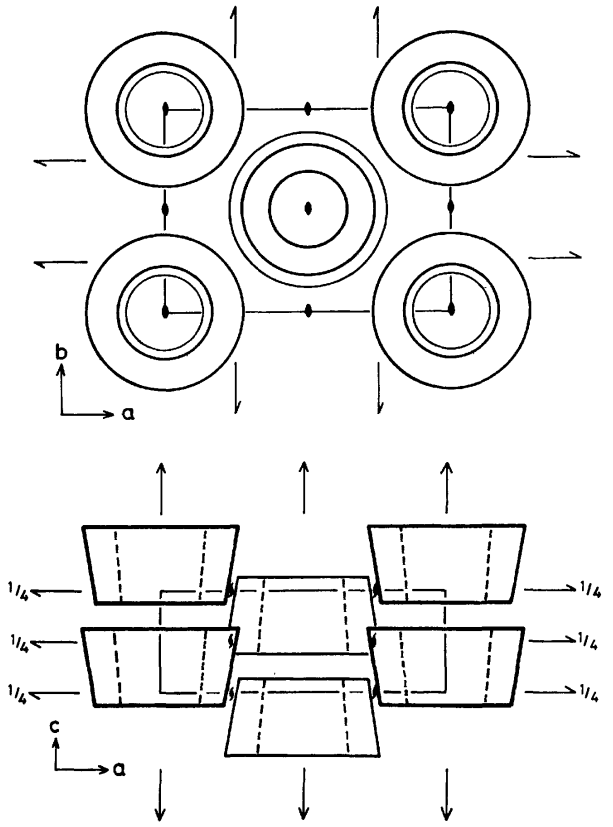

Fig. 5. A packing feature of α-CDx molecules in the crystal.

Schematic drawings of the arrangements of the guest molecules in the channel are shown in Fig. 4. A long molecule, as well as a small molecule, can be situated in the channel. In the ACK complex,[13] the acetate anion is so small that the empty space in the cavity is filled with two water molecules. On the other hand, a long guest anion extends through two α-CDx rings in the Methyl Orange complexes. For bulky guest molecules, the suitability of the guest molecule to the cavity may determine the geometry of the complex. In the interior of the cavity, the C(3)–H and C(5)–H groups are oriented at the center of the α-CDx cavity. The circle composed of six hydrogen atoms attached to the C(5) atoms forms the neck of the cavity. In the Methyl Orange complexes, the azo group is situated at the neck, but in the other complexes the guest molecules are not located at the neck. The conformation of the α-CDx ring in cage-type structures[5–9] changes remarkably with the dimension and the shape of the guest molecule. In channel-type structures,[13–15] however, the conformation change is quite small. This may be due to the fact that the framework of the α-CDx ring is held together by the hydrogen bonds between the α-CDx molecules and between α-CDx and the ionized group.

Crystal Structure and Hydrogen Bonds. The framework of the crystal is built up of endless cylinders formed by stacks of the α-CDx rings, as is shown in Fig. 5. The space outside the channel is filled with cations and water molecules (Fig. 6). The two adjacent α-CDx molecules are linked by O(2, G3)···O(W1)···O(5, G3), O(2, G1)···O(W2)···O(5, G1), and O(2, G2)···O(W3)···Na···O(5, G2) linkages except for O(3)···O(6) hydrogen bonds. The sodium ion is surrounded by five oxygen atoms, O(W1), O(W2), O(W3), O(W7), and O(5, G2), which form a distorted trigonal bipyramid (Fig. 7). The Na···O distance varies from 2.36 to 2.58 Å. These values are in good agreement with those of 2.34—2.55 Å found for the BSNa complex.[15] In the ACK complex[13] and the Methyl Orange complexes,[14] the cations are surrounded by six oxygen atoms which form a distorted octahedron (Fig. 8).

The hydrogen-bonding scheme is similar to that of the BSNa complex (Fig. 9). In the G1 residue, O(2, G1) and O(5, G1) are hydrogen-bonded to O(W2), while O(3, G1) is bonded to O(W5). Both of O(2,G3)

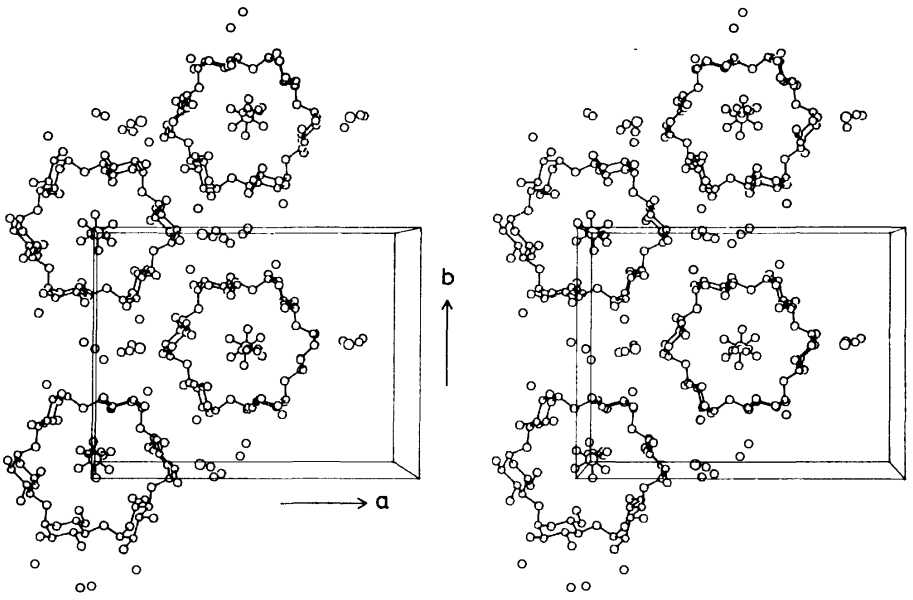

Fig. 6. A stereoview of the crystal structure viewed along the c axis.

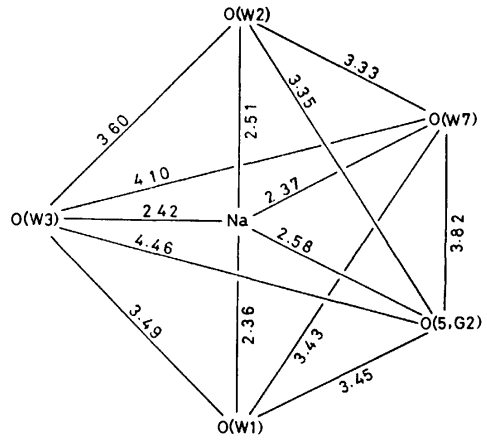

Fig. 7. Geometry of the sodium-ion coordination shell.

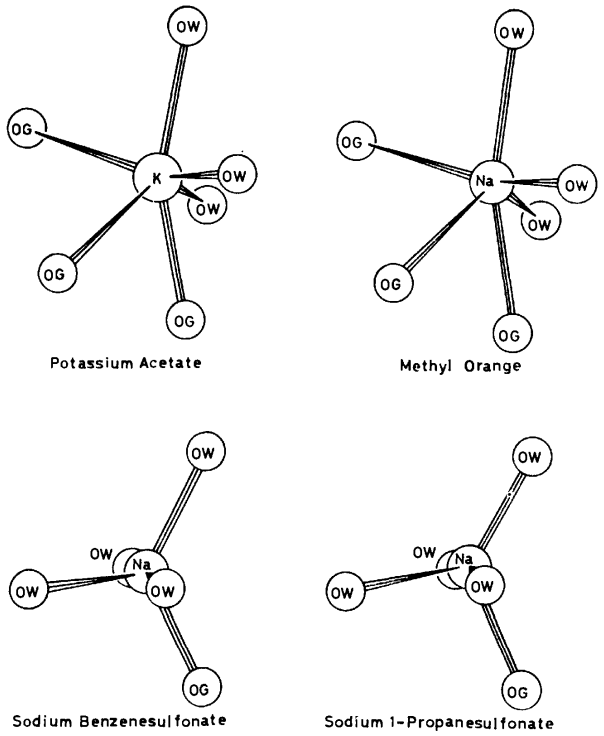

Fig. 8. Comparison of the geometry of the coordinations of alkali metal ions in the α-CDx complexes with the channel-type structure. OW and OG indicate oxygen atoms in water and glucose residue, respectively.

and O(5, G3) in the G3 residue form hydrogen bonds with O(W1). In the G2 residue, only O(2, G2) is involved in the hydrogen-bonding with water. The primary hydroxyl groups do not form hydrogen bonds with water, but they form hydrogen bonds with O(3) atoms in the adjacent α-CDx molecule.

Conclusions

So far, three channel-type structures with head-to-tail arrangement of α-CDx have been revealed; the ACK complex,[13] the Methyl Orange complex,[14] and the BSNa complex.[15] The PSNa complex has been

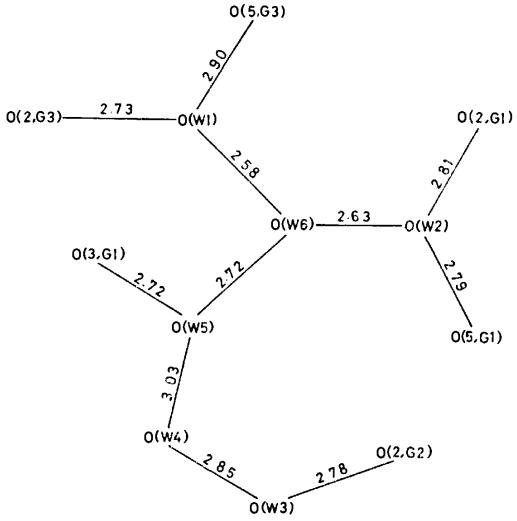

Fig. 9. The hydrogen-bonding scheme in crystals of α-CDx-PSNa nonahydrate.

shown to have the same crystal structure. It is noteworthy that these complexes crystallize in approximately isomorphous structures, although the shapes and dimensions of the guest molecules are quite different. The adjacent α-CDx molecules along the channel are connected by O(3)···O(6) hydrogen bonds. The hexagonal structure of α-CDx may be stabilized by hydrogen-bonding with the ionized group, which has a trigonal structures. The change in the macro-cyclic conformation of α-CDx, which is caused by the inclusion of the planar group, affects the lattice parameters. The elliptical α-CDx ring is parallel to the ac plane, and the long axis is oriented along the a axis. Therefore, the *a* dimensions of crystals of the Methyl Orange complexes and the BSNa complex are longer by 0.22—0.51 Å than that of the PSNa complex, while the *b* dimensions are shorter by 0.17—0.34 Å.

Another type of channel-type structure has been found in the α-CDx–polyiodide complexes.[16] In this case, the α-CDx molecules are arranged in a head-to-head fashion, that is, the O(2), O(3) side of the α-CDx ring is facing the same side of the adjacent α-CDx ring, and the O(6) side is facing the O(6) side. The conformation of the primary hydroxyl groups is *gauche-gauche*, and thus, these groups cannot form hydrogen bonds including the guest molecule. In the channel, the guest molecules are arranged with statistical disorder, forming an infinite polyiodide chain.

In both types of channel-type structures, the guest anions are included in the cavity, but the cations are located outside the α-CDx ring. This may be due to the fact that the α-CDx cavity has a relatively positively-charged character. The interior of the cavity contains C(3)–H, C(5)–H, H–C(6)–H, and O(4) whose charges were estimated to be 0.11, 0.14, 0.14, and −0.25, respectively.[15] Moreover, the C(3)–H and C-(5)–H groups are oriented to the center of the α-CDx ring. Therefore, it appears that the inclusion of an anion is more favorable than the inclusion of a cation. Outside the channel, the oxygen atoms surrounding the

TABLE 8. INTERMOLECULAR DISTANCES (l/Å) LESS THAN 3.0 Å

O (6, G2) -O (2, PS)	2.80	O (3, G1) -O (6, G1)	(i)	2.73
O (5, G2) -Na	2.58	O (3, G2) -O (6, G2)	(i)	2.78
O (W1) -Na	2.36	O (3, G3) -O (6, G3)	(i)	2.79
O (W2) -Na	2.51	O (6, G1) -O (1, PS)	(ii)	2.72
O (W7) -Na	2.37	O (6, G3) -O (3, PS)	(ii)	2.75
O (W1) -O (W6)	2.58	O (5, G1) -O (W2)	(iii)	2.79
O (W2) -O (W6)	2.63	O (W3) -O (W6)	(iii)	2.35[a]
O (W3) -O (W4)	2.85	O (2, G1) -O (W2)	(iv)	2.81
O (W5) -O (W6)	2.72	O (3, G1) -O (W5)	(iv)	2.72
O (W6) -Na	0.77[a]	Na -O (W3)	(v)	2.42
O (W5) -O (W7)	1.20[a]	O (5, G3) -O (W1)	(v)	2.90
O (W6) -O (W7)	2.04[a]	O (2, G2) -O (W3)	(vi)	2.78
		O (2, G3) -O (W1)	(vi)	2.73

Symmetry code	Symmetry operator		
None	x,	y,	z
i	x,	y,	$1+z$
ii	$-x$,	$-y$,	z
iii	$1/2-x$,	$1/2+y$,	$-z$
iv	$1/2-x$,	$1/2+y$,	$1-z$
v	$1/2-x$,	$-1/2+y$,	$-z$
vi	$1/2-x$,	$-1/2+y$,	$1-z$

a) The distance between disordered atoms.

cation form the coordination shell.

The geometry of the PSNa complex is similar to that of the BSNa complex. The hydrophobic propyl group is in contact with the O(2), O(3) side of the α-CDx ring, while the sulfonato group is hydrogen-bonded to the primary hydroxyl groups. When we consider a structure in an aqueous solution, the solvation effect is important as has been shown in a previous paper.[15] The transfer of the propyl group from the water environment to the interior of the cavity will reduce the solvation energy of PSNa, since the propyl group may be more likely to be found in the hydrophobic and nonpolar cavity than in the water environment. When the sulfonato group is included in the cavity, it may form hydrogen bonds with the primary hydroxyl groups. But, as has been suggested by Griffiths and Bender,[3] the hydrogen bonds do not appear to be important in the stabilization of the complex, since the sulfonato group may be hydrogen-bonded to water molecules in the uncomplexed state. Therefore, the inclusion of the propyl group will give a more stable complex than the inclusion of the sulfonato group in an aqueous solution.

The author would like to acknowledge the helpfull suggestions of Dr. Alfred D. French. The author also wishes to thank Dr. Hisashi Uedaira for supporting this study and for useful discussions. The stereoviews were drawn on a Hewlett-Packard 7200A graphic plotter. The computation was done on a HITAC 8450 computer in this laboratory.

References

1) J. A. Thoma and L. Stewart, "Starch: Chemistry and Technology," Vol. I, ed by R. L. Whistler and E. F. Pashall, Academic Press, New York (1965), pp. 209—249.
2) D. French, M. L. Levine, J. H. Pazur, and E. Norberg, *J. Am. Chem. Soc.*, **71**, 353 (1949).
3) D. W. Griffiths and M. L. Bender, *Adv. Catal.*, **23**, 209 (1973).
4) R. K. McMullan, W. Saenger, J. Fayos, and D. Mootz, *Carbohydr. Res.*, **31**, 37 (1973).
5) R. K. McMullan, W. Saenger, J. Fayos, and D. Mootz, *Carbohydr. Res.*, **31**, 211 (1973).
6) P. C. Manor and W. Saenger, *J. Am. Chem. Soc.*, **96**, 3630 (1974).
7) W. Saenger and M. Noltemeyer, *Chem. Ber.*, **109**, 503 (1976).
8) W. Saenger, R. K. McMullan, J. Fayos, and D. Mootz, *Acta Crystallogr., Sect. B*, **30**, 2019 (1974).
9) B. Hingerty and W. Saenger, *J. Am. Chem. Soc.*, **98**, 3357 (1976).
10) K. Harata, *Bull. Chem. Soc. Jpn.*, **48**, 2409 (1975).
11) W. Saenger, K. Beyer, and P. C. Manor, *Acta Crystallogr., Sect. B*, **32**, 120 (1976).
12) K. Harata, *Carbohydr. Res.*, **48**, 265 (1976).
13) A. Hybl, R. E. Rundle, and D. E. Williams, *J. Am. Chem. Soc.*, **87**, 2779 (1965).
14) K. Harata, *Bull. Chem. Soc. Jpn.*, **49**, 1493 (1976).
15) K. Harata, *Bull. Chem. Soc. Jpn.*, **49**, 2066 (1976).
16) M. Noltemeyer and W. Saenger, *Nature (London)*, **259**, 629 (1976).
17) "International Tables for X-Ray Crystallography," Vol. IV, Birmingham, Kynoch Press (1974), pp. 72—75.
18) S. Arnott and W. E. Scott, *J. Chem. Soc., Perkin Trans. 2*, **1972**, 324.
19) A. D. French and V. G. Murphy, *Carbohydr. Res.*, **27**, 391 (1973).
20) A. D. French and V. G. Murphy, Annual Meeting of Japanese Starch Society, Tokyo (1976).

Electronic Absorption and Fluorescence Spectra of 5-Hydroxytryptamine (Serotonin). Protonation in the Excited State

Tohru KISHI,* Masashi TANAKA, and Jiro TANAKA
Department of Chemistry, Faculty of Science, Nagoya University, Chikusa, Nagoya 464
(Received October 28, 1976)

The fluorescence spectra of 5-hydroxytryptamine (serotonin) in acidic media have been studied by means of fluorescence polarization, temperature dependence of fluorescence, and kinetics of the protonation in H_2O and D_2O. The red-shifted emission appearing by protonation in the excited state is ascribed to the protonated form of serotonin at C_4. In order to confirm the assignment of electronic spectra, the absorption spectra of the single crystal of 5-methoxyindole-3-acetic acid have been measured by means of reflection technique, the directions of transition moments being determined by polarization analysis. Calculation was carried out on the energy levels of the excited state for serotonin and its protonated forms, and the directions of transition moments were compared with the experimental results.

5-Hydroxytryptamine (serotonin) found in many mammal tissues has several unknown physiological effects, such as on nervous impulse transmission and mental activity.[1] The fluorescence assay of serotonin is important in biomedical analysis. Udenfriend *et al.*[2] found that the fluorescence of serotonin in a strongly acidic solution appears at 18000 cm^{-1} in the visible region, and at 30000 cm^{-1} in a neutral solution. Bridges and Williams,[3] and Chen[4] studied the mechanism of this anomalous fluorescence and postulated that the emitting species is the protonated excited state form of serotonin. However, no detail of the protonated structure was established, the postulate remaining unsettled.

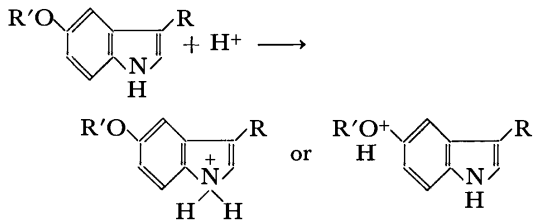

We have attempted to clarify the structure of the protonated form on the basis of (1) polarization measurement of the fluorescence, (2) temperature dependence of the fluorescence in the acidic media, (3) lifetime measurement of the fluorescence of both unprotonated and protonated serotonin in the acidic media, (4) polarization measurement of the reflection spectra of a crystal of serotonin derivative, and (5) theoretical calculation on serotonin and its protonated forms.

The electronic states and structures of serotonin and its protonated form were clarified from the results. The results are discussed in connection with the electronic spectra of the parent molecule, indole.

Experimental

Material. Serotonin creatinine sulfate (Nakarai Chemical Co.) was purified by repeated recrystallization from water. Ethylene glycol–water (7 : 3) (EGW) with 1.2 M HCl was used as a solvent for the fluorescence polarization measurement. The fluorescence lifetime were measured with solutions of 2×10^{-5} M in H_2O or D_2O by adding appropriate amounts of HCl or DCl. 5-Methoxyindole-3-acetic acid (pfs grade, Sigma Chemical Co.) was recrystallized from methanol–water. The compound was supplied by Prof. K. Tomita of Osaka University.

Methods. The temperature dependence of the fluorescence was measured in a thermostated cell with a Carl Zeiss spectrofluorometer in the temperature range −56—6 °C. A HTV-R446UR photomultiplier tube was used, no correction being made for the spectral responce of the detecting system. The polarization of the fluorescence was measured with the same apparatus combined with a calcite polarizer for excitation and a polacoat polarizer for analysis at −52 °C. The polarization characteristic of the polacoat polarizer was checked before the measurement, the stray light being less than 1%. The instrumental depolarization effect was corrected following the procedure of Azumi and McGlynn.[5] Fluorescence lifetimes were measured with an Ortec 9200 photon counting system. An Ortec nanosecond light pulser was used as an excitation source through a Toshiba DV-25 filter, with 20% $NiSO_4$ solution and 0.2% K_2CrO_4 solution of each 1 cm path. The fluorescence was detected through filters of a Toshiba UV-D1B and a Nd glass for the 29600 cm^{-1} band and a Fuji Color SC-52 for the 17800 cm^{-1} band. The reflection spectra were recorded by the microscopic reflecting system constructed in this laboratory.

Results and Discussion

The fluorescence spectra of indole in polar solvents exhibit a conspicuous red shift.[6–11] It is considered that the second excited level is stabilized and the fluorescence occurs from this state. The absorption and fluorescence spectra of serotonin are shown in Fig. 1 together with the polarization values for the excitation and emission. There are more than three absorption bands in the 31000—47000 cm^{-1} region. The first band appears in the 31000—34000 cm^{-1} range, the second band overlapping with it at 33000 cm^{-1} and extending to the 37000 cm^{-1} region, and the third band appearing with a maximum at 45300 cm^{-1}. Although the first and the second bands overlap in the 33000 cm^{-1} range, their maxima appear at different energies, differing from the case of indole where they overlap strongly.

The fluorescence spectra measured at −52 °C in an acidic media are shown in Fig. 1. The emission band with a maximum at 29800 cm^{-1} is ascribed to a neutral molecule and the band appearing at 17800 cm^{-1}

* Present address: National Research Institute of Police Science, 6, Sanban-cho, Chiyoda, Tokyo 102.

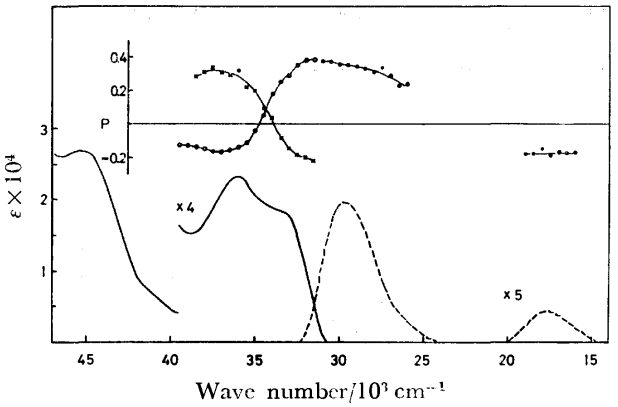

Fig. 1. The absorption (——), emission (---), and polarization spectra of serotonin in EGW with 1.2M HCl at −52 °C.
The fluorescence polarization (FP) spectra (-●-●-) were measured by exciting at 32500 cm^{-1}. The fluorescence excitation polarization (APF) spectra were recorded by monitoring the fluorescence at 30000 cm^{-1} (-O-O-) and at 18000 cm^{-1} (-×-×-).

is assigned to the protonated form. The maximum of this emission shifted to 17600 cm^{-1} when correction was made on the response of the photomultiplier tube.

Polarization Measurement of Fluorescence. The fluorescence excitation polarization (APF) spectra for the neutral molecule were measured by setting the detecting monochromator at 30000 cm^{-1}. It was found that the first absorption band shows p-values of 0.4—0.2. This indicates that the fluorescence originates from the first excited state. The second absorption band showed negative p-values of −0.12——0.17. Thus the direction of the transition moment is considered to be nearly perpendicular to the first band.

The fluorescence polarization (FP) of 29800 cm^{-1} emission band was measured by exciting at 32500 cm^{-1}, the p-valucs being always positive (0.4—0.25) in the range 31000—26000 cm^{-1}. This shows that the emission band consists of a unique origin, namely the fluorescence occurs from the lowest excited state.

The emission bands at 17800 cm^{-1} appearing in a strongly acidic solution showed a quite different polarization character as compared to the 29800 cm^{-1} band, its FP spectra measured by exciting at 32500 cm^{-1} showing a constant negative p-value of −0.18. In line with this results, the APF spectra in the first absorption region showed negative p-values of −0.2——0.1, while the second absorption band showed positive p-values of 0.2—0.3 in the 35000—39000 cm^{-1} range.

The 17800 cm^{-1} band is considered to be due to the protonated form of serotonin.[4] The present results show that the rotational motion of serotonin molecule in the excited state is frozen at −52 °C in EGW to give definite p-values, while the proton transfer occurs under these conditions and the protonated serotonin is formed consequently. The long wavelength fluorescence shows a different polarization character as compared to the parent molecule. The absorption spectra of serotonin in 1M HCl solution was almost the same as those in neutral solution. It was confirmed that the protonation occurs after the excitation of the neutral molecule, since a close correlation was found between the absorption and polarization spectra of the parent molecule and the protonated form. The direction of the transition moment of the protonated emitting species was shown to be nearly perpendicular to the first absorption band and parallel to the second absorption band.

Temperature Dependence of Fluorescence. The temperature dependence of the fluorescence in acidic media is shown in Fig. 2, the solution being excited at 33500 cm^{-1}. At 6 °C the peaks for neutral and protonated species were found at 29600 cm^{-1} and 17800 cm^{-1}, respectively. By lowering the temperature the intensity of the fluorescence from the neutral form increased, the peak showed a blue shift of 200 cm^{-1}, and the emission from the protonated form diminished. The results are explained by a retardation of the protonation in terms of increase in the viscosity of the solvent caused by fall of temperature. The disappearance of the visible fluorescence at −196 °C was reported by Chen.[4] This provides another evidence that the emission occurs from the protonated species.

Lifetime of Fluorescence. The rise and decay of fluorescence of the neutral and protonated forms are shown in Fig. 3. The lifetime of neutral species

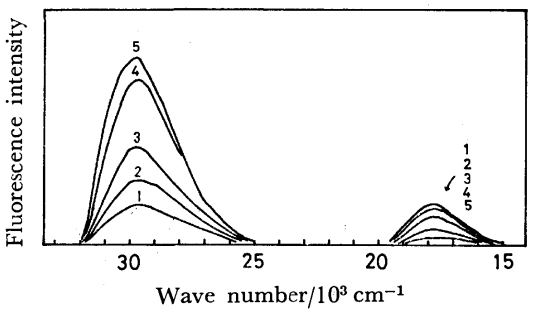

Fig. 2. The temperature dependence of the fluorescence of serotonin in EGW with 1.2 M HCl.
1. 6 °C; 2. −9 °C; 3. −19 °C; 4. −40 °C; 5. −56 °C.

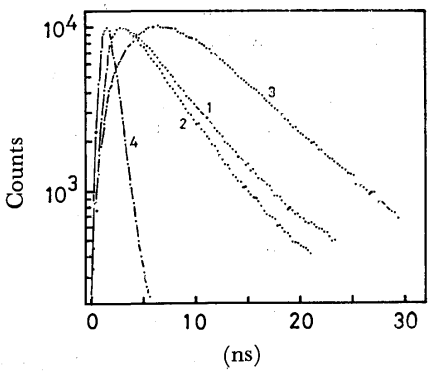

Fig. 3. The rise and decay curves of the fluorescence of the free and protonated serotonin in 0.04 M DCl.
1. Fluorescence intensity of serotonin measured at 30000 cm^{-1}, 2. Fluorescence intensity of serotonin with 0.04 M DCl measured at 30000 cm^{-1}, 3. Fluorescence intensity of protonated form of serotonin with 0.04 M DCl measured at 18000 cm^{-1}, 4. The flash profile.

decreases with increase in acid concentration. The rise and decay curves of the lower energy emission indicate that the excited species were produced after the excitation *via* the protonation of serotonin in the excited state.

Following Chen's[4] scheme, the reaction of the excited species is written as

$$\begin{array}{ccccc} S^* + H^+ & \underset{k_{-1}}{\overset{k_1}{\rightleftharpoons}} & SH^{+*} & & \\ \downarrow k_f \quad \searrow k_q & & \downarrow k_f' \quad \searrow k_q' & & \\ S + h\nu \qquad S & & SH^+ + h\nu' & & SH^+ \end{array} \tag{1}$$

where S* is the excited serotonin, k_1 and k_{-1} are the rate constants for the protonation and deprotonation reactions, respectively, k_f and k_f', and k_q and k_q' are the rate constants for radiative and radiationless processes of neutral and protonated species, respectively. If we assume that $k_1[H^+] \gg k_{-1}$, then the lifetime τ of the excited neutral molecule S* is given by

$$1/\tau = k_f + k_q + k_1[H^+]. \tag{2}$$

The change of the fluorescence lifetime at 20 °C with increase in the hydrogen ion concentration is given in Table 1. The fluorescence quenching by the counter ion Cl^- was examined. It was found that the effect is negligible in the concentration range of Cl^- less than 0.1 M. The plot of $1/\tau$ against $[H^+]$ or $[D^+]$ gives the rate constant, $k_1(H)$ and $k_1(D)$. The results are

$$k_1(H) = 2.9\times10^9\ s^{-1}\ M^{-1},$$
$$k_1(D) = 1.6\times10^9\ s^{-1}\ M^{-1},$$

and

$$k_1(H)/k_1(D) = 1.8.$$

The linear relation between $1/\tau$ and $[H^+]$ or $[D^+]$ supports Scheme 1 for the reaction of the excited species. The kinetic isotope effect found in these reactions can be correlated with the motion of the hydrogen ion in an aqueous solution, since the reaction seems to be a diffusion controlled process. The ratio of

Table 1. Fluorescence lifetime of serotonin in the acidic media

$[H^+]$	In H_2O	In D_2O
0 mM	4.65 ns	5.57 ns
40	3.72	4.81
60	3.30	4.43
80	2.99	4.13

the rate constants $k_1(H)/k_1(D)$ shows a normal isotope effect.[12] It is interesting that the value is close to the ratio of the mobilities of proton and deuteron, $\mu(H^+)/\mu(D^+)$ (1.44) at 25 °C.[13] It might imply that the proton transfer occurs in the charge-separated excited species through the Grotthuss mechanism.[14]

Theoretical Calculation of Electronic State. The electronic energy levels of serotonin and its protonated forms were calculated by the Pariser-Parr-Pople method[15,16] by using the Nishimoto-Mataga potential[17] and taking into account the configuration interaction. The calculated transition energy, size and direction of the transition moments are given in Table 2 and Fig. 4. The directions of ^1L_b and ^1L_a transitions

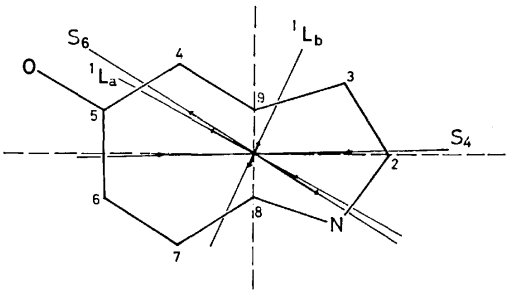

Fig. 4. The theoretical prediction of the direction of transition moments of the excited singlet states (^1L_a and ^1L_b) of serotonin and its protonated forms. S_4 or S_6 are is direction of the transition moment of the lowest singlet state of the protonated forms by adding proton at C_4 or C_6 positions, respectively.

Table 2. Theoretical calculations of the singlet excited states of serotonin and its protonated forms

	State symbols	State energy cm^{-1}	Transition-moment length R_x	Transition-moment length R_y	Oscillator strength f	Observed values cm^{-1} (f)
Serotonin	^1L_b	32940	0.079	0.174	0.013	33000 (0.054)
	^1L_a	38500	−0.694	0.395	0.267	36000 (0.098)
	^1B_b	43840	1.136	0.571	0.769	45300 (0.56)
	^1B_a	46390	−0.682	0.589	0.409	
Protonated at C_4		22750	1.553	0.028	0.596	20000
		28720	0.161	−0.059	0.009	
		39020	−0.028	0.464	0.091	
		43690	0.268	0.552	0.178	
Protonated at C_6		21890	−1.045	0.656	0.362	
		28730	0.662	0.576	0.240	
		37840	−0.143	−0.194	0.024	
		43130	0.947	0.155	0.431	

(Fig. 4) are given for serotonin; the transition moment to the ^1L_b state makes 85° with that of the ^1L_a, while the observed value estimated from the p-values and the relation between the p-value and the angle θ made of transition moments[18,19] given by

$$p = \frac{3\cos^2\theta - 1}{3 + \cos^2\theta} \qquad (3)$$

is 90°. The agreement between these two values is satisfactory, since the depolarization and other possible experimental errors might not be completely corrected.

Calculation for the protonated forms was carried out by assuming that the proton attack at C_4 or C_6 position of the indole ring and positive charge was put on oxygen atom (Table 2). The positions of proton attack were presumed since these protons are known to be easily deuterated in acidic media. The lowest energy transitions were calculated for C_4 and C_6 adducts at 22750 cm^{-1} and 21890 cm^{-1}, respectively. These values are in good agreement with the position of the fluorescence band when we consider a mirror image relationship between the absorption and emission spectra. The directions of transition moments from these levels to the ground state are along S_4 or S_6 (Fig. 4). A comparison of the calculated directions with the p-values suggests that the lowest state of the protonated form has a transition moment along S_4. As an example, from the observed p-values, the first and second transitions of parent molecule (^1L_b and ^1L_a) make 69° and 31°, respectively, with the direction of the emission of protonated form, while the calculated values with S_4 direction are 65° and 31°, respectively. In contrast, the transition moments to the ^1L_b and ^1L_a states makes 82° and 2°, respectively, with S_6 direction. Thus the position of proton attack may be assigned at C_4. However, an alternative choice remains at C_6 since a quantitative coincidence of p-values may not be easily realized, and the values can be affected by experimental artefact. Chen[4] presumed that the proton attack occurs at C_6 position, on the basis of the calculated charge density by DeVoe, who showed that the charge density in the excited state is the largest at this position. In spite of this the predicted p-values by the C_6 adduct are −0.32 and +0.5 for the first and the second bands, while the observed values are −0.18 and +0.32, respectively. The calculated values by the C_4 adduct are −0.15 and +0.33, respectively, the C_4 protonated form thus being more plausible than the C_6 adduct. We have calculated the charge density in the lowest excited state, the result of which is shown in Fig. 5. We see that the proton attack at C_4 is a reasonable process in view of charge distribution. The NMR spectra of serotonin in acidic media have been studied by Daly and Witkop[20] who found that the C_4 proton is most labile in an acidic media. This is in line with our conclusion that the proton attacks at C_4 position in the excited state of 5-hydroxyindole derivatives in an acidic media.

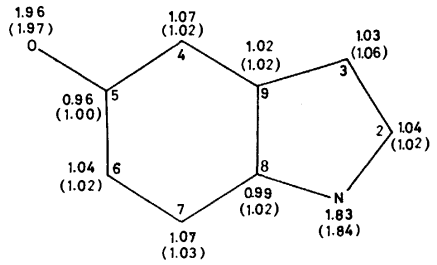

Fig. 5. The charge density of serotonin in the lowest excited state.
The charge density in the ground state was also shown in parenthesis.

Thus the excited-state reaction of 5-hydroxyindole derivatives can be depicted as:

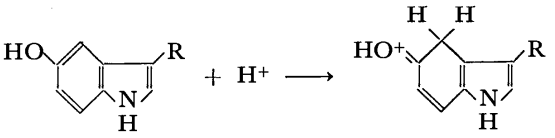

Reflection Spectra of 5-Methoxyindole-3-acetic Acid. In order to confirm the assignment of spectra of 5-hydroxyindole derivatives, the polarized reflection spectra were measured with a single crystal of 5-methoxyindole-3-acetic acid on its (100) plane. The crystalline structure was determined by Sakaki, Wakahara, Fujiwara, and Tomita.[21] Projection of the molecule on (100) plane is shown in Fig. 6. It is noted that the short molecular axis is nearly parallel to the crystalline c-axis while the long axis lies nearly perpendicular to this plane. The crystals used for spectral measurement were 0.8×2 mm×*ca.* 0.3 mm. The devel-

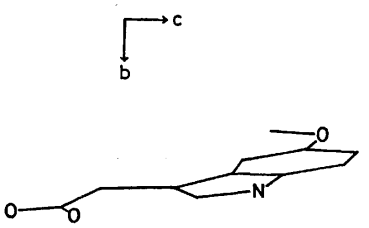

Fig. 6. Projection of 5-methoxyindole-3-acetic acid molecule onto the (100) plane of the crystal.

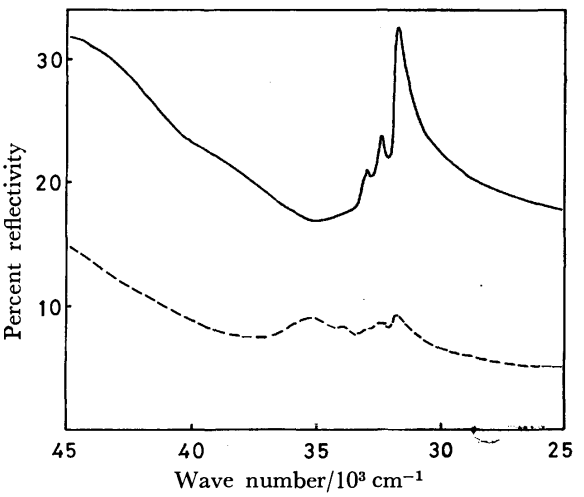

Fig. 7. Reflectivity of 5-methoxyindole-3-acetic acid crystal. Polarization of the light parallel to the b-axis (---) and the c-axis (——).

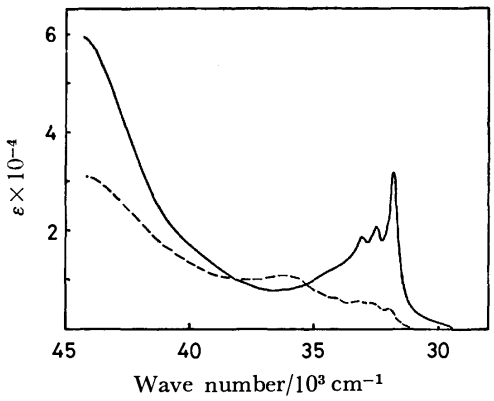

Fig. 8. Absorption spectra of 5-methoxyindole-3-acetic acid crystal obtained from Kramers-Kronig transformation. --- b-axis, —— c-axis.

oped plane was confirmed by X-ray photographs. The reflection spectra calibrated with SiC standard are shown in Fig. 7. The Kramers-Kronig transformation of reflectivity gives the absorption coefficient (Fig. 8).

The first band shows a vibronic structure at 31800, 32500, and 33100 cm^{-1}. Appearance of this structure peculiar to the first ^1L_b band has also been observed in the spectra of indole in the gaseous states.[22,23] The first absorption band shows a strong dichroism, strong along the c-axis. The direction of the transition moment obtained from the dichroic ratio confirms the calculated one shown in Fig. 4 and the band is thus assigned to the ^1L_b state. The second band observed at 36000 cm^{-1} is weak on this crystalline face, its dichroic ratio being $f_b/f_c=2$. The band is assigned to the ^1L_a band at 36000 cm^{-1} in solution spectra, its direction being consistent with that of the ^1L_a band deduced from theoretical calculation.

In their paper on indole derivatives, Yamamoto and Tanaka[24] estimated the directions of the transition moments of indole for ^1L_b and ^1L_a bands to make angles of 54 and −38°, respectively, to the long molecular axis. The present result confirms these assignments, *viz.*, although the present molecules have a hydroxyl or methoxyl substituent at C_5, the spectral features are very close to those of indole. Actually the calculated result on 5-hydroxyindole differs only by 9° rotation into anti-clockwise way from the result on indole by Yamamoto and Tanaka. Song and Kurtin[9] indicated that the transition moments of ^1L_b and ^1L_a states of indole are on the first and third quadrant and the second and fourth quadrant, respectively (Fig. 4). This is qualitatively in line with our result, but the directions are not in quantitative agreement with our assignment of indole and serotonin ^1L_b and ^1L_a bands.

As regards the oscillator strengths of ^1L_b and ^1L_a bands, whose relative intensity was discussed by Andrews and Forster,[11] the two bands overlap strongly but the whole band can be divided into two parts, *f*-values being estimated as 0.098 and 0.054 for ^1L_a and ^1L_b bands, respectively. From the crystalline spectra, the *f*-values for the ^1L_b band is estimated to be greater than 0.27, which is much greater than the value expected from the solution spectra (0.16), thus giving rise to a batho-chromic effect. The intensity ratio for $^1L_a/^1L_b$ bands is 1.8, whereas Andrews and Forster[11] estimated it to be 3—4 on indole and Yamamoto and Tanaka as 11. The effect of hydroxyl substituent is significant in enhancing the ^1L_b band.

The authors thank Mr. Tsutomu Kouyama, Physics Department, for his help in the fluorescence lifetime measurement and Dr. Tsuguhiro Kaneda of this laboratory for taking the X-ray photographs.

References

1) A number of review articles and monographs are available. For example, see H. E. Himwich, "Biochemistry, Schizophrenias, and Affective Illnesses," ed by H. E. Himwich, The Williams and Wilkins Co., Baltimore (1970), Chaps. IV and IX.
2) S. Udenfriend, D. F. Bogdanski, and H. Weissbach, *Science*, **122**, 972 (1955).
3) J. W. Bridges and R. T. Williams, *Biochem. J.*, **107**, 225 (1968).
4) R. F. Chen, *Proc. Natl. Acad. Sci. U.S.A.*, **60**, 598 (1968).
5) T. Azumi and S. P. McGlynn, *J. Chem. Phys.*, **37**, 2413 (1962).
6) H. Zimmermann and N. Joop, *Z. Elektrochem.*, **65**, 61 (1961).
7) N. Mataga, Y. Torihashi, and K. Ezumi, *Theoret. Chim. Acta*, **2**, 158 (1964).
8) J. Eisinger and G. Navon, *J. Chem. Phys.*, **50**, 2069 (1969).
9) P-S. Song and W. E. Kurtin, *J. Am. Chem. Soc.*, **91**, 4892 (1969).
10) C. Cazeau Dubroca, F. Dupuy, M. Martinand, and A. Lopez Campillo, *Chem. Phys. Lett.*, **23**, 397 (1973).
11) L. J. Andrews and L. S. Forster, *Photochem. Photobiol.*, **19**, 353 (1974).
12) R. A. More O'Ferrall, "Proton Transfer Reactions," ed by E. Caldin and V. Gold, Chapman and Hall, London (1975), p. 230.
13) J. O'M. Bockris and A. K. N. Reddy, "Modern Electrochemistry," Plenum Publishing Co., New York (1970), p. 472.
14) C. J. D. von Grotthuss, *Ann. Chim.*, **58**, 54 (1806).
15) R. Pariser and R. G. Parr, *J. Chem. Phys.*, **21**, 466 (1953).
16) J. A. Pople, *Proc. Phys. Soc. Ser., A*, **68**, 81 (1955).
17) K. Nishimoto and N. Mataga, *Z. Phys. Chem. (Frankfurt am Main)*, **13**, 140 (1957).
18) V. L. Levshin, *Z. Phys.*, **32**, 307 (1925).
19) F. Perrin, *Ann. Phys.*, **12**, 169 (1926).
20) J. W. Daly and B. Witkop, *J. Am. Chem. Soc.*, **89**, 1032 (1967).
21) T. Sakaki, A. Wakahara, T. Fujiwara, and K. Tomita, *Bull. Chem. Soc. Jpn.*, **48**, 536 (1975).
22) D. A. Chignell and W. B. Gratzer, *J. Phys. Chem.*, **72**, 2934 (1968).
23) E. M. Strickland, J. Horwitz, and C. Billups, *Biochemistry*, **9**, 4914 (1970).
24) Y. Yamamoto and J. Tanaka, *Bull. Chem. Soc. Jpn.*, **45**, 1362 (1972).

A Shock Tube Study of the Decomposition Mechanism of Chloroform in the Presence of Deuterium or Methane

Takayuki YANO

Institute of Space and Aeronautical Science, The University of Tokyo, Komaba, Meguro-ku, Tokyo 153

(Received November 10, 1976)

Chloroform was pyrolyzed in the absence and in the presence of one of three additives—D_2, CH_4, and CD_4, over the temperature range of 1000—1200 K in a single-pulse shock tube. The main products of the decomposition of chloroform by itself were tetrachloroethylene and hydrogen chloride. On the other hand, tetrachloroethylene, trichloroethylene, dichloromethane, and hydrogen chloride were the major products in the presence of D_2, while in the chloroform–methane systems they were tetrachloroethylene, trichloroethylene, 1,1-dichloroethylene, vinyl chloride, ethane, and hydrogen chloride. From the deuterium distribution of the products, as determined by mass spectrometry, it is found that the hydrogen atoms of trichloroethylene and 1,1-dichloroethylene mainly came from chloroform and methane respectively, while the hydrogen atoms of vinyl chloride came from both chloroform and methane. The change in the product distribution resulting from the addition of deuterium or methane and the hydrogen isotopic distribution suggest that the mechanism is composed of Cl atom elimination in the initiation step and successive reactions involving "hot" molecule reactions. The hydrogen isotopic distribution of vinyl chloride may indicate that the three-centered hydrogen elimination ($\alpha\alpha$) process competes with the four-centered ($\alpha\beta$) process in the decomposition of "hot" 1,1-dichloroethane.

The decomposition of chloroform has been investigated by several authors. Among them, the studies of Semeluk and Bernstein[1] and Shilov and Sabirova[2] have been detailed. However, they came to different conclusions about the initiation process.

Semeluk and Bernstein[1] investigated the decomposition of chloroform at about 800 K by the flow method; they found that hydrogen chloride and tetrachloroethylene (C_2Cl_4) were the main products and that the decomposition rate was first-order with respect to chloroform. They proposed the radical chain mechanism to explain the main product distribution and the kinetics;

$$CHCl_3 \longrightarrow CHCl_2\cdot + Cl\cdot, \quad (1)$$

$$Cl\cdot + CHCl_3 \longrightarrow CCl_3\cdot + HCl, \quad (2)$$

$$CCl_3\cdot \longrightarrow CCl_2{:} + Cl\cdot, \quad (3)$$

$$CCl_3\cdot + Cl\cdot \longrightarrow CCl_4, \quad (4)$$

$$CCl_2{:} + CHCl_3 \longrightarrow C_2Cl_4 + HCl. \quad (5)$$

On the other hand, Shilov and Sabirova[2] studied the decomposition in a toluene carrier and found no bibenzyl. From their results, they proposed another mechanism;

$$CHCl_3 \longrightarrow CCl_2{:} + HCl, \quad (6)$$

$$CCl_2{:} + CHCl_3 \longrightarrow C_2Cl_4 + HCl. \quad (5)$$

It is desirable to investigate further the initiation step of the chloroform decomposition by the shock-tube technique, which enables us to neglect the surface reaction. Although the two mechanisms mentioned above produce the same main products and give similar kinetics of the first order, they produce different radicals in the initiation step. This provides a possible way to check both mechanisms. In order to detect the radicals formed in the initiation step, we pyrolyze chloroform in the presence of a relatively large amount of methane or hydrogen, whose decomposition itself can be neglected at the reaction temperatures. We found the change in the product distribution to result from the interaction between the radicals and the added gas molecule. Further, by the use of deuterated chloroform or deuterated additives, we also found the hydrogen isotopic distribution to be dependent upon the characteristics of the interaction.

Experimental

Apparatus. The decomposition was studied in a 4-cm-i.d. single-pulse shock tube. The design and operation of the shock tube were fully described previously.[3]

Materials and Procedure. Chloroform of a research grade was purified as follows. In order to purge the trace of ethanol involved as a stabilizer, we first shook unpurified chloroform with concd H_2SO_4 in a separatory funnel, washed it with water, dehydrated it, and distilled it. Finally, we distilled chloroform three times under a vacuum. Deuterated chloroform obtained from E. Merck Co. was also distilled three times under a vacuum. Methane (99.5% purity) and deuterium of a research grade (99.5 D atom %) and argon of an ultra-high purity (99.999% purity) were used without further purification. A considerable amount of oxygen was present in the methane-d_4 (99.5 D atom %) of the Matheson Co.; it was removed by passing it through a reduced copper column.[4] Experiments were carried out with the gas mixtures listed in Table 1.

TABLE 1. THE REACTANT MIXTURES AND THEIR COMPOSITIONS

Series No.	Components	Composition in mol%
I	$CHCl_3/Ar$	1.5/98.5
II	$CHCl_3/D_2/Ar$	1.5/4.8/93.7
IIIa	$CHCl_3/CH_4/Ar$	2.4/4.6/93.0, 1.1/4.4/94.5
IIIb	$CHCl_3/CD_4/Ar$	1.8/3.7/94.5, 2.0/4.0/94.0
IIIc	$CDCl_3/CH_4/Ar$	1.0/7.8/91.2, 1.0/3.1/95.9
		1.9/5.8/92.3, 1.0/2.2/96.8

The hydrocarbons and chlorinated hydrocarbons were separated and analyzed on a Yanaco G-80 gas chromatograph equipped with a temperature programer. The gas sample was separated on a 2-m-long Porapak Q column, with He as the carrier gas; the separated components were detected by means of thermal-conductivity and flame-ionization detectors. As occasion demanded, we determined each eluted component by mass spectrometry in order to confirm the identification of each peak of the gas chromatography.

After the separation of the product gas mixture into com-

ponents on a gas chromatograph, we analyzed the separated elutant by mass spectrometry in order to determine the hydrogen isotopic distribution. For the simplification of the mass spectrum, a low ionization voltage was employed. At an ionization voltage of about 10 eV, only the parent peak remained except for chloroform. In the case of chloroform, $CHCl_3$, the peak intensity of $CHCl_2^+$ was much stronger than that of $CHCl_3^+$, even at a low ionization voltage.

Results

The dwell time was practically constant (1 ms), and the total density behind the reflected shock waves was about $(2.4—3.9)\times10^{-5}$ mol/cm^3. The reaction temperature range was about 1000—1200 K. It was true in all the series that chlorinated ethylene and hydrogen chloride were the main products and that the chlorinated ethane was not present or, occasionally, present in a very small amount.[5] When one of the reactants was deuterated, the hydrogen isotopic isomers of chloroform were analyzed by mass spectrometry after the shock heating. It was thus confirmed that the isomer of chloroform converted by H/D exchange reaction was negligibly small. The experimental results for each series are described below.

Series I. Tetrachloroethylene and hydrogen chloride were produced predominantly. The hydrogen chloride was not quantitatively analyzed, since an exact determination of the yield is difficult because of the surface reactions. As the minor products, four species were found; trichloroethylene, dichloromethane, 1,1,2,2-tetrachloroethane, and an unidentified species. The characteristics of the product distribution were consistent with those reported of Semeluk and Bernstein.[1] Table 2 shows the yields of C_2Cl_4 and C_2HCl_3, together with the conversion of chloroform.

Series II. When deuterium was added, much more species were produced than those obtained from the decomposition of chloroform alone. Fifteen species involving unidentified peaks were detected. Trichloroethylene, which has been a minor product in Series I, here appeared as the main product. Tetrachloroethylene, dichloromethane, 1,1-dichloroethylene, vinyl chloride, and chloroacetylene were identified, while as trace species methane, ethylene, ethyl chloride, and 1,1,-2,2-tetrachloroethane were detected. The yields of the principal products are plotted against the chloroform conversion in Fig. 1.

As is shown in Fig. 1, trichloroethylene, C_2Cl_4, and dichloromethane increase linearly with the increase in the conversion at relatively low conversions, but they show their maximum at higher conversions. On the other hand, 1,1-dichloroethylene, vinyl chloride, and chloroacetylene were hardly detected at all at low conversions; they increased remarkably at high conversions.

The deuterium content of trichloroethylene is shown in Table 3. It should be noted that the yield of C_2HCl_3 is much greater than that of C_2DCl_3 over a wide conversion range.

Series III. Many species (13 species) were observed, as in the case of Series II. The principal products of the Series IIIa were 1,1-$C_2H_2Cl_2$, C_2H_3Cl, C_2H_6, C_2H_4, C_2HCl_3, and C_2Cl_4. Their yields, except for that of C_2Cl_4, are plotted against the chloroform conversion in Fig. 2 (C_2Cl_4 was not determined by gas

Table 2. The concentrations of C_2Cl_4 and C_2HCl_3 in the product gas mixture and the conversion of chloroform

T/K	C_2Cl_4[a]	C_2HCl_3[a]	Chloroform conversion[b]
975	135	13	c)
1005	320	26	c)
1033	310	21	c)
1058	770	44	18
1073	2300	48	40
1090	1690	77	39
1093	1680	75	39
1103	2370	116	51
1105	1770	84	43
1155	3350	33	80

a) The concentration is expressed in ppm. b) The conversion is expressed in %. c) The values in this column were obtained from the analysis of chloroform. The value denoted by c is slightly negative due to the analytical error.

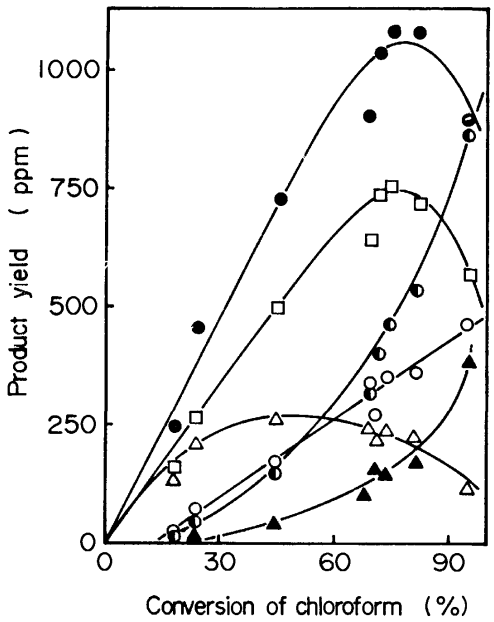

Fig. 1. Plots of product yield for series II, *vs.* chloroform conversion.
●: Trichloroethylene, □: C_2Cl_4, △: dichloromethane,
◐: 1,1-dichloroethylene, ▲: chloroacetylene,
○: vinyl chloride.

Table 3. Hydrogen isotopic distribution of trichloroethylene for series II

C_2HCl_3[a]	C_2DCl_3[a]	Chloroform conversion[a]
91.8	8.2	23.0
87.8	12.2	43.6
78.0	22.0	67.7
72.2	27.8	72.6

a) These values are expressed in percentages.

chromatography, but the mass spectra showed the yield of C_2Cl_4 was comparable with that of C_2HCl_3). The product distributions of Series IIIb and IIIc were similar to that of Series IIIa.

The main hydrogen isotopic isomers of each product for Series IIIb and IIIc are shown in Table 4. When the conversion of chloroform is smaller than 50%, 1,1-dichloroethylene and trichloroethylene almost always consist of only one hydrogen isotopic isomer; the other isomers form less than one tenth of the main isomer. Vinyl chloride consists of two hydrogen isotopic isomers of comparable amounts.

In Table 4, if we replace the H and D atoms of Series IIIc by D and H atoms respectively, we obtain the distributions of the isotopic isomers of Series IIIb. The hydrogen of trichloroethylene came mainly from the reactant chloroform. On the contrary, the hydrogens of 1,1-dichloroethylene came from the reactant methane. The hydrogens of vinyl chloride, like 1,1-dichloroethylene, were supplied mainly by the methane, but partly by the chloroform.

Figure 3 shows the hydrogen isotopic distribution of vinyl chloride, which is dependent upon the temperature for Series IIIb and IIIc. The ratios of $[CHCl=CD_2]/[CDCl=CD_2]$ and $[CDCl=CH_2]/[CHCl=CH_2]$ for Series IIIb and IIIc respectively are plotted against the temperature. In the following discussion, it will be shown that they are equal to the ratio of the rate of the $\alpha\beta$ process to that of the $\alpha\alpha$ process in the decomposition of "hot" 1,1-dichloroethane. The $R_{\alpha\beta}/R_{\alpha\alpha}$ ratio decreases with an increase in both the temperature and the [methane]/[chloroform] ratio. There is no detectable isotope effect in the IIIb and IIIc series.

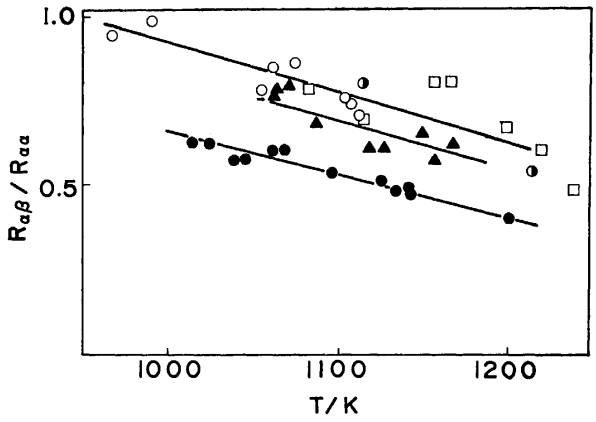

Fig. 3. Dependence of $R_{\alpha\beta}/R_{\alpha\alpha}$ on temperature and concentration ratio of r=[methane]/[chloroform] for series IIIb and IIIc. The ratio of $R_{\alpha\beta}/R_{\alpha\alpha}$ is equal to $[CHCl=CD_2]/[CDCl=CD_2]$ and $[CDCl=CH_2]/[CHCl=CH_2]$ for IIIb and IIIc, respectively.
□: r=2.0 (IIIb), ●: r=7.8 (IIIc), ▲: r=3.1 (IIIc), ○: r=3.0 (IIIc), ◑: r=2.2 (IIIc).

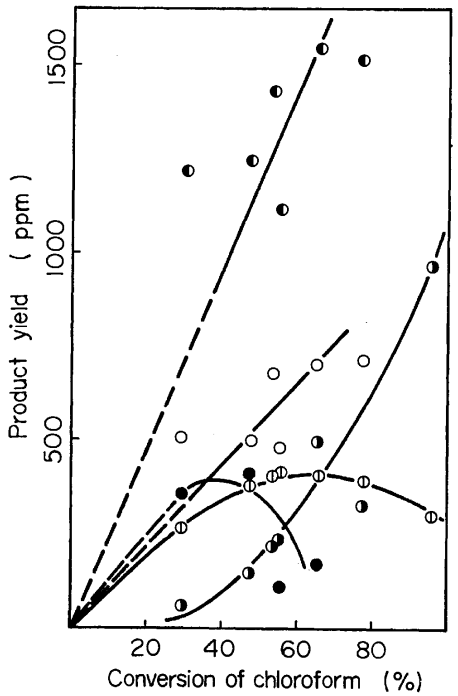

Fig. 2. Plots of product yield for series IIIa (1.1/4.4/94.5) *vs.* chloroform conversion.
◐: 1,1-Dichloroethylene, ○: vinyl chloride,
●: trichloroethylene, ⓘ: ethane, ◑: ethylene.

TABLE 4. MAIN HYDROGEN ISOTOPIC ISOMERS OF CHLORINATED ETHYLENE FOR SERIES III

Species	Series IIIb	Series IIIc
Dichloroethylene	$C_2D_2Cl_2$	$C_2H_2Cl_2$
Vinyl chloride	C_2D_3Cl, C_2HD_2Cl	C_2H_3Cl, C_2H_2DCl
Trichloroethylene	a)	C_2DCl_3

a) This was not determined by mass spectrometry, but it may be C_2HCl_3 in view of the results of Series II and IIIc.

Discussion

The product distribution was changed drastically by the addition of methane or hydrogen. One of the characteristic changes is the decrease in C_2Cl_4; another is the increase in trichloroethylene.

In the case of D_2 addition, trichloroethylene, C_2Cl_4, and dichloromethane are supposed to be the primary products, because, in Fig. 1, their yields are linear to the conversion[6] at a low conversion. In the case of methane addition, ethane, vinyl chloride, 1,1-dichloroethylene, trichloroethylene, and C_2Cl_4 are probably the primary products, while ethylene is a secondary product, as may be seen from Fig. 2, although their plots are somewhat scattered.

The change in the product distribution can be readily explained by the Cl atom elimination, proposed by Semeluk and Bernstein,[1] from the chloroform molecule in the initiation step. In the case of D_2 addition, the Cl atom formed by Step 1 may abstract the D atom from the D_2 present in a large amount; then DCl and the D atom are produced;

$$Cl\cdot + D_2 \longrightarrow DCl + D\cdot \quad (7)$$

The D atom produced in Reaction 7 then further reacts with chloroform;

$$D\cdot + CHCl_3 \longrightarrow CHCl_2\cdot + DCl \quad (8)$$

Since there is a competitive relation between Reactions

7 and 2, Reaction 7 retards the radical-chain reaction to yield C_2Cl_4. On the other hand, because of the participation of Reaction 8, the formation rate of the $CHCl_2$ radical is increased. The "hot" molecule of 1,1,2,2-tetrachloroethane may be produced *via* the combination reaction of the $CHCl_2$ radical;

$$2CHCl_2\cdot \longrightarrow CHCl_2CHCl_2^* . \quad (9)$$

The "hot" molecule is stabilized by collisions or decomposes to an ethylene-type molecule and hydrogen chloride *via* a unimolecular reaction;

$$CHCl_2CHCl_2^* \xrightarrow{+M} CHCl_2CHCl_2, \quad (10)$$

$$\longrightarrow C_2HCl_3 + HCl. \quad (11)$$

The fact that hardly no 1,1,2,2-tetrachloroethane is found may show that the "hot" molecule prefers the decomposition to the stabilization under our experimental conditions. Dichloromethane as a primary product may be formed *via* a hydrogen-abstraction reaction of the $CHCl_2$ radical;

$$CHCl_2\cdot + D_2 \longrightarrow CHDCl_2 + D\cdot. \quad (12)$$

The production of C_2Cl_4 can be explained by the partly surviving chain reaction proposed by Semeluk and Bernstein.[1] It is apparent that the trichloroethylene produced through Reactions 9 and 11 has the same hydrogen isomer as the reactant chloroform.

On the other hand, the assumption by Shilov and Sabirova[2] that the CCl_2 radical is formed in the initiation step is not reasonable. In explaining the formation of trichloroethylene, the following plausible reactions are assumed on the basis of analogy with the CH_2 radical;

$$CCl_2: + D_2 \longrightarrow CDCl_2\cdot + D\cdot, \quad (13)$$

$$D\cdot + CHCl_3 \longrightarrow CHCl_2\cdot + DCl . \quad (8)$$

The decrease in the formation rate of C_2Cl_4 can be explained by the competition between Reactions 5 and 13. However, the yields of C_2HCl_3 and C_2DCl_3 which are produced from "hot" tetrachloroethanes would then be equal, since the formation rates of the $CHCl_2$ and $CDCl_2$ radicals are supposed to be equal. This expectation is not consistent with the experimental result; that is ,the formation of the CCl_2 radical in the primary step is doubtful. The increase in the composition of C_2DCl_3 with the increase in the conversion (Table 3) may be the result of some secondary reactions.[7]

In the case of the methane addition, in the IIIc series for example, the Cl atom elimination reaction also agrees with the experimental results. The following reactions may give C_1 radicals;

$$CDCl_3 \longrightarrow CDCl_2\cdot + Cl\cdot, \quad (1)$$

$$Cl\cdot + CH_4 \longrightarrow CH_3\cdot + HCl , \quad (14)$$

$$Cl\cdot + CDCl_3 \longrightarrow CCl_3\cdot + DCl. \quad (2)$$

The "hot" ethane-type molecules are formed *via* the association of these C_1 radicals. These "hot" chlorinated ethanes decompose to ethylene-type molecules and hydrogen chloride. Ethane and C_2Cl_6 are only be stabilized by collisions;

$$2CDCl_2\cdot \longrightarrow CDCl_2CDCl_2^* \longrightarrow C_2DCl_3 + DCl, \quad (11)$$

$$CDCl_2\cdot + CH_3\cdot \longrightarrow CDCl_2CH_3^* ,$$

$$\xrightarrow{\alpha\beta} CDCl{=}CH_2 + HCl , \quad (15)$$

$$\xrightarrow{\alpha\alpha} CHCl{=}CH_2 + DCl , \quad (16)$$

$$CDCl_2\cdot + CCl_3\cdot \longrightarrow$$

$$CDCl_2CCl_3^* \longrightarrow C_2Cl_4 + DCl , \quad (17)$$

$$CH_3\cdot + CCl_3\cdot \longrightarrow$$

$$CH_3CCl_3^* \longrightarrow CH_2{=}CCl_2 + HCl , \quad (18)$$

$$2CH_3\cdot \longrightarrow C_2H_6^* \xrightarrow{+M} C_2H_6 , \quad (19)$$

$$2CCl_3\cdot \longrightarrow C_2Cl_6^* \xrightarrow{+M} C_2Cl_6 , \quad (20)$$

All the products formed by Reactions 11 and 15—20 except C_2Cl_6 were identified as the primary products. The partly surviving chain mechanism as well as Reaction 17 may be responsible for the formation of C_2Cl_4, as in the case of D_2 addition.

The hydrogen isotopic distributions of trichloroethylene and 1,1-dichloroethylene through Reactions 11 and 18 are in good agreement with the experimental results. The assumption that the "hot" $CDCl_2CH_3$ molecule decomposes not only through the $\alpha\beta$ process but also through the $\alpha\alpha$ process can well explain the isotope distribution of vinyl chloride. It is well known that the haloethane eliminates hydrogen chloride *via* the $\alpha\beta$ process. Recently, however, Perona *et al.*[8] found the $\alpha\alpha$ process in the chemical activation study of the "hot" CHF_2CD_3, and its occurrence has lately been confirmed by Kim *et al.*[9] Moreover, Perona *et al.*[8] suggested that the $\alpha\alpha$ process was competitive with the $\alpha\beta$ process only when two halogen atoms are attached to the same carbon atom. It was also found from the studies of "hot" 1,1,2-trichloroethane-1-d_1[10] that the $\alpha\alpha$ process competed with the $\alpha\beta$ process. Therefore, the fact that the vinyl chloride consists of two hydrogen isotopic isomers may be evidence in support of the proposal by Perona *et al.*[8] Figure 3 indicates that the rate ratio of $R_{\alpha\beta}/R_{\alpha\alpha}$ decreases with the increase in the temperature; behavior like this has already been described by Perona *et al.*[8] and Kim *et al.*[9] This temperature dependence can be qualitatively explained by the RRK theory.[8,11] The $R_{\alpha\beta}/R_{\alpha\alpha}$ ratio is expressed by the following equation;

$$R_{\alpha\beta}/R_{\alpha\alpha} = A_{\alpha\beta}(1-E^*_{\alpha\beta}/E)^{n-1}\{A_{\alpha\alpha}(1-E^*_{\alpha\alpha}/E)^{n-1}\}^{-1}.$$

The number of effective oscillators, n, is assumed to be the same for both eliminations, and a value of $n=12$ has been adopted.[11] The internal energy, E, was taken to vary between 85.4 kcal/mol at 298 K and 109.6 kcal/mol[12] at 1200 K. The temperature dependence is ascertained by the choice of $E^*_{\alpha\beta}=52$ kcal/mol[13] and $E^*_{\alpha\alpha}=62$ kcal/mol. The difference in the critical energies ($E^*_{\alpha\alpha}-E^*_{\alpha\beta}$) is similar to that obtained by Perona *et al.*,[8] but is somewhat larger than that for "hot" 1,1,2-trichloroethane-1-d_1.[10] A more exact study will be necessary for a quantitative discussion.

In conclusion, in the case of methane addition, the product distribution and hydrogen isotopic distributions support the Cl atom elimination in the initiation step. On the contrary, the assumption that the CCl_2 radical is formed in the initiation step does not agree

with the experimental results. If the following reactions were possible;

$$CCl_2: + CH_4 \longrightarrow CHCl_2\cdot + CH_3\cdot, \quad (21)$$

$$CCl_2: + CDCl_3 \longrightarrow CDCl_2\cdot + CCl_3\cdot, \quad (22)$$

the formation rate of C_2HCl_3 would be larger than that of C_2DCl_3, because Reaction 21 must be predominant over the Reaction 22 in the presence of excess methane. Vinyl chloride would be produced by the following reactions;

$$CHCl_2\cdot + CH_3\cdot \longrightarrow CHCl_2CH_3^* \longrightarrow CHCl{=}CH_2 + HCl, \quad (15')$$

$$CDCl_2\cdot + CH_3\cdot \longrightarrow CDCl_2CH_3^* \xrightarrow{\alpha\beta} CDCl{=}CH_2 + HCl, \quad (15)$$

$$\xrightarrow{\alpha\alpha} CHCl{=}CH_2 + DCl. \quad (16)$$

Reaction 15′ might be predominant over the others, and the yield of $CDCl{=}CH_2$ would be considerably small. These expectations are actually not in agreement with the experimental results. Further, the possibility of the insertion reaction of CCl_2 into C–H or a C–Cl bond and the successive elimination of hydrogen chloride may be considered. However, these reactions can not satisfactorily explain the variety of the products and the hydrogen isotopic distributions.

The reaction scheme based on the Cl atom elimination in the initiation step can well account for the variety of the products and their isotopic distributions. The scheme can not, however, explain the relative yields of the products without any modification. For the case of methane addition, 1,1-dichloroethylene was the main product, as is shown in Fig. 2. This can not be derived from the scheme. Under the experimental conditions, the formation rates of the C_1 radicals of $CDCl_2$, CH_3, and CCl_3 decrease in that order.[14] Therefore, the [vinyl chloride]>[1,1-dichloroethylene] relation might be expected. Perhaps this apparent contradiction can be solved by the assumption that there is another path to produced 1,1-dichloroethylene in addition to Reaction 18.

In the study of the chemical activation of CHF_2CD_3, Perona *et al.*[8] found the yield of $CF_2{=}CD_2$ to be about 1/2—1/10 of that of vinyl fluoride. They supposed a third unimolecular reaction path of "hot" CHF_2CD_3;

$$CHF_2CD_3^* \longrightarrow CF_2{=}CD_2 + HD. \quad (23)$$

Kim *et al.*[9] also found $CF_2{=}CD_2$ in a similar reaction system and confirmed the unimolecular pressure dependence of the yield. Although they did not agree with the third unimolecular path because of its unusual nature, they could not find out any evidence denying it. Perona *et al.*[8] thought that Process 23 had a larger critical energy than those of the $\alpha\beta$ and $\alpha\alpha$ processes. The importance of the third path may, then, become greater at higher temperatures. The following reaction is assumed by analogy with Reaction 23;

$$CDCl_2CH_3^* \longrightarrow CCl_2{=}CH_2 + HD. \quad (24)$$

Since Reaction 24 competes with the $\alpha\beta$ and the $\alpha\alpha$ processes, the formation rate of vinyl chloride decreases and that of 1,1-dichloroethylene increases.

Let us examine other possible paths yielding 1,1-dichloroethylene. Tschuikow-Roux *et al.*[15] found $CF_2{=}CH_2$ besides the main product $CHF{=}CH_2$ in their shock tube study of CHF_2CH_3. They suggested the following reactions for the formation of $CF_2{=}CH_2$;

$$CH_3\cdot + CH_3CHF_2 \longrightarrow CH_3CF_2\cdot + CH_4, \quad (25)$$

$$2CH_3CF_2\cdot \longrightarrow CF_2{=}CH_2 + CH_3CHF_2. \quad (26)$$

In the present case, 1,1-dichloroethylene may be produced by the following reactions analogous to Reactions 25 and 26;

$$CDCl_2\cdot \text{ (or } CH_3\cdot) + CH_3CDCl_2 \longrightarrow CH_3CCl_2\cdot + CD_2Cl_2 \text{ (or } CH_3D), \quad (27)$$

$$2CH_3CCl_2\cdot \longrightarrow CH_2{=}CCl_2 + CH_3CHCl_2. \quad (28)$$

In the present experiment, however, neither dichloroethane nor dichloromethane was found in the products. This indicates that Reactions 27 and 28 are not important for the formation of dichloroethylene. Next, let us consider the disproportionation of the $CDCl_2$ radical;

$$2CDCl_2\cdot \longrightarrow CD_2Cl_2 + CCl_2:, \quad (29)$$

$$CCl_2: + CH_3\cdot \longrightarrow CH_3CCl_2\cdot^* \longrightarrow CH_2{=}CCl_2 + H\cdot. \quad (30)$$

These reactions would produce a considerable amount of dichloromethane, which also is not compatible with the above observation. Therefore, it may be concluded that Reaction 24 is the most probable process for yielding dichloroethylene.

The author would like to express his grateful acknowledgments to Professor Kenji Kuratani, the University of Tokyo, for his encouragement and kind discussion throughout the work.

References

1) G. P. Semeluk and R. B. Bernstein, *J. Am. Chem. Soc.*, **75**, 3793 (1954); G. P. Semeluk and R. B. Bernstein, *ibid.*, **79**, 46 (1957).

2) A. E. Shilov and R. D. Sabirova, *Zh. Fiz. Khim.*, **34**, 860 (1960).

3) M. Tsuda and K. Kuratani, *Bull. Chem. Soc. Jpn.*, **41**, 53 (1968).

4) T. Yano, *Bull. Chem. Soc. Jpn.*, **46**, 1619 (1973).

5) All the chlorinated ethanes except the penta- and hexa-substituted ones were analyzed; only 1,1,2,2-tetrachloroethane was found in Series I, while 1,1,2,2-tetrachloroethane and ethyl chloride were found in Series II.

6) As can be seen from Figs. 1 and 2, the ratios among the main-product yields show little change in the range of conversion below 50%. This suggests that the same reaction mechanism is operative. When the conversions are reduced to the reaction temperatures, a wide conversion range corresponds to a very narrow temperature range, for example, a 20% conversion to less than 50 K. A change in mechanism is not likely to occur in this narrow temperature range. Therefore, the conversion may be regarded as the extent of the reaction in such a narrow temperature range.

7) In the case of the II series, dichloromethane is produced, but it seems to disappear at higher temperatures (Fig. 1). Therefore, the following secondary reactions may be supposed;

$$CHDCl_2 + \text{radical}(R\cdot) \text{ or } \text{atom}(X\cdot) \longrightarrow CDCl_2\cdot + RH \text{ or } XH,$$

$$CDCl_2\cdot + CHCl_2\cdot \longrightarrow CDCl_2CHCl_2^* \longrightarrow C_2DCl_3 + HCl.$$

8) M. J. Perona, J. T. Bryant, and G. O. Pritchard, *J. Am. Chem. Soc.*, **90**, 4782 (1968).

9) K. C. Kim, D. W. Setser, and B. E. Holmes, *J. Phys. Chem.*, **77**, 725 (1973).

10) K. C. Kim and D. W. Setser, *J. Phys. Chem.*, **76**, 283 (1972); K. C. Kim and D. W. Setser, *ibid.*, **78**, 2166 (1974).

11) S. W. Benson and G. Haugen, *J. Phys. Chem.*, **69**, 3898 (1965).

12) The change in the internal energy with the temperature was calculated from $C_v^{vib}(T-298)=3R(T-298)+[C_v^{vib}, CDCl_2(T)+C_v^{vib}, CH_3(T)]T-[C_v^{vib}, CDCl_2(298)+C_v^{vib}, CH_3(298)]298$. The same value of C_v^{vib} was assumed for $CDCl_2$ and $CHCl_2$. The vibrational contributions to the heat capacities of $CHCl_2$ and CH_3 were estimated from the heat capacities of CH_2Cl_2 and CH_3 respectively.

13) J. C. Hassler and D. W. Setser, *J. Chem. Phys.*, **45**, 3246 (1966).

14) In order to explain the greatest yield of 1,1-dichloroethylene, the change in the C_1 radical distribution due to the following hydrogen metathesis reactions are considered;

$$CDCl_2\cdot + CH_4 \longrightarrow CH_3\cdot + CHDCl_2,$$

$$CDCl_2\cdot + CDCl_3 \longrightarrow CCl_3\cdot + CD_2Cl_2.$$

However, the contributions of these reactions can be neglected for two reasons. The first is that there is no detectable amount of dichloromethane. The second is the kinetic one. Assuming the steady-state and the same recombination rate constants of the C_1 radicals, the steady-state rate is concluded to be considerably faster than that of the transformation among C_1 radicals. Thus, the disturbance of the C_1 radical distribution due to the above reactions is insignificant.

15) E. Tschuikow-Roux, W. J. Quiring, and J. M. Simmie, *J. Phys. Chem.*, **74**, 2449 (1970).

The Application of the Spin Trap, Phenyl *t*-Butyl Nitrone, to the Study of the γ-Radiolysis of Cyclohexane

Haruo IWAHASHI, Yo-ichi ISHIKAWA, Shin SATO, and Kinko KOYANO*

Department of Applied Physics, Tokyo Institute of Technology, Ookayama, Meguro-ku, Tokyo 152

**Institute of Chemistry, College of General Education, The University of Tokyo, Komaba, Meguro-ku, Tokyo 153*

(Received November 11, 1976)

It was shown that cyclohexyl radicals formed by the γ-radiolysis of cyclohexane were trapped by phenyl *t*-butyl nitrone (PBN) to give a nitroxide with a well defined ESR spectrum. We measured the yield of this nitroxide. In order to establish the radical and electron scavenging properties of PBN, we measured the effect of this compound on the yields of hydrogen and nitrogen by adding dinitrogen oxide in cyclohexane together with PBN. The results suggested that PBN is able to scavenge not only free radicals but also electrons. The following relative rates were obtained: $k(e^- + PBN \rightarrow PBN^-)/k(e^- + N_2O \rightarrow N_2O^-) = 0.7$ and $k(H + PBN \rightarrow HPBN)/k(H + C_6H_{12} \rightarrow H_2 + C_6H_{11}) \approx 200$ at room temperature. The *G*-value of the scavengeable hydrogen atoms from cyclohexane was estimated to be 3.4 ± 0.4.

The spin trapping technique has been applied to detect the short-lived free-radicals produced in various chemical reactions.[1] Since Eiben and Fessenden[2] used this technique in the study of the three primary species (e^-_{aq}, H, OH) produced in the radiolysis of water, this technique has been used in radiation chemistry, especially for the radiolysis of aqueous solutions,[3] water,[4] and alcohols.[5,6] So far, there seems to have been only one report about liquid alkanes.[7] Here, we wish to report the results obtained in the γ-radiolysis of cyclohexane using phenyl *t*-butyl nitrone (PBN) as a spin trap.

The radiolysis of cyclohexane has been studied extensively in many laboratories and it is now well known that the main radicals produced in the primary reaction are cyclohexyl radicals and hydrogen atoms. PBN as a spin trap reacts easily with free-radicals to produce relatively stable nitroxide and this nitroxide has a characteristic ESR spectrum.

$$\underset{\underset{\text{O}}{\downarrow}}{\text{PhCH=N-C(CH}_3)_3} + \text{R} \rightarrow \underset{\underset{\text{R}}{|}\ \ \underset{\text{O}}{|}}{\text{PhCH-N-C(CH}_3)_3} \qquad (1)$$

When we apply this technique to the study of the mechanism of the γ-radiolysis of liquid alkane, it is necessary to check the reactivity of PBN with free-radicals and electrons.

Experimental

PBN was prepared by the method of Emmons.[8] Cyclohexane (pure grade, Tokyo Kasei Kogyo Co.) was purified by being passed through an activated silica gel column.

For the ESR measurement, a constant volume (0.25 ml) of cyclohexane containing a certain concentration of PBN was sealed in a 4 mm i.d. Suprasil quartz tube in a mercury-free vacuum system. These samples were γ-irradiated with ^{60}Co γ-rays at a dose rate of 3.4×10^{17}—5.5×10^{18} eV g^{-1} h^{-1} at room temperature to a total dose 5×10^{15}—5×10^{17} eV g^{-1}. These samples were measured with a JEP-1 X-band ESR spectrometer with a field modulation of 100 kHz. The spin concentration was estimated by comparing integrated area of the spectrum with that of DPPH.

For the product analysis, 1 ml of cyclohexane-PBN solution was γ-irradiated. The yields of hydrogen and nitrogen were measured with a Toepler-McLeod gauge which was attached to a cuprous oxide furnace. The columns used for the gas chromatographic analysis were PEG-600: 2 m long for bicyclohexyl and dimethylsulfolane: 6 m long for cyclohexene.

Results

The γ-radiolysis of 0.1 M PBN solution in cyclohexane at room temperature gave the spectrum shown in Fig. 1. The spin adduct was quite stable at room temperature; no appreciable decay could be observed over one day. The spectrum was a triplet of doublets with $a^N \approx 14.5 \pm 0.2$ G and $a^H_\beta \approx 2.2 \pm 0.2$ G, which are characteristic to a cyclohexyl radical spin adduct. However, no hydrogen atom and electron spin adducts were detected.

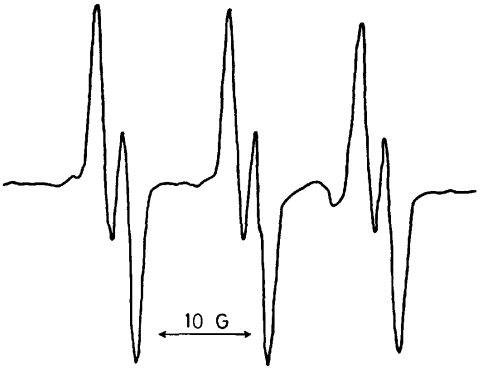

Fig. 1. A typical ESR spectrum of 0.1M PBN solution in cyclohexane after γ-radiolysis at room temperature.

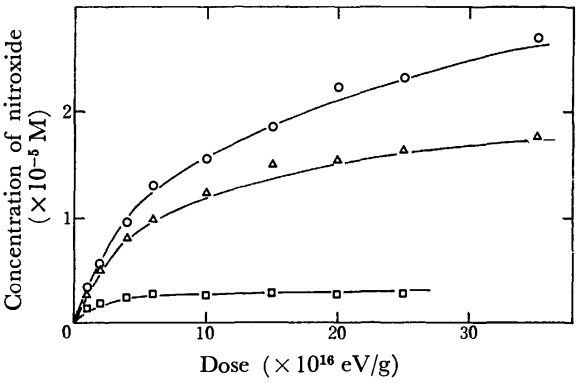

Fig. 2. The yield of nitroxide I as a function of radiation dose. PBN concentration; ○: 0.1 M, △: 0.05 M, □: 0.01 M.

Figure 2 shows the yields of the spin adduct as functions of the irradiation dose for 0.1, 0.05, and 0.01 M PBN solutions in cyclohexane. The yields are not linear with dose. This suggests that secondary reactions which destroy the spin adduct are occurring during the radiolysis. As the dose increases, the increasing rate of the yield decreases and the yield has a tendency to saturate. The saturating values are dependent on the PBN concentration.

Figure 3 shows the relation between the yield of the spin adduct and the dose rate for 0.1 M PBN solution. The yields show little dependence on the dose rate. This suggests that the reaction between two cyclohexyl radicals is not important compared with the reaction of cyclohexyl radicals with PBN to produce spin adducts.

Figure 4 shows the reciprocal of the G-value of spin adduct *vs.* the irradiation dose. Extrapolation to zero dose gives the results for the primary G-values of 3.1 ± 0.5, 2.9 ± 0.5, and 2.8 ± 0.5 respectively for 0.1, 0.05, and 0.01 M solutions.

In order to study the reaction of PBN in the radiolysis of cyclohexane, we measured the yields of several products from the γ-irradiated solutions. Figure 5 shows the yield of hydrogen. Figures 6 and 7 compare the yields of nitrogen and hydrogen respectively *vs.* the concentration of dinitrogen oxide in cyclohexane without PBN and with 0.1 M PBN. Solid lines are theoret-

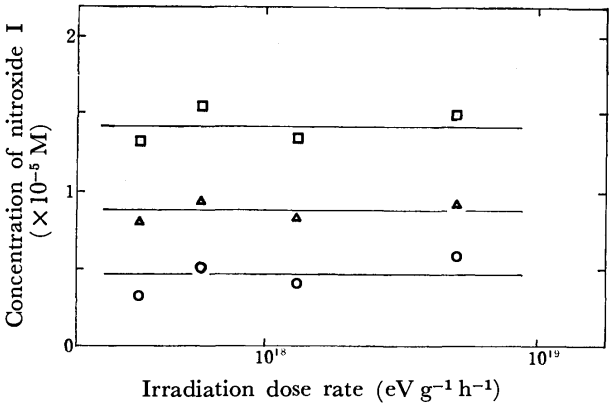

Fig. 3. The yield of nitroxide I as a function of radiation dose rate. Total dose; ○: 3.0×10^{16}, △: 5.0×10^{16}, □: 1.0×10^{17} eV g^{-1} at room temperature.

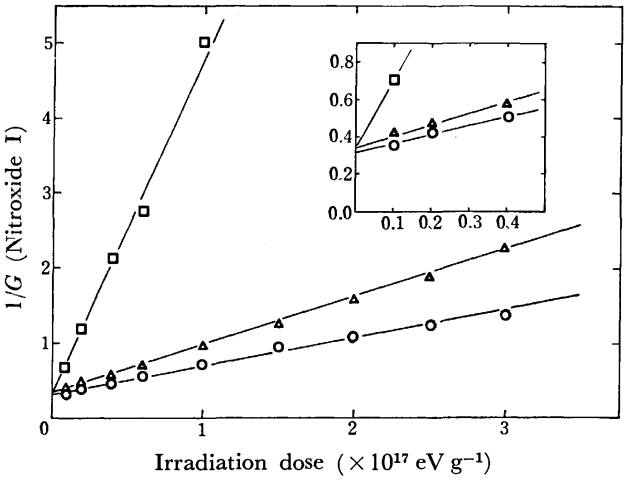

Fig. 4. The reciprocal of the G-value of nitroxide I as a function of radiation dose. PBN concentration; ○: 0.1 M, △: 0.05 M, □: 0.01 M.

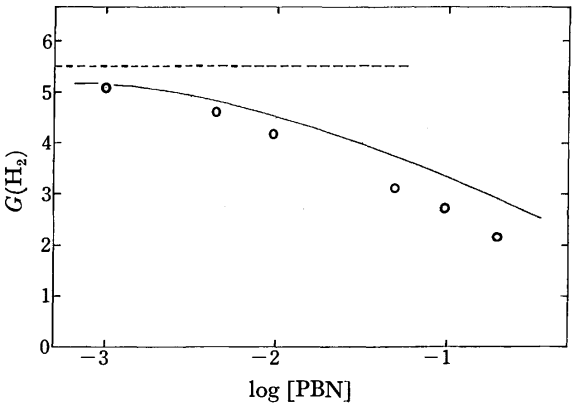

Fig. 5. The G-value of hydrogen molecule as a function of PBN concentration. The solid line is the theoretical fit (see in the text).

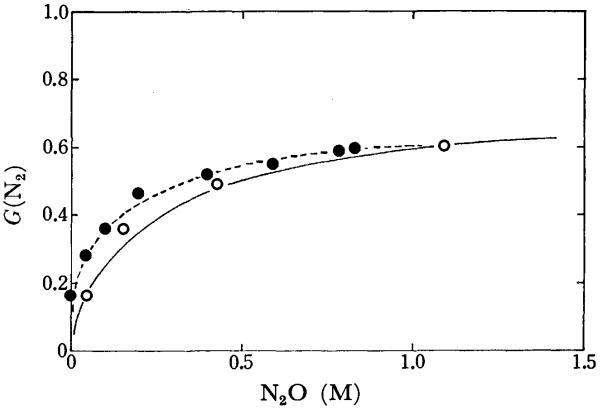

Fig. 6. The G-value of nitrogen as a function of the concentration of dinitrogen oxide. The total dose is 5.2×10^{19} eV g^{-1} at room temperature (○). The plots of cyclohexane without PBN refers to the paper of Takeuchi *et al.* (●).[13] The solid line is obtained from the relation proposed by Schuler *et al.*[11,12]

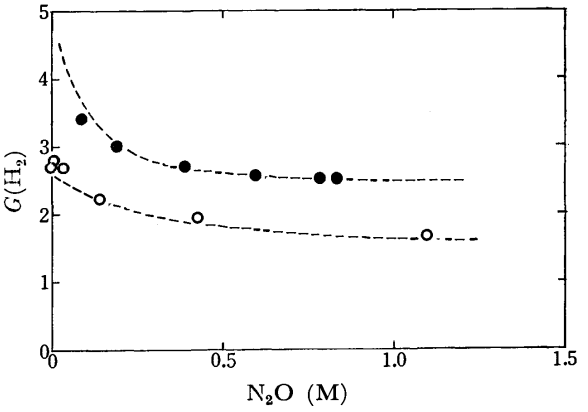

Fig. 7. The G-value of hydrogen molecule as a function of the concentration of dinitrogen oxide. The total dose is 5.2×10^{19} eV g^{-1} at room temperature (○). The plots of cyclohexane without PBN refers to the paper of Takeuchi *et al.* (●).[13]

Table 1. The effects of the radical scavengers on the G-values of products in the γ-radiolysis of cyclohexane

Radical scavenger	Total dose (eV g^{-1})	Products	
		$(c\text{-}C_6H_{11})_2$	$c\text{-}C_6H_{10}$
$C_3H_7SSC_3H_7$[17]	1.0×10^{19}	0.15	1.10
C_3H_7SH[18]	1.5×10^{19}	0.26	1.57
O_2[15]	$\geq2.5\times10^{19}$	0.29	1.49
p-Benzoquinone[15]	12.8×10^{19}	0.29	1.54
PBN (This work)	5.4×10^{19}	0.34	1.52

ical fits (see Discussion). Table 1 summarizes the yields of bicyclohexyl and cyclohexene in a γ-irradiated cyclohexane containing 0.1 M PBN together with the yields obtained by using different radical scavengers.

Discussion

The transient radicals produced in the radiolysis of cyclohexane are cyclohexane ion, electron, hydrogen atom, and cyclohexyl radical.[9] In the present experiment, the cyclohexyl radicals were identified as the nitroxide I:

$$C_6H_{11} + PBN \rightarrow (PBN)\text{-}C_6H_{11}. \qquad I \quad (2)$$

However, no other nitroxides could be observed, even though they were thought to be formed by the trapping of $C_6H_{12}^+$, e^-, and H by PBN. This does not necessarily mean that PBN does not react with them. In the study of the radiolysis of water in the presence of PBN, Sargent and Gardy suggested the existence of $(PBN)^-$.[4] On the other hand, the formation of (PBN)–H has been actually observed by ESR in the γ-radiolysis of methanol at low temperature[6] and during the radiolysis of water.[4] In the γ-radiolysis of hydrocarbon at room temperature, however, the formation of (PBN)–H has not been reported, except for the paper by Mao and Kevan.[7] Consequently, we think that nitroxides II and III are unstable and decay before the ESR measurement at room temperature:

$$e^- + PBN \rightarrow (PBN)^- \qquad II \quad (3)$$

$$H + PBN \rightarrow (PBN)\text{-}H. \qquad III \quad (4)$$

The curves shown in Fig. 2 have the same tendency as that obtained by Mao and Kevan in the γ-irradiated methanol containing PBN.[6] The nitroxide I may be attacked by cyclohexyl radicals or hydrogen atoms during the γ-irradiation:

$$(PBN)\text{-}C_6H_{11} + C_6H_{11} \rightarrow X, \qquad (5)$$

$$(PBN)\text{-}C_6H_{11} + H \rightarrow Y. \qquad (6)$$

As the concentration of PBN can be thought to change little during the γ-irradiation, the rate of formation of nitroxide I may be constant (Reaction 2). If this nitroxide I is consumed by the secondary reactions 5 and 6, we can derive the following relation for the steady-state treatment:

$$[(PBN)\text{-}C_6H_{11}] = A[PBN](1-\exp(-Bt)). \qquad (I)$$

Here, A stands for $k_2[C_6H_{11}]/(k_5[C_6H_{11}]+k_6[H])$ and B for $k_5[C_6H_{11}]+k_6[H]$. This relation can explain qualitatively the experimental result that saturating values are proportional to the concentration of PBN.

The hydrogen producing process in the γ-radiolysis of cyclohexane may be described as follows:

$$C_6H_{12} \sim\!\!\!\!\rightarrow C_6H_{12}^+ + e^- \rightarrow C_6H_{11} + H, \qquad (7)$$

$$\rightarrow C_6H_{10} + H_2, \qquad (8)$$

$$\rightarrow (C_6H_{11})_2 + H_2, \qquad (9)$$

$$\sim\!\!\!\!\rightarrow C_6H_{12}^* \rightarrow C_6H_{11} + H, \qquad (10)$$

$$\rightarrow C_6H_{10} + H_2, \qquad (11)$$

$$\rightarrow (C_6H_{11})_2 + H_2, \qquad (12)$$

$$H + C_6H_{12} \rightarrow H_2 + C_6H_{11}. \qquad (13)$$

Reactions 9 and 12 explain the formation of bicyclohexyl which is not suppressed by the presence of radical scavenger (Table 1). There are two processes in which PBN disturbs the formation of hydrogen: one is the capture of electrons produced in Reaction 7 and the other is the capture of hydrogen atoms produced in Reactions 7 and 10.

In order to determine the ability of PBN to capture electrons, we measured the yield of nitrogen from the 0.1 M PBN solution in the presence of dinitrogen oxide, which is a well known electron scavenger:[10]

$$e^- + N_2O \rightarrow N_2O^- \rightarrow \delta N_2. \qquad (14)$$

$$(1\leq\delta\leq2)$$

Figure 6 shows the results. Obviously, the yield of nitrogen was decreased by the presence of PBN. Schuler *et al.*[11,12] proposed an analytical treatment for the radiolysis system in which two electron scavengers are present. Using their technique, we estimated that $k_3=1.7\times10^{12}$ M^{-1} s^{-1}. Here, we assumed $k_{14}=2.4\times10^{12}$ M^{-1} s^{-1}.[13]

With k_3 estimated, we can calculate the G-value of hydrogen in the presence of PBN, if PBN does not scavenge hydrogen atoms. The calculated result is shown in Fig. 5 as the solid line. The difference between the solid line and the experimental plots must be due to the hydrogen-atom-scavenging by PBN.

The decrease in the G-value of hydrogen, $\Delta G(H_2)$, can easily be derived from the steady-state treatment of Reactions 4 and 7—13:

$$\Delta G(H_2) = \Delta G(H_2)_r + \Delta G(H_2)_i,$$

$$= G_0(H) - \frac{k_{13}[C_6H_{12}]}{k_4[PBN]}\Delta G(H_2)_r. \qquad (II)$$

Here, $G_0(H)$ stands for the G-value of hydrogen atoms in the γ-radiolysis of pure cyclohexane, $\Delta G(H_2)_i$ for the decrease of hydrogen due to the electron scavenging by PBN, and $\Delta G(H_2)_r$ for the decrease due to the hydrogen-atom-scavenging by PBN. $\Delta G(H_2)_i$ can be calculated with the value of k_3, while $\Delta G(H_2)_r$ can be estimated from the experimental data. Figure 8 shows the plots between $\Delta G(H_2)$ and $\Delta G(H_2)_r/[PBN]$. From this linear relationship, we can estimate the following values: $G_0(H)=3.4\pm0.4$ and $k_{13}/k_4=(6.0\pm0.6)\times10^{-3}$.

The decrease in the G-value of hydrogen in the presence of dinitrogen oxide together with PBN is shown in Fig. 7. The difference between the G-value with PBN and without PBN must be due to the hydrogen-atom-scavenging by PBN.

The effect of PBN on the yields of bicyclohexyl and cyclohexene is shown in Table 1, together with some

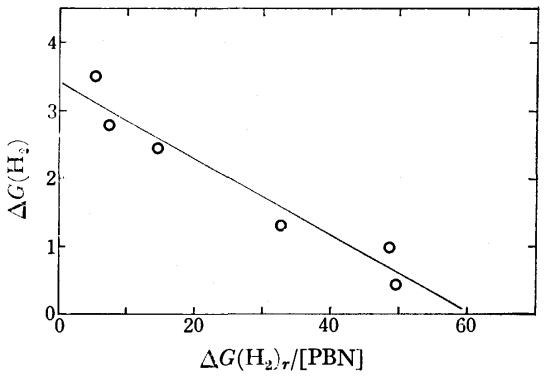

Fig. 8. The decrease in the G-value of hydrogen molecule as a function of $\Delta G(H_2)_r$/[PBN]. (Relation (II))

past data of radical scavengers. There is little difference between them, except in the case of di-*n*-propyl disulfide. It can thus be understood that PBN is one of the good radical scavengers.

Cyclohexane is probably the most popular hydrocarbon for the study of radiolysis. In spite of a large number of investigations, however, the quantitative assessment of the yields of the products from the radiolysis of cyclohexane such as the G-values of electrons, hydrogen atoms, and cyclohexyl radicals have not been settled yet. Only the G-value of hydrogen molecules seems to have reached a final assessment: $G(H_2)=5.7\pm0.2$.[14,15] For the G-value of electrons two values are proposed: One is about 4.0,[11] the other is around 5.2.[16] Both values were estimated by extrapolation to the infinite concentration of radical scavenger on the assumption of a certain reaction mechanism. The discrepancy between the two values is obviously beyond the experimental error. This difference is strongly connected to the fundamental interpretation of the radiolysis of hydrocarbons.

In the present study, we have estimated the G-value of hydrogen atoms. So far, this value has been estimated from the effect of the radical scavenger on the G-value of the hydrogen molecules produced; however, as is well known, the reaction of each radical scavenger is not clear cut. As has been stated above, the reaction of the spin trap, PBN, is also not clear cut; moreover, the spin adducts produced are not stable for reactive species. This fact complicates the analysis. Consequently, we regretfully have to say that the utilization of the spin trap for the quantitative estimation of the products in the radiolysis of hydrocarbons is not a very good technique.

References

1) a) E. G. Janzen and B. J. Blackburn, *J. Am. Chem. Soc.*, **90**, 5909 (1968); b) E. G. Janzen and J. L. Gerlock, *Nature (London)*, **222**, 867 (1969); c) E. G. Janzen and B. J. Blackburn, *J. Am. Chem. Soc.*, **91**, 4481 (1969); d) E. G. Janzen and J. L. Gerlock, *ibid.*, **91**, 3108 (1969); e) C. Lagercrantz, *J. Phys. Chem.*, **75**, 3466 (1971); f) E. G. Janzen, D. E. Nutter, Jr., and C. A. Evans, *ibid.*, **79**, 1983 (1975).

2) K. Eiben and R. W. Fessenden, *J. Phys. Chem.*, **72**, 3387 (1968).

3) D. Behar and R. W. Fessenden, *J. Phys. Chem.*, **76**, 1710 (1972).

4) F. P. Sargent and E. M. Gardy, *Can. J. Chem.*, **54**, 275 (1976).

5) a) J. A. Wargon and F. Williams, *J. Am. Chem. Soc.*, **94**, 7917 (1972); b) F. P. Sargent, E. M. Gardy, and H. R. Falle, *ibid.*, **24**, 120 (1974); c) F. P. Sargent and E. M. Gardy, *Can. J. Chem.*, **52**, 3645 (1974); e) F. P. Sargent and E. M. Gardy, *ibid.*, **53**, 3128 (1975).

6) S. W. Mao and L. Kevan, *Chem. Phys. Lett.*, **24**, 505 (1974).

7) S. W. Mao and L. Kevan, *J. Phys. Chem.*, **78**, 91 (1974).

8) W. D. Emmons, *J. Am. Chem. Soc.*, **79**, 5739 (1957).

9) J. W. T. Spinks and R. J. Woods, "An Introduction to Radiation Chemistry," John Wiley & Sons Inc., New York (1964), p. 319.

10) a) G. Scholes and M. Simić, *Nature (London)*, **202**, 895 (1964); b) S. Sato, R. Yugeta, K. Shinsaka, and T. Terao, *Bull. Chem. Soc. Jpn.*, **39**, 156 (1966).

11) a) P. P. Infelta and R. H. Schuler, *J. Phys. Chem.*, **76**, 987 (1972); b) G. W. Klein and R. H. Schuler, *ibid.*, **77**, 978 (1973).

12) P. P. Infelta and R. H. Schuler, *Int. J. Radiat. Phys. Chem.*, **5**, 41 (1973).

13) K. Takeuchi, K. Shinsaka, S. Takao, Y. Hatano, and S. Shida, *Bull. Chem. Soc. Jpn.*, **44**, 2004 (1971).

14) a) P. J. Dyne and J. A. Stone, *Can. J. Chem.*, **39**, 2381 (1961); b) K. M. Bansal and R. H. Schuler, *ibid.*, **74**, 3924 (1970).

15) S. K. Ho and G. R. Freeman, *J. Phys. Chem.*, **68**, 2189 (1964).

16) T. E. M. Sambrook and G. R. Freeman, *J. Phys. Chem.*, **78**, 32 (1974).

17) J. A. Stone and J. Esser, *Can. J. Chem.*, **52**, 1253 (1974).

18) J. Esser and J. A. Stone, *Can. J. Chem.*, **51**, 192 (1973).

Dichroism and Configuration Analysis of 2-Ethylthio-1,3-Diazaazulene

Hiroshi HIRATSUKA, Yoshie TANIZAKI, and Toshihiko HOSHI*

Department of Chemistry, Tokyo Institute of Technology, Meguro-ku, Tokyo 152

**Department of Chemistry, Aoyama Gakuin University, Setagaya-ku, Tokyo 157*

(Received November 19, 1976)

Electronic absorption spectrum of 2-ethylthio-1,3-diazaazulene (ESDA) is investigated by means of dichroism analysis using the stretched PVA film. Seven π-π^* bands and an allowed n-π^* band are assigned. The experimental assignment of π-π^* bands is in good agreement with the theoretical result using the PPP calculation. The effect of substituent groups on 1,3-diazaazulene (DA) is discussed by making use of a correlation diagram of SCF MO's of ESDA, 2-ethoxy-1,3-diazaazulene (EODA), DA, and the substituent groups. Configuration analysis of wave functions for ESDA and EODA is carried out, and the substituent effects of the ethylthio and ethoxyl groups are compared. The result shows that the ethylthio group perturbs the electronic structure of DA more strongly than the ethoxyl group.

To date we have investigated the electronic spectra, including n-π^* transition bands, of 1,3-diazaazulene (abbreviation, DA) and its derivatives, such as 2-ethoxy-1,3-diazaazulene (EODA).[1-3] We have determined that they have five π-π^* transition bands above 220 nm, which are correspondent to each other concerning the transition direction, the position, and the relative intensity. These bands also correspond in nature to the respective ones of azulene. The only difference is that all bands of DA (and EODA) are at shorter wavelengths than the corresponding bands of azulene.

In this series of study on the 1,3-diazaazulenes, we expected that 2-ethylthio-1,3-diazaazulene (ESDA) would also reveal a spectrum similar to EODA, but found that the ESDA spectrum does not always correspond to those of EODA and DA. This fact has already been noticed by Nozoe *et al.*;[4] they have pointed out that the absorption spectrum of 2-methylthio-1,3-diazaazulene as well as that of the 2-dimethylamino derivative does not resemble that of DA. The only difference in the chemical structure between EODA and ESDA is in the substituent group: ethoxyl and ethylthio. For that reason, their spectral characteristics must be attributed to the difference of the substituent effect between the ethoxyl and the ethylthio groups.

We will first analyze the absorption spectrum of ESDA theoretically and experimentally. Then, in order to clarify the distinction between the ethylthio and the ethoxyl groups for the substituent effect on the MO levels of DA, we will examine the correlation diagram of their MO levels, and also analyze the state wave functions of ESDA and EODA by means of the configuration analysis proposed by Baba *et al.*[5]

Experimental and Calculation

2-Ethylthio-1,3-diazaazulene (ESDA) was provided by the Sankyo Company Ltd. It was recrystallized from cyclohexane solution. The analytical values in percent were as follows:

Found: C, 63.28; H, 5.50; N, 14.80; S, 17.00%. Calcd for $C_{10}H_{10}N_2S$: C, 63.15; H, 5.30; N, 14.73; S, 16.72%.

The measurement of the solution spectrum was carried out by using a Shimadzu MPS-50L recording spectrophotometer. The details of measurement and analysis of the dichroic spectra are given in the previous paper.[1,3] In the figure of the dichroic spectra, $D_{/\!/}$ and $D_{\perp}$ indicate the absorbance for the plane polarized light whose electric vector is respectively parallel (//) and perpendicular ($\perp$) to the stretched direction of the film. The dichroic ratio R_d is defined as $D_{/\!/}/D_{\perp}$. R_s is the stretching ratio of the film.

We followed the Pariser-Parr-Pople method modified by the Nishimoto-Mataga approximation[6] including CI. The CI caluculation was limited to all the singly excited configurations. The one-center Coulomb repulsion integral was set equal to the valence state ionization potential (I_p) minus the valence state electron affinity (E_a) after Pariser and Parr.[7] The two-center repulsion was estimated by the Nishimoto-Mataga formula.[6] The core resonance integral ($\beta_{\mu\nu}$) was constant. Parameters used are listed in Table 1.

TABLE 1. PARAMETER VALUES USED

	C	S	N	O
Ionization potential (eV)	11.16	22.2	14.12	33.00
Electron affinity (eV)	0.03	9.15	1.78	11.47
	C-C	C-S	C-N	C-O
Core resonance integral (eV)	−2.32	−1.16	−2.38	−2.30

The molecular geometry of the diazaazulene skeleton used was the same as before.[2] The bond lengths of carbon-carbon and carbon-nitrogen were taken as 1.40Å, and those of carbon-oxygen and carbon-sulfur as 1.37Å and 1.70Å, respectively.

Assignment

The calculated result for ESDA is given in Table 2 and is compared with the absorption spectrum determined in cyclohexane solution in Fig. 1. It has already been shown that both 1,3-diazaazulene (DA) and 2-ethoxy-1,3-diazaazulene (EODA) have five electronic transitions (bands) in the region below 50000 cm^{-1}.[1] In the case of ESDA, however, eight transitions are computed in the same region.

From the comparison of the calculated result and the observed spectrum shown in Fig. 1, the following assignment is obtained. The shoulder in the region of 23000—25000 cm^{-1} corresponds to the first π-π^* transition (Y-polarization), the intense band with the double peak in the region of 26000—30000 cm^{-1} to the second transition (X), and the two peaks in 30000—34000 cm^{-1} to the third transition (Y). The intense bands at about 37000 and 41000 cm^{-1} are respectively correspondent to the fourth (X) and the sixth (X) transitions. An absorp-

Table 2. Calculated results and assignment for 2-ethylthio-1,3-diazaazulene (ESDA)

Number of Transition	Transition energy		Oscillator strength		Polarization[d]	
	calcd	obsd[a]	calcd	obsd[c]	calcd	obsd[e]
1	22480 cm^{-1} (445 nm)	23800 cm^{-1} [b] (420 nm)	0.007	0.001	Y	Y
2	26660 (375)	26500 (378)	0.323	0.267	X	X
3	31890 (314)	31500 (318)	0.154	0.099	Y	Y
4	35020 (286)	36630 (273)	0.279	0.263	X	X
5	40090 (249)		0.002		Y	Y
6	40900 (245)	41320 (242)	1.187	0.387	X	X
7	47030 (213)		0.565		Y	Y
8	48760 (205)		0.004		X	

a) Observed in cyclohexane solution. b) Shoulder. c) Estimated by the following equation using the component spectra obtained in the dichroism analysis: $f=4.32\times10^{-9}\times\varepsilon_{max}\times(\Delta\nu)_{1/2}$, where $(\Delta\nu)_{1/2}$ is the half value width in cm^{-1} units and for the extinction coefficient, ε_{max}, the value in ethanol is used instead of that in PVA film. Band shapes of IV and VI are determined by the optional way. d) X and Y are molecular long and short axes, respectively. e) Results of dichroism analysis using a stretched PVA film.

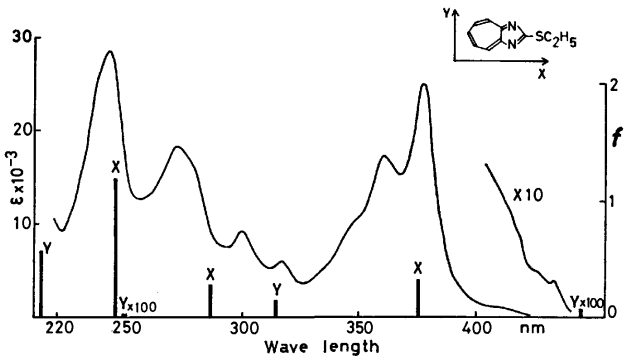

Fig. 1. Absorption spectrum of 2-ethylthio-1,3-diazaazulene (ESDA) in cyclohexane solution and the calculated result.

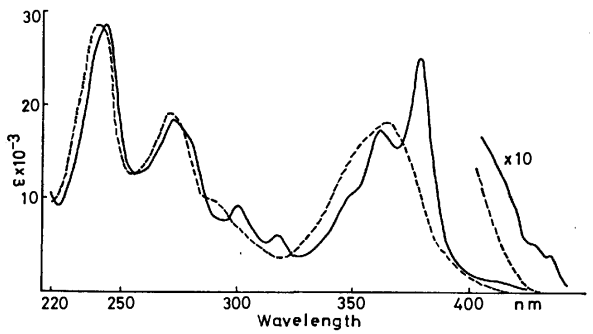

Fig. 2. Absorption spectra of 2-ethylthio-1,3-diazaazulene (ESDA) in cyclohexane (——) and ethanol solution (---).

tion band due to the fifth transition (Y) which is computed to be of very low intensity (see Table 2) should be hidden in the intense band which has been attributed to the sixth transition. The assignment thus deduced is tabulated in Table 2.

Figure 2 illustrates a solvent effect on the absorption spectrum of ESDA. The spectrum in ethanol solution loses its structure and undergoes a blue shift in comparison with that in cyclohexane solution. A similar situation is also observed for the spectrum in PVA film.

As above, we could characterize the absorption bands from the point of view of transition energy and intensity. However, in order to accomplish the assignment, it is desirable to examine the polarizations of the bands.

Dichroism Analysis

Since the symmetry of the π electron system of the ESDA molecule belongs to the point group C_{2v}, the possible π-π^* transitions must be along the long (X) or the short axis (Y) in the molecular plane. According to the dichroism-measurement using stretched PVA film, this is simply decided by the fact that the dichroic ratio ($R_d=D_{//}/D_{\perp}$) of a band polarized along the long axis of the molecule is larger than that along the short axis, because the orientation of the molecule by stretching is preferential in its longitudinal direction. Concerning the band polarizations in the quantitative sense, the dichroism analysis can provide the orientation angles of bands: the angles between an orientation axis of a molecule and the transition moments of bands. Since an orientation axis of a molecule must be a common axis to all the band polarizations which will determine orientation angles, the angle between any two band polarizations can be obtained by taking the sum or difference of the two experimental orientation angles, provided that the orientation axis and the two polarizations are in the same plane. In this case, when the two bands are both due to the transitions to the pure

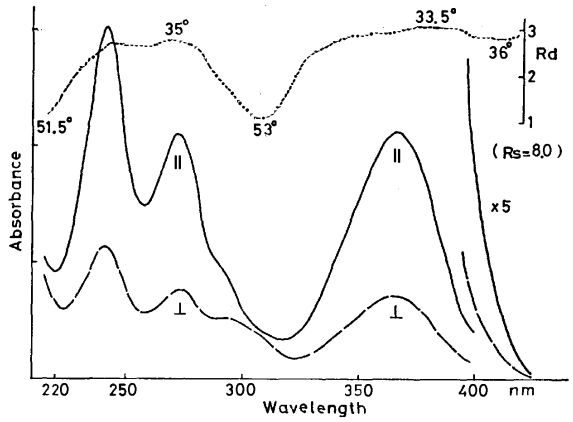

Fig. 3. Dichroic spectra and R_d curve of 2-ethylthio-1,3-diazaazulene (ESDA). R_s=8.0.

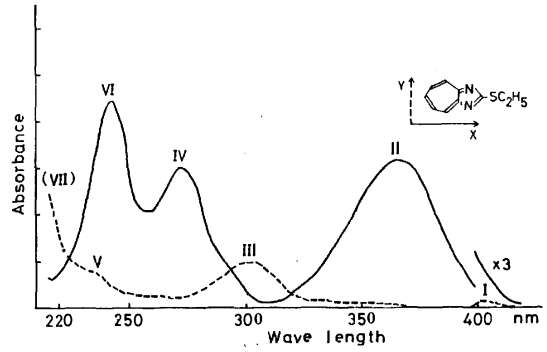

Fig. 4. Component spectra of 2-ethylthio-1,3-diazaazulene (ESDA). X(——) and Y(---) mean the components whose polarizations are along the molecular long and short axes, respectively.

electronic excited states, the sum of the orientation angles must be equal to 90° or the difference to 0° according to whether two band polarizations are orthogonal or parallel to each other, respectively. But it is rarely the case that the orthogonal-parallel relation is rigorously obtained under actual conditions, because there is often some mixing of other kinds of transitions and overlapping of other kinds of absorption bands with the band under consideration.

Figure 3 shows the dichroic spectra of ESDA in the stretched PVA film. The figures indicated along the R_d curve represent the orientation angles of the bands at the respective wavelengths. According to Fig. 3, the absorption band in the region 330—420 nm seems to be a single band. However, the R_d curve for the absorption above 400 nm falls slightly, indicating that a weak absorption is hidden. The presence of this weak absorption (the first band) is obvious from the absorption below 25000 cm^{-1} in Fig. 1.

The R_d value at 380 nm of the second band is the highest in the whole region observed (Fig. 3). It can be said, therefore, that the polarization of the second band is along the molecular long axis (X) and the first band which is hidden in the long wavelength tail of the second band must be polarized to the short axis (Y). The polarizations of other bands can be qualitatively discussed in the same way.

Incidentally, it should be noticed that the R_d curve is somewhat depressed (260 nm) between the strong fourth and sixth bands of X-polarization. This suggests the presence of a weak (fifth) band with Y-polarization.

In order to discuss in detail the polarization, in the next section, we will resolve the spectrum into the X- and Y-components.

Component Spectra of ESDA. The absorption spectrum of ESDA determined in a non-stretched PVA film could be decomposed into X- and Y-component spectra[1] using the R_d value in Fig. 3, assuming that the absorption at 380 nm, which shows the highest R_d value, has the pure X-polarization. The result is shown in Fig. 4.

From a comparison of the component spectra in Fig. 4 and the calculated results in Table 2, the absorption spectrum of ESDA in the PVA film is characterized in the following way. The second, fourth, and sixth bands which are polarized along the long axis (X) of the molecule can be attributed respecitvely to the second, fourth, and sixth transitions with X-polarizations. In addition, the observed bands and the calculated transitions correspond well to one another with respect to the relative intensities as well as the transition energies. Concerning the Y-component spectrum, the first, third, fifth, and seventh bands can be attributed to the first, third, fifth, and seventh transitions, respectively. In this assignment, however, the calculated oscillator strength of the fifth transition (Table 2) seems to be extremely small compared with the observed intensity of the fifth band (Fig. 4). Furthermore, the component spectra of Fig. 4 show that the shoulder due to the fifth band (Y) is at a shorter wavelength than the maximum of the sixth band (X). Therefore, the numbering of the order of the fifth (Y) and sixth (X) transitions by calculation must be reversed.

An extra weak absorption appears in the Y-component spectrum of Fig. 4, which extends from 320 to 365 nm. This is also suggested by the behavior of the R_d curve in Fig. 3, that is, the R_d curve shows some depression in that region. This extra band may be assigned to the forbidden character of the second π-π^* transition band and/or n-π^* transition band. However, since similar extra bands have been found in the Y-component spectrum of DA (1,3-diazaazulene) and EODA (2-ethoxy-1,3-diazaazulene) and have reasonably been assigned to allowed n-π^* transition bands polarized normal to the molecular plane (Z axis),[1] we may take the latter assignment here. (In the dichroism analysis, it must be noted that the Z- and Y-components cannot be distinguished from each other.[1,3])

Substituent Effect

Correlation Diagram of Molecular Orbitals. It has already been pointed out that the absorption spectrum of ESDA does not resemble that of DA, while that of EODA does.[4] That is to say, while all the bands observed for EODA keep the one-to-one correspondence to those of DA, in the case of ESDA, there appears an extra fourth and fifth band. The reason is to be

found in the difference of the substituent effect of the ethoxyl and ethylthio groups. In such a case, we can explain the substituent effect from the point of view of a one-electron molecular orbital. This is carried out by expanding the j-th SCF MO wave function ψ_j of EODA (or ESDA) into the SCF MO wave functions ψ°'s of DA and the ethoxyl (or ethylthio) group. Thus we have

$$\psi_j(\text{EODA}) = \sum_m C_m^j \psi_m^\circ(\text{DA}) + C_\circ^j \psi_\circ^\circ(\text{O}) . \quad (1)$$

Using the expansion coefficients, we can make a correlation among the SCF MO wave functions of EODA (or ESDA), DA, and the substituent. A correlation diagram of energy levels is shown in Fig. 5. The diagram consists of five sets of levels: from left to right, the energy levels for the MO's of substituent sulfur (S), ESDA, DA, EODA, and substituent oxygen (O). The levels are drawn by full and dotted lines which represent the symmetry species a_2 and b_1, respectively. For both ESDA and EODA, the occupied orbitals consist of four b_1 and two a_2 orbitals. DA has three b_1 and two a_2 occupied orbitals and three b_1 and two a_2 unoccupied ones. The substituents S and O have only one occupied orbital of b_1 symmetry, to which the substituents belong in the molecules.

Now, as is known from the symmetry consideration in the case of ESDA, for instance, the orbital of S cannot couple with a_2 type orbitals but only with b_1 type orbitals of DA. Actually, all four full lines (a_2) of ESDA or EODA keep nearly the same levels as the corresponding ones of DA. Furthermore, from the comparison of the unoccupied orbitals of ESDA (or EODA) and those of DA, it is recognized that even the b_1 orbitals are not perturbed by the substituent orbital. For that reason, in the correlation diagram, we can restrict the discussion to the relation between the substituent orbital and the occupied b_1 orbitals of DA.

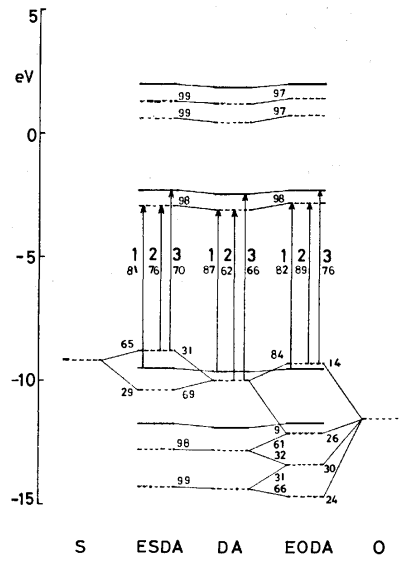

Fig. 5. Correlation diagram for SCF MO. From left to right, SCF MO's for sulfur, ESDA (2-ethylthio-1,3-diazaazulene), DA (1,3-diazaazulene), EODA (2-ethoxy-1,3-diazaazulene) and oxygen are arranged. a_2 and b_1 type SCF MO's are represented by the horizontal full and dotted lines, respectively. The figures along the joining fine lines are contribution weight from the MO's of sulfur, DA, oxygen to the MO's of ESDA and EODA. Each transition, being numbered by Roman numerals along the vertical arrow, is represented by the configuration which contains the two MO's connected with arrow and whose contribution weight is shown as the figure beneath the transition number.

The figures indicated on the correlation lines of Fig. 5 show the square values of the coefficients of Eq. 1 and represent the extent of the contribution from each of the wave functions. The highest occupied b_1 MO of ESDA, for instance, receives contributions of 65% and 31% from the MO of substituent S and the highest occupied b_1 MO of DA, respectively.

As the correlation diagram shows, the orbital of substituent S lies at around the highest occupied b_1 MO of DA, while the MO level of substituent O is much lower than that of the DA orbital. Consequently, the S MO couples strongly with the highest b_1 MO of DA to make two b_1 MO's of ESDA, while the O MO in EODA interacts more or less with all the occupied b_1 MO's of DA, but its interaction with the highest b_1 MO is especially weak (14%). This difference in the extent of interactions of the S and O orbitals with the DA orbitals could produce such differences in the spectra of ESDA and EODA as were described before; in comparison with the spectrum of DA, an extra band (either fourth or fifth band) is found in that of ESDA.

CA for Wave Functions of ESDA and EODA. The substituent effect can also be discussed from a point of view of CA (configuration analysis).[5] Making use of the CA method, any of the state wave functions of EODA or ESDA can be explained in terms of the wave functions of DA and the charge-transfer configurations which represent transitions from the π-orbital of the substituent to unoccupied molecular orbitals of DA. In short, we can write down the i-th state wavefunction Ψ_i (EODA) or Ψ_i (ESDA) by the reference configurations Ψ°'s as follows:

$$\Psi_i(\text{EODA}) = \sum_k C_k^i \Psi_k^\circ(\text{DA}) + \sum_l C_l^i \Psi_{\text{CT}l}^\circ , \quad (2)$$

where Ψ_k°(DA) stands for the k-th wave functions of DA and $\Psi_{\text{CT}l}^\circ$ stands for the l-th charge transfer configuration (electron excitation to the l-th molecular orbital of DA from the orbital of the subsituent).

By squaring the coefficients C_k^i and $C_{\text{CT}l}^i$, we can obtain the relative contribution of the respective configurations Ψ_k° and $\Psi_{\text{CT}l}^\circ$ to the state wave function Ψ_i (EODA) or Ψ_i (ESDA). The difference of the substituent effect of the ethoxyl and ethylthio groups can therefore be estimated by comparing the absolute values of $C_{\text{CT}l}^i$ of Ψ_i (EODA) and Ψ_i (ESDA).

Figure 6 shows the results of CA. The square values of the expansion coefficients are represented by circles which are drawn in such a way that their areas are proportional to the square values. Circles of values below 1% are omitted in Fig. 6. State wave functions (Ψ_i) are put on the tops of the columns and the reference configurations (Ψ_k°, $\Psi_{\text{CT}l}^\circ$) are arranged in the left column. Total weights are listed at the bottom of the columns.

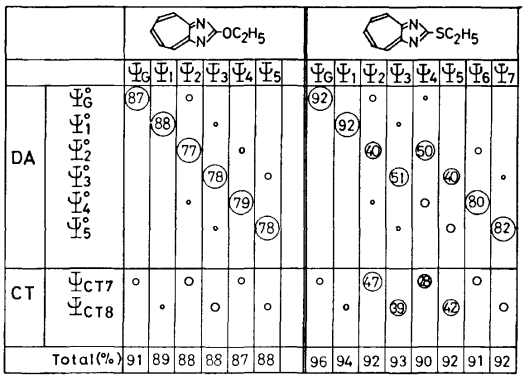

Fig. 6. The result of Configuration Analysis (CA). Top of each column is the state wave function of EODA and ESDA. Left hand side of each row is the reference configuration.

Since the total weight of the respective columns is nearly 90%, we may safely discuss the substituent effect without taking into account other wave functions such as doubly excited configurations. We can read any column in accordance with Eq. 2; for example, the ground (Ψ_G) and the first excited (Ψ_1) state wave functions of ESDA are as follows:

$$\Psi_G(\text{ESDA}) = (0.923)^{1/2}\Psi_G^\circ(\text{DA}) + \cdots + (0.033)^{1/2}\Psi_{CT7}^\circ , \quad (3)$$

$$\Psi_1(\text{ESDA}) = (0.917)^{1/2}\Psi_1^\circ(\text{DA}) + \cdots - (0.020)^{1/2}\Psi_{CT8}^\circ , \quad (4)$$

where Ψ_G° (DA) and Ψ_1° (DA) are the wave functions of the ground and first excited configurations of DA, respectively, and Ψ_{CT7}° and Ψ_{CT8}° mean respectively the transitions to the uncocupied DA orbitals 7th and 8th from the substituent orbital. In Eqs. 3 and 4, the absolute values of the coefficients of Ψ_G° (DA) and Ψ_1° (DA) are the largest and all the other coefficients are small enough to be neglected. In the first approximation, therefore, we can correlate Ψ_G (ESDA) and Ψ_1 (ESDA) to Ψ_G° (DA) and Ψ_1° (DA), respectively.

Any wave functions for ESDA and EODA in Fig. 6 can be read in the same manner as above. As shown in Fig. 6, all wave functions from Ψ_G to Ψ_5 of EODA are approximately equivalent to those from Ψ_G° to Ψ_5° of DA, respectively. As for ESDA, however, there is no one-to-one correspondence except for the pairs of Ψ_G–Ψ_G° and Ψ_1–Ψ_1°. In fact, all four wave functions, Ψ_2 to Ψ_5, of ESDA involve two kinds of predominant configurations: localized and charge transfer ones. Conversely, Ψ_2° of DA are distributed to Ψ_2 and Ψ_4 of ESDA, and Ψ_3° (DA) to Ψ_3 (ESDA) and Ψ_5 (ESDA). Therefore, the wave functions Ψ_2 to Ψ_5 of ESDA cannot be correlated by a one-to-one correspondence to Ψ_2° or Ψ_3° of DA. However, Ψ_6 and Ψ_7 of ESDA correspond well to Ψ_4° and Ψ_5° of DA.

From the above discussion, we can conclude as follows. The five transition bands of EODA correspond to each of the respective five bands of DA. Direct correspondence of the transition bands of ESDA and EODA exists between both of the first bands, between the sixth (ESDA) and fourth (EODA) bands and between the seventh (ESDA) and fifth (EODA) bands. But the second, third, fourth, and fifth bands of ESDA do not correspond directly to any single transition band of EODA.

The authors are greatly indebted to Dr. H. Negoro, Dr. G. Sunagawa, Dr. N. Soma, and Dr. H. Nakao of the Sankyo Company Ltd., for providing the sample.

References

1) H. Hiratsuka, Y. Tanizaki, and T. Hoshi, *Spectrochim. Acta, Part A*, **28**, 2375 (1972).
2) Y. Tanizaki, H. Hiratsuka, and T. Hoshi, *Bull. Chem. Soc. Jpn.*, **43**, 2283 (1970).
3) Y. Tanizaki, H. Hiratsuka, and T. Hoshi, *Spectrochim. Acta, Part A*, **28**, 2367 (1972).
4) T. Nozoe, T. Mukai, and I. Murata, *Proc. Jpn. Acad.*, **30**, 482 (1954).
5) H. Baba, S. Suzuki, and T. Takemura, *J. Chem. Phys.*, **50**, 2078 (1969).
6) K. Nishimoto and N. Mataga, *Z. Phys. Chem. (Frankfurt)*, **13**, 140 (1957).
7) R. Pariser and G. R. Parr, *J. Chem. Phys.*, **21**, 466, 767 (1953).

Vibrational Spectra and Normal Coordinate Calculations for Trimethylarsine–Borane

Fumio WATARI

Department of Applied Science, Faculty of Engineering, Tohoku University, Sendai 980

(Received November 19, 1976)

Studies were carried out on the infrared spectra (33—4000 cm^{-1}) of eight isotopic trimethylarsine–boranes, $(CH_3)_3AsBH_3$, $(CH_3)_3As^{10}BH_3$, $(CH_3)_3AsBD_3$, $(CH_3)_3As^{10}BD_3$, $(CD_3)_3AsBH_3$, $(CD_3)_3As^{10}BH_3$, $(CD_3)_3AsBD_3$, and $(CD_3)_3As^{10}BD_3$, in the solid state at low temperature, and on the Raman spectra (0—4000 cm^{-1}) in the solid state and in solution of dichloromethane at room temperature. The spectra were interpreted on the basis of C_{3v} molecular symmetry, complete assignments for all fundamentals except the internal torsion being made. Normal coordinate calculations were carried out utilizing a symmetry force field in order to confirm the assignments. One of the methyl rocks was found to be mixed with the borane rock, making the assignments of these frequencies complicated. The As–B and As–C force constants were found to have the values 1.849 and 3.087 mdyn/Å, respectively.

Group IIIb and Group Vb compounds form the so-called Lewis acid–base complexes. Reactions of diborane with several trialkyls of Group Vb elements and properties of the complexes were discussed by Hewitt and Holiday.[1] As regards phosphorus–boron and arsenic–boron bonding, Burg and Wagner,[2] and Stone and Burg[3] reported the preparation and properties of several phosphine–boranes and arsine–boranes. The arsine-borane compounds are less stable than the corresponding phosphine–boranes. Trimethylarsine–borane is slightly sensitive to water vapor, but stable at room temperature when kept in a vacuum or an inert gas atmosphere.

In studing these electron donor-acceptor complexes, the properties of the donor-acceptor bonds are of interest. Durig *et al.*[4] reported on microwave, vibrational, and NMR studies. During a course of vibrational studies on trimethylarsine oxide[5] and other trimethylarsine addition compounds, vibrational assignments obtained for trimethylarsine moiety were found to differ from the assignments of Durig *et al.* A detailed vibrational study was considered necessary for consistent assignments. A report is given herewith on infrared and Raman studies of trimethylarsine–borane for eight isotopic compounds prepared from $(CH_3)_3As$, $(CD_3)_3As$, B_2H_6, B_2D_6, $^{10}B_2H_6$, and $^{10}B_2D_6$ (the relative abundances of two isotopes in natural boron are 80.4% ^{11}B and 19.6% ^{10}B). The vibrational assignments were made by means of normal coordinate calculations.

Experimental

All the preparative work was carried out in a conventional vacuum-line. Spectral measurements were made in a vacuum. Trimethylarsine-d_0 and -d_9 were prepared by reactions of Grignard reagents, CH_3MgI and CD_3MgBr, with $AsCl_3$. B_2H_6 was prepared by the addition of BF_3–ether complex to $LiAlH_4$ suspension in ether.[6] B_2D_6 was prepared in a similar manner using $LiAlD_4$. In the preparation of ^{10}B isotopic diboranes, $^{10}BF_3$–ether complex was used, which was obtained by dissolving $^{10}BF_3$ gas in ether evolved by the thermal decomposition of $K^{10}BF_4$ at 750 °C.[7]

Trimethylarsine–borane complex was prepared by condensing trimethylarsine and diborane in a 2 : 1 mole ratio into a small reaction tube fitted with a stopcock at liquid nitrogen temperature. After closing the stopcock the tube was left to stand until it attained room temperature. It was then immersed in a −22 °C bath (carbon tetrachloride slush) and opened to the vacuum-line to remove volatile substances.

Infrared spectra were recorded on a Perkin-Elmer Model 337 in the region 400—4000 cm^{-1}. Frequencies were read on a Hitachi QPD-33 recorder by abscissa expansion with use of a Perkin-Elmer Expanded Scale Readout Kit. The instrument was calibrated in the ususal manner.[8] The spectra were obtained for the samples deposited onto a CsI plate cooled by liquid nitrogen. Before recording the spectra, the samples were annealed till there was a slight increase in intensity of absorption over that immediately after deposition.

Far infrared spectra were obtained between 33 and 400 cm^{-1} with a Hitachi FIS-III spectrophotometer which was evacuated in order to remove atmospheric water vapor. The instrument was calibrated with water vapor frequencies. The sample was sublimed onto a polyethylene window which was cooled by liquid nitrogen. The sample was annealed in a similar way to that for the mid-infrared study. The double chopping method was used to avoid the radiation effect resulting from the temperature difference between the sample and reference beam paths.

Raman spectra were recorded from 0 to 4000 cm^{-1} on a JEOL JRS-Sl laser Raman spectrophotometer equipped with a NEC GLG 108 He–Ne laser. The Raman spectrophotometer was calibrated with the emission lines of neon. The spectra were obtained at room temperature in the solid state and in CH_2Cl_2 solutions sealed into capillaries of about 1.5 mm o.d.

Results and Vibrational Assignments

The infrared spectra of ^{10}B complexes are shown in Fig. 1, and the Raman spectra of solid ^{10}B compounds in Fig. 2. In the far infrared spectra, only two absorptions were observed, one very weak and the other intense but broad. Since these frequencies are not sufficiently accurate because of high noise level and broadness, the spectra are not shown and no frequency data are used in this study.

If we assume a molecular symmetry of C_{3v}, we see from group theory that its 45 molecular vibrations are distributed as $10A_1+5A_2+15E$, in which A_1 and E vibrations are active in both infrared and Raman spectra, A_2 being inactive in both.

Nearly all the vibrations are observed in the region expected from trimethylarsine,[9] trimethylarsine addi-

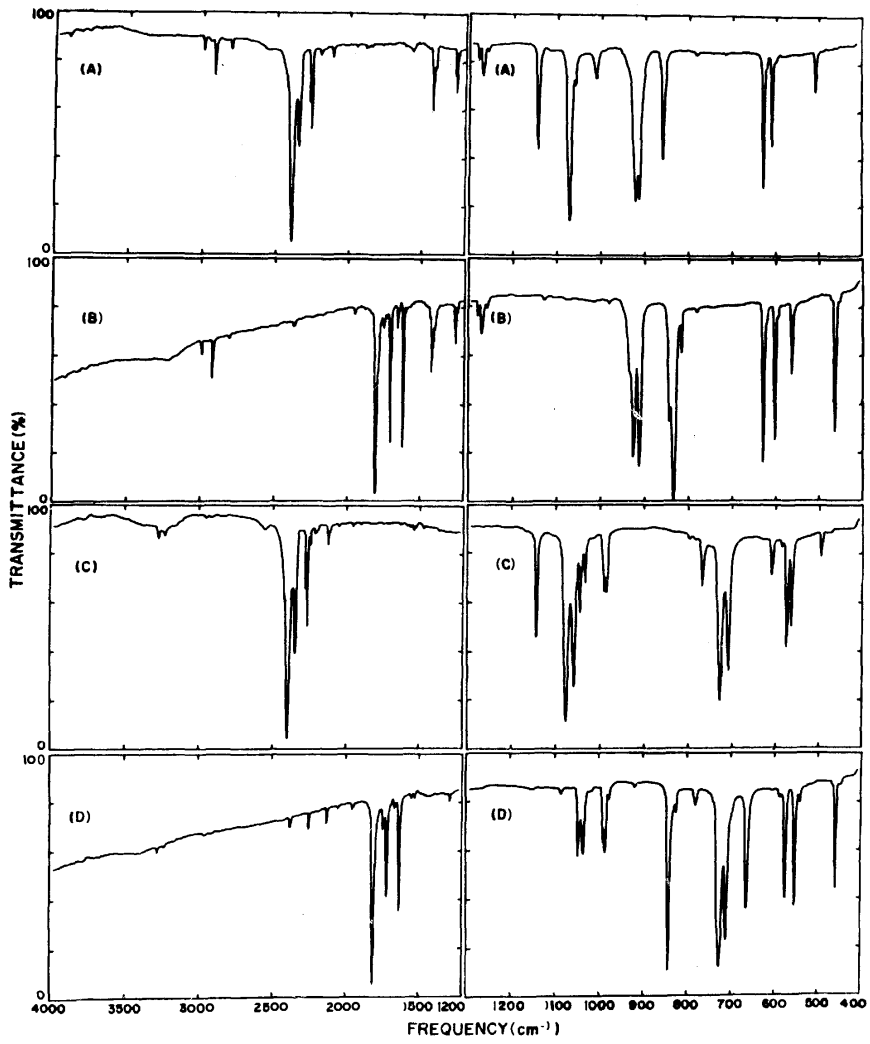

Fig. 1. Infrared spectra of (A) $(CH_3)_3As^{10}BH_3$, (B) $(CH_3)_3As^{10}BD_3$, (C) $(CD_3)_3As^{10}BH_3$, and (D) $(CD_3)_3As^{10}BD_3$ recorded at $-196°$.

tion compounds[10,11] and borane adducts.[12-17] For these vibrations, assignments are straightforward by comparison with the spectra for related compounds and taking into account of shifts upon deuteration. However, complexities are found in the region below 900 cm.$^{-1}$ The infrared spectra for all the eight isotopic compounds in this region are shown in Fig. 3. ^{10}B-^{11}B shifts are useful for assigning vibrational frequencies.

In the infrared spectrum of $(CH_3)_3As^{10}BH_3$ (Fig. 1), two absorptions are observed at 919 and 911 cm^{-1}, corresponding to 925 and 912 cm^{-1} absorptions of $(CH_3)_3As^{10}BD_3$. The E methyl rock is assigned to the higher frequency band and the A_1 rock, to the lower band. The two rocking frequencies shift on deuteration of the methyl groups to 728 and 710 cm^{-1} for $(CD_3)_3As^{10}BH_3$, and to 726 and 711 cm^{-1} for $(CD_3)_3As^{10}BD_3$.

The 857 cm^{-1} absorption in the infrared spectrum of $(CH_3)_3As^{10}BH_3$ was assigned to the BH_3 rock by Durig *et al.*[4] However, no absorption is found in the region 800—970 cm^{-1} in the spectrum of $(CD_3)_3As^{10}BH_3$. The corresponding absorption for $(CH_3)_3AsAuX$ (X=Cl, Br, I)[10] has been observed in the region 830—840 cm^{-1}. No absorption is expected from -AsAuX group in the region 830—840 cm^{-1}. It is very unlikely that the 857 cm^{-1} band of $(CH_3)_3As^{10}BH_3$ is due to the BH_3 rock as Durig *et al.* assigned it. Consequently this 857 cm^{-1} band is assigned to the CH_3 rock. The features of CD_3 rocking absorptions for $(CD_3)_3As^{10}BD_3$ are similar to those of $(CH_3)_3As^{10}BH_3$ except for the shifts toward lower frequencies. The 664 cm^{-1} band of $(CD_3)_3As^{10}BD_3$ is assigned to the CD_3 rock.

No absorption is found in the 850—900 cm^{-1} region in the spectrum of $(CH_3)_3As^{10}BD_3$. The CH_3 rock of this compound is assigned to the 844 cm^{-1} band. In the spectrum of $(CD_3)_3As^{10}BH_3$ also, no absorption is observed around 660 cm^{-1}, where the CD_3 rock of $(CD_3)_3As^{10}BD_3$ was assigned. The CD_3 rock of this compound is assigned to a low frequency band at 611 cm^{-1}.

The antisymmetric BH_3 and BD_3 deformations exhibit no resolvable ^{10}B-^{11}B isotopic shift. The symmetric deformation and the rocking of BH_3 and BD_3 groups have recognizable features of a ^{10}B-^{11}B isotopic shift in the infrared spctra (Fig. 3).

The symmetric BH_3 deformation indicates a clear

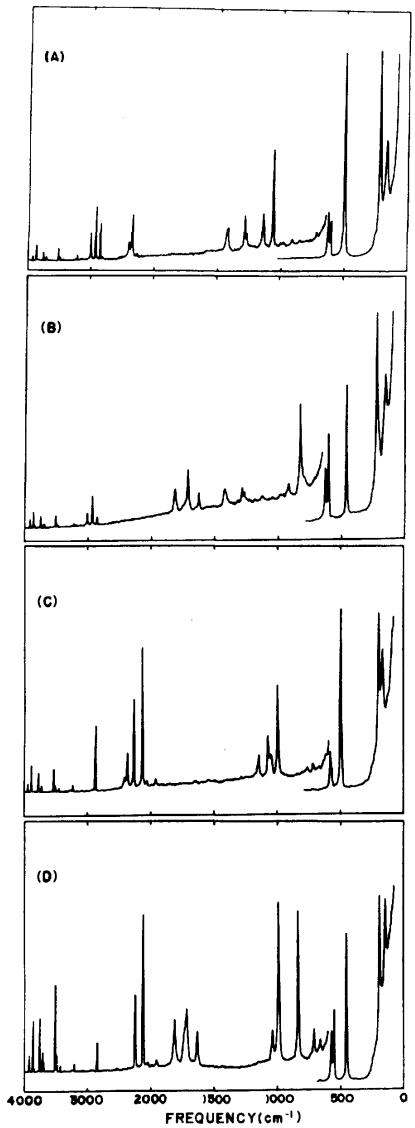

Fig. 2. Raman spectra of (A) $(CH_3)_3As^{10}BH_3$, (B) $(CH_3)_3As^{10}BD_3$, (C) $(CD_3)_3As^{10}BH_3$, and (D) $(CD_3)_3$-$As^{10}BD_3$ recorded in the solid state at room temperature.

^{10}B-^{11}B isotopic shift at 1070 and 1060 cm^{-1} for the $(CH_3)_3As$ adduct, and at 1076 and 1065 cm^{-1} for the $(CD_3)_3As$ adduct. The infrared spectrum of $(CD_3)_3$-$As^{10}BH_3$ represents curious features of a moderately strong absorption at 1059 cm^{-1}, which is lower by 6 cm^{-1} than the $^{11}BH_3$ symmetric deformation frequency (1065 cm^{-1}) and more intense than that expected from ^{11}B content (94% ^{10}B and 6% ^{11}B). The assignment of this absorption is still uncertain.

The symmetric BD_3 deformation for $(CD_3)_3As$ adducts are found at 842 cm^{-1} for $^{10}BD_3$ and at 827 cm^{-1} for $^{11}BD_3$. The antisymmetric BD_3 deformations are assigned to the bands at 842 cm^{-1} of the same frequency as that the symmetric $^{10}BD_3$ deformation. The symmetric BD_3 deformation for $(CH_3)_3As$ adducts is assigned to the absorption at 834 cm^{-1} for $^{10}BD_3$ and at 819 cm^{-1} for $^{11}BD_3$. Similarly the antisymmetric BD_3 deformation of $(CH_3)_3As$ adducts is assigned to the band at 834 cm^{-1} of the same frequency as the symmetric $^{10}BD_3$ deformation. We observe another

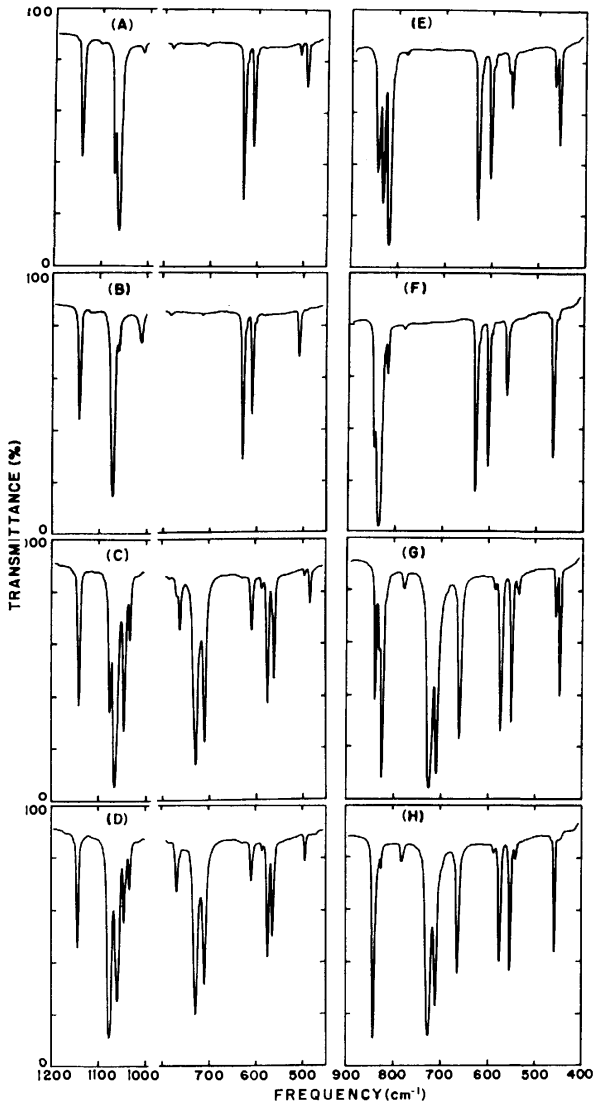

Fig. 3. Infrared spectra in the 1200—400 cm^{-1} region at −196 °. (A) $(CH_3)_3AsBH_3$, (B) $(CH_3)_3As^{10}BH_3$, (C) $(CD_3)_3AsBH_3$, (D) $(CD_3)_3As^{10}BH_3$, (E) $(CH_3)_3$-$AsBD_3$, (F) $(CH_3)_3As^{10}BD_3$, (G) $(CD_3)_3AsBD_3$, and (H) $(CD_3)_3As^{10}BD_3$.

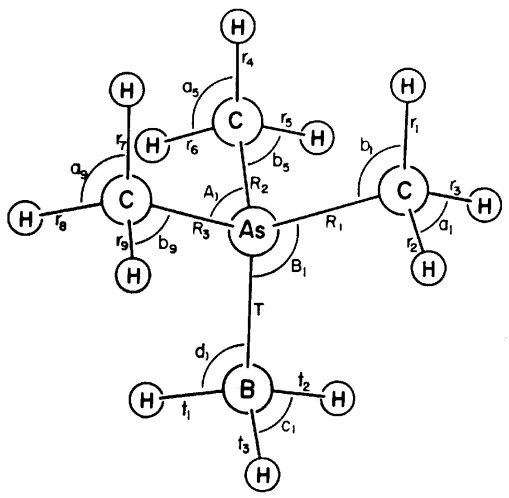

Fig. 4. Internal coordinates for trimethylarsine-borane.

absorption at 844 cm^{-1} in this region, which was previously assigned to the CH_3 rock.

A ^{10}B-^{11}B isotopic shift is also useful for the assignment of the BH_3 and BD_3 rocks. However, the rocks are rather weak and a coupling with the CH_3 or CD_3 rock makes the assignment more complicated. The $^{10}BH_3$ rock of $(CD_3)_3As^{10}BH_3$ is assigned to a band of weak intensity at 769 cm^{-1}. The $^{11}BH_3$ rocking frequency shifts by 6 cm^{-1} to 763 cm^{-1}. No absorptions assignable to the BH_3 rock are observed in the region 700—800 cm^{-1} in the infrared spectrum of $(CH_3)_3As^{10}BH_3$, but two very weak absorptions are found at 784 and 715 cm^{-1}. The latter band exhibits an isotopic shift, corresponding to the 710 cm^{-1} band for $(CH_3)_3AsBH_3$. Thus the 715 and 710 cm^{-1} bands are assigned to the $^{10}BH_3$ and $^{11}BH_3$ rocks, respectively for $(CH_3)_3AsBH_3$.

In the infrared spectrum of $(CH_3)_3As^{10}BD_3$, the 566 cm^{-1} band is assigned to the $^{10}BD_3$ rock, and the $^{11}BD_3$ rock is assigned to the 560 cm^{-1} absorption shifting by 6 cm^{-1}. For $(CD_3)_3AsBD_3$ adducts, the weak bands of low frequencies at 545 and 541 cm^{-1} are assigned to the $^{10}BD_3$ and $^{11}BD_3$ rocks, respectively.

Another absorption is observed in the region 450—500 cm^{-1} exhibiting a ^{10}B-^{11}B isotopic shift, which is assigned to the As–B stretching vibration. This vibration gives the most intense Raman band.

We should expect three skeletal deformations except the torsional modes in the region below 300 cm^{-1}. In the Raman spectra two strong Raman lines are observed. Durig *et al.*[4] resolved the higher frequency line into two at 232 and 217 cm^{-1} for $(CH_3)_3AsBH_3$, and at 232 and 216 cm^{-1} for $(CH_3)_3AsBD_3$, at liquid nitrogen temperature. We could not resolve the lines into two in either the infrared or Raman spectra under the experimental conditions. Consequently a higher frequency Raman line is assigned to the symmetric and the antisymmetric AsC_3 deformation. Finally a lower one is assigned to the AsC_3 rock which can be described as the CAsB bending mode.

One torsional mode should be observed, but no features ascribable to this mode were found in both the infrared and Raman spectra.

Normal Coordinate Analysis

Normal coordinate analysis was carried out in order to confirm the above assignments. The analysis was made by Wilson's *GF* matrix method on an ACOS 77/700 computer at the Computer Center, Tohoku

TABLE 1. SYMMETRY COORDINATES FOR TRIMETHYLARSINE-BORANE[a]

A_1	$S_1 = (2r_1-r_2-r_3) + (2r_4-r_5-r_6) + (2r_7-r_8-r_9)$	
	$S_2 = (r_1+r_2+r_3) + (r_4+r_5+r_6) + (r_7+r_8+r_9)$	
	$S_3 = (t_1+t_2+t_3)$	
	$S_4 = (2a_1-a_2-a_3) + (2a_4-a_5-a_6) + (2a_7-a_8-a_9)$	
	$S_5 = (a_1+a_2+a_3-b_1-b_2-b_3) + (a_4+a_5+a_6-b_4-b_5-b_6) + (a_7+a_8+a_9-b_7-b_8-b_9)$	
	$S_6 = m(c_1+c_2+c_3) - (d_1+d_2+d_3)$[b]	
	$S_7 = (2b_1-b_2-b_3) + (2b_4-b_5-b_6) + (2b_7-b_8-b_9)$	
	$S_8 = (R_1+R_2+R_3)$	
	$S_9 = T$	
	$S_{10} = n(A_1+A_2+A_3) - (B_1+B_2+B_3)$[c]	
	$S_{11} = (a_1+a_2+a_3+b_1+b_2+b_3) + (a_4+a_5+a_6+b_4+b_5+b_6) + (a_7+a_8+a_9+b_7+b_8+b_9)$	
	$S_{12} = (c_1+c_2+c_3) + m(d_1+d_2+d_3)$[b]	
	$S_{13} = (A_1+A_2+A_3) + n(B_1+B_2+B_3)$[c]	
A_2	$S_{14} = (r_2-r_3) + (r_5-r_6) + (r_8-r_9)$	
	$S_{15} = (a_2-a_3) + (a_5-a_6) + (a_8-a_9)$	
	$S_{16} = (b_2-b_3) + (b_5-b_6) + (b_8-b_9)$	
	$S_{17} = (p_1+p_2+p_3)$[d]	
	$S_{18} = p_4$[e]	
E	$S_{19} = 2(2r_1-r_2-r_3) - (2r_4-r_5-r_6) - (2r_7-r_8-r_9)$	
	$S_{20} = -(r_5-r_6) + (r_8-r_9)$	
	$S_{21} = 2(r_1+r_2+r_3) - (r_4+r_5+r_6) - (r_7+r_8+r_9)$	
	$S_{22} = (2t_1-t_2-t_3)$	
	$S_{23} = 2(2a_1-a_2-a_3) - (2a_4-a_5-a_6) - (2a_7-a_8-a_9)$	
	$S_{24} = -(a_5-a_6) + (a_8-a_9)$	
	$S_{25} = 2(a_1+a_2+a_3-b_1-b_2-b_3) - (a_4+a_5+a_6-b_4-b_5-b_6) - (a_7+a_8+a_9-b_7-b_8-b_9)$	
	$S_{26} = (2c_1-c_2-c_3)$	
	$S_{27} = 2(2b_1-b_2-b_3) - (2b_4-b_5-b_6) - (2b_7-b_8-b_9)$	
	$S_{28} = -(b_5-b_6) + (b_8-b_9)$	
	$S_{29} = (2d_1-d_2-d_3)$	
	$S_{30} = (2R_1-R_2-R_3)$	
	$S_{31} = (2A_1-A_2-A_3)$	
	$S_{32} = (2B_1-B_2-B_3)$	
	$S_{33} = -(p_2-p_3)$[d]	
	$S_{34} = 2(a_1+a_2+a_3+b_1+b_2+b_3) - (a_4+a_5+a_6+b_4+b_5+b_6) - (a_7+a_8+a_9+b_7+b_8+b_9)$	
E	$S_{35} = (2r_4-r_5-r_6)-(2r_7-r_8-r_9)$	
	$S_{36} = 2(r_2-r_3) - (r_5-r_6) - (r_8-r_9)$	
	$S_{37} = (r_4+r_5+r_6) - (r_7+r_8+r_9)$	
	$S_{38} = (t_2-t_3)$	
	$S_{39} = (2a_4-a_5-a_6) - (2a_7-a_8-a_9)$	
	$S_{40} = 2(a_2-a_3) - (a_5-a_6) - (a_8-a_9)$	
	$S_{41} = (a_4+a_5+a_6-b_4-b_5-b_6) - (a_7+a_8+a_9-b_7-b_8-b_9)$	
	$S_{42} = (c_2-c_3)$	
	$S_{43} = (2b_4-b_5-b_6) - (2b_7-b_8-b_9)$	
	$S_{44} = 2(b_2-b_3) - (b_5-b_6) - (b_8-b_9)$	
	$S_{45} = (d_2-d_3)$	
	$S_{46} = (R_2-R_3)$	
	$S_{47} = (A_2-A_3)$	
	$S_{48} = (B_2-B_3)$	
	$S_{49} = (2p_1-p_2-p_3)$[d]	
	$S_{50} = (a_4+a_5+a_6+b_4+b_5+b_6) - (a_7+a_8+a_9+b_7+b_8+b_9)$	

a) Normalization factors are omitted. b) $m=-\sqrt{3}\cos(d)/\cos(c/2)$. c) $n=-\sqrt{3}\cos(B)/\cos(A/2)$. d) The CH_3 torsions are p_1, p_2, and p_3. e) The BH_3 torsion is p_4.

Table 2. Vibrational numbers for the fundamentals of trimethylarsine-borane[a)]

Vibrational mode	Number		
	A_1	A_2	E
Stretching $(CH_3)_a$ or $(CD_3)_a$	1	11	16, 17
Stretching $(CH_3)_s$ or $(CD_3)_s$	2		18
Stretching (BH_3) or (BD_3)	3		19
Deformation $(CH_3)_a$ or $(CD_3)_a$	4	12	20, 21
Deformation $(CH_3)_s$ or $(CD_3)_s$	5		22
Deformation (BH_3) or (BD_3)	6		23
Rocking (CH_3) or (CD_3)	7	13	24, 25
Rocking (BH_3) or (BD_3)			26
Stretching (AsC_3)	8		27
Stretching (AsB)	9		
Deformation (AsC_3)	10		28
Rocking (AsC_3)			29
Torsion (CH_3) or (CD_3)		14	30
Torsion (BH_3) or (BD_3)		15	

a) Abbreviations used: a, antisymmetric; s, symmetric.

Table 3. Observed and calculated frequencies (cm^{-1}) for $(CH_3)_3As^{10}BH_3$[a)]

No.	Infrared solid	Raman solid	Raman solution	Calcd	PED[b)]
1	2994 w	3001 m		3002	$100F_1$
2	2919 m	2921 m	2924 m, p	2920	$94F_2$
3	2346 m	2350 m	2350 m, p	2347	$88F_3$
4	1427 w	1419 m		1430	$94F_4$
5	1278 w	1289 m	1286 m, p	1280	$86F_5, 13F_2$
6	1070 s	1067 s	1069 m, p	1074	$79F_6, 17F_3$
7	911 s	912 vw	900 w	919	$92F_7$
8	610 m	609 m	606 s, p	613	$83F_8, 13F_9$
9	510 w	506 vs	498 m, p	518	$83F_9, 14F_8$
10		226 vs	219 s	224	$97F_{10}$
16	2994 w	3001 m		3002	$78F_{16}, 22F_{17}$
17	2994 w	3001 m		3001	$78F_{17}, 22F_{16}$
18	2919 m	2921 m	2924 m	2922	$95F_{18}$
19	2393 s	2401 m	2402 s	2397	$99F_{19}$
20	1433 m	1431 m		1439	$94F_{20}$
21	1427 w			1429	$96F_{21}$
22	1269 m	1279 w	1269 m	1275	$88F_{22}$
23	1141 m	1144 m	1144 m	1146	$97F_{23}$
24	919 s	917 vw	900 w	930	$79F_{24}$
25	857 m	859 vw	854 vw	862	$67F_{25}, 15F_{26}$
26	715 vw	721 vw		725	$73F_{26}, 25F_{25}$
27	629 s	630 m	626 m	640	$85F_{27}, 13F_{24}$
28		226 vs	219 s	225	$96F_{28}$
29		175 m	166 s	173	$97F_{29}$

a) Abbreviations: v, very; w, weak; m, medium; s, strong; p, polarized. b) Values less than 10% in magnitude are omitted.

University, by means of the usual iterative least-squares procedure.

The 50 symmetry coordinates (Table 1) were constructed from the 50 internal coordinates (Fig. 4). The symmetry coordinates are mutually orthonormal, and by using them the G matrix is completely broken into

Table 4. Observed and calculated frequencies (cm^{-1}) for $(CH_3)_3As^{10}BD_3$[a)]

No.	Infrared solid	Raman solid	Raman solution	Calcd	PED[b)]
1	2994 w	3001 w		3002	$100F_1$
2	2920 m	2921 m	2924 m, p	2920	$94F_2$
3	1715 s	1715 m	1714 s, p	1717	$81F_3$
4	1425 w	1417 w		1430	$94F_4$
5	1278 w	1289 w	1286 m, p	1280	$86F_5, 10F_2$
6	834 s	827 m	827 s, p	836	$68F_6, 20F_3, 11F_9$
7	912 s	920 vw	917 w	919	$92F_7$
8	606 s	604 m	601 vs, p	608	$91F_8$
9	469 s	465 s	458 m, p	466	$78F_9$
10		226 s	219 s	223	$96F_{10}$
16	2994 w	3001 w		3002	$78F_{16}, 22F_{17}$
17	2994 w	3001 w		3001	$78F_{17}, 22F_{16}$
18	2920 m	2921 m	2924 m	2922	$95F_{18}$
19	1816 s	1815 m	1816 m	1809	$98F_{19}$
20	1434 m			1439	$94F_{20}$
21	1427 w	1428 w		1428	$96F_{21}$
22	1270 w	1270 w	1267 m	1275	$88F_{22}$
23	834 s	827 m	827 s	831	$84F_{23}, 13F_{25}$
24	925 s	920 vw		929	$80F_{24}$
25	844 m			844	$75F_{25}, 13F_{23}$
26	566 m	565 vw		551	$97F_{26}$
27	632 s	630 m	627 m	642	$85F_{27}, 13F_{24}$
28		226 s	219 s	224	$96F_{28}$
29		158 m	151 s	160	$96F_{29}$

a) For abbreviations, see Table 3.
b) Values less than 10% in magnitude are omitted.

a 10 by 10, a 5 by 5, two 15 by 15 matrices and 5 redundancies, not including non-zero cross terms between any two symmetry blocks. The corresponding terms of two degenerate pairs are equal to each other. In constructing the symmetry coordinates of C_{3v} $(XY_3)_3Z$ group, those of Kuroda and Kimura[18)] were often used. Care should be taken so that the matrix is completely broken into the symmetry blocks, and for the degenerate symmetry species in particular, each element of a matrix must be equal to the corresponding one of another degenerate pair.

The G matrix was calculated by use of the structural parameters determined from the microwave study[4)] assuming tetrahedral angle around carbon atoms: r(C–H)=1.09 Å, r(B–H)=1.212 Å, r(As–C)=1.945 Å, r(As–B)=2.035 Å, $\angle$(HBH)=113.5°, and $\angle$(CAsC)=105°.

In the calculations the infrared frequencies were used except for the AsC_3 deformation for which the Raman frequencies were taken and the observed frequencies were weighted by $(1/\lambda)$. Initial force constants for the borane group were taken from the values by Durig *et al.*,[4)] and for trimethylarsine moiety, from those for trimethylarsine oxide.[5)]

The least-squares refinement was carried out in terms of symmetry force constants, which were fitted to the observed frequencies for four ^{10}B compounds simultaneously.

The observed and calculated frequencies are given

TABLE 5. OBSERVED AND CALCULATED FREQUENCIES (cm^{-1}) FOR $(CD_3)_3As^{10}BH_3$[a]

No.	Infrared solid	Raman solid	Raman solution	Calcd	PED[b]
1	2248 w	2252 s	2252 m	2238	$98F_1$
2	2127 w	2129 s	2131 s, p	2126	$99F_2$
3	2346 m	2351 m	2351 m, p	2347	$88F_3$
4	1034 m	1039 m	1037 m	1031	$96F_4$
5	989 m	995 s	992 vs, p	987	$75F_5$, $13F_2$, $11F_8$
6	1076 s	1071 m	1070 m, p	1074	$79F_6$, $17F_3$
7	710 s	712 w		701	$89F_7$
8	567 m	565 m	561 m, p	564	$47F_8$, $38F_9$
9	499 w	496 vs	487 s, p	501	$56F_9$, $37F_8$
10		197 s	188 s	200	$95F_{10}$
16	2248 w	2252 s	2252 m	2238	$51F_{16}$, $47F_{17}$
17	2248 w	2252 s	2252 m	2236	$51F_{17}$, $47F_{16}$
18	2127 w	2129 s	2131 s	2124	$91F_{18}$
19	2392 s	2400 w	2400 w	2397	$99F_{19}$
20	1046 m	1054 m	1037 m	1038	$93F_{20}$
21	1034 m	1044 m	1037 m	1033	$95F_{21}$
22	984 m	990 sh	986 sh	978	$75F_{22}$, $12F_{27}$, $10F_{18}$
23	1143 m	1144 w	1144 m	1146	$97F_{23}$
24	728 s	712 w		712	$59F_{24}$, $12F_{27}$
25	611 w	614 vw		614	$79F_{25}$, $16F_{26}$
26	769 w	763 w		777	$76F_{26}$
27	577 m	576 w	573 m	564	$60F_{27}$, $28F_{24}$
28		197 s	188 s	197	$93F_{28}$
29		169 m	157 s	166	$97F_{29}$

a) Abbreviations: sh, shoulder. For the others, see Table 3.
b) Values less than 10% in magnitude are omitted.

TABLE 6. OBSERVED AND CALCULATED FREQUENCIES (cm^{-1}) FOR $(CD_3)_3As^{10}BD_3$[a]

No.	Infrared solid	Raman solid	Raman solution	Calcd	PED[b]
1	2248 w	2251 m	2251 m	2238	$98F_1$
2	2128 w	2128 s	2129 vs, p	2126	$90F_2$
3	1720 m	1718 m	1723 m, p	1717	$81F_3$
4	1035 m	1035 m	1035 m	1031	$96F_4$
5	990 m	995 s	992 vs, p	987	$75F_5$, $13F_2$, $11F_8$
6	842 s	838 s	835 s, p	837	$67F_6$, $20F_3$, $11F_9$
7	711 s	713 w		700	$90F_7$
8	556 m	555 m	553 s, p	551	$71F_8$, $11F_9$
9	463 m	457 s	451 s, p	459	$71F_9$, $13F_8$
10		195 m	188 s	199	$95F_{10}$
16	2248 w	2251 m	2251 m	2238	$51F_{16}$, $47F_{17}$
17	2248 w	2251 m	2251 m	2236	$51F_{17}$, $47F_{16}$
18	2128 w	2128 s	2129 vs	2124	$91F_{18}$
19	1815 s	1813 m	1816 m	1809	$98F_{19}$
20	1048 m	1041 m	1035 m	1038	$93F_{20}$
21	1035 m	1035 m	1035 m	1032	$95F_{21}$
22	985 m	988 sh	985 sh	978	$75F_{22}$, $12F_{27}$, $10F_{18}$
23	842 s	838 s	835 s	833	$97F_{23}$
24	726 s	713 w		720	$53F_{24}$, $16F_{27}$
25	664 w	663 w	662 w	652	$62F_{25}$, $13F_{24}$, $13F_{26}$
26	545 w			539	$75F_{26}$, $21F_{25}$
27	578 m	576 m	573 m	565	$62F_{27}$, $29F_{24}$
28		195 m	188 s	197	$94F_{28}$
29		150 m	142 s	152	$96F_{29}$

a) Abbreviations: sh, shoulder. For the others, see Table 3.
b) Values less than 10% in magnitude are omitted.

in Tables 3—6 for four ^{10}B isotopic species, in which the vibrational numbers refer to the vibrational modes (Table 2). The calculated frequencies have an average error of 0.52% for A_1 vibrations and 0.74% for E vibrations. The sum of the weighted squares of errors $\Sigma(\lambda_{obsd}-\lambda_{calcd})^2/\lambda_{obsd}$ was 2.24×10^{-3} for A_1 and 7.02×10^{-3} for E. The symmetry force constants together with the uncertainty from the last cycle of the least-squares refinement are given in Table 7. The observed frequencies of the ^{11}B compounds together with the frequencies calculated by use of the force constants (Table 7) are given in Table 8.

TABLE 7. SYMMETRY FORCE CONSTANTS AND THEIR UNCERTAINTIES FOR TRIMETHYLARSINE-BORANE[a]

		σ			σ
F_1	4.790	0.011	F_{16}	4.792	0.028
F_2	4.736	0.054	F_{17}	4.791	0.028
F_3	2.983	0.047	F_{18}	4.762	0.079
F_4	0.516	0.003	F_{19}	2.973	0.013
F_5	0.532	0.016	F_{20}	0.523	0.004
F_6	0.583	0.021	F_{21}	0.520	0.004
F_7	0.575	0.005	F_{22}	0.534	0.022
F_8	2.924	0.038	F_{23}	0.383	0.004
F_9	1.849	0.039	F_{24}	0.575	0.016
F_{10}	0.605	0.018	F_{25}	0.473	0.009
			F_{26}	0.465	0.009
$F_{2,5}$	−0.385	0.066	F_{27}	3.169	0.125
$F_{3,6}$	−0.442	0.048	F_{28}	0.713	0.030
$F_{5,8}$	−0.170	0.033	F_{29}	0.383	0.021
$F_{6,9}$	−0.159	0.030			
			$F_{18,22}$	−0.356	0.101
			$F_{22,27}$	−0.265	0.045
			$F_{24,27}$	−0.264	0.049
			$F_{25,26}$	0.065	0.007

a) The stretching force constants are given in mdyn/Å, the deformation force constants in mdyn Å, the stretching-deformation interaction constants in mdyn.

Discussion

As seen in the potential energy distributions, the BH_3 and BD_3 rocks couple with the CH_3 and CD_3 rocks, making the rocking frequency region complicated.

The valence force constants obtained from the symmetry force constants are compared with those of other borane and related compounds (Table 9). The force constant f_{N-B} of H_3NBH_3 is greater than that of $(CH_3)_3NBH_3$, whereas the force constant f_{P-B} of H_3PBH_3 is smaller than that of $(CH_3)_3PBH_3$. Arsine, AsH_3, forms no addition compound with borane. If arsine could form a borane adduct, f_{As-B} of arsine–borane would be smaller than 1.849 mdyn/Å obtained for

TABLE 8. OBSERVED AND CALCULATED FREQUENCIES (cm^{-1}) FOR ^{11}B ISOTOPIC SPECIES[a)]

No.	Observed (infrared)				Calculated			
	$(CH_3)_3As$		$(CD_3)_3As$		$(CH_3)_3As$		$(CD_3)_3As$	
	$^{11}BH_3$	$^{11}BD_3$	$^{11}BH_3$	$^{11}BD_3$	$^{11}BH_3$	$^{11}BD_3$	$^{11}BH_3$	$^{11}BD_3$
1	2995	2993	2248	2249	3002	3002	2238	2238
2	2920	2918	2128	2127	2920	2920	2126	2126
3	2346	1701	2346	1700	2340	1706	2340	1706
4	1427	1427	1034	1035	1430	1430	1031	1031
5	1279	1278	989	990	1280	1280	987	987
6	1060	819	1065	827	1065	823	1065	823
7	913	913	710	711	919	919	701	700
8	610	606	564	556	612	608	559	550
9	497	459	488	454	504	458	490	451
10	226	225	198	196	224	223	200	199
16	2995	2993	2248	2249	3002	3002	2238	2238
17	2995	2993	2248	2249	3002	3002	2236	2236
18	2920	2918	2128	2127	2922	2922	2124	2124
19	2380	1797	2382	1797	2383	1788	2383	1788
20	1433	1433	1046	1047	1439	1439	1038	1038
21	1427	1425	1035	1035	1429	1428	1033	1032
22	1270	1269	985	984	1275	1275	978	978
23	1140	834	1141	842	1143	827	1143	830
24	921	927	729	726	930	929	713	720
25	858	844	612	663	861	844	614	651
26	710	560	763	541	722	548	773	536
27	631	631	578	578	640	642	564	565
28	226	225	198	196	225	225	197	197
29	173	155	165	147	171	159	163	151

a) The force constants in Table 7 were used in frequency calculations. Observed frequencies for the vibrational number 10, 28, and 29 are taken from the Raman spectra.

TABLE 9. COMPARISON OF THE VALENCE FORCE CONSTANTS (mdyn/Å) FOR THE BORANE ADDITION COMPOUNDS (X=N, P, As)

	f_{B-X}	f_{As-C}	f_{B-H}	Ref.
H_3NBH_3	2.90		2.88	19
$(CH_3)_3NBH_3$	2.36		2.7	19
	2.59		2.49	13
F_3PBH_3	2.39			20
H_3PBH_3	1.78			15
	1.97		3.10	21
$CH_3PH_2BH_3$	2.44		3.07	14
$(CH_3)_3PBH_3$	2.37		2.987	12
$(CH_3)_3AsBH_3$	1.84	2.97	3.06	4
	1.849	3.087	2.976	This work
$(CH_3)_3AsO$		3.099		5
$(CH_3)_3As$		2.56		4, 22
		2.63		23

$(CH_3)_3AsBH_3$. As expected the stability of trimethylarsine–borane is less than that of N and P analogs. The trend is reflected in the stretching force constants of the donor-acceptor bonds.

The CAsC angle becomes larger by adduct formation toward the tetrahedral angle and s character increases in rehybridization around the arsenic atom. This accounts for the increase in the As–C force constant and in the As–C stretching frequencies.

The As–B force constant is in good agreement with the value obtained by Durig *et al.*,[4] the f_{As-C} value being slightly larger than theirs, but in accord with that in $(CH_3)_3AsO$. The B–H force constant is larger than that in amine–boranes, but smaller than that in phosphine–boranes. Accurate examination for other boranes would be necessary in order to compare the B–H force constant with the value obtained in this study.

The author wishes to express his sincere gratitude to Prof. K. Aida for his continued encouragement during this work.

References

1) F. Hewitt and A. K. Holiday, *J. Chem. Soc.*, **1953**, 530.
2) A. B. Burg and R. I. Wagner, *J. Am. Chem. Soc.*, **75**, 3872 (1953).
3) F. G. A. Stone and A. B. Burg, *J. Am. Chem. Soc.*, **76**, 386 (1954).
4) J. R. Durig, B. A. Hudgens, and J. D. Odom, *Inorg. Chem.*, **13**, 2306 (1974).
5) F. Watari, *Spectrochim. Acta, Part A*, **31**, 1143 (1975).
6) I. Shapiro, H. G. Weiss, M. Schmich, Sol Skolnik, and G. B. L. Smith, *J. Am. Chem. Soc.*, **74**, 901 (1952).
7) R. Amster and R. C. Taylor, *Spectrochim. Acta*, **20**, 1487 (1964).

8) R. N. Jones and A. Nadeau, *Spectrochim. Acta*, **20**, 1175 (1964).
9) P. T. D. Park and P. J. Hendra, *Spectrochim. Acta, Part A*, **24**, 2081 (1968); E. J. Rosenbaum, D. J. Rosenbaum, D. J. Rubin, and C. R. Sandberg, *J. Chem. Phys.*, **8**, 366 (1940).
10) D. A. Duddell, P. L. Goggin, R. J. Goodfellow, M. G. Norton, and J. G. Smith, *J. Chem. Soc., A*, **1970**, 545.
11) C. F. Shaw and R. S. Tobias, *Inorg. Chem.*, **12**, 965 (1973).
12) J. D. Odom, B. A. Hudgens, and J. R. Durig, *J. Phys. Chem.*, **77**, 1972 (1973).
13) J. D. Odom, J. A. Barnes, B. A. Hudgens, and J. R. Durig, *J. Phys. Chem.*, **78**, 1503 (1974).
14) J. R. Durig, V. F. Kalasinsky, Y. S. Li, and J. D. Odom, *J. Phys. Chem.*, **79**, 468 (1975).
15) J. Davis and J. E. Drake, *J. Chem. Soc., A*, **1970**, 2959.
16) J. R. Berschied, Jr. and K. F. Purcell, *Inorg. Chem.*, **11**, 930 (1972).
17) G. W. Bethke and M. K. Wilson, *J. Chem. Phys.*, **26**, 1119 (1957); R. C. Taylor, *ibid.*, **26**, 1131 (1957).
18) Y. Kuroda and M. Kimura, *Spectrochim. Acta*, **22**, 47 (1966).
19) R. C. Taylor, *Adv. Chem. Ser.*, **42**, 59 (1964).
20) W. Sawodney and J. Goubeau, *Z. Anorg. Allg. Chem.*, **356**, 289 (1968).
21) J. D. Odom, V. A. Karasinsky, and J. R. Durig, *J. Mol. Struct.*, **24**, 139 (1975).
22) G. Bougnet and M. Bigorgne, *Spectrochim. Acta, Part A*, **23**, 1231 (1967).
23) H. Siebert, *Z. Anorg. Allg. Chem.*, **273**, 11 (1953).

^{13}C Spin-Lattice Relaxation Times in Liquid Crystalline *p,p'*-Azoxyanisole

Kikuko HAYAMIZU and Osamu YAMAMOTO

National Chemical Laboratory for Industry, Honmachi, Shibuya-ku, Tokyo 151

(Received November 24, 1976)

The ^{13}C spin-lattice relaxation time T_1 in the liquid crystalline compound *p,p'*-azoxyanisole; (PAA; 4,4'-dimethoxyazoxybenzene) was observed in the nematic and isotropic liquid phases. From the obtained T_1's of the ring and the methyl carbons, the anisotropic rotational diffusion constants were determined. It is concluded that the rotational reorientation around the molecular axis is faster by an order of 10^3 than the rotational motion around the axis perpendicular to the molecular axis in the nematic and isotropic liquid states.

Nuclear relaxation time in the liquid crystals is known to give important information about molecular motions and intermolecular interactions of some interesting compounds. The nematic liquid crystal *p,p-'* azoxyanisole (PAA); 4,4'-dimethoxyazoxybenzene) and its deuterated species have been studied by observing ^1H, ^2D, ^{13}C and/or ^{14}N relaxation times.[1-9] Most of the relaxation studies were made by the ^1H resonance, but the ^1H relaxation time is affected by both intra- and intermolecular interactions. The spins of the other nucleus, however, relax predominantly by the intramolecular processes. In particular, the relaxation of ^{13}C nuclei, which is bonded by one or more protons, mainly takes place through the dipole-diploe interaction with the attached protons modulated by the molecular reorientations.

PAA contains two different types of carbons bearing protons, *i. e.*, the ring carbons and the methyl carbons. Clearly the relaxation times of the ring carbons can be expected to be affected by the motion of the nematic director. Although the motion of the methyl carbons is averaged by the internal rotation, the relaxation time will be also affected by the anisotropic motion of the elongated molecule in the nematic state. Here we would like to present the temperature dependence of ^{13}C spin-lattice relaxation times for the ring and the methyl carbons observed in the nematic liquid crystalline and in the isotropic liquid states, and to discuss the anisotropic rotation of the nematic molecule.

Experimental

PAA was purified by the zone melting method, degassed, and then sealed into a 12-mm sample tube under vacuum. The ^{13}C relaxation times were obtained by the 180°—τ—90° pulse method using a Varian XL-100-15 spectrometer operating at 25.16 MHz in the external ^{19}F lock mode with proton decoupling. The temperature range of the nematic liquid crystalline phase is 117—135 °C for PAA, and T_1's were observed both in the nematic and in the isotropic liquid states by varying the temperature from 118 to 175 °C. In the nematic phase the measurement was made without sample spinning in order to prevent the disturbance of the allignment of the nematic director along the external magnetic field.

Results and Discussion

The ^{13}C spectrum of PAA in $CDCl_3$ solution at ambient temperature consists of ten peaks arising from the 10 chemically non-equivalent carbons.[10] In the isotropic state at higher temperature, the ^{13}C spectrum shows a similar pattern to that for the $CDCl_3$ sloution, but only 8 peaks are observed due to the overlapping of two sets of two peaks, *i. e.*, the signals from two methyl carbons and from four ring carbons meta to OCH_3 group. Here four peaks are obtained from the carbons bearing protons. In the isotropic state the ^{13}C chemical shifts relative to that of the methyl carbons are nearly constant throughout the temperature range studied, and agree with those in $CDCl_3$ solution within 0.8 ppm. This fact suggests that the molecular structure of PAA does not significantly change from ambient to sufficient high temperatures.

In the nematic state where the molecules are in an anisotropic condition, the ^{13}C spectral lines for PAA are rather broad, probably due to insufficient proton decoupling. The lines of the two quaternary aromatic carbons bonded to nitrogen disappear, as shown by Pines and Chang.[11] But the change in the spectrum from the isotropic to the nematic states in the ^{13}C resonance is much smaller than that in the ^1H or ^2D resonances, so that the measurement of ^{13}C relaxation times is still possible by the usual high resolution technique.

In this paper, since the molecular motion of PAA will be discussed assuming the dipole-dipole mechanism as the relaxation process, T_1's are observed for the carbons bonded by protons, *i. e.*, three aromatic carbon peaks and one methyl carbon peak. The temperature dependences of these T_1's are shown in Fig. 1, which

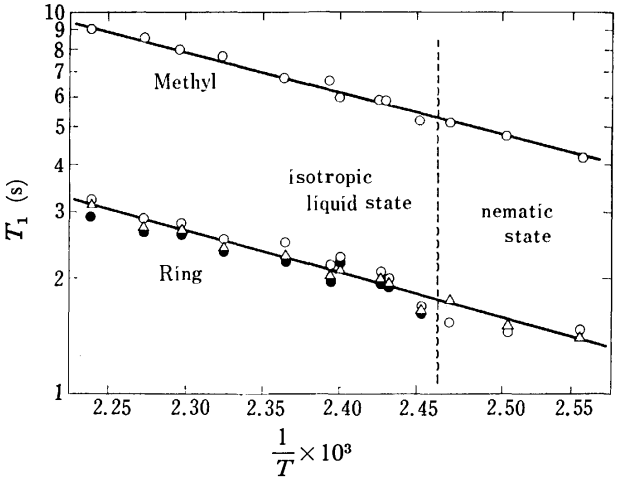

Fig. 1. The temperature dependences of ^{13}C relaxation times for PAA in the nematic and isotropic states. The ring carbons are expressed from a lower to a higher field by ○, ●, and △. In the nematic phase the two signals at the lower field collapses to a broad line which is shown by ○.

TABLE 1. NOE OF PAA IN THE ISOTROPIC LIQUID STATE

Temperature	Methyl	Ring		
137 °C	2.1	3.0	2.8	2.7
160 °C	2.3	2.6	2.7	2.6

have been observed both in the nematic and the isotropic liquid state. In order to estimate the contribution of the dipole-dipole relaxation mechanism to the observed ^{13}C relaxation times, NOE was determined in the isotropic state, as shown in Table 1. If we consider the experimental uncertainty, the observed NOE's are not very temperature dependent. Table 1 shows that the contribution of the dipole-dipole mechanism is a little larger in the ring carbons than in the methyl carbons, probably because the spin-rotation mechanism from the internal rotation may be effective in the ^{13}C relaxation of the methyl carbons. The dipole-diploe relaxation time T_{1d} can be calculated from the observed T_1 as follows[12]:

$$1/T_{1d} = \frac{\mathrm{NOE}-1}{1.988} \times 1/T_1.$$

A theoretical expression of nuclear magnetic relaxation in molecules with multiple internal rotations was first derived by Wallach.[13] In this derivation the molecular motion was treated as isotropic. It was shown that each internal rotation which is much faster than the overall molecular motion contributes a single factor $((3\cos^2\theta-1)/2)^2$ to the relaxation rate, where θ is the angle from the internal rotational axis of interest to the next internal rotational axis, or for the last internal rotational axis to the label axis of interset. Then Levine and his coworkers[14] have extended the theory to the dipolar relaxation for the case where the molecular motion is anisotropic, and presented the numerical results of the ^{13}C relaxation times in a hydrocarbon chain attached to an axially symmetric molecule.

The methyl groups of PAA are a dual rotation system which has internal rotations around the C–O bond and the three-fold axis. Possible mechanisms which are effective in the ^{13}C dipolar relaxation process for the methyl groups of PAA are molecular overall reorientation and the internal rotations. Since these dual internal rotations are reported to be activated in solid state,[19] it may be assumed that the methyl groups rotate freely around both bonds at higher temperatures in the nematic and isotropic states. We also assume that PAA is a symmetric rotor having two rotational diffusion constants, $D_{//}$ and $D_\perp$, where $D_{//}$ is the rotational diffusion constant for the motion about the molecular symmetry axis and $D_\perp$ is for the motion about an axis perpendicular to the molecular axis. According to the theory developed by Wallach and Levine *et al.*, and using the spectral density function for the internal rotation system attached to the molecule undergoing anisotropic molecular motion, the dipolar relaxation rate $1/T_{1d}$ for the methyl carbons of PAA can be derived as

$$\left(\frac{1}{T_{1d}}\right)_{Me} = \frac{3\gamma^2\gamma'^2\hbar^2}{2r^6} \times 3\left[\frac{1}{6D_\perp}\left(\frac{3\cos^2\theta-1}{2}\right)^2 + \frac{1}{2D_\perp+4D_{//}}\sin^4\theta\right] \times \left(\frac{3\cos^2\theta'-1}{2}\right)^2\left(\frac{3\cos^2\theta''-1}{2}\right)^2, \quad (1)$$

where θ is the angle between the molecular axis and the C–O axis, θ' is $\angle$COC, and θ'' is $\angle$OCH. The factor 3 corresponds to the three protons of the methyl groups. When $\theta=0°$, $D_{//}$ does not contribute to the relaxation rate of the methyl carbons. Even if θ is assumed to be 10°,[14] the contribution of $D_{//}$ will be negligibly small because of the term $\sin^4\theta$. In other words, the rotation around the molecular axis of PAA has little effect on the relaxation rate of the methyl carbons, and $(1/T_{1d})_{Me}$ may be assumed to be only a function of $D_\perp$. The angle $\angle$COC, θ' was determined to be 118° by the X-ray analysis.[16] Since the geometric factor $((3\cos^2\theta'-1)/2)^2$ is very sensitive to even small changes of this angle, the $D_\perp$ calculated using Eq. 1 contains some error due to the ambiguity of θ' in the nematic and isotropic states, in addition to the experimental error of $(1/T_{1d})_{Me}$.

On the other hand, since the ring carbons constitute the skeleton of the PAA molecule, the most important mechanism for the ^{13}C dipolar relaxation of the ring carbons bearing protons will be the molecular overall rotation. Huntress[17] has derived a theoretical expression for the relaxation rate of a nuclear spin in a molecule undergoing anisotropic diffusional rotation, which may be applied to the dipolar relaxation rate of the ring carbons of PAA. Then

$$\left(\frac{1}{T_{1d}}\right)_{Ring} = \frac{3}{2}\frac{\gamma^2\gamma'^2\hbar^2}{r^6}\frac{1}{6D_\perp}\left[1+\frac{3(D_\perp-D_{//})}{5D_\perp+D_{//}} \times \sin^2\alpha\left(1+\frac{3(D_\perp-D_{//})}{2(D_\perp+2D_{//})}\sin^2\alpha\right)\right], \quad (2)$$

where α is the angle between the molecular axis and the label axis of interest. For the dipole-dipole relaxation rate for the ring protons, $\alpha=58.7°$ (an average for two C–H bonds),[20] since the rotation around the molecular axis is expected. From Eq. 2, $D_{//}$ can be calculated using the $D_\perp$ value obtained from the relaxation time of the methyl carbons and Eq. 1. In Table 2 the calculated values of $D_{//}$ and $D_\perp$ are listed, together with those for D_{iso}, which are calculated from the assumption of isotropic motion.

TABLE 2. ROTATIONAL DIFFUSION CONSTANTS OF PAA

Temperature	$D_\perp$	$D_{//}$	D_{iso}	
			methyl	ring
137 °C	4.1×10^8	0.86×10^{11}	1.7×10^{11}	1.2×10^{10}
160 °C	4.8×10^8	1.7×10^{11}	2.0×10^{11}	1.8×10^{10}

Although Eqs. 1 and 2 are approximate equations for describing the internal and the anisotropic molecular rotations for an aligned molecule such as PAA in the nematic phase and in the isotropic phase near the transition point, where the short range order remains, they may be safely applied to the ^{13}C dipolar relaxation rate of PAA molecules at higher temperature in the isotropic state. The obtained rotational diffusion constants describe the molecular motion of PAA molecule in the isotropic state. The rotation around the

long molecular axis is much faster by an order of 10^3, than the rotation around the axis perpendicular to the molecular axis. Since the observed T_1 is continuous at the transition point from the nematic to the isotropic liquid states, as shown in Fig. 1, the same picture for the molecular motion of the PAA molecule will be almost true in the nematic state. The rotational motion expressed by the diffusion constant $D_\perp$ obtained from the ^{13}C relaxation time may be compared with the thermal fluctuation of the nematic director in the nematic state, which contributes to the ^1H relaxation rate as a frequency dependent phenomenon[1,2,9]. The order fluctuation of the director is shown to remain in the isotropic state,[5-7] and this is consistent with the fact that $D_\perp$ obtained in the isotropic state is still very small compared with the obtained $D_{//}$. Otherwise, in the usual isotropic liquid, $D_\perp$ and $D_{//}$ would have the values of the same order for a molecule about 18 Å in length and 6 Å in diameter, the approximate size of PAA.[16]

The measurement of ^2D relaxation time has been made by Orwoll *et al.*[8] for PAA-d_8 (ring positions are deuterated) in the nematic and isotropic liquid states. Although the relaxation mechanism is different for the ^{13}C and ^2D resonances, the direction of the interaction vector for the ^2D resonance in PAA-d_8 is the same as that for the ^{13}C resonance in the ring carbons of PAA. The correlation times calculated based on the assumption of the isotropic motion in the ^2D resonance are a little longer, by several percents, than thoes in the ^{13}C resonance at every temperature. Orwoll *et al.* also observed no frequency dependence of the ^2D relaxation time in the nematic and isotropic states. Since the correlation times and the observing frequencies are in a similar order for the ^{13}C and the ^2D resonances, it can be assumed that the ^{13}C relaxation time for the ring carbons is also frequency independent, and then the extreme narrowing condition will hold in the ^{13}C relaxation time when Eq. 2 is applied. From our measurement of ^2D relaxation times of PAA-d_6 (the methyl protons are deuterated) in the isotropic state[18], there is also the same trend in the correlation times of the methyl groups. The temperature dependences of the ^{13}C relaxation times in the ring and the methyl carbons shown in Fig. 1 are similar to those of the ^2D relaxation times in the ring position[8] and the methyl groups,[18] except that at the transition point there was observed the discontinuity in the T_1 of the ^2D resonance, while the T_1's of the ^{13}C resonance are continuous. Arrhenius plots of the ^{13}C relaxation times give the activation energies of 5.6 and 5.0 kcal/mol for the ring and the methyl carbons, respectively. The activation energy obtained for PAA-d_8 in the isotropic state is 5.5 kcal/mol,[8] and the agreement is good. Schwartz *et al.*[4] obtained the activation energy of 6.5 kcal/mol for the ^{13}C relaxation time for the ring carbons of PAA in a similar temperature region, and interpreted it by activation of the internal rotation about the C–N bond. But as discussed above and as also pointed out by Orwoll *et al.* from the results of the ^2D resonance, the main activation process which affects the temperature dependent ^{13}C and/or ^2D relaxation times from the nematic to the isotropic liquid phases may be concluded to be the anisotropic molecular rotational process.

References

1) R. Y. Dong, W. F. Forbes, and M. M. Pintar, *J. Chem., Phys.*, **55**, 145 (1971).
2) W. Wölfel, F. Noack, and M. Slohrer, *Z. Naturforsch.*, **30a** 437 (1975), and literature cited therein.
3) B. M. Fung, C. G. Wade, and R. D. Orwoll, *J. Chem. Phys.*, **64**, 148 (1976).
4) M. Schwartz, P. E. Fagerness, C, H. Wang, and D. M. Grant, *J. Chem. Phys.*, **60**, 5066 (1974).
5) B. Cabane and W. G. Clark, *Phys. Rev. Lett.*, **25**, 91 (1970)
6) R. Y. Dong, E. Tomchuk, J. J. Visintainer, and E. Bock, *Mol. Cryst. Liq. Cryst.*, **33**, 101 (1976).
7) B. Cabane, *Adv. Mol. Relaxation Process*, **3**, 341 (1972).
8) R. D. Orwoll, C. G. Wade, and B. M. Fung, *J. Chem. Phys.*, **63**, 986 (1975).
9) K. Hayamizu and O. Yamamoto, *J. Chem. Phys.*, **66**, 1720 (1977).
10) L. F. Johnson and W. C. Jankowski, "Carbon-13 NMR Spectra," Wiley, New York (1972).
11) A. Pines and J. J. Chang, *J. Am. Chem. Soc.*, **96**, 5590 (1974).
12) T. D. Alger, S. W. Collins, and D. M. Grant, *J. Chem. Phys.*, **54**, 2820 (1971).
13) D. Wallach, *J. Chem. Phys.*, **47**, 5258 (1967).
14) Y. K. Levine, N. J. M. Birdsall, A. G. Lee, J. C. Metcalbe, P. Partington, and G. C. K. Roberts, *J. Chem. Phys.*, **60**, 2890 (1974).
15) J. C. Rowell, W. D. Phillips, L. R. Melby, and M. Pamar, *J. Chem. Phys.*, **43**, 3442 (1965).
16) W. R. Krigbaum, Y. Chatani, and P. G. Barber, *Acta Crystallogr.*, **B26**, 97 (1970).
17) W. T. Huntress, Jr., *J. Chem. Phys.*, **48**, 3524 (1968).
18) K. Hayamizu and O. Yamamoto, unpublished data.
19) A. R. Sharp, W. F. Forbes, and M. M. Pintar, *J. Chem. Phys.*, **59**, 460 (1973).
20) P. Diehl and A. S. Tracey, *Mol. Phys.*, **30** 1917 (1975).

Activity Coefficients of Glycylglycine and α-Aminobutyric Acid in Aqueous Sucrose Solutions

Hatsuho UEDAIRA

Research Institute for Polymers and Textiles, Sawatari 4, Kanagawa-ku, Yokohama 221

(Received November 24, 1976)

The activity coefficients of glycylglycine and α-aminobutyric acid in aqueous sucrose solutions have been measured by the isopiestic vapor pressure method at 25 °C. α-Aminobutyric acid is salted-out by sucrose, the effect increasing with an increase in the concentration of sucrose and a decrease in the concentration of amino acid. However, in the glycylglycine–sucrose–water system at lower concentrations of solutes salting-in of glycylglycine by sucrose takes place and then salting-out predominates at concentrations higher than 1 mol kg^{-1} glycylglycine and 2 mol kg^{-1} sucrose. The pairwise interactions and the free energy of the transfer of amino acids from water to various concentractions of sucrose solutions are calculated. The results account for the stabilizing effect of sucrose on the higher structure of globular proteins.

Although sugars have long been observed to affect the stability and activity of proteins, the mechanism of the effect remains unclear. Beilinson[1] found that sucrose and glycerol inhibit the heat coagulation of ovalbumin. Ball *et al.*[2] reported that various sugars prevent heat coagulation of serum albumin. Gersma and Stuur[3] found that polyvalent alcohols show protective effects on the reversible thermal denaturation of lysozyme, ribonuclease, and chymotrypsinogen A.

Shimpson and Kauzman[4] found that sucrose and glycerol inhibit the denaturation of ovalbumin by urea. According to Shikama,[5] the bovin serum albumin molecule denaturated by urea has different conformations after the renaturation in 1 mol kg^{-1} sucrose solutions. Metral and Yon[6] showed that the inhibition caused by sucrose on triptic hydrolysis of β-lactoglobulin A is due to the fixation of sucrose on this protein and to the existence of strong stabilizing interactions. Furthermore, at low concentration the sugars accelerate the rate of subunit dissociation of the olygomeric enzyme L-asparaginase with urea, and at higher concentrations, sugars decrease the rate at which the enzyme dissociates in the presence of urea.[7]

In order to clarify the fundemantal mechanisms involved in these phenomena, a thermodynamic study with model compounds is one of the best approaches. Lakshimi and Nandi[8] obtained the activity coefficients of aromatic amino acids and their *N*-acetyl ethyl esters in sucrose and glucose solutions by means of solubility measurements.

In the present work, the activity coefficients of glycylglycine (glygly) and α-aminobutyric acid (αABA) in sucrose solutions were determined by the isopiestic vapor pressure methods. These amino acids were selected as models of peptide unit and amino acids having alkyl side chains. The isopiestic method is superior to the solubility method in that the change in interactions with both concentrations of amino acid and sucrose can be obtained.

Experimental

Materials. Glygly (G. R.) was decolorized and recrystallized twice from a water–ethanol solution. Sucrose and αABA were recrystallized from a water ethanol solution. The samples were dried *in vacuo* over phosphorus pentaoxide at room temperature. Potassium chloride (analytical grade, Merck Co.) was dried *in vacuo* over phosphorus pentaoxide at 110 °C. Solutions were prepared with deionized water freed of air by boiling.

Measurements and Calculation of the Activity Coefficients. Osmotic and activity coefficients were determined with the same apparatus as previously reported.[9] Several ternary solutions of amino acid and sucrose with varing compositions and reference potassium chloride solutions were put in silver dishes. The dishes were placed on a flat copper block in a glass vacuum dessicator set in a thermostat bath at 25 °C.[9] The initial concentrations in the ternary solutions were adjusted to be sufficiently close to their equilibrium concentrations.[10] The time required for attainment of equilibrium was 4—14 days. Equilibrium concentration was measured by weighing, all the weights being corrected to those in vacuum.

In the analysis of the results we use the function Δ, defined by[11]

$$\Delta = 2m_R\phi_R - m_1\phi_1 - m_2\phi_2 , \quad (1)$$

where m_1 and m_2 are the molalities of solute 1 (glygly or αABA) and solute 2 (sucrose), respectively, in aqueous ternary solutions; ϕ_1 and ϕ_2 are the osmotic coefficients of binary aqueous solutions of solutes 1 and 2 at a molality of m_1 and m_2, respectively; m_R and ϕ_R are the molality and osmotic coefficient, respectively, of the reference potassium chloride solution which is in vapor pressure equilibrium with a ternary solution containing solutes 1 and 2 at molalities m_1 and m_2.

The value of Δ/m_1m_2 is given by the equations

$$\Delta/m_1m_2 = \sum_{i=0}^{n}\sum_{j=0}^{n} A_{ij}m_1^i m_2^j \qquad (n=i+j=2 \text{ or } 3) \quad (2)$$

From Eqs. 1 and 2, the activity coefficient for solute 1 in the ternary solution is given[11,12] by

$$\ln \gamma_1 = \ln \gamma_{10} + A_{00}m_2 + A_{10}m_1m_2 + \frac{1}{2}A_{01}m_2^2 + A_{20}m_1^2m_2 + \frac{2}{3}A_{11}m_1m_2^2 + \frac{1}{3}A_{02}m_2^3 + A_{30}m_1^3m_2 + \frac{3}{4}A_{21}m_1^2m_2^2 + \frac{1}{2}A_{12}m_1m_2^3 + \frac{1}{4}A_{03}m_2^4 , \quad (3)$$

and that of solute 2 by

$$\ln \gamma_2 = \ln \gamma_{20} + A_{00}m_1 + \frac{1}{2}A_{10}m_1^2 + A_{01}m_1m_2 + \frac{1}{3}A_{20}m_1^3 + \frac{2}{3}A_{11}m_1^2m_2 + A_{02}m_1m_2^2 + \frac{1}{4}A_{30}m_1^4 + \frac{1}{2}A_{21}m_1^3m_2 + \frac{3}{4}A_{12}m_1^2m_2^2 + A_{03}m_1m_2^3 , \quad (4)$$

where γ_1 and γ_2 are the molal activity coefficients of solutes

TABLE 1. TERNARY ISOPIESTIC DATA AT 25 °C FOR THE SYSTEMS GLYCYLGLYCINE–SUCROSE–WATER AND α-AMINOBUTYRIC ACID–SUCROSE–WATER

m_R	m_1	m_2	Δ/m_1m_2 Exptl	Δ/m_1m_2 Calcd[a]	Diff. %[b]
		Glycylglycine–Sucrose–Water			
0.41292	0.17518	0.55396	-0.021_{54}	-0.023_{21}	−0.02
	0.26074	0.48299	-0.026_{12}	-0.024_{97}	0.02
	0.42168	0.34959	-0.023_{01}	-0.026_{94}	−0.08
	0.55101	0.24348	-0.026_{43}	-0.027_{52}	−0.02
	0.73539	0.091227	-0.037_{60}	-0.027_{70}	0.09
0.59975	0.25219	0.78754	-0.003_{77}	-0.005_{91}	−0.04
	0.44359	0.63745	-0.004_{98}	-0.006_{91}	−0.05
	0.65823	0.46967	-0.002_{82}	-0.006_{15}	−0.10
	0.86390	0.30841	-0.002_{42}	-0.004_{94}	−0.06
	1.0524	0.15741	0.000_{29}	-0.004_{75}	−0.08
0.81372	0.58512	0.86910	-0.002_{63}	-0.011_{47}	0.49
	0.88214	0.64024	0.017_{32}	0.014_{28}	−0.12
	1.1583	0.43184	0.016_{74}	0.015_{29}	−0.05
	1.3936	0.24999	0.008_{29}	0.012_{10}	0.09
1.1610	0.27866	1.5876	0.018_{51}	0.026_{77}	0.18
	0.57402	1.3735	0.032_{71}	0.029_{18}	−0.13
	0.87125	1.1631	0.037_{45}	0.033_{68}	−0.18
	1.2258	0.91511	0.035_{03}	0.036_{07}	0.06
	1.4723	0.73519	0.035_{02}	0.032_{15}	−0.15
1.5188	0.30159	2.0461	0.038_{00}	0.035_{47}	−0.06
	0.52929	1.8921	0.038_{31}	0.038_{13}	−0.01
	0.80052	1.7067	0.044_{58}	0.042_{97}	−0.08
	1.0730	1.5256	0.044_{76}	0.046_{84}	0.12
	1.3232	1.3569	0.044_{37}	0.046_{75}	0.16
2.1221	0.28058	2.8240	0.041_{21}	0.038_{25}	−0.06
	0.60993	2.6101	0.046_{47}	0.043_{59}	−0.12
	0.92873	2.4068	0.050_{01}	0.050_{06}	0.00
	1.2170	2.2253	0.050_{62}	0.052_{80}	0.15
	1.4622	2.0690	0.050_{56}	0.049_{96}	−0.05
3.0536	0.25757	3.9720	0.028_{15}	0.030_{84}	0.05
	0.83440	3.6171	0.043_{89}	0.043_{45}	−0.02
	1.1102	3.4518	0.046_{36}	0.048_{11}	0.12
	1.4335	3.2582	0.047_{59}	0.046_{61}	−0.08
3.8765	0.24079	4.9649	0.029_{35}	0.029_{11}	0.00
	0.51140	4.7984	0.037_{50}	0.035_{35}	−0.07
	0.82222	4.6149	0.040_{67}	0.044_{09}	0.17
	1.1378	4.4055	0.051_{77}	0.049_{87}	−0.13
		α-Aminobutyric Acid–Sucrose–Water			
0.41893	0.15289	0.56465	0.132_{34}	0.098_{44}	−0.39
	0.27378	0.45279	0.083_{34}	0.083_{99}	0.01
	0.36844	0.36689	0.040_{44}	0.075_{27}	0.62
	0.45887	0.27343	0.087_{31}	0.068_{99}	−0.30
	0.61716	0.12142	0.052_{02}	0.062_{11}	0.10
0.60585	0.20515	0.81427	0.072_{69}	0.089_{71}	0.26
	0.37736	0.65626	0.061_{24}	0.072_{97}	0.27
	0.57167	0.47473	0.051_{24}	0.061_{99}	0.27
	0.74552	0.30529	0.055_{71}	0.058_{15}	0.05
	0.91333	0.13887	0.059_{70}	0.058_{81}	−0.01
0.83636	0.19248	1.1680	0.092_{16}	0.089_{43}	−0.04
	0.48244	0.91170	0.067_{75}	0.065_{11}	−0.08
	0.72733	0.68513	0.067_{53}	0.057_{27}	−0.34
	1.0272	0.40075	0.063_{39}	0.058_{95}	−0.12
	1.2812	0.14770	0.079_{81}	0.066_{51}	−0.17

TABLE 1. (Continued)

m_R	m_1	m_2	Δ/m_1m_2 Exptl	Δ/m_1m_2 Calcd[a]	Diff. %[b]
0.87464	0.20041	1.2161	0.093_{17}	0.088_{27}	−0.08
	0.50305	0.95060	0.067_{91}	0.063_{97}	−0.12
	0.75888	0.71485	0.066_{60}	0.056_{85}	−0.34
	1.0716	0.41810	0.063_{99}	0.059_{69}	−0.12
1.1436	0.39163	1.4369	0.066_{35}	0.070_{08}	0.10
	0.68999	1.1789	0.061_{96}	0.057_{75}	−0.17
	0.97043	0.92902	0.057_{86}	0.057_{08}	−0.03
	1.3165	0.60988	0.049_{78}	0.064_{11}	0.56
	1.6161	0.31341	0.073_{10}	0.071_{53}	−0.04
1.5601	0.32964	2.0478	0.071_{68}	0.073_{67}	0.05
	0.63128	1.8023	0.066_{54}	0.059_{82}	−0.27
	1.1290	1.3856	0.059_{23}	0.059_{44}	0.01
	1.5484	1.0166	0.053_{21}	0.064_{68}	0.64
	1.8648	0.70963	0.061_{28}	0.062_{73}	0.07
2.0610	0.32614	2.6944	0.059_{28}	0.071_{88}	0.29
	0.64124	2.4470	0.063_{35}	0.060_{35}	−0.13
	1.0351	2.1369	0.060_{04}	0.059_{63}	−0.02
	1.3484	1.8829	0.057_{79}	0.061_{90}	0.28
	1.7479	1.5432	0.057_{04}	0.057_{53}	0.03
2.5831	0.19494	3.4234	0.072_{38}	0.074_{88}	0.03
	0.54857	3.1652	0.060_{54}	0.060_{55}	0.00
	0.80056	2.9752	0.060_{33}	0.058_{88}	−0.07
	1.1392	2.7143	0.060_{40}	0.060_{92}	0.03
	1.3856	2.5261	0.057_{78}	0.061_{16}	0.25
	1.6907	2.2794	0.058_{50}	0.054_{73}	−0.30
2.7287	0.20449	3.5911	0.070_{49}	0.071_{82}	0.02
	0.57545	3.3203	0.061_{14}	0.059_{16}	−0.07
	0.84047	3.1235	0.059_{53}	0.058_{60}	−0.05
	1.1971	2.8522	0.058_{90}	0.061_{00}	0.14
	1.4500	2.6435	0.063_{69}	0.060_{08}	−0.27
	1.7794	2.3989	0.056_{34}	0.049_{06}	−0.61
2.9161	0.35899	3.7005	0.067_{04}	0.061_{60}	−0.13
	0.66476	3.4811	0.059_{48}	0.057_{09}	−0.10
	0.94791	3.2676	0.060_{52}	0.058_{64}	−0.11
	1.2875	3.0172	0.056_{93}	0.060_{50}	0.25
	1.6002	2.7794	0.055_{31}	0.055_{38}	0.01
3.0421	0.37288	3.8437	0.062_{53}	0.059_{04}	−0.09
	0.69071	3.6170	0.056_{55}	0.055_{92}	−0.03
	0.98479	3.3948	0.058_{94}	0.058_{30}	−0.04
	1.6642	2.8906	0.053_{55}	0.051_{67}	−0.16
3.3771	0.35322	4.2703	0.046_{28}	0.052_{05}	0.14
	1.0433	3.7607	0.055_{42}	0.056_{08}	0.04
	1.3038	3.5743	0.052_{85}	0.057_{17}	0.31
3.6267	0.37633	4.5497	0.048_{34}	0.044_{86}	−0.09
	1.1130	4.0121	0.053_{65}	0.053_{64}	−0.00
	1.3920	3.8161	0.050_{45}	0.053_{23}	0.21

a) Calculated by the least-squares treatment of Eq. 20 and Table 2. b) Percentage error defined by Kelly *et al.*[16]

1 and 2 in a ternary solution containing solutes 1 and 2 with molalities m_1 and m_2, respectively; γ_{10} and γ_{20} are the molal activity coefficients, respectively, of binary solutions containing only solute 1 at molality m_1 or solute 2 at molality m_2. The values of osmotic and activity coefficients for reference potassium chloride solutions were taken from the values given by Robinson and Stokes.[13] The values of osmotic and activity coefficients for glygly and αABA solutions were taken from the data of Ellerton *et al.*,[14] and the values for sucrose solutions, from Robinson and Stokes.[15]

Results

The equilibrium molalities of solute 1 and 2 in ternary solutions and of potassium chloride in reference solutions for the systems, glygly–sucrose–water

Table 2. Coefficients in Eq. 2 for the ternary solutions glycylglycine–sucrose–water (I) and α-aminobutyric acid–sucrose–water (II) at 25 °C

Coefficients	I	II
$A_{00}\times 10$	−0.77385	1.3170
$A_{10}\times 10$	0.34859	−2.0566
$A_{01}\times 10$	1.0532	−0.15888
$A_{20}\times 10$	0.50339	1.8176
$A_{11}\times 10^2$	−3.2769	2.1159
$A_{02}\times 10^2$	−3.0133	0.4932
$A_{30}\times 10^2$	−2.6230	−4.6886
$A_{21}\times 10^2$	0.1266	−1.3365
$A_{12}\times 10^3$	5.098	0.668
$A_{03}\times 10^3$	2.647	1.012

and αABA–sucrose–water, are given in Table 1, together with the values of experimental quantities Δ/m_1m_2 defined by Eq. 1. In order to fit the experimental values of Δ/m_1m_2 to a power series in m_1 and m_2 with the form of Eq. 2, two polynomials involving terms up to squares or cubes in m_1 and m_2 were examined with a HITAC 8450 computer. In both systems, the better polynomials for representing the data are equations containing terms up to cubic. Their coefficients are given in Table 2.

From Eqs. 3 and 4 and Table 2, we obtain

$$\ln\gamma_1 = \ln\gamma_{10} - 0.077385m_2 + 0.034859m_1m_2 + 0.052662m_2^2 + 0.050339m_1^2m_2 - 0.021846m_1m_2^2 - 0.010044m_2^3 - 0.026230m_1^3m_2 + 0.000949m_1^2m_2^2 + 0.002549m_1m_2^3 + 0.000662m_2^4, \quad (5)$$

$$\ln\gamma_2 = \ln\gamma_{20} - 0.077385m_1 + 0.017429m_1^2 + 0.10532m_1m_2 + 0.016780m_1^3 - 0.021846m_1^2m_2 - 0.030133m_1m_2^2 - 0.006557m_1^4 + 0.000633m_1^3m_2 + 0.003824m_1^2m_2^2 + 0.002647m_1m_2^3, \quad (6)$$

for the system glygly–sucrose–water, and

$$\ln\gamma_1 = \ln\gamma_{10} + 0.13170m_2 - 0.20566m_1m_2 - 0.007944m_2^2 + 0.18176m_1^2m_2 + 0.014106m_1m_2^2 + 0.0016439m_2^3 - 0.046886m_1^3m_2 - 0.010024m_1^2m_2^2 + 0.000334m_1m_2^3 - 0.000253m_2^4, \quad (7)$$

$$\ln\gamma_2 = \ln\gamma_{20} + 0.13170m_1 - 0.10283m_1^2 - 0.015888m_1m_2 + 0.060588m_1^3 + 0.014106m_1^2m_2 + 0.004932m_1m_2^2 - 0.011721m_1^4 - 0.006683m_1^3m_2 + 0.000501m_1^2m_2^2 - 0.001012m_1m_2^3, \quad (8)$$

for the system αABA–sucrose–water.

The activity coefficients of glygly in binary solution and in ternary solutions containing several concentrations of sucrose are given in Fig. 1 and the activity coefficients of αABA in binary and in ternary solutions in Fig. 2. The activity coefficients of glygly and αABA increase with the concentration of sucrose. At lower concentrations, however, sucrose has a different effect on the activity coefficients of glygly and αABA. As shown in Fig. 1, when sucrose concentration is lower than 2 mol kg^{-1} glygly is salted-in by sucrose, but at higher concentrations of both glygly (>1 mol kg^{-1}) and sucrose (>2 mol kg^{-1}) sating-out predominates. The activity coefficient of αABA increases for all the concentrations studied, the increasing effect being greater at lower concentration of αABA.

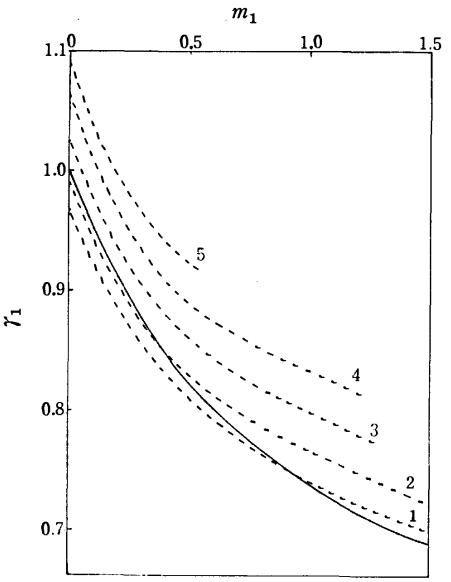

Fig. 1. Activity coefficients of glycylglycine in sucrose solutions: ——, in water; ----, in sucrose solutions at several concentrations of sucrose. The concentrations of sucrose (mol kg^{-1}): 1, 1.0; 2, 2.0; 3, 3.0; 4, 4.0; 5, 5.0.

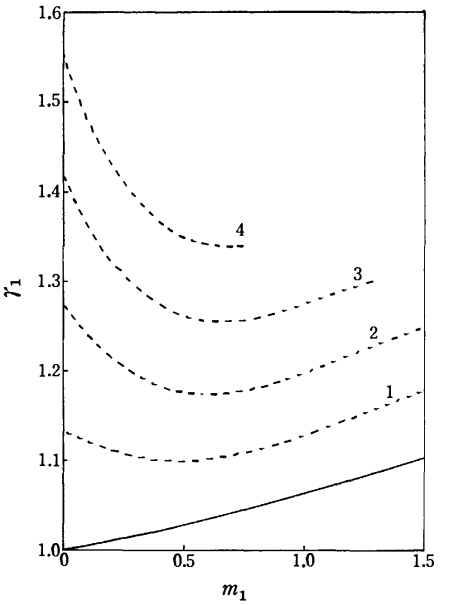

Fig. 2. Activity coefficients of α-aminobutyric acid in sucroes solutions: ——, in water; ----, in sucrose solutions at several concentrations of sucrose. The concentrations of sucrose (mol kg^{-1}): 1, 1.0; 2, 2.0; 3, 3.0; 4, 4.0.

Discussion

From the isopiestic data, the excess free energy of mixing per kilogram of solvent, $\Delta_m G_w^{ex}$, can be calculated. $\Delta_m G_w^{ex}$ for a mixture of two solutions of non-electrolytes A (concentration m_1) and B (m_2) is given

TABLE 3. FREE ENERGY EFFECTS OF PAIRWISE AND TRIPLET INTERACTIONS

A	B	$\{AB\}_g$[a] J mol^{-2} kg	$\{AAB\}_g$ J mol^{-3} kg^2	$\{ABB\}_g$ J mol^{-3} kg^2
α-Aminobutyric acid	Sucrose	160	−85	−6.6
Glycylglycine	Sucrose	−96	14	44
α-Aminobutyric acid	Urea	−54[b]	0.13	2.1
Glycylglycine	Urea	−123[b]	41	4.0
Sucrose	Urea	−155	7.5	6.2

a) $\{AB\}_g$ is $(2.303RT)$ times the "limiting interaction coefficients" which is defined by Schrier and Robinson[19] as a measure of the mutual interaction of the solutes (and the solvent) free of the contribution from concentration dependent terms. b) Lilley and Scott[20] obtained the values, −35 and −119 (J mol^{-2} kg), for αABA–urea and glygly–urea, respectively.

by Cassel and Wood[17] as follows:

$$\Delta_m G_w^{ex}/RT = (m_1+m_2)\phi_{mix} - m_1\phi_1 - m_2\phi_2 = [2\{AB\}_g m_1 m_2 + 6\{AAB\}_g m_1^2 m_2 + 6\{ABB\}_g m_1 m_2^2 + \cdots]/RT, \quad (9)$$

where ϕ_{mix} is the osmotic coefficient of a ternary solution, the species in brackets denoting the particles interacting, and subscript g the free energy of interaction. The values of the pairwise and triplet interactions calculated by Eq. 9 are given in Table 3, together with values for the systems αABA–urea–water,[18] glygly–urea–water,[9] and sucrose–urea–water.[12] Using an expression[17] similar to Eq. 9 and the data for binary solutions, the pairwise interactions for binary solutions of αABA,[14] glygly,[14] sucrose[15] and urea[12] are calculated to be 62, −660, 180 and −110 (J mol^{-2}kg), respectively.

Pairwise and triplet interactions formally depend only on the solute species, but they are affected by the interactions with the solvent water as Schrier and Robinson[19] pointed out.

It is interesting to classify the pairwise interactions by the effect of these solutes on water structure. Walrafen[21] showed from Raman spectral measurements that sucrose has a structure promoting effect on water. Taylor and Rowlinson[22] measured the heat of dilution of sucrose in water and concluded that strong hydrogen bonding exists between sucrose and surrounding water molecules. The self diffusion coefficients of water in aqueous solutions of glygly and αABA were measured at 25—50 °C by Altunina *et al.*[23] Glygly and αABA decrease the activation energy of self diffusion of water. On the other hand, the structure-making solutes cause the water near them to be more ice-like than normal; the melting of such a structure requires greater energy with the result that such solutes give rise to positive excess partial molal heat capacities.[24,25] Spink and Wadsö[26] measured the heat capacities of solid αABA and aqueous solution of the amino acid at 25 °C and also enthalpies of solution at several temperatures. By both direct and indirect measurements they determined the partial molal heat capacity, $\bar{C}^\circ_{p,2}$ and excess partial molal heat capacity, ΔC°_p, of αABA, 222—226 and 76—80 (J k^{-1}mol^{-1}), respectively. The corresponding values for glygly which are determined from the data of heat capacity of solid,[27] and of aqueous solutions[28] are 159 and −4.6 (J k^{-1}mol^{-1}) for $\bar{C}^\circ_{p,2}$, and ΔC°_p, respectively. The NMR and calorimetric data for αABA are not consistent as to the effect on the water structure, probably because αABA is near the borderline of the structure-making and structure-breaking solutes. We believe, however, that the precise calorimetric results by Spink and Wadsö are more reliable and thus, αABA is considered to be a weak structure maker. Many papers have appeared on the effect of urea on water structure, but it is generally accepted that urea behaves as a structure breaker.[29]

Thus, αABA and sucrose are ranked as structure makers (positive hydration) and glygly and urea as structure breakers (negative hydration). From Table 3, it is seen that the pairwise interactions between the two structure making solutes are positive (αABA+sucrose, sucrose+sucrose and αABA+αABA), and the interactions between the two structure breaking solutes are negative (glygly+urea, glygly+glygly and urea+urea). For the systems containing structure-making and structure-breaking solutes (sucrose+urea, glygly+sucrose and αABA+urea), the interactions are negative. The triplet interactions have signs opposite to the pairwise interactions between unlike solutes in the same systems.

The nature of the structure-making effect of hydrophylic sucrose on water structure differs from that of αABA having hydrophobic ethyl group, and the structure-breaking effects of glygly and urea are not the same. In spite of these differences, the signs of excess pairwise interactions entirely depend on the above classification by the effect on water structure.

In order to obtain the concentration dependency of the interaction quantitatively, the free energy of the transfer is calculated. The activity coefficients of the amino acids in sucrose solutions measured by the isopiestic method are referred to unity in the standard state in water, and not to the standard state in a water–sucrose solvent.[30] Thus the free energy of transfer at constant concentration of the solute is calculated from the change in activity coefficients. Consequently, the free energy of transfer, ΔG_t, of solute 1 from water to sucrose solution is given by[31]

$$\Delta G_t = RT \ln (f_1/f_{10}), \quad (10)$$

where f_{10} and f_1 are the activity coefficients in mole fraction scale of solute 1 in binary and ternary sucrose solutions, respectively, both at the same mole fraction; f_1 and f_{10} are defined as before.[31]

The values of ΔG_t of glygly and αABA from water to various concentrations of sucrose solutions are given

Table 4. Free energy of transfer (in J mol) of glycylglycine and α-aminobutyric acid from water to sucrose solutions

m_{10}[a]	m_2 0.5	1.0	2.0	3.0	4.0	5.0
			Glycylglycine			
0	−44.1	−40.3	53.3	190	320	431
0.2	−37.4	−31.3	57.5	183	303	414
0.5	−20.0	−2.6	95.7	223	347	
1.0	13.5	54.4	178	318	462	
1.5	30.2	76.7	188	297		
			α-Aminobutyric acid			
0	181	354	686	992	1260	
0.2	140	275	536	791	1020	
0.5	106	210	418	632	837	
1.0	97.5	194	388	590		
1.5	111	215	402			

a) The molality of solute 1 in a binary solution. The molalities in ternary solutions are slightly greater than m_{10} as the transfer is made at constant mole fraction.[31]

in Table 4. At higher concentrations of sucrose (>2 m), ΔG_t of both glygly and αABA increases with increasing concentration of sucrose, the increasing effect on αABA being much larger than that on glygly. The values of ΔG_t depend differently on the concentration of the amino acids. ΔG_t increases with increasing concentration of glygly and with decreasing concentration of αABA. At lower concentrations ($m_{10}<1.0$ and $m_2<2.0$), the sucrose solution is a more favorable solvent than water for glygly. The results indicate that the sucrose solution environment is much more unforable than water for αABA having an alkyl side chain as compared with glygly which has no side chain. It would require much more work for alkyl groups in the interior of the protein to be exposed in the sucrose solution than in water, they would thus be caused by the sucrose solution to enter into the interior of protein, as Lakshimi and Nandi[8] reported for amino acids with aromatic side chain.

The denaturing process can be considered to involve a dilution process of local concentrations of amino acid residues in a protein. The dilution process of a solute is accompanied by the decrease of its chemical potential since the term $RT \ln \gamma_1 m_1$ decreases with dilution. While γ_1 of glygly in a sucrose sloution increases with decreasing concentration more solwly than in water, γ_1 of αABA increases with decreasing concentration at a concentration lower than 0.5 mol kg^{-1} even though γ_{10} decreases with decreasing concentration. (Fig. 1 and 2).

Klotz[32] obtained values for the average molar local concentrations of peptide and low apolar residues (Ala +Val+Ileu+Phe) whihin molecular volume of proteins (insurine, ribonuclease, ovalbumin and bovin serum albumin) to be 12—13 M and 3—4 M, respectively. Though the concentration range of the present work is lower than the values estimated by Klotz, and it is difficult to determine the real local concentration of amino acid residues at the surface of the protein molecules, the results suggest that the decrease in chemical potential with denaturing (dilution) process is less in sucrose solutions than in water for apolar residues. When denaturant molecules cause the loosening of the globular structure of the protein resulting in a contact of the interior hydrophobic side chains to solutions, the decrease in chemical potential with the subsequent extending process would become less in sucrose+denaturant solution than in denaturant solution. This would also result in more stability of a protein molecule in a sucrose solution and would reduce the extent of denaturation of protein molecule induced thermally or by denaturants.

The results with glygly suggest that the interaction of sucrose on peptide group is somewhat complicated. A sucrose solution is a favorable solvent for glygly at low concentration of sucrose, becoming unfavorable at higher concentration. Shifrin and Parrott[7] have demonstrated that low concentrations of polyhydric alcohols (including glucose and sucrose) accelerate the rate of dissociation of tetrameric L-asparaginase by urea, and higher concentrations of polyols protect the enzyme against the dissociating effect of urea. The change in the effect of polyols on the protein with concentration might be related to the switch from salting-in to salting-out of glygly by sucrose with increase in sucrose concentration.

The author wishes to thank Dr. Hisashi Uedaira for his valuable discussions.

Refernces

1) A. Beilinson, *Biochem. Z.*, **213**, 399 (1929).
2) C. D. Ball, D. T. Hardt, and W. J. Duddles, *J. Biol. Chem.*, **151**, 163 (1943); C. R. Hardt, I. F. Huddelson, and C. D. Ball, *ibid.*, **163**, 211 (1946).
3) S. Y. Gersma and E. R. Stuur, *Int. J. Pept. Protein Res.*, **4**, 377 (1972); S. R. Gelsma, *Eur. J. Biochem.*, **14**, 150 (1970).
4) R. B. Simpson and W. Kauzmann, *J. Am. Chem. Soc.*, **75**, 5139 (1953).
5) K. Shikama, *J. Biochem.*, **64**, 55 (1968).
6) J. C. Metral and J. Yon, *Biochem. Biophys. Acta*, **160**, 340 (1968).
7) S. Shifrin and C. L. Parrot, *Arch. Biochem. Biophys.*, **166**, 426 (1975).
8) T. S. Lakshimi and P. K. Nandi, *J. Phys. Chem.*, **80**, 249 (1976).
9) H. Uedaira, *Bull. Chem. Soc. Jpn.*, **45**, 3068 (1972).
10) H. Uedaira and H. Uedaira, *J. Phys. Chem.*, **74**, 1931 (1970).
11) V. E. Bower and R. A. Robinson, *J. Phys. Chem.*, **67**, 1524 (1963).
12) H. D. Ellerton and P. J. Dunlop, *J. Phys. Chem.*, **70**, 1831 (1966).
13) R. A. Robinson and R. H. Stokes, "Electrolyte Solutions," 2nd ed., Butterworths, London (1959).
14) H. D. Ellerton, G. Reinfelds, D. E. Mulcahy, and P. J. Dunlop, *J. Phys. Chem.*, **68**, 400 (1964).
15) R. A. Robinson and R. H. Stokes, *J. Phys. Chem.*, **65**, 1954 (1961).
16) F. J. Kelly, R. A. Robinson, and R. H. Stokes, *J. Phys. Chem.*, **65**, 1958 (1961).
17) R. B. Cassel and R. H. Wood, *J. Phys. Chem.*, **78**, 2460, 2465 (1974).

18) E. L. Cussler, Jr., *J. Phys. Chem.*, **71**, 901 (1967).
19) E. E. Schrier and R. A. Robinson, *J. Biol. Chem.*, **245**, 2432 (1970).
20) T. H. Lilley and R. P. Scott, *J. Chem. Soc. Faraday Trans.*, **72**, 184 (1976).
21) G. E. Walrafen, *J. Chem. Phys.*, **44**, 3726 (1966).
22) J. B. Taylor and J. S. Rowlinson, *Trans. Faraday Soc.*, **51**, 1183 (1955).
23) L. K. Altunina, O. F. Bezrikov, N. A. Smirnova, I. A. Moskbicheva, and V. P. Fokanov, *Strukt. Rol' Vody Zhivom Org.*, **2**, 57 (1968).
24) H. S. Frank and W. Y. Wen, *Discuss. Faraday Soc.*, **24**, 133 (1957).
25) S. Subramanian, T. S. Sarma, D. Balasubramanian, and J. C. Ahluwalia, *J. Phys. Chem.*, **75**, 815 (1971).
26) C. H. Spink and I. Wadsö, *J. Chem. Thermodyn.*, **7**, 561 (1975).
27) H. M. Huffman, *J. Am. Chem. Soc.*, **63**, 688 (1941). Huffman measured the heat capacity of solid glygly at eighteen temperatures from −186.5 to 20.7 °C. The extraporated value to 25.0 °C is 163.5 J $k^{-1}mol^{-1}$.
28) G. C. Kresheck and L. Benjamin, *J. Phys. Chem.*, **68**, 2476 (1964).
29) For example, H. Uedaira, *Tampakushitsu Kakusan Koso*, **18** 62 (1973).
30) H. S. Harned and R. A. Robinson, "Multicomponent Electrolyte Solutions," Pergamon Press Inc., London (1968), p. 94.
31) H. Uedaira, *Bull. Chem. Soc. Jpn.*, **48**, 2006 (1975).
32) I. M. Klotz, *Brook Heaven Symposia in Biol.*, **13**, 25 (1960).

Dynamic Structure of Water in Aqueous Solutions of Chloroacetate. I. Temperature Dependence of Limiting Mobilities of Mono-, Di-, and Tri-chloroacetate Ions

Satoshi EBINA and Hisashi UEDAIRA*

Central Research Laboratory, Fukushima Medical College, Sugitsuma-cho 65, Fukushima 960

**Research Institute for Polymers and Textiles, Sawatari 4, Kanagawa-ku, Yokohama 221*

(Received December 24, 1976)

Electric conductivities of the sodium salts of mono-, di-, and tri-chloroacetic acids were measured in water at 15, 25, and 35 °C. The molar conductivities were analyzed by the Fuoss-Onsager equation to obtain the limiting mobility. On the basis of the temperature dependence of the limiting mobilities, the dynamic structure of water around these anions was investigated by means of Samoilov's theory. Chloroacetate ions are structure maker and the degree of the positive hydration is in the order TCA^- > acetate ion > DCA^- > MCA^-. From the results, it is shown that a competition between the different orientation of water molecules in the surroundings of $-CH_2Cl$ and $-CHCl_2$ groups occurs, and consequently, shown that the water molecules around DCA^- and MCA^- ions more mobile than those around TCA^- and acetate ions.

There have been many investigations on the hydration of aqueous solutions of organic electrolytes. The particular interest in the hydration is related to the interactions between water and the hydrophobic or ionized groups of these electrolytes.

The study of aqueous solutions of halogenized organic compounds is important from both theoretical and biochemical point of view. For example, trifluoroacetic and trichloroacetic acids cause denaturation of proteins and nucleic acids. The systematic investigations, however, have been scarecely made.

Robinson and Jencks[1] determined the activity coefficient of acetyltetraglycine ethyl ester in the presence of various organic electrolytes. According to their results, trichloroacetate ion behaves as the structure breaker in contrast to acetate ion. On the other hand, Engel and Hertz[2] showed that the trichloroacetate ion is structure maker by means of the measurement of proton relaxation rates in aqueous solutions of the various electrolytes. Recently, we have measured the turbidity of several proteins in aqueous solutions by some aromatic sulfonic acids and trichloroacetic acid.[3] Only trichloroacetic acid gave a common profile for all of the proteins examined, *i. e.*, the turbidity of protein solutions increases abruptly with increasing the concentration of trichloroacetic acid, and above 0.5 mol dm^{-3} of trichloroacetic acid goes through a maximum. The values of maximum turbidity are similar for all of the protein solutions.

It is thought that the peculiar interaction between trichloroacetic acid and protein may be related to the nature of hydration of the precipitant. But on the hydration of trichloroacetate ion the above mentioned contradictory results are obtained. In a series of our studies of the effects of organic electrolytes on the dynamic structure of water, it was shown that the water structure around organic ions is affected by the individual interactions between water and the ionized, hydrophobic, or hydrophilic groups.[4-7] From this point of view, in order to examine the interaction between trichloroacetate ion and water, we present here the electric conductivities of the sodium salts of mono-, di-, and trichloroacetate in water at 15, 25, and 35 °C. The dynamic structure of water around these anions are discussed on the basis of Samoilov's theory.[8]

Experimental

Monochloroacetic and trichloroacetic acids (G. R., Wako Pure Chemicals) without further purification were neutralized with NaOH (G. R., Wako Pure Chemicals). Dichloroacetic acid (E. P., Wako Pure Chemicals) was once distilled before neutralization with NaOH. These sodium salts (NaMCA, NaDCA, and NaTCA) were recrystallized five times from ethanol for NaMCA, and from ethanol-water for NaDCA and NaTCA, and dried at 55 °C *in vacuo* over phosphorus pentoxide.

Water was deionized, glass-distilled, and the electrolytic conductivity of water was about $1 \times 10^{-6}\ \Omega^{-1}\ cm^{-1}$ at 25 °C. All the solutions were prepared by weighing and all the weights were corrected to those in vacuum. The molar concentrations of these solutions were calculated from solution densities. Electric conductivities of all the solutions were measured at 15, 25, and 35±0.001 °C. The procedure of the measurements of the conductivity and density are described elesewhere.[9]

Results and Discussion

The molar conductivities of NaMCA, NaDCA, and NaTCA in water at 15, 25, and 35 °C are given in Tables 1, 2, and 3, respectively. The limiting molar conductivities of salts, Λ°, were determined by the Fuoss-Onsager equation,[10]

$$\Lambda = \Lambda^\circ - S\sqrt{c} + Ec\log c + Jc, \quad (1)$$

where c is a molar concentration and the other symbols are defined in Ref. 10. The plots of molar conductivities *vs.* $c^{1/2}$ at 25 °C are shown in Fig. 1, where the solid lines were calculated from Eq. 1.

The $\lambda_+^\circ(Na^+)$ used to calculate λ_-° from the Kohlraush rule were obtained from the literature.[11] The temperature dependence of λ_-° for MCA^-, DCA^-, and TCA^- ions are shown in Fig. 2.

According to Samoilov,[8,12] the dynamic structure of water around an ion is described by the quantities τ_1/τ_0 and ΔE_1, and the following relation approximately holds between these quantities:

$$\tau_1/\tau_0 = \exp(\Delta E_1/RT), \quad (2)$$

Table 1. Molar conductivities of sodium monochloroacetate in water as function of temperature

15 °C		25 °C		35 °C	
c (mol m^{-3})	Λ (cm^2 Ω^{-1} mol^{-1})	c (mol m^{-3})	Λ (cm^2 Ω^{-1} mol^{-1})	c (mol m^{-3})	Λ (cm^2 Ω^{-1} mol^{-1})
0	71.53	0	90.27	0	111.80
0.09446	70.62	0.18868	89.05	0.19857	110.44
0.20032	70.64	0.38206	88.83	0.35304	109.85
0.35782	70.43	0.55420	88.34	0.55159	109.83
0.55623	70.20	0.80334	88.11	0.79823	109.35
0.80029	70.04	1.08936	87.66	1.08461	108.91
1.10141	69.69	1.42188	87.59	1.41036	108.41
1.43009	69.63	2.22546	86.88	2.19660	107.83
2.21919	68.98	3.04732	86.66	3.18045	107.08
3.36991	68.55	4.43901	85.97		
4.37920	68.26	5.93186	85.26		
5.66748	67.82				

Table 2. Molar conductivities of sodium dichloroacetate in water as function of temperature

15 °C		25 °C		35 °C	
c (mol m^{-3})	Λ (cm^2 Ω^{-1} mol^{-1})	c (mol m^{-3})	Λ (cm^2 Ω^{-1} mol^{-1})	c (mol m^{-3})	Λ (cm^2 Ω^{-1} mol^{-1})
0	69.55	0	88.27	0	108.97
0.20595	68.61	0.19990	87.09	0.29099	107.10
0.35868	68.36	0.35322	86.72	0.47540	106.63
0.55703	68.11	0.55505	86.50	0.73606	106.31
0.80286	67.83	0.82304	86.13	1.06371	105.76
1.09032	67.61	1.08632	85.79	1.45131	104.97
1.42231	67.33	1.40913	85.39	1.90373	104.65
2.22863	66.82	2.221578	84.72	2.94811	103.85
3.20101	66.32	2.88883	84.23	4.20935	102.88
4.38957	65.80	4.36259	83.30		

Table 3. Molar conductivities of sodium trichloroacetate in water as function of temperature

15 °C		25 °C		35 °C	
c (mol m^{-1})	Λ (cm^2 Ω^{-1} mol^{-1})	c (mol m^{-3})	Λ (cm^2 Ω^{-1} mol^{-1})	c (mol m^{-3})	Λ (cm^2 Ω^{-1} mol^{-1})
0	67.39	0	85.76	0	106.33
0.08473	66.83	0.19128	84.27	0.19092	105.02
0.18446	66.82	0.33988	84.30	0.33748	104.33
0.33866	66.26	0.53254	83.90	0.52748	103.68
0.52955	65.92	0.75835	83.67	0.76188	103.21
0.76237	65.73	1.04199	83.29	1.03524	102.74
1.03783	65.51	1.32992	82.94	1.35195	102.14
1.35270	65.29	2.12819	82.30	1.97345	101.54
2.11642	64.94	2.87635	81.68	3.04430	100.52
2.98928	64.33	3.93795	81.03		
4.15373	63.91	5.15951	80.49		
5.38978	63.44				

where τ_1 and τ_0 are the mean residence times of a water molecule in the immediate neighbourhood of the ion in an aqueous solution and in the immediate vicinity of a water molecule in pure water, respectively. ΔE_1 is the difference of the activation energies for the removal of a water molecule from the immediate neighbourhoods of the ion and the water molecule.

The value of ΔE_1 is obtained from the temperature dependence of the limiting mobility of the ion. One of the authors (H. U.) together with Uedaira[4] obtained the following equation for organic ions and molecules by extending the Samoilov's equation,[8] which holds

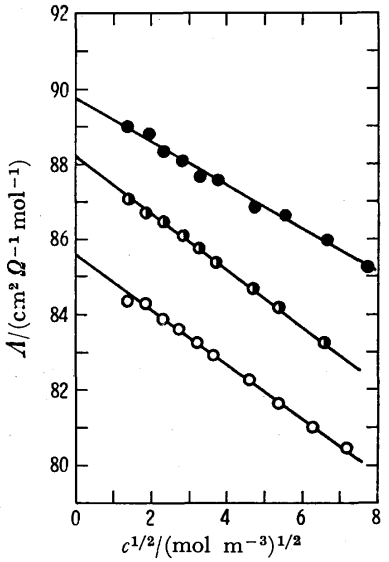

Fig. 1. Electric conductivities of NaMCA, NaDCA, and NaTCA in water at 25 °C.
—●— NaMCA, —◑— NaDCA, —○— NaTCA.

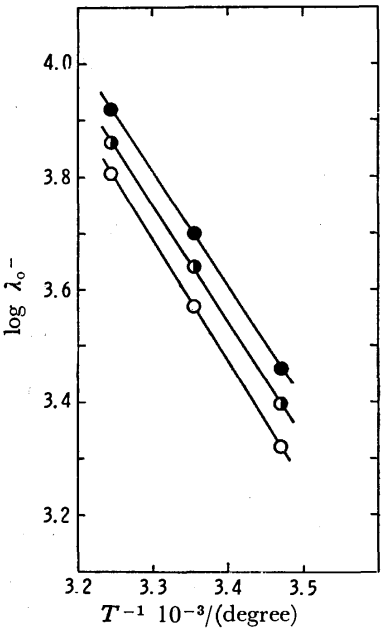

Fig. 2. Temperature dependence of limiting mobilities of MCA⁻, DCA⁻, and TCA⁻ ions.
—●— MCA⁻, —◑— DCA⁻, —○— TCA⁻.

for inorganic ions;

$$\frac{1}{\lambda_-^\circ}\frac{d\lambda_-^\circ}{dT}+\frac{1}{T}-\frac{1}{D_w}\frac{dD_w}{dT}=\frac{\Delta E_1}{RT^2}, \qquad (3)$$

where D_w is the self-diffusion coefficient of pure water. ΔE_1 consists of two terms,

$$\Delta E_1=\Delta E_1+\Delta E_2, \qquad (4)$$

where ΔE_1 and ΔE_2 represent the effects of the ionized and the hydrophobic groups on the thermal motion of water molecule around the organic ion, respectively. In general, ΔE_2 represents the effect of any group except the ionized group.

Table 4. The values of ΔE_1 and τ_1/τ_o for mono-, di-, and trichloroacetate ions at 25 °C

Ions	$r(10^{-10}\ m)$	$\Delta E_1(J/mol)$	τ_1/τ_o
MCA⁻	2.41	285	1.12
DCA⁻	2.54	582	1.26
TCA⁻	2.67	1247	1.65

From the results of Fig. 2 and the self-diffusion coefficient of water,[13] the values of ΔE_1 and τ_1/τ_o for MCA⁻, DCA⁻, and TCA⁻ ions at 25 °C were calculated by the Eqs. 2 and 3. The calculated results and the ionic radii estimated by the Pauling model[14] are presented in Table 4. The values of ΔE_1 and τ_1/τ_o for MCA⁻, DCA⁻, TCA⁻, and acetate ions[4] are shown in Fig. 3 as a function of the ionic radius.

It is seen from Table 4 that the residence times of a water molecule around MCA⁻, DCA⁻, and TCA⁻ ions are larger than that in pure water. That is to say, these anions are structure maker, and the structure making effect increases with an increase in the number of the chlorine atom.

As the result of the molecular motion, a water molecule change very rapidly its position and the momentary configurations between individual molecules. If the residence time of a water molecule in the hydration sphere of an ion is longer than that in pure water, also its reorientational time in the hydration sphere is longer than that in pure water. Hertz and Zeidler[15] showed that the residence time of the water molecule in the hydration sphere, τ_1, must be approximately equal to the reorientational correlation time. This concept was confirmed in the case of inorganic[16] and organic ions.[4] Engel and Hertz[2] obtained the value of 1.7, as the ratio of the reorientational correlation time in the hydration sphere to that in pure water

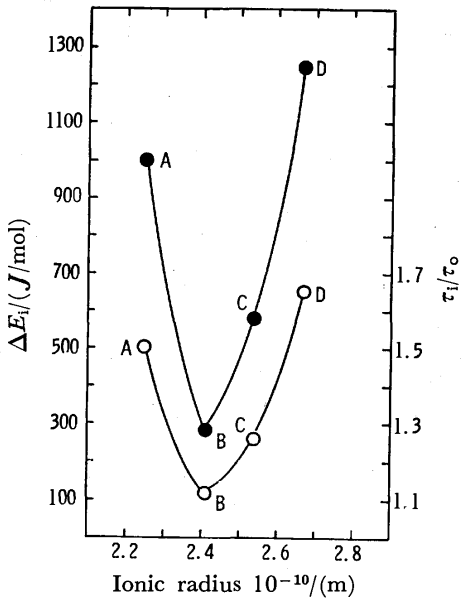

Fig. 3. The values of ΔE_1 and τ_1/τ_o of acetate, MCA⁻, DCA⁻, and TCA⁻ ions.
—●— ΔE_1, —○— τ_1/τ_o.
A; acetate ion, B; MCA⁻, C; DCA⁻, D; TCA⁻.

for TCA^- ion at 25 °C. Their result coincides very good with the result of Table 4.

From Fig. 3 one sees that ΔE_1 and τ_1/τ_0 for acetate ion are larger than those for MCA^- and DCA^- ions. Since ΔE_1 and τ_1/τ_0 are the characteristic quantities of the hydration at infinite dilution, the difference in ΔE_1 among acetate and chloroacetate ions is attributed to the difference in ΔE_2 in Eq. 4. Consequently, the thermal motion of the water molecule around $-CH_3$ group is slower than those around $-CH_2Cl$ and $-CHCl_2$ groups.

The possible explanation for this result is made as follows. At present, it is not yet clear what kind of water structure is formed around the alkyl groups in water. According to Wen,[17] there are two possibilities: ice-like and gashydrate-like types. The water molecule in the vicinity of the chlorine atom of MCA^-, DCA^-, and TCA^- ions may turn its proton preferentially towards the chlorine atom during the residence in the hydration sphere. This orientation is different from that of the water molecule around $-CH_3$ group. In the surroundings of $-CH_2Cl$ and $-CHCl_2$ groups, therefore, a competition between the different orientatins of water molecules occurs, and on account of this competitive action the water structure around these two groups may be in a state more disturbed than those around $-CH_3$ and $-CCl_3$ groups. As a result, the thermal motion of the water molecules around $-CH_2Cl$ and $-CHCl_2$ groups are faster than those around $-CH_3$ and $-CCl_3$ groups. Taking account of the fact that ΔE_1 of TCA^- ion is larger than that of acetate ion, the thermal motion of water molecule around $-CH_2Cl$ group is most vigorous (see Fig. 3).

If TCA^- ion and a compound with the hydrophobic group coexist in an aqueous solution, the water structure around the hydrophobic group may be disturbed by $-CCl_3$ group. That is, TCA^- ion behaves like a structure breaker and the hydrophobic compound is salted-in by TCA^- ion. The result of Robinson and Jencks[1] is accounted in this manner.

Both TCA^- and acetate ions are structure maker, but the water structure around them is very different from each other. Probably, the chlorine atom does not from the hydrogen bond with the water molecule, taking account of the values of τ_1/τ_0. Actually, Walrafen[18] found no evidence of the presence of the hydrogen bond between the water molecule and the chlorine atom by the measurement of Raman spectra of aqueous solution of NaTCA.

It is interesting to compare the dynamic structure of water around the chloro and methyl substituent groups of the protons in the methyl group of an acetate ion, since the van der Waals volume of the chlorine atom is equal to that of the methyl group. The limiting mobility is inversely proportional to both the ionic radius and the microviscosity of water around the ion, which depends on the water structure.[19] MCA^-, DCA^-, and TCA^- ions have the same volumes as propionate, isobutyrate, and trimethyl acetate ions, respectively. Therefore, the difference of the limiting mobilities of the ions can be ascribed in the difference in water structure around the ions. The limiting mobilities of propionate, isobutyrate, and trimethyl acetate ions at 25 °C are 35.82,[20] 24, and 23[4] Ω^{-1} cm^2 mol^{-1}, respectively.

From the values of the limiting mobilities, it is found that the microviscosities of water around MCA^-, DCA^-, and TCA^- ions are smaller than those around the corresponding methyl substituents of the acetate ion. Thus, the degree of the structure making effect of the chloroacetate ions is lower than that of the corresponding methyl substituents. Recently, we found that the degree of hydrophobic hydration of isobutyrate and trimethyl acetate ions is very strong.[4] These results support the existence of the competition between the different orientations of water molecules around $-CH_2Cl$ and $-CHCl_2$ groups.

The authors wish to acknowledge the helpful discussions and criticisms extended by Dr. Hatsuho Uedaira.

References

1) D. R. Robinson and W. P. Jencks, *J. Am. Chem. Soc.*, **86**, 2470 (1965).
2) G. Engel and H. G. Hertz, *Ber. Bunsenges. Phys. Chem.*, **72**, 808 (1968).
3) S. Ebina and H. Uedaira, The Annual Meeting of the Biophysical Society of Japan, Hiroshima, October 1976.
4) H. Uedaira and H. Uedaira, *Zh. Fiz. Khim.*, **42**, 3024 (1968).
5) H. Uedaira and H. Uedaira, *J. Phys. Chem.*, **74**, 1931 (1970).
6) H. Uedaira and H. Uedaira, *Zh. Fiz. Khim.*, **49**, 2306 (1975).
7) H. Uedaira and H. Uedaira, *Nippon Kagaku Kaishi*, **1975**, 2054.
8) O. Ya. Samoilov, "Struktura Vodn'kh Rastvorov Elektrolitov i Gidrataziya Ionov," Nauka, Moskow (1957); "Ion No Suiwa," (Translated from Russian), 2nd ed, Chigin Shokan (1976).
9) S. Ebina and H. Uedaira, *Chem. Lett.*, **1976**, 1015.
10) R. M. Fuoss and F. Accascina, "Electrolytic Conductances," Academic Press, N. Y. (1960).
11) R. A. Robinson and R. H. Stokes, "Electrolyte Solutions," 2nd ed, Butterworths, London (1959).
12) V. V. Goncharov, I. I. Romanova, O. Ya. Samoilov, and V. I. Yashikichev, *Zh. Strukt. Khim.*, **8**, 613 (1976).
13) G. A. Andreev, *Zh. Fiz. Khim.*, **37**, 361 (1963).
14) L. Pauling, "The Nature of the Chemical Bond," 3rd ed, Cornell University Press, Ithaca, N. Y. (1960).
15) H. G. Hertz and M. D. Zeidler, *Ber. Bunsenges. Phys. Chem.*, **67**, 774 (1963).
16) H. Uedaira, Symposium "Investigations on the Role of Liquid Structure of Solvent in Aqueous Solutions and the Interactions between Solute-Solute and Solute-Solvent," Nagoya, January 1975.
17) W. -Y. Wen, *J. Solution Chem.*, **2**, 253 (1973).
18) G. E. Walrafen, *J. Chem. Phys.*, **55**, 768 (1971).
19) H. Uedaira, *Zh. Fiz. Khim.*, **45**, 2550 (1971).
20) P. Saxton and L. S. Darkin, *J. Am. Chem. Soc.*, **62**, 846 (1940).

Microwave Spectrum, Dipole Moment, Structure, and Internal Motion of 1-Silabicyclo[2.2.1]heptane

Taso IKEURA,[1] Keiichi TANAKA, Eizi HIROTA,[2] Shin-ichi INABA,* and Yoichiro NAGAI*

Department of Chemistry, Faculty of Science, Kyushu University, Higashi-ku, Fukuoka 812

**Department of Applied Chemistry, Faculty of Engineering, Gunma University, Tenjin-cho, Kiryu 376*

(Received January 21, 1977)

The rotational constants of 1-silabicyclo[2.2.1]heptane in the ground vibrational state were determined to be A_0=2744.775 (2) MHz, B_0=2662.017 (2) MHz, and C_0=2145.994 (2) MHz, with the standard deviations in parentheses. Because the spectrum was very rich, the Stark effects of two transitions were analyzed by a simulation technique. The dipole moments thus obtained are μ_b=0.5±0.1 D, μ_c=0.05±0.01 D, and μ_t=0.5±0.1 D. The observed spectra did not exhibit any anomalies which were due to deviations of the molecular symmetry from C_s. Three structural parameters, Si–C(7), ∠C(2)–Si–C(6), and ∠Si–C(2)–C(3), were adjusted so as to reproduce the rotational constants observed for the ground state. The Si–C(7) bond was found to be longer than Si–C(2) by 0.07 Å. Two vibrational satellites were detected and were assigned to the v=1 and the v=2 states of a torsional mode of the skeleton. A relative-intensity measurement resulted in the excitation energies of 70±25 cm^{-1} and 160±60 cm^{-1} for v=1 and v=2, respectively. The molecular structure and the internal motions were discussed in terms of intramolecular forces.

Bicyclic compounds are often characterized by highly strained structures of their skeletons, which involve three-, four-, and/or five-membered rings in most cases. Because two or more such rings are condensed to constitute the skeleton of a bicyclic molecule, new aspects are often introduced in the resultant structure. Bicyclo[2.2.2]octane, for example, has cyclohexane rings as constituents, and may thus be free from the strain of the valence angles. However the cyclohexane rings are forced to be of the boat form in the bicyclo[2.2.2]-octane molecule, rather than of the more stable chair form. The conformation about the three C–C bonds is thus eclipsed, provided that the molecular symmetry is D_{3h}. We might, however, expect additional lowering in energy by twisting slightly the skeleton about the symmetry axis. In fact, we have shown in our previons papers[3,4] that simple derivatives of bicyclo[2.2.2]-octane have a double-minimum potential function to the torsion of the skeleton and the height of the potential barrier which is sensitive to the substituents is explained by balance of two forces due to the valence-angle strain and to the internal-rotation potential.

Bicyclo[2.2.1]heptane or norbornane is obtained by replacing one of the three ethylene bridges by a methylene bridge. We have thus here two C–C bonds with unstable conformation. Furthermore, the methylene bridge which is introduced will cause considerable strain in the molecular skeleton. These two facts will thus favor the C_{2v} symmetry much higher than C_2 or the twisted form. In fact, electron-diffraction data on norbornane[5] are consistent with C_{2v}. Unfortunately this molecule has too small dipole moment to observe its microwave spectrum. In the present work we investigated the 1-silabicyclo[2.2.1]heptane molecule by microwave spectroscopy.

Experimental

A sample of 1-silabicyclo[2.2.1]heptane was prepared by a procedure described in Ref. 6. It is a white crystalline solid with mp of 75 °C. Because this compound sublimes easily, the sample was purified by sublimation before use. However, the vapor pressure permitted observation of the microwave spectrum only at room temperature or higher. The microwave spectrometer which was used was of conventional Stark-modulation type with a 110 kHz sine-wave or square-wave oscillator as a modulator.

Rotational Spectra

By transferring appropriate structure parameters from norbornane,[5] dimethylsilane,[7] and trimethylsilane[8] we calculated the rotational constants of 1-silabicyclo-[2.2.1]heptane on an assumption of C_s symmetry. Bond-moment consideration indicated that the b component of the dipole moment was much larger than the c component, while the a component was zero because of symmetry (see Fig. 1, where the heavy atoms are given numbers for identification).

We first searched the spectra in the 20—30 GHz region. We observed a number of lines with nearly first-order Stark effects, which we subsequently assigned to the b-type Q-branches of high J and high K_{+1}. Figure 2 shows a portion of the observed spectra, which are assigned to K_{+1}=20←21. Because the members of the series are weak in the limit of $J \cong K_{+1}$, it is difficult to determine the J numbers unambiguously. We therefore searched the b-type R branches in higher-frequency region, where the R branches

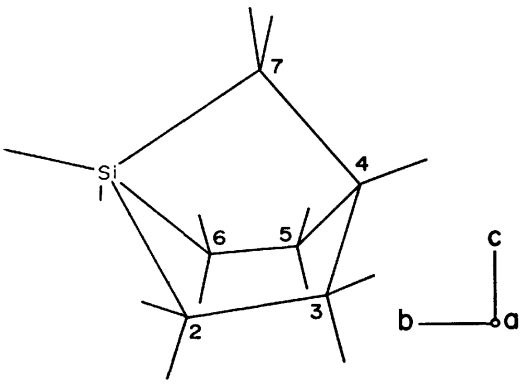

Fig. 1. 1-Silabicyclo[2.2.1]heptane. The heavy atoms are given numbers for identification.

TABLE 1. OBSERVED FREQUENCIES OF 1-SILABICYCLO[2.2.1]HEPTANE IN THE GROUND STATE (MHz)

Transition[a]	Obsd.	Δ[b]	Transition[a]	Obsd.	Δ[b]
21, 19—21, 20	21 671.60	−0.15	8, 8—7, 7	34 891.37	−0.04
22, 19—22, 20	21 666.90	0.22	8, 7—7, 6	36 003.37	0.00
23, 19—23, 20	21 660.95	0.01	8, 2, 6—7, 3, 5	37 116.18	0.02
24, 19—24, 20	21 654.44	−0.04	8, 3, 6—7, 2, 5		−0.12
25, 19—25, 20	21 647.07	−0.16	8, 8, 0—7, 7, 1	43 739.89	−0.02
26, 19—26, 20	21 639.25	0.11	8, 8, 1—7, 7, 0	43 641.89	−0.03
27, 19—27, 20	21 630.21	0.08	8, 7, 1—7, 6, 2	43 873.25	−0.01
28, 19—28, 20	21 620.06	−0.08	9, 9—8, 8	39 183.31	0.07
21, 20—21, 21	22 788.34	0.19	9, 8—8, 7	40 295.20	0.06
22, 20—22, 21	22 783.50	−0.16	9, 2, 7—8, 3, 6	41 407.60	0.00
23, 20—23, 21	22 778.52	−0.08	9, 3, 7—8, 2, 6		−0.01
24, 20—24, 21	22 772.87	−0.04	9, 3, 6—8, 4, 5	42 522.20	0.36
25, 20—25, 21	22 766.53	−0.02	9, 4, 6—8, 3, 5		−0.22
26, 20—26, 21	22 759.43	−0.02	9, 4, 5—8, 5, 4	43 634.58	−0.01
27, 20—27, 21	22 751.50	−0.06	9, 5, 5—8, 4, 4	43 653.92	−0.02
28, 20—28, 21	22 742.80	−0.02	9, 5, 4—8, 6, 3	44 645.12	−0.01
29, 20—29, 21	22 733.11	−0.06	9, 6, 4—8, 5, 3	44 943.67	0.02
30, 20—30, 21	22 722.56	0.01	9, 7, 3—8, 6, 2	46 682.80	−0.00
31, 20—31, 21	22 710.94	0.07	9, 8, 2—8, 7, 1	48 303.08	−0.01
32, 20—32, 21	22 698.14	0.06	10, 10—9, 9	43 475.00	−0.03
33, 20—33, 21	22 684.13	0.02	10, 9—9, 8	44 586.95	0.06
34, 20—34, 21	22 668.96	0.10	10, 8—9, 7	45 699.12	−0.02
35, 20—35, 21	22 652.25	−0.02	10, 3, 7—9, 4, 6	46 812.66	0.03
36, 20—36, 21	22 634.13	−0.12	10, 4, 7—9, 3, 6		−0.01
37, 20—37, 21	22 614.70	−0.01	10, 4, 6—9, 5, 5	47 929.00	−0.05
38, 20—38, 21	22 593.59	0.03	10, 5, 6—9, 4, 5	47 931.19	0.10
39, 20—39, 21	22 570.75	0.04	10, 10, 0—9, 9, 1	54 685.26	−0.03
40, 20—40, 21	22 546.08	0.03	10, 10, 1—9, 9, 0	54 654.92	0.03
41, 20—41, 21	22 519.42	−0.07	10, 9, 2—9, 8, 1	53 923.86	−0.01
23, 21—23, 22	23 895.59	0.01	10, 9, 1—9, 8, 2	54 507.37	−0.01
24, 21—24, 22	23 890.47	−0.05	10, 8, 2—9, 7, 3	55 379.70	0.05
25, 21—25, 25	23 884.97	0.10	10, 8, 3—9, 7, 2	52 386.10	−0.00
26, 21—26, 22	23 878.59	0.01	11, 11—10, 10	47 766.78	0.01
27, 21—27, 22	23 871.60	−0.00	11, 10—10, 9	48 878.63	0.01
28, 21—28, 22	23 863.89	0.00	11, 9—10, 8	49 990.78	0.05
29, 21—29, 22	23 855.44	0.07	11, 4, 7—10, 5, 6	52 218.93	0.04
30, 21—30, 22	23 845.90	−0.11	11, 5, 7—10, 4, 6		−0.14
31, 21—31, 22	23 835.72	−0.02	11, 6, 6—10, 5, 5	53 344.12	0.07
32, 21—32, 22	23 824.56	0.05	11, 5, 6—10, 6, 5	53 337.94	−0.04
33, 21—33, 22	23 812.14	−0.10	11, 6, 5—10, 7, 4	54 429.43	−0.01
34, 21—34, 22	23 799.05	0.17	11, 7, 5—10, 6, 4	54 542.58	0.04
35, 21—35, 22	23 784.38	0.03	11, 7, 4—10, 8, 3	55 174.74	0.01
23, 22—23, 23	25 012.15	0.09	11, 8, 4—10, 7, 3	56 142.70	−0.01
24, 22—24, 23	25 007.65	0.14	11, 9, 3—10, 8, 2	58 111.44	−0.04
25, 22—25, 23	25 002.55	0.10	11, 11, 1—10, 10, 0	60 151.39	0.07
26, 22—26, 23	24 996.78	−0.04	11, 11, 0—10, 10, 1	60 167.75	0.07
27, 22—27, 23	24 990.47	−0.12	11, 10, 2—10, 9, 1	59 515.76	0.03
28, 22—28, 23	24 983.80	0.09	11, 10, 1—10, 9, 2	59 889.97	−0.03
29, 22—29, 23	24 976.08	−0.05	11, 9, 2—10, 8, 3	60 510.81	0.15
30, 22—30, 23	24 967.62	−0.19	11, 8, 3—10, 7, 4	62 279.29	−0.06
31, 22—31, 23	24 958.55	−0.14	12, 12—11, 11	52 058.27	−0.20
32, 22—32, 23	24 948.68	−0.05	12, 11—11, 10	53 170.30	−0.01
33, 22—33, 23	24 937.88	0.02	12, 10—11, 9	54 282.27	−0.07
34, 22—34, 23	24 925.96	−0.08	12, 9—11, 8	55 394.80	−0.16
35, 22—35, 23	24 913.44	0.23	12, 4, 8—11, 5, 7	56 509.07	−0.02
			12, 5, 8—11, 4, 7		−0.04

Table 1. (Continued)

Transition[a]	Obsd.	Δ[b]	Transition[a]	Obsd.	Δ[b]
12, 5, 7—11, 6, 6	57 626.82	−0.02	13, 9—12, 8	60 799.67	−0.12
12, 6, 7—11, 5, 6	57 627.52	0.07	13, 5, 8—12, 6, 7	61 915.75	0.03
12, 7, 6—11, 6, 5	58 764.23	0.05	13, 6, 8—12, 5, 7		−0.02
12, 6, 6—11, 7, 5	58 748.06	−0.10	13, 6, 7—12, 7, 6	63 036.99	0.05
12, 7, 5—11, 8, 4	59 804.40	0.07	13, 7, 7—12, 6, 6	63 038.76	−0.00
12, 12, 1—11, 11, 0	65 644.36	−0.05	13, 8, 6—12, 7, 5	64 196.21	0.02
12, 12, 0—11, 11, 1	65 653.19	0.10	13, 7, 6—12, 8, 5	64 157.92	−0.07
12, 11, 2—11, 10, 1	65 077.92	−0.02	13, 8, 5—12, 9, 4	65 146.46	−0.10
12, 11, 1—11, 10, 2	65 307.95	−0.16	13, 9, 5—12, 8, 4	65 587.20	0.02
12, 10, 3—11, 9, 2	63 841.73	0.03	13, 9, 4—12, 10, 3	65 311.59	0.06
12, 9, 4—11, 8, 3	61 839.44	0.03	14, 14—13, 13	60 641.76	0.07
12, 8, 5—11, 7, 4	60 037.59	0.05	14, 13—13, 12	61 753.55	0.02
12, 8, 4—11, 9, 3	60 304.52	−0.08	14, 12—13, 11	62 865.44	−0.03
13, 13—12, 12	56 350.24	0.13	14, 11—13, 10	63 977.70	−0.03
13, 12—12, 11	57 461.88	−0.07	14, 10—13, 9	65 090.80	0.05
13, 11—12, 10	58 574.10	0.18	15, 15—14, 14	64 933.20	−0.02
13, 10—12, 9	59 686.38	0.05			

a) J', $K_{+1}'-J''$, K_{+1}'' for the degenerate transitions and J', K_{-1}' $K_{+1}'-J''$, K_{-1}'', K_{+1}'' for the non-degenerate transitions. b) Obsd−Calcd. The calculated frequencies are obtained using the constants listed in Table 2.

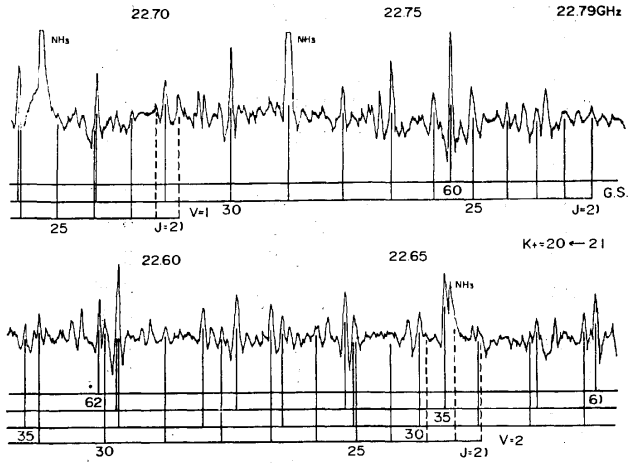

Fig. 2. A part of the *b*-type *Q*-branch spectra of 1-silabicyclo[2.2.1]heptane, recorded at room temperature with the AC modulation field of 20—40 V/cm superposed on the DC Stark field of 160—200 V/cm and with the time constant of 0.4 s.

were stronger than the *Q* branches. The *R* branches of $K_{+1}\cong J$ were degenerate and showed the first-order Stark effects. We observed peculiar lineshapes for transitions with small *K*-type splittings, that is, stronger Stark components between weaker zero-field doublets. This is due to Stark mixing of the *K* doublets, which induces forbidden transitions at finite Stark fields. Table 1 lists the observed frequencies of the assigned transitions, which we analyzed by a least-squares method taking into account the centrifugal distortion effects to the first order. In addition to those given in Table 1 we also observed the following transitions, but did not include them in a least-squares analysis; *Q* branches of $K_{+1}=19\leftarrow20$, $J=29$—44, of $K_{+1}=20\leftarrow21$, $J=42$—62, of $K_{+1}=21\leftarrow22$, $J=36$—67, of $K_{+1}=22\leftarrow23$, $J=36$—71, of $K_{+1}=23\leftarrow24$, $J=48$—75, of $K_{+1}=27\leftarrow28$, $J=29$—32, of $K_{+1}=52\leftarrow53$, $J=54$—83, of $K_{+1}=54\leftarrow55$, $J=66$—80, and of $K_{+1}=55\leftarrow56$, $J=57$—83, and four *R* branches, $5_{24}\leftarrow4_{13}$, $5_{14}\leftarrow4_{23}$, $5_{05}\leftarrow4_{14}$, and $5_{15}\leftarrow4_{04}$ (the latter two are degenerate). Table 2 lists the rotational constants and the centrifugal distortion constants which are thus derived. We set arbitrarily the τ_{aabb} constant to be zero. The transition frequencies which are calculated using the constants of Table 2 are compared with the observed frequencies in Table 1.

Table 2. Rotational constants and centrifugal distortion constants of 1-silabicyclo[2.2.1]-heptane (MHz)[a]

Constant	G. S.	$v=1$	$v=2$
A	2744.775 (2)	2745.94 (2)	2746.88 (5)
B	2662.017 (2)	2662.79 (2)	2663.59 (6)
C	2145.994 (2)	2148.779 (3)	2150.931 (6)
τ_{aaaa}	−0.00116 (4)	−0.0008 (4)	−0.0032 (7)
τ_{bbbb}	−0.00075 (3)	−0.0007 (2)	−0.0020 (4)
τ_{cccc}	−0.00075 (2)	−0.00078 (4)	−0.00060 (6)
τ_{bbcc}	0.0141 (3)	0.016 (4)	−0.014 (9)
τ_{aacc}	−0.0178 (4)	−0.020 (5)	0.02 (1)

a) Values in parentheses denote the standard deviations and apply to the last digits of the constants. The τ_{aabb} constant is fixed to zero.

In addition to the ground-state spectra we observed two prominent sets of the vibrational satellites. Based on the frequency shifts from the ground-state spectra and on the relative intensities, which are observed, we assigned these two to the first and the second excited states of the lowest normal mode, probably the skeletal torsion. We listed the observed transitions in Table 3, and the rotational constants and the centrifugal distortion constants, which were derived by a least-

TABLE 3. OBSERVED FREQUENCIES OF 1-SILABICYCLO[2.2.1]HEPTANE IN THE EXCITED VIBRATIONAL STATES (MHz)

Transition[a]	$v=1$ Obsd	$v=1$ Δ[b]	$v=2$ Obsd	$v=2$ Δ[b]
24, 20—24, 21			22 643.28	0.24
25, 20—25, 21			22 636.44	−0.07
26, 20—26, 21			22 628.94	−0.29
27, 20—27, 21			22 621.20	0.06
28, 20—28, 21			22 612.20	0.01
29, 20—29, 21			22 602.14	−0.16
30, 20—30, 21	22 647.50	−0.02	22 591.44	0.03
31, 20—31, 21	22 635.76	−0.01	22 579.34	−0.11
32, 20—32, 21	22 622.82	−0.08	22 566.34	−0.02
33, 20—33, 21	22 608.84	0.02	22 552.06	0.02
34, 20—34, 21	22 593.52	0.06	22 536.48	0.06
35, 20—35, 21	22 576.74	0.01	22 519.48	0.06
36, 20—36, 21	22 558.60	0.05	22 501.10	0.16
37, 20—37, 21	22 538.80	−0.04	22 481.04	0.13
38, 20—38, 21	22 517.46	−0.03	22 459.14	−0.07
39, 20—39, 21	22 494.40	−0.01	22 435.76	0.01
40, 20—40, 21	22 469.62	0.12	22 410.48	0.06
41, 20—41, 21	22 442.42	−0.23	22 382.80	−0.30
42, 20—42, 21	22 413.82	0.07	22 353.70	0.02
43, 20—43, 21	22 382.80	0.12	22 322.08	0.04
44, 20—44, 21	22 349.26	−0.06	22 288.04	0.02
45, 20—45, 21	22 313.50	−0.04	22 251.46	−0.05
46, 20—46, 21	22 275.26	0.06	22 212.38	0.05
48, 20—48, 21	22 190.24	−0.02		
10, 10—9, 9	43 528.93	0.07	43 571.00	0.23
10, 9—9, 8	44 637.02	−0.05	44 676.26	−0.09
10, 8—9, 7	45 745.61	−0.05	45 782.28	−0.04
10, 3, 7—9, 4, 6	46 855.52	0.00	46 889.50	−0.07
10, 4, 7—9, 3, 6		−0.04		−0.12
10, 4, 6—9, 5, 5	47 968.46	0.13	47 999.84	0.08
10, 5, 6—9, 4, 5	47 970.47	0.03	48 002.00	0.04
10, 6, 5—9, 5, 4	49 122.58	−0.05		
10, 5, 5—9, 6, 4	49 071.52	−0.08		
11, 11—10, 10	47 826.21	0.05	47 872.41	−0.02
11, 10—10, 9	48 934.39	0.04	48 978.08	0.09
11, 9—10, 8	50 042.82	0.00	50 083.79	−0.03
11, 8—10, 7			51 190.34	−0.17
11, 4, 7—10, 5, 6	52 263.81	0.09	52 299.48	−0.01
11, 5, 7—10, 4, 6		−0.10		−0.21
11, 5, 6—10, 6, 5	53 379.06	−0.14	53 412.28	−0.02
11, 6, 6—10, 5, 5	53 385.34	−0.15	53 419.04	0.18
11, 7, 5—10, 6, 4	54 582.51	0.28		
11, 6, 5—10, 7, 4	54 466.15	0.11		
12, 12—11, 11	52 123.39	−0.02	52 174.08	0.02
12, 11—11, 10	53 231.54	−0.06	53 279.53	−0.06
12, 10—11, 9	54 340.00	0.02	54 385.34	0.01
12, 9—11, 8	55 449.02	0.06	55 491.86	0.18
12, 4, 8—11, 5, 7	56 559.49	−0.02	56 599.50	−0.07
12, 5, 8—11, 4, 7		−0.03		−0.09
12, 5, 7—11, 6, 6	57 673.77	0.12	57 711.00	−0.14
12, 6, 7—11, 5, 6	57 674.40	0.11	57 711.90	0.08
12, 6, 6—11, 7, 5	58 791.20	−0.09	58 826.09	0.12
12, 7, 6—11, 6, 5	58 807.68	−0.20	58 843.53	0.27
12, 7, 5—11, 8, 4	59 841.69	−0.02		
12, 8, 5—11, 7, 4	60 081.00	−0.11		

Table 3. (Continued)

Transition[a]	$v=1$ Obsd	$v=1$ Δ[b]	$v=2$ Obsd	$v=2$ Δ[b]
13, 13—12, 12	56 420.63	0.03	56 475.60	−0.04
13, 12—12, 11	57 528.60	−0.19	57 581.09	−0.07
13, 11—12, 10	58 637.25	0.13	58 686.88	0.05
13, 10—12, 9	59 745.77	−0.12	59 792.91	−0.04
13, 9—12, 8	60 855.83	0.10	60 900.06	−0.09
13, 5, 8—12, 6, 7	61 968.15	0.08	62 010.00	0.12
13, 6, 8—12, 5, 7		0.03		0.06
13, 6, 7—12, 7, 6	63 085.74	0.00	63 125.06	0.12
13, 7, 7—12, 6, 6	63 087.49	−0.15	63 126.91	−0.05
13, 8, 6—12, 7, 5	64 242.51	0.05	64 279.94	−0.22
13, 7, 6—12, 8, 5	64 202.95	0.03	64 238.82	−0.15
14, 14—13, 13	60 717.80	0.06	60 777.07	−0.10
14, 13—13, 12	61 825.91	−0.03	61 882.50	−0.19
14, 12—13, 11	62 934.08	−0.15	62 988.30	−0.01
14, 11—13, 10	64 042.73	−0.12	64 094.18	−0.09
14, 10—13, 9	65 152.53	0.28	65 201.50	0.48

a) J', $K_{+1}'-J''$, K_{+1}'' for the degenerate transitions and J', K_{+1}', $K_{-1}'-J''$, K_{+1}'', K_{-1}'' for the non-degenerate transitions. b) Obsd−Calcd. The calculated frequencies are obtained using the constants listed in Table 2.

Table 4. Relative intensities of vibrational satellites[a]

Transition J', $K_{+1}'-J''$, K_{+1}''	$v=1$	$v=2$
14, 13—13, 12	0.75	
13, 13—12, 12	0.71	0.43
13, 12—12, 11	0.67	
13, 11—12, 10		0.45
13, 10—12, 9	0.75	
12, 11—11, 10	0.67	0.42
12, 10—11, 9	0.73	0.54
Av.	$0.71_3\pm0.093$	0.46±0.14
E_v(cm^{-1})[b]	70±25	160±60

a) Referred to the ground-state transitions, at room temperature. Errors are 2.5 times standard deviations. b) $kT=207$ cm^{-1} or $T=298$ K.

squares analysis, in Table 2. Although we included only the observed lines of $J\leqq48$ in a least-squares analysis, we measured additional lines which were mainly high J and K_{+1} transitions as in the case of the ground state. The intensities of the satellites were compared with those of the ground-state spectra at room temperature, as shown in Table 4. We thus determined the excitation energies to be 70±25 cm^{-1} and 160±60 cm^{-1} for $v=1$ and $v=2$, respectively. We did not observe any anomalies in the rotational spectra, even for the vibrational satellites, which were due to deviations of the molecular symmetry from C_s.

Dipole Moment

Because the spectrum is rich and weak, it is difficult to resolve the Stark components completely. We thus analyzed the Stark effects by a simulation technique similar to that described in our previous paper.[9] We made the following assumptions: (1) the linewidths of the Stark components are the same as that of the zero-field line, (2) the Stark components have the

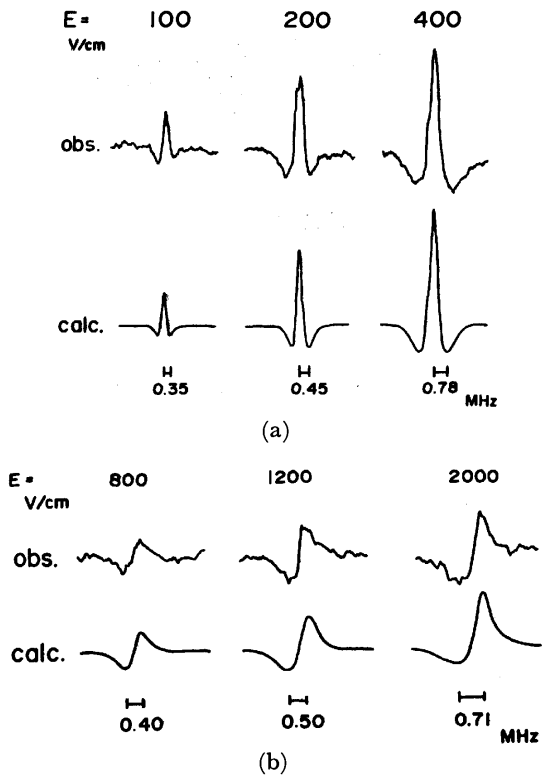

Fig. 3. Analysis of the Stark effects by a simulation method.
(a) J, $K_{+1}=13$, $13\leftarrow12$, 12. Calculated spectra are obtained using $\Delta\nu$(HWHM)=0.26 MHz and $\mu_c=0.05$ D.
(b) $J_{K_{-1},K_{+1}}=11_{11,1}\leftarrow10_{10,0}$. Calculated spectra are obtained using $\Delta\nu=0.25$ MHz, $\mu_b=0.5$ D, and $\mu_c=0.05$ D.

TABLE 5. MOLECULAR STRUCTURE OF 1-SILABICYCLO[2.2.1]HEPTANE[a)]

Assumed:	Si-C(2)	1.868 Å	∠C(2)-C(3)-C(4)	106.5°
	C(2)-C(3)	1.5527 Å	∠C(3)-C(4)-C(5)	111.0°
	C(3)-C(4)	1.5362 Å	∠H-Si-C(7)	109.4°
	C(4)-C(7)	1.5579 Å	∠H-C(4)-C(7)	109.4°
	C(4)-H	1.11 Å	∠H-C-H	109.4°
	other C-H	1.11 Å	CH_2 plane bisects C-C-C	
	Si-H	1.489 Å	or Si-C-C angles	
	C_s symmetry			
Fitted:	Si-C(7)	1.9431 Å	∠C(2)-Si-C(6)	104.1°
			∠Si-C(2)-C(3)	102.8°

a) See Fig. 1 for the atom numbers.

Lorentzian lineshape, and (3) the inhomogeneity of the Stark field may be neglected. We calibrated the Stark field using the $J=1\leftarrow0$ transition of OCS as a reference.

To determine the μ_c component we analyzed a K-degenerate transition J, $K_{+1}=13$, $13\leftarrow12$, 12. Its first-order Stark effect is determined by the μ_c component at low Stark fields. Overall fitting may be judged by two parameters, the intensity and the difference between the peak frequencies of the zero-field and of the Stark components. We obtained best fitting using the linewidth parameter $\Delta\nu$ (HWHM) of 0.26 MHz and μ_c of 0.05 D. The calculated spectrum thus obtained is compared with the observed in Fig. 3a. The error of μ_c is ±0.01 D. We determined the μ_b component from a similar analysis of the $11_{11,1}\leftarrow10_{10,0}$ transition. The two parameters which were derived are $\Delta\nu=0.25$ MHz and $\mu_b=0.5\pm0.1$ D. The total dipole moment is 0.5±0.1 D.

Molecular Structure

As stated above we did not observe any deviations of the molecular symmetry from C_s. An assumption of the C_s symmetry leaves nine parameters as independent to determine the heavy-atom skeleton. We adjusted three of the nine parameters, Si-C(7), ∠C(2)-Si-C(6), and ∠Si-C(2)-C(3), so as to reproduce the observed rotational constants, while others were fixed to the values of the related molecules.[5,7,8] Table 5 summarizes the fitted as well as the assumed parameters.

Discussion

We have recently shown[10] that the 1-silabicyclo[2.2.2]octane molecule has a double-minimum potential function to the skeletal torsion and the potential hump (212 cm^{-1}) is even higher than that (67 cm^{-1}) in 1-halogenobicyclo[2.2.2]octane.[3] The present work shows that replacement of one ethylene bridge by a methylene bridge removes the hump from the torsional potential function, and the 1-silabicyclo[2.2.1]heptane molecule actually belongs to C_s symmetry. This result is in accord with our expectation; the number of the C–C bonds with unstable *cis* conformation is decreased from three to two and the skeleton is more strained, and both factors favor the untwisted conformation. We have, however, still one silacyclohexane ring with unstable boat conformation. It may thus be easy to twist the molecular skeleton. In fact, we found that the frequency of the skeletal torsion was as low as 70 cm^{-1}. It may be interesting to compare this value with the torsional frequency of 132 cm^{-1} obtained for 7-thiabicyclo[2.2.1]heptane.[11]

We estimated only three structure parameters. The two angles, ∠C(2)-Si-C(6) and ∠Si-C(2)-C(3), may be compared with the corresponding angles, 103.5° and 104.3°, in norbornane.[5] It is interesting to note that Si–C(7) is considerably longer than Si–C(2) or the Si–C length (1.868 Å) in trimethylsilane.[8] The ∠Si-C(7)-C(4) angle is calculated to be 87.1° using the parameters of Table 5.

The dipole moment of 1-silabicyclo[2.2.1]heptane is close to that of trimethylsilane (0.525 D),[8] although methylsilane[12] and dimethylsilane[7] have the dipole moments of about 0.2 D larger.

The calculation in the present work is carried out at the Computation Center of Kyushu University.

References

1) Present address: Central Laboratory, S. S. Pharmaceutical Co., Narita, Chiba 286.
2) Present address: Institute for Molecular Science, Okazaki 444.
3) E. Hirota, *J. Mol. Spectrosc.*, **38**, 367 (1971).
4) E. Hirota and S. Suenaga, *J. Mol. Spectrosc.*, **42**, 127 (1972).
5) Y. Morino, K. Kuchitsu, and A. Yokozeki, *Bull. Chem. Soc. Jpn.*, **40**, 1552 (1967); G. Dallinga and L. H. Toneman, *Rec. Trav. Chim. Pays-Bas*, **87**, 795 (1968); J. F. Chiang, C. F. Wilcox, Jr., and S. H. Bauer, *J. Am. Chem. Soc.*, **90**, 3149 (1968); A. Yokozeki and K. Kuchitsu, *Bull. Chem. Soc. Jpn.*, **44**, 2356 (1971).
6) Y. Nagai, S. Inaba, H. Matsumoto, and H. Watanabe, *Bull. Chem. Soc. Jpn.*, **45**, 3224 (1972).
7) L. Pierce, *J. Chem. Phys.*, **34**, 498 (1961).
8) L. Pierce and D. H. Petersen, *J. Chem. Phys.*, **33**, 907 (1960).
9) E. Hirota and C. Matsumura, *J. Chem. Phys.*, **59**, 3038 (1973).
10) A. Kawaguchi, T. Tanaka, E. Hirota, K. Mochida, and H. Sakurai, to be published.
11) K. Irie, T. Tanaka, E. Hirota, Y. Tamaru, I. Tabushi, and Z. Yoshida, 27th National Meeting of the Chemical Society of Japan, Nagoya, 1972.
12) J. S. Muenter and V. W. Laurie, *J. Chem. Phys.*, **45**, 855 (1966).

Extraction of Nickel(II) in Aqueous Thiocyanate–Perchlorate Solutions with Trioctylphosphine Oxide in Hexane and with 4-Methyl-2-pentanone

Ryokichi MURAI, Shigehisa IWAHORI, and Tatsuya SEKINE

Department of Chemistry, Science University of Tokyo, Kagurazaka, Shinjuku-ku, Tokyo 162

(Received August 23, 1976)

The liquid-liquid partition of nickel(II) between hexane containing trioctylphosphine oxide or 4-methyl-2-pentanone and 1 mol dm^{-3} Na(SCN, ClO_4) solutions at 25 °C was measured. The absorption spectra of the organic and aqueous phases at equilibrium were also measured. From an analysis of these data, the extraction constant and absorption spectrum of each organic species were determined. By comparing the extraction and optical absorption of cobalt(II) complexes in the same systems with the above results for nickel(II), it was concluded that cobalt(II) thiocyanate complexes changed from octahedral to tetrahedral form upon extraction, but that nickel(II) thiocyanate complexes remained in octahedral form throughout.

It is known that cobalt(II) in thiocyanate solutions can be extracted with various oxygen-containing organic solvents. Since the extraction of cobalt(II) in these solutions is much better than that of nickel(II), this thiocyanate method has been recommended for the separation of trace amounts of cobalt(II) from large amounts of nickel(II).[1]

On the other hand, nickel(II) was found to form slightly more stable thiocyanate complexes in aqueous solutions than cobalt(II),[2] and the great difference in the extractability of these metal thiocyanates cannot be attributed to differences in the stabilities of the complexes in aqueous phase.

In order to learn further details of the thiocyanate extraction of these metal ions, solvent extraction and optical absorption measurements were made in aqueous phase for 1 mol dm^{-3} Na(SCN, ClO_4) and in organic phase for hexane containing trioctylphosphine oxide (TOPO) or for 4-metyl-2-pentanone at 25°C.

Experimental

All the reagents were of analytical grade. The TOPO was supplied by Dojindo & Co., Kumamoto. The sodium perchlorate was recrystallized three times from water.

All the distribution experiments and spectrophotometric measurements were performed in a thermostatically-controlled room at 25±0.3 °C. A portion of an aqueous 1 mol dm^{-3} Na(SCN, ClO_4) solution containing 10^{-5} to 10^{-2} mol dm^{-3} of nickel(II) or 10^{-4} to 10^{-2} mol dm^{-3} of cobalt(II) and the same volume of hexane containing TOPO or of 4-methyl-2-pentanone were placed in a stoppered glass tube and the tube was settled on a rotating frame (20 rpm). Since it was found that agitation for 2 h and for 24 h was sufficient to attain equilibrium distributions of cobalt(II) and nickel(II), respectively, agitation for the respective extractions were continued for these periods. The metal content in the organic phase was determined after back extraction into 0.1 mol dm^{-3} perchloric acid, while that in the aqueous phase was determined directly, in both cases, by the atomic absorption method. The optical absorption of the solutions was measured with a spectrophotometer (Hitachi type 139) using glass cells of 10-mm light paths.

Statistical

Throughout this paper, the subscript "org" denotes that in the organic phase while the lack of any subscript denotes that in the aqueous phase. The notation L^- represents the thiocyanate ion.

Since only the M^{2+}, ML^+, and ML_2 species are assumed to be present in the aqueous phase when extraction of higher complexes into the organic phase was possible, the following equation may be written for the distribution ratio:

$$D = ([M(ClO_4)_2]_{org} + [ML(ClO_4)]_{org} + [ML_2]_{org} + [ML_3Na]_{org} + [ML_4Na_2]_{org})([M^{2+}] + [ML^+] + [ML_2])^{-1},$$
$$= (\sum K_{ex,a}[L^-]^a[ClO_4^-]^b)(1+\beta_1[L^-]+\beta_2[L^-]^2)^{-1}, \quad (1)$$

where

$$\beta_n = [ML_n^{2-n}][M^{2+}]^{-1}[L^-]^{-n}, \quad (2)$$

$$K_{ex,a} = [ML_a(ClO_4)_bNa_c]_{org}[M^{2+}]^{-1}[L^-]^{-a}[ClO_4^-]^{-b}. \quad (3)$$

The sodium ion concentration was unity and thus the corresponding term was dropped. Here, $a+b-c=2$. Sodium ions were found in the extracted species only for $a>2$. Perchlorate ions were found only for $a<2$ and in such cases $a+b=2$.

The extraction data can be analyzed in a similar manner to that described in Ref. 3.

The optical absorption of the organic phase at a given wavelength can be written as;

$$E = \sum \varepsilon_a[ML_a(ClO_4)_bNa_c]_{org},$$
$$= \sum \varepsilon_a K_{ex,a}[M^{2+}][L^-]^a[ClO_4^-]^b, \quad (4)$$

where $0 \leq a \leq 4$. The total metal concentration in each phase was obtained by chemical analysis. The concentration of each species in each phase was calculated by Eq. 1 using these total metal concentrations and the stability and extraction constants which had been obtained from the distribution experiments. The molar extinction coefficient of the $M(ClO_4)_2$ species was obtained from an organic phase which was in contact with an aqueous solution containing no thiocyanate and those of the other metal species containing thiocyanate ions were obtained by analysis of the absorption curves of the organic phases which were in contact with aqueous thiocyanate solutions at various concentrations.

Results

Figure 1 gives the extraction curve of nickel(II) with 4-methyl-2-pentanone as a function of the thiocyanate concentration and also the curve for cobalt(II) extraction from a previous study.[4] As is seen in Fig. 1, the shape of the two curves is quite different

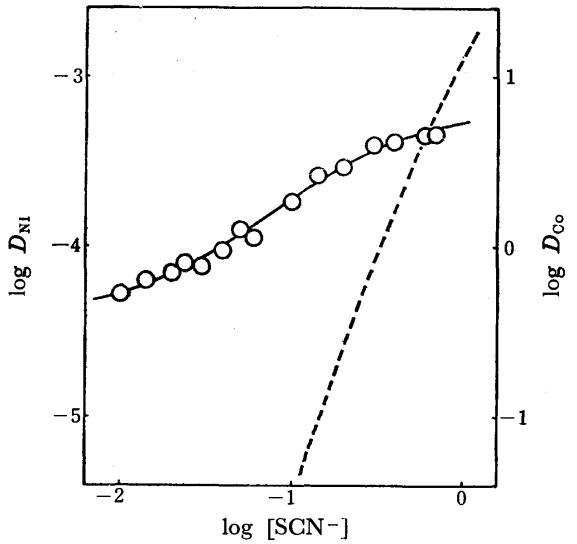

Fig. 1. Exrtaction curve of nickel(II) with 4-methyl-2-pentanone. The solid line was calculated by introducing the values in Table 1(a) and 1(b) into Eq. 1. The dotted curve is that of cobalt(II) in Ref. 4. The left ordinate is for the nickel(II) curve and the right ordinate is for the cobalt(II) curve.

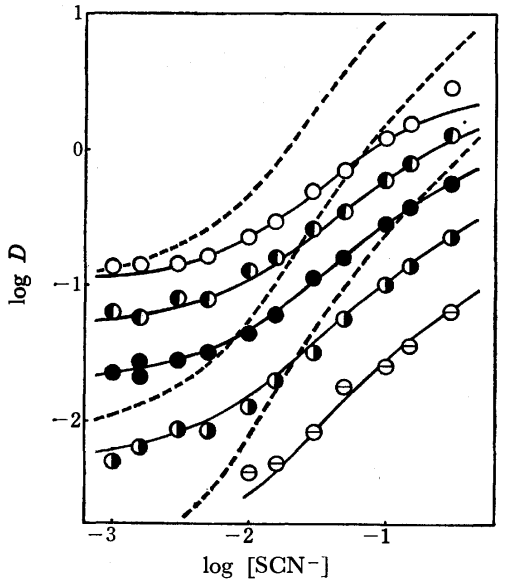

Fig. 2. Extraction curves of nickel(II) into hexane with 0.06 (○), 0.05 (◐), 0.04 (●), 0.03 (◑), and 0.02 (⊖) mol dm^{-3} of TOPO. The solid curves were calculated by introducing the values in Table 1(a) and 1(c) into Eq. 1. The dotted lines from the top to the bottom are curves of cobalt(II) into hexane with 0.04, 0.02, and 0.01 mol dm^{-3} of TOPO in Ref. 4.

and the extraction of nickel(II) is much poorer than that of cobalt(II). Figure 2 shows the extraction curves of nickel(II) with TOPO at various concentrations in hexane as a function of the thiocyanate concentration and also shows the curves for cobalt(II) from a previous study.[4] The shapes of the nickel(II) curves in this figure are similar to those of the curves of cobalt(II). However, the D values for nickel(II) are lower than those for cobalt(II), especially, in the higher thiocyanate concentration region. From an analysis of these distribution data, the extraction constants were obtained, as given in Table 1.

Table 1. Summary of equilibrium constants[a]

(a) Stability constants of aqueous thiocyanate complexes.

	$\log\beta_1$	$\log\beta_2$
Co(II)	1.00	1.32
Ni(II)	1.1	1.6

(b) Extraction constants with 4-methyl-2-pentanone.

	$\log K_{ex0}$	$\log K_{ex1}$	$\log K_{ex2}$	$\log K_{ex3}$	$\log K_{ex4}$
Co(II)	—	—	—	—	2.96
Ni(II)	−4.45	−2.66	−1.54	—	—

(c) Extraction constants with TOPO.

	$[TOPO]_{org}$	$\log K_{ex0}$	$\log K_{ex1}$	$\log K_{ex2}$	$\log K_{ex3}$
Co(II)	0.005	—	−1.00	1.10	0.49
	0.01	—	−0.43	1.80	1.48
	0.02	−2.06	−0.34	2.58	2.48
	0.04	−0.94	1.37	3.32	3.34
	0.08	0.00	2.18	4.00	—
Ni(II)	0.02	−2.62	0.63	0.66	—
	0.03	−2.36	1.10	1.24	—
	0.04	−1.72	1.30	1.64	—
	0.05	−1.18	1.43	1.90	—
	0.06	−0.84	1.58	2.20	—

a) The values in (a) were taken from Refs. 2 and 4, and the values for cobalt(II) in (b) and (c) from Ref. 4.

Table 2. Estimated solvation number of metal species for TOPO extracted into the hexane phase

	$M(ClO_4)_2$	$M(SCN)(ClO_4)$	$M(SCN)_2$	$M(SCN)_3Na$
Co(II)[a]	3	3	*ca.* 2	3
Ni(II)	4	4	3	not extracted

a) Taken from Ref. 4.

The extraction constant with TOPO for each metal species, $K_{ex,a}$, is dependent of the TOPO concentration. From the treatment described in Ref. 3, the solvation number of each species was obtained from the TOPO dependence of the constant, as listed in Table 2.

Figures 3a and 4a show the absorption curves for the organic phase obtained under the conditions described in the captions. Figures 3b and 4b show the absorbance per mole of complex for each extracted species calculated from the data in Figs. 3a and 4a using the procedures described in the statistical section. The absorption curve of cobalt(II) extracted into 4-methyl-2-pentanone has already been reported in Ref. 4(Fig. 7). This curve should be the absorption curve for the $Co(SCN)_4^{2-}$ species in 4-methyl-2-pentanone. The absorption of nickel(II) extracted into this solvent was too weak to be determined because of the low metal concentration due to poor extraction.

The absorption curves of the aqueous phases containing cobalt(II) or nickel(II) in 1 mol dm^{-3} Na(L, ClO_4) solutions were similar to those reported previously, for example (Ref. 6), the cobalt(II) solutions had an absorption peak at 510—520 nm, while the nickel(II) solutions had two peaks at 390—400 and 640—650 nm.

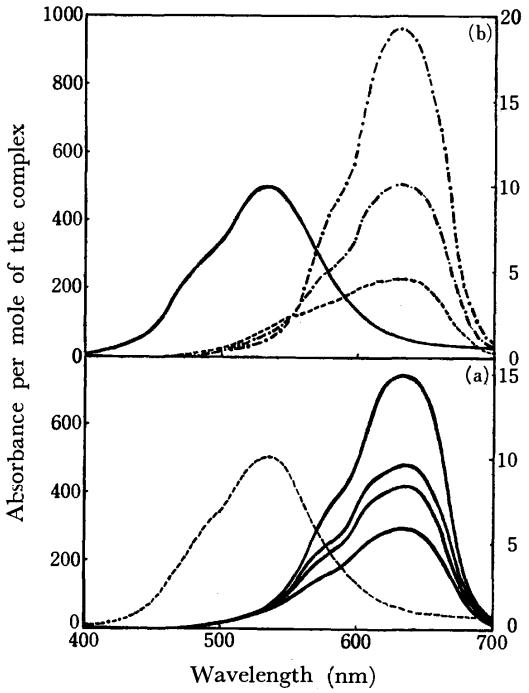

Fig. 3(a). Absorption curve of cobalt(II) extracted into hexane containing 0.04 mol dm^{-3} of TOPO from 1 mol dm^{-3} Na(SCN, ClO_4) aqueous solutions when [SCN^-] was 1, 0.1, 0.03, and 0.01 mol dm^{-3} from the top to the bottom (the absorbance per mole of the complex on the left ordinate). The dotted line is the curve when [SCN^-] was zero (the absorbance per mole of the complex on the right ordinate). Fig. 3(b). Absorption curve of $Co(ClO_4)_2$ ——, $Co(SCN)(ClO_4)$ ----, $Co(SCN)_2$ —·—·—, and $Co(SCN)_3^-$ —•—•— species combined with TOPO molecules in hexane obtained by analysis of the data in Fig. 3(a).

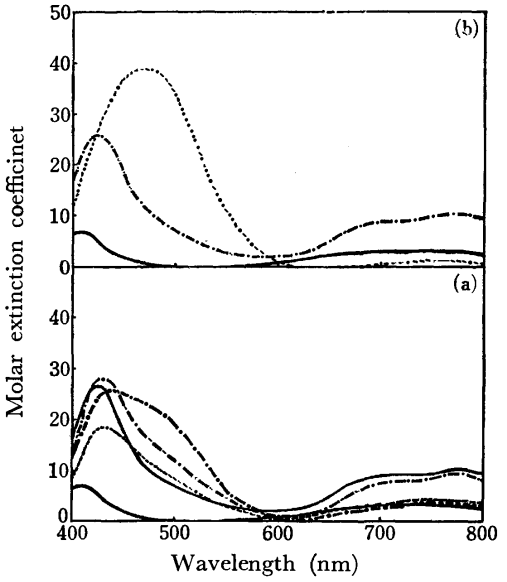

Fig. 4(a). Absorption curve of nickel(II) extracted into hexane containing 0.06 mol dm^{-3} of TOPO from 1 mol dm^{-3} Na(SCN, ClO_4) aqueous solutions when [SCN^-] was 1 ——, 0.3 —·—·—, 0.1 – – –, 0.03 —•—•—, and zero —— mol dm^{-3}. Fig. 4(b). Absorption curve of $Ni(ClO_4)_2$ ——, $Ni(SCN)(ClO_4)$ ----, and $Ni(SCN)_2$ —·—·— species combined with TOPO molecules in hexane obtained by analysis of the data in Fig. 4(a).

Discussion

It is known that cobalt(II) in aqueous solutions forms six-coordinated octahedral complexes which color the solution pink and four-coordinated tetrahedral ones which color the solution deep blue, while nickel(II) usually forms six-coordinated octahedral complexes in aqueous solutions except in some cases, such as those having chelating ligands (for example, see Ref. 6). The absorption for the aqueous phase in the present study ([L^-]<1 mol dm^{-3}), as described above, shows that both cobalt(II) and nickel(II) are present in six-coordinated octahedral form in the aqueous phase.

The absorption of the $Co(ClO_4)_2(TOPO)_3$ species in hexane, shown in Fig. 3, indicates that this cobalt(II) should also be in this form. However, it is notable that all the $CoL(ClO_4)(TOPO)_3$, $CoL_2(TOPO)_2$, $NaCoL_3(TOPO)_3$ species absorbed much more strongly and at higher wavelengths than the $Co(ClO_4)_2(TOPO)_3$ species and that all absorptions of these three thiocyanate species can usually assigned to a four-coordinated tetrahedral complex.[6] The absorption curve of the CoL_4^{2-} complex extracted into 4-methyl-2-pentanone together with two sodium ions in a previous study[4] also suggests the extraction of a four-coordinated tetrahedral species for this system.

The absorption curve of the organic phase which had extracted the $Ni(ClO_4)_2(TOPO)_4$, $NiL(ClO_4)(TOPO)_4$, and $NiL_2(TOPO)_3$ species are similar to that of the aqueous phase and thus these species in the organic phase should be of six-coordinated octahedral form.

The atom through which a thiocyanate ion coordinates with the metal ion has been discussed previously.[7] It is not possible to further discuss the position of the extractant in the coordination sphere or the details of the structure of the extracted species only on the basis of the present data. However, the extraction constants in Table 1 show that the extractabilities of the both perchlorates are similar, while the extractabilities of the other cobalt(II) thiocyanate complexes, which are assumed to be tetrahedral, are much higher than those of the other nickel(II) complexes, which are assumed to be octahedral.

An explanation for the higher extraction of the cobalt(II) tetrahedral species over that of the corresponding nickel(II) octahedral species may be that the latter accept water molecules more readily than the former and this stronger hydration hinders the extraction of the nickel(II) octahedral species more than that of the cobalt(II) tetrahedral species. However, much information appears to be necessary in order to explain this complicated phenomenon in more detail.

There have been some recent reports on the absorption spectra of cobalt(II) and nickel(II) perchlorates and thiocyanates in aqueous and nonaqueous solutions[8-10] and these as well as several previous reports[6,7] appear to support the conclusions of the present study.

Poor extraction of nickel(II) from thiocyanate solutions with various oxygen-containing solvents has been reported.[11–15] However, not much is known of the details of the nickel(II) distribution equilibria in these systems.

References

1) E. B. Sandell, "Colorimetric Determination of Traces of Metals," 3rd ed, Interscience, New York, (1959) p. 411.
2) R. Murai, K. Kurakane, and T. Sekine, *Bull. Chem. Soc. Jpn.*, **49**, 335 (1976).
3) H. Moriya and T. Sekine, *Bull. Chem. Soc. Jpn.*, **45**, 1626 (1972).
4) T. Sekine, R. Murai, and M. Iguchi, *Nippon Kagaku Zasshi*, **92**, 412 (1971).
5) T. Sekine and T. Ishii, *Bull. Chem. Soc. Jpn.*, **43**, 2422 (1970).
6) F. A. Cotton and G. Wilkinson, "Advanced Inorganic Chemistry," 2nd ed, John Wiley & Sons, Inc., New York (1972), Chap. 29
7) C. K. Jorgensen, "Inorganic Complexes," Academic Press, London (1963), p. 78.
8) O. Benali-Baitich and E. J. L. Wendling, *J. Inorg. Nucl. Chem.*, **37**, 1217 (1975).
9) Zs. Szabo-Akos, V. Izvekov, and E. Pungor, *Mikrochim. Acta.*, **20**, 187 (1974).
10) A. Miezis, *Acta Chem. Scand.*, **A28**, 407 (1974).
11) R. Rigamonti and E. Spaccamela-Marchetti, *Ann. Chim. (Rome)*, **49**, 106 (1959).
12) E. Spaccamela-Marchetti and M. T. C. Mazza, *Chem. Ind. (Milano)*, **43**, 133 (1961); *Chem. Abstr.*, **55**, 16100 (1961).
13) E. Jackwerth, *Z. Anal. Chem.*, **206**, 335 (1964).
14) A. K. De and A. K. Sen, *Separ. Sci.*, **1**, 641 (1966).
15) S. Tribalat and J. M. Caodero, *C. R. Acad. Sci.*, **258**, 2828 (1964).

Dialkylpalladium(II) Complexes. Syntheses, Characterizations, and Reactions with CO, I_2, and CH_3I

Takashi Ito, Hirotaka Tsuchiya, and Akio Yamamoto

Research Laboratory of Resources Utilization, Tokyo Institute of Technology, Ookayama, Meguro-ku, Tokyo 152

(Received October 12, 1976)

The reaction of bis(acetylacetonato)palladium(II), [Pd(acac)$_2$] with $AlR_2(OEt)$ in the presence of tertiary phosphine, L, in diethyl ether yields a series of dialkylpalladium(II) complexes, [PdR_2L_2], where R=Me, Et, and Pr^n; L=PEt_3, PPh_2Me, and $\frac{1}{2}Ph_2PCH_2CH_2PPh_2$ (dpe). These complexes were characterized by means of elemental analysis, IR and ^{1}H-NMR spectra and of some decomposition reaction such as thermolysis and acidolysis. The *trans*- and *cis*-configurations of [$PdMe_2L_2$] (L=PEt_3 and PPh_2Me, respectively) in solution were established on the basis of the ^{1}H-NMR spectra. The examination of ^{1}H-NMR spectra in the presence of tertiary phosphine suggests the ligand exchange processes promoted by the added phosphine. [PdR_2L_2] (L=PEt_3 and PPh_2Me) reacted with CO in toluene to yield the quantitative amounts of the corresponding dialkyl ketones. The reactions of the complexes [PdR_2L_2] with iodine afforded [PdI_2L_2] and RI, and of [PdR_2(dpe)] with MeI gave CH_3H, CH_3CH_3, R(−H), RH, R·CH_3, R·R, and RI together with [PdI_2L_2], suggesting the presence of a quadrivalent, six-coordinate intermediate palladium species.

Among the transition elements, palladium and its compounds are known to show the most versatile catalytic activities, which include olefin oxidation (Hoechst-Wacker process), oligomerization, carbonylation, vinylation, acetoxylation, isomerization, and hydrogenation of olefins, dienes and acetylenes.[1] In most of these catalytic reactions, formation of the intermediate species possessing an unstable palladium-carbon σ-bond is thought to constitute one of the key steps.[1] In this respect, the systematic studies of the alkylpalladium complexes are expected to provide the useful information related to the mechanistic aspect of the catalytic reactions and to the exploitation of the new catalytic processes.

Since the first syntheses of the methylpalladium complexes by Calvin and Coates in 1960,[2] various kinds of methylpalladium complexes have been prepared:[3] the preparation method includes alkylation of halogenopalladium(II) complex with methyl Grignard reagent or methyllithium,[2] and with dimethyl(1,5-cyclooctadiene)platinum(II),[4] and oxidative addition of methyl halide to the palladium(0) complex.[5,6] The isolation of the ethylpalladium complex, on the other hand, has been limited to only one example: diethyl{1,2-bis(dicyclohexylphosphino)ethane}palladium(II) which was prepared by the reaction of [Pd(acac)$_2$] (acac=acetylacetonato) with diethylaluminum monoethoxide in the presence of a tertiaryphosphine ligand under the atmosphere of ethylene.[7] Following our systematic studies on the preparations of series of alkyl complexes of Cr,[8] Fe,[9] Co,[10] Ni,[11] and Cu[12] by the use of alkylaluminum compounds as the alkylating agent, we succeeded in the isolation of the series of dialkylpalladium complexes by the analogous method. Alkylation of bis(acetylacetonato)palladium by alkylaluminum compounds has the advantage over the conventional alkylation reaction using palladium halides and alkyllithium or Grignard reagent in that the product can be isolated simply by the filtration and washing with some organic solvents such as hexane. This merit enables the reaction product isolable even if it is susceptible to water and is stable only at the low temperature.

Here we report the preparation, characterization and some reactions of the series of dialkylpalladium complexes with tertiary phosphine ligands. Zerovalent complexes, such as [$Pd(PPh_3)_4$],[13] [$Pd(CO)(PPh_3)_3$],[14] [$Pd(CO)PPh_3]_n$,[14] [$Pd_3(CO)_3(PPh_3)_4$],[14] [$Pd(C_2H_4)(PPh_3)_2$],[7] and [$Pd\{P(C_6H_{11})_3\}_2$],[15] and diethyl and dihydrido complexes, [$PdEt_2\{(C_6H_{11})_2PCH_2CH_2P(C_6H_{11})_2\}$][7] and [$PdH_2\{P(C_6H_{11})_3\}_2$],[15] have been hitherto reported as reaction products between palladium acetylacetonate and alkylaluminum compounds.

Results and Discussion

Preparation of Dialkylpalladium Complexes. The reaction of [Pd(acac)$_2$], tertiary phosphine, L, and dialkylaluminum monoethoxide (molar ratio, 1 : 2 : 3—5) in diethyl ether under a nitrogen atmosphere afforded a series of dialkylpalladium complexes.

$$[Pd(acac)_2] + 2L + AlR_2(OEt) \rightarrow [PdR_2L_2]$$

L = PEt_3, R = Me, **1a**; Et, **2a**; and Pr^n, **3a**.

L = PPh_2Me, R = Me, **1b**; Et, **2b**; and Pr^n, **3b**.

L = $\frac{1}{2}$dpe, R = Me, **1c**; Et, **2c**; and Pr^n, **3c**.

(dpe=$Ph_2PCH_2CH_2PPh_2$)

The results of the elemental analysis for these complexes are listed in Table 1 together with their decomposition points measured *in vacuo*. Among the complexes, [$PdMe_2(PEt_3)_2$](**1a**)and [$PdMe_2$(dpe)](**1c**) have been already prepared by Calvin and Coates by the method employing methyllithium as an alkylating agent.[2] The complexes, white solid except for complex **2c**, which is yellow, are diamagnetic and mostly sensitive to air. When L=PEt_3, ethyl and propyl complexes, **2a** and **3a**, are thermally unstable and decompose at room temperature even under a nitrogen atmosphere. Thermal stability increases in the order of PEt_3<PPh_2Me<dpe for the complexes with the same alkyl groups, and of Pr^n(*n*-C_3H_7)<Et<Me for those with the same phosphine ligands. The latter series of stability suggests that the mechanism involving β-hydrogen abstraction[16] is operative in the thermal decomposition of these complexes *(vide infra)*. The solubility of the complexes depends mostly on the phosphine ligand. On the whole the complexes with PEt_3 are soluble in most organic

Table 1. Analytical data and decomposition points of $[PdR_2L_2]$

Compounds		Analysis (%)[a] C	H	Pd	Dec. pt.[b] °C
$[PdMe_2(PEt_3)_2]$	**1a**	44.7(45.1)	10.4(9.7)	28.7(28.5)	56—64
$[PdEt_2(PEt_3)_2]$	**2a**	——[c]	——[c]	26.9(26.5)	<20
$[PdPr^n_2(PEt_3)_2]$	**3a**	——[c]	——[c]	24.4(24.8)	<20
$[PdMe_2(PPh_2Me)_2]$	**1b**	63.2(62.6)	6.5(6.0)	19.0(19.8)	110—115
$[PdEt_2(PPh_2Me)_2]$	**2b**	64.5(63.8)	7.2(6.4)	18.7(18.8)	73—76
$[PdPr^n_2(PPh_2Me)_2]$	**3b**	63.9(64.9)	6.9(6.8)	17.8(18.0)	58—63
[PdMe$_2$(dpe)]	**1c**	62.3(62.9)	6.0(5.6)	19.6(19.9)	166—168
[PdEt$_2$(dpe)]	**2c**	62.6(64.0)	6.3(6.1)	19.2(18.9)	144—148
[PdPr$^n_2$(dpe)]	**3c**	64.6(65.0)	7.1(6.5)	18.4(18.0)	132—140

a) Calculated values are in parentheses. b) Decomposition points were measured on a hot stage with a sample in a small capillary sealed under vacuum and are uncorrected. c) The complexes were too unstable to obtain good micro-analytical results.

Table 2. Gases evolved by the decomposition of $[PdR_2L_2]$

Compounds [PdR$_2$L$_2$] R	L		Thermolysis[a] Evolved gases Molar ratio Temp °C	R(−H)	RH	R·R	others	ΣR[c] %	Acidolysis[b] Evolved gases Molar ratio	ΣR[c] %
Me	PEt_3	**1a**	70	—	trace[f]	0.90[f]	C_2H_4(0.10)[f]	130	d)	
Et	PEt_3	**2a**	35	0.38	0.62	0	—	80	C_2H_6(1.0)	40
Pr^n	PEt_3	**3a**	40	0.50	0.50	d)	—	55[g]	C_3H_8(1.0), C_2H_6 (trace)[h]	25
Me	PPh_2Me	**1b**	100	0	0	1.00	—	75	d)	
Et	PPh_2Me	**2b**	70	0.50	0.50	0	—	95	C_2H_6(1.0)	60
Pr^n	PPh_2Me	**3b**	70	0.50	0.50	d)	—	85[g]	C_3H_8(1.0), C_2H_6 (trace)[h]	35
Me	$\frac{1}{2}$dpe	**1c**	170	—	0.01	0.92	C_2H_4(0.07)	70	CH_4(1.0)	100
Et	$\frac{1}{2}$dpe	**2c**	145	0.31	0.22	0.47	—	45	C_2H_6(1.0)	65
Pr^n	$\frac{1}{2}$dpe	**3c**	220	0.30	0.20	d)	C_2H_4(0.50)	10[g]	C_3H_8(0.8), C_3H_6(0.2) C_2H_6 (trace)[e,h]	15

a) Thermolysis *in vacuo*. b) Acidolysis by concd H_2SO_4. c) $\Sigma R = \{\text{moles}(R(-H)+RH+2R\cdot R+\text{others})/2\text{mol (complex)}\}\times 100$. d) Not investigated. e) Besides the hydrocarbons, the evolved gas contained H_2 (0.54 mol/mol of the complex). f) The similar results have been reported by Calvin and Coates, see Ref. 2. g) The figures do not include the possible non-gaseous product, R·R (hexane). h) Ethane might have come from the trace amounts of diethylpalladium impurities possibly produced by $AlEt_2(OEt)$ contaminated in $AlPr^n_2(OEt)$.

solvents while those with dpe are scarcely soluble. Thus, complex **1a** was recrystallized from hexane and **2a**, **3a**, **1b**, **3b**, and **1c** from acetone. The rest failed to be recrystallized.

Decomposition of the Complexes. Thermolysis of the dialkyl complexes released the corresponding alkene (R(−H)) and alkanes (RH and R·R) as are shown in Table 2. The formation of ethylene and methane in the thermolysis of dimethyl complexes, **1a** and **1c**, suggests the possibility of occurrence of the following α-elimination reaction as has been reported for $[FeMe_2(dpe)_2]$.[17]

$$2\rangle Pd\langle^{CH_3}_{CH_3} \rightarrow 2\rangle Pd(H)\langle^{CH_2}_{CH_3} \rightarrow CH_2{=}CH_2 + 2CH_4 \quad (1)$$

As the alternative source of ethylene, the alkyl groups in the tertiary phosphine ligand cannot be ruled out at present. In fact a high value of ΣR in the case of **1a** (130%) may be ascribed to the decomposition of triethylphosphine which might be catalyzed by Pd moiety.

Decomposition of the complexes with concd H_2SO_4 evolved mainly the corresponding alkane (R·H). The results are included in Table 2. The reason for evolution of smaller amounts of the gases as compared with the theoretical amount (except for methyl complex **1c**) may be ascribed to the dissolution of the product gases into sulfuric acid. The acidolysis of propyl complex **3c** evolved H_2 and propene, together with propane. The decomposition of **3c** with D_2SO_4 evolved hydrogen gas which was consisted mainly of HD (0.84) together

TABLE 3. IR[a] AND ^{1}H-NMR[b] SPECTRAL DATA OF $[PdR_2L_2]$

Compounds		IR data			^{1}H-NMR data[g]			
		νC-H[c]	δC-H[d]	νPd-C	Solvent	Temp/°C	Rd-R signals	PR_3' signals
$[PdMe_2(PEt_3)_2]$	**1a**	2900 s	1130 m	455 s	$(CD_3)_2CO$	25	−0.61 (t; J=5.5, 6H, Pd-C$\underline{H}_3$)	1.75 (m, 12H, P-C$\underline{H}_2$-) 1.10 (qu; J=8.0, 18H, P-C-C$\underline{H}_3$)
$[PdEt_2(PEt_3)_2]$	**2a**	2875 s 2825 s	1145 s 1360 m	455 s	$(CD_3)_2CO$	25	0.33 (q; J=8.0, 4H, Pd-C$\underline{H}_2$-) 1.12 (qu; J=8.0, 24H, Pd-C-C$\underline{H}_3$+P-C-C$\underline{H}_3$)	1.82 (m, 12H, P-C$\underline{H}_2$-)
$[PdPr^n_2(PEt_3)_2]$	**3a**	2855 s 2805 s	1125 s 1360 m 785 m	(560 s)[e]	$(CD_3)_2CO$	25	0.32 (m, Pd-C-(C$\underline{H}_2$-) 1.19 (qu; J=8.0, Pd-C$\underline{H}_2$-C-C$\underline{H}_3$+P-C-C$\underline{H}_3$)	1.75 (m, P-C$\underline{H}_2$-)
$[PdMe_2(PPh_2Me)_2]$	**1b**	2860 s	1125 s	475 s	$(CD_3)_2CO$	25	0.10 (q,[h] 6H, Pd-C$\underline{H}_3$)	1.58 (d; J=5.0, 6H, P-C$\underline{H}_3$)
$[PdEt_2(PPh_2Me)_2]$	**2b**	2890 s 2830 s	1140 m 1355 m	455 s	$C_6D_5CD_3$	−40	1.04 (br, Pd-C$_2\underline{H}_5$)	1.83 (s, P-C$\underline{H}_3$)
$[PdPr^n_2(PPh_2Me)_2]$	**3b**	2880 s 2850 w 2810 s	1120 s 1360 m	(560 s)[e]	$(CD_3)_2CO$	−40	0.27 (br, Pd-C$\underline{H}_2$-C-C$\underline{H}_3$) 0.90 (br, Pd-C-C$\underline{H}_2$-)	1.70 (br, P-C$\underline{H}_3$)
$[PdMe_2(dpe)]$	**1c**	2845 m	1130 m	f)	CH_2Cl_2	25	0.31 (t; J=7.0, 6H, Pd-C$\underline{H}_3$)	2.26 (d; J=18, 4H, P-C$\underline{H}_2$-)
$[PdEt_2(dpe)]$	**2c**	2900 s 2815 s	1140 s 1360 m	f)	C_5H_5N	25	1.96 (br, Pd-C$\underline{H}_2$-) 1.72 (br, Pd-C-C$\underline{H}_3$)	2.31 (d; J=18, P-C$\underline{H}_2$-)
$[PdPr^n_2(dpe)]$	**3c**	2900 s 2850 s 2810 m	1135 m 1360 w 785 m	f)	$C_6D_5CD_3$	−40	1.23 (br, Pd-C-C$\underline{H}_2$-C$\underline{H}_3$) 0.90 (br, Pd-C$\underline{H}_2$-)	1.68 (d; J=18, P-C$\underline{H}_2$-)

a) KBr disc, in cm^{-1}. b) 100 MHz, chemical shifts are in δ values (ppm) with respect to tetramethylsilane as an external standard (down field positive). Coupling constants, J, are in Hz. c) ν(C-H) of the coordinated alkyl group. d) The band due to the C-H deformation of the palladium-bonded methyl group and may contain contribution due to the other vibrations. e) The assignments are not certain, see text. f) ν(Pd-C) were not discernible from the complicated bands due to dpe. g) Multiplicity abbreviations are: s, singlet; t, triplet; q, quartet; qu, quintet, m, multiplet; br, broad singlet. h) An abnormal quartet, see Fig. 1 and text.

with minor amounts of H_2 (0.05) and D_2 (0.11) as analyzed by mass spectrometry. These results suggest the presence of such a β-elimination process as shown in Eq. 2, in addition to the normal protonation of propyl group with D_2SO_4 to yield propane-d_1.

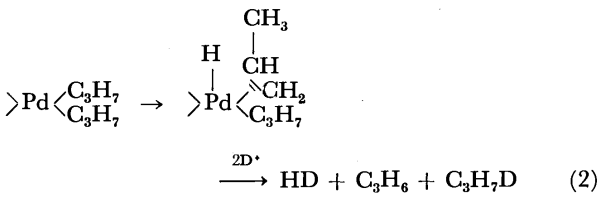

$$\xrightarrow{2D^+} HD + C_3H_6 + C_3H_7D \qquad (2)$$

Infrared Spectra of the Complexes. [PdR_2L_2]. The representative absorption assignable to ν(C–H), δ(C–H) *etc.* of the coordinated alkyl group are listed in Table 3 together with Pd–C stretching vibrations. These assignments were made by comparing the spectra each other and with those of the corresponding dichloro complexes, [$PdCl_2L_2$].

Somewhat different frequencies from those observed for our complexes were reported by Calvin and Coates for the methyl complex **1a**,[2] *i. e.*, δ(C–H)=1164 and ν(Pd–C)=491 and 457 cm^{-1}. The difference in the configuration of the complex might have caused such differences (as for the discussion about the configurations of the complexes, see the following section). The palladium-carbon stretching frequencies of the dimethyl and diethyl complexes with L=PEt_3 and $P(Ph_2Me)_3$ are observed in the region of 455—475 cm^{-1} which is lower than those of the corresponding Pt complexes (495—525 cm^{-1}),[18] reflecting the weaker Pd–C bond than Pt–C.

The ^{1}H-NMR Spectra of the Complexes, [PdR_2L_2]. The results of the ^{1}H-NMR measurements of the dialkyl complexes are included in Table 3. Some complexes are unstable in the solution even at low temperatures making their assignments somewhat tentative. The spectra of [$PdEt_2(PPh_2Me)_2$] (**2b**) and [$PdPr^n_2L_2$] (L=PEt_3, **3a** and PPh_2Me, **3b**) accompanied the weak signals due to ethane and propane, respectively, which may be formed by partial decomposition of the original complexes in solution. For the dimethyl complexes, [$PdMe_2L_2$], well resolved spectra were obtained and are reproduced in Fig. 1 for L=PEt_3 (**1a**) and PPh_2Me (**1b**).

The apparent doublet of the phosphine–methyl signal in **1b** suggests that the complex is in *cis* configuration.[19,20] This is further supported by observation of the complicated pattern of Pd–C$\underline{H}_3$ signal centered at 0.10 ppm, the pattern of which is very close to those of Pt–C$\underline{H}_3$ signals reported for *cis*-[$PtMe_2L_2$].[21–25] In contrast to the *cis* configuration of [$PdMe_2(PPh_2Me)_2$], **1b**, the triethylphosphine complex, [$PdMe_2(PEt_3)_2$], **1a**, was found to possess trans configuration. As is shown in Table 3 and Fig. 1, palladium-bonded methyl protons in **1a** resonates at −0.61 ppm as a triplet due to the coupling with two equivalent phosphorus atoms present in mutually trans positions. The apparent quintet pattern of the methyl protons in the phosphine ligand is also characteristic of the *trans*-bis(triethylphosphine) complexes.[26]

The same dimethyl complex as **1a** has been prepared by Calvin and Coates *via* methylation of [$PdCl_2(PEt_3)_2$] with methyllithium.[2] Although no ^{1}H-NMR spectral data have been reported, they assumed *cis* configuration for the complex through the dipole moment measurement. Furthermore, a slow isomerization in the solution from *cis* to trans as monitored by a decrease in the dipole moment has been suggested. In fact, the ^{1}H-NMR spectrum taken in $(CD_3)_2CO$ by us for [$PdMe_2(PEt_3)_2$] prepared by Calvin and Coates' method[2] showed two sets of Pd–C$\underline{H}_3$ signals, one at 0.01 ppm as a deformed quartet characteristic of the *cis*-dimethyl complex *(vide supra)* and the other at −0.67 ppm as a triplet corresponding to the *trans*-dimethyl isomer. These findings indicate that the product contains both cis and trans isomers in accord with the observation by Calvin and Coates.[2]

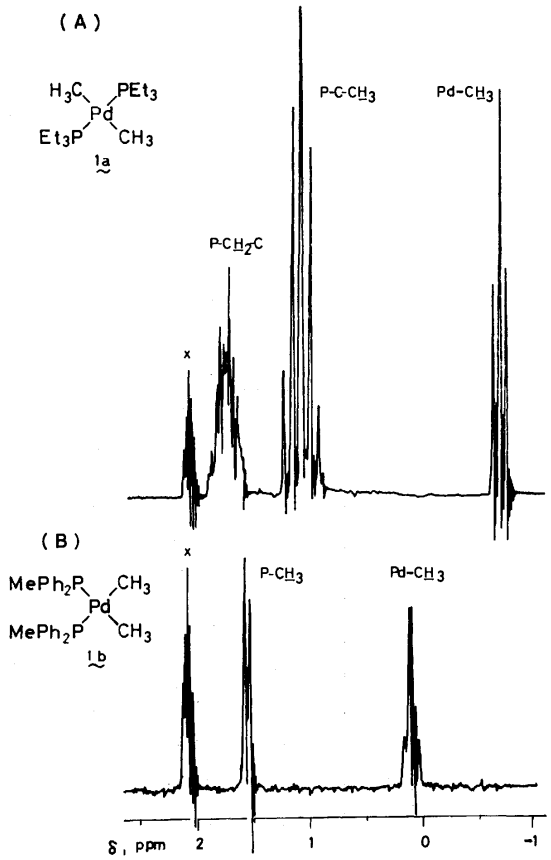

Fig. 1. ^{1}H–NMR spectra (100 MHz, methyl and methylene region) of the complexes, [$PdMe_2L_2$], L=PEt_3 **1a** (A) and PPh_2Me **1b** (B) in $(CD_3)_2CO$ at 25 °C. The sign x refers to the solvent impurities.

The ^{1}H-NMR spectra of the solutions of diethyl complexes, either after being heated at *ca.* 40 °C (for **2a**) or kept at room temperature for several days (for **2b**), indicated the formation of the ethylene-coordinated complex with the accompnaying evolution of ethane. As is shown in Fig. 2, the very small signals at 0.86 and 2.90 ppm observed in the spectrum of the freshly prepared acetone-d_6 solution of **2a** (Fig. 2A) grew considerably on heating the solution at the expense of the quartet at 0.33 ppm assigned to the palladium-attached methylene protons (Fig. 2B). A sharp singlet at 0.86 ppm in Fig. 2B can be assigned to ethane evolved

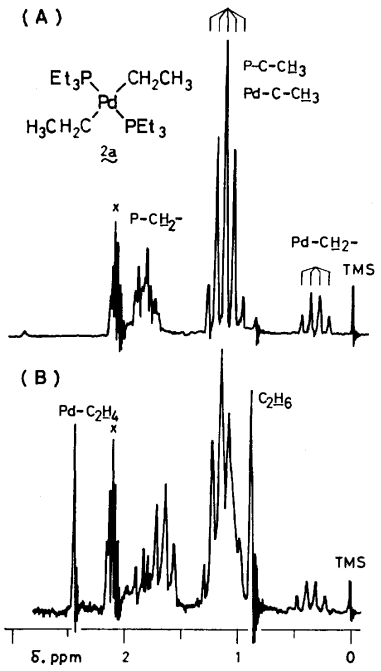

Fig. 2. ^{1}H-NMR spectra of $[PdEt_2(PEt_3)_2]$ **2a** in $(CD_3)_2CO$ at 25 °C. (A) Freshly prepared sample solution. (B) After being heated at 40 °C. The signals x refer to the solvent impurities.

whereas the one at 2.42 ppm (shifted upfield from the initial position of 2.90 ppm in Fig. 2A) to the coordinated ethylene protons. The similar values of the chemical shifts of the coordinated ethylene protons have been reported for $[Ni(C_2H_4)(PPh_3)_2]$ (2.55 ppm in toluene-d_8)[27] and $[Pt(C_2H_4)(PPh_3)_2]$ (2.41 ppm in toluene-d_8).[27] $[Pd(C_2H_4)(PPh_3)_2]$ prepared by the method reported by van der Linde and de Jongh[7] had the value of 2.88 ppm in acetone-d_6 at 25 °C. In the case of PPh_2Me complex **2b**, the proton resonance of the coordinated ethylene appeared at 3.64 ppm as a broad singlet, which is somewhat lower than the other coordinated ethylenes. The complete absence of the signal in the region of free ethylene (5.35 ppm in toluene-d_8)[27] suggests that ethylene, evolved by the decomposition of the diethyl complex according to the following equation, coordinates to palladium preferentially to form the zero-valuent ethylene complex.

$$L_2Pd(C_2H_5)_2 \rightarrow L_2Pd(H)(CH_2CH_2C_2H_5) \rightarrow L_2Pd(CH_2CH_2) + C_2H_6 \quad (3)$$

Attempted isolation of the ethylene complex by treatment of **2b** with excess ethylene in toluene failed.

Some evidence for the ligand exchange in the dimethyl complexes **1a** and **1b** was obtained by measuring the ^{1}H-NMR spectra in the presence of added phosphine ligand. Addition of PEt_3 to the solution of $[PdMe_2(PEt_3)_2]$ **1a** caused the ^{1}H-NMR spectral change from the triplet to a singlet for the Pd–C$\underline{H}_3$ signal, from the multiplet to a quartet for the P–C$\underline{H}_2$– signal and from the quintet to a triplet for the P–C–C$\underline{H}_3$ signal. The existence of a rapid exchange between the coordinated and dissociated PEt_3 has been demonstrated for $[CoMe_2(acac)(PEt_3)_2]$, where triplet, quintet and multiplet signals of the protons due to, respectively, Co–C$\underline{H}_3$, P–C–C$\underline{H}_3$, and P–C$\underline{H}_2$–, at −20 °C changes to singlet, triplet, and quartet, respectively, at 0 °C.[10c] The similar dissociation-exchange process has been observed for $[NiMe_2(PEt_3)_2]$ whose NMR at 25 °C consists of a siglet due to Ni–C$\underline{H}_3$, a triplet due to P–C–C$\underline{H}_3$, and a quartet assignable to P–C$\underline{H}_2$-protons.[28] The monomethyl complex $[PdMeCl(PEt_3)_2]$ also behaves quite similarly.

The ^{1}H-NMR spectrum of a mixture of $[PdMe_2(PPh_2Me)_2]$ and PPh_2Me at −40 °C in acetone-d_6 showed the resonances of the methyl protons of free $PPh_2\underline{Me}$ at 1.66 ppm as a singlet, of coordinated $PPh_2\underline{Me}$ at 1.49 ppm as a doublet (J=5 Hz) and of Pd–C$\underline{H}_3$ at 0.0 ppm, which appears as a distorted quartet as mentioned previously but is somewhat ill-resolved in the present spectrum. The reason for the absence of phosphorus coupling in the methyl proton signal of free PPh_2Me is uncertain. On raising the temperature to 25 °C, the methyl protons of the coordinated and uncoordinated PPh_2Me collapsed to a broad singlet at 1.6 ppm and the resonance due to Pd–C$\underline{H}_3$ also changed to a broad singlet at 0.04 ppm. The existence of the free phosphine ligand may be accelerating the exchange of the phosphine ligand and the exchange rate may be enhanced at the higher temperature. The similar ligand exchange process has been reproted for $[NiR(acac)(PPh_3)_{1\text{ or }2}]$.[29]

Reactions of Dialkylpalladium Complexes with Carbon Monoxide. Booth and Chatt have reported that the reaction of carbon monoxide with monomethyl complex, $[PdMeCl(PEt_3)_2]$, afforded the acyl complex $[Pd(COMe)Cl(PEt_3)_2]$, while the reactions with dimethyl complexes $[PdMe_2L_2]$ either gave uncharacterizable product (L=PEt_3) or led to decomposition (L=½ dpe).[30]

Introduction of carbon monoxide into the toluene solution of dialkyl complexes $[PdR_2L_2]$ (L=PEt_3 and PPh_2Me; R=Me, Et, and Pr^n) at *ca.* 1 atm afforded immediately a red clear solution, whose GLC analysis indicated the formation of a quantitative amount of the corresponding dialkyl ketone. None of alkanes, alkenes and α-diketones were detected in the system. The red solution was unstable in the absence of carbon monoxide and the removal of the solvent by evaporation *in vacuo* left a viscous yellow oil whose IR spectra showed the characteristic C≡O stretching band at 1800 and 1805 cm^{-1} for the PEt_3 and PPh_2Me complexes, respectively. This result suggests formation of carbonyl complexes, which may possibly be related to the reported palladium-carbonyl complexes, $[Pd(CO)(PPh_3)_3]$, $[Pd(CO)PPh_3]_n$ or $[Pd_3(CO)_3(PPh_3)_4]$[14]. However, purification and characterization of the complexes were not successful. Monitoring the reaction of $[PdEt_2(PPh_2Me)_2]$ with CO in toluene-d_8 by means of ^{1}H-NMR spectroscopy also supported the formation of a zero-valent palladium carbonyl complex as well as of diethyl ketone, since the spectrum consisted of the signals due to diethyl ketone (0.90 ppm, triplet, $J\approx7$ Hz, 4H, –C$\underline{H}_2$– and 1.87 ppm, quartet, $J\approx7$ Hz, 6H, –C$\underline{H}_3$) and the coordinated PPh_2Me (1.59 ppm, doublet, $J\approx7$ Hz, 6H, P–C$\underline{H}_3$).

$$[PdR_2L_2] + CO \rightarrow \{Pd(COR)RL_2\} \xrightarrow{CO} R_2CO + [Pd_x(CO)_yL_z]$$

Dialkylcobalt(III) complexes $[CoR_2(acac)(PR'_3)_2]$, have also been found to give the corresponding dialkyl ketones, $R_2C{=}O$, in a quantitative yield on the reaction with carbon monoxide,[10] while $[CuR(PR_3)_n]$ and $[NiR_2(bpy)]$ (bpy=2,2'-bipyridine) afforded ketones and/or diketones whose relative yield depended on the conditions employed.[12a,31] The formation of biacetyl by the reaction of CO with $[PtMe_2(PEt_3)_2]$ has been reported.[30] The acyl complexes which are considered to be the intermediates of the ketone or α-diketone formation have been isolated when $[NiR(acac)(PPh_3)_2]$,[32] $[CoMe(dpe)_2]$,[10a,33] and $[MRX(PEt_3)_2]$ (M=Pd and Pt, X=halogen, NCS, NO_2, and NO_3)[30] were allowed to react with carbon monoxide.

The reactions of $[PdR_2(dpe)]$ with carbon monoxide led to the decomposition of the complex evolving ethane (when R=Me) and ethylene and ethane (when R=Et). When R=Pr^n, dipropyl ketone was formed in 17% yield with concomitant evolution of propane.

Reactions of Dialkyl Palladium Complexes with Iodine. Diethyl and dipropyl complexes of palladium $[PdR_2L_2]$ in benzene reacted with excess amounts of iodine at room temperature to yield di-iodo complex $[PdI_2L_2]$ (as analyzed by IR spectra and elemental analyses), the corresponding alkyl iodide, RI, and the gases such as ethylene and ethane when R=Et and propylene and propane when R=Pr^n (Table 4). The analogous reaction involving dimethyl(bipyridine)palladium and iodine to produce methyl iodide and $[PdI_2(bpy)]$ has been reported by Maitlis and Stone.[34]

Table 4. The reaction products of $[PdR_2L_2]$ and I_2

Compounds		Molar ratio R(−H)	Molar ratio R·H	ΣR[a] %	RI %
$[PdEt_2(PEt_3)_2]$	**2a**	0.42	0.58	30	trace
$[PdPr^n_2(PEt_3)_2]$	**3a**	0.06	0.94	3	54
$[PdPr^n_2(PPh_2Me)_2]$	**3b**	0.33	0.67	9	37
$[PdEt_2(dpe)]$	**2c**	0.40	0.60	10[b]	74
$[PdPr^n_2(dpe)]$	**3c**	c)	c)	c)	18

a) $\Sigma R = \{mol(R(-H)+R\cdot H)/2\ mol(complex)\} \times 100$ where R(−H) corresponds to C_2H_4 (R=Et) and C_3H_6 (R=Pr^n) and R·H to C_2H_6 (R=Et) and C_3H_8 (R=Pr^n). b) R contained a trace amount of C_4H_{10}. c) Not measured.

Reactions of $[PdR_2(dpe)]$ with Methyl Iodide. Addition of methyl iodide to $[PdR_2(dpe)]$(R=Me, **1c**; Et, **2c**; and Pr^n, **3c**) *in vacuo* yielded a clear red solution from which a yellow solid precipitated with the accompanying evolution of gases and alkyl iodides. The yellow powder thus obtained was identified as $[PdI_2(dpe)]$ by means of IR spectroscopy. When R is CH_3, the evolved gas was mainly ethane containing a trace of methane. The amount of the produced RI (CH_3I) could not be measured because of the presence of the unreacted CH_3I. As is shown in Table 5, the gases evolved by the reactions of diethyl and dipropyl complexes (**2c** and **3c**) with CH_3I contained C_1 to C_4 hydrocarbons. The formation of propane as well as ethyl iodide in the case of diethyl complex and of ethane, butane, and propyl iodide in the case of dipropyl complex by the reactions with CH_3I, suggest the formation of intermediate Pd(IV) species as shown below.

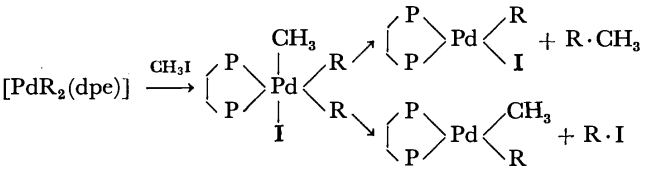

(5)

Beside the above equation, a number of processes may be postulated as the routes to yield the products listed in Table 5. Whichever process the reaction may follow, the six-coordinate palladium(IV) species seems to play an important role in these reactions. Although little has been known about the palladium(IV) compounds, quadrivalent platinum compounds have been amply reported including $[PtMe_2I_2(PEt_3)_2]$,[35] $[Pt(tolyl)RI_2(py)_2]$,[36] $[PtMeRX_2(PMe_2Ph)_2]$,[23,37] and $[PtMe_2RX(PMe_2Ph)_2]$[23,37,38] which were prepared by the oxidative addition of alkyl or aryl halide to the corresponding bivalent platinum-dialkyl or -alkyl halide complexes. Furthermore, the products of the thermal decomposition of series of platinum(IV) alkyl halide complexes have been studied[38,39] and the formation of ethane, methyl chloride and $[PtClMe(PMe_2Ph)_2]$ has

Table 5. The reaction products of $[PdR_2(dpe)]$ and excess CH_3I

Compounds		Products: CH_4 mol/mol·Pd	Molar ratio: C_2H_4	C_2H_6	C_3H_6	C_3H_8	C_4H_{10}	RI mol/mol·Pd
$[PdMe_2(dpe)]$	**1c**	trace	0	1.00 (R·R)	0	0	0	a)
$[PdEt_2(dpe)]$	**2c**	0.52	0.23 (R(−H))	0.36 (R·H, $CH_3\cdot CH_3$)	0	0.35 (R·CH_3)	0.06 (R·R)	0.22
$[PdPr^n_2(dpe)]$	**3c**	0.19	0	0.12 ($CH_3\cdot CH_3$)	0.34 (R(−H))	0.21 (R·H)	0.33 (R·CH_3)	0.26

a) Not measurable, see text.

been observed when $[PtClMe_3(PMe_2Ph)_2]$ was heated at 170 °C.[39] The attempted isolation of the intermediate Pd(IV) species in the reaction of $[PdEt_2(dpe)]$ **2c** with CH_3I by quenching the red clear solution by the addition of Et_2O was not successful, but the orange powder which may be a mixture of several kinds of Pd complexes including $[PdI_2(dpe)]$ was obtained. Evolution of CH_4 as well as C_2H_6 on decomposition of the orange powder with H_2SO_4 indicates the presence of Pd–CH_3 species in the mixture as the result of oxidative addition of CH_3I to **2c**.

In the metathesis reaction of $[PdMe_2(bpy)]$ with perfluoropropyl iodide to yield either $[PdMe(C_3F_7)(bpy)]$ (when equimolar amount of n-C_3F_7I was employed) or $[Pd(C_3F_7)_2(bpy)]$(excess C_3F_7I), Maitlis and Stone postulated the quadrivalent six-coordinate palladium intermediate, $[PdMe_2(C_3F_7)I(bpy)]$,[34] although the other possible by-products, MeI, $Me\cdot C_3F_7$, *etc.* have not been detected.

Experimental

All manipulations were carried out under an atmosphere of deoxygenated nitrogen or argon, or *in vacuo*. Solvents were dried in the usual manner, distilled, and stored under a nitrogen atmosphere.

Infrared spectra were recorded on Hitachi EPI-G3 and 295 spectrometers using KBr pellets prepared under an inert atmosphere. NMR spectra were measured on JEOL PS-100 spectrometer by Mr. Y. Nakamura of our reseach laboratory to whom we are indebted. ^{1}H-NMR signals are referred to tetramethylsilane as internal standard unless otherwise stated. Analysis of the gases evolved by the reaction or decomposition of the alkyl complexes was carried out by mass spectrometry and/or gas chromatography (Shimadzu GC-3BT) after collecting gases fractionally using a Toepler pump, by which the volumes of gases were also measured. Micro analyses (C, H, and halogens) were carried out by Mr. T. Saito of our laboratory using Yanagimoto CHN Autocorder Type MT-2 (for C and H analyses). Analysis of palladium content was performed by EDTA-back titration method using $Zn(NO_3)_2$ aqueous solution. The complete ionization of the palladium metal in the complex was achieved by treating the sample with a hot aqua regia.

Triethylphosphine (Strem) was used as purchased. Diphenylmethylphosphine[40] and 1,2-bis(diphenylphosphino)-ethane[41] were prepared by the literature method starting from PPh_2Cl (Strem) and PPh_3 (kindly donated by Ihara Chemical Industry Co. Ltd.), respectively. Dialkylmonoethoxyaluminums, $AlR_2(OEt)$ (R=Me, Et, and Pr^n), were prepared by the reactions of the corresponding trialkylaluminums and the equimolar amount of ethanol at a low temperature. $[PdCl_2L_2]$ (L=PEt_3 and PPh_2Me) were prepared by the analogous way as reported for $[PdCl_2\{tris(dimethylamino)phosphine\}_2]$.[42] $[PdCl_2(dpe)]$ was obtained from $PdCl_2$ and dpe according to the method described in the literature.[30] The monomethyl complex, $[PdMeCl(PEt_3)_2]$ was prepared by the methylation of $[PdCl_2(PEt_3)_2]$ with MeMgBr in Et_2O.[2]

Preparation of Dimethylbis(triethylphosphine)palladium(II), ***1a***. To a yellow heterogeneous mixture of $[Pd(acac)_2]$ (1.5 g, 5.0 mmol), PEt_3 (1.5 cm^3, 10 mmol) and 30 ml of diethyl ether cooled at −70 °C, $AlMe_2(OEt)$ (3.0 cm^3, 18 mmol) was added dropwise. On raising the temperature of the mixture gradually, it became homogeneous at −30 °C. The solution was stirred for several hours at 0 °C. Cooling the clear solution at −70 °C overnight yielded a white precipitate, which was filtered off, washed with a small amount of Et_2O at the same temperature and dried *in vacuo*. The product was recrystallized from cold hexane to yield colorless needles of $[PdMe_2(PEt_3)_2]$ **1a** (0.71 g, 40%). Similarly obtained were $[PdEt_2(PEt_3)_2]$ **2a** and $[PdPr^n{}_2(PEt_3)_2]$ **3a** by the use of, respectively, $AlEt_2(OEt)$ and $AlPr^n{}_2(OEt)$ in place of $AlMe_2(OEt)$. Complexes **2a** and **3a** were crystallized quickly from acetone at low temperatures. The low yields of crystallized complexes **2a** and **3a** (less than 15%) may be accounted for instability of the complexes in solution.

Preparation of Dimethylbis(diphenylmethylphosphine)palladium(II) ***1b***. To the heterogeneous yellow mixture of $[Pd(acac)_2]$ (1.5 g, 5 mmol), PPh_2Me (2.3 cm^3, 12 mmol) and diethyl ether (30 cm^3) cooled at −70 °C, was added 3 cm^3 (25 mmol) of $AlMe_2(OEt)$ dropwise. Gradual warming of the system to −20 °C with stirring afforded a clear red solution, and the solution was further stirred at 0 °C for several hours. Cooling the solution at −70 °C overnight yielded a white precipitate which was filtered off, washed with Et_2O and hexane at low temperature and dried *in vacuo*. The product was crystallized from cold acetone to give white crystals of $[PdMe_2(PPh_2Me)_2]$, **1b**, (0.23 g, 10%).

Similarly obtained were its ethyl and propyl analogs, **2b** and **3b**, using $AlEt_2(OEt)$ and $AlPr^n{}_2(OEt)$, respectively, in place of $AlMe_2(OEt)$. Crude complex **2b** (0.70 g, 25%) could not be crystallized due to its poor solubility. White crystals of **3b** (0.33 g, 10%) were obtained by the careful, low temperature crystallization from acetone.

Preparation of Dimethyl{1,2-bis(diphenylphosphino)ethane}palladium(II), ***1c***. Into the cooled (−70 °C) heterogeneous mixture of $[Pd(acac)_2]$ (1.5 g, 5 mmol), 1,2-bis(diphenylphosphino)ethane (dpe, 2.2 g, 5.5 mmol), and Et_2O (30 cm^3), was added dropwise 3 cm^3 (16 mmol) of $AlMe_2(OEt)$. Stirring the mixture at −20 to −30 °C yielded, at first, a sticky solid, and then finally a white precipitate, which was filtered off, washed with Et_2O and hexane, and dried *in vacuo*. Recrystallization of the product from acetone yielded white crystals of $[PdMe_2(dpe)]$ **1c** (1.6 g, 45%).

The analogous complexes, $[PdEt_2(dpe)]$ **2c** and $[PdPr^n{}_2(dpe)]$ **3c** were obtained by the similar method as above using $AlEt_2(OEt)$ and $AlPr^n{}_2(OEt)$, respectively, as alkylating agents in place of $AlMe_2(OEt)$. Complexes **2c** (2.1 g, 75%) and **3c** (2.5 g, 85%) could not be crystallized due to their poor solubility.

Reactions of Dialkylpalladium Complexes with Carbon Monoxide. To the pre-evacuated flask containing the mixture of $[PdMe_2(PEt_3)_2]$ **1a** (46.5 mg, 0.125 mmol) and toluene (1 cm^3) freezed at −198 °C, carbon monoxide was introduced. The system turned red instantly on melting by raising the temperature under carbon monoxide. At room temperature, a clear red solution resulted. No gas evolution was observed in the system. The formation of acetone (0.108 mmol, 90% on the basis of the amount of **1a** used) in the solution was confirmed by means of GLC.

The similar reactions of CO with complexes **2a**, **3a**, **1b**, **2b**, and **3b** yielded the corresponding ketones as shown in Table 6.

Reactions of Dialkylpalladium Complexes with Iodine. *$[PdEt_2(dpe)]$ (2c)*: Into the Schlenk flask fitted with a side arm, 74.1 mg (0.132 mmol) of $[PdEt_2(dpe)]$ was placed. The benzene (2 cm^3) solution of iodine (1.0 g) in a L-shaped tube was connected to the side arm of the flask. After being evacuated by freeze-thaw method, the contents were mixed together by rotating the L-shaped tube. The mixture was stirred at room temperature for several hours. The gases evolved by the reaction are listed in Table 4. From the solution, all volatile liquid was removed by a trap-to-trap distillation

Table 6. The amount of dialkylketones formed by the reactions of $[PdR_2L_2]$ with carbon monoxide

Complexes				Dialkylketones		
		mg	(mmol)		mmol	(%)
$[PdMe_2(PEt_3)_2]$	**1a**	46.5	(0.125)	Me_2CO,	0.108	(85)
$[PdEt_2(PEt_3)_2]$	**2a**	52.1	(0.130)	Et_2CO,	0.144	(110)
$[PdPr^n{}_2(PEt_3)_2]$	**3a**	21.1	(0.049)	$Pr^n{}_2CO$,	0.046	(95)
$[PdMe_2(PPh_2Me)_2]$	**1b**	77.0	(0.143)	Me_2CO,	0.129	(90)
$[PdEt_2(PPh_2Me)_2]$	**2b**	49.9	(0.088)	Et_2CO,	0.088	(100)
$[PdPr^n{}_2(PPh_2Me)_2]$	**3b**	25.2	(0.042)	$Pr^n{}_2CO$,	0.042	(100)

to leave a residual orange solid. The presence of methyl iodide (0.196 mmol, 74% on the basis of the amount of initially used complex) was confirmed by means of GLC. Recrystallization of the residue from acetone–hexane yielded orange crystals of $[PdI_2(dpe)]$ (Found: C, 41.6; H, 3.8; I, 33.0%. Calcd for $C_{26}H_{24}I_2P_2Pd$: C, 41.2; H, 3.2; I, 33.5%).

Similarly carried out were the reactions of $[PdEt_2(PEt_3)_2]$ and $[PdPr^n{}_2L_2]$ (L=PEt_3, PPh_2Me, and 1/2dpe) with iodine.

Reactions of $[PdR_2(dpe)]$ with methyl iodide. *$[PdMe_2(dpe)]$*: Methyl iodide (*ca.* 2 cm^3) was distilled over calcium hydride under a vacuum into a flask containing $[PdMe_2(dpe)]$ (69.6 mg, 0.13 mmol). On stirring the mixture at room temperature, the initial white suspension turned to a clear red solution and then finally to the suspension containing a yellow precipitate which was identified as $[PdI_2(dpe)]$ on the basis of the IR spectrum. The evolution of ethane containing a trace of methane was observed as analyzed by GLC. The amount of ethane can not be measured due to the coexistence of unreacted CH_3I. The reactions of diethyl and dipropyl complexes with methyl iodide were carried out similarly.

We thank the Kawakami Foundation for financial support.

References

1) P. M. Maitlis, "The Organic Chemistry of Palladium," Academic Press, Vol.2, New York and London (1971).
2) G. Calvin and G. E. Coates, *J. Chem. Soc.*, **1960**, 2008.
3) P. M. Maitlis, "The Organic Chemistry of Palladium," Academic Press, Vol.1, New York and London (1971).
4) J. P. Visser, W. W. Jagur, and C. Masters, *Recl. Trav. Chim. Pays-Bas*, **94**, 70 (1975); J. P. Visser and C. Masters, Abstr. No. 245, 7th International Conference on Organometallic Chemistry, Venice, September, 1975.
5) P. Fitton, M. P. Johnson, and J. E. McKeon, *Chem. Commun.*, **1968**, 6.
6) S. Otsuka, A. Nakamura, and T. Yoshida, *J. Am. Chem. Soc.*, **91**, 7196 (1969).
7) R. van der Linde and R. O. de Jongh, *Chem. Commun.*, **1971**, 563.
8) K. Nishimura, H. Kuribayashi, A. Yamamoto, and S. Ikeda, *J. Organomet. Chem.*, **37**, 317 (1972).
9) A. Yamamoto, K. Morifuji, S. Ikeda, T. Saito, Y. Uchida, and A. Misono, *J. Am. Chem. Soc.*, **87**, 4652 (1965); T. Yamamoto, A. Yamamoto, and S. Ikeda, *Bull. Chem. Soc. Jpn.*, **45**, 1104 (1972).
10) a) T. Ikariya, Ph. D. Thesis, Tokyo Institute of Technology, 1976. b) T. Ikariya and A. Yamamoto, *Chem. Lett.*, **1976**, 85. c) T. Ikariya and A. Yamamoto, *J. Organomet. Chem.*, **116**, 239 (1976). d) T. Ikariya and A. Yamamoto, *J. Organomet. Chem.*, **118**, 101 (1976).
11) T. Yamamoto, A. Yamamoto, and S. Ikeda, *J. Am. Chem. Soc.*, **93**, 3350 (1971).
12) a) A. Miyashita, Ph. D. Thesis, Tokyo Institute of Technology, 1975; A. Yamamoto, A. Miyashita, T. Yamamoto, and S. Ikeda, *Bull. Chem. Soc. Jpn.*, **45**, 1583 (1972) b) T. Ikariya and A. Yamamoto, *J. Organomet. Chem.*,**72**, 145 (1974).
13) E. O. Greaves, C. J. L. Lock, and P. M. Maitlis, *Can. J. Chem.*, **46**, 3879 (1968).
14) A. Misono, Y. Uchida, M. Hidai, and K. Kudo, *J. Organomet. Chem.*, **20**, P7 (1969).
15) K. Kudo, M. Hidai, and Y. Uchida, *J. Organomet. Chem.*, **56**, 413 (1973).
16) G. M. Whitesides, J. S. Filippo, Jr., E. R. Stedronsky, and C. P. Casey, *J. Am. Chem. Soc.*, **91**, 6542 (1969); **92**, 1426 (1970); G. Yagupsky, C. K. Brown, and G. Wilkinson, *J. Chem. Soc., A*, **1970**, 1392.
17) T. Ikariya and A. Yamamoto, *J. Chem. Soc., Chem. Commun.*, **1974**, 720; *J. Organomet. Chem.*, **118**, 65 (1976).
18) D. M. Adams, J. Chatt, and B. L. Shaw, *J. Chem. Soc.*, **1960**, 2047.
19) D. A. Redfield and J. H. Nelson, *Inorg. Chem.*, **12**, 15 (1973).
20) D. A. Redfield, L. W. Cary, and J. H. Nelson, *Inorg. Chem.*, **14**, 50 (1975).
21) R. J. Goodfellow, M. J. Hardy, and B. F. Taylor, *J. Chem. Soc., Dalton Trans.*, **1973**, 2450.
22) F. H. Allen and A. Pidcock, *J. Chem. Soc., A*, **1968**, 2700.
23) J. D. Ruddick and B. L. Shaw, *J, Chem. Soc., A*, **1969**, 2801.
24) A. J. Cheney, B. E. Mann, and B. L. Shaw, *Chem. Commun.*, **1971**, 431.
25) E. O. Greaves, R. Bruce, and P. M. Maitlis, *Chem. Commun.*, **1967**, 860.
26) (a) G. W. Parshall, *J. Am. Chem. Soc.*, **88**, 704 (1966). (b) H. C. Clark and W. S. Tsang, *ibid.*, **89**, 533 (1967). (c) R. G. Miller, R. D. Stauffer, D, R. Fahey, and D. R. Parnell, *ibid.*, **92**, 1511 (1970). (d) R. G. Miller, D. R. Fahey, H. J. Golden, and L. C. Satek, *J. Organomet. Chem.*, **82**, 127(1974).
27) P. -T. Cheng, C. D. Cook, S. C. Nyburg, and K. Y. Wan, *Inorg. Chem.*, **10**, 2210 (1971).
28) M. Takamatsu, T. Yamamoto, and A. Yamamoto, unpublished results.
29) T. Yamamoto, T. Saruyama, Y. Nakamura, and A. Yamamoto, *Bull. Chem. Soc. Jpn.*, **49**, 589 (1976).
30) G. Booth and J. Chatt, *J. Chem. Soc., A*, **1966**, 634.
31) T. Yamamoto, T. Kohara, and A. Yamamoto, *Chem. Lett.*, **1976**, 1217.
32) T. Saruyama, T. Yamamoto, and A. Yamamoto, *Bull. Chem. Soc. Jpn.*, **49**, 546 (1976).
33) T. Ikariya and A. Yamamoto, *J. Organomet. Chem.*,

116, 231 (1976).
34) P. M. Maitlis and F. G. A. Stone, *Chem. Ind. (London)*, **1962**, 1865.
35) J. Chatt and B. L. Shaw, *J. Chem. Soc.*, **1959**, 705.
36) C. R. Kistner, D. A. Drew, J. R. Doyle, and G. W. Rausch, *Inorg. Chem.*, **6**, 2036 (1967).
37) T. G. Appleton, H. C. Clark, and L. E. Manzer, *J. Organomet. Chem.*, **65**, 275 (1974).
38) M. P. Brown, R. J. Puddephatt, C. E. E. Upton, and S. W. Lavington, *J. Chem. Soc., Dalton Trans.*, **1974**, 1613
39) J. D. Ruddick B. L. Shaw, *J. Chem. Soc., A*, **1969**, 2969.
40) J. A. C. Allinson and F. G. Mann, *J. Chem. Soc.*, **1949**, 2915.
41) W. Hewertson and H. R. Watson, *J. Chem. Soc.*, **1962**, 1490.
42) J. M. Jenkins and J. G. Verkade, *Inorg. Synth.*, **11**, 108 (1968).

Kinetics of the Proton-Transfer Reaction of 4-(2,4-Dihydroxyphenylazo)-nitrobenzene in Dioxane–Water Media*

Noboru Yoshida and Masatoshi Fujimoto

Department of Chemistry, Faculty of Science, Hokkaido University, Sapporo 060

(Received October 30, 1976)

Kinetics of proton-transfer reactions in 4 to 50%(v/v) dioxane–water media between hydroxide ion and 4-(2,4-dihydroxyphenylazo)nitrobenzene (Magneson; MAG) having a strong OH···N intramolecular hydrogen-bond are studied by means of the temperature-jump method. The forward and the backward rate constants k_f and $k_r[H_2O]$ for the reaction $OH^- + HA^- \underset{k_r}{\overset{k_f}{\rightleftharpoons}} H_2O + A^{2-}$ are evaluated to be in the range of 9.2×10^5—1.3×10^5 $mol^{-1}\,dm^3\,s^{-1}$ and 5.5×10^3—$1.8\times10^3\,s^{-1}$, respectively. The dependence of the k_f and the acid dissociation constant K_a^c on the dioxane contents of the medium is interpreted on the basis of solute-solvent interactions.

The kinetic studies of proton-transfer reactions in mixed solvents are of particular importance for the interpretation of fast proton-transfer reactions in aqueous solutions, especially from the point of view of solute-solvent interactions.

1,4-Dioxane, a typical water-miscible aprotic solvent, can cover the wide range of dielectric constant of the medium on mixing with water. This characteristic is favorable for evaluating the solvent effects such as electrostatic effect in the fast proton-transfer reactions. Many investigations on the structure of dioxane–water solutions have so far been reported in detail.[1] However, it is necessary to get further information on the liquid structure of dioxane–water system at the periphery of a *bulky* solute molecule such as 4-(2,4-dihydroxyphenylazo)nitrobenzene (Magneson; MAG).

In a previous paper[2] we determined the overall rate constants k_f and k_r for the proton-transfer reactions between hydroxide ion and some *ortho*-hydroxy azo and azomethine compounds HA in 50%(v/v) dioxane–water medium and proposed the following reaction mechanism for this medium;

$$\underset{[1]}{\widehat{HA} + OH^-} \underset{k_{21}}{\overset{k_{12}}{\rightleftharpoons}} \underset{[2]}{HA^* + OH^-}$$

$$\overset{k_{23}}{\underset{k_{32}}{\rightleftharpoons}} \underset{[3]}{HA^* \cdots (H_2O)_n \cdots OH^-} \overset{k_{34}}{\underset{k_{43}}{\rightleftharpoons}} \underset{[4]}{A^- + H_2O}.$$

In the step [1]⇌[2], the hydrogen-bonded proton in $\widehat{HA}$ is set free from the azo-nitrogen atom and interacts with solvent *water* molecules to form HA*. Recently Jost and Liphard directly proved the existence of the first elementary step [1]⇌[2] from the activation volume of the overall reaction determined by the temperature-jump study under pressure.[3]

In the present study we found that for the uninegative acid HA^- of MAG the recombination rate constant k_f decreases with increasing dioxane contents in the medium. This dependence in the k_f was attributed to the change of the two terms, $K_{12}=k_{12}/k_{21}$ and k_{23}. From the dependence of $\log k_f$ on the value of the macroscopic dielectric constant of the medium, the number of intervening *water* molecules in the encounter complex, $HA^*\cdots(H_2O)_n\cdots OH^-$, was estimated to be $n=4$—5.

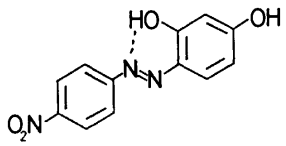

MAG: $\widehat{H_2A}$

Experimental

Reagents. The water used here was deionized and distilled. Guaranteed grade dioxane (Wako) was distilled and used without further purification.[2] 4-(2,4-Dihydroxyphenylazo)nitrobenzene was purified by repeated recrystallization from methanol. Dioxane solution of the dye (3×10^{-3} mol dm^{-3}) was stored in a well-stoppered bottle to avoid evaporation.

Measurements. *pH in the Mixed Solvent*: We used the following relationship[4] between pH-meter readings (pH*) and values of $-\log(C_H/\text{mol dm}^{-3}) = pC_H$

$$\log U_H = pC_H - pH^*,$$

where C_H denotes the analytical concentration of the solvated proton determined titrimetrically. The plot of pH* *vs.* pC_H shows a good linear relationship for any dioxane content in the medium. The values of $\log U_H$ were evaluated in the range of pH*=3—12 at 25 °C and I=0.1 mol dm^{-3} ($NaClO_4$) to be −0.07, −0.03, −0.06, −0.08, −0.11, and −0.14 for the mixed solvent containing 0, 10, 20, 30, 40, and 50%(v/v) dioxane, respectively. Hitachi-Horiba pH-meters Model P and Model M-7 were used throughout the study.

Equilibria and Kinetics: The acid dissociation constants of MAG were determined spectrophotometrically with a Hitachi recording spectrophotometer Model EPS-3T. The kinetic measurements were carried out with a Union Giken co-axial-cable temperature-jump apparatus Model RA-105. The temperature-jump cell was made of Teflon and equipped with gold electrodes. Temperature-rise was determined for discharge at 25 kV from the calibration curve between the light intensity and the temperature of the sample solution at I=0.1 mol dm^{-3} (KNO_3) to be 4.4 and 3.8 °C in the aqueous and the 50%(v/v) dioxane–water solution, respectively. The rise-time of the temperature in 50%(v/v) dioxane–water solution was *ca.* 5 μs.[5] To avoid partial decomposition of the dye after repeated discharges on the same sample solution, we often renewed the sample solution in the cell. As the

* Presented in part at the 26th Annual Meeting on Coordination Chemistry, Sapporo, August 30, 1976, Abstract p. 252.

noise-level in the signal was serious for dioxane-water system, the discharge voltage was carefully controlled below 25 kV. The reaction was followed on the screen of an oscilloscope Tektronix Type 545B at the absorption maximum of the conjugated base of the Brønsted acid. Temperature of the solution was kept constant by circulating the water thermostated with a regulator Lauda Type K2R or Coolnics Model CTR-1B.

Results

Equilibria of the Reaction. The apparent ionic product $K_w^c=[H][OH]$ of the water in dioxane–water mixture at 25 °C and $I=0.1$ mol dm^{-3} ($NaClO_4$) was calculated using the values of log U_H derived from the data of the potentiometric titrations as described in detail in a previous paper.[2] The values of K_w^c thus obtained were used for the evaluation of the acid dissociation constant K_a^c based on the kinetic data, according to the relation $K_a^c=[H][A]/[HA]=(k_f/k_r')[H][OH]=K_b^cK_w^c$, where K_b^c denotes the ratio k_f/k_r' and $k_r'=k_r\cdot[H_2O]$. Figure 1 shows the dependence of the pK_w^c ($=-\log(K_w^c/\text{mol}^2\,\text{dm}^{-6})$) on the mole fraction of dioxane in the medium, x_{dlox}, indicating the decrease in K_w^c with increasing dioxane content.

The absorption coefficient A of the solution at wavelength where the absorption of an acid form HA^- of MAG can be neglected is given by

$$A=\varepsilon_{HA}\bar{C}_{HA}+\varepsilon_A\bar{C}_A\simeq\varepsilon_A\bar{C}_A, \quad (1)$$

where ε and $\bar{C}$ denote the molar absorption coefficient and the equilibrium concentration, respectively. The acid dissociation constant $K_a^c=[H][A]/[HA]$ is derived from the following equation;

$$C/A_A=1/\varepsilon_A+\bar{C}_H/\varepsilon_AK_a^c, \quad (2)$$

where C denotes the total concentration, $C=C_{HA}+C_A$, and A_A the absorption coefficient of a basic form A^{2-}. The plot of C/A_A *vs.* $\bar{C}_H$ for each dioxane content of the medium gives a straight line as shown in Fig. 2. From the slope and the intercept of the straight line, the values of the K_a^c and ε_A are obtained, respectively. The acid dissociation constants K_a^c in the medium of varying dioxane content are summarized in Table 1.

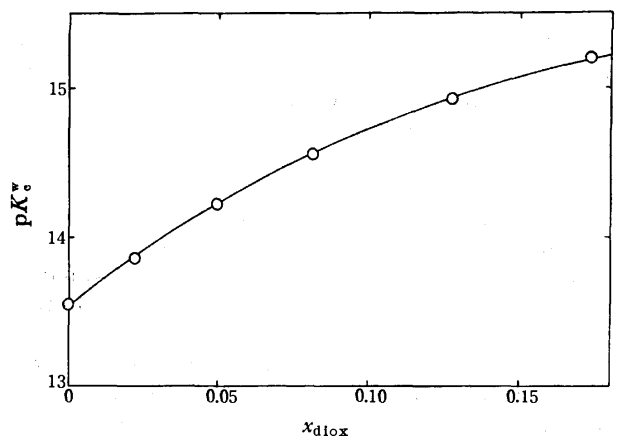

Fig. 1. Dependence of thep K_w^c on the mole fraction of dioxane, x_{dlox}. At 25 °C and $I=0.1$ mol dm^{-3} ($NaClO_4$).

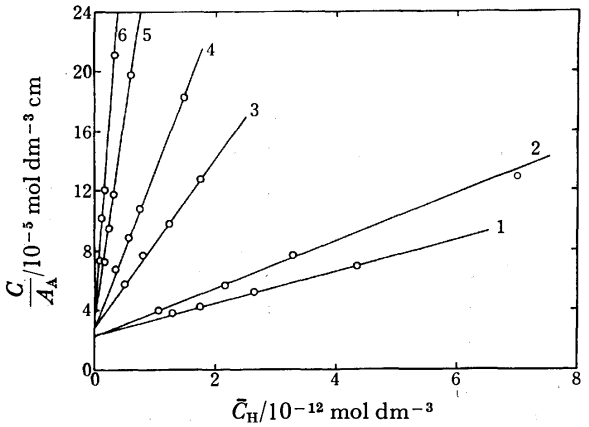

Fig. 2. Plots of C/A_A *vs.* $\bar{C}_H$ in dioxane-water media. Dioxane content: (1) 4, (2) 10, (3) 20, (4) 30, (5) 40, and (6) 50%(v/v). At 25 °C and $I=0.1$ mol dm^{-3} (KNO_3).

Table 1. Acid dissociation constants K_a^c of Magneson in dioxane-water medium at 25 °C determined from the spectrophotometric data

Dioxane/%(v/v)	pK_a^c ($=-\log(K_a^c/\text{mol dm}^{-3})$)[a]
4	11.66
10	11.88
20	12.26
30	12.60
40	12.98
50	13.23

a) $K_a^c=[A][H]/[HA]$, $I=0.1$ mol dm^{-3} (KNO_3).

In Fig. 4(a) the spectrophotometric acid dissociation constants are plotted against the mole fraction of dioxane, x_{dlox}. Increasing dioxane content in the medium would lead to a decrease in the acid dissociation constant of HA^-. A linear relationship between pK_a^c and x_{dlox} is observed in the range of x_{dlox} lower than 0.09, while for simple nonaromatic carboxylic acids such as acetic acid Van Uitert and Haas,[4] and Harned and Owen[6] reported the corresponding linear relationship in by far the wider range of the mole fraction of dioxane.

Kinetics. For the proton-transfer reactions of uninegative acid HA^- in the mixed solvent,

$$HA^- + OH^- \underset{k_r}{\overset{k_f}{\rightleftharpoons}} A^{2-} + H_2O$$

with the equilibrium constant $K_b^c=k_f/k_r'=\bar{C}_A/\bar{C}_{HA}\bar{C}_{OH}$, the relaxation time τ is expressed by

$$\tau^{-1}=k_f(\bar{C}_{OH}+\bar{C}_{HA})+k_r', \quad (3)$$

where k_r' involves the concentration of the water in the mixed solvent and equal to $k_r[H_2O]$. Figure 3 shows the plots of τ^{-1} *vs.* $\bar{C}_{HA}+\bar{C}_{OH}$, giving k_f and k_r' from the slope and the intercept, respectively. The values of k_f, k_r', and K_b^c are summarized in Table 2. In Fig. 4, pK_a^c evaluated as $K_a^c=K_b^cK_w^c$ from the kinetic data is plotted against x_{dlox} together with the spectrophotometric pK_a^c. Figure 5 shows a dependence of log k_f on x_{dlox}. At higher dioxane content, marked deviation from the linear dependence is observed.

Table 2. Rate constants for the proton-transfer reaction of Magneson $HA^- + OH^- \underset{k_r}{\overset{k_f}{\rightleftharpoons}} A^{2-} + H_2O$ in dioxane-water medium at 25 °C

Dioxane %(v/v)	k_f 10^5 mol^{-1} dm^3 s^{-1}	k'_r 10^3 s^{-1} a)	K_b^c 10^2 mol dm^{-3}	pK_a^c (=−log (K_a^c/mol dm^{-3}))b)
4	9.2	5.5	1.7	11.5
10	6.4	5.2	1.2	11.8
20	4.5	3.8	1.2	12.2
30	2.5	2.5	1.0	12.5
40	1.5	2.4	0.63	13.1
50	1.3	1.8	0.72	13.3

a) $k'_r = k_r[H_2O]$.
b) $K_a^c = K_b^c K_w^c$, I = 0.1 mol dm^{-3} (KNO_3).

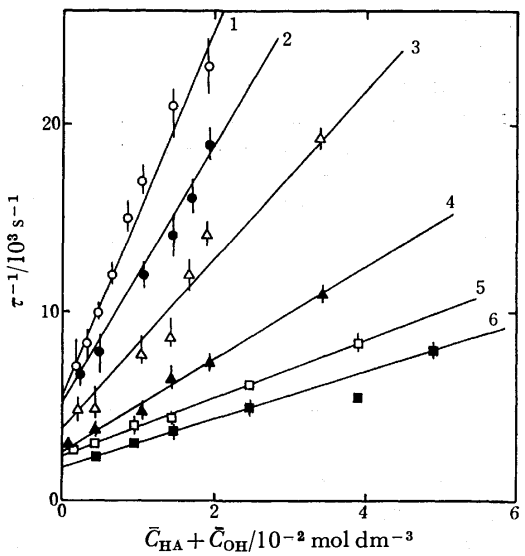

Fig. 3. Plots of the reciprocal relaxation time, τ^{-1}, *vs.* $\bar{C}_{HA}+\bar{C}_{OH}$ in dioxane-water media. Dioxane content: (1) 4, (2) 10, (3) 20, (4) 30, (5) 40, and (6) 50% (v/v). At 25 °C and I=0.1 mol dm^{-3} (KNO_3).

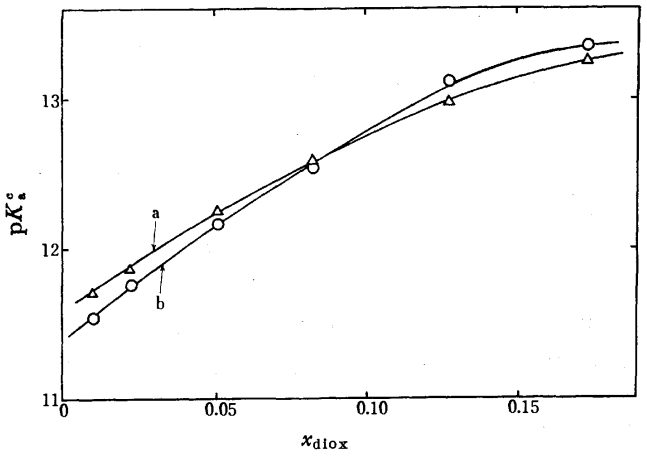

Fig. 4. Dependence of the acid dissociation constants K_a^c of MAG on the mole fraction of dioxane, x_{diox}. At 25 °C and I=0.1 mol dm^{-3} (KNO_3). (a) The plot of the spectrophotometric pK_a^c *vs.* x_{diox}. (b) The plot of the kinetic pK_a^c *vs.* x_{diox}.

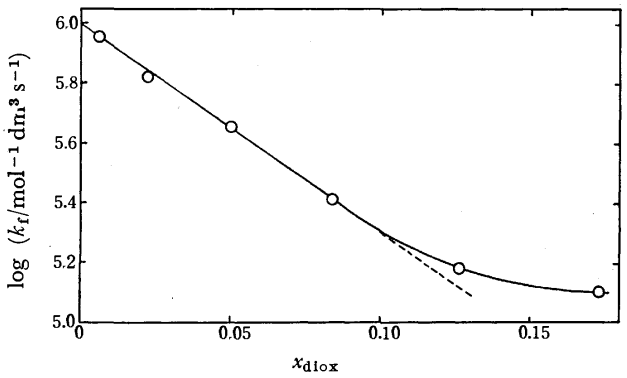

Fig. 5. Dependence of the recombination rate constants k_f on the x_{diox}. At 25 °C and I=0.1 mol dm^{-3} (KNO_3).

Discussion

In Fig. 6 the kinetic and the spectrophotometric pK_a^c are plotted against the inverse macroscopic dielectric constant of the medium.[7] Both pK_a^c's increase with decreasing dielectric constant of the medium, though the linear dependence of pK_a^c on D^{-1} as interpreted by Gilkerson in terms of electrostatic interactions[8] is observed only for the lower dioxane contents. The free energy of the acid dissociation is a sum of the energies required to break the O–H bond, the energies required to break the intramolecular hydrogen-bond, and the hydration energies of various species involved.[9] The decrease of K_a^c with increasing dioxane content in the medium shown in Fig. 6 would partly be ascribed to the difference in the energies of hydration of the reactants.[10]

The recombination of hydroxide ion with a uninegative 4-(2-hydroxy-4-ethylphenylazo)benzenesulfonate ion having no *para*-OH group was found to be almost diffusion-controlled,[11] and the value of pK_a^c for the hydrogen-bonded proton is by two orders of magnitude lower than that of a uninegative ion of 4-(2,4-dihydroxyphenylazo)nitrobenzene having a dissociated *para*-OH group. These facts would lead to the following conclusions: 1. The thermodynamic stability of the intramolecular hydrogen-bond increases mainly due to the presence of a *para*-O^- group which contributes to a resonance quinoidal form and enhances the electron density on the azo-nitrogen. 2. Increased

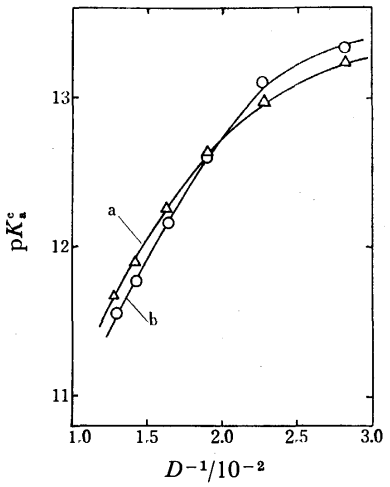

Fig. 6. Dependence of the acid dissociation constant K_a^c of MAG on the dielectric constant of the medium. At 25 °C and I=0.1 mol dm^{-3} (KNO_3). (a) The plot of the spectrophotometric pK_a^c *vs.* the dielectric constant of the medium. (b) The plot of the kinetic pK_a^c *vs.* the dielectric constant of the medium.

double-bond character of a C–N bond between an azo-nitrogen and the benzene ring owing to the resonance contribution from the *para*-O^- substituent may restrict the internal rotation about the C–N axis and further enhance the thermodynamic stability of the intramolecular hydrogen-bond. More recently, from the similar point of view Tōei[12] and Johnson and Florence[13] have also explained the stability of the complexes of *o*-hydroxyphenylazo multidentate ligands having a *para*-OH group in terms of a charge-quinone hypothesis.

For the proton-transfer reactions of a uninegative Brønsted acid ion $\widehat{HA}^- + OH^- \rightleftharpoons A^{2-} + H_2O$ in dioxane–water media, we propose the following mechanism which postulates the existence of the first pre-equilibrium between $\widehat{HA}^-$ and HA^{*-};

$$\underset{[1]}{\widehat{HA}^- + OH^-} \underset{k_{21}}{\overset{k_{12}}{\rightleftharpoons}} \underset{[2]}{HA^{*-} + OH^-}$$

$$\underset{k_{32}}{\overset{k_{23}}{\rightleftharpoons}} \underset{[3]}{HA^{*-}\cdots(H_2O)_n\cdots OH^-} \underset{k_{43}}{\overset{k_{34}}{\rightleftharpoons}} \underset{[4]}{A^{2-} + H_2O},$$

where $\widehat{HA}^-$ stands for the uninegative species having a *para*-O^- group and an intramolecular hydrogen-bond, and HA^{*-} an intermediate species without an intramolecular hydrogen-bond. The *ortho*-hydroxyl proton in $\widehat{HA}^-$ is set free from the intramolecular hydrogen-bond and associated with surrounding water molecules *via* hydrogen-bond to form HA^{*-}. If a proton-transfer reaction in dioxane-water media proceeds in accordance with the above mechanism, the relations between rate constants of the overall reaction and those for each elementary step are shown by Eqs. 4 and 5.

$$k_f = K_{12}k_{23}, \tag{4}$$

and

$$k_r = k_{32}/K_{34}, \tag{5}$$

where $K_{12}=k_{12}/k_{21}$ and $K_{34}=k_{34}/k_{43}$. The equilibrium constant K_{12} is characteristic of the structure of the Brønsted acid and may reflect the liquid structure of the water at the periphery of the reactant, namely, that in the vicinity of the hydroxyl proton. On the other hand, k_{23} is a function of the solvent composition and of the dielectric constant of the medium. Thus the value of K_{12} appears to be one of the measures of the differences in solute-solvent interactions for $\widehat{HA}^-$ and HA^{*-}. The values of k_f and k_r in dioxane–water media are found to be smaller than those in aqueous medium. As discussed above, this decrease in the recombination rate constant in the mixed solvent system is due to two terms K_{12} and k_{23}.

By neglecting the ionic-atmosphere term in Christiansen-Scatchard equation[14] we obtain

$$\ln (k_f/k_f^\circ) = -z_i z_j e^2/kTr^*D, \tag{6}$$

where z_i and z_j represent the charge of the reactants, D is the dielectric constant of the medium, k Boltzmann's constant, T the absolute temperature, r^* the reaction distance, e the elementary charge, and k_f° the rate constant at infinite dielectric constant. As shown in Fig. 7, the log k_f *vs.* D^{-1}-plot is linear in the region of higher dielectric constant (D=78—52). Since the decrease of log k_f in Fig. 7(a) is due to two terms K_{12} and k_{23}, and the term K_{12} is not constant[15] in this region, we obtain an unexpectedly small value of the reaction distance (2.9 Å) from the slope (a) in Fig. 7. In the region, where the term K_{12} is assumed to be nearly constant,[16] the slope in Fig. 7 is reduced to Eq. 7.

$$\mathrm{d}\log(k_f/\mathrm{mol}^{-1}\,\mathrm{dm}^3\,\mathrm{s}^{-1})/\mathrm{d}\,D^{-1} \simeq \mathrm{d}\log(k_{23}/\mathrm{mol}^{-1}\,\mathrm{dm}^3\,\mathrm{s}^{-1})/\mathrm{d}\,D^{-1}. \tag{7}$$

From the slope (b) of the log (k_f/mol^{-1} dm^3 s^{-1}) *vs.* D^{-1}-plot we obtain the value of r^*=18 Å as a phenomenological reaction distance. This value of the reaction distance would be reasonable in view of the charge and the size of the reactants, though further investigation is needed with respect to the phenomenological reaction distance derived from the assumption $K_{12}\simeq$constant. From the value 18 Å for r^*, the number of the inter-

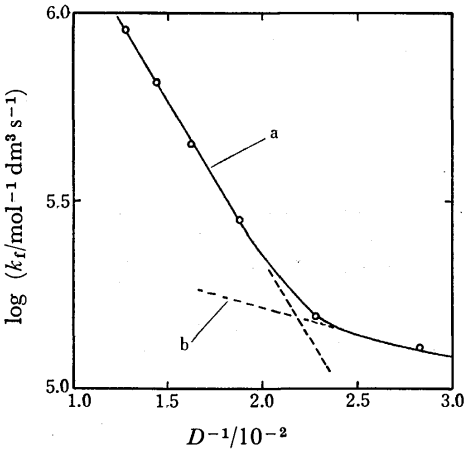

Fig. 7. Dependence of the log k_f on the dielectric constant of the medium. At 25 °C and I=0.1 mol dm^{-3} (KNO_3).

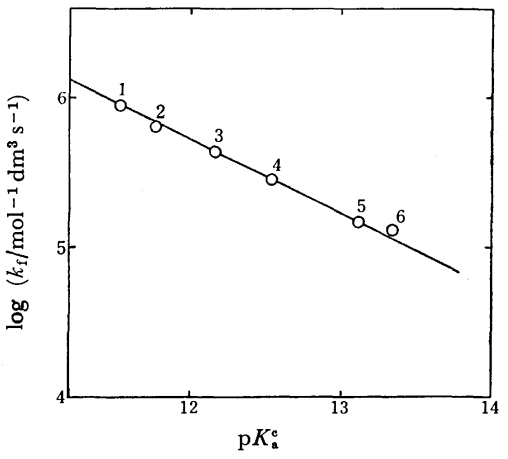

Fig. 8. Dependence of the recombination rate constants k_f on the acid dissociation constants K_a^c of MAG in dioxane-water media. Dioxane content: (1) 4, (2) 10, (3) 20, (4) 30, (5) 40, and (6) 50%(v/v). At 25 °C and I=0.1 mol dm^{-3} (KNO_3).

vening water molecules in the encounter complex, $HA^{*-}\cdots(H_2O)_n\cdots OH^-$ would be estimated to be n=4—5. The value is larger than that (n=2) for the neutralization reaction between the proton H_3O^+ and the hydroxide ion OH^- in aqueous solution.[17]

For a given solvent composition, it was found that the pK_a^c of the Brønsted acids of analogous structures shows a linear dependence on the value of log (k_f/mol^{-1} dm^3 s^{-1}).[2] Figure 8 shows the linear relationship between log (k_f/mol^{-1} dm^3 s^{-1}) and pK_a^c of MAG with respect to the medium effect. Since the variation of k_r' by varying solvent composition is small, the variation of $K_a^c=K_w^c(k_f/k_r')$ depends almost entirely on k_f and K_w^c. The plot of pK_w^c against pK_a^c for varying solvent composition shows a linear relationship, pK_w^c =0.8 pK_a^c+4.3. The plot in Fig. 8 gives a relationship, log (k_f/mol^{-1} dm^3 s^{-1}) = —0.5 pK_a^c + 11.5, or $k_f=G(K_a^c)^\alpha$, where G and α are constants. From Eq. 4 we have a simple relationship, $K_{12}k_{23}=G(K_a^c)^\alpha$. Considering the smaller variation in k_{23} than that in K_{12} we obtain

$$K_{12} = G'(K_a^c)^\alpha, \qquad (8)$$

where G' is a constant. Thus, the linear relationship between pK_a^c and log (k_f/mol^{-1} dm^3 s^{-1}) of MAG with respect to the medium effect could be explained by the linear relationship between pK_a^c and log K_{12}.

References

1) A. R. Tourky, H. A. Rezk, and Y. M. Gingis, *J. Phys. Chem.*, **56**, 40 (1961); C. J. Clemett, E. Forest, and C. P. Smyth, *J. Chem. Phys.*, **40**, 2123 (1964); S. K. Garg and C. P. Smyth, *ibid.*, **43**, 2925 (1965); E. Greinacher, W. Lüttke, and R. Mecke, *Z. Elektrochem.*, **59**, 23 (1955); A. Fratiello and D. C. Douglass, *J. Mol. Spectrosc.*, **11**, 465 (1963); K. Arakawa and N. Takanaka, *Bull. Chem. Soc. Jpn.*, **42**, 5 (1969).

2) N. Yoshida and M. Fujimoto, *Bull. Chem. Soc. Jpn.*, **49**, 1557 (1976).

3) K. G. Liphard and A. Jost, *Ber. Bunsenges. Physik. Chem.*, **80**, 125 (1976).

4) L. G. Van Uitert and C. G. Haas, *J. Am. Chem. Soc.*, **75**, 451 (1953).

5) In the case of 50%(v/v) dioxane-water solution, two relaxation processes were observed in the fast proton-transfer reaction between hydroxide ion and phenolphthalein. From the first relaxation process the rise-time of the temperature in dioxane-water solution was determined to be *ca.* 4—6 μs. In aqueous solution, the rise-time of the temperature was *ca.* 2—5 μs.

6) H. S. Harned and B. B. Owen, "The Physical Chemistry of Electrolytic Solutions," 3rd ed, Reinhold Publishing Corp., New York, N. Y. (1958).

7) The dielectric constant of the medium was calculated from the data of Åkerlöf and Short. See, G. Åkerlöf and O. A. Short, *J. Am. Chem. Soc.*, **58**, 1241 (1936).

8) W. Gilkerson, *J. Chem. Phys.*, **25**, 1199 (1956).

9) J. W. Larson and L. G. Hepler, "Solute-Solvent Interactions," ed by J. F. Coetzee and C. D. Ritchie, Marcel Dekker, New York, N. Y. (1968), p. 25.

10) In general the solvent effect on the acid-base equilibrium is explained on the basis of the change in the dielectric constant and the acid-base property of the solvent. Furthermore in the case of a bulky organic solute such as Magneson in dioxane-water medium, the preferential solvation by dioxane or water of the various species involved would play a significant role in the acid-base equilibrium.

11) N. Yoshida and M. Fujimoto, unpublished data.

12) See, S. Shibata and M. Furukawa, *Bunseki Kagaku*, **23**, 1412 (1974).

13) D. A. Johnson and T. M. Florence, *Talanta*, **22**, 253 (1975).

14) G. Scatchard, *Chem. Rev.*, **10**, 229 (1932); J. A. Christiansen, *Z. Phys. Chem.*, **113**, 35 (1924).

15) Since K_{12} is the equilibrium constant of the elementary process in which $\widehat{HA}^-$ interacts with surrounding water molecules *via* hydrogen-bond to form HA^{*-}, and since the unimolecular processes inherent to the properties of the reaction site itself, *viz.*, the rupture of the intramolecular hydrogen-bond and the rotation of OH-group around the C–O axis, are almost independent of the solvent composition, the increasing dioxane content of the medium would lead to the decrease in the value of K_{12}.

16) Since the process of dissolution of an ionic crystal is closely related to the process of solvation,[18] the large organic molecule ion $\widehat{HA}^-$ which dissolves readily in dioxane is strongly solvated by dioxane molecules in dioxane-water medium, namely, the preferential solvation of $\widehat{HA}^-$ by dioxane molecules is enhanced when the dioxane content in the medium is increased. The interaction of $\widehat{HA}^-$ with water molecules through hydrogen-bond is considerably restricted when the dioxane content in the medium is increased, and the change in the value of K_{12} due to the solvent composition[14] becomes smaller.

17) M. Eigen and L. De Maeyer, "The Structure of Electrolytic Solutions," ed by W. J. Hamer, Wiley, New York, N. Y. (1959), Chap. 5, p. 70; M. Eigen and L. De Maeyer, *Proc. R. Soc. London, Ser. A*, **247**, 505 (1958).

18) E. Price, "The Chemistry of Non-Aqueous Solvents," Vol. 1, ed by J. J. Lagowski, Academic Press, New York, N. Y. (1966), p. 67.

A Method for the Preparation of Potassium Hexafluorovanadate(III) and Its Polymorphic Transitions

Kōichirō Kōyama and Yasuhiko Hashimoto

Department of Materials Science, Himeji Institute of Technology, Shosya, Himeji 671-22

(Received December 13, 1976)

In order to determine the best conditions for the preparation of potassium hexafluorovanadate(III), the reaction of V_2O_3 with KHF_2 was studied by means of thermogravimetric analysis, differential thermal analysis, and X-ray diffraction analysis. The reaction begins at about 225 °C and terminates at about 300 °C, and the decomposition of excess KHF_2 terminates at from 300 to 450 °C, depending on the amount of the mixture of V_2O_3 and KHF_2. Potassium hexafluorovanadate(III) is stable in air up to about 300 °C and is oxidized at temperatures higher than 300 °C. Potassium hexafluorovanadate(III) has four polymorphic forms, and the transition points are 158, 200, and 218 °C. The transition from δ to γ or from γ to β on cooling is hindered by adding a small amount of sodium ion.

Previously we measured the freezing points of the KCl–VF_3, NaCl–VF_3, KCl–NaCl(equimolar)–VF_3, KCl–KF–K_3VF_6, NaCl–NaF–Na_3VF_6, KF–NaF–K_2NaVF_6, and KCl–NaCl–K_2NaVF_6 systems and pointed out that compositions in the vicinity of the minimum melting point of the KCl–NaCl–K_2NaVF_6 system are suitable as an electrolyte for the electrorefining or electroextraction of vanadium.[1,2] Most regions of the KCl–NaCl–K_2NaVF_6 system, shown by hatching in Fig. 1b, can be prepared by the use of K_3VF_6, which can be more easily prepared than K_2NaVF_6. Several methods for the preparation of K_3VF_6 have been reported by several groups of workers,[3–5] but none of these methods are practicable from the viewpoint of cost. In a previous paper,[6] we reported that $(NH_4)_3VF_6$ can be prepared by fusing a mixture of V_2O_3 and NH_4HF_2 in an inert atmosphere. By analogy with this preparation of $(NH_4)_3VF_6$, K_3VF_6 may be expected to be prepared by fusing a mixture of V_2O_3 and KHF_2. This work was undertaken to determine the conditions for the preparation of K_3VF_6 from V_2O_3 and KHF_2, and also to examine the polymorphic transition of K_3VF_6.

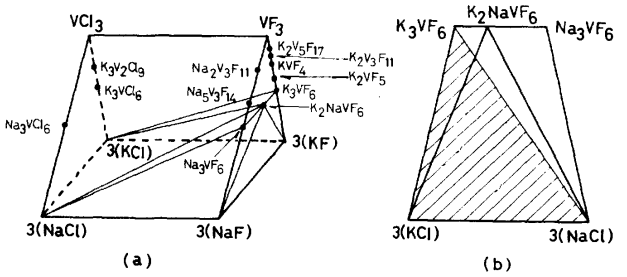

Fig. 1. (a) KCl–NaCl–VCl_3–KF–NaF–VF_3 system and (b) KCl–NaCl–K_3VF_6–Na_3VF_6 cross section.

Experimental

The vanadium(III) oxide used was prepared by the hydrogen reduction of V_2O_5 of a special reagent grade at 800—900 °C for 3 h. The potassium hydrogenfluoride and lithium fluoride used were of a special reagent grade, while the sodium hydrogenfluoride was reagent-grade. X-Ray diffraction patterns at elevated temperatures were taken with an X-ray diffractometer, Rigaku Denki Model SG-7, equipped with a high-temperature attachment, with a Ni-filtered Cu$K\alpha$ radiation. The diffraction angles were corrected by using the diffraction angles of silicon. The differential thermal analysis curves were taken with an apparatus constructed in our laboratory by using 10 mg of a sample at a heating rate of 5 °C/min. The thermocouple used was calibrated by the transition temperatures of KNO_3(129 °C) and $KClO_4$(299 °C). The thermogravimetric analysis curves were taken with a microthermobalance, Shimadzu Model TG-20, by using 10 mg of a sample and at a heating rate of 5 °C/min.

Results and Discussion

X-Ray Diffraction Analysis. A mixture (2.5844 g) of V_2O_3 and KHF_2 in a molar ratio of 1 : 8 was placed in a platinum boat and heated at a given temperature for 30 min in a stream of argon (20 ml/min). Figure 2 shows a schematic diagram of the apparatus used for this experiment. The reaction product was identified by X-ray diffraction analysis at room temperature. Potassium hexafluorovanadate(III) was identified on the basis of the set of interplanar spacings for the low-temperature form of K_3VF_6 reported by Cretenet.[7] Table 1 shows the compounds identified in the product. The reaction of V_2O_3 with KHF_2 began at 225 °C and was completely terminated at 300 °C. The decomposition of the excess KHF_2 was almost terminated at 400 °C and completely terminated at 450 °C. As is shown in Table 1, $KF \cdot 2H_2O$ was detected in the products. The thermogravimetric study of $KF \cdot 2H_2O$ showed that $KF \cdot 2H_2O$ released the water of crystallization at 200—300 °C and that the residue was KF. Therefore, the $KF \cdot 2H_2O$ detected in the products is considered to have been formed while the substance

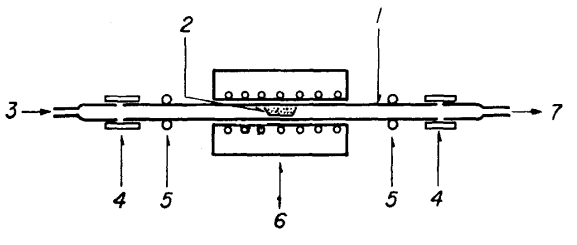

Fig. 2. Schematic diagram of the apparatus used for the preparation of K_3VF_6.
1. Nickel reaction tube, 2. platinum boat, 3. inlet of argon, 4. vinyl chloride tube, 5. copper cooling tube, 6. furnace, 7. outlet of argon.

was standing at room temperature by the reaction of KF with the moisture in air.

Differential Thermal Analysis. The differential thermal analysis curve for the reaction of V_2O_3 with KHF_2 is shown in Fig. 3. For comparison, the differential thermal analysis curve for the decomposition of KHF_2 is also shown in Fig. 3. Peaks a and b correspond to the transition(194 °C) and melting (225 °C) of KHF_2. Peak c is judged to correspond to the begining of the reaction of V_2O_3 with KHF_2 on the basis of the fact that the reaction of V_2O_3 with KHF_2 was observed with the naked eye to begin immediately after the melting of KHF_2, and the fact that K_3VF_6 was identified in the product obtained at 225 °C, as is shown in Table 1.

Thermogravimetric Analysis. The thermogravimetric analysis curve for the reaction of V_2O_3 with KHF_2 is shown in Fig. 4. For comparison, the thermogravimetric analysis curve for the decomposition of KHF_2 is also shown in Fig. 4. In curve a, the weight loss began at about 200 °C and terminated at about 300 °C; in curve b, while the weight loss also began at about 200 °C, it terminated at about 340 °C. The temperature at which the decomposition of excess KHF_2 terminated differs in Table 1 and Fig. 4. This can be ascribed to the difference in the weight of the samples

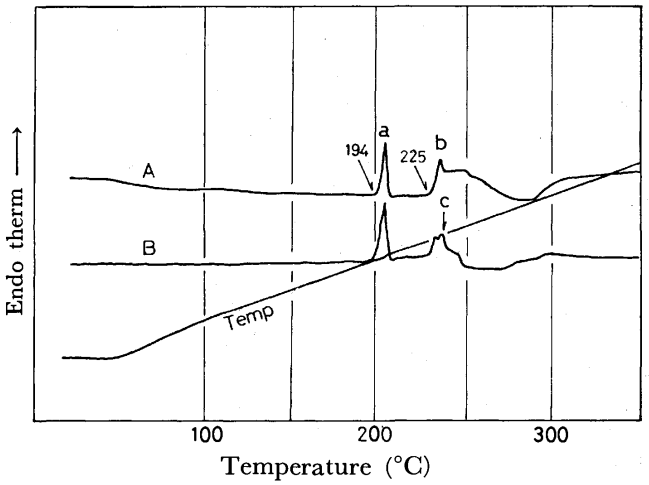

Fig. 3. DTA curves.
Curve A: KHF_2, curve B: a mixture of V_2O_3 and KHF_2 in a molar ratio of 1 : 8.

Table 1. Relationship between reaction temperature and compounds in the reaction product

Temperature (°C)	Compounds detected by X-ray diffraction analysis at room temperature
150	V_2O_3, KHF_2
200	V_2O_3, KHF_2
225	V_2O_3, KHF_2, K_3VF_6
250	V_2O_3, KHF_2, K_3VF_6
300	KHF_2, K_3VF_6, $KF\cdot 2H_2O$, KF
350	KHF_2, K_3VF_6, $KF\cdot 2H_2O$, KF
400	KHF_2, K_3VF_6, $KF\cdot 2H_2O$, KF
450	K_3VF_6, $KF\cdot 2H_2O$, KF
500	K_3VF_6, $KF\cdot 2H_2O$, KF
600	K_3VF_6, $KF\cdot 2H_2O$, KF

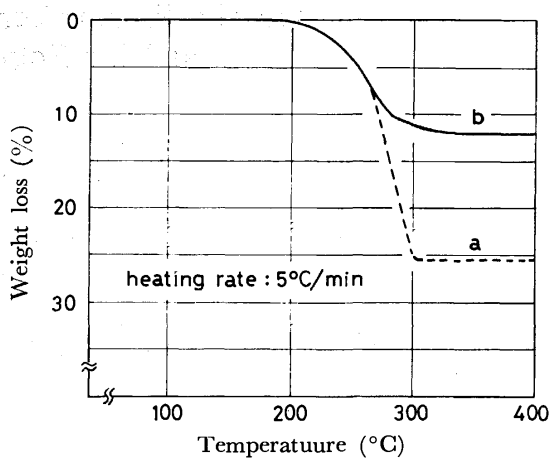

Fig. 4. TG curves.
Curve a: KHF_2, curve b: a mixture of V_2O_3 and KHF_2 in a molar ratio of 1 : 8.

used. The weight loss in the vicinity of 200 °C is considered to be due to the vaporization of HF from solid KHF_2, because the reaction of V_2O_3 with KHF_2 begins at about 225 °C.

From the results of the X-ray diffraction analysis, differential thermal analysis, and thermogravimetric analysis, it was found that the reaction of V_2O_3 with KHF_2 begins at about 225 °C and terminates at about 300 °C, and that the decomposition of excess KHF_2 terminates at 300—450 °C, depending on the weight of the mixture of V_2O_3 and KHF_2.

Molar Ratio of V_2O_3 to KHF_2. Since a part of the KHF_2 in a mixture decomposes without reacting with V_2O_3, an excess of KHF_2 is necessary for preparing

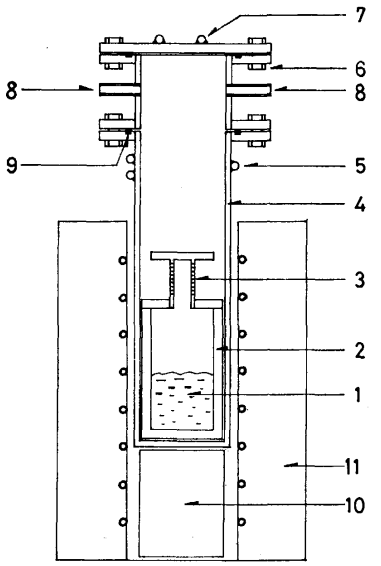

Fig. 5. Schematic diagram of the apparatus used for the preparation of K_3VF_6.
1: Mixture(about 300 g) of V_2O_3 and KHF_2, 2: graphite crucible(72 mm in inside diameter and 160 mm in height), 3: perforated lid, 4: stainless steel vessel, 5: copper cooling tube, 6: bolt and nut, 7: copper cooling tube, 8: inlet and outlet of argon, 9: O-ring.

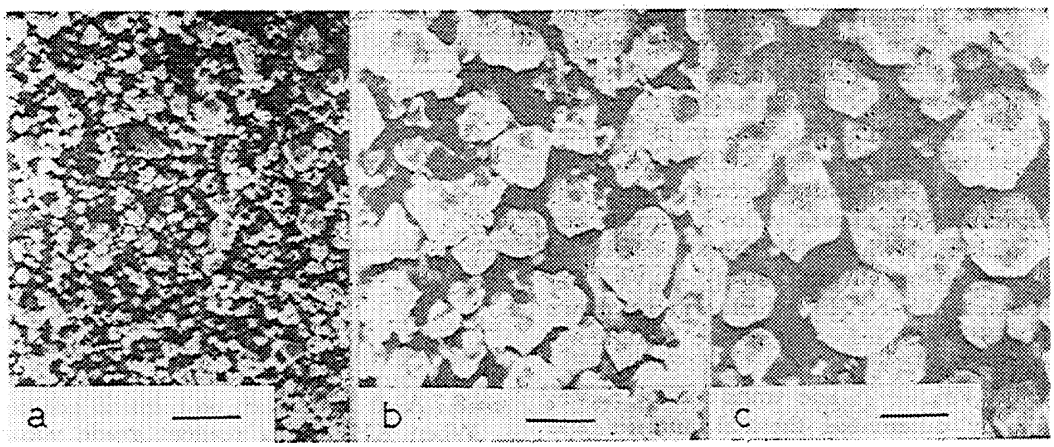

Fig. 6. Scanning electron micrographs of K_3VF_6. The bars represent 10 μm.
a: $V_2O_3/KHF_2=1/7$, b: $V_2O_3/KHF_2=1/8$, c: $V_2O_3/KHF_2=1/12$.

K_3VF_6 free from V_2O_3. In order to determine the lower limit of the excess of KHF_2, a 300-gram portion each of mixtures in the molar ratios 1 : 6, 1 : 6.5, 1 : 7, 1 : 8, 1 : 9, 1 : 10, 1 : 11, and 1 : 12 was heated at 600 °C in a stream of argon(200 ml/min) with the apparatus shown in Fig. 5. After having been cooled, the reaction products were leached with water, and the residue was examined with the naked eye and also analysed by an X-ray diffraction technique. Vanadium-(III) oxide is black or brown, while the color of K_3VF_6 is bright green. When a reaction product was leached with water, the remaining V_2O_3 particles, if any, could be well discriminated from the K_3VF_6 in water with the naked eye. The mixtures in the molar ratios of 1 : 6 and 1 : 6.5 gave K_3VF_6 contaminated with V_2O_3, but those in the molar ratios of 1 : 7—1 : 12 gave K_3VF_6 free from V_2O_3. Figure 6 shows the scanning-electron micrographs of K_3VF_6 prepared from the mixtures of V_2O_3 and KHF_2 in the molar ratios of 1 : 7, 1 : 8, and 1 : 12. As is shown in Fig. 6, the crystals of K_3VF_6 were fine at the molar ratios of 1 : 6—1 : 7 and coarse at 1 : 8—1 : 12. The growth feature observed at 1 : 8—1 : 12 indicates that the grain of K_3VF_6 somewhat dissolves in the KHF_2 melt.

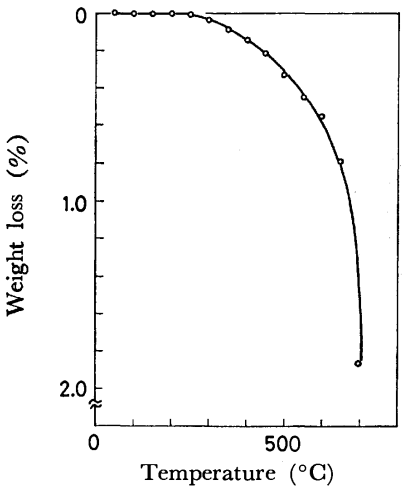

Fig. 7. Oxidation curve of K_3VF_6 in air.

Oxidation-resistance of K_3VF_6. A knowledge of the oxidation-resistance of K_3VF_6 is important for the synthesis of K_3VF_6 and also for the preparation of the electrolytic bath for the electroextraction of vanadium. One gram of K_3VF_6, the crystal sizes of which are shown in Fig. 6b, was heated at a given temperature for 30 min in air; then the product was weighed and analysed by means of an X-ray diffraction technique. The thermogravimetric analysis curve thus obtained is shown in Fig. 7. It may be seen that K_3VF_6 is

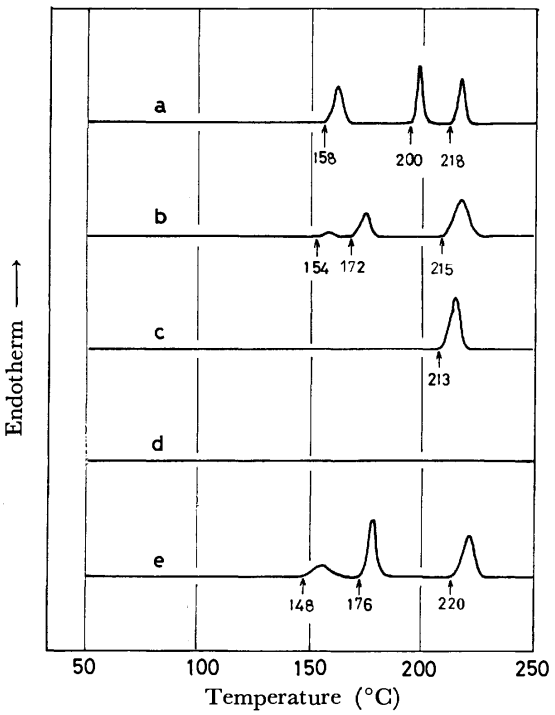

Fig. 8. DTA curves of K_3VF_6.
Curve a: K_3VF_6 prepared by using KHF_2 of a special reagent grade, curve b, c, d, e: K_3VF_6 prepared by using KHF_2 with the addition of a small amount of $NaHF_2$ or LiF.
b: $NaHF_2/KHF_2=1/999$, c: $NaHF_2/KHF_2=1/99$,
d: $NaHF_2/KHF_2=5/95$, e: $LiF/KHF_2=1/999$.
Heating rate: 5 °C/min.

stable in air up to about 300 °C and is oxidized at temperatures higher than 300 °C. Therefore, when a mixture of V_2O_3 and KHF_2 is heated at temperatures higher than 300 °C in order to decompose the excess KHF_2, heating must be done in a stream of an inert gas. The decomposition of excess KHF_2 to KF and HF makes the subsequent water-leaching easy. The product oxidized at 700 °C was yellowish green and was readily soluble in water. Its X-ray diffraction pattern was quite different from that of α-K_3VF_6, but was similar to that of γ-K_3VF_6, which will be shown below. This product is suspected to be tetrafluorodioxovanadate(V), $K_3VO_2F_4$.

Transition of K_3VF_6. The transition of K_3VF_6 was examined by differential thermal analysis and X-ray diffraction analysis. Curve a in Fig. 8. is the differential thermal analysis curve of the K_3VF_6 obtained by using KHF_2 of a special reagent grade. From curve a it may be seen that K_3VF_6 has four polymorphic forms and that the transition points are 158, 200, and 218 °C. These polymorphic forms will be called α, β, γ, and δ respectively as follows:

$$\alpha \overset{158}{\rightleftharpoons} \beta \overset{200}{\rightleftharpoons} \gamma \overset{218}{\rightleftharpoons} \delta$$

These transitions are all reversible. Figure 9 shows the X-ray diffraction patterns of α, β, γ, and δ. δ was found to be cubic with a lattice parameter of a=8.722Å at 235 °C. Cretenet[7] has found two polymorphic forms for K_3VF_6 and reported that the high-temperature form is cubic, with a lattice parameter of

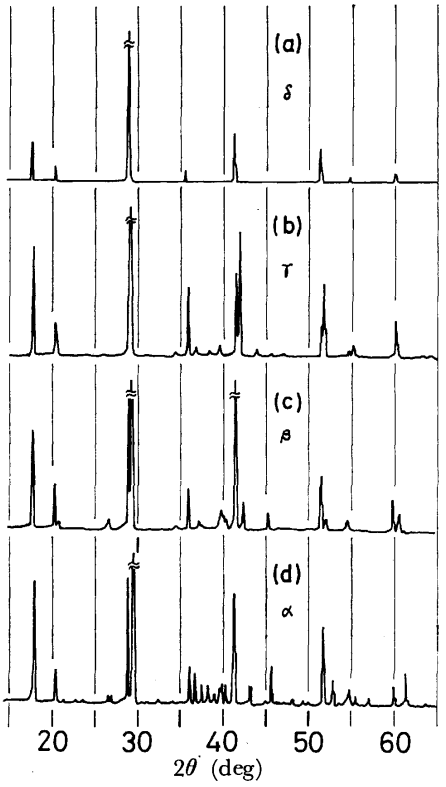

Fig. 9. X-Ray diffraction patterns of K_3VF_6(Cu$K\alpha$, Ni-filter). (a): 230 °C, (b): 210 °C, (c): 180 °C, (d): room temperature.

Table 2. The influence of sodium ion on the crystal transition of K_3VF_6

Molar ratio of $NaHF_2$ to KHF_2	1/999—3/997	8/992—20/980	30/970	50/950
Type of K_3VF_6	α γ	γ	γ δ K_2NaVF_6	δ K_2NaVF_6

K_3VF_6 was synthesized by heating a mixture of KHF_2 (with the addition of a small amount of $NaHF_2$) and V_2O_3 in a molar ratio 1 : 8 at 450 °C in a stream of argon.

a=8.7 Å at 250 °C.

When KHF_2 of a reagent grade was used in the synthesis of K_3VF_6, the X-ray diffraction pattern of the product showed some peaks of γ besides the peaks of α, or only the peaks of γ at room temperature. This was considered to be due to some impurity in the reagent used. Thus, $NaHF_2$ or LiF was deliberately added to KHF_2 of a special reagent grade in the synthesis of K_3VF_6. The K_3VF_6 thus obtained was examined by X-ray diffraction analysis and differential thermal analysis. Table 2 shows the relationship between the ratio of $NaHF_2$ to KHF_2 and the form of K_3VF_6. It may be seen that, on the addition of a small amount of Na^+, γ and δ remain stable, even at room temperature. Curve b, c, d, and e in Fig. 8 are the differential thermal analysis curves of the K_3VF_6 prepared by using the KHF_2 reagent with the addition of Na^+ or Li^+. With an increase in the amount of Na^+, first the β-γ transition temperature decreased, then the β-γ transition disappeared, and finally the γ-δ transition disappeared. These results show that a small amount of Na^+ stabilizes the high-temperature forms, γ and δ, at room temperature. This effect may be explained by the idea that Na^+, which has a smaller ionic radius than K^+, cancels the distortion of the lattice contraction caused by a lowering of the temperature. On the addition of a minute amount of Li^+, the β-γ transition temperature decreased, as in the case of Na^+. Lithium fluoride was almost insoluble in KHF_2, so the addition of more than 1/999 of LiF was not attempted.

The authors wish to express their thanks to Professor Tomoo Kirihara of Nagoya University for his helpful discussions.

References

1) K. Kōyama and Y. Hashimoto, *Trans. Jpn. Inst. Met.*, submitted for publication.
2) K. Kōyama and Y. Hashimoto, *Trans. Jpn. Inst. Met.*, submitted for publication.
3) B. M. Wanklyn, *J. Inorg. Nucl. Chem.*, **27**, 481 (1965).
4) R. S. Nyholm and A. G. Sharpe, *J. Chem. Soc.*, **1952**, 3579.
5) R. D. Peacock, "Progress in Inorganic Chemistry," ed by F. A. Cotton, Interscience, New York (1960).
6) K. Kōyama and Y. Hashimoto, *Trans. Jpn. Inst. Met.*, **17**, 287 (1976).
7) J. C. Cretenet, *Rev. Chim. Miner.*, **10**, 399 (1973).

NOTES

BULLETIN OF THE CHEMICAL SOCIETY OF JAPAN, VOL. 50 (5), 1337—1338 (1977)

Infrared Spectrum and Electronic State of *p*-Iodanil

Yôichi IIDA

Department of Chemistry, Faculty of Science, Hokkaido University, Sapporo 060

(Received September 9, 1976)

Synopsis. The infrared spectrum of *p*-iodanil was measured and the fundamental frequencies were assigned by using simple Urey-Bradley force field. The electronic state of *p*-iodanil was also discussed on the basis of those experimental results.

Halogen-substituted *p*-benzoquinones such as *p*-chloranil and *p*-bromanil (see Fig. 1) are known to be strong electron acceptor molecules, and much attention has been paid to the charge-transfer complexes with those acceptors.[1] However, only few attempts have been made to study the vibrational spectra of such acceptor molecules. In previous papers, we examined the infrared spectra of *p*-chloranil, *p*-bromanil, 2, 5-dibromo-3,6-dichloro-*p*-benzoquinone, and their anion radicals, and assigned their fundamental frequencies by using simple Urey-Bradley force fields (UBFF's).[2-4] This kind of investigation was found to be also very useful to study the electronic states of those π-conjugated *p*-benzoquinones, because the intramolecular force constants of those molecules are closely related to their electronic states. In the present paper, we examined the infrared spectrum and the electronic state of *p*-iodanil (see Fig. 1), which is one of the derivatives of iodo-substituted *p*-benzoquinones. It is interesting to compare the results of *p*-iodanil with those previously investigated for *p*-chloranil and *p*-bromanil.[2,3]

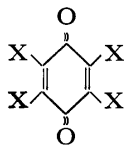

(a); X=Cl
(b); X=Br
(c); X=I

Fig. 1. Halogen-substituted *p*-benzoquinones; (a) *p*-chloranil, (b) *p*-bromanil, and (c) *p*-iodanil.

p-Iodanil was prepared by the reaction of *p*-bromanil with potassium iodide and sodium iodide and was crystallized from an ethyl acetate solution.[5] It was purified by sublimation *in vacuo*. The infrared spectrum of the solid *p*-iodanil was measured as Nujol mulls in the range from 400 to 4000 cm^{-1} using an IR-G infrared spectrophotometer (Japan Spectroscopic Co. Ltd.). The infrared spectrum in the regions where the absorption due to Nujol appears was measured using hexachlorobutadiene mulls. The observed absorptions are collected in Table 1.

Since only the intramolecular vibrations are expected to appear in the region from 400 to 4000 cm^{-1}, the vibrational spectrum of the solid compound can be approximately treated under the *p*-iodanil molecular point group D_{2h}. In order to understand the spectroscopic data, a normal coordinate treatment was made with *p*-iodanil molecule, and Wilson's ***GF*** matrix method was used for this purpose.[6] The structural data of *p*-iodanil were taken from those reported by Kobayashi *et al.*[7] Assuming that the *p*-iodanil molecule is planar, thirty normal modes of vibrations were reduced to the symmetry species:

$$\Gamma = 6A_g + 5B_{1g} + 5B_{2u} + 5B_{3u} + 1B_{2g} + 3B_{3g} + 2A_u + 3B_{1u}, \quad (1)$$

where the first four are the in-plane vibrations, and the rest, the out-of-plane vibrations. We calculated only the in-plane vibrations. A simple Urey-Bradley force field was employed as the potential function. The calculation process of the fundamentals of *p*-iodanil was very similar to the cases previously studied with *p*-chloranil and *p*-bromanil,[2,3] because the chloro-substituents or bromo-substituents were replaced by the iodo-substituents. Some of the force constants of *p*-iodanil could be transferred from those of *p*-chloranil or *p*-bromanil.[2,3] Refinements of the force constants were then carried out by the trial-and-error method making use of the Jacobian matrices. The calculated values of the *p*-iodanil fundamental vibrations with these force constants agreed well with the observed values. This is shown in Table 1 together with the assignments of the fundamental absorptions. In the following, we will only discuss the bond-stretching force constants, because the observed fundamentals arise mostly from the bond-stretching modes.

As for the C=O bond-stretching force constant, *K*-

Table 1. The observed and calculated frequencies (cm^{-1}) for the fundamental vibrations of *p*-iodanil

Obsd[a]	Calcd	Assignment
1659 (s)	1665	B_{2u}, ν(C=O)
1515 (s)	1506	B_{3u}, ν(C=C)
1192 (sh)		
1174 (s)	1167	B_{3u}, ν(C-C)
1161 (sh)		
1026 (sh), 1013 (s)	1024	B_{2u}, ν(C-C)
838 (w)		
833 (w)	838	B_{2u}, ν(C-C), ν(C-I)
824 (w)		
695 (s)		B_{1u}, out-of-plane
578 (sh), 567 (m)	562	B_{3u}, ν(C-I)

a) s: strong, m: medium, w: weak, sh: shoulder.

(C=O) of *p*-iodanil was estimated to be 9.56 mdyn/Å, whose value is close to the 9.7 value of *p*-chloranil or the 9.62 value of *p*-bromanil.[2,3] The C=C bond-stretching force constant, K(C=C), of *p*-iodanil was calculated to be 6.32 mdyn/Å, which is found to be somewhat smaller than the 6.6 value of *p*-chloranil or the 6.67 value of *p*-bromanil.[2,3] On the other hand, the C–C bond-stretching force constant, K(C–C), of *p*-iodanil was estimated to be 2.43 mdyn/Å. This value was found to be almost the same magnitude as those of the force constants for C–C single bonds of aliphatic hydrocarbons.[8] The C–C bond of *p*-iodanil appears to have more single bond character than have those of *p*-chloranil and *p*-bromanil. In fact, the C–C bond-stretching force constants of *p*-chloranil and *p*-bromanil have been estimated to be 3.0 mdyn/Å and 2.96, respectively[2,3]; these values are appreciably larger than the 2.43 mdyn/Å value for *p*-iodanil. In order to see this situation more quantitatively, the bond-stretching force constant, $K(12)$, in a π-conjugated system was related to the bond order, $p(12)$, and self-polarizability, $\pi(1212)$, of a bond (12) according to the Coulson and Longuet-Higgins formula:[9]

$$K(12) = \{(1-p(12))K_s + p(12)K_d\} + \left\{\frac{K_sK_d(s-d)}{K_s(1-p(12))+K_dp(12)}\right\}^2 \frac{\pi(1212)}{2}, \quad (2)$$

where s, d, K_s, and K_d are the bond lengths and the force constants associated with pure single and double bonds, respectively.

In a homopolar carbon-carbon bond, the second term involving the self-polarizability may be small.[2] By the use of the empirical relationship between $K(12)$ and $p(12)$ given in the previous paper,[2] we estimated the bond orders in *p*-iodanil as p(C=C)=0.82 and p(C–C) $\leq$0.15, respectively. Thus, the C–C bond of *p*-iodanil corresponds almost to pure single bond, and there is a strong alternation of the bond order between the C=C and C–C bonds. *p*-Iodanil appears to have more quinoid structure than has *p*-chloranil or *p*-bromanil.[2,3] This strong quinoid character of *p*-iodanil is also evidenced by the crystal structure analysis made by Kobayashi *et al.*[7] They reported the C–C bond length of *p*-iodanil to be 1.50 Å, which is as long as that of C–C pure single bond.

As for the heteropolar C=O bond, if we take, in Eq. 2, the values of K_s=5.0 mdyn/Å and K_d=10.7 proposed by Bratoz and Besnainou,[10] and if we neglect the contribution of the self-polarizability to K(C=O), the K (C=O) force constant of *p*-iodanil gives the value for the bond order of p(C=O)=0.80, which should be compared with p(C=O)=0.82 of *p*-chloranil or 0.81 of *p*-bromanil.[2,3]

The C–I bond-stretching force constant, K(C–I), of *p*-iodanil was estimated to be 1.43 mdyn/Å. This value was somewhat close to the value for the C–I bond-stretching force constant of alkyl iodides.[8]

We observed a strong absorption at 695 cm^{-1} in *p*-iodanil, but could not assign it to any of the in-plane fundamental vibrations. However, *p*-chloranil and *p*-bromanil have analogous absorptions at 715 cm^{-1} and 705, respectively,[2,3] and these absorptions show no appreciable frequency shifts in going from *p*-chloranil, *p*-bromanil to *p*-iodanil. Girlando *et al.* assigned the 715 cm^{-1} band of *p*-chloranil to the B_{1u} out-of-plane vibration of C=O bending mode.[11] Therefore, the same assignment is applicable to the 695 cm^{-1} absorption of *p*-iodanil.

In view of these results, the application of the infrared spectrum of *p*-iodanil is very useful to study the electronic states of the molecule. Kobayashi *et al.* have reported on some solid-state properties characteristic of *p*-iodanil.[7] In connection with the electronic states of the molecule, there remains a possibility that such properties may be induced by the strong quinoid structure of *p*-iodanil molecule.

References

1) See, for example, G. Briegleb, "Elektronen-Donator-Acceptor Komplexe," Springer-Verlag, Berlin-Göttingen-Heidelberg (1961).
2) Y. Iida, *Bull. Chem. Soc. Jpn.*, **43**, 345 (1970).
3) Y. Iida, *Bull. Chem. Soc. Jpn.*, **46**, 2955 (1973).
4) Y. Iida, *Bull. Chem. Soc. Jpn.*, **47**, 99 (1974).
5) H. A. Torrey and W. H. Hunter, *J. Am. Chem. Soc.*, **34**, 702 (1912).
6) E. B. Wilson, Jr., *J. Chem. Phys.*, **7**, 1047 (1939); **9**, 76 (1941).
7) H. Kobayashi, T. Danno, and I. Shirotani, *Bull. Chem. Soc. Jpn.*, **47**, 2333 (1974).
8) See, for example, Nippon Kagaku-kai, "Kagaku Binran," Maruzen, Tokyo (1966).
9) C. A. Coulson and H. C. Longuet-Higgins, *Proc. Roy. Soc.*, **A193**, 456 (1948).
10) S. Bratoz and M. S. Besnainou, *J. Chem. Phys.*, **34**, 1142 (1961).
11) A. Girlando and C. Pecile, *J. Chem. Soc., Faraday Trans. 2*, **69**, 1291 (1973).

BULLETIN OF THE CHEMICAL SOCIETY OF JAPAN, VOL. 50 (5), 1339—1340 (1977)

An MO-Theoretical Study of the Electronic Structures of Formyloxyl and Acetoxyl Radicals

Osamu KIKUCHI, Kayoko UTSUMI, and Keizo SUZUKI
Institute of Chemistry, The University of Tsukuba, Sakura-mura, Ibaraki 300-31

(Recived September 9, 1976)

Synopsis. A semi-empirical NDDO MO method was applied to formyloxyl(HCOO) and acetoxyl(CH_3COO) radicals in order to determine whether the ground-state electronic structure of the acyloxyl radical is of σ- or π-type. A σ-type state was found to be more stable than a π-type state over the entire range of values of the OCO angles of these radicals. This appears to be in agreement with the experimental facts which have been derived from the ESR spectra of several acyloxyl radicals.

Acyloxyl radicals are important intermediates in the thermal decomposition of acyl peroxides, although only a few acyloxyl radicals have directly been detected.[1-2] An important problem related to the acyloxyl radicals is to determine whether their ground-state electronic structures are of σ- or π-type. This problem is a key point in clarifying the role of acyloxyl radicals in the decomposition processes of acyl peroxides and has already been investigated both experimentally and theoretically. The observed principal values and directions of the g-tensors[1,2] appear to support a σ-type ground state for the acyloxyl radicals, while theoretical calculations performed up to now using INDO[3] and STO-3G[4] methods support a π-type state. This note presents theoretical results which were obtained using a semi-empirical NDDO MO method and which support a σ-type electronic structure for the ground-state of the acyloxyl radical.

The restricted SCF procedure for open-shell electronic systems proposed by Pople *et al.*[5] was applied to the simple acyloxyl radicals, the formyloxyl and acetoxyl radicals. In the SCF procedure, the MO of an open-shell system are divided into three parts, doubly-occupied, singly-occupied, and empty MO. A variational method was successively applied to two of the three groups, and the MO for a given electron configuration were determined by SCF iteration. The σ- and π-type electronic structrues for a given conformation of the acyloxyl radicals were obtained by assigning the singly-occupied MO to σ- and π-orbitals, respectively. In the evaluation of the matrix elements, the NDDO approximation,[6] which gives well-balanced molecular geometries and excitation energies, was employed.

The energetic dependence of σ- and π-states of the formyloxyl and acetoxyl radicals on their molecular geometries was calculated in detail. In the calculation of formyloxyl, a planar conformation was assumed. C_{2v} and C_s symmetries are possible geometries for the planar formyloxyl radical:

C_{2v} $\qquad$ C_s

The expected lower electronic states of C_{2v} symmetry are written as:

$$\cdots(b_2)^2(a_2)^2(a_1)^1;\ ^2A_1(\Sigma)$$
$$\cdots(a_2)^2(a_1)^2(b_2)^1;\ ^2B_2(\Sigma)$$
$$\cdots(a_1)^2(b_2)^2(a_2)^1;\ ^2A_2(\Pi)$$

and those of C_s symmetry as:

$$\cdots(a'')^2(a')^1;\ ^2A'\ (\Sigma)$$
$$\cdots(a')^2(a'')^1;\ ^2A''(\Pi)$$

The schematic shapes of the MO in the avove configurations are shown in Fig. 1. The energy variation of each electronic state on the OCO angle is shown in Fig. 2. The curves were obtained with CH and CO

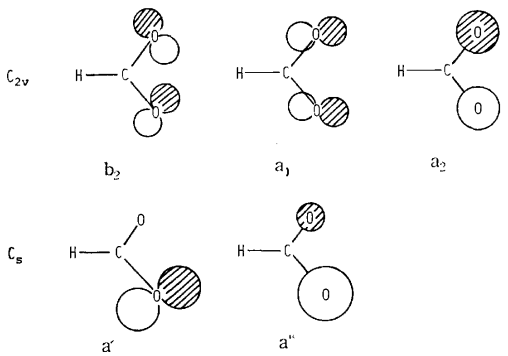

Fig. 1. Schematic representation of MO's which may be occupied by unpaired electron.

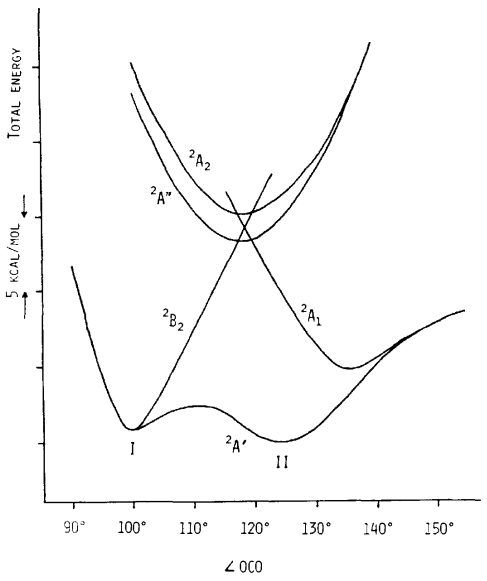

Fig. 2. Dependence of electronic states of formyloxyl radical upon the OCO angle. $^2B_2$, $^2A_1$, and $^2A'$ states correspond to the "σ-radical" and $^2A_2$ and $^2A''$ to the "π-radical".

bond lengths which were optimized for each OCO angle and each state.

A σ-type electronic structure is more stable than a π-type structure over the entire range of OCO angles. The most stable π-type radical lies 13 kcal/mol above the most stable σ-radical. This is contrary to the theoretical results obtained up to the resent[2-4] and agrees with the experimental results which were derived from the g-tensors of several acyloxyl radicals.[1,2] Two stable conformations are expected for the ground state of formyloxyl: one is of C_{2v} symmetry (I: $^2B_2$ with $\angle OCO=100°$) and the other is of C_s symmetry (II: $^2A'$ with $\angle OCO=125°$). Although the energy difference between I and II is very small, their electronic structures differ greatly. In radical I, more than 98% of the unpaired electrons are equally shared on two equivalent oxygen atoms, while about 90% of the unpaired electrons localized on oxygen atom in radical II. The geometrical changes of formyloxyl along the lowest curve are listed in Table 1.

Table 1. Geometry of the $^2\Sigma$-type formyloxyl radical

Total energy	∠OCO	C-O(1)	C-O(2)	C-H
−772.04 eV	90°	1.315 Å	1.375 Å	1.065 Å
−772.51	100	1.250	1.250	1.075
−772.43	110	1.210	1.290	1.085
−772.52	120	1.245	1.300	1.075
−772.50	130	1.240	1.290	1.148
−772.31	140	1.230	1.255	1.225
−772.20	150	1.220	1.220	1.320
−772.15	160	1.190	1.190	1.420

The results for the acetoxyl radical were almost identical to those of the formyloxyl radical. In the acetoxyl radical, as for the formyloxyl radical, the energy difference between the two σ-radicals corresponding to I and II of formyloxyl is very small (<2 kcal/mol) and the barrier for the conversion between them is also very small (<2 kcal/mol). This indicates that the conversion

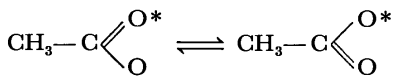

is very fast. In fact, the very fast scrambling between the two oxygen atoms, and the equivalence of the two oxygen atoms before the successive reactions involving the acetoxyl radical, have been confirmed experimentally.[7] A slight difference between formyloxyl and acetoxyl is the unpaired-electron distribution in radical II; 13% of the unpaired electrons delocalizes on the methyl-carbon atom in acetoxyl.

The question remains whether conventional MO methods can correctly predict the small energy difference between two closely adjacent electronic states. However, the present results are the first theoretical support for a σ-type ground state of the formyloxyl and acetoxyl radicals which appear to agree with the experimental facts derived from ESR spectra of several acyloxyl radicals.

References

1) K. Minakata and M. Iwasaki, *J. Chem. Phys.*, **57**, 4758 (1972); H. Muto, K. Toriyama, and M. Iwasaki, *ibid.*, **57**, 3016 (1972); H. C. Box, H. G. Freund, K. T. Liliga, and E. E. Budzinski, *J. Phys. Chem.*, **74**, 40 (1970).

2) N. J. Karch, E. T. Koh, B. L. Whitsel, and J. M. McBride, *J. Am. Chem. Soc.*, **97**, 6729 (1975).

3) T. Koenig, R. A. Wielesek, and J. G. Huntington, *Tetrahedron Lett.*, **1974**, 2283.

4) M. D. Newton, see Ref. 37 cited in Karch *et al.* (2).

5) J. S. Binkley, J. A. Pople, and P. A. Dobosh, *Molecular Phys.*, **28**, 1423 (1974).

6) O. Kikuchi, *Bull. Chem. Soc. Jpn.*, **50**, 593 (1977). Comparedwith the CNDO and INDO approximations, the NDDO approximation requires the evaluation of many additional two-center integrals. They were evaluated using the simple formulae derived from the corresponding theoretical equations. Empirical parameters involved in the two-electron integrals and in the core-core repulsion integrals were chosen so as to give well-valanced values of molecular geometries, heats of reactions, and excitation energies.

7) J. W. Taylor and J. C. Martin, *J. Am. Chem. Soc.*, **89**, 6904 (1967); T. Kashiwagi, S. Kozuka, and S. Oae, *Tetrahedron*, **26**, 3619 (1970); R. Kaptein, J. Brokken-Zijp, and F. J. J. de Kanter, J. *Am. Chem. Soc.*, **94**, 6280 (1972).

BULLETIN OF THE CHEMICAL SOCIETY OF JAPAN, VOL. 50 (5), 1341—1342 (1977)

ESR of F Center in $HgI_2 \cdot 2HgS$ Darkened with Sunlight

Kunio TAKEI, Hitoshi HAGIWARA, and Hiroshi TANAKA*

Department of Industrial Chemistry, Faculty of Engineering, Miyazaki University, Miyazaki 880

**Minami Kyushu Coca Cola Bottling Co., Kumamoto 860*

(Received October 25, 1976)

Synopsis. When yellow powders of $HgI_2 \cdot 2HgS$ turn black in sunlight in a few seconds, the black powders show an ESR signal, whose intensity increases with the time of irradiation; its *g*-value is 2.0046 ± 0.00028. The result of analysis shows that this signal is due to F centers, consisting of electrons captured by positive holes prepared at sites of S^{2-} ions in the crystal.

Twenty five years ago one of the authors[1] observed by means of Gouy's method that initially diamagnetic yellow powders of $HgI_2 \cdot 2HgS$ become paramagnetic after a darkening with sunlight. A print-out of mercury atoms and evolution of SO_2 and I_2 from these crystals during irradiation with sunlight were confirmed by chemical analysis[2] and the darkening process was considered to occur as follows. When electrons belonging to S^{2-} or I^- ions in the crystals absorb wavelengths shorter than 510 nm and are excited to upper states, these electrons leave behind neutral S or I atoms, which diffuse toward the crystal surface, resulting in the formation of gases of SO_2 or I_2. Some parts of the excited electrons neutralize Hg^{2+} ions in the crystal, resulting in the formation of Hg atoms, which diffuse toward the crystal surface and aggregate there to form colloidal mercury. Other excited electrons are captured by positive holes, which were created at the sites of S^{2-} or I^- ions in the crystals after neutral S or I atoms escaped thermally out of the crystals. These trapped electrons, *i. e.*, F center electrons exhibit a paramagnetic behavior.

In recent years the authors[3] found by means of a radioactive tracer technique that when the yellow $HgI_2 \cdot 2Hg^{35}S$ or $Hg^{131}I_2 \cdot 2HgS$ is darkened in sunlight, gases of $^{35}SO_2$ or $^{131}I_2$ evolve and that the evolution velocity of the former gases is larger than that of the latter. It was found that the longer the time of irradiation, the larger the quantity of $^{35}SO_2$. This fact suggests that S^{2-} ions are more sensitive to sunlight than I^- ions and the paramagnetism of the darkened crystals is chiefly due to the F center electrons, consisting of positive holes and electrons belonging to S^{2-} ions. These trapped electrons must show an ESR signal, the details of which will be discussed in the present paper.

The ESR measurements were carried out at liquid nitrogen temperature by using a JEOL X-band spectrometer. Yellow powders of $HgI_2 \cdot 2HgS$ were made by the action of purified H_2S on a methanol solution of mercury(II) iodide, which was purified three times by sublimation. If crude powders of mercury(II) iodide were used as the material, the yellow powders showed an ESR signal in the dark. When the yellow powders prepared from the purified mercury(II) iodide, which gave no ESR signal, were darkened black as much as possible in sunlight with stirring by a glass rod for 1 or 2 h, an ESR signal appeared, as is shown in Fig. 1. The obtained signal is not sharp and the intensity is weak. This is due to the fact that the samples are powders, the particles of which are not completely darkened with sunlight. If the signal is due to a formation of a color center, the density of the color center of the darkened powders must be larger than 10^{16} cm^{-3}, because in general a color center can be recognized as an ESR line when the density reaches this value. The *g*-value of the observed signal, with a mean value from about 8 measurements for 8 different samples, was estimated to be 2.0046 ± 0.00028. This signal intensity increased with the time of irradiation with sunlight. This relation is shown in Fig. 2. When the darkened samples were heated at 95 °C for 30 and 60 min, the

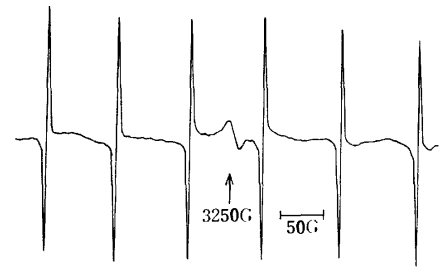

Fig. 1. ESR spectrum of $HgI_2 \cdot 2HgS$ irradiated by sunlight for 10 min.

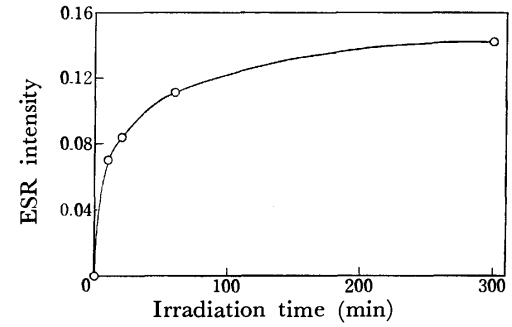

Fig. 2. ESR signal as a function of exposure time.

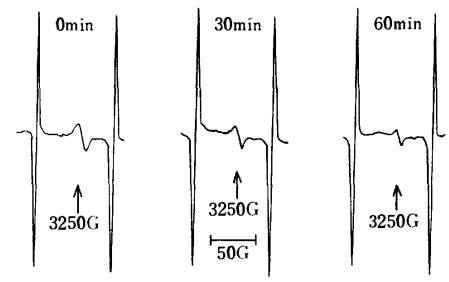

Fig. 3. ESR spectra of $(HgI_2 \cdot 2HgS)^*$ heated at 95 °C for some min.

intensity decreased with the time of heating and the sharpness increased, accompanied by a rapid recovery of the color. This relation is shown in Fig. 3. The *g*-value after thermal treatment, with a mean value of about 6 measurements for 6 different samples, was estimated to be 2.0026±0.00018.

The *g*-value obtained for the darkened $HgI_2 \cdot 2HgS$ is in agreement with the *g*-values of F centers presented by Alger[4] for different inorganic powder substances, and with the *g*-values of F centers for alkali halides given by Holton and Blum,[5] and with the *g*-value of the F center for MgO obtained by Wertz and his co-workers.[6] The F center ESR line often has some nuclear isotropic effects. Wertz and Auzins,[6] for example, found the F center ESR line for MgO with one or two ^{25}Mg ions around the negative ion vacancy, giving a six- or eleven-line hyperfine pattern centered upon the strong component. Similarly, Hausmann[7] found the F center ESR line for ZnO with one ^{67}Zn ion around the negative ion vacancy, giving a hyperfine pattern centered upon the strong component. In our sample, however, no effects of the nuclear spin of ^{199}Hg or ^{201}Hg on the pattern were observed, because of the complexity of the crystal structure of the sample. In 1972, Fujiwara and Isobe[8] showed that hot ions of the paramagnetic Hg(I) complex are formed by γ-irradiation of powders of $K_2[Hg(CN)_4]$ and that these ions are thermally very unstable at room temperature. All the spectra of the hot ions showed isotropic hyperfine splitting, which was recorded at K- or X-band frequency. The paramagnetism of the darkened $HgI_2 \cdot 2HgS$, however, is thermally very stable at room temperature and no isotropic hyperfine splitting appeared in spite of a sweep from 1000 to 10000 G. In 1966, Shields[9] reported that a reduction of silver ions in a pyrex glass by γ-rays induces an ESR spectra of Ag^0 accompanied with an isotropic hyperfine splitting. In our sample, the Hg^0 or Hg atom has nuclear spin, but no unpaired electrons. These discussions show that the ESR line in our sample cannot be explained by the mechanism of formation of Hg(I) or Hg^0.

Moran and his co-workers[10] reported that the bleaching of an F band produces a more rapid decrease in the density of magnetic centers than of the centers giving optical absorption in the F band; they suggested the presence of R, M, or N centers by a study of the temperature dependence of the relaxation time of F centers. Our complicated mercury complex exhibits a characteristic magnetic behavior, *i. e.*, a more rapid decrease in optical absorption centers than of the magnetic centers. This behavior is possible, because the results of thermal bleaching depend on the preparation methods of the F centers, as is reported by Alger.[11] If the signal in our sample is related to the existence of Hg^+ ions, or S or I neutral atoms in the crystal, the intensity of the signal should decrease rapidly when heated at 95 °C, because these ions or atoms are thermaly mobile in the crystal at 95 °C. It is conculded that the signal is not due to Hg^+ ions or S or I neutral atoms, but due to F centers, which are located at a deep energy level. When heated at 95 °C, the centers release slowly a small part of the trapped electrons, most of which are still captured, resulting in a formation of a new center, as is shown in Fig. 3. This new center has 2.0026±0.00018 as its *g*-value. The released electrons will be again captured by neutral atoms of S or I in the crystals to form S^{2-} or I^- ions, which react with Hg^{2+} ions to form HgS(black) or HgI_2, the existence of which was already chemically confirmed by the one of the authors.[2]

The authors with to thank Dr. S. Fujiwara, Dr. L. Shields, and Dr. A. Hausmann for many helpful discussions and suggestions during this work.

References

1) K. Takei, *Bull. Chem. Soc. Jpn.*, **28**, 403 (1955).
2) K. Takei, *Nippon Kagaku Zasshi*, **77**, 965 (1956).
3) K. Takei and H. Hagiwara, *Radioisotopes*, **24**, 715 (1975).
4) R. S. Alger, "Denshi Supin Kyomei" (Translated edition of Electron Paramagnetic Resonance : Tecnhiques and Applications by T. Isobe, M. Iwamizu, T. Okabe, A. Hanyu, and M. Hirayama), Yoshioka Publ. Co., Tokyo (1973), p. 409.
5) W. C. Holton and H. Blum, *Phys. Rev.*, **125**, 89 (1962).
6) J. E. Wertz, P. Auzins, R. A. Weeks, and R. H. Silsbee, *Phys. Rev.*, **107**, 1535 (1957).
7) A. Hausmann, *Z. Phys.*, **237**, 86 (1970).
8) S. Fujiwara and J. Isobe, *Bull. Chem. Soc. Jpn.*, **45**, 2182 (1972).
9) L. Shields, *J. Chem. Phys.*, **45**, 2332 (1966).
10) P. R. Moran, S. H. Christensen, and R. H. Silsbee, *Phys. Rev.*, **124**, 442 (1961).
11) R. S. Alger, Ref. 4, p. 391.

BULLETIN OF THE CHEMICAL SOCIETY OF JAPAN, VOL. 50 (5), 1343—1344 (1977)

Luminescence of Aminopyridines and Related Molecules

Ko KIMURA, Hideko TAKAOKA, and Ryo NAGAI

Department of Chemistry, Faculty of Science, Osaka City University, Sumiyoshi-ku, Osaka 558

(Received November 12, 1976)

Synopsis. Quantum yields and lifetimes of fluorescence and phosphorescence were measured for 2-, 3-, 4-aminopyridines, 2-, and 4-(dimethylamino)pyridines in ethanol–methanol, in an acidic ethanol–methanol mixture, and in a mixture of triethylamine and 2-methyltetrahydrofuran at 300 K and at 77 K. Quantum yields of fluorescence of 2- and 3-substituted pyridines are appreciable, while those of 4-substituted pyridines are as low as or less than 0.01 at 77 K. In view of the significant quantum yields of fluorescence for 2- and 3-substituted pyridines in the aprotic solvent, it may be concluded that the higher excited $^1(n\pi^*)$ or $^3(n\pi^*)$ states are not so close in energy to the lowest excited $^1(\pi\pi^*)$ states.

Quantum yields of fluorescence (Φ_f) of aminopyridines measured by Weisstuch and Testa[1] at room temperature suggest that the lowest excited singlet states (S_1) of 2- and 3-aminopyridines are assigned to $(\pi\pi^*)$, in contrast with that of 4-aminopyridine, which is assigned to $(n\pi^*)$ in nonpolar solvents or to the charge transfer type $(\pi\pi^*)$ in polar solvents. However, in view of the significant temperature dependence of Φ_f's for some nitrogen–heterocyclics,[2] measurements of Φ_f's and lifetimes of fluorescence (τ_f) at low temperature are desirable.

Φ_f's, τ_f's, quantum yields (Φ_p), and lifetimes (τ_p) of phosphorescence for 2-, 3-, 4-aminopyridines, 2-, and 4-(dimethylamino)pyridines are summarized in Tables 1 and 2. Solvents used were ethanol–methanol (A), an acidic (0.05 M H_2SO_4) ethanol–methanol mixture (H^+), and a mixture of triethylamine and 2-methyltetrahydrofuran (B). The first absorption bands of 2- and 3-substituted pyridines correspond fairly well to their fluorescence bands, as judged by the mirror symmetry relationship to each other. S_1's and the lowest excited triplet states (T_1) of 2- and 3-substituted pyridines are assigned unambiguously to $(\pi\pi^*)$ from Φ_f's and τ_p's in Table 1. The rate constants of the radiative transition (k_f) from S_1 are fairly independent of temperature and of protonation, while those of the radiationless deactivation (k_{nr}), which are composed of the rate constants of the internal conversion and the intersystem crossing from S_1, depend significantly on temperature and on protonation. If it is presumed that the k_f's are constant irrespective of the presence or absence of protons in solvents, then k_{nr}'s are estimated from Φ_f's without the observed τ_f's. k_{nr}'s at 77 K, designated in parentheses in Table 1, are calculated on this assumption, and those at 300 K on the assumption of the temperature-independent k_f's. As the Φ_p's of 2- and 3-substituted pyridinium cations used in this work are as low as or less than 0.01 at 77 K, their k_{nr}'s correspond

TABLE 1. QUANTUM YIELDS AND LIFETIMES OF FLUORESCENCE AND PHOSPHORESCENCE FOR 2-, 3-AMINOPYRIDINES, AND 2-(DIMETHYLAMINO)PYRIDINE

	$\lambda_{f\,max}$ (nm)	Φ_f	τ_f (ns)	$k_f \times 10^{-7}$ (s^{-1})	$k_{nr} \times 10^{-7}$ (s^{-1})	$\lambda_{p\,max}$ (nm)	ϕ_p	τ_p (s)
300 K								
2AMP(H^+)	366	0.63	14.8	4.3	2.5			
(A)	348	0.28			(12)			
(B)	338	0.06			(70)			
2DMAMP(H^+)		<0.01						
(A)	370	0.36	12.2	3.0	5.3			
(B)	351	0.23			(11)			
3AMP(H^+)	402	0.44	18.8	2.3	3.0			
(A)	352	0.24			(10)			
(B)	344	0.06			(52)			
77 K								
2AMP(H^+)	349	0.71	16.2	4.4	1.8	482	<0.01	1.8
(A)	346	0.52	11.7	4.4	4.1	441	0.10	2.0
(B)	341	0.35			(8)	435	0.19	1.4
2DMAMP(H^+)	389	0.47	15.0	3.1	3.5	472	<0.01	1.4
(A)	355	0.44	13.6	3.2	4.1	441	0.16	1.7
(B)	346	0.29			(8)	431	0.18	1.1
3AMP(H^+)	377	0.70	20.5	3.4	1.5	452	<0.01	1.3
(A)	352	0.54	16.3	3.3	2.8	465	0.33	3.0
(B)	344	0.15			(19)	442	0.41	2.7

2AMP, 3AMP, and 2DMAMP represent 2-, 3-aminopyridines, and 2-(dimethylamino)pyridine, respectively.
k_f's and k_{nr}'s are deduced from the following equations: $k_f = \Phi_f/\tau_f$ and $k_{nr} = (1-\Phi_f)/\tau_f$.

Table 2. Quantum yields and lifetimes of phosphorescence for 4-aminopyridine and 4-(dimethylamino)pyridine at 77 K

	$\lambda_{p\,max}$ (nm)	Φ_p	τ_p (s)
4AMP(H^+)	359	0.45	2.0
(A)	359	0.51	1.9
(B)	373	0.32	0.7
4DMAMP(H^+)	401	0.12	1.6
(A)	392	0.42	1.6
(B)	388	0.24	0.5

approximately to the rate constants of the internal conversion from S_1. However, the estimated k_{nr}'s in an aprotic solvent at 77 K are fairly large, and suggest a significant contribution of the rate constants of the intersystem crossing from S_1, in view of decrease in Φ_f's and the corresponding increase in Φ_p's. An increase in k_{nr}'s for 2- and 3-aminopyridines in the aprotic solvent at 300 K may arise from the temperature dependence of the rate constants of the intersystem crossing[3] as well as those of the internal conversion, in marked contrast with the almost temperature-independent k_{nr} of 2-(dimethylamino)pyridine in the same solvent. However, the fairly large k_{nr} for a 2-(dimethylamino)pyridinium cation might be deduced from the scarcely observed Φ_f at 300 K, which is quite opposed to the change in Φ_f's found in 2- and 3-aminopyridinium cations. In view of the large Φ_f's even in the aprotic solvent at 77 K, the singlet or triplet ($n\pi^*$) states of 2- and 3-substituted pyridines are not so close in energy to the S_1's.

The Φ_f's of 4-substituted pyridines are smaller than 0.01 at 77 K, irrespective of the solvents used in this work. The phosphorescence spectra of 4-aminopyridine show vibrational structures, in which a characteristic vibration at 850 cm^{-1}, indicative of the C–H out-of-plane deformation mode of aromatic rings, may be found, while those of 4-(dimethylamino)pyridine are without vibrational structures.[4] As is summarized in Table 2, the large Φ_p's and the long τ_p's suggest that the T_1's of 4-substituted pyridines are ($\pi\pi^*$) irrespective of solvents used. The small Φ_f's of 4-substituted pyridines in the aprotic and the acidic solvents at 77 K are consistent with the assignment of S_1's proposed by Weisstuch and Testa.[1]

Experimental

2-, 3-, 4-Aminopyridines, and 4-(dimethylamino)pyridine were recrystallized three times from ethanol-ligroin, then purified through a basic alumina column, and finally sublimed *in vacuo*. 2-(Dimethylamino)pyridine was distilled through a spinning band column, then purified through a basic alumina column, and finally distilled twice *in vacuo*. Triethylamine and 2-methyltetrahydrofuran were stored over sodium-potassium alloy after distillation through a stainless steel helices packed column, and used without exposure to air. The methods of purification of other solvents and reagents were described elsewhere.[5]

Measurements of Φ_f's, Φ_p's, τ_f's, and τ_p's were the same as those described elsewhere.[5] The concentrations used in the measurements of Φ_f's and Φ_p's and those of τ_f's and τ_p's were 10^{-2}—10^{-3} M and 10^{-4}—10^{-5} M, respectively. In the former case, the correction of concentration quenching, if necessary, was made by the use of the Stern-Volmer equation. All the samples were evacuated by the repeated cycles of freezing, pumping, and thawing. Then, the sample cells were sealed off from the evacuation system.

References

1) A. Weisstuch and A. C. Testa, *J. Phys. Chem.*, **72**, 1982 (1968); **74**, 2299 (1970).

2) Y. H. Li and E. C. Lim, *Chem. Phys. Lett.*, **9**, 279 (1971); M. Koyanagi, R. J. Zwarich, and L. Goodman, *J. Chem. Phys.*, **56**, 3044 (1972); R. Li and E. C. Lim, *J. Chem. Phys.*, **57**, 605 (1972).

3) E. W. Schlag, S. Schneider, and S. F. Fischer, *Ann. Rev. Phys. Chem.*, **22**, 490 (1971).

4) S. Hotchandani and A. C. Testa, *J. Chem. Phys.*, **59**, 596 (1973).

5) K. Kimura and R. Nagai, *Bull. Chem. Soc. Jpn.*, **49**, 3343 (1976).

BULLETIN OF THE CHEMICAL SOCIETY OF JAPAN, VOL. 50 (5), 1345—1346 (1977)

A Note on the Rates of Complex Formation of Indium(III) with Murexide and the Decomposition of Murexide in the Presence of Indium(III)

Yoshimi OHTANI, Shin-ichi YAGIHASHI,* and Masatoshi FUJIMOTO

Department of Chemistry, Faculty of Science, Hokkaido University, Sapporo 060

(Received November 11, 1976)

Synopsis. Kinetics of the complex formation between In(III) and murexide was studied by means of the temperature-jump method and the rate of decomposition of the ligand in acid nitrate media. The complex formation of $InOH^{2+}$ with murexide is about 10 times faster than that of In^{3+}. The stability constants indirectly obtained from the decomposition rate of murexide coincide with those from direct stopped-flow measurements.

Murexide, ammonium purpurate, is a useful metallochromic indicator except for the acid region where it decomposes to uramil and alloxan.[1] Kawai *et al.* studied the kinetics on the complex formation of murexide with In(III) and the decomposition of murexide in acid perchlorate media in the presence of In(III).[2] In this study no dependence of the rate of complex formation on hydrogen-ion concentration (0.001—0.5 M) could be observed. In addition a discrepancy in the stability constants was obtained from the two methods, the indirect calculation from the rate of decomposition of murexide giving a stability constant twice as large as that from the direct stopped-flow measurement. We have reexamined the questions with use of potassium nitrate instead of sodium perchlorate for adjusting the ionic strength in order to avoid the influence of the ion-pair formed between sodium ion and murexide anion.

Experimental

Materials. In order to prepare a stock solution of In(III) containing 1 M nitric acid, indium(III) oxide (Koso) was dissolved in excess of nitric acid by warming on a water bath. The concentration of In(III) was determined by titration with EDTA using Xylenol Orange as an indicator. The freshly prepared stock solution was used within a day in order to avoid undesired polymerization of In(III). Murexide was prepared and recrystallized.[3] A weighed amount of murexide was dissolved in water immediately before use. Acidity and ionic strength of the solution were adjusted with nitric acid and potassium nitrate.

Measurements. The rate of complex formation was measured with a Union Giken co-axial-cable temperature-jump apparatus Model RA-105. A Hitachi ESP-3T spectrophotometer equipped with a recorder was used to measure the rate of decomposition. Visible spectrum of unstable purpuric acid was obtained with a Union Giken rapid-scan spectrophotometer RA-1300, and the acid dissociation constant with a Yanagimoto SPS-1 stopped-flow apparatus.

Results and Discussion

Rate of Complex Formation. The rate of complex formation between In(III) and murexide was measured at the absorption peak of the complex, 460 nm, by means of the temperature-jump method at 20 °C and ionic strength 0.2 M (KNO_3). Acetic acid and potassium acetate were used to adjust pH. The results suggest the presence of a base-catalyzed path, the following mechanism being considered;

$$\begin{array}{ccc} In & + L \underset{k_2}{\overset{k_1}{\rightleftharpoons}} & InL \\ {\scriptstyle K_a}\downarrow\uparrow & & {\scriptstyle K_b}\downarrow\uparrow \\ In(OH) + H^+ & + L \underset{k_4}{\overset{k_3}{\rightleftharpoons}} & In(OH)L + H^+ \end{array}$$

$$\tau^{-1} = \frac{k_1[H]+k_3K_a}{[H]+K_a}\cdot C_{In} + \frac{k_2[H]+k_4K_b}{[H]+K_b},$$

where C_{In} is the total concentration of In(III) ($C_{In} \gg [L]$). The value of K_a in literature is adopted ($K_a = 10^{-4.42}$ M).[4] The values of rate constants are determined to be $k_1 = 6.0\times10^5$ M^{-1} s^{-1}, $k_2 = 50$ s^{-1}, $k_3 = 6.8\times10^6$ M^{-1} s^{-1}, and $k_4K_b = 2.3$ M s^{-1}. The hydrolyzed form, $InOH^{2+}$, reacts with the ligand about 10 times faster than the aquo form. This is in line with the tendency that the rate of complex formation of hydroxo metal ion is higher than that of the corresponding aquo metal ion.[5]

Acid Dissociation Constant of Purpuric Acid. Since murexide decomposes rapidly in an acid solution, the acid dissociation constant of protonated murexide or purpuric acid was measured by the stopped-flow method, giving $pK_1 = -0.24$. Rapid-scan spectroscopy gave $\lambda_{max} = 444$ nm, $\varepsilon = 2.2\times10^4$ l mol^{-1} cm^{-1} with an isosbestic point at 485 nm for purpuric acid.

Effect of [H] on the Decomposition Rate of Murexide. The decomposition of murexide is accelerated by acid. The reciprocal of the pseudo-first-order rate constant for the decomposition of murexide has a linear relationship with respect to $[H]^{-1}$, as shown in Fig. 1. The reaction mechanism is as follows;

$$MX + H \overset{K_H}{\rightleftharpoons} MXH \xrightarrow[+H_2O]{k} \text{Uramil} + \text{Alloxan},$$

$$k_{obsd}^{dec\,-1} = \frac{1}{k} + \frac{1}{kK_H}\cdot\frac{1}{[H]},$$

where MX and MXH denote purpurate anion and purpuric acid, respectively. Since the intercept of the straight line in Fig. 1 is too small for evaluation, the value obtained above is introduced into K_H ($K_H = K_1^{-1}$), giving the result $k = 0.13$ s^{-1}.

Rate of Decomposition of Murexide in the Presence of In(III). The rate of decomposition of murexide was measured at the absorption maximum of the complex. The rate decreases with increase in the concentration of In(III) (Fig. 2). The following reaction scheme is proposed:

* Present address: HOXAN Research Laboratories, Sapporo 060.

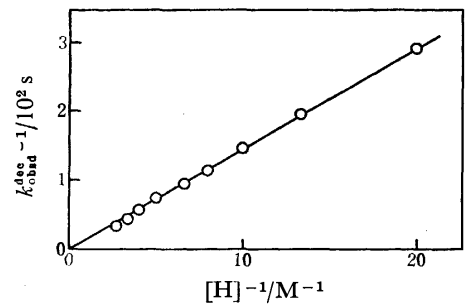

Fig. 1. Plot of $k_{obsd}^{dec\ -1}$ *vs.* inverse of hydrogen-ion concentration. At 520 nm, 10 °C, I=1.0 M (KNO_3), and $[MX]_0=5.0\times10^{-5}$ M.

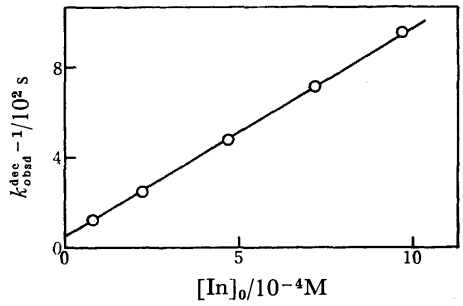

Fig. 2. Plot of $k_{obsd}^{dec\ -1}$ *vs.* total concentration of In(III). At 460 nm, 10 °C, [H]=0.25 M, I=1.0 M (KNO_3), and $[MX]_0=5.0\times10^{-5}$ M.

$$MX + In \overset{K_{In}}{\rightleftharpoons} InMX$$

$$MX + H \overset{K_H}{\rightleftharpoons} MXH \xrightarrow[+H_2O]{k} Uramil + Alloxan.$$

The rate of decomposition is given by

$$k_{obsd}^{dec\ -1} = \frac{[H]K_H + 1}{[H]kK_H} + \frac{K_{In}}{[H]kK_H}\cdot[In]_0.$$

Introduction of the above results into K_H and k leads to $K_{In}=1.5\times10^4\ M^{-1}$. The value coincides with the direct stopped-flow data, $K'_{In}=k_1/k_2=1.4\times10^4\ M^{-1}$, I=1 M (KNO_3) at 10 °C. Agreement of the two values indicates that the proposed mechanism is correct. The terdentate structure of the complex coordinated at the central nitrogen atom of the ligand stabilizes the ligand molecule against decomposition.[6]

The discrepancy in the two stability constants derived from the direct and the indirect measurements[2] would be clarified in terms of two effects of the sodium ion: (1) Sodium ion forms an ion-pair with purpurate anion, which is fairly stable against acid. (2) The ion-pair, $Na^+\cdots MX^-$, also forms a complex with In(III). Since the data on the ion-pair are very limited, no further discussion can be made.

The present work was supported by a grant-in-aid for Scientific Research from the Ministry of Education.

References

1) N. A. Ramaiah, S. L. Gupta, and J. Vishnu, *Z. Naturforsch.*, **12b**, 189 (1957); R. K. Chaturvedi, *Z. Phys. Chem. (Leipzig)*, **221**, 127 (1962).

2) Y. Kawai, T. Imamura, and M. Fujimoto, *Bull. Chem. Soc. Jpn.*, **48**, 3142 (1975).

3) D. Davidson, *J. Am. Chem. Soc.*, **58**, 1821 (1936).

4) G. Biedermann, *Arkiv Kemi*, **9**, 277 (1956).

5) J. Miceli and J. Stuehr, *J. Am. Chem. Soc.*, **90**, 6967 (1968); N. D. Lukomskaya, T. V. Malikova, and K. B. Yatsimirskii, *Zh. Neorg. Khim.*, **12**, 2462 (1967); Y. Kawai, T. Takahashi, K. Hayashi, T. Imamura, H. Nakayama, and M. Fujimoto, *Bull. Chem. Soc. Jpn.*, **45**, 1417 (1972).

6) G. L. Eichorn and N. D. Marchard, *J. Am. Chem. Soc.*, **78**, 2688 (1956); A. Nakahara, *Bull. Chem. Soc. Jpn.*, **32**, 308 (1959).

BULLETIN OF THE CHEMICAL SOCIETY OF JAPAN, VOL. 50 (5), 1347—1348 (1977)

Polarographic Studies of Several Metal Ions in the Molten Salts of KNO_3–$LiNO_3$–$NaNO_3$

Makoto SAITO and Tamio MIURA

Department of Chemistry, College of Liberal Arts, Toyama University, Gofuku, Toyama 930

(Received December 10, 1976)

Synopsis. The polarographic waves of Pb(II), Cd (II), Zn(II), and Tl(I) ions in molten salts of KNO_3–$LiNO_3$–$NaNO_3$ were measured by means of d.c. polarography, using an $Ag/AgNO_3$ reference electrode. The half-wave potential of metal ions was shifted toward more negative values in comparison with those in a nitrate melt containing no Li(I) ion.

The formation constants of several metal halide complexes in an alkali nitrate melt have been determined by means of d.c. polarography.[1-3] On the other hand, there have been only a few studies about the effect of the alkali metal ion as a component of the solvent on the half-wave potential of the reducible species. Kawamura[4-6] studied, by means of voltammetry and chronopotentiometry, the change in the diffusion coefficient of the Ag(I) ion over a wide composition range of molten salts of KNO_3–$NaNO_3$, KNO_3–$LiNO_3$, and KNO_3–$CsNO_3$. Francini and Martini reported that the peak potentials(E_p) of the oscillopolarogram of some metal ions in molten salts of KNO_3–$NaNO_3$ were shifted toward more positive values by adding variable quantities of $LiNO_3$ to the melt.[3]

The present authors have studied the half-wave potential($E_{1/2}$) of the polarographic wave of several metal ions in the molten salts of KNO_3–$LiNO_3$–$NaNO_3$, using the $Ag/AgNO_3$ reference electrode, and compared the obtained half-wave potential with the data obtained by Swofford and Holified[7] and by Tridot *et al.*[8]

Experimental

Reagent-grade chemicals were used in these experiments. The solvent used was the KNO_3–$LiNO_3$–$NaNO_3$(53 : 30 : 17 mol%, mp 120 °C) eutectic system. The eutectic materials were separately dried in a vacuum-oven at 100 °C for several days, and these mixed and gently fused in an argon gas atmosphere.

The metal salts used were $Pb(NO_3)_2$, $TlNO_3$, $Cd(NO_3)_2 \cdot 4H_2O$, and $Zn(NO_3)_2 \cdot 6H_2O$. The polarographic waves of the metal ions were not disturbed by the crystal water in metal salts. The concentration of the metal ions in a melt was determined by means of EDTA titration. The capillary used as the dropping mercury electrode(DME) was made of Pyrex glass. The drop time of the DME was about 3—5 s per drop at a height of 60—80 cmHg. The $Ag/AgNO_3$(0.05 mol/kg) electrode was used as the reference electode. Asbestos was used as a diaphragm between the reference electrode and the test solution. The temperature used in the experiments was 180 °C. The rest of the experimental procedure has been described elsewhere.[9]

Results and Discussion

The polarographic waves of some metal ions at 180 °C are shown in Fig. 1, in which curve(a) is a typical residual current curve and in which the useful potential range available to obtain polarographic waves is from 0 to −1.4 V *vs.* the $Ag/AgNO_3$ reference electrode; the maximum current obtained in this range was about 2 μA at −1.4 V. However, the final ascendent potential in the residual current was shifted toward a positive potential and the useful potential range was diminished about 100 mV, when the solution stood for a day and night. Curves(b), (c), (d), and (e) in Fig. 1 are the polarographic waves of the Pb(II), Cd(II), Tl(I), and Zn(II) ions. The polarographic waves of these metal ions indicated S-shaped waves. The plots of E *vs.* $\log[i/(i_d-i)]$ for polarographic waves are shown in Fig. 2, in which the plots give a straight line and the slope of the line was Pb(II): 45 mV, Cd(II): 41 mV, Tl(I): 80 mV, and Zn(II): 41 mV

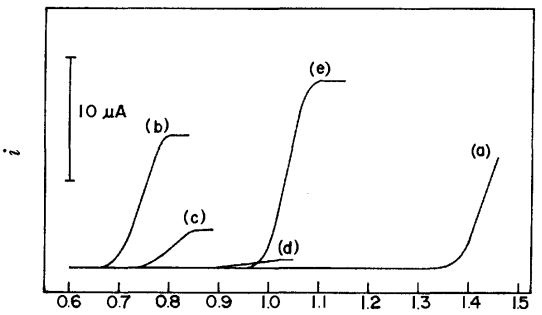

Fig. 1. Polarographic waves of some matel ions at 180 °C,
(a): Residual current curve of the molten salts of KNO_3–$LiNO_3$–$NaNO_3$, (b): Pb(II) ion, 2 mmol/kg, (c): Cd(II) ion, 1 mmol/kg, (d): Tl(I) ion, 0.2 mmol /kg, (e): Zn(II) ion, 3 mmol/kg.

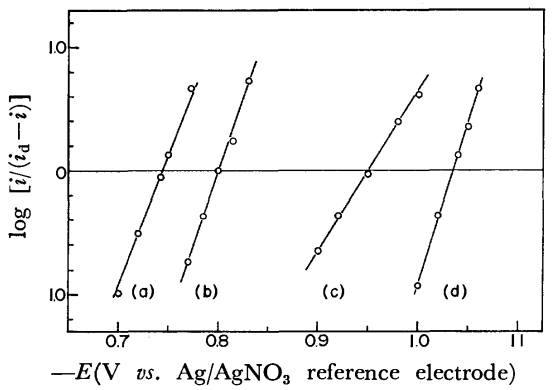

Fig. 2. Analyses of the polarographic waves of some metal ions at 180 °C. The slope of the line is 45, 41, 80, or 41 mV against $\log[i/(i_d-i)]$ for Pb(II), Cd(II), Tl(I), or Zn(II) ions.

TABLE 1. THE HALF-WAVE POTENTIALS OF SOME METAL IONS IN MOLTEN ALKALI NITRATES

	$-E_{1/2}$ (V *vs.* $Ag/AgNO_3$)				Ref.
	Pb(II)	Cd(II)	Tl(I)	Zn(II)	
Holifield and Swofford	—	0.665	0.828	—	(7)
Tridot *et al.*	0.560	0.565	0.730	0.820	(8)
Present authors	0.744	0.800	0.949	1.034	

($2.303RT/F$=90 mV at 180 °C). These polarographic waves are reversible, and the electrode reactions of metal ions are the transfer of two electrons(one electron in the case of the Tl(I) ion). The half-wave potentials of the metal ions were determined from the logarithm plots; they are tabulated in Table 1. As is evident from Table 1, the half-wave potentials of metal ions had more negative values than that obtained in the solvent containing the Li(I) ion and the useful potential range is diminished as compared with those obtained in the molten salts of KNO_3–$NaNO_3$ by Swofford *et al.* and by Tridot *et al.* The half-wave potentials of the metal ions obtained by Swofford *et al.* also differed from those obtained by Tridot *et al.* It is considered that the discrepancy in the half-wave potentials in their data reflects the difference in the concentration of $AgNO_3$ in the reference electrode.

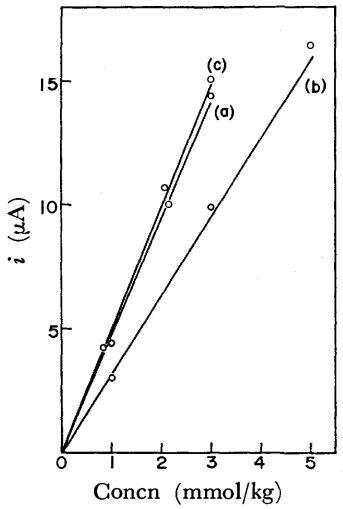

Fig. 3. Relationships between the limiting current and the concentrations of some metal ions at 180 °C.
(a): Pb(II) ion, (b): Cd(II) ion, (c): Zn(II) ion.

The linear dependence of the diffusion current on the metal ion concentration is shown in Fig. 3. The Ilkovic equation was applied in the ranges of 0.0—3.0 mmol/kg for Pb(II), 0.0—5.0 mmol/kg for Cd(II), and 0.0—3.0 mmol/kg for Zn(II). The diffusion current coefficients(I: $[\mu A]/[mg^{2/3}\,s^{-1/2}][mmol/kg]$) of the metal ions were Pb(II): 3.04, Cd(II): 3.11, Zn(II): 3.17. In the case of the Tl(I) ion, the maximum wave appeared in the concentration of the Tl(I) ion of more than 0.4 mmol/kg.

References

1) J. H. Christie and R. A. Osteryoung, *J. Am. Chem. Soc.*, **82**, 1841 (1961).
2) D. Inman, D. G. Lovering, and R. Narayan, *Trans. Faraday Soc.*, **64**, 2476 (1968).
3) M. Francini and S. Martini, *Electrochim. Metall.*, III 2, 136 (1968).
4) K. Kawamura, *Electrochim. Acta*, **12**, 1233 (1967).
5) K. Kawamura, *Denki Kagaku*, **38**, 12 (1970).
6) K. Kawamura, *Trans. Jpn. Inst. Met.*, **15**, 413 (1974).
7) H. S. Swofford and C. L. Holifield, *Anal. Chem.*, **37**, 1509 (1965).
8) G. Tridot, G. Nowogroki, J. Nicole, M. Wozniak, and J. Canonne, *C. R. Acad. Sci., Ser. C*, **270**, 240 (1970).
9) M. Saito and T. Miura, *Nippon Kagaku Kaishi*, **79**, 911 (1976).

BULLETIN OF THE CHEMICAL SOCIETY OF JAPAN, VOL. 50 (5), 1349—1350 (1977)

Photoreaction of Ferrocene with Some Acetylene Derivatives

Haruo WATANABE, Kazuo ITO, Fumio NAKANISHI, Takeo AKIYAMA, and Akira SUGIMORI

Department of Chemistry, Faculty of Science and Technology, Sophia University, Kioi-cho 7, Chiyoda-ku, Tokyo 102

(Received March 17, 1976)

Synopsis. The UV-irradiation of ferrocene and dimethyl acetylenedicarboxylate in acetic acid–water solution afforded dimethyl ferrocenylmaleate and dimethyl ferrocenylfumarate in 40 and 5% yield, respectively. Methyl 3-carbamoylpropiolate, dicyanoacetylene, and methyl propiolate were also reactive and the corresponding substituted ferrocenes were obtained. The reaction can be considered to proceed *via* the excitation of the charge transfer complex between ferrocene and acetylene derivatives.

As reported,[1] UV-irradiation of the ferrocene-halogenated hydrocarbon-ethanol system gave substituted ferrocene *via* the excitation of the charge transfer complex between ferrocene and halogenated hydrocarbon. We found a similar photo-substitution of ferrocene with some electron defficient acetylene derivatives.

When an acetic acid–water solution of ferrocene (**1**) and dimethyl acetylenedicarboxylate (**2a**) in a quartz vessel was irradiated with 254 nm light for 24 h under nitrogen atmosphere, dimethyl ferrocenylmaleate (**3a**) and dimethyl ferrocenylfumarate (**4a**) were obtained in 40 and 5% yield, respectively. When methyl 3-carbamoylpropiolate (**2b**), dicyanoacetylene (**2c**), and methyl propiolate (**2d**) were used instead of **2a**, photo-products similar to **3a** and **4a** were obtained. However, the yields of the photo-products were lower than those of **3a** and **4a**, and the isomer ratio, **3**/**4**, was different from that obtained in the case of **2a**. The results of the photoreactions are listed in Table 1. Other acetylene derivatives, such as phenylacetylene, diphenylacetylene, methyl 3-phenylpropiolate, phenylpropiolaldehyde, and acetylenedicarboxamide, were unreactive for this photoreaction and gave no substituted ferrocene under the UV-irradiations. The effect of additives and the wavelength of light used were examined for the **1**–**2a**–acetic acid–water systems which showed the highest yields of the photo-products. The results showed that the radical scavenger, cyclohexene, retarded the photo-substitution of ferrocene very little [yield of **3a**: without additive, 21%; with cyclohexene, 14%]. This result indicates that this photo-substitution does not proceed *via* the coupling of free, separate radicals as reported for the reaction of furan with **2a**,[2] but proceed *via* the geminate coupling of the radical pair in the solvent cage.[3] Benzophenone, a triplet sensitizer, was not effective for the formation of **3a** and **4a**. This result indicates that the contribution of the triplet state of **1** or **2a** for the photo-substitution is very small. In the irradiation with light of wavelength longer than 300 nm(high pressure mercury lamp with a Pyrex filter), only a trace amount of **3a** was obtained and more than 60% of **1** and **2a** were recovered.

The formation of the charge transfer complex between **1** and **2a** in the ground state was supported by the

TABLE 1. PHOTO-SUBSTITUTION OF FERROCENE WITH SOME ACETYLENE DERIVATIVES[1]

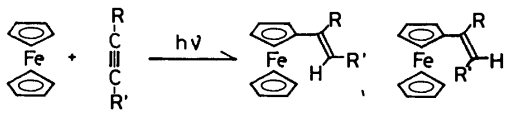

1 **2** **3** **4**

2a: R=R'=-CO_2Me **3a**, **4a**: R=R'=-CO_2Me

2b: R=-CO_2Me, R'=-$CONH_2$ **3b**, **4b**: R=-CO_2Me (or -$CONH_2$), R'=-$CONH_2$ (or -CO_2Me)

2c: R=R'=-CN **3c**, **4c**: R=R'=-CN

2d: R=-H, R'=-CO_2Me **4d**: R=-CO_2Me, R'=-CH_3

1 (mmol)	**2** (mmol)	Solvent (40 ml)	Light Source[3]/Time (h)	Conversion (%)	Products and yields[2] (%) **3**	**4**
0.2	**2a** 0.4	CH_3CO_2H-H_2O (3 : 1, v/v)	LP / 24	64	**3a** : 40.6(26)	**4a** : 4.7(3)
2.0	**2b** 2.0	CH_3CO_2H	LP / 24	60	**3b** : 7.4(4.4)	**4b** : 7.4(4.4)
4.0	**2c** 2.0	CH_3CO_2H	LP / 21[4]	6.4	**3c** : 16.1(1)	**4c** : 6.7(0.4)
1.0	**2d** 2.0	CH_3CO_2H-H_2O (3 : 1, v/v)	LP / 13	15	—	**4d** : 20.3(3)

1) These photoreactions were carried out below 25 °C. 2) Yields based on consumed ferrocene. The yields in parentheses are the net yields based on ferrocene used. 3) LP denotes a low pressure mercury lamp. 4) This reaction was carried out above 35 °C.

spectral data. The UV-spectra of **1** and **2a** in acetic acid showed an increment of absorption in the 250—300 nm region and the NMR spectra (measured at 90 MHz) of the mixed solution of **1** and **2a** in acetic acid showed a small downfield shift of the proton signals of **1** and an upperfield shift of those of **2a**, as compared to the corresponding proton signals measured independently. Based on these spectral data and on the effect of additives, the following processes can be considered for the present photo-substitution of ferrocene: i) The excitation of the charge transfer complex of **1** and **2a** to its singlet state. ii) One electron transfer from **1** to **2a**, followed by the formation of ferrocenium cation and anion radical of **2a**. iii) Coupling of the radical anion of **2a** with ferrocenium cation in the solvent cage. iv) Deprotonation and protonation to the anionic center of olefin,[4] or proton transfer.

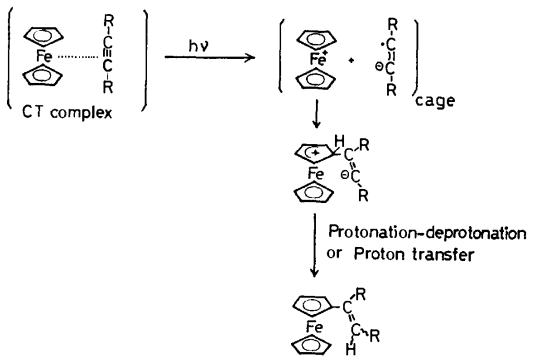

When acetone, acetonitrile, ethyl acetate, and methanol was used as the solvent, the yields of **3a** were much lower. This solvent effect indicates that the protic solvent with high polarity is necessary for this photo-substitution.

Experimental

Materials. Commercially available ferrocene (Wako Junyaku, GR-grade reagent) was used without further purification. Dimethyl acetylenedicarboxylate (Wako Junyaku, EP-grade reagent) was purified by column chromatography on silica gel (Merck, GF-254, Type 60) before use. Methyl 3-carbamoylpropiolate was prepared by mixing dimethyl acetylenedicarboxylate and ammonia–water for several hours. Dicyanoacetylene was prepared by the method described in the literature.[5] Commercial methyl propiolate (Wako Junyaku, EP-grade reagent) was used without further purification. Acetic acid and other solvents used in this reaction were all purified by distillation under nitrogen atmosphere and dried just before use.

Irradiation Procedure. The general execution of the photoreaction is represented by the procedure for the photo-substitution of ferrocene with dimethyl acetylenedicarboxylate.

Photoreaction of Ferrocene (1) with Dimethyl Acetylenedicarboxylate (2a). The acetic acid–water(3 : 1, v/v, 40 ml) solution of **1** (37 mg, 0.2 mmol) and **2a** (57 mg, 0.4 mmol) was degassed and then filled with nitrogen. This sample solution was irradiated in a quartz vessel with a low pressure lamp(Taika Kogyo, 16 W) for 24 h. After the irradiation, 100 ml of ethyl acetate was added to the reaction mixture and washed with water and then with aqueous sodium hydrogencarbonate solution. The ethyl acetate solution was dried and concentrated under reduced pressure. The residue was subjected to preparative TLC on silica gel (Merck, CF-254). **3a** and **4a** were obtained as a mixture. Further separation with TLC afforded 17.3 mg (40.6%) of **3a** as a red-purple oily solid. **3a**: IR(KBr) 1718, 1725 cm^{-1} (C=O), 1620 cm^{-1} (C=C), 1100, 1000 cm^{-1} (monosubstituted ferrocene); NMR(CCl_4), δ(ppm from TMS) 3.69 (s, 3H, $-CH_3$), 3.85 (s, 3H, $-CH_3$), 4.15 (s, 5H, C_5H_5), 4.32 (4H, C_5H_4), 5.86 (s, 1H, olefinic proton); MS(70 eV), *m/e*, 328(M^+). Found: C, 57.96; H, 5.00%. Calcd for $C_{16}H_{16}O_4Fe$: C, 58.57; H, 4.88%, M, 328. From another fraction, 2 mg (4.7%) of **4a** was obtained. **4a**: IR(direct) 1720, 1725 cm^{-1} (C=O), 1620 cm^{-1} (C=C), 1100, 1000 cm^{-1} (monosubstituted ferrocene); NMR(CCl_4), δ(ppm from TMS) 3.65 (s, 3H, $-CH_3$), 3.86 (s, 3H, $-CH_3$), 4.06 (s, 5H, C_5H_5), 4.30 (t, 2H, 3-, 4-position of C_5H_4–), 4.70 (t, 2H, 2-, 5-position of C_5H_4–), 6.37 (s, 1H, olefinic proton); MS(70 eV), *m/e*, 328(M^+). Found: C, 58.10; H, 4.95%. Calcd for $C_{16}H_{16}O_4Fe$: C, 58.57; H, 4.88%, M, 328.

3b and **4b** were obtained in the photoreaction of **1** with **2b**. **3b** and **4b** were obtained as a mixture and further separation was not possible. NMR(mixture in CCl_4), δ(ppm from TMS) 3.71(s, 3H, $-CH_3$ of ester **4b**), 3.87(s, 3H, $-CH_3$ of ester **3b**), 4.13(s, 5H, C_5H_5 of **4b**), 4.19(s, 5H, C_5H_5 of **3b**), 4.3—4.6(6H, C_5H_4– of **3b**, and H_2, and H_5 of C_5H_4– of **4b**), 4.74(t, 2H, H_3, H_4 of C_5H_4– of **4b**), 5.34 (s, 1H, olefinic proton of **3b**), 6.08(s, 1H, olefinic proton of **4b**); IR(mixture, KBr) 3490, 3390, 1630, 1550 cm^{-1} (NH_2 of primary amide), 1665 cm^{-1} (C=O of amide), 1715 cm^{-1} (C=O of ester), 3080, 1600, 780 cm^{-1} (C=C), 1100, 1000, 830 cm^{-1} (monosubstituted ferrocene).

3c and **4c** were obtained only when the acetic acid solution of **1** and **2c** was irradiated at 35—40 °C. As the isolation of **3c** and **4c** was not possible, the assignment and the quantitative analysis were done based on the NMR spectra of the mixture. NMR(mixture in CCl_4), δ(ppm from TMS) 4.24 (s, 5H, C_5H_5 of **4c**), 4.26(s, 5H, C_5H_5 of **3c**), 4.49 (t, 2H, H_2, H_5 of C_5H_4– of **4c**), 4.60(t, 2H, H_2, H_5 of C_5H_4– of **3c**), 4.94(t, 2H, H_3, H_4 of C_5H_4– of **4c**), 5.05(t, 2H, H_3, H_4 of C_5H_4– of **3c**), 5.72(s, 1H, olefinic proton of **3c**), 6.45(s, 1H, olefinic proton of **4c**); IR(direct) 3080, 1605, 770 cm^{-1} (C=C), 2210 cm^{-1} (–C≡N), 1105, 1030, 990(sh) cm^{-1} (monosubstituted ferrocene).

4d was obtained in the photoreaction of **1** with **2d** in acetic acid–water solution. As a main product, **4d** was obtained from TLC. NMR(CCl_4), δ(ppm from TMS) 2.12 (s, 3H, $-CH_3$), 3.81 (s, 3H, $-CH_3$ of ester), 4.10 (s, 5H, C_5H_5), 4.32 (s, 4H, C_5H_4–), 6.17 (s, 1H, olefinic proton). IR(KBr), 1725 cm^{-1} (C=O), 1580 cm^{-1} (C=C), 1100, 1000 cm^{-1} (ferrocene).

References

1) T. Akiyama, Y. Hoshi, S. Goto, and A. Sugimori, *Bull. Chem. Soc. Jpn.*, **46**, 1851 (1973).
2) P. Singh, *J. Org. Chem.*, **37**, 836 (1972).
3) T. Koenig and H. Fischer, "Free Radicals," Vol. 1, ed by J. K. Kochi, John Wiley & Sons, New York, N. Y. (1973), p. 157.
4) D. Bryce-Smith, R. Deshpande, A. Gilbert, and J. Grzonka, *J. Chem. Soc., Chem. Commun.*, **1970**, 561.
5) A. T. Bromquist and E. C. Winslow, *J. Org. Chem.*, **10**, 149 (1945).

BULLETIN OF THE CHEMICAL SOCIETY OF JAPAN, VOL. 50 (5), 1351—1352 (1977)

The Elimination Reaction of Chlorobutane over Some Molten Salts*

Shōichi KIKKAWA, Masakatsu NOMURA, and Takashi IKEUCHI
Department of Applied Chemistry, Faculty of Engineering, Osaka University, Yamadakami, Suita, Osaka 565

(Received September 16, 1976)

Synopsis. The elimination reactions of hydrogen chloride from 1-chlorobutane and 2-chlorobutane over molten salts ($ZnCl_2$, $SnCl_2$, CuCl melts) have been studied by using both a microreactor and a conventional flow reactor. The preferential formation of *cis*-2-butene in the reaction of 2-chlorobutane can be explained in terms of the stereochemistry of the surface-adsorbed carbonium ion.

Some molten salts, such as $SnCl_2$–KCl and $ZnCl_2$-containing melts, are known to assist the dehydrohalogenation of alkyl halides.[1–4] However, little is known about the stereochemistry of dehydrohalogenation over molten-salt catalysts. The present investigation was undertaken in order to obtain stereochemical information about the dehydrochlorination of chlorobutanes over $ZnCl_2$–KCl–NaCl melts, $SnCl_2$–KCl melts, and CuCl–KCl melts from the butene isomer-distribution and in order to discover a convenient method of using the pulse technique[5] for such a dehydrochlorination.

Results and Discussion

Elimination by Microcatalytic Reaction. The contact time of reactants with molten-salt catalysts was arbitrarily defined to be the reciprocal of the flow rate of hydrogen (F^{-1} s/ml), where various flow velocities were attained by varying the flow rate of the hydrogen carrier gas. The conversion percentage of 2-chlorobutane is plotted as a function of F^{-1} at 250 °C and 280 °C in Fig. 1, where the ratio of % conv with the $ZnCl_2$ melts to that with the $SnCl_2$ melts is shown to be about 10 to 1 (at 250 °C), while this conversion ratio is about 2—3 to 1 in the case of the ratio of the $SnCl_2$ melts to the CuCl melts (280 °C). Therefore, the relative activities for dehydrochlorination are $ZnCl_2 \gg SnCl_2 >$ CuCl melts.

The distribution of butene isomers over three kinds of molten salts are shown in Table 1, where the values of the thermal reaction and the equilibrium values are also cited for comparison. Although the % conv varied markedly from melt to melt, the *cis*/*trans* ratios (cited in Table 1) of 2-butene produced are much the same (1.3—1.4) over the series of melts. To examine the possibility of the isomerization of the olefins after elimination, the pulses of 1-butene and 2-butene isomers were passed over the $ZnCl_2$ melts.[6] However, no isomerization among the 1-, *cis*-2-, and *trans*-2-butenes was observed. The *cis*/*trans* ratio of the 2-butene produced over these salts is larger than the equilibrium values; this preferable formation of *cis*-2-butene is considered to be characteristic of this reaction.

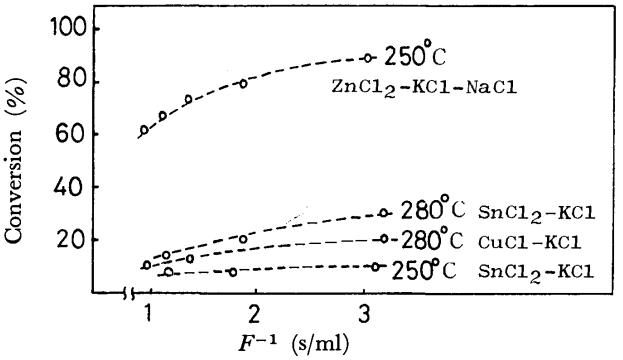

Fig. 1. Plots of % conv. of 2-chlorobutane *vs.* F^{-1}.

The reactivity of 1-chlorobutane over these molten salts becomes considerably lower than that of 2-chlorobutane. With $ZnCl_2$ melts, the % conv of 2-chlorobutane is 25 times as large as that of 1-chlorobutane, while the reactivity ratio of 2-chlorobutane/1-chlorobutane becomes about 9 in the case of the $SnCl_2$ melts. The relative catalytic activity of these melts for the de-

Table 1. Elimination reaction of 2-chlorobutane

Melts[a]		$ZnCl_2$-KCl-NaCl[b] (3 : 1 : 1)		$SnCl_2$-KCl[c] (1.5 : 1)		CuCl-KCl[d] (1.8 : 1)		Homogeneous reaction in gas phase[e]		Equilibrium		
Temp (°C)		205	250	290	350	280	320	400	450	200	300	400
Products (%)	1-butene (%)	9.8	10.8	7.9	12.8	11.1	11.9	39.3	37.4	13	19	23
	trans-2-butene (%)	37.4	37.3	39.8	38.6	38.1	37.3	38.6	36.3	55	50	46
	cis-2-butene (%)	52.8	51.9	52.3	48.6	50.8	50.7	22.1	26.3	32	31	31
cis/*trans*		1.4	1.4	1.3	1.3	1.3	1.4	0.57	0.72	0.58	0.62	0.67

a) The figures in parentheses indicate the molar ratio of the components. Hereafter, the melts will be denoted $ZnCl_2$ melts, $SnCl_2$ melts, and CuCl melts respectively. b) F^{-1}: 2.2 s/ml. c) F^{-1}: 3.3 s/ml. d) F^{-1}: 2.5 s/ml. e) F^{-1}: 2.5 s/ml.

* Organic Reaction in Fused Salts. XI.
Part X: S. Kikkawa, M. Nomura, and M. Shimizu, *Chem. Lett.*, **1977**, 317.

TABLE 2. ELIMINATION REACTION OF 1-CHLOROBUTANE

Melts		$ZnCl_2$ Melts[a]		$SnCl_2$ Melts[b]	
Temp (°C)		350	400	370	400
Products (%)	1-butene (%)	15.9	18.7	15.3	16.9
	trans-2-butene (%)	39.7	38.6	39.1	39.5
	cis-2-butene (%)	44.4	42.7	45.6	43.6
Conv (%)		18.8	51.0	15.5	31.9
cis/trans		1.1	1.1	1.2	1.1

a) F^{-1}: 2.78 s/ml. b) F^{-1}: 3.22 s/ml.

TABLE 3. ELIMINATION REACTION OF 1-CHLOROBUTANE AND 2-CHLOROBUTANE[a]

Melts		$ZnCl_2$ Melts	$SnCl_2$ Melts	CuCl-KCl-NaCl (3 : 1 : 1)
1-Chlorobutane (400 °C)				
Products (%)	1-butene (%)	22.2	31.1	41.2
	trans-2-butene (%)	39.4	32.3	27.3
	cis-2-butene (%)	38.4	36.6	31.5
Conv (%)		43.3	21.8	13.0
cis/trans		1.0	1.1	1.2
2-Chlorobutane (300°C)				
Products (%)	1-butene (%)	14.5	12.4	16.7
	trans-2-butene (%)	39.2	38.5	34.8
	cis-2-butene (%)	46.3	49.1	48.5
Conv (%)		62.8	20.9	0.7
cis/trans		1.2	1.3	1.4

a) Flow rate of Ar: 0.056 mol/h. Feed rate of reactant: 0.12 mol/h.

hydrochlorination of 1-chlorobutane was found to be different from that for 2-chlorobutane; that is, the ratio of % conv with the $ZnCl_2$ melts to that with the $SnCl_2$ melts is 2.5 to 1 (at 310 °C).

Table 2 shows the distribution of butene isomers resulting from the reaction of 1-chlorobutane over molten salts. In the last row of Table 2, the *cis/trans* ratios of 2-butene are presented. The preferable formation of 2-butene from 1-chlorobutane indicates that this elimination proceeds *via* a carbonium-ion mechanism involving rearrangement.[3,4]

The finding that *cis*-2-butene is formed in preference to *trans*-2-butene in the reaction of 2-chlorobutane over a series of molten salts can be explained in terms of the stereochemistry of the surface-adsorbed carbonium ion proposed by Noller, with the elimination of chlorobutane over CaO solid catalysts.[7] The secondary carbonium ion is attached to the molten-salt surface, where its most favorable conformation is as is shown in Fig. 2. Accordingly, *cis*-2-butene is preferably formed by sharing a free-electron pair resulting from the removal of H_b(by the chloride ion), with the vacant p orbital at C_2 (preferred path of the lower-energy barrier).

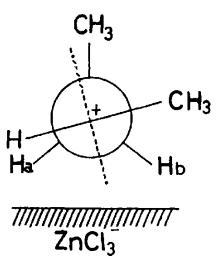

Fig. 2. Molten salts surface-adsorbed carbonium ion. Dotted line shows the vacant p orbital.

Elimination by Conventional Flow Method. Since the present elimination reaction is considered to be first-order, it was expected that the results from the pulse technique would be in agreement with those from the flow method. Table 3 shows the distribution of butene isomers obtained from both 1- and 2-chlorobutane, along with the values of % conv and the *cis/trans* ratios. As Table 3 clearly indicates, no notable differences were observed in the product distribution, the *cis/trans* ratio, or the % conv between the microcatalytic and the steady-state-flow reaction data. That is, in the study of such an elimination reaction over molten salts, the application of this microcatalytic method is of use experimentally. However, with the flow method, there was a tendency for the $ZnCl_2$ melts to have lower *cis/trans* ratios of the elimination of 2-chlorobutane compared with the results of the pulse method. This tendency may be explained by considering the small amount of the isomerization of products assisted by the considerable amounts of HCl dissolved in $ZnCl_2$ melts.

Experimental

Reagents. The 1-chlorobutane and 2-chlorobutane were obtained from Wako Pure Chemical Industries, Ltd. along with the three isomers of butene. The metal halides were guaranteed reagents from Nakarai Chemicals.

Apparatus and Procedure. A commercial gas chromatograph was arranged so as to record the amount of the pulse of the reactant (injected by means of a microsyringe, 1 μl) with a Silicone DC 550 column (75 cm) and to separate the products obtained after the reactant had passed over the melts in the reactor using a BMEE column (6 m) at 0 °C. A Pyrex-tube reactor containing the molten salts, immersed in a temperature-controlled salt bath, was connected to the gas chromatograph by means of a six-port valve which also served to dry the molten salt media by passing N_2 through before carrying out the pulse reaction.

For conventional flow experiments,[8] a vapor mixture of Ar and chlorobutane was bubbled up through dry molten salts for a period of 30 min. An Ar flow containing vaporized products was introduced, from the exit side, to the gas sampler once every 15 min. The gas-chromatographic separation of the products was done with a BMEE column (6 m).

References

1) W. Sundermeyer, *Angew. Chem. Int. Ed. Engl.*, **4**, 222 (1965).
2) S. Kikkawa, T. Hayashi, and T. Yamada, *Kogyo Kagaku Zasshi*, **74**, 1818 (1971).
3) C. N. Kenney and R. Takahashi, *J. Catal.*, 22, 16 (1971).
4) R. A. Bailey and S. F. Prest, *Can. J. Chem.*, **49**, 1 (1971).
5) T. Hattori and Y. Murakami, *J. Catal.*, **10**, 114 (1968).
6) In the elimination process of chlorobutane, HCl is produced; it might cause a higher isomerization rate than that observed with the olefins alone. This possibility was eliminated, however, by the finding using the pulse technique that isomerization did not occur among the three isomers under conditions such that HCl remained over the $ZnCl_2$ melts when two 10-μl pulses of the more reactive 2-chlorobutane were passed through.
7) H. Noller, H. Hantsche, and P. Andrew, *J. Catal.*, **4**, 354 (1965).
8) S. Kikkawa, M. Nomura, and M. Ikezaki, *Nippon Kagaku Kaishi*, **1976**, 472.

BULLETIN OF THE CHEMICAL SOCIETY OF JAPAN, VOL. 50 (5), 1353—1354 (1977)

Diorganostannylenes. II. Photolytic Reaction of Diphenyltin with Alkyl Halides

Kazuhiko KOBAYASHI, Kazuko KUNÔ, Mituyosi KAWANISI, and Sinpei KOZIMA*

Department of Industrial Chemistry, Faculty of Engineering, Kyoto University, Sakyo-ku, Kyoto 606

* *Department of Chemistry, School of Liberal Arts and Sciences, Kyoto University, Sakyo-ku, Kyoto 606*

(Received October 5, 1976)

Synopsis. Photolysis of diphenyltin polymer, $(Ph_2Sn)_m$, afforded diphenylstannylene, Ph_2Sn:, which was captured by alkyl halides, R'X, to give the insertion products, $Ph_2R'SnX$. The reactivity of Ph_2Sn: was found to be lower than that of dibutylstannylene, Bu_2Sn:.

In continuation of our investigations of diorganostannylenes,[1-3] the photolytic formation and some reactions of diphenylstannylene have been investigated. Diphenylstannylene, transiently formed, has been efficiently captured by several alkyl bromides and methyl iodide.

A solution of pale yellow diphenyltin, $(Ph_2Sn)_m$,[4] in a large excess of ethyl bromide was irradiated with a high pressure mercury lamp through a pyrex filter at 0 °C to give a mixture of distillable phenyltin bromides: *viz.*, $Ph_2EtSnBr$ (64%), Ph_2SnBr_2 (20%), $PhEtSnBr_2$ (3%), and Ph_3SnBr (2%), together with a trace of undistillable stannoxanes. The major product, $Ph_2EtSnBr$, should be produced by the insertion reaction of diphenyl stannylene, Ph_2Sn: (**2**), into the C–Br bond of ethyl bromide (Eq. 2). The minor disproportionation products, Ph_3SnBr and $PhEtSnBr_2$, could be formed by the photo-induced transposition[1] of the phenyl group and the scrambling of the phenyl and bromide groups, respectively.

$$(Ph_2Sn)_m \xrightarrow{h\nu} [Ph_2Sn:] + (Ph_2Sn)_{m-1} \quad (\mathbf{1} \rightarrow \mathbf{2} + \mathbf{1})$$

$$\text{or } \cdot Sn(Ph_2)-(Sn(Ph_2))_{m-3}-Sn(Ph_2)\cdot \quad (\mathbf{3}) \qquad (1)$$

$$[Ph_2Sn:] \xrightarrow{R'Br} Ph_2R'SnBr \quad (\mathbf{2}) \qquad (2)$$

It is important to note that a considerable amount (20%) of diphenyltin dibromide was obtained. In contrast, photochemical reactions of dibutyltin with alkyl bromides gave only a low yield of dibutyltin dibromide (4%).[1] There seem to be two possible pathways for the formation of diphenyltin dibromide. (i) A part of diphenylstannylene might possess a biradical character (*i. e.*, in a triplet state) and abstract two bromine atoms from ethyl bromide to give the dibromide. Although the spin state of the stannylene cannot be discussed from our present results, the idea of triplet diphenylstannylene could offer one explanation for the formation of diphenyltin dibromide. (ii) Diphenylbromostannyl radical (**5**) formed by the photochemical cleavage of the Sn–Sn bond of the compound (**4**) could

$$\cdot Sn(Ph_2)-(Sn(Ph_2))_{m-3}-Sn(Ph_2)\cdot \longrightarrow Br-Sn(Ph_2)-(Sn(Ph_2))_{m-3}-Sn(Ph_2)-Br \xrightarrow{h\nu}$$

(**3**) (**4**)

$$Br-Sn(Ph_2)-(Sn(Ph_2))_{m-3}\cdot + \cdot Sn(Ph)_2-Br \longrightarrow$$

(**5**)

$$Br-Sn(Ph_2)-(Sn(Ph_2))_{m-3}-Br + Br-Sn(Ph)_2-Br \qquad (3)$$

(**6**)

afford diphenyltin dibromide (Eq. 3). The possible intermediate, 1,2-dibromotetraphenylditin (**4**, $m=3$), could not be found in the reaction products. This compound could be completely consumed to give diphenyltin dibromide according to Eq. 3. This shows that the Sn–Sn bond of the tetraphenylditin compounds (**3**, **4**, $m=3$) could be cleaved by the UV irradiation in the case of diphenyltin derivatives. This is in sharp contrast to the case of dibutyltin, in which 1,2-dibromotetrabutylditin was formed in about 30% yield.[1]

Another noticeable observation in the photolytic reaction of diphenyltin is the lower reactivity of diphenylstannylene compared with that of dibutylstannylene. The lower reactivity of diphenylstannylene might be implied by the following facts: A longer irradiation time was needed to achieve a high conversion, and diphenyltin did not react with alkyl monochlorides. Even after the irradiation of diphenyltin in propyl chloride for 90 min, the insertion product, $Ph_2PrSnCl$, was not detected in the reaction mixture. A low yield (26

TABLE 1. PHOTOCHEMICAL REACTIONS OF $(Ph_2Sn)_m$ WITH R'X

R'X	Yields of products (%)			
	$Ph_2R'SnX$	Ph_2SnX_2	$PhR'SnX_2$	Ph_3SnX
MeI	77	16	0	0
EtBr	64	20	2.6	2.2
PrBr	63	20	3.3	1.8
$BrCH_2Br$[a]	71	27	0	1.7
$ClCH_2Cl$	26	14	11	27

a) Distribution was determined by the integral values in the ^1H-NMR spectrum.

Table 2. Chemical shifts of $Ph_2R'SnX$ in ^{13}C-NMR spectra

$Ph_2R'SnX$	Chemical shifts (ppm) ($CDCl_3$)						
	Ph				R′		
	C_1	C_2	C_3	C_4	C_1	C_2	C_3
Ph_2MeSnI	a)	135.5	128.6	129.8	−3.1	—	—
$Ph_2EtSnBr$	a)	135.8	128.9	130.0	9.6	10.3	—
$Ph_2PrSnBr$	a)	135.9	129.1	130.6	20.0	19.6	18.2
$Ph_2(BrCH_2)SnBr$	a)	136.0	129.1	130.6	10.7	—	—
$Ph_2(ClCH_2)SnCl$	137.6	136.0	129.1	130.8	28.7	—	—

a) Undetected.

%) of the insertion product, $Ph_2(ClCH_2)SnCl$, was obtained in the reaction with dichloromethane.[5]

All the results of the photochemical reactions of diphenyltin with alkyl halides and the ^{13}C-NMR spectral data of the insertion products are listed in Tables 1 and 2, respectively.

Photolysis of diphenyltin has been proved to be a more effective and facile method for the formation of diphenylstannylene than a thermal reaction of diphenyltin.[3] In the thermal reaction, formation of diphenylstannylene was a minor reaction path and various disproportionation reactions predominated.

Experimental

The ^{13}C-NMR spectra were recorded in the pulse Fourier transform mode using a JEOL-FX 60 spectrometer operating at a resonance frequency of 15.03 MHz. The parameters used were: pulse width 8 μs, spectral width 2500 Hz for 8 K data points. Chemical shifts are given in ppm downfield from internal TMS.

The ^1H-NMR spectra were measured in deuteriochloroform with a Varian EM 360 spectrometer operating at 60 MHz.

Gas-liquid chromatography (GLC) was carried out at 230 °C using Apiezon grease L as a stationary phase.

Photolytic Reaction of Diphenyltin with Ethyl Bromide. Yellow crystalline diphenyltin[4] (0.362 g) was dissolved in a large excess of ethyl bromide (8 ml) in a sealed pyrex glass ampoule, and was irradiated with a high pressure mercury lamp (450 W) at 0 °C under nitrogen atmosphere for 80 min. After irradiation, the excess of ethyl bromide was evaporated off to give a viscous liquid. The product was distilled *in vacuo* using a Kugelrohr (bath temperature was up to 200 °C) to give a trace of residue and a colorless distillate (0.813 g) containing $PhEtSnBr_2$, Ph_2SnBr_2, $Ph_2EtSnBr$, and Ph_3SnBr. These bromides were identified by the IR, ^1H-NMR,[3] and ^{13}C-NMR spectra. A part of the distillate was treated with a large excess of methylmagnesium iodide in ether to convert the phenyltin bromides quantitatively into the phenylmethyltin derivatives. Distribution of the products was determined by GLC: $PhEtSnMe_2$: Ph_2SnMe_2 : $Ph_2EtSnMe$: Ph_3SnMe = 2.8 : 24.1 : 69.5 : 2.7. It was confirmed that vacuum distillation caused no noticeable change in the distribution of the products.

The reactions with methyl iodide, propyl bromide, dichloromethane, and dibromomethane were carried out under similar conditions. In the reaction with methyl iodide, the product was treated with ethylmagnesium bromide for the determination of the distribution. In the reaction with dibromomethane, the product was distilled under high vacuum (0.02 Torr) to avoid the thermal decomposition. The distribution was determined by the integral values in the ^1H-NMR spectrum, since the methylation of $Ph_2(BrCH_2)SnBr$ with methylmagnesium iodide gave undetectable compounds on GLC analysis.

References

1) Part I: S. Kozima, K. Kobayashi, and M. Kawanisi, *Bull. Chem. Soc. Jpn.*, **49**, 2837 (1976).

2) K. Sisido, S. Kozima, and T. Isibasi, *J. Organomet. Chem.*, **10**, 439 (1967).

3) K. Sisido, T. Miyanisi, K. Nabika, and S. Kozima, *J. Organomet. Chem.*, **11**, 281 (1968).

4) H. G. Kuivila, A. K. Sawyer, and A. G. Armour, *J. Org. Chem.*, **26**, 1426 (1961).

5) Dichloromethane was found to be a more efficient trapping reagent of dibutylstannylene.[1]

BULLETIN OF THE CHEMICAL SOCIETY OF JAPAN, VOL. 50 (5), 1355—1356 (1977)

The Effect of Crown Ethers on the Reaction of Alkali Metal Trichloroacetate with Cyclohexene under Decarboxylative Conditions

Kenjiro IDEMORI, Makoto TAKAGI, and Tsutomu MATSUDA
Department of Organic Synthesis, Faculty of Engineering, Kyushu University, Hakozaki, Higashi-ku, Fukuoka 812

(Received October 20, 1976)

Synopsis. The reaction between alkali metal trichloroacetate and cyclohexene was studied in an aprotic medium in the presence and also in the absence of crown ethers. The crown ethers catalyzed decarboxylation but reduced the yield of the dichlorocarbene adduct.

Since the discovery of crown ethers and their metal complexes, numerous applications in organic chemistry have been worked out, in particular on the activation of anionic species as regards synthetic problems.[1] The anionic activation through complexation of alkali metal cations by crown ethers has been confirmed by the enhancement of nucleophilicity and basicity. However, recent studies show a variation of anionic activation, in which decarboxylation of certain alkali metal carboxylates is greatly accelerated. Hunter *et al.*[2] decarboxylated sodium 3-(9-fluorenylidene)-2-phenylacrylate in THF in the presence of dibenzo-18-crown-6 (I), and Smid *et al.*[3] described the decarboxylative rearrangement of potassium 6-nitrobenzisoxazole-3-carboxylate in aqueous media under the catalysis of a polymer crown, poly(vinylbenzo-18-crown-6). These works prompted us to examine the catalytic effect of crown ethers on the decarboxylation of alkali metal trichloroacetates, which has a synthetic utility to generate dichlorocarbene under neutral conditions.[4,5]

Results and Discussion

The reaction of alkali metal trichloroacetate with cyclohexene under decarboxylative conditions (Eq. 1) was studied in a suspension or solution in aprotic solvent using a thermostatted cell fitted with a small reflux condenser at 50—80 °C with and without added crown ether. The reaction was monitored by measuring

$$CCl_3COOM \xrightarrow[\Delta]{-CO_2} CCl_3M \xrightarrow{-MCl} :CCl_2$$

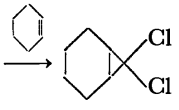

(M=Li, Na, K) (1)

the volume of evolved gas and analyzing the reaction mixture directly on GLC for 7,7-dichloronorcarane. In a typical run, 1.0 g of trichloroacetate salt, 2.6 g of cyclohexene (a large excess), 10 ml of appropriate solvent and 5—20 mol% (based on the salt) of crown ether (I, benzo-15-crown-5 (II) and dicyclohexyl-18-crown-6(III)) were utilized under anhydrous conditions. After the salt had been dried in the thermostatted cell under reduced pressure for 30 min, cyclohexene and the solvent were introduced into the cell, which was then connected to a gas burette, and the mixture was vigourously stirred magnetically. Crown ether dissolved in a solvent was used.

Reaction in the Absence of Crown Ether. The decarboxylation of potassium trichloroacetate at 80 °C was almost complete (>90% of the theoretical amount according to Eq. 1) within 30 min in acetonitrile and 1,2-dimethoxyethane (DME), while in benzene only 20% decarboxylation was observed after 5 h. As a solvent acetonitrile was at least four times more effective than DME when the reaction was carried out at 70 °C. Sulfolane behaved similarly to acetonitrile. The formation of dichloronorcarane paralleled the time course of the decarboxylation, but the yield remained at≈50% after 30 min (and for the rest of the reaction time) in acetonitrile and DME, and only at 2% (or 10% based on the salt decomposed) after 5 h in benzene. While the former yields are comparable to those originally reported by Wagner for the sodium salt in DME,[4] the extremely low yield in benzene is obviously caused by the insolubility of the salt, where decarboxylation took place in the suspended solid. The effect of cations (Li^+, Na^+, K^+) studied in acetonitrile (70 °C) and DME (80 °C)* showed that the initial rate of decarboxylation and the carbene adduct formation were in the increasing order of $K^+ > Na^+ > Li^+$ in line with previous results.[5] A difference of several times the magnitude of rates was observed between adjacent cations. Decomposition is accelerated when the anion is less tightly bound to cations of larger ionic radius. The enhanced reactivity in acetonitrile as compared with DME is also in line with the medium effect expected on the structure of ion pairs in aprotic medium.[2] However, it was noticeable that the final yield in the adduct was not proportional to the ease of decarboxylation. As an example, lithium salt in acetonitrile at 70 °C attained 80% decarboxylation and 60% yield of 7,7-dichloronorcarane in 5 h, and the reaction was still in progress. On the other hand, the reaction was complete for potassium and sodium salts well within a half hour, but the yields of the carbene adduct were 52 and 55% respectively.

Effect of Crown Ethers. The effect of added crown ethers in acetonitrile or DME was found to proceed in two ways, *i.e.*, a rate acceleration (both in decarboxylation and carbene adduct formation) and a decrease in the final yield of the carbene adduct. The rate increase in the initial phase of the reaction in the presence of 20 mol % of II ranged from two to

* Solubility of the salts in the solvents was in the order Li>Na>K. Lithium and sodium salts essentially gave uniform solutions.

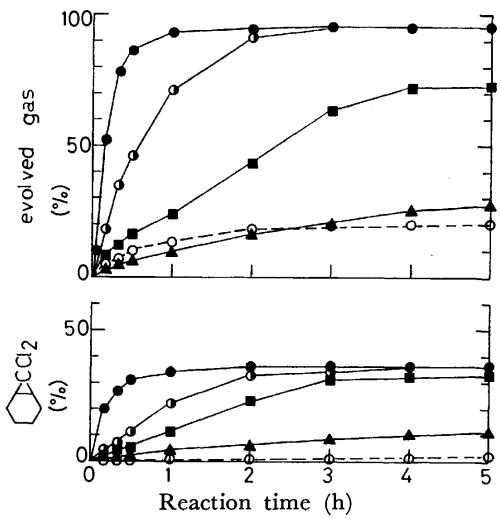

Fig. 1. Decarboxylation of potassium trichloroacetate in benzene (80 °C). Benzene, 10 ml; cyclohexene, 2.6 g; CCl_3CO_2K, 1.0 g(5.0 mmol). —▲— I(0.3 mmol); —■— II(1.0 mmol); —●— III(1.0 mmol); —◑— III(1.0 mmol), without benzene, cyclohexane 10 ml; --○-- without crown ether.

nine times of that in the case of its absence depending on the cation and the solvent. The rate increase was sufficient to lower the practical reaction temperature by 10—20 °C. However, the advantage was counterbalanced by the decrease in the yield of the adduct to two thirds of those in the case of the absence of crown ethers. The effect of crown ethers in benzene was much more pronounced. On addition of 20 mol % of III the reaction effectively approximated that in DME, as shown in Fig. 1. Even the reaction in cyclohexene (as both reactant and solvent) was successful. Obviously the crown ethers functioned as a solid-liquid phase-transfer catalyst.[1] In line with a similar observation on the effect of alkali metal ions, the trichloroacetate ion which is less tightly bound to the cation or freed from the cation by the intervention of crown ether decarboxylates more readily, but it introduces some unfavorable effects on the subsequent carbene formation and its reaction to form the adduct. The exact nature of these effects is not clear at present in view of the complexity of the side reactions involved in the carbene-generating system.[5,6] Decarboxylation on alkali metal trichloroacetate in aprotic medium was accelerated considerably by the cation complexation with crown ethers, but the extent was far less than the cases in which the resulting anions were strongly resonance-stabilized.[2,3,7,8] The acceleration of decarboxylation was counterbalanced by the reduced yield of dichlorocarbene adduct, thus diminishing the synthetic utility of crown ethers in the system.

References

1) G. W. Gokel and H. D. Durst, *Synthesis*, **1976**, 168.
2) D. H. Hunter, W. Lee, and S. K. Sim, *J. Chem. Soc., Chem. Commun.*, **1974**, 1018.
3) J. Smid, S. Shah, L. Wong, and J. Hurley, *J. Am. Chem. Soc.*, **97**, 5932 (1975).
4) W. M. Wagner, *Proc. Chem. Soc., London*, **1959**, 229.
5) W. Kirmse, "Carbene Chemistry," 2nd ed, Academic Press, New York, N. Y. (1971), p. 137.
6) E. V. Dehmlow, *Tetrahedron Lett.*, **1976**, 91, and the literature cited therein.
7) D. S. Kemp and K. G. Paul, *J. Am. Chem. Soc.*, **97**, 7305 (1975).
8) D. S. Kemp, D. D. Cox, and K. G. Paul, *J. Am. Chem. Soc.*, **97**, 7312 (1975).

BULLETIN OF THE CHEMICAL SOCIETY OF JAPAN, VOL. 50 (5), 1357—1358 (1977)

The Preparation of 3,5-Diacetoxy-1-cyclopentene[1)]

Seizi KUROZUMI, Takeshi TORU,* Toshio TANAKA, Shuji MIURA, Makiko KOBAYASHI, and Sachio ISHIMOTO

Institute for Biomedical Research, Teijin Ltd., Asahigaoka, Hino, Tokyo 191

(Received November 8, 1976)

Synopsis. The phase-transfer reaction of 3,5-dibromo-1-cyclopentene with potassium acetate was studied using trialkylamines and a trialkylphosphine as catalysts. Various metal acetates were examined for their effects in this reaction.

We recently reported[2)] on the nucleophilic substitution reaction of alkyl bromides with potassium acetate employing a quaternary ammonium ion catalyst in a heterogeneous system. This phase-transfer reaction provided a convenient synthetic method for acetates from the corresponding bromides besides previously developed methods using silver acetate, tetraethylammonium acetate, or potassium acetate in glacial acetic acid and acetic anhydride.[2)] Thus, *cis*-3,5-diacetoxy-1-cyclopentene **2** was prepared from *cis*-3,5-dibromo-1-cyclopentene **1**, 4-acetoxy-2-cyclohexen-1-one from 4-bromo-2-cyclohexen-1-one, and octyl acetate from octyl bromide. In the course of the study of the synthesis of prostaglandins, we succeeded

$$RX \xrightarrow[KOAc]{\text{phase-transfer catalyst}} ROAc$$

in converting the diacetate **2** into chiral 4-hydroxy-2-cyclopenten-1-one,[3,4)] which is a key intermediate to prostaglandins[5)] and their mimics.[6)] Furthermore, it was reported that the diacetate **2** was effectively transformed into a useful lactone intermediate for the synthesis of prostaglandins.[7)] 4-Cyclopentene-1,3-diol, which is easily accessible from the diacetate **2** is also a useful precursor for the synthesis of prostaglandins[8)] and their intermediates.[9)] These results led us to study the phase-transfer reaction of 3,5-dibromo-1-cyclopentene **1** indetail and to extend the scope of the reaction using i) various catalysts and ii) various metal acetates.

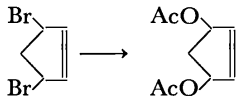

1 **2**

Quaternary ammonium and phosphonium salts are well known to be good catalysts in phase-transfer reactions.[10)] Tertiary amines have also been reported to be effective for the dichlorocarbene generation.[11)] More recently, it has been reported that tertiary amines as well as primary and secondary amines catalyzed the nucleophilic conversion of alkyl bromides into alkyl cyanides.[12)] Tertiary amines also catalyzed the alkylation of the α-carbon attached to the carbonyl group with alkyl halides.[13)] We first carried out the nucleophilic substitution reaction of 3,5-dibromo-1-cyclopentene[14)] with potassium acetate in mixtures of water and carbon tetrachloride, using either trioctyl- or tridecylamines. These reactions resulted in the formation of the diacetate **2** in moderate yields (see Table 1).

TABLE 1. PHASE-TRANSFER REACTIONS OF 3,5-DIBROMO-1-CYCLOPENTENE WITH POTASSIUM ACETATE

Catalyst	Yield[a)] of 3,5-diacetoxy-1-cyclopentene
Trioctylphoshine	58%
Trioctylamine	49
Tridecylamine	55

a) Isolated yield.

To our knowledge, it has not been reported that trialkylphosphines catalyze the nucleophilic substitution reaction in a heterogeneous system. We were interested to examine the possibility of trialkylphosphines as phase-transfer catalysts, because trialkylphosphines are known[15)] to react with alkyl halides, *e.g.*, in refluxing benzene, to form tetraalkylphosphonium salts, which could be catalysts for our reaction. In fact, the phase-transfer reaction of the dibromide **1** with potassium acetate, using trioctylphosphine as a catalyst, proceeded to give the acetate **2** in a 58% yield (Table 1).

In order to examine the effect of metal acetate, phase-transfer reactions were studied using various metal acetates, such as the Group I, II, VII, and VIII metal acetates. Trioctylpropylammonium chloride was used as the catalyst. The results are summarized in Table 2. It is interesting that magnesium acetate and alkali metal acetates were among the most effective acetates. Since magnesium, lithium, and sodium acetates have a higher solubility in water than the other acetates[16)] listed in Table 2, our results suggest that the solubility of the metal acetate in the aqueous phase plays an important role this phase-transfer reaction.

Experimental

Using Trioctylphosphine. A mixture of 3,5-dibromo-1-cyclopentene **1** (45.2 g, 0.2 mol), potassium acetate (99 g, 1 mol), and trioctylphosphine (14.8 g, 0.04 mol) in carbon tetrachloride (120 ml) and water (45 ml) was vigorously stirred at 60 °C for 5 h. The reaction mixture was then extracted with carbon tetrachloride (3×30 ml), dried, and evaporated. The residue was distilled to give 3,5-diacetoxy-1-cyclopentene **2** (21.3 g; 58% yield): bp 70.5 °C/0.08 Torr.

Using Trioctylamine. A mixture of the dibromide **1** (151 g, 0.67 mol), potassium acetate (300 g, 3 mol), and trioctylamine (10 g, 0.029 mol) in carbon tetrachloride (400 ml) and water (150 ml) was vigorously stirred at 60 °C for 12 h. The mixture was then treated as above to give the diacetate **2** (68.7 g; 55% yield).

Table 2. Phase-transfer reactions of dibromide **1** with various metal acetates in the presence of $(C_8H_{17})_3C_3H_7N^+Cl^-$ [a]

Metal acetate, g (mmol)		Solvent		Reaction conditions		Yield[b] of diacetate **2**	Solubility[c]
		H_2O	CCl_4				
$LiOAc \cdot 2H_2O$	10.2 (100)	6 ml	15 ml	70°C	5 h	52%	300
$NaOAc \cdot 3H_2O$	4.1 (30)	2	6	60	4	37	76
$Mg(OAc)_2 \cdot 4H_2O$	6.4 (30)	4	8	60	18	35	120
$Ca(OAc)_2$	2.6 (30)	3.5	6	60	6	8	37
$Ba(OAc)_2$	7.6 (15)	4	7	60	6	14	59
$Cu(OAc)_2 \cdot H_2O$	6.0 (30)	6	15	60	3	15	**7**
$Zn(OAc)_2 \cdot 2H_2O$	6.6 (30)	10	25	60	3	13	31
$Mn(OAc)_2 \cdot 4H_2O$	7.4 (30)	10	25	70	5	17	—
$Co(OAc)_2 \cdot 4H_2O$	7.5 (30)	10	25	70	3	15	—
$Pb(OAc)_2 \cdot 3H_2O$	11.4 (30)	3	7	60	6	9	46

a) All the reactions were carried out using 2.26 g (10 mmol) of 3,5-dibromo-1-cyclopentene **1** and 0.86 g (2 mmol) of trioctylammonium chloride. The reaction conditions and yields are not optimized.
b) Isolated yield. c) Solubility in grams per 100 ml in cold water.[16]

Using Tridecylamine. The dibromide **1** (54 g, 0.139 mol), potassium acetate (90 g, 0.9 mol), tridecylamine (5.9 g, 0.014 mol), water (45 ml), and carbon tetrachloride (120 ml) were used. The yield of the acetate **2** was 21.6 g (49%).

Using Various Metal Acetates. The reactions were carried out substantially as has been described above under the conditions summarized in Table 2.

The authors are grateful to Drs. T. Noguchi and S. Tsunoda of Teijin, Ltd., for their encouragement throughout the course of this work.

References

1) Prostaglandin Chemistry X. Part IX: *Chem. Lett.*, **1976**, 1341.
2) T. Toru, S. Kurozumi, T. Tanaka, S. Miura, M. Kobayashi, and S. Ishimoto, *Synthesis*, **1974**, 867, and references cited therein.
3) a) S. Miura, S. Kurozumi, T. Toru, T. Tanaka, M. Kobayashi, S. Ishimoto, and S. Matsubara, *Tetrahedron*, **32**, 1893 (1976); b) T. Tanaka, S. Kurozumi, T. Toru, S. Miura, M. Kobayashi, and S. Ishimoto, *ibid.*, **32**, 1713 (1976).
4) This chiral compound has also been prepared from a chiral precursor. K. Ogura, M. Yamashita, and G. Tsuchihashi, *Tetrahedron Lett.*, **1976**, 759.
5) G. Stork and M. Isobe, *J. Am. Chem. Soc.*, **97**, 4745, 6260 (1975).
6) a) T. Tanaka, S. Kurozumi, T. Toru, M. Kobayashi, S. Miura, and S. Ishimoto, *Tetrahedron Lett.*, **1975**, 1535; b) *Tetrahedron* in press.
7) S. Takano, K. Tanigawa, and K. Ogasawara, *J. Chem. Soc., Chem. Commun.*, **1976**, 189.
8) J. Fried, C. H. Lin, J. C. Sih, P. Dalven, and G. F. Cooper, *J. Am. Chem. Soc.*, **94**, 4342 (1972).
9) K. Kondo, M. Matsumoto, and F. Mori, *Angew. Chem.*, **87**, 109 (1975).
10) For a review, see J. Dockx, *Synthesis*, **1973**, 441.
11) a) K. Isagawa, Y. Kimura, and S. Kwon, *J. Org. Chem.*, **39**, 3171 (1974); b) M. Makosza, A. Kacprowica, and M. Fedorynski, *Tetrahedron Lett.*, **1976**, 2119.
12) W. P. Reeves and M. R. White, *Synth. Commun.*, **6**, 193 (1976).
13) R. Fornasier and F. Montanari, *Tetrahedron Lett.*, **1976**, 1381.
14) L. N. Owen and P. N. Smith, *J. Chem. Soc.*, **1952**, 4035.
15) A. Maercker, "Organic Reactions," Vol. 14, ed by A. C. Cope, J. Wiley & Sons (1965), p. 388.
16) R. C. Weast, "Handbook of Chemistry and Physics," 55th ed, 1974—1975, CRC Press, p. C-75.

BULLETIN OF THE CHEMICAL SOCIETY OF JAPAN, VOL. 50 (5), 1359—1360 (1977)

Synthesis of Some Imidazo[1,2-*c*][1,2,3]triazolo[4,5-*e*]pyrimidines

Takashi SUGIMOTO and Sadao MATSUURA

College of General Education, Nagoya University, Chikusa-ku, Nagoya 464

(Received December 13, 1976)

Synopsis. The reaction of 7-amino[1,2,3]triazolo-[4,5-*d*]pyrimidine (**1a**) with chloroacetaldehyde gave imidazo-[1,2-*c*][1,2,3]triazolo[4,5-*e*]pyrimidine (**2a**) which underwent facile ring opening in dilute hydrochloric acid. The methyl derivatives (**2b,c,d**) were similarly made from the appropriate triazolopyrimidine (**1b,c,d**) and chloroacetaldehyde.

The isolation and structural elucidation of the fluorescent imidazo[1,2-*a*]purines from baker's yeast ^{Phe}t-RNA[1] and *T. utilis* ^{Phe}t-RNA[2] has aroused considerable interest in the chemistry and biology of fused tricyclic compounds derived from the common base residues of nucleic acids. At about the same time, Kost and his co-workers reported that the reaction of 9-methyladenine with chloroacetaldehyde gave fluorescent 3-methylimidazo[2,1-*i*]purine.[3] The ribonucleoside and ribonucleotides of imidazo[2,1-*i*]purine have been synthesized and their activities in several enzymatic systems reported.[4] It has also been shown that two fluorescent substances derived from N^6-(3-methyl-2-butenyl)adenosine, a clinically useful antileukemic agent, were members of the imidazo[2,1-*i*]purine series.[5] This finding prompted us to investigate the synthesis of analogous ring systems with a view to possible biological activities. In the present paper, we describe the synthesis of certain imidazo[1,2-*c*]-[1,2,3]triazolo[4,5-*e*]pyrimidines.

Treatment of 7-amino[1,2,3]triazolo[4,5-*d*]pyrimidine (**1a**)[6] with chloroacetaldehyde in aqueous ethanol in the presence of sodium acetate gave the fluorescent imidazo[1,2-*c*][1,2,3]triazolo[4,5-*e*]pyrimidine (**2a**) in moderate yield. The ^{1}H NMR spectrum of **2a** in TFA exhibited a pair of doublets at δ 8.25 and 8.62 (J= 2.0 Hz) representing protons at the 7- and 8-position, and a singlet at δ 9.77 for 5-H. Similarly, the condensation of 7-amino-5-methyl[1,2,3]triazolo[4,5-*d*]pyrimidine (**1b**)[7] with chloroacetaldehyde gave 5-methylimidazo[1,2-*c*][1,2,3]triazolo[4,5-*e*]pyrimidine (**2b**). This compound showed UV spectra very similar to those of **2a**; also a singlet at δ 3.82 and a pair of doublets at δ 8.28 and 8.42 (J=2.0 Hz) in its ^{1}H NMR spectrum.

When **2a** was treated with dilute hydrochloric acid, its fluorescence disappeared and a ring-opened product, 4-amino-5-(2-imidazolyl)-1,2,3-triazole (**3**) was obtained. The same compound was formed also, but more slowly, when **2a** was boiled in water. The structure of **3** was derived from elemental analysis, UV spectra, and a ^{1}H NMR spectrum exhibiting a sharp singlet at δ 7.48 for both 4- and 5-H of the imidazole ring. This ring opening took place most probably by nucleophilic addition of water at the 5,4-double bond. Therefore, a compound such as **2b**, with a blocking methyl group[8] at the site of potential addition, is expected to resist ring opening. In fact, no ring opening was detected when **2b** was treated with hydrochloric acid as above.

3-Methyl-(**2c**) and 3,5-dimethyl-imidazotriazolopyrimidines(**2d**) were made similarly from 3-methyl- and 3,5-dimethyl-7-aminotriazolopyrimidine(**2c** or **d**) respectively.

We also investigated the reaction of **1a** with bromoacetone. Under a variety of conditions, the reaction gave 7-acetonylamino[1,2,3]triazolo[4,5-*d*]pyrimidine(**4a**) as a main product; several minor products were formed, but no imidazotriazolopyrimidine was detected. The structure of **4a** was confirmed by elemental analysis and by UV spectra which were very similar to those of **1a**. Its ^{1}H NMR spectrum showed singlets at δ 2.63(CH_3), δ 5.93(CH_2), and δ 8.80 (the aromatic proton of the pyrimidine ring). The reaction of **1b** with bromoacetone took place in a similar manner to give the 5-methyl compound(**4b**) without any imidazotriazolopyrimidine.

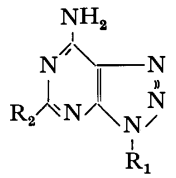

1

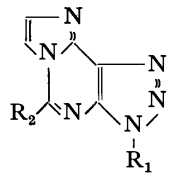

2

	a	b	c	d
R_1	H	H	CH_3	CH_3
R_2	H	CH_3	H	CH_3

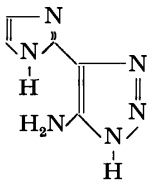

3

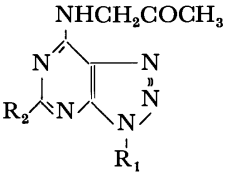

4

Experimental

The elemental analyses were done by the Analytical Section, Meijo University, Nagoya. The pK_a values were determined by a spectroscopic method and the UV spectra on a JASCO UVIDEC-1 spectrophotometer. The ^{1}H NMR spectra were determined on a JEOL JNM-MH-60 NMR spectrometer in TFA with TMS as an internal standard.

Imidazo[1,2-c][1,2,3]triazolo[4,5-e]pyrimidine (2a). One gram of **1a**, chloroacetaldehyde (0.50 g,) and NaOAc (1.0 g) were heated in 50% aq EtOH (200 ml) under reflux for 2 h. The solution was evaporated to dryness and the residue was chromatographed on a Florisil column (4×40 cm) by gradient elution using 0—1% ammonia (1.0 l). The fluorescent fractions were combined, concentrated to *ca.* 50 ml under reducted pressure, treated with charcoal, and chilled to give colorless needles (1.10 g) of **3a**; mp>300 °C (Found: C,

38.67; H, 3.55; N, 44.87%. Calcd for $C_6H_4N_6$–1.5H_2O: C, 38.50; H, 3.74; N, 44.92%); ^{1}H NMR: δ 8.25(d, J=2.0 Hz, 1), 8.62(d, J=2.0 Hz, 1), and 9.77(s, 1); pK_a 2.46±0.03; λ_{max} (log ε) at pH 0.44: 214(4.35), 270(sh, 3.83), 282(3.88); at pH 5.0: 219(4.32), 235(sh, 4.19), 284(3.82).

*5-Methylimidazo[1,2-c][1,2,3]triazolo[4,5-e]pyrimidine (**2b**).* A solution of **1b**[7] (2.5 g), chloroacetaldehyde (2.0 g), and NaOAc (4 g) were refluxed in 50% aq EtOH (400 ml) for 4 h. Evaporation under reduced pressure and subsequent crystallization from water gave colorless needles (2.0 g) of **2b**; mp>300 °C (Found: C, 48.09; H, 3.27; N, 48.55%. Calcd for $C_7H_6N_6$: C, 48.27; H, 3.45; N. 48.26%); ^{1}HNMR: δ 3.82(s, 3), 8.28(d, J=2.0 Hz, 1), and 8.42(d, J=2.0 Hz, 1); pK_a 2.57±0.02; λ_{max} (log ε) at pH 0.44: 212(4.38), 270(sh, 3.85), 279(3.90); at pH 5.0: 217(4.31), 240(sh, 3.97), 285(3.87).

*4-Amino-5-(2-imidazolyl)-1,2,3-triazole (**3**).* A solution of **2a** (270 mg) in 1M-HCl (20 ml) was kept at 20 °C for 10 h. Evaporation to dryness under reduced pressure and crystallization from EtOH gave colorless needles (145 mg) of **3** as hydrochloride; mp>300 °C (Found: C, 32.45; H, 3.66; N, 44.99%. Calcd for $C_5H_6N_6$–HCl: C, 32.17; H, 3.75; N, 45.04%); ^{1}HNMR: δ 7.48(s); pK_a 8.30±0.03, 5.24±0.03, and −1.39±0.05; λ_{max} (log ε) at H_0 −3.0: 251 (4.05), 295(sh, 3.41); at pH 2.0: 243(3.86), 278(4.10); at pH 6.5: 243(3.87), 277(4.08); at pH 10.5: 215(3.81), 273(4.15).

*3-Methylimidazo[1,2-c][1,2,3]triazolo[4,5-e]pyrimidine (**2c**) and the 3,5-Dimethyl Derivative (**2d**).* 7-Amino-3-methyltriazolopyrimidine[9] (1.0 g), chloroacetaldehyde (2 g) and NaOAc (2 g) were heated in water (300 ml) at 60 °C for 5 h. Evaporation under reduced pressure to *ca.* 20 ml gave **a** solid which was crystallized from MeOH to give colorless needles (0.45 g) of **2c**. The analytical sample was prepared by sublimation at 160 °C/1 Torr; mp 282—283 °C(decomp) (Found: C, 48.57; H, 3.27; N, 47.82%. Calcd for $C_7H_6N_6$: C, 48.27; H, 3.47; N, 48.26%); ^{1}H NMR: δ 4.67(s, 3), 8.25(d, J=2.0 Hz, 1), 8.60(d, J=2.0 Hz, 1), and 9.70(s, 1); pK_a 2.47±0.01; λ_{max} (log ε) at pH 0.44: 219.5(4.38), 263(3.74), 281(3.73); at pH 5.0: 229(4.35), 260(3.60), 298(3.50).

4-Amino-6-chloro-2-methyl-5-nitropyrimidine[10] and 30% methanolic methylamine under reflux gave *the 6-methylamino analogue* in 90% yield; mp 242—243.5 °C (from MeOH) (Found: C, 39.29; H, 4.82; N, 38.23%. Calcd for $C_6H_9N_5O_2$: C, 39.34; H, 4.92; N, 38.25%). The nitropyrimidine (2.0 g) was hydrogenated over Pd/C in 0.5M-HCl (50 ml), and subsequently treated with $NaNO_2$ to give *7-amino-3,5-dimethyl[1,2,3]triazolo[4,5-d]pyrimidine* (**1d**) (1.35 g; colorless needles when recrystallized from water); mp>300 °C (Found: C, 44.13; H, 4.95; N, 51.46%. Calcd for $C_6H_8N_6$: C, 43.89; H, 4.29; N, 51.19%). This compound was treated with chloroacetaldehyde as in the foregoing reaction to give **2d** (95% yield); mp 221—222 °C (sublimed at 160 °C/1 Torr) (Found: C, 51.23; H, 3.91; N, 44.35%. Calcd for $C_8H_8N_6$: C, 51.04; H, 4.29; N, 44.66%); ^{1}H NMR: δ 3.27(s, 3), 4.58(s, 3), 8.20(d, J=2.0 Hz, 1). and 8.37(d, J=2,0 Hz, 1); pK_a 2.65±0.01; λ_{max} (log ε) at pH 0.44: 219(4.41), 268.5 (3.79), 281(3.81); at pH 5.0: 219(4.35), 266.5(3.60), 295.5 (3.65).

*7-Acetonylamino[1,2,3]triazolo[4,5-d]pyrimidine (**4a**) and Its 5-Methyl Derivative(**4b**).* A solution of **1a** (1.0 g) and bromoacetone (2.5 g) in 50% aq EtOH (300 ml) was refluxed for 2 h. Evaporation under reduced pressure and subsequent crystallization from water gave colorless needles (0.50 g) of **4a**; mp> 300 °C (Found: C, 43.63; H, 4.03; N, 43.87%. Calcd for $C_7H_8N_6O$: C, 43.74; H, 4.20; N, 43.73%); ^{1}H NMR: δ 2.63(s, 3), 5.93(s, 2), and 8.80(s, 1), pK_a 2.42±0.01; λ_{max} (log ε) at pH 0.44: 205(4.27), 264(4.09); at pH 4.5: 214 (4.07), 279(4.06).

The 5-methyl derivative (**4b**) was similarly obtained from **1b** in 56% yield; mp>300 °C (Found: C, 46.32; H, 4.85; N, 40.62%. Calcd for $C_8H_{10}N_6O$: C, 46.59; H, 4.90; N, 40.76%); pK_a 3.08±0.02; λ_{max} (log ε) at pH 0.83: 205(4.30), 264(4.10); at pH 5.5: 215(4.22), 277(4.06); ^{1}H NMR: δ 5.82(s, 3), 2.88(s, 3), and 5.87(s, 2).

We thank Miss Noriko Itoh for measuring the pK_a values and UV spectra, Miss Keiko Shibata for measuring the ^{1}H NMR spectra, and Dr. D. J. Brown of Australian National University for discussion.

References

1) K. Nakanishi, N. Furutachi, M. Funamizu, D. Grundeger, and I. B. Weinstein, *J. Am. Chem. Soc.*, **92**, 7617 (1970).

2) H. Kasai, M. Goto, S. Takemura, T. Goto, and S. Matsuura, *Tetrahedron Lett.*, **1971**, 2725.

3) N. K. Kochetkov, V. N. Shibaev, and A. A. Kost, *Tetrahedron Lett.*, **1971**, 1993.

4) J. A. Secrist III, J. R. Barrio, and N. J. Leonard, *Science*, **175**, 646 (1972).

5) G. B. Chheda, S. P. Dutta, A. Mettelman, and L. Baczynskyj, *Tetrahedron Lett.*, **1974**, 433.

6) J. Davoll, *J. Chem. Soc.*, **1958**, 1593.

7) P. Bitterli and H. Erlenmeyer, *Helv. Chim. Acta*, **34**, 835 (1951).

8) for example, D. J. Brown and S. F. Mason, *J. Chem. Soc.*, **1956**, 3443; A. Albert and C. F. Howell, *ibid.*, **1962**, 1591.

9) R. Weiss, R. K. Robins, and C. W. Noell, *J. Org. Chem.*, **25**, 765 (1960).

10) W. R. Boon, W. G. M. Jones, and G. R. Ramage, *J. Chem. Soc.*, **1951**, 96.

Solid-state Reactions between CVD-TiO_2 and $BaCO_3$

Yoko SUYAMA and Akio KATO

Department of Applied Chemistry, Faculty of Engineering, Kyushu University, Hakozaki, Fukuoka 812

(Received July 17, 1976)

The solid-state reactions between CVD-TiO_2 powders of anatase- and rutile-forms with various particle sizes and $BaCO_3$ were investigated in O_2 and CO_2. The reactivity of the TiO_2 powders and the apparent activation energy for the reaction were independent of the crystal type of TiO_2. The reactivity of the TiO_2 powders increased remarkably as the particle sizes grew smaller than 0.15 μm. When such fine CVD-TiO_2 powders were used, the reaction proceeded to completion at temperatures below 1000 °C in both O_2 and CO_2 and gave fine $BaTiO_3$ powders. The particles of $BaTiO_3$ produced appeared single-crystalline and kept a shape similar to that of the starting TiO_2 particle. The sizes of the $BaTiO_3$ particles were controlled by those of the starting TiO_2 and were independent of those of $BaCO_3$.

On the solid-state reactions between TiO_2 and $BaCO_3$, there have been several investigations concerning the effects of the particle size and crystal type of the starting TiO_2 powders on the reactivity.[1,2] In these studies, anatase-TiO_2 powders were produced by wet methods and rutile-TiO_2 powders were prepared by the calcination of anatase-TiO_2 at temperatures above 900 °C. The primary TiO_2-particles aggregated in the powders, especially in calcined rutile-TiO_2 powders. Therefore, it is questionable whether or not the observed reactivities truly represent the effect of the size or crystal type of the primary TiO_2-particles.

On the other hand, both the anatase and rutile-TiO_2 powders produced by vapor-phase reactions (CVD-TiO_2) are characterized by high purity, a very closely controlled particle-size distribution, and easy dispersion, and consist of single-crystalline particles. Therefore, the effects of the size and crystal type of TiO_2-particles on the reactivity are expected to be caught more exactly by using CVD-TiO_2 powders. The present authors have reported that CVD-TiO_2 powders prepared from the $TiCl_4$-O_2 system show a high reactivity in the reaction with $BaCO_3$ and that the resulting $BaTiO_3$ powders consist of particles with the shape of the starting TiO_2 particles.[3]

In the present investigation, in order to elucidate the effects of the crystal type and particle size of TiO_2-particles on the reactivity and the properties of $BaTiO_3$ powders produced, the solid-state reaction between TiO_2 and $BaCO_3$ was carried out by using CVD-TiO_2 powders obtained from the reaction systems of $TiCl_4$-O_2, $TiCl_4$-H_2O, $TiCl_4$-H_2O-H_2, and $TiCl_4$-H_2-CO_2.

Experimental

Materials. The titanium dioxide powders were prepared by vapor-phase reactions, as has been described previously.[4,5] Their properties and electron micrographs are shown in Table 1 and Fig. 1, respectively. The TiO_2 powders obtained from the $TiCl_4$-H_2O-H_2 system consist of nealy spherical or cubic particles smaller than 0.1 μm in size (Figs. 1 (a) and (b)). The TiO_2 powders obtained from the $TiCl_4$-H_2-CO_2 system consist of plate-like particles grown preferentially in the plane perpendicular to the c-axis[5] (Figs. 1 (c) and (e)). The TiO_2 powders obtained from the $TiCl_4$-O_2 system consist of square and plate-like or square-bipyramidal particles grown in the plane perpendicular to the c-axis (Figs. 1 (d) and (f)).

TABLE 1. REACTION SYSTEMS AND THE CHARACTERISTICS OF TiO_2 POWDERS

No.	Reaction system	$D_{50}(D_{10}—D_{90})$ (μ)[a]	S_{BET} (m^2/g)[b]	W_A (%)[c]
a-20	$TiCl_4$-H_2O-H_2	0.05 (0.03—0.07)	—	0
a-15	$TiCl_4$-H_2O-H_2	0.06 (0.04—0.08)	21	5
a-13	$TiCl_4$-H_2O	0.09 (0.05—0.12)	—	52
a-7	$TiCl_4$-H_2O-H_2	0.09 (0.06—0.11)	17	100
A-11	$TiCl_4$-O_2	0.18 (0.13—0.24)	—	100
A-1	$TiCl_4$-O_2	0.37 (0.24—0.46)	8	100
R-22	$TiCl_4$-H_2-CO_2	0.42 (0.29—0.54)	3	0
R-7	$TiCl_4$-H_2-CO_2	1.0 (0.67—1.3)	—	5
D-1	$TiCl_4$-O_2	1.5 (1.1 —1.9)	1	100

a) D_{50}, D_{10}, and D_{90} are the particle sizes at which the weight of particles reaches 50, 10, and 90% respectively on the cumulative weight % distribution curve. b) Specific surface area obtained by the BET method. c) Content of the anatase form.

GR-grade $BaCO_3$ was obtained from Wako Pure Chemical Ind., Ltd. (purity>99.7%).[6] The particles of the $BaCO_3$ powder are needle-like and 0.5—10 μm long. They showed no weight loss when heated to 1000 °C at 5.4 °C/min in O_2.

Solid-state Reactions. Equimolar mixtures of TiO_2 and $BaCO_3$ were prepared by mixing with an ultrasonic wave in absolute ethanol. The mixture of 70—130 mg was heated in a platinum vessel up to 950—1100 °C at 5.4 °C/min in a flow of CO_2-free O_2 or CO_2. The flow rate was about 130—150 ml/min (the I.D. of the reactor was 17 mm). The weight loss caused by the reaction was followed by means of an electrobalance.[7] X-Ray diffraction [Co$K\alpha$] and electron-microscopic analyses of the products were done in the course of the reaction.

Results and Discussion

Thermogravimetric Analysis of Reactions between TiO_2 and $BaCO_3$. The TG curves of equimolar TiO_2-$BaCO_3$ mixtures are shown in Figs. 2 and 3. The reaction begins at about 530 °C, and the weight loss reaches 100% at 930—1010 °C in O_2. As the TiO_2 powders become finer, the reaction proceeds faster and the weight loss reaches 100% at a lower temperature; that is, the reactivity of the TiO_2 powders increases. The decrease in reactivity with the particle size of TiO_2, however, becomes smaller as the particles grow larger. In CO_2, the beginning and completion temperatures of the reaction are higher by 50 to 100 °C than those in

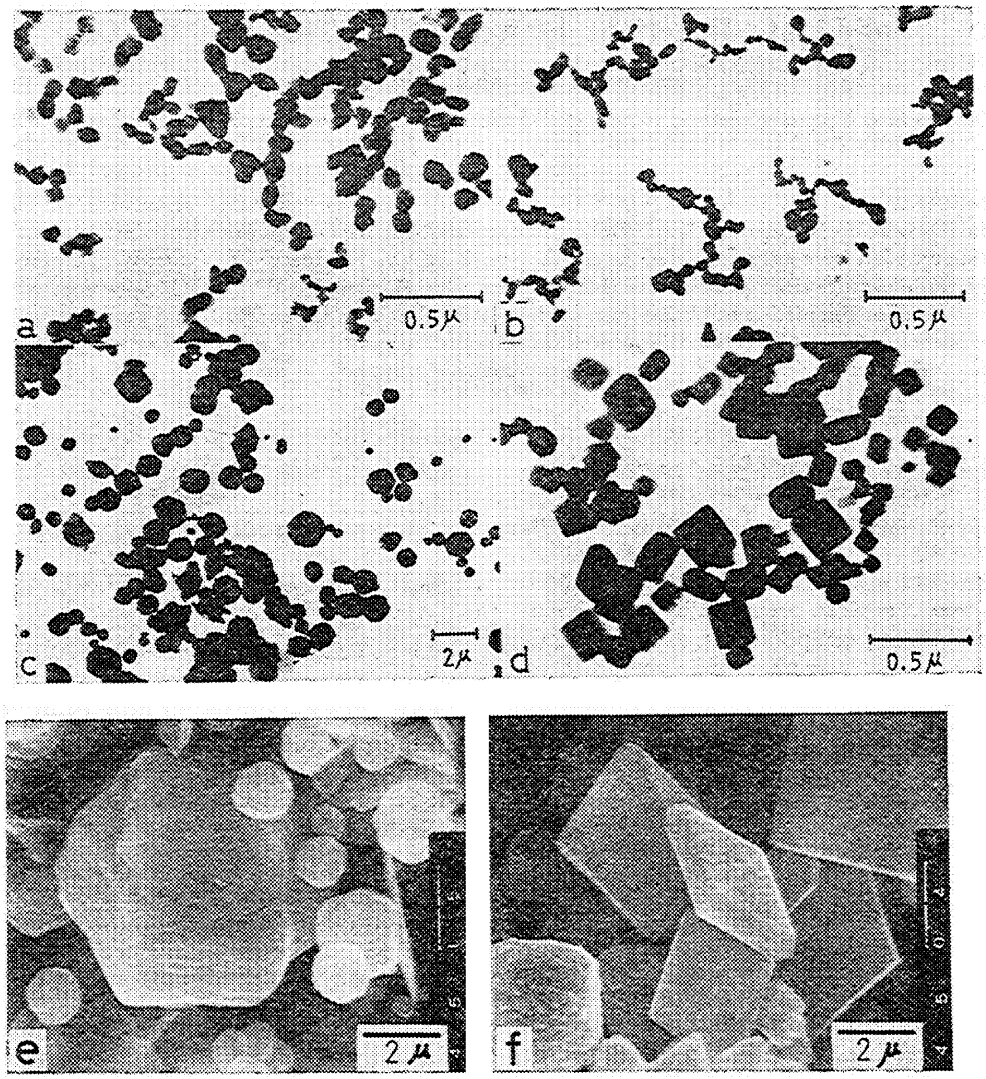

Fig. 1. Electron micrographs of TiO_2 powders.
(a), a-7; (b), a-15; (c) and (e), R-7; (d), A-11; (f), D-1.

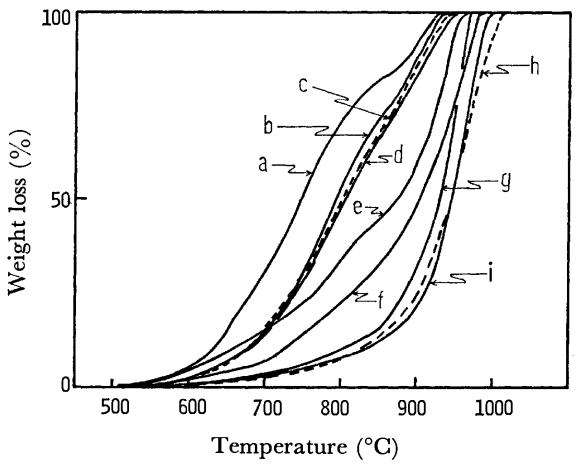

Fig. 2. TG curves of the reaction between TiO_2 and $BaCO_3$ in O_2.
TiO_2: (a), a-20; (b), a-15; (c), a-13; (d), a-7; (e), A-11; (f), R-22; (g), A-1; (h), R-7; (i), D-1.

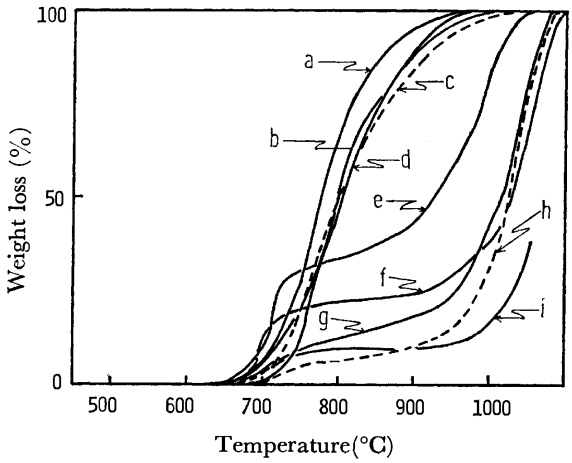

Fig. 3. TG curves of the reaction between TiO_2 and $BaCO_3$ in CO_2. Keys are the same as in Fig. 2.

O_2. The TG curves in CO_2 are classified into one- and two-step types. When the starting TiO_2 powders consist of particles smaller than 0.15 μm, the TG curves are of the first type and the reaction is completed below 1000 °C. When the TiO_2 powders contain particles larger than 0.15 μm, the TG curves are of the second type and the reaction is completed above 1000 °C. In the latter case, the rate of reaction in the first step is higher as the TiO_2 powders become richer in small particles. The difference in the TG curves between the reactions in O_2 and in CO_2 is due to the difference in the structure of the product layers.[3)]

In the reactions using other $BaCO_3$ powders which consisted of spherical particles finer than the present one,[3)] the TG curves changed with the particle size of TiO_2 in a manner similar to the present results, although the beginning and completion temperatures of the reaction were lower by 50—100 °C than in the present work. Therefore, the features of the TG curves in Figs. 2 and 3 may be considered to reflect the properties of the TiO_2 powders themselves.

The TG curves of a-15, a-13, and a-7, in which the

Table 2. Reaction products and activation energies for reactions in O_2

Group of TiO_2[a)]	Run	Former stage of reaction		Later stage of reaction	
		<850 °C Product[b)]	<840 °C E_a/kcal·mol^{-1}	>850 °C Product[b)]	>840 °C E_a/kcal·mol^{-1}
S	a-20	BT	55	BT	
	a-15	BT	56	BT	
	a-13	BT	56	BT	
	a-7	BT	56	BT	
L	A-11	BT	32	BT+B_2T	100
	R-22	BT	38	BT+B_2T	86
	A-1	BT	37	BT+B_2T	95
	R-7	BT	36	BT+B_2T	100
	D-1	BT	36	BT+B_2T	120

a) S, particle size <0.15 μm; L, the curves of the particle-size distributions extended above 0.15 μm.
b) BT, $BaTiO_3$; B_2T, Ba_2TiO_4.

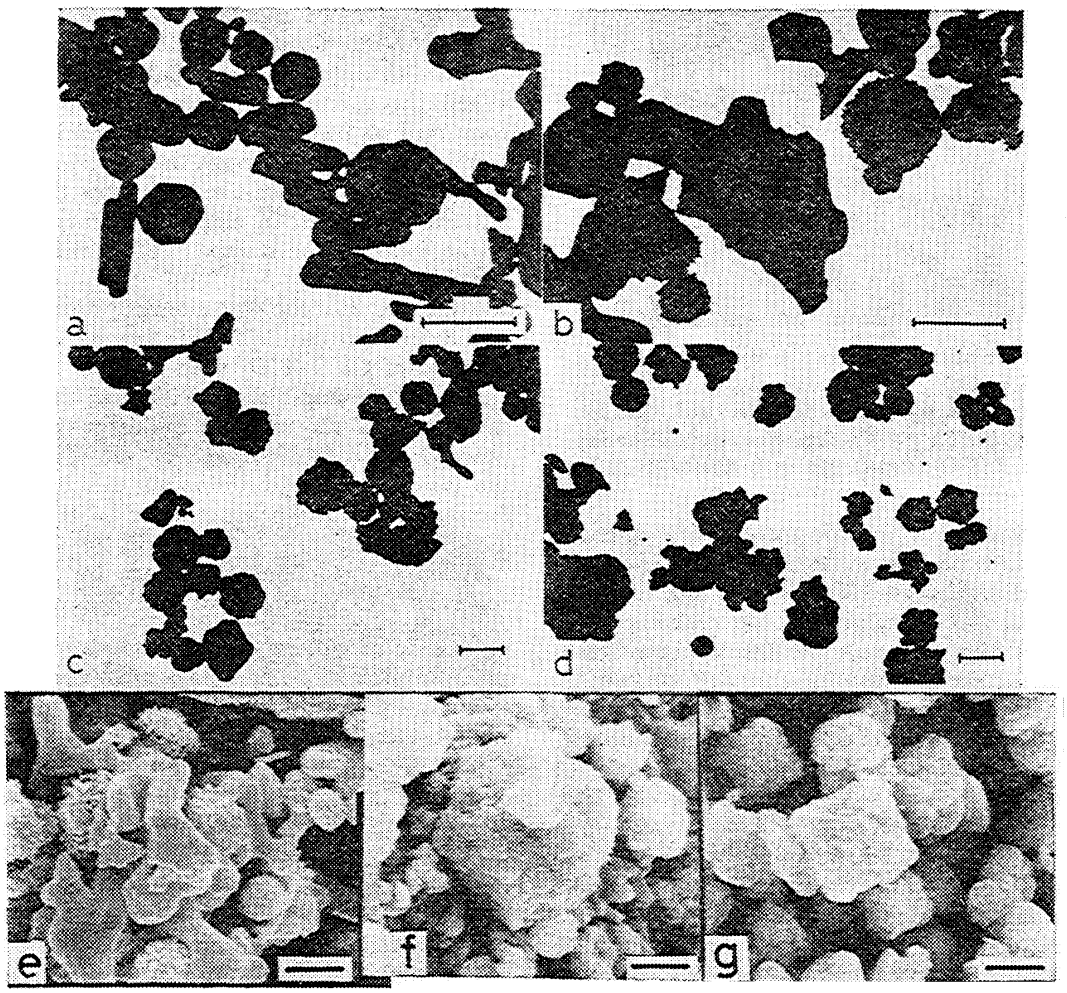

Fig. 4. Electron micrographs of the reaction products. (a), (b), (c), (d), (e), and (f), TiO_2: R-7, in O_2. Final temperature and % of reaction: (a), original mixture; (b) and (e), 905 °C, 25%; (c), 950 °C, 60%; (d) and (f), 1010 °C, 100%. (g), TiO_2: D-1, in O_2, 1062 °C, 100%. bar=2 μm.

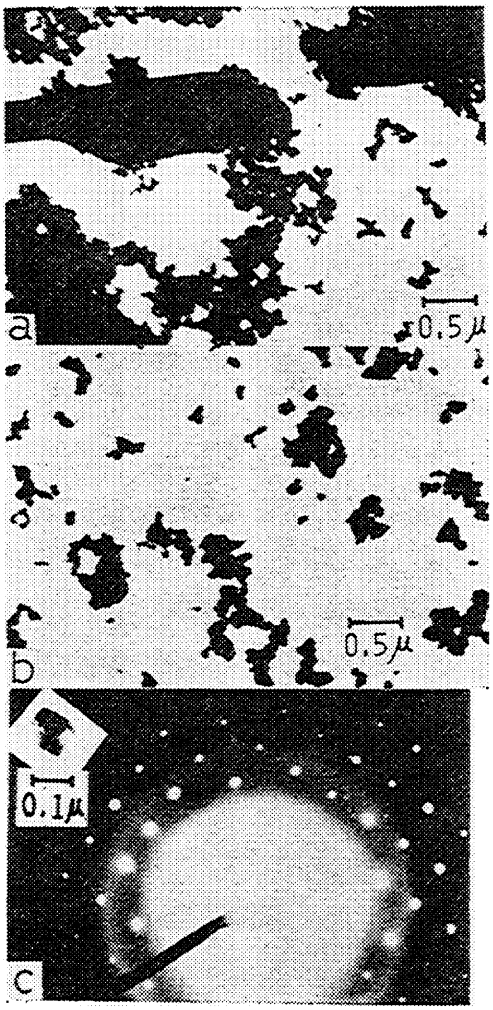

Fig. 5. Electron micrographs of the reaction products (TiO_2: a-15, in O_2).
Final temperature and % of reaction: (a), 780 °C, 50%; (b), 970 °C, 100%; (c), electron diffraction pattern of a $BaTiO_3$ particle shown in photo (b).

particle sizes of the TiO_2 powders are close, while the contents of the anatase-form differ, show little difference, indicating that the crystal form of TiO_2, whether anatase or rutile, does not affect the reactivity. It should be noted here that, in the course of the reaction of a-7, the unreacted TiO_2 consisted only of the anatase-form at 780 °C (the fraction reacted was 40%), although the anatase-rutile transition of the TiO_2 powders becomes appreciable above 900 °C when they are heated at 5.4 °C/min and the transition rate increases as the TiO_2 powders become finer.[3]

Reaction Products. The reaction products in O_2 are shown in Table 2, where the starting TiO_2 powders are classified into two groups according to the particle size: the TiO_2 powders consisting of particles smaller than 0.15 μm (S group) and the other TiO_2 powders (L group). In the S group, $BaTiO_3$ was the only product throughout the course of the reaction in both O_2 and CO_2. In the L group, $BaTiO_3$ was formed at first, and subsequently Ba_2TiO_4 was formed above 850 °C in O_2. The amount of Ba_2TiO_4 produced increased as the TiO_2 powders became coarser, in accord with the findings of a previous work.[1] In CO_2, the formation of Ba_2TiO_4 is suppressed thermodynamically up to 1145 °C.[8,9]

It is clear that the CVD–TiO_2 powders consisting of particles smaller than 0.15 μm show especially high reactivities and are converted into the $BaTiO_3$ powders at temperatures below 1000 °C.

Morphology of the Products. The electron micrographs of the products are shown in Figs. 4 and 5. Figure 4(a) shows the starting mixture of R-7. The particles of $BaCO_3$ are needle-like in shape. When a mixture is heated to 905 °C in O_2, products are formed on the surface of the TiO_2 particles consuming the neighboring $BaCO_3$ particles (Figs. 4(b) and (e)). The $BaCO_3$ particles become thinner with the progress of the reaction. When the mixture is finally heated to 1010 °C, all particles of the products maintain the outline of the starting TiO_2 particles (Figs. 4(d) and (f)). Figure 4(g) also shows the characteristic shape of the square and plate-like particles of the product in D-1 (compare with Fig. 1(f)). The change in the shape of particles in the course of the reaction of a-15 in O_2 is shown in Fig. 5. In this case, the change in the $BaCO_3$ particles is more significant. When the mixture is heated to 780 °C, large numbers of fine particles are attached to large particles of $BaCO_3$, as seen in Fig. 5(a). When the mixture is heated to 970 °C and wholly converted to $BaTiO_3$, the large particles disappear, as seen in Fig. 5(b). Although the particles are aggregated in part, they are cube-like and show the single-crystal pattern of $BaTiO_3$ in electron diffraction, the outline of the shape of the starting TiO_2 particles being held, too (Fig. 5(c)).

From the morphology mentioned above, it may be concluded that the $BaTiO_3$ is formed by a topotactical reaction of CVD–TiO_2 with $BaCO_3$. The manner of change in the shapes of the TiO_2 and $BaCO_3$ particles in the course of the reaction indicates that the reaction proceeds from the surface of the TiO_2-particle into the inside by the diffusion of the BaO component, forming a reaction-product layer on the surface of the TiO_2 particle.

When the reaction takes place by this model on a spherical TiO_2 particle with the radius of r_0, the fraction reacted α is given by:

$$\alpha = 1 - \left(\frac{r_0 - x}{r_0}\right)^3, \qquad (1)$$

where x is the thickness reacted. The values of α at 840 °C in Fig. 2, where $BaTiO_3$ is the only product, are compared in Fig. 6 with the ones calculated by means of Eq. 1. When the value of x at a given temperature is independent of r_0, the experimental and calculated values of α should agree. The agreement is not very good, but one can see that the present reaction model explains well the accelerated increase in the reactivity as the particle size of TiO_2 becomes smaller.

The particle-size distributions of the resulting $BaTiO_3$ and the starting TiO_2 are compared in Fig. 7. The average particle-size of the resulting $BaTiO_3$ is about 1.3 times that of the starting TiO_2. It is found that the TiO_2 powders with average particle-size of 1.3 μm were converted into the $BaTiO_3$ powders with that of

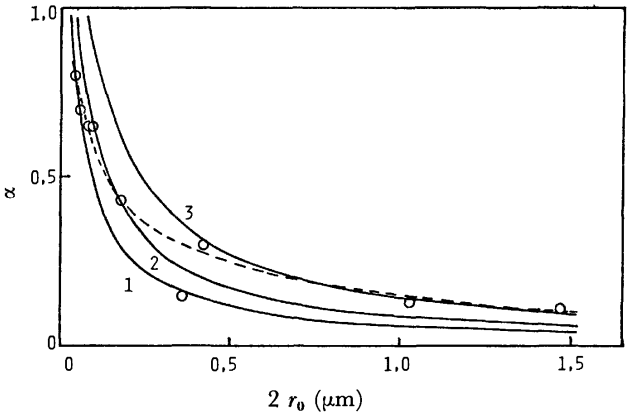

Fig. 6. Relation between the fraction reacted and particle size.
———, Calculated: 1, x=0.01 μm; 2, x=0.015 μm; 3, x=0.025 μm;
---○---, observed (at 840 °C).

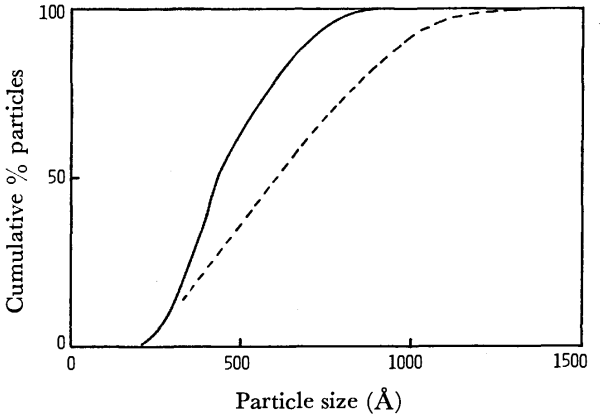

Fig. 7. Particle size distributions of the starting TiO_2 and the resulting $BaTiO_3$ powders of a-15.
——, TiO_2; ——, $BaTiO_3$.

$$(1-\sqrt[3]{1-\alpha})^2 = \frac{kt}{r_0^2} \quad (2)$$

where α is the fraction reacted at time t, k is the rate constant, and r_0 is the initial radius of the TiO_2 particle. We tried to analyze the TG curves in O_2 by the use of Jander's equation. To apply the equation to the TG data, it was modified as Eq. 3.[12-14]

$$K = \frac{2(1-\sqrt[3]{1-\alpha})}{3(1-\alpha)^{2/3}} \cdot \frac{\Delta\alpha}{\Delta T} = \frac{k_0}{ar_0^2} e^{-E/RT}, \quad (3)$$

where a is the heating rate. The values of K were calculated by taking ΔT=25 °C. Plots of log K *vs.* $1/T$ are shown in Fig. 8. Jander's equation holds well up to ≈770 °C for the S group and up to ≈840 °C for the L group. On the L group, the slope changes at ≈840 °C, suggesting that the reaction mechanism changes at this temperature. This may be caused by the appearance of Ba_2TiO_4 at ≈850 °C.

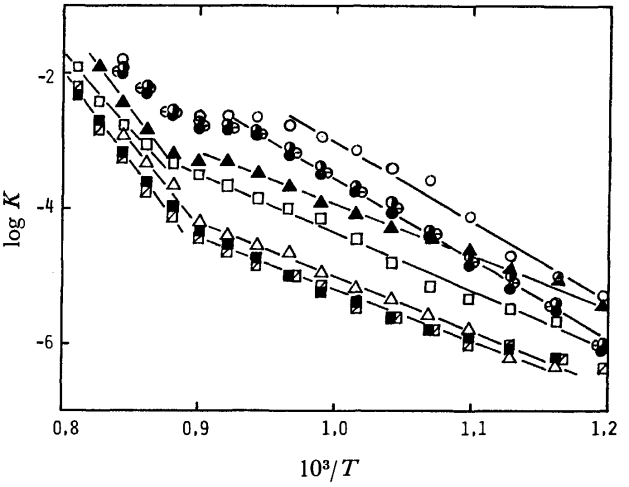

Fig. 8. Plots of log K *vs.* $10^3/T$ for the reactions in O_2.
○, a-20; ●, a-7; ◑, a-15; ⊖, a-13; △, A-1; ▲, A-11; □, R-22; ■, R-7; ⊠, D-1.

1.6 μm,[3] the ratio of the average particle sizes being 1.2. When a TiO_2 particle is converted into a $BaTiO_3$ particle, the particle size should increase by 1.26 times. The observed values are close to the calculated one. This supports also the reaction model mentioned above.

When reaction mixtures are heated up to 1100 °C, the resulting $BaTiO_3$ particles suffer sintering to a considerable extent. However, the reaction can be completed below 1000 °C by selecting appropriate reaction conditions such as the particle size of TiO_2 and $BaCO_3$, the heating rate, or the atmosphere. In this case, the particle sizes of the $BaTiO_3$ powders produced are controlled by those of the starting TiO_2 powders, and one can produce ultrafine $BaTiO_3$ powders, which have a fineness comparable with that obtained by the thermal decomposition of oxalate,[11] by a solid-state reaction.

Application of Jander's Equation. When the reaction between TiO_2 and $BaCO_3$ powders occurs in the manner mentioned above, the reaction rate may be controlled by the diffusion of the BaO component through the product layer and the kinetics may follow Jander's equation (2):

From the linear parts of the plots, the apparent activation energies are obtained (see Table 2). The activation energies for the former stage are different between the S and L groups. However, it should be noted that the activation energy is also independent of the crystal type of TiO_2 in each group. The activation energies reported hitherto are shown in Table 3. All of these activation energies are claimed for the diffusion process. When the diffusion of the BaO component in the $BaTiO_3$ layer is the rate-determining step, each experiment should give comparable activation energies independently of the crystal type of TiO_2. This is not the case, as may be seen in Table 3. However, it is interesting to note that, regardless of the crystal type of TiO_2, most of the values fall into two ranges: 34—36 and 54—60 kcal/mol; this is in good agreement with the results of the present work. The value of 99 kcal/mol is close to that of the L group in the higher-temperature range in the present work. This exceptionally high value, therefore, is considered to be due to the formation of Ba_2TiO_4 and not to the fact that TiO_2 has a rutile form.

Table 3. Activation energy for the formation of $BaTiO_3$

Workers	Crystal type of TiO_2	E_a kcal·mol^{-1}	Rate equation
Kubo and Shinriki[16]	Anatase	54	Jander
Kubo and Shinriki[15]	Rutile	99	modified
	Anatase	58	Jander
Kuno *et al.*[2]	Rutile	36	Tamman
	Anatase	34	
Arai *et al.*[14]	Anatase	60	Jander

The reason why the activation energies differ between the S and L groups, although both groups give the same reaction product, $BaTiO_3$, below 840 °C, is not clear at present. However, the following should be noted here.

It has been reported by Nakayama and Sasaki[10] that the activation energy of the diffusion of barium into the rutile-TiO_2 crystal is 59 kcal/mol for a direction perpendicular to the c-axis and 43 kcal/mol for a direction parallel to the c-axis. The activation energies obtained for the S and L groups in the lower-temperature range are of the same order of magnitude as the values of the former and the latter, respectively. The rutile-TiO_2 particles used in the present work are spherical or cubic in the S group and plate-like grown in the plane perpendicular to the c-axis in the L group. Accordingly, in the reaction of the L group, the diffusion of the BaO component may mainly occur along the direction of the c-axis of rutile-TiO_2 and give a lower activation energy. On the other hand, in the reaction of the S group, the diffusion may occur more isotropically and give a higher activation energy. On anatase-TiO_2 particles, the same interpretation may be applied in explaining the different behavior between the two groups.

Reactivity and Crystal Type of TiO_2. On the solid-state reaction of the TiO_2–$BaCO_3$ system, it has generally been accepted that anatase-TiO_2 shows a lower activation energy and a higher reactivity than rutile-TiO_2.[1] In the present study, however, there were no observable differences in the reactivity and activation energy between anatase- and rutile-forms. This is to be expected when the reaction is limited by a diffusion through the same reaction product. The particle size of TiO_2 governs the reactivity. In previous works, in which the differences in the reactivity and the activation energy between the two forms of TiO_2 were observed, the secondary properties of the TiO_2 powders such as the state of the agglomeration of primary particles, especially in the case of calcined rutile-TiO_2, would affect the reactivity and result in different reactivities between the two types of TiO_2.

This research was supported in part by the Science Foundation of the Ministry of Education (No. 885150).

References

1) For example, T. Kubo, M. Kato, and T. Fujita, *Kogyo Kagaku Zasshi*, **70**, 847 (1967).
2) H. Kuno, A. Suzuki, and M. Yokoyama, *Funtai Oyobi Funmatsu Yakin*, **13**, 47 (1966).
3) Y. Suyama and A. Kato, *Ceramurgia Intern.*, **1**, 5 (1975).
4) Y. Suyama and A. Kato, *J. Am. Ceram. Soc.*, **59**, 146 (1976).
5) Y. Suyama, K. Ohmura, and A. Kato, *Nippon Kagaku Kaishi*, **1976**, 584.
6) Impurities; chloride<0.002%, heavy metals<0.001%, iron<0.001%, calcium and alkalies<0.25%, sulphide<0.001 %.
7) Cahn RG electrobalance.
8) L. K. Templeton and J. A. Pask, *J. Am. Ceram. Soc.*, **42**, 212 (1959).
9) Y. Suyama and A. Kato, *Ceramurgia Intern.*, **1**, 123 (1975).
10) T. Nakayama and T. Sasaki, *Bull. Chem. Soc. Jpn.*, **36**, 569 (1963).
11) K. Kiss, J. Magder, M. S. Vukasovich, and R. J. Lockhart, *J. Am. Ceram. Soc.*, **49**, 291 (1966).
12) T. Kubo, S. Sirasaki, and M. Kato, *Kogyo Kagaku Zasshi*, **69**, 357 (1966).
13) A. Kato and Y. Suyama, *J. Therm. Anal.*, **7**, 149 (1975).
14) Y. Arai, T. Yasue, H. Takiguchi, and T. Kubo, *Nippon Kagaku Kaishi*, **1974**, 1611.
15) T. Kubo and K. Shinriki, *Kogyo Kagaku Zasshi*, **57**, 619 (1954).
16) T. Kubo and K. Shinriki, *Kogyo Kagaku Zasshi*, **55**, 49 (1952).

Photoreduction of Quinones. I. One-electron Transfer to *p*-Benzoquinone in Ethanol Studied by ESR during Continuous Photolysis

Yoshihiko KAMBARA* and Hiroshi YOSHIDA

Faculty of Engineering, Hokkaido University, Kita-ku, Sapporo 060

(Received August 7, 1976; in revised form December 21, 1976)

Electron spin resonance was examined during the continuous photolysis of a flowing solution of *p*-benzoquinone in ethanol at room temperature. It was found that both semiquinone anions and semiquinone radicals were generated, but their relative yields changed depending on the experimental conditions. The semiquinone anion was generated in a comparatively high yield at low concentrations of *p*-benzoquinone and at high flowing rates. Its formation was, however, quenched by the addition of acetic acid without transformation to the semiquinone radical. The semiquinone radical was generated efficiently at high *p*-benzoquinone concentrations and at low flowing rates. Its formation was enhanced by the addition of hydroquinone. These results, as well as the previous results on the effect of the wavelength of light, indicate, in contrast with the currently accepted view, that there is effectively no equilibrium in ethanol between the semiquinone radical and the semiquinone anion under the present experimental conditions, and that the latter is formed by a photoinduced one-electron transfer from solvent to *p*-benzoquinone. The semiquinone radical seems to arise from the hydrogen abstraction of excited *p*-benzoquinone from the hydroquinone formed as a product during photolysis.

One of the main interests in photobiology is associated with the naturally occuring quinones mediating in the electron-transport mechanism in photosynthesis.[1] Such a biological function of quinones seems to have attracted the interest of chemists in studying the photochemistry of simple quinones, such as *p*-benzoquinone and duroquinone, by means of the flash photolysis-optical absorption technique[2-7] as well as the photolysis-electron spin resonance (ESR) technique.[8-14] The flash photolysis studies have stressed the hydrogen-abstraction reaction of simple photoexcited quinones since the pioneering works by Bridge and Porter.[2] The transient optical absorption due to the semiquinone radical and the semiquinone anion was observed in hydrogen-donating solvents such as ethanol or in the presence of hydrogen donors; the formation of the latter has generally been attributed to its equilibrium with the former, generated primarily by the hydrogen-abstraction reaction:

$$Q^* + CH_3CH_2OH \longrightarrow \dot{Q}H + CH_3\dot{C}HOH \quad (1)$$

$$\dot{Q}H \longrightarrow Q^- + H^+. \quad (2)$$

This seems to be the currently accepted reaction mechanism,[15] and it seems to have been supported also by ESR studies,[10-13] because only the ESR spectrum of semiquinone radicals, presumed to be generated primarily through Reaction 1, has been detected from solutions of quinones in alcohols.

However, our previous ESR study seems to conflict with the above mechanism, because the ESR spectra of both semiquinone radicals and semiquinone anions were observed from a solution of *p*-benzoquinone and its methyl derivatives in ethanol or methanol during continuous photolysis and the effective wavelength of the photolyzing light was found to be different between the semiquinone anions and the semiquinone radicals.[16] The results suggested that the semiquinone anions might be generated primarily from photoexcited quinones, but not by Reaction 2. However, this was not conclusively proven, because the observed ESR signals depended very much on the experimental conditions and we could not verify the factors controlling the yields of both the semiquinone anions and the semiquinone radicals.

The previous study of detecting semiquinone intermediates by ESR has now been extended to verify the factors controlling their yields and to give firm indications against Reactions 1 and 2. The advantage of such an ESR study is that semiquinone anions and semiquinone radicals are clearly distinguished from each other,[16] while the spectra of semiquinone anions, radicals, and triplet quinones overlap each other, and so it is not easy to study the kinetic behavior of the semiquinone intermediates separately in flash photolysis-optical absorption studies.

Experimental

Chemicals. The *p*-benzoquinone (BQ) was purified by sublimation three times. The purified BQ showed a melting point of 387—389 K, identical with that quoted in chemical handbooks. The hydroquinone (BQH_2) was sublimed twice under a vacuum, volatile impurities being removed by means of a liquid nitrogen trap. Ethanol with a claimed purity of 99.5% was generally used without further purification. Occasionally, however, it was purified further by distilling it after reflux with sodium hydroxide and zinc powder to remove the acetaldehyde, by refluxing it with magnesium ethoxide prepared from magnesium and absolute ethanol in the presence of ethyl bromide to remove the water, and by then distilling it again. However, such additional purification of the ethanol caused no difference in the results. The acetic acid was used as received. All the chemicals used were of an SG grade and were supplied by Wako Pure Chemical Ind., Ltd.

Photolysis and ESR Measurements. The experimental instrument has already been described elsewhere:[17] it is essentially the same as that developed first by Livingston and Zeldes.[18] Sample solutions were purged with helium gas for at least half an hour under dimmed room light. This procedure was essential to obtaining reproducible results. The solutions were allowed to flow at a rate of from 0.014 to 5.0 $cm^3 s^{-1}$, which gave a resident time of 3.6 s to 10 ms of the flowing solution within the effective volume of the ESR

* Present address: Mitsui-Toatsu Co., Ltd., Mobara, Chiba 297.

resonant cavity. Photolysis was carried out at room temperature with unfiltered light of a wavelength longer than 270 nm from a super-high-pressure mercury lamp (Philips, SP-500). The intensity of light gradually changed in the shorter-wavelength region, thus causing a scattering of the results. Therefore, each series of data shown in one figure was obtained at one time. The solution was warmed during photolysis, but its temperature immediately after photolysis was found to be 290±2 K except when the flow rate was extremely slow.

Results

The ESR signal observed from the ethanol solution of BQ generally consisted of a spectrum of benzosemiquinone radicals (triplet of double triplet, with hyperfine separations of 0.51, 0.19, and 0.03 mT) and one of benzosemiquinone anions (quintet, with a separation of 0.24 mT). These spectra are essentially the same as those reported previously.[8,16,19] The most prominent finding was that the relative intensities of both spectra changed depending on the experimental conditions. For instance, Fig. 1 shows the ESR signals recorded for two different concentrations of BQ, the other experimental conditions being unchanged. The dependence of the observed yield for both the benzosemiquinone radical ($BQH\cdot$) and the benzosemiquinone anion (BQ^-) on the BQ concentration is shown in Fig. 2 for two different resident times of the solutions. $BQH\cdot$ was generated only at high BQ concentrations, whereas BQ^- was observed to form in a high yield even if the concentration was lowered to 0.01 mmol dm^{-3}.

Fig. 1. ESR signal recorded during photolysis of *p*-benzoquinone in ethanol flowing at a resident time of 0.5 s at 293 K. Concentration of quinone, (A) 10 and (B) 1.0 mmol dm^{-3}.

The observed yields of $BQH\cdot$ and BQ^- are plotted as functions of the resident time in Fig. 3 for particular BQ concentrations. $BQH\cdot$ was observed only at long resident times for the higher BQ concentrations; its yield increased with the resident time up to about 1 s. On the other hand, the BQ^- yield showed no increase with the resident time. Rather, it remained constant for the lower BQ concentrations, or it decreased from the highest value observed at the shortest resident time examined for the higher BQ concentrations.[20] These observations agree qualitatively with the results obtained

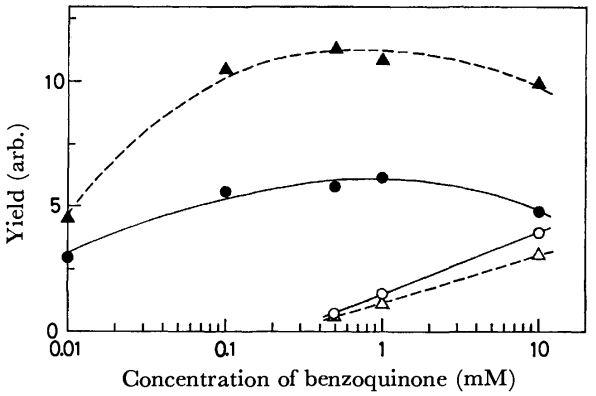

Fig. 2. Dependence of yield of benzosemiquinone anion and benzosemiquinone radical observed during photolysis of *p*-benzoquinone in ethanol on the benzoquinone concentration. Benzoquinone anion at resident time of (●) 1 s and (▲) 0.5 s, benzosemiquinone radical at resident time of (○) 1 s and (△) 0.5 s.

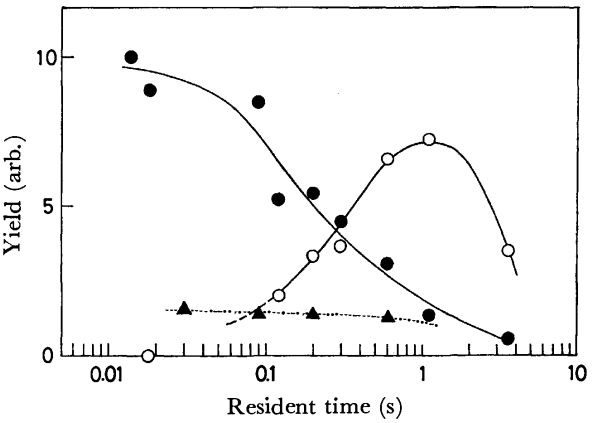

Fig. 3. Dependence of the yield of (●) benzosemiquinone anion and (○) benzosemiquinone radical observed during photolysis of flowing solution of 1.0 mmol dm^{-3} *p*-benzoquinone in ethanol, and (▲) that of the yield of benzosemiquinone anion from the solution of 0.01 mmol dm^{-3} *p*-benzoquinone on the resident time of the solutions within the effective volume of cell. No benzosemiquinone radical was detected from the diluted solution.

independently for the relationship between the yield and the BQ concentration, as is shown in Fig. 2.

Since $BQH\cdot$ is generated appreciably only at high BQ concentrations and at long photolysis times, it seems essential to study the effect of a photoproduct, BQH_2, on the formation of $BQH\cdot$ and on that of BQ^- as well. The yields of $BQH\cdot$ and BQ^- were examined by intentionally adding BQH_2 to a solution of 1 mmol dm^{-3} BQ under conditions where both $BQH\cdot$ and BQ^- were generated without added BQH_2. The yield of BQ^- remained unchanged, whereas that of $BQH\cdot$ increased with the concentration of the added BQH_2, as is shown in Fig. 4. Although both $BQH\cdot$ and BQ^- were found to form in the BQH_2 solution in ethanol, the increase in the $BQH\cdot$ yield shown in Fig. 4 cannot be attributed simply to the photodissociation of the added BQH_2 to $BQH\cdot$, because the effect of the added BQH_2 is prominent at its low concentrations. It should noted that the

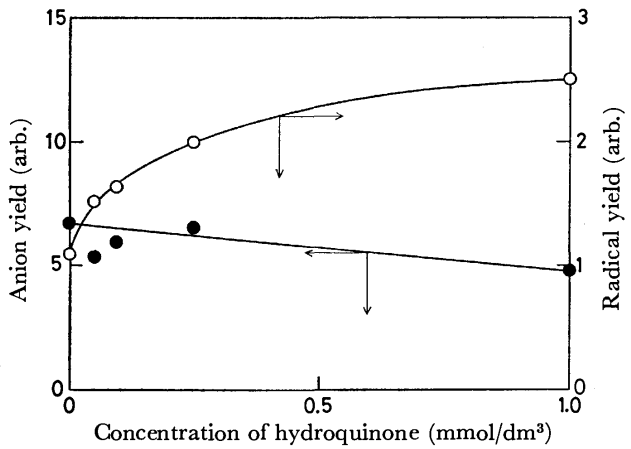

Fig. 4. Effect of the addition of hydroquinone into the solution of 1.0 mmol dm^{-3} *p*-benzoquinone in ethanol on the yield of (●) benzosemiquinone anion and (○) benzosemiquinone radical observed during photolysis at resident time of 1 s.

BQ^- formation from BQ is not affected by the addition of BQH_2.

Previously the addition of acids to the solution was found to eliminate the ESR spectrum of BQ^-. This was interpreted as being due to the protonation to BQ^-, resulting in the transformation of BQ^- into BQH·.[16] In the present study, however, it was found that the addition of acetic acid in increasing amounts up to 16 mmol dm^{-3} caused only a decrease in the BQ^- yield to zero, but no increase in the BQH· yield. When the BQ concentration was so low that only BQ^- was detected, the addition of acetic acid totally eliminated the ESR signal, indicating the absence of the transformation of BQ^- to BQH·.

Discussion

Although the ESR spectra of semiquinone anions have been recorded from halogenated benzoquinones[21,22] and anthraquinone,[9] the spectra recorded from BQ in fluid alcoholic solutions have been almost exclusively those of BQH·.[9,10,12,13,23,24] On the basis of the present results (Figs. 2 and 3), the absence of the BQ^- spectrum in the previous studies may be attributed to the effects of the BQ concentration and the photolysis time, since the solutions with comparatively high BQ concentrations were sealed in a sample tube and photolyzed for a long time or repeatedly by light pulses to overcome a poor signal-to-noise ratio. Pedersen *et al.* observed the coexistence of BQ^- and BQH· in an ethanol solution of BQ at a low concentration during photolysis by recycling a large volume of the solution.[14] This and our own previous studies[16] have been the only cases where evidence of the BQ^- formation was obtained by means of the ESR technique.

BQ^- was found to be generated at short resident times and/or at low BQ concentrations, while no BQH· at all was observed under the same experimental conditions. This strongly suggests that BQ^- is generated directly from BQ through a photoinduced one-electron transfer from the solvent ethanol. Although the above view of the BQ^- formation is not in accord with the currently accepted reaction mechanism for the photoreduction of quinones,[2,15] it is consistent with Tollin's interpretation of the observation of BQ^- by photolyzing BQ in a low-temperature ethanol matrix.[25] McLauchlan and Sealy applied the spin-trapping technique to the photochemical reaction of quinones including BQ in fluid alcoholic solutions and detected no 1-hydroxyethyl radical generated by Reaction 1, though they did detect alkoxyl radicals.[26] These radicals seem to have been generated through the deprotonation of the molecular cation of the alcohols primarily formed by the one-electron transfer between the quinones and the alcohols. The photoinduced electron transfer was demonstrated by Davis *et al.* by means of product analysis to occur from the alkoxide ion to amino anthraquinone derivatives.[27] They postulated that this reaction involves the charge-transfer lowest excited state.

One would anticipate that BQ^- might be generated from the primary intermediate, BQH·, by Reaction 2, which was so rapid that the primary intermediate could not be observed under the present experimental conditions. However, if the BQ^- formation is directly correlated to the BQH· formation by the rapid equilibration between these semiquinone intermediates, their relative yields should not depend on the BQ concentration. It can also be expected that the decrease in the BQ^- yield caused by the addition of acetic acid should be followed by an increase in the BQH· yield. Even if the equilibration was not rapid enough compared with the lifetime of the semiquinone intermediates, the primary intermediate should be observed comparatively more readily than the secondary one at short resident times. None of the present results, then, give any indication of a reaction mechanism comprising Reactions 1 and 2 for the BQ^- formation.

We found previously that BQH· was effectively generated with light of wavelengths of 260—300 nm, whereas BQ^- was generated with light of wavelengths around 460 nm.[16] The study of the wavelength effect on the formation of semiquinone intermediates is very undeveloped, but early in 1960 Bridge found, in his flash photolysis study, that the quantum yield of the durosemiquinone anion was the largest for the light of 350—400 nm, the longest wavelength examined.[28] This is consistent with our previous results.[16] The different wavelengths effective for the formation of BQ^- and BQH· support the view that the formation of the former is independent of that of the latter.

Some comments may be needed here on the BQH· formation, because it has thus far been believed to be the principal semiquinone intermediate in the photoreduction of BQ into BQH_2. The enhancement of the BQH· formation caused by the addition of a small amount of BQH_2 (see Fig. 4) seems to indicate that the hydrogen abstraction of photoexcited BQ from BQH_2 is one of the main sources of BQH·. This reaction reasonably interprets the observed dependence of the BQH· yield on the resident time and on the BQ concentration; the increase in the concentration of the photoproduct, BQH_2, during the photolysis of which the

rate is the higher for the higher BQ concentration, results in the observation of BQH· at long resident times from the solutions with higher BQ concentrations. It has been already observed in the flash photolysis study of duroquinone in ethanol[3,5,7] that the triplet excited quinone abstracts hydrogen from durohydroquinone with a diffusion-controlled rate, but from solvent ethanol only very slowly. However, we should reserve other possible sources for BQH·, especially for that observed at long resident times, because BQ is readily depleted under the present experimental conditions. In a separate experiment, for example, 1 mmol dm^{-3} BQ was found by optical absorption study to have been almost entirely transformed into BQH_2 and other unidentified stable products after the photolysis and ESR measurements at the resident time of 0.5 s. Therefore, the photodissociation of BQH_2 and the other products may be responsible for the BQH· formation in the later period of photolysis at a long resident time. Photolysis with light of selected wavelengths would give an insight into the detailed mechanism for the BQH· formation, but it could not be done mainly because of the limited sensitivity of the experimental method used.

In conclusion, the present ESR investigation revealed that the primary step in the photochemical reaction of BQ in ethanol is the one-electron transfer giving BQ^-:

$$BQ^* + CH_3CH_2OH \longrightarrow BQ^- + CH_3CH_2OH^+. \quad (3)$$

A question may arise as to the role of BQ^- in the photoreduction of BQ; is it really involved in the reduction process? In order to answer this question, we examined, though qualitatively, the optical absorption of the BQ solutions after the photolysis and ESR measurements under the conditions where BQ^- was exclusively formed, and found that a fraction of BQ had been transformed into BQH_2, giving an absorption band with its maximum at 295 nm. We are inclined to believe that BQ^- but not BQH· is involved in the photoreduction of BQ in ethanol, for which we propose the following reaction scheme based on the present results:

$$CH_3CH_2OH^+ + CH_3CH_2OH \longrightarrow CH_3CH_2\dot{O} + CH_3CH_2OH_2^+, \quad (4)$$

$$CH_3CH_2\dot{O} + CH_3CH_2OH \longrightarrow CH_3CH_2OH + CH_3\dot{C}HOH, \quad (5)$$

$$CH_3\dot{C}HOH + BQ \longrightarrow CH_3\overset{+}{C}HOH + BQ^-, \quad (6)$$

$$CH_3\overset{+}{C}HOH + CH_3CH_2OH \longrightarrow CH_3CHO + CH_3CH_2OH_2^+, \quad (7)$$

$$2BQ^- \longrightarrow BQ + BQ^{2-} \quad (8)$$

$$BQ^{2-} + 2CH_3CH_2OH_2^+ \longrightarrow BQH_2 + 2CH_3CH_2OH. \quad (9)$$

The above reaction scheme is only a matter of speculation. However, Reaction 4 is consistent with the detection of alkoxyl radicals by the spin-trapping technique applied to the photoreduction of quinones in alcohols.[26] Reaction 6 gives a reason why the hydroxyethyl radical was not observed in the present investigation, though it had been detected in a similar ESR study of the photoreduction of benzophenone in ethanol.[17] It was inferred in Willson's pulse radiolysis work[29] to occur as a route for the formation of the semiquinone anion. The disproportionation of semiquinone anion, Reaction 8, has been observed in the flash-photolysis study of duroquinone in an alkaline ethanol-water mixture.[2] This reaction, together with Reaction 9, explains the route without the participation of BQH· for the formation of BQH_2.

A part of this work was carried out at the Research Reactor Institute, Kyoto University, with the kind experimental assistance of Tetsuo Warashina, to whom we wish to express our sincere thanks.

References

1) R. Bentley and I. M. Campbell, "The Chemistry of the Quinonoid Compounds, Part 2," ed by S. Patai, Interscience, London (1974), p. 683.
2) N. K. Bridge and G. Porter, *Proc. R. Soc. London, Ser. A*, **244**, 259, 276 (1958).
3) F. Wilkinson, G. M. Seddon, and K. Tickle, *Ber. Bunsenges. Phys. Chem.*, **72**, 315 (1968).
4) E. J. Land, *Trans. Faraday Soc.*, **65**, 2815 (1969).
5) J. Nafisi-Movaghar and F. Wilkinson, *Trans. Faraday Soc.*, **66**, 2268 (1970).
6) D. R. Kemp and G. Porter, *Proc. R. Soc. London, Ser. A*, **326**, 117 (1971).
7) E. Amouyal and R. Bensasson, *J. Chem. Soc., Faraday Trans. 1*, **72**, 1274 (1976).
8) T. Warashina, O. Edlund, and H. Yoshida, *Bull. Chem. Soc. Jpn.*, **48**, 636 (1976), and the literature cited therein.
9) S. K. Wong, W. Sytnyk, and J. K. Wan, *Can. J. Chem.*, **50**, 3052 (1972).
10) P. B. Ayscough and R. C. Sealy, *J. Chem. Soc., Perkin Trans. 2*, **1973**, 543.
11) P. W. Atkins, A. J. Dobb, G. T. Evans, K. A. McLauchlan, and P. W. Percival, *Mol. Phys.*, **27**, 769 (1974).
12) H. M. Vyas, S. K. Wong, B. B. Adeleke, and J. K. S. Wan, *J. Am. Chem. Soc.*, **97**, 1385 (1975).
13) B. B. Adeleke, K. Y. Choo, and J. K. S. Wan, *J. Chem. Phys.*, **62**, 3822 (1975).
14) J. B. Pedersen, C. E. M. Hansen, H. Parbo, and L. T. Muus, *J. Chem. Phys.*, **63**, 2398 (1975).
15) J. M. Bruce, "The Chemistry of Quinonoid Compounds, Part 1," ed by S. Patai, Interscience, London (1974), p. 465.
16) H. Yoshida, K. Hayashi, and T. Warashina, *Bull. Chem. Soc. Jpn.*, **45**, 3515 (1972).
17) H. Yoshida and T. Warashina, *Bull. Chem. Soc. Jpn.*, **44**, 2950 (1971).
18) R. Livingston and H. Zeldes, *J. Chem. Phys.*, **44**, 1245 (1966).
19) B. Venkataraman, B. G. Segel, and G. K. Fraenkel, *J. Chem. Phys.*, **30**, 1006 (1959).
20) The dependence of the yields of BQ^- and BQH· on the resident time was wrongly presented in Fig. 4 of Reference 16 and was incorrectly interpreted as being due to their lifetime. In the figure caption, BQ^- should read BQH· and *vice versa*, so that the results are consistent with those of the present investigation.
21) A. Hudson and J. W. Lewis, *J. Chem. Soc., B*, **1967**, 531.
22) B. J. Hales and J. R. Bolton, *Photochem. Photobiol.*, **12**, 239 (1970).

23) T. E. Gough, *Trans. Faraday Soc.*, **62**, 2321 (1966).
24) T. E. Gough and G. A. Taylor, *Can. J. Chem.*, **47**, 3717 (1969).
25) J. R. Harbour and G. Tollin, *Photochem. Photobiol.*, **19**, 147 (1974).
26) K. A. McLauchlan and R. C. Sealy, *J. Chem. Soc., Chem. Commun.*, **1976**, 115.
27) A. K. Davis, J. F. McKeller, and G. O. Phillips, *Proc. R. Soc. London, Ser. A*, **323**, 69 (1971).
28) N. K. Bridge, *Trans. Faraday Soc.*, **56**, 1001 (1960).
29) R. L. Willson, *Trans. Faraday Soc.*, **67**, 3020 (1971).

Magnetic Properties and Low-Field ESR of Organic Free Radicals, Monochloroporphyrexide and Porphyrexide

Toshio YOSHIOKA*

Department of Chemistry, Faculty of Science, Kyoto University, Sakyo-ku, Kyoto 606

(Received August 9, 1976)

The static magnetic susceptibility, and ESR and proton NMR spectra of powder samples of monochloroporphyrexide were measured above 1 K and compared with those of porphyrexide. A broad maximum in the static susceptibility of monochloroporphyrexide, indicating an antiferromagnetic interaction, appeared at 22.5 K. The relative susceptibilities of the two radicals obtained from the ESR signal intensities and the proton NMR shifts agree qualitatively with the static susceptibilities. In the low-field ESR spectra (135 MHz) of each radical, broadening of the $g=2$ absorption line and distinct appearance of the $g=4$ absorption line were found in the temperature region below T_m, the temperature at which the susceptibility is maximum. The anisotropy of the g-value was estimated from Q-band ESR spectra. Furthermore, the unpaired electron-spin distribution over the ring was estimated from the X-band ESR and the proton NMR spectra. The results are interpreted assuming that the magnetic behavior of the two radicals is due to alternating antiferromagnetic Heisenberg linear chains with alternating parameters, $a=0.4$ and $a=0.6$, respectively.

At low temperatures, the magnetic susceptibility of many stable neutral radicals deviates from the Curie-Weiss law and sometimes has a broad maximum which indicates the presence of an antiferromagnetic exchange interaction J between unpaired electrons of the radicals.[1-5] This anomalous magnetic behavior has been interpreted in terms of the one-dimensional Heisenberg model with an antiferromagnetic exchange interaction.[3] Such an interaction is considered to be due to the overlap of the $2P_z\pi$-orbitals, each of which is occupied by an unpaired electron, and the one-dimensionality may be caused by the uniaxial characteristic of the π-orbital. It has been reported in previous papers, however, that for the porphyrexide radical the magnetic behavior is different from that for 2,2,6,6-tetramethyl-4-hydroxypiperidine-1-oxyl(TANOL),which is a one-dimensional Heisenberg antiferromagnet typical of organic neutral radicals.[3,4] Its magnetic susceptibility is better interpreted using the Ising model rather than the linear Heisenberg model. The difference between the magnetic properties of TANOL and porphyrexide has been considered to be due to their different molecular structures; the former has a non-planar molecular framework and a localized spin distribution, while the latter is somewhat planar with the unpaired electron expected to be over the ring. In order to clarify the magnetic properties of porphyrexide radicals, a chloroderivative of porphyrexide has been chosen as an appropriate sample. In this paper, the results of the magnetic susceptibility and ESR and proton NMR measurements of monochloroporphyrexide (Cl-porphyrexide) are reported for temperatures above 1 K, and the exchange interaction, spin correlation, and unpaired electron-spin distribution in porphyrexide radicals are discussed by comparing the results with those of porphyrexide and TANOL. Cl-porphyrexide has been suggested to have the molecular structure shown in Fig. 1.[6]

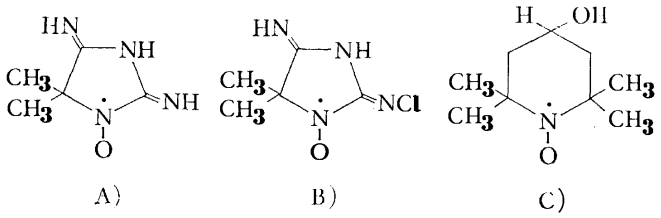

Fig. 1. Molecular structures of the radicals.
A) Porphyrexide, B) Cl-porphyrexide, C) TANOL.

* Present address: Fibers Research Laboratories, Toray Industries, Inc., Sonoyama, Otsu 520.

Experimental

The porphyrexide radical was obtained commercially and was used without further purification. The sample of monochloroporphyrexide was prepared according to the procedure of Piloty and Schwerin,[7] and was purified by recrystallization from methanol, mp 151—152 °C. The results of elemental analysis correspond closely to the calculated values. Found: C, 34.42; H, 4.61; N, 31.99; Cl, 20.10%. Calcd for $C_5H_8N_4OCl$: C, 34.18; H, 4.56; N, 31.91; Cl, 20.22%. TANOL was prepared by the oxidation of 2,2,6,6-tetramethyl-4-hydroxypiperidine according to the process of Rozantsev,[8] and was purified by recrystallization.

The magnetic susceptibilities were measured for powder samples of about 80 mg in a field of 8.8 kG from 1.7 to 300 K by means of a magnetic torsion balance described elsewhere.[9] The temperatures were measured with an AuCo–Cu thermocouple and a carbon resistor calibrated by measuring not only the magnetic susceptibility of Mn–Tutton salt, but also the vapor pressures of liquid helium, liquid hydrogen, and liquid nitrogen. The proton NMR measurements were carried out using a Robinson-type spectrometer operating at 35.0 MHz with an 80-Hz field modulation and with a field sweep. The magnetic field was calibrated by means of the proton absorption of H_2O. The low-field ESR (LF-ESR) spectra were observed using a Benedek-Kusida type spectrometer at 135 MHz.[10] Details of the apparatus for the low-field ESR measurements have been described elsewhere.[11] A conventional cryostat was used, and temperatures were determined using an Allen-Bradley carbon resistor calibrated against the vapor pressures of liquid helium, hydrogen, and nitrogen. The high-field ESR spectra in solution and in the crystalline state were obtained at room temperature, using JEOLCO X-band and Q-band spectrometers, respectively. The magnetic field was calibrated using the hyperfine splittings of Mn^{2+} doped in MgO.

Table 1. Results from susceptibility measurements

	χ_d (10^{-4} emu/mol)	θ (K)	T_m (K)	χ_m (10^{-4} emu/mol)	p	J/k(K)	a
Cl-porphyrexide	−1.08	−20	22.5	72	0.96	−18.2	0.4
Porphyrexide[a)]	−0.85	−8	7.2	207	0.91	−5.9	0.6
TANOL[b)]	−1.1	−6	6.5	226	1.00	−5.0	1.0

a) Ref. 4. b) Ref. 3.

Results

Susceptibility. The diamagnetic correction was made using Pascal's constant. The diamagnetic susceptibility, χ_d, is listed in Table 1. In the temperature range above 40 K, the paramagnetic susceptibility, χ_p, of Cl-porphyrexide follows the Curie-Weiss law, with a Weiss constant of $\theta=-20$ K and a spin concentration of 96.5%. As the temperature is lowered below 40 K, it deviates from the Curie-Weiss law and reaches a broad maximum at $T_m=22.5$ K, as is shown in Fig. 2. After passing through the maximum, it decreases gradually down to 3.5 K. However, below 3.5 K it increases again as the temperature is lowered. In the region from 1.7 to 2.3 K, the Curie-Weiss law was observed with a spin concentration of 0.5% and a Weiss constant of −0.4 K. When this low-temperature paramagnetic impurity curve is extrapolated to higher temperatures and subtracted from the experimental values, the corrected curve shown in Fig. 2 is obtained.

Proton NMR. In the proton NMR spectra of a powder sample of Cl-porphyrexide at 35.0 MHz, an assymetric single line was observed at a free proton position in the temperature range of 1.6—77 K. When the temperature was lowered below 77 K, the linewidth defined as the maximum slope width of signals obtained by 80-Hz field modulation increased and reached a maximum value of 8.0 G in the vicinity of $T_m=22.5$ K. Below T_m, it decreased as the temperature was lowered, and reached a value of 5.5 G at 4.2 K.

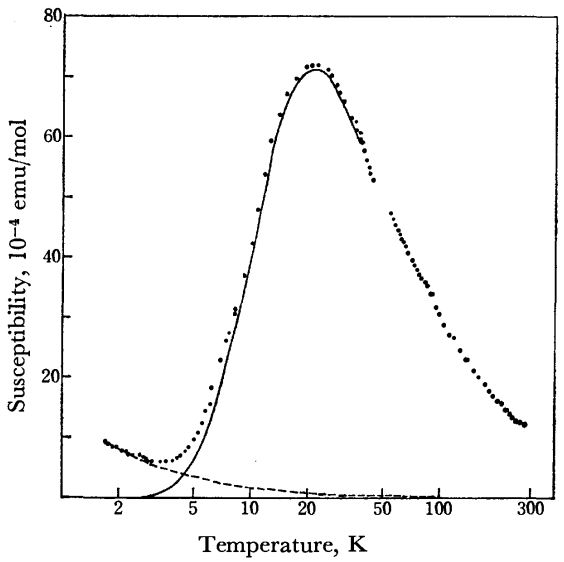

Fig. 2. Paramagnetic molar susceptibility of Cl-porphyrexide radical. The full circles represent the experimental values. The impurity curve indicated by the broken line is an extrapolation of the low temperature Curie-Weiss data. The solid line shows the difference between the experimental values and the impurity curve.

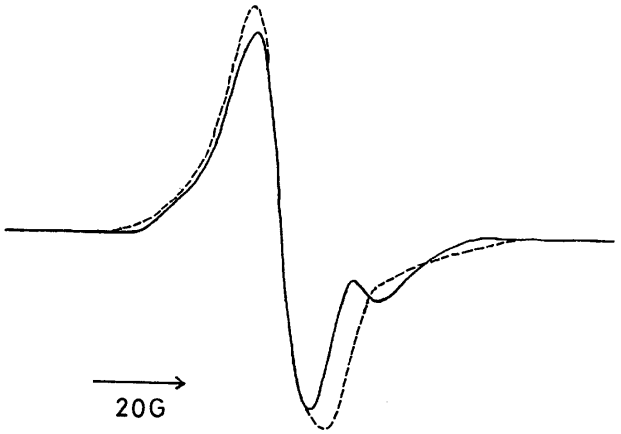

Fig. 3. Proton magnetic resonance spectra of porphyrexide, measured at 35 MHz. The solid line and the broken line represent the spectra at 20 K and 4.2 K, respectively.

The proton NMR spectra of a powder sample of porphyrexide at 35.0 MHz are shown in Fig. 3. In addition to the central unshifted line, one more absorption line shifted to higher magnetic field was observed in the temperature region 3.0—30 K. The magnitude of the shift was largest in the vicinity of $T_m=7.6$ K.[4] The resonance field of the unshifted line almost corresponded to the magnetic field of a free proton at that frequency.

X-Band ESR in Solution. The X-band ESR spectrum of Cl-porphyrexide in a chloroform solution is shown in Fig. 4. Triplet splitting ($a_N=8.5$ G), caused by the hyperfine interaction between an unpaired electron and a ^{14}N nucleus, and several subsplittings are observed. The g-value of Cl-porphyrexide in solution was determined to be 2.0060, which coincides with the values of other nitroxide radicals.

Fig. 4. The X-band ESR spectrum of Cl-porphyrexide in a chloroform solution.

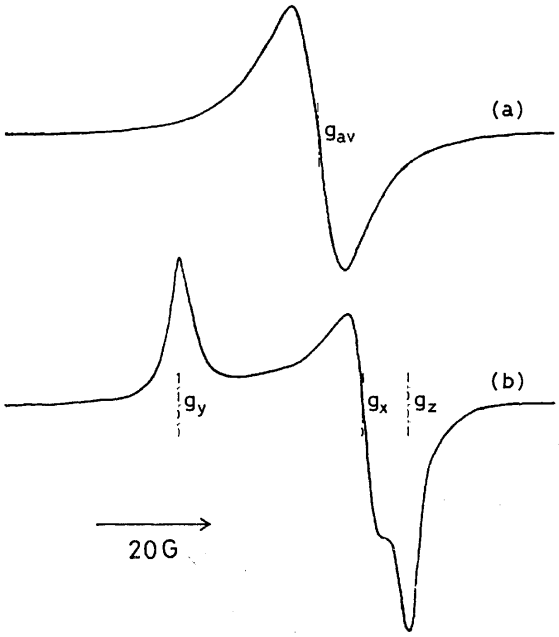

Fig. 5. The Q-band ESR spectra of porphyrexide (a) and Cl-porphyrexide (b) measured at room temperature.

Q-Band ESR. The *Q*-band ESR spectra for powder samples of porphyrexide and Cl-porphyrexide measured at room temperature are shown in Figs. 5(a) and (b), respectively. A relatively symmetrical single line was observed for porphyrexide. On the other hand, the spectrum of Cl-porphyrexide consists of three peaks. When single crystals of Cl-porphyrexide were used, a single line was obtained for any crystal orientation; the resonance field exhibited an angular dependence for an external magnetic field applied in a certain plane.

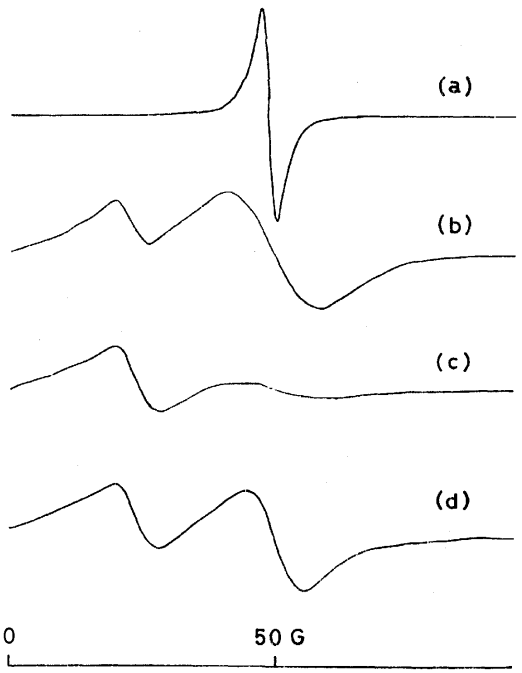

Fig. 6. The LF-ESR spectra of Cl-porphyrexide measured at 135 MHz.
(a) T=77 K, (b) T=6.3 K, (c) T=4.2 K, (d) T=2.0 K.

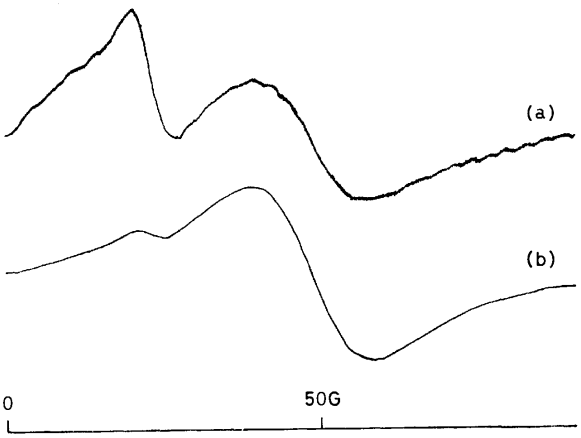

Fig. 7. The LF-ESR spectra of porphyrexide (a) and TANOL (b) measured at 135 MHz and at 1.4 K.

LF-ESR. The LF-ESR absorption spectra of powder samples of Cl-porphyrexide, porphyrexide, and TANOL all exhibit a single line which has an exchange-narrowed Lorentzian shape at room temperature. The temperature dependence of the LF-ESR spectrum for Cl-porphyrexide is shown in Fig. 6. Figures 7(a) and (b) show the LF-ESR spectra of porphyrexide and TANOL, respectively, measured at 1.4 K. When the temperature was lowered below room temperature, the linewidth of the g=2 absorption, defined as the peak-to-peak linewidth of the first derivative of the absorption spectrum, gradually decreased and exhibited a minimum in the vicinity of T_m. Then, it started to increase rapidly as the temperature was further decreased. Cl-porphyrexide and porphyrexide linewidths decreased again below given temperatures. The temperature dependence

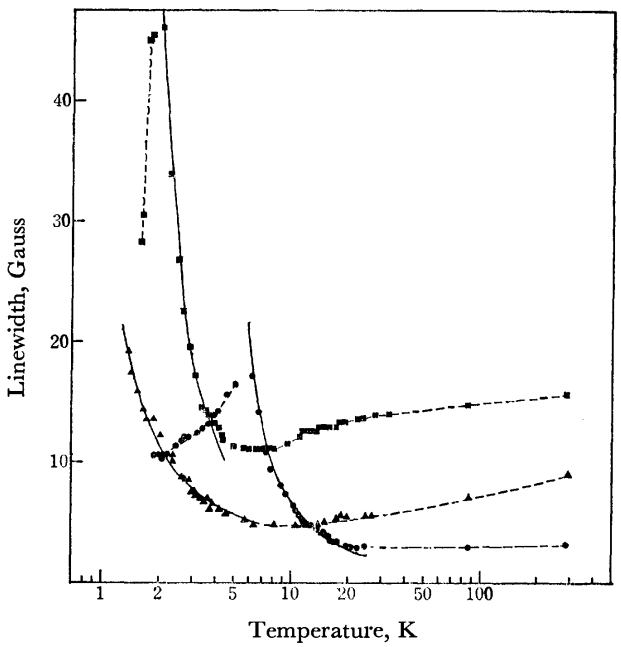

Fig. 8. The temperature dependence of the LF-ESR linewidth.
—●—, Cl-porphyrexide, —■— porphyrexide, —▲— TANOL.
The solid lines represent the curves calculated by Eq. 6.

of the linewidth for each sample is shown in Fig. 8. The relative susceptibility, obtained from the signal intensity, agreed qualitatively with the static susceptibility; it could not be treated quantitatively since the spectrometer sensitivity changed with temperature. The $g=4$ absorption could not be observed at room temperature or at liquid nitrogen temperature. Below the temperature at which the susceptibility deviated from the Curie-Weiss law, the $g=4$ ESR absorption was detected as the temperature was lowered. The linewidth of the $g=4$ ESR absorption was independent of the temperature within the experimental error. The ratio of the peak intensity of the $g=4$ resonance absorption to that of the $g=2$ absorption depended upon the angle between the direction of the radio-frequency field and that of the static magnetic field; it was the smallest when the radio-frequency field and the static magnetic field were perpendicular to each other.

Discussion

Susceptibility. The behavior of the magnetic susceptibility of Cl-porphyrexide is very similar to that of porphyrexide,[4] although the temperature T_m for the former is almost three times as high as that for the latter. The magnetic behavior cannot be explained quantitatively by the well-known pair model described by:

$$\chi_p = (Ng^2\beta^2S(S+1)/3kT)[1+(1/3)\exp(\Delta/kT)]^{-1}, \quad (1)$$

where Δ is the energy splitting between the ground singlet and the excited triplet states and is equal to $2J$. The maximum value of the observed susceptibility, χ_m, is about 15% smaller than the theoretical value calculated from Eq. 1. Moreover, the experimental values deviate from the theoretical χ_p-T curve as the temperature is decreased below T_m. These discrepancies can be reduced by introducing the alternating antiferromagnetic Heisenberg linear chain model[12] or the anisotropic regular chain model.[13] The susceptibility data of the nitroxide radical, TANOL, has been analyzed successfully on the basis of the regular Heisenberg model.[3] In the case of Cl-porphyrexide and porphyrexide, the g-values are nearly isotropic and are similar to those of nitroxide radicals, as is shown below, so that it is not appropriate to discuss their magnetic properties on the basis of the latter model. Therefore, the susceptibility data have been analyzed using the former model. The spin Hamiltonian for the former model is given by:

$$\mathcal{H} = -2J\sum_{i=1}^{N/2}(\boldsymbol{S}_{2i}\cdot\boldsymbol{S}_{2i-1}+a\boldsymbol{S}_{2i}\cdot\boldsymbol{S}_{2i+1}), \quad (2)$$

where J is the exchange integral coupling a certain spin with its nearest neighbor and aJ is the exchange integral of a spin with its next nearest neighbor. This model corresponds to the pair model when $a=0$ and to the regular Heisenberg model when $a=1$. The exact eigenvalue spectrum and thermodynamic properties of Eq. 2 have been calculated for short chains by Duffy and Barr.[12]

In Fig. 9, the (χ_p/p)-T data for Cl-porphyrexide and porphyrexide are given together with the "best fit"

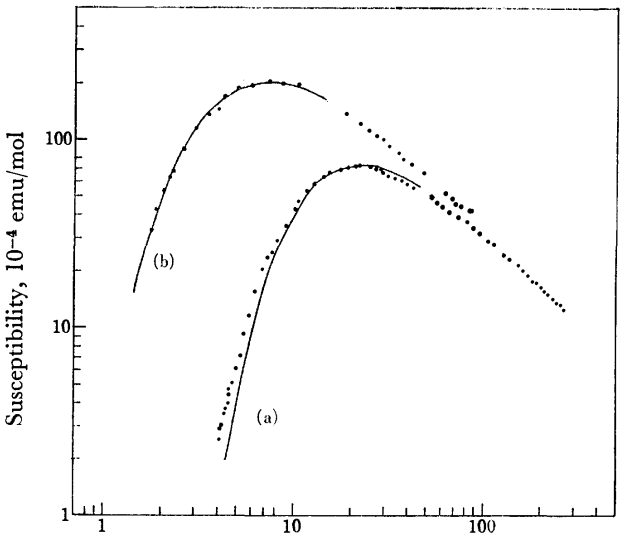

Fig. 9. Magnetic molar susceptibilities of Cl-porphyrexide (a) and porphyrexide (b). The full circles represent the experimental values of χ_p/p. The solid lines represent the theoretical χ_p-T curves with $a=0.4$ and $J/k=-18.2$ K (a), and $a=0.6$ and $J/k=-5.9$ K (b).

theoretical curves with $a=0.4$ and $J/k=-18.2$ K, and $a=0.6$ and $J/k=-5.9$ K, respectively. Here, p is the spin concentration which was found from the Curie-Weiss law observed at high temperature and is given in Table 1. The theoretical curves for $N=10$ were used, since it has been reported that the 10-spin chain values and ∞-spin chain estimates differ by less than 0.5% at $kT/|J|>0$, 0, 0.65, and 0.80 for $a=0.2$, 0.4, 0.6, and 0.8, respectively. The experimental results are in fairly good agreement with the theoretical curves. The interpretation based on this model may be tentative due to lack of a detailed crystal-structure determination. However, it may be concluded that the deviation of the susceptibility data from the pair-model curve is probably due to the existence of the second-strongest exchange interaction, since the curve for the pair model is described only by the strongest exchange interaction. The resulting parameters are summarized in Table 1, together with those for TANOL. The exchange parameter J for Cl-porphyrexide is relatively large in comparison with those of other neutral organic radicals and is the largest of the ring-iminoxyl radical exchange parameter investigated. The rise in the susceptibility of Cl-porphyrexide below 3.5 K is attributable to the impurity effect, as no abnormal behavior in the proton NMR spectra was found in this temperature range.

Recent specific heat and proton magnetic resonance measurements below 1 K, in the case of TANOL, revealed that the magnetic-phase transition occurs at about 0.4 K.[14,15] On the other hand, it may be impossible for Cl-porphyrexide and porphyrexide to change into a long-range ordered state even if the temperature is lowered below 1.4 K, since the magnitude of the susceptibilities is so small at 1.4 K that the exchange interaction leading to a long-range ordered state, such

as the interchain exchange interaction, is no longer effective.

Proton NMR. In the polycrystalline samples, the proton-resonance signal shift from the free-proton position in the direction of higher field can be approximately described by the following equation:[16,17]

$$\delta H = -a_H \chi H / g\beta g_N \beta_N. \quad (3)$$

The paramagnetic shift, δH, is proportional to the hyperfine coupling constant, a_H, and to the static magnetic susceptibility per molecule, χ. Taking the molecular framework of porphyrexide into account, the absorption line shifted to higher field can be roughly attributed to the three protons attached to the nitrogen atoms and the unshifted line to the six protons of the two methyl groups, since the spin density of the carbon atoms attached to the two methyl groups is expected to be very small. The hyperfine coupling constants of the three protons are evaluated to be −2.5 G using the susceptibility results.[4] From McConnell's relation, the unpaired electron-spin densities of the three nitrogen atoms are estimated to be +0.074 using $Q(\mathrm{NH}) = -33.7$ as obtained by Barton and Frenkel.[18] This assignment may be valid since the sign of the spin densities of the three nitrogen atoms is expected to be positive on the basis of electronic structure.

The resolved spectrum of Cl-porphyrexide could not be observed, since the static susceptibility is relatively small even at T_m. However, the asymmetric line shape may be due to the existence of a hyperfine interaction between the unpaired electron and the two protons attached to the nitrogen atoms. The temperature dependence of the linewidth may be explained by the hyperfine interaction which is related to the static susceptibility.[17] The susceptibility of TANOL obtained from the proton NMR shifts in single crystals agrees quantitatively with that of the one-dimensional Heisenberg model.[19]

X-Band ESR in Solution. The ^{14}N hyperfine constants, a_N, obtained in solution are shown in Table 2.[20,21] The hyperfine constants arising from the nitrogen nucleus of the NO group can be semiempirically described by the following equation:[22,23]

$$a_N = 134.8\rho_N - 35.8\rho_O, \quad (4)$$

where ρ_N and ρ_O are the unpaired π-electron spin densities at the nitrogen and oxygen atoms. In TANOL the values of $\rho_N+\rho_O$ is considered to be 1.0 since the unpaired electron is almost localized on the NO group masked by the four methyl groups. In porphyrexide the value of $\rho_N+\rho_O$ is estimated to be 0.78 using the NMR results neglecting the spin densities of the two carbon atoms attached to the nitrogen atoms which are expected to be negative and small on the basis of the electronic structure. Therefore, ρ_N and ρ_O were calculated from Eq. 4. In Cl-porphyrexide, they were calculated assuming that the value of ρ_N/ρ_O is equal to that of porphyrexide. The results are summarized in Table 2. The NMR and ESR results indicate that, in porphyrexide radicals, 20—30% of the unpaired electron from the NO group is distributed over the ring. Delocalization of the unpaired electron over the ring may play some role in the exchange interaction. Furthermore, it may be related to the high stabilization of these radicals, in addition to the steric hindrance of the two methyl groups.

Table 2. Hyperfine constants and spin densities

	a_N(G)	ρ_N	ρ_O
TANOL	15.5[a]	0.30	0.70
Porphyrexide	10.0[b]	0.22	0.56
Cl-porphyrexide	8.5	0.20	0.51

a) Ref. 20. b) Ref. 21.

Q-Band ESR. The Q-band ESR spectrum for powder samples of Cl-porphyrexide can be interpreted in terms of the g-factor anisotropy. The principal g-values obtained using the approximation of Kneübuhl[24] are shown in Table 3. Kikuchi has calculated the g-values of several nitroxide radicals using the CNDO/2 molecular-orbital calculation method.[25] The calculated principal g-values of H_2NO are cited in Table 3, along with the principal axes given by Kikuchi. The principal values are in fairly good agreement with those of Cl-porphyrexide. Furthermore, in the case of single crystals crystallized from methanol in rhombic plates, a single line was obtained for any crystalline orientation. These facts indicate that probably all the Cl-porphyrexide radicals are oriented with the N–O bond aligned along a unique direction in the crystalline state even if there is more than one site per unit cell. One-site ESR spectra were observed in the case of TANOL, as is expected from its crystal structure.[26] The principal velues are also given in Table 3.

On the other hand, a relatively symmetrical single line was observed for porphyrexide, with $g=2.0060$ which corresponds to the averaged g-value for the nitroxide radicals. The porphyrexide molecules have at least two different orientations in the crystalline state, so that the g-factor anisotropy may be averaged out by the exchange interaction between the unpaired electrons of two molecules oriented differently. The fact that Cl-porphyrexide has a large exchange interaction compared with that of porphyrexide can be ascribed to the difference in the crystal structure. The strongest exchange interaction of Cl-porphyrexide may arise from the overlap of the $P_z\pi$-orbitals between adjacent molecules

Table 3. Principle and averaged g-values

	g_x	g_y	g_z	g_{av}	Axis
Cl-porphyrexide	2.0048	2.0098	2.0034	2.0060	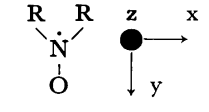
Porphyrexide	—	—	—	2.0061	
TANOL	2.0064	2.0096	2.0027	2.0062	
H_2NO[a]	2.0062	2.0091	2.0023	2.0059	

a) Calculated values (Ref. 25).

aligned in the z-direction. The decrease in the strongest exchange interaction of porphyrexide in comparison with that of Cl-porphyrexide is considered to be due to the increase in the distance between the two molecules or to the twisted overlap of the $P_z\pi$-obitals, which is caused by the existence of more than two molecular orientations.

LF-ESR. In the case of powder samples, the LF-ESR linewidths are more important since the contribution to the linewidth from the anisotropy of the g-values is excluded. The absorption lines observed at room temperature exhibit exchange-narrowed Lorentzian shapes. We can apply the usual three-dimensional Anderson-Weiss formula for a Lorentzian line:[27]

$$\Delta H = \Delta H_d^2/\sqrt{3}H_{ex}, \quad (5)$$

where ΔH is the peak-to-peak linewidth, ΔH_d^2 the second moment of the sum of the dipole-dipole interactions that would be observed in the absence of exchange, and H_{ex} the exchange field which is directly proportional to the exchange interaction J. In the low-field case, the so-called 10/3 effect is taken into account in Eq. 5. Since the crystal structures of Cl-porphyrexide and porphyrexide have not been determined, the second moment cannot be estimated from the Van Vleck formula. However, the second moment is the sum of the dipole-dipole interactions within the crystal, so that it is not as sensitive to changes in the crystal structure as is the exchange interaction. Therefore, the ratio of the exchange integrals J of Cl-porphyrexide and porphyrexide are evaluated from the ESR linewidths at 290 K and T_m to be 4.7 and 3.7, respectively, provided that the second moment of Cl-porphyrexide is approximately equal to that of porphyrexide. This ratio is consistent with the ratio 3.1 obtained from the magnetic susceptibility results (Table 1). This suggests that the ESR lines are narrowed predominantly by the strongest exchange interaction in the high-temperature range.

Table 4. Parameters for temperature dependent LF-ESR linewidth: $\Delta H=\alpha \exp(\beta J/kT)$

	α	β
Cl-porphyrexide	1.1	0.93
Porphyrexide	3.0	0.95
TANOL	3.6	0.48

The decrease in the linewidth from room temperature to T_m may be interpreted in terms of the contribution of spin-lattice relaxation to the linewidth since the spin-lattice relaxation time generally increases with decreasing temperature. The rapid broadening of the resonance is attributable to an increase in the correlation time for exchange motion because of spin ordering below the temperature of maximum susceptibility. As is shown in Fig. 7, the observed linewidth versus temperature below T_m can be fitted to the following empirical relation:

$$\Delta H = \alpha \exp(\beta J/kT). \quad (6)$$

The α and β values are summarized in Table 4. The β value is considered to be associated with the correlation mechanism of exchange motion which may be related to the magnetic behavior of the system. It is interesting that the β value for Cl-porphyrexide is roughly equal to that for porphyrexide and is almost twice as large as that for TANOL. These results indicate that the magnetic behavior of Cl-porphyrexide is similar to that of porphyrexide in spite of the difference in the crystal structures expected on the basis of the Q-band ESR spectra and is different from that of TANOL. Furthermore, they suggest that the exchange correlation time increases more rapidly in a pair-like system such as an alternating linear-chain system than in a regular linear-chain system. The narrowing of the resonance line below a certain temperature is probably due to paramagnetic impurities. Such behavior was also found in PAC and in Würster's blue perchlorate.[28]

The resonance line at $g=4$ is not due to the $\Delta M=2$ transition within the triplet levels caused by pairs of exchange coupling spins, since it has been found even for TANOL, in which no electron spin pairing occurs. It is probably caused by a forbidden transition due to dipolar interaction, as has been reported by Rhodes *et al.*[28] In the high-temperature region, the strong exchange interaction averages the dipolar coupling, so that the $g=4$ resonance cannot be detected.[29] The appearance of the $g=4$ resonance at low temperatures can be explained by an increase in the correlation time for exchange motion, as is expected from the linewidth of the $g=2$ resonance and the susceptibility data.

Summary

Because of the isotropic character of the g-factor, the susceptibility of Cl-porphyrexide was interpreted assuming that the magnetic behavior is due to alternating antiferromagnetic Heisenberg linear chains. The parameters derived from the susceptibility are $\theta=-20$ K, $T_m=22.5$ K, $\chi_m=72\times10^{-4}$ emu/mol, $J/k=-18.2$ K, and $a=0.4$. The fact that the strongest exchange interaction for Cl-porphyrexide is almost three times as large as that for porphyrexide is considered to be due to the difference of the crystal structures, as is expected from the Q-band ESR spectra. The LF-ESR lines are narrowed by the exchange interaction in the high-temperature region and the ratio of the strongest exchange integral J for Cl-porphyrexide to that for porphyrexide obtained from the linewidth is consistent with the ratio obtained from the susceptibility data. The rapid broadening of the $g=2$ absorption line and the distinct appearance of the $g=4$ absorption line are attributable to an increase in the correlation time for exchange motion resulting from spin ordering below the temperature of the susceptibility maximum. The susceptibility data and the temperature dependence of the LF-ESR linewidths indicate that the magnetic behavior of Cl-porphyrexide is similar to that of porphyrexide and is different from that of TANOL. In porphyrexide radicals, 20—30% of the unpaired electron is distributed over the ring from the NO group. More quantitative discussions concerning the magnetic interaction will be possible when detailed crystal-structure determinations are available in the future.

The author is deeply indebted to Professor Yasuo Deguchi for his continuous encouragement throughout this work, and also to Drs. Hiroaki Ohya-Nishiguchi, Jun Yamauchi, and Akira Nakajima for helpful advice and discussions. He also thanks Mr. Teruaki Fujito for supplying the susceptibility data of porphyrexide. Thanks are also due to Dr. Kohji Watanabe for his advice on the preparation of the samples.

References

1) W. Duffy, Jr., and D. L. Standburg, *J. Chem. Phys.*, **46**, 456 (1967).
2) W. Duffy, Jr., and K. P. Barr, *Phys. Rev.*, **165**, 647 (1968).
3) J. Yamauchi, *Bull. Chem. Soc. Jpn.*, **44**, 2301 (1971).
4) T. Fujito, H. Nishiguchi, Y. Deguchi, and J. Yamauchi, *Bull. Chem. Soc. Jpn.*, **42**, 3334 (1969).
5) N. Azuma, J. Yamauchi, K. Mukai, and H. Ohya-Nishiguchi, *Bull. Chem. Soc. Jpn.*, **46**, 2728 (1973).
6) A. R. Forrester, J. M. Hay, and R. H. Thomson, "Organic Chemistry of Stable Free Radicals," Academic Press, London (1968), p. 227.
7) O. Piloty and B. G. Schwerin, *Ber.*, **34**, 2354 (1901).
8) E. G. Rozantev, *Izv. Akad. Nauk. SSSR, Ser. Khim.*, **12**, 2218 (1964).
9) H. Mekata, *J. Phys. Soc. Jpn.*, **17**, 796 (1962).
10) G. B. Benedek and T. Kusida, *Phys. Rev.*, **118**, 46 (1960).
11) M. A. Garstens, L. S. Singer, and A. H. Ryan, *Phy. Rev.*, **96**, 53 (1954).
12) W. Duffy, Jr., and K. P. Barr, *Phy. Rev.*, **96**, 53 (1954).
13) J. C. Bonner and N. E. Fisher, *Phy. Rev. A*, **135**, 640 (1964).
14) S. Saito and T. Sato, *Phys. Lett. A*, **44**, 2301 (1971).
15) J. P. Boucher, M. Hechtschein, and M. Saint-Paul, *Phys. Lett. A*, **42**, 397 (1972).
16) T. Yoshioka, H. Ohya-Nishiguchi, and Y. Deguchi, *Bull. Chem. Soc. Jpn.*, **47**, 430 (1974).
17) T. Yoshioka, K. Watanabe, and H. Ohya-Nishiguchi, *Bull. Chem. Soc. Jpn.*, **48**, 2533 (1975).
18) B. L. Barton and G. K. Frenkel, *J. Chem. Phys.*, **41**, 1455 (1964).
19) T. Yoshioka, unpublished work.
20) K. Watanabe, J. Yamauchi, H. Takaki, H. Nishiguchi, and Y. Deguchi, *Bull. Inst. Chem. Res., Kyoto Univ.*, **48**, 264 (1970).
21) K. H. Hausser, *Z. Naturforsh*, **14a**, 425 (1959).
22) K. Mukai, H. Nishiguchi, K. Ishizu, Y. Deguchi, and H. Takaki, *Bull. Chem. Soc. Jpn.*, **40**, 2731 (1967).
23) P. H. Rieger and G. K. Fraenkl, *J. Chem. Phys.*, **39**, 609 (1963).
24) F. K. Kneubühl, *J. Chem. Phys.*, **33**, 1074 (1960).
25) O. Kikuchi, *Bull. Chem. Soc. Jpn.*, **40**, 704 (1967).
26) J. Lajzerowicz-Bonneteau, *Acta Crystallogr, Sect. B*, **24**, 196 (1968).
27) P. W. Anderson and P. R. Weiss, *Rev. Mod. Phys.*, **25**, 269 (1953).
28) R. S. Rhodes, J. H. Burgess, and A. S. Edelstein, *Phys. Rev. Lett.*, **6**, 462 (1961).
29) V. I. Konovalov and S. M. Ryabchenko, *Soviet Physics-Solid State*, **8**, 2833 (1967).

Simple Relations between Scattering Cross Sections and Molecular Diameters

Yoshitsugu OONO and Yukio NISHIMURA

Research Institute of Industrial Science, Kyushu University, Higashi-ku, Fukuoka 812

(Received August 12, 1976)

Empirical linear relations between the square roots of the electron-scattering cross sections for molecules and the cube roots of the van der Waals volumes for molecules due to Bondi are shown. The relations allow one to estimate, for example, the electron-impact ionization cross sections at 75 eV to within an error of ±15%. A dimensional analytic explanation of the relations is given.

It is a natural idea that the scattering cross section for a given collision process strongly depends on the size of the target. For example, in the case of electron collisions with molecules, Schmieder[1] has shown that there is a positive correlation between the molecular size and the collision probability P_c (*i.e.*, the number of collisions, per unit electron flux, per unit path length, per unit pressure at 0 °C). However, since the method for the evaluation of the size of the molecule was not systematic, it has not been possible to render this idea quantitative. Recently, Christophorou *et al.*[2] have shown that the cross section for the scattering of thermal electrons by normal alkanes is proportional to the mean square end-to-end distance, although the method for evaluating of the molecular size cannot be extended to molecules other than normal alkanes.

In this paper, it is shown that the following relation holds for several scattering processes involving molecules of molecular liquids:

$$\sigma^{1/2} = Av^{1/3} + B,$$

where σ is the scattering cross section, v the van der Waals volume of the molecule,[3] and A and B are numerical constants independent of the target molecule. Since the van der Waals volume is a good measure of the molecular size, this linear relation is a quantitative version of the natural idea mentioned above. There exist other measures of the molecular size, but the van der Waals volume is convenient for small molecules. For large molecules (or molecules with melting points higher than 150 K), the method of evaluation using the effective hard-core size of the molecule, proposed by one of the present authors,[4] can also be successfully used.

By using an empirical linear relation, rough estimations of the cross sections are possible. Such a relation reminds one of the Hammett rule, since the coefficients of the linear relation are independent of the target molecule and dependent only on the nature of process (or reaction).

A brief dimensional analytic account of the empirical relation will be given.

Empirical Relations

The van der Waals volumes for molecules, v, are calculated using the tables of Bondi.[3] Van der Waals volumes for rare gas atoms and hydrogen chloride are calculated from their critical volumes, V_c, using the crude relation, $v \simeq 0.18\ V_c$.

The relation between the ionization cross sections for 75-eV electrons σ_{ion}[5] and v is shown in Fig. 1. From Fig. 1 we get

$$\sigma_{ion}^{1/2} = 1.73v^{1/3} - 2.37, \quad (1)$$

where σ_{ion} is in Å^2 and v in cm^3/mol. Using Eq. 1, we can estimate σ_{ion}. The accuracy of the estimate is about ±15%, except for krypton, xenon, isobutane, and cyclohexane.

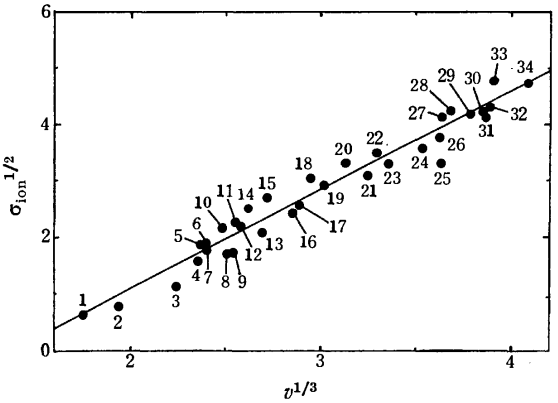

Fig. 1. The square root of the electron impact (75 eV) ionization cross section σ_{ion} (in Å^2)[5] *vs.* the cubic root of the van der Waals volume v (in cm^3/mol). The line denotes Eq. 1.
1: Helium, 2: neon, 3: hydrogen, 4: oxygen, 5: argon, 6: ammonia, 7: nitrogen oxide, 8: nitrogen, 9: carbon monoxide, 10: hydrogen chloride, 11: krypton, 12: methane, 13: carbon dioxide, 14: hydrogen sulfide, 15: xenon, 16: acetylene, 17: ethylene, 18: chloromethane, 19: ethane, 20: cyclopropane, 21: propene, 22: chloroethane, 23: propane, 24: isobutylene, 25: isobutane, 26: butane, 27: benzene, 28: cyclopentane, 29: isopentene (probably a mixture), 30: isopentene, 31: neopentane, 32: pentane, 33: cyclohexane, 34: hexane.

The linear relations between $P_c^{1/2}$ and $v^{1/3}$ for electron energies, E, of 49 and 25 eV are shown in Fig. 2. Even for E=4 eV this linear relation holds (Fig. 3). For 50 eV$\gtrsim E \gtrsim$15 eV these linear relations can be summarized as

$$P_c^{1/2} \simeq (5.56 - 0.22E^{1/2})(v^{1/3} - 1.0).$$

The linear relation between $P_c^{1/2}$ and $v^{1/3}$ also holds for much larger values of E, because the Born approximation is rather accurate for large E. However, the linear relation between $P_c^{1/2}$ and $E^{1/2}$ is crude and, for too large E, this linear relation ceases to hold.

For the case of monoatomic elements, it is known[6] that P_c is inversely proportional to the ionization

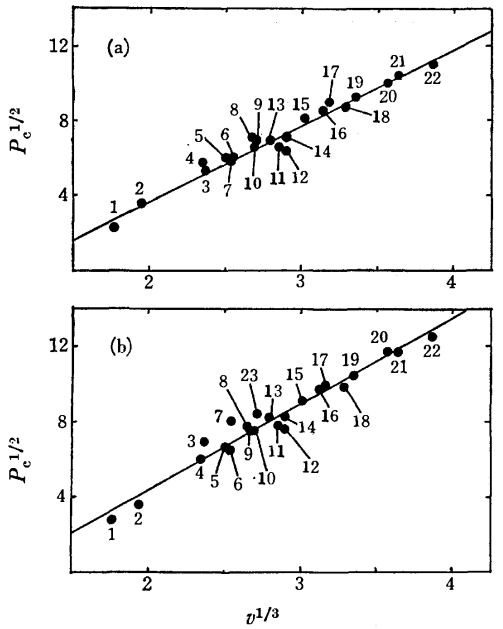

Fig. 2. The square root of the probability of collision P_c (in cm²/cm³ Torr)[1,6] *vs.* the cubic root of the van der Waals volume v (in cm³/mol). (a) is for the electron energy 49 eV, and (b) for 25 eV. The line in (a) denotes $P_c^{1/2}=4.02v^{1/3}-4.31$ and that in (b) $P_c^{1/2}=4.26v^{1/3}-4.49$.
1: Helium, 2: neon, 3: argon, 4: oxygen, 5: nitrogen, 6: krypton, 7: carbon monoxide, 8: dinitrogen oxide, 9: carbon dioxide, 10: fluoromethane, 11: acetylene, 12: hydrogen chloride, 13: methanol, 14: methylamine, 15: ethane, 16: dimethyl ether, 17: ethanol, 18: dimethylamine, 19: propane, 20: trimethylamine, 21: isobutane, 22: pentane, 23: xenon.

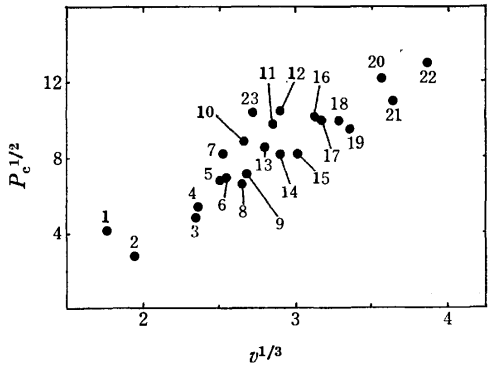

Fig. 3. The square root of the probability of collision P_c (in cm²/cm³ Torr) of electron[1,6] *vs.* the cubic root of the van der Waals volume v (in cm³/mol) at electron energy 4 eV. The numbers in the figure are the same as in Fig. 2.

potential, I. Although there is some correlation between the ionization potential and σ_{ion}^{-1} or P_c^{-1}, no clear relation similar to that shown above exists between them. According to Morrison (cited in Ref. 3) the van der Waals radii of atoms are proportional to $I^{-1/2}$, but this relation does not hold as accurately as the empirical relations proposed here. Lampe *et al.*[5] have shown that σ_{ion} is proportional to the polarizability, α. It is also

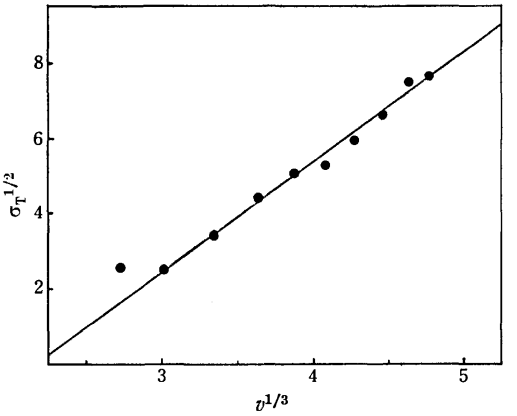

Fig. 4. The square root of the scattering cross section of thermal electrons with normal alkanes (methane to decane from left to right) σ_T (in Å²)[2] *vs.* the cubic root of the van der Waals volume v (in cm³/mol). The line denotes Eq. 2.

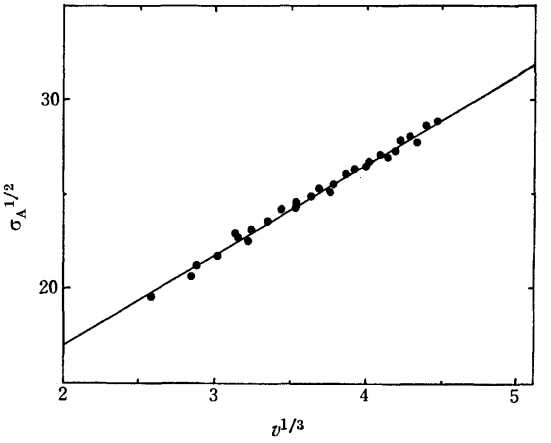

Fig. 5. The square root of the scattering cross section of thermal argon with hydrocarbons σ_A (in Å²)[8] *vs.* the cubic root of the van der Waals volume v (in cm³/mol). The line denotes Eq. 3.

known that P_c is proportional to α. However, it appears to be very difficult to explain these proportionalities. The explanation of Lampe *et al.* is based on the Born-approximation expression[7] of the cross sections, so that it is not conclusive.

The relation between the total cross section σ_T for the scattering of thermal electrons by normal alkanes[2] and v is shown in Fig. 4. The relation between the total cross section σ_A for the scattering of thermal argon atoms by hydrocarbons[8] and v is shown in Fig. 5. The empirical linear relations are as follows:

$$\sigma_T^{1/2} = 2.91v^{1/3} - 6.32 \quad (2)$$

and

$$\sigma_A^{1/2} = 4.79v^{1/3} + 7.38, \quad (3)$$

where σ_T and σ_A are in Å². For these very low-energy processes, the linear relations are valid only in a restricted group of compounds (*e.g.*, hydrocarbons), and hence are not very interesting, since we are interested in properties not strongly dependent on the electronic structure of the molecules.

Discussion

For higher-energy processes the Born approximation is valid, which suggests[7] that the cross sections are proportional to the geometrical cross sections of the target molecules. However, for lower-energy processes (for example, processes involving electrons having kinetic energy less than 100 eV), the Born approximation is not reliable. The theoretical calculation of the scattering cross sections for low-energy processes is very complicated. Thus, the derivation of the empirical relations above from scattering theory may be very difficult.

However, physical insight may be obtained from a dimensional analysis. All the relations obtained above are linear ones between $v^{1/3}+r_0$ and $\sigma^{1/2}$, where σ is the scattering cross section and r_0 is some constant. This suggests that the measure of the molecular diameter for collisional processes is not $v^{1/3}$, but $v^{1/3}+r_0$. The constant r_0 is considered, for example, to represent the Ramsauer-Townsend effect. Further considerations of r_0 are given below. Other relevant quantities with the dimension of length are σ, and the de Broglie wavelength of the projectile, λ. Hence we conclude that

$$\sigma^{1/2} = (v^{1/3}+r_0)f((v^{1/3}+r_0)/\lambda), \qquad (4)$$

where f is an appropriate function. In the high-energy limit, the scattering processes can be treated classically, so that $\lim_{\lambda\to 0} f((v^{1/3}+r_0)/\lambda)$ must be a finite constant. Therefore, for higher-energy scattering processes, f depends only slightly on $v^{1/3}+r_0$ and the empirical linear relation shown is obtained. As is seen in Figs. 1—5, r_0 is negative for σ_{ion}, P_c, and σ_T and is positive for σ_A. For the total cross sections for the scattering of positrons σ_P by rare gas atoms,[9] r_0 is also negative. Thus, we may concluded that r_0 is negative for charged particle scattering and positive for neutral particle scattering. For σ_T and σ_P, the negative r_0 can be explained by the Ramsauer-Townsend effect.[9] For impact ionization, an electron must strongly interact with the electron cloud of the target molecule, so that the length scale governing the cross section is not $v^{1/3}$ itself but the diameter of the electron cloud. Thus, the r_0 for σ_{ion} can be considered to represent the difference between the van der Waals diameter and the diameter of the electron cloud. For σ_{ion}, r_0 is *ca.* 1.8 Å and is about the twice the difference between the van der Waals radius and the covalent bond radius of Pauling. This may be a correct interpretation of r_0 for electron-impact ionization processes.

The square root of the (scattering) cross section *vs.* $v^{1/3}$ plot may be used to extract the specificity of molecules, since it has been implicitly assumed in deriving Eq. 4 that the electronic structure of the target molecules is relevant only through the van der Waals diameter. For example, the quenching cross sections of He (2^1S) by atoms and molecules[10] are shown in Fig. 6. From this, it may be concluded that ammonia, carbon dioxide, dinitrogen oxide, oxygen, and hydrogen have chemically specific properties in this reaction.

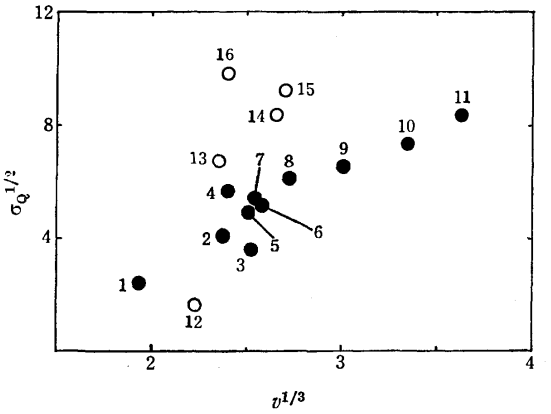

Fig. 6. The square root of the quenching cross section of He (2^1S) σ_Q (in Å^2)[10] *vs.* the cubic root of the van der Waals volume v (in cm^3/mol). ● Roughly satisfy a linear relation between $\sigma_Q^{1/2}$ and $v^{1/3}$, but ○ significantly deviate from this relation.
1: Neon, 2: argon, 3: nitrogen, 4: nitrogen oxide, 5: carbon monoxide, 6: methane, 7: krypton, 8: xenon, 9: ethane, 10: propane, 11: butane, 12: hydrogen, 13: oxygen, 14: dinitrogen oxide, 15: carbon dioxide, 16: ammonia.

One of the authors (Y. O.) would like to thank Dr. M. Tsuji for his encouragement.

References

1) F. Schmieder, *Z. Elektrochem.*, **36**, 700 (1930).
2) L. G. Christophorou, M. W. Grant, and D. Pittman, *Chem. Phys. Lett.*, **38**, 100 (1976).
3) A. Bondi, *J. Phys. Chem.*, **68**, 441 (1964).
4) Y. Oono, *Bull. Chem. Soc. Jpn.*, **48**, 2270 (1975).
5) F. W. Lampe, J. L. Franklin, and F. H. Field, *J. Am. Chem. Soc.*, **79**, 6129 (1957).
6) R. B. Brode, *Rev. Mod. Phys.*, **5**, 257 (1933).
7) H. Bethe, *Ann. Phys.*, **5**, 325 (1930).
8) T. Nenner, H. Tien, and J. B. Fenn, *J. Chem. Phys.*, **63**, 5439 (1975).
9) H. Massey, *Physics Today*, **29**, 3, 42 (1976).
10) A. L. Schmeltekopf and F. C. Fehsenfeld, *J. Chem. Phys.*, **53**, 3173 (1970).

The Raman Spectra of Solid and Liquid Tetramethylsilane

Takako SHINODA

National Chemical Laboratory for Industry, Shibuya-ku, Tokyo 151

(Received September 16, 1976)

Laser Raman spectra of tetramethylsilane in its three crystalline forms and in the liquid state have been observed for the lattice and intramolecular vibrational regions. The bands due to lattice vibrations increase as the transitions from α to β and to γ occur. The spectra of the β and γ forms exhibit crystal-field splittings of intramolecular bands. The observed spectra suggest that the β and γ forms are isomorphous with each other and the α form has a higher symmetry.

Solid $Si(CH_3)_4$ has been shown by calorimetric studies[1] to have three crystalline forms designated by α, β, and γ, their triple point temperatures being 165.91, 170.98, and 174.05 K, respectively. The transitions α-to-β-to-γ seem to be irreversible. The infrared and Raman spectra of the liquid state were measured and band assignments made by several authors,[2] but the crystal structures of the three forms have not been studied.

In the present investigation, the Raman spectra of $Si(CH_3)_4$ in its three crystalline phases and liquid state have been measured for the entire spectral region including lattice and intramolecular vibrations in order to obtain information on the crystal structure and molecular motions of the three forms.

Experimental

The sample of $Si(CH_3)_4$ was the same as that used in a previous calorimetric measurement,[1] the purity of which was determined to be 99.995_4 mol% by the measurement of melting point. The Raman spectra were obtained with a Raman spectrometer, Kawaguchi Electric Works Ltd. model RL-62. The exciting light was 488.0 or 514.5 nm line of the Ar^+ laser, NEC model GLG2003. The cryostat, experimental techniques and temperature measurements have been reported.[3] The crystals were grown from the liquid by careful cooling. The result of total thermal analysis obtained by using the apparatus for laser Raman measurements is shown in Fig. 1. After each measurement, the crystalline form was checked by observing its melting point.

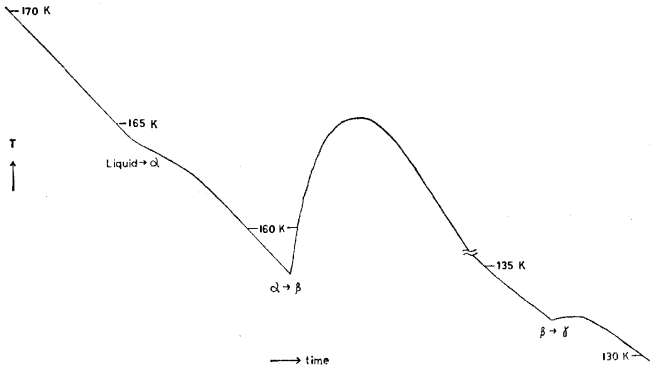

Fig. 1. Cooling curve (total thermal analysis) of $Si(CH_3)_4$.

Results and Discussion

Raman Spectrum in the Lattice Region. The observed spectrum in the lattice region consists of very weak and broad ghost bands. The lattice bands became very weak in the β and γ forms because a transparent crystal could not be obtained. The slitwidths of 3.1—3.6 cm^{-1} were used for reasonable intensities without too much background noise. The spectrum of the α-form in the lattice region is compared with corresponding spectrum of the γ-form in Fig. 2. The temperature measured was 163.9 K, which is about 2 K below the melting point of the α-form. The spectrum in the lattice vibrational region for the β-form at 152.7 K, about 18 K below its melting point, is shown in Fig. 3 together with the corresponding spectrum of the γ-form.

The Raman spectra of the β and γ forms have a pattern similar to each other with a large number of bands (Fig. 3). A similar spectral pattern suggests the two forms to be isomorphous with each other. Many bands in the lattice region suggest that the crystal contains many molecules of non-identical spatial position or orientation in a crystallographic unit cell with a low symmetry, as solid-CCl_4[4] and solid-CBr_4[5] in the low-temperature phases. In the Raman spectrum of the

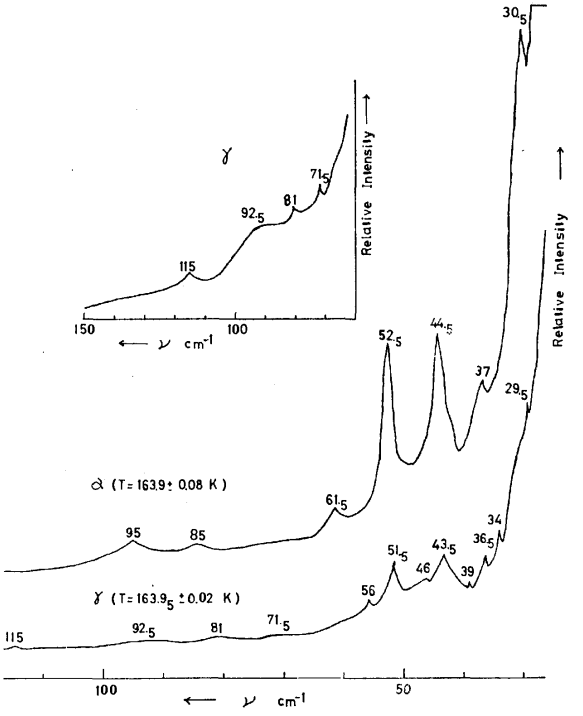

Fig. 2. Raman spectra in the lattice region of the α and γ forms at 163.9 K.

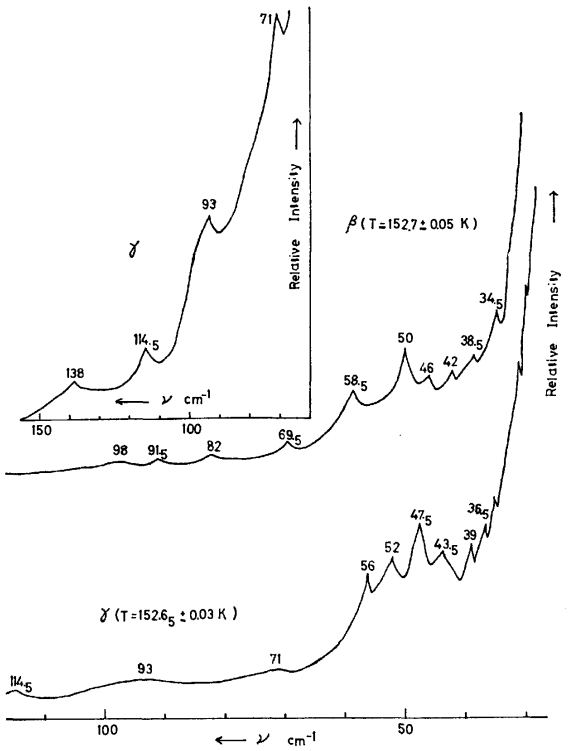

Fig. 3. Raman spectra in the lattice region of the β and γ forms at 152.7 K.

α-form the number of bands is smaller than that for the β and γ forms, probably owing to the high symmetry of the unit cell. We find no values in literature to compare with the ν values of lattice vibrations observed. The activation energies for the molecular reorientation or tumbling motion for γ-$Si(CH_3)_4$ were found to be 7.23 ± 0.40 and 8.7 ± 0.5 kcal mol^{-1} (above $\approx$140 K) by Smith[6] and Albert and Ripmeester[7] from their NMR studies. If molecules are assumed to be rigid rotators in a potential field of the type

$$V = (1/2)V_0(1-\cos n\theta), \quad (1)$$

the corresponding frequencies of librational lattice vibrations can be estimated from the above activation energies. The value of the moment of inertia of the molecule was calculated to be 27.20×10^{-39} g cm^2 by assuming the bond angle to be $\angle HCH=109°$ and interatomic distances $r_{CH}=1.10$ and $r_{CSi}=1.888$ Å.[8] The calculated results for $n=2$ and $n=3$ give values of frequencies of 32—35 and 48—53 cm^{-1}, respectively. Thus, the present values of lattice vibrations are reasonable.

Raman Spectrum of Intramolecular Vibrations. The Raman spectra of the liquid state and the three crystalline forms of $Si(CH_3)_4$ are shown in Fig. 4 for the intramolecular vibrational regions. The observed frequencies are given in Table 1 together with those reported.[2] The lines of the β and γ forms show a splitting of the degenerate fundamental of 7—26 cm^{-1}. In the crystal, the presence of some molecules of non-identical spatial position or orientation in the unit cell induces a splitting of the vibrational levels. In recent studies of other similar tetrahedral molecular crystals (CF_4[9] and CCl_4[10]) under high resolution, crystal splittings of the degenerate fundamentals were observed. The splittings observed for the degenerate fundamentals in the β and γ forms may be due to crystal effects.

The relative intensities of the lines obtained by integration are given in Table 1. We see that the relative intensities of the lines belonging to species e are large in α and those in β and γ are similar to each other. If only skeletal modes are taken into account, the vibrations $\nu_1(a_1)$, $\nu_2(e)$, $\nu_3(f_2)$, $\nu_4(f_2)$ are active in Raman scattering in the free molecule (T_d symmetry), The ratios of the intensity to that of the totally symmetric vibration, ν_1, for the liquid state, α, β and γ forms were estimated. The results are as follows, $I(\nu_2)/I(\nu_1)$: 1.3,

Table 1. Observed Raman active molecular vibrations of $Si(CH_3)_4$

Liquid[a]		Liquid			Solid(α)			Solid(β)			Solid(γ)			Sym. species
ν (cm^{-1})	Int	ν (cm^{-1})	Int	T(K)	ν (cm^{-1})	Int	T(K)	ν (cm^{-1})	Int	T(K)	ν (cm^{-1})	Int	T(K)	
199	80	199.$_5$	36(53)	176.6$_5$(295.2)	201.$_5$	98	163.9	205	45	152.6$_5$	181 207.$_5$	35	102.2	e
245	46	245	22(27)	176.5 (295.2)	243	58	163.9	232 248	29	152.7	235.5 248.5 249.5	19	102.2	f_2
593	40	594	24(30)	176.2 (295.1)	595	44	163.9	593	61	152.6	592	48	102.2	a_1
694	33	694	21(19)	176.2$_5$(295.0$_5$)	694.$_5$	37	163.9	694	21	152.6$_5$	694.$_5$	18	102.2	f_2
862	—	861.$_5$	7.7(4.9)	176.4 (295.1$_5$)	860.$_5$	18	164.0	853 862 866	10	152.6	854.5 864.5	9	102.1$_5$	f_2
1250	8	1250	2.7(1.5)	176.2 (295.2)	1251	5	163.9	1248	3.3	152.6	1247.$_5$	2.3	102.1	f_2
1263	8	1263	1.1(0.9)	176.2 (295.2)	1264	0.7	163.9	1257	2.5	152.6	1256.$_5$	1.9	102.1	a_1
1418	40	1418	14(11)	176.0 (295.0)	1418.$_5$	27	163.8$_5$	1418 1425	18	152.6	1418.5 1429.5	16	102.1$_5$	e
2900	100	2900	100(100)	176.2 (294.9)	2902	69	164.0	2901	100	152.6$_5$	2901	100	107.4$_5$	a_1
2957	88	2957.$_5$	88(76)	176.2 (294.9)	2958.$_5$	100	163.9$_5$	2961	77	152.6	2957 2959.5 2963	90	107.6	f_2

a) Ref. 2. The relative intensities are integrated intensities referred to the maximum intensity of 100. Correction in sensitivity dependent upon the exciting light is made.

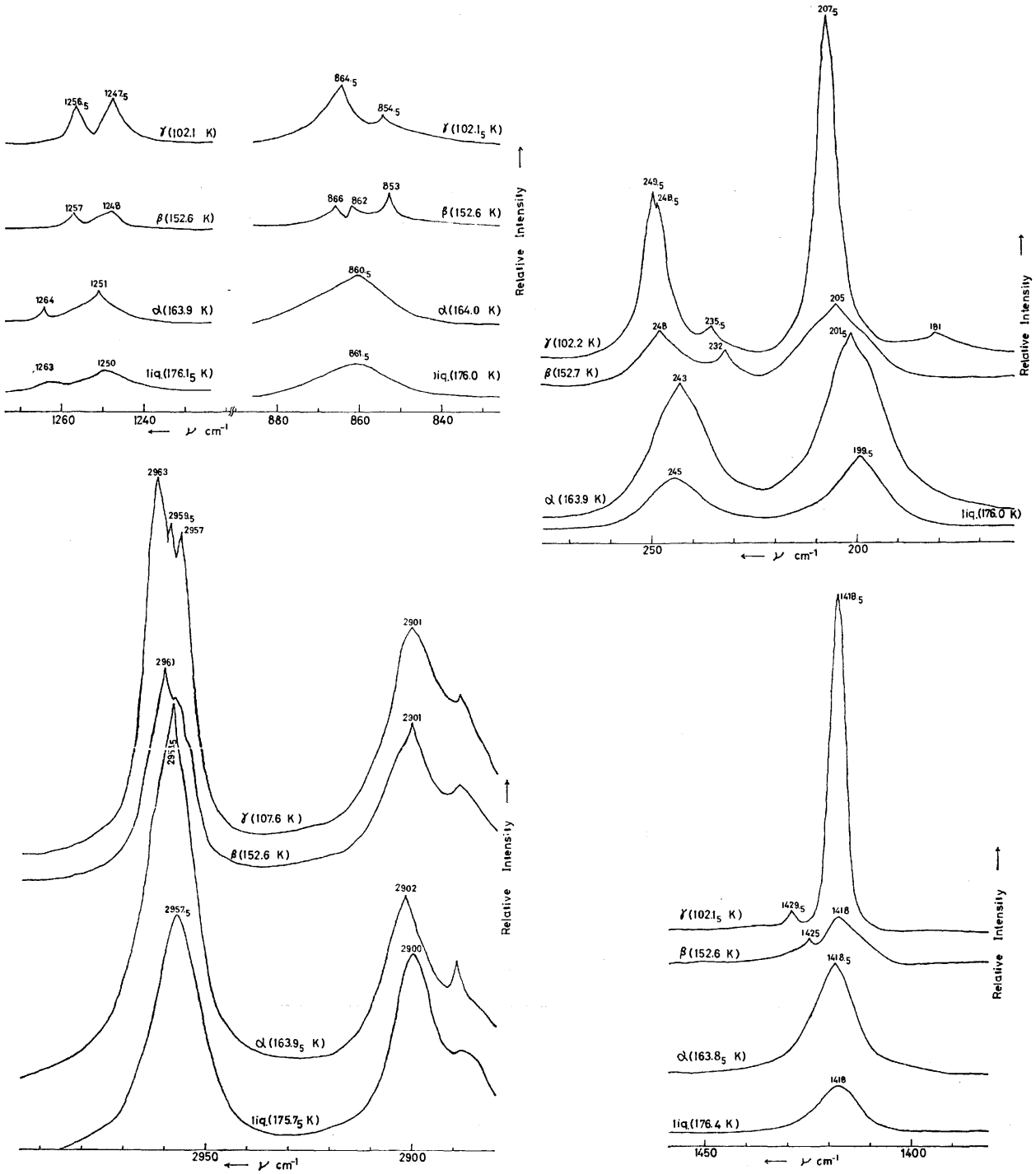

Fig. 4. Raman spectra in the intramolecular vibrational region of liquid and three crystalline forms. The temperatures observed are given in parentheses.

2.0, 0.67, 0.73; $I(\nu_3)/I(\nu_1)$: 0.87, 0.84, 0.35, 0.38; $I(\nu_4)/I(\nu_1)$: 0.81, 1.2, 0.44, 0.40, respectively.* The values for the β and γ forms are close to each other, the values for the α-form being nearer those for liquid than for the β and γ forms. On the assumption of the oriented gas model,[11] the derived polarizability tensor of the crystal related to the Raman intensity is obtained by the elements of the derived polarizability tensor of the free molecule and information on molecular orientation in crystal. It seems that the molecules of the α-form orientate in disorder favoring a high unit-cell symmetry, if we take into account the fact that the spectrum of the α-form exhibits on crystal-field splitting of intramolecular bands.

* The temperature dependence of the intensity is given by $I(T_1)/I(T_2)=[1-\exp(-h\nu/kT_2)]/[1-\exp(-h\nu/kT_1)]$. The present results are estimated at $T=102$ K.

References

1) J. G. Aston, R. M. Kennedy, and H. G. Messerly,

J. Am. Chem. Soc., **63**, 2343 (1941); T. Shinoda, H. Enokido, Y. Maeda, H. Tomita, and Y. Mashiko, *Bull. Chem. Soc. Jpn.*, **46**, 48 (1973); M. Harada, T. Atake, and H. Chihara, 9th Japanese Calorymetry Conf. 1973, Osaka.

2) D. H. Rank and E. R. Bordner, *J. Chem. Phys.*, **3**, 248 (1935); C. W. Young, J. S. Koehler, and D. S. Mckinney, *J. Am. Chem. Soc.*, **69**, 1410 (1947); E. R. Shull, T. S. Oakwood, and D. H. Rank, *J. Chem. Phys.*, **21**, 2024 (1953); K. Shimizu and H. Murata, *J. Mol. Spectrosc.*, **5**, 44 (1960); J. R. Durig, S. M. Craven, and J. Bragin, *J. Chem. Phys.*, **52**, 2046 (1970); S. C. Graham, *Spectrochim. Acta, Part A*, **26**, 345 (1970); A. M. Pyndyk, M. R. Aliev, and V. T. Aleksanyan, *Opt. Spektrosk.*, **36**, 393 (1974); S. Sunder and R. E. D. McClung, *Can. J. Phys.*, **54**, 211 (1976).

3) J. Hiraishi and T. Shinoda, *Bull. Chem. Soc. Jpn.*, **48**, 2732 (1975).

4) R. Rudman and B. Post, *Science*, **154**, 1009 (1966).

5) C. F. Finbak and O. Hassel, *Z. Phys. Chem.*, **36**, 301 (1937).

6) G. W. Smith, *J. Chem. Phys.*, **42**, 4229 (1965).

7) S. Albert and J. A. Ripmeester, *J. Chem. Phys.*, **57**, 2641 (1972).

8) L. E. Sutton, "Tables of Interatomic Distances and Configuration in Molecules and Ions," The Chemical Society, London (1958).

9) R. P. Fournier, R. Savoie, F. Bessette, and A. Cabana, *J. Chem. Phys.*, **49**, 1159 (1968).

10) H. F. Shurvell, *Spectrochim. Acta, Part A*, **27**, 2375 (1971).

11) M. Suzuki, T. Yokoyama, and M. Ito, *Spectrochim. Acta, Part A*, **24**, 1091 (1968).

Metal-ion Complexation of Noncyclic Poly(oxyethylene) Derivatives. I. Solvent Extraction of Alkali and Alkaline Earth Metal Thiocyanates and Iodides*

Shozo YANAGIDA, Kazutomo TAKAHASHI, and Mitsuo OKAHARA
Department of Applied Chemistry, Faculty of Engineering, Osaka University
Yamadakami, Suita, Osaka 565

(Received September 20, 1976)

The reaction of noncyclic poly(oxyethylene) derivatives with alkali and alkaline earth metal ions was investigated by means of the solvent extraction of their thiocyanates or iodides. Polyethylene glycols with more than 23 oxyethylene units showed a strong extracting power comparable to those of the crown ethers, and the power increased with the increasing number of oxyethylene units in them. Extraction studies using homogeneous poly(oxyethylene) monododecyl ethers revealed that more than 7 oxyethylene units were necessary to bind the potassium ion in the water phase and to transfer the complexed salt to the organic phase, and that the extracting ability of octa(oxyethylene) monododecyl ether was about one sixth of that of 18-crown-6. The monododecyl ether is fairly effective as a complexing agent for potassium picrate even below its critical micelle concentration; the stoichiometry of the extractable complex was found to be 0.8: 1 with respect to the ether and the picrate. There was no remarkable difference in the selectivity for alkali metal ions between noncyclic poly(oxyethylene) derivatives and 18-crown-6.

In comparison with cyclic polyethers, noncyclic polyethers seemed extraordinarily weak in ability of metal ion complexation,[1-3] while a search of the literature revealed that, before Pedersen's discovery of macrocyclic polyethers,[4] high-molecular-weight polyethylene glycols had been reported to form complexes with mercuric chloride[5] and with alkaline earth metal salts, especially in the presence of tetraphenylborate.[6-8]

Recently, in connection with the progress of the chemistry of macrocyclic polyethers, the interaction of open-chain poly(oxyethylene) derivatives with metal ions has attracted special interest; the unusual reaction of alkali metal in the presence of polyethylene glycol,[9] octopus molecules, and related compounds,[10,11] the isolation of the complexes with metal salts,[12,13] the crystalline structures of the complexes with mercuric and cadmium chlorides,[14-16] and solvent extraction using poly(oxyethylene) derivatives (POE) as extractants[17] are noteworthy.

The purpose of the present investigation is to clarify the effectiveness of noncyclic poly(oxyethylene) derivatives as complexing agents for metal ions. At first, solvent extraction was undertaken, because it is very convenient for the rapid screening of the complexing efficiency.

As regards the extraction of metal salts with cyclic polyethers, large hydrophobic anions such as picrate[18-21] and dipicrylaminate,[22] have been used as counter anions, since the ion-paired complexes formed are more extractable and can be easily determined colorimetrically. It has now been found, however, that thiocyanate and iodide salts form extractable salt–polyether complexes. Further, because they are stable and neutral in their aqueous solution, the thiocyanates and iodides were used in this extraction study.

Experimental

Materials. The following chemicals were obtained in the best available purity from the sources indicated: KSCN, $Ba(SCN)_2 \cdot 2H_2O$, $Ca(SCN)_2 \cdot 3H_2O$ (Pr. G. grade) NH_4SCN (G. R. grade), CsI (reagent grade) (Wako Pure Chemicals Industries, Ltd.); NaSCN, KI (G. R. grade), NH_4I, $Mg(SCN)_2 \cdot 4H_2O$ (E. P. Grade) (Nakarai Chemicals, Ltd.); LiI (G. R. grade) (Mitsuwa's Pure Chemicals), polyethylene glycols** 300 (n=7), 400 (n=9), 600 (n=14), 1000 (n=23), 4000 (n=90), 6000 (n=140), 20000 (n=450), polypropylene glycols** 1000; (diol type, n=17), 3000 (triol type, n=52), (Wako Pure Chemicals Industries, Ltd); penta(oxyethylene), hexa(oxyethylene), and octa(oxyethylene) monododecyl ethers (Tokyo Kasei Kogyo Co., Ltd.) (The purity was ascertained by NMR); and dicyclohexyl-18-crown-6 (Nakarai Chemicals, Ltd.). Block copolymers of propylene oxide (PO) and ethylene oxide (EO) (Pluronics), $PO_{34}EO_5$, $PO_{34}EO_{11}$, $PO_{34}EO_{45}$, and $PO_{34}EO_{232}$ were obtained from the Daiichi Kogyo Seiyaku Co., Ltd. The mole ratios of PO to EO were determined by means of both NMR and the molecular weight. Dibenzo-18-crown-6 and 18-crown-6 were prepared according to the methods of Pedersen[23] and Cram[24] respectively. Poly(oxyethylene) monododecyl ether with an average of 25 oxyethylene units was prepared by the reaction of dodecyl alcohol with ethylene oxide in the presence of sodium hydroxide. The average number of oxyethylene units was ascertained by NMR spectrometry.

Extraction Procedure. By preliminary experiments, halogenated solvents, such as dichloromethane, chloroform, and carbon tetrachloride, were found to be preferable, since other solvents, such as hexane and benzene, are readily emulsified in the presence of POE and are difficult to separate from the water phase. Considering the efficiency of dichloromethane for the extraction with cyclic polyethers,[19] we chose it as the solvent. An aqueous POE solution (0.02 M***, 25 cm^3), 25 cm^3 of a thiocyanate solution (1.0 M), and 50 cm^3

* A preliminary report of this work was presented at the 34th National Meeting of the Chemical Society of Japan, Hiratsuka, April, 1976.

** The figures indicate the nominal average molecular weight. The figures (n) in parentheses are the average numbers of oxyethylene units, calculated from the average molecular weight.

*** Throughout this paper, 1 M=1 mol dm^{-3}.

of dichloromethane saturated with water were transferred into 250-cm³ Erlenmeyer flask equipped with a well-grounded stopper. The mixture was placed in a thermostated water bath (25±0.5 °C) for ten minutes, and then shaken 200 times vigorously; this was found to be sufficient for equilibration. The stopper was replaced by the separation cock so as to use this Erlenmeyer flask as a separatory funnel in succession, and then the flask was turned upside down. With few exceptions, the phases separated clearly on standing. The dichloromethane layer was separated. After removing the dichloromethane by means of a rotary evaporator, the thiocyanate ion in the residue was determined by Volhard's method. In the extraction of potassium nitrate, the potassium ion in the residue was determined by means of Nippon Jarrell Ash Atomic Absorption Spectrometer AA-1. Duplicates agreed, usually to less than 5% from the mean, and were averaged for use in the calculation of the degree of extraction (Figs. 1, 2, 5, and 6.).

Percent Extraction of POE. According to the above-mentioned procedure, the extraction of the POE by dichloromethane was carried out in the absence of any salts. The residue of the dichloromethane layer was kept standing under a vacuum to a constant weight. The weight thus obtained was used in the calculation of the percentage of extraction (Table 1).

Extraction of Potassium Picrate. The extraction was worked out according to the procedure outlined by Frensdorf.[19] The picrate concentration in the water phase was measured by means of a Shimadzu Double-beam Spectrometer, UV-200, using as the extinction coefficient ($\lambda=357$ nm, $\varepsilon=1.46\times10^4$ in water).

Results and Discussion

The degree of extraction of potassium thiocyanate and the degree per oxyethylene unit are plotted against the number of oxyethylene units in each extractant in Figs. 1 and 2. Polyethylene glycols with more than about 23 oxyethylene units were found to have a strong power of extracting the potassium ion, one which was comparable to those of the macrocyclic polyethers. In addition, the extractability per oxyethylene unit was almost constant. The same is true of the poly(oxyethylene) monododecyl ethers with more than seven oxyethylene units (Fig. 2). While polypropylene glycols showed a low extracting power, a series of block copolymers of propylene oxide and ethylene oxide increased in their extracting power with the increase in the number of oxyethylene units (Fig. 1). The slope of the extraction curve was almost the same as that of polyethylene glycols, suggesting that the repeating oxyethylene is a factor governing the extraction. These facts indicate that even noncyclic poly(oxyethylene) derivatives have a remarkable complexing power for the potassium ion, even in an aqueous phase, if they have more than a definite number of oxyethylene units, and that the strength increases linearly with the number of repeating oxyethylenes.

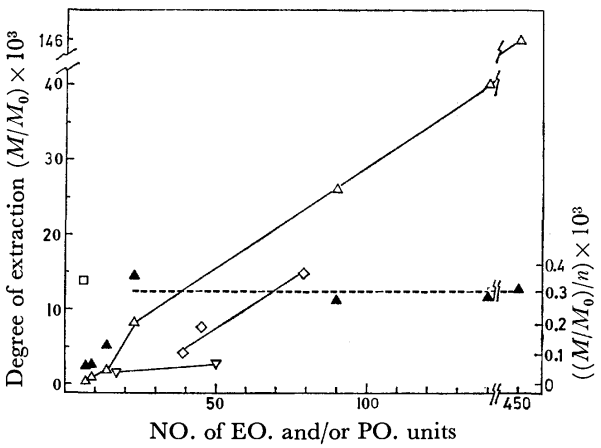

Fig. 1. Extraction of potassium thiocyanate into dichloromethane by poly(oxyethylene) derivatives. Thiocyanate concentration $[M_0]=0.5$ M. POE concentration: 0.01 M. △, Polyethylene glycols; ▽, polypropylene glycols; ◇, the block copolymers of PO and EO (Pluronics); □, 18-crown-6; ▲, the degree of extraction per one oxyethylene unit by polyethylene glycols. ----: Average value.

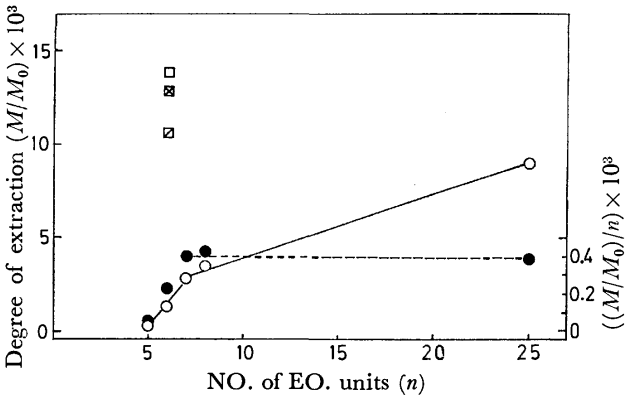

Fig. 2. Extraction of potassium thiocyanate into dichloromethane by homogeneous poly(oxyethylene) monododecyl ethers. Thiocyanate concentration $[M_0]=0.5$ M. Polyether concentration: 0.01 M. ○, homogeneous poly(oxyethylene) monododecyl ethers (The ether having 25 EO units is not homogeneous.); ●, the degree of extraction per one oxyethylene unit. ----: Average value; □, 18-crown-6; ▨, dicyclohexyl-18-crown-6; ⊠, dibenzo-18-crown-6.

As is shown in Table 1, the affinity of PEG to dichloromethane increased with the number of oxyethylene units. The rather hydrophobic property of the high-molecular-weight POE is worth noting.

Extraction properties are governed not only by the strenght of complex formation, but also by the solubility

Table 1. Percentage of extraction of poly(oxyethylene) derivatives by dichloromethane

Polyethylene glycols	Percentage of extraction	Pluronics of alkylated ether	Percentage of extraction
PEG 400 ($n=9$)[a]	6%	$PO_{34}EO_{11}$	91%
PEG 600 ($n=14$)[a]	14%	$PO_{34}EO_{45}$	95%
PEG 1000 ($n=23$)[a]	27%	$PO_{34}EO_{282}$	93%
PEG 4000 ($n=90$)[a]	*ca.* 100%	$C_{12}H_{25}EO_{25}$–H	93%

a) The figures indicate the nominal average molecular weight. The figures(n) in parentheses are the average numbers of oxyethylene units, calculated from the average molecular weight.

relation of the extractant and the formed complex.[19] The less efficient extraction of the short-chain polyethylene glycols is, thus, apparently due to their hydrophilic character.

The extraction using homogeneous poly(oxyethylene) monododecyl ethers as extractants has made it clear that seven repeating oxyethylenes are the minimum number to bind the potassium ion effectively in the water phase and to transfer the complexed salt to the dichloromethane phase (Fig. 2). This finding quite agreed with that of Liu,[25] who observed that the interaction of polyethylene glycols with potassium iodide in methanol became distinguished above heptaethylene glycol.[28]

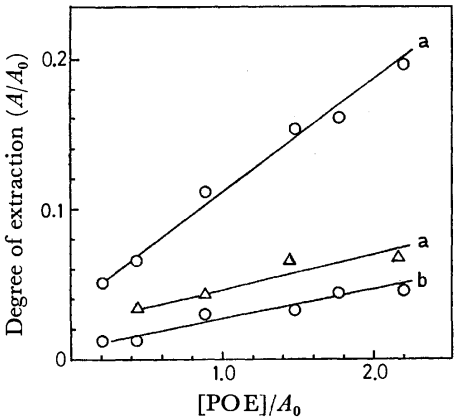

Fig. 3. Extraction of potassium picrate into dichloromehtane by homogeneous poly(oxyethylene) monododecyl ethers. Picrate concentration $[A_0]=7\times10^{-5}$ M. Potassium ion concentration $[M_0]=10^{-1}$ for a; 5×10^{-3} M for b.
○, Octa(oxyethylene) monododecyl ether;
△, hexa(oxyethylene) monododecyl ether.

However, the poly(oxyethylene) monododecyl ethers examined were all typical nonionic surfactants, and the effect of the micelle formation was conceivable under the conditions thus far discussed. To eliminate the influence of the micelle on the extracting properties as much as possible, the extraction of potassium picrate was undertaken when the extractants were diluted to around their critical micelle concentration.[26] Figure 3 shows that, even below the CMC, the extracting ability is fair for octa(oxyethylene) monododecyl ether, but very poor for the hexa(oxyethylene) ether. Compared with the results with dicyclohexyl-18-crown-6 under the same conditions,[19] the extracting ability of the octa(oxyethylene) ether was about one-sixth of that of the crown ether. This approximation is consistent with the results shown in Fig. 2. As expected, the extractability by the octa(oxyethylene) ether decreased much more drastically with a decrease in the potassium-ion concentration than by the crown ether.[19]

Assuming from the results shown in Table 1 that there is no complication due to the distribution of the ether between the two phases, the logarithm of the distribution ratio calculated from the degree of extraction by the octa(oxyethylene) ether was plotted against the logarithm of the total concentration of the ether (Fig. 4).

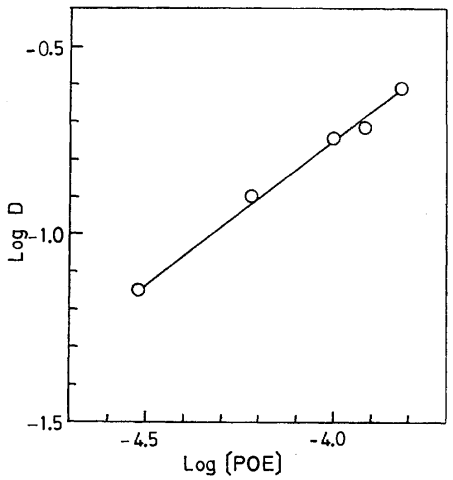

Fig. 4. Distribution ratio of potassium picrate *vs.* concentration of octa(oxyethylene) monododecyl ether. The conditions used are identical with those in Fig. 3. POE: Octa(oxyethylene) monododecyl ether.

This plot gave a straight line with a slope of about 0.8: 1 in respect to the ether and the picrate. The deviation from 1: 1 is probably due to a partial micelle formation, since the CMC's of these types of nonionic surfactants are generally lowered by the presence of an electrolyte.[27]

Calzolari *et al.*[12] recently reported the isolation of the complex formed by hexa(oxyethylene) diphenyl ether and sodium cobalt(II) thiocyanate. The composition of the complex indicates that the hexa(oxyethylene) coordinates with one sodium ion. Considering our result and this earlier finding, six to seven oxyethylene units seem critical for the complexation with alkali metal ions.[28] This conclusion contrasts with the 1: 2 and 1: 4 compositions needed in the $HgCl_2$–POE complexes.[14,15]

The extraction was also extended to other potassium salts. The iodide was found extractable to the same extent as the thiocyanate by both 18-crown-6 and noncyclic poly(oxyethylene) derivatives (Fig. 5). How-

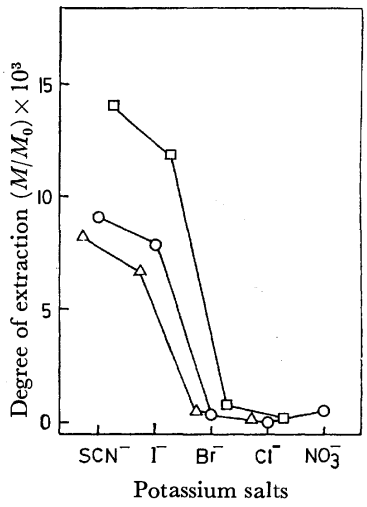

Fig. 5. Extraction of potassium salts into dichloromethane by poly(oxyethylene) derivatives. Concentration of each salt $[M_0]=0.5$ M. POE concentration: 0.01 M. □, 18-Crown-6; ○, $C_{12}H_{25}EO_{25}$–H; △, PEG 1000.

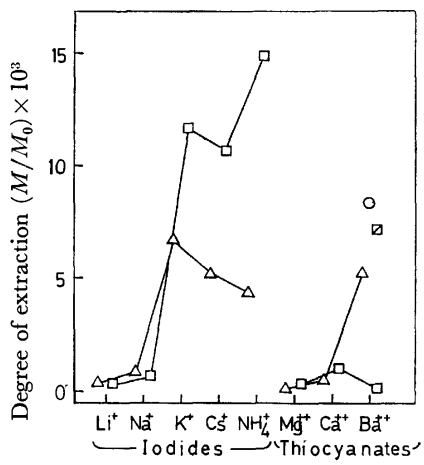

Fig. 6. Extraction of alkali metal iodides and alkaline earth metal thiocyanates into dichloromethane by poly(oxyethylene) derivatives. The conditions and symbols used are identical with those in Figs. 2 and 5.

ever, the nitrate, bromide, and chloride could not be extracted effectively by either of the extractants. The formation of extractable complexes with the thiocyanate and iodide may well be explained by the concept of water structure-enforced ion pairing.[29]

Figure 6 shows the extractions of other alkali and alkaline earth metal salts by polyethylene glycols (PEG) 1000 (n=23) and 18-crown-6. It is interesting to note that the selectivities for alkali metal ions are very similar to one another. On the other hand, ammonium iodide was found to be less extractable by PEG 1000.

As for barium thiocyanate, PEG 1000 was more effective than 18-crown-6. However, when dicyclohexyl-18-crown-6 was employed, the 1:1 complex[4] was precipitated during the extraction. The degree of extraction was found to be 7.2×10^{-3}, which corresponds to more than four times as much as that of 18-crown-6; it went up to 17.2×10^{-3} when the complex precipitated was included in the calculation of the degree of extraction. It should also be noted that 18-crown-6 extracted slightly more calcium thiocyanate than the barium salt; this is in contrast with their large differences in complexing stability constants reported by Izatt *et al.*[30] Recently, Rais *et al.* observed the synergistic effect of PEG in the extraction of alkaline earth metal ions by nitrobenzene.[31] In view of these findings, the solubility relation might exert much influence on the extraction of alkaline earth metal salts.

It was once concluded that the poly(oxyethylene) chain existed in a zigzag conformation at a low degree of polymerization and in a meander conformation at a high degree of polymerization.[32] Recently Tadokoro *et al.*[33] have established that the structure of poly(oxyethylene) in the crystalline state has a distorted helical structure containing seven oxyethylene units and two turns, and that it takes a planar zigzag structure only when it is elongated.[34] The molecular model (Corey-Pauling-Koltum model) based on this fact indicates that the helical structure is convenient for disposing the oxygen atoms of poly(oxyethylene) to the cationic species and can easily take a conformation very similar to 18-crown-6 by a slight rotation of each bonding. The hydrophobic property of high-molecular-weight poly(oxyethylene) derivatives, proved by the high-percent extraction by dichloromethane, implies that the helical conformation is energetically favorable in an organic solvent. In view of these points, noncyclic poly(oxyethylene) derivatives may take, on the average, a helical conformation even in the liquid state and may favorably complex with cations, or the cations may induce an energetically favorable helical structure and, as a result, show a fair extracting power for the cationic species. Polypropylene glycols were confirmed to have a nonplanar zigzag chain because of the steric effect of the methyl groups.[35] Their low extracting ability may be attributable to their nonplanar zigzag conformation.

A further investigation based on these results is now in progress.

The authors wish to express their thanks to Professor J. Shiokawa, Mr. Y. Hirashima, and Dr. M. Yokoyama (Department of Applied Chemistry of this Faculty) for their helpful discussions and kind advice. They also wish to acknowledge the generous gift of the Pluronics used in this work by Dr. H. Maki of the Daiichi Kogyo Seiyaku Co., Ltd.

References

1) H. K. Frensdorf, *J. Am. Chem. Soc.*, **93**, 600 (1971).
2) J. M. Timko, R. C. Helgeson, M. Newcomb, G. W. Gokel, and D. J. Cram, *J. Am. Chem. Soc.*, **96**, 7097 (1974).
3) G. Chaput, G. Jeminet, and J. Juillard, *Can. J. Chem.*, **53**, 2240 (1975).
4) C. J. Pedersen, *J. Am. Chem. Soc.*, **89**, 7017 (1967).
5) A. A. Blumberg and S. S. Pollack, *J. Polym. Sci., Part A*, **2**, 2499 (1964); A. A. Blumberg and J. Wyatt, *ibid., Part B*, **4**, 653 (1966).
6) T. M. Doscher, G. E. Myers, and D. C. Atkins, Jr., *J. Colloid Sci.*, **6**, 223 (1951).
7) R. Neu, *Fette, Seifen, Anstrichm.*, **59**, 823 (1957); *ibid.*, **61**, 585 (1959).
8) R. J. Levins and R. M. Ikeda, *Anal. Chem.*, **37**, 671 (1965), and the references cited therein.
9) I. M. Panayotov, D. T. Petrova, and C. B. Tsvetanov, *Makromol. Chem.*, **176**, 815 (1975).
10) F. Vögtle and E. Weber, *Angew. Chem. Int. Ed. Engl.*, **13**, 814 (1974).
11) R. Fornasier and F. Montanari, *Tetrahedron Lett.*, **1976**, 1381.
12) C. Calzolari, L. Favretto, G. Pertoldi Marletta, and L. Farvretto Gabrielli, *Ann. Chim. (Rome)*, **64**, 463 (1974); *Chem. Abstr.*, **84**, 38132s (1976).
13) E. Weber and F. Vögtle, *Tetrahedron Lett.*, **1975**, 2415.
14) R. Iwamoto, Y. Saito, H. Ishihara, and H. Tadokoro, *J. Polym. Sci., Part A-2*, **6**, 1509 (1968); M. Yokoyama, H. Ishihara, R. Iwamoto, and H. Tadokoro, *Macromolecules*, **2**, 184 (1969).
15) R. Iwamoto, *Bull. Chem. Soc. Jpn.*, **46**, 1114, 1118, 1123, 1127 (1973).
16) R. Iwamoto and H. Wakano, *J. Am. Chem. Soc.*, **98**, 3764 (1976).
17) T. Sotobayashi, T. Suzuki, and K. Yamada, *Chem. Lett.*, **1976**, 77; T. Sotobayashi, T. Suzuki, and K. Tanouchi. *ibid.*, **1976**, 585.
18) C. J. Pedersen, *Fed. Proc., Fed. Am. Soc. Exp. Biol.*, **27**, 1305 (1968).

19) H. K. Frensdorf, *J. Am. Chem. Soc.*, **93**, 4685 (1971).
20) A. Sadakane, T. Iwahido, and K. Toei, *Bull. Chem, Soc. Jpn.*, **48**, 60 (1975).
21) P. R. Danesi, H. Meider-Gorican, R. Chianizia, and G. Scibona, *J. Inorg. Nucl. Chem.*, **37**, 1479 (1975).
22) J. Rais, M. Kyrs, and L. Kadlecova, Proceedings International Solvent Extraction Conference (Lyon), Sept., 1974, Preprint, Vol. II, p. 1705.
23) C. J. Pedersen, *Org. Synth.*, **52**, 66 (1972).
24) G. W. Gokel and D. J. Cram., *J. Org. Chem.*, **39**, 2445 (1974).
25) K. Liu, *Macromolecules*, **1**, 308 (1968).
26) CMC of hexa(oxyethylene) monododecyl ether: 0.87×10^{-4} mol/l; J. M. Corkill, J. F. Goodman, and R. H. Ottewill, *Trans. Faraday. Soc.*, **57**, 1627 (1961). CMC of octa-(oxyethylene) monododecyl ether: 1.1×10^{-4} mol/dm^3, P. Becher, "Nonionic Surfactants," ed by M. J. Schick, Marcel Dekker, New York, N. Y. (1967), p. 480.
27) A. Ray and G. Neméthy, *J. Am. Chem. Soc.*, **93**, 6787 (1971).
28) Fenton *et al.* reported the isolation of KI and KSCN–PEG complexes from a methanolic solution in the molar proportion of 1:4 of salt and oxyethylene. However, the stoichiometry of the complexes is unsettled question; D. E. Fenton, J. M. Parker, and P. V. Wright, *Polymer*, **14**, 589 (1973).
29) R. M. Diamond, *J. Phys. Chem.*, **67**, 2513 (1963).
30) The stability constant of the Ba^{2+}–dicyclohexyl-18-crown-6 complex has been reported to be 10^3 times greater than that of the Ca^{2+}–crown complex; R. M. Izatt, D. P. Nelson, J. H. Rytting, B. L. Haymore, and J. J. Christensen, *J. Am. Chem. Soc.*, **93**, 1619 (1971); R. M. Izatte, D. J. Eatough, and J. J. Christensen, *Struct. Bonding (Berlin)*, **16**, 161 (1973).
31) J. Rais, E. Šebestovă, P. Seluckỳ, and M. Kyrš, *J. Inorg. Nucl. Chem.*, **38**, 1742 (1976).
32) M. Rosch, "Nonionic Surfactants," ed by M. J. Schick, Marcel Dekker, New York, N. Y. (1967), p. 753.
33) Y. Takahashi and H. Tadokoro, *Macromolecules*, **6**, 672 (1973); H. Tadokoro, Y. Chatani, T. Yoshihara, S. Tahara and S. Murahashi, *Makromol. Chem.*, **73**, 109 (1964).
34) Y. Takahashi, I. Sumida, and H. Tadokoro, *Polym. Preprints, Jpn.*, **21**, (1972), p. 497.
35) M. Cesari, G. Pergo, and W. Marconi, *Makromol. Chem.*, **94**, 194 (1966).

A Theoretical Study on Biradicals. I. Theoretical Characteristics of Biradicals

Kenichi FUKUI and Kazuyoshi TANAKA

Department of Hydrocarbon Chemistry, Faculty of Engineering, Kyoto University, Sakyo-ku, Kyoto 606

(Received October 28, 1976)

An interpretation is given on the characteristics of biradicaloids, such as the bonding, polar, and biradical characters of singlet biradicals. Systematization of the reactivity of singlet and triplet biradicals is based on the principle that 1) deformation takes place in the direction of bonding in singlet biradicals, and 2) deformation or bond formation occurs to separate unpaired-electrons from each other in triplet biradicals. Combination of the two principles is applied to the theory of orientation and stereoselection in excited-state reactions.

The word "biradical" in a chemical sense makes us think of a species having an odd electron on each of two sites of a molecule. This conforms to the interpretation of a biradical in the triplet state. However, problems may arise in the case of a singlet biradical.

The conversion of biradical species along the path of ground- and excited-state reactions has been treated theoretically.[1-4] Salem *et al.* discussed the nature of a singlet biradical by taking ionic states into account and explained a number of experimental results in regard to various reaction intermediates in photochemistry.[5-10] The present paper gives some new material.

Stabilization of Singlet Biradical by a Correlated Motion of Electrons

Consider a pair of two independent normalized one-electron space functions a and b whose overlap integral is s. In the case of biradical problems these two orbitals can be made to represent the two "unpaired"-electron orbitals essentially localized at each radical site. The following three configurations are here taken into consideration to treat the problem as a two-electron system:

a—o— —o—b $\Phi_1(1,2) = \frac{1}{\sqrt{2+2s^2}}\{a(1)b(2)+b(1)a(2)\}$

a-o-o- ——b $\Phi_2(1,2) = a(1)a(2)$ (1)

a—— -o-o-b $\Phi_3(1,2) = b(1)b(2)$

It is assumed that orbitals a and b are real and their signs are chosen in such a way that s becomes positive.

The electronic states of this two-electron system are then given by

$$\Psi = \frac{1}{\sqrt{N}}(C_1\Phi_1 + C_2\Phi_2 + C_3\Phi_3), \tag{2}$$

where C_1, C_2, and C_3 can be obtained by solving the eigenvalue problem of the Hamiltonian matrix, and $1/\sqrt{N}$ is the normalization factor. They are the usual energy-extremized wave functions in which the effect of correlation in electron motion is taken into account.

Direct consideration of the correlated motion of electrons might also be considered. The extent of correlation in orbital motion could roughly be represented by the averaged reciprocal interelectronic distance,

$$\overline{\frac{1}{r_{12}}} = \frac{2}{\nu(\nu-1)}\iint \rho(1,2|1,2)\frac{1}{r_{12}}\mathrm{d}v(1)\mathrm{d}v(2), \tag{3}$$

(ν: number of electrons)

where r_{12} is the distance of electrons 1 and 2, and

$$\rho(1',2'|1,2) = \frac{\nu(\nu-1)}{2}\int \Psi^*(r_1'\sigma_1, r_2'\sigma_2, r_3\sigma_3, \cdots) \times \Psi(r_1\sigma_1, r_2\sigma_2, r_3\sigma_3, \cdots)\mathrm{d}\sigma_1\mathrm{d}\sigma_2\mathrm{d}r_3\mathrm{d}\sigma_3\cdots \tag{4}$$

is the second-order spinless density matrix. For the present two-electron problem, we have

$$\gamma \equiv \overline{\frac{1}{r_{12}}} = \iint \Psi^*(1,2)\frac{1}{r_{12}}\Psi(1,2)\mathrm{d}v(1)\mathrm{d}v(2). \tag{5}$$

The extremization of $\overline{1/r_{12}}$ is achieved by obtaining the stationary values satisfying

$$\delta\gamma = 0. \tag{6}$$

The variation with respect to C_1, C_2, and C_3 leads to the secular equation

$$\begin{vmatrix} \gamma_{11}-\gamma & \gamma_{12}-S_{12}\gamma & \gamma_{13}-S_{13}\gamma \\ \gamma_{21}-S_{21}\gamma & \gamma_{22}-\gamma & \gamma_{23}-S_{23}\gamma \\ \gamma_{31}-S_{31}\gamma & \gamma_{32}-S_{32}\gamma & \gamma_{33}-\gamma \end{vmatrix} = 0, \tag{7}$$

where

$$\gamma_{jk} = \iint \Phi_j^*(1,2)\frac{1}{r_{12}}\Phi_k(1,2)\mathrm{d}v(1)\mathrm{d}v(2)$$

and

$$S_{jk} = \iint \Phi_j^*(1,2)\Phi_k(1,2)\mathrm{d}v(1)\mathrm{d}v(2)$$

($j, k = 1, 2$, and 3).

The coefficient of Φ_j in Eq. 2 can be obtained simultaneously, giving correlation-extremized wave functions $\{\Psi^{(i)}\}$ which are always mutually orthogonal. Both energy-extremization and correlation-extremization give wave functions with an essentially parallel trend in nonpolar species.[11] Thus in such favourable cases, we can use correlation-extremized wave functions as an approximate substitute of the usual energy-extremized functions. Such a consideration of the interaction of at least three configurations as mentioned above is essential in the theoretical interpretation of biradicals.

Bonding Character between Two Radical Sites

The bonding character between two radical sites each containing essentially one electron can be discussed by using Ψ of Eq. 2. A most reasonable scale of bonding

character[12] might be the magnitude of accumulation of electron population in the intermediate region between two radical sites.[13-15]

The distribution of electron density is given by

$$\rho(1) = 2\int \Psi^*(1,2)\Psi(1,2)\mathrm{d}v(2). \tag{8}$$

The density $\rho(1)$ is divided into three terms as

$$\rho(1) = A_{11}a(1)^2 + 2A_{12}a(1)b(1) + A_{22}b(1)^2. \tag{9}$$

The bonding strength can be determined by the second term of r.h.s. since the coefficient A_{12} of the cross term $a(1)b(1)$ contributes to the accumulation of electrons in the intermediate region.

It follows from Eq. 2 that

$$A_{12} = \frac{1}{N}\left\{\frac{s}{1+s^2}C_1^2 + \sqrt{\frac{2}{1+s^2}}C_1(C_2+C_3) + 2sC_2C_3\right\}, \tag{10}$$

where

$$N = C_1^2 + C_2^2 + C_3^2 + \frac{2\sqrt{2}s}{\sqrt{1+s^2}}C_1(C_2+C_3) + 2s^2C_2C_3.$$

In general, C_j may be complex. However, for the sake of simplicity, Eq. 9 is written for the real values of C_j. If we allow C_1, C_2, and C_3 of Eq. 2 to take *any* real values, the maximum and minimum values which A_{12} can take are $1/(1+s)$ and $-1/(1-s)$ corresponding to the wave functions

$$\left.\begin{aligned} \Psi^{(B)} &= \frac{1}{\sqrt{2}}\frac{1}{1+s}\left\{\sqrt{1+s^2}\Phi_1 + \frac{1}{\sqrt{2}}(\Phi_2+\Phi_3)\right\} \\ \text{and} \\ \Psi^{(AB)} &= \frac{1}{\sqrt{2}}\frac{1}{1-s}\left\{\sqrt{1+s^2}\Phi_1 - \frac{1}{\sqrt{2}}(\Phi_2+\Phi_3)\right\}, \end{aligned}\right\} \tag{11}$$

respectively. Thus, we see that the most bonding state ($\Psi^{(B)}$) or the most antibonding state ($\Psi^{(AB)}$) is obtained in the case of *moderate* mixing of three configurations Φ_1, Φ_2, and Φ_3. This implies that admixture of the ionic configuration Φ_2 or Φ_3 with the covalent configuration Φ_1, or the delocalization of each odd electron to the other radical site, serves as an effective origin of bonding character between two weakly interacting radical sites. The importance of such electron delocalization in the bond formation between molecules or radicals was early pointed out.[16-19] In particular, special importance of a cross term arising from two configurations, corresponding in the present case to the terms of C_1C_2 or C_1C_3 in A_{12}, was stressed.[20-22]

The bonding character of a singlet biradical is thus represented by sA_{12}. In the light of the relation

$$A_{11} + 2sA_{12} + A_{22} = 2,$$

we can also measure the less bonding character by the quantity $1/2(A_{11}+A_{22})$.

Polar Character of Two Radical Sites

The density $\rho(1)$ also provides information as to what extent the two radical sites are polar. Evidently, polarity parallels $|A_{11}-A_{22}|$. We tentatively define the polar character of a singlet biradical by means of

$$\Pi = \left|\frac{A_{11}-A_{22}}{A_{11}+A_{22}}\right|, \tag{12}$$

in which

$$\left.\begin{aligned} A_{11} &= \frac{1}{N}\left(\frac{1}{1+s^2}C_1^2 + \frac{2\sqrt{2}s}{\sqrt{1+s^2}}C_1C_2 + 2C_2^2\right), \\ A_{22} &= \frac{1}{N}\left(\frac{1}{1+s^2}C_1^2 + \frac{2\sqrt{2}s}{\sqrt{1+s^2}}C_1C_3 + 2C_3^2\right). \end{aligned}\right\} \tag{13}$$

These are the coefficients of the $a(1)^2$ and $b(1)^2$ terms in $\rho(1)$ of Eq. 9 which is derived from a wave function Ψ already *correlation-extremized* according to the procedure in previous section.

By this definition, we have

$$\Pi(\Phi_1) = 0, \quad \Pi(\Phi_2) = \Pi(\Phi_3) = 1,$$

provided that Φ_1, Φ_2, and Φ_3 are correlation-extremized states.

A change in electron distribution can be expected to arise causing bonding stabilization through a moderate mixing of ionic structures. In this connection the work of Wulfman and Kumei,[23] who first pointed out the high possibility of polarization in singlet excited states of alkenes, is of interest.

Biradical Character of Singlet Biradicals

Since the bonding character between two radical sites becomes maximum only in the case of moderate admixing of ionic configurations with a covalent configuration, the less ionic character can not be adopted for the measure of biradical character.

We must take into account the following requisites which qualify a biradical:

1) The bonding character between two radical ends should be small since a species with too large bonding character might be called a molecule, but not a biradical. The value $1/2(A_{11}+A_{22})$ should not be small.

2) The polar character should not be large since a species with a strong inequality in electron density at the radical ends should be called a zwitterion. Namely, $(1-\Pi)$ should not be small.

A conventional but reasonable definition of the biradical character $\mathfrak{B}$ may therefore be given by

$$\mathfrak{B} = \frac{1}{2}(A_{11}+A_{22})(1-\Pi) = \frac{1}{2}\{A_{11}+A_{22}-|A_{11}-A_{22}|\}$$
$$= (\text{the smaller of } A_{11} \text{ and } A_{22}). \tag{14}$$

Thus, the maximum possible biradical character in a *bonding* state is unity $(=1/(1+s))$, and the maximum biradical character in an *antibonding* state is larger than unity $(=1/(1-s))$. We also have

$$\mathfrak{B}(\Phi_1) = \frac{1}{1+s^2}, \quad \mathfrak{B}(\Phi_2) = 0, \quad \mathfrak{B}(\Phi_3) = 0,$$

in which Φ_1, Φ_2, and Φ_3 are the functions of Eq. 1, assuming that they are correlation-extremized ones.

The discussion can be easily extended to the case of complex wave functions.

Nonbonding Biradicals

It may happen that each odd electron occupies each of two orbitals orthogonal to each other so that the overlap integral s in Eq. 9 disappears. Hence, the

$\Psi^{(i)}$			γ	
$\frac{1}{\sqrt{2}}\{a(1)a(2)+b(1)b(2)\}$	$^1A_1$	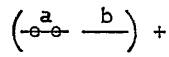	$(aa\|aa)+(ab\|ab)$	≈ 0.89120(a.u.)
$\frac{1}{\sqrt{2}}\{a(1)a(2)-b(1)b(2)\}$	$^1B_2$	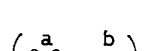	$(aa\|aa)-(ab\|ab)$	≈ 0.88969
$\frac{1}{\sqrt{2}}\{a(1)b(2)+b(1)a(2)\}$	$^1B_1$		$(aa\|bb)+(ab\|ab)$	≈ 0.39420
$\frac{1}{\sqrt{2}}\{a(1)b(2)-b(1)a(2)\}$	$^3A_2$	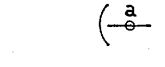	$(aa\|bb)-(ab\|ab)$	≈ 0.39268

maximal biradical character is unity.

An example is perpendicular ethylene in which two orthogonal radical orbitals a and b are $(2p_x)_A$ and $(2p_y)_B$, respectively, A and B denoting two carbon atoms. In this case, it follows from symmetry relations that

$$\gamma_{12}=\gamma_{13}=0,\quad S_{12}=S_{13}=0$$

in Eq. 7. Thus, $\Phi_1=1/\sqrt{2}\{a(1)b(2)+b(1)a(2)\}$ is already a correlation-extremized wave function with which Φ_2 or Φ_3 of different symmetry does not mix. From the definition of Eq. 14, the state $\Psi^{(1)}=\Phi_1$ has the $\mathfrak{B}$ value of unity and can be called "purely" biradical. The other two states ($\Psi^{(2)}=1/\sqrt{2}(\Phi_2+\Phi_3)$ and $\Psi^{(3)}=1/\sqrt{2}(\Phi_2-\Phi_3)$) also have the $\mathfrak{B}$ value of unity. Such a biradical species may be called a *nonbonding biradical.*

The level situation of three correlation-extremized states is given above, together with the value of γ. The result is qualitatively consistent with that of numerical calculations.[24]

It is to be noted that the level gap between $^1B_1$ and $^3A_2$ states is very small (*ca.* 1 kcal/mol) in this example. The small S–T separation is characteristic of nonbonding biradicals. From an energetic point of view, they are expected to interchange easily between singlet and triplet states.

Biradical with Cyclic Orbitals

Singlet Oxygen. Let two ($^1\pi_g$) orbitals of the oxygen molecule be

$$\phi_x=\frac{1}{\sqrt{2-2s}}\{(2p_x)_1-(2p_x)_2\},$$

$$\phi_y=\frac{1}{\sqrt{2-2s}}\{(2p_y)_1-(2p_y)_2\},$$

where O_1-O_2 axis is parallel to the z-axis and s is the overlap integral of $(2p_x)_1$ and $(2p_x)_2$ or that of $(2p_y)_1$ and $(2p_y)_2$. Three configurations are specified by

$$\Phi_1=\frac{1}{\sqrt{2}}\{\pi^+(1)\pi^-(2)+\pi^-(1)\pi^+(2)\},$$

$$\Phi_2=\pi^+(1)\pi^+(2),$$

$$\Phi_3=\pi^-(1)\pi^-(2),$$

where

$$\pi^+=\frac{1}{\sqrt{2}}(\phi_x+i\phi_y),$$

$$\pi^-=\frac{1}{\sqrt{2}}(\phi_x-i\phi_y).$$

Φ_1, Φ_2, and Φ_3 of different symmetries are correlation-extremized wave functions corresponding to the stationary values of γ.

$\Psi^{(i)}$		γ
$\Phi_1=\frac{1}{\sqrt{2}}\{\phi_x(1)\phi_x(2)+\phi_y(1)\phi_y(2)\}$	$^1\Sigma_g^+$	$(xx\|xx)+(xy\|xy)$,
$[\Phi_2,\Phi_3]=\left[\frac{1}{\sqrt{2}}\{\phi_x(1)\phi_x(2)-\phi_y(1)\phi_y(2)\},\ \frac{1}{\sqrt{2}}\{\phi_x(1)\phi_y(2)+\phi_y(1)\phi_x(2)\}\right]$	$^1\Delta_g$	$\frac{1}{2}(xx\|xx)+\frac{1}{2}(xx\|yy)$,
$\left(\frac{1}{\sqrt{2}}\{\phi_x(1)\phi_y(2)-\phi_y(1)\phi_x(2)\}\right.$	$^3\Sigma_g^-$	$\left.(xx\|yy)-(xy\|xy)\right)$

($(xy|xy)$, *etc.*, denote $(\phi_x\phi_y|\phi_x\phi_y)$, *etc.*).

The uppermost level corresponds to $^1\Sigma_g^+$ excited singlet state and the lower degenerate level to $^1\Delta_g$ state. The former stands for the configuration

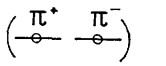

with $\mathfrak{B}=1$. The species can thus be called purely biradical.

In the latter state, the correlation-extremized wave functions consist of purely doubly-occupied configurations

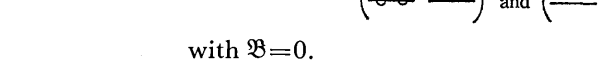

with $\mathfrak{B}=0$.

It should be noted that we have to employ the symmetry orbitals π^+ and π^- to construct wave functions with definite angular momenta.

Such cyclic orbitals, however, do not reflect the concept of radical site. The interpretation of $\mathfrak{B}$-values in this case should be made with certain reservation.

Cyclobutadiene (Planar Square). The orthogonal nonbonding orbitals can be taken as

$$\phi_1=\frac{1}{\sqrt{2-2s'}}\{(2p_z)_4-(2p_z)_2\},$$

$$\phi_2=\frac{1}{\sqrt{2-2s'}}\{(2p_z)_1-(2p_z)_3\},$$

where $(2p_z)_j$ ($j=1$, 2, 3, and 4) are the four $2p_z$ orbitals and s' is the overlap integral of $(2p_z)_1$ and $(2p_z)_3$. The three states are as follows.

$\Psi^{(i)}$		γ
$\frac{1}{\sqrt{2}}\{\phi_1(1)\phi_1(2)+\phi_2(1)\phi_2(2)\}$	$^1A_{1g}$	$(11\|11)+(12\|12)$,
$\frac{1}{\sqrt{2}}\{\phi_1(1)\phi_1(2)-\phi_2(1)\phi_2(2)\}$	$^1B_{1g}$	$(11\|11)-(12\|12)$,
$\frac{1}{\sqrt{2}}\{\phi_1(1)\phi_2(2)+\phi_2(1)\phi_1(2)\}$	$^1B_{2g}$	$(11\|22)+(12\|12)$,
$\frac{1}{\sqrt{2}}\{\phi_1(1)\phi_2(2)-\phi_2(1)\phi_1(2)\}$	$^3A_{2g}$	$(11\|22)-(12\|12)$,

($(11|22)$, *etc.*, denote $(\phi_1\phi_1|\phi_2\phi_2)$, *etc.*).

The level situation is consistent with the results of more elaborate calculations.[25]

Singlet Planar Trimethylenemethane.[26] The two orthogonal orbitals containing nonbonding electrons are written as

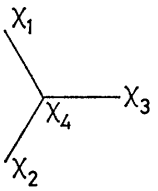

$$\phi_1 = \sqrt{\frac{2}{3(1-s')}}\left\{\chi_1-\frac{1}{2}(\chi_2+\chi_3)\right\},$$

$$\phi_2 = \frac{1}{\sqrt{2(1-s')}}(\chi_2-\chi_3),$$

where χ_j ($j=1$, 2, 3, and 4) are the four $2p_z$ orbitals, and s' is the overlap integral of χ_1 and χ_2. The resulting three states are

$$^1A_1' \quad \frac{1}{\sqrt{2}}\{\phi_1(1)\phi_1(2)+\phi_2(1)\phi_2(2)\},$$

$$^1E' \quad \begin{cases} \frac{1}{\sqrt{2}}\{\phi_1(1)\phi_2(2)+\phi_2(1)\phi_1(2)\}, \\ \frac{1}{\sqrt{2}}\{\phi_1(1)\phi_1(2)-\phi_2(1)\phi_2(2)\}, \end{cases}$$

$$\left(\ ^3A_2' \quad \frac{1}{\sqrt{2}}\{\phi_1(1)\phi_2(2)-\phi_2(1)\phi_1(2)\}\ \right).$$

The density of $^1E'$ ground state becomes

$$\rho(1) = \frac{2}{3(1-s')}[\{\chi_1(1)^2+\chi_2(1)^2+\chi_3(1)^2\} - \{\chi_1(1)\chi_2(1)+\chi_1(1)\chi_3(1)+\chi_2(1)\chi_3(1)\}]$$

showing that this is an antibonding biradical with $\mathfrak{B}=1/(1-s')$. The antibonding character might primarily cause the nonpolar geometry of singlet ground-state trimethylenemethane.[27]

General Characterization of Biradicals

The correlation-extremization approach developed in previous section is convenient for grasping a qualitative feature, but it can not be used in polar species where the potential field is partial to either one of the two radical sites. In such cases, the usual energy-extremization procedure, *viz.*, the configuration interaction (CI) approach, must be taken.

We use a CI wave function of n electron system $\Psi(1, 2, \cdots n)$ to construct the density distribution $\rho(1)$, which is decomposed in such a way as

$$\rho(1) = A_{11}a(1)^2 + 2A_{12}a(1)b(1) + A_{22}b(1)^2 + 2\sum_j\{B_{aj}a(1)+B_{bj}b(1)\}\chi_j(1) + \sum_{j,k}B_{jk}\chi_j(1)\chi_k(1), \quad (15)$$

The set of orbitals, a, b, and χ_j, in principle atomic hybrids or usual atomic orbitals, is obtained by a relevant transformation of the set of valence-shell atomic orbitals in such a way that orbitals a and b are appropriately associated with essentially located radical sites.

The bonding character and polar character can be represented by sA_{12} and Π of Eq. 12, respectively. We define a new concept, the delocalized character of a biradical, $\mathfrak{D}$, by

$$\mathfrak{D} = 2 - (A_{11}+2sA_{12}+A_{22}). \quad (16)$$

The biradical character of Eq. 14 can then be modified as

$$\mathfrak{B} = \frac{A_{11}+A_{22}}{2-\mathfrak{D}}(1-\Pi) = \frac{2}{2-\mathfrak{D}}(\text{the smaller of } A_{11} \text{ and } A_{22}). \quad (17)$$

Bonding Deformation of Singlet Biradicals

In the following examples, where the polar character Π can be put equal to zero, the biradical character $\mathfrak{B}$ depends only upon the overlapping between radical sites. Thus singlet biradicals stabilize with increasing overlapping between radical sites, which is in accordance with the direction of decreasing biradical character $\mathfrak{B}$. In contrast, the triplet species tend to decrease overlapping to stabilize.[29,30]

A molecular deformation in singlet biradicals to raise overlapping may even take place when stabilization overcomes destabilization, if it arises, due to the deformation. It may happen that a triplet biradical with minimal overlapping shifts to the singlet state through intersystem crossing to cause stabilization by bonding deformation. Let us discuss the bonding deformation in the direction of decreasing $\mathfrak{B}$ with regard to several examples of singlet biradicals.

The dependence of energy on the torsional angle θ in perpendicular ethylene discussed in previous section is shown below.[24] The lowest singlet has a deformation-instability in addition to the triplet-instability near $\theta=\pi/2$. The $^3A_2$ ground state of perpendicular geometry once formed may tend towards the planar form through the intersystem crossing to produce ^1A_g ground-state ethylene.

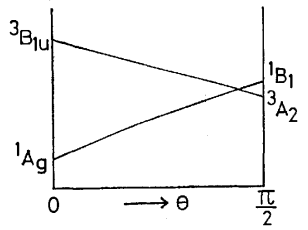

The direction of bonding deformation of perpendicular

species is simply represented by the following orbital phase scheme.[28]

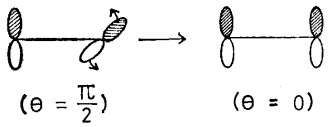

Similarly, the direction of deformation of square cyclobutadiene is given by the direction of in-phase overlapping of two odd-electron orbitals.

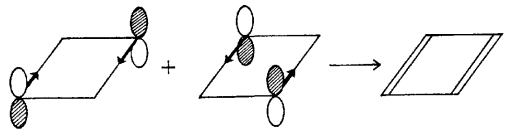

Also planar octagonal cyclooctatetraene will deform in the following way.

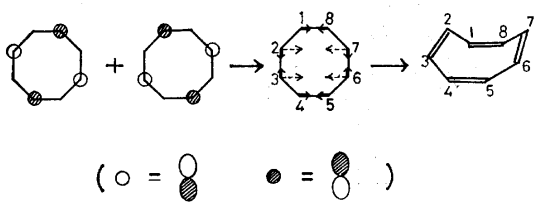

The bonding deformation consideration is employed to predict the geometry of stable intermediates in singlet radical reactions.

methylene-cyclopropane

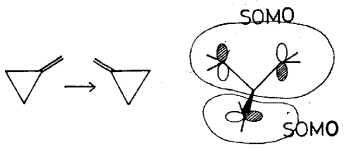

31)

methylene-cyclobutane

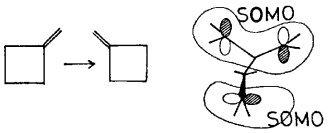

32)

1,2-dimethylene-cyclobutane

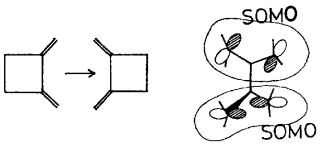

33)

SOMO denotes a singly occupied molecular orbital.

The bond alternation in carbon 2pπ chains can be explained by the following. The highest occupied (HO) and the lowest unoccupied (LU) MO's of a chain of equally distanced four p orbitals result approximately from the combination of the following two orbitals *a* and *b*.

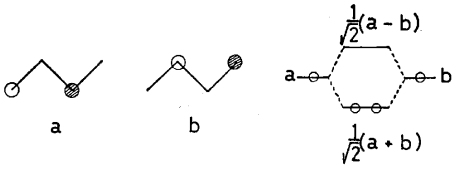

In this fictitious singlet biradical, the direction of deformation is also caused by the bonding overlapping of *a* and *b* to form a butadiene molecule, shown by

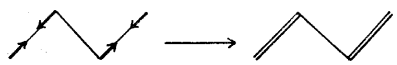

The lower occupied π orbital has hardly any connection with this deformation owing to its less nodal property.

Similarly, the difference in bond lengths in hexatriene, fulvene, naphthalene, *etc.*, is explained by considering the next HOMO's which contribute to the deformation less than HOMO because of their less nodal character.

An interesting application of the bonding deformation approach may be the prediction of the reaction path in excited states. In the π-π^* excited singlet state of hexatriene, the highest half-occupied orbital (a') and the lowest unoccupied orbital (b') are represented by

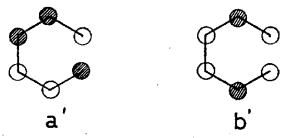

In order to consider bonding stabilization of the electron in orbital a', let us construct in the place of a' and b' the following quasiorthogonal orbitals.

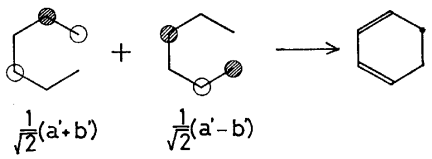

Combinations of these orbitals lead to orbitals a' and b', the former becoming occupied by a single electron to contribute to the bonding stabilization, and the direction of ring closure, if it occurs simultaneously, should be conrotatory. The conclusion is unchanged in the excited state with doubly occupied a'. In contrast, in the excited butadiene, the direction of hypothetical 1,4-bonding would be disrotatory.

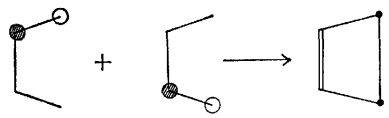

The lower singly occupied orbitals would contribute less by a similar discussion in terms of their less nodal property.

The simple approach is useful since it can be applied to a rough estimation of the direction of bonding in higher excited singlet states of a known electron configuration. The configuration might have several SOMO's. The general procedure is as follows:

i) By a linear combination of the HOMO (singly or doubly occupied) and the LUMO, say a' and b', we construct two MO's, *a* and *b*, which are mutually orthogonal and spatially separated from each other to construct a fictitious singlet biradical species.

ii) The direction of maximal overlapping of *a* and *b* to decrease the biradical character $\mathfrak{B}$, obtained by the usual procedure in the orbital interaction approach,[28] leads to a favourable reaction path.

In some cases, an excited state of the species before deformation may correlate to the ground state of the species after deformation, as in the following,

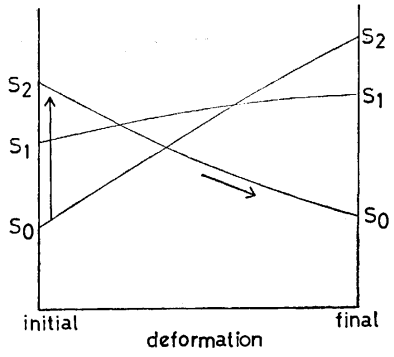

An example is the hypothetical disrotatory cyclization of S_2 excited butadiene to S_0 cyclobutene in the Longuet-Higgins-Abrahamson state correlation diagram.[34] The direction of such processes can be discussed by the method mentioned above.

Unpaired-Electron Isolating Deformation or Bonding in Triplet Biradicals

Once a triplet state is formed photochemically or thermally, a deformation or bond formation may be liable to take place to acquire stabilization in such a way that each of the two unpaired-electrons enters each of two orthogonal orbitals, or they become separated from each other by the newly formed bond as far away as possible.[9,30] In this connection Michl's conception of "loose" and "tight" biradicaloids is useful.[30c] The following examples are given for illustration.

Consider a π-π^* triplet hexatriene molecule. Twisting of the carbon chain would certainly diminish the overlapping of the two unpaired-electron orbitals. Two possibilities exist in regard to the twisting.

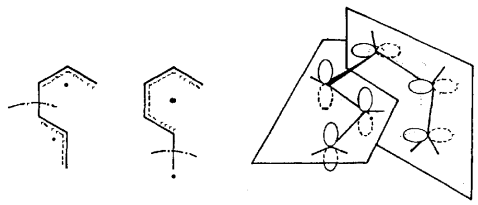

The sum of conjugation stabilization in the two separated parts in (I) is greater than in (II). The resulting geometry is shown in (III). Courtot and Salaün[35a] showed that sensitized photoreactions of hexatrienes preferentially cause the *cis-trans* isomerization of the *central* double bond, and that the singlet reaction causes isomerization of the terminal double bonds. The results are consistent with the theoretical prediction by Baird and West[35b] that the twisting of inner bonds should be preferred in the lowest triplet excited state of polyenes. In the singlet reaction a structure essentially like

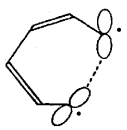

may be prevalent on account of the bonding nature of singlet biradicals, which will favour the terminal bond isomerization.

Geometries in which the planes associated with two unpaired-electron orbitals are perpendicular to each other might be expected more widely.[35c]

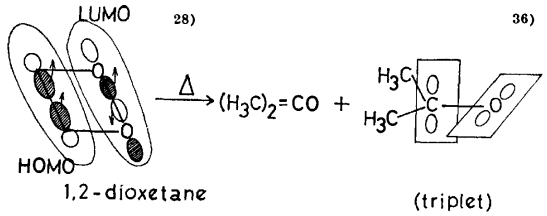

(Similar reactions are considered in chemiluminescent decomposition of 1,2-dioxetanone derivatives.[37])

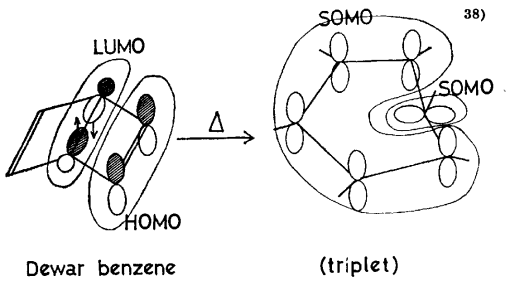

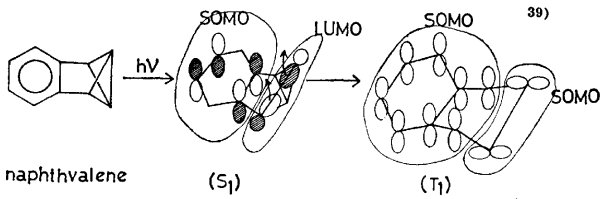

The above are examples of the separation of unpaired-electron orbitals by deformation. The isolation of unpaired-electrons also takes place by the formation of separating bonds.

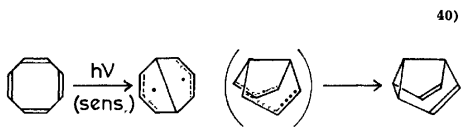

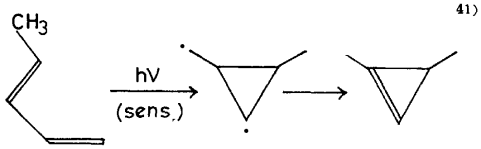

In the singlet-state reaction, a similar reaction takes place. In this case a certain concertedness may be mixed in the mechanism.[28]

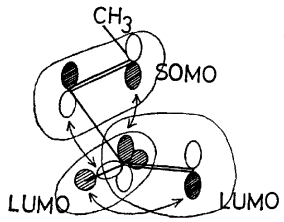

It appears that combination of the principle of unpaired-electron isolation in the triplet state with that of bonding deformation in the singlet state brings about a plausible mechanism occasionally prevalent in photochemical processes in which biradicaloid intermediates play an important role.

Suppose that the lowest triplet state (T_1) is produced, in some cases from higher excited singlet states (S_n) *via* S_1, through radiationless transitions (triplet biradical formation by a nonsensitized photoprocess). A possible deformation path might be composed of stages (I) and (II) as shown in Fig. 1.

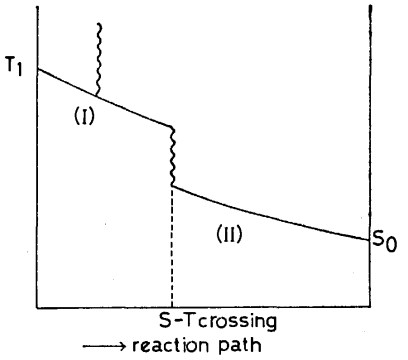

Fig. 1. A possible reaction path. (S_0: singlet ground state; T_1: first triplet state; ~~~~~: radiationless transition)

Stage (I) involves separation of unpaired-electron orbitals by orthogonally twisting deformation or bond formation, occuring in the first triplet state. Stage (II) is that of bonding deformation or bond formation in the singlet ground state, S_0.

By considering intermediate T_1, stereoselective phenomena can be explained by the augmenting chance to undergo further conversion due to the long lifetime of the triplet state.

This mechanism of the intermediation of triplet state is supported by Kushick and Rice[42] as regards the effectuation of the S-T transition by dynamical coupling of the torsional motion around the C_1–C_2 bond in the *cis-trans* photoisomerization of butadiene.

Let us consider excited-state reactions of benzene, six π MO's of which are given below.

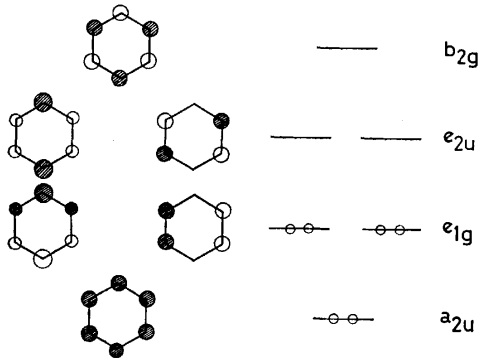

Thus, Dewar benzene might be produced from $e_{1g} \rightarrow e_{2u}$ excited singlet ($^1B_{1u}$),[43a]

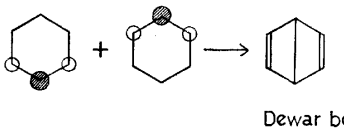

and the formation of benzvalene, prismane, and Dewar benzene would be favoured by triplet intermediation.

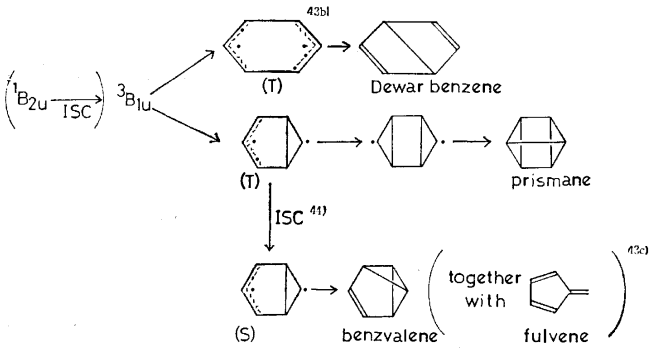

The mechanism involved might control the direction of reaction, giving a new principle of orientation or stereoselection in excited-state reactions.

This work was partly supported by Grants-in-Aid for Scientific Research from the Ministry of Education of Japan (No. 047068 and No. 139012). The authors express their appreciation to Prof. Hiroshi Kato, Nagoya University, for valuable discussions. One of the authors (K. F.) wished to thank Prof. P. Courtot for the interesting photochemical problem which stimulated him to carry out the present work.

References

1) R. B. Woodward and R. Hoffmann, *Angew. Chem. Int. Ed. Engl.*, **8**, 781 (1969).
2) J. A. Berson and L. Salem, *J. Am. Chem. Soc.*, **94**, 8917 (1972).
3) M. J. S. Dewar, S. Kirschner, and H. W. Kollmar, *J. Am. Chem. Soc.*, **96**, 7579 (1974).
4) D. R. Roberts, *J. Chem. Soc., Chem. Commun.*, **1974**, 683.
5) L. Salem and C. Rowland, *Angew. Chem. Int. Ed. Engl.*, **11**, 92 (1972); L. Salem, *Pure Appl. Chem.*, **33**, 317 (1973); L. Salem, W. G. Dauben, and N. J. Turro, *J. Chim. Phys.*, **70**, 694 (1973); L. Salem, *J. Am. Chem. Soc.*, **96**, 3486 (1974).
6) L. Salem, C. Leforestier, G. Segal, and R. Wetmore, *J. Am. Chem. Soc.*, **97**, 479 (1975).
7) V. Bonačić-Koutecký, P. Bruckmann, P. Hiberty, J. Koutecký, C. Leforestier, and L. Salem, *Angew. Chem.*, **87**, 599 (1975); *Angew. Chem. Int. Ed. Engl.*, **14**, 575 (1975).
8) W. G. Dauben, L. Salem, and N. J. Turro, *Acc. Chem. Res.*, **8**, 41 (1975).
9) L. Salem and P. Bruckmann, *Nature*, **258**, 526 (1975).
10) L. Salem, *Science*, **191**, 822 (1976).
11) The word "extremized" is used here only in the category of the present two-electron, two-orbital approximation. The parallel trend mentioned is evident for the systems with equivalent radical centres (see text). However, it is not necessarily guaranteed for general cases.
12) K. Ruedenberg, *Rev. Mod. Phys.*, **34**, 326 (1962).
13) H. Fujimoto, S. Yamabe, and K. Fukui, *Bull. Chem. Soc. Jpn.*, **44**, 2936 (1971).

14) K. Fukui, XXIII rd Internl. Congress of Pure and Applied Chemistry, Vol. 1, Butterworths, London (1971), p. 65.
15) H. Fujimoto, S. Yamabe, and K. Fukui, *Tetrahedron Lett.*, **1971**, 443.
16) S. Yamabe, T. Minato, H. Fujimoto, and K. Fukui, *Theoret. Chim. Acta*, **32**, 187 (1974).
17) S. Yamabe, S. Kato, H. Fujimoto, and K. Fukui, *Bull. Chem. Soc. Jpn.*, **46**, 3619 (1973).
18) H. Fujimoto, S. Yamabe, T. Minato, and K. Fukui, *J. Am. Chem. Soc.*, **94**, 9205 (1972).
19) K. Fukui, S. Kato, and H. Fujimoto, *J. Am. Chem. Soc.*, **97**, 1 (1975).
20) H. Fujimoto and K. Fukui, *Adv. Quantum Chem.*, **6**, 177 (1972).
21) H. Fujimoto and K. Fukui, in "Chemical Reactivity and Reaction Paths," ed by G. Klopman, John Wiley & Sons, Inc., New York (1974), p. 23.
22) S. Yamabe, S. Kato, H. Fujimoto, and K. Fukui, *Bull. Chem. Soc. Jpn.*, **48**, 1 (1975).
23) C. E. Wulfman and S. Kumei, *Science*, **172**, 1061 (1971).
24) R. J. Buenker, S. D. Peyerimhoff, and H. L. Hsu, *Chem. Phys. Lett.*, **11**, 65 (1971).
25) *E.g.* D. P. Craig, *Proc. R. Soc. London, Ser A*, **202**, 498 (1950).
26) cf. W. T. Borden, *J. Am. Chem. Soc.*, **98**, 2695 (1976).
27) M. J. S. Dewar and J. S. Wasson, *J. Am. Chem. Soc.*, **93**, 3081 (1971); D. R. Yarkony and H. F. Schaefer III, *ibid.*, **96**, 3754 (1974); W. J. Hehre, L. Salem, and M. R. Wilcott, *ibid.*, **96**, 4328 (1974).
28) K. Fukui, "Theory of Orientation and Stereoselection," Springer-Verlag, Berlin (1975).
29) See p. 81 of Ref. 28.
30) (a) S. Kita and K. Fukui, *Bull. Chem. Soc. Jpn.*, **42**, 66 (1969); (b) K. Fukui, *Acc. Chem. Res.*, **4**, 57 (1971); (c) J. Michl, *J. Am. Chem. Soc.*, **93**, 523 (1971); *Mol. Photochem.*, **4**, 257 (1972); "Chemical Reactivity and Reaction Paths," ed by G. Klopman, John Wiley & Sons, Inc., New York (1974), p. 301; (d) H. E. Zimmermann and G. A. Epling, *J. Am. Chem. Soc.*, **94**, 3647 (1972).
31) E. F. Ullman, *J. Am. Chem. Soc.*, **82**, 505 (1960); J. J. Gajewski, *J. Am. Chem. Soc.*, **93**, 4450 (1971); W. von E. Doering and H. D. Roth, *Tetrahedron*, **26**, 2825 (1970); W. von E. Doering and L. Birladeanu, *ibid.*, **29**, 499 (1973).
32) W. von E. Doering and J. C. Gilbert, *Tetrahedron Suppl.*, **7**, 397 (1966).
33) J. J. Gajewski and C. N. Shih, *J. Am. Chem. Soc.*, **89**, 4532 (1967); W. von E. Doering and W. R. Dolbier, Jr., *ibid.*, **89**, 4534 (1967).
34) H. C. Longuet-Higgins and E. W. Abrahamson, *J. Am. Chem. Soc.*, **87**, 2045 (1965).
35) (a) P. Courtot and J. Y. Salaün, *J. Chem. Soc., Chem. Commun.*, **1976**, 124; (b) N. C. Baird and R. M. West, *J. Am. Chem. Soc.*, **93**, 4427 (1971); (c) W. G. Dauben and J. S. Ritscher, *ibid.*, **92**, 2925 (1970).
36) N. J. Turro and P. Lechtken, *J. Am. Chem. Soc.*, **95**, 264 (1973); N. J. Turro, H. C. Steinmetzer, and A. Yetka, *ibid.*, **95**, 6468 (1973); N. J. Turro and P. Lechtken, *Pure Appl. Chem.*, **33**, 363 (1973); M. J. S. Dewar and S. Kirschner, *J. Am. Chem. Soc.*, **96**, 7578 (1974); N. J. Turro, P. Lechtken, N. E. Schore, G. Schuster, H. C. Steinmetzer, and A. Yetka, *Acc. Chem. Res.*, **7**, 97 (1974).
37) T. Goto and Y. Kishi, *Angew. Chem. Int. Ed. Engl.*, **7**, 407 (1968); W. D. McElroy, H. H. Seliger, and E. H. White, *Photochem. Photobiol.*, **10**, 153 (1969); E. H. White, J. D. Miano, C. J. Watkins, and E. J. Breaux, *Angew. Chem.*, **86**, 292 (1974).
38) P. Lechtken, R. Breslow, A. H. Schmidt, and N. J. Turro, *J. Am. Chem. Soc.*, **95**, 3025 (1973).
39) N. J. Turro, P. Lechtken, A. Lyons, R. R. Hautala, E. Carnahan, and T. J. Katz, *J. Am. Chem. Soc.*, **95**, 2035 (1973).
40) H. E. Zimmermann and H. Iwamura, *J. Am. Chem. Soc.*, **90**, 4763 (1968).
41) S. Boué and R. Srinivasan, *J. Am. Chem. Soc.*, **92**, 3226 (1970).
42) J. N. Kushick and S. A. Rice, *J. Chem. Phys.*, **64**, 1612 (1976).
43) (a) I. Haller., *J. Chem. Phys.*, **47**, 1117 (1967); (b) A. A. Gwaiz, M. A. El-Sayed, and D. S. Tinti, *Chem. Phys. Lett.*, **9**, 454 (1971); (c) H. R. Ward and J. S. Wishnok, *J. Am. Chem. Soc.*, **90**, 5353 (1968).
44) The possibility of the triplet intermediation in non-sensitized photolysis should be further examined. The sudden polarization of singlet biradicals[23] could be combined with the intersystem crossing $T_1 \rightarrow S_1$. The molecular geometry having minimum energy in the excited state is one with which the state T_1 has minimum energy. Such T_1 geometry would play some role in excited-state reactions (*e.g.*, see K. Yamaguchi, T. Fueno, and H. Fukutome, *Chem. Phys. Lett.*, **22**, 466 (1973)).

Large-Area (600 mm^2) Bimolecular Film in Aqueous Solutions. The Effect of an Amine-Ni^{2+} Complex on the Stability of *cis*-9-Octadecenylamine Bimolecular Film

Tadayoshi Yoshida, Masataka Okuyama, and Takahiro Itoh

Department of Engineering Chemistry, Nagoya Institute of Technology, Showa-ku, Nagoya 466

(Received October 29, 1976)

A large, planar, bimolecular film (bilayer, 600 mm^2) of *cis*-9-octadecenylamine (oleylamine) was found to be formed in an $NiCl_2$ solution. From the effect of the added metal ions on the proton magnetic resonance spectrum of octadecenylamine, it appears that the complex between the octadecenylamine molecule and the metal ion increases the stability of the bilayer. The thickness of the bilayer depended strongly on the kind of solvent in the film-forming solution. When decane, a normal alkane solvent, was used, the thickness of the bilayer was greatest (4.6 nm), and the temperature effect was smallest. The experimental results are explained in terms of (i) the influence of the solvent on the conformation of the octadecenyl chain and (ii) the amount of solvent remaining in the film.

A previously reported bilayer of 1-tetradecanol in an aqueous solution was stable, but not large (1 mm^2).[1,2] An increase in the bilayer size is essential to the improvement of the accuracy of electrical and optical measurements. Using a dipping technique, Tien *et al.* have prepared the largest planar bilayers thus far produced (*ca.* 100 mm^2).[3] Spherical bilayer has also been produced with areas up to *ca.* 100 mm^2 using a bubble technique.[4] For most measurements, however, a spherical bilayer is not as appropriate as a planar bilayer.

In order to prepare a large bilayer, it is necessary to increase the layer stability. The bonds between the constituent molecules and their surroundings may have a stabilizing effect on the bilayer. For example, it is expected that complex formation between the hydrophilic group of molecules in the bilayer and multivalent ions in the aqueous solution increases the stability of the bilayer.

On the other hand, it has been found empirically that no stable bilayer can be prepared from a dilute film-forming solution (surface-active molecule/organic solvent).[2]

Therefore, the molecules of an unsaturated hydrocarbon chain are more suitable than those of a saturated chain in view of the solubility. As a system which satisfies the above factors governing stability, a *cis*-9-octadecenylamine bilayer was formed in an $NiCl_2$ solution.

Experimental

Materials. The distilled *cis*-9-octadecenylamine (purity>99%) used in this study was purchased from the Tokyo Kagaku Seiki Co., Ltd. The aqueous solution surrounding the bilayer were prepared from redistilled water and guaranteed reagents (Wako Pure Chemical Industries, Ltd.). All solvents were of reagent grade.

Preparation of Large Bilayer Films. Bilayers were prepared by two methods (I and II), using the dipping technique. Method I: (1) Two compartments (F_1 and F_2) of the same volume were separated by a Teflon plate A (thickness: 2 mm) having a unique hole (width: 13 mm, length: 60 mm) at its center (Fig. 1). A 30 mM* $NiCl_2$ solution was introduced into both compartments through tubes (T_1 and T_2) until the water levels were raised to a point just below the hole in the Teflon plate (Fig. 1a). A small volume D (*ca.* 0.1 cm^3) of an octadecenylamine/alkane solution [*i.e.*, the film-forming solution, 0.2/1 (v/v)] was then delivered onto the rim around

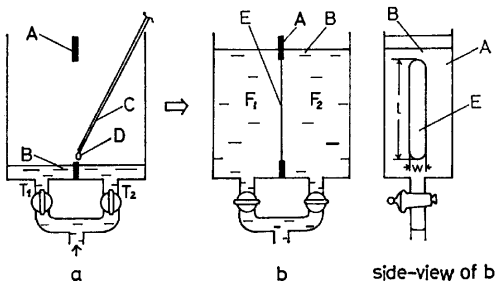

Fig. 1. Method (I) for the preparation of large bilayer. A: Teflon plate, B: aqueous solution, C: Teflon tube, D: a drop of the octadecenylamine/decane solution, E: large bilayer (width w=12 mm, length l=60 mm), T_1 and T_2: tube.

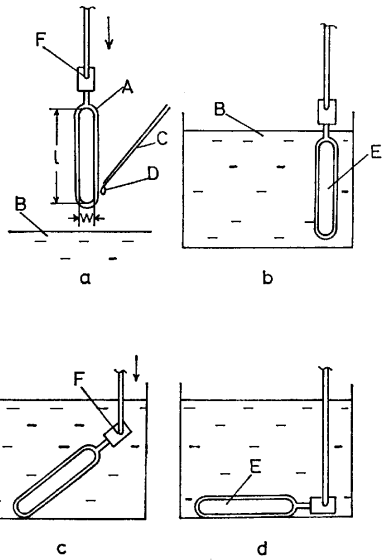

Fig. 2. Method (II) for the preparation of large bilayer. A: Frame of Teflon-coated wire (diameter: 2 mm), B, C, D, and E are the same as those of Method (I), F: joint.

* Throughout this paper, 1 M=1 mol/dm^3.

the hole with the help of a Teflon tube C (diameter: 1 mm) attached to a syringe. (2) The 30 mM $NiCl_2$ soultion was gradually added to both compartments. Two water levels were maintained at equal heights. The water levels were then raised until they reached *ca.* 5 mm above the hole (Fig. 1b). By this procedure, a colored film formed over the hole in the Teflon plate. After *ca.* 10 min, the colored film became black. Method II: A frame of Teflon-coated wire (diameter: 2 mm, Fig. 2a) was used in place of the Teflon plate. (1) A small volume D of the film-forming solution was delived onto the frame A in a manner similar to that described for Method I. (2) By lowering the frame into the aqueous solution (30 mM $NiCl_2$), a colored film formed on the frame (Fig. 2b). (3) After the frame had been further lowered, the major axis of the frame was rotated around the joint F through 90 ° (Figs. 2c and 2d). Thus, a longer film formed in the lateral direction, as well as in the vertical direction.

After *ca.* 10 min, these colored films became black. In order to improve the stability of the black film, care was taken to protect the film from vibration. The stability of the film was also increased by prepainting the frame with the sample solution.

Measurements. In order to estimate the thickness of the black film, the electrical capacitance of the film was measured by means of an AC bridge (Ando Electric Co., Ltd., Model TR-IC). Measurements were carried out in the frequency range from 30 Hz to 3MHz. The resistance of the black film was also obtained by the transient DC method. The potential across the film was measured using an electrometer of high-input impedance (Takeda Riken Industry Co., Ltd., Model TR-8651) by means of a pair of reversible Ag/AgCl electrodes. The area of the film was estimated from a photograph. The temperature of the film and its surrounding solution was maintained constant to within an accuracy of ± 0.5 °C by thermostatically-controlled water circulation. Proton magnetic resonance (PMR) spectra of metal octadecenylamine complexes were obtained at 60 MHz and 35 °C, using a Hitachi R-24 spectrometer. Monolayer characteristics of the octadecenylamine at the air–aqueous solution interface were obtained using the Wilhelmy method.

Results and Discussion

The black film formed by Method I is suitable for the measurement of electric properties, while that formed by Method II is suitable for the measurement of optical properties. The stability of the films was greatly influenced by the kind of solvent in the film-forming solution. When octane and dodecane were used as film-forming solution solvents, planar black films with areas up to 600 mm^2 were formed in the 30 mM $NiCl_2$ solution. In the case of decane as the solvent, the largest bilayer (5000 mm^2) was obtained. The films persisted over a period of one hour. When hexane, tetradecane, and hexadecane were used as solvents, however, the areas of the black films were less than 10 mm^2.

The stability of the bilayer was also influenced by the cation in the aqueous solution. The order of the stabilities of large black films was $Ni^{2+}>Co^{2+}>Mn^{2+}$. On the other hand, stable black films were not formed in NaCl, KCl, $CaCl_2$, and $MgCl_2$ solutions (30—100 mM). The addition of Ni^{2+} ions changed the PMR spectrum of the octadecenylamine (Fig. 3). The $-NH_2$ signal o octadecenylamine was no longer observable, as can be

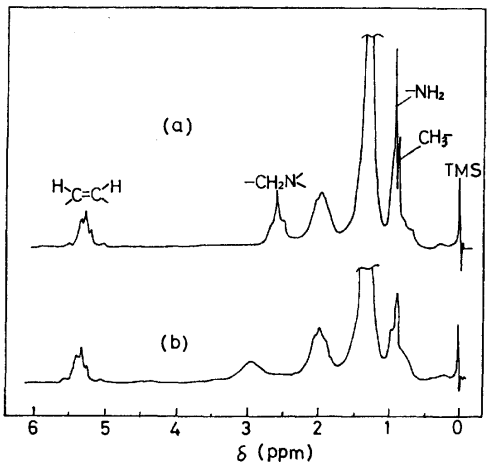

Fig. 3. Effect of added Ni^{2+} ion on the PMR spectrum of octadecenylamine; (a) octadecenylamine, (b) 1 dm^3 octadecenylamine plus 4 mM $NiCl_2 \cdot 6H_2O$. Internal reference: TMS.

seen in Fig. 3b. The $-CH_2N<$ signal is shifted downfield by 0.3 ppm and is also broadened. When ethyl glycinate was mixed in a 0.1 mM Cu^{2+} ion solution, the glycine–CH_2– signal changed in a manner similar to that for the $-CH_2N<$ signal.[5] The change in the glycine–CH_2– signal is accounted for by the proximity of the paramagnetic Cu^{2+} ion. Therefore, it appears that the proximity of the paramagnetic Ni^{2+} ion to the nitrogen atom of the octadecenylamine molecule is responsible for the change in the PMR spectrum (Fig. 3b). The magnitude of change in the $-CH_2N<$ signal was dependent on the kind of metal ion in the aqueous solution (Fig. 4). In particular, the addition of Ni^{2+} ions results in a remarkable change in the $-CH_2N<$ signal. The order of the change in magnitude of the $-CH_2N<$ signal was compatible with the Irving-Williams series ($Ni^{2+}>Co^{2+}>Mn^{2+}$), with respect to the stability of the complexation. The order of the stabilities of black films also agree with the Irving-Williams series.

From the above argument, it can be assumed that the interaction (complex formation) between the octadecenylamine molecule and metal ion (particularly,

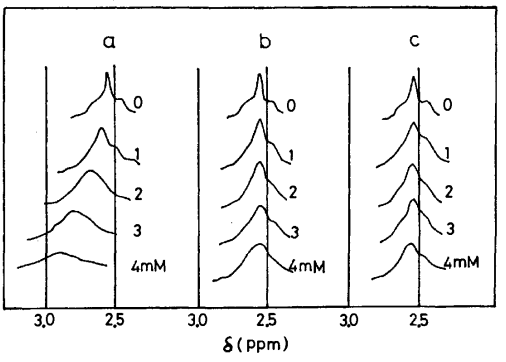

Fig. 4. Effect of the concentration of added metal ions on the $-CH_2N<$ signal of octadecenylamine; (a) $NiCl_2 \cdot 6H_2O$ plus octadecenylamine, (b) $CoCl_2 \cdot 6H_2O$ plus octadecenylamine, (c) $MnCl_2 \cdot 4H_2O$ plus octadecenylamine. Internal reference: TMS.

the Ni^{2+} ion) increases the stability of black film and that black films of large area are thus formed in aqueous solutions.

In accordance with the suggestion of Hanai *et al.*,[6] the static capacitance C_t (0 Hz) of the entire system (*i.e.*, the black film and its surrounding aqueous solution) is equal to the capacitance C_m of the black film itself, $C_t(0\text{ Hz})=C_m$. For several systems it was found that the static capacitance and the capacitance at 1 kHz agree with each other, $C_t(0\text{ Hz})=C_t(1\text{ kHz})$. Thus, the capacitance of the black film itself can be approximated by the observed capacitance of the entire system at 1 kHz. This approximation is the same as that which was used for 1-tetradecanol bilayers.[1] The capacitance of the black film itself depends strongly on the kind of hydrocarbon solvent used in its formation. In Fig. 5, it is seen that with decane as the film-forming solution solvent, the capacitance is smaller than that for any other alkane. In $CoCl_2$ solutions, as well as in $NiCl_2$ solutions, decane minimizes the capacitance.

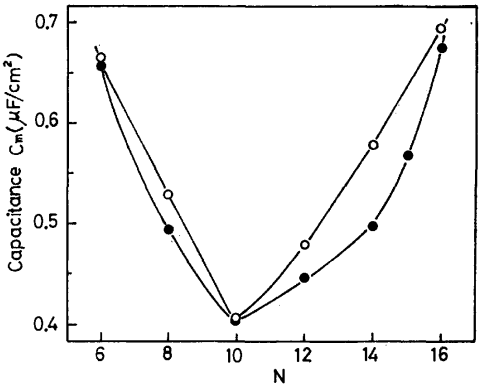

Fig. 5. Capacitance per unit area of black films of octadecenylamine dissolved in various alkanes. N is the number of carbon atoms of alkane used as solvent. ○: In 30 mM $NiCl_2$ solution, ●: in 30 mM $CoCl_2$ solution.

The capacitance of the black film is influenced both by the thickness and the dielectric constant of the hydrocarbon core of the film. Since the volume fraction of the solvent in core is not known, the dielectric constant of the core cannot be unequivocally estimated. Thus, the thickness of the black film cannot be accurately calculated from the capacitance measurement. Assuming, however, that the dielectric constant of the core has an intermediate value between that of the solvent of the sample solution and that of the octadecenyl chains, the thickness of the core may be estimated, as is shown in Fig. 6. The thickness of the film has a maximum value in the case of decane. The variation in thickness suggests that the hydrocarbon solvent greatly affects the conformation of the octadecenyl chains.

Fettiplace *et al.*[7] have reported the for hydrocarbon solvents of chain lengthgreater than decane, the thickness of black films (of glycerol monooleate or of lecithin) decrease with increasing solvent chain length. In addition, the following fact was observed. For solvents of chain length shorter than decane, the thickness of the octadecenylamine films decreases markedly with decreasing length of the hydrocarbon

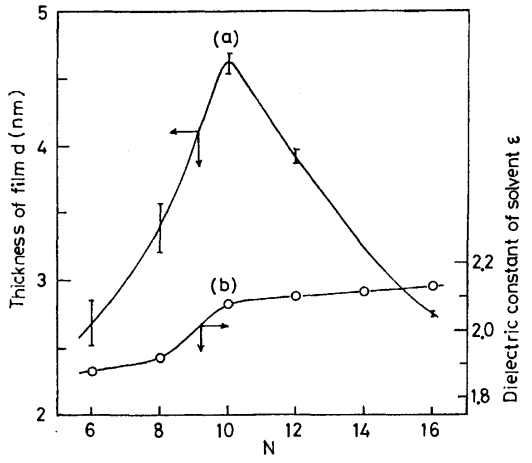

Fig. 6. Curve (a): calculated thickness of black film in the 30 mM $NiCl_2$ aqueous solution. N is the number of carbon atoms of alkane (solvent of the sample solution). The upper end of vertical line indicates the calculated value, assuming the dielectric constant of the core of black film to be equal to the value in curve (b) (*i.e.* the dielectric constant of normal alkane in the same solution). The lower end of vertical line indicates the calculated values, assuming the dielectric constant of the core to be that 1-octadecene, 2.15. The curve shows the mean value.

chain of the solvent (Fig. 6). This experimental, result can be accounted for both by (i) the influence of the solvent on the conformation of octadecenyl chain and (ii) that of the amount of solvent remaining in the film as described below. (i) The influence of the solvent on the conformation of the octadecenyl chain: The monolayer of octadecenylamine on the $NiCl_2$ solution (30 mM) is not condensed, but expanded. As a result, it appears that the molecular cavity (vacancy) between octadecenyl chains is larger than that between octadecyl chains, but that the octadecenyl chains are contiguous with each other due to the Van der Waals force which minimizes the molecular cavity. This property of octadecenylamine may appear also in black films of this molecule (note the properties of monolayers and bilayers of tetradecanoic acid[1]). Therefore, the effective length of a octadecenyl chain in a black film (*i.e.*, the thickness of the film) becomes shorter than the length of the fully extended form. Since the alkane molecules used as solvents occupy the molecular cavity of the octadecenyl chain, the conformation of the octadecenyl chain should be influenced by both the kind and the amount of solvent remaining in the film. In other words, the effective length of the octadecenyl chain (*i.e.*, the thickness of the black film) should be increased by the solvent remaining in the black film. (ii) The influence of the amount of solvent remaining in the film on the film thickness: Bewing and Zisman[8] have estimated the amount of normal alkanes in alkylamine–normal alkane mixed films adsorbed on platinum. Their conclusion is as follows. When both chains contain the same number of carbon atoms, the largest quantities of alkanes remain in the film. When the length of the alkane molecule is shorter or longer than that of the alkylamine molecule, the molar fraction of the alkane remaining in the films

decreases. Their conclusion was made on the basis of the alkane remaining in saturated hydrocarbons. On the other hand, Shah and Schulman[9] have suggested from the additivity of the surface areas of mixed lecithin–cholesterol monolayers that the stereochemical dimensions of cholesterol are appropriate for occupying the molecular cavities in lecithin monolayers. In the present case, it appears from curve (a) in Fig. 6 that decane rather than other normal alkanes tends to remain among the octadecenyl chains. The decrease in the molar fraction of alkane in the film increases the conformational change of the octadecenyl chains, and the film thus becomes thinner. Consequently, decane as a solvent results in maximum film thickness.

From the above argument, the change in the film thickness may be interpreted on the basis of the solvent in the film.

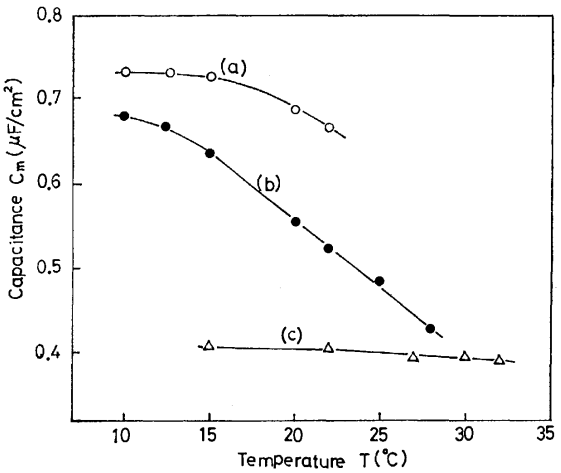

Fig. 7. Effect of temperature on the capacitance of black films in the 30 mM $CoCl_2$ solution.
(a): Film formed from octadecenylamine/hexane solution, (b): Film formed from octadecenylamine/tetradecane solution, (c): Film formed from octadecenylamine/decane solution.

Figure 7 shows the influence of temperature on the capacitance of the films. For films formed from an octadecenylamine/hexane or tetradecane solution, a marked effect of temperature on the capacitance of the film is found. It appears that the temperature dependence of the capacitance is associated with the molar fraction of the solvent in the films. That is to say, the molar fraction of the solvent in the films decreases with decreasing temperature, and then the octadecenyl chains in the film approach each other in order to reduce the molecular cavity from which the solvent molecules emerged. Consequently, the capacitance of the film increases with decreasing temperature. Since the capacitance of octadecenylamine and hexane films remains constant below 15 °C, it appears that hexane is almost completely excluded from the film. On the other hand, for black films produced in octadecenylamine/decane solutions, the capacitance also remains constant. However, the reason for the constancy of curve c in Fig. 6 differs from that for the flat part of curve a. As described above, it may be assumed from curve a that decane rather than other alkanes tends to remain in the octadecenyl chains. Therefore, since decane molecules in the film are hardly excluded, in spite of the decrease in temperature (from 32 to 15 °C), no temperature dependence of the capacitance is observed. The experimental results shown in Fig. 7 is, therefore, consistent with the assumption for curve a in Fig. 6.

For the film formed in an octadecenylamine/decane solution, the resistance of the $NiCl_2$ solution (30 mM) was in the range from 4 to $8\times10^6\,\Omega\,cm^2$. For films formed from octadecenylamine dissolved in other solvents, their resistances were from 1 to $5\times10^6\,\Omega\,cm^2$. In view of the uncertainties in the experimental results, it cannot be asserted that films formed with decane had higher resistances. The above result, however, suggests that a change in the film thickness has no significant effect on the film resistance. In other words, it appears that the rate-determining step for the permeation of ions across the black film is not the stage at which the ions move through the hydrocarbon core of the film, but the stage at which the ions enter from the aqueous solution into the hydrocarbon core of the film.

The authors wish to thank Dr. Hirofumi Okabayashi of this laboratory for valuable discussions. A part of this research was supported by a Scientific Research Grant from the Ministry of Education.

References

1) M. Okuyama, T. Yoshida, T. Tanii, M. Kunugi, and I. Ishizaki, *Bull. Chem. Soc. Jpn.*, **48**, 191 (1975).
2) M. Okuyama and T. Yoshida, *Maku (Membrane)*, **1**, 263 (1976).
3) H. T. Tien, S. Carbone, and E. A. Dawidowicz, *Kolloid-Z.*, **212**, 165 (1966).
4) R. Pagano and T. E. Thompson, *Biochim. Biophys. Acta*, **144**, 666 (1967).
5) R. Mathur and N. C. Li, *J. Am. Chem. Soc.*, **86**, 1289 (1964).
6) T. Hanai, D. A. Haydon, and J. Taylor, *Proc. R. Soc. London, Ser. A*, **281**, 377 (1964).
7) R. Fettiplace, D. M. Andrews, and D. A. Haydon, *J. Membr. Biol.*, **5**, 277 (1971).
8) K. W. Bewig and W. A. Zisman, *J. Phys. Chem.*, **67**, 130 (1963).
9) D. O. Shah and J. H. Schulman, *J. Lipid Res.*, **8**, 215 (1967).

On the Gibbs Adsorption Equation for Electrolyte Solutions

Shoichi IKEDA

Department of Chemistry, Faculty of Science, Nagoya University, Chikusa, Nagoya 464

(Received January 21, 1977)

A general method is developed to derive the Gibbs adsorption equation in the form applicable to aqueous solutions of electrolytes, either strong or weak, composed of multi-components. Assuming that the solution is ideal, the chemical potentials of solute electrolytes are represented by their concentrations, and the lowering of surface tension is calculated as a function of variations of these concentrations. Explicit expressions for surface excesses of various species are obtained on aqueous solutions of two strong electrolytes having a common cation, such as sodium dodecyl sulfate and NaCl, and on solutions containing a weak acid adjusted its ionization by addition of alkali, such as fatty acid or soap, in the presence of an added salt. The convention for drawing the Gibbs dividing plane is discussed when the Gibbs adsorption equation is represented in terms of all the species in solution.

For the experimental verification of the Gibbs adsorption isotherm, aqueous solutions of surface-active substances are the most appropriate to be examined, but, owing to the electrolytic nature of most of the well-defined surfactants, the Gibbs adsorption equation has to be cast into a form applicable to such multi-component systems. Nevertheless, considerable controversy has been raised about it, since Brady[1] and Hutchinson[2] first gave an equation for a solution of strong electrolyte, in which each constituent ionic species contributes to the lowering of surface tension.[3–7] Later it was shown, however, that when an excess amount of salt is added, the electric double layer reduces the contribution of counter ion, and only the surfactant ion is responsible for surface activity.[8–11] Davies[12] derived an approximate form of the Gibbs adsorption equation for a solution of strong electrolyte, which gave the results cited above in both extreme cases, *i.e.*, in the absence and excess presence of added salt.[13,14] Recently, Tajima[15] succeeded to find an exact equation for aqueous solution of strong electrolytes.

In the present work, we will develop a general method to derive the Gibbs adsorption equation in the form applicable to aqueous solutions of electrolytes, either strong or weak, composed of multi-components. This method is first adapted to a solution of two strong electrolytes having a common cation, *i.e.*, NaD and NaCl, where D^- may be any anion other than Cl^-. Then it is extended to treat aqueous solutions containing a weak electrolyte, HD, such as a solution of HD, NaOH and NaCl, or solutions of NaD, HCl, and NaCl, or NaD, NaOH, and NaCl, in the latter two of which HD is generated by hydrolysis. The binary system containing HD or NaD alone will appear as a limiting case of ternary or quaternary systems cited above.

Our approach is general and purely thermodynamic. The Gibbs adsorption equation is expressed in terms of chemical potentials of added solute components. The method is applicable to any multi-component systems. The assumption is made that the solution is dilute and ideal, in spite of electrolytes involved, so that the activity coefficients of solute components are put equal to unity. The lowering of surface tension is then given as a function of variations of concentrations of added solute components.

Principles of the Method

Our starting equation is given by

$$-\mathrm{d}\gamma = \sum_{\mathrm{i}} \Gamma_{\mathrm{i}} \mathrm{d}\mu_{\mathrm{i}}, \tag{1}$$

where γ is the surface tension, Γ_{i} is the surface excess referred to a dividing plane set at an unspecified position of the interface between two phases (vapor and solution), and μ_{i} is the chemical potential or may be the electrochemical potential (in the solution phase). The suffix, i, represents the chemical species, either nonionic or ionic, and the summation extends over all species actually present in the system (solution).[16–18] In the three-component system concerned, i stands for H_2O, Na^+, D^-, and Cl^-, and in the case of hydrolysis occurring, it should include HD, H^+, and OH^-. In the four-component systems, all these species must be taken into account.

It should be noticed that values of Γ_{i} thus given are not definite unless the position of the dividing plane is specified. When n_{i} moles of species i are distributed between vapor and solution phases, in which its molar concentrations are C_{i}' and C_{i}, respectively, the surface excess, Γ_{i}, is given by

$$A\Gamma_{\mathrm{i}} = n_{\mathrm{i}} - V'C_{\mathrm{i}}' - VC_{\mathrm{i}}, \tag{1a}$$

where A is the area of the plane interface. Volumes of the vapor phase and the solution phase, V' and V, are not definite as far as the location of dividing plane is unspecified, while the system is closed and $V'+V$ is constant. Consequently, values of Γ_{i} remain indefinite at this stage.[16–18]

Let ν neutral components be added to make up the solution, where ν is 3 or 4. When HD is involved, two ionization equilibria are set up. The condition for equilibrium is determined by

$$\mu_\lambda = \mu_{\mathrm{H}^+} + \mu_{\mathrm{a}}, \tag{2}$$

where λ is H_2O or HD and a is OH^- or D^-. It should be noticed that μ_λ stands for the chemical potential of water component or the weak acid added as well as that of unionized H_2O or HD.[17] Furthermore, the chemical potential of a (uni-univalent) strong electrolyte can also be represented by the sum of the potentials of its constituent ions:

$$\mu_\lambda = \mu_{\mathrm{k}} + \mu_{\mathrm{a}}, \tag{3}$$

where λ is NaD, HCl, NaOH, or NaCl, and k and a are

the corresponding cation and anion, respectively.

By means of Eqs. 2 and 3 we eliminate all the chemical potentials of ionic species except for one, and then we can express the decrease in surface tension in terms of the variations of chemical potentials of added neutral components and that of the single ionic species. As the chemical potential of a single ion cannot be altered by itself, the relevant term should not appear, and it is actually found that the condition is satisfied by the electroneutrality among surface excesses of ionic species. Equation 1 is then written in a form

$$-\mathrm{d}\gamma = \sum_{\lambda=1}^{\nu} \Gamma_\lambda \mathrm{d}\mu_\lambda, \tag{4}$$

where λ runs over all ν neutral components actually added, including water as 1. Γ_λ is here expressed by an algebraic sum of Γ_i, when started from Eq. 1, but it represents the surface excess of added neutral component, λ.

In a ν-component system composed of two phases (vapor and solution), the number of degrees of freedom is $\nu-1$ at constant temperature. Consequently, a term of Eq. 4 must vanish, and for dilute solutions the solvent, water, term is chosen, so that the coefficient of $\mathrm{d}\mu_{H_2O}$, *i.e.*, Γ_1, is put equal to zero.[18] This procedure is equivalent to set the dividing plane of the interface at a definite position, which makes the surface excesses of solute components definite. In Appendix an alternative definition of surface excesses is given, which eventually agrees with the above.

The Gibbs adsorption equation is now given by

$$-\mathrm{d}\gamma = \sum_{\lambda=2}^{\nu} \Gamma_\lambda^{(1)} \mathrm{d}\mu_\lambda, \tag{5}$$

where the superfix, (1), for Γ_λ implies that the dividing plane is placed at such a position that the surface excess of water, 1, is zero. An algebraic sum of $\Gamma_i^{(1)}$ will replace for $\Gamma_\lambda^{(1)}$. In the following we will omit the superfix, (1), for the sake of brevity, which will not cause any confusion.

It remains to express the chemical potentials of added neutral solutes by their concentrations. In the present work we make an assumption that the solution is ideal so that the activity coefficients of the solute components are unity. Then the chemical potential of an unionized solute species (or a weak electrolyte), λ=HD, has a form

$$\mu_\lambda = \mu_\lambda^\circ + RT \ln C_\lambda, \tag{6}$$

where C_λ is the molar concentration of λ and the superfix, O, refers to the standard state. The chemical potential of a strong electrolyte has a form

$$\mu_\lambda = \mu_\lambda^\circ + RT \ln C_k C_a, \tag{7}$$

where C_k and C_a are the molar concentrations of cation and anion, respectively. The concentrations, C_λ, C_k, and C_a, can be expressed by the concentrations of added neutral solutes and the degree of ionization.

Ternary System: H_2O+NaD+NaCl

We consider an aqueous solution of NaD and NaCl, where NaD may be an anionic surfactant. Hydrolysis of NaD is not taken into account, and accordingly, the ionization of water is not involved either. Then we have four chemical species in solution, and Eq. 1 is written as

$$-\mathrm{d}\gamma = \Gamma_{H_2O}\mathrm{d}\mu_{H_2O} + \Gamma_{Na^+}\mathrm{d}\mu_{Na^+} + \Gamma_{D^-}\mathrm{d}\mu_{D^-} + \Gamma_{Cl^-}\mathrm{d}\mu_{Cl^-}. \tag{8}$$

Using Eqs. 3 for chemical potentials of NaD and NaCl, Eq. 8 is converted into

$$-\mathrm{d}\gamma = \Gamma_{H_2O}\mathrm{d}\mu_{H_2O} + \Gamma_{D^-}\mathrm{d}\mu_{NaD} + \Gamma_{Cl^-}\mathrm{d}\mu_{NaCl} + (\Gamma_{Na^+} - \Gamma_{D^-} - \Gamma_{Cl^-})\mathrm{d}\mu_{Na^+}. \tag{9}$$

As the chemical potential of Na^+ cannot be varied by itself, the last term should not appear, but its coefficient vanishes owing to the electroneutrality condition

$$\Gamma_{Na^+} = \Gamma_{D^-} + \Gamma_{Cl^-}. \tag{10}$$

According to the phase rule, the system must have two degrees of freedom at constant temperature, so that we may put

$$\Gamma_{H_2O} = 0, \tag{11}$$

which defines the position of dividing plane and the surface excesses of solutes. Eq. 9 then becomes

$$-\mathrm{d}\gamma = \Gamma_{D^-}\mathrm{d}\mu_{NaD} + \Gamma_{Cl^-}\mathrm{d}\mu_{NaCl}. \tag{12}$$

It is evident that Γ_{D^-} is identical with the surface excess of NaD and Γ_{Cl^-} is that of NaCl.

If the molar concentrations of added NaD and NaCl are represented by C and C_S, respectively, the concentrations of ions are

$$\begin{aligned} C_{Na^+} &= C + C_S, \\ C_{D^-} &= C, \\ C_{Cl^-} &= C_S. \end{aligned} \tag{13}$$

Substituting Eqs. 13 into Eqs. 7 for NaD and NaCl, and putting them into Eq. 12, we obtain

$$-\mathrm{d}\gamma = RT[\Gamma_2 \mathrm{d} \ln C + \Gamma_3 \mathrm{d} \ln C_S], \tag{14}$$

where

$$\Gamma_2 = \left(1 + \frac{C}{C+C_S}\right)\Gamma_{D^-} + \frac{C}{C+C_S}\Gamma_{Cl^-}, \tag{14a}$$

$$\Gamma_3 = \frac{C_S}{C+C_S}\Gamma_{D^-} + \left(1 + \frac{C_S}{C+C_S}\right)\Gamma_{Cl^-}. \tag{14b}$$

Solving Eqs. 14a and b, we have the surface excesses or the adsorbed amounts of ions of NaD and NaCl:

$$\Gamma_{D^-} = \left(1 - \frac{C}{2(C+C_S)}\right)\Gamma_2 - \frac{C}{2(C+C_S)}\Gamma_3, \tag{15a}$$

$$\Gamma_{Cl^-} = -\frac{C_S}{2(C+C_S)}\Gamma_2 + \left(1 - \frac{C_S}{2(C+C_S)}\right)\Gamma_3. \tag{15b}$$

The surface excess of Na^+ is given by

$$\Gamma_{Na^+} = \Gamma_{D^-} + \Gamma_{Cl^-} = \frac{1}{2}(\Gamma_2 + \Gamma_3). \tag{15c}$$

The equations derived by Tajima[15] reduce to Eqs. 15a and 15b, if the activity coefficients of solutes are substituted by unity, instead of being given by the Debye-Hückel limiting law. Eqs. 14 and 15 are applicable to solutions of sodium dodecyl sulfate in the presence or absence of NaCl, provided that no (surface) hydrolysis occurs. It is easy to show that no surface hydrolysis occurs unless HCl is added, as far as HD is a strong acid.[19]

When HD is generated by hydrolysis, as in solutions

of sodium carboxylate, three additional species, HD, H^+, and OH^-, must be taken into account. Such a system will be treated as a special case of the quaternary systems below.

Quaternary Systems

When we consider an aqueous solution of HD, NaOH, and NaCl, in which HD is a weak acid such as fatty acid, there are seven chemical species in it. Clearly these species are also produced in solutions of NaD and NaCl, either in the presence or absence of HCl or NaOH. Then the Gibbs adsorption equation, Eq. 1, for these quaternary systems is commonly written as

$$-d\gamma = \Gamma_{H_2O}d\mu_{H_2O} + \Gamma_{HD}d\mu_{HD} + \Gamma_{H^+}d\mu_{H^+} + \Gamma_{OH^-}d\mu_{OH^-} + \Gamma_{Na^+}d\mu_{Na^+} + \Gamma_{D^-}d\mu_{D^-} + \Gamma_{Cl^-}d\mu_{Cl^-}, \quad (16)$$

For these systems the electroneutrality of surface excesses of ionic species

$$\Gamma_{H^+} + \Gamma_{Na^+} = \Gamma_{D^-} + \Gamma_{OH^-} + \Gamma_{Cl^-}. \quad (17)$$

holds.

There exist ionization equilibria given by Eqs. 2 for water and the weak acid, and these equilibrium conditions can be substantially represented by the molar concentrations of added HD or NaD, C, and of added NaCl, C_S, if the activity coefficients of solutes are assumed to be unity.

When the apparent ionic product of water is defined by K_W, Eq. 2 may be put as

$$C_{H^+}C_{OH^-} = K_W. \quad (18)$$

Similarly, when the degree of ionization of the weak acid is α and its ionization constant is K, then the concentrations of unionized and ionized acid species are given by

$$C_{HD} = (1-\alpha)C,$$
$$C_{D^-} = \alpha C, \quad (19)$$

and Eq. 2 reduces to

$$C_{H^+}\frac{\alpha}{1-\alpha} = K. \quad (20)$$

By means of the electroneutrality condition of the solution

$$C_{H^+} + C_{Na^+} = C_{D^-} + C_{OH^-} + C_{Cl^-}, \quad (21)$$

we can obtain C_{H^+} and α as a function of C and C_A or C_B for the individual systems, where C_A and C_B are the molar concentrations of added HCl and NaOH, respectively. It is ready to substitute the variations of solute concentrations, C, C_A or C_B, and C_S, for the differentials of chemical potentials.

(I) H_2O+HD+NaOH+NaCl

For this system Eqs. 3 are used for NaOH and NaCl, and Eq. 16 is modified into a form composed of terms for added neutral components and a term of $d\mu_{OH^-}$. It is found that the coefficient of the last term is equal to zero owing to Eq. 17, and we have

$$-d\gamma = (\Gamma_{H_2O}+\Gamma_{H^+}-\Gamma_{D^-})d\mu_{H_2O} + (\Gamma_{HD}+\Gamma_{D^-})d\mu_{HD} + (\Gamma_{Na^+}-\Gamma_{Cl^-})d\mu_{NaOH} + \Gamma_{Cl^-}d\mu_{NaCl} \quad (23)$$

As the number of degrees of freedom of the system should be 3 at constant temperature, the solvent, water, term is put equal to zero.

$$\Gamma_{H_2O} + \Gamma_{H^+} - \Gamma_{D^-} = 0 \quad (24)$$

Equation 24 implies that the dividing plane of two phases be drawn at such a position as to make the surface excess of added water zero. The left-hand side of Eq. 24 is equal to the surface excess of water component, since either H^+ or H_2O is generated by the dissociation of HD or the reaction of HD with OH^-, the amount of which being equal to that of D^- formed. The water component should be considered to contain H^+ or OH^- as well as H_2O, when weak electrolytic solute is present, and its surface excess should be $\Gamma_{H_2O}+\Gamma_{H^+}=\Gamma_{H_2O}+\Gamma_{OH^-}$, when the solute is absent. Thus we obtain

$$-d\gamma = (\Gamma_{HD}+\Gamma_{D^-})d\mu_{HD} + (\Gamma_{Na^+}-\Gamma_{Cl^-})d\mu_{NaOH} + \Gamma_{Cl^-}d\mu_{NaCl}, \quad (25)$$

where $\Gamma_{HD}+\Gamma_{D^-}$ is the total surface excess of the weak acid added, $\Gamma_{Na^+}-\Gamma_{Cl^-}$ is clearly equal to the surface excess of NaOH, and Γ_{Cl^-} is totally assignable to that of NaCl.

For the ideal solution, the chemical potential of HD is given by Eq. 6, and those of NaOH and NaCl are given by Eqs. 7, in which

$$C_{Na^+} = C_B + C_S,$$
$$C_{Cl^-} = C_S. \quad (26)$$

Replacing Eqs. 18, 19, and 26 into Eq. 21, and combining it with Eq. 20, we have an equation for C_{H^+} or α, which can give dC_{H^+} or $d\alpha$ in terms of dC and dC_B explicitly.

The final form of the Gibbs equation is then written as

$$-d\gamma = RT\{\Gamma_2 d\ln C + \Gamma_B d\ln C_B + \Gamma_3 d\ln C_S\}, \quad (27)$$

where

$$\Gamma_2 = \left(1+\frac{\alpha^2 C}{Q_B}\right)(\Gamma_{HD}+\Gamma_{D^-}) - \frac{\alpha C}{Q_B}(\Gamma_{Na^+}-\Gamma_{Cl^-}), \quad (27a)$$

$$\Gamma_B = -\frac{\alpha C_B}{Q_B}(\Gamma_{HD}+\Gamma_{D^-}) + \left(\frac{C_B}{Q_B}+\frac{C_B}{C_B+C_S}\right)\Gamma_{Na^+} - \frac{C_B}{Q_B}\Gamma_{Cl^-}, \quad (27b)$$

$$\Gamma_3 = \frac{C_S}{C_B+C_S}\Gamma_{Na^+} + \Gamma_{Cl^-}, \quad (27c)$$

and

$$Q_B = \alpha(2-\alpha)C - C_B + 2C_{OH^-} = -\alpha^2 C + C_B + 2C_{H^+}. \quad (27d)$$

Solving Eqs. 27a, b, and c, the surface excesses or the adsorbed amounts of the weak acid, Na^+ and Cl^- are obtained as follows:

$$\Gamma_{HD} + \Gamma_{D^-} = \frac{C_B+C_S}{H_B}\left\{\left(1+\frac{Q_B+C_S}{C_B+C_S}\right)\Gamma_2 + \left(\frac{Q_B}{C_B}+\frac{C_S}{C_B+C_S}\right)\frac{\alpha C}{C_B}\Gamma_B - \frac{\alpha C}{C_B+C_S}\Gamma_3\right\}, \quad (28a)$$

$$\Gamma_{Na^+} = \frac{C_B+C_S}{H_B}\left\{\alpha\Gamma_2 + \frac{Q_B+\alpha^2 C}{C_B}\Gamma_B + \Gamma_3\right\}, \quad (28b)$$

$$\Gamma_{Cl^-} = \frac{C_B+C_S}{H_B}\left\{-\frac{\alpha C_S}{C_B+C_S}\left(\alpha\Gamma_2 + \frac{Q_B+\alpha^2 C}{C_B}\Gamma_B\right) + \left(1+\frac{Q_B+\alpha^2 C}{C_B+C_S}\right)\Gamma_3\right\}, \quad (28c)$$

and

$$H_B = 2\alpha C + 2C_S + 2C_{OH^-} = 2C_B + 2C_S + 2C_{H^+}. \quad (28d)$$

This kind of equations is applicable to the solutions of monolauryl phosphoric acid in the presence of NaOH, as studied recently by Nakagaki, Handa, and Shimabayashi,[20] when it is modified for a uni-divalent acid instead of HD.

In particular, in the absence of added NaOH, $\Gamma_B = \Gamma_B/C_B = 0$, and also in the absence of added NaCl, $\Gamma_3 = 0$. Then we have

$$\Gamma_{HD} + \Gamma_{D^-} = \left(1 - \frac{\alpha^2 C}{2\alpha C + 2C_{OH^-}}\right)\Gamma_2. \quad (29)$$

This case corresponds to that often cited for illustration of the Traube's rule and Langmuir's deduction of fatty acid solutions,[21] which has been treated as $\alpha = 0$.

(II) H_2O+NaD+HCl+NaCl

For this system Eq. 16 is rearranged, by using Eqs. 3 for NaD, HCl, and NaCl, into a form composed of terms of added neutral components and a term of $d\mu_{Cl^-}$. The coefficient of the last term is found to vanish owing to Eq. 17. Thus we have

$$\begin{aligned} -d\gamma = {} & (\Gamma_{H_2O} + \Gamma_{OH^-})d\mu_{H_2O} + (\Gamma_{HD} + \Gamma_{D^-})d\mu_{NaD} \\ & + (\Gamma_{Cl^-} - \Gamma_{Na^+} + \Gamma_{HD} + \Gamma_{D^-})d\mu_{HCl} \\ & + (\Gamma_{Na^+} - \Gamma_{HD} - \Gamma_{D^-})d\mu_{NaCl}. \end{aligned} \quad (30)$$

By the requirement of phase rule, the number of variables must be 3 at constant temperature, and accordingly, the dividing plane should be set in such a way that

$$\Gamma_{H_2O} + \Gamma_{OH^-} = 0. \quad (31)$$

This means that the surface excess of added water, $\Gamma_{H_2O} + \Gamma_{OH^-}$, is zero, as OH^- has arisen from water by self ionization or by the reaction with D^- but H^+ is generated from HCl as well as from water. Then Eq. 30 becomes

$$\begin{aligned} -d\gamma = {} & (\Gamma_{HD} + \Gamma_{D^-})d\mu_{NaD} \\ & + (\Gamma_{Cl^-} - \Gamma_{Na^+} + \Gamma_{HD} + \Gamma_{D^-})d\mu_{HCl} \\ & + (\Gamma_{Na^+} - \Gamma_{HD} - \Gamma_{D^-})d\mu_{NaCl}. \end{aligned} \quad (32)$$

The chemical potentials of the three neutral components are given by Eqs. 7 in which

$$\begin{aligned} C_{Na^+} &= C + C_S, \\ C_{Cl^-} &= C_A + C_S. \end{aligned} \quad (33)$$

After straightforward calculation we have

$$-d\gamma = RT\{\Gamma_2 d\ln C + \Gamma_A d\ln C_A + \Gamma_3 d\ln C_S\} \quad (34)$$

where

$$\Gamma_2 = \left(1 - \frac{\alpha(1-\alpha)C}{Q_A}\right)(\Gamma_{HD} + \Gamma_{D^-}) + \left(\frac{(1-\alpha)C}{Q_A} + \frac{C}{C + C_S}\right)\Gamma_{Na^+} - \frac{(1-\alpha)C}{Q_A}\Gamma_{Cl^-}, \quad (34a)$$

$$\Gamma_A = \frac{\alpha C_A}{Q_A}(\Gamma_{HD} + \Gamma_{D^-}) - \frac{C_A}{Q_A}\Gamma_{Na^+} + \left(\frac{C_A}{Q_A} + \frac{C_A}{C_A + C_S}\right)\Gamma_{Cl^-}, \quad (34b)$$

$$\Gamma_3 = \frac{C_S}{C + C_S}\Gamma_{Na^+} + \frac{C_S}{C_A + C_S}\Gamma_{Cl^-}, \quad (34c)$$

and

$$Q_A = (1-\alpha^2)C - C_A + 2C_{H^+} = -(1-\alpha)^2 C + C_A + 2C_{OH^-}. \quad (34d)$$

No such system as that formed by neutralization of NaD by addition of HCl seems to have been dealt with experimentally. In the case of fatty acid, the formation of acid soap[22-24] would complicate the situation. Accordingly, we will not pursue this line further.

However, in the absence of added HCl and NaCl, *i.e.*, for $C_A = C_S = 0$, Eq. 34a yields

$$\Gamma_2 = \left(2 + \frac{(1-\alpha)^2 C}{(1-\alpha^2)C + 2C_{H^+}}\right)(\Gamma_{HD} + \Gamma_{D^-}) \quad (35)$$

Aqueous solutions of sodium carboxylate such as sodium laurate correspond to this system. Surface tension of such solutions has been measured by Powney.[25]

(III) H_2O+NaD+NaOH+NaCl

Equation 16 is now converted into a form of terms of neutral components, by the use of Eqs. 3 for NaD, NaOH, and NaCl, in such a way to leave the term of $d\mu_{Na^+}$ as a term of a single ion, which eventually vanishes by means of Eq. 17. As a result, we obtain

$$\begin{aligned} -d\gamma = {} & (\Gamma_{H_2O} + \Gamma_{H^+} + \Gamma_{HD})d\mu_{H_2O} + (\Gamma_{HD} + \Gamma_{D^-})d\mu_{NaD} \\ & + (\Gamma_{Na^+} - \Gamma_{Cl^-} - \Gamma_{HD} - \Gamma_{D^-})d\mu_{NaOH} \\ & + \Gamma_{Cl^-}d\mu_{NaCl}. \end{aligned} \quad (36)$$

Because of the condition imposed for the dividing plane, the coefficient of the first term must be zero:

$$\Gamma_{H_2O} + \Gamma_{H^+} + \Gamma_{HD} = 0. \quad (37)$$

The left-hand side of Eq. 37 comes from the fact that H_2O is consumed by reaction with D^- by the amount equal to that of HD formed, while H^+ remaining unaltered. Then Eq. 36 becomes

$$\begin{aligned} -d\gamma = {} & (\Gamma_{HD} + \Gamma_{D^-})d\mu_{NaD} \\ & + (\Gamma_{Na^+} - \Gamma_{Cl^-} - \Gamma_{HD} - \Gamma_{D^-})d\mu_{NaOH} \\ & + \Gamma_{Cl^-}d\mu_{NaCl}, \end{aligned} \quad (38)$$

where $\Gamma_{HD} + \Gamma_{D^-}$ is the surface excess of NaD, $\Gamma_{Na^+} - \Gamma_{Cl^-} - \Gamma_{HD^-} - \Gamma_{D^-} = \Gamma_{OH^-} - \Gamma_{H^+} - \Gamma_{HD}$ is that of NaOH, and Γ_{Cl^-} is that of NaCl.

The chemical potentials of the three solutes are given by Eqs. 3, for which

$$\begin{aligned} C_{Na^+} &= C + C_B + C_S, \\ C_{Cl^-} &= C_S. \end{aligned} \quad (39)$$

After direct calculations we reach the equation in a form

$$-d\gamma = RT\{\Gamma_2 d\ln C + \Gamma_B d\ln C_B + \Gamma_3 d\ln C_S\}, \quad (40)$$

where

$$\Gamma_2 = \left(1 - \frac{\alpha(1-\alpha)C}{P_B}\right)(\Gamma_{HD} + \Gamma_{D^-}) + \left(\frac{(1-\alpha)C}{P_B} + \frac{C}{C + C_B + C_S}\right)\Gamma_{Na^+} - \frac{(1-\alpha)C}{P_B}\Gamma_{Cl^-}, \quad (40a)$$

$$\Gamma_B = -\frac{\alpha C_B}{P_B}(\Gamma_{HD} + \Gamma_{D^-}) + \left(\frac{C_B}{P_B} + \frac{C_B}{C + C_B + C_S}\right)\Gamma_{Na^+} - \frac{C_B}{P_B}\Gamma_{Cl^-}, \quad (40b)$$

$$\Gamma_3 = \frac{C_S}{C+C_B+C_S}\Gamma_{Na^+} + \Gamma_{Cl^-}, \quad (40c)$$

and

$$P_B = (1-\alpha^2)C + C_B + 2C_{H^+}. \quad (40d)$$

Solving Eqs. 40a, b, c, the surface excesses or the adsorbed amounts of the salt, either ionic or hydrolyzed, and Na^+ and Cl^- are found to be

$$\Gamma_{HD} + \Gamma_{D^-} = \frac{1}{Z_B}\left\{(C+C_B+P_B+2C_S)\Gamma_2 - \frac{C}{C_B}[(1-\alpha)(C+C_B+2C_S)+P_B]\Gamma_B - \alpha C\Gamma_3\right\}, \quad (41a)$$

$$\Gamma_{Na^+} = \frac{C+C_B+C_S}{Z_B}\left\{\alpha\Gamma_2 - \frac{1}{C_B}[\alpha(1-\alpha)C-P_B]\Gamma_B + \Gamma_3\right\}, \quad (41b)$$

$$\Gamma_{Cl^-} = \frac{1}{Z_B}\left\{-\alpha C_S\Gamma_2 + \frac{C_S}{C_B}[\alpha(1-\alpha)C-P_B]\Gamma_B + [(1+\alpha^2)C+C_B+P_B+C_S]\Gamma_3\right\}, \quad (41c)$$

and

$$Z_B = 2C + 2C_B + 2C_S + 2C_{H^+}. \quad (41d)$$

These equations are applicable to the solutions of sodium carboxylate in the presence of NaOH, such as studied by Powney and Addison.[25] The effect of added K_2CO_3 on the surface tension of aqueous solutions of potassium laurate[26] may also be treated along the same line of consideration.[27]

In the absence of added NaOH and NaCl, *i.e.*, for $C_B=C_S=0$, again we can arrive at Eq. 35 from Eq. 40a.

Discussion

It was shown that the Gibbs adsorption equation for a plane surface of electrolyte solution can be represented either in terms of all species, both ionic and nonionic, present in the solution, as given by Eq. 1, or in terms of added neutral components, as shown by Eq. 4. The equivalence of both representations has not been well recognized so far, and the former representation has been preferred by most workers,[8–15,19,28] although the latter representation is more favorable and convenient for thermodynamic treatments. We have also followed the former.

To make the values of surface excess definite, a dividing plane has to be drawn at a definite position between two phases. The usual convention for dilute solutions is to set the plane in such a way as to extinguish the surface excess of added water component. As far as the solution of nonelectrolytes or strong electrolytes is concerned, this convention usually does not cause any confusion, irrespective of which kind of representation has been employed, because neither H^+ and OH^- nor the ionization of water need be taken into account. However, once a weak electrolyte is involved, the choice of the representation comes to have a serious effect on the formal expression of convention. While the representation in terms of the neutral components does not require any novel expression for the surface excess of water, the representaion in terms of all species in the solution distinguishes unionized water, H_2O, from total added water, because the ionization of water itself must be taken into account. Consequently, the surface excess of added water component, which should be put to be zero, is expressed by the sum of the surface excesses of unionized water, H_2O, and of H^+ or OH^- formed by the dissociation, in the absence of solutes. However, the significance of the setting of the dividing plane is nothing new but remains as usual, although the formal expression differs.

It is also noted that the measurements of surface tension on solutions containing a weak acid does not permit to estimate Γ_{HD} or Γ_{D^-} separately but only gives the values of $\Gamma_{HD}+\Gamma_{D^-}$. They are also limited in the evaluation of Γ_{H^+}, Γ_{OH^-} or even $\Gamma_{H^+}-\Gamma_{OH^-}$ and can give only the value of $\Gamma_{H^+}+\Gamma_{HD}-\Gamma_{OH^-}$.

For the rigorous treatment of experimental results, the postulate of ideal solution should be removed, but the introduction of the limiting expressions of the Debye-Hückel theory for activity coefficients of ions leads to explicit results with great difficulty, in general.

Appendix

For simplicity, we assume the concentrations of all species in the vapor phase to be negligible. In the solution phase the Gibbs-Duhem equation holds among chemical potentials of all species, and it can be written as

$$\sum_i C_i d\mu_i = 0. \quad (A1)$$

By means of Eqs. 2 and 3 and the condition of electroneutrality among concentrations of ionic species, Eq. A1 can be rewritten

$$\sum_{\lambda=1}^{\nu} C_\lambda d\mu_\lambda = 0. \quad (A2)$$

Equation A2 is the Gibbs-Duhem equation given in terms of all the neutral components added, and C_λ is actually expressed by an algebraic sum of C_i.

From Eq. A2 the variation of chemical potential of water component, 1, is represented by

$$d\mu_1 \equiv d\mu_{H_2O} = -\frac{1}{C_1}\sum_{\lambda=2}^{\nu} C_\lambda d\mu_\lambda. \quad (A3)$$

Substituting Eq. A3 into Eq. 4, we have Eq. 5, in which

$$\Gamma_\lambda^{(1)} = \Gamma_\lambda - \frac{C_\lambda}{C_1}\Gamma_1. \quad (A4)$$

Equation A4 gives $\Gamma_1^{(1)}=0$, which is equivalent to set the dividing plane at the definite position.

References

1) A. P. Brady, *J. Phys. Chem.*, **53**, 56 (1949).
2) E. Hutchinson, *J. Colloid Sci.*, **3**, 413 (1948).
3) J. Salley, A. J. Weith, Jr., A. A. Argyle, and J. K. Dixon, *Proc. R. Soc. London, Ser A*, **203**, 42 (1950).
4) E. G. Cockbain and A. I. McMullen, *Trans. Faraday Soc.*, **47**, 322 (1951).
5) J. T. Davies, *Trans. Faraday Soc.*, **48**, 1052 (1952).
6) G. Nilsson, *J. Phys. Chem.*, **61**, 1135 (1957).
7) R. Matuura, H. Kimizuka, S. Miyamoto, and R. Shimozawa, *Bull. Chem. Soc. Jpn.*, **31**, 532 (1958).
8) B. A. Pethica, *Trans. Faraday Soc.*, **50**, 412 (1954).
9) E. G. Cockbain, *Trans. Faraday Soc.*, **50**, 874 (1954).
10) K. Tajima, M. Muramatsu, and T. Sasaki, *Bull. Chem. Soc. Jpn.*, **43**, 1991 (1970).
11) K. Shinoda and H. Nakayama, *J. Colloid Sci.*, **18**, 705 (1963).
12) J. T. Davies, cited in E. Matijević, and B. A. Pethica, *Trans. Faraday Soc.*, **54**, 1382 (1958).

13) J. T. Davies and E. K. Rideal, "Interfacial Phenomena," Academic Press, New York and London (1961), Chap. 4, p. 197.
14) R. Defay, I. Prigogine, A. Bellemans, and D. H. Everett, "Surface Tension and Adsorption," Longmans, London (1966), Chap. XXI, p. 400.
15) K. Tajima, *Bull. Chem. Soc. Jpn.*, **44**, 1767 (1971).
16) N. K. Adam, "Physics and Chemistry of Surfaces," Dover Publications, New York (1968), Chap. III, p. 107 and Chap. VIII, p. 344.
17) J. G. Kirkwood and I. Oppenheim, "Chemical Thermodynamics," McGraw-Hill Book Co., New York (1961), Chap. 12, p. 189.
18) K. Motomura, "Yōeki Kagaku," Asakura Book Co., Tokyo (1974), Chap. 4, p. 109.
19) J. E. Bujake and E. D. Goddard, *Trans. Faraday Soc.*, **61**, 190 (1965).
20) M. Nakagaki, T. Handa, and D. Shimabayashi, *J. Colloid Interface Sci.*, **43**, 521 (1973).
21) A. W. Adamson, "Physical Chemistry of Surfaces," Interscience Publishers, New York (1960), Chap. 2, p. 94.
22) D. Eagland and F. Franks, *Trans. Faraday Soc.*, **61**, 2468 (1965).
23) J. Lucassen, *J. Phys. Chem.*, **70**, 1824 (1966).
24) M. E. Feinstein and H. L. Rosano, *J. Phys. Chem.*, **73**, 601 (1969).
25) J. Powney, *Trans. Faraday Soc.*, **31**, 1510 (1935).
26) J. Powney and C. C. Addison, *Trans. Faraday Soc.*, **34**, 372 (1938).
27) N. K. Adam, *Trans. Faraday Soc.*, **32**, 653 (1936).
28) E. A. Guggenheim, "Thermodynamics," North Holland Publishing Co., Amsterdam (1967), Chap. 7, p. 293.

The Theoretical Estimation of the *G*-Values for the Ionization and Excitation of Thirty-eight Gaseous Compounds Irradiated by 100 keV Electrons

Kiyoshi OKAZAKI, Masaki YAMABE, and Shin SATO

Department of Applied Physics, Tokyo Institute of Technology, Ookayama, Meguro-ku, Tokyo 152

(Received November 15, 1976)

The *G*-values for the ionization and excitation of thirty-eight gaseous compounds irradiated by 100 keV electrons have been calculated by combining the binary-encounter-collision theory with the theory of the degradation spectrum, which is based on the continuous-slowing-down approximation (CSDA). The thirty-eight compounds include C_2—C_6 alkanes, cycloalkanes, C_2—C_4 olefins, acetylene, 1,3-butadiene, benzene, toluene, phenol, pyrrole, furan, several alcohols, ethers, ketones, acetaldehyde, carbon dioxide, and hydrogen cyanide. Most of the calculated *G*-values of the electrons were in fair agreement with the experimental values. In the cases of several hydrocarbons, the dissociation from the superexcited state into the neutral fragments was taken into account, since the data for the fragmentation ratios were available. In the case of acetylene, the discrepancy in the *G*-values of electrons obtained experimentally and theoretically suggests that excited acetylene gives rise to a chemi-ionization reaction. In order to check the CSDA, the Fowler equation for helium has been calculated and the results compared with those obtained under the CSDA. The discrepancy in the *G*-values obtained by the two methods did not exceed 7%.

Three years ago we started the theoretical calculation of the *G*-values for the ionization and excitation of gaseous compounds irradiated by 100 keV electrons. Previously we have reported the results obtained with 5 rare gases (He, Ne, Ar, Kr, and Xe),[1,2] 5 diatomic molecules (H_2, N_2, CO, NO, and O_2),[3] and 3 ten-electron-containing molecules (H_2O, NH_3, and CH_4).[4,5] All of the *G*-values estimated were in fair agreement with the experimental ones. This agreement encouraged us to extend the calculation to other compounds. In this paper, we wish to report the results obtained with 38 gaseous compounds, which include most of the compounds whose *W*-values have been reported in the literature.

Method of Calculation

The details of the method of calculation have been reported in previous papers;[1—5] therefore, we will not repeat them here. In the present calculation, we do not take the double collision into account, since we know that the contribution of this process to the final *G*-values does not exceed 5% if the molecules consist of atoms with low atomic numbers.[5]

In the following calculation, all of the molecules excited to above their ionization potentials are assumed to ionize. Strictly speaking, this is not correct, for some of the superexcited states are known to dissociate into neutral fragments, as was mentioned by Platzman.[6] The correction for this process will be discussed in a later section.

Constants Used for Calculation

In order to perform the calculation, we need the constants belonging to each electron in the molecules; the binding energy (I_i), the average kinetic energy (E_i), and the energies of the lowest excited singlet and triplet states of the molecules (E_s and E_t).

The binding energy of an electron in the outermost shell is the ionization potential of the molecule. This value has been measured accurately by means of photoelectron spectroscopy.[7] For the binding energies

TABLE 1. THE ENERGIES OF THE LOWEST SINGLET AND TRIPLET STATES (eV)

	Compound	E_s	E_t
1.	Ethane	7.7[a]	6.3
2.	Propane	7.6	6.2
3.	Butane	7.5	6.1
4.	Isobutane	7.5	6.1
5.	Pentane	7.5	6.1
6.	Isopentane	7.5	6.1
7.	Neopentane	7.5	6.1
8.	Hexane	7.5	6.1
9.	Cyclopropane	7.8	6.4
10.	Cyclopentane	8.7	7.3
11.	Cyclopentene	6.2	4.2
12.	Cyclopentadiene	4.8[a]	3.4
13.	Cyclohexane	8.7[b]	7.3
14.	Spiro[2.2]pentane	7.8	6.4
15.	Ethylene	5.0[a]	3.6[a]
16.	Propylene	6.5[a]	5.1
17.	1-Butene	6.2	4.8
18.	*cis*-2-Butene	6.2	4.8
19.	*trans*-2-Butene	6.2	4.8
20.	2-Methyl-1-propene	6.2	4.8
21.	Acetylene	5.2[a]	4.0
22.	*s-trans*-1,3-Butadiene	6.0[a]	3.9
23.	Benzene	4.7[a]	3.6[a]
24.	Toluene	4.7	3.6
25.	Phenol	4.6	3.5
26.	Pyrrole	5.7[a]	4.5[a]
27.	Furan	5.9[a]	4.7
28.	Methanol	4.0	3.0
29.	Ethanol	4.0	3.0
30.	1-Propanol	4.0	3.0
31.	2-Propanol	4.0	3.0
32.	Dimethyl ether	3.8	2.8
33.	Diethyl ether	3.8	2.8
34.	Acetone	3.8[a]	2.8
35.	2-Butanone	3.8	2.8
36.	Acetaldehyde	3.6[a]	2.6
37.	Carbon dioxide	5.7[a]	4.5
38.	Hydrogen cyanide	6.5[a]	5.0

a) Ref. 10. b) Ref. 11.

Table 2. The G-value of ionization from each orbital

The binding energy of the electron in the orbital is I_i. The number in parentheses behind the value of I_i is the number of electrons in the orbital. The number in parentheses behind the value of G_i is the number of electrons ejected because of the Auger effect.

	Compound		I_i (eV) and G_i
1.	Ethane	I_i	11.51(2), 11.92(4), 14.15(4), 20.96(2), 28.84(2), 307(4)
		G_i	0.90, 1.67, 1.22, 0.33, 0.21, 0.020(6)
2.	Propane	I_i	11.06(4), 11.35(2), 12.67(2), 12.84(2), 13.91(2), 14.87(2), 19.71(2), 23.95(2), 30.63(2), 307(6)
		G_i	1.28, 0.61, 0.50, 0.49, 0.42, 0.38, 0.24, 0.18, 0.13, 0.021(6)
3.	Butane	I_i	10.67(2), 11.25(2), 11.66(2), 11.91(2), 12.04(2), 13.25(2), 13.41(2), 13.58(2), 15.29(2), 19.53(2), 21.25(2), 26.41(2), 31.62(2), 307(8)
		G_i	0.62, 0.55, 0.51, 0.48, 0.47, 0.39, 0.38, 0.37, 0.30, 0.20, 0.18, 0.13, 0.10, 0.022(9)
4.	Isobutane	I_i	10.69(4), 11.43(2), 12.27(2), 12.73(4), 13.73(4), 14.85(2), 18.75(2), 24.08(4), 32.05(2), 307(8)
		G_i	1.12, 0.49, 0.43, 0.79, 0.69, 0.30, 0.21, 0.29, 0.096, 0.022(7)
5.	Pentane	I_i	10.37(2), 11.21(2), 11.57(2), 11.66(2), 11.79(2), 12.24(2), 12.57(2), 12.96(2), 13.80(2), 13.99(2), 15.54(2), 19.57(2), 19.92(2), 23.42(2), 28.13(2), 32.22(2), 307(10)
		G_i	0.56, 0.50, 0.43, 0.42, 0.41, 0.38, 0.36, 0.33, 0.30, 0.29, 0.24, 0.17, 0.16, 0.13, 0.096, 0.080(2), 0.022(7)
6.	Isopentane	I_i	10.32(2), 10.68(2), 11.39(2), 11.80(2), 11.98(2), 12.41(2), 12.71(2), 13.21(2), 13.74(2), 14.25(2), 14.99(2), 18.65(2), 21.14(2), 24.15(2), 26.79(2), 32.83(2), 307(10)
		G_i	0.57, 0.52, 0.44, 0.41, 0.39, 0.37, 0.35, 0.32, 0.30, 0.28, 0.26, 0.18, 0.15, 0.12, 0.10, 0.078(2), 0.022(7)
7.	Neopentane	I_i	10.40(6), 12.31(6), 13.11(4), 14.25(6), 17.64(2), 24.22(6), 33.25(2), 307(10)
		G_i	1.40, 1.01, 0.60, 0.78, 0.18, 0.34, 0.073(2), 0.022(7)
8.	Hexane	I_i	10.43(2), 11.19(2), 11.20(2), 11.51(2), 11.65(2), 11.85(2), 12.17(2), 12.30(2), 13.03(2), 13.34(2), 13.60(2), 14.23(2), 15.06(2), 20.10(2), 20.43(2), 22.26(2), 24.76(2), 26.95(2), 28.39(2), 307(12)
		G_i	0.46, 0.38, 0.38, 0.36, 0.35, 0.33, 0.31, 0.31, 0.27, 0.26, 0.25, 0.23, 0.21, 0.13, 0.13, 0.11, 0.095, 0.084, 0.078, 0.022(7)
9.	Cyclopropane	I_i	10.06(4), 11.95(4), 12.64(2), 15.35(2), 20.17(4), 31.63(2), 307(6)
		G_i	1.73, 1.24, 0.56, 0.40, 0.53, 0.14(2), 0.023(7)
10.	Cyclopentane	I_i	10.49(4), 11.04(4), 11.34(4), 13.50(4), 14.21(2), 15.75(2), 18.58(4), 25.52(4), 33.30(2), 307(10)
		G_i	1.09, 0.97, 0.91, 0.65, 0.29, 0.25, 0.38, 0.23, 0.080(2), 0.024(7)
11.	Cyclopentene	I_i	9.00(2), 10.57(2), 10.60(2), 10.95(2), 11.33(2), 11.80(2), 12.92(2), 14.54(2), 15.03(2), 17.33(2), 18.60(2), 24.82(2), 25.05(2), 32.99(2), 307(10)
		G_i	0.80, 0.54, 0.54, 0.50, 0.47, 0.43, 0.36, 0.29, 0.28, 0.22, 0.20, 0.13, 0.13, 0.086(2), 0.025(7)
12.	Cyclopentadiene	I_i	8.55(2), 10.40(2), 10.45(2), 10.78(2), 10.85(2), 11.59(2), 13.86(2), 14.72(2), 16.97(2), 17.66(2), 24.14(2), 24.51(2), 32.78(2), 307(10)
		G_i	0.84, 0.55, 0.55, 0.51, 0.51, 0.45, 0.33, 0.29, 0.23, 0.22, 0.14, 0.14, 0.090(2), 0.026(7)
13.	Cyclohexane	I_i	9.81(4), 11.05(2), 11.43(2), 11.57(4), 12.39(4), 13.89(4), 14.31(2), 14.83(2), 18.67(2), 20.25(4), 26.95(4), 33.98(2), 307(6)
		G_i	1.15, 0.42, 0.39, 0.76, 0.65, 0.52, 0.25, 0.23, 0.16, 0.28, 0.18, 0.066(2), 0.024(7)
14.	Spiro[2.2]pentane	I_i	9.45(2), 9.82(4), 11.06(2), 11.82(2), 12.10(2), 12.71(2), 14.54(4), 17.53(2), 20.25(4), 27.44(2), 33.08(2), 307(10)
		G_i	0.76, 1.37, 0.51, 0.44, 0.42, 0.38, 0.60, 0.22, 0.35, 0.11, 0.086(2), 0.025(7)
15.	Ethylene	I_i	10.50(2), 11.47(2), 11.65(2), 14.37(2), 19.21(2), 20.01(2), 307(4)
		G_i	1.00, 0.86, 0.84, 0.60, 0.39, 0.23, 0.022(7)
16.	Propylene	I_i	9.69(2), 10.73(2), 11.45(2), 12.63(2), 13.30(2), 14.22(2), 18.31(2), 23.57(2),

TABLE 2. (continued)

Compound		I_1 (eV) and G_1
		29.82(2), 307(6)
	G_1	0.98, 0.79, 0.69, 0.57, 0.52, 0.47, 0.31, 0.21, 0.15(2), 0.023(7)
17. 1-Butene	I_1	9.59(2), 10.50(2), 11.39(2), 11.80(2), 11.98(2), 13.16(2), 13.58(2), 14.62(2), 18.34(2), 20.87(2), 26.04(2), 30.96(2), 307(8)
	G_1	0.78, 0.64, 0.54, 0.50, 0.49, 0.41, 0.38, 0.34, 0.23, 0.19, 0.14, 0.11(2), 0.023(7)
18. *cis*-2-Butene	I_1	9.12(2), 10.56(2), 11.76(2), 11.85(2), 12.74(2), 12.99(2), 13.61(2), 14.90(2), 17.10(2), 22.48(2), 25.25(2), 31.16(2), 307(8)
	G_1	0.90, 0.64, 0.51, 0.50, 0.44, 0.42, 0.39, 0.33, 0.26, 0.17, 0.15, 0.11(2), 0.023(7)
19. *trans*-2-Butene	I_1	9.12(2), 10.24(2), 11.42(2), 11.95(2), 13.03(2), 13.36(2), 13.44(2), 13.55(2), 18.16(2), 21.32(2), 26.08(2), 30.77(2), 307(8)
	G_1	0.89, 0.68, 0.54, 0.49, 0.42, 0.40, 0.39, 0.39, 0.24, 0.19, 0.14, 0.11(2), 0.023(7)
20. 2-Methyl-1-propene	I_1	9.17(2), 10.55(2), 10.91(2), 12.12(2), 12.68(2), 13.46(2), 13.90(2), 13.97(2), 17.05(2), 23.48(2), 24.32(2), 31.12(2), 307(8)
	G_1	0.88, 0.64, 0.59, 0.48, 0.44, 0.39, 0.37, 0.37, 0.26, 0.16, 0.15, 0.11(2), 0.023(7)
21. Acetylene	I_1	11.04(4), 17.86(2), 20.44(2), 27.34(2), 307(4)
	G_1	1.74, 0.43, 0.36, 0.24, 0.024(6)
22. *s-trans*-1,3-Butadiene	I_1	9.07(2), 10.30(2), 11.27(2), 11.38(2), 11.68(2), 13.47(2), 13.72(2), 18.00(2), 19.58(2), 25.81(2), 30.36(2), 307(8)
	G_1	0.92, 0.70, 0.58, 0.57, 0.54, 0.42, 0.40, 0.26, 0.23, 0.15, 0.12(2), 0.025(7)
23. Benzene	I_1	9.24(4), 10.07(4), 11.30(2), 12.29(4), 12.49(2), 14.80(2), 15.22(2), 19.24(4), 26.05(4), 32.75(2), 307(12)
	G_1	1.05, 0.90, 0.37, 0.63, 0.31, 0.23, 0.23, 0.32, 0.20, 0.075(2), 0.026(7)
24. Toluene	I_1	8.82(2), 9.58(2), 9.80(2), 10.12(2), 11.06(2), 11.74(2), 12.15(2), 12.29(2), 13.14(2), 13.51(2), 14.37(2), 15.07(2), 18.48(2), 19.42(2), 22.99(2), 26.12(2), 27.86(2), 33.15(2), 307(14)
	G_1	0.60, 0.50, 0.47, 0.44, 0.37, 0.33, 0.31, 0.30, 0.26, 0.25, 0.23, 0.21, 0.15, 0.14, 0.11, 0.090, 0.083(2), 0.064(2), 0.027(7)
25. Phenol	I_1	8.52(2), 9.80(2), 10.09(2), 10.48(2), 10.99(2), 12.03(2), 12.43(2), 12.45(2), 12.53(2), 13.62(2), 14.69(2), 15.17(2), 18.68(2), 19.48(2), 24.79(2), 26.27(2), 31.45(2), 34.55(2), 307(12), 540(2)
	G_1	0.66, 0.48, 0.45, 0.41, 0.37, 0.31, 0.30, 0.29, 0.29, 0.25, 0.22, 0.20, 0.15, 0.14, 0.098, 0.091(2), 0.070(2), 0.062(2), 0.023(8), 0.0019(10)
26. Pyrrole	I_1	8.2(2), 9.2(2), 12.6(2), 13.0(2), 13.7(2), 14.3(2), 14.8(2), 17.5(2), 18.1(2), 18.8(2), 22.3(2), 23.8(2), 29.5(2), 290.3(8), 406.1(2)
	G_1	1.11, 0.84, 0.43, 0.40, 0.37, 0.34, 0.32, 0.24, 0.23, 0.21, 0.16, 0.15, 0.11(2), 0.023(7), 0.0038(9)
27. Furan	I_1	8.9(2), 10.3(2), 13.0(2), 13.8(2), 14.4(2), 15.1(2), 15.6(2), 17.5(2), 18.6(2), 19.2(2), 23.5(2), 25.2(2), 34.1(2), 290.9(8), 539.4(2)
	G_1	0.98, 0.69, 0.42, 0.38, 0.35, 0.32, 0.30, 0.25, 0.22, 0.21, 0.16, 0.14, 0.091(2), 0.023(7), 0.0027(10)
28. Methanol	I_1	10.83(2), 11.98(2), 12.82(2), 13.97(2), 14.49(2), 22.88(2), 33.84(2), 307(2), 540(2)
	G_1	0.80, 0.68, 0.61, 0.53, 0.50, 0.26, 0.15(2), 0.0097(7), 0.0049(9)
29. Ethanol	I_1	10.46(2), 11.47(2), 11.96(2), 12.50(2), 13.00(2), 14.38(2), 14.65(2), 20.07(2), 26.83(2), 34.06(2), 307(4), 540(2)
	G_1	0.65, 0.55, 0.51, 0.48, 0.45, 0.38, 0.37, 0.23, 0.15, 0.11(2), 0.014(7), 0.0035(9)
30. 1-Propanol	I_1	10.25(2), 11.44(2), 11.45(2), 12.02(2), 12.13(2), 13.28(2), 13.68(2), 13.94(2), 15.20(2), 19.60(2), 22.53(2), 29.31(2), 34.17(2), 307(6), 540(2)
	G_1	0.55, 0.45, 0.45, 0.41, 0.40, 0.35, 0.33, 0.32, 0.28, 0.19, 0.15, 0.11, 0.085(2), 0.016(7), 0.0027(9)

Table 2. (continued)

Compound		I_i (eV) and G_i
31. 2-Propanol	I_i	10.18(2), 11.23(2), 11.78(2), 12.31(2), 12.69(2), 12.85(2), 13.66(2), 13.95(2), 14.93(2), 18.87(2), 24.21(2), 28.02(2), 34.53(2), 307(6), 540(2)
	G_i	0.57, 0.47, 0.43, 0.40, 0.38, 0.37, 0.33, 0.32, 0.29, 0.20, 0.14, 0.11, 0.084(2), 0.016(7), 0.0027(9)
32. Dimethyl ether	I_i	9.94(2), 11.73(2), 11.98(2), 12.89(2), 13.33(2), 14.27(2), 14.58(2), 22.37(2), 23.53(2), 34.83(2), 307(4), 540(2)
	G_i	0.71, 0.53, 0.51, 0.45, 0.43, 0.38, 0.37, 0.20, 0.18, 0.11(2), 0.014(7), 0.0035(9)
33. Diethyl ether	I_i	9.51(2), 11.02(2), 11.42(2), 11.79(2), 12.03(2), 12.40(2), 12.58(2), 13.27(2), 14.01(2), 14.28(2), 14.84(2), 19.88(2), 20.29(2), 26.07(2), 27.74(2), 35.17(2), 307(8), 540(2)
	G_i	0.55, 0.41, 0.38, 0.36, 0.34, 0.33, 0.32, 0.29, 0.26, 0.26, 0.24, 0.15, 0.15, 0.10, 0.093, 0.067(2), 0.018(7), 0.0022(10)
34. Acetone	I_i	9.68(2), 11.79(2), 12.12(2), 12.49(2), 13.28(2), 13.96(2), 14.05(2), 14.67(2), 17.46(2), 24.91(2), 27.53(2), 34.47(2), 307(6), 540(2)
	G_i	0.67, 0.46, 0.44, 0.42, 0.37, 0.34, 0.34, 0.32, 0.24, 0.14, 0.12, 0.091(2), 0.017(7), 0.0029(10)
35. 2-Butanone	I_i	9.51(2), 11.47(2), 11.86(2), 12.24(2), 12.51(2), 12.96(2), 13.21(2), 13.96(2), 14.59(2), 14.95(2), 17.37(2), 21.89(2), 25.90(2), 29.43(2), 34.64(2), 307(8), 540(2)
	G_i	0.59, 0.40, 0.38, 0.36, 0.34, 0.32, 0.31, 0.28, 0.26, 0.25, 0.20, 0.14, 0.11, 0.092(2), 0.074(2), 0.019(7), 0.0023(10)
36. Acetaldehyde	I_i	10.20(2), 12.23(2), 12.38(2), 13.17(2), 14.21(2), 14.58(2), 19.27(2), 26.66(2), 34.14(2), 307(4), 540(2)
	G_i	0.72, 0.53, 0.52, 0.47, 0.42, 0.40, 0.26, 0.17, 0.12(2), 0.015(7), 0.0038(9)
37. Carbon dioxide	I_i	13.79(4), 17.59(4), 18.07(2), 19.36(2), 33.73(2), 34.67(2), 307(2), 540(4)
	G_i	0.95, 0.66, 0.31, 0.28, 0.13, 0.13, 0.0082(6), 0.0082(8)
38. Hydrogen cyanide	I_i	13.0(2), 14.4(2), 21.1(2), 33.1(2), 308(2), 426(2)
	G_i	1.10, 0.93, 0.52, 0.27, 0.016(6), 0.011(7)

Table 3. Calculated G-values (G_s: singlet excitation, G_t: triplet excitation, G_e: electrons, G_e': electrons corrected for the neutral fragmentation of the superexcited state) and observed G-values of electrons (G_e^{exp})

Compound	G_s	G_t	G_e	G_e'	G_e^{exp}		Compound	G_s	G_t	G_e	G_e'	G_e^{exp}	
1. Ethane	1.94	0.93	4.45	3.88	4.24	a)	20. 2-Methyl-1-propene	2.26	1.54	5.12		4.20	c)
2. Propane	2.20	0.94	4.37	3.68	4.27	a)	21. Acetylene	6.52	0.91	2.92		3.95	a)
3. Butane	1.50	1.07	4.84	4.27	4.22	b)	22. *s-trans*-1,3-Butadiene	2.41	2.66	5.17	4.13	4.00	c)
4. Isobutane	1.97	1.01	4.56		4.35	a)	23. Benzene	4.91	1.61	4.57		4.29	c)
5. Pentane	1.35	1.08	5.03	4.26	4.26	b)	24. Toluene	3.87	2.03	5.22			
6. Isopentane	1.33	1.08	5.06		4.18	a)	25. Phenol	4.04	2.05	5.28			
7. Neopentane	2.05	1.01	4.61		4.31	c)	26. Pyrrole	2.54	1.60	5.22			
8. Hexane	1.25	1.06	4.88		4.27	b)	27. Furan	2.67	1.52	4.78			
9. Cyclopropane	1.75	0.92	4.91	4.11	4.22	c)	28. Methanol	7.38	1.37	3.78		4.24	c)
10. Cyclopentane	0.94	0.73	5.08		3.94	d)	29. Ethanol	6.74	1.60	4.12		3.98	b)
11. Cyclopentene	2.04	1.67	5.25				30. 1-Propanol	6.32	1.75	4.29		4.08	b)
12. Cyclopentadiene	3.87	2.44	5.11				31. 2-Propanol	6.38	1.77	4.30		4.13	b)
13. Cyclohexane	0.68	0.74	5.28		4.41	b)	32. Dimethyl ether	7.23	1.73	4.11		4.18	c)
14. Spiro[2.2]pentane	0.87	0.95	5.52				33. Diethyl ether	6.56	2.08	4.50		4.24	b)
15. Ethylene	5.07	1.68	4.06	3.22	3.92	c)	34. Acetone	6.96	1.85	4.20		3.88	c)
16. Propylene	2.29	1.36	5.00	4.17	4.03	a)	35. 2-Butanone	6.68	2.00	4.45			
17. 1-Butene	2.37	1.51	5.02	4.27	4.20	c)	36. Acetaldehyde	8.05	1.73	3.85		3.79	a)
18. *cis*-2-Butene	2.26	1.55	5.10	4.39	4.24	c)	37. Carbon dioxide	5.55	0.77	2.58		2.99	a)
19. *trans*-2-Butene	2.24	1.55	5.14	4.38	4.24	c)	38. Hydrogen cyanide	4.19	0.94	2.99			

a) G. G. Meisels, *J. Chem. Phys.*, **41**, 51 (1964). b) P. Adler and H. K. Bothe, *Z. Naturforschg.*, **20**a, 1700 (1965). c) R. M. Leblanc and J. A. Herman, *J. Chim. Phys.*, **63**, 1055 (1966). d) L. M. Hunter and R. H. Johnsen, *J. Phys. Chem.*, **71**, 3228 (1967).

of the other electrons in several molecules, the experimental data obtained by ESCA are available;[8] however, most of the binding energies of electrons in large molecules are not known. In this case, we use the values calculated by Dewar and Worley.[9] They obtained these values by using the MINDO approximation.

We previously calculated the average kinetic energies by using the SCF functions reported in the literature. In the present paper, we use the following relation to estimate them, since the SCF functions are not available for most of the molecules:

$$E_i = 2.34 I_i^{0.93}. \quad (1)$$

Equation 1 roughly satisfies the relation between the I_i and E_i values for rare gases, diatomic molecules, and ten-electron-containing molecules.

For the E_s and E_t values, we use the values reported by Herzberg[10] and Lassettre and Francis.[11] When no data are available, these values are tentatively assumed from those of similar compounds. The E_s and E_t values used in the present calculation are summarized in Table 1.

Results

The calculated results are summarized in Tables 2 and 3. Table 2 shows the G-values of ionization from each orbital in the molecules. This table can be used when discussing the initial process of energy absorption from high-energy electrons and also the properties of the ions initially produced. So far, such a discussion has been made for an only limited number of molecules.[3-5]

In Table 3, the total G-values of ionization and excitations are summarized; the experimental values are listed in the last column. Except for a few compounds, the calculated G-values of electrons are roughly equal to, or a little larger than, the observed ones.

Discussion

Neutral Fragmentation of the Superexcited State. In the present calculation, all compounds excited to above their ionization potentials are assumed to ionize; therefore, if the neutral fragmentation of the superexcited state is an important process, the G-values of the electrons listed in Table 3 may be overestimated. Since the amount of the neutral fragmentation is dependent upon the form and energy of the superexcited state, the estimation is not easy. However, we have a procedure to estimate them, although it is very rough—the optical approximation proposed by Platzman.[12]

According to the Bethe theory, the total cross section for ionization may be expressed as follows:

$$Q_i(T) = \frac{4\pi a_0^2 R}{T} M_i^2 \ln \frac{4c_i T}{R} \quad (2)$$

Here, a_0 is the Bohr radius, R is the Rydberg energy, c_i is a constant, and M_i^2 is the dipole matrix-element squared for ionization:

$$M_i^2 = \int_I^\infty \eta(E) \frac{R}{E} \frac{df}{dE} dE \quad (4)$$

where E is the excitation energy, I is the ionization potential, df/dE is the differential oscillator strength, and $\eta(E)$ is the probability of ionization upon excitation at E. On the other hand, the total cross section of dissociation into the neutral fragments may be expressed as follows:

$$Q_d(T) = \frac{4\pi a_0^2 R}{T} M_d^2 \ln \frac{4c_i T}{R}. \quad (4)$$

Here, M_d^2 is the dipole matrix-element squared for dissociation:

$$M_d^2 = \int_I^\infty [1-\eta(E)] \frac{R}{E} \frac{df}{dE} dE. \quad (5)$$

Therefore, if we can assume that these two total cross sections are applicable throughout the energy range of the incident electron, the ratio of neutral fragmentation/ionization may be expressed in this form:

$$F = M_d^2/M_i^2 = G_d'/G_e'. \quad (6)$$

Here, G_d' and G_e' are the G-values of neutral fragmentation and of ionization from the superexcited state respectively. In the present calculation, the sum of G_d' and G_e' should be equal to G_e.

Using the oscillator strengths reported in the literature,[13-15] Hatano estimated the F ratios for several hydrocarbons.[16] We can use these values for the calculation of G_d' and G_e'. The calculated results are included in Table 3. Except for a few compounds, the corrected G-values of the electrons, G_e', are in good agreement with those obtained experimentally. Most of the differences between calculation and experiment in the G-value of electrons, G_e and G_e^{exp}, seem to be explainable in terms of this fragmentation of the superexcited state. If this is true, Table 3 suggests that the neutral fragmentation from the superexcited state of oxygen-containing compounds is small compared with that of hydrocarbons.

Chemi-ionization. In the cases of a few compounds (C_2H_2, CH_3OH, and CO_2), the calculated G-values of electrons are smaller than the observed ones. In the case of acetylene especially, the difference in G-value amounts to 1.0.

It is well known that some of the excited states of rare gases give rise to the Hornbeck-Molnar process, which induces an extra ionization:[17]

$$M^* + M \longrightarrow M_2^+ + e^-$$

If a similar reaction should occur in acetylene, the difference in the G-value of electrons may be explainable. According to the mass-spectrometric study by Koyano *et al.*, acetylene excited by ultraviolet light at 121.6 nm gives rise to the following chemi-ionization:[18]

$$C_2H_2^* + C_2H_2 \longrightarrow C_4H_3^+ + H + e^-$$
$$\searrow\ C_4H_2^+ + H_2 + e^-$$

This process might be the cause of the difference in the G-value of electrons between calculation and experiment. Such processes, however, have not been reported with methanol and carbon dioxide.

G-value of Excitation. The calculated G-values for singlet and triplet excitations are summarized in Table 3; however, there are no available experimental data which they can be directly compared with. In Fig. 1,

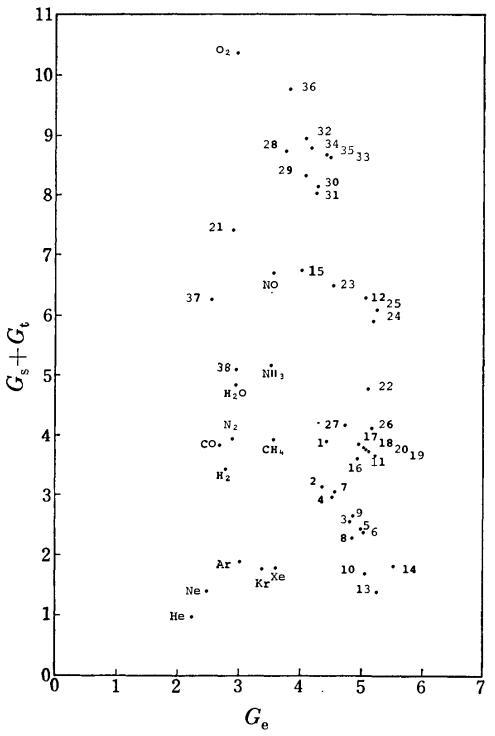

Fig. 1. Correlation between the Calculated G-values of Electrons (G_e) and Excited States (G_t+G_s). The number corresponds to the compounds listed in Table 3.

we plot all of the calculated G-values, including the results obtained in the previous papers.[1-5] The G-values of the electrons range from 2 to 6, while those of the excitations range from 1 to 11. Although the plots are widely scattered, there are some tendencies: the ratios of $G(\text{excitation})/G_e$ are smaller than unity for rare gases and saturated hydrocarbons, while those for oxygen-containing compounds and unsaturated hydrocarbons range from 1 to 4. This figure may provide useful information when the details of the radiolysis are discussed.

Appendix

In order to calculate the degradation spectrum, we have thus far used the CSDA. However, this approximation has not been justified quantitatively.[19] Before the concept of the degradation spectrum was developed, the W-values ($W=100/G_e$) had been calculated by using a more direct method.[20,21] The equation used for such calculations is called the Fowler equation. The actual calculation using the Fowler equation, however, is very tedious, even if an electronic computer is used. Consequently, only a few compounds have been subjected to the calculation.[22,23]

In the following, we will show the calculation for helium using the Fowler equation and compare its result with that obtained under the CSDA. Since both calculations use exactly the same cross sections for various inelastic collisions, the results may clarify the limits of the applicability of the CSDA in the calculation of the W-value.

The Fowler equation to be calculated may be written as follows:

$$N_m(T) = \sum_k \{N_m(T-E_k)+\delta_{km}\}p_k(T) + \sum_i \int_{I_i}^{T} \{N_m(T-E)+N_m(E-I_i)+\delta_{im}\}\frac{dp_i(T)}{dE}dE \quad (7)$$

Here, $N_m(T)$ is the number of atoms in the excited or ionized state, m, produced by the impinging of an electron with the energy, T, into a helium gas; I_i is the binding energy; E_k is the energy of the k-th excited state, and E is the energy loss. The suffixes i and k indicate the ionized and excited states respectively. $p_k(T)$ is the probability that an electron with the energy, T, loses its energy, E_k, in the first collision with the medium and excites the atom to the k-th state. When the medium absorbs the residual energy, $T-E_k$, of the electron, the number of the m-th excited state produced is $N_m(T-E_k)$. The $\{dp_i(T)/dE\}dE$ is the probability that an electron with the energy, T, loses its energy, $E\approx E+dE$, in collision with an atom and ionizes the atom to the i-th state. As a result of this collision, the energies of the scattered and ejected electrons are $T-E$ and $E-I_i$ respectively. Therefore, the numbers of the m-th excited states produced by absorbing the energies of $T-E$ and $E-I_i$ are $N_m(T-E)$ and $N_m(E-I_i)$. The δ_{km} and δ_{im} are Kronecker deltas. When m is equal to k, $\delta_{km}=1$; *i.e.*, an atom is excited to the m=k state in the first collision with the electron of energy, T. The formulation of $p_k(T)$ and $\{dp_i(T)/dE\}dE$ can easily be made as the ratios of the total cross section for ionization and excitations previously formulated.[1]

Equation 1 is a Volterra second-kind integral equation. In order actually to solve this equation, we must first calculate $N_m(T)$ numerically at an energy near the threshold energy. Then, using the obtained $N_m(T)$, we calculate $N_m(T)$ at a hi her energy. This calculating method is opposite to that used in the calculation of the degradation spectrum under CSDA, where the calculation is carried out from the higher energy to the lower energy.

For the estimation of the yields of ionization and excitations, we have to set up a Fowler equation for each process, one for ionization and two for the excitations, singlet and triplet. Since $N_m(T)$ at lower energies ($T<100$ eV) depends strongly upon T, the mesh of the calculation must be taken to be as small as possible. In the present calculations, we took 0.2 eV for the mesh. Consequently, the calculation time for the Fowler equation was about sixty times that of the method of the degradation spectrum under CSDA. These calculations were carried out by means of two computers, HITAC 8700 at the Tokyo Institute of Technology and HITAC 8800 at the University of Tokyo.

The $N_m(T)$ values for the ionization and singlet and triplet excitations in helium are shown in Fig. 2 as functions of the

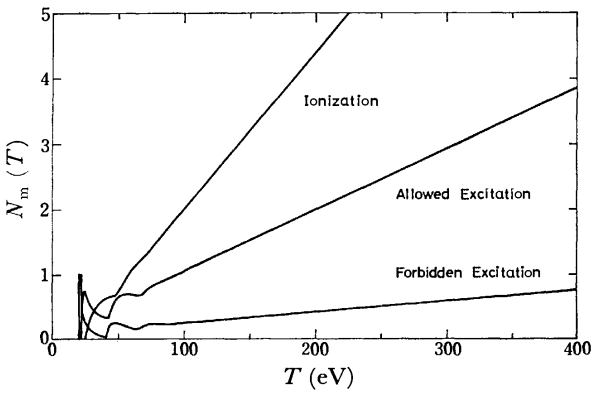

Fig. 2. The yields of ionization and excitations in helium as functions of the incident electron energy.

Table 4. Comparison of the G-values estimated by using the Fowler equation with those obtained by the method of the degradation spectrum under CSDA

Method of calculation	Incident electron energy (keV)	G_e	G_s	G_t
Fowler equation	1	2.35	0.94	0.18
	100	2.38	0.91	0.17
Degradation spectrum	1	2.23	0.88	0.17
	100	2.27	0.85	0.17

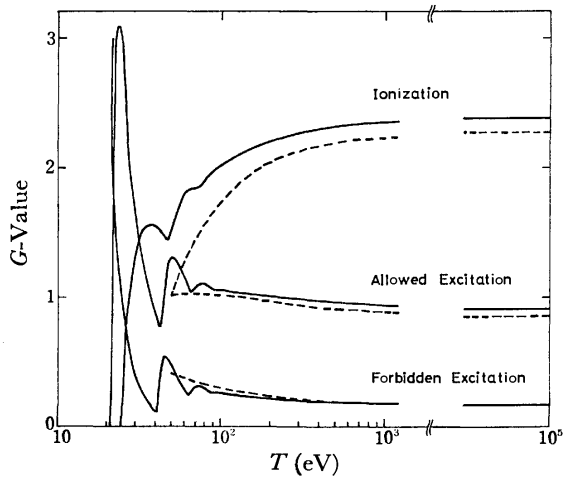

Fig. 3. The G-values for ionization and excitations as functions of ln T.
——: Estimated by using the Fowler equation,
----: estimated by the method of the degradation spectrum under CSDA.

Table 5. Comparison of the W-values obtained experimentally and theoretically

Theoretical:		
Method of calculation		W
Fowler equation	Present	42.0
	Miller[21]	46.5
	Alkhazov[22]	46.45±1.0
Degradation spectrum Douthat[24]		47.9
Degradation spectrum under CSDA		44.05
Experimental:		
Exciting source		W
Po-α		42.7 a)
Po-α		46.0 b)
Tritium-β		42.3 c)
Proton (3.6 MeV)		45.2 d)

a) W.P. Jesse and J. Sadauskis, *Phys. Rev.*, **90**, 1120 (1953). b) J. C. Bortner and G. S. Hurst, *Phys. Rev.*, **93**, 1236 (1954). c) W. P. Jesse and J. Sadauskis, *Phys. Rev.*, **107**, 766 (1957). d) J. E. Parks, G. S. Hurst, T. E. Stewart, and H. L. Weidner, *J. Chem. Phys.*, **57**, 5467 (1972).

electron energy, T. All the yields at the lower energies ($T<500$ eV) are strongly dependent on the energy of the incident electron. However, the yields at the higher energies ($T>1000$ eV) are nearly linear with T. Actually we have calculated the $N_m(T)$ from the threshold energy to 1200 eV, and then extrapolated it to 100 keV by using the linear relation between $N_m(T)$ and T.

Table 4 shows the G-values for ionization and two excitations estimated by the Fowler equation, together with those estimated by the degradation spectrum under CSDA. The values estimated by the two methods agree with each other within 7%. Figure 3 shows the incident electron-energy dependence of the G-values.

For comparison, the experimental and other theoretical W-values of helium are listed in Table 5. The W-value obtained in the present calculation (42.0 eV) seems to coincide with the experimental value (42.3 eV) reported by Jesse and Sadauskis, who used β-rays as the exciting source, while other experiments used heavier particles. This coincidence, however, should be taken as accidental, because the cross sections of ionization and excitations used in the present calculation cannot be more accurate than those used by Miller[21] and Alkhazov.[22] This point has already been discussed.[1]

References

1) S. Sato, K. Okazaki, and S. Ohno, *Bull. Chem. Soc. Jpn.*, **47**, 2174 (1974).
2) K. Okazaki, S. Sato, and S. Ohno, *Bull. Chem. Soc. Jpn.*, **48**, 1411 (1975).
3) K. Okazaki and S. Sato, *Bull. Chem. Soc. Jpn.*, **48**, 3523 (1975).
4) S. Ohno, H. Nagayama, K. Okazaki, and S. Sato, *Bull. Chem. Soc. Jpn.*, **48**, 2153 (1975).
5) K. Okazaki, S. Sato, and S. Ohno, *Bull. Chem. Soc. Jpn.*, **49**, 174 (1976).
6) R. L. Platzman, *J. Phys. Radium.*, **21**, 853 (1960).
7) "Handbook of Chemistry and Physics," The Chemical Rubber Co., 1975.
8) K. Siegbahn *et al.*, "ESCA Applied to Free Molecules," North-Holland, Amsterdam (1971).
9) M. J. S. Dewar and S. D. Worley, *J. Chem. Phys.*, **50**, 654 (1969).
10) G. Herzberg, "Molecular Spectra and Molecular Structure," Van Nostrand, Vol. III, Princeton, N. J. (1966).
11) E. N. Lassettre and S. A. Francis, *J. Chem. Phys.*, **40**, 1208 (1964).
12) R. L. Platzman, *Radiat. Res.*, **17**, 479 (1962).
13) R. L. Platzman, *Vortex*, **23**, 372 (1962).
14) R. I. Schoen, *J. Chem. Phys.*, **37**, 2032 (1962).
15) P. H. Metzger and G. R. Cook, *J. Chem. Phys.*, **41**, 642 (1964).
16) Y. Hatano, *Bull. Chem. Soc. Jpn.*, **41**, 1126 (1968).
17) J. A. Hornbeck and J. P. Molnar, *Phys. Rev.*, **84**, 621 (1951).
18) I. Koyano, I. Tanaka, and I. Omura, *J. Chem. Phys.*, **40**, 2734 (1964).
19) U. Fano and L. V. Spencer, *Int. J. Radiat. Phys. Chem.*, **7**, 63 (1975).
20) G. A. Erskine. *Proc. R. Soc. London, Ser. A*, **224**, 362 (1954).
21) W. F. Miller, *Bull. Am. Phys. Soc.*, **1**, 202 (1956).
22) G. D. Alkhazov, *Soviet Phys.-Tech. Phys.*, **16**, 1995 (1972).
23) M. Inokuti, *Radiat. Res.*, **64**, 6 (1975).
24) D. A. Douthat, *Radiat. Res.*, **61**, 1 (1975).

The Structure of the Cyclodextrin Complex. V. Crystal Structures of α-Cyclodextrin Complexes with *p*-Nitrophenol and *p*-Hydroxybenzoic Acid

Kazuaki HARATA

Research Institute for Polymers and Textiles, Sawatari 4, Kanagawa-ku, Yokohama 221

(Received November 30, 1976)

α-Cyclodextrin (α-CDx) forms a 1: 1 complex with *p*-nitrophenol (*p*-NP) and *p*-hydroxybenzoic acid (*p*-HB). The crystal structures were determined by the X-ray method. The crystals of both complexes are orthorhombic, and the space group is $P2_12_12_1$ with $Z=4$. The cell dimensions are $a=13.455(1)$, $b=15.296(1)$, and $c=24.740(3)$ Å for the *p*-NP complex, and $a=13.356(1)$, $b=15.342(1)$, and $c=24.896(2)$ Å for the *p*-HB complex. The crystal structures were determined on the basis of the isomorphous structure of the *p*-iodophenol complex by using 4811 reflections for the *p*-NP complex and 4692 reflections for the *p*-HB complex, and refined by the block-diagonal least-squares method to the final *R*-values of 0.066 and 0.067 respectively. In both complexes, the guest molecule is included in the α-CDx cavity, and the α-CDx ring is deformed from the regular hexagonal symmetry as a result of the inclusion of the planar molecule. The nitrophenyl or carboxyphenyl group is located in the cavity, while the phenolic hydroxyl group protrudes from the secondary hydroxyl side of the cavity. Several intermolecular hydrogen-hydrogen contacts shorter than the ideal van der Waals contact are observed between α-CDx and guest molecules, indicating that the guest molecule is rigidly fixed in the cavity. The nitro or carboxyl group is situated on the O(6) side and is hydrogen-bonded to water or a hydroxyl group of the adjacent α-CDx molecule. The geometry of the complex gives a reasonable model for the α-CDx-substrate complex in the hydrolysis of *p*-nitrophenyl acetate and *p*-carboxyphenyl acetate catalyzed by α-CDx.

α-Cyclodextrin (α-CDx) forms a number of inclusion complexes with a variety of molecules and ions,[1] and the inclusion process affects the reactivity of the guest molecule.[2] A remarkable stereospecific acceleration is caused by α-CDx in the hydrolysis of substituted phenyl esters.[3] The rate of phenol-release from *meta*-substituted phenyl esters is greatly enhanced, whereas the rate of phenol-release from the corresponding *para*-isomers is only slightly enhanced. It has been emphasized that the magnitude of the rate acceleration does not parallel the stabilities of the α-CDx-ester complex, but depends on the geometry of the complex. Moreover, the stereospecificity of the rate accerelation has been interpreted on the basis of the interaction of the secondary hydroxyl groups of α-CDx with the carbonyl carbon of the substrate in the α-CDx cavity.

The crystal structures of many α-CDx complexes have been determined by the X-ray method.[4-16] In the complexes with *p*-iodoaniline (*p*-IA)[14,15] and *p*-iodophenol (*p*-IP),[16] the hydrophobic iodophenyl group is located in the α-CDx cavity, while the amino or hydroxyl group protrudes from the secondary hydroxyl side. *p*-Nitrophenol (*p*-NP) and *p*-hydroxybenzoic acid (*p*-HB) forms a 1: 1 complex with α-CDx. In this case, the nitro or carboxyl group has been expected, from the kinetic study of the α-CDx-catalyzed hydrolysis of *p*-nitrophenyl acetate and *p*-carboxyphenyl acetate,[3] to be situated on the O(6) side of the cavity. The X-ray analysis of α-CDx complexes with *p*-NP and *p*-HB was carried out in order to investigate the geometry of the complexes in relation to the catalytic property of α-CDx.

Experimental

A yellowish and plate-like crystal of the α-CDx–*p*-NP complex was prepared by cooling an aqueous solution containing α-CDx and *p*-NP in a 1: 1 molar ratio. The crystals of the α-CDx–*p*-HB complex, which were obtained by the same procedure, are colorless needles. The determination of the lattice parameters and the intensity measurements were carried out on a Rigaku automatic four-circle diffractometer with graphite-monochromated Cu$K\alpha$ radiation. Intensity data were collected up to 150° in 2θ by using the 2θ-ω scan technique. 5765 independent reflections for the *p*-NP complex and 5410 for the *p*-HB complex were obtained, but reflections with $|F_o|<3\sigma(F)$, 954 for the *p*-NP complex and 718 for the *p*-HB complex, were treated as unobserved. No correction was made for absorption and extinction. The crystal data are shown in Table 1.

Table 1. Crystal data

	α-Cyclodextrin–*p*-nitrophenol $C_{36}H_{60}O_{30}\cdot C_6H_5NO_3\cdot 3H_2O$	α-Cyclodextrin–*p*-hydroxybenzoic acid $C_{36}H_{60}O_{30}\cdot C_7H_6O_3\cdot 3H_2O$
Molecular weight	1166.0	1165.0
Crystal system	Orthorhombic	Orthorhombic
Cell dimensions	*a* 13.455(1)Å	13.356(1)Å
	b 15.296(1)Å	15.342(1)Å
	c 24.740(3)Å	24.896(2)Å
Cell volume	*V* 5092.1(8)Å^3	5101.4(6)Å^3
Space group	$P2_12_12_1$	$P2_12_12_1$
	Z 4	4
Density	D_m 1.53 g cm^{-3}	1.53 g cm^{-3}
	D_x 1.52	1.52

Determination and Refinement of the Structure

The crystals of the α-CDx–*p*-NP complex and the α-CDx–*p*-HB complex are isomorphous with the crystals of the α-CDx–*p*-IA complex[14,15] and the α-CDx–*p*-IP complex.[16] A set of coordinates of α-CDx found in the α-CDx–*p*-IP complex was used to calculate the initial phases for the *p*-NP complex and the *p*-HB complex. The phases were refined by the block-diagonal least-squares method. Then, an electron-density map was

Table 2. Final atomic parameters ($\times 10^4$) for the non-hydrogen atoms
The anisotropic thermal factors are of the form: $\exp[-(B_{11}h^2+B_{22}k^2+B_{33}l^2+B_{12}hk+B_{23}kl+B_{31}lh)]$.
OC indicates the occupancy factor of the disordered atom.

α-Cyclodextrin-*p*-Nitrophenol Complex

	x	y	z	B_{11}	B_{22}	B_{33}	B_{12}	B_{23}	B_{31}	OC
C(1,G1)	1491(5)	-491(4)	6957(3)	44(4)	29(3)	11(1)	-2(6)	2(3)	0(4)	
C(2,G1)	1237(5)	-1215(4)	6562(3)	42(4)	28(3)	10(1)	-10(6)	1(3)	-1(4)	
C(3,G1)	1880(5)	-1131(4)	6061(2)	44(4)	22(3)	8(1)	-4(5)	-2(3)	-7(3)	
C(4,G1)	1749(5)	-214(4)	5813(2)	35(4)	19(2)	10(1)	-1(5)	3(3)	0(3)	
C(5,G1)	1988(6)	474(4)	6239(3)	62(5)	21(3)	11(1)	2(6)	-3(3)	-4(4)	
C(6,G1)	1794(8)	1400(5)	6037(3)	134(9)	20(3)	14(1)	3(9)	10(4)	-16(6)	
O(2,G1)	1434(5)	-2034(3)	6830(2)	85(4)	27(2)	10(1)	-42(5)	9(2)	-16(3)	
O(3,G1)	1549(4)	-1750(3)	5658(2)	82(4)	21(2)	10(1)	-9(5)	-2(2)	-15(3)	
O(4,G1)	2456(4)	-138(3)	5378(2)	39(3)	31(2)	7(1)	2(4)	6(2)	-1(2)	
O(5,G1)	1349(4)	332(3)	6702(2)	58(3)	28(2)	9(1)	23(5)	-5(2)	0(3)	
O(6,G1)	826(5)	1510(4)	5815(3)	101(6)	45(3)	23(1)	75(7)	17(3)	6(5)	
C(1,G2)	2089(5)	122(4)	4857(3)	39(4)	29(3)	10(1)	5(6)	10(3)	-2(3)	
C(2,G2)	2297(5)	-625(4)	4469(2)	45(4)	25(3)	9(1)	-12(6)	3(3)	-9(3)	
C(3,G2)	3422(5)	-795(4)	4453(3)	46(4)	20(2)	10(1)	-11(6)	-8(3)	2(3)	
C(4,G2)	3931(5)	42(4)	4290(2)	37(4)	15(2)	9(1)	4(5)	3(2)	2(3)	
C(5,G2)	3646(5)	803(4)	4664(3)	45(4)	19(3)	13(1)	2(6)	-8(3)	3(4)	
C(6,G2)	4042(6)	1672(4)	4468(3)	60(5)	17(3)	22(2)	-3(6)	-5(4)	13(5)	
O(2,G2)	1745(4)	-1393(3)	4615(2)	58(3)	35(2)	10(1)	-43(5)	5(2)	-10(3)	
O(3,G2)	3662(4)	-1442(3)	4049(2)	62(4)	20(2)	14(1)	-10(5)	-12(2)	16(3)	
O(4,G2)	4980(3)	-123(3)	4351(2)	32(2)	21(2)	8(1)	11(4)	4(2)	-1(2)	
O(5,G2)	2577(3)	887(3)	4688(2)	35(3)	20(2)	13(1)	7(4)	8(2)	7(3)	
O(6,G2)	3798(5)	1817(4)	3909(3)	70(4)	34(3)	26(1)	2(6)	31(3)	12(4)	
C(1,G3)	5630(5)	84(4)	3915(2)	36(4)	24(3)	7(1)	1(5)	5(3)	0(3)	
C(2,G3)	6263(5)	-729(4)	3808(2)	37(4)	24(3)	7(1)	1(5)	0(3)	-1(3)	
C(3,G3)	6798(5)	-974(4)	4318(2)	40(4)	14(2)	9(1)	16(5)	-2(2)	2(3)	
C(4,G3)	7374(5)	-207(4)	4560(2)	36(4)	20(2)	8(1)	6(5)	3(3)	-4(3)	
C(5,G3)	6767(5)	652(4)	4570(2)	37(4)	18(2)	8(1)	-5(5)	-1(3)	1(3)	
C(6,G3)	7410(6)	1456(4)	4658(3)	52(5)	18(2)	14(1)	-6(6)	-4(3)	-9(4)	
O(2,G3)	5628(3)	-1436(3)	3625(2)	40(3)	26(2)	9(1)	-3(4)	-7(2)	-2(2)	
O(3,G3)	7487(4)	-1693(3)	4229(2)	42(3)	20(2)	11(1)	6(4)	-5(2)	0(3)	
O(4,G3)	7597(3)	-477(3)	5100(2)	34(3)	27(2)	7(1)	-3(4)	4(2)	-5(2)	
O(5,G3)	6269(3)	777(3)	4063(2)	43(3)	19(2)	9(1)	4(4)	8(2)	-1(2)	
O(6,G3)	8221(4)	1501(3)	4293(2)	60(4)	37(3)	18(1)	-41(5)	12(3)	-1(3)	
C(1,G4)	8568(5)	-320(4)	5311(2)	37(4)	28(3)	9(1)	-9(6)	-10(3)	-3(3)	
C(2,G4)	8888(6)	-1150(4)	5622(3)	53(5)	28(3)	8(1)	20(6)	-7(3)	-11(4)	
C(3,G4)	8302(6)	-1253(4)	6134(2)	58(5)	17(2)	9(1)	5(6)	-3(3)	-13(4)	
C(4,G4)	8309(5)	-426(4)	6474(2)	45(4)	17(2)	8(1)	1(5)	-4(3)	1(3)	
C(5,G4)	7913(5)	334(4)	6117(2)	51(4)	16(2)	8(1)	3(5)	-3(3)	4(3)	
C(6,G4)	7960(7)	1215(4)	6414(3)	90(6)	15(3)	10(1)	8(7)	-5(3)	-14(4)	
O(2,G4)	8778(4)	-1905(3)	5276(2)	79(4)	31(2)	11(1)	40(5)	-16(2)	-14(3)	
O(3,G4)	8761(4)	-1949(3)	6432(2)	80(4)	19(2)	12(1)	24(5)	2(2)	-1(3)	
O(4,G4)	7650(3)	-576(3)	6915(2)	35(3)	22(2)	7(1)	-7(4)	-3(2)	-1(2)	
O(5,G4)	8580(3)	417(3)	5658(2)	42(3)	24(2)	9(1)	-13(4)	-1(2)	1(2)	
O(6A,G4)	9053(14)	1458(9)	6516(6)	119(15)	28(6)	17(3)	-9(16)	-23(7)	12(11)	0.4
O(6B,G4)	7400(6)	1851(4)	6087(3)	40(5)	12(3)	9(1)	5(6)	3(3)	-2(4)	0.6
C(1,G5)	8019(5)	-417(4)	7442(2)	45(4)	19(2)	9(1)	0(6)	0(3)	-3(3)	
C(2,G5)	7801(5)	-1234(4)	7793(2)	41(4)	21(3)	10(1)	13(5)	-4(3)	-2(3)	
C(3,G5)	6674(5)	-1391(4)	7829(3)	44(4)	21(3)	9(1)	1(6)	4(3)	2(3)	
C(4,G5)	6147(5)	-561(4)	8013(2)	34(4)	22(3)	9(1)	-1(5)	4(3)	-4(3)	
C(5,G5)	6457(5)	239(4)	7677(2)	28(3)	23(3)	10(1)	2(5)	3(3)	-3(3)	
C(6,G5)	6055(5)	1098(4)	7895(3)	48(4)	19(3)	12(1)	16(6)	-3(3)	2(4)	
O(2,G5)	8280(4)	-1972(3)	7559(2)	58(3)	25(2)	13(1)	25(5)	-2(2)	5(3)	
O(3,G5)	6476(4)	-2082(3)	8202(2)	70(4)	23(2)	14(1)	-7(5)	13(2)	14(3)	
O(4,G5)	5108(3)	-715(3)	7930(2)	34(3)	31(2)	8(1)	-3(4)	-4(2)	2(2)	
O(5,G5)	7524(3)	316(2)	7674(2)	39(3)	16(2)	8(1)	4(4)	-6(2)	-3(2)	
O(6,G5)	6211(4)	1168(3)	8466(2)	44(3)	33(2)	14(1)	9(5)	-16(2)	-4(3)	
C(1,G6)	4440(5)	-589(4)	8362(2)	45(4)	27(3)	7(1)	4(6)	7(3)	5(3)	
C(2,G6)	3740(5)	-1378(4)	8361(3)	46(4)	24(3)	12(1)	-3(6)	9(3)	-3(4)	
C(3,G6)	3239(5)	-1438(4)	7812(3)	39(4)	22(3)	12(1)	-11(6)	6(3)	-3(4)	
C(4,G6)	2734(5)	-563(4)	7682(2)	31(4)	22(3)	9(1)	-4(5)	-1(3)	-1(3)	
C(5,G6)	3404(5)	238(4)	7767(2)	45(4)	18(2)	8(1)	-6(5)	-4(3)	-3(3)	
C(6,G6)	2812(6)	1087(4)	7751(3)	61(5)	23(3)	14(1)	1(6)	1(3)	-11(4)	
O(2,G6)	4261(4)	-2155(3)	8493(3)	55(4)	29(2)	26(1)	1(5)	18(3)	-19(4)	
O(3,G6)	2522(4)	-2126(3)	7821(2)	55(3)	20(2)	17(1)	-26(5)	6(2)	-10(3)	
O(4,G6)	2500(3)	-599(3)	7117(2)	33(3)	24(2)	8(1)	0(4)	-3(2)	-3(2)	
O(5,G6)	3880(3)	185(3)	8291(3)	41(3)	25(2)	7(1)	1(4)	-6(2)	-1(2)	
O(6,G6)	1870(4)	1025(4)	8007(2)	65(4)	37(3)	17(1)	30(5)	-8(3)	9(3)	
C(1,NP)	5286(6)	-2209(4)	6068(3)	50(5)	23(3)	13(1)	10(6)	8(3)	16(4)	
C(2,NP)	5046(7)	-1823(5)	6563(3)	81(6)	32(3)	10(1)	1(8)	1(3)	16(5)	
C(3,NP)	4917(7)	-938(5)	6589(3)	78(6)	35(3)	11(1)	-11(8)	-5(3)	20(5)	
C(4,NP)	5059(5)	-437(4)	6125(3)	41(4)	25(3)	9(1)	-4(6)	1(3)	-4(3)	
C(5,NP)	5302(6)	-804(5)	5636(3)	75(6)	30(3)	11(1)	-2(7)	2(3)	10(4)	
C(6,NP)	5415(7)	-1709(5)	5604(3)	70(6)	41(4)	11(1)	12(8)	-2(4)	19(5)	
N(NP)	4967(5)	517(4)	6160(3)	57(4)	28(3)	15(1)	-2(6)	-6(3)	-3(4)	
O(1,NP)	5430(4)	-3091(3)	6074(2)	71(4)	26(2)	16(1)	16(5)	9(3)	29(3)	
O(2,NP)	4742(6)	849(4)	6597(3)	144(7)	31(3)	21(1)	-5(7)	-11(3)	29(5)	
O(3,NP)	5149(6)	951(4)	5748(2)	121(6)	33(3)	17(1)	-1(7)	16(3)	3(5)	
O(W1)	5077(6)	-1109(5)	2510(3)	80(5)	74(4)	16(1)	-6(8)	16(4)	-18(4)	
O(W2A)	4859(6)	-1541(6)	9688(3)	48(5)	79(5)	25(2)	27(9)	28(5)	23(5)	0.8
O(W2B)	3571(25)	-2527(19)	9381(12)	84(25)	45(15)	20(6)	9(33)	44(16)	18(21)	0.2
O(W3A)	190(14)	-1713(13)	7923(8)	75(13)	87(12)	29(4)	12(21)	-10(12)	8(13)	0.4
O(W3B)	9798(7)	-2574(7)	8219(4)	57(7)	58(5)	19(2)	30(10)	-11(5)	-20(6)	0.6

α-Cyclodextrin-*p*-Hydroxybenzoic Acid Complex

	x	y	z	B_{11}	B_{22}	B_{33}	B_{12}	B_{23}	B_{31}	OC
C(1,G1)	1502(5)	-473(4)	6944(3)	46(4)	31(3)	11(1)	-6(6)	-2(3)	11(4)	
C(2,G1)	1260(5)	-1199(4)	6549(3)	46(4)	27(3)	12(1)	-9(6)	1(3)	-14(4)	
C(3,G1)	1892(5)	-1114(4)	6044(2)	49(4)	29(3)	9(1)	0(6)	-4(3)	-9(3)	
C(3,G1)	1737(5)	-206(4)	5803(2)	42(4)	27(3)	9(1)	-4(6)	-1(3)	3(3)	
C(5,G1)	1968(6)	496(5)	6227(3)	80(6)	32(3)	10(1)	-14(7)	-6(3)	12(4)	
C(6,G1)	1702(8)	1408(5)	6021(3)	123(9)	30(3)	16(1)	-26(9)	-1(4)	10(6)	
O(2,G1)	1447(4)	-2016(3)	6812(2)	85(4)	30(2)	11(1)	-34(5)	2(2)	-25(3)	
O(3,G1)	1564(4)	-1739(3)	5652(2)	87(4)	23(2)	12(1)	8(5)	-3(2)	-15(3)	
O(4,G1)	2434(4)	-122(3)	5366(2)	42(3)	39(2)	10(1)	6(5)	1(2)	2(3)	
O(5,G1)	1334(4)	334(3)	6686(2)	73(4)	28(2)	11(1)	17(5)	-2(2)	12(3)	
O(6,G1)	732(5)	1467(4)	5771(3)	108(6)	50(3)	26(1)	68(7)	17(4)	18(5)	
C(1,G2)	2043(5)	139(5)	4854(3)	44(5)	43(4)	12(1)	16(7)	5(3)	1(4)	
C(2,G2)	2234(6)	-597(5)	4462(3)	52(5)	38(3)	11(1)	-3(7)	3(3)	-6(4)	
C(3,G2)	3346(5)	-780(4)	4435(3)	50(4)	24(3)	11(1)	4(6)	-2(3)	-1(4)	
C(4,G2)	3891(5)	39(4)	4278(2)	46(4)	16(2)	10(1)	10(5)	-1(2)	3(3)	
C(5,G2)	3637(6)	799(4)	4650(3)	51(5)	22(3)	16(1)	13(6)	-7(3)	14(4)	
C(6,G2)	4041(7)	1665(5)	4463(4)	83(7)	34(4)	29(2)	8(9)	-7(5)	11(7)	
O(2,G2)	1663(4)	-1357(4)	4605(2)	62(4)	55(3)	10(1)	-48(6)	1(3)	-14(3)	
O(3,G2)	3569(4)	-1420(3)	4025(2)	76(4)	23(2)	14(1)	-4(5)	-7(2)	7(3)	
O(4,G2)	4933(3)	-149(3)	4329(2)	44(3)	26(2)	7(1)	13(4)	6(2)	2(2)	
O(5,G2)	2549(4)	900(3)	4679(2)	50(3)	28(2)	17(1)	23(5)	5(2)	12(3)	
O(6,G2)	3805(7)	1813(4)	3906(4)	142(8)	46(3)	47(2)	8(9)	43(5)	8(8)	
C(1,G3)	5589(5)	55(4)	3905(2)	52(4)	28(3)	7(1)	13(6)	4(3)	5(3)	
C(2,G3)	6225(5)	-762(4)	3802(2)	49(4)	24(3)	9(1)	-4(6)	2(3)	3(3)	
C(3,G3)	6786(5)	-995(4)	4317(2)	47(4)	19(2)	10(1)	-3(5)	1(3)	3(4)	
C(4,G3)	7364(5)	-221(4)	4543(2)	52(4)	24(3)	7(1)	-15(6)	2(3)	-3(3)	
C(5,G3)	6744(6)	622(4)	4555(2)	63(5)	24(3)	9(1)	1(6)	3(3)	-4(4)	
C(6,G3)	7387(7)	1433(4)	4640(3)	88(6)	22(3)	14(1)	-19(7)	-1(3)	-16(5)	
O(2,G3)	5606(3)	-1465(3)	3626(2)	41(3)	29(2)	9(1)	3(4)	-8(2)	2(2)	
O(3,G3)	7465(4)	-1708(3)	4232(2)	46(3)	21(2)	11(1)	0(4)	1(2)	-4(3)	
O(4,G3)	7590(4)	-467(3)	5090(2)	47(3)	30(2)	8(1)	-5(4)	1(2)	-5(2)	
O(5,G3)	6242(4)	745(3)	4046(2)	61(3)	23(2)	10(1)	-1(4)	10(2)	-3(3)	
O(6,G3)	8192(4)	1497(4)	4260(2)	68(4)	50(3)	18(1)	-43(6)	11(3)	-3(4)	
C(1,G4)	8572(5)	-339(4)	5288(2)	41(4)	35(3)	10(1)	-6(6)	-7(3)	-7(3)	
C(2,G4)	8875(6)	-1169(4)	5593(3)	60(5)	30(3)	11(1)	14(6)	-9(3)	-13(4)	
C(3,G4)	8296(6)	-1261(4)	6118(3)	60(5)	22(3)	13(1)	5(6)	-9(3)	-10(4)	
C(4,G4)	8368(5)	-422(4)	6447(2)	48(4)	24(3)	9(1)	-6(6)	-4(3)	3(3)	
C(5,G4)	7985(5)	336(4)	6102(2)	62(5)	22(3)	9(1)	-6(6)	-2(3)	4(4)	
C(6,G4)	8063(7)	1216(4)	6389(3)	93(7)	16(3)	14(1)	-4(7)	-8(3)	-7(5)	
O(2,G4)	8741(5)	-1933(3)	5270(2)	87(5)	43(3)	12(1)	46(6)	-17(3)	-23(3)	
O(3,G4)	8749(4)	-1964(3)	6409(2)	92(4)	22(2)	11(1)	19(5)	1(2)	-1(3)	
O(4,G4)	7723(3)	-544(3)	6899(2)	38(3)	27(2)	10(1)	-4(4)	-5(2)	-5(2)	
O(5,G4)	8627(4)	396(3)	6527(2)	52(3)	32(2)	10(1)	-34(5)	-4(2)	2(3)	
O(6A,G4)	9128(6)	1450(5)	6509(3)	82(6)	33(3)	15(1)	33(8)	-18(4)	5(5)	0.7
O(6B,G4)	7442(15)	1861(9)	6098(7)	90(15)	22(6)	17(3)	-34(17)	-25(8)	29(12)	0.3
C(1,G5)	8111(5)	-382(4)	7419(3)	56(5)	27(3)	10(1)	1(6)	-3(3)	-6(4)	
C(2,G5)	7910(6)	-1193(5)	7764(3)	55(5)	32(3)	11(1)	11(7)	0(3)	-5(4)	
C(3,G5)	6782(6)	-1353(4)	7814(3)	68(5)	20(3)	11(1)	3(6)	1(3)	-4(4)	
C(4,G5)	6231(5)	-541(4)	7993(2)	50(4)	21(3)	11(1)	-7(6)	-2(3)	-11(4)	
C(5,G5)	6532(5)	265(4)	7663(3)	43(4)	27(3)	11(1)	-3(6)	-1(3)	-3(4)	
C(6,G5)	6119(5)	1117(4)	7882(3)	49(5)	27(3)	14(1)	10(6)	3(3)	-1(4)	
O(2,G5)	8380(4)	-1939(3)	7535(2)	77(4)	36(2)	14(1)	40(5)	-7(3)	-9(3)	
O(3,G5)	6593(4)	-2041(3)	8189(2)	75(4)	28(2)	17(1)	5(5)	16(2)	1(3)	
O(4,G5)	5188(4)	-691(3)	7895(2)	44(3)	35(2)	8(1)	-10(4)	-3(2)	-4(2)	
O(5,G5)	7625(4)	345(3)	7653(2)	43(3)	22(2)	12(1)	2(4)	-9(2)	-2(3)	
O(6,G5)	6262(4)	1174(3)	8454(2)	44(3)	41(2)	16(1)	18(5)	-19(3)	-5(3)	
C(1,G6)	4491(6)	-617(5)	8325(3)	60(5)	33(3)	9(1)	-15(7)	1(3)	2(4)	
C(2,G6)	3829(6)	-1433(5)	8294(3)	65(5)	39(3)	14(1)	-40(7)	6(4)	-14(4)	
C(3,G6)	3286(6)	-1434(5)	7762(3)	51(5)	30(3)	14(1)	-25(6)	4(3)	3(4)	
C(4,G6)	2766(5)	-570(4)	7652(2)	44(4)	27(3)	10(1)	-14(6)	-5(3)	9(3)	
C(5,G6)	3434(5)	219(4)	7748(2)	49(4)	32(3)	9(1)	-8(6)	-6(3)	-6(4)	
C(6,G6)	2858(6)	1076(5)	7738(3)	64(6)	35(3)	17(1)	-7(7)	-1(4)	-13(5)	
O(2,G6)	4465(5)	-2187(3)	8349(3)	103(5)	29(2)	29(1)	-19(6)	11(3)	-41(5)	
O(3,G6)	2574(4)	-2136(3)	7769(2)	74(4)	34(2)	16(1)	-43(5)	3(3)	-5(3)	
O(4,G6)	2510(3)	-575(3)	7091(2)	38(3)	38(2)	8(1)	-14(4)	-8(2)	-1(2)	
O(5,G6)	3912(4)	147(3)	8275(2)	56(3)	32(2)	8(1)	-2(5)	-8(2)	-6(3)	
O(6,G6)	1907(4)	1012(4)	7994(2)	70(4)	56(3)	16(1)	20(6)	-22(3)	12(3)	
C(1,HB)	5261(5)	-2175(4)	6073(3)	38(4)	29(3)	12(1)	-10(6)	3(3)	15(4)	
C(2,HB)	5110(6)	-1737(5)	6552(3)	56(5)	44(4)	10(1)	8(7)	11(3)	16(4)	
C(3,HB)	5032(7)	-847(5)	6558(3)	80(6)	39(3)	9(1)	14(8)	-8(3)	9(4)	
C(4,HB)	5151(6)	-366(5)	6092(3)	53(5)	39(3)	11(1)	-1(7)	-9(3)	-1(4)	
C(5,HB)	5268(7)	-797(5)	5604(3)	85(6)	36(3)	8(1)	-17(8)	1(3)	4(4)	
C(6,HB)	5334(6)	-1708(5)	5592(3)	73(6)	43(4)	10(1)	-29(8)	-6(3)	17(4)	
C(7,HB)	5177(7)	602(5)	6103(3)	91(7)	39(4)	14(1)	7(9)	-13(4)	2(5)	
O(1,HB)	5368(4)	-3057(3)	6079(2)	68(4)	34(2)	15(1)	9(5)	4(3)	32(3)	
O(2,HB)	5168(7)	969(4)	6561(2)	205(9)	31(3)	16(1)	35(9)	-9(3)	9(6)	
O(3,HB)	5312(7)	1017(4)	5676(2)	181(8)	48(3)	13(1)	-72(9)	14(3)	-5(5)	
O(W1)	5047(6)	-1151(5)	2507(3)	81(5)	101(5)	18(1)	-39(9)	27(4)	-28(4)	
O(W2A)	4932(7)	-1677(10)	9690(4)	45(6)	222(14)	22(2)	31(16)	69(9)	0(6)	0.7
O(W2B)	3716(12)	-2467(10)	9383(8)	40(11)	34(8)	25(4)	19(15)	13(9)	23(11)	0.3
O(W3A)	277(7)	-1713(8)	7950(5)	60(7)	113(8)	36(3)	-14(12)	-26(8)	35(7)	0.7
O(W3B)	9798(15)	-2594(13)	8201(7)	71(14)	58(10)	18(4)	29(21)	-4(10)	-7(12)	0.3

Table 3. Fractional coordinates ($\times 10^3$) and isotropic thermal factors (B/Å^2) for hydrogen atoms

α-Cyclodextrin-*p*-Nitrophenol Complex

	x	y	z	B		x	y	z	B
H(C1,G1)	109(6)	-48(5)	735(3)	2.8	H(C5,G4)	710(6)	18(5)	598(3)	2.5
H(C2,G1)	42(6)	-116(5)	644(3)	2.6	H(O2,G4)	866(7)	-180(5)	484(3)	3.1
H(C3,G1)	275(6)	-128(5)	618(3)	2.6	H(O3,G4)	867(6)	-209(6)	680(3)	3.1
H(C4,G1)	93(6)	-15(5)	563(3)	2.2	H(C1,G5)	882(6)	-23(5)	741(3)	2.0
H(C5,G1)	285(6)	44(5)	636(3)	2.9	H(C2,G5)	809(6)	-117(5)	823(3)	2.2
H(C6A,G1)	238(7)	157(6)	575(3)	4.0	H(C3,G5)	632(6)	-153(5)	741(3)	2.4
H(C6B,G1)	185(7)	185(6)	638(4)	4.0	H(C4,G5)	631(6)	-49(5)	843(3)	2.1
H(O2,G1)	100(6)	-230(6)	654(3)	3.2	H(C5,G3)	616(6)	12(5)	726(3)	2.4
H(O3,G1)	193(6)	-203(6)	565(3)	3.1	H(C6A,G5)	645(6)	160(5)	769(3)	2.6
H(C1,G2)	128(6)	29(5)	490(3)	2.5	H(C6B,G5)	528(6)	118(5)	780(3)	2.6
H(C2,G2)	207(6)	-45(5)	406(3)	2.5	H(O2,G5)	900(6)	-218(5)	779(3)	2.9
H(C3,G2)	367(6)	-102(5)	486(3)	2.4	H(O3,G5)	670(6)	-213(6)	849(3)	3.2
H(C4,G2)	371(6)	17(5)	386(3)	1.8	H(O6,G5)	574(6)	127(6)	865(3)	3.2
H(C5,G2)	389(6)	67(5)	507(3)	2.6	H(C1,G6)	481(6)	-50(5)	875(3)	2.3
H(C6A,G2)	485(6)	168(5)	458(3)	3.2	H(C2,G6)	315(6)	-133(5)	868(3)	2.7
H(C6B,G2)	379(7)	214(5)	471(3)	3.2	H(C3,G6)	384(6)	-158(5)	750(3)	2.5
H(O2,G2)	192(6)	-160(6)	501(3)	3.1	H(C4,G6)	199(6)	-52(5)	792(3)	2.2
H(O3,G2)	308(6)	-134(5)	415(3)	2.9	H(C5,G6)	399(6)	24(5)	743(3)	2.2
H(C1,G3)	527(6)	29(5)	356(3)	2.1	H(C6A,G6)	329(6)	161(5)	796(3)	3.1
H(C2,G3)	679(6)	-58(5)	351(3)	2.3	H(C6B,G6)	273(6)	124(6)	730(3)	3.1
H(C3,G3)	624(6)	-116(5)	466(3)	2.2	H(O2,G6)	491(7)	-215(6)	825(3)	3.8
H(C4,G3)	809(6)	-10(5)	433(3)	2.1	H(O3,G6)	224(7)	-214(6)	751(3)	3.1
H(C5,G3)	624(6)	59(5)	492(3)	1.9	H(O6,G6)	170(7)	112(6)	837(3)	3.8
H(C6A,G3)	765(6)	144(5)	503(3)	2.8	H(C2,NP)	495(7)	-215(6)	699(3)	3.7
H(C6B,G3)	695(6)	199(5)	462(3)	2.8	H(C3,NP)	480(7)	-64(6)	701(4)	3.8
H(O2,G3)	502(6)	-152(5)	379(3)	2.4	H(C5,NP)	534(7)	-49(6)	520(3)	3.4
H(O3,G3)	775(6)	-169(5)	386(3)	2.4	H(C6,NP)	561(7)	-207(6)	523(3)	3.5
H(O6,G3)	824(7)	170(6)	407(4)	4.0	H(O1,NP)	535(7)	-330(6)	567(4)	3.9
H(C1,G4)	910(6)	-18(5)	502(3)	2.4	H(OA,W1)	465(7)	-87(6)	266(4)	5.0
H(C2,G4)	971(6)	-109(5)	572(3)	2.6	H(OB,W1)	522(7)	-123(6)	281(4)	5.0
H(C3,G4)	739(6)	-138(5)	605(3)	2.2	H(OA,W2A)	480(8)	-152(7)	994(4)	6.1
H(C4,G4)	910(6)	-33(5)	667(3)	1.9					

α-Cyclodextrin-*p*-Hydroxybenzoic Acid Complex

	x	y	z	B		x	y	z	B
H(C1,G1)	95(6)	-46(5)	731(3)	3.0	H(C5,G4)	707(6)	22(5)	599(3)	2.6
H(C2,G1)	43(6)	-117(5)	645(3)	2.8	H(O2,G4)	865(7)	-177(6)	501(3)	3.6
H(C3,G1)	276(6)	-126(5)	613(3)	2.7	H(O3,G4)	868(6)	-198(5)	679(3)	3.1
H(C4,G1)	92(6)	-10(5)	565(3)	2.5	H(C1,G5)	895(6)	-24(5)	739(3)	2.6
H(C5,G1)	278(6)	49(6)	635(3)	3.8	H(C2,G5)	815(6)	-115(5)	817(3)	2.9
H(C6A,G1)	238(7)	160(6)	582(3)	4.2	H(C3,G5)	648(6)	-153(5)	743(3)	2.9
H(C6B,G1)	172(7)	181(6)	634(3)	4.2	H(C4,G5)	641(6)	-44(5)	843(3)	2.3
H(O2,G1)	122(6)	-246(6)	659(3)	3.2	H(C5,G5)	623(6)	19(5)	723(3)	2.8
H(O3,G1)	196(6)	-228(6)	568(3)	3.3	H(C6A,G5)	646(6)	163(5)	770(3)	3.3
H(O6,G1)	31(7)	162(6)	619(4)	5.3	H(C6B,G5)	534(6)	114(5)	778(3)	3.3
H(C1,G2)	121(6)	37(5)	488(3)	3.5	H(O2,G5)	906(6)	-205(5)	779(3)	3.5
H(C2,G2)	189(6)	-43(5)	407(3)	3.2	H(O3,G5)	646(7)	-219(6)	868(3)	3.9
H(C3,G2)	360(6)	-99(5)	481(3)	2.4	H(O6,C5)	575(6)	131(5)	861(3)	3.3
H(C4,G2)	369(5)	21(5)	385(3)	2.0	H(C1,G6)	494(6)	-54(5)	867(3)	2.8
H(C5,G2)	399(6)	68(5)	507(3)	3.3	H(C2,G6)	326(6)	-141(6)	861(3)	3.7
H(C6A,G2)	492(7)	174(6)	457(4)	5.3	H(C3,G6)	393(6)	-157(5)	745(3)	2.8
H(C6B,G2)	363(7)	227(6)	469(4)	5.3	H(C4,G6)	207(6)	-48(5)	791(3)	2.7
H(O2,G2)	166(6)	-138(6)	500(3)	3.5	H(C5,G6)	407(6)	23(5)	743(3)	2.5
H(O3,G2)	341(6)	-192(5)	417(3)	3.1	H(C6A,G6)	329(7)	161(6)	793(3)	4.0
H(C1,G3)	514(6)	28(4)	356(3)	2.6	H(C6B,G6)	272(7)	125(6)	729(3)	4.0
H(C2,G3)	674(6)	-63(5)	346(3)	2.6	H(O2,G6)	489(7)	-267(6)	818(4)	5.4
H(C3,G3)	621(6)	-116(5)	461(3)	2.6	H(O3,G6)	224(7)	-202(6)	751(3)	3.9
H(C4,G3)	807(6)	-13(5)	432(3)	2.4	H(O6,G6)	177(7)	113(6)	831(3)	4.6
H(C5,G3)	616(6)	59(5)	492(3)	2.9	H(C2,HB)	503(6)	-209(5)	695(3)	3.3
H(C6A,G3)	768(6)	146(6)	498(3)	3.6	H(C3,HB)	492(6)	-52(5)	698(3)	3.7
H(C6B,G3)	696(6)	205(6)	462(3)	3.6	H(C5,HB)	527(6)	-39(5)	525(3)	3.5
H(O2,G3)	500(6)	-152(5)	381(3)	2.4	H(C6,HB)	538(6)	-204(6)	523(3)	3.6
H(O3,G3)	792(6)	-154(5)	384(3)	2.5	H(O1,HB)	576(6)	-327(6)	577(3)	3.5
H(O6,G3)	890(7)	170(6)	414(4)	4.7	H(O2,HB)	432(8)	111(6)	671(4)	5.8
H(C1,G4)	916(6)	-19(5)	496(3)	2.8	H(OA,W1)	473(7)	-91(6)	266(4)	5.6
H(C2,G4)	971(6)	-115(5)	567(3)	2.8	H(OB,W1)	540(7)	-126(6)	273(4)	5.6
H(C3,G4)	736(6)	-140(5)	600(3)	2.8	H(OA,W2A)	493(7)	-142(6)	996(4)	5.0
H(C4,G4)	920(6)	-29(5)	663(3)	2.4					

calculated. The guest molecule and water molecules were found on the map. The hydrogen atoms were found on a difference-Fourier map. In both complexes, O(6,G4), O(W2), and O(W3) were revealed to be statistically disordered. The occupancy was estimated on the electron-density map, but they were not refined. The refinement of the crystal structures was carried out by the block-diagonal least-squares method. The quantity minimized was $\sum w(|F_o|-|F_c|)^2$, with $w=1.0$ for the all reflections used. The thermal factors of the hydrogen atoms were not refined, but they were fixed as equal to the isotropic ones of the carbon or oxygen atoms to which the hydrogen atoms are bonded. The final R-values were 0.066 for the *p*-NP complex and 0.067 for the *p*-HB complex. The atomic scattering factors were taken from "International Tables for X-ray Crystallography."[17] The atomic parameters are listed in Tables 2 and 3. The observed and calculated structure factors are given in Table 4.*

Description of the Structure and Discussion

The structure and numbering schemes of the complexes are shown in Figs. 1 and 2. The atom numbering for α-CDx is the same as that used in the *p*-IA complex[14] and the *p*-IP complex.[16] The bond distances, angles, and conformation angles are shown in Figs. 3—6 and Tables 5* and 6. The geometrical data for the complex are shown in Tables 7 and 8. The crystal structure and hydrogen-bonding schemes are given in Figs. 7—9 and Table 9.

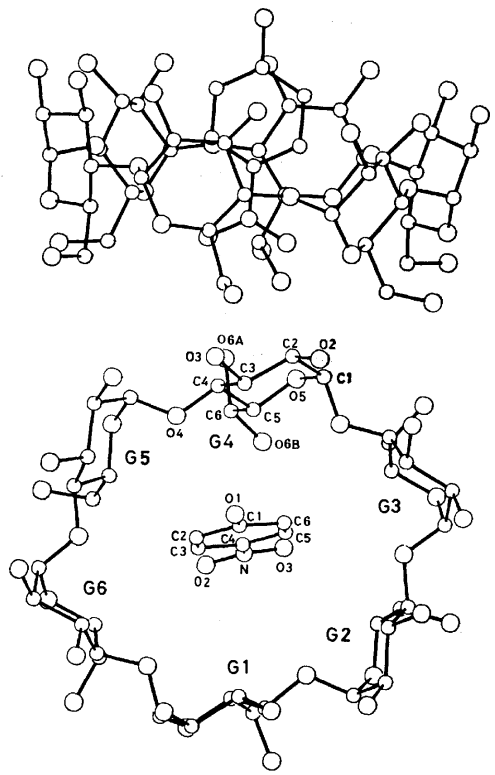

Fig. 1. The structure and numbering scheme of the α-cyclodextrin–*p*-nitrophenol complex.

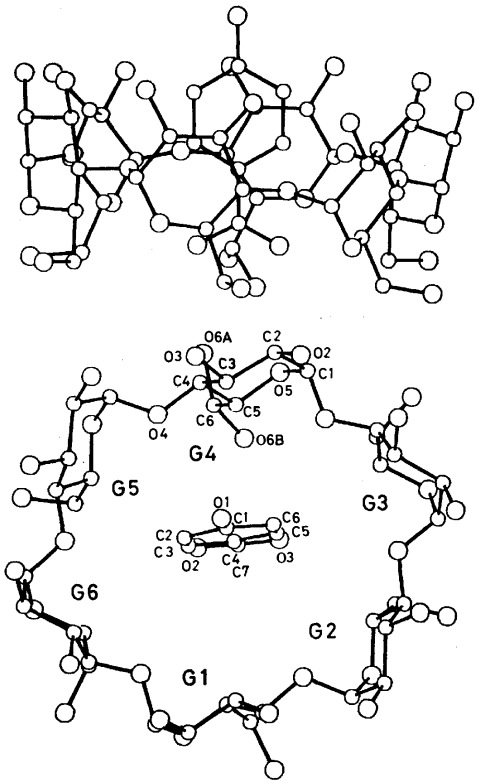

Fig. 2. The structure and numbering scheme of the α-cyclodextrin–*p*-hydroxybenzoic acid complex.

Structure of α-CDx. In both the α-CDx–*p*-NP complex and the α-CDx–*p*-HB complex, the conformation of α-CDx is nearly identical with the conformation found in the complexes with *p*-IA and *p*-IP. The distances of the C(1)–C(2) and C(4)–C(5) bonds are slightly longer than the C(2)–C(3) and C(3)–C(4) distances, while the contrary tendancy is observed in α-D-glucose monohydrate.[18] The C(4)–O(4) bond of the glycosidic linkage is longer than the C(1)–O(4) bond. In the pyranose ring, the C(5)–O(5) bond is longer than the C(1)–O(5) bond; a similar effect is observed in α-D-glucose monohydrate. The C(1)–O(5)–C(5) angles are in good agreement with the values found in the α-D-glucose derivatives[18,19] and in the maltose derivatives.[20-22] The α-1,4-linking oxygen angles of C(4)–O(4)–C(1′) are a little larger than those found in the maltose derivatives, but such large values are commonly observed in other α-CDx complexes.

A small conformational difference is observed among the glucose residues. One of the indices which represent the conformational change of glucose residues is the O(4)···O(4′) distance.[23] The O(4)···O(4′) distance in the *p*-NP complex and the *p*-HB complex (Table 7) are quite small compared with that found in α-D-glucose monohydrate. This may be due to the cyclic structure of α-CDx. The distance of the C(4) atom from the plane through C(2), C(3), C(5), and O(5) also indicates the conformational change in the pyranose ring (Table 8). The C(4) atom approaches to the plane slightly when the O(4)···O(4′) distance is shortened.

* Tables 4 and 5 are kept in the office of The Chemical Society of Japan (Document No. 7707).

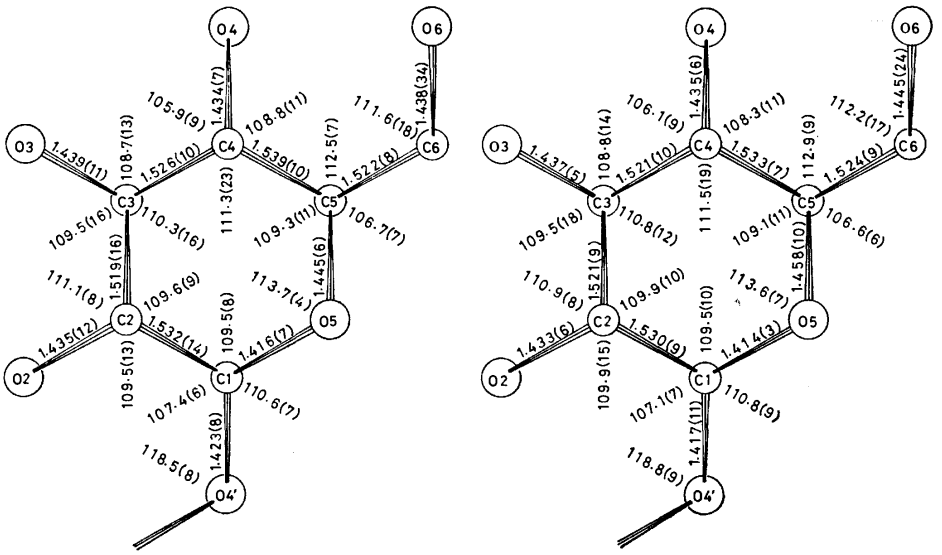

Fig. 3. Average bond distances and angles for the glucose residue in the α-cyclodextrin–*p*-nitrophenol complex (left) and the α-cyclodextrin–*p*-hydroxybenzoic acid complex (right). Standard deviations given in parentheses were estimated according to $\sigma=[\sum_{i=1}^{6}(x_i-\bar{x})^2/5]^{1/2}$, where x_i is the bond distance or angle in the i-th glucose residue and $\bar{x}$ is the average value.

Table 6. Conformation angles (ϕ/°) in α-cyclodextrin

A prime (′) indicates the atom in the adjacent glucose residue.

	G1	G2	G3	G4	G5	G6	AVERAGE
α-Cyclodextrin–*p*-Nitrophenol Complex							
C(1)–C(2)–C(3)–C(4)	−56.0	−57.2	−52.5	−51.1	−52.6	−54.2	−53.9
C(2)–C(3)–C(4)–C(5)	56.0	55.2	45.1	56.0	50.5	48.9	52.0
C(3)–C(4)–C(5)–O(5)	−57.0	−54.0	−44.8	−60.6	−53.0	−48.4	−53.0
C(4)–C(5)–O(5)–C(1)	62.3	56.8	57.3	65.4	60.9	57.0	60.0
C(5)–O(5)–C(1)–C(2)	−62.5	−60.9	−66.4	−60.3	−63.5	−65.5	−63.2
O(5)–C(1)–C(2)–C(3)	57.9	60.1	61.8	51.2	58.0	63.1	58.7
O(4′)–C(1)–C(2)–O(2)	56.9	64.7	64.6	52.7	59.7	66.5	60.9
O(2)–C(2)–C(3)–O(3)	69.4	62.1	65.0	67.1	66.2	61.9	65.3
O(3)–C(3)–C(4)–O(4)	−67.9	−67.9	−71.6	−67.9	−70.4	−73.5	−69.9
O(4)–C(4)–C(5)–C(6)	68.0	71.5	79.8	68.1	71.1	75.9	72.4
O(5)–C(5)–C(6)–O(6)	−67.4	−70.0	−69.2	−50.9* 74.2**	−73.8	−81.6	−68.8
C(4)–C(5)–C(6)–O(6)	51.7	50.6	51.9	65.5* −169.4**	47.3	39.0	51.0
C(2)–C(1)–O(4′)–C(4′)	−131.9	−118.0	−129.1	−137.5	−129.3	−135.1	−130.2
O(5)–C(1)–O(4′)–C(4′)	108.3	122.0	113.2	101.4	112.2	106.0	110.5
C(1)–O(4′)–C(4′)–C(3′)	122.4	127.2	129.9	136.6	128.0	126.9	128.5
C(1)–O(4′)–C(4′)–C(5′)	−115.7	−114.9	−110.4	−101.8	−115.3	−112.6	−111.8
α-Cyclodextrin–*p*-Hydroxybenzoic Acid Complex							
	G1	G2	G3	G4	G5	G6	AVERAGE
C(1)–C(2)–C(3)–C(4)	−55.6	−57.0	−52.0	−51.4	−51.3	−50.3	−52.9
C(2)–C(3)–C(4)–C(5)	55.2	54.3	46.0	56.5	48.7	47.9	51.4
C(3)–C(4)–C(5)–O(5)	−56.7	−52.8	−46.9	−60.9	−51.2	−49.6	−53.0
C(4)–C(5)–O(5)–C(1)	62.7	57.0	59.1	64.4	60.4	58.7	60.4
C(5)–O(5)–C(1)–C(2)	−63.0	−61.4	−66.7	−59.0	−63.9	−64.6	−63.1
O(5)–C(1)–C(2)–C(3)	57.7	60.3	61.0	51.5	57.9	59.4	58.0
O(4′)–C(1)–C(2)–O(2)	58.8	66.1	63.7	53.0	59.5	59.6	60.1
O(2)–C(2)–C(3)–O(3)	67.4	62.1	63.4	65.2	65.4	68.4	65.3
O(3)–C(3)–C(4)–O(4)	−67.9	−67.3	−72.4	−68.4	−72.4	−73.9	−70.4
O(4)–C(4)–C(5)–C(6)	69.9	71.6	79.8	66.9	71.9	73.8	72.3
O(5)–C(5)–C(6)–O(6)	−70.5	−71.5	−67.1	−54.9* 77.2**	−75.2	−81.3	−72.4
C(4)–C(5)–C(6)–O(6)	46.7	49.0	53.4	62.9* −165.0**	46.2	39.7	49.7
C(2)–C(1)–O(4′)–C(4′)	−130.3	−117.5	−131.3	−135.2	−128.8	−132.4	−129.2
O(5)–C(1)–O(4′)–C(4′)	111.4	123.5	111.2	103.3	113.7	117.1	113.4
C(1)–O(4′)–C(4′)–C(3′)	122.1	127.8	130.6	133.7	128.8	123.7	127.8
C(1)–O(4′)–C(4′)–C(5′)	−116.4	−113.6	−108.9	−105.6	−114.2	−116.1	−112.5

* The angles of O(5,G4)–C(5,G4)–C(6,G4)–O(6A,G4) and C(4,G4)–C(5,G4)–C(6,G4)–O(6A,G4).
** The angles of O(5,G4)–C(5,G4)–C(6,G4)–O(6B,G4) and C(4,G4)–C(5,G4)–C(6,G4)–O(6B,G4).

Table 7. Geometrical data for α-cyclodextrin

I. Distances (l/Å) between glycosidic oxygen atoms in the *p*-NP complex (A) and in the *p*-HB complex (B).

	A	B
O(4, G1)–O(4, G6)	4.361	4.351
O(4, G1)–O(4, G2)	4.241	4.219
O(4, G2)–O(4, G3)	4.016	4.053
O(4, G3)–O(4, G4)	4.493	4.509
O(4, G4)–O(4, G5)	4.249	4.201
O(4, G5)–O(4, G6)	4.049	4.103
Average value	4.235	4.239
O(4, G1)–O(4, G4)	7.984	8.055
O(4, G2)–O(4, G5)	8.902	8.923
O(4, G3)–O(4, G6)	8.457	8.418
Average value	8.457	8.465

II. Torsion-angle index[a] (ϕ/°) in the *p*-NP complex (A) and in the *p*-HB complex (B).

Residue	Index A	Index B	Residue	Index A	Index B
G1	125.7	127.1	G4	111.4	108.9
G2	125.8	128.6	G5	131.5	133.6
G3	148.1	145.9	G6	142.5	135.5
			Average value	130.8	129.9

a) The torsion-angle index is defined as follows: $|\phi(C(1)-C(2))|+|\phi(C(2)-C(3))|+|\phi(C(5)-O(5))|+|\phi(O(5)-C(1))|-|\phi(C(3)-C(4))|-|\phi(C(4)-C(5))|$, if the conformation angle of C(1)–C(2)–C(3)–C(4) is expressed as $\phi(C(2)-C(3))$.

The conformation angles in the G4 residue, which gives the largest O(4)···O(4′) distance are in agreement with those of α-D-glucose monohydrate within 3.0° in the *p*-NP complex and within 4.0° in the *p*-HB complex. A small difference in the pyranose-ring conformation is observed between the G3 residue and the G4 residue. The C(3)–C(4)–C(5)–O(5) conformation angle of the G3 residue is greater by 15.8° in the *p*-NP complex and by 14.0° in the *p*-HB complex than the values found in the G4 residue. The change in the pyranose-ring conformation is also clearly shown by means of the torsion-angle index defined by French and Murphy.[23] The torsion-angle indices in the *p*-NP complex and the *p*-HB complex, except for that in the G4 residue, are

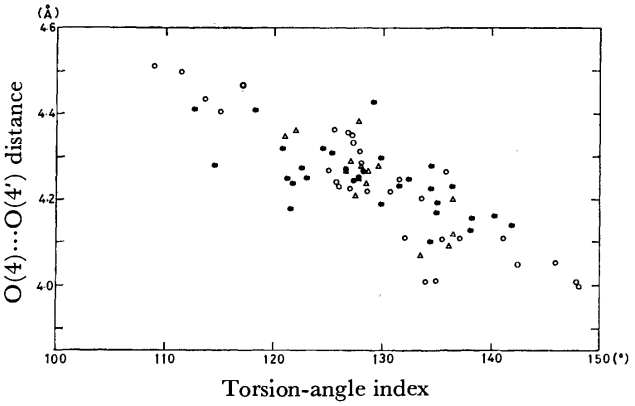

Fig. 4. Plot of the O(4)···O(4′) distance against the torsion-angle index in the α-cyclodextrin complexes with *para*-disubstituted benzenes (○), the complexes with the cage-type structure (●), and the complexes with the channel-type structure (△).

greater than that found in α-D-glucose monohydrate. The glucose residue, which has a small O(4)—O(4′) distance, gives a large torsion-angle index, and *vice versa*. The value found in the G3 residue is considerably larger than the values of 112.6—134.6° found in the α-CDx–water complex. This suggests that the pyranose ring changes its conformation when α-CDx includes the planar molecule.

The O(4)···O(4′) distance is plotted against the torsion-angle index for the three types of crystal structures in Fig. 4. In the complexes with *para*-disubstituted benzenes, a correlation similar to that found in mono-, di-, and trisaccharides[23] is found between the two variables, while in the complexes with the cage-type structure[4-8] or the channel-type structure[9-12] the correlation is not clear. In the channel-type structure, the O(4)···O(4′) distance and the torsion-angle index are found in a relatively small region, although the dimension and shape of the guest molecule are quite flexible. This indicates that the geometrical freedom of the pyranose ring is restricted not only by the guest molecule, but also by the crystal structure.

The α-CDx ring shows a distorted hexagon. The diagonal distances measured between the glycosidic oxygen atoms vary from 7.984 to 8.902 Å in the *p*-NP complex and from 8.055 to 8.923 Å in the *p*-HB complex (Table 7). On the other hand, the PSNa complex[12] gives 8.40—8.59 Å, showing a nearly regular hexagon. A distorted hexagon was also observed in the other α-CDx complexes with phenyl derivatives. The planarity of the six O(4) atoms is quite good (Table 8).

TABLE 8. LEAST-SQUARES PLANES AND DEVIATIONS OF ATOMS FROM THE PLANE (l/Å)
An asterisk (*) indicates an atom not included in the plane.

I. α-Cyclodextrin–*p*-nitrophenol complex.

(i) The plane through C(2), C(3), C(5), and O(5). The plane equation is of the $AX+BY+CZ=D$ form.

Residue	A	B	C	D
G1	0.8120	−0.1425	0.5660	10.7960
G2	0.0029	−0.2186	0.9758	11.0176
G3	0.8801	0.1257	−0.4578	2.9684
G4	0.8015	0.1501	0.5789	17.4115
G5	0.0166	0.1393	0.9901	19.0157
G6	0.8920	−0.0991	−0.4411	−4.4224

Deviations of atoms from the plane.

Residue	C(1)*	C(2)	C(3)	C(4)*	C(5)	O(5)
G1	−0.682	−0.009	0.009	0.699	−0.009	0.010
G2	−0.676	−0.012	0.011	0.660	−0.012	0.013
G3	−0.768	−0.004	0.004	0.559	−0.004	0.004
G4	−0.638	−0.039	0.039	0.723	−0.040	0.041
G5	−0.698	−0.015	0.014	0.630	−0.015	0.016
G6	−0.716	−0.004	0.003	0.592	−0.004	0.004

(ii) The plane through six O(4) atoms.

$0.0432X+0.9942Y+0.0988Z=1.1267$

O(4, G1)	0.121	O(4, G4)	0.133
O(4, G2)	0.040	O(4, G5)	0.022
O(4, G3)	−0.163	O(4, G6)	−0.152

(iii) The benzene plane.

$0.9711X+0.1004Y+0.2163Z=9.8172$

C(1, NP)	−0.001	C(6, NP)	−0.004
C(2, NP)	0.008	N(NP)*	0.050
C(3, NP)	−0.010	O(1, NP)*	0.053
C(4, NP)	0.004	O(2, NP)*	0.040
C(5, NP)	0.004	O(3, NP)*	0.133

II. α-Cyclodextrin–*p*-hydroxybenzoic acid complex,

(i) The plane through C(2), C(3), C(5), and O(5), The plane equation is of the $AX+BY+CZ=D$ form.

Residue	A	B	C	D
G1	0.8205	−0.1266	0.5574	10.6892
G2	0.0136	−0.2242	0.9744	11.0791
G3	0.8777	0.1223	−0.4633	2.7799
G4	0.8255	0.1224	0.5510	17.2970
G5	0.0327	0.1384	0.9898	19.2449
G6	0.8854	−0.0630	−0.4606	−4.8608

Deviations of atoms from the plane.

Residue	C(1)*	C(2)	C(3)	C(4)*	C(5)	O(5)
G1	−0.685	−0.013	0.012	0.693	−0.013	0.014
G2	−0.686	−0.009	0.008	0.644	−0.009	0.009
G3	−0.721	−0.011	0.010	0.571	−0.011	0.011
G4	−0.629	−0.033	0.032	0.720	−0.033	0.034
G5	−0.698	−0.020	0.019	0.610	−0.020	0.021
G6	−0.685	−0.017	0.016	0.587	−0.017	0.017

(ii) The plane through six O(4) atoms.

$0.0422X+0.9950Y+0.0908Z=1.0190$

O(4, G1)	0.145	O(4, G4)	0.145
O(4, G2)	0.011	O(4, G5)	0.004
O(4, G3)	−0.154	O(4, G6)	−0.152

(iii) The benzene plane.

$0.9892X+0.0585Y+0.1345Z=8.7861$

C(1, HB)	0.003	C(6, HB)	0.007
C(2, HB)	0.003	C(7, HB)*	0.151
C(3, HB)	−0.018	O(1, HB)*	0.067
C(4, HB)	0.027	O(2, HB)*	0.326
C(5, HB)	−0.021	O(3, HB)*	0.225

The intramolecular O(2)···O(3) hydrogen bonds are observed between the adjacent glucose residues (Table 9). Not all of these hydrogen bonds are oriented in the same direction, but both O(2)→O(3) and O(3)→O(2) hydrogen bonds are found. In the G4 and G6 residues, both of the secondary hydroxyl groups act as donors, but in the G1 residue, they are acceptors. The O(2) hydroxyl group in the G2 and G3 residues donates the hydrogen atom. O(2,G4)···O(3,G3) in the *p*-NP complex and O(2,G6)···O(3,G5) in the *p*-HB complex are rather doubtful hydrogen bonds since the O–H···O angles are too small.

Structures of p-*NP and* p-*HB.* The bond distances and angles in *p*-NP (Fig. 5) are in good agreement with those found in the crystal structure of *p*-NP.[24,25] The inequality in the C(2)–C(1)–O(1) and C(6)–C(1)–O(1) angles which is found in *p*-NP is not found in *p*-HB (Fig. 6). The bond distances of C(7)–O(2) and C(7)–O(3) in *p*-HB agree with those found in *p*-chlorobenzoic acid.[26] In both *p*-NP and *p*-HB, the benzene ring shows a good planarity (Table 8).

α-CDx-Guest Interaction. The nitrophenyl or carboxyphenyl group is located in the α-CDx cavity, while the phenolic hydroxyl group protrudes from the O(2),

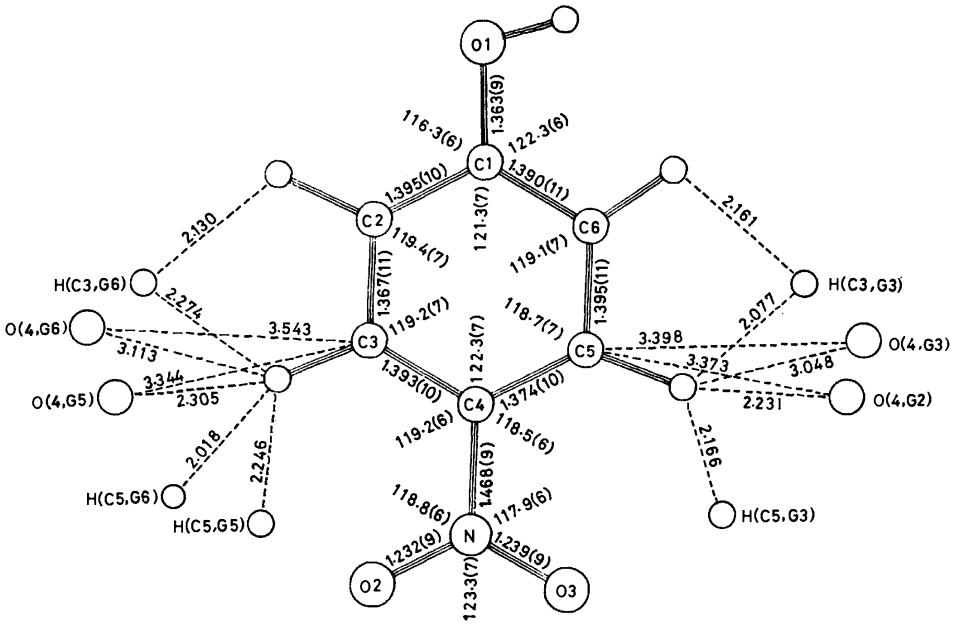

Fig. 5. Bond distances (*l*/Å) and angles (*φ*/°) in *p*-nitrophenol. Intermolecular distances between *p*-nitrophenol and α-cyclodextrin are shown by dashed lines.

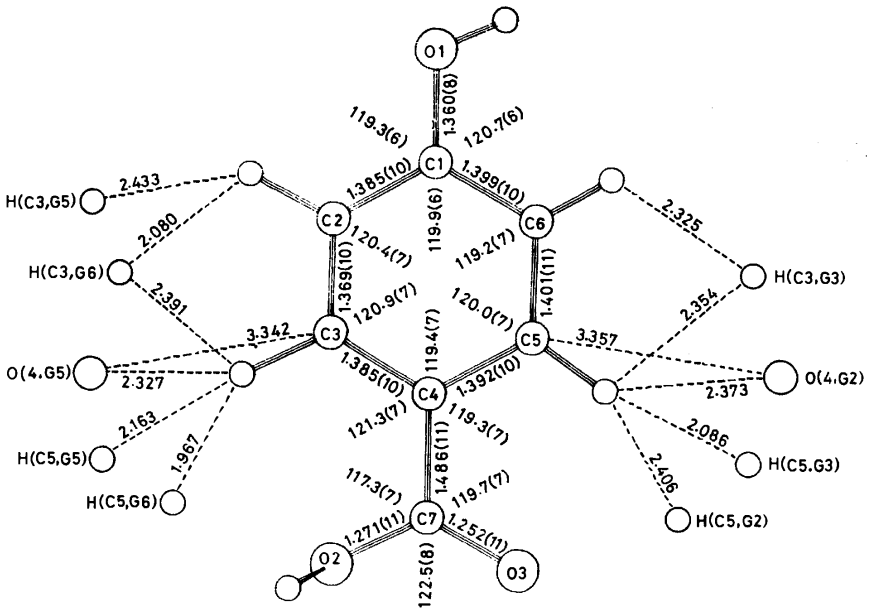

Fig. 6. Bond distances (*l*/Å) and angles (*φ*/°) in *p*-hydroxybenzoic acid. Intermolecular distances between *p*-hydroxybenzoic acid and α-cyclodextrin are shown by dashed lines.

TABLE 9. HYDROGEN BOND DISTANCES (l/Å) AND ANGLES (ϕ/°)

α-Cyclodextrin-*p*-Nitrophenol Complex

O	H	O		DISTANCE O-H	H···O	O···O	ANGLE O-H···O
O(3,G6)	H(O3,G6)	O(2,G1)		0.852	2.015	2.860	171.2
O(2,G2)	H(O2,G2)	O(3,G1)		1.054	1.693	2.650	148.6
O(2,G3)	H(O2,G3)	O(3,G2)		0.921	1.943	2.847	166.6
O(2,G4)	H(O2,G4)	O(3,G3)		1.104	2.189	2.736	107.8
O(3,G4)	H(O3,G4)	O(2,G5)		0.942	1.960	2.863	159.9
O(2,G6)	H(O2,G6)	O(3,G5)		1.052	2.116	3.068	149.3
O(W1)	H(OB,W1)	O(2,G3)		0.791	2.111	2.901	176.6
O(2,G5)	H(O2,G5)	O(W3B)		1.174	1.620	2.771	165.1
O(2,G6)		O(W2B)				2.453	
O(2,G5)	H(O2,G5)	O(W3A)	(a)	1.174	1.783	2.751	136.0
O(6,G1)		O(6A,G4)	(b)			2.950	
O(W2A)	H(OA,W2A)	O(6,G1)	(c)	0.628	2.326	2.938	165.4
O(6,G6)	H(O6,G6)	O(3,G2)	(c)	0.931	1.826	2.753	173.5
O(6A,G4)		O(W1)	(d)			2.774	
O(3,G5)	H(O3,G5)	O(6,G3)	(d)	0.787	2.201	2.871	143.3
O(W1)	H(OA,W1)	O(6,G6)	(e)	0.771	2.236	2.897	144.3
O(6,G2)		O(W3A)	(e)			2.800	
O(6,G2)		O(W3B)	(f)			2.798	
O(3,G3)	H(O3,G3)	O(6,G5)	(f)	0.972	1.889	2.697	138.7
O(6,G3)		O(W2A)	(f)			2.764	
O(1,NP)	H(O1,NP)	O(2,G2)	(g)	1.045	2.057	2.580	108.1
O(6,G2)		O(6A,G4)	(h)			2.861	
O(6,G2)		O(6B,G4)	(h)			2.773	
O(2,G1)	H(O2,G1)	O(2,G3)	(i)	1.004	2.036	2.814	132.6
O(3,G1)	H(O3,G1)	O(3,G3)	(i)	0.667	2.114	2.709	149.3
O(3,G2)		O(3,G4)	(i)			2.737	
O(W1)		O(W3B)	(i)			2.730	
O(6,G1)		O(W3B)	(j)			2.894	
O(6B,G4)		O(2,G6)	(j)			2.896	
O(6,G5)	H(O6,G5)	O(1,NP)	(j)	0.798	1.969	2.730	159.3
O(3,NP)		O(W2B)	(j)			2.914	

α-Cyclodextrin-*p*-Hydroxybenzoic Acid Complex

O	H	O		DISTANCE O-H	H···O	O···O	ANGLE O-H···O
O(3,G6)	H(O3,G6)	O(2,G1)		0.792	2.046	2.824	167.3
O(2,G2)	H(O2,G2)	O(3,G1)		0.986	1.715	2.674	163.2
O(2,G3)	H(O2,G3)	O(3,G2)		0.936	1.991	2.897	162.4
O(2,G4)	H(O2,G4)	O(3,G3)		0.716	2.491	3.114	146.6
O(3,G4)	H(O3,G4)	O(2,G5)		0.944	1.908	2.845	171.5
O(2,G6)	H(O2,G6)	O(3,G5)		1.018	2.474	2.878	102.9
O(W1)	H(OB,W1)	O(2,G3)		0.740	2.279	2.926	146.7
O(2,G5)	H(O2,G5)	O(W3B)		1.126	1.643	2.709	155.7
O(2,G6)		O(W2B)				2.795	
O(2,G5)	H(O2,G5)	O(W3A)	(a)	1.126	1.746	2.757	146.7
O(6,G1)	H(O6,G1)	O(6A,G4)	(b)	1.218	1.778	2.824	140.3
O(W2A)	H(OA,W2A)	O(6,G1)	(c)	0.784	2.196	2.851	141.4
O(6,G6)	H(O6,G6)	O(3,G2)	(c)	0.839	1.879	2.718	180.0
O(3,G5)	H(O3,G5)	O(6,G3)	(d)	1.246	1.863	2.808	128.1
O(6A,G4)		O(W1)	(d)			2.756	
O(W1)	H(OA,W1)	O(6,G6)	(e)	0.686	2.338	2.886	138.2
O(6,G2)		O(W3A)	(e)			2.682	
O(6,G2)		O(W3B)	(f)			2.829	
O(3,G3)	H(O3,G3)	O(6,G5)	(f)	1.174	1.563	2.706	162.6
O(6,G3)	H(O6,G3)	O(W2A)	(f)	1.037	2.087	2.739	118.6
O(2,G1)	H(O2,G1)	O(2,G3)	(g)	0.928	1.916	2.809	160.8
O(3,G1)	H(O3,G1)	O(3,G3)	(g)	0.995	1.699	2.685	170.3
O(6,G2)		O(6A,G4)	(h)			2.891	
O(6,G2)		O(6B,G4)	(h)			2.730	
O(W1)		O(W3B)	(i)			2.629	
O(1,HB)	H(O1,HB)	O(2,G2)	(i)	0.978	1.634	2.588	163.9
O(3,G2)	H(O3,G2)	O(3,G4)	(i)	0.876	2.281	2.715	110.5
O(3,HB)		O(W2B)	(j)			2.667	
O(6,G1)	H(O6,G1)	O(W3B)	(j)	1.218	1.939	3.023	145.6
O(6,G5)	H(O6,G5)	O(1,HB)	(j)	0.816	1.941	2.736	164.5
O(2,G6)	H(O2,G6)	O(2,HB)	(k)	1.018	2.183	2.880	124.1

Code	Symmetry Operator	Code	Symmetry Operator
None	x, y, z	f	$3/2-x$, $-y$, $1/2+z$
a	$1+x$, y, z	g	$1/2+x$, $-1/2-y$, $1-z$
b	$-1+x$, y, z	h	$-1/2+x$, $1/2-y$, $1-z$
c	$1/2-x$, $-y$, $1/2+z$	i	$-1/2+x$, $-1/2-y$, $1-z$
d	$3/2-x$, $-y$, $1/2+z$	j	$1-x$, $1/2+y$, $3/2-z$
e	$1/2-x$, $-y$, $-1/2+z$	k	$1-x$, $-1/2+y$, $3/2-z$

O(3) side. The relative orientation of the guest molecule in the cavity is similar to that found in the *p*-IA complex and the *p*-IP complex. In the channel-type structure and the cage-type structure, the hydroxyl group or sulfonato group of the guest molecule is hydrogen-bonded to the primary hydroxyl group with the *gauche-trans* conformation. However, in the complexes with *p*-NP and *p*-HB, the nitro or carboxyl group does not form the hydrogen bond with O(6B,G4), although the C(6,G4)–O(6B,G4) bond shows the *gauche-trans* conformation. It is noteworthy that the location of the benzene ring is the same as in the other α-CDx complexes with the aromatic guest molecule, such as *p*-IA,[14,15] *p*-IP,[16] Methyl Orange,[10] and BSNa.[11] This may be due to the fact that this position is sterically most favorable for the benzene ring. The plane of the guest molecule is nearly parallel to the longest diagonal line which passes through O(4,G2) and O(4,G5). The benzene ring makes angles of 80.6 and 83.6° against the plane through the six O(4) atoms in the *p*-NP complex and the *p*-HB complex respectively, while in the BSNa complex the benzene plane is perpendicular to the O(4) plane. The distances of O(4,G2)···C(5,NP), O(4,G5)···C(3,NP), O(4,G2)···C(5,HB), and O(4,G5)···C(3,HB) are in good agreement with the corresponding distances found in the *p*-IA complex, the *p*-IP complex, and the BSNa complex. Several hydrogen-hydrogen contacts shorter than the ideal van der Waals contact[27] are found between α-CDx and the benzene ring, as is shown in Figs. 5 and 6. This indicates that the guest molecule is tightly packed in the α-CDx ring. The hydrogen atoms attached to C(3) and C(5) of α-CDx are located inside the cavity, and are in contact with the guest molecule. The six hydrogen atoms bonded to C(5) form a neck of the cavity. The C(4)–C(7) bond of *p*-HB and C(4)–N bond of *p*-NP are located at the neck, showing a good fit of the guest molecule to the cavity. A similar geometrical fitness is observed in the complexes with *p*-IA, *p*-IP, Methyl Orange, and iodine.[4]

In the *p*-IA complex and the *p*-IP complex, the iodine atom is found at the position where the nitro or carboxyl group is located. In this case, the inclusion of the iodophenyl group has been interpreted as being mainly due to the hydrophobic interaction, since the interior of the cavity is relatively hydrophobic. It has also been shown by the theoretical calculation of the complex formation energy[11] that the inclusion of the hydrophobic group gives a more stable complex than the inclusion of the hydrophilic group when the guest molecule consists of hydrophobic and hydrophilic groups. In the complexes with *p*-NP and *p*-HB, the nitro or carboxyl groups are hydrophilic, and they form hydrogen bonds with water and the hydroxyl group of the adjacent α-CDx molecule (Table 9). It is geometrically possible that the *p*-NP and *p*-HB molecules are situated upside down in the cavity, that is, the nitro or carboxyl group protrudes from the secondary hydroxyl side of the cavity, and the phenolic hydroxyl group is situated at the primary hydroxyl side in the cavity. However, this structure may be unfavorable in view of the fit of the guest molecule to the α-CDx cavity. The guest molecule seems to be more loosely packed in the cavity. Moreover, the phenolic hydroxyl group can not be in contact with water or hydroxyl groups outside the cavity, since it is buried in the cavity. Thus, the geometry of inclusion may be determined by the fit of the guest molecule and the hydrogen bonds.

Crystal Structure and Hydrogen Bonds. The α-CDx molecules are arranged nearly parallel to the ac plane, forming a molecular layer (Fig. 7). The least-squares plane through the six O(4) atoms makes an angle of 6.2° in the *p*-NP complex and one of 5.7° in the *p*-HB complex against the ac plane. This type of the crystal structure is different from the cage-type structure,[4–8] since both ends of the cavity are open to the space between the layers. The α-CDx molecule, which lies in the next layer, is slipped so that the overlap of the annular aperture is quite small. Therefore, this arrange-

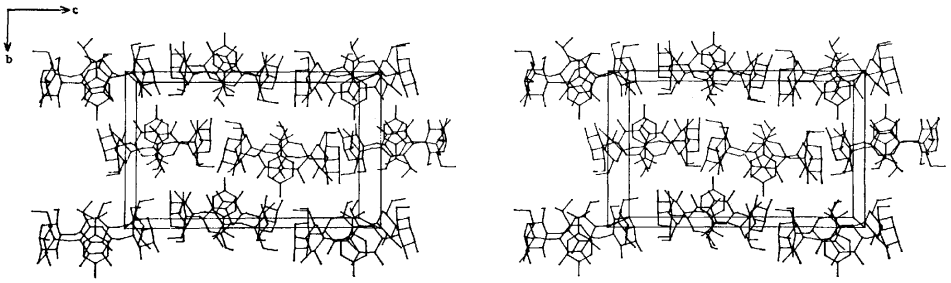

Fig. 7. A stereo drawing of the packing of the complex, viewed down along the a axis.

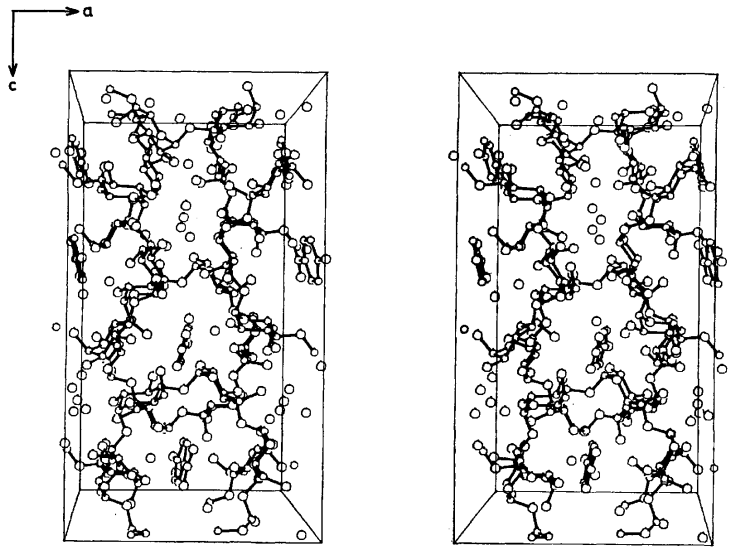

Fig. 8. A stereo drawing of the crystal structure of the α-cyclodextrin–*p*-nitrophenol complex, viewed down along the b axis.

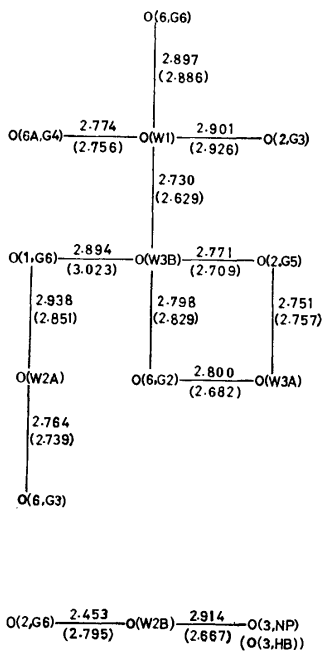

Fig. 9. A hydrogen-bonding scheme involving water molecules in the α-cyclodextrin complexes with *p*-nitrophenol and *p*-hydroxybenzoic acid. Hydrogen bond distances (*l*/Å) in the *p*-hydroxybenzoic acid complex are shown in parentheses.

ment of α-CDx molecules does not form a continuous channel such as is found in the channel-type structure.[9–12] The guest molecules are situated nearly parallel to the bc plane. The empty space between the α-CDx molecules is filled with three water molecules, two of which are statistically disordered.

A complete explanation of the hydrogen-bonding scheme is impossible since not all of the hydrogen atoms have been determined, but intermolecular oxygen-oxygen contacts less than 3.0 Å were considered as hydrogen bonds. All of the primary or secondary hydroxyl groups except for O(2,G4) and O(3,G6) are involved in the intermolecular hydrogen bonds in both the *p*-NP complex and the *p*-HB complex (Table 9). The phenolic hydroxyl groups of *p*-NP and *p*-HB donate the hydrogen atom to the O(2,G2) of α-CDx in the next layer, and accept it from O(6,G5) of the symmetry-related α-CDx by the two-fold screw axis parallel to the b axis. The hydrogen bonds of the same type are also found in the *p*-IA complex,[14,15] and the *p*-IP complex.[16] However, different hydrogen bonds are observed between the α-CDx and guest molecules. The carboxyl group of *p*-HB forms the two hydrogen bonds with O(W2B) and O(2,G6) in the next layer, while the nitro group is hydrogen-bonded to only O(W2B). In the *p*-IA complex and the *p*-IP complex, O(W2) is not disordered, but occupies the same position as O(W2A). Therefore, the hydrogen bonds involving

O(W2B) are not found in these complexes. O(W1) forms the four hydrogen bonds with O(2,G3), O(6A,G4), O(6,G6), and O(W3A), as is shown in Fig. 9. Both O(W3A) and O(W3B) are hydrogen-bonded to O(2,G5) and O(6,G2).

Structure and Catalytic Ability of α-CDx. α-CDx catalyzes the hydrolysis of *p*-nitrophenyl acetate and *p*-carboxyphenyl acetate.[3] The reaction mechanism has been interpreted on the basis of the α-CDx-substrate inclusion complex and the nucleophilic attack of the secondary hydroxyl group on the carbonyl carbon atom of the substrate. The structures of the *p*-NP complex and the *p*-HB complex support this reaction mechanism. If the *p*-nitrophenyl group or *p*-carboxyphenyl group is included in the same manner as in the crystal, the carbonyl group of the ester will be situated near the secondary hydroxyl side of α-CDx. However, the carbonyl carbon atom is expected for geometrical considerations to be more than 5 Å apart from the secondary hydroxyl groups. The phenyl group is rigidly fixed in the cavity so that the severe restriction is imposed on the translational and rotational freedom of the included substrate. Therefore, a considerable strain energy may be required to the α-CDx molecule to bring the carbonyl group in close contact with the secondary hydroxyl groups. As has been suggested by VanEtten *et al.*,[3] this seems to be the reason why the catalytic ability of α-CDx is low in the hydrolysis of *para*-substituted phenyl acetates.

The author wishes to thank Dr. Hisashi Uedaira for supporting this study and for his helpful discussions. The computation was carried out on a HITAC 8450 computer in our laboratory.

References

1) J. A. Thoma and L. Stewart, "Starch: Chemistry and Technology," Vol. I, ed by R. L. Whistler and E. F. Pashall, Academic Press, New York (1965), pp. 209—249.
2) D. W. Griffiths and M. L. Bender, *Adv. Catal.*, **23**, 209 (1973).
3) R. L. VanEtten, J. F. Sebastian, C. A. Clows, and M. L. Bender, *J. Am. Chem. Soc.*, **89**, 3242 (1967).
4) R. K. McMullan, W. Saenger, J. Fayos, and D. Mootz, *Carbohydr. Res.*, **31**, 211 (1973).
5) P. C. Manor and W. Saenger, *J. Am. Chem. Soc.*, **96**, 3630 (1974).
6) W. Saenger, R. K. McMullan, J. Fayos, and D. Mootz, *Acta Crystallogr., Sect. B*, **30**, 2019 (1974).
7) W. Saenger and M. Noltemeyer, *Chem. Ber.*, **109**, 503 (1976).
8) B. Hingerty and W. Saenger, *J. Am. Chem. Soc.*, **98**, 3357 (1976).
9) A. Hybl, R. E. Rundle, and D. E. Williams, *J. Am. Chem. Soc.*, **87**, 2779 (1965).
10) K. Harata, *Bull. Chem. Soc. Jpn.*, **49**, 1493 (1976).
11) K. Harata, *Bull. Chem. Soc. Jpn.*, **49**, 2066 (1976).
12) K. Harata, Part IV of this series, to be published.
13) M. Noltemeyer and W. Saenger, *Nature (London)*, **259**, 629 (1976).
14) K. Harata, *Bull. Chem. Soc. Jpn.*, **48**, 2409 (1975).
15) W. Saenger, K. Beyer, and P. C. Manor, *Acta Crystallogr., Sect. B*, **32**, 120 (1976).
16) K. Harata, *Carbohydr. Res.*, **48**, 265 (1976).
17) "International Tables for X-Ray Crystallography," Vol. IV, Birmingham: Kynoch Press (1974), pp. 72—75.
18) E. Hough, S. Neidle, D. Rogers, and P. G. H. Troughton, *Acta Crystallogr., Sect. B*, **29**, 365 (1973).
19) H. M. Berman and S. H. Kim, *Acta Crystallogr., Sect. B*, **24**, 897 (1968).
20) S. S. C. Chu and G. A. Jeffrey, *Acta Crystallogr.*, **23**, 1038 (1967).
21) G. J. Quigley, A. Sarko, and R. H. Marchessault, *J. Am. Chem. Soc.*, **92**, 5834 (1970).
22) I. Tanaka, N. Tanaka, T. Ashida, and M. Kakudo, *Acta Crystallogr., Sect. B*, **32**, 155 (1976).
23) A. D. French and V. G. Murphy, *Carbohydr. Res.*, **27**, 391 (1973).
24) P. Coppens and G. M. Schmidt, *Acta Crystallogr.*, **18**, 62 (1965).
25) P. Coppens and G. M. Schmidt, *Acta Crystallogr.*, **18**, 654 (1965).
26) R. S. Miller, I. C. Paul, and D. Y. Curtin, *J. Am. Chem. Soc.*, **96**, 6334 (1974).
27) A. Bondi, *J. Phys. Chem.*, **68**, 441 (1964).

Conductance of Some High Valence Type Electrolytes in Mixed Solvents. II. Conductance of Pentaamminenitrocobalt(III) and Tris(1,10-phenanthroline)iron(II) Sulfates in Water-Ethylene Glycol Mixtures at 25 °C*

Eiji KUBOTA and Masatoki YOKOI

Department of Chemistry, Faculty of Science, Shinshu University, Asahi, Matsumoto 390

(Received December 3, 1976)

Conductance data are reported for dilute solutions of pentaamminenitrocobalt(III) sulfate, $[Co(NO_2)(NH_3)_5]SO_4$, and tris(1,10-phenanthroline)iron(II) sulfate, $[Fe(phen)_3]SO_4$ in water–ethylene glycol mixed solvents at 25 °C. The conductance data were analyzed in terms of the 1957 Fuoss-Onsager and Fuoss-Hsia equations. While the application of the 1957 Fuoss-Onsager equation to $[Fe(phen)_3]SO_4$ data suggested a complete dissociation of the salt over the entire range of solvent compositions, the Fuoss-Hsia equation fitted the data better and yielded K_A values which are in accord with the ion association theories. $[Co(NO_2)(NH_3)_5]SO_4$ had a higher association constant in the range of solvent composition studied (0 to 40% ethylene glycol) than the predictions of the ion association theories.

In a previous paper[1] we reported the conductance data of $[Fe(phen)_3]SO_4$ in a water–methanol mixed solvent at 25 °C. The association constant of the salt was estimated to be 40 in water by the analysis of the data with the Fuoss-Hsia equation[2] in the form developed by Fernandez-Prini.[3]

Masterton and Biery[4] reported that $[Co(NO_2)(NH_3)_5]SO_4$ is much more ion-paired than has been calculated from the ion association theory, the association constants being 400 in water at 25 °C. Since the values of the association constants of bivalent metal sulfates are 150—250 in water and those of the *m*-benzenedisufonates of bivalent metals are much lower than the constants of the corresponding sulfate, the complex salt seems to be the most highly associated 2:2-type sulfate in water.[5]

It seemed interesting to study the association equilibiria of the complex salts in water–organic solvent systems. Thus, the conductance of $[Co(NO_2)(NH_3)_5]SO_4$ and $[Fe(phen)_3]SO_4$ in water–ethylene glycol mixtures was measured at 25 °C, and the association constants thus derived were compared with the predictions of the ion association theories.

Experimental

Materials. The $[Co(NO_2)(NH_3)_5]SO_4$ was synthesized as has been described in the literature.[6] The $[Co(NO_2)(NH_3)_5]Cl_2$ was prepared by reaction between $[CoCl(NH_3)_5]Cl_2$ and sodium nitrate; it was then converted to $[Co(NO_2)(NH_3)_5]SO_4$. The raw crystals were recrystallized repeatedly from a hot aqueous solution by adding ethanol and then dried at 105 °C. The procedure was carried out in the dark as far as possible to avoid nitrito-form contamination. The purity of the sample was checked by means of its UV and IR spectra, by elementary analysis (Found: N, 29.25; H, 5.32%. Calcd: N, 29.37; H, 5.28%), and by a total-cation determination untilizing cation-exchange resin.

The $[Fe(phen)_3]SO_4$ was prepared and purified as has been described in the previous paper.[1]

The ethylene glycol was dried with anhydrous sodium sulfate and fractionally distilled at 5 Torr. The specific conductivity was less than 7×10^{-8} ohm^{-1} cm^{-1}.

Apparatus and Measurement. The conductance measurement was performed by a transformer bridge (with a reproducibility of 0.005%) and a 3—10 kHz audio oscillator. Two flask-type cells with constants of 0.11631 and 0.09695 cm^{-1} were used. The temperature of the liquid paraffin bath was controlled at 25.000±0.005 °C.

The dilution method of a stock solution was not suitable for the preparation of $[Co(NO_2)(NH_3)_5]SO_4$ solutions because of the low solubility of the salt. The samples (10—20 mg) were weighed in small polyethylene dishes 10 mm in diameter, and the dishes were thrown into the cell. The conductivity was measured after each dissolution of samples.

$[Fe(phen)_3]SO_4$ had enough solubility for preparin the stock solution over the complete range of solvent compositions.

Results and Discussion

The conductance data of $[Co(NO_2)(NH_3)_5]SO_4$ and $[Fe(phen)_3]SO_4$ in water–ethylene glycol are given in Tables 1 and 2 respectively.

The data were analyzed by means of the Fuoss-Onsager (1957) equation:[7]

$$\Lambda = \Lambda_0 - Sc^{1/2}\gamma^{1/2} + Ec\gamma\log c\gamma + Jc\gamma - K_A c\gamma\Lambda f_\pm^2, \quad (1)$$

where the symbols have their usual meanings.[1] The f's were calculated from the extended Debye-Hückel theory, including the ion-size parameter, $\mathring{a}$. The coefficient, J, is also a function of $\mathring{a}$; the adjustable parameters are thus Λ_0, K_A, and $\mathring{a}$. The results of the computer analysis of the $[Co(NO_2)(NH_3)_5]SO_4$ data are summarized in Table 3.

The application of Eq. 1 to the $[Fe(phen)_3]SO_4$ data gave negative K_A values, as in the data for the salt in a water–methanol mixture.[1] Thus, the data were fitted by means of Eq. 2 for unassociated electrolytes:[7]

$$\Lambda = \Lambda_0 - Sc^{1/2} + Ec\log c + Jc. \quad (2)$$

Here, the adjustable parameters are Λ_0 and $\mathring{a}$. The results are given in Table 4.

For the $[Fe(phen)_3]SO_4$ data in water–methanol, the Fuoss-Hsia[2] equation was applied in the form of Eq. 3 developed by Fernandez-Prini:[3]

$$\Lambda = \Lambda_0 - Sc^{1/2}\gamma^{1/2} + Ec\gamma\log c\gamma + J_1c\gamma - J_2c^{3/2}\gamma^{3/2} - K_A c\gamma\Lambda f_\pm^2. \quad (3)$$

* Presented in part at the 29th National Meeting of the Chemical Society of Japan, Nagoya, October 1974.

TABLE 1. EQUIVALENT CONDUCTANCES AND CONCENTRATIONS OF $[Co(NO_2)(NH_3)_5]SO_4$ IN WATER–ETHYLENE GLYCOL AT 25 °C[a,b]

0% Ethylene glycol $D=78.30$ $10^3\eta=8.903$		10% Ethylene glycol $D=75.93$ $10^3\eta=11.40$		20% Ethylene glycol $D=73.25$ $10^3\eta=14.50$		30% Ethylene glycol $D=70.43$ $10^3\eta=18.30$		40% Ethylene glycol $D=67.30$ $10^4\eta=23.90$	
10^4c	Λ	10^4c	Λ	10^4c	Λ	10^4c	Λ	10^4c	Λ
0.81562	135.06	0.75060	108.60	1.3390	83.099	0.73736	66.446	1.4415	48.393
1.1627	133.15	1.4165	105.50	2.2305	79.931	1.4932	63.524	2.2746	46.024
1.3006	132.60	2.1559	102.61	3.1271	77.296	2.2686	61.087	3.1991	43.946
1.7636	130.34	2.9798	99.815	4.1033	74.948	3.0706	59.083	4.2445	42.053
2.0948	128.92	3.7614	97.718	4.9826	73.116	3.9176	57.304	5.0779	40.761
2.7598	126.54	4.7133	95.305	5.8667	71.558	4.8122	55.566	6.0095	39.496
3.1299	125.20	5.7809	93.017	7.0449	69.621	5.8846	53.972	7.0822	38.257
3.3635	124.59	6.8444	90.973	8.3689	67.753	7.0000	52.488	7.9862	37.351
4.0820	122.43	8.2655	88.610	9.3785	66.490	8.3381	50.860	8.9833	36.430
4.5080	121.28	9.2510	87.129	10.442	65.189	9.7533	49.318	10.063	35.554
5.2253	119.49	10.513	85.366	11.545	64.103	10.831	48.336	11.222	34.693
5.7822	118.10	11.472	84.153	12.692	62.922	11.843	47.469	12.412	33.908
6.3016	116.98	12.438	83.100	13.929	61.853	12.726	46.781	13.609	33.181
7.2328	115.08	14.499	80.944	15.301	60.718				
7.3927	114.78								
8.1406	113.36								
8.3004	113.07								
9.1147	111.68								
10.104	110.13								
10.259	109.91								
11.109	108.61								
11.319	108.26								

a) c, in mol dm^{-3}; Λ, in ohm^{-1} cm^2 equiv^{-1}. b) D, dielectric constant; η, viscosity(poise), Ref. 19).

TABLE 2. EQUIVALENT CONDUCTANCES AND CONCENTRATIONS OF $[Fe(phen)_3]SO_4$ IN WATER–ETHYLENE GLYCOL AT 25 °C[a]

20% Ethylene glycol $D=73.25$ $10^3\eta=14.50$		40% Ethylene glycol $D=67.30$ $10^3\eta=23.90$		60% Ethylene glycol $D=60.50$ $10^3\eta=41.30$		80% Ethylene glycol $D=51.80$ $10^3\eta=79.50$		100% Ethylene glycol $D=37.70$ $10^3\eta=169.0$	
10^4c	Λ	10^4c	Λ	10^4c	Λ	10^4c	Λ	10^4c	Λ
1.3565	69.889	2.0101	40.173	2.6545	23.226	2.6402	11.507	2.0997	4.7133
2.0994	69.111	2.3156	40.029	4.0023	22.871	3.4761	11.333	2.4603	4.6467
2.9888	68.402	2.8292	39.749	5.2773	22.522	5.0588	11.110	3.1656	4.5532
4.3533	67.492	3.8810	39.249	6.3007	22.294	6.1119	10.970	3.9743	4.4689
5.3797	66.965	4.8364	38.832	7.4408	22.054	7.8546	10.770	4.7148	4.4076
5.9415	66.698	6.3137	38.307	8.5096	21.852	9.1025	10.637	5.3202	4.3476
6.6305	66.399	8.7512	37.672	9.6793	21.662	9.9287	10.571	6.1617	4.2938
6.9474	66.254	12.326	36.853	12.167	21.281	13.255	10.304	6.9619	4.2440
7.4935	66.064							7.8798	4.1923
8.2785	65.779							9.1063	4.1298
								10.007	4.0910
								10.752	4.0559

a) Table 1, a) and b).

The application improved $\sigma\Lambda$ and gave reasonable K_A values. Therefore, the fitting of the present data to Eq. 3 was examined.

The best-fit values of Λ_0, K_A, and $\mathring{a}$ were calculated by a successive approximation for the series of initial values of the ion-size parameter, $\mathring{a}_i$, between 1—28 Å with 0.05 Å intervals. $\sigma\Lambda$ is defined as:

$$\sigma\Lambda = \left[\frac{\sum(\Lambda_{expti}-\Lambda_{calcd})^2}{N-3}\right]^{1/2}, \quad (4)$$

where N is the number of experimental points.

An example of the results is shown graphically in Fig. 1 for the $[Co(NO_2)(NH_3)_5]SO_4$ data in water. The solid lines of Fig. 1 indicate the variation in Λ_0, K_A, $\sigma\Lambda$,

Table 3. Conductance parameters for $[Co(NO_2)(NH_3)_5]SO_4$ in water–ethylene glycol at 25 °C, calculated from the Fuoss-Onsager equation[a)]

Solvents (wt %)	Λ_0	$\mathring{a}_J$	K_A	$\sigma\Lambda$	N
0	142.64±0.06	7.9±0.3	281±6	0.06	22
10	115.09±0.06	7.7±0.3	363±3	0.05	14
20	91.50±0.08	7.9±0.3	480±9	0.05	14
30	71.54±0.08	7.5±0.5	610±15	0.06	13
40	55.96±0.04	8.2±0.2	923±8	0.02	13

a) Λ_0, limiting conductance (ohm^{-1} cm^2 equiv^{-1}); $\mathring{a}_J$, ion-size parameter(Å); K_A, ion association constant (dm^3 mol^{-1}); $\sigma\Lambda$, standard deviation of N, experimental points.

Table 4. Conductance parameters for $[Fe(phen)_3]SO_4$ in water–ethylene glycol at 25 °C, calculated from the Fuoss-Onsager equation[a)]

Solvents (wt %)	Λ_0	$\mathring{a}_J$	$\sigma\Lambda$	N
0[b)]	114.58 ±0.06	7.06±0.08	0.14	17
20	73.61 ±0.03	8.9 ±0.2	0.04	10
40	43.29 ±0.05	7.6 ±0.2	0.08	8
60	25.70 ±0.07	7.3 ±0.2	0.07	8
80	13.06 ±0.05	7.6 ±0.2	0.06	8
100	5.712±0.026	8.1 ±0.2	0.04	12

a) Table 1, a). b) Ref. 1.

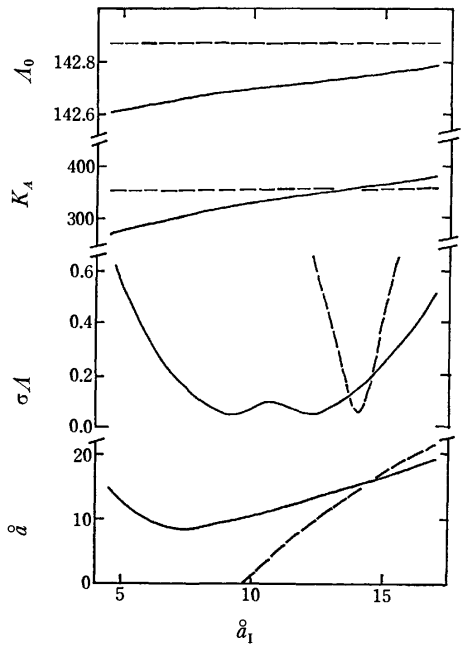

Fig. 1-A. Values of parameters and standard deviations as a function of $\mathring{a}_I$ for $[Co(NO_2)(NH_3)_5]SO_4$ in water. The units of Λ_0 and $\sigma\Lambda$ are ohm^{-1} cm^2 equiv^{-1} and those of K_A are dm^3 mol^{-1}. The broken lines are calculated by fixing $\mathring{a}=q$ in the J_1 and $f_\pm$ terms.

and $\mathring{a}$ with the change in $\mathring{a}_I$. While the K_A and Λ_0 values increase with the $\mathring{a}_I$, $\sigma\Lambda$ has two similar minima corresponding to the $\mathring{a}$ values of 9.0 and 12.0 Å. In Fig. 2, the $\sigma\Lambda$ values are shown as contour lines with the

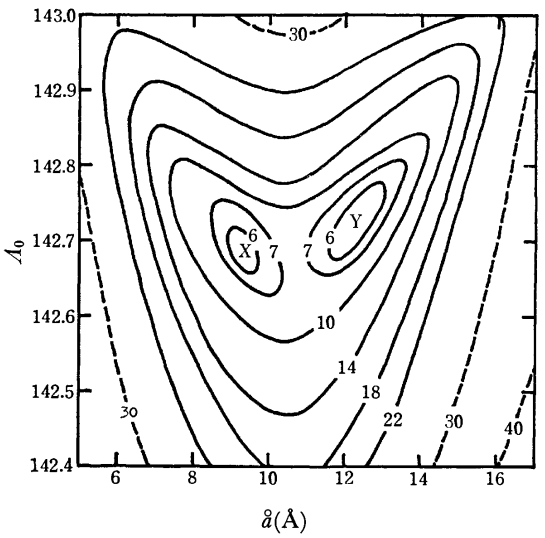

Fig. 1-B. Contour diagram for the $[Co(NO_2)(NH_3)_5]SO_4$ in water. The contour lines illustrate how $\sigma\Lambda$ depends on different conbinations of the Λ_0 and $\mathring{a}$. The figures on the contours represent the values of $10^2\sigma\Lambda$. The minimum at point X, $\sigma\Lambda=0.06$, corresponds to the parameters, $\Lambda_0=142.68$, $K_A=316$, $\mathring{a}=9.2$Å, while the minimum at point Y, $\sigma\Lambda=0.06$, corresponds to $\Lambda_0=142.72$, $K_A=343$, $\mathring{a}=12.4$Å.

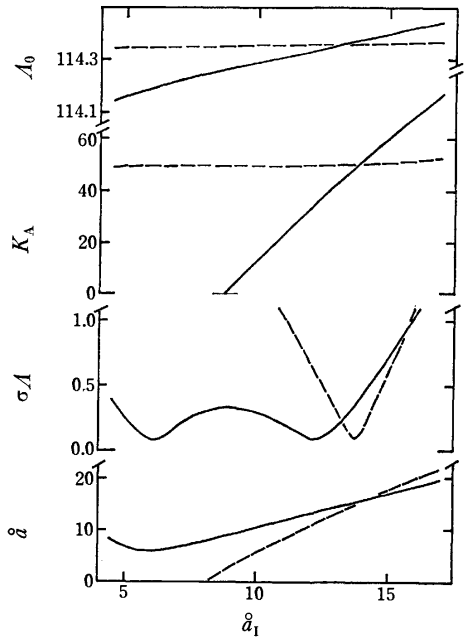

Fig. 2. Values of parameters and $\sigma\Lambda$ as a function of $\mathring{a}_I$ for $[Fe(phen)_3]SO_4$ in water. The broken lines are calculated by fixing $\mathring{a}=q$ in the J_1 and $f_\pm$ terms.

variation in the $\mathring{a}_I$ and Λ_0 values. It is apparent that two sets of parameter values were obtained by the above computation method. For the $[Co(NO_2)(NH_3)_5]SO_4$ data in other water–ethylene glycol solvent systems, two sets of parameter values of the minimum $\sigma\Lambda$ with different $\mathring{a}$ values are obtained. The appearance of the two minima in fitting the conductance data to the Fuoss-Hsia equation were observed for some 1 : 1-type electrolytes.[8)] It is rather difficult to decide which

TABLE 5-A. CONDUCTANCE PARAMETERS FOR $[Co(NO_2)(NH_3)_5]SO_4$ IN WATER–ETHYLENE GLYCOL AT 25 °C, CALCULATED FROM THE FUOSS-HSIA EQUATION IN THE FERNANDEZ-PRINI FORM[a)]

Solvents (wt %)	q	Λ_0	$\mathring{a}_{J_2}$	K_A	$\sigma\Lambda$	N
0	14.3	142.68±0.05	9.2±0.6	316±3	0.06	22
		142.72±0.05	12.4±0.5	343±3	0.06	
10	14.8	115.15±0.06	8.8±0.7	400±4	0.06	14
		115.20±0.07	12.7±0.5	437±5	0.07	
20	15.3	91.57±0.07	9.5±0.6	527±5	0.05	14
		91.62±0.07	12.5±0.5	560±5	0.05	
30	15.9	71.56±0.08	7.5±1.5	705±10	0.06	13
		71.64±0.10	15.7±0.9	736±12	0.08	
40	16.6	56.03±0.04	9.1±0.5	976±6	0.02	13
		56.10±0.05	14.2±0.4	1047±7	0.02	

TABLE 5-B. CONDUCTANCE PARAMETERS FOR $[Co(NO_2)(NH_3)_5]SO_4$ IN WATER–ETHYLENE GLYCOL CALCULATED FROM THE FUOSS-HSIA EQUATION IN THE FERNANDEZ-PRINI FORM, FIXING $\mathring{a}_1=q$ IN THE J_1 AND $f_\pm$ TERMS[a)]

Solvents (wt %)	q	Λ_0	$\mathring{a}_{J_2}$	K_A	$\sigma\Lambda$	N
0	14.3	142.74±0.05	14.0±0.4	358±3	0.06	22
10	14.8	115.22±0.08	14.4±0.6	455±5	0.07	14
20	15.3	91.68±0.07	14.6±0.4	589±5	0.04	14
30	15.9	71.62±0.08	16.1±0.8	734±11	0.06	13
40	16.6	56.14±0.05	16.1±0.4	1077±7	0.03	13

a) q, Bjerrum's distance (Å); $\mathring{a}_{J_2}$, ion-size parameter (Å); Table 1, a).

minimum is preferable. Thus, both sets of parameters are given in Table 5-A, which summarizes the results for $[Co(NO_2)(NH_3)_5]SO_4$.

For the $[Fe(phen)_3]SO_4$ data also, two minima with the lowest $\sigma\Lambda$ value are obtained, but the one corresponding to the lower $\mathring{a}$ has a negative K_A value. The results obtained for the data in water are shown as solid lines in Fig. 3. Similar results were obtained for the data in water–ethylene glycol solvents and for the data[1)] of the $[Fe(phen)_3]SO_4$ in water–methanol. In this case, the minimum $\sigma\Lambda$ values with a negative K_A are disregarded; the results are summarized in Table 6-A.

As another method of fitting the data to Eq. 4, the ion-size parameters appearing in the J_1 and $f_\pm$ terms were fixed as equal to the Bjerrum q values,[9)] and the best-fit $\mathring{a}$ values for the J_2 term were calculated. The results of the calculation are shown as broken lines in Figs. 1 and 3. In this case, a single minimum of $\sigma\Lambda$ was obtained; the corresponding $\mathring{a}_{J_2}$ was close to the q values. Tables 5-B and 6-B summarize the results for $[Co(NO_2)(NH_3)_5]SO_4$ and $[Fe(phen)_3]SO_4$ respectively.

Tables 5-A and 5-B show that, in comparison with the parameters listed in Table 3, the Fuoss-Hsia equation gives the same values of Λ_0 within the limits of error, but the values of K_A and $\mathring{a}$ are a little larger than those obtained by means of the Fuoss-Onsager equation. On the other hand, Tables 6-A and 6-B show that the application of the Fuoss-Hsia equation to the

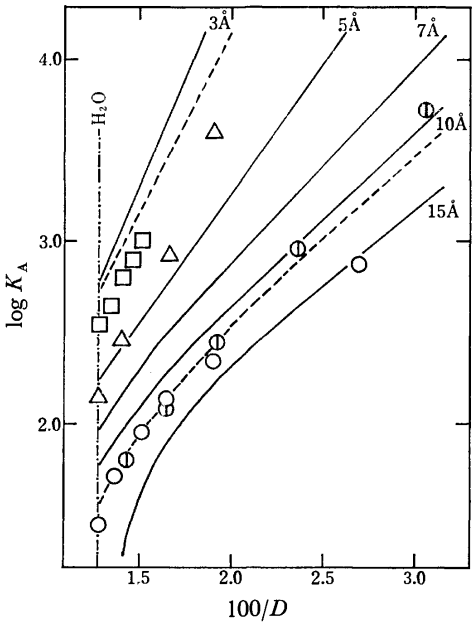

Fig. 3. Plot of log K_A *vs.* $1/D$.
□, $[Co(NO_2)(NH_3)_5]SO_4$ and ○, $[Fe(phen)_3]SO_4$, the present work at 25 °C. △, $MnSO_4$ in water–ethylene glycol and ⓘ, $[Fe(phen)_3]SO_4$ in water–methanol at 25 °C. Curves are theoretical curves due to Bjerrum's (——) and Yokoyama-Yamatera's (----) theories[9,16)] with each ion sizes.

$[Fe(phen)_3]SO_4$ data gives apparently better data, just fitting the results on the data of the salts in water–methanol. The association constant is estimated to increase with a decrease in the solvent dielectric constant. A conductance equation which contains higher terms than c seems to be required as the reference function in the analysis of the conductance data of slightly associated 2:2 electrolytes.

Fuoss has revised his conductance equation recently;[7)] also, an extended conductance equation[10)] including the $c^{3/2}$ term has been proposed by Pitts.[11,12)] These equations will have to be examined for the conductance data of a slightly associated 2:2 electrolyte. At present, the discussion is based on the results obtained by means of the Fuoss-Hsia equation.

Λ_0 value of $[Co(NO_2)(NH_3)_5]SO_4$ obtained here in water, 144.9, is about 2 units lower than that reported by Masterton and Bierly; the association constant obtained is also a little lower than their value. The ionic conductances of $[Co(NO_2)(NH_3)_5]^{2+}$ and $[Fe(phen)_3]^{2+}$ ions in water are obtained as 63.1 and 34.6 by subtracting the $\lambda_0^-=80.0$[13)] of the SO_4^{2-} ion from the Λ_0 values. The latter values are in accord with values, 34.8—34.9, reported by Yamamoto *et al.* in their conductance measurements of the chloride and the bromide in water.[14)] The ionic conductance of the aquo Co^{2+} ion has been reported as 52.8,[15)] while those of the $[Ni(en)_3]^{2+}$ and aquo Ni^{2+} ions were estimated as 58.9 and 49.4[16)] respectively. The substitution of the first hydration-sphere by a ligand gives the ion higher mobility. A large ligand like phenanthroline, which may cover more than the second hydration sphere, will decrease the mobility of the ion.

Table 6-A. Conductance parameters for $[Fe(phen)_3]SO_4$ in water–ethylene glycol at 25 °C, calculated from the Fuoss-Hsia equation in the Fernandez-Prini form

Solvents (wt %)	q	Λ_0	$\mathring{a}_{J_1}$	K_A	$\sigma\Lambda$	N
0[b]	14.3	114.18 ±0.10	6.0±1.0	−28± 5	0.09	17
		114.33 ±0.10	12.9±0.5	35± 5	0.09	
20	15.3	73.20 ±0.05	4.6±2.0	−87± 6	0.02	10
		73.45 ±0.03	15.4±0.4	40± 3	0.01	
40	16.6	42.96 ±0.05	5.1±1.3	−85± 8	0.03	8
		43.09 ±0.06	17.5±0.6	82±10	0.03	
60	18.5	25.15 ±0.05	4.1±1.4	−178±15	0.02	8
		25.39 ±0.08	20.8±0.7	128±20	0.03	
80	21.6	12.65 ±0.02	5.2±0.5	−272±11	0.001	8
		12.86 ±0.04	20.8±0.4	207±19	0.01	
100	29.7	5.354±0.022	6.8±0.4	−696±42	0.007	12
		5.616±0.014	23.0±0.2	759±27	0.05	

Table 6-B. Conductance parameters for $[Fe(phen)_3]SO_4$ in water–ethylene glycol at 25 °C, calculated from the Fuoss-Hsia equation in the Fernandez-Prini form, fixing $\mathring{a}_1=q$ in the J_1 and $f_\pm$ terms[a]

Solvents (wt %)	q	Λ_0	$\mathring{a}_{J_1}$	K_A	$\sigma\Lambda$	N
0[b]	14.3	114.37 ±0.10	13.8±0.5	51± 5	0.09	17
20	15.3	73.45 ±0.03	15.3±0.4	39± 3	0.01	10
40	16.6	43.09 ±0.06	17.1±0.6	72± 9	0.03	8
60	18.5	25.37 ±0.08	19.8±0.7	95±18	0.03	8
80	21.6	12.86 ±0.04	21.1±0.4	228±19	0.01	8
100	29.7	5.650±0.017	25.5±0.2	1131±34	0.005	12

a) q, Bjerrum's distance (Å); $\mathring{a}_{J_1}$, ion-size parameter (Å); Table 1, a). b) Ref. 1.

In Fig. 3 the log K_A's of $[Co(NO_2)(NH_3)_5]SO_4$ and $[Fe(phen)_3]SO_4$ in water–ethylene glycol are plotted against the reciprocal of the dielectric constants of the solvents. The predictions of the ion association theories of Bjerrum[9] and Yokoyama-Yamatera[17] are shown as solid and dotted lines respectively for the specific contact distances. The data of $[Co(NO_2)(NH_3)_5]SO_4$ are on a straight line, which is located on Bjerrum's prediction corresponding to about 3.7 Å.

The size of the $[Co(NO_2)(NH_3)_5]^{2+}$ ion could be estimated from the X-ray crystal analysis data of $[CoCl(NH_3)_5]Cl_2$.[18] The minimum distance of the approach of the cobalt atom and chloride in the crystal is 4.2 Å. The crystal analysis data[19] of anhydrous sulfates of alkaline earth and first-transition metals gave effective radii of the sulfate ions ranging 2.3 to 2.5 Å. If the effective radius of $[Co(NO_2)(NH_3)_5]^{2+}$ is close to that of $[CoCl(NH_3)_5]^{2+}$, the closest distance of approach in the sulfate would be about 4.8 Å. This is larger than the distance found from the location of the log K_A-1/D plot in Fig. 3. The plot of the $MnSO_4$ data in the same solvent system[20] corresponds to a contact distance of 4.6 Å, judging from a comparison with Bjerrum's theory. The minimum distance of Mn^{2+} and SO_4^{2-} separation in the anhydrous $MnSO_4$ crystal is 3.3 Å.[19]

The above results suggest that the main species of association in the $MnSO_4$ solution might be a solvent-separated ion pair. The Mn–SO_4 distance separated by one water molecule would be about 4.8 Å, which is found as the closest distance between metal and sulfur in the $[Ni(OH_2)_6]SO_4$ crystal. On the other hand, in the $[Co(NO_2)(NH_3)_5]SO_4$ solution, the main species of association would be a contact-ion pair, as was suggested by Osugi *et al.* in their interpretation of the pressure dependence of the ion association constant.[12] Interaction between opposite-charged ions other than the coulombic attraction of opposite charges stabilizes the contact-ion pair. Masterton *et al.* suggested that the extra stability of the associated species comes from a dispersion interaction. D'Aproano and Fuoss[22] interpreted the high association constant of TlCl in water–dioxane mixture by calculating the energies due to the interaction between the charges and the induced dipoles. In a 1:1 cobalt complex salt solution, an extra stability of associated species sometimes promotes the K_A value to an order higher.[4] In a 2:2 electrolyte, however, the effect of extrastabilization is not so remarkable as in the 1:1 salt solution, since the charge-charge interaction energy is larger; yet it is clear that the effect is maintained independently of the macroscopic dielectric constant of the solvent.

The data of the log K_A of $[Fe(phen)_3]SO_4$ in water–methanol are plotted in Fig. 3 for purposes of comparison. The plots for the two solvent systems coincide with each other in the water-rich solvent range, but deviate in a high organic solvent content medium. This suggests that solvent-separated association species may contribute by some extent. The overall data points are located close the Yokoyama-Yamatera theory of 10 Å.

In this case, the cation is large enough and is not easily polarizable, and the specific interaction with the sulfate ion contributes little to the extra stability of the contact-ion pair.

All the calculations were performed on HITAC 10-II remote-batch system, FACOM 230-60, and HITAC 8800/8700 computers using the program of FORTRAN IV. The authors wish to thank the staffs of the Shinshu University Remote Batch Computation Center, Nagoya University Computation Center, and Tokyo University Computation Center for the use of the computers.

References

1) E. Kubota and M. Yokoi, *Bull. Chem. Soc. Jpn.*, **49**, 2674 (1976).

2) a) R. M. Fuoss and K. L. Hsia, *Proc. Natl. Acad. Sci. U.S.A.*, **57**, 1550 (1966); *ibid.*, **58**, 1818 (1967); b) K. L. Hsia and R. M. Fuoss, *J. Am. Chem. Soc.*, **90**, 3055 (1968).

3) R. Fernandez-Prini, *Trans. Faraday Soc.*, **65**, 3311 (1969).

4) W. L. Masterton and T. Biery, *J. Phys. Chem.*, **74**, 139 (1970).

5) a) G. Atkinson and C. J. Hallada, *J. Am. Chem. Soc.*, **84**, 721 (1962); G. Atkinson and S. Petrucci, *ibid.*, **86**, 7 (1964); H. Tsubota and G. Atkinson, *ibid.*, **86**, 164 (1965); *J. Phys. Chem.*, **71**, 1131 (1967); b) E. Kubota, M. Yokoi, and S. Shikata, *Nippon Kagaku Zasshi*, **85**, 89 (1964); M. Yokoi and E. Kubota, *ibid.*, **86**, 894 (1965); Ref. 15; c) S. Petrucci, P. Hemmes, and M. Battistini, *J. Am. Chem. Soc.*, **89**, 5552 (1967); P. Hemmes and S. Petrucci, *ibid.*, **91**, 275 (1969); d) E. M. Hanna, A. D. Pethybridge, and J. E. Prue, *Electrochim. Acta*, **16**, 677 (1971); Ref. 19.

6) S. M. Jörgensen, *Z. Anorg. Chem.*, **5**, 172 (1894).

7) a) R. M. Fuoss and L. Onsager, *J. Phys. Chem.*, **61**, 668 (1957); b) R. M. Fuoss and F. Accacina, "Electrolytic Conductance," Interscience Publishers, New York, N. Y. (1959), Chap. VIII—XVII.

8) a) R. Fernandez-Prini, "Physical Chemistry of Organic Solvent Systems," ed by A. K. Convington and T. Dickinson, Prenum Press, London-New York (1973), p. 588; b) J. C. Justice, T. Bury, and C. Treiner, *J. Chim. Phys. Phys.-Chim. Biol.*, **65**, 1780 (1968); c) Derossi, B. Sesta, M. Battistini, and S. Petrucci, *J. Am. Chem. Soc.*, **94**, 2961 (1972); d) M. L. Jansen and H. L. Yeager, *J. Phys. Chem.*, **77**, 3089 (1973); *ibid.*, **78**, 1380 (1974); e) J. Barthal, J. C. Justice, and R. Wachter, *Z. Phys. Chem.*, **bd. 84**, 100 (1973); E. Reard and J. C. Justice, *J. Solution Chem.*, **3**, 633 (1974); f) P. Beronius, *Acta Chem. Scand.*, **A28**, 77 (1974); *ibid.*, **A29**, 289 (1975); g) E. M. Hanna, A. D. Pethybridge, J. E. Prue, and D. J. Spiers, *ibid.*, **3**, 563 (1974); h) A. D. Pethybridge and D. J. Spiers, *J. Chem. Soc., Faraday Trans. 1*, **72**, 64 (1976); *ibid.*, **72**, 73 (1976).

9) Bjerrum's critical distance, $q=Z^2e^2/(2DkT)$; Ref. 13.

10) a) R. M. Fuoss, *J. Phys. Chem.*, **79**, 525 (1975); b) C. F. Mattina and R. M. Fuoss, *ibid.*, **79**, 1604 (1975).

11) E. Pitts, *Proc. R. Soc. London, Ser. A*, **217**, 43 (1953).

12) R. Fernandez-Prini and J. E. Prue, *Z. Phys. Chem. (Leipzig), A*, **228**, 372 (1965); E. Pitts, B. E. Tabor, and J. Daly, *Trans. Faraday Soc.*, **65**, 849 (1969); *ibid.*, **66**, 693 (1970); Ref. 8b, p. 525.

13) R. A. Robinson and R. H. Stokes, "Electrolyte Solutions," Butterworths, London (1965), 2nd ed, p. 392.

14) Y. Yamamoto, E. Sumimura, K. Miyoshi, and T. Tominaga, *Anal. Chim. Acta*, **64**, 225 (1973).

15) S. Katayama, *J. Solution Chem.*, **5**, 241 (1976).

16) M. Yokoi, Y. Mori, E. Kubota, and K. Murata, *Nippon Kagaku Zasshi*, **89**, 1192 (1968).

17) H. Yokoyama and H. Yamatera, *Bull. Chem. Soc. Jpn.*, **48**, 1770 (1975).

18) a) Y. Shigeta, Y. Komiyama, and H. Kuroya, *Bull. Chem. Soc. Jpn.*, **36**, 1159 (1963); b) K. Matsumoto, S. Ooi, and H. Kuroya, *ibid.*, **43**, 3801 (1970).

19) R. W. G. Wyckoff, "Crystal Structures," Vol. 3, Interscience Publishers, New York (1965), 2nd ed, Chap. VIIIA—B.

20) R. Lovas, G. Macri, and S. Petrucci, *J. Am. Chem. Soc.*, **92**, 6502 (1970).

21) J. Osugi, K. Shimizu, M. Nakamura, E. Hirayama, Y. Yasuhiko, and M. Ueno, "Proceeding of The 4th International Conference on High Pressures," Kyoto (1974), p. 610.

22) A. A'Daprano and R. M. Fuoss, *J. Am. Chem. Soc.*, **91**, 279 (1969).

Mechanism of the Reduction of Nitric Oxide with Ammonia over Cu(II) Ion-Exchanged Zeolites

Tsuyoshi ARAKAWA, Mamoru MIZUMOTO, Yusaku TAKITA, Noboru YAMAZOE, and Tetsuro SEIYAMA

Department of Materials Science and Technology, Faculty of Engineering, Kyushu University, Higashi-ku, Fukuoka 812

(Received December 6, 1976)

The catalytic NO reduction with NH_3 over Cu(II) ion-exchanged zeolite was studied with special attention to the temperature dependence of catalytic activity which reaches maximum at *ca.* 120 °C. ESR study showed that in the catalytic system all the exchanged copper ions exist as Cu(II) up to *ca.* 120 °C, above which Cu(II) ions decrease with a rise in temperature. The reaction rates measured at 110 and 140 °C were found to show similar dependence on both NO and NH_3 partial pressures, indicating that the reaction mechanism does not differ much. By lowering temperature the Cu(I) ions formed at higher temperatures were reoxidized to Cu(II), accompanied by N_2O formation due to the disproportionation of NO. From the results and the IR spectroscopic data a reaction mechanism was proposed. It includes a step in which NO reacts with NH_3 adsorbed to Cu(II) ions to give rise to the evolution of N_2 and the reduction of Cu(II) ions, and steps in which Cu(II) ions are regenerated accompanying the evolution of N_2+N_2O.

The catalytic reduction of nitrogen oxide with ammonia is important from the standpoint of removal of air pollutants. For the reduction we found that Cu(II) ion-exchanged zeolite exhibits pronounced unique catalytic activity.[1,2] In addition to the significant catalytic activity shown at temperatures below 100 °C, a characteristic bell-shaped temperature dependence with a maximum appearing at *ca.* 120 °C was observed. This catalytic reaction is not only of practical importance with its low temperature performance, but it also gives a case in which complex formation and redox change of the exchanged metal ions within the zeolite framework take place reversibly. These are in marked contrast to the case of Co(II) ion-exchanged zeolites, first reported by Windhorst and Lunsford,[3] in which Co(II) ions are reactive to the mixture of NO and NH_3 in a similar temperature region but are irreversibly oxidized to unreactive Co(III).

The catalytic NO reduction with NH_3 over Cu(II) ion-exchanged zeolite, however, remains unclarified as regards the path and mechanism of the reaction and the role of copper ions. We have investigated the problems by means of ESR spectroscopy, IR spectroscopy, and reaction kinetics. Efforts were made to elucidate the bell-shaped correlation between the catalytic activity and temperature. A kind of temperature jump method was applied to pursue the transient phenomena observed when the catalytic system was forced to shift from one stationary state to another, especially in relation to the regeneration step of Cu(II) ions from Cu(I).

Experimental

Partly Cu(II) ion-exchanged zeolites, Cu(II)NaY and Cu(II)NaX, were prepared by treating Linde Y and X zeolites with aqueous $CuSO_4$ solutions. The ion-exchanged samples were thoroughly washed with deionized water and dried at 100 °C. The ion-exchange levels of Cu(II) were determined by X-ray fluorometry.

The ESR spectra of Cu(II) ions were recorded in the X-band region at room temperature with a Hitachi 771 spectrometer, by using 2,2-diphenyl-1-picrylhydrazyl (DPPH) standard ($g=2.0036$).

IR spectra were recorded with a JASCO-IR-G spectrophotometer in the double beam absorbance mode. The infrared cell consists of a Pyrex glass fitted with potassium bromide windows. The cell allowed heating of the sample wafer at elevated temperatures measured with a thermocouple in contact with the wafer. The sample wafer, 20 mm diameter, was prepared by pressing the exchanged zeolite powder (*ca.* 10 mg) at 100 kg/cm^2.

Stationary as well as non-stationary reactions between NO and NH_3 were carried out in a fixed bed flow reactor under an atmospheric pressure. The gas composition was analyzed by gas chromatography.

Results

Oxidation State of Copper Ions. For the catalytic NO reduction with NH_3, Cu(II) ion-exchanged zeolite exhibits catalytic activity with unique temperature dependence.[1,2] A typical activity *vs.* temperature profile of a convex bell-shape is exemplified by curve (a) in Fig. 1 where activity is given in terms of the conversion of NO. The reaction products are N_2, N_2O, and H_2O.

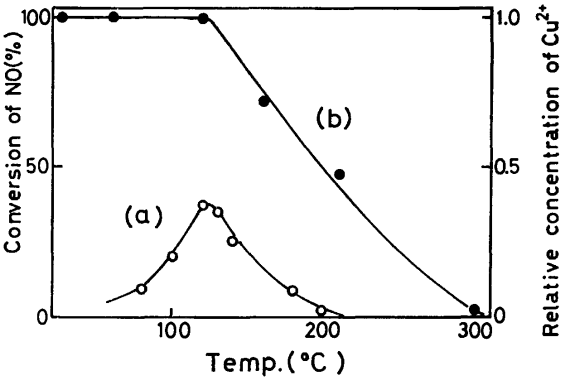

Fig. 1. Changes in catalytic activity (a) and in Cu(II) concentration (b) with temperature in the catalytic NO–NH_3 reaction over copper ion-exchanged Y zeolites.
Feed; NO (3%)+NH_3 (2%)+He,
Contact time; 1.0 g·s/mol.

The selectivity for N_2O ($N_2O/(N_2+N_2O)$) is little influenced by the reaction temperature. It seems that such an activity profile is correlated with the change in oxidation state of the copper ions present in the zeolite framework, as observed by the change in the coloration of catalysts. The correlation was first examined by ESR study as follows.

Cu(II)NaY zeolite with 60% cation exchange (150 mg) was loaded as a catalyst bed in a Pyrex glass tube of o.d. 3.5 mm, which was thereafter connected to a gas flow system. After heating the catalyst bed to the desired temperature, a stream (10 cm^3/min) of gas mixture of NO (3%), NH_3 (2%), and He (95%) was introduced. The same composition and contact time as those used to obtain curve (a) in Fig. 1 were selected. After treatment for 4 h, which was found to be sufficient for the catalytic system to reach a stationary state, the catalyst was purged of the gaseous compounds at the same temperature for 15 min by He stream. The Pyrex glass tube containing the catalyst was then removed from the flow system, and the catalyst was subjected to ESR measurement at room temperature. Figure 2

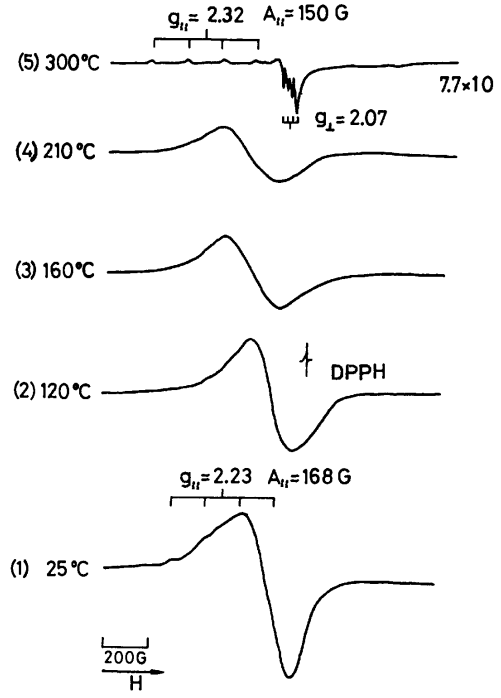

Fig. 2. ESR spectra of Cu(II) ions for a 60% copper ion-exchanged Y zeolites treated by NO (3%)+NH_3 (2%) at various temperatures.

shows ESR spectra of Cu(II) ions recorded after the treatment at various temperatures. All the spectra were taken for one and the same sample by subjecting it to repeated treatment. The signals except (5) turned or nearly turned in to symmetric ones due to high Cu(II) concentrations. Spectra (1) and (2) can be ascribed to square planer Cu(II)$(NH_3)_4$ ($g_{//}$=2.23, $A_{//}$=1.68 G),[4] while (3) and (4) agree with the spectra recorded for partially dehydrated Cu(II)NaY. The decrease in Cu(II) concentration at elevated temperatures made the hyperfine structure of the signal to appear in spectrum (5); g values ($g_\perp$=2.07, $g_{//}$=2.32, $A_{//}$=150 G) show that the Cu(II) center is dehydrated and probably located at site I or I'.[5] It is evident that the Cu(II) ions exchanged in the zeolite exist mostly as tetraammine complexes below 120 °C, above which the complexes are replaced by partially or entirely dehydrated Cu(II) ions. No particular evidence was obtained for the formation of distorted tetrahedral Cu(II)–NH_3 complexes reported by Vansant and Lunsford.[5]

By double integration of the ESR signals the concentrations of Cu(II) ions were determined relative to that obtained after the treatment at 25 °C. They are plotted against temperatures (curve (b), Fig. 1). The Cu(II) concentration remains up to 120 °C, but decreases monotonously at higher temperatures. The decrease in Cu(II) concentration is related to that in catalytic activity shown by curve (a). However, agreement of the two curves is not satisfactory in detail. With rise in temperature, the activity falls more rapidly than Cu(II) concentration. At 200 °C, the activity is almost completely lost but the Cu(II) concentration remains near 50% level. The discrepancy seems to be correlated to the distribution of Cu(II) ions over several sites in the zeolite framework; the Cu(II) ions present above 200 °C are mostly located at inactive "locked-in" sites within the sodalite cage or hexagonal prism.

In dehydrated Cu(II)NaY zeolite, Cu(II) ions show rather strong preference to the "locked-in" sites.[6,7] In the presence of water or ammonia, however, the the Cu(II) ions are pulled toward the supercage by complex formation as reported by Huang and Vansant.[8] Under the present reaction conditions, the catalytic activity of Cu(II)NaY catalyst at 120 °C has been found to be proportional to the Cu(II) ion-exchanged level.[2] This indicates that at temperatures below 120 °C the Cu(II) ions are dominantly present in the supercage and act as active catalytic sites. Above 120 °C, however, the present ESR study shows that complex formation of Cu(II) with NH_3 or water molecules becomes increasingly difficult. This might be the reason for the Cu(II) ions returning to the "locked-in" sites at higher temperatures. The decrease in catalytic activity above 120 °C (curve (a)) results from a decrease in Cu(II) concentration within the supercage, which is caused partly by the reduction of Cu(II) ions to Cu(I) and partly by the migration of Cu(II) ions towards the "locked-in" site.

Reaction Kinetics. The reaction kinetics of the NO reduction with NH_3 over Cu(II)NaY catalysts was studied at 110 and 140 °C in a flow system. The temperatures were so chosen as to include the temperature for maximum activity (120 °C). As a result, the reaction rates at both temperatures were found to be expressed by empirical equations of the following form;

$$r = -\frac{dP_{NO}}{dt} = k_1 P_{NO}^n P_{NH_3}^m, \quad (1)$$

where P_{NO} and P_{NH_3} denote the partial pressures of nitrogen oxide and ammonia, respectively, and k_1 is a rate constant. P_{NO} and P_{NH_3} were varied in the range 0.01—0.08 atm. The reaction orders, n and m, obtained at 110 and 140 °C are given in Table 1. The difference in reaction temperature affects both n and m only slightly.

Table 1. Reaction orders on NO and NH_3 (Eq. 1) in the NO and NH_3 reaction over a Cu(II)NaY catalyst (Contact time; 1.0 g · s/cm³)

Temp (°C)	n	m	k[a]
110	1.0	0.63	2.45×10^{-4}
140	0.92	0.53	0.79×10^{-4}

a) Mols NO/s · (atm)$^{n+m}$ · g.

The rate data were found to satisfy the following expression within experimental errors at both temperatures.

$$r = \frac{k_2 P_{NO} P_{NH_3}}{(1+K_{NH_3}P_{NH_3})^2}. \quad (2)$$

This was derived by assuming a Langmuir-Hinshelwood type of reaction between weakly adsorbed NO and strongly adsorbed NH_3. Here, K_{NH_3} is the adsorption equilibrium constant and k_2 is a constant. It turned out subsequently, however, that the rate data also satisfy the equation

$$r = \frac{k_3 P_{NO} P_{NH_3}}{(1+K_{NH_3}P_{NH_3})}, \quad (3)$$

which implies that NO weakly adsorbs on sites different from those for NH_3 or that a Redeal type of reaction takes place between NO and adsorbed NH_3. Differentiation between (2) and (3) was difficult on the basis of kinetic data only. However, the results of IR study suggest that (3) appears to be more appropriate. The kinetic scheme does not change much for the two temperatures. Kinetic study also revealed that selectivity of the N_2O formation is slightly dependent upon the contact time as shown in Fig. 3. The selectivity ratio N_2/N_2O was extrapolated to exactly 2: 1 at contact time 0. The increase of the ratio at longer contact times indicates a consecutive reduction of N_2O to N_2.

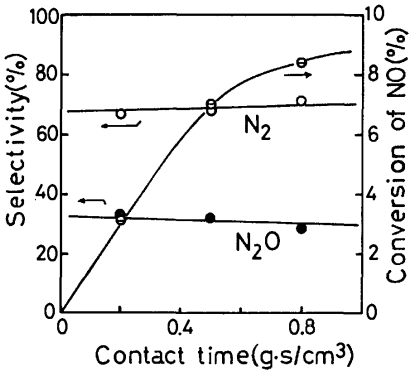

Fig. 3. Effect of the contact time on the conversion and selectivity of the NO-NH_3 reaction.

IR Study on NO-NH_3 Reaction. IR study was carried out to pursue *in situ* the reaction between NO and NH_3 over Cu(II)NaY catalysts. NH_3 undergoes adsorption on both the zeolite skeleton and the Cu(II) ions exchanged. The latter amounts to 3—4 NH_3 molecules per Cu(II) ion at room temperature in agreement with the result of Lunsford *et al.* who reported the formation of tetraammine complexes of Cu(II) ions in the zeolite cavity.[4] As for the NO adsorption, *ca.* one NO molecule is adsorbed per Cu(II) ion at room temperature with no detectable adsorption on the zeolite skeleton.

The results of IR spectroscopic study of the reaction at room temperature are shown in Figs. 4 and 5. A 32% Cu(II) ion-exchanged zeolite was used. The zeolite wafers were evacuated for 4 h at 400 °C in the IR cell before experiments. Introduction of NO over Cu(II)NaY gave curve 2 in Fig. 4. A strong absorption band at 1910 cm^{-1} is attributable to the stretching of the

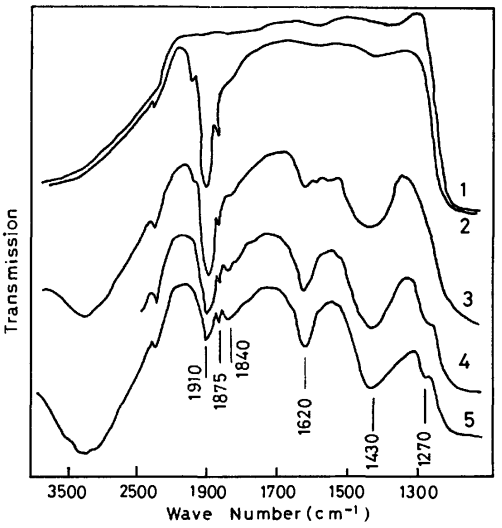

Fig. 4. Infrared spectra produced on introduction of NH_3 over a Cu(II)NaY preadsorbing NO (recorded at 25 °C). (1) Cu(II)NaY after evacuation at 400 °C for 4 h. (2) 30 min after the exposure to NO (49.5 Torr) at 25 °C. (3), (4), and (5) 30, 60, 180 min after the introduction of NH_3 (8 Torr) to (2), respectively.

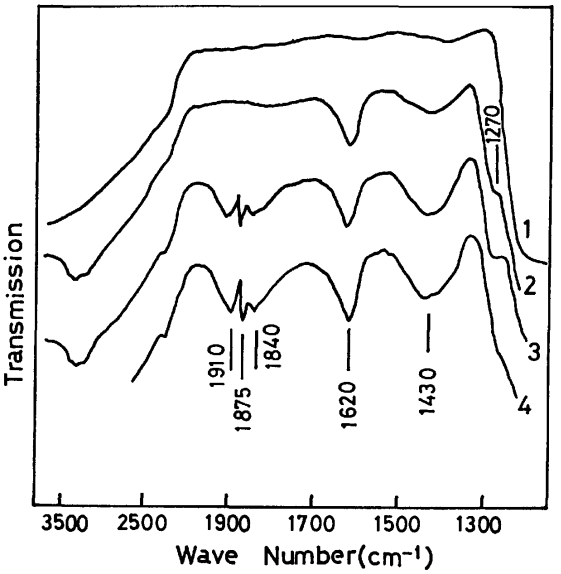

Fig. 5. Infrared spectra produced on introduction of NO over a Cu(II)NaY preadsorbing NH_3.
(1) Cu(II)NaY after evacuation at 400 °C for 4 h. (recorded at 25 °C). (2) Cu(II)NaY evacuated for 30 min after the adsorption of NH_3 (0.75 Torr) at 25 °C. (3) 60 min after the introduction of NO (64 Torr) to (2) at 25 °C. (4) After heating of (3) to 80 °C.

adsorbed NO, as first reported by Tarrit *et al.*[9] Bands at 1875 cm^{-1} are ascribable to gaseous NO. Gaseous NO shows a typical rotation-vibration spectrum with its Q branch centered at 1875 cm^{-1}, as exemplified by curve 2 or 3 in Fig. 5. A band at 2240 cm^{-1} is due to gaseous N_2O, mainly brought about as an impurity contained in NO gas. Curves 3, 4, and 5 in Fig. 4 were recorded 30, 60, and 180 min respectively after the addition of NH_3 (8 Torr). The band at 1910 cm^{-1} became weaker with the elapse of time while the intensities of the band at 1620 cm^{-1} and a broad one at 1430 cm^{-1} increased. A shoulder at 1270 cm^{-1} is a characteristic band due to the symmetric deformation vibration of NH_3 contained in $Cu(II)(NH_3)_4$.

NH_3 was adsorbed prior to the introduction of NO (Fig. 5). In curve 1, bands at 1270 and 1620 cm^{-1} and a broad band around 3300 cm^{-1} are ascribable to adsorbed NH_3, while a broad band around 1430 cm^{-1} is due to the deformation vibration of NH_4^+ formed. Major changes in the spectra caused by the introduction of gaseous NO (64 Torr) were the increase of the broad band centered at 1430 cm^{-1} and the slight increase of the band at 1620 cm^{-1}. Bands in 1910—1840 cm^{-1} of curves 2 and 3 are attributed to gaseous NO. Throughout Figs. 4 and 5, there is no evidence for the formation of nitrosyl ammine complex of Cu(II) ions. The NO adsorption is much weaker as compared with NH_3 adsorption. The adsorbed NO is easily replaced by NH_3. This makes the Langmuir-Hinshelwood type of reaction between adsorbed NO and adsorbed NH_3 (Eq. 2) less plausible. The reaction between NO and NH_3 gives rise to a remarkable increase in intensity of the broad band around 1430 cm^{-1}. It is probable that this band is in fact a composite of bands responsible for NH_4^+ and some other adsorbates. It seems that in this case the absorption of NO_2^- overlaps that for NH_4^+. NO_2^- shows absorption at 1430 and 1330 cm^{-1} in $[Co(NH_3)_nNO_2]^{2+}$, and at 1630, 1420, 1332, and 1260 cm^{-1} in $K_2Ba[Cu(NO_2)_6]$.[10,11]

Regeneration of Cu(II) from Cu(I). The bell-shaped dependence of the catalytic activity of Cu(II)-NaY catalysts implies that a reversible redox change occurs between Cu(II) and Cu(I) with the change in reaction temperature. Elucidation of the redox step is considered to contribute to the understanding of the catalytic reaction. A study was made on how the Cu(I) ions produced in the catalytic reaction at high temperature were reoxidized by lowering temperature in the same system. The experiments were performed in a flow system as well as in a pulse reactor. In the flow experiments, either a gas of NO (3%), NH_3 (2%), and He (95%) or a purge gas of He was allowed to flow (60 cm^3/min) over the catalyst bed. Cu(II)NaY with 60% cation exchange were first treated in a stream of the gas mixture at 300 °C for 4 h and then purged by He stream for 15 min. Almost all the Cu(II) ions were reduced to Cu(I) as revealed by ESR. The reduced sample was then cooled to the desired temperature and brough again into contact with the flow of the gas mixture. This caused a transient reaction to occur until a stationary catalytic reaction between NO and NH_3 was reached. The stationary state was reached

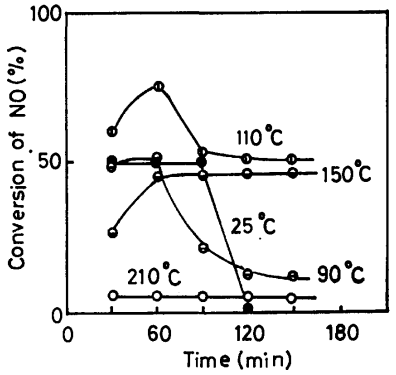

Fig. 6. Time course of NO conversion observed when gas mixture NO (3%)+NH_3 (2%) was contacted to reduced copper ion-exchanged Y zeolites at various temperatures.

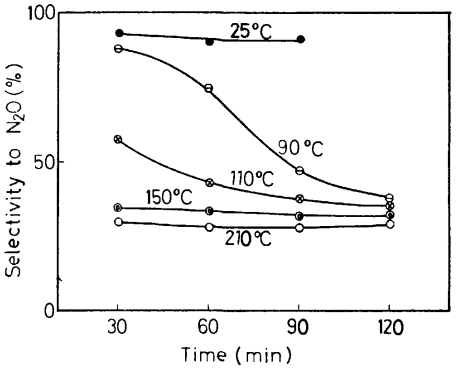

Fig. 7. Time course of the slectivity to N_2O, corresponding to Fig. 6.

within 60 min at 150 °C and above, while a period longer than 2 h was required at 90 °C and below.

The transients in conversion of NO and in selectivity for N_2O formation are shown in Figs. 6 and 7, respectively. The former transients are complicated. Selectivity for N_2O formation, on the contrary, showed monotonous decreases with time from the initial values to the stationary ones near 1/3 except for the case at 25 °C, where no stationary reaction proceeded at a

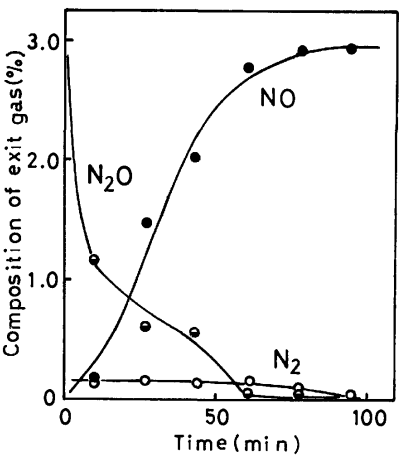

Fig. 8. Time course of N_2O and NO formation observed when NO (3%)+NH_3 (2%) was contacted to a reduced copper ion-exchanged 13X zeolites at 15 °C. Contact time; 1.0 g·s/cm^3.

significant rate. The high N_2O selectivity at the initial period, especially at lower temperatures, suggests that the transient reaction is connected to the reoxidation of Cu(I) to Cu(II). The transients at 15 °C are described in more detail in Fig. 8. In this case, Cu(II)Na 13X with 66% Cu(II) ion-exchanged was used after the reduction. The consumption of NO decreased rapidly with time until it ceased within *ca.* 1 h. A corresponding change took place in the evolution of N_2O, while N_2 formation in small quantities decreased more gradually over a longer reaction period. The color of the catalyst turned rapidly into pale greyish blue on contact with the gas mixture, and then gradually into blue developing from an upstream end of the catalyst bed to another. When the catalyst became entirely blue, N_2O formation stopped. The greyish blue might be due to the complex formation of a trace amount of unreduced Cu(II) ions with NH_3. The blue coloration is ascribable to the ammine complex of the Cu(II) ions regenerated.

The transient reaction at 15 °C was examined by a pulse reaction technique in order to obtain quantitative information. It was found that 2.7 mol of NO and 0.8 mol of N_2O are consumed and formed, respectively, to regenerate 1.0 mol of Cu(II). This strongly indicates the following disproportionation reaction.

$$Cu(I)(NH_3)_m \xrightarrow{+3NO} Cu(II)(NH_3)_mNO_2^- + N_2O \quad (4)$$

The reaction was found to proceed only in the presence of NH_3. After the completion of reaction, the catalyst, when heated at 150 °C in the same atmosphere, evolved a large amount of N_2 presumably by the following reaction.

$$Cu(II)(NH_3)_mNO_2^- + NH_4^+{}_{ad} \longrightarrow Cu(II)(NH_3)_m + N_2 + 2H_2O \quad (5)$$

Nitrite ion NO_2^- is known to react with NH_4^+ to produce N_2. Reaction (5) is considered to be slow at 25 °C, judging from the prolonged evolution of a small amount of N_2 (Fig. 8).

Discussion

From the results, we propose the following reaction path for the steady reaction between NO and NH_3 over Cu(II)NaY catalysts.

$$Cu(II)(NH_3)_n + NO \longrightarrow Cu(I)(NH_3)_m + N_2 + H_2O + (n-m-1)NH_3 + H^+{}_{ad} \quad (6)$$

$$H^+{}_{ad} + NH_3 \longrightarrow NH_4^+{}_{ad} \quad (7)$$

$$Cu(I)(NH_3)_m + 3NO \longrightarrow Cu(II)(NH_3)_mNO_2^- + N_2O \quad (8)$$

$$Cu(II)(NH_3)_mNO_2^- + NH_4^+{}_{ad} \longrightarrow Cu(II)(NH_3)_m + N_2 + 2H_2O \quad (9)$$

$$Cu(II)(NH_3)_m + (n-m)NH_3 \longrightarrow Cu(II)(NH_3)_n \quad (10)$$

$$4NO + 2NH_3 \longrightarrow 2N_2 + N_2O + 3H_2O \quad (11)$$

Here, n and m are the numbers of NH_3 molecules coordinating to a Cu(II) ion, probably 4 and 2, respectively, because of the complexes $Cu(II)(NH_3)_4$ and $Cu(I)(NH_3)_2$. Reaction (6), initiated between NO and coordinated NH_3, produces N_2, H_2O, and an atomic hydrogen, the last species of which reduces a Cu(II) ion to Cu(I) through a electron transfer. The H^+ produced is adsorbed on the framework oxygen of zeolite, being ammoniated to form NH_4^+ according to Reaction (7). Reactions (6) and (7) are supported by the result of IR study which shows that the band intensity of NH_4^+ at 1430 cm^{-1} for NH_3-preadsorbed Cu(II)-NaY increases on contact with NO. Reaction (8), which is identical with Reaction (4), is applied to regenerate Cu(II) ions. The NO_2^- produced then reacts with NH_4^+ by Reaction (9) to evolve N_2. The overall reaction is reduced to Reaction (11) which explains the observed N_2O selectivity at zero contact time.

The bell-shaped temperature dependence of catalytic activity is explained as follows. At temperatures lower than 120 °C, Reaction (6) is slow and rate-determining. Above 120 °C, on the other hand, it is presumed that Reaction (8) becomes less and less favored with an increase in temperature, causing the stationary Cu(II) concentration and therefore the steady reaction rate also to decrease with increasing temperature.

Reaction (8) can formally be separated into the following two reactions.

$$3NO \longrightarrow NO_2 + N_2O \quad (12)$$

$$Cu(I)(NH_3)_m + NO_2 \longrightarrow Cu(II)(NH_3)_mNO_2^- \quad (13)$$

The disproportionation reaction of NO on zeolites was first reported by Addison and Barrer.[12] They found that over unexchanged zeolites the reaction is fast at dry ice temperature or at 0 °C but very slow at 25 °C. Regarding Reaction(13), Kasai and Bishop reported that addition of NO_2 to Cu(I)NaY at room temperature restores the ESR signal of Cu(II) instantaneously.[13] The important result in the present study is that Reaction (8) proceeds only in the presence of NH_3. This implies that Reaction(8) can not be separated into Reactions(12) and (13). The crucial role of NH_3 for Reaction (8) may come from two possible effects.

(1) The redox potential between Cu(I) and Cu(II) is lowered by the formation of ammine complexes; it is 0.153 eV for $Cu(I) \rightarrow Cu(II) + e$, whereas −0.01 eV for $Cu(I)(NH_3)_2 + 2NH_3 \rightarrow Cu(II)(NH_3)_4 + e$.

(2) The location of copper ions in the zeolite framework is affected by the presence of NH_3. As a result of coordination, NH_3 pulls out copper ions from the sodalite cage or hexagonal prism toward the supercage in which the copper ion becomes more easily accessible for reactants.

Which of the two effects is more dominant can not be distinguished at present. However, the same effects can be operative for the depression of the reaction rate above 120 °C. The dissociation pressure of NH_3 for $CuSO_4 \cdot 4NH_3 \rightarrow CuSO_4 \cdot 2NH_3 + 2NH_3$ is 0.08 atm at 120 °C.[14]

It is of interest to compare the present reaction with the oxidation of ammonia with oxygen over Cu(II)NaY catalyst reported by Williamson *et al.*[15] In the latter reaction, the rate was found to show first and zero orders with respect to NH_3 and O_2, respectively, and was concluded to be solely determined by a step in which Cu(II) ions are reduced to Cu(I) by NH_3. There are several marked contrasts between the reactions of

NH_3–NO and NH_3–O_2.

(1) The dependence of the rate on the NH_3 partial pressure differs entirely for the two reaction. This reflects that, unlike the NH_3–O_2 reaction, the NH_3–NO reaction does not follow a simple redox mechanism.

(2) The NH_3–NO reaction is characterized by the bell-shaped temperature dependence, whereas the rate of the NH_3–O_2 reaction shows a normal increase with increasing temperature. This indicates that, at higher temperatures, the reoxidation of Cu(I) to Cu(II) is much slower in the former case. This would be important when the NH_3–NO reaction is carried out in the presence of oxygen.

The present work was partially supported by a Grant-in-Aid for Scientific Research from the Ministry of Education (No. 110306)

References

1) T. Seiyama, T. Arakawa, T. Matsuda, N. Yamazoe, and Y. Takita, *Chem. Lett.*, **1975**, 781.

2) T. Seiyama, T. Arakawa, T. Matsuda, and N. Yamazoe, Preprints of Papers for the Japan-U.S.A. Seminar on Catalytic NO_x Reactions, Susono, Japan, November 2—4, 1975.

3) K. A. Windhorst and J. H. Lunsford, *J. Am. Chem. Soc.*, **97**, 1407 (1975).

4) D. R. Flentge, J. H. Lunsford, P. A. Jacobs, and J. B. Uytterhoeven, *J. Phys. Chem.*, **79**, 354 (1975).

5) E. F. Vansant and J. H. Lunsford, *J. Phys. Chem.*, **76**, 2860 (1972).

6) I. E. Maxwell and J. J. de Boer, *J. Phys. Chem.*, **79**, 1874 (1975).

7) P. Gallezot, Y. B. Tarrit, and B. Imelik, *J. Catal.*, **26**, 295 (1973).

8) Yung-Yang Huang and E. F. Vansant, *J. Phys. Chem.*, **77**, 663 (1973).

9) Y. B. Tarrit, C. Naccache, and B. Imelik, *J. Chim. Phys.*, **70**, 728 (1973).

10) K. A. Windhorst and J. H. Lunsford, *J. Am. Chem. Soc.*, **97**, 1407 (1975).

11) K. Nakamoto "Infrared Spectra of Inorganic and Coordination Compounds," John Wiley and Sons, New York (1970), p. 160.

12) W. E. Addison and R. M. Barrer, *J. Chem. Soc.*, **1955**, 757.

13) P. H. Kasai and R. J. Bishop, Jr., *J. Phys. Chem.*, **77**, 2308 (1973).

14) C. J. Westand and N. E. Dorsey, "International Critical Table," McGraw-Hill Book Company, Vol. 7, New York (1930), p. 263.

15) W. B. Williamson, D. R. Flentge, and J. H. Lunsford, *J. Catal.*, **37**, 258 (1975).

ESR of Hot Ions: Low Spin Pt(III) Complex Ions Produced by γ-Irradiation

Chikara AMANO* and Shizuo FUJIWARA

Department of Chemistry, Faculty of Science, The University of Tokyo, Hongo, Bunkyo-ku, Tokyo 113

(Received December 9, 1976)

Tervalent platinum complex ions have been observed by the electron spin resonance method upon γ-irradiation of both bivalent and quadrivalent complexes. From their g-values, the tervalent complex ions can be classified into two types, one axially symmetric and the other rhombic, the former having typical g-values of 2 ($g_{//}$) and 2.4($g_{\perp}$), and the latter a g_1-value slightly lower than the free electron value of 2.0023. It has been shown by means of ligand field theory that both types have $5d^7$ low spin electron configuration. The hyperfine interaction due to ^{195}Pt is one order of magnitude larger than that in cobalt complexes with $3d^7$ low spin configuration, indicating that the configuration interaction involving 6s-orbital is more important than that for 3d transition metal complexes involving 4s-orbital, and that 5d electrons penetrate deeply into inner shells, resulting in core polarizarion.

γ-Irradiation produces metal complex ions with unusual valence states, Co^{2+}, Ni^{+}, Pd^{+}, Zn^{+}, Cd^{+} *etc.*[1-4] All these hot ions are produced through reduction of original complexes having the usual valence. Thus univalent platinum complexes which seem to have $5d^9$ electron configuration are expected to be produced by γ-irradiation of bivalent complexes. The electronic states of transition metal ions belonging to the 5d group remain unclarified. Neither visible nor ultraviolet absorption spectra have been assigned to any transitions between multiplet states, and the order of one-electron energy levels has not been established. Almost all the complexes with d^9 electron configuration studied thus far show the same type of g-value: $g_{//}>g_{\perp}>2$. It has not been clarified whether univalent platinum complexes show this type of g-value.

In the present work eleven bivalent platinum complexes and three quadrivalent ones were γ-irradiated at 77 K and their ESR spectra were recorded. The present paper reports on a new valence state of tervalent platinum complex ions along with a discussion on their electronic state.

Experimental

Both platinum metal and hydrogen hexachloroplatinate(VI) ($H_2PtCl_6 \cdot 6H_2O$) were used to synthesize bivalent and quadrivalent platinum complexes. Copper(II) ions contained in commercial $H_2PtCl_6 \cdot 6H_2O$ were removed in synthetic processes; they were not found in potassium tetrachloroplatinate(II). The complexes subjected to γ-irradiation are summarized in Table 1. Each complex of polycrystalline state was put into a radiation-protected sample tube for ESR measurement, in 50—100 mg amount. The sample tubes were immersed in liquid nitrogen and subjected to γ-irradiation at 77 K. They were inverted on γ-irradiation, the upper half of the tubes shielded with lead blocks to prevent production of paramagnetic centers. The tubes were again inverted before ESR measurement. The total dose was 10^6 R with a 5×10^4 R/h dose rate at 77 K, and 10^7 R with a 5×10^5 R/h dose rate at room temperature. ESR spectra were recorded with a JEOL 3BSX spectrometer.

Results and Discussion

$[Pt(py)_4]Cl_2 \cdot 3H_2O$. The ESR absorption shown in Fig. 1 was obtained on γ-irradiation of a polycrystalline sample. The strong absorption at about 2800 G shows a large g-shift ($\Delta g=g-2.0023$), which suggests that the paramagnetic center is due to a platinum complex; the large g-shift is caused mainly by the strong spin-orbit interaction. Platinum has a large spin-orbit coupling constant, *e.g.* 3368 cm^{-1} for Pt^+ ion.[5] The strong singlet line is accompanied by weak doublet satellite lines at 2300 and 3100 G. The doublet

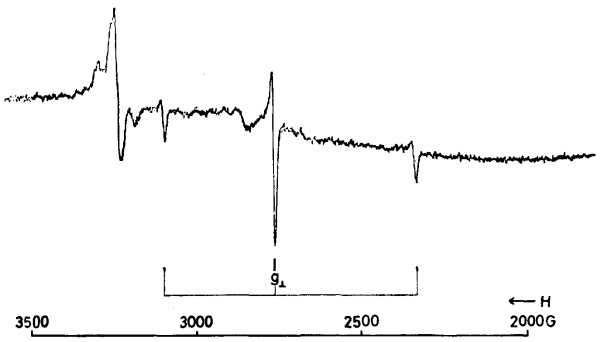

Fig. 1. The ESR spectrum of $[Pt(py)_4]^{3+}$ produced by γ-irradiation.

TABLE 1. BIVALENT AND QUADRIVALENT PLATINUM COMPLEXES

Pt(II):	$K_2[Pt(NO_2)_4] \cdot 2H_2O$, $K_2[Pt(CN)_4] \cdot 3H_2O$, $K_2[Pt(C_2O_4)_2]$, $[Pt(NH_3)_4]Cl_2$, $[Pt(py)_4]Cl_2 \cdot 3H_2O$, $[Pt(acac)_2]$, *cis*-$[Pt(py)_2Cl_2]$, $[Pt(gly)_2]$, $[Pt(dmgH)_2]$, $[Pt(xant)_2]$, *trans*-$[Pt(Py)_2Cl_2]$
Pt(IV):	$K_2[PtCl_6]$, $K_2[PtI_6]$, $K_2[Pt(SCN)_6]$
	C_2O_4: oxalate, py: pyridine, acac: acetylacetonate, gly: glycinate, dmgH: dimethylglyoximate, xant: ethylxanthate

* Present address: Department of Engineering Physics, The University of Electro-Communications, Chofugaoka, Chofu, Tokyo 182.

Table 2. Predicted g-values for four cases

Case	Configuration	Multiplet	$g_{//}$	$g_{\perp}$	Order
A	d^9	$^2B_{1g}$	$2+8\zeta/E(^2B_{2g})$[a]	$2+2\zeta/E(^2E_g)$	$g_{//}>g_{\perp}>2$
B	d^9	$^2A_{1g}$	2	$2+6\zeta/E(^2E_g)$	$g_{\perp}>g_{//}=2$
C	d^7	$^2A_{1g}$	2	$2+(3+6a_1b_1)\zeta/E(^2E_g{}^a)$ $+(3+6a_2b_2)\zeta/E(^2E_g{}^b)$	$g_{\perp}>g_{//}=2$
D	d^7	$^2B_{1g}$	$2+(4+8a_1b_1)\zeta/E(^2B_{2g})^a)$ $+(4+8a_2b_2)\zeta/E(^2B_{2g}{}^b)$[b]	$2+(1+2a_1b_1)\zeta/E(^2E_g{}^a)$ $+(1+2a_2b_2)\zeta/E(^2E_g{}^b)$	$g_{//}>g_{\perp}>2$

a) Energy value of multiplet when that of the ground multiplet is set to zero. b) $a_1=-10B/\{(4B+C+A)^2+100B^2\}^{1/2}$, $b_1=(4B+C+A)/\{(4B+C+A)^2+100B^2\}^{1/2}$, $a_2=-10B/\{(4B+C-A)^2+100B^2\}^{1/2}$, $b_2=(4B+C-A)/\{(4B+C-A)^2+100B^2\}^{1/2}$, $A=(116B^2+8BC+C^2)^{1/2}$. A, B, and C are Racah's parameters.

has a large splitting of *ca.* 800 G, presumably due to the hyperfine interaction with ^{195}Pt, only one stable isotope with nonzero nuclear spin 1/2. Since the natural abundance of ^{195}Pt is 33.8%, the relative absorption strength of one of the doublets to the main singlet should be 1/4 (Fig. 1). The shift of the singlet from the center of the doublet toward upper field is due to the large hyperfine interaction with ^{195}Pt nucleus.[6] The spectral feature shows that the paramagnetic platinum complex ion produced takes axial symmetry and the absorption at 2800 G is a perpendicular component. The parallel component should be much weaker than the perpendicular one. It would be observed near 3300 G, where the strong absorption of unidentified radicals obscures the observation of the parallel component. Careful investigation shows that no parallel component was found at any other magnetic field strength.

The value of $g_{\perp}$ was found to be 2.377 ± 0.002, which can be directly calculated from the main singlet line, that of $g_{//}$ being probably 2. The principal value of the hyperfine splitting tensor due to ^{195}Pt, $A_{\perp}$, also obtained by use of the usual second order perturbation formula, is 877×10^{-4} cm^{-1}.[6]

As regards the valence state of paramagnetic platinum complexes, two possibilities should be considered, univalent complexes with $5d^9$ electron configuration and tervalent complexes with $5d^7$ electron configuration. The g-values for possible ground states for these two valences have been calculated by means of ligand field theory (Table 2).[2] The experimental g-values are consistent in cases B and C. However, B corresponds to the structure of uniaxially compressed D_{4h}, found to be very rare for d^9 configuration, while C corresponds to the uniaxially elongated structure, which seems reasonable in consideration of the tetragonaly four-coordinated structure of the original complex. The complexes having d^7 low spin configuration have been shown to take this multiplet in several cases.[7,8] Thus, the paramagnetic center observed can be assigned to a tervalent platinum complex ion which takes $^2A_{1g}$ as the ground multiplet, having one unpaired electron in $5d_{z^2}$ orbital.

In contrast to the transition metal complexes of the 3d group, no systematic studies have been made on the electronic state of the 5d group. Optical absorption spectra of some Pt(II) complexes were studied by Chatt, Gamlen, and Orgel.[9] The order of the one electron energy level for $[PtCl_4]^{2-}$ was determined: $5d_{x^2-y^2}>5d_{xy}>5d_{yz,zx}>5d_{z^2}$, though the position of $5d_{z^2}$ was uncertain. However, it seems difficult to assign an absorption band to a certain transition between multiplets because of the presence of strong spin-orbit coupling. Krigas and Rogers studied γ-irradiation of $K_2[PtCl_4]$ by the ESR method and found the formation of $[PtCl_5]^{2-}$ with $5d^7$ electron configuration.[10] Since the original $[PtCl_4]^{2-}$ takes a tetragonally four-coordinated structure, one chlorine ion appears to be attached to the axial position in the course of oxidation. It is concluded that one electron energy level of $[PtCl_5]^{2-}$ has the order: $5d_{x^2-y^2}>5d_{z^2}>5d_{xy}>5d_{yz,zx}$. The unusually high energy of $5d_{z^2}$ was explained to be caused by the presence of the axial chloride ion. The present g-values of $[Pt(py)_4]^{3+}$ are also in line with this order. However, there can be no chloride ion at the axial position, since the absorption of the perpendicular part (Fig. 1) has a very narrow width of about 20 G, showing neither hyperfine splitting by chlorine nucleus nor line broadening due to unresolved structure by chlorine.

Let us compare the hyperfine splitting of $[Pt(py)_4]^{3+}$ with that of bivalent cobalt complexes having $3d^7$ low spin configuration. A comparison between tervalent nickel and tervalent palladium and tervalent platinum complexes would have been preferable, but we could not obtain the A-values of either tervalent nickel or tervalent palladium of low spin type. We chose β-cobaltphthalocyanine as an example, since this is one of the few bivalent cobalt complexes taking low spin configuration. A-values of β-cobaltphthalocyanine have been reported to be 160×10^{-4} cm^{-1} ($A_{//}$) and 280×10^{-4} cm^{-1} ($A_{\perp}$).[7] In order to see the effect of electron orbitals, we compared the values which can be obtained by dividing the experimental A-values by nuclear moment of each isotope. They are 60.3 for the cobalt complex and 1480 for the platinum complex on a ceartin scale, which shows that the latter is about twenty times greater than the former. In 5d transition metal complexes the valence electrons mainly in metal 5d orbitals could penetrate deeply near the metal nucleus because of the incomplete shielding of the nuclear potential by the other inner closed shell electrons, resulting in large core polarization.

$K_2[Pt(NO_2)_4]\cdot2H_2O$. There is a strong absorption at 2500 G with a weak satellite at 1900 G (Fig. 2). This should be due to platinum complexes because of the large g-shift and the large hyperfine splitting. From the line shape this can be ascribed to the perpendicular component, which splits slightly to form g_2 and g_3 component. A parallel component is also observed at

Table 3. ESR parameters of low spin Pt^{3+} complexes

A) Axial symmetry

Complexes	$g_{//}$	$g_{\perp}$	$A_{//}$	$A_{\perp}$ (10^{-4} cm^{-1})
$[Pt(py)_4]^{3+}$	(≈2)	2.377	—	877
$[Pt(NH_3)_4]^{3+}$	(≈2)	2.395	—	940
cis-$[Pt(py)_2Cl_2]^{+}$	(≈2)	2.544	—	768
$[PtCl_6]^{3-}$	(≈2)	2.659	—	591

B) Rhombic symmetry

Complexes	g_1	g_2	g_3	A_1	A_2	A_3 (10^{-4} cm^{-1})
$[Pt(gly)_2]^{+}$	1.939	2.338	2.674	1025	—	1210
$[Pt(NO_2)_4]^{-}$	1.910	2.572	2.622	1690	—	—

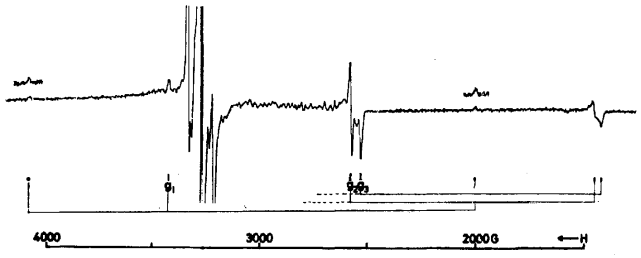

Fig. 2. The ESR spectrum of $[Pt(NO_2)_4]^{-}$ produced by γ-irradiation. The splitting of $g_{\perp}$ part shows the small distortion of ligand configuration.

slightly upper field than that of strong absorptions due to unidentified radicals with *g*-value of 2. Very weak satellites are observed at both 2000 and 1400 G. The ESR parameters obtained are given in Table 3.

Since original $[Pt(NO_2)_4]^{2-}$ has square-planar configuration of ligand ions, the tervalent platinum complex produced through oxidation should show a line with axial symmetry, if the original configuration is maintained. However, the line shape (Fig. 2) indicates that the tervalent platinum has a slightly deformed ligand configuration. Some of the complexes having d^7 low spin configuration have been shown to have smaller $g_{//}$- or g_1-value like this. As an example, β-cobaltphthalocyanine has $g_{//}$ of 1.91.[7] Griffith tried to explain this by means of ligand field theory.[11] He assumed several ground multiplets which arise from different orders of one electron energy levels, and concluded that the ground state is $|d_{zx}\bar{d}_{zx}d_{yz}\bar{d}_{yz}d_{xy}\bar{d}_{xy}d_{z^2}|$ and that the smaller $g_{//}$ than 2 is due to the third order terms of spin-orbit interaction. It is uncertain, however, whether the sum of many spin-orbit terms can result in $g_{//}$ smaller than 2. On the other hand, we presume that g_1 smaller than 2 is caused by the lowering of symmetry from D_{4h}. In D_{2h} symmetry, $5d_{z^2}$ orbital mixes with $5d_{x^2-z^2}$ to form new one-electron eigenfunctions. It can be assumed from the small splitting of $g_{\perp}$ component observed that the distortion from D_{4h} to D_{2h} is small. We obtained one-electron eigenfuctions in D_{2h} ligand field $5d_{xy}$, $5d_{yz}$, $5d_{zx}$, $5d_{z^2}'=(1+a^2)^{-1/2}(5d_{z^2}+a5d_{x^2-y^2})$ and $5d_{x^2-y^2}'=(1+a^2)^{-1/2}(5d_{x^2-y^2}-a5d_{z^2})$, where *a* is a small mixing coefficient. Considering electron-electron repulsion, the ground multiplet becomes $|^2A_{1g}1/2>=|5d_{yz}\bar{5}d_{yz}5d_{zx}\bar{5}d_{zx}5d_{xy}\bar{5}d_{xy}5d_{z^2}'|$. Applying the usual perturbation formula to calculate *g*-values, we have $g_1=2+8a^2(1+a^2)^{-1}/E(^2B_{1g}-{}^2A_{1g})$. This predicts that g_1 is slightly greater than 2, a disappointing result. The simple model presented here gives no reasonable explanation of the observed *g*-value.

cis-*[Pt(py)$_2$Cl$_2$]*. Although this complex does not have a fourfold axis, the electronic state can be explained approximately in terms of D_{4h}. The ligand field of *cis*-type complexes has D_{4h} symmetry contrary to their geometrical symmetry.[12] The ESR spectrum which can be assigned to $[Pt(py)_2Cl_2]^{+}$ from its large *g*-shift showed that the complex has D_{4h} or C_{4v} symmetry in spite of the lack of a fourfold axis in geometrical structure. This suggests that the tervalent platinum complex ion does not suffer from distortion through oxidation. $g_{//}$ is probably 2, though it was not observable in the superposition of the strong absorption of unidentified radicals. *trans*-$[Pt(py)_2Cl_2]$ was also examined, but it gave no ESR absorption other than that of radicals at 3300 G. This indicates that the tervalent complex of the *cis*-type is produced in a greater amount than the *trans*-type by a factor of at least 100.

trans-*[Pt(gly)$_2$]*. This complex has a asymmetry between the axis of N–Pt–N and that of O–Pt–O in the plane formed by ligand and a central platinum ion. Thus, the ESR spectrum of the tervalent platinum complex produced by oxidation should show asymmetric shape with three different principal values of *g*-tensor (Fig. 3). The g_1-value less than 2, 1.939 also obtained in this case, suggests that a g_1-value smaller than 2 may be due to the lack of a fourfold axis.

K_2[PtCl$_6$]. A tervalent platinum complex was produced on γ-irradiation at room temperature. This tervalent platinum has different ESR parameters from

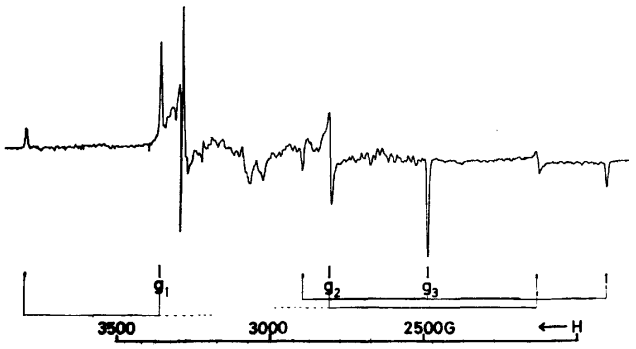

Fig. 3. The typical rhombic ESR spectrum of $[Pt(gly)_2]^{+}$ produced by γ-irradiation.

the paramagnetic chlorine-coordinated platinum complexes reported by Krigas and Rogers.[10] $g_{//}$ was not observable, but it is probably 2, considering that ESR absorption was not observed at any other position than near 3300 G where unidentified absorption of complex structure was observed. On the other hand, γ-irradiation at 77 K gave ESR absorption, which may come from platinum complexes by considering its large g-shift, +0.379. However, the hyperfine splitting due to ^{195}Pt was not clearly observed. The $g_{\perp}$-value is similar to that of the $[PtCl_5]^{2-}$ reported by the above authors.

In contrast to the formation of univalent complexes upon γ-irradiation of bivalent nickel and bivalent palladium complexes, γ-irradiation of bivalent platinum complexes gives tervalent complexes but not univalent ones. Since ionization probability is proportional to electronic density, it seems reasonable that the tervalent platinum complexes are produced in a greater amount than tervalent nickel or palladium complexes. The tervalent platinum complexes usually take $5d^7$ low spin electron configuration and show typical g-values like those of 3d complexes: $g_{\perp} > g_{//} \approx 2$. The $g_{\perp}$-value smaller than 2 observed in rhombic complexes seems to come from the lack of a fourfold axis, but no simple explanation can be given. The A-values of the tervalent platinum complexes are usually one order greater than those of the cobalt complexes, suggesting that 5d electrons penetrate deeply into the closed shell and result in the large core polarization. The yield of the tervalent platinum complexes varies from complex to complex, as shown typical between *cis*- and *trans*-$[Pt(py)_2Cl_2]$. It is interesting to see whether univalent platinum complexes would show the typical g-values of $3d^9$ and $4d^9$ complexes: $g_{//} > g_{\perp} > 2$.

We wish to thank Dr. Yoji Arata for reading this manuscript.

References

1) S. Fujiwara, T. Watanabe, and H. Tadano, *J. Coord. Chem.*, **1**, 196 (1971).
2) C. Amano and S. Fujiwara, *Bull. Chem. Soc. Jpn.*, **46**, 1379 (1973).
3) M. Nakamura and S. Fujiwara, *J. Coord. Chem.*, **1**, 221 (1971).
4) J. Isoya and S. Fujiwara, *Bull. Chem. Soc. Jpn.*, **45**, 2182 (1972).
5) J. S. Griffith, "The Theory of Transition-Metal Ions," Cambridge University Press (1961), p. 438.
6) B. Bleaney, *Philos. Mag.*, **42**, 441 (1951); By using the second order perturbation formula, the resonant field is shown to be

$$H_{du} = [h\nu + A_{\perp}/2 + \{(h\nu + A_{\perp}/2)^2 - (A_{//}^2 + A_{\perp}^2)/2\}^{1/2}]/2g_{\perp}\beta$$

for the upper component of the hf doublet,

$$H_{dl} = [h\nu - A_{\perp}/2 + \{(h\nu - A_{\perp}/2)^2 - (A_{//}^2 + A_{\perp}^2)/2\}^{1/2}]/2g_{\perp}\beta$$

for the lower component and $H_s = h\nu/g_{\perp}\beta$ for that of the singlet.
7) J. M. Assour and W. K. Kahn, *J. Am. Chem. Soc.*, **87**, 207 (1965).
8) S. Geschwind and J. P. Rameika, *J. Appl. Phys.*, **33**, 721 (1961).
9) J. Chatt, G. A. Gamlen, and L. E. Orgel, *J. Chem. Soc.*, **1958**, 486.
10) T. Krigas and M. T. Rogers, *J. Chem. Phys.*, **55**, 3035 (1971).
11) J. S. Griffith, *Nature*, **182**, 81 (1959).
12) C. J. Ballhausen, "Introduction to Ligand Field Theory," McGraw-Hill Book Company Inc. (1962).

The Effect of NCS^- on the Radiation-induced Decoloration of Azo and Anthraquinone Dyes in N_2O-saturated Aqueous Solutions

Nobutake SUZUKI and Hiroshi HOTTA

Japan Atomic Energy Research Institute, Takasaki Radiation Chemistry Research Establishment, Takasaki, Gunma 370-12

(Received December 13, 1976)

The radiation-induced decoloration of azo and anthraquinone dyes was studied in N_2O-saturated aqueous solutions containing NCS^-. In the N_2O-saturated solutions, the decoloration yield, $G(-\text{Dye})$, increased markedly upon the addition of NCS^-, which is an efficient scavenger of the OH radical—that is, from 1.46 up to 2.10 for Acid Red 265 and from 0.51 up to 1.51 for Acid Blue 40 upon the addition of 1 mM NCS^-. In the nitrogen-saturated solutions, however, the $G(-\text{Dye})$ decreased upon the addition of NCS^-. It is concluded that the increase in the $G(-\text{Dye})$ upon the addition of NCS^- in the N_2O-saturated solutions is mainly attributable to the attack of the radical anion $(NCS)_2^-$ on the ring structure of the dyes. This radical anion is formed through the following path: $NCS^- + OH \rightarrow NCS + OH^-$ and $NCS + NCS^- \rightleftarrows (NCS)_2^-$. At low NCS^- concentrations, the $G(-\text{Dye})$ decreased for Acid Red 265 and increased for Acid Blue 40. This may be attributable to the larger reactivity of $(NCS)_2^-$ on Acid Blue 40 than on Acid Red 265.

As has been described in preceding papers,[1,2] the radiation-induced decoloration of Acid Red 265 (azo dye) in aqueous solutions is mainly attributable to the attack of the OH radicals on the aromatic rings connected directly to the azo group, while that of Acid Blue 40 (anthraquinone dye) is attributable to the attack of the hydrated electrons on the carbonyl group in the anthraquinone ring, in addition to the attack of the OH radicals on the anthraquinone ring. In both cases, the decoloration is promoted in the N_2O-saturated solutions; that is, this increase in the $G(-\text{Dye})$ is due to the conversion of the hydrated electrons into the OH radicals by means of the following reaction;[3]

$$N_2O + e_{aq}^- \longrightarrow OH + OH^- + N_2. \qquad (1)$$

The yield of the OH radical in the N_2O-saturated aqueous solution $(G(OH) + G(e_{aq}^-) = 5.5)$[4] becomes about twice as large as that in the nitrogen-saturated aqueous solution $(G(OH) = 2.74)$.[4]

In such systems, the rate constants of the reactions of the hydrated electron with N_2O and Acid Blue 40 are 8.7×10^9 M^{-1} s^{-1} at pH 7[5] and 1.5×10^{10} M^{-1} s^{-1} at pH 6.3—5.1[2] respectively. In the N_2O-saturated 0.1 mM Acid Blue 40 solution, since the N_2O concentration (about 3×10^{-2} M) is about 300 times larger than the dye concentration, a large portion of the hydrated electrons are converted into OH radicals because $(8.7 \times 10^9\ M^{-1}\ s^{-1}) \times (3 \times 10^{-2}\ M) \gg (1.5 \times 10^{10}\ M^{-1}\ s^{-1}) \times (1 \times 10^{-4}\ M)$. Therefore, in the N_2O-saturated solution, the OH radical is considered to be the only active species. In the present study, the effect of NCS^-, which is an efficient scavenger of the OH radical, on the radiation-induced decoloration of azo and anthraquinone dyes was investigated in order to demonstrate the above scheme more clearly.

Experimental

The experimental procedures were the same as in the preceding works.[1,2] The dye solutions were prepared by dissolving recrystallized Acid Red 265[1] or Acid Blue 40[2] in triply distilled water. The solutions were bubbled with N_2O for 20 min prior to irradiation and were then irradiated with cobalt-60 gamma rays at room temperature.

The absorption spectra were measured with a Shimadzu UV-200 spectrophotometer. The decoloration yield was determined by measuring the optical density at 542 nm for Acid Red 265 and at 610 nm for Acid Blue 40. The NCS^- concentration was determined by the iron-thiocyanate method.[6]

Results and Discussion

N_2O-saturated NCS^- Solutions without Dye. In order to study the effect of NCS^- on the radiation-induced decoloration of the dyes in N_2O-saturated solutions, it is necessary first to elucidate the behavior of the consumption of NCS^- in a solution without the dye. Thus, the NCS^- concentration in N_2O- and nitrogen-saturated solutions without the dye was measured after irradiation.

The reduction of NCS^-, $G(-NCS^-)$, for the N_2O- and nitrogen-saturated solutions without the dye (initial pH 7.2) is shown as a function of the NCS^- concentration in Fig. 1. The $G(-NCS^-)$ for the N_2O-saturated solution increased steeply with an increase in the NCS^- concentration up to about 0.4 mM, and then it increased gradually above about 0.4 mM. The $G(-NCS^-)$ increased up to 1.72 from 0.96 in the NCS^- concentration

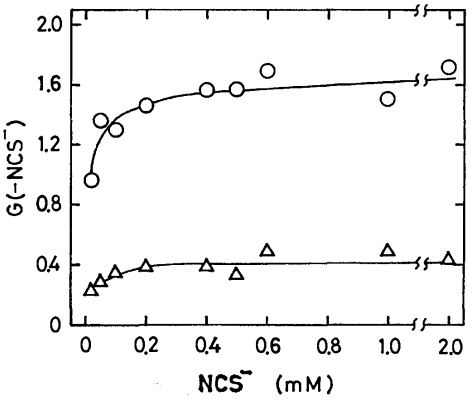

Fig. 1. $G(-NCS^-)$ as a function of NCS^- concentration in the N_2O- and nitrogen-saturated NCS^- solutions without the dye.
Dose: 1.8×10^4 rad. N_2O saturation (○) and N_2 saturation (△).

range from 0.02 to 2 mM. On the other hand, the $G(-NCS^-)$ for the nitrogen-saturated solution increased with an increase in the NCS^- concentration up to about 0.2 mM, and then it was kept nearly constant above about 0.2 mM. The $G(-NCS^-)$ increased up to 0.43 from 0.22 in the NCS^- concentration range from 0.02 to 2 mM. The ratio of $G(-NCS^-)_{N_2O}/G(-NCS^-)_{N_2}$ is about 4 ± 1 in this NCS^- concentration range.

In the irradiated N_2O-saturated solution, the hydrated electrons are converted into the OH radicals as Reaction 1. The OH radical reacts rapidly with NCS^- to form the NCS radical, following the formation of the radical anion $(NCS)_2^-$;[7,8]

$$NCS^- + OH \xrightarrow{k_2} NCS + OH^-, \quad (2)$$

$$NCS + NCS^- \underset{k_{3b}}{\overset{k_{3a}}{\rightleftharpoons}} (NCS)_2^-. \quad (3)$$

Then;[7,9]

$$2(NCS)_2^- \longrightarrow (NCS)_2 + 2NCS^-, \quad (4)$$

$$NCS + NCS \longrightarrow (NCS)_2. \quad (5)$$

Baxendale *et al.* determined the value of k_2 (2.8×10^{10} $M^{-1}s^{-1}$) from a kinetic study of the equilibrium of Reaction 3 at pH 7 by pulse radiolysis ($k_{3a}=7.0\times10^9$ $M^{-1}s^{-1}$ and $k_{3b}=3.4\times10^4$ s^{-1}).[7] On the other hand, Willson *et al.* concluded that the most reasonable value of k_2 was 1.03×10^{10} $M^{-1}s^{-1}$, since the above value was significantly higher than the values obtained by other methods.[10]

Since the ratio of $G(OH)_{N_2O}/G(OH)_{N_2}$ equals about 2, as has been described already, the ratio of $G(-NCS^-)_{N_2O}/G(-NCS^-)_{N_2}$ should equal about 2. However, the ratio of $G(-NCS^-)_{N_2O}/G(-NCS^-)_{N_2}$ (about 4 ± 1) obtained from Fig. 1 is larger than the above ratio. This may be mainly attributable to the consumption of the NCS radical by the hydrated electron in the nitrogen-saturated solution as Reaction 6:[9]

$$NCS + e^-_{aq} \longrightarrow NCS^- \quad (6)$$

N_2O-saturated Acid Blue 40 Solutions. The $G(-Dye)$ for the N_2O-saturated 0.1 mM Acid Blue 40 solutions containing NCS^- (initial pH 6.3) is shown as a function of the NCS^- concentration in Fig. 2. The $G(-Dye)$ increased steeply with an increase in the NCS^- concentration up to about 0.4 mM, and then it increased gradually above about 0.4 mM. The $G(-Dye)$ increased up to 1.51 upon the addition of 1 mM NCS^- from 0.51 for the N_2O-saturated solution without NCS^-. It is noteworthy that the tendency of the $G(-Dye)$-NCS^- concentration curve is similar to that of the $G(-NCS^-)$-NCS^- concentration curve for the N_2O-saturated NCS^- solution without the dye in Fig. 1. In the case of an unirradiated N_2O-saturated solution, the absorption spectrum was not changed upon the addition of NCS^-. On the other hand, in a nitrogen-saturated solution, the $G(-Dye)$ decreased to 0.06 upon the addition of 1 mM NCS^- from 0.18 for the solution without NCS^-.[2]

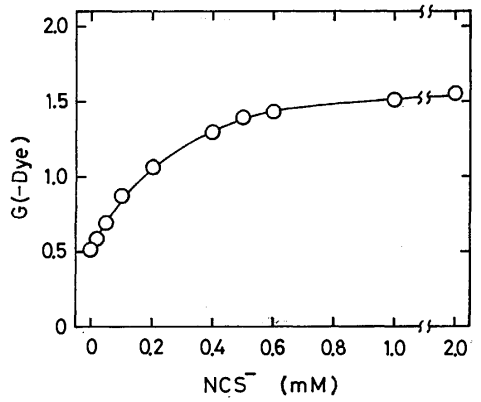

Fig. 2. Effect of NCS^- on $G(-Dye)$ in the N_2O-saturated Acid Blue 40 solutions.
Dye concentration: 0.1 mM. Dose: 1.8×10^4 rad.

The radiation-induced decoloration scheme of Acid Blue 40 in the nitrogen-saturated solution has been represented in a preceding paper[2] as follows:

$$AB + OH \xrightarrow{k_7} ABOH \text{ (decolored product)}, \quad (7)$$

$$AB + OH \longrightarrow ABOH' \text{ (colored product)}, \quad (8)$$

$$AB + e^-_{aq} \longrightarrow AB_{red} \text{ (decolored product)}, \quad (9)$$

$$AB + e^-_{aq} \longrightarrow AB_{red}' \text{ (colored product)}, \quad (10)$$

where AB, ABOH, and AB_{red} are Acid Blue 40, its OH adduct, and its reduction product by the attack of the hydrated electron respectively. In the N_2O-saturated solution, however, since the hydrated electrons are converted into the OH radicals as Reaction 1, Acid Blue 40 is decolored only by Reaction 7.

According to the earlier studies of the radiation-induced inactivation of lysozyme in the N_2O-saturated solution containing NCS^-,[8,11] the inactivation was caused by a reaction between lysozyme and $(NCS)_2^-$:

$$\text{lysozyme} + (NCS)_2^- \longrightarrow \text{inactive product} \quad (11)$$

The site of the $(NCS)_2^-$ attack is the ring structure of tryptophan in lysozyme; that is, the reaction with $(NCS)_2^-$ is a direct addition to the ring structure of tryptophan (T);

$$T + (NCS)_2^- \longrightarrow (T(NCS)_2)^-. \quad (12)$$

In the Acid Blue 40 solution containing NCS^-, most of the OH radicals react rapidly with NCS^- to form the NCS radical at NCS^- concentrations above about 0.2 mM, because k_2 is larger than k_7 (6.6×10^9 $M^{-1}s^{-1}$ at pH 6.3—5.1).[2] Therefore, it may be concluded from these facts that the increase in the $G(-Dye)$ upon the addition of NCS^- in the N_2O-saturated solution is mainly attributable to the attack of the radical anion $(NCS)_2^-$ formed through Reactions 2 and 3 on the Acid Blue 40 molecule as follows:

$$AB + (NCS)_2^- \longrightarrow (AB(NCS)_2)^- \text{ (decolored product)}, \quad (13)$$

$$AB + (NCS)_2^- \longrightarrow (AB(NCS)_2)^{-\prime} \text{ (colored product)}. \quad (14)$$

The Acid Blue 40 molecule has two kinds of reaction sites for Reactions 13 and 14; (a) the anthraquinone ring and (b) the substituted benzene ring, not conjugated to the carbonyl group in the anthraquinone ring. The attack of the radical anion $(NCS)_2^-$ on Site b is independent of the decoloration reaction. The increase in the $G(-Dye)$ in Fig. 2 indicates that the radical anion

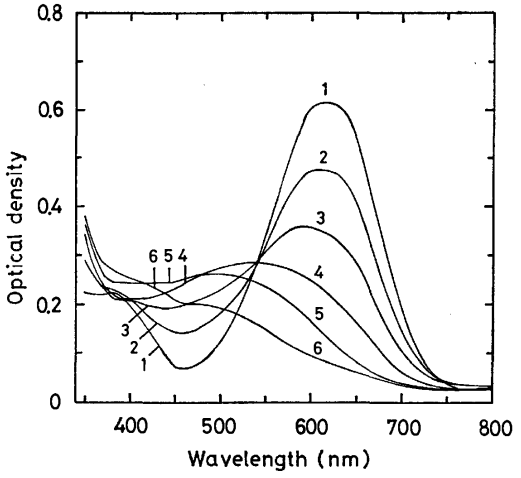

Fig. 3. Absorption spectra of unirradiated and irradiated N_2O-saturated Acid Blue 40 solutions containing 1 mM NCS^-.
Dye concentration: 0.1 mM. Doses (rad): 0 (Curve 1), 1.8×10^4 (Curve 2), 3.7×10^4 (Curve 3), 5.5×10^4 (Curve 4), 1.1×10^5 (Curve 5), and 3.9×10^5 (Curve 6).

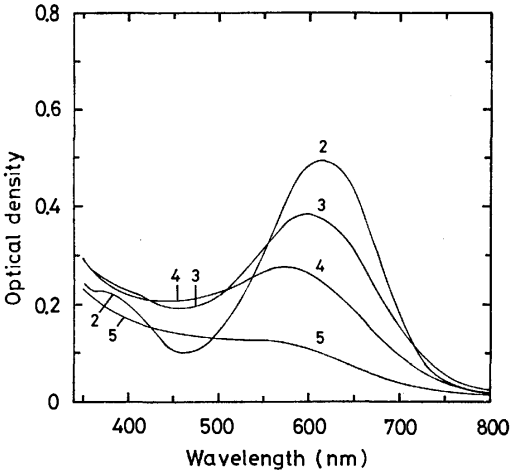

Fig. 4. Absorption spectra of irradiated N_2O-saturated Acid Blue 40 solutions without NCS^-.
Dye concentration: 0.1 mM. Doses (rad): 3.7×10^4 (Curve 2), 1.7×10^5 (Curve 3), 3.9×10^5 (Curve 4), and 5.5×10^5 (Curve 5).

$(NCS)_2^-$ destroys the dye chromophore more efficiently than the OH radical does.

The absorption spectra for the unirradiated and irradiated N_2O-saturated solution containing 1 mM NCS^- are shown in Fig. 3. The absorption band at 610 nm disappeared with an increase in the dose, and at the same time, the new absorption band near 460—490 nm seems to appear at a slightly higher dose (Curves 5 and 6 in Fig. 3). This new absorption band hardly appeared at all in the N_2O-saturated solution without NCS^-, as is shown in Fig. 4. The absorption band near 460—490 nm coincides approximately with that for the reduction products of Acid Blue 40 formed by the attacks of the hydrated electron and the alcohol radical on the carbonyl group in the anthraquinone ring.[2] It is known that quinones are easily reduced by such reducing species as alcohol radicals.[12,13] Therefore, it is assumed that a part of the Acid Blue 40 is reduced by the attack of the radical anion $(NCS)_2^-$ on the carbonyl group in the anthraquinone ring, thus forming the reduction product as follows:

$$AB + (NCS)_2^- \longrightarrow AB_{red}\text{ (decolored product)} + (NCS)_2 \quad (15)$$

On the other hand, the G(–Dye) for the nitrogen-saturated solution decreased upon the addition of NCS^-,[2] in contrast to that for the N_2O-saturated solution. The decrease in the G(–Dye) upon the addition of NCS^- in the nitrogen-saturated solution may be mainly attributable to the consumption of the NCS radical by Reaction 6, without forming $(NCS)_2^-$.

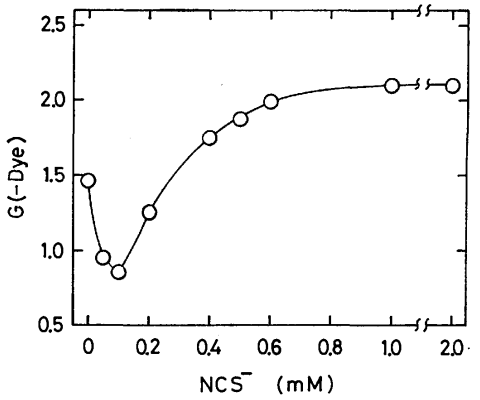

Fig. 5. Effect of NCS^- on G(–Dye) in the N_2O-saturated Acid Red 265 solutions.
Dye concentration: 0.1 mM. Dose: 1.8×10^4 rad.

N_2O-saturated Acid Red 265 Solutions. The G(–Dye) for the N_2O-saturated 0.1 mM Acid Red 265 solutions containing NCS^- (initial pH 6.4) is shown as a function of the NCS^- concentration in Fig. 5. The G(–Dye) decreased at first to 0.85 upon the addition of 0.1 mM NCS^-, and then it increased steeply with an increase in the NCS^- concentration up to about 0.6 mM NCS^-, in contrast to the result for the Acid Blue 40 solution in Fig. 2. The G(–Dye) increased up to 2.10 upon the addition of 1 mM NCS^- from 1.46 for the N_2O-saturated solution without NCS^-. In the case of the unirradiated N_2O-saturated solution, the absorption spectrum was also unchanged upon the addition of NCS^-. On the other hand, in the nitrogen-saturated solution the G(–Dye) decreased to 0.22 upon the addition of 1 mM NCS^- from 1.00 for the solution without NCS^-.[1]

The radiation-induced decoloration scheme of Acid Red 265 in the nitrogen-saturated solution has been represented in a preceding paper[1] as follows:

$$AR + OH \longrightarrow AROH\text{ (decolored product)} \quad (16)$$

$$AR + OH \longrightarrow AROH'\text{ (colored product)} \quad (17)$$

where AR and AROH are Acid Red 265 and its OH adduct respectively.

In the N_2O-saturated solution containing NCS^-, the increase in the G(–Dye) is also mainly attributable to the attack of the radical anion $(NCS)_2^-$ formed through Reactions 2 and 3 on the Acid Red 265 molecule as follows:

$$AR + (NCS)_2^- \longrightarrow (AR(NCS)_2)^- \text{ (decolored product)}, \quad (18)$$

$$AR + (NCS)_2^- \longrightarrow (AR(NCS)_2)^{-\prime} \text{ (colored product)}. \quad (19)$$

The Acid Red 265 molecule has two kinds of reaction sites for Reactions 18 and 19; (a) the aromatic rings connected directly to the azo group, and (b) the substituted benzene ring, not conjugated to the azo group. The attack of the radical anion $(NCS)_2^-$ on Site b is independent of the decoloration reaction. It is difficult for the direct attack of the radical anion $(NCS)_2^-$ on the azo group to take place because the azo group is stabilized by the hydrogen bonding with an adjacent OH group in a naphthalene ring.[1] Furthermore, the masking of the azo group can be expected because of the steric effect of the adjacent SO_3Na and CH_3 groups.[1]

The decrease in the G(–Dye) upon the addition of NCS^- up to 0.1 mM in Fig. 5 may be explained as follows. At low NCS^- concentrations, since the equilibrium of Reaction 3 may be rather shifted to the left side, a part of the NCS radical is consumed by Reaction 5, thus decreasing the G(–Dye). As the NCS^- concentration increases, the OH radicals are scavenged efficiently by NCS^- and the equilibrium of Reaction 3 is shifted to the right side. Therefore, the G(–Dye) increases at high NCS^- concentrations, as has previously been described.

The decrease in the G(–Dye) upon the addition of NCS^- was not observed in the N_2O-saturated Acid Blue 40 solution. This may be attributable to the larger reactivity of the radical anion $(NCS)_2^-$ on Acid Blue 40 than on Acid Red 265, because the increase in the G(–Dye) upon the addition of NCS^- is larger for Acid Blue 40 than for Acid Red 265 in spite of the smaller G(–Dye) value for the Acid Blue 40 solution without NCS^- than for the Acid Red 265 one.

The authors wish to thank Mr. Masamitsu Washino of JAERI for his encouragement and support.

References

1) N. Suzuki, T. Nagai, H. Hotta, and M. Washino, *Bull. Chem. Soc. Jpn.*, **48**, 2158 (1975).
2) N. Suzuki, T. Nagai, H. Hotta, and M. Washino, *Bull. Chem. Soc. Jpn.*, **49**, 600 (1976).
3) F. S. Dainton and S. R. Logan, *Trans. Faraday Soc.*, **61**, 715 (1965).
4) B. H. J. Bielski and A. O. Allen, *Int. J. Radiat. Phys. Chem.*, **1**, 153 (1969).
5) M. Anbar, M. Bambenek, and A. B. Ross, NSRDS-NBS 43 (1973).
6) I. Iwasaki, S. Utsumi, T. Ozawa, and R. Hasegawa, *Nippon Kagaku Zasshi*, **78**, 468 (1957).
7) J. H. Baxendale, P. L. T. Bevan, and D. A. Stott, *Trans. Faraday Soc.*, **64**, 2389 (1968).
8) G. E. Adams, J. E. Aldrich, R. H. Bisby, R. B. Cundal, J. L. Redpath, and R. L. Willson, *Radiat. Res.*, **49**, 278 (1972).
9) G. E. Adams, J. W. Boag, J. Currant, and B. D. Michael, "Pulse Radiolysis," Proceedings of the International Symposium held at Manchester, April 1965, Academic Press, London (1965), pp. 117—129.
10) R. L. Willson, C. L. Greenstock, G. E. Adams, R. Wageman, and L. M. Dorfman, *Int. J. Radiat. Phys. Chem.*, **3**, 211 (1971).
11) G. E. Adams, *Adv. Radiat. Chem.*, **3**, 125 (1972).
12) G. O. Phillips, N. W. Worthington, J. F. McKellar, and R. R. Sharpe, *J. Chem. Soc., A*, **1969**, 767.
13) E. Hayon and M. Simic, *J. Am. Chem. Soc.*, **95**, 1029 (1973).

Charge-Transfer Absorption of Solid Ion Radical Salts. Application of One-Dimensional Hubbard Model

Yôichi IIDA

Departmebt of Chemistry, Faculty of Science, Hokkaido University, Sapporo 060

(Received December 24, 1976)

The electronic spectrum of solid ion radical salt is known to be different from the monomer spectrum of the radical ion and to show an intermolecular charge-transfer band in the low-energy region. In order to understand the character of this charge-transfer absorption, one-dimensional Hubbard model was applied to such solid ion radical salt. The transition energy and the theoretical line shape of the charge-transfer absorption were derived and were compared with those of certain TCNQ anion radical salts.

The prominent magnetic, electrical, and optical properties of a number of solid ion radical salts have been the subject of many theoretical and experimental investigations over the past fifteen years.[1-5] In such ion radical salts, the planar ion radical molecules are known to form, in themselves, a plane-to-plane stacking into infinite one-dimensional columns so as to make a large overlap between their half-filled molecular orbitals.[6,7] In this case, since any individual radical molecule interacts through charge-transfer most strongly with two other neighboring radicals, the electronic spectrum of the solid salt differs distinctly from the monomer spectrum of the radical ion in solution but shows a charge-transfer transition between ion radicals in the low-energy region.[3-5]

In the present paper, we applied one-dimensional Hubbard model to the columns of ion radical molecules, and investigated the optical properties of solid ion radical salts. We attempted to explain the character of such charge-transfer absorptions on the basis of Green's function method. The transition energy and the theoretical absorption shape were compared with those observed for K^+ $TCNQ^-$ anion radical salt, where TCNQ is 7,7,8,8-tetracyanoquinodimethane.

Theoretical

In a narrow energy band with strong electron correlation, an electron transfers from one site to another site, but a strong repulsive force will take place when an electron happens to come onto a site which is already occupied by another electron with opposite spin. Let us denote the intra-site Coulomb repulsive energy as I, and consider a system of electrons described by the following Hamiltonian, which is often called the Hubbard Hamiltonian;[8,9]

$$\mathcal{H} = \sum_{i,j,\sigma} t_{ij} C_{i\sigma}^{+} C_{j\sigma} + I \sum_{i} n_{i\downarrow} n_{i\uparrow}, \tag{1}$$

where $n_{i\sigma}=C_{i\sigma}^{+}C_{i\sigma}$, and $C_{i\sigma}^{+}$ and $C_{i\sigma}$ are the creation and annihilation operators of an electron with σ-spin at the i-th site, respectively, and where t_{ij} is the transfer matrix element between the i-th and j-th sites, and the repulsive potential, I, appears only when two electrons are at the same site. We put $t_{ii}=0$ without loss of generality. The unperturbed band energy, ε_k, of the system is related to t_{ij} by

$$\varepsilon_k = \sum_j t_{ij} e^{ik\cdot(R_i-R_j)}. \tag{2}$$

Hubbard studied, in his first paper (it is often referred to as Hubbard I),[8] the one-particle Green's function of this system by using decoupling method of equation of motion. The Green function is given by

$$G_{k\sigma}(E) = \frac{1}{2\pi}\left\{\frac{E_{k\sigma}^{U}-I(1-n_{-\sigma})}{E_{k\sigma}^{U}-E_{k\sigma}^{L}}\frac{1}{E-E_{k\sigma}^{U}} + \frac{I(1-n_{-\sigma})-E_{k\sigma}^{L}}{E_{k\sigma}^{U}-E_{k\sigma}^{L}}\frac{1}{E-E_{k\sigma}^{L}}\right\}, \tag{3}$$

where

$$n_\sigma = \langle n_{i\sigma}\rangle,$$

$$E_{k\sigma}^{U} = \frac{1}{2}(\varepsilon_k + I + \sqrt{\varepsilon_k^2 + 2(2n_{-\sigma}-1)\varepsilon_k I + I^2}),$$

$$E_{k\sigma}^{L} = \frac{1}{2}(\varepsilon_k + I - \sqrt{\varepsilon_k^2 + 2(2n_{-\sigma}-1)\varepsilon_k I + I^2}).$$

Here $E_{k\sigma}{}^{L}$ is the energy of an electron with σ-spin which moves about avoiding other electrons with $-\sigma$-spin, while $E_{k\sigma}{}^{U}$ is the energy of an electron which propagates mainly among sites already occupied with electrons with $-\sigma$-spin.

On the other hand, starting from Kubo's formula,[10] Kubo expressed the conductivity tensor of the Hubbard Hamiltonian in terms of two-time Green's function.[11] The spectrum of optical absorption from $E_{k\sigma}{}^{L}$ to $E_{k\sigma}{}^{U}$ (*i.e.*, the intermolecular charge-transfer absorption) is given by the real part of the diagonal element of the frequency-dependent conductivity tensor, $\mathrm{Re}\sigma_{xx}(\omega)$, that is,

$$\mathrm{Re}\sigma_{xx}(\omega) = \frac{e^2}{\pi V}\frac{1}{\omega}\sum_{k,\sigma}\delta(\omega - E_{k\sigma}^{U} + E_{k\sigma}^{L}) \times \frac{\delta E_{k\sigma}^{U}}{\delta k_x}\frac{\delta E_{k\sigma}^{L}}{\delta k_x}\{f(E_{k\sigma}^{U}) - f(E_{k\sigma}^{L})\}, \tag{4}$$

where V is the volume of the system, and $f(E)$ is the Fermi distribution function.

In order to apply this theory to one-dimensional stacks of ion radical molecules, we consider non-alternant linear chain of sites for which the transfer matrix elements are assumed to exist only between nearest neighbor sites. In this case, the unperturbed band energy is given by

$$\varepsilon_k = 2T\cos ka, \quad \left(-\frac{\pi}{a}\leq k\leq\frac{\pi}{a}\right), \tag{5}$$

where $T(<0)$ is the transfer matrix element between nearest neighbors and a is the lattice separation. Re $\sigma_{xx}(\omega)$ in Eq. 4 is composed of two contributions from the transitions of electrons with up and down spins. In the following, we only consider the contribution of electrons with up spin, but the optical absorption by

electrons with up spin depends strongly upon $n_\downarrow$ through correlation effect. From the δ-function of Eq. 4, an electron with a wave vector $\boldsymbol{k}$ absorbs the electromagnetic wave with the frequency ω;

$$\omega^2 = \varepsilon_k{}^2 + 2(2n_\downarrow - 1)I\varepsilon_k + I^2. \quad (6)$$

This leads to

$$\varepsilon_k = \varepsilon^{\pm}(\omega) = -I(2n_\downarrow - 1) \pm \sqrt{\omega^2 - 4I^2 n_\downarrow (1-n_\downarrow)}. \quad (7)$$

The optical transition from $E_{k\sigma}{}^L$ to $E_{k\sigma}{}^U$ with the wave vector $\boldsymbol{k}$, which satisfies $\varepsilon_k = \varepsilon^+(\omega)$, gives the absorption

$$\mathrm{Re}\sigma^+(\omega) = \frac{e^2}{2} \frac{I^2 n_\downarrow (1-n_\downarrow)}{\omega^2 \sqrt{\omega^2 - 4I^2 n_\downarrow (1-n_\downarrow)}}$$
$$\times \sqrt{4T^2 - \{-(2n_\downarrow - 1)I + \sqrt{\omega^2 - 4I^2 n_\downarrow (1-n_\downarrow)}\}^2}\, \theta_+(\omega), \quad (8)$$

where

$$\theta_\pm(\omega) = f(E_\pm{}^L) - f(E_\pm{}^U),$$

$$E_\pm{}^L = \frac{1}{2}\{\varepsilon^\pm(\omega) + I - \sqrt{(\varepsilon^\pm(\omega) + I)^2 - 4I(1-n_\downarrow)\varepsilon^\pm(\omega)}\},$$

$$E_\pm{}^U = \frac{1}{2}\{\varepsilon^\pm(\omega) + I + \sqrt{(\varepsilon^\pm(\omega) + I)^2 - 4I(1-n_\downarrow)\varepsilon^\pm(\omega)}\}.$$

In a similar way, the transition between the two states with the wave vector $\boldsymbol{k}$, which satisfies $\varepsilon_k = \varepsilon^-(\omega)$, gives the absorption

$$\mathrm{Re}\sigma^-(\omega) = \frac{e^2}{2} \frac{I^2 n_\downarrow (1-n_\downarrow)}{\omega^2 \sqrt{\omega^2 - 4I^2 n_\downarrow (1-n_\downarrow)}}$$
$$\times \sqrt{4T^2 - \{-(2n_\downarrow - 1)I - \sqrt{\omega^2 - 4I^2 n_\downarrow (1-n_\downarrow)}\}^2}\, \theta_-(\omega). \quad (9)$$

Therefore, the total contribution to the optical absorption, $\mathrm{Re}\sigma_{xx}(\omega)$, due to the electrons with up spin is given by $\mathrm{Re}\sigma^+(\omega) + \mathrm{Re}\sigma^-(\omega)$.

Discussion

In this section, we shall apply this theory to the optical properties of certain crystalline TCNQ anion radical salts. Let us consider, for example, a system of simple anion radical salt of K^+TCNQ^-. According to Anderson and Fritchie's X-ray analysis data,[6] the crystal structure of K^+TCNQ^- belongs to the monoclinic system with space group $P2_1/n$. The structure consists of one-dimensional columns of $TCNQ^-$ ions parallel to the a (needle) axis with a plane-to-plane stacking; the molecular normal vectors nearly coincide with the column axes. Each column is surrounded by four columns in which the $TCNQ^-$ ions are rotated by 90° from those in the central column. The potassium ions occupy sites between $TCNQ^-$ columns in such a manner that each K^+ ion is surrounded by eight nitrogen atoms at the corners of a distorted cube.

On the other hand, each TCNQ anion radical molecule is almost planar, and has sixteen molecular orbitals for seventeen $2p\pi$ electrons.[12] Therefore, in the ground state, the molecular orbitals from the lowest to the 8 th are fully occupied, while an unpaired electron is in the 9 th molecular orbital. The other molecular orbitals are vacant orbitals.

In order to apply Hubbard model of Eq. 1 to the crystalline K^+ $TCNQ^-$ anion radical salt, we consider the column of TCNQ anion radicals. We take only the 9 th molecular orbital of the unpaired electron for one site of TCNQ anion radical, and assume a model of non-alternant one-dimensional column composed of infinite number of such sites. From the crystallographic data,[6] the intermolecular distance between nearest neighbor sites, a in Eq. 5, is of the order of 3.4 Å. Therefore, in this model, each TCNQ anion radical site has one identical molecular orbital with equal energy level, and there is one electron per each site. Then, we have $n_\downarrow = 0.5$ if we assume a paramagnetic state for our system. Under these situations, we consider the optical absorption (charge-transfer absorption) of the crystalline K^+TCNQ^- anion radical salt as expressed by Eqs. 8 and 9. By using $n_\downarrow = 0.5$, we can easily obtain

$$\mathrm{Re}\sigma^+(\omega) = \frac{e^2}{8} \frac{I^2}{\omega^2 \sqrt{\omega^2 - I^2}} \sqrt{4T^2 - \omega^2 + I^2}\, \theta_+(\omega), \quad (10)$$

$$\mathrm{Re}\sigma^-(\omega) = \frac{e^2}{8} \frac{I^2}{\omega^2 \sqrt{\omega^2 - I^2}} \sqrt{4T^2 - \omega^2 + I^2}\, \theta_-(\omega). \quad (11)$$

Here we assume, for the sake of simplicity, that the Coulomb repulsion potential is much greater than the band width, or we consider the absorption spectrum at very low temperature. In this case, $\theta_\pm(\omega) = 1$ so that both $\mathrm{Re}\sigma^+(\omega)$ and $\mathrm{Re}\sigma^-(\omega)$ in Eqs. 10 and 11 have the same absorption spectrum. Fig. 1 shows a schematic description of $\mathrm{Re}\sigma^+(\omega)$ or $\mathrm{Re}\sigma^-(\omega)$ *versus* ω for this case, as is shown by the (a) line. Therefore, the total contribution to the absorption spectrum, $\mathrm{Re}\sigma^+(\omega) + \mathrm{Re}\sigma^-(\omega)$, is given by the (b) line of Fig. 1.

As is shown in Fig. 1, the theoretical optical absorption due to the charge-transfer transition between TCNQ anion radical sites has a sharp divergent peak at the energy $\omega = I$, where the spectrum has a van Hove singularity in the lower energy side.[11] The spectrum has no absorption in the energy region $\omega < I$, but has an absorption intensity in the region $\omega > I$. The absorption intensity is the greatest at $\omega = I$, and decreases progressively with the increase of ω. The highest energy of the absorption takes place at $\omega = \sqrt{I^2 + 4T^2}$,

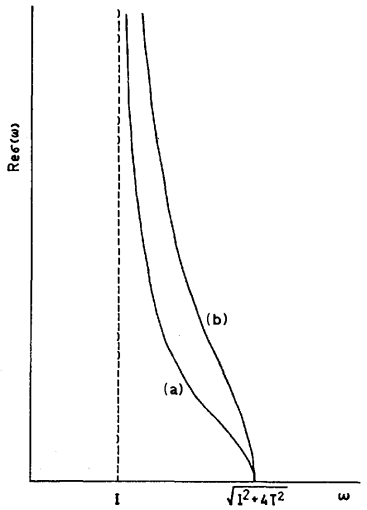

Fig. 1. The theoretical absorption line shape due to the charge-transfer transition between ion radical molecules in one-dimensional Hubbard model. Curve (a) indicates the spectrum of $\mathrm{Re}\sigma^+(w)$ of Eq. 10 or $\mathrm{Re}\,\sigma^-(w)$ of Eq. 11 with $\theta_\pm(w) = 1$, while curve (b), that of $\mathrm{Re}\sigma^+(w) + \mathrm{Re}\sigma^-(w)$. See text.

where the intensity falls down to zero. The spectrum has a shoulder in the region $I<\omega<\sqrt{I^2+4T^2}$. Therefore, the charge-transfer absorption has a width of $\sqrt{I^2+4T^2}-I$. This width is caused by the existence of non-zero transfer matrix element of T in the unperturbed energy band of Eq. 5. In fact, if we assume $T=0$, that is, if we assume an independent site model in the unperturbed energy band, the absorption spectrum, $\mathrm{Re}\sigma^+(\omega)+\mathrm{Re}\sigma^-(\omega)$, is only a δ-function at $\omega=I$ with no width, as this model requires.

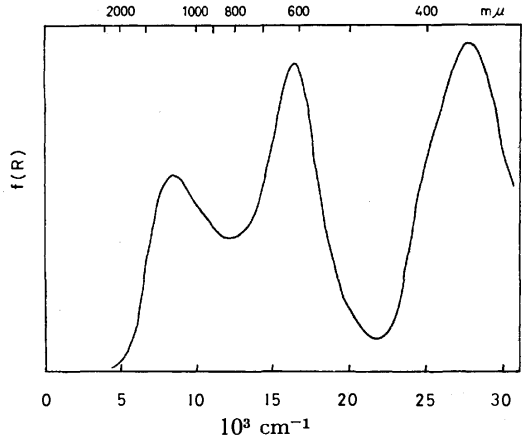

Fig. 2. The experimental result on the diffuse reflection spectrum of solid K^+ $TCNQ^-$ anion radical salt, where the value of Kubelka-Munk function, $f(R)=(1-R)^2/2R$, was plotted *versus* wave number (10^3 cm^{-1} unit). See Ref. 3.

Let us compare these theoretical predictions with the experimental electronic spectrum of crystalline K^+ $TCNQ^-$ anion radical salt. In a previous paper,[3] we measured the electronic spectrum of this salt by means of diffuse reflection method. The observed spectrum is reproduced in Fig. 2. The Kubelka-Munk function, $f(R)=(1-R)^2/2R$, where R is the reflectance and $f(R)$ is proportional to the absorbance, was plotted against the wave number (10^3 cm^{-1} unit). In the energy region from 5000 to 30000 cm^{-1} the solid-state spectrum of K^+ $TCNQ^-$ anion radical salt has three absorptions. The absorptions at 16400 and 27800 cm^{-1} are the shifted bands of the monomer spectrum of the TCNQ anion radical at 11900 and 25300 cm^{-1}, respectively, while the low-energy band at 8500 cm^{-1} characteristic of the solid salt has been assigned to the charge-transfer transition between TCNQ anion radicals in one-dimensional column.[3] If the theoretical absorption of Fig. 1 is applied to this characteristic low-energy band, the observed absorption peak value, 8500 cm^{-1}, should correspond to $\omega=I$, so that the intra-site Coulomb repulsive energy for the system of TCNQ anion radicals is estimated to be $I=8500$ cm^{-1}. As for the line shape and the line width, the theoretical spectrum has no absorption in the region $\omega<I$, while the observed charge-transfer absorption has a considerable width even in the energy region lower than its peak position. Moreover, the theoretical spectrum has absorption only in the region $I\leq\omega\leq\sqrt{I^2+4T^2}$ so that the line shape should be asymmetrical with respect to $\omega=I$. However, this asymmetric character is not obvious in the observed charge-transfer absorption, although the charge-transfer band overlaps with the higher-energy band of 16400 cm^{-1}. There may be several reasons for these discrepancies:

(1) An important one is that in our theory we assumed, as is shown in Eq. 4, a δ-function for the elementary transition from $E_{k\sigma}{}^L$ to $E_{k\sigma}{}^U$ at each wave vector, while the actual elementary transition is not a δ-function but involves finite width. In fact, the individual site in our Hubbard model is the TCNQ anion radical molecule composed of 20 atoms. Then, the elementary absorption may involve a width of vibrational structures due to the vibronic effect of the molecule.

(2) Another reason for the broadening of elementary transition at each wave vector comes from two electronic effects in the scattering process of an electron by those with opposite spin.[9] One is the effect of the randomness in the spacial distribution of electrons with opposite spin; Hubbard called it as the scattering correction. Another is the effect of the motion of electrons with opposite spin; he called it as the resonance broadening correction. These two electronic effects will also influence significantly the shape of charge-transfer absorption spectrum. We can make these corrections if we use the method proposed by Hubbard in his third paper.[9] There has been a relevant work made by Sadakata and Hanamura,[13] who examined the optical properties of three-dimensional half-filled band system for certain transition metal compounds.

(3) In the theoretical absorption spectrum of Fig. 1, we neglected the temperature effect and only considered the extreme case of $\theta_\pm(\omega)=1$. However, the experimental spectrum of Fig. 2 was observed at room temperature. Therefore, if we consider the effect of Fermi distribution term, $\theta_\pm(\omega)$, at finite temperature, the theoretical spectrum of Fig. 1 will become more smoothed.

At any rate, in the charge-transfer absorption of K^+ $TCNQ^-$ system, the observed line shape is almost symmetrical with respect to $\omega=I$. In this respect, the absorption line width due to the transfer matrix element, $\sqrt{I^2+4T^2}-I$, seems to be very narrow compared to the width due to the elementary transition, 3500 cm^{-1}, so that the $|T|$ value may be much less than 4200 cm^{-1}. As this $|T|$ value appears much less than the I value, we can well see that a narrow band system with strong electron correlation takes place in such one-dimensional column of TCNQ anion radicals. On the other hand, however, it is very important to find certain crystalline ion radical salts where transfer matrix element is comparable to or larger than the width of elementary transition, because they will show asymmetric charge-transfer absorption with a shoulder in the high-energy region. Then we can estimate the magnitude of T directly by analyzing such asymmetric line shape with our theoretical model, as long as the approximation for the Green function of Eq. 3 is applicable to our system.

So far, in order to apply simple one-dimensional Hubbard Hamiltonian of Eq. 1 to the crystalline K^+ $TCNQ^-$ salt, we have only considered the 9 th molecular

orbital of the unpaired electron as one site of TCNQ anion radical, and neglected the other occupied and vacant molecular orbitals. This simple model solely leads to the optical properties of the charge-transfer transition between TCNQ anion radicals, but cannot explain the character of other higher-energy electronic transitions which arise mostly from local excitations of TCNQ anion radical molecules. Therefore, further theoretical treatment including all of the molecular orbitals is required to explain those higher-energy transitions as well as the low-energy charge-transfer transition in such crystalline ion radical salts.

In the present paper, we have only discussed the one-dimensional system of simple TCNQ anion radical salts, where each TCNQ anion radical has one unpaired electron so that each TCNQ site is equivalent. However, there are a number of complex TCNQ anion radical salts,[1,2] which include not only TCNQ anion radicals but also formally neutral TCNQ molecules so that each TCNQ site is no longer equivalent. In order to take into account this inequivalence, Soos and Klein modified the Hubbard Hamiltonian of Eq. 1 and studied the electronic states of less than half-filled band system for those complex TCNQ anion radical salts.[14] Therefore, we will also attempt to investigate, by extending our present method, the optical properties of such complex TCNQ anion radical salts.

The author wishes to express his thanks to Dr. Kenn Kubo of Tokyo Kyoiku University for his valuable discussion regarding this work.

References

1) L. R. Melby, R. J. Harder, W. R. Hertler, W. Mahler, R. E. Benson, and W. E. Mochel, *J. Am. Chem. Soc.*, **84**, 3374 (1962).
2) W. J. Siemons, P. E. Bierstedt, and R. G. Kepler, *J. Chem. Phys.*, **39**, 3523 (1963); R. G. Kepler, *ibid.*, **39**, 3528 (1963).
3) Y. Iida, *Bull. Chem. Soc. Jpn.*, **42**, 71, 637 (1969).
4) Y. Iida, *Bull. Chem. Soc. Jpn.*, **43**, 2772 (1970); **44**, 663, 1777 (1971); **45**, 105, 624 (1972).
5) J. Tanaka, M. Tanaka, T. Kawai, T. Takabe, and O. Maki, *Bull. Chem. Soc. Jpn.*, **49**, 2358 (1976), and the references cited therein.
6) G. R. Anderson and C. J. Fritchie, Jr., Second National Meeting for Applied Spectroscopy, San Diego, Paper 111 (1963).
7) H. Kobayashi, Y. Ohashi, F. Marumo, and Y. Saito, *Acta Crystallogr., Sect. B*, **26**, 459 (1970), and the references cited therein.
8) J. Hubbard, *Proc. R. Soc., Ser. A*, **276**, 238 (1963).
9) J. Hubbard, *Proc. R. Soc., Ser. A*, **281**, 401 (1964).
10) N. Ohata and R. Kubo, *J. Phys. Soc. Jpn.*, **28**, 1402 (1970).
11) K. Kubo, *J. Phys. Soc. Jpn.*, **31**, 30 (1971).
12) D. A. Lowitz, *J. Chem. Phys.*, **46**, 4698 (1967).
13) I. Sadakata and E. Hanamura, *J. Phys. Soc. Jpn.*, **34**, 882 (1973).
14) Z. G. Soos and D. J. Klein, *J. Chem. Phys.*, **55**, 3284 (1971).

Formation of CN($B^2\Sigma^+$) in the Reaction of Acetonitrile with Metastable Ar($^3P_{2,0}$) Atoms

Kaoru SUZUKI and Kozo KUCHITSU

Department of Chemistry, Faculty of Science, The University of Tokyo, Hongo, Bunkyo-ku, Tokyo 113

(Received January 7, 1977)

A flowing-afterglow method was applied to the formation of CN($B^2\Sigma^+$) from CH_3CN by impact of metastable argon atoms, Ar($^3P_{2,0}$). Emission spectra of CN $B^2\Sigma^+$-$X^2\Sigma^+$ (violet band) were analyzed to estimate the energies distributed to the vibrational and rotational motions of CN($B^2\Sigma^+$). In comparison with the CN($B^2\Sigma^+$) produced from HCN under similar experimental conditions, relative populations in excited vibrational states are smaller. The effective rotational temperatures range from 5000±1000 K (v=0—2) to 2000±1500 K (v=5—10). An intensity anomaly caused by the rotational perturbation with $A^2\Pi$ is used for estimating the ratio of the formation rates of CN $B^2\Sigma^+$ and $A^2\Pi$, F_B/F_A, to be 0.19±0.05.

Metastable argon atoms, Ar($^3P_{2,0}$), are known to react with cyanides (XCN, X=H, Cl, Br, I, CN, and CH_3) and produce CN radicals in electronically excited states. Studies on light emission from the CN radicals thus formed have been reported.[1-6] The vibrational and rotational distributions of the CN($A^2\Pi$) and CN($B^2\Sigma^+$) radicals produced by photodissociation[7,8] and electron impact[9,10] have also been studied in detail. A comparison of the results shows that the distributions resulting from the metastable reactions extend more broadly among different internal states and that the production of CN($A^2\Pi$) is more favored than that in the other reactions.

The emission from CN($B^2\Sigma^+$) formed in the reaction of metastable argon atoms with CH_3CN has previously been studied; spectra were reported in Refs. 1 and 5, and an analysis of a vibrational distribution was made on a spectrum taken with medium resolution,[3] where no rotational structure was observed. In the present paper a detailed analysis of the CN violet emission from acetonitrile based on a spectrum taken with higher resolution is presented. Rotational and vibrational distributions are obtained by a band envelope analysis for $\Delta v=0$ and -1 sequences. In addition, quantitative information on the formation rate to the CN $A^2\Pi$ and $B^2\Sigma^+$ states is obtained by an analysis of anomalies in the rotational distribution caused by the rotational perturbation between the two states.

Experimental

A flowing afterglow apparatus[1] was used. The flow tube was evacuated by a mechanical booster pump (500 l/s). Argon gas (99.99% nominal purity) was admitted into the flow tube after passing through a liquid nitrogen trap and is subjected to microwave discharge (2450 MHz, 500 W). Ionic species generated in the discharge section were collected on grids, and neutral atoms were led into the reaction zone. Acetonitrile (extra pure) was introduced into the flow about 15 cm downstream from the discharge section. The time of flight of argon atoms from the discharge section to the reaction zone was estimated to be of the order of 1 ms. The flame in the reaction region was observed through a quartz window and focused by a lens on a Spex 1704 monochromator. A photomultiplier (HTV R585) and a photon counting unit were used. The CN violet system ($B^2\Sigma^+$-$X^2\Sigma^+$) was observed for $\Delta v=+1$, 0, and -1 sequences.

The pressures of argon and the sample were monitored at the reaction zone by a Pirani gauge, which was calibrated against a McLeod gauge. Typical pressures were 0.3 and 0.01 Torr for argon and acetonitrile, respectively.

The effect of the light generated in the discharge section was checked by a time-of-flight experiment[13] and was found to be negligible.

Vibrational and Rotational Distributions

Provided the CN($B^2\Sigma^+$) formed has thermal velocity, the effect of collisional relaxation on the rotational distribution can be ignored, since the mean time between effective collisions (200 ns, as estimated from the cross section of rotationally inelastic collision, 85 Å^2)[4] is appreciably longer than the radiative lifetime of CN($B^2\Sigma^+$) (60 ns[14]). It is not known, however, whether the CN($B^2\Sigma^+$) produced is thermal. Therefore, the effect of collisional relaxation was tested by taking spectra at different argon pressures (Fig. 1). Since the spectra were essentially pressure-independent, the effect of rotational relaxation was ignored in the present analysis of relative intensities.

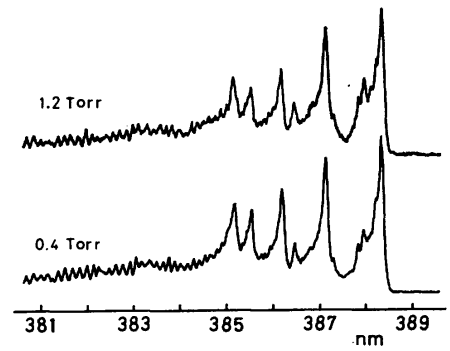

Fig. 1. Check of dependence of the spectra on argon pressure, CN $B^2\Sigma^+$-$X^2\Sigma^+$ 0-0 sequence. No appreciable collisional relaxation with argon is observed.

The CN $B^2\Sigma^+$-$X^2\Sigma^+$ $\Delta v=0$ and -1 sequences were used for analysis. Since transitions from different vibrational states, especially from higher vibrational states, were heavily overlapped by one another in these sequences, their band envelopes were analyzed by simulation. Relative vibrational populations and effective rotational temperatures were taken as parameters. The intensity of a transition is given by

$$I_{v'N'}^{v''N''} \propto P_{v'N'} q_{v'v''} \nu^3 S_{N'N''} R_{v'N'} / Q_{v'}, \quad (1)$$

where $P_{v'N'}$ is the population in the level v' and N', ν is the transition frequency, $q_{v'v''}$ is the Franck-Condon factor, $S_{N'N''}$ is the rotational line-strength, $Q_{v'}$ is the rotational state sum, and $R_{v'N'}$ is the rotational distribution, which is assumed to follow the Boltzmann statistics. The intensities were superposed to obtain a band envelope. Molecular constants[15,16] and the Franck-Condon factors[17] were taken from the literature. Rotational line-strengths were calculated according to Mulliken's formulas.[18]

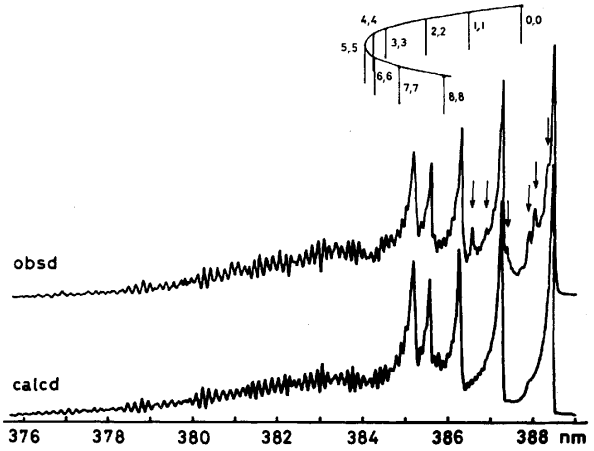

Fig. 2. Observed and simulated spectra of the CN $B^2\Sigma^+$-$X^2\Sigma^+$ 0-0 sequence. Those lines in the observed spectrum for which rotational perturbations with the $A^2\Pi$ state are known (indicated by arrows) are enhanced.

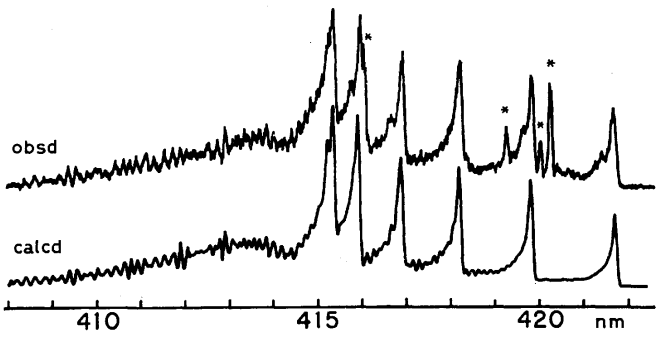

Fig. 3. Observed and simulated spectra of the CN $B^2\Sigma^+$-$X^2\Sigma^+$ 0-1 sequence. Asterisks indicate argon stray lines.

Simulated spectra are shown in Figs. 2 and 3 for the $\Delta v=0$ and -1 sequences, respectively. The observed and simulated spectra agree well except in the region where the intensities of the observed spectra are enhanced by the rotational perturbation with the $A^2\Pi$ state. The parameters used are listed in Table 1. The available energy, which is calculated from the argon metastable energies (11.55 and 11.72 eV[19]) and the C–C bond dissociation energy (5.2[20] or 5.32 eV[21]), is such that CN radicals can be excited up to $v'=14$ in the $B^2\Sigma^+$ state. Nevertheless, levels higher than $v'=11$, which are expected to appear as tail bands, were not observed.

Excess energy is defined as $E_{\text{excess}}=E_{\text{Ar}(^3P_{2,0})}-D_0-E_{\text{CN(B)}}$, where $E_{\text{Ar}(^3P_{2,0})}$ is the excitation energies of $\text{Ar}(^3P_{2,0})$, D_0 is the dissociation energies for H–CN and CH_3–CN, and $E_{\text{CN(B)}}$ is the electronic excitation energy of the $CN(B^2\Sigma^+)$. Then, excess energies for HCN and CH_3CN are nearly equal, since the dissociation energies, D_0, for H–CN (5.2[22] or 5.5 eV[20]) and CH_3CN (5.2[20] or 5.32 eV[21]) are nearly equal. The excess energy is distributed to vibration and rotation of $CN(B^2\Sigma^+)$ and the translational motions of the fragments. For CH_3CN, energy is also consumed in the internal degrees of freedom of the methyl radical.

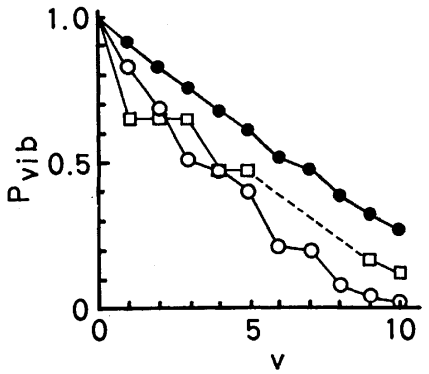

Fig. 4. Relative vibrational populations of the CN ($B^2\Sigma^+$) formed by impact of argon metastable atoms from CH_3CN (○, this work), HCN (●, Ref. 2), and HCN (□, Ref. 5).

Relative vibrational populations for the $CN(B^2\Sigma^+)$ from CH_3CN are compared with those from HCN[2,3,5] in Fig. 4. In spite of a slight discrepancy existing in the published populations for HCN, a clear difference is observed in the CH_3CN and HCN cases; populations in higher vibrational states are lower in the former case. The rotational excitation in the $CN(B^2\Sigma^+)$ from CH_3CN is higher than that from HCN (Table 1) in the $v'=0$—3 states.

Table 1. Relative vibrational populations, P_{vib}, and effective rotational temperatures, T_{rot}, of $CN(B^2\Sigma^+)$ formed in $Ar(^3P_{2,0})$ reactions

v	from CH_3CN[a]		from HCN[b]	
	P_{vib}	T_{rot}/K	P_{vib}	T_{rot}/K
0	0.23	5000	0.137	2400
1	0.19	5000	0.126	
2	0.15	5000	0.114	
3	0.12	4000	0.105	1900
4	0.11	3000	0.094	
5	0.09	2000	0.084	
6	0.05	2000	0.073	
7	0.04	2000	0.066	
8	0.02	2000	0.054	
9	0.01	2000	0.045	
10	$\lesssim$0.01	2000	0.038	

a) Errors in P_{vib} are about 0.02 for $v<5$ and about 0.01 for $v\gtrsim 5$. Errors in T_{rot} are estimated to be about 1000 K for $v<4$ and about 1500 K for $v\gtrsim 4$. b) Ref. 2.

Average energies distributed to vibration and rotation are 0.79 ± 0.10 and 0.35 ± 0.09 eV, respectively, for the CN($B^2\Sigma^+$) from CH_3CN, to be contrasted with those for HCN,[2] 1.2 and 0.2 eV, respectively. Accordingly, the CN($B^2\Sigma^+$) produced from CH_3CN is vibrationally less populated than that produced from HCN. This trend may be explained as that the methyl radical acts as an energy absorber,[3] *i.e.*, the residual energy may be used to excite the internal motions of the methyl radical. A similar trend was observed in the reaction of active nitrogen with organic compounds.[23]

Rotational Perturbation

The CN $A^2\Pi$ and $B^2\Sigma^+$ states are coupled through rotational perturbation,[24] and extra lines and anomalies in emission intensities have been observed. In order to estimate the ratio of the formation rates to the $A^2\Pi$ and $B^2\Sigma^+$ states, relative intensities for rotationally perturbed lines were analyzed. The analysis followed the scheme used in the analyses of the CN radicals formed in the reaction of active nitrogen with organic compounds,[25] in the electron impact on XCN (X=H, Br, and CN),[11] in the metastable-Ar impact on HCN and BrCN,[5] and in the photodissociation of ICN.[12]

Enhancement of intensities of the transitions from $N'=4$, 7, 11, and 15 in the $v'=0$ state were observed in a low resolution spectrum (Fig. 2). These states are known to be rotationally perturbed by the corresponding rotational levels in the $v=10$ level of the $A^2\Pi$ state. The R(14) transition was used for the analysis as the most suitable case.

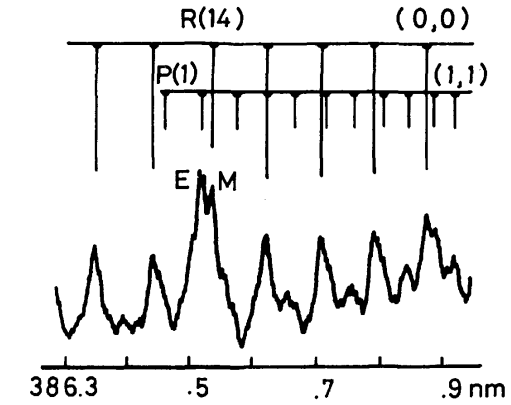

Fig. 5. A portion of the CN violet 0-0 band showing the rotationally perturbed R(14) lines (indicated as E and M).

A typical observed spectrum showing a rotationally perturbed line is given in Fig. 5. The spectrum was taken with a slit width of 10 μm. An extra line and a main line, which is overlapped by an unperturbed line, were observed. The relative intensities of the extra and main lines were essentially independent of the argon pressure between 0.3 and 0.8 Torr. Therefore, the effect of collisional relaxation is ignored in the following analysis.

The energy-level relations relevant to the rotational perturbation at the $B^2\Sigma^+$, $v=0$, $N=15$ level are shown in Fig. 6. The rate equations for the states shown in Fig. 6 lead to

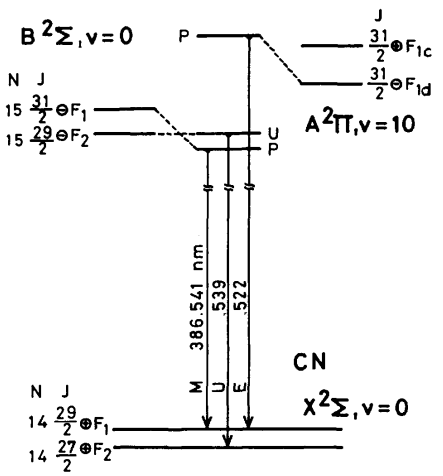

Fig. 6. Energy level diagram (schematic) for the rotational perturbation at the $B^2\Sigma^+$, $v=0$, $N=15$ level, drawn after Refs. 11, 24, and 26.

$$\frac{I_E}{I_M+I_U} = \frac{1+\beta\rho^2/(1-\rho^2)}{1+\beta(1-\rho^2)/\rho^2} \times \frac{1-\rho^2+\alpha\rho^2}{\rho^2+\alpha\{2-\rho^2+\beta\rho^2/(1-\rho^2)\}}, \quad (2)$$

where α is the ratio of formation rates to the $B^2\Sigma^+$ and $A^2\Pi$ states, F_B/F_A, β is the ratio of the radiative lifetimes of the states, τ_B/τ_A, and ρ^2 is a parameter representing the degree of mixing of the states. The values for β and ρ^2 are characteristic of the states and reported to be 0.14 and 0.22 respectively. Thus, the relative formation rate, α, is a function of the observable value, $I_E/(I_M+I_U)$. In deriving Eq. 2 the following assumptions are made: 1) Collisional transitions to and from the states shown in Fig. 6 are negligible. This implies that Eq. 2 is an exact expression for the low pressure limit. 2) The rates of formation of the different spin sublevels are equal. 3) A steady state is established. 4) The transition moment for the $A^2\Pi$ to $X^2\Sigma^+$ states is negligible in comparison with that for the $B^2\Sigma^+$-$X^2\Sigma^+$ transition. In addition, the difference in the transition frequencies between the extra and main lines is disregarded.

Since the rotational temperatures of the CN($B^2\Sigma^+$) levels obtained by a band envelope analysis are several thousand kelvins, the R(14) line is overlapped by the P-branches of $v'=0$ and 1. The intensities, I_E and I_M+I_U, are estimated by subtracting the overlapping band intensities estimated from the rotational temperatures.

The α value is then estimated from I_E and I_M+I_U to range between 0.14 and 0.23. In other words, the $A^2\Pi$ state is formed 4—7 times faster than the $B^2\Sigma^+$ state. This value is consistent with those produced from BrCN ($\alpha\simeq0.08$ obtained by extrapolating the values in Ref. 5 to zero pressure) and from HCN ($\alpha<0.18$).[5] Accordingly, a typical value of α in metastable argon reactions seems to be of the order of 0.1. This is in striking contrast with the corresponding values in electron-impact dissociative excitations of HCN, BrCN, and C_2N_2 ($0.5\lesssim\alpha\lesssim1.3$)[11] and in photodissociation of HCN

and BrCN ($\alpha \gg 1$)[7] by rare-gas (Xe, Kr), Hg (184.9 nm), and Br (145—170 nm) lamps. (Note, however, that a recent photodissociation experiment with the hydrogen Lyman-α line (10.2 eV) on ICN gave $\alpha=0.3$—0.5.[12]) The difference in α by different methods of excitation indicates a difference in the excited states of the parent molecules from which CN $A^2\Pi$ and $B^2\Sigma^+$ are produced.

Note added in proof. According to a recent report by Ashfold and Simons (*Chem. Phys. Lett.*, **47**, 65 (1977)), CN-($A^2\Pi$) as well as CN($B^2\Sigma^+$) was formed in the vacuum UV photodissociation of BrCN. See also Luk and Bersohn, *J. Chem. Phys.*, **58**, 2153 (1973).

References

1) T. Urisu and K. Kuchitsu, *Chem. Lett.*, **1972**, 813.
2) T. Urisu and K. Kuchitsu, *Chem. Phys. Lett.*, **18**, 337 (1973).
3) T. Urisu and K. Kuchitsu, *J. Photochem.*, **2**, 409 (1974).
4) W. H. Duewer, J. A. Coxon, and D. W. Setser, *J. Chem. Phys.*, **56**, 4355 (1972).
5) J. A. Coxon, D. W. Setser, and W. H. Duewer, *J. Chem. Phys.*, **58**, 2244 (1973).
6) J. A. Coxon, D. A. Ramsay, and D. W. Setser, *Can. J. Phys.*, **53**, 1587 (1975).
7) A. Mele and H. Okabe, *J. Chem. Phys.*, **51**, 4798 (1969).
8) G. A. West and M. J. Berry, *J. Chem. Phys.*, **61**, 4700 (1974).
9) I. Tokue, T. Urisu, and K. Kuchitsu, *J. Photochem.*, **3**, 273 (1974).
10) I. Tokue and K. Kuchitsu, *Chem. Phys. Lett.*, **34**, 369 (1975).
11) I. Tokue and K. Kuchitsu, *Chem. Phys. Lett.*, **36**, 207 (1975).
12) S. Tatematsu and K. Kuchitsu, to be published.
13) T. Urisu, Ph. D. Thesis, The University of Tokyo, 1972.
14) W. M. Jackson, *J. Chem. Phys.*, **61**, 4177 (1974).
15) L. Wallace, *Astrophys. J. Suppl.*, **7**, 165 (1962).
16) R. Engleman, Jr., *J. Mol. Spectrosc.*, **49**, 106 (1974).
17) R. J. Spindler, *J. Quant. Spectrosc. Radiat. Transfer*, **5**, 165 (1965).
18) R. S. Mulliken, *Rev. Mod. Phys.*, **3**, 89 (1931).
19) C. E. Moore, "Atomic Energy Levels," Vol. I, NBS Circular 467, U. S. Government Printing Office, Washington, D. C. (1949).
20) B. deB. Darwent, "Bond Dissociation Energies in Simple Molecules," NSRDS-NBS 31, U. S. Government Printing Office, Washington, D. C. (1970).
21) H. Okabe and V. H. Dibeler, *J. Chem. Phys.*, **59**, 2430 (1973).
22) D. D. Davis and H. Okabe, *J. Chem. Phys.*, **49**, 5526 (1968).
23) T. Iwai, M. I. Savadatti, and H. P. Broida, *J. Chem. Phys.*, **47**, 3861 (1967).
24) N. H. Kiess and H. P. Broida, *J. Mol. Spectrosc.*, **7**, 194 (1961).
25) H. E. Radford and H. P. Broida, *J. Chem. Phys.*, **38**, 644 (1963).
26) H. E. Radford and H. P. Broida, *Phys. Rev.*, **128**, 231 (1962).

Kinetic Study of Oxidative Addition and Replacement Reactions of Chlorotris(triphenylphosphine)rhodium(I) in Benzene

Yoshimi OHTANI, Masatoshi FUJIMOTO, and Akihiko YAMAGISHI

Department of Chemistry, Faculty of Science, Hokkaido University, Sapporo 060

(Received August 7, 1976)

Chlorotris(triphenylphosphine)rhodium(I) exists in benzene as $RhCl(PPh_3)_3$, a dimeric species $[RhCl(PPh_3)_2]_2$ and a reaction intermediate $RhCl(PPh_3)_2$. The rates of oxidative addition and replacement reactions were examined in benzene. For the oxidative addition reaction, $RhCl(PPh_3)_3$, $RhCl(PPh_3)_2$, or $[RhCl(PPh_3)_2]_2$+ $X_1 \overset{k_{add}}{\rightleftarrows}$Products ($X_1=H_2$, O_2, C_2H_4, $CHCl=CCl_2$, CH_3I), it was found that the reaction intermediate $RhCl(PPh_3)_2$ is most reactive, the degree of its reactivity depending largely on the reactants (X_1). A significant enhancement of the rate ($k_{sub}>k_{add}$) was observed for the ligand substitution reaction, $RhClX_1(PPh_3)_m+X_2 \overset{k_{sub}}{\rightleftarrows} RhClX_2(PPh_3)_n+X_1$ (m, $n=3$ or 2), where $X_1=H_2$ and $X_2=$olefin and *vice versa*. The results are discussed in relation to the mechanism of hydrogenation.

In recent years homogeneous reactions catalyzed by metal complexes have attracted attention and have been studied extensively.[1] Wilkinson's complex, chlorotris(triphenylphosphine)rhodium(I), is well known owing to its high reactivity in hydrogenation reactions.[2-6] A number of works have appeared on the mechanisms of the hydrogenation reactions catalyzed by this complex. In most works the overall rate of the reactions was determined by following the rate of H_2 gas absorption[3,4] or the change in concentration of the reactant and the product by gas-liquid chromatography.[7,8] The mechanisms of the hydrogenation of olefins were assumed by the dependence of the overall rate on the reactant concentrations. However, this sometimes leads to erroneous conclusions. There is another method in which the concentration change of the identified species of metal complexes or metal-reactant complexes is followed in solution. From the transient change of the species, it would be possible to establish the sequence of the reaction steps leading to the final hydrogenation products. Halpern and Wong studied the H_2 addition on Wilkinson's complex in benzene with a stopped-flow apparatus.[9] They determined the rate constant for several elementary steps with little ambiguity. We applied a similar method to study monomer$\rightleftarrows$dimer reactions of Wilkinson's complex, $2RhCl(PPh_3)_3 \rightleftarrows [RhCl(PPh_3)_2]_2+2PPh_3$, in benzene,[10] and identified the total mechanisms of the above reaction taking the intermediate species $RhCl(PPh_3)_2$ into consideration.

As an extension of the above work we report on the results of kinetic studies on the reactivities of the three species for the addition and the replacement reactions,

$$\underset{\text{Products}}{RhCl(PPh_3)_3,\ RhCl(PPh_3)_2,\ [RhCl(PPh_3)_2]_2} + X_1 \underset{\text{(addition)}}{\rightleftarrows}$$

$$RhClX_1(PPh_3)_m + X_2 \underset{\text{(replacement)},}{\rightleftarrows} RhClX_2(PPh_3)_n + X_1,$$

where X denotes a substrate and m, $n=3$ or 2. The intermediate structure of Wilkinson's complex during the course of hydrogenation is also discussed.

Experimental

Chlorotris(triphenylphosphine)rhodium(I) was prepared by the method described by Osborn *et al.*[3] Di-μ-chloro-tetrakis(triphenylphosphine)dirhodium(I) $[RhCl(PPh_3)_2]_2$ was obtained by dissolving Wilkinson's complex in benzene *in vacuo* and heating at *ca.* 60 °C. The precipitate was rapidly filtered and stored *in vacuo*. For the kinetic measurements it was solubilized in benzene by warming at 60 °C *in vacuo*. Triphenylphosphine was recrystallized from ethanol. Benzene, trichloroethylene, and acrylonitrile were distilled. Hydrogen, oxygen, ethylene, and methyl iodide were used without purification. The concentrations of H_2, O_2, and C_2H_4 at 1 atm were calculated from the solubility data.[11] The concentrations of H_2 and C_2H_4 were obtained by the gas-chromatography with a Molecular sieve 5A.

All the reactions were studied at 20 °C in oxygen-free benzene. The addition reactions of $CHCl=CCl_2$ and CH_3I were slow enough to measure with a Hitachi recording spectrophotometer model EPS-3T *in vacuo*. The progress of the reaction was followed by the absorbance change at 400 nm for $CHCl=CCl_2$ and 430 nm for CH_3I. The experiments of the addition and the replacement reactions involving C_2H_4, $CH_2=CHCN$, H_2, and O_2 were carried out with a Union Giken RA-1300 stopped-flow apparatus. The addition and the replacement reactions of C_2H_4 and $CH_2=CHCN$ were followed by the absorbance change at 422 nm and 400 nm, respectively. The addition reaction of O_2 was followed at 400 nm or 440 nm. The replacement reactions, $RhClX_1(PPh_3)_m+X_2 \rightleftarrows RhClX_2(PPh_3)_n+X_1$ (m, $n=3$ or 2), were observed by mixing an X_2 solution with an $RhClX_1(PPh_3)_m$ solution, where $X_1=H_2$ and $X_2=$olefin and *vice versa*. Above reactions were followed either by the decrease of $RhClX_1(PPh_3)_m$ or by the increase of $RhClX_2(PPh_3)_n$.

Results and Discussion

Oxidative Addition Reactions. Figure 1 shows the visible spectra of the addition products between $RhCl(PPh_3)_3$ (5.0×10^{-4} M) and H_2 (1.4×10^{-3} M), O_2(4.6×10^{-3} M), C_2H_4 (7.5×10^{-2} M), $CH_2=CHCN$(1.5×10^{-1} M), $CHCl=CCl_2$ (0.56 M), and CH_3I (2.5×10^{-2} M). The values in parentheses are the initial concentrations of the reactants.

Addition of Ethylene: Ethylene reacts reversibly with Wilkinson's complex to produce $RhCl(C_2H_4)L_2$, where $L=PPh_3$.[3,12] The stoichiometry of the reaction is

$$RhClL_3 + C_2H_4 \rightleftarrows RhCl(C_2H_4)L_2 + L. \quad (1)$$

The equilibrium constant of Eq. 1 is calculated to be $K=0.4$, which agrees with the value obtained by Tolman and co-workers.[12] The pseudo-first-order rate constant

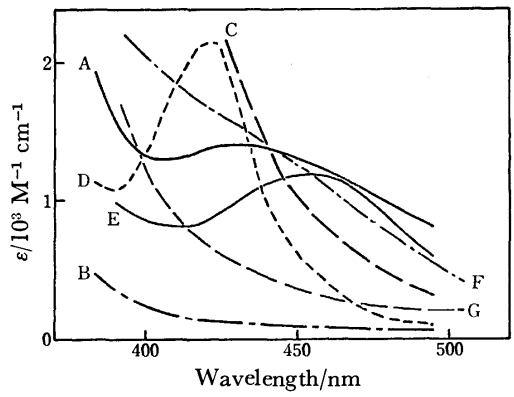

Fig. 1. Visible spectra of the equilibrium addition products on $RhClL_3$. $[RhClL_3]=5.0\times10^{-4}$ M, and $[PPh_3]=3\times10^{-3}$ M was added to exclude dimer formation. (A) none, (B) H_2 (1.4×10^{-3} M), (C) O_2 (4.6×10^{-3} M), (D) C_2H_4 (7.5×10^{-2} M), (E) CH_2=CHCN (1.5×10^{-1} M), (F) CHCl=CCl_2 (5.6×10^{-1} M), (G) CH_3I (2.5×10^{-2} M). The values in the parentheses are the initial concentrations of the reactants.

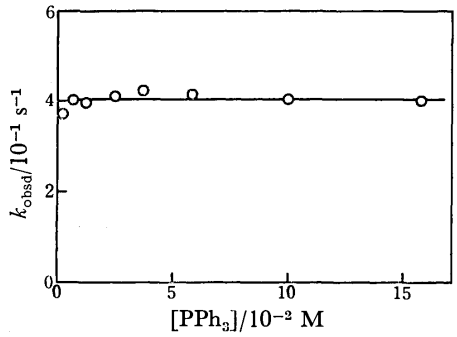

Fig. 2. Dependence of the observed rate constant of the ethylene addition reaction on the concentration of PPh_3. $[RhCl(PPh_3)_3]_0=5.0\times10^{-4}$ M, $[C_2H_4]=7.5\times10^{-2}$ M, and at 422 nm.

of the ethylene addition, k_{obsd}, is dependent neither on the concentration of L (0.002—0.16 M) (Fig. 2) nor on that of ethylene (0.025—0.075 M) added. The rate of the dissociation of ethylene from $RhCl(C_2H_4)L_2$ was measured by mixing the solution of L with the solution of the ethylene complex, $RhCl(C_2H_4)L_2$. The dissociation rate constant is also independent of the concentrations of L (0.012—0.081 M) (Fig. 3a) and ethylene (0.012—0.075 M) (Fig. 3b). The results are consistent with the following mechanism:

$$RhClL_3 + C_2H_4 \underset{k_{-1}}{\overset{k_1}{\rightleftharpoons}} RhClL_2 + L + C_2H_4$$

$$\underset{k_{-2}}{\overset{k_2}{\rightleftharpoons}} RhCl(C_2H_4)L_2 + L. \quad (2)$$

The value of k_{obsd} is expressed in terms of k_1, k_{-1}, k_2, and k_{-2} as

$$k_{obsd} = \frac{k_1k_2[C_2H_4]+k_{-1}k_{-2}[L]}{k_2[C_2H_4]+k_{-1}[L]}. \quad (3)$$

Since the rate of addition and dissociation show no dependence on the concentration of either C_2H_4 or L,

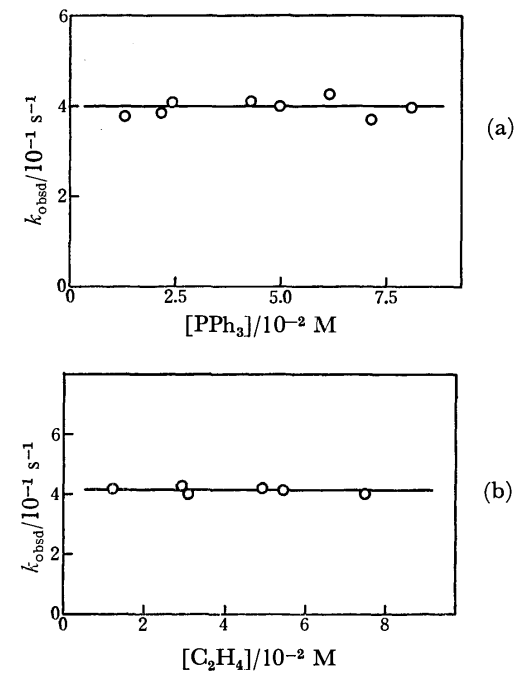

Fig. 3. Dissociation rate of ethylene from $RhCl(C_2H_4)(PPh_3)_2$. (a) Plot of k_{obsd} *vs.* $[PPh_3]$. $[RhCl(C_2H_4)(PPh_3)_2]_0=5\times10^{-4}$ M, $[C_2H_4]=7.5\times10^{-2}$ M, and at 422 nm. (b) Plot of k_{obsd} *vs.* $[C_2H_4]$. $[RhCl(C_2H_4)(PPh_3)_2]_0=5\times10^{-4}$ M, $[PPh_3]=5.2\times10^{-2}$ M, and at 422 nm.

we have $k_1=k_{-2}$; that is, $k_{obsd}=k_1=k_{-2}=0.4$ s^{-1} from Figs. 2 and 3. The value of the ratio $k_1k_2/k_{-1}=0.16$ s^{-1} since $K=k_1k_2/k_{-1}k_{-2}=0.4$. It is found that C_2H_4 reacts with only $RhClL_2$, whereas $RhClL_3$ is inactive for C_2H_4 addition.

Addition of Oxygen. Molecular oxygen adds to the Wilkinson's complex,[3,13] followed by the oxidation of the ligand PPh_3 in the Wilkinson's complex with coordinated active oxygen. In the present work, the fast addition reactions were studied:

$$RhClL_{3,2} + O_2 \longrightarrow RhCl(O_2)L_n \quad (n=3 \text{ or } 2)$$
$$(RhClL_2)_2 + O_2 \longrightarrow \text{Product}. \quad (4)$$

When a solution of Wilkinson's complex (5.0×10^{-4} M) was mixed with a solution of O_2 (9.1×10^{-3} M) under the conditions where the concentration of L is lower than 3×10^{-3} M, a two-step increase in absorbance was observed at 400 nm, the faster process terminating within 2 s and the slower one within 20 s. At 440 nm, the isosbestic point for $RhClL_3$ and $RhCl(O_2)L_n$ in equilibrium,[14] only the faster increase of the absorbance was observed. When the concentration of L exceeded 3×10^{-3} M, the faster process disappeared. This indicates that the slower step consists of the reaction between monomeric species $RhClL_3$ ($RhClL_2$ partly participates) and molecular oxygen. The faster one consists of the reaction between the dimer $(RhClL_2)_2$ and O_2. This was confirmed by a study of the solution containing only di-μ-chloro-terakis(triphenylphosphine)dirhodium (I) and oxygen.

The rate of the slower step is proportional to the concentration of O_2 ($(0.9—4.1)\times10^{-3}$ M). Figure 4

shows the dependence of the observed rate constant, k_{obsd}, on the concentration of L added. The value of k_{obsd} decreases until the concentration of L becomes *ca.* 1×10^{-2} M, attaining a constant value beyond this value. This trend is similar to that of the addition reaction of H_2 to the same complex reported by Halpern and Wong.[9] As in the case of the H_2 addition, the decrease of k_{obsd} with the addition of L may arise from the decrease of an active intermediate, $RhClL_2$, which is produced from $RhClL_3$ according to

$$RhClL_3 \rightleftharpoons RhClL_2 + L. \quad (5)$$

The mechanism for the O_2 addition to the monomeric species $RhClL_3$ is thus expressed by

$$\begin{array}{ccc} RhClL_3 + O_2 & \xrightarrow{k_M} & RhCl(O_2)L \\ k_1 \uparrow\downarrow k_{-1} & & \uparrow\downarrow \text{fast} \\ RhClL_2 + O_2 & \xrightarrow{k_I} & RhCl(O_2)L \\ + & & + \\ L & & L \end{array} \quad (6)$$

Application of the steady state approximation to $RhClL_2$ gives the following rate law:

$$-\frac{d[RhClL_3]}{dt} = \left\{k_M + \frac{k_1k_I}{k_{-1}[L]+k_I[O_2]}\right\}[O_2][RhClL_3]. \quad (7)$$

The ratio k_1/k_{-1} is less than 1×10^{-5} M.[9] k_1 was found to be 0.4 s^{-1} from the experiments of ethylene.[15] Thus $k_{-1}>4\times10^4$ M^{-1} s^{-1}. The value of k_M is found to be 26 M^{-1} s^{-1} by means of Eq. 7 from the constant value in Fig. 4. Introducing the above values of k_{-1} and k_M into Eq. 7 and applying the curve-fitting method to the results given in Fig. 4, we get the following rate constants: $k_1k_I/k_{-1}=1.7\times10^{-2}$ s^{-1}, $k_I>1.7\times10^3$ M^{-1} s^{-1}.

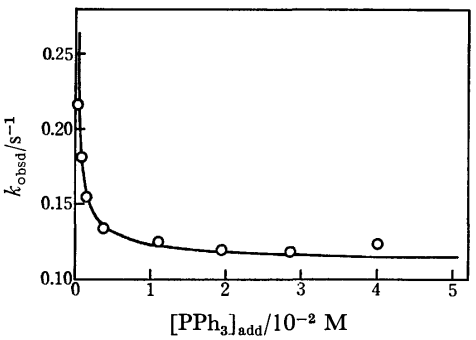

Fig. 4. Plot of the observed rate constant of the addition of O_2 *vs.* $[PPh_3]$. A solid curve is calculated from Eq. 7. $[RhCl(PPh_3)_3]_0=2.5\times10^{-4}$ M, $[O_2]=4.6\times10^{-3}$ M, and at 400 nm.

The rate of the following dimerization is negligibly small as compared to the rates of the O_2 addition (4).[10]

$$2RhClL_3 \rightleftharpoons (RhClL_2)_2 + 2L \quad (8)$$

The rate constant of the O_2 addition on the dimer which initially exists in Eq. 8 can thus be obtained by observing the decrease of the initial concentration of the dimer estimated from Eq. 8. The result is given in Fig. 5: $k_D=7.5\times10^2$ M^{-1} s^{-1}, where k_D is the addition rate constant on the dimer. The figure also contains the result involving only the dimer and O_2. It is seen

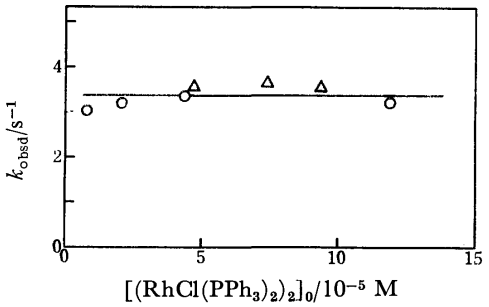

Fig. 5. Addition rate constant of O_2 on the dimer. ○; using Wilkinson's complex, △: using a pure dimer solution. $[O_2]=4.6\times10^{-3}$ M, at 440 nm.

that the faster process mentioned above corresponds to the O_2 addition on the dimer. Ethylene does not react with the monomer, while oxygen reacts with the monomer. The order of the rate constants is $k_I>k_D>k_M$ for the O_2 addition. The order corresponds to that for the H_2 addition reported by Halpern and Wong.[9]

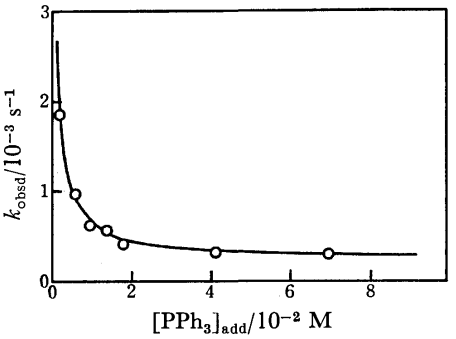

Fig. 6. Addition rate of $CHCl=CCl_2$. Plot of k_{obsd} *vs.* $[PPh_3]$. $[RhCl(PPh_3)_3]_0=5.0\times10^{-4}$ M, $[CHCl=CCl_2]=5.4\times10^{-2}$ M, and at 400 nm.

Addition of Trichloroethylene. The observed rate constant for the addition of $CHCl=CCl_2$ on Wilkinson's complex depends on the concentration of L as shown in Fig. 6. The trends of k_{obsd} are similar to those for the O_2 addition (Fig. 4), analysis thus being carried out in a similar way to that for oxygen. The results $k_M=4.6\times10^{-3}$ M^{-1} s^{-1}, $k_1k_I/k_{-1}=6.5\times10^{-5}$ s^{-1} and $k_I>6.5$ $M^{-1}\cdot s^{-1}$ were obtained.

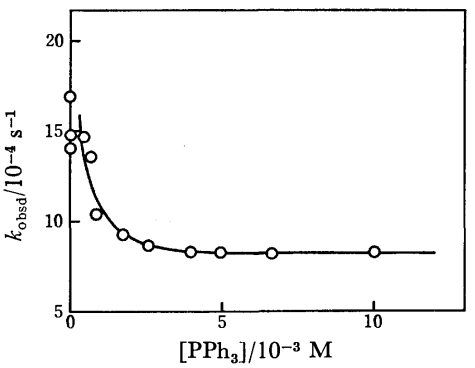

Fig. 7. Addition rate of CH_3I. Plot of k_{obsd} *vs.* concentration of PPh_3. The curve is calculated from Eq. 9. $[RhCl(PPh_3)_3]_0=5.1\times10^{-4}$ M, $[CH_3I]=2.5\times10^{-2}$ M, anda at 400 nm.

Addition of Methyl Iodide. Figure 7 shows the dependence of k_{obsd} for the addition of CH_3I on the concentration of L. When $[L]>1\times10^{-2}$ M, phosphonium salt precipitates during the course of measurement. However the CH_3I addition rate is not affected.[16] The value of k_{obsd} decreases with the addition of L as in the case of O_2 and $CHCl{=}CCl_2$.

By assuming the following mechanism involving the fast monomer-dimer equilibrium we obtained the curve given in Fig. 7.

$$\begin{array}{ccc} RhClL_3 + RhClL_3 & \overset{K}{\rightleftharpoons} & (RhClL_2)_2 + 2L \\ + & & + \\ CH_3I & & CH_3I \\ \downarrow k_M & & \downarrow k_D \\ \text{Product A} & & \text{Product B} \end{array} \quad (9)$$

$$-\frac{d[RhClL_3]}{dt} = k_M[RhClL_3][CH_3I] + k_D[(RhClL_2)_2][CH_3I], \quad (10)$$

$$= k_M[RhClL_3][CH_3I] + k_DK\frac{[RhClL_3]^2}{[L]^2}[CH_3I], \quad (10')$$

$$k_{obsd} = \left\{k_M + k_DK\frac{[RhClL_3]}{[L]^2}\right\}[CH_3I], \quad (11)$$

where k_M is the rate constant under the higher L concentration ($>3\times10^{-3}$ M) and k_D the rate constant obtained for the solution of di-μ-chloro-tetrakis(triphenylphosphine)dirhodium(I) and CH_3I. The curve shows that the decrease of k_{obsd} is interpreted by the monomer-dimer equilibrium species alone. No contribution of the reaction intermediate, $RhClL_2$, is observed. This is confirmed by the dependence of k_{obsd} on the concentration of $RhClL_3$ ($(2—15)\times10^{-4}$ M) observed without L added ($[CH_3I]=0.025$ M=const.) (Fig. 8). The fact that k_{obsd} increases with the increase in the total concentration of Rh complex even under the conditions of $[CH_3I]\gg$[Rh complex] indicates that the aggregated form of Rh complex (dimer) is more active than a monomer for the addition of CH_3I.

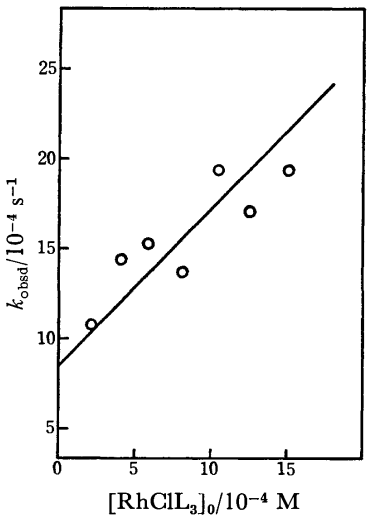

Fig. 8. Addition rate of CH_3I. Plot of k_{obsd} *vs.* $[RhCl(PPh_3)_3]_0$. $[CH_3I]=2.5\times10^{-2}$ M, $[PPh_3]_{add}=0$ M, and at 400 nm.

If the dimerization process is rate-determining in the reaction path of product B, Eq. 10 is modified as Eq. 13:

$$\begin{array}{ccc} RhClL_3 + RhClL_3 & \overset{K_1}{\rightleftharpoons} & RhClL_3 + RhClL_2 + L \\ + & & \overset{k_2}{\longrightarrow} (RhClL_2)_2 + 2L \\ CH_3I & & + \\ \downarrow k_M & & CH_3I \\ \text{Product A} & & \downarrow k_D \\ & & \text{Product B} \end{array} \quad (12)$$

$$-\frac{d[RhClL_3]}{dt} = k_M[RhClL_3][CH_3I] + K_1k_2\frac{[RhClL_3]^2}{[L]}, \quad (13)$$

$$k_{obsd} = k_M[CH_3I] + K_1k_2\frac{[RhClL_3]}{[L]},$$

where $K_1k_2=1.1\times10^{-3}$ s^{-1}.[10] The intercept of the curve in Fig. 8 gives 8×10^{-4} s^{-1} which is equal to the value in the higher concentration of L in Fig. 7. Thus the value 8×10^{-4} s^{-1} corresponds to the observed rate constant of the reaction of CH_3I with the monomer.

Conclusion of the Addition Reactions: The results are summarized in Table 1. The main findings are as follows.

(i) Except for CH_3I, an intermediate complex ($RhClL_2$) is the most reactive among the three species, $RhClL_3$, $RhClL_2$, and $(RhClL_2)_2$.

(ii) The values of k_M and k_D increase in the sequence of $CHCl{=}CCl_2<CH_3I<H_2<O_2$ and k_I in the sequence of $CHCl{=}CCl_2<O_2<C_2H_4<H_2$.

$RhClL_2$ might be a solvated species obtained by replacing one L of $RhClL_3$ with a solvent molecule. Thus the first finding implies that the main factor in determining the reactivity of the metal complex for oxidative addition is the presence of the labile site occupied by a solvent molecule. If the addition rate were determined by the dissociation of L from $RhClL_3$ (Eq. 5), k_I would be constant irrespective of the kind of substrate. However, as stated in (ii), k_I varies over several orders of magnitude for the substrates studied. k_I is remarkably large for C_2H_4 and H_2 but not for O_2. Therefore the addition reaction on $RhClL_2$ may be of an

Table 1. Rate constants of oxidative addition

	k_M / M^{-1} s^{-1}	k_D / M^{-1} s^{-1}	k_1k_I/k_{-1} / s^{-1}	k_I / M^{-1} s^{-1}	k_I/k_M
C_2H_4	small[b]	—	1.6×10^{-1}	$>1.6\times10^4$	very large
H_2[a]	4.8	5.4	4.8×10^{-1}	$>4.8\times10^4$	$>1\times10^4$
O_2	2.6×10	7.5×10^2	1.7×10^{-2}	$>1.7\times10^3$	$>6.3\times10$
$CHCl{=}CCl_2$	4.6×10^{-3}	1.0×10^{-2}	6.5×10^{-5}	>6.5	$>1.4\times10^3$
CH_3I	3.3×10^{-2}	2.5×10^{-1}	small[b]	small[b]	small[b]

a) From Ref. 9, at 25 °C. b) The exact values could not be estimated.

associative character proceeding through a five coordinated complex, $RhClL_2SYZ$, where S and YZ are the solvent molecule and the reactant, respectively.

The kinetic nature of Wilkinson's complex becomes more evident when the present results are compared with those for Vaska's complex, $IrCl(CO)L_2$. Vaska's complex undergoes the oxidative addition reaction as follows.

$$IrCl(CO)L_2 + X \rightleftarrows IrClX(CO)L_2.$$

For Vaska's complex, the rates of the addition of various substrates follow the order $C_2H_4 < O_2 < H_2$ in chlorobenzene at 30 °C.[17] Probably because of the presence of a labile site in Wilkinson's complex, the magnitude of k_1 is generally much higher than for Vaska's complex.[18] Comparing the reactivities with C_2H_4 and O_2 of Wilkinson's complex with those of Vaska's complex we find that their reactivities are reversed. The difference in the reactivities for both complexes may also be related to the bond nature of metal-substrate, but not entirely to the electronic property intrinsic to the substrate such as electron affinity.

Chock and Halpern[18] suggested that for the addition reaction of CH_3I to the $IrCl(CO)L_2$ complex the transition-state configuration would be

$$L_2(CO)ClIr^{\delta+}\cdots CH_3\cdots I^{\delta-}.$$

The present reaction for CH_3I may proceed through a similar transition-state configuration. Thus the change in the polarity both in a central metal and CH_3I plays a more important role than the substitution lability in $RhClL_2$. The labile site is not highly effective also in the case of the addition reaction of CH_3I on Pt complex. The rate constants are reported to be 3.5×10^{-3} $M^{-1}s^{-1}$ and 2.0×10^{-2} $M^{-1}s^{-1}$ for $Pt(PPh_3)_3$ and $Pt(PPh_3)_2$, respectively.[16]

Replacement Reactions. $RhCl(C_2H_4)L_2+H_2+L$ and $RhClH_2L_3+C_2H_4$: When a solution of $RhCl(C_2H_4)L_2$ ($[C_2H_4]=7.5\times10^{-2}$ M) is mixed with a solution of H_2 ($[H_2]=1.4\times10^{-3}$ M), a rapid decrease of $RhCl(C_2H_4)L_2$ occurs. No hydrogenation of C_2H_4 takes place within the time range[3] studied. There is no free Rh complex present under the given H_2 and C_2H_4 concentrations. The reaction of $RhCl(C_2H_4)L_2$ and H_2 thus seems to proceed as follows:

$$RhCl(C_2H_4)L_2 + H_2 + L \rightleftarrows RhClH_2L_3 + C_2H_4. \quad (14)$$

The equilibration is confirmed by the same spectra of $RhCl(C_2H_4)L_2+H_2+L$ and of $RhClH_2L_3+C_2H_4$, irrespective of the mode of mixing. Figures 9(a) and (b) give the dependence of k_{obsd} on [L] for the reaction of $RhCl(C_2H_4)L_2+H_2+L$ and $RhClH_2L_3+C_2H_4$, respectively. Increase of k_{obsd} with decreasing [L] suggests that in the replacement reaction $RhClH_2L_3$ is activated by dissociation of an L molecule. Thus the mechanism of the replacement reaction is

$$RhCl(C_2H_4)L_2 + H_2 + L \underset{k_{-1}}{\overset{k_1}{\rightleftarrows}} RhClH_2L_2 + C_2H_4 + L \underset{K}{\rightleftarrows} RhClH_2L_3 + C_2H_4, \quad (15)$$

$$k_{obsd} = k_1[H_2] + k_{-1}\frac{[C_2H_4]}{1+[L]/K}, \quad (16)$$

where K is the equilibrium constant for the dissociation of L from $RhClH_2L_3$. It is assumed in the derivation of the equation that the dissociation of L from $RhClH_2L_3$ is much faster than the replacement reaction of $RhCl(C_2H_4)L_2$ with H_2.[19] Equation 16 shows that the value of k_{obsd} in the plateau region of Figs. 9 (a) and (b) ($20\ s^{-1}$) corresponds to the forward reaction rate of Eq. 14 (when $[L]>5\times10^{-3}$ M, $k_{obsd}=k_1[H_2]$). Figures 10(a) and (b) show the dependence of k_{obsd} on the concentration of H_2 and C_2H_4 for the reactions $RhCl(C_2H_4)L_2+H_2+L$ and $RhClH_2L_3+C_2H_4$, respectively ($[L]=7.0\times10^{-3}$ M). The fact that k_{obsd} is independent of $[C_2H_4]$ is in line with the conclusion that k_{obsd} corresponds to the forward reaction rate. It will be expected from Eq. 16 that k_{obsd} is proportional to $[H_2]$. The dependence of k_{obsd} on the H_2 concentration, however, does not follow the relation $k_{obsd}=k_1[H_2]$. The results in Fig. 10(a) imply that the forward rate consists of at least two terms, one independent of $[H_2]$ and the other proportional to $[H_2]$. Thus we assume two parallel paths for the replacement of $RhCl(C_2H_4)L_2$ with H_2.

$$RhCl(C_2H_4)L_2 + H_2 \xrightarrow[A]{L} RhClH_2L_3 + C_2H_4 \text{ (path 1)}$$
$$\xrightarrow[B]{} Rh^*Cl(C_2H_4)L_2 + H_2 \xrightarrow{L} RhClH_2L_3 + C_2H_4 \text{ (path 2)} \quad (17)$$

Path 1 is the direct exchange between H_2 and the coordinated C_2H_4 ($k=7.8\times10^3$ M^{-1} s^{-1}). Path 2 involves the uni-molecular step (B) in which $RhCl(C_2H_4)L_2$ is

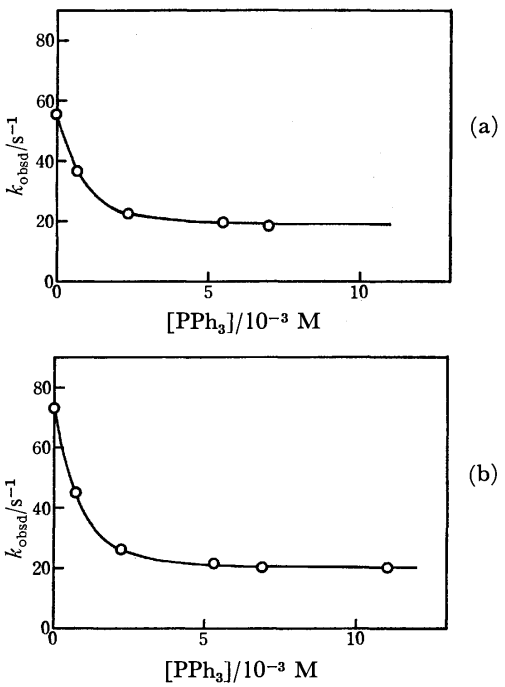

Fig. 9. Replacement reactions. Plot of k_{obsd} *vs.* $[PPh_3]$. (a) $RhCl(C_2H_4)(PPh_3)_2+H_2+PPh_3$; $[RhCl(C_2H_4)(PPh_3)_2]=2.5\times10^{-4}$ M, $[C_2H_4]=7.5\times10^{-2}$ M, $[H_2]=1.4\times10^{-3}$ M, and at 422 nm. (b) $RhClH_2(PPh_3)_3+C_2H_4$; $[RhClH_2(PPh_3)_3]_0=2.5\times10^{-4}$ M, $[H_2]=1.4\times10^{-3}$ M, $[C_2H_4]=7.5\times10^{-2}$ M, and at 422 nm.

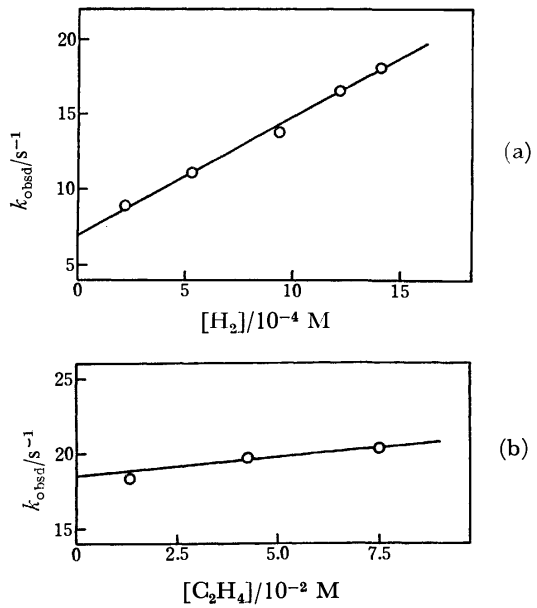

Fig. 10. Replacement reactions. Plots of k_{obsd} *vs.* concentration of the reactants. (a) $RhCl(C_2H_4)(PPh_3)_2+H_2+PPh_3$; dependence of k_{obsd} on the concentration of H_2. $[RhCl(C_2H_4)(PPh_3)_2]_0=1.6\times10^{-4}$ M, $[C_2H_4]=7.5\times10^{-2}$ M, $[PPh_3]=7.0\times10^{-3}$ M, and at 422 nm. (b) $RhClH_2(PPh_3)_3+C_2H_4$; dependence of k_{obsd} on the concentration of C_2H_4. $[RhClH_2(PPh_3)_3]_0=2.5\times10^{-4}$ M, $[H_2]_0=1.4\times10^{-3}$ M, $[PPh_3]=7.0\times10^{-3}$ M, and at 422 nm.

activated ($k=7\ s^{-1}$). Process B does not involve the dissociation of C_2H_4. The rate constant of the dissociation of C_2H_4, k_{diss}, is $0.4\ s^{-1}$ as determined previously. On the other hand the intercept in Fig. 10(a) gives $7\ s^{-1}$ to the rate constant of the uni-molecular process in path 2, which is much greater than k_{diss}. The uni-molecular process seems to be the dissociation process of a solvent molecule which is loosely coordinated to the central metal above or below the plane of $RhCl(C_2H_4)L_2$ complex.

$RhCl(CH_2=CHCN)L_2+H_2+L$ and $RhClH_2L_3+CH_2=CHCN$: The results of kinetic studies on this system are very similar to those obtained for $RhCl(C_2H_4)L_2+H_2+L$ and $RhClH_2L_3+C_2H_4$. The results are summarized in Table 2.

TABLE 2. OBSERVED RATE CONSTANTS OF THE REPLACEMENT REACTIONS ($RhClX_1L_m+X_2\rightleftarrows RhClX_2L_n+X_1$; $m, n=3$ or 2)

k_{obsd}/s^{-1}

$RhClX_1L_m$	X_2		
	H_2	C_2H_4	$CH_2=CHCN$
H_2	—	20	32
C_2H_4	18	—	310
$CH_2=CHCN$	20	250	—
None[a]	0.071	0.4	0.5

a) Observed rate constants of the addition reactions under comparable conditions. $[RhCl(PPh_3)_3]_0=2.5\times10^{-4}$ M, $[PPh_3]=7\times10^{-3}$ M, $[H_2]_0=1.4\times10^{-3}$ M, and $[C_2H_4]=[CH_2=CHCN]=7.5\times10^{-2}$ M.

Conclusion on the Replacement Reactions: In the replacement reaction the rate of replacement of the coordinated olefin by H_2 is greater by about two orders of magnitude than the rate of the oxidative addition of H_2 on Rh complex under comparable conditions. The acceleration effect observed implies that the approach of H_2 to Rh(olefin) complex makes the coordinated olefin labile. In other words, a strong interaction exists through the central metal between H_2 and the coordinated olefin. It strongly supports the presence of an associative intermediate $RhClH_2(olefin)L_2$. The hydrogenation of the olefins proceeds much more slowly than the replacement reaction.[3] However, it is probable that on hydrogenation of the olefins the same associative intermediate exists, on which 2H migrate on olefin to produce paraffin. If that is the case the complex formation step is considered to be a pre-equilibrium in the hydrogenation of olefins. If this conclusion is correct, there is no question as to whether H_2 or olefin adds first on the Rh complex during the course of hydrogenation, that is the hydride route or the unsaturate route.[3,4,6,7]

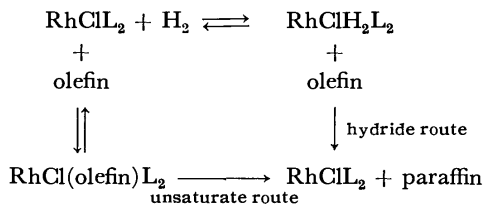

We consider that the high activity of Wilkinson's complex may arise from the existence of both the intermediates $RhClL_2$ and $RhClH_2(olefin)L_2$ through which hydrogenation of the olefin proceeds.

We wish to express our thanks to Dr. Tokio Iizuka of this department for the supply of ethylene. The present work was supported by the Grant-in-Aid for Scientific Research from the Ministry of Education.

References

1) B. R. James, "Homogeneous Hydrogenation," Wiley, New York, N. Y. (1973), pp. 204—250; G. N. Schrauzer, "Transition Metals in Homogeneous Catalysis," Marcell Dekker, New York, N. Y. (1971), pp. 31—36; M. M. T. Khan and A. E. Martell, "Homogeneous Catalysis by Metal Complexes," Vol. 1, Academic Press, New York, N. Y. (1974), pp. 46—56.

2) L. A. Osborn, G. Wilkinson, and J. F. Young, *Chem. Commun.*, **1965**, 17.

3) J. A. Osborn, F. H. Jardine, J. F. Young, and G. Wilkinson, *J. Chem. Soc., A*, **1966**, 1711.

4) F. H. Jardine, J. A. Osborn, and G. Wilkinson, *J. Chem. Soc., A*, **1967**, 1574; S. Montelatici, A. van der Ent, J. A. Osborn, and G. Wilkinson, *ibid., A*, **1968**, 1054.

5) A. J. Birch and K. A. M. Walker, *J. Chem. Soc., C*, **1966**, 1894; A. J. Birch and K. A. M. Walker, *Aust. J. Chem.*, **24**, 513 (1971).

6) W. Voelter and C. Djerassi, *Chem. Ber.*, **101**, 58 (1968).

7) J. P. Candlin and A. R. Oldham, *Discuss. Faraday Soc.*, **46**, 60 (1968).

8) G. C. Bond and R. A. Hillyard, *Discuss. Faraday Soc.*, **46**, 20 (1968).

9) J. Halpern and C. S. Wong, *J. Chem. Soc., Chem. Commun.*, **1973**, 629.
10) Y. Ohtani, M. Fujimoto, and A. Yamagishi, *Bull. Chem. Soc. Jpn.*, **49**, 1871 (1976).
11) Landolt-Börnstein, "Zahlenwerte und Funktionen," Vol. II, 6th ed, Part 2b, Springer-Verlag, Berlin, 1962.
12) C. A. Tolman, P. Z. Meakin, D. L. Lindner, and J. P. Jesson, *J. Am. Chem. Soc.*, **96**, 2762 (1974).
13) J. P. Birk, J. Halpern, and A. L. Pickard, *J. Am. Chem. Soc.*, **90**, 4491 (1968).
14) Y. Ohtani, M. Fujimoto, and A. Yamagishi, unpublished result.
15) Halpern and Wong obtained 0.7 s^{-1} as k_1 at 25 °C from the H_2 addition (Ref. 9).
16) R. G. Pearson and J. Rajaram, *Inorg. Chem.*, **13**, 246 (1974).
17) L. Vaska, *Acc. Chem. Res.*, **1**, 335 (1968).
18) P. B. Chock and J. Halpern, *J. Am. Chem. Soc.*, **88**, 3511 (1966).
19) P. Meakin, J. P. Jesson, and C. A. Tolman, *J. Am. Chem. Soc.*, **94**, 3240 (1972).

The Fluorometric Determination of Indium with 8-Quinolinethiol[1)]

Kunihiro WATANABE, Akio FUJIWARA, and Kyōzō KAWAGAKI
Faculty of Science and Technology, Science University of Tokyo, Yamazaki, Noda-shi, Chiba 278
(Received October 7, 1976)

8-Quinolinethiol reacts with indium in the presence of acetic acid to give a yellow ternary complex. The complex, which has a greenish-yellow fluorescence with an emission maximum at 515 nm, can be extracted into chloroform at pH 2—4. In the ternary complex, the fluorescence intensity was about two times as large as that of the indium 8-quinolinethiolato complex containing no acetate ion. The fluorescence was stable for at least 1 h. By the use of a 0.2 μg/ml uranine solution as the setting reagent, 0—25 μg of indium in 10 ml of chloroform was determined. The coefficient of the variation was 3% for 12 μg of indium. The extractability of the ternary complex from 50 ml of an aqueous solution into 10 ml of chloroform was 99%. Iron, mercury, and silver, which interfere with the determination of indium, were masked with ascorbic acid, potassium iodide, and thiourea. Other interfering elements, including zinc, cadmium, gallium, nickel, palladium, cobalt, antimony, gold, copper, bismuth, and vanadium, must be removed before any analysis.

8-Quinolinethiol reacts with metal ions to form water-insoluble chelates, and they are extracted into some organic solvents. The indium 8-quinolinethiolato chelate extracted into chloroform or benzene has been used in spectrophotometric[2)] and fluorometric[3,4)] determination methods. The spectra and the composition of the indium chelate have also been obtained by Davis.[3)] Suprunovich *et al.*[5)] found that the indium 8-quinolinethiolato chelate reacts with acetic acid to form a ternary complex. However, the determination of indium in terms of the ternary-complex formation has not yet been studied. Recently, the present authors have found the ternary complex of indium–8-quinolinethiol–acetic acid to have a stronger fluorescence than the indium 8-quinolinethiolato chelate containing no acetate ion.

The present paper will report on the fundamental conditions for the fluorometric determination of indium with 8-quinolinethiol in the presence of acetic acid. Chloroform and methyl isobutyl ketone (MIBK) were used as the extraction solvents.

Experimental

Reagents. Standard solution of indium: 0.2502 g of 99.99% indium metal (Mitsubishi Kinzoku) was dissolved in 25 ml of hydrochloric acid, and then the solution was diluted to 250 ml with water. The solution was diluted further as a more diluted solution was required.

0.2% 8-Quinolinethiol Solutiol: In 50 ml of 6 M (M=mol dm^{-3}) hydrochloric acid, 0.1 g of 8-quinolinethiol hydrochloride (Dojin Yakukagaku) was dissolved.

Buffer Solution: A 2% ammonium acetate solution was prepared. The pH of the buffer solution was adjusted with hydrochloric acid or ammonia.

Acetic Acid: Glacial acetic acid of an analytical grade (Wako Chemicals Co.) was used.

A 0.2 μg/ml Uranine Solution: 0.1 g of uranine was dissolved in water, and the solution was diluted to 100 ml. The solution was then further diluted with water to obtain a solution containing 0.20 μg uranine per ml.

Other Reagents: The chloroform and MIBK used as extraction solvents and the other chemicals used were all of an analytical reagent grade.

Apparatus. The fluorometric measurements were carried out using a Hitachi fluorescence spectrophotometer, Model 203, with a mercury lamp. A 120-W Xenon lamp was used as the exciting source for the measurements of the fluorescence and excitation spectra. A 1 cm × 1 cm quartz cell was used. The pH was measured with a Toa Denpa Model HM-5 pH meter. An Iwaki KM shaker was used.

Procedure. To a sample solution containing 0.5—25 μg of indium, we added 10 ml of glacial acetic acid and 0.2 ml of a 0.2% 8-quinolinethiol solution. After the solution had then been diluted to 50 ml with water, the pH of the solution was adjusted to 2.5 with diluted hydrochloric acid or ammonia. The resultant aqueous solution was then transferred into a separatory funnel. The indium complex was extracted with 10 ml of chloroform or MIBK by shaking it vigorously for 2 min. After the separation of the mixture into two phases, the organic phase was transferred into a quartz cell and the fluorescence intensity of the extract was measured using a 0.2 μg-per-ml uranine solution as the reference standard. The excitation and fluorescence wavelengths used were 365 and 515 nm respectively. The content of indium was calculated using the calibration curve.

Results and Discussion

Excitation and Fluorescence Spectra. The apparent excitation and fluorescence spectra of the ternary complex and the indium 8-quinolinethiolato chelate extracted into chloroform and MIBK are given in Fig. 1. The ternary complex had an excitation maximum at 395 nm and a fluorescence maximum at 515 nm, while the indium 8-quinolinethiolato chelate had an excitation maximum at 395 nm and a fluorescence maximum at 505 nm. No shift of these maximum wavelengths due to extraction solvents was observed. The ternary complex, however, had a fluorescence intensity about two times as large as that of the indium 8-quinolinethiolato chelate. The fluorescence intensity of the complex extracted into chloroform was greater than that of the complex extracted into MIBK.

Effect of the pH. The effect of the pH of the aqueous phase on the fluorescence intensity is shown in Fig. 2. The optimum pH for the extraction of the indium 8-quinolinethiolato chelate was 1.6. The maximum extractability of the ternary complex into chloroform was, however, obtained at pH values from 2 to 4 and the fluorescence intensity of the complex in MIBK gave a maximum at pH 1.8—2.2. Therefore, the extractions of the ternary complex were carried out at pH 2.5 in chloroform and at pH 2.0 in MIBK.

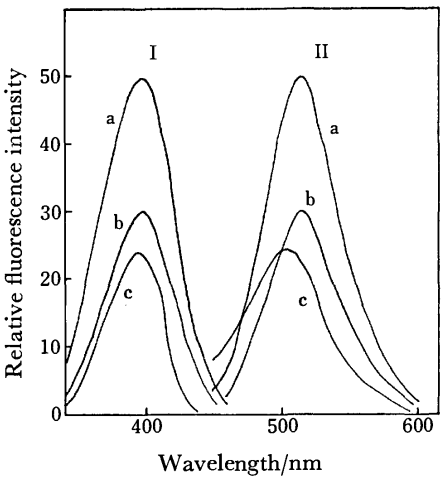

Fig. 1. Excitation and fluorescence spectra of indium complexes. Excitation spectra (I): Excited with xenon lamp and analyzed at wavelength for maximum fluorescence intensity. Emission spectra (II): Excited at 395 nm, a: acetic acid 10 ml, chloroform extraction, pH: 2.5, b: acetic acid 10 ml, MIBK extraction, pH: 2.0, c: acetic acid 0 ml, chloroform extraction, pH: 1.6, In 12 μg.

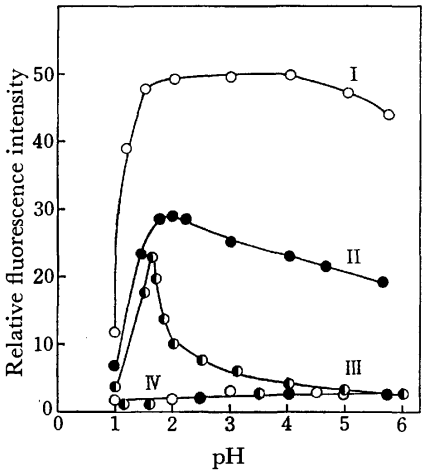

Fig. 2. Effect of pH on fluorescence intensity. In: 12 μg, I: acetic acid 10 ml, chloroform extraction, II: acetic acid 10 ml, MIBK extraction, III: acetic acid 0 ml, chloroform extraction, IV: reagent blanks.

Effect of the Acetic Acid Concentration. The effect of the acetic acid concentration in the aqueous phase on the extraction of ternary complex was examined by varying the acetic acid concentration. As the concentration of the acetic acid increased, the fluorescence intensity of the extract increased remarkably. However, above 3.4 M (10 ml acetic acid/50 ml) the fluorescence intensity increased gradually with the amount of acetic acid, as is shown in Fig. 3. On the other hand, since acetic acid in concentrations higher than 6.8 M gave difficulties in the pH adjustment and in the separation of the aqueous and MIBK phases, the concentration of acetic acid was kept at 3.4 M.

Effect of the Concentration of 8-Quinolinethiol. The effect of the 8-quinolinethiol concentration in the aqueous phase on the extractability of the ternary

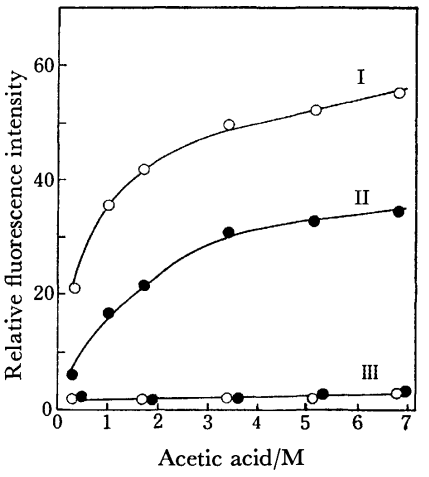

Fig. 3. Effect of the concentration of acetic acid on fluorescence intensity. In: 12 μg, I: chloroform extraction, II: MIBK extraction, III: reagent blanks.

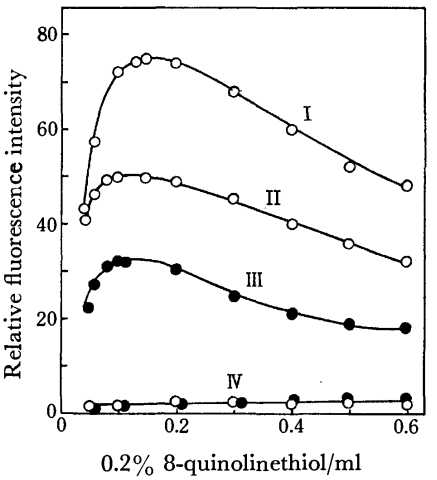

Fig. 4. Effect of amount of 8-quinolinethiol on fluorescence intensity. I: chloroform extraction, In: 18 μg, II: chloroform extraction, In: 12 μg, III: MIBK extraction, In: 12 μg, IV: reagent blanks, Acetic acid: 10 ml.

complex was examined by varying the amount of the 0.2% 8-quinolinethiol solution added, while the other variables were held constant. The results shown in Fig. 4 indicate that the optimum amount of the reagent was 0.1 ml of the 0.2% solution for 12 μg of indium, and from 0.1 to 0.2 ml for 18 μg of indium. The fluorescence intensity of the extracts decreased gradually with the increase in the reagent. The reagent blank was constant. Therefore, the amount of the 0.2% 8-quinolinethiol solution was kept at 0.2 ml.

Effect of the Volume of the Aqueous Solution. For the investigation of the effect, the volume of the organic phase was kept at 10 ml, while that of the aqueous phase was varied from 30 to 150 ml. When the concentration of acetic acid added was kept at 3.4 M, the fluorescence intensity in chloroform was nearly constant regardless of the increase in the volume of the aqueous phase. On the other hand, when MIBK was used for the extraction of the complex, a small amount of MIBK dissolved in the aqueous phase, so that the fluorescence

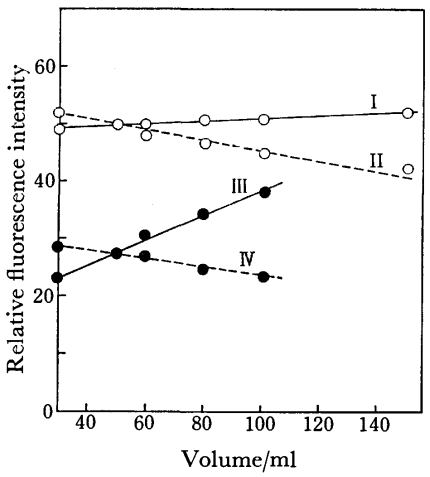

Fig. 5. Effect of volume of aqueous solution on fluorescence intensity. I, III: Concentration of acetic acid was kept at 3.4 M, II, IV: amount of acetic acid added was kept at 10 ml, I, II: chloroform extraction, III, IV: MIBK extraction.

intensity gradually increased with the volume of the aqueous phase. However, when the amount of acetic acid added was kept at 10 ml, the fluorescence intensities in organic solvents decreased with a decrease in the concentration of acetic acid. The results are shown in Fig. 5.

Effect of the Shaking Time, and the Stability of the Ternary Complex. The shaking time was varied from 0.25 to 30 min. It was found that shaking for 1 min was, in most cases, long enough for the extraction. A shaking time of 2 min was chosen, however, taking into consideration the possibility of accidental failure in extractability.

The fluorescence intensity of the ternary complex in a closed quartz cell was measured at 5 min intervals. The fluorescence intensity was constant until 10 min, past which point it increased gradually with the decrease in the amount of the solvent because of evaporation. However, after the ternary complex had been extracted, the fluorescence was stable at least for 60 min in a separatory funnel. It is recommended, therefore, to measure the fluorescence intensity of the complex within 10 min after it is transferred into a quartz cell.

TABLE 1. RELATIVE FLUORESCENCE INTENSITIES OF THE INDIUM–8-QUINOLINETHIOL–ACETIC ACID COMPLEX IN VARIOUS ORGANIC SOLVENTS

Solvent (10 ml)	Relative fluorescence intensity		
	Complex	Reagent blank	Difference
Chloroform	49.1	2.0	47.1
Benzene	31.8	1.2	30.6
MIBK	30.7	2.2	28.5
Toluene	27.0	1.8	25.2
Carbon tetrachloride	24.8	1.2	23.6
Xylene	26.1	2.9	23.2
Diisopropyl ether	23.0	1.2	21.8
Cyclohexane	4.0	1.2	2.8

In: 12 μg.

Extractability. A 50 ml portion of the aqueous phase containing the indium complex was shaken with 10 ml of chloroform, and the fluorescence intensity of the extract was measured. Then the indium remaining in the aqueous phase was extracted twice with chloroform. Extractability was calculated from the sum of the fluorescence intensities of the extracts and that of the first extract. It was found that 99% of indium was extracted by a single extraction.

Choice of Solvent. Chloroform was used as the extraction solvent of indium 8-quinolinethiolato chelate by Davis,[3] while benzene was used by Korenman *et al.*[4] The ternary complex of indium–8-quinolinethiol–acetic acid can also be extracted into many organic solvents. Therefore, the relative fluorescence intensities of the ternary complex extracted into several organic solvents were examined. The experimental results showed that chloroform and benzene, as well as MIBK, were excellent solvents, as is shown in Table 1. Chloro-

TABLE 2. EFFECTS OF DIVERSE IONS

Ion	(mg)	Added as	In found (μg)
Al^{3+}	8.0	$Al(NO_3)_3 \cdot 9H_2O$	12.0
Na^{+}	8.0	NaCl	12.0
Mg^{2+}	8.0	$Mg(NO_3)_2 \cdot 6H_2O$	12.0
Ca^{2+}	8.0	$Ca(NO_3)_2 \cdot 4H_2O$	12.0
Ba^{2+}	8.0	$BaCl_2 \cdot 2H_2O$	12.0
Cr^{3+}	8.0	$Cr(NO_3)_3 \cdot 9H_2O$	12.0
Sr^{2+}	8.0	$Sr(NO_3)_2$	11.9
Zr^{4+}	4.0	$ZrOCl_2 \cdot 8H_2O$	12.0
Cu^{2+}	0.01	$CuSO_4 \cdot 5H_2O$	12.0
	0.02	$CuSO_4 \cdot 5H_2O$	10.5
Ag^{+}	0.061	$AgNO_3$	10.9
	1.0	$AgNO_3$+10% thiourea 1 ml	12.0
Hg^{2+}	0.1	$Hg(NO_3)_2 \cdot 1/2H_2O$	5.0
	0.1	$Hg(NO_3)_2 \cdot 1/2H_2O$+10% ascorbic acid 1 ml+2N KI 2 ml	11.8
Fe^{3+}	0.042	Fe+HNO_3	9.5
	1.0	Fe+HNO_3+10% ascorbic acid 1 ml	12.0
Ni^{2+}	0.023	Ni+HNO_3	9.8
Co^{2+}	0.011	$Co(NO_3)_2 \cdot 6H_2O$	9.5
Cd^{2+}	0.06	Cd+HNO_3	12.0
	0.148	Cd+HNO_3	13.2
Zn^{2+}	0.006	Zn+HCl	17.6
Ga^{3+}	0.015	Ga_2O_3+HCl	24.3
Mn^{2+}	1.0	$MnCl_2$	12.0
Tl^{+}	8.0	$TlNO_3$	12.4
Pb^{2+}	5.0	Pb+HNO_3	12.5
Sn^{2+}	0.2	$SnCl_2 \cdot 2H_2O$+HCl	11.9
Bi^{3+}	0.05	$Bi(NO_3)_3 \cdot 5H_2O$	9.9
	0.1	$Bi(NO_3)_3 \cdot 5H_2O$	6.3
Sb^{3+}	0.07	Sb+H_2SO_4	12.0
	0.3	Sb+H_2SO_4	6.6
As^{3+}	5.0	As_2O_3+NaOH	12.0
Pd^{2+}	0.04	$PdCl_2$+HCl	3.0
La^{3+}	0.6	La_2O_3+HCl	12.4
Au^{3+}	0.046	$HAuCl_4 \cdot 4H_2O$	6.5
W^{6+}	8.0	$Na_2WO_4 \cdot 2H_2O$	12.0
V^{5+}	0.04	NH_4VO_3	5.2

In taken: 12.0 μg; 0.2% 8-quinolinethiol 0.2 ml; pH 2.5.

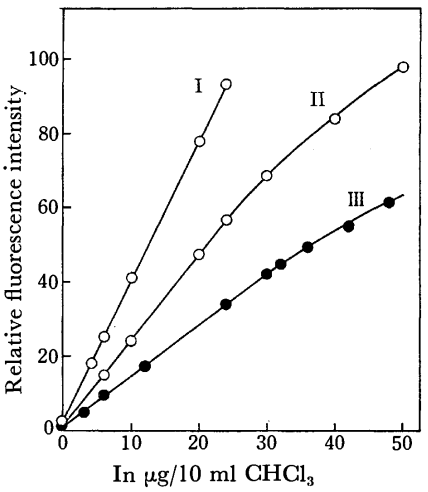

Fig. 6. Calibration curves for indium. Fluorometer reading was set at 50 div. (curve I) or 30 div. (curves II, III) with the uranine reference solution (0.2 μg/ml). I, II: chloroform extraction, III: MIBK extraction.

form and MIBK have been chosen as the solvents.

Calibration Curves. Figure 6 shows the calibration curves for indium, which were obtained by the described procedure above, based on the experimental results. However, the pH's of extraction were 2.5 in the chloroform extraction and 2.0 in the MIBK extraction. The sensitivity of the fluorometer was adjusted by setting the fluorescence of the standard uranine solution (0.2 μg/ml) at 30 or 50 on the fluorometer scale.

A good linear relationship was obtained over the concentration ranges from 0 to 25 μg per 10 ml of chloroform, and from 0 to 32 μg per 10 ml of MIBK. The coefficient of the variation obtained in 25 measurements was 3% for 12 μg of indium.

Effects of Diverse Ions and of Masking. The effects of 29 cations on the determination of indium were studied under optimum conditions. The results are shown in Table 2. Gallium, zinc, and cadmium gave positive errors in the determination of indium, and copper, cobalt, iron, nickel, palladium, mercury, bismuth, antimony, gold, vanadium, and silver ions reduced the fluorescence, but the other ions presented in Table 2 did not interfere.

The interference of ions such as iron (up to 1 mg), mercury (up to 100 μg), and silver (up to 1 mg) can be masked by using ascorbic acid, a mixture of ascorbic acid and potassium iodide, and thiourea respectively.

Composition of the Ternary Complex. By using the variation method fluorometrically, the molar ratio of indium to 8-quinolinethiol was found to be 1 : 2. However, the molar ratio of indium to acetic acid was not determined.

References

1) Determination of metals with thiooxine. VI. Part V of this series: K. Watanabe and K. Kawagaki, *Bunseki Kagaku*, **25**, 246 (1976).

2) J. Bankovskis, J. Cirule, and A. Ievins, *Zh. Anal. Khim.*, **16**, 562 (1961).

3) R. Davis, *Univ. Microfilms* (Ann Arbor. Mich.), Order No. 66-7874.

4) I. M. Korenman, F. R. Sheyanova, and N. I. Starodubova, *Tr. Po Khim. i Khim. Tekhnol.*, **1963**, 243.

5) V. I. Suprunovich and Yu. I. Usatenko, *Ukr. Khim. Zh.*, **34**, 120 (1968).

The Effect of Steric Condition on the Structure of Cobalt(II), Nickel(II), and Copper(II) Complexes with Schiff Bases Obtained from Salicylaldehyde Derivatives and 9-Aminofluorene

Shoichiro YAMADA, Hideaki TANAKA, and Kuniko YAMANOUCHI

Institute of Chemistry, College of General Education, Osaka University, Toyonaka, Osaka 560

(Received November 1, 1976)

Cobalt(II), nickel(II), and copper(II) complexes with *N*-(9-fluorenyl)salicylideneaminates (abbreviated as X-sal-fl) have been examined in relation to the effect of steric condition on the structure of the metal complexes. Compounds of the type $M(X\text{-sal-fl})_2$ and their pyridine adducts were isolated as crystals. Complexes of the type Cu(X-sal-fl)Cl were also obtained. Both in the solid state and in non-donor solvents, the complexes $Co(X\text{-sal-fl})_2$ have a tetrahedral configuration, and $Ni(X\text{-sal-fl})_2$ and $Cu(X\text{-sal-fl})_2$ have a square-planar configuration. Possible structures of the pyridine adducts are discussed. The results indicate that the steric hindrance caused by fluorenyl is greater than that by diphenylmethyl.

Transition metal complexes with *N*-substituted salicylideneaminates (abbreviated as X-sal-R, a) vary widely in structure, depending upon the steric conditions arising from the substituent R.[1-3] Many 3d metal complexes with *N*-isopropyl- and *N*-diphenylmethylsalicylideneaminates (b, c)[4] were synthesized and the steric effect of the substituents on the structure of the metal complexes was discussed. The present work deals with cobalt(II), nickel(II), and copper(II) complexes with *N*-(9-fluorenyl)salicylideneaminates (d), whose steric condition is expected to differ slightly from that of the *N*-diphenylmethyl-derivatives.

Experimental

Materials. Analytical data of the new complexes are given in Tables 1 and 2.

Bis[N-*(9-fluorenyl)salicylideneaminato]metal(II) Complexes, M-(X-sal-fl)*$_2$ *(M=Co, Ni, Cu).* These complexes were obtained as crystals by methods similar to those reported previously.[1,2,4] Two methods were used. (A) To a suspension of bis(salicylaldehydato)metal(II) (0.01 mol) in ethanol (20 ml) was added 9-aminofluorene (0.02 mol) at 60 °C under stirring. (B) To a solution of X-salicyldehyde (0.01 mol) in ethanol (25 ml) was added 9-aminofluorene (0.01 mol) at 60 °C and the mixture was stirred for 30 min. A solution of the appropriate metal(II) salt (0.005 mol) in ethanol (15 ml) was added to the resulting solution and stirred for 15 min, followed by addition of an aqueous solution of sodium carbonate (0.01 mol).

In both cases the reaction mixture was heated on a water-bath at 60 °C for about 2h. The resulting precipitate was recrystallized from chloroform.

The cobalt(II), nickel(II), and copper(II) complexes obtained are orange, olive-green and olive-green, respectively. They are moderately soluble in chloroform and benzene with the exception of bis[*N*-(9-fluorenyl)-2-hydroxy-1-naphthylmethyleneaminato]nickel(II), abbreviated as Ni(5,6-benzo-sal-fl)$_2$, which is less soluble than the others. They are almost insoluble in methanol, ethanol and acetone. The cobalt(II) and nickel(II) complexes are almost insoluble in cold pyridine but soluble in hot pyridine, accompanied by colour change. The copper(II) complexes are soluble in pyridine at room temperature, the colour of the solution changing gradually with time.

Bis[N-*(9-fluorenyl)salicylideneaminato]metal(II) Monopyridine Adducts, M(X-sal-fl)*$_2$*·py (M=Co, Ni, Cu).* These adducts were obtained as crystals when a hot saturated solution of the parent complex was allowed to stand overnight in a

TABLE 1. ANALYTICAL DATA OF NICKEL(II) AND COBALT(II) COMPLEXES

Compound	Calcd, %			Found, %			μ	Mp °C
	C	H	N	C	H	N		
$Ni(H\text{-sal-fl})_2$	76.58	4.50	4.47	76.45	4.51	4.36	dia	263
$Ni(5\text{-Br-sal-fl})_2$[a]	58.70	3.22	3.40	58.41	3.37	3.55	dia	269
$Ni(5\text{-Cl-sal-fl})_2$	69.00	3.77	4.02	68.89	3.84	4.01	dia	288
$Ni(3\text{-}CH_3O\text{-sal-fl})_2$[b]	72.44	4.78	4.02	72.64	4.92	4.43	dia	206
$Ni(5,6\text{-benzo-sal-fl})_2$	79.25	4.43	3.85	79.08	4.41	3.87	dia	195
$Co(H\text{-sal-fl})_2$	76.55	4.50	4.46	76.51	4.48	4.38	4.06	185
$Co(5\text{-Br-sal-fl})_2$	61.17	3.34	3.57	60.84	3.37	3.75	4.23	235
$Co(5\text{-Cl-sal-fl})_2$	68.97	3.76	4.02	68.55	3.79	4.16	4.23	217
$Co(5,6\text{-benzo-sal-fl})_2$	79.22	4.43	3.85	78.99	4.47	3.83	4.21	236
$Ni(5\text{-Br-sal-fl})_2\cdot py$[c]	62.53	3.62	4.86	62.11	3.82	4.89	dia	dec
$Ni(5\text{-Cl-sal-fl})_2\cdot py$	69.71	4.03	5.42	69.62	3.95	5.45	dia	dec
$Ni(5,6\text{-benzo-sal-fl})_2\cdot py$	79.32	4.64	5.23	78.91	4.58	5.15	dia	dec
$Co(5\text{-Cl-sal-fl})_2\cdot py$	70.27	4.03	5.42	69.99	4.03	5.89	4.25	dec
$Co(5,6\text{-benzo-sal-fl})_2\cdot py$	78.69	4.62	5.22	78.90	4.62	5.28	2.52	dec

μ: BM at room temperature. a) With 1/3 $CHCl_3$. b) With 1/2H_2O. c) Notation py denotes a pyridine molecule.

Table 2. Analytical data of copper(II) complexes

Compound	Calcd, %			Found, %			Mp °C
	C	H	N	C	H	N	
Cu(H-sal-fl)$_2$	75.99	4.46	4.43	75.91	4.45	4.46	205
Cu(5-Br-sal-fl)$_2$[a]	58.08	3.14	3.36	58.13	3.29	3.39	217
Cu(5-Cl-sal-fl)$_2$[a]	65.13	3.69	3.80	65.34	3.81	3.90	207
Cu(5-NO$_2$-sal-fl)$_2$[b]	64.90	3.81	7.56	64.42	3.84	7.55	239
Cu(5,6-benzo-sal-fl)$_2$	78.92	4.41	3.85	78.68	4.39	3.84	220
Cu(5,6-benzo-sal-fl)$_2$·py	78.45	4.60	5.18	78.91	4.50	5.17	dec
Cu(H-sal-fl)Cl	62.66	3.68	3.65	62.84	3.83	3.60	174
Cu(5-Br-sal-fl)Cl	51.97	2.84	3.03	52.26	2.95	3.12	177
Cu(5-Cl-sal-fl)Cl	57.68	3.14	3.35	57.68	3.23	3.54	179

a) 1/3 $CHCl_3$. b) 1/2H_2O.

refrigerator. The cobalt(II) and nickel (II) complexes are reddish brown, and the copper(II) complex is dark green. They are soluble in cold pyridine, chloroform and acetone and almost insoluble in methanol and ethanol. They do not lose a pyridine molecule in the atmosphere at room temperature.

Cu(X-sal-fl)Cl (X=H, 5-Br, 5-Cl). Salicylaldehyde (0.01 mol) was added to a solution of copper(II) chloride hydrate (0.01 mol) in ethanol (20 ml) under stirring at 70 °C. After 10 min a solution of sodium carbonate (0.005 mol) in water (5 ml) was added to the resulting solution; a yellowish green precipitate appeared in the solution. To this mixture was added 9-aminofluorene (0.01 mol), and stirred for 1 h at 70 °C. Brown microcrystals were filtered off and washed with ethanol. Recrystallization was unsuccessful.

They are insoluble in benzene, methanol, ethanol and water but are soluble in chloroform, undergoing decomposition.

Measurements. Electronic absorption spectra of the complexes were measured on a Shimadzu MPS 50L spectrophotometer. Solubility of some complexes in appropriate solvents was too low for spectral measurements. Infrared spectra of the complexes were recorded as Nujol mulls using a Hitachi EPI-S2 infrared spectrophotometer and a Hitachi 215 infrared spectrophotometer.

Magnetic measurements were carried out at room temperature by the Gouy method. Powder diffraction patterns were obtained with a Rigakudenki 4001-A2 diffractometer using Co$K\alpha$ radiation and an iron filter.

Results and Discussion

Nickel(II) and Cobalt(II) Complexes. Complexes of the type Ni(X-sal-fl)$_2$ are diamagnetic in the solid state, indicating that they have a four-coordinate, square-planar structure. They show electronic absorption spectra typical of the square-planar nickel(II) complexes in non-donor solvents or in the solid state (Table 3). A d-d band with a maximum at about 16000 cm^{-1}, which may be ascribed to a $d_{x^2-y^2} \leftarrow d_{xy}$ transition, is slightly lower than that of the *N*-diphenylmethyl analogue,[4] implying that the ligand field produced by X-sal-fl is weaker than that by X-sal-dpm (dpm, diphenylmethyl).

In spite of the steric hindrance, the tetrahedral species has neither been isolated as crystals nor detected in solution at room temperature for the nickel(II) complexes of the type Ni(X-sal-fl)$_2$. This finding is similar to that for Ni(X-sal-dpm)$_2$ but contrary to that for Ni(X-sal-*i*-C_3H_7)$_2$.[4]

Table 3. Main d-d absorption maxima of nickel(II) and cobalt(II) complexes of the type M(X-sal-fl)$_2$

Compound	Solvent	ν (log ε)
Ni(H-sal-fl)$_2$	$CHCl_3$	15.9(1.95)
	Nujol	16.0
	pyridine[a]	17.5(2.45)
Ni(5-Br-sal-fl)$_2$	$CHCl_3$	16.0(1.90)
	pyridine[a]	17.5(2.38)
Ni(5-Cl-sal-fl)$_2$	$CHCl_3$	15.9(1.90)
Ni(3-CH_3O-sal-fl)$_2$	$CHCl_3$	15.7(1.91)
Ni(5,6-benzo-sal-fl)$_2$	Nujol	16.0
Co(H-sal-fl)$_2$	$CHCl_3$	7.5(1.78),10.6(1.56)sh, 17.5(1.88)
	pyridine[a]	6.4(1.30), 10.5(0.81)
Co(5-Br-sal-fl)$_2$	$CHCl_3$	7.5(1.81),10.3(1.63)sh, 17.5(1.82)
Co(5,6-benzo-sal-fl)$_2$	$CHCl_3$	7.8(1.90),10.4(1.50)sh

ν: 10^3 cm^{-1}. a) With the solution obtained by heating at 70 °C for a few hours.

It has not been possible to isolate tris(Schiff base)-cobalt(III) complexes so far, probably owing to the steric condition. The cobalt(II) complexes Co(X-sal-fl)$_2$ are paramagnetic with magnetic moments of 4.0—4.3 BM, which lie in the range expected for the tetrahedral cobalt(II) complex. They also show electronic absorption spectra typical of the tetrahedral cobalt(II) complex (Table 3). The d-d band at 7500—8000 cm^{-1} with a shoulder at 10300—10600 cm^{-1} may be assigned to a transition $^4T_1(F) \leftarrow {}^4A_2$.

Monopyridine adducts of the type M(X-sal-fl)$_2$·py were isolated as crystals. Six-coordinate bis(pyridine)-adducts have neither been isolated in crystals nor detected in solution, in contrast to the *N*-diphenylmethyl analogues.[4] The steric hindrance due to the ligands X-sal-fl is thus greater than that due to X-sal-dmp.

The pyridine molecule in M(X-sal-fl)$_2$·py is not readily lost. No weight loss was observed when the adducts were heated at 100 °C for several hours. It is likely that the pyridine molecule is bound with the metal(II) ion in the adducts. This presumption seems to be borne out by the observation that the parent complexes are not soluble in pyridine at room temperature, and that the adducts M(X-sal-fl)$_2$·py isolated from hot pyridine are readily soluble in cold pyridine. Since the pyridine adducts show infrared ν(C–O)

(1520—1530 cm^{-1}) and ν(C=N) bands (1600—1610 cm^{-1}) at almost the same frequencies as those of the parent complexes, it is presumed that the ligands X-sal-fl in the pyridine adducts function as bidentates, as in the parent complexes. All these findings indicate that the pyridine adducts with cobalt(II) and nickel(II) complexes have a five-coordinate structure.

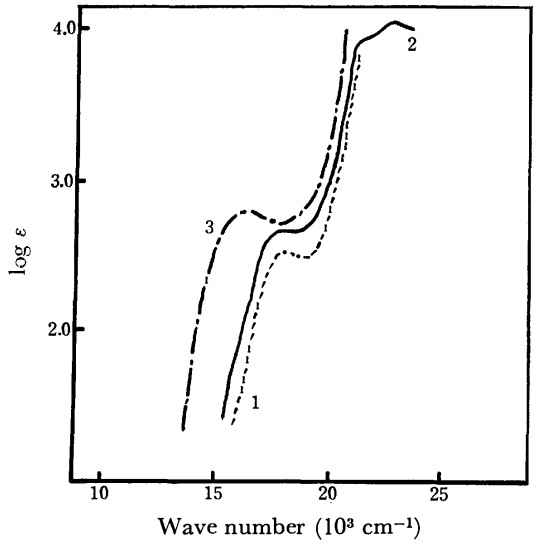

Fig. 1. Electronic absorption spectra of nickel(II) complexes: 1. Ni(5,6-benzo-sal-fl)$_2$·py, in Nujol, scale arbitrary; 2. Ni(5,6-benzo-sal-fl)$_2$·py, in pyridine; 3. Ni(5,6-benzo-sal-fl)$_2$, in Nujol, scale arbitrary.

Since the nickel(II) complexes Ni(X-sal-fl)$_2$·py are diamagnetic, they are considered to be spin-paired, five-coordinate complexes. As shown in Fig. 1, the solid state spectra of Ni(X-sal-fl)$_2$·py, which are essentially similar to the spectra of their pyridine solutions, have a main d-d band at 17400—17800 cm^{-1}. The band maxima are much higher than those (15700—16000 cm^{-1}) of the parent complexes, which have a diamagnetic square-planar structure, and the intensity of the d-d bands for the pyridine adducts is significantly higher than of the parent complexes. These findings are also in agreement with the five-coordinate structure for the pyridine adducts. The principal spectral data are summarized in Table 4.

Table 4. Main d-d absorption maxima of M(X-sal-fl)$_2$·py, M^{II} being Co and Ni

Compound	Solvent	ν (log ε)
Ni(5-Br-sal-fl)$_2$·py	Nujol	17.6
	pyridine	17.5(2.38)
Ni(5-Cl-sal-fl)$_2$·py	Nujol	17.6
	pyridine	17.4(2.37)
	$CHCl_3$	17.5(2.32)
Ni(5,6-benzo-sal-fl)$_2$·py	Nujol	17.8
	pyridine	18.0(2.62)
	$CHCl_3$	18.0(2.62)
Co(5-Cl-sal-fl)$_2$·py	Nujol	6.6, 11.7
	pyridine	6.7(1.38), 11.5(1.14)
	$CHCl_3$	5.3(1.20), 8.1(1.33)
Co(5,6-benzo-sal-fl)$_2$·py	Nujol	5.3, 8.3
	pyridine	5.5(1.42), 8.1(1.28)
	$CHCl_3$	5.5(1.50), 8.2(1.47)

ν: 10^3 cm^{-1}.

Two types of structure may be considered for the five-coordinate complexes, trigonal-bipyramidal and square-pyramidal. Spin-paired, five-coordinate, trigonal-bipyramidal nickel(II) complexes having NP_3Cl, NP_3Br, and NAs_3Br donors sets[6] were reported to show a d-d band at a much lower frequency than the pyridine adducts (N_3O_2 set) obtained in the present work (about 18000 cm^{-1}). Even the trigonal bipyramidal complex with the P_4Cl donor set shows the band at 17500 cm^{-1}, although the P_4Cl donor set is expected to produce considerably stronger ligand field than the N_3O_2 set. The trigonal-bipyramidal structure, therefore, seems to be unlikely. On the contrary, the spectra of Ni(X-sal-fl)$_2$·py may reasonably be interpreted on the basis of the model of spin-paired, five-coordinate, square-pyramidal stereochemistry.[5] For the square-pyramidal structure II rather than structure I (Fig. 2)

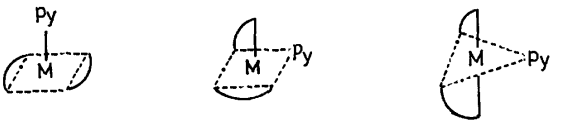

(I) (II) (III)

Fig. 2. Some possible structures for M(5,6-benzo-sal-fl)$_2$·py (M=Co, Ni, and Cu).

is considered to be more likely, judging from their formation reaction; the pyridine adducts are obtained only on heating the parent complexes in pyridine. Simple axial addition of a pyridine molecule to the square-planar complex would readily produce structure I, for instance, without heating, if this species were stable enough at all. This, however, is not the case. The very high frequencies of the d-d band maxima for Ni(X-sal-fl)$_2$·py also favor structure II, suggesting that the bond between the nickel(II) ion and the axial fifth donor atom is weak.

The d-d band maxima in the spectra of the pyridine adducts in chloroform are almost the same as those of the pyridine adducts in pyridine or in the solid state, indicating that the structure of the adducts in the solid state is retained in the chloroform solution.

Table 5. X-Ray powder diffraction data of M(5,6-benzo-sal-fl)$_2$·py, using Co$K\alpha$ radiation with an iron filter

M=Co		M=Ni	
d, Å	I	d, Å	I
11.41	100	11.41	100
8.81	15	8.78	12
6.94	12	6.94	10
5.69	40	5.71	45
4.95	6	4.95	6
4.77	7	4.77	7
4.38	7	4.38	7
4.14	8	4.12	7
3.65	4	3.65	4

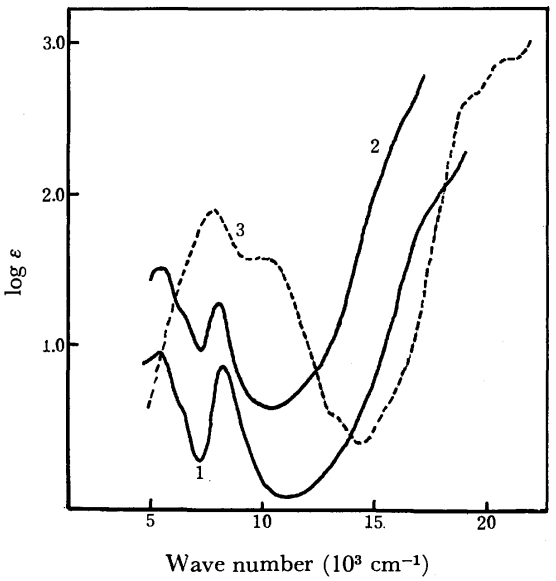

Fig. 3. Electronic absorption spectra of cobalt(II) complexes: 1. Co(5,6-benzo-sal-fl)$_2$·py, in Nujol, scale arbitrary; 2. Co(5,6-benzo-sal-fl)$_2$·py, in pyridine; 3. Co(5,6-benzo-sal-fl)$_2$, in chloroform.

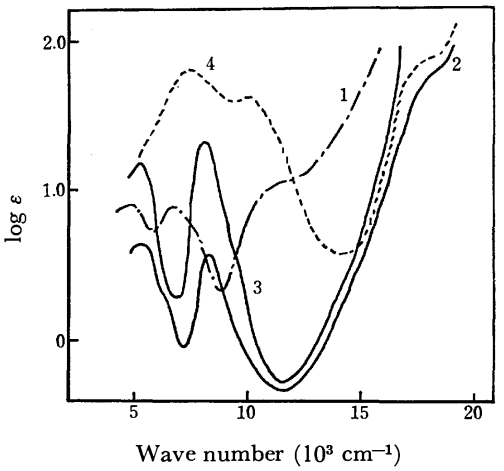

Fig. 4. Electronic absorption spectra of cobalt(II) complexes: 1. Co(5-Cl-sal-fl)$_2$·py, in Nujol, scale arbitrary; 2. Co(5-Cl-sal-fl)$_2$·py, in Nujol; 3. Co-(5-Cl-sal-fl)$_2$·py, in chloroform; 4. Co(5-Cl-sal-fl)$_2$, in chloroform.

Two types of cobalt(II) pyridine adducts were isolated as a solid, one being spin-paired and the other spin-free. One of them, Co(5,6-benzo-sal-fl)$_2$·py, is paramagnetic with a moment of 2.53 BM and is thus regarded to be a spin-paired, five-coordinate complex. Its X-ray powder diffraction pattern (Table 5) is almost the same as that of Ni(5,6-benzo-sal-fl)$_2$·py, which was presumed to consist of a spin-paired, five-coordinate complex. This is also borne out by the infrared spectrum in the whole 250—4000 cm^{-1} region of the cobalt(II) complex, which is slmost the same as that of the nickel-(II) analogue. It is thus presumed that Co(5,6-benzo-sal-fl)$_2$·py has the same structure as that of Ni(5,6-benzo-sal-fl)$_2$·py, possibly a spin-paired, square-pyramidal structure. The solid state spectrum of this cobalt(II) compound is essentially similar to the spectrum of its pyridine solution having a rather narrow band at 8400 cm^{-1}, in addition to a band at about 5300 cm^{-1} (Fig. 3). The spectrum is found to be correlated with that of a spin-paired, five-coordinate, square-planar cobalt(II) complex.[7] A remarkable similarity of its solid spectrum to that of the spin-paired, square-planar cobalt(II) complex indicates that the bond between the cobalt(II) ion and the axial fifth donor atom is weak, as in the corresponding nickel(II) analogue.

In contrast to Co(5,6-benzo-sal-fl)$_2$·py, Co(5-Cl-sal-fl)$_2$·py is paramagnetic with a moment of 4.25 BM, indicating that the latter is a spin-free, five-coordinate cobalt(II) complex. The solid state spectrum of Co(5-Cl-sal-fl)$_2$·py, which is very similar to the spectrum of its pyridine solution, differs a great deal from that of the tetrahedral cobalt(II) complex as well as from that of the six-coordinate, octahedral compex. lIn contrast, the solid spectrum is similar to the spectra of the spin-free, five-coordinate cobalt(II) complexes.[8]

The spectrum of Co(5-Cl-sal-fl)$_2$·py in chloroform differs considerably from its solid state spectrum, but is remarkably similar to the solid spectrum of Co(5,6-benzo-sal-fl)$_2$·py, which was presumed to have a spin-paired, five-coordinate structure (Fig. 4). It is interesting to note that the conversion of the spin state, probably accompanied by configurational change, occurs in this pyridine adduct on going from the solid state to the chloroform solution. If the pyridine molecule were lost from Co(5-Cl-sal-fl)$_2$·py on dissolution in chloroform, remaining complex Co(5-Cl-sal-fl)$_2$ would assume a tetrahedral configuration.

The pyridine solutions of Co(H-sal-fl)$_2$ and Co(5-Br-sal-fl)$_2$, obtained by heating the complexes in pyridine, show electronic absorption spectra similar to the solid spectrum of Co(5-Cl-sal-fl)$_2$·py, which was presumed to have a spin-free, five-coordinate complex.

Copper(II) Complexes. Electronic absorption spectra of copper(II) complexes of the type Cu(X-sal-fl)$_2$ in non-donor solvents have a d-d band at about 16000 cm^{-1}. From the frequency of the band, it may be reasonable to assume that these copper(II) complexes in non-donor solvents have an essentially square-planar configuration.

The complexes Cu(X-sal-fl)$_2$ are soluble in pyridine at room temperature, but the colour of the solution changes with time. The complexes, which are originally olive-green, turn bluish green immediately upon dissolution in pyridine, becoming greenish brown by reflected light (orangish brown by transmitted light) after more than 24 h. Absorption spectra of Cu(5-Cl-sal-fl)$_2$ in pyridine are shown as representative data in Fig. 5.

The spectrum obtained within 8 min after dissolution in pyridine (curve 2) has a broad d-d band, which shifts toward significantly lower frequencies than the d-d band of the original complex. It is recognized that curve 2 is similar to the spectrum expected for the five-coordinate species formed by axial addition of a pyridine molecule to the square-planar copper(II) complexes.[9] When dissolved in pyridine the first d-d band of the copper(II) complex shifts toward considerably lower frequencies, becoming also much broader than that of the complexes in non-donor solvents. In fact, curve 2

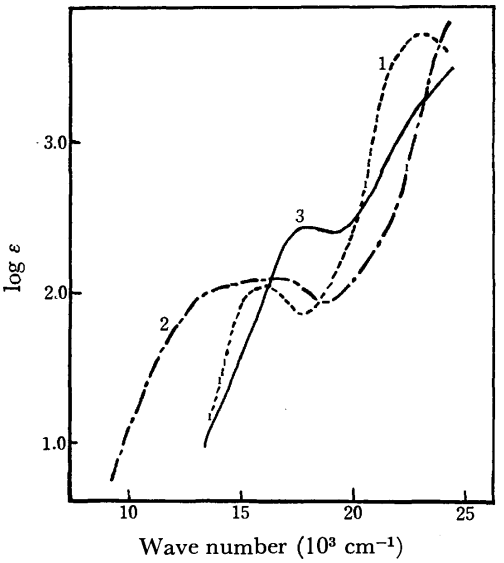

Fig. 5. Electronic absorption spectra of Cu(5-Cl-sal-fl)$_2$: 1. in chloroform; 2. in pyridine (measured within 8 min after dissolution); 3. in pyridine (measured after 24 h).

is very similar to the spectra of Cu(X-sal-dpm)$_2$ in pyridine.[4] The species corresponding to curve 2, therefore, may be assumed to have structure I in Fig. 2, or a structure slightly distorted from it.

The spectrum recorded after more than 24 h (curve 3), which differs entirely from curves 1 and 2, has a d-d band with a distinct maximum at about 18000 cm^{-1}. The pyridine adduct Cu(5,6-benzo-sal-fl)$_2$·py also shows a similar solid state spectrum having a d-d band at nearly the same frequency as that of curve 3. It is most likely that the main species existing after 24 h in pyridine may have the same structure as that of Cu(5,6-benzo-sal-fl)$_2$·py in the solid state. The pyridine adduct shows infrared ν(C–O) (1530 cm^{-1}) and ν(C=N) (1610 cm^{-1}), which are almost the same frequencies as those of the parent complexes. It is thus very likely that the ligand functions as a bidentate, as in the parent complexes.

It seems that one of the most probable structures of the species corresponding to curve 3 is structure II in Fig. 2. The considerably high frequency of the d-d band maximum seems to exclude a trigonal-bipyramidal structure,[10] which would show the corresponding band at a much lower frequency. The bond between the copper(II) and the axial fifth donor atom would not be strong.

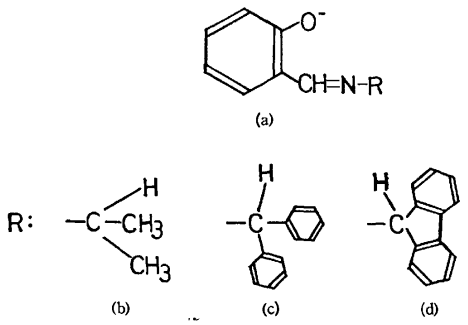

Complexes of the type Cu(X-sal-fl)Cl (X=H, 5-Br, 5-Cl) at room temperature have subnormal magnetic moments of 1.35, 1.34 and 1.39 BM, respectively, which are much lower than the normal magnetic moments expected for the d^9 system. A sort of interaction, therefore, may be expected to exist between two copper(II) ions, as in complexes of a similar type.[11–13] Their infrared ν(C–O) bands appear at 1550 (X=H), 1535 (X=5-Br) and 1540 cm^{-1} (X=5-Cl), respectively. They are significantly higher than those of Cu(X-sal-fl)$_2$, which appear at 1525 cm^{-1} for X=H, 5-Br and 5-Cl. Based upon the criteria proposed previously,[11–13] the present finding on the infrared spectra seems to indicate that these complexes have a binuclear structure with the phenolic oxygen atom bridging two copper(II) ions.

Their solid state electronic spectra, which are similar to each other, show the first d-d band as a shoulder at about 11500 cm^{-1} and the next shoulder at 15600 cm^{-1}, more intense absorption rising up in the higher frequency region. Kato *et al.*[12] classified the spectra of the Cu(X-sal-alkyl)Cl type complexes into two groups, designating them as B- and Y-type. The spectra of Cu(X-sal-fl)Cl are similar to those of B-type, their magnetic moments also being in the range expected for B-type complexes.

The authors are grateful to Professor Shoichi Kume and Dr. Yoshinari Miyamoto, Institute of Geology, Osaka University, for X-ray powder diffraction patterns. Thanks are also due to Mr. Hiro Kuma for valuable discussions.

References

1) R. H. Holm and M. J. O'Connor, *Prog. Inorg. Chem.*, **14**, 241 (1971).
2) S. Yamada, *Coord. Chem. Rev.*, **1**, 415 (1966); S. Yamada, "Novel in Coordination Chemistry. Section Lectures of XIII. I. C. C. C.," ed by B. J. -Trzebiatowska and M. Rudolph, Polish Academy of Sciences (1974), p. 189.
3) L. Sacconi, *Coord. Chem. Rev.*, **1**, 192 (1966).
4) K. Yamanouchi and S. Yamada, *Bull. Chem. Soc. Jpn.*, **49**, 163 (1976).
5) L. Sacconi and R. Morassi, *J. Chem. Soc., A*, **1969**, 2904.
6) L. Sacconi and I. Bertini, *J. Am. Chem. Soc.*, **89**, 2235 (1967); L. Sacconi, *Pure Appl. Chem.*, **17**, 95 (1968).
7) G. Busetto, F. Cariati, A. Fusi, M. Gullotti, F. Morazzoni, A. Pasini, R. Ugo, and V. Valenti, *J. Chem. Soc., Dalton*, **1973**, 754.
8) L. Sacconi, M. Ciampolini, and G. P. Speroni, *Inorg. Chem.*, **4**, 1116 (1965); S. Yamada and H. Nishikawa, *Bull. Chem. Soc. Jpn.*, **38**, 683 (1965); S. Yamada and E. Yoshida, *ibid.*, **40**, 1298 (1967).
9) S. Yamada, H. Nishikawa, and E. Yoshida, *Bull. Chem. Soc. Jpn.*, **39**, 994 (1966); S. Yamada, H. Nishikawa, Y. Kuge, and K. Yamanouchi, *Sci. Repts. Coll. Gen. Educ. Osaka Univ.*, **16**, 11 (1967); S. Yamada, A. Takeuchi, K. Yamanouchi, and K. Iwasaki, *Bull. Chem. Soc. Jpn.*, **42**, 131 (1969).
10) B. J. Hathaway and A. A. G. Tomlinson, *Coord. Chem. Rev.*, **5**, 1 (1970).
11) R. B. Coles, C. M. Harris, and E. Sinn, *Inorg. Chem.*, **8**, 2607 (1969).
12) M. Kato, K. Imai, Y. Muto, T. Tokii, and H. B. Jonassen, *J. Inorg. Nucl. Chem.*, **35**, 109 (1973).
13) S. Yamada, K. Yamanouchi, W. Mori, and M. Kishita, *Bull. Chem. Soc. Jpn.*, **49**, 2111 (1976).

Secondary Ion Mass Spectrometry for Diffusion Studies in Glass

Atsushi MIZUIKE and Akira IINO
Faculty of Engineering, Nagoya University, Chikusa-ku, Nagoya 464
(Received December 24, 1976)

A procedure has been established for obtaining quantitative diffusion profiles by means of an ion microanalyzer in the narrow region within 1 μm of the glass surface. The interdiffusion of silver and sodium ions in Pyrex glass immersed in molten silver nitrate was studied as an example.

Diffusion kinetics during ion exchange in various glasses has been studied by many workers[1] from purely physicochemical points of view (*e.g.*, to get a better understanding of the basic mechanism of ionic transport in glass and the structure of glass) and in connection with industrial problems (*e.g.*, the strengthening of glass). The radioactive tracer technique and electron microprobe X-ray analysis have been employed extensively in these studies to obtain diffusion profiles (concentration *vs.* depth curves).

Secondary ion mass spectrometry (SIMS) offers a new means for obtaining profiles in the near-surface region (within 1 μm of the surface). In this technique, the sample surface is bombarded with a beam of high-energy primary ions, and the resulting ions from the sample are analyzed by means of a mass spectrometer. The successive removal by sputtering of the surface layers enables one to obtain the profiles by monitoring the ion intensity at the appropriate mass *vs.* sputtering time. This technique, however, is still semiquantitative,[2] because there remain three unresolved problems. First is the quantification of the SIMS intensities, *i.e.*, the conversion of the ion intensity at the appropriate mass into the concentration of the corresponding element. The large variations in the secondary ion yields and the matrix effects complicate the quantification. Although a theoretical correction procedure based on the local thermal equilibrium model has been proposed by Andersen and Hinthorne,[3] standard samples are still generally required for an accurate quantification. These standards have to shape both the chemical and physical nature of the sample as much as possible; therefore, their preparation is often very difficult. Second is the depth assignment, *i.e.*, the conversion of the sputtering time into depth. The rate of material removal depends on the sample matrix as well as the primary ion characteristics. Third, ion migration induced by ion bombardment may distort the diffusion profiles.[4]

The present work has been undertaken in order to resolve these problems and to establish a procedure for obtaining quantitative diffusion profiles in the near-surface region by SIMS. Experiments have been carried out on the interdiffusion of silver and sodium ions in Pyrex glass immersed in molten silver nitrate.

Experimental

Apparatus. A Hitachi IMA-2 ion microanalyzer was operated under the following conditions unless otherwise stated: primary ion-source gas, 99.99% argon; primary ion-accelerating voltage, 15 kV; primary beam current, 0.1 μA; spot diameter, 250 μm; sample chamber pressure, 3×10^{-5} Pa; secondary ion-accelerating voltage, 3 kV; electron-multiplier voltage, 2 kV. The electric charges accumulated on the glass surfaces were eliminated by means of the electron-spray method. The SIMS peak ratios—$^{109}Ag^+/^{30}Si^+$, $^{23}Na^+/^{28}Si^+$, and $^{39}K^+/^{28}Si^+$—were measured after rastering the primary beam (total number of scanning lines, 500; line frequency, 100 Hz) over an area 0.8 mm square around the spot to be measured. A Mizojiri Kogaku model II multiple-beam interferometer (Hg 546.1 nm, magnification 40X) was used to measure the depth of craters formed on glass surfaces by ion etching (ion sputtering) and the thickness of the chemically etched glass-surface layers. A Nippon Jarrell-Ash AA-1 MK II atomic-absorption flame-emission spectrophotometer with an SA-61 slit burner (acetylene 2 l/min, air 7 l/min) and a Hitachi model QPD53 recorder was employed for the atomic-absorption spectrophotometric determination of silver at 328.1 nm and the flame-photometric determination of sodium at 589.3 nm.

Material. Pyrex glass sheets (81% SiO_2, 13% B_2O_3, 4% Na_2O, 2% Al_2O_3, 0.5% or 0.04% K_2O; density, 2.2 g/cm^3) were annealed at 550 °C for 30 min and then cooled to room temperature at a rate of 1—2 °C/min. They were then washed with a detergent solution, followed by water, at room temperature, and subsequently dried.

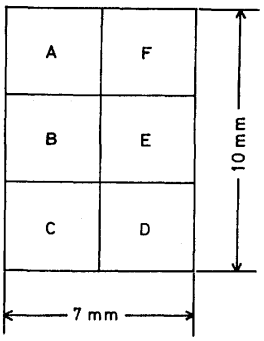

Fig. 1. Standard sample.

Preparation of Standard Sample. A 30-mm-square glass piece was immersed in molten silver nitrate at 335 °C for 90 min to effect the interdiffusion of silver and sodium ions into the glass. The piece was then withdrawn, cooled, washed in water, and dried. A 10×7 mm piece was cut from the above piece, and after covering Part A of the piece (see Fig. 1) with paraffin wax, we immersed it in 5% hydrofluoric acid at 19 °C for 15 min, withdrew it, washed it in water, and dried it. Parts B to E of the piece were successively covered with paraffin wax, and the above chemical etching was repeated. Finally, all the paraffin was removed with benzene. The piece thereafter served as a standard sample with 6 different surface concentrations of silver and sodium.

The surface concentrations were determined as follows. Another 10×7 mm piece was cut from the 30-mm-square

piece, and after its edges had been covered with paraffin wax, immersed in 5% hydrofluoric acid at 19 °C for 15 min, withdrawn, washed in water, and dried. The hydrofluoric acid and the washings were analyzed for silver and sodium by atomic absorption spectrometry and flame photometry. The above procedure was then repeated. The means of the concentrations of silver (or sodium) in two adjacent etched layers correspond to the surface concentrations of the standard sample.

Results and Discussion

Construction of Concentration Calibration Curves. A standard sample was prepared by the interdiffusion of silver and sodium ions in Pyrex glass, followed by chemical etching as has been described above. The corresponding diffusion profiles, obtained by chemical etching and chemical analysis, are shown in Fig. 2. The potassium profile was measured by SIMS, the details of which will be published elsewhere. The sum of the atomic concentrations of silver and sodium, as well as the potassium concentration, remained nearly constant over the whole range. Figure 3 illustrates the concentration calibration curves constructed by the use of the standard sample. Before each SIMS measurement, the surface layer (about 30 nm) of the standard sample was removed by ion etching (0.1 μA, 7-min rastering). The SIMS peak ratios were proportional to the atomic concentrations of the corresponding ions, with maximum deviations of about ±10%. There was no day-to-day variation in the calibration curves.

Depth Resolution and Depth Scale Assignment. When the primary beam was continuously focused on a spot on the glass surface, a conical crater was produced by ion sputtering and the signal from the crater walls deteriorated the depth resolution. To overcome this difficulty, the primary beam (0.3 μA) was rastered over an area 0.8 mm square in order to produce a flat-bottomed crater; then the beam (0.1 μA) was focused for 1 min on the center of the area for SIMS measurements. A fresh spot on the glass surface was used for each measurement. Thus, a depth resolution of the order of 10 nm was achieved.

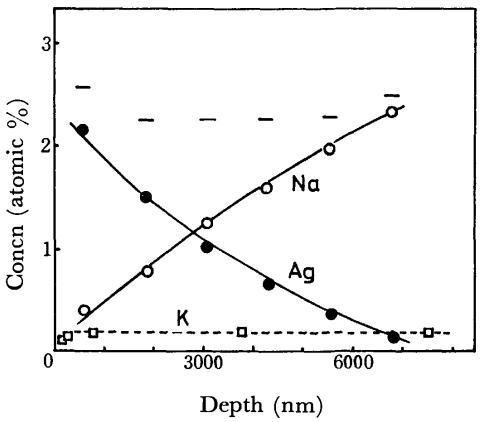

Fig. 2. Diffusion profiles. Pyrex (0.5% K_2O). 335 °C, 90 min. —: Sum of Ag and Na.

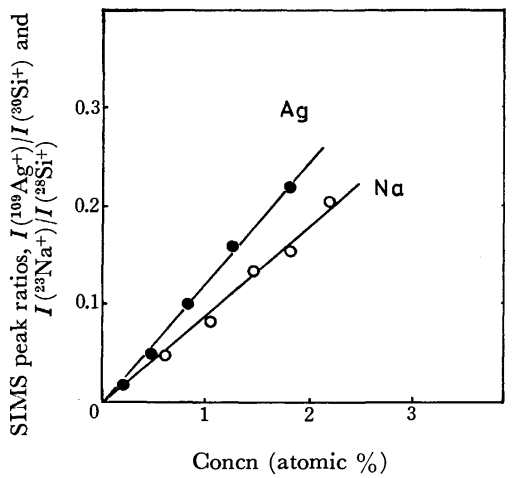

Fig. 3. Concentration calibration curves. Pyrex (0.5% K_2O).

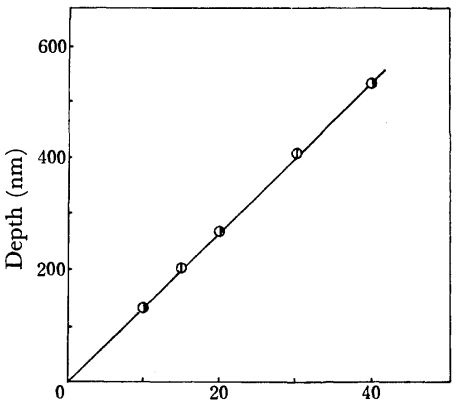

Fig. 4. Plots of crater depth *vs.* sputtering time. ⓘ: Pyrex (0.5% K_2O), ◑: Pyrex (0.5% K_2O) in which Na is nearly completely replaced by Ag.

The rate of material removal by ion sputtering under the above conditions was independent of the possible variation in composition of the glass under study, as is shown in Fig. 4. In addition, the day-to-day instrumental fluctuation was negligible. Therefore, the sputtering time can be readily converted to the depth.

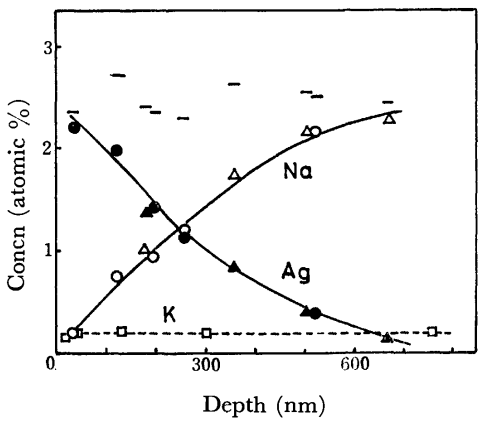

Fig. 5. Diffusion profiles. Pyrex (0.5% K_2O). 335 °C, 1 min. ●○: Ion etching, ▲△: chemical etching. —: Sum of Ag and Na.

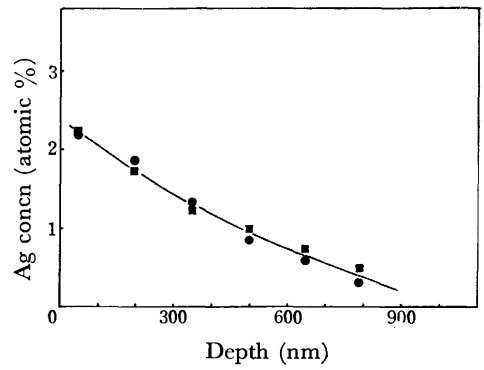

Fig. 6. Diffusion profile. Pyrex (0.04% K_2O). 335 °C, 1 min. ●■: Data on two separately prepared samples.

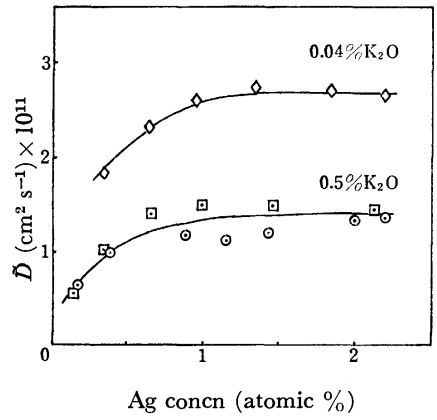

Fig. 7. Interdiffusion coefficients $\tilde{D}$ *vs.* silver concentration. Data from Fig. 2 (⊡), Fig. 5 (⊙), and Fig. 6 (◇).

Diffusion Profiles in the Near-Surface Region. The interdiffusion of silver and sodium ions was effected at 335 °C for 1 min, after which the diffusion profiles were obtained by SIMS. The results are shown in Figs. 5 and 6. The distortion of the diffusion profiles due to ion migration during the ion etching is negligible, because there is no appreciable difference from the profiles obtained by chemical etching with 0.8% hydrofluoric acid instead of ion etching prior to SIMS measurements.

Interdiffusion Coefficients. The interdiffusion coefficients at 335 °C were obtained from the profiles shown in Figs. 2, 5, and 6 by the Boltzmann-Matano method.[5] The results are illustrated in Fig. 7. The interdiffusion coefficients (between 1 and 2.4 atomic% Ag) are 1.4×10^{-11} cm^2 s^{-1} for Pyrex glass containing 0.5% K_2O and 2.7×10^{-11} cm^2 s^{-1} for Pyrex glass containing 0.04% K_2O, showing the mixed alkali effect.[6] The latter value is in reasonable agreement with the values obtained for Pyrex glass containing a negligible amount of potassium by Sjöblom and Andersson (2.6×10^{-11} cm^2 s^{-1})[7] and by Doremus (3.0×10^{-11} cm^2 s^{-1}).[8]

References

1) R. H. Doremus, "Ion Exchange," Vol. 2, ed by J. A. Marinsky, Marcel Dekker, New York (1969), p. 1.
2) P. Heyndryckx, *Glastechn. Ber.*, **44**, 543 (1971).
3) C. A. Andersen and J. R. Hinthorne, *Anal. Chem.*, **45**, 1421 (1973).
4) D. V. McCaughan and R. A. Kushner, "Characterization of Solid Surfaces," ed by P. F. Kane and G. B. Larrabee, Plenum Press, New York (1974), p. 627.
5) J. Crank, "The Mathematics of Diffusion," 2nd ed, Clarendon Press, Oxford (1975), p. 230.
6) D. E. Day, *J. Non-Cryst. Solids*, **21**, 343 (1976).
7) C. A. Sjöblom and J. Andersson, *Z. Naturforsch., Teil A*, **21**, 274 (1966).
8) R. H. Doremus, *Phys. Chem. Glasses*, **9**, 128 (1968).

Ionic Equilibria in Mixed Solvents. XII. Hydrolysis of Cadmium(II) Ion in Dioxane-Water and Methanol-Water Mixtures

Haruo MATSUI and Hitoshi OHTAKI*,**

Government Industrial Research Institute, Nagoya, Hirate-machi, Kita-ku, Nagoya 462
**Department of Electronic Chemistry, Tokyo Institute of Technology, O-okayama Meguro-ku, Tokyo 152*

(Received December 25, 1976)

The hydrolytic reactions of cadmium(II) ions were studied at 25 °C in dioxane–water and methanol–water mixtures with varying compositions of the organic solvents, each mixture containing 3 mol dm^{-3} (Li)ClO_4 as an ionic medium. Emf measurements were carried out over the range of the total cadmium(II) concentrations of 0.2 to 0.8 mol dm^{-3} in all the systems. Two complexes Cd_2OH^{3+} and $CdOH^+$ were found in the dioxane–water mixtures, but the latter complex was not detected in the methanol–water system. The formation constant of the $Cd_2OH_4^{3+}$ complex was slightly larger in the methanol–water mixtures than in the dioxane–water mixtures at the same mole-fraction concentration of the organic solvents.

The formation of the mononuclear complex $CdOH^+$ was reported by many authors[1–6] in the hydrolytic reactions of cadmium(II) ion in aqueous solutions. The formation of the dinuclear Cd_2OH^{3+} complex, which has been first reported by Biedermann and Ciavatta,[7] was confirmed by us in a previous work.[8] However, the existence of the tetranuclear $Cd_4(OH)_4^{4+}$ complex was doubtful as an equilibrium species of hydrolyzed cadmium ions.[8]

The solvent effects on the hydrolytic reactions of various metal ions such as beryllium,[9–11] copper,[12,13] nickel,[14] and aluminium[15] have so far been studied in various aqueous–organic mixtures and the results can be summarized as follows: 1) The formation constants of the complexes, most of which were large polynuclear complexes, were little affected by the solvent composition even though the dioxane concentration changed widely, *e.g.*, 0—83% w/w, in contrast with the dissociation constants of carboxylic acids[16] and phenols,[17] which markedly changed with the solvent composition. 2) Similar results were found in other solvent systems, water–methanol, water–ethanol, and water–acetone mixtures. 3) The solvent effects on the hydrolytic reactions of metal ions were qualitatively explained by Kawai[18] in terms of the changes in the activity coefficients of the ions in solutions.

However, Wada and his coworkers[19,20] have shown that the formation constant $*\beta_{1,1}$ of the mononuclear hydroxo complex of Fe^{3+} monotonously increased with the increase of the concentration of methanol in which 0.5 mol dm^{-3} (Na,H)ClO_4 was contained as an ionic medium, as well as the formation constant of the $FeCl^{2+}$ complex in the same ionic medium, containing methanol up to 0.52 mole fraction (about 66% w/w).

In order to find if the formation constant of a mononuclear hydroxo complex would be affected by the solvent composition of aqueous mixed solvents in a different manner from that of a polynuclear complex, we have examined the hydrolysis of cadmium(II) ions in dioxane–water and methanol–water mixtures, because both mononuclear and polynuclear complexes are formed in this system and their formation constants can be determined with reasonable accuracies in various mixed media.

Experimental

Reagents. *Cadmium(II) Perchlorate*: Cadmium oxide (99.99%, Mitsuwa Pure Chemicals Co., Osaka) was dissolved in 1:1 $HClO_4$ (Super special grade, Wako Pure Chemical Ind., Osaka) and cadmium perchlorate thus prepared was recrystallized three times from water. The purity of the cadmium oxide had been checked by emission spectroscopy.

Lithium perchlorate and *lithium hydroxide* were prepared by the same procedures as described in the previous paper.[8] *Dioxane* purified by the ordinary method[13] was stored in a refrigerator and melted just before preparation of a test solution. *Methanol* of reagent grade was distilled twice.

Apparatus. Beckman (No. 40498) glass electrodes were used in combination with an Orion Digital pH Meter Model 801. A cadmium-ion selective electrode Model 94-48A (Orion Research Inc., Mass., USA) was used, and the potentials were measured by use of Takeda Riken Digital Multimeter 6854. The potentials were reproducible within ± 0.1 mV in the mixed solvents used. A Metrohm E211 type Coulometer was employed as a current source for generation of hydrogen ions in a solution during the course of titrations. Silver–silver chloride electrodes set in the Kawai type[11] of the half-cell were prepared according to Brown.[21]

Preparation of the Test Solutions. A slightly acid cadmium(II) perchlorate solution in a mixed solvent was placed in a glass vessel and bubbled with nitrogen gas to remove carbon dioxide, and then a small amount of CdO powder was added to the solution. White precipitates appeared in the solution while agitating for several hours. The agitation was continued for a day passing nitrogen gas through the mixture and then the glass vessel was tightly sealed. The mixture was still continuously agitated for about 20 days in a thermostated room at 25 ± 1.5 °C. Then the solution was filtered through G-3 and G-4 glass filters and the filtrate was left to stand for one day at 25 °C in a liquid paraffin thermostat. This solution was filtered again through a G-4 glass filter to a measuring vessel. The volume of the test solution was determined from the weight and density of the test solution in the vessel. The total concentration of cadmium ion in the test solution was determined gravimetrically as $Cd_2P_2O_7$.

The method of emf measurements was essentially the same as that used in the previous works of this series.

All the measurements were carried out at 25.00 ± 0.02 °C in a liquid paraffin bath set in a room thermostated at 25.0 ± 1.5 °C.

** To whom correspondence should be addressed.

Results and Discussion

When cadmium(II) ions hydrolyze in a solution, the reaction equilibrium may be written as follows:

$$qCd^{2+} + pH_2O = Cd_q(OH)_p^{(2q-p)+} + pH^+. \quad (1)$$

The average number of hydrogen ion set free per metal ion Z is given as follows:

$$Z = \sum_q \sum_p p{*\beta}_{p,q} b^q h^{-p}/B, \quad (2)$$

where ${*\beta}_{p,q}$ is the formation constant of a species defined by Eq. 3

$${*\beta}_{p,q} = [Cd_q(OH)_p^{(2q-p)+}]h^p/b^q, \quad (3)$$

and B stands for the total concentration of cadmium ion, $b=[Cd^{2+}]$ and $h=[H^+]$ at equilibrium.

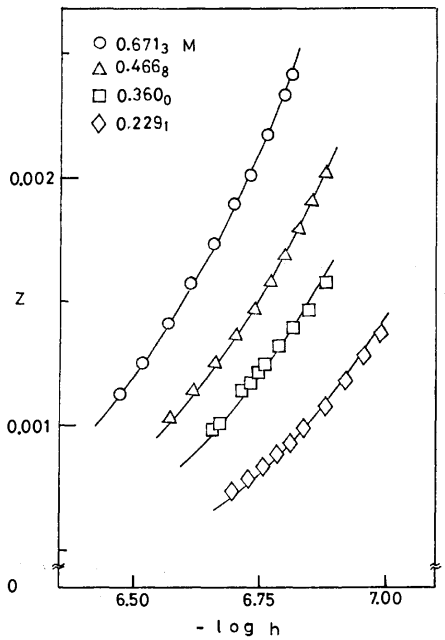

Fig. 1. Values of Z *vs.* $-\log h$ in the 0.10 mole fraction dioxane–water mixture. Solid lines show calculated curves of Z with the formation constants listed in Table 1.

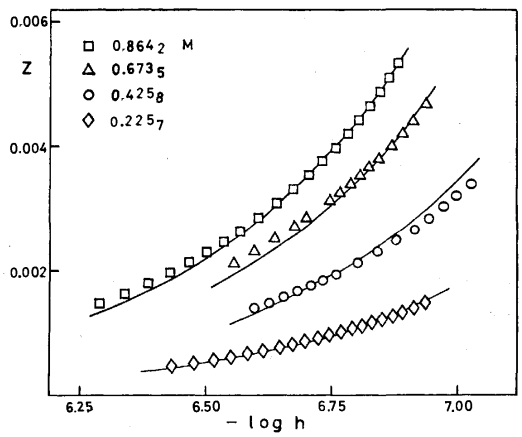

Fig. 2. Values of Z *vs.* $-\log h$ in the 0.10 mole fraction methanol–water mixture. Solid lines show calculated curves of Z with the formation constant listed in Table 1.

Typical results represented by Z plotted against $-\log h$ are graphically shown in Figs. 1 and 2 for the 0.1 mole fraction dioxane–water and methanol–water systems, respectively. According to the same procedure described in the previous paper,[8] we obtained a set of horizontal lines of Zh *vs.* h^{-1} and the intercepts which were dependent on B in each solvent. Thus we concluded that homoligandic complexes, $p=1$, were formed and the equilibrium species were Cd_2OH^{3+} and $CdOH^+$.

Table 1. Formation constants ($\log {*\beta}_{p,q}$) of the $Cd_q(OH)_p^{(2q-p)+}$ complex in dioxane–water and methanol–water mixtures at 25 °C

Solvent	Dioxane–Water		Methanol–Water
	Cd_2OH^{3+}	$CdOH^+$	Cd_2OH^{3+}
Aqueous	−9.13±0.01	−10.3±0.1	−9.13±0.01
0.05 mole fraction	−9.23±0.02	−9.9±0.1	−9.07±0.02
0.10 mole fraction	−9.28±0.02	−10.7±0.1	−9.08±0.02
0.15 mole fraction	−9.37±0.02	−11.0±0.1	—
0.20 mole fraction	−9.3±0.2	−10.7±0.5	−9.3 ±0.2

Table 1 lists the values of $\log {*\beta}_{p,q}$ determined by the least squares method[18] with a help of an electronic computer HITAC 8700 situated at the Tokyo Institute of Technology. The solid lines in Figs. 1 and 2 show calculated Z values with the constants which are inserted into Eq. 4.

$$Z = ({*\beta}_{1,1} bh^{-1} + {*\beta}_{1,2} b^2 h^{-1})/B \quad (4)$$

In the methanol–water mixtures, the values of ${*\beta}_{1,1}$ were so small in all the solvents that the values were not evaluated with reasonable accuracies.

The solvent effect of the organic solvents on the formation constants of cadmium(II) hydroxo complexes is rather small as is expected from the results obtained previously of this series.

The formation constant of the Cd_2OH^{3+} complex monotonously decreases with the increase of the dioxane concentration. In the methanol–water mixtures ${*\beta}_{1,2}$ is slightly larger than that in aqueous solution, but the change in ${*\beta}_{1,2}$ is not systematic. The formation constant of the $CdOH^+$ complex in the dioxane–water mixtures first increases with increasing concentration of dioxane up to 0.05 mole fraction and then decreases. The similar change in the formation constants, *i.e.*, ${*\beta}_{p,q}$ increases with the dioxane concentration and then decreases after passing through a broad maximum at around 0.1 mole fraction dioxane, has been observed in ${*\beta}_{3,3}$ of beryllium,[10] ${*\beta}_{1,1}$ of copper,[13] ${*\beta}_{4,4}$ of nickel,[14] and ${*\beta}_{4,4}$ and ${*\beta}_{8,6}$ of lead hydroxo complexes.[18] The values of ${*\beta}_{1,1}$ of the mononuclear $CdOH^+$ complex changed in a different manner from that of ${*\beta}_{1,1}$ of Fe^{3+} observed by Wada and his coworkers.[19,20]

Since the changes in ${*\beta}_{p,q}$ in a constant ionic medium with the solvent composition are caused by the changes of the ratios of activity coefficients of relevant ions in Eq. 1 and the concentration of water, the changes of the activity coefficients of the metal and hydrogen ions

were measured with varying solvent compositions by means of emf measurements of the cells,

Cd(selective electrode)|test solution|Ref (5)

and GE|test solution|Ref. (6)

The potentials of the cells may be written as follows: for cell (5)

$$E_{Cd} = E^{\circ}_{Cd} + 29.58 \log b + 29.58 \log y_{Cd} + E_j \quad (7)$$

and for cell (6)

$$E_H = E^{\circ}_H + 59.15 \log h + 59.15 \log y_H + E_j \quad (8)$$

where y denotes the activity coefficient of a species in the solution. In an acid solution where no hydrolysis of cadmium ion occurs, $B=b$. At low and constant b and h, the potential changes of cells 5 and 6 with the solvent composition are proportional to the values of log $\{y_{Cd(mix)}/y_{Cd(aq)}\}$ and log $\{y_{H(mix)}/y_{H(aq)}\}$, respectively, and the change of the liquid junction potentials is negligible in a high ionic medium.[22] Thus, the changes of the activity coefficients of cadmium and hydrogen ions in a 3 mol dm^{-3} $LiClO_4$ can be described with a good approximation as follows:

$$\log \{y_{Cd(mix)}/y_{Cd(aq)}\} = \Delta E_{Cd}/29.58, \quad (9)$$

and

$$\log \{y_{H(mix)}/y_{H(aq)}\} = \Delta E_H/59.15, \quad (10)$$

where ΔE_{Cd} and ΔE_H represent the potential changes of cells (5) and (6), respectively, with the solvent composition.

If the standard state of any reacting species is so chosen that the activity coefficient of the species approaches unity when the solution approaches 3 mol dm^{-3} $LiClO_4$ aqueous solution, the activity coefficient of the reacting species y in the aqueous medium is regarded as unity. Therefore, Eqs. 9 and 10 may be simplified as Eqs. 11 and 12, respectively.

$$\log y_{Cd} = \Delta E_{Cd}/29.58 \quad (11)$$

and

$$\log y_H = \Delta E_H/59.15 \quad (12)$$

The values of log y_{Cd} and log y_H thus evaluated in dioxane–water and methanol–water mixtures are plotted against the concentration of the organic solvents in Figs. 3 and 4, respectively.

The formation constant of the $Cd_q(OH)_p^{(2q-p)+}$ complex is given in terms of activities as follows:

$$*\beta^{\circ}_{p,q} = \frac{a_{Cd_q(OH)_p} \cdot a_H^p}{a_{Cd}^q \cdot a_{H_2O}^p} = \frac{[Cd_q(OH)_p^{(2q-p)+}] \cdot h^p}{b^q} \cdot \frac{1}{[H_2O]^p} \cdot \frac{y_{Cd_q(OH)_p} \cdot y_H^p}{y_{Cd}^q \cdot f_{H_2O}^p} \quad (13)$$

$*\beta^{\circ}_{p,q}$ is the formation constant thermodynamically defined, which is independent of the solvent composition at a given temperature. The activity coefficient y is defined in terms of molarity and is independent of the concentration of the relevant species in a constant ionic medium, but is dependent on the solvent composition. f_{H_2O} is the activity coefficient of water in a mixed solvent expressed by the mole fraction scale of the solvent component. Since the value $[Cd_q(OH)_p^{(2q-p)+}]h^p/b^q = *\beta_{p,q}$ is experimentally determinable for the complex $Cd_q(OH)_p^{(2q-p)+}$ in a given solvent and $*\beta^{\circ}_{p,q}$ is the formation constant of the complex in the aqueous medium according to definition stated above, the difference between the formation constants obtained in a mixed solvent and in the aqueous solution may be given as follows:

$$\Delta \log *\beta_{p,q} = \log *\beta_{p,q}(mix) - \log *\beta_{p,q}(aq) = \log [H_2O]^p + \log \{y_{Cd}^q/y_H^p\} - \log \{y_{Cd_q(OH)_p}/f_{H_2O}^p\}. \quad (14)$$

The first two terms of the right hand side of Eq. 14 can be determined experimentally and log $\{y_{Cd_q(OH)_p}/f_{H_2O}^p\}$ is thus determined. The values of log $\{y_{Cd_q(OH)_p}/f_{H_2O}^p\}$ are plotted for the Cd_2OH^{3+} complex against the mole

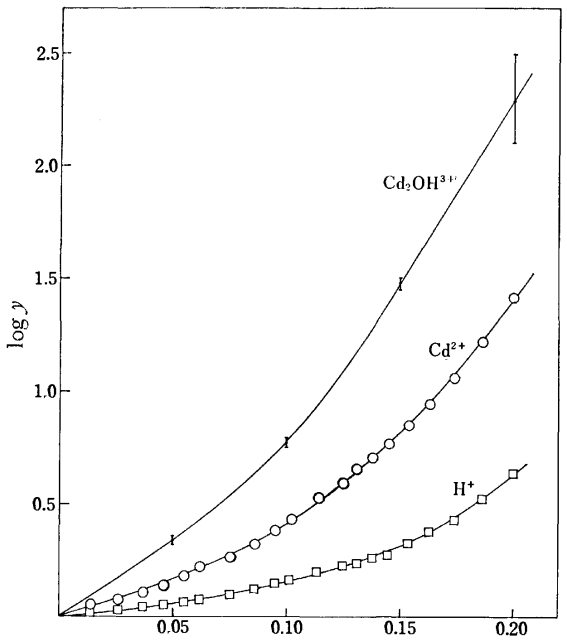

Fig. 3. Variations of log y for H^+, Cd^{2+}, and Cd_2OH^{3+} ions with the concentration of dioxane–water mixtures. The error bar shown for the Cd_2OH^{3+} curve represents an estimated error in log y_{Cd_2OH} from the uncertainty of the log $*\beta_{1,2}$ value.

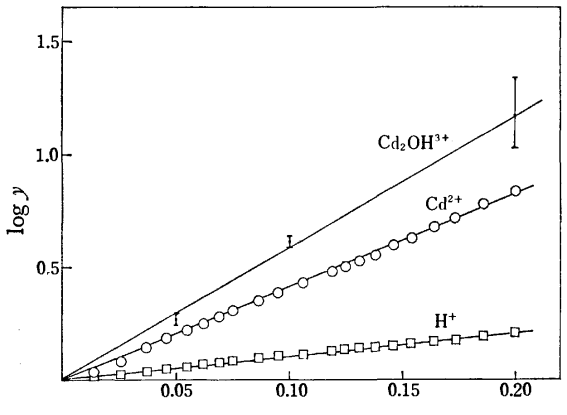

Fig. 4. Variations of log y for H^+, Cd^{2+}, and Cd_2OH^{3+} ions with the concentration of methanol in methanol–water mixtures. The error bar shown for the Cd_2OH^{3+} curve represents an estimated error in log y_{Cd_2OH} from the uncertainty of the log $*\beta_{1,2}$ value.

fractions of dioxane and methanol at $[H_2O]=0.95$, 0.90, 0.85, and 0.80 in Figs. 3 and 4, respectively. If we can assume that $f_{H_2O}=1$ as a first approach over the range of the solvent composition examined here, the curves thus drawn may represent the variations of the activity coefficients of the Cd_2OH^{3+} complex in the dioxane–water and methanol–water mixtures containing 3 mol dm^{-3} $LiClO_4$ at 25 °C. It seems reasonable that the activity coefficient of the Cd_2OH^{3+} ion, as well as those of Cd^{2+} and H^+ ions, was more sensitive to the solvent composition in the dioxane–water mixtures than that in the methanol–water mixtures, because it is expected that the dielectric constants of the former solvent may be lower than that of the latter at the same mole-fraction composition. The change in the activity coefficient of the Cd_2OH^{3+} ion was much larger than those of Cd^{2+} and H^+ ions in the both solvents as is expected from the larger charge of the complex ion.

The authors wish to thank Dr. T. Kawai for his technical assistance during the work. The work is financially supported by the Ministry of Education and, in part, by the Ministry of International Trade and Industry.

References

1) C. Kullgren, *Z. Phys. Chem.*, **85**, 446 (1913).
2) N. Löfman, *Z. Anorg. Chem.*, **107**, 241 (1919).
3) Y. Marcus, *Acta Chem. Scand.*, **11**, 690 (1957).
4) K. H. Gayer and L. J. Wootner, *J. Phys. Chem.*, **61**, 364 (1957).
5) P. Schindler, *Helv. Chim. Acta*, **42**, 2736 (1959).
6) D. Dyrssen and P. Lumme, *Acta Chem. Scand.*, **16**, 1785 (1962).
7) G. Biedermann and L. Ciavatta, *Acta Chem. Scand.*, **16**, 2221 (1962).
8) H. Matsui and H. Ohtaki, *Bull. Chem. Soc. Jpn.*, **47**, 2603 (1974).
9) H. Ohtaki, *Inorg. Chem.*, **6**, 808 (1967).
10) H. Ohtaki and H. Kato, *Inorg. Chem.*, **6**, 1935 (1967).
11) H. Tsukuda, T. Kawai, M. Maeda, and H. Ohtaki, *Bull. Chem. Soc. Jpn.*, **48**, 691 (1975).
12) H. Ohtaki, *Inorg. Chem.*, **7**, 1205 (1968).
13) H. Ohtaki and T. Kawai, *Bull. Chem. Soc. Jpn.*, **45**, 1735 (1972).
14) T. Kawai, H. Otsuka, and H. Ohtaki, *Bull. Chem. Soc. Jpn.*, **46**, 3753 (1973).
15) H. Ohtaki, *Bull. Chem. Soc. Jpn.*, **43**, 2463 (1970).
16) H. Ohtaki, *Bull. Chem. Soc. Jpn.*, **42**, 1573 (1969).
17) M. Yasuda, *Bull. Chem. Soc. Jpn.*, **32**, 429 (1959).
18) T. Kawai, The doctoral thesis, Tokyo Institute of Technology (1975).
19) G. Wada and A. Endo, *Bull. Chem. Soc. Jpn.*, **45**, 1073 (1972).
20) G. Wada and Y. Kobayashi, *Bull. Chem. Soc. Jpn.*, **48** 2451 (1975).
21) A. S. Brown, *J. Am. Chem. Soc.*, **56**, 646 (1934).
22) H. Ohtaki, unpublished results.

Enhancement of the Pfeiffer Effect Arising from the Cation-Cation Interaction*

Katsuhiko MIYOSHI, Yasushige KURODA, Hiroshi OKAZAKI, and Hayami YONEDA

Department of Chemistry, Faculty of Science, Hiroshima University Higashi-senda-machi, Hiroshima 730

(Received January 5, 1977)

The influence of added sodium and potassium chloride, bromide, and sulfate was examined on the Pfeiffer effect of the $[Co(phen)_3]^{2+}$– and $[Ni(phen)_3]^{2+}$–*d*-cinchoH$^+$ systems in water (phen=1,10-phenanthroline, and *d*-cinchoH$^+$=*dextro*-cinchoninium ion). It was found that the added anions enhance the circular dichroism (CD) induced in the d-d transition region of $[Co(phen)_3]^{2+}$ and $[Ni(phen)_3]^{2+}$ ions, and that the CD-enhancing order is $Br^- > Cl^- > SO_4^{2-}/2$. These findings were well interpreted in terms of reduced electrostatic repulsion between $[Co(phen)_3]^{2+}$ or $[Ni(phen)_3]^{2+}$ and *d*-cinchoH$^+$ by the added anions, and of the resulting enhanced enantiomerization of these cationic complexes in favor of Δ-isomers in the presence of *d*-cinchoH$^+$. Logarithm of the magnitude of the induced CD was found to be a linear function of logarithm of the total anion concentration in all the systems examined. This fact gives a strong support to the above interpretation, and suggests a close resemblance of these Pfeiffer-active systems to aqueous cationic surfactant solutions.

When a racemic mixture of a labile metal complex is added to a solution containing a certain chiral molecule called an environment compound, additional optical activity is sometimes developed. This phenomenon is known as the Pfeiffer effect,[1] and several possible mechanisms have been proposed, *e.g.*, configurational activity,[2] differential association,[1c,3] equilibrium shift (enantiomerization),[4] hydrogen bonding,[5] and hydrophobic bonding.[1c,6] The fact that partial resolution of some metal complexes is performed by exploiting this phenomenon,[4a,4b,7] provides decisive evidence for the equilibrium shift mechanism by which metal complexes enantiomerize in favor of either *d*- or *l*-isomer, depending on the spacial demand of the chiral environment compound present. As a result, the Pfeiffer effect is successfully applied to assign the absolute configuration of metal complexes,[5,7-9] in particular for those which are so labile that conventional resolution techniques fail to isolate them as antipodes.[10,11]

It seems convenient to classify the Pfeiffer-active systems into three groups according to their charge type as far as tris-phen or tris-bpy complexes are concerned; i) systems of the same charge, *e.g.*, $[M(phen)_3]^{2+}$–*l*-stryH$^+$ and –*d*-cinchoH$^+$ in water, ii) systems of opposite charge, *e.g.*, $[M(phen)_3]^{2+}$–*d*-BCS$^-$ in water, and iii) systems containing nonelectrolytes, *e.g.*, $[M(phen)_3]^{2+}$–*l*-malic acid and –*d*-tartaric acid in water, and $[Ni(phen)_3]^{2+}$ in *l*-2,3-butanediol[4b] (M(II)=Co(II) or Ni(II), phen=1,10-phenanthroline, bpy=2,2′-bipyridine, *l*-stryH$^+$ = *levo*-strychninium ion, *d*-cinchoH$^+$ = *dextro*-cinchoninium ion, and *d*-BCS$^-$ = *dextro*-3-bromocamphor-9-sulfonate ion). Among these groups, the first group is seemingly unusual in the sense that the Pfeiffer effect is well observed despite the inevitable electrostatic repulsion between cationic complexes and cationic environment compounds even at a low concentration in water. Thus, some mechanisms must operate which force these cations to attract each other against their mutual repulsion. In this paper, we present some experimental results suggesting a close resemblance of these Pfeiffer systems to aqueous ionic surfactant solutions in which hydrophobic ions of the same charge associate to form aggregates called micelles.

Experimental

Sample solutions containing both $[Co(phen)_3]Cl_2$ and *d*-cinchoHCl were prepared by diluting respective stock solutions with water in volumetric flasks. To prevent the decomposition of the complex, a small amount of free phen was added.[4b] To these solutions were added varying amounts of NaCl or KCl. Completely the same operation was employed to prepare the corresponding bromide and sulfate solutions, and NaBr or KBr, and Na_2SO_4 or K_2SO_4 were added respectively in place of NaCl or KCl. Tetraalkylammonium bromides R_4NBr (R=methyl to butyl) were also added to the bromide solution in place of NaBr or KBr. A similar procedure was applied to the $[Ni(phen)_3]^{2+}$–*d*-cinchoH$^+$ system, but the sample solutions thus prepared were allowed to stand for two weeks at room temperature to attain an enantiomerization equilibrium.[4a] Absorption (AB) and circular dichroism (CD) spectra were recorded on a Shimadzu UV-200 and a Jasco J-40CS spectrometer at ambient temperature, and optical rotations were measured with a Union-Giken PM-71 polarimeter in a 5 cm cell. All chemicals used were of reagent grade.

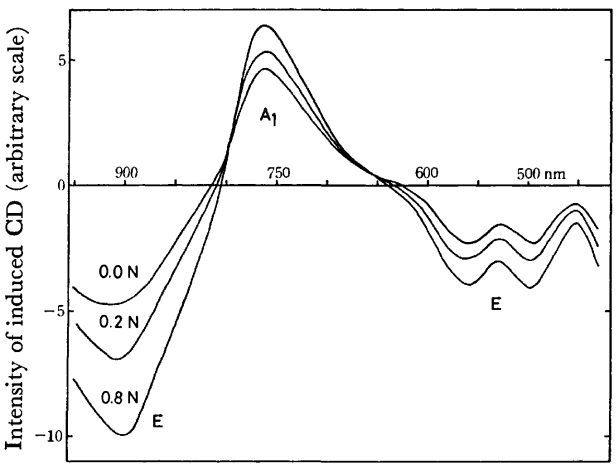

Fig. 1. CD spectra induced in the $[Ni(phen)_3]SO_4$ (0.03 M)–*d*-cinchoH1/2SO_4(0.03 M) systems containing various amounts of Na_2SO_4.

* Preliminary results of this work were reported in, H. Yoneda, K. Miyoshi, and S. Suzuki, *Chem. Lett.*, **1974**, 349; K. Miyoshi, K. Sakata, and H. Yoneda, *ibid.*, **1974**, 1087.

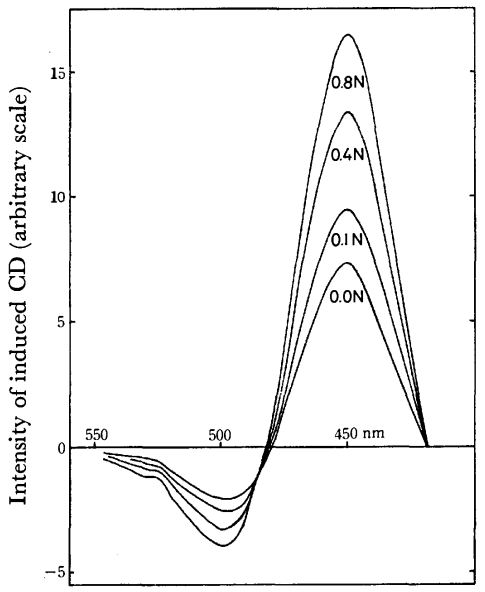

Fig. 2. CD spectra induced in the $[Co(phen)_3]Cl_2$(0.015 M)-*d*-cinchoHCl (0.03 M) systems containing various amounts of NaCl.

Results and Discussion

Figures 1 and 2 show the CD induced in the d-d transition region for the $[Ni(phen)_3]SO_4$-*d*-cinchoHl/$2SO_4$ and the $[Co(phen)_3]Cl_2$-*d*-cinchoHCl systems in water, where varying amounts of Na_2SO_4 and NaCl are added respectively. It is seen that the CD spectrum for the former system is almost the same in shape as that of *levo*-$[Ni(phen)_3]^{2+}$ ion,[4b,12] and that its intensity is enhanced uniformly throughout the spectrum upon the addition of Na_2SO_4. These facts mean that an enantiomerization of $[Ni(phen)_3]^{2+}$ ion actually takes place in favor of its *levo*- or Λ-isomer[13] in the presence of *d*-cinchoH$^+$ and is enhanced by added Na_2SO_4, and that the same will be true for the $[Co(phen)_3]Cl_2$-*d*-cinchoHCl system. Similar results obtained in other systems are summarized in Table 1, which clearly indicates that the intensities of the induced CD are dependent on the kind of the added anions, but not of cations when they are compared at a fixed concentration of added salts. Therefore, it is concluded that the added anions are responsible for the enhancement of the Pfeiffer effect shown in Figs. 1 and 2 and Table 1.

The influence of added inert counter-ions on the optical activity of metal complexes has been extensively studied[14] and has been usually attributed to outer-sphere association of the complexes with added counter-ions. However, the anion effect shown in Figs. 1 and 2 and Table 1 is not ascribed to usual ion association, because each component of the induced CD in $[Ni(phen)_3]^{2+}$ and $[Co(phen)_3]^{2+}$ ions is affected uniformly but not differently by the added anions.[12c,14] Instead, it is attributed to reduced electrostatic repulsion between these cationic complexes and *d*-cinchoH$^+$ by the added anions and to the resulting enhanced enantiomerization of $[Ni(phen)_3]^{2+}$ or $[Co(phen)_3]^{2+}$ ion in the presence of *d*-cinchoH$^+$.

In order to confirm the above interpretation, an

Table 1. Intensities of the induced CD

$[Ni(phen)_3]SO_4$(0.03M)-*d*-cinchoHl/$2SO_4$(0.03M)			
Na_2SO_4	$\Delta\varepsilon_{497}$		$\Delta\varepsilon_{560}$
0.05N	9.1×10^{-4}		8.6×10^{-4}
0.1 N	9.9×10^{-4}		9.3×10^{-4}
0.2 N	10.6×10^{-4}		10.1×10^{-4}
0.4 N	12.3×10^{-4}		11.5×10^{-4}
0.8 N	14.1×10^{-4}		13.1×10^{-4}
slope	0.23		0.23
K_2SO_4	$\Delta\varepsilon_{497}$		$\Delta\varepsilon_{560}$
0.05N	9.4×10^{-4}		8.6×10^{-4}
0.1 N	10.1×10^{-4}		9.1×10^{-4}
0.2 N	10.8×10^{-4}		9.9×10^{-4}
0.4 N	12.5×10^{-4}		11.6×10^{-4}
0.8 N	14.1×10^{-4}		13.3×10^{-4}
slope	0.23		0.24
$[Co(phen)_3]SO_4$(0.015M)-*d*-cinchoHl/$2SO_4$ (0.03M)			
Na_2SO_4	$\Delta\varepsilon_{450}$	K_2SO_4	$\Delta\varepsilon_{450}$
0.05N	1.66×10^{-2}	0.05N	1.68×10^{-2}
0.1 N	1.82×10^{-2}	0.1 N	1.82×10^{-2}
0.2 N	2.04×10^{-2}	0.2 N	2.06×10^{-2}
0.4 N	2.34×10^{-2}	0.4 N	2.34×10^{-2}
0.6 N	2.59×10^{-2}	0.6 N	2.57×10^{-2}
0.8 N	—	0.8 N	2.79×10^{-2}
slope	0.24	slope	0.25
$[Co(phen)_3]Cl_2$(0.015M)-*d*-cinchoHCl(0.03M)			
NaCl	$\Delta\varepsilon_{450}$	KCl	$\Delta\varepsilon_{450}$
0.05N	1.74×10^{-2}	0.05N	1.76×10^{-2}
0.1 N	1.96×10^{-2}	0.1 N	1.98×10^{-2}
0.2 N	2.22×10^{-2}	0.2 N	2.26×10^{-2}
0.4 N	2.77×10^{-2}	0.4 N	2.71×10^{-2}
0.8 N	3.42×10^{-2}	0.8 N	3.38×10^{-2}
slope	0.32	slope	0.31
$[Co(phen)_3]Br_2$(0.015M)-*d*-cinchoHBr(0.03M)			
NaBr	$\Delta\varepsilon_{450}$	KBr	$\Delta\varepsilon_{450}$
0.05N	1.86×10^{-2}	0.05N	1.80×10^{-2}
0.1 N	2.04×10^{-2}	0.1 N	1.98×10^{-2}
0.2 N	2.34×10^{-2}	0.2 N	2.32×10^{-2}

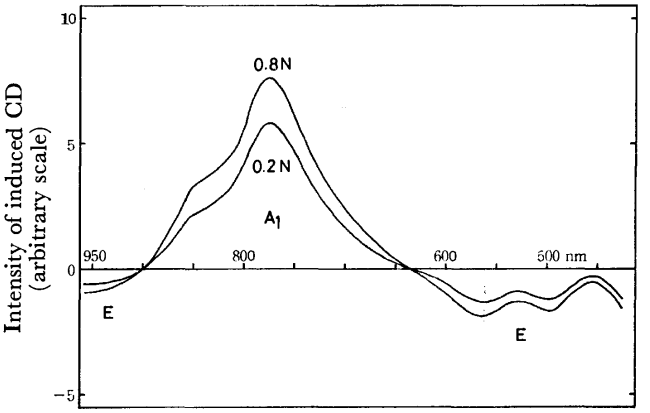

Fig. 3. CD spectra of the $[Ni(phen)_3]SO_4$ (0.03 M)-*d*-cinchoHl/$2SO_4$ (0.03 M) systems containing various amounts of Na_2SO_4, measured after they are re-dissolved in acetone–water mixtures (1 : 1 volume ratio).

Table 2. Degree of optical resolution

$[Ni(phen)_3]SO_4$(0.03M)–*d*-cinchoHl/$2SO_4$(0.03M)[a]			
0.2N	Na_2SO_4	2.2%(497 nm)	2.0%(562 nm)
0.8N	Na_2SO_4	3.0%(497 nm)	2.9%(562 nm)
$[Co(phen)_3]Cl_2$(0.015M)–*d*-cinchoHCl(0.03M)[b]			
0.2N	NaCl	1.1%(492 nm)	
0.4N	NaCl	1.4%(492 nm)	

a) $\Delta\varepsilon_{497}=-4.57\times10^{-2}$ and $\Delta\varepsilon_{562}=-5.12\times10^{-2}$ for optically-pure Λ-$[Ni(phen)_3]^{2+}$ in an acetone–water mixture. Racemization of $[Ni(phen)_3]^{2+}$ in this mixed solvent is not taken into account. See, N. R. Davies and F. P. Dwyer, *Trans. Faraday Soc.*, **50**, 1325 (1954). b) $\Delta\varepsilon_{492}=-1.29$ for optically-pure Λ-$[Co(phen)_3]^{3+}$ in water. See, Ref. 18. Oxidation of $[Co(phen)_3]^{2+}$ with H_2O_2 to $[Co(phen)_3]^{3+}$ is not necessarily quantitative.

excess amount of $NaClO_4$ was added to the $[Ni(phen)_3]$-SO_4–*d*-cinchoHl/$2SO_4$ system and resulting precipitates containing both $[Ni(phen)_3](ClO_4)_2$ and *d*-cinchoHClO_4 were re-dissolved in acetone–water mixtures (1 : 1 volume ratio). In Fig. 3 are shown their CD spectra, which are completely the same in shape as that of Λ-$[Ni(phen)_3]^{2+}$ ion in an acetone–water mixture.[12c] Since the Pfeiffer effect is not exhibited in this mixed solvent, our interpretation is verified, and the degree of optical resolution estimated is given in Table 2. However, a detailed examination of Fig. 1 reveals that the CD induced in the $[Ni(phen)_3]SO_4$–*d*-cinchoHl/$2SO_4$ system is somewhat different in shape from that of Λ-$[Ni(phen)_3]^{2+}$ ion resolved by a usual method,[12c] in particular at a long wavelength region, *e.g.*, the $^3A_{2g}\rightarrow{}^3T_{2g}$ transition in an Oh approximation. That is, the E($^3T_{2g}$) component is greater in magnitude than the $A_1(^3T_{2g})$ component in the Pfeiffer system,[15] while the corresponding E component of resolved $[Ni(phen)_3]^{2+}$ ion is not detected in water unless acetone or some polyoxyanions are added.[12c] This difference is attributed to marked association of $[Ni(phen)_3]^{2+}$ ion with *d*-cinchoH$^+$, because the Pfeiffer effect is not exhibited unless the complex comes into direct contact with chiral environment compounds.[16]

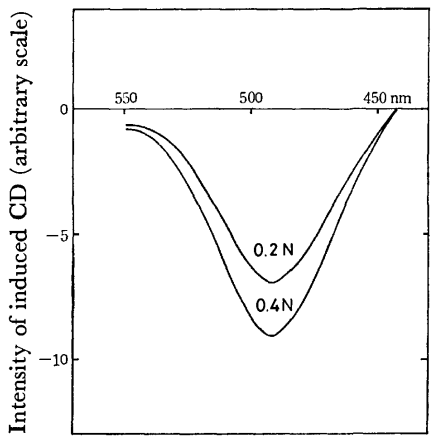

Fig. 4. CD spectra of the $[Co(phen)_3]Cl_2$ (0.015 M)–*d*-cinchoHCl (0.03 M) systems containing various amounts of NaCl after oxidation with H_2O_2.

Figure 4 shows the CD spectra of the $[Co(phen)_3]Cl_2$–*d*-cinchoHCl systems containing varying amounts of NaCl after they are oxidized with H_2O_2 in the presence of MnO_2. It is seen that their CD spectra are the same in shape as that of resolved *levo*- or Λ-$[Co(phen)_3]^{3+}$ ion,[12b,17,18] and that their intensity is increased as the amount of NaCl added to these systems is increased. Since $[Co(phen)_3]^{3+}$ ion does not exhibit the Pfeiffer effect with *d*-cinchoH$^+$, it is confirmed that $[Co(phen)_3]^{2+}$ ion also enantiomerizes[7] in favor of its Λ-isomer in the presence of *d*-cinchoH$^+$ like $[Ni(phen)_3]^{2+}$ ion does. By comparing the CD intensities, the degree of optical resolution is estimated as before for the $[Co(phen)_3]Cl_2$–*d*-cinchoHCl systems and is included in Table 2.

It is now well known that ionic surfactants associate to form aggregates called micelles at relatively low concentrations against their mutual electrostatic repulsion in water. In the process of micellization, two opposing factors[19] are usually taken into account, *i.e.*, electrostatic repulsion between surfactant ions of the same charge, and the hydrophobic interaction[20] which is regarded as a main driving force for the aggregation of surfactants in water. If anions (or cations) are added to cationic (or anionic) surfactant solutions, the resulting reduced electrostatic repulsion leads to increased micelle

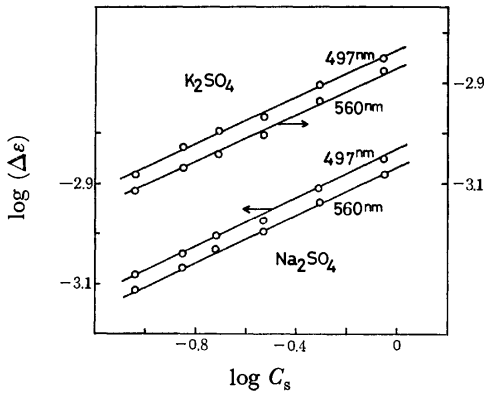

Fig. 5. Plots of log ($\Delta\varepsilon$) at 497 and 560 nm *vs.* log C_s for the $[Ni(phen)_3]SO_4$(0.03 M)–*d*-cinchoHl/$2SO_4$(0.03 M) system.

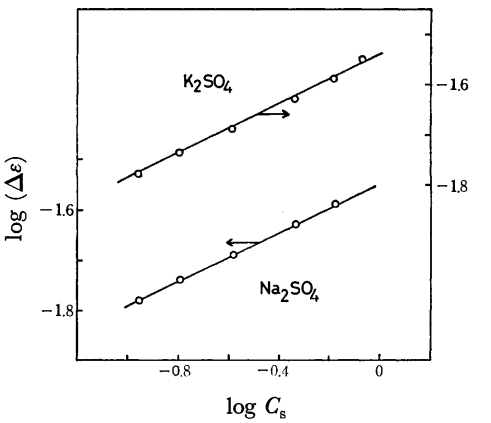

Fig. 6. Plots of log ($\Delta\varepsilon$) at 450 nm *vs.* log C_s for the $[Co(phen)_3]SO_4$ (0.015 M)–*d*-cinchoHl/$2SO_4$ (0.03 M) system.

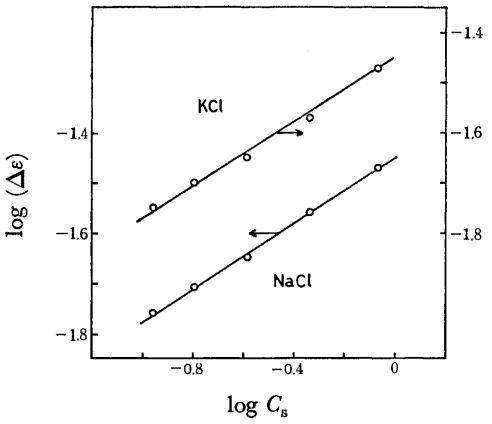

Fig. 7. Plots of log(Δε) at 450 nm *vs.* log C_s for the $[Co(phen)_3]Cl_2$(0.015 M)-*d*-cinchoHCl(0.03 M) system.

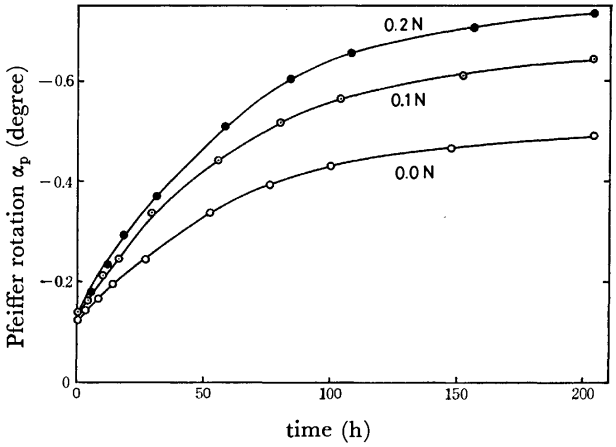

Fig. 8. Plots of the Pfeiffer rotation α_p *vs.* time (h) for the $[Ni(phen)_3]Cl_2$ (0.016 M)-*d*-cinchoHCl (0.016 M) systems containing various amounts of NaCl, measured at 436 nm in a 5 cm cell. 0.0 N NaCl; α_p (0)= −0.122°, α_p (∞)= −0.505°, 0.1 N NaCl; α_p (0)= −0.138°, α_p (∞)= −0.661°, 0.2 N NaCl; α_p (0)= −0.135°, α_p (∞)= −0.759°.

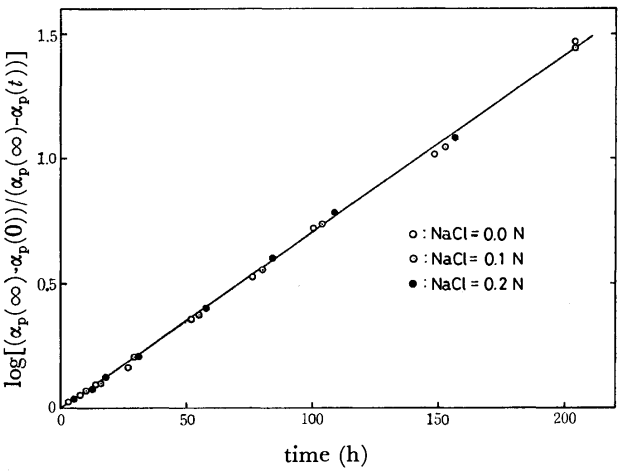

Fig. 9. Plots of $\log[(\alpha_p(\infty)-\alpha_p(0))/(\alpha_p(\infty)-\alpha_p(t))]$ *vs.* time (h) for the $[Ni(phen)_3]Cl_2$(0.016M)-*d*-cinchoHCl (0.016M) systems containing various amounts of NaCl.

stability.[21] That is, the CMC (critical micelle concentration) is greatly lowered by added ions possessing charges opposite in sign to those of surfactant ions. According to the theory of micellization for ionic surfactants,[21] the CMC is expressed as a function of the total equivalent counter-ion concentration C_s by

$$\log (CMC) = -K_g \log C_s + \text{constant},$$

where K_g is a measure of the degree of charge neutralization on the micelle surface. Since *d*-cinchoH$^+$ is a bulky organic ion with its positive charge localized on its nitrogen atom like usual cationic surfactant molecules, and since tris-phen complexes are surrounded by bulky organic ligands, they are all regarded as hydrophobic. In fact, the hydrophobic nature of $[Fe(phen)_3]^{2+}$ ion[22,23] and some compounds[24] like *d*-cinchoH$^+$ or *l*-stryH$^+$ has been recently examined by some workers. Consequently, it is fairly plausible for these hydrophobic cations to attract each other through the hydrophobic interaction to form aggregates in water like cationic surfactants. Though the structure and the aggregation number of the aggregates are not known, highly aggregated species are improbable, judging from the molecular structures of $[M(phen)_3]^{2+}$ and *d*-cinchoH$^+$. Then, by analogy with aqueous ionic surfactant solutions, log (Δε) is plotted against log C_s for both the $[Co(phen)_3]^{2+}$- and $[Ni(phen)_3]^{2+}$-*d*-cinchoH$^+$ systems in Figs. 5—7. Good linear relationships are observed in these plots, derived slopes of which are listed in Table 1. It should be noted here that these plots have an almost constant slope for a given system irrespective of the kind of added cations and of the wavelength chosen for the CD measurement, and that the slope is constant for sulfate systems whether the central metal ion is Co(II) or Ni(II). These findings are completely consistent with the above interpretation for the anion effect shown in Figs. 1 and 2 and Table 1. Furthermore, the increasing order of the degree of charge neutralization, *i.e.*, the increasing order of the induced CD is $Br^- > Cl^- > SO_4^{2-}$/2,[25] which is in agreement with the decreasing order of the CMC of usual cationic surfactants in water (Hofmeister or lyotropic series).[26] This order is also consistent with the influence of the added anions on the chemical potential of cationic tris-phen complexes in aqueous solutions.[27] That is, hydrophobic cations like these complexes are more stable when their counter-ions are structure-breaking anions like Br^- than when they are structure-making anions like SO_4^{2-}.[28]

In order to elucidate the anion effect more clearly, we examined the influence of the added NaCl on the time-dependence[4a,11] of the Pfeiffer rotation α_p.[1] Figure 8 shows the plots of α_p *vs.* time after mixing $[Ni(phen)_3]Cl_2$ with *d*-cinchoHCl in water, where varying amounts of NaCl are added. It is seen that α_p increases exponentially with time,[1,4a] and is enhanced by the added NaCl. In Fig. 9 is plotted $\log[(\alpha_p(\infty)-\alpha_p(0))/(\alpha_p(\infty)-\alpha_p(t))]$ against time t, $\alpha_p(0)$ and $\alpha_p(t)$ being the Pfeiffer rotation immediately after mixing and at a time t after mixing, respectively, and $\alpha_p(\infty)$ the Pfeiffer rotation at enantiomerization equilibrium. It is seen that the value of $\log[(\alpha_p(\infty)-\alpha_p(0))/(\alpha_p(\infty)-\alpha_p(t))]$ is almost constant at a given time after mixing whether NaCl is added or not. This suggests that added NaCl has no effect at all on the rate constant of the

enantiomerization of $[Ni(phen)_3]^{2+}$ in the presence of *d*-cinchoH$^+$, but increases the number of $[Ni(phen)_3]^{2+}$ ion interacting with *d*-cinchoH$^+$, thereby enhancing the Pfeiffer effect. The same will be true for the sulfate system as well as for the $[Co(phen)_3]^{2+}$–*d*-cinchoH$^+$ systems, though the enantiomerization is too rapid[7] to be measured for the latter systems under our experimental conditions.

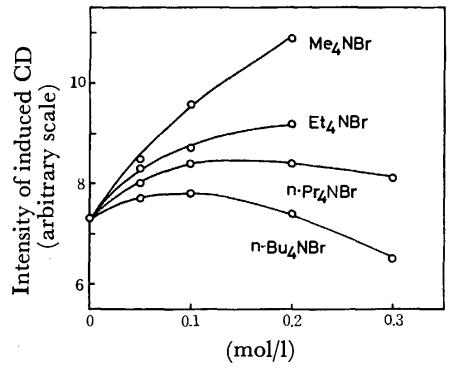

Fig. 10. Plots of the intensity of induced CD at 450 nm *vs.* molar concentration of added R_4NBr (R=methyl to butyl) for the $[Co(phen)_3]Br_2$(0.0075M)–*d*-cinchoHBr (0.03M) system.

In Fig. 10 is plotted the intensity of the induced CD at 450 nm as a function of molar concentration of added tetraalkylammonium bromides R_4NBr (R=methyl to butyl) for the $[Co(phen)_3]Br_2$–*d*-cinchoHBr system. It is seen that the intensity of the induced CD ceases to increase and finally decreases as the alkyl group of added R_4N^+ ion becomes bulky, in other words, as the R_4N^+ ion bears hydrophobic character.[29] This may be interpreted to mean that, when the added R_4N^+ ion is hydrophobic, the hydrophobic bond is formed between R_4N^+[23,30] and $[Co(phen)_3]^{2+}$ or *d*-cinchoH$^+$, and that as a result, the hydrophobic bonding between the complex and *d*-cinchoH$^+$ giving rise to the Pfeiffer effect, is thereby prohibited. Interestingly enough, Steigman *et al.*[31] have found the addition of hydrophobic R_4NBr to raise the CMC of a cationic surfactant, hexadecyltrimethylammonium bromide in aqueous solutions despite the accompanying increase in the counter-ion (Br^-) concentration. They attributed this anomalous cation effect to highly organized water-structure brought about by the added R_4N^+ ion. However, it is still difficult at this stage to decide which explanation is more probable.[26d,32]

Finally, Kirschner and Ahmad,[1b] and Kan and Brewer[33] have reported that *Λ*-isomer[13,34,35] is enriched in both the $[Co(ox)_3]^{3-}$– and $[Cr(ox)_3]^{3-}$–*d*-cinchoH$^+$ systems in water (ox=oxalate anion). On the other hand, *Λ*-isomer is enriched in the present $[Co(phen)_3]^{2+}$– and $[Ni(phen)_3]^{2+}$–*d*-cinchoH$^+$ systems, though the same environment compound as above is used. Consequently, the Pfeiffer effect does not work as an absolute tool for the determination of the absolute configuration of labile metal complexes.[9]

In conclusion, $[Co(phen)_3]^{2+}$ or $[Ni(phen)_3]^{2+}$ ion comes into contact with *d*-cinchoH$^+$ to enantiomerize in favor of its *Λ*-isomer, and added anions reduce the electrostatic repulsion between the cationic complexes and *d*-cinchoH$^+$, thereby enhancing the enantiomerization of these complexes. This situation is similar to that encountered in aqueous cationic surfactant solutions in which ions of the same charge associate to form aggregates against their mutual electrostatic repulsion and added anions facilitate their aggregation greatly. Therefore, so-called long-range interaction is not important to the chiral discrimination even in the Pfeiffer-active systems of the same charge, contrary to the speculation of Schipper.[1d]

References

1) For reviews, a) S. Kirschner and K. R. Magnell, *Adv. Chem. Ser.*, **62**, 366 (1967); b) S. Kirschner, N. Ahmad, and K. R. Magnell, *Coord. Chem. Rev.*, **3**, 201 (1968); S. Kirschner, *Rec. Chem. Prog.*, **32**, 29 (1971); S. Kirschner and N. Ahmad, "Coordination Chemistry," ed by S. Kirschner, Plenum Press, New York (1969), p. 42; c) R. C. Brasted, V. Landis, E. J. Kuhajek, P. E. R. Nordquist, and L. Mayer, *ibid.*, p. 64; d) P. E. Schipper, *Inorg. Chim. Acta*, **12**, 199 (1975).

2) F. P. Dwyer, E. C. Gyarfas, and M. F. O'Dwyer, *Nature*, **167**, 1036 (1951); F. P. Dwyer and E. C. Gyarfas, *ibid.*, **168**, 29 (1951); P. E. Schipper, *Aust. J. Chem.*, **28**, 1161 (1975); D. P. Craig, *Proc. R. Aust. Chem. Inst.*, **41**, 1 (1974).

3) V. Landis, Ph. D. Thesis, University of Minnesota, Minneapolis, Minn., 1956.

4) a) S. Kirschner and N. Ahmad, *J. Am. Chem. Soc.*, **90**, 1910 (1968); b) B. Bosnich and D. W. Watts, *Inorg. Chem.*, **14**, 47 (1975); c) B. Bosnich, "Fundamental Aspects and Recent Developments in Optical Rotatory Dispersion and Circular Dichroism," ed by F. Ciardelli and P. Salvadori, Heydon and Sons, New York (1973), Chap. 3.8.

5) S. Kirschner, *J. Indian Chem. Soc.*, **51**, 28 (1974); R. J. Pollock, Ph. D. Thesis, Wayne State University, Detroit, Michigan, 1972.

6) P. E. R. Nordquist, Ph. D. Thesis, University of Minnesota, Minneapolis, Minn., 1964.

7) N. A. P. Kane-Maguire and D. E. Richardson, *J. Am. Chem. Soc.*, **97**, 7195 (1975).

8) L. Mayer and R. C. Brasted, *J. Coord. Chem.*, **3**, 85 (1973).

9) J. P. Gunter and A. F. Schreiner, *Inorg. Chim. Acta*, **15**, 117 (1975).

10) N. Ahmad and S. Kirschner, *Inorg. Chim. Acta*, **14**, 215 (1975).

11) K. Ogino and T. Kumagai, *Bull. Chem. Soc. Jpn.*, **47**, 855 (1974).

12) a) J. Hidaka and B. E. Douglas, *Inorg. Chem.*, **3**, 1180 (1964); b) J. Ferguson, C. J. Hawkins, N. A. P. Kane-Maguire, and H. Lip, *ibid.*, **8**, 771 (1969); c) M. J. Harding, S. F. Mason, and B. J. Peart, *J. Chem. Soc., Dalton Trans.*, **1973**, 955.

13) K. R. Butler and M. R. Snow, *J. Chem. Soc., A*, **1971**, 565.

14) For example, H. L. Smith and B. E. Douglas, *Inorg. Chem.*, **5**, 784 (1966); S. F. Mason and B. J. Norman, *Proc. Chem. Soc.*, **1964**, 339; *Chem. Commun.*, **1965**, 73; R. Larsson, S. F. Mason, and B. J. Norman, *J. Chem. Soc., A*, **1966**, 301; S. F. Mason and B. J. Norman, *ibid.*, **1966**, 307; J. E. Sarneski and F. L. Urbach, *J. Am. Chem. Soc.*, **93**, 884 (1971).

15) Similar trends are also observed in the $[Ni(phen)_3]^{2+}$–*l*-stryH$^+$, –*l*-malic acid and –*d*-tartaric acid systems in water.

16) K. Miyoshi, Y. Kuroda, and H. Yoneda, *J. Phys. Chem.*, **80**, 270 (1976).
17) S. F. Mason and B. J. Norman, *Inorg. Nucl. Chem. Lett.*, **3**, 285 (1967); S. F. Mason and B. J. Peart, *J. Chem. Soc., Dalton Trans.*, **1973**, 949.
18) L. S. Dollimore and R. D. Gillard, *J. Chem. Soc., Dalton Trans.*, **1973**, 933.
19) See, for example, P. Mukerjee, *Adv. Colloid Interface Sci.*, **1**, 241 (1967); *J. Phys. Chem.*, **73**, 2054 (1969) and references cited therein; D. C. Poland and H. A. Scheraga, *J. Colloid Sci.*, **21**, 273 (1966).
20) W. Kauzmann, *Adv. Protein Chem.*, **14**, 1 (1959); G. Nemethy, *Angew. Chem., Int. Ed. Engl.*, **6**, 195 (1967); F. Franks, "Water, Comprehensive Treatise," Vol. 4, Plenum Press, New York (1975), p. 1; C. Tanford, "The Hydrophobic Effect," Wiley-Interscience, New York (1973).
21) K. Shinoda, "Colloidal Surfactants," ed by K. Shinoda, T. Nakagawa, B. Tamamushi, and T. Isemura, Academic Press, New York (1963), Chap. 1.
22) B. Krotachil and J. Knoeck, *J. Phys. Chem.*, **70**, 944 (1966); Y. Yamamoto, T. Tominaga, and S. Tagashira, *Inorg. Nucl. Chem. Lett.*, **11**, 825 (1975). See also, G. N. LaMar and G. R. Van Hecke, *Inorg. Chem.*, **12**, 1767 (1973); F. M. Van Meter and H. M. Neumann, *J. Am. Chem. Soc.*, **98**, 1382 (1976); *ibid.*, **98**, 1388 (1976).
23) K. Miyoshi, C. Shimada, and H. Yoneda, *Bull. Chem. Soc. Jpn.*, **48**, 3403 (1975).
24) P. Mukerjee, *J. Pharm. Sci.*, **63**, 972 (1974).
25) The slope of log ($\Delta\varepsilon$)-log C_s plot could not be obtained for the bromide solutions because of low solubility of [Co(phen)$_3$]Br$_2$ in water. However, if $\Delta\varepsilon$ values are compared at the same concentration of added salts, it is confirmed that Br^- ion is certainly a more effective charge-neutralizer than Cl^- or SO_4^{2-} ion.
26) For example, a) E. W. Anacker and H. M. Ghose, *J. Phys. Chem.*, **67**, 1713 (1963); *J. Am. Chem. Soc.*, **90**, 3161 (1968); b) P. Mukerjee and A. Ray, *J. Phys. Chem.*, **70**, 2150 (1966); c) M. F. Emerson and A. Holtzer, *ibid.*, **71**, 1898 (1967); d) J. W. Larsen and L. J. Magid, *J. Am. Chem. Soc.*, **96**, 5774 (1974).
27) K. Miyoshi, T. Taura, C. Shimada, and H. Yoneda, *Bull. Chem. Soc. Jpn.*, **48**, 1783 (1975).
28) J. E. Desnoyers, M. Arel, G. Perron, and C. Jolicoeur, *J. Phys. Chem.*, **73**, 3346 (1969).
29) W. -Y. Wen, "Water and Aqueous Solutions," ed by R. A. Horne, Wiley-Interscience, New York (1972), p. 613; *J. Solution Chem.*, **2**, 253 (1973).
30) Cation-cation interactions in R_4N^+ solutions are recently reviewed by J. E. Gordon, "The Organic Chemistry of Electrolyte Solutions," Wiley-Interscience, New York (1975), Chap. 3.
31) J. Steigman, I. Cohen, and F. Spingola, *J. Colloid Sci.*, **20**, 732 (1965).
32) A. Ray and G. Nemethy, *J. Am. Chem. Soc.*, **93**, 6787 (1971); R. Tenne and A. Ben-Naim, *J. Phys. Chem.*, **80**, 1120 (1976).
33) K. T. Kan and D. G. Brewer, *Can. J. Chem.*, **49**, 2161 (1971).
34) A. J. McCaffery, S. F. Mason, and R. E. Ballard, *J. Chem. Soc.*, **1965**, 2883.
35) K. R. Butler and M. R. Snow, *Chem. Commun.*, **1971**, 550; *J. Chem. Soc., Dalton Trans.*, **1976**, 251.

Reactions of Aminoalkanols with Some Copper(II) Complexes of the Mixed and Non-mixed Bis(Schiff base) Ligands

V. B. MOHANKUMAR, B. T. THAKER, Rakesh K. KOHLI, and P. K. BHATTACHARYA
Chemistry Department, Faculty of Science, M. S. Universiry of Baroda, Baroda 390-002, India
(Received March 22, 1976; in revised form January 18, 1977)

Reactions of aminoalkanols have been carried out with mixed and non-mixed bis(Schiff base) complexes of copper(II). In these reactions one of the ligands combines with the aminoalcohol forming a tridentate ligand, wheras another ligand is removed. From the resulting complexes the tendency to form the Schiff base is found to be in the order 2-hydroxybenzophenone≈2-hydroxy-1-naphthaldehyde>salicylaldehyde>2-hydroxyacetophenone. The complexes formed have been characterized by analytical, spectral, and magnetic studies.

Tridentate Schiff bases of amino acids with salicylaldehyde, and other similar tridentate Schiff base ligands form 1 : 1 complexes with copper(II),[1-6] the fourth site being occupied by a water molecule[2,3]. Aminoalkanols are also known to form tridentate Schiff base with aromatic aldehydes or ketones.[7] It has been shown by X-ray studies that the tridentate ligand occupies three positions around the metal ion.[2] Chakravorty and co-workers[8] have recently observed that mixed-ligand complexes of copper(II) containing salicylaldehyde, and the Schiff base of *N,N*-diethylethylenediamine with salicylaldehyde react with acids to lose the salicylaldehyde part, and that a complex of tridentate Schiff base is formed with water at the forth position. These facts suggest that the tridentate Schiff bases have a great tendency to form stable copper(II) complexes. An attempt was, therefore, made to study the reactions of aminoalkanols with bis(bidentate Schiff base)complexes of copper(II), and to confirm the formation of copper(II) complexes with tridentate Schiff bases through an amine-exchange reaction.[9] The reactions were also carried out on the mixed Schiff base complexes of copper(II) reported by us earlier[10-12] to compare the relative reactivity among the tridentate ligands. The structures of the resulting tridentate Schiff base complexes have been discussed, and the machanism of the formation of the 1 : 1 complex has been suggested.

Experimental

All the complexes used for the reactions with aminoalkanols were prepared according to the published procedures.[10-16] Aminoalkanols used were 2-aminoethanol(mea) and 1-amino-2-propanol(ipa) of A. R. quality.

Reactions with Bis(imine) Complexes of Copper(II). The following bis-complexes have been used:

(a) Bis(salicylideneaminato)copper(II),
(b) bis(2-hydroxy-1-naphthylmethyleneaminato)copper(II),
(c) bis[1-(*o*-hydroxyphenyl)ethyleneaminato]copper(II),
(d) bis[α-(*o*-hydroxyphenyl)benzylideneaminato]copper(II).

The complexes (a), (b), (c), or (d) (1 g) was taken in suspension in ethanol (30 ml), and to this was added mea (2 ml) or ipa (2 ml), and the mixture was refluxed for 3 h. The reaction mixture was stirred well, and water was added when a solid separated out. It was filtered, washed and dried.

Reactions with the Mixed Schiff Base Complexes of Copper(II). The reactions were carried out with the following mixed complexes:

(a′) (Salicylideneaminato)(2-hydroxy-1-naphthylmethyleneaminato)copper(II),
(b′) (salicylideneaminato)[1-(*o*-hydroxyphenyl)ethylideneaminato]copper(II),
(c′) (salicylideneaminato)[α-(*o*-hydroxyphenyl)benzylideneaminato]copper(II),
(d′) (2-hydroxy-1-naphthylmethyleneaminato)[α-(*o*-hydroxyphenyl)benzylideneaminato]copper(II).

An ethanolic (30 ml) suspension of the complex (a′), (b′), (c′), or (d′) (1 g) was refluxed for 3 h with 2-aminoethanol (2 ml) or 1-amino-2-propanol (2 ml). The reaction mixture was stirred well and water was added to obtain the compound. The complex was filtered, washed, and dried.

The complexes have been analysed for metal, N, C, and H (in some cases). The results have been tabulated in Table 1. Conductivity measurements were carried out in chloroform using a Toshniwal conductivity bridge Type CLOI/OIA. The magnetic susceptibilities of the complexes were determined at room temperature by the Gouy method using $Hg[Co(NCS)_4]$ as the calibrant. Infrared spectra of the complexes were recorded on a Perkin Elmer 427 infrared grating spectrophotometer in the form of KBr pellets. The electronic spectra of the complexes in chloroform solutions were taken on a Beckman DU-2 spectrophotometer at room temperature using 1 cm quartz cells in the range of 400—1000 nm. The reflectance spectra in the LiF medium have been obtained for some of the complexes.

The molar conductances of all the copper(II) complexes in chloroform show them to be non-electrolytes. The magnetic and spectral data have been presented in Table 1. The important IR bands of some of the complexes are listed in Table 2.

Results and Discussion

The reactions of 2-aminoethanol with the complexes (a), (b), (c), and (d) gave the products (A), (B), (C), and (D), respectively. Similar reactions take place with 1-amino-2-propanol and, the products obtained are (E), (F), (G), and (H). The reaction schemes proposed are as follows:

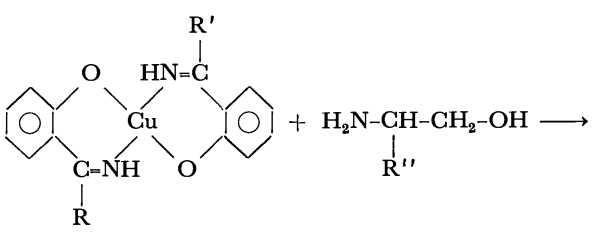

TABLE 1. ANALYTICAL DATA

Sample	Complex	Metal %		C and H %		N%		λ_{max} (nm)	μ_{eff} (B.M)
		Calcd	Found	Calcd	Found	Calcd	Found		
(A)	[*N*-(Hydroxyethyl)salicylideneaminato]Cu(II)H_2O	25.98	25.58	39.25 4.49	39.15 4.25	5.72	5.85	610	1.50
(B)	[*N*-(2-Hydroxyethyl)-2-hydroxy-1-naphthylmethyleneaminato]Cu(II)H_2O	21.57	21.25	—	—	4.75	4.85	630	1.72
(C)	[*N*-(2-Hydroxyethyl)-1-(*o*-hydroxyphenyl)ethylideneaminato]Cu(II)H_2O	24.54	24.62	41.77 5.02	41.52 4.92	5.41	5.54	600	2.01
(D)	[*N*-(2-Hydroxyethyl)-α-(*o*-hydroxyphenyl)benzylideneaminato]Cu(II)H_2O	19.82	19.69	56.16 4.68	55.82 4.48	4.37	4.40	620	1.97
(E)	[*N*-(2-Hydroxy-1-methylethyl)salicylideneaminato]Cu(II)H_2O	24.58	24.21	—	—	5.41	5.81	610	1.44
(F)	[*N*-(2-Hydroxy-1-methylethyl)-2-hydroxy-1-naphthylmethyleneaminato]Cu(II)H_2O	19.88	19.50	—	—	4.38	4.52	620	1.75
(G)	[*N*-(2-Hydroxy-1-methylethyl)-1-(*o*-hydroxyphenyl)-ethylideneaminato]Cu(II)H_2O	23.22	23.00	—	—	5.11	5.24	610	1.95
(H)	[*N*-(2-Hydroxy-1-methylethyl)-α-(hydroxyphenyl)benzylideneaminato]Cu(II)H_2O	18.99	18.75	—	—	4.18	3.85	620	1.90
(A′)	[*N*-(2-Hydroxyethyl)-2-hydroxy-1-naphthylmethyleneaminato]Cu(II)H_2O	21.57	21.32	—	—	4.75	5.41	620	1.78
(B′)	[*N*-(2-Hydroxyethyl)salicylideneaminato]Cu(II)H_2O	25.98	25.70	—	—	5.72	5.30	600	1.52
(C′)	[*N*-(2-Hydroxyethyl)-α-(*o*-hydroxyphenyl)benzylideneaminato]Cu(II)H_2O	19.82	19.58	—	—	4.37	4.50	620	1.96
(D′)	[*N*-(2-hydroxy-1-methylethyl)-2-hydroxy-1-naphthylmethyleneaminato]Cu(II)H_2O	19.88	19.60	—	—	4.38	4.80	620	1.74
(E′)	[*N*-(2-hydroxy-1-methylethyl)salicylideneaminato]Cu(II)H_2O	24.58	24.56	—	—	5.39	5.50	610	1.50

TABLE 2. IR SPECTRAL DATA

	Complex	C=N stretch (cm^{-1})	O-H stretch (cm^{-1})	O-H deformation mode (cm^{-1})
(A)	[*N*-(2-Hydroxyethyl)salicylideneaminato]Cu(II)H_2O	1600	3350	900
(B)	[*N*-(2-Hydroxyethyl)-2-hydroxy-1-naphthyl-methyleneaminato]Cu(II)H_2O	1600	3400	880
(C)	[*N*-(2-Hydroxyethyl)-1-(*o*-hydroxyphenyl)-ethylideneaminato]Cu(II)H_2O	1600	3300	890
(D)	[*N*-(2-Hydroxyethyl)-α-(*o*-hydroxyphenyl)-benzylideneaminato]Cu(II)H_2O	1600	3400	900
(E)	[*N*-(2-Hydroxy-1-methylethyl)salicylideneaminato]Cu(II)H_2O	1600	3400	910
(F)	[*N*-(2-Hydroxy-1-methylethyl)-2-hydroxy-1-naphthylmethyleneaminato]Cu(II)H_2O	1590	3400	880
(G)	[*N*-(2-Hydroxy-1-methylethyl)-1-(*o*-hydroxyphenyl)-ethylideneaminato]Cu(II)H_2O	1600	3400	900
(H)	[*N*-(2-Hydroxy-1-methylethyl)-α-(*o*-hydroxyphenyl)-benzylideneaminato]Cu(II)H_2O	1590	3400	880

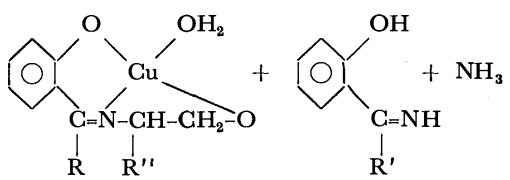

R=R′=H, CH_3, or C_6H_5
R″=H or CH_3

Thus it is observed that the aminoalkanols replace ammonia from of the Schiff base molecule, and the resulting tridentate Schiff base occupies three positions around the metal ion, the other Schiff base molecule being removed. The fourth position may be occupied by a water molecule.

The reaction can be explained by analogy with the Schiff base copper(II) complex of *N*,*N*-diethylethylene-

diamine.[8] It can be considered that the OH of the aminoalkanol liberates on coordination the H^+ ion which attacks the phenolic-O of the other Schiff base molecule reforming OH, and that a Schiff base molecule is detached.

The reactions of 2-aminoethanol with the mixed complexes (a'), (b'), and (c') gave the products (A'), (B'), and (C'), respectively, salicylideneamine or 1-(*o*-hydroxyphenyl)ethylideneamine being removed. Similar reactions take place with 1-amino-2-propanol. Reactions of 1-amino-2-propanol with (c') gave no definite compound. The reactions can be shown by the same scheme as above where R is H and R' is CH_3.

Thus it is observed that for the mixed ligand complexes also aminoalkanol replaces ammonia from one of the ligands forming a tridentate Schiff base and another ligand molecule is removed.

The above reaction is a confirmation of the fact that the mixed Schiff base complex (CuLL') is really a mixed ligand complex. If it were a mixture of the two bis-compounds, CuL_2 and CuL_2', a mixture of complexes of tridentate Schiff base from both the ligands (L and L') would have been obtained. In the cases of reactions of mea and ipa on mixed Schiff base complexes, it is also interesting to observe which ligand forms the tridentate Schiff base, and which one is displaced. For the copper(II) complexes (b'), salicylaldehyde is retained, and 1-(*o*-hydroxyphenyl)ethylideneamine is removed. This shows that salicylaldehyde has a stronger tendency to form the Schiff base. For the complex (c'), 2-hydroxybenzophenone is retained, and salicylideneamine is removed. It is indicated that 2-hydroxybenzophenone has a stronger tendency to form the Schiff base than salicylaldehyde. Thus the order found is as follows:

2-hydroxybenzophenone>salicylaldehyde>
2-hydroxyacetophenone.

Similarly with complex (a'), 2-hydroxy-1-naphthaldehyde is retained, salicylideneamine being removed. For the complex (d'), no definite compound was obtained on reaction with 2-aminoethanol. The composition of the compound obtained is very close to the complex in which both 2-hydroxy-1-naphthaldehyde and 2-hydroxybenzophenone form Schiff bases and remain with copper(II). This shows that 2-hydroxy-1-naphthaldehyde and hydroxybenzophenone have similar tendencies to form a Schiff base. Thus the order of forming Schiff base is 2-hydroxybenzophenone ≈2-hydroxy-1-naphthaldehyde>salicylaldehyde> 2-hydroxyacetophenone

This is expected from theoretical considerations also. Schiff base formation or amine exchange is due to the nucleophilic attack of an amine on the positively charged carbonyl carbon atom.[17] Attachment of a methyl group with the +I effect lowers the positive charge on the carbon atom, reducing the nucleophilic attack. Thus 2-hydroxyacetophenone is less susceptible to Schiff base formation. The attachment of a phenyl group with the −I effect to C=O group increases the possibility of the nucleophilic attack of 2-hydroxybenzophenone. Similarly the naphthalene ring in 2-hydroxy-1-naphthaldehyde makes the carbonyl carbon atom more positive.

Above reactions with mixed and non-mixed Schiff base complexes show that copper(II) prefers to form a 1 : 1 complex with the tridentate Schiff base. All the copper(II) complexes formed are paramagnetic, corresponding to the nearly spin-only value of one unpaired electron. This shows that a water molecule is in the coordination sphere, and it is a monomeric complex. In some copper(II) complexes the magnetic moment is slightly lower than the spin-only value of one unpaired electron. This may be due to the fact that the complexes are anhydrous and dimeric, leading to the Cu–Cu interaction and the lowering of paramagnetism.[18] The electronic spectra of all the copper (II) complexes are similar and show a peak at ≈620 nm expected for the $Cu(N)(O)_3$ type complexes[19]. This broad band is a combination of three bands corresponding to

$$^2B_{1g} \longrightarrow 2A_{1g},\ ^2B_{1g} \longrightarrow {}^2B_{2g} \text{ and } {}^2B_{1g} \longrightarrow {}^2E_g \text{ transitions.}^{20}$$

The IR spectra of copper(II) complexes exhibit a broad band at 3400 cm^{-1} showing the presence of water. Since there is a band at 900 cm^{-1} corresponding to the O–H out-of-plane deformation mode, this suggests the coordinated water molecule[21]. The absence of the N–H stretching frequency at about 3300 cm^{-1} is also in keeping with the structure of the complexes.

Authors' thanks are due to Prof. S. M. Sethna, former Head, Department of Chemistry, for providing all the laboratory facilities. Two of the authors (V.B.M) and (R.K.K) are also grateful to M. S. University, Baroda, and U.G.C. New-Delhi for providing fellowships.

References

1) R. H. Holm, "Inorganic Biochemistry," Vol. 2, p. 1137.
2) T. Ueki, T. Ashida, Y. Sasada, and M. Kakudo, *Acta Crystallogr.*, **22**, 870, (1967).
3) M. Kubo, Y. Kuroda, M. Kishita, and Y. Muto, *Aust. J. Chem.*, **16**, 7, (1963).
4) G. L. Eichhorn and N. D. Marchand, *J. Am. Chem. Soc.*, **78**, 2688, (1956).
5) A. Nakahara, *Bull. Chem. Soc. Jpn.*, **32**, 1195 (1959).
6) Y. Nakao, K. Sakurai, and A. Nakahara, *Bull. Chem. Soc. Jpn.*, **40**, 1536 (1967).
7) S. Yamada, Y. Kuge, and K. Yamanouchi, *Bull. Chem. Soc. Jpn.*, **40**, 1864 (1967).
8) R. H. Balundgi and A. Chakravorty, *Inorg. Chem.*, **12**, 981, (1973).
9) D. H. Martin, *Adv. Chem. Ser.*, **37**, 192 (1963).
10) B. T. Thaker and P. K. Bhattacharya, *J. Inorg. Nucl. Chem.*, **37**, 615 (1975).
11) V. B. Mohankumar and P. K. Bhattacharya, Accepted in *Indian J. Chem.*
12) R. K. Kohli and P. K. Bhattacharya, *Bull. Chem. Soc. Jpn.*, **49**, 2872 (1976).
13) P. Pfeiffer, E. Buchholz, and O. Baueve, *J. Prakt. Chem.*, **129**, 163 (1931).
14) P. Pfeiffer and H. Glaser, *J. Prakt. Chem.*, **153**, 265 (1939).
15) B. T. Thaker and P. K. Bhattacharya, *J. Indian Chem. Soc.*, **52**, 454 (1975).

16) V. B. Mohankumar and P. K. Bhattacharya, *Indian J. Chem.*, **13**, 928 (1975).
17) W. P. Jencks, *Prog. Phys. Org. Chem.*, **2**, 63 (1964).
18) M. Kishita, A. Nakahara, and M. Kubo, *Aust. J. Chem.*, **17**, 810 (1964).
19) R. H. Balundgi and A. Chakravorty, *Inorg. Chem.*, **12**, 981 (1973).
20) C. J. Ballhausen, "Introduction to Ligand Field Theory," McGraw Hill, New York (1962), p. 268.
21) K. Nakamoto, "Infrared Spectra of Inorganic and Coordination Compounds," Wiley & Sons, Inc., New York (1962), p. 156.

Lead(II) Butanedioate–Pentanedioate Mixed Complexes

S. C. BAGHEL, K. K. CHOUDHARY, and J. N. GAUR
Department of Chemistry, University of Rajasthan, Jaipur 302004, India
(Received June 21, 1976)

Butanedioate and pentanedioate form 1 : 3 highest complexes separately with lead(II) in aqueous medium, three mixed complexes of these two ligands with the metal ion expected in solution being observed. The formation constants of mixed complexes have been evaluated on the basis of polarographic measurements by the method of Schaap and McMasters. The formation constants of the mixed complexes $[Pb(X)(Y)]^{2-}$, $[Pb(X)(Y)_2]^{4-}$, and $[Pb(X)_2(Y)]^{4-}$ are 3.57, 4.22, and 4.49 respectively in their logarithmic form at 303 K, where X^{2-} and Y^{2-} stand for butanedioate and pentanedioate ion, respectively. The statistically calculated values of logarithm of formation constants are 3.43, 4.43, and 4.49 in the above order. The small differences in the observed and calculated values may be due to electrostatic, steric *etc.* factors. The relative probability of the existence of these mixed complexes and also simple complexes has been explained.

When two or more complexing species are added to a solution containing a metal ion, it has been observed that metal ion forms complex with all the ligand molecules simultaneously. The complexes so formed in the solution are called mixed complexes. Such species have been found as components in natural waters and biological fluids.

Many workers have reported the existence of mixed complexes.[1-4] Polarographic measurements have also shown the formation of mixed complexes in solution.[5-8]

Discussion of the Schaap and McMasters method has been given in detail in our previous publication.[5]

Experimental

All the chemicals used were of reagent grade purity. The sodium salts of butanedioic and pentanedioic acids were used as complexing species at pH 6.8±0.1. The capillary of DME had the following characteristics, $m=2.14$ mg s^{-1} and $t=4.65$ s, where m is the mass of mercury in milligram falling from capillary per second and t is the drop life in seconds. Ionic base strength was kept constant at 2.0 mol dm^{-3} using KNO_3 as electrolyte. At 5×10^{-4} mol dm^{-3} metal ion concentration no maximum suppressor was required. Potentials were measured with reference to SCE. All solutions were prepared in twice distilled water. The temperature was maintained constant at 303±0.1 K using a U_3 Ger. Nr. 8954 type thermostat.

Results

Polarographic Behavior. *Simple Systems*: In each case a single well defined reversible and diffusion controlled reduction wave was obtained. Reversibility and the diffusion controlled nature of reduction were revealed from the slope (31±1) mV of the E_{de} *vs.* $\log(i/(i_d-i))$ plots and the i *vs.* $h^{1/2}$ straight line plots, respectively, where E_{de} is applied potential, i_d is diffusion current, i is current at any potential and h, is effective height of mercury head of DME. The method of DeFord and Hume[10] was used to calculate the overall formation constants (β's) of complexes formed by butanedioate and pentanedioate ions individually with lead(II). The results are as follows:

Equilibria with Butanedioate:

$[Pb(H_2O)_6]^{2+} + X^{2-} \rightleftharpoons [Pb(H_2O)_4X]$; β_{10} (230)

$[Pb(H_2O)_6]^{2+} + 2X^{2-} \rightleftharpoons [Pb(H_2O)_2(X)_2]^{2-}$; β_{20} (3250)

$[Pb(H_2O)_6]^{2+} + 3X^{2-} \rightleftharpoons [Pb(X)_3]^{4-}$; β_{30} (11700)

Equilibria with Pentanedioate:

$[Pb(H_2O)_6]^{2+} + Y^{2-} \rightleftharpoons [Pb(H_2O)_4Y]$; β_{01} (200)

$[Pb(H_2O)_6]^{2+} + 2Y^{2-} \rightleftharpoons [Pb(H_2O)_2(Y)_2]^{2-}$; β_{02} (2950)

$[Pb(H_2O)_6]^{2+} + 3Y^{2-} \rightleftharpoons [Pb(Y)_3]^{4-}$; β_{03} (7850)

where the numerals in parentheses are the overall formation constant at 303 K.

Mixed Systems: The lead(II) butanedioate–pentanedioate mixed complexes were found to reduce reversibly at DME with the involvement of two electrons. The ions reaching the electrode were solely due to diffusion. The above conclusions were drawn from the slopes of the log plots (30—32) mV and the constancy of the ratio of diffusion current and square root of the effective height of mercury column.

In the first set of observations the fixed concentration of pentanedioate ion was 0.075 mol dm^{-3} in all the solutions. The varying quantities of butanedioate were added to the solutions. A cathodic shift in the half wave potential was observed as a function of butanedioate concentration. The shift was greater in the presence of pentanedioate than the one obtained for the simple lead(II) butanedioate system. This indicates the mixed ligand complex formation of butanedioate and pentanedioate with lead(II). In the second set of observations the pentanedioate ion concentration was fixed at 0.2 mol dm^{-3}.

The Schaap and McMasters functions F_{10} given in the theory were computed. The graphical extrapolation of the plots of F_{10} *vs.* C_X gave the values of A, B, C, and D; A, B, C, and D are constants and are the intercepts of the plots of F_{00}, F_{10}, F_{20}, and F_{30} *vs.* C_X on the F_{10} axis, respectively. C_X is the butanedioate concentration which is varied. The functions F_{10} and the constants A, B, C, and D have been defined in our previous publication.[5] The values of A, B, C, and D for the two fixed concentrations of pentanedioate are recorded below:

[Pentanedioate] in mol dm^{-3}	Temperature 303 K			
	A	B	C	D_{av}
0.075	35	600	5550	12200
0.20	200	1850	9400	14100

The values of β_{11} and β_{12} were calculated using values of B at two fixed concentrations of pentanedioate by means of the equation

$$B = \beta_{10} + \beta_{11}[Y] + \beta_{12}[Y]^2,$$

Table 1. Polarographic measurements and F_{10} function values of lead(II) butanedioate-pentanedioate system at 303 K[a)]

C_X[b)]	$-E_{1/2}$[c)] (V *vs.* SCE)	i_d[d)] (Divs.)	F_{00}	F_{10}	F_{20}	F_{30}
0.025	0.4215	51.0	53.70	748.0	5920	14800
0.05	0.4265	50.5	80.23	904.6	6092	10840
0.10	0.4355	50.0	161.60	1266.0	6660	11100
0.15	0.4425	48.0	288.00	1686.6	7244	11293
0.20	0.4490	47.5	479.30	2221.5	8107	12787
0.30	0.4585	45.5	1037.00	3340.0	9133	11944
0.40	0.4665	44.0	1983.00	4870.0	10675	12812

$m=2.14$ mg s^{-1}, $t=4.6$ s, and $\mu=2.0$ mol dm^{-3}.
μ is ionic strength of the electrolyte solution.
a) Concentration of Pentanedioate = 0.075 mol dm^{-3} (fixed). b) C_X=Butanedioate concentration in mol dm^{-3}. c) $-E_{1/2}$ of simple metal ion=0.3695 volts. d) i_d of simple metal ion=51 Divisions.

Table 2. Polarographic measurements and F_{10} eunction values of lead(II) butanedioate-pentanedioate system at 303 K[a)]

C_X[b)]	$-E_{1/2}$[c)] (V *vs.* SCE)	i_d[d)] (Divs.)	F_{00}	F_{10}	F_{20}	F_{30}
0.025	0.4400	50.0	228.3	1132	9280	—
0.05	0.4420	49.5	268.7	1374	9480	—
0.10	0.4495	48.0	494.0	2940	10900	15000
0.15	0.4545	47.0	739.1	3594	11626	14840
0.20	0.4590	47.0	1044.0	4220	11850	12250
0.25	0.4635	46.5	1189.0	5156	13224	15296
0.30	0.4670	46.0	1970.0	5900	13500	13666
0.40	0.4735	45.0	3318.0	7795	14862	13656

a) Concentration of Pentanedioate = 0.20 mol dm^{-3} (fixed). b), c), d) See footnotes b), c), d) of Table 1.

from which we get β_{11} and β_{12} to be 3.57 and 4.22, respectively, in their logarithmic form. The β's are overall formation constants of the corresponding simple and mixed complexes.

The two values of C gave two values of log β_{21}, both of which are 4.49. The relation between β_{21} and C is given by

$$C = \beta_{20} + \beta_{21}[Y].$$

The polarographic measurements and the values of F_{10} functions values are given in Tables 1 and 2 at pentanedioate concentrations 0.075 and 0.20 mol dm^{-3}, respectively.

Discussion

The structures of butanedioate and pentanedioate are as follows:

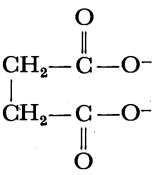

Butanedioate

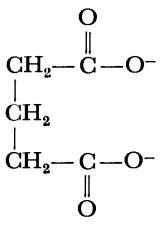

Pentanedioate

As is evident from their structures the butanedioate complexes are more stable than the pentanedioate complexes (see results of the simple complexes). The highest complex formed with lead(II) is 1 : 3 with each ligand which shows the formation of three mixed complexes, *viz.* $[Pb(X)(Y)]^{2-}$, $[Pb(X)_2(Y)]^{4-}$, and $[Pb(X)(Y)_2]^{4-}$, where X^{2-} and Y^{2-} stand for butanedioate and pentanedioate ion, respectively. The schematic representation of all the complexes (simple as well as mixed) present in the system and the equlibria between them are:

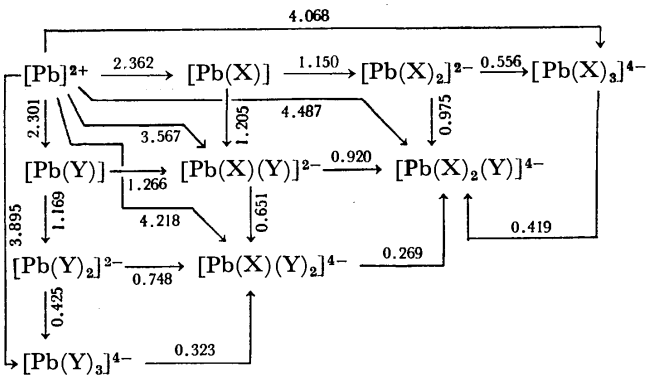

The numerical values in the scheme above are log K values for the step indicated where K is the equilibrium constant for that step.

Statistical calculations[9)] suggest that

$$\beta_{11} = 2.\ 3.\ \beta_{30}^{1/3}.\ \beta_{03}^{1/3},$$
$$\beta_{12} = 3.\ \beta_{30}^{1/3}.\ \beta_{03}^{2/3},$$
and $$\beta_{21} = 3.\ \beta_{30}^{2/3}.\ \beta_{03}^{1/3}.$$

The statistically calculated values of log β_{11}, log β_{12} and log β_{21} are 3.43, 4.43, and 4.49, respectively. The observed and calculated values of log β_{21} agree well, while those of log β_{11} and log β_{12} slightly differ. The deviations in the values of β_{11} and β_{12} may be due to steric or electrostatic factors and also to different approaches for getting these values. From the theory it is seen that log D equals log β_{30} as was observed in our results.

we can compare the tendency of various unsaturated complex species to add another ligand with that of saturated complex species to substitute another ligand. The complexes [Pb(X)] and [Pb(Y)] have a tendency to add Y^{2-} and X^{2-}, respectively. The equilibrium constants in the logarithmic form for these addition reactions are 1.205 and 1.266, respectively. These values show greater probability of the formation of the mixed complex $[Pb(X)(Y)]^{2-}$ from [Pb(Y)] than from [Pb(X)] and hence a slightly greater complexing tendency of X^{2-} than of Y^{2-}. The tendency of [Pb(X)] to add X^{2-} and Y^{2-} shows that there is a greater probability of a mixed ligand complex formation than a

simple complex formation. The same is also concluded from the relative tendency of $[Pb(Y)]$ to add X^{2-} and Y^{2-}. The equilibrium constants for all the above addition reactions are nearly equal, showing a nearly equal complexing tendency of the two ligands, as seen from their nearly equal size.

The tendency of $[Pb(X)_2]^{2-}$ to add X^{2-} and Y^{2-} favor the formation of mixed complexes. Similarly X^{2-} is more easily added to $[Pb(Y_2)]^{2-}$ than Y^{2-}. It is also seen that $[Pb(X)_3]^{4-}$ has a tendency to substitute Y^{2-} and $[Pb(Y)_3]^{4-}$ to substitute X^{2-}. These substitution reactions prove that formation of mixed complexes is favored.

The unsaturated mixed complex $[Pb(X)(Y)]^{2-}$ has a greater tendency to add X^{2-} than Y^{2-}, which shows that the approach of Y^{2-} to $[Pb(X)(Y)]^{2-}$ is hindered to a greater extent. The saturated mixed complex $[Pb(X)(Y)_2]^{4-}$ can substitute X^{2-} but not Y^{2-}. The saturated mixed complex $[Pb(X)_2(Y)]^{4-}$ can substitute neither X^{2-} nor Y^{2-}.

References

1) W. B. Schaap and D. L. McMasters, *J. Am. Chem. Soc.*, **83**, 4699 (1961).
2) S. C. Shrivastava and L. Newmann, *Inorg. Chem.*, **11**, 2855 (1972).
3) L. Newmann and D. N. Hume, *J. Am. Chem. Soc.*, **79**, 457, 4581 (1957).
4) J. I. Watters and J. Mason, *J. Am. Chem. Soc.*, **78**, 285 (1956).
5) S. C. Baghel, K. K. Choudhary, and J. N. Gaur, *J. Inorg. Nucl. Chem.*, **37**, 2513 (1975).
6) S. C. Khurana and C. M. Gupta, *Talanta*, **19**, 1235 (1972).
7) S. C. Baghel and J. N. Gaur, Proc. 14th Seminar on electrochemistry, Karaikudi (India).
8) S. C. Khurana and C. M. Gupta, *J. Inorg. Nucl. Chem.*, **35**, 209 (1973).
9) J. I. Watters and R. Dewitt, *J. Am. Chem. Soc.*, **82**, 1333 (1960).
10) D. D. DeFord and D. N. Hume, *J. Am. Chem. Soc.*, **73**, 5321 (1951).

Metal Complexes of Sulfur–Nitrogen Chelating Agents. IV. Complexes of Ni(II), Pd(II), Pt(II), and Rh(III) with Methyl Ester of 2-Amino-1-cyclopentene-1-carbodithioic Acid

D. S. JOARDAR, S. K. MONDAL, and K. NAG*

Department of Inorganic Chemistry, Indian Association for the Cultivation of Science, Calcutta 700032, India

(Received August 23, 1976)

The methyl ester of 2-amino-1-cyclopentene-1-carbodithioic acid (HE) acts both as an unidentate and a bidentate ligand. With Ni(II) and Pd(II) the deprotonated chelates of the ME_2 type are obtained readily, the corresponding Pt(II) complex being obtained on the addition of an equivalent amount of alkali. In these compounds, bond formation takes place from the nitrogen and the sulfur atoms and there is strong delocalization in the chelate ring. Unidentate bonding behavior of the ligand is observed in the complexes $Pt(HE)_2Cl_2$ and $Rh(HE)_3Cl_3$, where the bonding takes place through the nitrogen atom only.

Coordination compounds with ligands showing linkage isomerism are a topic of interest. We have shown[1–4] that in the complexes of 2-amino-1-cyclopentene-1-carbodithioic acid (ACDA) and its *N*-ethyl derivative the metal-ligand bonding takes place either from the amino nitrogen and the deprotonated thiol sulfur or from the dithiocarboxylic moiety depending on the type of a metal ion. The methyl ester of ACDA

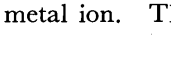

which contains the skeletal unit $H_2N–CH=CH–C(SCH_3)=S$ is also capable of forming linkage isomers with metal ions. There are several possibilities for the ligand to bind a metal ion, *e. g.* (i) through NH_2 and C=S, (ii) through NH_2 and the deprotonated thiol sulfur or through the deprotonated amino nitrogen and C=S, (iii) through NH_2 only, (iv) through C=S only, and (v) interaction of SCH_3 in combination with the other donor atoms.

We wish to report here the preparation and characterization of Ni(II), Pd(II), Pt(II), and Rh(III) complexes with the methyl ester of 2-amino-1-cyclopentene-1-carbodithioic acid (hereafter abbreviated as HE).

Experimental

The ligand was prepared by the method of Bordăs *et al.*[5] and recrystallized from (1 : 1) ethanol–water mixture (mp 75 °C, lit,[5] 77—79 °C). Satisfactory results in the elemental analysis of the compound were obtained (Table 1). Other chemicals used were of reagent grade.

Preparation of the Complexes. *NiE_2*: To an ethanolic solution of the ligand (4 mmol) was slowly added an ethanolic solution of hydrated nickel chloride (2 mmol) with stirring. The complex began to separate almost immediately, but to ensure the completion of reaction the mixture was stirred for 30 min. The olive green crystals were collected by filtration, washed with ethanol, and recrystallized from chloroform; yield 90%.

PdE_2: On slow addition of an ethanolic solution of the ligand (4 mmol) to an ethanolic solution of sodium tetrachloropalladate(II) (2 mmol), a brownish yellow compound was formed. This was filtered and washed first with ethanol and then with water till the filtrate showed negative test for chloride ion. The compound was recrystallized from chloroform; yield 80%.

$Pt(HE)_2Cl_2$: A mixture of potassium tetrachloroplatinite (II) (2 mmol) and HE (4 mmol) in acetone was stirred for 2 h. The brownish red product was filtered, washed with ethanol and warm water, and finally recrystallized from chloroform; yield 70%.

$PtE_2 \cdot H_2O$: To a solution of potassium tetrachloroplatinite (2 mmol) in acetone was added dropwise a mixture of 4 mmol of the ligand and 5 mmol of sodium hydroxide in ethanol. The brick red product was filtered and washed successively with petroleum ether, 1 : 1 aqueous ethanol, and warm water. The compound was recrystallized from chloroform; yield 70%.

$Rh(HE)_3Cl_3 \cdot 2H_2O$: A mixture of hydrated rhodium chloride (2 mmol) and the ligand (6.5 mmol) in acetone was stirred for 4 h. A brown compound precipitated slowly was collected on a glass frit, and washed with acetone and water. The compound was dried over fused calcium chloride but could not be recrystallized due to the lack of solvent; yield 50%.

Physical Measurements. Infrared spectra were recorded in nujol mulls on a Perkin-Elmer 457 spectrophotometer in the frequency range 4000—250 cm^{-1}. The NMR spectrum of the ligand in carbon tetrachloride was recorded on a Varian T 60 spectrometer using TMS as a reference. Electronic spectral measurements were made on a Hilger UV-spek spectrophotometer. Conductivity measurements were carried out using a Philips PR 9500 conductivity bridge. Magnetic measurements were performed on a Guoy balance. Thermal analysis was carried out in a Derivatograph (MOM). Molecular weight determination was made with a Mechrolab vapor phase osmometer.

Analyses. C and H were determined by micro combustion analysis, nitrogen by semimicro combustion analysis, and sulfur and metal ions as described earlier.[1]

Results and Discussion

The analytical data (Table 1) indicate that with HE two types of compounds are obtained, *viz.* (a) type ME_2(Ni, Pd, Pt) in which the ligand is in the deprotonated form, and (b) type $M(HE)_mX_n$(Pt, Rh) in which the ligand is in the uncharged form. With Ni(II) and Pd(II), compounds of the type $M(HE)_2Cl_2$ could not be prepared; NiE_2 is formed even in slightly acidic solution (pH≈2). Of the compounds, NiE_2 is soluble in chloroform, acetone, and DMF; PdE_2 in chloroform, nitrobenzene, and DMSO, $PtE_2 \cdot H_2O$ in chloroform and DMF, $Pt(HE)_2Cl_2$ in acetone, chloroform, and nitrobenzene, and $Rh(HE)_3Cl_3 \cdot 2H_2O$ in DMF. The diamagnetic nature of the compounds under investigation indicates the square planar configuration of Ni(II), Pd(II), and Pt(II) complexes and the octahedral configuration of the Rh(III) complex. Both $Pt(HE)_2Cl_2$ and $Rh(HE)_3Cl_3$ act as non-electrolytes (in nitro-

* Responsible coauthor.

TABLE 1. ANALYTICAL DATA

Compound	Decomposes at °C	%C		%H		%Cl		%M		%N		%S	
		Calcd	Found	Calcd	Found	Calcd	Found	Calcd	Found	Calcd	Found	Calcd	Found
$C_7H_{11}NS_2$	75	48.56	48.48	6.36	6.28					8.09	8.20	37.00	36.81
$C_{14}H_{20}N_2S_4Ni$	250							14.58	14.61	7.01	6.94	31.71	31.65
$C_{14}H_{20}N_2S_4Pd$	240							23.62	23.54	6.22	6.30	28.42	28.31
$C_{14}H_{22}ON_2S_4Pt$	220	30.16	30.32	3.95	4.05					5.02	5.10		
$C_{14}H_{22}N_2S_4Cl_2Pt$	200	27.45	27.60	3.59	3.65	11.58	11.40			4.57	4.61		
$C_{21}H_{37}O_2N_3S_6Cl_3Rh$	250	32.97	33.12	4.32	4.45	13.67	13.51			5.50	5.43		

TABLE 2. SOME STRUCTURALLY IMPORTANT INFRARED BANDS IN THE DEPROTONATED CHELATES OF HE

HE	NiE_2	PdE_2	$PtE_2 \cdot H_2O$	Assignments
3240 (b, w)	3260 (m)	3255 (w)	3280 (b, w)	ν(N-H)
1595 (s)	1580 (s)	1585 (s)	1585 (m)	δ(N-H) + ν(C=C)
1410 (w)	1420 (m)	1420 (m)	1410 (w)	ν(C=C) + ν(C=N)
1305 (w)	1305 (w)	1310 (w)	1310 (w)	ν(S-CH_3)
1260 (w, b)	1290 (w) 1255 (m) 1225 (w)	1290 (w) 1245 (b)	1290 (w) 1245 (w) 1215 (w)	ν(C=N) + ν(C=S)
1155 (w, b)	1130 (w)	1140 (w)	1130 (w)	ν(C=S) + ν(C=N)
970 (m)	980 (m) 965 (m)	975 (w) 960 (w)	980 (w)	CH_2 rocking
905 (m)	910 (s) 860 (w)	900 (s) 840 (w)	915 (s) 860 (w)	assym($CSSCH_3$)
610 (m)	630 (w)	630 (w)	630 (w)	sym($CSSCH_3$) or ν(C-S)
—	490 (w)	520 (m) 490 (w)	500 (w)	ν(M-N)
—	380 (m)	350 (m)	355 (w)	ν(M-S)

benzene) which indicate the unidentate behavior of the ligand in these compounds.

In order to confirm the coordination sites involved in bond formation, the structure of the ligand itself requires prior consideration. The PMR spectrum of the ligand has the following characteristics: 4-CH_2 (δ 1.78 ppm; quintet), SCH_3 (δ 2.50 ppm; singlet), 3,5-CH_2 (δ 2.33—2.93; multiplet), NH (δ 5.66 ppm; broad, slowly exchanged with D_2O). The above assignments are compatible with structures I and II, excluding other structures which could be envisaged. The hydrogen bonded structures are also supported by the IR spectra of the ligand (in the solid state and in chloroform) which show the presence of a weak broad band due to ν(N-H) at 3240 cm^{-1}, and the absence of a band due to ν(S-H). It appears that both the tautomeric forms coexist in solution.

In the ME_2 type chelates bond formation may take place as in III or IV. If the bond type is III, bands due to C=C and C=S stretching should be expected in the IR spectra. In the bond type IV both ν(C=C) and ν(C=N) vibrations will be observed but no band due to ν(C=S). For substituted cyclopentenes ν(C=C) is observed in the range 1670—1620 cm^{-1}, and for non-conjugated systems ν(C=N) is usually observed in the range 1690—1640 cm^{-1}. For a series of esters of carbodithioic acid Bellamy and Rogasch[6] reported ν(C=S) in the range 1200—1170 cm^{-1}. Thus, a band around 1650 cm^{-1} is expected in both III and IV. However, if a delocalized chelate ring (V) results from the conjugation of 1,3-double bonds present in III and IV, bond orders of C=C, C=N, and C=S will decrease to a great extent. As a result, the stretching vibrations will be observed at lower frequencies. This was actually the case as shown in Table 2. It can be seen that the ν(N-H) band of the ligand at 3240 cm^{-1} remains almost in the same position as in the chelates. The lowering of ν(N-H) frequency in the ligand is shown to be due to hydrogen bonding and in the chelates the lowering of this band to a similar extent is also justified with the bond type (V). Two new bands appearing at 500 cm^{-1} and in the 380—350 cm^{-1} range are assigned to ν(M-N) and ν(M-S) respectively. In Table 2 assignments, based on observations made in several other related systems,[1-4,6-9] have been made to several other vibrations which are structurally important.

Bond formation may take place either as VI or VII in $Pt(HE)_2Cl_2$ and in $Rh(HE)_3Cl_3$ where the unidentate nature of the ligand has been indicated. If bond formation takes place through the thione sulfur atom, ν(N-H) should be expected to occur in the 3500—3300 cm^{-1} range (the usual range for primary amines), whereas bond formation through the amino nitrogen atom would result in its displacement to lower frequency. In the Pt(II) complex two weak bands appear at 3220 and 3150 cm^{-1}, and in the Rh(III) complex these two bands are observed at 3240 and 3140 cm^{-1}. The presence of two bands and their shift to lower frequency indicates bond formation through the nitrogen atom. The band due to (N-H) deformation ap-

pears as a shoulder in the Pt(II) complex and as a band of medium intensity in the Rh(III) complex at 1580 cm^{-1}. In these two compounds a new band observed at 1630 cm^{-1} is absent in the ligand as well as in the deprotonated chelates. On the basis of the preceding arguments we assign this band due to ν(C=C). Moreover, a band due to ν(C=S) as required in VI is observed in the expected range, *viz.* at 1200 cm^{-1} in the Pt(II) complex and at 1215 cm^{-1} in the Rh(III) complex. Although ν(M–N) appears in both compounds at 500 cm^{-1}, ν(M–Cl) which is usually observed at 350—300 cm^{-1} probably gets merged with the ligand band at 320 cm^{-1}. Except for these bands no other significant variation in the spectral features of these compounds from the deprotonated chelates could be observed.

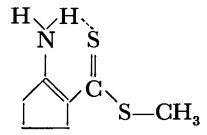

I

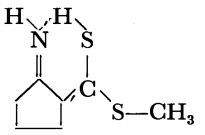

II

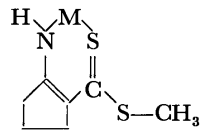

III

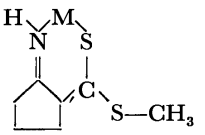

IV

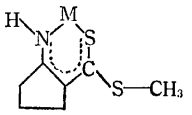

V

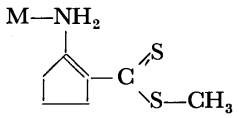

VI

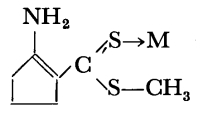

VII

The electronic spectra of the compounds proved to be less useful in confirming the bond types because of the presence of high intensity ligand bands in the UV region. In methanol, the ligand shows the presence of two bands at 25840 and 32050 cm^{-1} with the extinctions (log ε) 4.38 and 4.10, respectively (in chloroform these bands are shifted slightly to lower energy). The spectra of the complexes were measured in chloroform solution except for the Rh(III) compound for which a dimethylformamide solution was used. In the nickel complex the lowest energy band at 15870 cm^{-1} (log ε=1.98) is the ν_1 band ($^1A_{1g} \rightarrow {}^1A_{2g}$) of the square planar complexes. The next higher energy band observed at 22730 cm^{-1} (log ε=3.72) appears to be the ν_2 band ($^1A_{1g} \rightarrow {}^1B_{1g}$), but the high extinction indicates that it is mixed with the ligand band in this region. A third band at 33560 cm^{-1} (log ε=4.68) arises due to internal ligand transition. It is interesting to note that in complexes containing the chromophore [NiS_4], the ν_1 band is observed in the range 14500—16000 cm^{-1},[10] whereas for[NiN_2S_2] chromophore, it is usually observed at 18000 cm^{-1}.[11,12] The energy of the ν_1 band in our complex (15870 cm^{-1}) on this basis would indicate disulfur chelated species. However, molceular weight determination in chloroform established the monomeric nature of the complex and the infrared data showed that chelation takes place from the nitrogen and the sulfur atoms. There are increasing evidences[13,14] to show that in [NiN_2S_2] chromophores having strong delocalization in the chelate ring the energy range for the ν_1 band is 15500—16500 cm^{-1}.

No band due to d-d transition could be noted in the Pd(II), Pt(II), and Rh(III) complexes. This is not unexpected since the energy range at which such transitions occur is masked by the ligand band. The Pd(II) complex shows two bands at 24510 cm^{-1} (log ε=3.93) and 32680 cm^{-1} (log ε=4.38) due to the ligand, however a band at 41150 cm^{-1} (log ε=4.55) appears to be due to charge transfer transition. Similar is the case with $PtE_2 \cdot H_2O$ whose bands are located at 26320 cm^{-1} (log ε=3.87), 31250 cm^{-1} (log ε=4.25) and 41150 cm^{-1} (log ε=4.24). $Pt(HE)_2Cl_2$ shows only two bands at 30770 cm^{-1} (log ε=4.33) and 41490 cm^{-1} (log ε=4.34). In the Rh(III) complex also only the ligand bands at 25840 cm^{-1} (log ε=4.28) and 36360 cm^{-1} (log ε=4.59) are observed.

Thanks are due to Dr. T. Seshadri, Institut für anorganische Chemie, Technische Hochschule, Karlsruhe for some of the infrared spectra and to Prof. G. B. Singh of Beneras Hindu University, India for molecular weight measurement. One of us (DSJ) is indebted to CSIR, India, for awarding a PDF.

References

1) K. Nag and D. S. Joardar, *Inorg. Chim. Acta*, **14**, 133 (1975).
2) K. Nag and D. S. Joardar, *Z. Naturforsch.*, **30b**, 107 (1975).
3) K. Nag and D. S. Joardar, *Inorg. Chim. Acta*, **17**, 111 (1976).
4) K. Nag and D. S. Joardar, *Can. J. Chem.*, **54**, 2827 (1976).
5) B. Bordàs, P. Sohar, G. Matolosy, and P. Berencsi, *J. Org. Chem.*, **37**, 1727 (1972).
6) L. J. Bellamy and P. E. Rogasch, *J. Chem. Soc.*, **1960**, 2218.
7) M. F. Iskander and L. El-Sayed, *J. Inorg. Nucl. Chem.*, **33**, 4253 (1971).
8) M. Akbar Ali, S. E. Livingstone, and D. J. Phillips, *Inorg. Chim. Acta*, **5**, 119 (1971).
9) C. Battistoni, G. Matogno, A. Monaci, and F. Tarli, *J. Inorg. Nucl. Chem.*, **33**, 3915 (1971).
10) A. B. P. Lever, "Inorganic Electronic Spectroscopy," Elsevier, Amsterdam (1968), p. 344.
11) R. Gronback and S. E. Rasmunssen, *Acta Chem. Scand.*, **16**, 2325 (1962).
12) R. A. Haines and K. K. W. Sun, *Can. J. Chem.*, **46**, 3241 (1968).
13) P. R. Blum, R. M. C. Wei, and S. C. Cummings, *Inorg. Chem.*, **13**, 450 (1974).
14) S. K. Mondal, D. S. Joardar, and K. Nag, under publication.

The Correlation between Photo-electrochemical Cell Reactions and Photocatalytic Reactions on Illuminated Rutile

Mikio MIYAKE, Hiroshi YONEYAMA, and Hideo TAMURA

Department of Applied Chemistry, Faculty of Engineering, Osaka University, Yamadakami, Suita, Osaka 565

(Received October 29, 1976)

Photocatalytic reductions of MnO_4^-, $Cr_2O_7^{2-}$, and Fe^{3+} on illuminated rutile were demonstrated. The suitability of a method to analyze the reduction process of the photocatalytic reaction was discussed. It was concluded that a high utilization of light energy could not be expected for photocatalytic reactions because both bands of the semiconductor participated in the reaction. In such a case, the development of the photocatalytic process into a photoelectrochemical cell has a great advantage from the point of view of energy utilization.

Recently, electrochemical reactions on semiconductor electrodes have been investigated extensively.[1-3] The "Photo-sensitized electrolytic reaction" on an illuminated semiconductor electrode is one of the most interesting features of semiconductor electrochemistry.[4] Fujishima and Honda reported a photo-electrochemical cell with a decomposition of water,[5,6] and the cells of this type have been investigated intensively.[7-9] On the other hand, photocatalytic reactions on illuminated semiconductor catalysts seem to be another feature of the "photo-sensitized electrolytic reaction."[10,11] Some attempts have been made to analyze a photocatalytic reaction on an illuminated semiconductor catalyst by electrochemical methods.[11]

It has been reported that electrochemical measurements based on the local cell process are useful for analyses of the reaction rates and mechanisms of the reduction of Methylene Blue[12] and quinones[13] dissolved in methanol on illuminated rutile catalysts. The local cells of these reactions were found to be composed of the "photo-sensitized electrolytic oxidation" and the cathode process of a reaction which obeys usual thermodynamics.[10]

When the local cell is established on an illuminated semiconductor catalyst, a photo-electrochemical cell can be constructed in which the cell reaction is composed of the two individual reactions. This idea was successfuly demonstrated in a previous paper.[10]

It is well known that water is oxidized to oxygen on an illuminated rutile anode in the following way:[4-7]

$$2H_2O + 4p^+ \longrightarrow O_2 + 4H^+, \qquad (1)$$

where p^+ denotes a positive hole in the valence band of rutile. If one chooses an oxidizing agent whose redox-potential is more noble than the potential at which the oxidation of water commences on an illuminated rutile electrode, then one can easily construct a photo-electrochemical cell by using a rutile anode and a Pt cathode. The performance of the cell will be different depending on the redox-potentials of the oxidizing agents chosen so long as the anode process is not heavily disturbed by the existence of the oxidizing agent, which may cause a partial cathodic current.

If the Pt cathode is taken out from the cell, and the rutile electrode is illuminated at the open-circuit condition, then a local cell must be established on the illuminated rutile surface with the same reaction as that in the photo-electrochemical cell. The reaction in this case may be termed a photocatalytic reaction, as in the cases of the reduction of Methylene Blue[12] and quinones[13] on illuminated rutile in methanol solutions. It is quite natural to expect, however, that the reaction behavior will be different between the photo-electrochemical cell and the photocatalytic process.

The purpose of this paper is to present the difference in the behavior between the two kind of reactions by using several kinds of oxidizing agents.

Experimental

A commercial single crystal of rutile ($1 \times 1 \times 0.2$ cm) was used as the electrode material. It was reduced in an argon atmosphere at 800 °C for 2 h. Before being mounted in a glass tube with epoxy resin, the rutile was etched in a concd H_2SO_4 solution containing the same weight of $(NH_4)_2SO_4$ at 240 °C for 0.5 h. The (100) face was chosen as the electrode surface. Its carrier concentration (N_D), as estimated from Mott-Shottky plots in the dark, was about $10^{19}/cm^3$. Before measurements, the rutile electrode was dipped in a concd HNO_3 solution for 2 min, washed with de-ionized water for about 0.5 h, and then dried by hot air. A Pt electrode (1×1 cm) as the cathode of a photo-electrochemical cell and rutile powder as the catalyst were prepared in a manner described previously.[13]

The solution used in this study was 0.5 mol dm^{-3} H_2SO_4 containing an oxidizing agent. The oixdizing agents chosen were $KMnO_4$, $K_2Cr_2O_7$, and $Fe_2(SO_4)_3$. The water used as the solvent was distilled twice, and the H_2SO_4 solution was pre-electrolyzed for 48 h. All the chemicals were of a guaranteed reagent grade. Nitrogen gas was bubbled into the solution during all the electrochemical and chemical experiments.

A 500 W ultra-high pressure Hg arc lamp (Ushio Electric, Inc.; model UI-501) was used as the light source. The light of wavelengths shorter than 350 nm was cut off by setting a convex glass lens in front of the quartz window of the measurement cell. In the case of the experiment using the $KMnO_4$ solution, a $CoSO_4$-solution filter was set in front of the cell to prevent the photo-excitation of MnO_4^-.[14]

Polarization curves were obtained in a steady-state condition by means of a potentiostat (Hokuto Denko Co.; model ps-500B). The potentials were measured against the SCE. The concentration of chemical species in the solution was determined by means of absorptiometry. A Hitachi 124 spectrophotometer was used for this purpose.

The other details such as the purification of the gas, the construction of the measurement cell, and the procedure for the chemical analysis, have been described before.[13]

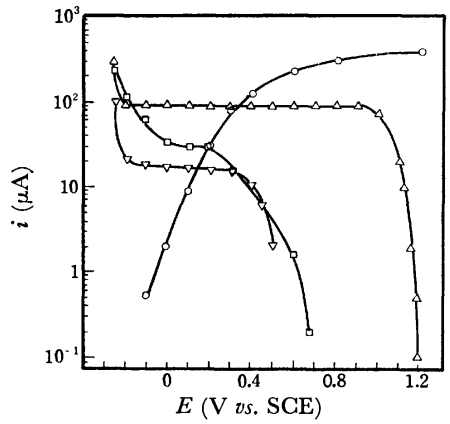

Fig. 1. Polarization curves of the illuminated rutile and the Pt electrodes in 0.5 mol dm^{-3} H_2SO_4 solution with and without 5×10^{-4} mol dm^{-3} of the oxidizing agent. (○) Anodic curve at rutile without the oxidizing agent, and cathodic curves at Pt with (△) $KMnO_4$, (□) $K_2Cr_2O_7$, and (▽) $Fe_2(SO_4)_3$.

Results and Discussion

Photo-electrochemical Cells. Figure 1 shows the polarization curves of the photo-electrochemical cells of

rutile|0.5 mol dm^{-3} H_2SO_4|Ox, 0.5 mol dm^{-3} H_2SO_4|Pt,

where Ox denotes the oxidizing agent. This figure suggests that if the cell of

rutile|Ox, 0.5 mol dm^{-3} H_2SO_4|Pt

works ideally, the cell reaction is composed of the oxidation of water and the reduction of the oxidizing agent. The term "ideally" means that the partial cathodic reduction of Ox and the oxidation of the product formed at the Pt cathode are negligible at the rutile electrode. The establishment of this ideal condition was confirmed, at least in the cases of the reduction of MnO_4^- to MnO_2 and of $Cr_2O_7^{2-}$ to Cr^{3+}, by analyzing the concentration of the oxidizing agent in the cell as a function of the quantity of electricity drawn under short-circuited conditions.

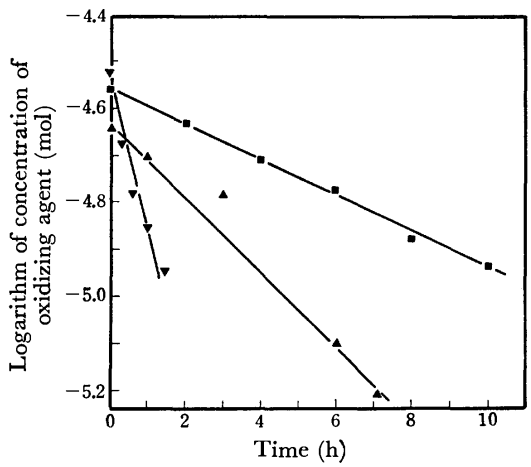

Fig. 2. Change of the concentration of oxidizing agents in 0.5 mol dm^{-3} H_2SO_4 with the reaction time on the illuminated rutile powder catalyst. The solutions containing (▼) Fe^{3+}, (■) $1/2Cr_2O_7^{2-}$, and (▲) MnO_4^-, respectively.

Chemical Analysis of Photocatalytic Reactions. When a rutile powder catalyst was suspended in a 0.5 mol dm^{-3} H_2SO_4 solution (50 cm^3) containing an oxidizing agent, the concentration of the oxidizing agent was decreased by illumination. The results are shown in Fig. 2.

The solutions retained their original absorbance when they were illuminated without the rutile catalyst for 20 h. By the reaction, the solution containing $KMnO_4$ produced a brown precipitate and the purple solution turned light yellow. The other solutions became transparent, and no deposit was detected on the catalyst. Accordingly, the cathode processes of the photocatalytic reactions are the reductions of MnO_4^-, $Cr_2O_7^{2-}$, and Fe^{3+} to MnO_2, Cr^{3+}, and Fe^{2+} respectively. On the other hand, the anodic process is the oxidation of water.[4-7] These results suggest that illuminated rutile worked effectively as a catalyst, causing the same reaction as in the photo-electrochemical cell.

The reaction in Fig. 2 seems to be first-order with respect to the oxidizing agent chosen, since linear relations were established between the logarithm of the concentration of the oxidizing agent and the reaction time. The rate constant calculated from the slopes of the lines are summarized in Table 1.

Table 1. Reaction rates determined by electrochemical analysis and reaction rate constants determined by chemical analysis

Solution	$K_2Cr_2O_7$	$KMnO_4$	$Fe_2(SO_4)_3$
Electrochemical analysis (μA)	0.26	0.73	2.2
Chemical analysis ($\times10^{-4}$, 1/s)	1.1	1.5	6.0

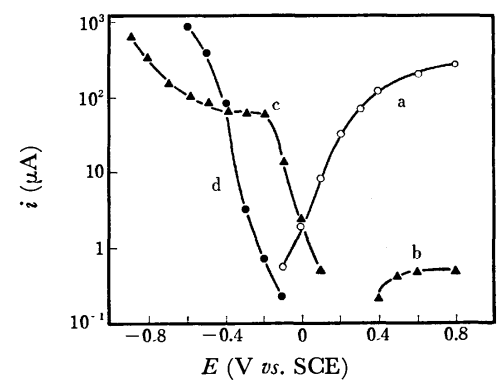

Fig. 3. Polarization curves of the rutile electrode in 0.5 mol dm^{-3} H_2SO_4 solution with and without 5×10^{-4} mol dm^{-3} $KMnO_4$. (a): Anodic curve without $KMnO_4$ under illumination, (b): anodic curve with $KMnO_4$ in the dark, (c): cathodic curve with $KMnO_4$ in the dark, (d): cathodic curve without $KMnO_4$ in the dark.

Electrochemical Analysis of Photocatalytic Reactions. Figure 3 shows the polarization curves of the rutile electrode in 0.5 mol dm^{-3} H_2SO_4 solutions with and without 5×10^{-4} mol dm^{-3} $KMnO_4$. The anodic curve (a), obtained under illumination in a solution without $KMnO_4$, is the same as the curve at the rutile anode in

Fig. 1, and indicates the anodic oxidation of water by positive holes.[4-7] This curve was little affected by the presence of $KMnO_4$ in the solution. On the other hand, it can be noticed, from a comparison of the two cathodic curves (c) and (d), that the cathodic current was distinctly increased by addition of $KMnO_4$ to the solution. This increase in the cathodic current may be ascribed to the participation of the reduction of $KMnO_4$ to MnO_2. The magnitude of the current in the presence of the oxidizing agent was by far larger than that in the absence of it. This means that the polarization curve of the oxidizing agent was eventually the same as curve (c). The stagnation of the cathodic current in curve (c) under a relatively high cathodic polarization is attributable to the deposition of MnO_2 onto the rutile surface. The cathodic process is based on the conduction-band electrons, since the cathodic current increased exponentially with an increase in the cathodic polarization.[1-3]

Similar results were obtained for the solutions with the other oxidizing agents. The reduction curves of these oxidizing agents are summarized in Fig. 4, together with the oxidation curve of water.

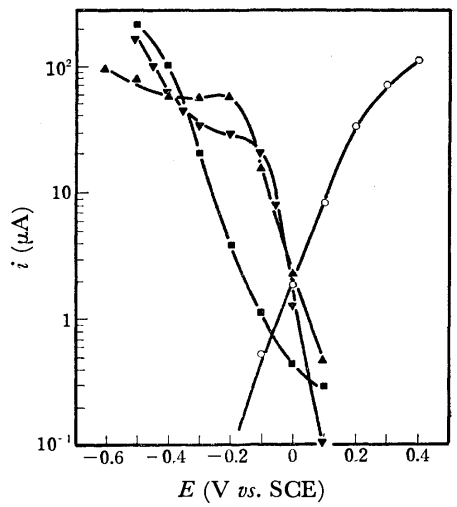

Fig. 4. Polarization curves of the rutile electrode in 0.5 mol dm^{-3} H_2SO_4 solution with and without the oxidizing agent. (○) Anodic curve without the oxidizing agent under illumination. Cathodic curves with 5×10^{-4} mol dm^{-3} (▲) $KMnO_4$, and 2.5×10^{-4} mol dm^{-3} (▼) $Fe_2(SO_4)_3$ and (■) $K_2Cr_2O_7$ in the dark.

When the cathodic polarization curves obtained in the dark are not changed by the illumination, the rate of the catalytic reaction on illuminated rutile can be estimated as the current value at the intersection point of the anodic and the cathodic curves in Fig. 4; this procedure is widely adopted in the estimation of the corrosion rates of metals.[15] The illumination has a negligible influence on the cathodic polarization curves when the electron concentration at the rutile surface is almost unchanged by the illumination. Therefore, it is necessary to discuss whether or not such a condition is fulfilled in the present study.

The electron concentration at equilibrium in the rutile electrode at room temperature (n_0) was about $10^{19}/cm^3$, as stated in the experimental section. The concentration of excited electrons by the illumination (n^*) is given as a function of the distance x from the illuminated surface by[16]

$$dn^*(x)/dt = \alpha f' \exp(-\alpha x) - di/dx - n^*(x)/\tau,$$
$$i = -Ddn^*(x)/dx \qquad (2)$$

where α, f', τ, and D denote the absorption coefficient of rutile, the numbers of incident photons per cm^2 per second on the crystal, the lifetime of the carrier in rutile, and the diffusion constant of the carrier in rutile respectively. In a steady state, Eq. 2 becomes

$$\alpha f' \exp(-\alpha x) + Dd^2n^*(x)/dx^2 - n^*(x)/\tau = 0 \qquad (3)$$

since $dn^*(x)/dt=0$.[16] By applying the conditions that $n^*(x)$ becomes 0 when x is infinitely large, and that carriers which diffuse to the surface can escape from the crystal to cause the current to flow, that is, $i=-D\{dn^*(x)/dx\}_{x\to0}=n^*(x\to0)$, Eq. 3 gives the following equation:

$$n^*(x) = \alpha f'\tau\{\exp(-\alpha x)\}/(1-D\tau\alpha^2) + K\exp\{-x/(D\tau)^{1/2}\}$$
$$K = \alpha f'\tau^{3/2}(D\alpha-1)/\{(D\alpha^2\tau-1)(D^{1/2}-\tau^{1/2})\} \qquad (4)$$

α is judged to be $10^3/cm$ for the light of 400 nm,[17,18] which gives the maximum photo-response at the rutile electrode.[19,20] τ has been reported to be 5×10^{-6} s and almost independent of the applied electric field and temperature.[21] If a value of 1 cm^2/V s is chosen as the electron mobility,[22,23] then we can obtain 3×10^{-2} cm^2/s for D from the well-known Einstein relation.[24]

The quantum yield of the "photo-sensitized electrolytic oxidation" of water is dependent on the wavelength and N_D, and is around 0.3 ± 0.2 in an rutile anode having 10^{19} carriers/cm^3 at 2 V *vs.* SCE for the light of 400 nm.[19] If it is assumed that the numbers of holes reached at the electrode surface per second are a 0.1 fraction of that of the incident photons, we can get a rough measure of f' from a knowledge of the saturated photo-current. We use here the smallest value of the quantum yield, 0.1, because we have to estimate the upper limit of n^*. In the present study, the saturated hole current at 2 V *vs.* SCE in a 0.5 mol dm^{-3} H_2SO_4 solution was 875 $\mu A/cm^2$. Accordingly, f' was estimated to be less than $10^{17}/cm^2$ s.

In order to get information on the concentration of photo-generated electrons at the surface, Eq. 4 was simplified with the condition of $x\to0$:

$$n^*(x\to0) = \alpha f'\tau/(1-D\tau\alpha^2) + K. \qquad (4')$$

By substituting the just-estimated values into Eq. 4', $n^*(x\to0)$ was determined to be smaller than $10^{15}/cm^3$.

Now it is possible to get information on the relative measure of the numbers of photo-generated electrons at the surface of rutile to those of electrons at equilibrium in the dark. The electron concentration at the surface of the electrode n_s in the dark is given by Eq. 5:[25]

$$n_s = n_o \exp\{-e(E-E_{fb})/kT\} \qquad (5)$$

where E and E_{fb} are the electrode potential and the flat-band potential of rutile respectively. The E_{fb} of rutile in a 0.5 mol dm^{-3} H_2SO_4 solution was reported to be −0.1 V *vs.* SCE.[26] A similar argument can also be applied to $n^*(x\to0)$ when the effect of the band

bending is taken into consideration for $n^*(x\rightarrow 0)$. Anyway, comparing the value of n_s with that of $n^*(x\rightarrow 0)$, $n^*(x\rightarrow 0)$ is too small to give a distinct change in the numbers of electrons at the rutile surface.

It may also be valuable to discuss the effect of the photovoltage on cathodic polarization curves obtained in the dark. A depletion layer is formed when an *n*-type semiconductor electrode such as rutile is placed in contact with a solution containing a chemical species which has a more noble redox-potential than E_{fb}. By illumination, the degree of the band bending is reduced, and this effect causes the so-called photovoltage.[27] According to Gerischer, the electron-energy level in the semiconductor is changed by illumination by the magnitude of the photovoltage, and the change is equal to $e(E_F^*-E_F)$ eV, where E_F^* and E_F denote the Fermi levels of the semiconductor under illumination and in the dark respectively. By the illumination, the electrode potential is shifted toward a cathodic direction by the magnitude of the change in the band bending. If the illuminated electrode is polarized anodically by $|E_F^*-E_F|$, the electrode potential is brought back to the same value as before illumination, and simultaneously the band bending also returns to the same situation as before illumination. It is concluded from this discussion that the same band situation is realized at rutile electrodes both with and without illumination if the electrodes are polarized at the same potential.

It is, therefore, believed that the reduction curves obtained in the dark in Fig. 4 represent the behavior of the reduction of the oxidizing agents on the illuminated rutile catalyst.

It is, then, possible to determine the rates of the photocatalytic reactions as the current values of the intersection points in Fig. 4.[12,13] In the cases of MnO_4^- and $Cr_2O_7^{2-}$, three and six Faradays are needed to produce 1 mol of MnO_2 and 2 mol of Cr^{3+} respectively. One-third of the current values at the intersection points in Fig. 4 thus correspond to the reaction rates for these systems. The reaction rates estimated from the electrochemical measurements are summarized in Table 1, together with the reaction rate constants determined by the chemical analysis described above.

The rutile powder catalyst used in the chemical analysis had an unidentified N_D and various crystal planes exposed to the solution. On the other hand, the electrochemical analysis was performed on the single crystal which had a fixed N_D and crystal plane. Nevertheless, the results in Table 1 show that the reaction rates determined by the two kinds of methods had a similar tendency in their relative magnitudes. The important influence of N_D on the rate of the photoelectrochemical reaction was theoretically predicted[27] and was also experimentally found on the photoelectrolytic decomposition of water at rutile anodes and GaP cathodes.[19] However, the ambiguity of N_D does not cause any serious problem in the qualitative comparison of the reaction rates determined by the two kinds of methods, because the dimensions of the reaction rates are completely different between the two kinds of methods, and the same powder catalyst was used in the series of the experiments, by which the effect of N_D was fixed in various systems of the photocatalytic reactions.

The value of the reaction rates on the illuminated rutile catalyst is determined by the feasibility of electron exchange between the semiconductor and the species in the solution, as has been discussed in a previous paper in the case of quinones dissolved in methanol.[13] The feasibility is determined by the positions of the energy levels of the band edges of semiconductor relative to the electron-energy levels of the chemical species, which are distributed with a specified rearrangement energy.[2,3] Accordingly, the difference in the reaction rates of the oxidizing agents in Table 1 seems to be due to this factor. No detailed discussion of the difference in the reactivity could be done, however, since we have no data on the rearrangement energy of MnO_4^- and $Cr_2O_7^{2-}$, which are reduced by three-step processes.

Difference in the Behavior of the Cathodic Polarization Curves between Photo-electrochemical Cells and Photocatalytic Reactions. It can be noticed by comparing Figs. 1 and 4 that the main difference lies in the cathodic polarization behavior of the oxidizing agents.

The cathodic curves on the rutile electrode given in Fig. 4 commenced at almost the same potential of 0.1 V *vs.* SCE. This means that the overpotential was different depending on the kind of oxidizing agent. In the case of a semiconductor electrode, an externally applied potential causes a change in the band bending in the semiconductor.[1-3] When the semiconductor electrode is polarized at potentials anodic to E_{fb}, the bands bend up toward the surface.[1-3] Consequently, the cathodic current should be controlled by this energy barrier, and it shoud eventually be independent of the redox-potentials of the oxidizing agents used as long as the cathodic process is affected only by the electron density at the semiconductor surface. The validity of this view has already been reported in connection with ZnO.[25] In that case, the potential barrier to bringing the cathodic current flow of an order of 0.1 $\mu A/cm^2$ was 0.6 eV at most.[25] Therefore, the cathodic polarization curves in Fig. 4 are judged to be reasonable, since the E_{fb} values of rutile in 0.5 mol dm^{-3} H_2SO_4 has been reported to be -0.1 V *vs.* SCE.[26]

On the other hand, the polarization of the rutile electrode at a potential cathodic to E_{fb} causes an energy barrier for the positive holes reaching the electrode surface in the same manner as electrons for the anodic process.[1-3]

When both electrons and positive holes transfer from the electrode to the chemical species in the solution, as is the case in the present photocatalytic reaction, the flat-band condition will be feasible for the transfer of both carriers. The potential where the reaction proceeds reflects this situation and is located around E_{fb}, as Fig. 4 shows. Under these conditions, the quantum yield of the reaction should be quite low, since electron-hole recombination predominates,[19,27,28] and the reaction rate is low, as is shown in Fig. 4. Therefore, it can be confirmed in the present study that a good utilization of light energy can not be expected for a photocatalyst where both bands participate in the reaction.

In the case of photo-electrochemical cells using the

illuminated rutile anode and metal cathode, it is necessary to take the energy barrier into consideration only for positive holes in the anode. When the energy bands bend up enough to accelerate positive holes effectively to the semiconductor surface, a larger reaction rate can be expected than that of the photocatalytic reaction.

References

1) V. A. Myamlin and Y. V. Pleskov, "Electrochemistry of Semiconductors," Plenum Press, New York (1967), pp. 1—277.
2) H. Gerischer, "Physical Chemistry," Vol. 1XA, ed by H. Eyring *et al.*, Academic Press, New York (1970), pp. 463—542.
3) A. K. Vijh, "Electrochemistry of Metals and Semiconductors," Marcel Dekker, New York (1973), pp. 1—123.
4) A. Fujishima, K. Honda, and S. Kikuchi, *Kogyo Kagaku Zasshi*, **72**, 108 (1969).
5) A. Fujishima and K. Honda, *Nature*, **238**, 37 (1972).
6) A. Fujishima and K. Honda, *Bull. Chem. Soc. Jpn.*, **44**, 1148 (1971).
7) H. Yoneyama, H. Sakamoto, and H. Tamura, *Electrochim. Acta*, **20**, 341 (1975).
8) J. G. Mavroides, J. A. Kafalas, and D. F. Kolesar, *Appl. Phys. Lett.*, **28**, 241 (1976).
9) A. Fujishima, K. Kohayakawa, and K. Honda, *Bull. Chem. Soc. Jpn.*, **48**, 1041 (1975).
10) M. Miyake, H. Yoneyama, and H. Tamura, *Electrochim. Acta*, **21**, 1065 (1976).
11) T. Freund and W. P. Gomes, "Catalysis Reviews," Vol. 3, ed by H. Heinemann, Marcel Dekker, New York (1969), pp. 1—36.
12) H. Yoneyama, Y. Toyoguchi, and H. Tamura, *J. Phys. Chem.*, **76**, 3460 (1972).
13) M. Miyake, H. Yoneyama, and H. Tamura, *Electrochim. Acta*, **22**, 319 (1977).
14) "Butsuri Jyosuhyo," ed by S. Iida *et al.*, Asakura, Tokyo (1969), p. 227.
15) N. Sato, "Kagaku Sosetsu," Vol. 7, ed by H. Kamata *et al.*, Tokyo Daigaku Shyuppankai, Tokyo (1975), p. 226.
16) R. H. Bube, "Physical Chemistry," Vol. X, ed by H. Eyring *et al.*, Academic Press, New York (1970), p. 515.
17) D. C. Cronemeyer, *Phys. Rev.*, **87**, 876 (1952).
18) F. Möllers, H. J. Tolle, and R. Memming, *J. Electrochem. Soc.*, **121**, 1160 (1974).
19) H. Tamura, H. Yoneyama, C. Iwakura, H. Sakamoto, and S. Murakami, *J. Electroanal. Chem.*, in press.
20) J. G. Mavroides, D. I. Tchernav, J. A. Kafalas, and D. F. Kolesar, *Mat. Res. Bull.*, **10**, 1023 (1975).
21) Y. Tsuchiya and H. Segawa, *J. Phys. Soc. Jpn.*, **36**, 1566 (1974).
22) R. G. Breckenridge and W. R. Hosler, *Phys. Rev.*, **91**, 793 (1953).
23) H. P. R. Frederikse, *J. Appl. Phys. Suppl.*, **32**, 2211 (1961).
24) M. Haratome, "Handotai Busseikogaku No Kiso," Kogyochosakai, Tokyo (1967), p. 134.
25) S. R. Morrison, *Surface Sci.*, **15**, 363 (1969).
26) E. C. Dutoit, F. Cardon, and W. P. Gomes, *Ber. Bunsenges. Phys. Chem.*, **80**, 475 (1976).
27) H. Gerischer, *J. Electroanal. Chem.*, **58**, 263 (1975).
28) T. Ohnishi, Y. Nakato, and H. Tsubomura, *Ber. Bunsenges. Phys. Chem.*, **79**, 523 (1975).

Studies on the Thermal Separation Column. V. Thermal Separation Column Having Horizontal Barriers

Kazuo SASAKI, Seiji TAO, and Yoshio HIRANO

Department of Applied Chemistry, Hiroshima University, Sendamachi, Hiroshima 730

(Received November 29, 1976)

The performance of a hot wire type thermal separation column in which many horizontal barriers of Teflon or copper plates are installed has been examined. At the optimum spacing of barrier plates, the quality factor defined by $(2AL)_{barrier}/(2AL)_{open}$ exceeds 3. This means that a barrier column constructed properly has a performance equivalent to that of an open column of three times taller in height. Visualization of a stream line in the barrier assembly indicates that a helical transverse motion takes place in the space partitioned by two adjacent barrier plates.

We have studied the effect of installing flow barriers inside the gas chamber of a thermal separation column.[1-3] It was concluded that the presence of a flow barrier retards the convectional velocity of separating gas mixture and the largest separation is attainable when convectional velocity is minimized. A similar conclusion was also obtained from the study of a tilted column.[4]

Although the use of a vertical barrier has been proved effective to improve the performance of thermal separation, there are some difficulties as regards the construction of the vertical barrier system.

This paper deals with the effect caused by the use of horizontal barriers in place of vertical ones. The structural difficulty in the vertical system can mostly be eliminated by use of the horizontal barrier system for which there is no difficulty in selecting the standard of comparison.[3] Utilization of horizontal barriers was first studied by Treacy and Rich[5] who claimed the merit of the barriers. However, the procedure of the experiment and the data do not seem convincing.

Experimental

Apparatus. An outline of the column is shown in Fig. 1. A straight column employing an iron tube for the outer wall of the gas chamber is fixed vertically as accurately as possible. Inclination of a column seriously affects the degree of equilibrium separation.[4] The upper end of the center wire (diam. 0.23 mm, nichrome) (9) is tightly fixed to the column top which is electrically insulated from the column body. A micalex rod (1) was used for this part. At the lower end of the heater wire, a copper rod (10), 99 g, is connected to assure the verticality and tautness of the heater wire. A mercury pool (11) is provided in contact with the tail end of the weight to make allowance for the thermal elongation of heating wire. The elongation is measured with a travelling microscope in order to estimate the heater temperature. The length of the column as measured by the distance between two sampling ports (5) at top and bottom is 54 cm.

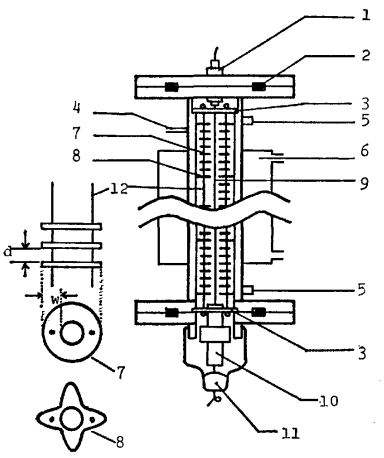

Fig. 1. Illustration of barrier-column.
1: Micalex rod, 2: O-ring seal, 3: terminal plates, 4: gas inlet, 5: sampling port, 6: water jacket, 7: flat doughnut barrier, 8: cruciform barrier, 9: nichrome heater, 10: weight, 11: mercury pool, 12: fine wire.

Barriers. The horizontal barrier assembly consists of many plane parallel plates made from Teflon (0.8 mm thick) or copper sheets (0.55 mm thick). Each barrier plate is in the form of a flat doughnut (7) having outer and inner diameter of 12.0 and 4.7 mm, respectively. The desired number of barrier plates are assembled into one unit by keeping the plates plane parallel with a regular distance. This was done by sewing the plates with two pieces of fine wire (12). At least 89 and at most 260 plates were fitted over the whole length of the barrier assembly (52 cm). Regardless of the number of barrier plates fitted, twelve cruciform barriers (8), slightly larger than the doughnut barriers, were placed every 4.7 cm in place of the doughnut barrier. This was necessary for assuring the installation of the barrier assembly in the proper position inside the column space. When copper was used as barrier material, the contact point between the plate and sewing wire was cemented by epoxy resin, while no cement was necessary for Teflon plates. The barrier assembly built up outside the column was carefully transferred into the column space and fixed to the terminal plates (3) located at the top and bottom of the gas chamber.

Operation of the Column. Operation of the column was more or less the same as described previously.[2] A d.c. power source with stabilized voltage was used for heating the nichrome wire. The column was filled with test gas before heating current was supplied. After steady temperature difference had been set up the column was evacuated and filled with fresh gas in order to start the measurement. The gas pressure was kept at 785±4 Torr throughout the experiment. The test gas was an equimolar mixture of argon and nitrogen.

Results and Discussion

Theoretical Value of q_e for the Open Column. So far we have no reliable means to predict a theoretical value of q_e attainable in a column having a horizontal barrier

Table 1. Calculated values of transport coefficients and equilibrium separation factor

ΔT (°C)	$h\times10^3$	$k_c\times10^2$	k_d	$H\times10^4$ (g/s)	$K_c\times10^2$ (g cm/s)	$K_d\times10^4$ (g cm/s)	$A^{a)}\times10^3$ (cm^{-1})	$q_e^{b)}$
221	4.10	1.74	0.52	1.60	1.97	6.17	3.93	1.53
310.4	6.30	2.15	0.53	2.46	2.44	6.28	4.91	1.70
419	8.53	2.48	0.54	3.33	2.81	6.47	5.80	1.87
527.7	10.5	2.51	0.56	4.11	2.84	6.66	7.05	2.14

a) $A=\dfrac{H}{2(K_c+K_d)}$. b) $q_e=\exp(2AL)$.

assembly. A theoretical value can be obtained only for the open column.

The basic equation derived by Jones and Furry[6] was used for calculation. The following values were used for basic parameters;

$$\alpha = 0.127-13.6/T,^{7)}\quad (D_{12})_1 = 0.20\ \mathrm{cm^2\ s^{-1}},$$

$$(\bar{\rho})_1 = 1.53\times10^{-3}\ \mathrm{g\ cm^{-3}},\quad (\bar{\eta})_1 = 1.97\times10^{-4}\ \mathrm{pois}.$$

Subscript 1 outside the parentheses refers to the temperature of the cold wall taken to be 289 K. The numerical tables by Saxena and Raman[8] were used for the corrections as regards the cylindricity of the column. This is equivalent to assuming both argon and nitrogen molecules to be rigid spheres. The calculated values of equilibrium separation factor, q_e, as well as the transport coefficients are given in Table 1.

Experimental Results. Measurements were carried out (1) with an open column in which no barrier was installed, (2) with a column having Teflon barriers, and (3) with a column having copper barriers. In the measurements with barrier-columns the effect of barrier distance, *i.e.* vertical distance between two adjacent plates, was also studied. Altogether, seven series of experiments were made, the results of which are summarized in Table 2.

The progress of separation with time for the initial 15 min of each measurement is shown in Fig. 2. The curves are numbered according to the series of experiments and correspond to those in Table 2.

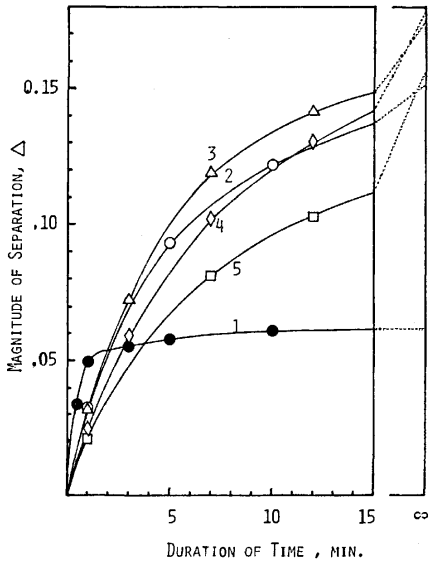

Fig. 2. Progress of separation with time.
The magnitude of separation is the difference in mole fractions of component 1 between top and bottom of the column.

Variations of equilibrium separation, q_e, with temperature difference, ΔT, are shown in Fig. 3. We see that in each series of experiments with the barrier-column, q_e increases linearly with increasing ΔT.

The dotted line connects theoretical values calculated for the open column. The experimental values for q_e for the open column are much lower than those of theoretical prediction. In contrast, the q_e values

Table 2. Experimental results

Series	Barrier	Barrier spacing, d (mm)	ΔT(°C)	$q_e^{a)}$	t_r (min)	f
1	None	—	200±5	1.205	2.1	1
			400±10	1.279	0.6	1
2	Teflon	5.3	200±5	1.463	7.6	2.04
			400±10	1.845	5.4	2.49
3		3.5	200±5	1.534	10.6	2.29
			400±10	2.027	6.2	2.87
4		2.1	200±5	1.527	13.6	2.27
			400±10	2.059	8.8	2.93
5		1.0	200±5	1.460	16.7	2.03
			400±10	1.885	11.1	2.58
6	Copper	5.3	200±5	1.521	12.9	2.25
			400±10	1.963	7.5	2.74
7		2.8	200±5	1.61	18.3	2.55
			400±10	2.15	10.4	3.11

a) Average of at least three measurements.

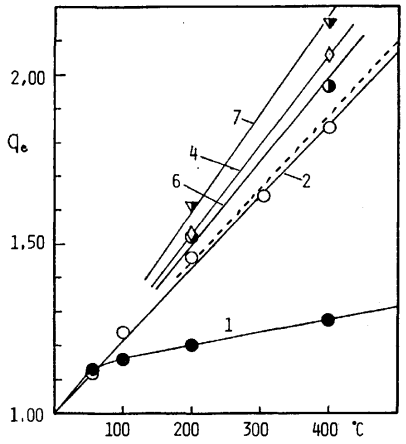

Fig. 3. Equilibrium separation factor, q_e, against the temperature difference applied. Numerical figures attached are serial number of experiments.

observed with barrier-columns are always larger than those with the open column even in comparison with theoretical prediction. The quality factor, f,[2] defined by

$$f = (\ln q_e)_{\text{barrier}}/(\ln q_e)_{\text{open}}$$

takes values greater than two (Table 2). In this equation, q_e is defined by

$$\ln q_e = 2AL,$$

where A is the characteristic constant of each individual column and L the column length. The two fold increase in the quality factor is equivalent to using an open column of two times taller in height. The quality factor seems to be affected largely by spacer distance. This is shown in Fig. 4, where the solid curve stands for Teflon barriers and the dotted curve for copper barriers. An optimum appears at about 2.8 mm.

Effect of Barrier Material. The barrier material affects the equilibrium separation, copper being superior

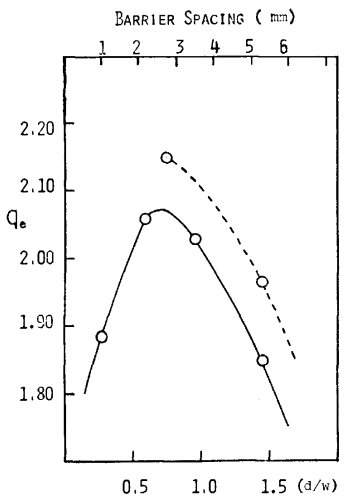

Fig. 4. Change in q_e against the barrier spacing, d, as well as the ratio of d to the barrier width, w. Full line; Teflon plates, Dotted line; copper plates.

to Teflon. Prior to the experiment we surmised that q_e would be reduced by the local disturbance of uniform temperature gradient caused by the metallic heat conductor. The result was contrary to expectation but it is understandable if we take the temperature gradient in a field of forced convection into consideration. The temperature is thought to fall steeply at the surface region of the central heater, never changing linearly. It seems that, in the column studied, most part of the temperature gradient is set up in a restricted region near the heater surface and the space in which barrier plates are located is almost isothermal. If this is the case, the barrier material would have no effect. Actually, however, copper enhances the equilibrium separation. The enhancing effect of metallic barriers can be attributed to the enhancement of net heat conduction through the column. The primary driving force of thermal diffusion is undoubtedly the heat flux. The presence of a heat conductor inside the gas chamber, even in the isothermal region, would increase the net heat flux giving rise to an enhanced separation. This is in accordance with the fact that when the barrier assembly of copper plates was used approximately 10% larger power dissipation was necessary for maintaining a given temperature difference as compared to the case in which Teflon plates were used. Teflon plate is also a better heat conductor when compared with separating gas. As a result, power dissipation always increases when barriers are used.

Effect of Barrier on the Rate of Separation. Use of horizontal barriers resulted in an appreciable increase in q_e (Table 2). This is reflected in the retardation of the rate of separation. If we assume that the separation proceeds by the exponential function[10]

$$\Delta = \Delta_e(1-e^{-t/t_r}),$$

we can estimate the relaxation time, t_r, experimentally. The values of t_r thus determined are given in Table 2. We see that the use of barriers increases the transition time a great deal; the denser the barrier spacing, the greater the transition time (Fig. 5). This is in line with what we found in the case of vartical barrier, that the retardation of convectional velocity is the primary factor for the enhancement of equilibrium separation.[1] In the present case, however, it should be emphasized that too dense installation of barrier plates reduces q_e and an optimum appears in the relation between q_e and barrier spacing (Fig. 4). This suggests that the enhancement in equilibrium separation can not be entirely attributed to the retardation of convectional velocity (Fig. 2). The rate of separation (tangential slope of each curve at $t=0$) varies with curve. However, the slopes have no simple correlation with the relaxation time. It seems that the greater the equilibrium separation the faster the intial rate of separation.

Visualization of Stream Line. Let us consider the question of why the use of the barrier assembly increases the magnitude of q_e. Each barrier plate serves to disturb the stream line of flowing gas making the flow turbulent. A turbulent flow would act to mix rather than to separate the mixed components. Actually, this was not the case and the use of barrier was unexpectedly effective for

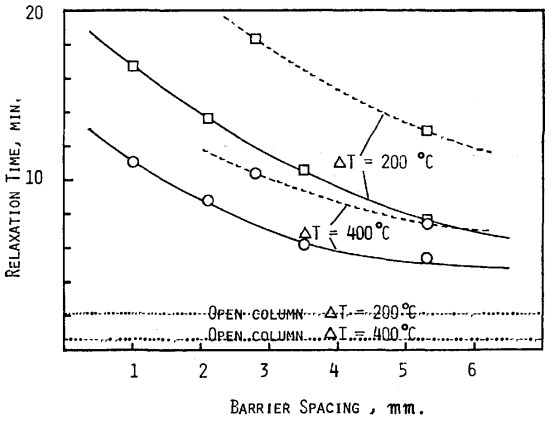

Fig. 5. Relaxation time against the barrier spacing. Full line, Teflon plates, Broken line, copper plates, Dotted straight line, open column.

attaining a larger separation. We thus attempted to visualize the flow pattern inside the barrier-column. Attempts in a gas sample using several kinds of aerosols were unsuccessful. We then carried out the experiment with use of a solid suspension in a liquid. Fine powder of polyethylene suspended in a water–isopropyl alcohol mixture was employed. A model column of a glass tube, in which a barrier assembly and a central heater wire were installed, was filled with the indicator solution. The whole apparatus was immersed vertically in a thermostatted water bath (25 °C). The temperature of the heater wire was not measured but the heating current was so controlled as to make the flow pattern visible.

A typical example of stream line is shown in the photograph attached. It is evident that the flow of fluid occurs in a regular manner. The path of particle movement as observed in a vertical cross section is a circle. It is unlikely that indicator particles move only in a fixed vertical plane. The path of each particle must be continuous in the transverse direction. It is highly probable that the path of stream line forms a doughnut-shaped circular helical coil surrounding the central heater wire. Although the picture was taken in a dummy column with a liquid sample which might differ from gaseous sample in many respects, a rough concept on the nature of flow pattern can be attained.

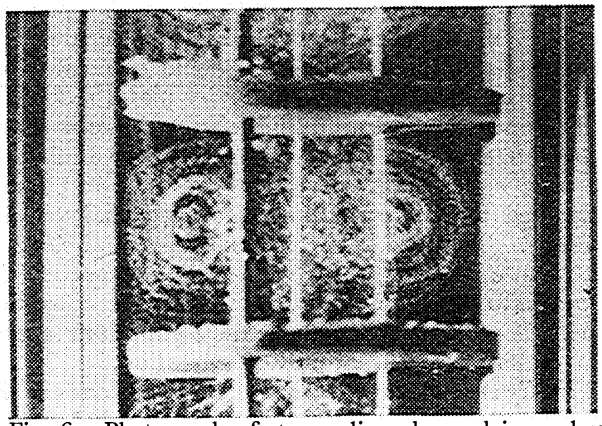

Fig. 6. Photograph of stream line observed in a glass column. Moving particles are polyethylene powder suspended in a water–isopropyl alcohol mixture. Inner diameter of glass tude; 18 mm, Outer and Inner diameters of barrier; 14 and 5 mm, Barrier spacing; 8 mm.

The flight length of a particle in upward convection stream should be L, the length of column, in the open column. The flight length should be elongated in the barrier column by involvement in the helical transverse motion. Involvement in the helical transverse motion might be rationalized from the view that the value of the quality factor, f, can be considered as an effective elongation of column length.

Optimum Spacing of Barriers. We see in Fig. 4 that an optimum barrier distance exists for the largest separation. The scale of abscissa is also expressed tentatively in terms of the ratio of spacer distance, d, against the width of barrier plate, w. The optimum lies at about 0.75 of this scale. The optimum distance should be a function of the relative dimension of inner and outer diameters of barrier plate relative to those of column and heater wire.

Conclusion

1. Installation of a horizontal barrier assembly, consisting of many plates with the form of a flat doughnut, remarkably increases the equilibrium separation as compared with the open column. The spacing between two adjacent barrier plates has an appreciable effect on the eqilibrium separation. There is an optimum spacing for the largest separation. Almost three times greater separation can be obtained by suitable choice of horizontal barriers.

2. As the barrier material, copper was found to be superior to Teflon. The presence of the barrier assembly, which is a better heat conductor as compared with gaseous material, increases the effective heat conductivity of the whole apparatus and the increase in heat flux enhances the separation. The enhanced separation would be partly due to this effect. The power dissipation per unit time increases by using barriers.

3. Installation of a barrier assembly reduces the rate of separation and elongates the relaxation time for separation. The relaxation time is a simple function of the barrier spacing, increasing monotonously with decreasing barrier spacing (increasing number of barrier plates). However, the actual rate of separation determined from the tangential slope of separation-time curve has no simple correlation with the relaxation time. The rate so determined varies in line with the statement "the greater the separation, the greater the rate."

4. Attempts were made to visualize the flow pattern in the barrier column with use of a dummy column. The movement of polyethylene powder suspended in a water–isopropyl alcohol mixture in the field of forced convection was recorded in order to show that the stream line forms a helical coil at each space partitioned by barrier plates. It is suggested that the use of horizontal barriers is equivalent to lengthening the open column. The situation is similar to that observed in

a tilted column.[4]

5. In contrast to the vertical barrier, the enhancement of separation in a horizontal barrier system can not be attributed solely to the retardation of convectional velocity. The regular helical motion of molecules would have an important effect.

References

1) K. Sasaki, T. Yoshitomi, and N. Miura, *Bull. Chem. Soc. Jpn.*, **49**, 363 (1976).
2) K. Sasaki, N. Miura, and T. Yoshitomi, *Bull. Chem. Soc. Jpn.*, **49**, 367 (1976).
3) K. Sasaki, Y. Hirano, and S. Tao, *Bull. Chem. Soc. Jpn.*, **50**, 788 (1977).
4) N. Miura, S. Tao, and K. Sasaki, *Nippon Kagaku Kaishi*, **1976**, 185.
5) R. C. Treacy and R. E. Rich, *Ind. Eng. Chem.*, **47**, 1544 (1954).
6) R. C. Jones and W. H. Furry, *Rev. Mod. Phys.*, **18**, 151 (1946).
7) This empirical equation was tentatively derived from the data.[9]
8) S. C. Saxena and S. Raman, *J. Chem. Phys.*, **36**, 3345 (1962).
9) Chemical Society of Japan, "Kagaku Binran," Maruzen (1966), p. 497.
10) A precise examination of experimental data shows that this function does not hold exactly.

Nanosecond Fluorescence Anisotropy of the DNA-Acridine Complexes

Yukio KUBOTA* and Robert F. STEINER

Department of Chemistry, University of Maryland, Baltimore County, Baltimore, Maryland 21228, U.S.A.

(Received November 30, 1976)

The rotational motions of various acridine dyes bound to DNA were investigated by the measurements of nanosecond fluorescence anisotropy. It was found that the total decay of fluorescence is a single exponential, whereas the decay of fluorescence anisotropy is a sum of an exponential function and a constant. The apparent values of the rotational relaxation time of the complexes calculated from anisotropy data range from 21 to 31 ns. The results are discussed by comparing with those obtained from the measurements of steady-state fluorescence depolarization.

Since Lerman[1,2] proposed the intercalation model in which the dye molecule is sandwiched between the adjacent base pairs of DNA by extension and local unwinding of the helix, the general features of the model have been widely accepted.[3,4] However, the exact location of the intercalated dye is not yet definitely known. One of the approaches to elucidate the possible location of the dye is a systematic investigation of the dependence of the binding nature on the dye structure.[5-7]

In a previous paper,[6] it was found that the mean rotational relaxation times of the DNA-acridine complexes obtained from the measurements of steady-state fluorescence depolarization depend on the dye structure. In this paper, nanosecond fluorescence anisotropy and viscosity studies have been undertaken to obtain further information on the rotational motions of the dye bound to DNA, using various acridine dyes.

Experimental

Materials. Calf thymus DNA was purchased from Worthington Biochemical Corporation. The concentration of DNA was determined spectrophotometrically at 260 nm with the extinction coefficient per mol of DNA phosphate ($\varepsilon_p = 6600\ M^{-1}\ cm^{-1}$).[8] Acridine Orange (AO), Proflavine (PF), 3,6-bis(methylamino)acridine (Ac[NHMe]$_2$), 3,6-bis(ethylamino)acridine (Ac[NHEt]$_2$), 3,6-bis(diethylamino)acridine (Ac[NEt$_2$]$_2$), 3,6-bis(dimethylamino)-10-propylacridinium chloride (AO-propyl) and 3,6-bis(dimethylamino)-10-isopropylacridinium chloride (AO-isopropyl) were the same as previously reported.[6,7]

Nanosecond Fluorescence Anisotropy. Fluorescence decay curves were measured with an Ortec 9200 single photon counting nanosecond fluorometer.[9] In the measurements of fluorescence anisotropy, the exciting light was vertically polarized. A polarizer was also placed in the emission beam, which could be rotated by 90 ° to permit the measurements of the intensities of the vertically and horizontally polarized components. The time-dependent anisotropy $r(t)$ is defined as:

$$r(t) = \frac{I_{//}(t) - I_{\perp}(t)}{I_{//}(t) + 2I_{\perp}(t)} = \frac{d(t)}{s(t)}, \tag{1}$$

where $I_{//}(t)$ and $I_{\perp}(t)$ are the fluorescence intensities observed with the analyzer parallel and perpendicular to the direction of polarization of the exciting light. Unequal response of the detector system to the polarized light was corrected using an aqueous dilute solution of 9-aminoacridine.[9] The total decay of fluorescence $s(t)$ was determined independently. This was achieved by orienting the polarization axis of the analyzer at 35.3 ° from the vertical direction and using unpolarized exciting light.[10] In the measurements of the fluorescence decay curves, there was a small contribution of the scattered light; this was subtracted from the decay curves prior to analysis.

In agreement with previous observations,[6,11] the polarization of fluorescence was constant above *ca.* 400 nm and showed a minimum around 320—340 nm. Therefore, the complexes were excited at 430 nm for the measurements of nanosecond anisotropy.

All the measurements were carried out in 5 mM phosphate buffer (pH 6.9, ionic strength of 0.01) at room temperature (23±1 °C). The molar ratio of DNA phosphate to dye (P/D) was about 200, and the dye concentration ranged from 5×10^{-6} to 10^{-5} M. In such conditions, the concentration of free dye and energy transfer between bound dye molecules were negligible.[7,11]

Analysis of Nanosecond Anisotropy Decay Curves. The fluorescence decay functions $S(t)$ and $D(t)$ are related to the observed decay curves $s(t)$ and $d(t)$ by the following convolution integrals;

$$s(t) = \int_0^t S(t-u)E(u)\mathrm{d}u, \tag{2}$$

$$d(t) = \int_0^t D(t-u)E(u)\mathrm{d}u, \tag{3}$$

where $E(t)$ is the response function of the apparatus to the exciting pulse. First, $S(t)$ was determined by deconvolution of Eq. 2. In every case, $S(t)$ was found to be a single exponetial;

$$S(t) = S_0 e^{-t/\tau}, \tag{4}$$

where τ is the fluorescence lifetime. Next, the result was checked by a synthetic method.[12] The anisotropy decay function is given by

$$R(t) = \frac{D(t)}{S(t)}, \tag{5}$$

where $S(t)$ is the function given by Eq. 4. Several $R(t)$ functions were tested so that the numerically computed convolution of $D(t)$ with $E(t)$ may fit the experimental decay curve. The computed curve, $f^{\circ}(k)$, was then visually compared with the experimental curve, $f(k)$, and the weighed residue (χ^2) was calculated according to the method of Knight and Selinger.[13] Here, k denotes channel number.

$$\chi^2 = \frac{1}{n}\sum_{k=1}^{n}\frac{1}{f(k)}[f(k) - f^{\circ}(k)]^2. \tag{6}$$

The best fit between the computed and experimental decay curves was achieved by minimizing the χ^2 value.

* Present address: Department of Chemistry, Yamaguchi University, Yamaguchi 753.

Deconvolution was made with the aid of the methods of moments[14,15] and Laplace transformation.[16] Both methods yielded very similar results. Copies of the computer programs for these methods were kindly supplied to us by Dr. D. R. Dyson and Dr. L. Brand. All the analyses were carried out with a Univac 1108 computer.

Viscosity Measurements. Viscosity measurements of the sonicated DNA-acridine complexes were performed at 25± 0.05 °C by means of a Ubbelohde viscometer. The flow time of the solvent (5 mM phosphate buffer) was 270 s. We limited our study to r values smaller than 0.12 to avoid the errors due to the possible presence of the weakly bound dye molecules; r represents the number of moles of dye bound per DNA phosphate. The r value was determined by using data of equilibrium dialysis reported previously.[7]

Sonication of DNA was carried out with a Kubota ultrasonicator (200 W, 9 kHz). Immediately prior to irradiation, the sample solution was flushed with nitrogen gas, and during irradiation, ice-cold water was circulated through the jacket sorrounding the steel cup of a sonic oscillator. The molecular weight of sonicated DNA was determined to be 5.2×10^5 from the viscosity measurements; this value means that the sonicated DNA behaves almost like a rigid rod.[17]

Results and Discussion

A typical set of anisotropy data is shown in Fig. 1 for the DNA–AO complex, where the observed $s(t)$, $d(t)$, and $E(t)$ values are plotted every five channels. After deconvolution using the methods of moments[14,15] and Laplace transformation,[16] the function $S(t)$ was found to be a single exponential. On the other hand, the function $D(t)$ was found to be a sum of two exponential functions whose decay constants are very close. Figure 1 shows that, at large channel numbers, $s(t)$ and $d(t)$ are superposable on each other upon translation. As can be seen in Figs. 1 and 2, the anisotropy curves $r(t)=d(t)/s(t)$ obtained by point by point division exhibit non-exponential decays. They tend to decay exponentially at the initial stage and then to become constant, although the calculated points are somewhat scattered after channel 200. In view of these findings, it seems reasonable to assume that $R(t)$ and $D(t)$ are expressed by the following equations:[12,18]

$$R(t) = R_0(\alpha e^{-t/\phi} + 1-\alpha), \quad (7)$$

$$D(t) = R(t)S(t) = S_0R_0\alpha e^{-t/\tau'} + S_0R_0(1-\alpha)e^{-t/\tau}, \quad (8)$$

where

$$\tau' = \frac{\phi\tau}{\phi+\tau}, \quad (9)$$

and where ϕ corresponds to the rotational correlation time of the dye. This is a rather general result for the dye–macromolecule and dye–membrane systems in which the motion of the dye is locally limited.[12,18,19] Since two decay constants are very close in our case ($\tau/\tau'\simeq1.5$), we can not accurately deconvolute the observed $d(t)$ curves.[16,20] Therefore, using the deconvoluted $S(t)$ function which is a single exponential like Eq. 4 and assuming appropriate α and ϕ in Eq. 7, several $R(t)$ functions were tested so that the numerically computed convolution of $D(t)$ with $E(t)$ may fit the experimental curve. The solid line for $d(t)$ in Fig. 1 shows the calculated best-fit curves.

Table 1 summarizes the results of nanosecond anisotropy. The two different methods were used for deconvolution of the observed $s(t)$ curves. Both methods give almost the same lifetimes, which are in fairly good agreement with the lifetimes obtained by phase-shift method.[6] All anisotropy decay curves for the complexes are expressed by a function like Eq. 7. It should be noted that acridine dyes bound to DNA behave similarly to ethidium bromide (another intercalative dye) with respect to the anisotropy decay.[18] The values of limiting anisotropy ($R_0=0.31$—0.36) are comparable to those obtained from the measurements of steady-state depolarization.[6,21] The apparent values of the rotational relaxation time ($\rho_a=3\phi$) were calculated using decon-

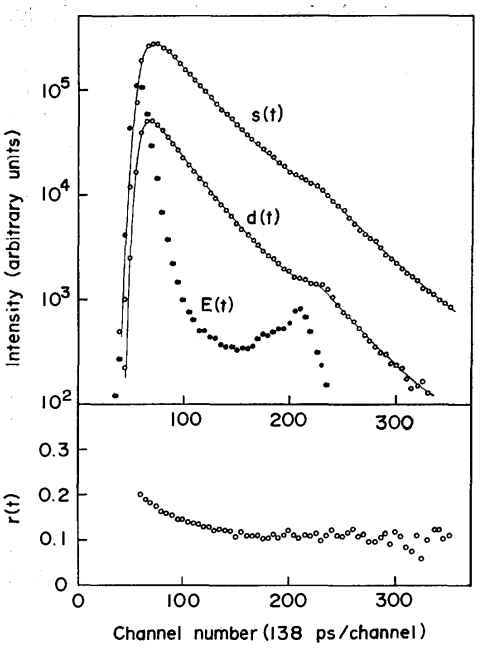

Fig. 1. Fluorescence decay curves of DNA–AO complex ($P/D=204$) in 5 mM phosphate buffer (pH 6.9) at 22°C. Open circles are observed decay curves, and solid lines are the best-fit curves. Excitation wavelength: 430 nm. Emission wavelength: 520 nm.

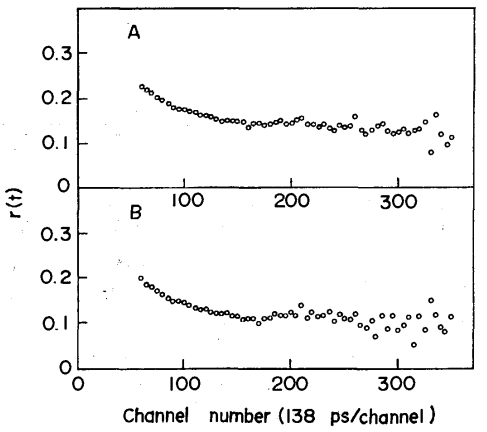

Fig. 2. Observed anisotropy decay curves at 22°C. (A) DNA–PF complex ($P/D=204$). Excitation wavelength: 430 nm. Emission wavelength: 500 nm. (B) DNA–Ac[NEt_2]$_2$ complex ($P/D=242$). Excitation wavelength: 430 nm. Emission wavelength: 520 nm.

TABLE 1. RESULTS OF NANOSECOND ANISOTROPY AND VISCOSITY

Dye	P/D	τ/ns		R(t)	ρa/ns			β
		a)	b)		c)	d)	e)	
PF	204	6.5_0	6.5_4	$0.34\ (0.62e^{-t/10.0}+0.38)$	31	60	52	1.30
$Ac[NHMe]_2$	201	4.1_9	4.1_5	$0.36\ (0.60e^{-t/10.0}+0.40)$	28	55	48	1.25
$Ac[NHEt]_2$	205	4.4_9	4.4_4	$0.34\ (0.60e^{-t/9.47}+0.40)$	27	52	45	1.05
$Ac[NEt_2]_2$	242	4.7_3	4.7_1	$0.32\ (0.72e^{-t/7.55}+0.28)$	21	35	32	0.60
AO	204	5.6_3	5.6_1	$0.33\ (0.71e^{-t/10.1}+0.29)$	28	50	48	1.30
AO-propyl	201	4.9_7	4.9_7	$0.32\ (0.71e^{-t/10.0}+0.29)$	28	48		1.15
AO-isopropyl	201	4.6_4	4.6_3	$0.31\ (0.70e^{-t/7.91}+0.30)$	22	37		0.70

a) Analyzed by the method of moments.[14,15] b) Analyzed by the method of Laplace transformation.[16]
c) The apparent value of the rotational relaxation time ($\rho_a=3\phi$) for the aqueous solution at 25 °C.
d) Calculated using Eq.14 ($\rho_a=3\phi'$). e) Obtained from the measurements of steady-state depolarization.

voluted $R(t)$ functions; the results are listed in Table 1. The ρ_a values are much smaller when compared to the values obtained by a steady-state study (Table 1).[6]

A continuous light source may be considered as a sum of an infinite number of pulses. Therefore, the observed static anisotropy is the mean value of $R(t)$.

$$\langle R\rangle = \frac{\int_0^\infty D(t)\mathrm{d}t}{\int_0^\infty S(t)\mathrm{d}t}. \tag{10}$$

If $S(t)$ is a single exponential like Eq. 4, Eq. 10 gives

$$\langle R\rangle = \frac{1}{\tau}\int_0^\infty R(t)\mathrm{e}^{-t/\tau}\mathrm{d}t. \tag{11}$$

Put the case that $R(t)$ is an exponential function like $R(t)=R_0\mathrm{e}^{-t/\phi}$, Eq. 11 leads to

$$\langle R\rangle = \frac{R_0}{1+\tau/\phi}. \tag{12}$$

Equation 12 is equivalent to Perrin's well-known formula.[22] When $R(t)$ is a function like Eq. 7, which is the present case, one obtains

$$\langle R\rangle = \frac{R_0\{\phi+(1-\alpha)\tau\}}{\phi+\tau} = \frac{R_0}{1+\tau/\phi'}, \tag{13}$$

where

$$\phi' = \frac{1}{\alpha}\{\phi+(1-\alpha)\tau\}. \tag{14}$$

According to Eq. 13, Perrin's plot in the steady-state study gives us ϕ' instead of ϕ. If Eq. 14 is applied to the deconvoluted $R(t)$ functions for the DNA–acridine complexes, the ρ_a values ($\rho_a=3\phi'$) listed in Table 1 are obtained. These values are in agreement with those obtained from the steady-state measurements (Table 1).[6] Thus, the discrepancy between steady-state and nanosecond anisotropy results can be understood.

It should be noted that the ρ_a values reported here are comparable to the rotational correlation times for the DNA–ethidium bromide[18] and *Cl. perfringens* DNA–PF[23] complexes which were obtained by nanosecond fluorometry. However, the ρ_a values are too much small to correspond to the rotation of the whole DNA molecule.[24] The most probable origin for the observed depolarization appears to be a local deformation motion of DNA base pairs.[18,21]

As is seen in Table 1, the ρ_a values for acridine dyes with bulky substituents ($Ac[NEt_2]_2$ and AO-isopropyl) are a little smaller than those obtained with the other dyes. Further, fluorescence quenching[5] and equilibrium dialysis[7] studies showed that the binding constant and the maximum number of binding sites per DNA phosphate are much smaller for acridine dyes with bulky substituents. This implies that the bulky groups attached to the acridine ring (*e.g.*, diethylamino and isopropyl) produce some steric hindrance to the binding.

Due to the presence of bulky substituents on the acridine ring, some changes in hydrodynamic properties of DNA may arise when acridine dyes are bound to it. Cohen and Eisenberg[25] showed that for short, almost rodlike fragments of DNA, the ratio of the contour length at the binding ratio r to that in the absence of dye (L/L_0) can be calculated from the viscosity data:

$$\frac{L}{L_0} = \left\{\frac{[\eta]f(p)_0}{[\eta]_0 f(p)}\right\}^{1/3}. \tag{15}$$

where $f(p)$, a function of the axial ratio p of the DNA rod, is insensitive to variations in p for large p, and $[\eta]$ and $[\eta]_0$ are intrinsic viscosities, respectively, in the

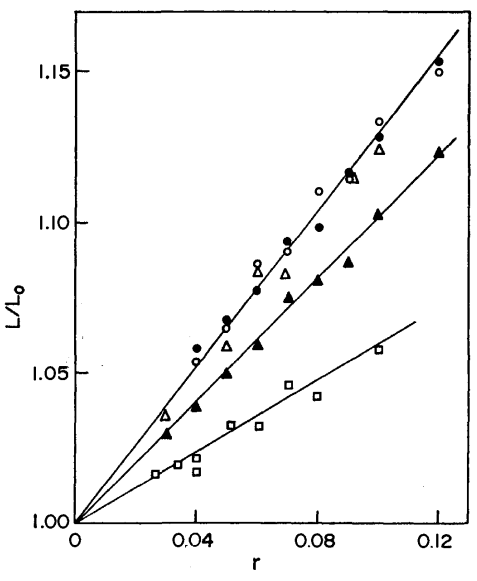

Fig. 3. Variation of L/L_0 as a function of r for sonicated DNA–acridine complexes. The molar concentration of DNA phosphate: 3.7×10^{-4} M. Acridine dyes: ○PF, ● AO, △ $Ac[NHMe]_2$, ▲ $Ac[NHEt]_2$, □ $Ac[NEt_2]_2$.

presence and absence of dye. The results obtained with various acridines are plotted in Fig. 3. In all cases, L/L_0 varies linearly with the binding ratio r.

$$\frac{L}{L_0} = 1 + \beta r. \tag{16}$$

The values of the slope β are listed in Table 1. The result obtained with PF is in good agreement with that previously reported.[25] As is clearly seen in Fig. 3 and Table 1, β is dependent on the dye structure; the β values for $Ac[NEt_2]_2$ and AO-isopropyl are much smaller than those for the other dyes.

Lerman's intercalation model[1,2] predicts that the DNA molecule is lengthened by 3.35 Å per intercalated dye molecule. If all bound molecules are completely intercalated, the slope of the L/L_0 *vs.* r plot should be 2.[1,25] From temperature jump relaxation studies of the DNA–PF complex, Crothers *et al.*[26,27] showed that most of bound PF molecules are intercalated, but some of those are bound outside of the DNA helix even at low binding ratios. On the other hand, Müller *et al.*[28] and Bontemps *et al.*[29] showed that a derivative of PF with bulky side chains, 3,6-diamino-2,7-di-*t*-butylacridine, binds to DNA but not by intercalation; they concluded that an outside bound complex is formed. In view of these, our viscosity results can be interpreted as follows: (1) the β values smaller than 2 result from the existence of the outside bound complex which would not contribute to an increase in the length of DNA[25–27] and (2) there exists a higher fraction of the outside bound complex in the case of $Ac[NEt_2]_2$ and AO-isopropyl because of the presence of bulky substituents.

Hydrodynamic and thermodynamic properties of outside bound dye are different from those of intercalated dye, while their optical properties are very similar.[26,27] In practice, the fluorescence decay of the complex could be characterized by a single exponential function (Fig. 1; Table 1). However, the structure of the outside bound complex is not yet well-defined.[26,27] In conclusion, the interpretation of the anisotropy results may be complicated by the heterogeneity of binding sites (intercalating and outside binding sites). If we assume that the local movement of the outside bound dye is more rapid compared to that of the intercalated dye which is restricted between adjacent base pairs, the smaller ρ_a values obtained with $Ac[NEt_2]_2$ and AO-isopropyl may be qualitatively understood. Further study would be necessary to clarify the origin for depolarization of the DNA–acridine complexes.

The authors are indebted to Dr. Ming S. Tung and Dr. Lih-Heng Tang for valuable advice and helpful discussions. We also thank Mr. Masaaki Wakita for viscosity measurements.

References

1) L. S. Lerman, *J. Mol. Biol.*, **3**, 18 (1961).
2) L. S. Lerman, *Proc. Natl. Acad. Sci. U.S.A.*, **49**, 94 (1963).
3) A. R. Peacocke, "Acridines," 2nd ed, ed by R. M. Acheson, Interscience Publishers, New York (1973), p. 723.
4) E. R. Lochmann and A. Micheler, "Physico-Chemical Properties of Nucleic Acids," Vol. 1, ed by J. Duchesne, Academic Press, New York (1973), p. 223.
5) G. Löber and G. Achtert, *Biopolymers*, **8**, 595 (1969).
6) Y. Kubota, *Bull. Chem. Soc. Jpn.*, **46**, 2630 (1973).
7) Y. Kubota, Y. Eguchi, K. Hashimoto, M. Wakita, Y. Honda, and Y. Fujisaki, *Bull. Chem. Soc. Jpn.*, **49**, 2424 (1976).
8) H. R. Mahler, B. Kline, and B. D. Mehrotra, *J. Mol. Biol.*, **9**, 801 (1964).
9) L. H. Tang, Y. Kubota, and R. F. Steiner, *Biophys. Chem.*, **4**, 203 (1976).
10) R. D. Spencer and G. Weber, *J. Chem. Phys.*, **52**, 1654 (1970).
11) G. Weill and M. Calvin, *Biopolymers*, **1**, 401 (1963).
12) Ph. Wahl, "Biochemical Fluorescence: Concepts," Vol. 1, ed by R. F. Chen and H. Edelhoch, Marcel Dekker, New York (1975), p. 1.
13) A. E. W. Knight and B. K. Selinger, *Spectrochim. Acta*, **27A**, 1223 (1971).
14) I. Isenberg and R. D. Dyson, *Biophys. J.*, **9**, 1337 (1969).
15) I. Isenberg, R. D. Dyson, and R. Hanson, *Biophys. J.*, **13**, 1090 (1973).
16) A. Gafni, R. L. Modlin, and L. Brand, *Biophys. J.*, **15**, 263 (1975).
17) J. Eigner and P. Doty, *J. Mol. Biol.*, **12**, 549 (1965).
18) Ph. Wahl, J. Paoletti, and J. B. Le Pecq, *Proc. Natl. Acad. Sci. U.S.A.*, **65**, 417 (1970).
19) Ph. Wahl, M. Kasai, and J. P. Changeux, *Eur. J. Biochem.*, **18**, 332 (1971).
20) I. Isenberg, *J. Chem. Phys.*, **59**, 5708 (1973).
21) N. F. Ellerton and I. Isenberg, *Biopolymers*, **8**, 767 (1969).
22) F. Perrin, *J. Phys. Radium*, **7**, 390 (1926).
23) S. Georghiou, *Photochem. Photobiol.*, **22**, 103 (1975).
24) P. K. Callis and N. Davidson, *Biopolymers*, **7**, 335 (1969).
25) G. Cohen and H. Eisenberg, *Biopolymers*, **8**, 45 (1969).
26) H. J. Li and D. M. Crothers, *J. Mol. Biol.*, **39**, 461 (1969).
27) D. E. V. Schmechel and D. M. Crothers, *Biopolymers*, **10**, 465 (1971).
28) W. Müller, D. M. Crothers, and M. J. Waring, *Eur. J. Biochem.*, **39**, 223 (1973).
29) J. Bontemps, C. Houssier, and E. Fredericq, *Biophys. Chem.*, **2**, 301 (1974).

The Crystal and Molecular Structure of *dl*-2-*cis*-4-*trans*-Abscisic Acid

Hideo UEDA* and Jiro TANAKA

Department of Chemistry, Faculty of Science, Nagoya University, Chikusa, Nagoya 464

(Received December 22, 1976)

The crystal and molecular structure of *dl*-2-*cis*-4-*trans*-abscisic acid has been determined by the X-ray method. The crystal is monoclinic, $P2_1/c$, with lattice parameters $a=6.316(1)$, $b=33.575(3)$, $c=7.607(1)$ Å, and $\beta=118.42(1)°$. The molecule has two independent conjugated systems forming respective planes which are orthogonal to each other. The molecules form a dimer by the hydrogen bonding and are connected by the other hydrogen bonding along the c-axis.

Abscisic acid is an important plant hormone which promotes abscission of leaves and dormancy in buds and seeds. Ohkuma, Lyon, and Adicott[1] isolated abscisic acid and determined its chemical structure. Cornforth and his co-workers[2,3] synthesized and determined the absolute configuration of natural (+) abscisic acid as (I) by applying Mill's empirical rule to the diols obtained through the reduction of optically active abscisic acid.

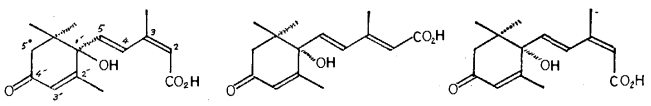

I II III

Burden and Taylor[4] reported that $(+)_{589}$-2-*trans*-4-*trans*-abscisic acid(II) obtained from violaxanthine shows a positive Cotton effect, which is in contradiction with the result of Cornforth and his co-workers. Oritani and Yamashita,[5–7] Ryback,[8] Mori,[9] and Weiss, Koreda, and Nakanishi[10] showed that the natural $(+)_{589}$-abscisic acid has *S*-configuration(III) at C_1'.

The crystal structure of *dl*-2-*trans*-4-*trans*-abscisic acid has been determined recently by Swaminathan, Vijayalakshmi, and Srinivasan;[11] the acid has only 1% activity as compared to the natural (*S*)-2-*cis*-4-*trans*-abscisic acid.[2,12]

In this paper we report on the crystal and molecular structure of *dl*-2-*cis*-4-*trans*-abscisic acid, which has the most efficient hormonal activity.

Experimental

The crystals were obtained as transparent thin plates from ethanol solution in the dark in a refrigerator.

The space group was determined as $P2_1/c$ from the oscillation and Weissenberg photographs. The density was measured by the floatation method in KI aqueous solution. The unit-cell parameters were determined by the least-squares method, using twelve reflections carefully measured on Hilger & Watts four circle diffractometer with Ni-filtered Cu$K\alpha$ radiation ($\lambda=1.5418$ Å). The intensity data were collected on the diffractometer with the 2θ-ω scanning mode ($2\theta\leqq 57°$). The size of the crystal used was $0.2\times0.1\times0.3$ mm. The crystal used for the X-ray measurement was mounted in a glass capillary. In order to confirm the stability of the crystal and the counting system, the intensities of three standard reflections were measured every 50 reflections. The fluctuation and decay of standard reflections were within 5%. No absorption nor extinction correction was made. The crystal data are given in Table 1.

Table 1. Crystal data

$C_{15}H_{20}O_4$
Mol wt: 264.32
Crystal system: $P2_1/c$; $Z=4$
$a=6.316(1)$, $b=33.575(3)$, $c=7.607(1)$ Å;
$\beta=118.42(1)°$
$D_m=1.232$, $D_c=1.237$ g cm^{-3}
$\mu=7.37$ cm^{-1} (for Cu$K\alpha$ radiation)

Determination and Refinement of the Structure

The structure was determined by the direct method with the program MULTAN[13] using 162 reflections with $|E|\geqq1.70$. An E map computed from the phase set with the highest figures of merit ($FOM=1.16$) revealed the positons of 16 atoms. Other atoms were found by the successive Fourier synthesis. Refinement of the structure was performed by the block-diagonal least-squares method with 1315 independent reflections of $|F°|\geqq3\sigma$. The final refinement was carried out with anisotropic thermal parameters for non-hydrogen atoms and isotropic thermal factors for hydrogen atoms. The R-index converged to 0.071 with an equal weight for each reflection. The atomic scattering factors were

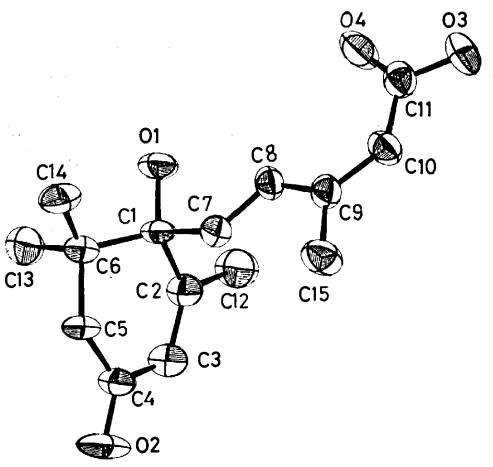

Fig. 1. The atomic labelings of abscisic acid. Carbon and oxygen atoms are represented as thermal ellipsoids of a size such that the vibrating atoms have a 50% probability of being found within them.

* Present address: Central Research Laboratory, Ube Industries Ltd., Nishihon-machi, Ube, Yamaguchi 755.

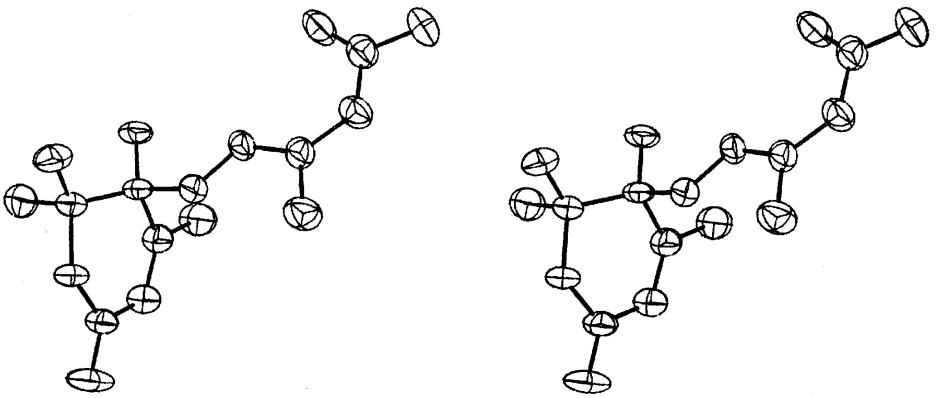

Fig. 2. A stereoscopic view of abscisic acid. The criterion to the themal ellipsoids of carbon and oxygen atoms are the same as in Fig. 1.

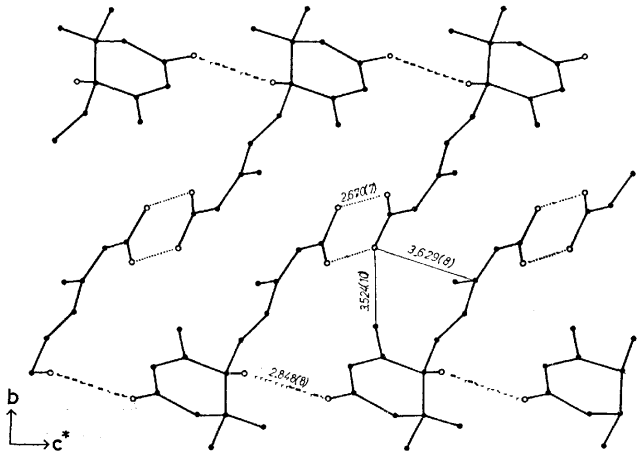

Fig. 3. Hydrogen bond network viewed along the a-axis. Carbon atoms are depicted as filled circles and oxygen atoms as open circles. Hydrogen bonds are represented with both dotted and broken lines.

taken from the International Tables for X-Ray Crystallography.[14] The program HBLS-IV coded by Ashida in UNICS was utilized for the refinement. The program ORTEP coded by Johnson was used for drawing of Figs. 1 and 3. A part of the computation was performed at the Nagoya University Computation Center. The observed and calculated structure factors are given in Table 2.[20]

Results and Discussion

The molecular structure, atomic labelings, and thermal ellipsoids are shown in Fig. 1. It can be seen that the conformation around C–C double bonds is *cis-trans*. The positional and thermal parameters of non-hydrogen atoms with their standard deviations are given in Tables 3 and 4, respectively. The coordinates and isotropic thermal parameters of hydrogen atoms are given in Table 5.

Molecular Structure. The bond lengths and bond angles with their standard deviations are given in Tables 6 and 7, respectively. The bond distances are normal. The C=O bond of the carboxylic group takes the *cis*-conformation with respect to the diene group. The angles, C(1)C(7)C(8), C(7)C(8)C(9), C(8)C(9)-C(10), and C(9)C(10)C(11), are larger than 120°, having values 128, 123, 126, and 128°, respectively. The conjugated double bond of the diene group forms plane A. Deviations of atoms from the plane and equations of the planes are given in Table 8. The carboxylic group forms plane B, at 9° to plane A.

The six-membered ring is puckered, C(1) and C(6) being out of plane C formed by the remaining atoms, C(2), C(3), C(4), C(5), C(12), and O(2). The planarity of plane C is fairly good, the largest deviation being 0.016 Å of C(3).

Planes A and C are orthogonal; the dihedral angle is 91°. A stereoscopic projection of the (*S*)-isomer is shown in Fig. 2. Two independent chromophores take a chiral configuration, the strong optical rotatory power of the $(+)_{589}$-abscisic acid thus being explained.

Crystal Structure. The crystal structure projected along the a-axis is shown in Fig. 3. The molecule is connected with neighboring ones by the hydrogen bonds; two molecules related by a center of symmetry form a dimer through the hydrogen bonds of carboxylic groups.

Table 3. Atomic coordinates and their standard deviations of heavy-atoms

	x	*y*	*z*
O(1)	0.7982(8)	0.1463(1)	0.0594(6)
O(2)	0.5798(10)	0.1750(2)	0.6589(7)
O(3)	0.3078(9)	−0.0211(1)	−0.4123(6)
O(4)	0.5107(8)	0.0363(1)	−0.3416(6)
C(1)	0.6629(11)	0.1460(2)	0.1663(8)
C(2)	0.8387(11)	0.1314(2)	0.3769(8)
C(3)	0.8011(12)	0.1408(2)	0.5332(9)
C(4)	0.6163(14)	0.1678(2)	0.5158(8)
C(5)	0.4581(12)	0.1874(2)	0.3191(8)
C(6)	0.5644(12)	0.1878(2)	0.1716(8)
C(7)	0.4714(11)	0.1143(2)	0.0868(8)
C(8)	0.4473(10)	0.0849(2)	−0.0385(8)
C(9)	0.2706(10)	0.0535(2)	−0.0896(8)
C(10)	0.2421(11)	0.0222(2)	−0.2077(9)
C(11)	0.3681(11)	0.0139(2)	−0.3252(8)
C(12)	1.0300(13)	0.1034(2)	0.3986(10)
C(13)	0.7673(14)	0.2189(2)	0.2437(10)
C(14)	0.3582(14)	0.2002(2)	−0.0331(10)
C(15)	0.1037(11)	0.0554(2)	0.0032(9)

TABLE 4. ANISOTROPIC THERMAL FACTORS[a] ($\times 10^4$) AND THEIR STANDARD DEVIATIONS OF HEAVY-ATOMS

	B_{11}	B_{22}	B_{33}	B_{12}	B_{23}	B_{31}
O(1)	424(18)	9(1)	163(10)	−8(5)	−2(4)	382(23)
O(2)	898(32)	19(1)	220(12)	26(8)	−4(5)	747(35)
O(3)	560(22)	9(1)	274(13)	−24(5)	−42(4)	462(29)
O(4)	472(20)	10(1)	276(12)	−30(5)	−47(4)	455(28)
C(1)	390(25)	7(1)	126(13)	−20(6)	−9(5)	323(31)
C(2)	378(27)	7(1)	187(15)	−5(6)	−1(5)	249(35)
C(3)	521(32)	9(1)	159(15)	3(8)	6(5)	343(37)
C(4)	580(33)	9(1)	177(15)	−26(8)	−14(5)	432(39)
C(5)	508(24)	8(1)	188(15)	−6(7)	−7(5)	444(38)
C(6)	512(31)	7(1)	166(15)	9(7)	4(5)	409(36)
C(7)	335(24)	7(1)	161(14)	7(6)	3(5)	282(31)
C(8)	336(24)	6(1)	141(13)	17(6)	1(4)	224(30)
C(9)	299(23)	6(1)	158(14)	6(6)	−2(5)	173(31)
C(10)	301(24)	6(1)	216(16)	3(6)	−7(5)	240(33)
C(11)	310(25)	7(1)	172(15)	15(6)	−7(5)	128(32)
C(12)	445(32)	13(1)	222(18)	38(9)	24(7)	299(40)
C(13)	691(39)	8(1)	308(20)	−36(8)	−14(6)	620(49)
C(14)	655(39)	10(1)	222(18)	17(8)	16(6)	496(45)
C(15)	312(26)	10(1)	248(17)	−18(7)	−24(6)	304(36)

a) The anisotropic thermal factors are of the form $\exp\{-(h^2B_{11}+k^2B_{22}+l^2B_{33}+hkB_{12}+hlB_{31}+klB_{23})\}$.

TABLE 5. HYDROGEN ATOM PARAMETERS AND THEIR STANDARD DEVIATIONS

	x	y	z	B/Å^2
H(O1)	0.375(12)	−0.026(2)	−0.473(10)	4.8(1.8)
H(O3)	0.699(11)	0.159(2)	−0.039(9)	3.3(1.5)
H(C3)	0.905(12)	0.125(2)	0.662(10)	3.3(1.9)
H(C5a)	0.420(10)	0.219(2)	0.338(8)	1.8(1.3)
H(C5b)	0.296(11)	0.176(2)	0.257(9)	3.5(1.6)
H(C7)	0.372(10)	0.113(2)	0.662(9)	3.3(1.6)
H(C8)	0.546(10)	0.083(2)	−0.093(8)	1.5(1.3)
H(C10)	0.125(9)	0.000(2)	−0.234(7)	0.6(1.1)
H(C12a)	0.957(11)	0.077(2)	0.342(11)	7.3(2.1)
H(C12b)	1.135(11)	0.112(2)	0.349(11)	7.2(2.1)
H(C12c)	1.122(11)	0.095(2)	0.508(9)	4.1(1.7)
H(C13a)	0.832(11)	0.224(2)	0.134(9)	3.8(1.6)
H(C13b)	0.705(11)	0.250(2)	0.241(10)	3.2(1.6)
H(C13c)	0.924(12)	0.211(2)	0.380(10)	4.3(1.7)
H(C14a)	0.324(10)	0.233(2)	−0.019(8)	2.6(1.4)
H(C14b)	0.254(10)	0.178(2)	−0.077(8)	1.9(1.3)
H(C14c)	0.427(11)	0.206(2)	−0.109(9)	3.6(1.6)
H(C15a)	0.204(11)	0.054(2)	0.134(9)	4.1(1.6)
H(C15b)	−0.024(10)	0.038(2)	−0.058(8)	2.3(1.4)
H(C15c)	0.014(10)	0.083(2)	−0.025(8)	2.2(1.3)

TABLE 6. BOND LENGTHS AND THEIR STANDARD DEVIATIONS

O(1)–C(1)	1.433(8) Å	O(2)–C(4)	1.239(10)Å
O(3)–C(11)	1.312(9)	O(4)–C(11)	1.224(9)
C(1)–C(2)	1.532(10)	C(1)–C(6)	1.545(10)
C(1)–C(7)	1.503(10)	C(2)–C(3)	1.356(11)
C(2)–C(12)	1.476(11)	C(3)–C(4)	1.433(11)
C(4)–C(5)	1.499(11)	C(5)–C(6)	1.558(11)
C(6)–C(13)	1.538(12)	C(6)–C(14)	1.537(12)
C(7)–C(8)	1.330(9)	C(8)–C(9)	1.449(9)
C(9)–C(10)	1.337(9)	C(9)–C(15)	1.524(10)
C(10)–C(11)	1.479(9)		
C(i)–H(i)			
Average	0.99		
Range	0.81—1.15		

TABLE 7. BOND ANGLES AND THEIR STANDARD DEVIATIONS

O(1)–C(1)–C(2)	105.8(5)°	O(1)–C(1)–C(6)	111.3(6)°
O(1)–C(1)–C(7)	110.9(5)	C(2)–C(1)–C(6)	111.1(6)
C(2)–C(1)–C(7)	103.9(6)	C(6)–C(1)–C(7)	113.4(6)
C(1)–C(2)–C(3)	120.4(7)	C(1)–C(2)–C(12)	117.6(6)
C(3)–C(2)–C(12)	121.6(7)	O(2)–C(3)–C(4)	121.6(8)
C(2)–C(3)–C(4)	122.7(7)	O(2)–C(4)–C(5)	119.0(7)
C(3)–C(4)–C(5)	119.4(7)	C(4)–C(5)–C(6)	114.8(6)
C(1)–C(6)–C(5)	109.1(6)	C(1)–C(6)–C(13)	110.5(6)
C(1)–C(6)–C(14)	111.9(6)	C(5)–C(6)–C(13)	108.5(6)
C(5)–C(6)–C(14)	107.0(6)	C(13)–C(6)–C(14)	109.7(7)
C(1)–C(7)–C(8)	127.5(6)	C(7)–C(8)–C(9)	123.0(6)
C(8)–C(9)–C(10)	126.3(6)	C(8)–C(9)–C(15)	117.1(6)
C(10)–C(9)–C(15)	116.6(6)	C(9)–C(10)–C(11)	128.2(6)
O(3)–C(11)–O(4)	123.1(6)	O(3)–C(11)–C(10)	111.5(6)
O(4)–C(11)–C(10)	125.4(6)		

TABLE 8. DEVIATIONS OF NONHYDROGEN ATOMS FROM LEAST-SQUARES PLANES CONTAINING THE CONJUGATED DOUBLE BONDS

Plane A[a]		Plane B[b]		Plane C[c]	
C(7)	0.008Å	O(3)	0.000Å	C(2)	−0.008Å
C(8)	−0.006	O(4)	0.000	C(3)	0.016
C(9)	−0.003	C(10)	0.000	C(4)	0.010
C(10)	0.036	C(11)	0.000	C(5)	0.000
C(11)	−0.020	C(9)[d]	0.088	C(12)	−0.004
C(15)	−0.015			O(2)	−0.014
C(1)[d]	0.147			C(1)[d]	−0.205
O(1)[d]	−0.005			C(6)[d]	0.484
O(3)[d]	0.144				
O(4)[d]	−0.197				

a) The equation of the plane is: $0.3286X-0.5420Y+0.5238Z-3.220=0$. b) The equation of the plane is: $0.4212X-0.4217Y+0.5057Z-3.378=0$. c) The equation of the plane is: $0.6007X+0.7577Y-0.0618Z-5.885=0$. d) Omitted from the least-squares plane calculation.

TABLE 9. HYDROGEN BONDS AND SHORT VAN DER WAALS CONTACTS

The Roman numerals represent the symmetry operators relevant to the atoms listed second.

Hydrogen bonds

Donor	Aceptor	Distance D···A	Distance H···A	Angle D–H···A
O(1)—H(O1)···O(2)^{I}		2.848(8)Å	2.14(7)Å	147(6)°
O(3)—H(O3)···O(4)^{II}		2.670(7)	1.91(8)	171(8)

Short van der Waals contacts

O(2)–C(14)^{III}	3.360(11)Å	O(3)–C(9)^{IV}	3.629(8)Å
O(3)–C(10)^{V}	3.296(9)	O(3)–C(11)^{II}	3.482(9)
O(3)–C(12)^{IV}	3.524(10)	O(4)–C(11)^{II}	3.421(9)
O(4)–C(12)^{VI}	3.534(10)	O(4)–C(15)^{VII}	3.459(9)
C(9)–C(11)^{IV}	3.664(9)	C(10)–C(10)^{IIx}	3.608(9)
C(12)–C(15)^{VII}	3.632(11)		

Symmetry code

Superscript	Symmetry operator		
i)	x	y	$1+z$
ii)	$1-x$	$-y$	$-1-z$
iii)	x	y	$-1+z$
iv)	$1-x$	$-y$	$-z$
v)	$-x$	$-y$	$-1-z$
vi)	$1+x$	y	$1+z$
vii)	$-1+x$	y	z
iix)	$-1-x$	$-y$	$-z$

The O(3)–H···O(4) distance is 2.67 Å, the angle O(3)–H···O(4) is 171°, and the H atom is nearly on the line O(3)···O(4). Another hydrogen bond exists between the hydroxyl group attached to the cyclohexenone ring and the carbonyl group of the ring of the adjacent molecule. The O(1)–H···O(2) distance is 2.85 Å and the angle O(1)–H···O(2) is 147°. The hydrogen bond is not linear, but the distance is within the range of the O–H···O hydrogen bond.[15]

Other short contacts are given in Table 9. Most of them are in the range of van der Waals contact, but O(3)···C(10) 3.30 Å is slightly shorter than the sum of van der Waals radii (3.40 Å). Close C···O contacts have been reported and several types of molecular interaction have been recognized.[16–19] In one type the C–H group is attached to the electronegative oxygen atom. In another type the C=O group interacts with aromatic rings or C=C groups. In the present crystal the oxygen atom of the carboxylic group is close to the carbon atom of the diene group and situated antiparallel.

The authors are grateful to Dr. Takayuki Oritani, Tohoku University, for the supply of the sample. They also thank Mr. Chuji Katayama for his help in collection of the data.

References

1) K. Ohkuma, J. C. Lyon, and F. T. Adicott, *Science*, **142**, 1592 (1963).
2) J. W. Cornforth, B. V. Millborrow, and G. Ryback, *Nature*, **206**, 715 (1965).
3) J. W. Cornforth, W. Draber, B. V. Millborrow, and G. Ryback, *Chem. Commun.*, **1967**, 114.
4) R. S. Burden and H. R. Taylor, *Tetrahedron Lett.*, **1970**, 4071.
5) T. Oritani and K. Yamashita, *Agric. Biol. Chem.*, **34**, 1184 (1970).
6) T. Oritani and K. Yamashita, *Tetrahedron Lett.*, **1972**, 2521.
7) T. Oritani and K. Yamashita, *Agric. Biol. Chem.*, **36**, 362 (1972).
8) G. Ryback, *J. Chem. Soc., Chem. Commun.*, **1972**, 1190.
9) K. Mori, *Tetrahedron Lett.*, **1973**, 2635.
10) G. Weiss, M. Koreda, and K. Nakanishi, *J. Chem. Soc., Chem. Commun.*, **1973**, 565.
11) P. Swaminathan, J. Vijayalakshmi, and R. Srinivasan, *Acta Crystallogr., Sect. B*, **32**, 2351 (1976).
12) K. Ohkuma, *Agric. Biol. Chem.*, **29**, 962 (1965); **30**, 434 (1966).
13) G. Germain, P. Main, and M. M. Woolfson, *Acta Crystallogr., Sect. A*, **27**, 368 (1971).
14) "International Tables for X-Ray Crystallography," Vol. III, Birmingham, Kynoch Press (1968), p. 201.
15) G. C. Pimental and A. L. McClellan, "The Hydrogen Bond," W. H. Freeman and Co., San Francisco (1960), pp. 268, 271.
16) G. J. Palenik, *Acta Crystallogr.*, **19**, 47 (1965).
17) D. J. Sutor, *J. Chem. Soc.*, **1963**, 1105.
18) J. C. Calabrese, A. T. McPhail, and G. A. Sim, *J. Chem. Soc.*, **1970**, 282.
19) C. K. Prout and S. C. Wallwork, *Acta Crystallogr.*, **21**, 449 (1966).
20) Table 2 is kept at the Chemical Society of Japan, Kanda, Surugadai, Chiyodaku, Tokyo (Document No. 7709).

N-Alkylation of Nitrogen Heterocyclic Compounds with Dialkyl Phosphites

Masahiro HAYASHI, Kiyoshi YAMAUCHI, and Masayoshi KINOSHITA

Department of Applied Chemistry, Osaka City University, Sumiyoshi-ku, Osaka 558

(Received August 26, 1976)

Dialkyl phosphites were found to be efficient alkylating agents for various nitrogen heterocyclic compounds, especially for imidazole analogs and pyridones, producing the corresponding *N*-alkyl derivatives.

Generally, *N*-alkylation of nitrogen heterocyclic compounds has been attempted with dialkyl sulfates or alkyl halides. Recently, trialkyl phosphate, dialkyl phosphonate, and alkyl phosphinate were found to alkylate nitrogen heterocyclic compounds to give the corresponding *N*-alkyl derivatives in good yields.[1-4]

On the other hand, there are a few reports which show the addition of a dialkyl phosphite to the carbonyl groups of various heterocyclic compounds[5,6] and to etherify cholesterols.[7] However, there has been no report on the use of a dialkyl phosphite as an alkylating agent. The present paper shows a new method for the alkylation of imidazoles, 2,4-pyrimidinediols, and pyridones by means of a dialkyl phosphite.

Results and Discussion

Reactions were carried out by heating a mixture of a heterocyclic compound and a dimethyl, diethyl, diisopropyl, or dibutyl ester of phosphorus acid. The products were isolated by distillation or extraction after neutralization of the reaction mixtures. In the reaction

TABLE 1. REACTIONS OF NITROGEN HETEROCYCLIC COMPOUNDS WITH DIALKYL PHOSPHITES

Heterocyclic Compd	R of $(RO)_2P(O)H$	Time (h)	Temp (°C)	Product	Yield (%)
Imidazole (Im, Ia)	Me	1	155	1-Methyl-Im (Ib)	58
Benzotriazole (Bztri, IIa)	Me	1	165	1-Methyl-Bztri (IIb)	46
				2-Methyl-Bztri (III)	4
Pyrazole (Pyra, IVa)	Me	1	130	1-Methyl-Pyra (IVb)	69
Theophylline (TP, Va)	Me	4.5	130	7-Methyl-TP (Vb) (Caffeine)	71
	Et	7	180	7-Ethyl-TP	60
Uracil (U, VIa)	Me	4	170	1,3-Dimethyl-U (VIb)	12
				3-Methyl-U (VIc)	29
				1-Methyl-U (VId)	11
	Me	11[a]	140	1,3-Dimethyl-U (VIb)	19
				3-Methyl-U (VIc)	13
				1-Methyl-U (VId)	26
	Et	5	196	1,3-Diethyl-U	7
				3-Ethyl-U	4
Thymine (T, VIIa)	Me	4	172	1,3-Dimethyl-T (VIIb)	10
				3-Methyl-T (VIIc)	4
				1-Methyl-T (VIId)	35
	Me	11[a]	140	1,3-Dimethyl-T (VIIb)	6
				1-Methyl-T (VIId)	25
	Et	12	176	1,3-Diethyl-T	2
				3-Ethyl-T	1
				1-Ethyl-T	30
	Isopropyl	13	182	1-Isopropyl-T	1
	Bu	13	180	3-Butyl-T	1
				1-Butyl-T	4
2-Pyridone (2-Py, VIIIa)	Me	6	171	*N*-Methyl-2-Py (VIIIb)	81
	Me	11.5	100	*N*-Methyl-2-Py (VIIIb)	52
				2-Methoxypyridine (IX)	5
	Et	6	171	*N*-Ethyl-2-Py	80
	Et	44.5	100	*N*-Ethyl-2-Py	5
				2-Ethoxypyridine	10
4-Pyridone (4-Py, Xa)	Me	5.5	169	*N*-Methyl-4-Py (Xb)	98
	Et	5.75	173	*N*-Ethyl-4-Py	86

a) Tributylamine was added.

of uracil and thymine, the yields of products were obtained spectrometrically. The results are summarized in Table 1.

The reaction of imidazole (Ia) with dimethyl phosphite proceeded smoothly at 155 °C to give 1-methylimidazole (Ib) as a liquid with the coformation of monomethyl phosphite or phosphorus acid. Facile alkylations were also observed in theophylline (Va) and pyrazole (VIa) giving 7-alkyl and 1-alkyl derivatives, respectively. Selective alkylation took place in benzotriazole (IIa) in which alkylation occurred at the N-1 position preferentially to the N-2 position producing 1-methylbenzotriazole (IIb) and 2-methylbenzotriazole (III) at an approximately 11 to 1 molar ratio. Other alkylating agents, such as dialkyl sulfates, alkyl halides, and diazomethane, are known to give N-1 and N-2 derivatives at less selective ratios (2: 1, 5: 3, and 3: 10, respectively).[8-14]

In 2,4-pyrimidinediols, the yields of *N*-alkyl derivatives was rather low, *e.g.*, in the reaction with uracil (VIa) at 170 °C, 1,3-dimethyluracil (VIb), 3-methyluracil (VIc), and 1-methyluracil (VId) were obtained in 12, 29, and 11% yields, respectively. But when a large amount of a tertiary amine was used in the reaction, the conversion of uracil to methylated derivatives increased even at low reaction temperature (140 °C), *e.g.*, for tributylamine, 1,3-dimethyluracil (VIb), 3-methyluracil (VIc), and 1-methyluracil (VId) were obtained in 19, 13, and 26% yields, respectively, with no other product. The employment of solvents, such as *N*,*N*-dimethylformamide, ethanol, and diglyme,

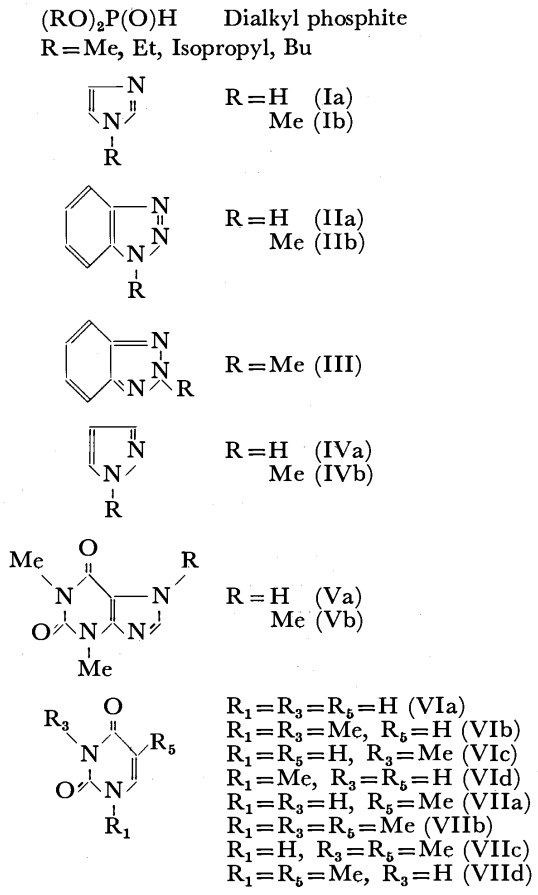

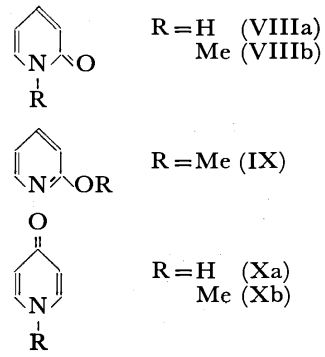

lowered the yield of the *N*-alkyl derivatives by about one-third, but tended to increase the relative yield of the 1-alkyl derivatives produced. In the reaction of thymine (VIIa), alkylation occurred mainly at the N-1 position giving 1-alkyl derivatives along with small amounts of 3-alkyl and 1,3-dialkyl derivatives. In this case, the reaction was not appreciably affected by the addition of a tertiary amine. The yield of the 1,3-dialkyl derivative increased with the reaction temperature and no *O*-alkylation was observed for these 2,4-pyrimidinediols (VIa, VIIa). At higher temperature (about 200 °C), the yields of alkylated products from VIa and VIIa decreased and relatively large amounts of unknown products were obtained, which appeared to be derived from decomposition of the pyrimidine ring, since no absorption was observed in the aromatic region of complex NMR spectra.

However, for 2-pyridone (VIIIa), alkylation occurred very smoothly giving the corresponding *N*-alkyl derivative. Here, the *O*-alkyl derivative was isolated only when the reaction was carried out at low temperature and was found to undergo rapid thermal rearrangement to the corresponding *N*-alkyl derivative upon heating at high temperature. Similar facile alkylation was observed in 4-pyridone (Xa) although the *O*-alkyl derivative was neither isolated nor detected even at low temperature (97 °C).

For the above reactions, the reactivities of the dialkyl phosphites were found to be in the following general order; methyl>ethyl>butyl>isopropyl as shown in Table 1. The present results suggest that dialkyl phosphites may be utilized as covenient alkylating agents, especially for imidazole analogs and pyridones.

Experimental

UV and IR spectra were measured with Hitachi 3-T and Jasco IR-G spectrometers, respectively. NMR spectra were recorded on a Hitachi-Perkin Elmer R-20 spectrometer with a dilute solution in deuterochloroform and deuterium oxide using tetramethylsilane as an internal and external standard.

Preparative thin-layer chromatography (aluminium oxide, Merck Art 1064) was used to analyze the reaction products.

All materials are commercially available and were used without further purification. The reaction conditions are given in Table 1. The following experiments are typical. Other compounds in the table were prepared similarly and their physical constants agreed with the literature values.

Methylation of Imidazole (Ia). A mixture of Ia (1.00 g, 0.015 mol) and dimethyl phosphite (0.81 g, 0.70 mol) was

heated at 155 °C with stirring for 1 h. After the reaction mixture had been neutralized by aqueous sodium hydrogencarbonate, it was extracted with tetrahydrofuran. Upon concentration of the organic extract, 1-methylimidazole (Ib) was obtained as a liquid; (0.70 g, 58%). bp 76—77 °C/11 Torr (lit,[11] 94—95 °C/13 Torr). IR and NMR spectra of the product are identical with those of an authentic sample.

Methylation of Theophylline (Va). 1.01 g (0.0056 mol) of Va and 1.20 g (0.0109 mol) of dimethyl phosphite were heated at 130 °C for 4.5 h with stirring. The reaction mixture was neutralized and extracted with chloroform. The organic layer gave 7-methyltheophylline (Vb, caffeine, 0.775 g, 71%). IR, NMR, UV, and mp measurements were consistent with those of an authentic sample.

Methylation of Pyrazole (IVa). A mixture of IVa (1.00 g, 0.0147 mol) and dimethyl phosphite (0.81 g, 0.0073 mol) was heated at 130 °C for one hour with stirring. 1-Methylpyrazole (IVb) was distilled at 127 °C during the reaction through a distillation column; (0.85 g, 69%). bp 127 °C (lit,[15] 127 °C); NMR: τ($CDCl_3$): 2.60 (d, J=3 Hz, 2H, ring), 3.81 (t, J=3 Hz, 1H, ring), and 6.20 (s, 3H, $-CH_3$).

Methylation of Benzotriazole (IIa). A mixture of IIa (2.00 g, 0.0168 mol) and dimethyl phosphite (0.93 g, 0.0084 mol) was heated at 165 °C with stirring for one hour. The reaction mixture was neutralized with aqueous sodium hydrogencarbonate and extracted with chloroform. The organic layer was concentrated to give the residue (1.44 g), the NMR spectrum of which showed only peaks attributable to 1-methylbenzotriazole (IIb), 2-methylbenzotriazole (III), and benzotriazole (IIa). From the area ratio (34: 3: 4) of the singlet peaks of the CH_3 groups of both isomers (τ=5.83 for IIb and τ=5.60 for III), and the NH group of IIa (τ=−5.50), the yields of IIb, III, and IIa were calculated to be 46, 4, and 16%, respectively. Isolation of these products was carried out in a manner similar to that mentioned in a previous paper.[4] The values of the physical constants agree with those of authentic samples.

Methylation of Uracil (VIa). A mixture of VIa (3.01 g, 0.0268 mol), dimethyl phosphite (6.00 g, 0.0545 mol), and tributylamine (10.0 g) was heated at 140 °C for 11 h with stirring. After one hour of heating, VIa was a thoroughly mixed solution. The reaction mixture was diluted with water to 50 ml, then separated using preparative aluminium oxide thin-layer chromatography (eluted with $CHCl_3$: MeOH=10: 1). This gave four ultraviolet absorbing spots [R_f and λ_{max} (mμ): **a**= 0.97, 267.5, **b**=0.57, 260.0, **c**=0.38, 268.0, and **d**=0.10, 259.5], which were identified to be **a**=1,3-dimethyluracil (VIb), **b**=3-methyluracil (VIc), **c**=1-methyluracil (VId), and **d**=uracil (VIa), from a comparison of the physical constants (from IR, UV, NMR, and mp determinations) with literature values[7,16,17] and authentic samples. The yields for the reaction products were calculated to be VIb=19, VIc=26, and VId=30%.

Methylation of Thymine (VIIa). A mixture of VIIa (0.50 g, 0.0039 mol) and dimethyl phosphite (2.40 g, 0.0218 mol) was heated at 172 °C for 4 h with stirring. The reaction mixture was neutralized with sodium hydrogencarbonate and diluted to 80 ml and then separated in a manner similar to that described above. The following products were obtained (their physical constants are consistent with those of authentic samples and literature values): *N*-Alkyl derivatives, yield, R_f ($CHCl_3$: MeOH=10: 1), and λ_{max}(H_2O): 1,3-dimethylthymine (VIIb), 10, 0.98, 272, 3-methylthymine (VIIc), 4, 0.72, 265, and 1-methylthymine (VIId), 35%, 0.47, 273 mμ, respectively; (lit,[18] VIIb, 272, VIIc, 264.5, and VIId, 273 mμ).

Methylation of 2-Pyridone (VIIIa). A mixture of VIIIa (3.00 g, 0.0316 mol) and dimethyl phosphite (3.60 g, 0.0327 mol) was heated at 100 °C for 11.5 h. Then the mixture was made alkaline with aqueous sodium hydroxide and then extracted with chloroform. Thin-layer chromatography (eluted with $CHCl_3$: MeOH=10: 1) showed three spots (R_f, **e**=0.77, **f**=0.44, **g**=0.33). The spots **e** and **g** were identified from authentic samples to be *N*-methyl-2-pyridone (VIIIb) and 2-pyridone (VIIIa), respectively. The residue (1.97 g) from the organic layer dissolved with deuterochloroform in order to obtaine the NMR spectrum. From the area ratio (20: 2.1) of the singlet peaks of the CH_3 groups of both isomers [τ=6.62 for VIIIb and τ=6.27 for 2-methoxypyridine (IX)], the yield of *N*-methyl and *O*-methyl derivatives were calculated to be 52 and 5%, respectively. Distillation of this mixture gave IX (trace) and VIIIb (1.44 g, 42%): 2-methoxypyridine (IX); bp 60 °C/50 Torr (lit,[20] 142.4 °C), picrate (acetone–H_2O); mp 141—143 °C (lit,[20] 145—146 °C): *N*-methyl-2-pyridone (VIIIb); bp 92 °C/4 Torr (lit,[19] 250 °C).

Methylation of 4-Pyridone (Xa). 1.74 g (0.0183 mol) of Xa and 2.04 g (0.0185 mol) of dimethyl phosphite reacted at 169 °C for 5.5 h. The reaction mixture produced only one thin-layer chromatographic product; R_f=0.72 (Xb) and R_f= 0.41 (Xa) (eluted with $CHCl_3$: MeOH=10: 1). Making the solution alkaline with aqueous sodium hydroxide and extracting with chloroform gave *N*-methyl-4-pyridone (Xb, 1.95 g, 98%); picrate (acetone–H_2O), mp 183.5—184.5 °C, NMR; τ ($CDCl_3$) 2.49 (d, J=7 Hz, 2H, ring), 3.77 (d, J= 7 Hz, 2H, ring), and 6.36 (s, 3H, $-CH_3$).

References

1) K. Yamauchi and M. Kinoshita, *J. Chem. Soc., Perkin Trans. 1*, **1973**, 391.
2) K. Yamauchi and M. Kinoshita, *J. Chem. Soc., Perkin Trans. 1*, **1973**, 2506.
3) K. Yamauchi, M. Hayashi, and M. Kinoshita, *J. Org. Chem.*, **40**, 385 (1975).
4) M. Hayashi, K. Yamauchi, and M. Kinoshita, *Bull. Chem. Soc. Jpn.*, **49**, 283 (1976).
5) D. Redmore, *Chem. Rev.*, **71**, 315 (1971) and references cited therein.
6) K. J. M. Andrews and F. R. Atherton, *J. Chem. Soc.*, **1960**, 4682.
7) Y. Kashman, *J. Org. Chem.*, **37**, 912 (1972).
8) F. R. Benson and W. L. Savell, *Chem. Rev.*, **46**, 1 (1950).
9) M. A. Phillips, *J. Chem. Soc.*, **1921**, 2920 and **1931**, 1143.
10) M. R. Atkinson and J. B. Polya, *J. Chem. Soc.*, **1954**, 141.
11) L. P. Kyrides, F. B. Zienty, G. W. Steahly, and H. L. Morril, *J. Org. Chem.*, **12**, 577 (1947).
12) F. L. Pyman and L. Light, *J. Chem. Soc.*, **121**, 2616 (1922).
13) J. G. Buchman, A. W. Johnson, J. A. Mills, and A. R. Todd, *J. Chem. Soc.*, **1950**, 2845.
14) F. Krollpfeiffer, *Ber.*, **71B**, 596 (1938).
15) K. v. Auwers, *Ann.*, **437**, 52 (1924).
16) C. W. Whitehead, *J. Am. Chem. Soc.*, **74**, 4267 (1952).
17) D. Shugar and J. J. Fox, *Biochim. Biophys., Acta*, **9**, 199 (1952).
18) E. Wittenburg, *Chem. Ber.*, **99**, 2391 (1966).
19) A. H. Blatt, *Org. Synth.*, Coll. Vol. II, 419 (1943).
20) H. J. den Hertog, *Recl. Trav. Chim., Pays-Bas*, **74**, 1160 (1955).

Isolation of Enammonium Salt and Its Rearrangement to the Corresponding Iminium Salt

Hajime MATSUSHITA, Yasuko TSUJINO, Masao NOGUCHI, and Sadao YOSHIKAWA*

Central Research Institute, The Japan Tobacco and Salt Public Corporation, 6-2 Umegaoka, Midori-ku, Yokohama, Kanagawa 227

**Department of Synthetic Chemistry, Faculty of Engineering, The University of Tokyo, Hongo, Bunkyo-ku, Tokyo 113*

(Received October 14, 1976)

Enammonium salt of 2-methyl-1-(β-methylstyryl)piperidine (**1**) was isolated for the first time and characterized. The enammonium salt, 2-methyl-1-(β-methylstyryl)piperidinium chloride (**2**), was found to change easily to the corresponding iminium salt, 2-methyl-1-(2-phenylpropylidene)piperidinium chloride (**3**), at room temperature. The structure of the salts derived from 1-(β-methylstyryl)piperidine (**4**), 2-methyl-1-(β-methylstyryl)pyrrolidine (**5**), 1-(β-methylstyryl)pyrrolidine (**6**), 1-(2-methyl-1-propenyl)pyrrolidine (**7**), and 2-methyl-1-(2-methyl-1-propenyl)piperidine (**8**) were also examined.

Enamines are useful as a starting material for various organic syntheses, and their reactivities have been investigated by many workers.[1] One of the reactions is the formation of salts with acids. Protonation on the nitrogen or the β-carbon of the enamine to give the salt (I) or (II) is possible.

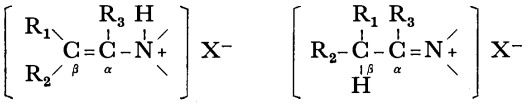

Enammonium salt (I) Iminium salt (II)

It has been shown that the protonation takes place rapidly on nitrogen and is followed by a transfer of the proton to the carbon. The evidence for *N*-protonation has been based on the reaction of ozone, diazomethane or lithium aluminum hydride with *N*-protonated salts under cooling.[2] Existence of the enammonium salt and its rearrangement to the corresponding iminium salt were also suggested kinetically.[3] However, the enamine salts so far isolated have the iminium salt structure (II).[4] This paper deals with the isolation and identification of *N*-protonated salt derived from 2-methyl-1-(β-methylstyryl)piperidine (**1**), 2-methyl-1-(β-methylstyryl)piperidinium chloride (**2**), and its rearrangement to the corresponding iminium salt (**3**). Structures of the salts derived from 1-(β-methylstyryl)piperidine (**4**),[5] 2-methyl-1-(β-methylstyryl)pyrrolidine (**5**),[6] 1-(β-methylstyryl)pyrrolidine (**6**),[5] 1-(2-methyl-1-propenyl)-pyrrolidine (**7**)[3] and 2-methyl-1-(2-methyl-1-propenyl)piperidine (**8**) were also examined.

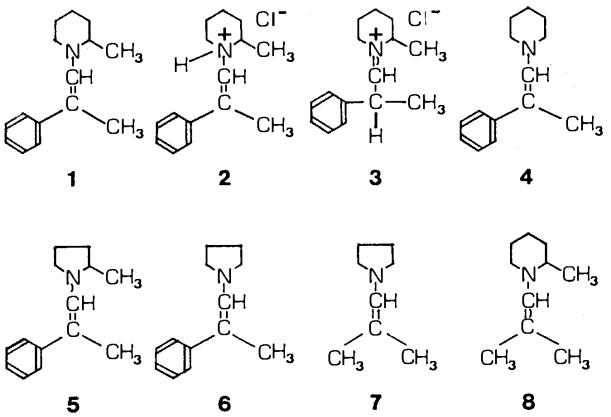

1 **2** **3** **4**

5 **6** **7** **8**

Experimental

Proton magnetic resonance spectra were obtained with a JNM-PS-100 Spectrometer. Chemical shifts are indicated in δ value using TMS as an internal standard. The IR spectra were recorded with a JASCO IR-S Spectrometer. Gas chromatographic analyses were carried out on a 2 m column of 20% Carbowax 20 M on Cromosorb W with a Hitachi Gas Chromatograph, Model K 53.

Materials. Enamines, **1**, **4**, **5**, **6**, **7**, and **8** were prepared by the usual azeotropic procedures with benzene as a solvent. **8**; bp 66.5—67 °C (17 Torr).

Preparation of the Salts. The preparation of the salts was carried out as follows. Dry hydrogen chloride gas was bubbled into a benzene solution (60 ml) of each enamine (0.1 mol) under cooling in an ice-salt bath. White very fine needles precipitated out gradually. The needles were separated from the solution by filtration, washed with benzene completely in a dry box, and dried under vacuum. The data of PMR spectra and IR spectra are summarized in Tables 1 and 2, respectively.

PMR Spectra of Enamines and Their Salts. The solutions for PMR spectral measurements were prepared by dissolving about 30 mg of the enamines or their salts in 0.5 ml CD_3OD or $CDCl_3$ in a dry box. They are easily soluble in both solvents. The spectra of the salts were obtained immediately after preparation of the samples.

Results and Discussion

The salts derived from **1**, **4**, **5**, and **6** are highly hydroscopic and decompose into 2-phenylpropanal and the amine hydrochlorides on exposure to air. No elemental analyses of these salts could be carried out. The salts were hydrolyzed and the resulting 2-phenylpropanal was estimated gas-chromatographically. (The 2-phenylpropanal obtained from the hydrolyzates of the salts: 0.93 mol/1 mol salt of **1**, 0.91 mol/1 mol salt of **4**, 0.97 mol/1 mol salt of **5**, 0.95 mol/1 mol salt of **6**). The results show that one mol of 2-phenylpropanal is obtained from one mol of each salt within experimental error.

PMR spectra of **1**, **2**, and **3** in CD_3OD and those of **2** and **3** in $CDCl_3$ are shown in Fig. 1. The spectrum of **1** in $CDCl_3$ was essentially the same as that of **1** in CD_3OD.

Two olefin proton signals (5.75 and 5.99 ppm) and

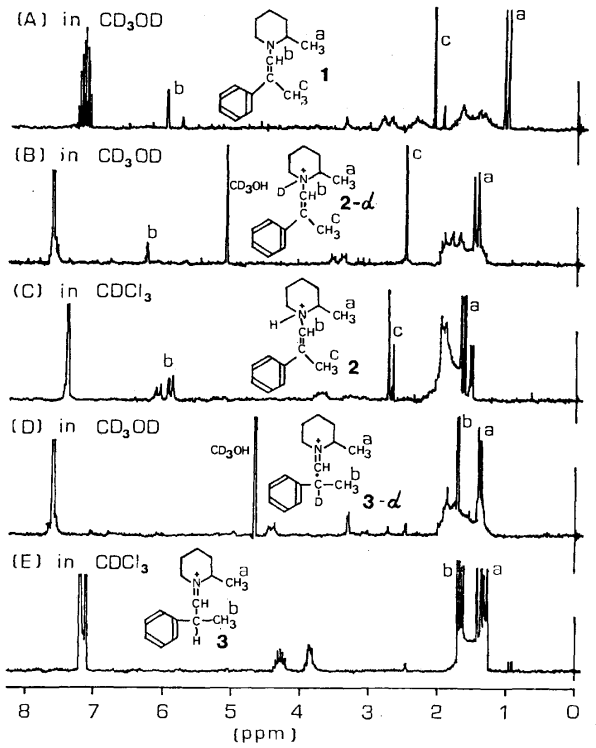

Fig. 1. 100 MHz PMR spectra of **1**, **2**, and **3** in CD_3OD or $CDCl_3$.

two propenyl methyl proton signals (1.95 and 2.10 ppm) were observed (Fig. 1-(A)). The area ratio of the former signals 5.75 ppm: 5.99 ppm is 8: 92, coinciding with that of the latter 1.95 ppm: 2.10 ppm (10: 90). This shows that **1** is a mixture of two geometrical isomers, one of which predominantes over the other. The existence ratio of the isomers in $CDCl_3$ is essentially the same as that in CD_3OD. The predominant one seems to have a structure where the phenyl and the 2-methylpiperidino groups are situated in trans position to each other judging from the steric models of the two geometrical isomers. Allyl couplings (1.5 Hz) are observed between the corresponding olefin and methyl protons. The allyl coupling constant, 1.5 Hz, was also observed between the olefin proton (6.27 ppm) and the propenyl methyl protons (2.48 ppm) (Fig. 1-(B)). This shows that **2** has the same partial structure, N–CH=C–CH_3, as enamine, **1**. The propenyl methyl signals at 2.10 ppm in spectrum (A) shift toward lower field, 2.48 ppm, in spectrum (B). This also supports the partial structure of the enammonium salt, N^+H–CH=C–CH_3. The occurrence of the proton exchange between CD_3OD and N^+H–CH=C–CH_3 or HCl is shown by the appearance of the signal at 5.10 ppm assignable to CD_3OH in spectrum (B). The hydrochloric acid might be derived from that of crystallization. The PMR signals of the two geometrical isomers in CD_3OD are considered to completely overlap each other, because of the existence of the isomers as shown in Fig. 1-(C). The existence ratio of the geometrical isomers was determined as 2: 3 based on the area ratio of the respective signals. This suggests that the formation of the enammonium salt is accompanied by geometrical isomerization. The isomerization was also observed in the case of **4**.[5] The signal of the olefin proton seems to be the A part of a nearly pure first-order AMX_3 pattern; major isomer (J=8.0, 1.2 Hz), minor isomer (J=9.1, 1.5 Hz). The coupling constant, 1.2 or 1.5 Hz, is due to the allyl coupling between the olefin proton and the propenyl methyl protons. The coupling constant, 8.0 or 9.1 Hz, may be due to the coupling between this olefin proton and the proton attached to the nitrogen atom. The major one seems to have a structure in which the phenyl and the 2-methylpiperidino groups are situated in trans position to each other. The smaller allyl coupling constant of the major isomer (1.2 Hz) suggests that the propenyl methyl group is situated in trans position of the olefin proton, because J_{cisoid} is usually larger than $J_{transoid}$.[7]

When the CD_3OD solution of **2** was heated up to 50 °C, the signals of the PMR spectrum of **2** (spectrum B) changed to those of **3** in a CD_3OD solution (Fig. 1-(D)). The methyl proton signal at 2.48 ppm in spectrum B is shifted to the higher field (at 1.70 ppm) in spectrum D. This suggests that the enammonium structure, CH_3–C=C–N^+–, was converted in solution into the iminium structure, CH_3–C–C=N^+. The signal at 1.70 ppm was singlet, and no allyl coupling could be observed, indicating that **3** in CD_3OD had been deuterated at the β-carbon. This shows that **2** is easily deuterated in CD_3OD to the N-deuterated salt which is subsequently rearranged to the corresponding iminium salt. The sequence of the reactions (Scheme 1) is in line with the generally accepted mechanism of the iminium salt formation.

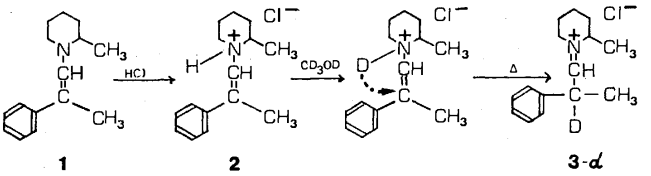

Scheme 1.

In the case of a $CDCl_3$ solution, the signals of the PMR spectrum of **2** (Fig. 1-(C)) also changed to those of **3** (Fig. 1-(E)).[8] Addition of CD_3OD to the $CDCl_3$ solution of **2** is recognized to accelerate the rearrangement, giving **3-d** (Fig. 1-(D)). Possibility of the existence of two geometrical isomers of **3** can be neglected by consideration of the steric interaction using models (Corey-Pauling-Kaltum type and Dreiding type).[6] PMR spectra of the salts derived from **4** and **5** were also obtained. As shown in Table 1, the produced salts have the iminium salt structures. Bubbling of dry hydrogen chloride gas into the solution of **4** or **5** under cooling also gave the corresponding enammonium salts although their amounts were much smaller in comparison with those of the iminium salts.

From the PMR spectral data of the enamines and their salts, **1**—**8** (Table 1), we see that the salts except for **2** have an iminium salt structure.

The complex bands observed in 2350—2600 cm^{-1} in the IR spectrum of **2** were assignable to the ammonium

Table 1. PMR Spectral data of enamines, enammonium and iminium salts (in $CDCl_3$)

1	major: 1.03 (d, J=6.70 Hz, N-CH-C$\underline{H}_3$), 2.10 (d, J=1.5 Hz, CH=C-C$\underline{H}_3$), 5.99 (d, J=1.5 Hz, C$\underline{H}$=C-CH_3), minor: 1.09 (d, J=6.70 Hz, N-CH-C$\underline{H}_3$), 1.95 (d, J=1.5 Hz, CH=C-C$\underline{H}_3$), 5.75 (d, J=1.5 Hz, C$\underline{H}$=C-CH_3).
2	major: 1.63 (d, J=6.0 Hz, $\overset{+}{N}$H-CH-C$\underline{H}_3$), 2.72 (d, J=1.2 Hz, CH=C-C$\underline{H}_3$), 5.90 (dq, J=8.0, 1.2 Hz, C$\underline{H}$=C-CH_3), minor: 1.51 (d, J=6.0 Hz, $\overset{+}{N}$H-CH-C$\underline{H}_3$), 2.66 (d, J=1.5 Hz, CH=C-C$\underline{H}_3$), 6.09 (dq, J=9.1, 1.5 Hz, C$\underline{H}$=C-CH_3).
3	major: 1.40 (d, J=7.0 Hz, $\overset{+}{N}$-CH-C$\underline{H}_3$), 1.69 (d, J=7.5 Hz, CH-CH-C$\underline{H}_3$), 9.00 (m, $\overset{+}{N}$=C$\underline{H}$-C), minor: 1.29 (d, J=6.5 Hz, $\overset{+}{N}$-CH-C$\underline{H}_3$), 1.66 (d, J=7.5 Hz, CH-CH-C$\underline{H}_3$), 9.08 (m, $\overset{+}{N}$=C$\underline{H}$-C).
4	major: 2.09 (d, J=1.2 Hz, CH=C-C$\underline{H}_3$), 6.11 (d, J=1.2 Hz, C$\underline{H}$=C-CH_3), minor: 1.97 (d, J=1.6 Hz, CH=C-C$\underline{H}_3$), 5.82 (d, J=1.6 Hz, C$\underline{H}$=C-CH_3).
Salt of **4**	1.46 (d, J=7.0 Hz, CH-CH-C$\underline{H}_3$), 9.65 (m, $\overset{+}{N}$=C$\underline{H}$-C).
5	major: 1.17 (d, J=6.3 Hz, N-CH-C$\underline{H}_3$), 2.15 (d, J=1.3 Hz, CH=C-C$\underline{H}_3$), 6.40 (d, J=1.3 Hz, C$\underline{H}$=C-CH_3), minor: 1.17 (d, J=6.3 Hz, N-CH-C$\underline{H}_3$), 2.04 (d, J=1.5 Hz, CH= C-C$\underline{H}_3$), 6.11 (d, J=1.5 Hz, C$\underline{H}$=C-CH_3).
Salt of **5**	major: 1.55 (d, J=7.0 Hz, $\overset{+}{N}$-CH-C$\underline{H}_3$), 1.80 (d, J=7.5 Hz, -CH-C$\underline{H}_3$), 8.86 (m, $\overset{+}{N}$=C$\underline{H}$-C), minor: 1.55 (d, J=7.0 Hz, $\overset{+}{N}$-CH-C$\underline{H}_3$), 1.78 (d, J=6.5 Hz, -CH-C$\underline{H}_3$), 8.86 (m, $\overset{+}{N}$=C$\underline{H}$-C).
6	major: 2.07 (d, J=1.2 Hz, CH=C-C$\underline{H}_3$), 6.38 (d, J=1.2 Hz, C$\underline{H}$=C-CH_3), minor: 1.95 (d, J=1.6 Hz, CH=C-C$\underline{H}_3$), 6.07 (d, J=1.6 Hz, C$\underline{H}$=C-CH_3).
Salt of **6**	1.80 (d, J=7.5 Hz, -CH-C$\underline{H}_3$), 9.76 (m, $\overset{+}{N}$=C$\underline{H}$-C).
7	major: 1.75 (s, -C$\underline{H}_3$), 5.67 (m, C$\underline{H}$=C-CH_3), minor: 1.68 (s, -C$\underline{H}_3$), 5.67 (m, C$\underline{H}$=C-CH_3).
Salt of **7**	1.32 (C-C$\underline{H}_3$), 8.15 (d, J=9.0 Hz, $\overset{+}{N}$=C$\underline{H}$-).
8	mixture of two geometrical isomers (1 : 1) 0.97 (d, J=6.2 Hz, N-C-C$\underline{H}_3$), 1.67 (d, J=1.6 Hz, C=C-C$\underline{H}_3$), 1.72 (d, J=1.4 Hz, C= C-C$\underline{H}_3$), 5.24 (m, N-C$\underline{H}$=C).
Salt of **8**	1.37 (d, J=6.8 Hz, $\overset{+}{N}$-C-C$\underline{H}_3$), 1.61 (d, J=7.2 Hz, $\overset{+}{N}$=C-C-C$\underline{H}_3$), 9.14 (d, J=8.0 Hz, $\overset{+}{N}$=C$\underline{H}$).

structure, N^+–H. In the case of nicotine hydrochloride, it was reported that the band attributable to the ammonium structure was observed in the region of 2350—2440 cm^{-1}.[9] The IR spectrum of **3** was obtained after concentration of its $CDCl_3$ solution. The absorption band, 1637 cm^{-1}, due to the double bond stretching of the enamine shifts by 21 and 34 cm^{-1} toward higher frequencies in those of **2** and **3**, respectively. Leonard and Gash reported a shift of 20—50 cm^{-1} toward higher frequencies when an enamine was converted into its iminium salt.[4] The salts derived from enamines except for **2** have an iminium salt structure, since the band due to ν_{NH} connot be observed in the spectra of these salts (Table 2).

Table 2. Infrared frequencies of enamines, enammonium and iminium salts

	$\nu_{C=C}$	$\nu_{C=N}$	ν_{N-H}	Lit
1	1637			
2	1658		2350—2600	
3		1671		
4	1637			
Salt of **4**		1677		
5	1631			6
6	1633			
Salt of **6**		1679		
7	1672			2
Salt of **7**		1715		10
8	1675			
Salt of **8**		1690		
Nicotine HCl			2353—2439	9
Nicotine 2HCl			2353—2439	9

It seems that the enammonium salt is too labile to be isolated. Salt **2** seems to be the first case of the isolation of the enammonium salt. Preparation of the salts of **4**, **5**, and **6** under cooling also gave the enammonium salts although their contents were low. This shows that **4**, **5**, and **6** as well as **1** have a possibility of giving their corresponding enammonium salt. No enammonium salts could be detected in the salts derived from **7** and **8**. The stability of the enammonium salt can be attributed to the conjugation of the C=C double bond with benzene ring. The salt isolated as crystals derived from **1** was enammonium salt **2**, and iminium salt **3** could be obtained as the product of the rearrangement of **2**. On the other hand, the salts of **4**, **5**, and **6** isolated as crystals were iminium salts. It seems that enammonium salt of **1** is sparingly soluble in benzene, but those of **4**—**5** are readily soluble and subsequently converted into the corresponding less soluble iminium salts. Thus, it is concluded that in the case of the salt of **1**, rearrangement from **2** to **3** would be interfered by the immediate precipitation of **2** out of the solution. This may be the reason why the salt derived from **1** has the enammonium salt structure.

References

1) A. G. Cook, "Enamines," Marcel Dekker, New York and London (1969).
2) G. Optiz and A. Griesinger, *Ann.*, **665**, 101 (1963).
3) E. J. Stamhuis and W. Maas, *J. Org. Chem.*, **30**, 2156 (1965).
4) N. J. Leonard and V. W. Gash, *J. Am. Chem. Soc.*, **76**, 2781 (1954).
5) H. Matsushita, M. Noguchi, M. Saburi, and S. Yoshikawa, *Bull. Chem. Soc. Jpn.*, **48**, 3715 (1975).
6) H. Matsushita, M. Noguchi, and S. Yoshikawa, *Bull. Chem. Soc. Jpn.*, **49**, 1928 (1976).
7) Jackman and Sternhell, "Applications of Nuclear Magnetic Resonance Spectroscopy in Organic Chemistry," Pergamon Press (1969), p. 316.
8) H. Matsushita, Y. Tsujino, M. Noguchi, and S. Yoshikawa, in press.
9) B. Witkop, *J. Am. Chem. Soc.*, **76**, 5597 (1954).
10) N. J. Leonard and K. Jann, *J. Am. Chem. Soc.*, **84**, 4806 (1962).

Photolysis of Ethyl Azidoformate in Ethers and in Alcohols

Noboru TORIMOTO, Tadao SHINGAKI,* and Toshikazu NAGAI*

Science Education Institute of Osaka Prefecture, Karita-cho, Sumiyoshi-ku, Osaka 558

**College of General Education, Osaka University, Toyonaka, Osaka 560*

(Received October 18, 1976)

Ethoxycarbonyl nitrene, generated by the photolysis of ethyl azidoformate (I), was inserted preferentially into the α C–H bonds of acyclic ethers. Each of the reactions with acyclic ethers gave *N*-alkoxyurethane *via* a cleavage of the C–O bond, indicating that an O–N ylide is an intermediate of the nitrene reaction. Comparing sensitized photolysis with direct photolysis of I in ethers and in alcohols, it was found that the nitrene insertion into the α C–H bonds of ethers proceeds for both singlet and triplet and that the insertion into the β and γ C–H bonds of ethers and the O–H bonds of alcohols proceeds only for the singlet.

In a previous paper,[1] the photolysis of ethyl azidoformate (I) in cyclic ethers was reported. The ethoxycarbonyl nitrene, generated by the photolysis of I, was inserted preferentially into the α C–H bonds of cyclic ethers. The reactions with cyclic ethers bearing an alkyl group at the α-position gave unsaturated alkoxyurethane *via* a cleavage of the ring C–O bond. In addition, the nitrene insertion into the α C–H bonds of *cis*- and *trans*-2,5-dimethyltetrahydrofurans proceeded non-stereospecifically. From these results, a mechanism which included an O–N ylide intermediate for the insertion reaction was proposed, although the hydrogen abstraction-recombination mechanism was not ruled out.

The present paper reports further information about the mechanism based on a study of the photolyses of I carried out in acyclic ethers and in alcohols. Furthermore, the sensitized photolysis of I was examined and compared with direct photolysis in the ethers and alcohols.

Results and Discussion

Direct Photolysis of Ethyl Azidoformate in Acyclic Ethers. Ethyl azidoformate (I) in acyclic ether (III) was irradiated by the light (mainly of 2537 Å) from a low-pressure mercury arc at 0 °C with stirring in an atmosphere of nitrogen. Insertion products (IV) of ethoxycarbonyl nitrene (II) into the C–H bonds of the acyclic ethers were obtained, accompanied by the hydrogen abstraction product, urethane (VI), and small amounts (0.3—1.3%) of diethyl hydrazodiformate (VII). In addition, *N*-alkoxyurethanes (V) were obtained for each reaction.

TABLE 1. DIRECT PHOTOLYSIS OF ETHYL AZIDOFORMATE IN ACYCLIC ETHERS

Ether (III)	Product (%)[a]				
	Insertion (IV)		C–O Cleavage (V)		Abstraction (VI)
(a) Diethyl	(a) $CH_3CHOC_2H_5$ (NHR)	31.2	(a) CH_3CH_2ONHR[b]	3.9	17.6
(b) Dipropyl	(b$_1$) $CH_3CH_2CHOC_3H_7$ (NHR)	32.3	(b) $CH_3CH_2CH_2ONHR$	5.6	20.5
	(b$_2$) $CH_3CHCH_2OC_3H_7$ (NHR)	3.1			
(c) Dibutyl	(c$_1$) $CH_3CH_2CH_2CHOC_4H_9$ (NHR)	25.0	(c) $CH_3CH_2CH_2CH_2ONHR$	4.1	17.4
	(c$_2$) $CH_3CH_2CHCH_2OC_4H_9$ (NHR)	3.8			
	(c$_3$) $CH_3CHCH_2CH_2OC_4H_9$ (NHR)	3.9			
(d) Diisopentyl	(d$_1$) $(CH_3)_2CHCH_2CHOC_5H_{11}$ (NHR)	17.1	(d) $(CH_3)_2CHCH_2CH_2ONHR$	2.4	15.1
	(d$_2$) $(CH_3)_2CCH_2CH_2OC_5H_{11}$ (NHR)	5.7			
(e) Isobutyl methyl	(e$_1$) $(CH_3)_2CHCHOCH_3$ (NHR)	16.5	(e$_1$) $(CH_3)_2CHCH_2ONHR$	2.6	20.3
	(e$_2$) $(CH_3)_2CHCH_2OCH_2$ (NHR)	5.7	(e$_2$) CH_3ONHR	trace	
(f) 2-Methoxyethanol	ND[c]		(f) $CH_3OCH_2CH_2ONHR$[d]	37.8	21.2

a) Calculated on the basis of the azide used. b) R: COOEt. c) ND: not detected. d) This compound is the O–H insertion product.

$$N_3COOEt \xrightarrow[-N_2]{h\nu} :NCOOEt \xrightarrow{R\text{-}O\text{-}C_nH_{2n+1}}$$

(I) (II)

$$R\text{-}O\text{-}C_nH_{2n}NHCOOEt + R\text{-}ONHCOOEt$$

(IV) (V)

$$+ NH_2COOEt + \begin{matrix} NHCOOEt \\ | \\ NHCOOEt \end{matrix}$$

(VI) (VII)

The yields of the products mentioned above are listed in Table 1.

The insertion occurred preferentially at the C–H bonds of the α-position. In the reaction with an unsymmetrical ether, isobutyl methyl ether, insertion into the secondary α C–H bond predominated over insertion into the primary α C–H bond. In the reaction with 2-methoxyethanol (methylcellosolve), however, the product of O–H insertion was isolated instead of that of C–H insertion. The formation of *N*-alkoxyurethane (V) shows that cleavage of the C–O bonds occurs during the reactions. Olefins, although not detected, might be formed concomittantly by V, in analogy to the formation of an unsaturated product of the cleavage of the ring C–O bonds of cyclic ethers.[1,2]

Relative Reactivities. As mentioned above, the α C–H bonds of the acyclic ethers were more reactive for nitrene insertion than the other C–H bonds. In order to compare the insertion reactivities of the α C–H bonds with those of the cyclohexane C–H bonds, direct photolysis of I was carried out in a mixture of equimolar amounts of an acyclic ether and cyclohexane. The yields of the products and the reactivities are summarized in Table 2, with the reactivities of primary (1°), secondary (2°), and tertiary (3°) C–H bonds in 2-methylbutane.[3]

Table 2. Direct photolysis of I in a mixture of an acyclic ether and cyclohexane

	Product (%)[a]		Type of C–H bond	Relative reactivity[b]	2-Methylbutane		
	Insertion (IV)	Cyclohexylurethane			1°	2°	3°
(c_1)	17.8	12.0	2°(α)	4.5			
(c_2)	2.8		2°(β)	0.7			
(c_3)	3.0		2°(γ)	0.8			
(d_1)	13.2	9.2	2°(α)	4.4			
(d_2)	4.5		3°(γ)	2.9			
					0.09	0.8	3.0

a) Calculated on the basis of the azide used.
b) Relative reactivity: per C–H bond of cyclohexane.

The secondary C–H bonds at the α-position of the acyclic ethers were much more reactive for nitrene insertion than the corresponding C–H bonds of hydrocarbons. Such unusually high reactivities and the formation of *N*-alkoxyurethanes (V) are very similar to reactions with cyclic ether.[1] Thus the reaction of nitrene with acyclic ethers may involve the O–N ylide, which has been proposed for the reaction with cyclic ethers.[1]

Sensitized Photolysis in Ethers. As has been pointed out in a previous paper,[1] the abstraction-recombination mechanism due to the triplet nitrene was not ruled out for insertion into the α C–H bonds of the ethers. Thus, the decomposition of I was carried out under conditions involving no singlet nitrene. Ethyl azidoformate (I) in ether was irradiated with the light from a high-pressure mercury lamp in the presence of a sensitizer, acetophenone, in an atmosphere of nitrogen. A 1.5 M-$CuSO_4$ aqueous solution was circulated as a filter. The filter completely inhibited the direct excitation of I. The yields of the products are listed in Table 3, in which they are compared with those for reactions using a low-pressure mercury lamp (direct photolysis).

Table 3. Sensitized photolysis of I in ethers

Ether	Product (%)[a]		
	Insertion into α C–H bond (IV)	Abstraction (VI)	Ratio VI/IV
	27.0(32.8)	44.6(22.2)	1.7(0.7)
	27.8(25.0)[b]	72.5(16.0)	2.6(0.6)
	16.5[c] (12.0)[b,c]	65.2(34.0)	4.0(2.8)
$(CH_3CH_2CH_2\text{-}CH_2)_2O$	8.4(25.0)	50.5(17.4)	6.0(0.7)

( ) Indicates the values for direct photolysis.
a) Calculated on the basis of the azide used.
b) From Ref. 1.
c) Insertion into the tertiary C–H bond.

The nitrene species involved in these sensitized photolysis reactions must be in the triplet state.[4] The molar ratios of VI/IV for sensitized photolysis are larger than those for direct photolysis. The findings for dioxane are similar to those reported by Nozaki *et al.*[5] In the sensitized photolysis with dibutyl ether, neither the products of insertion into the β and γ C–H bonds nor *N*-butoxyurethane were detected in contrast to direct photolysis, as is shown in Table 1. Furthermore, neither the product of insertion into the β C–H bonds of tetrahydropyran nor the C–O cleavage product in 2-methyltetrahydropyran was detected, although both were isolated for direct photolysis.[1] It is noteworthy that both singlet and triplet ethoxycarbonyl nitrenes are inserted into the C–H bonds adjacent to the oxygen atom, in contrast to insertion by only the singlet into the C–H bonds of hydrocarbons.[6-8]

The insertion of the triplet nitrene is initiated by hydrogen abstraction from the etheral α-position, followed by the radical recombination, as shown in Scheme 1.

$$R\text{-}\dot{N}\cdot \xrightarrow{-\underline{O}\text{-}\underset{H}{\underset{|}{C}}\text{-}CH_2-} -\underline{O}\text{-}\underset{\cdot}{\underset{|}{C}}\text{-}CH_2- + H\dot{N}R$$

(II)
triplet nitrene

$$\longrightarrow -\underline{O}\text{-}\underset{HNR}{\underset{|}{C}}\text{-}CH_2-$$

Scheme 1.

Concerning hydrocarbons, such a radical recombination mechanism has been ruled out because of no insertion by the triplet.[6-8] For ethers, however, the α-carbon radical is stabilized by the adjacent oxygen atom, permitting recombination with the HNR radical. As is seen in Table 3, the molar ratios of VI/IV for direct photolysis are much smaller than those for sensitized photolysis. This means that the singlet nitrene participates in the insertion into the α C–H bonds. Judging from the view point of non-stereospecific insertion,[1] the singlet nitrene is not inserted into the α C–H bonds by a one-step mechanism.

The insertion of the singlet nitrene, which results only from direct photolysis, is initiated by the formation of an O–N ylide (VIII) with the ethereal oxygen. The ylide VIII abstracts a proton from the α C–H bond, followed by homolytic cleavage of the O–N bond giving

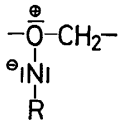

(VIII)

the radical species, the α-carbon radical, and HNR. The recombination of these two radicals results in the α-insertion product as has been reported in a preceding paper.[1] On the other hand, VIII leads to V *via* hydrogen abstraction and cleavage of the C–O bond.[1]

Insertion into the β and γ- C–H bonds, however, may proceed by the one-step mechanism proposed for the reaction with hydrocarbons,[6-8] since the β- and γ-carbon radicals, whose resonances with the oxygen lone pair are insulated by the methylenes, are not as stable as the α-carbon radical. These two distinct mechanisms can explain the difference in reactivity between the α C–H bond and the β or γ C–H bond shown in Table 2.

In the reaction with isobutyl methyl ether, as shown in Table 1, preferential insertion into the α-methylene group may be due to the difference between the radical stabilities of $-\dot{C}HOCH_3$ and $-CH_2O\dot{C}H_2$.

Direct and Sensitized Photolysis in Alcohols. To obtain further information about the behavior of the nitrene for other oxygen compounds, direct and sensitized photolysis of I were carried out in alcohols. The results are shown in Table 4. Direct photolysis gave products for nitrene insertion into the O–H bonds, while sensitized photolysis gave no such insertion products. Therefore, it is concluded that the O–H insertion products are formed only by the singlet nitrene as shown in Scheme 2.[9] The O–H insertion can be considered to proceed by a one-step of the singlet nitrene.

Table 4. Photolysis of I in alcohols

Alcohol	Product (%)[a,b] Insertion into O–H bond		Abstraction (VI)	
	Direct	Sensitized	Direct	Sensitized
CH_3CH_2OH	11.0	ND[c]	71.0	64.6
$CH_3CH_2CH_2OH$	15.0	ND	46.0	80.5
$CH_3CH_2CH_2CH_2OH$	27.0	ND	47.0	74.9

a) Calculated on the basis of the azide used.
b) Photolysis gave the corresponding aldehydes in addition to the insertion and abstraction products.
c) ND: not detected.

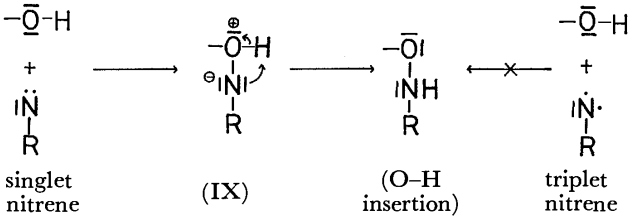

Scheme 2.

However, it is more reasonable that O–H inserion proceeds *via* an O–N ylide intermediate (IX), in analogy to reactions of ethers with the singlet nitrene, as mentioned above.

Reaction Course. The facts observed for the reactions of nitrene with ethers and alcohols can be accommodated into Scheme 3.

Experimental

Most of the equipment and techniques have been described in preceding papers.[1,10] In addition, a Nippon Bunko (JASCO) Model A-3 photometer was used for the IR measurements and a 20% mixture Apiezone Grease L on Neosorb NC (60—80 mesh) was employed as the absorbent for VPC.

Materials. Ethyl azidoformate (I) was prepared by the method of Lwowski and Mattingly.[4] Cyclohexane, dioxane, alcohols, and most of the ethers were used after the

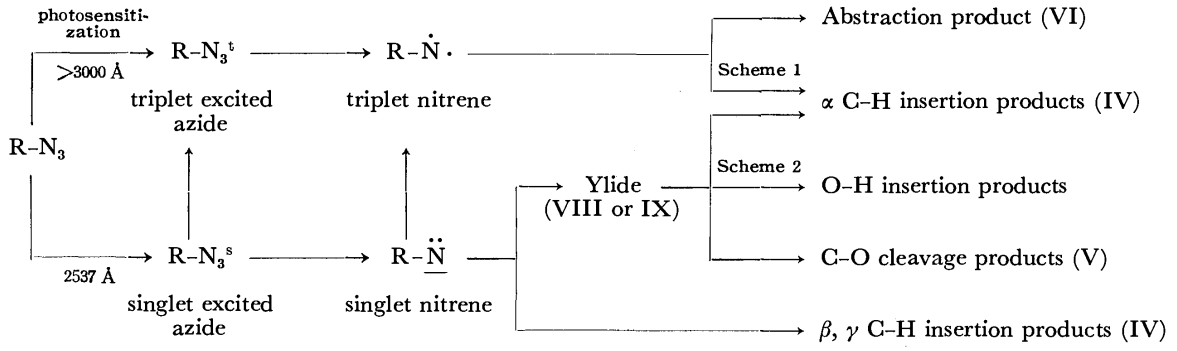

Scheme 3.

commercial reagents had been purified according to published directions.[11] All the acyclic ethers were purified by boiling with sodium and by distillation. The absence of alcohols in the ethers was confirmed by VPC. Isobutyl methyl ether was prepared from sodium isopropoxide and methyl iodide using the Williamson procedure; bp 58.5 °C (lit,[12] 59 °C); yield, 73%. Diisobutyl ether was prepared from isobutyl alcohol and concentrated sulfuric acid. A mixture of 100 ml of concentrated sulfuric acid and 400 ml of isobutyl alcohol was refluxed in a flask equipped with a distillation column. A fraction, bp 82—91 °C, was collected and dried over anhydrous calcium chloride. After the solid part had been removed by filtration, the filtrate was washed with water, dried over anhydrous calcium chloride, and distilled; bp 120—123 °C (lit, 122—124 °C). To prepare the authentic IVc_2, amino ether was prepared from 2-amino-1-butanol and butyl iodide using the Williamson procedure; bp 96 °C/25 Torr; yield, 76%. A solution of 10 g of the amino ether in diethyl ether was cooled and 7 g of ethyl chloroformate was added dropwise to the solution. The solution was washed with 10% sodium carbonate and with water. The ether layer was dried over anhydrous sodium sulfate, the solvent was evaporated, and the residue was distilled; bp 124 °C/3 Torr; yield, 56%.

Direct Photolysis of I in Acylic Ethers. A solution of 5.0 g (0.043 mol) of ethyl azidoformate in 0.5 mol of acyclic ether was irradiated using a low-pressure mercury lamp, with stirring and cooling at 0 °C, until the evolution of nitrogen was no longer observed. The nitrogen evolved then gave almost the theoretical amount based on the azide used. The excess substrate was removed by distillation at 25—85 °C and 20—30 Torr. The residue was analyzed by VPC on columns. The IR and NMR spectra and VPC retention time of urethane (VI) were identical to those of an authentic sample, and a mixed melting point test with the authentic sample was undepressed. Diethyl hydrazodiformate (VII) was obtained in yields of 0.01—0.05 g for each experiment. The IR and NMR spectral, and elemental analysis data of VII have been described previously.[1] The insertion products (IV) and *N*-alkoxyurethanes (V) displayed strong absorptions in the 3260—3360 and 1700—1730 cm^{-1} regions due to the NH groups and the ester C=O groups, respectively. The NMR spectra of IV and V were measured in carbon tetrachloride and the chemical shifts were given in τ values. The IR and NMR spectral data, and the VPC retention times of V are identical to those of the products obtained by nitrene insertion into the O–H bonds when I was photolyzed in alcohols.[13]

(a) In Diethyl Ether (IIIa): *N*-(1-ethoxyethyl)urethane (IVa, 2.16 g) and *N*-ethoxyurethane (Va, 0.22 g) were isolated. IVa: NMR: 4.25 (NH, 1H, bs), 5.00 (CH, 1H, m), 5.94 (ester-CH_2, 2H, q), 6.50 (OCH_2, 2H, m), 8.70 (CH_3, 3H, d), 8.76 (ester-CH_3, 3H, t), 8.86 (CH_3, 3H, t). Found: C, 52.58; H, 9.51; N, 8.46%. Calcd for $C_7H_{15}O_3N$: C, 52.15; H, 9.38; N, 8.69%. Va: NMR: 1.97 (NH, 1H, bs), 5.85 (ester-CH_2, 2H, q), 6.14 (CH_2, 2H, q), 8.70 (CH_3, 3H, t), 8.73 (ester-CH_3, 3H, t). Found: C, 45.62; H, 8.08; N, 10.91%. Calcd for $C_5H_{11}O_3N$: C, 45.10; H, 8.33; N, 10.52%.

(b) In Dipropyl Ether (IIIb): *N*-(1-propoxypropyl)urethane (IVb_1, 2.62 g), *N*-[1-(propoxymethyl)ethyl]urethane (IVb_2, 0.25 g), and *N*-propoxyurethane (Vb, 0.35 g) were isolated. IVb_1: NMR: 4.65 (NH, 1H, bs), 5.25 (CH, 1H, m), 5.93 (ester-CH_2, 2H, q), 6.57 (OCH_2, 2H, m), 8.40 (CH_2, 4H, m), 8.76 (ester-CH_3, 3H, t), 9.08 (CH_3, 6H, t). Found: C, 56.98; H, 10.01; N, 7.62%. Calcd for $C_9H_{19}O_3N$: C, 57.11; H, 10.12; N, 7.40%. IVb_2: NMR: 5.29 (NH, 1H, bs), 5.97 (ester-CH_2, 2H, q), 6.06 (CH, 1H, m), 6.64 (OCH_2, 2H, bt), 6.68 (CH_2, 2H, d), 8.40 (CH_2, 2H, m), 8.84 (CH_3, 3H, d), 8.78 (ester-CH_3, 3H, t), 9.07 (CH_3, 3H, t). Found: C, 57.37; H, 10.28; N, 7.15%. Calcd for $C_9H_{19}O_3N$: C, 57.11; H, 10.12; N, 7.40%. Vb: NMR: 2.00 (NH, 1H, bs), 5.86 (ester-CH_2, 2H, q), 6.25 (OCH_2, 2H, t), 8.37 (CH_2, 2H, six), 8.71 (ester-CH_3, 3H, t), 9.03 (CH_3, 3H, t). Found: C, 49.15; H, 9.12; N, 9.81%. Calcd for $C_6H_{13}O_3N$: C, 48.96; H, 8.90; N, 9.52%.

(c) In Dibutyl Ether (IVc): *N*-(1-butoxybutyl)urethane (IVc_1, 2.33 g), *N*-[1-(butoxymethyl)propyl]urethane (IVc_2, 0.35 g), *N*-(3-butoxy-1-methylpropyl)urethane (IVc_3, 0.36 g), and *N*-butoxyurethane (Vc, 0.28 g) were isolated. IVc_1: NMR: 5.15 (NH, 1H, bs), 5.16 (CH, 1H, m), 5.94 (ester-CH_2, 2H, q), 6.56 (OCH_2, 2H, t), 8.53 (CH_2, 8H, m), 8.74 (ester-CH_3, 3H, t), 9.05 (CH_3, 6H, t). Found: C, 61.08; H, 10.35; N, 6.18%. Calcd for $C_{11}H_{23}O_3N$: C, 60.80; H, 10.67; N, 6.45%. IVc_2: NMR: 5.30 (NH, 1H, bs), 5.96 (ester-CH_2, 2H, q), 6.40 (CH, 1H, m), 6.62 (OCH_2, 4H, bt), 8.25 ($CHCH_2$, 2H, m), 8.52 (CH_2, 4H, m), 8.77 (ester-CH_3, 3H, t), 9.06 (CH_3, 6H, t). Found: C, 61.18; H, 10.42; N, 6.08%. Calcd for $C_{11}H_{23}O_3N$: C, 60.80; H, 10.67; N, 6.45%. IVc_3: NMR: 4.85 (NH, 1H, bs), 5.98 (ester-CH_2, 2H, q), 6.33 (CH, 1H, m), 6.56 and 6.65 (OCH_2, 4H, t), 8.50 (CH_2, 6H, m), 8.58 (CH_3, 3H, d), 8.79 (ester-CH_3, 3H, t), 9.07 (CH_3, 3H, t). Found: C, 60.98; H, 10.38; N, 6.11%. Calcd for $C_{11}H_{23}O_3N$: C, 60.80; H, 10.67; N, 6.45%. Vc: NMR: 1.97 (NH, 1H, bs), 5.86 (ester-CH_2, 2H, q), 6.22 (OCH_2, 2H, t), 8.2—8.9 (CH_2, 4H, m), 8.71 (ester-CH_3, 3H, t), 9.05 (CH_3, 3H, t). Found: C, 52.51; H, 9.19; N, 8.44%. Calcd for $C_7H_{15}O_3N$: C, 52.15; H, 9.38; N, 8.69%. The insertion product, IVc_2, exhibited IR and NMR spectra and a VPC retention time identical with those of an authentic sample.

(d) In Diisopentyl Ether (IIId): *N*-(3-methyl-1-isopentyloxybutyl)urethane (IVd_1, 1.80 g), *N*-(1,1-dimethyl-3-isopentyloxypropyl)urethane (IVd_2, 0.60 g), and *N*-isopentyloxy urethane (Vd, 0.18 g) were isolated. IVd_1: NMR: 5.14 (NH, 1H, bs), 5.14 (OCH, 1H, t), 5.94 (ester-CH_2, 2H, q), 6.57 (OCH_2, 2H, t), 8.15 and 8.30 (CH, 2H, m), 8.70 (CH_2, 4H, m), 8.75 (ester-CH_3, 3H, t), 9.06 and 9.10 (CH_3, 12H, d). Found: C, 63.69; H, 10.92; N, 5.58%. Calcd for $C_{13}H_{27}O_3N$: C, 63.64; H, 11.09; N, 5.71%. IVd_2: NMR: 4.55 (NH, 1H, bs), 6.04 (ester-CH_2, 2H, q), 6.50 and 6.60 (OCH_2, 4H, t), 8.39 (two CH_2 and CH, 5H, m), 8.66 (CH_3, 6H, s), 8.80 (ester-CH_3, 3H, t), 9.08 (CH_3, 6H, d). Found: C, 63.23; H, 10.98; N, 5.95%. Calcd for $C_{13}H_{27}O_3N$: C, 63.64; H, 11.09; N, 5.71%. Vd: NMR: 2.08 (NH, 1H, bs), 5.85 (ester-CH_2, 2H, q), 6.18 (OCH_2, 2H, t), 8.1—8.6 (CH_2 and CH, 3H, m), 8.71 (ester-CH_3, 3H, t), 9.06 (CH_3, 6H, d). Found: C, 54.52; H, 9.54; N, 8.27%. Calcd for $C_8H_{17}O_3N$: C, 54.83; H, 9.78; N, 7.99%.

(e) In Isobutyl Methyl Ether (IIIe): *N*-(1-methoxy-2-methylpropyl)urethane (IVe_1, 1.24 g), *N*-(isobutoxymethyl)-urethane (IVe_2, 0.43 g), and *N*-isobutoxyurethane (Ve_1, 0.18 g) were isolated. IVe_1: NMR: 4.68 (NH, 1H, bs), 5.45 (OCH, 1H, m), 5.90 (ester-CH_2, 2H, q), 6.71 (OCH_3, 3H, s), 8.26 (CH, 1H, m), 8.75 (ester-CH_3, 3H, t), 9.08 (CH_3, 6H, d). Found: C, 55.12; H, 9.92; N, 7.69%. Calcd for $C_8H_{17}O_3N$: C, 54.83; H, 9.78; N, 7.99%. IVe_2: NMR: 4.19 (NH, 1H, bs), 5.14 (NCH_2, 2H, d), 5.87 (ester-CH_2, 2H, q), 6.77 (OCH_2, 2H, d), 8.10 (CH, 1H, m), 8.74 (ester-CH_3, 3H, t), 9.10 (CH_3, 6H, d). Found: C, 55.05; H, 9.98; N, 7.70%. Calcd for $C_8H_{17}O_3N$: C, 54.83; H, 9.78; N, 7.99%. Ve_1: NMR: 2.04 (NH, 1H, bs), 5.85 (ester-CH_2, 2H, q), 6.42 (OCH_2, 2H, d), 7.63—8.57 (CH, 1H, m), 8.71 (ester-CH_3, 3H, t), 9.05 (CH_3, 6H, d). Found: C, 52.51; H, 9.12; N, 8.81%. Calcd for $C_7H_{15}O_3N$: C, 52.15; H, 9.38; N, 8.69%.

The VPC retention time for methoxyurethane (Ve_2) was identical with that of an authentic sample.

(f) In 2-Methoxyethanol (IIIf): *N*-(2-methoxyethoxy)-urethane (Vf, 2.39 g) was isolated. Vf: NMR: 1.37 (NH, 1H, bs), 5.84 (ester-CH_2, 2H, q), 5.81—6.21 (CH_2ON, 2H, m), 6.26—6.58 (CH_2, 2H, m), 6.62 (CH_3, 3H, s), 8.72 (ester-CH_3, 3H, t). Found: C, 49.25; H, 9.12; N, 9.28%. Calcd for $C_6H_{13}O_3N$: C, 48.96; H, 8.90; N, 9.52%.

Direct Photolysis of I in Dioxane and Alcohols. In dioxane, ethyl 1,4-dioxan-2-ylcarbamate was obtained in yield of 2.47 g. NMR: 4.37 (NH, 1H, bs), 4.87—5.27 (CH, 1H, m), 5.82 (ester-CH_2, 2H, q), 5.97—6.77 (CH_2, 6H, m), 8.74 (ester-CH_3, 3H, t). Found: C, 47.46; H, 7.62; N, 8.21%. Calcd for $C_7H_{13}O_4N$: C, 47.99; H, 7.48; N, 8.00%. The NMR spectrum was in good agreement with that reported in Ref. 8. In the alcohols, Va, Vb, and Vc were obtained in yields of 0.63, 0.95, and 1.87 g, respectively.

Sensitized Photolysis of I in Ethers and Alcohols. A solution of 2.3 g (0.02 mol) of ethyl azidoformate (I) and 3.12 g (0.026 mol) of acetophenone in 0.5 mol of a substrate was irradiated, with stirring at 25 °C, using a high-pressure mercury lamp until the evolution of nitrogen was no longer observed. The reaction mixture was treated as in the case of direct photolysis. In addition, for each of the reactions with alcohols, the excess substrate and a volatile product, aldehyde, were trapped in a flask immersed in a Dry Ice–methanol bath under reduced pressure. The trapped solution was added to a 2,4-dinitrophenylhydrazine solution and the aldehyde was converted to hydrazone. For ethanol, 1-propanol, and 1-butanol, acetaldehyde, propionaldehyde, and butyraldehyde were isolated as hydrazones in yields of 0.43, 0.58, and 0.53 g, respectively. For the reactions with IIIc, dioxane, tetrahydropyran, and 2-methyltetrahydrofuran, IVc_1, ethyl 1,4-dioxan-2-ylcarbamate, ethyl 2-tetrahydropyranylcarbamate, and ethyl 2-methyl-2-tetrahydrofurylcarbamate were isolated in yields of 0.36, 0.95, 0.96, and 0.57 g, respectively. The identification procedure for the third and fourth products has been reported elsewhere.[1)]

Direct Photolyses of I in a Mixture of Acyclic Ether and Cyclohexane. A solution of I (5.0 g, 0.043 mol) in III (0.25 mol) and cyclohexane (21 g, 0.25 mol) was irradiated internally as described above. The excess substrate was removed by distillation, and the residue was analyzed by VPC. The *N*-cyclohexylurethane was identified by comparison with an authentic sample. The yields of the insertion products and urethane are displayed in Table 2.

The authors are particulary indebted to Dr. Hisao Arakawa of the Science Education Institute of Osaka Prefecture for help in the preparation of this paper and for many useful suggestions.

References

1) N. Torimoto, T. Shingaki, and T. Nagai, *Bull. Chem. Soc. Jpn.*, **49**, 2572 (1976).

2) The reaction of methylene with ether gave methyl ether and an olefin. G. Ayrey, E. Buncel, and A. N. Bourns, *Proc. Chem. Soc.*, **1961**, 458. F. Weygand, H. Daniel, and H. Simon, *Ann.*, **654**, 111 (1962).

3) T. Shingaki, M. Inagaki, N. Torimoto, and M. Takebayashi, *Chem. Lett.*, **1972**, 1181.

4) W. Lwowski and T. W. Mattingly, Jr., *J. Am. Chem. Soc.*, **87**, 1947 (1965).

5) H. Nozaki, S. Fujita, H. Takaya, and R. Noyori, *Tetrahedron*, **23**, 45 (1967).

6) D. S. Breslow, E. I. Edward, R. Leone, and P. von R. Schleyer, *J. Am. Chem. Soc.*, **90**, 7097 (1968).

7) W. Lwowski, "Carbonylnitrenes," in "Nitrenes," ed by W. Lwowski, Interscience Publishers, New York (1970). p. 185, and references quoted therein.

8) W. Lwowski, *Angew. Chem.*, **79**, 922 (1967),; *Angew, Chem. Int. Ed. Engl.*, **6**, 897 (1967).

9) This finding is in accordance with the report: that the S–N ylide is not formed by the triplet nitrene, but by the singlet nitrene. W. Ando, N. Ogino, and T. Migita, *Bull. Chem. Soc. Jpn.*, **44**, 2278 (1971).

10) T. Shingaki, M. Inagaki, M. Takebayashi, and W. Lwowski, *Bull. Chem. Soc. Jpn.*, **45**, 3567 (1967).

11) J. A. Riddic and W. B. Bunger, "Organic Solvents," in "Techniques of Chemistry," Vol. VII, ed by A. Weissberger, Wiley-Interscience, New York, N. Y. (1970).

12) A. W. Smith and C. E. Boord, *J. Am. Chem. Soc.*, **48**, 1512 (1926).

13) T. Shingaki, M. Inagaki, N. Torimoto, and M. Takebayashi, Symposium of Organic Free Radical Reactions, Nagoya, Japan, October (1971), Abstract, p. 9.

The Benzannelated Annulenones. Syntheses and Properties of 10-Methylbenzo[*d*]- and Dibenzo[*d,j*]-6,8-bisdehydro[13]annulenone

Jūro Ojima,* Yōji Yokoyama, and Michiko Enkaku

Department of Chemistry, Faculty of Science, Toyama University, Gofuku, Toyama 930

(Received October 21, 1976)

In order to examine the paratropic nature expected for a thirteen-membered ring system arising from polarization of the carbonyl group, the two benzannelated bisdehydro[13]annulenones, VI and IX, were prepared respectively by the aldol condensation of an appropriate aldehyde and an appropriate ketone followed by the oxidative coupling of the resulting acyclic ketone containing terminal acetylene groups. The NMR spectra indicate that both of VI and IX, as well as the respective protonated species, VII and X, are paratropic and paratropicities decrease in the sequence of VI>IX with the increasing number of fused benzene ring. The dibenzannelated annulenone (IX) and its precursor (VIII) were converted into the corresponding alcohols or ethers (XIIa, XIIb and XIa, XIb), respectively, to test the presence of the paratropic nature of IX. The NMR spectra of XIa, XIb and XIIa, XIIb, in addition to those of VIII and IX, suggested that IX seemed to be weakly paratropic. An attempt made to prepare the dibenzannelated bisdehydro[13]annulenyl anion (XIII) was unsuccessful.

A series of fully conjugated monocyclic monoketones (annulenones) are expected to be diatropic or paratropic owing to polarization of a carbonyl group provided they contain a $(4n+3)$-membered ring or $(4n+1)$-membered ring, respectively.[1]

In connection with the studies to confirm this prediction Howes *et al.* have reported a simple general approach to bisdehydro[13]- (I), [15]-, and [17]-annulenones in which the carbonyl group is flanked by ethylenic bonds on both sides.[2] The method consists in employing an aldol condensation of an appropriate aldehyde and ketone, containing terminal acetylene group, followed an intramolecular oxidative coupling of the resulting acyclic ketone.

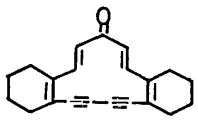

I

We have now applied with advantage the method to the synthesis of benzannelated bisdehydro[13]annulenones (VI and IX) by using *o*-ethynylbenzaldehyde (II) as the starting material and essentially by the same approach as that of Howes *et al.* It is now established[3] that the annelated benzenoid nuclei such as benzene or naphthalene reduce the diatropic nature of a $(4n+2)$-membered annulene. However, when this work was commenced, little reports had yet appeared concerning the effect of annelation of benzene nuclei on annulenones.[4] Some aspect of this work have appeared in the preliminary form.[5] In this paper, we present a full account of our investigation on the synthesis and properties of monobenzo and dibenzo analogues of I, *i.e.*, 10-methylbenzo[*d*]- (VI) and dibenzo[*d,j*]-6,8-bisdehydro[13]annulenone (IX).

The preparation of VI and IX was carried out as follows. The ketone (III) was obtained by treatment of *o*-ethynylbenzaldehyde (II) with excess acetone in the presence of aqueous sodium hydroxide as previously

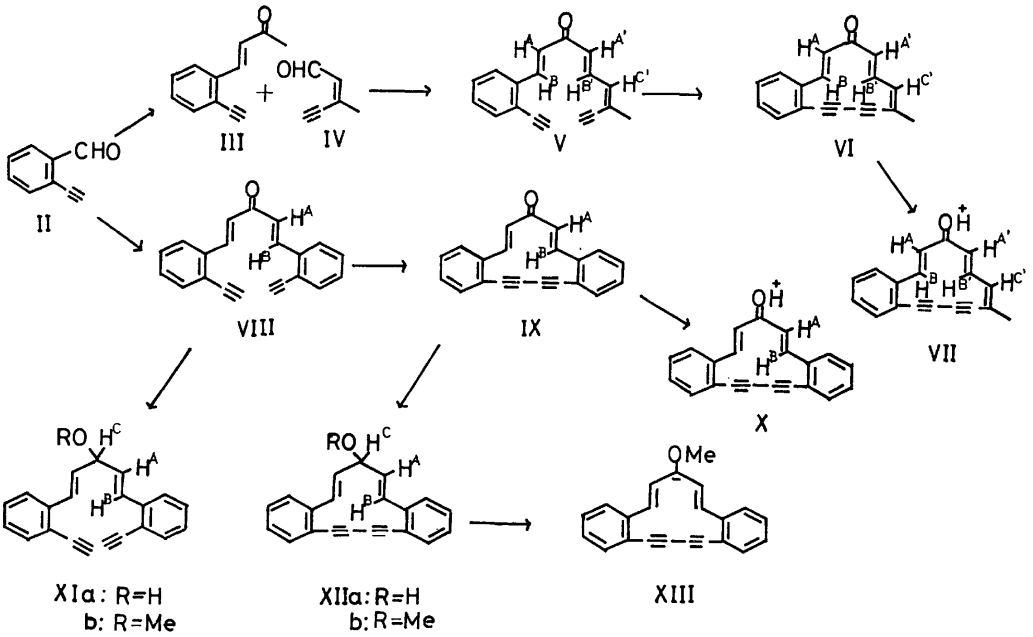

* Author to whom correspondence should be addressed.

Table 1. ^{1}H-NMR parameters of V, VI, VIII, IX, XIV, and XV in $CDCl_3$ at 60 MHz (τ-values; Internal standard, TMS; J values in Hz in parentheses)

Proton	V[a]	VI	VIII[b]	IX	XIV[b]	XV	ΔVI–V[c]	ΔIX–VIII[c]	ΔXV–XIV[c]
H^A	3.68d(17)[d]	3.90d(16)[e]	2.84d(16)	3.24d(16)	3.55d(16)	3.90d(17)	+0.22	+0.40	+0.35
H^B	1.98d(17)	1.45d(16)	1.82d(16)	1.53d(16)	2.32dd(16,11)	0.61dd(17,10)	−0.53	−0.29	−1.71
H^C	—	—	—	—	3.54d(11)	3.71d(10)	—	—	+0.17
$H^{A'}$	3.42d(17)[d]	3.68d(16)[e]	—	—	—	—	+0.26	—	—
$H^{B'}$	2.13dd(17,11)	1.26dd(16,10)	—	—	—	—	−0.87	—	—
$H^{C'}$	3.32d(11)	3.60d(10)	—	—	—	—	+0.28	—	—
CH_3	8.07s	8.17s	—	—	7.98s	8.26s	+0.10	—	+0.28
Benzenoid H	2.47—3.10m	2.73—2.92m	2.22—2.76m	2.5—2.8m	—	—			

a) In addition, a singlet at 6.87 (–C≡CH). b) In addition, a singlet at 6.54 (–C≡CH). c) This shows the chemical shift differences. d), e) These assignments may be reversed in each group. However, most probable values are given in Table 1 by referring to the chemical shifts of the related compounds.[9]

reported.[6] Aldol coupling of III and *cis*-3-methyl-2-penten-4-ynal (IV)[7] by methanolic potassium hydroxide gave the acyclic ketone (V) in a 10% yield, upon chromatographic purification of the product over alumina, as an unstable orange liquid. Both of the aldehyde (IV) and the ketone (V) were unstable at room temperature. Oxidative coupling of V, under Eglinton's conditions using copper(II) acetate in pyridine,[8] gave the cyclic ketone, the desired annulenone (VI), in a 20% yield as relatively stable crystals. While, condensation of 2 molar equivalents of II with 1 molar equivalent of acetone, under the same conditions as indicated for the reaction of III and IV, afforded a 44% yield of the acyclic ketone (VIII). Oxidation of VIII with copper(II) acetate as before, gave the dibenzannelated annulenone (IX) in a 61% yield. The assigned conformations were given to the annulenones (VI) and (IX) in analogy with the compound (I) which was shown to have the conformation based on NMR spectroscopy of dideutrio compound of I.[2] Treatment of VI or IX with trifluoroacetic acid gave the corresponding carbonyl protonated species, VII (dark red; λ_{max} 277 sh, 292, 350 sh, with absorption>700 nm) or X (yellow brown; λ_{max} 285 sh, 301, 348, 413 sh, with absorption>700 nm), respectively.

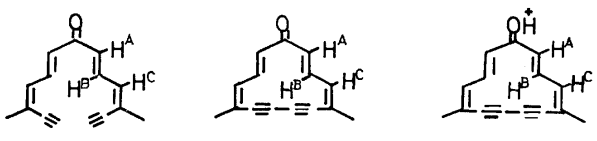

XIV XV XVI

The ^{1}H-NMR parameters of the obtained compounds, V and VI, are listed in Table 1, as well as the chemical shift differences for various resonances on passing from V to VI, indicating the magnitude of the upfield shift of the outer proton signals and the downfield shift of the inner proton signals.

The comparison of the NMR spectra of V and VI (Table 1) reveals the compound VI to be paratropic, as expected for a potential 12π-electron system by the polarization of the carbonyl group, since the inner proton (H^B, $H^{B'}$) resonances of VI have moved to a lower field, the outer (H^A, $H^{A'}$, $H^{C'}$) and methyl proton resonances to a higher field, as compared with those of the corresponding proton of V.

In order to obtain an approximate measure regarding the effect of benzannelation on thirteen-membered ring system, the NMR spectral data of VIII and IX, and the chemical shift differences are also given in Table 1, together with those of XIV and XV which were prepared by Ojima and Sondheimer.[9] The data (Table 1) suggests that IX is also paratropic as VI, because the inner proton (H^B) signal has moved to a lower field, and the outer proton (H^A) signal to a higher field as compared with that of the respective proton of VIII.

As indicated in Table 1, an examination of the NMR spectra demonstrated that the thirteen-membered ring system in dimethyl compound XV is paratropic, in monobenzo-fused compound VI, it is less paratropic, in dibenzo-fused compound IX, it is at most weakly paratropic. This can be seen in particular by the downfield shifts, as compared with the respective models (XV, VI, IX), of the inner proton (H^B, $H^{B'}$) bands [−1.71, (−0.53 and −0.87), −0.29 ppm, respectively],

Table 2. ^{1}H-NMR parameters of XVI, VII, and X in CF_3COOD at 60 MHz (τ-values; Internal standard, TMS; J values in Hz in parentheses)

	XVI	VII	X	ΔXVI–XIV	ΔVII–V	ΔX–VIII
H^A	3.85 d(16)	3.75[a] d(17)	3.00 d(16)	+0.30	+0.07	+0.16
H^B	−0.79 dd(16,10)	0.65 d(17)	0.98 d(16)	−3.11	−1.33	−0.84
H^C	3.88 d(10)			+0.34		
$H^{A'}$		3.47[a] d(17)			+0.05	
$H^{B'}$		0.19 dd(17,11)			−1.94	
$H^{C'}$		3.42 d(11)			+0.10	
CH_3	8.33s	8.20s		+0.35	+0.13	
Benzenoid H		2.80—2.97m	2.6—2.8m			

a) These assignments may be reversed in this group, as described in Table 1.

Table 3. ^{1}H-NMR parameters of XIa, XIb, XIIa, and XIIb in $CDCl_3$
(τ-values; Internal standard, TMS; J values in Hz in parentheses)

	XIa[a]	XIb[b]	XIIa[b]	XIIb[a]	ΔIX−VIII	ΔXIIa−XIa	ΔXIIb−XIb
H^A	3.87 dd(16,6)	3.85 dd(16,7)	4.10 dd(16,6)	4.23 dd(17,7)	+0.40	+0.23	+0.38
H^B	3.07 d(16)	2.95 d(16)	3.27 d(16)	3.18 d(17)	−0.29	+0.20	+0.23
H^C	5.65 t (6)	6.08 t (7)	4.91 t (6)	5.43 t (7)			
-OH	7.13 broad s		8.10 broad s				
-OMe		6.69 s		6.50 s			
-C≡CH	6.80 s	6.70 s					
Benzenoid H	2.6—2.9 m	2.40—2.85 m	2.50—2.87 m	2.4—2.8 m			

a) At 60 MHz. b) At 100 MHz.

and the chemical shifts [0.61, (1.45 and 1.26), 1.53 τ, respectively].

Furthermore, the result analogous to the above is also obtained by the comparison of the NMR spectra in CF_3COOD (Table 2); the same trend is observed in the downfield shifts and the chemical shifts of the inner proton (H^B, $H^{B'}$) bands [−3.11, (−1.94 and −1.33), −0.84 ppm], [−0.79, (0.65 and 0.19), 0.98 τ] of the respective models (XVI, VII, X).[9,10]

As described above, it was concluded that the dibenzannelated [13]annulenone (IX) is paratropic. This conclusion was derived by comparing the chemical shifts of H^A and H^B protons of IX with those of the acyclic ketone (VIII) which is an atropic compound. However, the chemical shift differences between VIII and IX are so small that we attempted to examine these differences in the corresponding atropic models.[11] Along this line we undertook to prepare the alcohols (XIa, XIIa) and the methyl ethers (XIb, XIIb) which are the corresponding atropic models of VIII and IX.

Reduction of the acyclic ketone (VIII) in ether with sodium borohydride gave a 57% yield of the alcohol (XIa) as a pale yellow liquid. The methylation of XIa with methyl iodide and silver oxide gave fruitless results. However, methylation of XIa could be effected with methy iodide and sodium hydride[12] to afford a 51% yield of the ether (XIb) as a pale yellow liquid. The cyclic ketone (IX) was reduced more readily than the acyclic ketone (VIII) by sodium borohydride to afford alcohol (XIIa) in a 91% yield. Methylation of XIIa with methyl iodide and silver oxide in ether gave a 67% yield of the ether (XIIb) as crystals.

The ^{1}H-NMR data of the compounds thus obtained are given in Table 3, as well as the chemical shift differences. As illustrated in Table 3, we can see the chemical shift differences between XIa and XIIa, or between XIb and XIIb, which are definitely atropic. The chemical shift differences of H^A proton between XIa and XIIa, and that between XIb and XIIb, respectively, (+0.23 and +0.38) are smaller than that of H^A between VIII and IX (+0.40). Whereas, as for H^B proton the reverse is observed (+0.20 and +0.23, −0.29).

This result seems to suggest that the compound IX is weakly paratropic although the differences in chemical shifts of both H^A and H^B are small.

We have also attempted without success to prepare the dibenzannelated [13]annulenyl anion (XIII) by abstraction of ^{1}H from XIIb with dimsyl sodium in DMSO,[13] as reported by LeGoff and Sondheimer.[14] Under conditions performed, XIIb afforded a deep green solution, however all attempts to obtain a satisfactory NMR spectrum were failed owing to the unstability of the product.

Experimental

Freshly deoxygenated ether, methanol, and acetone were used to minimize an oxidation of the compounds used for aldol condensation. The ether was freed from a peroxide by passing through a short column of basic alumina (Act. I) followed by flushing with nitrogen. The methanol and acetone were flushed by nitrogen. All 20% methanolic potassium hydroxide solutions were prepared by dissolving 10 g of potassium hydroxide in 50 ml of methanol and by flushing the solution with nitrogen immediately prior to use. All the melting points are uncorrected. Brockmann alumina (Act. II—III) was used for column chromatography. The ^{1}H-NMR, IR, UV, and mass spectra were taken using the instruments JEOL-JNM-MH-60 or Varian XL-100, Hitachi EPI-S2, Hitachi-124, and JEOL-MS-OI-SG-2, respectively. Shoulders in UV spectra are denoted by sh.

o-Ethynylbenzaldehyde (II) and 4-(o-Ethynylphenyl)-1-buten-2-one (III). The aldehyde (II) and the ketone (III) were prepared as reported previously.[6]

cis-3-Methyl-2-penten-4-ynal (IV). The aldehyde (IV) was obtained by the reported method.[7]

9-(o-Ethynylphenyl)-3-methyl-3,5,8-nonatrien-1-yn-7-one (V). A mixture of the ketone (III, 3.6 g, 21.2 mmol) and the aldehyde (IV, 2.0 g, 21.3 mmol) in deoxygenated ether (85 ml) was treated with a 20% methanolic potassium hydroxide (3.1 ml). The mixture was further stirred at room temp for 2 h. Neutralization with acetic acid (4.0 ml) followed by addition of water (100 ml), and extraction with ether, and work up in the usual manner gave a dark red liquid. Chromatography of the liquid over alumina (80 g) with light petroleum–ether (8:2) as eluent gave the desired ketone (V, 0.5 g, 10%) as an unstable organge liquid: MS: *m/e* 246 (M^+, 40), 149 (100); mol wt, 246.29; IR (neat): 3250 (–C≡CH), 2100 (–C≡C–), 1660, 1615, 1600 (C=O, C=C), 980 cm^{-1}

(*trans* C=C); UV: λ_{max}^{EtOH} 226 (11000), 248 (9230), 321 nm (8830); NMR: see Table 1.

10-Methylbenzo[d]-*6,8-bisdehydro*[*13*]*annulenone (VI).* A soln of V (0.5 g, 2.0 mmol) in pyridine (11 ml) was added dropwise to a stirred soln of copper(II) acetate monohydrate (5.5 g) in pyridine (19 ml) for 10 min at 50—55 °C, and the reaction mixture was stirred for further 2 h at 55—65 °C. The ppt formed on cooling and diluting with benzene (100 ml) was washed with benzene (50 ml×2). Then the filtrate was washed with 6% hydrochloric acid until it was slightly acidic, saturated aq sodium hydrogencarbonate, and sodium chloride solutions successively, and dried over sodium sulfate. The residual dark red liquid obtained after evaporation of the solvent was chromatographed on alumina (80 g) with light petroleum–ether (7: 3) to afford VI (0.1 g, 20%) as relatively stable solid. Recrystallization from hexane gave pure VI as orange needles: mp *ca.* 160 °C (dec); IR (KBr disk): 2150 (–C≡C–), 1630, 1610, 1590 (C=O, C=C), 980 cm^{-1} (*trans* C=C); UV: λ_{max}^{EtOH} 236 (9880), 258 (15800), 388 nm (2100); MS: *m/e* 244 (M^+, 20), 215 (100); mol wt, 244.28; NMR: see Table 1.

1,5-Bis(o-ethynylphenyl)-1,4-pentadien-3-one (VIII). To a stirred soln of *o*-ethynylbenzaldehyde (II, 4.0 g, 0.031 mol) and acetone (0.94 g, 0.016 mol) in deoxygenated ether (48 ml) was added a 20% methanolic potassium hydroxide soln (1.5 ml) at 15—16 °C. After stirring for 3 h at the same temp, the reaction was quenched with acetic acid (1.5 ml). A dark red liquid obtained by usual work up of the ethereal extracts was purified by chromatography over alumina (150 g) using light petroleum–ether (95: 5—90: 10) as eluent. The fractions containing VIII were collected and evaporated, yielding the ketone (1.9 g, 44%) as a partly crystalline oil. Crystallization from light petroleum–benzene formed yellow cubes: mp 101.3—101.7 °C; MS: *m/e* 282 (M^+, 20), 155 (100); mol wt, 282.32; IR (KBr disk): 3250 (–C≡CH), 2100 (–C≡C–), 1660 (C=O), 1595 (C=C), 985, 965 cm^{-1} (*trans* C=C); UV: λ_{max}^{EtOH} 250 (24400), 332 nm (24500); NMR: see Table 1.

Found: C, 89.18; H, 4.76%. Calcd for $C_{21}H_{14}O$: C, 89.33; H, 5.00%.

Dibenzo[d,j]-*6,8-bisdehydro*[*13*]*annulenone (IX).* A soln of the ketone (VIII, 1.15 g, 4.07 mmol) dissolved in pyridine (25 ml) was added dropwise to a stirred soln of copper(II) acetate monohydrate (12.0 g) in pyridine (40 ml) for 10 min at 50 °C, and the reaction mixture was stirred for further 3 h at 60—65 °C. The mixture was cooled, diluted with benzene (300 ml), and the resulting mixture was filtered through Hyflo Super-Cel and washed with benzene (100 ml×2). Work up of the filtrate, as described for the isolation of VI, gave a dark red solid. The solid was chromatographed on alumina (70 g) and the ketone (IX, 0.7 g, 61%) was eluted with light petroleum–ether (9: 1—8: 2). Recrystallization from benzene gave pure IX as yellow cubes: mp 194 °C (dec); MS: *m/e* 280 (M^+, 100); mol wt, 280.31; IR (KBr disk): 2150 (–C≡C–), 1640, 1620, 1590 (C=O, C=C), 975 cm^{-1} (*trans* C=C); UV: λ_{max}^{EtOH} 284 (39000), 298 (46000), 379 sh (3820), 468 sh (1380), NMR: see Table 1.

Found: C, 90.03; H, 4.59%. Calcd for $C_{21}H_{12}O$: C, 89.98; H, 4.32%.

1,5-Bis(o-ethynylphenyl)-1,4-pentadien-3-ol (IXa). To a stirred soln of the ketone (VIII, 3.5 g, 0.012 mol) in dry ether (300 ml) was added a soln of sodium borohydride (8.5 g, 0.22 mol) in absolute ethanol (400 ml). After stirring at 20—23 °C for 20 h the reaction mixture was poured into water (900 ml) containing acetic acid (6 ml). The organic layer combined with the ethereal extracts was washed with dilute acetic acid, water, saturated aq sodium hydrogencarbonate, and sodium chloride successively, and dried over sodium sulfate. The residual yellow liquid obtained after evaporation of the solvent was chromatographed on alumina (100 g) and the fractions eluted with light petroleum–ether (4: 6—2: 8) gave the desired alcohol (XIa, 2.0 g, 56%) as a pale yellow liquid: MS: *m/e* 284 (M^+, 10), 129 (100); mol wt, 284.34; IR (neat): 3300 (–OH), 3250 (–C≡CH), 2100 (–C≡C–) 1700, 1640, 1595 (C=C), 965 cm^{-1} (*trans* C=C); UV: λ_{max}^{EtOH} 226 sh (12100), 233 (15000), 239 (12800), 249 (8550), 264 (8430), 276 nm (6350); NMR: see Table 3.

4,5 : 10,11-Dibenzocyclotrideca-2,12-diene-6,8-diyn-1-ol (XIIa). To a stirred soln of the ketone (IX, 0.60 g, 2.14 mmol) in dry ether (600 ml) was added a soln of sodium borohydride (900 mg, 0.024 mol) in absolute ethanol (120 ml) at room temp, and the reaction mixture was allowed to stir at the same temp for 2 h. Then the mixture was poured into water (450 ml) containing acetic acid (3 ml) and worked up as described for the isolation of XIa. The residual, partly crystallized, pale yellow liquid was chromatographed on alumina (100 g) with benzene–chloroform (1: 1) to give the alcohol (XIIa, 0.55 , 91%). Recrystallization from benzene formed white needles: mp *ca.* 150 °C (dec); MS: *m/e* 282 (M^+, 25), 253 (100); mol wt, 282.32; IR (KBr disk): 3350, 3250 (–OH), 2150 (–C≡C–), 1640 (C=C), 975, 965 cm^{-1} (*trans* C=C); UV: λ_{max}^{EtOH} 257 (20700), 268 (20000), 297 (13200), 322 (16500), 343 (17500), 368 sh nm (3310); NMR: see Table 3.

1,5-Bis(o-ethynylphenyl)-3-methoxy-1,4-pentadiene (XIb). To a slurry of sodium hydride (derived from washing 0.065 g of 53% NaH in oil) was added a soln of the alcohol (XIa, 0.24 g, 0.85 mmol) in dry tetrahydrofuran (20 ml) and methyl iodide (5 ml) at room temp under a nitrogen atmosphere. The reaction mixture was stirred at the same temp and the reaction was monitored at appropriate intervals by TLC. After stirring for 20 h additional methyl iodide (2 ml) and sodium hydride (30 mg) was added. After stirring for a total 26 h, the mixture was poured into water (200 ml) and extracted with ether. The extracts were washed with saturated aq sodium chloride soln and dried over sodium sulfate. The residue obtained after the evaporation of the solvent was chromatographed on alumina (130 g) with light petroleum to give the ether (XIb, 0.13 g, 51%) as a pale yellow liquid: IR (neat): 3300 (–C≡CH), 2100 (–C≡C–), 1145, 1110, 1080 (C–O–C), 970 cm^{-1} (*trans* C=C); UV: λ_{max}^{EtOH} 231 (59900), 238 (47900), 256 (33900), 265 (35300), 274 nm (23100); NMR: see Table 3.

1-Methoxy-4,5: 10,11-dibenzocyclotrideca-2,12-diene-6,8-diyne (XIIb). To a stirred soln of the alcohol (XIa, 0.25 g, 0.90 mmol) in dry ether (40 ml) was added methyl iodide (10 ml) and silver oxide (2 g), and the mixture was allowed to stir for 7 h at the same temp. A second silver oxide (2 g) was added and stirring was continued for another 8 h at the same temp. Then the mixture was filtered and the filtrate was concentrated under reduced pressure to give a pale yellow liquid. Chromatography of the liquid on alumina (100 g) with light petroleum–ether (95: 5—90: 10) afforded the ether (XIIb, 0.15 g, 57%) as yellow liquid which gave white crystals (mp 79—82 °C) on strong cooling. Attempts to recrystallize this material were failed. MS: *m/e* 296 (M^+, 40), 266 (100); mol wt, 296.35; IR (KBr disk): 2200 (–C≡C–), 1105, 1080 (C–O–C), 970 cm^{-1} (*trans* C=C); UV: λ_{max}^{EtOH} 231 (40200), 257 (19000), 268 (17900), 300 (8730), 320 (13100), 342 nm (13400); NMR: see Table 3.

Attempts to Prepare the Anion XIII. To a soln of the ether (XIIb, 252 mg) in dimethyl-d_6 sulfoxide (4 ml) was added a dimsyl anion (0.6 ml, prepared from dimethyl-d_6 sulfoxide and sodium hydride)[13] with stirring at room temp. A deep green color developed. However, no satisfactory

NMR spectrum could be obtained although we performed several runs under similar conditions for various elapse of time.

We wish to thank Professor Franz Sondheimer, University College, London, for useful suggestions, and Dr. Shuzo Akiyama and Professor Masazumi Nakagawa, Osaka University, for measurement of NMR spectra at 100 MHz. This research was supported by a Grant-in-Aid for Scientific Research from the Ministry of Education (054103, 1975), which is gratefully acknowledged.

References

1) F. Sondheimer, a) *Pure Appl. Chem.*, **28**, 331 (1971); b) *Acc. Chem. Res.*, **5**, 81 (1972).

2) P. D. Howes, E. LeGoff, and F. Sondheimer, *Tetrahedron Lett.*, **1972**, 3691, 3695.

3) *Inter alia*, a) K. Endo, Y. Sakata, and S. Misumi, *Tetrahedron Lett.*, **1970**, 2557; *Bull. Chem. Soc. Jpn.*, **44**, 2465 (1971); b) M. Iyoda, M. Morigaki, and M. Nakagawa, *Tetrahedron Lett.*, **1974**, 817, 3677; c) A. Yasuhara, T. Satake, M. Iyoda, and M. Nakagawa, *ibid.*, **1975**, 815; d) M. Iyoda and M. Nakagawa, *Chem. Lett.*, **1975**, 815; e) A. Yasuhara, M. Iyoda, T. Satake, M. Nakagawa, *Tetrahedron Lett.*, **1975**, 3931.

4) a) H. Ogawa, H. Kato, and M. Yoshida, *Tetrahedron Lett.*, **1971**, 1795; b) R. T. Weavers, R. R. Jones, and F. Sondheimer, *ibid.*, **1975**, 1043.

5) a) J. Ojima, Y. Yokoyama, and T. Yokoyama, *Chem. Lett.*, **1974**, 1261; b) J. Ojima, M. Ishiyama, A. Kimura, and Y. Yokoyama, *Tetrahedron Lett.*, **1975**, 1909; c) J. Ojima, Y. Yokoyama, and T. Yokoyama, *Chem. Lett.*, **1975**, 487.

6) J. Ojima, T. Yokomachi, and A. Kimura, *Bull. Chem. Soc. Jpn.*, **49**, 2840 (1976).

7) a) E. R. H. Jones and B. C. L. Weedon, *J. Chem. Soc.*, **1946**, 937. b) J. Ojima, T. Katakami, G. Nakaminami, and M. Nakagawa, *Bull. Chem. Soc. Jpn.*, **49**, 292 (1976).

8) G. Eglinton and A. R. Galbraith, *Chem. Ind. (London)*, **1956**, 737; *J. Chem. Soc.*, **1959**, 889.

9) J. Ojima and F. Sondheimer, Abstracts of Papers, 30th National Meeting of the Chemical Society of Japan, Osaka, April 1974; R. L. Wife and F. Sondheimer, *J. Am, Chem. Soc.*, **97**, 640 (1975).

10) The small downfield shift of all protons expected to be caused by the positive charge does not significantly affect the argument.

11) After a preliminary report (Ref. 5a), Professor F. Sondheimer cast a doubt on our interpretation that IX is weakly paratropic and suggested to examine the chemical shift differences between XIa and XIIa in order to normalize the difference between an acyclic atropic compond and a cyclic atropic compound. (F. Sondheimer, private communication (1974)).

12) B. A. Stochnoff and N. L. Benoiton, *Tetrahedron Lett.*, **1973**, 21.

13) E. J. Corey and M. Chaykovsky, *J. Am. Chem. Soc.*, **87**, 1345 (1965).

14) E. LeGoff and F. Sondheimer, *Angew. Chem. Int. Ed. Engl.*, **11**, 926 (1972).

Formose Reactions. III. Evaluation of Various Factors Affecting the Formose Reaction

Yoshihiro SHIGEMASA, Takashi FUJITANI, Chikahiro SAKAZAWA, and Teruo MATSUURA*

Department of Industrial Chemistry, Faculty of Engineering, Tottori University, Tottori 680
**Department of Synthetic Chemistry, Faculty of Engineering, Kyoto University, Kyoto 606*

(Received November 4, 1976)

By an analytical method using oxidation-reduction potential measurements of the formose reaction, which were previously shown to be useful for separately analyzing the induction and the formose-forming steps, the influence of various factors on each step and on the sugar yield were examined. It was found for the batch-system formose reaction that the rate of both steps and the sugar yield are affected by the concentration of formaldehyde, the amount of calcium hydroxide, and also by the ratio of the two. The dissolved calcium ion is believed to be an essential catalyst for either the induction or the formose-forming step, with the hydroxy anion playing significant role as the catalyst for the latter step. The optimum conditions necessary for obtaining the sugars in high yields are discussed.

Since Butlerow[1] found in 1861 that various saccharides are formed from an aqueous formaldehyde solution in the presence of $Ca(OH)_2$, many investigations concerning the formose reaction have been undertaken concerning many aspects,[2] such as the catalytic effect of organic and inorganic bases,[3-5] the function of a co-catalyst having enediol-forming ability,[6] and analytical techniques for the products.[7] The formose reaction is considered to proceed *via* the following two steps.[2] The first step is an induction period involving most probably formaldehyde condensation forming glycolaldehyde, and this induction period can be reduced by the addition of substances capable of forming an enediol, *e.g.*, various monosaccharides and benzoins.[8] In the subsequent step, rapid aldol condensation, a Cannizzaro reaction, and a cross-Cannizzaro reaction take place simultaneously resulting in formaldehyde condensation to saccharides. Some other reactions such as the interconversion of intermediates (the Lobry de Bruyn-Alberda van Eckenstein rearrangement) and the decomposition of various products also accompany the above reactions.

There are two important unsolved problems concerning the formose reaction which has rather complex features. One is to provide a convenient method for separately analyzing the induction step and the formose-forming step, and the other is to separately examine the roles of the dissolved and undissolved amounts of the $Ca(OH)_2$ catalyst. Although many approaches have been made to understanding the mechanism of the formose reaction and a number of workers have proposed the mechanism of $Ca(OH)_2$ catalytic action,[4,9,10] there are still ambiguities to be clarified with respect to these two points. Weiss *et al.* have reported important aspects of the kinetics of the formose reaction using a continuously stirred tank reactor (CSTR) which was desinged to maintain the reaction in steady-state conditions. They observed inevitable instabilities caused by varying the formaldehyde concentration, the calcium hydroxide concentration,** or the reaction pH.[9,11,12] However, as far as their method is concerned, no discussion of the induction-step mechanism is possible because they allowed the reaction to start by adding an endiol initiator, in which case the formose-forming step occurred instantly without any induction period.

In an approach to the investigation of the formose reaction, the measurement of the oxidation-reduction potential (ORP) during the $Ca(OH)_2$-catalyzed reaction in the batch system has proven useful for the separate analysis of each reaction step.[13,14] This showed that whenever the formose reaction occurs, the ORP curve invariably shows a minimum at the beginning of the formose-forming step and a maximum near the end point of the reaction (the so-called yellowing point[5,15]), at which the highest sugar yield is usually obtained. In a continuation of this study using the ORP method, this paper reports detailed examinations of various factors affecting the induction step, the sugar-forming step, and the sugar yield. Particular attention is placed on the following factors; the formaldehyde concentration, the $Ca(OH)_2$ quantity and particle size, the dissolved $Ca(OH)_2$, and the initial pH.

Experimental

A formaldehyde solution was prepared as follows: 200 g of paraformaldehyde (Merck) was suspended in 400 ml of distilled water, refluxed for 4 h, and filtered through a sintered glass disk. The filtrate containing *ca.* 30 wt-% of formaldehyde was stored in a brown bottle at the dark and was used for experiments within a few days, in order that no substances accelerating the formose reaction be produced. Commercial grade $Ca(OH)_2$ was used as a catalyst and the ground powder was passed through a 200 mesh sieve. When other $Ca(OH)_2$ particle sizes were required, the $Ca(OH)_2$ was prepared by a method similar to that described by Huttig and Arbes[16] and fractionated into the desired sizes by sieving.

The formose reaction was started without adding any initiator but by adding $Ca(OH)_2$ to a formaldehyde solution pre-heated to 60±1 °C. The procedure and apparatus used in the present experiments, the methods for determining the formaldehyde consumption and sugar yield, and the manner of measuring the ORP were essentially the same as those

** The term "concentration," which was used by Weiss *et al.* for $Ca(OH)_2$, is not relevant, because their reaction system (CSTR) was not initially homogeneous, but can accurately be called heterogeneous, in view of the coexistence of dissolved and undissolved calcium hydroxide in the system.

described in a previous paper.[14] The dissolved calcium ion concentration was determined by the EDTA method with an NN-reagent as the indictator.[17]

The sugar composition of the formose product for several runs was determined by GLC after trimethylsilylation.[18] The chromatographic patterns obtained were virtually identical in all cases.

Results and Discussion

Throughout the present paper, the following terms are adopted: [HCHO] is the formaldehyde concentration, $[Ca(OH)_2]$ the quantity of calcium hydroxide added as catalyst, T_{min} the length of the induction period, which is the time from the start of the formose reaction to the ORP minimum,[14] T_{max} the time from the start to the ORP maximum,[14] and $T_{max}-T_{min}$ the length of the formose-forming period. T_{min} and $T_{max}-T_{min}$ can be used for evaluating the rate of each step.

Effects of [HCHO] and $[Ca(OH)_2]$. As has been observed by Weiss *et al.*, the formose reaction is sensitive to [HCHO] and $[Ca(OH)_2]$. In the present work, this sensitivity to concentration is shown to occur in both the induction and formose-forming steps and to affect the sugar yield.

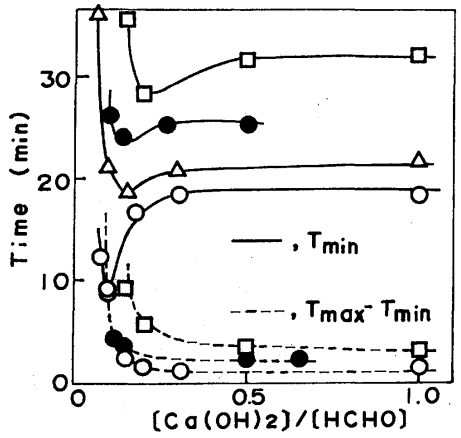

Fig. 1. Effect of $[Ca(OH)_2]$ on T_{min} and $T_{max}-T_{min}$. [HCHO]: □, 0.1 M; ●, 0.5 M; △, 1.0 M; ○, 2.2 M; $Ca(OH)_2$: 200 mesh.

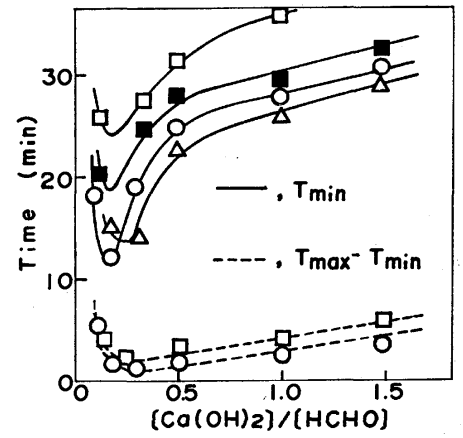

Fig. 2. Effect of [HCHO] on T_{min} and $T_{max}-T_{min}$. $Ca(OH)_2$: 200 mesh; □, 0.05 M; ■, 0.13 M; ○, 0.25 M; △, 0.33 M.

The Effect on the Induction Period: These are shown in Figs. 1 and 2. Figure 1 shows that, for increased $[Ca(OH)_2]$ at constant [HCHO], T_{min} decreases, passes through a minimum and then at about $[Ca(OH)_2]/[HCHO]=0.1—0.2$ becomes constant. Similar behavior is observed for decreased [HCHO] at constant $[Ca(OH)_2]$, however, T_{min} tends to be prolonged (Fig. 2). In both cases, the formose reaction did not occur when the $[Ca(OH)_2]/[HCHO]$ ratio was set to less than 0.05. As is seen in Table 1, which shows the effects of $[Ca(OH)_2]/[HCHO]$ on the initial pH, the $Ca(OH)_2$ solubility and the amount of HCHO adsorbed on solid $Ca(OH)_2$, the pH decreases at lower $[Ca(OH)_2]/[HCHO]$ ratios; for example, it is as low as 10.5 at $[Ca(OH)_2]/[HCHO]=0.05$. It is known that the formose reaction does not occur such a low pH value.[9]

TABLE 1. THE EFFECTS OF [HCHO] AND $[Ca(OH)_2]$ ON pH AND $Ca(OH)_2$ SOLUBILITY AT 60 °C

[HCHO] (M)	$[Ca(OH)_2]$ (M)	$[Ca(OH)_2]/[HCHO]$	pH	Dissolved $Ca(OH)_2$	HCHO adsorbed on solid $Ca(OH)_2$ (mg/ml)
1.90	0.60	0.32	11.3	0.11	10.9
1.90	0.40	0.21	11.2	0.12	6.8
1.90	0.20	0.11	11.0	0.12	3.3
1.90	0.16	0.08	11.0	0.12	1.4
1.53	0.30	0.20	11.4	0.09	1.0
2.99	0.30	0.10	11.0	0.14	4.2
5.94	0.30	0.05	10.5	0.21	8.4

In spite of the fact that Weiss *et al.* have observed in their CSTR experiments that the reaction does not occur when the $[Ca(OH)_2]/[HCHO]$ ratio is more than 2, it was demonstrated that the reaction did occur for the appearance of the ORP minimum and maximum even at $[Ca(OH)_2]/[HCHO]=5$. Furthermore, experiments at extremely low or high [HCHO] showed that such conditions are not appropriate for the formose reaction. Thus, when the [HCHO] is set to less than 0.01 M, neither did the ORP minimum appear nor did the reaction occur even for an extension of the reaction time up to 90 min. At high [HCHO] (*ca.* 10 M), the reaction occurred whenever an adequate amount of $Ca(OH)_2$ was used. However, because of a highly exothermic reaction, the mixture became too viscous to control properly.

The Effect on the Formose Forming Step. These effects were examined at constant [HCHO] and $[Ca(OH)_2]$ and are shown as dotted curves in Figs. 1 and 2, respectively. At constant [HCHO], $T_{max}-T_{min}$ is sharply reduced with increased $[Ca(OH)_2]$ in the range of $[Ca(OH)_2]/[HCHO]$ ratios between 0.1 and 0.3, and remains constant at higher ratios. For constant $[Ca(OH)_2]$, it also decreases with decreasing [HCHO] for lower $[Ca(OH)_2]/[HCHO]$ ratios but increases with decreasing [HCHO] for higher ratios.

In comparison with the effects on the induction period (Figs. 1 and 2), the kinetics for the formose-

forming step apparently differ from those for the induction step. However, when a comparison is made in the region of $[Ca(OH)_2]/[HCHO]$ ratios greater than 0.3, for both steps the rate increases with increasing [HCHO] at constant $[Ca(OH)_2]$ (Fig. 2), but the rate remains unchanged with increasing $[Ca(OH)_2]$ at constant [HCHO] (Fig. 1). These results suggest that, under certain conditions ($[Ca(OH)_2]/[HCHO] \geq 0.3$), the reactions for both the induction and formose-forming steps are of zeroth order for $Ca(OH)_2$ and probably of first order for formaldehyde. This is contrary to the concept of Weiss and Lapierre[12] that, at intermediate conversion levels, the formose reaction is of first order for $Ca(OH)_2$ and of zeroth order for the organics. Although there are some difficulties in accounting for the discrepancy between their and the present results, it is reasonable to assume that this is due to a difference between the CSTR kinetics and those of the present study.

The Effect on Sugar Yield: As shown in Figs. 3 and 4, the sugar yield is considerably altered by varying the [HCHO] and $[Ca(OH)_2]$. In summarizing the results, it can generally be said that the sugar yield increases with a decrease in either the [HCHO] or $[Ca(OH)_2]$. This may be partly explained in terms of the Cannizzaro reaction for formaldehyde. The consumption of formaldehyde in the induction period is known to be largely caused by the Cannizzaro reaction,[11] the rate of which is expressed by $-d[HCHO]/dt = k[OH^-]^{1-2}[HCHO]^{1-2}$.[2,19-21] Therefore, a higher [HCHO] or $[Ca(OH)_2]$ is not recommended for obtaining sugar products in a high yield. As discussed below, a higher $[Ca(OH)_2]$ also causes facile decomposition of the sugars formed.

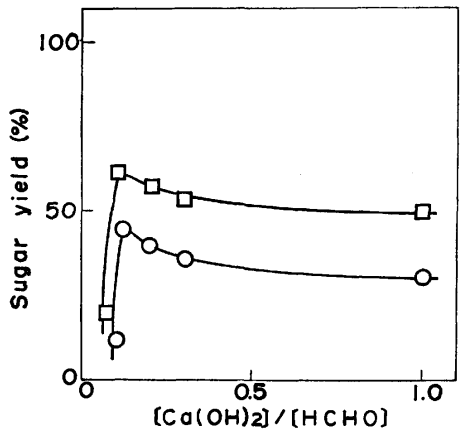

Fig. 3. Effect of $[Ca(OH)_2]$ on the sugar yield.
[HCHO]: □, 1.0 M; ○, 2.2 M; $Ca(OH)_2$: 200 mesh.
The sugar yield is based on the used formaldehyde.

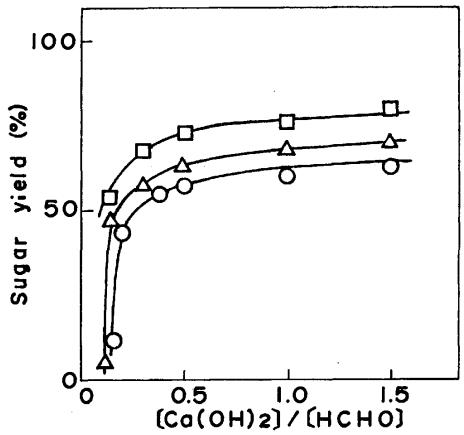

Fig. 4. Effect of [HCHO] on the sugar yield.
$Ca(OH)_2$: 200 mesh; □, 0.13 M; △, 0.25 M; ○, 0.33 M. The sugar yield is based on the used formaldehyde.

Effect of $Ca(OH)_2$ Particle Size. As a probe of the catalytic action of $Ca(OH)_2$, which exists in several forms, *e.g.*, dissolved, undissolved, or free and bound to organic materials, the influence of $Ca(OH)_2$ particle size was examined. The results are shown in Table 2. For a constant $[Ca(OH)_2]$ (0.22 or 0.33 M), an increase in particle size led to an increase of both T_{min} and $T_{max} - T_{min}$.

Since, in general, the particle size of a solid is inversely proportional to the specific surface area, the increase in the $Ca(OH)_2$ particle size causes a lowering of the dissolved rate. Thus, as shown in Table 3 (Runs 2, 5, and 6), the dissolved calcium ions at the beginning (T_s) decrease with increasing $Ca(OH)_2$ particle size. The delay in the induction period caused by the increase in $Ca(OH)_2$ size suggests that the dissolved calcium species plays an important role in the catalysis of this step. Conversely, undissolved $Ca(OH)_2$ may not be an essential catalyst but may play the role of either continuously supplying the dissolved calcium species or maintaining the pH range required for the induction period.

The delay effect on the rate of the formose-forming step for the larger $Ca(OH)_2$ particles can also be explained in terms of the slow dissolution rate. The particle size did not have any appreciable influence on the sugar yield, even when the formose reaction proceed-

Table 2. The influence of $Ca(OH)_2$ particle-size on the formose reaction[a]

$[Ca(OH)_2]$ (M)	Particle size (mesh)	T_{min} (min)	T_{max} (min)	$T_{max} - T_{min}$ (min)	Sugar yield at T_{max} (%)	Sugar yield 3 min after T_{max}
0.22	200	12.5	23.0	10.5	39.6[b]	48.4[b]
0.22	60—100	19.0	unknown	—	3.8[c]	—
0.22	20—30	unknown	unknown	—	0.6[c]	—
0.33	200	13.2	15.3	2.1	48.5	16.4
0.33	60—100	15.2	18.7	3.5	48.0	24.3
0.33	20—30	38.6	47.5	8.9	49.1	31.3

a) [HCHO]; 2.2M. b) T_{max} was somewhat obscure. c) Sugar yield at 30 min.

TABLE 3. THE EFFECTS OF INITIAL CONDITIONS ON THE FORMOSE REACTION[a)]

Run No.	[HCHO] (M)	[Ca-(OH)$_2$] (M)	T_{min} (min)	T_{max} (min)	pH at T_s	pH at T_{min}	pH at T_{max}	HCHO consumption (%) at T_{min}	HCHO consumption (%) at T_{max}	Dissolved Ca^{2+} (mM) at T_s	Dissolved Ca^{2+} (mM) at T_{min}	Dissolved Ca^{2+} (mM) at T_{max}	Sugar yield (%) at T_{max}	Sugar yield (%) at T_3[f)]
1	2.0	0.16	—[d)]	—[d)]	11.0	$(10.6)_{10}$[e)]	$(10.2)_{30}$	$(18)_{10}$	$(25)_{30}$	110	$(140)_{30}$		—	—
2	2.0	0.22	14.6	18.5	11.2	10.9	9.8	30	98	116	182	196	48.4	40.4
3	2.0	0.60	16.8	20.5	11.3	11.1	10.9	34	98	112	262	425	36.5	14.6
4	2.0	1.00	17.0	18.5	11.4	11.1	10.9	28	98	108	220	368	33.0	7.5
5[b)]	2.0	0.22	22.0	—[d)]	11.1	10.7	$(9.1)_{30}$	34	$(55)_{30}$	89	192	$(205)_{30}$	$(15.0)_{30}$	
6[c)]	2.0	0.22	—[d)]	—[d)]	11.2	$(11.1)_{10}$	$(10.8)_{30}$	$(14)_{30}$	$(33)_{30}$	30	$(175)_{30}$		—	—
7	0.5	0.25	19.4	21.6	11.2	11.5	11.5	23	99	35	53	195	58.7	27.0
8	1.3	0.25	15.0	17.0	11.4	11.2	11.0	25	98	72	133	210	48.7	18.8
9	2.5	0.25	11.8	—[d)]	11.1	10.8	$(9.0)_{30}$	26	$(85)_{30}$	121	212	$(220)_{30}$	$(23.1)_{30}$	
10	5.0	0.25	—[d)]	—[d)]	10.8	$(10.3)_{10}$	$(9.5)_{30}$	$(13)_{10}$	$(18)_{30}$	150	$(232)_{30}$		—	—
11	1.0	0.10	21.0	28.8	11.3[g)]	11.0	10.2	28	98	53	80	85	52.4	48.6
12	1.0	0.10	33.7	37.7	11.5[g)]	11.2	10.9	42	99	32	69	86	50.5	15.8
13	1.0	0.10	41.5	44.2	11.7[g)]	11.3	11.3	42	99	16	50	86	46.7	12.9
14	1.0	0.10	—[d)]	—[d)]	12.0[g)]	$(11.9)_{30}$	$(11.6)_{60}$	$(41)_{30}$	$(52)_{60}$	9	$(14)_{30}$	$(19)_{60}$	—	—

a) Reaction temp, 60 °C; $Ca(OH)_2$, 200 mesh. b) $Ca(OH)_2$, 60—100 mesh. c) $Ca(OH)_2$, 20—35 mesh. d) The minimum ORP and/or maximum ORP were obscure. e) In cases when T_{min} and T_{max} were obscure, the measurement were performed for reaction times of 10 and 30 min respectively, the results of which are shown in parenthesis with a subscript number. f) T_3=3 min after T_{max}. g) The pH was adjusted with concd KOH.

ed slowly (see Table 2, for a 0.33 M [$Ca(OH)_2$]). However, the decomposition of sugar products after T_{max} was found to be suppressed with increased $Ca(OH)_2$ size, although the $T_{max}-T_{min}$ was prolonged. This may also be due to the slow dissolution rate of $Ca(OH)_2$ which is considered to accelerate the decomposition of sugar in dissolved form.

Effects of the pH and the Dissolved Calcium Ions. The above results led us to the preliminary conclusion that the pH and the dissolved calcium species may be important factors in the formose reaction, in addition to the effect of the [HCHO] and [$Ca(OH)_2$]. The importance of the pH effect has already been pointed out.[9,22,23)] Weiss and John have shown that the consumption rate of formaldehyde using CSTR is highly pH-dependent at constant [HCHO] and [$Ca(OH)_2$]: for example, the highest rate is observed for a pH of *ca.* 11.0 for 1.3 M [HCHO] and 0.45 M [$Ca(OH)_2$] and for a pH of *ca.* 11.5 for 1.3 M [HCHO] and 0.35 M [$Ca(OH)_2$].[9)]

In order to gain more insight into the nature of the formose reaction, the effects of the initial conditions were examined while measuring the initial pH and dissolved calcium ion and the T_{min} and T_{max} points, as well as the formaldehyde consumption and the sugar yield. The results are summarized in Table 3. The most typical standard conditions that give good sugar yields are Runs 2, 8, and 11, which will be compared with other Runs in the following discussion.

The Effect of [$Ca(OH)_2$] (Runs 1—4). At the same [HCHO] and $Ca(OH)_2$ particle size, the initial pH (at T_S) increases with increasing [$Ca(OH)_2$], in accord with the results shown in Table 1, however, the initial concentration of the dissolved calcium ion is virtually independent of the [$Ca(OH)_2$] which has a significant effect on the yield and the sugar decomposition rate.

The Effect of the $Ca(OH)_2$ Particle Size (Runs 2, 5, and 6). Delayed effects similar to those described above were observed for T_{min} and $T_{max}-T_{min}$ (Table 2). It should be noted that the initial concentration of the dissolved calcium ion decreases significantly with increased particle size despite the fact that the initial pH is practically the same in all cases.

The Effect of [HCHO] (Runs 7—10). For the same [$Ca(OH)_2$] and $Ca(OH)_2$ particle size, the initial pH showed a tendency to decrease with increasing [HCHO], while the initial dissolved calcium ion increased.

The Effect of the Initial pH (Runs 11—14). For constant [HCHO] and [$Ca(OH)_2$], the effect of the initial pH was examined, as adjusted to the desired value by the addition of potassium hydroxide. For increased pH, the initial concentration of dissolved calcium ions decreased and, in proportion to this decrease, T_{min} increased while $T_{max}-T_{min}$ decreased.

Other Significant Observations. T_{min} is increased with decreasing initial concentration of the dissolved calcium ion. Also, $T_{max}-T_{min}$ is prolonged with decreasing pH at T_{min}. A lowering of the pH was observed throughout the induction and formose-forming steps; this was more significant in the latter step. The pH lowering near the end of the formose-forming step has previously been reported.[5,6)] This may be largely due to the facile complex formation between sugars and $Ca(OH)_2$.[5,9)] In fact, when an aqueous $Ca(OH)_2$ solution was titrated with a solution of several sugars, an appreciable fall in the pH was observed, as is shown in Fig. 5. However, for titration with 0.1 M glucose, the pH of a $Ca(OH)_2$ solution showed no tendency to decrease. It should be noted that the formation of organic acids by the Cannizzaro reaction may also contribute to the pH lowering either in the induction or the formose-forming step, and it has been shown that the rate of organic-acid formation in the induction period is similar to that for the formose-

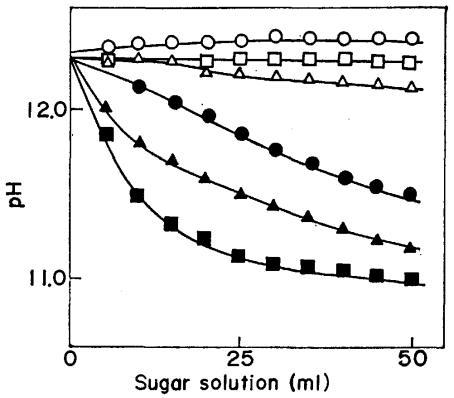

Fig. 5. pH change of 0.1 M $Ca(OH)_2$ solution (50 ml) by titration with an aqueous sugar solution. Temp, 26°C; Sugar solution: □, Blank; ○, 0.1 M glucose; △, 0.1 M xylose; ●, 1.0 M glucose; ▲, 1.0 M xylose; ■, 1.0 M fructose.

forming step.[3,14]

Conclusion. From these observations, one can draw the following conclusions. First, the formose reaction does not occur for low $[Ca(OH)_2]/[HCHO]$ ratios (<0.05). Under such conditions, the induction step is not initiated because of the low pH (<10.5). Second, the dissolved calcium ion may act as an active catalyst in the induction step when the pH is maintained at the appropriate range (approximately 10.8—11.7) and when the $[Ca(OH)_2]/[HCHO]$ ratio is not extremely low (<0.1). The undissolved $Ca(OH)_2$ may not play a significant role in the catalysis during the induction period, but may serve as a supplier of dissolved calcium ions, which are consumed by the Cannizzaro reaction for formaldehyde, and for maintaining the neccessary pH. Third, the dissolved calcium ion is considered to be essential for catalyzing the formose-forming step. However, due to the fact that the rate of this step is accelerated with increasing initial pH (T_{min}), it is suggested that the OH^- ion plays a significant role in the catalysis of the formose-forming step.

There are some discrepancies between the results of Weiss *et al.*[9,11,12] and those presented here regarding the kinetic behavior of the formose reaction. However, the above conclusions are not inconsistent with those of Weiss *et al.* such as the suggestion that $CaOH^+$ might be the true catalyst in the overall formose reaction, in view of the pH dependence and the sensitivities to the $[Ca(OH)_2]$ and [HCHO]. More details on the nature of the catalyst will be reported in a subsequent paper.

Finally, the present investigation provides the following guide-lines for obtaining high sugar yield in batch-reaction systems. The amount of formaldehyde consumed by the Cannizzaro reaction must be minimized. This may be done at low formaldehyde concentrations ($[HCHO]<1$ M), at relatively low pH values, such as *ca.* 11.2 (Table 3, Runs 7 and 11) and at high $[Ca(OH)_2]/[HCHO]$ ratios with low $[Ca(OH)_2]$ (Fig. 4). In order to prevent sugar decomposition, it is strongly recommended to stop the reaction exactly at T_{max} and to set the pH as low as possible. For example, under the conditions described here, when the $[Ca(OH)_2]/[HCHO]$ ratio was set in the range from 0.11 to 0.15, the sugar yields were 45 and 58% at 2.2 and 1.0 M [HCHO], respectively (Fig. 3). When the $[Ca(OH)_2]/[HCHO]$ ratio was set to 1.5, the sugar yields were 60 and 77% at 0.33 and 0.13 M $[Ca(OH)_2]$, respectively (Fig. 4). However, when the [HCHO] was less than 0.01 M for any $[Ca(OH)_2]/[HCHO]$ ratio, the formose reaction could not occur.

References

1) A. Butlerow, *Ann. Chem.*, **120**, 295 (1861).
2) T. Mizuno and A. H. Weiss, *Adv. Carbohydr. Chem. Biochem.*, **29**, 137 (1974).
3) R. Mayer and L. Jäschke, *Ann. Chem.*, **635**, 145 (1960).
4) K. Runge and R. Mayer, *Ann. Chem.*, **707**, 161 (1967).
5) T. Mizuno, T. Mori, N. Shiomi, and H. Nakatsuji, *Nippon Nogei Kagaku Kaishi*, **44**, 324 (1970).
6) A. Kusin, *Chem. Ber.*, **68**, 1494 (1935).
7) H. Ruckert, E. Pfeil, and G. Scharf, *Chem. Ber.*, **98**, 2558 (1965).
8) W. Langenbeck, *Naturwissenschaften*, **30**, 30 (1942).
9) A. H. Weiss and T. John, *J. Catal.*, **32**, 216 (1974).
10) K. Fujino, J. Kobayashi, and I. Higuchi, *Nippon Kagaku Kaishi*, **1972**, 2287, 2292.
11) H. Tambawala and A. H. Weiss, *J. Catal.*, **26**, 388 (1972).
12) A. H. Weiss and R. B. Lapierre, *J. Catal.*, **16**, 332 (1970).
13) T. Matsuura, Y. Shigemasa, and C. Sakazawa, *Chem. Lett.*, **1974**, 713.
14) Y. Shigemasa, M. Shimao, C. Sakazawa, and T. Matsuura, *Bull. Chem. Soc. Jpn.*, **48**, 2099 (1975).
15) E. Pfeil and H. Ruckert, *Ann. Chem.*, **641**, 121 (1961).
16) G. F. Huttig and U. A. Arbes, *Z. Anorg. Allg. Chem.*, **191**, 161 (1930).
17) J. Patton and W. Reeder, *Anal. Chem.*, **28**, 1026 (1956).
18) T. Mizuno, M. Asai, A. Misaki, and Y. Fujihara, *Nippon Nogei Kagaku Kaishi*, **45**, 344 (1971).
19) H. V. Euler and T. Lovgren, *Z. Anorg. Chem.*, **127**, 123 (1925).
20) I. I. Paul, *J. Gen. Chem.*, **11**, 1121 (1941).
21) J. March, "Advanced Organic Chemistry," McGraw-Hill, New York (1968), p. 692.
22) H. Schmalfuss, *Biochem. Z.*, **185**, 70 (1927).
23) A. Kusin, *Chem. Ber.*, **68**, 619 (1935).

Asymmetric Reactions. II. Asymmetric Synthesis of Methyl α-Phenylpropionate by Means of Chiral Polymers

Tetsushi YAMASHITA, Hiroshi YASUEDA, Yasushi MIYAUCHI, and Nobuo NAKAMURA

Department of Chemistry, Faculty of Science, Osaka City University, Sumiyoshi-ku, Osaka 558

(Received November 8, 1976)

The asymmetric addition of methanol to phenylmethylketene was carried out in the presence of propionylcinchonine and poly(acryloylcinchonine). The use of poly(acryloylcinchonine) produced additional products with higher optical yields than that of propionylcinchonine. The highest optical yield (35%) was obtained with the above polymeric catalyst at −78 °C. An insoluble, cross-linked polymer obtained by the co-polymerization of acryloylcinchonine with *N,N'*-diacryloylhexamethylenediamine, was also used as a catalyst. The products obtained for the cross-linked polymer showed a linear correlation between log k_R/k_S and $1/T$ while those with non-cross-linked poly(acryloylcinchonine) exhibited a relationship deviating somewhat from linearity. A linear relationship was also observed using insoluble, cross-linked poly(acryloylquinine).

The use of chiral synthetic polymers for asymmetric synthesis has been attempted by several workers[1-8] because of the interest in the study of asymmetric reactions, new catalysts, enzyme models, and polymer effects.

In a previous paper,[1] the asymmetric addition of methanol to phenylmethylketene (PMK) was examined in the presence of optically-active polymers and their corresponding monomeric model compounds.

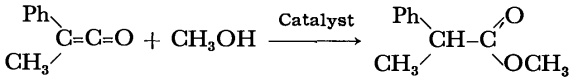

A distinct polymer effect with regard to stereoselectivity was observed with poly(*N*-benzyl-2-pyrrolidinylmethyl acrylate) (**P-1**) and poly(acryloylquinine) (**P-2**).

Figure 1 indicates the result of the addition reaction obtained with **P-1** and *N*-benzyl-2-pyrrolidinylmethyl propionate in plots of log k_R/k_S against $1/T$ [$k_R(k_S)$: the rate constant for the *R*(*S*)-isomer]. The addition products with **P-1** showed a linear relationship between log k_R/k_S and $1/T$.

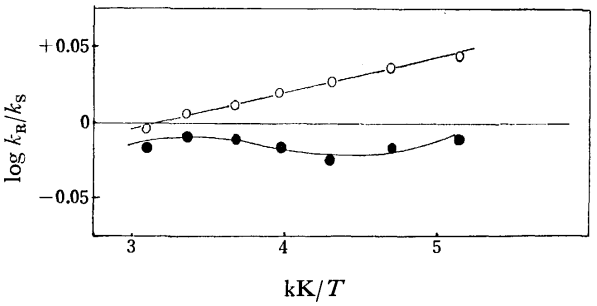

Fig. 1. Plots of log k_R/k_S against $1/T$ in case of **P-1** (—○) and *N*-benzyl-2-pyrrolidinylmethyl propionate (—●).

Pracejus and his co-workers[9] have previously reported that a linear correlation between log k_R/k_S and $1/T$ was observed with α-isocinchonine[9c] (**B**) (a cyclic ether derived from cinchonine) rather than with acetylcinchonine[9b] (**A-1**) (see Fig. 2).

Pracejus *et al.* explained their results using the effect of molecular immobility. Rotation about the carbon-carbon bond (C_8–C_9) of **B** is strongly restricted, and the conformation of **B** is more rigid than that of **A-1**.

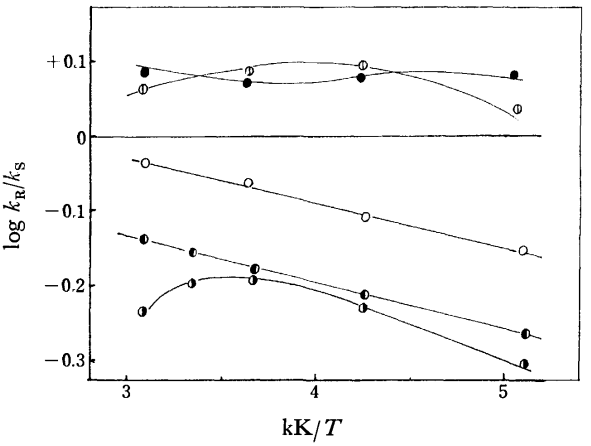

Fig. 2. Plots of log k_R/k_S against $1/T$ in case of cinchonine catalysts
A-1 —●, **A-2** —◐, **B** —○, **P-3** —◑, **P-4** —◐.

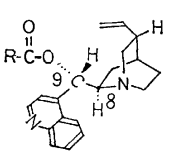

Acylcinchonine (**A**)
A-1, CH_3
A-2, CH_2CH_3
A-3, $CH{=}CH_2$

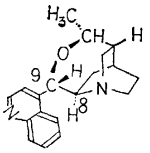

α-Isocinchonine (**B**)

The results obtained with **P-1** are interpreted on the basis of the concept of Pracejus *et al.* The steric bulkiness of the back-bone of the polymer restricts the mobility of the side chain and increases the degree of conformational rigidity of the molecules in the side chain.

In the present work, this sort of polymer effect was examined in detail with cinchonine and quinine derivatives as catalysts. The reactions of cinchonine with acetic anhydride, propionic anhydride and acryloyl chloride was carried out in the presence of triethylamine producing **A-1**, **A-2**, and **A-3**, respectively.

Acryloylcinchonine (**A-3**) was polymerized using azobisisobutyronitrile as an initiator in dry benzene under reflux giving a polymer (**P-3**) soluble in common organic solvents.

An insoluble, cross-linked polymer (**P-4**) was obtained

by the co-polymerization of **A-3** with *N,N'*-diacryloylhexamethylenediamine.[10] Acryloylquinine[1] was similarly co-polymerized with *N,N'*-diacryloylhexamethylenediamine and *N,N'*-diacryloyldodecamethylenediamine to give **P-5** and **P-6**, respectively. These insoluble, polymeric catalysts were easily separated from the reaction mixture by filtration.

The asymmetric addition of methanol to PMK was carried out with the above catalysts in a manner similar to that reported earlier.[1] To one equivalent amount of PMK and a small excess of methanol was added a 0.01 molar equivalent of the catalyst.

The molar equivalent amount of the polymeric catalyst was calculated on the basis of that of the monomer used in the polymerization (*e.g.*, 10 mg of **P-3** corresponds to 10 mg of **A-3**).

Table 1. The specific rotations, optical yields and configurations of the addition products

Catalyst	T (°C) −78 $[\alpha]_D$	−78 O.Y.[a]	0 $[\alpha]_D$	0 O.Y.	+50 $[\alpha]_D$	+50 O.Y.	Conf[b]
A-2	−4.8	4.4	−10.5	9.6	−8.9	8.2	*R*
P-3	+38.1	35.0	+23.6	21.7	+29.6	27.2	*S*
P-4	+33.1	30.4	+23.3	21.4	+17.5	16.1	*S*
P-5	−16.2	14.9	−11.4	10.5	−8.4	7.7	*R*
P-6	−12.9	11.8	−11.3	10.4	−10.1	9.3	*R*

a) The O.Y. (optical yield, %) was calculated from the specific rotation of the product and that of optically pure methyl α-phenylpropionate[9a] (*S*-form, $[\alpha]_D^{22}=+109°$, *c* 6.2, toluene). b) Configuration of the predominant isomer.

Table 1 gives the specific rotations, optical yields and configurations of the addition products obtained with cinchonine and quinine catalysts at −78, 0 and +50 °C.

Figure 2 shows the log (k_R/k_S) *vs.* $1/T$ relation of the addition products obtained for the cinchonine catalysts (**A-2**, **P-3**, and **P-4**).

The products for **P-4** (cross-linked) showed a linear relationship between log k_R/k_S and $1/T$ while those with **P-3** (non-cross-linked) showed a relation deviating from linearity.

In Figure 3 are shown plots of log k_R/k_S against $1/T$ in the case of the quinine catalysts (**P-2**, **P-5**, and **P-6**).

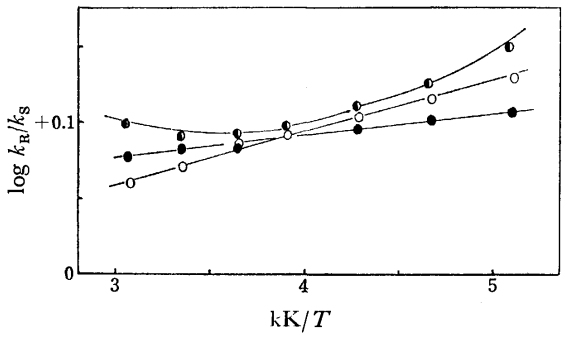

Fig. 3. Plots of log k_R/k_S against $1/T$ in case of **P-2** (—◐), **P-5** (—○), **P-6** (—●).

The products for the cross-linked polymer (**P-5** and **P-6**) showed a linear correlation between log k_R/k_S and $1/T$.

Figures 2 and 3 suggest that the cross-linking of polymers, which further restricts the mobility of the side chain, resulted in the linear relationship for the addition products of the cinchonine and quinine catalysts.

Experimental

Propionylcinchonine (A-2). A solution of cinchonine (1.5 g), propionic anhydride (0.7 g) and triethylamine (0.8 g) in dry benzene (100 ml) was stirred under refluxing. After 4 h, the solution was cooled to room temperature, and poured into water (100 ml). The organic layer separated out was washed with saturated sodium hydrogencarbonate and water, and dried over anhydrous sodium sulfate. After removal of the solvent, the residue was recrystallized from ether. Yield, 90%. Mp 46 °C. $[\alpha]_D^{20}=+101°$ (*c* 2, chloroform). Found: C, 75.60; H, 7.50; N, 8.15%. Calcd for $C_{22}H_{26}O_2N_2$: C, 75.42; H, 7.42; N, 8.00%. IR (cm^{-1}): 1720, 1180: NMR (ppm): 1.1, 2.4 (propionyl group proton), 5.5—6.5 (olefinic proton), 7.5, 8.1, 8.8 (quinoline ring proton).

Acryloylcinchonine (A-3). To a solution of cinchonine (3 g) and triethylamine (1.5 g) in dichloromethane (100 ml) a solution of freshly distilled acryloyl chloride (1.3 g) in dichloromethane (50 ml) at −20 °C was dropwise added with stirring. After standing overnight, the reaction mixture was poured into water (200 ml). The organic layer separated out was washed with saturated sodium hydrogencarbonate and water, and dried over anhydrous sodium sulfate.

The solution was concentrated, and subjected to chromatography on alumina (2×30 cm, 200 mesh, neutral). Elution with ethyl acetate gave **A-3** as a clear oil in a 94% yield. $[\alpha]_D^{20}=+80°$ (*c* 2, chloroform). TLC of **A-3** gave only one spot for several solvent systems. IR (cm^{-1}): 1720, 1180, 990. NMR (ppm): 5.6—6.5 (olefinic proton), 7.5, 8.1, 8.8 (quinoline ring proton).

Poly(acryloylcinchonine) (P-3). A solution of **A-3** (1 g) and azobisisobutyronitrile (10 mg) in dry benzene (10 ml) was refluxed with stirring in an argon atmosphere. After 20 h, the solution was cooled to room temperature and poured into ether. A precipitate (**P-3**) was filtered off and washed thoroughly with ether. Yield, 74%. $[\alpha]_D^{20}=+50°$ (*c* 1, chloroform). Mol wt 13000 (dichloromethane).

Acryloylquinine[1] was similarly polymerized to give **P-2**.[1] Yield, 56%. $[\alpha]_D^{20}=-14°$ (*c* 1, chloroform). Mol wt 14000 (dichloromethane).

Cross-linking Agents. 1) *N,N'*-diacryloylhexamethylenediamaine (**CA-1**) was prepared by the reaction of hexamethylenediamine with acryloyl chloride according to the method reported previously.[10] Mp 147 °C. Found: C, 64.45; H, 9.00; N, 12.11%. Calcd for $C_{12}H_{20}N_2O_2$: C, 64.28; H, 8.92; N, 12.50%. IR (cm^{-1}): 3300, 1660, 1610. NMR (ppm): 5.5—6.5 (olefinic proton). 2) *N,N'*-Diacryloyldodecamethylenediamine (**CA-2**) was obtained similarly by the reaction of dodecamethylenediamine with acryloyl chloride. Mp 123—125 °C. Found: C, 69.90; H, 10.50; N, 8.70%. Calcd for $C_{18}H_{32}N_2O_2$: C, 70.12; H, 10.38; N, 9.09%. IR (cm^{-1}): 3300, 1665. NMR (ppm): 5.6—6.6 (olefinic proton).

Co-polymers. A solution of **A-3** (700 mg), **CA-1** (224 mg) and azobisisobutyronitrile (10 mg) in dry benzene (10 ml) was refluxed with stirring in an argon atmosphere. After 40 h, a white precipitate was filtered off and washed thoroughly with acetone, benzene, chloroform, ethanol and ethyl acetate, successively. An insoluble polymer (**P-4**) was

obtained in an 80% yield. Acryloylquinine was similarly co-polymerized with **CA-1** (**CA-2**) to give **P-5** (**P-6**) in an 80—90% yield.

Poly(N-benzyl-2-pyrrolidinylmethyl acrylate) (P-1).

N-Benzyl-2-pyrrolidinylmethyl acrylate[1] (2.1 g) containing azobisisobutylronitrile (21 mg) was polymerized without solvents in a sealed tube at 80 °C for 70 h and cooled to room temperature. The product was dissolved in benzene and the solution was poured into methanol. A yellow precipitate was filtered off and washed with methanol. Yield, 50%. $[\alpha]_D^{15} = -43°$ (*c* 1.6, benzene). Mol wt 5300 (dichloromethane).

The polymerization of *N*-benzyl-2-pyrrolidinylmethyl acrylate was not successful under the conditions described for the cases of **P-2** and **P-3**.

The co-polymerization of *N*-benzyl-2-pyrrolidinylmethyl acrylate with **CA-1** and **CA-2** was also unsuccessful and gave only polymers of **CA-1** and **CA-2**. The *N*-benzyl-2-pyrrolidinylmethyl acrylate was largely recovered. The shapes of the ORD and CD curves for **P-1** were similar to those of *N*-benzyl-2-pyrrolidinylmethyl propionate. The hydrolyzed **P-1** showed no optical activity.

These facts suggest that there was no occurrence of asymmetric induction to the main chain configuration of **P-1**.

Similar results[11] were also observed for **P-2**[11a] and **P-3**.

The Addition Reaction of Methanol with PMK. (A)Freshly distilled PMK (330 mg) and **P-5** (11 mg) were added to 25 ml of dry toluene at −78 °C in an argon atmosphere. After addition of methanol (82 mg), the mixture was stirred at the same temperature for 20 h. The end point of the reaction was confirmed by the absence of the yellow color of PMK. After the removsl of **P-5** by filtration, the toluene solution was washed with saturated sodium hydrogencarbonate and water, and dried over anhydrous sodium sulfate. The solution was evaporated to dryness under reduced pressure. The residue was distilled to give a colorless oil in a 70% yield. Bp 69—71 °C at 2 mmHg. $[\alpha]_D^{20} = -16.2°$ (*c* 10, toluene).

TLC and GLC of the product showed it to be a single material. The IR and NMR spectra of the product were completely in agreement with those of authentic methyl α-phenylpropionate. The addition of methanol to PMK was carried out similarly in the presence of other insoluble catalysts (**P-4** and **P-6**) at various reaction temperatures.

(B) Freshly distilled PMK (330 mg) and **A-2** (8 mg) were added to 25 ml of dry toluene at −78 °C in an argon atmosphere. After the addition of methanol (82 mg), the mixture was stirred at the same temperature for 10 h. The toluene solution was poured into dilute hydrochloric acid. The organic layer separated out was washed with saturated sodium hydrogencarbonate, water, and dried over anhydrous sodium sulfate. After removal of the solvent, the residue was distilled to give an oil in a 72% yield. $[\alpha]_D^{20} = -4.8°$ (*c* 10, toluene).

The structure of this oil was confirmed in the manner described in (A).

The use of other soluble catalysts was similarly attempted at various reaction temperatures.

For the measurement of the samples, a Jasco IRA-1 (IR), a Jeol-60 MC (NMR), a Varian M920 (GLC), a Jasco J-20(ORD,CD), a Rex-automatic polarimeter (specific rotation, length of sample: 10 cm) and a Knauer vapor-pressure osmometer (molecular weight) were used in this experiment.

References

1) T. Yamashita, H. Yasueda, and N. Nakamura, *Chem, Lett.*, **1974**, 585.
2) S. Tsuboyama, *Bull. Chem. Soc. Jpn.*, **39**, 698 (1966).
3) H. Fukushima and S. Inoue, *Makromol. Chem.*, **176**, 3609 (1975).
4) T. Nozawa, Y. Akimoto, and M. Hatano, *Makromol. Chem.*, **158**, 21 (1972).
5) K. Harada and T. Yoshida, *Naturwissenschaften*, **57**, 306 (1970).
6) R. L. Beamer and W. D. Brown, *J. Pharm. Sci.*, **60**, 583 (1971).
7) M. Kawana and E. Emoto, *Tetrahedron Lett.*, **1972**, 4855.
8) W. Dumont, J. C. Poulin, T. P. Dang, and H. B. Kagan, *J. Am. Chem. Soc.*, **95**, 8295 (1973).
9) a) H. Pracejus, *Ann. Chem.*, **634**, 9 (1960); b) H. Pracejus and H. Matje, *J. Prakt. Chem.*, **24**, 195 (1964); c) H. Pracejus and G. Kohl, *Ann. Chem.*, **722**, 1 (1969).
10) T. Yamashita and N. Nakamura, *Bull. Chem. Soc. Jpn.*, **43**, 1809 (1970).
11) a) K. Yamauchi, Y. Mitsuda, and M. Kinoshita, No, 3103, 29th National Meeting of the Chemical Society of Japan, Hiroshima, October 1973; b) K. Matsuzaki and T. Sugimoto, *Makromol. Chem.*, **164**, 127 (1973); c) Y. Izumi, T. Oguni, and K. Takemoto, *Kagaku Sōsetsu*, **4**, 200 (1974).

Reduction by a Model of NAD(P)H. XIV. Mechanistic Consideration on the Role of Metal Ion

Atsuyoshi OHNO, Takahide KIMURA, Hiroyuki YAMAMOTO, Seung Geon KIM,* Shinzaburo OKA, and Yutaka OHNISHI**

Institute for Chemical Research, Kyoto University, Uji, Kyoto 611

***Sagami Chemical Research Center, 4-4-1 Nishiohnuma, Sagamihara-shi, Kanagawa 229*

(Received November 18, 1976)

The driving force for the catalytic activity of metal ions on the reduction of α-keto esters with an NAD(P)H-model compound has been discussed. The scope of the reaction and spectroscopic investigations as well as molecular orbital consideration have revealed that the transition state of the reaction consists of a ternary complex in analogy with a coenzyme-enzye-substrate complex in an enzymic system. It is concluded that, at the transition state, one electron migrates from a model compound to a substrate through a metal ion, which is followed by the transfer of a proton.

Dihydropyridine nucleotides, NADH and NADPH, are coenzymes which are widely co-operating with dehydrogenases. It has been acepted that the reaction with NAD(P)H proceeds with a one-step hydride transfer from the coenzyme to a substrate.[1,2] On the other hand, recent model reactions revealed that the reduction involves at least one intermediate,[3,4] and that there appear ion-radicals during the reduction.[5,6] ESR signals were also observed with enzymic systems.[7] Yet, the mechanism or the driving force of the reduction with NAD(P)H or its model compounds has not been understood.

In a series of investigations, we found that 1-benzyl-1,4-dihydronicotinamide (BNAH) or its analogs reduces α-keto esters in acetonitrile in the presence of a bivalent metal ion such as magnesium or zinc perchlorate.[8] When the amide-nitrogen is substituted by a chiral group, asymmetric reduction takes place.[8] The ratio of the concentration of metal perchlorate to that of the model compound, but not the absolute concentration of metal perchlorate, influences the optical yield of the product.[9]

The metal ion in the present model reaction may be regarded as a mimetic enzyme in the sense that it catalyzes the reaction as does an enzyme in biological reactions, and the information for the mechanism of the model reaction may provide an insight into the mechanism of enzymic reactions. The purpose of the present paper is focused to elucidate the role of metal-ion catalysts.

Results

Reaction. As was reported, the reaction of methyl benzoylformate (**1**) with *R*-(−)- or *S*-(+)-*N*-(α-methylbenzyl)-1-propyl-1,4-dihydronicotinamide (**2**) afforded *R*-(−)- or *S*-(+)-methyl mandelate, respectively, in quantitative chemical yield with about 15% enantiomeric excess, in the presence of equimolar amount of magnesium perchlorate.[10] When magnesium perchlorate was substituted by lithium perchlorate, the catalytic efficiency decreased remarkably and 6 to 8 molar excess of the lithium salt resulted in the formation

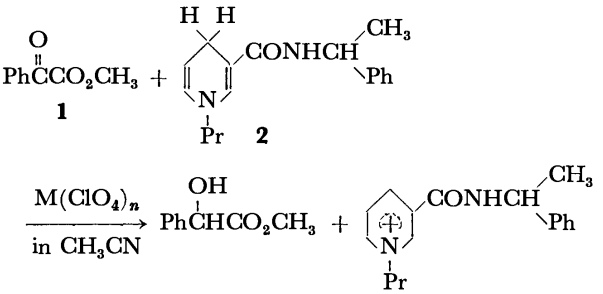

of methyl mandelate in only 60—70% yield. Moreover, it is surprising that the reaction with lithium perchlorate is non-stereospecific. Although less than 1% of enantiomeric excess was observed with the lithium salt, the value was well within the experimental error of ±2%. Tetraethylammonium perchlorate was ineffective to promote the reaction. The reaction was not catalyzed by acetylacetonate magnesium or tris(3-trifluoroacetyl-*d*-camphor)europium, Eu(TFAC)$_3$, effectively; 10 and 12% reductions were observed with these catalysts, respectively.

TABLE 1. ELECTRONIC SPECTRA OF *N*-(α-METHYLBENZYL)-1-PROPYL-1,4-DIHYDRONICOTINAMIDE (**2**) IN ACETONITRILE IN THE ABSENCE OR PRESENCE OF MAGNESIUM PERCHLORATE

$([Mg^{2+}]/[2]$	λ_{max}, nm	ε_{max}
0	351	7765
0.25	352	7647
0.50	352	7718
1.0	353	7605
2.0	354	7824
3.0	354	8047
4.0	355	7906
6.0	356	8194
8.0	357	8194
400	367	—

Spectroscopy. The absorption maximum of **2** at 351 nm shifted toward the region of longer wave-length with the addition of magnesium perchlorate as listed in Table 1. With lithium perchlorate, no shift was observed up to the ratio of 10. However, 18 nm of the shift was recorded at the point of $[Li^+]/[2]=400$. Tetraethylammonium perchlorate did not change the

* Department of Chemistry, Faculty of Science, Tokai University.

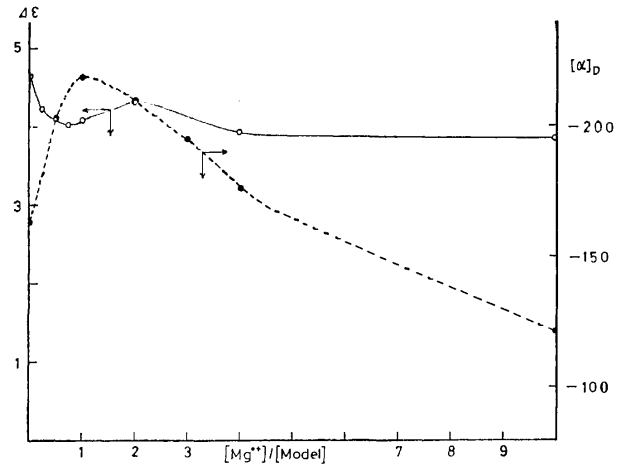

Fig. 1. Variations of $[\alpha]_D$ (----) and maximum intensity in CD spectrum (——) of *N*-(α-methylbenzyl)-1-propyl-1,4-dihydronicotinamide (**2**) as a function of $[Mg^{2+}]/[2]$ (in CH_3CN).

spectrum even at its saturated concentration. The dependencies of the intensity of the CD spectrum, observed at around 350 nm, and $[\alpha]_D$ of **2** on the molar ratio are illustrated in Fig. 1. Chemical shifts of protons in NMR spectrum of **2** were not altered significantly by the addition of magnesium perchlorate.[11] Remarkable shift was observed, however, with the addition of chiral shift reagents, $Eu(TFAC)_3$ and its ytterbium analog. Nevertheless, the protons at the chiral and prochiral centers in *R*- and *S*-**2** behaved similarly (Fig. 2). No appreciable difference was detected from IR spectra of **2** with and without magnesium perchlorate.

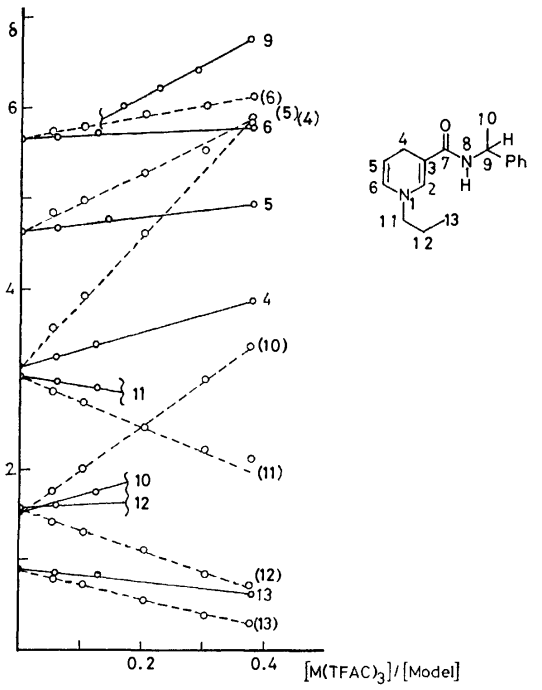

Fig. 2. Variations of chemical shift of protons in *N*-(α-methylbenzyl)-1-propyl-1,4-dihydronicotinamide (**2**) as functions of $[Eu(TFAC)_3]/[2]$ (——) and $[Yb(TFAC)_3]/[2]$ (----) (in $CDCl_3$).

All spectra were recorded with acetonitrile solutions and were not affected by the addition of **1**. The electronic and vibrational spectra of **1** remained unchanged in the presence of magnesium ion.

Discussion

The absorption at around 350 nm is attributed to the π,π^* transition of the dihydropyridine moiety.[12,13] It should be noted that only closed (ring) enamine-structure can account for the absorption at such a long wavelength as 350 nm.[12] All spectral data are in accord with the concept that the metal ion coordinates onto the dihydropyridine moiety instead of the amide-carbonyl; the absorption at 350 nm was affected by the addition of magnesium ion; but not by the addition of tetraethylammonium ion; only slight difference was observed in the CD spectrum; the chiral NMR shift reagent did not discriminate the chiral protons; no shift was observed for the stretching frequencies of the amide–C–O, C=N, and N–H groups; the fact that the band at 350 nm is the longest-wavelength absorption indicates that the π-orbital of the dihydropyridine ring is the highest-occupied molecular orbital (HOMO) of **2**. Coordination of metal ions onto the pyridine ring of nicotinamide has also been witnessed.[14,15] The meaning of minimum and maxima in curves shown in Fig. 1 is equivocal because the absorption spectra did not show an isosbestic point to calculate the dissociation constant of the complex. A complex containing four moelcules of BNAH coordinated onto a magnesium ion has been isolated from an acetonitrile solution.[11] It is also reported that the rate *vs.* molar ratio, $[Mg^{2+}]/[BNAH]$, profile for the reaction of BNAH with 2-benzoylpyridine has a maximum at the ratio of 0.4.[11]

Since the prochiral C_4-protons were shifted in the same extent by the chiral NMR shift reagent, it is apparent that the coordination does not introduce the chirality at the C_4-position, or the C_4-protons still remain to be prochiral in the coordination complex.

The red-shift of the absorption maximum at 350 nm indicates that the decrease of the energy level of the lowest-unoccupied molecular orbital (LUMO) of **2**, by the influence of magnesium ion, is larger than that of the HOMO.[17] Consequently, the hyperconjugative participation of the C_4–H σ-bond to the π-orbital of the dihydropyridine moiety (or, more precisely, the contribution of the C_4–H σ-bond to the molecular orbital which is mainly constituted by π-orbitals of dihydropyridine moiety) becomes larger when magnesium ion coordinates onto the ring. The importance of the C_4-moiety was emphasized at the beginning of this discussion. Under such a circumstance, it is highly unlikely to expect that a hydride ion dissociates from the C_4-position, whereas a proton may easily dissociate because of the developing positive charge on the dihydropyridine ring in the complex. The localization of large positive-charge density on the C_4-protons is also proved by the large down-field shift of the corresponding NMR signal on complexation of **2** with $Yb(TFAC)_3$.[16]

On the other hand, molecular orbital theories have proposed that a positive charge operates to decrease

the energy level of the LUMO of a carbonyl group so that the carbonyl group is activated to accept an electron.[17-19] Since magnesium ion is a bivalent cation, a one-to-one complex of **2** and magnesium ion remains one more positive charge on the magnesium ion formally, which, in the present reaction, may play to activate the substrate, **1**.[20] In other words, an electron migrates from **2** to **1** in the transition-state ternary-complex, **2**-Mg^{2+}-**1**, which is followed by the migration of a proton from the cation-radical of **2** to the anion-radical of **1**.[21,22] The transfer of an electron may or may not precede the migration of a proton. What is the most important here is that an electron and proton move separately and the movement of an electron triggers the migration of a proton. Catalytic activity of alkali and alkaline earth metal ions in an electron-transfer process has been reported and discussed in relation to the polarizabilities of metal ions and ligands.[23] The same kinetic deuterium isotope effect for an electron-transfer process[25] and for the reduction of an organic substrate ($\approx$1.7)[4] as well as large and similar isotope partitioning ratios in products from various reductions ($\approx$4)[1,3,4] also suggest the existence of two distinguishable processes for electron- and proton-migrations.[25] The migration of a second electron seems to take place almost spontaneously, because the pyridinyl radical can gain large stabilization energy by converting into the pyridinium ion.[26] Thus, the chirality in **2** is recognized by **1** in a complex, or with intramolecular fashion. When magnesium ion is substituted by univalent lithium ion, on the other hand, the corresponding binary complex, **2**-Li^+, remains no positive charge on the metal ion and another lithium ion (or ions) has to be used to activate the substrate. In this case, therefore, the reaction takes place bimolecularly and the transition state is so loose that the chirarity in **2** cannot be recognized by **1**. The idea of a positive-charge-promoted reaction discussed above is supported by the inability of tetraethylammonium and chelated metal ions to catalyze the reaction.[20] The dependency of the optical yield on the molar ratio of $[Mg^{2+}]/[\mathbf{2}]$[9] can also be interpreted with the present proposal: under the condition of $[Mg^{2+}]/[\mathbf{2}]<1$, is favored the formation of complexes composed of a magnesium ion and more than two molecules of **2**. The positive charge in such a complex is so diffused that it has no facility to activate the substrate and the situation becomes similar to that with lithium perchlorate.

The scheme for the stereospecific reaction may be represented as follows:

$$MgX_2 \rightleftharpoons MgX^+ + X^-,$$

$$NH + MgX^+ \rightleftharpoons (NH\cdot MgX)^+,$$

$$(NH\cdot MgX)^+ + S \longrightarrow [(NH\cdot Mg\cdot S)^{2+}]^{2+} + X^-$$

$$\downarrow$$

$$N^+ + HSMg^+$$

$$2HSMg^+ + 2X^- \rightleftharpoons Mg(SH)_2 + MgX_2$$

where X, NH, N^+, S, and SH are perchlorate ion, reduced form of a coenzyme-model, oxidized form of a coenzyme-model, α-keto ester, and the anion of α-hydroxy ester, respectively. The double dagger stands for the transition state, which may be depicted as shown in Fig. 3. It seems better, as a minor effect, to take into account the interaction between the amide-carbonyl group and magnesium ion, because the stereospecificity of the reaction depends on the basisity of the carbonyl-oxygen.[27]

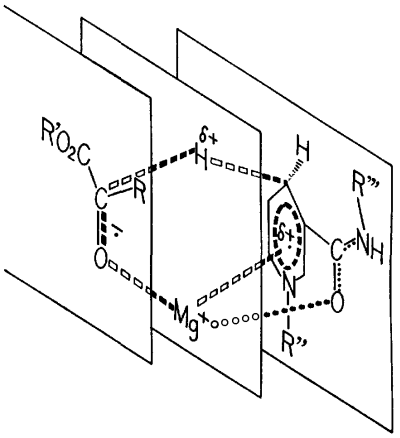

Fig. 3. Schematic representation of the transition state of the reaction.

Mechanistic studies so far reported have had no facility to discriminate the one-step hydride transfer and three-step electron-proton-electron transfer mechanisms and the present paper is the first one to deal with the detailed interaction of molecules at the transition state of the reaction in favor of the latter process. Kinetic studies will provide further support for the discussed concept and the research in our laboratories is in progress toward this end.

Experimental

Preparation and purification of materials and general procedure of the reduction were described previously.[10] Tris(3-trifluoroacetyl-*d*-camphor)-europium and -ytterbium were prepared according to the literature.[28]

UV, IR, NMR, and CD spectra were recorded on Union Giken SM-401, Hitachi EPI-S2, Varian T-60, and Union Giken CD-1000 spectrometers, respectively. Optical rotations were observed with a JASCO DIP-180 automatic polarimeter.

Support for a part of this research by the Ministry of Education, Japanese Government, with a Scientific Research Grant is acknowledged. The authors also wish to thank Dr. S. Inagaki of Gifu University for fruitful discussions on molecular orbital theory.

References

1) R. H. Abeles, R. F. Hutton, and F. H. Westheimer, *J. Am. Chem. Soc.*, **79**, 712 (1957).

2) F. H. Westheimer, H. F. Fisher, E. E. Conn, and B. Veenesland, *J. Am. Chem. Soc.*, **73**, 2403 (1951).

3) J. J. Steffens and D. M. Chipman, *J. Am. Chem. Soc.*, **93**, 6694 (1971).

4) (a) D. J. Creighton, J. Hajdu, and D. S. Sigman, *J. Am. Chem. Soc.*, **98**, 4619 (1976); (b) J. Hajdu and D. S. Sigman, *ibid.*, **98**, 6060 (1976).

5) A. Ohno and N. Kito, *Chem. Lett.*, **1972**, 369.
6) R. J. Kill and D. A. Widdowson, *J. Chem. Soc., Chem, Commun.*, **1976**, 755.
7) B. Commoner, J. J. Heise, B. B. Lippincott, R. E. Norberg, J. V. Passonneau, and J. Townsend, *Science*, **126**, 57 (1957).
8) Y. Ohnishi, M. Kagami, and A. Ohno, *J. Am. Chem. Soc.*, **97**, 4766 (1975).
9) Y. Ohnishi, T. Numakunai, T. Kimura, and A. Ohno, *Tetrahedron Lett.*, **1976**, 2699.
10) A. Ohno, T. Kimura, S. G. Kim, H. Yamamoto, S. Oka, and Y. Ohnishi, *Bioorg. Chem.*, **6**, 21 (1977).
11) *Cf.*, R. A. Gase, G. Boxhoorn, and U. K. Pandit, *Tetrahedron Lett.*, **1976**, 2889.
12) E. M. Evleth, *J. Am. Chem. Soc.*, **89**, 6445 (1967).
13) G. Maggiora, H. Johansen, and L. L. Ingraham, *Arch. Biochem. Biophys.*, **131**, 352 (1969).
14) F. C. Paul, H. Arora, and S. I. Chadha, *Inorg. Nucl. Chem. Lett.*, **6**, 469 (1970).
15) However, *cf.* M. Hughes and R. H. Prince, *Chem. Ind. (London)*, **1975**, 648, and Refs. 3a and 11. Substrates used by authors contain a pyridine moiety, which may interact with magnesium ion.
16) Ytterbium reagents do not cause appreciable contact shift. Therefore, the observed chemical shift may safely regarded as a measure of positive-charge density on the proton. See (a) J. D. Roberts, G. E. Hawkes, J. Husar, A. W. Roberts, and D. W. Roberts, *Tetrahedron*, **30**, 1833 (1974); (b) G. R. Sullivan, Ph. D. Thesis, Stanford University, Stanford, Calif., 1975.
17) K. Fukui and H. Fujimoto, *Annu. Rep. Res. Inst. Chem. Fibers. Jpn.*, **29**, 27 (1972).
18) H. Fujimoto and R. Hoffmann, *J. Phys. Chem.*, **78**, 1874 (1974).
19) A. Imamura and T. Hirano, *J. Am. Chem. Soc.*, **97**, 4192 (1975).
20) General-acid catalysis has been suggested for the reduction of α,α,α-trifluoroscetophenone. P. van Eikeren and D. L. Grier, *J. Am. Chem. Soc.*, **98**, 4655 (1976).
21) For interpretation of this phenomenon from the viewpoint of MO theory of catalysis, see K. Fukui and S. Inagaki, *J. Am. Chem. Soc.*, **97**, 4445 (1975).
22) It is likely that the magnesium ion in the ternary complex function as an electron-conductor. See Ref. 23.
23) M. Shporer, G. Ron, A. Loewenstein, and G. Navon, *Inorg. Chem.*, **4**, 361 (1965), and references cited therein.
24) T. Okamoto, A. Ohno, and S. Oka, *J. Chem. Soc., Chem. Commun.*, **1977**, 181.
25) When the enthalpy of activation for the proton-transfer is comparable to or higher than that for the electron-transfer, the isotope partitioning ratio and kinetic isotope effect appear to be comparable. See D. C. Dittmer, A. Lombardo, F. H. Batzold, and C. S. Greene, *J. Org. Chem.*, **41**, 2976 (1976).
26) The reduction potential of 1-methyl-3-carbamidepyridinium salt to its corresponding free radical is −1.1 V. See (a) J. N. Burnett and A. L. Underwood, *J. Org. Chem.*, **30**, 1154 (1965); (b) A. J. Cunningham and A. L. Underwood, *Biochemistry*, **6**, 266 (1967).
27) A. Ohno, H. Yamamoto, T. Kimura, S. Oka, and Y. Ohnishi, *Tetrahedron Lett.*, **1976**, 4585.
28) (a) V. Schuring, *Tetrahedron Lett.*, **1972**, 3297; (b) V. Schuring, *Inorg. Chem.*, **11**, 736 (1972).

Direct Synthesis of Methyl Isobutyl Ketone by Reductive Aldol Condensation. III. Kinetics

Yoshiaki WATANABE, Masato OKADA, Yusuke IZUMI, and Yukio MIZUTANI
Tokuyama Soda Co., Ltd., Mikage-cho, Tokuyama, Yamaguchi 745
(Received November 19, 1976)

The kinetics of the direct catalytic conversion of acetone and hydrogen into methyl isobutyl ketone (MIBK) were investigated in the liquid phase using palladium-zirconium phosphate as a catalyst. Kinetic studies on the conversion of acetone into mesityl oxide (4-methyl-3-pentene-2-one) and its hydrogenation were separately carried out using the same catalyst. It was found that the direct reaction proceeded *via* a sequence of processes: mesityl oxide was first formed by condensation of acetone on acid sites of the catalyst and MIBK was then produced by hydrogenation of the mesityl oxide on palladium metal in the catalyst. Moreover, the experimental results were well interpreted by assuming that the condensation of acetone was controlled by a surface reaction between the acetone molecules adsorbed on the catalyst surface and that the rate of hydrogenation of mesityl oxide was determined by a surface reaction between dissociated hydrogen atoms and adsorbed mesityl oxide molecules.

Recently, several processes have been developed for the production of methyl isobutyl ketone (MIBK) by the direct catalytic reaction of acetone with hydrogen on palladium metal supported on solid acids such as cation-exchange resins,[1-5] alumina,[6-8] and zeolite.[9-10]

Some kinetic studies on the catalytic conversion of acetone into mesityl oxide[11] and on the hydrogenation of mesityl oxide[12] have been reported independently, but little work has been done on the kinetics of the direct catalytic reaction of acetone with hydrogen to form MIBK.

In a previous paper,[13] zirconium phosphate containing dispersed metallic palladium was shown to be a highly-active bifuctional catalyst for direct MIBK synthesis.

The present paper deals with the kinetics of the direct reaction using a palladium-zirconium phosphate catalyst (Pd-ZrP Cat). The direct reaction may involve the reversible condensation of acetone to mesityl oxide on the acid sites of zirconium phosphate and consecutive hydrogenation of mesityl oxide to MIBK on the palladium metal:

$$2CH_3COCH_3 \rightleftharpoons (CH_3)_2C{=}CHCOCH_3 + H_2O \quad (1)$$

$$(CH_3)_2C{=}CHCOCH_3 + H_2 \longrightarrow (CH_3)_2CHCH_2COCH_3 \quad (2)$$

The above mechanism was investigated in detail by comparing the rate constants for the direct reaction with those for acetone condensation and hydrogenation of mesityl oxide measured independently.

Experimental

Catalyst and Reagents. Pd-ZrP cat was prepared according to the method described in a previous paper.[13] After being treated with hydrogen, the catalyst was ground to fine powder in order to pass through a 100 mesh sieve. Before use, the catalyst was dried in a stream of nitrogen at 400 °C for 3 h. Acetone and hexane were purified by distillation after the dehydration with P_2O_5 and a molecular sieve 5A, respectively. Commercial mesityl oxide (reagent grade) was used without further purification.

Apparatus and Procedure. Figure 1-A shows the apparatus for the condensation of acetone. The reaction vessel was equipped with a Dry Ice-methanol condenser and a sampling tube with a rubber stopper. The upper part of the reactor

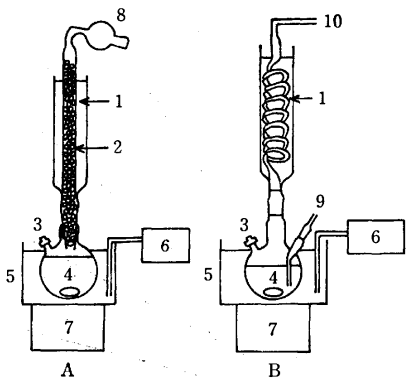

Fig. 1. Apparatus. 1: Dry Ice-methanol condenser, 2: Glass beads, 3: sampling tube, 4: rotator, 5: water bath, 6: water heater and circulator, 7: magnetic stirrer, 8: $CaCl_2$ tube, 9: hydrogen delivery tube, 10: hydrogen gas outlet.

was filled with glass beads to prevent gasification of the reactant, as is shown in Fig. 1-A. The direct conversion of acetone as well as the hydrogenation of mesityl oxide was carried out using the apparatus shown in Fig. 1-B. The reaction vessel was fitted with a hydrogen-delivery tube, a Dry Ice-methanol condenser and a sampling tube. The reaction vessel containing the catalyst (0.1—2.0 g) was filled with hexane, and immersed in a water bath maintained at a given temperature (±0.5 °C). The reaction was initiated by injecting the reactant through the rubber stopper into the reaction vessel with a syringe. The total volume of the reactant and the solvent was maintained constant (50 ml). The reactants were vigorously stirred in order to reduce physical effects to a negligible level. All of the experiments were carried out at a temperature between 30 and 50 °C at atmospheric pressure. Except during the condensation of acetone, hydrogen was continuously introduced into the vessel at a rate of 20 ml/min through the delivery tube, and the vapor of the reactants contained in the exhaust hydrogen gas completely condensed in the Dry Ice-methanol condenser. The product was sampled using a syringe and analyzed by gas chromatography on a column of PEG-1000; the operating conditions were identical to those described previously.[13] In all experiments in the present study, no by-products, such as 4-hydroxy-4-methyl-2-pentanone, 4-methyl-2-pentanol and other high-boiling point products, were detected.

Results and Discussion

Condensation of Acetone to Mesityl Oxide. In order to determine the rate-determining step of the condensation of acetone, the changes in conversion with reaction time at constant volume were measured for different initial concentrations of acetone in hexane (Fig. 2). The conversion rate was approximately proportional to the reaction time. Accordingly, the initial reaction rates for mesityl oxide formation can be determined from the slopes of the straight lines in Fig. 2 and are given in Table 1.

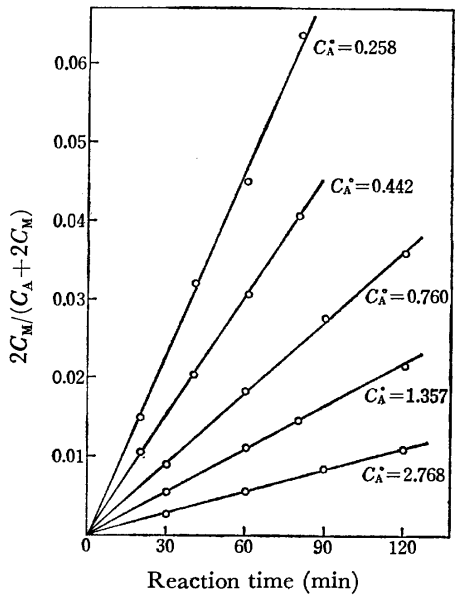

Fig. 2. Effect of the initial concentration of acetone in hexane on the charge in conversion with reaction time. Conditions: temp; 45 °C, catalyst; 1.000 g.

TABLE 1. THE EFFECT OF THE INITIAL CONCENTRATION ON THE INITIAL RATE

Initial concentration of acetone (C_A°) (mol/l)	Initial rate (r_0) (mol/l h g-cat)	$1/C_A^\circ$	$1/\sqrt{r_0}$
0.258	0.01225	3.876	9.03
0.442	0.01358	2.262	8.58
0.760	0.0144	1.316	8.33
1.357	0.0148	0.737	8.22
2.768	0.0153	0.361	8.08

Temp: 45 °C, catalyst: 1000 g.

The over-all reaction is shown by reaction 1. If the reaction between acetone molecules adsorbed on the catalyst surface is rate-determining, the rate equation should be:

$$r = \frac{k_c(C_A^2 - C_M C_W/K)}{(1+K_A C_A + K_M C_M + K_W C_W + K_S C_S)^2}, \quad (3)$$

where k_C denotes the rate constant for acetone condensation, K_A, K_M, K_W, K_S are the adsorption equilibrium constants for acetone, mesityl oxide, water and hexane, respectively, K is the equilibrium constant and C_A, C_M, C_W, and C_S are the concentrations of acetone, mesityl oxide, water and hexane, respectively.

For lower conversion rates, the reverse reaction of acetone condensation and the adsorption terms for mesityl oxide and water in the rate equation are negligible. Assuming that the hexane used as a solvent is not appreciably adsorbed on the catalyst, the adsorption term may be also omitted from the rate equation.[14] Consequently, the initial rate can be expressed in terms of the initial concentration of acetone:

$$r_0 = \frac{k_c C_A^2}{(1+K_A C_A)^2} \quad (4)$$

If the assumptions described above are a reasonable interpretation of the results given in Table 1, the plot of $1/C_A$ *vs.* $1/\sqrt{r_0}$ should be a straight line. In reality, Fig. 3 shows a linear relationship between $1/C_A$ and $1/\sqrt{r_0}$, which suggests that the surface reaction between adsorbed acetone molecules is rate-controlling.

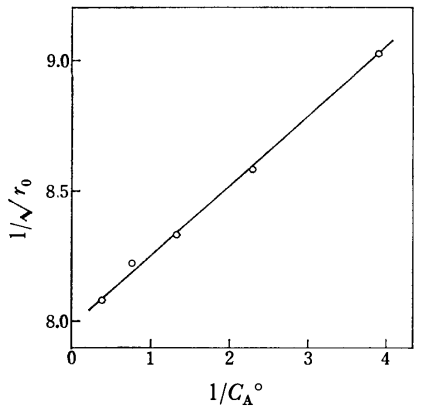

Fig. 3. $1/r_0^{1/2}$ *vs.* $1/C_A^\circ$.

The rate constant and the adsorption equilibrium constant for acetone at unit catalyst concentration calculated from Fig. 3 are shown in Table 2.

TABLE 2. VALUE OF THE RATE PARAMETERS OBTAINED BY FITTING Eq. 3 TO THE DATA SHOWN IN Fig. 2 AT 45 °C

Rate parameter	Value
k_C	17.8 mol/l h g-cat
K_A	33.9 l/mol

Another possible mechanism that the rate-determining step might be the adsorption of acetone, the desorption of mesityl oxide or the desorption of water is unsatisfactory in interpreting the results.

The effect of temperature on the initial reaction rate was examined at an acetone concentration of 2.768 mol/l in the temperature range of between 35 and 50 °C. The relation between the logarithm of r_0 and the reciprocal of the absolute temperature is shown in Fig. 4. The apparent activation energy was calculated to be 18.4 kcal/mol. This value indicates that probably diffusion of the reactants does not control the reaction rate. The activation energy for the formation of 4-hydroxy-4-methyl-2-pentanone from acetone with a base catalyst has been reported to be 17.3 kcal/mol by

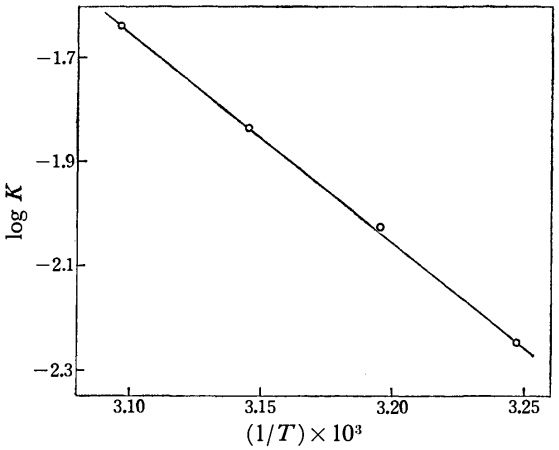

Fig. 4. Arrhenius plot.

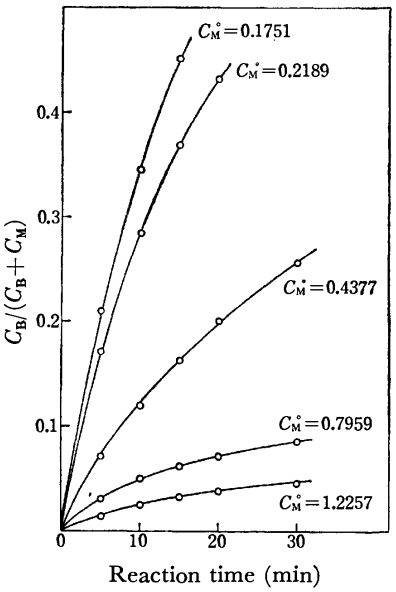

Fig. 5. Effect of the initial concentration of mesityl oxide in hexane on the charge in conversion with reaction time. Conditions: temp; 45 °C, catalyst; 0.500 g.

Lemcoff *et al.*[15]

Hydrogenation of Mesityl Oxide. The changes in the conversion rate with reaction time at constant volume were measured with different initial concentrations of mesityl oxide in hexane, as is shown in Fig. 5. The rate of hydrogenation of mesityl oxide decreases gradually with reaction time.

In order to estimate the initial rates with accuracy, the time-conversion curve shown in Fig. 5 can be empirically represented by the following third-order equation:

$$B = Xt^3 + Yt^2 + Zt, \tag{5}$$

where B denotes $C_B/(C_B+C_M)$ after reaction time t and X, Y, and Z are constants. The rate after reaction time t is derived from Eq. 5 and is found to be:

$$\frac{dB}{dt} = 3Xt^2 + 2Yt + Z \tag{6}$$

Thus, the initial rate is given by

$$\left(\frac{dB}{dt}\right)_{t=0} = Z. \tag{7}$$

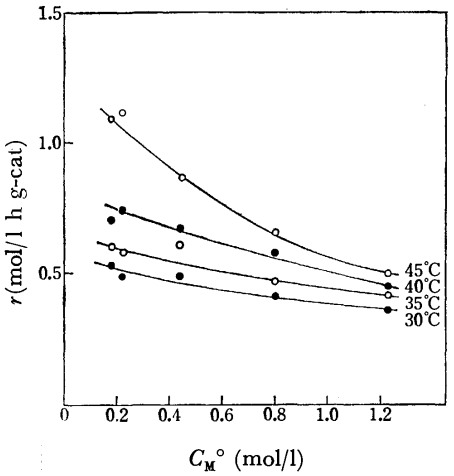

Fig. 6. Effect of the initial concentration of mesityl oxide on the initial rate at various reaction temperatures.

The initial rates for hydrogenation of mesityl oxide are plotted against the initial concentration of mesityl oxide in Fig. 6. The results suggest that the reaction proceeds according to the Langmuir-Hinshelwood mechanism, in which hydrogen and mesityl oxide are absorbed competitively. The rate equation corresponding to the mechanism is

$$r = k_H \cdot \theta_H \cdot \theta_M, \tag{8}$$

where k_H denotes the rate constant of the surface reaction, θ_H the fractional surface coverage of hydrogen, and θ_M that of mesityl oxide. From Eq. 8 Teranishi *et al.*[14] and Kubomatsu *et al.*[16] have obtained

$$r_0 = \frac{k_H \cdot b \cdot C_M}{(1+bC_M)^2}, \tag{9}$$

where C_M denotes the concentration of mesityl oxide, and b is a function of the hydrogen concentration.

When the rate of hydrogenation is measured at constant hydrogen pressure, and the solubility of hydrogen is considered to be independent of the composition of the reaction mixture, b has a constant value at a given temperature. The adsorption of hexane is negligible.

Equation 9 can be rearranged to

$$\left(\frac{C_M}{r_0}\right)^{1/2} = \left(\frac{1}{k_H \cdot b}\right)^{1/2} + \left(\frac{b}{k_H}\right)^{1/2} C_M. \tag{10}$$

Plots of $(C_M/r_0)^{1/2}$ *vs.* C_M at various reaction temperatures are straight lines, as is shown in Fig. 7.

Assuming that hydrogenation occurs between the dissociated hydrogen atoms and the molecules of mesityl oxide adsorbed on the catalyst surface, the plot of $(C_M/r_0)^{1/3}$ *vs.* C_M should be a straight line. However, such plots actually deviate from straight lines, as is shown in Fig. 8.

The adsorption of mesityl oxide, the adsorption of hydrogen with or without dissociation, or the desorption of MIBK might be considered as the rate-controlling step, although they do not reasonably explain the data.

On the other hand, the fact that the rate of formation of MIBK decreases gradually with reaction time, as is shown in Fig. 5, suggests that the rate is retarded by the

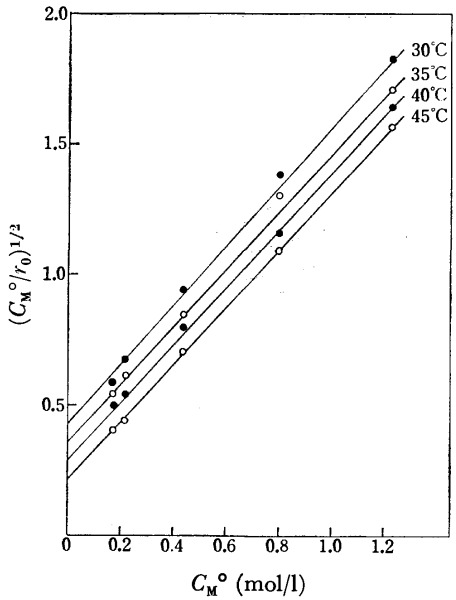

Fig. 7. $(C_M°/r_0)^{1/2}$ *vs.* $C_M°$.

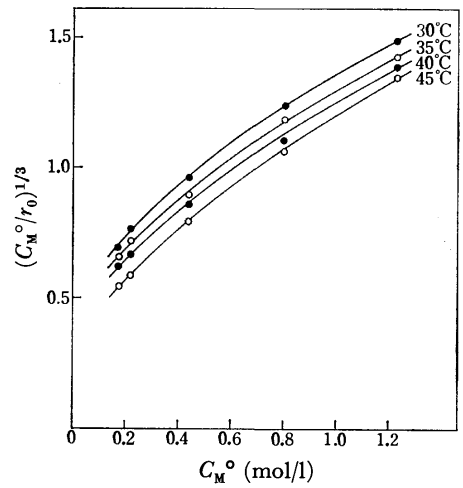

Fig. 8. $(C_M°/r_0)^{1/3}$ *vs.* $C_M°$.

adsorption of MIBK onto the catalyst. By introducing the MIBK adsorption term into Eq. 9, we obtain

$$r = \frac{k_H \cdot b \cdot C_M}{(1+bC_M+K_BC_B)^2} \tag{11}$$

Using Eq. 11, the values of k_H, b, and K_B obtained from the data shown in Fig. 5 are given in Table 3.

TABLE 3. VALUES OF THE RATE PARAMETERS OBTAINED BY FITTING Eq. 11 TO THE DATA SHOWN IN Fig. 5 AT 45 °C

Rate parameter	Value
k_H	3.70 mol/l h g-cat
b	4.75 l/mol
K_B	19.65 l/mol

The relation between the logarithm of k_H calculated from the plots in Fig. 7 and the reciprocal of the absolute temperature is shown in Fig. 9. The apparent activation energy for the hydrogenation of mesityl oxide is 8.1 kcal/mol. This value is considered to be reasonable

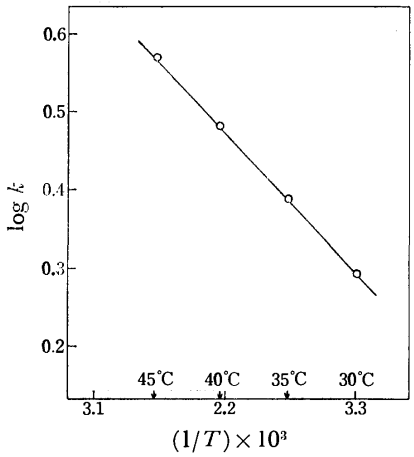

Fig. 9. Arrhenius plot.

compared with those reported by other authors.[14,16]

Direct conversion of Acetone and Hydrogen to MIBK.

In the direct conversion of acetone and hydrogen to MIBK using a bifuctional catalyst, it appears probable that the condensation of acetone on the acid sites of the catalyst and hydrogenation of the resultant mesityl oxide on palladium metal occur in succession.

The rate equations for the consecutive reactions are obtained by combining the individual rate equations obtained from studies of acetone condensation and of the hydrogenation of mesityl oxide. Considering that the direct synthesis of MIBK was carried out in an acetone medium and that the hydrogenation was separately investigated in a medium of mesityl oxide–hexane, the rate equation for hydrogenation of mesityl oxide by direct synthesis may include an adsorption term for acetone:

$$-\frac{dC_A}{dt} = 2\frac{dC_M}{dt} = 2\frac{dC_W}{dt} = \frac{K_1C_A^2}{(1+33.9C_A)^2}, \tag{12}$$

$$\frac{dC_B}{dt} = \frac{17.8C_M}{(1+4.75C_M+K_A'C_A+19.65C_B)^2} \tag{13}$$

where k_1 denotes the apparent rate constant for acetone condensation.

The above differential equations were integrated using the Runge-Kutta-Gill method. The minimum value of the sum of the square of the difference between the experimental and the calculated concentration distributions was chosen as the parameter using Hill-Climbing, as is given in Table 4.

The apparent rate constant for acetone condensation and the adsorption equilibrium constant for acetone at unit catalyst concentration were calculated from the data in Table 4 as given in Table 5.

The molar fractions of mesityl oxide and MIBK for various reaction times were calculated from Eqs. 12 and 13 by substituting the numerical values for k_1 and K_A'. The solid curves shown in Fig. 10 are in good agreement with the data.

The value of k_1 is about 1.6 times larger than that of the rate constant K_C obtained independently from the study of acetone condensation. The reason for this is not obvious at the present time. However, the difference appears to be due to experimental error.

Table 4. Data for the direct conversion of acetone and hydrogen to MIBK
Conditions: $C_A°$: 2.768 mol/l; catalyst: 1.000 g; H_2 flow rate: 20 ml/min; temp: 45 °C

Time	Experimental results			Computed results		
	y_A	y_M	y_B	y_A	y_M	y_B
0.0	1.00000	0.00000	0.00000	1.00000	0.00000	0.00000
0.5	0.99631	0.00110	0.00075	0.99561	0.00137	0.00082
1.0	0.99581	0.00185	0.00235	0.99122	0.00192	0.00247
1.5	0.99259	0.00220	0.00485	0.98683	0.00221	0.00437
2.0	0.99072	0.00255	0.00675	0.98244	0.00242	0.00636
2.5	0.98845	0.00295	0.00860	0.97630	0.00259	0.00838
3.0	0.98610	0.00301	0.01090	0.97366	0.00276	0.01041
3.5	0.98425	0.00310	0.01265	0.96927	0.00293	0.01243
4.0	0.98210	0.00310	0.01480	0.96488	0.00310	0.01445
4.5	0.97970	0.00326	0.01705	0.96049	0.00328	0.01647
5.0	0.97770	0.00328	0.01910	0.95611	0.00346	0.01848

Table 5. Value of the rate parameters obtained for direct conversion of acetone and hydrogen to MIBK

Rate parameter	Value
k_1	28.48 mol/l h g-cat
K'_A	0.686 l/mol

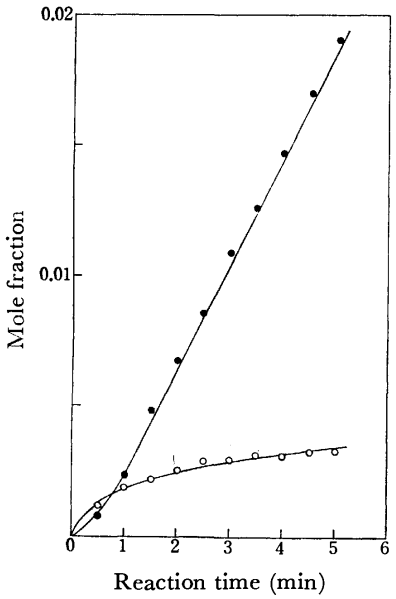

Fig. 10. Comparison of calculated curves with experimental data.
●: y_B, ○: $y_{M'}$, ——: calculated curve.

When the condensation reaction of acetone to mesityl oxide and the direct reaction of acetone and hydrogen to MIBK are carried out in acetone alone using the apparatus shown in Fig. 1-B, both rate constants are approximately equal. On the other hand, when the condensation of acetone to mesityl oxide is carried out using the apparatus shown in Fig. 1-B or when direct conversion of acetone to MIBK is carried out in a mixture of acetone and hexane, reproducible data cannot always be obtained.

In conclusion, the direct reaction by reductive aldol condensation over a Pd–ZrP catalyst involves the condensation of acetone to mesityl oxide on the acid sites of the catalyst and subsequent hydrogenation of the mesityl oxide to MIBK on the palladium metal dispersed over the catalyst.

The authors express their sincere thanks to Prof. Yoshinobu Takegami of Kyoto University and to Dr. Yasuharu Onoue, Director of the Tokuyama Soda Co. for valuable discussion and advise.

Nomenclature

k	Reaction rate constant (mol/l h g-cat).
K	Equilibrium constant (1/mol).
K_1	Adsorption equilibrium constant of component i (1/mol).
r	Reaction rate (mol/l h g-cat).
t	Time.
C_i	Concentration of component i (mol/l).
C_t	Total concentration of reactants.
θ_i	Fractional surface coverages of component i.
y_i	Molar fraction of component i.
T	Temperature (K).
b, X, Y, Z	Constant.
Suffixes	
A	Acetone.
M	Mesityl oxide.
W	Water.
B	MIBK.
H	Hydrogen.
i	General component.
o	Initial rate of reaction.
t	Total.
c	Condensation.
h	Hydrogenation.

References

1) Rheinpreussen A. G., Ger. Pat. 1193931 (1965).
2) Rheinpreussen A. G., Ger .Pat. 1238453 (1967).
3) Rheinpreussen A. G., Ger. Pat. 1260454 (1968).
4) H. Giehring, *Brennstoff Chem.*, **49** (8), 229 (1968).
5) Scholven-Chemie A. G., Neth, Pat. 6812327 (1969).
6) Sumitomo Chemical Ind., U.S. Pat. 3666816 (1972).
7) Sumitomo Chemical Ind., Japan Pat. 47-15809 (1972).
8) Sumitomo Chemical Ind., Japan Pat. 47-15810 (1972).
9) Showa Denko Co., Japan Pat. 46-2009 (1971).

10) Showa Denko Co., Japan Pat. 46-2643 (1971).
11) F. G. Klein and J. T. Banchero, *Ind. Eng. Chem.*, **48**, 1278 (1956).
12) S. Nagata, K. Hashimoto, K. Tsuto, K. Miyamoto, N. Hashimoto, N. Goto, and T. Tada, *J. Chem. Eng. Jpn.*, **2**, 158 (1969).
13) Y. Watanabe, Y. Matsumura, Y. Izumi, and Y. Mizutani, *Bull. Chem. Soc. Jpn.*, **47**, 2922 (1974).
14) S. Kishida and S. Teranishi, *J. Catal.*, **12**, 90 (1968).
15) N. O. Lemcoff and R. E. Cunninggham, *J. Catal.*, **23**, 81 (1971).
16) K. Hotta and T. Kubomatsu, *Bull. Chem. Soc. Jpn.*, **44**. 1348 (1971).

A One-step Synthesis of 2,7-Dimethyl-5-silaspiro[4.4]nona-2,7-diene and the Synthesis of Its Derivatives

Daiyo TERUNUMA, Satoshi HATTA, Tsunao ARAKI,* Tadashi UEKI, Tsutomu OKAZAKI, and Yasutaka SUZUKI

Department of Applied Chemistry, Faculty of Engineering, Saitama University, Urawa, Saitama 338

(Received November 27, 1976)

The *in situ* reaction of dialkoxydichlorosilanes, such as dimethoxy-, diethoxy-, dipropoxy-, dibutoxy-, and diisobutoxydichlorosilane, with isoprene and magnesium in tetrahydrofuran (THF) was investigated. It was found that the double annelation product, *i.e.*, 2,7-dimethyl-5-silaspiro[4.4]nona-2,7-diene (**1**), was obtained from diethoxy-, dipropoxy-, and dibutoxydichlorosilane in 87.0, 65.2, and 66.5% yields respectively. On the other hand, the reaction of dimethoxy- and diethoxydichlorosilane with butadiene and magnesium in THF gave 5-silaspiro[4.4]nona-2,7-diene (**7**) in 20.7 and 35.4% yields respectively. Several silaspirononane derivatives were synthesized from **1**.

Recently, Salomon reported on the synthesis of 5-silaspiro[4.4]nona-2,7-diene by a one-step reaction[1] from silicon tetrachloride and the butadiene-magnesium complex prepared from active-magnesium[2] and butadiene. Takase *et al.* reported independently on the preparation of silaspiro compounds by treating silicon tetrachloride with diene-magnesium compound in a step-by-step manner.[3] In a preliminary communication,[4] we have reported on a convenient method for the preparation of 2,7-dimethyl-5-silaspiro[4.4]nona-2,7-diene (**1**). The double annelation product was obtained in a high yield when a mixture of diethoxydichlorosilane and isoprene in a molar ratio of 1/2 was refluxed in the presence of magnesium in THF. In this paper we wish to describe further details of the double annelation reaction and the synthesis of the derivatives of **1**.

Results and Discussion

Reaction of Dialkoxydichlorosilanes with Isoprene and Magnesium. Dialkoxydichlorosilanes, such as dimethoxy-(**2**), diethoxy-(**3**), dipropoxy-(**4**), dibutoxy-(**5**), and diisobutoxydichlorosilane(**6**), were obtained by means of disproportionation reactions between the appropriate tetraalkoxysilane and silicon tetrachloride in a manner described by Kumada[5] [Table 1].

$$Si(OR)_4 + SiCl_4 \xrightarrow[30\,h]{160^\circ C} ROSiCl_3 + (RO)_2SiCl_2 + (RO)_3SiCl$$

R=Me, Et, *n*-Pr, *n*-Bu, *i*-Bu

To investigate the effect of the varieties of alkoxyl groups of dialkoxydichlorosilanes in the preparation of **1**, the reactions of dialkoxydichlorosilanes (R=Me, Et, Pr, Bu) with two mole equivalents of isoprene and magnesium were carried out in THF [Table 2]. It was observed that the magnesium dichloride precipitated at the beginning of the exthothermic reaction dissolved gradually as the reaction proceeded. The reaction mixture became homogenous at the end of the reaction. These observations presumably indicate that the isoprene-magnesium complex reacts with dialkoxydichlorosilanes in 2 steps, *i.e.*, a first reaction with chloride groups, and a second reaction with alkoxide groups. In this reaction it was found that **3** was the best agent for the preparation of the double annelation product(**1**). In contrast, **2**, like silicon tetrachloride, was found to be less effective for the preparation of **1**. The predominance of the yield of **1** in the reaction using **3** as the starting material may be considered to be because **3** contains Si–Cl and Si–OR bonds which have a suitable reactivity difference from the isoprene-magnesium complex without decreasing the reactivity of the alkoxy group itself.

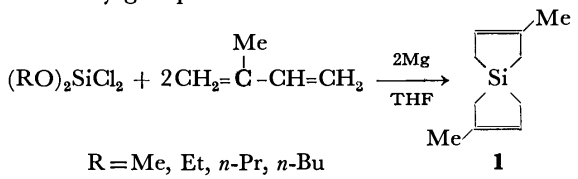

R=Me, Et, *n*-Pr, *n*-Bu **1**

The reactions of the dialkoxydichlorosilanes with equimolar amounts of isoprene and magnesium were then carried out. When such dialkoxydichlorosilanes as **3**, **4**, **5**, and **6** were employed in the reaction, it was found, by GLC analysis of the reaction mixture, that not only the mono annelation product, *i.e.*, 1,1-dialkoxy-

TABLE 1. THE PREPARATION OF DIALKOXYDICHLOLOROSILANE

R	$Si(OR)_4$ g(mol)	$SiCl_4$ g(mol)	Temp °C	Time h	$(RO)_2SiCl_2$ Bp °C/Torr	$(RO)_2SiCl_2$ Yield, g(%)
Me	70.4(0.46)	78.7(0.46)	150	30	96—100	89.6(60.1)
Et	55.0(0.26)	44.9(0.26)	160	30	135—137	61.6(60.0)
n-Pr	156.6(0.59)	100.7(0.59)	160	30	173—175	151.1(58.7)
n-Bu	70.0(0.22)	37.2(0.22)	160	30	115/20	69.6(64.9)
i-Bu	64.0(0.20)	34.0(0.20)	160	30	119—198	53.4(54.5)

* Present address: Department of Environmental Engineering, Saitama Institute of Technology, Okabe, Saitama 369-02.

Table 2. Reaction of dialkoxydichlorosilanes with two mole equivalents of isoprene and magnesium

R	$(RO)_2SiCl_2$ g(mol)	Mg g(mol)	Isoprene g(mol)	Yield of **1** g(%)
Me	16.1(0.1)	5.3(0.22)	17.0(0.25)	0.8(5)
Et	75.5(0.4)	21.4(0.88)	68.0(1.0)	57.2(87.0)
n-Pr	21.7(0.1)	5.3(0.22)	17.0(0.25)	10.7(65.2)
n-Bu	24.5(0.1)	5.3(0.22)	17.0(0.25)	10.9(66.5)

3-methyl-1-sila-3-cyclopentene(**7**), but also the double annelation product(**1**) and tetraalkoxysilanes were formed [Table 3]. These results may support the above consideration that the 2-mole-equivalent reaction of isoprene-magnesium complex with unimolar dialkoxydichlorosilanes proceeds in 2 steps:

$$(RO)_2SiCl_2 + CH_2{=}\overset{\overset{Me}{|}}{C}{-}CH{=}CH_2 \xrightarrow[THF]{Mg} \mathbf{7} + \mathbf{1} + Si(OR)_4$$

R=Et, *n*-Pr, *n*-Bu, *i*-Bu

Table 3. Reaction of dialkoxydichlorosilanes with equimolar amounts of isoprene and magnesium

$(RO)_2SiCl_2$ R=	Yield[a] (%)		
	7	**1**	$Si(OR)_4$
Me	5	5	5
Et	32.5	23.2	23.1
n-Pr	40.0	20.1	25.0
n-Bu	49.4	18.9	18.4
i-Bu	36.5	10.1	15.4

a) The yields were estimated by GLC.

It may be considered that the tetraalkoxysilanes found in the above experiment resulted from the reaction of magnesium dialkoxides with dialkoxydichlorosilanes as follows:

$$\mathbf{7} \xrightarrow[\text{isoprene}]{Mg} \mathbf{1} + Mg(OR)_2$$

$$Mg(OR)_2 + (RO)_2SiCl_2 \longrightarrow Si(OR)_4 + MgCl_2$$

When butadiene was used as an annelating agent, **2** and **3** gave 5-silaspiro[4.4]nona-2,7-diene(**8**) in 20.7 and 35.4% yields respectively.

$$(RO)_2SiCl_2 + CH_2{=}CH{-}CH{=}CH_2 \xrightarrow[THF]{Mg} \underset{\mathbf{8}}{Si} + Si(OR)_4$$

R=Me, Et

On the other hand, when the reaction of **3** and the Grignard reagent prepared from 1,4-dibromobutane in a molar ratio of 1/2 was carried out, 5-silaspiro[4.4]nonane(**9**) was obtained in a 61.6% yield.

$$2Br(CH_2)_4Br + (EtO)_2SiCl_2 \xrightarrow[Et_2O]{Mg} \underset{\mathbf{9}}{Si}$$

West[6] obtained **9** in a 26.5% yield by the treatment of silicon tetrachloride with the same Grignard reagent, followed by treatment with the organolithium reagent prepared from 1,4-dibromobutane. These results indicate that **3** is also useful for the one-step synthesis of **9**.

Preparation of the Derivatives of **1**. The new derivatives of silaspirononane synthesized in the present work are 2,7-dimethyl-2,3: 7,8-dimethylene-5-silaspiro-[4.4]nonane(**10**), 2,7-dimethyl-2,3: 7,8-diepoxy-5-silaspiro[4.4]nonane(**11**), 2,7-dimethyl-5-silaspiro[4.4]-nonane(**12**), 2,7-dimethyl-5-silaspiro[4.4]nonane-3,8-diol(**13**), and 2,7-dimethyl-5-silaspiro[4.4]nonane-3,8-diamine (**14**). The silaspirononane **10** was obtained in a 54.9% yield by using the Simmons-Smith agent.[7] The silaspirononane **11** was obtained in a 65.4% yield by the treatment of **1** with perbenzoic acid in chloroform.[8] The structural assignment was done by the analysis of the IR and NMR spectra. (**10**, IR spectrum; -CH- in the cyclopropane ring, 3030 cm^{-1}; skeletal vibration, 1030, 1010 cm^{-1}: **11**, IR spectrum; skeletal vibration, 1040, 1005 cm^{-1}; NMR spectrum; (δ) 3.0—3.1 $\diagup O \diagdown H$).

The hydrogenation of **1** by using Pd-C catalyst in hexane gave **12** in a 78.8% yield. Although the hydrogenation of 1,1,3-trimethyl-1-sila-3-cyclopentene(**15**) using Pd-C catalyst in methanol afforded only a ring-opening product, *i.e.*, dimethylmethoxyisopentylsilane,[7b] that of **1** in the presence of methanol gave **12** in a 64.4% yield. The hydroboration of **1**, followed by treatment with hydrogen peroxide in the presence of sodium hydroxide[8b,9] or with hydroxylamine-*O*-sulfonic acid,[10] gave **13** and **14** in 46.0 and 46.8% yields respectively. A large excess of diborane was required to attain the complete hydroboration of the bifunctional compound (**1**). The diol **13** and the diamine **14** were identified by the analysis of the IR and NMR spectra. (**13**, IR spectrum; skeletal vibration, 1075, 1040, 1030 cm^{-1}; NMR spectrum; (δ) 3.6 (CH-O): **14**, IR spectrum; skeletal vibration, 1075, 1040, 1030 cm^{-1}; NMR spectrum; (δ) 2.7 (CH-N)).

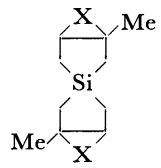

10: X=CH_2
11: X=O

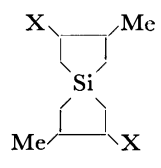

12: X=H
13: X=OH
14: X=NH_2

The interfacial polycondensation reaction[11] of the diamine(**14**) with adipoyl dichloride was carried out, and a white solid polymer (**16**) ([η]=1.07) was thus obtained in a 69.8% yield. The polymer was soluble in methanol and ethanol, but insoluble in such solvents as ether, benzene, and acetone.

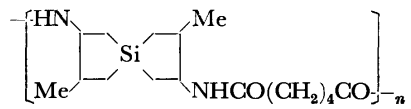

16

Experimental

All the boiling and melting points are uncorrected. The IR and mass spectra were recorded on a JASCO IR-2A spectrometer and on a JEOL-01SG instrument respectively. The NMR spectra were recorded on a Varian A-60 spectrometer in CCl_4 using TMS as the internal standard. The analytical GLC was carried out with a Shimadzu GC-3A chromatograph [1.5 m, 15% SE-30 on Chromosorb W (60—80 mesh)].

Preparation of Dialkoxydichlorosilanes. A mixture consisting of the appropriate tetraalkoxysilane and silicon tetrachloride was placed into a sealed glass tube. The reaction tube was then maintained at 160 °C (at 150 °C for tetramethoxysilane) for 30 h. The fractional distillation of the reaction mixture by using a 1×60 cm column packed with Fenske ring gave the dialkoxydichlorosilanes in about a 60% yield. The results are shown in Table 1.

*Reaction of **3** with Two Mole Equivalents of Isoprene and Mg.* A mixture of **3** (75.5 g, 0.4 mol), isoprene (68.0 g, 1.0 mol), and Mg (21.4 g, 0.88 mol) in dry THF (300 ml) was refluxed with stirring for 30 h under a nitrogen atmosphere. During the reaction, the internal temperature gradually rose from 60 to 69 °C. After the removal of the solvent from the reaction mixture, dry hexane (150 ml) was added to the residue, and then the deposited magnesium salts was separated by filtration. The distillation of the mixture gave **1** in a 87.0% (57.2 g) yield. NMR: (δ) 1.1—1.4 (m, 8H, Si-CH_2) 1.5—1.7 (m, 6H, C-CH_3) 4.9—5.2 (m, 2H, =CH). IR (neat): 2900, 1640, 1450, 1430, 1400, 1220, 1160, 1100, 1030, 1010, 760 cm^{-1}. Mass, *m/e* 164 (M^+). Bp 140 °C/105 Torr, n_D^{20} 1.5062, d_4^{25} 0.9897. Found: Si, 17.1%. Calcd for $C_{10}H_{16}Si$: Si, 17.2%.

The reaction of **4** and **5** with isoprene and Mg was carried out in THF under the reaction conditions described above. These results are shown in Table 2.

*Reaction of **3** with Equimolar Amounts of Isoprene and Mg.* A mixture of **3** (25 g, 0.13 mol), isoprene (16.5 g, 0.24 mol), and Mg (3.2 g, 0.13 mol) in dry THF (160 ml) was refluxed with stirring for 30 h under a nitrogen atmosphere. After the removal of the solvent, dry hexane (150 ml) was added to the residue, and the deposited magnesium salts were filtered off. The resulting solution was evaporated to give 1,1-diethoxy-3-methyl-1-sila-3-cyclopentene (**17**), **1**, and tetraethoxysilane in 32.5, 23.2, and 23.1% yields respectively, as determined by GLC analysis. **17**, NMR: (δ) 1.1 (t, 6H, CH_3), 0.9—1.2 (m, 1H, Si-CH_2), 1.5—1.6 (m, 3H, =C-CH_3), 3.4 (q, 4H, O-CH_2), 5.0 (m, 1H, =CH). IR (neat): 2900, 1640, 1440, 1400, 1160, 1080, 1030, 1010, 780 cm^{-1}. Mass, *m/e* 172 (M^+). Bp 190 °C, n_D^{25}1.4389.

The reaction of **4**, **5**, and **6** with isoprene and Mg was carried out in THF under the reaction conditions described above, and the yields of the products were estimated by GLC. These results are shown in Table 3.

*Reaction of **3** with Butadiene and Mg.* A mixture of **3** (18.9 g, 0.1 mol), Mg (8.2 g, 0.3 mol), and dry THF (150 ml) was placed in a flask equipped with a magnetic stirrer and a Dry Ice trap. Butadiene was then introduced into the mixture at room temperature under a nitrogen atmosphere. After stirring for 30 h, saturated aq NH_4Cl (100 ml) was added to the mixture. The organic layer was separated and then treated with 4M NaOH at room temperature for 24 h in order to hydrolyze the side reaction product, *i.e.*, tetraethoxysilane. Then the mixture was washed with two 50 ml portions of water, and dried over Na_2SO_4. Evaporation and distillation gave **8** in a 35.4% (4.8 g) yield. Bp 102 °C/72 Torr (lit, 65—68 °C/13 Torr).[1] In a similar manner, when **2** was employed in place of **3**, **8** was obtained in a 20% yield.

*Preparation of **9**.* A mixture of **3** (23.2 g, 0.12 mol) and 1,4-dibromobutane (53.0 g, 0.25 mol) in diethyl ether (100 ml) was added, over a 3-h period to magnesium (14.2 g, 0.58 mol) in diethyl ether (400 ml). After stirring had been continued for an additional 8 h, 150 ml of water was added to the mixture. The organic layer was separated, washed with water, and then dried over $CaCl_2$. Evaporation and distillation gave **9** in a 61.6% (10.6 g) yield. Bp 103 °C/90 Torr (lit, 178.5 °C).[6]

*Preparation of **10**.* A mixture of **1** (3.3 g, 0.02 mol) and diiodomethane (26.8 g, 0.1 mol) in dry ether was refluxed in the presence of a Zinc-Copper couple (6.5 g) with stirring for 30 h. The ether slution was decanted from the unreacted couple, washed with two 30 ml portions of saturated aq NH_4Cl, and then dried over Na_2SO_4. Fractional distillation gave **10** in a 54.9% (2.1 g) yield. NMR: (δ) −0.2, 0.5 (m, 4H, $\angle CH_2 \rangle$), 0.7—1.2 (m, 8H, Si-CH_2), 1.2—1.5 (m, 6H, C-CH_3). IR (neat): 3030, 2900, 1440, 1400, 1250, 1180, 1160, 1120, 1060, 1030, 1010, 930, 850, 750 cm^{-1}. Bp 110—112 °C/34 Torr, n_D^{20} 1.5033, d_4^{25} 0.9802. Found: Si, 14.6%. Calcd for $C_{12}H_{20}Si$: Si, 14.9%.

*Preparation of **11**.* To a solution of perbenzoic acid (0.09 mol) in chloroform (157 ml), **1** (4.9 g, 0.03 mol) was added at 5 °C over 1 h. After the mixture had been maintained at 5 °C for two days, benzoic acid and excess perbenzoic acid were extracted with 1M NaOH (200 ml). The chloroform solution was washed with two 60 ml portions of water, and then dried. The removal of the solvent under reduced pressure at room temperature, followed by distillation, gave **11** in a 65.3% (3.8 g) yield. NMR: (δ) 0.7—1.3 (m, 8H, Si-CH_2), 1.2—1.5 (m, 6H, C-CH_3), 3.0—3.1 (m, 2H, $\overline{O}\wedge H$); IR (neat): 2950, 1450, 1390, 1260, 1180, 1040, 1005, 950, 900, 830, 780, 760 cm^{-1}. Bp 80 °C/0.45 Torr, n_D^{20} 1.4969, d_4^{25} 0.9974. Found: Si, 14.3%. Calcd for $C_{10}H_{16}O_2Si$: Si, 14.9%.

*Preparation of **12**.* Compound **1** (6.6 g, 0.04 mol) was hydrogenated in a catalytic hydrogenating apparatus in hexane, using palladium charcoal (0.3 g) as the catalyst, at room temperature. The hydrogen up-take was almost theoretical. After the removal of the solvent, distillation gave **12** in a 78.7% (5.3 g) yield. NMR: (δ) 0.2—1.0 (m, 8H, Si-CH_2), 1.0 (d, 6H, -CH_3), 1.1—2.0 (m, 6H, -CH_2-CH-). IR (neat): 2940, 1450, 1405, 1370, 1180, 1080, 1040, 1030, 970, 840, 780, 750, 720 cm^{-1}. Bp 105—107 °C/45 Torr, n_D^{20} 1.4079, d_4^{20} 0.8682. Found: Si, 16.9%. Calcd for $C_{10}H_{20}$-Si: Si, 16.7%.

*Preparation of **13**.* Gaseous diborance generated from $NaBH_4$ (2.8 g) in diglyme and BF_3OEt_2 was added to a solution of **1** (8.2 g, 0.05 mol) in THF (125 ml) at 0 °C over a period of 2 h. After the mixture had then been stood for 2 h at room temperature, small chips of ice were added to hydrolyze the excess diborane. The solution was then immersed in an ice bath, and 3M NaOH (11 ml) was added, followed by 30% H_2O_2 (11 ml) over a period of 1 h. One hour later the organic layer was extracted with ether. The combined organic layer was dried and distilled to yield 4.6 g (46.0%) of **13**. NMR: (δ) 0.25—0.6 (m, 4H, Si-CH_2), 0.95 (d, 6H, C-CH_3), 0.7—1.3 (m, 4H, Si-CH_2-C-O), 1.5—2.1 (m, 2H, CH), 2.4 (s, 2H, OH), 3.6 (q, 2H, CH-O). IR (neat): 3300, 2900, 1450, 1400, 1330, 1250, 1190, 1130, 1075, 1040, 1030, 1000, 900, 840, 800, 780 cm^{-1}. Bp 122 °C/0.1 Torr. Found: Si, 14.9%. Calcd for $C_{10}H_{20}Si$: Si, 14.0%.

*Preparation of **14**.* Gaseous diborane generated from $NaBH_4$ (4.5 g, 0.12 mol) in diglyme and BF_3OEt_2 was added

to a solution of **1** (6.6 g, 0.04 mol) in diglyme (100 ml) at 0 °C over a period of 3 h. After the mixture was stood for 2 h at room temperature, a solution of NH_2OSO_3H (18.1 g, 0.16 mol) in diglyme (30 ml) was added. The solution was then refluxed for 4 h. The mixture was cooled, treated with concd HCl (32 ml), and poured into water (200 ml). The acidic solution was then made strongly alkaline with a concd NaOH solution, and the liberated amine was extracted with ether. The extracts was dried over KOH, and the solvent was evaporated. The residual solid product was distilled to yield 3.7 g (46.8%) of **14**. NMR: (δ) 0.25—0.7 (m, 4H, Si-CH_2), 0.95 (d, 6H, C-CH_3), 0.8—1.3 (m, 4H, Si-CH_2-CN), 1.0 (s, 4H, NH_2), 1.3—1.9 (m, 2H, CH), 2.7 (q, 2H, CH-N). IR (neat): 3350, 2900, 1560, 1450, 1360, 1100, 1075, 1040, 1030, 800, 760 cm^{-1}. Mass: *m/e* 198 (M^+). Mp 53 °C, Bp 79 °C/0.5 Torr. Found: N, 13.90, Si, 13.9%. Calcd for $C_{10}H_{22}N_2Si$: N, 14.11, Si, 14.2%.

*Polycondensation of **14** with Adipoyl Dichloride.* A solution of adipoyl dichloride (0.17 g, 0.93 mmol) in CCl_4 (7 ml) was placed in beaker. A solution of **14** (0.5 g, 2.5 mmol) in 3.3 ml of water was then carefully poured over the acid chloride solution. The polymeric film which formed at the interface of the two solutions was grasped with tweezers and raised from the beaker. Yield 0.2 g (69.8%). IR(KBr): 3250, 2950, 1640, 1540, 1460, 1400, 1280, 1160, 1075, 1010, 770 cm^{-1}. $[\eta]=1.07$ (MeOH). Found: N, 8.73%. Calcd for $C_{16}H_{28}N_2O_2Si$: N, 9.80%.

The authors wish to thank Professor Nohira for his many helpful discussions and the Nihon Gosei-Gomu Co. for providing the isoprene.

References

1) R. G. Salomon, *J. Org. Chem.*, **39**, 3602 (1974).
2) R. D. Rieke and S. E. Bales, *J. Am. Chem. Soc.*, **96**, 1775 (1974).
3) a) T. Terasawa, K. Takahashi, and K. Takase, Preprints of the XXXVth Annual Meeting of the Chemical Society of Japan, p. 672, Sapporo, August 28, 1976; b) M. Yang, M. Ando, and K. Takase, *Tetrahedron Lett.*, **38**, 3529 (1971).
4) D. Terunuma, S. Hatta, and T. Araki, *Chem. Lett.*, **1974**, 1321.
5) M. Kumada, *J. Inst. Polytech. Osaka City Univ. Ser. C*, **2**, 139 (1952).
6) R. West, *J. Am. Chem. Soc.*, **76**, 6012 (1954).
7) a) H. E. Simmons and R. D. Smith, *J. Am. Chem. Soc.*, **81**, 4256 (1959); b) T. Araki, D. Terunuma, and T. Fuse, *Bull. Chem. Soc. Jpn.*, **45**, 293 (1972).
8) a) M. Tiffeneau, *Org. Synth.*, Coll. Vol. I, 422 (1941). b) G. Manuel, P. Mazerolles, and J. C. Florence, *J. Organomet. Chem.*, **30**, 5 (1971).
9) H. C. Brown and G. Zweifel, *J. Am. Chem. Soc.*, **81**, 247 (1959).
10) a) H. C. Brown and G. Zweifel, *J. Am. Chem. Soc.*, **82**, 4708 (1960); b) T. Araki, D. Terunuma, F. Kato, H. Kaneda, and A. Iino, *Bull. Chem. Soc. Jpn.*, **46**, 644 (1973).
11) E. L. Wittbeker and P. W. Morgan, *J. Polym. Sci.*, **40**, 289 (1960).

Chemistry of 1,3-Glycol Derivatives. II. Lithium Aluminium Hydride and Meerwein-Ponndorf-Verly Reductions of 6,6-Dimethylspiro[2.5]octane-4,8-dione

Osamu Itoh, Tsutomu Okita, Makoto Umezu, Masashi Inoue, and Katsuhiko Ichikawa*

Department of Hydrocarbon Chemistry, Faculty of Engineering, Kyoto University, Yoshida, Kyoto 606

(Received December 6, 1976)

Lithium aluminium hydride reduction of 6,6-dimethylspiro[2.5]octane-4,8-dione in tetrahydrofuran gave *cis*- and *trans*-6,6-dimethylspiro[2.5]octane-4,8-diols. Almost the same ratio of *cis*: *trans*=1: 2 was obtained with various substrate-reagent ratios. In the case of Meerwein-Ponndorf-Verly reduction, however, *cis*-diol was obtained almost exclusively. It is clear that the former reduction gave kinetically-controlled products and that the latter gave thermodynamically-stable products. Unusual results were obtained by changing the hydrolysis conditions for the lithium aluminium hydride reduction products and these are explained assuming that the intermediate aluminium alkoxide is oxidized by acid.

The reduction of 6,6-dimethylspiro[2.5]octane-4,8-dione (**1**) produces *cis*- and *trans*-6,6-dimethylspiro[2.5]-octane-4,8-diols (*cis*- and *trans*-**2**). Because of the special structure of **1**, a study of the steric course will provide a convenient tool for examining the mechanism for various reducing reagents and the spectral data of the resulting diol will be useful in stereochemistry. In this article, the results of lithium aluminium hydride and Meerwein-Ponndorf-Verly reductions of **1** are reported.

Lithium aluminium hydride reduction of **1** in tetrahydrofuran at 0 °C gave two kinds of diols, A and B, which were separated by fractional recrystallization from chloroform. As mentioned below, it was concluded that A (mp 166—168 °C) is *cis*-**2** and B (mp 119—121 °C) is *trans*-**2**.

The melting points of the *cis*- and *trans*-isomers of 1,3-cyclohexanediols appear to be related to the conformations. The melting points of the *cis*-isomers which can form intramolecular hydrogen bonds are higher than those of the *trans*-isomers, but this relation is reversed in cases where the intramolecular hydrogen bond is difficult to form due to steric repulsion. Related data are shown in Table 1. Applying this conclusion to the present case, it appears likely that A and B are *cis*- and *trans*-**2** respectively.

Finegold and Kwart have discussed the conformation of the 1,3-cyclohexanediol system and concluded that the hydroxyl groups of the *cis*-isomer are diaxial forming an intramolecular hydrogen bond when C-5 has no substituent, and are diequatorial when C-5 is substituted with two methyl groups because of the 1,3-diaxial repulsion between the hydroxyl and methyl groups.[1] Therefore, two hydroxyl groups of the present *cis*-**2** should also be diequatorial.

The NMR spectra can be explained reasonably well in terms of the above conformations. Protons of the two methyl groups at the C-6 position of *trans*-**2** gave only one singlet at δ=1.09, since rapid ring-inversion renders the two methyl groups equivalent. In the case of *cis*-**2**, two singlets were observed at δ=1.00 (axial) and at δ=1.13 (equatorial), since ring inversion is restricted. Cyclopropane ring protons of *trans*-**2** gave a multiplet of A_2B_2 type centered at δ=0.52. The same protons of *cis*-**2** gave a singlet at δ=0.54, since the cyclopropane ring is perpendicular and symmetrical to the plane of C-1, C-4, and C-8 which includes the two C–OH bonds. Assignments of the signals due to the cyclohexane ring protons are as follows. In the case of *cis*-**2**, a doublet (J=12.0 Hz) of doublets (J=8 Hz) centered at δ=1.45 can be assigned to the signals of the two axial

Table 1. Melting points and IR absorptions due to the hydroxyl group of 1,3-diols

Diol			Mp, °C	IR absorption, cm^{-1}
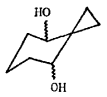	a)	*cis*	166—168	3610 (free)
		trans	119—121	3610 (free)
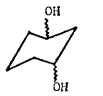	b)	*cis*	86—87	3619 (free), 3544 (bonded)
		trans	116—116.5	3625 (free)
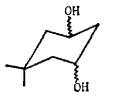	c)	*cis*	147—148	
		trans	102—104	
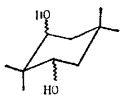	d)	*cis*	205—206	3635 (free)
		trans	107—108	3637 (free)
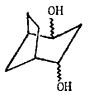	e)	*cis*		3615 (free), 3575 (bonded)
		trans		3615 (free)
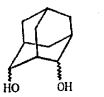	f)	*cis*		3616 (free), 3530 (bonded)

a) Determined in carbon tetrachloride. b) L. P. Kuhn, *J. Am. Chem. Soc.*, **74**, 2492 (1956). c) H. Finegold and H. Kwart, *J. Org. Chem.*, **27**, 2361 (1962). d) H. Favre and J. C. Richer, *Can. J. Chem.*, **37**, 411 (1959). A. W. Allan, R. P. A. Sneeden, and J. M. Wilson, *J. Chem. Soc.*, **1959**, 2186. e) J. G. Durocher and H. Favre, *Can. J. Chem.*, **42**, 260 (1964). f) D. Lenoir and P. von R. Schleyer, *Chem. Commun.*, **1971**, 26.

hydrogens at C-5 and C-7, a doublet (J=12 Hz) of doublets (J=4 Hz) centered at δ=1.65 to those of the two equatorial hydrogens, and a doublet (J=8 Hz) of doublets (J=4 Hz) centered at δ=3.67 to the two methine protons at C-4 and C-8, respectively. In the case of *trans*-**2**, a doublet (J=13 Hz) of doublets (J=7 Hz) centered at δ=1.45 can be assigned to the two axial protons at C-5 and C-7, a doublet (J=13 Hz) of doublets (J=4 Hz) centered at δ=1.16 to those of the two equatorial protons, and a doublet (J=7 Hz) of doublets (J=4 Hz) centered at δ=3.77 to the two methine protons, respectively. The protons of the hydroxyl groups gave a rather sharp singlet at δ=1.54 in the case of *cis*-**2**, and a rather broad singlet at δ=1.61 which overlapped with the signals of the axial protons in the case of *trans*-**2**.

Lithium aluminium hydride reduction of **1** in tetrahydrofuran at 0 °C followed by hydrolysis gave *cis*- and *trans*-**2** in a ratio of 37: 63. In contrast, aluminium isopropoxide reduction in 2-propanol under reflux followed by hydrolysis gave *cis*-**2** almost exclusively (the *cis*- to *trans*-**2** ratio was 99: 1). These results are in accordance with the conclusions of Dauben *et al.* that the Meerwein-Ponndorf-Verly reduction gives thermodynamically more stable products (product development-control) and that lithium aluminium hydride reduction gives sterically approach-controlled products.[2]

Attacks by aluminium isopropoxide on **1** appear to occur to form the less hindered diequatorial intermediate leading to *cis*-**2**. Because the reduction is reversible, thermodynamic stabilities of the products determine the product distribution. The possibility that one aluminium isopropoxide molecule reacts with two carbonyl groups of the same molecule leading to *cis*-**2** appears to be unlikely because of the steric repulsion with cyclopropyl group.

In the case of lithium aluminium hydride, the reduction process is not reversible. In the intermediate of the attack on the first carbonyl, the $-OAlH_3^-$ group will take the equatorial position, prohibit ring inversion, and fix the conformation. The less hindered reaction path for second carbonyl group reduction appears to proceed from the opposite side of the axial methyl group at C-5 and results in *trans*-**2** preferentially.

Unusual results were obtained during the course of the attempts to obtain the hydroxy ketone by the half reduction of dione **1**. In tetrahydrofuran at 0 °C, **1** was treated with a 1/3 mole equivalent of lithium aluminium hydride. After one hour, 2 M-HCl was added. In one experiment, the reaction mixture was heated to 40—50 °C to remove the solvent using a rotary evaporator immediately after the addition of hydrochloric acid. In another experiment, the solvent was evaporated after standing at room temperature for two days. The former experiment gave 2-(2-chloroethyl)-3-hydroxy-5,5-dimethyl-2-cyclohexanone (**3**), which is the enol form of 2-(2-chloroethyl)-5,5-dimethyl-1,3-cyclohexanedione (**4**) and is the cleaved product of the cyclopropane ring of **1** with hydrochloric acid. The latter gave diol **2**. Related results are shown in Table 2. Since the experiments were carried out on a small scale because of the limited amount of **1** available and the product separations were performed by column chromatography, the data are not quantitative.

These results show that the reduction intermediate, aluminium alkoxide, decomposes to give **3** at a higher temperature, 40—50 °C, and hydrolyzes slowly to give **2** at room temperature. The addition of hydrochloric acid to the intermediate alkoxide results in the rapid hydrolysis of the hydrides bonded to aluminium. The hydrolysis of the Al–O bond, however, appears to be not always fast. For example, it is well known that the B–O bond in the borohydride reduction intermediate is sometimes hydrolyzed only slowly with acid. Rickborn and Quartucci have suggested the possibility that the intermediate of lithium aluminium hydride reduction of epoxide could be oxidized to ketone by a hydride acceptor (AlH_3).[3] In the present case, oxidation back to ketone **1** and its subsequent decomposition by hydrochloric acid cannot explain the results, because **1** does not react with hydrochloric acid under the same conditions, but does react giving 6,6-dimethyl-2,3,4,5,-6,7-hexahydrofuran-4-one (**5**) instead of **3** under tetrahydrofuran refluxing. The formation of **3**, therefore, follows some other reaction path. The most probable scheme is depicted in Fig. 1 together with those of related reactions. The oxidation step with hydrochloric acid might be intramolecular, if both or either of the H^+ and Cl^- ions come from the ligands of aluminium. However, further detailed experiments are required to examine this interesting possibility.

The unusual results were obtained only in runs with smaller lithium aluminium hydride to **1** ratios (1 : 2—1 : 3), and no formation of the expected hydroxy ketone was observed. These results appear to show that the oxdation of alkoxide with acid occurs only in the case of an $RO–AlH_2–OR$ type alkoxide where the hydrolysis of Al–O bond is strongly hindered by two bulky R groups.

Some of the chemical properties of **3** were investigated. The reaction with equimolar sodium carbonate in 75% ethanol at 40 °C for 24 h gave **1**. The changes of **3** in pyridine were followed by NMR at 40 °C (NMR-probe temperature). Into 0.5 ml of pyridine were dissolved 30 mg of **3** and the spectra were determined immediately

Table 2. The effects of hydrolysis condition on the product distribution[a]

Run No.	$1/LiAlH_4$ mole ratio	Duration time of hydrolysis	Product
1	0.6/1	10 min	**2**
2	3.0/1	48 h	**2**
3	3.0/1	40 min	**3** and a trace of **2**
4	3.0/1	10 min	**3**
5[b]	2.3/1	1 h	**3**

a) **1** (3 mmol in runs 1 and 5 and 5 mmol in runs 2, 3, and 4, respectively) was reduced with lithium aluminium hydride in 30 ml of tetrahydrofuran at 0 °C for 1 h. The reaction mixtures were treated with 4 ml of 2M-HCl to hydrolyze the products at room temperature for the duration times given in the table. b) Diethyl ether (30 ml) was used in place of tetrahydrofuran.

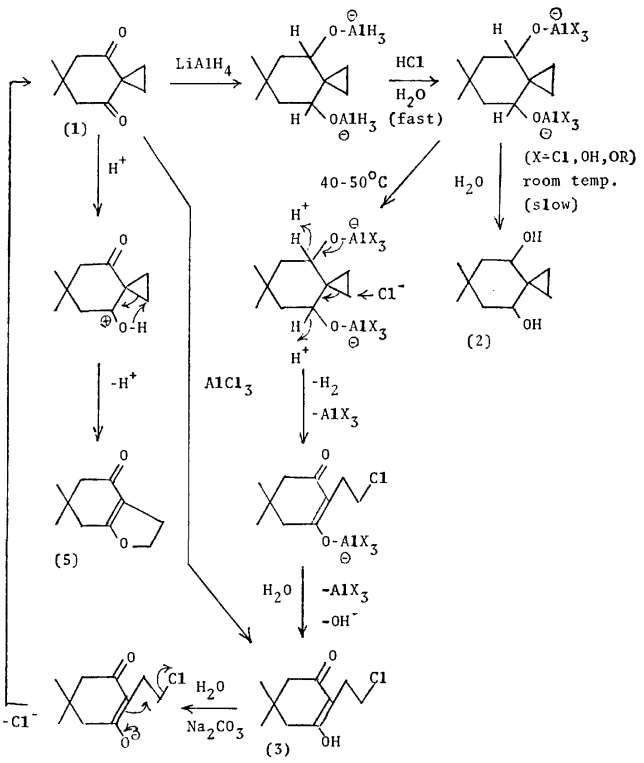

Fig. 1. Reaction of **1** and related reaction scheme.

after preparation of the solution, and at 24 and 48 h after preparation. When one drop of D_2O was added to the sample, the spectra showed that **3** was transformed to **1** after 24 h and further to **5** after another 24 h. When no D_2O was added, the changes were much slower. The reaction of **1** with a half mol of aluminium chloride in chloroform at room temperature gave **3**.

Experimental

Materials. The preparation of **1** has been reported previously.[4] Aluminium isopropoxide was prepared by a method reported in the literature.[5] Commercial tetrahydrofuran and 2-propanol were dried over calcium hydride and distilled before use. Other reagents were commercial ones of analytical grade.

*Reduction of **1** with Lithium Aluminium Hydride.* The following examples show typical experimental procedures. Into a tetrahydrofuran (20 ml) solution of lithium aluminium hydride (0.379 g, 10 mmol) was added a tetrahydrofuran (10 ml) solution of **1** (1.68 g, 10 mmol) over a period of 5 min at 0 °C. After 2 h, 2 M-HCl (5 ml) was added. After standing for 24 h, the solvent was evaporated with a rotary evaporator (bath temperature, 40—50 °C) and the residue was dissolved in ethyl ether, washed with a saturated aqueous sodium chloride solution, and dried over anhydrous sodium sulfate. After evaporation of the ether, a colorless solid of **2** (1.58 g) was obtained. The *cis-* to *trans-* **2** ratio in the crude **2** was determined to be about 1: 2 by measuring the proton ratio of the NMR spectra in pyridine. The solid was dissolved in ether and passed through Wakogel C-200, $2\phi \times 3$ cm, to remove inorganic salts. After evaporating the solvent the product was recrystallized from chloroform (20 ml) to give fraction A, mp 166—168 °C (Found: C, 70.54; H, 10.54%. Calcd for $C_{10}H_{18}O_2$: C, 69.93; H, 10.54%) and fraction B, mp 119—121 °C (Found: C, 69.85; H, 10.56%).

1 (0.83 g, 5 mmol) was reduced with lithium aluminium hydride (0.062 g, 1.63 mmol) by the same procedure as described above, except that tetrahydrofuran was removed from the reaction mixture just after the addition of 2 M-HCl using a rotary evaporator at 45—50 °C. The evaporation required about 10 min. A work-up gave crystals of **3**, mp 144—145 °C (0.524 g, 52% yield). Found: C, 58.83; H, 7.21; Cl, 17.21%. Calcd for $C_{10}H_{15}ClO_2$: C, 59.26; H, 7.46; Cl, 17.59%. NMR in dimethyl-d_6 sulfoxide δ: 0.95 (s, 6H, methyl), 2.23 (s, 4H, cyclohexane ring methylene), 2.62 (t, J=7.0 Hz, 2H, branched α-methylene), 3.49 (*t*, J=7.0 Hz, 2H, branched β-methylene), and 4.10 (s, broad, 1H, hydroxyl). IR (KBr disc): 3350 (ν_{O-H}), 2470 ($\nu_{C=O\cdots H-O}$), 1635 ($\nu_{C=O}$), and 1558 cm^{-1} ($\nu_{C=C}$).

*Meerwein-Ponndorf-Verly Reduction of **1**.* According to the reported method,[5] **1** (1.0 g, 6 mmol) was reduced with aluminium isopropoxide (4.08 g, 20 mmol) in dry 2-propanol (9.0 g, 150 mmol). **2** was obtained in a yield of 98% (0.98 g). Gas-chromatographic analysis could not be applied to **2**. However, application of the trimethylsilylation method[6] gave satisfactory results, although the detector was damaged after repeated analyses. The ratio of *cis-* to *trans-***2** was found to be 99: 1.

The NMR spectra were recorded on a Varian Associates HR-220 spectrometer at 220 MHz at room temperature or on a Jeol PMX-60 spectrometer. The IR spectra were recorded on a Hitachi EPI-G2 spectrometer. The gas-chromatographic analyses were carried out by Yanaco GC-550 TPH chromatograph with a 1.5 m OV-17 column.

This work was partially supported by a Grant-in-Aid for Scientific Research (No. 911503) from the Ministry of Education, Japan.

References

1) H. Finegold and H. Kwart, *J. Org. Chem.*, **27**, 2361 (1962).
2) W. G. Dauben, G. J. Fonken, and D. S. Noyes, *J. Am. Chem. Soc.*, **78**, 2579 (1956).
2) W. G. Dauben, G. J. Fonken, and D. S. Noyes, *J. Am. Chem. Soc.*, **78**, 2579 (1956).
3) B. Rickborn and J. Quartucci, *J. Org. Chem.*, **29**, 3185 (1964).
4) K. Ichikawa, O. Itoh, and T. Kawamura, *Bull. Chem. Soc. Jpn.*, **41**, 1240 (1968).
5) A. L. Wilds, *Org. React.*, **2**, 178 (1944).

Boron Trifluoride Etherate-Catalyzed Backbone Rearrangement of 3β,4β-Epoxyshionane and the Synthesis of Dihydrobaccharis Oxide

Kazuo TACHIBANA, Motoo TORI, Yoshihiko MORIYAMA, Takahiko TSUYUKI, and Takeyoshi TAKAHASHI

Department of Chemistry, Faculty of Science, The University of Tokyo, Hongo, Bunkyo-ku, Tokyo 113

(Received December 10, 1976)

3β,4β-Epoxyshionane (**15**) was treated with boron trifluoride etherate in ether at −30 °C to give dihydrobaccharis oxide (**4**; yield 17%), 4α-fluoroshionan-3β-ol (**17**; 10%), D: B-friedo-bacchar-5-en-3β-ol (**18**; 18%), D: B-friedo-bacchar-5(10)-en-3β-ol (**20**; 15%), and D: C-friedo-bacchar-7-en-3β-ol (**21**; 15%). The reaction in benzene, toluene, cyclohexane, or in hexane at −5 °C or at room temperature yielded bacchar-12-en-3β-ol (**5**), D: C-friedo-bacchar-8-en-3β-ol (**25**), **18**, **20**, and **21**. The reaction product ratios in the same reaction in various solvents are listed in Table 1.

Baccharis oxide (**1**)[2] is a triterpene oxide isolated from *Baccharis halimifolia* L. and shionone (**2**)[3] is a tetracyclic triterpene ketone contained in *Aster tataricus* L. These two triterpenes are biogenetically considered to be derived from a common intermediate (**3**) (or its equivalent species) and closely related to each other.[2,3] Baccharis oxide (**1**) may be formed from **3** by an attack of an oxygen atom on C-3 to the cationic center at C-10.

It has been reported that a boron trifluoride etherate-catalyzed rearrangement of dihydrobaccharis oxide (**4**) gives bacchar-12-en-3β-ol (**5**).[2b,4] In view of a correlation between compounds with shionane (D: A-friedobaccharane) and baccharane skeletons, we previously investigated[5] a backbone rearrangement of 3α,4α-epoxyshionane (**6**)[5] to afford bacchar-12-en-3α-ol (**7**) and D: B-friedo-bacchar-5(10)-en-3α-ol (**8**). We also reported[6] a transformation of friedelin (**9**) into dendropanoxide (**10**).[7] 3β,4β-Epoxyfriedelane (**11**) prepared from **9** was treated, according to Halsall's procedures,[8] with boron trifluoride etherate to give **10** together with D: B-friedo-olean-5(10)-en-3β-ol (**12**), D: B-friedo-olean-5-en-3β-ol (**13**), and β-amyrin (**14**).[6]

Backbone rearrangements in the steroid and terpenoid fields are well documented.[9] Intracyclic tension in the rigid polycyclic ring provokes of backbone rearrangements to give the products less constrained. Electronic effects resulting from the presence of functional groups and kinetic effects due to the nature of reagents can modify the development of rearrangement.[10] The shionane skeleton is considered to be 3α-(4-methylpentyl)-3β,5α,8β,17aβ-tetramethyl-D-homoandrostane, in which there exists an intracyclic tension due to 1,3-diaxial interactions among the alkyl substituents. The backbone rearrangements in **6** were shown to proceed from ring A towards ring D;[5] a 1,3-diaxial interaction between the side chain and the 13α-methyl group is released in **7**. The present paper deals with a reaction of 3β,4β-epoxyshionane (**15**) with boron trifluoride etherate and a preparation of dihydrobaccharis oxide (**4**).[2] Solvent effects on this reaction were also examined.

Shionone (**2**) was converted *via* shionan-3-one (**16**),[3b,c] shionan-3β-ol,[3b,c] and shion-3-ene,[3c] into 3β,4β-epoxyshionane (**15**)[5] by known procedures. Treatment of the β-epoxide (**15**) with boron trifluoride etherate in anhydrous ether at −30 °C for 1 h gave a complex mixture which was separated by column chromatography over silica gel, recrystallization, preparative thin-layer chromatography (TLC), column chromatography on silica gel impregnated with silver nitrate, and by high performance liquid chromatography (HPLC) (*cf.* Experimental).

The reaction mixture was separated into five components (**a**—**e**; designated in an order of the elution) by column chromatography (Column I). The least polar component **a** (yield: *ca.* 17%) was shown to be identical with dihydrobaccharis oxide (**4**),[2] mp 127—128.5 °C, by direct comparison with an authentic specimen, which was prepared by hydrogenation of baccharis oxide (**1**) over palladium charcoal.[2b] The second component **b** (y: *ca.* 1%) was found to be the starting β-epoxide (**15**).

The third component **c** (**17**; y: *ca.* 10%), $C_{30}H_{53}OF$, mp 174—175 °C, was suggested to be a fluoro alcohol based on the spectral data and elemental analysis. The IR spectrum showed a band attributable to a hydroxyl group and the PMR spectrum showed a quintet centered at δ 3.70 due to a proton on a carbon atom ($C_{(3)}$) bearing the hydroxyl group. In the PMR

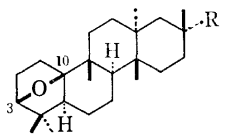

1 R=$(CH_2)_2CH=C(CH_3)_2$

4 R=$(CH_2)_3CH(CH_3)_2$

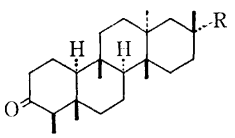

2 R=$(CH_2)_2CH=C(CH_3)_2$

16 R=$(CH_2)_3CH(CH_3)_2$

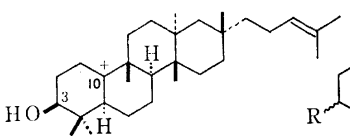

3

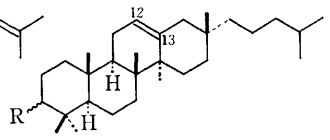

5 R=β-OH

7 R=α-OH

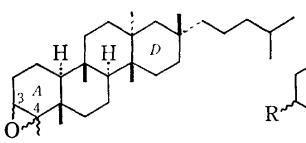

6 3α,4α-epoxide

15 3β,4β-epoxide

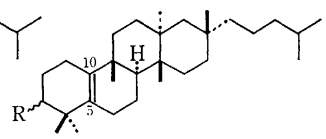

8 R=α-OH

20 R=β-OH

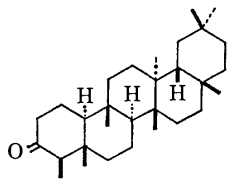

9

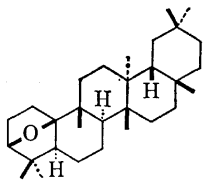

10

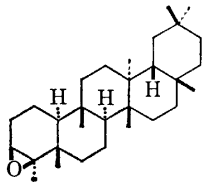

11

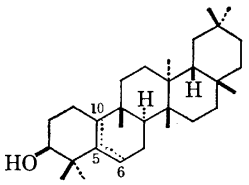

12 5(10)-ene

13 5-ene

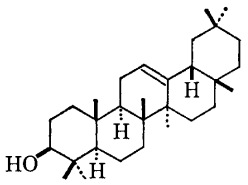

14

measurement using Eu(fod)$_3$-d_{27} as a shift reagent, signals due to a methyl group on a carbon atom bearing a fluorine atom ($C\underline{H}_3$–C(–F)) suffered a considerable downfield shift and were observed as a doublet (J=23 Hz). The fluoro alcohol (**17**) was treated with potassium hydroxide in methanol under reflux to generate the starting 3β,4β-epoxide (**15**). The reaction of an epoxide with boron trifluoride etherate to give a fluorohydrin is often encountered.[11] These observations together with the mechanistic consideration[11] led to the conclusion that the fluoro alcohol should be formulated as 4α-fluoroshionan-3β-ol (**17**).

The presence of a secondary hydroxyl group [IR 3450 cm^{-1}; PMR δ 3.47 (1H, t-like; $C_{(3)}$–H)] and a trisubstituted double bond [IR 820 cm^{-1}; PMR δ 5.62 (1H, m; $C_{(6)}$–H)] was shown for the fourth component **d** (**18**; y: *ca.* 18%), $C_{30}H_{52}O$, mp 124—125 °C, by its IR and PMR spectra. The appearance of peaks at *m/e* 276 and *m/e* 152 due to a retro-Diels-Alder fragmentation[12] in the mass spectrum showed the presence of the double bond between C-5 and C-6. Thus the structure of D: B-friedo-bacchar-5-en-3β-ol (**18**) was proposed for the fourth component **d**. This was substantiated by the following transformation. The unsaturated alcohol (**18**) was converted by a usual procedure into a corresponding acetate. Oxidation of the acetate with selenium dioxide in acetic acid under reflux gave a diene identical with a known D: B-friedo-bacchara-1(10),5-dien-3β-yl acetate (**19**).[5]

The fifth component **e** was found to be a mixture of two compounds (**20** and **21**) containing a small amount of **17** and **18** by HPLC examination. The component **e** was chromatographed on silica gel impregnated with silver nitrate (Column II) to give a mixture of two compounds (**20** and **21**). This mixture could not be separated into pure compounds by repeated column and thin layer chromatography and by recrystallization. Application of HPLC however gave a satisfactory separation: D: B-friedo-bacchar-5(10)-en-3β-ol (**20**; y: 15%) and D: C-friedo-bacchar-7-en-3β-ol (**21**; y: 15%) were obtained. Their structures were characterized as follows.

The former compound (**20**), mp 142—143 °C, showed the same spectral data and melting point (and mixed mp) as those of an authentic D: B-friedo-bacchar-5(10)-en-3β-ol (**20**)[13] prepared from shionanone (**16**) *via* D: B-friedo-bacchara-1,5(10)-dien-3-one.[13]

The latter compound was inferred to be **21** by the following evidence. The compound (**21**) had mp 136.5—137.5 °C and a molecular formula $C_{30}H_{52}O$. The presence of a secondary hydroxyl group [IR 3350 cm^{-1}; PMR δ 3.26 (1H, dd, $J_{2\beta,3\alpha}$=8 and $J_{2\alpha,3\alpha}$=5 Hz; $C_{(3\alpha)}$–H)] and a trisubstituted double bond [IR 820 cm^{-1}; PMR δ 5.39 (1H, quartet, $J_{6\beta,7}$=3, $J_{6\alpha,7}$=3, and $J_{7,9\alpha}$=3 Hz; $C_{(7)}$–H)] was indicated by the IR and PMR spectra. In the PMR spectrum using Eu(fod)$_3$-d_{27} as a shift reagent, signals due to the olefinic and allylic protons and the methyl protons at C-10 shifted to downfield and were easily assignable (Fig. 1). The magnitude and tendency of the shift of these protons were found to be similar to those (Fig. 2) of α-spinasterol (**22**).[14] The position of the trisubstituted double bond between C-7 and C-8 was supported by fragment ion peaks at *m/e* 247 and *m/e* 229. The peak at *m/e* 247 is characteristic for Δ^7- and Δ^8-triterpenoids[15] and the latter peak at *m/e* 229 is corresponding to the dehydration peak of the former ion. It is therefore concluded that the compound (**21**) should be formulated as D: C-friedo-bacchar-7-en-3β-ol. The proposed structure was further supported by the following transformations (a and b).

a) The compound (**21**) was acetylated in a usual manner to give an acetate (**23**), $C_{32}H_{54}O_2$, which also showed a characteristic fragment ion peak at *m/e* 289 due to a retro-Diels-Alder fragmentation of Δ^7- and Δ^8-triterpenoids[15] accompanied with a peak at *m/e* 229 due to loss of acetic acid from the ion at *m/e* 289. In the PMR and IR spectra, the presence of an acetoxyl group and an olefinic proton [PMR δ 5.39 (1H, quartet, $J_{6\beta,7}$=3, $J_{6\alpha,7}$=3, and $J_{7,9\alpha}$=3 Hz; $C_{(7)}$–H)] was observed. On allylic oxidation with *t*-butyl chromate,[16] the acetate (**23**) afforded an enone acetate (**24**), $C_{32}H_{52}O_3$, as an oil. Its IR, UV [λ_{max} 248 nm (ε 12000)], and PMR [δ 2.17 (s, $C_{(5)}$–H) and 5.81 (d, $J_{7,9\alpha}$=2.4 Hz; $C_{(7)}$–H)] spectral data may best be interpreted by a structure of D: C-friedo-bacchar-7-en-6-on-3β-yl acetate (**24**).[17]

b) Treatment of the acetate (**23**) with hydrogen chloride in chloroform, followed by alkaline hydrolysis and purification by HPLC, gave an isomerized product (**25**), $C_{30}H_{52}O$, as an oil. The presence of a hydroxyl group and the absence of olefinic proton in **25** were shown by the IR and PMR spectra. Prominent peaks at *m/e* 247 and 229 characteristic for Δ^7- and Δ^8-triterpenoids[15] were observed in the mass spectrum. When **23** was treated with hydrochloric acid in acetic acid at

60 °C and then subjected to alkaline hydrolysis, the 12-ene (**5**)[2b,4] was formed together with **25**. These observations suggest the structure of D: C-friedo-bacchar-8-en-3β-ol for the isomerized alcohol (**25**) and

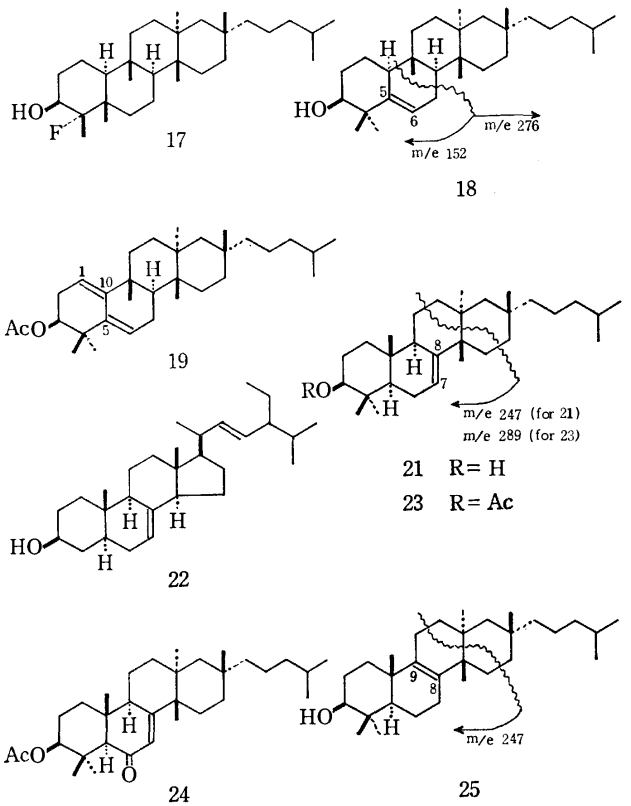

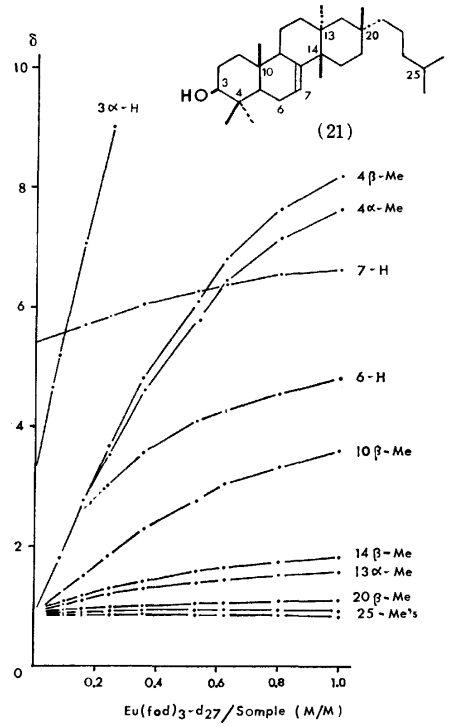

Fig. 1. Induced paramagnetic shifts for D: C-friedo-bacchar-7-en-3β-ol (**21**) in a 3% (w/v) solution in $CDCl_3$.

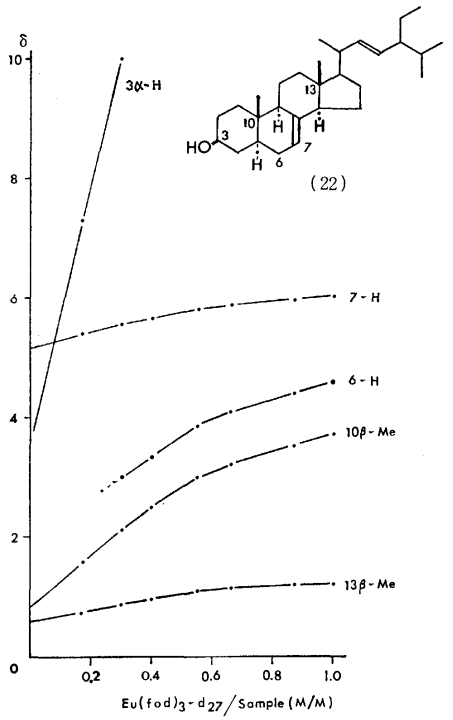

Fig. 2. Induced paramagnetic shifts for α-spinasterol (**22**) in a 3% (w/v) solution in $CDCl_3$.

that of D: C-friedo-bacchar-7-en-3β-ol for the alcohol (**21**).

Solvent effects on the formation of these reaction products were then investigated. The small scale reaction using 1—3 mg of the 3β,4β-epoxide (**15**) and boron trifluoride etherate (2 drops) in a solvent (2—10 ml) was carried out at room temperature or at —5 °C. The reaction mixture, after the usual treatment, was extracted with ether to give a residue. This residue was dissolved in 10% ether–hexane and the identification of each component and the determination of its relative amount were carried out by HPLC (Table 1).

In the reaction conditions listed in Table 1, five alcohols were detected besides dihydrobaccharis oxide (**4**) and the fluorohydrin (**17**), and four of the alcohols were identified to be **18**, **20**, **21**, and **25** by HPLC. The fifth alcohol was found to be bacchar-12-en-3β-ol (**5**) by direct comparison (IR, mass spectrum, TLC, and HPLC) with an authentic specimen[2b] prepared by the acid-catalyzed rearrangement of dihydrobaccharis oxide (**4**).

In the rearrangement of the 3β,4β-epoxide (**15**), the cationic center at C-4 was initially formed by boron trifluoride etherate-attack to an oxygen atom of the epoxide. A sequence of 1,2-shifts of methyl group(s) and hydrogen atom(s) were then followed. From the derived cations in various rearranged stages, the rearranged alcohols (**5**, **18**, **20**, **21**, and **25**) would be produced after deprotonation in the last step.[18]

It is obvious that the rearrangement in solvents with low nucleophilicity *e.g.* such as nitromethane, proceeds up to C/D rings because the cationic centers survive longer in these solvents and spread over the whole skeleton; therefore the formation of bacchar-12-en-3β-ol

Table 1. Relative amount ratios of the products in the reaction of **15** with boron trifluoride etherate[a)]

Solvents	Temp (°C)	Time (min)	**17**	**4**	**18** (5-ene)	**20** [5(10)-ene]	**25** (8-ene)	**21** (7-ene)	**5** (12-ene)
CH_3NO_2	r.t.[b)]	5	0	0	0	0	30	0	70
CH_2Cl_2	r.t.	5	0	0	20	trace	25	trace	55
Benzene	r.t.	5	0	0	15	20	20	15	30
Toluene	r.t.	5	0	0	10	15	25	15	35
Cyclohexane	r.t.	5	0	0	15	25	25	15	20
Hexane	r.t.	5	0	0	25	25	20	5	25
CH_3CN	r.t.	5	0	0	15	35	25	15	10
Ether	r.t.	5	40	25	5	15	0	15	trace
DME	r.t.	5	0	15	30	40	0	15	0
THF	r.t.	5	0	0	45	50	0	5	0
CH_3NO_2	−5	15	0	0	trace	0	35	30	35
CH_2Cl_2	−5	10	0	0	10	20	25	10	35
Toluene	−5	15	0	0	10	10	25	20	35
Hexane	−5	5	0	0	25	25	15	25	10
CH_3CN	−5	10	0	0	15	50	20	15	trace
Ether	−5	50	30	25	10	20	0	15	trace
DME	−5	20	0	15	30	30	0	25	0
THF[c)]	−5	5	0	0	10	10	0	0	0
Ether	−30	60	10	25	20	15	0	30	0
Ether[d,e)]	−30	60	10	17	18	15	0	15	0

a) Relative yields were determined by HPLC. Measurements were carried out at room temperature using a Liquid Chromatograph Model ALC/GPC 202/401 (Waters Assoc.) with an RI detector; column: μ-PORASIL 1/8 (inch)×1 (foot); solvent system: 1 or 10% ether–hexane; flow rate: 1.0 or 1.2 ml/min; pressure: *ca.* 500 psi. Under the conditions (1% ether–hexane; 1.0 ml/min), retention time for **17**, **4**, **18**, **20**, and **21** was shown to be 54.7, 8.3, 51.7, 69.7, and 81.7 min, respectively. Under the other conditions (10% ether–hexane; 1.2 ml/min), retention time for **18**, **20**, **25**, **21**, and **5** was found to be 11.0, 14.6, 17.0, 15.6, and 18.3 min, respectively. b) Room temperature (r.t.) refers to a temperature range between 20 and 28 °C. c) The epoxide (**15**) was recovered in about 80% yield. d) Yields in this line are expressed as isolated yields (in %). e) A small quantity (*ca.* 1%) of the starting material (**15**) was recovered.

(**5**), derived from a species with a cationic center at C-13, was observed. On the contrary, in a solvent apt to coordinate with a cation such as dimethoxyethane (DME), tetrahydrofuran, or ether, the rearrangement reaction was interrupted in early stages; *e.g.* the D: B-friedo-type alcohols (**18** and **20**) were formed preferentially in the rearrangement in the former two solvents (DME and THF) (*vide infra* for the reaction in ether).

In the reaction of the 3β,4β-epoxide (**15**) in ether or in dimethoxyethane, dihydrobaccharis oxide (**4**) was formed together with the other reaction products, while no **4** was produced in the reaction in nitromethane, dichloromethane, benzene, toluene, cyclohexane, hexane, acetonitrile, and in tetrahydrofuran.

Dihydrobaccharis oxide (**4**) was then treated with boron trifluoride etherate in ether at various temperatures. No reaction occurred at a temperature range between −40 and 0 °C; this shows that the intermediacy of the oxide (**4**) for the formation of the rearranged alcohols (**18**, **20**, and **21**) from 3β,4β-epoxyshionane (**15**) under the similar conditions (at −30 and at −5 °C) is improbable. The reaction of **4** in ether at room temperature for 1 h gave **18** (relative yield determined by HPLC: 10%), **20** (8%), and **21** (2%), besides the starting material (**4**; 80%).

According to Anthonsen's procedure,[2b)] dihydrobaccharis oxide (**4**) was treated with boron trifluoride etherate in benzene at room temperature for 10 min. An examination of the reaction mixture by HPLC showed that bacchar-12-en-3β-ol (**5**; 50%) was the main product and that minor products were **18** (10%), **20** (10%), **21** (10%), and **25** (20%).

The conversion of shionone (**2**) into dihydrobaccharis oxide (**4**) *via* the 3β,4β-epoxide (**15**) was thus shown. As the total synthesis of shionone (**2**) was recently achieved,[19)] the present report constitutes formally the total synthesis of dihydrobaccharis oxide (**4**).

Experimental

Melting points were measured on a Mel-temp capillary melting point apparatus (Laboratory Devices) and were uncorrected. IR and UV spectra were determined on a Hitachi EPI-G2 and EPS-2 spectrometer, respectively. Mass spectra were taken on a Hitachi RMU-6-Tokugata mass spectrometer and high resolution mass spectra on a Hitachi RMH-2 mass spectrometer operating at 70 eV with a direct inlet system. PMR spectra were measured using a JEOL JNM PS-100 (100 MHz), a Hitachi R-20B (60 MHz), or a JEOL JNM FX-60 (Fourier Transform) spectrometer in deuteriochloroform. Measurements of optical rotations were carried out using a JASCO polarimeter DIP-SL. Thin layer chromatography (TLC) was carried out on Kieselgel PF_{254} (E. Merck) in 0.25 or 0.5 mm thickness or Wako Alumina B-10F (Wako). Wakogel C-200 (Wako) was used for column chromatography.

*Reaction of 3β,4β-Epoxyshionane (**15**) with Boron Trifluoride Etherate in Ether.* To a solution of 3β,4β-epoxyshionane (**15**; 384 mg)[5)] in ether (30 ml, distilled from sodium wire) at −30 °C was added boron trifluoride etherate (1.0 ml) with stirring. After 1 h the starting material mostly disappeared and several spots were observed on TLC. The reaction was stopped by addition of 5% methanolic potassium hydroxide (10 ml) kept at the same temperature. The reaction products were extracted with ether twice (each 50 ml) and the organic layer was washed with water (50 ml) and brine, dried over magnesium sulfate, and evaporated to give a colorless oil (384 mg).

The resulting oil was dissolved in petroleum ether–ether (10: 1), absorbed on silica gel (200 g), and eluted with the following solvent system (each fraction 100 ml; Column I): frs. 1—6, petroleum ether–ether (10: 1); frs. 7—12, (5: 1); frs. 13—35, (10: 3).

From frs. 5—8 was obtained dihydrobaccharis oxide (**4**; 42 mg)[2)] after purification by preparative TLC and crystallization from ethyl acetate–methanol, mp 127—128.5 °C (lit, 127—128 °C)[2b)]; IR (KBr) 1000 and 910 cm^{-1}; PMR δ 3.73 (1H, d, $J_{2\beta,3\alpha}$=5 Hz; $C_{(3\alpha)}$–H); mass spectrum *m/e* (relative intensity %) 428 (23; M^+), 413 (73), and 137 (base peak); $[\alpha]_D$ +45 ° (*c* 1.7, chloroform) [lit, +44 ° (*c* 2.30)][2b)]; Found: C, 84.00; H, 12.31%. Calcd for $C_{30}H_{52}O$: C, 84.02; H, 12.23%.

Fr. 9 gave the starting material (**15**; 4 mg).

From frs. 10—12 was obtained a mixture of dihydrobaccharis oxide (**4**) and 4α-fluoroshionan-3β-ol (**17**), which was further separated by preparative TLC to give **17** (35 mg), mp 174—175 °C (crystallized from methanol); IR (KBr) 3450 cm^{-1}; PMR δ 3.70 (1H, quintet, $J_{2\beta,3\alpha}=3$, $J_{2\alpha,3\alpha}=3$, and $J_{3\alpha,F}=6$ Hz; $C_{(3\alpha)}$-H); mass spectrum *m/e* 448 (11; M^+), 433 (8), 428 [18; $(M-HF)^+$], 413 (11), 343 (46), 275 (33), 247 (33), 229 (28), 220 (31), and 95 (base peak); Found: C, 80.29; H, 11.87%. Calcd for $C_{30}H_{53}OF$: C, 80.30; H, 11.90%.

From frs. 13—15 was obtained a mixture of 4α-fluoroshionan-3β-ol (**17**) and D: B-friedo-bacchar-5-en-3β-ol (**18**), which was passed through a short column of silica gel (4 g) impregnated with silver nitrate (20%, 1 g) and eluted with benzene to afford **17** (0.5 mg) and **18** (63 mg), mp 124—125 °C (crystallized from acetone); IR (KBr) 3450, 1630, 1100, 830, and 820 cm^{-1}; PMR δ 3.47 (1H, t-like, $W_{1/2}$ 6 Hz; $C_{(3\alpha)}$-H and 5.62 (1H, m, $C_{(6)}$-H); mass spectrum *m/e* 428 (8; M^+), 413 (10), 410 (5), 395 (8), 276 (39), 261 (base peak), 152 (21), and 134 (79); Found: C, 84.07; H, 12.62%. Calcd for $C_{30}H_{52}O$: C, 84.04; H, 12.23%.

Fractions 16—22 gave a mixture (194 mg) of D: B-friedo-bacchar-5(10)-on-3β-ol (**20**) and D: C-friedo-bacchar-7-en-3β-ol (**21**) containing a small amount of **17** and **18**. This mixture was dissolved in benzene, absorbed on silica gel (34 g) impregnated with silver nitrate (20%, 8 g), and eluted with the same solvent (Column II, each 100 ml). Frs. 1 and 2 gave **17** (4 mg), while **18** (6 mg) was obtained from frs. 13—18. Since frs. 3—12 afforded a mixture of **20** and **21** in a various ratio, these fractions were combined and subjected to separation by HPLC (*vide infra*).

Frs. 23—35 afforded a mixture of **20** and **21**, which was also subjected to HPLC separation (*vide infra*).

Separation of D: B-Friedo-bacchar-5(10)-en-3β-ol (20) and D: C-Friedo-bacchar-7-en-3β-ol (21) by High Performance Liquid Chromatography (HPLC). The above fractions (Column I, frs. 23—35 and Column II, frs. 3—12) were subjected to separation by HPLC to give D: B-friedo-bacchar-5(10)-en-3β-ol (**20**) and D: C-friedo-bacchar-7-en-3β-ol (**21**). Each compound was collected by repeating the procedure to afford **20** (59 mg), mp 142—143 °C (crystallized from acetone) (lit, 141.5—142 °C)[13]; IR (KBr) 3350 cm^{-1}: PMR δ 3.48 (1H, dd, $J_{2\beta,3\alpha}=10$ and $J_{2\alpha,3\alpha}=4$ Hz, $C_{(3\alpha)}$-H); mass spectrum *m/e* 428 (17; M^+) and 135 (base peak), and **21** (59 mg), mp 136.5—137.5 °C (crystallized from petroleum ether); IR (liquid) 3350, 1630, 1035, and 820 cm^{-1}; PMR δ 3.26 (1H, dd, $J_{2\beta,3\alpha}=8$ and $J_{2\alpha,3\alpha}=5$ Hz, $C_{(3\alpha)}$-H) and 5.39 (1H, quartet, $J_{6\beta,7}=3$, $J_{6\alpha,7}=3$, and $J_{7,9\alpha}=3$ Hz, $C_{(7)}$-H); mass spectrum *m/e* 428 (25, M^+), 413 (base peak), 395 (51), 247 (14), 229 (28), and 135 (46); high resolution mass spectrum, Found: 428.4000. Calcd for $C_{30}H_{52}O$: 428.4015. Found: 247.2045. Calcd for $C_{17}H_{27}O$: 247.2060. Found: 229.1928. Calcd for $C_{17}H_{25}$: 229.1954.

Base Treatment of 4α-Fluoroshionan-3β-ol (17). 4α-Fluoroshionan-3β-ol (**17**; 64 mg) was treated with 5% methanolic potassium hydroxide (15 ml) for 21 h under reflux temperature. The reaction mixture was extracted with chloroform followed by the usual work-up to give a residue (62 mg), which was crystallized from acetone to afford 3β,4β-epoxyshionane (**15**; 34 mg) as white needles, mp 152.5—153.5 °C (lit, 154—155 °C)[5]; IR, PMR, and mass spectrum were superimposable with those of an authentic specimen.

D: B-Friedo-bacchara-1(10),5-dien-3β-yl Acetate (19). D: B-Friedo-bacchar-5-en-3β-ol (**18**; 23 mg) was treated with acetic anhydride (1.5 ml) in pyridine (2 ml) at room temperature and was allowed to stand overnight. After usual work-up, the corresponding acetate (24 mg) was obtained. A mixture of this acetate (11 mg) in acetic acid (3 ml) and selenium dioxide (11 mg) in water (0.5 ml) was heated under reflux for 5 h. After the similar work-up according to Ref. 5b, an oil was obtained. The dehydrogenation reaction of the acetate (5 mg) was repeated once more and the resulting oil was combined and passed through a short column of silica gel to afford a residue (16 mg). Purification by preparative TLC and crystallization from methanol gave white crystalline D: B-friedo-bacchara-1(10),5-dien-3β-yl acetate (**19**; 7 mg), mp 123—124 °C (lit, 123—123.5 °C).[5]

Acetylation of D: C-Friedo-bacchar-7-en-3β-ol (21). A solution of D: C-friedo-bacchar-7-en-3β-ol (**21**; 32 mg) in pyridine (2 ml) and acetic anhydride (1 ml) was allowed to stand overnight at room temperature. Methanol was added and the reaction mixture was poured into water and extracted with ether three times. On usual work-up, a colorless gum (**23**; 31 mg) was obtained. IR (liquid) 1730, 1240, 1030, 820, and 760 cm^{-1}; PMR δ 2.04 (3H, s, $-OCOCH_3$), 4.51 (1H, dd, $J_{2\beta,3\alpha}=9$ and $J_{2\alpha,3\alpha}=5$ Hz; $C_{(3\alpha)}$-H), and 5.39 (1H, quartet, $J_{6\beta,7}=3$, $J_{6\alpha,7}=3$, and $J_{7,9\alpha}=3$ Hz; $C_{(7)}$-H); mass spectrum *m/e* 470 (36; M^+), 455 (base peak), 395 (57), 289 (7), and 229 (28); molecular weight (by high resolution mass spectrometry), Found: 470.4121. Calcd for $C_{32}H_{54}O_2$: 470.4121.

Allylic Oxidation of D: C-Friedo-bacchar-7-en-3β-yl Acetate (23). A solution of D: C-friedo-bacchar-7-en-3β-yl acetate (**23**; 19 mg) in benzene (1 ml) was treated with *t*-butyl chromate in benzene [0.1 ml; prepared from *t*-butyl alcohol (24.6 g), chromium trioxide (11.1 g), and benzene (50 ml)] and was allowed to stand overnight at room temperature. Saturated aqueous formic acid solution was added and the reaction mixture was poured into water and extracted with ether three times. On usual work-up, a pale yellow oil was obtained, which was separated by TLC to give D: C-friedo-bacchar-7-en-6-on-3β-yl acetate (**24**; 0.5 mg) and the starting material (**23**; 14 mg). This procedure was repeated twice and the enone-acetate fractions were combined (1.8 mg), and purified by silica gel TLC, alumina TLC, and then by HPLC. D: C-Friedo-bacchar-7-en-6-on-3β-yl acetate (**24**; *ca.* 1.5 mg) was obtained as an oil, IR (liquid) 1730, 1660, 1610, and 1245 cm^{-1}; UV λ_{max}^{EtOH} 248 nm (ε 12000); PMR δ 2.17 (s, $C_{(5\alpha)}$-H) and 5.81 (d, $J_{7,9\alpha}=2.4$ Hz, $C_{(7)}$-H); mass spectrum *m/e* 484 (13; M^+), 469 (4), 424 (23), 409 (17), 302 (43), 277 (9), 243 (9), 217 (25), 196 (50), and 121 (base peak); molecular weight (by high resolution mass spectrometry), Found: 484.3902. Calcd for $C_{32}H_{52}O_3$: 484.3913.

Isomerization of D: C-Friedo-bacchar-7-en-3β-yl Acetate (23). a) Hydrogen chloride was bubbled for 5 min through a solution of D: C-friedo-bacchar-7-en-3β-yl acetate (**23**; 7 mg) in chloroform (3 ml) at 0 °C. The solution was kept for 10 min at the same temperature, poured into water, extracted with chloroform, washed with 10% aqueous sodium carbonate, and brine, and then evaporated. A resulting residue was treated with 5% methanolic potassium hydroxide (10 ml) at 60 °C for 2 h. The reaction mixture was diluted with water and extracted with ether. After usual work-up and purification by preparative TLC, D: C-friedo-bacchar-8-en-3β-ol (**25**; 1.8 mg) was obtained as an oil, which was subjected to examination by HPLC and proved to be pure. IR (liquid) 3400 cm^{-1}; PMR δ 3.28 (1H, m, $C_{(3\alpha)}$-H), no olefinic proton was observed; mass spectrum *m/e* 428 (29; M^+), 413 (base peak), 395 (50), 247 (13), and 229 (40); high resolution mass spectrum, Found: 428.4018. Calcd for $C_{30}H_{52}O$: 428.4015, Found: 247.2056. Calcd for $C_{17}H_{27}O$: 247.2059. Found: 229.1929. Calcd for $C_{17}H_{25}$: 229.1954.

b) To a solution of D: C-friedo-bacchar-7-en-3β-yl acetate (**23**; 1.5 mg) in acetic acid (2 ml) was added concd hydro-

chloric acid (0.2 ml) and the mixture was heated at 60 °C for 19 h. The reaction mixture, after usual treatment, was extracted with ether to give a residue, which was treated with 5% methanolic potassium hydroxide (2 ml) at room temperature overnight. The usual work-up gave an oil, which was subjected to examination by HPLC and was found to be a mixture of the 7-ene (**21**), the 8-ene (**25**), and the 12-ene (**5**)[2b,4] in a ratio of 6: 9: 5.

Reaction of Dihydrobaccharis Oxide (4) with Boron Trifluoride Etherate in Ether and in Benzene. Boron trifluoride etherate (4 drops) was added to a solution of dihydrobaccharis oxide (**4**; 5 mg)[2] in ether (1 ml), and the solution was kept at room temperature for 1 h. The reaction mixture was treated as usual to give a residue. An examination of this residue by HPLC showed that it consisted of the 5-ene (**18**; relative amount ratio 10%), the 5(10)-ene (**20**; 8%), the 7-ene (**21**; 2%), and of the oxide (**4**; 80%).

The small scale reaction of **4** (9 mg) with boron trifluoride etherate (5 drops) in benzene[2b] (2 ml) was effected at room temperature for 10 min. The product was found to be a mixture of the 12-ene (**5**; relative amount ratio 10%), **18** (10%), **20** (10%), **21** (10%), and the 8-ene (**25**; 20%), by HPLC examination.

The authors wish to thank Dr. Torger Bruun, Norges Teckniske Hφgskole, Trondheim, Norway, for a generous gift of an authentic sample of baccharis oxide. The authors also wish to thank Dr. Nobuo Nakamura, Dr. Hidehiro Ishizuka, and Dr. Kazuyuki Aizawa for the measurements of PMR (FT), PMR (100 MHz), and high resolution mass spectra, respectively.

References

1) Preliminary accounts of this paper: K. Tachibana and T. Takahashi, *Tetrahedron Lett.*, **1975**, 1857; M. Tori, K. Tachibana, Y. Moriyama, T. Tsuyuki, and T. Takahashi, *Chem. Lett.*, **1976**, 1359.

2) a) F. Mo, T. Anthonsen, and T. Bruun, *Acta Chem. Scand.*, **26**, 1287 (1972); b) T. Anthonsen, T. Bruun, E. Hemmer, D. Holme, A. Lamvik, E. Sunde, and N. A. Sφrensen, *ibid.*, **24**, 2479 (1970).

3) a) Y. Moriyama, Y. Tanahashi, T. Takahashi, and G. Ourisson, *Bull. Soc. Chim. Fr.*, **1968**, 2890; T. Tsuyuki, T. Hoshino, M. Ito, and T. Takahashi, *ibid.*, **1968**, 2895. And references cited therein; b) M. Takahashi, W. Kamisako, S. Ishimasa, and K. Miyamura, *Yakugaku Zasshi*, **79**, 1281 (1959); W. Kamisako and M. Takahashi, *ibid.*, **84**, 318 (1964); c) Y. Tanahashi, T. Takahashi, F. Patil, and G. Ourisson, *Bull. Soc. Chim. Fr.*, **1964**, 584.

4) E. Suokas and T. Hase, *Acta Chem. Scand.*, **25**, 2359 (1971).

5) S. Yamada, S. Yamada, K. Tachibana, Y. Moriyama, Y. Tanahashi, T. Tsuyuki, and T. Takahashi, *Bull. Chem. Soc. Jpn.*, **49**, 1134 (1976). And references cited therein.

6) T. Torii, K. Tachibana, S. Yamada, T. Tsuyuki, and T. Takahashi, *Tetrahedron Lett.*, **1975**, 2283; M. Tori, T. Torii, K. Tachibana, S. Yamada, T. Tsuyuki, and T. Takahashi, *Bull. Chem. Soc. Jpn.*, **50**, 469 (1977).

7) a) J. D. White, J. Fayos, and J. Clardy, *J. Chem. Soc., Chem. Commun.*, **1973**, 357; b) G. H. Constantine, Jr. and J. H. Block, *Phytochemistry*, **9**, 1659 (1970); c) J. H. Block and G. H. Constantine, Jr., *ibid.*, **11**, 3279 (1972). And references cited therein.

8) M. S. Hadley and T. G. Halsall, *J. Chem. Soc., Perkin Trans. 1*, **1974**, 1334.

9) *E.g.*, D. N. Kirk and M. P. Hartshorn, "Steroid Reaction Mechanism," Elsevier Publishing Company, Amsterdam (1968), pp. 290, 353; P. de Mayo, "Molecular Rearrangements," Vol. 2, John Wiley & Sons, Inc., New York (1964), p. 821; D. N. Kirk and P. M. Shaw, *Chem. Commun.*, **1971**, 948.

10) *E.g.*, J. Bascoul, B. Cocton, and A. Crastes de Paulet, *Tetrahedron Lett.*, **1969**, 2401; J. Bascoul, E. Noyer, and A. Crastes de Paulet, *Bull. Soc. Chim. Fr.*, **1972**, 2744; J. C. Jacquesy, J. Levisalles, and J. Wagnon, *ibid.*, **1970**, 670.

11) *E.g.*, L. H. Knox, J. A. Zderic, J. P. Ruelas, C. Djerassi, and H. J. Ringold, *J. Am. Chem. Soc.*, **82**, 1230 (1960); J. M. Coxon, M. P. Hartshorn, and D. N. Kirk, *Tetrahedron*, **20**, 2547 (1964); J. W. Blunt, M. P. Hartshorn, and D. N. Kirk, *ibid.*, **21**, 559 (1965); J. M. Coxon, M. P. Hartshorn, and D. N. Kirk, *ibid.*, **21**, 2489 (1965); J. R. Bull, *Tetrahedron Lett.*, **1968**, 5959; P. A. Diassi and J. Fried, U. S. P. 3 364 204 (1964), *Chem. Abstr.*, **69**, 27638a (1968).

12) In the mass spectrum of the 5-ene (**13**), a peak at *m/e* 274 due to a retro-Diels-Alder fragmentation was observed as a base peak.

13) K. Tachibana, S. Yamada, S. Yamada, T. Tsuyuki, and T. Takahashi, *Bull. Chem. Soc. Jpn.*, **48**, 3425 (1975).

14) L. F. Fieser and M. Fieser, "Steroids," Reinhold, New York (1959), p. 352; J. W. Clark-Lewis and I. Dainis, *Aust. J. Chem.*, **20**, 1961 (1967); M. Tada, T. Takahashi, and H. Koyama, *Phytochemistry*, **13**, 670 (1974).

15) H. Budzikiewicz, J. M. Wilson, and C. Djerassi, *J. Am. Chem. Soc.*, **85**, 3688 (1963).

16) K. Fujita, *Nippon Kagaku Zasshi*, **78**, 1112 (1957).

17) A proton at C-7 of 3β-acetoxybauer-7-en-6-one resonated at δ 5.72 as a doublet ($J_{7,9\alpha}$=3 Hz), while the corresponding proton ($C_{(7)}$-H) of 3β-acetoxy-9βH-bauer-7-en-6-one at δ 5.57 as a singlet: M. Fukuoka and S. Natori, *Chem. Pharm. Bull.*, **20**, 974 (1972). This provided support for the 9αH configuration of **24** (and of **21**).

18) *Cf.*, A. Eschenmoser, L. Ruzicka, O. Jeger, and D. Arigoni, *Helv. Chim. Acta*, **38**, 1890 (1955).

19) R. E. Ireland, C. A. Lipinski, C. J. Kowalski, J. W. Tilley, and D. M. Walba, *J. Am. Chem. Soc.*, **96**, 3333 (1974); R. E. Ireland, M. I. Dawson, C. J. Kowalski, C. A. Lipinski, D. R. Marshall, J. W. Tilley, J. Bordner, and B. L. Trus, *J. Org. Chem.*, **40**, 973 (1975); R. E. Ireland, C. J. Kowalski, J. W. Tilley, and D. M. Walba, *ibid.*, **40**, 990 (1975).

Reactions of a Variety of Diazoalkanes with *o*-Sulfobenzoic Anhydride

Takumi OSHIMA and Toshikazu NAGAI

Institute of Chemistry, College of General Education, Osaka University, Toyonaka, Osaka 560

(Received December 13, 1976)

It was found that a number of diazoalkanes (I) bearing a relatively small substituent reacted with *o*-sulfobenzoic anhydride (II) in acetonitrile at an ordinary temperature to give the *o*-(substituted glycoloyl)benzenesulfonic acid sultones (IV), which correspond formally to the products from the insertion into the C–O bond of II by the carbenes, while diaryldiazomethanes underwent decomposition under the same conditions to produce the corresponding tetraarylethylenes (V) instead of the inserted products (IV). The olefin formation reaction was very fast compared to the sultone formation and was considered to be the result of the acid-catalyzed decomposition caused by the contaminant *o*-sulfobenzoic acid (III) which was derived from II. The kinetics and the mechanism of these reactions were discussed on the basis of the nature of diazoalkanes.

It is well known that diazoalkanes(I) undergo decomposition in the presence of protic acids,[1] a variety of metalic halides,[2] or other Lewis acids[3]—*e.g.*, $ZnCl_2$, Hg_2Cl_2, and BF_3—involving intermediate diazonium ions or carbenoids. However, the decomposition of I under the influence of an organic Lewis acid has not been widely investigated.[4] During our recent study of a mixed sulfonic carboxylic anhydride such as *o*-sulfobenzoic anhydride(II), we found that II can act as an electron acceptor toward tertiary amines, thus giving rise to their radical cations.[5] This Lewis acid behavior of II led us to investigate the decomposition of diazoalkanes using it. We now wish to report that *o*-sulfobenzoic anhydride(II) reacts under ordinary conditions with a variety of diazoalkanes(I) to afford the keto sultones(IV), and that, in the case of diaryldiazomethanes, a trace amount of contaminant *o*-sulfobenzoic acid(III) rather than II preferentially causes the acid-catalyzed decomposition to yield the olefins(V).

Results and Discussion

The reactions of a variety of diazoalkanes(I) with II in dry acetonitrile gave the keto sultones(IV) or the tetraarylethylenes(V) depending on the nature of I (Scheme 1 and Table 1).

As may be seen in Table 1, the diazoalkanes (I-1—5) which bear a relatively small substituent, R_1, such as H or CH_3, gave the keto sultones(IV), while when the R_1 and R_2 substituents were both aryl rings (I-6—9), the olefins(V) were isolated instead of the keto sultones

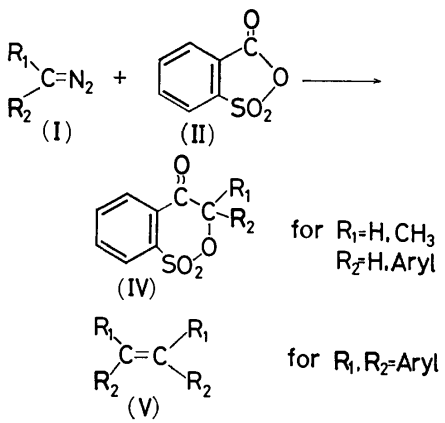

Scheme 1.

Table 1. Product distributions from the reactions of a number of diazoalkanes(I) with *o*-sulfobenzoic anhydride(II) in acetonitrile at room temperature[a]

	R_1	R_2	Products (Yield[b])	
I-1	H	H	IV-1 (74)	—
I-2	H	C_6H_5	IV-2 (71)	—
I-3	H	*p*-$C_6H_4CH_3$	IV-3 (81)	—
I-4	H	*p*-C_6H_4Cl	IV-4 (95)	—
I-5	CH_3	C_6H_5	IV-5 (67)	—
I-6	C_6H_5	C_6H_5	—	V-6 (96)
I-7	C_6H_5	*p*-$C_6H_4CH_3$	—	V-7 (97)
I-8	*p*-$C_6H_4OCH_3$	*p*-$C_6H_4OCH_3$	—	V-8 (≈100)
I-9	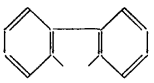		—	V-9 (75)

a) Reaction time: 1 h. b) The yield is in mol% based on the I used.

In the course of these reactions it was noticed that the disappearance of diazo-color and the evolution of nitrogen gas occurred very much more rapidly and vigorously in the case of the diaryldiazomethanes (I-6—9) than in the case of the monoaryldiazomethanes (I-2—5). The marked difference in the product distributions and the reaction velocities suggests that these reactions proceed by way of a different mechanism between the monoaryldiazomethanes and the diaryldiazomethanes.

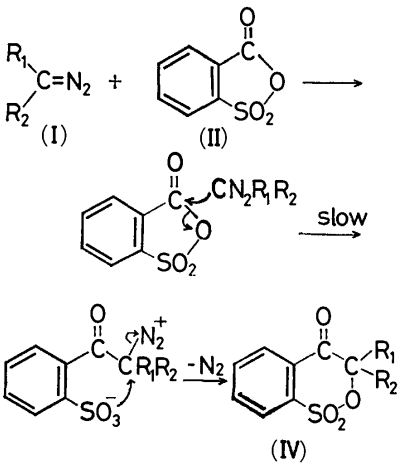

Scheme 2.

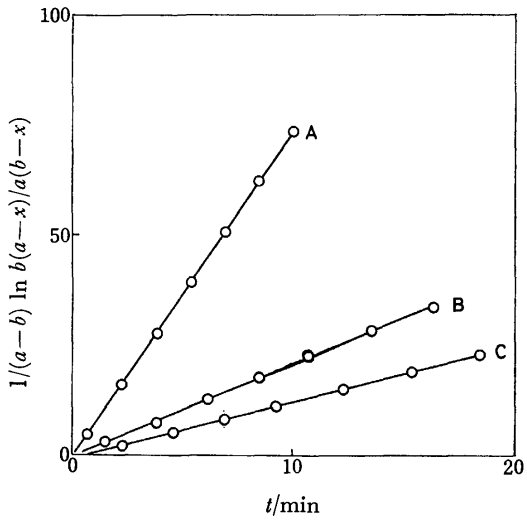

Fig. 1. Second-order kinetic behavior in the reactions of aryldiazomethanes with *o*-sulfobenzoic anhydride (II) in acetonitrile at 23 °C; a plot of the integrated form $[1/(a-b)\ \ln b(a-x)/a(b-x)]$ against time, where a and b are the initial concentrations of II and I respectively, x being the concentration of product IV.
A: *p*-Tolyldiazomethane (I-3); 2.71×10^{-2} M, II; 8.43×10^{-2} M, B: phenyldiazomethane (I-2); 2.54×10^{-2} M, II; 9.50×10^{-2} M, C: *p*-chlorophenyldiazomethane (I-4); 2.21×10^{-2} M, II; 9.00×10^{-2} M.

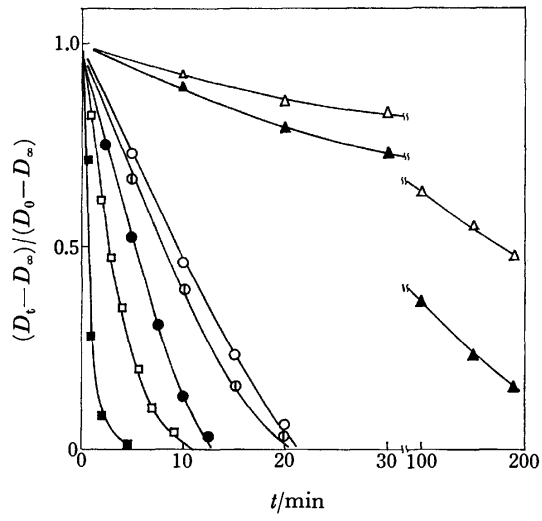

Fig. 2. Decay curves for aryl- and diaryldiazomethanes under the influence of *o*-sulfobenzoic anhydride (II) or *o*-sulfobenzoic acid (III) in acetonitrile. D_0 is the initial optical density, D_t and D_∞ being the values when the reaction time is t and when the reaction was complete respectively.
△: Phenyldiazomethane (I-2); 2.44×10^{-2} M, III; 1.15×10^{-3} M, 23 °C, ▲: *p*-tolyldiazomethane (I-3); 3.38×10^{-2} M, III; 1.15×10^{-3} M, 21 °C, ○: diphenyldiazomethane (I-6); 1.01×10^{-2} M, II; 2.10×10^{-4} M, 20 °C, ●: I-6; 1.01×10^{-2} M, III; 9.7×10^{-5} M, 20 °C, □: *p*-tolylphenyldiazomethane (I-7); 8.34×10^{-3} M, II; 2.10×10^{-4} M, 20 °C, ■: I-7; 8.34×10^{-3} M, III; 9.7×10^{-5} M, 20 °C, ⦶: I-6; 1.01×10^{-2} M, II; 2.1×10^{-4} M,* 20 °C.
* *o*-Sulfobenzoic anhydride solution used here is identical to that used in the case of marked ○ but has been stood for 1 day in glass stoppered flask.

The kinetic measurements of these reactions provided some information about the mechanism. Keto sultone formation reactions obeyed a clean second order, as is shown in Fig. 1, suggesting a rate-determining nucleophilic attack of diazoalkanes at the carbonyl position of II (Scheme 2). This is also supported by the tendency for the rate constants to increase with the electron-donating ability of the aryl substituents of these monoaryldiazomethanes: $k=1.25$ (1 mol^{-1} min^{-1}) (*p*-Cl), $k=2.48$ (*p*-H), and $k=6.85$ (*p*-CH_3). Taking into account the fact that II is a good acylating reagent,[6] it is reasonable to account for this insertion reaction in terms of the nucleophilic attack of the diazo-carbon at the carbonyl position of II.

On the other hand, as Fig. 2 shows, the olefin-formation reactions progressed quickly even in the presence of a catalytic amount of II. Here, it is noteworthy that I-7, bearing an electron-donating *p*-substituent (CH_3), decomposes much faster than I-6. In addition, the IR spectra of equimolar I and II in acetonitrile showed no change in the two characteristic carbonyl absorptions at 1818 and 1836 cm^{-1} of II after the reactions. These facts imply that the decomposition of diaryldiazomethanes does not consume II and that it proceeds through a catalytic mechanism.

Considering that II invariably contains a trace amount of free acid,[7,8] *o*-sulfobenzoic acid (III), it seems possible that this free acid induces the decomposition of diazoalkanes. The quantitative formation of the tetraarylethylenes in our present reaction is well consistent with that in the acid-catalyzed decompositions of diaryldiazomethanes in aprotic solvents with such strong acids as *p*-toluenesulfonic acid.[1b,9,10,11] Keeping this in mind, we examined the decompositions of I by III, which had been prepared independently, and compared the decompositions with those by II (Fig. 2).

As for the reaction leading to V, the kinetic order by authentic III was very similar to that by II: the kinetic order was close to zero up to the final stage of the reaction, in analogy with that of the *p*-toluenesulfonic acid-catalyzed decomposition of diaryldiazomethanes in dry acetonitrile.[12] Furthermore, a rate acceleration was observed when we employed a solution of II which had been stored for one day (Fig. 2). This phenomenon is due to the partial transformation of II to III by the action of atmospheric moisture, as was confirmed by the UV spectra of II, as may be seen in Fig. 3. When the measurement was done one day later, the intensity in the UV spectrum of II (Curve b) decreased at $\lambda_{max}=286.5$ nm and had new absorption maxima at 237 and 278.5 nm instead of at 239 and 279 nm, with two isosbestic points at 254 and 284 nm. Therefore, it is apparent that the decomposition of diaryldiazomethanes was induced by the trace amount of III instead of by II.

As is well known, the acid-catalyzed reaction of diaryldiazomethanes, involving a rate-determining proton transfer and obeying a pseudo-first order, proceeds by way of intermediate diazonium ions[1b,9,10,11] (or carbonium ions derived from them). Bethell and Callister[11] studied the decomposition of diphenyl-

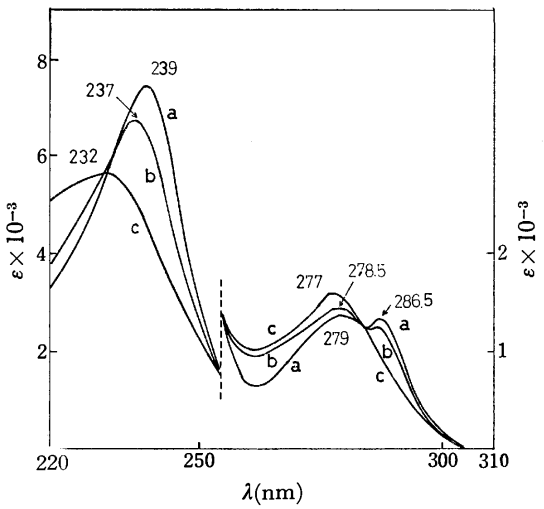

Fig. 3. UV spectra of II under the various conditions. a: Measured immediately after preparation, b: measured after 1 day, c: measured after hydrolysis.

diazomethane in dry acetonitrile with perchloric acid, which is fully ionized in this solvent,[13] and found the kinetic order to be pseudo-first, as is formulated in Scheme 3:

$$Ph_2CN_2 \xrightarrow[k_1]{H^+ \text{ slow}} Ph_2CHN_2^+ \xrightarrow{-N_2}$$

$$Ph_2CH^+ \xrightarrow[k_2]{Ph_2CN_2} Ph_2C{=}CPh_2 + N_2 + H^+$$

Kinetic equation:

$$\frac{-d[Ph_2CN_2]}{dt} = 2k_1[H^+][Ph_2CN_2] = k_1'[Ph_2CN_2]$$

Scheme 3.

However, at the same time they found that the kinetic order changes to zero when perchloric acid is replaced by *p*-toluenesulfonic acid, which reacts in an undissociated form in dry acetonitrile.[12] As to this zero order decomposition, they thought that the diphenyldiazomethane reacts first to form the benzhydryltoluenesulfonate intermediate, which subsequently undergoes a slow solvolysis to form tetraphenylethylene, as is formulated in Scheme 4:

$$Ph_2CN_2 + HOTs \underset{k_{-3}}{\overset{k_3}{\rightleftharpoons}} [Ph_2CHN_2^+ \ ^-OTs \longrightarrow$$

$$Ph_2CHOTs] \xrightarrow[k_4 \text{ slow}]{} Ph_2CH^+ + {}^-OTs \xrightarrow{Ph_2CN_2}$$

$$Ph_2C{=}CPh_2 + HOTs + N_2$$

Kinetic equation:

$$\text{if } (k_3/k_{-3})[Ph_2CN_2] \gg 1, \quad \frac{-d[Ph_2CN_2]}{dt} = k_4[HOTs]_{st}$$

$[HOTs]_{st}$: the stoicheiometric acid concentration

Scheme 4.

In the present system, *o*-sulfobenzoic acid (III) has both carboxyl and sulfo groups, and its behavior toward diazoalkanes can be regarded as being comparable to *p*-toluenesulfonic acid because the two acids similarly bring about a quantitative olefin formation under zero order kinetics.

The decompositions of monoaryldiazomethanes by the action of III were quite slow compared with those of diaryldiazomethanes, even in the presence of about a ten-fold concentration of III (Fig. 2). This marked change in the decomposition rate between the monoaryldiazomethanes and the diaryl ones may be attributed to the differences in the stabilities of the intermediate sulfonates. The sulfonates derived from diaryldiazomethanes seem to be much more subject to solvolysis than the corresponding sulfonates from monoaryldiazomethanes.

Consequently, it is concluded that, in the cases of diazomethane and monoaryldiazomethanes, the insertion reaction is preferential because these diazoalkanes have an effective nucleophilicity toward II; even if the reaction could occur with a trace amount of III, it would essentially stop at the stage of the sulfonate formation because of its stability against solvolysis. On the other hand, in the cases of diaryldiazomethanes, the lesser nucleophilicity of the diazo-carbon atom toward II resulting from the conjugation with the two aromatic rings as well as the steric effects and the readier solvolysis of the sulfonates make the acid-catalyzed decomposition predominant. From these observations, the present decomposition reactions are formulated as follows (Scheme 5):

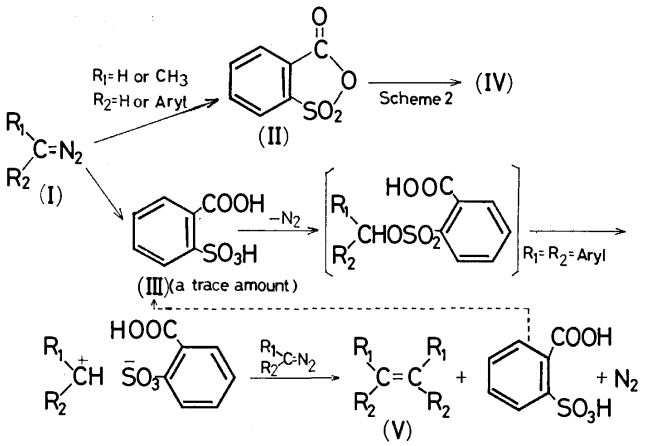

Scheme 5.

Experimental

The NMR spectra were obtained with a Varian EM-360 (60 MHz) instrument, with tetramethylsilane as the internal standard. The IR spectra were recorded on a Hitachi 215 Grating Infrared Spectrophotometer; a 0.1 mm NaCl cell was used for the measurement in solution. The UV spectra were taken with a Union SM-401 spectrophotometer.

Materials. The acetonitrile was purified by careful distillation from phosphorus pentoxide through a 10-in helix-packed column. The middle fractions were collected and stored in a glass-stoppered flask. The *o*-sulfobenzoic anhydride (II) was prepared by the method of Clarke and Dreger,[14] and recrystd from benzene; mp 126—127 °C, (lit,[14] 126—127 °C); IR (in CH_3CN): 1836 and 1818 (C=O), 1206, 996, 810 cm^{-1}. The anhyd *o*-sulfobenzoic acid (III) was given on the hydrolysis of II and was dried *in vacuo* above 105 °C; mp 140—141 °C; IR (Nujol): 3500—2500 (COOH

and SO_3H), 1720 (C=O), 1160 and 1020 cm^{-1} (SO_2). Because of moisture-sensitive substances, the anhydride and the acid, placed in a bottle fitted with a sealing cap, were stored in a desiccator, with silica gel as the desiccant. The diazomethane was prepared by the procedure in the literature,[15] and its ethereal solution was dried over potassium hydroxide. The monoaryldiazomethanes and diaryldiazomethanes were synthesized by the methods of Closs and Moss[16] and Smith and Howard[17] respectively. $\lambda_{max}(\varepsilon)$ in CH_3CN: 488 nm (25) for phenyldiazomethane (I-2), 495 (25) for *p*-tolyldiazomethane (I-3), 484 (32) for *p*-chlorophenyldiazomethane (I-4), 525 (95) for diphenyldiazomethane (I-6); these values are essentially identical with those in the literature.[11,16]

p-Tolylphenyldiazomethane (I-7); mp 51—53 °C, reddish purple needles (from petroleum ether), (lit,[18] 53—55 °C), $\lambda_{max}(\varepsilon)$ in CH_3CN: 530 nm (98). Bis(*p*-methoxyphenyl)-diazomethane (I-8); mp 99 °C (dec), purple needles (from ether), (lit,[11] 99—100 °C (dec)). 9-Diazofluorene (I-9); mp 94—95 °C (from EtOH), (lit,[19] 94—95 °C). Because of the unstability of the diazo compounds, they were prepared just before use for the aryldiazomethanes and were purified before use by recrystallization for the diaryldiazomethanes.

Kinetic Measurements. The temperature during the measurements was not especially controlled, but its change was within ±0.5 °C. As a rule, solutions of I, II, and III were made up separately just before use. The change in the optical density at the wavelength of the absorption maximum of I in the visible region was followed spectrophotometrically. The second order rate constants, k, were determined graphically from the plots of $1/(a-b)\ln b(a-x)/a(b-x)$ against the time.

General Procedure. To a three-necked flask (100 ml) equipped with a dropping funnel, a thermometer, and a drying tube of calcium chloride, we added II (5 m mol) in dry acetonitrile (25 ml), and then I (5 m mol) in dry acetonitrile (25 ml) was stirred in over a 10-min period. Stirring was then continued for 50 min. In the case of diazomethane, its excess in an ether solution dried over potassium hydroxide was dropped in. The addition of I caused the evolution of nitrogen gas. The removal of the solvent *in vacuo* gave oily reaction mixtures in the cases of I-1—5 or solid ones in the cases of I-6—9. The same procedure was used for the *o*-sulfobenzoic acid-catalyzed decomposition of diaryldiazomethanes (I-6—8) by employing a catalytic amount of III instead of II. These catalytic decompositions also gave almost quantitative olefins for I-6—8. These reaction mixtures were submitted to chromatography, using silica gel as the adsorbent. Elution with a petroleum ether–ether gave the olefins (V), while elution with chloroform gave the keto sultones (IV). The olefins, V-6, 8, were identified by comparison with authentic specimens,[11] while the V-7 and V-9 were confirmed by elemental analyses: V-7; Found: C, 93.11; H, 6.79%. Calcd for $C_{28}H_{24}$: C, 93.29; H, 6.71%. V-9; Found: C, 94.74; H, 5.11%. Calcd for $C_{26}H_{16}$: C, 95.09; H, 4.91%. 1,2-Di-*p*-tolyl-1,2-diphenylethylene (V-7) showed two kinds of methyl signals to the same extent, centered at δ 2.2 and due to the *cis* and *trans* isomers. The structures of the keto sultones (IV-1—5) were determined by means of elemental analyses and by measurements of the IR, NMR, and Mass spectra.

o-*Glycoloylbenzenesulfonic Acid Sultone (IV-1)*: Mp 93—94 °C, colorless needles (from CH_3OH), (lit,[20] 93—94 °C). IR (Nujol): 1700 (C=O), 1367 and 1195 cm^{-1} (SO_2). MS: m/e=198 (M^+). NMR (δ, $CDCl_3$): 7.7—8.2 (m, 4H), 5.25 (s, 2H). Found: C, 48.27; H, 3.17%. Calcd for $C_8H_6O_4S$: C, 48.49; H, 3.05%.

o-*(Phenylglycoloyl)benzenesulfonic Acid Sultone (IV-2)*: Mp 54—55 °C, colorless needles (from CH_3OH). IR (Nujol): 1703 (C=O), 1370 and 1195 cm^{-1} (SO_2). MS: m/e=274 (M^+). NMR (δ, $CDCl_3$): 7.67—8.17 (m, 4H), 7.40 (s, 5H), 6.38 (s, 1H). Found: C, 61.22; H, 3.77%. Calcd for $C_{14}H_{10}O_4S$: C, 61.32; H, 3.68%.

o-*(Tolylglycoloyl)benzenesulfonic Acid Sultone (IV-3)*: Mp 123—124 °C, pale yellow needles (from CH_3OH). IR (Nujol): 1700 (C=O), 1365 and 1195 cm^{-1} (SO_2). MS: m/e=288 (M^+). NMR (δ, $CDCl_3$): 7.67—8.17 (m, 4H), 7.25 (s, 4H), 6.37 (s, 1H), 2.37 (s, 3H). Found: C, 62.52; H, 4.23%. Calcd for $C_{15}H_{12}O_4S$: C, 62.50; H, 4.20%.

o-*(p-Chlorophenylglycoloyl)benzenesulfonic Acid Sultone (IV-4)*: Mp 89—90 °C, colorless needles (from CH_3OH). IR (Nujol): 1705 (C=O), 1360 and 1195 cm^{-1} (SO_2). MS: m/e=308, 310 (3:1) (M^+). NMR (δ, $CDCl_3$): 7.73—8.33 (m, 4H), 7.40 (s, 4H), 6.40 (s, 1H). Found: C, 54.21; H, 3.35%. Calcd for $C_{14}H_9O_4SCl$: C, 54.40; H, 3.01%.

o-*(Methylphenylglycoloyl)benzenesulfonic Acid Sultone (IV-5)*: Mp 80—81 °C. Colorless needles (from CH_3OH). IR (Nujol): 1700 (C=O), 1365 and 1194 cm^{-1} (SO_2). MS: m/e=288 (M^+). NMR (δ, $CDCl_3$): 7.67—8.07 (m, 4H), 7.27—7.57 (m, 5H), 2.28 (s, 3H). Found: C, 62.41; H, 4.59%. Calcd for $C_{15}H_{12}O_4S$: C, 62.50; H, 4.20%.

References

1) a) R. A. More O'Ferrall, "The Reactions of Aliphatic Diazocompounds with Acids," in "Advances in Physical Organic Chemistry," ed by V. Gold, Academic Press, Vol. 5, London (1967), p. 331; b) D. Bethell and R. D. Howard, *J. Chem. Soc., B*, **1968**, 430; c) N. B. Chapman, D. J. Newman, J. Shorter, and H. M. Wall, *J. Chem. Soc., Perkin Trans. 2*, **1976**, 847.

2) a) D. Bethell and K. C. Brown, *J. Chem. Soc., Perkin Trans. 2*, **1972**, 895; b) R. G. Salomon and J. K. Kochi, *J. Am. Chem. Soc.*, **95**, 3300 (1973); c) D. S. Crumrine, T. J. Haberkamp, and D. J. Suther, *J. Org. Chem.*, **40**, 2274 (1975).

3) J. K. Chakrabarti, S. S. Szinai, and A. Todd, *J. Chem. Soc., C*, **1970**, 1303.

4) Recently, J. E. Franz *et al.* have reported the decomposition of diazoalkanes in the presence of tetracyanoethylene. J. E. Franz, R. K. Howe, and H. K. Pearl, *J. Org. Chem.*, **41**, 620 (1976).

5) T. Nagai, T. Shingaki, and H. Yamada, *Bull. Chem. Soc. Jpn.*, **50**, 248 (1977).

6) V. Iyer and N. K. Mathur, *Anal. Chim. Acta*, **33**, 554 (1965).

7) S. Siggia and N. A. Floramo, *Anal. Chem.*, **25**, 797 (1953).

8) V. Iyer and N. K. Mathur, *Talanta*, **13**, 1592 (1966).

9) J. D. Roberts and W. Watanabe, *J. Am. Chem. Soc.*, **72**, 4869 (1950).

10) J. D. Roberts, W. Watanabe, and R. E. McMahon, *J. Am. Chem. Soc.*, **73**, 760 (1951).

11) D. Bethell and J. D. Callister, *J. Chem. Soc.*, **1963**, 3801.

12) D. Bethell and J. D. Callister, *J. Chem. Soc.*, **1963**, 3808.

13) I. M. Kolthoff, S. Bruckenstein, and M. K. Chantooni, *J. Am. Chem. Soc.*, **83**, 3927 (1961).

14) H. T. Clarke and E. E. Dreger, *Org. Synth.*, Coll. Vol. I, p. 495.

15) F. Arndt, *Org. Synth.*, Coll. Vol. II, p. 165.

16) G. L. Closs and R. A. Moss, *J. Am. Chem. Soc.*, **86**, 4042 (1964).

17) L. I. Smith and K. L. Howard, *Org. Synth.*, Coll. Vol. III, p. 351.

18) H. Staudinger and J. Goldstein, *Ber.*, **49**, 1923 (1916).

19) H. Staudinger and O. Kupfer, *Ber.*, **44**, 2207 (1911).

20) A. L. Crowther and G. Holt, *J. Chem. Soc.*, **1963**, 2926.

Photochemistry of 1,2-Diphenylcyclobutene in Protic Solvents. Addition of Alcohols, Acetic Acid, and Water

Masako SAKURAGI, Hirochika SAKURAGI,* and Masaki HASEGAWA

Research Institute for Polymers and Textiles, 4 Sawatari, Kanagawa-ku, Yokohama 221

**Department of Chemistry, Faculty of Science, The University of Tokyo, Hongo, Bunkyo-ku, Tokyo 113*

(Received December 14, 1976)

Irradiation of 1,2-diphenylcyclobutene (**1**) in methanol affords the methyl ethers, 1,2-diphenyl-1-methoxycyclobutane (**2a**) and 1-(α-methoxybenzyl)-1-phenylcyclopropane (**3a**). In acetic acid and in a mixture of water and dioxane, the corresponding esters (**2b** and **3b**) and alcohols (**2c** and **3c**) are formed, respectively. Evidence supporting the involvement of a singlet species was obtained upon finding that the fluorescence of **1** is substantially quenched upon the addition of methanol or acetic acid to a solution of **1** in hexane.

One of the simplest organic chromophores is the carbon-carbon double bond. However, its photochemical behavior is not at all simple. This chromophore undergoes, on direct or sensitized irradiation, *cis-trans* isomerization, cycloaddition, reduction, and the addition of protic solvents depending on the nature of the double bond, the solvent, and the sensitizer.[1] Even for the photochemical behavior of cyclic olefins in protic solvents, no consistent explanation has been given. The behavior of six- and seven-membered cycloalkenes are the best documented and most studied.[2] Direct or sensitized irradiation of cyclohexenes and cycloheptenes in an (acidic) alcoholic solution affords ethers arising from the addition of the alcohol to the double bond.[2] In these cases, the orthogonal excited triplet olefin or a highly-strained ground state of *trans*-olefin is considered to be the reactive species.[2]

Eight-membered cycloalkenes, which easily isomerize through the triplet state upon irradiation, also undergo this polar addition, but less efficiently.[2b,2d,2j,3] Polar addition disappears on going to smaller ring sizes. Cyclopentenes undergo reduction of the double bond, but do not undergo the addition of protic solvents.[2d,2e,2j] However, bicyclic olefins containing a five-membered ring, such as 2-phenylbicyclo[2.2.1]hept-2-ene and its 1,7,7-trimethyl derivative, have been reported to undergo polar addition of methanol under illumination.[4] The reaction products are apparently similar to those from cyclohexenes, cycloheptenes, and cyclooctenes, but the reaction course is unequivocally different because the bicyclic olefins fail to transform to the orthogonal triplet states or to the *trans*-configurations. The polar addition of the bicyclic olefins as well as styrene derivatives has been interpreted in terms of a reactive singlet excited state displaying a charge-transfer character.[4]

In a previous communication,[5] the first example of the photochemical ionic addition to the rigid cyclobutene system was reported and evidence supporting the involvement of a singlet excited species in the addition was presented by showing that the irradiation of 1,2-diphenylcyclobutene (**1**) in methanol and acetic acid affords polar addition products, methyl ethers and acetates and that the fluorescence of **1** is quenched substantially by methanol. In the present paper, the details of these results will be described.

Results and Discussion

A solution of 1,2-diphenylcyclobutene (**1**, 5×10^{-5} M) in methanol, ethanol, acetic acid, or in a mixture of water and dioxane was irradiated with 330 nm light. The bands of **1** at 227 and 297 nm decreased in intensity during the irradiation. A typical example is shown for methanol in Fig. 1. Three isosbestic points maintained

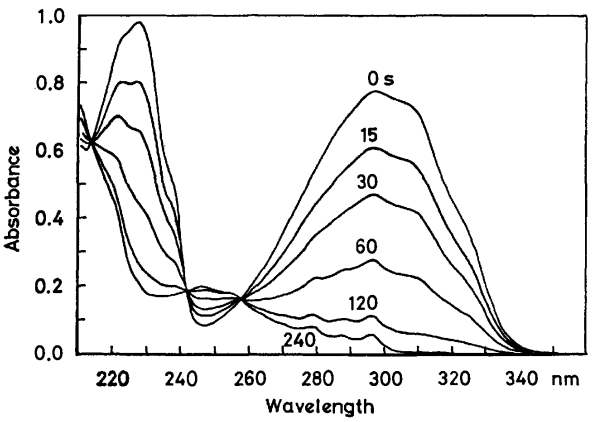

Fig. 1. Spectral change of a solution of 1,2-diphenylcyclobutene (**1**) in methanol (4×10^{-5} M) during irradiation with 330 nm light.

their positions during the reaction, suggesting that this reaction is straightforward. In order to obtain the reaction products, **1** in methanol (7×10^{-3} M) was irradiated by a 500 W xenon lamp through a filter (Corning glass filter 0—54, nominally wavelengths longer than 300 nm). The reaction mixture was separated by column chromatography on silica gel into two components in addition to the recovered starting material. One component was a colorless liquid which was identified as 1-(α-methoxybenzyl)-1-phenylcyclopropane (**3a**) by the presence in the NMR spectrum of a four-proton multiplet at δ 0.65—1.15 which is characteristic of methylene protons attached to a cyclopropane ring and by elemental analysis (*cf.* Experimental). The other component was a white crystalline solid which was characterized as 1,2-diphenyl-1-methoxycyclobutane (**2a**) from the spectral data and elemental analysis (*cf.* Experimental). Gas chromatographic analysis and the NMR spectrum show that **2a** consists of only one isomer.

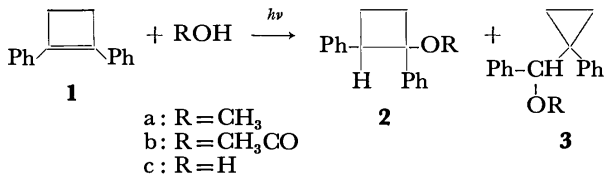

Similar irradiation of **1** in acetic acid afforded 1,2-diphenylcyclobutyl acetate (**2b**) and α-(1-phenylcyclopropyl)benzyl acetate (**3b**). Their structures were established from spectral data and elemental analysis (*cf.* Experimental). Compound **2b** was also found to consist of one isomer from gas chromatographic analysis and NMR data. The addition products, **2a** and **2b**, as well as *N,N*-disubstituted 1,2-diphenylcyclobutanamines, the adducts of **1** with *s*-amines, displayed a multiplet due to a methine proton at the same region (δ 3.7—4.2) as did *cis*-1,2-diphenylcyclobutane, while *trans*-1,2-diphenylcyclobutane exhibited a multiplet at a somewhat higher field (δ 3.2—3.6).[6] Taking into account the small effect of the β-substituents on the chemical shift of a methine proton,[7] **2a** and **2b** can safely be assigned to the *cis*-configuration. The results are summarized in Table 1.

Table 1. Products from the irradiation of 1,2-diphenylcyclobutene (**1**) in polar solvents

Solvent	Irradiation time (h)	Product yield (%)[a]	
		2	**3**
MeOH	18	25	43
AcOH	100	50	17
H_2O[b]	80	12	44
D_2O[b]	90	16	34

a) The yield based on the amount of **1** reacting.
b) In dioxane.

α,1-Diphenylcyclopropanemethanol (**3c**) and 1,2-diphenylcyclobutanol (**2c**)[8] were similarly obtained upon irradiation of **1** in a mixture of water and dioxane (1 : 4 by volume), as is summarized in Table 1. These products, **2c** and **3c**, were characterized by their spectral data and by comparing the spectral data of their acetates with those of **2b** and **3b**.

The possibility that **2** and **3** could have arisen non-photochemically from **1** was eliminated by leaving solutions of **1** in methanol, acetic acid, and water–dioxane in the dark for 3 days.

The formation of **3**, as well as **2**, from **1** suggests that these products arise from an initial photoprotonation of **1** with the formation of a cyclobutyl cation, which in turn undergoes three competing reactions: a) nucleophilic capture by the solvent to afford **2**, b) skeletal rearrangement to a cyclopropylmethyl cation, with subsequent capture by the solvent affording **3**, and c) deprotonation which regenerates the starting olefin **1**.

Although a protonated bicyclobutane has been proposed as an intermediate in the deamination of cyclobutanamine and cyclopropylmethanamine producing the same mixture of cyclobutanol and cyclopropanemethanol in each case,[9] there is no need to postulate a nonclassical cation in this photochemical process, and the product ratio is attributable to kinetic control in the nucleophilic capture by the solvent. This assumption

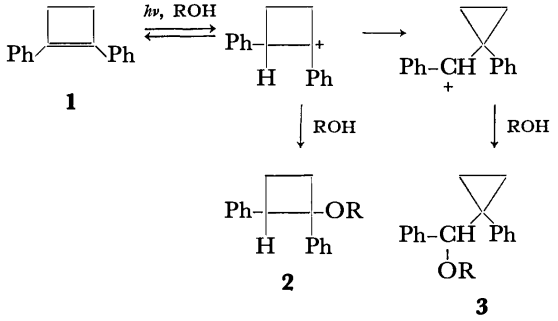

is consistent with the sole formation of the *cis*-cyclobutane derivatives since the nucleophile would preferentially attack the 1,2-diphenylcyclobutyl cation from the less hindered side. The behavior of the diphenylcyclobutyl cation upon rearrangement to the cyclopropylmethyl cation is in remarkable contrast to that of the 1-phenylcyclobutyl cation, which shows no tendency to rearrange in superacid solutions.[10] For the photoreaction of 2,3-diphenyl-1,3-butadiene in methanol, Baldry[11] has isolated **2a** and **3a** together with **1** and other products, and postulated a mechanism for the ether formation involving a bicyclobutane intermediate.[12] However, the possibility that **2a** and **3a** arise from the photoprotonation of primarily formed **1** can not be ruled out completely in view of the photolability of **1**.

Table 2. Kinetic data for the photoprotonation of 1,2-diphenylcyclobutene (**1**) in hexane[a]

Quencher	$k_q\tau_0$ (M^{-1})		k_d/k_r
	From fluorescence quenching experiment	From quantum-yield measurement	
EtOH	0.36	0.41	12
AcOH	0.38	0.40	9

a) Conducted under aerated conditions.

In order to gain more insight into the mechanism for the polar addition, a labeling study using deuterated water as the additive was undertaken. 1,2-Diphenylcyclobutene (**1**) was irradiated in a mixture of deuterated water and dioxane (1 : 4 by volume), and the products were isolated in a manner similar to that described above. The deuteration position for each product was determined by comparing its NMR spectrum with that of the non-deuterated product; 1,2-diphenylcyclobutanol (**2c-d**) undergoes deuteration at the 2-position and α,1-diphenylcyclopropanemethanol (**3c-d**) at the α-position. These results confirm the assumption that the addition proceeds from the initial photoprotonation of the cyclobutene (**1**).

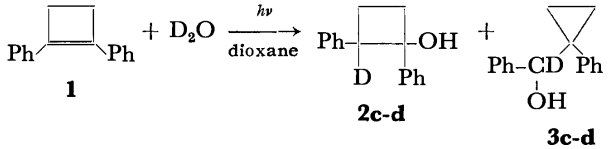

Since the quantum yield for fluorescence of **1** is

reported to be almost as high as unity in a diluted solution,[13] photoprotonation is assumed to proceed from the excited singlet state of **1**. Evidence supporting the involvement of a singlet species was obtained from the finding that the fluorescence of **1** is substantially quenched upon the addition of methanol, ethanol, and acetic acid to the solution of **1** in hexane. Plots of the reciprocals of the relative fluorescence intensities against the quencher concentrations are linear and can be fitted to the Stern-Volmer equation,

$$I_0/I = 1 + k_q\tau_0[Q],$$

where I_0 and I denote the intensities of the fluorescence of **1** in the absence of and in the presence of the quencher, respectively, in the concentration [Q], k_q is the rate constant of the bimolecular quenching process, and τ_0 denotes the average lifetime of the excited singlet state of **1** in the absence of the quencher. The quenching constants, $k_q\tau_0$, obtained from the slopes of these plots are 0.42, 0.36, and 0.38 M^{-1} for methanol, ethanol, and acetic acid, respectively. The singlet lifetime of **1** (τ_0) has been reported to be shorter than 5 ns,[13] and thus the k_q values are estimated to be larger than 8×10^7 M^{-1} s^{-1}, and are probably about 10^8 M^{-1} s^{-1}, suggesting that the excited singlet state of **1** interacts with the ground state of the alcohols and acetic acid.

The quantum yield of the photochemical polar addition of ethanol and acetic acid to **1** was determined under aerated conditions in hexane by monitoring the decrease of **1** upon irradiation with 330 ± 7 nm light. A linear relationship is found between the reciprocal of the quantum yield (Φ) for the decrease of **1** and the reciprocal of the concentration of the additive. The intercepts and the slopes were estimated to be 13 and 32 for ethanol, and 10 and 25 for acetic acid, respectively.

The simplest mechanism which accounts for all the above results can be written as follows,

$$\mathbf{1} + h\nu \longrightarrow \mathbf{1}^*$$

$$\mathbf{1}^* \xrightarrow{k_f} \mathbf{1} + h\nu'$$

$$\mathbf{1}^* + O_2 \xrightarrow{k_0} \mathbf{1} + O_2$$

$$\mathbf{1}^* + HOR \xrightarrow{k_q} [\mathbf{1}\cdots HOR]^*$$

$$[\mathbf{1}\cdots HOR]^* \xrightarrow{k_d} \mathbf{1} + HOR$$

$$[\mathbf{1}\cdots HOR]^* \xrightarrow{k_r} [\mathbf{1}\text{–}H^+ + {}^-OR] \longrightarrow \text{products},$$

where **1*** denotes the excited singlet state of **1**. At infinite dilution under degassed conditions, the quantum yield for the fluorescence of **1** is unity,[13] and therefore, intersystem crossing to the triplet state can be neglected. By making the usual steady-state assumption, the quantum yield for the decrease of **1** is written as follows;

$$1/\Phi = (1+k_d/k_r)(1+1/k_q\tau_0[Q]).$$

The k_d/k_r values, *i.e.*, the ratio of rates for the decay process and the protonation in the interaction of excited **1** and the polar solvent, can be estimated to be 12 for ethanol and 9 for acetic acid, and the $k_q\tau_0$ values were found to be 0.41 M^{-1} for ethanol and 0.40 M^{-1} for acetic acid. These values are in good agreement with those obtained in the fluorescence quenching experiments: 0.36 M^{-1} for ethanol and 0.38 M^{-1} for acetic acid. These results substantiate the above mechanism.

When 1-phenylcyclobutene was irradiated in methanol no addition products resulted. This, combined with the results for 1,2-diphenylcyclobutene, suggests that substituents on the cyclobutene ring play important roles in the reactivity of cyclobutenes. These substituent effects upon the reactivity will be discussed in a future publication. 1,2-Diphenylcyclopentene was also irradiated in methanol giving no polar addition products but a phenanthrene derivative, the formation of which was so efficient that it was observed in the course of the fluorescence measurement.

The only previously observed ring system for photoprotonation from the excited singlet state is the case of 2-phenylbicyclo[2.2.1]hept-2-ene derivatives,[4] and thus 1,2-diphenylcyclobutene is the first example for a four-membered cycloalkene. For three-membered cycloalkenes, 1,2-diphenyl-3,3-dimethylcyclopropene has been reported to give open-ring products, 1,2-diphenyl-1-methoxy-3-methyl-2-butene and *cis*-1,2-diphenyl-3-methoxy-3-methyl-2-butene, upon irradiation in methanol, through a carbene intermediate arising from the excited singlet state with subsequent capture by methanol.[14] It is interesting that the cyclobutene system has almost the same strain energy as the bicyclo[2.2.1]hept-2-ene system, the cyclopropene system having a much higher energy.[15]

Recently, the reactive intermediate in the photoprotonation of 1-phenylcyclohexene was shown to be *trans*-phenylcyclohexene, which must be very twisted, by more than 90°.[16] This is assumed to be the case for the phenylcycloheptene photoprotonation. These *trans*-cycloalkenes are singlet in nature and possess a partial singlet diradical character if the twist is not completed to 180°.[16] This may be common to the excited singlet states of highly-strained cycloalkenes, such as the phenylbicyclo[2.2.1]heptenes and diphenylcyclobutene. Thus, protonation in the highly-strained *cis*-cycloalkenes, as well as in the highly-twisted *trans*-cycloalkenes, would be effected by the simultaneous release of strain in those intermediates.

Experimental

The IR and UV spectra were recorded on a Hitachi EPI-G3 grating infrared spectrophotometer and a Hitachi EPS-3 recording spectrophotometer, respectively. The NMR spectra were recorded on a JEOL C-60HL spectrometer. GLPC analysis was performed on a Hitachi 163 gas chromatograph equipped with a flame ionization detector.

Materials. 1,2-Diphenylcyclobutene,[17] 1-phenylcyclobutene,[18] and 1,2-diphenylcyclopentene[19] were prepared according to reported methods. Solvents were purified by distillation.

Irradiation of 1,2-Diphenylcyclobutene (1) in Methanol. A solution of **1** (300 mg) in methanol (200 ml) was irradiated in a nitrogen atmosphere for 18 h using a 500-W xenon lamp and a Corning 0—54 filter. This procedure was repeated six times. The reaction mixtures were combined, and the solvent was removed by rotary evaporation. The residue was subjected to chromatography on silica gel using hexane–benzene eluants affording a colorless liquid (540 mg), a white crystalline solid (310 mg), and the starting olefin (720 mg).

The colorless liquid was identified to be 1-(α-methoxybenzyl)-1-phenylcyclopropane (**3a**) from the spectral data and elemental analysis. Bp *ca.* 270 °C. IR (liquid film) 1090 cm^{-1}. NMR δ 0.65—1.15 (m, 4H, cyclopropyl CH_2-CH_2), 3.22 (s, 3H, OCH_3), 4.02 (s, 1H, methine H), 6.8—7.4 (m, 10H, aromatic H). Found: C, 85.47; H, 7.44%. Calcd for $C_{17}H_{18}O$: C, 85.67; H, 7.61%.

The white solid was deduced to be 1,2-diphenyl-1-methoxycyclobutane (**2a**) from the spectral data and elemental analysis. The GLPC analysis and NMR data showed that **2a** consists of only one isomer. Mp 91.5—92.0 °C (from petroleum ether). IR (KBr) 1080 cm^{-1}. NMR ($CDCl_3$) δ 1.7—2.3 (m, 4H, CH_2CH_2), 2.93 (s, 3H, OCH_3), 3.7—4.1 (m, 1H, methine H), 6.6—7.3 (m, 10H, aromatic H). Found: C, 86.09; H, 7.54%. Calcd for $C_{17}H_{18}O$: C, 85.67; H, 7.61%.

Irradiation of 1,2-Diphenylcyclobutene (1) in Acetic Acid. A solution of **1** (2.0 g) in acetic acid (200 ml) was similarly irradiated for 100 h using a 500-W xenon lamp. The solvent was removed by rotary evaporation, and the residue was subjected to chromatography on silica gel with hexane-benzene eluants resulting in three components: the first white solid (640 mg) was found to be the starting olefin, and the second colorless liquid (300 mg) was identified as α-(1-phenylcyclopropyl)benzyl acetate (**3b**) from spectral data and elemental analysis. Bp *ca.* 300 °C. IR (liquid film) 1740, 1240 cm^{-1}. NMR (CCl_4) δ 0.6—1.4 (m, 4H, cyclopropyl CH_2CH_2), 1.95 (s, 3H, $OCOCH_3$), 5.40 (s, 1H, methine H), 6.6—7.2 (m, 10H, aromatic H). Found: C, 81.17; H, 6.74%. Calcd for $C_{18}H_{18}O$: C, 81.17; H, 6.81%.

The third colorless liquid (870 mg) was characterized as 1,2-diphenylcyclobutyl acetate (**2b**) from spectral data and elemental analysis. The GLPC analysis and NMR data showed that **2b** consists of only one isomer. Bp *ca.* 235 °C. IR (liquid film) 1745, 1240 cm^{-1}. NMR (CCl_4) δ 1.90 (s, 3H, $OCOCH_3$), 1.7—3.35 (m, 4H, CH_2CH_2), 3.7—4.1 (m, 1H, methine H), 6.4—7.2 (m, 10H, aromatic H). Found: C, 81.01; H, 6.90%. Calcd for $C_{18}H_{18}O$: C, 81.17; H, 6.81%.

Irradiation of 1,2-Diphenylcyclobutene (1) in a Mixture of Water and Dioxane. A solution of **1** (300 mg) in a mixture of water (40 ml) and dioxane (160 ml) was similarly irradiated by a 500-W xenon lamp for 80 h. This procedure was repeated twice. The reaction mixtures were combined, and the solvent was removed by rotary evaporation. The residue was subjected to chromatography on silica gel. The products obtained were diphenylacetylene[20] (20 mg), α,1-diphenylcyclopropanemethanol (**3c**, 235 mg), 1,2-diphenylcyclobutanol (**2c**, 65 mg), and 1,2-dibenzoylethane[21] (40 mg). The starting olefin (10 mg) was recovered. **3c** and **2c** were identified upon esterification with acetic anhydride to the corresponding acetates, **3b** and **2b**, respectively.

α,1-Diphenylcyclopropanemethanol (**3c**). NMR (CD_3COCD_3) δ 0.6—1.4 (m, 4H, cyclopropyl CH_2CH_2), 4.45 (s, 1H, OH, exchanged with D_2O), 4.75 (s, 1H, methine H), 7.2—7.7 (m, 10H, aromatic H).

1,2-Diphenylcyclobutanol (**2c**).[8] NMR (CD_3COCD_3) δ 2.0—3.0 (m, 4H, CH_2CH_2), 3.9—4.4 (m, 1H, methine H), 5.15 (s, 1H, OH, exchanged with D_2O), 6.9—7.9 (m, 10H, aromatic H).

Irradiation of 1,2-Diphenylcyclobutene (1) in a Mixture of Deuterated Water and Dioxane. The irradiation of **1** (500 mg) in a mixture of deuterated water (40 ml) and dioxane (160 ml) was performed under otherwise similar conditions. Deuterated products, α,1-diphenylcyclopropanemethanol-α-*d* (**3c-d**, 140 mg) and 1,2-diphenylcyclobutanol-2-*d* (**2c-d**, 70 mg), were isolated in a similar manner together with 1,2,5,6-tetraphenyltricyclo[4.2.0.$0^{2,5}$]octane[13,20] (35 mg), 1,2,5,6-tetraphenylcycloocta-1,5-diene[13,20] (10 mg), and the recovered starting olefin (120 mg). The position of deuteration in the products, **2c-d** and **3c-d**, was determined by comparing their NMR spectra with those for non-deuterated products, **2c** and **3c**, respectively.

Quenching of the Fluorescence of 1,2-Diphenylcyclobutene (1). The fluorescence of **1** (4×10^{-4} M) in hexane containing various concentrations of alcohols or acetic acid (0—0.8 M) was determined using a Hitachi MPF-2A fluorescence spectrophotometer.

Quantum-yield Measurements. The exciting light for the quantum-yield measurements was furnished by a JASCO CRM-FA spectroirradiator. Hexane solutions of **1** (10^{-3} M) and ethanol or acetic acid (0—1 M) were irradiarted with 330 ± 7 nm light for 3 min. The reaction mixture was diluted twenty times with the same solvent and its UV spectrum was measured. The light intensity was measured by potassium ferrioxalate actinometry.

References

1) See for example, K. J. Crowley and P. M. Mazzocchi, in "The Chemistry of Alkenes," Vol. 2, ed by J. Zabicky, Interscience Publishers, London (1970), p. 267; T. Matsuura, "Organic Photochemistry," Kagakudojin, Kyoto (1970), p. 83.

2) a) J. A. Marshall, *Acc. Chem. Res.*, **2**, 33 (1969), and references cited therein; b) P. J. Kropp, *J. Am. Chem. Soc.*, **91**, 5783 (1969); c) S. Fujita, T. Nomi, and H. Nozaki, *Tetrahedron Lett.*, **1969**, 3557; d) M. Tada and H. Shinozaki, *Bull. Chem. Soc. Jpn.*, **43**, 1270 (1970); e) P. J. Kropp, *Pure Appl. Chem.*, **24**, 585 (1970); f) M. Kawanisi and H. Kato, *Tetrahedron Lett.*, **1970**, 721; g) T. Okada, K. Shibata, M. Kawanisi, and H. Nozaki, *ibid.*, **1970**, 859; h) M. P. Servé and A. W. Bryant, *ibid.*, **1972**, 2663; i) H. M. Rosenberg and M. P. Servé, *J. Org. Chem.*, **37**, 141 (1972); j) P. J. Kropp, E. J. Reardon, Jr., Z. L. F. Gaibel, K. F. Williard, and J. H. Hattaway, Jr., *J. Am. Chem. Soc.*, **95**, 7058 (1973).

3) H. Kato and M. Kawanisi, *Tetrahedron Lett.*, **1970**, 865.

4) P. J. Kropp, *J. Am. Chem. Soc.*, **95**, 4611 (1973).

5) M. Sakuragi and M. Hasegawa, *Chem. Lett.*, **1974**, 29.

6) M. Sakuragi and H. Sakuragi, *Bull. Chem. Soc. Jpn.*, in press.

7) L. M. Jackman and S. Sternhell, "Applications of Nuclear Magnetic Resonance Spectroscopy in Organic Chemistry," 2nd ed, Pergamon Press, London (1969), p. 159; S. L. Murov, "Handbook of Photochemistry," Marcel Dekker, Inc., New York, N. Y. (1973), p. 179.

8) R. B. LaCount and C. E. Griffin, *Tetrahedron Lett.*, **1965**, 1549.

9) T. H. Lowry and K. S. Richardson, "Mechanism and Theory in Organic Chemistry," Harper and Row, Publishers, Inc., New York, N. Y. (1976), p. 293.

10) G. A. Olah, C. L. Jeuell, D. P. Kelly, and R. D. Porter, *J. Am. Chem. Soc.*, **94**, 146 (1972).

11) P. J. Baldry, *J. Chem. Soc., Perkin Trans. 1*, **1975**, 1913.

12) W. G. Dauben, J. H. Smith, and J. Saltiel, *J. Org. Chem.*, **34**, 261 (1969); K. B. Wiberg and G. Szeimies, *J. Am. Chem. Soc.*, **92**, 571 (1970).

13) C. D. DeBoer and R. H. Schlessinger, *J. Am. Chem. Soc.*, **90**, 803 (1968).

14) J. A. Pincock, R. Morchat, and D. R. Arnold, *J. Am. Chem. Soc.*, **95**, 7536 (1973).

15) The strain energies of 1,2-dimethylcyclopropene (47.0 kcal/mol), 1,2-dimethylcyclobutene (25.3), and bicyclo[2.2.1]-hept-2-ene (22.8) are reported: R. B. Turner, P. Goebel,

B. J. Mallon, W. von E. Doering, J. F. Coburn, Jr., and M. Pomerantz, *J. Am. Chem. Soc.*, **90**, 4315 (1968).
16) R. Bonneau, J. Joussot-Dubien, L. Salem, and A. J. Yarwood, *J. Am. Chem. Soc.*, **98**, 4329 (1976).
17) R. M. Dodson and A. G. Zielske, *J. Org. Chem.*, **32**, 28 (1967).
18) F. Gerson, G. Moshuk, and M. Schwyzer, *Helv. Chim. Acta*, **54**, 361 (1971).
19) R. Criegee, A. Kerckow, and H. Zinke, *Chem. Ber.*, **88**, 1878 (1955).
20) E. H. White and J. P. Anhalt, *Tetrahedron Lett.*, **1965**, 3937.
21) A. G. Schultz and R. H. Schlessinger, *Tetrahedron Lett.*, **1970**, 2731.

The Highly Selective Sulfonylation of Cycloheptaamylose and Syntheses of Its Pure Amino Derivatives

Kenji TSUJIHARA, Hironori KURITA, and Mitsutaka KAWAZU

Organic Chemistry Research Laboratory, Tanabe Seiyaku Co., Ltd., Toda Saitama 335

(Received December 14, 1976)

Mesitylenesulfonyl chloride reacted selectively with primary hydroxyl groups of cycloheptaamylose to give hexakis(6-*O*-mesitylsulfonyl)cycloheptaamylose (II) and heptakis(mesitylsulfonyl)cycloheptaamylose (I). The selectivity of mesitylenesulfonyl chloride in the preferential sulfonylation is 24 times larger than that of tosyl chloride. Pure hexakis(6-azido-6-deoxy)cycloheptaamylose (III) and hexakis(6-amino-6-deoxy)cycloheptaamylose (IV) were synthesized from II. Pure heptakis(6-amino-6-deoxy)cycloheptaamylose (VII) and mixture of positional isomers of hexakis(6-amino-6-deoxy)mesitylsulfonylcycloheptaamylose (VIII)* were obtained by the catalytic hydrogenation of the corresponding azido compounds V and VI,* which were themselves given by the reaction of I with sodium azide. These amino derivatives, IV, VII, and VIII,* showed significant antimicrobial activities against such gram-negative bacteria as Escherichia, Shigella, and Pseudomonas. These compounds also exhibited hypocholesterolemic effects in the chick when added in the diet for two weeks, probably through sequestration of intestinal bile acids.

Cycloamyloses have attracted increased interest in recent years[1] because of their ability to include a compound into their cavity utilizing hydrophobic interaction in an aqueous solution. In this respect, a variety of cycloamylose derivatives have been prepared as models of enzymes.[2] Therefore, the pure sulfonylesters of cycloamylose have been required as important key intermediates.

Lautsch and his co-workers[3] were the first to attempt the selective modification of one position in each D-glucose residue. They attempted to prepare heptakis(6-*O*-tosyl) and heptakis(6-*O*-mesyl)cycloheptaamyloses by using one molar equivalent of the corresponding sulfonyl chlorides per D-glucose residue.

Recently, Cramer and his co-workers[4] studied in detail the specific modification of each D-glucose residue of cycloamyloses at a primary carbon atom and claimed that hexakis- and heptakis(6-*O*-tosyl)cyclohexa and cycloheptaamyloses were obtained by the reaction of a 50% excess of tosyl chloride and the corresponding cycloamyloses.

Using this method with a 50% excess of tosyl cloride, Umezawa and Tatsuta[5] reported that the product was a mixture of tosylated cyclohexaamyloses and that pure hexakis(6-*O*-tosyl)cyclohexaamylose was obtained after purification on a silica gel column.

However, it is still uncertain whether tosylation occurred exclusively at the primary hydroxyl groups in all the residues as claimed by these workers, because the tosylation of monosaccharides, such as α-D-glucose[6] and methyl α-D-glucopyranoside,[7] and polysaccharides, such as amylose[8] and cellulose,[9] under similar conditions has been reported to cause further tosylation at some secondary hydroxyl groups. The tosyl esters in which all the tosyloxyl groups are attached to primary carbon atoms are obtained only by purification in the case of monosaccharides, while such tosyl esters can not be obtained in the case of polysaccharides. Thus, a functional modification of cycloamyloses has been prevented by difficulties in purifying the products and it has been practically impossible to obtain the pure products by the usual methods.

Pure sulfonylesters of cycloamyloses must have definitive numbers and established positions of sulfonyloxyl groups such as all at the C-2, C-3, or C-6 positions.

Both the number and the position of sulfonyloxyl groups are equivocal in Cramer's work, in which the term "hexakis" or "heptakis" represents only the average number of the tosyl groups of a complex mixture of the products. In Umezawa's work the number is evident upon the separation of the products, but the position has not been established. It seems most likely that they obtained a mixture of the positional isomers of hexakis(tosyl)cyclohexaamyloses, as we have clarified in the present work that the heptasulfonyl ester of cycloheptaamylose with a single spot in its thin-layer chromatography was found to be still a mixture of the positional isomers.

It seems almost impossible to obtain the pure sulfonyl esters without utilizing more highly selective sulfonylating agents than tosyl chloride or mesyl chloride.

Meanwhile, the use of mesitylenesulfonyl chloride (MstCl) as a selective sulfonylating agent has been reported. Palmer and his co-workers[10] reported that MstCl was a preferable sulfonylating agent in the case of secondary and tertiary hydroxyl groups of a steroid system. Furthermore, Creasey and Guthrie[11] found that MstCl reacted more selectively with one hydroxyl group of a vicinal secondary diol of α-D-glucopyranoside than did tosyl chloride, though Johnson *et al.*[12] showed in their aldosterone synthesis that the use of MstCl offered no significant advantage over the use of tosyl chloride for the selective esterification of a primary hydroxyl group in the presence of a secondary one.

In this paper we wish to report a highly selective sulfonylation of the primary hydroxyl groups of cycloheptaamylose using MstCl and describe the synthesis of some pure derivatives of cycloheptaamylose.

Results and Discussion

The selective esterification was carried out by adding a 20% excess of MstCl to a solution of cycloheptaamylose in dry pyridine at 0—5 °C and by then allowing the mixture to stand at room temperature for 3 days. The product was obtained as a white powder, and its

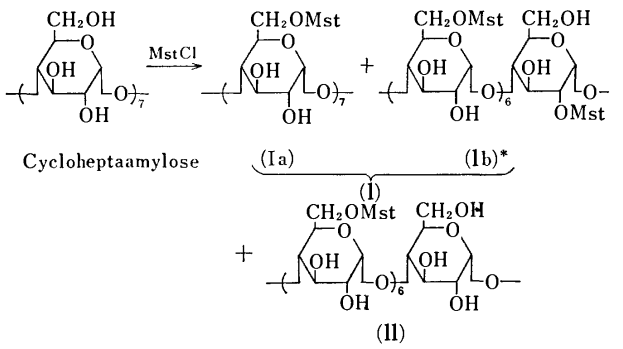

I: A mixture of Ia and Ib*.
Mst: 2,4,6-trimethylbenzenesulfonyl.
* This represents one of many kinds of possible positional isomers with regard to one secondary sulfonyl group.

thin-layer chromatography (TLC) gave only three spots (R_f; 0.79, 0.41, 0.02).

Compound Ib*, with an R_f value of 0.79, was separated on silica gel column and was established to be heptakis(mesitylsulfonyl)cycloheptaamylose by analyzing the sulfur content, while the one(II) with an R_f value of 0.41 was determined to be hexakis(mesitylsulfonyl)cycloheptaamylose in the same manner. A small amount of the compound with an R_f value of 0.02 may be pentakis(mesitylsulfonyl)cycloheptaamylose, though it was not further examined. The reaction of compound II with sodium azide in DMF at 80—85 °C, instead of at the 135 °C previously reported,[5] for 7 h led to the complete replacement of all the mesitylsulfonyloxyl groups by the azido groups.

The IR absorption bands at 1600, 1350, 1190, and 1170 cm^{-1} due to the mesitylsulfonyloxyl group disappeared completely, while the one at 2100 cm^{-1} due to the azido group appeared. The azido compound obtained in this way was determined to be pure hexakis(6-azido-6-deoxy)cycloheptaamylose (III) with satisfactory physical properties. This indicates that II contains sulfonyloxyl groups only at the primary carbon atoms and none at the secondary ones, since a sulfonyloxyl group attached to a secondary carbon atom can hardly be replaced by an azido group under these reaction conditions.[13] Therefore, II must be pure hexakis(6-*O*-mesitylsulfonyl)-cycloheptaamylose.

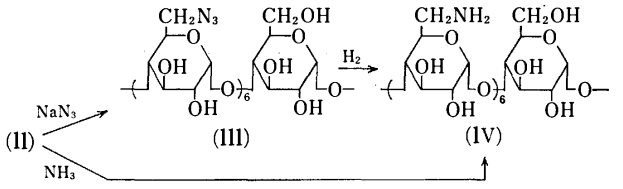

The catalytic hydrogenation of III gave pure hexakis-(6-amino-6-deoxy)cycloheptaamylose (IV) as a hexahydrochloride with satisfactory physical properties. IV was also obtained directly by the reaction of II with ammonia in methanol.

On the other hand, Ib* gave an azido compound (VI)* upon heating with sodium azide in DMF at 85—90 °C for 7 h. The product VI*, whose TLC gave almost a single spot (R_f=0.37), had the IR absorption bands due to the mesitylsulfonyloxyl group together with the band due to the azido group and gave a satisfactory analysis for a mixture of the positional isomers of hexakis(6-azido-6-deoxy)mesitylsulfonylcycloheptaamylose, in which the mesitylsulfonyl group is considered to bind with one among the fourteen secondary hydroxyl groups. Thus, Ib* was determined to be the positional isomers of hexakis(6-*O*-mesitylsulfonyl)-mesitylsulfonylcycloheptaamylose, in which six sulfonyl groups are attached to six primary hydroxyl groups, while one is attached to one among the fourteen secondary hydroxyl groups.

Meanwhile, Compound I, with the same R_f value as that of Ib*, was also obtained by washing the crude sulfonylation product with an appropriate solvent (see Experimental section). The azido compound obtained from I in the manner described above gave two spots in its TLC (R_f=0.01, 0.37); each component was separated on treatment with an appropriate solvent. The compound with an R_f value of 0.37 proved to be identical with the VI* previously obtained from Ib*. On the contrary, Compound V, with an R_f value of 0.01, had the IR absorption bands at 2100 cm^{-1} due to the azido group, with no sulfonate band, and had seven azido groups, as evidenced by its elemental analysis. Therefore, V was determined to be pure heptakis(6-azido-6-deoxy)cycloheptaamylose. Thus, from these results, I, with the same R_f value as that of Ib*, was found to be a mixture of heptakis(6-*O*-mesitylsulfonyl)cycloheptaamylose (Ia) and Ib*. The latter had previously been obtained by the separation of the crude sulfonylation product by column chromatography. These results suggest that Ia, with its highly crowded and strained structure, may be easily hydrolyzed to the more stable II during separation on a silica gel column. Actually, the sulfonyl esters of cycloheptaamylose were not stable, and their TLC figures were changed almost completely when methanol solutions of the esters were allowed to stand at room temperature for two weeks.

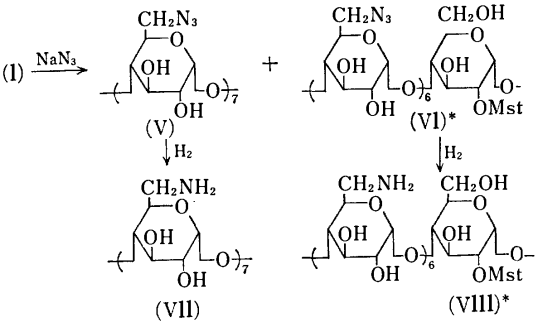

The catalytic hydrogenation of V and VI* gave hydrochlorides of heptakis(6-amino-6-deoxy)cycloheptaamylose (VII) and positional isomers of hexakis (6-amino-6-deoxy) mesitylsulfonylcycloheptaamylose (VIII)* respectively.

The more highly selective sulfonylation of cycloheptaamylose with MstCl than with TsCl was clearly revealed by plotting the average number of the sulfonyloxyl groups against the reaction time. In dry pyridine,

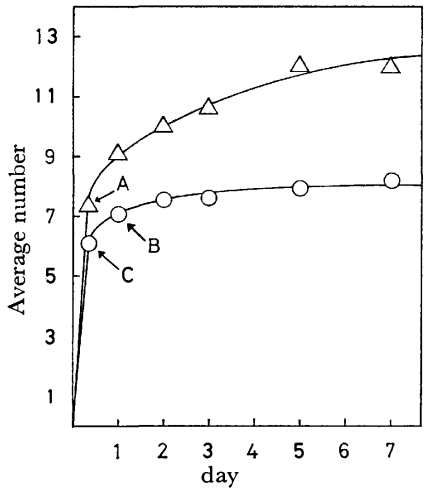

Fig. 1. Relation between average numbers of entered sulfonyloxyl groups and reaction time.
○: MstCl, △: TsCl.
[Numbers of primary, and secondary RSO_3; A: 6.2, 1.1; B: 6.6, 0.5; C: 6.1, 0].

cycloheptaamylose was esterified by the use of 4 eq-moles of the corresponding sulfonyl chlorides for the D-glucose residue at 15 °C.

The average number of the sulfonyloxyl groups introduced was determined by analyzing the sulfur content of the products which has been obtained from an aliquot of the reaction mixture. Furthermore, the positions of the sulfonyloxyl groups were determined by the transformation of the samples (A, B, and C) to azido compounds by the usual method. The number of the sulfonyloxyl groups remaining after this treatment should correspond to the number of the secondary sulfonyloxyl groups. The results are shown in Fig. 1. These data indicate that the preparation of pure heptakis(6-*O*-tosyl)cycloheptaamylose is almost impossible, while that of Ia or II is possible. As can be seen from the figure, both the sulfonylating reagents react with the six hydroxyl groups of cycloheptaamylose at a similar rate. After the six primary hydroxyl groups are esterified, however, subsequent sulfonylation becomes very slow in the case of MstCl, while TsCl reacts rapidly until eight hydroxyl groups are esterified. After 7 days, MstCl had reacted with eight hydroxyl groups, probably corresponding to seven primary and one secondary groups, while TsCl esterifies twelve hydroxyl groups, which may consist of seven primary and five secondary groups. This result indicates that bulky MstCl reacts less readily with a secondary hydroxyl group than does TsCl. It takes 5 h for TsCl and 120 h for MstCl to increase the sulfonylation number from six to eight; the latter process may involve one or two secondary hydroxyl groups. In conclusion, the selectivity of MstCl in the preferential sulfonylation of the primary hydroxyl groups is 24 times larger than that of TsCl. The surprisingly large selectivity may be due to the doughnut-shaped structure[14] of cycloheptaamylose, where the primary hydroxyl groups are located apart from the side of the torus, while the secondary hydroxyls are located directly on the other side of the torus.

Preliminary Biological Tests

It has been found that the amino compounds, IV, VII, and VIII*, showed significant antimicrobial activities, as tested by the two-fold dilution method in a heart-infusion agar medium, though it was earlier reported[5] that hexakis(6-amino-6-deoxy)cyclohexaamylose inhibited the growth of Bacillus subtilis PCI 219 at the concentration of 2000 μg/ml. These amino derivatives inhibited the growth of Staphylococcus aureus at concentrations of 25—100 μg/ml, of Escherichia coli at 12.5—50 μg/ml, of Shigella flexneri and sonnei at 1.56—100 μg/ml, and of Pseudomonas aeruginosa at 6.25—50 μg/ml.

It is also noteworthy that some of these compounds exhibited hypocholesterolemic activities, which were tested by feeding groups of 10 male one-day old chicks with a diet containing 0.2% cholesterol and a 1% test compound for two weeks, and by then determining the serum cholesterol using the method of Zak *et al.*,[15] with blood samples obtained through heart puncture. In this method, a mixture of IV and VII depressed the cholesterol level by 10—15% in comparison with the control groups. The details of the results will be reported elsewhere.

Experimental

All the melting points are uncorrected. The solutions were concentrated under reduced pressure at a bath temperature not exceeding 50 °C. The IR spectra were taken in Nujol mull on a Hitachi 215 spectrometer. The optical rotations were measured in a 0.5-dm tube with a Jasco DIP-180 polarimeter and were corrected as an anhydrous form if a compound had several molecules of adherent water. The TLC was performed on Merck TLC plate silica gel 60 F_{254}. Concentrated sulfuric acid was used as the spray reagent. The column chromatography was carried out by the use of Merck silica gel 60. The paper chromatography was conducted by using Merck Pre-Coated TLC Plates cellulose as a substitute for paper, and the substances were detected by the use of ninhydrin spray. The following solvent systems were used: for TLC, methanol–chloroform (3: 7) (Solvent A); for column chromatography, methanol–chloroform (1: 5) (Solvent B); for paper chromatography, 1-butanol–pyridine–acetic acid–water (1: 5: 2: 4) (Solvent C) and 1-propanol–pyridine–acetic acid–water (6: 4: 1: 3) (Solvent D).

Selective Sulfonylation of Cycloheptaamylose; Heptakis(mesitylsulfonyl)cycloheptaamylose (I and Ib); Hexakis(6-O-mesitylsulfonyl)cycloheptaamylose (II).* Into a solution of cycloheptaamylose (32.7 g, containing 0.8% water) in dry pyridine (320 ml), we stirred MstCl (55.6 g, 1.2 eq-moles for the D-glucose residue) at 0—5 °C. After 3 h, the mixture was allowed to stand for 3 days at room temp. To the mixture 20 ml of cold water was stirred in, drop by drop, under cooling after which the new mixture was allowed to stand for 1 h at room temp. The mixture was then poured into a large volume of a dil-HCl solution under cooling to obtained a white precipitate which was collected and washed with water; yield, 66.0 g (S, 9.07%). TLC with Solvent A proved the product to be composed of three components with R_f values of 0.79, 0.41, and 0.02. These products (33.0 g) were chromatographed on a silica gel column (60×700 mm) with Solvent B. The substance with an R_f value of 0.79 was obtained as a white powder and

was determined to be Ib*; yield, 5.0 g; mp 187.0 °C (decomp), $[\alpha]_D^{20}$ +70.8 ° (*c* 1.0, chloroform), IR spectrum: 1600 (phenyl), 1350, 1185, 1170 (sulfonate) cm^{-1}. Found: C, 52.20; H, 5.89; S, 9.40%. Calcd for $C_{105}H_{140}O_{49}S_7$: C, 52.33; H, 5.81; S, 9.30%.

The substance with an R_f value of 0.41 was also obtained as a white powder and was determined to be II; yield, 12.5 g; mp 189.5 °C (decomp), $[\alpha]_D^{20}$ +76.2 ° (*c* 1.0, chloroform), IR spectrum; 1600 (phenyl), 1355, 1185, 1180 (sulfonate) cm^{-1}. Found: C, 51.64; H, 5.91; S, 8.76%. Calcd for $C_{96}H_{130}O_{47}S_6$: C, 51.75; H, 5.84; S, 8.63%.

The powdered mixture of the crude sulfonyl esters (33.0 g) described above was suspended in a mixture of ethyl acetate (800 ml) and ethanol (200 ml) at 50 °C for 1 h. To the mixture, ethyl acetate (500 ml) was then added, and the mixture was stirred for 10 h at room temperature and subsequently filtered. The remaining powder was suspended in a mixture of the same solvent; to the mixture we then added ethyl acetate, and then we stirred and filtered the solution. This treatment was repeated two more times. The filtrate (about 5 l) was then concentrated, and the residue was suspended in a hot ethyl acetate (2 l) for 30 min, stirred at room temperature overnight, and filtered. To the filtrate ether was added, drop by drop, until the clear solution became slightly cloudy after which it was allowed to stand overnight. After the precipitate had then been filtered off, the filtrate was concentrated, the residue was dissolved in hot ethyl acetate (1.5 l), and ether was added. These procedures were repeated two further times, after which the white precipitate I was obtained by adding ether to the last residue. This was practically pure heptakis(mesitylsulfonyl)cycloheptaamylose, as determined by TLC (R_f=0.79), though a trace of II (R_f=0.41) was still present; yield, 1.4 g; mp 177—181 °C (decomp), $[\alpha]_D^{20}$ +69.8 ° (*c* 1.0 chloroform). Found: C, 52.66; H, 6.06; S, 9.38%. The substance with an R_f value of 0.02 was not further examined.

Hexakis(6-azido-6-deoxy)cycloheptaamylose (III). To a solution of II (3.0 g) in dry *N,N*-dimethylformamide (30 ml), sodium azide (3.0 g) was added after which the mixture was heated with stirring at 80—85 °C for 7 h. The reaction mixture was then poured into a large volume of cold water the white precipitate thus obtained was collected and washed with water; yield, 1.60 g (92.5%); mp above 230 °C (decomposed slowly); IR spectrum: 2100 (azido) cm^{-1}, no sulfonate band. Found: C, 39.07; H, 5.26; N, 19.24%. Calcd for $C_{42}H_{64}N_{18}O_{29}$: C, 39.25; H, 4.98; N, 19.63%.

Heating of I and Ib with Sodium Azide: Heptakis(6-azido-6-deoxy)cycloheptaamylose (V) and Hexakis(6-azido-6-deoxy)mesitylsulfonylcycloheptaamylose (VI)*.* To a solution of I (1.2 g) in dry *N,N*-dimethylformamide (20 ml) sodium azide (1.2 g) was added; there after the mixture was heated with stirring at 85—90 °C for 7 h and then poured into a large volume of cold water. A white precipitate (0.60 g) was collected, washed with water, and dried; it showed two spots in its TLC with Solvent A (R_f 0.37 and 0.01). The precipitate was dissolved in a mixture of methanol (20 ml) and *N,N*-dimethylformamide (20 ml), and then diisopropyl ether was added slowly. The white precipitate which separated was collected. This treatment was repeated twice more. A white powder (0.20 g) thus obtained was determined to be V; mp above 220 °C (decomposed slowly); IR spectrum: 2100 (azido) cm^{-1}, no sulfonate band. Found: C, 38.24; H, 5.04; N, 21.54%. Calcd for $C_{42}H_{63}N_{21}O_{28}$: C, 38.50; H, 4.81; N, 22.46%.

The filtrate was concentrated, the residue was dissolved in ethyl acetate, and the solution was treated with active charcoal and filtered. To the filtrate, diisopropyl ether was added, and the white precipitate VI*, whose TLC gave only one spot (R_f=0.37), was collected; yield, 0.3 g; mp 211—216 °C (decomp). IR spectrum; 2100 (azido), 1600 (phenyl), 1185, 1175 (shoulder) (sulfonate) cm^{-1}. Found: C, 41.41; H, 5.16; N, 17.74; S, 2.23%. Calcd for $C_{51}H_{74}O_{31}N_{18}S$: C, 41.75; H, 5.05; N, 17.19; S, 2.18%. Compound VI* was also obtained by heating Ib* with sodium azide in *N,N*-dimethylformamide at 85—90 °C for 7 h.

Hexakis(6-amino-6-deoxy)cycloheptaamylose (IV). A sample (1.20 g) of III was suspended in methanol (200 ml) containing 5%-HCl aq (20 ml), and the mixture was hydrogenated with platinum dioxide (300 mg) under 3 atm of hydrogen pressure at 10—20 °C for 2 days. After the removal of the catalyst, the filtrate was concentrated. To the residue ethanol was added, and the precipitate which was thus separated was collected and dissolved in a small amount of water. The solution was lyophilized, and the hexahydrochloride of IV was obtained as a white powder; yield, 1.15 g (91%); mp 190.5—191.5 °C (decomp). $[\alpha]_D^{20}$ +136.4 ° (*c* 1.0, H_2O), R_f=0.37 with Solvent C. IR spectrum; 3300 (*ν* OH, NH, broad), 1600 (*δ* as NH_3^+), 1550 (*δ* s NH_3^+) cm^{-1}. Found: C, 34.05; H, 6.13; N, 5.64; Cl, 14.23%. Calcd for $C_{42}H_{82}O_{29}N_6Cl_6 \cdot 7H_2O$: C, 34.22; H, 6.52; N, 5.70; Cl, 14.46%.

A small quantity of IV was hydrolyzed with 3M hydrochloric acid in a sealed tube for 4 h at 100 °C, and the mixture was concentrated. The hydrolyzate was then paper-chromatographed with Solvent D and detected by ninhydrin. The chromatogram was completely identical (R_f=0.27, violet; R_f=0.63, yellow) with that obtained from the hydrolysis of 6-amino-6-deoxy-α-methylglucoside (mp 200—201 °C, lit,[16] mp 195—200 °C, R_f=0.41 with Solvent D).

Heptakis(6-amino-6-deoxy)cycloheptaamylose (VII). A sample (200 mg) of V was subjected to catalytic hydrogenation with platinum dioxide (100 mg) in a mixture of methanol (200 ml) and 3%-HCl aq (5 ml) and then treated in a manner similar to that described above. The heptahydrochloride of VII was obtained as a white powder; yield, 150 mg (70%); mp 182—185 °C (decomp). $[\alpha]_D^{20}$ +131 °C (*c* 1.0, H_2O). R_f=0.30 with Solvent C. IR spectrum: 3300 (*ν* OH, NH, broad), 1600 (*δ* as NH_3^+), 1500 (*δ* s NH_3^+) cm^{-1}. Found: C, 33.41; H, 6.32; N, 6.21; Cl, 16.03%. Calcd for $C_{42}H_{84}O_{28}N_7Cl_7 \cdot 8H_2O$: C, 33.02; H, 6.55; N, 6.42; Cl, 16.28%.

Positional Isomers of Hexakis(6-amino-6-deoxy)mesitylsulfonylcycloheptaamylose (VIII). A sample (600 mg) of VI* was hydrogenated with platinum dioxide (150 mg) in methanol (50 ml) containing 5%-HCl aq (10 ml) in a manner similar to that described above; the hexahydrochloride of VIII* was thus obtained as a white powder; yield, 550 mg (88%); mp 187—188 °C (decomp). $[\alpha]_D^{20}$ +112 ° (*c* 1.0, H_2O). R_f=0.69 with Solvent C. IR spectrum: 3300 (broad, *ν* OH, NH), 1605 (*δ* as NH_3^+), 1505 (*δ* s NH_3^+), 1195, 1175 (shoulder) (sulfonate) cm^{-1}. Found: C, 36.20; H, 5.91; N, 5.24; Cl, 13.51; S, 1.94%. Calcd for $C_{51}H_{92}O_{31}N_6Cl_6S \cdot 7H_2O$: C, 36.98; H, 6.40; N, 5.08; Cl, 12.87; S, 1.93%.

Reaction of II with Ammonia in a Methanol Solution. A sample (6.0 g) of II was dissolved in a 10%-NH_3–methanol solution (100 ml), and the mixture was heated at 70—75 °C in a sealed tube for 3 days. After the reaction mixture had then been cooled to 0—10 °C, the slightly yellow crystals which were thus separated were collected and washed with methanol. The crystals were dissolved in water (30 ml), treated with active charcoal, and lyophilized. The free base of IV was thus obtained as a white powder; yield, 2.7 g (89%); mp above 230 °C. IR spectrum; 3300, 3350 (*ν* OH, NH), 1600 (*δ* NH_2) cm^{-1}. Found: C, 42.75; H, 6.52; N, 6.79%. Calcd for $C_{42}H_{76}O_{29}N_6 \cdot 3H_2O$: C, 42.64; H, 6.94; N, 7.11%.

The aqueous solution of the base was neutralized with hydrochloric acid to pH 2 and then concentrated. The white precipitate of the hexahydrochloride was obtained by adding ethanol to the residue. The physical properties of the hexahydrochloride thus obtained were identical with those of the hexahydrochloride which was obtained by the hydrogenation of III.

More Highly Selective Sulfonylation of Cycloheptaamylose with MstCl than with TsCl. Into a solution of cycloheptaamylose (9.97 g, containing 2.5% water) in dry pyridine (200 ml) we quickly stirred a solution of the corresponding sulfonylating agent (MstCl, 55.47 g, TsCl 48.36 g; 4.0 eq-moles respectively) in dry pyridine (100 ml) at 15.0 °C; the mixture was then kept at 15.0±0.5 °C during experiments. An aliquot portion (10—15 ml) of the reaction mixture was taken up from time to time and was quenched with 1 ml of cold water. After 3 h the aliquot was poured into a large volume of water to give a white precipitate, which was collected. The average number of entering sulfonyloxyl groups was determined by analyzing the sulfur content of the precipitate. The results are shown in Fig. 1. The samples (A, B, and C) were all heated with sodium azide in DMF at 80 °C for 7 h, and the average numbers of the sulfonyloxy groups remaining and of the azido group replacing them were analyzed. The average number of the azido groups introduced corresponds to the number of the primary sulfonyloxyl groups, while that of the sulfonyloxy groups remaining represents the number of secondary sulfonyloxy groups in the samples (A, B, and C).

The authors wish to express their thanks to Mr. Michio Yamazaki, Director of this Laboratory, for his encouragement and to Dr. Tomishige Mizoguchi for his kind advice. Thanks are also due to Dr. Shigeyuki Takeyama for the hypocholesterolemic activity tests and to Dr. Totaro Yamaguchi for the antimicrobial activity tests.

References

1) For a recent review, see D. W. Griffiths and M. L. Bender, *Adv. Catal.*, **23**, 209 (1973).
2) For example, see J. Emert and R. Breslow, *J. Am. Chem. Soc.*, **97**, 670 (1975).
3) W. Lautsch, R. Wiechert, and H. Lehmann, *Kolloid-Z.*, **135**, 134 (1954).
4) F. Cramer, G. Mackensen, and K. Sensse, *Chem. Ber.*, **102**, 494 (1969).
5) S. Umezawa and K. Tatsuta, *Bull. Chem. Soc. Jpn.*, **41**, 464 (1968).
6) E. Hardegger, R. M. Montavon, and O. Jucker, *Helv. Chim. Acta*, **31**, 1863 (1948).
7) J. Asselineau, *Bull. Soc. Chim. Fr.*, **1955**, 937.
8) M. L. Wolfrom, M. I. Taha, and D. Horton, *J. Org. Chem.*, **28**, 3553 (1963).
9) E. Heuser, M. Health, and W. H. Shockley, *J. Am. Chem. Soc.*, **72**, 670 (1950).
10) K. H. Palmer, C. E. Cook, F. T. Ross, J. Dolar, M. E. Twine, and M. E. Wall, *Steroids*, **14**, 55 (1969).
11) S. E. Creasey and R. D. Guthrie, *J. Chem. Soc., Chem. Commun.*, **1971**, 801; *J. Chem. Soc.*, **1974**, 1373.
12) W. S. Johnson, J. C. Collines, Jr., R. Pappo, M. B. Rubin, R. J. Kropp, W. F. Johns, J. E. Pike, and W. Bartmann, *J. Am. Chem. Soc.*, **85**, 1409 (1963).
13) R. S. Tipson, *Adv. Carbohydr. Chem.*, **8**, 107 (1953).
14) D. French, *Adv. Carbohydr. Chem.*, **12**, 190 (1957).
15) B. Zak, R. C. Dickenman, E. G. White, H. Burnett, and P. J. Cherney, *Am. J. Clin. Pathol.*, **24**, 1307 (1954).
16) F. Cramer, H. Otterbach, and H. Springmann, *Chem. Ber.*, **92**, 384 (1959).

Nucleoside Analogs. 4. Synthesis of 3′-Amino-3′-deoxyadenosine Analogs

Kin-ichi TADANO, Yasufumi EMORI, Mitsukuni AYABE, and Tetsuo SUAMI

Department of Applied Chemistry, Faculty of Engineering, Keio University, Hiyoshi, Yokohama 223

(Received December 15, 1976)

Three 9-(3-amino-2,4,5-trihydroxycyclopentyl)adenines and their *N*-acyl derivatives were prepared as carbocyclic analogs of 3′-amino and 3′-acetamido-3′-deoxyadenosine from the three diastereomers of diaminocyclopentanetriol and 4-amino-6-chloro-5-nitropyrimidine.

We have been working on a synthesis of nucleoside analogs, in which the ribofuranosyl moiety of adenosine is replaced by a cyclopentane ring stable against hydrolysis and enzymic action. In connection with the preceding paper,[1] we wish to report a synthesis of carbocyclic analogs of 3′-amino-3′-deoxyadenosine.

3′-Amino-3′-deoxyadenosine (**1**) has been found in a fermentation broth of *Helminthosporium*,[2] *Cordyceps militaris*,[3] and *Aspergillus nidulans*.[4] The compound has antitumor and antimitotic activity, inhibiting growth of *Cryptococcus neoformans* 4806 and *Candida albicans*.[4] 3′-Acetamido-3′-deoxyadenosine (**2**)[5] was found in a culture filtrate of *Helminthosporium* together with **1**, but inhibited growth of neither Ehrlich carcinoma nor of bacteria.[5]

The structural requirements in puromycin analogs for inhibition of protein synthesis were demonstrated by Daluge and Vince[6] in a synthesis of carbocyclic analogs of puromycin. They suggested that the ribofuranosyl ring can be replaced by the cyclopentyl ring without loss of activity, and that removal of the hydroxymethyl group is not detrimental to the activity, its removal being desirable for reducing toxicity.

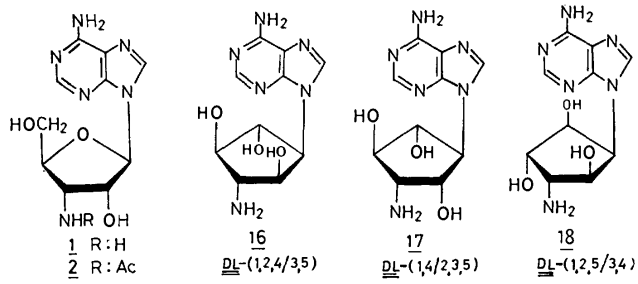

Scheme 1.*

We were prompted to attempt the synthesis of a carbocyclic analog retaining the structural features suggested so far. We have prepared 9-(3-amino-2,4,5-trihydroxycyclopentyl)adenines (**16**, **17**, and **18**) and their *N*-acyl derivatives (**13**, **14**, and **15**) by the following reaction routes (Scheme 2).

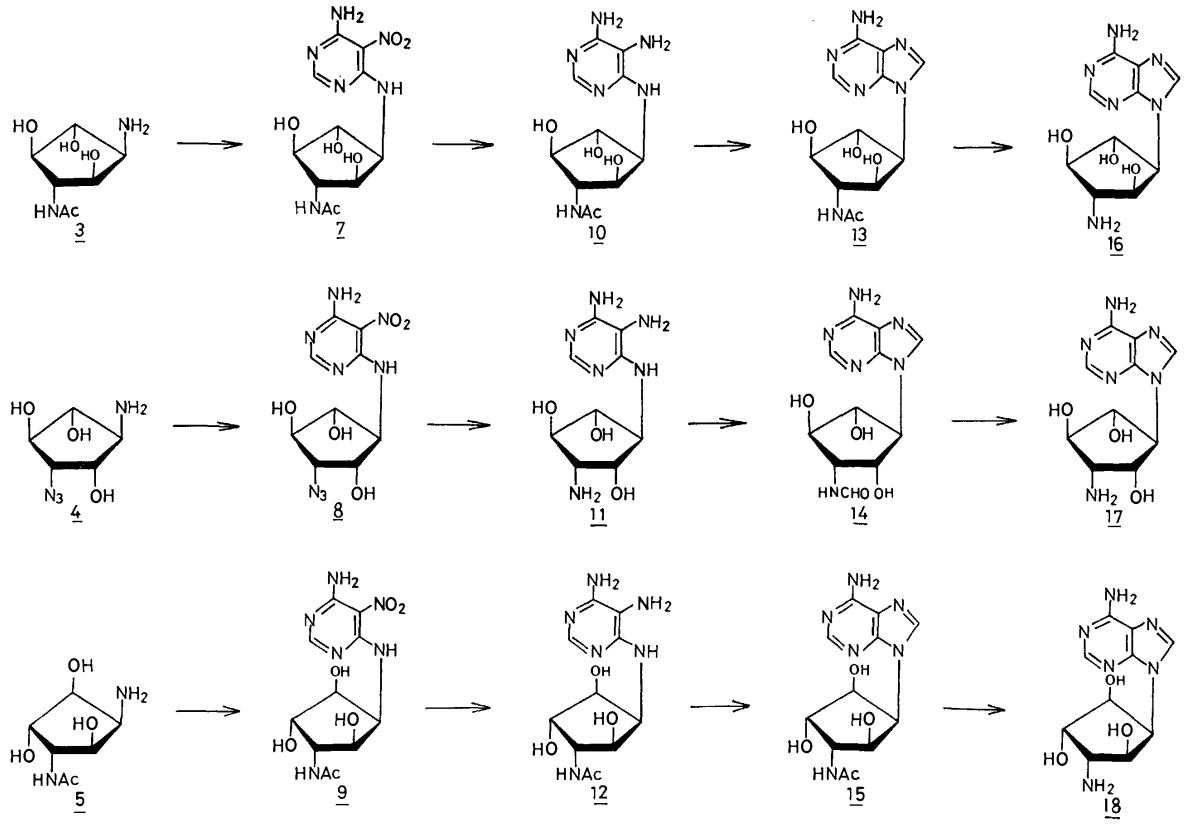

Scheme 2.*

* Structures in Schemes 1 and 2 dipict only one enantiomer of the racemic form actually obtained in the present experiment.

Tri-*O*-acetyl-DL-(1,2,4/3,5)-5-acetamido-2-azido-1,3,4-cyclopentanetriol[7] was selectively *O*-deacetylated, and subsequently hydrogenated to give DL-(1,3,5/2,4)-2-acetamido-5-amino-1,3,4-cyclopentanetriol (**3**).

Hydrolysis of the starting material in 3 M hydrochloric acid, followed by removal of the chloride ion, gave 5-amino-2-azido-1,3,4-cyclopentanetriol (**4**). Another diastereomer: tri-*O*-acetyl-DL-(1,2,3/4,5)-5-acetamido-2-azido-1,3,4-cyclopentanetriol[7] was *O*-deacetylated, and subsequently hydrogenated catalytically to give DL-(1,4,5/2,3)-2-acetamido-5-amino-1,3,4-cyclopentanetriol (**5**).

Compounds **3**, **4**, and **5** were condensed with 4-amino-6-chloro-5-nitropyrimidine[8] (**6**) to give the corresponding pyrimidine derivatives (**7**), (**8**), and (**9**), respectively. Reduction of the nitro group, followed by ring closure of the respective pyrimidine derivatives (**10**), (**11**), and (**12**) with formamide, gave the corresponding 3′-*N*-acyl adenine derivatives (**13**), (**14**), and (**15**), respectively. Hydrolysis of **13**, **14**, and **15** in barium hydroxide solution yielded the corresponding adenine analogs (**16**), (**17**), and (**18**), respectively. These compounds showed no biological activity against HeLa S3 cell.

Experimental

Melting points were determined in capillary tubes in a liquid bath and are uncorrected. Solutions were evaporated under reduced pressure at 40—50 °C. TLC was performed on a silica gel plate (Wakogel B-10, Wako Pure Chemical Industries Ltd.). Elemental analyses were performed by Mr. Saburo Nakada to whom our thanks are due.

DL-(1,3,5/2,4)-2-Acetamido-5-amino-1,3,4-cyclopentanetriol (3). A 4.94 g portion of DL-1,3,4-tri-*O*-acetyl-(1,2,4/3,5)-5-acetamido-2-azido-1,3,4-cyclopentanetriol[7] was *O*-deacetylated in methanolic ammonia. The product was catalytically hydrogenated in 50% aqueous ethanol in the presence of Raney nickel to give 2.48 g of crude **3**, which was recrystallized from aqueous ethanol to give 0.98 g (36%) of pure **3**, mp 199—200 °C.

Found: C, 44.16; H, 7.39; N, 14.72%. Calcd for $C_7H_{14}N_2O_4$: C, 44.20; H, 7.42; N, 14.73%.

DL-(1,2,4/3,5)-5-Amino-2-azido-1,3,4-cyclopentanetriol (4). DL-1,3,4-tri-*O*-acetyl-(1,2,4/3,5)-5-acetamido-2-azido-1,3,4-cyclopentanetriol[7] (5.39 g) was hydrolyzed in 3 M hydrochloric acid (100 ml) at 100 °C for 3 h, and the solution was evaporated. The residue was dissolved in water and the solution was treated with Amberlite IRA-400 (OH^-) resin in a column. The effluent was evaporated and the residue was recrystallized from isopropyl alcohol to give 2.40 g (88%) of **4**, mp 115—116 °C.

Found: C, 34.73; H, 5.78: N, 32.02%. Calcd for $C_5H_{10}N_4O_3$: C, 34.48; H, 5.79; N, 32.17%.

DL-(1,4,5/2,3)-2-Acetamido-5-amino-1,3,4-cyclopentanetriol (5). DL-1,3,4-Tri-*O*-acetyl-(1,2,3/4,5)-5-acetamido-2-azido-1,3,4-cyclopentanetriol[7] (3.35 g) was *O*-deacetylated in methanolic ammonia to give 2.45 g of crude product. The product was triturated in ethanol to give 1.97 g (93%) of *O*-deacetylated derivative, mp 168—169 °C.

Found: C, 38.77; H, 5.74; N, 25.60%. Calcd for $C_7H_{12}N_4O_4$: C, 38.89; H, 5.60; N, 25.92%.

The above product (1.38 g) was catalytically hydrogenated in water (32 ml) overnight to give 1.17 g (97%) of crude **5**, which was recrystallized from ethanol to give an analytical sample, mp 175—176 °C (dec).

Found: C, 43.90; H, 7.36; N, 14.56%. Calcd for $C_7H_{14}N_2O_4$: C, 44.20; H, 7.42; N, 14.73%.

The hydrochloride melted at 194—195 °C.

Found: C, 37.29; H, 6.61; N, 12.13; Cl, 15.72%. Calcd for $C_7H_{15}N_2O_4Cl$: C, 37.09; H, 6.67; N, 12.36; Cl, 15.64%.

6-[DL-(1,2,4/3,5)-3-Acetamido-2,4,5-trihydroxycyclopentyl]-amino-4-amino-5-nitropyrimidine (7). A mixture of **3** (1.00 g), 4-amino-6-chloro-5-nitropyrimidine[8] (**6**) (1.10 g) and triethylamine (1 ml) was heated in 2-methoxyethanol (50 ml) at 90—95 °C for 1.5 h. After being cooled to ambient temperature, the resulting crystalline product was collected by filtration. The product was recrystallized from hot water and subsequently washed with warm ethanol to give 1.58 g (92%) of **7**, 275—285 °C (dec).

Found: C, 40.34; H 4.89; N, 25.72%. Calcd for $C_{11}H_{16}N_6O_6$; C, 40.25; H, 4.91; N, 25.60%.

4-Amino-6-[DL-(1,4/2,3,5)-3-azido-2,4,5-trihydroxycyclopentyl]-amino-5-nitropyrimidine (8). A mixture of **4** (1.00 g), 4-amino-6-chloro-5-nitropyrimidine[8] (1.10 g) and triethylamine (1 ml) was heated at 80 °C in 2-methoxyethanol (30 ml) for 1 h. The reaction mixture was evaporated and the residue was triturated with warm benzene. The residual solid was recrystallized from hot water to give 1.70 g (95%) of **8** as yellow crystals, mp 206—207 °C (dec).

Found: C, 34.68; H, 3.88; N, 35.66%. Calcd for $C_9H_{12}N_8O_5$: C, 34.62; H, 3.88; N, 35.89%.

6-[DL-(1,2,5/3,4)-3-Acetamido-2,4,5-trihydroxycyclopentyl]amino-4-amino-5-nitropyrimidine (9). A mixture of **5** (1.17 g), 4-amino-6-chloro-5-nitropyrimidine[8] (1.29 g) and triethylamine (2.4 ml) was heated in 2-methoxyethanol (59 ml) at 85 °C for 3 h. The reaction mixture was evaporated and the residue was triturated with warm ethanol to give 1.43 g (71%) of **9** as yellow crystals, mp 237—238 °C (dec).

Found: C, 40.31; H, 4.93; N, 25.28%. Calcd for $C_{11}H_{16}N_6O_6$: C, 40.25; H, 4.91; N, 25.60%.

6-[DL-(1,2,4/3,5)-3-Acetamido-2,4,5-trihydroxycyclopentyl]amino-4,5-diaminopyrimidine (10). Compound **7** was dissolved in hot water (80 ml) and to the resulting solution zinc powder (15 g) was added. The mixture was heated under reflux for 7.5 h, and filtered. The filtrate was evaporated and the residue was washed with ethanol to give 455 mg (100%) of **10**, which was acetylated in the usual way to give a hexa-*N*,*O*-acetyl derivative. The product was recrystallized from ethyl acetate–ethanol (1:1 v/v%) to give an analytical sample, mp 232—233 °C (dec).

Found: C, 49.69; H, 5.73; N, 16.68%. Calcd for $C_{21}H_{28}N_6O_9$: C, 49.60; H, 5.55; N, 16.53%.

6-[DL-(1,2,5/3,4)-3-Acetamido-2,4,5-trihydroxycyclopentyl]amino-4,5-diaminopyrimidine (12). Compound **9** (504 mg) was reduced with zinc powder in boiling water as in the preparation of **10**. The crude product was recrystallized from ethanol to give 402 mg (88%) of **12**. An analytically pure sample was obtained by further recrystallization from water as pale yellow crystals, mp 237—238 °C (dec).

Found: C, 44.40; H, 6.17; N, 27.84%. Calcd for $C_{11}H_{18}N_6O_4$: C, 44.29; H, 6.08; N, 28.17%.

9-[DL-(1,2,4/3,5)-3-Acetamido-2,4,5-trihydroxycyclopentyl]-adenine (13). Compound **10** was heated at 175—180 °C in formamide (10 ml) for 1.5 h, and evaporated. The residue was recrystallized from hot water (3 ml) to give 131 mg (37%) of **13** as colorless needles, mp 290—300 °C (dec).

UV: $\lambda_{max}^{0.1\ M\ HCl}$ 259 nm (ε=12400), $\lambda_{max}^{H_2O}$ 261 nm (ε=12900), $\lambda_{max}^{0.1\ M\ NaOH}$ 259 nm (ε=6450).

Acetylation of **13** in the usual way gave 9-[DL-(1,2,4/3,5)-3-acetamido-2,4,5-triacetoxycyclopentyl]-6-diacetylaminopurine, mp 201—203 °C.

Found: C, 50.90; H, 5.10; N, 16.13%. Calcd for $C_{22}H_{26}$-

N_6O_9: C, 50.96; H, 5.06; N, 16.21%.

9-[DL-(1,4/2,3,5)-3-Formamido-2,4,5-trihydroxycyclopentyl]-adenine (14). Compound **8** (600 mg) was hydrogenated in the presence of Raney nickel under hydrogen atmosphere (3.4 kg/cm²) for 18 h in a Parr apparatus. After the catalyst had been filtered off, the filtrate was evaporated. The residue (484 mg) was heated at 170 °C for 1 h in formamide (20 ml) and subsequently evaporated. The residue was dissolved in hot water and decolorized with active charcoal. The solution was evaporated, and the residue was recrystallized from hot water to give 235 mg (42%) of **14**, mp 277—278 °C (dec).

Found: C, 44.64; H, 5.07; N, 28.77%. Calcd for $C_{11}H_{14}N_6O_4$: C, 44.90; H, 4.79; N, 28.56%.

9-[DL-(1,2,5/3,4)-3-Acetamido-2,4,5-trihydroxycyclopentyl]-adenine (15). Compound **12** was heated at 175 °C for 2 h in formamide (30 ml), and evaporated. The residue was decolorized with active charcoal in boiling water to give 381 mg (42%) of crude product. Recrystallization from hot water gave 318 mg (34%) of **15**, mp 278—280 °C (dec). **15** was acetylated in the usual way to give penta-*N,O*-acetyl derivative. The product was recrystallized from ethyl acetate to give an analytical pure sample, mp 219—220 °C (dec).

Found: C, 50.15; H, 4.99; N, 17.72%. Calcd for $C_{20}H_{24}N_6O_8$: C, 50.42; H, 5.08; N, 17.64%.

9-[DL-(1,2,4/3,5)-3-Amino-2,4,5-trihydroxycyclopentyl]adenine (16). Compound **13** (150 mg) was heated at 85 °C for 3 h in a barium hydroxide [$Ba(OH)_2 \cdot 8H_2O$, 300 mg] solution (water, 23 ml). Carbon dioxide was bubbled into the solution and the resulting precipitate was filtered off. The filtrate was evaporated to a small volume and the residue was allowed to stand in a refrigerator to give 114 mg (88%) of crystals. The product was recrystallized from hot water to give an analytical sample of **16**, mp 280—290 °C (dec).

Found: C, 45.09; H, 5.34; N, 31.19%. Calcd for $C_{10}H_{14}N_6O_3$: C, 45.11; H, 5.30; N, 31.56%.

UV: $\lambda_{max}^{0.1\,M\ HCl}$ 259 nm (ε=14200), $\lambda_{max}^{H_2O}$ 260 nm (ε=12400), $\lambda_{max}^{0.1\,M\ NaOH}$ 261 nm (ε=6700).

9-[DL-(1,4/2,3,5)-3-Amino-2,4,5-trihydroxycyclopentyl]adenine (17). Compound **14** (230 mg) was treated with Dowex IX-2 (OH^-) (5 ml) in water (180 ml) at 50 °C for 3 h with agitation. After the resin had been filtered off, the solution was evaporated. The residue was recrystallized from hot water to give 176 mg (85%) of **17**, mp 255—256 °C (dec).

Found: C, 44.81; H, 5.25; N, 30.99%. Calcd for $C_{10}H_{14}N_6O_3$: C, 45.11; H, 5.30; N, 31.56%.

UV: $\lambda_{max}^{0.1\,M\ HCl}$ 258 nm (δ=15000), $\lambda_{max}^{H_2O}$ 260 nm (ε=16000), $\lambda_{max}^{0.1\,M\ NaOH}$ 261 nm (ε=16000).

The hydrochloride melts at 250 °C (dec).

Found: C, 39.49; H, 4.97; N, 27.49; Cl, 11.75%. Calcd for $C_{10}H_{15}N_6O_3Cl$: C, 39.68; H, 4.99; N, 27.76; Cl, 11.71%.

9-[DL-(1,2,5/3,4)-3-Amino-2,4,5-trihydroxycyclopentyl]adenine (18). Compound **15** (200 mg) was hydrolyzed by treating in the barium hydroxide solution for 6 h as in the preparation of **16** to give 105 mg (61%) of **18**, mp 264—266 °C (dec).

Found: C, 44.69; H, 5.25; N, 30.69%. Calcd for $C_{10}H_{14}N_6O_3 \cdot 1/4\ H_2O$: C, 44.36; H, 5.40; N, 31.04%.

UV: $\lambda_{max}^{0.1\,M\ HCl}$ 258 nm (ε=14300), $\lambda_{max}^{H_2O}$ 259 nm (ε=14600), $\lambda_{max}^{0.1\,M\ NaOH}$ 259 nm (ε=14500).

References

1) T. Suami, S. Nishiyama, K. Tadano, and F. W. Lichtenthaler, *Bull. Chem. Soc. Jpn.*, **46**, 2562 (1973).

2) C. A. Ammann and R. S. Safferman, *Antibiot. Chemother.*, **8**, 1 (1958).

3) A. J. Guarino and N. M. Kredich, *Biochem. Biophys. Acta*, **58**, 317 (1963).

4) R. J. Suhadolnik, "Nucleoside Antibiotics," Wiley Interscience, New York (1970), pp. 76—85.

5) R. J. Suhadolnik, B. M. Chassy, and G. R. Waller, *Biochem. Biophys. Acta*, **179**, 258 (1969).

6) S. Daluge and R. Vince, *J. Med. Chem.*, **15**, 171 (1972).

7) K. Tadano, Y. Emori, M. Ayabe, and T. Suami, *Bull. Chem. Soc. Jpn.*, **49**, 1108 (1976).

8) W. R. Boon, W. G. M. Johnes, and G. E. Ramege, *J. Chem. Soc.*, **1951**, 99.

A Convenient Synthesis of (±)-Taxodione, (±)-Ferruginol, and (±)-Sugiol

Takashi MATSUMOTO, Shuji USUI, and Toshitaka MORIMOTO

Department of Chemistry, Faculty of Science, Hiroshima University, Higashisenda-machi, Hiroshima 730

(Received December 24, 1976)

The condensation of β-cyclocitral (**4**) with 3-isopropyl-4-methoxybenzyl chloride (**5**) in the presence of lithium naphthalenide gave an alcohol (**6**), which was then oxidized to the corresponding α,β-unsaturated ketone (**7**). The Intramolecular cyclization of **7** with polyphosphoric acid yielded (±)-12-methoxyabieta-8,11,13-trien-6-one (**8**) and its *cis*-isomer (**9**), which was then successfully converted into **8** *via* an enol acetate (**11**). The **8** ketone was demethylated with boron tribromide to give a phenol (**18**), and this was then reduced with lithium aluminium hydride to yield the corresponding alcohol (**19**). The oxidation of the C-11 position in **19** with benzoyl peroxide gave (±)-12-benzoyloxyabieta-8,11,13-trien-6β,11-diol (**20**), which, on reduction with lithium aluminium hydride and subsequent oxidation with Jones reagent, afforded (±)-taxodione (**1**). The reductive cleavage of the hydroxyl group in **6** with dichloroaluminium hydride, followed by cyclization, gave (±)-ferruginyl methyl ether (**12**), which was then demethylated with boron tribromide to produce (±)-ferruginol (**2**). Further, the oxidation of **12** with chromium trioxide, followed by demethylation, gave (±)-sugiol (**3**).

Taxodione (**1**), a tumor-inhibitory diterpene quinone methide, was isolated from Taxodium distichum Rich by Kupchan *et al.*[1] In a previous paper, Matsumoto *et al.*[2] reported the total synthesis of (±)-**1** by the route of C→B→A ring construction. However, this synthetic route involves eighteen reaction steps and affords a low over-all yield (*ca.* 0.3%). Very recently, Matsumoto and Harada[3] also reported the syntheses of highly-oxygenated tricyclic diterpenes, taxoquinone, 7α-acetoxyroyleanone, dehydroroyleanone, horminone, 7-oxoroyleanone, and inuroyleanol, all starting from ferruginol (**2**). In conjunction with these previous works, we studied a general synthetic route for the naturally-occurring tricyclic diterpenes (C_{20} unit). This paper[4] will describe the simple and short-step syntheses of (±)-**1**, (±)-**2**, and (±)-sugiol (**3**) starting from two C_{10} units, β-cyclocitral (**4**)[5] and 3-isopropyl-4-methoxybenzyl chloride (**5**).

The condensation of **4** with **5** in the presence of lithium naphthalenide in tetrahydrofuran in a stream of nitrogen afforded the desired alcohol (**6**), which was then oxidized with the chromium trioxide–pyridine complex to yield an α,β-unsaturated ketone (**7**). The intramolecular cyclization of **7** with polyphosphoric acid afforded (±)-12-methoxyabieta-8,11,13-trien-6-one (**8**) as the minor product and its *cis*-isomer (**9**) as the major one, along with a small amount of (±)-xanthoperyl methyl ether (**10**),[6] which must have been produced by the air-oxidation of **9** during chromatographic purification. The *cis*-configuration of an A/B ring junction in **9** and **10** was supported by their NMR spectra, which showed signals due to the $C_{4\alpha}$ methyl group[7] at δ 0.32 and 0.44 ppm respectively. Since all natural compounds (**1**, **2**, and **3**) possess a *trans* A/B ring junction, the **9** *cis*-isomer was then converted into the **8** *trans*-isomer in the following manner. The oxidation of **9** with the Jones reagent readily produced **10**, which, on being refluxed with acetic anhydride in the presence of sodium acetate, gave the corresponding enol acetate (**11**) in a good yield. The **11** acetate in ethyl acetate was then submitted to catalytic hydrogenation over Pd–C in the presence of perchloric acid to afford a mixture of (±)-ferruginyl methyl ether (**12**, 33%), **8** (2%), (±)-6α- and (±)-6β-acetoxy-12-methoxyabieta-8,11,13-triene (**13**) (*ca.* 3:2, 42%), and (±)-12-methoxyabieta-8,11,13-trien-6α-ol (**14**, 5%). The treatment of **13** with lithium aluminium hydride in refluxing ether, followed by the oxidation of the resulting alcohols with the Jones reagent, afforded **8**. Further, the oxidation of **12** with lead tetraacetate in acetic acid afforded a mixture of 7α- and 7β-acetoxy compounds (**15**), which were then refluxed with dilute hydrochloric acid to yield (±)-12-methoxyabieta-6,8,11,13-tetraene (**16**). The **16** tetraene was then oxidized with *m*-chloroperoxybenzoic acid and the epoxide (**17**) was treated with dilute hydrochloric acid to give **8**. Subsequently, the **8** *trans*-ketone was demethylated with boron tribromide in dichloromethane, giving the corresponding phenol (**18**). The reduction of the carbonyl group in **18** was carried out with lithium aluminium hydride; (±)-abieta-8,11,13-trien-6β,12-diol (**19**) was thus obtained. The oxidation of the C-11 position in **19** with benzoyl peroxide in chloroform yielded (±)-12-benzoyloxyabieta-8,11,13-trien-6β,11-diol (**20**), which responded positively to the Gibbs test,[8] suggesting the presence of an aromatic proton para to a phenolic hydroxyl group. The reductive cleavage of the benzoyl group in **20** with lithium aluminium hydride and the subsequent oxidation of the crude product with the Jones reagent afforded (±)-**1**. The IR and NMR spectra of the synthetic **1** were identical with those of natural taxodione. Thus, (±)-**1** was synthesized starting from β-cyclocitral (**4**) in eight steps, giving an over-all yield of *ca.* 7%.

As has been described above, ferruginol (**2**) is an important intermediate for the syntheses of the highly-oxygenated tricyclic diterpenes.[3] Therefore, it is worthwhile to synthesize **2** by a simple and short-step procedure, although several synthetic routes have already been reported by other workers.[9–13] For this purpose, the hydroxyl group in **6** was reductively removed with dichloroaluminium hydride in ether, and the resulting phenethyl derivative (**21**) was cyclized with anhydrous aluminium chloride in refluxing benzene, thus producing **12**. The demethylation of **12** with boron tribromide in dichloromethane gave (±)-ferruginol (**2**), which was characterized as its benzoate (**22**).[9,10,13] Subsequently, **12** was oxidized with chromium trioxide in acetic acid to afford the corresponding 7-oxo com-

pound (**23**).[6] The demethylation of **23** with boron tribromide yielded (±)-sugiol (**3**),[11] which was also characterized as its acetate (**24**) and benzoate (**25**).

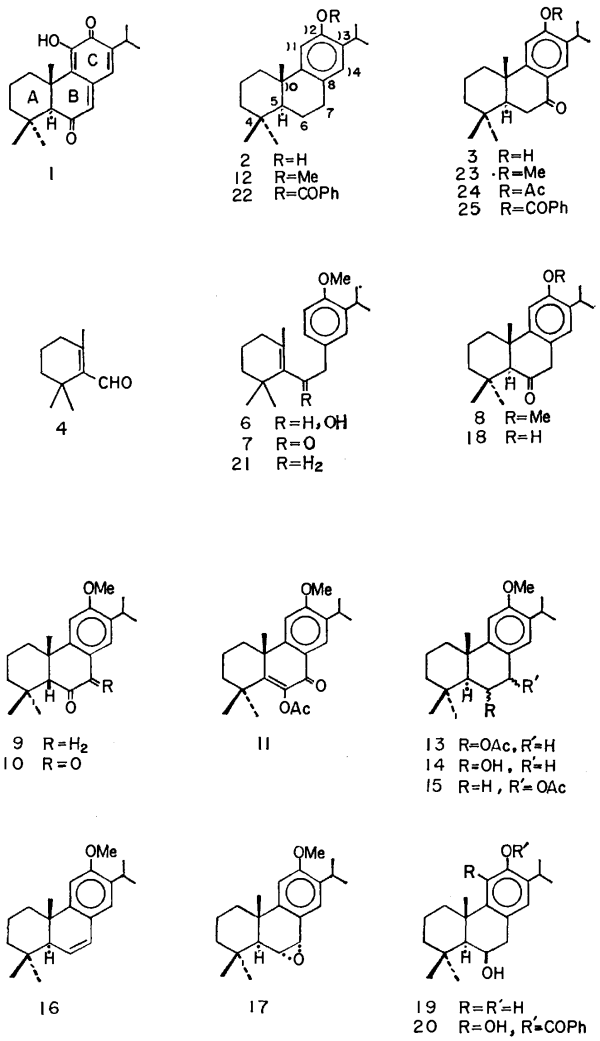

Experimental

All melting points are uncorrected. The IR spectra were taken in chloroform, and the NMR spectra in carbon tetrachloride at 60 MHz, with tetramethylsilane as the internal standard, unless otherwise stated. The chemical shifts are presented in terms of δ values. Column chromatography was performed using Merck silica gel (0.063 mm).

3-Isopropyl-4-methoxybenzyl Chloride (5). A solution of methyl 3-isopropyl-4-methoxybenzoate (2.48 g)[14] in dry ether (7 ml) was added, drop by drop, to a suspension of lithium aluminium hydride (500 mg) in dry ether (20 ml) over a 20-min period. The mixture was then refluxed for 1 h, poured into an iced aqueous ammonium chloride solution, and extracted with ether. The extract was washed with brine. The dried extract was evaporated *in vacuo* to give 3-isopropyl-4-methoxybenzyl alcohol as an oil; NMR: 1.18 (d, 6, J=7 Hz, $-CH(C\underline{H}_3)_2$), 2.72 (s, 1, -OH), 3.28 (m, 1, $-C\underline{H}(CH_3)_2$), 3.78 (s, 3, $-OCH_3$), 4.42 (s, 2, $-CH_2-$), 6.65 (d, 1, J=8 Hz), 7.00 (dd, 1, J=8 and 2 Hz), and 7.07 (bs, 1) (aromatic protons).

A solution of the above alcohol in thionyl chloride (2.0 ml) was stirred at 0 °C for 30 min and then at room temperature for 1 h, decomposed with ice water, and extracted with ether. The dried extract was evaporated *in vacuo* to give **5** as an oil (1.82 g: 77%); NMR: 1.20 (d. 6, J=7 Hz, $-CH(C\underline{H}_3)_2$), 3.28 (m, 1, $-C\underline{H}(CH_3)_2$), 3.80 (s, 3, $-OCH_3$), 4.48 (s, 2, $-CH_2-$), 6.67 (d, 1, J=9 Hz), 7.08 (dd, 1, J=9 and 2 Hz), and 7.10 (d, 1, J=2 Hz) (aromatic protons).

In another experiment, the above benzyl alcohol derivative was prepared from 3-isopropyl-4-methoxybenzaldehyde[15] by a similar reduction.

Condensation of β-Cyclocitarl (4) and 3-Isopropyl-4-methoxybenzyl Chloride (5). A mixture of naphthalene (1.92 g) and small pieces of lithium (103 mg) in dry tetrahydrofuran (15 ml) was stirred for 1.5 h at room temperature under an atmosphere of nitrogen. Into the above solution we then stirred, drop by drop, a solution of β-cyclocitral (610 mg) and 3-isopropyl-4-methoxybenzyl chloride (890 mg) in dry tetrahydrofuran (3.0 ml) at 0—10 °C over a 15-min period. The mixture was then stirred at room temperature for 2.5 h in a stream of nitrogen, diluted with ether and then with aqueous ammonium chloride, and extracted with ether, and the extract was washed with brine. The dried extract was evaporated *in vacuo* to give a crude product which was subsequently purified by column chromatography on silica gel, using benzene–ether (98: 2) as the eluent, to afford an oily alcohol (**6**) (1.10 g: 87%); IR: 3580 cm^{-1}, NMR: 0.94 and 1.08 (each s, 6, $-C(CH_3)_2$), 1.20 (d, 6, J=7 Hz, $-CH(C\underline{H}_3)_2$), 1.88 (s, 3, $=CCH_3$), 3.15 (m, 1, $-C\underline{H}(CH_3)_2$), 3.77 (s, 3, $-OCH_3$), 4.27 (dd, 1, J=4 and 9 Hz, $-C\underline{H}OH$), 6.63 (d, 1, J=9 Hz), 6.90 (dd, 1, J=9 and 2 Hz), and 6.92 (d, 1, J=2 Hz), (aromatic protons). Found: C, 79.93; H, 10.32%. Calcd for $C_{21}H_{32}O_2$: C, 79.70; H, 10.19%.

2,6,6-Trimethyl-1-cyclohexenyl 3-Isopropyl-4-methoxybenzyl Ketone (7). A solution of the **6** alcohol (5.424 g) in pyridine (10 ml) was added, drop by drop at 7—10 °C, to a chromium trioxide–pyridine complex prepared from chromium trioxide (5.0 g) and pyridine (50 ml). The mixture was stirred at 10—20 °C for 3.5 h, poured into ice–dilute hydrochloric acid, and extracted with ether. The ether extract was washed with brine, dried, and then evaporated. The crude product was purified by column chromatography on silica gel (500 g), using benzene–ether (99: 1) as the eluent, to give an α,β-unsaturated ketone **7** as an oil (3.507 g: 65%); IR: 1690 cm^{-1}, NMR: 1.02 (s, 6, $-C(CH_3)_2$), 1.19 (d, 6, J=7 Hz, $-CH(C\underline{H}_3)_2$), 1.52 (s, 3, $=CCH_3$), 3.29 (m, 1, $-C\underline{H}(CH_3)_2$), 3.65 (s, 2, $-COCH_2-$), 3.80 (s, 3, $-OCH_3$), 6.65 (d, 1, J=8.5 Hz), 6.91 (dd, 1, J=8.5 and 2 Hz), and 6.93 (d, 1, J=2 Hz) (aromatic protons). Found: C, 79.98; H, 9.43%. Calcd for $C_{21}H_{30}O_2$: C, 80.21; H, 9.62%.

Intramolecular Cyclization of 7. A mixture of **7** (879 mg) and polyphosphoric acid prepared, from 85% phosphoric acid (9 ml) and phosphorus pentaoxide (13 g) at 100 °C for 1 h, was heated at 100 °C for 1.5 h. After cooling, the mixture was diluted with water and extracted with ether, and the dried extract was evaporated to dryness. The crude product was purified by column chromatography on silica gel (90 g) using benzene–ether (99: 1 and then 97: 3) as the eluent, to give three ketones (**8**—**10**).

a) (±)-12-Methoxyabieta-8,11,13-trien-6-one (**8**) as an oil (182 mg: 21%); IR: 1708 cm^{-1}, NMR: 1.06 and 1.13 (each s, 6, $-C(CH_3)_2$), 1.14 and 1.16 (each d and J=7 Hz, 6, $-CH(C\underline{H}_3)_2$), 1.28 (s, 3, $C_{10}-CH_3$), 2.29 (s, 1, C_5–H), 3.22 (m, 1, $-C\underline{H}(CH_3)_2$), 3.43 (s, 2, $-COCH_2-$), 3.78 (s, 3, $-OCH_3$) 6.67 and 6.75 (each s, 2, C_{11}–H and C_{14}–H). Found: C, 80.09; H, 9.32%. Calcd for $C_{21}H_{30}O_2$: C, 80.21; H, 9.62%

b) (±)-12-Methoxy-5βH-abieta-8,11,13-trien-6-one (**9**).

(341 mg: 39%); mp 94—95 °C (from methanol), IR: 1692 cm^{-1}, NMR: 0.33 (s, 3, $C_{4\alpha}$-CH_3), 0.92 (s, 3, $C_{4\beta}$-CH_3), 1.07 (s, 3, C_{10}-CH_3), 1.18 (d, 6, J=7 Hz, -CH($C\underline{H}_3$)$_2$), 1.99 (s, 1, C_5-H), 3.10 (m, 1, -C$\underline{H}$(CH_3)$_2$), 3.42 (s, 2, -$COCH_2$-), 3.83 (s, 3, -OCH_3), 6.70 and 6.78 (each s, 2, C_{11}-H and C_{14}-H). Found: C, 80.11; H, 9.54%. Calcd for $C_{21}H_{30}O_2$: C, 80.21; H, 9.62%.

c) (±)-Xanthoperyl methyl ether (**10**) (13 mg: 1%), which has been obtained from benzene–ether (97: 3) fraction; mp 204—207 °C (from methanol) (lit,[6] mp 205 °C), IR: 1715, 1668 cm^{-1}, NMR ($CDCl_3$): 0.44 (s, 3, $C_{4\alpha}$-CH_3), 0.98 (s, 3, $C_{4\beta}$-CH_3), 1.23 (s, 3, C_{10}-CH_3), 1.24 (d, 6, J= 7 Hz, -CH($C\underline{H}_3$)$_2$), 2.66 (s, 1, C_5-H), 3.28 (m, 1, -C$\underline{H}$(CH_3)$_2$), 3.98 (s, 3, -OCH_3), 6.82 (s, 1, C_{11}-H), 7.96 (s, 1, C_{14}-H). Found: C, 76.73; H, 8.69%. Calcd for $C_{21}H_{28}O_3$: C, 76.79; H, 8.59%.

The **10** diketone was also obtained in a 92% yield by the oxidation of **9** in acetone with the Jones reagent at room temperature for 30 min.

(±)-6-Acetoxy-12-methoxyabieta-5,8,11,13-tetraen-7-one (11). A mixture of **10** (511 mg) and anhydrous sodium acetate (2.0 g) in acetic anhydride (20 ml) was refluxed for 33 h, and then filtered. After the filtrate had been evaporated to dryness, the residue was extracted with ether and the extract was washed with aqueous sodium hydrogencarbonate and water. The dried extract was evaporated to yield a crude product which was subsequently purified by column chromatography on silica gel (70 g), using benzene–ether (97: 3) as the eluent, to give **11** (556 mg: 96%), which was then recrystallized from methanol; mp 126—126.5 °C, IR: 1755, 1648 cm^{-1}, NMR: 1.22 and 1.26 (each d and J=7 Hz, 6, -CH($C\underline{H}_3$)$_2$), 1.31 and 1.36 (each s, 6, -C(CH_3)$_2$), 1.57 (s, 3, C_{10}-CH_3), 2.27 (s, 3, -$OCOCH_3$), 3.23 (m, 1, -C$\underline{H}$-(CH_3)$_2$), 3.88 (s, 3, -OCH_3), 6.78 (s, 1, C_{11}-H), 7.79 (s, 1, C_{14}-H). Found: C, 74.70; H, 8.19%. Calcd for $C_{23}H_{30}O_4$: C, 74.56; H, 8.16%.

Catalytic Hydrogenation of the Enol Acetate (11). A mixture of **11** (283 mg), 5% Pd-C (250 mg), and 70% perchloric acid (10 drops) in ethyl acetate (10 ml) was subjected to catalytic hydrogenation at room temperature. After the usual work-up, the crude product was purified by column chromatography on silica gel (25 g), using hexane–benzene (1: 1) and benzene–ether (97: 3) as eluents, to yield **12**, **8**, **13**, and **14** (in the order of elution).

a) (±)-12-Methoxyabieta-8,11,13-triene (ferruginyl methyl ether) (**12**) as an oil (76 mg: 33%); NMR: 0.94 (s, 6, -C(CH_3)$_2$), 1.14 (d, 6, J=7 Hz, -CH($C\underline{H}_3$)$_2$), 1.18 (s, 3, C_{10}-CH_3), 3.15 (m, 1, -C$\underline{H}$(CH_3)$_2$), 3.72 (s, 3, -OCH_3), 6.53 and 6.67 (each s, 2, C_{11}-H and C_{14}-H). Found: C, 84.17; H, 10.76%. Calcd for $C_{21}H_{32}O$: C, 83.94; H, 10.73%.

b) **8** (4.3 mg: 2%), whose IR and NMR spectra were identical with those of (±)-12-methoxyabieta-8,11,13-trien-6-one.

c) (±)-6α- and 6β-Acetoxy-12-methoxyabieta-8,11,13-triene (**13**) as an oil (115 mg: 42%); IR: 1721 cm^{-1}. The ratio of 6α- and 6β-acetoxy compounds was found to be *ca.* 3: 2 by NMR analysis of the mixture, using signals due to C_6-H at δ 5.35 (m, $W_{1/2}$=19 Hz) and 5.65 (m, $W_{1/2}$=10 Hz) ppm.

d) (±)-12-Methoxyabieta-8,11,13-trien-6α-ol (**14**) as an oil (13 mg: 5%); IR: 3600 cm^{-1}, NMR: 1.10, 1.10, and 1.15 (each s, 9, -C(CH_3)$_2$ and C_{10}-CH_3), 1.16 (d, 6, J=7 Hz, -CH($C\underline{H}_3$)$_2$), 4.20 (m, 1, $W_{1/2}$=16 Hz, C_6-H), 3.77 (s, 3, -OCH_3), 6.58 and 6.78 (each s, 2, C_{11}-H and C_{14}-H).

(±)-12-Methoxyabieta-8,11,13-trien-6-one (8). *a*) A mixture of **13** (177 mg) and lithium aluminium hydride (20 mg) in dry ether (10 ml) was refluxed for 1 h. After the usual work-up, the crude alcohol was immediately oxidized at 0 °C for 5 min with the Jones reagent (8N, 12 drops) in acetone (3.0 ml). The mixture was diluted with water, and the ether extract was washed with brine, dried, and evaporated. The product was then chromatographed on silica gel (15 g), using benzene as the eluent, to give a ketone (127 mg: 82%), whose IR and NMR spectra were identical with those of the *trans*-ketone **8**.

b) A solution of **12** (110 mg) and 85% lead tetraacetate (290 mg) in acetic acid (1.0 ml) was heated at 42—47 °C for 1 h in a stream of nitrogen. The solution was then diluted with water and extracted with ether, and the extract was washed successively with water, aqueous sodium hydrogencarbonate, and water. The dried extract was evaporated to give a crude acetate (**15**) (129 mg); IR: 1720 cm^{-1}, NMR: 1.97 and 2.06 (each s, C_7-$OCOCH_3$).

The above crude acetate (129 mg) was dissolved in ethanol (5.0 ml) containing 10% hydrochloric acid (1.0 ml) and refluxed for 2 h. After the solution had been diluted with ether, the ether solution was washed with brine, dried, and then evaporated to give (±)-12-methoxyabieta-6,8,11,13-tetraene (**16**) as an oil (109 mg); NMR: 0.97, 1.01, and 1.04 (each s, 9, -C(CH_3)$_2$ and C_{10}-CH_3), 1.15 and 1.19 (each d and J=7 Hz, 6, -CH($C\underline{H}_3$)$_2$), 3.21 (m, 1, -C$\underline{H}$(CH_3)$_2$, 3.79 (s, 3, -OCH_3), 5.78 (dd, 1, J=3 and 10 Hz, C_6-H), 6.42 (dd, 1, J=3 and 10 Hz, C_7-H), 6.57 and 6.77 (each s, 2, C_{11}-H and C_{14}-H).

A solution of **16** and 85% *m*-chloroperoxybenzoic acid (90 mg) in chloroform (3.0 ml) was allowed to stand at room temperature for 6 h and then diluted with ether. The solution was washed successively with aqueous potassium iodide, aqueous sodium hydrogencarbonate, and brine. After the removal of the solvent, the crude epoxide (**17**) was refluxed with dilute hydrochloric acid in ethanol (5.0 ml) for 1 h and then diluted with ether. The ether solution was washed with brine, dried, and evaporated. The chromatographic purification of the crude product afforded **8** (39 mg: 34% from **12**).

(±)-12-Hydroxyabieta-8,11,13-trien-6-one (18). A solution of **8** (143 mg) and boron tribromide (0.2 ml) in dichloromethane (2.0 ml) was stirred at 0 °C for 30 min, diluted with ether, and then poured into ice water. The mixture was extracted with ether, and the extract was washed successively with aqueous sodium thiosulfate and brine. The dried ether solution was then evaporated to dryness and purified by column chromatography on silica gel (15 g), using benzene–ether (97: 3) as the eluent, to produce **18** (117 mg: 85%), which was subsequently recrystallized from hexane–acetone; mp 134—135 °C, IR: 3605, 3360, 1707 cm^{-1}, NMR: 1.08 and 1.10 (each s, 6, -C(CH_3)$_2$), 1.20 (d, 6, J=7 Hz, -CH-($C\underline{H}_3$)$_2$), 1.29 (s, 3, C_{10}-CH_3), 2.33 (s, 1, C_5-H), 3.51 (s, 2, -$COCH_2$-), 6.15 (bs, 1, -OH), 6.67 and 6.73 (each s, 2, C_{11}-H and C_{14}-H). Found: C, 80.08; H, 9.34%. Calcd for $C_{20}H_{28}O_2$: C, 79.95; H, 9.39%.

(±)-Abieta-8,11,13-trien-6β,12-diol (19). A mixture of **18** (117 mg) and lithium aluminium hydride (20 mg) in dry ether (10 ml) was refluxed for 1 h. The mixture was then poured into ice–aqueous ammonium chloride and extracted with ether. The extract was washed with brine. The dried extract was evaporated to give **19** (108 mg: 92%), which was subsequently recrystallized from hexane–acetone; mp 174—176 °C, IR: 3610, 3350 cm^{-1}, NMR ($CDCl_3$): 1.03 and 1.28 (each s, 6, -C(CH_3)$_2$), 1.22 (d, 6, J=7 Hz, -CH($C\underline{H}_3$)$_2$), 1.53 (s, 3, C_{10}-CH_3), 4.5—4.9 (m, 2, -OH and C_6-H), 6.67 and 6.82 (each s, 2, C_{11}-H and C_{14}-H). Found: C, 79.24; H, 9.94%. Calcd for $C_{20}H_{30}O_2$: C, 79.42; H, 10.00%.

(±)-12-Benzoyloxyabieta-8,11,13-trien-6β,11-diol (20).

A solution of **19** (185 mg) and benzoyl peroxide (160 mg) in chloroform (10 ml) was allowed to stand at room temperature for 5 h, diluted with ether containing a small amount of acetic acid, and washed successively with aqueous potassium iodide, aqueous sodium thiosulfate, aqueous sodium hydrogencarbonate, and water. After drying over sodium sulfate, the solvent was removed and the residue was chromatographed on silica gel (35 g), using benzene–ether (98: 2) as the eluent, to yield **20** (152 mg: 59%), which responded positively to the Gibbs test;[8] mp 201—201.5 °C (from hexane–acetone), IR: 3580, 3400, 1743 cm^{-1}, NMR ($CDCl_3$): 1.04 and 1.23 (each s, 6, $-\dot{C}(CH_3)_2$), 1.20 (d, 6, $J=7$ Hz, $-CH(C\underline{H}_3)_2$), 1.70 (s, 3, $C_{10}-CH_3$), 4.64 (m, 1, $W_{1/2}=9$ Hz, C_6-H), 6.62 (s, 1, $C_{14}-H$), 7.4—8.3 (m, 5, $-C_6H_5$). Found: C, 76.96; H, 8.20%. Calcd for $C_{27}H_{34}O_4$: C, 76.74; H, 8.11%.

(±)-Taxodione (1). A mixture of **20** (70.0 mg) and lithium aluminium hydride (30 mg) in dry tetrahydrofuran (10 ml) was refluxed for 1.5 h and then treated by **a** method similar to that used for **19**. The crude product was immediately oxidized with the Jones reagent (3 drops) in acetone (2.0 ml) at 0 °C for 2 min. After the usual work-up, the product was purified by column chromatography on silica gel (10 g), using hexane–benzene (1: 4) as the eluent, to yield an oil (**1**) (19.6 mg: 38%); IR: 3344, 1670, 1641, 1625, 1616, 1598 cm^{-1}, NMR: 1.10, 1.26, and 1.26 (each s, 9, $-\dot{C}(CH_3)_2$ and $C_{10}-CH_3$), 1.18 (d, 6, $J=7$ Hz, $-CH(C\underline{H}_3)_2$), 2.50 (s, 1, C_5-H), 6.13 (s, 1, C_7-H), 6.85 (s, 1, $C_{14}-H$), 7.50 (s, 1, -OH). The IR and NMR spectra of (±)-**1** were identical with those of natural taxodione.

2-(2,6,6-Trimethyl-1-cyclohexenyl)-1-(3-isopropyl-4-methoxypheny)ethane (21). Lithium aluminium hydride (110 mg) was added to a solution of anhydrous aluminium chloride (1.2 g) in dry ether (18 ml), and then the mixture was stirred at room temperature for 100 min. To the above solution we then added, drop by drop, a solution of **6** (315 mg) in dry ether (4.0 ml) at 5—6 °C over an 8-min period. The mixture was further stirred at this temperature for 30 min, poured into ice–dilute hydrochloric acid, and extracted with ether. The ether extract was washed with brine, dried over sodium sulfate, and evaporated to give an oil which was purified by column chromatography on silica gel (30 g), using hexane as the eluent, to yield **21** (142 mg: 47%); NMR: 1.04 (s, 6, $-\dot{C}(CH_3)_2$), 1.20 (d, 6, $J=7$ Hz, $-CH(CH_3)_2$), 1.65 (s, 3, $=\dot{C}CH_3$), 3.23 (m, 1, $-C\underline{H}(CH_3)_2$), 3.74 (s, 3, $-OCH_3$), 6.58 (d, 1, $J=9$ Hz), 6.86 (dd, 1, $J=9$ and 3 Hz), and 6.9 (d, 1, $J=3$ Hz) (aromatic protons). Found: C, 84.14; H, 10.43%. Calcd for $C_{21}H_{32}O$: C, 83.94; H, 10.73%.

(±)-12-Methoxyabieta-8,11,13-triene (12). A mixture of **21** (298 mg), anhydrous aluminium chloride (140 mg), and dry benzene (10 ml) was refluxed for 3 h. The mixture was then poured into water and extracted with ether. The extract was washed with water, dried, and then evaporated. The chromatographic purification on silica gel (30 g) yielded **12** (155 mg: 52%), whose IR and NMR spectra were identical with those of an authentic sample.

(±)-Ferruginol (2). A solution of **12** (138 mg) and boron tribromide (0.2 ml) in dichloromethane (2.0 ml) was allowed to stand at room temperature for 2 h. The solution was then poured into water and extracted with ether. The extract was washed with brine, dried, and then evaporated to dryness. The crude product was purified by column chromatography on silica gel (15 g), using hexane–benzene (6: 4) as the eluent, to give **2** as an oil (127 mg: 96%); IR: 3605, 3355 cm^{-1}, NMR: 0.93 (s, 6, $-\dot{C}(CH_3)_2$), 1.11 (s, 3, $C_{10}-CH_3$), 1.19 (d, 6, $J=7$ Hz, $-CH(C\underline{H}_3)_2$), 3.08 (m, 1, $-C\underline{H}(CH_3)_2$), 4.70 (s, 1, -OH), 6.42 and 6.67 (each s, 2, $C_{11}-H$ and $C_{14}-H$). The IR and NMR spectra of the synthetic **2** were identical with those of authentic ferruginol.

(±)-Ferruginyl Benzoate (22). A mixture of **2** (127 mg) and benzoyl chloride (0.1 ml) in pyridine (1.0 ml) was heated at 50 °C for 1 h. After the usual work-up, the crude product was chromatographed on silica gel (20 g), using benzene as the eluent, to yield **22** (146 mg: 85%), which was subsequently recrystallized from methanol; mp 125—126 °C (lit,[13] mp 127—130 °C), IR: 1728 cm^{-1}, NMR: 0.95 (s, 6, $-\dot{C}(CH_3)_2$), 1.19 (d, 6, $J=7$ Hz, $-CH(C\underline{H}_3)_2$), 1.21 (s, 3, $C_{10}-CH_3$), 6.82 and 6.86 (each s, 2, $C_{11}-H$ and $C_{14}-H$), 7.3—8.2 (m, 5, $-C_6H_5$). Found: C, 83.01; H, 8.75%. Calcd for $C_{27}H_{34}O_2$: C, 83.03; H, 8.78%.

(±)-12-Methoxyabieta-8,11,13-trien-7-one (23). A mixture of **12** (161 mg) and chromium trioxide (160 mg) in acetic acid (5.0 ml) was stirred at room temperature for 11 h. After the usual work-up, the product was purified by column chromatography on silica gel (15 g), using benzene as the eluent, to yield **23** (110 mg: 65%), which was subsequently recrystallized from methanol; mp 125—126 °C (lit,[6] mp 125—126 °C), IR: 1660 cm^{-1}, NMR 0.95 and 1.00 (each s, 6, $-\dot{C}(CH_3)_2$), 1.21 (d, 6, $J=7$ Hz, $-C\underline{H}(CH_3)_2$), 1.24 (s, 3, $C_{10}-CH_3$), 3.21 (m, 1, $-C\underline{H}(CH_3)_2$), 3.87 (s, 3, $-OCH_3$), 6.66 (s, 1, $C_{11}-H$), 7.69 (s, 1, $C_{14}-H$). Found: 80.01; H, 9.48%. Calcd for $C_{21}H_{30}O_2$: C, 80.21; H, 9.62%.

(±)-Sugiol (3). A solution of **23** (110 mg) and boron tribromide (0.3 ml) in dichloromethane (2.0 ml) was allowed to stand at room temperature for 4 h and then treated as has been described for **2**. The crude product was chromatographed on silica gel (15 g) and eluted with benzene–ether (99: 1) to give **3** (84 mg: 80%), which was then recrystallized from methanol; mp 246.5—247 °C, IR (KBr): 3120, 1643 cm^{-1}, NMR (pyridine-d_5): 0.83 and 0.87 (each s, 6, $-\dot{C}(CH_3)_2$), 1.14 (s, 3, $C_{10}-CH_3$), 1.35 (d, 6, $J=7$ Hz, $-CH(C\underline{H}_3)_2$), 3.60 (m, 1, $-C\underline{H}(CH_3)_2$), 7.05 (s, 1, $C_{11}-H$), 8.30 (s, 1, $C_{14}-H$). Found: C, 79.73; H, 9.25%. Calcd for $C_{20}H_{28}O_2$: C, 79.95; H, 9.39%.

(±)-Sugiyl Acetate (24). A solution of **3** (49 mg) and acetic anhydride (0.2 ml) in pyridine (2.0 ml) was heated at 50—55 °C for 3 h. The crude product was then chromatographed on silica gel (10 g) and eluted with benzene to afford **24** as an oil (47 mg: 85%); IR: 1753, 1675 cm^{-1}, NMR ($CDCl_3$): 0.93 and 1.01 (each s, 6, $-\dot{C}(CH_3)_2$), 1.22 (d, 6, $J=7$ Hz, $-CH(C\underline{H}_3)_2$), 1.25 (s, 3, $C_{10}-CH_3$), 2.32 (s, 3, $-OCOCH_3$), 2.99 (m, 1, $-C\underline{H}(CH_3)_2$), 6.96 (s, 1, $C_{11}-H$), 7.94 (s, 1, $C_{14}-H$). Found: C, 77.44; H, 8.88%. Calcd for $C_{22}H_{30}O_3$: C, 77.15; H, 8.83%. The NMR spectrum was identical with that published[7] for (+)-sugiyl acetate.

(±)-Sugiyl Benzoate (25). A solution of **3** (48 mg), benzoyl chloride (0.1 ml), and pyridine (1.0 ml) was heated at 50—55 °C for 1 h. The crude product was then chromatographed on silica gel (15 g) and eluted with benzene–ether (99: 1) to give **25** (57 mg: 88%), which was subsequently recrystallized from methanol; mp 164—166 °C, IR: 1734, 1673 cm^{-1}, NMR: 0.97 and 1.02 (each s, 6, $-\dot{C}(CH_3)_2$), 1.25 and 1.27 (each d and $J=7$ Hz, 6, $-CH(C\underline{H}_3)_2$), 1.28 (s, 3, $C_{10}-CH_3$), 3.06 (m, 1, $-C\underline{H}(CH_3)_2$), 7.02 (s, 1, $C_{11}-H$), 7.89 (s, 1, $C_{14}-H$). Found: C, 80.05; H, 8.11%. Calcd for $C_{27}H_{32}O_3$: C, 80.16; H, 7.97%.

References

1) S. M. Kupchan, A. Karim, and C. Marcks, *J. Am. Chem. Soc.*, **90**, 5923 (1968); *J. Org. Chem.*, **34**, 3912 (1969).

2) T. Matsumoto, Y. Tachibana, J. Uchida, and K. Fukui, *Bull. Chem. Soc. Jpn.*, **44**, 2766 (1971).

3) T. Matsumoto and S. Harada, *Chem. Lett.*, **1976**, 1311.

4) Although the formulas depicted represent only one

enantiomer, they should be taken to indicate racemates.

5) R. N. Gedye, P. C. Arora, and K. Deck, *Can. J. Chem.*, **49**, 1764 (1971); W. M. Könst, L. M. van der Linde, and H. Boelens, *Tetrahedron Lett.*, **1974**, 3175.

6) D. Nasipuri and M. Guha, *J. Chem. Soc.*, **1962**, 4248.

7) Y. Kondo, T. Ikenoue, and T. Takemoto, *Chem. Pharm. Bull.*, **11**, 678 (1963).

8) F. E. King, T. J. King, and L. C. Manning, *J. Chem. Soc.*, **1957**, 563.

9) F. E. King, T. J. King, and J. G. Topliss, *J. Chem. Soc.*, **1957**, 573.

10) R. N. Rao and K. Raman, *Tetrahedron*, **4**, 294 (1958).

11) W. L. Meyer, G. B. Clemans, and R. W. Huffman, *Tetrahedron Lett.*, **1966**, 4255; W. L. Meyer, G. B. Clemans, and R. A. Manning, *J. Org. Chem.*, **40**, 3686 (1975).

12) M. Ohashi, T. Maruishi, and H. Kakisawa, *Tetrahedron Lett.*, **1968**, 719.

13) J. Wolinsky, R. Lau, J. J. Hamsher, and C. M. Cimarusti, *Synth. Commun.*, **2**, 327 (1972).

14) H. Gilman and N. O. Calloway, *J. Am. Chem. Soc*,. **55**, 4197 (1933).

15) H. Gilman and R. R. Burtner, *J. Am. Chem. Soc.*, **57**, 909 (1935).

A Synthesis of 3′,4′-Dideoxykanamycin B

Tomo NISHIMURA, Tsutomu TSUCHIYA, Sumio UMEZAWA, and Hamao UMEZAWA*

Institute of Bioorganic Chemistry, 1614 Ida, Nakahara-ku, Kawasaki 211

**Institute of Microbial Chemistry, Kamiosaki, Shinagawa-ku, Tokyo 141*

(Received December 25, 1976)

3′,4′-Dideoxykanamycin B was prepared from kanamycin B *via* 4″,6″-*O*-cyclohexylidenation, *N*-benzyloxycarbonylation, 3′,4′,2″-tri-*O*-benzylsulfonylation, double bond formation at C-3′,4′, removal of the cyclohexylidene group, simultaneous removal of the *N*,*O*-protecting groups with sodium metal in liquid ammonia and hydrogenation of the resulting 3′,4′-dideoxy-3′-eno-kanamycin B.

3′,4′-Dideoxykanamycin B[1] (Dibekacin) (**10**) has strong antibacterial activities against usual and resistant bacteria including *Pseudomonas aeruginosa*. The first[1] and an improved synthesis[2] have been reported. This paper describes another synthesis of **10**.

In this synthesis, various protecting groups used in transformation of aminoglycoside antibiotics were first studied to increase the yield of **10**.

In order to prepare kanamycin derivatives, protection of the amino groups is generally the requisite step which comes first, but we tried, in this paper, to protect the 4″- and 6″-hydroxyl groups in advance to the protection of the amino groups. In this attempt, kanamycin B (KMB) was converted to its penta-*p*-toluenesulfonate (**1**) in order to raise the solubility of kanamycin B in organic solvents. The pentasulfonate was treated with 1,1-dimethoxycyclohexane in *N*,*N*-dimethylformamide (DMF) in the presence of *p*-toluenesulfonic acid in a manner as described in a previous paper[2] to give 4″,6″-*O*-cyclohexylidene-kanamycin B (**2**) in 85% yield. Similar treatment of the pentasulfonate (**1**) with 2,2-dimethoxypropane gave the corresponding 4″,6″-*O*-isopropylidene derivative (**3**). The low yield (48%) of the latter compound will be due to[3] the low boiling point of the ketal reagent. It was surprising that **2** and **3** (especially **3**) retained antibacterial activity as shown in Table 1. As already reported, even minor modifications of 6-amino-6-deoxyglucose and 2,6-diamino-2,6-dideoxyglucose moieties of kanamycin (3′-*O*-methylkanamycin[4]) and neamine (3′- and 4′-*O*-methylneamines[5]) gave derivatives almost devoid of antibacterial activity. However, it seems that the antibacterial activity is not strongly reduced by minor modifications of the 3-amino-3-deoxyglucose moiety of kanamycins or other related antibiotics.

The amino groups of **2** were protected with benzyl chloroformate in a usual manner to give **4** in 94% yield. To carry out 3′,4′-di-*O*-sulfonylation, which is the requisite step for making 3′,4′-unsaturation bond, benzylsulfonylation was adopted from the following reason. In *N*-tosyl derivatives[2] of kanamycin B, 3′,4′-dibenzylsulfonylation can smoothly be carried out and the 2″-*O*-benzylsulfonyl group, which is simultaneously formed, can readily be removed in addition to the *N*-tosyl groups in a later step without formation of 2″,3″-epimine. On the other hand, 3′,4′-di-*O*-tosylation was shown to be difficult to attain on account of steric hindrance caused by the first tosyl group introduced at C-3′ or C-4′ of the *N*-ethoxycarbonyl derivative[6] of kanamycin B. Instead of tosylation, 3′,4′-di-*O*-

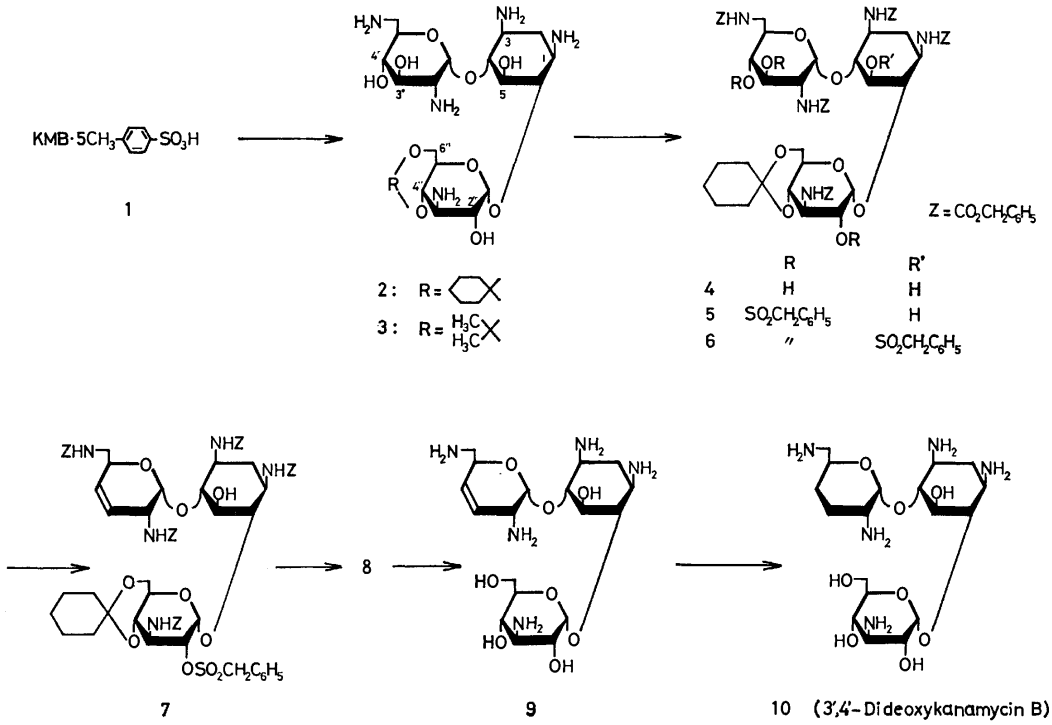

Table 1. Antibacterial spectra of **2**, **3**, **9**, **10**, authentic sample of **10**, and kanamycin B (KMB)

Test organisms[a]	Minimal inhibitory concentration (mcg/ml)					
	KMB	**2**	**3**	**9**	**10**	**10** (authentic)
Staphylococcus aureus FDA 209P	0.39	1.56	0.78	1.56	<0.2	<0.2
Sarcina lutea PCI 1001	12.5	50	12.5	>100	12.5	12.5
Bacillus subtilis NRRL B-558	<0.2	0.78	0.4	0.78	<0.2	<0.2
Klebsiella pneumoniae PCI 602	0.39	6.25	1.56	12.5	0.78	0.78
Salmonella typhi T-63	<0.2	0.39	0.78	12.5	0.78	0.39
Escherichia coli K-12	0.78	1.56	0.78	12.5	0.39	0.39
Escherichia coli K-12 ML 1629[b]	>100	>100	>100	25	0.78	0.78
Pseudomonas aeruginosa A3	25	>100	>100	12.5	0.39	0.39
Mycobacterium smegmatis ATCC 607[c]	1.56	25	12.5	3.12	0.39	0.39

a) Agar dilution streak method (nutrient agar, 37 °C, 18 h). b) A strain of clinical origin having the ability of phosphorylating the 3′-hydroxyl group of kanamycin B. c) 48 h.

mesylation is also possible, however, 2″-*O*-mesyl group, which is simultaneously formed, resists[7] sometimes to elimination in treatment with sodium metal in liquid ammonia in comparison to the 2″-*O*-benzylsulfonyl group. In view of these results benzylsulfonylation was selected. When **4** was treated with benzylsulfonyl chloride in pyridine–collidine (1: 1), 3′,4′,2″-tri-*O*- (**5**) and 5,3′,4′,2″-tetra-*O*-benzylsulfonyl (**6**) derivatives were formed. The formation of the 5-*O*-sulfonate was unexpected, because 5-*O*-acylation of kanamycins in pyridine occurs scarcely, in general. Since **6** gave, in the next unsaturation step, an unidentified product, **5** was selected for the precursor for unsaturation and an effort was made to increase the yield of **5**. When **4** was treated with four equivalents of benzylsulfonyl chloride for **4** at −20 °C for 4.5 h, **5** was obtained in 98% yield.

3′,4′-Unsaturation of **5** was tried firstly with sodium iodide in DMF in a similar fashion as described[2] for 3′,4′-di-*O*-benzylsulfonyl-penta-*N*-tosylkanamycin B derivative, however, no unsaturated compound was obtained as previously[2] experienced. Raising the reaction temperature or prolongation of the reaction period also failed to give the desired product. Addition of zinc dust, however, readily gave the 3′,4′-unsaturated derivative (**7**) in 86% yield. The presence of the 3′,4′-unsaturation bond was supported by the optical rotation[1,2,8] and also by the PMR spectrum, in which a 2-proton AB quartet ($J \approx 11$ Hz) assignable to protons of *cis* double bond[8] was observed. In this reaction, no 2″,3″-aziridine as experienced in the above-described *N*-tosyl derivative[2] of kanamycin B was formed. These features of reactions may be due to the nature of the *N*-protecting groups, *i.e.* the benzyloxycarbonyl and tosyl groups.

Acidic hydrolysis of **7** gave the decyclohexylidenated product (**8**). Treatment of **8**, which has been carefully purified to remove inorganic impurities,[9] with sodium metal in liquid ammonia at −50 °C for 1 h gave the desired 3′,4′-unsaturated derivative (**9**), both the *N*-benzyloxycarbonyl[10] and *O*-benzylsulfonyl groups being readily removed. Catalytic hydrogenation of **9** gave 3′,4′-dideoxykanamycin B (**10**) in 95% yield. The physical constants, IR and PMR spectra, and antibacterial activity were identical with those of specimen previously prepared.[1,2] Overall yield of **10** from kanamycin B was over than 50% of the theoretical.

Antibacterial activities of the synthesized products and related antibiotics are ahown in Table 1. The antibacterial activity of **9** was found to be fairly weaker than that of 3′,4′-dideoxykanamycin B (**10**), although **9** inhibited growth of resistant bacteria and *pseudomonas*

Experimental

PMR spectra were recorded at 60, 90, and 100 MHz with Hitachi R-24A, Varian EM-390, and Varian XL-100 spectrometers, respectively. Thin-layer chromatography (TLC) was performed on Wakogel B-5 with sulfuric acid spray for detection. Paper chromatography (PPC) was carried out on Toyo-Roshi No. 50 descending with 1-butanol–pyridine–water–acetic acid=6: 4: 3: 1 and detected by 0.5% ninhydrin in pyridine. For column chromatography, silica gel (Wakogel C-200) was used. For experiments at lower than 0 °C, cooling assembly of Haake constant temperature circulator KS60W was used.

*Kanamycin B Penta-*p*-toluenesulfonate (**1**).* To an aqueous solution (5 ml) of kanamycin B monocarbonate (4.1 g), *p*-toluenesulfonic acid monohydrate (8.5 g) was added and to the acidic solution (pH≈1), acetone (300 ml) was added. Precipitates were collected, washed thoroughly with acetone and dried *in vacuo* in a desiccator to give kanamycin B penta-*p*-toluenesulfonate as tetrahydrate, 10.17 g (96%), $[\alpha]_D^{25}$ +55° (*c* 1, water).

Found: C, 45.15; H, 5.65; N, 4.83; S, 11.29%. Calcd for $C_{18}H_{37}N_5O_{10}\cdot 5C_7H_8O_3S\cdot 4H_2O$: C, 44.94; H, 6.05; N, 4.94; S, 11.32%.

*4″,6″-O-Cyclohexylidenekanamycin B (**2**).* Compound **1** tetrahydrate (5.16 g) was dried at 60 °C *in vacuo* in the presence of CaH_2 for 2.5 h and the dried **1** was dissolved in dry DMF (26 ml). To the solution, anhydrous *p*-toluenesulfonic acid (1.85 g) and 1,1-dimethoxycyclohexane (4.2 ml) were added and the solution was kept at room temperature overnight, further at 50 °C for 30 min and at 65 °C for 15 min *in vacuo* (both at 20 Torr). The solution contained two components, **2** (major, TLC, R_f 0.38 with 1-BuOH–EtOH–$CHCl_3$–17% NH_4OH=4: 4: 2: 3, doubly developed; *cf.* **1**, R_f 0.05) and dicyclohexylidene derivative (R_f 0.52). Water (0.015 ml) was added and the solution was kept at room temperature overnight. Dicyclohexylidene derivative almost disappeared. The solution was poured into 8 M ammonia solution (20 ml) with vigorous stirring and concentrated *in vacuo*. The residue

was dissolved in water and the solution was passed through a column of Amberlite IRA 900 (OH form, 50 ml) with water. The ninhydrin-positive fractions were concentrated to give a solid (2.8 g), which was further chromatographed over CM-Sephadex C-25 (NH_4 form, 300 ml) with 0.03→0.15 M ammonia (gradually changed). After minor product was eluted (≈0.2 g), **2** was eluted, 1.93 g (85% as monocarbonate), $[\alpha]_D^{25}$ +114° (*c* 1, water); PMR (D_2O) δ: 1.0—2.2 (12H, H-2,2 and cyclohexylidene), 4.98 and 5.32 (each 1H d, $J\approx$ 3 Hz, anomeric).

Found: C, 48.31; H, 7.77; N, 11.31%. Calcd for $C_{24}H_{45}N_5O_{10}\cdot H_2CO_3$: C, 47.97; H, 7.57; N, 11.20%.

4'',6''-O-Isopropylidenekanamycin B (3). Compound **1** tetrahydrate (100 mg) was treated with 2,2-dimethoxypropane (0.1 ml) similarly as described for **2** to give **3** as a solid of monocarbonate, 20.0 mg (48%). Recovered **2** was 13 mg.

Compound **3**: $[\alpha]_D^{25}$ +110° (*c* 0.5, water); PMR (D_2O) δ: 1.94 and 2.07 (each 3H s, $(CH_3)_2C$).

Found: C, 45.10; H, 7.47; N, 11.74%. Calcd for $C_{21}H_{41}N_5O_{10}\cdot H_2CO_3$: C, 45.12; H, 7.40; N, 11.96%.

Penta-N-benzyloxycarbonyl-4'',6''-O-cyclohexylidenekanamycin B (4). To a stirred mixture of **2** (1.60 g) and anhydrous sodium carbonate (1.57 g) in acetone (16 ml)–water (16 ml)–methanol (1.6 ml), benzyl chloroformate (2.05 ml) was added and the mixture was stirred at room temperature for 2 h. After concentration, the residue was washed successively with ether and water and dried, 2.97 g (94%), $[\alpha]_D^{25}$ +47° (*c* 1, pyridine); IR (KBr): 1700, 1520 cm^{-1}.

Found: C, 62.06; H, 6.11; N, 5.61%. Calcd for $C_{64}H_{75}N_5O_{20}$: C, 62.28; H, 6.12; N, 5.67%.

Penta-N-benzyloxycarbonyl-3',4',2''-tri-O- and 5,3',4',2''-tetra-O-benzylsulfonyl-4'',6''-O-cyclohexylidenekanamycin B (6 and 5). Reaction 1. To a cold solution (−20 °C) of **4** (1.00 g) in dry pyridine–collidine (1: 1, 20 ml), benzylsulfonyl chloride (925 mg, 6 equivalents for **4**) was added and the solution was kept at −20 °C for 20 h. The solution was gradually warmed to 3 °C in 20 min and further kept at the temperature for 2 h. Water (0.1 ml) was added to stop the reaction and the solution was allowed to stand at 3 °C for 1 h. The solution was poured into aqueous 0.05% sodium carbonate solution. Slightly yellow precipitates were collected, washed with water, and dissolved in chloroform. The solution was washed with water, dried (Na_2SO_4), and concentrated to give a solid (1.67 g). The solid was chromatographed over silica gel with chloroform–acetone=12: 1 to give **5** (847 mg, 62%, R_f 0.5 with benzene–ethyl acetate=2: 1) and **6** (327 mg, 22%, R_f 0.77).

5: mp 198—205 °C (dec), $[\alpha]_D^{25}$ +59° (*c* 0.8, dioxane).

Found: C, 59.90; H, 5.45; N, 4.03; S, 5.67%. Calcd for $C_{85}H_{93}N_5O_{26}S_3$: C, 60.17; H, 5.52; N, 4.13; S, 5.67%.

6: mp 110—114 °C, $[\alpha]_D^{25}$ +52° (*c* 0.8, dioxane).

Found: C, 59.68; H, 5.40; N, 3.69; S, 6.79%. Calcd for $C_{92}H_{99}N_5O_{28}S_4$: C, 59.70; H, 5.39; N, 3.78; S, 6.93%.

Reaction 2. To a cold solution (−20 °C) of **4** (200 mg) in dry pyridine (4 ml), benzylsulfonyl chloride (123 mg, 4 equivalents for **4**) was added and the solution was kept at −20 °C for 4.5 h. After addition of water (0.02 ml), the solution was further kept at the temperature for 1 h. The solution contained, on checked by TLC, **5** accompanied by only a slight amont of **6**. The solution was poured into aqueous 0.05% sodium carbonate solution. Colorless solid precipitated was then treated similarly as described in Reaction 1 (but without column chromatography) to give a solid, which was purified by reprecipitation with chloroform–hexane to give **5**, 270 mg (98%).

Penta-N-benzyloxycarbonyl-2''-O-benzylsulfonyl-4'',6''-O-cyclohexylidene-3',4'-dideoxy-3'-eno-kanamycin B (7). A mixture of **5** (169 mg), sodium iodide (1.7 g), and zinc dust (840 mg) in dry DMF (3.4 ml) was stirred at 95 °C for 35 min. The solution, which soon solidified on cooling, was extracted with chloroform (7 ml×6). The solution was washed with water, dried (Na_2SO_4), and concentrated. The resulting syrup was dissolved in a mixture of hot chloroform (16 ml) and hexane (6 ml) and gradually cooled to give precipitates. After filtration, hexane was added to the filtrate to give additional precipitates. The process was further repeated three times. Precipitates combined were chromatographically homogeneous colorless solid, 115 mg (86%), $[\alpha]_D^{25}$ +12.5° (*c* 0.8, dioxane); PMR ($CDCl_3$): δ 1.1—1.9 (12H, H-2,2 and cyclohexylidene), $\delta\approx$5.5 (12H, CH_2Ph), a deformed AB quartet (2H, $J\approx$11 Hz) centered at δ 5.6 (H-3',4').

Found: C, 62.73; H, 5.96; N, 5.04; S, 2.32%. Calcd for $C_{71}H_{79}N_5O_{20}S$: C, 62.96; H, 5.88; N, 5.17; S, 2.32%.

Penta-N-benzyloxycarbonyl-2''-O-benzylsulfonyl-3',4'-dideoxy-3'-eno-kanamycin B (8). A suspension of **7** (115 mg) in a mixture of dioxane (0.25 ml)–water (0.15 ml)–acetic acid (1.6 ml) was heated at 80 °C for 2.5 h. The solution showed, on TLC with chloroform–acetone=2: 1, a spot at R_f 0.15 (**8**), and the spot of R_f 0.85 (**7**) disappeared. The solution was concentrated with several additions of toluene to give a residue, which was dissolved in dioxane. Addition of water gave precipitates, which were washed with hexane and with water to give a solid, 104 mg (96%), $[\alpha]_D^{25}$ +10° (*c* 0.2, dioxane).

Found: C, 61.43; H, 5.71; N, 5.70; S, 2.78%. Calcd for $C_{65}H_{71}N_5O_{20}S$: C, 61.26; H, 5.62; N, 5.50; S, 2.52%.

3',4'-Dideoxy-3'-eno-kanamycin B (9). A hot solution of **8** (61 mg) in dioxane (4 ml) was filtered with aid of absorbent cotton in close distance of a bar magnet, and to the filtrate, Dowex 50W X2 resin (H form, 1 ml) pretreated with dioxane was added. After agitation for a while, the mixture was filtered and the filtrate was concentrated. The residual solid was dried at 65 °C *in vacuo* for 2 h. An air-proof vessel containing the above solid was cooled to −60 °C and to it, ammonia was introduced. To the resulting solution (≈18 ml), a piece of sodium metal (≈120 mg) was added and the solution was warmed to −50 °C with stirring within 15 min. The deep-blue solution was kept at the temperature for 1 h. After addition of methanol, ammonia was evaporated with gradual warming to room temperature. To an aqueous solution of the residue, Dowex 50W X2 resin (H form, 4 ml) was added and after agitation for a while, the mixture was poured into a column containing the same resin (3.5 ml). The column was washed thoroughly with water and the product was eluted with 1 M aqueous ammonia. The ninhydrin-positive fractions were collected and concentrated to give a solid, which was thoroughly dried *in vacuo* to give **9** as monocarbonate, 23.8 mg (97%), $[\alpha]_D^{25}$ +44° (*c* 0.4, water); **9** has slightly slower mobility than that of **10** on PPC, and **9** gives bluish brown coloration (*cf.* **10**, blue) with ninhydrin in pyridine. PMR (D_2O+slight DCl) δ: 1.3 (1H q, $J\approx$12 Hz, H-2_{ax}), 2.0 (1H double t, J=3—4, 3—4, and 12 Hz, H-2_{eq}), 5.0 (1H m, H-1'), 5.4 (1H, d, J=3 Hz, H-1''), 5.82 (2H, slightly broadened s, H-3',4').

Found: C, 44.76; H, 7.51; N, 13.75%. Calcd for $C_{18}H_{35}N_5O_8\cdot H_2CO_3$: C, 44.61; H, 7.29; N, 13.69%.

3',4'-Dideoxykanamycin B (10). To an aqueous solution (0.3 ml) of **9** monocarbonate (12.1 mg), platinum oxide (≈3 mg) was added and the mixture was hydrogenated with hydrogen under pressure (3.5 kg/cm^2) at room temperature for 1.5 h. Filtration followed by concentration gave a solid, which was dried thoroughly to give **10** as monocarbonate, 11.5 mg (95%), $[\alpha]_D^{25}$ +109° (*c* 1, water) (lit,[1] +132° as free base).

Found: C, 44.91; H, 7.96; N, 13.63%. Calcd for $C_{18}H_{37}N_5O_8 \cdot H_2CO_3$: C, 44.44; H, 7.65; N, 13.64%.

References

1) H. Umezawa, S. Umezawa, T. Tsuchiya, and Y. Okazaki, *J. Antibiot.*, **24**, 485 (1971); S. Umezawa, H. Umezawa, Y. Okazaki, and T. Tsuchiya, *Bull. Chem. Soc. Jpn.*, **45**, 3624 (1972).

2) T. Miyake, T. Tsuchiya, S. Umezawa, and H. Umezawa, *Carbohydr. Res.*, **49**, 141 (1976).

3) F. H. Bissett, M. E. Evans, and F. W. Parrish, *Carbohydr. Res.*, **5**, 184 (1967).

4) H. Umezawa, T. Tsuchiya, R. Muto, and S. Umezawa, *Bull. Chem. Soc. Jpn.*, **45**, 2842 (1972).

5) S. Umezawa, T. Jikihara, T. Tsuchiya, and H. Umezawa, *J. Antibiot.*, **25**, 322 (1972).

6) Y. Takagi, T. Miyake, T. Tsuchiya, S. Umezawa, and H. Umezawa, *J. Antibiot.*, **26**, 403 (1973); *Bull. Chem. Soc. Jpn.*, **49**, 3649 (1976).

7) The 2″-*O*-mesyl group of 4″,6″-*O*-cyclohexylidene-3′,4′-dideoxy-3′-eno-2″-*O*-mesylpenta-*N*-tosylkanamycin B[2] sometimes resists to elimination by unknown reasons in treatment with sodium in liquid ammonia giving rise to some impurities.

8) S. Umezawa, T. Tsuchiya, and Y. Okazaki, *Bull. Chem. Soc. Jpn.*, **44**, 3494 (1971); *ibid.*, **45**, 3619 (1972).

9) Some inorganic salts seem to destroy sodium radical. Without deironation with bar magnet and successive resin treatment as described in the experimental, the yield of **9** was fluctuating.

10) R. H. Sifferd, V. du Vigneaud, *J. Biol. Chem.*, **108**, 753 (1935).

The Benzannelated Annulenones. Syntheses and Properties of 12-Methylbenzo[*f*]- and Dibenzo[*f,l*]-8,10-bisdehydro[17]annulenone

Jūro Ojima,* Miyako Ishiyama, and Akihiko Kimura

Department of Chemistry, Faculty of Science, Toyama University, Gofuku, Toyama 930

(Received December 27, 1976)

The benzannelated annulenones VII and XI have been synthesized to establish the effect of annelation of benzene ring on the seventeen-membered ring system. An examination of the NMR spectra suggested that both of VII and XI are paratropic and the paratropicities decrease in the order of VII>XI with the number of benzene ring fused to seventeen-membered ring system.

As reported in the previous papers,[1] the monobenzo- (I) and dibenzobisdehydro[13]annulenone (II) were prepared by an aldol condensation of an appropriate aldehyde and ketone containing terminal acetylene group, followed by an oxidative coupling of the resulting acyclic ketone. The same approach has been now extended to synthesis of a next higher $(4n+1)$-membered ring system. The present paper deals with the synthesis and properties of the respective vinylogues of I and II, *i.e.*, 12-methylbenzo[*f*]- (VII) and dibenzo[*f,l*]-8,10-bisdehydro[17]annulenone (XI).[2]

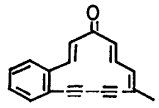

I

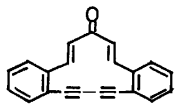

II

As outlined in Scheme, the methylbenzo[17]-annulenone (VII) was synthesized as follows. The starting material was the available *cis*-3-methyl-2-penten-4-ynal (III).[3] This substance was converted to the vinylogue (IV) in an 88% overall yield by transformation to the diethyl acetal of III followed by condensation with ethyl vinyl ether in the presence of zinc chloride and treatment of the ethoxy acetal of the resulting vinylogue with sodium acetate in acetic acid according to the method of Isler *et al.*[4,5] *o*-Ethynylcinnamaldehyde (IX), prepared from *o*-ethynylbenzaldehyde (VIII) as has been reported previously,[6] was condensed with acetone in the presence of aqueous sodium hydroxide to afford the ketone (V) in a high yield. Aldol condensation of the dienyne aldehyde (IV) and the ketone (V) by means of methanolic potassium

Table 1. ^{1}H-NMR parameters of VI and VII in $CDCl_3$ at 100 MHz (τ-values; internal standard, TMS; J in Hz in parentheses)

Proton	VI[a]	VII	ΔVII−VI[i]
H^A	3.53d(15)[b]	4.03d(16)[e]	+0.50
H^B	2.48dd(15,11)[c]	2.28—2.78[f,h]	
H^C	3.05dd(15,11)[d]	3.51dd(16,11)[g]	+0.46
H^D	2.49d(15)	1.94d(16)	−0.55
$H^{A'}$	3.44(15)[b]	4.00d(16)[e]	+0.56
$H^{B'}$	2.53dd(15,11)[c]	2.10dd(16,11)[f]	−0.43
$H^{C'}$	3.54dd(15,11)[d]	3.76dd(16,11)[g]	+0.22
$H^{D'}$	2.45dd(15,11)[c]	1.85dd(16,11)[f]	−0.60
$H^{E'}$	2.95d(11)	3.50d(11)	+0.55
CH_3	8.10s	8.13s	+0.03
Benzenoid H	2.52—2.78m	2.28—2.78m	

a) In addition, two singlets at 6.57 and 6.61 (-C≡CH). b),c),d),e),f),g) These assignments may be reversed in each group, but most probable values are given by referring to the NMR spectra of the related compounds.[1] h) This proton signal is submerged by those of benzenoid protons. i) This exhibits the chemical shift differences for the resonances on passing from IV to V.

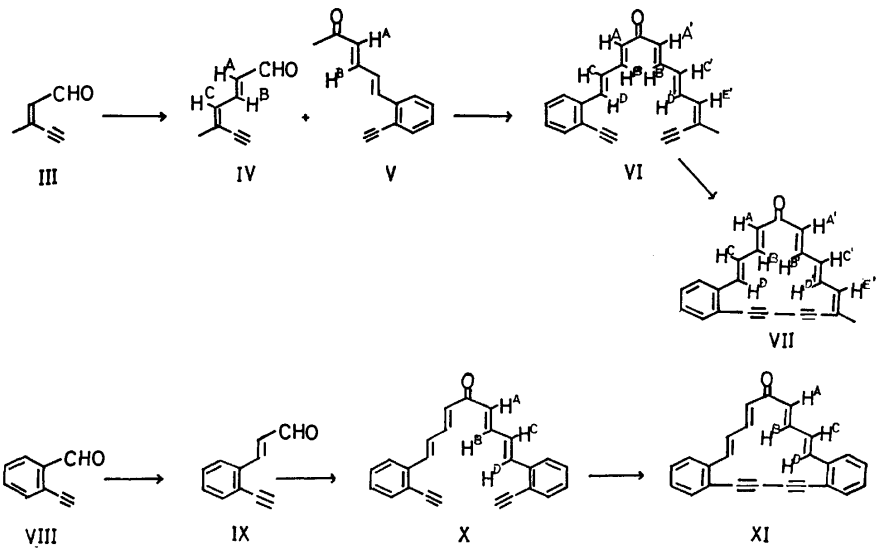

* The author to whom correspondence should be addressed.

Table 2. ^{1}H-NMR parameters of X and XI at 90 MHz (τ-values; Internal Standard, TMS; J in Hz in Parentheses)

Proton	X in $CDCl_3$[a]	XI in $CDCl_3$	XI in CF_3COOD	ΔXI−X
H^A	3.43d(15)	3.92d(16)	3.60d(16)	+0.49
H^B	3.05dd(15,11)	2.28dd(16,11)	1.18dd(16,11)	−0.77
H^C		3.33dd(16,11)	3.20dd(16,11)	(+1.0—+0.53)
H^D		2.08d(16)	1.03d(16)	(−0.72——0.22)
	2.3—2.8m[b]			
Benzenoid H		2.5—2.8m	2.45—2.70m	

a) In addition, a singlet at 6.63 (-C≡CH).
b) The resonances of H^C and H^D protons are submerged by those of benzenoid protons.

hydroxide gave the acyclic ketone (VI) in a 38% yield. Oxidation of VI with copper(II) acetate in pyridine[7] afforded the monobenzannelated annulenone (VII) as yellow crystals in a low yield.

While, a condensation of 2 molar equivalents of IX with 1 molar equivalent of acetone, under the same conditions as indicated for the reaction of IV and V, afforded the acyclic ketone (X) in a 28% yield as orange crystals. Oxidation of X as before yielded the dibenzannelated annulenone (XI) as yellow crystals.

An inspection of the Dreiding molecular model reveals that the title compounds VII and XI should have the assigned conformations corresponding to those for I and II, respectively.

The ^{1}H-NMR parameters of the compounds thus obtained are shown in Tables 1 and 2. The comparison of VI and VII (Table 1) suggests that the compound VII is paratropic, as expected for a potential 16π-electron system due to the polarization of the carbonyl group, since the inner proton (H^B, $H^{B'}$, H^D, $H^{D'}$) resonances have moved to a lower field, and the outer (H^A, $H^{A'}$, H^C, $H^{C'}$, $H^{E'}$) and methyl ones to a higher field, as compared with those of the corresponding protons of the acyclic analogue (VI), respectively.

The similar result as above is obtained for the comparison of the parameters between X and XI (Table 2),[8] although the chemical shift differences are smaller than those between VI and VII. Furthermore, the chemical shifts of the olefinic protons of XI in CF_3-COOD (the carbonyl protonated species) also suggest that XI is paratropic, if we consider the small downfield shift of all protons may be caused by introduction of the positive charge.

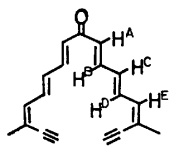

XII

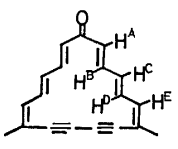

XIII

In order to obtain an approximate measure of the effect of benzannelation on seventeen-membered ring system, the ^{1}H-NMR parameters of the model compounds (XII and XIII) synthesized by Ojima and Sondheimer,[9] are listed in Table 3.

As shown in Tables (1, 2, 3), an examination of the NMR spectra demonstrated that the seventeen-membered ring system in dimethyl compound XIII is paratropic, in monobenzo-fused compound VII, it is less paratropic, and in dibenzo-fused compound XI, it is at most weakly paratropic. The sequence can be seen in particular by the downfield shifts, as compared with the respective models (XIII, VII, XI), of the inner proton (H^B, $H^{B'}$, H^D, $H^{D'}$) bands [(−1.24——1.55), (−0.43——0.60), (−0.22——0.77) ppm, respectively], and the chemical shifts [(1.37—1.40), (1.85—),[10] (2.08—2.28) τ, respectively].

Table 3. ^{1}H-NMR parameters of XII and XIII at 60 MHz (τ-values; internal standard, TMS; J in Hz inparentheses)

Proton	XII[a]	XIII	ΔXIII−XII
H^A	3.57d(16)	4.20d(16)	+0.63
H^B	2.64dd(16,11) or 2.92dd(16,11)	1.37dd(16,11) or 1.40dd(16,11)	−1.24——1.55
H^C	3.61dd(16,11)	3.98dd(16,11)	+0.37
H^D	2.64dd(16,11) or 2.92dd(16,11)	1.37dd(16,11) or 1.40dd(16,11)	−1.24——1.55
H^E	3.60d(11)	3.67d(11)	+0.07
CH_3	8.01s	8.23s	+0.22

a) In addition, a singlet at 6.59 (-C≡CH).

The result obtained in the above is accord with that on thirteen-membered ring system obtained by us.[1]

Experimental

The deoxygenated ether, methanol, and acetone were used to minimize an oxidation of the compounds used for aldol condensation and prepared immediately before use. The ether was freed from a peroxide by passing through a short column of basic alumina (Woelm, Act. I) followed by flushing with nitrogen. The methanol and acetone were flushed by nitrogen immediately prior to use. All 20% methanolic potassium hydroxide solutions were prepared before each use by dissolving 10g of potassium hydroxide in 50 ml of methanol and flushing the solution with nitrogen. All the melting points are uncorrected. Brockmann alumina (Act. II—III) was used for column chromatography unless otherwise indicated. The IR, UV, and mass spectra were taken on a Hitachi EPI-S2 or a Unicam SP-200, a Hitachi 124 or a Unicam SP-800, and a JEOL-JMS-SG-2 or an AEI MS-12 spectrometers, respectively. Shoulders in UV spectra are denoted by sh, and wavelength of absorption maximum is recorded in nm and ε-values are given in parentheses. NMR

spectra were taken on a Varian XL-100, a Varian EM-930, a JEOL-JNM-MH-60 or a Varian T-60 spectrometer. Chemical shifts are given in τ-values with respect to TMS as an internal standard, while the coupling constants (J) are given in Hz.

5-Methyl-2,4-heptadien-6-ynal (IV)[5] A 1% solution of *p*-toluenesulfonic acid monohydrate in absolute ethanol (9 drops) was added to a solution of the aldehyde (III, 3.0 g, 0.032 mol) and ethyl orthoformate (6.0 g, 0.04 mol) in absolute ethanol (5 ml). After being stirred at room temperature for 24 h, the mixture was treated with pyridine (0.5 ml) and poured into 2% aqueous sodium hydrogencarbonate (50 ml). Extraction with ether, drying over magnesium sulfate, and evaporation of the solvent yielded the crude diethyl acetal of III as a red liquid. The liquid was dissolved in ethyl acetate (5 ml) and warmed to 35 °C in a flask equipped with two dropping funnels, a condenser, and a magnetic stirrer. A 10% solution of zinc chloride in ethyl acetate (10 drops) was added, and then simultaneously this solution (5 ml) and ethyl vinyl ether (20 ml) during 15 min with stirring at 35 °C. The mixture was stirred for 2 h at room temperature, stoppered, and allowed to stand for 17 h. A solution of sodium acetate (10 g) in water (7 ml) and acetic acid (100 ml) was then added, and the mixture was heated to 90 °C for 2 h. Dilution with water (500 ml), extraction with ether, drying over magnesium sulfate, and evaporation gave a residue, which was chromatographed on alumina (100 g, Woelm, Act. III). Elution with pentane–ether (96: 4—94: 6) and evaporation of the solvents gave the aldehyde (IV, 3.4 g, 88%) as pale yellow liquid, IR (neat): 3250 (–C≡CH), 2100 (–C≡C–), 1675, 1615 (C=O, C=C), 980 cm^{-1} (*trans* C=C), UV: λ_{max}^{ether} 290 (24100), 300 sh nm (23100), NMR ($CDCl_3$, 60 MHz): 0.33 (d, J=8, 1H, –CHO), 2.47 (dd, J=15, 11, 1H, H^B), 3.47 (d, J=11, 1H, H^C), 3.83 (dd, J=15, 8, 1H, H^A), 6.32 (s, 1H, –C≡CH), 7.95 (s, 3H, $-CH_3$), MS: *m/e* 120 (M^+), 119 (M^+–1), 105 (M^+–15), 91 (M^+–29); mol wt, 120.14.

6-(o-Ethynylphenyl)-3,5-hexadien-2-one (V). To a stirred solution of *o*-ethynylcinnamaldehyde (IX, 4.7 g, 0.031 mol) in acetone (250 ml) was added under a nitrogen atmosphere a 5% aqueous sodium hydroxide solution (135 ml) over a period of 15 min at room temperature and stirring was continued for further 2 h at the same temperature. Neutralization with acetic acid and addition of water (250 ml) was followed by extraction with ether. The extracts were washed successively with saturated aqueous sodium hydrogencarbonate and sodium chloride solutions, dried over sodium sulfate and evaporated. The residue was chromatographed on alumina (130 g), eluting with 30% ether in light petroleum to give the ketone (V, 4.8 g, 81%) as crystals. Recrystallization from hexane–benzene afforded pure V as yellow cubes, mp 75.0—76.5 °C, IR (KBr disk): 3250 (–C≡CH), 2100 (–C≡C–), 1655, 1620, 1595 (C=O, C=C), 1000, 970 cm^{-1} (*trans* C=C), MS: *m/e* 196 (M^+, 55), 153 (100); mol wt, 196.24, UV: λ_{max}^{THF} 246 (11000), 254 (15000), 320 nm (29500), NMR ($CDCl_3$, 60 MHz): 2.47—3.05 (m, 6H, phenyl and olefinic H), 3.25 (dd, J=16, 10, 1H, H^B), 3.85 (d, J=16, 1H, H^A), 6.55 (s, 1H, –C≡CH), 7.82 (s, 3H, Me).

Found: C, 85.42; H, 6.09%. Calcd for $C_{14}H_{12}O$: C, 85.68; H, 6.16%.

1-(o-Ethynylphenyl)-11-methyl-1,3,6,8,10-tridecapentaen-12-yn-5-one (VI). To a mixture of the dienyne aldehyde (IV, 1.5 g, 0.0125 mol) and the ketone (V, 1.2 g, 0.0061 mol) in deoxygenated ether (80 ml) was added a 20% methanolic potassium hydroxide solution (4.5 ml) with stirring on ice-bath. The mixture was then stirred at room temperature for 90 min. Neutralization with acetic acid (5 ml) followed by pouring into water (1000 ml) and extraction with benzene gave an organic extract which was washed successively with saturated sodium hydrogencarbonate and sodium chloride solutions, and dried over sodium sulfate. The residue obtained by evaporation of the solvent was chromatographed on alumina (100 g) with light petroleum–ether (7: 3) to give the ketone (VI, 0.7 g, 38%) as unstable solids. Recrystallization from hexane–benzene formed yellow-brown needles, mp 121.5—122.5 °C, MS: *m/e* 298 (M^+, 80), 154 (100); mol wt, 198.36, IR (KBr disk): 3300, 3250 (–C≡CH), 2100 (–C≡C–), 1660, 1605, 1600 (C=O, C=C), 1010 cm^{-1} (*trans* C=C), UV: λ_{max}^{THF} 258 (20200), 267 (21800), 288 sh (18500), 378 nm ((40700), NMR: see Table 1.

12-Methylbenzo[f]-8,10-bisdehydro[17]annulenone (VII). A solution of VI (0.6 g, 0.002 mol) in pyridine (26 ml) was added, drop by drop, with stirring over a period of 10 min into a solution of copper(II) acetate monohydrate (9.0 g) in pyridine (19 ml) kept at 55 °C; the mixture was stirred for further 2 h at 60—65 °C. Then the mixture was chilled, diluted with benzene (200 ml), and poured into 6% hydrochloric acid (1000 ml). The layers were separated, and the aqueous layer was extracted with benzene. The combined benzene layer was washed successively with aqueous sodium hydrogencarbonate and saturated sodium chloride solutions, dried over sodium sulfate, and evaporated *in vacuo*. The residue was chromatographed on alumina (100 g) with light petroleum–ether (1: 1) to give VII (0.07 g, 12%) as relatively stable solids. Recrystallization from hexane–benzene afforded pure VII as yellow cubes, mp *ca.* 180 °C (dec), MS: *m/e* 296 (M^+, 45), 252 (100); mol wt, 296.35, IR (KBr disk): 2200 (–C≡C–), 1630 (C=O), 1595 (C=C), 995 cm^{-1} (*trans* C=C), UV: λ_{max}^{THF} 285 sh (28500), 299 (35500), 317 (30400), 400 nm (2760), NMR: see Table 1.

1,10-Bis(o-ethynylphenyl)-1,3,6,8-decatetraen-5-one (X). A 20% methanolic potassium hydroxide solution (2 ml) was added dropwise to a stirred solution of *o*-ethynylcinnamaldehyde (IX, 5.0 g, 32.0 mmol) and acetone (1.14 g, 19.6 mmol) in deoxygenated ether (103 ml) at room temperature over a period of 15 min. After had been stirred for 2 h at the same temperature, the reaction mixture was neutralized with acetic acid (2 ml) and mixed with water (300 ml). The mixture was extracted with benzene. After work up of the extracts in the standard way, a dark red liquid obtained was chromatographed on alumina (150 g) with light petroleum–ether (75: 25—55: 45) to give X (1.49 g, 28%) as solids. Recrystallization from light petroleum–benzene gave pure X as orange needles, mp 149.0—149.8 °C,[11] MS: *m/e* 334 (M^+, 85), 154 (100); mol wt, 334.39, IR (KBr disk): 3250 (–C≡CH), 2100 (–C≡C–), 1660, 1620, 1595 (C=O, C=C), 995 cm^{-1} (*trans* C=C), UV: λ_{max}^{THF} 236 (42200), 259 (29500), 267 (29800), 369 nm (57400), NMR: see Table 2.

Found: C, 89.59; H, 5.18%. Calcd for $C_{25}H_{18}O$: C, 89.79; H, 5.43%.

Dibenzo[f,l]-8,10-bisdehydro[17]annulenone (XI). A solution of the ketone (X, 2.08 g, 6.22 mmol) in pyridine (35 ml) was added to a stirred solution of copper(II) acetate monohydrate (17.0 g) in pyridine (56 ml) at 50 °C over a period of 30 min, and the reaction mixture was stirred for further 3 h at 60—65 °C. The precipitate formed on cooling and diluted with benzene (300 ml) was washed with benzene (50 ml × 3). Then the filtrate was washed with 6% hydrochloric acid until it was slightly acidic, and saturated aqueous sodium hydrogencarbonate and sodium chloride solutions successively, and dried over sodium sulfate. The residual dark red liquid obtained after evaporation of the solvent was chromatographed on alumina (130 g) with light petroleum–ether (1: 1) to give the ketone (XI, 348 mg, 17%) as crystals.

Recrystallization from benzene gave pure XI as yellow cubes, mp 209—210.5 °C (dec),[11] MS: *m/e* 332 (M^+, 60), 313 (100); mol wt, 332.38, IR (KBr disk): 2200 (–C≡C–), 1640, 1606, 1594 (C=O, C=C), 1000, 960 cm^{-1} (*trans* C=C), UV: λ_{max}^{THF} 224 (63300), 297 (63300), 313 nm (70000); λ_{max} (CF_3-COOH): 275 sh, 292, 309, 328, 355 sh, 395 sh, 572 nm, NMR: see Table 2.

Found: C, 90.33; H, 4.79%. Calcd for $C_{25}H_{16}O$: C, 90.33; H, 4.85%.

The authors wish to thank Professor F. Sondheimer, University College London, for kindly providing unpublished result. We also thank Dr. S. Akiyama and Prof. M. Nakagawa, Osaka University, for measuring NMR spectra at 100 MHz, and Mr. M. Ikeguchi for his experimental help. This research was financially supported by a Grant-in-Aid for Scientific Research from the Ministry of Education (974151, 1974), which is gratefully acknowledged.

References

1) a) J. Ojima, Y. Yokoyama, and T. Yokoyama, *Chem. Lett.*, **1974**, 1261. b) J. Ojima, M. Ishiyama, A. Kimura, and Y. Yokoyama, *Tetrahedrom Lett.*, **1975**, 1909. c) J. Ojima, Y. Yokoyama, and M. Enkaku, *Bull. Chem. Soc. Jpn.*, **50**, 1522 (1977).

2) For preliminary reports, see a) J. Ojima, A. Kimura, and T. Yokoyama, *Chem. Lett.*, **1975**, 207. b) Ref. 1b.

3) E. R. H. Jones and B. C. L. Weedon, *J. Chem. Soc.*, **1946**, 937; J. Ojima, T. Katakami, G. Nakaminami, and M. Nakagawa, *Bull. Chem. Soc. Jpn.*, **49**, 292 (1976).

4) O. Isler, H. Linder, M. Montavon, H. Rüegg, and P. Zeller, *Helv. Chim. Acta.*, **39**, 249 (1956); H. Rüegg, H. Montavon, G. Saucy, H. Schwieter, and O. Isler, *ibid.*, **42**, 854 (1959).

5) This experiment was carried out in the Prof. Sondheimer's laboratory at University College London.

6) J. Ojima, A. Kimura, Y. Yokoyama, and T. Yokoyama, *Bull. Chem. Soc. Jpn.*, **48**, 367 (1975).

7) G. Eglinton and A. R. Galbraith, *Chem. Ind.*, **1956**, 737; *J. Chem. Soc.*, **1959**, 889.

8) These ^{1}H-NMR spectra were reexamined by measuring at 90 MHz spectrometer after a preliminary report (Ref. 2a).

9) J. Ojima and F. Sondheimer, The Proceedings of the 30th Annual Meeting of the Chemical Society of Japan, Osaka, April, Vol. III (1974), p. 1531.

10) It is unable to determine the value because the signal of H^B proton of VII is submerged by those of benzenoid protons.

11) The melting points of X and XI given in the preliminary report (Ref. 2a) were erroneous.

A Practical Synthesis of Polyhalomethyllithium-Carbonyl Adducts[1)]

Hiroaki TAGUCHI, Hisashi YAMAMOTO, and Hitosi NOZAKI
Department of Industrial Chemistry, Kyoto University, Yoshida, Kyoto 606
(Received January 5, 1977)

The title adducts are produced upon treatment of a mixture of polyhalomethane and a carbonyl compound with a hindered lithium amide. The kinetically controlled, selective lithiation of the halide enables us to avoid a troublesome procedure involving preformed lithium carbenoid. The halide components examined are dichloromethane, dibromomethane, diiodomethane, chloroform, and bromoform, while the carbonyl ones are ubiquitous ketones and nonanal. A *gem*-dichloroallyllithium is generated similarly from 3,3-dichloropropene and, furthermore, the procedure is successfully extended to the Darzens-type reaction of α-halo esters.

Polyhalomethyllithiums have proved to be extremely useful in organic synthesis as shown in the accompanying scheme.[2,3,4)] For example, nucleophilic addition of dichloromethyllithium to ketones, followed by α-chloro aldehyde formation and dehydrochlorination, gives one carbon homologated α,β-unsaturated aldehydes.[4b)]

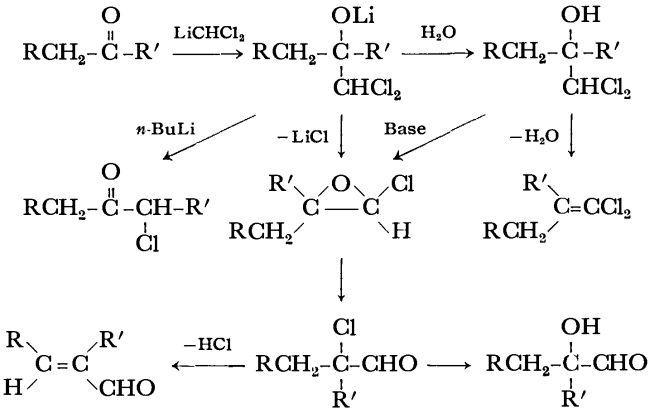

Difficulties arise from the extreme thermolability of the carbenoids[2,3)] in generating them on a large scale. Slow and constant addition of butyllithium under vigorous stirring of the halide solution is essential even at −78 °C in order to prevent the local heating, which causes the rapid decomposition of the resulting lithium reagent. The optimum reaction temperature, which is normally between −70 and −120 °C (internal temperature), is limited at the lower end of the range by the rate of formation, and the upper end by the tendency of the carbenoids to decompose.

We have disclosed that the *in situ* reaction of a polyhalomethyllithium with carbonyl compounds offers a simple and direct solution to this problem. Treatment of a mixture of polyhalomethane and carbonyl component with an *N,N*-disubstituted lithium amide[5)] results in the preferential formation of polyhalomethyllithium instead of the expected enolate. The carbenoid attacks instantaneously the carbonyl group prior to its thermal decomposition. With this new technique in hand, we can prepare dichloromethyllithium–cyclohexanone adduct even at the reaction temperature of 0 °C in an 89% isolation yield. Table 1 summarizes the fairly extensive scope of this technique.

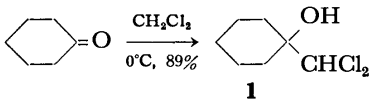

1

Obvious side reaction is the formation of 2-halooxirane, whose rearrangement produces α-halo aldehyde. The extent of such consecutive reactions was not significant upon treatment of simple ketones or aldehydes with dichloro- or dibromomethyllithium. However, the rate of ring closure was found to be greatly enhanced in the reaction of dibromomethyllithium with carbonyl componenents having bulky group directly attached to C=O moiety, probably owing to the steric acceleration. Minimizing this pathway has been attained by performing the reaction in less polar solvents and at lower temperatures. Ether was found to be a favorable solvent for the isolation of hydroxylic adducts, while tetrahydrofuran (THF) gave poor yields. Although the safe upper limit of the reaction temperature was found to be −78 °C, the reaction of crowded carbonyl components should preferably be performed at −95 °C.

Both diiodomethyllithium and tribromomethyllithium are extremely unstable even at −110 °C.[6)] The carbonyl adducts of these carbenoids could, however, be prepared in good to excellent yields by means of the present *in situ* technique at −78 °C (external cooling). Although cyclopentanone is known as one of the readily enolizable ketones, the generation of polyhalomethyllithium proceeded in preference of the enolate formation to afford the desired adducts in good yields. With respect to the basic reagent, lithium diisopropylamide, lithium dicyclohexylamide, and lithium 2,2,6,6-tetramethylpiperidine all gave satisfactory results.

Seyferth and co-workers previously prepared *gem*-dichloroallyllithium from $Ph_3PbCH_2CH{=}CCl_2$ by the action of butyllithium.[7)] In extention of the present method, the carbenoid-carbonyl adduct was synthesized directly from 3,3-dichloropropene in a single step. Addition of lithium diisopropylamide to a mixture of cyclododecanone and the dichloride furnished 1-(3,3-dichloropropenyl)cyclododecanol **2** in 66% yield.

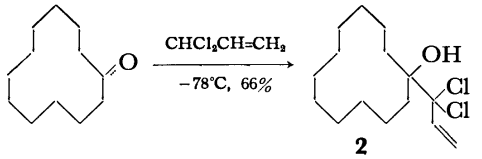

2

Attempts to obtain a carbonyl adduct of monohalomethyllithium derived from allyl bromide or methyl iodide failed to success. The halides containing –COOR moiety on the α-carbon afforded the desired adducts almost quantitatively. Treatment of a mixture of methyl bromoacetate and cyclohexanone with lithium

Table 1. Preparations of polyhalomethyllithium-carbonyl adducts

Polyhalomethane	Carbonyl	Method[c]	Temp, °C	% Yield[b]
CH_2Cl_2	Cyclohexanone	A	−78	quant.
CH_2Cl_2	Cyclohexanone	B	0	89
CH_2Cl_2	Cyclohexanone	C	−78	86
CH_2Cl_2	Cyclopentanone	A	0	66
CH_2Cl_2	Cyclopentanone	A	−20	90
CH_2Cl_2	Cycloheptanone	A	−20	88
CH_2Cl_2	6-Methyl-5-hepten-2-one	A	0	84
CH_2Cl_2	Nonanal	C	0	73
CH_2Br_2	Cyclopentanone	C	−78	82
CH_2Br_2	Cyclohexanone	C	−78	91
CH_2Br_2	Cycloheptanone	C	−78	76
CH_2Br_2	Cyclooctanone	D	−78	70
CH_2Br_2	Cyclododecanone	E	−95	81
CH_2Br_2	2-Methyl-cyclohexanone	E	−78	75
CH_2Br_2	2-Methyl-cyclododecanone	E	−78	66
CH_2Br_2	2-Methylcyclo-tetradecanone	E	−78	78
CH_2Br_2	2-Cyclohexanone	D	−78	67
CH_2Br_2	2-Cycloheptanone	D	−78	75
CH_2Br_2	Nonanal	C	−78	77
CH_2I_2	Nonanal	C	−78	79
$CHCl_3$	Cyclopentanone	F	−78	91
$CHCl_3$	Cyclohexanone	C	−78	92
$CHCl_3$	Cyclohexanone	F	−78	94
$CHBr_3$	Cyclohexanone	C	−78	91

a) For details, see experimental part. b) Yields are based on material isolated by column or thin layer chromatography. c) *Method A*: Lithium dicyclohexylamide (2 equiv) was added to a polyhalomethane solution of carbonyl compound over a period of 1 h; *Method B*: Lithium dicyclohexylamide (2 equiv) was added to a polyhalomethane solution of carbonyl compound over a period of 10 min; *Method C*: Lithium dicyclohexylamide (2 equiv) was added to a THF solution of carbonyl compound and polyhalomethane (24 equiv) over 1 h; *Method D*: Lithium 2,2,6,6-tetramethylpiperidine (2.2 equiv) was added to a THF solution of carbonyl compound and polyhalomethane (2.2 equiv) over a period of 1 h; *Method E*: Lithium 2,2,6,6-tetramethylpiperidine (2.2 equiv) was added to an ether solution of carbonyl compound and polyhalomethane (2.2 equiv) over a period of 1 h; *Method F*: Lithium dicyclohexylamide (2 equiv) was added to a THF solution of carbonyl compound and polyhalomethane (2 equiv) over a period of 1 h.

dicyclohexylamide afforded a Darzens-type product, methyl α,β-epoxycyclohexylacetate **3**, in 93% yield.[8] In contrast, ethyl dichloroacetate gave an aldol, ethyl dichloro(1-hydroxycyclohexyl)acetate **4**, in 91% yield. This variation provides a simple and efficient means of preparing two carbon homologated esters.

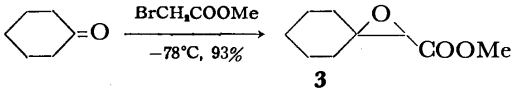

3

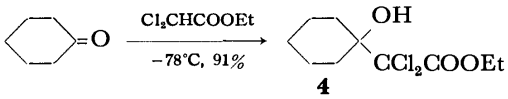

4

Experimental

The IR spectra were determined on a Shimadzu IR-27-G spectrometer; the mass spectra, on a Hitachi RMU-6L mass spectrometer; and the NMR spectra, on a JEOL C-60-H or a Varian EM-360 spectrometer. The chemical shifts are given in δ, with TMS as the internal standard. The analyses were carried out by the staff at the Elemental Analyses Center of Kyoto University. All the experiments were carried out under an atmosphere of dry nitrogen, by preparative thin-layer chromatography (PLC) on silica gel PF-254 plates (Merck) with benzene as an eluent, and by preparative column chromatography on silica gel Wakogel C-100 (Wako).

Preparation of Polyhalomethylcarbinols. Method A: Lithium dicyclohexylamide (50 mmol) was prepared from dicyclohexylamine (9.05 g, 50 mmol) in dry THF (50 ml) with butyllithium (50 mmol, 33 ml of 1.5 M hexane solution) at 0 °C. This solution was added dropwise into a well-stirred polyhalomethane (50 ml) solution of carbonyl compound (25 mmol) under a nitrogen atmosphere over a period of 1 h at the low temperature described in Table 1. The mixture was then allowed to stand for 1 h at the same low temperature. After hydrolysis at that temperature, the resulting organic layer was extracted with ether, and the extract was washed with water and dried over anhydrous Na_2SO_4. The solution was condensed under reduced pressure, and the residue was purified by column chromatography using benzene as an eluent.

Method B: A well-stirred solution of carbonyl compound (1.0 mmol) in polyhalomethane (2.0 ml) was cooled to the temperature listed in Table 1. To the mixture was added a THF solution of lithium dicyclohexylamide (2.0 mmol) dropwise over a period of 10 min, and the resulting solution was stirred for 5 min at the same temperature. After extractive work up, polyhalomethylcarbinol was obtained by PLC using benzene as an eluent.

Method C: A well-stirred solution of polyhalomethane (50 mmol) and carbonyl compound (25 mmol) in dry THF (50 ml) was cooled to the temperature described in Table 1. To the mixture was added a THF solution of lithium dicyclohexylamide (50 mmol) dropwise over a period of 1 h. The mixture was stirred for 1 h at that temperature. After extractive work up, polyhalomethylcarbinol was obtained by column chromatography using benzene as an eluent.

Method D: A THF solution of lithium 2,2,6,6-tetramethylpiperidide (2.2 mmol) was added to a stirred solution of polyhalomethane (2.2 mmol) and carbonyl compound (1.0 mmol) in dry THF over a period of 1 h at low temperature. Polyhalomethylcarbinol was obtained according to the similar procedure.

Method E: To an ether solution of polyhalomethane (2.2 mmol) and carbonyl compound (1.0 mmol) was added a THF solution of lithium 2,2,6,6-tetramethylpiperidine (2.2 mmol) mmol) over a period of 1 h at low temperature, and the solution was stirred for 1 h at the same temperature. Polyhalomethylcarbinol was obtained according to the similar procedure.

Method F: A well-stirred solution of polyhalomethane (24 mmol) and carbonyl compound (1 mmol) in dry THF was cooled to low temperature. To the mixture was added a THF solution of lithium dicyclohexylamide (2 mmol) over a period of 1 h and the resulting solution was stirred for 1 h at

the same temperature. After extractive work up, polyhalomethylcarbinol was obtained by PLC using benzene as an eluent.

1-Dichloromethylcyclopentanol: Bp 110 °C (bath temp 14 Torr); IR (neat) 3450, 790, 760 cm^{-1}; NMR (CCl_4) δ 1.46—2.15 (m, 8H), 2.25 (s, 1H), 5.65 (s, 1H); MS: *m/e* (%) 139 (11), 85 (100). Found: C, 42.9; H, 6.2%. Calcd for $C_6H_{10}Cl_2O$: C, 42.6; H, 6.0%.

1-Dichloromethylcyclohexanol: Bp 118 °C (20 Torr); IR (neat) 3460, 980, 785, 750 cm^{-1}; NMR (CCl_4) δ 1.10—2.10 (m, 10H), 2.20 (s, 1H), 5.49 (s, 1H); mass *m/e* (%) 149 (1), 139 (4), 99 (100). Found: C, 46.0; H, 6.9%. Calcd for $C_7H_{12}Cl_2O$: C, 45.9; H, 6.6%.

1-Dichloromethylcycloheptanol: Bp 155 °C (bath temp 14 Torr); IR (neat) 3460, 805, 780, 732 cm^{-1}; NMR (CCl_4) δ 1.35—2.30 (m, 12H), 2.18 (s, 1H), 5.54 (s, 1H); mass *m/e* (%) 173 (trace), 113 (100). Found: C, 48.9; H, 7.4%. Calcd for $C_8H_{14}Cl_2O$: C, 48.8; H, 7.2%.

1,1-Dichloro-2,6-dimethyl-5-hepten-2-ol: Bp 110 °C (bath temp 2 Torr); IR (neat) 3470, 796, 770 cm^{-1}; NMR (CCl_4) δ 1.36 (s, 3H), 1.58 (s, 3H), 1.64 (s, 3H), 1.70—2.45 (m, 4H), 5.07 (m, 1H); mass *m/e* (%) 212 (3), 210 (5), 109 (68). Found: C, 51.3; H, 7.8%. Calcd for $C_9H_{16}Cl_2O$: C, 51.2; H, 7.6%.

1,1-Dichloro-2-decanol: Bp 130 °C (bath temp 2 Torr); IR (neat) 3500, 780 cm^{-1}; NMR (CCl_4) δ 0.75—1.10 (m, 3H), 1.10—1.85 (m, 14H), 2.65 (m, 1H), 3.75 (m, 1H), 5.54 (d, J=4, 1H); mass *m/e* (%) 143 (18), 83 (45). Found: C, 52.6; H, 9.0%. Calcd for $C_{10}H_{20}Cl_2O$: C, 52.9; H, 8.9%.

1-Dibromomethylcyclopentanol: Bp 140 °C (bath temp 2 Torr); IR (neat) 3450, 745, 688 cm^{-1}; NMR (CCl_4) δ 1.55—2.25 (m, 8H), 2.30 (s, 1H) 5.68 (s, 1H); mass *m/e* (%) 137 (6), 135 (6), 85 (100). Found: C, 28.0; H, 3.7%. Calcd for $C_6H_{10}Br_2O$: C, 27.9; H, 3.9%.

1-Dibromomethylcyclohexanol: Bp 74 °C (2 Torr); IR (neat) 3570, 974, 745 cm^{-1}; NMR (CCl_4) δ 1.30—2.20 (m, 10H), 1.98 (s, 1H), 5.59 (s, 1H); mass *m/e* (%) 231 (trace), 229 (trace), 227 (trace), 99 (100). Found: C, 31.0; H, 4.5%. Calcd for $C_7H_{12}Br_2O$: C, 30.9; H, 4.5%.

1-Dibromomethylcycloheptanol: Bp 152 °C (bath temp 2 Torr); IR (neat) 3460, 800, 720 cm^{-1}; NMR (CCl_4) δ 1.30—2.27 (m, 12H), 2.31 (s, 1H), 5.62 (s, 1H); mass *m/e* (%) 288 (trace), 286 (trace), 284 (trace), 113 (100). Found: C, 33.8; H, 4.9%. Calcd for $C_8H_{14}Br_2O$: C, 33.6; H, 4.9%.

1-Dibromomethylcyclooctanol: Bp 150 °C (bath temp 1 Torr); IR (neat) 3460, 787, 688 cm^{-1}; NMR (CCl_4) δ 1.10—2.23 (m, 14H), 2.33 (s, 1H), 5.68 (s, 1H); mass *m/e* (%) 302 (1), 300 (2), 298 (1), 127 (100). Found: C, 36.3; H, 5.4%. Calcd for $C_9H_{16}Br_2O$: C, 36.0; H, 5.4%.

1-Dibromomethylcyclododecanol: Mp 61 °C; IR (Nujol) 3450, 693 cm^{-1}; NMR ($CDCl_3$) δ 0.77—2.00 (m, 22H), 2.08 (s, 1H), 5.73 (s, 1H); mass *m/e* (%) 279 (3), 277 (3), 183 (100). Found: C, 43.9; H, 6.8%. Calcd for $C_{13}H_{24}Br_2O$: C, 43.8. H, 6.8%.

1-Dibromomethyl-2-methylcyclohexanol: Bp 156 °C (bath temp 15 Torr); IR (neat) 3560, 737, 684 cm^{-1}; NMR (CCl_4) δ 0.90 (d, J=6, 3H), 1.07—2.36 (m, 9H), 2.47 (s, 1H), 5.70 (s, 1H); mass *m/e* (%) 288 (1), 286 (2), 284 (1), 95 (100); Found: C, 33.8; H, 5.0%. Calcd for $C_8H_{14}Br_2O$: C, 33.6; H, 4.9%.

1-Dibromomethyl-2-methylcyclododecanol: Mp 61 °C; IR (Nujol) 3500, 958, 700 cm^{-1}; NMR ($CDCl_3$) δ 5.73 (s, C<u>H</u>Br_2 of major isomer), 5.81 (s, C<u>H</u>Br_2 of minor isomer); mass *m/e* (%) 380 (2), 197 (100). Found: C, 45.6; H, 7.3%. Calcd for $C_{14}H_{26}Br_2O$: C, 45.4; H, 7.1%.

1-Dibromomethyl-2-methylcyclotetradecanol: Bp 190 °C (bath temp 2 Torr); IR (neat) 3580, 978, 702 cm^{-1}; NMR (CCl_4) δ 5.78 (s, C<u>H</u>Br_2 of major isomer), 5.86 (s, C<u>H</u>Br_2 of minor isomer); mass *m/e* (%) 398 (trace), 225 (51), 55 (100). Found: C, 48.1; H, 7.6%. Calcd for $C_{16}H_{30}Br_2O$: C, 48.3; H, 7.6%.

1-Dibromomethyl-2-cyclohexenol: Bp 110 °C (bath temp 2 Torr); IR (neat) 3450, 850, 736 cm^{-1}; NMR (CCl_4) δ 1.52—2.30 (m, 6H), 2.38 (m, 1H), 5.63 (s, 1H), 5.70—6.16 (m, 2H); mass *m/e* (%) 272 (1), 270 (2), 268 (1), 97 (100). Found: C, 31.1; H, 3.9%. Calcd for $C_7H_{10}Br_2O$: C, 31.1; H, 3.7%.

1-Dibromomethyl-2-cycloheptenol: Bp 125 °C (bath temp 1 Torr); IR (neat) 3450, 861, 757 cm^{-1}: NMR (CCl_4) δ 1.30—2.50 (m, 8H), 1.62 (s, 1H), 5.69 (s, 1H), 5.60—6.20 (m, 2H); mass *m/e* (%) 286 (trace), 284 (trace), 282 (trace), 111 (100). Found: C, 33.9; H, 4.4%. Calcd for $C_8H_{12}Br_2O$: C, 33.8; H, 4.3%.

1,1-Dibromo-2-decanol: Bp 165 °C (bath temp 4 Torr); IR (neat), 3450, 708 cm^{-1}; NMR (CCl_4) δ 0.66—1.06 (m, 3H), 1.06—1.97 (m, 14H), 2.77 (m, 1H), 3.75 (m, 1H), 5.64 (d, J=4, 1H); mass *m/e* (%) 205 (trace), 203 (1), 201 (trace), 143 (40), 69 (100). Found: C, 38.2; H, 6.6%. Calcd for $C_{10}H_{20}Br_2O$: C, 38.0; H, 6.4%.

1,1-Diiodo-2-decanol: Bp 180 °C (bath temp 0.1 Torr); IR (neat) 3440, 758, 677 cm^{-1}; NMR (CCl_4) δ 0.65—1.05 (m, 3H), 1.05—2.00 (m, 14H), 2.96 (m, 1H), 3.05 (m, 1H), 5.22 (d, J=4, 1H); mass *m/e* (%) 410 (M^+, 1), 283 (10), 268 (15), 170 (15).

1-Trichloromethylcyclopentanol: Bp 135 °C (bath temp 14 Torr); IR (neat) 3470, 886, 830, 786 cm^{-1}; NMR (CCl_4) δ (1.50—2.80 (m, 8H), 2.58 (s, 1H); mass *m/e* (%) 186 (1), 85 (100). Found: C, 35.6; H, 4.7%. Calcd for $C_6H_9Cl_3O$: C, 35.4; H, 4.5%.

1-Trichloromethylcyclohexanol: Mp 56 °C; IR (Nujol) 3480, 812, 780 cm^{-1}; NMR (CCl_4) δ 1.30—2.50 (m, 10H), 2.06 (s, 1H); mass *m/e* (%) 198 (3), 99 (46).

1-Tribromomethylcyclohexanol: Mp 74 °C; IR (Nujol) 3450, 760, 696 cm^{-1}; NMR (CCl_4) δ 1.40—2.80 (m, 10H), 2.13 (s, 1H); mass *m/e* (%) 273 (1), 271 (3), 269 (1). 99 (100). Found: C, 24.0; H, 3.2%. Calcd for $C_7H_{11}Br_3O$: C, 23.9; H, 3.0%.

Preparation of Methyl α,β-Epoxycyclohexylideneacetate. To a solution of methyl bromoacetate (168 mg, 1.1 mmol) and cyclohexanone (98 mg, 1.0 mmol) in dry THF (2 ml) was added dropwise a solution of lithium dicyclohexylamide (2.0 mmol) in THF over a period of 30 min at −78 °C. The reaction mixture was then stirred for 1 h at the same temperature, and for 3 h at room temperature. After extractive work-up 158 mg (93%) of methyl α,β-epoxycyclohexylacetate was obtained by preparative TLC using benzene as an eluent.

Preparation of Ethyl Dichloro(1-hydroxycyclohexyl)acetate. To a stirred solution of cyclohexanone (98 mg, 1.0 mmol) and ethyl dichloroacetate (0.246 ml, 2.0 mmol) was added dropwise lithium dicyclohexylamide (2.0 mmol) over a period of 30 min at −78 °C, and the reaction mixture was stirred for 30 min at the same temperature. According to the usual procedure 234 mg (92%) of ethyl dichloro(1-hydroxycyclohexyl)acetate was obtained by PLC using benzene as an eluent: Bp 165 °C (bath temp 5 Torr); IR (neat) 3475, 872, 694, 666 cm^{-1}; NMR (CCl_4) δ 1.36 (t, J=8, 3H), 1.20—2.20 (m, 10H), 3.71 (s, 1H), 4.03 (q, J=8, 2H); mass *m/e* (%) 218 (10), 98 (100). Found: C, 47.4; H, 6.6%. Calcd for $C_{10}H_{16}Cl_2O_3$: C, 47.1; H, 6.3%.

Preparation of 1-(3,3-Dichloropropenyl)cyclododecanol. To a solution of cyclododecanone (3.64 g, 20 mmol) and 3,3-dichloropropene (2.42 g, 22 mmol) in dry THF (40 ml) was added dropwise lithium diisopropylamide (30 mmol) at −78 °C over a period of 30 min, and stirred for 30 min at the same temperature. After extractive work-up 3.83 g (66%) of 1-(3,3-dichloropropenyl)cyclododecanol was obtained by column chromatography using benzene as an eluent: Mp

89 °C; IR (Nujol) 3480, 840, 794 cm^{-1}; NMR (CCl_4) δ 1.20—2.00 (m, 22H), 2.08 (s, 1H), 5.26 (d, $J=10$, d, $J=1$, 1H), 5.76 (d, $J=16$, d, $J=1$, 1H), 6.30 (d, $J=16$, d, $J=10$, 1H); mass *m/e* (%) 292 (4), 243 (32). Found: C, 61.7; H, 9.2%. Calcd for $C_{15}H_{26}Cl_2O$: C, 61.4; H, 8.9%.

The authors wish to thank the Ministry of Education Japan, for a Grant-in-Aid (No. 911506).

References

1) A preliminary account of this work has appeared: H. Taguchi, H. Yamamoto, and H. Nozaki, *J. Am. Chem. Soc.*, **96**, 3010 (1974).

2) W. Kirmse, "Carbene Chemistry," 2nd ed, Academic Press, New York, N. Y. (1971).

3) a) G. Kobrich, *Angew. Chem. Int. Ed. Engl.*, **6**, 41 (1967); **11**, 473 (1972), and references therein; b) D. F. Hoeg and D. I. Lusk, *J. Am. Chem. Soc.*, **86**, 928 (1964); D. F. Hoeg, D. I. Lusk, and A. L. Crumbliss, *ibid.*, **87**, 4147 (1965); D. F. Hoeg, and D. I. Lusk, *J. Organomet. Chem.*, **5**, 1 (1966).

4) a) α-Chloro ketones, H. Taguchi, H. Yamamoto, and H. Nozaki, *Tetrahedron Lett.*, **1972**, 4661; J. Villieras, C. Bacquet, and J. F. Normant, *J. Organomet. Chem.*, **40**, C, (1972); G. Köbrich and J. Grosser, *Tetrahedron Lett.*, **1972**, 2181; I. Kuwajima and Y. Fukuda, *Chem. Lett.*, **1973**, 327; G. Köbrich and J. Grosser, *Chem. Ber.*, **106**, 2626 (1973); b) α,β-Unsaturated aldehydes, H. Taguchi, S. Tanaka, H. Yamamoto, and H. Nozaki, *Tetrahedron Lett.*, **1973**, 2465; c) α-Chloro aldehydes, G. Kobrich and W. Werner, *ibid.*, **1969**, 2181; d) α-Hydroxy aldehydes, J. I. Stevents, *J. Org. Chem.*, **37**, 1248 (1972), and references cited therein: e) Dichloroolefins, G. Köbrich, H. Trapp, and I. Hornke, *Chem. Ber.*, **100**, 961 (1967); G. Köbrich, H. Trapp, K. Flory, and W. Drischel, *ibid.*, **99**, 689 (1966).

5) R. A. Olofson and C. M. Dougherty, *J. Am. Chem. Soc.*, **95**, 582 (1973). Villieras also reported the generation of dibromomethyllithium solution using lithium diisopropylamide at low temperature: J. Villieras, *J. Organomet. Chem.*, **50**, C7 (1973).

6) Diiodomethyllithium: G. Köbrich and R. von Nagel, *Chem. Z., Chem. Appl.*, **94**, 984 (1970); tribromomethyllithium: R. H. Fischer and G. Köbrich, *Chem. Ber.*, **101**, 3230 (1968).

7) a) D. Seyferth, G. J. Murphy, and R. A. Woodruff, *J. Organomet. Chem.*, **66**, C29 (1974); b) D. Seyferth, G. J. Murphy, and R. A. Woodruff, *J. Am. Chem. Soc.*, **96**, 5011 (1974).

8) Attempted isolation of the corresponding hydroxybromide was unsuccessful.

A Facile Ring Enlargement Reaction *via* β-Oxido Carbenoid[1)]

Hiroaki TAGUCHI, Hisashi YAMAMOTO, and Hitosi NOZAKI
Department of Industrial Chemistry, Kyoto University, Yoshida, Kyoto 606
(Received Jannuary, 5, 1977)

A general method of transforming a cyclic ketone to the next higher ring homolog chlorinated at the α-carbon or alternatively to its parent ketone is described. Treatment of a dichloromethyllithium-carbonyl adduct **2** with butyllithium affords a β-oxido carbenoid **3** at low temperature. Upon warming, **3** decomposes to a lithium enolate **4**, which is quenched with diluted hydrochloric acid to give the α-chloro ketone **5**. Cycloalkanone is converted to a one-carbon ring enlarged halogenated ketone. Meanwhile, dibromomethylcarbinol **7** is transformed to the halogen-free ketone **8** *via* monobromo β-oxido carbenoid upon treatment with butyllithium. α-Methyl substituted ketone is exclusively converted to the β-methyl substituted homolog and therefore *dl*-muscone is synthesized from cyclotetradecanone according to this new method.

The construction of the desired medium or large ring structure can be performed easily by ring enlargement of readily available cyclic compounds.[2)] The one-carbon ring expansion is most important and has been attained by either (a) diazomethane reaction[3)] or (b) the Tiffeneau-Demjanov rearrangement.[4)] However, preparative disadvantages arise from either the complex mixture being formed in the method (a) or from the number of steps required in the method (b).[5)] In addition, regioselectivity can hardly be expected when these methods are applied to an α-substituted or an α,β-unsaturated cyclic ketone. In this report we describe a new method, which is not only simple and convenient, but is highly regioselective. The method is based on smooth decomposition of a β-oxido carbenoid to a lithium enolate.

Synthesis of α-Chloro Ketones.[1a,6)] Nucleophilic addition of dichloromethyllithium to a carbonyl component **1** proceeds smoothly at low temperature to afford a lithium (dichloromethyl)alkoxide **2**. Treatment of the solution with butyllithium at −95 °C, gradual warming to 0 °C, and quenching with diluted hydrochloric acid yielded a one-carbon homologated α-chloro ketone **5**. The reaction obviously involves initial formation of the dilithiated intermediate, β-oxido carbenoid **3**, followed by decomposition to the enolate **4** as shown in Scheme 1.

From benzaldehyde (**1a**), phenacyl chloride (**5a**) was obtained in 72% yield. The possible phenyl migration

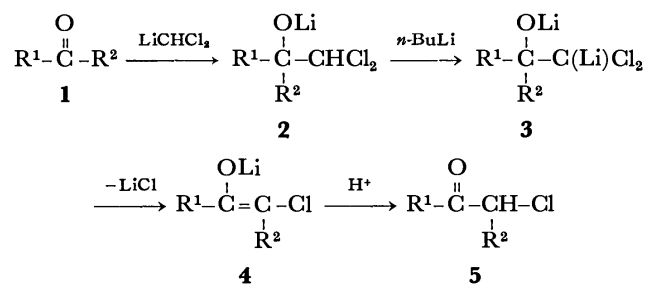

a: R^1=Ph, R^2=H
b: R^1=*n*-C_8H_{17}, R^2=H
c: R^1=2-furyl, R^2=H
d: R^1=$(CH_3)_2C{=}CH(CH_2)_2C(CH_3){=}CH$–, R^2=H
e: R^1, R^2=$-(CH_2)_{11}-$
f: R^1, R^2=$-(CH_2)_4-$

Scheme 1.

producing PhCHClCHO was anticipated, but the NMR assay of the reaction product indicated the absence of any isomer other than **5a** before and after purification.

The reaction of PhCDO (98% D content)[7)] gave PhCOCHDCl (97% D content) after recrystallization from the crude product. This is a token indicating the intermediacy of the enolate **4a** resulting from intramolecular carbene insertion to the adjacent C–H bond of β-oxido carbenoid.

The conversion of cyclic ketones to the one-carbon ring enlarged chloro ketones was performed under similar conditions. Sequential treatment of cyclododecanone (**1e**) with dichloromethyllithium at −78 °C and then with butyllithium at −30 °C afforded 46% of 2-chlorocyclotridecanone (**5e**).

Similarly, nonanal (**1b**), furfural (**1c**), citral (**1d**), and cyclopentanone (**1f**) gave the one-carbon homologated chloro ketones in the yield as shown in Table 1.

TABLE 1. PREPARATION OF α-CHLORO KETONE

Carbonyl compd	α-Chloro ketone	Yield, %
PhCHO **1a**	$PhCOCH_2Cl$ **5a**	72
$CH_3(CH_2)_7CHO$ **1b**	$CH_3(CH_2)_7COCH_2Cl$ **5b**	62
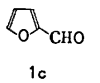 **1c**	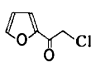 **5c**	62
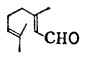 **1d**	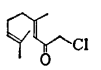 **5d**	51
 **1e**	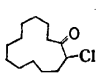 **5e**	46
 **1f**	 **5f**	64

One-Carbon Ring Enlargement of Cyclic Ketones. The next problem was the synthesis of halogen-free ketones under one-carbon homologation, which required generation of monohalo β-oxido carbenoids. This was attained by the lithium-halogen exchange proceeding upon treatment of lithium (dibromomethyl)alkoxide with

butyllithium.

The dibromides **7** were readily prepared from cyclic ketones **6** by the previous method.[8] Treatment with butyllithium in tetrahydrofuran (THF) gave the homologous ketones **8** as shown in Table 2. Thus a two step, facile transformation of a cyclic ketone to a next higher ring homolog has been established.

Table 2. Preparation of cycloalkanones from 1-dibromomethylcycloalkanols

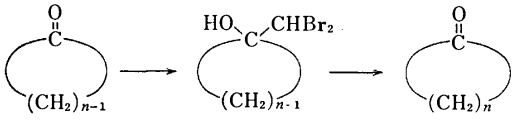

6 **7** **8**

Dibromide	n	Product	Yield, %
7a	12	**8a**	89
7b	8	**8b**	87
7c	7	**8c**	80
7d	6	**8d**	70
7e	5	**8e**	92

Regioselectivity in the Ring Enlargement Reaction. 2-Methylcyclohexanone gives the dibromide **9b**, whose treatment with butyllithium afforded methylcycloheptanone. Yields and isomer ratios under various reaction conditions are listed in Table 3. Thus, the regioselectivity is highly dependent upon the nature of solvent and the reaction temperature. When the reaction was conducted at −95 °C in ether, 3-methylcycloheptanone (**10b**) was obtained with high selectvity (97: 3). At −45 °C a significant amount of 2-methylcycloheptanone was produced. THF as a solvent was characterized by higher selectivity giving 3-methyl ketone **10b** almost exclusively. In ether, **10b** still dominated, but significant amount of 2-methyl ketone **11b** was produced at −78 °C. In hexane solvent the regioselectivity was scarcely observed, and the yield was poor. The low yield in THF was ascribed to the thermal lability of dibromide **9b** even at −78 °C.

The high selectivity was observed as well in the larger ring system. Under similar procedure the dibromide **9c** (n=12) afforded 96% isolated yield of 3-methylcyclotridecanone (**10c**) in 99% selectivity.

The regioselectivity is rationalized by assuming the contribution of β-oxido carbenoid **12** and **13** (from the dibromide **9b**) to be in equilibrium. The absence of repulsion between bulky bromine and methyl group should favor **12** thermodynamically over **13**. Curved arrows indicate that simultaneous elimination of Br^- and selective migration of methyl substituted carbon should afford the observed 3-methylcycloheptanone (**10b**) in preference.

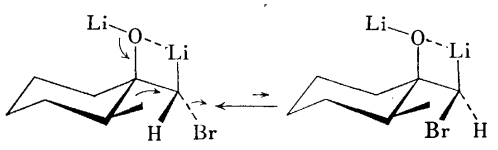

12 **13**

Table 3. Product distribution of ring expansion reaction of 1-dibromomethyl-2-methylcycloalkanol

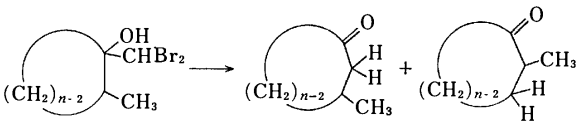

9 **10** **11**

Dibromide	n	Temp[b] °C	Solvent	Isomer distribution **10:11**	Yield[d] % (**10**+**11**)
9a-*trans*[e]	5	−78	THF	69:31	90
9a-*cis*[e]	5	−78	THF	49:51	73
9b[f]	6	−78	THF	98:2	29[g]
9b	6	−95	THF	99:1	51
9b	6	−45	ether	86:14	62
9b	6	−78	ether	95:5	82
9b	6	−95	ether	97:3	86
9b	6	−78	hexane	66:34	71
9b	6	−95	hexane	65:35	68
9c[h]	12	−78	THF	99:1	(96)
9d[i]	14	−78	THF	97:3[j]	(79)

a) Prepared according to the previously reported procedure.[8] b) Cooling bath temperature. c) Determined by GLPC assay on analytical samples before bulk purification. d) The yields were determined by analytical GLPC using an internal standard: isolated yields in parentheses. e) Reaction of cyclopentanone with dibromomethyllithium afforded **9a** in a ratio of *trans*: *cis*=7: 3. The isomers were separated by preparative TLC. The stereochemical course of the reaction was estimated by the analogy in similar systems. See, for example, E.C. Ashby and J. T. Laemmle, *Chem. Rev.*, **75**, 521 (1975). f) Only one isomer was detected from the reaction of dibromomethyllithium and 2-methylcyclohexanone. 2-Methylcyclohexanone is known to be attacked from the equatrial side to a large extent. It has been suggested that the 2-methyl group introduces a pseudo-axial hydrogen into the molecule which increases hindrance of attack from the axial side; see G. Chauviere, Z. Welvart, D. Eugene, and J. Richer, *Can. J. Chem.*, **47**, 3285 (1969). g) Low yield of this reaction was due to the thermal lability of dibromide **9b** even at −78 °C. h) Mixture of stereoisomers (≈4:1 by NMR assay). i) Mixture of stereoisomers (≈8: 1 by NMR assay). j) Estimated by NMR analysis.

The effectiveness of THF may be attributed to the increased stability of the β-oxido carbenoid because of the solvation of THF for lithium atom.[5] Since the β-oxido carbenoid is stabilized more in THF than in less polar solvent such as ether or hexane, the species is supposed to have enough time for establishment of the equilibrium **12**⇄**13**, which should result in the observed high regioselectivity.

The novel reaction of remarkable regioselectivity has a wide applicability as exemplified by the following *dl*-muscone synthesis.[9] Addition of dibromomethyllithium to 2-methylcyclotetradecanone (**14**) afforded 1-

dibromomethyl-2-methylcyclotetradecanol (**9d**) in 78% yield. The dibromide **9d** was transformed into *dl*-muscone (**10d**) exclusively (≈97% of selectivity) in 79% yield by the reaction with butyllithium.

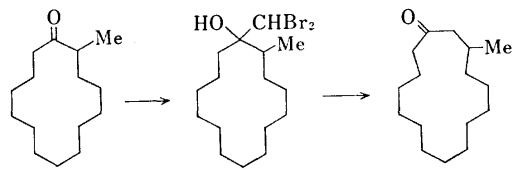

14 **9d** **10d**

The present method is successfully applied also to the regioselective ring enlargement of α,β-unsaturated cyclic ketone affording β,γ-unsaturated ketone. Treatment of the dibromide **15a** and **15b** with butyllithium gave 3-cyclooctenone (**16a**) (85% yield, 98% of selectivity) and 3-cycloheptenone (**16b**) (76% yield, 95% of selectivity) respectively.

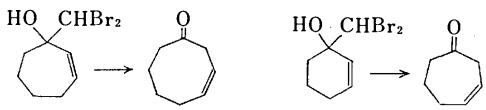

15a **16a** **15b** **16b**

Experimental

The IR spectra were determined on a Shimadzu IR-27-G spectrometer; the mass spectra on a Hitachi RMU-6L mass spectrometer; the GLPC analyses on a Yanagimoto GCG-550F; and NMR spectra on a Varian EM-360 spectrometer. The chemical shifts are given in δ with TMS as the internal standard. The analyses were carried out by the staff at the the Elemental Analyses Center of Kyoto University. All the experiments were carried out under an atmosphere of dry nitrogen, preparative thin layer chromatography (PLC) on silica gel PF-254 plates (Merck) with benzene as an eluent, and preparative column chromatography on silica gel Wakogel C-100 (Wako). THF was purified by distillation from $LiAlH_4$. Ether and hexane were dried over Na metal.

Preparation of Dichloromethyllithium. To a stirred solution of dichloromethane (0.18 ml, 2.8 mmol) in dry THF (5 ml) butyllithium (2.4 mmol) was added drop by drop at −95°C. The resulting solution was stirred for 0.5 h at the same temperature and used immediately.

Preparation of Phenacyl Chloride. Benzaldehyde (212 mg, 2.0 mmol) was added slowly to a stirred solution of dichloromethyllithium (2.4 mmol) at −95 °C. The reaction mixture was stirred for 2 h at the same temperature. To the solution, butyllithium (3.6 mmol) was added dropwise at −95 °C. The resulting mixture was warmed gradually to 0 °C for 20 min, and then quenched with 1M hydrochloric acid. The aqueous layer was separated and extracted with ether 3 times. All organic layers were combined, washed with brine, dried over Na_2SO_4, and concentrated *in vacuo*. Preparative TLC of the residue gave 223 mg (72%) of phenacyl chloride: IR (KBr) 1699, 1600 cm^{-1}; NMR (CCl_4) δ 4.52 (s, 2H), 7.30—8.05 (m, 5H); mass *m/e* (%) 156 (1), 105 (100).

PhCDO was obtained from benzil by the method of Burgstahler.[7]

PhCOCHDCl: NMR (CCl_4) δ 4.52 (s, 1H); mass *m/e* (%) 157 (1), 105 (100).

The reactions of aldehydes, such as furfural, nonanal, and citral, were carried out according to the above procedure, and the yields of the corresponding chloromethyl ketones are summarized in Table 1. The spectral and analytical data of the products are listed below.

1-Chloro-2-decanone: IR (neat) 1719 cm^{-1}; NMR (CCl_4) δ 3.89 (s, 2H); mass *m/e* (%) 190 (1), 141 (59), 57 (100).

2-(Chloroacetyl)furan: IR (neat) 1682 cm^{-1}; NMR (CCl_4) δ 4.46 (s, 2H), 7.23—7.72 (m, 3H); mass *m/e* (%) 146 (8), 95 (100); Found: C, 50.0; H, 3.6%. Calcd for $C_6H_5ClO_2$: C, 49.9; H, 3.5%.

1-Chloro-4,8-dimethyl-3,7-nonadien-2-one: IR (neat) 1710 cm^{-1}; NMR (CCl_4) δ 3.84 (s, 2H); mass *m/e* (%) 202 (1), 69 (100); Found: C, 65.5; H, 8.7%. Calcd for $C_{11}H_{17}ClO$: C, 65.8; H, 8.5%.

Preparation of 2-Chlorocyclotridecanone. To a stirred solution of dichloromethyllithium (2.4 mmol), a solution of cyclododecanone (364 mg, 2.0 mmol) in dry THF (2 ml) was added slowly at −78 °C. The resulting solution was stirred for 1.5 h at the same temperature, and for 0.5 h at −26 °C. To the solution butyllithium (6.0 mmol) was added at the same temperature. The resulting mixture was warmed gradually to 0 °C for 20 min, and then quenched with 1M hydrochloric acid. After extraction with ether, the combined organic layers were washed, dried, and then concentrated under reduced pressure. The residue was purified by preparative TLC affording 212 mg (46%) of 2-chlorocyclotridecanone: IR (neat) 1715 cm^{-1}; NMR (CCl_4) δ 4.20 (m, 1H); mass *m/e* (%) 232 (3), 98 (74), 55 (100). The preparation of 2-chlorocyclohexanone was carried out under the same procedure, and the yield is given in Table 1.

2-Chlorocyclohexanone: IR (neat) 1720 cm^{-1}; NMR (CCl_4) δ 4.32 (m, 1H); mass *m/e* (%) 134 (10), 117 (50), 55 (100).

Preparation of Cyclotridecanone. 1-Dibromomethylcyclododecanol (365 mg, 1.0 mmol) was dissolved in dry THF (3 ml) under nitrogen and cooled to −78 °C. To the stirred solution butyllithium (1.3 ml of a 1.6M hexane solution, 2.1 mmol) was added dropwise over a period of 30 min. The resulting pale yellow solution was stirred for 30 min at −78 °C and 5 min at 0 °C, quenched by pouring into ice cold 1 M hydrochloric acid, and extracted with ether 3 times. The ethereal layers were washed with brine, dried over Na_2SO_4, and concentrated *in vacuo* to afford cyclotridecanone in 89% yield after preparative TLC on silica gel using benzene as an eluent: IR (neat) 1715 cm^{-1}; mass *m/e* (%) 196 (26), 55 (100).

The preparations of cycloalkanones, such as cyclohexanone, cycloheptanone, cyclooctanone, and cyclononanone were carried out according to the above procedure, and the yields of cycloalkanones are listed in Table 2. The product was identified by the comparison of its spectral data or mp of 2,4-dinitrophenylhydrazone derivative with those of the authentic specimen.

Reaction of 1-Dibromomethyl-2-methylcyclopentanol with Butyllithium. To a THF (5 ml) solution of 1-dibromomethyl-2-methylcyclopentanol (272 mg, 1.0 mmol), butyllithium (2.2 mmol) was added dropwise over a period of 10 min at −78°C. The resulting pale yellow solution was stirred for 1 h at −78 °C and 5 min at 0 °C, quenched by pouring into ice cold 1M hydrochloric acid, and extracted with ether. The GLPC analysis of the ethereal layers was performed using cycloheptanone as an internal standard. The yields and isomer ratios are given in Table 3.

Reaction of 1-Dibromomethyl-2-methylcyclohexanol with Butyllithium. The reactions under various conditions were carried out similarly as described above. The GLPC analyses of the ethereal layers were performed using cyclooctanone as an internal standard, and the results are summarized in Table 3.

Preparation of 3-Methylcyclotridecanone. To a solution of 1-dibromomethyl-2-methylcyclododecanol (370 mg, 1.0 mmol) butyllithium (2.2 mmol) was added dropwise over a period of 10 min at −95 °C. The resulting solution was stirred for 1 h at the same temperature and 5 min at 0 °C. Usual work up afforded a colorless oil after preparative TLC on silica gel using benzene as an eluent. Before and after purification, GLPC analyses showed that the oil contains 99% of 3-methylcyclotridecanone (yield 96%): IR (neat) 1710, 1370, 1124, 780 cm^{-1}; NMR (CCl_4) δ 0.95 (d, J=6, 3H), 1.06—1.88 (m, 18H), 2.00—2.60 (m, 5H); mass *m/e* (1) 210 (22), 125 (23), 110 (42), 55 (100).

Preparation of 2-Methylcyclotetradecanone. To a solution of diisopropylamine (0.77 ml, 5.5 mmol) in dry THF (5 ml) butyllithium (5.5 mmol) was added at 0°C and the resulting solution was stirred for 10 min. A solution of cyclotetradecanone (1.05 g, 5.0 mmol) in dry THF (3 ml) was added to the solution, and the reaction mixture was stirred for 30 min at 0°C. To the solution, hexamethylphosphoric triamide (HMPA) (1 ml) and methyl iodide (0.62 ml, 10 mmol) was added at −78 °C. The mixture was stirred for 30 min at the same temperature, and 2 h at room temperature. After extraction with ether, the ethereal layer was concentrated to afford 2-methylcyclotetradecanone (820 mg, 73%) after preparative TLC using benzene as an eluent: IR (neat) 1710, 1020, 720 cm^{-1}; NMR (CCl_4) δ 1.01—2.86 (m, 25H); mass *m/e* (%) 224 (22), 166 (15), 98 (30), 55 (100).

Preparation of 1-Dibromomethyl-2-methylcyclotetradecanol. A well-stirred solution of dibromomethane (0.73 ml) and 2-methylcyclotetradecanone (819 mg, 3.7 mmol) dissolved in dry ether (18 ml) cyclotetradecanone (819 mg, 3.7 mmol), dissolved in dry ether (18 ml) and dry THF (2 ml) was cooled to −78 °C. To the mixture, lithium 2,2,6,6-tetramethylpiperidide (prepared from 2,2,6,6-tetramethylpiperidine (1.14 g, 8.1 mmol) and butyllithium (3.3 ml of 2.4 M hexane solution at 0 °C) was added dropwise over a period of 2 h. The mixture was stirred for 30 min at that temperature. After hydrolysis at −78 °C, the resulting organic layer was extracted with ether, and the extract was washed with 1M hydrochloric acid 3 times and water. The mixture was dried over anhydrous Na_2SO_4, and condensed under reduced pressure to afford 1-dibromomethyl-2-methylcyclotetradecanol (1.14 g, 78%) after preparative TLC using hexane and ether mixture (15: 2) as an eluent: bp 190 °C (bath temp 2 Torr); IR (neat) 3580, 1460, 1154, 978, 708 cm^{-1}; NMR (CCl_4) δ 0.93 (d, J=6, $C\underline{H}_3$ of major isomer), 1.02 (d, J=6, $C\underline{H}_3$ of minor isomer), 5.78 (s, $C\underline{H}Br_2$ of major isomer), 5.86 (s, $C\underline{H}Br_2$ of minor isomer); mass *m/e* (%) 398 (trace), 225 (51), 55 (100). Found: C, 48.1; H, 7.6%. Calcd for $C_{16}H_{30}Br_2O$: C, 48.3; H, 7.6%.

Preparation of dl-*Muscone.* 1-Dibromomethyl-2-methylcyclotetradecanol (183 mg, 0.46 mmol) was dissolved in dry THF (2.5 ml) and cooled to −78 °C. The stirred solution, butyllithium (0.65 ml of a 1.6 M solution, 1.0 mmol) was added dropwise over a period of 10 min. The resulting solution was stirred for 1 h at −78 °C and 5 min at 0 °C, quenched by pouring into ice cold 1M hydrochloric acid, and extracted with ether. The ethereal layer was concentrated to afford *dl*-muscone (86 mg, 79%) after preparative TLC. Before purification, the product was shown by NMR analysis to contain 97% of 3-methylcyclopentadecanone (*dl*-muscone): bp 140 °C (bath temp 2 Torr); IR (neat) 1710, 1370, 1280, 1125, 1055, 790 cm^{-1}; NMR (CCl_4) δ 0.92 (d, J=6.5, 3H), 1.01—1.85 (m, 22H), 1.90—2.50 (m, 5H); mass *m/e* (%) 238 (21), 223 (9), 55 (100). Found: C, 80.4; H, 12.4%. Calcd for $C_{16}H_{30}O$: C, 80.6; H, 12.7%.

Preparations of 3-Cyclooctenone and 3-Cycloheptenone. These β,γ-unsaturated ketones were prepared from 1-dibromomethyl-2-cycloheptenol and 1-dibromomethyl-2-cyclohexenol respectively by the method similar to the preparation of 3-methylcyclotridecanone.

The authors wish to thank the Ministry of Education, Japan, for a Grant-in Aid (No. 911506).

References

1) A preliminary account of this work has appeared: (a) H. Taguchi, H. Yamamoto, and H. Nozaki, *Tetrahedron Lett.*, **1972**, 4661; (b) H. Taguchi, H. Yamamoto, and H. Nozaki, *J. Am. Chem. Soc.*, **96**, 6510 (1974); (c) H. Taguchi, H. Yamamoto, and H. Nozaki, *Tetrahedron Lett.*, **1976**, 2617.

2) (a) C. D. Gutche and D. Redmore, "Carbocyclic Ring Expansion Reactions," Academic Press, New York, N. Y. (1968); (b) P. R. Story and P. Busch, *Adv. Org. Chem.*, **8**, 67 (1972); (c) G. Wilke, *Pure Appl. Chem.*, **17**, 179 (1968).

3) (a) C. D. Gutche, *Org. React.*, **8**, 364 (1954); (b) Ref. 2a, Chap. 4.

4) P. A. S. Smith and D. R. Baer, *Org. React.*, **11**, 154 (1967); see also, D. A. Evans, G. L. Carroll, and L. K. Truesdale, *J. Org. Chem.*, **39**, 914 (1974).

5) For example, U. Schöllkopf and P. Böhme, *Angew. Chem. Int. Ed. Engl.*, **10**, 491 (1969).

6) This novel rearragement was also found by three other groups; (a) J. Villieras, C. Bacquet, and J. F. Normant, *J. Organomet. Chem.*, **40**, C1 (1972); (b) I. Kuwajima and Y. Fukuda, *Chem. Lett.*, **1973**, 372; (d) G. Köbrich and J. Grosser, *Chem. Ber.*, **106**, 2626 (1973).

7) A. W. Burgstahler, D. E. Walker, Jr., J. P. Kuebrich, and R. L. Schowen, *J. Org. Chem.*, **37**, 1272 (1972).

8) H. Taguchi, H. Yamamoto, and H. Nozaki, *J. Am. Chem. Soc.*, **96**, 3010 (1974); H, Taguchi, H. Yamamoto, and H. Nozaki, *Bull. Chem. Soc. Jpn.*, **50**, 1588 (1977).

9) For recent *dl*-muscone synthesis, see (a) G. Stork and T. L. MacDonald, *J. Am. Chem. Soc.*, **97**, 1265 (1975); (b) T. Hiyama, T. Mishima, K. Kitatani, and H. Nozaki, *Tetrahedron Lett.*, **1974**, 3297; (c) H. Nozaki, H. Yamamoto, and T. Mori, *Can. J. Chem.*, **47**, 1107 (1969); (d) R. Baker, R. C. Cookson, and J. R. Vinson, *J. Chem. Soc., Chem. Commun.*, **1974**, 515; (e) R. Baker, B. N. Blackett, and R. C. Cookson, *J. Chem. Soc., Chem. Commun.*, **1972**, 802; (f) B. C. Mookherjee, R. W. Trenkle, and R. R. Patel, *J. Org. Chem.*, **36**, 326, (1971); (g) R. D. Mookherjee, R. R. Patel, and W. O. Ledig, *J. Org. Chem.*, **36**, 4124 (1971); (h) D. Felix, J. Schrieber, G. Ohloff, and A. Eschenmoser, *Helv. Chim. Acta*, **54**, 2896 (1971); (i) G. Ohloff, J. Becker, and K. Schulte-Elte, *ibid.*, **50**, 705 (1967); (j) A. Eschenmoser, D. Felix, and G. Ohloff, *ibid.*, **50**, 708 (1967); (k) E. Yoshii and S. Kimoto, *Chem. Pharm. Bull.*, **17**, 629 (1969).

Synthesis of Mesoionic Triazolopyridine. I. *N*-Alkylation of 1,2,4-Triazolo[4,3-*a*]pyridin-3(2*H*)-one

Akio SAITO and Bunji SHIMIZU

Central Research Laboratories, Sankyo Co., Ltd., Hiromachi, Shinagawa-ku, Tokyo 140

(Received January 6, 1977)

Mesoionic *anhydro*-1-alkyl-3-hydroxy-1,2,4-triazolo[4,3-*a*]pyridinium hydroxide (**6**) was synthesized by selective alkylation at the N^1-position of 1,2,4-triazolo[4,3-*a*]pyridin-3(2*H*)-one (**8**). The selectively depends on the use of a mercuric salt catalyst in combination with the trimethylsilyl derivative of **8**, and its mechanistic features were also studied with reference to the benzylation of **8**.

During the course of an investigation on nucleoside and nucleotide synthesis we found that the mercuric salt catalyzed silyl procedure* is an excellent method for the glycosylation of purine and pyrimidine bases.[1] In this procedure, the reaction proceeds under mild conditions, the yield being satisfactory. The procedure has been widely applied[4] to the glycosylation of a variety of *N*-heterocycles.

In a series of studies on the application, we attempted the glycosylation of 2-trimethylsilyl-1,2,4-triazolo[4,3-*a*]-pyridin-3(2*H*)-one (**1**) with *O*-acyl-glycosyl halide (**2**) expecting to obtain N^2-glycosyltriazolopyridine (**4**). However, an unusual glycoside which showed strong fluorescence in an aprotic solvent in day light, exhibiting polar behavior as compared with **4** on TLC, was obtained as the main product along with a small amount of **4**. By comparison of its IR, UV, and NMR spectra with those of authentic samples of *anhydro*-1-benzyl-3-hydroxy-1,2,4-triazolo[4,3-*a*]pyridinium hydroxide (**6**, R=benzyl), the glycoside was found to have mesoionic structure (**3**), which was the first example of a mesoionic triazole glycoside.

Mesoionic 1,2,4-triazoles were prepared by cyclization of appropriate hydrazidine derivatives.[5] Mesoionic triazolopyridines (**6**, R=alkyl) have also been obtained[6] in this way from 1-alkyl-1-(2-pyridyl)hydrazine (**7**). It may be possible to obtain the mesoionic compound (**6**) if the reaction occurs exclusively at the N^1-position in the alkylation of 1,2,4-triazolo[4,3-*a*]pyridin-3(2*H*)-one (**8**). In the alkylation of **8** an N^2-alkylated product (**9**) was known[7] to be obtained predominantly. Our findings in the glycosylation of **1** suggested the possibility of this approach. By applying the "mercuric salt catalyzed silyl procedure" to the alkylation, we found it possible to obtain the mesoionic compounds (**6**) from **8**.

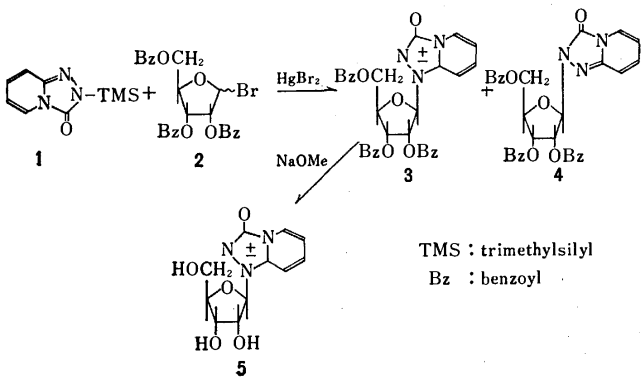

1 2 3 4 5

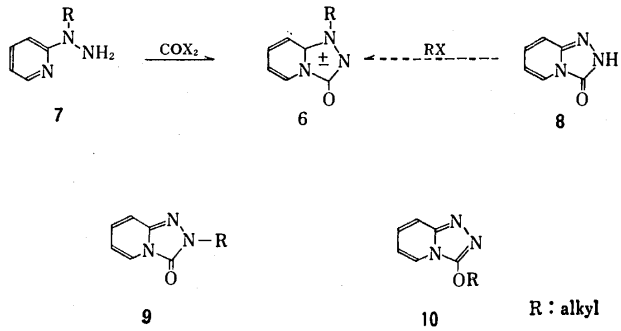

7 6 8 9 10

This report deals with a novel synthesis of mesoionic triazolopyridines (**6**). A detailed study of benzylation of **8** or **1** was also carried out under various conditions in order to clarify the procedure.

Result and Discussion

The synthesis of mesoionic compound (**6**) by an alkylation of **8** was conducted as follows.

The reaction of the trimethylsilyl derivative of **8** with an equimolar amount of alkyl halide or alkyl tosylate in the presence of mercury(II) bromide in nitrobenzene at 60—90 °C gave **6** as the $HgBr_2$-complex in moderate yield. The other alkylated products, **9** and **10**, were obtained in a negligible amount.

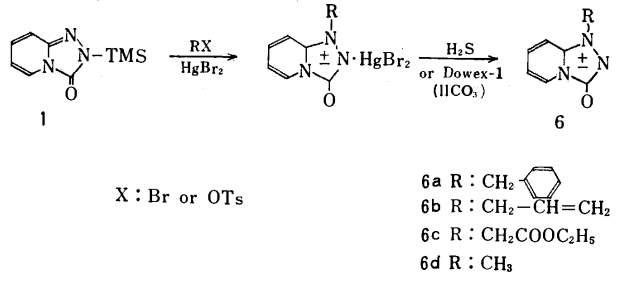

1 6

* The term "silyl solvent method" was proposed in a previous paper.[1b] It refers to an improved silyl procedure in which the glycosylation of trimethylsilylated purine or pyrimidine bases with *O*-acyl-glycosyl halide is conducted in the presence of a mercuric salt, *e.g.* mercury(II) chloride or mercury(II) bromide, in a solvent. An analogous procedure, in which the mercuric salt was used in combination with mercury(II) oxide, was reported independently by Wittenburg.[2] Several Lewis acids have been surveyed[3] as an alternative to the mercuric salt in this procedure, tin(IV) chloride being most widely employed.

Table 1. Yields and physical data of mesoionic triazolopyridines (**6**)

Compound	Mp °C	Yield[a] %	Found % C	Found % H	Found % N	Calcd % C	Calcd % H	Calcd % N	UV: λ_{max}^{MeOH} (nm)
6a	163—164	79	69.36	4.92	18.59	69.31	4.92	18.66	236,285,348
6b	108—109	74	61.71	5.36	23.89	61.70	5.17	23.98	235,282,341
6c	190	85	54.36	5.04	18.97	54.29	5.01	18.99	235,282,340
6d	220	78	56.34	4.73	28.16	56.55	4.71	27.93	235,281,342

a) Based on the products isolated.

The physical properties of the free mesoionic compounds (**6**) obtained by treating the complex with hydrogen sulfide or ion exchange resin (Dowex-1, HCO_3^-) are given in Table 1.

Detailed studies on the benzylation of **8** were carried out in order to elucidate the factor inducing the remarkable selectivity on alkylation.

Since **8** includes three active sites for alkylation N^1,N^2, and O), a number of products would be expected. In fact, three monoalkylated products, **6a**, **9a** (R=benzyl), and **10a** (R=benzyl) were obtained by the reaction of Ag-salt of **8** with benzyl bromide under mild conditions (80 °C, in nitrobenzene). The reaction of **8** with benzyl bromide at relatively high temperature gave **9a** predominantly with a small amount of **6a**. The reaction was accelerated by the addition of mercury(II) bromide, the main product being **6a**. Trimethylsilyl substitution at the N^2-position of **8** afforded a result similar to that obtained by the use of **8** itself on benzylation with regard to the distribution of the products. Sufficient selectivity to give **6a** on the benzylation was obtained by the use of **1** in combination with mercury(II) bromide. The results on the benzylation of **1** or **8** are given in Table 2.

Table 2. Benzylation[a] of **1** or **8**: reaction conditions and products

Exp No.	Starting material	React temp (°C)	React time (h)	Cat ($HgBr_2$)	Yield[b] (%) of the product **10a**	**6a**	**9a**
1	Ag-salt of **8**	80	3	—	19	38	29
2	**8**	125	12	—	—	12	78
3	**8**	125	3	1-eq.	—	68	20
4	**1**	125	5	—	—	21	68
5	**1**	85	20	1-eq.	—	79	trace

a) Carried out using 1-eq. of benzyl bromide in nitrobenzene. b) Based on the product isolated.

The results indicate that products can be selected by varying the reaction conditions appropriately. Previous studies[8] on the alkylation of purine bases revealed that alkyl migration plays an important role in determination of the reaction product. The following experiments suggest that the benzyl moiety attached to the triazolopyridine ring easily migrates under the same reaction conditions as described above, the migration proceeding successively in the order $O \rightarrow N^1 \rightarrow N^2$.

Heating of **10a** in nitrobenzene (100—110 °C, 23 h) gave **6a** exclusively. The conversion was accelerated by the addition of a mercuric salt catalyst, *e.g.* $HgBr_2$ or $Hg(CN)_2$. Conversion of **6a** into **9a** was observed in the presence of mercury(II) bromide, but not in the absence of the catalyst even at high temperature (150 °C).

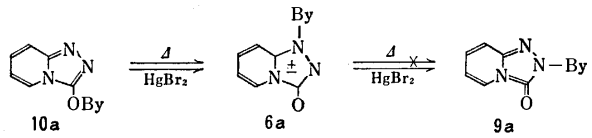

10a 6a 9a

By : benzyl

Benzyl bromide was found to act as a more efficient catalyst for these conversions. Treatment of **10a** with a catalytic amount of benzyl bromide in nitrobenzene at

Table 3. Benzyl migration[a]: reaction conditions and products

Exp No.	Starting material	Cat	React temp (°C)	React time (h)	Yield (%) of the product **10a**	**6a**	**9a**	**11**	**12**
1	**10a**	—	100—110	23	15	76	—	—	—
2	**10a**	1-eq. $Hg(CN)_2$	100—110	15	17	73	—	—	—
3	**10a**	1-eq. ByBr	80	5.5	2	93	—	—	—
4	**10a**	0.1-eq. ByBr	80	25	33	63	—	—	—
5	**10a**	1-eq. ByBr +1-eq. $HgBr_2$	25	25					52[c]
6	**6a**	—	150	50	no reaction				
7	**6a**	1-eq. $HgBr_2$	150	50	—	8	55	trace	
8	**6a**	1-eq. ByBr	125	1	—	trace	90	—	—
9	**6a**	0.1-eq. ByBr	125	20	—	19	76	—	—
10	**6a**	1-eq. ByBr +1-eq. $HgBr_2$	125	3					37[c]

a) Conducted in nitrobenzene. b) Based on the product isolated. c) $HgBr_2$-complex.

80 °C for 5 h gave **6a** almost quantitatively. Conversion of **6a** into **9a** took place by a similar treatment of **6a** with benzyl bromide at 120 °C

Quaternary salts (**11**) and (**12**), assumed to be the intermediates of these conversions, could be isolated as $HgBr_2$-complexes. Detailed results are given in Table 3.

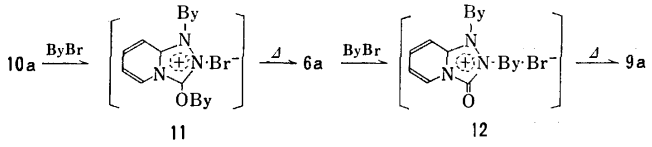

Demercuration of the complex of **12** gave a free quaternary salt which decomposed easily to give **9a** in nitrobenzene at 80 °C. On treatment with hydrogen sulfide, the $HgBr_2$-complex of **11** gave **6a** as a result of the instability of the free quaternary salt.

The results suggest that the primary factor determining the products of benzylation is the benzyl migration under the reaction conditions employed. Presumably, the initial product is either **6a** or **10a**. However, the formation of the latter is uncertain in the reaction of **8** with benzyl bromide since conversion of **10a** into **6a** is very rapid. When the reaction is carried out at high temperature, these compounds are transformed easily into thermodynamically more stable **9a** by benzyl migration. The migration seems to proceed mainly through intermediates **11** and **12**. In order to obtain the mesoionic compound (**6a**) by the benzylation of **8**, it is apparent that further benzylation of **6a** should be suppressed. The use of trimethylsilyl substituent with mercury(II) bromide for the benzylation makes the formation of **6a** under mild conditions possible, **6a** not undergoing further benzylation. The metal probably not only acts as a Friedel-Crafts catalyst but also suppresses the nucleophilic capability of the N^2-atom by the complex formation with **6a**.

By applying the mercuric salt catalyzed silyl procedure to the alkylation of **8**, the reaction was controlled sufficiently to give the mesoionic compound as a product. An analogous controlled acylation of **8** was found to give a new mesoionic *N*-acyltriazolopyridine (**6**, R= acyl).

Experimental

Melting points were determined on a Yazawa hot-stage apparatus and are uncorrected. Infrared, UV and NMR spectra were recorded on Hitachi EPI-S2, Hitachi-124 and Varian T-60 spectrometers respectively.

Triazolopyridine (**8**) was prepared by the method of Potts and Burton.[9] An authentic sample of **6a** was prepared by ring closure of 1-benzyl-1-(2-pyridyl)hydrazine with urea and that of **10a** by the reaction of 3-bromo-1,2,4-triazolo[4,3-*a*]-pyridine with sodium benzyl alcoholate.

2-Trimethylsilyl-1,2,4-triazolo[4,3-a]pyridin-3(2H)-one (**1**). To a mixture of **8** (13.6 g), trimethylchlorosilane (13.0 g) in dry benzene (200 ml) under stirring was added dropwise a solution of triethylamine (12.1 g) in dry benzene (50 ml). After being stirred at room temperature for 2 h, the reaction mixture was filtered, and the cake was washed with a small amount of dry benzene. The combined filtrate and washings were evaporated to give a solid product: yield 20.65 g (99.7%). UV: $\lambda_{max}^{Dioxane}$ 252, 268, 279, 345 nm. Found: C, 51.95; H, 6.45; N, 20.03%. Calcd for $C_{19}H_{13}N_3OSi$: C, 52.10; H, 6.31; N, 20.05%. (Owing to the instability of the product toward water, all the operation had to be performed under the conditions protected from atmospheric moisture.)

Anhydro-*1-(β-D-ribofranos-1-yl)-3-hydroxy-1,2,4-triazolo[4,3-a]pyridinium Hydroxide* (**5**) *and Its* N^2-*Isomer*. Acetic anhydride (0.05 ml) and acetic acid (5 ml) saturated with hydrogen bromide were added to a solution of 1-*O*-acetyl-2,3,5-tri-*O*-benzoyl-β-*D*-ribofranoside (2.52 g) in dry chloroform (5 ml). The resulting solution was allowed to stand at room temperature for 45 min, and then evaporated *in vacuo* to give a thick sirup at a temperature below 40 °C. Co-evaporation with dry toluene was repeated three times. The residual sirup was dissolved in dry benzene (10 ml), and mercury(II) bromide (1.80 g) and **1** (1.04 g) were added. The mixture was stirred at room temperature for 2 h, then evaporated *in vacuo*, and the residue was extracted with chloroform. The extract was washed successively with 25% potassium iodide (2 times) and with water, dried over anhydrous sodium sulfate, and evaporated to give an amorphous solid (3.169 g). The protected glycoside thus obtained was heated in methanol (70 ml) containing sodium methoxide (216 mg) under reflux for 60 min. The reaction solution was cooled, then evaporated *in vacuo* to dryness, and the residue was dissolved in water (10 ml). The aqueous solution was washed with ether, rendered neutral with 1M HCl, and applied to a column of 50 ml of Dowex-1×4 (OH^-, 100—200 mesh) anion exchange resin. The column was washed with water (200 ml) and eluted with 40% methanol. The eluate could be separated into two fractions. Evaporation of the first fraction gave **5**, which was recrystallized from aqueous ethanol. Yield 989 mg (74%); fine needles, mp 204—206 °C. UV λ_{max}^{MeOH} 236, 283, 339 nm. IR (Nujol): 1660 cm^{-1} (C=O). NMR (D_2O); δ: 8.18 (d, J=7 Hz, 1, H-5), 7.7—8.0 (m, 2, H-7 and H-8), 7.1—7.4 (m, 1, H-6), 6.12 (d, J=5 Hz, 1, H-1′), 3.8—4.9 ppm (m, 5, ribose ring protons). Found: C, 49.60; H, 5.07; N, 15.85%. Calcd for $C_{11}H_{13}N_3O_5$: C, 49.47; H, 4.91; N, 15.73%. On evaporation, the second fraction yielded 2-(β-*D*-ribofranos-1-yl)-1,2,4-triazolo[4,3-*a*]-pyridin-3(2*H*)-one; 57 mg (4.3%) mp 172—173 °C. UV: λ_{max}^{MeOH} 220, 259(sh), 275, 328 nm. IR (Nujol); 1710 cm^{-1} (C=O). Found: C, 49.70; H, 4.92; N, 15.65%. Calcd for $C_{11}H_{13}N_3O_5$: C, 49.47; H, 4.91; N, 15.73%.

Anhydro-*1-benzyl-3-hydroxy-1,2,4-triazolo[4,3-a]pyridinium Hydroxide* (**6a**). A mixture of **1** (2.08 g), benzyl bromide (1.75 g) and mercury(II) bromide (3.60 g) in nitrobenzene (10 ml) was stirred at 85 °C for 20 h. 2-Propanol was then added. The crystals deposited were collected by filtration to give $HgBr_2$-complex of **6a**: yield 4.878 g (83.5%); mp 116—117 °C. The complex was suspended in methanol (300 ml), and then treated with hydrogen sulfide stream until the starting white crystals disappeared. The resulting precipitate of mercury sulfide was filtered off. The filtrate was evaporated to give a yellow powder, which was crystallized from 2-propanol. Yield 1.79 g (79.5%, based on **1**); yellow needles; mp 163—164 °C. UV; λ_{max}^{MeOH} 236, 285, 348 nm. IR (Nujol); 1660 cm^{-1} (C=O). NMR (DMSO-d_6); δ: 8.21 (m, 1, H-5), 7.5—7.9 (m, 2, H-7 and H-8), 7.02 (m, 1, H-6), 5.41 ppm (s, 2, CH_2-Ph). Found: C, 69.36; H, 4.92; N, 18.59%. Calcd for $C_{13}H_{11}N_3O$: C, 69.31; H, 4.93; N, 18.66%.

General Procedure for the Preparation of **6**. A mixture of **1** (10 mmol), alkyl halide (or alkyl tosylate) (10—11 mmol) and mercury(II) bromide in nitrobenzene (10 ml) was stirred at 60—90 °C under monitoring with TLC until the starting material disappeared, and then evaporated *in vacuo*. The residue was dissolved in methanol. The resulting solution

was neutralized with Dowex-1 (HCO_3^-), and the resin was filtered off. The filtrate was evaporated *in vacuo* to give a yellow powder, which was crystallized from appropriate solvent. Yields and physical constants of the products are given in Table 2.

Reaction of the Ag-salt of 8 with Benzyl Bromide. A suspension of the Ag-salt of **8** (121 mg) in nitrobenzene (1 ml) containing benzyl bromide (81 mg) was stirred at 80 °C for 3 h, and then evaporated *in vacuo* to give sirupy residue which was extracted with chloroform. Chromatographic separation of the extract on a silica gel plate yielded three isolated products: **9a** (31.1 mg), **10a** (20.3 mg) and **6a** (40.5 mg). Physical constants of **9a**: mp 114—115 °C. UV λ_{max}^{MeOH} 222, 260 (sh), 268, 278, 331 nm. IR (Nujol); 1720 cm^{-1} (C=O). NMR (DMSO-d_6); δ: 7.89 (m, 1, H-5), 7.36 (s, 5, C_6H_5), 7.15—7.3 (m, 2, H-7 and H-8), 6.63 (m, 1, H-6), 5.15 ppm (s, 2, $C\underline{H}_2$-Ph). Found: C, 69.22; H, 5.02; N, 18.69%. Calcd for $C_{13}H_{11}N_3O$: C, 69.31; H, 4.93; N, 18.66%. Physical constant of **10a**: oil. UV λ_{max}^{MeOH} 227, 256 (sh), 260, 271, 301 nm. NMR (DMSO-d_6); δ: 8.08 (m, 1, H-5), 7.2—7.7 (m, 2, H-7 and H-8), 7.43 (s, 5, C_6H_5), 6.85 (m, 1, H-6), 5.70 ppm (s, 2, $C\underline{H}_2$-Ph).

Reaction of 8 with Benzyl Bromide. a) A mixture of **8** (1.35 g) and benzyl bromide (1.80 g) in nitrobenzene (10 ml) was stirred at 125 °C for 12 h, and then evaporated *in vacuo*. The residue was dissolved in methanol, neutralized with Dowex-1 (HCO_3^-), and the resin was filtered off. The filtrate was concentrated *in vacuo* giving a crystalline mass, which was recrystallized from 2-propanol to give pure **9a**: yield 1.482 g (66%); mp 114—115 °C. A further crop of **9a** (280 mg, 12.4%) and **6a** were isolated from the mother liquor by column chromatography on silica gel.

b) In the Presence of $HgBr_2$. A mixture of **8** (1.35 g), benzyl bromide (1.80 g) and mercury(II) bromide (3.60 g) in nitrobenzene (10 ml) was stirred at 125 °C for 3 h, then evaporated *in vacuo*, and the residue was dissolved in methanol. The solution was neutralized with Dowex-1 (HCO_3^-), filtered, and the filtrate was evaporated to give a sirupy residue. Chromatographic separation of the residue on silica gel (40 g, 1% methanol in chloroform was used as eluent) yielded two isolated product: **6a** (1.537 g, 68.3%) and **9a** (450 mg, 20%).

1-Benzyl-3-benzyloxy-1,2,4-triazolo[4,3-a]pyridinium Bromide (11). A solution of **10a** (678 mg), benzyl bromide (513 mg) and mercury(II) bromide (1.08 g) in nitrobenzene (3 ml) was stirred at room temperature for 20 h, and then poured into a large amount of ethanol. The precipitate formed was crystallized from methanol to give $HgBr_2$-complex of **11**: yield 1.175 g (51.7%); mp 78—80 °C. UV λ_{max}^{MeOH} 218, 260 (sh), 299 nm. NMR (DMSO-d_6); δ: 7.4—8.8 (m, 14, pyridine and phenyl ring H), 5.83 and 5.74 ppm (two s, 4, $C\underline{H}_2$-Ph). Found: C, 31.75; H, 2.40; N, 5.55; Br, 10.56%. Calcd for $C_{20}H_{18}N_3OBr \cdot HgBr_2$: C, 31.90; H, 2.70; N, 5.49; Br, 10.72%.

1,2-Di-benzyl-3-oxo-1,2,4-triazolo[4,3-a]pyridinium Bromide (12). A solution of **6a** (1.13 g), benzyl bromide (90 mg) and mercury(II) bromide (1.80 g) in nitrobenzene (5 ml) was stirred at 125 °C for 3 h. Methanol was added to the reaction solution giving a crystalline solid. On filtration, the pure $HgBr_2$-complex of **12** was obtained: yield 1.39 g (36.8%); mp 157—158 °C. Found: C, 41.77; H, 3.31; N, 7.16; Br, 14.08%. Calcd for $C_{20}H_{18}N_3OBr \cdot 1/2HgBr_2$: C, 41.73; H, 3.49; N, 7.77; Br, 13.82%.

The complex (577 mg) was dissolved in methanol. Hydrogen sulfide was bubbled through the solution until the precipitation of mercury sulfide was complete. The precipitate was then filtered off. Evaporation of the filtrate gave white powder which was crystallized from ethanol–ether to give pure **12**: yield 376 mg (95%); mp 157—158 °C. UV λ_{max}^{MeOH} 212, 230 (sh), 260 (sh), 328 nm. IR (Nujol); 1770 cm^{-1} (C=O). NMR (DMSO-d_6); δ: 8.79 (m, 1, H-5), 8.2—8.5 (m, 2, H-7 and H-8), 7.56 (m, 1, H-6), 5.85 and 5.41 ppm (two s, 4, $C\underline{H}_2$-Ph). Found: C, 60.41; H, 4.60; N, 10.55; Br, 20.05%. Calcd for $C_{20}H_{18}N_3OBr$: C, 61.60; H, 4.58; N, 10.60; Br, 20.16%.

Benzyl Migration. A solution of the starting material (**10a** or **6a**, 10 mmol) in nitrobenzene (10 ml) was heated with (or without) a catalyst ($HgBr_2$ or benzyl bromide) in the desired temperature range. The reaction mixture was worked up in the manner described above.

The author thank Dr. Y. Baba of these Laboratories for helpful discussions.

References

1) a) B. Shimizu and A. Saito, *Agric. Biol. Chem.*, **13**, 199 (1969); b) B. Shimizu, *Yuki Gosei Kagaku Kyokai Shi*, **28**, 860 (1970).

2) a) E. Wittenburg, *Chem. Ber.*, **101**, 1095 (1968); b) E. Wittenburg, *ibid.*, **101**, 1614 (1968); c) E. Wittenburg, *ibid.*, **101**, 2132 (1968).

3) a) U. Niedballa and H. Vorbrueggen, *Angew. Chem. Int. Ed. Engl.*, **9**, 461 (1970); b) H. Vorbrueggen and U. Niedballa, *ibid.*, **10**, 657 (1971); c) U. Niedballa and H. Vorbrueggen, *J. Org. Chem.*, **39**, 3654 (1974); d) T. Ogawa, M. Yasui, and M. Matsui, *Agric. Biol. Chem.*, **36**, 913 (1972); e) H. Vorbrueggen and K. Krolikiewicz, *Angew. Chem. Int. Ed. Engl.*, **14**, 421 (1975).

4) a) B. Shimizu and A. Saito, Jpn. Patent Provisional publication, 49-86372 (1974); b) Y. D. Patil, D. S. Wise, and L. B. Townsend, *J. Med. Chem.*, **1974**, 1282.

5) M. Ohta and H. Kato in "Nonbenzenoid Aromatics," Vol. 1, ed by J. P. Synder, Academic Press, Inc., New York (1969), Chap. 4.

6) a) G. Palazzo and L. Baiocchi, *Ann. Chim. (Rome)*, **55**, 935 (1965); b) K. T. Potts, S. K. Roy, and R. M. Huseby, *J. Org. Chem.*, **33**, 2559, (1968).

7) G. Plazzo, *Curr. Ther. Res. Clin. Exp.*, **15**, 745 (1973).

8) a) B. Shimizu and M. Miyaki, *Tetrahedron Lett.*, **1968**, 855; b) B. Shimizu and M. Miyaki, *Chem. Pharm. Bull.*, **18**, 570 (1970); c) M. Miyaki and B. Shimizu, *ibid.*, **18**, 732 (1970); d) M. Miyaki and B. Shimizu, *ibid.*, **18**, 1446 (1970); e) M. Miyaki, A. Saito, and B. Shimizu, *ibid.*, **18**, 2459 (1970).

9) K. T. Potts and H. R. Burton, *J. Org. Chem.*, **31**, 251 (1966).

Stereoselective One-pot Dialkylation of *gem*-Dihalocyclopropanes by Means of Dialkylcopperlithiums

Katuzi KITATANI, Tamejiro HIYAMA, and Hitosi NOZAKI
Department of Industrial Chemistry, Kyoto University, Yoshida, Kyoto 606
(Received January, 17, 1977)

The transformation of *gem*-dihalocyclopropanes (**1**) into 1-alkyl-1-butylcyclopropanes (**2** and **3**) is established by successive treatment with dibutylcopperlithium and several electrophiles. This sequence is found to be stereochemically controllable and is successfully applied to *dl*-sirenin synthesis. In contrast to the reaction of dibutylcopperlithium, dimethyl- and divinylcopperlithiums convert 1,1-dibromo-2-phenylcyclopropane (**1a**) into 1-bromo-1-methyl- and 1-bromo-1-vinyl-2-phenylcyclopropanes (**15a**, **16a** and **15b**, **16b**) respectively.

It is remarkable that a class of natural products commonly possess a substituted cyclopropane ring[1] in spite of the large strain energy therein involved. One of the most facile routes to the smallest carbocyclic ring is dihalocyclopropanation of olefins[2] by phase-transfer technique, but unfortunately efficient methodology has never been recorded for replacing each halogen atom of the dihalocarbene-adducts with two different alkyl groups successively. Although monoalkylation of *gem*-dihalocyclopropanes proceeds effectively and stereoselectively,[3] the second alkylation of the resulting α-alkylcyclopropyl halides has turned out extremely arduous. Remarkably, it is known that the reaction of *gem*-dihalides with dimethylcopperlithium results in *gem*-dimethylation.[4,5] Being interested in this particular observation we have carefully investigated the interaction of *gem*-dihalocyclopropanes with dibutylcopperlithium to find that α-butylcyclopropylcopper compounds thus initially produced react with methyl iodide giving stereoselectively the desired dialkylated products which have the methyl group always on the more hindered (*cis* or *endo*) site. On the basis of this finding a novel approach to sirenin synthesis has been exploited.[6]

Reaction of gem-*Dihalocyclopropanes with Dibutylcopperlithium.* Upon treatment with 5 mol of dibutylcopperlithium the dibromocyclopropane **1a**, for example, produced a stereoisomeric mixture of organometallic species, which after workup with excess methyl

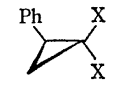

1a: X=Br
1b: X=Cl

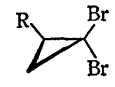

1c: R=*n*-C_6H_{13}
1d: R=$PhCH_2OCH_2$

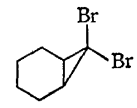

1e

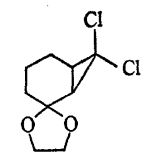

1f

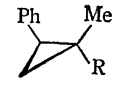

2a: R=*n*-Bu
2b; R=*s*-Bu
2c: R=*t*-Bu

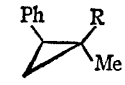

3a: R=*n*-Bu
3b: R=*s*-Bu
3c: R=*t*-Bu

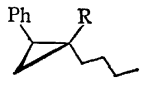

2d: R=Et
2e: R=Ac
2f: R=H
2g: R=I

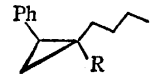

3d: R=Et
3e: R=Ac
3f: R=H
3g: R=I

TABLE 1. STEREOSELECTIVE DIALKYLATION OF *gem*-DIHALOCYCLOPROPANES

Entry	*gem*-Dihalocyclopropane	R^1[a]	R^2-Y[b]	Reaction temp (°C)	Products	Yield (%) of **2** and **3**	**2**:**3**
1	**1a**	*n*-Bu	MeI	−48	**2a** and **3a**	100	80:20
2	**1a**	*n*-Bu	MeI	−78	**2a** and **3a**	64	86:14
3	**1a**	*s*-Bu	MeI	−78	**2b** and **3b**	43	93:7
4	**1a**	*t*-Bu	MeI	−55	**2c**	20	100:0
5	**1a**	*n*-Bu	EtI	−48	**2d** and **3d**	65	51:49
6	**1a**	*n*-Bu	AcBr	−48	**2e** and **3e**	34	80:20
7	**1a**	*n*-Bu	HOEt	−48	**2f** and **3f**	96	81:19
8	**1a**	*n*-Bu	I_2	−48	**2g** and **3g**	79	66:34[c]
9	**1b**	*n*-Bu	MeI	−60	**2a** and **3a**	71	41:59[d]
10	**1c**	*n*-Bu	MeI	−48	**2h** and **3h**	50	76:24
11	**1d**	*n*-Bu	MeI	−48	**2i** and **3i**	50	70:30
12	**1e**	*n*-Bu	MeI	−48	**2j** and **3j**	82	99:1
13	**1f**	*n*-Bu	MeI	−48	**2k**[e]	78	100:0

a) Butyl group in dibutylcopperlithium. b) Electrophiles (see Scheme 1). c) 1,1-Dibutyl-2-phenylcyclopropane (**17c**) was obtained as a by-product (see Experimental). d) The reason for the inverted isomer-preference is not clear. e) After deacetalization of the primary product.

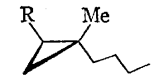

2h: R=*n*-C_6H_{13}
2i: R=$PhCH_2OCH_2$

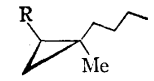

3h: R=*n*-C_6H_{13}
3i: R=$PhCH_2OCH_2$

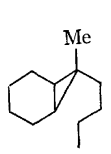

2j

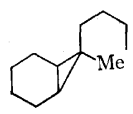

3j

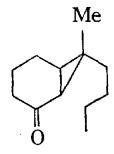

2k

iodide afforded a 4: 1 mixture of **2a** and **3a** in a quantitative yield. Various *gem*-dihalocyclopropanes were allowed to react first with some dibutylcopperlithiums and then with a variety of electrophiles including methyl iodide. The results are summarized in Table 1. Preliminary experiments revealed, however, that the yields were very much influenced by the reaction conditions. Among solvent systems examined (hexane, hexane–ether, ether, tetrahydrofuran (THF), THF–hexamethylphosphoric triamide (HMPA)) hexane–ether gave the best results. The strict absence of unchanged butyllithium should be assured and therefore a slight excess of cuprous iodide was used for the preparation of the cuprate. Finally, the reaction temperature should be controlled carefully: the temperature during the reaction of the cuprate with dihalocyclopropanes being adjusted at −40 to −78 °C and the second alkylation at −20 °C.

Of importance in the alkylation is the stereochemical consequence. The reaction of **1a** under the condition cited above resulted in the preferred formation of *cis*-methyl isomer (entry 1). The ratio was better at low temperatures, while the use of more polar solvent systems (THF or THF–HMPA) or the presence of *n*-Bu_3P as a ligand gave no improvement. Reaction of **1a** with di-*s*-butylcopperlithium or di-*t*-butylcopperlithium followed by methylation afforded predominantly *cis*-methylated **2b** and **2c** albeit in lower yields (entry 3, 4). Noteworthy is the reaction of 7,7-dibromonorcarane (**1e**) and its derivative **1f**, in which *endo*-methyl isomers (**2j** and **2k**) were formed exclusively (entry 12 and 13).

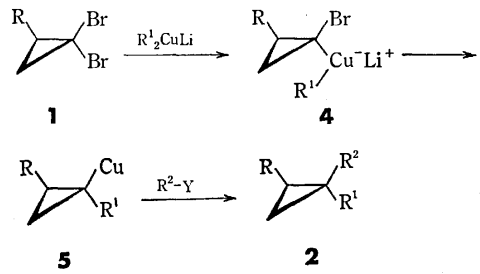

Scheme 1.

These stereochemical results are explained by Scheme 1 which involves halogen-copper exchange *at the less hindered halogen*, the consecutive S_N2 type alkyl migration (*inversion on the cyclopropane carbon*), and the second alkylation by R^2–Y with *retention of configuration*. The steric hindrance of large substituent(s) and/or the bulkiness of the copper reagent would strongly direct the dialkylcuprate to attack the less hindered halogen.

The configurational stability of α-alkylcyclopropylcopper reagent of type 5 was verified as follows. At −78 °C the dibromocyclopropane **1a** was treated with 5 mol of dibutylcopperlithium which had been prepared at −48 °C, and then the reaction mixture was gradually warmed up finally to −10 °C in *ca.* 3 h. Aliquots of the sample at various temperatures were withdrawn, quenched with methanol and the products, 1-butyl-2-phenylcyclopropanes (**2f** and **3f**), were analyzed by GLC to give a nearly invariable ratio of 4: 1 of **2f**/**3f** throughout the period of experiment. This indicates that the species **5** is configurationally stable at the temperature range examined.

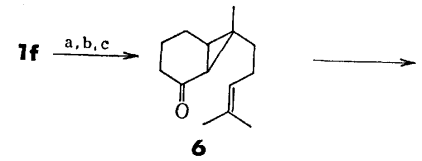

6

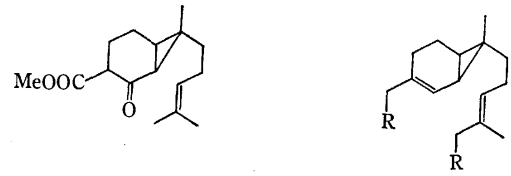

a: $(Me_2C{=}CHCH_2CH_2)_2CuLi$; b: MeI; c: H_2SO_4–H_2O; d: NaH-$(MeO)_2CO$.

8a: R=H
8b: R=OH

Application to dl-*Sirenin Synthesis.*[7] With these observations in hand we extended the reaction to the preparation of a key intermediate of *dl*-sesquicarene and *dl*-sirenin syntheses. As attempted preparation of the dibromocarbene adduct of cyclohexenone ethylene acetal failed to success, we were compelled to start with the dichlorocarbene adduct **1f** which was obtained by the phase-transfer technique.[2] Treatment of **1f** with bis-(4-methyl-3-pentenyl)copperlithium and then with excess methyl iodide, followed by deacetalization, afforded **6** in 44% yield. The GLC and PMR analyses showed no contamination of the stereoisomer. The configuration was established by the methoxycarbonyla-

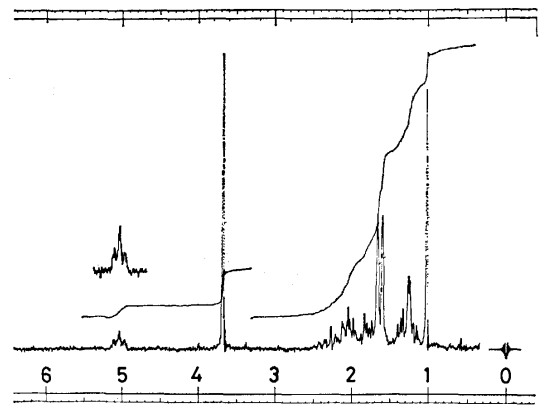

Fig. 1. The PMR spectrum of the keto ester **7** (CCl_4, 100 MHz).

tion of **6**. The methyl chemical shift (δ 1.02) of the product **7** (Fig. 1) was strictly the same as that of the 7-*endo*-methyl keto ester and clearly different from that of 7-*exo*-methyl isomer (δ 1.14).[7a] Further transformation of **7** to *dl*-sesquicarene (**8a**) and *dl*-sirenin (**8b**) has been already established.[7a]

Stereochemistry of Dialkylated Cyclopropanes. The configuration of each phenyl substituted cyclopropane (**2a—g**, **3a—g**) was identified by the comparison of PMR spectra. In general, the methyl signal *cis* to phenyl group appeared at higher field than that of *trans* isomer (see Experimental).[3] For example, the methyl signal of **2a** appeared at δ 0.73, whereas that of its stereoisomer **3a** appeared at δ 1.18. Similarly, *cis*-acetylated cyclopropane **2e** showed acetyl signal at δ 1.61 and its *trans* isomer **3e** at δ 2.12. The peak shape analysis of butyl signal also afforded a basis for the stereochemical determination of **2d** and **2f**. The α-methylene proton peak of butyl group *cis* to phenyl group appeared at slightly higher field than that of the *trans* isomer due to the shielding effect of the benzene ring. The stereochemical assignment is also possible from the fact that proton(s) *cis* to butyl group on the three membered ring generally appeared at higher field than the *trans* proton(s) probably due to the deshielding effect by σ bond(s).[8] This criterion was applied to the determination of the iodinated cyclopropanes: benzylic proton of **2g** at δ 2.16 and that of **3g** at δ 2.78.

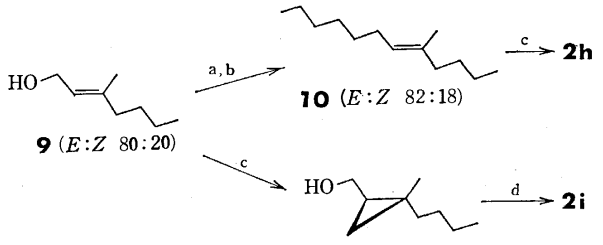

a: PBr_3; b: *n*-AmMgBr; c:CH_2I_2/Zn–Cu; d: NaH/$PhCH_2Cl$.

Scheme 2.

Stereochemistry of **2h** and **2i** was unambiguously determined by the independent syntheses as shown in Scheme 2. An allyl alcohol **9**[9] was converted into a trisubstituted olefin **10**, which was subjected to the Simmons-Smith reaction[10] to give **2h** and **3h** (84: 16). The authentic samples of **2i** and **3i** were obtained by cyclopropanation on **9** and the successive benzylation. Scheme 3 shows the syntheses of the authentic specimens of **2j** and **2k**. The route involves a well-established diazoketone cyclization.[11] Copper catalyzed thermal decomposition of **14** afforded **2k** and its stereoisomer (71: 29). The Wolff-Kishner reduction[12] of **2k** gave the hydrocarbon **2j**.

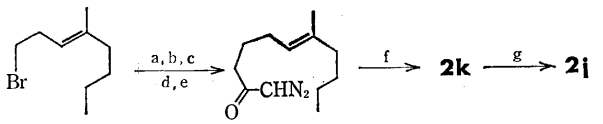

12 (*E*:*Z* 77:23) **14**

a: $NaCH(COOEt)_2$; b: NaOH; c: H_3O^+, Δ; d: $SOCl_2$; e: CH_2N_2; f: $CuSO_4$, Δ; g: NH_2NH_2, KOH, $HO(CH_2CH_2O)_3H$.

Scheme 3.

Further Extention and Possible Reaction Mcehanism. In sharp contrast to the above reaction of dibutylcuprates, dimethylcopperlithium reacted with **1a** in THF at —78 °C to afford dimethylated product **17a** (48%). Remarkably, the same procedure at —38 °C in ether gave a mixture (43: 57) of mono-methylated products **15a** and **16a** (49% yield) along with **17a** (17%). More drastic change of the reaction path was achieved only by temperature control in the reaction of divinylcopperlithium. Whereas at —48 °C in ether divinylcyclopropane **17b** was obtained in 47% yield, the reaction at —78 °C afforded 1-bromo-1-vinylcyclopropanes **15b** and **16b** (26: 74) in 80% yield. It should be noted that the reaction of **1a** with dibutylcopperlithium gave no **17c**.

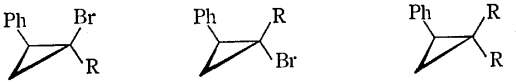

15 **16** **17**

a: R=Me; **b**: R=vinyl; **c**: R=*n*-Bu

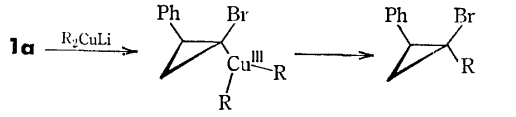

R=Me or vinyl **18** **15** or **16**

Scheme 4.

We do not believe that all these three cuprates react with **1a** by a single mechanism. The initial step in the reaction of dibutylcopperlithium shown in Scheme 1 is copper-halogen exchange (two-electron transfer process)[5a] to afford a mixed cuprate **4** which easily rearranges to an α-alkylated cyclopropylcopper **5** under S_N2 type alkyl migration. Another possibility is shown in Scheme 4 in which a trivalent copper species is assumed in the initial step. Reductive elimination of this unstable transient affords an α-alkylated cyclopro pyl bromide. The reaction of dimethyl- ;or divinylcopperlithium should be explained by this scheme, which is quite similar to the one proposed for the coupling of dialkylcuprates with alkyl halides and tosylates.[13]

The Scheme 1 is supported by the related observations as follows. When *trans*-1-bromo-2-phenylcyclopropane (**19**) was treated with 4 mol of dibutylcopperlithium in THF and successively with allyl bromide, *trans*-1-allyl-2-phenylcyclopropane (**20**) was obtained in 97% yield. No butylated product was detected and, therefore, the copper intermediate is probably the one as shown below. It should be noted that **19** was more susceptible to the reaction than its *cis* isomer.[14]

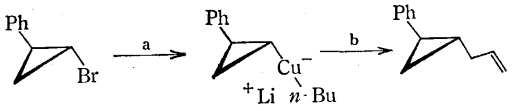

19 **20**

a: *n*-Bu_2CuLi/THF; b: CH_2=$CHCH_2Br$.

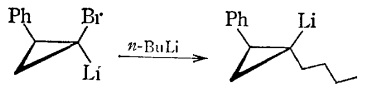

The second step in Scheme 1 is the intramolecular S_N2 type alkyl migration which is exemplified by the following experiment. A solution of **1a** in THF was added to a solution of butyllithium (3.3 mol) in THF at −95 °C. Aqueous workup afforded *trans*-1-butyl-2-phenylcyclopropane.[15] Introduction of butyl group is attributed to nucleophilic attack of butyl anion as illustrated below.[16]

Experimental

All the temperatures are uncorrected. The IR spectra were obtained on a Shimadzu spectrometer 27-G, MS on a Hitachi RMU-6L, and PMR on JEOL JNM-PMX 60, Varian EM-360, or Varian HA-100D spectrometers. Butyllithium and *t*-butyllithium were purchased from Aldrich Co. Ltd. Vinyllithium in ether,[17] methyllithium in ether,[18] and *s*-butyllithium in pentane[19] were prepared according to the literature. Commercial cuprous iodide was purified according to the literature.[20] Ether and hexane were distilled and dried on sodium metal. THF was dried on benzophenone ketyl and distilled. All the reactions were performed under a nitrogen atmosphere. The cold bath of −48 °C was prepared by mixing Dry Ice and *m*-xylene.

gem-*Dihalocyclopropanes.* These were prepared by the reaction of the corresponding olefins with bromoform/*t*-BuOK. *gem*-Dichlorocyclopropanes were prepared by the phase transfer method. A typical procedure is illustrated in the synthesis of **1f**.

*7,7-Dichloronorcaran-2-one Ethylene Acetal (**1f**).* A solution of cyclohexenone ethylene acetal (11.2 g, 80 mmol) in benzene (10 ml) was mixed with 120 ml of 50% aqueous sodium hydroxide. The mixture was warmed to 40 °C and under vigorous stirring 80 ml of chloroform was added during 4 h. After the addition was completed, the reaction mixture was stirred at 40 °C for 2 h. Extraction with hexane and subsequent fractionation through a 15 cm Vigreux column gave **1f** (88—90 °C/1 Torr, 11.6 g, 71% based on the consumed starting olefin). IR (neat): 1107, 1020, 948, 784 cm^{-1}; MS: *m/e* (%), 226 (M^++4, 0.5), 224 (M^+ +2, 2), 222 (M^+, 3.4), 187 (32), 99 (100), 86 (37); PMR (CCl_4): δ 1.0—2.3 (m, 8H), 3.7—4.2 (m, 4H). Found: C, 48.7; H, 5.7%. Calcd for $C_9H_{12}Cl_2O_2$: C, 48.5; H, 5.4%.

*1-Butyl-1-methyl-2-phenylcyclopropane (**2a** and **3a**).* Dibutylcopperlithium was prepared by the treatment of butyllithium (5.7 ml of 1.75 M hexane solution) with cuprous iodide (0.96 g, 5.0 mmol) suspended in ether (10 ml) at −48 °C. A solution of **1a** (0.28 g, 1.0 mmol) in ether (1 ml) was added dropwise to this solution. The reaction mixture was gradually warmed up to −20 °C in 1 h, treated with excess methyl iodide (1 ml), and further warmed to room temperature during 15 h. Workup followed by short path distillation at 82—92 °C/26 Torr gave a mixture of **2a** and **3a** (0.19 g, quantitative yield). Each isomer was separated by preparative GLC (20% Silicone HV grease on Celite 545, 1 m, 160 °C, He, 1.2 kg/cm^2).

r-*1-Butyl-1-methyl*-t-*2-phenylcyclopropane (**2a**)*: R_t 25 min; bp 84—89 °C (bath temp)/2 Torr; IR (neat): 3070, 3040, 1605, 1580, 1498, 1450, 1385, 1070, 1030, 780, 735, 700 cm^{-1}; MS: *m/e* (%), 188 (M^+, 16), 173 (2), 131 (100), 117 (15), 104 (32), 91 (34); PMR (CCl_4): δ 0.6—1.7 (m, 11H), 0.73 (s, 3H, Me), 1.83 (t, J=7 Hz, 1H, PhCH), 6.8—7.4 (m, 5H, Ph). Found: C, 89.3; H, 10.9%. Calcd for $C_{14}H_{20}$: C, 89.3; H, 10.7%.

r-*1-Butyl-1-methyl*-c-*2-phenylcyclopropane (**3a**)*: R_t 20 min; bp 85—95 °C (bath temp)/1 Torr; IR (neat): 3070, 3040, 1605, 1497, 1460, 1380, 1025, 777, 699 cm^{-1}: MS: *m/e* (%), 188 (M^+, 14), 173 (2), 131 (100), 117 (18), 104 (39), 91 (37); PMR (CCl_4): δ 0.5—1.6 (m, 11H), 1.18 (s, 3H, Me), 1.83 (dd, J=6, 8 Hz, 1H, PhC*H*), 6.9—7.4 (m, 5H, Ph). Found: C, 89.5; H, 10.7%. Calcd for $C_{14}H_{20}$: C, 89.3; H, 10.7%.

r-*1*-s-*Butyl-1-methyl*-t-*2-phenylcyclopropane (**2b**).* A cooled solution of *s*-butyllithium (16 ml of 0.62 M pentane solution, 10 mmol) was added to a suspension of cuprous iodide (0.95 g, 5.0 mmol) in ether (10 ml) at −78 °C. The suspension immediately turned to black, and after 5 min a solution of **1a** (0.28 g, 1.0 mmol) in ether (1 ml) was added. The reaction mixture was gradually warmed to −20 °C in 3 h, treated with methyl iodide (1 ml) and further warmed to room temp during the period of 5 h. Aqueous workup and subsequent preparative TLC (silica gel, hexane, R_f 0.7—0.8) afforded 83 mg of **2b** (93% pure on GLC assay). Analytical sample was obtained by preparative GLC. Bp 84—92 °C (bath temp)/23 Torr; IR (neat): 3060, 3040, 1603, 1575, 1498, 1450, 1370, 1075, 1020, 775, 733, 700 cm^{-1}: MS: *m/e* (%), 188 (M^+, 4), 131 (100), 117 (11), 104 (45); PMR (CCl_4): δ 0.3—1.7 (m, 11H), 0.61 (s, 3H, Me), 1.83 (dd, J=6, 8 Hz, 1H, PhC*H*), 6.7—7.3 (m, 5H, Ph). Found: C, 89.0; H, 10.6%. Calcd for $C_{14}H_{20}$: C, 89.3; H, 10.7%. GLC separation of minor components gave **3b** which was identified by MS: *m/e* 188 (M^+).

r-*1*-t-*Butyl-1-methyl*-t-*2-phenylcyclopropane (**2c**).* To di-*t*-butylcopperlithium, prepared from *t*-butyllithium (3.1 ml of 1.6 M pentane solution, 5.0 mmol) and cuprous iodide (0.48 g, 2.5 mmol) in ether (5 ml) at −55 °C, **1a** (0.14 g, 0.5 mmol) in ether (1 ml) was added, and the reaction mixture was gradually warmed up to −20 °C in 3 h, then treated with methyl iodide (1 ml) and further warmed up to room temp during the period of 15 h. Workup followed by preparative TLC (silica gel, hexane, R_f 0.7—0.8) gave **2c** (19 mg, 20% yield). Any isomer was not detected by GLC or PMR assay. Bp 95—100 °C (bath temp)/24 Torr; IR (neat): 3090, 3050, 1605, 1580, 1500, 1383, 1363, 1172, 1080, 1028, 773, 734, 699 cm^{-1}; MS: *m/e* (%), 188 (M^+, 3), 131 (78), 84 (100), 69 (73), 57 (46), 41 (38); PMR (CCl_4): δ 0.66 (s, 3H, Me), 0.7—1.3 (m, 2H), 0.93 (s, 9H, *t*-Bu), 2.10 (dd, J=5, 9 Hz, 1H, PhC*H*), 6.8—7.3 (m, 5H, Ph). Found: C, 89.6; H, 11.0%. Calcd for $C_{14}H_{20}$: C, 89.3; H, 10.7%.

*1-Butyl-1-ethyl-2-phenylcyclopropanes (**2d** and **3d**).* A solution of **1a** (0.28 g, 1.0 mmol) in ether (1 ml) was added to *n*-Bu_2CuLi (5.0 mmol) prepared at −48 °C. Stirring was continued for 1 h and ethyl iodide (1 ml) was added. Then the mixture was gradually warmed to room temp during 15 h. Workup and preparative TLC (silica gel, hexane, R_f 0.8—0.9) afforded an isomeric mixture of **2d** and **3d** (0.14 g, 65%). Each isomer was separated by GLC (Silicone HV grease, 150 °C He, 1.7 kg/cm^2).

r-*1-Butyl-1-ethyl*-t-*2-phenylcyclopropane (**2d**)*: R_f 16 min; bp 87—95 °C (bath temp)/27 Torr; IR (neat): 3060; 3040, 1605, 1580, 1497, 1453, 1378, 1070, 1029, 774, 730, 699 cm^{-1}; MS: *m/e* (%), 202 (M^+, 18), 173 (28), 145 (100), 117 (78), 104 (52), 91 (76); PMR (CCl_4): δ 0.5—1.6 (m, 16H), 1.87 (dd, J=6, 8 Hz, 1H, PhC*H*), 6.9—7.4 (m, 5H, Ph). Found: C, 88.8; H, 10.9%. Calcd for $C_{15}H_{22}$: C, 89.0; H, 11.0%.

r-*1-Butyl-1-ethyl*-c-*2-phenylcyclopropane (**3d**)*: R_t 13 min; bp 82—89 °C (bath temp)/20 Torr; IR (neat): 3070, 3040, 1605, 1580, 1499, 1450, 1380, 1070, 1029, 778, 730 cm^{-1}; MS: *m/e* (%), 202 (M^+, 19), 173 (28), 145 (100), 117 (76),

104 (57), 91 (61); PMR (CCl_4): δ 0.5—1.6 (m, 16H), 1.82 (dd, J=6, 8 Hz, 1H, PhCH), 6.8—7.4 (m, 5H, Ph). Found: C, 88.8; H, 11.0%. Calcd for $C_{15}H_{22}$: C, 89.0; H, 11.0%.

*1-Acetyl-1-butyl-2-phenylcyclopropanes (**2e** and **3e**).* A solution of **1a** (0.28 g, 1.0 mmol) in ether (1 ml) was treated with *n*-Bu_2CuLi (5.0 mmol) in ether (10 ml) at −48 °C. The reaction mixture was warmed to −20 °C during 1 h and then cooled again to −78 °C. Acetyl bromide (1.0 ml) was added and the reaction mixture was gradually warmed to room temp during 15 h. Workup and preparative TLC (silica gel, hexane–ether (4: 1) gave **2e** and **3e**.

r-*1-Acetyl-1-butyl*-c-*2-phenylcyclopropane (**2e**)*: R_f 0.4—0.5; bp 70—75 °C (bath temp)/0.07 Torr; IR (neat): 1690, 1600, 1580, 1498, 1450, 1355, 1196, 1134, 1025, 958, 768, 730, 695 cm^{-1}: MS: *m/e* (%), 216 (M^+, 18), 173 (26), 129 (17), 117 (19), 91 (20), 43 (100); PMR (CCl_4): δ 0.7—2.5 (m, 12H), 1.61 (s, 3H, Ac), 6.9—7.4 (m, 5H, Ph). Found: C, 83.2; H, 9.4%. Calcd for $C_{15}H_{20}O$: C, 83.3; H, 9.3%.

r-*1-Acetyl-1-butyl*-t-*2-phenylcyclopropane (**3e**)*: R_f 0.3—0.4; bp 66—70 °C (bath temp)/0.06 Torr; IR (neat): 1688, 1605, 1580, 1500, 1450, 1380, 1356, 1200, 1142, 778, 732, 700 cm^{-1}; MS: *m/e* (%), 216 (M^+, 16), 173 (24), 129 (13), 117 (27), 91 (19), 43 (100); PMR (CCl_4): δ 0.5—1.9 (m, 11H), 2.12 (s, 3H, Ac), 2.57 (dd, J=7, 9 Hz, 1H, PhCH), 6.9—7.3 (m, 5H, Ph). Found: C, 83.0; H, 9.5%. Calcd for $C_{15}H_{20}O$: C 83.3; H, 9.3%.

*1-Butyl-2-phenylcyclopropanes (**2f** and **3f**).* A solution of **1a** (0.28 g, 1.0 mmol) in ether (1 ml) was treated with *n*-Bu_2CuLi (5.0 mmol) in ether (10 ml) at −48 °C. The reaction mixture was warmed up tp −20 °C during 1 h, and ethanol (2 ml) was added. Workup and subsequent preparative TLC purification gave a mixture of **2f** and **3f** (0.17 g, 96% yield). Each isomer was separated by preparative GLC (Silicone HV grease, 150 °C, 0.7 kg/cm^2).

trans-*1-Butyl-2-phenylcyclopropane (**2f**)*: R_t 12 min; bp 82—83 °C/21 Torr; IR (neat): 1605, 1500, 1465, 1084, 1020, 750, 695 cm^{-1}; MS: *m/e* (%), 174 (M^+, 22), 117 (77), 104 (100), 91 (33); PMR (CCl_4): δ 0.5—1.7 (m, 13H), 6.7—7.3 (m, 5H, Ph). Found: C, 89.5; H, 10.3%. Calcd for $C_{13}H_{18}$: C, 89.6; H, 10.4%.

cis-*1-Butyl-2-phenylcyclopropane (**3f**)*: R_t 11 min; bp 70—74 °C (bath temp)/4 Torr; IR (neat): 1600, 1495, 1025, 770, 723, 700 cm^{-1}; MS: *m/e* (%), 174 (M^+, 17), 117 (72), 104 (100), 91 (32); PMR (CCl_4) δ 0.4—1.7 (m, 12H), 1.7—2.3 (m, 1H), 7.0—7.2 (m, 5H, Ph). Found: C, 89.5; H, 10.7%. Calcd for $C_{13}H_{18}$: C, 89.6; H, 10.4%.

*Reaction of 1,1-Dichloro-2-phenylcyclopropane (**1b**) with Dibutylcopperlithium.* A solution of **1b** (0.19 g, 1.0 mmol) in ether (1 ml) was added to a solution of *n*-Bu_2CuLi (5.0 mmol) prepared at −48 °C, and the reaction mixture was warmed to 0 °C in 3.5 h, treated with methyl iodide (1 ml), and allowed to warm to room temp (15 h). Workup and preparative TLC afforded a mixture of **2a** and **3a** (97 mg, 71% yield) besides a recovered starting material (49 mg).

*1-Iodo-1-butyl-2-phenylcyclopropane (**2g** and **3g**).* A solution of **1a** (0.28 g, 1.0 mmol) in ether (1 ml) was treated with *n*-Bu_2CuLi (5.0 mmol) in ether (10 ml) at −48 °C. The reaction mixture was warmed to −30 °C in 1 h and then treated with iodine (2.5 g, 10 mmol) dissolved in THF (4 ml), and further warmed up to room temp. Usual workup involving reduction of the excess iodine with aq. sodium thiosulfate, followed by preparative TLC (silica gel, hexane), gave **2g** (R_f 0.5—0.6, 0.16 g, 52%) and **3g** (R_f 0.6—0.7, 81 mg, 27%) along with **17c** (R_f 0.7—0.8, 22 mg, 10%).

r-*1-Iodo-1-butyl*-c-*2-phenylcyclopropane (**2g**)*: Bp 123—128 °C (bath temp)/3 Torr; IR (neat): 3090, 3060, 3040, 1602, 1580, 1497, 1450, 1370, 1150, 1022, 780, 756, 722, 690 cm^{-1}; MS: *m/e* (%), 300 (M^+, 2), 217 (5), 173 (38), 131 (22), 117 (100) 91 (68); PMR (CCl_4): δ 0.6—2.2 (m, 12H), 6.8—7.4 (m, 5H, Ph). Found: C, 52.3; H, 5.8%. Calcd for $C_{13}H_{17}I$: C, 52.0; H, 5.7%.

r-*1-Iodo-1-butyl*-t-*2-phenylcyclopropane (**3g**)*: Bp 118—124 °C (bath temp)/3 Torr; IR (neat): 3090, 3070, 3040, 1600, 1580, 1499, 1450, 1370, 1195, 1142, 770, 725, 695 cm^{-1}; MS: *m/e* (%), 300 (M^+, 2), 217 (1), 173 (37), 131 (23), 117 (100), 91 (68); PMR (CCl_4): δ 0.5—1.8 (m, 11H), 2.78 (dd, J=7, 10 Hz, 1H, PhC*H*), 7.0—7.4 (m, 5H, Ph). Found: C, 52.3; H, 5.8%. Calcd for $C_{13}H_{17}I$: C, 52.0; H, 5.7%.

*1,1-Dibutyl-2-phenylcyclopropane (**17c**)*: Bp 80—86 °C (bath temp)/2 Torr; IR (neat): 3040, 1600, 1495, 1460, 1027, 780, 727, 700 cm^{-1}; MS: *m/e* (%), 230, (M^+, 17), 173 (66), 117 (100), 104 (55), 91 (68); PMR (CCl_4): δ 0.5—1.7 (m, 20H), 1.83 (dd, J=7, 10 Hz, 1H, PhC*H*), 6.8—7.3 (m, 5H, Ph). Found: C, 88.4; H, 11.4%. Calcd for $C_{17}H_{26}$: C, 88.6; H, 11.4%.

*Air Oxidation of the Cyclopropylcopper Reagent Prepared from **1a** and Dibutylcopperlithium.* A solution of **1a** (0.28 g, 1.0 mmol) in ether (1 ml) was treated with *n*-Bu_2CuLi (5.0 mmol) in ether (10 ml) at −48 °C. After 1 h dry air (passed through $CaCl_2$ and silica gel) was introduced into the reaction mixture which was subsequently allowed to warm to 0 °C in 3 h. Workup and subsequent TLC purification (silica gel, hexane) gave **17c** (R_f 0.7—0.8, 80 mg, 34%), **3g** (R_f 0.6—0.7, 38 mg, 12%), and **2g** (R_f 0.5—0.6, 54 mg, 18%).

*1-Butyl-1-methyl-2-hexylcyclopropane (**2h** and **3h**).* Dibromocyclopropane **1c** (0.30 g, 1.0 mmol) in ether (1 ml) was treated with *n*-Bu_2CuLi (5.0 mmol) in ether (10 ml) at −48 °C to −20 °C for 1 h. Addition of methyl iodide (1 ml) at −20 °C, followed by usual workup and preparative TLC (silica gel, hexane, R_f 0.8—0.9), gave a mixture of **2h** and **3h** (0.10 g, 50% yield). Each product was separated by GLC (Silicone HV grease, 150 °C, 0.8 kg/cm^2).

r-*1-Butyl-1-methyl*-t-*2-hexylcyclopropane (**2h**)*: R_t 58 min; bp 75—80 °C (bath temp)/4 Torr; IR (neat): 3050, 2930 2860, 1465, 1375, 1020, 730 cm^{-1}; MS: *m/e* (%), 196 (M^+, 4) 154 (6), 139 (11), 126 (4), 111 (8), 97 (24), 83 (55), 69 (98), 55 (100); PMR (CCl_4): δ −0.3—0.5 (m, 3H), 0.97 (s, 3H, Me), 0.7—1.9 (m, 22H). Found: C, 85.8; H, 14.5%. Calcd for $C_{14}H_{28}$: C, 85.6; H, 14.4%.

r-*1-Butyl-1-methyl*-c-*2-hexylcyclopropane (**3h**)*: R_t 38 min; bp 60—65 °C (bath temp)/3 Torr; IR (neat): 3050, 2930, 1460, 1370, 1255, 1015 cm^{-1}; MS: *m/e* (%), 196 (M^+, 3), 154 (5), 139 (8), 126 (3), 111 (11), 97 (17), 83 (41), 69 (79), 55 (78), 44 (100); PMR (CCl_4): δ −0.3—0.6 (m, 3H), 0.99 (s, 3H, Me), 0.6—1.7 (m, 22H). Found: C, 85.6; H, 14.4%. Calcd for $C_{14}H_{28}$: C, 85.6; H, 14.4%.

*1-Butyl-1-methyl-2-benzyloxymethylcyclopropanes (**2i** and **3i**).* A solution of **1d** (0.32 g, 1.0 mmol) in ether (1 ml) was treated with *n*-Bu_2CuLi (5.0 mmol) in ether (10 ml) at −48 °C. The reaction mixture was gradually warmed up to −20 °C during 1 h and treated with methyl iodide (1 ml), and then further warmed to room temp in 15 h. Workup and preparative TLC (silica gel, hexane–ether 1: 1) gave a mixture of **2i** and **3i** (0.12 g, 50% yield). Each product was separated by preparative GLC (Apiezon L (30%) and KOH (10%) on Chromosorb W, 2 m, 150 °C, 1.0 kg/cm^2 of He gas).

r-*1-Butyl-1-methyl*-t-*2-benzyloxymethylcyclopropane (**2i**)*: R_t 35 min; bp 73—80 °C (bath temp)/0.06 Torr; IR (neat): 1492, 1450, 1374, 1254, 1090, 1025, 790, 734, 700 cm^{-1}; MS: *m/e* (%), 232 (M^+, 0.2), 217 (0.1), 191 (2), 188 (1), 175 (2), 91 (100); PMR (CCl_4): δ 0.3—0.6 (m, 1H), 0.7—1.7 (m, 11H), 1.03 (s, 3H, Me), 3.17 (dd, J=8, 10 Hz, 1H, OCH_aH_b), 3.53 (dd, J=6, 10 Hz, 1H, OCH_aH_b), 4.43 (s, 2H, $PhCH_2$), 7.2—7.3 (m, 5H, Ph). Found: C, 82.9; H, 10.6%. Calcd

for $C_{16}H_{24}O$: C, 82.7; H, 10.4%.

r-*1-Butyl-1-methyl*-c-*2-benzyloxymethylcyclopropane (3i)*: R_t 30 min; bp 75—83 °C (bath temp)/0.06 Torr; IR (neat): 1494, 1451, 1375, 1255, 1090, 1027, 805, 736, 700 cm^{-1}; MS: *m/e* (%), 232 (M^+, 0.05), 217 (0.1), 191 (0.5), 188 (0.5), 175 (0.5), 91 (100); PMR (CCl_4): δ 0.3—0.5 (m, 1H), 0.7—1.7 (m, 11H), 1.03 (s, 3H, Me), 3.22 (dd, J=8, 10 Hz, 1H, OCH_aH_b), 3.50 (dd, J=6, 10 Hz, 1H, OCH_aH_b), 4.41 (s, 2H, $PhCH_2$), 7.2—7.4 (m, 5H, Ph). Found: C, 82.6; H, 10.5%. Calcd for $C_{16}H_{24}O$: C, 82.7; H, 10.4%.

7-exo-*Butyl*-*7*-endo-*methylnorcarane (2j)*. A solution of 7,7-dibromonorcarane (**1e**) (0.26 g, 1.0 mmol) in ether (1 ml) was treated with *n*-Bu_2CuLi (5.0 mmol) in ether (10 ml) at −48 °C. After 1 h methyl iodide (1.0 ml) was added and the reaction mixture was gradually warmed up to room temp in 3 h. Workup and subsequent preparative TLC (silica gel, hexane, R_f 0.8—0.9) afforded **2j** (0.14 g, 82% yield). Bp 100—106 °C (bath temp)/15 Torr; IR (neat): 3000, 1465, 1449, 1380, 785 cm^{-1}; MS: *m/e* (%), 166 (M^+, 5), 152 (3), 151 (3), 123 (9), 110 (54), 109 (100), 95 (26); PMR (CCl_4): δ 0.4—0.6 (m, 2H), 0.93 (s, 3H, Me), 0.6—2.6 (m, 17H). Found: C, 86.6; H, 13.6%. Calcd for $C_{12}H_{22}$: C, 86.7; H, 13.3%.

exo-*7-Butyl*-endo-*7-methylnorcaran-2-one (2k)*. Dichlorocarbene adduct **1f** (0.22 g, 1.0 mmol) in ether (1 ml) was treated with *n*-Bu_2CuLi (5.0 mmol) in ether (10 ml) at −48 °C to 0 °C for 3 h and at 0 °C for 1 h. After the addition of methyl iodide (1 ml) the reaction mixture was gradually warmed to room temp (3 h). Workup and concentration *in vacuo* afforded an oil which was subsequently treated with a mixture of THF (1 ml) and 1.5 M aq H_2SO_4 at room temp for 1 h. Workup and subsequent TLC (silica gel, hexane–ether 3: 1, R_f 0.3—0.4) afforded **2k** (0.14 g, 78% yield). Bp 90—97 °C (bath temp)/15 Torr; IR (neat): 1690, 1470, 1320, 1240, 1180, 1110, 890 cm^{-1}; MS: *m/e* (%), 180 (M^+, 8), 124 (42), 95 (100), 82 (84); PMR (CCl_4): δ 0.6—2.6 (m, 17H), 1.09 (s, 3H, Me). Found: C, 80.0; H, 11.3%. Calcd for $C_{12}H_{20}O$: C, 79.9; H, 11.2%.

exo-*7-(4-Methyl-3-pentenyl)*-endo-*7-methylnorcaran-2-one (6)*. An ethereal solution of 4-methyl-3-pentenyllithium (14 ml of 0.86 M solution, 12 mmol) was added to cuprous iodide (1.1 g, 6.0 mmol) suspended in a mixture of hexane (15 ml) and ether (5 ml) at −78 °C. During the period of 40 min the reaction mixture was warmed to −70 °C and then a solution of **1f** (0.27 g, 1.2 mmol) in ether (1 ml) was added to the resulting dark gray slurry. The reaction mixture was gradually warmed to −20 °C in 1 h, treated with methyl iodide (2 ml) and allowed to warm to room temp (16 h). Usual workup gave an oil which was subsequently treated with a mixture of THF (1 ml) and 1.5 M aq H_2SO_4 (1 ml) at room temp for 40 min. Workup and preparative TLC purification (silica gel, CH_2Cl_2, R_f 0.3—0.4) gave **6** (0.11 g, 44%). Bp 95—105 °C (bath temp)/0.1 Torr; IR (neat): 1685, 1445, 1380, 1349, 1330, 1245, 895, 790 cm^{-1}; MS: *m/e* (%), 206 (M^+, 5), 137 (22), 69 (87), 41 (100); PMR (CCl_4): δ 1.115 (s, 3H, Me), 1.59 (s, 3H, Me), 1.67 (s, 3H, Me), 1.2—2.3 (m, 12H), 4.9—5.2 (m, 1H). The product **6** was converted into 3-carbomethoxy-*exo*-7-(4-methyl-3-pentenyl)-*endo*-7-methylnorcaran-2-one (**7**) according to the literature.[7a] Bp 110—120 °C (bath temp)/0.3 Torr; IR (neat): 1744, 1689, 1644, 1610 cm^{-1}; MS: *m/e* (%), 264 (M^+, 3), 69 (82), 55 (48), 41 (100); PMR: Fig. 1.

Authentic Samples of 2h and 3h. A solution of 3-methylhept-2-en-1-ol (**9**) (0.74 g, 5.7 mmol, *E*: *Z* 80: 20) in ether (5 ml) was treated with phosphorous tribromide (0.52 g, 1.9 mmol) at −78 °C. The solution was stirred at room temp for 3 h and worked up. Distillation (80—90 °C/18 Torr) of the crude product gave 1-bromo-3-methylhept-2-ene (0.78 g, 71%). The bromide was directly treated with amylmagnesium bromide (5.0 mmol) in ether (4 ml) at room temp for 2 h. Workup and GLC separation (Silicone HV grease, 150 °C, 0.8 kg/cm^2, R_t 30 min) gave an isomeric mixture of 5-methyl-5-dodecene (**10**) (15 mg, *E*: *Z* 82: 18), which was converted to a mixture of **2h** and **3h** (ratio 84: 16) upon heating with methylene iodide (85 mg, 0.32 mmol), zinc powder (42 mg, 0.64 mmol), and cuprous chloride (10 mg, 0.10 mmol) for 15 h.[10] GLC separation of the products gave the authentic samples of **2h** and **3h**, both of which showed the identical GLC retention times (5% Apiezon L grease and 1% KOH on Chromosorb W, 2 m, 104 °C, 0.6 kg/cm^2; R_t of **2h**, 27 min; R_t of **3h**, 25 min) and MS spectra with the samples prepared by the cuprate reaction.

Authentic Samples of 2i and 3i. The allyl alcohol **9** (0.13 g, 1.0 mmol, *E*: *Z* 80: 20) was transformed, upon heating with methylene iodide (0.41 g, 1.5 mmol), zinc powder (0.20 g, 3.0 mmol) and cuprous chloride (30 mg, 0.30 mmol) in ether (2 ml) for 15 h,[10] to the cyclopropyl carbinol **11**: bp 85—95 °C (bath temp)/56 Torr; IR (neat): 3340, 1020 cm^{-1}: MS: *m/e* 124 (M^+-H_2O); PMR (CCl_4): δ 1.05 (s, 3H, Me), 3.1—3.8 (m, 2H, CH_2O). The crude cyclopropyl carbinol **11** in *N*,*N*-dimethylformamide (DMF) (0.5 ml) was mixed with sodium hydride (50 mg) in DMF (1 ml) and the whole was stirred at room temp for 1 h, treated with benzyl chloride (0.15 ml) and worked up after 30 min. Preparative TLC of the crude product (silica gel, ether–hexane 1: 3, R_f 0.8) gave a mixture of **2i** and **3i** (92 mg, 40% overall yield from **9**, 76: 28 ratio). GLC separation afforded each isomer which was identical with the samples prepared by cuprate reaction.

Authentic Samples of 2k. A solution of **12** (0.76 g, 3.7 mmol, *E*: *Z* 77: 23) in ethanol (1 ml) was treated with diethyl sodiomalonate (prepared from 1.2 g of diethyl malonate, 7.4 mmol) according to the literature.[7d] Workup and short path distillation at 124—134 °C/6 Torr gave crude diethyl 4-methyl-3-octenylmalonate (0.49 g) which was directly hydrolyzed (KOH, ethanol reflux) and decarboxylated (acetic acid, reflux for 2 days).[7d] Short path distillation at 106—116 °C/4 Torr gave 6-methyl-5-decenoic acid (**13**) (0.24 g); IR (neat): 3600—3200, 1710, 1410, 1240, 930 cm^{-1}; PMR (CCl_4): δ 1.60 and 1.68 (s, 3H, vinylic methyl of *E* and *Z* isomers), 5.06 (t, J=6 Hz, 1H); *E*: *Z* 70: 30. The acid **13** (0.24 g, 1.3 mmol) was heated with $SOCl_2$ (0.18 g, 1.5 mmol) in dry benzene (5 ml) to reflux for 1 h and the mixture was concentrated. The residue was distilled at 90—100 °C/0.2 Torr and the distillate was treated with excess diazomethane in ether at 0 °C and left over night. The solvent and the excess diazomethane were removed by passing a nitrogen stream over the surface. The concentrated crude diazoketone **14** was dissolved in cyclohexane (1 ml) and added dropwise to a suspension of cupric sulfate (0.30 g, 1.9 mmol) in refluxing cyclohexane (110 ml). After 2 h reflux the reaction mixture was filtered and concentrated *in vacuo*. Short path distillation of the residue at 100—115 °C/5 Torr afforded an oil (0.18 g, 78% overall yield from **13**). Although the product showed identical IR and MS spectra with that of **2k** prepared by cuprate reaction, GLC (3% Apiezol L grease and 10% KOH on Neosorb NC, 154 °C, 1.0 kg/cm^2 of He) and PMR revealed that it was a mixture (71: 29) of **2k** (R_t 6.9 min, methyl signal at δ 1.09) and its stereoisomer (R_t 5.6 min, methyl signal at δ 1.11).

Authentic Samples of 2j. A mixture of **2k** (0.14 g, 0.78 mmol), 80% hydrazine hydrate (3.2 g, 51 mmol) and hydrazine dihydrochloride (0.65 g, 6.2 mmol) in triethylene glycol (15 ml) was heated at 130 °C. After 3 h potassium hydroxide

(0.96 g, 17 mmol) was added and the mixture was heated at 210 °C for 3 h during which volatile products were distilled off. Preparative TLC (silica gel, hexane) of the distillate gave an oil (R_f 0.9, 24 mg) which was further purified by preparative GLC (Silicone HV grease, 130 °C, He, 0.8 kg/cm^2) giving an authentic sample of **2j**.

*Reaction of **1a** with Dimethylcopperlithium in Ether.* Methyllithium (20 ml of 0.5 M ether solution, 10 mmol) was added to cuprous iodide (0.95 g, 5.0 mmol) suspended in ether (5 ml) and hexane (15 ml) at 0 °C. After cooling to −38 °C **1a** (0.28 g, 1.0 mmol) in ether (1 ml) was added and the reaction mixture was gradually warmed to 0 °C in 3 h. Workup and preparative TLC (silica gel, hexane) afforded 1,1-dimethyl-2-phenylcyclopropane (**17a**) (R_f 0.6—0.7, 26 mg, 17%) and a mixture of **15a** (R_f 0.4—0.5, 46 mg, 21%) and **16a** (R_f 0.5—0.6, 60 mg, 28%). Physical properties of **17a**: bp 69—76 °C (bath temp)/20 Torr; IR (neat): 1609, 1580, 1499, 1451, 1375, 1028, 779, 730, 700 cm^{-1}; MS: *m/e* (%), 146, (M$^+$, 38), 131 (100), 117 (20), 91 (50); PMR (CCl_4): δ 0.5—2.0 (m, 3H), 0.78 (s, 3H, Me), 1.22 (s, 3H, Me), 6.7—7.3 (m, 5H, Ph). Found: C, 90.6; H, 9.4%. Calcd for $C_{11}H_{14}$: C, 90.4; H, 9.7%.

*Conversion of **1a** to **17a**.* A solution of methyllithium (3.2 ml of 1.9 M ether solution, 6.0 mmol) was added to a suspension of cuprous iodide (0.58 g, 3.0 mmol) in THF (10 ml) at 0 °C. The reaction mixture was cooled at −78 °C, treated with **1a** (0.28 g, 1.0 mmol) in THF (1 ml) and warmed to room temp in 15 h. Workup and preparative TLC (silica gel, hexane, R_f 0.7—0.8) afforded **17a** (69 mg, 48% yield).

*Reaction of **1a** with Divinylcopperlithium.* A solution of vinyllithium (35 ml of 0.85 M ether solution, 30 mmol) was added to a suspension of cuprous iodide (2.9 g, 15 mmol) in hexane (18 ml) at −48 °C. After 5 min the cuprate solution was cooled to −78 °C and a solution of **1a** (1.4 g, 5.0 mmol) in hexane (2 ml) was added. After 2 h the reaction mixture was quenched with ethanol (1 ml) and allowed to warm to room temp. Workup and subsequent preparative TLC (silica gel, hexane) afforded **15b** and **16b**.

r-*1-Bromo-c-2-phenyl-1-vinylcyclopropane (**15b**)*: R_f 0.7—0.8, 0.23 g, 20% yield; bp 80—87 °C (bath temp)/3 Torr; IR (neat): 1630, 1604, 1500, 1450, 1120, 1020, 970, 903, 698 cm^{-1}; MS: *m/e* (%), 222 (M$^+$, 1), 195 (1), 143 (89), 141 (24), 128 (100), 115 (35), 91 (24), 65 (15); PMR (CCl_4): δ 1.5—1.9 (m, 2H), 2.23 (dd, J=8, 10 Hz, 1H, PhCH), 4.9—6.1 (m, 3H), 7.0—7.4 (m, 5H, Ph). Found: C, 59.2; H, 4.9%. Calcd for $C_{11}H_{11}Br$: C, 59.2; H, 5.0%.

r-*1-Bromo-t-2-phenyl-1-vinylcyclopropane (**16**)*: R_f 0.8—0.9, 0.66 g, 59%; bp 75—82 °C (bath temp)/2 Torr; IR (neat): 1630, 1602, 1496, 1450, 1160, 970, 903, 697 cm^{-1}; MS: *m/e* (%), 222 (M$^+$, 1), 195 (1), 143 (86), 141 (26), 128 (100), 115 (45), 91 (21), 65 (16); PMR (CCl_4): δ 1.4—2.0 (m, 2H), 2.91 (dd, J=8, 9 Hz, 1H, PhC*H*), 4.9—5.5 (m, 3H), 7.0—7.3 (m, 5H, Ph). Found: C, 59.3; H, 5.0%. Calcd for $C_{11}H_{11}Br$: C, 59.2; H, 5.0%.

*1-Phenyl-2,2-divinylcyclopropane (**17b**).* A solution of **1a** (0.14 g, 0.50 mmol) in ether (0.5 ml) was added to a solution of divinylcopperlithium (2.5 mmol) in a mixture of ether (6 ml) and hexane (4 ml) at −48 °C. The reaction mixture was gradually warmed to 0 °C during the period of 3 h. Workup followed by preparative TLC (silica gel, hexane, R_f 0.3—0.4) gave **17b** (40 mg, 47%). Bp 61—66 °C (bath temp)/3 Torr; IR (neat): 1634, 1623, 1600, 1492, 985, 895, 773, 733, 695 cm^{-1}; MS: *m/e* (%), 170 (M$^+$, 58), 155 (82), 141 (46), 128 (85), 115 (80), 91 (100); PMR (CCl_4): δ 0.8—1.7 (m, 2H), 2.35 (dd, J=6, 9 Hz, 1H, PhC*H*), 4.7—6.3 (m, 6H), 6.9—7.3 (m, 5H, Ph). Found: C, 91.9; H, 8.4%. Calcd for $C_{13}H_{14}$: C, 91.7; H, 8.3%.

trans-*1-Allyl-2-phenylcyclopropane (**20**).* A solution of *n*-BuLi (7.2 ml of 1.7 M hexane solution, 12 mmol) was added slowly to a stirred suspension of cuprous iodide (1.1 g, 6.0 mmol) in THF (20 ml) at −48 °C. After 10 min a solution of *trans*-1-bromo-2-phenylcyclopropane (**19**) (0.29 g, 1.5 mmol) in THF (2 ml) was added and stirring was continued further 49 min at this temp. Allyl bromide (1.5 ml) in HMPA (1 ml) was then added and after 30 min the reaction mixture was worked up as usual. Preparative TLC (silica gel, hexane, R_f 0.3—0.4) of the crude oil gave **20** (0.22 g, 97%). Bp 55—60 °C (bath temp)/15 Torr; IR (neat): 1639, 1605, 1497, 1460, 1030, 995, 913, 790, 756, 700 cm^{-1}; MS: *m/e* (%), 158 (M$^+$, 6), 143 (4), 129 (9), 117 (100), 104 (36), 91 (35); PMR (CCl_4): δ 0.6—1.5 (m, 3H), 1.5—1.9 (m, 1H, PhCH), 2.0—2.4 (m, 2H, allylic H), 4.9—6.3 (m, 3H), 6.8—7.4 (m, 5H). Found: C, 90.8; H, 9.0%. Calcd for $C_{12}H_{14}$: C, 91.1; H, 8.9%.

The authors wish to thank the Ministry of Education, Japanese Government, for a Grant-in-Aid (011010).

References

1) T. K. Devon and A. I. Scott, "Handbook of Naturally Occurring Compounds," Vol. II, Academic Press, New York and London (1972), see *e.g.* p. 56.

2) Recently regioselective dihalocyclopropanation was reported: T. Hiyama, H. Sawada, M. Tsukanaka, and H. Nozaki, *Tetrahedron Lett.*, **1975**, 3013.

3) K. Kitatani, T. Hiyama, and H. Nozaki, *J. Am. Chem. Soc.*, **97**, 949 (1975).

4) a) G. H. Posner and D. J. Brunelle, *Tetrahedron Lett.*, **1972**, 293; b) J. Villieras, J. R. Disnar, D. Masure, and J. F. Normant, *J. Organomet. Chem.*, **57**, C95 (1973); c) J. Klein and R. Levene, *Tetrahedron Lett.*, **1974**, 2935; d) G. H. Posner, G. L. Loomis, and H. S. Sawaya, *ibid.*, **1975**, 1373; e) J. E. Dubois and C. Lion, *C. R. Acad. Sci., Ser. C*, **280**, 217 (1975).

5) a) E. J. Corey and G. H. Posner, *J. Am. Chem. Soc.*, **89**, 3911 (1967); **90**, 5615 (1968); b) J. A. Marshall and J. A. Ruth, *J. Org. Chem.*, **39**, 1971 (1974).

6) A part of this work was published in a communication form: K. Kitatani, T. Hiyama, and H. Nozaki, *J. Am. Chem. Soc.*, **98**, 2362 (1976).

7) a) U. T. Bhalerao, J. J. Plattner, and H. Rapoport, *J. Am. Chem. Soc.*, **92**, 3429 (1970); b) E. J. Corey and K. Achiwa, *Tetrahedron Lett.*, **1969**, 1837, 3257; **1970**, 2245; E. J. Corey, K. Achiwa, and J. A. Katzenellenbogen, *J. Am. Chem. Soc.*, **91**, 4318 (1969); c) R. M. Coates and R. M. Freidinger, *Tetrahedron*, **26**, 3487 (1970); d) K. Mori and M. Matsui, *ibid.*, **26**, 2801 (1970); e) P. A. Grieco, *J. Am. Chem. Soc.*, **91**, 5660 (1969).

8) L. M. Jackman and S. Sternhell, "Applications of Nuclear Magnetic Resonance Spectroscopy in Organic Chemistry," 2nd ed, Pergamon Press, Oxford and New York (1969), p. 229.

9) K. Ogura, T. Nishino, T. Koyama, and S. Seto, *J. Am. Chem. Soc.*, **92**, 6036 (1970).

10) R. J. Rawson and I. T. Harrison, *J. Org. Chem.*, **35**, 2057 (1970).

11) W. Kirmse, "Carbene Chemistry," 2nd ed Academic Press, New York and London (1971), p. 339.

12) W. Nagata and H. Itazaki, *Chem. Ind. (London)*, **1964**, 1194.

13) G. H. Posner, "Organic Reactions," Vol. 22 ed. by W. G. Dauben, John Wiley & Sons, Inc., New York (1975),

p. 259 and references cited therein.

14) Remarkably THF solvent is prerequisite to this reaction in contrast to the case of *gem*-dihalocyclopropanes which have an activating geminal halogen atom and undergo copper-halogen exchange even in ether. Probably THF strongly coordinates to the cuprate to increase the electron density on the copper atom enough to reduce even monohalocyclopropanes.

15) K. Kitatani, H. Yamamoto, M. Shinoda, T. Hiyama, and H. Nozaki, Abstracts of Papers presented at the 24th Symposium on Organometallic Chemistry, Kyoto, Japan, October 13—15, 1976, p. 1.

16) The intermediacy of 1-bromo-1-butyl-2-phenylcyclopropane is readily excluded because the carbenoid does not react with butyl bromide under the condition.

17) D. Seyferth and M. A. Weiner, *J. Am. Chem. Soc.*, **83**, 3583 (1961).

18) U. Schölkopf, J. Paust, and M. R. Patsch, "Organic Syntheses," Coll. Vol. V, (1973), p. 859.

19) H. Gilman, F. W. Moore, and O. Baine, *J. Am. Chem. Soc.*, **63**, 2479 (1941).

20) G. H. Posner, C. E. Whitten, and J. J. Sterling, *J. Am. Chem. Soc.*, **95**, 7788 (1973).

21) S. F. Brady, M. A. Ilton, and W. S. Johnson, *J. Am. Chem. Soc.*, **90**, 2882 (1968).

Carbon-13 NMR Spectra of π-Allyl Palladium Chloride Complexes

Yasuhisa SENDA, Hiroshi SUDA, Jun-ichi ISHIYAMA, Shin IMAIZUMI, Akira KASAHARA,* Taeko IZUMI,* and Takao KATO*

Department of Applied Science, Faculty of Engineering, Tohoku University, Aoba, Sendai 980
**Department of Applied Chemistry, Faculty of Engineering, Yamagata University, Yonezawa 992*

(Received January 26, 1977)

The ^{13}C NMR spectra of thirteen acyclic and cyclohexenyl π-allyl palladium chloride dimers are examined and their chemical shifts are compared with those of the corresponding olefins. The signals for the central carbons of the π-allyl palladium moiety were displaced upfield by 8.0—25.5 ppm and those for the terminal carbons by 34.9—55.9 ppm compared to the corresponding carbons of the corresponding olefins.

In recent years, considerable effort has been directed towards the elucidation of the molecular structures of organic compounds using ^{13}C NMR spectroscopy. However, its application to organometallic compounds has so far been limited. Although there have been a number of ^{1}H NMR studies on π-allyl palladium chloride dimers, the ^{13}C NMR spectra of only a few simple chain compounds are to be found in the literature.[1] Here ^{13}C NMR spectra of π-allyl palladium chloride dimers of simple acyclic olefins and substituted cyclohexenes are reported. The carbon chemical shifts are compared with those of the corresponding olefins.

Results and Discussion

The π-allyl palladium chloride complexes of acyclic olefins were prepared from the corresponding allylic chlorides[2] and those of cyclic olefins from the corresponding olefins.[3] Natural abundance 25.15-MHz ^{13}C FT-NMR spectra were obtained using the ^{1}H noise-decoupling technique. The spectra were obtained in $CDCl_3$ as a primary solvent. Since 2- (**4**) and 1-phenyl-π-allyl palladium chloride (**5**) were not sufficiently soluble in this solvent, DMSO-d_6 was also used. The signals were assigned by comparing the signal shifts due to the structural differences between closely-related compounds and by using the ^{1}H off-resonance decoupling technique. The carbon chemical shifts obtained are listed in the table together with those of the corresponding olefins. The butenyl palladium chloride complex (**3**) and **5** are assumed to be composed predominantly of *syn*-isomers.[4] Although each of the cyclohexenyl palladium chloride complexes, **9**, **10**, and **12**, can exist as two stereoisomers, it was impossible to determine the stereochemistry of the complexes obtained here.

For the carbon chemical shifts of the π-allyl palladium moiety, the resonances for the tertiary central carbons of the *endo*-cyclic complexes appeared at fields slightly higher than those of the *exo*-cyclic complexes, while the resonances for the secondary terminal carbons of the *endo*-cyclic complexes appeared at fields lower than those of the *exo*-cyclic isomers. The carbon resonances for the acyclic compounds appeared at fields lower than those of the corresponding cyclic complexes.

The ^{13}C chemical shift of π-allyl palladium complexes were compared with those of the corresponding olefins. The chemical shifts of **3** and **5** were compared with those of the corresponding internal olefins and only the chemical shifts for the primary terminal carbons were compared with those of the terminal olefins. For cyclic π-allyl palladium complexes, the ^{13}C chemical shifts were compared with those of the corresponding cyclohexenes. Only the primary terminal carbons were compared with those of the corresponding methylenecyclohexanes. In order to evaluate the solvent shifts by DMSO, the ^{13}C spectra of the π-allyl (**1**), 2-methylallyl (**2**), **3** and cyclohexenyl palladium chloride complexes (**6**) were also measured in the DMSO-d_6 solvent. The carbon resonances for the central carbons moved downfield by 6.4—7.6 ppm and those of the terminal carbons by 4.1—4.7 ppm. It has been reported that the bridged π-allyl palladium chloride dimers in DMSO are converted to form solvent adducts[5] and that the ^{1}H resonances of the allyl part of the adducts moved downfield compared to the parent bridged dimers.[6] A similar trend was observed for the ^{13}C NMR spectra. If the averaged values of such solvent shifts are applied to the ^{13}C chemical shifts of **4** and **5**, the values for $CDCl_3$ can be estimated. These values are tabulated in the table.

The signals for the secondary central carbons revealed upfield shifts of 14.4—25.5 ppm, while those of the tertiary carbons shifts of 8.0—19.3 ppm. For the terminal carbons, the signals for the primary position moved upfield by 47.1—55.9 ppm, for the secondary ones by 42.7—52.5 ppm and for the tertiary one by 34.9 ppm. Such upfield shifts of the carbon resonances of these π-allylic ligands are generally observed in the ^{13}C NMR spectra of π-allylic-type transition metal complexes.[7] The bonding of the π-allyl metal complexes involves two components: forward donation from the φ_1 orbital to an empty metal d orbital, which causes the electron density to decrease around all three carbon atoms, and interaction of the φ_2 and φ_3 orbitals, which increases the electron density only for the terminal carbon atoms of the π-allylic ligand.[8] This results in larger upfield shifts for the terminal carbons in the π-allyl palladium moiety than for the central carbon atoms.

The ^{13}C NMR spectra of 1-phenylcyclohexene revealed that the resonances corresponding to the carbons of the phenyl group, excepting that of the substituted carbons moved downfield for the π-allylic complex **13**, especially those corresponding to the para- and ortho-related carbons. This implies that the electrons, as a whole, are shifted by the complex formation from the ligand to the metal.

For the carbons of the remaining π-cyclohexenyl ligands, the C-3 and C-5 signals of the *endo*-cyclic

TABLE 1. CARBON-13 CHEMICAL SHIFTS FOR π-ALLYL PALLADIUM CHLORIDE DIMERS AND FREE LIGANDS

No.	Compound	Solvent	C-1	C-2	C-3	C-4	C-5	C-6	C-7	C-8	C_6H_5–
1		$CDCl_3$	62.91	111.08							
		DMSO-d_6	67.58	118.67							
		CH_2Cl_2	63.2	111.9[a]							
		neat	115.4	135.7	18.7[b]						
	$\Delta\delta$[c]		−52.1	−22.0							
2	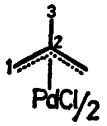	$CDCl_3$	61.88	126.92	22.75						
		DMSO-d_6	66.49	134.14	22.75						
		CH_2Cl_2	61.7	127.9	23.1[a]						
			109.8	141.2	23.3[d]						
	$\Delta\delta$		−47.9	−14.3	−0.6						
3	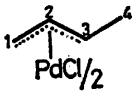	$CDCl_3$	58.30	111.39	81.42	18.01					
		$CDCl_3$	59	111	81	18[e]					
		DMSO-d_6	62.43	117.82	86.27	17.29					
			17.3	125.8[d]							
		neat	112.8	140.2[b]							
	$\Delta\delta$		−54.5	−14.4	−44.4	0.7					
4	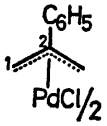										s-C[f]; 135.52
		DMSO-d_6	63.87	132.86							o-C; 126.55
		$CDCl_3$	[59.5]	[125.9][g]							m-C; 128.85
											p-C; 129.94
		$CDCl_3$	112.36	141.36	21.78						s-C; 143.36
											o-C; 125.58
											m-C; 128.25
											p-C; 127.46
	$\Delta\delta$		−53.0	−15.5							
5	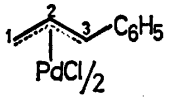	DMSO-d_6	64.18	112.60	86.57						s-C; 136.87
		$CDCl_3$	[59.8]	[105.6]	[82.1]						o-C; 128.01
											m-C; 128.62
											p-C; 128.01
		$CDCl_3$	18.26	128.95	131.37						s-C; 138.05
											o-C; 125.98
											m-C; 128.50
											p-C; 126.56
	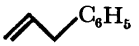	$CDCl_3$	115.63	128.50	40.34						s-C; 143.79
											o-C; 128.50
											m-C; 128.68
											p-C; 126.13
	$\Delta\delta$		−55.9	−22.9	−49.3						
6	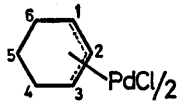	$CDCl_3$	78.81	101.74	78.81	28.81	19.41	28.81			
		DMSO-d_6	83.42	108.17	83.42	28.27	18.56	28.27			
		$CDCl_3$	127.28	127.28	25.54	23.11	23.11	25.54			
	$\Delta\delta$		−48.5	−25.5		5.7	−3.7	3.3			
7	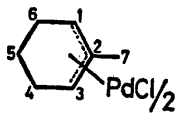	$CDCl_3$	77.90	116.18	77.90	29.06	20.08	19.06	22.56		
		$CDCl_3$	121.34	133.96	30.33	24.02	23.35	25.54	22.69		
	$\Delta\delta$		−43.3	−17.8		5.0	−3.3	3.5	−0.1		
8	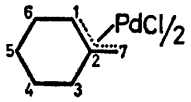	$CDCl_3$	68.80	126.01	(28.81)[h]	(21.05)	(17.59)	(26.93)	58.24		

TABLE 1. (Continued)

No.	Compound	Solvent	C-1	C-2	C-3	C-4	C-5	C-6	C-7	C-8	C_6H_5–
		$CDCl_3$	121.34	133.96	30.33	24.02	23.35	25.54	22.69		
	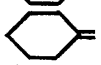	$CDCl_3$	35.55	149.97	35.55	28.45	26.51	28.45	106.65		
	$\Delta\delta$		−52.5	−8.0					−48.4		
9	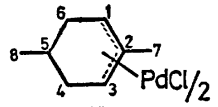	$CDCl_3$	78.20	114.99	78.20	35.91	31.48	35.91	(22.44)	(20.99)	
	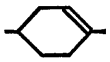	$CDCl_3$	120.91	133.53	31.54	30.39	28.51	34.15	23.60	21.90	
	$\Delta\delta$		−42.7	−18.5		5.5	3.0	1.8			
10	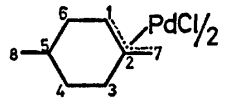	$CDCl_3$	71.40	123.10	(31.36)	(29.49)	27.47	(35.24)	55.87	21.59	
	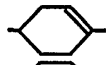	$CDCl_3$	120.91	133.53	31.54	30.39	28.51	34.15	23.60	21.90	
	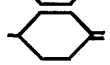	$CDCl_3$	36.58	149.43	36.58	34.82	32.39	34.82	106.78	22.02	
	$\Delta\delta$		−49.5	−10.4			−1.0		−50.9	−0.3	
11	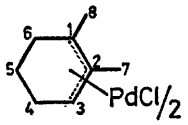	$CDCl_3$	90.70	113.33	75.71	29.00	20.87	36.34	(22.14)	(19.29)	
	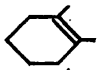	$CDCl_3$	125.64	125.64	31.39	23.72	23.72	31.91	19.17	19.17	
	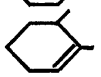	$CDCl_3$	33.67	138.03	121.76	25.96	22.02	31.85	20.02	19.65	
	$\Delta\delta$		−34.9	−12.3	−46.1	5.3	−2.9	4.4			
12	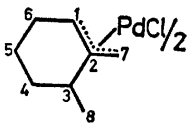	$CDCl_3$	71.71	121.76	20.99	(29.30)	(16.01)	(26.81)	57.27	18.74	
		$CDCl_3$	121.76	138.03	33.67	31.85	22.02	25.96	20.02	19.65	
		$CDCl_3$	36.88	154.18	37.73	36.22	26.08	28.87	104.35	18.68	
	$\Delta\delta$		−50.1	−16.3	−12.7				−47.1	−0.9	
13	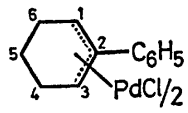	$CDCl_3$	75.96	117.39	75.96	29.36	19.96	29.36			*s*-C; 136.75 *o*-C; 126.13 *m*-C; 128.56 *p*-C; 128.56
	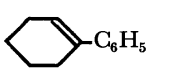	$CDCl_3$	124.43	136.69	27.54	23.23	22.38	26.02			*s*-C; 142.63 *o*-C; 124.98 *m*-C; 128.13 *p*-C; 126.49
	$\Delta\delta$		−48.5	−19.3		6.1	−2.4	3.3			*s*-C; −5.9 *o*-C; 1.2 *m*-C; 0.4 *p*-C; 2.1

a) These values are taken from Ref. 1a. b) These values are taken from G. B. Savitsky, P. D. Ellis, K. Namikawa, and G. E. Maciel, *J. Chem. Phys.*, **49**, 2395 (1968). c) The value for the complex minus that for the olefin. Positive values represent shifts toward lower field. d) These values are taken from J. B. Stothers, "Carbon-13 NMR Speetroscopy," Academic Press, New York (1972), p. 70. The solvent used was not indicated. e) These values are taken from Ref. 1e. f) Substituted. g) The values in brackets are estimated. See text. h) The values in parenthesis may be interchanged.

complexes are usually shifted downfield, while the C-4 signal is shifted upfield relative to the corresponding carbons of the corresponding olefins. Such a downfield shift of the C-3 and C-5 signals implies that these carbons are closer to the palladium atom than C-4 and the nonbonding paramagnetic shielding effect of a palladium atom which is a function of $(r_{M-C})^{-3}$,[9] plays a major role in the shift to lower field for complex formation. The exception is the case of C-4 for complex **9**. The deformation of the six-membered ring due to the replacement of the hydrogen at the C-4 position with the methyl group may result in a net decrease in the shielding of this carbon. In the *exo*-cyclic complexes, it was impossible to assign the carbon signals other than that for the π-allyl palladium moiety to specific carbon atoms. The resonances for the substituted methyl groups revealed no appreciable shift due to complex formation.

Experimental

NMR Spectra. ^{13}C FT-NMR spectra were obtained at 25.15 MHz using a JEOL JNM-MH-100 instrument equipped with a JNM-MFT-100 Fourier transform accessory; the instrument was controlled by a JEC-6 spectrum computer. The samples were in 5-mm spining tubes in $20\pm10\%$ solutions of $CDCl_3$ or DMSO-d_6 at 26 °C. The solvents provided the internal lock signal. Measurement conditions were as follows: pulse width, 27.5 μs (*ca.* 45°); reptition time, 4 s; spectral width, 6250 Hz; data points, 8192; and acquisition time, 0.65 s. Noise-modulated proton decoupling was carried out at a nominal power of 20 W. All chemical shifts are expressed in δ (ppm downfield from internal Me_4Si). Each observed chemical shift is estimated to be accurate to within ±0.06 ppm.

Materials. π-Allylic palladium complexes, **1**—**5** were prepared by the method of Dent *et al.*[2a] or Hüttel *et al.*[2b] The complexes, **6**—**13** were prepared by the method of Trost and Strege.[3] For the synthesis of the new compounds (**9**—**13**), the following general procedure was used; sodium acetate (6.0 g, 0.073 mol), sodium chloride (4.2 g, 0.072 mol), cupric chloride (4.6 g, 0.034 mol) and palladium chloride (1.0 g, 0.006 mol) were stirred for 2 h at 95 °C in 62 ml of glacial acetic acid and 1.3 ml of acetic anhydride. The solution was cooled and 0.013 mol of the corresponding cyclohexene in 4 ml of acetic acid was added. The solution was heated for several hours. The reaction temperature and time were as follows: **9** from 1,4-dimethylcyclohexene, 60 °C, 4 h; **10** from 1,4-dimethylcyclohexene, 60 °C, 27 h; **11** from 1,2-dimethylcyclohexene, 55 °C, 5 h; **12** from 2,3-dimethylcyclohexene, 60 °C, 44 h; and **13** from 1-phenylcyclohexene, 55 °C, 24 h. The solution was cooled to room temperature and filtered. After an aqueous work-up and extraction with benzene, the crude yellow oil was purified by chromatography on SiO_2 with chloroform as the eluting solvent. The addition of pentane to the purified yellow oil and refrigeration (at 5 °C) for 2 days induced crystallization giving pure yellow crystals. Since compounds **10** and **11** were obtained in a mixture with **9** and **12**, respectively, separation was performed using SiO_2 chromatography with benzene. Compound **10** was only partially separated (80% purity). Compound **9**; yield, 0.36 g (26%); mp 82—86 °C (dec) (Found: C, 38.01; H, 5.02 %. Calcd for $C_{16}H_{26}Pd_2Cl_2$: C, 38.26; H, 5.18%); ^1H NMR ($CDCl_3$); δ 4.86 (bs, 2H), δ 2.07 (s, 3H), δ 0.91 (d, J=6.8 Hz, 3H), δ 1.5—2.3 (5H): compound **10**; yield, 0.22 g (16%); mp 114—118 °C (dec) (Found: C, 38.19; H, 5.15%. Calcd for $C_{16}H_{26}Pd_2Cl_2$: C, 38.26, H, 5.18%); ^1H NMR ($CDCl_3$); δ 4.16 (bs, 1H), δ 3.62 (bs, 1H), δ 2.63 (bs, 1H), δ 0.92 (d, J=6.8 Hz, 3H), δ 1.5—2.2 (7H): compound **11**, yield, 0.65 g (46%); mp 79—81 °C (dec) (Found; C, 37.91; H, 5.02%. Calcd for $C_{16}H_{26}Pd_2Cl_2$: C, 38.26; H, 5.18%); ^1H NMR ($CDCl_3$); δ 5.23 (bs, 1H), δ 2.08 (s, 3H), δ 1.23 (s, 3H), δ 1.0—2.3 (6H): compound **12**; yield, 0.60 g (43%); mp 98—100 °C (dec) (Found; C, 38.49; H, 5.08%. Calcd for $C_{16}H_{26}Pd_2Cl_2$: C, 38.26; H, 5.18%); ^1H NMR ($CDCl_3$); δ 4.43 (bs, 1H), δ 3.76 (bs, 1H), δ 2.67 (bs, 1H), δ 1.23 (d, J=6.5 Hz, 3H), δ 1.2—2.2 (7H): compound **13**, yield, 0.28 g (17%); mp 188—190 °C (dec) (Found; C, 48.29; H, 4.07%. Calcd for $C_{24}H_{26}Pd_2Cl_2$: C, 48.18; H, 4.35%); ^1H NMR ($CDCl_3$); δ 7.27 (m, 5H), δ 5.30 (bs, 2H), δ 1.0—2.3 (6H).

References

1) a) B. E. Mann, R. Pietropaolo, and B. L. Shaw, *Chem. Commun.*, **1971**, 790; b) B. E. Mann, R. Pietropaolo, and B. L. Shaw, *J. Chem. Soc., Dalton Trans.*, **1973**, 2390; c) L. F. Farnell, E. W. Randall, and E. Rosenberg, *Chem. Commun.*, **1971**, 1078; d) V. N. Sokolov, G. M. Khvostic, I. Ya. Poddubnyi, and P. K. Kondratenkov, *J. Organomet. Chem.*, **53**, 361, 375 (1973).

2) a) W. T. Dent, R. Long, and A. J. Wilkinson, *J. Chem. Soc.*, **1964**, 1585; b) R. Hüttel, J. Kratzer, and M. Bechter, *Chem. Ber.*, **94**, 766 (1961).

3) B. M. Trost and P. E. Strege, *Tetrahedron Lett.*, **1974**, 2603.

4) H. L. Clarke, *J. Organomet. Chem.*, **80**, 155 (1974).

5) G. L. Statton and K. C. Ramey, *J. Am. Chem. Soc.*, **88**, 1327 (1966).

6) K. C. Ramey and G. L. Statton, *J. Am. Chem. Soc.*, **88**, 4387 (1966).

7) B. E. Mann, *Adv. Organomet. Chem.*, **12**, 135 (1974).

8) P. W. Jolly and G. Wilke, "The Organic Chemistry of Nickel," Vol. 1, Academic Press, New York (1974), p. 332.

9) D. G. Cooper, R. P. Hughes, and J. Powell, *J. Am. Chem. Soc.*, **94**, 9244 (1972).

Synthesis of Mono-*O*-tritylraffinoses and Deca-*O*-acetylraffinoses

Tetsuo SUAMI,* Toshiki OTAKE, Toshihide IKEDA, and Ryoichi ADACHI

Department of Applied Chemistry, Faculty of Engineering, Keio University, Hiyoshi, Yokohama 223

(Received February 8, 1977)

Starting from raffinose (**1**), its 6″-*O*-trityl (**2**) and 6′-*O*-trityl derivative (**6**) have been prepared. Acetylation of **2** and **6** gave deca-*O*-acetyl-6″-*O*-tritylraffinose (**3**) and deca-*O*-acetyl-6′-*O*-tritylraffinose (**7**) respectively. Detritrylation of **3** gave two products: 1′,2,2″,3,3′,3″,4,4′,4″,6′-deca-*O*-acetylraffinose (**4**) as a main product and 1′,2,2″,3,-3′,3″,4,4′,6′,6″-deca-*O*-acetylraffinose (**5**) as a minor product, which were successfully separated by a column chromatography. On the other hand, detritylation of **7** gave 1′,2,2″,3,3′,3″,4,4′,4″,6″-deca-*O*-acetylraffinose (**8**) as a sole product. Their structures were established by NMR spectra, together with a chemical evidence.

Tri-*O*-tritylraffinose has been described by Josephson[1] in 1929, but mono-*O*-tritylraffinose has never been described in a literature. In connection with our previous studies on sucrochemistry,[2-6] mono-*O*-trityl derivatives of raffinose have been prepared in our laboratory. By acetylation and subsequent detritylation, mono-*O*-tritylraffinose was readily converted to deca-*O*-acetylraffinose, which is an attractive key compound for a synthesis of a tetrasaccharide. For instance, a naturally occurring tetrasaccharide: stachyose will be prepared from 1′,2,2″,3,3′,3″,4,4′,4″,6′-deca-*O*-acetylraffinose (**4**), since α-D-galactopyranosyl group is linked to the 6″-*OH* of raffinose in this tetrasaccharide.

Results and Discussion

A reaction between raffinose (**1**) and trityl chloride in pyridine afforded a mixture of mono-, di-, and tri-*O*-tritylraffinoses. The di- and tri-*O*-tritylraffinoses are considerably less soluble in cold water, compared to the mono-*O*-tritylraffinoses. The mono-*O*-tritylraffinoses were able to be separated from the others by means of this solubility difference in an aqueous solution. The mono-*O*-tritylraffinoses thus obtained consisted of two components of 6″-*O*-trityl (**2**) and 6′-*O*-tritylraffinose (**6**). After acetylating, the intact mixture of **2** and **6** revealed two peaks in a ratio of 4: 1 on a high performance liquid chromatogram. The major component was assumed to be deca-*O*-acetyl-6″-*O*-tritylraffinose (**3**) and the minor component was assumed to be deca-*O*-acetyl-6′-*O*-tritylraffinose (**7**), since in the case of sucrose,[7] the hydroxyl group on C-6 of the D-glucopyranosyl moiety is most reactive and the hydroxyl group on C-1′ of the D-fructofuranosyl moiety is least reactive among the three primary hydroxyl groups against tritylation.

Compounds **2** and **6** were successfully separated by a column chromatography, and subsequently acetylated to give **3** and **7** respectively.

The assumed structure of **3** was confirmed by the following evidence. The ^{1}H NMR spectrum of **3** revealed the signals of the two methylene groups (4 protons) in a region between δ 2.9 and 3.9. These signals were regarded as two AB parts of ABM-systems, and each of them consisted of eight-line-signals. The signal pattern in a lower field was almost superposable on the signal pattern of the bridge methylene protons (C-6) of raffinose undecaacetate (**9**). The signal pattern in a higher field was coincident in the chemical shifts and coupling constants with that of the methylene protons of methyl 2,3,4-tri-*O*-acetyl-6-*O*-trityl-α-D-galactopyranoside (**10**). Therefore, the signal pattern was attributable to the methylene protons on C-6″ of **3**, on which the trityloxyl group was attached (Fig. 1).

The structure of **7** was deduced from carbon-13 nuclear magnetic resonance (^{13}C NMR) spectrum of its detritylation product. That is, detritylation of **7** with

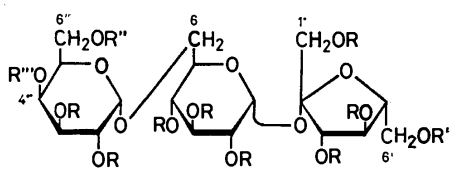

1: R=R′=R″=R‴=H **2**: R=R′=R‴=H,R″=Tr
3: R=R′=R‴=Ac,R″=Tr **4**: R=R′=R‴=Ac,R″=H
5: R=R′=R″=Ac,R‴=H **6**: R=R″=R‴=H,R′=Tr
7: R=R″=R‴=Ac,R′=Tr **8**: R=R″=R‴=Ac,
R′=H **9**: R=R′=R″=R‴=Ac

Ac: $COCH_3$, Tr: $C(C_6H_5)_3$

Scheme 1.

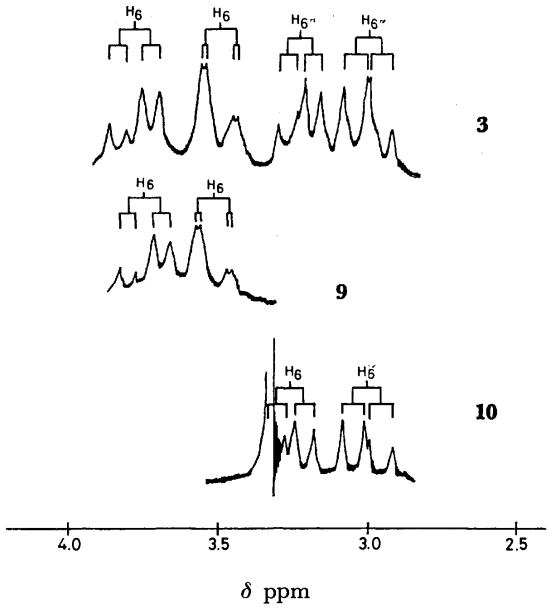

Fig. 1. ^{1}H NMR signals of *O*-methylene groups of **3**, **9**, and **10**.

* To whom correspondence should be addressed.

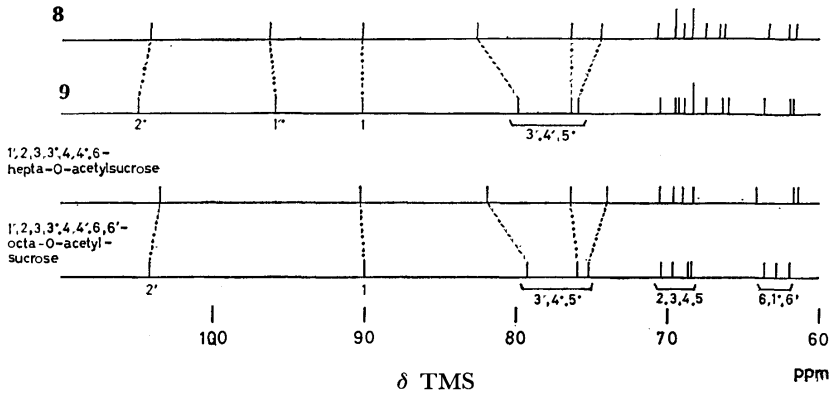

Fig. 2. Correlation map of ^{13}C NMR spectra of **8**, **9**, 1,2,3,3',4,4',6-hepta-*O*-acetylsucrose,[8] and 1',2,3,4,4',6,6'-octa-*O*-acetylsucrose.[12]

hydrogen bromide in glacial acetic acid gave 1',2,2'',3,-3',3'',4,4',4'',6''-deca-*O*-acetylraffinose (**8**) as a sole product. ^{13}C NMR spectrum of **8** revealed the signals of the three methine carbons of C-3', 4' and 5' in the D-fructofuranosyl moiety in a region between 74 and 82 ppm, which were shifted remarkably from the signals of the corresponding three methine carbons of **9** and were almost the same as those revealed by these carbons of 1',2,3,3',4,4',6-hepta-*O*-acetylsucrose[8] (Fig. 2).

On the other hand, detritylation of **3** with hydrogen bromide in glacial acetic acid under ice cooling gave a mixture of two products. These products were separated by a column chromatography, and the major component was assumed to be 1',2,2'',3,3',3'',4,4',4'',6'-deca-*O*-acetylraffinose (**4**). The minor component was assumed to be 1',2,2'',3,3',3'',4,4',6',6''-deca-*O*-acetylraffinose (**5**).

To establish the structure of **4**, a deuteration technique for an individual acetyl group[9] was applied. When ^1H NMR spectrum of a deuterioacetyl derivative of **4** was compared with the spectrum of **9**, it was readily observed that an intensity of the signal (6 protons) at δ 2.05 in the spectrum of **9** was reduced to one half (3 protons) in the spectrum of the deuterioacetyl derivative. The missing half of the signal was attributed to the acetoxyl group on C-6'' of **9**, since the acetoxyl group on C-6 of methyl 2,3,4,6-tetra-*O*-acetyl-α-D-galactopyranoside[11] (**12**) revealed its signal at δ 2.04. Furthermore, this assignment of the signal of **12** was achieved by comparing the ^1H NMR spectrum of methyl 2,3,4-tri-*O*-acetyl-6-*O*-trideuterioacetyl-α-D-galactopyranoside (**11**) with that of **12**. Therefore, the structure of **4** was reasonably established.

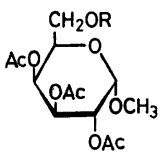

10: R=Tr **11**: R=$COCD_3$ **12**: R=Ac
Ac: $COCH_3$, Tr: $C(C_6H_5)_3$

Scheme 2.

Meanwhile, **5** might be formed from **4** by an acetyl group migration from 4''-*OH* to 6''-*OH* during a course of the reaction, and this has been verified by the fact that detritylation of **3** in an aqueous acetic acid solution at elevated temperature yielded **5** as a main product.

Experimental

General Methods. Raffinose was purchased from a commercial source. Melting points were determined in capillary tubes and are uncorrected. Solutions were evaporated under diminished pressure below 40 °C. Optical rotations were measured on a Japan Spectroscopic DIP-SL polarimeter. ^1H NMR spectra were recorded on a Varian A-60D spectrometer at 60 MHz or a Varian XL-100 spectrometer at 100 MHz. ^{13}C NMR spectra were recorded by the Fourier transform technique on a Varian CFT-20 spectrometer at 20 MHz. In both spectra, deuteriochloroform was used as a solvent and tetramethylsilane was used as an internal standard, and the peak positions are given in δ values. A high performance liquid chromatogram was obtained on a Varian Model 8520 liquid chromatograph equipped with a MicroPak Si-10 column using dichloromethane as an eluting solvent. Acetylation was carried out with acetic anhydride in pyridine in the usual manner. TLC was performed on Wakogel B-10 (Wako Pure Chemical Co., Ltd.) plates, and silica gel (Wakogel C-300) was employed for a column chromatography. Elemental analyses were performed by Mr. Saburo Nakada.

6''-O-Tritylraffinose (2) and 6'-O-Tritylraffinose (6). After drying over phosphorous pentoxide at 50 °C for several days, raffinose (**1**, 7.45 g, 14.8 mmol) was treated with trityl chloride (7.00 g, 25.1 mmol) in dry pyridine (60 ml) for 64 h under mild stirring at ambient temperature. The reaction mixture was poured into ice cold water (1 l), and an insoluble matter was filtered off. The filtrate was evaporated to one tenth of the original volume to give 2.74 g of amorphous precipitates which were collected by filtration. The product consisted mainly of mono-*O*-tritylraffinoses. The product was fractionated on a column using 4:9:4:1 (v/v) acetone–chloroform–methanol–water as an eluant, and each fraction was monitored on TLC in the same solvent system.

The fractions which showed a single spot at R_f 0.40 were combined and evaporated. The residue was recrystallized from ethanol to give 1.04 g (9.4%) of **2**, mp 221—222 °C, $[\alpha]_D^{21}$ +70.9° (*c* 1.03, pyridine).

Found: C, 59.66; H, 6.17%. Calcd for $C_{37}H_{46}O_{16}$: C, 59.51; H, 6.21%.

The fractions having a single spot at R_f 0.31 were combined

and evaporated to give 0.19 g (1.7%) of **6** as a glassy solid, $[\alpha]_D^{21}$ +88° (*c* 0.5, pyridine).

*1′2,2″3′,3″,4′,4″,6′,-Deca-*O*-acetyl-6″-*O*-tritylraffinose (3).* Compound **2** (1.04 g) was acetylated, and the product was recrystallized from isopropyl alcohol to give 1.07 g (66%) of **3**, mp 96—98 °C, $[\alpha]_D^{22}$ +73.8° (*c* 0.84, chloroform). ^{1}H NMR: δ 1.87 (s, OAc), 1.95 (s, 3, OAc), 2.04 (s, 12, 4OAc), 2.09 (s, 6, 2OAc), 2.12 (s, 3, OAc), 2.15 (s, 3, OAc), 4.77 (dd, 1, $J_{1,2}$ 3.5 Hz, $J_{2,3}$ 10.5 Hz, H-2), 5.72 (d, 1, H-1).

Found: C, 58.64; H, 5.80%. Calcd for $C_{57}H_{66}O_{26}$: C, 58.66; H, 5.70%.

*1′,2,2″,3,3′,3″,4,4′,4″,6″,-Deca-*O*-acetyl-6′-*O*-tritylraffinose (7).* Compound **6** (186 mg) was acetylated, and the product was recrystallized from isopropyl alcohol to give 187 mg (64%) of **7**, mp 96—97.5 °C, $[\alpha]_D^{23}$ +98.1° (*c* 1.05, chloroform). ^{1}H NMR: δ 1.78 (s, 3, OAc), 1.88 (s, 3, OAc), 1.96 (s, 3, OAc), 2.02 (s, 6, 2OAc), 2.04 (s, 3, OAc), 2.09 (s, 9, 3OAc), 2.14 (s, 3, OAc), 4.70 (dd, 1, $J_{1,2}$ 3.7 Hz, $J_{2,3}$ 10.5 Hz, H-2), 5.04 (dd, 1, $J_{3,4}$ 9.5 Hz, $J_{4,5}$ 9.5 Hz, H-4), 4.65 (d, 1, H-1).

Found: C, 58.43; H, 5.75%. Calcd for $C_{57}H_{66}O_{26}$: C, 58.66; H, 5.70%.

Detritylation of 3. To a solution of **3** (1.12 g) in glacial acetic acid (10 ml), a 0.5 ml portion of glacial acetic acid saturated with hydrogen bromide was added under ice cooling with agitation. After two min, the mixture was quenched into ice cold water, and the solution was extracted with chloroform repeatedly. The chloroform solution was washed with sodium hydrogencarbonate solution and water. After drying over sodium sulfate, the solution was evaporated to give 1.05 g of a crude product, which showed two spots on TLC at R_f 0.54 (major component) and 0.50 (minor component) in 20: 1 (v/v) chloroform–ethanol with a ratio of approximately 4: 1.

The major component: 1′,2,2″,3,3′,3″,4,4′,4″,6′-deca-*O*-acetylraffinose (**4**, 110 mg, 12%) was obtained from the mixture by a column chromatography with 1: 5 (v/v) acetone–benzene as an eluant. The amorphous product of **4** had $[\alpha]_D^{23}$ +101.8° (*c* 0.56, chloroform). ^{1}H NMR: δ 1.97 (s, 3, OAc), 2.00 (s, 3, OAc), 2.05 (s, 3, OAc), 2.08 (s, 3, OAc), 2.10 (s, 6, 2OAc), 2.12 (s, 3, OAc), 4.80 (dd, 1, $J_{1,2}$ 3.5 Hz, $J_{2,3}$ 10.5 Hz, H-2), 5.06 (dd, 1, $J_{1'',2''}$ 5.0 Hz, $J_{2'',3''}$ 10.5 Hz, H-2″), 5.10 (dd, 1, $J_{3,4}$ 10.0 Hz, $J_{4,5}$ 10.0 Hz, H-4), 5.24 (d, 1, H-1″), 5.26 (dd, 1, $J_{3'',4''}$ 4.5 or 3.5 Hz, $J_{4'',5''}$ 3.5 or 4.5 Hz, H-4″), 5.66 (d, 1, H-1).

Found: C, 49.31; H, 5.69%. Calcd for $C_{38}H_{52}O_{26}$: C, 49.35; H, 5.67%.

Compound **4** (45 mg) was acylated with acetic anhydride-d_6 in pyridine to give 46 mg of 1′,2,2″,3,3′,3″,4,,4′,4″,6′-deca-*O*-acetyl-6″-*O*-trideuterioacetylraffinose as a glassy solid, $[\alpha]_D^{20}$ +88.9° (*c* 2.07, chloroform). ^{1}H NMR: δ 1.955 (s, 3, OAc), 2.015 (s, 3, OAc), 2.055 (s, 3, OAc), 2.10 (s, 6, 2OAc), 2.105 (s, 3, OAc), 2.11 (s, 3, OAc), 2.12 (s, 3, OAc), 2.135 (s, 3, OAc), 2.175 (s, 3, OAc).

The minor component: 1′,2,2″,3,3′,3″,4,4′,6′,6″-deca-*O*-acetylraffinose (**5**, 100 mg, 11%) was obtained by the column chromatography as described above. The amorphous product of **5** had $[\alpha]_D^{21}$ +101.0° (c 1.00, chloroform). ^{1}H NMR: δ 2.02 (s, 3, OAc), 2.06 (s, 3, OAc), 2.075 (s, 3, OAc), 2.095 (s, 6, 2OAc), 2.12 (s, 9, 3OAc), 2.15 (s, 3, OAc), 2.18 (s, 3, OAc), 3.50 (dd, 1, $J_{6''a,6''b}$ 10.0 Hz, $J_{6''a,5''}$ 1.3 Hz, H-6″a), 3.75 (dd, 1, $J_{6''b,5''}$ 5.0 Hz, H-6″b), 4.78 (dd, 1, $J_{1,2}$ 3.5 Hz, $J_{2,3}$ 10 Hz, H-2), 5.66 (d, 1, H-1).

Found: C, 49.08; H, 5.50%. Calcd for $C_{38}H_{52}O_{26}$: C, 49.35; H, 5.67%.

Besides **4** and **5**, a mixture of **4** and **5** (340 mg, 38%) was recovered from the column.

Detritylation of 3 in 98% Acetic Acid. Compound **3** (120 mg) was heated in 98% acetic acid (5 ml) on a boiling water bath. After 70 min, the solution was evaporated, and the residue was purified by a column chromatography with 1: 5 (v/v) acetone–benzene as an eluant to give 48 mg (51%) of **5** as a main product.

Detritylation of 7. Compound **7** (166 mg) was detritylated with hydrogen bromide in glacial acetic acid under ice cooling as described in the case of **5**, to give 159 mg of a crude product. The product was purified by a column chromatography with 1: 5 (v/v) acetone–benzene as an eluant. The fractions that showed a single spot at R_f 0.53 on TLC in 20: 1 (v/v) chloroform–ethanol were combined and evaporated to give 107 mg (81%) of 1′,2,2″,3,3′,3″,4,4′,-4″,6″-deca-*O*-acetylraffinose (**8**) as a glassy solid, $[\alpha]_D^{21}$ +101.0° (*c* 1.00, chloroform). ^{1}H NMR: δ 1.97 (s, 3, OAc), 2.02 (s, 3, OAc), 2.08 (s, 6, 2OAc), 2.13 (s, 15, 5OAc), 2.20 (s, 3, OAc), 4.79 (dd, 1, $J_{1,2}$ 3.5 Hz, $J_{2,3}$ 10.5 Hz, H-2), 5.70 (d, 1, $J_{1,2}$ 3.5 Hz, H-1).

Found: C, 48.84; H, 5.49%. Calcd for $C_{38}H_{52}O_{26}$: C, 49.35; H, 5.67%.

*Methyl 2,3,4-Tri-*O*-acetyl-6-*O*-trityl-α-*D*-galactopyranoside (10).* Methyl α-D-galactopyranoside[10] (1.6 g) was treated with trityl chloride (6.5 g) in pyridine for 47 h, and subsequently acetylated in the conventional method. The product was purified by a column chromatography with 1: 40 (v/v) acetone–benzene to give 3.6 g of a crude product. Recrystallization from ethanol gave 2.9 g (63%) of **10**, mp 179—180 °C, $[\alpha]_D^{25}$ +69.2° (*c* 1.71, chloroform).

Found: C, 68.39; H, 6.09%. Calcd for $C_{32}H_{34}O_9$: C, 68.31; H, 6.09%.

*Methyl 2,3,4-Tri-*O*-acetyl-6-*O*-trideuterioacetyl-α-*D*-galactopyranoside (11).* Compound **10** (0.5 g) was detritylated with hydrogen bromide in glacial acetic acid under ice cooling analogously as described above and the product was purified by a column chromatography with 1: 5 (v/v) acetone–benzene to give 0.24 g (86%) of methyl 2,3,4-tri-*O*-acetyl-α-D-galactopyranoside as a glassy solid, $[\alpha]_D^{20}$ +56.8 °C (*c* 0.67, chloroform).

The product (60 mg) was acylated with acetic anhydride-d_6 in pyridine, and the product was purified by a column chromatography to give 62 mg (91%) of **11** as a glassy solid, $[\alpha]_D^{20}$ +130 °C (*c* 1.6 chloroform).

^{1}H NMR: δ 1.97 (s, 3, OAc), 2.07 (s, 3, OAc), 2.13 (s, 3, OAc), 3.40 (s, 3, OCH_3).

^{1}H NMR spectrum of methyl 2,3,4,6-tetra-*O*-acetyl-α-D-galactopyranoside (**12**) was determined by Rathbone and his coworkers[11] [δ 1.97 (s, 3, OAc), 2.035 (s, 3, OAc), 2.07 (s, 3, OAc), 2.13 (s, 3, OAc), 3.40 (s, 3, OCH_3)].

References

1) K. Josephson, *Justus Liebigs Ann. Chem.*, **472**, 230 (1929).
2) T. Suami, T. Ikeda, S. Nishiyama, and R. Adachi, *Bull. Chem. Soc. Jpn.*, **48**, 1953 (1975).
3) T. Suami, T. Otake, T. Nishiyama, and T. Ikeda, *Bull. Chem. Soc. Jpn.*, **46**, 1014 (1973).
4) T. Suami, T. Otake, T. Nishiyama, and T. Ikeda, *Carbohydr. Res.*, **26**, 234 (1973).
5) T. Suami, T. Otake, N. Kato, T. Nishiyama, and T. Ikeda, *Carbohydr. Res.*, **21**, 451 (1972).
6) T. Suami, N. Kato, M. Kawamura, and T. Nishiyama, *Cabohydr. Res.*, **19**, 407 (1971).
7) T. Otake, *Bull. Chem. Soc. Jpn.*, **45**, 2895 (1972).
8) T. Suami, T. Otake, S. Ogawa, T. Shoji, and N. Kato, *Bull. Chem. Soc. Jpn.*, **43**, 1219 (1970).
9) D. Horton, J. B. Hughes, J. S. Jewell, K. D. Philips, and W. N. Turner, *J. Org. Chem.*, **32**, 1073 (1967); D. Horton

and J. H. Lauterback, *J. Org. Chem.*, **34**, 86 (1969).
10) F. Reber and T. Reichstein, *Helv. Chim. Acta*, **28**, 1164 (1945); R. G. Ault, W. N. Haworth, and E. L. Hirst, *J. Chem. Soc.*, **1935**, 1012.
11) E. B. Rathbone, A. M. Stephen, and K. G. R. Pachler, *Carbohydr. Res.*, **20**, 357 (1971).
12) A. Allerhand and D. Doddrell, *J. Am. Chem. Soc.*, **93**, 2777 (1971); R. Khan, *Adnavs. Carbohydr. Chem. Biochem.*, **33**, 278 (1976). The chemical shift values of the methylene and methine carbon atoms of the sucrose octaacetate and the raffinose undecaacetate (**9**) compare well with those of sucrose and raffinose.

Kinetics and Mechanism of the Oxidation of Substituted Benzyl Alcohols by Chloramine-T in Acid Solution

Kalyan K. BANERJI

Department of Chemistry, University of Jodhpur, Jodhpur 342001, India

(Received August 16, 1976)

The oxidation of benzyl alcohol and eight monosubstituted benzyl alcohols by chloramine-T in acid solution has been studied. The reaction is of first order with respect to the concentration of alcohol and oxidant. The rate constant is proportional to the square of hydrogen ion concentration. The kinetic isotope effect (k_H/k_D) is 4.13 at 303 K. The solvent isotope effect ($k(D_2O)/k(H_2O)$) is 5.93 at 303 K. The activation enthalpies and entropies are linearly related. The reaction exhibited a reaction constant $\rho^+ = -2.08 \pm 0.08$ at 303 K. The active oxidizing species is considered to be $(H_2OCl)^+$. A mechanism involving transfer of a hydride ion to the oxidant is suggested.

Chloramine-T (CAT) acts as an oxidizing agent in both acid and alkaline solutions. The kinetics of the oxidation by alkaline CAT has received much attention.[1,2] The reports on the oxidation by CAT in acid solutions are rather scanty. Mushran *et al.*[3] studied the oxidation of some primary alcohols in the pH range 4.0—5.2. Mahadevappa and Naidu[4] reported the oxidation of allyl alcohol by CAT in aqueous HCl medium.

This paper deals with the oxidation of monosubstituted benzyl alcohols by CAT in acid solution and the evaluation of the reaction constant. During the course of this investigation the oxidation of 2-propanol in acid solutions was reported by Natarajan and Thiagarajan.[5] Their results are also discussed.

Results

The oxidation of benzyl alcohol by CAT in acetic acid–water (1 : 1 (v/v)), in the presence of perchloric acid, results in the formation of benzaldehyde as the main product.

Stoichiometry. Excess of CAT was allowed to react with 0.02 M benzyl alcohol at various acidities. For some runs the carbonyl product was determined using an excess of benzyl alcohol. Values of $\Delta[CAT]/\Delta[alcohol]$ and $\Delta[CAT]/\Delta[benzaldehyde]$ in Table 1 show that the overall reaction corresponds to

$$PhCH_2OH + MeC_6H_4SO_2NCl^- \rightarrow PhCHO + MeC_6H_4SO_2NH_2 + Cl^- \quad (1)$$

Rate Laws. The rate laws were determined for the oxidation of benzyl alcohol and the eight monosubstituted benzyl alcohols. Since the results are similar, only those of benzyl alcohol are reproduced.

When the alcohol is in excess, the rate of disappearence of CAT follows the first-order rate laws. The rate constant is independent of the initial concentration of CAT (Table 2), confirming that the order with respect to CAT is one. The reaction is of first order with respect to the alcohol concentration also (Table 3). The rate constant is proportional to the square of hydrogen ion concentration (Table 4). The rate law for the oxidation is therefore given as follows:

$$\text{Rate} = k[CAT][Alcohol][H^+]^2. \quad (2)$$

The rate law differs from those reported for the oxidation of primary alcohols and allyl alcohol in aqueous solutions.[3,4] However, it agrees with the results of Natarajan and Thiagarajan[5] obtained in the oxidation of 2-propanol in acetic acid–water (1 : 4 (v/v)).

The rate constants for the oxidation of benzyl alcohol and α,α-dideuteriobenzyl alcohol in acetic acid–water (1 : 1 (v/v)) at 303 K, are $10^6 k = 6.32$ and $1.53\ l^3 m^{-3} s^{-1}$, respectively. The kinetic isotope effect (k_H/k_D) is 4.13 at 303 K.

Benzyl alcohol was oxidized in 95% deuterium oxide and the rate constant was $16.7 \times 10^{-6}\ l^3 m^{-3} s^{-1}$ at 303 K. The rate constant under similar conditions in water is $2.81 \times 10^{-6}\ l^3 m^{-3} s^{-1}$. The solvent isotope effect ($k(D_2O)/k(H_2O)$) is 5.93 at 303 K. In this set of experiments no acetic acid was present.

The oxidation of benzyl alcohol in an atmosphere of nitrogen failed to induce polymerisation of acrylo-

Table 1. Stoichiometry of the oxidation of benzyl alcohol (BA) by CAT

$[H^+]$M	$\Delta[CAT]/\Delta[BA]$	$\Delta[CAT]/\Delta[Benzaldehyde]$
0.2	1.01	—
0.5	0.97	—
1.0	0.96	—
1.2	1.03	—
0.5	—	0.91
1.0	—	0.88
1.2	—	0.91

Table 2. Oxidant dependence of the reaction rate

[BA] 0.20 M	$[H^+]$ 0.5 M		Temp 303 K	
[CAT] M	0.01	0.02	0.04	0.06
$10^7 k_1\ s^{-1}$	3.15	3.20	3.15	3.11

Table 3. Substrate dependence of the reaction rate

[CAT] 0.02 M	$[H^+]$ 0.5 M		Temp 303 K		
[BA] M	0.10	0.20	0.40	0.60	1.0
$10^7 k_1\ s^{-1}$	1.60	3.15	6.31	9.50	15.8

Table 4. Acidity dependence of the reaction rate

[BA] 0.20 M	[CAT] 0.02 M		Temp 303 K		
$[H^+]$ M	0.1	0.2	0.5	0.8	1.0
$10^8 k_1\ s^{-1}$	1.29	5.10	31.5	80.0	125
$10^6 k_1/[H^+]^2$	1.29	1.27	1.26	1.25	1.25

Table 5. Oxidation of benzyl methyl ether by chloramine-T at 303 K in 1 : 1 (v/v) acetic acid-water

[Substrate] M	[CAT] M	[H$^+$] M	$10^7 k_1$ s^{-1}
0.10	0.02	1.0	5.01
0.20	0.02	1.0	10.0
0.40	0.02	1.0	20.2
0.20	0.01	1.0	10.1
0.20	0.04	1.0	9.90
0.20	0.02	0.5	2.43
0.20	0.02	0.8	6.50
0.20	0.02	1.6	26.2

$10^6 k = 5.04 \pm 0.07$ l^3 mol^{-3} s^{-1}.

Table 6. Rate constants for the oxidation of substituted benzyl alcohol by chloramine-T

Substituent	$10^8 k$ l^3 mol^{-3} s^{-1}				
	298	300	308	313	318 K
H	431	631	900	1410	1780
m-Me	596	850	1200	1680	2290
p-Et	1740	2400	3230	4360	5820
p-Me	1950	2630	3540	4680	6200
p-OMe	20000	23900	30200	37100	—
p-Cl	278	363	556	759	1050
m-Br	51.3	95.5	123	185	275
p-NO_2	8.95	15.1	24.8	40.3	64.6
m-NO_2	15.8	26.3	42.7	68.4	1.9

Table 7. Activation parameters for the oxidation

Substituent	H	*m*-Me	*p*-Et	*p*-Me	*p*-OMe
ΔH^* kJ mol^{-1}	55.4	52.0	47.0	45.8	34.4
$-\Delta S^*$ J mol^{-1} K^{-1}	165	169	182	184	203
Substiutent	*p*-Cl	*m*-Br	*p*-NO_2	*m*-NO_2	
ΔH^* kJ mol^{-1}	59.6	66.4	77.7	75.6	
$-\Delta S^*$ J mol^{-1} K^{-1}	158	145	123	124	

nitrile. Thus a hydrogen abstraction giving rise to free radicals is unlikely.

The oxidation of benzyl methyl ether also follows similar rate laws, the ease of its oxidation being comparable to that of benzyl alcohol (Table 5).

The oxidation of benzyl alcohol and the monosubstituted benzyl alcohols was determined at various temperatures (Table 6) and the activation parameters were evaluated (Table 7). The average errors in the values of ΔH^* and ΔS^* are ± 4 kJ mol^{-1} and ± 11 J mol^{-1}K^{-1}, respectively.

Discussion

Chloramine-T is a strong electrolyte dissociating into ions in aqueous solution;[6]

$$RNClNa \rightleftharpoons RNCl^- + Na^+, \quad (3)$$

where R=*p*-$MeC_6H_4SO_2$. The anion is protonated in acid solution to give the acid. No free acid could be isolated since it undergoes hydrolysis;[4]

$$RNCl^- + H_3O^+ \rightleftharpoons RNHCl + H_2O, \quad (4)$$

$$RNHCl + H_2O \rightleftharpoons RNH_2 + HOCl. \quad (5)$$

However, the second order dependence on acidity and the magnitude of the solvent isotope effect suggest that a protonated species is involved in the rate-determining step. Thus Eq. 5 is followed by a protonation

$$HOCl + H_3O^+ \rightleftharpoons H_2OCl^+ + H_2O. \quad (6)$$

This accords well with the suggestion of earlier workers[4,5] that in the oxidation by CAT in acid solution, the active oxidizing species is $(H_2OCl)^+$. Natarajan and Thiagarajan[5] have suggested an alternate oxidizing species $(RNH_2Cl)^+$ in the oxidation of 2-propanol. Some earlier workers[7] however, have preferred HOCl as the oxidizing species in a weak acid solution. The sulfonamide group is not likely to be sufficiently basic to accept another proton.

The kinetic isotope effect, $k_H/k_D=4.13$, is very close to the value obtained in the oxidation of benzyl alcohol by bromine.[8] The mechanistic conclusion is that the rate-determining step involves a C–H bond rupture from the carbinol carbon.

The difference in the rate laws of the oxidation of allyl alcohol[4] and benzyl alcohol can be explained on the basis of different reactivities of the two alcohols towards the oxidant. In the case of allyl alcohol, the oxidation is a fast step following the slow formation of HOCl or H_2OCl^+ (depending upon the reaction conditions), wheras the oxidation of benzyl alcohol is solwer than the formation of the oxidizing species. Thus the oxidation of benzyl alcohol should be slower than that of allyl alcohol. This is actually the case. The oxidation of allyl alcohol is so fast that it has been studied at 273 K.

The activation enthalpies and entropies of the nine compounds are linearly related ($r=0.991$). The correlation was tested and found genuine by applying Exner's criterion.[9] The isokinetic temperature computed from the plot is 540 ± 35 K. Current views do not attach much physical significance to isokinetic temperature,[10] though a linear relation is usually a necessary condition for the validity of the Hammett equation.

No systematic study of the effect of substituents on the oxidation of alcohols by CAT is available. The rates of the oxidation of monosubstituted benzyl alcohols correlate well with σ^+ values ($r=0.996$). The reaction constant was $\rho^+ = -2.08 \pm 0.08$ at 303 K. The negative value of the reaction constant indicates an electron-deficient carbon center in the transition state.

Natarajan and Thiagarajan[5] have suggested an initial formation of a hypochlorite in the oxidation of 2-propanol. However, the ester formation is unlikely in view of the almost equal ease of the oxidation of benzyl alcohol and its methyl ether. The large negative reaction constant thus arises only out of the differential effects of the substituents in the rate-determining step. The correlation with σ^+, together with the substantial deuterium isotope effect suggest a considerable carbonium ion character in the transition state.

From the results, a mechanism involving transfer of a hydride ion from the alcohol to the oxidant is suggested. Simultaneous release of hydroxylic proton is

unlikely in view of the observed solvent isotope effect and the magnitude of the reaction constant. The polar requirement on the alcohol carbon for hydride release from C–H is opposite to that for proton release from O–H, the reaction constant being likely to be nearly zero in a concerted process:

$$PhCH_2OH + (H_2OCl)^+ \xrightarrow{slow} \overset{+}{P}HCHOH + H_3O^+ + Cl^- \quad (7)$$

$$\overset{+}{P}hCHOH \xrightarrow{fast} PhCHO + H^+. \quad (8)$$

It is of interest to recall here that in the oxidation of substituted benzyl alcohols by bromine[8] and acid permanganate,[11] which involve rate-determining transfer of a hydride ion, the reported values of ρ are -2.3 and -1.76 respectively.

Experimental

Materials. The preparation and specification of the alcohols used have been described earlier.[11] Isotopic purity of α,α-dideuteriobenzyl alcohol, as determined by NMR, was 92±5%. Commercial benzyl methyl ether was purified by distillation from all glass apparatus. Aqueous solution of chloramine-T (E. Merck, pro analysi) was stored in dark bottles. Acetic acid was purified by the usual methods.[12] Perchloric acid was used as a source of hydrogen ions.

Product Analysis. Benzaldehyde was characterized and estimated by the isolation of its 2,4-dinitrophenylhydrazone.

Kinetic Measurements. The reactions were carried out under pseudo-first-order conditions by keeping a large excess of the alcohol over CAT. The temperature was kept constant to ±0.1 K. The solvent used was acetic acid–water (1 : 1 (v/v)), unless otherwise stated. The reactions were followed iodometrically up to nearly three half-lives, the reactions being found smooth. The rate constants were evaluated from the plots of log [oxidant] against time and were reproducible within ±3%. Preliminary experiments showed that the oxidation is not sensitive to ionic strength, hence no attempt was made to keep it constant. The rate for the deuterated alcohol was corrected for the ordinary alcohol present. The usual concentration of the reactants in the reaction mixture was: the alcohol 0.05—1.0 M, CAT 0.01—0.08 M, and perchloric acid 0.1—1.5 M.

References

1) S. P. Mushran, M. C. Agarwal, and B. Prasad, *J. Chem. Soc., B*, **1971**, 1712.
2) S. P. Mushran and M. C. Agarwal, *J. Chem. Soc., Perkin Trans. 2*, **1973**, 762 and references therein.
3) S. P. Mushran, R. M. Mehrotra, and R. Sanehi, *J. Indian Chem. Soc.*, **51**, 594 (1974).
4) D. S. Mahadevappa and H. M. K. Naidu, *Aust. J. Chem.*, **27**, 1203 (1974); **28**, 899 (1975).
5) M. M. Natarajan and V. Thiagarajan, *J. Chem. Soc., Perkin Trans. 2*, **1975**, 1590.
6) E. Bishop and V. J. Jennings, *Talanta*, **1**, 197 (1958).
7) T. Higuchi and A. Hussain, *J. Chem. Soc., B*, **1967**, 549.
8) P. Aukett and I. R. L. Barker, *J. Chem. Soc., Perkin Trans. 2*, **1972**, 568.
9) O. Exner, *Coll. Czeck. Chem. Commun.*, **29**, 1094 (1964).
10) J. E. Leffler, *J. Org. Chem.*, **31**, 533 (1966).
11) K. K. Banerji, *J. Chem. Soc., Perkin Trans. 2*, **1973**, 435.
12) K. J. P. Orton and A. E. Bradfield, *J. Chem. Soc.*, **1924**, 960; **1927**, 983.

Branched-Chain Deoxy Nitro and Amino Sugar Derivatives from Ketose

M. M. A. ABDEL-RAHMAN

Department of Chemistry, Faculty of Science, Alexandria University, Alexandria, Egypt

(Received September 22, 1976)

The nitromethane addition to 1,2-*O*-isopropylidene-5-*O*-trityl-α-D-*erythro*-pentofuranos-3-ulose (**1**) proceeded smoothly to give the corresponding branched-chain sugar (**2**), which on acetylation afforded (**3**) followed by elimination of acetic acid in presence of a base catalyst, resulted in the formation of the corresponding nitro olefin (**4**). The nitro olefin when subjected to borohydride reduction gave 5-*O*-acetyl-3-deoxy-1,2-*O*-isopropylidene-3-(nitromethyl)-α-D-ribofuranose (**5**), which on catalytic hydrogenation followed by acetylation yielded the 3-(acetamidomethyl)-5-*O*-acetyl-3-deoxy-1,2-*O*-isopropylidene-α-D-ribofuranose (**6**). By the study of the NMR spectra of 3-deoxy derivatives (**5**) and (**6**), their D-ribo configurations were established.

The synthesis of various branched-chain carbohydrates was the aim of several investigators in recent years.[1,2] These syntheses usually utilise the required oxo sugars as intermediates, which then condense with diazomethane,[3] organolithium compounds,[1,4] Grignard reagents,[1,4,5] sulfur ylides,[6] and phosphorane.[7,8]

The synthesis of amino sugars by the method of nitromethane-sugar dialdehyde[9] has been modified,[10] by using nitroethane to afford branched-chain amino deoxy sugars, in which branching is on the carbon atom having the amino group.

A recent method[8] described the synthesis of deoxy sugars having a nitrile or an amino group on the branched-chain. The synthesis of branched-chain nitro sugars[11] was carried out by the addition of nitryl iodide to a branched-chain unsaturated sugars, whereas Michael addition of nitro-alkanes to unsaturated nitro sugars produced branched-chain dinitro sugar derivatives.[12] The nitromethane method[9] has now been applied to oxo sugar to produce sugar derivatives with a nitro group on the branch, which could be readily converted into deoxy sugars having a nitro or an amino group on the branched-chain. This mehtod and others[13] led to the direct introduction of a functionalized one-carbon branch into carbohydrates.

Results and Discussion

The reaction of 1,2-*O*-isopropylidene-5-*O*-trityl-α-D-*erythro*-pentofuranos-3-ulose[14] (**1**) with a suspension of the sodium salt of nitromethane (prepared by careful addition of sodium hydride to nitromethane)in nitromethane afforded 1,2-*O*-isopropylidene-3-(nitromethyl)--5-*O*-trityl-α-D-ribofuranose (**2**) in 76% yield.
Its NMR spectrum showed the existence of an exchangeable proton (3-OH) and an AB quartet of the two methylene protons of the branch. The IR spectrum showed the presence of a nitro group.

Acetylation of **2** with acetic anhydride in the presence of *p*-toluenesulfonic acid resulted in acetolysis of the 5-trityl ether in addition to acetylation of the 3-hydroxyl group, to produce 3,5-di-*O*-acetyl-1,2-*O*-isopropylidene-3(nitromethyl)-α-D-ribofuranose (**3**).

β-Acetoxynitroalkanes are useful precursors for α-nitroalkene synthesis, since they easily undergo base-catalyzed elimination of acetic acid.[15] Thus, treatment of **3** with anhydrous sodium carbonate in dry benzene readily gave the nitro olefin (**4**), which was then reduced

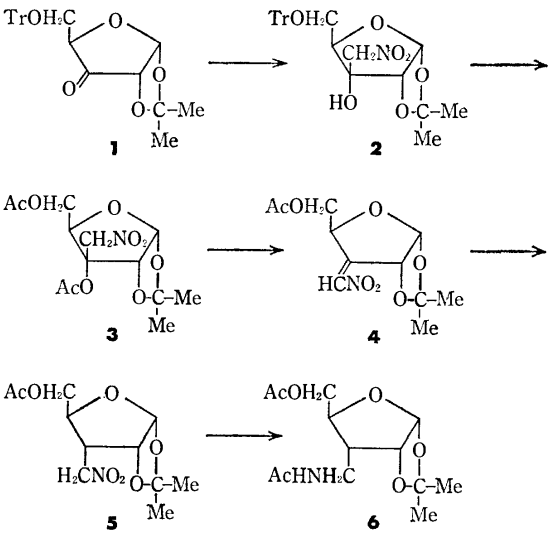

using sodium borohydride in aqueous acetonitrile,[16] to give the corresponding branched-chain deoxy nitro sugar (**5**) in a good overall yield. The 1,2-*O*-isopropylidene group, as expected, controlled the reaction sterically. From the NMR data of **5**, the configuration at C-3 was deduced. It showed a doublet at τ 4.14 (H-1) and a triplet at 5.19 (H-2), indicating that it was also coupled to H-3 . Since there was no coupling between H-2 and H-3 in 1,2-*O*-isopropylidene -α-D-xylo-furanose,[17] the product should have the deoxy-D-ribo configuration.

Catalytic reduction of **5** followed by acetylation afforded 3-(acetamidomethyl)-5-*O*-acetyl-3-doxy-1,2-*O*-isopropylidene-α-D-ribofuranose (**6**). Its NMR spectral data also confirmed the deoxy-D-ribo configuration.

This series of reactions describes the synthesis of functionalized branched-chain deoxy sugars from a branched-chain sugar with inversion of configuration at the center of branching, which is achieved by the steric influence of the 1,2-*O*-isopropylidene group.

Experimental

Melting points were determined with a Fischer-Jones apparatus and were uncorrected. NMR spectra were observed on a Varian HA-100 spectrometer using TMS as an internal standard. IR spectra were recorded with a Unican SP 200 spectrometer. Optical rotations were determined with a Perkin-Elmer 141 recording polarimeter. Solutions were concentrated on a rotary evaporator at below 20 °C under

reduced pressure.

1,2-O-Isopropylidene-3-(nitromethyl)-5-O-trityl-α-D-ribofuranose (2). A suspension of sodium hydride (0.15 g) in nitromethane (10 ml) was added dropwise to a cooled (Dry Ice bath below −20 °C) and stirred solution of 1,2-*O*-isopropylidene-5-*O*-trityl-α-D-*erythro*-pentofuranos-3-ulose[14] (1.1 g) in nitromethane (10 ml). The reaction mixture was stirred for one additional hour at room temperature and neutralized with glacial acetic acid, and the solvent was evaporated. The residue was dissolved in water (60 ml) and extracted with chloroform (3×50 ml), washed with water and dried. The syrup obtained on evaporation of the extract was crystallised from acetone–hexane to give the title compound **2** (0.9 g, *Y*= 76%); mp 120—122 °C, $[\alpha]_D^{20}$ +29° (*c* 1, $CHCl_3$), IR ν_{max}^{KBr} 3450 (OH), 1560 cm^{-1} (NO_2); NMR ($CHCl_3$): τ 3.98 (1H, d, $J_{1,2}$ 4.0 Hz); 5.13 (2H, d), 5.88 (4H, t, $J_{4,5}$ 5 Hz); 6.68 (5H, m); 5.59 (CH_2NO_2, q, $J_{a,b}$ 12.5 Hz); 8.40, 8.60 (CMe_2, s); 6.83 (OH, s, disappeared on deuteration with D_2O).

Found: C, 68.5; H, 5.7; N, 3.0%. Calcd for $C_{28}H_{29}NO_7$: C, 68.4; H, 5.9; N, 2.8%.

3,5-Di-O-acetyl-1,2-O-isopropylidene-3-(nitromethyl)-α-D-ribofuranose (3). A solution of **2** (0.6 g) in acetic anhydride (6 ml) was stirred overnight at room temperature in the presence of anhydrous *p*-toluenesulfonic acid (0.1 g). The reaction mixture was then slowly poured onto an aqueous solution of sodium hydrogencarbonate and the gummy product was decanted, washed several times with cold water and dissolved in chloroform, which was washed with water and dried (Na_2SO_4). On evaporation of the dried chloroform, compound **3** was obtained as a pale yellow syrup (0.4 g); IR ν_{max} 1760 (OAc); 1510 cm^{-1} (NO_2).

Found: C, 45.1; H, 4.8; N, 4.6%. Calcd for $C_{12}H_{16}NO_9$: C, 45.3; H, 5.0; N, 4.4%.

5-O-Acetyl-3-deoxy-1,2-O-isopropylidene-3-(nitromethyl)-α-D-ribofuranose (5). Powdered potassium carbonate (0.5 g) was added to a solution of **3** (1.8 g) in dry benzene (25 ml) and the suspension was stirred magnetically for 6 h at room temperature. The mixture was filtered using Celite pad and the filtrate was evaporated to give **4** as yellow viscous syrup. It was dissolved in acetonitrile (25 m), cooled in an ice bath, stirred. To this was added a solution of sodium borohydride (0.2 g) in water (2 ml). After one hour stirring, the reaction mixture was diluted with water (100 ml) and extracted with chloroform (4×25 ml). The extracts were washed with water and dried (Na_2SO_4). On evaporation, the residue obtained (0.8 g, *Y*=58%) was crystallised from acetone–hexane, mp 127—129 °C; $[\alpha]_D^{20}$ +62° (*c* 1, $CHCl_3$), IR ν_{max}^{KBr} 1750 (OAc), 1565 cm^{-1} (NO_2), NMR ($CDCl_3$): τ 4.14 (1H, d, $J_{1.2}$ 4.0 Hz); 5.14 (2H, t); 7.32 (3H, m); 5.70—6.07 (3-proton, m, 4H, 5H); 5.39 (CH_2NO_2, q); 8.52, 8.72 (CMe_2, 2 s); 7.96 (Ac, s).

Found: C, 48.2; H, 6.3; N, 4.9%. Calcd for $C_{11}H_{17}NO_7$: C, 48.0; H, 6.2; N, 5.1%.

3-(Acetamidomethyl)-5-O-acetyl-3-deoxy-1,2-O-isopropylidene-α-D-ribofuranose (6). A solution of **5** (0.14 g) in ethanol (20 ml) was reduced with hydrogen in the presence of platinum oxide (0.1 g) at room temperature under atmospheric pressure for 2 h, during which the calculated amount of hydrogen was consumed. The reaction mixture was filtered and evaporated to give the corresponding amine as a syrup. It was dissolved in dry pyridine (2 ml) and acetic anhydride (2 ml) was added, and the solution was stirred for 2 h. The reaction mixture was then poured onto ice, and extracted with chloroform (4× 20 ml). The extracts were then washed with cold dilute hydrochloric acid, aqueous sodium hydrogencarbonate and water, and dried (Na_2SO_4). On evaporation of the dried extract compound **6** was obtained as a syrup, (0.11 g, *Y*= 82%) $[\alpha]_D^{20}$+57° (*c* 1, $CHCl_3$); IR ν_{max} 3450 (NH), 1750 (OAc), 1680, 1525 cm^{-1} (NHAc); NMR ($CDCl_3$): τ 4.20 (1H, *d*, $J_{1,2}$ 4.0 Hz); 5.34 (2H, t); 3.74 (NH, broad);7.93, 8.04 (Ac, two s); 8.50, 8.70 (CMe_2, two s).

Found: C, 54.4; H, 7.6; N, 4.7%. Calcd for $C_{13}H_{21}NO_6$: C, 54.3; H, 7.4; N, 4.9%.

References

1) W. G. Overend, *Chem. Ind. (London)*, **1963**, 342.
2) L. Hough and A. C. Richardson, "Rodd's Chemistry of Carbon Compounds," **1F** ed by S. Coffey, Elsevier, Amsterdam (1967) pp. 529—543.
3) R. J. Ferrier, W. G. Overend, W. G. Rafferty, H. M. Wall, and N. R. Williams, *J. Chem. Soc., C*, **1968**, 1091.
4) R. D. Ress, K. James, A. R. Tatchebl, and R. H. Williams, *J. Chem. Soc., C*, **1968**, 2716.
5) R. F. Nutt, M. J. Dickenson, F. W. Holly, and E. Walton, *J. Org. Chem.*, **33**, 1789 (1968).
6) R. D. King, W. G. Overend, and N. R. Williams, *Chem. Commun.*, **1967**, 726.
7) A. Rosenthal and L. Nguyen, *J. Org. Chem.*, **34**, 1029 (1969).
8) A. Rosenthal and D. A. Baker, *Tetrahedron Lett.*, **1969**, 397.
9) F. W. Lichtenthaler, *Angew. Chem. Int. Ed. Engl.*, **3**, 211 (1964); H. H. Baer, *Adv. Carbohydr. Chem. Biochem.*, **24**, 67 (1969).
10) S. W. Gunner, W. G. Overend, and N. R. Williams, *Chem. Ind. (London)*, **1964**, 1523; H. H. Baer and G. V. Rao, *Ann. Chem.*, **686**, 210 (1965); F. W. Lichtenthaler, *Fortsch. Chem. Forschg.*, **14**, 556 (1970).
11) W. A. Szarek, J. S. Jewell, I. Szczerek, and J. K. N. Jones, *Can. J. Chem.*, **47**, 4473 (1969).
12) H. H. Baer and K. S. Ong, *Can. J. Chem.*, **46**, 2511 (1968).
13) A. Rosenthal and K. S. Ong, *Tetrahedron Lett.*, **1969**, 3981; A. Rosenthal, K. S. Ong, and D. Baker, *Carbohydr. Res.*, **13**, 113 (1970).
14) W. Sowa, *Can. J. Chem.*, **46**, 1586 (1968).
15) H. B. Hass, A. G. Susie, and R. L. Heider, *J. Org. Chem.*, **15**, 8 (1950); H. H. Baer, T. Neilson, and W. Rank, *Can. J. Chem.*, **45**, 991 (1967).
16) A. I. Meyers and J. C. Sircar, *J. Org. Chem.*, **32**, 4134 (1967).
17) R. J. Abraham, L. D. Hall, L. Hough, and K. A. McLauchlan, *J. Chem. Soc.*, **1962**, 3699.

NOTES

BULLETIN OF THE CHEMICAL SOCIETY OF JAPAN, VOL. 50 (6), 1621—1622 (1977)

Accordionlike Skeletal Motions of $CH_3NHCONH(CH_2)_nCH_3$ (n=1—15)

Yoshiyuki MIDO, Fumiko FUJITA, and Teizo KITAGAWA*

Department of Chemistry, Faculty of Science, Kobe University, Nada, Kobe 657
**Institute for Protein Research, Osaka University, Yamadakami, Suita, Osaka 565*

(Received December 6, 1976)

Synopsis. Solid $CH_3NHCONH(CH_2)_nCH_3$ (n=1—15) gave two intense Raman lines in the 100—500 cm^{-1} region. The frequency of one of them varied with n, but that of the other was unvarying. The n-dependent frequencies fit the theoretical ν-δ curve of C–C–C deformation of polyethylene and were, therefore, assigned to the accordion modes.

In early Raman studies of normal paraffin crystals, Mizushima and Shimanouchi[1] found sharp Raman lines which appeared at frequencies inversely proportional to the number of carbon atoms; they assigned them to the accordion-like motion of the totally symmetric skeletal deformation. Schaufele and Shimanouchi[2] elucidated the frequencies (ν) of the accordion modes of C_nH_{2n+2} molecules in terms of the phase difference (δ) of the vibrational displacements between two adjacent methylene groups.

We ourselves have previously studied the vibrational spectra of alkylureas[3-5] and pointed out that the C–N–C–N–C skeleton of the $CH_3NHCONHCH_2$– group is of a planar zigzag structure.[3] In the present study we examined the accordion modes of dialkylureas of $CH_3NHCONH(CH_2)_nCH_3$ (n=1—15). These compounds were prepared by a standard method[4] and were purified through repeated crystallization. The laser Raman spectra were excited by the 514.5 nm line and recorded on a JEOL-400D Raman spectrometer.

Two prominent Raman lines were found in the region between 100 and 500 cm^{-1}. One of them appeared around 230 cm^{-1} irrespective of n, but the other was located at a frequency which varied sensitively with n, although it became a shoulder of the libration band at about 100 cm^{-1} when $n \geqq 6$. The frequencies of the latter group of the Raman lines were approximately inversely-proportional to $n+5$ and were thus assigned to the accordion mode.

The n-dependent frequencies observed for solid $CH_3NHCONH(CH_2)_nCH_3$ are plotted against the phase difference in Fig. 1, where $\delta = 2\pi/(n+5)$ (instead of $\pi/n+5$) is used to refer to the theoretical ν-δ curve of the polyethylene crystal. The observed frequencies fit closely the theoretical curve (solid line) calculated for the ν_5 branch of the polyethylene crystal by Kitagawa and Miyazawa.[6] The ν-δ curve used has also been applied satisfactorily to the analysis of the skeletal modes of $CH_3(CH_2)_nCONH_2$.[7] Furthermore, the corresponding ν-δ plots observed for various polyethers of the $[-(CH_2)_m-O-]_n$ type have been reported to fit the theoretical ν-δ curve of the infinite polymethylene chain.[8]

Upon the determination of δ for the skeletal deformation vibrations of chain molecules with a *trans* zigzag structure, the number of constituent atoms is taken, in general, as the denominator.[2] In the present case, if the plane of the C–N–C–N–C of $CH_3NHCONHCH_2$– coincides with the *trans* zigzag plane of $-(CH_2)_nCH_3$, there will be $n+5$ atoms as the constituents of the *trans* zigzag chain of $CH_3NHCONH(CH_2)_nCH_3$ molecule; therefore $n+5$ was adopted for the denominator in the plot of Fig. 1.

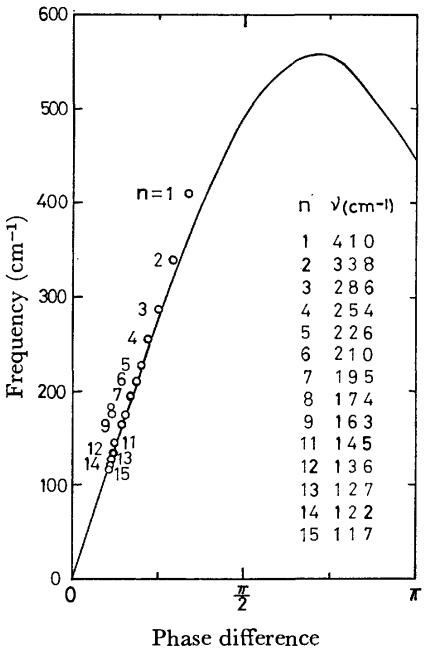

Fig. 1. The ν-δ plots for the accordionlike motion of $CH_3NHCONH(CH_2)_nCH_3$.

Usually, when n is small, the experimental ν-δ plots deviate considerably from the theoretical ν-δ curve and a correction for the effect of the end group is required.[7] Nevertheless, it is surprising that the present data for small n values fall closely on the theoretical curve without any correction for the end group. This fact may imply that all the skeletal atoms constitute a *trans* zigzag plane, and also that the deformations of NH–CO–NH and CO–NH–CH_2 (or CH_3) are effectively coupled with other skeletal deformations of the molecule just as where those parts are replaced with CH_2–CH_2–CH_2. If this consideration is correct, then it is not unexpected that the present data for n=2 fall on the theoretical ν-δ curve, because it corresponds to the case of the n=7 of C_nH_{2n+2}, for which the observed frequency fits the theoretical curve fairly well.

The authors wish to express their gratitude to Mr. Shuuichi Muraishi of Japan Electric Co., Ltd., for his measurements of the Raman spectra.

References

1) S. Mizushima and T. Shimanouchi, *J. Am. Chem. Soc.*, **71**, 1320 (1949).
2) R. F. Schaufele and T. Shimanouchi, *J. Chem. Phys.*, **47**, 3605 (1967).
3) Y. Mido and H. Murata, *Bull. Chem. Soc. Jpn.*, **42**, 3372 (1969).
4) Y. Mido, *Spectrochim. Acta, Part A*, **28**, 1503 (1972).
5) Y. Mido and H. Murata, *Nippon Kagaku Zasshi*, **90**, 254 (1969); Y. Mido, *Spectrochim. Acta, Part A*, **29**, 1, 431. (1973); Y. Mido, *Bull. Chem. Soc. Jpn.*, **47**, 1833 (1974); **48**, 2704 (1975).
6) T. Kitagawa and T. Miyazawa, *Adv. Polym. Sci.*, **9**, 335 (1972).
7) K. Machida, S. Kojima, and T. Uno, *Spectrochim. Acta, Part A*, **28**, 235 (1972).
8) D. Makino, M. Kobayashi, and H. Tadokoro, *Spectrochim. Acta, Part A*, **31**, 1481 (1975).

BULLETIN OF THE CHEMICAL SOCIETY OF JAPAN, VOL. 50 (6), 1623—1624 (1977)

X-Ray Diffraction Studies of the Metal Soaps of Fatty Acids of Odd Carbon Numbers

Keizo OGINO and Toshio SAITO

Faculty of Science and Technology, Science University of Tokyo, Noda, Chiba 278

(Received September 20, 1976)

Synopsis. X-Ray diffraction patterns have been observed for metal soaps of fatty acids with odd carbon numbers. The soaps of Pb, Cd, Ba, and Zn were prepared from the fatty acids of hexanoic, heptanoic, nonanoic, decanoic, undecanoic, dodecanoic, tridecanoic, tetradecanoic, pentadecanoic, hexadecanoic, heptadecanoic, and octadecanoic, the long spacings of which were studied in comparison with those of sodium soaps. The most prominent characteristic of these soaps is the presence of a definite order of long spacing which is directly proportional to the number of carbon atoms in the hydrocarbon chains, this is in contrast to the sodium soaps, which show a zigzag relation.

Although many reports have been presented on X-Ray diffraction studies on metal soaps, they have been concerned with the fatty acid salts of even carbon numbers originating from natural fatty oils.[1-6]

Recently, though the advance of organic synthesis has made the fatty acids of odd carbon numbers readily available for technical uses. It is important to investigate the properties of metal soaps of fatty acids with odd carbon numbers to facilitate the present industrial activity. With this in view, X-Ray diffraction patterns have been obtained for the metal soaps of fatty acids of odd carbon numbers in this study.

Experimental

Materials. *Fatty Acids*: The fatty acids, from hexanoic acid (C_6) to octadecanoic acid (C_{18}), used in this investigation were supplied from the Ajinomoto Co., Ltd. The purities of the fatty acids were confirmed to be over 98.5 per cent by gas chromatography.

Metal Salts: The inorganic chemicals used in the preparation of metal soaps were a reagent grade: lead acetate $Pb(CH_3COO)_2$, cadmium sulfate $CdSO_4$, barium nitrate $Ba(NO_3)_2$, and zinc acetate $Zn(CH_3COO)_2$.

Preparation of Metal Soaps. The soaps of Pb, Cd, Ba, and Zn were prepared by the addition of aqueous solutions of sodium soaps to a large excess of solutions of the metal salts. The precipitates were washed with water and then with ethanol, and successively extracted with boiling acetone. The purified metal soaps were dried *in vacuo* and then stored in a desiccator at room temperature for two months.

Apparatus. The X-ray diffraction measurements were performed with a Rigaku Denki Geiger Spectrometer D-9C instrument, using copper K_α radiation through a nickel filter, under the following conditions: voltage, 30 kV; 10 mA; count full scale, 1000 c/s; scanning speed, 2/min; time constant, 2 cm/min.

Results and Discussion

X-Ray diffraction patterns were obtained for a series of metal soaps made from straight-chain fatty acids containing 6, 7, 8, 9, 10, 11, 12, 13, 14, 15, 16, 17, and 18 carbon atoms. Figure 1 shows the X-Ray diffraction patterns of the metal soaps of tridecanoic acid in comparison with the sodium soap.

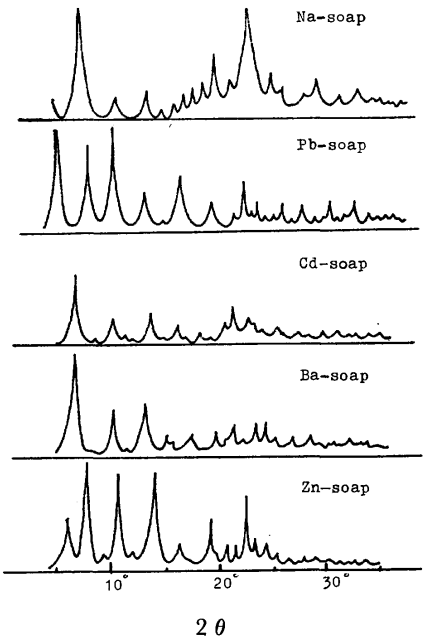

Fig. 1. X-Ray diffraction pattern of metal soaps of tridecanoic acid.

All of the metal soaps showed several strong diffraction patterns corresponding to the spacings. It is noticed that sodium soap diffracts strongly, showing the higher crystallinity of sodium soaps than those of the other metal soaps. Similar results were also obtained for the metal soaps of the other fatty acids.

In Table 1, the long spacings for the metal soaps of

Table 1. Long spacing (Å) of metal soaps

Carbon number of fatty acid	Na-soap	Pb-soap	Cd-soap	Ba-soap	Zn-soap
C_{18}	48.21	51.27	50.01	48.10	42.70
C_{17}	45.17	48.87	47.90	46.35	41.88
C_{16}	42.75	46.50	45.72	44.17	38.46
C_{15}	39.00	43.47	42.46	40.56	36.05
C_{14}	37.35	41.43	40.17	38.43	34.02
C_{13}	33.99	37.89	36.84	35.85	33.12
C_{12}	32.34	35.37	34.47	32.72	—
C_{11}	29.16	33.00	32.37	30.48	27.98
C_{10}	27.83	30.84	30.15	28.53	26.01
C_9	24.57	28.23	26.01	25.77	23.49
C_8	23.28	25.77	22.68	—	20.91
C_7	20.28	23.28	20.91	—	—
C_6	20.13	20.70	20.58	—	—

Table 2. Short spacing of metal soaps

	Short spacing (Å)				
	(i) C_{16}-soaps				
Na-soa&	4.60(m)	4.17(m)	3.87(ss)	3.56(m)	—
Pb-soap	4.10(ss)	3.93(m)	3.82(m)	3.66(s)	—
Cd-soap	4.08(ss)	3.90(m)	3.19(s)	3.68(m)	—
Ba-soap	4.57(s)	4.04(m)	3.90(s)	3.72(s)	—
Zn-soap	4.55(s)	4.33(m)	4.04(m)	3.85(ss)	—
	(ii) C_{13}-soaps				
Na-soap	4.91(s)	4.19(m)	3.87(ss)	3.56(m)	—
Pb-soap	4.21(m)	4.08(ss)	3.85(m)	3.79(w)	3.65(m)
Cd-soap	4.12(m)	3.78(m)	3.53(w)	—	—
Ba-soap	4.60(m)	4.42(m)	4.35(m)	4.01(m)	3.80(m)
Zn-soap	4.62(ss)	4.27(m)	4.15(m)	4.10(ss)	3.80(m)

fatty acids with even and odd carbon numbers from C_6 to C_{18} are shown. The short spacings for metal soaps of hexadecanoic and tridecanoic acid are shown in Table 2. The short spacings permit the identification of the soaps.

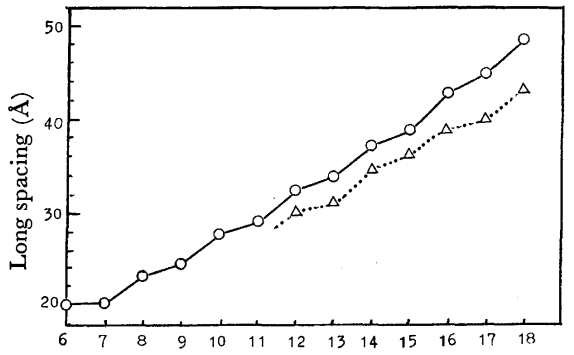

Fig. 2. Long spacing of sodium soaps in reference with those of fatty acids.
○; Sodium soap, △; fatty acid.

Figure 2 shows the long spacings of the sodium soaps and the fatty acids. The data for the fatty acids are taken from the literature.[7,8] Here, the crystalline forms of the acids are denoted as the B-form for even-carbon-number acids and as the B'-form for odd-carbon-number acids.

When the long spacings of the sodium soaps of saturated fatty acids are plotted against the number of carbon atoms, as in Fig. 2, one obtains a zigzag curve (high at even carbon numbers and low at odd). It is also well known that the long spacings of fatty acids are related to the carbon numbers of the fatty acids in a zigzag curve.

On the other hand, the melting points of saturated fatty acids with even and odd numbers of carbon atoms are known to be related to the carbon number in a zigzag curve with higher melting points for the even fatty acids than those for the odd ones. This is because fatty acids with odd carbon numbers have structures of the *cis*-form, by analogy with other organic compounds showing long and short terminal distances between two adjacent molecules when the molecules are declined, while the fatty acids with even carbon numbers have structures of the *trans*-form showing a short terminal distance only. Therefore, the packings of fatty acids with odd carbon numbers are more loose than those of even ones.

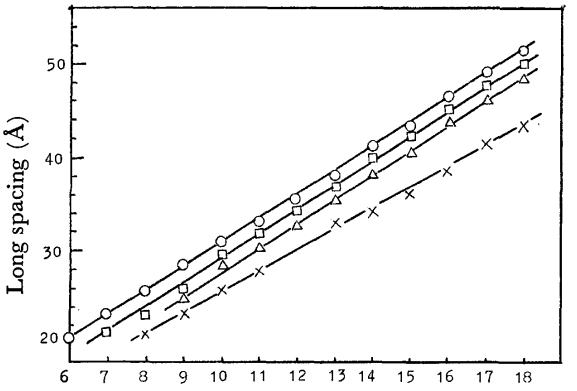

Fig. 3. Long spacing of metal soaps.
○; Pb-soap, □; Cd-soap,
△; Ba-soap, ×; Zn-soap.

Figure 3 shows plots of the long spacings of the metal soaps against the carbon numbers of the fatty acids. It may be noted in the figure that the long spacings of these metal soaps increase linearly with the number of carbon atoms in the fatty acids.

Vold *et al.*[4] have reported that the long spacings of heavy metal soaps are correlated with their structures, in which the cations are separated in parallel planes at a distance somewhat less than the length of two fatty acid radicals. In this work, it was found that the regular increase in spacing (about 2.5 Å per additional carbon atom) corresponds to twice the size of the CH_2 unit.

However, the slope of the linear relation for Zn-soap differs from those of the other metal soaps. Matuura[6] found that the long spacings for the soaps of fatty acids with most of the light metals in the periodic table appear to be peculiar. The peculiarity of Zn-soaps seems to be related to Matuura's result. The theoretical approaches to the details of this evidence will be here after studied.

References

1) G. H. Smith, *J. Am. Oil Chem. Soc.*, **24**, 353 (1947).
2) R. D. Vold and M. J. Vold, *J. Phys. Colloid Chem.*, **52**, 1424 (1948).
3) M. J. Vold, G. S. Hattiangdi, and R. D. Vold, *J. Colloid Sci.*, **4**, 93 (1949).
4) R. D. Vold and G. S. Hattiangdi, *Ind. Eng. Chem.*, **41**, 2311 (1949).
5) H. Kambe, *Bull. Chem. Soc. Jpn.*, **35**, 78 (1962).
6) R. Matsuura, *Nippon Kagaku Kaishi*, **86**, 560 (1965).
7) "Yushi Kagaku Binran," Maruzen (1965), p. 305.
8) F. Francis and S. H. Piper, *J. Am. Chem. Soc.*, **61**, 577 (1939).

BULLETIN OF THE CHEMICAL SOCIETY OF JAPAN, VOL. 50 (6), 1625—1626 (1977)

The Channeling of Hot H Atoms in the Radiolysis and Photolysis of Crystalline Alkane

Tetsuo MIYAZAKI

Department of Synthetic Chemistry, Faculty of Engineering, Nagoya University, Chikusa-ku, Nagoya 464

(Received December 16, 1976)

Synopsis. The possibility of a long migration of hot H atoms through crystalline alkane is discussed in terms of a simple channeling theory. The potential energy surface for an H atom in crystalline neopentane shows that the channeling directions are perpendicular to the [110] and [100] planes. The energy dependence of the channeling of hot H atoms is discussed.

Recently Miyazaki *et al.* found that H atoms, which are produced by the radiolysis of solvent neopentane or by the photolysis of hydrogen halide, react selectively with a small amount of solute alkane in a neopentane matrix at 77 K.[1] A similar phenomenon has also been observed in isobutane, 2,2,3,3-tetramethylbutane and cyclopropane matrices at 77 K.[1] At present, we cannot give a clear answer to the question whether the reactive H atoms are thermal or hot.

The following observations, however, favor the hypothesis of the hot H atoms: (1) The competitive reaction between *c*-C_6H_{12} and HI for H atoms was studied in the radiolysis and photolysis of a *neo*-C_5H_{12}–*c*-C_6H_{12}–HI mixture at 77 K. The rate constants of these reactions in the neopentane matrix are quite different from those of the thermal H atom reaction.[1] (2) When a H atom is produced by the photolysis of HBr with a 185 nm light, the hot H atom has initially a kinetic energy of 67 kcal/mol. When C_3H_8 is present in the *i*-C_4H_{10} matrix, the hot H atom reacts selectively with solute C_3H_8 to form the C_3H_7 radical.[1] (3) The selective hydrogen atom abstraction by H atoms occurs even at 4 K in *neo*-C_5H_{12} matrix and the H atoms cannot be detected at all by ESR spectroscopy.[2]

There is, however, a dogmatic conception that a long migration of a hot H atom through solid alkane is quite improbable. In this report the author will discuss the possibility of a long migration of the hot H atom by means of the channeling phenomenon.[3]

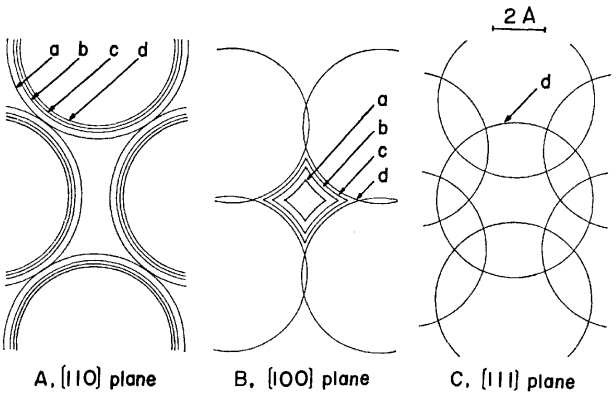

Fig. 1. Projections of potential energy distribution in neopentane crystal.
Contour lines are : a, 1.0 kcal/mol; b, 3.0 kcal/mol; c, 5.0 kcal/mol; d, 9.3 kcal/mol. Position of the contour map represents the position of mass center of H atom.

Potential Energy Surface for H Atoms in Crystalline Neopentane. The occurrence of the channeling in the crystal depends on the existence of the channeling region, which is decided by the potential energy distribution in the crystal. Since the calculation of the potential energy between *neo*-C_5H_{12} and an H atom is quite difficult, the potential energy between an H atom and CH_4, which is a very similar compound to *neo*-C_5H_{12}, is applied here to the neopentane crystal as an approximation. Recently Raff has calculated the potential energy surface between CH_4 and a T atom.[4] He considered the energy for an angular displacement of C–H bonds in addition to the energy calculated by London-Eyring-Polanyi-Sato's method. The potential energy, $V(R_i, \theta_i)$, is given by:

$$V(R_i, \theta_i) = T(R_1, R_5, R_6) + T(R_2, R_5, R_7) + T(R_3, R_5, R_8) + T(R_4, R_5, R_7) + \frac{1}{2}\sum_{j=1}^{6} k_j(\theta_j - \theta_j^0)^2 \quad (1)$$

where R_i represents the interparticle distance between C, H, and T atoms. The θ_i are the six H–C–H angles of CH_4. The bending-force constant for the θ_j angle is k_j, with θ_j^0 representing the equilibrium angle. The four terms $(T(R_i, R_j, R_k))$ in Eq. 1 represent the energies of three-body interaction among C, H, and T atoms.

Raff calculated the potential energy surface of the CH_4–T system by means of the above procedure. Here the potential energy surface calculated by him is applied to the crystalline *neo*-C_5H_{12}–H atom system. The crystalline structure of neopentane at 77 K consists of face-centered cubic unit cells with a lattice constant of 11.4 A.[5] Since the chemical structure of neopentane is symmetrical, the structure is depicted as a sphere. Since an overall rotation of the neopentane molecule occurs even at 77 K,[6] the positions of the H atoms of the methyl group are not fixed in the lattice. Therefore, the depiction of the neopentane molecule as a sphere is reasonable. The energy of the abstraction saddle point on the potential energy surface is normalized to 9.3 kcal/mol,[7] which is the observed activation energy for an H atom-abstraction reaction from neopentane by an H atom. Projections of the potential energy distributions of the three principal planes of the f.c.c. lattice of neopentane are shown in Fig. 1. The potential energy surface in Fig. 1 is based on the energy of the H and CH_4 pair, and the distance between the reactive H atom and the H atom of the methyl group is 1.08 Å at the saddle point of the potential energy surface. The distances between the reactive H atom and the nearest H atoms

of the other methyl groups are 1.9 Å for the other methyl group of the same neopentane molecule and 2.9 Å for the methyl group of the neighboring neopentane molecule. Therefore, the interaction energies of the reactive H atom and these nearest H atoms may be negligible as compared with the energy at the saddle point.

It is clear that the layers of the [110] and [100] orientations exhibit low potential regions to the incident H atoms, which are produced by the radiolysis of neopentane or by the photolysis of hydrogen halide. If the energy in the transverse motion of a hot H atom is larger than the 9.3 kcal/mol shown in Fig. 1A and B, the H atom reacts with neopentane. If, on the other hand, the energy in the transverse motion is smaller than 9.3 kcal/mol, the hot H atom travels a long distance by a succession of glancing collisions with the channel walls of neopentane molecules and then reacts with a solute alkane, which may exist as a defect in the neopentane crystal. When hot H atoms are incident upon the [111] plane, however, they react with neopentane molecules in the first collision (Fig. 1C).

The selective hydrogen atom abstraction reaction by H atoms in neopentane-alkane mixtures is not observed in the liquid phase.[1] This phenomenon can be explained by the channeling hypothesis. Since a random arrangement of molecules in the liquid phase does not contain channels, the hot H atom collides head-on with a solvent molecule in the liquid phase and loses its energy by chemical reaction or deactivation.

Energy Dependence of the Channeling of Hot H Atoms. When the channeling of H atoms takes place, the intervals of glancing collisions of H atoms with the channel wall are much longer than in the lattice period. It is a good approximation[3] to assume that the potential distribution of Fig. 1A or B continues in a direction perpendicular to the [110] or [100] plane. The collision in the channeling is depicted in Fig. 2A, where E is the kinetic energy of an H atom. If the energy of an H atom in its x-direction motion is smaller than 9.3 kcal/mol, then:

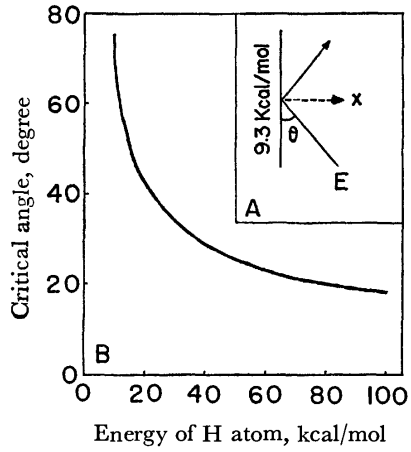

Fig. 2. Critical angle of channeling of hot H atom. A, Glancing collision of hot H atom with channel wall of 9.3 kcal/mol. B, Dependence of critical angle of channeling upon kinetic energy of H atom.

$$E \sin^2\theta < 9.3 \text{ kcal/mol} \quad (2)$$

where θ is the angle between the H-atom motion and the channel direction.

Though the thermalization process of the hot H atom may be important, only the hydrogen-atom-abstraction reaction is considered in this model for the following two reasons: (1) The cross section of the H atom abstraction reaction by hot H atoms in the 3-methylpentane matrix at 77 K is three times as large as that of the thermalization.[8] (2) Though the H atom abstraction reaction by hot H atoms takes place in the neopentane matrix at 4 K, trapped H atoms are not observed at 4 K by ESR spectroscopy.[2]

The substitution reaction of hot H atoms is neglected also in this treatment for the following reasons. The activation energy for the substitution reaction is about 35 kcal/mol,[9] which is much higher than that for the H-atom-abstraction reaction. The cross section for the abstraction from methane by a 65 kcal/mol tritium atom is 3.7 times as large as that for the substitution reaction.[9]

The critical angle for the channeling of the hot H atoms can be calculated by means of Eq. 2; it is shown in Fig. 2B. The H atoms easily undergo a channeling with a decrease in the kinetic energies, when they converse upon the crystal from all directions.

When hot H atoms are produced by the photolysis of hydrogen halide or by the radiolysis of the solvent alkane, the direction of the initial motion of the H atoms is also important. If hydrogen halide is dissolved in a void space of the lattice, as is shown in Fig. 1A, the H atoms easily converse upon the channeling region.

It can be concluded that the channeling phenomenon of hot H atoms can take place in the organic crystal if the conditions are optimum. We cannot reject *a priori* the possibility of long migrations of hot H atoms in the organic crystal.

The author wishes to express his appreciation to Professor Noriaki Ito, Professor Kenji Fueki, and Dr. Kenji Morita of Nagoya University for their fruitful discussions.

References

1) T. Miyazaki, K. Kinugawa, M. Eguchi, and S. M. L. Guedes, *Bull. Chem. Soc. Jpn.*, **49**, 2970 (1976). Previous papers concerning selective hydrogen atom abstraction by H atoms are cited therein.

2) K. Kinugawa, T. Miyazaki, and H. Hase, to be published.

3) P. S. Nelson, "The Observation of Atomic Collisions in Crystalline Solids," North-Holland Publ. Co., (1968).

4) L. M. Raff, *J. Chem. Phys.*, **60**, 2220 (1974).

5) A. H. Mones and B. Post, *J. Chem. Phys.*, **20**, 755 (1952).

6) J. G. Powles and H. S. Gutowsky, *J. Chem. Phys.*, **21**, 1695 (1953).

7) T. Kagiya, Y. Sumida, I. Inoue, and F. S. Dyachkovskii, *Bull. Chem. Soc. Jpn.*, **42**, 1812 (1969).

8) L. Perkey and J. E. Willard, *J. Chem. Phys.*, **60**, 2732 (1974).

9) C. C. Chou and F. S. Rowland, *J. Chem. Phys.*, **50**, 2763 (1969).

BULLETIN OF THE CHEMICAL SOCIETY OF JAPAN, VOL. 50 (6), 1627—1628 (1977)

The Reactions of the Nitrogen Atom with Ethylene and Ethylene-d_4

Saku TAKAHASHI and Shozo MIYAZAKI

Department of Chemistry, Defense Academy, Hashirimizu, Yokosuka-shi, Kanagawa 239

(Received December 24, 1976)

Synopsis. In the N–C_2H_4 system, the main final product was HCN, and the stoichiometry (ΔN/HCN) of the reaction was about 1.3. In the N–C_2D_4 system, CD_2 and CD_2N were found as the reactive intermediates. We suggested a mechanism different from that proposed by Herron.

On the reaction of N with C_2H_4, the following reaction mechanism was postulated by Herron:[1]

$$N + C_2H_4 \longrightarrow HCN + CH_3 \quad (1)$$

$$N + CH_3 \longrightarrow HCN + 2H \quad (2)$$

$$H + C_2H_4 \longrightarrow C_2H_5 \quad (3)$$

$$H + C_2H_5 \longrightarrow 2CH_3 \quad (4)$$

$$N + C_2H_5 \longrightarrow NH + C_2H_4 \quad (5)$$

$$N + NH \longrightarrow N_2 + H \quad (6)$$

The features of this mechanism are that the amount of CH_3 produced through the reaction depends on the competition between H and N for C_2H_5 and that the formation of HCN is mainly due to the reaction of N with CH_3. This list of reactions is not meant to be inclusive. For instance, it does not account for the recombination of CH_3 which proceeds with a rate constant of 3.6×10^{-11} ml/molecure·s.[2] This rate is so fast that, in order to produce HCN in Reaction 2, the rate constant, k_{N-CH_3}, between N and CH_3 needs to have a value greater than 10^{-11} ml/molecule·s. The value of k_{N-CH_3} has not been evaluated experimentally; however, 10^{-11} ml/molecule·s for k_{N-CH_3} seems to be too large.

In order to define the intermediate compounds and to determine the reaction mechanism, the reactions of N with C_2H_4 and C_2D_4 were reinvestigated.

Experimental

The apparatus and procedure were almost the same as those used by Herron and Klein.[3] N was generated by a 2450 MHz electrodeless discharge in N_2. A reaction tube of Pyrex glass, 20 mm i.d. and 100 cm long, formed a part of the fast-flow system. C_2H_4 and C_2D_4 diluted with Ar were added through a movable central inlet tube in the reaction tube. At the end of the reaction tube, the sampling orifice of a mass spectrometer was located. The mass spectra were recorded on a quadrupole mass spectrometer. The pressure in the reaction tube was about 4 Torr and the linear velocity of the gas was 200 cm/s. The materials used in this experiment were research-grade. The observation was carried out at room temperature. The initial concentration of N was measured by means of a gas-phase titration with NO.[4] The HCN was determined by titration with $AgNO_3$. The reaction time was calculated from the linear velocity of the gas and from the distance between the tip of the inlet of the hydrocarbon reactants and the sampling orifice.

The quantities of reactants and products were followed by the ion current with ionization by 23 eV. As to the intermediate products, assuming that they had the same mass spectrometric sensitivity as N, the quantities were determined. The measurements were done in both the N–C_2H_4 and N–C_2D_4 systems.

Results and Discussion

Substracting the background ion current from the observed value in the reaction, the detectable species and their concentrations are determined. The atoms and free radicals investigated in these observations are as follows:

m/e	14	15	16	27	29	30	34
Species	N,CH_2	CH_3	CD_2	HCN	C_2H_5	CD_2N,C_2H_6	C_2D_5

In the N–C_2H_4 system, the quantities of species of *m/e* 14, 15 and 27 are plotted as functions of the reaction time. They are shown in Fig. 1. In this figure, the quantity of species of *m/e* 14 shows a maximum at the beginning of the reaction, and the maximum moves in the direction of the increase in the reaction time with the decrease in the initial concentration of C_2H_4. This fact suggests that CH_2 is formed in the course of the reaction. The quantities of species of *m/e* 15 and 29 produced through the reactions are small and about equal in amount. The species of *m/e* 30 is not found as a product. The stoichiometry of the reaction (ΔN/HCN) is evaluated to be about 1.3.

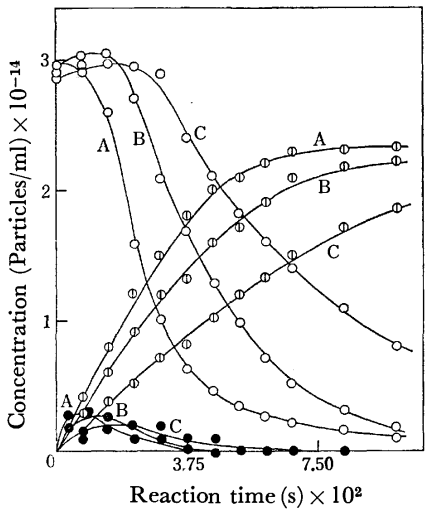

Fig. 1. Kinetics of the reaction of N with C_2H_4.
○: *m/e* 14, ◑: *m/e* 27, ●: *m/e* 15.

Initial concentration

	$[N]_0\times10^{-14}$ atoms ml^{-1}	$[C_2H_4]_0\times10^{-14}$ molecules ml^{-1}
A	2.90	3.25
B	2.90	2.66
C	2·90	1.42

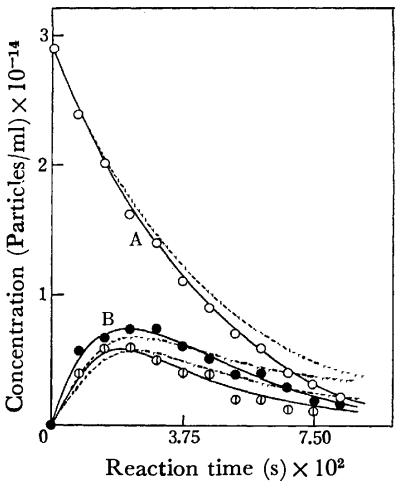

Fig. 2. Kinetics of the reaction of N with C_2D_4.
○: *m/e* 14, ●: *m/e* 16, ◑: *m/e* 30.
Initial concentration
$[N]_0$: 2.90×10^{14} atoms ml^{-1},
$[C_2D_4]_0$: 2.66×10^{14} molecules ml^{-1}.
——: Experimental results, ·····: calculated results.

As a supplementary method to determine the formation of CH_2, the reaction was studied in the N–C_2D_4 system. The results are shown in Fig. 2 in the same manner as in Fig. 1. In this case, the decrease in the quantity of the species of *m/e* 14 with the reaction time is shown by a monotonous curve, Curve A, and the concentrations of species of *m/e* 16 and 30 are varied with the time, having these maximum values in the course of the reaction, shown as Curve B. No species of *m/e* 34 was found.

At the same initial concentrations of reactions in the N–C_2H_4 and N–C_2D_4 systems, assuming that the quantity of N (*m/e* 14) in the N–C_2H_4 system represented as a function of the reaction time is equal to that in the N–C_2D_4 system, we can estimate the quantity of CH_2 produced in the N–C_2H_4 system. It is shown in Fig. 3. It is impossible, though, to measure the quantity of CH_2N produced in the reaction, because CH_2N has the same *m/e* value as N_2.

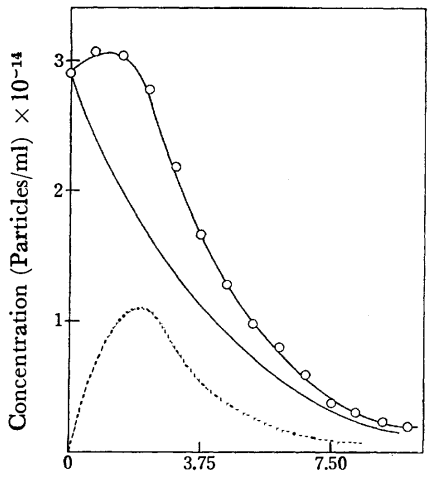

Fig. 3. Kinetics of the reaction of N with C_2H_4.
–○–: *m/e* 14, ——: *m/e* 14 (N),
----: *m/e* 14 (estimated value of CH_2).
Initial concentration
$[N]_0$: 2.90×10^{14} atoms ml^{-1},
$[C_2H_4]_0$: 2.66×10^{14} molecules ml^{-1}.

Comparing these results obtained in the N–C_2H_4 system with those in the N–C_2D_4 system, we can suggest that CH_2 and CH_2N are produced as intermediate compounds in the course of reactions in the N–C_2H_4 system.

In the N–C_2H_4 system, it seems possible that CH_2 and CH_2N might be formed at the beginning of the reaction:

$$N + C_2H_4 \longrightarrow CH_2 + CH_2N \quad (1)$$
$$N + CH_2 \longrightarrow CH_2N \quad (2)$$
$$CH_2N \longrightarrow HCN + H \quad (3)$$
$$N + CH_2N \longrightarrow N_2 + CH_2 \quad (4)$$
$$H + CH_2N \longrightarrow H_2 + HCN \quad (5)$$
$$CH_2 + CH_2 \longrightarrow C_2H_4 \quad (6)$$
$$N + N + M \longrightarrow N_2 + M \quad (7)$$
$$H + H + M \longrightarrow H_2 + M \quad (8)$$
$$CH_2 + \text{wall} \longrightarrow \frac{1}{2}C_2H_4 \quad (9)$$

In the N–C_2D_4 system, the reaction mechanism is almost the same as that considered in the N–C_2H_4 system. The main feature of the mechanism is the competition reaction between N and H for CH_2N in Steps 4 and 5. This competition roughly determines whether N will be detected as HCN or will remain undetected as N_2. An increase in the concentration of H would favor Reaction 5 relative to Reaction 4 and, hence, bring about a decrease in the ΔN/HCN ratio. It is known that the ΔN/HCN ratio approaches unity[1] with the introduction of H into the reactor.

Table 1. Evaluated rate constants in the N–C_2D_4 system (at room temperature)

Step	k ml molecule^{-1} s^{-1}	Step	k ml molecule^{-1} s^{-1}
1	1.0×10^{-13}	6	2.0×10^{-12}
2	5.0×10^{-14}	7	5.0×10^{-16}
3	6.0×10	8	5.0×10^{-16}
4	5.0×10^{-14}	9	3.0×10
5	1.0×10^{-14}		

In the N–C_2D_4 system, the rate constants are evaluated by a computer simulation of the experimental data. The rate constants for the reactions are listed in Table 1. With these values, the quantities of N, CD_2, and CD_2N are calculated as function of the reaction time. The results are shown by dotted lines in Fig. 2. The curves are seen to be identical within the limits of experimental uncertainty.

References

1) J. T. Herron, *J. Phys. Chem.*, **69**, 2736 (1965).
2) a) L. Endrenly and D. J. Le Roy, *J. Phys. Chem.*, **71**, 1334 (1967); b) A. Shepp, *J. Chem. Phys.*, **24**, 939 (1956); c) J. K. Kochi, "Free Radicals," Vol. 1, John Wiley & Sons, New York (1972).
3) a) F. S. Klein and J. T. Herron, *J. Chem. Phys.*, **33**, 1275 (1960); b) E. M. Levy and C. A. Winkler, *Can. J. Chem.*, **40**, 686 (1962).
4) G. B. Kistiakowsky and G. G. Volpi, *J. Chem. Phys.*, **27**, 1141 (1957).

BULLETIN OF THE CHEMICAL SOCIETY OF JAPAN, VOL. 50 (6), 1629—1630 (1977)

Self-Consistent Renormalized RPA: The Electronic Excited States of Benzene in the INDO/S Method

Hirotoshi Ito and Yasumasa J. I'Haya

Department of Materials Science, The University of Electro-Communications, Chofu-shi, Tokyo 182

(Received January 24, 1977)

Synopsis. A self-consistent renormalized RPA and its approximated analogues are compared in the calculation of the electronic excited states of benzene by using the INDO/S method.

In previous papers,[1,2] we have presented an approximate self-consistent renormalized random-phase approximation (SCrRPA) with the CNDO/S method and shown that making use of a well-correlated ground state charge density the rRPA equation can be self-consistently solved though approximately. In this note, we like to present the result of the complete SCrRPA calculation for benzene and compare it with those of the approximate SCrRPA ones. We use the INDO/S basis, since the CNDO method has a deficiency that energy separations between the singlet and triplet levels of both $\sigma\pi^*$ and $\pi\sigma^*$ states are calculated to be zero in high-symmetry molecules like benzene.

For the real basis, the rRPA equation is given by[3,4]

$$\begin{pmatrix} \tilde{A}(S) & -\tilde{B}(S) \\ -\tilde{B}^*(S) & -\tilde{A}^*(S) \end{pmatrix} \begin{pmatrix} \tilde{Y}(\lambda S) \\ \tilde{Z}(\lambda S) \end{pmatrix} = \omega_\lambda \begin{pmatrix} (\tilde{Y}\lambda S) \\ \tilde{Z}(\lambda S) \end{pmatrix}, \quad (1)$$

where

$$\tilde{A}_{\mathrm{ph,vf}}(S) = \delta_{\mathrm{pv}}\delta_{\mathrm{hf}}(E_{\mathrm{p}}-E_{\mathrm{h}}) + (1/2)(\rho_{\mathrm{h}}-\rho_{\mathrm{p}})^{1/2}(\rho_{\mathrm{f}}-\rho_{\mathrm{v}})^{1/2} \times (A^0_{\mathrm{ph,vf}}(S)-\delta_{\mathrm{pv}}\delta_{\mathrm{hf}}(E_{\mathrm{h}}-E_{\mathrm{p}})),$$

$$\tilde{B}_{\mathrm{ph,vf}}(S) = (1/2)(\rho_{\mathrm{h}}-\rho_{\mathrm{p}})^{1/2}(\rho_{\mathrm{f}}-\rho_{\mathrm{v}})^{1/2}B^0_{\mathrm{ph,vf}}(S).$$

A^0 and B^0 are the well-known normal RPA(nRPA) matrices for the HF ground state, E_i the ith HF orbital energy, ρ_i the charge density (non-integral occupation number) of the ith MO in the correlated RPA ground state. Subscripts *ph* and *vf* are used for the particle-hole and vacant-filled MO pair states, respectively. We are interested in the cases except $\rho_{\mathrm{h}}=\rho_{\mathrm{f}}=2$ and $\rho_{\mathrm{p}}=\rho_{\mathrm{v}}=0$ (nRPA), which correspond to a higher RPA and are referred to merely as RPA in the following. The renormalized transition amplitudes matrices $\tilde{\boldsymbol{Y}}$ and $\tilde{\boldsymbol{Z}}$ are given by the unrenormalized ones $\boldsymbol{Y}$ and $\boldsymbol{Z}$.[5] The λth excited state creation operator $O^+_{\lambda SM}$ which satisfies $O^+_{\lambda SM}|0\rangle=|\lambda SM\rangle$ is expanded in terms of the singly excited unrenormalized amplitudes $Y_{\mathrm{ph}}(\lambda S)$ and $Z_{\mathrm{ph}}(\lambda S)$ and the particle-hole pair creation and annihilation operators $C^+_{\mathrm{ph}}(SM)$ and $C_{\mathrm{ph}}(\overline{SM})$. The correlated RPA ground state is unknown before solving Eq. 1 and is assumed to take the form

$$|0\rangle = N_0 e^U|\mathrm{HF}\rangle \quad (2)$$

with

$$U = (1/2)\sum_{S=0,1}\sum_{i}\sum_{\mathrm{ph}\in\Gamma_i}\sum_{\mathrm{vf}\in\Gamma_i} C_{\mathrm{ph,vf}}(S)C^+_{\mathrm{ph}}(S0)C^+_{\mathrm{vf}}(\overline{S0}), \quad (3)$$

$$\Gamma_i \times \Gamma_i \in \Gamma_{\mathrm{HF}},$$

Γ being denote the irreducible representation of a certain set of the excited states under consideration, and N_0 the normalization constant. $C_{\mathrm{ph,vf}}(S)$ in Eq. 3 is then given by a solution of the equation

$$O_{\lambda SM}|0\rangle = 0 \quad (\text{all } \lambda SM), \quad (4)$$

leading to the equation $\boldsymbol{Z}=\boldsymbol{CY}$ and/or $\tilde{\boldsymbol{Z}}=\boldsymbol{C}\tilde{\boldsymbol{Y}}$. Assuming the starting value of $C_{\mathrm{ph,vf}}(S)$ under this constraint, we can determine by an iterative prodecure the occupation number of the ith MO averaged with respect to a trial ground state. Invoking the identity, operator $\times e^U$, we can derive the correlated charge densities of the uth particle and oth hole states averaged according to the correlated RPA ground state as follows;

$$\rho_{\mathrm{u}} = 2^{1/2}\langle 0|C^+_{\mathrm{uu}}(00)|0\rangle = (1/2)\sum_{s}\sum_{\mathrm{h}}\sum_{\mathrm{vf}}|C_{\mathrm{uh,vf}}(S)|^2, \quad (\text{for all } \Gamma_i) \quad (5)$$

and

$$\rho_{\mathrm{o}} = 2^{1/2}\langle 0|C^+_{\mathrm{oo}}(00)|0\rangle = 2-(1/2)\sum_{s}\sum_{\mathrm{p}}\sum_{\mathrm{vf}}|C_{\mathrm{po,vf}}(S)|^2. \quad (\text{for all } \Gamma_i) \quad (6)$$

In order to circumbent the triplet instability at an initial stage, we start a computation by making use of the following trial correlated coefficients of a ground state wavefunction,[6] so as to satisfy the equation $\tilde{\boldsymbol{Z}}=\boldsymbol{C}\tilde{\boldsymbol{Y}}$;

$$C^{\mathrm{trial}}_{\mathrm{ph,vf}}(S) = (E_{\mathrm{p}}+E_{\mathrm{v}}-E_{\mathrm{h}}-E_{\mathrm{f}})^{-1}B^0_{\mathrm{ph,vf}}(S). \quad (7)$$

We can then iteratively determine new renormalized coefficients as[7,8]

$$\boldsymbol{C}^{\mathrm{new}}(S) \approx (\tilde{\boldsymbol{Y}}^{-1}(S)\tilde{\boldsymbol{Z}}(S))^{\mathrm{trial}}. \quad (8)$$

The convergence criterion used is $|\rho_i(\mathrm{new})-\rho_i(\mathrm{old})|\leqq 10^{-5}$ (i for all the MO's).

The summation over i of Γ_i indicates that the excited states of different symmetry groups affect the correlated ground state. Therefore, if possible, it is better to solve such an rRPA equation that all the possible particle-hole pair configurations are involved in a one matrix, without paying attention to a special symmetry representation. At least for the RPA equation of limited particle-hole pairs this may play a considerable role in the computation of ρ's.

In our previous SCF calculation of benzene by the INDO/S method,[9] the ground-state electronic configuration was given by

$$(1a_{1g})^2(2,3e_{1u})^4(4,5e_{2g})^4(6a_{1g})^2(7b_{1u})^2(8b_{2u})^2(9,10e_{1u})^4 (11\pi a_{2u})^2(12,13e_{2g})^4(14\pi,15\pi e_{1g})^4(16\pi,17\pi e_{2u})^0 (18b_{2u})^0(19\pi b_{2g})^0(20,21e_{2g})^0(22a_{1g})^0(23,24e_{1u})^0 (25b_{1u})^0(26,27e_{1u})^0(28,29e_{2g})^0(30a_{1g})^0.$$

From this, we take *thirty* particle-hole pair configuration, in which we promote an electron from *five* MO's below the highest occupied orbital to *six* MO's above the lowest unoccupied orbital. Then, we solve a 60×60 matrix of the rRPA equation involving $\sigma\pi^*$, $\pi\sigma^*$, $\sigma\sigma^*$, and $\pi\pi^*$ particle-hole pairs, iteratively. For comparison,

TABLE 1. EXCITATION ENERGIES (eV) OF BENZENE COMPUTED BY THE RPA EQUATIONS CONSTRUCTED FROM THIRTY SIGMA-PI PARTICLE HOLE PAIRS[a]

State	SCrRPA	rRPA/CI	rRPA/RS	TDA	nRPA	Obsd[c]
$^1B_{2u}(\pi\pi^*)$[b]	5.07	4.97	4.86	4.90	4.76	4.93
$^1B_{1u}(\pi\pi^*)$	5.46	5.36	5.27	5.21	5.18	6.21
$^1E_{1u}(\pi\pi^*)$	6.92 (1.324)[d]	6.84 (1.321)	6.76 (1.316)	7.23 (2.070)	6.68 (1.310)	6.96 (0.690)
$^1A_{2u}(\sigma\pi^*)$	7.97 (0.003)	7.92 (0.003)	7.86 (0.003)	7.82 (0.003)	7.82 (0.003)	
$^1F_{2u}(\pi\sigma^*)$	8.00	7.95	7.89	7.88	7.84	
$^1E_{2u}(\pi\sigma^*)$	8.10	8.05	7.99	7.95	7.95	
$^1A_{1u}(\sigma\pi^*)$	8.17	8.12	8.07	8.02	8.02	
$^1E_{2g}(\pi\pi^*)$	8.20	8.13	8.07	8.15	8.03	
$^3B_{1u}(\pi\pi^*)$	2.90	2.72	2.55	3.04	2.39	3.95
$^3E_{1u}(\pi\pi^*)$	4.58	4.46	4.35	4.26	4.25	4.75
$^3B_{2u}(\pi\pi^*)$	5.07	4.97	4.86	4.90	4.76	5.60
$^3E_{2g}(\pi\pi^*)$	6.33	6.22	6.15	6.11	6.08	6.75
$^3E_{2u}(\pi\sigma^*)$	7.30	7.24	7.18	7.16	7.13	

a) Geometry: C–C 1.40 Å; C–H 1.10 Å. b) Symbols in braces show the main contribution. c) J. Karwowski, *Acta Phys. Pol. A*, **37**, 417 (1970). d) Figures in braces are the values of oscillator strength.

TABLE 2. PURE $\pi\pi^*$ EXCITATION ENERGIES (eV) OF BENZENE, FOR WHICH NINE $\pi\pi^*$ PARTICLE-HOLE PAIR CONFIGURATIONS ARE TAKEN FROM THE INDO/S BASIS MO'S[a]

State	SCrRPA	rRPA/CI	rRPA/RS	TDA	nRPA
$^1B_{2u}$	5.06	4.98	4.85	4.90	4.76
$^1B_{1u}$	5.45	5.37	5.26	5.21	5.18
$^1E_{1u}$	7.07 (1.572)	7.00 (1.565)	6.91 (1.554)	7.44 (2.553)	6.84 (1.545)
$^1E_{2g}$	8.25	8.21	8.13	8.22	8.08
$^1E_{2g}$	10.48	10.44	10.37	10.39	10.33
$^1B_{1u}$	12.82	12.81	12.77	12.79	12.76
$^3B_{1u}$	2.88	2.74	2.53	3.04	2.39
$^3E_{1u}$	4.56	4.47	4.34	4.26	4.25
$^3B_{2u}$	5.06	4.98	4.85	4.90	4.76
$^3E_{2g}$	6.32	6.26	6.15	6.12	6.08
$^3E_{2g}$	10.07	10.03	9.96	9.92	9.92
$^3B_{1u}$	12.42	12.41	12.37	12.36	12.36

a) See the footnotes of Table 1.

we calculate pure $\pi\pi^*$ excitations taking nine $\pi\pi^*$ particle-hole pair configurations.

Without solving Eq. 1 iteratively, the coefficients $C_{\mathrm{ph,vf}}(S)$ can be approximately determined either (i) by using the perturbation theory in the CI language to include doubly excited configurations which mix with the HF ground state (referred to as rRPA/CI), or (ii) by relating $C_{\mathrm{ph.vf}}(S)$ with $B^0_{\mathrm{ph.vf}}(S)$ matrix in the basis of Rayleigh-Schrödinger perturbation theory (Eq. 7) (as rRPA/RS). With the trial RPA ground state to be obtained in such ways, we can bypass the problem of solving Eq. 4, in case when the trial coefficients satisfy Eq. 4 approximately. These methods have been called an approximate SCrRPA in our previous paper.[5]

The numerical results are summarized in Tables 1 and 2. The SCrRPA results satisfactorily agree with the experimental values except for the lowest $^3B_{1u}$ state. The self-consistency has been attained after nine iterations. It should be mentioned that we have fixed the correlated charge densities as $\rho(\mathrm{new}')=(1/2)\times\{\rho(\mathrm{new})+\rho(\mathrm{old})\}$ at every iterative step in order to get a quick convergence. It is observed that the following relationship holds for most cases:

$$\omega(\mathrm{rRPA}) > \omega(\mathrm{TDA}) > \omega(\mathrm{nRPA}) \quad (9)$$

or in more detail

$$\omega(\mathrm{SCrRPA}) > \omega(\mathrm{rRPA/CI}) > \omega(\mathrm{rRPA/RS}) > \omega(\mathrm{TDA}) > \omega(\mathrm{nRPA}). \quad (10)$$

The $^1E_{1u}$ and $^3B_{1u}$ transition energies fall out of this sequence, for which $\omega(\mathrm{TDA})>\omega(\mathrm{SCrRPA})$. It has been numerically ascertained that this sequence also holds for the electronic excited states of DNA bases in the CNDO/S method.[5] The treatment including σ electrons (Table 1) gives rise to the considerable lowering of the transition energy and oscillator strength of the dipole-allowed $^1E_{1u}$ transition, compared with that of the π electrons only (Table 2). This can be ascribed to the sigma-pi coupling; *i.e.*, the so-called dynamical screening effect of the $\pi\pi^*$ transition by σ electrons which has been pointed out previously by several authors.[10,11]

The sequence of Eq. 10 and Table 1 indicates that rRPA/CI promises to give a good approximation to SCrRPA, and that the correlated ground-state wavefunction (HF+doubly excited CI's) takes in the triplet correlation effect through $B^0_{\mathrm{ph.vf}}(S)$ matrix elements in a somewhat skillful way. It might also be concluded that to solve the nRPA equation with a partinent choice of parameters in the semiempirical MO methods rivals a higher RPA, fully accounting the correlation effect in large conjugated systems. This can also be visualized in a Green's function language; *i.e.*, the use of the CNDO/S and/or INDO/S parametrization together with nRPA has a drastic effect upon the self-energy part, leaving the zero-order polarization propagator unaffected.[12]

Comparison of the present semiempirical results with the *ab initio* ones computed by Rose *et al.*[10] suggests that if the present restricted configurational space is extended the lowest $^3B_{1u}$ state will be refined. This possibility can be observed from the inspection of Tables 1 and 2, where the sigma-pi coupling effect puts the lowest $^3B_{1u}$ state a little bit up. Extensive calculation including a larger particle-hole pair space is now in progress.

References

1) O. Matsuoka and H. Ito, *Theor. Chim. Acta*, **39**, 111 (1975).
2) H. Ito and Y. J. I'Haya, *Chem. Phys. Lett.*, **38**, 271 (1976).
3) D. J. Rowe, *Rev. Mod. Phys.*, **40**, 153 (1968).
4) J. Simons, *J. Chem. Phys.*, **55**, 1218 (1971).
5) H. Ito and Y. J. I'Haya, *Bull. Chem. Soc. Jpn.*, **49**, 3466 (1976).
6) T. Shibuya and V. McKoy, *J. Chem. Phys.*, **54**, 1738 (1971).
7) E. A. Sanderson, *Phys. Lett.*, **19**, 141 (1965).
8) J. da Providência, *Phys. Lett.*, **21**, 668 (1966).
9) H. Ito and Y. J. I'Haya, *Bull. Chem. Soc. Jpn.*, **49**, 940 (1976).
10) J. B. Rose, T. Shibuya, and V. McKoy, *J. Chem. Phys.*, **60**, 2700 (1974).
11) T. Shibuya, Y. J. I'Haya, and V. McKoy, *Intern. J. Quantum Chem.*, **9**, 505 (1975).
12) Y. J. I'Haya, S. Narita, K. Yamaguchi, and M. Nakayama, *Prog. Theor. Phys.*, **55**, 1685 (1976).

BULLETIN OF THE CHEMICAL SOCIETY OF JAPAN, VOL. 50 (6), 1631—1632 (1977)

The Behavior of Aerosol OT in Organic Solvents

Masaharu UENO and Hiroshi KISHIMOTO

Faculty of Pharmaceutical Sciences, Nagoya City University, Tanabe-dori, Mizuho-ku, Nagoya 467

(Received January 28, 1977)

Synopsis. The parameters concerning the micelle formation of Aerosol OT in organic solvents were determined. In order to determine CMC, an apparatus was constructed for the measurement of the interfacial tension between mercury and organic media. The association numbers were estimated by vapor pressure depression measurements.

The behavior of oil-soluble surfactants in organic solvents has been studied from the stand-point of micelle formation,[1,2] but more data are needed for its elucidation as compared with the behavior of surfactants in water. We have carried out the following experiments on Aerosol OT (sodium 1,2-bis(2-ethylhexyloxycarbonyl)ethane-1-sulfonate, American Cyanamid Co., Ltd.) in benzene, cyclohexane, and carbon tetrachloride. In order to determine CMC, a new method and apparatus based on interfacial tension measurement between mercury and organic media were devised. The number average association numbers were estimated by vapor pressure depression measurements.

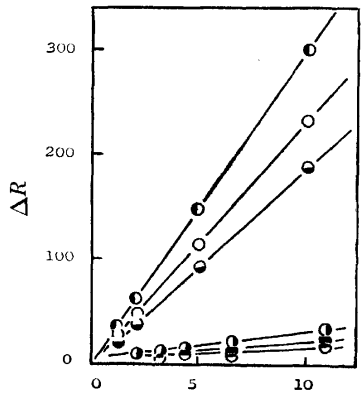

Fig. 1. Thermister bridge reading (ΔR) *vs.* solute concentration in benzene.
◑: Aerosol OT as solute at 25 °C.
●: Aerosol OT as solute at 37 °C.
◓: Aerosol OT as solute at 45 °C.
◐: Triphehylmethane as solute at 25 °C.
○: Triphenylmethane as solute at 37 °C.
◒: Triphenylmethane as solute at 45 °C.

(1) Vapor Pressure Depression Measurement: For this a molecular weight apparatus (Hitachi-Perkin-Elmer, Type 115) was used. The thermister bridge reading, ΔR, which depends only on the vapor pressure, is plotted against the solute concentration in benzene in Fig. 1. The results for other solvents are similar to those shown in Fig. 1. In each measurement, triphenylmethane was used as a standard substance for calibration. The relationship of thermister bridge reading, ΔR, *vs.* solute concentration in benzene was linear above 1×10^{-3} mol kg^{-1}. As the ratio of the slope for Aerosol OT to that for reference, the number average association number was estimated to be 13. The values in other solvents are summarized in Table 1. The temperatue dependence of association numbers was small.

Table 1. CMC and association number (N) of Aerosol OT in organic solvents

		CMC (mol kg^{-1})	N
CCl_4	25 °C	1×10^{-4}	17
	30 °C	1.5×10^{-4}	17
	37 °C	2.5×10^{-4}	17
	45 °C		17
C_6H_6	25 °C		13
	37 °C	4×10^{-4}	13
	45 °C		13
C_6H_{12}	25 °C		17
	37 °C	5×10^{-4}	17
	45 °C		17

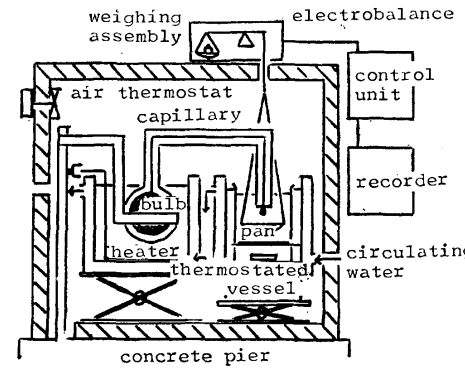

Fig. 2. The apparatus for the interfacial tension measurement between mercury and organic media.

(2) Interfacial Tension Measurements between Mercury and Organic Media: The measurements were carried out by the drop weight method. The apparatus is shown in Fig. 2. In order to drop mercury without vibration, the thermal expansion of mercury was employed according to the method of Sonntag and Strenge.[3] The bulb is heated just a little for the mercury to expand and fall into the platinum pan after a long interval. The weight of falling mercury drop in the organic media containing various amounts of Aerosol OT was measured *in situ* with the accuracy of $\pm 10^{-5}$ g by means of the load added to the electrobalance (Cahn RG Electrobalance, Cahn Instrument Co., Ltd.) holding the pan. The interfacial tension was calculated according to the method of Harkins and Brown.[4] The radius of the tip (0.045 cm) was obtained by calculation using the data[5] between mercury and

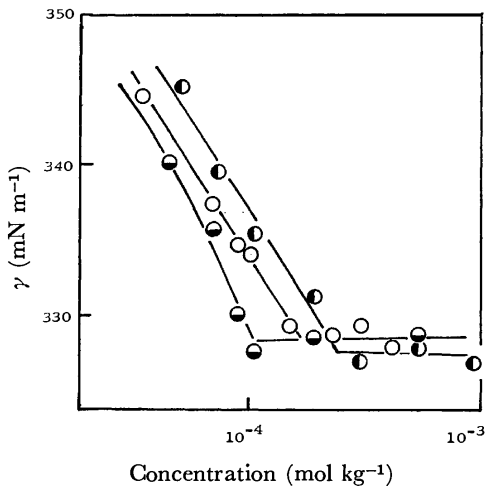

Fig. 3. Interfacial tension between mercury and carbon tetrachloride *vs.* solute concentration in logarithmic scale.
◒: at 25°C. ○: at 30°C. ◐: at 37°C.

benzene. As shown in Fig. 3, the plots of interfacial tension between mercury and carbon tetrachloride solution show a behavior similar to that of the surface or interfacial tension of aqueous solution of surfactant near CMC. From the equation of adsorption isotherm (Eq. 1), surface (or interfacial) tension against solute concentration in logarithmic scale breaks when the relationship between activity and concentration of surface active solute has a breaking point or CMC.

$$-d\gamma = RT\Gamma d \ln a_1 \quad (1)$$

Since the depression (Fig. 3) indicates the surface activity of solute to mercury/organic medium interface and relatively large association numbers were obtained (Table 1), we identified the breaking points in Fig. 3 as the CMC of Aerosol OT in carbon tetrachloride, also given in Table 1 with those in benzene and cyclohexane.

References

1) C. R. Singleterry, *J. Am. Oil Chem. Soc.*, **32**, 446 (1955).
2) A. Kitahara, *Kogyo Kagaku Zasshi*, **68**, 2019 (1965).
3) H. Sonntag and K. Strenge, *J. Colloid Sci.*, **32**, 159 (1970).
4) W. D. Harkins and F. E. Brown, *J. Am. Chem. Soc.*, **41**, 499 (1919).
5) F. M. Fowkes, *J. Phys. Chem.*, **67**, 2538 (1963).

BULLETIN OF THE CHEMICAL SOCIETY OF JAPAN, VOL. 50 (6), 1633—1634 (1977)

The Microwave Spectra, Molecular Structures, and Quadrupole Coupling Constants of Methyltrichlorosilane and Trichlorosilane

Harutoshi TAKEO and Chi MATSUMURA

National Chemical Laboratory for Industry, Honmachi-1, Shibuya-ku, Tokyo 151

(Received January 31, 1977)

Synopsis. The microwave spectrum of methyltrichlorosilane has been re-examined in order to determine the precise molecular structure by observing the spectra due to the isotopic species. The previously reported value of the nuclear quadrupole coupling constant of trichlorosilane has been corrected by the reinvestigation of the hyperfine structure.

The microwave spectra of methyltrichlorosilane and its isotopic species have been investigated first by Mockler *et al.*[1] and recently by Mitzlaff *et al.*[2] In both cases, the spectrum arising from the silicon isotopic species has not been observed, and therefore the precise molecular structure has not been determined. We reinvestigated the microwave spectrum of this molecule in order to obtain the spectrum of the silicon isotopic species, and succeeded in observing it. Furthermore, we found the spectrum of the ^{13}C species at frequencies different from the previously reported values. In their paper[2] Mitzlaff *et al.* have also reported the quadrupole coupling constant of trichlorosilane. Their value, however, seemed too small compared with that of chlorosilane. We reinvestigated the spectrum of this molecule and corrected their value. In this paper we report the newly determined molecular constants and the precise molecular structures of methyltrichlorosilane and trichlorosilane.

Methyltrichlorosilane. The spectra were examined with a conventional 100 kHz Stark-modulation spectrometer, with a 3-m X-band waveguide cell. Both ^{29}Si and ^{13}C species were measured in natural abundances. To obtain the spectrum due to the ^{29}Si species, the regions near the high-J transitions of normal species were searched, because the low-J transitions have fairly broad linewidths and low intensities. Very low modulation voltages (*ca.* 10 V/cm) were used to prevent disturbances by the Stark lobes of the normal species and its strong excited states. The transitions of the ^{29}Si species were assigned on the basis of the intensity ratio to the lines of normal species, and the assignment was confirmed by the measurement of the intensity change between room and Dry Ice temperatures. Unfortunately, the line due to the ^{30}Si species could not be obtained, since the predicted positions were overlapped by the strong vibrational satellites. The observed transition frequencies are listed in Table 1. For the precise determination of the rotational constants, several transitions of normal species including low-J transitions were also measured. Since the observed peak positions differ from the hypothetical unsplit values because of the hyperfine structure due to the chlorine nuclei, the observed peak values were corrected to unsplit values[3] using the calculated frequency differences on the assumptions of $eqQ=-40$ MHz and $\angle ClSiCl=108.6°$. The rotational constant and the centrifugal distortion constant, D_J, were obtained by a least-squares fit of all the corrected transition frequencies in Table 1. The rotational constant of the ^{29}Si species listed in the table was determined from the high-J transitions, assuming the same D_J value.

The obtained rotational constants lead to the C–Si bond distance of 1.865 Å by the use of Kraitchman's equation, if the previously reported rotational constant of ^{13}C species[2] is included. This C–Si distance, which is close to that of methylsilane (1.867 Å), seemed too long considering that the substitution of the hydrogen atoms by the halogen atoms should cause a fairly large bong shortening;[4] in fact the C–Si distance in CH_3SiF_3 is 1.812 Å. Therefore, a reinvestigation of the spectrum of the ^{13}C species was undertaken. We tried to observe a few high-J transitions of the ^{13}C species, but we could not find them at the frequencies calculated from the B value reported in Ref. 2 except for the $J=9\leftarrow8$ transition, which is the only transition observed by Mitzlaff *et al.* Furthermore, the intensity measurements at room and Dry Ice temperatures showed that it was impossible that this transition belongs to the ground state line. Presumably it is to be ascribed to one of the excited vibrational states of the $^{35}Cl_2{}^{37}Cl$ species, since this region is near to its ground state transitions. We found several lines which should be ascribed to the spectrum of the ^{13}C species at slightly lower frequencies, as calculated from the reported value. The assignment was confirmed by a comparison of the intensities with those of the ^{29}Si species and by the change in the intensities between room and Dry Ice temperatures. The molecular structure, except for the methyl group, was determined by the substitution method, as Table 1 shows. The coordinates of the chlorine atoms were obtained by combining the A and B rotational constants of $^{35}Cl_2{}^{37}Cl$ species and the B rotational constants of the $^{35}Cl_3$ and $^{37}Cl_3$ species with a modification of Kraitchman's equation.[5] The obtained Si–C bond distance shows a clear bond shortening upon the substitution of chlorine atoms for hydrogen atoms attached to the silicon. The amount of the shortening is about a half of that by fluorine substitution, as has been estimated from the results for other molecules.[6]

Trichlorosilane. Mitzlaff *et al.* have also investigated the microwave spectrum of trichlorosilane. They have reported the eQV_{zz} to be +12.8 MHz, which was obtained from the measurement of the two strong lines in the $J=2\leftarrow1$ transition on the basis of the theory presented by Wolfe.[7] This theory, however, was found to be incorrect and was amended by Wolf *et al.* recently.[3] If we analyze the reported frequencies by means of the new theory, the eQV_{zz} of trichlorosilane becomes 8

TABLE 1. THE OBSERVED AND CALCULATED FREQUENCIES, ROTATIONAL PARAMETERS, AND MOLECULAR STRUCTURES OF TRICHLOROMETHYLSILANE AND TRICHLOROSILANE (MHz)

CH_3SiCl_3		$^{12}CH_3{}^{28}Si^{35}Cl_3$			$CH_3{}^{29}SiCl_3$	$^{13}CH_3SiCl_3$
J'	J	Obsd	Corr[a]	Obsd − Calcd		
4	3	14157.85	14158.32	0.01		
5	4	17697.54	17697.81	−0.03		
6	5	21237.05	21237.23	−0.09		
7	6	24776.70	24776.82	0.02		
8	7	28316.24	28316.33	0.11		
9	8	31855.67	b	0.09		31350.10
10	9	35394.13	b	0.03	35383.51	34832.78
11	10	38934.13	b	0.00		38315.98
12	11					41798.92
13	12	46012.36	b	−0.05		45281.90
14	13	49551.38	b	−0.04	49535.46	48764.91
B		1769.797			1769.228	1741.700
D_J		0.00026				
		r_s(Si–Cl) = 2.026 Å		∠Cl–Si–Cl = 108.6°		
		r_s(Si–C) = 1.848 Å		∠C–Si–Cl = 110.3°		

$SiHCl_3$		$HSi^{35}Cl_3$			$HSi^{37}Cl_3$	$H^{29}SiCl_3$
J'	J	Obsd	Corr[a]	Obsd − Calcd		
2	1	9888.07[c] 9890.19[c]	9889.89	−0.03		
3	2	14833.95	14834.84	0.02		
4	3	19779.23	19779.68	0.01		
5	4	24724.22	24724.49	0.06		
6	5	29668.86	29669.03	−0.06		
7	6	34613.57	34613.69	0.05	32845.83	34568.78
8	7	39558.00	b	−0.03	37537.65	39506.68
B		2472.468			2346.213	2469.279
D_J		0.00085				
eQq		−37.0				
		r_s(Si–H) = 1.464 Å		∠Cl–Si–Cl = 109.4°		
		r_s(Si–Cl) = 2.020 Å		∠H–Si–Cl = 109.5°		

a) The corrected frequencies considering the shift resulting from the nuclear quadrupole interaction. b) The correction was neglected. c) $K=1$ component.

MHz; this leads to −25 MHz of eQV_{aa}, by assuming ∠ClSiCl = 109.6°. This eQV_{aa} seemed too small compared with the eQq of −40 MHz in SiH_3Cl. Therefore, we reinvestigated the hyperfine structure of trichlorosilane.

The $J=2\leftarrow1$ transition was measured carefully and repeatedly, and two strong components were found at the values calculated from the high-J transitions and a reasonable eQV_{aa} value. We did not find strong lines at the frequencies reported by Mitzlaff *et al.* From these two components, the eQV_{zz} is determined to be 12 MHz, which leads to an eQV_{aa} value of −37 MHz. This value is quite reasonable as the quadrupole coupling constant of the chlorine atom attached to silicon. The rotational constants obtained by Mitzlaff *et al.* were also refined using the quadrupole coupling constant newly determined by the method used for the analysis of methyltrichlorosilane; they were determined to be as listed in the table. The molecular structure was also recalculated with these rotational constants by means of the substitution method. However, the change in the molecular structure is small, since the changes in the rotational constants are very small.

References

1) R. C. Mockler, J. H. Bailey, and W. Gordy, *J. Chem. Phys.*, **21**, 1710 (1953).
2) M. Mitzlaff, R. Holm, and H. Hartmann, *Z. Naturforsch.*, **22a**, 1415 (1967).
3) A. A. Wolf, Q. Williams, and T. L. Weatherly, *J. Chem. Phys.*, **47**, 5101 (1967).
4) J. R. Durig, Y. S. Li, and C. C. Tong, *J. Mol. Struct.*, **14**, 225 (1972).
5) Y. S. Li, M. M. Chen, and J. R. Durig, *J. Mol. Struct.*, **14**, 261 (1972).
6) D. R. Lide, Jr., *J. Am. Chem. Soc.*, **74**, 3548 (1952).
7) P. N. Wolfe, *J. Chem. Phys.*, **25**, 976 (1956).

BULLETIN OF THE CHEMICAL SOCIETY OF JAPAN, VOL. 50 (6), 1635—1636 (1977)

The Coercive Force of γ-Fe_2O_3 Prepared from γ-FeOOH

Shuichi HAMADA and Kenshi KUMA

Department of Chemistry, Faculty of Science, Science University of Tokyo, Kagurazaka, Shinjuku-ku, Tokyo 162

(Received October 22, 1976)

Synopsis. The γ-Fe_2O_3 with a high coercive force was prepared by reducing the acicular γ-FeOOH at 300 °C and by then reoxidizing it at 250 °C. A conversion from γ-FeOOH to γ-Fe_2O_3 at lower temperatures was effective in obtaining acicular particles without pores because of the large mobilities of ions in the crystal.

The γ-Fe_2O_3 with a high coercive force has usually been prepared from the acicular α-FeOOH through complex processes: dehydration, reduction, and reoxidation, especially by the heat treatment of the α-Fe_2O_3 before the reduction.[1] These three processes were also effective in obtaining the γ-Fe_2O_3 with a high coercive force when the γ-FeOOH was used as the starting material, while the γ-Fe_2O_3 obtained by only the dehydration of the γ-FeOOH exhibited a very low coercive force. In this work, the effect of this heat treatment on the coercive force was examined for the γ-FeOOH.

Experimental

Two kinds of γ-FeOOH were prepared as the starting materials by the method described in a previous paper.[2] Three kinds of α-FeOOH were also prepared by the method reported by Nakajima *et al.*[1] in order to compare them with the γ-FeOOH as follows: a solution of iron(II) chloride or sulfate was made alkaline (pH 13.1—13.7) after the dissolved oxygen had been removed, and then the iron(II) ions were oxidized at 45 °C by bubbling air at the flow rate of 2.5 l/min, while the pH value of the reaction mixture was not controlled. The preparative conditions are shown as follows:

Sample No.	Product	Initial concn mol/l	pH	Temp °C
L-1	γ-FeOOH	0.064 ($FeCl_2$)	6.5	25
L-2	γ-FeOOH	0.096 ($FeCl_2$)	6.5	25
G-1	α-FeOOH	0.064 ($FeCl_2$)	13.7→12.8	45
G-2	α-FeOOH	0.064 ($FeSO_4$)	13.5→12.5	45
G-3	α-FeOOH	0.257 ($FeCl_2$)	13.1→12.2	45

These iron(III) hydroxide oxides were then converted to γ-Fe_2O_3 in the following manners:

Process 1.

$$\left.\begin{matrix}\gamma\text{-FeOOH}\\ \alpha\text{-FeOOH}\end{matrix}\right\} \xrightarrow[440\text{—}800\text{°C (60 min)}]{\text{Heat treatment, in air}} \alpha\text{-}Fe_2O_3$$

$$\xrightarrow[360\text{°C (30 min)}]{\text{Reduction in } H_2} Fe_3O_4 \xrightarrow[250\text{°C (30 min)}]{\text{Reoxidation in air}} \gamma\text{-}Fe_2O_3$$

Process 2.

$$\left.\begin{matrix}\gamma\text{-FeOOH}\\ \alpha\text{-FeOOH}\end{matrix}\right\} \xrightarrow[300\text{—}340\text{°C (30 min)}]{\text{Dehydration and reduction in } H_2}$$

$$Fe_3O_4 \xrightarrow[250\text{°C (30 min)}]{\text{Reoxidation in air}} \gamma\text{-}Fe_2O_3$$

The coercive force, ${}_BH_C$ (maximum applied field; H_m= 2 KOe), of the γ-Fe_2O_3 was measured at 25 °C at the packing density of 0.1 with an automatic B-H curve tracer, model BHH-5, from the Riken Denshi Co.; the packing density, p, was expressed as follows: $p=d/d_0$, where d is the apparent density of a cylindrical specimen, and d_0, the intrinsic density of γ-Fe_2O_3 (5.24 g/cm³).[3]

The particles were observed at magnifications of from 24000 to 36000 times with an electron microscope, model HU-200F, from Hitachi Seisakusho.

The crystallite sizes of the heat-treated α-Fe_2O_3 were estimated by the Scherrer method[4] at the directions of [012], [104], [110], and [113] by using Fe$K\alpha$ radiation.

Results and Discussion

Figure 1 shows the relationships between the coercive force of the γ-Fe_2O_3 and the reduction temperature in Process 2 or the heat-treatment temperature in Process 1. The γ-Fe_2O_3 was found to exhibit sufficiently high coercive forces when the samples were prepared from the γ-FeOOH by Process 2 at the reduction temperature of 300 °C. The γ-FeOOH was not reduced completely into the Fe_3O_4 below 300 °C. The coercive force, however, was lowered abruptly with the rise in the reduction temperature in Process 2 and in the heat-treatment temperature in Process 1. On the contrary, a remarkable effect on the coercive force was observed by heat treatment at 600 or 700 °C in Process 1 when the α-FeOOH was used as the starting material. This effect has previously been reported by Nakajima *et al.*[1]

The DTA pattern of the γ-FeOOH showed an endothermic peak near 270 °C based on the dehydration of structural water and an exothermic peak near 440 °C based on the transformation to α-Fe_2O_3 from γ-Fe_2O_3.

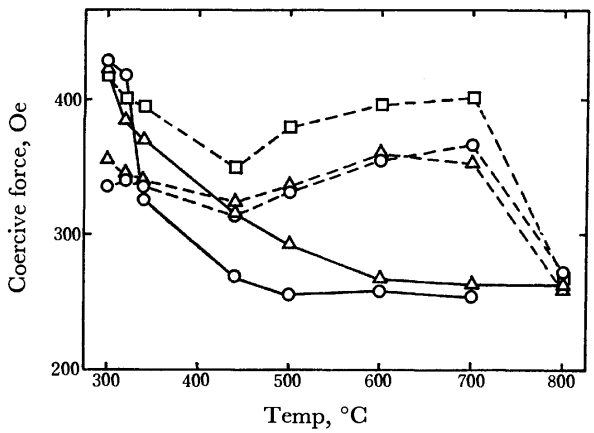

Fig. 1. Relationships between coercive force of γ-Fe_2O_3 and reduction or heat-treatment temperature.
—○—: L-1, —△—: L-2, ---○---: G-1, ---△---: G-2, ---□---: G-3.

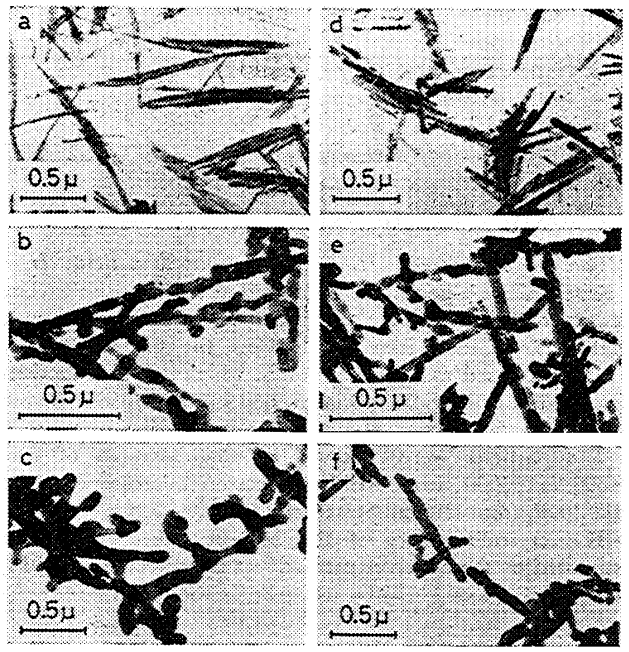

Fig. 2. Particles of γ-, α-FeOOH and γ-Fe_2O_3.
a: γ-FeOOH(L-1), b: γ-Fe_2O_3, reduced L-1 at 300°C in Process 2, c: γ-Fe_2O_3, heat-treated L-1 at 600°C in Process 1, d: α-FeOOH(G-1), e: γ-Fe_2O_3 reduced G-1 at 300°C in Process 2, f: γ-Fe_2O_3, heat-treated G-1 at 600°C in Process 1.

Figures 2a and 2d show the original γ- and α-FeOOH particles with acicular shapes. When the γ-Fe_2O_3 was obtained only by the dehydration at 300 °C, countless number of fine pores were observed, while the particles kept the original shapes of the γ-FeOOH. This γ-Fe_2O_3 exhibited very low values of the coercive force, 126 and 129 Oe.

Figure 2b shows the γ-Fe_2O_3 particles obtained from the γ-FeOOH by Process 2. Few pores were observed in the particles thus prepared, while the shapes were deformed in some degree compared with the original ones. Much deformation and sintering were, however, observed among the particles prepared by the heat treatment at 600 °C in Process 1, as is shown in Fig. 2c. On the contrary, several pores were observed in the particles, though there was less deformation, when the γ-Fe_2O_3 was prepared from the α-FeOOH by Process 2, as is shown in Fig. 2e. The pores, however, were scarcely detectable by heat treatment, especially at 600 or 700 °C, in Process 1, as is shown in Fig. 2f. Remarkable deformation and sintering among the particles were observed by heat treatment at 800 °C, even when the α-FeOOH was used as the starting material as well as the γ-FeOOH.

In the acicular particles of γ-Fe_2O_3 with a single domain size,[5] the shape anisotropy is well known to dominate their coercive force; $H_c=(1/2)\Delta N \cdot M_s$ in random-oriented powders,[6] where ΔN is the difference between the demagnetizing factors along the minor and major axes of the acicular particles, which can take 2π as the maximum value in the CGS-Gauss unit system,

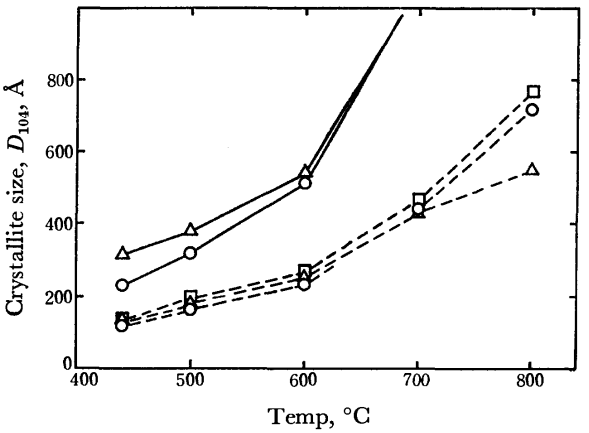

Fig. 3. Plots of crystallite size, D_{104}, of α-Fe_2O_3 against heat-treatment temperature.
—○—: L-1, —△—: L-2, ---○---: G-1, ---△---: G-2, ---□---: G-3.

and M_s, the saturation magnetization. Therefore, the coercive force depends mainly on the acicularity of the particles. On the other hand, the existence of pores in the particles lowers the coercive force.[5] The coercive force of the γ-Fe_2O_3 varies reasonably according to the degree of deformation and the existence of the pores, as Figs. 1 and 2 show.

The crystallite size, D_{104}, for [104] of the α-Fe_2O_3, the intermediate in Process 1, grew as the heat-treatment temperature increased, as is shown in Fig. 3. The crystallite of the α-Fe_2O_3 obtained from the γ-FeOOH grew much extensively than that obtained from the α-FeOOH. Similar tendencies were confirmed for the other directions of the α-Fe_2O_3 lattice. Such a clear difference between them is considered to be due not to the absorbed Cl^- ions, but to the difference in the structural arrays of ions in the iron(III) hydroxide oxides, judging from the corresponding results between the G-1 and G-2 samples. This fact indicates that the ions in the lattice moved easily when the α-Fe_2O_3 was obtained from the γ-FeOOH. It can be considered that the large mobilities of ions in the lattice carry a positive effect which serves to abolish the pores, but also a negative effect which serves to keep the acicularity of the particles, when the γ-FeOOH is converted into the γ-Fe_2O_3.

References

1) T. Nakajima and S. Ogawa, *Trans. IECE Jpn.*, **56-C**, 99 (1973).
2) S. Hamada and K. Kuma, *Bull. Chem. Soc. Jpn.*, **49**, 3695 (1976).
3) G. Bate and J. K. Alstad, *IEEE Trans. Mag.*, **Mag-5**, 821 (1969).
4) R. C. Rau, "Advances in X-Ray Analysis," Vol. 5, ed by W. Mueller, Plenum Press, New York (1961), p. 104.
5) A. H. Morrish and S. P. Yu, *J. Appl. Phys.*, **26**, 1049 (1955).
6) E. C. Stoner and E. P. Wohlfarth, *Phil. Trans. Roy. Soc. London*, **A-240**, 599 (1965).

BULLETIN OF THE CHEMICAL SOCIETY OF JAPAN, VOL. 50 (6), 1637—1638 (1977)

Preparation and the Acid Hydrolysis of *N*-(2-Hydroxyethyl)ethylenediamine-*N*,*N*′,*N*′-triacetate Complex of Di-μ-oxo-bis(oxomolybdenum(V))

Yoichi SASAKI and Tomoji S. MORITA

Chemistry Department, Faculty of Science, Tohoku University, Aoba, Aramaki, Sendai 980

(Received October 30, 1976)

Synopsis. A hedta (H_3hedta = *N*-(2-hydroxyethyl)-ethylenediamine-*N*,*N*′,*N*′-triacetic acid) complex of molybdenum(V), Mo_2O_4(hedta)$(H_2O)^-$, has been prepared and characterized. The rate of acid hydrolysis of this complex in an aqueous perchloric acid solution ($[H^+]=0.5$—2.0 mol dm^{-3}; $I=2.0$) is of similar magnitude to that of $Mo_2O_4(edta)^{2-}$ (H_4edta = ethylenediaminetetraacetic acid), increasing with increase in $[H^+]$.

A dimeric unit, $Mo_2O_4^{2+}$, di-μ-oxo-bis(oxomolybdenum(V)) is common in molybdenum(V) chemistry in aqueous media. The ligand substitution reactions on the $Mo_2O_4^{2+}$ center have been studied with various ligands such as $edta^{4-}$,[1] ida^{2-} (H_2ida = iminodiacetic acid),[2] $C_2O_4^{2-}$,[2] and NCS^-.[3] The results show that the rate of substitution reactions on the $Mo_2O_4^{2+}$ center varies remarkably with ligand, spanning six orders of magnitude. The number of ligating atoms of a ligand, and/or the location on the oxo metal moiety at which substitution occurs (*cis* or *trans* to oxo ligand) would be important factors controlling the substitution rate. In order to obtain further information on the substitution reactions on the $Mo_2O_4^{2+}$ center, we used $hedta^{3-}$ as a ligand, the structure of which is similar to that of $edta^{4-}$.

Experimental

Material. *Sodium Salt of Aqua*[N-*(2-hydroxyethyl)ethylenediamine*-N,N′,N′-*triacetato*]-*di*-μ-*oxo*-*bis*(*oxomolybdate(V)*) *Complex*, *Na*[Mo_2O_4(*hedta*)(H_2O)]·$2H_2O$: Nine grams of dipyridinium pentachlorooxomolybdate(V), $(pyH)_2[MoOCl_5]$,[4] and 2.8 g of H_3hedta were dissolved in 100 cm^3 of water. The solution was warmed at 90 °C for about 3 h with constant stirring, and then cooled to room temperature. To this solution were added 5 g of $NaClO_4$ and then 100 cm^3 of ethanol, and the solution was kept in a refrigerator for a day. Orange crystals were filtered off, washed with ethanol, and dried in air. They were recrystallized from water. Found: C, 19.53; H, 3.62; N, 4.74; Mo, 31.15%. Calcd for $C_{10}H_{21}N_2O_{11}NaMo_2$: C, 19.75; H, 3.48; N, 4.61; Mo, 31.55%.

Measurements. Ultraviolet and visible absorption spectra were recorded with a Hitachi 323 spectrophotometer. For kinetic studies, a Hitachi 124 spectrophotometer with a Hitachi recorder QPD-34 was used. The acid dissociation constant of the complex was determined by pH titration with a pH-meter E300B of Metrohm Herisau. The meter was standardized against perchloric acid solutions in 2 M $LiClO_4$ (M = mol dm^{-3}) so that H^+ concentration rather than activity was measured. Thermal decomposition curves of the complexes were obtained with a Shinku Riko TGD-3000 differential thermal microbalance with a heating rate of 10 K/min.

Kinetic Runs. All the solutions used for kinetic runs were prethermostatted at a given temperature for at least 20 min. A solution of the complex was mixed with a perchloric acid solution for starting the kinetic run. The solutions contained appropriate amounts of lithium perchlorate to adjust ionic strength. The change of absorbance was followed at a fixed wavelength (mostly at 295 nm). Rate constants were evaluated from the first-order plots of absorbance changes. Since the aqua ion of molybdenum(V), $Mo_2O_4(aq)^{2+}$,[5] undergoes slow oxidation by oxygen,[1] some runs were carried out under a nitrogen atmosphere.

Results and Discussion

It was suggested that the two peaks at *ca.* 300 nm ($\varepsilon = 3000$—10000 l mol^{-1} cm^{-1} per dimer) and at *ca.* 390 nm (100—400) are characteristic of complexes containing the dimeric unit, $Mo_2O_4^{2+}$.[2,6] The present complex has two peaks in these two regions, indicating the presence of $Mo_2O_4^{2+}$ group. The complex liberates two water molecules at 20—90 °C and one at 100—140 °C. We assigned the former to the water of crystallization and the latter to the coordinated water. This was supported by the patterns of thermal decomposition of other molybdenum(V) complexes, $Ba[Mo_2O_4(C_2O_4)_2(H_2O)_2]\cdot 3H_2O$ (liberate three water molecules at 20—100 °C and two at 140—180 °C)[7] and $Na[Mo_2O_4(edta)]$ (no weight loss up to 370 °C). On the basis of these findings, the structure of the present complex is considered as follows.

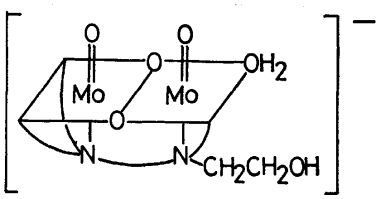

The pH of an aqueous solution of the hedta complex (*ca.* 5×10^{-3} mol dm^{-3}) is *ca.* 2. The solution was titrate with 0.1 M sodium hydroxide. There was one sharp break for one equivalent sodium hydroxide to the complex, no further inflection being observed up to pH = 11. The sharp break would be associated with the deprotonation of the coordinated water as follows.

$$\underset{\text{(aqua form)}}{Mo_2O_4(hedta)(H_2O)^-} \overset{K_a}{\rightleftharpoons} \underset{\text{(hydroxo form)}}{Mo_2O_4(hedta)(OH)^{2-}} + H^+ \qquad (1)$$

The pK_a value for this process was estimated from the pH titration curve; 3.02 ± 0.03 at 25 °C and $I=2.0$ M. The absorption spectrum of the aqua complex was measured in 0.1 M perchloric acid in the presence of the ligand added in order to avoid dissociation of the ligand from the complex. The spectrum of the hydroxo

complex was measured in an acetate buffer at pH 5. Peak positions (and intensities) are 383 nm (ε=300) and 295 nm (9200) for the aqua complex, and 393 nm (300) and 305 nm (9500) for the hydroxo complex.

In acidic aqueous solution, the complex decomposed to give $Mo_2O_4(aq)^{2+}$ and the protonated forms of the free ligand.

$$Mo_2O_4(hedta)(H_2O)^- + nH^+ \xrightarrow{k_f} Mo_2O_4(aq)^{2+} + H_nhedta^{(3-n)-} \quad (2)$$

The rate of this reaction was measured at $[H^+]$=0.5—2.0 M, I=2.0 M and at 20—35 °C. (The k_f was not obtained accurately at $[H^+]<0.5$ M since reaction (2) did not proceed completely.) The observed first-order rate constant (k_f) was of similar magnitude to that of the acid hydrolysis of $Mo_2O_4(edta)^{2-}$,[1] and much smaller than that of other complexes of $Mo_2O_4^{2+}$.[2,3] The dependence of k_f on $[H^+]$ is not simple (Fig. 1).

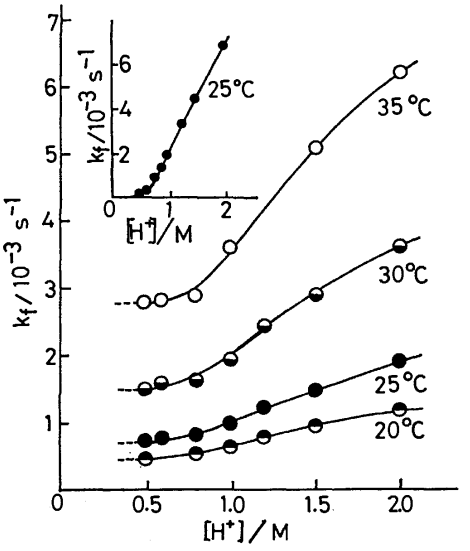

Fig. 1. $[H^+]$-Dependence of k_f for the acid hydrolysis of $Mo_2O_4(hedta)(H_2O)^-$ in aqueous perchloric acid solutions. Each point represents the average of at least 3 runs. The inset is a similar plot for $Mo_2O_4(edta)^{2-}$.[2]

As in the case of the edta complex, k_f increases when $[H^+]$ exceeds 1.0 M. There is a slight tendency for the k_f value to saturate when $[H^+]$ increases. For the edta complex, it was suggested from the analysis of $[H^+]$ dependence that the cleavage of the last acetate group, *viz.* the dissociation of H_3edta^- (uni- or bidentate), is rate-determining, its rate being of similar magnitude to that of the overall rate.[1] A similar rate-determining process would be possible for the hedta complex at least in a higher $[H^+]$ region. It should be noted that the multi-step preequilibria would not be necessarily responsible for the slow rate of acid hydrolysis of these complexes.

In a lower $[H^+]$ region ($[H^+]<1.0$ M), unlike the edta complex, k_f does not approach zero. The difference can be explained by considering equilibrium (1) of the hedta complex. If both aqua and hydroxo forms of the complex contribute to the dissociation reaction (rate constants are expressed as k_{H_2O} and k_{OH}, respectively), k_f is written as follows under the conditions $K_a \ll [H^+]$.

$$k_f = K_a k_{OH}[H^+]^{-1} + k_{H_2O} \quad (3)$$

Here both k_{H_2O} and k_{OH} may change with $[H^+]$. No path corresponding to k_{OH} is expected for the edta complex in which no coordinated water exists. No discussion will be given on the mechanism as for the edta complex,[1] since we cannot estimate each term of (3) accurately.

The sequence of the apparent rate of acid hydrolysis of various ligands from the $Mo_2O_4^{2+}$ center is given in the following, with order of rate (s^{-1}) at 25 °C and at $[H^+]$=1.0 M in parentheses.[1-3]

$$edta^{4-} \approx hedta^{3-} < ida^{2-} < C_2O_4^{2-} < NCS^-$$
$$(10^{-3}) \quad (10^{-3}) \quad (10^{-2} \text{ at } 0°C) \quad (10^0) \quad (10^2)$$

The rate decreases remarkably as the dentate number of the ligand increases.

We are grateful to Professor K. Saito for his helpful discussion and to Dr. K. Nagase for the measurement of thermal decomposition of the complexes and his helpful discussion.

References

1) Y. Sasaki and A. G. Sykes, *J. Chem. Soc., Dalton Trans.*, **1974**, 1468.
2) Y. Sasaki and A. G. Sykes, *J. Less-common Metals*, **36**, 125 (1974); unpublished data.
3) Y. Sasaki, R. S. Taylor, and A. G. Sykes, *J. Chem. Soc., Dalton Trans.*, **1975**, 396.
4) H. Sabat, M. F. Rudolf, and B. Jezowska-Trzebiatowska *Inorg. Chim. Acta*, **7**, 365 (1973).
5) M. Ardon and A. Pernick, *Inorg. Chem.*, **12**, 2484 (1973).
6) D. T. Brown, P. G. Perkins, and J. T. Stewart, *J. Chem. Soc., Dalton Trans.*, **1972**, 1105.
7) P. C. H. Mitchell, *J. Inorg. Nucl. Chem.*, **26**, 1967 (1964).

BULLETIN OF THE CHEMICAL SOCIETY OF JAPAN, VOL. 50 (6), 1639—1640 (1977)

A Palladium-catalyzed Alkoxycarbonylation of Ethynylmercury Compounds

Akira KASAHARA, Taeko IZUMI, and Akio SUZUKI

Department of Applied Chemistry, Faculty of Engineering, Yamagata University, Yonezawa 992

(Received November 15, 1976)

Synopsis. Bis(phenylethynyl)mercury reacts with carbon monoxide and alcohol at room temperature in the presence of palladium(II) salt to form dialkyl phenylmaleate, accompanied by small amounts of alkyl phenylpropiolate and dialkyl phenylfumarate. An alkoxycarbonylation at 100 °C afforded a trialkoxycarbonylation product, accompanied by dialkoxycarbonylation products. The alkoxycarbonylation of bis(ethylethynyl)mercury proceeds similarly.

The palladium-promoted alkoxycarbonylation of alkyl,[1] aryl,[2] and vinyl-mercury compounds[3] has been described. Heck[4] has also reported the palladium-catalyzed carbonylation of olefins and acetylenes with methoxycarbonylmercuric chloride. In this paper, we wish to report the palladium-catalyzed alkoxycarbonylation of bis(phenylethynyl)mercury (**1**) and bis(ethylethynyl)mercury (**2**).

The methoxycarbonylation of **1** was carried out at room temperature under a carbon monoxide pressure of 20 atm in the presence of lithium tetrachloropalladate(II) in methanol to give dimethyl phenylmaleate (**3a**) as the main product. Small amounts of methyl phenylpropiolate (**4a**) and dimethyl phenylfumarate (**5a**) were also produced. The methoxycarbonylation of **1** at 100 °C resulted in the formation of **3a**, **4a**, **5a**, and trimethyl 2-phenyl-1,1,2-ethanetricarboxylate (**6a**). In ethanol, the corresponding ethyl esters were obtained. Similarly, the alkoxycarbonylation of **2** at room temperature afforded dialkoxycarbonylated products, and the reaction at 100 °C led to the formation of trialkoxycarbonylation products. These results are presented in Table 1.

The palladium-catalyzed alkoxycarbonylation of **1** and **2** undoubtedly proceeds by means of an initial mercury-palladium exchange reaction, carbon monoxide insertion into the resultant ethynyl palladium compounds, and subsequent alcoholysis to give **4** and [HPdCl]. The formation of **3** and **5** could be explained by considering the re-addition of [HPdCl] to **4**. A proposed reaction mechanism is shown in Scheme 1. That the elimination and addition of [HPdCl] on unsaturated carbon-carbon bond proceed *via* a *cis* stereochemistry is well-known.[5] Consequently, the

Table 1. Alkoxycarbonylation of bis(phenylethynyl)-mercury (**1**) and bis(ethylethynyl)mercury (**2**)

Mercurial	ROH	Temp °C	Product	Yield %[a]
1	CH_3OH	25	Methyl phenylpropiolate (**4a**)	4
			Dimethyl phenylmaleate (**3a**)	58
			Dimethyl phenylfumarate (**5a**)	4
1	CH_3OH	100	**4a**	3
			3a	43
			5a	10
			Trimethyl 2-phenyl-1,1,2-ethanetricarboxylate (**6a**)	12
1	C_2H_5OH	25	Ethyl phenylpropiolate (**4b**)	5
			Diethyl phenylmaleate (**3b**)	62
			Diethyl phenylfumarate (**5b**)	6
1	C_2H_5OH	100	**4b**	2
			3b	48
			5b	11
			Triethyl 2-phenyl-1,1,2-ethanetricarboxylate (**6b**)	8
2	C_2H_5OH	25	Ethyl 2-pentynoate (**4c**)	6
			Diethyl ethylmaleate (**3c**)	40
			Diethyl ethylfumarate (**5c**)	10
2	C_2H_5OH	100	**4c**	1
			3c	46
			5c	4
			Triethyl 1,1,2-butanetricarboxylate (**6c**)	6
			Triethyl 1,2,2-butanetricarboxylate (**8**)	2

a) Yields are based on the mercurial used.

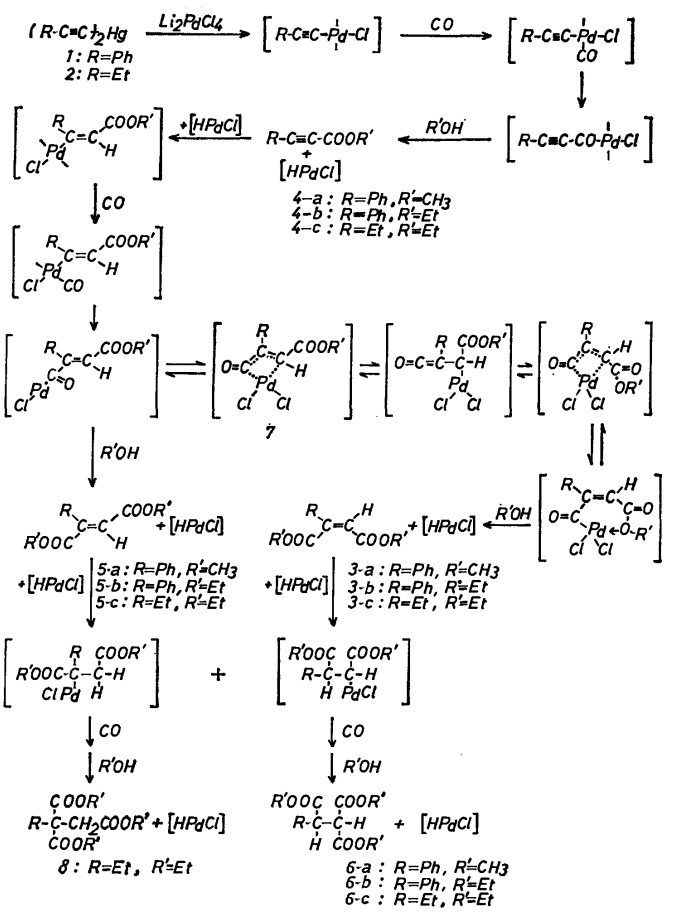

Scheme 1.

reaction pathway of the formation of **5** may very probably include a *cis* addition of [HPdCl] to **4**, but the *cis-trans* isomerization (**5**→**3**) can not be explained only in terms of a palladium-hydride addition-elimination mechanism in the present case. Furthermore, the product, **5**, did not isomerize to **3** under the present reaction conditions.

Schoenberg *et al.*[6] reported that the palladium-catalyzed butoxycarbonylation of (*Z*)-β-bromostyrene gave a mixture of (*E*)- and (*Z*)-butyl cinnamate, and, with reference to the formation of the (*E*)-isomer, they suggested that the *cis-trans* isomerization proceeds probably *via* a ionic carbene-type intermediate or a π-acryloylpalladium-type intermediate. As they have pointed out, the mechanism of the formation of **3** probably involves a π-acryloylpalladium-type intermediate (**7**), and the overwhelming formation of **3** compared with **5** is consistent with this process, because a coordination of the palladium atom to the alkoxycarbonyl group occurs. In the alkoxycarbonylation of **1** and **2** at 100 °C, the formation of **6** and/or **8** proceeds *via* a re-addition of [HPdCl] to **3** and/or **5**. **8a** and **8b** could not be detected because of their poor yields.

Experimental

Materials. The bis(phenylethynyl)mercury (**1**) and bis(ethylethynyl)mercury (**2**) were prepared according to the method described by Johnson and McEwen.[7]

General Procedure for the Alkoxycarbonylation of 1 and 2.

A lithium tetrachloropalladate(II) solution was prepared by stirring 0.82 g (20 mmol) of lithium chloride with 1.77 g (10 mmol) of palladium(II) chloride overnight at room temperature in 80 ml of methanol or ethanol. In this solution, 5 mmol of mercurial (**1** or **2**) was then carbonylated under a carbon monoxide pressure of 20 atm for 6 h with shaking. The reaction mixture was then filtered to remove a precipitated palladium and distilled under reduced pressure to remove the solvent. The products were isolated by preparative gas chromatography or column chromatography (Al_2O_3–hexane), analysed by gas chromatography on 1-m SE 30 (5% on celite) column with a Hitachi K-53 gas-chromatograph, and identified by comparing their retention time and IR and NMR spectra with those of an authentic sample. The reactions carried out are listed in Table 1.

References

1) J. K. Stille and P. K. Wong, *J. Org. Chem.*, **40**, 335 (1975).

2) a) P. M. Henry, *Tetrahedron Lett.*, **1968**, 2285; b) R. F. Heck, *J. Am. Chem. Soc.*, **90**, 5546 (1968); c) A. Kasahara, T. Izumi, and S. Ohnishi, *Bull. Chem. Soc. Jpn.*, **45**, 951 (1972); d) T. Izumi, T. Iino, and A. Kasahara, *ibid.*, **46**, 2251 (1973).

3) R. C. Larock, *J. Org. Chem.*, **40**, 3237 (1975).

4) R. F. Heck, *J. Am. Chem. Soc.*, **94**, 2712 (1972).

5) a) P. M. Henry and G. A. Ward, *J. Am. Chem. Soc.*, **93**, 1494 (1971); *ibid.*, **94**, 673 (1972); b) S. Wolfe and P. G. C. Campbell, *ibid.*, **93**, 1497 (1971).

6) A. Schoenberg, I. Bartoletti, and R. F. Heck, *J. Org. Chem.*, **39**, 3318 (1974).

7) J. R. Johnson and W. L. McEwen, *J. Am. Chem. Soc.*, **48**, 469 (1926).

BULLETIN OF THE CHEMICAL SOCIETY OF JAPAN, VOL. 50 (6), 1641—1642 (1977)

Additions of Dibenzyl Selenoxides and Selenonium Ylides to an Electron-Deficient Ethylene and Acetylene

Seizo TAMAGAKI, Ryuji AKATSUKA, and Seizi KOZUKA

Department of Applied Chemistry, Faculty of Engineering, Osaka City University, Sugimoto-cho, Sumiyoshi-ku, Osaka 558

(Received November 19, 1976)

Synopsis. Dibenzyl selenoxides reacted with dimethyl acetylenedicarboxylate and tetracyanoethylene to give new ylides, while the reaction of selenonium ylides produced new ylides or cyclopropane derivatives.

Although the reactions of selenoxides and selenomium ylides have attracted attention over the last few years,[1] no systematic study seems to have appeared on their reactions with unsaturated C–C bonds. We wish to report on the reactions obtained by use of dimethyl acetylenedicarboxylate and tetracyanoethylene (TCNE) representing an electron-deficient olefin and acetylene, respectively.

Results and Discussion

A number of addition reactions to dimethyl acetylenedicarboxylate affording ylides, known as the reverse Wittig reactions, were reported with regard to various oxides such as amine and arsine oxides,[2,3] and sulfoxides.[4] We have observed new examples of such reaction type, giving new ylides.

The reaction of dibenzyl selenoxide (**1**) with the carboxylate ester was found to produce the corresponding stable ylide (**2**) in a good yield.[5] The structure of the product was easily assigned on the basis of

$$(PhCH_2)_2Se{=}O + (MeOOCC{\equiv})_2 \xrightarrow[2\,h,\ quant.]{r.t.,\ CHCl_3} (PhCH_2)_2Se{=}C(COOMe)(CCOOMe)(=O)$$

(**1**) (**2**)

some spectral evidence and by the independent synthesis from the correspoding selenoxide and the active methylene compound.[6]

$$(PhCH_2)_2Se{=}O + MeOOCCH_2COCOOMe \xrightarrow[5\,min]{r.t.,\ CHCl_3} \mathbf{2}$$

Similarly, dibenzylselenonium cyano(methoxycarbonyl)methylides, **3a** and **3b**, were allowed to react with the carboxylate at room temperature in $CHCl_3$ to afford the unstable oily ylides, **4a** and **4b**, respectively. The NMR spectrum of **4a** in $CDCl_3$ shows a multiplet between 3 and 4 ppm due to the three methoxycarbonyl methyl groups and a quartet centered at 4.2 ppm due to the benzyl protons characteristic of the dibenzylselenonium ylide, its IR spectrum displaying moderately intense bands at 2200, 1655, and 1720 cm^{-1} due to the C=N and C=O's, respectively.

$$R_2Se{=}C(CN)(COOMe) + (MeOOCC{\equiv})_2$$

3a: R = $PhCH_2$
3b: R = $MeC_6H_4CH_2$

$$\xrightarrow[24\,h]{r.t.,\ CHCl_3} R_2Se{=}C(COOMe)(CCOOMe)(C(=O)CCN)$$

4a: 78%
4b: 90%

A suspension of TCNE in a $CHCl_3$ solution of **3a** at room temperature immediately afforded a violet-colored solution. On being stirred vigorously for 1 h, the cyclopropane derivative (**5**) was obtained as a precipitate in an excellent yield.

$$R_2Se{=}C(CN)(COOMe) + TCNE$$

3a (**3b**)

$$\xrightarrow[2\,h]{r.t.,\ CHCl_3} R_2Se + (NC)_2C(COOMe)C(CN)_2$$

82% (90%) **5**: 98% (82%)

Trost reported on a similar decomposition reaction of dimethylsulfonium ylides in the presence of olefins to yield cyclopropane derivatives.[7] The results can thus be explained in terms of initial addition of the starting ylide to the olefinic carbon atom to form the zwitter-ion intermediate, with subsequent three-membered ring closure on the ylide carbon to give the products.

The treatment of dibenzyl selenoxide with an equivalent of TCNE at room temperature in polar aprotic solvents such as CH_3CN and THF afforded the precipitation of dibenzylselenonium dicyanomethylide (**6**). Yields greater than 14% were not attained.
(*Reaction A*)

$$R_2Se{=}O + TCNE \xrightarrow[30\,min]{r.t.,}$$

1a: $PhCH_2$
1b: $MeC_6H_4CH_2$

$$R_2Se{=}C(CN)_2 + RSeCN + R_2Se$$

(**6**) (**7**)

From the reaction mixture two additional products were isolated and identified as selenocyanates (**7**) and selenides. The results are summarized in Table 1 together with those for reaction B of the selenides with TCNE oxide (Table 2).[8]

(*Reaction B*)

$$R_2Se + (NC)_2C\overset{O}{\diagdown\diagup}C(CN)_2 \longrightarrow R_2Se{=}C(CN)_2 + RSeCN$$

Several pathways to these products are possible. One of them is the formation of a selenide and TCNE oxide at the initial stage.

$$R_2Se{=}O + TCNE \longrightarrow R_2\overset{\oplus}{S}e{-}O{-}C(CN)_2\,{}^{\ominus}\!\overset{|}{C}(CN)_2$$

$$\longrightarrow Re_2Se + (NC)_2C\overset{O}{\diagdown\diagup}C(CN)_2$$

The mechanism bringing about such a cyclization has been found in the reaction of ylides affording cyclopropane derivatives, referred to above. However, this pathway is highly unlikely and, even if operative, would be a minor one. The two related reactions A, and B, give the same products having markedly different ratios in the distribution of ylides and selenocyanates especially in non-polar solvents such as benzene and $CHCl_3$. The ylide formation is nil in the reaction of a selenoxide with TCNE, while it exceeds 50% in that of selenides with TCNE oxide, the yields of the selenocyanates being far higher in the latter in all solvents employed.

The results can only be rationalized by the assumption that the reaction proceeds *via* at least two common intermediates which are not so rapidly equilibrated as to give an identical product distribution for the two reactions.

Table 1. Reaction (A) of dibenzyl selenoxides with TCNE at room temperature

Selenoxide (R)	Solvent	Yield, isolated %		
		$R_2Se{=}C(CN)_2$	RSeCN	R_2Se
$MeC_6H_4CH_2$	Benzene	0	56	0
$MeC_6H_4CH_2$	$CHCl_3$	0	87	3
$MeC_6H_4CH_2$	THF	14	57	17
$MeC_6H_4CH_2$	CH_3CN	5	64	18
$PhCH_2$	THF	14	52	11
$PhCH_2$	CH_3CN	6	56	14

Table 2. Reaction (B) of dibenzyl selenides with TCNE oxide at room temperature

Selenide (R)	Solvent	Yield, isolated %		
		$R_2Se{=}C(CN)_2$	RSeCN	R_2Se
$MeC_6H_4CH_2$	Benzene	52	trace	16
$MeC_6H_4CH_2$	$CHCl_3$	65	9	4
$PhCH_2$	THF	14	15	44
$PhCH_2$	CH_3CN	10	11	43

Experimental

All the reactions were performed at room temperature in the mole ratios of 1: 1. Products except **5** and **6** were isolated by preparative TLC using $CHCl_3$ as eluant. Physical properties of products are as follows.

2: IR(KBr) 1725 (C=O), 1655 cm^{-1} (C=O); NMR ($CDCl_3$) δ=4.10 (s, 3H), 4.60 (s, 3H), 5.64 (q, 4H), 8.74 ppm (s, 10H).

4a: IR (neat) 1720 (C=O), 1655 cm^{-1} (C=O); NMR ($CDCl_3$) δ=3.78—3.93 (m, 9H), 4.87 (q. 4H), 7.44 ppm (s, 10H).

4b: IR (neat) 1725 (C=O), 1660 cm^{-1} (C=O); NMR ($CDCl_3$) δ=2.29 (s, 6H), 3.62—3.78 (m, 9H), 4.66 (q, 4H), 7.10 (s, 9H).

5: IR (KBr) 2200 (C≡N), 1775 (C=O), 1280 cm^{-1} (C–O); Found: C, 53.21; H, 1.99; N, 29.84%; M^+, 225. Calcd for $C_{10}H_3N_5O_2$: C, 53.34; H, 1.34; N, 31.10%; mol wt, 225. Mp 175—177 °C.

7a: Found: C, 48.78; H, 3.64; N, 7.17%.

7b: IR (neat) 2145 cm^{-1} (C≡N); NMR ($CDCl_3$) δ= 2.32 (s, 6H), 4.26 (s, 4H), 7.25 ppm (s, 8H); Found: C, 51.28; H, 4.22; N, 6.60%. Calcd for C_9H_9NSe: C, 51.43; H, 4.28; N, 6.67%. Mp 53—55 °C.

References

1) S. Tamagaki and I. Hatanaka, *Chem. Lett.*, **1976**, 301; S. Tamagaki, I. Hatanaka, and K. Tamura, *ibid.*, 81 (1976); S. Tamagaki and I. Hatanaka, *ibid.*, 1303 (1976).

2) H. Seidl, R. Huisgen, and R. Knorr, *Chem. Ber.*, **102**, 904 (1969).

3) E. Ciganek, *J. Org. Chem.*, **35**, 1725 (1970).

4) E. Winterfield, *Chem. Ber.*, **95**, 1581 (1965).

5) The reaction of 3,3-dimethyl dihydrobenzoselenophene oxide with dimethyl acetylenedicarboxylate has recently been reported: H. J. Reich and J. E. Trend, *J. Org. Chem.*, **41**, 2503 (1976).

7) B. M. Trost, *J. Am. Chem. Soc.*, **89**, 138 (1967).

8) W. J. Linn, O. W. Webster, and R. E. Benson, *J. Am. Chem. Soc.*, **87**, 3651 (1965).

BULLETIN OF THE CHEMICAL SOCIETY OF JAPAN, VOL. 50 (6), 1643—1644 (1977)

Synthesis of 3-(Alkoxycarbonylmethylthio)coumarins from Thiocyanatoacetic Esters and Salicylaldehydes

Satoshi KAMBE, Tokiharu TAKAJO, Toshio HAYASHI,* and Hiroshi MIDORIKAWA**

Oyama Technical College, Oyama-shi, Tochigi 323

**The Institute of Physical and Chemical Research, Wako-shi Saitama 351*

***Department of Domestic Science, Showa Women's University, Tokyo 154*

(Received December 8, 1976)

Synopsis. A number of 3-(alkoxycarbonylmethylthio)-coumarins (**3**) were prepared by reactions of thiocyanatoacetic esters (**1**) with salicylaldehydes in the presence of potassium carbonate.

In previous papers,[1-5] it has been shown that thiocyanatoacetic ester (**1**) is available for the synthesis of sulfur-containing heterocycles. Here, the direct synthesis of the hitherto unknown coumarin derivatives from **1** and salicylaldehydes are reported. The reaction of **1b** with salicylaldehyde was carried out in the presence of potassium carbonate at room temperature giving 3-(methoxycarbonylmethylthio)coumarin (**3b**) as the major product and 3,3′-thiodicoumarin (**4**) as a minor product. The structural elucidation of the products are based on elemental analysis and spectral studies. Further confirmation of the structure (**3b**) was made by a comparison with an authentic sample prepared from 2-mercapto-3-(*o*-hydroxyphenyl)acrylic acid (**5**) and **1b** or ethyl chloroacetate (**6**). On the other hand, **4** was also obtained by the reaction of **3** with **2** in the presence of potassium carbonate. In this reaction, **1** and substituted salicylaldehydes also gave similar coumarin derivatives (**3**), but the product corresponding to **4** could not be found.

Although an investigation of the reaction mechanism was not undertaken, the reaction is considered to proceed

TABLE 1. COMPOUNDS **3a—f**, **4**, AND **5**

Compound	Yield (%)	Mp (°C)	Formula	Found %			Calcd %		
				C	H	S	C	H	S
3a	29	143—144	$C_{12}H_{10}O_4S$	57.22	3.92	12.79	57.60	4.03	12.81
3b	36	113—114	$C_{13}H_{12}O_4S$	59.19	4.64	12.13	59.08	4.58	12.13
3c	17	118—119	$C_{13}H_{12}O_5S$	55.72	4.32	11.40	55.72	4.53	11.42
3d	20	129—130	$C_{14}H_{14}O_5S$	57.27	4.55	10.64	57.14	4.80	10.87
3e	7	158—159	$C_{12}H_8O_4SBr_2$	35.15	2.01	7.78	35.29	1.96	7.84
3f	12	155—156	$C_{13}H_{10}O_4SBr_2$	37.11	2.39	7.60	36.96	2.36	7.58
4	4[a], 6[b]	271—273	$C_{18}H_{10}O_4S$	66.98	2.98	9.95	67.08	3.13	9.92
5	81	134—135	$C_9H_8O_3S$	54.75	4.11	16.50	55.10	4.11	16.31

a) From **1a** and **2a**. b) From **1d** and **2a**.

TABLE 2. IR AND NMR DATA FOR THE COMPOUNDS **3a—f**, **4**, AND **5**

Compound	IR[a] (ν_{max}, cm^{-1})	NMR[b] δ, (ppm)
3a	1745, 1706, 1600	7.90 (s, 1H, -C<u>H</u>=C=), 7.15—7.75 (m, $4H_{arom}$), 4.30 (s, 2H, -S-C<u>H_2</u>-), 3.69 (s, 3H, -COOC<u>H_3</u>)
3b	1734, 1706, 1610	7.90 (s, 1H, -C<u>H</u>=CH=), 7.26—7.66 (m, $4H_{arom}$), 3.81—4.31 (m, 4H, -COOC<u>H_2</u>-CH_3, -S-C<u>H_2</u>-), 1.20 (t, 3H, -COOCH_2-C<u>H_3</u>)
3c	1740, 1705, 1610	7.86 (s, 1H, -C<u>H</u>=C=), 7.00—7.47 (m, $3H_{arom}$), 4.02 (s, 2H, -S-C<u>H_2</u>-), 3.90 (s, 3H, -OC<u>H_3</u>), 3.67 (s, 3H, -COOC<u>H_3</u>)
3d	1728, 1698, 1610	7.86 (s, 1H, -C<u>H</u>=C=), 7.15—7.35 (m, $3H_{arom}$), 3.80—4.30 (m, 7H, -COOC<u>H_2</u>-CH_3, -S-C<u>H_2</u>-, -OC<u>H_3</u>)
3e	1728, 1698, 1610	8.00 (s, 1H, -C<u>H</u>=C=), 7.65—7.95 (m, $2H_{arom}$), 4.00 (s, 2H, -S-C<u>H_2</u>-), 3.68 (s, 3H, -COOC<u>H_3</u>)
3f	1760, 1730, 1600	8.06 (s, 1H, -C<u>H</u>=C=), 7.70—7.96 (m, $2H_{arom}$), 4.00—4.17 (m, 4H, -COOC<u>H_2</u>-CH_3, -S-C<u>H_2</u>-), 1.20 (t, 3H, -COOCH_2-C<u>H_3</u>)
4	1697, 1605	8.33 (s, 2H, 2×-C<u>H</u>=C=), 7.35—7.75 (m, $8H_{arom}$)
5	3400, 3150, 2570, 1680, 1615	9.10 (b, 3H, -S<u>H</u>, -O<u>H</u>, -COO<u>H</u>), 8.10 (s, 1H, -C<u>H</u>=C=), 7.70 (q, 1H, aromatic H relative to the OH group), 6.70—7.30 (m, $3H_{arom}$)

a) The IR spectra were recorded for Nujol mulls. b) The NMR spectra were determined in DMSO-d_6 for **3a—3f**, CF_3COOH for **4**, solution of $CDCl_3$:DMSO-d_6=3:1 for **5** with tetramthylsilane as internal reference; s, singlet; d, doublet; t, triplet; q, quartet; m, multiplet; b, broad.

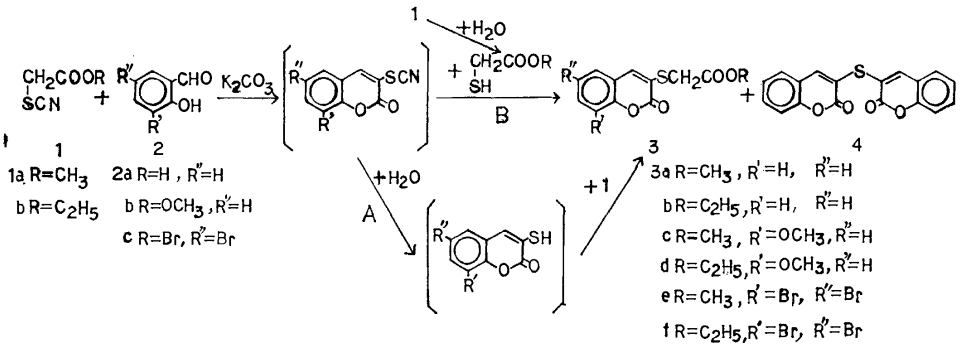

Scheme 1.

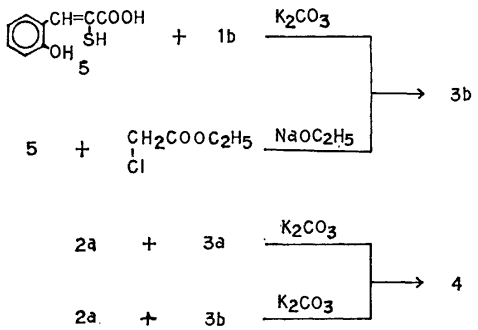

Scheme 2.

via route A or B. Product **4** may form upon further condensation of **3** with **2** as depicted above.

Experimental

*Preparation of **3** and **4**.* A mixture of **1** (0.02 mol), salicylaldehyde (0.01 mol) and potassium carbonate (0.01 mol) was stirred in 10 ml of acetone at room temperature for 6—7 h. Upon cooling to room temperature, crystals precipitated; the precipitate was washed with water, dried, and then washed with hot ethanol. The residue was recrystallized from dioxane to give **4**. To the ethanolic washing was added a small amount of water, and then the solution, when allowed to stand overnight at room temperature, gave pale yellow crystals (**3**) which were recrystallized from alcohol. Substituted coumarines (**3c—f**) are also obtained similarly, but no compound of type **4** could be found.

Preparation of 2-Mercapto-3-(o-hydroxyphenyl)acrylic Acid (5). The title acid was prepared by a modification of the reported method.[6] 5-(*o*-Hydroxybenzylidene)-2-thioxothiazolidin-4-one (0.01 mol) was hydrolyzed with 8% sodium hydroxide (20 ml) by heating to 50—60 °C. The mixture was well stirred until a clear solution was obtained. After cooling with an ice-salt mixture, the solution was acidified with 3M-hydrochloric acid, and the stirring was continued for 30 min. The resulting acid was washed with water, dried in air, and recrystallized from dichloromethane.

Preparation of an Authentic Sample from 2-Mercapto-3-(o-hydroxyphenyl)acrylic Acid (5) and Ethyl Chloroacetate. To a solution of sodium 2-mercapto-3-(*o*-hydroxyphenyl)acrylate (0.005 mol) in absolute ethanol (10 ml) was added ethyl chloroacetate (0.005 mol). The solution was stirred for 4 h and then allowed to stand overnight in a refrigerator. The resulting crystals were collected on a filter, washed with water, and dried. Recrystallization from ethanol gave **3b**; yield: 0.6 g (45%); mp 113—114 °C.

*Preparation of an Authentic Sample from 2-Mercapto-3-(o-hydroxyphenyl)acrylic Acid and **1b**.* A mixture of 2-mercapto-3-(*o*-hydroxyphenyl)acrylic acid (0.005 mol), **1b** (0.005 mol) and potassium carbonate (0.005 mol) in acetone (10 ml) was stirred at room temperature for 5 h. After the mixture was allowed to stand overnight in a refrigerator, crystalline matter separated out. Recrystallization from ethanol gave **3b**; yield: 0.5 g (38%); mp 113—114 °C.

*Preparation of **4** from **3** and Salicylaldehyde.* A mixture of **3** (0.005 mol), salicylaldehyde (0.005 mol), and potassium carbonate (0.005 mol) in acetone (10 ml) was stirred for 1 h. Crystalline matter precipitated out during the reaction; this was recrystallized from dioxane affording **4**; yield 0.9 g (56%) from **3a** and salicylaldehyde; 1.1 g (69%) from **3b** and salicylaldehyde: mp 271—272 °C.

References

1) S. Kambe, T. Hayashi, H. Yasuda, and H. Midorikawa, *Bull. Chem. Soc. Jpn.*, **44**, 1357 (1971).
2) S. Kambe, T. Hayashi, H. Yasuda, and A. Sakurai, *Nippon Kagaku Zasshi*, **92**, 867 (1971).
3) S. Kambe and T. Hayashi, *Bull. Chem. Soc. Jpn.*, **45**, 952 (1972).
4) S. Kambe and T. Hayashi, *Bull. Chem. Soc. Jpn.*, **45**, 3192 (1972).
5) S. Kambe, *Bull. Chem. Soc. Jpn.*, **46**, 2926 (1973).
6) N. Campbell and J. E. McKall, *J. Chem. Soc.*, **1948**, 1251.

BULLETIN OF THE CHEMICAL SOCIETY OF JAPAN, VOL. 50 (6), 1645—1646 (1977)

A New Synthetic Approach to Esters of β-Keto Thiocarboxylic *S*-Acids

Toshimitsu WAKUI, Haruzo YAMAGUCHI, and Shinichi MOTOKI

Department of Chemistry, Faculty of Science, Science University of Tokyo, Kagurazaka, Shinjuku-ku, Tokyo 162

(Received December 23, 1976)

Synopsis. Esters of β-keto thiocarboxylic *S*-acids (**5**) were synthesized from *S*-ethyl bromothioacetate (**1**), through a reaction sequence involving the reduction of sulfonium ylides (**4**) with zinc in acetic acid.

S-Ethyl acetothioacetate (**5a**) reacts with mercury(II) oxide to afford diacetylacetone and mercury(II) ethanethiolate, along with carbon dioxide.[1] Since the corresponding oxygen ester dose not react with mercury(II) oxide in a similar way, we thought it of interest to develop a general method of preparing esters of β-keto thiocarboxylic *S*-acids.

Esters of acetothioacetic *S*-acid, representative esters of β-keto thiocarboxylic *S*-acid, are readily prepared by the Claisen ester condensation[2] or by the reaction of alkanethiols with diketene.[1,3] However, no other esters of β-keto thiocarboxylic *S*-acids can be obtained. In this paper, we wish to report a new general route for the preparation of esters of β-keto thiocarboxylic *S*-acids (**5**) starting from *S*-ethyl bromothioacetate (**1**).

S-Ethyl bromothioacetate **1**, obtained from bromoacetyl bromide and ethanethiol in the presence of triethylamine, was treated with dimethyl sulfide at room temperature for 24 h to afford [(ethylthio)carbonylmethyl]dimethylsulfonium bromide (**2**, 70%), which was deprotonated with sodium hydride in a tetrahydrofuran solution affording [(ethylthio)carbonylmethylene]dimethylsulfurane (**3**, 85%). **3** was obtained as a yellow solid (mp 50—52 °C) after evaporation of the solvent, while sulfonium ylide of the corresponding oxygen ester was obtained as a yellowish oily substance.[4] Acylation of **3** with a half-equivalent amount of acid chlorides gave new ylides, [[(ethylthio)carbonyl]acyl(or benzoyl)methylene]dimethylsulfuranes (**4**, Table 1). Ylides **4** were readily reduced with zinc in acetic acid as in the case of sulfoxonium ylides,[5] affording esters of β-keto thiocarboxylic *S*-acids (**5**, R=alkyl, Table 2)

$$\mathrm{BrCH_2COSEt} \xrightarrow{\mathrm{CH_3SCH_3}} \underset{\mathbf{2}}{(\mathrm{CH_3})_2\overset{+}{\mathrm{S}}\mathrm{CH_2COSEt\ Br^-}} \xrightarrow{\mathrm{NaH}} \underset{\mathbf{3}}{(\mathrm{CH_3})_2\mathrm{S{=}CHCOSEt}} \xrightarrow{\mathrm{RCOCl}} \underset{\mathbf{4}}{(\mathrm{CH_3})_2\mathrm{S{=}C(COR)COSEt}}$$

R=alkyl or Ph

$$\xrightarrow{\mathrm{Zn\text{-}AcOH}} \underset{\mathbf{5}}{\mathrm{RCOCH_2COSEt}}$$

R=alkyl

Table 1. Yields and physical data for sulfonium ylides (**4**)

	R	Yield[a] (%)	Mp (°C)	IR[b] (C=O) (cm^{-1})	NMR (δ) in $CDCl_3$	Anal, S% Found	Anal, S% Calcd
4a	Me	53	107—108	1640 1590	1.28 (t, 3H), 2.44 (s, 3H) 2.90 (q, 2H), 3.03 (s, 6H)	31.32	31.08
4b	Et	46	78—79	1620 1585	1.09 (t, 3H), 1.27 (t, 3H) 2.84 (q, 2H), 2.88 (q, 2H) 3.02 (s, 6H)	29.18	29.10
4c	iso-Pr	69	137—138	1600 1570	1.07 (d, 6H), 1.25 (t, 3H) 2.85 (q, 2H), 3.01 (s, 6H) 3.55 (m, 1H)	27.14	27.36
4d	*t*-Bu	52	188—189	1590 1560	1.26 (t, 3H), 1.28 (s, 9H) 2.83 (q, 2H), 3.00 (s, 6H)	26.01	25.81
4e	Ph	77	169—170	1590 1550	1.24 (t, 3H), 2.83 (q, 2H) 2.94 (s, 6H), 7.35 (s, 5H)	23.71	23.89

a) Based on acid chlorides used. b) In Nujol.

Table 2. Yields and physical data for esters of β-keto thiocarboxylic *S*-acids (**5**)

	R	Yield[a] (%)	Bp (°C/Torr)	IR[b] (C=O) (cm^{-1})	Enol %[c]	Anal, S% Found	Anal, S% Calcd
5a	Me	50	80/8	1725 1680 1625	33[d]		
5b	Et	43	81/5	1730 1680 1620	33	19.75	20.01
5c	iso-Pr	57	88—90/6	1720 1685 1605	56	18.46	18.40
5d	*t*-Bu	53	85/6	1725 1680 1620	63	17.03	17.03

a) Based on sulfonium ylides **4** used. b) In liquid film. c) Estimated from integration of the NMR signal. d) Lit,[2] 30.8%.

in moderate yields.

On the other hand, reduction of ylide **4e** (R=Ph) did not give the expected compound *S*-ethyl benzoylthioacetate (**6**), but afforded *S*-ethyl 3-hydroxy-3-phenylpropanethioate (**7**, 15%) and *S*-ethyl 3-acetoxy-3-phenylpropanethioate (**8**, 38%).

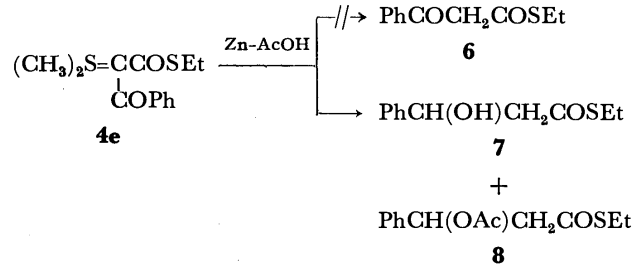

Experimental

All the melting points and boiling points are uncorrected. The IR spectra were obtained on a Hitachi EPI-G2 spectrometer and the NMR spectra on a Varian A-60 spectrometer, using tetramethylsilane as an internal standard. Mass spectra were taken with a Hitachi RMU-7M mass spectrometer at 70 eV by a direct insertion technique.

S-Ethyl Bromothioacetate (1). Bromoacetyl bromide (101 g, 0.5 mol) was added dropwise over a 1 h-period at 0—5 °C with stirring to a solution of ethanethiol (37.3 g, 0.6 mol) and triethylamine (50.5 g, 0.5 mol) in ether (200 ml). The reaction mixture was stirred at the same temperature for 5 h and then poured into water (200 ml). The organic layer was separated and the aqueous layer was extracted with ether. The combined ether solution was dried over anhydrous sodium sulfate and evaporated under reduced pressure. Distillation of the residue gave 65.9 g (72%) of **1**. Bp 60 °C/5 Torr; IR (liquid film): 1685 cm^{-1} (COS). Found: S, 17.63%. Calcd for C_4H_7OSBr: S, 17.51%.

Sulfonium Bromide 2. Treatment of *S*-ethyl ester **1** (54.9 g, 0.3 mol) with dimethyl sulfide (27.9 g, 0.45 mol) at room temperature for 24 h afforded 51.5 g (70%) of **2**. Recrystallization from ether-ethanol gave a pure sample. Mp 117—118 °C; IR (Nujol): 1670 cm^{-1} (COS); NMR (trifluoroacetic acid): δ 1.36 (t, 3H), 3.15 (s, 6H), 3.16 (q, 2H), 4.75 (s, 2H). Found: C, 26.15%. Calcd for $C_6H_{13}OS_2Br$: S, 25.97%.

Sulfonium Ylide 3. Sodium hydride (5.76 g, 0.2 mol), free of mineral oil, was added portionwise with stirring to a suspension of sulfonium bromide **2** (49 g, 0.2 mol) in tetrahydrofuran (150 ml). After stirring for 10 h at room temperature, the precipitate was filtered off and the filtrate was concentrated to afford 27.9 g (85%) of crude ylide **3**. Mp 50—52 °C; IR (Nujol): 1600 cm^{-1} (COS); NMR ($CDCl_3$): δ 1.24 (t, 3H), 2.83 (q, 2H), 2.88 (s, 6H), 3.58 (s, 1H).

General Procedure for Acylation of 3. An acid chloride (0.1 mol) was added dropwise to a solution of *S*-ethyl ester ylide **3** (0.2 mol) in benzene (250 ml), the temperature being kept below 30 °C by occasional cooling. After being stirred at room temperature for 24 h, the precipitate ([(ethylthio)-carbonylmethyl] dimethylsulfonium chloride, mp 150—151 °C) was filtered off. Addition of hexane to the filtrate resulted in the precipitation of a new ylide **4** (Table 1).

General Procedure for Reduction of 4. Zinc powder (0.25 mol) was added in many portions to a solution of a ylide **4** (0.05 mol) in acetic acid (50 ml), the temperature being kept below 20 °C with external cooling. The reaction mixture was stirred at 15—20 °C for 30 h. The insoluble material was filtered and washed with ether. Concentration of the filtrate afforded a crude product, which was purified by distillation. Yields and physical properties of **5** thus obtained are shown in Table 2. The NMR data (in CCl_4, δ) of **5** are as follows: **5a**: 1.25 (t), 1.92 (s), 2.19 (s), 2.90 (q), 3.63 (s), 5.43 (s), 12.66 (s). **5b**: 1.02 (t), 1.27 (t), 2.20 (q), 2.54 (q), 2.90 (q), 3.59 (s), 5.38 (s), 12.70 (s). **5c**:[6] 1.08 (d), 1.14 (d), 1.28 (t), 2.89 (q), 3.60 (s), 5.32 (s), 12.73 (s). **5d**: 1.15 (s), 1.28 (t), 2.89 (q), 3.65 (s), 5.37 (s), 12.94 (s).

Reduction of 4e. Zinc powder (4.9 g, 75 mmol) was added portionwise at 15—20 °C with stirring to a solution of **4e** (1.34 g, 5 mmol) in acetic acid (20 ml). The reaction mixture was stirred at the same temperature for 24 h and the insoluble material was filtered off. Concentration of the filtrate gave a colorless liquid which was subjected to column chromatography on silica gel (Wakogel C-200) to afford 158 mg (15%) of **7** and 475 mg (38%) of **8** by eluting with benzene. **7**: IR (liquid film): 1685 cm^{-1} (COS); NMR (CCl_4): δ 1.22 (t, 3H), 2.83 (d, 2H), 2.84 (q, 2H), 3.31 (s, 1H), 5.06 (t, 1H), 7.22 (s, 5H); MS *m/e*, 210 (M^+). **8**: IR (liqid film): 1745 (COO) and 1685 cm^{-1} (COS); NMR (CCl_4): δ 1.18 (t, 3H), 1.98 (s, 3H), 2.81 (m, 4H), 6.20 (m, 1H), 7.28 (s, 5H); MS *m/e* 252 (M^+).

References

1) S. Motoki and T. Sato, *Bull. Chem. Soc. Jpn.*, **42**, 1322 (1969).

2) a) R. B. Baker and E. E. Reid, *J. Am. Chem. Soc.*, **51**, 1567 (1929); b) J. C. Sheehan and C. W. Beck, *ibid.*, **77**, 4875 (1955); c) M. W. Cronyn, M. P. Chang and R. A. Wall, *ibid.*, **77**, 3031 (1955).

3) T. Wieland and L. Rueff, *Angew. Chem.*, **65**, 186 (1953).

4) A. W. Johnson and R. T. Amel, *J. Org. Chem.*, **34**, 1240 (1969).

5) a) E. J. Corey and M. Chaykovsky, *J. Am. Chem. Soc.*, **86**, 1640 (1964); b) J. Ide and Y. Kishida, *Bull. Chem. Soc. Jpn.*, **49**, 3239 (1976).

6) Absorption due to the methine proton of **5c** could not be assigned.

BULLETIN OF THE CHEMICAL SOCIETY OF JAPAN, VOL. 50 (6), 1647—1648 (1977)

Tungsten Hexachloride-catalyzed Decomposition of Diazo Compounds. A Novel Oxazole Synthesis

Katuzi KITATANI, Tamejiro HIYAMA, and Hitosi NOZAKI
Department of Industrial Chemistry, Kyoto University, Yoshida, Kyoto 606

(Received January 28, 1977)

Synopsis. Benzoylphenyldiazomethane and diazoacetophenone react with several nitriles in the presence of WCl_6 catalyst to produce 2-substituted 4,5-diphenyloxazoles (**1a—d**) and 2-methyl-5-phenyloxazole (**2**) in good yields. The remarkable catalysis is ascribed to the good affinity of tungsten with carbenes. The catalytic decomposition of diphenyldiazomethane yields diphenylcarbenium ion, which is transformed into triarylmethanes in aromatic solvents.

Lewis acid-catalyzed decomposition of diazo compounds gives intermediary carbene complexes, which are often too much reactive for synthetic applications.[1] The requisite selectivity should be attained by proper choice of the metal salt catalyst in which the central metal atom has good affinity with carbenes and therefore stabilizing the intermediate carbene complex. Among them tungsten salt seems to be a candidate since low valent tungstens give very stable carbene complexes.[2] On this account we have investigated the catalytic activity of tungsten hexachloride in the thermal decomposition of diazo compounds.

Decomposition of Diazo Ketones in Nitriles. When benzoylphenyldiazomethane was treated with tungsten hexachloride suspended in benzonitrile at room temperature, immediate decomposition occurred. Work-up gave 2,4,5-triphenyloxazole (**1a**). Similarly upon the catalytic decomposition in several nitriles the diazo ketone afforded oxazoles **1b—d** in good to moderate yields. Diazoacetophenone was also converted into 2-methyl-5-phenyloxazole (**2**).

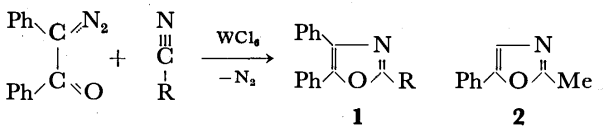

1 **2**

a: R=Ph; **d**: R=Me
c; R=Et; **d**: R=CH_2=CH

The results are in sharp contrast to the thermal, photochemical or copper(II)-catalyzed decomposition which give only negligible yields of oxazoles.[3] The remarkable catalysis by WCl_6 can be attributed to the Lewis acidity of the salt[4] coupled with its good affinity with carbenes.[2,5] The dual character would probably account for the assumption that both α-keto carbenes and nitriles are assembled together within the ligand sphere of W(VI) and are cyclocoupled effectively. Another noteworthy facet is the formation of 2-vinyl-4,5-diphenyloxazole (**1d**) in the reaction of benzoylphenyldiazomethane with acrylonitrile, where none of the cyclopropanation product has been detected. This suggests the electrophilic nature of carbenic center.[6] These observations are in accord with the following mechanistic postulation.[7]

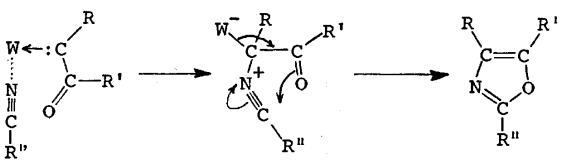

Decomposition of Diphenyldiazomethane. Tungsten hexachloride catalyzes the decomposition of diphenyldiazomethane (**3**) in another way. *N*-Benzhydrylacetamide was produced in the reaction with acetonitrile. When **3** was treated with WCl_6 dissolved in *N,N*-dimethylformamide (DMF), immediate decomposition was again observed and a light green solution was obtained which upon hydrolysis gave benzhydrol and upon methanolysis benzhydryl methyl ether (see Experimental). Deuterium oxide quenching of this solution resulted in no deuterated benzhydrol. Obviously the aliphatic proton of diphenylcarbenium ion intermediate originates from the catalyst, but the proton source could not be eliminated in spite of repeated sublimations.[8] The catalytic decomposition of **3** in aromatic solvents (benzene, toluene, and anisole) gave Friedel-Crafts type products, triarylmethanes (Ph_3CH, 58%; $Ph_2CHC_6H_4Me$, 47%; $Ph_2CHC_6H_4$-*p*-OMe, 76% respectively).

Experimental

All the temperatures were uncorrected. The IR spectra were obtained on a Shimadzu spectrometer 27-G, mass spectra on a Hitachi RMU-6L, and PMR spectra on JEOL JNM-PMX 60, JEOL C-60-H, or Varian EM-360 spectrometer. Unless otherwise stated, commercial tungsten hexachloride was sublimed once (160 °C/0.2 Torr). All the experiments were performed under a nitrogen atmosphere and at room temperature.

*Triphenyloxazole (**1a**).* A solution of benzoylphenyldiazomethane (0.11 g, 0.50 mmol) in benzonitrile (3 ml) was added to a suspension of WCl_6 (0.20 g, 0.49 mmol) in the same solvent (2 ml). Nitrogen evolution immediately occurred and after 5 min the solution turned to light brown, then to dark blue after 2 h. After the addition of water the reaction mixture was extracted (AcOEt), dried (Na_2SO_4), and concentrated *in vacuo*. Preparative TLC (alumina, benzene, R_f 0.6—0.8) afforded **2a** (80 mg, 66%). Mp 113—115 °C (lit,[9] 114—115 °C); IR (Nujol): 3050; 1602, 1595, 1555, 1490, 1450, 968, 770, 694, cm^{-1}; MS: *m/e* 297 (M^+); PMR (CCl_4): δ 7.2—8.1 (m, Ph). Byproducts were diphenylethanedione (**4**) (13 mg, 12%) and 2-chloro-1,2-diphenylethanone (**5**) (21 mg, 18%).

*2-Methyl-4,5-diphenyloxazole (**1b**):*[9] 65% yield; bp 80—90 °C (bath temp)/0.1 Torr; IR (neat): 3060, 2940, 1602, 1585, 1500, 1443, 1270, 1226, 1051, 1020, 967, 767, 699 cm^{-1}; MS: *m/e* 235 (M^+); PMR (CCl_4): δ 2.50 (s, 3H, Me), 7.1—7.6 (m, 10H, Ph).

*2-Ethyl-4,5-diphenyloxazole (**1a**)*:[9] 45% yield; bp 110—125 °C (bath temp)/0.3 Torr; IR (neat): 3060, 1603, 1570, 1500, 1450, 1211, 1060, 1024, 965, 761, 692 cm^{-1}; MS: *m/e* 249 (M^+); PMR (CCl_4): δ 1.43 (t, J=9 Hz, 3H, Me), 2.85 (q, J=9 Hz, 2H, CH_2), 7.0—8.1 (m, 10H, Ph). **4** was a by-product (7%).

*4,5-Diphenyl-2-vinyloxazole (**1d**)*:[10] 50% yield; bp 150—168 °C (bath temp)/0.2 Torr; IR (neat): 1600, 1530, 1180, 1070, 1029, 980, 760, 695 cm^{-1}; MS: *m/e* 247 (M^+); PMR (CCl_4): δ 5.3—6.9 (m, 3H, $CH{=}CH_2$), 7.0—8.2 (m, 10H, Ph). By-products were **4** (19%), **5** (13%) and 2-hydroxy-1,2-diphenylethanone (15%).

*2-Methyl-5-phenyloxazole (**2**)*: 66% yield; mp 56—58 °C (lit,[11] 58 °C); IR (Nujol): 1580, 1560, 1215, 1132, 1060, 940, 839, 830, 764, 698, 676 cm^{-1}; MS: *m/e* 159 (M^+); PMR (CCl_4): δ 2.48 (s, 3H, Me), 7.1—7.8 (m, 6H, aromatic protons). 2-Chloro-1-phenylethanone (41%) was also obtained.

*Decomposition of **3** in Acetonitrile.* A solution of **3** (97 mg, 0.50 mmol) in acetonitrile (1 ml) was added to a suspension of WCl_6 (0.20 g, 1.5 mmol) in the same solvent (5 ml). After 10 h the reaction mixture was worked up. Preparative TLC (silica gel, benzene) afforded *N*-benzhydrylacetamide[12] (R_f 0.3—0.4, 38 mg, 32%) along with 9,10-diphenylphenanthrene[13] (R_f 0.9—0.95, 57 mg, 64%).

*Decomposition of **3** in DMF.* A solution of **3** (97 mg, 0.50 mmol) in DMF (1 ml) was added to a solution of WCl_6 (0.20 g, 0.50 mmol) in DMF (5 ml). After 1 h the reaction mixture was quenched (H_2O) and extracted (ether). Preparative TLC (silica gel, benzene, R_f 0.2—0.3) of the crude product afforded benzhydrol (63 mg, 77%) along with tetraphenylethylene (R_f 0.8—0.9, 13 mg, 9%). Quenching with methanol afforded benzhydryl methyl ether in 60% yield.[14]

*Decomposition of **3** in Anisole.* A solution of **3** (0.10 g, 0.53 mmol) in anisole (1 ml) was added to a brown solution of WCl_6 (0.20 g, 0.51 mmol) in anisole (5 ml). After 5 h the reaction mixture was quenched with water and extracted with ether. The organic layer was dried (Na_2SO_4), concentrated *in vacuo*, and the residue was purified by preparative TLC (silica gel, benzene, R_f 0.8—0.9, 0.10 g, 76%). Mp 61—62 °C (lit,[15] 61 °C); IR (Nujol): 1610, 1510, 1250, 1030, 700 cm^{-1}; MS: *m/e* 274 (M^+); PMR (CCl_4): δ 3.73 (s, 3H, OMe), 5.47 (s, 1H, CH), 6.6—7.1 (ABq, 4H, C_6H_4-OMe), 7.0—7.5 (m, 10H, Ph).

References

1) W. Kirmse, "Carbene Chemistry," 2nd ed, Academic Press, New York (1971), p. 85. See also R. Noyori, *Tetrahedron Lett.*, **1973**, 1691.

2) C. P. Casey and T. J. Burkhardt, *J. Am. Chem. Soc.*, **95**, 5833 (1973) and references cited therein.

3) In these reactions Wolff rearrangement predominates over the dipolar cycloaddition. R. Huisgen, G. Binsch, and L. Ghosez, *Chem. Ber.*, **97**, 2628 (1964). A preliminary results of the present note have been published in K. Kitatani, T. Hiyama, and H. Nozaki, *Tetrahedron Lett.*, **1974**, 1531.

4) In order to check the contribution of Lewis acidity to the catalysis, benzoylphenyldiazomethane was treated with such halides as $ZnCl_2$, $SnCl_4$, $TiCl_4$, and $AlCl_3$ in acetonitrile. The major product was 2-chloro-1,2-diphenylethanone (**5**) in each case ($ZnCl_2$, 33%; $SnCl_4$, 22%; $TiCl_4$, 48%; $AlCl_3$, 41%), although the desired product **1b** was obtained as follows: $ZnCl_2$, 12%; $SnCl_4$, 6%; $TiCl_4$, 16%; $AlCl_3$, 8%.

5) T.-L. Ho, *Chem. Rev.*, **75**, 1 (1975).

6) In contrast, thermal reaction of electron-deficient diazo compounds (*e.g.* 10-diazoanthrone) with acrylonitrile affords cyanocyclopropanes. N. Filipescu and J. W. Pavlik, *J. Chem. Soc., C*, **1970**, 1851.

7) The intermediacy of **5** is readily excluded because it does not react with acetonitrile even in the presence of WCl_6 at room temperature.

8) The addition of deuterium oxide prior to the reaction resulted in the formation of the products derived from diphenyldeuteriomethyl cation. In the reaction of benzoylphenyldiazomethane with acetonitrile, however, the presence of water in the reaction mixture strongly depressed the oxazole formation (17% yield).

9) M. Lora-Tamayo, R. Madronero, and H. Leiprand, *Chem. Ber.*, **97**, 2230 (1964).

10) Y. Kurusu, H. Nishiyama, and M. Okawara, *Kogyo Kagaku Zasshi*, **71**, 1741 (1968).

11) R. Pfleger and H. Vogt, *Chem. Ber.*, **90**, 1467 (1957).

12) H. L. Wheeler, *Am. Chem. J.*, **26**, 345 (1901).

13) W. A. Mosher, F. W. Steffgen, and P. T. Lansbury, *J. Org. Chem.*, **26**, 670 (1961).

14) The nature of the reactive species responsible for these products is still obscure. A possible explanation might involve diphenylcarbenium ion (protonated carbene) probably complexed with tungsten.

15) A. Bistrzycki and C. Herbst, *Ber.*, **35**, 3133 (1902).

BULLETIN OF THE CHEMICAL SOCIETY OF JAPAN, VOL. 50 (6), 1649—1650 (1977)

Synthesis of 2-Alkoxy-3,4,6-trihydroxyacetophenones

Kiyotaka HATAKEDA, Norio SAITO, Shota ITO, and Takashi ASANO

Government Industrial Research Institute, Tohoku, Nigatake, Harano-machi, Sendai 983

(Received November 12, 1976)

Synopsis. 2-Alkoxy-3,4,6-trihydroxyacetophenones have been prepared from 2,3,4,6-tetrakis(benzyloxy)acetophenone (II) in good yields by the following reactions: hydrolysis of II to 2-hydroxy-3,4,6-tris(benzyloxy)acetophenone (IIIa), alkylation of IIIa to 2-isopropoxy and 2-ethoxy-3,4,6-tris(benzyloxy)acetophenones (IVa and VIb), and hydrogenolysis of IVa and IVb to the corresponding 2-alkoxy-3,4,6-trihydroxyacetophenones (Va and Vb).

Synthsis of two kinds of monomethyl ether of 2,3,4,6-tetrahydroxyacetophenone (I) (3 and 4 position) was reported by Phadke[1] and Krishna.[2] However, 2-alkoxy-3,4,6-trihydroxyacetophenones have not been reported in literature.

In the synthetic course of flavonoid compounds, we found a new synthetic method of 2-alkoxy-3,4,6-trihydroxyacetophenones from 2-hydroxy-3,4,6-tris(benzyloxy)acetophenone (IIIa) which was obtained by the selective hydrolysis of 2,3,4,6-tetrakis(benzyloxy)acetophenone (II). Recently, several polyhydroxy flavonoids (and/or their ether derivatives) have been found in nature.[3,4] Therefore our method offers a good starting material for these flavonoid synthesis.

IIIa was obtained when II was hydrolyzed by 90% acetic acid. The signal of hydrogen bonding OH (13.98 ppm) with ketone in its NMR spectrum and hydrogen bonded ketone (1620 cm^{-1}) in its IR spectrum are observed. IIIa gave isopropoxy-tris(benzyloxy)acetophenone (IVa) by isopropylation. Hydrogenolysis of IVa gave isopropoxy-trihydroxyacetophenone (Va). The compound Va was transformed to the corresponding trimethyl ether (VI) which was also obtained from the known compound, 2-hydroxy-3,4,6-trimethoxyacetophenone (IIIb).[5]

IIIa is an useful compound as a starting material in the synthesis of 2-alkoxy-3,4,6-trihydroxyacetophenones. For example, 2-ethoxy-3,4,6-trihydroxyacetophenone (Vb) was synthesized from IIIa in the same manner as described above.

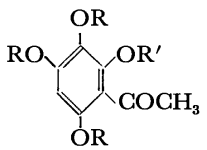

I, R=R'=H
II, R=R'=CH_2Ph
IIIa, R=CH_2Ph, R'=H
b, R=Me, R'=H
IVa, R=CH_2Ph, R'=Pr(*i*)
b, R=CH_2Ph, R'=Et
Va, R=H, R'=Pr(*i*)
b, R=H, R'=Et
VI, R=Me, R'=Pr(*i*)

Experimental

All the melting points are uncorrected. The IR spectra were recorded with a Hitachi Model 285 infrared spectrophotometer. The mass spectra were recorded with a JEOL Model JMS-OMS mass spectrometer. The NMR spectra were determined at 100 MHz with a JEOL Model 4H-100 NMR spectrometer, using tetramethylsilane as the internal standard. 2,3,4,6-Tetrahydroxyacetophenone (I)[6] was prepared from 1,2,3,5-benzenetetrol which was obtained by hydrogenolysis of 1,3-bis(benzyloxy)-2,5-benzenediol.[7]

2,3,4,6-Tetrakis(benzyloxy)acetophenone (II). A mixture of 2,3,4,6-tetrahydroxyacetophenone (I)[6] (0.68 g, 3.7 mmol), benzyl chloride (3.14 g, 22 mmol) and potassium carbonate (anhyd 22 g) in *N,N*-dimethylformamide (DMF) (30 ml) was heated for 1 h at 190 °C. The reaction mixture was poured into ice–water, and then extracted with benzene. The benzene layer was chromatographed over silica gel and eluted with benzene to give 0.81 g of crystals of II, mp 81 °C. IR (KBr): 1680 cm^{-1} (C=O); MS *m/e*: 544 (M^+); NMR δ ($CDCl_3$): 2.35 (3H, s, acetyl methyl), 4.98—5.08 (8H, benzyl methylene), 6.36 (1H, s, phenyl) and 7.15—7.45 (20H, phenyl). Found: C, 79.37; H, 5.99%. Calcd for $C_{36}H_{32}O_5$: C, 79.41; H, 5.88%.

2-Hydroxy-3,4,6-tris(benzyloxy)acetophenone (IIIa). A solution of II (1 g, 2 mmol) in 90% acetic acid (65 ml) was refluxed for 17 h. The reaction mixture was poured into ice–water, and then extracted with 300 ml of benzene. The benzene layer was washed with aqueous sodium hydrogencarbonate and water, dried and then evaporated to give IIIa as yellow crystals. Recrystallization from ethanol gave pale yellow needles of IIIa (0.65 g, 78%); mp 141—142 °C. IR (KBr): 1620 cm^{-1} (C=O, hydrogen bonded); NMR δ ($CDCl_3$): 2.50 (3H, s, acetyl methyl), 4.93—5.02 (6H, benzyl methylene), 5.98 (1H, s, phenyl), 7.20—7.50 (15H, phenyl) and 13.98 (1H, s, hydrogen bonding OH). Found: C, 76.41; H, 5.72%. Calcd for $C_{29}H_{26}O_5$: C, 76.65; H, 5.73%.

2-Isopropoxy-3,4,6-tris(benzyloxy)acetophenone (IVa). A mixture of IIIa (0.33 g, 0.7 mmol), isopropyl bromide (0.17 g, 1.4 mmol) and potassium carbonate (anhyd 20 g) in DMF (30 ml) was heated for 1 h at 150 °C. The reaction mixture was poured into ice–water, and then extracted with benzene. The benzene layer was washed with water, dried, and then evaporated. Recrystallization of the residue from hexane gave 0.29 g (80%) of IVa as colorless needles; mp 114 °C. IR (KBr): 1685 cm^{-1}; MS *m/e*: 496 (M^+); NMR δ ($CDCl_3$): 1.16 (6H, d, isopropyl methyl, J=7 Hz), 2.41 (3H, s, acetyl methyl), 4.65 (1H, septet, isopropyl methine, J=7 Hz), 4.93—4.99 (6H, benzyl methylene), 6.32 (1H, s, phenyl) and 7.10—7.45 (15H, phenyl). Found: C, 77.55; H, 6.61%. Calcd for $C_{32}H_{32}O_5$: C, 77.42; H, 6.45%.

2-Ethoxy-3,4,6-tris(benzyloxy)acetophenone (IVb). IVb was prepared according to the procedure described above. In place of isopropyl bromide, ethyl iodide (0.22 g, 1.4 mmol) was used to give 0.3 g (86%) of IVb; mp 87 °C (from hexane). IR (KBr): 1695 cm^{-1}; MS *m/e*: 482 (M^+): NMR δ ($CDCl_3$): 1.28 (3H, t, ethoxyl methyl, J=7.5 Hz), 2.40 (3H, s, acetyl methyl), 4.09 (2H, quartet, ethoxyl methylene, J=7,5 Hz), 4.93—4.99 (6H, benzyl methylene), 6.29 (1H, s, phenyl), 7.20—7.48 (15H, phenyl). Found: C, 77.26; H, 6.26%. Calcd for $C_{31}H_{30}O_5$: C, 77.18; 6.22%.

2-Isopropoxy-3,4,6-trihydroxyacetophenone (Va). A mixture of IVa (0.2 g, 0.4 mmol), 5% palladium–charcoal (3 g), and ethanol (50 ml) was shaken under hydrogen atmosphere for 5 h at room temp. After the removal of the catalyst, ethanol was evaporated to give Va. Recrystallization from

water gave yellow plates of Va (86 mg, 94%); mp 137 °C. IR (KBr): 3450 (OH) and 1630 cm^{-1} (C=O, hydrogen bonded); MS *m/e*: 226 (M^+); NMR δ (CD_3COCD_3): 1.32 (6H, d, isopropyl methyl, J=7 Hz), 2.61 (3H, s, acetyl methine, J=7 Hz), 6.17 (1H, s, phenyl), and 12.87 (1H, s, hydrogen bonding OH). Found: C, 58.69; H, 6.37%. Calcd for $C_{11}H_{14}O_5$: C, 58.40; H, 6.19%

2-Ethoxy-3,4,6-trihydroxyacetophenone (Vb). Vb was prepared according to the procedure described above. Recrystallization from 30% ethanol gave yellow plates of Vb (96%); mp 169 °C. IR (KBr): 3350 (OH) and 1610 cm^{-1} (C=O, hydrogen bonded); NMR δ (DMSO-d_6): 1.45 (3H, t, ethoxy methyl, J=7.5 Hz), 4.21 (2H, quartet, ethoxyl methylene, J=7.5 Hz) 6.18 (1H, s, phenyl), 9.80 (2H, broad, s, OH), and 13.42 (1H, s, hydrogen bonding OH). Found: C, 56.76; 5.81%. Calcd for $C_{10}H_{12}O_5$: C, 56.60; H, 5.66%.

2-Isopropoxy-3,4,6-trimethoxyacetophenone (VI). A solution of 2,4-dihydroxy-3,6-dimethoxyacetophenone[8] (1 g, 4.7 mmol) in ether (10 ml) was treated with excess of etheral diazomethane for 1 h. Evaporation of ether gave a residue which was recrystallized from diisopropyl ether. 2-Hydroxy-3,4,6-trimethoxyacetophenone (IIIb) thereby separated as yellow needles, mp 110—111 °C (lit,[5] mp 112—113 °C). IR (KBr): 1630 cm^{-1} (C=O, hydrogen bonded); NMR δ ($CDCl_3$): 3.64, 3.78 and 3.80 (methoxyl methyl), and 13.60 (1H, s, hydrogen bonding OH). A mixture of IIIb (0.2 g, 0.88 mmol), potassium carbonate (anhyd 5 g) and isopropyl bromide (0.2 g, 1.6 mmol) in DMF (20 ml) was heated for 1 h at 150 °C. The product VI was recrystallized from hexane as colorless needles (0.19 g, 80%); mp 60 °C. IR (KBr): 1710 cm^{-1} (C=O); MS *m/e*: 268 (M^+); NMR δ ($CDCl_3$); 1.26 (6H, d, isopropyl methyl, J=7 Hz), 2.44 (3H, s, acetyl methyl), 3.79—3.88 (9H, methoxyl methyl), 4.56 (1H, septet, isopropyl methine, J=7 Hz), and 6.22 (1H, s, phenyl). Found: C, 62.29; H, 7.78%. Calcd for $C_{14}H_{20}O_5$: C, 62.69; H, 7.46%.

References

1) P. S. Phadke, A. V. Rama Rao, and K. Venkataramane, *Indian J. Chem.*, **5**, (4), 130 (1967); *Chem. Abstr.*, **67**, 116792x (1967).

2) G. S. Krishna Rao, K. Visweswara Rao, and T. R. Seshadri, *Proc. Indian Acad. Sci.*, **27A**, 245 (1948); *Chem. Abstr.*, **43**, 181f (1949).

3) N. P. Beshko, E. V. Gella, V. I. Litvinenko, I. P. Kovalev, and V. G. Gordienko, *Khim. Prir. Soedin.*, **11**, (4), 514 (1975); *Chem. Abstr.*, **84**, 27991 (1976).

4) A. J. Faik, S. J. Smolenski, L. Bauer, and C. L. Bell, *J. Pharm. Sci.*, **64**, 1838 (1975); *Chem. Abstr.*, **84**, 14697 (1976).

5) G. Bargellini, *Atti X° Conger. Inter. Chim.*, **3**, 32 (1939); *Chem. Abstr.*, **34**, 1018[1] (1940).

6) M. Nierenstein, *J. Chem. Soc.*, III, 4 (1917).

7) J. F. W. McOmie, "Advance in Organic Chemistry," Vol. 3, ed by R. A. Raphael, E. C. Talor, and H. Wynberg, Interscience Publishers, New York, N. Y. (1963), p. 321.

8) V. D. Nageswara Sastri and T. R. Seshadri, *Proc. Indian Acad. Sci.*, **24A**, 243 (1946); *Chem. Abstr.*, **41**, 2417i (1947).

An MO Calculation of the Reaction Path of a Symmetry-Disfavored 1,3-Sigmatropic Rearrangement

Tsutomu MINATO, Satoshi INAGAKI, Hiroshi FUJIMOTO, and Kenichi FUKUI

Faculty of Engineering, Kyoto University, Sakyo-ku, Kyoto 606

(Received September 8, 1976)

The path of suprafacial 1,3-sigmatropic rearrangement is studied with the INDO-CI and INDO LMO methods. The methyl migration has been found to be represented by successive 1,2-shifts with a biradicaloid transition state. The interaction between the singly occupied MO's of allyl and methyl fragments is suggested to be responsible for the determination of the path. A subsidiary orbital also plays a part. On the other hand, the chlorine migration has been shown to be a direct 1,3-shift. The interaction between the lowest unoccupied MO of the allyl cationic part and the highest occupied MO of the remaining part, chloride anion, has been found to govern the path of chlorine migration. The lone pair electrons of the migrating fragment makes the successive 1,2-shifts quite unlikely in the 1,3-suprafacial chlorine rearrangements.

The frontier orbital theory[1] and Woodward-Hoffmann rule[2] have been demonstrated to be useful in disclosing the electronic control of chemical reaction paths. On the other hand, some interesting suggestions[3] have been presented on the mechanism of the reactions which do not obey the prediction obtained from the usual orbital symmetry considerations. In this paper, the mechanistic difference between the suprafacial 1,3-sigmatropic migrations of a methyl group and a chlorine atom over the allylic framework will be studied on the basis of a semiempirical all-valence electron MO calculation.

Recently, there have been several notable developments in the study of 1,3-sigmatropic rearrangements. According to the Woodward-Hoffmann rule, 1,3-sigmatropic rearrangements should occur in a suprafacial fashion over the allylic framework with the inversion of the configuration of the migrating group, or in an antarafacial fashion with the retention of the configuration of the migrating species. Experiments do show, however, that some thermal suprafacial 1,3-sigmatropic reactions take place with retention.[4] On the other hand, intramolecular chlorine migration was observed in allyl chloride.[5] If the single chlorine p orbital participates in the rearrangement, the 1,3-migration would be a symmetry-disfavored process. There have been some MO calculations[6] on the mechanisms of the 1,3-migrations. However, the reaction paths have not been discussed in detail as yet. Accordingly it may be worthwhile to study the mechanism of the 1,3-sigmatropic rearrangements based on the detailed information on the possible course of the migration.

We studied first the paths of the 1,3-methyl and chlorine migrations over the allylic framework by the use of the INDO MO method. Then, the bond interchange along the reaction path was examined in terms of the localized molecular orbital (LMO) to get a clearer insight into the formation and breaking of chemical bonds which are characteristic of the migrations.

Method

The INDO approximation[7] is employed in the present MO calculation. The reaction system consists of an allyl and a methyl fragment and of an allyl and a chlorine fragment. The geometrical parameters of allyl and methyl fragment were taken after the standard values proposed by Pople.[7a] Three typical pathways of a suprafacial 1,3-sigmatropic reaction, depicted in Fig. 1, have been examined tentatively. In the first model, Route 1, the migration occurs along the line connecting C_1 and C_3 of the allylic framework. The second is Route 2 in which the migrating group (M) approaches first to C_2, and then moves on to C_3. In Route 3, M transfers from C_1 to C_3 far away from C_2. The energies of the two reaction steps, Step 1 and Step 2, for each of the models, Route 1—3, were compared. Figure 1 illustrates the variables representing the reaction systems. Two independent parameters, R_1 and R_2 were selected. R_1 represents the height of M above the plane of the allylic framework. R_2 stands for the vertical distance between the point of the projection of M onto the allylic plane and the line connecting the two terminal carbons (C_1 and C_3) of the allylic framework. The origin of the coordinate system is taken at the midpoint of C_1 and C_3. The minus sign of R_2 means that M moves away from the origin in the opposite direction to C_2. Step 1 corresponds to the initial stage of the reaction. Namely, M is above the

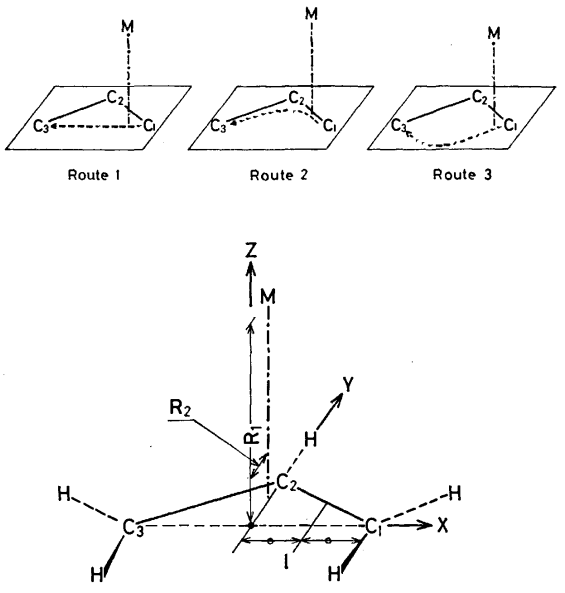

Fig. 1. Assumed reaction models. The origin of the coordinate system is on the center of C_1–C_3 line.

TABLE 1. TOTAL ENERGY OF METHYL MIGRATION

	R_1	R_2	Total energy	Total energy with CI
Step 1	1.50 Å	0.00 Å	−907.46 eV	−907.75 eV
	1.50	0.175	−907.56	−907.84
	1.50	0.35	−907.32	−907.57
	1.40	0.00	−907.45	−907.76
	1.40	0.175	−907.45	−907.77
	1.40	0.35	−907.15	−907.46
Step 2	1.50	0.00	−904.93	−905.36
	1.50	0.35	−905.22	−906.07
	1.50	0.70	−904.25	−905.31
	1.40	0.00	−905.37	−905.86
	1.40	0.35	−904.97	−905.79
	1.40	0.70	−903.68	−904.75

TABLE 2. TOTAL ENERGY OF CHLORINE MIGRATION

	R_1	R_2	Total energy
Step 1	1.80 Å	−0.35 Å	−1073.45 eV
	1.80	−0.175	−1073.46
	1.80	0.0	−1073.37
	1.80	0.175	−1073.18
Step 2	1.80	−0.70	−1071.51
	1.80	−0.525	−1071·59
	1.80	−0.35	−1071.52
	1.80	0.0	−1070.95

line (l) which is perpendicular to the line connecting C_1 and C_3 with X= one-fourth of C_1–C_3 length. Step 2 represents the transition state, and M is placed above the Y-axis. Total energies of the system are listed in Tables 1 and 2.

The Reudenberg-Edmiston LMO's[8] used in Steps 1 and 2 were calculated to investigate the change in the chemical bonds during the reaction. The bond orbitals obtained visualize the appearance and disappearance of specific bonds along the reaction process, as will be seen in the next section.[9]

Results

From the results of the INDO calculation without configuration interaction (CI) given in Table 1 it is seen that Route 2 is adequate for representing the methyl migration at the initial stage but is not suitable for describing the transition state. However, the result with CI suggests that the reaction path would be close to Route 2 throughout the migration. These results indicate that the inclusion of the CI is of essential significance in obtaining reasonable results in regard to the loosely bound transition state. The gross atomic charges given in Table 3 show that the methyl and allyl fragments tend to be neutral at the transition state (R_1=1.50 Å, R_2=0.35 Å).

The most stable geometry for the chlorine migration was found to be R_1=1.80 Å and R_2=−0.175 Å in Step 1, and R_1=1.80 Å, R_2=−0.525 Å in Step 2, as shown in Table 2: that is, the reaction path is close to Route 3. It should be noted that the path is very

The methyl migration. The chlorine migration.

different from that of the methyl migration mentioned above. The chlorine migrates along the pathway as to minimize the interaction with C_2 of the allylic framework. In the chlorine migration the inclusion of the CI did not show any serious change in our conclusion, so the CI result was omitted in Table 2. The electron populations given in Table 3 show that the transition state of the chlorine migration is likely to be an ion-pair.

The LMO's of the methyl migration are illustrated in Fig. 2. It is found that the LMO's localized in C–H bonds do not change markedly throughout the migration. The methyl carbon (C_M)–C_1 bond which disappears in the reaction is transformed into a three-centered bond, C_1–C_M–C_2, and the double bond (C_2=C_3) is represented by two bent bonds in Step 1. In Step 2 one of the bent bonds of C_2=C_3 is transformed into the three-centered bond (C_2–C_M–C_3), and the other bent bond is converted to a σ-bond (C_2–C_3). Accordingly, two three-centered bonds appear in Step 2. The LMO's of the doubly-excited configuration were also calculated. The doubly-excited configuration in which a pair of electrons are promoted from the highest occupied (HO) MO to the lowest unoccupied (LU) MO of the whole system was found to be the most important one from the CI calculation. Figure 3 illustrates several LMO's of the doubly-excited configuration in Step 2. One of the two three-centered bond orbitals is converted to the C_M–C_2 bond and the other is transformed to the orbital which localizes at C_1 and C_3. This localized orbital at C_1 and C_3 seems to represent the biradical nature of the system. The transition state has been found from the CI calculation to be described sufficiently well by the linear combination of the ground configuration and the doubly-excited configuration mentioned above. It is concluded, therefore, that the transition state of the methyl migration possesses a biradical character to a certain extent.

The LMO's for the chlorine migration are illustrated in Figs. 4 and 5. It is seen that the LMO's localized in the C–H bonds are not changed markedly throughout the migration. Figure 4 demonstrates that the mode

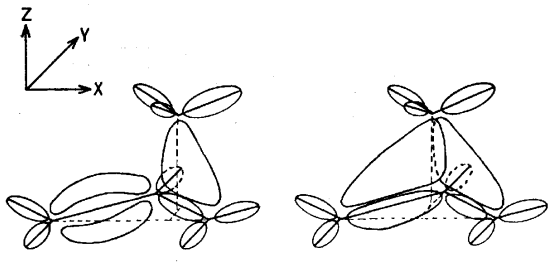

Fig. 2. The schematic presentation of the LMO's of the methyl migration. (a): Step 1. (b): Step 2.

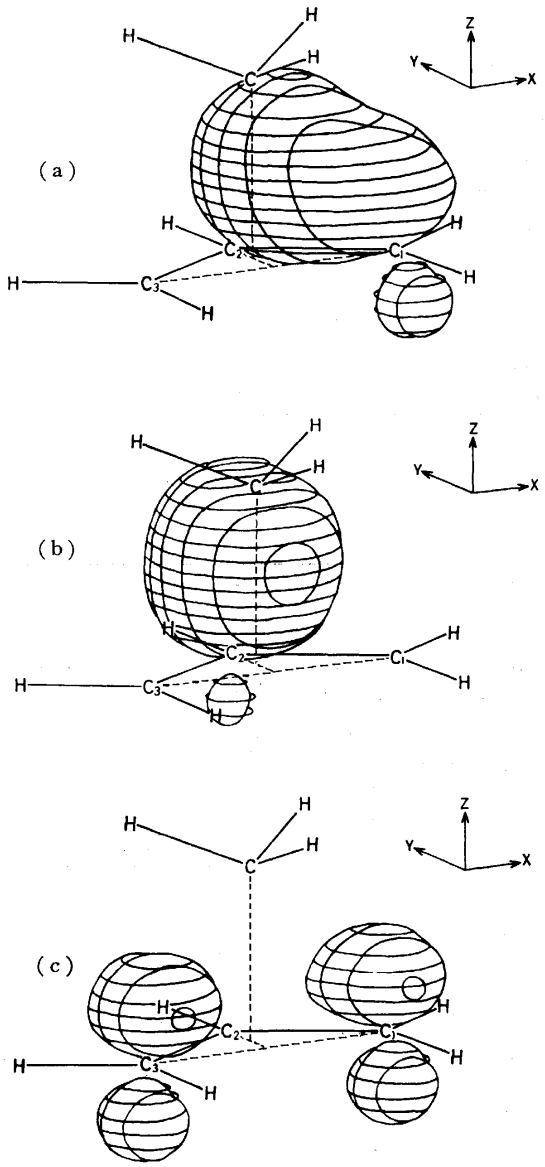

Fig. 3. The particular LMO shapes of the methyl migration. The density line is 0.3 e/Å^3. (a): One of the three-centered bonds of the ground configuration at the transition state. (b): One of the LMO's of the doubly-excited configuration at the transition state. (c): Another LMO of the doubly-excited configuration at the transition state.

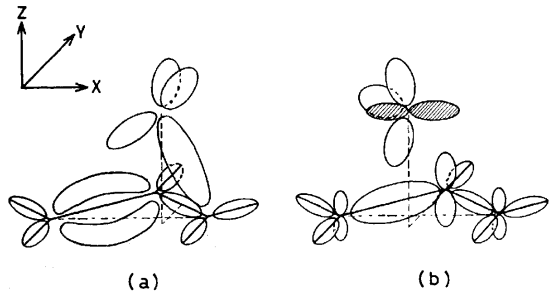

Fig. 4. The schematic presentation of the LMO's of the chlorine migration. (a): Step 1. (b): Step 2. Two shaded lobes which are nearly equal to chlorine $3p_x$ AO represent one of the chloride anion lone pairs, and one LMO is composed of three $2p_z$ Ao's of the allyl carbons.

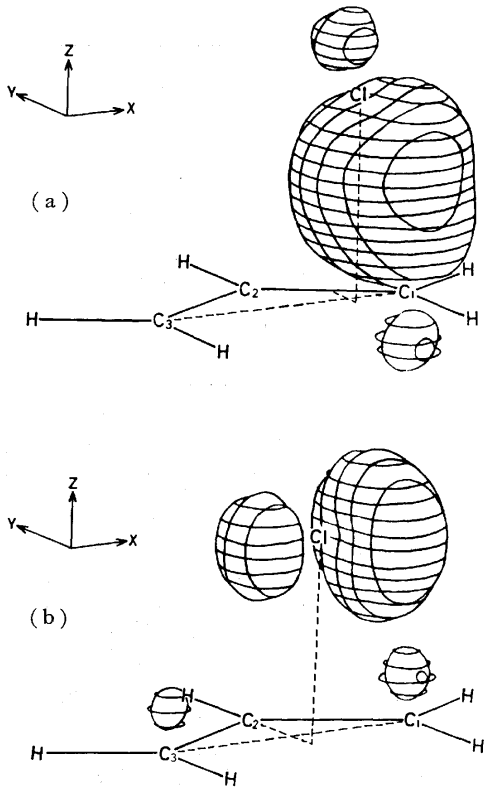

Fig. 5. The particular LMO shapes of the chlorine migration. The density line is 0.3 e/Å^3. (a): C_1–Cl bond orbital of Step 1. (b): C_1–Cl–C_3 bond orbital of Step 2.

of bond interchange in the chlorine migration is different from that in the methyl migration. In the case of the chlorine migration, one of the bent LMO's representing C_2–C_3 bond is transformed into the LMO composed of three $2p_z$ atomic orbitals (AO's) of allyl carbons. The chlorine atom is bonded to C_1 and C_3 of the allylic framework by the LMO corresponding to the chlorine lone pair at the transition state. However, the LMO representing C_1–Cl–C_3 three-centered bond is almost exclusively localized at the chlorine $3p_x$ AO and, hence, the migrating chlorine is bound to the allylic framework very weak in the neighborhood of the transition state. The gross charges on the composed atoms and groups shown in Table 3 indicate that the transition state should be described as an ion-pair between the allyl cation and chloride ion, in agreement with the result of the LMO calculation.

We may conclude here from our INDO-CI and LMO calculations that the suprafacial migration of methyl with retention of the configuration of the migrating center, takes place *via* successive 1,2-shifts. However, the migration possesses a single symmetrical transition state and, hence, it should be classified as a one-step process. On the contrary, the chlorine migration is concluded to occur by way of a direct 1,3-shift with an ion-pair transition state.

TABLE 3. ATOMIC GROSS CHARGE AT THE TRANSITION STATE

The optimized geometry without CI ($R_1=1.40$ and $R_2=0.0$) of the methyl migration.

	Allyl carbon			Allyl group	Methyl carbon	Methyl group
	C_1	C_2	C_3			
Gross charge	−0.187	0.229	−0.187	−0.153	0.394	0.153

The optimized geometry with CI ($R_1=1.50$ and $R_2=0.35$) of the methyl migration.

	Allyl carbon			Allyl group	Methyl carbon	Methyl group
	C_1	C_2	C_3			
Gross charge without CI	−0.172	0.211	−0.172	−0.142	0.333	0.142
Gross charge with CI	−0.162	0.203	−0.162	−0.131	0.311	0.131

The optimized geometry ($R_1=1.80$ and $R_2=-0.525$) of the chlorine migration.

	Allyl carbon			Allyl group	Chlorine
	C_1	C_2	C_3		
Gross charge	0.143	0.043	0.143	0.400	−0.400

Discussion

Let us interpret here the reaction mechanisms of the methyl and chlorine migrations by means of the orbital interaction in order to disclose the reason why the paths of the migrations are different from each other.

Methyl Migration. The principal orbital interactions involve the three π orbitals (π_1, π_2, and π_3) of the allyl group, and a σ-type (ϕ_σ) and a π-type (ϕ_π) orbitals of the methyl group as shown in Fig. 6. The interaction of ϕ_σ with π_1 and π_3 gives ϕ_1, ϕ_4, and ϕ_5, and that between π_2 and ϕ_π gives ϕ_2 and ϕ_3. The CI coefficients of the lowest closed-shell configuration and the $\phi_3\rightarrow\phi_4$ doubly-excited configuration are listed in Table 4, as well as the orbital energies of ϕ_3 and ϕ_4. The contributions of the other excited configurations are found to be negligibly small. The MO ϕ_4 has a bonding nature between C_2 and C_M, but the MO ϕ_3 is antibonding. Accordingly, the mixing in of the $\phi_3\rightarrow\phi_4$ doubly-excited configuration gives rise to the strengthening of both the σ and π type bondings in the reaction system. Table 4 clearly indicates that the effect of the CI becomes more significant as the separation between the methyl carbon and C_2 gets smaller.

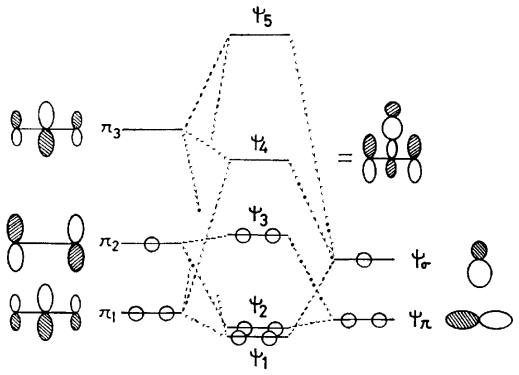

Fig. 6. The MO interaction diagram at the transition state of the methyl migration.

TABLE 4. THE CI BOEFFICIENTS AND ORBITAL ENERGY AT THE TRANSITION STATE OF THE METHYL MIGRATION

R_1	R_2	C_0	$C_{3\rightarrow4}$	ϕ_3	ϕ_4
1.50 Å	0.70 Å	0.934	0.352	−6.99 eV	2.39 eV
1.50	0.35	0.950	0.309	−6.72	3.31
1.50	0.0	0.979	0.192	−6.31	4.14

The enhancement of mixing in of the diexcited configuration is attributable to the decrease in the energy gap between ϕ_3 and ϕ_4. The interaction between ϕ_σ and π_1 stabilizes the system.[3a] On the other hand, the interaction between ϕ_σ and π_3 leads to the lowering of the ϕ_4 orbital. It is obvious that the dominant component of ϕ_4 is π_3. The interaction between ϕ_σ and π_3 contributes to the stabilization of the transition state, as well as the interaction between ϕ_σ and π_1, through the lowering of the composite MO ϕ_1.

Berson and Salem introduced the subjacent orbital effect in order to explain the occurrence of the formally symmetry-disfavored 1,3-migrations. They claimed that this resulted not from an effect on the HOMO but instead from the interaction of the carbon p orbital with a subjacent, bonding allyl orbital.[3a] We feel, however, that the interaction of the carbon p orbital with a subjacent orbital (π_1) was over-emphasized in their discussion. Since the carbon p orbital can interact both with π_1 and π_3, the role of π_3 orbital should be clearly recognized.[10] Our INDO-CI calculation disclosed not only the importance of the depression of ϕ_1 as the major stabilization through the direct overlap interaction between ϕ_σ and π_1 but also that of ϕ_4 for lifting the destabilization due to ϕ_3 through the mixing in of the $\phi_3\rightarrow\phi_4$ doubly-excited configuration to facilitate the occurrence of the migration.

The mechanism of 1,3-sigmatropic shift was rationalized above as a successive 1,2-shift. The interaction between the singly occupied (SO) MO of the allyl and the SOMO of the methyl is considered to have a key importance in stabilizing the reaction system at the

initial stage of the migration. As the migration proceeds, however, the stabilization decreases because of the out-of-phase overlapping of ψ_σ with the C_3 lobe of the antisymmetric π_2 becomes large. Accordingly, the reaction would proceed along the pathway in which the C_3 lobe and ψ_σ tend to overlap as little as possible. That is, the migration seems to take the pathway in which the destabilization due to the weakening of the SOMO-SOMO interaction is as small as possible. Furthermore, the reaction should take place in a way as to give a large overlapping between ψ_σ and π_1. At the transition state the interaction of ψ_σ with π_1 and π_3 orbitals is important. Since the π_1 and π_3 MO's possess the largest amplitudes at the central carbon, the methyl group comes closer to C_2 to create larger overlaps of ψ_σ with π_1 and with π_3. The reason why Route 2 is the most favorable pathway is thus clarified.

The preference of the 1,2-shift to the direct 1,3-shift is explained in another way by considering the orbital interaction between the π bond (C_2–C_3) and the σ-bond (C_1–C_M) to be broken.[11] The reaction may be initiated by the charge-transfer interaction from the former to the latter and *vice versa*. The mode of the orbital interaction between the HOMO and the LUMO of the two localized bonding regions is depicted in Fig. 7. It

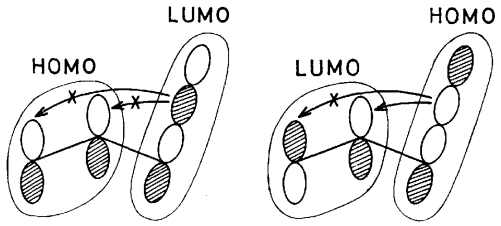

Fig. 7. The mode of the orbital interaction between the two bonding region.

is seen that the overlapping of the HOMO of the C_2–C_3 π bond with the LUMO of the C_1–C_M σ bond is ineffective, while the overlapping of the LUMO of the former with the HOMO of the latter is effective. It is now obvious that the overlap interaction between the HOMO of the C_1–C_M bond and the LUMO of the C_2–C_3 π bond in this migration makes a successive 1,2-shift more likely than a direct 1,3-shift. This explanation leads to an important prediction that the 1,3-sigmatropic rearrangement with retention will occur easily when the migrating group has an electron donating group.[12]

The mechanism presented here (a successive 1,2-shift) agrees with the experimental results in regard to the stereoselectivity of the migrating center.[4c] The rate ratio of the 1,3-suprafacial rearrangement with retention to the rearrangement with inversion increases in the order bicyclo[2.1.1]hexene series (1)<bicyclo[3.2.0]-heptene series (2)<bicyclo[4.2.0]octene series (3)< monocyclic series (4).[13]

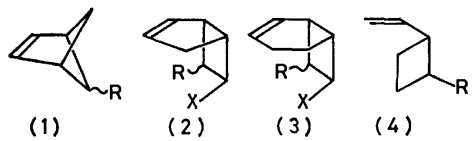

Berson and Holder[4c] proposed that this rate ratio might depend on the reactant structures. Namely, they suggested that the overlap between the front lobe of the migrating carbon and the suprafacial lobe of the central carbon of the allylic framework would stabilize the transition state of the symmetry-disfavored reactions. The Berson's interpretation is consistent with our conclusion derived here, *i.e.*, the suprafacial 1,3-shift with retention of the configuration can be interpreted in terms of a successive 1,2-shift, because the facility of a 1,2-shift is also dependent upon the reactant structure.

Chlorine Migration. The orbital interaction of Step 2 was examined in a similar way as that of the methyl migration. The principal orbital interaction seems to include the three π orbitals of the allylic framework and chlorine $3p_x$ and $3p_z$ AO's. From the gross charges in Table 3, it is appropriate to consider here the orbital interaction between an allyl cation and a chloride anion. The MO interaction diagram is presented in Fig. 8. It is noted that the ψ_3 and ψ_4 MO's are interchanged in chlorine migration in comparison with the case of methyl migration. This is a reason why the inclusion of the CI does not change seriously the conclusion derived from the results of calculation without CI. The MO ψ_3 of the chlorine migration was found to have antibonding character between Cl and C_2 in the transition state. This means that the interaction between $3p_z$ AO and π_1 is greater than that between $3p_z$ AO and π_3. The difference in the ordering of the ψ_3 and ψ_4 levels between methyl and chlorine migrations is attributed to the lower energy of the chlorine $3p_z$ AO than that of the ψ_σ MO of the methyl group. Figure 8 shows that the interaction between the HOMO ($3p_x$ AO) of the chloride anion and the LUMO (π_2) of the allyl cation stabilizes the transition state effectively.

The path of the 1,3-migration of chlorine is rationalized in the following manner. The interaction between the π_2 MO and the $3p_z$ AO has a key importance in stabilizing the reaction system at the initial stage of the migration. As the migration proceeds, however, the stabilization decreases because the out-of-phase overlapping of $3p_z$ AO with the C_3 lobe of the antisymmetric π_2 becomes large. However, throughout the chlorine migration reaction, unlike the methyl migration, the interaction between π_2 and $3p_x$ AO is bonding in character to stabilize the system efficiently. The interaction between π_1 and $3p_z$ AO is larger than that be-

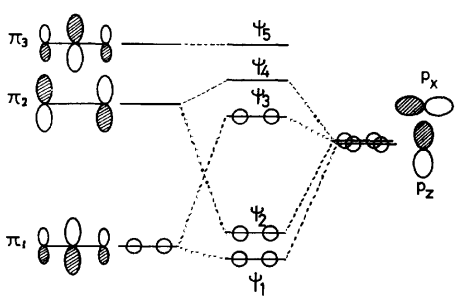

Fig. 8. The MO interaction diagram at the transition state of the chlorine migration.

tween π_3 and $3p_z$ AO as mentioned above. Consequently, the interaction of $3p_z$ with π_1 and π_3 leads to the destabilization of the reaction system. The destabilization makes the chloride anion migrate in such a way as to minimize the overlap with C_2. The reason why Route 3 is the most favorable pathway is clarified. The difference between the mechanism of the methyl migration and that of the chlorine migration can be ascribed to the presence of a low-lying pair of electrons in the migrating species in the latter case.

It is interesting to examine the intramolecular acid-catalyzed isomerization of allyl alcohols[14] in relation to the chlorine migration described above.

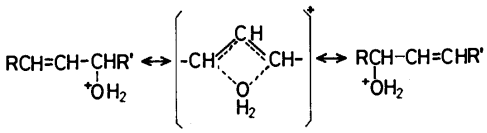

In this case, the transfer of the double-bond and the migration of the hydroxyl group as a neutral water molecule are supposed to take place simultaneously.[14b] It is considered that the path of isomerization may be similar to the chlorine migration, water molecule being bonded to two terminal carbons of the allylic framework at the transition state, because the migrating species has a lone pair orbital relevant to the orbital interaction with the π_1 and π_3 MO's and another lone pair orbital to the interaction with π_2 MO of the allyl fragment.

Conclusion

It is concluded here that 1,3-sigmatropic rearrangement may occur suprafacially on the allylic framework with retention of the configuration of the migrating center as the result of a successive 1,2-shift with a radical nature. This is interpreted by the SOMO-SOMO interaction between the allyl radical and the methyl radical in the initial stage and the subsidiary orbital effect near the transition state. In the chlorine migration the HOMO-LUMO interaction between the allyl cation and the chloride anion provides the dominant stabilization to the reaction system. From the present calculation, it is clarified that the mechanism of 1,3-migration in allylic framework depends on the property of the migrating species.

We would like to express our gratitude to the Data Processing Center, Kyoto University, for its generous permission to use the FACOM 230-75 computer. Our MO calculation was carried out under the financial support of the Ministry of Education (Grant-in-Aid 047068).

References

1) (a) K. Fukui, "Molecular Orbitals in Chemistry, Physics, and Biology," P.-O. Löwdin and B. Pullmann, Ed., Academic Press, New York, N. Y. (1964), p. 513; (b) K. Fukui and H. Fujimoto, "Mechanisms of Molecular Migration," ed by B. S. Thyagarajan, Interscience, Vol. 2, New York, N. Y. (1969), p. 118; (c) K. Fukui, "Theory of Orientation and Stereoselection," Springer-Verlag, Heidelberg (1970).

2) R. B. Woodward and R. Hoffmann, "The Conservation of Orbital Symmetry," Academic Press, New York, N. Y. (1970).

3) (a) J. A. Berson and L. Salem, *J. Am. Chem. Soc.*, **94**, 8917 (1972); (b) J. A. Berson, *Acc. Chem. Res.*, **5**, 406 (1972); (c) S. Inagaki, H. Fujimoto, and K. Fukui, *J. Am. Chem. Soc.*, **97**, 6108 (1975); (d) N. D. Epiotis, *ibid.*, **94**, 1924 (1972); (e) K. Yamaguchi, T. Fueno, and H. Fukutome, *Chem. Phys. Lett.*, **22**, 461 (1973); (f) W. Schmidt, *Tetrahedron Lett.*, **1972**, 581.

4) (a) J. A. Berson and G. L. Nelson, *J. Am. Chem. Soc.*, **92**, 1096 (1970); (b) J. A. Berson and P. B. Dervan, *ibid.*, **95**, 269 (1973); (c) J. A. Berson and R. W. Holder, *ibid.*, **95**, 2073 (1973); (d) J. A. Berson, T. Miyashi, and G. Jones, II, *ibid.*, **96**, 3468 (1974); (e) J. Meinwald and D. Schmidt, *ibid.*, **91**, 5877 (1969); (f) H. E. Zimmerman, J. D. Robbins, and J. Schantl, *ibid.*, **91**, 5878 (1969); (g) R. C. Cookson and J. E. Kemp, *Chem. Commun.*, **1971**, 385.

5) W. G. Young, S. Winstein, and H. L. Goering, *J. Am. Chem. Soc.*, **73**, 1958 (1951).

6) (a) H. M. Niemeyer and P. Ahlberg, *Chem. Commun.*, **1974**, 799; (b) H. M. Niemeyer, O. Goscinski, and P. Ahlberg, *Tetrahedron*, **31**, 1699 (1975); (c) F. Bernardi, N. D. Epiotis, and R. L. Yates, *J. Am. Chem. Soc.*, **97**, 1334 (1975); (d) N. D. Epiotis, R. L. Yates, and F. Bernardi, *ibid.*, **97**, 4198 (1974).

7) (a) J. A. Pople and D. L. Beveridge, "Approximate Molecular Orbital Theory," McGraw-Hill, New York, N. Y. (1970); (b) P. E. Stevenson and D. L. Burkey, *J. Am. Chem. Soc.*, **96**, 3061 (1974).

8) C. Edmiston and K. Reudenberg, *Rev. Mod. Phys.*, **35**, 457 (1963).

9) D. A. Dixon and W. N. Lipscomb, *J. Am. Chem. Soc.*, **95**, 2854 (1973).

10) We shall examine the interaction of the carbon p orbital having one electron with the occupied π_1 orbital and the unoccupied π_3 orbital. This interaction gives three orbitals. The lowest energy level orbital given by the interaction is depressed relative to the π_1 by the interaction between the p and π_1. The new radical orbital energy level is not remarkably affected, because the interaction between the p and π_1 raises the new radical orbital but that between the p and π_3 depresses the radical orbital. Thus the transition state is considered to be stabilized. Similar discussion is implicitly included in Ref. 3a.

11) K. Fukui, *Acc. Chem. Res.*, **4**, 57 (1971).

12) The rate ratio of the suprafacial 1,3-sigmatropic rearrangement with retention to that with inversion was observed to be greater on *endo*-7-*exo*-methylbicyclo[3.2.0]heptenyl acetate than on *endo*-7-*exo*-D-bicyclo[3.2.0]heptenyl acetate.[4c] This observation seems to show that the migrating group with an electron donating group would make the 1,3-rearrangement occur easily since the methyl group is considered to be an electron donating one.

13) The high stereospecificity was observed in the case of bisallyl system.[4d,4e,4f] In this case there is another factor, a multi-cyclic interaction. *C.f.*, S. Inagaki, T. Minato, H. Fujimoto, and K. Fukui, *Chem. Lett.*, **1976**, 89.

14) (a) R. Huisgen, R. Grashey, and J. Sauer, "The Chemistry of Alkenes," ed by S. Patai, Interscience, New York (1964), Chap. 10; (b) E. A. Braude and E. R. Jones, *J. Chem. Soc.*, **1944**, 436; (c) W. G. Young, K. Nozaki, and R. Warner, *J. Am. Chem. Soc.*, **61**, 2564 (1939); (d) H. L. Georing and R. R. Josephson, *ibid.*, **84**, 2779 (1962).

Determination of the $6^3P_1 \rightarrow 6^3P_0$ Transition Rate of Hg in CO and NO by a Modulation Technique

Hiroyuki HORIGUCHI and Soji TSUCHIYA

Department of Pure and Applied Sciences, College of General Education, University of Tokyo, Meguro-ku, Tokyo 153

(Received November 1, 1976)

In order to determine the branching ratio for $Hg(6^3P_1)$ deactivation to the 6^3P_0 and 6^1S_0 states in CO or NO, a modulation technique was utilized. The intensity of 253.7-nm radiation was modulated at a frequency in the range from 0.1 to 20 kHz, and the resulting a.c. component of the $Hg(6^3P_1$ or $6^3P_0)$ concentration was measured by monitoring the absorption of the 435.8- or the 404.7-nm emission line from an Hg discharge lamp. The lower detection limit of excited Hg atoms was 10^7 cm^{-3} in this experimental method. On the basis of the $Hg(6^3P_0)$ concentration relative to that of $Hg(6^3P_1)$ in an Ar+CO or NO mixture including information on the phase delay, the $6^3P_1 \rightarrow 6^3P_0$ transition rate could be determined; the $6^3P_1 \rightarrow 6^3P_0$ cross section was found to be 22.4 Å^2 for CO and 7.1 Å^2 for NO and the $6^3P_0 \rightarrow 6^1S_0$ cross section to be 1.80 Å^2 for CO and 37 Å^2 for NO at room temperature.

A number of studies[1] have been reported on the lifetime measurement of $Hg(6^3P_1)$ atoms, which gives the sum of the rate constants for the collisional processes, $6^3P_1 \rightarrow 6^3P_0$ and $\rightarrow 6^1S_0$. In order to separate these two processes, it is necessary to monitor a transient or stationary concentration of $Hg(6^3P_0)$ atoms through an energy transfer process. (Hereafter, $Hg(6^3P_1)$, Hg (6^3P_0) and $Hg(6^1S_0)$ will be denoted by Hg_1*, Hg_0* and Hg, respectively.) Three reports have appeared on the determination of the $Hg_1^* \rightarrow Hg_0^*$ spin-orbit relaxation rate. The method employed by Callear and McGurk[2] is based on the fact that the Hg_0* concentration in a quenching gas relative to that in N_2 just after the flash excitation of Hg results in the quantum yield of Hg_0* (=the spin-orbit relaxation rate divided by the Hg_1* deactivation rate), since N_2 deactivates Hg_1* only to Hg_0*. In a previous experiment by Horiguchi and Tsuchiya,[3] a stationary concentration of Hg_0* atoms yields the spin-orbit relaxation rate if the Hg_0* deactivation rate is known. Vikis *et al.*[4] have also determined this rate by detecting the Hg_0* atoms through the amount of H_2 formed by the reaction of ethylene with Hg_0*. In these experiments, however, if the collisional transition from the 6^3P_1 state is mostly to the 6^1S_0 state or if the deactivation rate of Hg_0* is of the same order of magnitude as that of Hg_1*, the Hg_0* concentration becomes very small, and it is difficult to determine it to high accuracy. In this paper, a modulation technique is introduced in order to improve the detectivity of the Hg_0* atoms as well as to obtain information on the kinetics of excited Hg atoms.

Experimental

The apparatus was essentially the same as that described in a previous paper.[5] A quartz cell (3 cm in diameter and 24 cm in length) containing a gaseous mixture of Ar+a quenching gas containing Hg vapor at 1.9×10^{-4} Torr was illuminated by six low-pressure Hg discharge lamps (Toshiba 10-W germicidal lamps). A 200-W oscillator (Elger, 251) with a frequency variable in the range from 0.01 to 10 kHz supplied the power for the lamps through ballast resistors. Then, the intensity of 253.7-nm radiation was modulated at twice the frequency of the power source with a waveform that was approximately triangular rather than sinusoidal. An example of the waveform is shown in Fig. 1. The waveform is composed mainly of the fundamental component, the harmonic contribution being less than 10% of the fundamentals. For the present experiment, only the fundamental component is considered. This is justified if the rate equation for Hg* deactivation is of first order with respect to [Hg*], since the harmonic components may be separated from the fundamentals.

For detection of the Hg* atoms, the 404.7- or 435.8-nm emission line from a d.c.-operated Hg discharge lamp was passed through the cell, and then into a monochromator (Spex, 1700III) equipped with a photomultiplier. The output was analyzed by a lock-in amplifier (P. A. R. 186), the reference signal of which was supplied from a photo-tube that monitored 253.7-nm radiation. A quadrature output from the lock-in amplifier divided by an in-phase output gave the tangent of the phase-shift angle for the a.c. component of the Hg* concentration. Since the absorption intensity is not proportional to the Hg* concentration at higher densities, a condition of a low Hg* concentration was chosen in order to meet the requirement that the optical density for absorption be less than 0.02. The signal-to-noise ratio was greatly improved by using a lock-in amplifier, so that absorptions with optical densities as small as 10^{-4} could be detected. This absorption corresponds to 10^7 cm^{-3} of Hg_0* or Hg_1* atoms under the present conditions. In a previous experiment,[3] the lower detection limit of [Hg_0*] was *ca.* 10^9 cm^{-3}. This can be expected from the atomic absorption spectrometry for analyses of atoms having *f*-numbers similar to Hg_0*. Thus, the sensitivity is improved by a factor of 10^2 in the present modulation technique.

The nominal purities of the sample gases, Ar, N_2, CO, and NO, were 99.999, 99.995, 99.5, and 98.5%, respectively. The first two gases were used without further treatment.

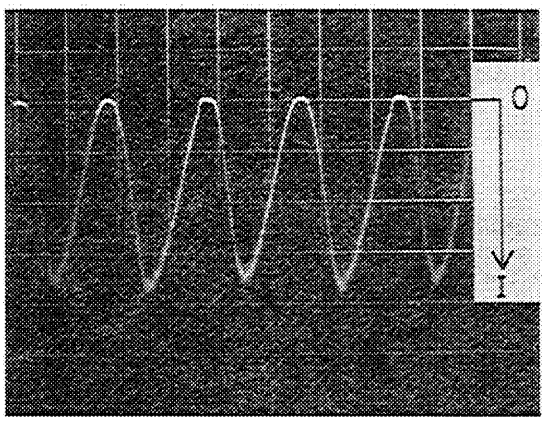

Fig. 1. Waveform of the 253.7-nm radiation intensity from an Hg discharge lamp powered by an oscillator whose frequency is 500 Hz (0.5 ms/div.).

CO was purified by repeated adsorption and desorption on molecular sieve 5A at liquid N_2 temperature, and NO was first passed through a column containing molecular sieve 5A and solidified several times for further purification. The fraction of Ar or CO in an Ar+CO mixture was determined by pressure measurement in a mixing vessel of calibrated volume. Hg vapor in the gas mixture was once removed by passing the gas through a spiral trap at 77 K, and later, the gas was fed into the cell through an Hg saturator at 0 °C. Since Hg-sensitized decomposition of NO was expected, a flow technique was adopted for measurements in an Ar+NO mixture. A capacitance manometer (M.K.S. 210) was employed for the pressure measurements; the fraction of NO in the mixture was determined from the pressure increase which was measured differentially.

Principle of the Modulation Technique

The application of the modulation technique to studies on chemical kinetics has been reviwed by Phillips.[6] Here, the modulation spectroscopy to elucidate the initial stage of Hg-photosensitized reactions will be discussed. If excited Hg atoms are formed in an Ar+CO mixture, the following energy transfer processes should be taken into account:

$$\mathrm{Hg} + h\nu(253.7\text{-nm}) \rightleftharpoons \mathrm{Hg_1}^*, \quad (1)$$

$$\mathrm{Hg_1}^* + \mathrm{CO}(v=0) \rightleftharpoons \mathrm{Hg_0}^* + \mathrm{CO}(v=1), \quad (2)$$

$$\mathrm{Hg_1}^* + \mathrm{CO}(v=0) \longrightarrow \mathrm{Hg} + \mathrm{CO}(v\geq 0), \quad (3)$$

$$\mathrm{Hg_0}^* + \mathrm{CO}(v=0) \longrightarrow \mathrm{Hg} + \mathrm{CO}(v\geq 0), \quad (4)$$

$$\mathrm{Hg_0}^* \longrightarrow \mathrm{Hg}, \quad (5)$$

$$\mathrm{CO}(v=1) \longrightarrow \mathrm{CO}(v=0), \quad (6)$$

of which Reaction 5 is the sum of all deactivation processes including wall collisions and those with impurity molecules, and Reaction 6 represents similar processes for the deactivation of $CO(v=1)$. Vibrational excitation of CO in Reactions 3 and 4 has been demonstrated by the infrared emission measurements of Polanyi and coworkers.[7] However, direct experimental evidence for vibrational excitation in Reaction 2 has not yet appeared. However, since the spin-orbit relaxation in N_2 accompanies vibrational excitation of N_2,[5] it is reasonable to suppose a similar reaction for Hg_1*-CO collisions.

The modulated intensity of 253.7-nm radiation may be represented as

$$I = \bar{I} + I_0 e^{i\omega t}, \quad (7)$$

where ω is the angular frequency of modulation. Corresponding to the above equation, the excited species formed make a cycle of appearance and dissipation, *i.e.*,

$$x_0 = [\mathrm{Hg}] = \bar{x},$$
$$x_1 = [\mathrm{Hg_1}^*] = \bar{x}_1 + \boldsymbol{x}_1 e^{i\omega t},$$
$$x_2 = [\mathrm{Hg_0}^*] = \bar{x}_2 + \boldsymbol{x}_2 e^{i\omega t},$$
$$y_0 = [\mathrm{CO}(v=0)] = \bar{y}_0,$$
$$y_1 = [\mathrm{CO}(v=1)] = \bar{y}_1 + \boldsymbol{y}_1 e^{i\omega t},$$

where the first term of the right-hand side in each case represents the d.c. component of the respective concentration and the second term the a.c. component, except for ground-state atoms or molecules whose a.c. components are disregarded since they are much more abundant than the excited species. The amplitude of the a.c. component must be a complex number since a phase delay is expected.

On the basis of the mechanism involving Reactions 1—6, the rate equations can be written as

$$dx_1/dt = k_1 I_0 x_0 - k_{-1}x_1 - k_2 y_0 x_1 - k_3 y_0 x_1 + k_{-2}x_2 y_1, \quad (8)$$

and

$$dx_2/dt = k_2 x_1 y_0 - k_{-2}x_2 y_1 - k_4 x_2 y_0 - k_5 x_2, \quad (9)$$

where the rate constant for Reaction j is denoted by k_j and the reverse reaction rate by k_{-j}. If the a.c. parts of these equations are separated, the following equations can be derived:

$$i\omega \boldsymbol{x}_1 = k_1 I_0 \bar{x}_0 - (k_{-1} + k_2\bar{y}_0 + k_3\bar{y}_0)\boldsymbol{x}_1 + k_{-2}\bar{y}_1 \boldsymbol{x}_2, \quad (10)$$

and

$$i\omega \boldsymbol{x}_2 = k_2 \bar{y}_0 \boldsymbol{x}_1 - (k_{-2}\bar{y}_1 + k_4\bar{y}_0 + k_5)\boldsymbol{x}_2. \quad (11)$$

In these equations, it is assumed that $\bar{y}_1 \gg |\boldsymbol{y}_1|$, since the lifetime of $CO(v=1)$ is much longer than ω^{-1}, which is less than 1.3 ms. The imaginary part of Eq. 10 results in the equation,

$$-\boldsymbol{x}_1^i/\boldsymbol{x}_1^r = \tan\phi_1 = [1/(k_{-1} + k_2\bar{y}_0 + k_3\bar{y}_0)][\omega + k_{-2}\bar{y}_1(-\boldsymbol{x}_2^i/\boldsymbol{x}_1^r)]. \quad (12)$$

The corresponding equation derived from Eq. 11 is

$$-\boldsymbol{x}_2^i/\boldsymbol{x}_2^r = \tan\phi_2 = [1/(k_{-2}\bar{y}_1 + k_4\bar{y}_0 + k_5)][\omega + k_2\bar{y}_0(-\boldsymbol{x}_1^i/\boldsymbol{x}_2^r)]. \quad (13)$$

Here, ϕ_1 and ϕ_2 are defined as phase delay angles for the a.c. components of $[Hg_1^*]$ and $[Hg_0^*]$, respectively, and $\boldsymbol{x}_j^r$ and $\boldsymbol{x}_j^i$ are the real and imaginary parts, respectively, of $\boldsymbol{x}_j$. The real part may be obtained from the in-phase signal of the absorption and the imaginary from the quadrature.

The reciprocal radiative lifetime of Hg_1* is estimated to be 3.5×10^6 s^{-1} which is calculated according to the Milne-Samson equation[8] for the correction of radiation imprisonment effect. This value is much larger than the angular frequency of modulation in this experiment. Therefore, the phase delay for the Hg_1* concentration may not be of detectable magnitude, *i.e.*, $\tan\phi_1 \fallingdotseq 0$. Hence, Eq. 13 can be approximated by

$$\tan\phi_2 = \omega/(k_{-2}\bar{y}_1 + k_4\bar{y}_0 + k_5). \quad (13')$$

In addition, the real part of Eq. 11 results in the relation,

$$k_2 y_0 = \omega(\boldsymbol{x}_2^r/\boldsymbol{x}_1^r)(\tan\phi_2 + \cot\phi_2). \quad (14)$$

Thus, the spin-orbit relaxation rate of $Hg_1^* \rightarrow Hg_0^*$ can be determined if the phase-delay angle and the a.c. component of the Hg_0* concentration relative to that of Hg_1* are measured.

Results and Discussion

In Fig. 2, the observed phase-delay angle, ϕ_2, for the a.c. component of the Hg_0* concentration in an Ar+CO mixture is plotted as a function of the modulation frequency. The results are in good agreement with the relation

$$\tan\phi_2 = \omega\tau, \quad (15)$$

where τ is the lifetime of Hg_0* and is defined by Eq. 13′ as

$$\tau = (k_{-2}\bar{y}_1 + k_4\bar{y}_0 + k_5)^{-1}. \quad (16)$$

This equation shows that the lifetime is dependent on the concentration of vibrationally excited CO as well as on that of ground-state CO. If the spin-orbit relaxation accompanies the vibrational excitation, an excess amount of $CO(v=1)$ is formed. Hence, it is expected that strong 253.7-nm radiation causes an ac-

Table 1. The reciprocal lifetime of $Hg(6^3P_0)$ in an Ar+CO mixture at 10 Torr as a function of the 253.7-nm photon intensity

p(CO) (Torr)	253.7-nm photon intensity (photon $cm^{-3}\ s^{-1}$)				
	3.85×10^{15}	2.70×10^{15}	1.33×10^{15}	6.65×10^{14}	3.40×10^{13}
0.20	6.42	6.28	5.76	6.28	$6.22\times10^4\ s^{-1}$
0.01	5.03	5.46	4.83	4.70	$4.79\times10^3\ s^{-1}$

Table 2. A part of the experimental results for determination of $Hg_1^* \rightarrow Hg_0^*$ and $Hg_0^* \rightarrow Hg$ transition rates

p(CO) (Torr)	f (Hz)	x_2^r/x_1^r	$\tan\phi_2$	k_2y_0 (s^{-1})	$k_4y_0+k_5$ (s^{-1})
a) Data for Ar+CO mixtures at 10 Torr.					
0.045	2×10^3	6.71	0.923	1.69×10^5	1.36×10^4
0.106	2	9.47	0.401	3.44	3.13
	4	7.03	0.865	3.57	2.90
	8	4.12	1.679	4.71	2.99
0.20	1	11.7	0.106	7.01	5.93
	2	9.82	0.196	6.54	6.41
	4	9.45	0.434	6.50	5.79
0.37	2	13.3	0.118	14.4	10.65
				$k_2=(1.13\pm0.04)\times10^{-10}\ cm^3\ s^{-1}$	$k_4=(8.89\pm0.27)\times10^{-12}\ cm^3\ s^{-1}$
b) Data for Ar+NO mixtures at 1 Torr.					
2.20×10^{-4}	200	0.116	0.36	351	3490
2.34	600	0.173	0.74	399	5090
4.00	200	0.071	0.33	241	3810
5.60	200	0.089	0.21	509	5980
5.88	600	0.084	0.43	596	8710
10.2	200	0.111	0.15	909	8380
				$k_2=(3.5\pm0.9)\times10^{-11}\ cm^3\ s^{-1}$	$k_4=(1.8\pm0.5)\times10^{-10}\ cm^3\ s^{-1}$

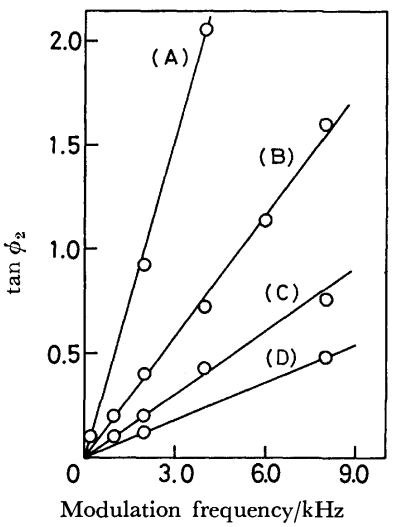

Fig. 2. Plots of $\tan\phi_2$ against modulation frequencies; p(CO)=0.045 (A),=0.106 (B),=0.20 (C),=0.37 Torr (D), and p(CO)+p(Ar)=10 Torr for all mixtures.

cumulation of vibrationally excited CO which shortens the Hg_0^* lifetime through Reaction 2 in the reverse direction. This has been confirmed in the lifetime measurements of Hg_0^* in Ar+N_2 mixtures.[5] However, in an Ar+CO mixture, the lifetime of Hg_0^* does not depend on the intensity of 253.7-nm radiation, as is shown in Table 1, which lists the observed lifetimes as a function of the 253.7-nm photon intensity entering the cell. The latter quantity was varied by changing the number of illuminating lamps and their distance from the cell; the intensity was estimated from the observed value of Hg_1^* concentration in pure Ar, since Ar does not deactivate Hg_1^* and its concentration is given by $x_1=k_1I_0x_0/k_{-1}$. The results in Table 1 leads to the conclusion that there is no accumulation of CO (v=1) in the present system, which is probably due to the relatively short lifetime of CO(v=1). Thus, the vibrational temperature of CO must be room temperature and the reverse of Reaction 2 may be disregarded. This estimate should be valid for other quenching gases, since these gases have relaxation times shorter than those of CO and N_2.

The reciprocal lifetime determined from the data in Fig. 2 is proportional to the CO partial pressure and, thus, gives the rate constant for Hg_0^* deactivation, k_4, which is $(8.89\pm0.27)\times10^{-12}\ cm^3\ s^{-1}$. The spin-orbit relaxation rate, k_2, was determined to be $(1.13\pm0.04)\times10^{-10}\ cm^3\ s^{-1}$ using Eq. 14 and the data listed in Table 2. The rates thus determined may be converted to

Table 3. Collision cross section for Hg* in Å²

Process	Investigator	Collision partner: CO	Collision partner: NO
Hg_1*→ Hg_0*, Hg	DPK[a]	21.7	—
	MS[b]	23.2	88.9
Hg_1*→Hg_0*	this work	22.4±0.8	7.0±1.8
	CM[c]	19.5	—
	VTL[d]	16.1	—
Hg_0*→Hg	this work	1.80±0.05	37±10(35±2)[f]
	CM[c]	2.06	50.1
	FMCP[e]	7.8	41

a) Deech *et al.*[9] b) Michael and Suess.[10] c) Callear and McGurk.[2] d) Vikis *et al.*[4] e) Freeman *et al.*[11] f) Observed in N_2+NO mixtures.

collision cross sections as summarized in Table 3 together with the results for NO and literature values. The total deactivation cross section of Hg_1* by a collision with CO (Reactions 2 and 3) has been measured accurately by Deech *et al.*[9] and found to be 21.7 Å² at room temperature. This value was determined from a measurement of the 253.7-nm fluorescence decay after pulsed excitation of Hg to Hg_1*. The value agrees well with the present measurement of 22.4 Å² for Reaction 2 within the error limits. This means that the deactivation of Hg_1* by collisions with CO leads mainly to formation of Hg_0* and not to ground-state Hg; the latter process may occur with a probability of less than 2% of the Hg_1* deactivation. Clear evidence for vibrat onal excitation of CO by the spin-orbit relaxation was not obtained in the present experiment. However, since CO is isoelectronic with N_2 and the resonance is improved ($\Delta E = -373$ cm^{-1} for CO compared with -563 cm^{-1} for N_2) in Reaction 2, vibrational excitation is expected to be accompanied by the spin-orbit relaxation.[5]

Formerly, it was difficult to detect Hg_0* atoms produced in Hg_1*-NO collisions, and, thus, the rate constant, k_2, could not be determined. However, the present modulation technique makes it possible to detect the a.c. component of [Hg_0*] which has been so small that rate constants, k_2 and k_4, cannot be determined accurately. A more reliable value for k_4 was obtained from phase-shift measurements of Hg_0* in a mixture of N_2+NO; the cross section is given in Table 3. Contrary to the case of Hg_1*-CO collisions, NO deactivates Hg_1* mainly to the ground state, with only 10% of the Hg_1* deactivation proceeding *via* spin-orbit relaxation.

The energy transfer mechanism for Hg*-CO collisions can be understood if the non-adiabatic coupling between spin-orbit states is complete in the course of the collisional interaction *via* the simultaneous vibrational excitation of CO, while adiabaticity is preserved between the 6^3P and 6^1S states of Hg. Contrary to this, in Hg*-NO collisions, a large probability for crossing from the 6^3P surface to the 6^1S surface significantly reduces the relative importance of the transition from the 6^3P_1 state to the 6^3P_0 state.

Appendix

For the readers' convenience, the equivalence of the sine or cosine formulation to the vector notation in the complex plane is explained. According to the radiation intensity expressed as

$$I = \bar{I} + I_0 \sin \omega t, \tag{A1}$$

the Hg_1* and Hg_0* concentrations are described as

$$x_1 = \bar{x}_1 + \tilde{x}_1 \sin(\omega t - \phi_1) \tag{A2}$$

and

$$x_2 = \bar{x}_2 + \tilde{x}_2 \sin(\omega t - \phi_2). \tag{A3}$$

If these equations are substituted into Eqs. 8 and 9, and the coefficients of $\cos \omega t$ are taken, the following two equations can be derived:

$$\tan \phi_1 = [1/(k_{-1} + k_2\bar{y}_0 + k_3\bar{y}_0)] \times [\omega + k_{-2}\bar{y}_1(\tilde{x}_2 \sin \phi_2/\tilde{x}_1 \cos \phi_1)] \tag{A4}$$

and

$$\tan \phi_2 = [1/(k_{-2}\bar{y}_1 + k_4\bar{y}_0 + k_5)] \times [\omega + k_2\bar{y}_0(\tilde{x}_1 \sin \phi_1/\tilde{x}_2 \cos \phi_2)]. \tag{A5}$$

These equations are equivalent to Eqs. 12 and 13 assuming that

$$x^r = \tilde{x} \cos \phi \quad \text{and} \quad x^i = \tilde{x} \sin(-\phi).$$

References

1) For example, R. J. Cvetanovic, "Progress in Reaction Kinetics," Vol. 2, Pergamon Press, London (1964), p. 39, and J. G. Calvert and J. N. Pitts, Jr., "Photochemistry," John Wiley & Sons, New York (1967), p. 71.

2) A. B. Callear and J. C. McGurk, *J. Chem. Soc., Faraday Trans. 2*, **69**, 97 (1973).

3) H. Horiguchi and S. Tsuchiya, *Bull. Chem. Soc. Jpn.*, **44**, 1213 (1971).

4) A. C. Vikis, G. Torrie, and D. J. Le Roy, *Can. J. Chem.*, **50**, 176 (1972).

5) H. Horiguchi and S. Tsuchiya, *J. Chem. Soc., Faraday Trans. 2*, **71**, 1164 (1975).

6) L. F. Phillips, "Progress in Reaction Kinetics," Vol. 7, Pergamon Press, London (1973), Part 2.

7) G. Karl, P. Kruus, and J. C. Polanyi, *J. Chem. Phys.*, **46**, 224 (1967).

8) E. W. Samson, *Phys. Rev.*, **40**, 940 (1932).

9) J. S. Deech, J. Pitre, and L. Krause, *Can. J. Phys.*, **49**, 1976 (1971).

10) J. V. Michael and G. N. Suess, *J. Phys. Chem.*, **78**, 482 (1974).

11) C. G. Freeman, M. J. McEwan, R. F. C. Clarigde, and L. F. Phillips, *Trans. Faraday Soc.*, **67**, 2004 (1971).

The Detection of Hg(6^3P_1 and 6^3P_0) Atoms by an Atomic Absorption Method and Their Quenching Cross Sections

Hiroyuki HORIGUCHI and Soji TSUCHIYA

Department of Pure and Applied Sciences, College of General Education, The University of Tokyo, Meguro-ku, Tokyo 153

(Received November 1, 1976)

The absorption intensities of the 435.8- and 404.7-nm lines by Hg(6^3P_1 and 6^3P_0) atoms were calculated taking into account the hyperfine structure under the assumption of a Doppler spectral line shape. The calculated values were tested by comparison with experimental absorption of the line in an Ar+N_2+Hg mixture illuminated by 253.7-nm radiation. This procedure led to the conclusion that the ratio of the spectral half-width of the 404.7-nm line from a low-pressure Hg lamp to that of the Hg(6^3P_0) absorption line should be 2.25±0.25 instead of the value of 5 determined in the previous experiment. On the basis of this value, the quenching cross sections of the excited Hg atoms reported in the previous paper were revised. The corrections are generally less than 20%, so that it is not necessary to change the previous conclusions.

In a previous paper,[1] a method was described to determine the quenching rate of excited Hg atoms for the processes $6^3P_1 \rightarrow 6^3P_0$ and $\rightarrow 6^1S_0$ from the observation of a stationary concentration of Hg(6^3P_0) atoms in a gaseous mixture of quencher +Hg vapor illuminated by 253.7-nm radiation. (Hereafter, Hg_1*, Hg_0*, and Hg stand for Hg atoms in the 6^3P_1, 6^3P_0, and 6^1S_0 states, respectively.) The Hg_0* concentration [Hg_0*], was estimated by the absorption measurement of the 404.7-nm line emitted from a low-pressure Hg discharge lamp. In this procedure, care was paid to verify that the absorption intensity was a function of [Hg_0*] as well as of the ratio of the spectral line half-width from the light source to that of the absorption line. In order to determine this ratio (denoted here by α), it was assumed that the [Hg_0*] in the mixture of Ar+N_2 is proportional to the intensity of the 253.7-nm radiation and that the 404.7-nm line is composed of a single spectral line. However, according to recent results,[2] the [Hg_0*] in the Ar+N_2 mixture is proportional to the square root of the 253.7-nm radiation intensity. Moreover, the 404.7-nm line has 9 hyperfine components resulting from the isotope shift and the nuclear-spin coupling. Therefore, the value of α reported previously must be corrected. In addition, the quenching cross sections[3] of the excited Hg atoms determined from the observed decay of the absorption at 404.7-nm must also be revised.

Experimental

The apparatus is essentially the same as that described in Ref. 1. In a quartz cell (3 cm in diameter and 24 cm in length) containing an Ar+N_2 mixture with an Hg pressure of 1.9×10^{-4} Torr, excited Hg atoms were formed by illumination with 253.7-nm radiation from 6 low-pressure Hg discharge lamps (Toshiba, 10-W germicidal lamp) surrounding the cell. The cell has an outer jacket filled with a 0.6 M $NiSO_4$ aq solution to avoid excitation of the Hg atoms to levels higher than the 6^3P_1 state. Another low-pressure Hg discharge lamp was employed as a light source for the 404.7- and 435.8-nm lines which were modulated by a chopper at 125 Hz before entering the cell. A d.c. source supplied the power for the Hg discharge lamps. A monochromator (Spex, 1700) and a lock-in amplifier (P. A. R. 186) were used to monitor the line intensity. The absorption due to [Hg_1*] was very weak, so that the 253.7-nm radiation intensity was modulated at a frequency of 0.12—3 kHz and the resulting a.c. component of the absorption at 435.8-nm was measured without the chopper; the signal obtained divided by the d.c. intensity of the 435.8-nm line from the source gives the absorbance. This procedure makes it possible to detect optical densities for absorption as small as 10^{-4}.

The rotational (=translational) temperature of the sample gas in the cell under the irradiation of 253.7-nm radiation was 292±15 K. This was estimated from the observed rotational temperature of CO, added as a tracer to the mixture.[4]

The nominal purities of the sample gases, Ar and N_2, were 99.999% and 99.99%, respectively. The method of gas handling is the same as that described previously.

Results and Discussion

Calculation of the Absorption Intensities of Excited Atoms. Taking the hyperfine splitting of 404.7- and 435.8-nm lines into account, the intensities for absorption by Hg_0* and Hg_1* atoms were calculated. For the calculation, the fine structure of the Hg lines observed by Schüler and Keyston[5] were adopted; the 404.7- and 435.8-nm lines are composed of 9 and 15 hyperfine components, respectively. It can be assumed that the line profile of each component of the 404.7- and 435.8-nm absorption lines is Doppler broadened with a common F. W. H. M. denoted by $\Delta\nu_D$. Though the line profile for radiation from a discharge lamp is dependent on many factors such as Doppler and collisional broadening, the Stark effect, *etc.*, it can be approximated by a Doppler-broadened line with a F. W. H. M. of α times that of the absorption line, *i.e.*, $\alpha\Delta\nu_D$. Thus, the spectral profile of the i-th component of the line from an Hg discharge lamp is given by

$$E^{(i)}(\nu) = E_0{}^{(i)}\exp\{-(\ln 2)[2(\nu-\nu_0{}^{(i)})/\alpha\Delta\nu_D]^2\}, \quad (1)$$

where $\nu_0{}^{(i)}$ is the frequency at the line center of the i-th component and $E_0{}^{(i)}$ is the peak intensity at $\nu_0{}^{(i)}$. Similarly, the absorption coefficient of the i-th component is

$$k^{(i)}(\nu) = k_0{}^{(i)}\exp\{-(\ln 2)[2(\nu-\nu_0{}^{(i)})/\Delta\nu_D]^2\}. \quad (2)$$

Since the absorbance A is defined as 1−(transmitted radiation, I)/(incident radiation, I_0), the observed absorption which should be the sum of those for the individual hyperfine components is described as

$$A = \int\sum_i E^{(i)}(\nu)[1-\exp(-k^{(i)}(\nu)l)]\mathrm{d}\nu \Big/ \int\sum_i E^{(i)}(\nu)\mathrm{d}\nu, \quad (3)$$

where l is the absorption length. The Hg discharge

lamp emits spectral lines under optically-thin conditions, so that the relative intensity of each hyperfine component is equal to that for the absorption coefficient;

$$k_0^{(i)}/k_0 = E_0^{(i)}/E_0,$$

where $E_0=\sum_i E_0^{(i)}$ and $k_0=\sum_i k_0^{(i)}$. This last quantity is described as

$$k_0 = (2/\Delta\nu_D)(\ln 2/\pi)^{1/2}(\pi e^2/mc)fN,$$

where e and m are the charge and mass of electron, respectively, and c is the velocity of light, f the f-number, and N the number density of excited atoms; $k_0=5.905\times10^{-12}N\,\mathrm{cm}^{-1}$ for Hg_0^* and $6.207\times10^{-12}N\,\mathrm{cm}^{-1}$ for Hg_1^* atoms.

Numerical integration of Eq. 3 was carried out for various α and k_0l values. In Figs. 1 and 2, the calculated values of $\log(1-A)^{-1}$ which is equal to $\log(I_0/I)$ are plotted as a function of k_0l. It is obvious that the optical density calculated with the hyperfine splittings is smaller than that calculated assuming a single line. In the region of small optical densities (<0.1) the calculation assuming a single line for the 404.7-nm line gives 4.6 times the value with the hyperfine splittings for $\alpha=1$ and decreases to 3.4 for $\alpha=2$ and 2.7 for $\alpha=3$. This may be interpreted to a very rough approximation as a 404.7-nm line having 3 to 4 lines with equal intensities; a large α causes a dense overlapping of hyperfine lines resulting in a reduction in the effective number of lines.

Determination of the Ratio of the Emission Line Width to the Absorption Line Width. Previously, it was assumed that the $[Hg_0^*]$ in an $Ar+N_2$ mixture is proportional to the intensity of 253.7-nm radiation. This is based on the processes for the Hg_0^* production:

$$Hg + h\nu \rightarrow Hg_1^*, \quad \text{(i)}$$

$$Hg_1^* \rightarrow Hg + h\nu, \quad \text{(ii)}$$

$$Hg_1^* + N_2 \rightarrow Hg_0^* + N_2, \quad \text{(iii)}$$

$$Hg_0^* \rightarrow Hg. \quad \text{(iv)}$$

However, the recent measurement[2] of the Hg_0^* lifetime indicates that the above processes cannot explain the formation and deactivation of Hg_0^*, and that reaction (iii) must be replaced by

$$Hg_1^* + N_2(v=0) \rightarrow Hg_0^* + N_2(v=1), \quad \text{(v)}$$

where $N_2(v=1)$ is vibrationally-excited N_2. Moreover, the inverse of this reaction and the deactivation of N_2 $(v=1)$ must be added:

$$Hg_0^* + N_2(v=1) \rightarrow Hg_1^* + N_2(v=0), \quad \text{(vi)}$$

and

$$N_2(v=1) \rightarrow N_2(v=0). \quad \text{(vii)}$$

A steady-state analysis of reactions (i)—(vii), excepting (iii), leads to the relation

$$[Hg_0^*] = \frac{k_7}{2k_6}\left\{\left[\left(\frac{k_5}{k_2}[N_2]+1\right)^2+4\frac{k_1k_5k_6}{k_2k_4k_7}I[Hg][N_2]\right]^{1/2} - \left(\frac{k_5}{k_2}[N_2]+1\right)\right\}, \quad (4)$$

where I is the intensity of the 253.7-nm radiation and k_1 is the rate constant for reaction (i). Equation 4 may be simplified to a good approximation as

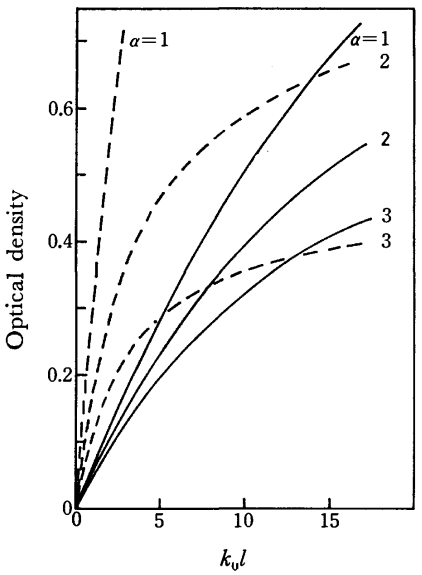

Fig. 1. Absorption intensity of the 404.7-nm line by $Hg(6^3P_0)$ atoms as a function of α; solid line: calculation with the hyperfine line structure, broken line: calculation assuming a single line.

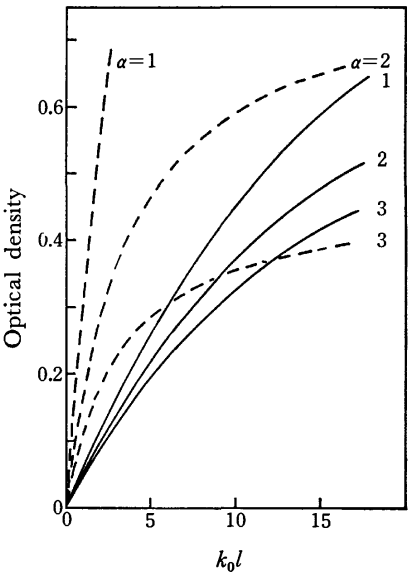

Fig. 2. Absorption intensity of the 435.8-nm line by $Hg(6^3P_1)$ atoms as a function of α; solid line: calculation with the hyperfine line structure, broken line: calculation assuming a single line.

$$[Hg_0^*] = (k_1k_5k_7[Hg][N_2]/k_2k_4k_6)^{1/2} \quad (5)$$

under the condition that $k_2>k_5[N_2]\gg k_4$. This condition is satisfied if the N_2 pressure is in the range from 1 to 30 Torr.

In order to determine α, the optical density of the 404.7-nm absorption was measured as a function of the relative intensity of the 253.7-nm radiation, as well as of the N_2 partial pressure. The intensity was estimated from the absorption of the 435.8-nm line caused by the formation of Hg_1^* in pure Ar, *i.e.*,

$$[Hg_1^*]_0 = k_1I[Hg]/k_2. \quad (6)$$

Substituting this equation into Eq. 5, the relation

TABLE 1. THE CROSS SECTIONS ($\pi\sigma^2$ IN Å^2) FOR THE QUENCHING OF Hg (6^3P_1 AND 6^3P_0) BY VARIOUS MOLECULES[a]

Quencher	$6^3P_1 \rightarrow 6^3P_0, {}^1S_0$	$6^3P_1 \rightarrow 6^3P_0$			$6^3P_0 \rightarrow 6^1S_0$		
		This work	CM[b]	VTL[c]	This work	FECP[d]	CM[e]
N_2O	53.6[k]	<6	<7		35(44)	14	26.7
O_2	60.5[f]	<6	<6		35(50)	57	37.7
C_2H_4	151[g]	<16	<15		129		82.5
C_3H_6	179[j]	<16			135(157)		
C_2H_2	135[j]	<13			91(113)		
H_2	24.6[f]	<0.3	<0.7		6.0(6.6)	5.1	3.0
D_2	22.7[f]	<0.3			8.5(9.1)		
C_3H_8	6.9[g]	3.0(3.7)	1.4	0.87	0.15(0.23)		0.105
n-C_4H_{10}	18[h]	11		2.2	2.0(2.9)		
i-C_4H_{10}	29[i]	19(14)		1.06	4.2(4.4)		
$C(CH_3)_4$	6.0[g]	5.7(5.0)		3.8	0.30(0.35)		
CO	21.7[f]	22(12)	19.5	16.1	1.8(2.2)	7.8	2.06
NO	71.6[k]	7.1(16)	<11		37(25)	41	50.1
NH_3	12.7[h]	3.5(4.1)	8.1	14.2	0.038(0.05)	0.05	0.049
CO_2	10.2[f]	0.19(0.06)	0.2	0.12	0.093(0.1)		0.104
CH_4	0.25[h]	0.016(0.03)	0.03		4.1×10^{-4} (4.4×10^{-4})		9.0×10^{-4}
C_2H_6	1.8[h]	0.66(0.53)	1.2	0.29	5.3×10^{-3} (6.3×10^{-3})	0.091	0.018
N_2	0.73[f]	0.77			$<1\times10^{-3}$		

a) Previous values are given in parentheses if corrected. b) Calculated from quantum yields of Hg_0* determined by Callear and McGurk.[7] c) Vikis, Torrie and LeRoy.[8] d) Freeman, McEwan, Claridge, and Phillips.[9] e) Callear and McGurk.[7] f) Deech, Pitre and Krause.[10] g) Kang Yang.[11] h) The data of Zemansky[12] multiplied by 1.379 a correction factor which is explained in Ref. 3. i) The value calculated from $\sigma^2(i\text{-}C_4H_{10})/\sigma^2(n\text{-}C_4H_{10})$ determined by Darwent.[13] j) The data of Darwent[14] multiplied by a correction factor of 1.85. k) the data of Michael and Suess[15] multiplied by a correction factor of 0.805.

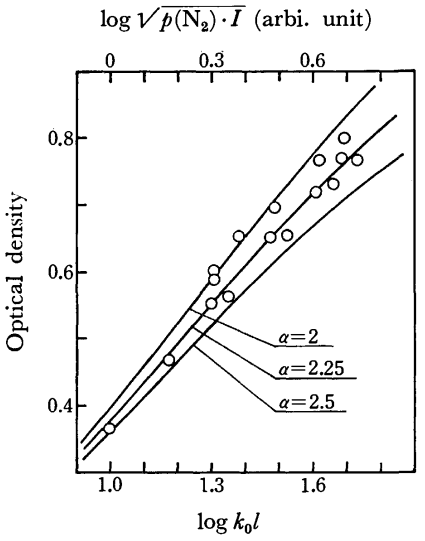

Fig. 3. Comparison of the calculated absorption intensities (solid line) of the 404.7-nm line with the experimental ones(circle) as a function of the N_2 partial pressure and the 253.7-nm radiation intensity.

$$[Hg_0^*] = [(k_5[N_2]/k_4)[Hg_1^*]_0(k_7/k_6)]^{1/2} \quad (5')$$

is obtained. Here, the absorption at 435.8-nm is so weak that the optical density can be assumed to be proportional to $[Hg_1^*]$ for any value of α. In Fig. 3, the optical density of the 404.7-nm absoption is plotted against $\log([N_2]I)^{1/2}$, together with the theoretical optical density, as a function of $\log k_0l$. The best fit to the experimental points is obtained for

$$\alpha = 2.25 \pm 0.25.$$

With this value of α, the optical density of the absorption at 404.7-nm gives the absolute magnitude of k_0l or $[Hg_0^*]$. The same value of α is assumed for the 435.8-nm line in the absence of experimental evidence. However, only a very weak absorption appears at 435.8-nm in the Hg* quenching experiment, so that the error caused by this assumption is rather small as can be understood from Fig. 2, in which the optical density is seen to be almost proportional to k_0l.

Quenching Cross Sections of Hg(6^3P_1 and 6^3P_0). The decay of the 404.7-nm absorption after a short pulse of 253.7-nm radiation was measured to estimate the Hg_0* quenching cross section as well as the spin-orbit relaxation rate of $Hg_1^* \rightarrow Hg_0^*$.[3] The new value of α, which is 2.25 instead of 5, as found previously, changes the conversion from the optical density to the $[Hg_0^*]$. Thus, the reported quenching cross sections are revised to new values as summarized in Table 1, in which the data for collision partners of CO and NO are given from the new measurement employing a phase-shift method.[6] There are minor changes in the cross sections: most of the Hg_0* deactivation cross sections are smaller by 10—20% than the previous values. This is due to the fact that the deactivation rate is deduced from the normalized quantity, $[Hg_0^*]/[Hg_1^*]_0$, which is not very sensitive to the value of α, especially for cases of weak absorption intensity. Thus, it is not necessary to change the conclusion derived in Ref. 3.

References

1) H. Horiguchi and S. Tsuchiya, *Bull. Chem. Soc. Jpn.*, **44**, 1213 (1971).
2) H. Horiguchi and S. Tsuchiya, *J. Chem. Soc., Faraday Trans. 2*, **71**, 1164 (1975).
3) H. Horiguchi and S. Tsuchiya, *Bull. Chem. Soc. Jpn.*, **47**, 2768 (1974).
4) Y. Fushiki and S. Tsuchiya, *Jpn. J. Appl. Phys.*, **13**, 1043 (1974).
5) H. Schüler and J. E. Keyston, *Z. Phys.*, **72**, 423 (1931).
6) H. Horiguchi and S. Tsuchiya, *Bull. Chem. Soc. Jpn.*, **50**, 1657 (1977).
7) A. B. Callear and J. C. McGurk, *J. Chem., Soc., Faraday Trans. 2*, **69**, 97 (1973).
8) A. C. Vikis, G. Torrie, and D. J. LeRoy, *Can. J. Chem.*, **50**, 176 (1972).
9) C. G. Freeman, M. C. McEwan, R. F. C. Claridge, and L. F. Phillips, *Trans. Faraday Soc.*, **67**, 2004 (1971).
10) J. S. Deech, J. Pitre, and L. Krause, *Can. J. Phys.*, **49**, 1976 (1971).
11) Kang Yang, *J. Am. Chem. Soc.*, **89**, 5344 (1967).
12) M. W. Zemansky, *Phys. Rev.*, **36**, 919 (1930).
13) B. deB. Darwent, *J. Chem. Phys.*, **18**, 1532 (1950).
14) B. deB. Darwent, *J. Chem. Phys.*, **22**, 859 (1954).
15) J. V. Michael and G. N. Suess, *J. Phys. Chem.*, **78**, 482 (1974).

Electronic Interactions in Triple Exciplex of the 1,4-Dicyanobenzene and Naphthalene System

Tsutomu MIMURA, Michiya ITOH,* Toshiaki OHTA,** and Toshihiko OKAMOTO

Faculty of Pharmaceutical Sciences, The University of Tokyo, Bunkyo-ku, Tokyo 113

**Faculty of Pharmaceutical Sciences, Kanazawa University, Takara-machi, Kanazawa 920*

***Department of Chemistry, Faculty of Science, The University of Tokyo, Bunkyo-ku, Tokyo 113*

(Received November 22, 1976)

Semiempirical SCF-MO-CI caluculation was carried out for the 1,4-dicyanobenzene (DCB) and naphthalene system which is known to form exciplex (DA)* and triple exciplex (D_2A)*. Potential energy curves of the electronic interactions between excimer and electron acceptor molecule, and between exciplex and electron donor molecule were constructed. The results show that the array of component molecules in the triple exciplex is DDA, and the stabilization energy of triple exciplex is $\approx$0.4 eV from the excimer and $\approx$0.2 eV from the exciplex. They are in line with results reported on the experiment of exciplex and triple exciplex formation.

The system of 1,4-dicyanobenzene (DCB) and naphthalene exhibits exciplex fluorescence and also triple exciplex fluorescence as reported by Beens and Weller. They suggested from the solvent effect of the fluorescence spectra that the array of component molecules in the triple exciplex is not DAD but DDA.[1] Mimura and Itoh also reported the triple exciplex formation in 1,4-dicyanobenzene and dinaphthylpropane(DNP) where an array of the triple exciplex was proposed to be DDA from a steric factor of the trimethylene chain in DNP.[2] They reported on the mechanism of triple exciplex formation in the DCB and several alkylnaphthalene systems. In high concentration of electron donor ($>10^{-2}$ M), the triple exciplex was formed from excimer of alkylnaphthalene and DCB as well as from exciplex and alkylnaphthalene, while the triple exciplex formation from exciplex and electron donor in the concentration below $\approx 10^{-2}$ M is predominant in another process.[3] The dissociation process from the triple exciplex to the exciplex is so fast that the fluorescence rise of the triple exciplex and double exponential decay of the exciplex fluorescence are observed. The fluorescence rise as well as two-component decay of the exciplex was observed in the system of DCB and alkylnaphthalene which exhibits no triple exciplex fluorescence. This was explained by the exciplex formation through triple exciplex *via* the excimer in high concentration of electron donor.[3] A similar investigation was reported by Grellman and and Suckow in connection with the formation of triplet state of anthracene in the diethylaniline and anthracene system.[4]

Most molecular orbital calculations of the electron-donor-acceptor (EDA) complex as well as the exciplex are based on the configuration interaction between the ground and locally excited states of each component molecule, including the charge transfer interaction (CT) which is called the method of "composite molecules." On the other hand, some attempts have been made to calculate the electronic structure of the EDA complex as a single conjugate system of π-electrons.[5-7] The method of calculation of molecular orbital is almost the same as reported, namely the Pariser-Parr-Pople type semiempirical LCAO-SCF-MO method including CI.[7] We have calculated the trimolecular system as well as bimolecular system as a single molecule.

In this paper we discuss the electronic structure of triple complex in both the ground state and the excited state. The potential energy curves obtained revealed the correlation between four excited species, excited monomer, exciplex, excimer and triple exciplex.

Method of Calculation

The method of calculation and the parameters used are the same as in the previous paper.[7] It was also assumed that π-electron approximation is applicable to the triple complex. Two center resonance integrals were evaluated for the two molecules neighboring each other in the triple complex, but neglected for the two molecules far from each other. Two center resonance integrals were evaluated by following the Katagiri-Sandorfy formula:[8]

$$H_{\mu\nu} = \frac{1}{4}(C_\mu + C_\nu + \gamma_{\mu\mu} + \gamma_{\nu\nu} - 2_{\mu\nu})S_{\mu\nu}, \quad (1)$$

where C_μ is one center penetration integral and $S_{\mu\nu}$ is the overlap integral between atomic orbitals and evaluated from single Slater atomic orbitals. When two atomic orbitals are associated with different molecules, we use SCF-atomic orbitals.[9] Two center repulsion integrals $\gamma_{\mu\mu}$ were evaluated by the Nishimoto-Mataga formula,[10] and $\gamma_{\mu\mu}$ were estimated according to the Pariser-Parr method.[11] Core energy, $H_{\mu\mu}$ is assumed to be the negative of the ionization potential, given by Hinze and Jaffé.[12] Intermolecular core-core repulsion integrals $\gamma^c_{\mu\nu}$ were estimated by following the Dewar-Klopman formula[13] modified by Ohta *et al.*[6]

$$\gamma^c_{\mu\nu} = \gamma_{\mu\nu} + \left(\frac{1}{R_{\mu\nu}} - \gamma_{\mu\mu}\right)\exp\left[\alpha(R_{\mu\nu} - D_\mu - D_\nu)\right]. \quad (2)$$

Parameters used in this calculation (Table 1) are the same as those previously reported. The nature of electronic transition was estimated by the following equations which are almost the same as reported.[7]

$$\mathrm{LE}(\mathrm{M_1{}^*M_2M_3}) = \sum_{ij} b^{s_2}_{ij} m^1_i m^1_j, \quad (3)$$

$$\mathrm{CT}(\mathrm{M_1^+M_2^-M_3}) = \sum_{ij} b^{s_3}_{ij} m^1_i m^3_j, \quad (4)$$

where M_i is i-th molecule in the complex and b^s_{ij}, m^1_i are given by Eqs. 5 and 6, respectively.

$$m^1_i = \sum_{\mu=1}^{n_1} c^2_{i\mu} \quad (5)$$

$$\Phi_a = \sum_{ij} b^a_{ij} \Psi_{ij} \quad (6)$$

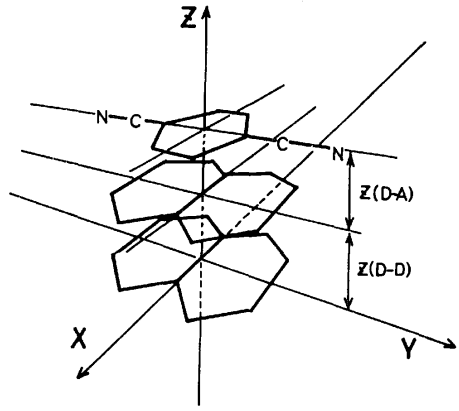

Fig. 1. The conformation and the geometrical parameters used for these calculations where Z(D–D) and Z(D–A) are distances between the molecular planes (parallel) of these component molecules.

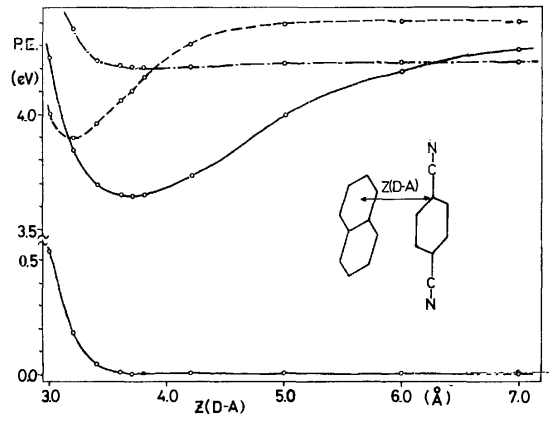

Fig. 2. Potential curves of complex (DA). In the excited state, ——, – – –, and ---- indicate mainly (D^+A^-), (D*A) ^1L_b, and (DA*), respectively.

TABLE 1. PARAMETERS USED IN THE CALCULATION

	$H_{\mu\mu}$(eV)	$\gamma_{\mu\mu}$(eV)	C_μ(eV)	D_μ(a.u.)	ζ
C^+	−11.16	11.13	14.5	2.0	1.625
N^+	−16.18	11.52	20.0	1.0	1.950
		$\alpha=-1.75$			

where n_1 indicates the number of atoms in molecule 1, Φ_a the wave function of a-th electronic excited state, and Ψ_{ij} a configuration promoting an electron from i-th MO to j-th MO.

In the actual calculation of the electronic structures, molecular planes of each component molecule in the complex were assumed to be both parallel to each other and also to the long axes of each component molecule as shown in Fig. 1. The geometrical change from the standard conformation, such as component molecules being twisted together around an axis perpendicular to the molecular planes, did not affect so much the energy of the excited state of molecular complex. The iteration of SCF-MO calculation was repeated until the deviation in the total electronic energy became less than 10^{-4}%. For evaluation of the electronic transition energy and the oscillator strength of each transition, forty lowest singly excited configurations were taken into account. The calculation was carried out by the HITAC 8700/8800 operating system of the University of Tokyo.

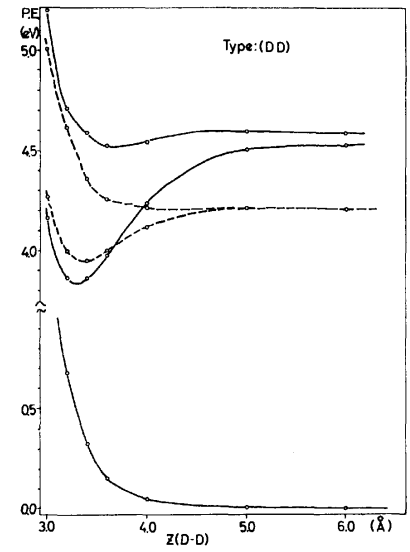

Fig. 3. Potential curves of dimer (DD). In the excited state, —— indicates levels including ^1L_a exciton interaction and charge resonance interaction, and ---- indicates levels including ^1L_b exciton interaction and charge resonance interaction.

Results and Discussion

Potential energy curves of the ground state and the excited state of complex (DA) are shown in Fig. 2. The abscissa indicates the distance between electron donor D and electron acceptor A. The complex in the ground state is unstable between D and A. With decreasing distance of each component molecule (D and A), a charge transfer state (CT-state) is stabilized in the potential energy surface, crossing a potential energy curve of locally excited state (LE-state) of the electron donor at 6.2 Å. This indicates that an electron transfer state mixes with the LE state at 6.2 Å in association with the excited electron donor D and the electron acceptor A to form the exciplex (DA)*. A prominent feature of (DA)* is that the CT character of the first excited state amounts to 98—100% at any distance below ≈6 Å of Z(D–A).

The potential energy curves of the naphthalene dimer, (DD), both in the ground and excited states are shown in Fig. 3. The abscissa indicate the distance between two naphthalene molecules. The dimer (DD) is unstable in the ground state, while it is stabilized by the exciton interaction mixed with the charge resonance interaction. The mixing ratio of the molecular exciton interaction with the charge resonance interaction is 1 : 1 for all the excited states. The first excited state of the dimer stabilized from the monomer is the state including ^1L_a exciton interaction (not ^1L_b exciton interaction) in a D_{2h} symmetry.[14]

The potential energy curves of the ground state and the excited state are shown in Fig. 4 for the case of an interaction of the exciplex and the donor molecule to form the array of DDA of the triple exciplex. The intermolecular distance between a centered electron

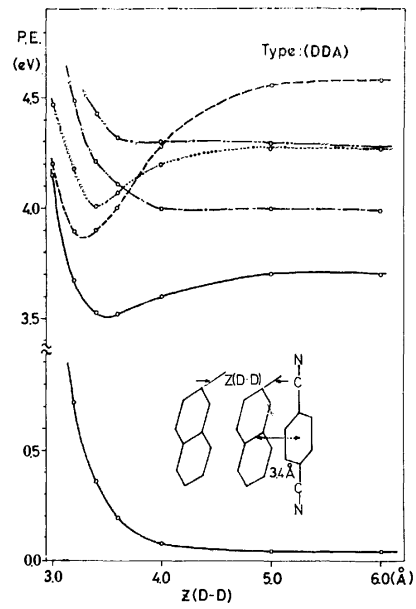

Fig. 4. Potential curves of complex (DDA). Variable parameter is Z(D–D) and Z(D–A) is constant (3.4 Å). In the excited state, ——, ———, – – –, and ····· indicate mainly (D···D$^+$A$^-$), (D···DA*), excimer (^1L_a) and excimer (^1L_b) levels, respectively.

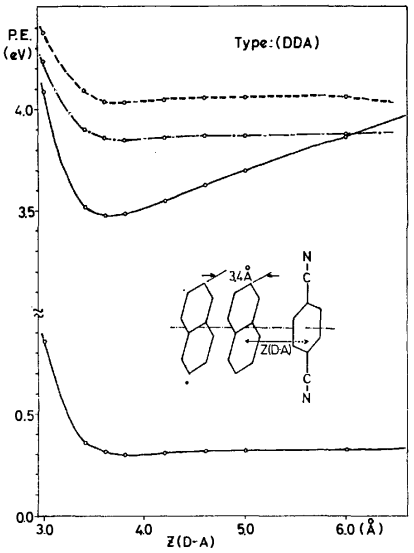

Fig. 5. Potential curves of complex (DDA). Variable parameter is Z(D–A) and Z(D–D) is constant (3.4 Å). In the excited state, ——, ———, and – – – – indicate mainly (D$^+$D···A$^-$)↔(DD$^+$···A$^-$), excimer (^1L_a), and excimer (^1L_b) levels, respectively.

donor and a terminal electron acceptor is set to be constant (3.4 Å), and the intermolecular distance between two electron donors as is variable (Z(D–D) as abscissa). The triple complex is repulsive in the ground state. However, there is a shallow minimum in the first excited state of DDA which implies the triple exciplex formation in the excited state.

Figure 5 shows the potential energy curves of the ground state and the excited state of electronic interaction between the excimer and the electron acceptor to also form the array of DDA, where the intermolecular distance between electron donors in the dimer is constant (3.4 Å) and the intermolecular distance between centered electron donor and terminal electron acceptor changes (Z(D–A) as abscissa). The first excited singlet state (S_1 state) of this triple complex at the distance between D and A of 7.0 Å is almost first LE state of naphthalene dimer, namely excimer state. The charge transfer from the excimer to the electron acceptor occurs at the D–A distance ≈6 Å, then the CT state is stabilized by coulomb interaction between (DD)$^+$ and A$^-$. The energy gap of the triple exciplex from the excimer state of naphthalene was found to be *ca.* 0.4 eV.

It was suggested in the nano-second time resolved fluorescence investigation on the triple exciplex formation in the intermolecular system of DCB-alkylnaphthalene that the triple exciplex is formed *via* exciplex in a dilute solution of the electron donor ($<10^{-2}$ M), and the triple exciplex is also formed *via* excimer in a high concentration of the electron donor ($>10^{-1}$ M) (see Scheme 1).

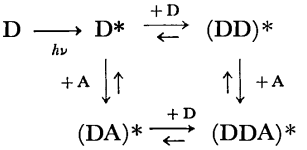

Scheme 1.

It was also verified that the dissociation process from the triple exciplex, (DDA)*, to the exciplex, (DA)*, is significant at room temperature. These results are clarified by the MO calculations described above. Since the energy gap of the stable triple exciplex, (DDA)*, from the exciplex, (DA)*, is 0.2 eV (≈4.6 kcal/mol), the triple exciplex (DDA)* and the exciplex (DA)* might coexist at room temperature, and the stable triple exciplex (Type: DDA) would be formed from the exciplex even in the considerably dilute solution of electron donor. On the other hand, the energy gap between the excimer state of naphthalene and the more stable triple exciplex (Type: DDA) in the excited state is 0.4 eV (≈9.2 kcal/mol) as shown in Fig. 5. The energy gap calculated is so great that the naphthalene excimer can not coexist thermodynamically with the triple exciplex of the array of DDA at room temperature. The triple exciplex formation *via* the excimer as well as *via* the exciplex with increasing concentration of electron donor greater than 10^{-1} M was mentioned. Subsequently, the triple exciplex *via* the excimer may dissociate easily to the exciplex at room temperature due to the small stabilization energy (≈0.2 eV) of the triple exciplex.

The potential energy curves of the ground state and the excited states for the array of component molecules, DAD, are given in Fig. 6. The intermolecular distance between a centered electron acceptor and one of two electron donors is constant (3.4 Å), while that between A and D varies (Z(A–D) as abscissa). The triple complex in the array of DAD is stable neither in the ground state nor in the first excited state. The exciplex (DA)* seems to be unperturbed by the approach of another

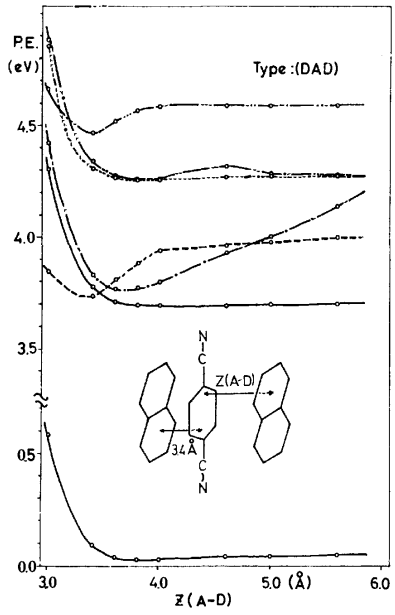

Fig. 6. Potential curves of complex (DAD). Variable parameter is Z(A–D), and Z(D–A) is constant (3.4 Å). In the excited state, ——, ——, ----, ——, and —·—·— indicate mainly ($D^+A^-\cdots D$), ($DA^-\cdots D^+$), ($DA^*\cdots D$), ($D^*A\cdots D$)↔($DA\cdots D^*$) (^1L_b) and ($D^*A\cdots D$) (^1L_a), respectively.

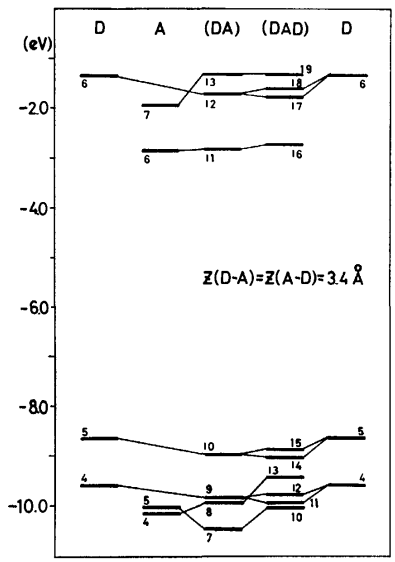

Fig. 7. Origins of SCF-MOs of complexes (DA) and (DAD) from SCF-MOs of component molecules.

D molecule leading to the formation of DAD. The calculated results concerning with the array of the triple exciplex are in line with the experimental results of the intramolecular triple exciplex formation in 1,3-dinaphthylpropane (DNP) and DCB system and also with the suggestion by Beens and Weller.[1] In the intramolecular system, it is impossible that triple exciplex takes an array of DAD because of trimethylene chain of DNP.[2]

The first electronic transition energies calculated in D, (DD), (DA) and (DDA) are summarized in Table 2 in comparison with the results from their fluorescence

Table 2. The first electronic transition energies (eV)

	D[a]	(DA)[a]	(DD)	(DDA)
Calcd	4.11	3.65	3.53	3.16
Obsd[b]	3.68	2.95	3.09	2.58

a) D and A are naphthalene and 1,4-dicyanobenzene, respectively. b) Obtained from the fluorescence maxima of respective excited species in 2-MN and DCB system.

Table 3. Characters of first electronic transition in several D–D distances of the triple complex (Type; D···DA)

Character of transition	Z(D-D)/Å			
	3.4	4.0	5.0	6.0
($D^*\cdots DA$)	0.03%	0.01%	0.00%	0.00%
($D^+\cdots D^-A$)	0.75	0.72	0.26	0.02
($D^+\cdots DA^-$)	55.00	55.69	20.82	1.35
($D^-\cdots D^+A$)	0.03	0.01	0.00	0.00
($D\cdots D^*A$)	0.60	0.56	1.00	1.24
($D\cdots D^+A^-$)	43.15	42.57	77.20	96.53
($D^-\cdots DA^+$)	0.01	0.00	0.00	0.00
($D\cdots D^-A^+$)	0.02	0.02	0.03	0.04
($D\cdots DA^*$)	0.42	0.42	0.69	0.82

Table 4. Characters of first electronic transition in several A–D distances of the triple complex (Type; DA···D)

Character of transition	Z(A-D)/Å			
	3.4	4.0	5.0	6.0
($D^*A\cdots D$)	0.39%	1.14%	1.26%	1.26
($D^+A^-\cdots D$)	19.54	88.53	97.71	97.88
($D^+A\cdots D^-$)	0.39	0.23	0.01	0.00
($D^-A^+\cdots D$)	0.69	0.03	0.04	0.04
($DA^*\cdots D$)	57.99	0.80	0.83	0.82
($DA^+\cdots D^-$)	0.69	0.01	0.00	0.00
($D^-A\cdots D^+$)	0.39	0.12	0.00	0.00
($DA^-\cdots D^+$)	19.54	9.12	0.14	0.01
($DA\cdots D^*$)	0.39	0.02	0.00	0.00

spectra, where the molecular distance of component molecules are all 3.4 Å. The calculated transition energies are compared with those of fluorescence maxima, transition energy obtained in this kind of MO calculation being usually compared with that of electronic absorption spectra. Decrease in the transition energy in the order D>(DA)>(DD)>(DDA) is in line with that of transition energy from their fluorescence spectra, though all the energies were calculated to be *ca.* 0.5—0.6 eV greater than those of the corresponding fluorescence maxima, and the observed energy of (DD) is a little greater than that of (DA). Characters of the electronic transition of the lowest excitation in several D–D distance of the triple complex of DDA are given in Table 3. When donor molecule approaches the exciplex which has great CT-character (D^+A^-), the electronic configuration ($D^+\cdots DA^-$) gradually mixes with ($D\cdots$

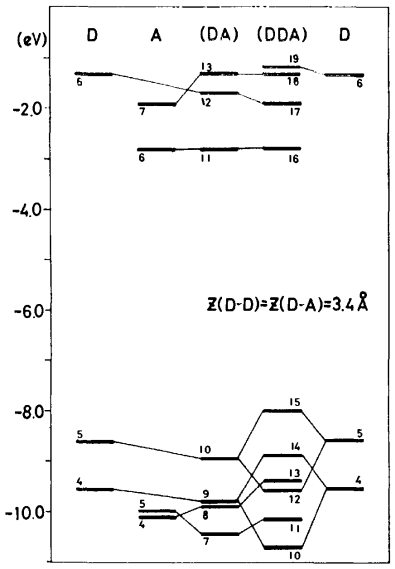

Fig. 8. Origins of SCF-MOs of complexes (DA) and (DDA) from SCF-MOs of component molecules.

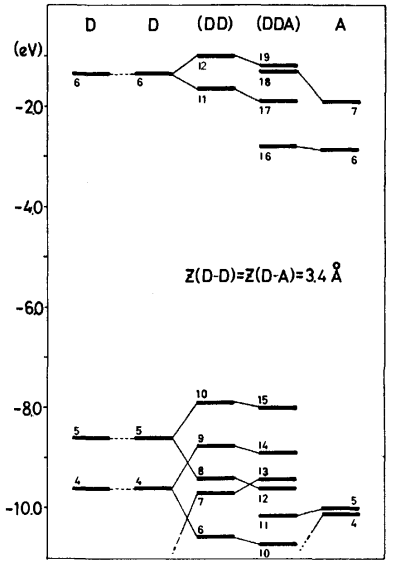

Fig. 9. Origins of SCF-MOs of dimer (DD) and complex (DDA) from SCF-MOs of component molecules.

D^+A^-). The dipole moment of the exciplex was calculated to be 16.16 D, while that of the triple exciplex was 18.13 D at the most stable molecular distance shown in Figs. 2 and 4. If the donor molecule approaches the exciplex to form (DDA)*, the donor molecule shares a positive charge with the another D molecule in the (D^+A^-) of the exciplex leading to form ($(DD)^+A^-$). It is necessary to stabilize the triple exciplex that two electron donors interact with each other effectively when the exciplex associates with another electron donor. In the symmetric triple exciplex (DAD)* formation (Fig. 6), however, the CT state of ($DA^-\cdots D^+$) does not mix with ($D^+A^-\cdots D$), the electronic structure of which is almost the same as that of the initial exciplex (D^+A^-) (Table 4). The first excited state of triple complex ($DA\cdots D$) maintains the CT character of the exciplex (DA)* in approaching another D molecule. Figures 7—9 show the molecular orbitals and their correlations obtained in each conformation. Higher occupied orbitals of triple complexes (DDA) and (DAD) and the complex (DA) are supplied from electron donor molecule. In (DAD) alignment, the interaction between the highest occupied molecular orbital (HOMO, 5th MO) of electron donor and HOMO (10th MO) of the complex (DA) which consists of mostly HOMO (5th MO) of electron donor is not so great. They form 14 and 15th MO's (Fig. 7). However, the great interaction occurs between 5th MO of D molecule and 10th MO of the complex (DA) which is supplied from the electron donor (Fig. 8) in DDA alignment. In the electronic interaction between (DD) and A, the electronic attribution of MO's of component molecules to MO's of the triple complex in DDA alignment is obvious (Fig. 9). The 14 and 15th MO's of the triple complex are supplied from the dimer. Since there is no chance for the two electron donors interacting with each other in DAD alignment, the symmetric exciplex of (DAD) would be unstable.

References

1) H. Beens and A. Weller, *Chem. Phys. Lett.*, **2**, 82 (1968).
2) T. Mimura and M. Itoh, *J. Am. Chem. Soc.*, **98**, 1095 (1976).
3) T. Mimura and M. Itoh, *Bull. Chem. Soc. Jpn.*, **50**, 1739 (1977); 34th National Meeting of the Chemical Society of Japan, Kanagawa, April (1976).
4) K. H. Grellmann and U. Suckow, *Chem. Phys. Lett.*, **32**, 250 (1975).
5) T. Shida and S. Iwata, *J. Chem. Phys.*, **56**, 2858 (1972).
6) T. Ohta, H. Kuroda, and T. L. Kunii, *Theor. Chim. Acta (Berl.)*, **19**, 167 (1970).
7) T. Mimura, M. Itoh, T. Ohta, and T. Okamoto, *Bull. Chem. Soc. Jpn.*, **48**, 2245 (1975).
8) S. Katagiri and C. Sandorfy, *Theor. Chim. Acta, (Berl.)*, **4**, 203 (1966).
9) E. Clementi, C. C. J. Roothaan, and M. Yoshimine, *Phys. Rev.*, **127**, 1618 (1962).
10) K. Nishimoto and N. Mataga, *Z. Phys. Chem. (Frankfurt)*, **13**, 140 (1957).
11) R. Pariser and R. G. Parr, *J. Chem. Phys.*, **21**, 466 (1953).
12) J. Hinze and H. H. Jaffé, *J. Am. Chem. Soc.*, **84**, 540 (1962).
13) M. J. S. Dewar and G. Klopman, *J. Am. Chem. Soc.*, **89**, 3089 (1967).
14) N. Mataga and T. Kubota, "Molecular Interactions and Electronic Spectra", Marcel Dekker, New York (1970), and references cited therein.

The Electron Capture by Bromobenzene in the γ-Radiolyses of Cyclohexane and 2,2,4-Trimethylpentane

Hidetoshi KARASAWA, Eung-Ryul KIM, and Shin SATO

Department of Applied Physics, Tokyo Institute of Technology, Ookayama, Meguro-ku, Tokyo 152

(Received November 22, 1976)

The γ-radiolyses of cyclohexane and 2,2,4-trimethylpentane have been reinvestigated. Bromobenzene was used as the electron scavenger. The analysis of the *G*-values of benzene obtained at high concentrations of bromobenzene showed that the empirical formula proposed by Hummel for the electron scavenging

$$G = G_{fi} + G_{gi}\{1-\exp(-\sqrt{\alpha S})\}$$

is better than that proposed by Warman *et al.* The values of $G_{fi}+G_{gi}$ thus obtained were 3.7±0.3 for cyclohexane and 3.5±0.2 for 2,2,4-trimethylpentane. The bromobenzene-concentration dependence of the *G*-values of hydrogen and methane from 2,2,4-trimethylpentane was well explained by the hypothesis that the lifetimes of the 2,2,4-trimethylpentane ion for the decomposition are in the same order as the time needed for the geminate recombination.

Bromobenzene is an efficient electron scavenger in the radiolysis of hydrocarbon. As the product of the electron scavenging reaction, benzene is formed, in amounts which can easily be estimated by gas chromatography.[1] In this paper we wish to report the *G*-values of benzene, hydrogen, and methane from cyclohexane and 2,2,4-trimethylpentane solutions as functions of the concentration of bromobenzene.

Such studies have been carried out by many radiation chemists in order to clarify the initial process of the radiation chemistry of hydrocarbons. Although many aspects of the initial process have been clarified by this method, one of the most interesting values has not yet been finally assessed—the total *G*-value of electrons. In the gas phase, the *G*-value of electrons can easily be measured by the current-saturation-method. However, in the liquid phase, this method cannot easily be applied. Moreover, the definition of the ionization in the liquid phase itself is somewhat obscure; *i.e.*, the ionized state and the highly excited state are not clearly distinguishable in the liquid phase.

When we use the electron-scavenging method, the value we can determine is the *G*-value of scavengeable electrons, which might not equal the total *G*-value of the electrons. For example, a certain highly excited state might be quenched by the electron transfer to the scavenger.[2,3] Moreover, when we use the electron-scavenging method, we have to face the problem of extrapolation. If there are two different equations which fit the data at low concentrations of the scavenger, the extrapolation to an infinite concentration would give two different values of the total *G*-value of the scavengeable electrons. From this point of view, bromobenzene is one of the most useful electron scavengers, because we can make experiments with pure bromobenzene and, therefore, can apply the extrapolation technique from both sides, from lower concentrations and from higher concentrations, when the direct radiolysis of bromobenzene becomes important. In this paper, we wish to show that, in order to obtain a self-consistent value, the empirical formula proposed by Hummel[4] for the electron scavenging is better than that proposed by Warman *et al.*[5]

Experimental

The cyclohexane (Wako Pure Chemical Co. and Tokyo Kagaku Seiki Co.) and 2,2,4-trimethylpentane (Koso Chemical Co. and Tokyo Kagaku Seiki Co.) were used after being passed through 1-m-long silica gel columns. The bromobenzene (Wako Pure Chemical Co.) was purified by fractional distillation before use.

The 2-ml solutions *in vacuo* were irradiated by ^{60}Co γ-rays. The dose rate was $3—9\times10^{19}$ eV/g h, and the total dose ranged from 1 to 15×10^{19} eV.

The products noncondensable at the temperature of liquid nitrogen, hydrogen and methane, were collected in a Toepler-McLeod apparatus and the amount measured by means of a gas buret. The gas was circulated through a cuprous oxide furnace maintained at 260 °C and a liquid nitrogen trap to convert the hydrogen into water. The residual gas, methane, was then collected again, and its amount was measured.

The condensable products were measured gas-chromatographically. The following columns were used: the 4-m tricresyl phosphate column at 60 °C for benzene, the 5-m dimethylsulfolane column at room temperature for cyclohexene, and the 2-m polyethylene glycol column at 80 °C for bicyclohexyl. As the standard compound, toluene or hexane was used.

Results

Figures 1 and 2 show the *G*-values of benzene, hydrogen, and methane from the bromobenzene solutions in cyclohexane and 2,2,4-trimethylpentane as functions of the concentration of bromobenzene, where the concentration of bromobenzene is lower than 1 mol l^{-1}.

In order to subtract the contribution of the direct

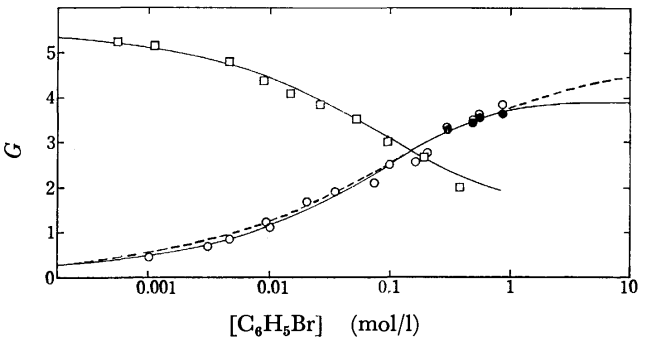

Fig. 1. The *G*-values of benzene (○) and hydrogen (□) from the bromobenzene solution in cyclohexane. For the filled circles and the curves, see the text.

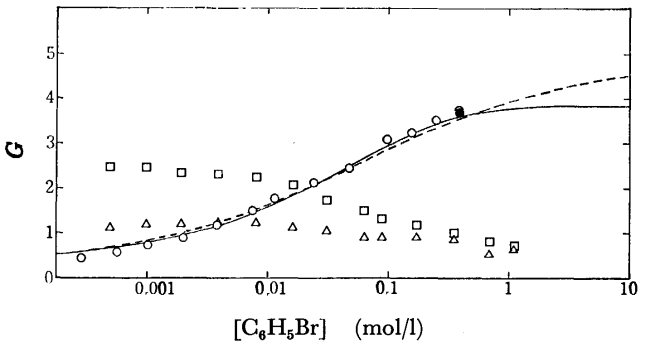

Fig. 2. The G-values of benzene (○), hydrogen (□), and methane (△) from the bromobenzene solution in 2,2,4-trimethylpentane. For the filled circle and the curves, see the text.

radiolysis of bromobenzene, we assumed that the G-value of benzene from pure bromobenzene is 1.2 (see below) and that the energy absorption occurs proportionally to the electron fraction. The filled signs in Figs. 1 and 2 represent the corrected values.

The two kinds of curves for the G-values of benzene, solid and dashed, shown in Figs. 1 and 2, were drawn by using the following two empirical equations; for the solid curves,

$$G(C_6H_6) = G_{fi} + G_{gi}\{1-\exp(-\sqrt{\alpha S})\} \quad (1)$$

and for the dashed curves,

$$G(C_6H_6) = G_{fi} + G_{gi}\frac{\sqrt{\alpha S}}{1+\sqrt{\alpha S}}. \quad (2)$$

Here, S is the concentration of bromobenzene. G_{fi}, G_{gi}, and α are empirical constants, whose values are summarized in Table 1. Since the two equations coincide with each other at the low-concentration limit, the G_{fi}'s in both equations should be the same.

Figures 3 and 4 show the G-values of benzene observed at the concentrations higher than 1 mol l^{-1}. The abscissa is the electron fraction of bromobenzene. Obviously, the G-value of benzene has its maximum value at about 1 mol l^{-1} of bromobenzene. The solid lines correspond to the equation

$$G(C_6H_6) = g_B(C_6H_6)\varepsilon_B + g_H(C_6H_6)\varepsilon_H, \quad (3)$$

where ε_B and ε_H are the electron fractions of bromobenzene and the hydrocarbon used. The g_B and g_H values thus obtained may be summarized as follows; $g_B=1.2\pm0.3$, $g_H=3.7\pm0.3$ for cyclohexane and $g_B=1.0\pm0.2$, $g_H=3.5\pm0.2$ for 2,2,4-trimethylpentane. Since g_H corresponds to the total G-value of benzene when ideal electron scavenging occurs in a pure hydrocarbon, the g_H should be equal to the sum of G_{fi} and G_{gi}.

Table 1. Empirical constants obtained by fitting the data to Eq. 1 and to Eq. 2.

Equation	Cyclohexane			2,2,4-Trimethylpentane		
	G_{fi}[a]	G_{gi}	α[b]	G_{fi}[a]	G_{gi}	α[b]
(1)	0.15	3.8	10	0.33	3.5	18
(2)	0.15	4.8	10	0.33	4.5	16

a) Determined by the conductivity method.[10]
b) 1 mol^{-1}.

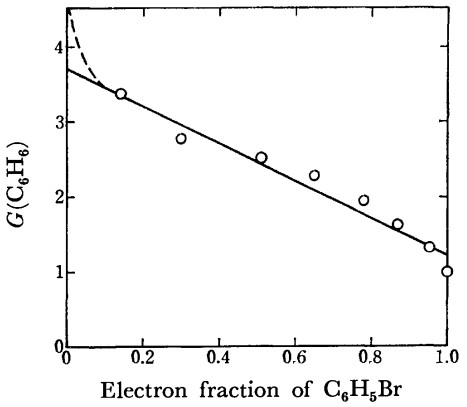

Fig. 3. The G-values of benzene from the bromobenzene solution in cyclohexane at the high concentrations of bromobenzene. For the solid and dashed lines, see the text.

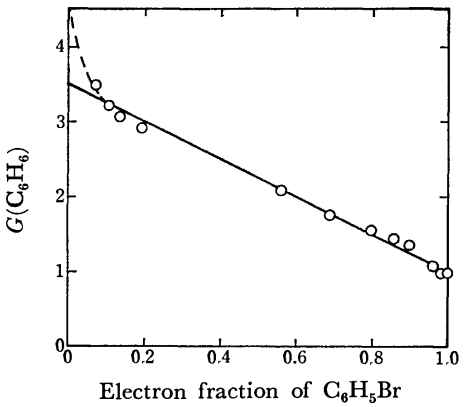

Fig. 4. The G-values of benzene from the bromobenzene solution in 2,2,4-trimethylpentane at the high concentrations of bromobenzene. For the solid and dashed lines, see the text.

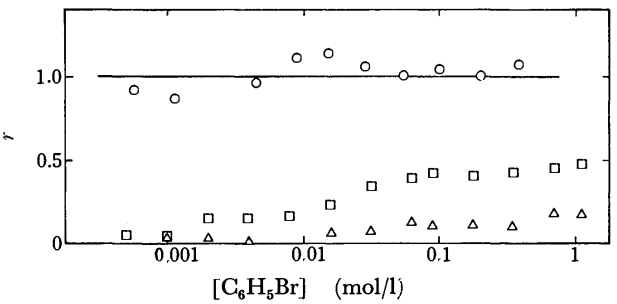

Fig. 5. Compensation between the G-value of benzene and the G-value of noncondensable products. ○: r_{H_2} from cyclohexane solution, □: r_{H_2} from 2,2,4-trimethylpentane solution, and △: r_{CH_4} from 2,2,4-trimethylpentane solution.

Comparing the g_H's shown above with the values in Table 1, we can conclude that Eq. 1 gives more self-consistent values than does Eq. 2.

Figure 5 shows the following ratios;

$$r_{H_2} = \{G_0(H_2) - G(H_2)\}/G(C_6H_6), \quad (4)$$

and

$$r_{CH_4} = \{G_0(CH_4) - G(CH_4)\}/G(C_6H_6). \quad (5)$$

TABLE 2. G-VALUES OF CYCLOHEXENE, BICYCLOHEXYL, AND CYCLOHEXYL BROMIDE FROM THE BROMOBENZENE SOLUTION IN CYCLOHEXANE

Bromobenzene (mol l^{-1})	$G(C_6H_{10})$	$G(C_{12}H_{22})$	$G(C_6H_{11}Br)$
0	3.01	1.95	
0.00045	0	0.49	
0.42	0	0.31	0.75
1.06	0	0.23	0.72

Here, G_0 stands for the G-value from a pure hydrocarbon. Obviously, in the case of cyclohexane, the $G(H_2)$ are compensated by the $G(C_6H_6)$. The G-values of hydrogen and methane from 2,2,4-trimethylpentane solution will be discussed later.

A few experiments were made in the measurement of the G-values of cyclohexene, bicyclohexyl, and cyclohexyl bromide in the presence of bromobenzene. The results obtained are summarized in Table 2.

Discussion

When Warman *et al.* proposed Eq. 2 for expressing the G-values of the methyl radicals formed by the electron scavenging of methyl bromide in cyclohexane, they compared Eq. 2 with Eq. 1,[6] which had been proposed by Hummel. Since their data beautifully fit Eq. 2, they abandoned Eq. 1. However, the highest concentration they used was 0.5 mol l^{-1}, and the G-value obtained at this concentration was 2.8, which corresponds to 72% of the value of G_{gi} they estimated by applying Eq. 2 to their data. In other words, the G_{gi} value they determined is based on a long extrapolation. Consequently, it is doubtful that the sum of G_{fi} and G_{gi} thus obtained is the true total G-value of scavengeable electrons.

As is shown in Figs. 1 and 2, the present data obtained at lower concentrations of bromobenzene are not reproducible enough to discriminate Eq. 1 from Eq. 2. However, as has been shown above, the extrapolation from the high-scavenger-concentration side seems to be more consistent with Eq. 1 than with Eq. 2.

Theoretically we cannot discuss the merits of the two empirical equations. All we can say at present is that the sum of G_{fi} and G_{gi} obtained by the use of Eq. 1 is closer to the total G-value of scavengeable electrons estimated by the extrapolation from the high-concentration side than that estimated by the use of Eq. 2. Of course, Eq. 3 is also an empirical equation. Therefore, $G(C_6H_6)$ might deviate from Eq. 3 at the low-electron fraction of bromobenzene, as is shown by dashed lines in Figs. 3 and 4. However, we do not think this is plausible.

As Fig. 5 shows, the $G(H_2)$ from the cyclohexane solution are compensated by $G(C_6H_6)$. This seems to substantiate the idea that one neutralization reaction between the cyclohexane ion and electron leads to the formation of one hydrogen molecule. The curve for $G(H_2)$ in Fig. 3 was drawn by the use of the equation

$$G(H_2) = 5.6 - [G_{fi} + G_{gi}\{1-\exp(-\sqrt{\alpha S})\}]. \quad (6)$$

Here, the value of 5.6 is the G-value of hydrogen from pure cyclohexane.

On the other hand, in the case of 2,2,4-trimethylpentane, the situation is much more complex. The ratios, r, for hydrogen and methane depend on the concentration of bromobenzene. In order to explain this dependence, we propose the following reaction mechanism.

According to the mass-spectrometric analysis, the parent ion of 2,2,4-trimethylpentane is not stable, but easily decomposes into a butyl ion and a butyl radical. If this type of decomposition competes with the geminate recombination between the parent ion and an electron, and if the neutralization reaction between a butyl ion and an electron does not lead to the formation of hydrogen or methane, then we can derive the concentration-dependences of $G(H_2)$ and $G(CH_4)$.

The probability of the electron scavenging by bromobenzene by the time t may be expressed as follows:

$$\int_0^t kSe^{-kSt'}dt' = 1 - e^{-kSt}. \quad (7)$$

Here, k is the rate constant of the electron scavenging by bromobenzene. Then, the fraction of electrons which react with the electron scavenger should be expressed by the equation

$$F(\phi) = \int_0^\infty f(t)(1-e^{-kSt})dt = 1 - \int_0^\infty f(t)e^{-kSt}dt. \quad (8)$$

Here, $f(t)$ is the time distribution function of the geminate electrons. If Hummel's empirical equation can be used for expressing the electron scavenging in the present system, the $f(t)$ function should satisfy the following equation:

$$\int_0^\infty f(t)e^{-kSt}dt = \exp(-\sqrt{\alpha S}). \quad (9)$$

The $F(\phi)$ fraction corresponds to the yield of benzene produced by the reaction between bromobenzene and geminate electrons.

When the electron scavenger is absent, the formation of hydrogen depends on the decomposition lifetime of the parent ion ($\tau = 1/k_0$) and on the efficiency of the hydrogen formation from the neutralization reaction (γ):

$$F(H_2) = \gamma\int_0^\infty e^{-k_0t}f(t)dt. \quad (10)$$

In the presence of bromobenzene, this fraction should be modified as follows:

$$F(H_2)_S = \gamma\int_0^\infty e^{-k_0t}f(t)e^{-kSt}dt. \quad (11)$$

Therefore, we can easily derive the following equations:

$$r'_{H_2} = \frac{G(H_2)_0 - G(H_2)}{G(\phi) - G_{fi}} = \gamma\frac{\int_0^\infty f(t)\{e^{-k_0t} - e^{-(k_0+kS)t}\}dt}{1-\int_0^\infty f(t)e^{-kSt}dt} = \gamma\frac{\exp(-\sqrt{\beta}) - \exp(-\sqrt{\beta+\alpha S})}{1-\exp(-\sqrt{\alpha S})}. \quad (12)$$

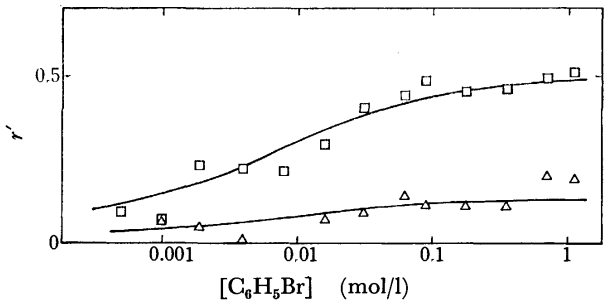

Fig. 6. The interpretation of the formation of hydrogen and methane from 2,2,4-trimethylpentane solution. □: r'_{H_2} and △: r'_{CH_4}.

Here, $\beta=k_0\alpha/k$. The curve for r'_{H_2} in Fig. 6 was drawn by using the following values; $\alpha=18$ l mol^{-1}, $\beta=0.052$, and $\gamma=0.61$. A similar treatment can be applied to r'_{CH_4} ratio. The value of γ used for drawing the curve for methane was 0.16.

In order to estimate the decomposition lifetime of the 2,2,4-trimethylpentane ion, let us assume that $k=10^{13}$ l mol^{-1} s^{-1}.[7] Then, the lifetime can be estimated to be 2×10^{-11} s.

Freeman and Sambrook commented that, when one uses a bromide compound as an electron scavenger, one has to pay attention to the effect of the product, especially hydrogen bromide, on the electron scavenging process.[8] According to the radiolysis study of pure bromobenzene, the G-value of hydrogen bromide is not small, but ranges from 1.0 to 2.0.[9]

When we measured the G-value of benzene from the bromobenzene solution in cyclohexane, we observed the formation of cyclohexyl bromide as is shown in Table 2. Upon the addition of bromobenzene, the formation of cyclohexene was completely suppressed. This is probably due to the reaction of cyclohexene with the hydrogen bromide eventually produced.

Although we could not clarify the fate of all of the bromine atoms, the final form of bromine atoms may be alkyl bromide. If such products as alkyl bromide should seriously affect the electron scavenging process of bromobenzene, some changes would be needed in the present treatment, especially for the absolute value of G_{gl}. However, since the absolute amount of any product is much smaller than that of bromobenzene added to the solution, we do not think that the effect of a product such as alkyl bromide on the electron-scavenging process of bromobenzene is serious.

References

1) T. Kimura, K. Fueki, and Z. Kuri, *Bull. Chem. Soc. Jpn.*, **43**, 3090 (1970); M. Baba and K. Fueki, *ibid.*, **48**, 3039 (1975).
2) S. Sato and T. Oka, *Bull. Chem. Soc. Jpn.*, **44**, 856 (1971).
3) T. Wada and Y. Hatano, *J. Phys. Chem.*, **79**, 2210 (1975).
4) A. Hummel *J. Chem. Phys.*, **49**, 4840 (1968).
5) J. M. Warman, K. D. Asmus, and R. H. Schuler, *J. Phys. Chem.*, **73**, 931 (1969).
6) S. J. Rzad, P. P. Infelta, J. M. Warman, and R. H. Schuler, *J. Chem. Phys.*, **52**, 3971 (1970).
7) A. O. Allen, T. E. Gangwer, and R. A. Holroyd, *J. Phys. Chem.*, **79**, 25 (1975).
8) G. R. Freeman and T. E. M. Sambrook, *J. Phys. Chem.*, **78**, 102 (1974).
9) S. S. Kumar and J. F. Merklin, *J. Chem. Soc., Faraday Trans. 1*, **69**, 577 (1973); A. F. Everard, J. D. Parrack, G. A. Swan, and P. S. Timmons, *J. Chem. Soc.*, **169**, 905 (1962); R. E. Buhler and J. M. Bossy, *Int. J. Radiat. Phys. Chem.*, **6**, 95 (1974).
10) W. F. Schmidt and A. O. Allen, *J. Chem. Phys.*, **52**, 2345 (1970).

Cation Distribution in Mixed Formates. I. Change in Lattice Constants and in Infrared Spectra with the Chemical Constitution of $(Cu,M^{II})(HCOO)_2 \cdot 2H_2O$

Toshiko OGATA,* Tooru TAGA, and Kenji OSAKI

Faculty of Pharmaceutical Sciences, Kyoto University, Sakyo-ku, Kyoto 606

(Received November 22, 1976)

Mixed crystals of formates, with the general formula of $(Cu,M^{II})(HCOO)_2 \cdot 2H_2O$, were found to show non-uniform changes in lattice constants with the change in the chemical constitution. The reason for this unusual change was sought in relation to a possible non-uniform distribution of the cations over the two non-equivalent sites for metal ions. A simple model based merely on the difference in the radii of metallic ions did not agree with the results of IR measurements nor with those of an ESR study by Wagner *et al.* Another model, incorporating the change in the direction of the longest axis of the octahedron coordinating to the Cu^{2+} ion at the M1-site, as suggested from the results of a related work (Part II), was found not only to explain the changes in lattice constants, but also to conform with other evidences; it seems to be an essentially correct interpretation.

It has been reported that formates of divalent transitional metals, such as Mn, Fe, Co, Ni, Cu, Zn, and Cd, form isomorphous crystals with the general formula of $M^{II}(HCOO)_2 \cdot 2H_2O$.[1-7] Figure 1 shows the crystal structure of the copper salt as an example. The crystals are monoclinic, with a space group of $P2_1/c$, and the metal ions occupy two sets of non-equivalent centers of symmetry: the M1-site at 0,0,0, *etc.* and the M2-site at 1/2, 1/2, 1/2, *etc.* The metal ion at the M1-site is coordinated by an octahedron of six oxygen atoms, all from formate ions, while that at the M2-site is coordinated by a second octahedron of four water molecules and two oxygen atoms from formate ions.

The existence of the two sets of metal sites with different surroundings suggested the possibility that, when mixed crystals were prepared among the members of this series, cations of different chemical species might occupy different sites with different occupancy. Such a phenomenon would be interesting not only because it has been observed frequently in minerals, but also because it reminds us of the selectivity of biologically important substances to metal ions.[8]

From a series of preliminary experiments made in this laboratory,[9] it has been found that mixed crystals containing copper ions as one of the components exhibit an unusual behavior in the change of lattice constants with the change in the molar ratio of cations. A systematic study was thus undertaken of copper-containing mixed crystals of dihydrated formates.

Description of the Results

Preparation and Chemical Constitution. Mixed crystals with various molar ratios were prepared for the Cu–Zn, Cu–Ni, and Cu–Mn systems by the slow evaporation of the corresponding mixed solution at 55±2 °C. Only a small portion from a large quantity of each solution was crystallized out so as not to cause a substantial change in the composition of the solutions during crystallization. The relative amount of metallic ions in mixed crystals and in the mother liquor, both before and after the crystallization, were determined by absorptiometric methods. Figure 2 shows the relations between the compositions of the solution and the mixed crystals obtained in this way.

Powder X-Ray Pattern and Lattice Constants. The mixed crystals obtained were studied by X-ray powder diffractometry; the results are shown diagrammatically in Fig. 3. It may be noted that the 2θ values of some of the reflections do not change uniformly, indicating that the change in the lattice constants with the chemical constitution is not uniform; this can be seen more clearly in Fig. 4. The results obtained here seem to indicate a non-uniform distribution of the metal ions over the two possible sites, but a detailed interpretation will be given later.

Study by Infrared Absorption. IR measurements were made in order to get some additional clue as to the possibility that either one of the two sites, M1 or M2, might be preferentially occupied by Cu^{2+} ions. The spectra that were found to be most useful for this purpose are those assigned to the wagging vibrations of the water molecules, as is shown in Table 1, where the assignment was obtained by studying the IR spectra

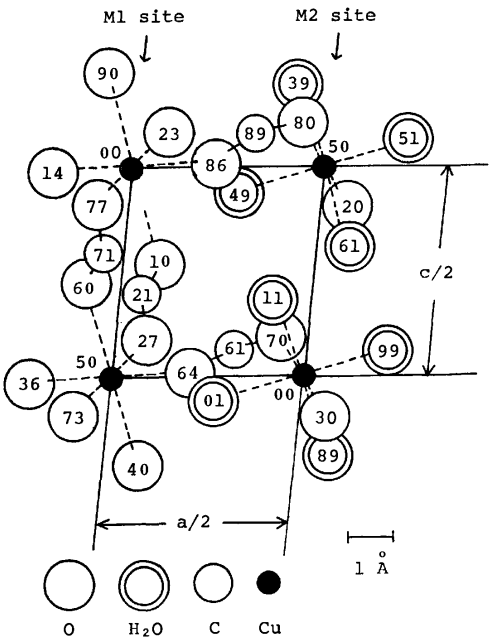

Fig. 1. Crystal structure of $Cu(HCOO)_2 \cdot 2H_2O$ projected on (010).

* Present address: Medical Research Institute, Tokyo Medical and Dental University, Yushima, Bunkyo-ku, Tokyo 113.

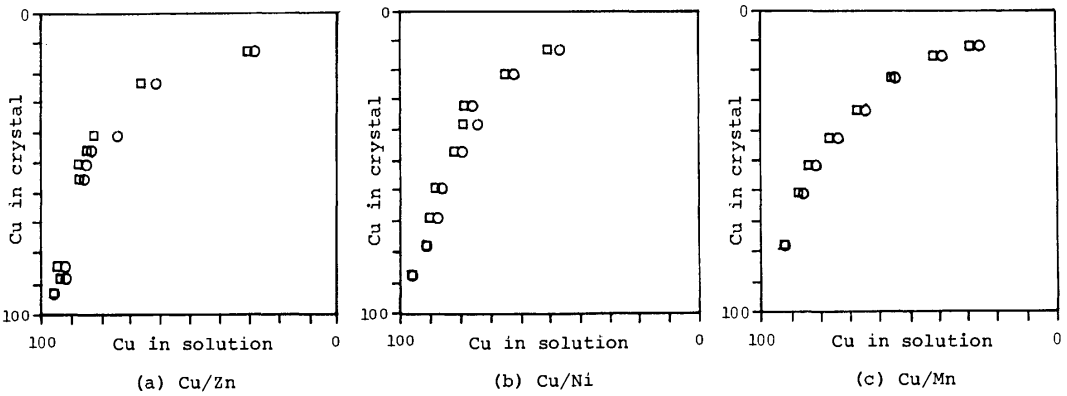

Fig. 2. Relative concentrations of the metal ions in mixed crystals plotted against those in solutions before (○) and after (□) the crystallization. Ordinate and abscissa represent molar percentage of Cu ions in crystal and in solution, respectively.

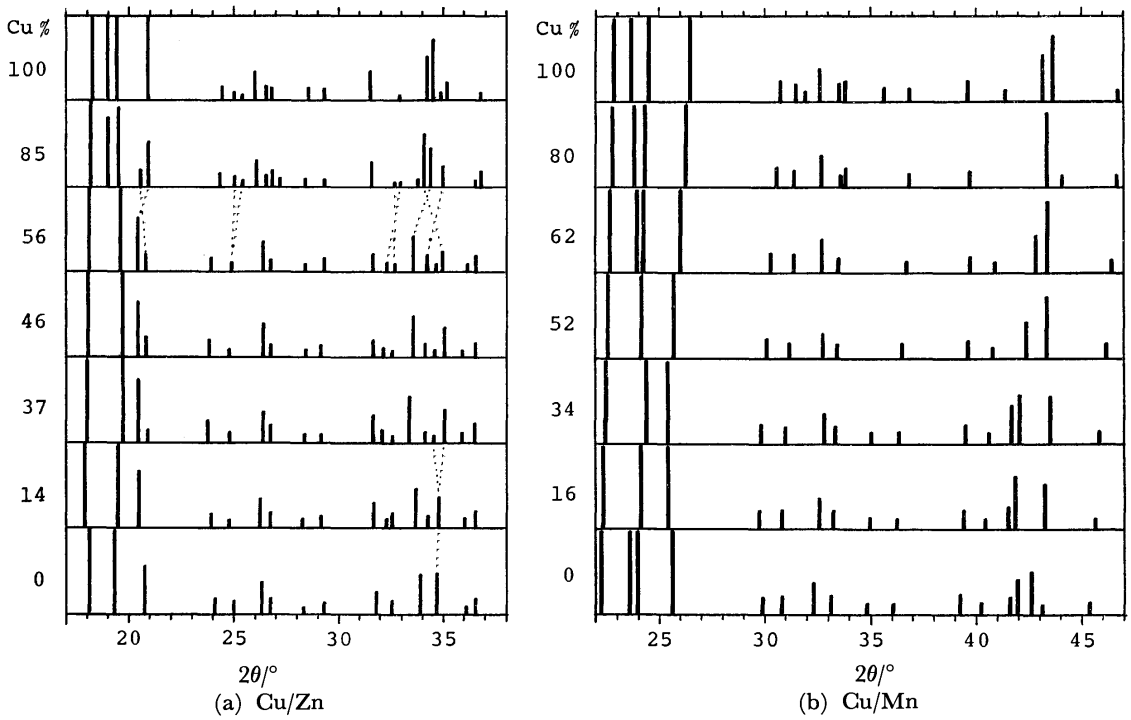

Fig. 3. Powder X-ray diffraction patterns of the mixed crystals.

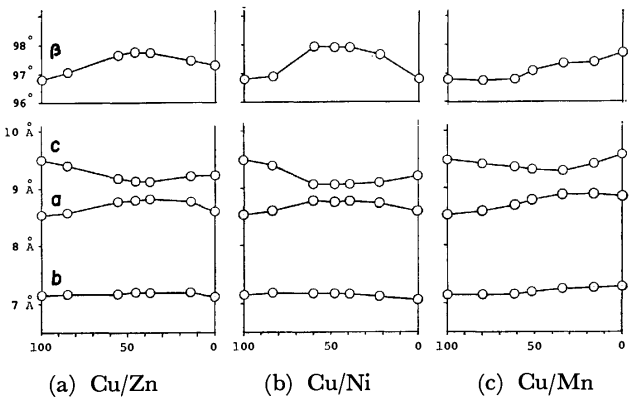

Fig. 4. Change of lattice constants with the chemical constitution.

Table 1. IR absorption frequencies ($\nu \times$ cm) of $M^{II}(HCOO)_2 \cdot 2H_2O$ and their assignments

Salts in which M^{II} are				Assignments
Cu	Zn	Ni	Mn	
1580	1575	1580	1580	antisym. CO stretching
1390	1395	1400	1395	CH stretching in-plane
1325	1355	1355	1360	sym. CO stretching
	1380	1375	1375	
910	870	890	820	$M-H_2O$ rocking
875	830	850		
		795?		
785	765	770	750	OCO bending
600	555	550	568	$M-H_2O$ wagging
470	375	410	400	M-O stretching
400		360	365	
350			310	lattice deformation

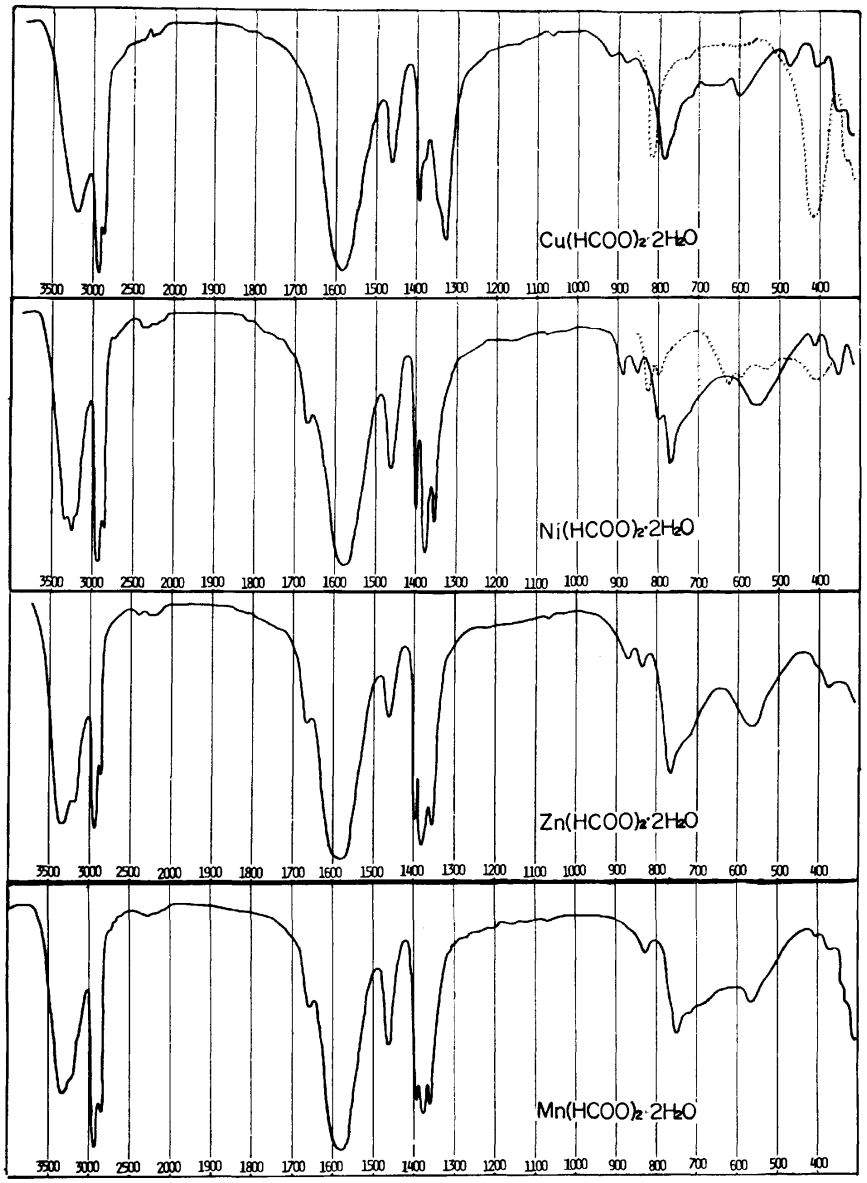

Fig. 5. Infrared absorption spectra of pure dihydrated formates. Dotted curves shown for Cu salt and for Ni salt are those of the anhydrous salt and of the deuterated salt, respectively.

reproduced in Fig. 5 with reference to some reports on related substances.[10,11]

Figure 6 shows how the spectra in this region change with the molar ratio of the cations. The relative amounts of the two kinds of metal ions occupying the M2-sites were determined from these spectra by comparing the optical densities at appropriate wavelengths (600, 555, 550, and 568 cm^{-1} for Cu, Zn, Ni, and Mn, respectively), assuming a 100% transmission at about 430 cm^{-1} and making use of the calibration curves prepared by mixing known amounts of the two kinds of pure substances corresponding to Fig. 5.

The results are shown in Fig. 7, in which the dotted lines, A, B, and C, correspond to the simple models described in the next section. Although there is some scattering of the observed points, it may be concluded that there is a definite tendency for the Cu^{2+} ions to occupy the M1-site rather than the M2-site.

Discussion

As has already been stated, the observed characteristic change of the lattice constants shown in Fig. 3 can not be explained by the uniform replacement of the metal ions in both M1- and M2-sites; some kind of structural change must be taken into account in order to explain the results obtained.

Model calculations were attempted of the lattice constants, a and c, of the Cu–Ni and Cu–Mn systems, for which the two extreme structures are shown in Fig. 8 in superposed projections. We assumed that the change in the lattice constants is mainly the result of the dif-

ference in metal-oxygen distances observed in Fig. 8. In the first place, calculations were made for the three simplest models:

(Model A) The two kinds of ions occupy the two sites without any preference;

(Model B) The Cu^{2+} ions occupy the M2-sites, and the other ions occupy the M1-sites, both with a 100% preference;

(Model C) The same as in model B, except that the M1- and M2-sites are interchanged.

In all three cases, it was assumed that the orientations of the Cu-octahedra at the M1- and M2-sites are the same as those found in the crystal structure of the pure Cu salt.[6]

The results of these model calculations are shown in Fig. 9. Of the three models given above, Model B appears to be in better agreement with the observed points than does A or C. However, this is just the opposite of the results of the IR measurements given above, and also contradicts the results of the ESR study by Wagner *et al.*[12] Moreover, it is noticed that the change in *a* in Fig. 9 (a) is too big to be explained even with Model B.

As a matter of fact, it has been shown, from the single crystal study described in Part II,[13] that, in the 1 : 1 mixed crystal of Cu and Zn salts, most of the Cu-octahedra occupying the M1-site have their longest axis pointing normal to the $[Cu(HCOO)_2]$ sheet, unlike those in the pure Cu salt. This is a possibility that has not been taken into account thus far, so model calculations were also tried for the following two models:

(Model D) Similar to Model C, except that the orientation of the Cu-octahedron at the M1-site is varied according to the Zn/Cu ratio; the longest axis of the Cu octahedron mostly lies along the bc-plane, while the Zn/Cu ratio is low, but as the Zn/Cu ratio increases the proportion of the longest axis pointing normal to the bc-plane becomes larger, attaining to a 70 to 80% orientation at Zn/Cu=1 : 1 (Part II);

(Model E) Both ions occupy both M1- and M2-sites without any preference, as in Model A, but the longest axis of the Cu-octahedron at the M1-site changes its direction, just as in Model D.

In both cases, the longest axis of the Cu-octahedron at the M2-site always corresponds to M2–O3′. The results for these models, also shown in Fig. 9, seem to indicate that the best model lies somewhere between D and E. This result is also in accord with that of the IR measurements and seems to be the most reasonable interpretation of the mixed crystal formation in the $(Cu,M^{II})(HCOO)_2 \cdot 2H_2O$ system.

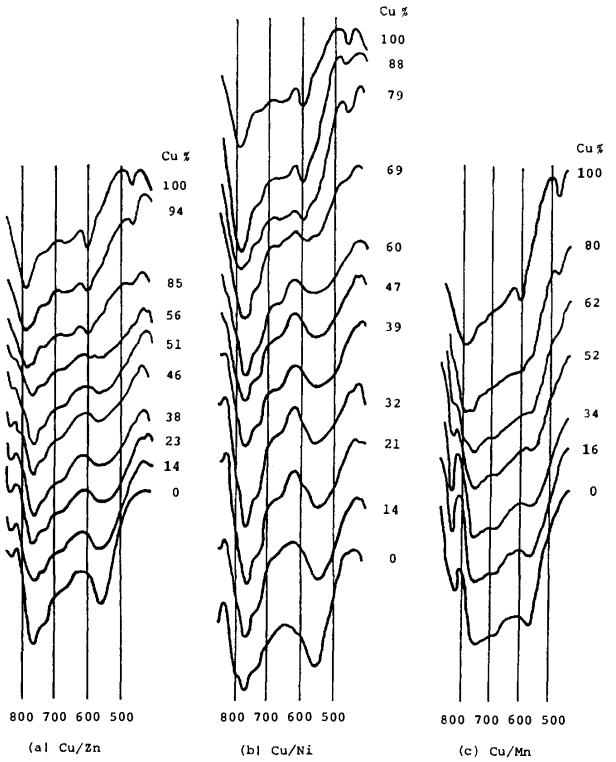

Fig. 6. Changes of the IR spectra assigned to wagging vibrations of water molecules, caused by the change in the molar ratio of metal ions. The abscissa are the wavelengths ($\nu \times$ cm).

Experimental and Calculational Details

Preparation of Mixed Crystals. A mixture of calculated amounts of the starting substances, carbonates for Zn and Mn or basic carbonates for Cu and Ni, was decomposed in water with a slight excess of formic acid. The solution thus obtained (pH 3—4) was then evaporated in a constant-temperature box at 55±2 °C.

Chemical Analysis. Mixed crystals from each batch were dissolved in water and analyzed by absorptiometric methods,

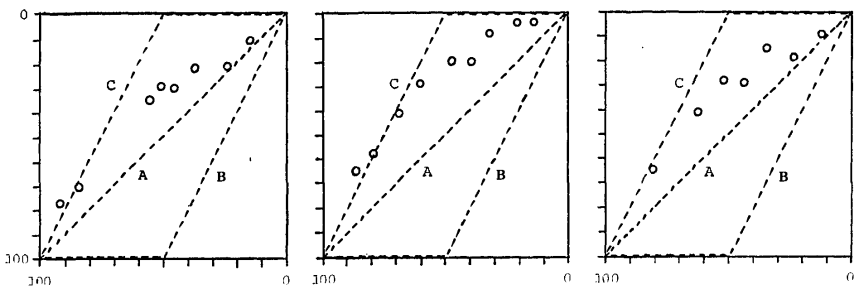

Fig. 7. Relative amount of metal ions coordinated by water molecules (in M2-sites) against the total amount contained in the mixed crystals.

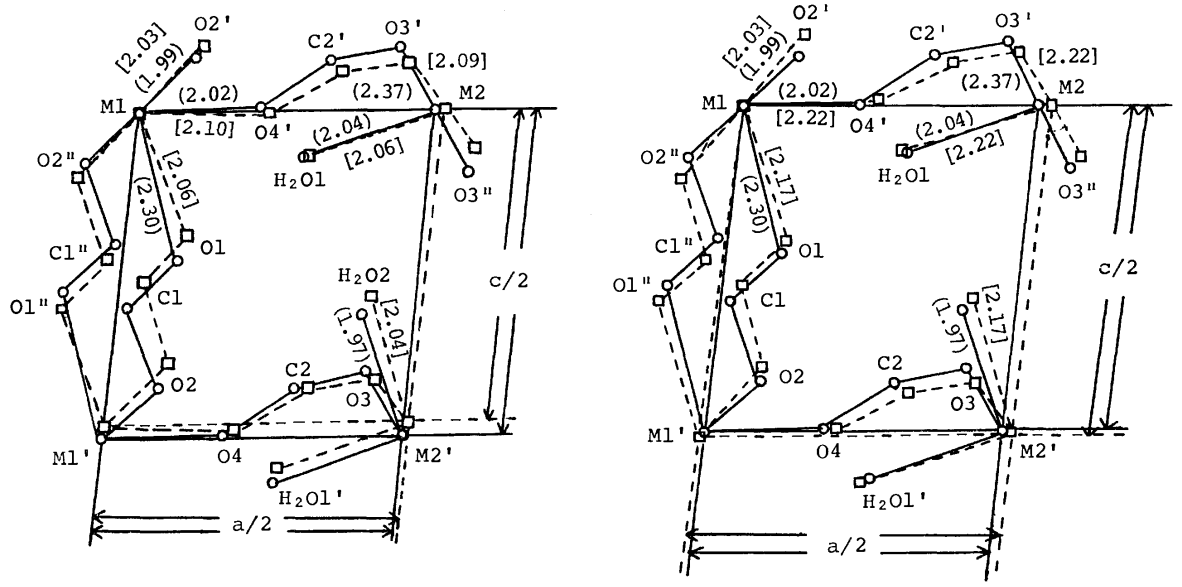

Fig. 8. Crystal structures of $Cu(HCOO)_2 \cdot 2H_2O$ and of $M^{II}(HCOO)_2 \cdot 2H_2O$, shown superposed in b-axis projections. Figures in ( ) and in [ ] are those for the Cu salt and for the salt of the other metals, respectively.

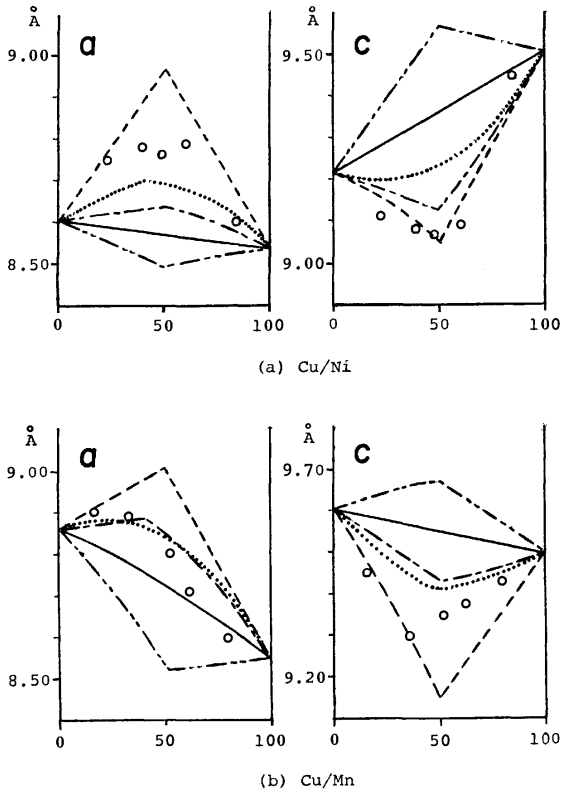

Fig. 9. Model calculations on the lattice constants a and c.
——— model A, ------ model D,
—— — model B, ····· model E.
—— — model C,

as will be described below. The same method was used also for the analysis of the mother liquor.

For the case of Cu–Zn, the zincon method[14,15] was used. For the case of Cu–Ni, the absorbance of the solutions colored by EDTA (pH≈6) was measured at two suitable wavelengths selected from 740, 590, and 385 mμ according to the concentration adopted (from 10^{-3} to 4×10^{-2} mol/l). For the case of Cu–Mn, Mn was measured using the permanganic-acid method[16], while Cu was measured as in the case of Cu–Ni.

X-Ray Powder Diffractometry. The conditions of powder diffractometry were, for the Cu–Zn and Cu–Ni systems: Rigaku Geigerflex; Ni-filtered CuK radiation; 30 kV; 15 mA; receiving slit, 0.15 mm; scanning speed, 1°/min; time constant, 4 s; for the Cu–Mn system: Norelco Diffractometer; Mn-filtered FeK radiation, 35 kV; 10 mA; receiving slit, 0.006 inch; scanning speed, 1°/min; time constant, 8 s.

No signs of unusual line broadening were detected in the powder diagrams of mixed crystals; this suggests that the compositions of the powdered crystal grains in the same batch were fairly uniform and that local fluctuations in the lattice constants were not appreciable.

Indices were given at first only to lower-order, non-overlapping reflections, making use of the similarity in the powder patterns of the mixed crystals and of individual pure substances. The lattice constants calculated by the least-squares method from the observed spacings of these reflections made possible the indexing of additional reflections. This process was repeated until it became difficult to add new reflections.

Infrared Absorption Measurements. The IR spectra shown in Fig. 5 were obtained with a Perkin-Elmer Model 521, and those in Fig. 6, with a Koken DS-301, both using the nujol mull method. In Fig. 5, the spectra shown by dotted lines are those of the anhydrous salt in the case of $Cu(HCOO)_2 \cdot 2H_2O$ and those of the deuterates in the case of $Ni(HCOO)_2 \cdot 2H_2O$.

Model Calculations of the Lattice Constants. The following assumptions were also made:

1) The change in β can be ignored;

2) The change in the axial length, a, is mainly determined by the a-axis component of the variations in the M1–O4′ bond distances, though some additional corrections were also applied taking into consideration the differences in the M2–

O4′ distances which were actually observed in the Cu, Ni, and Mn salts;

3) The change in the axial length, c, is mainly determined by the c-axis component of the difference in the M1–O1 bond distances, though corrections similar to those above were also made for the change in the M1′–O1 distance.

The authors are indebted to Professor Emeritus Eiji Suito, Institute for Chemical Research, Kyoto University, and to Professor Katsunosuke Machida of this Faculty for their helpful advice in doing the IR measurements. The preliminary part of this work has been participated in by Miss Yoko Kokado (Mrs. Taga), Miss Miyako Yasuda (Mrs. Hoshiai), Miss Ouko Hamada (Mrs. Umemura), Miss Noriko Okudaira, Miss Yuriko Tanaka (Mrs. Ohno), Miss Yasuko Matsuo and Miss Yumiko Sumida, to all of whom the authors' thanks are also due.

One of the authors (K. O.) is also especially indebted to Professor Emeritus Isamu Nitta and Professor Emeritus Tokunosuké Watanabé, in the atmosphere of whose laboratories in the Faculty of Science, Osaka University, the idea of this work has emerged.

Most of the computations were performed on the HITAC 5020 at the Kyoto University Computation Center or on the FACOM 230-60 at the Data Process ing Center, Kyoto University, using UNICS programs and those written by the authors.

References

1) K. Osaki, Y. Nakai, and T. Watanabé, *J. Phys. Soc. Jpn.*, **18**, 919 (1963); *ibid.*, **19**, 717 (1964).

2) G. R. Hoy, S. Barros, F. Barros, and S. A. Friedberg, *J. Appl. Phys.*, **36**, 936 (1965).

3) A. S. Antsyshkina, M. K. Guseinova, and M. A. Porai-Koshitz, *Zh. Strukt. Khim.*, **8**, 365 (1967).

4) K. Krogmann and R. Mattes, *Z. Kristallogr.*, **118**, 291 (1963).

5) M. Bukowska-Strzyzewska, *Acta Crystallogr.*, **19**, 357 (1965).

6) M. I. Kay, I. Almodovar, and S. F. Kaplan, *Acta Crystallogr., Sect. B*, **24**, 1312 (1968).

7) M. L. Post and J. Trotter, *Acta Crystallogr., Sect. B*, **30**, 1880 (1974).

8) "The Biochemistry of Copper," ed by J. Peisach, P. Aisen, and W. E. Blumberg, Academic Press, New York and London (1966).

9) Unpublished work by the same authors read at the annual meetings of the Pharmaceutical Society of Japan: Kyoto, 1966, and Osaka, 1972.

10) I. Nakagawa and T. Shimanouchi, *Spectrochim. Acta*, **20**, 429 (1964).

11) Y. Kuroda and M. Kubo, *Spectrochim. Acta*, **23A**, 2779 (1967).

12) G. R. Wagner, R. T. Schumacher, and S. A. Friedberg, *Phys. Rev.*, **150**, 226 (1966).

13) T. Ogata, T. Taga, and K. Osaki, *Bull. Chem. Soc. Jpn.*, **50**, 1680 (1977).

14) R. M. Rush and J. H. Yoe, *Anal. Chem.*, **26**, 1345 (1954).

15) R. H. Maier and J. S. Bullock, *Anal. Chim. Acta*, **19**, 354 (1958).

16) E. B. Sandell, "Colorimetric Determination of Traces of Metals," Interscience Publishers, New York, N. Y. (1959), p. 606.

Cation Distribution in Mixed Formates. II. The Structure of the Mixed Crystal $Cu_{0.5}Zn_{0.5}(HCOO)_2 \cdot 2H_2O$

Toshiko OGATA,* Tooru TAGA, and Kenji OSAKI
Faculty of Pharmaceutical Sciences, Kyoto University, Sakyo-ku, Kyoto 606
(Received November 22, 1976)

The structure of the 1 : 1 mixed crystal between $Cu(HCOO)_2 \cdot 2H_2O$ and $Zn(HCOO)_2 \cdot 2H_2O$ has been determined on the basis of 878 visual intensity data. The space group is $P2_1/c$, with $a=8.77$, $b=7.25$, $c=9.17$ Å, $\beta=98.0°$, and $Z=4$. The structure is similar to that of $Cu(HCOO)_2 \cdot 2H_2O$, except that the two metal ions are distributed over two metal ion sites, the Cu^{2+} ions being mostly localized in the $[Cu(HCOO)_2]$ sheet, and except that the longest axis of the coordination octahedron around the Cu^{2+} ion in this sheet is nearly perpendicular to it. It is suggested that the type of sheet found in the mixed crystal as well as in $Cu(HCOO)_2 \cdot 4H_2O$ is more favorable than that in $Cu(HCOO)_2 \cdot 2H_2O$ for an independent $[Cu(HCOO)_2]$ sheet.

In Part I of this series,[1] it has been shown that the lattice constants of the mixed crystals with the general formula of $(Cu,M^{II})(HCOO)_2 \cdot 2H_2O$ do not change uniformly with the change in the chemical constitution, and that simple models based merely on the preferential occupation of the two non-equivalent sites by different metal ions were unsatisfactory in explaining the observed results. It was, therefore, hoped that a detailed structure study of a 1 : 1 mixed crystal of this series would provide some evidence which might help elucidate the problem.

Structure Determination

Apparently single crystals containing approximately equal amounts of Cu^{2+} and Zn^{2+} ions were obtained by the slow evaporation of a mixed solution with an appropriate molar ratio, as determined from Fig. 2 of Part I.

The lattice constants obtained from Weissenberg photographs are $a=8.77\pm0.03$, $b=7.25\pm0.02$, $c=9.17\pm0.02$ Å, and $\beta=98.0\pm0.5°$. There are four formula units in this unit cell with the space group of $P2_1/c$, just as in $Cu(HCOO)_2 \cdot 2H_2O$.[2] The intensity data, visually estimated on Weissenberg photographs and put on a common scale after necessary corrections, amounted to 878, excluding non-observed reflections.

An approximate structure was easily obtained with reference to those of related formates,[2,3] assuming averaged atoms at both metal sites. Refinements were performed with full-matrix least-squares for the two cases: one with Zn^{2+} at the M1-site and Cu^{2+} at the M2-site (case 1), and the other in which they are interchanged (case 2), in the hope that the slight difference in the number of electrons in the metal ions might give evidence as to which of these two cases corresponds to the true structure. The results are given in Table 1. The R value was 0.110 for both cases. No significant difference was found in the positions of the lighter atoms. From the smaller difference in the thermal parameters for the two metal sites, it might seem that Case 1 could be the correct structure. As a matter of fact, it turned out that the final model adopted after a detailed examination of the structure (to be described later) was closer to Case 2, though the localization of the metal ions was found to be incomplete. A reasonable interpretation of the above contradiction is that the large difference in the thermal parameters has upset the effect of the small difference in electron density.

The atomic scattering factors used were taken from the International Tables for X-ray Crystallography (Vol. 3), and dispersion corrections were applied to the real parts of the scattering factors for Cu^{2+} and Zn^{2+}. The

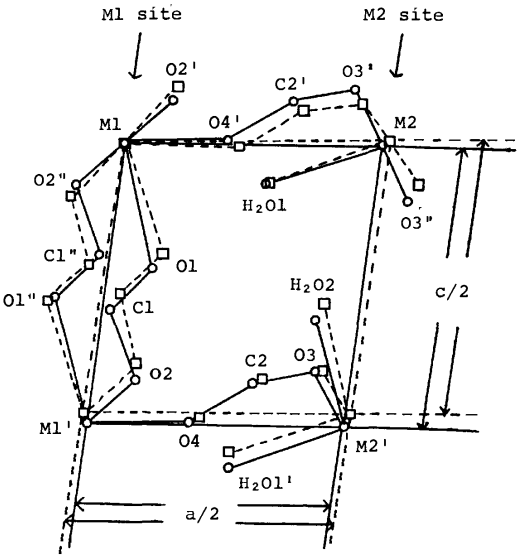

Fig. 1. Crystal structures of $Cu_{0.5}Zn_{0.5}(HCOO)_2 \cdot 2H_2O$ and $Cu(HCOO)_2 \cdot 2H_2O$ seen superposed in projection down the b-axis.

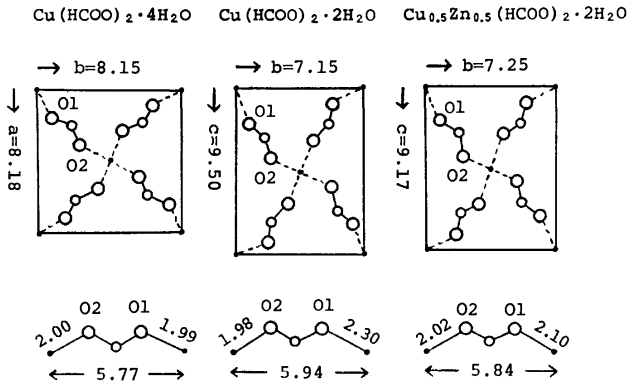

Fig. 2. The structure of the $[Cu(HCOO)_2]$ sheets in the three related compounds.

* Present address: Medical Research Institute, Tokyo Medical and Dental University, Yushima, Bunkyo-ku, Tokyo 113.

Table 1. Positional and thermal parameters

Atom	x	y	z	B/Å²	
				Case 1	Case 2
M1	0	0	0	1.72(05)	1.21(04)
M2	0.5	0.5	0	1.48(05)	2.07(05)
C1	0.034(1)	0.226(1)	0.277(1)	1.96(18)	1.97(18)
C2	0.324(1)	0.612(1)	0.438(1)	1.96(18)	2.01(18)
O1	0.095(1)	0.103(1)	0.207(1)	2.22(16)	2.16(13)
O2	0.087(1)	0.279(1)	0.405(1)	1.99(13)	2.00(13)
O3	0.436(1)	0.722(1)	0.420(1)	2.87(16)	2.90(16)
O4	0.214(1)	0.664(1)	0.502(1)	2.11(13)	2.17(13)
$(H_2O)1$	0.284(1)	0.474(1)	0.073(1)	2.19(13)	2.13(13)
$(H_2O)2$	0.413(1)	0.107(1)	0.300(1)	3.06(16)	3.15(16)

Case 1: Zn^{2+} in M1 and Cu^{2+} in M2, Case 2: Cu^{2+} in M1 and Zn^{2+} in M2.

Table 3. Interatomic distances and angles

Atom pairs[a)]	$Cu_{0.5}Zn_{0.5}$-$(HCOO)_2 \cdot 2H_2O$	Cu-$(HCOO)_2 \cdot 2H_2O$
M1-O1	2.10(2) Å	2.30(2) Å
M1-O2′	2.02(1)	1.98(2)
M1-O4′	2.22(1)	2.02(2)
M2-W1	2.10(1)	2.04(2)
M2-O3′	2.19(1)	2.37(2)
M2′-W2	2.04(1)	1.97(2)
O4-M1′-O1″	92.8(4)°	91.5(6)°
O1″-M1′-O2	91.2(6)°	89.2(7)°
O4-M1′-O2	93.4(7)°	93.2(7)°
O3-M2′-W1′	89.3(4)°	87.6(6)°
W1′-M2′-W2	90.5(8)°	87.5(7)°
O3-M2′-W2	90.1(5)°	86.9(6)°
C1-O1	1.26(1) Å	1.26(3) Å
C1-O2	1.27(1)	1.30(3)
C2-O3	1.29(1)	1.26(3)
C2-O4	1.25(1)	1.24(3)
O1-C1-O2	124(1)°	121(2)°
O3-C2-O4	121(1)°	130(2)°
W1′-O2	2.82(2) Å	2.82(2) Å
W1′-O4	2.75(1)	2.78(2)
W2-O1	2.79(2)	2.77(3)
W2-O3″	2.70(2)	2.67(2)

a) W in this column represents (H_2O).

observed and calculated structure factors are given in Table 2.**

Description and Interpretation of the Structure

The crystal structure of $Cu_{0.5}Zn_{0.5}(HCOO)_2 \cdot 2H_2O$ is similar to that of $Cu(HCOO)_2 \cdot 2H_2O$,[2)] as is shown in Fig. 1 in superposed projections along the b-axis. They both contain parallel sheets with the composition of $[M^{II}(HCOO)_2]$, interleaved with another kind of sheet with the composition of $[M^{II}(H_2O)_4]$ and linked together by a second formate ion. However, closer study shows that, in the mixed crystal, both the M1–O4′ and M2–O3′ listed in Table 3 are definitely longer than those to be expected for a Zn–O bond (0.74+1.40=2.14 Å), and that the longest axis (M1–O4′) of the coordination octahedron at the M1-site points almost normal to the $[M^{II}(HCOO)_2]$ sheet, which is quite different from that found in $Cu(HCOO)_2 \cdot 2H_2O$, where the longest axis M1–O1 lies along the sheet. The latter observation suggests that the longest axis of the Cu-octahedron at the M1-site changes its direction in relation with the relative concentration of the Cu atom and opens the possibility of some new models for the relation between lattice constants and chemical constitution which has been discussed in Part I.

Table 4. Observed and calculated M–O distances

Bond	Observed	Calcd[a)]		
		70%	80%	100%
M1-O4′	2.22 Å	2.20 Å	2.23 Å	2.27 Å
M1-O1	2.10	2.10	2.08	2.03
M1-O2′	2.02	2.03	2.03	2.03
M2-O3′	2.19	2.18	2.18	2.18
M2-W1	2.10	2.07	2.07	2.07
M2′-W2	2.04	2.07	2.07	2.07

a) The percentages given for the calculated values are the proportions of the longest axis orientated along M1–O4′.

The observed length of M1–O4′ and M2–O3′ can only be explained if it is assumed that both M1 and M2 sites are occupied by Cu^{2+} ions to some extent and that the two bond lengths mentioned above are the average values including the contributions from the longest axis of the Cu octahedron. If we adopt the findings of our IR study described in Part I, that in a 1 : 1 mixed crystal between the Cu and Zn salts about 70% of the M1-site is occupied by Cu^{2+} ions, and make the further assumption that from about 70 to 100% of the Cu-octahedra occupying the M1-site are orientated with their longest axis along M1–O4′, we obtain the calculated M–O distances given in Table 4.

It will be seen that a satisfactory agreement between observed and calculated M–O lengths is obtained with

** Table 2 is kept at the office of the Chemical Society of Japan, 1-5 Kanda-Surugadai, Chiyoda-ku, Tokyo 113 (Document No. 7708).

a 70 to 80% orientation. In this calculation, it was further assumed that all the Zn–O bond is 2.10 Å, while for Cu–O, the longest axis is 2.35 Å and the shorter ones are 2.00 Å.

The conclusions obtained here, that in the 1 : 1 mixed crystals between Cu and Zn salts, the M1-site is preferentially occupied by Cu^{2+} ions and that most of the longest axes of the Cu-octahedra at the M1-site point to M1–O4′, while those at the M2-site point to M2–O3′, not only explain the observed changes in the lattice constants with respect to the chemical constitution (Part I), but are in agreement with the results of an ESR study of the Cu-doped $Zn(HCOO)_2 \cdot 2H_2O$ by Wagner *et al.*[4] if the principal axis of the magnetic field at the Cu^{2+} ion found by ESR coincides with the longest axis of the Cu-octahedron.

The structure of the 1 : 1 mixed crystal between Cu and Zn salts has now been elucidated including the distribution of the cations, but questions still remain as to why the Cu^{2+} ion occupies the M1-site preferentially and why the longest axis of the Cu-octahedron at the M1-site points to M1–O4′ and not to M1–O1, as in the pure Cu salt.

A sheet with the composition of $[M^{II}(HCOO)_2]$, similar to that found in the mixed crystal, is also found in $Cu(HCOO)_2 \cdot 4H_2O$;[5] it resembles the one in the mixed crystal also with respect to the orientation of the longest axis of the Cu-octahedron. The sheet in the tetrahydrate has been the subject of many investigations because of its remarkable anti-ferromagnetic nature,[6–15] and it seems generally accepted that the superexchange interaction by way of the delocalized π-electron cloud of the formate ion is responsible for the magnetic interaction between the neighboring Cu^{2+} ions in the sheet.[4,16,17] Since the Cu^{2+} ion is coordinated with an elongated octahedron, an arrangement with the long axis almost normal to the sheet will be most favorable for a better overlapping between the copper d-orbitals and oxygen π-orbitals of the formate ion. The very large exchange integrals observed for the tetrahydrate ($-54\ cm^{-1}$)[12] and for the Cu^{2+} ions in $Zn(HCOO)_2 \cdot 2H_2O$ ($-33\ cm^{-1}$)[4], as compared with the corresponding values for $Cu(HCOO)_2 \cdot 2H_2O$ (1.5 K),[18] seem to support this view.

A comparison among the $[Cu(HCOO)_2]$ sheets found in the three compounds discussed shows that the sheet in the mixed crystal is, in a sense, intermediate between those in $Cu(HCOO)_2 \cdot 4H_2O$ and in $Cu(HCOO)_2 \cdot 2H_2O$ (Fig. 2). Perhaps it may be said that the sheets found in $Cu(HCOO)_2 \cdot 4H_2O$ and in the mixed crystal represent the most stable structure for a single $[Cu(HCOO)_2]$ sheet, while that of the other type, found in $Cu(HCOO)_2 \cdot 2H_2O$, is probably a result of some additional interaction through the second formate linkages.

Most of the computations were made on the HITAC 5020 at the Kyoto University Computation Center, using programs written by the present authors.

References

1) T. Ogata, T. Taga, and K. Osaki, *Bull. Chem. Soc. Jpn.*, **50**, 1674 (1977).
2) M. I. Kay, I. Almodovar, and S. F. Kaplan, *Acta Crystallogr., Sect. B*, **24**, 1312 (1968); M. Bukowska-Strzyzewska, *Acta Crystallogr.*, **19**, 357 (1965).
3) K. Osaki, Y. Nakai, and T. Watanabé, *J. Phys. Soc. Jpn.*, **19**, 717 (1964).
4) G. R. Wagner, R. T. Schumacher, and S. A. Friedberg, *Phys. Rev.*, **150**, 226 (1966).
5) R. Kiriyama, H. Ibamoto, and K. Matsuo, *Acta Crystallogr.*, **7**, 482 (1954).
6) H. Kobayashi and T. Haseda, *J. Phys. Soc. Jpn.*, **18**, 541 (1963).
7) R. B. Flippen and S. A. Friedberg, *J. Chem. Phys.*, **38**, 2652 (1963).
8) K. Okada, M. I. Kay, D. T. Cromer, and I. Almodovar, *J. Chem. Phys.*, **44**, 1648 (1966).
9) K. C. Turberfield, *Solid State Commun.*, **5**, 887 (1967).
10) G. Soda and T. Chiba, *J. Phys. Soc. Jpn.*, **26**, 249 (1969).
11) M. S. Seehra and S. Mohindar, *Phys. Lett. A*, **28**, 754 (1969).
12) A. K. Gregson and S. Mitra, *J. Chem. Phys.*, **51**, 5226 (1969).
13) M. J. Bird and T. R. Lomer, *Acta Crystallogr., Sect. B*, **27**, 859 (1971).
14) K. Yamagata, M. Hayama, and T. Okada, *J. Phys. Soc. Jpn.*, **31**, 1279 (1971).
15) T. G. Castner and M. S. Seehra, *Phys. Rev. B*, **4**, 38 (1971).
16) R. L. Martin and H. Waterman, *J. Chem. Soc.*, **1959**, 1359.
17) M. Inoue and M. Kubo, *Inorg. Chem.*, **9**, 2310 (1970).
18) M. Matsuura, K. Takeda, T. Satoh, Y. Sawada, and J. M. Machado da Silva, *Solid State Commun.*, **13**, 467 (1973).

Radiative Lifetimes of $NH_2(^2A_1)$ Produced by Photodissociation of NH_3 on Irradiation with Vacuum Ultraviolet Light

Seiichiro KODA

Department of Reaction Chemistry, Faculty of Engineering, The University of Tokyo, Bunkyo-ku, Tokyo 113

(Received December 1, 1976)

$NH_2(\tilde{A}^2A_1)$ was produced by photolysis of NH_3 on irradiation with vacuum ultraviolet light. The zero pressure lifetimes were evaluated to be *ca.* 15 μs from the phase lag of the emission excited by modulated Xe and Kr resonance lamps. The quenching rate coefficient of $NH_2(^2A_1)$ for NH_3 was determined to be *ca.* $(1.6\pm0.3)\times10^{-10}$ cm³/molecule·s.

Emission from NH_2* (* denotes $^2A_1$) in the visible region was observed from various sources in discharges and flames.[1] Steady state fluorescence was measured following the production of the excited state radical by photodissociation of NH_3 on irradiation with vacuum ultraviolet light from a hydrogen discharge lamp.[2] Rare gas resonance lamps have been rarely used as an exciting light source.

The radiative lifetimes and the quenching rate of the fluorescence for NH_3 was studied by Lenzi *et al.*[3] by a static method. No absolute values could be determined. Only the product value $\tau_0 k_q$ could be obtained, where τ_0 is the zero pressure lifetime and k_q the quenching rate coefficient for NH_3. Halpern *et al.*[4] observed the time resolved fluorescence from NH_2* following the excitation of the radical in its ground state by means of a pulsed tunable dye laser, and measured zero pressure lifetimes and collisional de-excitation rate constants for several rovibronic levels of NH_2*. The calculated values of $\tau_0 k_q$ from their data disagreed with the values in the UV photolysis experiment.[3]

This work was undertaken with the object of measuring τ_0 and k_q, separately, for NH_2* produced in the UV photolysis by using modulated resonance lamps. Through this work deals only with the lifetime measurement of NH_2*, it has a wide applicability. Recently, the pulse method seems to be much more popular than the modulation method for measuring emission lifetimes. This seems to be mainly due to the usefulness of pulsed lasers with a very short pulse width. It is not easy to find a good pulsed light source in the vacuum UV region. Thus the method using modulated resonance lamps and digital lock-in detection of feeble emission light should be utilized for the lifetime measurement of various excited species produced by vacuum UV photolysis.

Experimental

The apparatus is shown in Fig. 1. The fluorescence cell with several appropriate light horns is made of glass, the outside being blackened; the total volume is *ca.* 600 cm³.

The sample gas, NH_3, is illuminated with light from a 2450 MHz microwave discharge lamp inserted directly into the fluorescence cell. The Xe (CaF_2 window) and Kr(LiF window) lamps were of the type described by Loewenstein *et al.*[5] The microwave power was modulated by a circuit similar to that described by Phillips.[6] The light from the discharge lamp could be modulated as nearly a sine-wave form, judging from its oscilloscope trace. Observation was restricted to the UV-visible light from the lamp.

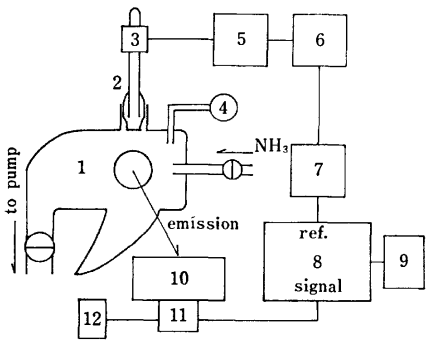

Fig. 1. Reaction apparatus.
1: Fluorescence cell, 2: vuv resonance lamp, 3: microwave cavity, 4: oil manometer, 5: microwave generator, 6: modulation circuit, 7: sine wave generator, 8: photon-counter with a synchronous sampler, 9: chart recorder, 10: monochromator, 11: photomultiplier, 12: high voltage power supply.

Emission from NH_2* was observed at right angles to the exciting beam with a *f*/4.5 monochromator (Nikon P-250). The emission light was then converted into electron pulses by H.T.V. R464 and/or R456 photomultipliers and fed to a Brookdeal 5 Cl photon counter. For lifetime measurements, the reference signal in each cycle from the modulation circuit was fed to the synchronous sampler 5C21. The data of "*A*"−"*B*" were recorded, where "*A*" is the photon count number during a small sampling interval lagging from the reference signal by an arbitrary degree ϕ and "*B*" is that by $\phi+180$ degree. The percent duty, 2×(sampling interval)/(time for one cycle), was set to be 5%.

Ammonia (Matheson Co., 99.99%) was purified by freeze-thaw cycles. The pressure of NH_3 in the cell was measured with an oil manometer.

Results and Discussion

When NH_3 was irradiated by a Xe lamp with a CaF_2 window (147 nm), a weak emission was observed in the range 380—650 nm. The cut-off wavelength at the longer wavelength side could not be determined accurately because of the poorer response of the detector system at longer wavelengths. The Xe lamp with a LiF window (147, 129.6 nm) and a Kr lamp (123.6 nm) eventually gave the same emission besides a much stronger NH (c→a) emission at 327 nm. Because of the weakness of emission, it could only be detected under relatively poor resolution of the monochromator (a band path width above 1.2 nm was adopted) and we could not determine whether the emission was of continuous or many-line type. However, it was evident

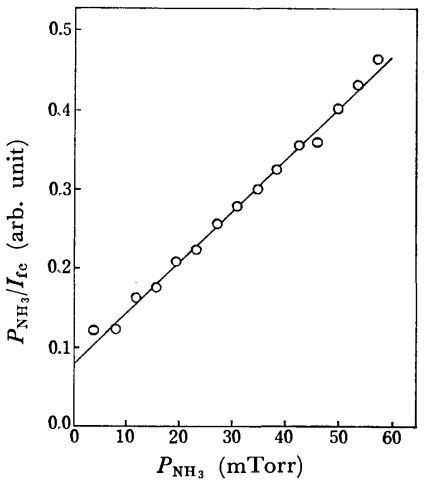

Fig. 2. A typical relationship between P_{NH_3}/I_{fc} and P_{NH_3}.
Excitation by Xe lamp, observation at 520±6 nm. $k_q/k_B=(2.6\pm0.4)\times10^{-15}$ cm^3/molecule is obtained.

from its behavior and the quenching experiments that the emission was from the electronically excited NH_2. Becker and Welge[7] failed to observe this emission with similar resonance lamps. This might be due to the fact that the emission lines were buried in the background under their relatively higher resolution, as suggested by Okabe and Lenzi.[2]

A typical plot is given in Fig. 2 which shows the quenching of NH_2* due to NH_3. The data for the quenching was treated according to the usual mechanism.

$$NH_3 + h\nu \longrightarrow NH_2^* + H$$
$$NH_2^* \longrightarrow NH_2(X) + \text{fluorescence} \quad k_B = \tau_0^{-1}$$
$$NH_2^* + NH_3 \longrightarrow NH_2(X) + NH_3 \quad k_q$$

The fluorescence intensity, I_{fc}, is related to NH_3 pressure, P_{NH_3}, by the equation

$$P_{NH_3}/I_{fc} \propto k_B + k_q P_{NH_3}. \quad (1)$$

Under higher NH_3 pressures, the effect of NH_3 pressure on the light absorption should be considered. Necessary corrections were made on the basis of the geometry of the cell and the extinction coefficient of NH_3 against the exciting lines.[8] The maximum correction was *ca.* 4%.

TABLE 1. THE RATIO k_q/k_B

Exciting light (nm)	Observation wavelength (nm)	k_q/k_B (10^{-15} cm^3/molecule)	Lit
151.8	≥350	2.9±0.5	3
147 (Xe)	400±6[a]	2.4±0.5	this work
	440±6	2.3±0.4	this work
	520±6	2.6±0.4	this work
	560±6	3.0±0.4	this work
139.7	≥350	2.2±0.3	3
125.3	≥350	3.0±0.3	3
123.6 (Kr)	460±9	3.1±0.4	this work
	530±9	2.9±0.4	this work

a) Band path width.

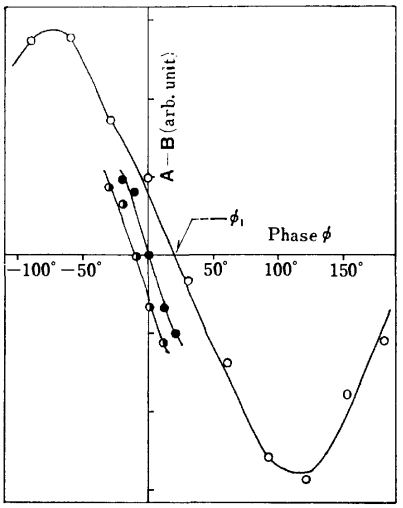

Fig. 3. The data of "A"—"B" at various phases in a modulation experiment.
Excitation by modulated Kr lamp (50 kHz), observation at 520±12 nm. P_{NH_3}=450 mTorr (○), 110 mTorr (●), 50 mTorr (◑). As for ϕ_1, see text.

The fluorescence was observed at several wavelengths. k_p/k_B were evaluated from similar plots to those in Fig. 2 and are given in Table 1. The values are almost independent of the observation wavelength, though allowance should be made for the fact that the fluorescence was observed under relatively low resolution. These values seem to be in good agreement with those of Lenzi *et al.*[3]

Direct lifetime measurements were carried out by means of a modulation technique. The exciting light was modulated as $I_0=\bar{I}_0+\tilde{I}_0\sin(2\pi ft)$, where $\bar{I}_0$ is the d.c. part and $\tilde{I}_0$ is the amplitude of the a.c. part. The possible phase lag of the fluorescence is related to the kinetic process by the equation

$$\theta = \tan^{-1}[2\pi f(k_B+k_qP_{NH_3})^{-1}]. \quad (2)$$

The value "A"—"B" could be measured against any desired phase of degree ϕ (Fig. 3). If we find the degree ϕ_1 at which "A"—"B" is zero, ϕ_1 is equal to $\theta+\phi_0$, where ϕ_0 is the common, though unknown, phase lag of the exciting light from the reference signal of the modulation circuit. ϕ_0 was not measured directly. However, it was so selected that it might give the best linearity as indicated in Eq. 2 between $\theta(=\phi_1-\phi_0)$ and P_{NH_3} at various NH_3 pressures.

The experiments were carried out with several modulation frequencies. Figures 4 and 5 show the results in the case of Xe and Kr lamp excitation, respectively. Because of the weakness of emission, the slightly different wave form of the a.c. part of the exciting light from a precise sine wave, and the relatively large duty factor in measuring "A"—"B", the precision in the measurements of the phase lag was only within ±5 degree. The data do not lie exactly on the straight line, the error limit at the zero pressure limit not being small. In order to confirm the reliability of this technique, measurement was made of the zero pressure lifetime of the c state of NH produced by the Kr lamp excitation. The lifetime of 530 ns ($k_B=1.9\times10^6$/s) was

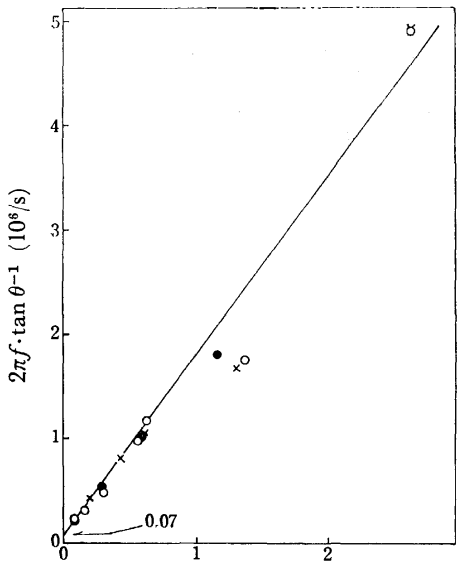

Fig. 4. Emission lifetimes of NH_2* produced by modulated Xe lamp at various pressures of NH_3.
Excitation by Xe lamp, observation at 530±12 nm. Modulation frequency, 54.3 kHz (○), 87.7 kHz (●), 96.2 kHz (×). $k_B=(0.7\pm0.3)\times10^5$/s, $k_q=(1.7\pm0.3)\times10^{-10}$ cm^3/molecule·s are obtained.

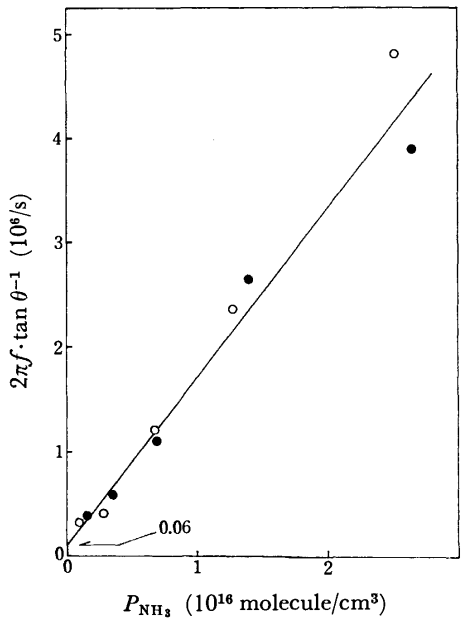

Fig. 5. Emission lifetimes of NH_2* produced by modulated Kr lamp at various pressures of NH_3.
Excitation by Kr lamp, observation at 520±12 nm. Modulation frequency, 54.1 kHz (●), 87.7 kHz (○). $k_B=(0.6\pm0.3)\times10^5$/s, $k_q=(1.6\pm0.3)\times10^{-10}$ cm^3/molecule·s are obtained.

obtained by the same procedure (Fig. 6). The result agrees with the reported value 480±90 ns.[9]

The zero pressure lifetime 14 μs [$k_B=(0.7\pm0.3)\times10^5$ /s] for Xe lamp and 16 μs [$k_B=(0.6\pm0.3)\times10^5$/s] for Kr lamp excitation are near the lifetime 10 μs for the (0,9,0) state obtained by laser light excitation.[4]

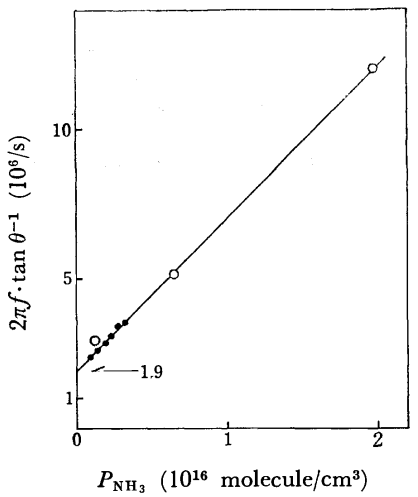

Fig. 6. Emission lifetimes of NH (c) produced by Kr lamp at various pressures of NH_3.
○: $2\pi f \cdot \tan\theta^{-1}$ *vs.* P_{NH_3}, excitation by modulated Kr lamp, observation at 327±3 nm, modulation frequency, 87.7 kHz.
●: P_{NH_3}/I_{fc} *vs.* P_{NH_3}, obtained by steady illumination of Kr lamp, observation at 327±3 nm. In this case, the unknown k_B value (for NH) is assumed to be 1.9×10^6/s in order to plot the value of P_{NH_3}/I_{fc} in the same scale as the data of $2\pi f \cdot \tan\theta^{-1}$.

The k_q values were $(1.7\pm0.3)\times10^{-10}$ (Xe lamp) and $(1.6\pm0.3)\times10^{-10}$ cm^3/molecule·s (Kr lamp). The product values $\tau_0 k_q$ of 2.4×10^{-15} (Xe lamp) and 2.7×10^{-15} cm^3/molecule are in good agreement with the values given in Table 1.

The k_q values are much smaller than the value 10×10^{-10} cm^3/molecule·s for the (0,9,0) state. Thus the discrepancy between the $\tau_0 k_q$ value given by Halpern *et al.*[4] and by Lenzi *et al.*[3] seems to be mainly due to the large difference in the k_q value. The present values as well as those of Lenzi *et al.*[3] are the average of the quenching coefficients for various different vibronic levels of NH_2* produced by the dissociation of NH_3. Fluorescence under low resolution was observed. It should thus consist of the primary emission from the excited NH_2* before any relaxation plus a secondary emission from the relaxed but still electronically excited NH_2. The relatively small k_q values in our case as compared with those of Halpern *et al.*[4] indicates an appreciably efficient vibrational relaxation within the upper electronic state of NH_2 against electronic relaxation to the ground state NH_2.

The author is grateful to Professors S. Tsuchiya and K. Akita, Tokyo University, for their encouragement and valuable suggestions. Thanks are due to Dr. S. Tsunashima, Tokyo Institute of Technology, for his valuable comments as regards the construction of the modulation circuit.

References

1) D. A. Ramsay, *Ann. N. Y. Acad. Sci.*, **67**, 485 (1957).
2) H. Okabe and M. Lenzi, *J. Chem. Phys.*, **47**, 5241 (1967).

3) M. Lenzi, J. R. McNesby, A. Mele, and C. Nguyen Xuan, *J. Chem. Phys.*, **57**, 319 (1972).
4) J. B. Halpern, G. Hancock, M. Lenzi, and K. H. Welge, *J. Chem. Phys.*, **63**, 4808 (1975).
5) M. Loewenstein, J. Heimerl, and E. C. Y. Inn, *Rev. Sci. Instrum.*, **41**, 1908 (1970).
6) L. F. Phillips, *Prog. React. Kinet.*, **7**, 83 (1973).
7) K. H. Becker and K. H. Welge, *Z. Naturforsch., Teil A*, **18**, 600 (1963).
8) R. L. Lilly, R. E. Rebbert, and P. Ausloos, *J. Photochem.*, **2**, 49 (1973/74).
9) S. N. Suchard, Ed., "Spectroscopic Data," Vol. 1, IFI/Plenum Data Co., N. Y. (1975), p. 709.

Heat Capacities of Aqueous Solutions of Glutaric and Malonic Acids*

Fumio KAWAIZUMI, Tuneyuki NOGUCHI, and Yutaka MIYAHARA

Department of Chemical Engineering, Faculty of Engineering, Nagoya University, Chikusa-ku, Nagoya 464

(Received December 6, 1976)

Using a calorimeter composed of a Dewar vessel and a Beckmann thermometer, the specific heat capacities of aqueous solutions of glutaric and malonic acids were measured at 30 °C. Techniques for establishing the temperature gadient between the solution in the Dewar and the outer air bath were adopted. The partial molar heat capacities at infinite dilution were estimated assuming a relation of the form $m\phi_{Cp}=bm+cm^2$. The contributions of the $-CH_2-$ and $-COOH$ groups to the partial molar heat capacities in aqueous solution are roughly additive: for $-CH_2-$ a positive contribution and for $-COOH$ a negative one. The $\Delta(=\overline{Cp}_2^\circ-Cp_2(\text{pure state}))$ were also calculated and positive and negative values were obtained for $\Delta(-CH_2-)$ and $\Delta(-COOH)$, respectively.

It is widely recognized that the heat capacity of a solution is one of the essential quantities which characterizes the solute in solution, especially for solutes containing both hydrophobic and hydrophilic groups.[1-4] From this point of view, the determination of the heat capacities of an aqueous solution of 1,2-ethanediol, 1,2-propanediol, and 1,3-butanediol at 30 °C has been reported.[5]

The present study deals with similar work on aqueous solutions of glutaric and malonic acids using a laboratory-constructed calorimeter composed of a Dewar vessel and a Beckmann thermometer. The heat capacities of aqueous solutions of monocarboxylic acids and their sodium salts have been reported many years ago with sufficient precision,[6] but the situation is completely different for the dicarboxylic series.

Experimental

The calorimeter vessel used is shown in Fig. 1. Although the experimental procedures for determining the heat capacities of solutions are essentially the same as reported previously,[5] the following should be mentioned regarding the calorimeter and the manipulations in the present study. 1) The entire Dewar, except for the upper part of the stirrer and the Beckmann thermometer, is placed in a constant-temperature air bath, while in a previous work,[5] the Dewar was immersed up to the neck in a water bath. 2) In order to obtain more favorable adiabatic conditions, a magnetic stirring system was used in the Dewar. The rotational speed of the stirrer is slow but no heat conduction delay due to the viscosity of the solution was observed. 3) The temperature of the air bath was maintained at a temperature lower than that of the solution in the Dewar. This latter temperature was set near 30 °C and thus the temperature gradient between the solution in the Dewar and the air bath was established. Preliminary experiments showed that with the air bath maintained at 28 °C the most satisfactory results, *i.e.* the temperature variations as a function of time for the solution in the calorimeter before and after the heating are nearly "parallel" to each other (see Fig. 2), are obtained.

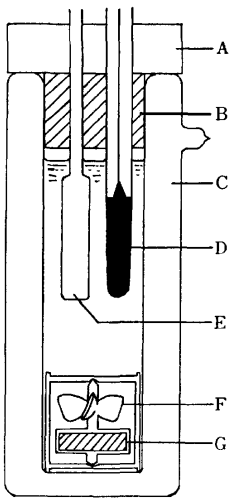

Fig. 1. Calorimeter.
A: Wood plate, B: cork cap,
C: Dewar vessel, D: Beckmann thermometer,
E: glass tube containing heater(manganin wire),
F: glass stirrer,
G: stirring magnet driven externally.

The contact between the cork cap and the Dewar was not so tight as to prevent the passage of vapor from the solution. Other parts of the experimental equipment, such as the electric heating circuit, the circuit for the measurement of the supplied electric power, and the details of the manipulations for determining the heat capacities of the solutions are the same as reported previously.[5]

The heat capacities of the Dewar determined using 100 ml of water are 24.8 cal/K (1 cal=4.184 J) and the reproducibility relative to this value was within ±2.5%. Therefore, the errors due to this uncertainty are *ca.* 0.5% for measurements of 100 g solutions. The precision of the experiments using this calorimeter was checked with the aid of an aqueous solution of Na_2CO_3 at 30 °C, the results being as shown in

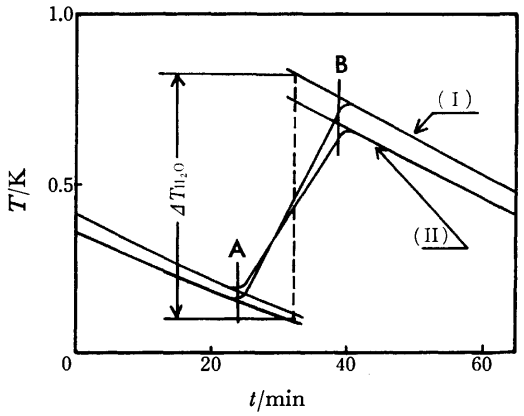

Fig. 2. Temperature variations of the calorimeter with time.
A; on, B; off.
(I); H_2O, (II); Na_2CO_3 15 wt%.

* Heat Capacities of Aqueous Solutions. II.

Table 1. Specific heat capacities of aqueous Na_2CO_3 solutions at 30 °C

Concentration (wt%)	Cp (This work) (cal/g K)	Cp (Literature)[a] (cal/g K)	Ratio
15.26	0.867	0.8835	0.981
14.86	0.874	0.8855	0.987
9.48	0.900	0.9138	0.985
5.64	0.932	0.9445	0.987
5.46	0.941	0.9462	0.994
3.14	0.967	0.9685	0.998

a) Estimated from the data in "Kagaku Binran," Maruzen, Tokyo (1966), p. 775.

Table 1. There was no special reason for choosing Na_2CO_3 as a standard sample, except that it is easy to handle. As shown in Table 1, the values obtained are always smaller than those found in the literature and the differences increase with concentration. These differences might arise from differences in the degree of vaporization in pure water and that in the aqueous solution.

On taking account of the uncertainty of the heat capacity relative to the Dewar, and the deviations shown in Table 1, in order to determine the specific heat capacity within a precision of 1%, the use of the present calorimeter should be limited to solutions whose specific heat capacities exceed *ca.* 0.9 cal/g K.

Guaranteed pure-grade reagents were used without further purification.

Results and Discussion

The values of the specific heat capacities of the solutions Cp are listed in Tables 2 and 3. The quantity which is of greatest importance in the discussion of the solute-solvent interaction in solution is the partial molar heat capacity, which is defined as

$$\phi_{Cp} = \frac{1}{m}\{(1000+mM_2)Cp-1000Cp_1\}, \qquad (1)$$

where M_2 is the molar mass of the dissolved solute, m the molality, and the subscript 1 refers to the solvent. The limiting partial molar heat capacities, $\phi^\circ_{Cp}=\overline{Cp}^\circ_2$, can be estimated by extrapolating the relationship between ϕ_{Cp} and m. Carboxylic acids are electrolytes but the variation of the ϕ_{Cp} for the carboxylic acids with concentration is linear.[6] Hence $\overline{Cp}^\circ_2$ was obtained from least-squares calculation of the relation

$$m\phi_{Cp} = bm+cm^2, \qquad (2)$$

on taking account of the uncertainties of the Cp data which increase as the concentration becomes more dilute. The relation between $m\phi_{Cp}$ and m is shown in Fig. 3. The coefficients b and c obtained are, for glutaric acid, $b=37.2\pm4.6$ and $c=17.8\pm4.0$, and for malonic acid, $b=0.2\pm3.4$ and $c=18.8\pm2.4$. In Table 4 are summarized the values of $\overline{Cp}^\circ_2(=b)$ thus obtained, along with the results reported by Ackermann *et al.*[6,7] Table 4 also includes the values of $\Delta=\overline{Cp}^\circ_2-Cp_2$(pure state), which are considered to represent the degree of structural change caused by the dissolution of the solutes.

From the data shown in Table 4, the contribution of the $-CH_2-$ and $-COOH$ groups to the $\overline{Cp}^\circ_2$ values can be evaluated;

for $-CH_2-$,

$$1/2\{(CH_2)_3(COOH)_2-CH_2(COOH)_2\} = 18.5$$

monocarboxylc acids: 16.7—20.5

and for $-COOH$,

$$(CH_2)_3(COOH)_2-n\text{-}C_3H_7COOH = -38.3$$

$$CH_2(COOH)_2-CH_3COOH = -41.8.$$

Table 2. Specific heat capacities of aqueous malonic acid solutions at 30 °C

Concentration (mol/kg)	Cp (cal/g K)	Concentration (mol/kg)	Cp (cal/g K)
1.715	0.898	0.5141	0.952
1.696	0.896	0.5065	0.956
1.069	0.916	0.4008	0.968
1.065	0.909	0.2972	0.975
0.7787	0.933	0.2936	0.973
0.6127	0.949		

Table 3. Specific heat capacities of aqueous glutaric acid solutions at 30 °C

Concentration (mol/kg)	Cp (cal/g K)	Concentration (mol/kg)	Cp (cal/g K)
1.337	0.918	0.8412	0.933
1.335	0.914	0.8403	0.942
1.324	0.919	0.7029	0.942
1.252	0.923	0.6119	0.949
1.229	0.914	0.5040	0.961
1.193	0.933	0.4755	0.955
1.129	0.926	0.3991	0.963
1.106	0.921	0.3978	0.966
1.032	0.937	0.3173	0.975
0.9326	0.930	0.3138	0.977
0.8479	0.940	0.2331	0.983

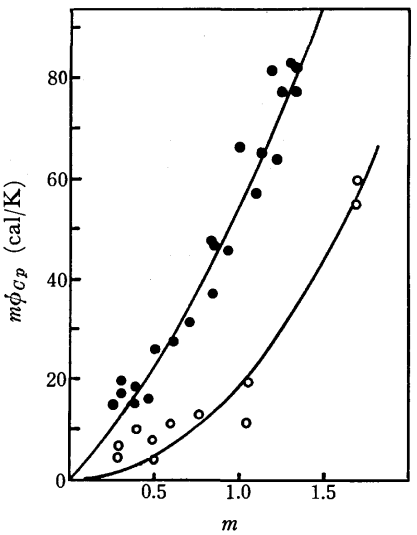

Fig. 3. Relation between apparent molar heat capacities and concentration.
●: Glutaric acid, $m\phi_{Cp}=37.2m+17.8m^2$.
○: Malonic acid, $m\phi_{Cp}=0.2m+18.8m^2$.

Table 4. Partial molar heat capacities of aqueous solutions of mono- and dicarboxylic acids

Molecule	Cp_2- (pure state) (cal/mol K)	$\overline{Cp}_2^\circ$ (cal/mol K)	Δ (cal/mol K)
$(CH_2)_3(COOH)_2$	39.5[a]	37.2±4.6	−2.3
$CH_2(COOH)_2$	28.6[a]	0.2±3.4	−28.4
HCOOH	23.7[b]	21.5[b]	−2.2
CH_3COOH	29.5[b]	42.0[b]	12.5
C_2H_5COOH	38.1[b]	58.8[b]	20.7
n-C_3H_7COOH	45.3[b]	75.5[b]	30.2

a) "International Critical Tables," Vol. 5, McGraw-Hill, New York (1928), p. 102. b) Cited in Ref. 7.

The values of $\overline{Cp}_2^\circ(-CH_2-)$ for an aqueous system obtained in the present work are compatible with those reported previously,[5] (14.9—20.9 cal/mol K) from diols. The $\overline{Cp}_2^\circ(-CH_2-)$ values have been determined for carboxylic acids by Ackermann *et al.*[6,7] and Konicek and Wadsö[8] (20.1), for amines[8] (21.5), for *N*-substituted amines[8] (20.6), for alcohols[9] (22.7), for *n*-alkylamine hydrobromide[3] (21.1), for bolaform electrolytes[10] (19.4—23.7), and for alkyl-substituted ammonium chlorides[4] (12—18).

Similar calculations for Δ result in the following values:

for $-CH_2-$,

$$1/2\{(CH_2)_3(COOH)_2-CH_2(COOH)_2\} = 13.1$$

monocarboxylic acids: 8.2—14.4

and for $-COOH$,

$$(CH_2)_3(COOH)_2-n\text{-}C_3H_7COOH = -32.5$$

$$CH_2(COOH)_2-CH_3COOH = -40.9.$$

In Ref. 5, 8.1 and −1.6 cal/mol K were reported for $\Delta(-CH_2-)$ and $\Delta(-OH)$, respectively. As mentioned above, Δ is a measure of the structural change accompanying the dissolution of a solute and positive values of $\Delta(-CH_2-)$ have been ascribed to the hydrophobic interaction between water and the $-CH_2-$ group, or iceberg formation.

While the values of ϕ_V°, the apparent molar volume, appear to be precise to within ±0.05 cm^3/mol or better at all temperatures, the situation is quite unfavorable for ϕ_{Cp}°. For instance, Ackermann *et al.*[7] have given, for $MeNH_3Cl$ and $EtNH_3Cl$, −2.0 and 14.6 cal/mol K, respectively, at 25 °C, while Desnoyers *et al.*[10] have reported, for the corresponding bromides, 1.9 and 24.3 cal/mol K, respectively. These differences are too large even after taking account of the difference between $\phi_{Cp}^\circ(Cl^-)$ and $\phi_{Cp}^\circ(Br^-)$. It is highly questionable, at least at the present stage of experimental accuracy inherent in the determination of $\overline{Cp}_2^\circ$, whether the small differences in the $\overline{Cp}_2^\circ(-CH_2-)$ and $\Delta(-CH_2-)$ observed for different homologs, and also for the same homolog, can be related to the neighboring organic groups.

References

1) J. E. Desnoyers, R. Pagé, G. Perron, J-L. Fortier, P-A. Leduc, and R. F. Platford, *Can. J. Chem.*, **51**, 2129 (1973).
2) P-A. Leduc and J. E. Desnoyers, *Can. J. Chem.*, **51**, 2993 (1973).
3) P-A. Leduc, J-L. Fortier, and J. E. Desnoyers, *J. Phys. Chem.*, **78**, 1217 (1974).
4) K. Tamaki, S. Yoshikawa, and M. Kushida, *Bull. Chem. Soc. Jpn.*, **48**, 3018 (1975).
5) F. Kawaizumi, T. Otake, H. Nomura, and Y. Miyahara, *Nippon Kagaku Kaishi*, **1972**, 1773.
6) Th. Ackermann and F. Schreiner, *Z. Elektrochem.*, **62**, 1143 (1958).
7) H. Rüterjans, F. Schreiner, U. Sage, and Th. Ackermann, *J. Phys. Chem.*, **73**, 986 (1969). In Ref. 6, the values at standard state (298 K, $\gamma=1$) are shown, while in Ref. 7, the values refer to the state at infinite dilution. In Table 4, the values in Ref. 7 are adopted.
8) J. Konicek and I. Wadsö, *Acta Chem. Scand.*, **25**, 1541 (1971).
9) E. M. Arnett, W. B. Kover, and J. V. Carter, *J. Am. Chem. Soc.*, **91**, 4028 (1969).
10) C. Jolicoeur and J. Boileau, *J. Solution Chem.*, **3**, 889 (1974).

The Effect of Added Inorganic Salts on the Micelle Formation of Nonionic Surfactants in Aqueous Solutions

Nagamune NISHIKIDO and Ryohei MATUURA

Department of Chemistry, Faculty of Science, Kyushu University, Fukuoka 812

(Received December 20, 1976)

In order to divide the inorganic salt effect on the micelle formation of nonionic surfactants into the effects on the hydrocarbon and on the hydrophilic moieties of the surfactant, the critical micelle concentrations(CMC) of nonionic surfactant homologs (8,10,12 methylene and 6 oxyethylene groups) were determined in aqueous salt solutions. The salt-effect parameters of methylene and hexa(oxyethylene) groups were calculated from the CMC data. The orders of both the parameters with respect to the anion obeyed the Hofmeister series. The variation in the extent of the parameters with respect to the cation was much less than that with respect to the anion. These phenomena were discussed in terms of the direct and indirect effects of ions on the water structure around the hydrocarbon and hydrophilic moieties of the surfactants. In addition, the salt effect on the cloud point (CP) and the amount of solubilization toward the Yellow OB dyestuff in aqueous solutions were discussed in connection with the salt effect on the hydrophilic moiety.

The critical micelle concentrations (CMC) of nonionic surfactants in aqueous solutions are lowered by the addition of most inorganic salts.[1-5] In explaining this phenomenon, it has been suggested that salts bring about the dehydration of the hydrophilic moiety of the surfactant "monomer," causing the enhancement of the tendency toward micelle formation, *i.e.*, CMC lowering.[2,3] This mechanism has thus far been the standard view, although others have been suggested.[6,7] However, the micelle formation, *i.e.*, the CMC, is determined by the balance of surfactant stability between that in the monomer and that in the micelle state. Salts have influence not only on the dissolved state of monomers, but also on that of micelles in the solution, and so the dehydration mechanism is questionable. Recently, Mukerjee proposed a salting-out mechanism of the hydrocarbon moiety of surfactant, in which the salt effects on the hydrophilic moieties of the monomer and micelle were assumed to be almost equal in magnitude and to cancel each other out in determining the CMC.[7,8] More recently, Ray and Nemethy[9] and Kresheck[10] examined Mukerjee's suggestion. However, their discussion is insufficient because Mukerjee's assumption of the cancellation of the salt effect on the hydrophilic moiety was not fully taken into consideration. In order to get rid of this ambiguity, it is necessary to estimate separately the salt effects on hydrocarbon and hydrophilic moieties.

In this study, the salt-effect parameter of each moiety during micellization was estimated. Also, we discussed qualitatively the salt effect on the dissolved state of nonionic surfactants in an aqueous solution, since there have been no theories concerning the quantitative clarification of the salt effect on aqueous polar or nonpolar substances.[11-17] In this connection, the cloud points (CP) and the amount of solubilization toward Yellow OB in aqueous salt-nonionic surfactant mixed solutions were determined and discussed.

Experimental

Materials. The nonionic surfactants, poly(oxyethylene) alkyl ethers (abbreviated as C_mE_n; m: the number of methylene groups; n: the number of ethylene oxide groups), were the same materials as those used in a previous paper.[18] All the inorganic salts were of a reagent grade (min 99.0 or 99.5% pure), supplied by the Wako Pure Chemical Co., and were used without further purification. The purification of the Yellow OB dyestuff (1-(o-tolylazo)-2-naphthylamine) as a solubilizate was described in the previous paper.[18]

Method. The CMC values of C_8E_6, $C_{10}E_6$ and $C_{12}E_6$ in aqueous salt solutions at 20 °C were determined by plotting the surface tension against the logarithm of the concentration. The surface tensions were measured with the Dû Noüy tensiometer. In Table 1 are tabulated the CMC values of C_8E_6, $C_{10}E_6$ and $C_{12}E_6$ in a pure aqueous solution. The cloud points were determined as the temperatures at which a sudden turbidity appeared or disappeared in the 1 wt% $C_{12}E_6$ aqueous solutions containing salts, when the solutions were heated or cooled at a constant rate of 0.5 °C/min under stirring. The change in the transparency of the solutions was observed with the naked eye. The procedure for determining the amount of solubilized Yellow OB in the aqueous $C_{12}E_{10}$-salt solutions at 30 °C has been described elsewhere.[18]

TABLE 1. THE VALUES OF THE CMC OF NONIONIC SURFACTANTS USED IN THIS STUDY IN AN AQUEOUS SOLUTION AT 20 °C

Surfactant	CMC (10^{-3} mol/dm^3)
C_8E_6	8.3
$C_{10}E_6$	0.86
$C_{12}E_6$	0.074

Results and Discussion

Salt-effect Estimation from CMC Measurements. By considering the equilibrium between N' surfactant monomers and a micelle in an aqueous salt solution, it is shown that the molar standard free energy for micelle formation, $\Delta G_m^{(c)0}$, is expressed by the following equation:

$$\Delta G_m^{(c)0} = \frac{1}{N'}(\mu_m^{(c)0} - N'\mu_2^{(c)0})$$

$$= kT \ln c_2' f_2' - \frac{kT}{N'} \ln c_m' f_m', \qquad (1)$$

where $\mu^{(c)0}$ denotes a molar standard chemical potential; the subscripts m and 2 refer to the micelle and the monomer respectively, and where c' and f' denote a molar-concentration and a molar-activity coefficients

respectively. The molar activity coefficients of the monomer and the micelle are expressed by the well-known Setschnow equation:

$$\log f'_1 = k_2 C_s, \qquad \log f'_m = k_m C_s, \tag{2}$$

where k is a salt-effect parameter and C_s is the molar concentration of salts. Here, it may be assumed that the concentrations of the monomer and the micelle are low enough and, therefore, that ideality holds near the CMC in the aqueous solution free of salts.[15] By introducing Eq. 2 into Eq. 1, and by using Phillips' definition for CMC in the mass-action model,[19] the following equation is derived:

$$\Delta G_m^{(c)0} \simeq kT \ln C' + 2.303 kTk_2 C_s - \frac{2.303kT}{N'} k_m C_s, \tag{3}$$

where C' is the CMC in the aqueous salt solution. In the aqueous solution free of salts, the molar standard free energy, $\Delta G_m^{(c)0}$, is expressed as follows:

$$\Delta G_m^{(c)0} \simeq kT \ln C, \tag{4}$$

where C is the CMC in the aqueous solution. From the standpoint of the pseudo-phase separation model,[20] the following CMC equation holds:[21]

$$kT \ln C = -m\omega + \Delta + K(T, P), \tag{5}$$

where ω and Δ denote the free energy difference of methylene and poly(oxyethylene) groups between in the monomer state and in the micelle state respectively; K is a constant at constant temperature and pressure, and m is the number of methylene groups in the hydrocarbon chain of the surfactant. We assume the additivity for the salt-effect parameters to be as follows:

$$k_2 = mk_{CH_2} + k_{p,2}, \qquad k_m = N'k_{p,m}, \tag{6}$$

where k_{CH_2} and $k_{p,2}$ are the salt-effect parameters of the methylene and poly(oxyethylene) groups in the monomer respectively and where $k_{p,m}$ is that of the poly(oxyethylene) group in the micelle, because the hydrocarbon moieties form the micelle core and are shielded from the aqueous environment containing salts if we neglect the exposure of some of the hydrocarbon tails to the solvent near the micelle surface.[22] Then, the following equation is derived formally from Eqs. 3—6:

$$kT \ln C' = -m\omega' + \Delta' + K, \tag{7}$$

where

$$\omega' = \omega + 2.303 kTk_{CH_2} C_s, \tag{7a}$$

and

$$\Delta' = \Delta + 2.303 kT(k_{p,m} - k_{p,2}) C_s. \tag{7b}$$

The values of the salt-effect parameters, k_{CH_2} and $k_{p,m} - k_{p,2}$, can be determined by the use of Eqs. 7, 7a, and 7b as follows. The value of ω' can be determined from the slope in the log C' *vs.* m plots at a constant salt concentration C_s; a representative example is shown in Fig. 1 for the case of the sodium chloride additive. These plots form a straight line and then give a well-defined ω' value. The value of ω' thus determined is plotted in Fig. 2 against C_s. These plots also form a straight line, and the value of k_{CH_2} can be determined from the slope of the line. The value of Δ' at a constant C_s can be calculated by introducing the value of ω' and the experimental C' into Eq. 7. Figure 3 shows the plots of Δ' *vs.* C_s, whose slope gives the value of $k_{p,m} - k_{p,2}$. The calculated respective salt-effect param-

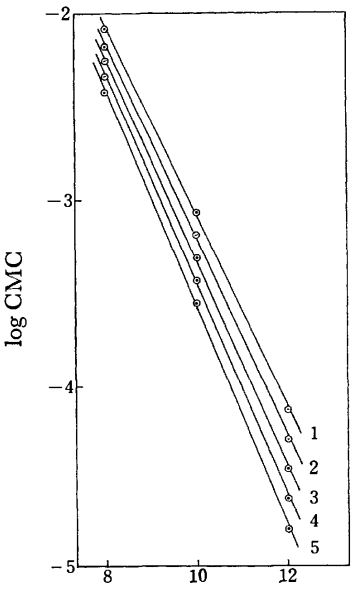

Fig. 1. log CMC *vs.* the number of methylene groups in C_mE_6 in aqueous sodium chloride solutions at 20 °C. Sodium chloride conc.: (1) 0, (2) 0.38 M*), (3) 0.75 M, (4) 1.28 M, (5) 1.50 M.
*) Throughout this paper, 1 M=1 mol dm^{-3}.

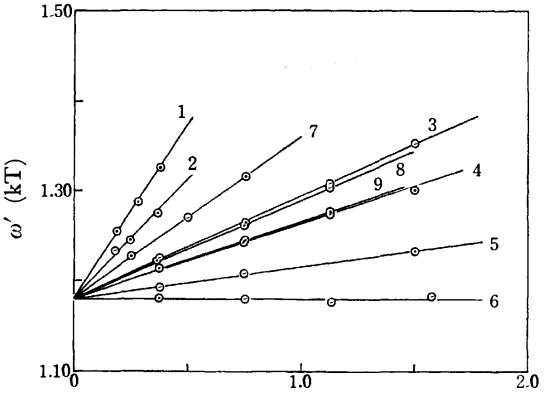

Fig. 2. The plots of ω' against the concentration of salts at 20 °C.
(1) Na_2SO_4, (2) $NaIO_3$, (3) NaCl, (4) NaBr, (5) NaI, (6) NaSCN, (7) $MgCl_2$, (8) KCl, (9) LiCl.

Table 2. Calculated salt-effect parameters of methylene and hexaoxyethylene groups for nonionic surfactants' micellization at 20 °C

Salt	k_{CH_2} (dm^3/mol)	$k_{p,m} - k_{p,2}$ (dm^3/mol)
Na_2SO_4	0.17_0	0.76_2
$NaIO_3$	0.11_6	0.51_2
NaCl	0.05_0	0.17_4
NaBr	0.03_6	0.07_4
NaI	0.01_5	-0.01_3
NaSCN	0.00_0	-0.18_4
KCl	0.04_8	0.18_2
LiCl	0.03_7	0.16_9
$MgCl_2$	0.07_9	0.36_0

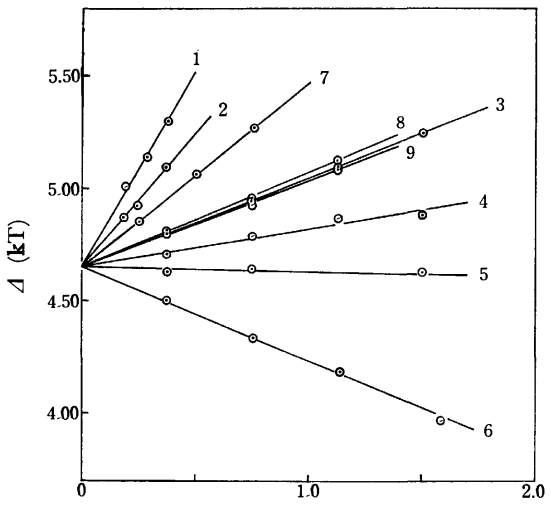

Fig. 3. The plots of Δ' against the concentration of salts at 20 °C.
(1) Na_2SO_4, (2) $NaIO_3$, (3) NaCl, (4) NaBr, (5) NaI, (6) NaSCN, (7) $MgCl_2$, (8) KCl, (9) LiCl.

eters are tabulated in Table 2. As may be seen from Table 2, the salt effect on the hydrophilic moiety during micellization is found not to cancel out; *i.e.*, $k_{p,m}-k_{p,2}\neq 0$. The positive value of $k_{p,m}-k_{p,2}$ means that $k_{p,m}>k_{p,2}>0$. That is, a salting-out effect occurs on the hydrophilic moieties in the monomer and micelle states, and the extent of the effect on the micelle is greater than that on the monomer state. This salting-out effect, $k_{p,m}-k_{p,2}>0$, contributes to raising the CMC, as can be seen from Eqs. 7 and 7b. Therefore, in this case, the CMC lowering is caused by the salting-out effect on the hydrocarbon moiety, $k_{CH_2}>0$, which overcomes the $k_{p,m}-k_{p,2}>0$ effect from Eqs. 7 and 7a. On the contrary, the negative $k_{p,m}-k_{p,2}$ means that $k_{p,m}<k_{p,2}<0$; *i. e.* it is a salting-in effect, which contributes to lowering the CMC. Especially in the solution containing sodium thiocyanate, the CMC lowering is attributable to the salting-in effect on hydrophilic moieties, because the value of k_{CH_2} is nearly zero. As has been mentioned above, the various modes for the salt effect on the micelle formation are shown according to the kind of salts.

In addition, two features are found in Table 2; (1) the salt effects on the hydrocarbon and hydrophilic moieties give the same order with respect to the relative efficiency, and (2) the variation in the extent of the salt effect with respect to the anion is larger than that with respect to the cation. By considering the above two features, the salt effect can be explained qualitatively as follows. In the case of sodium salts, the order of the salt effect follows the Hofmeister series or the order of the water-structure-making or -breaking capacity of salts.[23-26] That is, the more strongly water-structure-making salt gives the greater, positive k-value, whereas the more strongly water-structure-breaking salt gives the smaller, negative k-value. Water molecules are oriented around the water-structure-making ions, which leads to the reduction of the hydrophobic or hydrophilic hydration of the surfactants as a salting-out effect. On the contrary, the water-structure-breaking ions increase the ratio of monomeric water molecules in the bulk and promote the hydration of the surfactants as a salting-in effect. However, the second feature suggests another source for the salt effect. The following fact is suggestive in considering the second tendency; an air– or hydrocarbon–water interfacial tension is increased by the kind of anion to a greater extent than in the case of cations.[12,27-30] This fact shows that cations are almost completely excluded from an air– or hydrocarbon–water interface because of their requirement for hydration, whereas the less hydrated anions exhibit a large variation in the degree of their exclusion, and may even be concentrated at the interface. This situation may be applied to the exclusion of ions from the water region around the hydrocarbon moiety of a surfactant. That is, the more weakly hydrated anions are excluded to a less extent and then directly disturb the hydrophobic hydration around hydrocarbon moieties to a greater extent, which leads to salting-out. On the contrary, the more strongly hydrated anions are excluded to a greater extent and so exhibit a less direct effect on hydration. Cations also exhibit a less direct effect. As a result of the two factors inferred from the above two features, (1) and (2), the more strongly water-structure-making (more strongly hydrated) anions and cations have, for the most part, an indirect salting-out effect. The more strongly water-structure-breaking (more weakly hydrated) anions have an indirect salting-in and a direct salting-out effect, which cancel each other out for the most part in the overall salt effect, *e.g.*, $k_{CH_2}\simeq 0$ for sodium thiocyanate. As for the water region near the polar poly(oxyethylene) moiety of a surfactant, ions will be less excluded from this region than in the case of the water region near the hydrocarbon moiety. The weakly hydrated anions, *e.g.*, thiocyanate and iodide anions, may even be concentrated in this region; especially, the magnesium cation forms an oxonium compound with the lone-pair electrons of ether oxygen atoms in the poly(oxyethylene) moiety[31] to cause salting-in. It may be because of these factors that we find the experimental $k_{p,m}-k_{p,2}<0$ for sodium thiocyanate and iodide, and the large difference between the value of $k_{p,m}-k_{p,2}$ for magnesium chloride and that for sodium sulfate, in which the two salts have nearly equal water-structure-making capacities. As we have mentioned, the salt effect includes two types of effects on the hydrophobic and hydrophilic hydration of surfactants: the direct effect by the accessibility of ions to the water region near the monomers and the micelles, and the indirect effect.

Salt Effect on Cloud Points and Solubilization. The cloud points of 1 wt% $C_{12}E_6$ in aqueous salt solutions were measured; results similar to those reported in the literature were obtained.[2,31-34] Cloud points can be regarded as a measure of the affinity of the oxyethylene groups in a nonionic surfactant for the water environment.[35] Then, the limiting slope in the plots of the cloud point *vs.* the salt concentration, $\lim_{C_s\to 0}(d\,CP/dC_s)$, may be regarded as the variation of this affinity by salt. These slopes are plotted in Fig. 4 against the values of $k_{p,m}-k_{p,2}$ for various salts. The plots give

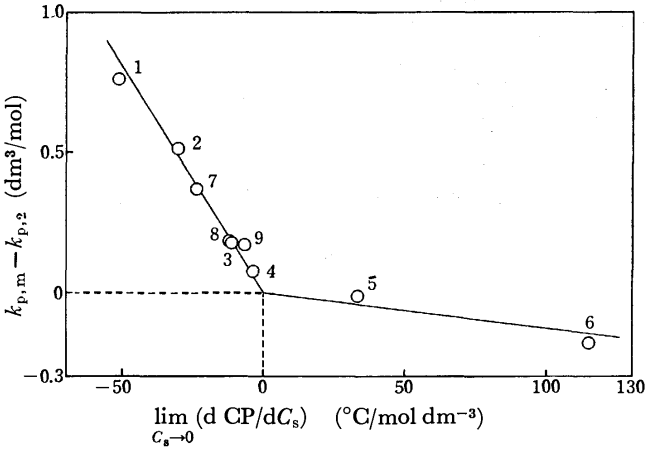

Fig. 4. $k_{p,m}-k_{p,2}$ *vs.* $\lim_{C_s\to 0}$(d CP/dC_s) plots for various salts.
(1) Na_2SO_4, (2) $NaIO_3$, (3) NaCl, (4) NaBr, (5) NaI, (6) NaSCN, (7) $MgCl_2$, (8) KCl, (9) LiCl.

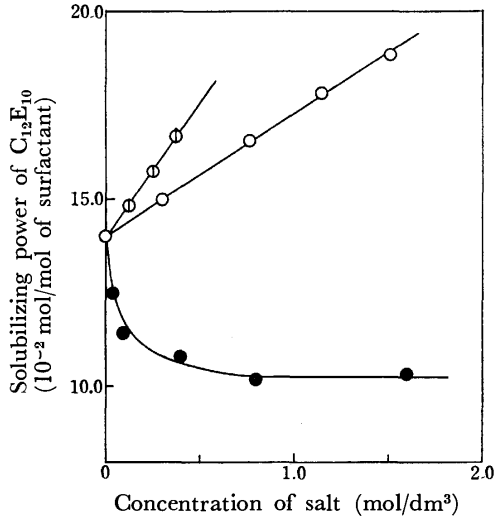

Fig. 5. Solubilizing power of $C_{12}E_{10}$ in aqueous salt solutions at 30 °C.
(Ⓓ) Na_2SO_4, (○) NaCl, (●) NaSCN.

two straight lines, which cross at the point that $\lim_{C_s\to 0}$(d CP/d C_s)$=k_{p,m}-k_{p,2}=0$ and which divide the salts into the two groups, salting-out and -in. From the discussion in the previous section, this correlation shows that the strengthening or weakening of the affinity of oxyethylene groups for the water environment by salts is brought about through the promotion or reduction of the hydration of oxyethylene groups respectively. The strengthening of the affinity is also caused by the ion concentration in the water region near oxyethylene groups.

Next, the amount of solubilization toward Yellow OB was determined at 30 °C in the aqueous $C_{12}E_{10}$ solutions containing sodium chloride, sulfate, and thiocyanate; it was found to increase linearly with the concentration of $C_{12}E_{10}$. The slopes of the lines, referred to as the solubilizing power,[36] are plotted in Fig. 5 against the concentrations of three representative salts. It may be found from Fig. 5 that the salts exhibiting a salting-out or -in effect on oxyethylene groups give an increased or decreased solubilizing power respectively with the salt concentration as compared with that in the salt-free solution. The solubilizing power depends sensitively on the compactness of the poly(oxyethylene) shell of the micelle,[18,36] and so the following explanation is possible. The oxyethylene groups on the micelle cohere as a result of the weakening of the hydration of these groups, and then this increased compactness brings about the increased solubilizing power. On the contrary, the enhancement of the hydration of the oxyethylene groups on the micelle leads to a decreased compactness, which causes a decrease in the solubilizing power.

We wish to express our hearty thanks to the Kaō Soap Co., Ltd., and to Dr. Noboru Moriyama for supplying the nonionic surfactants used in the present study.

References

1) P. Becher, *J. Colloid Sci.*, **17**, 325 (1962).
2) M. J. Schick, *J. Colloid. Sci.*, **17**, 801 (1962).
3) M. J. Schick, *J. Phys. Chem.*, **68**, 3585 (1964).
4) W. U. Malik and S. M. Saleem, *J. Am. Oil Chem. Soc.*, **45**, 670 (1968).
5) W. U. Malik and O. P. Jhamb, *Kolloid Z. Z. Polym.*, **242**, 1209 (1970).
6) P. Becher, "Nonionic Surfactants," ed by M. J. Schick, Marcel Dekker, New York, N. Y. (1967), p. 500.
7) P. Mukerjee, *Adv., Colloid Interface Sci.*, **1**, 241 (1967).
8) P. Mukerjee, *J. Phys. Chem.*, **69**, 4038 (1965).
9) A. Ray and G. Nemethy, *J. Am. Chem. Soc.*, **93**, 6787 (1971).
10) G. C. Kresheck, "Water," Vol. 4, ed by F. Frank, Plenum, New York (1973), Chap. 2.
11) P. H. von Hippel and T. Schleich, "Biopolymers," ed by A. G. Walton and J. Blackwell, Academic Press, New York (1973), Chap. 6.
12) D. R. Robinson and W. P. Jencks, *J. Am. Chem. Soc.*, **87**, 2470 (1965).
13) J. E. Desnoyers and C. Jolicoeur, "Modern Aspects of Electrochemistry," No. 5, ed by J. O'M. Bockris and B. E. Conway, Plenum, New York (1969), Chap. 1.
14) G. Wada and C. Itō, *Nippon Kagaku Zasshi*, **78**, 1500 (1957); **80**, 705 (1959).
15) F. A. Long and W. F. McDevit, *Chem. Rev.*, **51**, 119 (1952).
16) H. Schneider, "Solute-Solvent Interactions," ed by J. F. Coetzee and C. D. Ritch, Marcel Dekker, New York (1969), Chap. 5.
17) R. Aveyard and R. Heselden, *J. Chem. Soc., Faraday Trans. 1*, **71**, 312 (1975).
18) N. Nishikido, *J. Colloid Interface Sci.*, in press.
19) J. N. Phillips, *Trans. Faraday Soc.*, **51**, 561 (1955).
20) K. Shinoda and E. Hutchinson, *J. Phys. Chem.*, **66**, 577 (1962).
21) N. Nishikido, Y. Moroi, and R. Matuura, *Bull. Chem. Soc. Jpn.*, **48**, 1387 (1975).
22) D. C. Poland and H. A. Scheraga, *J. Phys. Chem.*, **69**, 2431 (1965).
23) J. E. Desnoyers and G. Perron, *J. Solution Chem.*, **1**, 199 (1972).
24) F. J. Millero, "Water and Aqueous Solutions," ed by R. A. Horne, John Wiley & Sons, New York (1972), Chap. 13.
25) M. Kaminsky, *Discuss. Faraday Soc.*, **24**, 171 (1957);

R. M. Gurney, "Ionic Processes in Solution," McGraw-Hill, New York (1953), Chap. 9; R. L. Kay, T. Vituccio, C. Zawoyski, and D. F. Evans, *J. Phys. Chem.*, **70**, 2336 (1966).
26) H. G. Hertz, "Water," Vol. 3, ed by F. Franks, Plenum, New York (1973), Chap. 7.
27) J. J. Bikerman, "Physical Surfaces," Academic Press, New York, N. Y. (1970), p. 73.
28) J. Ralston and T. W. Healy, *J. Colloid Interface Sci.*, **42**, 629 (1973).
29) J. E. B. Randles, *Discuss. Faraday Soc.*, **24**, 194 (1957).
30) R. Aveyard and S. M. Saleem, *J. Chem. Soc., Faraday Trans. 1*, **71**, 1609 (1975).
31) H. Schott, *J. Colloid Interface Sci.*, **43**, 150 (1973).
32) K. Deguchi and K. Meguro, *J. Colloid Interface Sci.*, **50**, 223 (1975).
33) K. Kuriyama, *Kolloid Z. Z. Polym.*, **181**, 144 (1961).
34) W. N. Maclay, *J. Colloid Sci.*, **11**, 272 (1956).
35) T. Nakagawa, "Nonionic Surfactants," ed by M. J. Schick, Marcel Dekker, New York, N. Y. (1967), p. 571.
36) F. Tokiwa, *J. Phys. Chem.*, **72**, 1214 (1968).

The Nuclear Quadrupole Resonance of Dibromoiodate Ions

Tsutomu OKUDA, Isamu TOMOYASU, Koji YAMADA, and Hisao NEGITA
Department of Chemistry, Faculty of Science, Hiroshima University, Hiroshima 730
(Received January 10, 1977)

The NQR sepctra due to ^{81}Br and ^{127}I in potassium dibromoiodate and its monohydrate were observed, and the Zeeman effect of ^{81}Br NQR in the monohydrate was examined. The resonance lines indicate that both compounds have two kinds of dibromoiodate ions and that these ions in the anhydride are slightly asymmetric, while those in the monohydrate are symmetric. The difference in frequency between the two resonance lines due to each resonant nucleus in the monohydrate is explained in terms of the I···Br intermolecular interaction. The charge distributions in both compounds were evaluated to be about $-0.6e$ and $0.2e$ on the terminal and central atoms respectively.

In general, trihalide ions are almost linear and the iodine atom occupies the center of the ion.[1] The reported halogen-halogen length is considerably larger than the sum of the covalent bond radii. The bonding in these ions is considered to result from the overlap of the valence np_σ orbitals of the constituting atoms. Trihalide compounds have been studied so far by means of the nuclear quadrupole resonance,[2-9] since they can give more useful information about the bond character and the charge distribution.

According to the crystal structure of $KIBr_2 \cdot H_2O$ as determined by X-ray analysis,[10] the space group is Pnnm and all atoms lie on the mirror planes at $z=0$ $z=1/2$. The structure consists of nearly linear chains of halogen atoms extending infinitely along the b axis, as is shown in Fig. 1. The two independent IBr_2^- anions are linear and symmetric. The closest O···Br and I···Br distances are 3.60 Å and 3.87 Å respectively, indicative of weak hydrogen bonding and intermolecular interaction. Therefore, it is interesting to examine not only the charge distribution on halogen atoms but also the influence of the intermolecular interaction on the electric field gradient of the halogen atom.

Experimental

The potassium dibromoiodate monohydrate was prepared by heating an aqueous solution of potassium bromide, bromine, and iodine. Its anhydride was obtained by dehydrating the monohydrate. The single crystal of the monohydrate was obtained by slowly lowering an ampoul filled with a saturated aqueous solution of potassium dibromoiodate through an electric furnace. The single crystal of the anhydride could not be obtained.

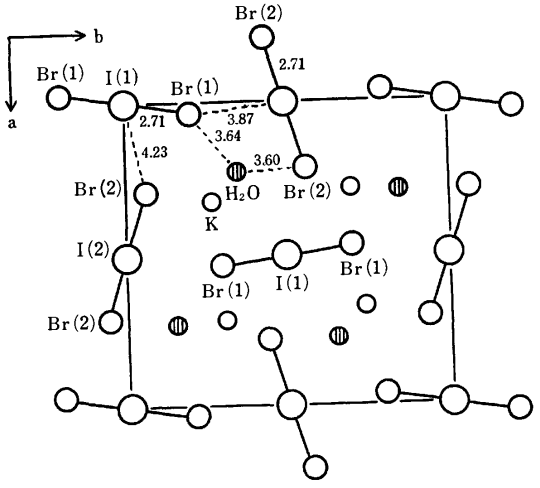

Fig. 1. The crystal structure of $KIBr_2 \cdot H_2O$ projected onto the ab plane.

A super-regenerative oscillator was used for the detection of the NQR line. The absorption lines were displayed on an oscilloscope. The resonance frequencies were determined by the use of a universal counter, TR-5578, of the Takeda Riken Industry Co. Ltd. The Zeeman effect was measured by means of the zero-splitting cone method. The magnetic field was provided by a Helmholtz coil with a field strength of about 200 G.

Results and Discussion

Table 1 shows ^{81}Br and ^{127}I NQR frequencies of $KIBr_2 \cdot H_2O$ and $KIBr_2$. Since ^{127}I has a nuclear spin equal to 5/2, it shows two NQR lines. However, we could not observe the resonance line due to the transition between the $\pm 3/2$ and $\pm 5/2$ levels, because the resonance frequency was too high to be detected with a conventional NQR spectrometer. Two resonance lines each were observed for ^{81}Br and ^{127}I nuclei in the monohydrate. On the other hand, four and two resonance lines were observed for ^{81}Br and ^{127}I respectively in the anhydride. These findings indicate that both compounds have two kinds of IBr_2^- ions in the crystals, and that the IBr_2^- ions are symmetric in the monohydrate, while those in the anhydride are slightly asymmetric. In general, it is accepted that the trihalide ions are symmetric only when the cation in a trihalide compound is as large as a tetralkylammonium ion.[8] In the present case, the IBr_2^- ions seem to become symmetric in spite of having a small cation because the crystal includes a water of crystallization. The two resonance frequencies of ^{81}Br in the mono-

TABLE 1. ^{81}Br AND ^{127}I NQR FREQUENCIES IN $KIBr_2 \cdot H_2O$ AND $KIBr_2$ AT 300 K

Compound	Resonance frequency (MHz)	
	$\nu(^{81}Br)$	$\nu_{(1/2\leftrightarrow 3/2)}(^{127}I)$
$KIBr_2 \cdot H_2O$	124.17	421.51
	128.41	438.77
$KIBr_2$	123.54	425.83
	129.33	433.24
	129.63	
	130.22	

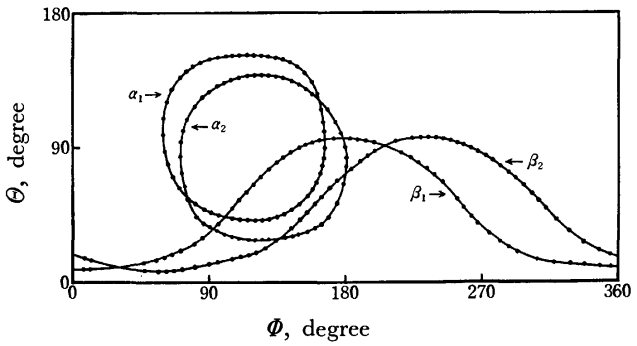

Fig. 2. Zero-splitting patterns of ^{81}Br Zeeman lines in $KIBr_2 \cdot H_2O$.

Table 2. Angles between dibromoiodate ions in $KIBr_2 \cdot H_2O$

	$IBr_2^-(\alpha_1)$	$IBr_2^-(\alpha_2)$	$IBr_2^-(\beta_1)$
$IBr_2^-(\alpha_2)$	17.21°		
$IBr_2^-(\beta_1)$	80.87°	63.66°	
$IBr_2^-(\beta_2)$	116.77°	99.56°	35.90°

hydrate are so different that the interactions between the resonant nucleus and the surrounding atoms are quite different. This must be clarified by the assignment of the Br atoms. Therefore, we observed the Zeeman effect on ^{81}Br NQR. The results are shown in Fig. 2. Each resonance line gives two zero-splitting patterns, indicating that the monohydrate crystal belongs to a monoclinic or a higher symmetric system. The Br atom was assigned on the basis of the angles between the IBr_2^- ions, assuming that the principal z axis of the Br atom is parallel to the linear ion. The angles thus obtained are listed in Table 2. The X-ray analysis indicates that the angles between the chemically equivalent ions are 17.66° for the ions with Br(1) and 35.92° for those with Br(2). Therefore, the Br atoms contributing to the lower and higher resonance lines were assigned to Br(1) and Br(2) respectively.

Fortunately, the I atoms could be assigned from the intensities of the resonance lines on the single crystal. The principal z axis of the I atom is considered to be parallel to the linear IBr_2^- ion, that is, parallel to that of the Br atom. The Zeeman analysis indicates that the angles between the principal z axis of the Br atoms and the rf coil axis are about 90° for Br(1) and about 45° for Br(2). Therefore, the strong resonance line is assigned to the I atoms bonded to Br(1), and the weak line, to those bonded to Br(2). The observed intensity ratio of the higher resonance line to the lower was nearly 2 : 1, indicating that the former line is due to I(1) and the latter to I(2).

The resonance frequency of Br(1) is considerably lower than that of Br(2). Therefore, Br(1) seems to be strongly affected by the intermolecular interaction. This is obvious from the temperature dependence of the resonance frequency shown in Fig. 3. The intermolecular interactions which affect the Br atoms include the OH···Br hydrogen bonding and the Br···I interaction. The hydrogen bondings at both Br atoms are considered to affect the nuclei to almost the same

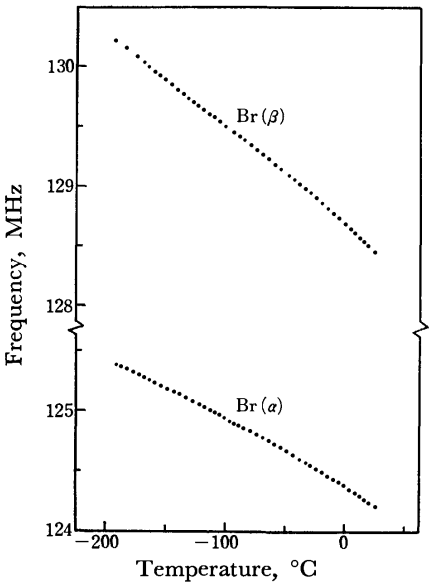

Fig. 3. Temperature dependences of ^{81}Br NQR frequencies in $KIBr_2 \cdot H_2O$.

Table 3. ^{81}Br NQR parameters of $KIBr_2 \cdot H_2O$ at 300 K

Resonance line	ν(MHz)	η(%)	e^2Qq/h(MHz)
$^{81}Br(\alpha)$	124.17	0.5±0.3	248.34
$^{81}Br(\beta)$	128.41	3.4±1.1	256.77

extent, because the X-ray analysis[10] indicates that the O···Br(1) and O···Br(2) distances are 3.60 Å and 3.64 Å respectively. On the other hand, the I(1)···Br(2) distance is 4.23 Å and the I(2)···Br(1) distance is 3.87 Å, which is about 0.2 Å less than the sum of the van der Waals radii. Therefore, the difference in the resonance frequencies between Br(1) and Br(2) is mainly to be ascribed to the I···Br interaction. In this case, the I(2)···Br(1) interaction is considered to be formed by the charge transfer from I to Br. The charge from the lone-pair orbital of I(2) enters the bonding orbital of Br(1), and the quadrupole coupling constant of Br(1) decreases and that of I(2) increases.

The asymmetry parameters of the electric field gradient are obtained from the zero-splitting loci; they are listed in Table 3. The asymmetry parameters of both Br atoms are so small that the electric field gradients are almost axially symmetric. This may be seen from the fact that the IBr_2^- ions are symmetric and the Br–I bond has little double-bond character.

The charge on the Br atom can be obtained from the quadrupole coupling constant. All the asymmetry parameters of Br in $KIBr_2 \cdot H_2O$ and those of I in the trihalide ions are so small (up to 4%)[5] that they can be neglected. Furthermore, s hybridization does not seem to participate in the halogen-halogen bond. Using the Townes-Dailey method,[11] the following equations are obtained for the terminal and the central halogen atoms.

For a terminal atom:

$$\frac{(e^2Qq)_{obsd}}{(e^2Qq)_{atom}} = 1 - i = 2 - N_z \qquad (1)$$

Table 4. Electron populations and charge distributions in linear trihalide ions

Compound	N_z		$Q_x(e)$		Total charge (e)
	Terminal	Central	Terminal	Central	
$KIBr_2 \cdot H_2O$	1.61	0.78	−0.61	0.22	−1.00
	1.60	0.82	−0.60	0.18	−1.02
$KIBr_2$	1.60	0.80	−0.60	0.20	−1.00
$KICl_2 \cdot H_2O$	1.66	0.70	−0.66	0.30	−1.02
$KICl_2$	1.65	0.71	−0.65	0.29	−1.01

For a central atom:

$$\frac{(e^2Qq)_{obsd}}{(e^2Qq)_{atom}} = (1-i) + 2i(1+\varepsilon) = 1 + (1-N_z)(1+2\varepsilon), \quad (2)$$

where $(e^2Qq)_{obsd}$ is the observed quadrupole coupling constant and $(e^2Qq)_{atom}$ is that due to one p_z electron, *i.e.*, 643.03 MHz for ^{81}Br and 2292.71 MHz for ^{127}I.[12,13] ε is a correction factor for a positively charged resonant atom and 0.12 for ^{127}I.[11] N_z is the electron number of the p_z orbital. Using the N_z values obtained from Eqs. 1 and 2, the charges, Q_x, on the halogen atoms are readily calculated by means of the following relation: $Q_x = 1 - N_z$. The values thus obtained are listed in Table 4, in which the values for the ICl_2^- ions are given for purposes of comparison. Since no resonance lines except those in $KIBr_2 \cdot H_2O$ are assigned, the charges on the halogen atoms were calculated for the averaged resonance frequency. The charges of the terminal and central halogen atoms in the ICl_2^- ions are larger than those in the IBr_2^- ions. This can be explained by the difference in electronegativity between Br and Cl. In any case, the calculated total charges are equal to the theoretical value, $-e$. Therefore, the approximation used in the present work is reasonable.

References

1) E. H. Wiebenga, E. E. Havinga, and K. H. Boswijk, *Adv. Inorg. Radiochem.*, **3**, 133 (1961).
2) C. D. Cornwell and R. S. Yamasaki, *J. Chem. Phys.*, **72**, 1060 (1957).
3) Y. Kurita, D. Nakamura, and N. Hayakawa, *Nippon Kagaku Zasshi*, **79**, 1093 (1958).
4) R. S. Yamasaki and C. D. Cornwell, *J. Chem. Phys.*, **30**, 1265 (1959).
5) A. Sasane, D. Nakamura, and M. Kubo, *J. Phys. Chem.*, **71**, 3249 (1967).
6) G. L. Breneman and R. D. Willett, *J. Phys. Chem.*, **71**, 3684 (1967).
7) G. A. Bowmaker and S. Hacobian, *Aust. J. Chem.*, **21**, 551 (1968).
8) W. Gabes, D. J. Stufkens, and H. Gerding, *J. Mol. Struct.*, **20**, 343 (1974).
9) Y. Kume and D. Nakamura, *J. Magn. Reson.*, **21**, 235 (1976).
10) S. Soled and G. B. Carpenter, *Acta Crystallogr., Sect. B*, **29**, 2556 (1973).
11) B. P. Dailey and C. H. Townes, *J. Chem. Phys.*, **23**, 118 (1955).
12) V. Jaccarino and J. G. King, *Phys. Rev.*, **94**, 1610 (1954).
13) V. Jaccarino, J. G. King, R. H. Satten, and H. H. Stoke, *Phys. Rev.*, **94**, 1798 (1954).

An Interpretation of Delayed Fluorescence Behavior of Naphthalene in Biphenyl Host in the Lower Temperature Region

Yoshihumi KUSUMOTO, Yasuhiko GONDO,* Hiroyasu SATO, and Yoshiya KANDA*

Chemical Institute, College of Liberal Arts, Kagoshima University, Korimoto, Kagoshima 890

**Department of Chemistry, Faculty of Science, Kyushu University, Hakozaki, Higashi-ku, Fukuoka 812*

(Received January 20, 1977)

Temperature and concentration dependences of the delayed luminescence observed in the naphthalene (guest)–biphenyl (host) mixed crystal system have been studied. The presence of the temperature-independent delayed fluorescence (TIDF) and its significance in the evaluation of activation energy have also been confirmed in this system as in the case of the benzo[*f*]quinoline–biphenyl system previously reported, and the generality of the existence of TIDF as well as its significance in relation to activation energy has been suggested. In addition, some remarks have been made on the nature of TIDF and the decay behavior.

We have observed TIDF of benzo[*f*]quinoline in biphenyl host in the low temperature region from 90 K down to liquid helium temperature and showed that subtraction of this temperature-independent contribution (I_{TIDF}) from the observed total delayed fluorescence intensity ($(I_{DF})_{total}$) above 90 K gave straight-line fits of both $\log I_{DF}/I_P^2$ and $\log I_{DF}$ *vs.* $1/T$ plots, where I_{DF} and I_P stand for the delayed fluorescence (DF) and phosphorescence (P) intensities, respectively, in good agreement with the usual temperature-dependent model.[1-3] Moreover, it has been shown that the decay behavior of TIDF may be responsible for the unusual decay behavior of DF around 77 K, the decay of which deviates considerably from exponentiality in the lower temperature region where the exponential behavior is expected from the usual temperature-dependent model.[2] The investigation on the temperature and concentration dependences of both the intensity and the decay of the delayed luminescence (P and DF) of naphthalene in biphenyl host has been made in order to examine the existence and its significance of TIDF as found in the benzo[*f*]quinoline–biphenyl system. Incidentally, Misra[4] reported an observation of TIDF in the same system. In the present work, therefore, we will mainly discuss whether this temperature-independent portion of DF plays an important role for the anomaly of DF observed in the lower temperature region in the naphthalene–biphenyl system. Benzo[*f*]quinoline has overlapping phosphorescence and triplet-triplet absorption bands,[5] whereas it is not the case in naphthalene.[6] Since this type of overlapping might be significant in the triplet-triplet annihilation,[7] it seems interesting to choose naphthalene as another guest to be compared with benzo[*f*]quinoline.

Experimental

Chemicals were obtained from Tokyo Kasei Kogyo Co., Ltd. Biphenyl was recrystallized twice from ethanol, and was further purified by the method of repeated zone refining and abstraction of the non-emissive portions of the specimen. Naphthalene of the UP grade (zone refined, number of passes: 23) was used without further purification. The polycrystalline samples used were prepared from the melts between two fused-silica plates which were mounted in a brass block holder. Concentration of the samples studied ranges from 10^{-2} to 10^{-4} mol/mol. All apparatus and techniques were identical to those already described.[2]

Results and Discussion

Spectra. As shown in Fig. 1, the normal and delayed fluorescence spectra obtained at 77 K with a guest concentration of 1.0×10^{-3} mol/mol are in good correspondence with each other in any of the mixed crystal samples, giving a confirmation that the observed DF is genuine. The temperature dependence of the delayed luminescence was studied for bands b, c, and d in Fig. 1. The phosphorescence spectrum obtained at 77 K from the mixed crystals is given in Fig. 2, where "a" stands for the 0,0-band of P. The delayed luminescence spectrum of the naphthalene–biphenyl mixed crystals has been reported, particularly by Misra and McGlynn.[8] Comparing our observed spectrum with theirs, the naphthalene guest is identified to be the emitting species.

Temperature Dependence of Intensity. The results of the temperature dependence of the delayed luminescence with a guest concentration of 1.0×10^{-2} mol/mol in the

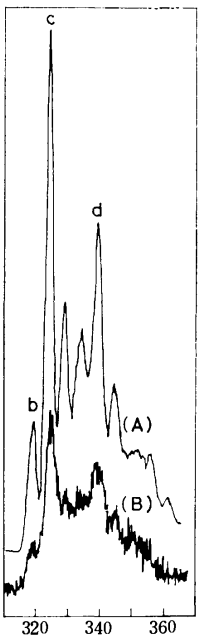

Fig. 1. Comparison of (A) normal and (B) delayed fluorescence of naphthalene in biphenyl host at 77 K. Concn: 1.0×10^{-3} mol/mol.

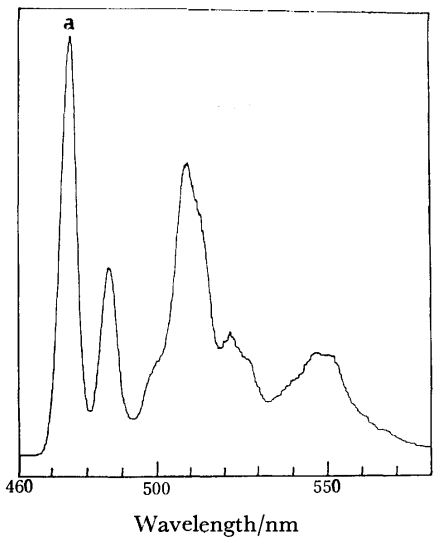

Fig. 2. Phosphorescence spectrum of naphthalene in biphenyl host at 77 K. Concn: 1.0×10^{-3} mol/mol.

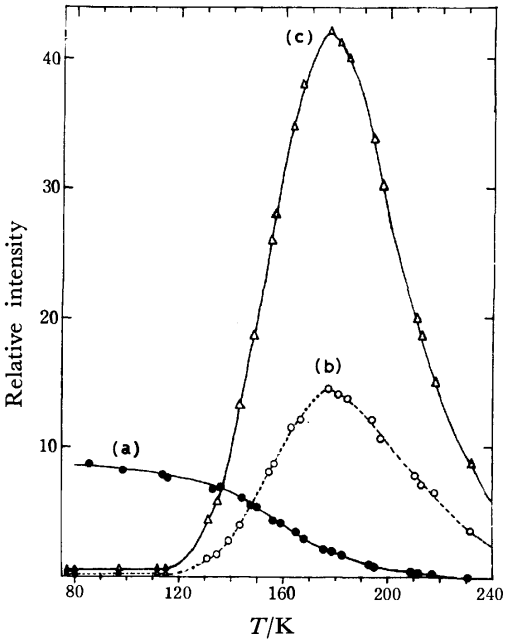

Fig. 3. Temperature dependence of the delayed luminescence of naphthalene in biphenyl host in the temperature region above 77 K. Concn: 1.0×10^{-2} mol/mol. (a): Phosphorescence intensity observed at 475 nm, *i.e.*, the 0,0-band shown in Fig. 2; (b) and (c): delayed fluorescence intensities observed at 318 nm (the 0,0-band) and the corresponding band shown in Fig. 1, respectively. No correction was made for the spectral response of the apparatus.

temperature region above 77 K are shown in Fig. 3. The results on DF observed at band d are not shown in the figure because it is similar to those of bands b and c as far as the temperature dependence is concerned. The results obtained with the guest concentrations of 1.0×10^{-3} and 1.0×10^{-4} mol/mol were also similar to those obtained with the guest concentration of 1.0×10^{-2} mol/mol just mentioned above. As can be seen in Fig. 3, the DF intensities observed at bands b and c remain constant at least in the temperature range of 77—110 K. This thermal behavior is quite similar to that in the benzo[*f*]quinoline–biphenyl system[2] except that T_{max} (the temperature at which maximum intensity of DF occurs) shifts to the higher temperature. These suggest that I_{DF} below 77 K may be independent of temperature. This system has very weak delayed luminescence at temperatures below 77 K, which we were not able to study quantitatively even by use of an NF LI-572B auto lock-in amplifier, partly because of the use of glass dewars. Incidentally, Misra[4] has reported that I_{DF} observed in the same system remains fairly constant in the temperature range from 6 to 77 K, 77 K being the highest temperature in their study. On the other hand, we also observed TIDF in the range of 77—105 K. Combining these results obtained in the different temperature regions, it may be concluded that TIDF exists over a wide range of temperature in this system just as in the case of the benzo[*f*]quinoline–biphenyl system. Hence, the important features of TIDF may be investigated in the region above 77 K. In this system, a rather peculiar temperature dependence of I_{DF}, as was already pointed out by Misra and McGlynn,[8] was found in the lower temperature region where an exponential temperature dependence is expected. This peculiarity may be correlated to the DF decay behavior at the same lower temperature region[2] and we emphasize that this peculiarity is due to the existence of TIDF over a wide range of temperature.

Evaluation of Activation Energy from Intensity Analyses. We have emphasized in the previous papers[1,2] that the peculiarity of DF in the lower temperature region can be understood well in accodance with the kinetic model if we take into consideration the temperature-independent portion of DF in a process of estimation of I_{DF}. We use the following three Arrhenius plots[2,9] in order to estimate the activation energy ΔE from the intensity analyses:

(1) In the higher temperature region, $\log I_P$ *vs.* $1/T$ (plot (1))
(2) in the lower temperature region, $\log I_{DF}$ *vs.* $1/T$ (plot (2))
(3) in the whole temperature region, $\log I_{DF}/I_P^2$ *vs.* $1/T$ (plot (3)).

In Fig. 4 are shown plots (1) and (2) obtained with three different concentrations, together with the plot obtained using corrected values of I_{DF}, *i.e.*, $[(I_{DF})_{total}-I_{TIDF}]$. Among the plots, only the latter one gave good fits to straight lines in all the concentrations studied. Figure 5 shows the results obtained with plot (3) in the three different concentrations. Here also, only the plot obtained with the corrected values of I_{DF} gave a straight line over the whole temperature range. In the naphthalene–biphenyl system, however, the effect of the correction is found to be smaller than that in the benzo[*f*]quinoline–biphenyl system, reflecting the fact that the temperature-independent fraction is much smaller, as can be seen in Fig. 3. The slopes of the straight-line portions shown in Figs. 4 and 5 give the activation energies listed in Table 1, which are comparable with the spectroscopic value[8] of 1940 cm^{-1}. Misra and McGlynn[8] obtained the ac-

TABLE 1. ACTIVATION ENERGIES[a] AND RATIOS $I_{TIDF}/(I_{DF})_m$

Guest concn (mol/mol)	Band[c]	ΔE (cm^{-1})[b]				$\frac{I_{TIDF}}{(I_{DF})_m}$[f]
		$\log I_{DF}/I_P^2$ *vs.* $1/T$		$\log I_{DF}$ *vs.* $1/T$	$\log I_P$ *vs.* $1/T$	
		Uncorrected[d]	Corrected[d]	Corrected[e]		
1.0×10^{-2}	c	1755	1770	1900	1950	0.012
1.0×10^{-3}	c	1970	2040	1980	2030	0.004
1.0×10^{-4}	c	2340	2400	1910	1950	0.004

a) The spectroscopic energy gap of host triplet-guest triplet state is 1940 cm^{-1} for the naphthalene-biphenyl system.[8] b) Activation energy calculated from the temperature dependence of the delayed luminescence. See text. c) See Fig. 1. d) See text. e) Only the corrected plot gives a good fit to a straight line. See text. f) $(I_{DF})_m$ denotes the maximum I_{DF} at T_{max}.

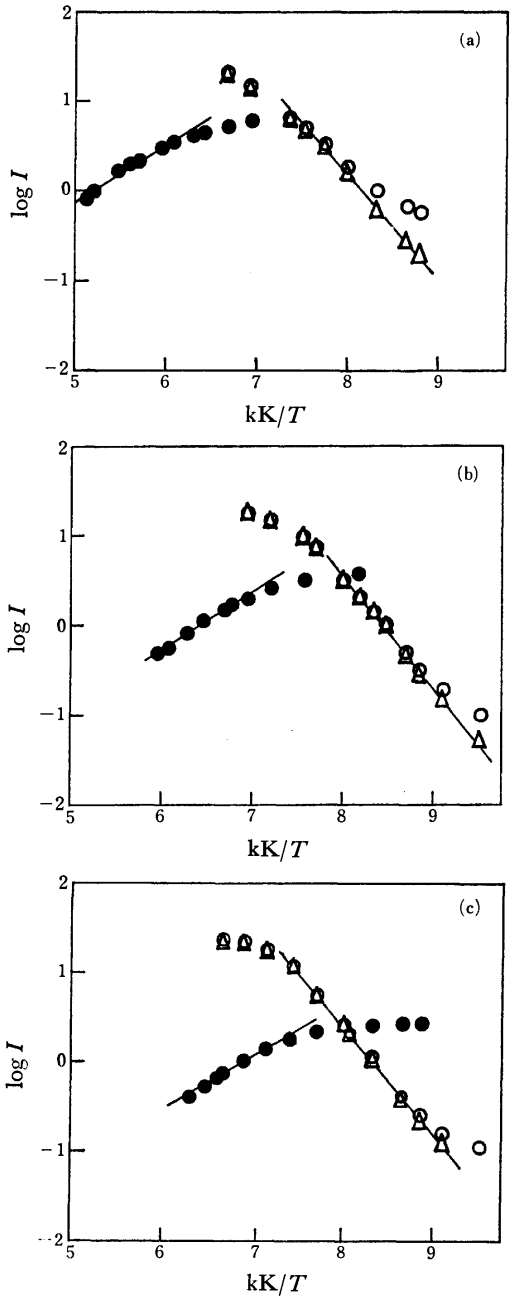

Fig. 4. Plots of log $(I_{DF})_{total}$ (○), log $[(I_{DF})_{total}-I_{TIDF}]$ (△), and log I_P (●) *vs.* $1/T$ with I_{DF} at band c shown in Fig. 1. Concn: (a) 1.0×10^{-2}, (b) 1.0×10^{-3}, (c) 1.0×10^{-4} mol/mol.

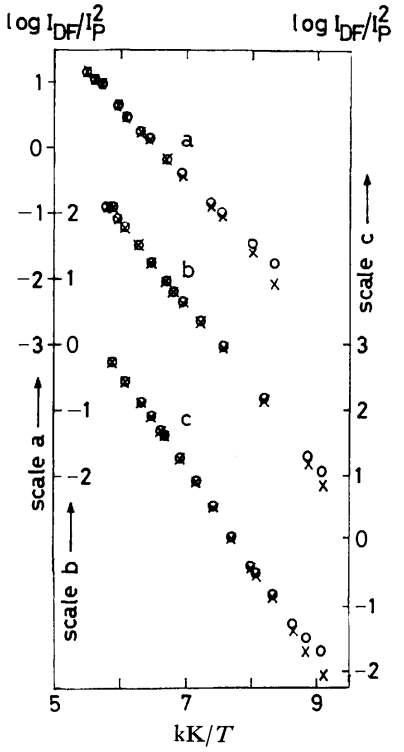

Fig. 5. Plots of log $(I_{DF})_{total}/I_P^2$ (○) and log $[(I_{DF})_{total}-I_{TIDF}]/I_P^2$ (×) *vs.* $1/T$ with I_{DF} at band c. Concn: (a) 1.0×10^{-2}, (b) 1.0×10^{-3}, (c) 1.0×10^{-4} mol/mol.

tivation energy of 1760 cm^{-1} from the "uncorrected" part of plot (3) and 175 K for T_{max}. Our uncorrected results are in good agreement with theirs. We would like to emphasize here that, according to our results, the existence of shallow traps in host crystal lattices suggested by Misra and McGlynn[8] as an interpretation of DF in the lower temperature region is in doubt and that it should be re-interpreted as due to the existence of TIDF as has been detailed on the benzo-[*f*]quinoline-biphenyl system.[1,2] The activation energies obtained from plot (3) with a very low guest concentration of 10^{-4} mol/mol seem too large to fall within the experimental error in either of the spectroscopic value or the other thermal activation energies. As was already suggested in the previous paper,[2] this may be due to an influence of a very weak trap-DF observed at such a very low concentration. Judging from the thermal values obtained from the other sources (*i.e.*, plots (1) and (2)) and from the discussion in the previous

paper,[2] it may be concluded that the thermal activation energy is independent of concentration.

Decay Behavior. We have observed exponential or nearly exponential decays of DF of naphthalene in biphenyl host crystals in the temperature range of 120—130 K,[3] just as have been reported by Hirota[9] and by McGlynn *et al.*[8,10,11] in the vicinity of the so-called characteristic temperature (*i.e.*, the temperature at which deviations from exponential decay behavior of P begin to occur). These experimental observations indeed seem to be in accordance with our suggestion[2] that when the contribution of TIDF is negligible and the decay of temperature-dependent DF remains exponential, the exponential decay behavior of DF to be observed will be expected at least in the vicinity of the characteristic temperature. Detailed results on the decay behavior will be presented elsewhere.

Some Remarks on the Nature of TIDF. In the last column of Table 1 are given the ratios of I_{TIDF} to I_{DF} at T_{max}, that is, $I_{TIDF}/(I_{DF})_m$. For naphthalene in biphenyl host, Misra obtained a value of 0.12 for the above ratio from the temperature dependence of I_{DF},[4] while our values are lower by one order as listed in Table 1. These ratios seem to exhibit the concentration dependence, as have already been suggested by us, and are much smaller than those obtained in the benzo[*f*]quinoline–biphenyl system.[1,2] In any event, considering the fact that we have observed TIDF, it may be concluded that the overlap of the P and T-T absorption bands is not necessarily significant for the occurrence of TIDF. Recently, Gondo *et al.*[12] have suggested, on the sound basis of the results on the concentration depolarization in P and normal fluorescence of some aromatic compounds in ethanol glass at 77 K, that formation of the molecular complexes might be responsible for the energy transfer observed in the benzophenone-naphthalene-in-rigid-glass system by Terenin and Ermolaev.[13] Namely, the experimental results that the triplet-triplet energy transfer is inefficient and is of the short range phenomenon,[12] and that TIDF has been observed at the low concentrations of the order of 10^{-4} mol/mol, suggest that the formation of molecular aggregates in mixed crystals may be responsible for the existence of TIDF.[2,14]

Similar TIDF has also been observed for naphthalenes and phenanthrenes in biphenyl host crystals,[4,9] for perprotobenzene in perdeuterobenzene host crystals,[15] and in the crystalline 1,2,4,5-tetracyanobenzene–biphenyl complex,[16] as well as for the naphthalene– and benzo[*f*]quinoline–biphenyl systems. Very recently, in the benzo[*h*]quinoline–biphenyl system, TIDF has also been observed and the above-mentioned correction has been carried out successfully.[17] Therefore, it may be allowed to state that the existence of TIDF in organic mixed crystals is a general phenomenon and the correction should be carried out in those systems where TIDF is observed.

References

1) (a) Y. Kusumoto, Y. Gondo, and Y. Kanda, *Chem. Lett.*, **1974**, 81; (b) Y. Kusumoto, Y. Gondo, and Y. Kanda, Preprint of the 7th Molecular Crystal Symposium, Nikko, Japan (1975), A-27, p. 79.

2) Y. Kusumoto, Y. Gondo, and Y. Kanda, *Bull. Chem. Soc. Jpn.*, **49**, 2706 (1976).

3) Y. Kusumoto, Thesis, Kyushu University, Fukuoka, Japan, 1976.

4) T. N. Misra, *J. Chem. Phys.*, **58**, 1235 (1973).

5) J. L. Kropp and J. J. Lou, *J. Phys. Chem.*, **75**, 2690 (1971); B. R. Henry and E. A. Lawler, *J. Mol. Spectrosc.*, **51**, 385 (1974).

6) D. P. Craig and I. G. Ross, *J. Chem. Soc.*, **1954**, 1589; D. P. Craig and G. Fischer, *Trans. Faraday Soc.*, **63**, 530 (1967); R. Astier and Y. H. Meyer, *Chem. Phys. Lett.*, **11**, 523 (1971); E. B. Priestly and G. W. Robinson, *Mol. Phys.*, **26**, 159 (1973).

7) R. E. Kellogg, *J. Chem. Phys.*, **41**, 3046 (1964), and other papers in this series.

8) T. N. Misra and S. P. McGlynn, *J. Chem. Phys.*, **44**, 3816 (1966).

9) N. Hirota, *J. Chem. Phys.*, **43**, 3354 (1965).

10) M. Kinoshita, T. N. Misra, and S. P. McGlynn, *J. Chem. Phys.*, **45**, 817 (1966).

11) (a) M. Kinoshita and S. P. McGlynn, *Mol. Cryst.*, **3**, 163 (1967); (b) M. Kinoshita and S. P. McGlynn, *ibid.*, **4**, 231 (1968).

12) (a) Y. Gondo, M. Hirai, T. Iwao, T. Kakibaya, T. Kuroi, H. Nagatomo, and Y. Kanda, *Chem. Lett.*, **1975**, 463; (b) Y. Gondo, M. Hirai, T. Iwao, T. Kakibaya, Y. Kanda, T. Kuroi, and H. Nagatomo, *J. Lumin.*, **12/13**, 825 (1976).

13) A. Terenin and V. Ermolaev, *Trans. Faraday Soc.*, **52**, 1042 (1956).

14) M. Schwoerer and H. C. Wolf, *Mol. Cryst.*, **3**, 177 (1967).

15) G. F. Hatch and G. C. Nieman, *J. Chem. Phys.*, **48**, 4116 (1968).

16) M. Yagi, S. Nagakura, and H. Hayashi, *Chem. Phys. Lett.*, **18**, 272 (1973).

17) S. Taen, Y. Gondo, and Y. Kanda, unpublished results.

Construction of a ^{3}He Calorimeter and Heat Capacity Measurement of the 1965 Calorimetry Conference Copper Standard between 0.4 and 20 K

Naoto Arai, Michio Sorai, Hiroshi Suga, and Syûzô Seki

Department of Chemistry, Faculty of Science, Osaka University, Toyonaka, Osaka 560

(Received January 21, 1977)

Construction of an isoperibol-type calorimeter with a ^{3}He cryostat is described. A system of charcoal-adsorption-pump is adopted. A Ge-thermometer used in the heat capacity measurements is calibrated in the temperature range from 0.4 to 1.5 K against the magnetic susceptibility of chromium potassium alum. The precision and the accuracy of the calorimeter is ascertained by the heat capacity measurement of the 1965 Calorimetry Conference Copper Standard (T-8.6) in the temperature range from 0.420 to 19.46 K. The deviation of the experimental points from the "copper reference equation" is within the experimental error of $\pm 2.5\%$ between 0.4 and 0.9 K, $\pm 1.5\%$ between 0.9 and 1.5 K, $\pm 1.2\%$ between 1.5 and 4 K, and $\pm 0.6\%$ between 4 and 20 K. The highest deviation of absolute value of the present heat capacity data of copper is 1.86% smaller than the "selected values (Furukawa *et al.*)" around 6 K. This difference may be primarily attributable to the NBS-65 temperature scale adopted in the present experiment.

In the field of magnetism, weak interactions among the magnetic moments are unambiguously interpreted based on the heat capacity measurements at extremely low temperatures where the lattice contribution is negligibly small. In the temperature region below 1 K, there are known considerable number of inorganic and metallic substances on which magnetic heat capacity measurements are performed. However, precise heat capacity measurements of organometallic and complex compounds are very scanty because these compounds are usually obtained as a polycrystalline form. In this work we constructed a calorimeter capable of measuring precisely the heat capacity of polycrystalline sample in the temperature range from 0.4 to 20 K. Two kinds of calorimeter cell suitable for this purpose were also designed.

The calorimeter constructed here is an isoperibol ^{3}He evaporation-type. To attain temperature significantly below 1 K there are two possible ways for evaporation; one is to pump out ^{3}He vapor by use of a diffusion pump or a rotary pump[1,2] and the other is to use a charcoal adsorption pump.[3,4] The latter is superior to the former due to the following three reasons. (i) The evaporation rate by an adsorption pump is much larger than that by an oil diffusion pump because it is possible to connect an adsorption pump to a ^{3}He pot *via* the extremely short pumping line which is everywhere near 1 K. (ii) In case of an adsorption pump one can avoid the heat generation arising from mechanical vibration of a rotary pump. Mechanical vibration causes very large temperature drift of a calorimeter cell at very low temperatures. (iii) A gas handling system using an adsorption pump is much simpler and securer than that consisting of a rotary pump. Based on our design Oxford Instrument Co., Ltd. constructed a part of the evaporation system of the present ^{3}He cryostat. In the present investigation a charcoal adsorption pump is adopted to avoid mechanical vibrations. A germanium resistance thermometer used here was calibrated against the magnetic temperature scale derived from the magnetic susceptibility of chromium potassium alum. For this end, an a.c. Hartshorn mutual inductance bridge and a coil assembly were constructed. The working principle of the ^{3}He cryostat and the calibration of Ge-thermometer will be described rather in detail.

Any physical quantity can exhibit its exact meaning only when the precision and the accuracy are critically evaluated. A convenient method of their estimation is to compare particular physical quantity with a well-established "standard" value. As to the low temperature calorimetry, heat capacity of high purity copper has been recommended as the calorimetry standard since last decade or so. At the 19th Annual Calorimetry Conference (U. S. A.), it was recommended to use a specially prepared and characterized copper sample for this purpose. In response to this recommendation, standard samples were prepared by Osborne *et al.*, and these samples are now available from Argonne National Laboratory.[5]

To estimate the precision and the accuracy for the present low temperature calorimetry, we measured the heat capacity of the 1965 Calorimetry Conference Copper Standard (Argonne Designation "T-8.6") in the temperature range from 0.4 to 20 K. The results and comparison with those by other investigators will be described below.

Experimental

1. Construction of Apparatus. The calorimeter consists of four major parts, namely a ^{3}He cryostat of isoperibol type, calorimeter cell, temperature measuring circuit, and energy measuring circuit.

1.1 ^{3}He Cryostat: The cryostat consists of three precooling steps and the innermost ^{3}He refrigerant system. The three precoolants are liquid N_2 and liquid ^{4}He at 4.2 and 1.2 K, respectively. The liquid containers for these coolants are designated hereafter as the N_2 reservoir, the ^{4}He main bath and 1.2 K pot, respectively. In order to minimize a heat evolution caused by mechanical vibration due to both a rotary pump used for a vacuum system and the laboratory building, the metal frame supporting the cryostat has been installed on rubber-dampers "Rubloc" and suitable bellows are inserted into the pipings, which cut off the vibration conducted from the building.

Figure 1 illustrates a schematic drawing of the main part of the ^{3}He evaporation cryostat. In this figure the drawing of a part of the dewar vessel and the N_2 reservoir is omitted. A gold-plated copper vacuum jacket (G) immersed in the ^{4}He main bath (C) houses the 1.2 K pot (K), a charcoal adsorption pump (N), a ^{3}He evaporator or the ^{3}He pot (P)

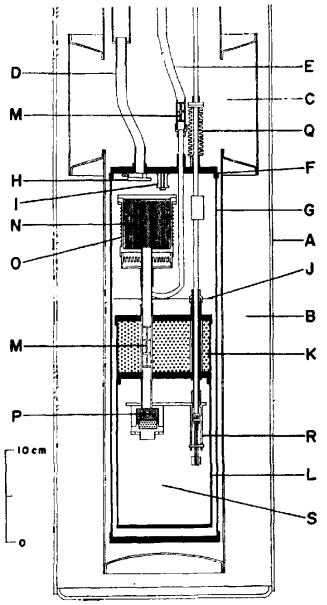

Fig. 1. Schematic drawing of the main part of ^{3}He evaporation-type cryostat (0.4—20 K): (A) aluminium jacket (liquid N_2 temperature), (B) vacuum space, (C) ^{4}He main bath, (D) vacuum pumping tube, (E) ^{3}He filling tube, (F) Wood's alloy joint, (G) gold-plated copper vacuum jacket, (H) radiation shield, (I) thermal anchor for leads, (J) radiation shield, (K) 1.2 K pot, (L) 1.2 K shield, (M) flow-impedance, (N) charcoal adsorption pump, (O) heater, (P) ^{3}He evaporator, (Q) bellows, (R) mechanical thermal switch, (S) experimental space.

and a mechanical thermal switch (R). The 1.2 K pot (inner volume of 400 cm^3) is filled with the liquid ^{4}He in the main bath *via* a needle valve. The 1.2 K pot is pumped down slowly to 1.2 K. The charcoal adsorption pump is heated to about 30 K by use of a heater (O) wound around it. The ^{3}He gas admitted through a flow-impedance (M) from an external storage tank is liquefied by passing it through a tube which is in thermal contact with the 1.2 K pot. The liquid ^{3}He drops into the ^{3}He pot. Then the heater is switched off and at the same time a compartment attached to the bottom of the adsorption pump is filled with liquid ^{4}He *via* a needle valve. The adsorption pump is cooled down to 4.2 K and the ^{3}He evaporator reaches rapidly its lowest temperature (0.26 K). The lowest temperature is sustained for more than ten hours in the heat capacity measurements.

The mechanical thermal switch has the gold-plated copper jaws, which are anchored to the ^{3}He evaporator by the copper braids. A stainless steel frame for sample mounting, which is not drawn in Fig. 1, is set in an experimental space (S) and supports a calorimeter cell with fine nylon threads. All the leads between the hermetic seals at the top of the cryostat at room temperature and the tag located under the 1.2 K pot are 46 S.W.G. enamelled copper and are thermally anchored at the 4.2 K spot (I) and at the 1.2 K pot, respectively.

Figure 2 is a sketch of the experimental space inside the 1.2 K shield. Here, a calorimeter cell is already mounted.

1.2 Calorimeter Cells: Tow kinds of calorimeter cells were constructed for the heat capacity measurements of polycrystalline specimen in the low temperature region. One is to use a small amount of ^{3}He gas as a heat exchanger, while the other is to use an organic material (Apiezon-N grease) forming a glassy state for good thermal contact. For convenience, these two cells are designated hereafter the calorimeter cell-type 1 and -type 2, respectively.

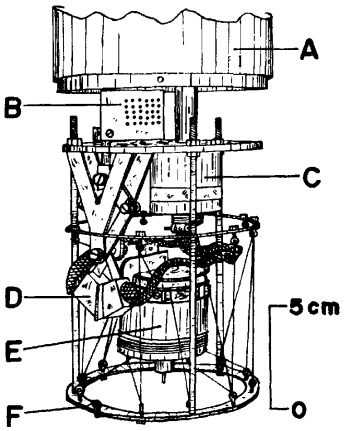

Fig. 2. Sketch of experimental space. The 1.2 K shield is dismantled and a calorimeter cell of type-1 is mounted: (A) 1.2 K pot, (B) tag for leads, (C) ^{3}He evaporator, (D) mechanical thermal switch, (E) calorimeter cell, (F) sample mounting frame.

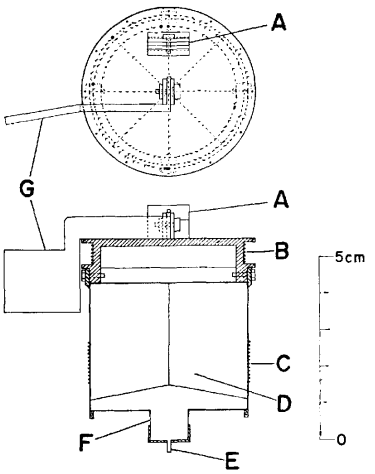

Fig. 3. Schematic diagram of calorimeter cell-type 1: (A) germanium thermometer holder, (B) leads for germanium thermometer, (C) heater, (D) eight vertical radial vanes, (E) ^{3}He gas filling tube, (F) sample filling tube, (G) clamping post.

1.2.1 Calorimeter Cell-Type 1: The calorimeter cell-type 1 (Fig. 3) consists of two parts: the upper part made of gold-plated copper is equipped with a clamping post (G) and a germanium thermometer holder (A), while the lower part is a sample container made of 20 carat gold which has a cylindrical form with the dimension of 4.2 cm in diameter, 3.5 cm in height and *ca.* 42 cm^3 of capacity. Both parts are connected mechanically. This device is necessary to protect the Ge-thermometer from contamination and mechanical vibration when the sample is loaded. Eight vertical radial vanes (D) in the cell makes the thermal equilibration within the cell easier and to the same end a small amount of ^{3}He gas (*ca.* 2 kPa at room temperature) is also sealed. The heater (C) is formed of a strain-free manganin wire of about 1.5 kΩ (49 S.W.G.) wound non-inductively. The heater is wound directly on to the periphery of the cell for assurance of good thermal contact at very low temperatures. For improvement of electric insulation and thermal contact between

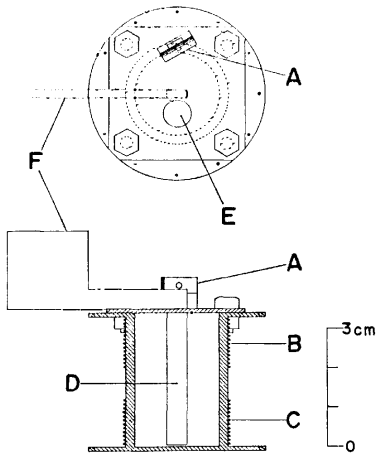

Fig. 4. Schematic diagram of calorimeter cell-type 2: (A) germanium thermometer holder, (B) thermometer leads, (C) heater, (D) copper stirring rod, (E) evacuating hole, (F) clamping post.

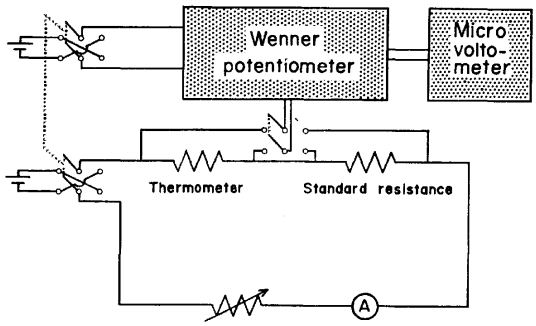

Fig. 5. Block-diagram of temperature measuring circuit.

the cell and the heater, the manganin wire is coated with GE7031 varnish. Thermal contact between the Ge-thermometer and the holder is increased by use of a small quantity of Apiezon-N grease between them. A part of the leads is thermally anchored to the upper part of the cell by means of GE7031 varnish. The cell is fixed to the sample mounting frame by fine nylon threads. The clamping post is adjusted to locate symmetrically between the jaws of the mechanical thermal switch (see Fig. 2).

1.2.2 Calorimeter Cell-Type 2: Figure 4 shows the calorimeter cell-type 2. In this case a polycrystalline sample is mixed with Apiezon-N grease. Heat transfer within the cell is promoted by a copper stirring rod (D) attached to one end of the clamping post. The cell is a copper cylinder of 2.5 cm in diameter, 3.5 cm in length and *ca.* 12 cm^3 of capacity. The clamping post (F), the thermometer holder (A) and so on are similar to those of the type 1.

1.3 Temperature Measuring Circuit: The measurement of temperature is achieved by the potential drops across both a germanium resistance thermometer (CryoCal, Inc., type CR100) and a standard resistor (1 kΩ, Shimadzu Electrical Measuring Instruments Co., Ltd.) arranged in series with it (see Fig. 5). These measurements are made by use of a Wenner-type potentiometer (Leeds & Northrup Co.). The degree of imbalance of the potentiometer is monitored by a d.c. micro voltmeter (Ohkura Electric Co., model AM-1001). The electric current used for the resistance measurements of the Ge-thermometer is selected to be 3.6—46 μA in the temperature range from 0.9 to 20 K, while below 0.9 K 1 μA or less is used so that the self-heating effect can be

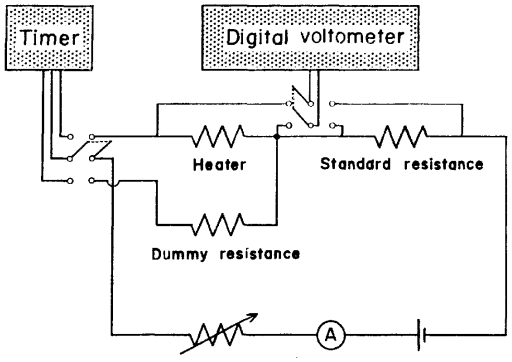

Fig. 6. Block-diagram of heating circuit.

minimized. The thermal electromotive force generated in the circuit is compensated by the reversion of the electric current. The apparent temperature difference caused by the current reversion were, *e.g.*, 0.6 mK at 0.61 K and 1.0 mK at 1.3 K. The standard resistor and an unsaturated-type standard cell (Epply Laboratory, Inc.) necessary for the potentiometer are kept at constant temperature.

1.4 Heating Circuit: Figure 6 shows the heating circuit. The heater current is supplied from a bank of low discharge lead storage batteries. The circuit is arranged to give a continuously variable current from 20 μA to 3.7 mA. The electric current flowing through the heater is determined by the potential drop across a standard resistor (1 kΩ). The heating element consists of a 49 S.W.G. manganin wire whose resistance is *ca.* 1.5 kΩ at room temperature. The d.c. voltages across the heater and the standard resistor are displayed on an integrating digital voltmeter (Takeda Riken Industry Co., Ltd., model TR-6515D, 5 digits). A dummy resistor having a similar resistance to the heater is placed in parallel to the heater. This dummy circuit enables the batteries to supply a stable current for a long period. The duration of the heating period is determined by an electronic counter (Takeda Riken Industry Co., Ltd., model TR-5104/04F, 6 digits).

2. Calibration of Ge-thermometer between 0.4 and 1.5 K. The germanium resistance thermometer (CryoCal, Inc., type CR100) used for the present heat capacity measurements has been already calibrated in the temperature range from 1.5 to 20 K at CryoCal, Inc. The temperature scale between 1.5 and 2.0 K is based on the helium-4 vapor pressure scale of 1958 (T_{58}). The 2.25 to 13 K readings are traceable to the National Bureau of Standards Provisional Scale 2—20 (1965) through a secondary standard. The temperature scale between 14 and 20 K is based on the International Practical Temperature Scale of 1968 (T_{68}) through a secondary standard.

Then the calibration below 1.5 K is made against the magnetic temperature scale derived from our measurement of magnetic susceptibility for chromium potassium alum. For this end, an a.c. Hartshorn mutual inductance bridge and a coil assembly for it were constructed. The oscillator is a commercially available audio-frequency signal generator (General Radio Co., type 1301-A). The frequency used here is 100 Hz. The inductive unbalance of the measuring secondary coil can be resolved into two components; the first component corresponds to the real part of the magnetic susceptibility of the paramagnetic salt and can be compensated by a variable mutual inductor (H. Tinsley & Co., Ltd., type 4229). The second component corresponds to the imaginary part of the susceptibility and can be compensated by taking off a small voltage from a potentiometer. The null balance of the circuit is attained by visual observation on the oscil-

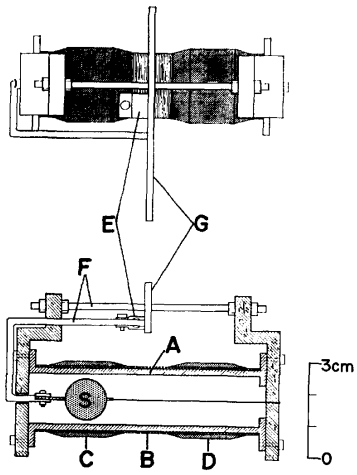

Fig. 7. Schematic diagram of the coil assembly: (S) paramagnetic salt, (A) nylon bobbin, (B) primary coil, (C) measuring secondary coil, (D) compensating secondary coil, (E) germanium thermometer holder, (F) copper rod, (G) clamping post.

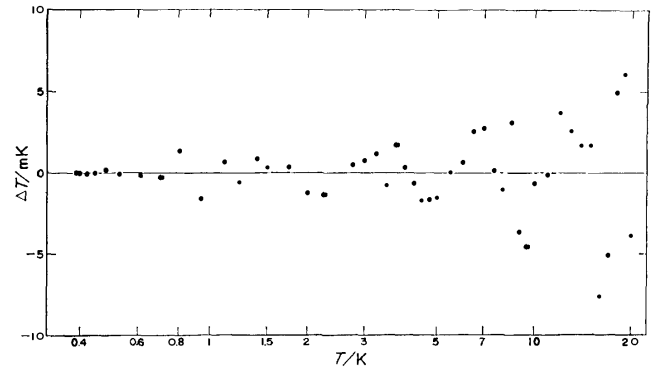

Fig. 8. Deviation plot for the germanium thermometer. $\Delta T = T_{\text{calcd}} - T_{\text{obsd}}$, where T_{obsd} is the calibrated temperature and T_{calcd} is the temperature calculated from the observed resistance R and the polynomial of the form given by Eq. 1.

lograph.

In the coil assembly (see Fig. 7), the Nb–Ti superconducting wire is wound on a nylon bobbin as a primary coil. The use of superconducting wire prevents the heat evolution due to Joule-effect in the primary coil at low temperatures. The measuring and the compensating secondary coils (copper wire) are wound directly onto the primary coil in opposite directions so that the mutual inductance due to the empty coil may be reduced to a conveniently small value. A single crystal of chromium potassium alum (*ca.* 2 g) is mounted in the bobbin.

The calibration procedure is as follows; in the first place, the magnetic susceptibility of the specimen was measured in the range from 1.5 to 7.0 K by use of the temperature scale of the Ge-thermometer. Based on these measurements we determined the Curie constant, the geometry factor of the salt, and the constant mutual inductance characteristic of the present apparatus. By assuming that these factors would not change below 1.5 K the Ge-thermometer was calibrated against the magnetic susceptibility in this temperature region. At each temperature the readings of the mutual inductor and the resistance of the thermometer were recorded over a period of 15—30 min. Twenty-seven sets of the experimental points were determined in the range between *ca.* 0.4 and 7 K. During the calibration the temperature of the coil assembly was controlled by both the mechanical thermal switch and the heater.

The calibration data, together with those above 1.5 K, were fitted to the following polynomial by using the method of least squares in the fractional deviations with equal weight:

$$\ln R = \sum_{i=0}^{13} A_i (\ln T)^i. \qquad (1)$$

This polynomial with fourteen parameters can reproduce the calibration points within ±2 mK below 6 K, within ±5 mK between 6 and 15 K, and within ±8 mK between 15 and 20 K (see Fig. 8).

The main source of experimental errors lies in the inaccuracy of the measurement of the mutual inductance. Its readings have an uncertainty of ±0.1 μH owing to the small current in the primary coil. On the other hand, the lowest range of the mutual inductor showed different values of the reading taken in the clockwise and the counterclockwise directions. This may be caused by the external electromagnetic coupling around the mutual inductor.

The validity of temperature calibration will be discussed later in connection with the heat capacity data of the 1965 Calorimetry Conference Copper Standard.

3. Heat Capacity Measurement of Standard Copper Sample. To evaluate the precision and the accuracy for the present low temperature calorimetry, we measured the heat capacity of the 1965 Calorimetry Conference Copper Standard (Argonne Designation "T-8.6")[5] in the temperature range from 0.4 to 20 K. The purity of the present copper sample is guaranteed to be better than 99.999%.

3.1 Preparation of Standard Copper Sample: The standard copper sample employed for the present purpose was the 1965 Calorimetry Conference Copper Standard (T-8.6), which was prepared in Argonne National Laboratory by vacuum casting 99.999+% High Purity Copper (American Smelting and Refining Co.) into rods. The sample has a cylindrical form of 5.3 cm in height and 3.1 cm in diameter. It was cleaned first with nitric acid and then with hydrochloric acid, rinsed with distilled water and dried *in vacuo*. After the surface treatments was over it was annealed in H_2 atmosphere for 2 h at 670 K, in ^{4}He atmosphere for 4.5 h at 720 K, and cooled *in vacuo* overnight in a Pyrex vessel. The final mass of the sample was 376.605 g (≙5.92649 mol).

For the heat capacity measurement the sample was mounted in a sample holder (Fig. 9). The sample holder consists of two flat copper disks (B) and (C); the upper one (B) is equipped with a clamping post (D) and a germanium thermometer holder (A). The sample (E) was interposed mechanically between these two disks. The calibrated germanium thermometer was inserted into the thermometer holder. Small amount of Apiezon-N grease was used for the attainment of good thermal contact between each part. A heater consists of a manganin wire (49 S.W.G.) with about 1.5 kΩ, which was wound directly onto the periphery of the sample rod and glued with GE7031 varnish. The sample holder was tightly hung in the calorimeter mounting frame in the cryostat by fine nylon threads. The clamping post was adjusted to locate centrally between the pair of jaws of the mechanical thermal switch. The weight of the sample holder and other addenda was 84.333 g.

3.2 Heat Capacity Measurement of Standard Copper Sample: The heat capacity measurement was made by an impulse method. The principle of this method is to measure a tem-

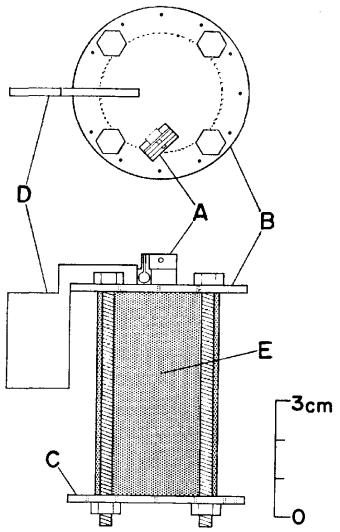

Fig. 9. Schematic diagram of the sample holder for standard copper: (A) germanium thermometer holder, (B) upper disk, (C) lower disk, (D) clamping post, (E) copper sample.

perature increment ΔT after a known quantity of heat ΔQ is introduced to a sample at a temperature T. The average heat capacity C_{av} in the temperature interval between T and $T+\Delta T$ may be given by $C_{av}=\Delta Q/\Delta T$. On the other hand, the true heat capacity (C) is defined as $C=\lim_{\Delta T\to 0}(\Delta Q/\Delta T)=dQ/dT$. When the ΔT is small enough, C_{av} approximates well to C and can be regarded as the true heat capacity at the average temperature T_{av} ($=T+\Delta T/2$). However, in the temperature region where the heat capacity is largely varied with temperature, the curvature correction should be made.

The temperature drift was monitored over a period of *ca.* 8 min and the attainment of thermal equilibrium in the sample was confirmed. The heat leak into the sample was estimated to be 20 nW at 0.45 K and −21 nW at 0.68 K. On the other hand, a breaking-off operation of the thermal switch brought about a temperature rise of 50 mK from the realized lowest temperature (*ca.* 0.32 K). This heat evolution is caused by the friction between the clamping post and the jaws of the thermal switch.

The heat capacity of the copper plus addenda was first measured in the temperature range from 0.391 to 20.02 K. Then the auxiliary measurement of the heat capacity of addenda was made between 0.456 and 19.18 K. The same amount of Apiezon-N grease was used for both sets of measurements. The ratio of the heat capacity of the addenda to the total amounts to about 20% at 0.42 K and becomes smaller with increasing temperature.

Results and Discussion

The experimental heat capacities, average temperatures and temperature increments are given in Table 1. The curvature correction has been applied for the determination of the heat capacity over the whole temperature region investigated. The experimental values below 2.0 K are compared in Fig. 10 with the results of previous measurements on copper in this temperature region. The open triangle and square represent the individual experimental points of previous measurements,[5,9] while a solid line is a smoothed curve calculated as an average of the data obtained by other two groups.[6-8] The present data (solid circle) agree well with these previous results except for several points around 1.0 K, which are scattered within ±2%. It may be mainly caused by rather small temperature increments in the present heat capacity measurement in this temperature region. On the whole, however, the calibration accuracy of the present thermometer below 1.5 K seems to be satisfactory.

Table 1. Heat capacity of the sample T-8.6 from the 1965 calorimetry conference copper standard (atomic weight=63.546)

T / K	C_p / mJ K^{-1} mol^{-1}	ΔT / K	T / K	C_p / mJ K^{-1} mol^{-1}	ΔT / K
0.420	0.2934	0.024	1.161	0.8840	0.056
0.448	0.3182	0.026	1.210	0.9247	0.064
0.481	0.3484	0.033	1.291	1.001	0.071
0.520	0.3645	0.037	1.348	1.058	0.067
0.554	0.4024	0.028	1.406	1.114	0.064
0.581	0.4264	0.026	1.465	1.171	0.076
0.607	0.4359	0.025	1.529	1.234	0.072
0.631	0.4542	0.024	1.600	1.308	0.121
0.656	0.4742	0.026	1.767	1.478	0.231
0.678	0.4974	0.022	1.971	1.711	0.200
0.702	0.5071	0.029	2.224	2.030	0.339
0.729	0.5188	0.030	2.506	2.457	0.332
0.748	0.5414	0.022	2.794	2.937	0.278
0.767	0.5575	0.022	3.113	3.577	0.392
0.786	0.5648	0.024	3.514	4.500	0.451
0.816	0.5819	0.024	3.981	5.694	0.589
0.834	0.6026	0.025	4.523	7.374	0.549
0.852	0.6274	0.023	4.961	9.083	0.440
0.859	0.6294	0.022	5.400	11.10	0.481
0.873	0.6366	0.022	5.941	13.86	0.647
0.889	0.6468	0.024	6.574	17.91	0.667
0.905	0.6525	0.022	7.151	22.23	0.534
0.920	0.6601	0.024	7.616	26.13	0.445
0.935	0.6816	0.023	8.068	30.27	0.510
0.950	0.7017	0.022	8.518	35.35	0.442
0.965	0.7184	0.025	8.913	39.89	0.393
0.978	0.7314	0.023	9.217	43.71	0.362
0.992	0.7316	0.023	9.600	48.84	0.436
1.007	0.7433	0.028	11.06	72.93	2.538
1.007	0.7474	0.029	12.93	116.1	1.239
1.024	0.7660	0.024	14.10	150.6	1.135
1.044	0.7751	0.036	15.13	187.6	1.003
1.058	0.7994	0.026	16.04	226.5	0.835
1.076	0.8126	0.033	16.97	269.4	1.052
1.101	0.8363	0.035	18.19	334.9	1.414
1.126	0.8537	0.033	19.46	423.0	1.119

The heat capacities of copper were fitted to the following equation proposed by Barron and Morrison[10] for the heat capacity of metallic solids,

$$C_p=\sum_{i=1}^{n}A_iT^{2i-1}, \qquad (2)$$

by using the method of least squares weighted with $1/C_p^2$, so that the sum of squares of the fractional deviations of the observed C_p values from the calculated ones may be minimized. Here, the first term propor-

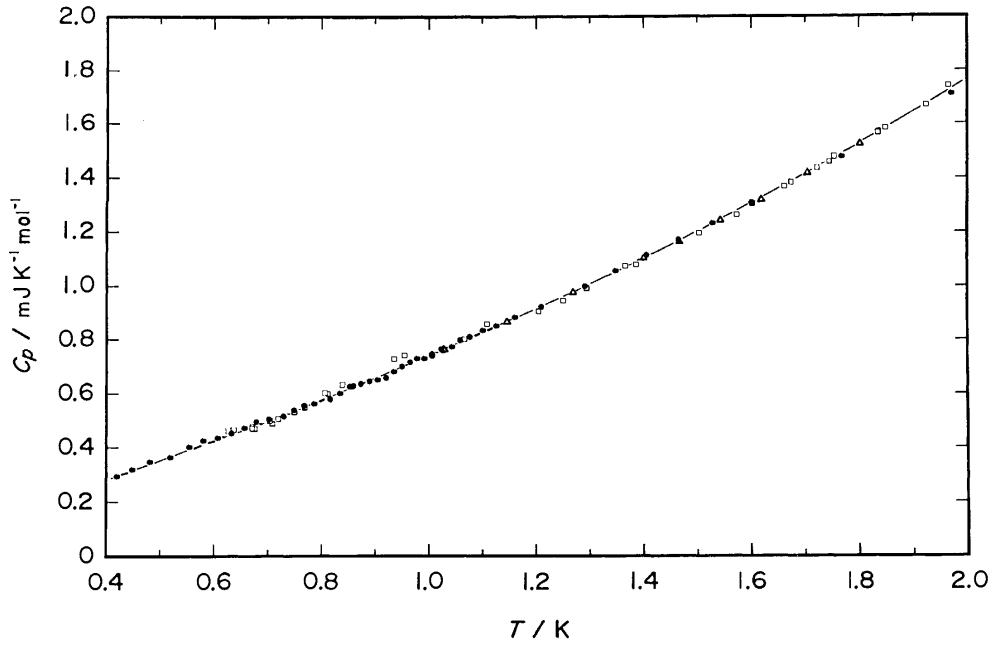

Fig. 10. Heat capacity of copper below 2.0 K: solid curve, Martin,[6,7] and Gmelin and Gobrecht;[8] □, Hurley and Gerstein;[9] △, Osborne *et al.*;[5] ●, present work.

tional to T is the "electronic heat capacity" due to conduction electrons and the remaining higher terms such as T^3, T^5 and so on correspond to the contributions from lattice heat capacity. Osborne *et al.*[5] designated the polynomial as "the copper reference equation" and used it for the purpose of interlaboratory comparison of heat capacity measurements. For the calculation the higher terms greater than $n=6$ were truncated. The "best fit" values of the coefficients were determined to be

$$A_1/\text{mJ K}^{-2}\,\text{mol}^{-1} = 0.69783,$$
$$A_2/\text{mJ K}^{-4}\,\text{mol}^{-1} = 0.45586 \times 10^{-1},$$
$$A_3/\text{mJ K}^{-6}\,\text{mol}^{-1} = 0.26336 \times 10^{-4},$$
$$A_4/\text{mJ K}^{-8}\,\text{mol}^{-1} = -0.39043 \times 10^{-7},$$
$$A_5/\text{mJ K}^{-10}\,\text{mol}^{-1} = 0.16039 \times 10^{-9},$$

and

$$A_6/\text{mJ K}^{-12}\,\text{mol}^{-1} = -0.15882 \times 10^{-12}.$$

The percentage deviations of the present results from the polynomial are shown in Fig. 11. The deviation of the experimental points is within the experimental error of ±0.6% above 4 K, ±1.2% between 4 and 1.5 K, ±1.5% in the range from 1.5 to 0.9 K, and ±2.5% below 0.9 K. As described above, the rather large scatter between 0.9 and 1.5 K may attributable to the small temperature increment in the heat capacity measurement, while the systematic deviation between 1.5 and 4 K may be caused by the discrepancy between the NBS-65 and the T_{58} scales. This problem will be discussed below together with the effect of both temperature scales upon the heat capacity values of copper.

A_1 is the coefficient of electronic heat capacity. The coefficient A_2 corresponds to $12\pi^4R/5[\theta_D(0)]^3$ and thus yields the Debye characteristic temperature $\theta_D(0)$ at 0 K, where R is the gas constant. In Table 2, both

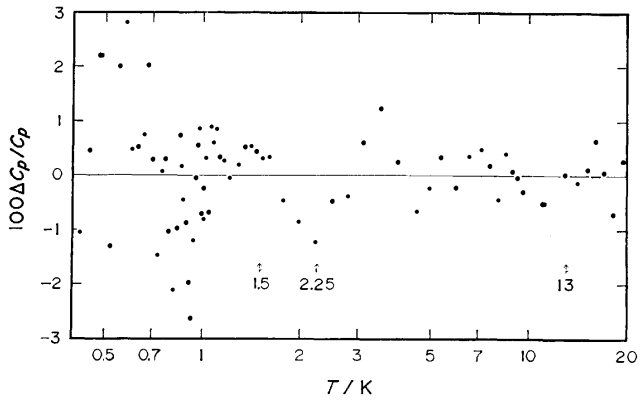

Fig. 11. Percentage deviations of the experimental C_p values from the calculated values, C_p(calcd), by the aid of the copper reference equation; $\Delta C_p = C_p - C_p$(calcd).

values are compared with those reported in recent years by a number of workers.[5-9,11-15] Almost all the measurements have been made by using thermometers calibrated against the T_{58} scale, except for the case of Bloom *et al.*[14] They have used the thermometer based on a combination of the T_{58} and the NBS-65 acoustic scales, as is in our case. The present value of $\theta_D(0)$ is slightly larger than the previous results. The difference may be primarily attributed to the temperature scale above 1.5 K because the data below 1.5 K coincide well with the reported values (see Fig. 10). In the present case, the calibration of the germanium thermometer between 1.5 and 2.0 K is based on the helium-4 vapor pressure scale of 1958 and that between 2.25 and 13 K on the National Bureau of Standards Provisional Scale 2—20 (1965). The temperature scale between 14 and 20 K is based on the International Practical Temperature Scale of 1968. The NBS-65 scale was determined on the assumption that the speed of sound

Table 2. Comparison of the electronic coefficient and the Debye temperature of copper at 0 K with the reported values by several workers

	A_1 / $\mu J\,K^{-2}\,mol^{-1}$	$\theta_D(0)$ / K	Temperature range / K	Sample	Ref.
Furukawa *et al.*	695±5	344.5±1.5	0—5	Selected value	(11)
Martin (1968)	691.5	345.8	0.3—3	ASARCO	(6)
Martin (1969)	689.0	347.7	0.4—3	Single crystal	(7)
	689.9	346.6	0.4—3	ASARCO	
Osborne *et al.*	694.3	344.5	1—25	T-1.1	(5)
Ahlers	696.0	343.8	1.3—20	T-1.2	(12)
Boerstoel *et al.*	696.8	344.4	1—30	T-3.4	(13)
Gmelin and Gobrecht	696.0	344.4	0.4—2.2	T-4.4	(8)
	696.9	344.6	2—30	T-4.4	
Bloom *et al.*	690.3	345.4	1.5—20	T-5.4	(14)
Holste *et al.*	694.5	343.7	1.5—30	ASARCO (degassed)	(15)
	696.5	343.3	1.5—30	ASARCO	
Hurley and Gerstein	691.4	343.9	0.6—28	T-6.2	(9)
Present work	697.8	349.4	0.4—20	T-8.6	
	698.1	348.5	1—5	T-8.6	
	697.3	346.5	1—5 (corrected)	T-8.6	

in helium gas is proportional to the square root of thermodynamic temperature. The NBS-65 scale is known to be higher than the T_{58} scale.[11,16] Therefore, in order to investigate more critically the dependence of the heat capacity of copper on both temperature scales, we should convert the present data based on the NBS-65 scale into those based on the T_{58} scale in the temperature range between 1 and 5 K.

To do this, we estimated the relationship between the T_{58} and the $T_{NBS\text{-}65}$ scales by use of the numerical values listed in reference (11) and obtained the following equation;

$$T_{58} = -0.1534\times10^{-2} + 0.9982\ (T_{NBS\text{-}65}) - 0.5340\times10^{-4}\ (T_{NBS\text{-}65})^2. \quad (3)$$

For examination of the dependence of heat capacity on the two different temperature scales, two sets of values concerning A_1 and $\theta_D(0)$ were calculated by use of the heat capacity data in the range from 1 to 5 K. Firstly, the data due to the $T_{NBS\text{-}65}$ scale were fitted to the equation,

$$C_p = A_1T + A_2T^3, \quad (4)$$

by the method of least squares with a weight of $1/C_p^2$ and A_1 and $\theta_D(0)$ were determined. Secondly, the heat capacity data recalculated based on the T_{58} scale (Eq. 3) were also fitted to Eq. 4. Two sets of the parameters A_1 and $\theta_D(0)$ are given in Table 2. The corrected values show evidently a tendency to approach the reported values. The $T_{NBS\text{-}65}$ scale itself is smoother than the T_{58} scale as previously described, but it is, for the moment, realized by use of only the acoustic thermometer in U. S. National Bureau of Standards. The present germanium thermometer has been calibrated above 2.25 K not directly against the $T_{NBS\text{-}65}$ scale but through a secondary thermometer possessed by CryoCal Co. It is, therefore, plausible to consider that the extra errors have been included in the process of calibration. Another possible reason for the deviation of the heat capacity of copper may be caused by different qualities of copper from sample to sample, because the original data for the evaluation of the standard values[11] include heat capacity measurements on a variety of coppers other than the calorimetry standard copper. At any rate, the temperature scales at low temperatures are hoped to be unified internationally as soon as possible.

By use of this calorimeter, we have measured the heat capacity of a five-coordinated ferromagnet, Fe-$[S_2CN(C_2H_5)_2]_2Cl$, in the temperature range from 0.4 to 20 K. The detailed results will be published in due course.[17]

This work was partially supported by Grant-in-Aid for Fundamental Scientific Research from the Ministry of Education. The authors thank Dr. Darrell W. Osborne for providing them the 1965 Calorimetry Conference Copper. Experimental assistance by Mr. Masanori Yoshikawa is also gratefully acknowledged.

References

1) G. Seidel and P. H. Keesom, *Rev. Sci. Instrum.*, **29**, 606 (1958).
2) D. L. Martin, *Proc. R. Soc. London, Ser. A*, **263**, 378 (1961).
3) B. N. Esel'son, B. G. Lazarev, and A. D. Shvets, *Cryogenics*, **3**, 207 (1963).
4) C. F. Mate, R. Harris-Lowe, W. L. Davis, and J. G. Daunt, *Rev. Sci. Instrum.*, **36**, 369 (1965).
5) D. W. Osborne, H. E. Flotow, and F. Schreiner, *Rev. Sci. Instrum.*, **38**, 159 (1967).
6) D. L. Martin, *Phys. Rev. Ser. II*, **170**, 650 (1968).
7) D. L. Martin, *Can. J. Phys.*, **47**, 1253 (1969).
8) E. Gmelin and K. H. Gobrecht, *Z. Angew. Phys.*, **24**, 21 (1967).
9) M. Hurley and B. C. Gerstein, *J. Chem. Thermodyn.*, **6**, 787 (1974).
10) T. H. K. Barron and J. A. Morrison, *Can. J. Phys.*,

35, 799 (1957).
11) G. T. Furukawa, W. G. Saba, and M. L. Reilly, Critical Analysis of the Heat-Capacity Data of the Literature and Evaluation of Thermodynamic Properties of Copper, Silver, and Gold from 0 to 300 K (U. S. Government Printing Office, Washington, D. C., 1968), NSRDS-NBS 18.
12) G. Ahlers, *Rev. Sci. Instrum.*, **37**, 477 (1966).
13) B. M. Boerstoel, W. J. J. van Dissel, and M. B. M. Jacobs, *Physica (Utrecht)*, **38**, 287 (1968).
14) D. W. Bloom, D. H. Lowndes, Jr., and L. Finegold, *Rev. Sci. Instrum.*, **41**, 690 (1970).
15) J. C. Holste, T. C. Cetas, and C. A. Swenson, *Rev. Sci. Instrum.*, **43**, 670 (1972).
16) H. Plumb and G. Cataland, *Metrologia*, **2**, 127 (1966).
17) N. Arai, M. Sorai, H. Suga, and S. Seki, *J. Phys. Chem. Solids.*, to be published in 1977.

Structural Studies of Asymmetric Hydrogenation. II*. The Crystal Structure of Methyl(R(+)-α-methylbenzylamine)-bis(dimethylglyoximato)cobalt(III) Benzene Solvate

Yuji Ohashi and Yoshio Sasada

Laboratory of Chemistry for Natural Products, Tokyo Institute of Technology, O-okayama, Meguro-ku, Tokyo 152

(Received January 28, 1977)

The structure of methyl(R(+)-α-methylbenzylamine)bis(dimethylglyoximato)cobalt(III) benzene solvate has been determined by X-ray crystal analysis. The crystal is orthorhombic; space group, $P2_12_12_1$; $Z=4$ with $a=14.074(1)$, $b=14.390(1)$, and $c=12.202(1)$ Å. The structure was deduced by the heavy-atom method and refined by the block-diagonal least-squares method to a final R value of 0.063 for 1413 observed reflections. The symmetry of the bis(dimethylglyoximato)cobalt moiety has been lowered from D_{2h} to C_{2h} as a result of the steric repulsion from optically active amine. It is proposed that this deformation is a factor inducing the asymmetry in the hydrogenation catalyzed by the complex of bis(dimethylglyoximato)cobalt and the active amine.

It has recently been shown that the complexes of bis(dimethylglyoximato)cobalt (abbreviated to Co(dmg)$_2$ or cobaloxime) and optically active amine catalyze the asymmetric hydrogenation of olefins with the CH_2=CXY formula, where X and Y are nucleophilic and electrophilic substituents respectively.[2-7] The hydrogenation proceeds according to the scheme shown in Fig. 1. We explored the mechanism of inducing the asymmetry by analyzing the structures I, II, and III. In the first place, the title complex was chosen because it is the simplest crystallized complex of the methylcobaloxime and the asymmetric amine. The methyl group does not seem bulky enough to change the structural features of the Co(dmg)$_2$ moiety, and it can be expected that the effect of the optically active amine on the structure of Co(dmg)$_2$ will be revealed.

Experimental

Dark red crystals of the title complex were obtained from a benzene solution. They are unstable in the air. The unit-cell dimensions were determined from zero-layer Weissenberg photographs, using Co$K\alpha$ radiation about the a and c axes. Spacing of 80 high-angle reflections ($\theta \geqq 70°$), calibrated with superposed silicon powder lines, were subjected to the least-squares treatment. The crystal data are summarized in Table 1.

Using a crystal with dimensions of $0.3\times0.2\times0.3$ mm, coated with nail enamel, the intensities for the layers from $hk0$ to $hk15$ and $0kl$ were collected on a Hilger-Watts linear diffractometer with Mo$K\alpha$ radiation. The balanced Y/Zr filter pair was used. Out of 3190 independent reflections ($3° \leqq 2\theta \leqq 55°$), 1418 were observed, those of $I<2.5\,\sigma(I)$ being regarded as unobserved. Only 65 reflections between 50° and 55°(2θ) had non-zero intensities. The usual Lorentz and polarization, but no absorption, corrections were made.

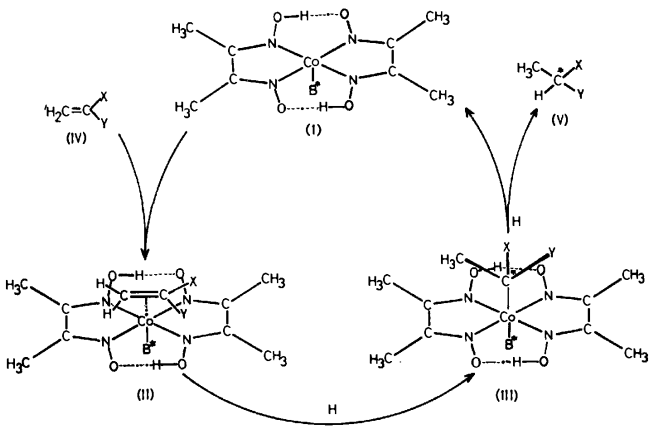

Fig. 1. The reaction path of the asymmetric hydrogenation, where B* is the optically active amine; (I) the catalyzer, (II) the π-complex, (III) the σ-complex, (IV) the substrate, and (V) the product.

* Part I of this series[1] deals with the crystal structure of β-cyanoethyl(D(−)-*erythro*-1,2-diphenyl-2-hydroxyethylamine)bis(dimethylglyoximato)cobalt(III).

Structure Determination

The positions of the cobalt and the six coordinated atoms were obtained from the three-dimensional Patterson function. The other atoms were revealed on the first Fourier map phased with those seven atoms.

The structure was refined by the block-diagonal least-squares methods. After several cycles of the refinement, the five strongest reflections were excluded because they seemed to be affected by secondary extinction. All the hydrogen atoms were found on the three-dimensional difference Fourier map. The final refinement was performed including these hydrogen atoms, with isotropic temperature factors which were assumed to be equal to those of the directly bonded atoms. The weighting

Table 1. Crystal data

Formula	$C_{17}H_{28}N_5O_4Co\cdot C_6H_6$
F. W.	503.5
Crystal system	Orthorhombic
a	14.074(1) Å
b	14.390(1)
c	12.202(1)
Volume of a unit-cell	2471.3 Å^3
Systematic absences	$h00$, h odd
	$0k0$, k odd
	$00l$, l odd
Space group	$P2_12_12_1$
Z	4
Density measured	1.353 g/cm^3
Density calculated	1.353 g/cm^3
μ(Mo$K\alpha$)	7.57 cm^{-1}

Table 2. Fractional atomic coordinates ($\times 10^4$) and thermal parameters ($\times 10^5$) for the non-hydrogen atoms

The anisotropic thermal parameters are of this form:

$$T=\exp\left[-(B_{11}h^2+B_{22}k^2+B_{33}l^2+B_{12}hk+B_{13}hl+B_{23}kl)\right].$$

The estimated standard deviations are in parentheses.

Atom	x	y	z	B_{11}	B_{22}	B_{33}	B_{12}	B_{13}	B_{23}
Co	1869(1)	2399(1)	1149(1)	0302(5)	0336(6)	0419(7)	0050(17)	0040(16)	0068(19)
N(1)	2453(6)	3303(5)	0267(7)	0478(54)	0210(48)	0417(68)	0029(84)	0176(96)	0202(89)
N(2)	2411(6)	1598(6)	0097(8)	0519(57)	0512(64)	0458(71)	0273(102)	−0642(105)	−0229(117)
N(3)	1217(7)	1521(8)	2010(9)	0507(62)	0682(72)	0735(85)	0225(113)	−0445(116)	−0009(135)
N(4)	1298(6)	3218(6)	2185(8)	0409(52)	0338(52)	0697(80)	0445(91)	−0152(106)	−0307(108)
C(1)	2903(7)	3028(9)	−0562(10)	0322(67)	0833(86)	0582(93)	0024(120)	−0055(121)	0534(150)
C(2)	2926(8)	2001(8)	−0655(9)	0490(73)	0479(61)	0273(69)	0432(110)	−0212(113)	0142(107)
C(3)	0738(7)	1814(9)	2831(11)	0185(54)	0621(78)	0877(111)	0261(113)	−0563(128)	0004(162)
C(4)	0757(7)	2817(10)	2916(10)	0300(59)	1111(115)	0577(87)	0494(139)	0212(118)	−0151(170)
C(5)	3450(8)	3623(9)	−1368(10)	0348(66)	0744(83)	0783(116)	−0117(120)	−0021(136)	0546(162)
C(6)	3341(9)	1411(11)	−1526(11)	0412(86)	1142(115)	0849(120)	−0020(156)	0111(147)	−0401(191)
C(7)	0231(10)	1212(12)	3626(11)	0711(100)	1190(117)	0654(124)	−0735(184)	0106(175)	0443(205)
C(8)	0213(11)	3389(11)	3780(12)	0815(103)	1259(121)	0485(101)	0337(190)	0176(190)	−0279(214)
O(1)	2404(6)	4204(5)	0453(7)	0663(55)	0411(46)	0833(75)	0037(86)	−0185(108)	0115(105)
O(2)	2282(6)	0672(5)	0184(7)	0630(52)	0262(41)	0823(75)	0025(76)	−0397(104)	−0339(95)
O(3)	1291(7)	0612(6)	1837(8)	0892(67)	0546(55)	0876(81)	−0363(104)	−0162(127)	0103(113)
O(4)	1401(6)	4148(6)	2117(7)	0500(50)	0687(57)	0752(70)	0287(92)	−0007(101)	−0308(112)
N(5)	3142(6)	2220(5)	1999(6)	0328(42)	0437(52)	0448(58)	−0059(105)	−0231(105)	−0033(87)
C(9)	3493(8)	2824(7)	2875(10)	0458(65)	0241(59)	0699(91)	−0131(95)	0217(130)	0066(116)
C(10)	4570(7)	2688(9)	3052(10)	0335(60)	0682(84)	0783(94)	−0073(147)	0121(127)	0288(180)
C(11)	2984(6)	2683(8)	3981(8)	0255(50)	0633(66)	0333(64)	0007(119)	−0050(100)	−0105(147)
C(12)	2804(9)	1810(8)	4393(10)	0756(90)	0303(63)	0600(96)	−0098(122)	0276(151)	0079(131)
C(13)	2395(10)	1721(10)	5404(13)	0763(95)	0629(95)	1062(139)	−0334(161)	0045(188)	0502(188)
C(14)	2141(7)	2476(13)	6008(9)	0510(66)	1198(101)	0563(84)	0435(211)	0094(125)	0382(281)
C(15)	2346(10)	3348(10)	5597(11)	0785(94)	0761(100)	0610(106)	0383(165)	0432(164)	−0397(174)
C(16)	2786(9)	3455(9)	4594(11)	0584(81)	0720(91)	0629(100)	−0002(141)	0073(149)	−0375(163)
C(17)	0730(6)	2515(13)	0194(8)	0320(55)	0734(75)	0699(97)	0045(170)	−0205(113)	0651(219)
C(18)	5561(10)	4843(8)	1688(13)	0654(92)	0289(63)	1341(147)	0494(137)	0941(209)	0028(164)
C(19)	4604(12)	5019(10)	1673(13)	1232(149)	0654(89)	0969(137)	−0043(200)	−0725(254)	0278(196)
C(20)	4122(9)	5244(9)	2579(14)	0304(67)	0455(71)	1850(190)	0194(126)	−0284(186)	0863(210)
C(21)	4638(11)	5296(7)	3544(11)	1070(122)	0237(58)	0892(131)	−0012(146)	0678(208)	0214(141)
C(22)	5570(9)	5172(9)	3579(11)	0435(72)	0640(79)	0886(130)	−0519(133)	0184(160)	0299(168)
C(23)	6048(9)	4966(10)	2651(13)	0401(79)	0818(98)	1308(163)	−0364(153)	0063(188)	0764(224)

Table 3. Fractional coordinates ($\times 10^3$) and thermal parameters for hydrogen atoms

The estimated standard deviations are in parentheses.

Atom	x	y	z	B/Å^2	Atom	x	y	z	B/Å^2
H(N51)	356(7)	209(7)	130(9)	2.52	H(21)	413(9)	558(8)	427(10)	4.42
H(N52)	308(8)	163(7)	223(9)	2.52	H(22)	611(9)	518(9)	421(11)	4.45
H(9)	349(8)	343(8)	258(10)	3.32	H(23)	683(10)	482(8)	256(10)	4.42
H(101)	473(8)	215(7)	330(9)	3.52	H(51)	334(8)	430(8)	−106(11)	4.02
H(102)	489(8)	283(7)	242(10)	3.52	H(52)	303(9)	355(8)	−229(10)	4.02
H(103)	472(8)	314(7)	355(10)	3.52	H(53)	406(9)	346(8)	−143(10)	4.02
H(12)	294(8)	121(8)	408(10)	3.62	H(61)	385(9)	177(9)	−174(12)	5.32
H(13)	219(9)	101(9)	568(11)	4.72	H(62)	383(9)	095(9)	−126(11)	5.32
H(14)	192(8)	228(9)	662(10)	5.42	H(63)	272(10)	091(9)	−196(11)	5.32
H(15)	230(9)	395(9)	609(12)	5.52	H(71)	047(9)	068(8)	382(12)	5.02
H(16)	309(9)	418(8)	429(10)	4.82	H(72)	−016(9)	087(9)	342(11)	5.02
H(171)	040(8)	212(8)	037(10)	4.22	H(73)	031(9)	157(9)	410(12)	5.02
H(172)	094(7)	264(9)	−059(9)	4.22	H(81)	−015(9)	305(8)	415(12)	5.32
H(173)	033(9)	304(8)	042(10)	4.22	H(82)	069(9)	386(9)	421(11)	5.32
H(18)	583(9)	454(8)	106(11)	4.42	H(83)	007(10)	420(9)	329(11)	5.32
H(19)	419(9)	494(8)	107(11)	4.42	H(O1)	187(9)	433(8)	151(10)	4.42
H(20)	351(9)	542(9)	257(10)	4.42	H(O2)	184(9)	072(8)	099(10)	4.42

scheme of $w=(13.8/|F_o|)^2$ if $|F_o|>13.8$, $w=1.0$ if $13.8\geqq|F_o|\geqq4.6$, and $w=0.2$ if $|F_o|<4.6$ was employed. The final R became 0.063 for 1413 observed reflections. At the final stage, no peaks higher than 0.03 e Å^{-3}, except for the peaks of 0.05 e Å^{-3} around the cobalt atom, were observed on the difference map. The atomic scattering factors were taken from International Tables for X-Ray Crystallography.[8] The final atomic parameters and their standard deviations are given in Table 2 for non-hydrogen atoms and in Table 3 for hydrogen

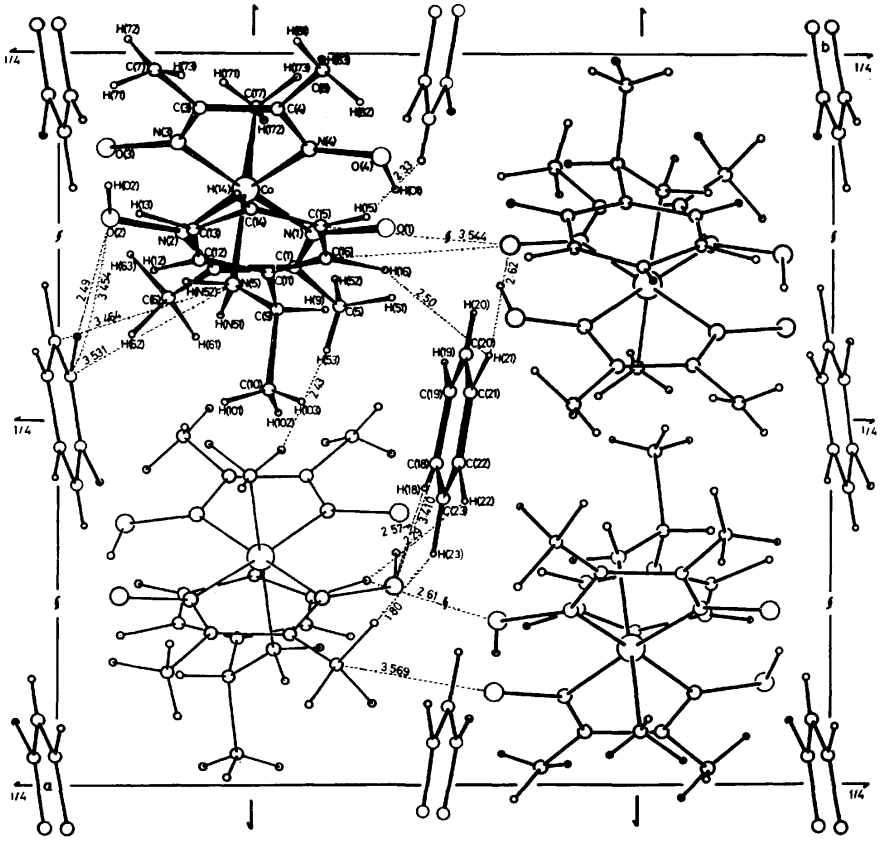

Fig. 2. Projection of the structure along the c axis and the interatomic distances between the Co-complexes and between the Co-complex and benzene. Along the c axis the contacts, 3.775 Å for C(14)···C(6), 2.77 Å for C(15)···H(52), and 2.30 Å for H(15)··· H(52), are observed.

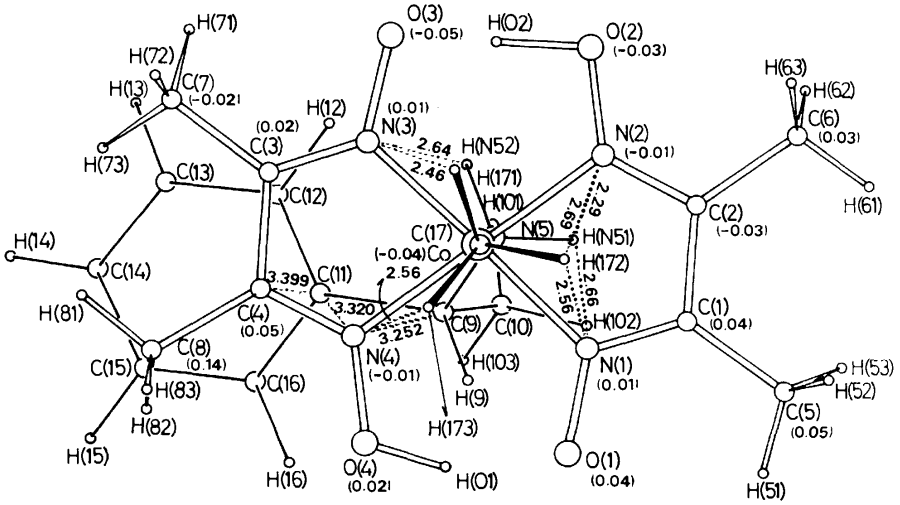

Fig. 3. Projection of the complex to the mean plane of four nitrogen atoms of $Co(dmg)_2$ and the short contacts between non-bonded atoms (l/Å), their threshold values being 3.400 Å for distances between the non-hydrogen atoms and 2.70 Å for those including hydrogen atoms. The deviations of the non-hydrogen atoms of $Co(dmg)_2$ from the plane are in parentheses.

atoms. A list of the observed and calculated structure factors is kept in the office of the Chemical Society of Japan (Document No. 7711).

The computation was done on the HITAC 8800 computer at the University of Tokyo and on the HITAC 8700 computer at Tokyo Institute of Technology. The programs, PROC for the data reduction and TLSU for the determination of the cell dimensions, were used. The other programs used were those in the UNICS Program System[9] with some modification.

Description of the Structure

The crystal structure viewed along the c axis is shown in Fig. 2, in which the short interatomic distances are also given. There are no unusual short contacts between the Co-complexes, or between the Co-complex and the benzene molecule. The mean plane of the

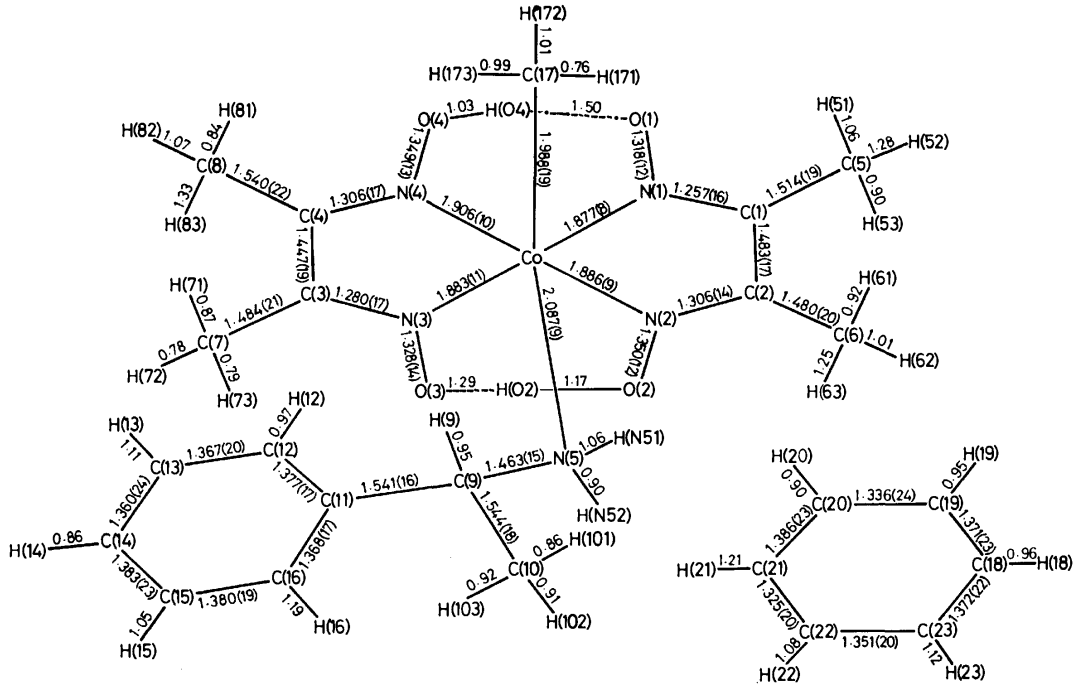

Fig. 4. Bond distances (l/Å). Their standard deviations are in parentheses, while those involving hydrogen atoms are 0.11—0.15 Å and are omitted for clarity.

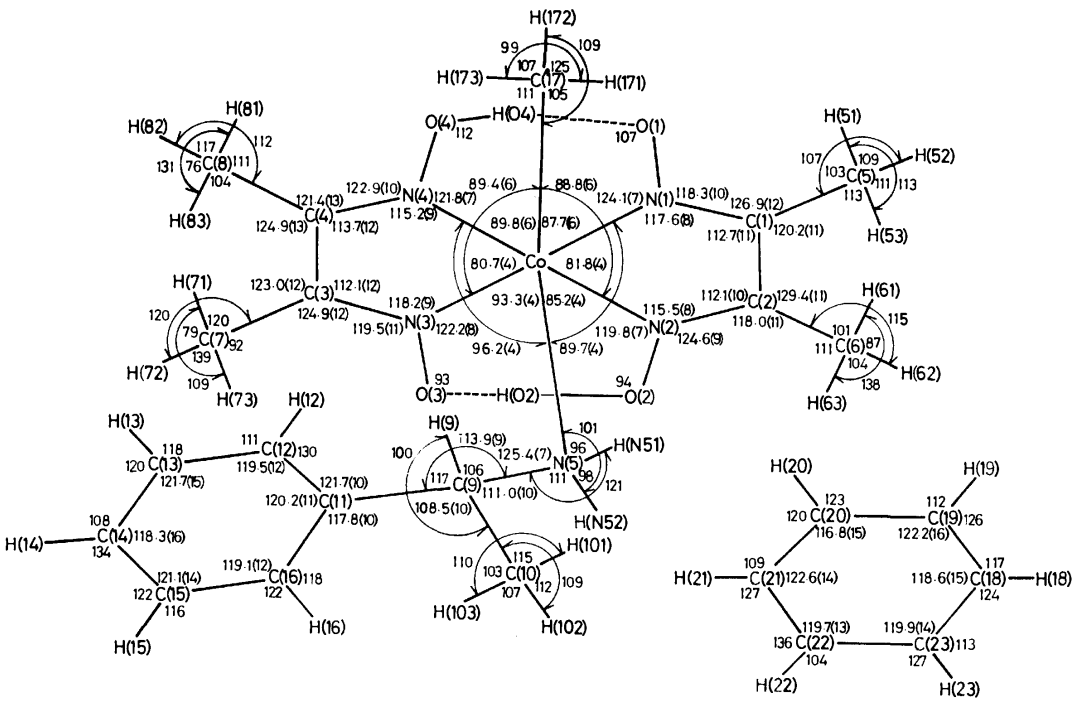

Fig. 5. Bond angles (ϕ/°). Their standard deviations are in parentheses, while those involving hydrogen atoms are 6—14° and are omitted for clarity.

benzene ring is about at right angles to that of $Co(dmg)_2$ and to that of the phenyl ring of α-methylbenzylamine (abbreviated as mba).

The four nitrogen atoms in $Co(dmg)_2$ are coplanar within the limits of 0.01 Å, and the equation of the best plane is given by:

$$-0.8157X + 0.0781Y - 0.5731Z + 2.6438 = 0,$$

where X, Y, and Z are the coordinates (in Å units) referred to the crystal axes. The deviations of the atoms from the plane and the distances between the non-bonded atoms in the complex are shown in Fig. 3. The C(8) atom over the phenyl ring is significantly out of the best plane, probably to avoid the short contact with the phenyl ring. The cobalt atom is slightly displaced from the plane toward mba. The short contact, N(4)···C(9), which is also observed in the complex reported in Part I (abbreviated as β-cne(dphyea)cobaloxime), seems to represent a fairly strong steric repulsion. The Co–N(5) bond makes an angle of 84° with the average plane.

The bond distances and angles are shown in Figs. 4 and 5 respectively. The $Co(dmg)_2$ moieties of aquomethylcobaloxime,[10,11] methylpyridinecobaloxime,[12] and methyl(3-*N*-methylimidazolyl)cobaloxime[12] have the D_{2h} symmetry. Bigotto *et al.*[12] have suggested, on the basis of all the reported structures of the alkylcobaloxime complexes, that the standard values for Co–N, N–O, N–C, and C–CH_3 are 1.879, 1.343, 1.297, and 1.500 Å respectively. In the present complex, however, the bonds of Co–N, N–O, and N–C around N(2) and N(4) are longer than the standard lengths, whereas those around N(1) and N(3) are shorter except for Co–N(3). The hydrogen atoms, H(O1) and H(O2), do not exist at the mid-point of O···O, but come close to O(2) and O(4) respectively. The three angles of Co–N–O, Co–N–C and O–N–C around N(1) are in fair agreement with the corresponding angles of N(3), but are distinct from those of N(2), which, on the other hand, are close to those of N(4). These dimensions indicate that $Co(dmg)_2$ has a two-fold axis perpendicular to its plane and that the symmetry is approximately C_{2h}.

The Co–C distance coincides with those of the related methyl–Co(III) complexes.[10–14]

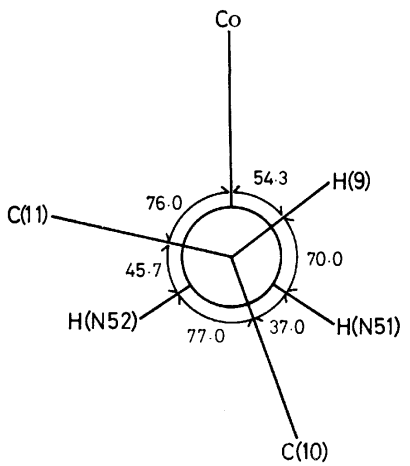

Fig. 6. Newman projection of mba along C(9)–N(5) with the angles (ϕ/°) between the projected bonds.

The values of Co–N(5) and Co–N(5)–C(9) (2.087 Å and 125.4°) are nearly equal to those in β-cne(dphyea)-cobaloxime (2.08 Å and 126°), but significantly greater than the corresponding distance and angle of 2.001 Å and 119.5° in bis(aniline)cobaloxime chloride.[15] This is probably because of the steric repulsion between Co-$(dmg)_2$ and the pheny ring of mba; the 'trans-influence' suggested by Brückner and Randaccio[16] would also be included. The conformation of mba is a staggered form as shown in Fig. 6. The N(5)–C(9) length of 1.463 Å is close to the usual C–N(amine) distance (1.472±0.005 Å),[17] and the C(9)–C(11) value of 1.541 Å is slightly longer than the usual C–C(aromatic) bond (1.505±0.005 Å).[17] The phenyl ring is planar within an error of 0.02 Å, and makes an angle of 10° with the $Co(dmg)_2$ plane. The deviation of C(9) from the phenyl ring plane is 0.04 Å, C(9)–C(11) making an angle of 2.2° with the plane.

Discussion

A fairly strong steric repulsion between $Co(dmg)_2$ and the axial ligand of the asymmetric amine was observed in the present complex. The $Co(dmg)_2$ moiety is deformed significantly, and its symmetry changes from D_{2h} to C_{2h} as a result of the repulsion. In order to explore the reaction mechanism, it is necessary to examine whether or not such a deformation can exist in the solution.

In conformation analysis to solve the problem, we made some simplifying assumptions which will not lead to any serious errors:

(1) The structure of $Co(dmg)_2$ has the D_{2h} symmetry and the dimensions suggested by Bigotto *et al.*;[12]

(2) the dimensions and the conformation of mba are the same as those in the crystal, because the conformation around N(5)–C(9) is a stable staggered form and the rotation around C(9)–C(11) is prevented by the $Co(dmg)_2$ plane when the amine enters into coordination;

(3) the bond of Co–N(5) is perpendicular to the $Co(dmg)_2$ plane and has the same length as that in the crystal;

(4) the formulae and the parameters for the van der Waals energy are those proposed by Giglio,[18] because his parameters were deduced from the crystal of dimethylglyoxime;

(5) the parameters of the methyl groups of $Co(dmg)_2$ are the same as those of the nitrogen atom, because the methyl groups probably rotate freely around the C–CH_3 bonds.[19]

On such simplifications, the van der Waals energy was calculated by changing the rotation angle, ϕ, around Co–N(5), as shown in Fig. 7. The minimum energy was obtained at the angle of −13°, which is in good agreement with the observed dihedral angle of N(4)–Co–N(5)–C(9), −17.6°, in the crystal. The N(4)···C(9) distance in the structure of the miniumm energy was 2.239 Å, which is shorter than that of the crystalline state. To avoid such short contact, N(5) should be driven toward N(2) and Co–N(4) should be lengthened, as observed in the crystal. It is reasonable to assume

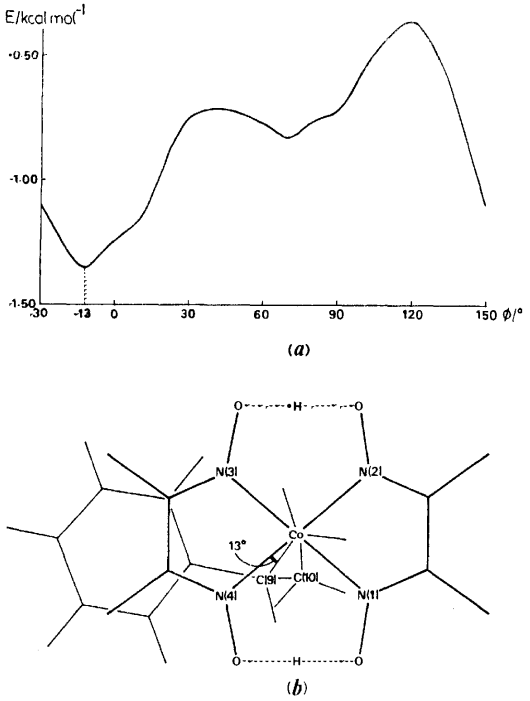

Fig. 7. (a) The variation of van der Waals energy, E, with the rotation angle, ϕ, around Co–N(5), $Co(dmg)_2$ being fixed. The axial ligand of mba is rotated clockwise from the position in which the dihedral angle of N(4)–Co–N(5)–C(9) is zero. (b) The conformation with the minimum energy.

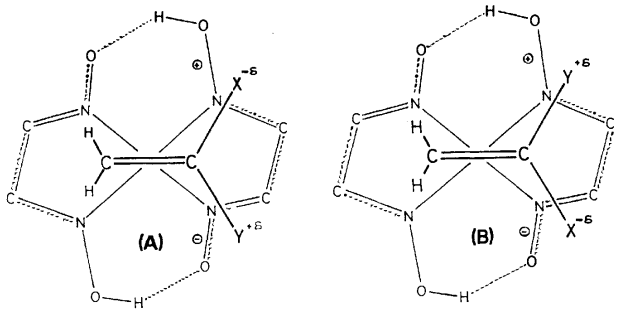

Fig. 8. Two possible ways in which the substrate approaches the active site of the catalyzer.

that such an elongation of Co–N(4) causes the change of the π-electron distribution and the geometry of dmg from D_{2h} to C_{2h}. The negative charge in dmg is localized on the shorter bonds.

The hydrogenation proceeds when the substrate has the nucleophilic and electrophilic substituents adjacent to the C=C double bond.[2] These observations suggest that the electrostatic force controls the way in which the substrate comes close to the active site of the catalyzer. As shown in Fig. 8, the mode of approaching, (A), is more favorable than (B) in view of the electrostatic interaction, so that one configuration of the asymmetric carbon in the intermediate σ-complex (termed (III) in Fig. 1) should be preferable to the other. We propose that this is a factor for inducing the asymmetry in the hydrogenation. Besides the factor proposed above, some others, for example, the van der Waals force, probably affect the overall optical yield in the step of π-bond formation and in the following steps illustrated in Fig. 1. We intend to examine those factors and correlate the optical yield to each factor in further studies of this series.

The authors are grateful to Dr. Yoshiaki Ohgo and Professor Juji Yoshimura for kindly supplying the specimens and for their valuable discussions.

References

1) Y. Ohashi, Y. Sasada, Y. Tashiro, Y. Ohgo, S. Takeuchi, and J. Yoshimura, *Bull. Chem. Soc. Jpn.*, **46**, 2589 (1973).
2) Y. Ohgo, S. Takeuchi, and J. Yoshimura, *Bull. Chem. Soc. Jpn.*, **44**, 283 (1971).
3) Y. Ohgo, S. Takeuchi, and J. Yoshimura, *Bull. Chem. Soc. Jpn.*, **44**, 583 (1971).
4) S. Takeuchi, Y. Ohgo, J. Yoshimura, *Chem. Lett.*, **1973**, 265.
5) Y. Ohgo, S. Takeuchi, Y. Natori, and J. Yoshimura, *Chem. Lett.*, **1974**, 33.
6) Y. Ohgo, Y. Natori, S. Takeuchi, and J. Yoshimura, *Chem. Lett.*, **1974**, 709.
7) Y. Ohgo, Y. Natori, S. Takeuchi, and J. Yoshimura, *Chem. Lett.*, **1974**, 1327.
8) "International Tables for X-Ray Crystallography," Vol. IV, The Kynoch Press, Birmingham (1974), p. 72.
9) UNICS Program System, ed by T. Sakurai, The Crystallographic Society of Japan (1967).
10) D. L. McFadden and A. T. McPhail, *J. Chem. Soc., Dalton Trans.*, **1974**, 363.
11) P. D. Ginderow, *Acta Crystallogr., Sect. B*, **31**, 1092 (1975).
12) A. Bigotto, E. Zangrando, and L. Randaccio, *J. Chem. Soc., Dalton Trans.*, **1976**, 96.
13) S. Brückner, M. Calligaris, G. Nardin, and L. Randaccio, *Inorg. Chim. Acta*, **2**, 416 (1968).
14) S. Brückner, M. Calligaris, G. Nardin, and L. Randaccio, *Inorg. Chim. Acta*, **3**, 278 (1969).
15) L. P. Battaglia, A. B. Corradi, C. G. Palmieri, M. Nardelli, and M. E. V. Tani, *Acta Crystallogr., Sect. B*, **30**, 1114 (1974).
16) S. Brückner and L. Randaccio, *J. Chem. Soc., Dalton Trans.*, **1974**, 1017.
17) L. E. Sutton, "Tables of Interatomic Distances and Configuration in Molecules and Ions. Supplement," Special Publication No. 18, The Chemical Society, London (1965).
18) E. Giglio, *Nature*, **222**, 339 (1969).
19) Giglio's parameters for the methyl group are overestimeted at the distance of short contact, probably because they are deduced from the crystal structure of the trans-dmg molecule.

Ultrasonic Study of Aqueous Solutions of Amines

Sadakatsu NISHIKAWA, Unpei OTANI, and Mitsuo MASHIMA

Department of Chemistry, Faculty of Science and Engineering, Saga University, Honjo-machi, Saga 840

(Received January 31, 1977)

Ultrasonic absorptions in aqueous solutions of allylamine have been measured in the frequency range from 8.5 to 220 MHz at 20 °C. Only a single relaxational absorption has been observed in the concentration range from 0.0562 to 4.00 M; this absorption has been attributed to the proton-transfer reaction. The rate constants and the standard volume change due to the reaction have been determined, and the results are compared with those for aqueous solutions of other amines previously published. It has been elucidated from the ultrasonic absorption data that the presence of the intermediate in the proton-transfer reaction is required in order to analyze the ultrasonic absorption mechanisms quantitatively. The hydrophobic effect in the aqueous solutions of amines has also been discussed.

Ultrasonic absorptions in aqueous solutions of amines are characterized by two kinds of relaxation processes. One is the phenonemon associated with the Peak Sound Absorption Concentration, which is observed in relatively concentrated solutions. Barfield and Schneider,[1] and Andreae *et al.*[2] have attributed the phenomenon to the solute-solvent interactions. However, on the basis of ultrasonic studies in aqueous solutions of several amines, the present authors[3,4] have concluded that the phenomenon is, rather, due to the aggregation reaction of amine molecules not ionized.

The other is the relaxation phenomenon due to the proton-transfer reaction. Maass *et al.*[5,6] have reported the kinetic data of the proton-transfer reaction for various amines; also there have been several discussions for the role of the perturbation of the proton-transfer equilibria of the basic residues of proteins in aqueous solutions.[7,8]

The present authors intend to investigate the correlations between these two kinds of phenomena in ultrasonic absorptions. In this paper the experimental results in an aqueous solution of allylamine will be reported, and the results will be compared with those for other amines.

Experimental

The ultrasonic absorption measurements were made at the odd harmonics of 0.5, 5, and 20 MHz x-cut quartz transducers by using the pulse technique. The frequency range was from 8.5 to 220 MHz. The sound velocity was measured by a sing-around method operated at 1.92 MHz. The major mechanical features of the apparatus have been shown elsewhere.[9] The values of pH were determined by means of Hitachi-Horiba F-5 pH-meter. A saturated solution of $Ca(OH)_2$ was used as the standard reference of the electrode of the pH-meter. All the measurement were made in a dry nitrogen gas atmosphere in order to prevent the contamination of air, for the aqueous solutions of amines are highly basic. The allylamine was distilled once from a commercial product of a G. R. grade. The purity was confirmed by the gas-chromatographic method to be more than 99.9%. NaOH and HCl (guaranteed reagent) were used to obtain the desirable hydroxide concentrations. The measurement cells were immersed in a water bath mantained at a constant temperature within ±0.002 °C. All the measurements were made at 20 °C.

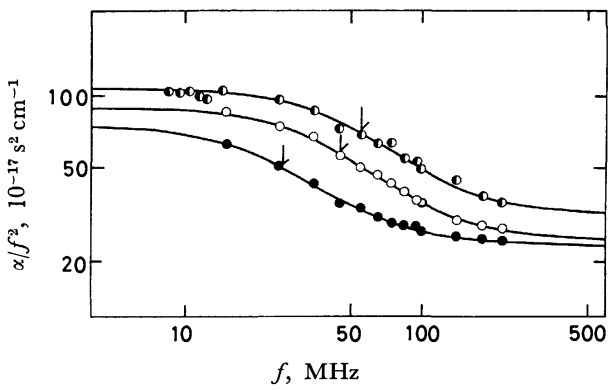

Fig. 1. Representative ultrasonic absorption spectra in aqueous solutions of allylamine at 20 °C. The arrow shows the relaxation frequency. ◐: 2.86 M, ○: 0.435 M, ●: 0.0562 M.

Results

The sound absorption caused by a single relaxation process can generally be expressed by

$$\alpha/f^2 = A/[1+(f/f_r)^2] + B, \quad (1)$$

where α is the sound absorption coefficient; f, the frequency; f_r, the relaxation frequency; and A and B, the constants. Figure 1 shows some representative ultrasonic absorption spectra in an aqueous solution of allylamine. The spectra in the concentration range up to 4.00 M are all characteristic of a single relaxation process; the ultrasonic parameters, A, B, and f_r, were determined so as to obtain the best fit of the experimental data to Eq. 1. The parameters are listed in Table 1, along with the values of the density, the pH, and the activity coefficient of the solutions used. The activity coefficients were calculated by means of Daviss' equation, $-\log\gamma = 0.5[(\sqrt{I}/(1+\sqrt{I})) - 0.3I]$, where I is the ionic strength. The relaxation frequencies and the excess absorptions increase continuously with the solute concentrations, and finally both of them reach their constant values. From these facts it is expected that only a single relaxation process is observed in the frequency range measured. The excess absorption is observed even in relatively dilute solution; thus, the perturbation of the following equilibrium will be considered as the excess absorption mechanism:

$$R\text{-}NH_3^+ + OH^- \underset{k_b}{\overset{k_f}{\rightleftharpoons}} R\text{-}NH_2 + H_2O, \quad (2)$$

where k_f and k_b are the forward and backward rate

Table 1. Ultrasonic parameters, density, and activity coefficients in aqueous solutions of allylamine

C_0 M	pH	ρ (g cm^{-3})	γ	A (10^{-17} s^2 cm^{-1})	B (10^{-17} s^2 cm^{-1})	f_r (MHz)	c (10^5 cm s^{-1})
0.0562	11.16	0.9966	0.966	52.3	23.3	26	1.497
0.107	11.43	0.9958	0.966	58.6	24.4	30	1.502
0.247	11.62	0.9950	0.944	63.3	24.4	40	1.507
0.311	11.68	0.9943	0.941	65.6	24.2	40	1.512
0.435	11.80	0.9930	0.933	65.6	24.2	45	1.520
0.508	11.84	0.9927	0.930	70.6	23.1	47	1.524
0.636	11.90	0.9913	0.926	66.2	23.0	55	1.532
0.749	11.95	0.9903	0.922	72.5	23.6	53	1.539
1.15	12.02	0.9873	0.912	75.9	24.9	55	1.561
1.76	12.23	0.9818	0.898	70.3	22.9	65	1.596
2.02	—	—	—	78.1	26.9	54.5	—
2.86	—	—	—	76.6	31.1	55	—
3.00	—	—	—	80.6	36.8	60	—
4.00	—	—	—	81.2	73.0	50	—

Throughout this paper 1 M=1 mol/dm^3.

constants respectively. The concentration dependences of the relaxation frequency and the maximum excess absorption per wavelength, μ_{max}, for the above mechanism can be written as follows:

$$2\pi f_r = 2k_f\gamma^2[OH^-] + k_b, \quad (3)$$

and

$$\mu_{max} = Af_r c/2 = \pi\rho c^2(\Delta V)^2\Gamma_c/2RT, \quad (4)$$

where

$$\Gamma_c = (1/[OH^-] + 1/[R\text{-}NH_3^+] + 1/[R\text{-}NH_2])^{-1}, \quad (5)$$

and where γ is the activity coefficient; ρ, the density; c, the sound velocity; ΔV, the standard volume change associated with the reaction. The relaxation frequencies are plotted in Fig. 2 as functions of $\gamma^2[OH^-]$; the straight line drawn provides the rate constants from the slope and intercept, which are determined by using the least-mean square method. For determining the rate constants, the experimental values in the concentration range below 0.749 M were used because in the concentrated solutions the Daviss equation might not hold and another reaction, such as molecular aggregation with hydrogen-bonding, might affect the reaction of Eq. 2. The standard volume change is determined by Eqs. 4 and 5. The obtained values are listed in Table 2 along with the results of other amines. The equilibrium constants obtained by the $K=k_b/k_f$ relation are abnormally larger than the dissociation constants in the literature, as may be seen in Table 2. The dissociation constant, K_b, was calculated from the pH dependence on the analytical concentration by the equation, $K_b=\gamma^2[OH^-]/(C_o-[OH^-])$; we obtained the value of 3.75×10^{-5} M[10] for K_b which was in agreement with that in the literature (see Table 2).

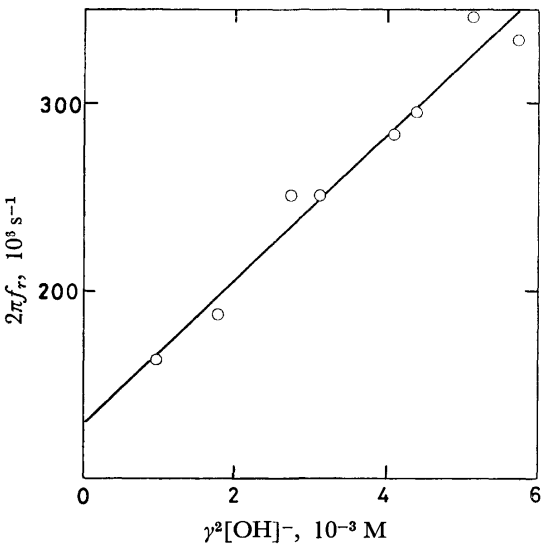

Fig. 2. The plots of $2\pi f_r$ *vs.* $\gamma^2[OH^-]$ in aqueous solutions of allylamine at 20 °C.

In order to ascertain the excess absorption mechanism associated with the reaction expressed by Eq. 2, the pH dependence of the absorption at a constant concentration of allylamine has been investigated by adding small amounts of NaOH or HCl. However, the relaxation frequencies obtained did not agree with those calculated by means of Eq. 3; also the pH dependence of μ_{max} was not in accordance with the theory. These facts indicate the presence of another equilibrium in the aqueous solutions of amines.

Discussion

The investigations of a number of proton-transfer reactions of compounds containing the $-NH_2$ group have been performed and the kinetics have been rationalized in terms of the following mechanism:[7,8,13]

$$R\text{-}NH_3^+ + OH^- \underset{k_{21}}{\overset{k_{12}}{\rightleftharpoons}} R\text{-}NH_3^+\cdots OH^- \underset{k_{32}}{\overset{k_{23}}{\rightleftharpoons}} R\text{-}NH_2 + H_2O. \quad (6)$$

If the second step is faster than the first one, we get the following relations for each process:

$$2\pi f_{r1} = k_{12}\gamma^2([R\text{-}NH_3^+] + [OH^-]) + k_{21}(1+K_{23}^{-1})^{-1}, \quad (7)$$

TABLE 2. RATE CONSTANTS AND STANDARD VOLUME CHANGE OF PROTON-TRANSFER REACTIONS IN AQUEOUS SOLUTIONS OF AMINES

Solute	k_f (10^{10} M s^{-1})	k_b (10^7 s^{-1})	$K(k_b/k_f)$ (10^{-3} M^{-1})	ΔV (cm^3 mol^{-1})	K_b[a] (10^{-4} M^{-1})	Ref.
Propylamine	2.5	3.7	1.5	21	3.73	5)
	3.0	1.2	0.4	24	3.73	4)
Allylamine	1.9	13	6.8	29	0.368	This work
Butylamine	4.1	12	2.9	32	4.44	16)
Pentylamine	3.0	7.5	2.5	25	4.94	4)
Octylamine	1.0	7.6	7.6	32	4.5	17)

a) The dissociation constants, K_b, are taken from Refs. 10 and 11.

TABLE 3. REEXAMINED RATE AND EQUILIBRIUM CONSTANTS OF PROTON-TRANSFER REACTIONS

Solute	k_{12} (10^{10} M s^{-1})	k_{21} (10^7 s^{-1})	K_{12} (10^3 M)	K_{23}
Propylamine	2.5	4.7	0.53	4.0
Allylamine	1.9	13	0.15	190
Butylamine	4.1	14	0.30	6.5
Pentylamine	3.0	8.8	0.33	5.1
Octylamine	1.0	8.1	0.12	17

$$2\pi f_{r2} = k_{23} + k_{32}, \tag{8}$$

where f_{r1} and f_{r2} are the relaxation frequencies associated with the first and second step respectively, and where $K_{23}=k_{23}/k_{32}$. Comparing Eq. 3 with Eq. 7, the rate constants obtained from the plots of $2\pi f_r$ *vs.* γ^2-[OH$^-$] may easily be written as follows:

$$k_f = k_{12}, \quad k_b = k_{21}(1+K_{23}^{-1})^{-1}. \tag{9}$$

The dissociation constant, K_b, which is determined by the static method, may be expressed by the following equation, considering the detailed equilibrium of Eq. 6:

$$K_b^{-1} = K_{12} + K_{12}K_{23}, \tag{10}$$

where $K_{12}=k_{12}/k_{21}$. The following relation is derived from Eqs. 9 and 10:

$$K_{23} = k_b K_b^{-1}/k_f. \tag{11}$$

The values of the rate constants, k_{12} and k_{21}, and the equilibrium constants, K_{12} and K_{23}, as calculated from Eqs. 9 and 11, are listed in Table 3. The absorption data in aqueous solutions of other amines reported previously[4,16,17] were reexamined by using the above treatment; these results are also listed in Table 3. The values of K_{23} are larger than unity, which reflects the fact that the intermediate of the hydrolysis of amines is not very stable.

Debye[14] has derived an expression for the diffusion-controlled rate of the reactions of ions in solutions and Eigen[15] has considered the reverse process of dissociation to form ions. The rate constant, k_{12}, of the first step in Eq. 6 is reasonable for the diffusion-controlled reaction, because the rate constant determined agrees very closely with the results obtained experimentally and theoretically for other compounds.[4,7] However, the rate constant of the reverse process is too low because its order should be 10^{10} s^{-1} according to Eigen's theory;[7] the similar discrepancies have also been found by Applegate *et al.*[7] for some aminoacids and polypeptides.

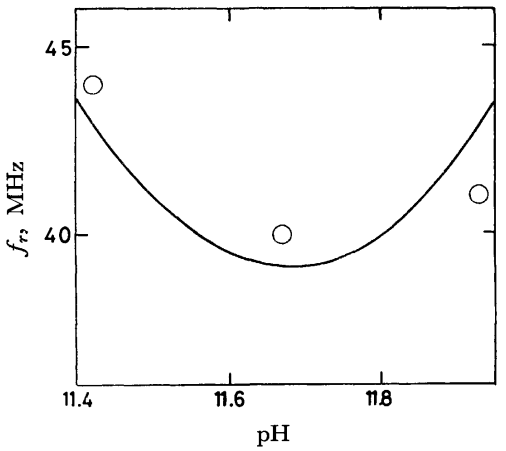

Fig. 3. The pH dependence of the relaxation frequency associated with the proton-transfer reaction. The solid curve is the theoretical value.

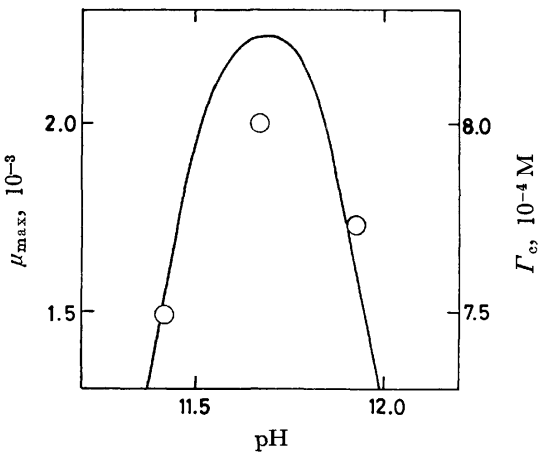

Fig. 4. The pH dependence of μ_{max} and Γ_c. The solid curve is the calculated value of Γ_c.

Though the pH dependences of f_r and μ_{max} are difficult to be interpreted only in terms of the process of Eq. 2, the introduction of the intermediate expressed by Eq. 6 allows us to analyze the dependences quantitatively. Figure 3 shows the pH dependences of the relaxation frequencies. The solid line represents the relaxation frequencies calculated by Eq. 7, where the analytical concentration has to be written as $C_0=[R\text{-}NH_3^+]+[R\text{-}NH_3^+\cdots OH^-]+[R\text{-}NH_2]$. The pH dependence of μ_{max} is also shown in Fig. 4, along with that of Γ_c

which is nearly dependent on μ_{max} (see Eqs. 4 and 5). Though the contribution from the fast process to the slow one for μ_{max} should be taken into account, the effects were very small. As may be seen in Fig. 4, the tendency of the pH dependence of μ_{max} is similar to that of Γ_c. These facts confirm that the excess absorption mechanism in the aqueous solution of allylamine is due to the perturbation of the equilibrium of Eq. 6.

In aqueous solutions of allylamine, only one kind of excess absorption is found in the frequency range investigated here; the character of the excess absorption is similar to that obtained for propylamine.[4] However, another excess absorption in aqueous solutions of butyl,[3] pentyl,[4] and octylamine[18] has been observed in addition to that due to the proton-transfer reaction. The cause of the latter excess absorption has quantitatively interpreted by the molecular aggregation theory,[4,18] and this excess absorption may be the main cause of the phenomenon associated with the Peak Sound Absorption Concentration. These results lead us to predict that the characteristic ultrasonic absorption due to the molecular aggregation reaction is associated with the hydrophobicity in amine molecules; that is, the aggregate may be formed by hydrophobic effects. With decrease in the hydrophobic effects, the excess absorption disappears in the frequency range measured except for the absorption due to the proton-transfer reaction.

The background absorption, B, in Eq. 1 increases with the analytical concentration. This means that the other excess absorption, *e. g.*, that due to the aggregation reaction with hydrogen-bondings, may exist in the higher-frequency range. However, this is beyond the scope of this paper.

In conclusion, the present ultrasonic study has revealed that the excess absorption mechanism in aqueous solutions of allylamine is attributable to the hydrolysis which proceeds through an intermediate, and the excess absorption associated with the Peak Sound Absorption Concentration has not been observed.

This work was partially supported by the Sakkokai Foundation.

References

1) R. N. Barfield and W. G. Schneider, *J. Chem. Phys.*, **31**, 488 (1959).
2) J. H. Andreae, P. D. Edmonds, and J. F. McKellar, *Acustica*, **15**, 74 (1965).
3) S. Nishikawa and T. Yasunaga, *Bull. Chem. Soc. Jpn.*, **45**, 1262 (1972).
4) S. Nishikawa, T. Yasunaga, and K. Takahashi, *Bull. Chem. Soc. Jpn.*, **46**, 2992 (1973).
5) G. Maass, Ph. D. Thesis, Univ. of Göttingen (1962).
6) M. Eigen, G. Maass, and G. Schwarz, *Z. Phys. Chem. (Frankfurt am Main)*, **74**, 319 (1971).
7) K. Applegate, L. J. Slutsky, and R. C. Parker, *J. Am. Chem. Soc.*, **90**, 6909 (1968).
8) R. D. White, L. J. Slutsky, and S. Pattion, *J. Phys. Chem.*, **75**, 161 (1971).
9) N. Tatsumoto, *J. Chem. Phys.*, **47**, 4561 (1967).
10) This dissociation constant was calculated in the concentration range below 0.749 M.
11) M. C. Cox, D. H. Everett, D. A. Lansman, and R. J. Munn, *J. Chem. Soc., B*, **1968**, 1373.
12) J. J. Christensen, R. M. Izatt, D. P. Wrathall, and L. D. Hansen, *J. Chem. Soc., B*, **1969**, 1212.
13) M. Eigen and L. DeMaeyer, "Technique of Organic Chemistry," Vol. VIII, Part 2, ed by A. Weissberger, Jr., Wiley, New York, N. Y. (1961).
14) P. Debye, *Trans. Electrochem.*, **82**, 256 (1942).
15) M. Eigen, *Z. Phys. Chem. (Frankfurt am Main)*, **1**, 176 (1954).
16) S. Nishikawa, T. Nakamoto, and T. Yasunaga, *Bull. Chem. Soc. Jpn.*, **46**, 324 (1973).
17) S. Nishikawa, T. Yasunaga, and N. Tatsumoto, *Bull. Chem. Soc. Jpn.*, **46**, 1657 (1973).
18) S. Nishikawa, *J. Colloid Interface Sci.*, **45**, 259 (1973).

The Effective π-Electron Hamiltonian for the Excited State. The Effect of Σ-Π Interaction*

Izumi MAKI, Kazuo KITAURA, and Kichisuke NISHIMOTO

Department of Chemistry, Faculty of Science, Osaka City University, Sumiyoshi-ku, Osaka 558

(Received February 2, 1977)

The effective π-electron Hamiltonian for the excited molecule has been derived from the singly excited configuration interaction method (SECI) considering Σ-Π interaction. In this paper, the zero-differential overlap (ZDO) approximation has been employed. Then, in SECI scheme, π-π^* and σ-σ^* configurations interact through the exchange type MO-integrals over π- and σ-MO's. As the result, only the excited singlet states are modified by Σ-Π interaction. So that the triplet states remain unchanged by this type of interaction.

When the ZDO approximation is employed, the effective electron interaction over AO's, $\tilde{\gamma}_{\mu\nu}$, can be derived. It is found that $\tilde{\gamma}_{\mu\nu}$'s are represented approximately in terms of topological matrix, so named 'bond index matrix'.

Semiempirical LCAO-SCF-MO method for the π-electron systems, namely P-P-P method,[1] has been succeeded for both the ground and excited states. However, there are still some problems left behind. For the calculations of the excitation energies, there is no good formula of the electron repulsion integrals for both the triplet and singlet states. It is generally known that Nishimoto-Mataga approximation[2] gives good results for the calculation of the excited singlet states but not good for the triplet states. On the other hand, Ohno-Klopman[3] and P-P[4] approximations calculate the satisfactory energy separation between the first singlet state and triplet state, but not good for the excited singlet states. These problems seem to be mainly caused by the difference in the Σ-Π interaction at the singlet and triplet states and also that in the electron correlation between each state. In this paper, we treat only the former problem. Concerning the Σ-Π interaction, there are some approaches based on MO techniques,[5] one approach is the MO-CI method considering all valence electrons, such as CNDO approximation.[6] However, CNDO method is suitable for the calculations of the ground state properties, but not appropriate for the excited state. In order to improve this point, Bene and Jaffe introduced a σ-π separation parameter and obtained good results of n-π^* and π-π^* excitation energies.[7] Recently, Lipari and Duke modified CNDO/2 by introducing empirical formula for the electron repulsion integrals and using different bonding parameters.[8]

In this paper, we analyze the Σ-Π interaction explicitly from the standpoint of the π-electron approximation. We also derive the effective π-electron interaction at the excited state considering its effect and derive the effective electron repulsion integrals, $\tilde{\gamma}_{\mu\nu}$.

Theoretical

The Effective π-Electron Hamiltonian for the Excited State. We are concerning with a closed system in the ground state and assume that the Hartree-Fock orbitals are already obtained. We use the following notation; i, j, k, l,···for the occupied molecular orbitals and α, β, γ, δ,···for the unoccupied ones.

Singly excited configuration interaction (SECI) method is our starting point.[9] The excited state is expressed as follows;

$$\Phi = \sum_{i\alpha} C_{i\alpha} |{}^{\alpha}_{i}>, \tag{1}$$

where, $|{}^{\alpha}_{i}>$ represents the singly excited configuration associated with the excitation of an electron from i to α $C_{i\alpha}$'s are coefficients to be determined by the variation method. The variation of the expectation value of the total Hamiltonian $\boldsymbol{H}$ leads to the following seqular equation,

$$[\boldsymbol{H} - \boldsymbol{E}\boldsymbol{I}]\boldsymbol{C} = 0, \tag{2}$$

where, $\boldsymbol{H}$ is Hamiltonian matrix represented by singly excited configurations. $\boldsymbol{C}$ is the coefficient vector. For the Simplicity, we use the ZDO approximation in this paper. Then configurations $|{}^{\pi}_{\pi}>$ and $|{}^{\sigma}_{\sigma}>$ do not interact with $|{}^{\sigma}_{\pi}>$ or $|{}^{\pi}_{\sigma}>$. So that the matrix can be divided into two mutually independent groups; one is made from $|{}^{\pi}_{\pi}>$ and $|{}^{\sigma}_{\sigma}>$ and another is made from $|{}^{\sigma}_{\pi}>$ and $|{}^{\pi}_{\sigma}>$. As we are interested in the π-π^* excited state, hereafter we treat only the former group. In order to get the effective π-electron Hamiltonian for the excited state, we divide the configurations into two subgroups. One is a subgroup containing $|{}^{\pi}_{\pi}>$ and another is one containing $|{}^{\sigma}_{\sigma}>$. Then Eq. 2 is written as follows;

$$[\boldsymbol{H}^{\Pi\Pi} - \boldsymbol{E}\boldsymbol{I}]\boldsymbol{C}^{\Pi} + \boldsymbol{H}^{\Pi\Sigma}\boldsymbol{C}^{\Sigma} = 0, \tag{3-a}$$

$$\boldsymbol{H}^{\Sigma\Pi}\boldsymbol{C}^{\Pi} + [\boldsymbol{H}^{\Sigma\Sigma} - \boldsymbol{E}\boldsymbol{I}]\boldsymbol{C}^{\Sigma} = 0, \tag{3-b}$$

where, $\boldsymbol{H}^{\Pi\Pi}$, $\boldsymbol{H}^{\Sigma\Sigma}$, and $\boldsymbol{H}^{\Sigma\Pi}$ mean the submatrices with elements $<{}^{\pi}_{\pi}|\boldsymbol{H}|{}^{\pi}_{\pi}>$, $<{}^{\sigma}_{\sigma}|\boldsymbol{H}|{}^{\sigma}_{\sigma}>$ and $<{}^{\sigma}_{\sigma}|\boldsymbol{H}|{}^{\pi}_{\pi}>$, respectively. $\boldsymbol{C}^{\Pi}$ and $\boldsymbol{C}^{\Sigma}$ are coefficient vectors corresponding to π-π^* and σ-σ^* subspaces, respectively. If the matrix $[\boldsymbol{H}^{\Sigma\Sigma} - \boldsymbol{E}\boldsymbol{I}]^{-1}$ has no singularities at π-π^* excitation energies, $\boldsymbol{C}^{\Sigma}$ can be given as follows from Eq. 3-b,

$$\boldsymbol{C}^{\Sigma} = -[\boldsymbol{H}^{\Sigma\Sigma} - \boldsymbol{E}\boldsymbol{I}]^{-1}\boldsymbol{H}^{\Sigma\Pi}\boldsymbol{C}^{\Pi}. \tag{4}$$

Substituting this equation into Eq. 3-a, we obtain the equation containing only $\boldsymbol{C}^{\Pi}$ explicitly.

$$[\boldsymbol{H}^{\Pi\Pi} - \boldsymbol{H}^{\Pi\Sigma}(\boldsymbol{H}^{\Sigma\Sigma} - \boldsymbol{E}\boldsymbol{I})^{-1}\boldsymbol{H}^{\Sigma\Pi} - \boldsymbol{E}\boldsymbol{I}]\boldsymbol{C}^{\Pi} = 0, \tag{5}$$

or;

$$|\boldsymbol{H}^{\Pi\Pi} - \boldsymbol{H}^{\Pi\Sigma}(\boldsymbol{H}^{\Sigma\Sigma} - \boldsymbol{E}\boldsymbol{I})^{-1}\boldsymbol{H}^{\Sigma\Pi} - \boldsymbol{E}\boldsymbol{I}| = 0. \tag{6}$$

* A preliminary report of this work was presented at the Oji International Seminar on Theories and *Ab Initio* Computations of Molecular Electronic Structure, Hokkaido, September 1976

When we write,

$$\tilde{\boldsymbol{H}}^{\Pi\Pi} = \boldsymbol{H}^{\Pi\Pi} - \boldsymbol{H}^{\Pi\Sigma}[\boldsymbol{H}^{\Sigma\Sigma} - \boldsymbol{EI}]^{-1}\boldsymbol{H}^{\Sigma\Pi}, \tag{7}$$

then, the eigenvalue problem to be solved becomes as follows;

$$|\tilde{\boldsymbol{H}}^{\Pi\Pi} - \boldsymbol{EI}| = 0. \tag{8}$$

Thus, $\tilde{\boldsymbol{H}}^{\Pi\Pi}$ represents the matrix associated with the effective π-electron Hamiltonian of the excited state, $\tilde{\boldsymbol{H}}(\pi)$. And $\tilde{\boldsymbol{H}}(\pi)$ can be expressed in the operator form, referring to the partitioning technique proposed by Löwdin,[10]

$$\tilde{\boldsymbol{H}}(\pi) = \boldsymbol{H} - \boldsymbol{VP}\frac{1}{\boldsymbol{H}-\boldsymbol{E}}\boldsymbol{PV}. \tag{9}$$

Where, $\tilde{\boldsymbol{H}}(\pi)$ is defined only in the subspace spanned by π-π^* configurations and V means the operator associated with the electron repulsions. As we use the Hartree-Fock basis, Σ-Π interaction appears through the electron repulsions. $\boldsymbol{P}$ in Eq. 9 represents the projection operator defined by Eq. 10, which picks up σ-σ^* configurations.

$$\boldsymbol{P} = \sum_{\sigma\sigma^*} |{}^{\sigma^*}_{\sigma}><{}^{\sigma^*}_{\sigma}|. \tag{10}$$

Thus the matrix elements associated with $\tilde{\boldsymbol{H}}(\pi)$ coincide with Eq. 7. Referring to Eq. 9, the effective π-electron interaction $\tilde{\boldsymbol{V}}(\pi)$ can be defined as follows;

$$\tilde{\boldsymbol{V}}(\pi) = \boldsymbol{V} - \boldsymbol{VP}\frac{1}{\boldsymbol{H}-\boldsymbol{E}}\boldsymbol{PV}. \tag{11-a}$$

$$\tilde{\boldsymbol{V}}(\pi) = \sum_{\xi\eta}\tilde{v}_{\xi\eta} \tag{11-b}$$

$$\boldsymbol{V}(\pi) = \sum_{\xi\eta} v_{\xi\eta}, \tag{11-c}$$

$v_{\xi\eta}$ means potential between ξ and η electrons and $\tilde{v}_{\xi\eta}$ is corresponding modified potential which is not given in the explicit form.

As σ-MO may be considered to be approximately localized in the particular bond, the off-diagonal matrix elements of $\boldsymbol{H}^{\Sigma\Sigma}$ in Eq. 5 may be negligibly small. So, the matrix element, $<{}^{\alpha}_{i}|\tilde{\boldsymbol{H}}|{}^{\beta}_{j}>$, becomes as follows;

For the singlet state,

$$\langle {}^{\alpha}_{i}|\tilde{\boldsymbol{H}}|{}^{\beta}_{j}\rangle = (\varepsilon_\alpha - \varepsilon_i)\delta_{ij}\delta_{\alpha\beta} - V_{i\alpha j\beta} + 2V_{ij\alpha\beta} - 4\sum_{k\gamma} V_{ik\alpha\gamma}V_{kj\gamma\beta}\, e_{k\gamma}, \tag{12-a}$$

$$e_{k\gamma} = [(\boldsymbol{H}^{\Sigma\Sigma} - \boldsymbol{EI})^{-1}]_{k\gamma,k\gamma}.$$

For the triplet state,

$$\langle {}^{\alpha}_{i}|\tilde{\boldsymbol{H}}|{}^{\beta}_{j}\rangle = (\varepsilon_\alpha - \varepsilon_i)\delta_{ij}\delta_{\alpha\beta} - V_{i\alpha j\beta}, \tag{12-b}$$

$$V_{i\alpha j\beta} = \iint i^*(1)\alpha^*(2)\; v_{12}\, j(1)\beta(2)\; d\tau_1 d\tau_2.$$

Where, i, j, α, and β are used for the π-MO's and k, l, γ, and δ are for the σ-MO's. Comparing Eqs.12-a and 12-b, it is seen that π-π^* configurations interact with σ-σ^* ones only in the excited singlet state, but not in the triplet state.[11] The matrix elements of the effective interaction of the excited singlet state can be divided into two parts,

Exchange type interaction

$$\tilde{V}_{ij\alpha\beta} = V_{ij\alpha\beta} - \frac{1}{2}\sum_{k\gamma} 4V_{ik\alpha\gamma}V_{kj\gamma\beta}\, e_{k\gamma}. \tag{13-a}$$

Coulomb type interaction

$$\tilde{V}_{i\alpha j\beta} = V_{i\alpha j\beta} \tag{13-b}$$

From Eqs. 13-a and 13-b, it is seen that only the exchange type interaction between π-electrons is modified by Σ-Π interaction. From the standpoint of the π-electron approximation, it means that π-electron excitation makes σ-field polarize and π-electrons in the excited state interact each other through the polarized σ-field, in addition to direct coulomb potential. Such kind of interaction appears only on exchange interaction between π-electrons. So that only the exchange type integrals over MO's are modified.

In the present study, $\boldsymbol{E}$ in the inverse matrix is treated as a parameter so that the calculated excitation energies agree with those of experiments.

Using the LCAO approximation as,

$$\psi = \sum_t d_{it}\phi_t,$$

the effective π-electron repulsion integral, $\tilde{\gamma}_{\mu\nu}$, can be written as,

$$\tilde{\gamma}_{\mu\nu} = \gamma_{\mu\nu} + \frac{1}{2}\sum_{rs}\gamma_{\mu r}\Pi_{rs}\gamma_{s\nu}, \tag{15}$$

where,

$$\Pi_{rs} = -4\sum_{k\gamma} d_{kr}d_{\gamma r}d_{ks}d_{\gamma s}e_{k\gamma}, \tag{16}$$

$\tilde{\gamma}_{\mu\nu}$ and $\gamma_{\mu\nu}$ are defined as follows,

$$\tilde{\gamma}_{\mu\nu} = \iint \phi^*_\mu(1)\phi^*_\nu(2)\; \tilde{v}_{12}\phi_\nu(1)\phi_\mu(2)\; d\tau_1 d\tau_2,$$

$$\gamma_{\mu\nu} = \iint \phi^*_\mu(1)\phi^*_\nu(2)\; v_{12}\phi_\nu(1)\phi_\mu(2)\; d\tau_1 d\tau_2,$$

where, μ and ν are used for the π-AO's and r and s for the σ-AO's. Π_{rs} represents the mutual polarizability associated with σ-electrons. Therefore, the second term of Eq.15 indicates the effect of the polarized σ-field on the π-electron-electron interaction. It is interesting to note that the formula of $\tilde{\gamma}_{\mu\nu}$ is similar to that of Little's which was derived by the RPA method.[12]

An Improvement of P-P-P Method Including σ-Electrons as the Field. Following the result mentioned above, P-P-P method can be improved from the standpoint of Σ-Π interaction, including the σ-electron as the field.

Employing the avaraged energy parameter $1/\tilde{e}$ instead of $e_{k\gamma}$ in Eq.16, $\tilde{\gamma}_{\mu\nu}$ of Eq. 15 can be written as follows;

$$\tilde{\gamma}_{\mu\nu} = \gamma_{\mu\nu} + \Delta_{\mu\nu}, \tag{17-a}$$

$$\Delta_{\mu\nu} = \frac{1}{2\tilde{e}}\sum_r\sum_s \gamma_{\mu r}Q_{rs}\gamma_{s\nu}, \tag{17-b}$$

$$Q_{rs} = -4\sum_{k\gamma} d_{kr}d_{\gamma r}d_{ks}d_{\gamma s}. \tag{17-c}$$

It is convenient to divide the correction term, $\Delta_{\mu\nu}$, into two terms,

$$\Delta_{\mu\nu} = \Delta^1_{\mu\nu} + \Delta^2_{\mu\nu}.$$

When r and s belong to the same atom A, the contribution is collected into the term $\Delta^1_{\mu\nu}$. On the other hand, if r and s belong to the different atoms, respectively, we collect the contribution into the term $\Delta^2_{\mu\nu}$. Using the bond order P_{rs} and the virtual bond order P^*_{rs} defined by

$$P_{rs} = 2\sum_{k}^{\text{occ.}} d_{kr}d_{ks}, \tag{18-a}$$

$$P^{*}_{rs} = 2\sum_{r}^{\text{unocc.}} d_{\gamma r}d_{\gamma s} = 2\delta_{rs} - P_{rs}. \tag{18-b}$$

$\Delta^{1}_{\mu\nu}$ and $\Delta^{2}_{\mu\nu}$ can be written as follows;

$$\Delta^{1}_{\mu\nu} = \frac{-1}{2\tilde{e}}\sum_{A}[\sum_{r}^{A}\gamma_{\mu r}(2P_{rr}-P^{2}_{rr})\gamma_{r\nu} - \sum_{\substack{r\\(r\neq s)}}^{A}\sum_{s}^{A}\gamma_{\mu r}P^{2}_{rs}\gamma_{s\nu}], \tag{19}$$

$$\Delta^{2}_{\mu\nu} = \frac{1}{2\tilde{e}}\sum_{B}\sum_{C}\sum_{r}^{B}\sum_{s}^{C}\gamma_{\mu r}P^{2}_{rs}\gamma_{s\nu}. \tag{20}$$

When CNDO scheme is adopted, the electron repulsion integrals, $\gamma_{\mu\nu}$'s depend only on the nature of atoms A, B, and C. Therefore, after the summation over r and s for each atom, Eqs. 19 and 20 become as follows:

$$\Delta^{1}_{\mu\nu} = \frac{-1}{2\tilde{e}}\sum_{A}\gamma_{\mu A}[\sum_{\substack{r,s\\(s\neq r)}}^{A}(2P_{rr}-P^{2}_{rr}-P^{2}_{rs})]\gamma_{A\nu}, \tag{21}$$

$$\Delta^{2}_{\mu\nu} = \frac{1}{2\tilde{e}}\sum_{B}\sum_{C}\gamma_{\mu B}(\sum_{r}^{B}\sum_{s}^{C}P^{2}_{rs})\gamma_{C\nu}. \tag{22}$$

The terms, $\sum(2P_{rr}-P^{2}_{rr}-P^{2}_{rs})$ in Eq. 21 and $\sum_{rs}(P^{2}_{rs})$ in Eq. 22 correspond to the bond index proposed by Wiberg.[13] These terms are easily understood by the concept of hybrid orbitals. The hibrid orbital, X^{A}_{h}, is constructed from the adequate unitary transformation of the basis AO's, ϕ_{p}'s, which are s, p_x, p_y, and p_z; $X^{A}_{h}=\sum_{p}d_{hp}\phi_{p}$. Where, X^{A}_{h} means a hybrid orbital of the atom A. The bonding orbital ϕ and antibonding orbital ϕ^{*} associated with nonpolar σ-bond between atoms A and B can be approximately written in terms of the hybrid orbitals X^{A}_{h} and $X^{B}_{h'}$;

$$\phi = \frac{1}{\sqrt{2}}(X^{A}_{h}+X^{B}_{h'}), \qquad \phi^{*} = \frac{1}{\sqrt{2}}(X^{A}_{h}-X^{B}_{h'}).$$

A lone pair orbital of the atom A can be approximately written as $\phi=X^{A}_{h}$. The values of Eqs. 21 and 22 are invariant to the unitary transformation, so that we can express approximately,

$$\sum_{rs}^{A}(2P_{rr}-P^{2}_{rr}-P^{2}_{rs}) = \sum_{h}^{A}(2P_{hh}-P^{2}_{hh}), \tag{23}$$

$$\sum_{r}^{B}\sum_{s}^{C}(P^{2}_{rs}) = \sum_{h}^{B}\sum_{h'}^{C}(P^{2}_{hh'}). \tag{24}$$

When X_h and $X_{h'}$, belong to the same atom, P_{hh} is equal to 1.0, except for the lone pair orbital. If X_h represents a lone pair orbital, P_{hh} becomes 2.0. If there exists a nonpolar σ-bond between B and C, $P_{hh'}$ becomes 1.0. Otherwise, $P_{hh'}$ is equal to zero. Therefore, the following simple relations are visualized.

$$\sum_{\substack{r,s\\(s\neq r)}}^{A}(2P_{rr}-P^{2}_{rr}-P^{2}_{rs}) = \boxed{\text{Number of valence electrons of the atom A}} - \boxed{\text{Number of lone pair electrons of the atom A}} - \boxed{\text{Number of } \pi\text{-electrons of the atom A}} = N_A\,[\text{Number of } \sigma\text{-bond of the atom A}] \tag{25}$$

$$\sum_{r}^{B}\sum_{s}^{C}(P^{2}_{rs}) = \begin{cases}1 & \begin{pmatrix}\text{If there exists } \sigma\text{-bond between atoms}\\ \text{B and C}\end{pmatrix}\\ 0 & \text{(Otherwise)}\end{cases}$$

$$B = \begin{pmatrix} -1 & 0 & 0 & 0 & 1 & 0\\ 0 & -1 & 0 & 0 & 1 & 0\\ 0 & 0 & -1 & 0 & 0 & 1\\ 0 & 0 & 0 & -1 & 0 & 1\\ 1 & 1 & 0 & 0 & -3 & 1\\ 0 & 0 & 1 & 1 & 1 & -3 \end{pmatrix}$$

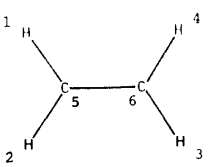

Fig. 1. The bond index matrix for ethylene and the numbering of the atoms.

Combining Eqs.21 and 22, the following relation is obtained.

$$\Delta_{\mu\nu} = \frac{1}{2\tilde{e}}[\sum_{A}(-N_A)\gamma_{\mu A}\gamma_{A\nu} + \sum_{B-C}^{\text{Bond}}\gamma_{\mu B}\gamma_{C\nu}], \tag{27}$$

where, the summation, $\sum_{B-C}^{\text{bond}}$, runs over all the σ-bonding atomic pairs.

Using Eq. 27, the effective electron repulsion integrals given by Eq. 15 can be rewritten by the matrix representation introducing a new matrix $\boldsymbol{B}$, as follows;

$$\tilde{\boldsymbol{\gamma}}^{\Pi} = \boldsymbol{\gamma}^{\Pi} + \boldsymbol{\Delta}^{\Pi}, \tag{28-a}$$

$$\boldsymbol{\Delta}^{\Pi} = \frac{1}{2\tilde{e}}\boldsymbol{\gamma}^{\Pi\Sigma}\boldsymbol{B}\boldsymbol{\gamma}^{\Sigma\Pi}, \tag{28-b}$$

$$\boldsymbol{\gamma}^{\Pi\Sigma} = (\boldsymbol{\gamma}^{\Sigma\Pi})^{+}. \tag{28-c}$$

$\tilde{\boldsymbol{\gamma}}^{\Pi}$, $\boldsymbol{\gamma}^{\Pi}$, and $\boldsymbol{\Delta}^{\Pi}$ are $N\times N$ square matrices and $\boldsymbol{\gamma}^{\Sigma\Pi}$, $N\times M$ rectangular matrix and $\boldsymbol{B}$, $M\times M$ square matrix. Here N and M are number of π-AO's and that of atoms, respectively. The value of the diagonal term of the matrix $\boldsymbol{B}$ is equal to $(-N_A)$. The value of the off-diagonal term is equal to $P_{hh'}$, namely 0 or 1. This matrix is named bond index matrix and is easily made from the structural formula of the molecule. As an example, $\boldsymbol{B}$ matrix of ethylene is shown in Fig. 1. This matrix reflects bonding relations of atoms in the molecule. So that the correction terms, $\Delta_{\mu\nu}$, depend on the topological nature of the molecule.

From these results we conclude that the most important effect of Σ-Π interaction on the π-electron-electron interactions depends on the topology and conformation of the molecule. Using Eqs. 28-a and 28-b, we can take into account the effect of σ-electrons explicitly in the π-electron approximation.

Calculational Procedure. π-π^{*} Excitation energies are calculated, considering Σ-Π interaction by the method mentioned above. According to the present theory, all valence electrons are taken into account, however, only the SCF-MO-CI calculation based on P-P-P scheme is needed, because σ-electrons are treated as it forms a field.

The calculational procedure is summarized as follows. First of all, we carry out the usual P-P-P calculation for the ground state. Secondly, we evaluate the effective $\tilde{\gamma}_{\mu\nu}$, using Eq. 28-a and an appropriate bare $\gamma_{\mu\nu}$. Lastly, we perform the SECI calculation, in which we use $\tilde{\gamma}_{\mu\nu}$ instead of $\gamma_{\mu\nu}$, only in the evaluation of the exchange type integrals over MO's in CI matrix elements.

In the present calculation, Ohno-Klopman formula[3] is applied for the standard (or bare) electron repulsion integrals,

$$\gamma_{\mu\nu} = \frac{14.40}{\sqrt{(R_{\mu\nu}^2 + a_{\mu\nu}^2)}} \text{(eV)},$$

where $R_{\mu\nu}$ is the interatomic distance between μth and νth atoms.

One center repulsion integrals, $\gamma_{\mu\mu}$, are evaluated by the approximation suggested by Pariser and Parr,[14]

$$\gamma_{\mu\mu} = I_\mu - A_\mu,$$

where A_μ and I_μ are the valence state electron affinity and the valence state ionization potential of the μth atom, respectively. These values are found in the work of Hinze and Jaffé.[15] Two center core integrals $\beta_{\mu\nu}$ are approximated by the formula given by Nishimoto and Forster,[16]

$$\beta_{\mu\nu} = A_0 + A_1 P_{\mu\nu}$$

where, $P_{\mu\nu}$'s are bond order which depend on each iteration. Standard values of parameters for A_0 and A_1 are summarized by Younkin *et al.*[17]

In order to estimate the correction term $\Delta_{\mu\nu}$ in Eq. 27, the electron repulsion integrals between π and σ AO's are required, which does not come out in the usual π-electron theory. For the calculation of these integrals we employ the same approximations as used for the π-electrons, namely, Pariser-Parr prescription for the one center electron repulsion integrals and Ohno-Klopman formula for the two center ones. Iwata[18] have pointed out that Pariser-Parr approximation for the one center electron repulsion integral includes Σ-Π interaction. Therefore, in this paper, we did not apply the present method to one center electron repulsion integrals.

We use 13.0 eV as the value of the averaged energy parameter $\bar{e}$ to reproduce the lower excitation energies of benzene. We consider whether the approximation $\bar{e}$ and the value of 13.0 eV are reasonable or not by the following manner: The mutual polarizability of σ-cores, Π_{rs}, is written by the atomic suffix as follows,

$$\Pi_{AB} = \sum_r^A \sum_s^B \Pi_{rs},$$

and Π_{AB} is related to the matrix element of the bond index matrix B_{AB} by

$$\Pi_{AB} = \frac{1}{2\bar{e}} B_{AB}.$$

In Tables 1 and 2, the calculated values of Π_{AB} and $(B_{AB}/2\bar{e})$ are listed, respectively. The atom-atom mutual polarizabilities associated with σ-electrons of ethylene are calculated by CNDO/2. From these Tables, it is found that the present approximation is reasonable and the parametrized value, 13.0 eV, is also admittable in spite of the drastic approximation was introduced. There are small discrepancies among the values in these Tables, which are caused by the approximation of averaging e_{kr} and neglecting the off-diagonal terms of the inverse matrix in Eq. 7.

Results and Discussion

In Tables 3—6, the calculated excitation energies of polyacenes are summarized. As seen from these Tables, the agreement between calculations and experiments is satisfactory.

Table 1. Atom-atom mutual polarizability (Π_{AB})[a] associated with σ-electrons calculated by CNDO/2; ethylene molecule

B \ A	1	2	3	4	5	6
1	−0.099	−0.006	0.016	0.012	0.092	−0.008
2		−0.099	0.012	0.016	0.092	−0.008
3			−0.099	−0.006	−0.008	0.092
4				−0.099	−0.008	0.092
5					−0.231	0.069
6						−0.231

a) Numbering of atoms is shown in Fig. 1.

Table 2. The values of the bond index matrix (B_{AB}) of ethylene divided by the energy parameter 13.0 eV

B \ A	1[a]	2	3	4	5	6
1	−0.077	0	0	0	0.077	0
2		−0.077	0	0	0.077	0
3			−0.077	0	0	0.077
4				−0.077	0	0.077
5					−0.231	0.077
6						−0.231

a) Numbering of atoms is shown in Fig. 1.

Table 3. Benzene. Excitation energies (eV) and oscillator strength (in parenthese)

	Nishimoto-Mataga[e]	Ohno[f]	This calc.	Exptl
$^3B_{1u}$	3.08	3.95	3.95	3.66[a]
$^3E_{1u}$	3.99	4.46	4.46	4.59[a]
$^1B_{2u}$	4.89 (0)	4.96 (0)	4.96 (0)	4.9[b] (0)
$^1B_{1u}$	6.18 (0)	4.96 (0)	6.05 (0)	6.07[c] (0.1)
$^1E_{1u}$	7.00 (2.36)	7.38 (2.44)	7.00 (2.40)	6.95[c]

a) Ref. 22. b) Ref. 19. c) Ref. 20. e) Nishimoto-Mataga formula was used for $\gamma_{\mu\nu}$. f) Ohno-Klopman formula was used for $\gamma_{\mu\nu}$.

Table 4. Naphthalene. Excitation energies (eV) and oscillator strength (in parenthese)

	Nishimoto-Mataga	Ohno	This calc.	Exptl
$^3B_{2u}$	2.04	2.36	2.36	2.64[a]
$^3B_{3u}$	3.03	3.38	3.38	3.82[a]
$^1B_{3u}$	4.03 (0)	4.03 (0)	4.03 (0)	3.97[b] (0.002)
$^1B_{2u}$	4.42 (0.20)	3.92 (0.08)	4.68 (0.23)	4.51[b] (0.18)
$^1B_{2u}$	5.46 (0)	5.26 (0)	5.67 (0)	
$^1B_{3u}$	5.58 (1.96)	6.10 (2.16)	5.80 (2.00)	5.63[b] (1.70)

a) Ref. 22. b) Ref. 21.

TABLE 5. ANTHRACENE. EXCITATION ENERGIES (eV) AND OSCILLATOR STRENGTH (in parenthese)

	Nishimoto-Mataga	Ohno	This calc.	Exptl
$^3B_{2u}$	0.99	1.75	1.75	1.82[a]
$^3B_{3u}$	1.98	2.69	2.69	3.22[a]
$^1B_{3u}$	3.39 (0)	3.51 (0)	3.51 (0)	
$^1B_{2u}$	3.41 (0.26)	3.33 (0.18)	3.79 (0.30)	3.34[b] (0.1)
$^1B_{3u}$	4.76 (2.60)	5.33 (2.96)	5.11 (2.72)	4.83[b] (2.5)
$^1B_{2u}$	5.69 (0.10)	5.77 (0.38)	6.13 (0.72)	5.61[b] (0.3)

a) Ref. 22. b) Ref. 21.

TABLE 6. NAPHTHACENE. EXCITATION ENERGIES (eV) AND OSCILLATOR STRENGTH (in paraenthese)

	Nishimoto-Mataga	Ohno	This calc.	Exptl
$^3B_{2u}$	0.86	1.43	1.43	1.28[a]
$^3B_{3u}$	2.00	2.60	2.60	2.57[a]
$^1B_{2u}$	2.89 (0.29)	3.04 (0.29)	3.25 (0.40)	2.63[a]
$^1B_{3u}$	3.28 (0)	3.49 (0)	3.49 (0)	
$^1B_{3u}$	4.41 (3.30)	4.97 (3.73)	4.81 (3.49)	4.51[a]
$^1B_{2u}$	4.82 (0.05)	4.75 (0.03)	5.14 (0.07)	

a) Ref. 22.

TABLE 7. CORRECTION TERMS ($\Delta_{\mu\nu}$)[a] OF NAPHTHALENE (eV)

μ \ ν	2	3	4	5	6	7	8	9	10
1	−0.89	−0.04	0.07	0.34	0.40	0.27	−0.33	−1.22	−0.26
2		−0.83	−0.04	0.40	0.47	0.44	0.27	−0.21	−0.02
9									−1.43

a) Numbering is shown in Fig. 2.

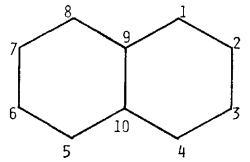

Fig. 2. The numbering of the atoms of naphthalene.

It is seen from Table 3, $^1B_{2u}$ excited state of benzene is unchanged by the Σ-Π interaction. The $^1B_{2u}$ excited state is much improved compared to that of Ohno's.

It is also found from Tables 4—6 that Σ-Π interaction has an effect of increasing the excitation energies of $^1B_{2u}$($^1B_{1u}$ in benzene) states which are polarized to the direction of molecular short axis. On the other hand, the excitation energies of $^1B_{3u}$($^1B_{2u}$ in benzene) states which are polarized to the direction of molecular long axis, remain unchanged or slightly decrease. These very interesting effect of Σ-Π interaction can be understood from the point of view of the polarization of the σ-framework caused by π-π^* excitation. It should be noted that the calculated excitation energies of the singlet state by the present method are similar to the Nishimoto-Mataga's.

In Table 7, the correction terms, $\Delta_{\mu\nu}$, of naphthalene are given. From this Table, it is found that the magnitude of $\Delta_{\mu\nu}$ depends considerably on the interatomic distance and also on the relative atomic sites in the molecule. Moreover, it can be generally said that the correction is larger at the inner part than at the outer part in the molecule.

We will apply the present theory to linear polyenes, aromatic derivatives, heterocycles and interaction of two aromatic systems connected by aliphatic chain in our next papers.

References

1) R. G. Parr, "The Quantum Theory of Molecular Electronic Structure," Benjamine, New York (1961).
2) K. Nishimoto and N. Mataga, *Z. Phys. Chem.* (*Frankfurt am Main*), **12**, 335 (1957).
3) K. Ohno, *Theor. Chim. Acta*, **2**, 219 (1964).
4) R. Pariser and R. G. Parr, *J. Chem. Phys.*, **21**, 466, 767 (1953).
5) P. G. Lykos and R. G. Parr, *J. Chem. Phys.*, **24**, 1166 (1956); R. A. Harris, *ibid.*, **47**, 3967 (1967); J. Koutecky, *ibid.*, **47**, 1501 (1967); P. A. Clark and J. L. Ragle, *ibid.*, **46**, 4235 (1967); K. F. Freed, *ibid.*, **60**, 1765 (1974); S. Iwata and K. F. Freed, *ibid.*, **64**, 500 (1974).
6) J. A. Pople and D. L. Beveridge, "Approximate Molecular Orbital Theory," McGraw-Hill, New York (1970).
7) J. D. Bene and H. H. Jaffe, *J. Chem. Phys.*, **48**, 1807 (1968).
8) P. O. Lipari and C. B. Duke, *J. Chem. Phys.*, **63**, 1748, 1758, 1768, (1975).
9) A low-lying excited state affected dominantly by doubly excited configurations cannot be treated within SECI approximation. The examples are the lower ^1A_g state of polyene and the $^1E_{2g}$ state of benzene molecule. See, for example, K. Schulten and M. Karplus, *Chem. Phys. Lett.*, **14**, 305 (1972).
10) P. O. Löwdin, in C. H. Wilcox, Ed., "Perturbation Theory and its Application in Quantum Mechanics," Wiley, New York (1966).
11) Since the MO integral V_{iakr} becomes zero by the ZDO approximation, we obtain Eqs. 12-a and 12-b.
12) H. Gutfreund and W. A. Little, *Phys. Rev.*, **183**, 68 (1969); H. Gutfreund and W. A. Little, *J. Chem. Phys.*, **50**, 4468, 4478 (1969).
13) K. B. Wiberg, *Tetrahedron*, **24**, 1083 (1968); C. Trindle,

J. Am. Chem. Soc., **91**, 220 (1969).
14) R. Pariser, *J. Chem. Phys.*, **21**, 568 (1953).
15) J. Hinze and H. H. Jaffe, *J. Am. Chem. Soc.*, **84**, 540 (1962).
16) L. S. Forster and K. Nishimoto, *J. Am. Chem. Soc.*, **87**, 1459 (1965).
17) J. M. Younkin, L. J. Smith, and R. G. Compton, *Theor. Chim. Acta*, **41**, 157 (1976).
18) S. Iwata, *Kagaku No Ryoiki*, **30**, 41 (1976).
19) F. Helverson and R. C. Hirt, *J. Chem. Phys.*, **19**, 711 (1951).
20) M. A. El-Sayed, *J. Chem. Phys.*, **36**, 552 (1962).
21) J. N. Murrel, "The theory of the Electronic Spectra of Organic Molecules," Methuen, London (1963).
22) J. B. Birks, Ed., "Organic Molecular Photophysics," John Wiley & Sons, Vol. 1, New York (1973).

Electrical Conductivity of Single Crystals of *N*-Methylphenazinium-TCNQ and Rb-TCNQ

Genshiro Fujii, Ichimin Shirotani, and Hiroshi Nagano

The Institute for Solid State Physics, The University of Tokyo, Roppongi, Minato-ku, Tokyo 106

(Received February 5, 1977)

Temperature and pressure dependence of the electrical conductivity of NMP(I)-, NMP(II)-, Rb(I)- and Rb(II)-TCNQ single crystals was studied. NMP(I)-TCNQ showing diffuse streaks was found to have a semiconductive behavior at atmospheric pressure and no conductive maximum appeared at low temperatures. Moreover the metallic behavior was not shown even at 100 kbar. The crystal structure of NMP(II)-TCNQ is not similar to that of NMP(I)-TCNQ. The difference of physical properties of two phases is discussed. The anomalous electrical behavior in the pressure range from 1 bar to 40 kbar was observed for Rb(I)-TCNQ. The resistivity of Rb(II)-TCNQ decreased monotonously with increasing pressure. The magnitude of their activation energies was 0.15 eV for Rb(I) salt and 0.11 eV for Rb(II) salt at 100 kbar. The insulator to metal transition could not be observed at least up to 100 kbar.

Physical properties of TCNQ (tetracyanoquinodimethane) salts which are quasi one-dimensional conductors have been a subject of considerable interest in recent years. NMP (*N*-Methylphenazininum)-TCNQ and Rb-TCNQ are polymorphic having two crystalline forms at room temperature. One is a triclinic phase (NMP(I)-TCNQ, Rb(II)-TCNQ) and the other is a monoclinic phase (NMP(II)-TCNQ, Rb(I)-TCNQ).

The crystal structure of NMP(I)-TCNQ consists of linear chains of $TCNQ^-$ anions and parallel chains of NMP^+ cations.[1,2] The crystals of this phase are one of the most highly conductive ion-radical salts. The electrical,[3-5] magnetic,[6] and optical[7,8] properties have been intensively studied. The conduction mechanism in NMP(I)-TCNQ crystal has been particularly discussed by many authors.

The monoclinic phase of NMP(II)-TCNQ shows semiconductive behavior; $\rho \approx 10^4\ \Omega$ cm at room temperature with an activation energy of 0.4 eV.[9] NMP^+ cations and $TCNQ^-$ anions alternate in columns parallel to the c axis.[10] The columnar structure of NMP(II)-TCNQ is remarkably different from that of NMP(I)-TCNQ.

Rb(I)-TCNQ has monoclinic symmetry and the $TCNQ^-$ anions are stacked face to face to form columns of diadic units of a $TCNQ^-$. Within a column, two different intermolecular spacings, 3.159 and 3.484 Å, appear alternately.[11]

The X-ray study of Rb(II)-TCNQ shows a triclinic structure consisting of linear chains of identical TCNQ molecules stacked face to face and equally separated from one another.[12] This columnar structure is very similar to that found in the crystal of NMP(I)-TCNQ. However, the electronic structure of Rb(II)-TCNQ is remarkably different from that of NMP(I)-TCNQ. The differences of the physical properties in both Rb-TCNQ have already been discussed in previous papers.[13-15]

In this paper, we present some findings on the temperature and pressure dependence of electrical conductivity in single crystals of NMP- and Rb-TCNQ and discuss the conduction mechanism for these salts.

Experimental

Preparation of Single Crystals. The acetonitrile solvent (Donin Yaku Kagaku, Spectro Grade) was refluxed over P_2O_5 and fractionally distilled. TCNQ (Tokyo Kasei Company) was recrystallized twice from pure acetonitrile and sublimed three times at 120 °C and 10^{-5} Torr. Only brilliant yellow orange TCNQ crystals from the center zone were collected for usage. NMP-TCNQ was prepared by treatment of *N*-methylphenazinium methyl sulfate in hot alcohol with a boiling solution of Li-TCNQ in ethanol.[16] Li-TCNQ was prepared by the reaction of TCNQ and anhydrous LiI provided by Hashimoto.[17] The phenazine provided by Anzai was purified by zone refining and sublimation.

Black needle single crystals of NMP(I)-TCNQ were grown from saturated acetonitrile solutions by fast recrystallization. The largest crystal obtained was $0.6 \times 0.08 \times 5$ mm^3. Single crystals prepared by us showed the diffuse streaks along the c* direction.[2] Crystals of NMP(II)-TCNQ were grown from dilute acetonitrile solutions by very slow recrystallization.

The preparation of Rb-TCNQ has been reported in detail previously.[13]

Electrical Measurements. DC four-probe resistance measurements were made on single crystals of NMP-TCNQ and Rb-TCNQ along the needle axis parallel to the TCNQ stacks. The gold wires (0.02 mm diameter) were used for electrical lead wires. Electrical contact with the crystals was made by wetting the electrical lead wires with a silver paste paint. Using this arrangement, the crystals could be thermally cycled without damage. The sample holder, in which the sample was already placed, was mounted in a vacuum can of a temperature-variable cryostat. The temperature, which was controlled by helium exchange gas and a heater, was determined by means of a copper-constantan thermocouple.

Measurements of electrical resistance as a function of pressure were made using a clamped-type high-pressure anvils-apparatus as previously described.[18]

Optical measurements have been made by the same manner as described previously.[13]

Results and Discussion

NMP(I)-TCNQ. Fritchie's average structure of NMP(I)-TCNQ shows that NMP^+ cation is located at the position (1/2, 1/2, 1/2) in unit cell, taking either of the two possible orientations of the methyl groups as equally probable[1]. On the basis of this structure, Bloch *et al.*[5] have tried to apply the theory of hopping in disordered systems to the conductivity of NMP(I)-TCNQ. The hopping theory for one dimensional disordered system predicts $\ln\sigma(T) = \ln\sigma_0 - (T_0/T)^{1/2}$. They have found that the temperature dependence of the conductivity could be approximately fitted by $\ln\sigma \approx$

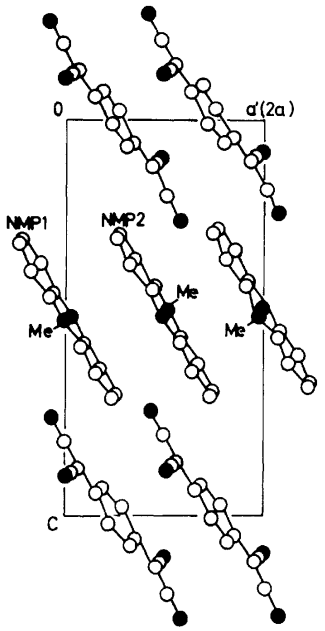

Fig. 1 (a). Crystal structure of NMP(I)–TCNQ showing diffuse streaks along b axis.[2]

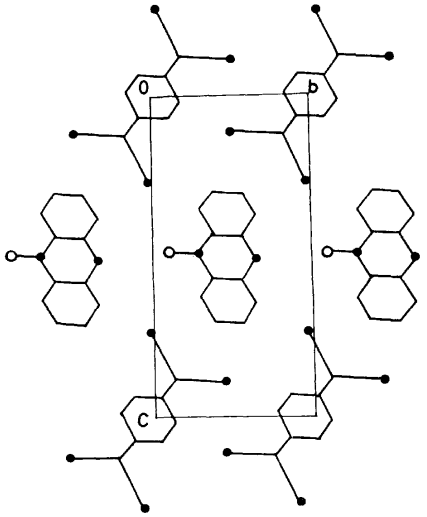

Fig. 1 (b). Crystal structure of NMP(I)–TCNQ showing diffuse streaks along a axis.[2]

$(T_0/T)^{1/2}$. On the other hand, Coleman *et al.*[4] have emphasized that the electronic and magnetic properties can be quantitatively described in terms of the one-dimensional Mott-Hubbard model. The temperature dependence of the conductivity of high purity single crystals has revealed that the plot of $\ln(\sigma/\sigma_0)$ *vs.* $1/T$ shows straight-line; this is not consistent with the analysis of Bloch *et al.*

Recently, Kobayashi[2] has studied an X-ray analysis of high purity single crystal of NMP(I)–TCNQ prepared by us. The X-ray diffraction patterns of this crystal show diffuse streaks along the c* direction. The analysis of the intensities of these streaks reveals that the orientation of NMP^+ cation is one-dimensionally disordered along the c axis as is shown in Fig. 1. The structure obtained indicates that the potential exerted on an electron moving in a column of TCNQ is not random, but can be expressed by a periodic function.

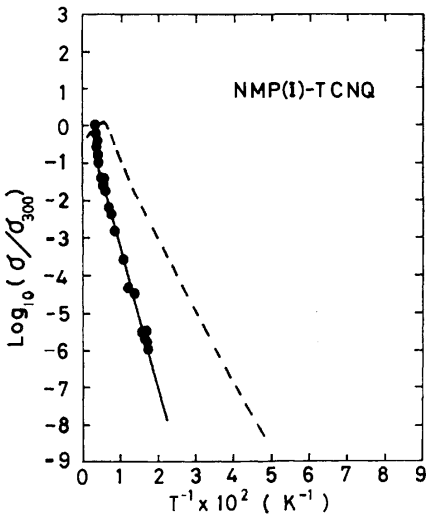

Fig. 2. Temperature dependence of the electrical conductivity for NMP(I)–TCNQ.
●: Present work, ----: Ref. 4.

Table 1. Physical properties of NMP- and Rb-TCNQ.

	NMP — TCNQ		Rb — TCNQ	
Polymorphic form	I	II	I	II
Crystal symmetry	triclinic[a]	monoclinic[b]	monoclinic[c]	triclinic[d]
Space group	$P\bar{1}$[a]	$P2_1/n$[b]	$P2_1/c$[c]	$P\bar{1}$[d]
Unit of TCNQ	monadic[a]		diadic[c]	monadic[d]
Interplanarspcing between TCNQ(Å)	3.26[a]		3.159[c] 3.484[c]	3.43[d]
Model of overlap between nearest molecule	[a]	[e]	[c]	[d]
Resistivity at 1 bar (Ω-cm)	7.7×10^{-3}[h] 2.63×10^{-3}[f]	1.3×10^{4}[g]	3×10^{5}[g]	1×10^{2}[g]
Activation energy at 1 bar (eV)	0.06[h] 0.037[f]	0.405[b]	0.44 ~ 0.53[g]	0.16 ~ 0.22[g]
Resistivity at 100 kbar (Ω-cm)	1.38×10^{-4}[h]	5.75×10^{2}[h]	7.5×10^{2}[h]	1.5×10^{-2}[h]
Activation energy at 100 kbar (eV)	0.02[h]	0.07[h]	0.15[h]	0.11[h]

a) Ref. 1. b) Ref. 9. c) Ref. 11. d) Ref. 12. e) Ref. 10. f) Ref. 4. g) Ref. 13. h) Present work.

The temperature and pressure dependence of the conductivity of single crystals of NMP(I)–TCNQ showing the diffuse streaks were studied. The conductivity data are presented in Fig. 2, where $\log(\sigma/\sigma_{300})$ is plotted as a function of T^{-1}. The room temperature conductivity was 130 Ω^{-1} cm^{-1}. The activation energy was 0.06 eV as shown in Table 1. No conductivity maximum appeared. This behavior is not consistent with the data reported by Coleman *et al.*[4]

Morosin[19] has pointed out that the single crystals supplied by Heeger did not show diffuse streaks. The conductivity of those crystals indicates a metallic state above 200 K with a continuous transition to an insulator below 200 K.[3,4] Morosin has conjectured that Kobayashi's observation on NMP(I)–TCNQ arose from the disordered regions formed between the twin boundaries of two different phases of NMP–TCNQ. If single crystals are grown from saturated acetonitrile solution by fast recrystallization, crystals of the triclinic phase (NMP(I)–TCNQ) are only found. Crystals prepared by us showed diffuse streaks. Therefore, Kobayashi's observation does not arise from the twin

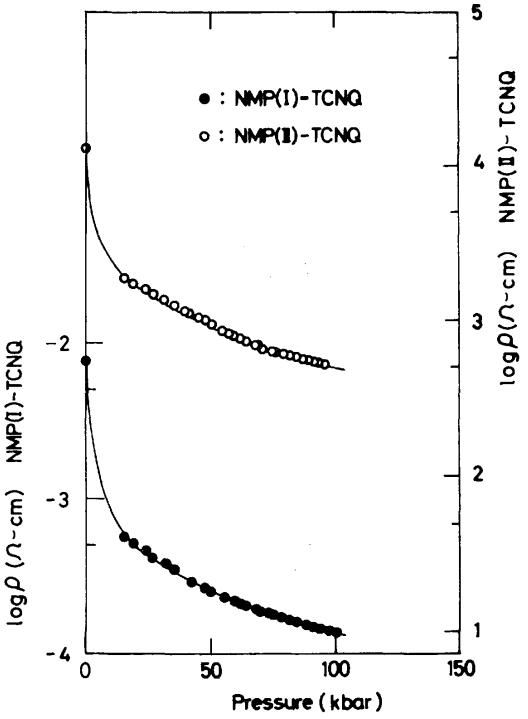

Fig. 3. Pressure dependence of the electrical resistivity for NMP-TCNQ.
●: NMP(I)-TCNQ, ○: NMP(II)-TCNQ.

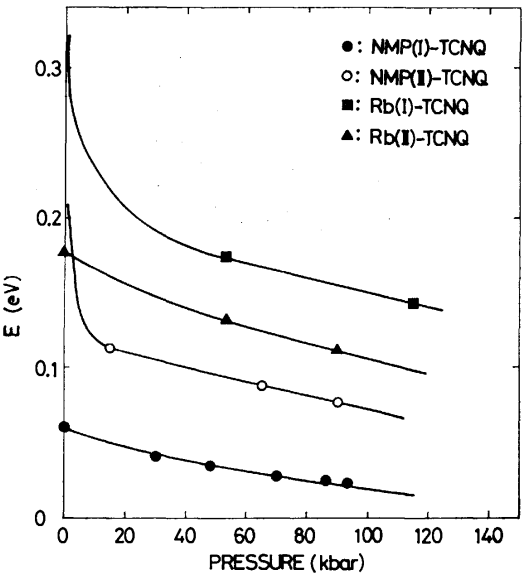

Fig. 4. Pressure dependence of activation energy for NMP- and Rb-TCNQ.
●: NMP(I)-TCNQ, ○: NMP(II)-TCNQ, ■: Rb(I)-TCNQ, ▲: Rb(II)-TCNQ.

boundaries of two phases, but is the intrinsic property of NMP(I)-TCNQ. There is an apparent difference in the columnar structure of NMP^+ between Heeger's crystals and ours. This inconsistency may be due to the difference of the method of sample preparation.

As is shown in Fig. 1, the positive potential exerting on an electron moving in a column of TCNQ can be expressed by the periodic function. Therefore, the corresponding energy band has not to be a half-filled band, but a filled band.[2] It seems to be reasonable that the

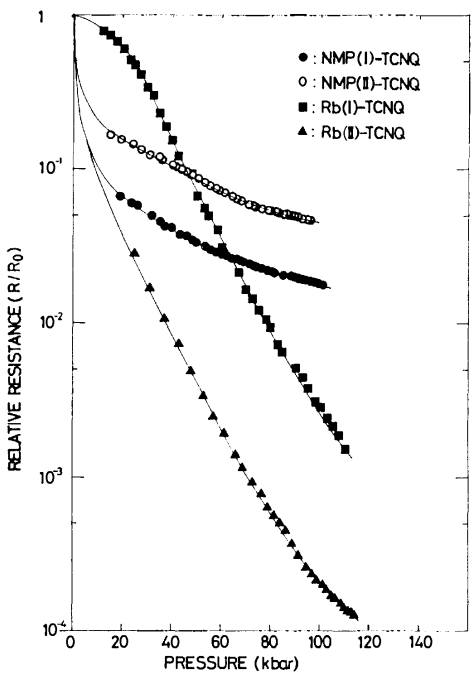

Fig. 5. Pressure dependence of relative resistance for NMP- and Rb-TCNQ.
●: NMP(I)-TCNQ, ○: NMP(II)-TCNQ, ■: Rb(I)-TCNQ, ▲: Rb(II)-TCNQ.

electrical behavior in NMP(I)-TCNQ showing diffuse streaks is semiconductive.

The pressure effect on electrical resistivity of this single crystals was measured along the conductive axis up to 100 kbar at room temperature. The result is shown in Fig. 3. The electrical resistivity decreased with increasing pressure. The resistivity at 100 kbar was 1.38×10^{-4} Ωcm. Figure 4 exhibits the pressure dependence of the activation energies of the TCNQ salts. The activation energy of NMP(I)-TCNQ rapidly decreased up to 20 kbar. It was 0.02 eV at 100 kbar. NMP(I)-TCNQ showing diffuse streaks did not show the metallic behavior even at 100 kbar.

NMP(II)-TCNQ. This compound crystallizes in space group $P2_1/n$ with $a=10.558$, $b=25.952$, $c=7.0872$ Å, $\alpha=90.68°$, and $z=4$.[10] The anion and cation alternate in the column parallel to the c axis with slightly unequal interplanar spacings. This structure does not resemble that of NMP(I)-TCNQ. Coleman *et al.*[9] have already studied the temperature dependence of the electrical conductivity for NMP(II)-TCNQ; this monoclinic phase is semiconductive with a room temperature conductivity of 7.67×10^{-5} Ω^{-1} cm^{-1} and an energy gap of 0.81 ± 0.02 eV.

Recently the absorption spectra of two crystalline forms have been studied by Tanaka *et al.*[8] Their absorption spectra are very different. The lowest energy transition in NMP(I)-TCNQ appears along the a axis at 5500 cm^{-1}. This band is assigned to an intermolecular transition between TCNQ molecules. On the other hand, the CT band in NMP(II)-TCNQ is observed at near 8000 cm^{-1}. This band corresponds to a charge transfer of an electron from the NMP molecule to TCNQ. The large difference between electrical and optical properties of such two-phase salts indicates

a crucial role of crystal structure of an organic salt. Mulliken[20] discussed the effect of pressure on electronic state of D^+A^- complexes and predicted a red shift and an increase of absorption intensity of a CT band and a decreased resistivity with increasing pressure. The majority of D^+A^- complexes show a decrease in resistivity with increasing pressure.[21,22] As shown in Figs. 3 and 4 the electrical resistivity and the activation energy in NMP(II)–TCNQ single crystals rapidly droped in the low pressure region and above 30 kbar decreased monotonously with increasing pressure. Figure 5 exhibits the ratio of the resistance, $\log R/R_0$, for both NMP–TCNQ. Above 30 kbar the rate of the pressure change of resistivity for the NMP(I) salt is approximately equal to that for the NMP(II) salt.

The values of their activation energies (ΔE_{I} and ΔE_{II}) decrease in the rate of

$$(\partial \Delta E_{\mathrm{I}}/\partial P)_T = -3.5\times10^{-4}\ \mathrm{eV/kbar}$$
$$(\partial \Delta E_{\mathrm{II}}/\partial P)_T = -4.4\times10^{-4}\ \mathrm{eV/kbar}.$$

These values are nearly equal, though the crystal structures of both NMP–TCNQ are significantly different. This may have arisen from the comparable compressibility between the two phases. Similar electrical behavior was found for both Rb–TCNQ salts, as discussed in the next section.

We suggest that the electrical behavior of these salts above 30 kbar may mainly be due to the increase of interchain interactions.

Rb(I)- and Rb(II)-TCNQ. Phase transitions and electrical and optical properties in both Rb salts have been already studied.[13] The relation between those properties and crystal structures have been discussed in the previous paper.[14] The electrical resistance of powdered Rb–TCNQ has been measured up to 500 kbar at room temperature.[15] The lowest resistivity for the Rb(I) salt is 1 Ωcm at 135 kbar, while that for the Rb(II) salt is 0.06 Ωcm at 170 kbar.

Figure 6 shows the effect of pressure on the resistance of single crystals of Rb(I)- and Rb(II)–TCNQ. The positive slope of the electrical resistance in the pressure range from 1 bar to 40 kbar was observed for the Rb(I) salt. Since the pressure induced phase transition in Rb(I)–TCNQ has been found at about 3.5 kbar,[13] this positive slope may be due to the appearance of a high pressure phase at quasi hydrostatic pressure. The activation energy was 0.15 eV at 100 kbar. A phase transition to a metallic state was not observed.

The resistivity of Rb(II)–TCNQ decreased monotonically with increasing pressure. The resistivity along the conductive axis was 1.5×10^{-2} Ωcm and the activation energy was 0.11 eV at 100 kbar. The compressibility of Rb(II)–TCNQ has not been measured, but it is probably comparable to that of aromatic crystals. From the relation between the pressure and the volume for molecular solid given by Samara and Drickamer,[23] the average intermolecular distance at 100 kbar was estimated to be about 90% of that at atmospheric pressure. Therefore, we can estimate the interplanar spacings between TCNQ molecules in the Rb(II) salt around at 100 kbar to be shorter than that in metallic TCNQ salts at 1 bar.[21] However, metallic behavior could not be observed in Rb(II)–TCNQ at 100 kbar

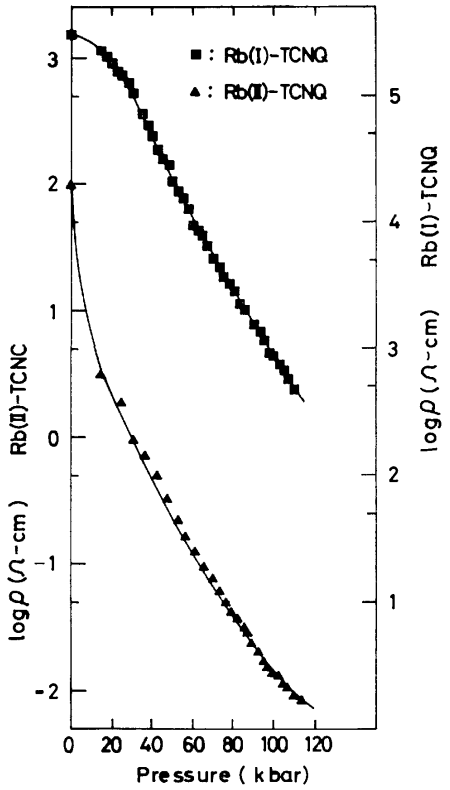

Fig. 6. Pressure dependence of electrical resistivity for Rb–TCNQ.
■: Rb(I)–TCNQ, ▲: Rb(II)–TCNQ.

The large difference in the conductivity of Rb(II)- and NMP(I)–TCNQ at atmospheric pressure has been mainly explained by two models. LeBlanc[25] suggested that the excitonic polarizability of the cation is the more important determinant of the variation in conductivities. On the other hand, Torrance *et al.*[7] proposed the new model in which the large conductivity of NMP(I)–TCNQ is attributed to incomplete charge transfer from the aromatic cation to TCNQ.

Figure 7 shows the effect of pressure on the absorption spectra of NMP(I)–TCNQ at room temperature. The absorption spectrum of NMP(I)–TCNQ is similar to that of complex salts such as Q- and Ad–$TCNQ_2$. The absorption bands have been assigned by Torrance *et al.*[7] and Tanaka *et al.*[8]

The pressure induced absorption band observed at around $20\times10^3\ \mathrm{cm^{-1}}$ for NMP(I)–TCNQ has also been found many complex salts.[26] Oohashi and Sakata[27] have suggested that the new band at high pressure may be assigned to the 8→9′ CT transition from $TCNQ^-$ to $TCNQ^0$. This shows that there may be neutral TCNQ molecules in NMP(I)–TCNQ. The incomplete charge transfer from NMP to TCNQ has been discussed by Butler *et al.*[28] and Kwak *et al.*[29] Ukei[30] has observed new weak X-ray diffuse streaks in addition to Kobayashi's observation. These diffuse lines can be interpreted in terms of a Kohn anomaly. From the observed superperiod the degree of charge transfer is estimated. The characteristic electrical and optical behavior in NMP(I)–TCNQ arises from the incomplete charge transfer from NMP to TCNQ.

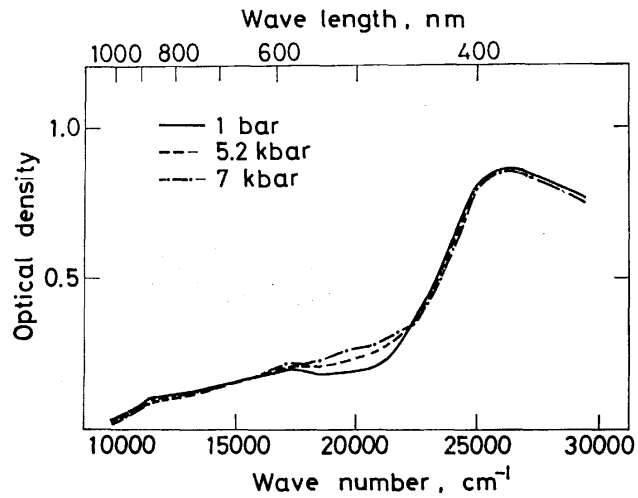

Fig. 7. Effect of pressure on the absorption spectra for NMP(I)-TCNQ.
——: 1 bar, ----: 5.2 kbar, ——: 7 kbar.

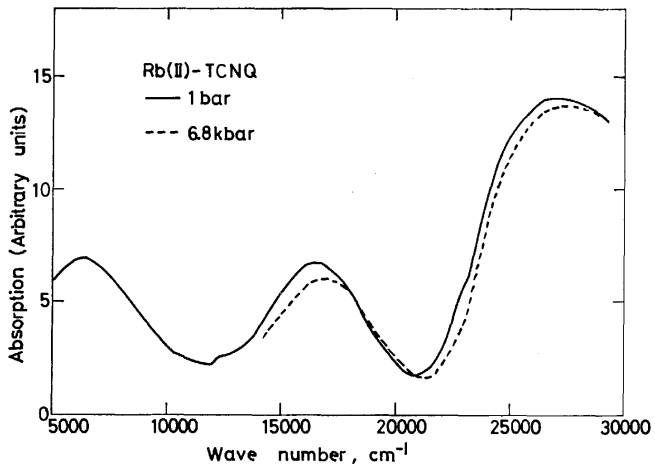

Fig. 8. Pressure effect on absorption spectra for Rb(II)-TCNQ.
——: 1 bar, ----: 6.8 kbar.

Figure 8 illustrates the pressure effect on absorption spectra of Rb(II)-TCNQ at room temperature. The absorption bands in the visible region are the locally excited (LE) bands within the $TCNQ^-$ anion. These exhibit the spectral blue shift with increasing pressure. The rate of pressure shift was $+67\ cm^{-1}$/kbar for $26.2 \times 10^3 cm^{-1}$ band and $+62\ cm^{-1}$/kbar for $16.1 \times 10^3\ cm^{-1}$ band. The near-infrared band at around $5.5 \times 10^3\ cm^{-1}$ is assigned to the charge transfer band between $TCNQ^-$ anions. The pressure effect on the CT band could not be observed because of interference by the pressure-transmitting fluid. The absorption spectrum of Rb(II)-TCNQ is markedly different from that of NMP(I)-TCNQ.

Rb(II)-TCNQ is fully charge transferred from Rb to TCNQ. Torrance *et al.*[8] have pointed out that in the case of complete charge transfer the lower Hubbard band was full; such a compound was a Mott insulator. Though NMP- and Rb-TCNQ are 1 : 1 simple salts, their electronic structures are essentially different. The conductivity along the conductive axis for the Rb(II) salt at 100 kbar is smaller than that of the NMP(I) salt at 1 bar, and the Rb(II) salt does not indicate the metallic behavior at 100 kbar though we can expect the interplanar distance between TCNQ molecules in the Rb(II) salt at 100 kbar to be shorter than 3.26 Å in NMP(I)-TCNQ at 1 bar. These results indicate that the electrical conductivity depends not only on the molecular distance between TCNQ molecule but also to a good extent on the electronic structure of TCNQ salts.

The authors wish to thank Dr. Y. Oda, Mr. H. Mukaida and Mr. K. Masuda in our institute for their kind help throughout this work. Their thanks are also due to Dr. S. Hashimoto, Kyoto University of Education and Dr. H. Anzai, Electrotechnical Laboratory for providing the materials.

References

1) C. J. Fritchie, Jr., *Acta Crystallogr.*, **20**, 982 (1966).
2) H. Kobayashi, *Bull. Chem. Soc. Jpn.*, **48**, 1373 (1975).
3) A. J. Epstein, S. Etemad, A. F. Garito, and A. J. Heeger, *Phys. Rev. B*, **5**, 952 (1972).
4) L. B. Coleman, J. A. Cohen, A. F. Garito and A. J. Heeger, *Phys. Rev. B*, **9**, 2122 (1973).
5) A. N. Bloch, R. B. Weisman, and C. M. Varma, *Phys. Rev. Lett.*, **28**, 753 (1972).
6) G. Theodorou and M. H. Cohen, *Phys. Rev. Lett.*, **37**, 1014 (1976).
7) J. B. Torrance, B. A. Scott, and F. B. Kaufman, *Solid State Commun.*, **17**, 1369 (1975).
8) J. Tanaka, M. Tanaka, T. Kawai, T. Takabe, and O. Maki, *Bull. Chem. Soc. Jpn.*, **49**, 2358 (1976).
9) L. B. Coleman, S. K. Kanna, A. F. Garito, and A. J. Heeger, *Phys. Lett. A*, **42**, 15 (1972).
10) B. Morosin, *Acta Crystallogr., Sect. B*, **32**, 1176 (1976).
11) A. Hoekstra, T. Spoelder, and A. Vos, *Acta Crystallogr., Sect. B*, **28**, 14 (1972).
12) I. Shirotani and H. Kobayashi, *Bull. Chem. Soc. Jpn.*, **46**, 2595 (1973).
13) N. Sakai, I. Shirotani, and S. Minomura, *Bull. Chem. Soc. Jpn.*, **45**, 3314, 3321 (1972).
14) I. Shirotani and N. Sakai, *J. Solid State Chem.*, **18**, 17 (1976).
15) I. Shirotani, A. Onodera, and N. Sakai, *Bull. Chem. Soc. Jpn.*, **48**, 167 (1975).
16) L. R. Melby, *Can. J. Chem.*, **43**, 1448 (1965)
17) S. Hashimoto and H. Kanzaki, *Phys. Lett. A*, **49**, 299 (1974)
18) G. Fujii, Y. Oda, and H. Nagano, *Jpn. J. Appl. Phys.*, **11**, 591 (1972).
19) B. Morosin, *Phys. Lett. A*, **53**, 455 (1975).
20) R. S. Mulliken, *J. Am. Chem. Soc.*, **74**, 811 (1952).
21) M. Schwarz, H. W. Davies, and B. J. Dobriansky, *J. Chem. Phys.*, **40**, 3257 (1964).
22) I. Shirotani, H. Inokuchi, and S. Minomura, *Bull. Chem. Soc. Jpn.*, **30**, 386 (1966).
23) G. A. Samara and H. G. Drickamer, *J. Chem. Phys.*, **37**, 474 (1962).
24) The interplanar spacings between TCNQ molecules in Q-$TCNQ_2$, Ad-$TCNQ_2$ and TTF-TCNQ are 3.22, 3.25, and 3.17 Å, respectively.
25) O. H. LeBlanc, *J. Chem. Phys.*, **42**, 4307 (1965).
26) N. Sakai, I. Shirotani, and S. Minomura, *Bull. Chem. Soc. Jpn.*, **43**, 57 (1970).
27) Y. Oohashi and T. Sakata, *Bull. Chem. Soc. Jpn.*, **48**, 1725 (1975).
28) M. A. Butler, F. Wudl, and Z. G. Soos, *Phys. Rev. B*, **12**, 4708 (1975).
29) J. F. Kwak, G. Beni, and P. M. Chaikin, *Phys. Rev. B*, **13**, 641 (1976).
30) K. Ukei, private communication.

Studies of the Interaction of Excited Chloranil with Acrylonitrile, Methyl Methacrylate, and Styrene by Means of Laser Photolysis

Harumichi KOBASHI, Hitoshi GYODA, and Toshifumi MORITA

Department of Chemistry, Faculty of Technology, Gunma University, Kiryu, Gunma 376

(Received February 5, 1977)

The behavior of electronically excited chloranil interacting with the titled vinyl compounds and solvents has been studied by means of the nanosecond laser photolysis technique. Semiquinone radicals and/or chloranil anions have been detected as transients except in the system containing styrene. Careful observation and analysis of the kinetic behavior of the transient absorptions reveal that these transients are brought about by the interaction of excited triplet state of chloranil with vinyl monomers and/or solvents. The logarithms of the quenching rate constants and rate constants of the formation of transients are linearly related to the ionization potentials of the vinyl monomers and solvents used. The mechanisms of the triplet quenching and transient formation can reasonably be interpreted by taking the relaxed triplet-state complex with a charge-transfer character into account as the precursor leading to the production of semiquinone radicals, chloranil anions, and other intermediate compounds.

Several investigations of the behavior of the chloranil (CA) molecule, as a representative quinone, have been performed with reference to electron donor–acceptor (EDA) complex formations,[1] photochemical reactions,[2] electronic states,[3] and electrical conductivities.[4] Among these, the photopolymerization mechanism in which the excited state of CA plays an important role is one of the most interesting. Mikawa and his co-workers[5,6] have reported, in their studies concerning the photosensitized polymerization mechanism of *N*-vinylcarbazole (VCZ) by CA, that electron transfer occurs from VCZ to excited CA, producing the CA anion (CA^-) and the VCZ cation, and that VCZ cations behave differently depending as the polarity of the solvents used; in a polar solvent such as acetone cyclodimerization occurs,[5,6] but in a nonpolar solvent such as benzene catonic polymerization occurs without any induction period.[6] In contrast to their studies, we have confirmed[7] that acrylonitrile (AN), methyl methacrylate (MMA), and styrene (ST) react with excited CA and that radical polymerization occurs after a well-defined induction period, during which addition compounds between CA and the vinyl monomers used are produced both in polar and in nonpolar solvents. The difference in the polymerization mechanisms between the two series of systems mentioned above seems to be originally attributable to a difference in the ionization potentials of the vinyl monomers. Mikawa and his co-workers used vinyl monomers with relatively small ionization potential values, while we used vinyl monomers with relatively large ionization potentials. It is well known that, because of their strong electron-accepting and hydrogen-abstracting properties, CA molecules in the excited states interact with various electron and/or hydrogen donors, even with some solvents as well, to produce semiquinone anions and/or radicals.[9–14] Furthermore, the presence of the excited triplet state EDA complex has been suggested by Tsubomura and his co-workers,[10] who used a microsecond flach-photolysis technique in a fluid solution of CA–benzene and CA–acetone systems.

Since the excited CA behaves, as has been mentioned above, in very different ways as systems studied vary, very careful experiments should be performed to determine the photosensitized polymerization mechanisms, with special attention paid to the interaction between the excited CA and the vinyl monomers in both the presence and absence of solvents.

In this work, as a part of our studies of the polymerization mechanisms photosensitized by CA, nanosecond ruby laser photolysis has been carried out, with special attention paid to the detection of transients, tracing their origins, and making sure of the kinetic behavior of the transients produced by the interactions between excited CA and AN, MMA, ST, and tetrachlorohydroquinone in the presence and absence of dichloroethane, trichlorotrifluoroethane, and acetonitrile as solvents. The interactions of excited CA with dichloroethane, trichlorotrifluoroethane, and acetonitrile have also been studied in order to obtain further knowledge.

Experimental

Apparatus and Measurements. The nanosecond laser photolysis apparatus used in the present study is shown schematically in Fig. 1. A giant pulse of 694 nm, with an output of *ca.* 2 J, was generated with a ruby laser (JEOL, JLS-R3A) Q-switched by a rotating prism and passed through an ADP frequency doubler to obtain a second harmonic for excitation. After the elimination of an undoubled fundamental pulse with a 10-mm cell containing a saturated cupric sulfate solution, the doubled laser pulse of a 23 ns half-duration, with a wavelength of 347 nm, was supplied into a sample in a 10-mm quartz cell mounted on a cell holder. The output energy of this laser pulse was measured with a thermopile (TRG, Model 107) combined with a recorder (Hitachi, Model 056) through a microvolt meter (Ohkura Electric Co., AM-1001). The power of the pulse through the sample cell was also measured with the same thermopile each time photolysis was done. In each measurement, the spectra of the transients were easily corrected to the same laser intensity by this way after confirmation of the absorption arising through the one-photon process. Since the laser intensity effect on the absorption intensities of transients should be checked beforehand, a small part of the exciting pulse, which was reflected with a beam splitter placed between the solution filter and the sample cell, was simultaneously monitored by means of a photomultiplier, PM-1 (HTV, 1P28) with a high response. Glass plates were employed to reduce the intensity of the exciting pulse. A xenon flash of *ca.* 600 μs half-width from a stroboscope (SUNPACK, Model 107) was used as an analysis flash for the detection of the transients; its peak

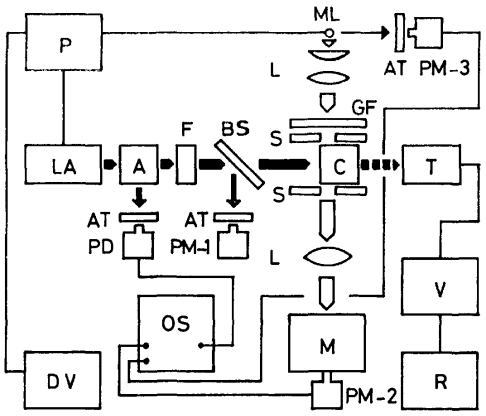

Fig. 1. Schematic diagram of the apparatus for nanosecond laser photolysis. LA: ruby laser, P: power supply and timing circuit, DV: degital voltmeter (Hitachi, Type 028-0010) by which supplied voltage to a pumping flash is externally read out. A: ADP frequency doubler, F: $CuSO_4$ aq filter, BS: beam splitter which is removed in ordinary experiments, C: sample cell, T: thermopile, V: μV meter, R: recorder, ML: monitor flash lamp, L: lens, GF: glass filter, S: variable slit, M: monochromater, PM-1, 2, and 3: photomultipliers, PD: photodiode, AT: light attenuator, OS: oscilloscope.

was synchronized electronically with the laser pulse. After crossing through the sample cell at right angles with respect to the laser beam, this analyzing light was collected by a lens and focussed onto the slit of a grating monochromator which was a part of a Hitachi UV-VIS spectrophotometer (model 139). An appropriate combination of glass filters at the front of the cell was used not only to remove the second-order stray light, but also to prevent the sample solution from being illuminated undesirably. The exit light from the monochromator was received by a photomultiplier tube, PM-2 (HTV, R446), loaded with a 75Ω resistor. The output signal from this tube was displayed on a 200 MHz oscilloscope (Iwatsu, SS-6200) which was triggered externally by the pulse from a photodiode (EG & G, SGD-100A) monitoring the laser pulse scattered from the ADP crystal. The rise and decay profile of a single sweep of the signal was photographed on X-ray films. Further, a third photomultiplier tube, PM-3 (HTV, 1P28), was used to correct the intensity fluctuation of the analysis lamp. The response of the photomultiplier which was exposed to the analyzing flash, attenuated by half-transparent papers, was guided into the second channel of the oscilloscope; thus, a reference signal to the signal corresponding to a 100% transmittance of the analyzing light was obtained. Operation using the chopped-sweep function of the oscilloscope made it possible to photograph this reference signal and the decay of the transient absorption simultaneously. Then decay patterns of the long-life transients could be analyzed accurately, even in a time region where the intensity of the analyzing flash was no longer 'steady.' In addition, air conditioning was needed to obtain a constant output of second harmonics, because the best matched axis of the ADP crystal to the fundamental laser beam was quite sensitive to room temperature. The variation in the temperature in an operating room was controlled in the range of ±1.0 °C during laser photolysis. Thus, the nanosecond time resolution was obtained by the use of this instrumental system and the transient spectra, and the rise and/or decay curves could be followed up quantitatively over the time range from the starting time of laser oscillation to *ca.* 200 μs.

When samples were photolyzed at the temperature of liquid nitrogen, the cell holder was replaced by a quartz vessel with three flat windows at right angles with each other. In the present study, all the experiments, except for the system of CA and MMA in EPA (ethylether : isopentane : ethanol=5 : 5 : 2 in volume), were carried out at room temperature.

The EDA complex formation in the ground state between CA and the vinyl compounds was examined by measurements of the absorption spectra using Hitachi 124 and 139 spectrophotometers. To describe the results briefly in this section, spectroscopic evidence for complexing in 1,2-dichloroethane was not observed in the CA–AN system. On the other hand, in the CA–MMA system a new broad band appeared around 315 nm as a shoulder of the falling branch of the intense π-π^* transition of uncomplexed CA, which has a maximum at 292 nm, and in the CA–ST system a band having its maximum at 420 nm was remarkably observed. Both of the latter bands can be reasonably interpreted as charge-transfer (CT) bands by the aid of the Benesi-Hildebrand equation, the Ketelaar equation, and the linear relation of CT-band energies against the ionization potentials of the donors.

Materials. The chloranil (Tokyo Kasei, G. R. grade) was purified by a recommended method,[15] *i.e.*, recrystallized twice from benzene and chromatographed on freshly baked calcium carbonate, using purified benzene as the eluant in order to eliminate any acidic impurities. After one more recrystallization, a vacuum sublimation was undertaken just before use. The acrylonitrile (Wako, G. R. grade) was washed with 5% NaOHaq, phosphoric acid, and distilled water, three times each. After drying over potassium carbonate, it was fractionally distilled twice in an atmosphere of nitrogen under reduced pressure. Methyl methacrylate (Wako, G. R. grade) was purified by the method described elsewhere.[16a] The styrene (Wako, Practical grade) was treated with 5% NaOHaq, washed with distilled water, dried over calcium chloride and barium oxide, and purified twice by fractional distillation in a nitrogen atmosphere under reduced pressure. These vinyl monomers were passed through a short column of molecular sieves *(Zeolite)* and silica gel immediately before use. The tetrachlorohydroquinone (CA-H_2) (Tokyo Kasei, C. P. grade) was purified as follows. The faint pink substance which was obtained by two recrystallizations from glacial acetic acid and successive washing with hot water was treated with an aqueous solution of sodium sulfite in order to reduce, chemically, a little amount of contaminated CA to the corresponding hydroquinone. The precipitates which were obtained by adding an adequate amount of hydrochloric acid to the aqueous solution were washed throughly with ethanolic water and dried. The raw product was sublimed under a vacuum. A pure white material was thus obtained; it was found by usual analytic methods, to be tetrachlorohydroquinone. The benzophenone, which was used as a standard to estimate the extinction coefficient of the triplet chloranil, CA(T), was purified by the method described elsewhere.[16b] The 1,2-dichloroethane (DCE), acetonitrile, trichlorotrifluoroethane, ethyl ether, and isopentane used as solvents were purified by ordinary methods,[17] while the ethanol (Kanto Chemical Co., G. R. grade) was used without further purification. The solutions subject to laser photolysis were deaerated carefully by the freeze-pump-thaw cycle method. The concentration of CA in the solution was controlled in the range of $(1—3)\times10^{-3}$ mol dm^{-3}.

Results and Discussion

Identification of Transients. CA–DCE System:

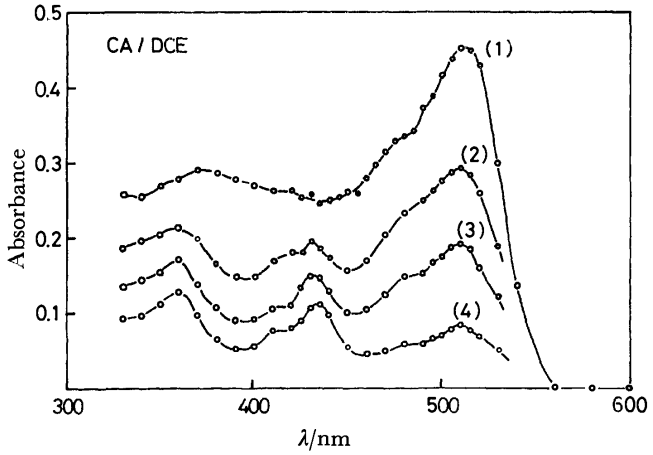

Fig. 2. Time resolved transient spectra for CA–DCE system: $[CA]=2\times10^{-3}$ mol dm^{-3}. The delay time from the laser pulsing, (1) 0, (2) 2, (3) 4, (4) 8 μs.

Figure 2 shows the time-resolved spectra after laser excitation for the system of CA alone in DCE. Observed bands with maxima at 510 and 370 nm in the spectrum immediately after pulsing closely resemble those of CA(T) in several solvents illustrated in Fig. 1 of Ref. 10 and discussed in Ref. 9. From an examination of the exponential decay of the 510 nm band, its lifetime was determined to be 5.6 μs in the deaerated solution and 0.45 μs in the aerated solution. These values are nearly equal to those for other solvent systems previously reported.[9a,9c] This is other evidence that this band belongs to CA(T). According to the investigation by the authors of Ref. 10, the 370 nm band is also attributable to CA(T). From the standpoint of these authors, we may also regard this band as belonging to CA(T), although, in our case, the band around 370 nm behaves, after a lapse of time, in the somewhat complicated manner to be described below. With the lapse of time, the spectrum is gradually replaced by another with band maxima at 430 and 360 nm. As regards these two bands, we obtained the following information: (a) Both of these bands had a relatively long life, and they decayed with similar time profiles. (b) Both the shape of the 430 nm band and the position of the 360 nm band closely resemble those studied in Ref. 10, which were attributed to semiquinone radicals. (c) Our experiments, performed by replacing the DCE by trichlorotrifluoroethane (with no hydrogen atom), revealed the non-existence of these bands. Using the microsecond-flash-photolysis technique, in which the irradiation of light over a broader range of wavelengths than in the case of nanosecond-laser photolysis is not avoided, Tsubomura and his co-workers[10] have reported the appearance of the bands attributable to the semiquinone radicals produced by the chlorine atom transfer to CA(T) from the Diflon S3 used as a solvent. This seems to indicate that the quite high excess vibrational energy in the lowest excited electronic state might be required for the abstraction of a 'heavy' chlorine atom in this system. An inspection of this information allows us to consider these two bands as belonging to semiquinone radicals of CA, CAH·, which have been produced by hydrogen-atom abstraction from the solvent.

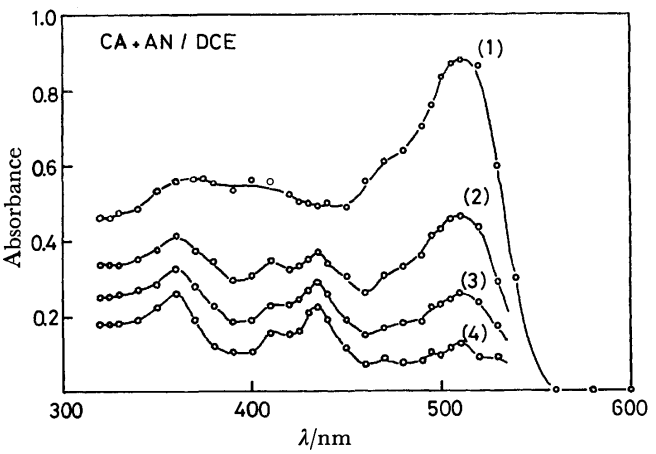

Fig. 3. Time resolved transient spectra for CA–AN–DCE system: $[CA]=2\times10^{-3}$ mol dm^{-3}, $[AN]=0.76$ mol dm^{-3}. The delay time from the laser pulsing, (1) 0, (2) 2, (3) 4, (4) 8 μs.

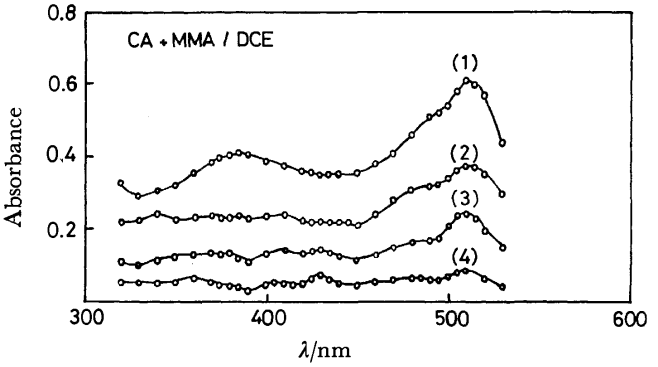

Fig. 4. Time resolved transient spectra for CA–MMA–DCE system: $[CA]=2\times10^{-3}$ mol dm^{-3}, $[MMA]=0.94$ mol dm^{-3}. The delay time from the laser pulsing, (1) 0, (2) 0.1, (3) 0.2, (4) 0.4 μs.

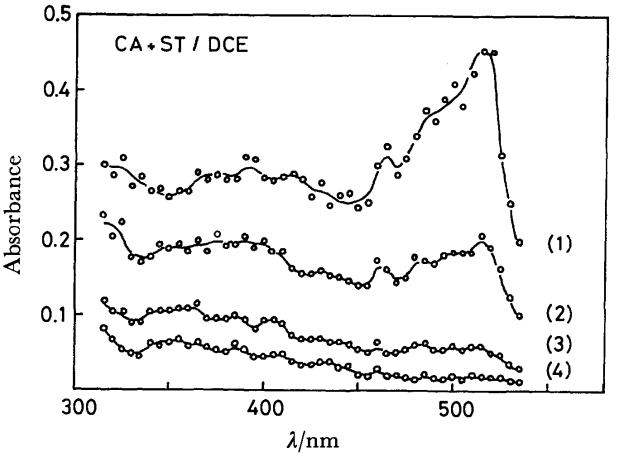

Fig. 5. Time resolved transient spectra for CA–ST–DCE system: $[CA]=1.7\times10^{-3}$ mol dm^{-3}, $[ST]=0.87\times10^{-3}$ mol dm^{-3}. The delay time from the laser pulsing, (1) 0, (2) 0.2, (3) 0.7, (4) 1.5 μs.

CA–Vinyl Monomer–DCE Systems: The transient absorption spectra changing with the lapse of time are exemplified for several systems in Fig. 3 (CA–AN–DCE), Fig. 4 (CA–MMA–DCE) and Fig. 5 (CA–ST–DCE).

The spectral features of the CA–AN–DCE system closely resemble those of the CA–DCE system (Figs. 2 and 3). In the CA–MMA–DCE system containing a high concentration of MMA the 510 nm absorption of CA(T) decays rapidly and scarcely no spectral components of CAH· remain (Fig. 4). In the CA–ST–DCE system containing a high concentration of ST ($\geq$0.1 mol dm^{-3}), no transient could be observed at all. However, in the same system containing a low concentration of ST, where ground-state EDA-complex formation is negligible, the initial spectrum rapidly disappears, keeping its spectral aspects without any bands attributable to semiquinone radicals being distinguishable (Fig. 5).

Kinetic Behavior of the 425 nm Band. The behavior of the absorption band monitored at 425 nm in the CA–DCE and CA–AN–DCE systems was followed from the time just after pulsing to *ca.* 10 μs (Fig. 7a). The decay of this absorption apparently obeyed the second-order kinetics after a rapid rise just after pulsing. The absorption intensity at the pulse end was recognized to be linearly related with the power of the laser for excitation. This means that this band arose through a one-photon process. It was observed that the 510 nm band also arose through a one-photon process. Since species bearing the 425 nm absorption in our systems are CA(T) and CAH·, it is important to check if CAH· comes from the singlet excited state of CA, CA(S) or from CA(T). This problem can be clarified by observing and analyzing the addition effect of ST, CAH_2, and MMA, as will be described below.

(a) As has previously been suggested for the CA–ST–DCE system, CA(T) is quenched rapidly, keeping its spectral features, and no observable transient like CAH· exists during the quanching process. This indicates that the initial appearance of the 425 nm band is due to CA(T). We will further discuss what would happen if CAH· is assumed to be produced in CA(S). The disappearance of CAH· might occur following self-disproportionation:[11a]

$$\text{CAH}\cdot + \text{CAH}\cdot \longrightarrow \text{CA} + \text{CAH}_2 \qquad k_d, \qquad (1)$$

and/or the conventional mechanism[19] described below, which is generally accepted for a radical polymerization with an induction period:

$$\text{CAH}\cdot\ (\text{or } \sim\text{CA}\cdot) + \text{ST} \longrightarrow \sim\text{ST}\cdot \qquad k_o, \qquad (2)$$

$$\sim\text{ST}\cdot + \text{CA} \longrightarrow \sim\text{CA}\cdot \qquad k_z, \qquad (3)$$

$$\sim\text{ST}\cdot + \text{ST} \longrightarrow \sim\text{ST}\cdot \qquad k_p. \qquad (4)$$

Here, k_d, k_o, k_z, and k_p are the rate constants of Reactions 1, 2, 3, and 4 respectively, and $k_d=1.4\times10^9$ mol^{-1} dm^3 s^{-1} (to be described in detail later), $k_p=123$ mol^{-1} dm^3 s^{-1},[18] $k_z/k_p=2040$ at 50 °C,[18] and $k_o<k_p$.[19] An inspection of the values of those rate constants and the relation between them indicates that the disappearance of CAH· would be efficiently subject to self-disproportionation, which, in turn, is very slow compared to the disappearance of CA(T) under our experimental conditions. On the assumption that CAH· would be produced from CA(S), therefore, the 425 nm band due to CAH· should remain during the spectral change in question. This contradicts the experiments and suggests that CAH· is not produced from CA(S).

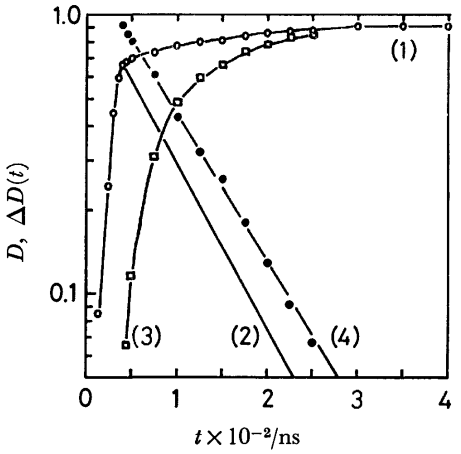

Fig. 6. Graphical analysis of the decay function of transient observed at 425 nm in CA–CAH_2–DCE system: [CA]$=2.36\times10^{-3}$ mol dm^{-3}, [CAH_2]$=2.58\times10^{-3}$ mol dm^{-3}. Curve (1): observed, (2) triplet decay, (3): CAH· rise, $D(t)=(1)-(2)$, (4): rate determining curve for CAH· formation, $\Delta D(t)=D_p-D(t)$; $D_p=0.92$.

(b) In order to clarify more distinctly the kinetic behavior of the absorption at 425 nm, we examined the addition effect of CAH_2 to the CA–DCE system. The decay profile followed up at 425 nm was analyzed kinetically for this system containing a small amount of CAH_2 (2.6×10^{-3} mol dm^{-3}), where no spectroscopic evidence exists as to a ground-state complex formation between CA and CAH_2. The analyzed results regarding the kinetic behavior of the 425 nm absorption can be reasonably explained by considering that the CA(T) which is generated at first will be quenched dynamically by CAH_2 and that the CAH· will increase through the CA(T) + CAH_2 → 2CAH· reaction. In fact, in our experiments, the increase in the 425 nm band was shown directly on the oscilloscope. Furthermore, this band was distinctly confirmed to belong to CAH· by an examination of its position and band shape as distinguished from all others in the spectrum. Figure 6 shows the results analyzed carefully. When the contribution of CA(T) to the absorbance at this wavelength, (2), is subtracted from the observed signal, (1), Curve (3) results; this curve refers to the growth of CAH· itself. Since the decay rate of the radical is much lower than that of the triplet (its decay time, $\tau_T=73$ ns in the present system), the disappearance of the former can reasonably be neglected during such a short time interval as in our experiments. Then, the subtraction of Curve (3), $D(t)$, from the peak value, D_p, of the observed curve gives Curve (4), $\Delta D(t)$, from which the time constant of CAH· formation can be obtained. By these procedures, it was quantitatively ascertained that the initial absorption at 425 nm was certainly due to CA(T) and that the rise time of CAH· ($\tau_r=83$ ns) was equal to the decay time of CA(T), within our limits of experimental accuracy. That is to say, CAH· is certainly produced *via* CA(T). Another support to this reasoning is also obtained from a comparison of the decay patterns of the 425 nm absorption between the CA–DCE and CA–CAH_2–DEC systems. Figure 7

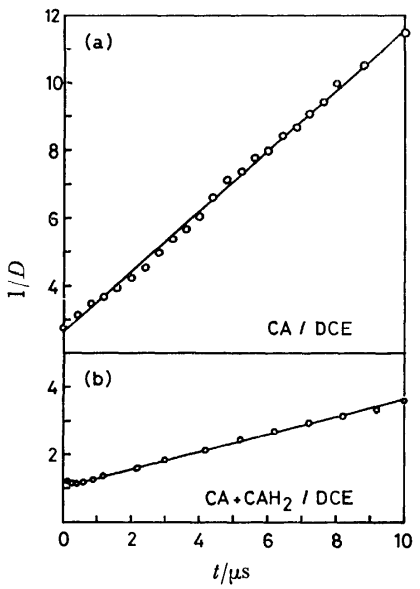

Fig. 7. Plots of second-order kinetics for the decay observed at 425 nm. a: CA–DCE, b: CA–CAH_2–DCE system.

shows the curves obtained by plotting the reciprocal of the optical density (D) against the lapse of time for these two systems. In the CA–CAH_2–DCE system (Fig. 7b), after the complete disappearance of CA(T) and the complete rising of CAH· at the initial stage of time lapse, the decay of the 425 nm band with reference to CAH· proceeds along a good straight line (Line *b*). In the CA–DCE system, there is apparently a straight line (Line *a*) following the second-order kinetics (Fig. 7a). If the transients were the same for both systems, their decay constants and, accordingly, the slopes of Line *a* and Line *b* would have to be identical. However there is a remarkable discrepancy between these two slopes, as may be seen in Fig. 7. Since Line *b* is the very realization of the kinetic behavior of CAH·, Line *a* does not embody the kinetic behavior of only CAH·. Moreover, a close inspection of Fig. 7a shows the string of circles to form a slightly S-shaped curve. We observed, further, a little more striking S-shaped curve for this system when the kinetic behavior was followed at 430 nm. This decay picture is characteristic when the absorption of a long-life transient, obeying the second-order decay kinetics, overlaps that of another transient decaying exponentially. Therefore, the observations can be understood by reasoning that, because of the superpostion of the CAH· rise and decay on the CA(T) decay, the absorption at 425 nm in the CA–DCE system apparently behaves as if the initially formed CAH· has decayed alone and smoothly with the second-order kinetics. As has been mentioned in the previous section, the 425 nm band in the CA–AN–DCE system also decayed apparently following the second-order kinetics from the time immediately after pulsing. This feature is the reflex of the same situation as that of Fig. 7a. These interpretations well correspond to those of Kemp and Porter[9b] as to the origin of the durosemiquinone radical produced by microsecond-flash photolysis in liquid paraffin.[20] Now, we can estimate the decay constant of CAH· accurately from Fig. 7b. From the slope of Line *b*, which strictly obeys the second-order kinetics, the decay constant was determined to be $2.8\times10^5\varepsilon l$ mol^{-1} dm^3 s^{-1}, where ε is the molar extinction coefficient of CAH· at 425 nm and where l is the width of the photolyzed part, which was estimated as 0.70 cm from the size of the second harmonics for excitation. The estimated value, 1.4×10^9 mol^{-1} dm^3 s^{-1}, was obtained using the reference value of ε, 7.3×10^3 mol^{-1} dm^3 cm^{-1}.[11a]

(c) In the system containing a high concentration of MMA, the absorption at 425 nm due to CA(T) early disappears exponentially, and after this rapid decay the remaining transient, CAH·, gradually decays with a long life. Although no exact analysis on the growth of CAH· was done in the DCE solvent, the above behavior and the results of kinetic analysis for CA^- and CAH· in the CA–MMA–CH_3CN system described in the next section may allows us to consider that the formation of CAH· arises from CA(T). It is noteworthy that CAH· is surely generated in this system, also through interaction between CA(T) and MMA.

Therefore, from the above discussions it can safely be concluded that the origin of CAH· in the CA–DCE system, regardless of the presence or absence of the additives (ST, CAH_2, AN, and MMA), is the triplet state of CA.

Production of the Chloranil Anion in the Polar Solvent.

The time-resolved spectra obtained by the laser photolysis for the CA–CH_3CN system are shown in Fig. 8a. CA(T), with maxima at 510 and 370 nm, decays relatively fast, and the absorption bands of maxima at 450, 430, and 360 nm become conspicuous 5 μs after flashing. These aspects closely resemble those obtained by the microsecond-flash photolysis for the same system.[10] It has already been known that CA^- has absorption bands at 448, 422, and 321 nm.[23] From this knowledge and from a comparison with the results for the CA–DCE system (Fig. 2), it is possible to deduce that, among the bands observed, the 450 nm band is brought about mainly from CA^-, the 360 nm band mainly from CAH·, and the 430 nm band from both CA^- and CAH·. On adding ST to this solution, CA(T) decayed rapidly, keeping its original aspects and without producing any transients, in the same way as in the case of the DCE solution. On the other hand, however, as may be seen in Fig. 8b, the addition of 1.0 mol dm^{-3} MMA to the solution causes a rapid decrease in CA(T) and does not prevent CA^- and CAH· from being produced and living for a relatively long time. The kinetic behavior of the band with its maximum at 450 nm was analyzed carefully in the same manner as in the CA–CAH_2–DCE system. The results revealed that CA^- grow simultaneously with the decay of CA(T). The kinetic analysis at 420 nm also led to the same result. Therefore, which one of the two species, CA^- or CAH·, is the primary transient is not proven, but it is elucidated that both of them come from CA(T).

Some observations have now established that the weak EDA complex in a polar solvent is photolyzed to produce the anion of an electron acceptor due to ionic dissociation in the first excited singlet state.[21] However, for the CA–MMA complex in acetonitrile, no

TABLE 1. QUENCHING RATE CONSTANTS FOR TRIPLET CHLORANIL BY VINYL MONOMERS AND THEIR IONIZATION POTENTIALS (I)

Quencher	I/eV	Solvent	k_q/mol^{-1} dm^3 s^{-1}
AN	10.91	DCE	3.1×10^4
MMA	9.8	DCE	5.1×10^6
		CH_3CN	6.7×10^6
ST	8.47	DCE	2.5×10^9
		CH_3CN	8.0×10^9

indication of the direct production of the anion *via* the excited singlet state has been obtained. This may be interpreted as follows. As the CT band maximum of the CA–MMA complex is located at a higher energy than its locally excited band within the CA molecule, the lowest excited singlet state of the complex is probably similar in nature to that of uncomplexed CA. Accordingly, a rapid intersystem crossing in the complex may occur, as in CA, immediately after pumping to the singlet state, this crossing being then followed by ionic dissociation.

The Mechanism of Triplet Quenching and Semiquinone Formation. As is illustrated in Figs. 3, 4, and 5, CA(T) is quenched by each of the vinyl monomers. The rate of decay at 510 nm obeyed a Stern-Volmer-type relation in the relatively low concentration range of quenchers: $1/\tau=1/\tau_0+k_q[Q]$, where τ and τ_0 are the decay times of CA(T) in the presence and absence of a quencher, Q, respectively, where [Q] is the concentration of Q, and where k_q is the quenching rate constant. The values of the rate constants are listed in Table 1. The values of k_q increase with a decrease in the ionization potentials of the quenchers, and an increase in the solvent polarity tends to enhance the quenching by vinyl monomers, especially by ST. This means that the CT interaction between CA(T) and ST is quite responsible for the quenching.

For the purpose of estimating the quantum yields of the transients, we estimated the molar extinction coefficient of CA(T) at 510 nm by comparison with that of the benzophenone triplet at 532.5 nm in benzene,[22] assuming the triplet yield of CA to be unity. The estimated value was $(7.2\pm1.3)\times10^3$ mol^{-1} dm^3 cm^{-1} in DCE, nearly equal to that of duroquinone triplet in cyclohexane or benzene.[22] Using this value and that of CAH·[11] or CA$^-$,[23] the yield, ϕ, of the CAH· or CA$^-$ formed from CA(T) can be approximately evaluated from the time-resolved spectra for the systems shown in Figs. 2, 3, 4, and 8 and for the system of CA in neat AN or MMA as well. In this estimation, the triplet yield of CA has already been assumed to be unity, and it was assumed that there was no effect of the solvent change upon the absorptivity of CA(T). Since the observed ϕ value corresponds approximately to $k_{ri}[M_i]\tau$, where k_{ri} is the second-order rate constant for the transient arising from the interactions between CA(T) and the reactant, M_i (the vinyl compound and/or solvent), where $[M_i]$ is the concentration of M_i, and where τ is the lifetime of CA(T) under the examining conditions, one can estimate k_r easily. These results

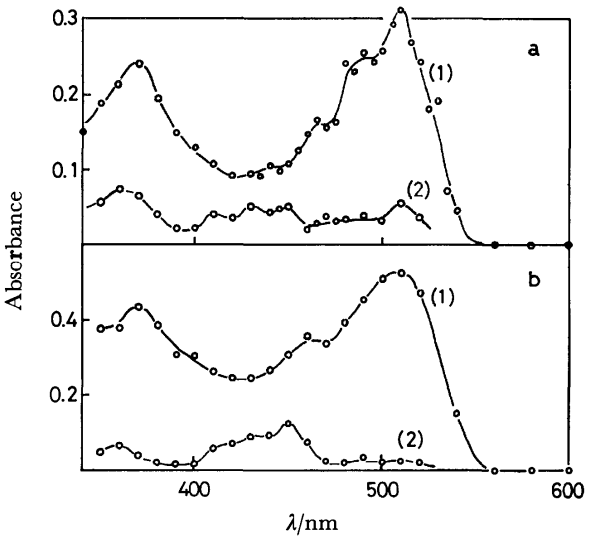

Fig. 8. Transient absorption spectra obtained by nanosecond laser photolysis for CA–CH_3CN and CA–MMA–CH_3CN systems. a: [CA]$=1.5\times10^{-3}$ mol dm^{-3}, b: [CA]$=3\times10^{-3}$ mol dm^{-3}, [MMA]$=1.0\times10^{-3}$ mol dm^{-3} in acetonitrile.

TABLE 2. YIELD OF CAH· AND CA$^-$ FOR SEVERAL SYSTEMS AND RATE CONSTANTS FOR THEIR FORMATION

Transient	System	ϕ	k_r/mol^{-1} dm^3 s^{-1}
CAH·[a]	CA-DCE	0.19	3×10^3
	CA-AN	0.20	7×10^3
	CA-MMA	0.08	4×10^5
CA$^-$ [b]	CA-CH_3CN	0.08	9×10^2
	CA-MMA-CH_3CN	0.15	9×10^5

a) The molar extinction coefficients at 435 and 420 nm in dioxane[11] were used for all our systems: $\varepsilon(435)=7.7\times10^3$ mol^{-1} dm^3 cm^{-1}, $\varepsilon(425)=7.3\times10^3$ mol^{-1} dm^3 cm^{-1}. b) $\varepsilon(450)=9.7\times10^3$ mol^{-1} dm^3 cm^{-1} [23] was used.

are summarized in Table 2, along with the corresponding ϕ values. The low yields of CAH· and CA$^-$ imply that other quanching processes are efficiently competing with their formation. One of the competing processes is the rather efficient production of an intermediate compound during the induction period of the ST or MMA polymerization photosensitized by CA.[7] That is to say, the quenching of CA(T) by vinyl monomers results mainly in the production of adducts between CA and monomers, and partly in the formation of CAH· and/or CA$^-$.

When the logarithms of the formation-rate constants (k_r) of CAH· are plotted against the ionization potentials of the reactants, a linear relationship is obtained. Plots of log k_q against the ionization potentials of the quenchers also show a linearity (Fig. 9). An inspection of these results reveals that the hydrogen transfer as well as the triplet quenching may be swayed by the CT interaction.[25] Accordingly, the existence of a triplet state complex as a precursor may be safely assumed, from which the electron transfer, the hydrogen transfer, the formation of intermediate componds for polymerization, and a return to the ground state may be thought to take place. In this connection, the next

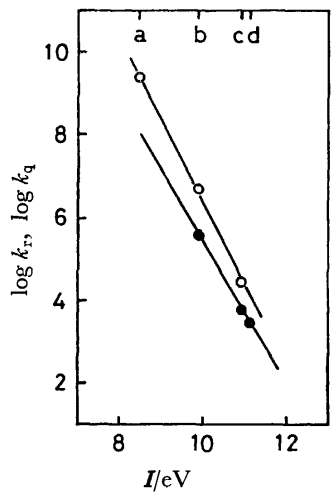

Fig. 9. Plots of log k_r and log k_q, respectively, against ionization potentials (I). The horizontal scale a, b, c, and d refer to I values of ST, MMA, AN, and DCE, respectively.
●: log k_r, ○: log k_q.

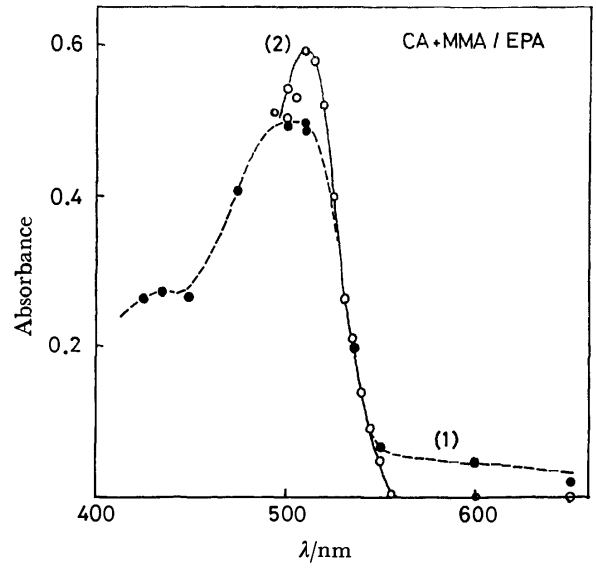

Fig. 10. Transient absorption spectra immediately after pulsing for CA–MMA–EPA and CA–MMA–DCE systems. (1): CA–MMA–EPA system at 77 K, [MMA]=0.48 mol dm^{-3}, (2): CA–MMA–DCE system at room temperature, [MMA]=0.94 mol dm^{-3}.

observation seems to supply additional support for the CT character of the triplet intermediate. The photolysis for the CA–MMA complex at 77 K in EPA, where the ground-state conformation of the complex may be almost frozen, gave a new, weak, transient absorption in the 550—650 nm region like that of the triplet EDA complex between CA(T) and benzene or between CA(T) and acetone,[10] although at room temperature such a broad band was not found, not even in a more concentrated MMA solution. These aspects are shown in Fig. 10. As the ionization potential of MMA is not very different from that of acetone, it may be possible to regard that absorption as the band arising from the CT interaction between CA(T) and MMA.

The observations and considerations described above allow us to explain the interaction mechanisms of the excited state of CA with the vinyl monomers used in the present work by assuming the following scheme:

$$CA(T) + M \rightarrow {}^3(CA^{\delta-}\cdots M^{\delta+}) \rightarrow CAH\cdot + M'\cdot$$

$$(TC) \quad \text{and/or}$$

$$\swarrow \quad \searrow \quad CA^- + M^+$$

$$CA(S_0) + M \qquad P$$

where M means the vinyl monomer; TC, the triplet complex, and P, the intermediate compound which relates to polymerization. The main features of this scheme resemble that proposed for the photoreduction of benzophenone by amines.[25,26] Whether the semiquinones appear or not may be determined by the relative efficiency of each process under the effect of surrounding solvent molecules upon the triplet-state complex. In so far as our present systems are concerned, both electron transfer and hydrogen abstraction by CA(T) should take place from a relaxed equilibrium state of the triplet intermediate after solvent reorientation is realized, because the triplet quenching is rather slow compared to the diffusion-controlled rate.

This conclusion is very interesting compared to the assumption[26] of the existence of a non-relaxed triplet-state encounter complex from which hydrogen-atom abstraction occurs, competing with the ionic dissociation, for the benzophenone-tertiary amine systems with relatively low ionization potentials.

The authors wish to thank Mr. Norihito Suzuki and Mr. Kazuo Maeda for their experimental assistance. One of the authors (H. K.) would like to acknowledge the award of a Grant-in-Aid for Scientific Research from the Ministry of Education.

References

1) a) G. Briegleb, "Electronen-Donator-Acceptor-Komplexe," Springer-Verlag, Berlin (1962); b) R. Foster, "Organic Charge-Transfer Complexes," Academic Press, London (1969); c) R. S. Mulliken and W. B. Person, "Molecular Complexes," Wiley-Interscience, New York (1969).

2) a) G. O. Schenck, *Z. Electrochem.*, **64**, 997 (1960); b) D. Bryce-Smith and A. Gilbert, *Tetrahedron Lett.*, **1964**, 3471; c) J. A. Barltrop and B. Hesp, *J. Chem. Soc. C*, **1967**, 1625; d) T. Nogami, K. Yoshihara, H. Hosoya, and S. Nagakura, *J. Phys. Chem.*, **73**, 2670 (1969); T. Nogami, K. Yoshihara, and S. Nagakura, *Bull. Chem. Soc. Jpn.*, **45**, 122 (1972); T. Yamaoka and S. Nagakura, *ibid.*, **44**, 2971 (1971); e) R. Foster, *J. Chem. Soc., Perkin Trans. 1*, **1974**, 1318.

3) a) G. Giacometti, P. L. Nordio, and G. Rigatti, *Nuovo Cimento*, **23**, 433 (1962); b) A. Bieber and J. J. Andre, *Chem. Phys.*, **5**, 166 (1974); c) M. Sebti, F. Dupuy, J. Mégel, and G. Nouchi, *C. R. Acad. Sci., Ser. B*, **272**, 123 (1971); d) H. P. Trommsdorff, P. Sahy, and J. Kahane-Paillous, *Spectrochim. Acta, Part A*, **26**, 1135 (1970); H. P. Trommsdorff, *J. Chem. Phys.*, **56**, 5358 (1972); e) E. A. Braude, *J. Chem. Soc.*, **1945**, 490.

4) D. D. Eley, H. Inokuchi, and M. R. Willis, *Discuss. Faraday Soc.*, **28**, 54 (1959).

5) Y. Shirota, K. Kawai, N. Yamamoto, K. Tada, T. Shida, H. Mikawa, and H. Tsubomura, *Bull. Chem. Soc. Jpn.*,

45, 2683 (1972).

6) K. Tada, Y. Shirota, S. Kusabayashi, and H. Mikawa, *Chem. Commun.*, **1971**, 1169; K. Tada, Y. Shirota, and H. Mikawa, *Macromolecules*, **6**, 9 (1973).

7) Detailed results should be published soon.

8) a) K. Watanabe, T. Nakayama, and J. Mottl, *J. Quant. Spectrosc. Radiat. Transfer*, **2**, 369 (1962) ; b) D. W. Turner, C. Baker, A. D. Baker, and C. R. Brundle, "Molecular Photoelectron Spectroscopy," John Wiley and Sons, London (1970). The ionization potential (I) of MMA was assumed to be almost equal to that of methacrylaldehyde[8b] (I=9.8 eV). The ionization potential of VCZ was estimated to be about 7.9 eV from the energy of its charge-transfer band with CA [T. Nasuume, M. Nishimura, H. Fujimatsu, M. Shimizu, Y. Shirota, H. Hirata, S. Kusabayashi, and H. Mikawa, *Polymer J.*, **1**, 181 (1970)] by using the linear relation between the charge-transfer-band energies and the ionization potentials of the donors.[2b]

9) a) D. R. Kemp and G. Porter, *Chem. Commun.*, **1969**, 1029; b) D. R. Kemp and G. Porter, *Proc. R. Soc. London, Ser. A*, **326**, 117 (1971); c) G. Porter and M. R. Topp, *ibid.*, **315**, 163 (1970).

10) K. Kawai, Y. Shirota, H. Tsubomura, and H. Mikawa, *Bull. Chem. Soc. Jpn.*, **45**, 77 (1972).

11) a) S. K. Wong, L. Fabes, W. J. Green, and J. K. S. Wan, *J. Chem. Soc., Faraday Trans. 1*, **68**, 2211 (1972); b) S. K. Wong, W. Sytnyk, and J. K. S. Wan, *Can, J. Chem.*, **50**, 3052 (1972).

12) B. J. Hales and J. Bolton, *Photochem. Photobiol.*, **12**, 239 (1970).

13) A.-I. Kryukov and V. A. Krasnova, *Theor. Eksp. Khim.* **8**, 478 (1972); *Chem., Abstr.*, **78**, 130553d (1973).

14) a) H. Yoshida, Y. Kambara, and B. Rånby, *Bull. Chem. Soc. Jpn.*, **47**, 2599 (1974); b) Y. Kambara and H. Yoshida, Preprint for 34th Annual Meeting of Chemical Society of Japan, I, 282 (1976).

15) T. Natsuume, M. Nishimura, M. Fujimatsu, M. Shimizu, Y. Shirota, H. Hirata, S. Kusabayashi, and H. Mikawa, *Polymer J.*, **1**, 181 (1970).

16) a) N. Mataga, H. Kobashi, and T. Okada, *J. Phys. Chem.*, **73**, 370 (1969); b) H. Kobashi, T. Morita, and N. Mataga, *Chem. Phys. Lett.*, **20**, 376 (1973).

17) J. A. Riddick and W. B. Bunger, "Organic Solvents," in "Techniques of Chemistry," Vol. II, 3rd ed, ed by A. Weisberger, Wiley-Interscience, New York (1970).

18) J. Ulbricht, "Polymer Handbook," 2nd ed, ed by J. Brandrup and E. H. Immergut, Wiley-Interscience, New York (1975), p. 53.

19) For example, P. J. Flory, "Principles of Polymer Chemistry," Cornell University Press, New York (1953).

20) N. K. Bridge and G. Porter, *Proc. R. Soc. London, Ser A*, **244**, 276 (1958).

21) a) H. Masuhara, M. Shimada, and N. Mataga, *Bull. Chem. Soc. Jpn.*, **43**, 3316 (1970); b) H. Masuhara, M. Shimada, N. Tsujino, and N. Mataga, *ibid.*, **44**, 3310 (1971).

22) E. J. Land, *Trans Faraday Soc.*, **65**, 2815 (1969); R. Bensasson and E. J. Land, *ibid.*, **67**, 1904 (1971). We used the value of 7630 $mol^{-1}\,dm^3\,cm^{-1}$ as the molar extinction coefficient, ε, of triplet benzophenone. In the latter article, the ε values of triplet duroquinone are given as 5330 and 6950 $mol^{-1}\,dm^3\,cm^{-1}$ in cyclohexane and benzene respectively.

23) J. J. Andre and G. Weil, *Mol. Phys.*, **15**, 97 (1968).

24) In Fig. 9, when the straight line for the CAH· formation is extrapolated to the ionization potential of ST, it leads to an estimated value of $k_r \leq 10^8$ $mol^{-1}\,dm^3\,s^{-1}$ for the CA–ST system. Therefore, even if CAH· should be generated, its detection might be impossible because of the low yield, too low to register on our apparatus.

25) S. G. Cohen, A. Parola, and H. Parson, Jr., *Chem. Rev.*, **73**, 141 (1973).

26) S. Arimitsu, H. Masuhara, N. Mataga, and H. Tsubomura, *J. Phys. Chem.*, **79**, 1255 (1975).

Time-Resolved Fluorescence Study of Exciplex and Triple Exciplex in 1,4-Dicyanobenzene and Alkylnaphthalenes

Tsutomu MIMURA and Michiya ITOH*,[1]

Faculty of Pharmaceutical Sciences, The University of Tokyo, Bunkyo-ku, Tokyo 113

**Faculty of Pharmaceutical Sciences, Kanazawa University, Takara-machi, Kanazawa 920*

(Received February 7, 1977)

Exciplex (DA)* and triple exciplex (DDA)* formation between 1,4-dicyanobenzene (DCB) and alkylnaphthalenes was investigated by steady-state and nanosecond time-resolved fluorescence spectroscopies at room temperature. Typical two-component decay of the exciplex and the fluorescence rise of the triple exciplex were observed in dioxane solutions of DCB and several alkylnaphthalenes. The results imply a significant dissociation process of (DDA)* to (DA)*. Triple exciplex formation *via* excimer (DD)* was proposed to be significant in a concentrated solution of alkylnaphthalene ($>10^{-1}$ M), while the triple exciplex was formed *via* the exciplex in a dilute solution of the electron donor.

Triple exciplex formation was reported first by Beens and Weller in the 1,4-dicyanobenzene (DCB) and naphthalene system. They reported the fluorescence lifetime of the exciplex ($\approx$30 ns) and an extraordinary rate constant (1.8×10^{8} $s^{-1}M^{-1}$) of triple exciplex formation from the exciplex.[2] Recently, Saltiel *et al.* reported triple exciplex emission in the system of 9,10-dichloroanthracene and 2,5-dimethyl-2,4-hexadiene in a polar solvent such as acetonitrile.[3] On the other hand, Grellmann and Suckow have reported triple exciplex formation in the anthracene–diethylaniline system in the temperature region of $\approx$230—180 K and discussed its intersystem crossing to the triplet state of anthracene.[4] More recently, Mimura and Itoh reported an intramolecular triple exciplex formation between two naphthyl moieties of 1,3-dinaphthylpropane (DNP) and DCB, and they suggested that the triple exciplex was not formed *via* intramolecular excimer of DNP, but *via* exciplex (DA)* formed between DCB and DNP.[5] Preliminary results of the exciplex and the triple exciplex were also reported for the DCB and alkylnaphthalene system. The dissociation process from the triple exciplex to the exciplex was so significant that this system exhibits typical two-component decay of the exciplex and fluorescence rise of the triple exciplex.[6] Although two-component decay of D*(or A*) and also fluorescence rise of (DA)* has been reported,[7] there are no reports of lifetime measurements which bear on the transformation between the exciplex, (DA)*, and the triple exciplex, (DDA)*.

This paper reports steady-state and nanosecond time-resolved fluorescence studies of the triple exciplex as well as the exciplex in several solvents of the DCB and several alkylnaphthalene systems at room temperature. Typical two-component decay of the exciplex fluorescence and the fluorescence rise of the triple exciplex were observed in the dilute solution of alkylnaphthalenes and DCB in dioxane. Concentrated solutions ($>10^{-1}$ M) of acenaphthene (AcN) and DCB in dioxane or THF exhibit fluorescence rise of the exciplex, which is not attributable to exciplex formation from DCB and AcN, but to dissociation of the triple exciplex. Since a time-dependent exciplex concentration in the system cannot show any fluorescence rise of the exciplex (see Eq. 1),[7,8] the triple exciplex formation *via* the excimer is suggested not to be negligible. This is consistent with the fact that the fluorescence quenching of alkylnaphthalene by DCB depends remarkably on the concentration of alkylnaphthalene above $\approx10^{-1}$ M. The triple exciplex formation and dissociation in the intermolecular system of alkylnaphthalene and DCB are discussed in comparison with the results of the intramolecular system of DNP and DCB mentioned above.

Experimental

Commercially available 2-methylnaphthalene (2-MN), 1,5-dimethylnaphthalene (1,5-DMN) and 2,3,6-trimethylnaphthalene (2,3,6-TMN)(Tokyo Kasei) were purified by silica gel chromatography and recrystallized from methanol (spectrograde) several times. Zone-refined acenaphthene (AcN) which was available commercially (Tokyo Kasei) was also purified in a manner similar to that described above. The fluorescence spectra were recorded with a Hitachi MPF-2A spectrophotometer with an exciting light of 310 nm. Good commercial solvents (Dotite spectrosols) were used, and chloroform was used after purification through an alumina colum (Woelm, Activity I) for removal of methanol which was present as a stabilizer. Solutions were contained in squartz cells (1 cm) equipped with graded seals, and were degassed by freeze-thaw cycles at 10^{-4}—10^{-5} Torr. Rectangular quartz cells with lightpath length 0.1 mm and 1 mm were also used for the concentrated solution. The time-resolved fluorescence spectra and the fluorescence lifetimes were determined by analyzing exponential decay curves measured by an oscilloscope (Tektronix 465), and a photomultiplier, HTV-R342 or R666, and by excitation with a coaxial N_2 gas laser which has a maximum 20-kW photon peak intensity at 3371 Å.

Results and Discussion

Steady-State Fluorescence Study. Fluorescence spectra of dioxane solutions of alkylnaphthalene, $<10^{-4}$ M, and in the presence of several concentrations of DCB at room temperature exhibit ordinary fluorescence behavior as expected for the electron donor-acceptor system. The fluorescence intensity of alkylnaphthalene decreases and the exciplex fluorescence intensity ($\lambda_{max}=$ 420—440 nm, $\tau=\approx$10—15 ns) increases when the DCB concentration increases. Apparent rate constants for exciplex formation were obtained from linear Stern-Volmer plots of the fluorescence quenching of 2-MN by DCB, and found to be 1.6×10^{10} $s^{-1}M^{-1}$ in dioxane and 2.5×10^{9} $s^{-1}M^{-1}$ in chloroform assuming negligible reversal of exciplex formation (Scheme 1).

Excitation spectra monitored at 450 nm (concentration of electron donor $<10^{-1}$ M, where fluorescence was determined from front surface of the sample cell in the concentrated solution) and the absorption spectra of dioxane solutions of 2-MN and DCB by using 1 mm and 1 cm quartz cells indicate no complex formation in the ground state. Figure 1 shows fluorescence spectra of dioxane solutions of DCB (concentration, $\approx 10^{-2}$ M) and several concentrations of 2-MN. The fluorescence of both exciplex and alkylnaphthalene are quenched with increasing 2-MN concentration up to 10^{-3} M. In highly concentrated solution of electron donor, $>\approx 10^{-1}$ M, fluorescence intensity at the longer wavelength region increases and an isoemissive point is observed at $\approx$480 nm. The fluorescence at 490 nm region may be ascribed to the triple exciplex, as mentioned in the previous paper.[5,6] In the concentrated solution ($>10^{-1}$ M) of 2-MN, however, it is difficult to determine an exact stoichiometry of the triple complex from fluorescence intensity.

The Stern-Volmer plots of the fluorescence quenching of 2-MN show a linear relationship against DCB concentration, as mentioned above. The slope of the Stern-Volmer plots increases markedly with increasing 2-MN concentration $>\approx 10^{-1}$ M, as shown in Fig. 2. On the other hand, excimer fluorescence is known to be observed for alkylnaphthalene such as [2-MN] $>\approx 10^{-1}$ M, while excimer formation is negligible in more dilute solution of alkylnaphthalene.[9] However, unless triple exciplex formation *via* the excimer is taken into account, the fluorescence quenching of 2-MN by DCB cannot depend on the concentration of 2-MN (Scheme 1). This argument is still valid even if dissociation of the long lived excimer to D* might be significant in the concentrated solution of 2-MN. Anomalous fluorescence quenching by DCB was observed for other alkylnaphthalenes such as AcN in the concentrated solutions, [AcN]$>\approx 10^{-1}$ M. Therefore, the concentration dependence of the slope of the Stern-Volmer plot shown in Fig. 2 may be attributable to the triple exciplex formation *via* the excimer. These transformations of the excited species are shown in Scheme 1. The anomalous fluorescence quenching of alkylnaphthalene evident in this steady-state fluorescence measurement agrees well with results of the time-resolved fluorescence studies in the following section.

Time-Resolved Fluorescence Study. Figure 3 shows time-resolved fluorescence spectra of a dioxane solution of DCB and 2-MN. The fluorescence spectra cen-

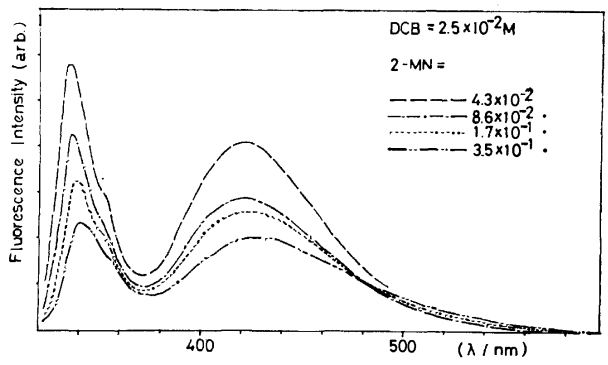

Fig. 1. Fluorescence spectra of dioxane solutions of DCB and several concentrations of 2-MN at room temperature.

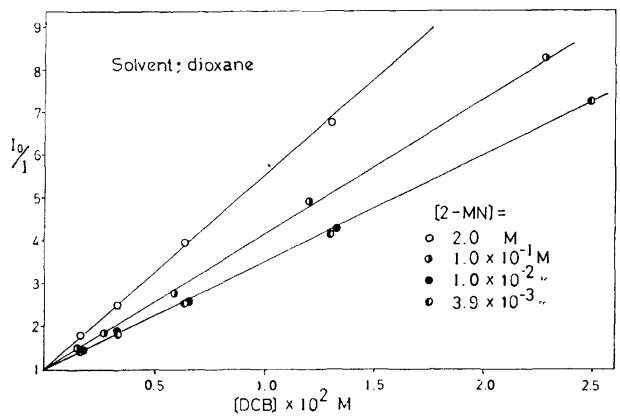

Fig. 2. Stern-Volmer plots of fluorescence quenching of 2-MN by DCB in several concentrations of 2-MN at room temperature.

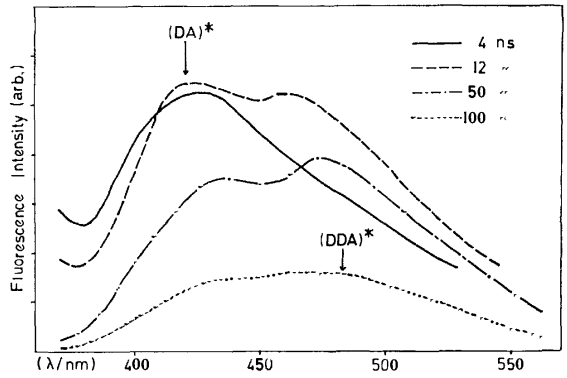

Fig. 3. Time-resolved fluorescence spectra of the intermolecular system of 2-MN (2×10^{-1}M) and DCB (2×10^{-2}M) in dioxane (extracted from the previous paper, Ref. 6).

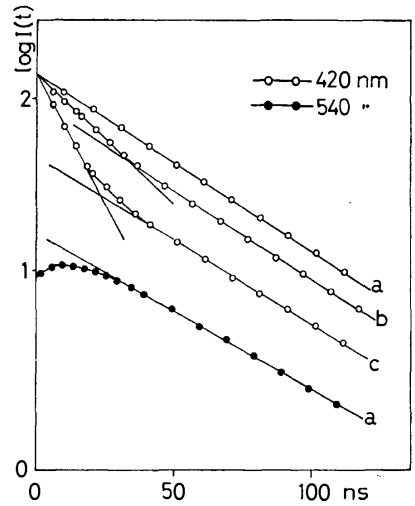

Fig. 4. Time development of the fluorescence of the exciplex, (DA),* and the triple exciplex, (DDA),* in dioxane solutions of 2-MN and DCB (2×10^{-1}M). The concentrations of 2-MN are 2.0×10^{-1}M (a), 3.5×10^{-3}M (b), and 8.8×10^{-4}M (c), respectively.

tered at 420 and 490 nm are ascribed to the exciplex and the triple exciplex, respectively. The fluorescence spectrum of the exciplex with a maximum at the 420—430 nm region was observed at 4 ns after laser pulse, while the fluorescence spectra of the exciplex as well as the triple exciplex were observed at 50—100 ns after a laser pulse. Figure 4 shows semilogarithmic plots of the fluorescence decay monitored at 420 nm in dioxane solutions of DCB and several concentrations of 2-MN. The fluorescence at 420 nm shows a single exponential decay in a high concentration of 2-MN, while the fluorescence at 420 nm exhibits a double exponential decay with decreasing concentration of 2-MN. On the other hand, fluorescence rise when the emission is monitored in the 470—580 nm region was observed from a concentrated solution of 2-MN and DCB (Fig. 4).

The photochemical interactions in the excited states are as follows:

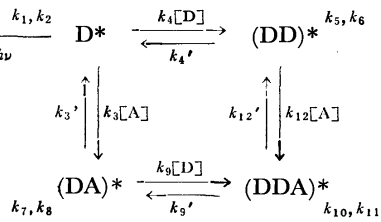

Scheme 1.

where D and A are alkylnaphthalene and DCB, respectively. The rate constants k_1,k_5,k_7, and k_{10} are the radiative rate constants of each excited species, and k_2, k_6,k_8, and k_{11} are nonradiative rate constants. The rate constants k_3,k_4,k_9, and k_{12}, and their primed counter parts are for the association and dissociation of the excimer, the exciplex and the triple exciplex, respectively. If excimer formation is neglected in a dilute concentration of alkylnaphthalene,[2] the time dependent concentrations of the exciplex (DA)* and the triple exciplex (DDA)* are expressed by the following well known equations:[4,8]

$$[(DA)^*] = c_1 \exp(-\lambda_1 t) + c_2 \exp(-\lambda_2 t), \quad (1)$$

$$[(DDA)^*] = c_3\{\exp(-\lambda_1 t) - \exp(-\lambda_2 t)\}, \quad (2)$$

where

$$\lambda_{1,2} = 1/2[k_7+k_8+k_9[D]+k_9'+k_{10}+k_{11}+k_{12}' \mp\{(k_9'+k_{10}+k_{11}+k_{12}'-k_7-k_8-k_9[D])^2 + 4k_9k_9'[D]\}^{1/2}]. \quad (3)$$

The time lag (t_L) between a response curve of the triple exciplex fluorescence and the exciting laser pulse is given by[8]

$$t_L = \ln(\lambda_2/\lambda_1)/(\lambda_2-\lambda_1). \quad (4)$$

The value of λ_2 was obtained from t_L and decay of the triple exciplex for several concentrations of the electron donor in dioxane solution. The association rate constant (k_9) was obtained from a slope of $\lambda_1+\lambda_2$ against alkylnaphthalene concentration, and the dissociation rate constant (k'_9) was obtained from λ_2 and fluorescence lifetimes of the exciplex, $(k'_3+k_7+k_8)^{-1}$, in a very dilute solution of electron donor compared with that of DCB. The rate constant k_9 and k'_9 obtained here for the 2,3,6-TMN and DCB system are 2.1×10^9 $s^{-1}M^{-1}$ and 1.5×10^7 s^{-1}, respectively as reported in a previous paper.[5] These rate constants demonstrate a significant dissociation process of the triple exciplex to the exciplex, which are in good agreement with results obtained from the typical two-component decay of the exciplex fluorescence. However, the values of k_9 determined in the concentrated solutions of alkylnaphthalene, $>\approx10^{-1}$ M, appear to be considerably smaller than those determined in dilute solution. This is attributed to formation of the triple exciplex *via* the excimer as well as the exciplex in concentrated solutions of alkylnaphthalenes.

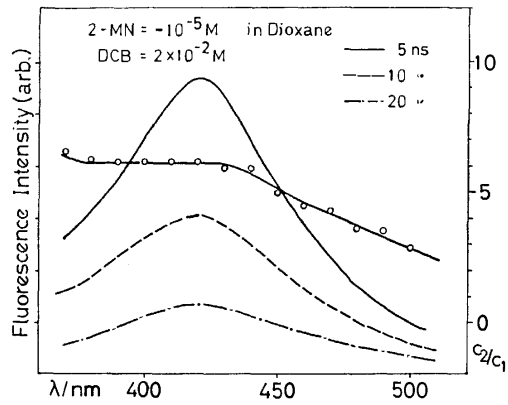

Fig. 5. Time-resolved fluorescence spectra of the intermolecular system 2-MN ($\approx10^{-5}$M) and DCB (2×10^{-2}M) in dioxane at room temperature and plots of c_2/c_1 at several wavelengths.

In order to exclude the ambiguity that the double-exponential decay curve of the exciplex may overlap the decay of the triple exciplex, ratios of c_2 and c_1, in Eq. 1, were plotted *vs.* the wavelength. The values of c_1 and c_2 were obtained by a deconvolution method from the decay curves of the exciplex. Figure 5 shows these plots and time-resolved fluorescence spectra in the dilute solution of 2-MN and DCB. The ratio of c_2/c_1 does not depend on the wavelength in the 380—440 nm region in dioxane solution. The fact implies real two-exponential decay of the exciplex fluorescence. Time-resolved fluorescence spectra in dilute solution shown in Fig. 5 reveal no significant triple exciplex but two-component decay of the exciplex fluorescence. Similar behavior of the fluorescence decay of the exciplex was observed for DCB associated with other alkylnaphthalenes. The results are summarized in Table 1.

The AcN–DCB system in a polar solvent such as THF does not exhibit triple exciplex fluorescence in either steady-state fluorescence or in time-resolved fluorescence spectra. The plots of c_2/c_1 also indicate no triple exciplex fluorescence even in 500—590 nm. Nevertheless, the double exponential decay of the exciplex fluorescence was observed at low concentration of the electron donor ($<10^{-5}$ M). A short lifetime component in the double exponential decay decreased and a long lifetime component increased with increasing AcN concentration. Furthermore, the fluorescence rise of the exciplex was observed in concentrated solutions of AcN $>\approx10^{-1}$ M. Semilogarithmic plots of these exciplex fluorescence decay for several concentrations of AcN are shown in Fig. 6.

TABLE 1. FLUORESCENCE MAXIMA OF EXCIPLEX (DA)* AND TRIPLE EXCIPLEX (DDA)*, THEIR LIFETIMES AND TIME LAGS t_L

Electron donor	Fluorescence maxima		Fluorescence lifetimes		
	(DA)* (nm)	(DDA)* (nm)	t_L [a] (ns)	(DA)* [b] (ns)	(DDA)* [a] (ns)
2-MN	425	480	6	10 (49)	56
1,5-DMN	435	490	8	6 (40)	38
2,3,6-TMN	440	510	12	8 (49)	55

Concentration of DCB is constant (2×10^{-2} M). Concentrations of electron donors are $10^{-1}\approx10^{-2}$ M (a) and $\approx10^{-4}$ M (b), respectively. Values in parentheses are long lifetime components in exciplex fluorescence decay curves.

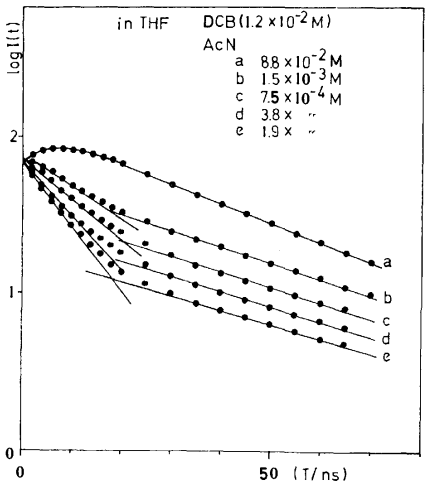

Fig. 6. Time developments of the fluorescence of the exciplex in the DCB-AcN system at room temperature.

In the dioxane solution of AcN and DCB, slope of Stern–Volmer plots of the AcN fluorescence against DCB concentration increased with increasing AcN concentration, $>\approx10^{-1}$ M, as mentioned for the 2-MN and DCB system. The experimental fact was accounted for by a postulate of significant triple exciplex formation *via* excimer and dissociation to the exciplex in high concentration of AcN, as mentioned above. This is consistent with the observation of fluorescence rise for the exciplex in a concentrated solution of AcN, as shown in Fig. 6. The excimer is implicated in the triple exciplex formation because the time dependent exciplex concentration as expressed by Eq. 1 cannot show any fluorescence rise, nor is fluorescence rise from the direct formation of exciplex between excited AcN and DCB molecules detected.

In the DCB and 1,3-dinaphthylpropane (DNP) system, the absence of concentration dependence of the fluorescence lifetimes of the excimer on the DCB concentration suggested that the intramolecular triple exciplex is not formed *via* excimer but formed *via* exciplex, as reported in the previous papers.[5,6] However, similar concentration dependence of the excimer fluorescence lifetimes was difficult to determine in the DCB and alkylnaphthalene systems. This is because the weak excimer fluorescence (lifetime $\tau=\approx35$ ns) was hardly distinguishable from the emission of the exciplex ($\tau=\approx10$ and ≈45 ns). In the concentrated solution of alkylnaphthalene where the excimer formation occurs,[9] the triple exciplex formation *via* the excimer as well as the exciplex was suggested in this paper. On the other hand, the intramolecular excimer formation is well known in symmetric DNP ($\beta\beta$- and $\alpha\alpha$-DNP).[10] Therefore, if the triple exciplex formation from the excimer and DCB is significant as mentioned above, the triple exciplex formation *via* the excimer can be also observed in the DNP and DCB system. The results of no triple exciplex formation *via* excimer in the DCB and DNP systems were ascribed to the different geometrical arrangement of two naphthyl moieties in the triple exciplex from that of the excimer. The favorable intramolecular excimer of DNP was regarded as a parallel sandwich structure of the long axis in the naphthyl moiety,[10] while two naphthyl moieties were regarded to be twisted in the molecular plane by a small angle around an axis perpendicular to the plane (a twisted model[6]). These two models cannot be transformed into each other while retaining the distance between the two aromatic moieties which is imposed by the steric requirements of the trimethylene chain. In the formation of the triple exciplex from the excimer of alkylnaphthalene and DCB which is suggested here, no steric hindrance in the transformation between a parallel sandwich model and a twisted model is anticipated.

The authors are indebted to Prof. Keitaro Yoshihara of Institute for Molecular Science, Okazaki, and Dr. Takayoshi Kobayashi of Institute of Physical and Chemical Research, Wako, for valuable discussions. The authors are also indebted to Prof. Toshihiko Okamoto for his kind encouragement and financial support.

References

1) To whom correspondence should be addressed, Kanazawa University.
2) H. Beens and A. Weller, *Chem Phys. Lett.*, **2**, 82 (1968).
3) J. Saltiel, D. E. Townsent, B. D. Watson, and P. Shannon, *J. Am. Chem. Soc.*, **97**, 5688 (1975).
4) K. H. Grellmann and U. Suckow, *Chem. Phys. Lett.*, **32**, 250 (1975).
5) T. Mimura and M. Itoh, Proceeding of International Conference on Luminescence in Tokyo (1975), *J. Luminescence*, **12/13**, 836 (1976).
6) T. Mimura and M. Itoh, *J. Am. Chem. Soc.*, **98**, 1095 (1976).
7) W. R. Ware and H. P. Richter, *J. Chem. Phys.*, **48**, 1595 (1968).
8) J. B. Birks, "Photophysics of Aromatic Molecules," Wiley Interscience, New York (1970).
9) N. Mataga, M. Tomura and H. Nishimura, *Mol. Phys.*, **9**, 367 (1965).
10) E. A. Chandross and C. J. Dempster, *J. Am. Chem Soc.*, **92**, 3586 (1970).

Bimolecular Quenching of Triplet Exciton in Crystalline *p*-Dibromobenzene

Takayoshi Kobayashi and Noboru Hirota*†
The Institute of Physical and Chemical Research, Wako, Saitama, 351
**The Institute for Solid State Physics, The University of Tokyo, Minato-ku, Tokyo, 106*
(Received February 7, 1977)

The rate constants of the bimolecular quenching (γ), the hopping rate (λ), and the diffusion coefficient (D) of triplet exciton in crystalline *p*-dibromobenzene at temperatures between 160 and 77 K were obtained by analyzing the phosphorescence decay curves at high and low density excitations with the use of an N_2 laser as an exciting pulsed light source. Estimated values of γ, λ, and D at room temperature (300 K) are $(2\pm1)\times10^{-12}$ cm^3 s^{-1}, $9\pm4\times10^9$ s^{-1}, and $2\pm1\times10^{-4}$ cm^2 s^{-1}, respectively. The activation energy of the exciton hopping was obtained to be 290 ± 50 cm^{-1}. This implies that the triplet exciton in *p*-dibromobenzene crystal is described in terms of a localized exciton model.

One of the most important properties of excitons is their ability to transport electronic excitation energy without transport of charge. The diffusion constant of a triplet exciton in aromatic crystals has been obtained by several methods: *i.e.* (1) the dependence of an integrated intensity of delayed fluorescence in an aromatic crystal on the spatial distribution of excitons created by spatially inhomogeneous excitation,[1] (2) the absorption spectrum for generation of a triplet exciton by polarized light,[2] (3) surface quenching of a triplet exciton,[3] (4) diffusion of the excitons out of the tracks where they were formed by ionizing radiation,[4] (5) the magnetic field dependence of the effect of triplet excitons on the proton spin-lattice relaxation.[5] In the present paper we determined the diffusion constant of the triplet exciton by observing the phosphorescence decay curve at high and low density excitations using an intense N_2 laser light source in crystalline *p*-dibromobenzene (hereafter abbreviated to DBB). The present method of the determination of exciton migration rate has been applied to the singlet exciton in aromatic crystals[6-8] and the triplet exciton in uranyl salts.[9,10]

Experimental

The determination method of the rate constants of the bimolecular quenching and exciton migration is the same as that described in a previous paper.[8] The excitation pulsed light source is an N_2 laser (Avco Everett Model 950) with the peak power of 48 kW and the pulse width of 10 ns.

DBB was purified by repeated zone meltings. DBB single crystal in a Bridgman tube was cut in a size of $5\times4\times2$ mm^3 ($b\times c\times a$, respectively). Incident laser light was focused on the bc cleavage surface of the crystalline sample. The normal line of the surface and the incident light beam make an angle of about 45° with each other. Cooled nitrogen gas obtained from liquid nitrogen was used to control the tempetarure of the sample crystal between 97 and 160 K.

Results and Discussion

Phosphorescence Decay Curve. The phosphorescence decay curve at low density excitation observed at several temperatures between 77 and 160 K was exponential and was independent of the observing wavelength. This implies that the phosphorescence emission from the crystalline DBB sample used in the present work is not contaminated with the impurity emission. The phosphorescence intensity of DBB deviated from the exponential one at high density excitation at temperature between 77 and 160 K. The phosphorescence decay curves at low and high density excitations at 77 K are shown in Fig. 1. If the faster decay of phosphorescence at high density excitation is due to the biexcitonic quenching, the exciton concentration $n(t)$ at time t after excitation can be given by the following equation:[6,7]

$$1/n(t) = \{1/n(0) + \gamma/\alpha\}\exp(\alpha t) - \gamma/\alpha, \qquad (1)$$

where α and γ are the rate constants of monomolecular and bimolecular anihilation processes, respectively. α is obtained from the decay curve of phosphorescence at low density excitation.

The inverse of the exciton density in an arbitrary unit at high density excitation at 77 K is plotted against $\exp(\alpha t)$, the result being shown in Fig. 2. As is shown in this figure, the existence of a good linear relationship between the two quantities is consistent with the quenching mechanism given by Eq.1. Therefore the shortening of the phosphorescence decay time observed at high density excitation can be explained in terms of biexcitonic quenching. From the estimation of the initial concentration of the exciton ($n(0)$) and the intercept of the plot of $n(t)^{-1}$ *versus* $\exp(\alpha t)$, γ can be obtained. The initial concentration of the triplet exciton can be

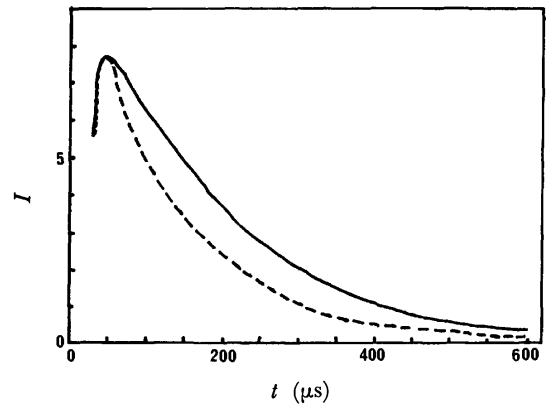

Fig. 1. Phosphorescence decay curves of crystalline DBB at 77 K at low (——) and high (----) density excitations.

† On leave from Department of Chemistry, State University of New York at Stony Brook, New York, U. S. A.; present adress Department of Chemistry, Kyoto University, Kyoto.

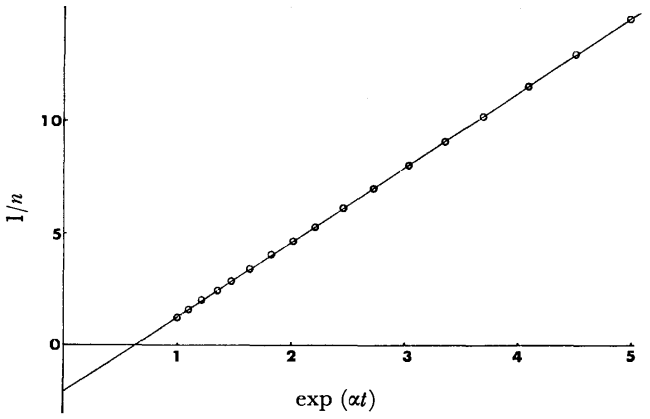

Fig. 2. The plot of $1/n$ *versus* $\exp(\alpha t)$ for the triplet exciton in crystalline DBB at 77 K at high density excitation. n is in an arbitrary unit. The initial concentration, $n(0)$, is estimated to be 1×10^{-3} M ($=6\times10^{17}$ cm^{-3}).

obtained by the $T_1\leftarrow S_0$ absorption cross section of the DBB crystal at the wavelength of the excitation laser pulse.

Estimation of the Initial Concentration of Triplet Exciton. The initial concentration of the triplet exciton, $n(0)$, is estimated by using the following equation:[8]

$$n(0) = \frac{N_0(1-e^{-1})L}{\Delta S\Delta l} = \frac{0.632N_0L}{\Delta S}\times 2.303\,\varepsilon c = \frac{1.455N_0\varepsilon cL}{\Delta S}, \quad (2)$$

where N_0 and ΔS are the number of photons irradiated and the irradiated area on the sample crystal, respectively. ε and Δl are the molar extinction coefficient and absorption depth of the $T_1\leftarrow S_0$ transition in the DBB crystal at the wavelength of the N_2 laser oscillation, respectively, and L and c are the light transmittance of lenses and dewar and the molar concentration of the DBB crystal, respectively. Crystal data[11] were used to estimate c to be 9.96 M. From the data on the $T_1\leftarrow S_0$ absorption spectrum of the DBB crystal measured by Castro and Hochstrasser,[12] molar extinction coefficients parallel to b and c axes at 337.1 nm are estimated to be 5.0 and 7.5 M^{-1} cm^{-1}, respectively. The average of the two values were used for the estimation of $n(0)$ using Eq. 2. By applying these values to Eq. 2, $n(0)$ is estimated to be *ca.* 1×10^{-3} M($=6\times10^{17}$cm^{-3}).

Estimation of γ and Hopping Rate (λ) of Triplet Exciton in DBB Crystal. From the estimated value of $n(0)$ and the intercept of the plot, γ is obtained to be $(4\pm2)\times10^{-14}$ cm^3 s^{-1} at 77 K. The relationship between the biexcitonic quenching rate constant γ and the hopping rate, λ, of the exciton is expressed by the following equation[10]:

$$\gamma = (2-A)\frac{V_0z_n}{V_{tot}z_u}\frac{\lambda\mu}{\lambda+\mu}. \quad (3)$$

Here A, z_n, and z_u are the quantum yield of the formation of a triplet exciton from a pair of two nearest neighboring excitons, the number of sites in the nearest neighbor, and the number of molecules in a unit cell of the DBB crystal with volume V_0, respectively, and

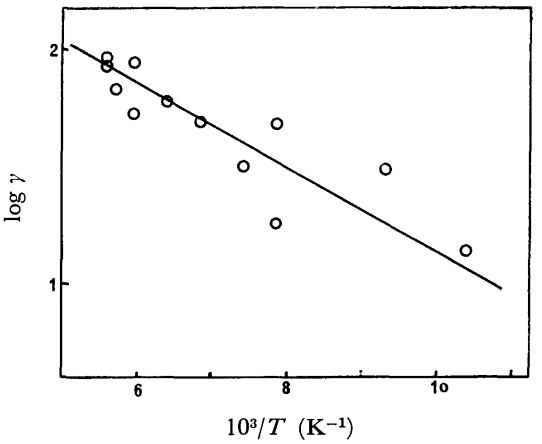

Fig. 3. The logarithmic plot of γ *versus* $1/T$ for the triplet exciton in crystalline DBB.

μ represents the rate of the quenching for a pair of two nearest neighboring excitons.

Now we consider two extreme cases: (1) The rate of bimolecular quenching is determined by that of the transition to the final higher excited state and therefore is thought to be temperature independent. In this case,

$$\gamma = (2-A)\frac{V_0z_n}{z_u}\mu. \quad (4)$$

(2) The bimolecular quenching rate is determined by the migration rate of the exciton and γ increases or decreases with the increasing temperature dependeng upon the mechanism of exciton migration. With increasing temperature the rate of the exciton migration in the hopping model (Case (b-1): $\lambda=\lambda_h$) increases, while the rate in the coherent model (Case (b-2): $\lambda=\lambda_c$) decreases. In this case,

$$\gamma = (2-A)\frac{V_0z_n}{z_u}\lambda. \quad (5)$$

The temperature dependence of γ of the triplet exciton in crystalline DBB shows that it can be described in the hopping model (Fig. 3). The activation energy of exciton hopping in DBB is obtained to be 290 ± 50 cm^{-1} from the temperature dependence of γ shown in Fig. 3.

Since it is difficult to determine A experimentally, it is tentatively assumed to be unity. The assumption makes the γ value different by factor of only 2 from that obtained by the assumption of $A=0$. The difference is smaller than the experimental error in the determination of $n(0)$ and hence of γ. The obtained value of γ is listed in Table 1 together with the data of the triplet exciton in crystalline anthracene and pyrene previously reported by Avakian and Merrifield,[13] and Ern *et al.*,[14] respectively. The values of γ and D of triplet exciton in crystalline DBB are quite similar to those in crystalline anthracene and pyrene. The similarity in the magnitude of D and hence γ of triplet exciton in anthracene, pyrene, and DBB is in contrast with the difference in the magnitude of γ of singlet exciton in crystalline anthracene ($\gamma=1.25\times10^{13}$ cm^3 s^{-1})[15] and pyrene ($\gamma=5\times10^{10}$ cm^3 s^{-1}).[16] This may be interpreted in terms of the expected smaller difference in the ex-

Table 1. The rate of bimolecular quenching, hopping rate and diffusion coefficient of exciton (γ, λ, and D, respectively) in DBB in the comparison with those of anthracene and pyrene

Crystal	DBB		Anthracene[b]	Pyrene[c]
Temperature	77 K	300 K	room temperature	room temperature
γ/cm^3 s^{-1}	$(4\pm2)\times10^{-14}$	$(2\pm1)\times10^{-12}$	2×10^{-12}	$(7.5\pm4.0)\times10^{-12}$
λ/s^{-1}	$(2\pm1)\times10^{8}$	$(9\pm4)\times10^{9}$		
D/cm^2 s^{-1}	$(3\pm1.5)\times10^{-5}$	$(2\pm1)\times10^{-4}$	2×10^{-4}	$(8\ \pm4\ )\times10^{-4}$

a) The values of γ, λ, and D at 300 K are estimated by the extrapolation from those values between 77 and 180 K, with use of the activation energy of exciton migration. b) Ref. 15. c) Ref. 16.

change integral than in the electronic coupling among anthracene, pyrene, and DBB.

The authors wish to thank Professor S. Nagakura for his kind encouragement and helpful discussions. N. H. wishes to thank the support of his stay by the US-Japan science collaboration program of the U. S. National Science Foundation.

References

1) P. Avakian and R. E. Merrifield, *Phys. Rev. Lett.*, **13**, 541 (1964).
2) P. Avakian, V. Ern, R. E. Merrifield, and A. Suna, *Phys. Rev.* **165**, 974 (1968).
3) R. G. Kepler and A. C. Switendick, *Phys. Rev. Lett.*, **15**, 56 (1965).
4) T. A. King and R. Voltz, *Proc. R. Soc. London, Ser A*, **289**, 424 (1966).
5) G. Maier, U. Haeberlen, and H. C. Wolf, *Phys. Lett.*, **25A**, 323 (1967).
6) A. Bergman, M. Levine, and J. Jortner, *Phys. Rev. Lett.*, **18**, 593 (1967).
7) A. Inoue, K. Yoshihara, and S. Nagakura, *Bull. Chem. Soc. Jpn.*, **45**, 1973 (1972).
8) T. Kobayashi and S. Nagakura, *Mol. Phys.*, **24**, 695 (1972).
9) N. A. Tolstoi, A. P. Abramov, and I. N. Abramova, *Sov. Phys.-Solid State*, **9**, 1516 (1968).
10) T. Kobayashi to be published.
11) S. Bezzi and V. Croatts, *Gazz. Chim. Ital.*, **12**, 318 (1942).
12) G. Castro and R. M. Hochstrasser, *J. Chem. Phys.*, **46**, 3617 (1967).
13) P. Avakian and R. E. Merrifield, *Mol. Cryst.*, **5**, 37 (1968).
14) V. Ern, H. Bonchriha, M. Bisceglia, S. Arnold, and M. Schott, *Phys. Rev. B*, **8**, 6038 (1973).
15) N. A. Tolstoi and A. P. Abramov, *Sov. Phys.-Solid State*, **9**, 255 (1967).
16) W. Klöpffer and H. Bauser, *Chem. Phys. Lett.*, **6**, 275 (1970).

A Chlorine NQR Study of Trichloromethyl Derivatives. I

Masao HASHIMOTO

Department of Chemistry, Faculty of Science, Kobe University, Nada-ku, Kobe 657

(Received February 9, 1977)

The chlorine NQR frequencies of several benzene derivatives with $-CCl_3$ groups were measured at temperatures above 77 K. For all the compounds studied, the NQR signals of the $-CCl_3$ groups were observed to fade out; the fade-out temperatures (T_f) were in the temperature range of 130—370 K. It was found that the most important factors involved in determining the T_f value are the intramolecular steric hindrance, hyperconjugation, and intermolecular interactions. In some compounds, an increase in the NQR frequency was found to be caused by the intramolecular steric hindrance.

It is well known that the chlorine NQR signals of the trichloromethyl ($-CCl_3$) group often fade out at temperatures far below the melting point. The fade-out temperatures (T_f) reported so far for several compounds are distributed over a fairly wide temperature range.[1-7] The object of this work is to explore the role of the various factors involved in determining the T_f value. For this purpose, several tens of compounds with $-CCl_3$ group(s) were investigated; of them, a series of benzene derivatives will be discussed here. Of the benzene derivatives, trichloromethylbenzene (I)[1,7] and 1-trichloromethyl-4-chlorobenzene (II)[5] have already been studied in detail. In this work, therefore, NQR measurements were carried out for the materials shown below.

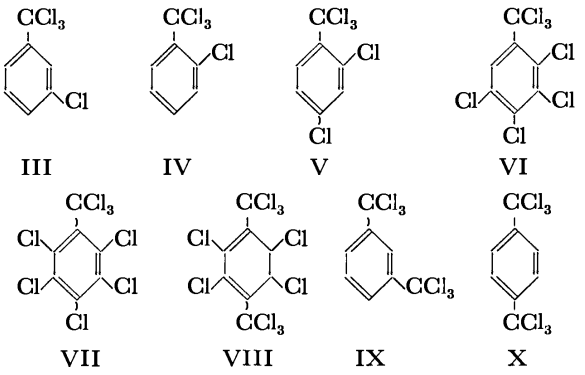

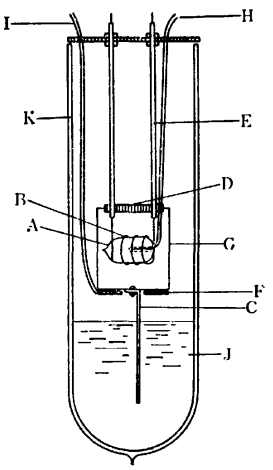

Fig. 1. Cryostat for the NQR measurement. A: Sample. B: Sample coil. C: Copper plate. D: Teflon. E: Transmission line (stainless steel pipe). F: Electric heater. G: Copper case. H: Thermocouple. I: Heater leads. J: Liquid nitrogen. K: Glass Dewar flask.

Experimental

The NQR signals of ^{35}Cl were detected by a LC-push-pull type superregenerative spectrometer.[8] For the measurement of the temperature dependence of the NQR frequency, the simple cryostat shown in Fig. 1 was employed. The temperature was controlled by changing both the amount of liquid nitrogen and the heater current. The temperature was measured with a calibrated copper-constantan thermocouple.

A commercial compound (Tokyo Kasei) of 1-trichloromethyl-3-chlorobenzene (III) was purified by vacuum distillation (3 Torr, 120 °C). Commercial reagents (Tokyo Kasei) of 1-trichloromethyl-2-chlorobenzene (IV), 1-trichloromethyl-2,4-dichlorobenzene (V), 1,3-bis(trichloromethyl)benzene (IX), and 1,4-bis(trichloromethyl)benzene (X) were purified by recrystallization from ethyl ether. The 1-trichloromethyl-2,3,4,5-tetrachlorobenzene (VI), 1-trichloromethyl-2,3,4,5,6-pentachlorobenzene (VII), and 1,4-bis(trichloromethyl)-2,3,5,6-tetrachlorobenzene (VIII) were supplied by Professor Akira Fujino, Osaka City University.

Results and Discussion

The ^{35}Cl NQR frequencies of III, IV, V, VI, VII, VIII, IX, and X were measured at temperatures above 77 K. The NQR frequencies of these compounds at 77 K are listed in Table 1. The results obtained for III, IV, IX, and X at 77 K in good agreement with the data reported by Ardalan and Lucken,[9] except for slight differences in the data for IV and IX (see footnotes of Table 1). The NQR signals corresponding to the chlorine atoms of the $-CCl_3$ group (α-chlorine atoms) of each compound were found to fade out at temperatures below the melting point of the compound. The fade-out temperatures (T_f) are summerized in Table 2, together with the melting points (T_m).

Four NQR lines were observed for V at 77 K. As judged by the value of the resonance frequency, two of them (39.733 and 39.405 MHz) are assigned to α-chlorine atoms, and, as the intensity of the line at 39.405 MHz is stronger than that at 39.733 MHz, the lower-frequency line is assigned to two equivalent α-chlorine atoms.

The NQR spectrum of VI consists of twelve lines. The number of resonance lines indicates that there are two crystallographically nonequivalent molecules in a unit cell and that each molecule has a mirror plane which coincides with the benzene ring. The most energetically favorable arrangement for the $-CCl_3$

Table 1. The ^{35}Cl NQR frequencies of some benzen derivatives with $-CCl_3$ group(s) at 77 K

Compound	Frequency/MHz			
III[a]	39.510	39.065	39.045	35.010*[b]
IV[c]	39.613	39.602	39.155	35.798*
V[d]	39.733	39.405	36.816*	35.296*
VI	40.093	39.909	39.851	39.709
	38.430*	38.071*	38.049*	37.990*
	37.907*	37.850*	37.588*	37.274*
VII	41.744	41.034	39.794	39.361*
	38.954*	38.878*	38.467*	38.377*
VIII	41.649	41.214	41.169	40.491
	39.689	39.381	39.204*	38.874*
	38.830*	38.825*		
IX[e]	39.492	39.470	39.097	38.993
	38.921	38.783	38.698	38.590
	38.472			
X[f]	39.628	39.408	39.343	39.322
	39.276	39.196	38.907	38.716
	38.300			

a) By thermal analysis, this compound was found to form a glassy state from a supercooled liquid (T_g=166 K and T_c=201 K). For a quenched specimen, no NQR signals were observed because of the formation of the glassy state. b) The NQR frequencies corresponding to chlorine atoms attached to the benzene ring are denoted by asterisks. c) Aldaran and Lucken (A & L) reported three frequencies, 39.602, 39.158, and 35.794 MHz, at 77 K and assigned the highest one to two equivalent α-chlorine atoms.[9] The existenec of the four lines was confirmed in this work by the temperature dependence of the NQR frequencies. d) Sasikala and Murty reported three NQR frequencies, 38.76, 36.40, and 34.87 MHz, at room temperature.[10] e) A & L reported twelve frequencies, 39.481, 39.461, 39.307, 39.084, 38.987, 38.913, 38.761, 38.692, 38.640, 38.570 38.462, and 38.440 MHz, at 77 K.[9] Nine of these frequencies agreed with the present data, but the rest of them (39.307, 38.640, and 38.440 MHz) were not detected, even in spite of careful measurement. f) By thermal analysis it was found that the room-temperature modification of X is transformed into a high temperature phase at 362 K. The frequencies given in this table correspond to the room-temperature modification. A supercooled high-temperature modification gave fairly broad NQR signals at 77 K, their frequencies being 39.54, 39.42, 39.34, 39.23, and 38.82 MHz.

groups in these molecules appears to be the one in which two α-chlorine atoms are located symmetrically above and below the plane of the benzene ring, while the third one lies on it, pointing away from the ortho chlorine atom. Therefore, the two crystallographically nonequivalent molecules have the same molecular configuration. Four of the twelve lines of VI (40.093, 39.909, 39.851, and 39.709 MHz at 77 K) were found to fade out; they are assigned to the two $-CCl_3$ groups of the two crystallographically nonequivalent molecules. Since the intensities of the signals at 40.093 and 39.851 MHz are approximately twice as strong as those at 39.909 and 39.709 MHz, each of the former two lines corresponds to two equivalent α-chlorine atoms in a molecule.

Table 2. Fade-out temperatures (T_f) of the NQR signals of $-CCl_3$ groups and melting points (T_m) of several benzene derivatives

Compound	T_f/K	T_m/K
I[a]	130 and 215	265
II[b]	250	270
III	260	270
IV	260	303
V	320	323
VI	330 and 370	395
VII	260	345
VIII	300	380
IX	145—160	308
X	160—170 and 255	383

a) Ref. 7. b) Ref. 5.

Three of the eight NQR lines of VII (41.744, 41.034, and 39.794 MHz) and six of the ten NQR lines of VIII (41.649, 41.214, 41.169, 40.491, 39.689, and 39.381 MHz) are undoubtedly to be assigned to α-chlorine atoms, because of the fade-out phenomena of these lines.

Ballester *et al.* pointed out that the $-CCl_3$ group of VII is arranged in such a way that two α-chlorine atoms lie on one side, and the third one on the other side, of the plane of the benzene ring, and that the benzene ring is distorted as the result of a strong steric repulsion between the α-chlorine atom and the ortho substituent.[11] As is shown in Table 1, the $-CCl_3$ group of VII gives three NQR lines, two of them with relatively high resonance frequencies (41.744 and 41.034 MHz) as compared to the third one (39.794 MHz). The two higher frequency lines are probably to be assigned to the two α-chlorine atoms, which interact with the ortho substituents. The reason for this assignment is as follows: the steric repulsion between the chlorine atoms causes a decrease in the ionic character of the C–Cl bond in the $-CCl_3$ group, and, according to the theory of Townes-Daily,[12] the decrease in the ionic character increases the resonance frequency.

For the chlorine atoms attached to the benzene ring (olefinic chlorine atoms) of VII, the mean NQR frequency is 38.80 MHz, while that of hexachlorobenzene is 38.45 MHz.[13] The rise in the NQR frequency in VII is also to be attributed to the steric repulsion between chlorine atoms. In the case of VIII, the mean NQR frequency (38.93 MHz) of the olefinic chlorine atom is higher than that of VII, in accord with the fact that, in VIII, all of the olefinic chlorine atoms are repelled.

The fade-out phenomenon of the NQR signals of the $-CCl_3$ group is known to be due to the reorientation of the group around its three-fold axis.[14] Recently, several authors have reported both the values of the potential barriers (V_0) for the reorientation of the group and the T_f's for some compounds.[1-3,5,6] These data show that the values of V_0 and T_f vary widely from compound to compound and that the T_f value tends to rise with an increase in the V_0 value. Of the benzene derivatives studied in this work, the substances with a

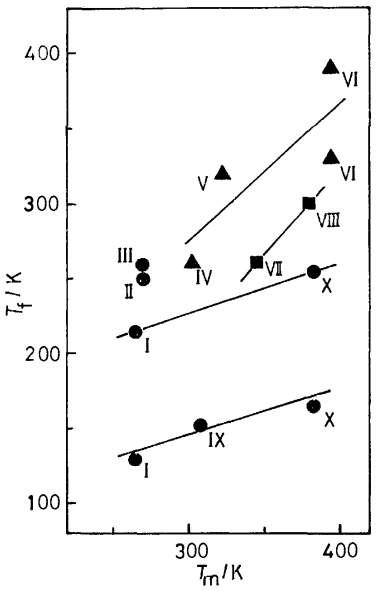

Fig. 2. Fade-out temperature (T_f) *vs.* melting point (T_m) plots of benzene derivatives.
●: Substances without ortho-substituent,
▲: substances with ortho-substituent(s),
■: perchloro-compounds.

$-CCl_3$ group with ortho substituent(s) show considerably high T_f values. Since the intramolecular steric hindrance between the $-CCl_3$ group and ortho substituent(s) raises a potential barrier for the reorientation of the $-CCl_3$ group, it seems reasonable that the substances with ortho substituent(s) show high T_f values. It is worth noting that the fade-out phenomenon was observed even for the $-CCl_3$ groups of VII and VIII, in which the groups are flanked by two ortho chlorine atoms. Moreover, despite the presence of the two ortho substituents, the T_f values of VII and VIII are comparable with those of other compounds with one ortho substituent. Therefore, the distortion of the benzene ring in VII and VIII relieves the steric hindrance, thus decreasing the value of V_0.

In the single-crystal NQR study of II, Kiichi *et al.* reported the presence of hyperconjugation between the $-CCl_3$ group and the π-systems of the benzene ring.[5] According to them, the hyperconjugation tends to lower both the NQR frequency and the magnitude of the temperature coefficient of the α-chlorine atom associated with the hyperconjugation. The $-CCl_3$ group of III gives the NQR frequencies of 39.510, 39.065, and 39.045 MHz at 77 K; their mean temperature coefficients are -3.00, -3.23, and -2.51 kHz/K respectively. The possibility of the hyperconjugation in III is suggested by the fact that the lowest frequency line exhibits the smallest absolute value of the temperature coefficient. In addition, the high T_f value of III seems to support the possibility of the hyperconjugation.[5,6]

Quite different T_f values were found for the $-CCl_3$ groups of the two crystallographically nonequivalent molecules of VI. Among the nine NQR signals of X, three signals (39.343, 39.276, and 38.716 MHz at 77 K) were observed up to 255 K, while the others faded out in the temperature region of 160—170 K. The large differences in T_f evidently indicate that, in each of these compounds, there exist two kinds of $-CCl_3$ groups with different potential barriers for the reoricntation of the group. The cause of the difference in T_f for VI is probably of intermolecular nature, because the two crystallographically nonequivalent molecules have almost the same molecular configuration.

For the benzene derivatives studied, T_f *vs.* T_m plots are shown in Fig. 2. In the series of the substances without an ortho substituent (denoted by ● in Fig. 2), T_f tends to increase with an increase in T_m.[15] The same trend can be seen for the compounds with an ortho substituent (denoted by ▲) and also for the perchloro compounds (denoted by ■). Since T_m reflects the degree of intermolecular interaction, this tendency implies that T_f (in other words, V_0) is affected not only by intramolecular interactions, but also by intermolecular ones.

The author would like to express his gratitude to Professor Ryôiti Kiriyama for his helpful discussion. The author also wishes to thank Professor Akira Fujino for the generous gift of authentic samples of 1-trichloromethyl-2,3,4,5-tetrachlorobenzene (VI), perchlorotoluene (VII), and perchloro *p*-xylene (VIII). Thanks are due to Dr. Koichi Mano for his thermal analyses.

References

1) I. V. Izmest'ev and V. S. Grechishkin, *Zh. Strukt. Khim.*, **11**, 927 (1970).
2) I. V. Izmest'ev and G. B. Soifer, *Opt. Spectrosk.*, **30**, 479 (1971).
3) N. E. Ainbinder, B. F. Amirkhanov, I. V. Izmest'ev, A. N. Osipenko and G. B. Soifer, *Soviet Physics-Solid State*, **13**, 344, (1971).
4) M. Hashimoto and K. Mano, *Bull. Chem. Soc. Jpn.*, **45**, 706 (1972); M. Hashimoto, *Chem. Lett.*, **1975**, 1325.
5) T. Kiichi, N. Nakamura, and H. Chihara, *J. Magn. Reson.*, **6**, 516 (1972).
6) H. Chihara and N. Nakamura, *Bull. Chem. Soc. Jpn.*, **45**, 3530, (1972).
7) T. Yoshii, S. Murata, and M. Suhara, *Sci. Rep. Kanazawa Univ.*, **19**, 113 (1974).
8) A. Hirai, H. Abe, and H. Yasuoka, *Bussei*, **1967**, 697.
9) Z. Ardalan and E. A. C. Lucken, *Helv. Chim. Acta*, **56**, 1724 (1973).
10) D. Sasikala and C. R. K. Murty, *J. Phys. Chem.*, **58**, 2955 (1973).
11) M. Ballester, C. Molinet, and J. Castaner, *J. Am. Chem. Soc.*, **82**, 4254 (1960); M. Ballester and J. Castaner, *ibid.*, **82**, 4259 (1960).
12) C. H. Townes and B. P. Dailey, *J. Chem. Phys.*, **17**, 782 (1949); B. P. Dailey and C. H. Townes, *ibid.* **23**, 118 (1955).
13) I. P. Biryukov, M. G. Voronkov, and I. A. Safin, "Tables of Nuclear Quadrupole Resonance Frequencies," Israel Program for Scientific Translations, Jerusalem (1967), p. 49.
14) M. Buyle-Bodin, *Ann. Phys. (Paris)*, **10**, 533 (1955).
15) The points for II and III deviate from this trend. The unexpectedly high T_f values of II and III are due to the hyperconjugation mentioned above.

The Microwave Spectrum of 1-Propanethiol

Osamu OHASHI, Mamoru OHNISHI, Akira TAGUI, Takeshi SAKAIZUMI, and Ichiro YAMAGUCHI

Department of Chemistry, Faculty of Science and Technology, Sophia University, Chiyoda-ku, Tokyo 102

(Received March 1, 1977)

The microwave spectra of 1-propanethiol and its deuterated species ($CH_3CH_2CH_2SD$) were measured in the frequency region from 8.5 to 35 GHz. Several a-type R-branch transitions for the ground and excited vibrational states of the normal species and for the ground state of the deuterated species were identified, and the following rotational constants in MHz were obtained: $A=23429\pm653$, $B=2345.29\pm0.03$, and $C=2250.18\pm0.03$ for the ground state of the normal species; $A=24483\pm945$, $B=2346.30\pm0.04$, and $C=2253.91\pm0.04$ for the excited state of the normal species, and $A=21758\pm461$, $B=2306.71\pm0.03$, and $C=2217.79\pm0.03$ for the ground state of the deuterated species. The spectrum assigned to the ground vibrational states has been attributed to the T–G rotational isomer, and the excited vibrational state has been ascribed to the $-CH_2-CH_2-$ torsional motion.

The chemical thermodynamic properties and rotational isomerism of 1-propanethiol have been reported by Pennington *et al.*[1] In the gas phase, the potential energy of the *trans* form, a conformer with respect to the central C–C bond, is only about 400 cal mol^{-1} lower than that of the *gauche* form.[1] The vibrational assignment and rotational isomerism of 1-propanethiol have been reported by Hayashi *et al.*[2] Taking account of the additional rotational isomerism around the C–S bond, we would expect the five possible rotational isomers, T-T, T-G, G-T, G-G, and G-G′, shown in Fig. 1, where the first symbol refers to the isomerism around the central C–C bond, and the second, to the one around the C–S bond.[2] In the gaseous and liquid states, the T-T isomer, the more stable one, and the G-T isomer have been confirmed to exist.[2]

Microwave spectroscopic studies have shown that the *gauche* form is more stable than the *trans* form for 1-fluoropropane[3] and 1-chloropropane.[4] The 1-propanol molecule has been confirmed by microwave spectroscopy to exist in both *trans* and *gauche* forms.[5] The relative intensity measurement has shown that the *gauche* form is more stable than the *trans* form by 0.29 ± 0.15 kcal mol^{-1}.[5]

The relative intensity measurement of the microwave spectral lines of ethanethiol showed that the *gauche* isomer is more stable than the *trans* isomer by 142 ± 15 cm^{-1} in their lowest vibrational states.[6]

We are interested in the rotational isomerism of 1-propanethiol, and so we examined the microwave spectra of the normal and deuterated ($CH_3CH_2CH_2SD$) species.

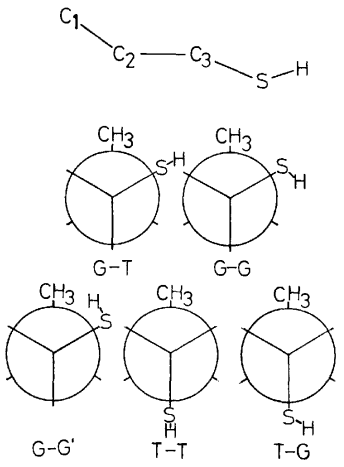

Fig. 1. Five possible rotational isomers and the numbering of carbon atoms.

Experimental

The sample of 1-propanethiol was obtained commercially (Tokyo Kasei Kogyo Co., Ltd.) and was purified by trap-to-trap distillation *in vacuo*. The deuterated species was prepared in the absorption cell by the following procedures. First, the cell was filled with D_2O vapor. It was then evacuated by means of a vacuum pump for about 20 min. At the end of this time, 1-propanethiol, purified beforehand, was admitted into the cell.

The spectrometer used was a conventional 100 kHz sinusoidal and square-wave Stark modulation type, with a phase-sensitive detector. The measurements of the transition frequencies were made with a Hewlett-Packard Model 5245 L frequency counter.

The rotational spectra were observed in the frequency region from 8.5 to 35 GHz at about −40 °C. The measurement of the relative intensity was made at about −40 °C and at room temperature. The sample was renewed about every 30 min.

Results and Discussion

Normal Species. It has been reported that 1-propanethiol exists in the T-T and G-T forms and that the T-T form is more stable than the G-T form in the gaseous and liquid states.[1,2] Consequently, the spectrum of the T-T rotational isomer was searched for at first. The moments of inertia calculated from the assumed structural parameters in Table 1 indicated that the T-T form was nearly prolate symmetric top with Ray's asymmetric parameter of −0.989. A large component of the dipole moment in this molecule was expected to lie close to the a axis. Consequently, strong a-type R-branch absorption lines were expected.

Many groups of relatively strong absorption lines were observed at intervals of about 4600 MHz. The strong

Table 1. Structural parameters assumed for 1-propanethiol

r(C–C)	1.534 Å	∠CCS	111.0°
r(C–S)	1.819	∠CSH	96.5°
r(S–H)	1.336	$\angle C_2C_1H$	110.1°
r(C–H)	1.094	$\angle C_3C_2H$	109.6°
∠CCC	110.5°	∠HCH	108.8°

Table 2. Observed frequencies of 1-propanethiol

Transition	Normal species				D species	
	Ground state		Excited state		Ground state	
	Obsd	$\Delta\nu$[a)]	Obsd	$\Delta\nu$[a)]	Obsd	$\Delta\nu$[a)]
2_{02}-1_{01}	9191.36	0.08	9200.31	0.17	9048.81	0.10
2_{11}-1_{10}	9286.88	−0.07	9292.76	−0.06		
2_{12}-1_{11}	9096.26	0.13	9108.14	0.10	8960.02	−0.07
3_{03}-2_{02}	13786.41	0.39	13799.05	−0.44	13572.58	0.28
3_{12}-2_{11}	13930.31	0.08	13939.16	0.11	13706.65	−0.06
3_{13}-2_{12}	13644.39	0.39	13662.10	0.22	13440.20	0.25
3_{21}-2_{20}	13789.57	0.96	13801.64	−0.16		
3_{22}-2_{21}	13787.77	0.46	13799.95	−0.70		
4_{04}-3_{03}	18379.98	0.11	18398.26	0.28	18095.03	0.05
4_{13}-3_{12}	18573.19	−0.07	18584.58	−0.49	18275.27	0.03
4_{14}-3_{13}	18191.78	0.16	18215.70	0.20	17919.69	0.11
4_{22}-3_{21}	18385.97	−0.10	18403.49	−0.03		
4_{23}-3_{22}	18383.10	0.26	18401.12	0.48		
4_{31}-3_{30}, 4_{32}-3_{31}	18383.79	0.06	18401.93	0.49		
5_{05}-4_{04}	22972.57	0.17	22995.28	−0.03	22616.49	0.04
5_{14}-4_{13}	23215.84	−0.12	23230.95	0.16	22843.44	−0.05
5_{15}-4_{14}	22738.79	−0.14	22768.94	0.10	22398.93	0.02
5_{23}-4_{22}	22984.45	−0.15	23006.66	0.41		
5_{24}-4_{23}	22978.46	0.32	23001.52	1.08		
5_{32}-4_{31}		−0.32		1.14		
5_{33}-4_{32}	22979.66	−0.30	23003.22	1.16		
5_{41}-4_{40}, 5_{42}-4_{41}		0.08		1.50		
6_{06}-5_{05}	27563.42	0.08	27590.92	−0.28	27136.40	0.00
6_{15}-5_{14}	27858.24	−0.03	27876.14	−0.01	27411.48	0.13
6_{16}-5_{15}	27285.81	−0.04	27321.77	−0.05	26877.66	−0.20
6_{24}-5_{23}	27584.18	−0.30	27610.57	0.48		
6_{25}-5_{24}	27573.22	0.04	27600.17	0.18		
6_{33}-5_{32}		−0.39	27603.14	0.24		
6_{34}-5_{33}		−0.35		0.28		
6_{42}-5_{41}, 6_{43}-5_{42}	27576.04	0.31	27602.51	0.24		
6_{51}-5_{50}		0.60	27602.25	0.24		
6_{52}-5_{51}				0.23		
7_{07}-6_{06}	32152.28	−0.04	32185.52	0.16	31654.55	0.03
7_{16}-6_{15}	32499.99	−0.07	32521.24	0.18	31978.55	−0.18
7_{17}-6_{16}	31831.90	−0.37	31874.15	−0.23	31356.26	−0.11
7_{25}-6_{24}	32185.52	−0.45	32216.35	0.93		
7_{26}-6_{25}	32167.83	−0.06	32199.58	0.32		
7_{34}-6_{33}	32172.90	−0.23		−0.27		
7_{35}-6_{34}		−0.14		−0.20		
7_{43}-6_{42}, 7_{44}-6_{43}		−0.12	32203.67	−0.62		
7_{52}-6_{51}, 7_{53}-6_{52}	32171.89	0.34		1.14		
7_{61}-6_{60}, 7_{62}-6_{61}		0.58		1.35		

Only the frequencies of the transitions with $K_{-1}=1,0$ were fitted to the rigid rotor Hamiltonian. a) Obsd−Calcd. The calculated frequencies were obtained using the constants in Table 3.

Table 3. Rotational constants of 1-propanethiol (MHz)

	Normal species		D species
	Ground state	Excited state	Ground state
A	23429(649)	24483(934)	21758(461)
B	2345.591(35)	2346.314(43)	2306.713(25)
C	2250.181(35)	2253.911(42)	2217.793(25)
Δ(amu Å^2)[a]	12.43(61)	11.81(79)	14.44(49)

Values in parentheses denote the standard deviations and apply to the last significant digits. a) $I_a+I_b-I_c$.

lines in a group were preliminarily assigned to the T-T isomer in the ground vibrational state and fitted to the rigid rotor Hamiltonian by the least-squares method. These assigned absorption lines are accompanied by the several satellite lines. It seems reasonable to ascribe some of these satellite lines to the excited vibrational states. One set of the absorption lines, picked up from the bushes of the satellite lines, could be fitted to the rigid rotor Hamiltonian by the least-squares method and assigned to the first excited vibrational state. The observation of the temperature dependence of the lines led to the confirmation of the assignments of the sets of lines to the ground and excited vibrational states. The other sets of satellite lines were partly observed. The observed and calculated frequencies of the transition lines, assigned to the ground and excited states, are given in Table 2 and are in good agreement. The rotational constants obtained by the least-squares fit are given in Table 3.

The $\Delta(=I_a+I_b-I_c)$ value of 12.4 amu Å^2 calculated from the rotational constants for the ground states is very different from that of 9.569 amu Å^2 predicted from the T-T model. This indicates that the molecular structure in question deviates from the T-T form which has a plane of symmetry.

Table 4 shows a comparison of the observed rotational constants, Ray's asymmetry parameters, and the values of $\Delta(I_a+I_b-I_c)$ with those calculated from the assumed structural parameters for the five possible rotational isomers. A comparison of the observed constants with the calculated ones in Table 4 reveals that the observed spectrum assigned to the ground vibrational state can reasonably be attributed to the T-G rotational isomer. Although the existence of the T-T and G-T forms has been confirmed in the gaseous and liquid states,[2] that of the T-G rotational isomer has not yet been reported. The exsitence of the T-G isomer of 1-propanethiol in the gas phase is consistent with the following facts: the *trans* form of 1-propanethiol around the central C–C bond is more stable than the *gauche* form in the gas phase[1,2] and the *gauche* isomer of ethanethiol with respect to the C–S bond is more stable than the *trans* isomer in the gaseous state.[6]

There are two possible equivalent configurations in the T-G form which can interchange with each other through thiol internal motion. The spectrum of the T-G form, therefore, can be expected to be split into doublets due to the tunneling effect of the thiol internal rotation, as is observed in the spectrum of ethanethiol.[6] Therefore, the counterpart lines of the doublets were searched for in the vicinity of the lines assigned to the rigid T-G rotor, but there was no absorption line to be assigned as a counterpart line. Consequently, the analysis of the spectrum was done assuming the rigid T-G form.

Deuterated Species. The transitions of the deuterated species were predicted from the assumed T-G model with the same structural parameters as for the normal species. The observed transition lines in Table 2 were identified by measurements of their Stark effects and fitted to the rigid rotor Hamiltonian in order to obtain the rotational constants in Table 3. Table 2 indicates that the observed and calculated transition frequencies are in good agreement. Table 4 shows that the observed Δ value of 14.44 amu Å^2 is in good agreement with the value of 14.016 amu Å^2 calculated from the T-G model.

Conformation of 1-Propanethiol. The r_s coordinates of the thiol hydrogen atom were calculated from the observed rotational constants of the normal and deuterated species in Table 3, using the expressions given by Kraitchman.[7] Table 5 shows that the r_s coordinates obtained from the observed rotational constants are in good agreement with the coordinates calculated from the T-G model. This is consistent with the result ob-

Table 4. Observed and calculated rotational constants (MHz) of 1-propanethiol

	A	B	C	κ	Δ[a] (amu Å^2)
Model			Normal species		
G-T	11222	3448.28	2915.87	−0.87180	18.273
G-G′	10869	3500.00	2980.33	−0.86826	21.316
G-G	10867	3571.76	2971.11	−0.84748	17.983
T-T	24153	2374.03	2253.81	−0.98902	9.569
T-G	23341	2393.03	2288.57	−0.99008	12.012
Obsd (Ground state)	23429	2345.59	2250.18	−0.99099	12.43
			D species		
T-T	23004	2316.74	2316.74	−0.99393	9.570
T-G	21580	2354.90	2256.05	−0.98977	14.016
Obsd (Ground state)	21758	2306.71	2217.79	−0.99089	14.44

The calculations of the rotational constants for the models were based upon the assumption that the *gauche* form has the dihedral angle of 120°. a) $I_a+I_b-I_c$.

Table 5. r_s coordinates of the thiol hydrogen atom (Å)

Coordinate	Obsd	Calcd	
		T-G	T-T
a	1.585 (85)	1.553	2.296
b	0.83 (15)	0.836	1.040
c	1.11 (13)	1.050	0

Values in parentheses denote the uncertainties estimated from the standard deviations of the rotational constants.

tained above from Table 4.

Dipole Moment. The dipole moments of the molecules were determined from the measurements of the Stark effect of the absorption lines for the ground and excited vibrational states of the normal species and for the ground state of the deuterated species. The observed Stark coefficients are listed in the third, sixth, and eighth columns in Table 6 for the ground and excited vibrational states of the normal species, and for the ground state of the deuterated species, respectively. The electric field inside the absorption cell was calibrated by observing the Stark shifts of the transitions, $1\leftarrow0$ and $2\leftarrow1$, of OCS, whose dipole moment is 0.71521 D.[8]

In the T-T form, the component of μ_c along the c principal axis should be zero due to the plane of symmetry. The T-G rotational isomer, however, has no electronic plane of symmetry, and it is expected that all three components of μ will be nonzero. Schmidt and Quade[6] have report d that, in the *gauche* isomer of ethanethiol, the inclusion of the tunneling energy in the denominator of the Stark coefficient of μ_c^2 gave the correct variation of $\Delta\nu/E^2$ for the doublet split due to the tunneling motion of the thiol hydrogen in the normal spectrum. We proceeded, however, to analyze the observed Stark coefficients without taking account of the tunneling motion of the thiol hydrogen atom, because we could not observe the doublet lines split due to the tunneling effect described above.

The least-squares fit to obtain μ_a and μ_b, assuming $\mu_c=0$, for the ground state gave the results presented in the fourth column (Calcd I) of Table 6. The calculated Stark coefficients for the M=0 components of the transitions, $3_{12}\leftarrow2_{11}$, $4_{04}\leftarrow3_{03}$, and $4_{13}\leftarrow3_{12}$, are very different from the observed ones. These deviations may be attributed to the assumption of the μ_c component being zero, since the μ_c component of the dipole moment in this molecule, if there is one, should give rise to a large effect on the Stark coefficients of these transitions. This fact indicates that the molecule in question is not in the T-T form. This result is consistent with the one deduced from the observed and calculated rotational constants.

Since the T-G isomer was likely to exist in the gaseous state, as has been described above, the observed Stark coefficients were fitted to obtain all three components of the dipole moment by the following procedures. First, since the μ_b and μ_c components have a smaller

Table 6. Stark coefficients ($\Delta\nu/E^2$[MHz/(V/cm)^2]$\times10^{-5}$) and dipole moments of 1-propanethiol

Transition	|M|	Normal species					D species	
		Ground state			Excited state		Ground state	
		Obsd	Calcd I	Calcd II	Obsd	Calcd	Obsd	Calcd
2_{02}-1_{01}	0	−2.19	−2.05	−1.99	−2.05	−2.06		
	1	2.04	1.67	1.64	2.07	1.68		
2_{12}-1_{11}	0	1.89	1.68	1.61	1.83	1.68		
2_{11}-1_{10}	0	1.46	1.65	1.56	1.41	1.64		
3_{03}-2_{02}	0	−0.40	−0.35	−0.39	−0.42	−0.36	−0.40	−0.38
	1	−0.14	−0.10	−0.13	−0.11	−0.11	−0.13	−0.13
	2	0.63	0.64	0.62	0.50	0.65	0.63	0.63
3_{13}-2_{12}	0	−0.10	−0.07	−0.08	−0.10	−0.09	−0.10	−0.10
	1	5.02	5.33	5.02	5.15	5.47	5.75	5.49
	2	19.9	21.5	20.3	20.1	22.2	23.1	22.2
3_{12}-2_{11}	0	0.18	−0.10	0.12			0.19	0.19
	1	−5.27	−5.18	−4.69	−4.38	−5.30	−5.20	−5.10
	2	−19.1	−20.4	−19.1			−19.9	−21.0
4_{04}-3_{03}	0	−0.39	−0.15	−0.35	−0.19	−0.19		
	2	−0.14	0.05	−0.10				
	3				0.34	0.29		
4_{14}-3_{13}	0	−0.12	−0.16	−0.10				
	1	0.52	0.47	0.48				
	2	2.23	2.36	2.24				
4_{13}-3_{12}	0	−1.37	−0.08	−1.68				
μ_a(D)			1.56	1.52±0.01		1.56±0.01		1.53±0.03
μ_b(D)			0.2	0.12±0.08		0.15±0.10		0 ±0.2
μ_c(D)			0(Assumed)	0.73±0.08		0.4 ±0.3		0.53±0.40
μ_{total}(D)			1.57	1.69±0.05		1.62±0.20		1.62±0.30

effect on the Stark coefficients for the a-type R-branch transitions than the μ_a component, the observed Stark coefficients of the M=0 components of the transitions, $3_{03}\leftarrow 2_{02}$, $3_{12}\leftarrow 2_{11}$, $3_{13}\leftarrow 2_{12}$, and $4_{14}\leftarrow 3_{13}$, all sensitive to the μ_b and μ_c components, were fitted to obtain all three components, μ_a, μ_b, and μ_c respectively. The values of μ_b and μ_c obtained are shown in the fifth column (Calcd II) of Table 6. Next, the values of μ_b and μ_c obtained above were kept fixed, and all the observed Stark coefficients were fitted to obtain the μ_a component. The results are listed in the fifth column of Table 6. The observed and calculated Stark coefficients are in good agreement, as a whole.

The observed Stark coefficients for the excited vibrational state of the normal species and for the ground state of the deuterated species were fitted to obtain all three components, μ_a, μ_b, and μ_c, by the same procedure as was used for the ground state of the normal species. The results are given in the seventh and last columns of Table 6 respectively.

The value of the total dipole moment of 1-propanethiol in the gas phase obtained in this work, 1.69 D, is considerably larger than the value of 1.33 D determined in a benzene solution.[9] This difference may be compared with that reported for ethanethiol; the dipole moments determined by microwave spectroscopic investigation, were 1.58 and 1.61 D in the gas phase for the *trans* form and for the *gauche* form respectively,[6] and 1.39 D in a benzene solution.[10]

The values of μ_a, μ_b, and μ_c for the T-G isomer of 1-propanethiol determined in this work can be compared with the values of μ_a (1.49 D), μ_b (0.19 D), and μ_c (0.59 D) for the *gauche* isomer of ethanethiol in the gas phase.[6]

Excited Vibrational State. Our measurements of the intensities of the transition lines, $J=2\leftarrow 1$, $3\leftarrow 2$, and $4\leftarrow 3$, in the excited state relative to the lines in the ground state yielded the vibrational frequency of 136 ± 35 cm^{-1}. This value is very close to the $-CH_2-CH_2-$ torsional frequency of 130 cm^{-1} calculated using the Urey-Bradley force field.[2] Therefore, the assigned vibrational satellite can reasonably be ascribed to the excited state of the $-CH_2-CH_2-$ torsional mode.

References

1) R. E. Pennington, D. W. Scott, H. L. Finke, J. P. McCullough, J. F. Messerly, I. A. Hossenlopp, and Guy Waddington, *J. Am. Chem. Soc.*, **78**, 3266 (1956).
2) M. Hayashi, Y. Shiro, and H. Murata, *Bull. Chem. Soc. Jpn.*, **39**, 112 (1966).
3) E. Hirota, *J. Chem. Phys.*, **32**, 283 (1962).
4) T. N. Sarachman, *J. Chem. Phys.*, **39**, 469 (1963).
5) A. A. Abdurahmanov, R. A. Rahimova, and L. M. Imanov, *Phys. Lett. A*, **32**, 123 (1970).
6) R. E. Schmidt and C. R. Quade, *J. Chem. Phys.*, **62**, 3864 (1975).
7) J. Kraitchman, *Am. J. Phys.*, **21**, 17 (1953).
8) J. S. Muenter, *J. Chem. Phys.*, **48**, 4544 (1968).
9) E. C. E. Hunter and J. R. Partington, *J. Chem. Soc.*, **1932**, 2812.
10) E. C. E. Hunter and J. R. Partington, *J. Chem. Soc.*, **1931**, 2062.

Thermal Decomposition of Hydrogen Cyanide in Shock Waves

Kiyohiko TABAYASHI, Takayuki FUENO, Kenji TAKASA, Okitsugu KAJIMOTO, and Kazuo OKADA

Department of Chemistry, Faculty of Engineering Science, Osaka University, Toyonaka, Osaka 560

(Received December 17, 1976)

The thermal decomposition of hydrogen cyanide diluted to 0.2, 0.5, and 1.0 mol% in argon was studied behind incident shock waves over the temperature range 2600—3600 K. The decomposition process was followed by monitoring the CN $X^2\Sigma^+$-$B^2\Sigma^+$ (0-0) absorption centered at 3883 Å. The bimolecular rate constants for the reaction HCN+Ar→H+CN+Ar were obtained from the initial slopes of absorption; $k_1=(1.26\pm0.28)\times10^{16}$ exp[$-(99.69\pm1.39)$kcal mol$^{-1}/RT$] cm^3 mol^{-1} s^{-1}. The kinetic results are well fitted by the classical collision-theory expression, $k_1=\lambda(Z/n!)(E/RT)^n\exp(-E/RT)$, with $\lambda=0.22$, $n=3.5$, and $E=D_0$(H-CN)$=118.7$ kcal/mol. The overall absorption profiles were found to be explicable on the basis of the reaction scheme involving the homorecombinations of H and CN as well as the chain reaction with H and CN as carrier species.

Precise kinetic studies of the thermal decomposition of cyano compounds in shock waves have already been reported for cyanogen (C_2N_2)[1,2] chlorocyanogen (ClCN),[3] and bromocyanogen (BrCN).[4,5] The primary step of the overall decomposition process is established to be the bimolecular reaction of these compounds with diluent gas, to give CN radicals. The rate parameters obtained for this primary process over specified temperature ranges were rationalized reasonably well in terms of the classical collision theory.[6]

In this work, we extend our absorption studies[2,5] to the decomposition of hydrogen cyanide in argon behind incident shock waves. As in the cases of ClCN[3] and BrCN,[4,5] the overall kinetics of the HCN decomposition is expected to conform to the following reaction scheme:

$$HCN + Ar \rightleftharpoons H + CN + Ar \qquad \Delta H_0^\circ = 118.7 \text{ kcal/mol}, \quad (1)$$

$$C_2N_2 + Ar \rightleftharpoons 2CN + Ar \qquad \Delta H_0^\circ = 125.5 \text{ kcal/mol}, \quad (2)$$

$$H_2 + Ar \rightleftharpoons 2H + Ar \qquad \Delta H_0^\circ = 103.3 \text{ kcal/mol}, \quad (3)$$

$$CN + HCN \rightleftharpoons C_2N_2 + H \qquad \Delta H_0^\circ = -6.9 \text{ kcal/mol}, \quad (4)$$

$$H + HCN \rightleftharpoons H_2 + CN \qquad \Delta H_0^\circ = 15.5 \text{ kcal/mol}. \quad (5)$$

(1 kcal=4.184 kJ)

Our primary purpose is to obtain accurate rate constant k_1 for the forward process of Reaction 1. Examination of the validity of the assumed mechanism (1)—(5) is also an aim of this work.

Experimental

Material. Hydrogen cyanide was generated[7] by pouring a saturated aqueous solution of sodium cyanide onto the surface of sulfuric acid and dried by passing through anhydrous calcium chloride. It was distilled over diphosphorus pentaoxide under a dry nitrogen atmosphere. The material was solidified at the temperature of Dry Ice-acetone bath and degassed several times by the freeze-thaw method. Mass spectrometric analysis of the purified sample showed no indication of impurities. Argon, from the Osaka Sanso Kogyo Corp., having a purity of 99.99% was used as a diluent gas without further purification. Reaction mixtures of 0.2, 0.5, and 1 mol% HCN in Ar were prepared at a total pressure of 600 Torr and stored in 10-l glass flasks. Mixing was allowed to proceed by diffusion for at least 12 h before use.

Procedure. Experiments were carried out in a stainless-steel cylindrical shock tube having an internal diameter of 10.4 cm. Variations in concentration of the CN radicals formed behind incident shock waves were followed by means of specific absorption spectroscopy. Details of the shock tube and associated equipments have been described previously.[2]

Shock waves were generated with hydrogen as driver gas. Mylar diaphragms of 0.1 and 0.188 mm in thickness, which corresponded to the burst driver pressures of 4 and 7.5 atm (1 atm=101325 Pa), respectively, were used. Prior to filling the test gas, the driven section was evacuated to a pressure less than 10^{-5} Torr. The leak rate was no greater than 8.5×10^{-6} Torr/min (1 Torr=(101325/760) Pa). The initial pressure, P_1, of the gas mixture was varied from 6.0 to 30 Torr to produce a given temperature condition for operation. The temperature range studied was 2600 to 3600 K.

For measuring the CN concentrations, portions of CN $X^2\Sigma^+$-$B^2\Sigma^+$ (0-0) absorption (P branch, head at 3883 Å, 1 Å=10^{-10} m) were utilized. A Rikotsusho MC-50 grating monochromator with 0.27-mm entrance and exit slits was set to isolate the spectral bandwidth 3880.6—3884.4 Å. This region encompasses the overlapping rotational lines $J=12$—44 of the ground state CN ($X^2\Sigma^+$, $v=0$).

Thermodynamic properties of the shock-heated gas immediately behind the shock front were calculated from the initial temperature and pressure in conjunction with the measured incident shock velocity. The gases were assumed to be ideal; no correction was made for the reaction heat behind the shock wave. Boundary layer effects[8] on the gas properties were estimated to be small under our experimental conditions and hence were ignored throughout. All calculations were carried out on a NEAC N-2200 digital computer.

Results

Equilibrium. The oscillographic records of the CN absorption generally showed a fast initial rise, followed by a gradual rise to a steady level. This final constancy in absorption intensity is an indication that the overall decomposition attains an equilibrium within the observation time.

Concentrations of the five species HCN, H, CN, H_2, and C_2N_2 at any given time should bear the following constraints:

$$[HCN]_0 = [HCN] + [CN] + 2[C_2N_2], \quad (6)$$

$$[HCN]_0 = [HCN] + [H] + 2[H_2], \quad (7)$$

where $[HCN]_0$ denotes the concentration of hydrogen cyanide at zero time. It follows that the concentra-

Table 1. HCN dissociation rate data

m mol%	P_1 Torr	U_s mm/μs	ρ_{21}	T_2 K	$[Ar]_0$ 10^{-6} mol/cm^3	x_e	x_e-y_e	x_e-z_e	k_1 cm^3 mol^{-1} s^{-1}
0.217	28.5	1.60	3.57	2577	5.49	0.360	0.240	0.198	4.43×10^7
0.217	22.1	1.70	3.61	2861	4.32	0.650	0.590	0.529	3.05×10^8
0.217	13.8	1.92	3.69	3590	2.74	0.989	0.987	0.982	8.59×10^9
0.515	23.0	1.69	3.61	2846	4.47	0.519	0.432	0.364	2.55×10^8
0.498	8.53	1.75	3.63	3016	1.66	0.805	0.773	0.726	5.96×10^8
0.515	15.0	1.82	3.66	3235	2.96	0.877	0.858	0.820	2.38×10^9
0.498	6.45	1.92	3.69	3591	1.28	0.988	0.986	0.981	8.43×10^9
1.02	11.4	1.73	3.62	2968	2.19	0.633	0.570	0.500	6.46×10^8
1.02	6.90	1.86	3.67	3368	1.35	0.935	0.925	0.901	5.70×10^9
1.02	6.18	1.92	3.69	3570	1.22	0.975	0.971	0.961	1.05×10^{10}

tions of only three of the five species can be regarded as independent unknown quantities. Thus, the overall equilibrium can be represented by the scheme comprising the three independent local equilibria as follows:

$$\underset{(1-x_e)}{HCN} \rightleftharpoons \underset{(x_e-z_e)}{H} + \underset{(x_e-y_e)}{CN}, \quad (8)$$

$$\underset{(y_e/2)}{C_2N_2} \rightleftharpoons \underset{(x_e-y_e)}{2CN}, \quad (9)$$

$$\underset{(z_e/2)}{H_2} \rightleftharpoons \underset{(x_e-z_e)}{2H}. \quad (10)$$

The fractions of dissociation at equilibrium, x_e, y_e, and z_e, which are defined as in the above scheme, can be obtained by solving the following set of simultaneous equations:

$$K_1 = m(x_e-y_e)(x_e-z_e)P/(1-x_e)S, \quad (11)$$

$$K_2 = m(x_e-y_e)^2P/(y_e/2)S, \quad (12)$$

$$K_3 = m(x_e-z_e)^2P/(z_e/2)S. \quad (13)$$

where K_1, K_2, and K_3 are the pressure-based equilibrium constants for Reactions 8—10, respectively; m is the initial molar fraction of HCN; P is the total pressure of the shock-heated gas mixture; and S is the quantity defined by

$$S = 1 + m(x_e-y_e/2-z_e/2). \quad (14)$$

Evaluations of the equilibrium constants were based on the thermodynamic data listed in the JANAF Tables[9] except for the new values $\Delta H_f^\circ(CN)=99.5$ kcal/mol[2] and $\Delta H_f^\circ(HCN)=32.4$ kcal/mol.[10] The values of x_e, x_e-y_e, and x_e-z_e thus calculated for some representative runs are shown in Table 1.

The equilibrium concentration of CN radicals is given by

$$[CN]_e = m(x_e-y_e)[Ar]_0. \quad (15)$$

$[Ar]_0$ being the concentration of argon heated by the shock. $[CN]_e$ should be related with the observed absorbance at equilibrium by

$$\ln(I_0/I_e) = \beta_{00}lF_{ab}(T)[CN]_e, \quad (16)$$

where β_{00} is the effective absorption coefficient for CN radicals in the absorbing levels ($X^2\Sigma^+$, $v=0$, $J=12-44$); $l=10.4$ cm is the length of optical path across the tube diameter; and $F_{ab}(T)$ is the fractional population of the absorbing CN($X^2\Sigma^+$) radicals at temperature T. In the present work, $F_{ab}(T)$ is given by

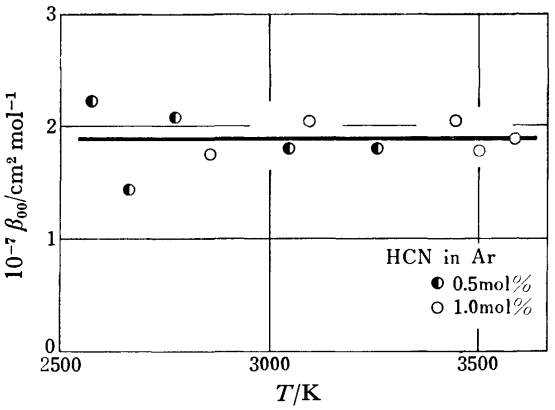

Fig. 1. Temperature variation of the CN absorption coefficient β_{00} at 3883 Å.

$$F_{ab}(T) = \frac{\sum_{J=12}^{44}(2J+1)\exp[-J(J+1)\varepsilon_{rot}/kT]}{Q_{rot}Q_{vib}}, \quad (17)$$

where ε_{rot} denotes the rotational quantum of the CN radical and where Q_{rot} and Q_{vib} respectively stand for its rotational and vibrational partition functions.

The absorption coefficient β_{00} which is related with the absorbance by Eq. 16 should by least temperature-dependent.[2] As is shown in Fig. 1, the values of β_{00} calculated from Eq. 16 for different runs were indeed nearly constant over the entire temperature range studied. The results assure that the assumption concerning the complete equilibration of Reactions 1—5 is basically correct and that the influence of CN emission on the absorbance is not significant below 3600 K. The average β_{00} value was $(1.90\pm0.12)\times10^7$ cm^2/mol.

Dissociation Kinetics. At the initial stage of reaction, disappearance of hydrogen cyanide by Reaction 1 is the only process to be considered. Thus, the bimolecular dissociation rate constants k_1 can be evaluated from the initial slopes of the CN absorption traces. Guided by Eq. 16, we may write:

$$k_1 \equiv (d[CN]/dt)_0/[HCN]_0[Ar]_0$$
$$= r_0/\beta_{00}lF_{ab}(T)[HCN]_0[Ar]_0, \quad (18)$$

where r_0 is the initial slope of the absorbance

$$r_0 = \{d\ln(I_0/I)/dt\}_0. \quad (19)$$

We set $\beta_{00}=1.90\times10^7$ cm^2/mol as has been determined

Table 2. Rate constants selected for integration

Reaction	Rate constant ($cm^3\ mol^{-1}\ s^{-1}$)	Reference
(1)	$k_1=1.26\times10^{16}\exp(-99.69\ kcal\ mol^{-1}/RT)$	This work
(2)	$k_2=6.66\times10^{16}\exp(-98.64\ kcal\ mol^{-1}/RT)$	2
(3)	$k_3=2.23\times10^{12}\ T^{1/2}\exp(-92.60\ kcal\ mol^{-1}/RT)$	12
(4)	$k_{-4}=8.0\times10^{13}\exp(-6.0\ kcal\ mol^{-1}/RT)$	—
(5)	$k_5=5.0\times10^{13}\exp(-12.0\ kcal\ mol^{-1}/RT)$	—

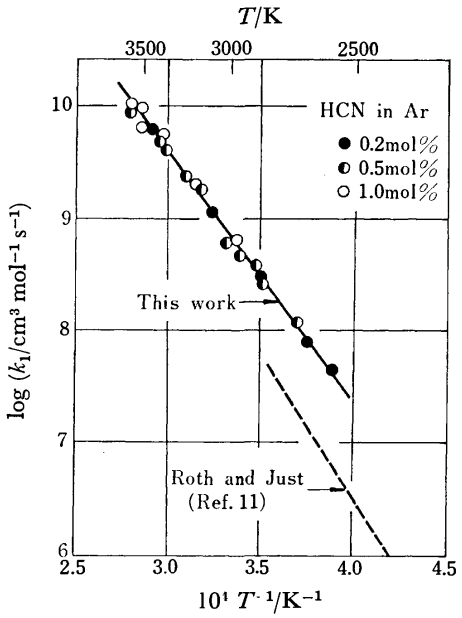

Fig. 2. Arrhenius plots of k_1.
$k_1=1.26\times10^{16}\exp(-99.69\ kcal\ mol^{-1}/RT)\ cm^3\ mol^{-1}\ s^{-1}$.

in the preceding section.

Kinetic data were taken for 0.2, 0.5, and 1.0% HCN-Ar mixtures at the total pressures between 0.353 and 1.16 atm. The temperature range was limited by immeasurably small initial rise of the absorption intensities below 2600 K and by significant influence of the CN emission on the absorption trace above 3600 K. The values of k_1 obtained for representative runs are listed in Table 1, together with pertinent experimental data, *i.e.*, the initial pressure of the test gas, P_1, the measured shock velocity, U_s, the density ratio across the shock front, ρ_{21}, the reaction temperature, T_2, and the concentration of Ar behind the incident shock.

Figure 2 shows Arrhenius plots of k_1 obtained for a total of 21 experiments. A single straight line fits the plots, irrespective of the $[HCN]_0/[Ar]_0$ ratio. Least-squares treatment of the data led to the Arrhenius expression:

$$k_1 = (1.26\pm0.28)\times10^{16}\times\exp[-(99.69\pm1.39)\ kcal\ mol^{-1}/RT]\ cm^3\ mol^{-1}\ s^{-1}. \quad (20)$$

In Fig. 2, the rate constants which Roth and Just[11] have recently obtained by the H-atom resonance absorption spectroscopy are compared with our results. Their rate constants are expressed by

$$k_1^{RJ} = 5.7\times10^{16}\times\exp(-117.1\ kcal\ mol^{-1}/RT)\ cm^3\ mol^{-1}\ s^{-1}, \quad (21)$$

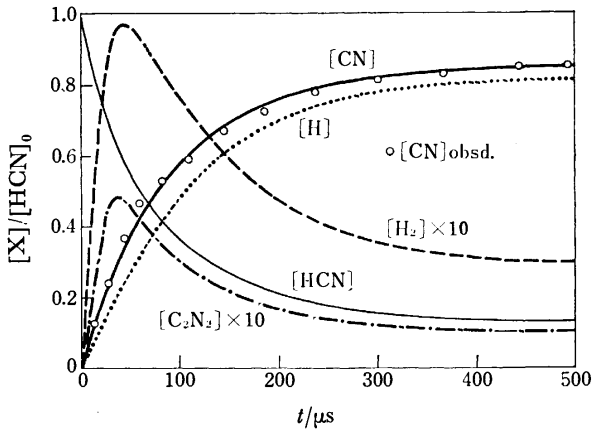

Fig. 3. Relative concentrations *vs.* particle time.
$T_2=3235$ K, $m=0.5$ mol%, $[HCN]_0=1.53\times10^{-8}$ mol/cm³, $[CN]_e=1.31\times10^{-8}$ mol/cm³.

in the temperature range 2200—2700 K. Their results are uniformly smaller than ours by a factor of *ca.* 6 in the overlapping temperature region.

Overall kinetics. The rate equations pertinent to the entire mechanism (1)—(5) were subjected to numerical (Runge-Kutta-Gill) integration on a computer. Table 2 presents the rate parameters used for computation. The rate constants k_1, k_2, and k_3 are those determined at high temperatures (~3000 K) behind shock waves.[2,12] The rate constant k_{-4} at room temperature was found to be $5.2\times10^8\ cm^3\ mol^{-1}\ s^{-1}$ in a cyanogen flow.[13] Assuming the activation energy for this reaction to be close to its endothermicity, we estimated the preexponatial factor of k_{-4} to be $8\times10^{13}\ cm^3\ mol^{-1}\ s^{-1}$. For Reaction 5, we estimated the rate parameters by analogy with other metathetic reactions of the X+XCN type.[3,5] Rate constants for the reverse reactions were all calculated from those for the forward reactions and the equilibrium constants. The time step used for integration was 0.2 μs.

The results of computation for the case of $T_2=3235$ K as an example are shown in Fig. 3. The abscissa expresses the concentrations of the various species relative to $[HCN]_0$ while the ordinate, the particle time t. The experimental concentrations of CN radicals read from the CN absorption records are indicated with open circles. The agreement between the calculated and experimental concentration profiles of CN radicals is excellent.

The computation results for other temperatures were qualitatively much the same as those shown in Fig. 3. In all cases, the concentrations of H_2 and C_2N_2 reached their maxima at a relatively early stage of reaction while those of both H and CN increased monotonously. Im-

portantly, however, these initial spikes of the H_2 and C_2N_2 concentrations were not so large as to affect the initial slope of the CN concentration curve which was calculated separately for Reaction 1 alone. The only rate constants which are adjustable for the present computations are k_{-4} and k_5. We varied these rate constants over a wide range (by a factor of 5), but the computed concentration profiles remained essentially unaltered at least in the initial 20% region of the HCN decomposition. It was also verified that Reactions 2 and 3 exert virtually no influence on the initial portion of the CN concentration profile. Evaluation of k_1 from the initial slope of absorption is thus confirmed to be perfectly legitimate.

Discussion

The apparent activation energy of 99.7 kcal/mol observed for Reaction 1 is clearly below the dissociation energy of HCN (118.7 kcal/mol). The results indicate that the internal energy of the molecule should participate in the activation process. The situation can most conveniently be represented by the Fowler-Guggenheim expression:[6]

$$k_1 = \lambda(Z/n!)(E/RT)^n \exp(-E/RT). \quad (22)$$

Under the assumption that E is equal to $D_0(\mathrm{H-CN}) = 118.7$ kcal/mol, the best fit of the temperature variation is obtained when $n=3.5$. The least-squares fit of Eq. 22 with $n=3.5$ to the experimental values of k_1 led to the expression

$$k_1 = [(1.88\pm0.26)\times 10^{12}/3.5!]T^{1/2} \times (E/RT)^{3.5} \exp(-E/RT)\ \mathrm{cm^3\ mol^{-1}\ s^{-1}}. \quad (23)$$

The value of $n=3.5$ obtained indicates that the number of the squared terms contributing to the dissociation process is 9, a nearly maximal value permissible from a classical point of view. Assuming a mean HCN–Ar collision diameter of 3.54 Å, we obtain the steric factor $\lambda=0.22$. These results do not appear unreasonable.

The results reported by Roth and Just[11] are somewhat anomalous in the sense delineated above. Their activation energy 117.1 kcal/mol for Reaction 1 is only slightly below the bond dissociation energy $D_0=118.7$ kcal/mol. If their rate constants, Eq. 21, are to be expressed in the Fowler-Guggenheim form, it is required to set $n=1$, which in itself may not be quite unreasonable. However, use of $n=1$ leads to the steric factor $\lambda=9.2$. Such an anomalously *large* λ has never been met with in the existing literature. Even when we set D_0 equal to 122.4 kcal/mol as these authors have done in their work, the results are still $n=1.5$ and $\lambda=4.0$. Perhaps, their resonance absorption technique involves some systematic errors.

It is interesting to note that, although HCN bears similarities to BrCN and ClCN in both the number of atoms and the kind of bonds involved, its activation invokes apparently more internal degrees of freedom than in the cases of its halogen homologs. More specifically, the rotational energy contributes to activation in the case of HCN only. This would not be surprising in view of the small momentum of inertia for HCN, a linear molecule which carries a hydrogen atom, an extremely light atom, at its terminal.

This work was supported in part by a Scientific Research Grant from the Ministry of Education (No. 011002).

References

1) W. Tsang, S. H. Bauer, and Cowperthwaite, *J. Chem. Phys.*, **36**, 1768 (1962).
2) T. Fueno, K. Tabayashi, and O. Kajimoto, *J. Phys. Chem.*, **77**, 575 (1973).
3) D. Schofield, W. Tsang, and S. H. Bauer, *J. Chem. Phys.* **42**, 2132 (1965).
4) P. J. Kayes and B. P. Levitt, *J. Chem. Soc. Faraday Trans. 1*, **69**, 1415 (1973).
5) K. Tabayashi, O. Kajimoto, and T. Fueno, *J. Phys. Chem.*, **79**, 204 (1975).
6) R. Fowler and E. A. Guggenheim, "Statistical Thermodynamics," Cambridge University Press, Cambridge (1952), pp. 495—499.
7) C. S. Marvel, Ed., "Organic Syntheses," Vol. 1, John Wiley & Sons, Inc., New York, N. Y. (1931), p. 314.
8) R. L. Belfold and R. A. Strehlow, *Ann. Rev. Phys. Chem.*, **20**, 247 (1969).
9) D. R. Stull, Ed., "JANAF Thermochemical Tables," Dow Chemical Co., Midland, Mich. (1965).
10) D. D. Wagman, W. H. Evans, V. B. Parker, I. Halow, S. M. Balley, and R. M. Schumm, "Selected Values of Chemical Thermodynamic Properties," Natl. Bur. Std. (U. S.) Tech. Note 270—3 (1968).
11) P. Roth and Th. Just, *Ber. Bunsenges. Phys. Chem.*, **80**, 171 (1976).
12) A. L. Myerson and W. S. Watt, *J. Chem. Phys.*, **49**, 425 (1968).
13) M. R. Dunn, C. G. Freeman, M. J. McEwav, and L. F. Phillips, *J. Phys. Chem.*, **75**, 2662 (1971).

Color and Precipitation Reactions of Lanthanoids with Chlorophosphonazo III

Tomitsugu TAKETATSU

Laboratory of Chemistry, College of General Education, Kyushu University, Ropponmatsu, Chuo-ku, Fukuoka 810

(Received August 16, 1976)

Aqueous solutions of pH 1—3 containing Chlorophosphonazo III chelates of lanthanoids give an absorption spectrum of the α-type, the spectrum showing two maximum peaks at approximately 620 and 670 nm, in the presence of an excessive amount of the reagent. However, the chelates of heavier lanthanoids give an absorption band of the β-type, which extends from 700 to 800 nm with a maximum at 745 nm, with an increase in the mole ratio of the metal against the reagent. A dark-violet precipitate forms from the solution, giving the β-type spectrum under certain experimental conditions. The combining ratio of the metal against the reagent in the precipitate is estimated to be 1:1. Since a reaction rate from the α-type to the β-type corresponds to the second order, the combining form between the metal and the reagent in the β-type chelate is assumed to be 2 : 2, *i.e.*, a dimer. The chelates of lanthanum to samarium do not give the β-type spectrum under the same conditions.

The Chlorophosphonazo III [2,7-bis(4-chloro-2-phosphonophenylazo)-1,8-dihydroxynaphthalene-3,6-disulfonic acid] reagent, which is one of the symmetrical bisazo derivatives of chromotropic acid, was used by O'Laughlin and Jensen to determine a micro-amount of the lanthanoids.[1] The determination was carried out by the measurement of the absorbance at a maximum peak near 670 nm of the absorption spectrum. The pattern of the spectrum was previously defined as α-type by the present author.[2] O'Laughlin *et al.* reported that, when the lutetium and ytterbium concentrations were increased to approximately half of the reagent concentration of 6×10^{-6}M at pH 3.0, a precipitate was formed and the solution became colorless.[1] The present author found the heavier lanthanoid chelates gave an absorption band, defined as of the β-type, which extends from 700 to 800 nm with a maximum at 745 nm, and a dark-violet precipitate is formed in the solution containing the β-type chelate under certain experimental conditions.[2]

In the present paper, the equilibrium relationship between the α-type and β-type chelates, the reaction rate of the change from the α-type to the β-type chelate, and the combining ratio of a metal against the reagent in the precipitate and the β-type chelate are investigated.

Experimental

Apparatus. All the absorption spectra were measured with a Hitachi EPS-3T automatic recording spectrophotometer. The hydrogen-ion concentration was determined by means of a Hitachi model M-4 pH meter.

Reagents. Standard aqueous solutions of lanthanoid chlorides were prepared from the respective oxides in a 99.9% purity.

Chlorophosphonazo III obtained from the Dojindo Co., Ltd., was used without further purification. The concentration was represented by multiplying the amount weighed by 0.76 because the purity of this reagent was 76%.[3]

Procedure. The absorption spectra were recorded after the prepared solutions had been allowed to stand for more than 50 h, unless otherwise indicated. Since the precipitate formed in the solution was readily dispersed by shaking, the measurement could be carried out by using the resulting solution.

The concentration of lanthanoid and phosphorus in the precipitate was estimated by the following procedure: the precipitate was obtained by adding 10 ml of a 2.4×10^{-4} M thulium, ytterbium, or lutetium chloride solution to 10 ml of a 2.4×10^{-4} M Chlorophosphonazo III solution at pH 1—2. The precipitate was then separated from the solution by centrifuging, and the supernatant was removed from the tube. An acidic solution of pH 1 containing a samll amount of magnesium chloride, used for preventing deflocculation of the precipitate, was added to the precipitate in the tube. The centrifuge tube was then shaked to disperse the precipitate into the solution. Again, the solution was removed from the precipitate by centrifuging. The dispersing and centrifuging was repeated 3—5 times. A part of the precipitate was then transferred into a conical beaker and decomposed by concentrated perchloric and nitric acids. After a clear solution had been obtained, the lanthanoid and phosphorus were determined spectrophotometrically by the O'Laughlin[1] and Lucena-Conde[4] methods respectively.

Results and Discussion

Absorption Spectra of the Lanthanoid Chelates. Figure 1 shows the absorption spectra of the aqueous

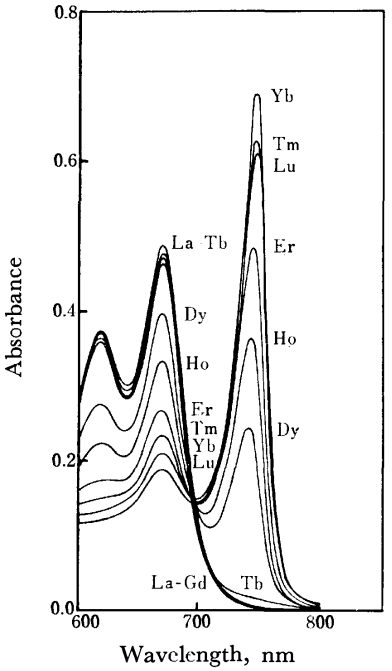

Fig. 1. Absorption spectra of lanthanoid Chlorophosphonazo III Chelates. Concentration of lanthanoids: 7.50×10^{-6}M. Concentration of reagent: 7.50×10^{-6} M. pH 1.6.

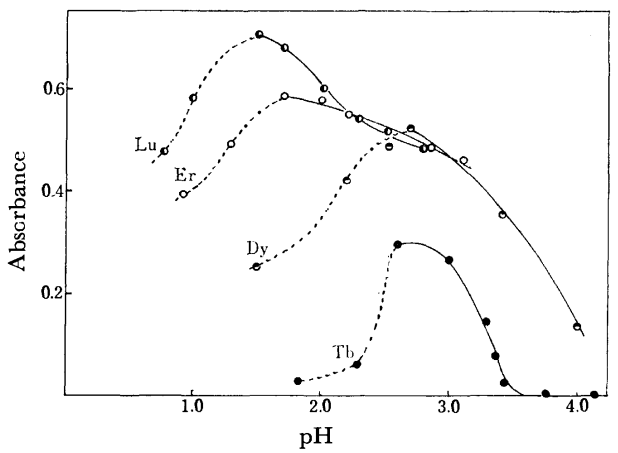

Fig. 2. Flariation of absorbance at 745 nm as a function of pH. Concentration of lanthanoids: 7.50×10^{-6}M. Concentration of reagent: 7.50×10^{-6}M.

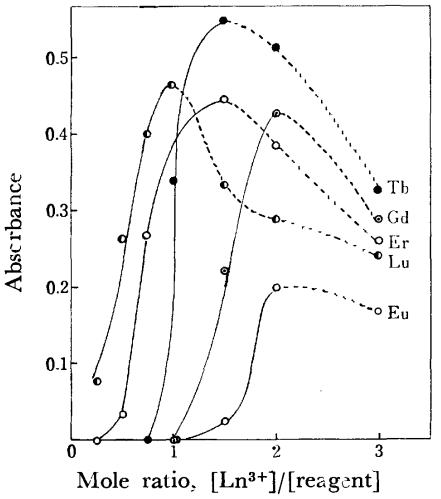

Fig. 3. Variation of absorbance at 745 nm as a function of mole ratio, $[Ln^{3+}]/[reagent]$.
Concentration of lanthanoids: 7.50×10^{-6}M. pH 2.5.

solution of pH 1.6 containing an equimole of each lanthanoid and Chlorophosphonazo III. The spectra of the chelates of lanthanum to terbium give an similar pattern and correspond to that of the α-type. On the other hand, the chelates of dysprosium to lutetium give a maximum absorption band at 745 nm, which is characteristic of the β-type. The tendency for the conversion from the α-type into the β-type increases with an increase in the atomic number, except in the case of lutetium.

Figure 2 shows the variation in the absorbance at 745 nm for the chelates of several lanthanoids as a function of the pH. The height of the maximum peaks and the degree of the transfer of the maximum position to the lower region increase with an increase in the atomic number. The precipitate was observed in a lower pH range than each maximum position; the dotted line indicates the range. The chelates of lanthanum to gadolinium do not give the β-type spectrum in the pH range between 1.0 and 4.0.

Figure 3 shows the variation in the absorbance at 745 nm as a function of the mole ratio of each lanthanoid

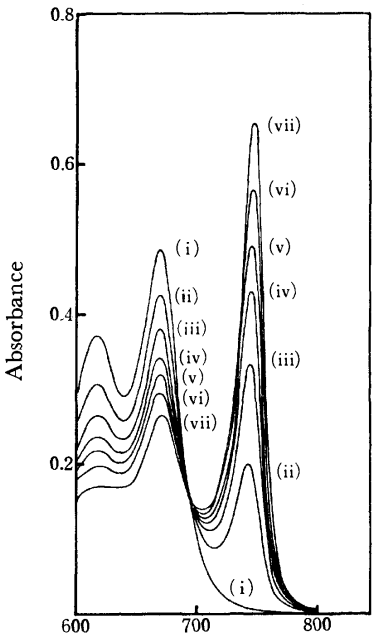

Fig. 4. Variation of absorption spectra of thulium chelate as a function of elapsing time.
Concentration of thulium: 7.50×10^{-6}M.
Concentration of reagent: 7.50×10^{-6}M. pH 2.0.
(i) 0.0, (ii) 0.25, (iii) 0.5, (iv) 1.0, (v) 2.0, (vi) 6.0, (vii) 72 h.

to the reagent. The intensity of the absorption band first increases and then decreases with an increase in the mole ratio. The maximum values of the ratio for thulium to lutetium, for terbium to erbium, and for europium to gadolinium were observed at the mole ratios of approximately 1 : 1, 1.5 : 1, and 2 : 1 respectively. However, the absorption band of the β-type was not observed in the case of lanthanum to samarium even when the mole ratio of [metal]/[reagent] attained 15 : 1.

Reaction Rate of the Variation from the α-Type to the β-Type Chelate. Figure 4 shows the variation in the absorption spectrum of the thulium chelate from the α-type to the β-type as a function of the elapsed time. The spectrum gives the typical α-type at first, and then the pattern changes to the β-type with time. An isosbestic point is observed at approximately 700 nm. This fact suggests that an equilibrium relationship exists between the α-type and β-type chelates. The order of the reaction rate was investigated, and the following results were obtained; (i) the concentration of the β-type chelate follows Beer's law at 745 nm, and (ii) x and a, which represent the absorbance at 745 nm after t and 72 h respectively, are proportional to the reacting and initial concentration of the α-type chelate respectively. Figure 5 shows that the reaction rate for the thulium chelate is second-order, because the $1/(a-x)$ *vs.* t diagram gives a straight line.

Composition of the β-Type Chelate. Figure 6 shows the the continuous-variation plots at 745 nm for the holmium chelate. The peak at the mole fraction [Ho]/([Ho]+[reagent]) of 0.5 indicates that the combining ratio is 1 : 1. Moreover, the mole ratio of the lantha-

TABLE 1. ESTIMATION OF THE COMBINING RATIO OF LANTHANOID TO A REAGENT BY MEANS OF AN ANALYSIS OF THE LANTHANOID AND PHOSPHORUS IN THE PRECIPITATE

Lanthanoid used as precipitants	Phosphorus in the precipitate (mmol)	Lanthanoid in the precipitate (mmol)	Combining ratio, [lanthanoid]/[reagent]
Lu^{3+}	3.390×10^{-4}	1.686×10^{-4}	1.00
Lu^{3+}	2.658×10^{-4}	1.354×10^{-4}	1.02
Lu^{3+}	1.665×10^{-4}	0.920×10^{-4}	1.10
Lu^{3+}	1.795×10^{-4}	0.917×10^{-4}	1.02
Yb^{3+}	2.950×10^{-4}	1.518×10^{-4}	1.03
Yb^{3+}	5.525×10^{-4}	2.642×10^{-4}	0.96
Tm^{3+}	2.458×10^{-4}	1.180×10^{-4}	0.96
		Average	1.01

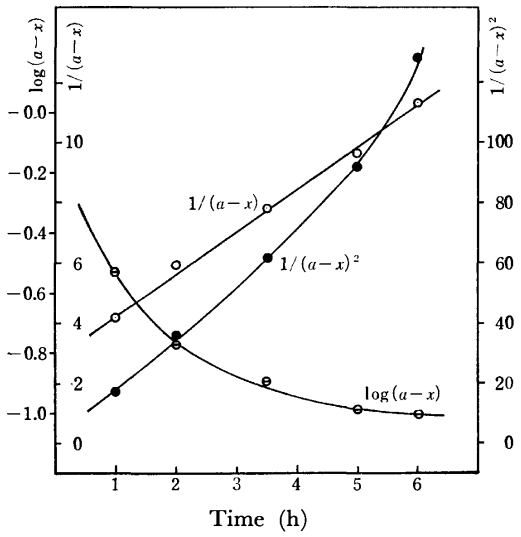

Fig. 5. Determination of order of reaction rate.

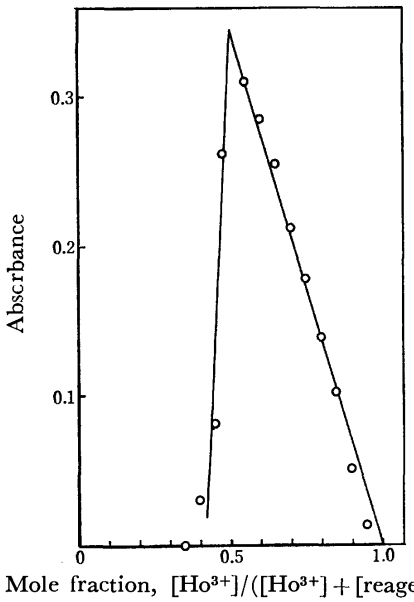

Fig. 6. Continuous variation plots at 745 nm for holmium chelate.
$[Ho^{3+}]+[\text{reagent}]=1.25\times10^{-5}$M. pH 2.2.

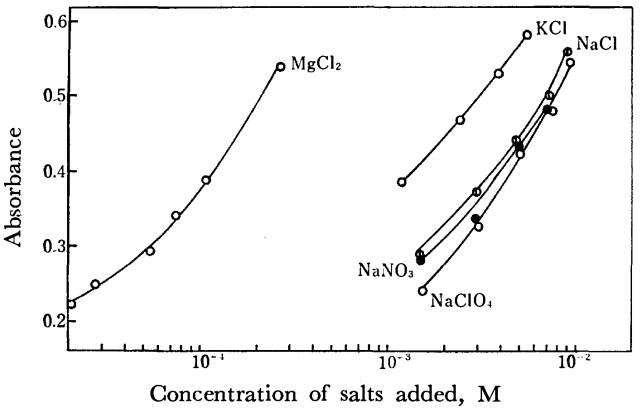

Fig. 7. Variation of absorbance of dysprosium chelate at 745 nm with increasing of coexisting salts.
Concentration of Dy^{3+}: 6.25×10^{-6}M,
Concentration of reagent: 6.25×10^{-6}M, pH 3.0.

noid to phosphorus in the precipitate obtained from the solution of the β-type chelate was estimated by the method described above. Table 1 shows that the mole ratio of lanthanoid against phosphorus is 1 : 2; *i.e.*, the combining ratio of lanthanoid against the reagent is 1 : 1. The impurities in the Chlorophosphonazo III used were presumed to be mono- and bisazo derivatives of chromotropic acid and unreacted chromotropic acid.[5] However, it is considered that these materials do not react to lanthanoids under the present experimental conditions.

Savvin reported[6] that only one functional group in Arsenazo III, which is one of the symmetrical derivatives of chromotropic acid, participates in the 1 : 1 chelate formation with lanthanoids. It is expected that the form of the α-type chelate of Chlorophosphonazo III resembles that of the Arsenazo III chelate, because the ratio of the metal against Chlorophosphonazo III is known[1] to be 1 : 1 and the spectrum of the α-type is similar to that of the Arsenazo III chelate. Thus, it may be concluded from the results of the reaction rate that the β-type chelate is a 2 : 2 dimer. The present author previously reported[2] that the β-type chelate may be supposed to be a chained-form in which two functional groups of Chlorophosphonazo III interact with the lanthanoids. However, the recent work

shows that the β-type chelate is not the chained-form, but the 2 : 2 form.

Figure 7 shows the variation in the absorbance of the dysprosium chelate as 745 nm as a function of the concentration of the coexisting metal ions. The absorbance increases with an increase in the concentration of the coexisting metal ions, and finally the precipitate is formed. The effects of the metals on the intensity of the absorbance are in the following increasing order: sodium, potassium, and magnesium. However, it seems that anions do not contribute to the intensity. The formation of the precipitate may be explained by a coagulation of the anionic β-type chelate as a result of the influence of the coexisting cations.

The β-type spectrum was not observed in the Chlorophosphonazo III chelates of iron(III), aluminum, gallium, indium, scandium, zirconium, thorium, and uranium(VI), nor in the Arsenazo III chelates of these metals, including all of the lathanoids. On the other hand, it has been reported by several investigators that the chelate formed between a lighter lanthanoid and Carboxynitrazo[7] or Arsenazo-*p*-NO_2,[8,9] which is an unsymmetrical bisazo derivative of chromotropic acid, gives an absorption spectrum which is similar to the β-type. It is interesting to study the reason why the β-type spectrum appears considering the relationship between the positions or sorts of functional groups in the reagent and the ionic radius or coordination number of the metals.

References

1) J. W. O'Laughlin and D. F. Jensen, *Talanta*, **17**, 329 (1970).
2) T. Taketatsu and N. Kono, *Chem. Lett.*, **1974**, 989.
3) T. Taketatsu, M. Noda, and M. Takasugi, *Bunseki Kagaku*, **25**, 134 (1976).
4) F. Lucena-Conde and L. Prat, *Anal. Chim. Acta*, **16**, 473 (1957).
5) E. Kamata, K. Goto, and S. Shibata, *J. Chromatogr.*, **115**, 660 (1975).
6) S. B. Savvin, *Talanta*, **11**, 7 (1964).
7) S. B. Savvin, T. V. Petrova, and P. N. Romanov, *Talanta*, **19**, 1437 (1972).
8) N. U. Perisic-Janjic, A. A. Muk, and V. D. Canic, *Anal. Chem.*, **45**, 798 (1973).
9) A. A. Muk and M. B. Pravica, *Anal. Chem.*, **46**, 1121 (1974).

Reactions of ^{125}I Activated by $^{125}Xe(EC)^{125}I$ Process with Methane

Masakatsu SAEKI and Enzo TACHIKAWA

Division of Chemistry, Japan Atomic Energy Research Institute, Tokai-Mura, Ibaraki 319-11

(Received September 24, 1976)

The reactions of ^{125}I obtained from the $^{125}Xe(EC)^{125}I$ process with methane have been investigated. It was confirmed that electron scavengers, such as I_2, SF_6, and O_2, play an important role. The main product is only $CH_3{}^{125}I$, the yield decreasing significantly with the concentration of Xe. By adding various additives, the yield of $CH_3{}^{125}I$ in the presence of trace amount of I_2 was assigned as follows: $8.7\pm6.7\%$ by the hot atom reaction, $35.8\pm8.0\%$ by $^{125}I^+$ in the $^1D_2$ state, and $31.5\pm2.0\%$ by $^{125}I^+$ in the ^3P states. The results are discussed in comparison with those reported on similar reactions utilizing different activation processes. Chemical sequences of the formation of $CH_3{}^{125}I$ are proposed.

Many papers have appeared on the reactions of recoil iodine from various nuclear transformations[1-12] with simple alkanes. Iodine ions in excited states always play important roles in the reactions. A number of experiments were carried out dealing with the systematics of the role of excited iodine ions.

Rack and Gordus investigated the reactions of ^{128}I obtained from the $^{127}I(n,\gamma)^{128}I$ reaction with gaseous methane, and they concluded that about 18.4% of the 54.4% organic ^{128}I is formed as a result of hot ^{128}I reactions, 11% as a result of excited iodine ions in $^3P_2$, $^3P_1$, and/or $^3P_0$ states, and 25% as a result of reactions of $I^+(^1D_2)$ ions.[3,4] Nicholas *et al.* reached a similar conclusion in the reactions of ^{130}I activated by the (n,γ) or (IT) process with methanes (CH_4 and CD_4).[5] Due to rather high yield of hot reactions, the recoils, ^{128}I and ^{130}I, however, are not necessarily suitable for a specific study of the role of excited iodine ions.

Loberg and Welch chose ^{123}Xe formed by the $^{122}Te(^3He,2n)^{123}Xe$ reaction as nuclide to give iodine, and studied the ionic reactions of $^{123}I^+$ with CH_4.[10] The nuclide, ^{123}Xe, decays in two modes, electron capture and β^+ decay.[13] In the latter mode, 14% of the ^{123}I recoils are formed initially in the I^- state.[10] This indicates that for a detailed analysis the role of the negative ion should be taken into account. The ^{125}I recoil from $^{125}Xe(EC)^{123}I$ process is preferable to other recoils for a specific investigation of iodine ions, since the nuclide, ^{125}Xe, decays only by electron capture and the resulting ^{125}I has a maximum kinetic energy of 15.6 eV.[13]

Schroth and Adloff examined the reactions of ^{125}I obtained from ^{125}Xe with methane.[6] Schleiffer and Certout also investigated the same reaction system.[11] However, they reached different conclusions.

We have studied the reactions of ^{125}I obtained from ^{125}Xe with methane in gaseous phases. The reaction yield was carefully investigated by adding various gases to the reaction system. The results are discussed in comparison with those reported from the viewpoint of the role of iodine ions in the excited state.

Experimental

Chemicals. Xenon gas with natural composition (Nippon Sanso Co., purity 99.9%) and methane (Takachiho Chem. Co., purity 99.95%) were used. Other reagents used as additives had the highest purity among those available.

Sample Preparation. Xenon gas with natural composition was introduced in a silica ampoule (18.5 ml) equipped with a breakable seal. The pressure was kept at around 700 Torr. The ampoule was irradiated in the T-pipe of a JRR-4 reactor of JAERI for 30—120 min; the neutron flux at the irradiation port was 4×10^{13} n cm^{-2} s^{-1}. After 4—12 h from the end of irradiation, the radioactive xenon mixture was purified by passing the mixture through a column packed with granular silver in order to remove ^{125}I formed in the ampoule.

Pyrex glass ampoules, with volume either 6.5 or 10.5 ml, were used as the reaction vessels. The irradiated and purified xenon gas, additive gas, when necessary, and methane were introduced into the reaction vessel by means of a vacuum line. The pressure of the reaction system was usually kept constant at 500 Torr, but it was widely varied for investigation of the dependence of the product yields on pressure. The pressure of radioactive xenon was usually kept at 20 Torr [0.04 m.f. (mole fraction)]. For the addition of excess iodine, a small amount of solid iodine was placed in an ampoule. Subsequently, air was pumped off and the radioactive xenon and methane were introduced. The samples were stored in the dark at room temperature for more than 4 days. Some samples were exposed to a 45 kCi ^{60}Co source immediately after their preparation.

Sample Processing. The reaction products were separated by means of a radio-gas chromatograph. The sample was directly injected into a radio-gas chromatograph by means of a vacuum line. A potassium hexacyanoferrate(II) 16/20 mesh precolumn of $4\phi\times100$ mm was placed in front of the separation column in order to prevent the introduction of inorganic iodides such as HI and I_2.[14] The separation column was 2.8 m D.O.P. column, Neopak 1A of 60/80 mesh coated with 15% dioctyl phthalate. In the operation, the temperature of the column was raised from room temperature to 115 °C at a rate of 8 °C min^{-1}. The effluent was collected by bubbling through a trap filled with liquid scintillator, after its activities had been continuously measured with a NaI(Tl) counter. The traps were radio-assayed with a liquid scintillation counter.

Total organic yield in the reaction system of Xe(0.04 m.f.) and CH_4 was determined to be 60.7% by the conventional solvent extraction method. This particular reaction system was chosen as a reference in determining the total organic yield in other reaction systems. In the solvent extraction method, toluene with iodine carrier (10^{-3} M) was used as an organic layer and 0.5 M Na_2SO_3 solution as an inorganic layer. The radioactivity of each layer was measured with a NaI scintillation counter and a liquid scintillation counter.

The absolute yields (AY) in other systems were determined according to the equation

$$AY(\%) = 60.7\ (A_{Xe}/A_{CH_3I})_{ref}\cdot(A_P/A_{Xe})_{sam},$$

where 60.7 is the absolute yield in the reference sample.

A_{Xe}, A_P, and A_{CH_3I} denote the activities of xenon, some product of interest and methyl iodide, respectively, in a radio-gas chromatogram (A_{CH_3I} and A_P were also measured with a liquid scintillation counter). Subscripts "ref" and "sam" denote the reference system (Xe(0.04 m.f.) and CH_4) and any other reaction systems, respectively.

Results

The vacuum line used in most of the experiments was previously utilized for sampling gases including iodine. The iodine adsorbed on the surface can not be removed completely. Thus, almost all reaction systems will have been contaminated with iodine vapor, unless otherwise stated.

The total organic yield in the reaction system, Xe (20 Torr) and CH_4(480 Torr), was 60.7±4.5%. The results based on the two different measurements, NaI and liquid scintillation counters, agree. The organic yield product in the gaseous phase was only $CH_3{}^{125}I$, unless other additives such as C_2H_6, C_2H_5Cl, and solid-I_2 were present.

When the pressure was changed from 16 to 923 Torr, the Xe/CH_4 ratio being kept at 0.10, the yield of $CH_3{}^{125}I$ remained at 54.8±4.1%. The results obtained at various temperatures are given in Table 1. The yield of $CH_3{}^{125}I$ remained unchanged, showing no temperature-effect. No wall effect was observed. Addition of 0.5 g of quartz wool (1−5 μ) inside a pyrex ampoule of similar size hardly affected the results.

The variation of $CH_3{}^{125}I$-yield with the concentration of Xe is given in Table 2. The yields decreased with an increase in the concentration of Xe, from 74.0 ±5.0% (0.011 m.f. of Xe) to 31.5±2.0% (1.0 m.f. of Xe).

The effects of additives on the reaction system of 0.04 m.f. of Xe and CH_4 containing a trace amount of I_2 are shown in Fig. 1. The yield of $CH_3{}^{125}I$ decreased monotonically with an increase in the concentration of Kr, Ar, and N_2. It was extrapolated to be 52.0±5.0 % at 1.0 m.f. of additives. When O_2 or SF_6 was chosen as an additive, the yield increased at the beginning, but decreased with a further increase in the concentrations. The extrapolated value at 1.0 m.f. of O_2 is also 52.0±5.0%, but 31.5±2.0% for the case of SF_6. With the addition of CH_3Cl, C_2H_5Cl, and C_2H_6, the yield of $CH_3{}^{125}I$ decreased with an increase in the concentrations of additives, the limiting values being 4.9± 0.8%, almost 0%, and 2.4±0.4%, respectively. A small amount of $C_2H_5{}^{125}I$ was detected in the case of C_2H_5Cl and C_2H_6 additives.

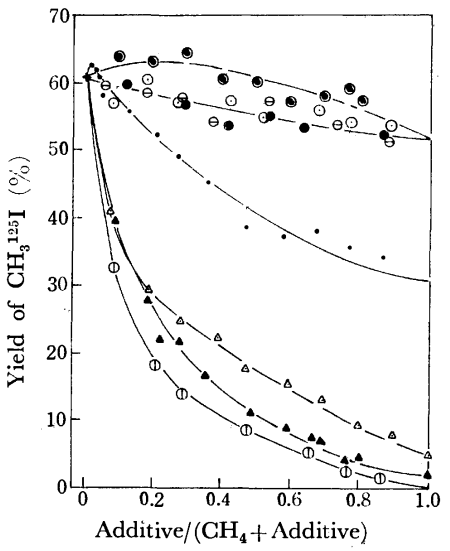

Fig. 1. Variation of the $CH_3{}^{125}I$-yield with the concentrations of various additives.
●: O_2, ⊙: Ar, ●: Kr, ⊖: N_2, ●: SF_6, △: CH_3Cl, ▲: C_2H_6, ⊕: C_2H_5Cl.

Addition of Br_2 significantly influenced the $CH_3{}^{125}I$ yield; less than 0.5 mol % of Br_2 reduced the yield below 1%. However, the addition of a macroscopic amount of I_2 has no definite effect on the $CH_3{}^{125}I$ yield (Table 1). A concomitant formation of $CH_2{}^{125}II$ scarcely occurred; the yield was less than 1%.

Some experiments with CD_4 were performed. The yield of methyl iodide, $CD_3{}^{125}I$, was 59.9±6.9% at the concentration of Xe, 0.04 m.f. The effects of pressure and Xe-concentration were similar to the case of the

Table 1. Effect of reaction temperature on the yield of $CH_3{}^{125}I$

Temperature (°C)	Iodine	
	Trace	Macroscopic
Room	60.7±4.5%	63.3±7.1%
0	61.2±5.0%	62.3±4.6%
−86	57.9±4.3%	56.7±5.2%

Table 2. Variation of $CH_3{}^{125}I$-yield with the concentration of Xe

Mole fraction of Xe	Yield of $CH_3{}^{125}I$ (%)	Mole fraction of Xe	Yield of $CH_3{}^{125}I$ (%)
0.00	(76.0±6.0)	0.21	46.3±3.4
0.011	74.0±5.5	0.31	39.2±2.8
0.021	71.9±5.3	0.40	35.5±2.6
0.03	67.6±5.0	0.53	31.3±2.3
0.04	60.7±4.5	0.62	31.5±2.3
0.054	59.7±4.4	0.70	31.4±2.3
0.10	54.8±4.1	0.80	31.4±2.2
0.15	51.9±3.8	0.90	31.6±2.3
		1.00	(31.5±2.0)

Table 3. Yields of $CH_3{}^{125}I$ observed in the reaction system exposed to a ^{60}CO source[a)]

Reaction system	yield of $CH_3{}^{125}I$(%)
CH_4+Xe(0.04 m.f.)	<0.5
CH_4+Xe(0.04 m.f.) +SF_6(0.02 m.f.)[b)]	38.5±1.6

a) Dose rate 2.1×10^6 R/h, exposing time 20 h.
b) Other products: $C_2H_5{}^{125}I$: 12.3±1.2%, i-$C_3H_7{}^{125}I$: 2.1±1.0%, n-$C_3H_7{}^{125}I$: 1.3±0.5%, and n-$C_4H_9{}^{125}I$: 1.2±0.6%.

reaction with CH_4.

Some samples were exposed to a ^{60}Co source of 45 kCi for 20 h within 30 min after preparation in a similar manner to that of other samples. The results are summarized in Table 3 with experimental conditions.

Discussion

Formation of $CH_3{}^{125}I$ via Energetic Process. Schroth and Adloff[6] and Schleiffer and Certout[11] studied similar reaction systems to those in the present experiments, although no reference was made to the hot atom reaction. The latter gave the extrapolated value of 55±3% at 1.0 m.f. of additives of He, Ne, Ar, and Kr.[11] This is in good agreement with our results, 52.0±5.0 %. Schleiffer and Certout maintained the concentration of Xe at 0.025 m.f. throughout their experiments.

Loberg and Welch investigated the reaction of ^{123}I from ^{123}Xe with methane and mentioned the following for the hot atom reactions: "this lack of reactivity due to kinetically hot species indicates that by the time the iodine ion has attained a charge of +1 it has come to thermal equilibrium with its surroundings."[10] However, they observed the hot atom reactions with ethane and neopentane as reactants. The ^{123}I atom from ^{123}Xe has the maximum kinetic energy of 34.4 eV as a result of the electron capture decay.[13] The excess kinetic energy corresponds to the median kinetic energies of ^{80}Br and ^{82}Br from the isomeric transition processes.[15] In the reactions of these recoil bromines with alkanes, it has been confirmed that the reactivity of methane was higher than that of other alkanes.[16,17] From the chemical similarity between bromine and iodine, the trend may be maintained also in the energetic reaction of recoil iodine. Thus, the failure of detection of energetic yield in the reaction of ^{123}I with methane[10] would not necessarily indicate the absence of the hot atom reactions.

The nuclide of ^{125}I decays only by electron capture, and the Q value of the decay is reported as 1.9 MeV.[13] From this value, the maximum recoil energy possessed by the ^{125}I atom is calculated to be 15.6 eV. The limiting yield of $CH_3{}^{125}I$ at 1.0 m.f. of additives is 52.0 ±5.0% for Kr, Ar, N_2, and O_2 (Fig. 1). The difference between the yield at 0.04 m.f. of Xe, 60.7±4.5%, and this limiting value, 52.0±5.0%, should be considered to result from hot atom reactions. Although the presence of 0.04 m.f. of Xe may influence the yield dependence on kinetic energy, its extent is considered to be unimportant, being less than 1% as referred to the results of bromine hot atom reaction.[18] Thus, the yield of hot atom reaction is assigned to be 8.7±6.7%.

Main Mechanisms of $CH_3{}^{125}I$-formation via Ionic Process. The absence of the wall effect of vessel indicates that the reactions mainly occur in gaseous phase and the reactions are not catalyzed by the wall.

The yield of $CH_3{}^{125}I$ decreased with an increase in the concentration of Xe (Table 2). The value extrapolated to zero m.f. of Xe is 76.0±6.0% and the limiting value at 1.0 m.f. of Xe is 31.5±2.0%. This reduction of the yield is due to the near resonant charge exchange between xenon and I^+ in the $^1D_2$ state, and the limiting yield, 31.5±2.0%, should be ascribed to reactions of I^+ in the ^3P states.[3,4,10,11]

Table 4. Effects of electron scavengers on the yield of $CH_3{}^{125}I$

Additive[1]	Yield of $CH_3{}^{125}I$(%)	
	By new line	By old line
no	47.8±4.8	60.7±4.5
SF_6(0.07 m.f.)	57.3±4.8	60.1±5.9
O_2 (0.30 m.f.)	59.3±4.3	64.0±6.0

1) All reaction systems contain 0.04 m.f. of Xe.

The yield of $CH_3{}^{125}I$ increases first with an increase in the concentration of O_2 and SF_6(Fig. 1). This suggests that an electron scavenger plays an important role in the mechanism of $CH_3{}^{125}I$-formation. Since I_2 is also an excellent electron scavenger, experiments were carried out with a new vacuum line in order to investigate of the effect of trace amout of I_2 in the reaction. The results are shown in Table 4. The yield obtained by the new line was significantly lower than that by the old line contaminated with iodine vapor, the yield increasing by about 10%, on addition of SF_6 or O_2 to the system.

This trend was not observed with use of the old line. We see that the presence of electron scavengers raises the yield of $CH_3{}^{125}I$. The following finding also supports the result.

Samples prepared in a similar way using the old line were exposed to a ^{60}Co source. The yield of $CH_3{}^{125}I$ in the system of CH_4±0.04 m.f. of Xe was reduced to less than 0.5% (Table 3). However, in the system containing SF_6, the yield was 38.5±1.6% under the same conditions. The trace amount of I_2 originally contained in the system would have been consumed by the reactions with radiolysis-products of CH_4 and stabilized to either HI or organic iodides. As a result, the system would be cleaned from I_2 in the early stage of the reactions. Thus, we see that $CH_3{}^{125}I$ can not be produced in the system with carrier free ^{125}I unless some other electron scavenger is present, and that the samples prepared by the new line are still contaminated by a trace amount of I_2, although the extent is much less than with the old line. (Pumps and reagents were used in common in both experiments.)

Schleiffer and Certout proposed the following reaction sequences:

$$CH_4 + {}^{125}I^+ \rightarrow CH_3{}^{125}I^+ + H \quad (1)$$

$$CH_3{}^{125}I^+ + I_2 \rightarrow CH_3{}^{125}I + I_2{}^+ \quad (2)$$

$$CH_3{}^{125}I + e^- \rightarrow CH_3 + {}^{125}I^- \quad (3)$$

The mechanism involves a neutralization process of $CH_3{}^{125}I^+$ with additives and is consistent with the results. If the neutralization of $CH_3{}^{125}I^+$ is the working process, the role of SF_6 observed in the systems exposed to ^{60}Co-source can be ascribed to the following scheme in analogy with Reaction 2:

$$CH_3{}^{125}I^+ + SF_6 \rightarrow CH_3{}^{125}I + SF_6{}^+ \quad (4)$$

However, a similarity in the effects of Xe and SF_6 on the $CH_3{}^{125}I$ yield (Fig. 1 and Table 2) predicts that the ionization potential of SF_6 is in the same range of

TABLE 5. COMPARISON OF THE PRESENT RESULTS WITH THOSE REPORTED

Reaction system	Iodine carrier	Yield of CH_3I(%)				Reference
		Total	Hot	$^1D_2$	^3P	
$^{127}I(n,\gamma)^{128}I+CH_4$	yes	54.4±2.0	18.4±2.0	25.0±2.0	11.0±2.0	3
$^{129}I(n,\gamma)^{130,130m}I+CH_4$	yes	42.5±2.0	16.5±2.0	9.5±2.0	16.3±2.0	5
$^{130m}I(IT)^{130}I+CH_4$	yes	25.6±2.0	9.7±2.0	5.6±2.0	10.3±2.0	5
$^{129}I(n,\gamma)^{130,130m}I+CD_4$	yes	41.3±2.0	15.3±2.0	9.5±2.0	16.5±2.0	5
$^{130m}I(IT)^{130}I+CD_4$	yes	26.4±2.0	10.5±2.0	5.6±2.0	10.3±2.0	5
$^{123}Xe(EC,\beta^+)^{123}I+CH_4$	no	51.8±2.9	0	21.2	30.6	10
$^{123}Xe(EC,\beta^+)^{123}I+CH_4$	yes	53.8	0	27.0	25.4	10
$^{125}Xe(EC)^{125}I+CH_4$	—	58±6	0	40±7	18±2[a]	6
$^{125}Xe(EC)^{125}I+CH_4$	yes	75	0	55	20	11
$^{125}Xe(EC)^{125}I+CH_4$	yes	76.0±6.0	8.7±6.7	35.8±8.0	31.5±2.0	present work

a) Assigned as the yield resulting from the reaction of I^+ in the $^1S_0$ state.

Xe, both being higher than that of CH_3I. This implies that Reaction 4 is unimportant. Loberg and Welch reported that the reaction to form $CH_3{}^{125}I^+$ is exothermic only with $I^+(^1D_2)$.

Reaction 3 would not be important under the low electron density as in the present case. When samples which had been stored for more than 4 days after their preparation were exposed to a ^{60}Co-source up to the total dose 6.6×10^5 R, more than 10% of $CH_3{}^{125}I$ still survived, even in the absence of an electron scavenger.

The reaction sequences proposed by Schleiffer and Certout do not seem to be able to explain our results. Let us introduce the following reaction mechanisms:

$$^{125}I^+ + CH_4 \rightarrow (CH_4{}^{125}I)^+ \quad (5)$$

$$(CH_4{}^{125}I)^+ + CH_4 \rightarrow CH_3{}^{125}I + CH_5^+ \quad (6)$$

$$(CH_4{}^{125}I)^+ + e^- \rightarrow CH_4 + {}^{125}I \quad (7)$$

$$SF_6,\ I_2,\ \text{or}\ O_2 + e^- \rightarrow SF_6^-,\ I + I^-,\ \text{or}\ O_2^- \quad (8)$$

According to the reaction sequences, $CH_3{}^{125}I$ is formed by Reactions 5 and 6. However, the formation will be interferred by Reaction 7. In the presence of SF_6, O_2, or I_2, Reaction 8 occurs in competition with Reaction 7. As a result the yield of $CH_3{}^{125}I$ would increase.

As is shown in Table 1, no temperature effect was observed within experimental error. $CH_3{}^{125}I$ will be predominantly produced by Reactions 5 and 6, and hot atom reactions. These reactions usually occur adiabatically in a very short period. The energy required for the reactions is supplied by the excitation energy of I^+ ions or the kinetic energy of recoils. This explains the fact that the yield is independent of temperature.

In the reactions of ^{123}I obtained from the decay of ^{123}Xe, Loberg and Welch stressed the importance of a molecular ion complex, AI^+, where A can be any molecule involved in the system, for the formation of $CH_3{}^{123}I$, based on the observation that the yield increased with some additives such as Kr, Ar, and Ne.[10] However, we have observed no such characteristic behavior of the yield. This suggests that the role of AI^+ is much less important in the reactions of ^{125}I as compared with those of ^{123}I.

Effects of Reactive Additives. When the additives CH_3Cl, C_2H_5Cl, and C_2H_6 were added to the reaction system, the yield of $CH_3{}^{125}I$ decreased with an increase in the concentration of additives and continuously approached the values found in the absence of CH_4, *i.e.*, 480 Torr of additive gas and 20 Torr of Xe (4.9±0.8 % for CH_3Cl, almost zero % for C_2H_5Cl, and 2.4±0.4% for C_2H_6).

The results indicate that the $CH_3{}^{125}I$-yield resulting from the reaction with CH_4 can be suppressed by any of the additives. The ionization potentials (IP) of the reagents are 11.28±0.01 eV for CH_3Cl, 10.97±0.02 eV for C_2H_5Cl, and 11.65±0.03 eV for C_2H_6.[20] Thus, the IP alone as a determining factor of the yield can not explain the efficient reduction of the yield by C_2H_6, since the I.P. of C_2H_6 is higher than that of I^+ state, 11.34 eV. Thus, an alternative reaction pathway for the reaction of $^{125}I^+$ will be present, such as the one suggested by Loberg and Welch.[10]

$$^{125}I^+(^3P_2) + C_2H_6 \rightarrow (C_2H_6{}^{125}I)^+ \rightarrow H^{125}I + C_2H_5^+ \quad (9)$$

Similarly in the presence of CH_3Cl, Reaction 10 would be important.

$$^{125}I^+(^3P_2) + CH_3Cl \rightarrow (CH_3Cl^{125}I)^+ \rightarrow {}^{125}ICl + CH_3^+ \quad (10)$$

The addition of Br_2 remarkably reduced the yield. However, when Br_2 was added to the reaction system after the completion of the reactions (after more than 4 days from the preparation of the sample), the yield was also reduced to less than 1%. This is due to the fact that Br_2 undergoes exchange with ^{125}I in $CH_3{}^{125}I$ as follows:

$$Br_2 + CH_3{}^{125}I \rightarrow CH_3Br + {}^{125}IBr \quad (11)$$

Comparison of the Results. The present results as well as previous ones are summarized in Table 5. A general trend exists in the reactivities of excited iodine. Hot yields show a remarkable dependence on the initial kinetic energies possessed by the recoil iodines, decreasing in the order $(n,\gamma)>(IT)\geq(EC)$. The maximum kinetic energies imparted to the recoils are 194 eV for ^{128}I and 177 eV for ^{139}I from the (n,γ) process[21] and 15.6 eV for ^{125}I from the (EC) process.[13] From these values and experimental findings, the kinetic energy for ^{130}I from the (IT) process is assumed to be *ca.* 20 eV when $CH_3{}^{130m}I$ is used as an iodine source.

In contrast, the thermal ionic yield was the highest for ^{125}I obtained from the (EC) process. It can be

concluded that the population of the iodine ion in each excited state depends on the decay mode of precursors. We found that the population of $^{125}I^+(^1D_2)$ is slightly higher than that of $^{125}I^+$ in the ^3P states. This is in line with the results by Schleiffer and Certout[12] and by Loberg and Welch[10] in the presence of a macroscopic amount of I_2. However, Schroth and Adloff[6] and Schleiffer and Certout[12] reported lower yields for ^3P states than ours. This discrepancy may be due to the amount of I_2 in the reaction system. In the former cases, they examined the system with saturated vapor pressure of I_2. We see from the results by Loberg and Welch[10] that the presence of a macroscopic amount of I_2 would protect I^+ in the $^1D_2$ state.

As regards the reactant-isotope-effect between CH_4 and CD_4, the present results, together with those reported by Nicholas *et al.*[5] provide no positive evidence, indicating that the effect, if it exists at all, should be very small. In the reactions of ^{80}Br obtained from $^{79}Br(n,\gamma)^{80}Br$ process with methane the large reactivity-isotope-effect was observed in the hot yields.[18,22] However, it has been confirmed that the isotope effect is not present in the yield due to ionic processes.[23,24] In the present system, over 80% of $CH_3{}^{125}I$ is formed by the reaction of I^+ in the excited states. Thus, the expected isotope effect in hot reactions might have been overlooked because of large fluctuations in experimental conditions.

References

1) J. F. Hornig, G. Levey, and J. E. Willard, *J. Chem. Phys.*, **20**, 1556 (1952).
2) G. Levey and J. H. Willard, *J. Chem. Phys.*, **25**, 904 (1956).
3) E. P. Rack and A. A. Gordus, *J. Chem. Phys.*, **34**, 1855 (1961).
4) E. P. Rack and A. A. Gordus, *J. Chem. Phys.*, **36**, 287 (1962).
5) J. B. Nicholas, M. Yoog, and E. P. Rack, *Radiochim. Acta*, **19**, 124 (1973).
6) F. Schroth and J. P. Adloff, *J. Chim. Phys.*, **61**, 1373 (1964).
7) V. M. Zaitsez, I. S. Kirin, V. A. Serova, and V. I. Tikhonov, *Soviet Radiochem.*, **14**, 900 (1972).
8) V. M. Zaitsev, V. A. Serova, and V. I. Tikhonov, *Soviet Radiochem.*, **15**, 768 (1973).
9) V. M. Zaitsev, V. A. Serova, and V. I. Tikhonov, *Radiochem. Radioanal. Lett.*, **16**, 231 (1974).
10) M. D. Loberg and M. J. Welch, *J. Am. Chem. Soc.*, **95**, 1073 (1973).
11) J. J. Schleiffer and G. Certout, *Radiochim. Acta.*, **20**, 59 (1973).
12) J. J. Schleiffer and G. Certout, *Radiochim. Acta.*, **20**, 66 (1973).
13) C. M. Lederer, J. M. Hollander, and I. Perlman, "Table of Isotopes," 6th ed., John Willy and Sons, Inc., New York.
14) W. E. Harris, "Chemical Effects of Nuclear Transformations," Vol. 1, IAEA, Vienna (1961), p. 229.
15) A. R. Kazanjian and W. F. Libby, *J. Chem. Phys.*, **42**, 2778 (1965).
16) L. D. Spicer and A. A. Gordus, "Chemical Effects of Nuclear Transformations," Vol. 1, IAEA, Vienna (1965), p. 185.
17) M. Saeki and E. Tachikawa, *Radiochim. Acta*, **20**, 27 (1973).
18) M. Saeki, K. Numakura, and E. Tachikawa, *Bull. Chem. Soc. Jpn.*, **45**, 1715 (1972).
19) M. Saeki and E. Tachikawa, *J. Nucl. Sci. Technol.*, in press.
20) K. Watanabe, *J. Chem. Phys.*, **26**, 542 (1957).
21) J. H. E. Mattauch, W. Thiele, and A. H. Wapstra, *Nucl. Phys.*, **67**, 32 (1965).
22) E. Tachikawa and T. Kahara, *Bull. Chem. Soc. Jpn.*, **43**, 1293 (1970).
23) E. Tachikawa and K. Yanai, *Radiochim. Acta*, **17**, 138 (1972).
24) M. Saeki and E. Tachikawa, *Bull. Chem. Soc. Jpn.*, **46**, 839 (1973).

Kinetics of the Oxidation of Formate by Iodine in the Water–Methanol and the Water–Ethanol Mixed Solvents

Katumitu HAYAKAWA and Makoto SATO

Department of Chemistry, Faculty of Science, Kagoshima University, Koorimoto, Kagoshima 890

(Received December 9, 1976)

The kinetics of the iodine–formate reaction gives an identical rate equation in several water–alcohol mixed solvents: rate$=k[HCOO^-]\,[I_3^-]/(a[I^-]+1)$. The values of $k/M^{-1}\,s^{-1}$ and $10^{-3}\,a/M^{-1}$ are 5.5 and 16 in ethanol at 35 °C, 3.6 and 12 in methanol at 30 °C, and 0.06 and 0.7 in water at 30 °C, respectively. The values of a are comparable to the formation constants of I_3^- in the water–alcohol mixtures. The rate-determining step is the reaction between an iodine molecule and a formate ion. The activation parameters, $\Delta H^*/kJ\,mol^{-1}$ and $\Delta S^*/J\,K^{-1}\,mol^{-1}$, are 71 and −1 in the 0.95 mole fraction of methanol, 60 and −32 in the 0.92 mole fraction of ethanol, and 75 and −20 in water, respectively. The entropy term contributes to the acceleration by alcohol in the water–methanol mixtures, whereas both the entropy term and the enthalpy term contribute to the acceleration in the water–ethanol mixtures. These effects of the mixed solvents suggest that the specific interactions of the solvent molecule with the reactants and the activated complex, such as a specific solvation or a hydrogen bond, play an important role in the rate-determining step.

The iodine–formate reaction 1 is remarkably accelerated by the addition of dimetyl sulfoxide(DMSO) to water:[1]

$$I_3^- + HCOO^- \longrightarrow 3I^- + H^+ + CO_2 \qquad (1)$$

According to the electron-transfer theory,[2] changes in dielectric properties are expected to affect the reorganization of a solvent molecule around the reactants and the activated complex. The water–alcohol solvent mixtures exhibit pronounced structural and dielectric changes at different component ratios.[3] In the present paper, we will deal with the kinetics of Reaction 1 and will determine the activation parameters in the water–methanol and water–ethanol mixed solvents. The dependence of the rate and the activation parameters on the changes in such bulk properties as the dielectric property will be discussed quantitatively. The changes in the microscopic properties around the reactants and the activated complex, such as the specific solvation or the hydrogen bond, play an important role in the rate-determining step in Reaction 1.

Experimental

Reagents. The iodine, potassium iodide, sodium formate, methanol, and ethanol were obtained commercially. The ethanol was of Wako's super special grade, while the other substances were of a guaranteed grade. The iodine was purified by sublimation, and the solutions were prepared by dissolving the iodine in the potassium iodide solution in each measurement. The potassium iodide and sodium formate were dried at 120 °C overnight. The sodium perchlorate was obtained from BDH Chemicals, Ltd. It was recrystallized from water and used as a control of the ionic strength of the solutions. The pH of the aqueous solution was controlled using a phosphate buffer. In the water–alcohol mixed solvents, the pH and ionic strength of the solution were uncontrolled.

Measurements. The reaction was followed by measuring the absorbance at 350 nm at different times, using a Hitachi 101 spectrophotometer with quartz cells in a thermostated holder. When high iodide concentrations are employed, the iodine is completely converted into the triiodide ion. The ion is the only species which absorbs appreciably at 350 nm. Independent experiments showed that Beer's law was obeyed in water–alcohol mixed solvents. The reaction was also followed by measuring the concentration of total iodine in the aqueous solution by iodometry. Both methods give the same rate constant.

When mixtures of iodine and potassium iodide in several mixed solvents were left standing for 25 h, the absorbance of the solutions changed slightly (below 5%). The change was neglected compared with the rate of the reaction of iodine with formate. Irradiation with light of 350 nm had no effect on the rate.

Results and Discussion

Kinetics and the Mechanism. The rate depended on the concentrations of iodine, iodide, and formate, and in the aqueous solution it was independent of the pH at 4—9 and of the ionic strength below 0.6 M, as is shown in Table 1.

In all the kinetic runs, the initial concentrations of iodide and of formate were chosen to be much greater than the initial total iodine concentration. Under these conditions, the reaction was found to be a first-order reaction of the triiodide ion. The apparent first-order rate constant, k_{app}, is proportional to the formate concentration (Fig. 1). Figure 2 shows that the plot of $1/k'$ *vs.* $[I^-]$, where $k'=k_{app}/[HCOO^-]$, gives a straight line with an intercept. Thus, the following rate law describes the kinetics in the present solvents:

$$\text{Rate} = -d[I_3^-]/dt = k[I_3^-][HCOO^-]/(a[I^-]+1). \qquad (2)$$

Table 2 shows the kinetic parameters, k and a, in the various solvents.

TABLE 1. THE EFFECTS OF THE pH AND THE IONIC STRENGTH ON THE RATE IN AN AQUEOUS SOLUTION AT 30 °C

pH	$10^3\,k_{app}/s^{-1}$	I_c	$10^4\,k_{app}/s^{-1}$
8.8	2.1	0.035	0.77
7.5	2.0	0.055	0.81
6.7	2.2	0.085	0.85
5.9	1.9	0.12	0.84
5.7	2.1	0.32	0.74
[HCOONa]/M=0.39		0.62	0.81
[KI]/M=0.015		[HCOONa]/M=0.02	
		[KI]/M=0.02	

TABLE 2. THE KINETIC PARAMETERS IN VARIOUS SOLVENTS

Solvent	k/M^{-1} s^{-1}	10^{-3} a/M^{-1}	10^{-3} K_f/M^{-1}	t/°C
EtOH (0.98)	5.5±0.1	16±1	17	35
EtOH-H_2O (0.24)	1.1±0.6	7±4	7.6	30
H_2O (0.00)	0.11±0.01	0.57±0.03	0.59	35
H_2O (0.00)	0.06±0.02	0.7±0.2	0.66	30
MeOH-H_2O (0.31)	0.37±0.08	2.3±0.4	2.7	30
MeOH (0.99)	3.6±1.0	12±3	11	30

( ): mole fraction of alcohol.

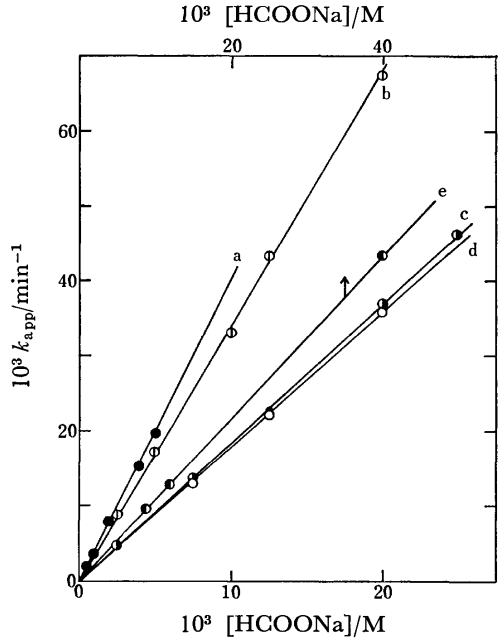

Fig. 1. Dependence of the apparent first-order rate constant on the formate concentration in various solvents: a. EtOH, b. MeOH, c. EtOH-H_2O, d. MeOH-H_2O, e. H_2O.

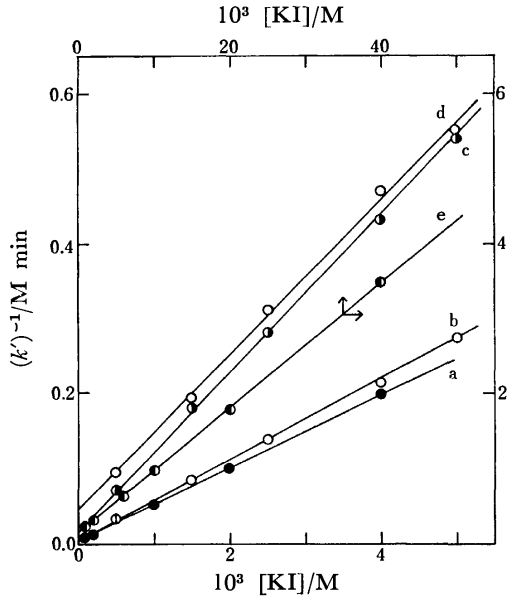

Fig. 2. Dependence of $k'(=k_{app}/[HCOO^-])$ on the iodide concentration in various solvents: a. EtOH, b. MeOH, c. EtOH-H_2O, d. MeOH-H_2O, e. H_2O.

The rate equation is derived from the following mechanism:[1]

$$I_3^- \underset{k_{3-}}{\overset{k_{3+}}{\rightleftharpoons}} I_2 + I^-, \quad (3)$$

$$I_2 + HCOO^- \xrightarrow{k_4} \text{Products}. \quad (4)$$

When k_4, k_{3+}, and k_{3-} are the rate constants of the respective reactions,

$$-d[I_2]/dt = k_4[I_2][HCOO^-] - k_{3+}[I_3^-] + k_{3-}[I_2][I^-], \quad (5)$$

$$-d[I_3^-]/dt = k_{3+}[I_3^-] - k_{3-}[I_2][I^-] = d[I_2]/dt + k_4[I_2][HCOO^-]. \quad (6)$$

Assuming that Reaction 4 is slow and Reaction 3 is in pseudo-equilibrium,

$$[I_2] = [I_3^-]/(K_f[I^-]), \quad (7)$$

where K_f is the formation constant of I_3^-.

$$\frac{d[I_2]}{dt} = \frac{1}{K_f[I^-]}\left(\frac{d[I_3^-]}{dt} - \frac{[I_3^-]}{[I^-]}\frac{d[I^-]}{dt}\right) \approx \frac{1}{K_f[I^-]}\frac{d[I_3^-]}{dt}, \quad (8)$$

because $[I_3^-]/[I^-] \ll 1$ and $|d[I^-]/dt| \leqslant |3d[I_3^-]/dt|$. When Eqs. 7 and 8 are substituted into Eq. 6,

$$-d[I_3^-]/dt = k_4[I_3^-][HCOO^-]/(K_f[I^-]+1). \quad (9)$$

Thus, the experimental kinetic parameters, k and a, equal k_4 and K_f respectively. The fourth column in Table 2 shows the K_f values obtained by the spectrophotometric method.[4] The finding that K_f is comparable to a supports the mechanism proposed in the present study. The mechanism involving the iodine atom[5,6] is eliminated because the rate must be proportional to the root of the iodine concentration in the mechanism. The effects of the pH and the water content of the solvent on the rate eliminate the mechanism involving hypoiodous acid.[7] The fact that the rate was independent of the ionic strength of the solution indicates that the rate-determining step involves a non-ionic species[8-12] and supports the mechanism proposed in the present study.

The slow step involves an iodine attack on the formate anion, although one can only speculate about the nature of the following intermediate. Hiller and Krueger[1] proposed a rate-determining step involving a transfer of a hydride ion from carbon to iodine, as is shown in Eq. 10, because $DCOO^-$ has a considerable effect on the rate $(k(HCOO^-)/k(DCOO^-)=3.8$ in water and 2.2 in DMSO).

$$I_2 + HCOO^- \longrightarrow I_2H^- + CO_2 \quad \text{(slow)}, \quad (10)$$

$$I_2H^- \longrightarrow 2I^- + H^+ \quad \text{(fast)}. \qquad (11)$$

In order to estimate the srtucture of the activated complex, the MO's energy and the formal charge for $HCOO^-$ were calculated by means of the CNDO method. The calculation indicated that the energy level of the highest occupied orbital of $HCOO^-$ (−2.26 eV) is higher than that of the lowest vacant orbital in I_2 (−7.0 eV[13]). It seems that the iodine molecule is an electrophilic reagent in the reaction with the formate ion.[14] The formal charge and the frontier electron density[15] of $HCOO^-$ shown in Table 3 suggest

Table 3. The formal charge and the frontier electron density in the $HCOO^-$ ion

Atom	Formal charge	Frontier electron density
H	+0.20	0.0
C	−0.27	0.0
O	−0.47	1.0

that an iodine molecule attacks the O-atom in $HCOO^-$. The kinetic isotope data[1] suggest that the H–C bond is loosened or severed by the attack of the iodine molecule. Thus, the activated complex may be proposed to be **1**, in which the C–H bond is greater than those in a formate ion.

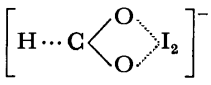

1

Table 2 shows that the rate in alcohol is much faster than that in water. The dependence of the rate on the solvents is, clearly, not caused by the change in the mechanism in the water–alcohol mixed solvents.

The Activation Parameters in the Mixed Solvents. The apparent first-order rate constants were determined at various temperatures in mixed solvents of various alcohol contents. The rate constant, k, was calculated using the formation constant of the triiodide ion, K_f, which was determined by the spectrophotometric method.[4] Table 4 shows the values of k, ΔH^*, ΔS^*, and the relative thermodynamic functions of activation, $\Delta(\Delta H^*)$ and $\Delta(-T\Delta S^*)$. The small maximum in ΔH^* appears near the 0.1 mole fraction of methanol, and the entropy term contributes to the acceleration by alcohol in the water-methanol system, whereas the maximum in ΔH^* disappears and both the entropy term and the enthalpy term contribute to the acceleration in the water–ethanol system.

For the reaction between an ion and a neutral molecule, the rate constant is given by Eq. 12:[16]

$$\ln k = \ln k_0 + (Az^2/2RT\varepsilon_r)(r^{-1} - r_*^{-1}), \qquad (12)$$

where $A = N_A e^2/4\pi\varepsilon_0$. In Eq. 12, ε_r is a relative permittivity; r and r_*, the respective radii of the ion and the activated complex; z, a charge of the ion, and the others, the usual constants. Since $r_* > r$, the rate constant increases with a decrease in the permittivity of the solution. When r and r_* are independent of the temperature of reaction, the activation energy is given by:

$$E_a = E_0 - (Az^2/2)(r^{-1} - r_*^{-1})(1 - bT)/\varepsilon_r, \qquad (13)$$

where b is given by $\varepsilon_r = c\exp(-bT)$ and where $E_0 = -R\mathrm{d}(\ln k_0)/\mathrm{d}(1/T)$. When b is calculated by means of the data of Albright and Gosting[17] and Akerlöf,[18] $(1-bT)/\varepsilon_r$ is negative and decreases with an increase in the alcohol contents. Thus, Eq. 13 indicates that E_a increases with an increase in the alcohol content. This prediction does not agree with the present results.

The changes in the solvation properties also have an important influence on the rate. Laidler and Eyring[19] and Scatchard[20] recognized the possible importance of specific solvation as a determining factor in the behavior of the rate constant. Hyne[21] ascribed the appearance of the maximum or the minimum in an activation energy to a specific solvation. According to him, the maximum appears as a result of the specific solvation

Table 4. The values of the rate constant and the activation parameters

Mole fraction of alcohol	$k/M^{-1}s^{-1}$ 40 °C	30 °C	20 °C	10 °C	ΔH^* kJ mol^{-1}	ΔS^* J K^{-1} mol^{-1}	$\Delta(\Delta H^*)$[a] kJ mol^{-1}	$\Delta(-T\Delta S^*)$[b] kJ mol^{-1}
MeOH								
0.00	0.19	0.068	0.024	0.008	75±1	−20±1	—	—
0.10	0.27	0.094	0.031	0.009	80±1	−1±1	+5	−6
0.15	0.39	0.14	0.045	0.014	80±1	+1±1	+5	−6
0.22	0.61	0.22	0.075	0.024	77±1	−3±1	+2	−5
0.28	0.89	0.33	0.11	0.037	76±1	−5±1	+1	−5
0.47	2.5	0.95	0.33	0.11	75±1	+1±1	0	−6
0.95	8.0	3.2	1.2	0.40	71±1	−1±0	−4	−6
EtOH								
0.05	0.31	0.11	0.040	0.013	75±1	−15±3	0	−2
0.10	0.76	0.28	0.10	0.034	74±0	−12±1	−1	−2
0.17	1.8	0.72	0.26	0.086	73±1	−8±2	−2	−4
0.30	5.2	2.0	0.73	0.26	72±1	−4±3	−3	−5
0.52	9.4	3.8	1.6	0.64	63±1	−25±4	−12	+2
0.92	18	7.8	3.4	1.4	60±1	−32±3	−15	+4

a) $\Delta(\Delta H^*) = \Delta H^* - \Delta H^*(\text{in } H_2O)$. b) $\Delta(-T\Delta S^*) = -T\Delta S^* + T\Delta S^*(\text{in } H_2O)$.

when the reactant is an ionic species and when the transition state is a "dipole," which means also a charge-delocalized species. In the transition state, **1**, the negative charge must undergo delocalization preliminary to the electron transfer. A consideration of the transition state, **1**, as a "dipole" seems, therefore, a valid approximation. Then, the appearance of a maximum in ΔH^* can be expected. The small maximum in ΔH^* is possibly to be ascribed to the specific solvation in the water-methanol system. Though the relative permittivity suggests a larger maximum in the water–ethanol system than that in the water–methanol system,[21] the experimental results indicate that the maximum disappears in the former system.

Water forms a strong hydrogen bond to the O-atom in $HCOO^-$ and interferes with the approach of the iodine molecule to the ion. Since alcohol has a weak hydrogen-bonding property, the rate may be faster in alcohol than in water. Though DMSO has a greater permittivity than alcohols, it does not form a hydrogen bond, so the rate constant in DMSO is the largest among them.[1]

Hiller and Krueger observed that the ion-pairing of formate lowers the rate.[1] Since the ion-pair association constant increases with a decrease in the permittivity of a solvent, the ion-pairing effect lowers the rate with an increase in the alcohol content. This is not consistent with the present results.

Thus, the specific interactions of the solvent molecule with the reactants and the activated complex, such as the specific solvation or the hydrogen bond, possibly play an important role in the rate-determining step of Reaction 1.

References

1) F. W. Hiller and J. H. Krueger, *Inorg. Chem.*, **6**, 528 (1967).
2) R. A. Marcus, *J. Chem. Phys.*, **24**, 966 (1956).
3) F. Franks and J. G. Ives, *Quart. Rev. Chem. Soc.*, **20**, 1 (1966).
4) K. Hayakawa and S. Nakamura, *Bull. Chem. Soc. Jpn.*, **50**, 566 (1977).
5) R. O. Griffith and A. Mckeown, *Trans. Faraday Soc.*, **28**, 752 (1932).
6) E. Abel and K. Hilferding, *Z. Phys. Chem.*, **A172**, 353 (1935).
7) Hypohalous acid has been proposed for the oxidation of oxalate by bromine or chlorine; R. O. Griffith, A. Mckeown, and A. G. Winn, *Trans. Faraday Soc.*, **28**, 107 (1932); R. O. Griffith and A. Mckeown, *ibid.*, **28**, 518, 616 (1932).
8) J. N. Brønsted, *Z. Phys. Chem.*, **102**, 169 (1922).
9) N. Bjerrum, *Z. Phys. Chem.*, **108**, 82 (1924).
10) J. A. Christiansen, *Z. Phys. Chem.*, **113**, 35 (1924).
11) G. Scatchard, *Chem. Rev.*, **10**, 229 (1932).
12) C. W. Davies, "Progress in Reaction Kinetics," ed by G. Porter, Pergamon Press, New York (1961), p. 161.
13) J. D. Morrison, *J. Chem. Phys.*, **19**, 1305 (1951).
14) S. Nagakura and J. Tanaka, *Bull. Chem. Soc. Jpn.*, **32**, 734 (1959). The theory by which this conclusion is derived was proposed for the aromatic substitution reaction.
15) K. Fukui, T. Yonezawa, and H. Shingu, *J. Chem. Phys.*, **20**, 722 (1952); K. Fukui, T. Yonezawa, C. Nagata, and H. Shingu, *J. Chem. Phys.*, **22**, 1433 (1954).
16) A. A. Frost and R. G. Pearson, "Kinetics and Mechanism," 2nd ed, John Wiley and Sons, New York (1961), p. 149.
17) P. S. Albright and L. J. Gosting, *J. Am. Chem. Soc.*, **68**, 1061 (1946).
18) G. Akerlöf, *J. Am. Chem. Soc.*, **54**, 4125 (1932).
19) K. J. Laidler and H. Eyring, *Ann. N. Y. Acad. Sci.*, **39**, 303 (1940).
20) G. Scatchard, *Ann. N. Y. Acad. Sci.*, **39**, 341 (1940).
21) J. B. Hyne, *J. Am. Chem. Soc.*, **82**, 5129 (1960).

Crystal and Molecular Structure of a Chelating Ylide Complex of Palladium : [(Benzoylmethylene)diphenyl-2-(diphenylphosphino)-ethylphosphorane]dichloropalladium(II) Toluene Solvate

Hirofumi Takahashi, Yoshinao Oosawa, Akiko Kobayashi, Taro Saito, and Yukiyoshi Sasaki*

Department of Chemistry, Faculty of Science, The University of Tokyo, Hongo, Tokyo 113

(Received December 13, 1976)

The crystal structure of the title compound was solved by single-crystal X-ray diffraction techniques. Crystals are monoclinic, space group $P2_1/c$, with cell dimensions $a=13.39(5)$, $b=16.88(1)$, $c=19.85(6)$ Å, $\beta=123.54(1)°$, $Z=4$. The final R was 0.065. The ylide ligand coordinates to palladium through the ylide carbon Pd–C, 2.115(15) Å and phosphine phosphorus Pd–P, 2.230(8)Å forming a six-membered chelate ring. The chelating ligand together with two chlorine atoms forms a square-planar geometry around the palladium. The Pd–Cl distances are discussed in terms of *trans*-influence of the ylide carbon.

We have reported syntheses of chelating ylide ligands derived from 1,2-bis(diphenylphosphino)ethane and bis-(diphenylphosphino)methane and their palladium(II) and platinum(II) complexes.[1-4] The coordination of the ylide carbon to the metal has been inferred from infrared, ^1H and ^{31}P NMR spectra.[4] The present X-ray structure determination of one of the ylide complexes, [(benzoylmethylene)diphenyl-2-(diphenylphosphino)ethylphosphorane]dichloropalladium(II) (formulated as $[PdCl_2(bdep)]$† in this paper), has confirmed that the ylide carbon and phosphine phosphorus coordinate to palladium. This paper describes the details of the X-ray study, the preliminary results of which have been published.[5]

Experimental

The chelating ylide ligand and its complex, $[PdCl_2(bdep)]$, were prepared as described in an earlier report.[4]

Preparation of the Crystal. $[PdCl_2(bdep)]$ (0.1 g) was dissolved in nitromethane (7 ml), and toluene (15 ml) was added to the solution. The solution was kept at 20 °C for three days. Yellow crystals were filtered, washed with diethyl ether, and dried *in vacuo*. A ^1H NMR spectrum and elemental analyses indicated that the crystals contained a toluene molecule per palladium atom as a crystallization solvent. A single crystal with dimensions *ca.* $0.25\times0.25\times0.10$ mm was used for measurement of diffraction intensities.

Crystal Data. $C_{34}H_{30}Cl_2P_2Pd\cdot C_7H_8$, $M=786.0$, monoclinic, $a=13.39(5)$, $b=16.88(1)$, $c=19.85(6)$ Å, $\beta=123.54(1)°$, $V=3740$ Å^3, $Z=4$, $D_m=1.42$ and $D_x=1.40$ g/cm^3, $\mu=7.47$ cm^{-1} (Mo-$K\alpha$). Space group $P2_1/c$ from systematic absences,, $h0l$, $l=2n+1$ and $0k0$, $k=2n+1$.

Intensity data were recorded on a Rigaku automated four-circle diffractometer, by use of graphite-monochromatized Mo-$K\alpha$ radiation. By the $\omega-2\theta$ scan technique, diffraction intensities were measured up to $2\theta=55°$ and 2652 independent reflections ($|F_o|\geq3\sigma$) were used for the structure analysis. Intensities were corrected for Lorentz and polarization effects but not for absorption and extinction.

Determination of the Structure. The position of the palladium atom was deduced from a three-dimensional Patterson map, and the positions of non-hydrogen atoms including carbon atoms of toluene were determined by the usual heavy-atom method. The structure was refined by block-diagonal least-squares, first with isotropic and then with anisotropic temperature factors. Of the 38 hydrogen atoms, 23 atoms were located from a difference Fourier map, and were refined with isotropic temperature factors. After inclusion of the rest of the hydrogen atoms whose positions were obtained by calculation, the final R value was reduced to 0.065.

Atomic scattering factors were taken from ref. 6. A weighting scheme adopted was $w=1.0$ for $|F_o|\geq36.19$ on an absolute scale and $w=0.5$ otherwise was employed. The calculation was performed on a HITAC 8800/8700 computer at the Computer Center of the University of Tokyo using a local version of UNICS programs.[7]**

Final positional and thermal parameters are given in Table 1, with their estimated standard deviations.

Results and Discussion

Molecular Structure. Final positional and thermal parameters are given in Table 1, with their estimated standard deviations. The molecular structure with the numbering scheme of atoms and a stereoview are

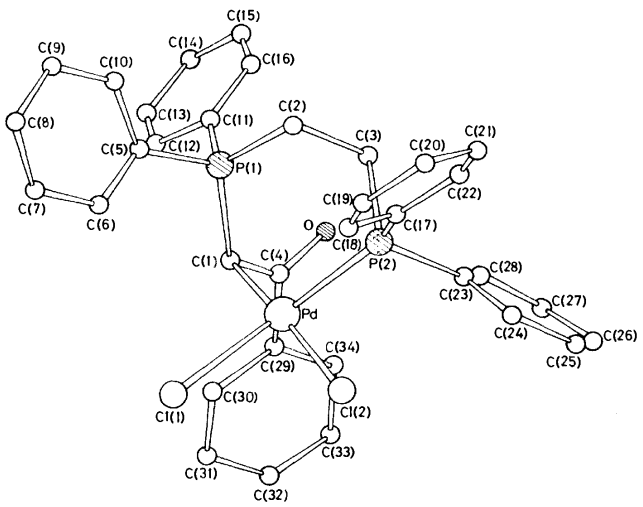

Fig. 1. Molecular structure of $[PdCl_2(bdep)]$ and numbering scheme of non-hydrogen atoms.

† bdep = C_6H_5–C(=O)–C$^-$–H–P$^+$–$(CH_2)_2$–P–$(C_6H_5)_2$, with $(C_6H_5)_2$ on P

** Observed and calculated structure factors are held by the office of the Chemical Society of Japan as Document No. 7710.

Table 1a. Final atomic coordinates ($\times 10^4$) and anisotropic thermal parameters ($\times 10^3$) of the non-hydrogen atoms with their estimated standard deviations in parentheses

The U_{ij}'s are defined by

$$\exp[-2\pi^2(h^2a^{*2}U_{11}+k^2b^{*2}U_{22}+l^2c^{*2}U_{33}+2hka^*b^*U_{12}+2hla^*c^*U_{13}+2klb^*c^*U_{23}]$$

	x	y	z	U_{11}	U_{22}	U_{33}	U_{12}	U_{13}	U_{23}
Pd	839(1)	1247(1)	3111(1)	51(1)	32(0)	43(1)	0(1)	33(0)	3(1)
Cl(1)	−922(4)	493(2)	2698(2)	74(3)	40(2)	66(3)	−11(2)	51(2)	−3(2)
Cl(2)	1898(4)	582(2)	4352(2)	71(3)	46(2)	55(2)	16(2)	41(2)	41(2)
P(1)	−183(3)	2784(2)	1875(2)	47(2)	33(2)	43(2)	2(2)	30(2)	5(2)
P(2)	2473(3)	1994(2)	3603(2)	51(2)	36(2)	42(2)	2(2)	30(2)	1(2)
O	1332(8)	1798(5)	1568(6)	56(7)	43(6)	60(6)	3(5)	36(6)	1(5)
C(1)	−99(12)	1723(7)	1929(7)	65(10)	23(7)	35(8)	12(7)	30(8)	4(6)
C(2)	1129(12)	3288(7)	2694(8)	58(10)	29(7)	52(9)	−7(7)	28(8)	−12(7)
C(3)	2305(12)	2865(8)	2995(8)	44(9)	44(8)	41(8)	6(7)	24(7)	17(7)
C(4)	583(12)	1411(7)	1597(8)	60(9)	35(8)	49(8)	−3(7)	35(8)	0(7)
C(5)	−1415(12)	3104(7)	1919(8)	51(9)	28(7)	49(8)	−4(7)	35(8)	−3(6)
C(6)	−2006(14)	2589(9)	2135(10)	63(11)	66(11)	78(12)	0(9)	52(10)	−1(9)
C(7)	−2982(16)	2882(11)	2183(11)	83(13)	82(13)	101(14)	2(11)	61(12)	−9(12)
C(8)	−3256(14)	3670(11)	2045(10)	73(11)	78(12)	89(12)	6(11)	56(10)	−7(11)
C(9)	−2690(15)	4177(9)	1814(9)	83(13)	59(10)	67(11)	24(9)	48(10)	2(9)
C(10)	−1732(13)	3895(8)	1787(8)	67(10)	34(9)	62(9)	−9(7)	43(8)	−3(7)
C(11)	−450(12)	3121(8)	924(8)	49(9)	52(9)	54(9)	19(8)	33(8)	17(8)
C(12)	−1422(18)	2816(13)	243(10)	114(17)	146(20)	47(11)	−38(15)	35(12)	17(12)
C(13)	−1641(23)	3012(15)	−538(12)	170(24)	167(24)	68(14)	−48(20)	52(16)	6(16)
C(14)	−946(16)	3553(11)	−575(11)	98(14)	84(14)	88(13)	29(11)	59(12)	28(11)
C(15)	−15(18)	3879(12)	101(12)	124(16)	106(16)	131(16)	−2(14)	103(14)	30(14)
C(16)	231(18)	3669(11)	877(10)	143(17)	67(12)	90(13)	−3(13)	84(13)	0(12)
C(17)	2952(13)	2467(8)	4581(8)	65(11)	49(9)	32(8)	3(8)	23(8)	−7(7)
C(18)	2230(15)	2452(9)	4874(8)	91(12)	55(9)	46(9)	3(9)	46(9)	1(8)
C(19)	2619(16)	2855(11)	5596(10)	100(14)	98(14)	62(11)	28(12)	56(11)	10(11)
C(20)	3657(17)	3255(10)	5975(9)	125(16)	79(12)	29(9)	11(11)	31(10)	2(9)
C(21)	4423(17)	3271(11)	5711(10)	101(15)	86(13)	51(11)	−14(11)	26(11)	−26(10)
C(22)	4001(14)	2876(10)	4978(9)	71(12)	70(11)	54(10)	−15(10)	25(10)	−20(9)
C(23)	3774(11)	1491(7)	3767(8)	37(8)	36(8)	51(9)	2(6)	23(7)	8(6)
C(24)	4590(13)	1133(10)	4499(8)	64(10)	68(11)	56(9)	3(10)	33(9)	−3(9)
C(25)	5581(14)	730(10)	4644(9)	63(12)	77(12)	68(11)	17(10)	40(10)	10(10)
C(26)	5735(15)	620(11)	4007(10)	79(14)	106(15)	84(13)	36(12)	57(12)	9(11)
C(27)	4868(17)	932(12)	3259(10)	101(14)	138(18)	73(12)	72(13)	65(12)	31(12)
C(28)	3932(15)	1365(11)	3123(9)	92(13)	89(13)	69(11)	44(12)	59(10)	11(11)
C(29)	404(14)	555(8)	1312(7)	79(12)	47(9)	24(7)	2(8)	25(8)	3(7)
C(30)	−618(16)	129(9)	1108(9)	105(14)	49(10)	91(10)	−13(10)	40(10)	−7(8)
C(31)	−807(17)	−641(9)	776(10)	130(17)	55(11)	66(11)	−20(11)	59(12)	−8(9)
C(32)	111(17)	−978(9)	729(10)	122(16)	53(10)	69(11)	11(10)	59(12)	−6(9)
C(33)	1118(18)	−584(10)	947(10)	120(17)	63(12)	74(12)	12(11)	55(12)	2(10)
C(34)	1277(15)	210(9)	1231(9)	73(12)	60(10)	68(11)	12(9)	35(10)	−11(9)
C(35)	5084(22)	4176(18)	3657(17)	116(21)	228(33)	188(26)	−97(21)	83(20)	−2(23)
C(36)	4171(23)	4700(15)	3228(17)	158(24)	109(19)	232(29)	−69(18)	127(24)	−38(20)
C(37)	3455(22)	4571(15)	2401(17)	145(23)	131(21)	243(30)	−40(18)	144(24)	9(21)
C(38)	3628(22)	3924(15)	2001(17)	141(21)	122(21)	236(28)	−14(17)	141(22)	10(20)
C(39)	4574(22)	3450(16)	2576(17)	135(20)	196(29)	212(26)	−33(19)	144(21)	−11(22)
C(40)	5395(25)	3454(17)	3445(20)	186(27)	173(28)	295(37)	−35(22)	193(29)	−65(26)
C(41)	5948(32)	4254(29)	4519(21)	192(35)	467(73)	194(33)	−159(41)	66(28)	31(39)

Table 1b. Final atomic coordinates ($\times 10^3$) and isotropic thermal parameters of the hydrogen atoms with their estimated standard deviations in parentheses

	x	y	z	B (Å^2)
H(2)	109(9)	378(7)	269(6)	2.8(27)
H(3)	115(9)	323(6)	321(6)	1.8(26)
H(4)	306(8)	314(6)	330(6)	0.4(22)
H(5)	223(10)	285(7)	253(7)	3.4(31)
H(6)	−176(10)	204(7)	227(6)	2.4(28)
H(8)	−402(11)	401(8)	205(7)	5.0(37)
H(9)	−279(9)	483(6)	185(6)	1.9(27)
H(10)	−121(10)	424(6)	159(6)	2.4(28)
H(12)	−195(14)	230(10)	15(9)	8.2(49)
H(13)	−217(15)	262(11)	−94(10)	10.0(56)
H(14)	−131(13)	365(10)	−121(9)	8.0(44)
H(15)	59(10)	429(7)	14(7)	2.6(30)
H(16)	81(11)	400(8)	134(7)	4.9(37)
H(18)	137(10)	210(7)	455(7)	2.9(30)
H(19)	207(12)	281(8)	580(8)	5.4(38)
H(20)	396(11)	345(7)	656(7)	3.8(34)
H(22)	460(10)	274(7)	484(6)	2.4(28)
H(24)	466(9)	130(7)	494(6)	2.5(26)
H(26)	639(9)	18(6)	410(6)	1.8(27)
H(27)	509(14)	62(9)	293(9)	8.3(49)
H(30)	−134(11)	38(8)	99(7)	4.3(34)
H(32)	−5(13)	−162(6)	78(9)	6.9(43)
H(34)	219(11)	57(7)	150(7)	3.7(32)

illustrated in Figs. 1 and 2, respectively. Bond lengths and bond angles are listed in Tables 2 and 3. The results show that [$PdCl_2$(bdep)] is an ylide complex in which the ylide carbon coordinates to palladium with Pd-C bond length of 2.115(15) Å. This value is slightly larger than the metal-ylide carbon bond lengths (1.91—2.10 Å) determined by X-ray diffraction for some other ylide complexes.[8-10] Although the ylide methine hydrogen atom could not be located, the bond angles around the ylide carbon ∠Pd-C(1)-P(1) (115.1 (6)°), ∠Pd-C(1)-C(4) (102.9(9)°), and ∠P(1)-C(1)-C(4) (111.2(12)°), suggest that the C(1) carbon orbital is nearly sp^3 hybrid. This provides another example of the conversion of sp^2 hybridized ylide carbon to sp^3 state on coordination to the metal.[8,11] The phosphine P also is coordinated to palladium with the Pd-P(2) bond length of 2.230(8) Å, and a six-membered chelate ring is formed. The five atoms, Pd, C(1), P(2), Cl(1), and Cl(2), are approximately coplanar and the coordination around the palladium has square-planar geometry with the angles, ∠C(1)-Pd-P(2) (86.2(1)°), ∠C(1)-Pd-Cl(1) (87.3(4)°), ∠Cl(1)-Pd-Cl(2) (90.8 (1)°), and ∠Cl(2)-Pd-P(2) (96.2(4)°).

The bond lengths of the ylide system in the present complexes, P(1)-C(1) (1.795(12) Å), C(4)-O (1.225(21) Å, and C(4)-C(1) (1.486(27) Å), indicate that the complex presumably takes the betaine structure (I) in contrast with the significant contribution of the betaine structure (II) in the free ligand which can be inferred from the lower ν(CO) frequency in an infrared spectrum.[4] The X-ray structure determination of a benzoyl stabilized ylide, benzoylchlorotriphenylphosphorane, has shown that the main contribution in the bonding is the betaine structure (II).[12]

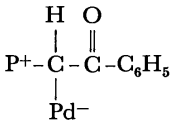

(I)

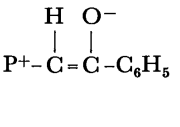

(II)

It seems significant to compare the properties of ylides as ligands with those of phosphines, because both ylides (C ligands) and phosphines (P ligands) coordinate to the metal in similar fashion formally. Bdep which has both ylide and phosphine parts in a molecule appears to be a suitable ligand for the comparison of such properties as trans-influence (or -effect) simulta-

Table 2. Bond lengths (l/Å) with their estimated standard deviations in parentheses

Pd-C(1)	2.115(15)	C(9)-C(10)	1.397(29)	C(28)-C(23)	1.424(29)	H(6)-C(6)	0.97(11)
Pd-P(2)	2.230(8)	C(10)-C(5)	1.382(18)	C(29)-C(30)	1.393(26)	H(8)-C(8)	1.18(17)
Pd-Cl(1)	2.390(8)	C(11)-C(12)	1.358(20)	C(30)-C(31)	1.415(22)	H(9)-C(9)	1.12(11)
Pd-Cl(2)	2.340(9)	C(12)-C(13)	1.447(35)	C(31)-C(32)	1.403(34)	H(10)-C(10)	1.13(15)
P(1)-C(1)	1.795(12)	C(13)-C(14)	1.337(38)	C(32)-C(33)	1.343(30)	H(12)-C(12)	1.08(17)
P(1)-C(2)	1.816(14)	C(14)-C(15)	1.345(23)	C(33)-C(34)	1.423(23)	H(13)-C(13)	0.97(16)
P(1)-C(5)	1.783(19)	C(15)-C(16)	1.430(34)	C(34)-C(29)	1.391(29)	H(14)-C(14)	1.09(16)
P(1)-C(11)	1.808(19)	C(16)-C(11)	1.337(29)	C(35)-C(36)	1.361(35)	H(15)-C(15)	1.04(13)
P(2)-C(3)	1.836(15)	C(17)-C(18)	1.377(31)	C(36)-C(37)	1.387(40)	H(16)-C(16)	0.98(11)
P(2)-C(17)	1.856(17)	C(18)-C(19)	1.401(25)	C(37)-C(38)	1.442(45)	H(18)-C(18)	1.14(11)
P(2)-C(23)	1.797(17)	C(19)-C(20)	1.341(27)	C(38)-C(39)	1.396(32)	H(19)-C(19)	1.02(19)
C(1)-C(4)	1.486(27)	C(20)-C(21)	1.386(37)	C(39)-C(40)	1.445(41)	H(20(-C(20)	1.05(13)
C(2)-C(3)	1.519(22)	C(21)-C(22)	1.406(25)	C(40)-C(35)	1.425(47)	H(22)-C(22)	1.01(16)
C(4)-C(29)	1.522(19)	C(22)-C(17)	1.359(22)	C(41)-C(35)	1.447(40)	H(24)-C(24)	0.87(14)
C(4)-O	1.225(21)	C(23)-C(24)	1.384(18)			H(26)-C(26)	1.08(12)
C(5)-C(6)	1.394(26)	C(24)-C(25)	1.373(27)	H(2)-C(2)	0.84(12)	H(27)-C(27)	1.00(21)
C(6)-C(7)	1.448(32)	C(25)-C(26)	1.402(33)	H(3)-C(2)	1.02(14)	H(30)-C(30)	0.97(15)
C(7)-C(8)	1.367(25)	C(26)-C(27)	1.388(22)	H(4)-C(3)	0.97(9)	H(32)-C(32)	1.11(15)
C(8)-C(9)	1.380(30)	C(27)-C(28)	1.343(30)	H(5)-C(3)	0.87(15)	H(34)-C(34)	1.21(13)

Table 3. Bond angles (ϕ/°) with their estimated standard deviations in parentheses

Cl(1)-Pd-Cl(2)	90.8(1)	P(1)-C(5)-C(6)	121.6(12)	P(2)-C(23)-C(24)	121.4(13)
Cl(1)-Pd-C(1)	87.3(4)	P(1)-C(5)-C(10)	118.6(12)	P(2)-C(23)-C(28)	121.1(11)
Cl(2)-Pd-P(2)	96.2(4)	C(6)-C(5)-C(11)	139.4(14)	C(24)-C(23)-C(28)	117.1(15)
P(2)-Pd-C(1)	86.2(1)	C(5)-C(6)-C(7)	119.5(16)	C(23)-C(24)-C(25)	123.2(18)
Cl(1)-Pd-P(2)	174.1(2)	C(6)-C(7)-C(8)	118.2(20)	C(24)-C(25)-C(26)	118.9(16)
Cl(2)-Pd-C(1)	173.2(4)	C(7)-C(8)-C(9)	122.3(20)	C(25)-C(26)-C(27)	117.5(19)
Pd-C(1)-P(1)	115.1(6)	C(8)-C(9)-C(10)	119.1(16)	C(26)-C(27)-C(28)	124.0(21)
Pd-C(1)-C(4)	102.9(9)	C(5)-C(10)-C(9)	121.0(16)	C(23)-C(28)-C(27)	119.1(16)
P(1)-C(1)-C(4)	111.2(12)	P(1)-C(11)-C(12)	116.6(13)	C(4)-C(29)-C(30)	121.7(16)
C(1)-P(1)-C(2)	114.6(5)	P(1)-C(11)-C(16)	122.8(13)	C(4)-C(29)-C(34)	118.1(15)
C(1)-P(1)-C(5)	109.2(7)	C(12)-C(11)-C(16)	120.6(17)	C(30)-C(29)-C(34)	120.2(16)
C(1)-P(1)-C(11)	110.3(7)	C(11)-C(12)-C(13)	119.7(21)	C(29)-C(30)-C(31)	120.2(19)
C(2)-P(1)-C(5)	106.1(7)	C(12)-C(13)-C(14)	118.8(19)	C(30)-C(31)-C(32)	117.7(18)
C(2)-P(1)-C(11)	108.9(7)	C(13)-C(14)-C(15)	120.9(22)	C(31)-C(32)-C(33)	122.6(18)
C(5)-P(1)-C(11)	107.5(8)	C(14)-C(15)-C(16)	120.7(22)	C(32)-C(33)-C(34)	119.8(21)
Pd-P(2)-C(3)	115.6(5)	C(11)-C(16)-C(15)	119.1(17)	C(29)-C(34)-C(33)	119.2(17)
Pd-P(2)-C(17)	112.9(5)	P(2)-C(17)-C(18)	121.1(12)	C(36)-C(35)-C(40)	132.8(26)
Pd-P(2)-C(23)	115.5(5)	P(2)-C(17)-C(22)	118.3(14)	C(36)-C(35)-C(41)	122.4(29)
C(3)-P(2)-C(17)	100.9(7)	C(18)-C(17)-C(22)	120.5(16)	C(40)-C(35)-C(41)	104.7(24)
C(3)-P(2)-C(23)	104.7(7)	C(17)-C(18)-C(19)	118.2(16)	C(35)-C(36)-C(37)	115.7(28)
C(17)-P(2)-C(23)	105.8(7)	C(18)-C(19)-C(20)	120.2(21)	C(36)-C(37)-C(38)	123.7(24)
P(1)-C(2)-C(3)	114.3(10)	C(19)-C(20)-C(21)	123.4(19)	C(37)-C(38)-C(39)	109.5(24)
P(2)-C(3)-C(2)	111.1(12)	C(20)-C(21)-C(22)	115.2(18)	C(38)-C(39)-C(40)	136.2(29)
C(1)-C(4)-C(29)	119.5(14)	C(17)-C(22)-C(21)	122.4(19)	C(35)-C(40)-C(39)	101.7(23)
C(1)-C(4)-O	123.4(14)				
C(29)-C(4)-O	117.0(15)				

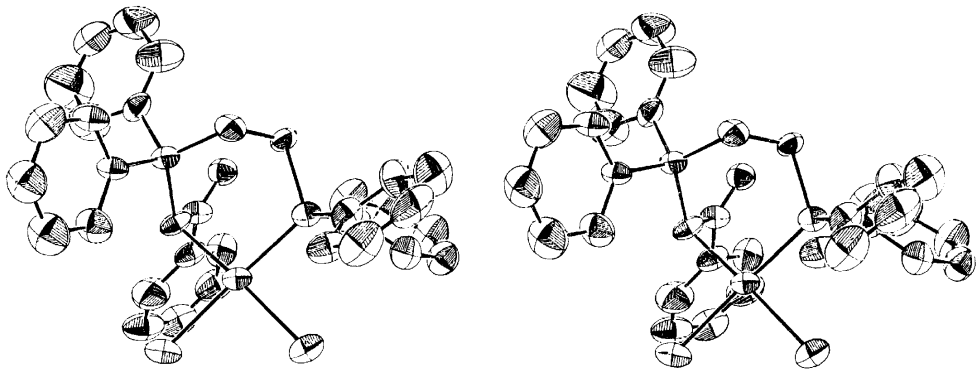

Fig. 2. A stereoscopic view of the molecule; the thermal ellipsoids are drawn at the 50% probability level (ORTEP).

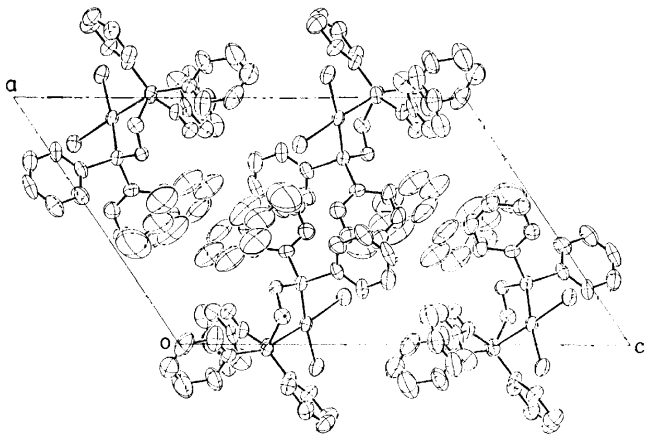

Fig. 3. Crystal structure projected along the b axis.

neously. Chlorine atoms in $[PdCl_2(bdep)]$ are bonded to palladium with bond lengths of Pd–Cl(1) (2.390(8) Å) and Pd–Cl(2) (2.340(8) Å). The Pd-Cl(2) which is trans to the ylide C is somewhat shorter than the other Pd–Cl(1) which is *trans* to the phosphine P. Since longer bond length of the bond *trans* to a ligand can be regarded as an indication of larger *trans*-influence of the ligand,[13] it is likely that the *trans*-influecne of the ylide C is comparable with, but slightly smaller than, that of the phosphine P in bdep.

Crystal Structure. The crystal structure projected along b axis is shown in Fig. 3. Toluene molecules are packed in voids formed by $[PdCl_2(bdep)]$ molecules, but the molecular interaction seems to be rather loose judging from the intermolecular contacts which are larger than 4 Å.

References

1) Y. Oosawa, T. Miyamoto, T. Saito, and Y. Sasaki, *Chem. Lett.*, **1975**, 33.
2) Y. Oosawa, T. Saito, and Y.Sasaki, *Chem. Lett.*, **1975**, 1259.
3) M. Kato, H. Urabe, Y. Oosawa, T. Saito, and Y. Sasaki, *Chem. Lett.*, **1976**, 51.
4) Y. Oosawa, H. Urabe, T. Saito, and Y. Sasaki, *J. Organometal. Chem.*, **122**, 113 (1976).
5) H. Takahashi, Y. Oosawa, A. Kobayashi, T. Saito, and Y. Sasaki, *Chem. Lett.*, **1976**, 15.
6) "International Tables for X-Ray Crystallography," Vol. III, 3rd ed., Kynoch Press, Birmingham (1969), pp. 202.
7) "The Universal Crystallographic Computation Program System," Crystallographic Society of Japan (1969).
8) F. Heydenreich, A. Mollbach, G. Wilke, H. Dreeskamp, E. G. Hoffmann, G. Schroth, K. Seevogel, and W. Stemple, *Israel J. Chem.*, **10**, 293 (1972).
9) D. J. Brauer, C. Krüger, P. J. Roberts, and Y-H. Tsay, *Chem. Ber.*, **107**, 3706 (1974).
10) M. Keeton, R. Mason, and D. R. Russell, *J. Organometal. Chem.*, **33**, 259 (1971).
11) H. Schmidbaur, W. Buchner, and D. Sheutzow, *Chem. Ber.*, **106**, 1351 (1973).
12) A. J. Speziale and K. W. Ratts, *J. Am. Chem. Soc.*, **87**, 5603 (1965).
13) T. G. Appleton, H. C. Clark, and L. E. Manzer, *Coord. Chem. Rev.*, **10**, 335 (1973).

Stereoselectivity in Mixed Ligand Copper(II) Complexes with Electrostatic Ligand-Ligand Interactions. Application to Optical Resolution of α-Amino Acids with a Charged Side Chain

Osamu YAMAUCHI, Takeshi SAKURAI, and Akitsugu NAKAHARA

Institute of Chemistry, College of General Education, Osaka University, Toyonaka, Osaka 560

(Received January 14, 1977)

Optical resolution of DL-aspartic acid and DL-glutamic acid (abbreviated as DL-A) has been achieved *via* formation of ternary copper(II) complexes composed of a DL-A and L-arginine, L-lysine, or L-ornithine (L-B). For every pair of ligands DL-A and L-B, a neutralized solution containing $Cu(ClO_4)_2$, DL-A, and L-B in the molar ratio of 1 : 2 : 1 gave the mixed ligand complex abounding in [Cu(D-A)(L-B)] as crystals, from which incorporated A was isolated through a Dowex CCR-2 column after treating with H_2S. In a very similar manner D-enantiomer-rich B was obtained from DL-B by using an L-A. The optical purities of the resolved amino acids were as high as 90 and 70% for aspartic acid and glutamic acid, respectively, and 40—50% for the basic amino acids. The finding shows that the electrostatic ligand-ligand interactions in the mixed ligand complexes give rise to geometric isomerism around copper(II) and hence preferential formation and crystallization of the *meso* complexes, [Cu(L-A)(D-B)] and [Cu(D-A)(L-B)], probably with a *cis* configuration.

Stereoselectivity has been reported recently for kinetically labile transition metal complexes containing simple amino acids[1,2] and *N*-carboxymethyl[3] and *N*-benzyl[4] derivatives of amino acids, and in most cases the selectivity has been attributed to the steric hindrance arising from two bulky ligands coordinated around a metal ion. In our previous studies electrostatic ligand-ligand interactions between the oppositely charged groups in the side chains of coordinated amino acids and related compounds have been inferred from the CD (circular dichroism) spectral magnitude enhancements in the d-d region, and interpreted as one of the driving forces leading to the formation of mixed ligand copper(II) complexes.[5,6] Because of the steric requirements for such interactions around the central atom, they were expected to give rise to geometric isomerism in the ternary copper(II) complexes, Cu(A)(B), where A refers to the ionized form of aspartic acid (Asp) or glutamic acid (Glu) and B to the protonated form of arginine (Arg), lysine (Lys), or ornithine (Orn).[7] In fact,the infrared spectra of the isolated complexes indicated the existence of the geometric isomerism,[6a] and molecular models suggested a *trans* structure (**1**) for Cu(L-A)(L-B) and a *cis* structure (**2**) for Cu(D-A)(L-B).

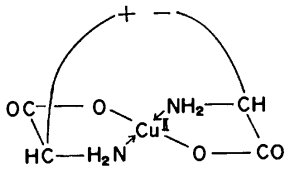

Cu(L-A)(L-B)

1

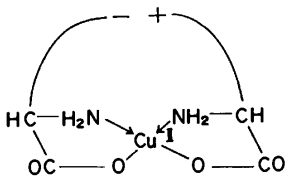

Cu(D-A)(L-B)

2

The stereoselectivity attributable to steric interactions between the side chains of the ligands in the coordination sphere has been applied to optical resolution of amino acids with a bulky side chain by ligand-exchange chromatography in the presence of copper(II) and other metal ions.[8] Since the selectivity is purely due to steric hindrance, resolvable amino acids have been confined to those having a bulky group, such as proline, valine, and leucine.

On the other hand, the stereoselectivity due to the electrostatic ligand-ligand interactions suggested the possibility of optical resolution of amino acids with a charged side chain, such as aspartic acid, glutamic acid, arginine, and lysine, which have been excluded from the resolution based on the bulkiness of the side chains. We reported in a previous communication[9] that racemic aspartic acid and glutamic acid could be resolved into enantiomers by using copper(II) and an optically active basic amino acid, L-B, and now we have investigated the stereoselectivity in detail to explore a novel approach to optical resolution of the enantiomers of the mentioned amino acids *via* formation of mixed ligand copper(II) complexes.

Experimental

Materials. D-Arginine hydrochloride and D-lysine hydrochloride were obtained from Fluka AG and D-ornithine hydrochloride from Sigma Chemical Co. All other amino acids were purchased from Nakarai Chemicals Ltd. Their purity was checked by the specific rotations, $[\alpha]_{589}^{20}$ (in 3M HCl; $c=1$), which were +25.7° (L-Asp), −24.9° (D-Asp), +31.9° (L-Glu), −30.9° (D-Glu), +22.8° (L-Arg·HCl), −21.7° (D-Arg·HCl), +20.8° (L-Lys·HCl), −20.5° (D-Lys·HCl), +22.9° (L-Orn·HCl), and −22.5° (D-Orn·HCl). All the materials used were of reagent grade or of highest grade available.

Measurements. Absorption spectra of the complexes were measured with a Union Giken SM-401 High-Sensitivity recording spectrophotometer and CD spectra with a JASCO MOE-1 spectropolarimeter in a 1-cm or a 2-cm quartz cell. The spectral measurements were made in the range 400—800 nm at a constant copper(II) concentration of 5.0×10^{-3} M in water at room temperature. The pH values (7.5—8.5) of the solutions were roughly adjusted with aqueous sodium hydroxide and dilute perchloric acid and finally determined immediately after the spectroscopic measurements. Optical rotations of amino acids were measured on a Yanagimoto OR-10 polarimeter at 589 nm in a 5-cm quartz cell at 20 ±0.1 °C. Infrared spectra of the isolated mixed ligand copper(II) complexes were obtained in the range 4000—650 cm^{-1} with a Hitachi 215 grating infrared spectrophotometer with the KBr disk method.

Optical Resolution of Racemic Aspartic Acid and Glutamic Acid. For every pair of DL-A and L-B, optical resolution of an

acidic amino acid was performed by essentially the same method as typically described for the Cu(II)–DL-Asp–L-Arg system. Copper(II) perchlorate hexahydrate (3.70 g, 10 mmol), DL-aspartic acid (2.66 g, 20 mmol), and L-arginine hydrochloride (2.10 g, 10 mmol) were dissolved in *ca.* 50 ml of water, and the pH of the resulting solution was adjusted to *ca.* 7 with aqueous sodium hydroxide. After stirring for 1 h at room temperature, the reaction mixture was concentrated *in vacuo* to a small volume at temperatures below 50 °C. Addition of ethanol to the residue gave [Cu(asp)(L-argH)]·$2H_2O$ as blue crystals (0.68 g, 1.7 mmol; 17% based on the amount of copper(II) used). Found: C, 29.29; H, 5.51; N, 17.27%. Calcd for $C_{10}H_{19}N_5O_6Cu \cdot 2H_2O$: C, 29.66; H, 5.73; N, 17.30%.

After copper(II) had been removed by treating an aqueous solution of the isolated complex with hydrogen sulfide, the incorporated aspartic acid was separated from L-arginine through a 1×100 cm column of Dowex CCR-2 (mesh 20—50) in the H^+ form by eluting with water. Isolated aspartic acid was recrystallized from aqueous ethanol to give a salt-free product (0.16 g, 1.2 mmol; 12% based on the half amount of DL-aspartic acid used). The specific rotation of −22.9° (in 3M HCl; $c=1$) demonstrates that D-aspartic acid was preferentially incorporated into the ternary complex. Its optical purity (89%) was substantiated by an estimation made from the CD curve of the isolated ternary complex in aqueous solution (pH 8.0) according to the method described below.

In order to determine the optical purities of the acidic amino acids incorporated into [Cu(asp)(L-lysH)], [Cu(asp)(L-ornH)], and [Cu(glu)(L-ornH)], the first crops, which were nearly pure, were recrystallized once from aqueous ethanol.

Optical Resolution of Racemic Arginine, Lysine, and Ornithine. According to a procedure very similar to that described above, racemic basic amino acids were resolved into enantiomers by using a different Cu(II) : L-A : DL-B molar ratio of 1 : 1 : 1.5 to avoid precipitation of less soluble binary complexes $Cu(B)_2$. The amino acids B incorporated into Cu(L-A)(B) were separated from L-A through a 1×100 cm column of Amberlite IR-45 in the Cl^- form by eluting with water and obtained as hydrochlorides.

Determination of Optical Purity by CD Spectral Curves. The optical purities of the incorporated amino acids were also determined by the CD calibration curves, which were based on either the magnitude or the maximum wavelength and set up for the Cu(A)(L-B) and Cu(L-A)(B) systems with five different enantiomer contents of A and B, respectively, at the molar ratio of 1 : 1 : 1. The measurements were made at selected pH values where the complex formation was nearly complete. The enantiomer contents of the Cu(glu)(L-B) and Cu(L-A)(B) systems were found to be linearly correlated with the CD magnitudes ($\Delta\varepsilon$) at fixed wavelengths around 600 nm. Because the magnitudes for the Cu(asp)-(L-B) systems changed only slightly at different L- or D-Asp contents, the calibration curves were made by plotting the enantiomer contents against the maximum wavelengths that shifted with the contents.

Results and Discussion

Stereoselective Incorporation of Amino Acids into Ternary Complexes. Yields and optical purities of the acidic and the basic amino acids obtained *via* the ternary complex formation are summarized in Tables 1 and 2. The specific rotations clearly indicated that the D-enantiomers of the racemic amino acids used were preferentially incorporated into the ternary copper(II) complexes each containing an L-A or an L-B. Another line of evidence supporting the incorporation of the D-enantiomers is given by the optical purities of A and B estimated directly from the CD spectra of the complexes in the d-d region according to the calibration curves, such as are shown in Figs. 1 and 2. The optical purities determined by the two methods are in reasonable agreement with each other, and the differences between the correspoding values may be due to the inaccuracies pertaining to the calibration curves based on the CD spectra. The IR spectra of the isolated complexes, [Cu(A)(L-B)], showed the patterns that were more closely related to [Cu(D-A)(L-B)] than to [Cu(L-A)(L-B)], further substantiating that the *meso* complexes were preferentially obtained as crystals under the conditions employed.

It is interesting to note that, whereas X-ray structure analyses[10,11] have revealed that some bis(amino acidato)-

Table 1. Yields and optical purities of the D-enantiomers of acidic amino acids isolated *via* formation of the ternary complexes, Cu(A)(L-B)

Ligand A	Ligand B	Cu(A)(L-B) isolated: Yield (%)[a]	Cu(A)(L-B) isolated: Optical purity (%)[b]	A isolated: Yield (%)[c]	A isolated: Optical purity (%)[d]
DL-Asp	L-Arg	17	93	12	89
	L-Lys	28	79	11	89
	L-Orn	28	50	14	44
DL-Glu	L-Arg	61	42	53	33
	L-Lys	18	75	14	70
	L-Orn	21	39	12	35

a) Yield of the isolated complex based on the amount of copper(II) used. b) Optical purity of A estimated from the calibration curves shown in Fig. 1. c) Yield of isolated A based on the half amount of DL-A used. d) Estimated from the specific rotation, $[\alpha]_{589}^{20}$ (in 3 M HCl; $c=1$).

Table 2. Yields and optical purities of the D-enantiomers of basic amino acids isolated *via* formation of the ternary complexes, Cu(L-A)(B)

Ligand B	Ligand A	Cu(L-A)(B) isolated: Yield (%)[a]	Cu(L-A)(B) isolated: Optical purity (%)[b]	B isolated: Yield (%)[c]	B isolated: Optical purity (%)[d]
DL-Arg	L-Glu	36	46	14	41
	L-Asp	63	42	30	38
DL-Lys	L-Glu	18	56	7	50
	L-Asp	39	16	21	11
DL-Orn	L-Glu	36	12	19	17
	L-Asp	34	42	29	36

a) Yield of the isolated complex based on the amount of copper(II) used. b) Optical purity of B estimated from the calibration curves shown in Fig. 2. c) Yield of isolated B based on two-thirds of the amount of DL-B used. d) Estimated from the specific rotation, $[\alpha]_{589}^{20}$ (in 3 M HCl; $c=1$).

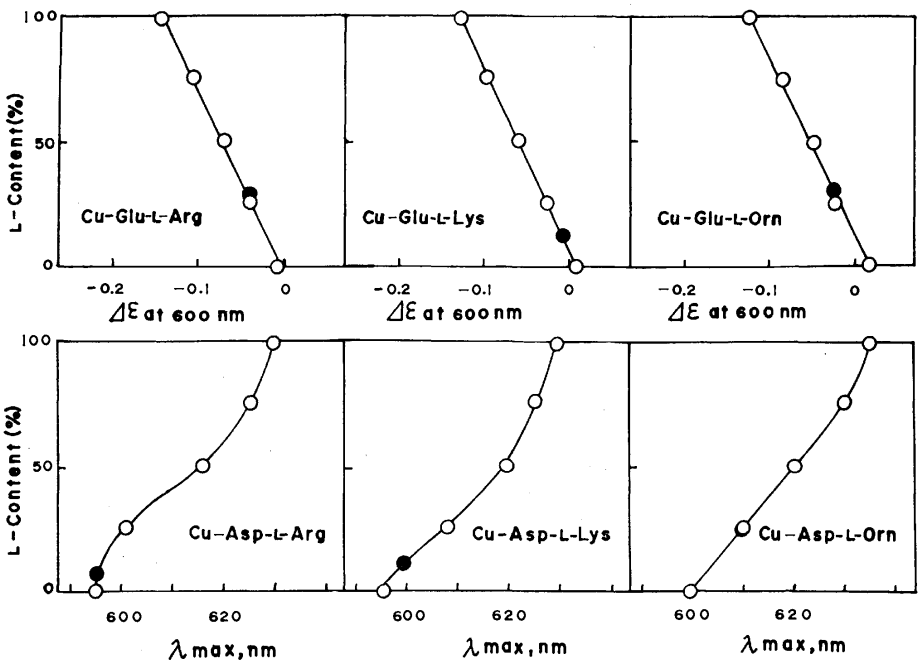

Fig. 1. Determination of the optical purities of acidic amino acids incorporated into Cu(A)(L-B) (●) from the calibration curves based on the CD spectra of the standard samples (○).

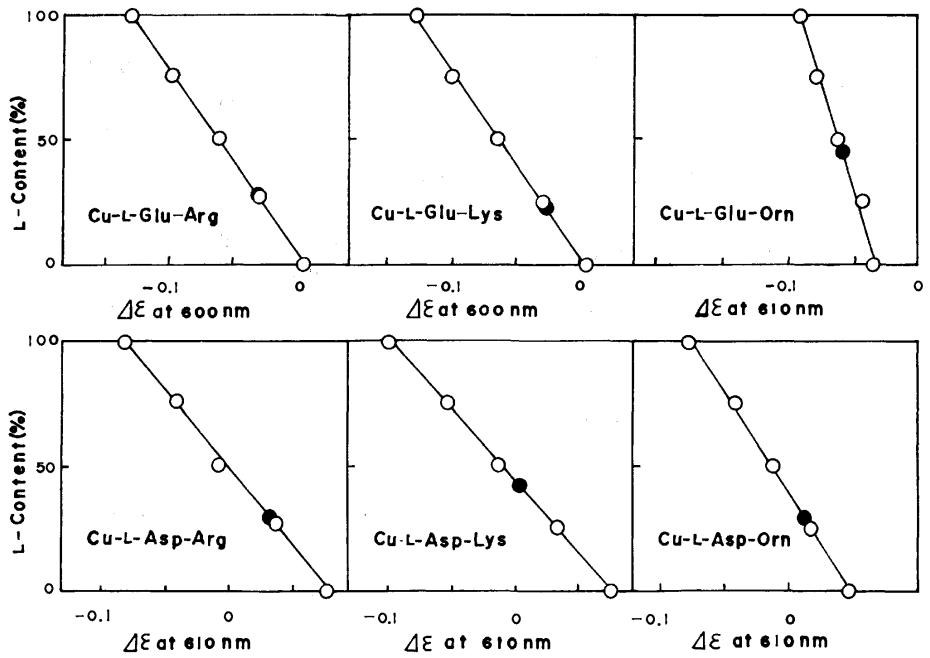

Fig. 2. Determination of the optical purities of basic amino acids incorporated into Cu(L-A)(B) (●) from the calibration curves based on the CD spectra of the standard samples (○).

copper(II) complexes assume a *cis* structure while others assume a *trans* one, every possible combination of A and B invariably gives as the main product a *meso* complex probably with a *cis* structure.[6a]

Factors Affecting the Optical Resolution. Probably owing to the electrostatic ligand-ligand interactions, the protonated ternary copper(II) complexes containing L-histidine and a basic amino acid, such as L-arginine and L-lysine, have been reported to have slightly higher stability constants than those containing D-histidine in place of L-histidine.[2b,2c] Although equilibrium constants are a reliable source of information about the species distribution and hence the stereoselectivity in solution, it seems difficult to detect the selectivity in solution in the present cases, because the electrostatic ligand-ligand interactions are seriously affected by the ionic strength of the solution, whose influence has been found to be reflected in the CD magnitudes of the

ternary systems.[5,6] A preliminary potentiometric study showed that the enantiomeric pairs of the ternary systems give almost identical titration curves at the ionic strength of 0.1(KNO_3). Accordingly, it may be unrealistic to expect large stability differences between the enantiomeric species present in the reaction media. No significant difference was observed between the CD spectra in the d-d region of 1 : 1 : 1 and 1 : 2 : 1 mixtures of Cu(II), DL-A, and L-B, which indicates that there exists no remarkable preference of *cis*-[Cu(D-A)(L-B)] over *trans*-[Cu(L-A)(L-B)] in solution and that the two isomers are approximately equally present. In contrast to this, the ternary complex isolated from a 1 : 1 : 1 mixture of Cu(II), L-Glu, and DL-Orn had incorporated D-Orn with 17% enantiomeric excess. These findings suggest that the solubility factor rather than the stability factor plays an important role in the optical resolution *via* complex formation.

In conclusion, the electrostatic interactions between the ligands within a complex molecule serve as an essential force fixing the structure of the complex in a particular configuration, and the resulting *cis-trans* isomerism makes optical resolution of racemic ligands feasible under favorable conditions.

This work was supported in part by a grant from the Ministry of Education, which is gratefully acknowledged. We also wish to thank Miss Teruko Kuroe for elemental analysis.

References

1) a) K. Harada and S. V. Fox, *Nature*, **194**, 768 (1962); b) K. Harada, *ibid.*, **205**, 590 (1965); c) K. Harada and T. Iwasaki, *Chem. Lett.*, **1972**, 1057.

2) a) G. Brookes and L. D. Pettit, *J. Chem. Soc., Chem. Commun.*, **1974**, 813; b) G. Brookes and L. D. Pettit, *ibid.*, **1975**, 385; c) P. J. Morris and R. B. Martin, *J. Inorg. Nucl. Chem.*, **32**, 2891 (1970); d) L. D. Pettit and J. L. M. Swash, *J. Chem. Soc., Dalton Trans.*, **1976**, 588.

3) a) B. E. Leach and R. J. Angelici, *J. Am. Chem. Soc.*, **91**, 6296 (1969); b) R. V. Snyder and R. J. Angelici, *J. Inorg. Nucl. Chem.*, **35**, 523 (1973).

4) a) V. A. Davankov, S. V. Rogozhin, and A. A. Kurganov, *Izv. Akad. Nauk SSSR, Ser. Khim.*, **1971**, 204; b) G. G. Alexandrov, Yu. T. Struchkov, A. A. Kurganov, S. V. Rogozhin, and V. A. Davankov, *J. Chem. Soc., Chem. Commun.*, **1972**, 1328; c) V. A. Davankov and P. R. Mitchell, *J. Chem. Soc., Dalton Trans.*, **1972**, 1012; d) V. A. Davankov, S. V. Rogozhin, A. A. Kurganov, and L. Ya. Zhuchkova, *J. Inorg. Nucl. Chem.*, **37**, 369 (1975); e) V. A. Davankov, S. V. Rogozhin, Yu. T. Struchkov, G. G. Alexandrov, and A. A. Kurganov, *ibid.*, **38**, 631 (1976); f) E. Tsuchida, H. Nishikawa, and E. Terada, *Eur. Polym. J.*, **12**, 611 (1976).

5) O. Yamauchi, Y. Nakao, and A. Nakahara, *Bull. Chem. Soc. Jpn.*, **48**, 2572 (1975).

6) a) T. Sakurai, O. Yamauchi, and A. Nakahara, *Bull. Chem. Soc. Jpn.*, **49**, 169 (1976); b) T. Sakurai, O. Yamauchi, and A. Nakahara, *ibid.*, **49**, 1579 (1976).

7) The abbreviations such as Asp, Glu, and Arg denote the neutral, uncomplexed forms of amino acids. The fully ionized amino acids in coordination are described in small letters, *e.g.* asp for Asp and glu for Glu, and a dissociable hydrogen ion contained in a coordinated amino acid is expressed by H as in argH and ornH.

8) a) C. W. Roberts and D. H. Haigh, *J. Org. Chem.*, **27**, 3375 (1962); b) R. V. Snyder, R. J. Angelici, and R. B. Meck, *J. Am. Chem. Soc.*, **94**, 2660 (1972); c) V. A. Davankov and S. V. Rogozhin, *Dokl. Akad. Nauk SSSR*, **193**, 94 (1970); d) I. I. Peslyakas, S. V. Rogozhin, and V. A. Davankov, *Izv. Akad. Nauk SSSR, Ser. Khim.*, **1974**, 174.

9) T. Sakurai, O. Yamauchi, and A. Nakahara, *J. Chem. Soc., Chem. Commun.*, **1976**, 553.

10) a) H. C. Freeman, *Adv. Protein Chem.*, **22**, 257 (1967); b) H. C. Freeman, "Inorganic Biochemistry," Vol. 1, ed by G. L. Eichhorn, Elsevier, Amsterdam (1973), Chap. 4.

11) a) K. Tomita and K. Nitta, *Bull. Chem. Soc. Jpn.*, **34**, 286 (1961); b) R. D. Gillard, R. Mason, N. C. Payne, and G. B. Robertson, *Chem. Commun.*, **1966**, 155; c) A. McL. Mathieson and H. A. Welsh, *Acta Crystallogr.*, **5**, 599 (1952); d) B. Evertsson, *ibid., Sect. B*, **25**, 30 (1969); e) C. M. Weeks, A. Cooper, and D. A. Norton, *ibid., Sect. B*, **25**, 443 (1969).

Preparation and Stereochemistry of *trans*-Dianionocobalt(III) Complexes with (*S*)-2-(Methylaminomethyl)pyrrolidine

Taku KITAMURA, Yoshiko SATO, Masahiko SABURI, and Sadao YOSHIKAWA

Department of Synthetic Chemistry, Faculty of Engineering, The University of Tokyo, Hongo, Bunkyo-ku, Tokyo 113

(Received January 22, 1977)

trans-Dinitro and dichloro cobalt(III) complexes containing (*S*)-2-(methylaminomethyl)pyrrolidine (*N*-Me-ampr) were prepared. Their stereochemistry differs a great deal from that of other *N*-methylated 1,2-diamines. The *N*-Me-ampr complexes prefer the *trans,cis* instead of the *trans,trans* configuration, the axial *N*-methyl groups being fairly stabilized. In the case of the dinitro complex, only one isomer which has the axial *N*-methyl groups, was isolated, but in the case of the *trans*-dichloro complex two diastereomers (*trans,cis(RR)* and *trans,cis(SS)*) were obtained. These dichloro isomers were slowly converted into an equilibrium mixture in methanol. The CD spectral data of the equilibrium mixture show that the *trans,cis(RR)* is more stable than the *trans,cis(SS)* isomer ($-\Delta G=0.4$ kcal/mol).

Substituents introduced into polyamine ligands have been seen to regulate the configuration of their metal complexes. For example, the dianionobis(diamine)cobalt (III) complexes (diamine=*N*-substituted 1,2-diamine) sterospecifically adopt the *trans* configuration with respect to the unidentate anionic ligands, and the *N*-substituents take *trans* position to each other. Thus the structures of these complexes are not *trans,cis* but *trans, trans* configuration.[1] The *C*- and *N*-substituents in the chelate rings generally prefer the equatorial position[2] and cnsequently the chelate rings are fixed to the δ or λ gauche conformation.

(*S*)-2-(Methylaminomethyl)pyrrolidine (*N*-Me-ampr) has some characteristics differing from other *C*- and *N*-substituted diamines. The absolute configuration of the asymmetric carbon in the five membered chelate ring is *S* and the gauche chelate conformation should be fixed to δ.[3] The asymmetric nitrogen in the pyrrolidine ring is considered to coordinate with the *S* configration.[4] On the other hand, the absolute configuration of the asymmetric nitrogen center with the *N*-methyl groups is capable of having either the *S* or the *R* configuration, corresponding to the axial or the equatorial *N*-methyl groups, respectively.

For the cobalt(III) complexes of the type $[CoX_2(N\text{-Me-ampr})_2]^+$ (X=Cl^- or NO_2^-), we have observed some stereochemical features differing from the complexes of other *N*-methyl diamines. First, the *N*-Me-ampr complexes have the *trans,cis* configuration instead of the *trans,trans*. Second, the axial *N*-methyl groups are fairly stabilized. Third, equilibrium between the isomer having the axial and that having the equatorial *N*-methyl groups is influenced by the kind of apical anionic ligands.

Experimental

trans,cis(SS)-[*Co(NO$_2$)$_2$(N-Me-ampr)$_2$]ClO$_4$*. *Air Oxidation Method*: To an aqueous solution of $CoCl_2\cdot 6H_2O$ (1.19 g in 10 cm^3 of water) was added a solution of *N*-Me-ampr (1.14 g in 5 cm^3 of water containing 0.41 cm^3 of concentrated hydrochloric acid), and $NaNO_2$ (0.69 g) then being added quickly. The resulting solution was vigorously aerated in an ice cold bath for 20 min, and then for 2 h at room temperature. The solution was warmed and evaporated to half its volume at 60 °C on a water bath. Yellow crystals appeared on addition of large excess of $NaClO_4$. The crystals were filtered off and washed with a small volume of cold water, and ethanol and then ether, and air dried. The compound was recrystallized from a small volume of hot water. Yield; 0.5 g. Found: C, 30.13; H, 5.59; N, 17.42%. Calcd for $C_{12}H_{28}N_6O_8ClCo$: C, 30.00; H, 6.06; N, 17.13%.

Derivation from Sodium Hexanitrocobaltate (Na$_3$[Co(NO$_2$)$_6$]): A solution of $Na_3[Co(NO_2)_6]$ (4.04 g in 30 cm^3 of water) was mixed with *N*-Me-ampr (2.28 g), warmed on a water bath at 70 °C for 15 min and then filtered. Yellow crystals appeared on addition of an excess of $NaClO_4$ (3 g) to the filtrate, and the mixture was warmed on a water bath at 60 °C for about 5 min. After being stored in a refrigerator overnight, the precipitate was filtered off, washed with a small volume of cold water and ethanol, and dried under reduced pressure. The compound was recrystallized from a small volume of water. Yield; 3.15 g. Found: C, 30.24; H, 5.89; N, 17.56%. Calcd for $C_{12}H_{28}N_6O_8ClCo$: C, 30.00; H, 6.06; N, 17.13%.

The visible absorption, CD and ^{1}H NMR spectral data indicate that the dinitro complexes prepared by two methods are identical.

trans,cis(SS)-[*CoCl(NO$_2$)(N-Me-ampr)$_2$]ClO$_4$*. A solution of *trans,cis(SS)*-$[Co(NO_2)_2(N\text{-Me-ampr})_2]ClO_4$ (2.0 g) in concentrated hydrochloric acid (4 cm^3) was warmed at 40 °C on a water bath for 1 h. Excess $LiClO_4$ (0.5 g) was added and the solution was cooled to room temperature. Red crystals were filtered off and washed with a small volume of cold water and ethanol and dried under reduced pressure. The product was recrystallized from methanol. Yield; 1.6 g. Found: C, 30.54; H, 6.14; N, 14.35%. Calcd for $C_{12}H_{28}N_5O_6Cl_2Co$: C, 30.78; H, 6.03; N, 14.96%.

trans,cis(SS)-[*CoCl$_2$(N-Me-ampr)$_2$]ClO$_4$*. *trans,cis(SS)*-$[CoCl(NO_2)(N\text{-Me-ampr})_2]ClO_4$ (0.4 g) was dissolved in hydrochloric acid (10 cm^3) and the solution was heated on a water bath at 80 °C until the color of the solution turned from red to deep green. Green crystals formed by the addition of perchloric acid (60% 3 cm^3), were filtered off, washed with a small volume of cold water, ethanol and ether, and air dried. The product was recrystallized from methanol. Yield; 0.3 g. Found: C, 31.41; H, 6.15; N, 12.45%. Calcd for $C_{12}H_{28}N_4O_4Cl_3Co$: C, 31.49, H; 6.17; N, 12.24%.

trans,cis(RR)-[*CoCl$_2$(N-Me-ampr)$_2$]ClO$_4$*. To an aqueous solution of $CoCl_2\cdot 6H_2O$ (2.39 g in 15 cm^3 of water) was added *N*-Me-ampr (2.28 g in 10 cm^3 of water) and the resulting solution was aerated for 5 h with carbon dioxide free air. After concentrated hydrochloric acid (15 cm^3) had been added, the solution was heated on a boiling water bath and concentrated to about half of its original volume. Green crystalline powder of the *trans*-dichloro complex was formed by the addition of perchloric acid (60% 10 cm^3), was filtered off, washed with a small amount of ethanol and ether, and air dried.

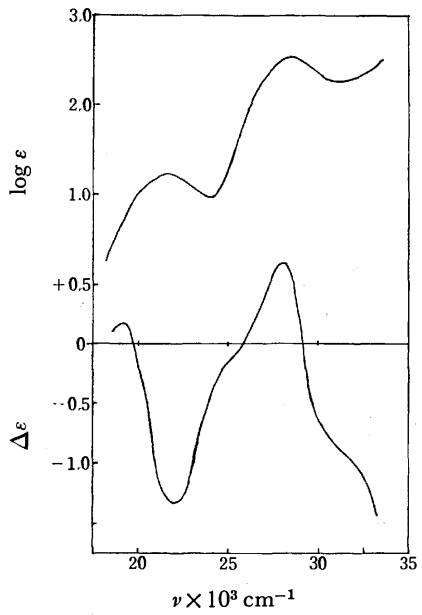

Fig. 1. Absorption (upper) and CD spectra (lower) of *trans*-$[Co(NO_2)_2(N\text{-Me-ampr})_2]ClO_4$.

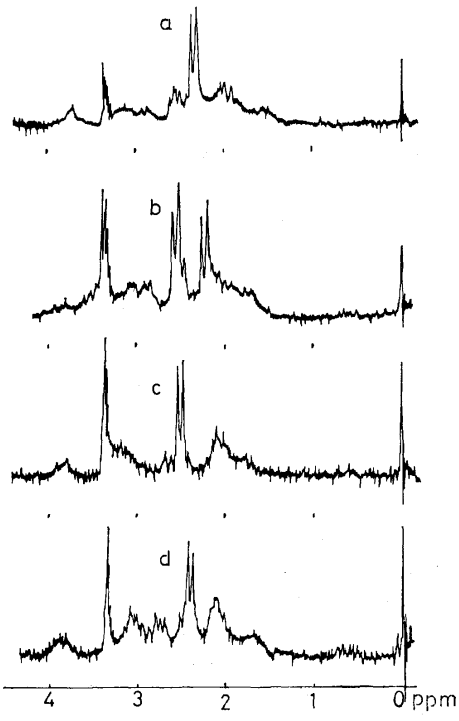

Fig. 2. ^1H NMR spectra of *N*-Me-ampr complexes. a) *trans*-$[Co(NO_2)_2(N\text{-Me-ampr})_2]ClO_4$, b) *trans,cis*-$[CoCl(NO_2)(N\text{-Me-ampr})_2]ClO_4$, c) *trans,cis(SS)*-$[CoCl_2(N\text{-Me-ampr})_2]ClO_4$, d) *trans,cis(RR)*-$[CoCl_2(N\text{-Me-ampr})_2]ClO_4$.

This product was found to be a mixture of two isomers of *trans,cis(SS)* and *trans,cis(RR)* on the basis of ^1H NMR and CD spectral data. The pure *trans,cis(RR)* isomer was obtained by repeated recrystallization from methanol (less soluble part). Yield; 2.0 g. Found: C, 30.93; H, 6.06; N, 12.49%. Calcd for $C_{12}H_{28}N_4O_4Cl_3Co$: C, 31.49; H, 6.17; N, 12.24%.

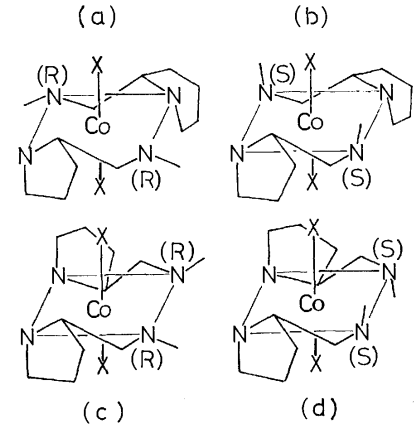

Fig. 3. Four possible structures of *trans*-$[Co(NO_2)_2(N\text{-Me-ampr})_2]^+$ ions.
a) *trans,trans(RR)*, b) *trans,trans(SS)*, c) *trans,cis(RR)*, d) *trans,cis(SS)*.

Results and Discussion

trans-$[Co(NO_2)_2(N\text{-Me-ampr})_2]ClO_4$ was prepared by two methods (usual air oxidation and a reaction of diamine with $[Co(NO_2)_6]^{3-}$ ion). The absorption, circular dichroism (CD) and ^1H NMR spectra of the products obtained by the two methods were identical with each other, indicating the identity of the complexes. The absorption spectrum (Fig. 1) shows two absorption maxima at 465 nm (ε=189.7) and 354 nm (ε=3720), indicating that the complex has *trans* configuration with regard to the nitrite ions.[1,5] In the ^1H NMR spectrum of this complex (in CD_3OD), one doublet assignable to the *N*-methyl groups was observed at 2.36 ppm, indicating that the two *N*-Me-ampr are chemically equivalent (Fig. 2). Since the CD spectrum of *N*-Me-ampr complex (Fig. 1) differs a great deal from the other complexes of *N*-substituted diamines with fixed δ conformations, the vicinal contribution from the asymmetric nitrogens would affect the CD pattern.

Four possible structures of the *trans*-$[Co(NO_2)_2(N\text{-Me-ampr})_2]^+$ ion, with equivalent *N*-Me-ampr, are shown in Fig. 3. Two forms (a,b) have the *trans,trans* configuration and the others (c,d) the *trans,cis* configuration. The structures of this type were assigned by converting them into chloronitro complexes in hydrochloric acid.[5] When the dinitro isomer has the *trans,trans* configuration, the chloronitro complex should be composed of two diastereomers, the yields of which would differ. In such diastereomers, however, both chelate rings are situated in identical chemical environment. Consequently, the ^1H NMR spectra of the *trans,trans* isomers would show two kinds of *N*-methyl signals with different intensities. On the other hand, the *trans,cis* isomer should give rise to only one isomer of chloronitro complex. However, the two chelate rings are affected by distinct circumstances of anionic ligands, which will result in two *N*-methyl resonances with equal intensities.

The ^1H NMR spectrum of the $[CoCl(NO_2)(N\text{-Me-ampr})_2]^+$ ion (in CD_3OD) showed two *N*-methyl doublets at 2.24 ppm and 2.58 ppm (Fig. 2). The intensities of these methyl signals could be regraded as practically equal. The spectral pattern did not change after

repeated recrystallization from methanol or 1M HCl solution. This indicates that the chloronitro complex adopts the *trans,cis* configuration, though the absolute configuration of the *N*-methyl centers, either the *RR* or the *SS*, can not be determined from the ^{1}H NMR data. The orientation of the *N*-methyl group was clarified by examining the CD curves of dichloro complexes.

The *trans,cis*-$[Co(NO_2)_2(N\text{-Me-ampr})_2]^+$ ion was converted into the *trans,cis*-$[CoCl_2(N\text{-Me-ampr})_2]^+$ ion in hydrochloric acid, where no stereochemical change including the inversion of the *N*-methyl centers should occur. The ^{1}H NMR spectrum of the dichloro complex has a single doublet at 2.51 ppm assignable to the *N*-methyl resonances, as expected (Fig. 2). The *trans*-dichloro complex prepared by the usual air oxidation showed a CD curve differing a great deal from that of the *trans,cis*-dichloro complex derived from the *trans,cis*-dinitro complex (Fig. 4). This indicates that the *trans*-(Cl)-$[CoCl_2(N\text{-Me-ampr})_2]^+$ ion exist in at least two isomeric forms. The ^{1}H NMR spectrum of the dichloro complex prepared by air oxidation showed only one doublet at 2.45 ppm assignable to the *N*-methyl groups (Fig. 2), which shows that the *N*-Me-ampr chelates are situated in equivalent circumstances.

Two isomers of the *trans*-dichloro complex show mutarotation in methanol solution, and the CD spectra of both isomers converge to the same curve. This suggests that these complexes isomerize and give rise to the same equilibrium mixture. The configurational rearrangement from *trans,cis* to *trans,trans* and *vice versa* seems to be unlikely. However, it is possible that the inversion of asymmetric nitrogen of *N*-methyl group takes place to contribute to the mutarotation. We thus conclude that the *trans*-dichloro complex prepared from air oxidation also has the *trans,cis* configuration. One of the dichloro isomers should adopt the *RR* configuration and the other the *SS* configuration with respect to the *N*-methyl centers (Fig. 3).

The CD spectrum is considered to arise from the configurational, the conformational and the vicinal effects[6]. In the case of *trans*-dianiono complexes, only the latter two effects should be taken into consideration. It is assumed that the contribution from the δ conformations and asymmetric *S*-nitrogens in pyrrolidine rings are equal for both of the *trans*-dichloro isomers, and that the vicinal contributions from the *S* and the *R* methylated nitrogens are opposite in sign and have approximately equal intensities. Half of the subtract of the CD of *trans,cis(SS)* from that of the *trans,cis(RR)* would be regarded as the vicinal contribution of *R* nitrogens. The half of the CD curve obtained by subtracting the curve of the former dichloro isomer (from dinitro complex) from that of the latter (by air oxidation) are given in Fig. 4 ($1/2$*(trans,cis(RR)—trans,cis(SS))* or *vice versa*). The vicinal contribution of the *R* nitrogens is known to have a positive and a negative Cotton effect dominating the E_g and the A_{2g} (D_{4h}) components, respectively, in the first d-d transition region[6]. From a positive (E_g) and a negative (A_{2g}) maxima in the subtracted CD curve (Fig. 4), it is considered that the absolute configuration of *N*-methyl centers in the dichloro complex obtained by air oxidation is *R* (equatorially disposed

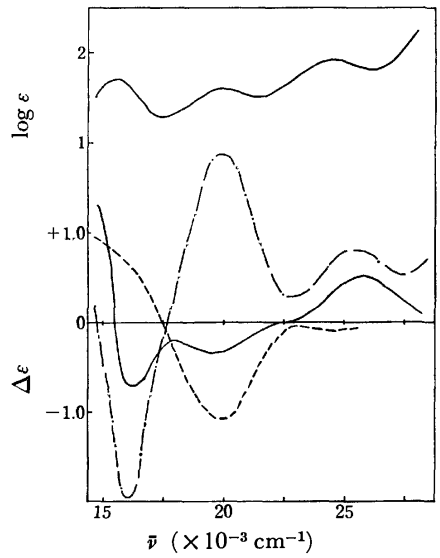

Fig. 4. Absorption (upper) and CD (lower) curves of *traas*-dichloro isomers of *N*-Me-ampr complexes *SS* (——) and *RR*(——), and the differential CD spectrum ($1/2\times(RR-SS)$) (——).

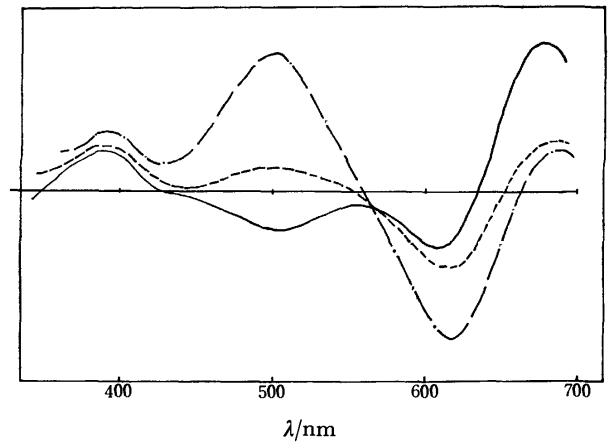

Fig. 5. CD spectra of *trans*-dichloro isomers and the equilibrium mixture (——).

N-methyl groups), and that of the dichloro complex prepared from the dinitro complex as well as the parent dinitro complex is *S* (axial *N*-methyl groups).

From CD spectral data of an equilibrium mixture, the free energy difference between the axial and the equatorial *N*-methyl groups is calculated to be *ca.* 0.4 kcal/mol (axial(*S*): equatorial (*R*)=1 : 2)(Fig. 5). In *trans*-dianiono complexes *N*-methyl groups in the axial orientation are known to interact with the apical ligands more strongly than those in the equatorial orientation. DeHayes and Busch calculated the free energy difference between the axial and the equatorial *N*-methyl groups to be 0.49 kcal/mol from conformational analysis.[7] However, the experimental data obtained so far show that the equatorial *N*-methyl groups are far more profitable than the axial ones in octahedral Co(III) complexes.

The stereochemistry of *N*-Me-ampr complexes is quite different from that of other *N*-methyl substituted diamines. The *N*-Me-ampr complexes prefer the *trans,cis*

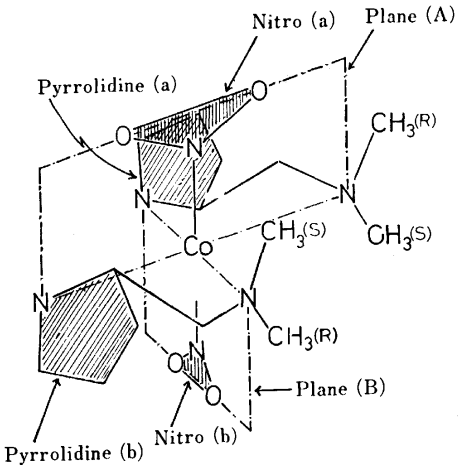

Fig. 6. Illustrative structure of *trans,cis(SS)*-$[Co(NO_2)_2$-(*N*-Me-ampr)$_2]^+$ ion.

rather than the *trans,trans* configuration. The *N*-methyl groups orientate to the axial position more easily than other *N*-methylated diamine complexes. In the *trans*-dinitro complex, the *N*-methyl groups adopt stereospecifically axial positions, and in the *trans*-dichloro complex, two isomers arise due to the difference of the absolute configuration of asymmetric nitrogen centers (axial and equatorial *N*-methyl groups).

The predominance of the axial *N*-methyl groups in the *trans*-dinitro complexes in comparison with the *trans*-dichloro complexes indicates that the orientation of *N*-methyl groups is affected by the kind of apical ligand. The characteristic orientation of the *N*-methyl groups would be attributed to the geometry of apical ligands as well as the steric interaction among the pyrrolidine rings, the apical ligands and the *N*-methyl groups. A possible structure of *trans,cis*-$[Co(NO_2)_2$(*N*-Me-ampr)$_2]^+$ is illustrated in Fig. 6. The triangular nitro groups[8] result in rotational isomers around the NO_2^-–Co–NO_2^- axis. When the nitro group (a) is situated on the plane (A) (Fig. 6), the steric repulsion between nitro group (a) and pyrrolidine ring (a) can be reduced, and another nitro group (b) will locate on the plane (B) for the same reason. The equatorial methyl groups will produce more strict steric repulsions than the axial ones. This may be the reason why the *N*-methyl groups prefer to axial position in the dinitro complex.

Since the chloride ion has spherical symmetry, the *trans*-dichloro complexes has no rotamer around the Cl^-–Co–Cl^- axis. The orientation of *N*-methyl groups depends only on stereochemical interactions between the Cl^- and the *N*-methyl groups. The equatorial *N*-methyl groups in the *trans*-dichloro complex are stabilized to a great extent than the axial ones as well as other *N*-methylated diamine complexes. However, the reason why the axial *N*-methyl group is more stabilized than other *N*-methyl derivatives is not clear.

According to the conformational analysis of some *C*- and/or *N*-methyl substituted diamine complexes,[7] the axial *N*- and *C*-methyl groups flatten the chelate ring conformations. It was demonstrated by X-ray crystal structure analysis[9] that a remarkable flattening of the chelate rings takes place in the *cis*-$[Co(NO_2)_2(ampr)_2]^+$, (ampr=(*S*)-2-(aminomethyl)pyrrolidine) relative to ethylenediamine chelate rings. The averaged dihedral angle of N–C–C–N moieties in the ampr complex was 46°, that for ethylenediamine chelate 55°. It is possible that the asymmetric *S*-nitrogen in the pyrrolidine rings of *N*-Me-ampr complexes would also flatten the chelate rings, reducing the energy difference between the axial and the equatorial *N*-methyl groups.

References

1) D. A. Buckingham, L. G. Marzilli, and A. M. Sargeson, *Inorg. Chem.*, **7**, 915 (1968).
2) S. Yano, M. Saburi, S. Yoshikawa, and J. Fujita, *Bull. Chem. Soc. Jpn.*, **49**, 101 (1976).
3) C. J. Hawkins, E. Larsen, and I. Olsen, *Acta Chem. Scand.*, **19**, 1915 (1965),
4) T. Murakami, S. Kitagawa, and M. Hatano, *Bull. Chem. Soc. Jpn.*, **49**, 2631 (1976).
5) M. Saburi, Y. Tsujito, and S. Yoshikawa, *Inorg. Chem.*, **9**, 1476 (1970).
6) C. J. Hawkins, *Chem. Commun.*, **1969**, 777.
7) L. J. DeHayes and D. H. Busch, *Inorg. Chem.*, **12**, 1506. (1973).
8) G. A. Barlay, E. Goldschmid, and N. C. Stephenson *Acta Crystallogr.*, **B26**, 1558 (1970).
9) Y. Sato, M. Saburi, and S. Yoshikawa, Presented at the 25th Symposium on Coordination Chemistry, Tokyo, Japan (1975).

^{13}C NMR Spectroscopy. Substituent Effects in the Ethyl *trans*-2-Substituted Cyclopropanecarboxylates

Yoshiaki KUSUYAMA and Yoshitsugu IKEDA

Department of Chemistry, Faculty of Education, Wakayama University, Masagocho, Wakayama 640

(Received August 14, 1976)

^{13}CFT NMR spectra have been obtained for ethyl *trans*-2-substituted cyclopropanecarboxylates. The chemical shifts have been compared with those of saturated and unsaturated compounds and with substituent constants. The chemical shifts of the methylene carbon of the ethyl group have been correlated linearly with σ_m.

A substantial body of evidence supporting resonance interactions between the cyclopropane ring and the p-orbital of substituents has been obtained from spectroscopic measurements and chemical reactions.[1] However, there has been little work suggesting such interactions based on ^{13}C NMR spectroscopy, which is a useful source of information on the nature of chemical bonds.[2] This paper will describe some characteristic results for the ^{13}C chemical shifts of ethyl *trans*-2-substituted cyclopropanecarboxylates. It is hoped that the effects of the substituents at the 2-position of the ring on the chemical shifts of ^{13}C of the ethyl group will provide a convenient tool for estimating the transmitting ability of the polar effect through a cyclopropane ring.

Results and Discussion

Proton-decoupled natural-abundance ^{13}CFT NMR spectra were obtained at 25.15 MHz at 30 °C. The samples were run as a 1.5±0.1 M solution in $CDCl_3$ containing tetramethylsilane as an internal reference. The signals have been assigned on the basis of the peak intensities and the chemical shifts reported in the literature.[3-5] The assignments of the ^{13}C resonances of the ethyl cyclopropanecarboxylates investigated in this work are shown in Table 1.

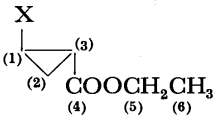

Ring carbons are strongly affected by the substituents. The screening at the carbons of the α and β positions relative to the substituents is influenced by several factors (inductive, steric, magnetic anisotropy, *etc.*) contributed by the substituents. One of the most common methods to interpret the substituent effects is a comparison with other similarly substituted compounds.

The best agreement of the cyclopropyl α-carbon shieldings of the monosubstituted cyclopropanes *vs.* the shieldings of substituted methanes was found by Weiner and Malinowski.[3] In addition to their results, a very high correlation of $C_{(1)}$ chemical shifts with the chemical shifts of substituted methanes[2a,3,6] or those of the α-position of 1-substituted pentanes[2a,2b] was obtained by others (slope, 0.80; Fig. 1.). Spiesecke and Schneider[6,7] reported that the chemical shifts of ^{13}C, to which substituents were attached, were correlated by the electronegativity (Ex) of the substituents. In Table 2, the relations of the relative substituent-induced chemical shifts of α-carbons to substituents(C_α-scs) and Ex[8] are

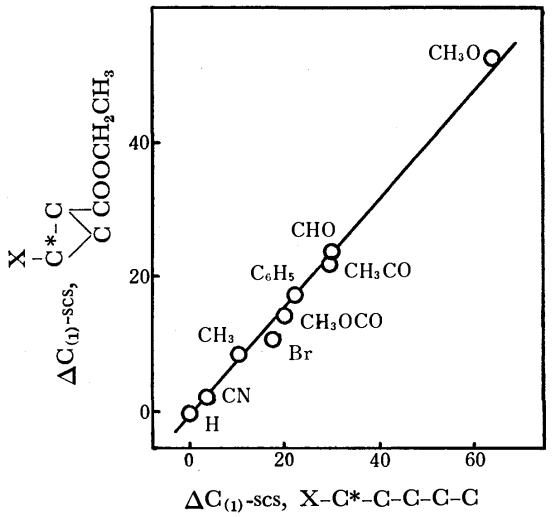

Fig. 1. Comparison of relative substituent-induced ^{13}C chemical shifts of the substituted carbons ($\Delta C_{(1)}$-scs) in 1-substituted pentanes and ethyl *trans*-2-substituted cyclopropanecarboxylates.

summarized. The electronegativity of the group substituents, OCH_3, NH_2, and CH_3, was assumed to be that of the first atom in the group. Good correlations of C_α-scs with Ex were obtained except for the X-vinyl derivative. In the case of the X-vinyl derivative, neighbor-anisotropy may contribute considerably.[2,7] In all five series, bromine deviated from the correlation line because of the contribution of the heavy-atom effect.[2b,9,10] The ($C_{(\alpha)}$-scs *vs.* C_{X-Me}-scs) slopes were parallel to the ($C_{(\alpha)}$-scs *vs.* Ex) slopes. Thus, the electronegativity of the substituents is the most important factor in the ^{13}C chemical shifts of α-carbons.[6] It may be though that the hydridization of α-carbons is a result of the susceptibility of the electronegativity.

The chemical shifts of $C_{(3)}$ were slightly larger than those of $C_{(2)}$. There is a good linear relation between the shifts of $C_{(3)}$ and those of the β-carbons of 1-substituted pentanes for the methyl, bromo, and methoxyl groups,[11] while the cyano, formyl, methylcarbonyl, and acetyl groups are scattered (Fig. 2). Also the chemical shifts of $C_{(3)}$ can not be correlated by those of the β-carbons of substituted ethylenes.[2,12]

For the β-carbons to the substituents in the unsaturated frameworks, the substituent effects exhibit a much wider range of shifts than those observed in saturated frameworks.[2] The chemical shitfs may be indicated by the kinds of canonical resonance structures:

TABLE 1. ^{13}C CHEMICAL SHIFTS FOR ETHYL *trans*-2-SUBSTITUTED CYCLOPROPANECARBOXYLATES
(The shifts are in PPM downfield from TMS)

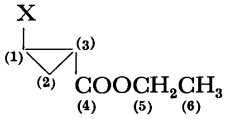

X	$C_{(1)}$	$C_{(2)}$	$C_{(3)}$	$C_{(4)}$	$C_{(5)}$	$C_{(6)}$
H	8.25(8.4)[a]	8.25(8.4)[a]	12.92(13.2)[a]	174.86(174.1)[a]	60.37(60.8)[a]	14.26(14.7)[a]
CH_3	17.87	17.05	21.30	174.32	60.19	14.26
C_6H_5	26.15(26.4)[a]	17.05(16.9)[a]	24.15(24.3)[a]	173.22(172.1)[a]	60.61(60.6)[a]	14.32(14.5)[a]
CH_3O	62.13	15.72	20.87	172.49	60.49	14.26
C_2H_5O	66.62	15.05	21.17	172.62	60.49	14.32
C_6H_5O	57.15	15.59	21.66	172.06	60.85	14.26
Br	15.17	18.87	23.78	171.46	61.10	14.20
CH_3OCO	22.45	15.35	22.15	171.65	61.10	14.20
C_2H_5OCO	22.33	15.23	22.33	171.65	60.97	14.20
CHO	30.70	14.80	22.15	171.09	61.28	14.14
CH_3CO	30.70	17.05	24.15	171.89	61.04	14.20
COCl	31.73	17.96	25.24	170.01	61.64	14.14
CN	5.64	14.50	21.05	170.06	61.70	14.08

a) O. A. Subbotin, A. S. Kozmin, Yu. K. Grishin, N. M. Sergeyev, and I. G. Bolesov, *Org. Magn. Reson.*, **4**, 53 (1972).

TABLE 2. COMPARISON OF THE SUBSTITUENT-INDUCED CHEMICAL SHIFTS OF α-CARBON ($C_{(\alpha)}$-SCS) AND THE RELATION OF $C_{(\alpha)}$-SCS TO THE ELECTRONEGATIVITY (Ex)[a]

	α-Carbon	($C_{(\alpha)}$-scs *vs.* C_{X-Me}-scs)Slope	($C_{(\alpha)}$-scs *vs.* Ex)Slope	f[b]
(1)	X-Me	1.00	43.4(0.940, H, Me, Cl, Br, NH_2, MeO)[c]	1.00
(2)	X-*c*-Pr	0.82[d]	31.1(0.983, H, Cl, Br, NH_2)	0.72
(3)	X-vinyl	0.88[d]	15.7(0.738, H, Me, Cl, Br, F, MeO)	
			21.3(0.998, H, Me, MeO)	0.49
(4)	X-Ph	0.54[d]	20.45(0.846, H, Me, Cl, Br, F, NH_2, MeO)	
			18.9(0.994, H, Me, F, NH_2, MeO)	0.44
(5)	*trans*-2-X-*c*-Pr-CO_2Et	0.80	37.7(0.923, H, Me, Cl, Br, MeO)[e]	
			38.0(0.979, H, Me, Cl, MeO)	0.82

a) Ref. 8. b) Relative value of the ($C_{(\alpha)}$-scs *vs.* Ex)Slope. c) Correlation coefficient and the substituents included for the calculation. d) Ref. 3. e) The value of the methyl ester (δ 33.25) was used for chlorine.

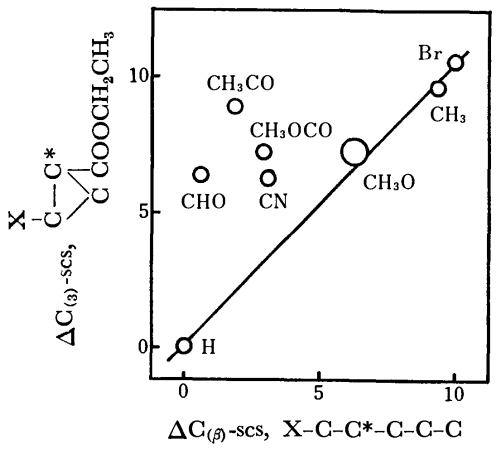

Fig. 2. Plots of the relative substituent-induced ^{13}C chmical shifts of $C_{(3)}$ ($\Delta C_{(3)}$-scs) in ethyl *trans*-2-substituted cyclopropanecarboxylates *vs.* the relative substituent-induced ^{13}C chemical shifts of β-carbons ($\Delta C_{(\beta)}$-scs) in 1-substituted pentanes.

$$X\text{-}C{=}C \leftrightarrow \overset{\delta-}{X}{=}C\text{-}\overset{\delta+}{C} \leftrightarrow \overset{\delta+}{X}{=}C\text{-}\overset{\delta-}{C}. \quad (1)$$

The cyclopropane ring exhibits a considerable degree of π-bond character and interacts with the p-orbitals of the substituents, especially releasing electrons to substituents:[1,2]

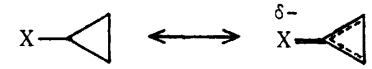

(2)

The cyano, formyl, methoxycarbonyl, and acetyl groups are electron-attracting groups by means of their resonance and decrease the electron densities of $C_{(2)}$ and $C_{(3)}$, as is shown in (2). Accordingly, $C_{(2)}$ and $C_{(3)}$ shift downfield from those expected from the shift of the saturated frameworks. It may be thought that the interaction is responsible for the appreciable differences between the observed values and the predicted values (Table 3.) which were calculated by the simple additive rule.[5] The shift differences in $C_{(2)}$ is largest in the three ring carbons except for the $C_{(1)}$ of the bromo derivative, to which the heavy halogen atom effect may contribute.[2] In order to estimate semiquantitatively

TABLE 3. SHIFT DIFFERENCES BETWEEN THE OBSERVED VALUES AND THE PREDICTED ONE

	$\delta_{pred}-\delta_{obsd}$ (in ppm)		
	$C_{(1)}$	$C_{(2)}$	$C_{(3)}$
C_6H_5	0.75	3.55	1.25
Br	6.13	5.03	1.22
$COCH_3$	2.20	4.35	2.05
COCl	3.77	5.64	3.16
CN	2.41	4.32	2.15

TABLE 4. Δ_R VALUES FOR THE $C_{(3)}$ OF ETHYL *trans*-2-SUBSTITUTED CYCLOPROPANECARBOXYLATES

Substituent	Δ_R
H	0.0
CH_3	−1.0
CH_3O	1.9
Cl	0.7
Br	0.9
CH_3OCO	6.3
CH_3CO	9.1
CHO	8.5
CN	4.9

the contribution of the ionic canonical form in (2), the differences (Δ_R) in the chemical shifts between $C_{(3)}$ (ethyl *trans*-2-substituted cyclopropanecarboxylate) and $C_{(\beta)}$ (1-substituted pentane) were calculated (Table 4). For unsaturated frameworks, the substituent effects may be designated as follows:

$$\Delta\delta = \Delta\delta_{saturated} + \Delta_R. \quad (3)$$

A linear correlation was obtained between Δ_R and σ_R^- for the electron-attracting groups by means of the resonance (slope, 15.97; r: correlation coefficient, 0.980). On the basis of these results, it seemed reasonable to assume that the resonance interaction of a cyclopropane with electron-attracting substituents plays an important role in the chemical shifts of $C_{(2)}$ and $C_{(3)}$.

The most striking result in the present investigation is a measurable chemical shift of $C_{(5)}$. In general, chemical shifts of the carbon of the δ position to substituents are correlated by a Hammett-type equation because of the absence of steric interaction between the substituents and δ-carbon. The present chemical shifts of $C_{(5)}$ are correlated with σ_m (slope, 2.07; r=0.985), and a more excellent correlation was obtained with σ_m° (slope, 2.17; r=0.994)[13] although σ_m and σ_m° were obtained from the reaction in hydroxylic solvents, and solvent-variable substituent constants are included in the calculations.

$$\Delta\delta_{(C5)} = 2.07\sigma_m,$$
$$\Delta\delta_{(C5)} = 2.17\sigma_m^\circ.$$

It is noteworthy that σ_m and σ_m° include considerable contributions of the resonance effects.[1,14]

$$\sigma_m = \sigma_I + 0.33\sigma_R,$$
$$\Delta\delta_{(C5)} = 2.1\sigma_I + 0.72\sigma_R.$$

On the basis of this correlation of $^{13}C_{(5)}$ chemical shifts, it seemed reasonable to assume that the cyclopropane ring can transmit the resonance effect, although its influence is rather small. The pK_a values of *trans*-2-substituted cyclopropanecarboxylic acids in water or in 50% aqueous alcohol were correlated by σ_m:[15]

$$\Delta pK_a = 1.99\sigma_m = 0.96\Delta\delta(C_{(5)}) \text{ (in water)}$$
$$\Delta pK_a = 2.92\sigma_m = 1.41\Delta\delta(C_{(5)}) \text{ (in 50\% alcohol)}$$

Thus, the relative acidities of carboxylic acids may be estimated by means of the ^{13}C chemical shifts of alkoxyl carbons of appropriate esters, in which substituents are sufficiently remote from the carboxyl group.

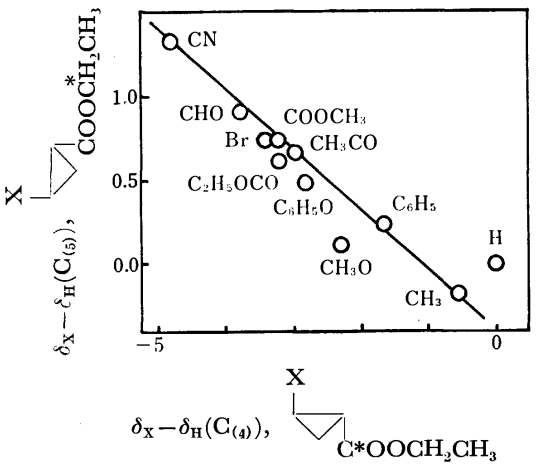

Fig. 3. Correlation between the ^{13}C chemical shifts of carbonyl carbons and those of alkoxy carbons in ethyl *trans*-2-substituted cyclopropanecarboxylates.

A linear correlation was observed between the ^{13}C chemical shifts of $C_{(4)}$ and those of $C_{(5)}$ (Fig. 3). The unsaturated compound, however, deviated from the correlation line. The direction of the chemical shifts of $C_{(4)}$ is reversed in terms of the substituent electronic properties. A "reverse" correlation has previously been reported for the chemical shifts of carboxyl carbons in the substituted benzoic acids[16] and benzocaine hydrochlorides[17] and of cyanide carbons in the substituted benzonitriles.[18] It appears that the large charge separation in the carboxyl group is responsible for the reversal in this direction of the substituent effects.

The $C_{(6)}$, which is most remote from the site of substitution, is practically not influenced at all by the substituent and has a chemical shift equal to 14.2±0.1 ppm from tetramethylsilane. This carbon seems too distant from the substituent for any substituent effect to be detected.

Experimental

^{13}C NMR Spectra. The ^{13}CFT NMR spectra were obtained at 25.15 MHz on a JEOL-JNM-PFT-100 apparatus at 30 °C. Samples were dissolved in $CDCl_3$ containing tetramethylsilane as the internal reference. The concentrations were 1.5±0.1 M. The measurement conditions were as follows: puls width, 15 μs(90°); repetition time, 2.5 s; frequency range, 6.25 KHz; data points, 8192. The accuracy is at least ±0.06 ppm.

Materials. The materials were identified on the basis of spectroscopic and gas-chromatographic measurement and elemental analysis. The NMR spectra were measured on a JEOL-JNM-C-60HL(60 MHz) spectrometer, with tetrameth-

Table 5. Boiling points of ethyl *trans*-2-substituted cyclopropanecarboxylate (°C/Torr)

Substituent	Observed[a]	Lit, value
H	127	134—135[b], 50—51/4[c]
CH_3	144	76/70
C_6H_5	132—135/7	94—95.5/0.65[d]
		105—106/0.2[e]
CH_3O	76—77/30	61—63/15[f]
C_2H_5O	95/32	66/9[f]
C_6H_5O[g]	87—90/1.5	
Br[h]	98/40	
CH_3OCO[i]	109/28	101—114/15[j]
C_2H_5OCO	101—103/5	117/17
CHO	97/20	45/<1[k]
CH_3CO	83/6	105/19[f]
COCl[l]	110/22	
CN	82/5	80—82/3

a) Uncorrected. b) S. R. Landor and N. Punja, *J. Chem. Soc., C*, **1967**, 2495. c) A. F. Ferris, *J. Org. Chem.*, **20**, 780 (1955). d) C. H. Depuy, G. M. Duppen, K. L. Eilers, and R. A. Klein, *J. Org. Chem.*, **29**, 2813 (1964). e) M. Julia, S. Julia, and B. Bemont, *C. R. Acad. Sci.*, **245**, 2304 (1957). f) Ref. 15. g) Found: C, 69.28; H, 6.88%. Calcd for: C, 69.89; H, 6.84%, NMR (CCl_4) δ 0.75—1.58 (2H, m, CH_2, ring), 1,26(3H, t, J= 7 Hz, CH_3), 1.68—2.02(1H, m, CHCO), 3.75—4.10(1H, m, OCH), 4.09(2H, q, J=7 Hz, OCH_2), 6.6—7.3(5H, m, C_6H_5). h) NMR(CCl_4) δ 1.27(3H, t, J=7Hz, CH_3), 1.2—1.7(2H, m, CH_2, ring), 1.80—2.20(1H, m, CHCO), 2.95—3.35(1H, m, CHBr), 4.16(2H, q, J=7 Hz, OCH_2). i) NMR(CCl_4) δ 2.25(3H, t, J=7 Hz, CCH_3), 1.30—1.50(2H, m, CH_2, ring), 1.86—2.20(2H, m, CH, ring), 3.61(3H, s, OCH_3), 4.06(2H, q, J=7 Hz. OCH_2C). j)Mixture of *cis-trans* isomers, L. L. McCoy, *J. Am. Chem. Soc.*, **80**, 6568(1958). k) Ref. 25. l) NMR(CCl_4) δ 1.27(3H, t, J=7 Hz, CH_3), 1.4—1.8(2H, m, CH_2, ring), 2.16—2.75(2H, m, CH), 4.11(2H, q, J=7 Hz, OCH_2).

ylsilane employed as the internal standard. Two geometrical isomers of ethyl 2-substituted cyclopropanecarboxylates were isolated by fractional distillation and/or by GLC. For the 2-phenyl derivative, the *trans*-isomer in a mixture of the two isomers was hydrolyzed to *trans*-2-phenylcyclopropanecarboxylic acid, which was then converted to the appropriate ethyl ester by the usual method.[19] The GLC analyses were carried out on a Yanaco GCG-550T, using a 1-m column of Silicone DC 550 or Silicone XF 1150. The *trans*-isomer always showed the shorter retention time. The separation of the two isomers were carried out on a Yanaco G80 apparatus equipped with AP11. The structure assignments for the geometrical isomers were made by means of the ^1H NMR spectra using shift reagents based on a generalization[20] that the tendency of the shift of the signal of the *cis* proton to ethoxycarbonyl is larger than that of the shift of the *trans* protons.

The ethyl 2-phenyl-, methoxy-, ethoxy-, phenoxy-, cyano-, and ethoxycarbonyl-cyclopropanecarboxylates were prepared by the reaction of ethyl diazoacetate with the appropriate alkene.[15] Ethyl *trans*-2-methylcyclopropanecarboxylate was obtained by the ethanolysis of the appropriate acid chloride,[21] itself prepared by the chlorination of *trans*-2-methylcyclopropanecarboxylic acid[21,22] with thionyl chloride. The ethyl 2-bromocyclopropanecarboxylate was synthesized by a Hunsdicker reaction[23,24] of silver *trans*-2-ethoxycarbonylcyclopropanecarboxylate using bromine. The *trans*-2-ethoxycarbonylcyclopropanecarboxylic acid[24] was chlorinated by thionyl chloride to *trans*-2-ethoxycarbonylcyclopropanecarbonyl chloride. The methanolysis of *trans*-2-ethoxycarbonylcyclopropanecarbonyl chloride afforded methyl ethyl cyclopropane-1,2-dicarboxylate. Ethyl 2-formyl- and 2-cyanocyclopropanecarboxylates were obtained by the reaction of ethyl (dimethylsulfuranylidene) acetate with acrolein and acrylonitrile respectively.[25] The boiling points of the ethyl *trans*-2-substituted cyclopropanecarboxylates are summarized in Table 5.

The authors wish to thank Professor Teijiro Yonezawa and Mr. Toshiro Inubushi (Kyoto Univ.) for their ^{13}CFT NMR measurements.

References

1) M. Charton, "The Chemistry of Alkenes," Vol. 2, ed by J. Zabicky, Wiley-Interscience (1970), Chap. 10, p. 530, and the literature cited therein.
2) a) J. B. Stothers, "Carbon-13 NMR Spectroscopy," Academic Press, New York (1972), Chap. 5; b) G. E. Maciel, "Topics in Carbon-13 NMR Spectroscopy," ed by George C. Levy, pp. 1, 53.
3) P. H. Weiner and E. R. Malinowski, *J. Phys. Chem.*, **71**, 2791 (1967).
4) K. M. Crecely, R. W. Crecely, and J. H. Goldstein, *J. Phys. Chem.*, **74**, 2680 (1970).
5) O. A. Subbotin, A. S. Kozmin, Yu. K. Grishin, N. M. Sergeyer, and I. G. Bolesov, *Org. Magn. Reson.*, **4**, 53 (1972).
6) H. Spiesecke and W. G. Schneider, *J. Chem. Phys.*, **35**, 722 (1961).
7) H. Spiesecke and W. G. Schneider, *J. Chem. Phys.*, **35**, 73 (1961).
8) L. Pauling, "The Nature of the Chemical Bond," 2nd ed, Cornell University Press., Ithaca (1940).
9) T. Shefer, W. F. Reynolds, and T. Yonemoto, *Can. J. Chem.*, **41**, 2969 (1963).
10) I. Morishima, K. Endo, and T. Yonezawa, *J. Chem. Phys.*, **59**, 3356 (1973).
11) The exact interaction between cyclopropane and electron-releasing substituents caused by resonance remains to be elucidated.
12) G. E. Macial, *J. Phys. Chem.*, **69**, 1947 (1965).
13) M. Sawada, Y. Tsuno, and Y. Yukawa, *Bull. Chem. Soc. Jpn.*, **45**, 1198 (1972).
14) R. W. Taft Jr., and I. C. Lewis, *J. Am. Chem. Soc.*, **80**, 2436 (1958); *ibid.*, **81**, 5343 (1959); R. W. Taft Jr., S. Ehrenson, I. C. Lewis, and R. E. Glick, *ibid.*, **81**, 5354 (1959).
15) Y. Kusuyama and Y. Ikeda, *Bull. Chem. Soc. Jpn.*, **49**, 724 (1976).
16) J. Niwa and M. Yamazaki, *Chem. Lett.*, **1974**, 765; C. Nagata, H. Nagata, and S. Tanaka, *Nippon Kagaku Kaishi*, **1975**, 2045.
17) G. A. Gansow, W. M. Bekenbaugh, and R. L. Sass, *Tetrahedron*, **28**, 2691 (1972).
18) J. Bromilow and R. T. C. Brownlee, *Tetrahedron Lett.*, **1975**, 2113.
19) C. Kaiser *et al.*, *Org. Synth.*, Vol. 50, p. 94.
20) Y. Kusuyama and Y. Ikeda, *Bull. Fac. Edu., Wakayama Univ., Natural Science*, **24**, 13 (1974).
21) G. W. Cannon, A. A. Santilli, and F. Shenian, *J. Am. Chem. Soc.*, **81**, 1660 (1959).
22) J. E. Cloke, E. Stehr, T. R. Steadman, and L. C. Westcott, *J. Am. Chem. Soc.*, **67**, 1587 (1958).
23) D. E. Applequist and A. H. Peterson, *J. Am. Chem. Soc.*, **82**, 2372 (1960).
24) K. B. Wiberg, R. K. Barnes, and J. Albin, *J. Am. Chem. Soc.*, **79**, 4994 (1957).
25) G. B. Payne, *J. Org. Chem.*, **32**, 3351 (1967).

α,β-Unsaturated Carboxylic Acid Derivatives. XII. A Convenient Synthesis of Oxazole-4-carboxylic and 3,3-Dibromo-2,2-diamino Acids[1]

Chung-gi SHIN,* Yoshiaki SATO, Hidetoshi SUGIYAMA, Katsumi NANJO, and Juji YOSHIMURA**

Laboratory of Organic Chemistry, Faculty of Technology, Kanagawa University, Rokkakubashi, Kanagawa-ku, Yokohama 221

***Laboratory of Chemistry for Natural Products, Faculty of Science, Tokyo Institute of Technology, Ōkayama, Meguro-ku, Tokyo 152*

(Received November 16, 1976)

Treatment of *t*-butyl 2-acetylamino-3-bromo-2-alkenoate with triethylamine gave *t*-butyl 5-alkyl-2-methyloxazole-4-carboxylate by dehydrobromination, but no reaction occurred with primary amines. While treatment of *t*-butyl 2-acetylimino-3,3-dibromoalkanoate with hydroxylamine or several aliphatic and aromatic primary amines gave addition products, *t*-butyl 2-acetylamino-3,3-dibromo-2-(hydroxyamino)- and 2-(substituted amino)-alkanoate, respectively, in fairly good yields.

Previously, Shin *et al.* have reported on the facile synthesis of *t*-butyl 2-(*N*-bromoacetylamino)-2-alkenoate by the reaction of *t*-butyl 2-acetylamino-2-alkenoate with *N*-bromosuccinimide (NBS), and its bromine migration into *t*-butyl 2-acetylamino-3-bromo-2-alkenoate (**1**).[2] Repeated bromination of **1** and its migration gave *t*-butyl 2-acetylimino-3,3-dibromoalkanoate (**4**), to which water or several kinds of alcohol were added readily to give the corresponding 2-hydroxy- and alkoxy derivatives.[1]

Recently, it has been described that the same addition reaction of aliphatic primary and some secondary amines to methyl 2-acylamino-3,3-dichloroacrylate gave a mixture of methyl 2-acylamino-2-(substituted amino)-3,3-dichloropropanoate and oxazole derivatives.[3,4] However, not only has the suppositional imino-form intermediate, methyl 2-acylimino-3,3-dichloropropanoate, not been isolated, but also there was no evidence for the presence of the intermediate.

In order to ascertain and extend the above addition reaction, the reaction of **4** with several aliphatic and aromatic primary amines and that of **1** with triethylamine was carried out and these resulted in the convenient synthesis of 3,3-dibromo-2,2-diamino acid derivatives and oxazole-4-carboxylic acids, respectively.[5]

Results and Discussion

*Reaction of **1** with Triethylamine.* When a solution of **1a,b** (**a**; R=CH_3, **b**; R=C_2H_5) and triethylamine in benzene was refluxed for 2.5 h, a colorless syrup, which gradually crystallized during distillation under reduced pressure, was obtained in a *ca.* 40% yield. The colorless crystals isolated were determined to be *t*-butyl 5-alkyl-2-methyloxazole-4-carboxylate (**2a, b**) from elemental analysis and spectroscopic data. A similar treatment of ethyl 2-acetylamino-3-bromo-2-butenoate (**1c**), derived from the reaction of ethyl 2-acetylamino-2-butenoate with NBS, also gave ethyl 2,5-dimethyloxazole-4-carboxylate (**2c**). An independent preparation of **2c**, by the reaction of ethyl 2-acetylamino-3-oxobutanoate with phosphoryl chloride,[6] demonstrated the structure unambiguously.

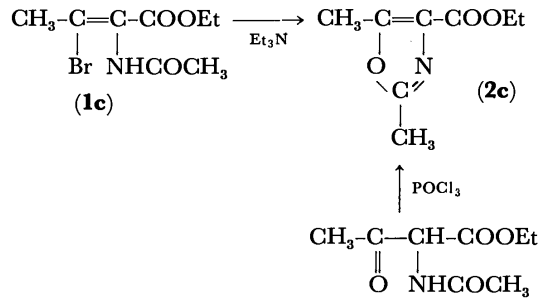

Although the assignment of the proper configuration (*E*-, *Z*-) was not successful in this work, the geometric isomer of **1** was subjected to the cyclization reaction (Table 1). Moreover, **2a** was converted into colorless, crystalline, 2,5-dimethyloxazole-4-carboxylic acid (**3a**) in a 57% yield, by treatment with hydrogen chloride in chloroform at room temperature. On the other hand, it was found that conversion of **1** into **2** by ammonia or benzylamine did not occur.

The yields, physical properties, and spectral data of **2** and **3** are summarized in Table 1.

*Reaction of **4** with Several Amines.* The compound **4a,b** (**a**; R=CH_3, **b**; R=C_2H_5) used was prepared according to the method previously reported.[1] Treatment of **4** with excess gaseous ammonia in ether with stirring below 10 °C gave only *t*-butyl 2-acetylamino-2-amino-3,3-dibromoalkanoate (**5**) as colorless crystals in a *ca.* 70% yield. The subsequent acylation of **5** with acetic anhydride and benzoyl chloride in pyridine at room temperature or below, respectively, gave *t*-butyl 2,2-diacetylamino- and 2-acetylamino-2-benzoylamino-3,3-dibromoalkanoates (**12** and **13**), which could not be obtained independently from the direct addition of the acid amide to **4**. Furthermore, a similar addition reaction of almost equimolar **4** and alkylamines (benzylamine and phenylhydrazine) or arylamines (aniline, ethyl *p*-aminobenzoate, 2-aminopyridine and 2-aminothiazole) in ethanol below 10 °C or at room temperature also gave *t*-butyl 2-acetylamino-2-(substituted amino)-3,3-dibromoalkanoates (**6**—**11**) as colorless crystals in *ca.* 85% yields, without the accompaniment of the expected oxazoline derivatives (**19** and **20**).

From the above results, it was found that the amino group added readily and dominatly to the carbon-nitrogen double bond in **4**, even in the presence of ethanol.

* To whom all correspondence should be addressed.

TABLE 1. 5-ALKYL-2-METHYLOXAZOLE-4-CARBOXYLIC ACIDS (**2** AND **3**)

Compd No.	Yield (%)	Bp °C/Torr (mp °C)	Formula	Found (Calcd), % C	H	N	IR spectrum, cm^{-1} in KBr	NMR spectrum, δ 5-RCH_2	2-CH_3	COOH
2a	58[a] 25[b]	70—73/1.5 (33—35)	$C_{10}H_{15}NO_3$	60.91 (60.89	7.61 7.69	7.11 7.10)	1735, 1710, 1625	2.57 s (R=H)	2.44[h]	
2b	23[c] 37[d]	85—86.5/2 (28.5—30)	$C_{11}H_{17}NO_3$	62.44 (62.54	8.34 8.11	6.74 6.63)	1727, 1705, 1616	2.75 t J=8.0 Hz	2.45[h]	
2c[e]	41[f]	82—83/2[g]	$C_8H_{11}NO_3$	56.77 (56.79	6.28 6.55	8.32 8.28)	1715, 1623	2.56 s (R=H)	2.45[h]	
3a	57	(182.5—184.5)	$C_6H_7NO_3$	50.96 (51.06	4.94 5.00	9.85 9.93)	1716, 1640	2.60 s (R=H)	2.46	8.87[i]

a) From **1a** (mp 138—139 °C).[e] b) From **1a** (mp 101—102.5 °C).[e] c) From **1b** (mp 84—87 °C).[e] d) From **1b** (syrup).[e] e) Ref. 2. f) From a 1 : 1 mixture of *E*- and *Z*-isomer. g) Ref. 4 (bp 110—115 °C/10 Torr). h) Measured in $CDCl_3$. i) Measured in DMSO-d_6.

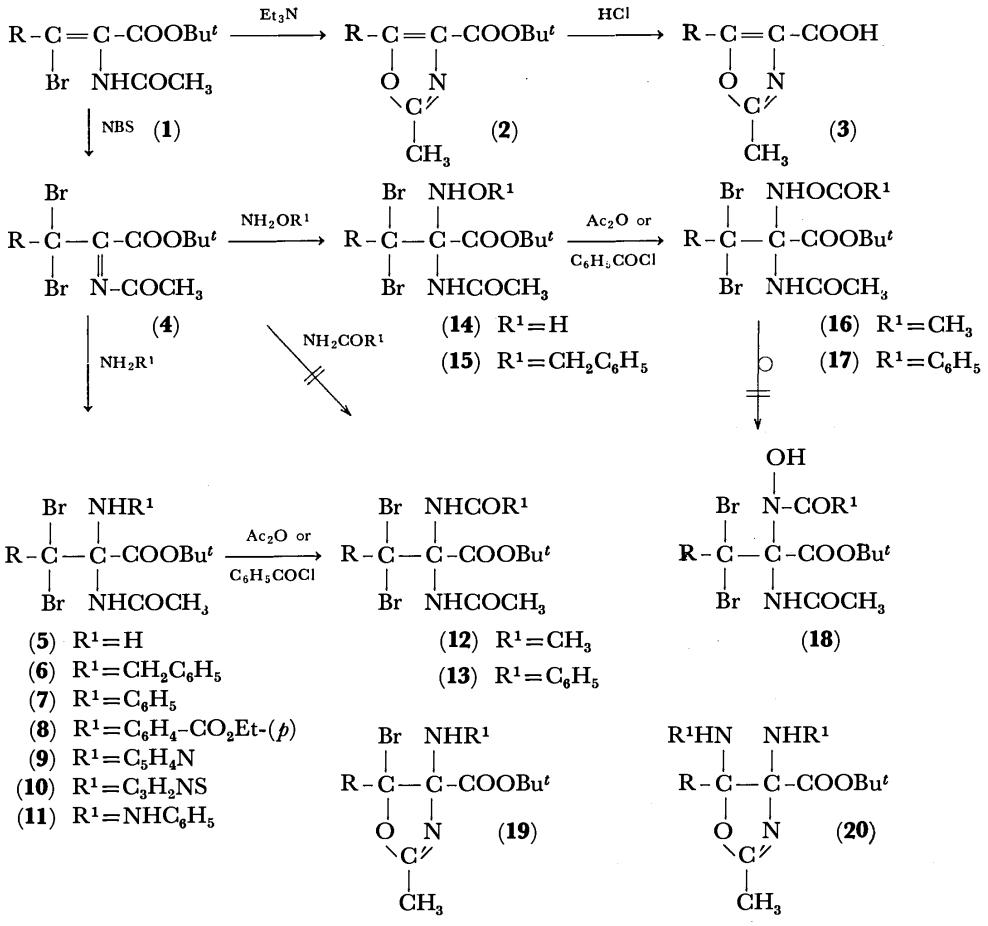

Scheme 1.

Moreover, the reaction of **4** with hydroxylamine in ethanol below 10 °C gave the expected *t*-butyl 2-acetylamino-3,3-dibromo-2-(hydroxyamino)alkanoate (**14**) in an unstable crystalline state. The structure of **14** was assigned, on the basis of the appearance of the hydroxyl group absorption band at 3360—3370 cm^{-1} in the IR spectrum and the subsequent acylation of **14**. The acylation of **14** with acetic anhydride and benzoyl chloride in pyridine gave *t*-butyl 2-acetylamino-2-acetoxyamino- and 2-benzoyloxyamino-3,3-dibromoalkanoates (**16** and **17**) as colorless crystals in *ca.* 87% yields. Compounds **16** and **17** showed no coloration with methanolic ferric chloride, indicating the absence of hydroxamic acid structures. However, migration of the acyl group on an oxygen in **16** or **17** to a nitrogen atom, as reported an earlier paper,[7] was not observed. Moreover, a similar treatment of **4** with *O*-benzylhydroxylamine gave *t*-butyl 2-acetylamino-2-benzyloxyamino-3,3-dibromoalkanoate (**15**). In this work, however, the conversion of **15** into **14** was unsuccessful. Although reactions of **4** with other primary amines, for example, butylamine, cyclohexylamine and 2-aminoethanol, occurred, the un-

TABLE 2. *t*-BUTYL 3,3-DIBROMO-2-(SUBSTITUTED AMINO)-2-ACETAMIDO-2-ALKANOATES $\left(\begin{array}{c} Br \quad NH\text{-}R^1 \\ | \quad | \\ R\text{-}C\text{-}C\text{-}COOBu^t \\ | \quad | \\ Br \quad NHCOCH_3 \end{array}\right)$

Compd No.	R^1	Yield (%)	Mp °C	Formula	Found (Calcd), % C	H	N	IR, cm^{-1}, in KBr NH, (OH), COO, NCO	NMR[b] NH, (OH)
5a	-H	76.6	137—138.5[a,c]	$C_{10}H_{18}N_2O_3Br_2$	32.14 (32.11)	4.80 (4.84)	7.49 (7.51)	3380, 3340, 1730, 1670	2.79, 6.62
5b	-H	67.7	133—134[a,c]	$C_{11}H_{20}N_2O_3Br_2$	34.11 (34.04)	5.13 (5.19)	7.12 (7.22)	3380, 3340, 1730, 1670	
6a	$-CH_2C_6H_5$	94.0	91.5—92.5[d]	$C_{17}H_{24}N_2O_3Br_2$	43.92 (43.99)	5.30 (5.21)	5.91 (6.03)	3380, 3310, 1730, 1680	4.02, 6.76
7a	$-C_6H_5$	97.0	121—122[a,d]	$C_{16}H_{22}N_2O_3Br_2$	42.45 (42.69)	4.97 (4.93)	6.12 (6.22)	3350, 1720, 1690	5.60
7b	$-C_6H_5$	92.5	123.5—124[a,d]	$C_{17}H_{24}N_2O_3Br_2$	44.12 (43.99)	5.24 (5.21)	6.16 (6.03)	3330, 1710, 1680	5.62
8a	$-C_6H_4CO_2Et(p)$	97.6	126—127[a,d]	$C_{19}H_{26}N_2O_5Br_2$	43.63 (43.70)	5.01 (5.02)	5.30 (5.36)	3350, 1710, 1690	
8b	$-C_6H_4CO_2Et(p)$	75.0	111—116[a,d]	$C_{20}H_{28}N_2O_5Br_2$	45.16 (44.80)	5.26 (5.26)	5.29 (5.22)	3350, 1710, 1690	
9a		87.6	138—139[a,e]	$C_{15}H_{21}N_3O_3Br_2$	39.86 (39.93)	4.70 (4.69)	9.05 (9.31)	3350, 1730, 1690	5.99, 8.00
9b		76.0	130—130.5[a,f]	$C_{16}H_{23}N_3O_3Br_2$	41.28 (41.30)	5.08 (4.98)	8.88 (9.03)	3350, 1730, 1690	
10a		73.1	145—146[a,g]	$C_{13}H_{19}N_3O_3SBr_2$	34.38 (34.15)	4.23 (4.19)	9.16 (9.19)	3320, 1730, 1690	
10b		42.9	138—139[a,g]	$C_{14}H_{21}N_3O_3SBr_2$	35.87 (35.69)	4.58 (4.49)	8.89 (8.92)	3300, 1730, 1690	
11a	$-NHC_6H_5$	96.7	127—127.5[a,d]	$C_{16}H_{23}N_3O_3Br_2$	41.08 (41.31)	4.96 (4.98)	8.96 (9.03)	3370, 3260, 1730, 1680	5.74
11b	$-NHC_6H_5$	85.1	124—125[a,d]	$C_{17}H_{25}N_3O_3Br_2$	42.73 (42.61)	5.28 (5.26)	8.94 (8.77)	3320, 3250, 1720, 1660	5.74
12a	$-COCH_3$	60.3	135—136[a,h]	$C_{12}H_{20}N_2O_4Br_2$	34.70 (34.64)	4.88 (4.84)	6.82 (6.73)	3330, 3320, 1740, 1700 1670	
12b	$-COCH_3$	67.5	131—132[c]	$C_{13}H_{22}N_2O_4Br_2$	36.29 (36.30)	5.23 (5.16)	6.49 (6.51)	3310, 3280, 1730, 1670	
13a	$-COC_6H_5$	57.0	133—133.5[a,c]	$C_{16}H_{22}N_2O_4Br_2$	41.31 (41.22)	4.77 (4.76)	5.99 (6.01)	3320, 3300, 1730, 1690 1650	7.02
14a	-OH	87.9	crystals[j]		—	—	—	(3360), 3330, 1740, 1650 3230	
14b	-OH	83.0	crystals[j]		—	—	—	(3370), 3330, 1730, 1650 3220	(7.95) 5.36
15a	$-OCH_2C_6H_5$	82.1	99.5—100.5[i]	$C_{17}H_{24}N_2O_4Br_2$	42.77 (42.52)	5.01 (5.04)	5.85 (5.83)	3360, 3160, 1730, 1680	
15b	$-OCH_2C_6H_5$	78.9	124—125[e]	$C_{18}H_{26}N_2O_4Br_2$	43.88 (43.75)	5.31 (5.30)	5.70 (5.67)	3370, 3200, 1730, 1680	
16a	$-OCOCH_3$	85.6	139—141[a,h]	$C_{12}H_{20}N_2O_5Br_2$	33.62 (33.36)	4.70 (4.67)	6.57 (6.48)	3280, 3220, 1750, 1650	
16b	$-OCOCH_3$	87.4	124—125[c]	$C_{13}H_{22}N_2O_5Br_2$	34.66 (35.00)	4.88 (4.97)	6.21 (6.28)	3380, 3220, 1750, 1690 1730	
17a	$-OCOC_6H_5$	84.3	132.5—133[c]	$C_{17}H_{22}N_2O_5Br_2$	41.51 (41.32)	4.55 (4.49)	5.61 (5.67)	3340, 3200, 1730, 1680 1720	
17b	$-OCOC_6H_5$	91.1	121—122[e]	$C_{18}H_{24}N_2O_5Br_2$	42.97 (42.54)	4.74 (4.76)	5.58 (5.51)	3360, 3190, 1720, 1680	

a) Decomposition. b) δ, in $CDCl_3$. c) Colorless needles from dibutyl ether. d) Colorless needles from ethanol-H_2O. e) Colorless prisms from dibutyl ether. f) Colorless needles from hexane. g) Colorless needles from ethanol. h) Colorless prisms from benzene-petroleum ether. i) Colorless prisms from hexane. j) Unstable.

stable crystalline products obtained could not be confirmed.

The yields, physical properties, and spectral data of **5**—**17** are summarized in Table 2.

Experimental

All boiling and melting points are uncorrected. The IR spectra were recorded with a Hitachi EPI-G3 Spectrometer.

The NMR spectra were measured using a JNM-PS-100 Spectrometer (Japan Electron Optics Laboratory Co., Ltd.) with tetramethylsilane as the internal standard.

Materials. The *E*- and *Z*-isomers of **1a,b** were prepared by the method recently reported.[2] Similarly, **1c** was also obtained by the reaction of ethyl 2-acetylamino-2-butenoate (0.0304 mol) and NBS (0.0335 mol) in carbon tetrachloride (30 ml). Colorless needles from dibutyl ether, yield 55%, mp 108—109 °C. IR (KBr): 3245 (NH), 1720 (COO), 1660 and 1520 (NHCO) cm^{-1}. NMR (δ): 2.34, 2.55 (two s, $COCH_3$), 2.04, 2.07 (two s, CH_3–C=), 7.47, 8.20 (two broad s, NH), contributing to the mixture of the *E*- and *Z*-isomers of **1c**. From the intensity of the amide proton, **1c** was found to be composed of the *E*- and *Z*-isomers in a ratio of 1 : 1. Found: C, 38.52; H, 4.81; N, 5.60%. Calcd for $C_8H_{12}NO_3Br$: C, 38.40; H, 4.80; N, 5.60%.

*Preparation of **2a,b,c**.* A solution of **1a,b,c** (0.0036 mol) and triethylamine (0.0072 mol) in dry benzene (20 ml) was refluxed for 2.5 h. The triethylamine hydrobromide separated out was filtered off, and then the benzene solution was washed three times with water (30 ml). The benzene layer was dried over anhydrous magnesium sulfate and then evaporated under reduced pressure to give a colorless syrup. The residual syrup was distilled under reduced pressure to give crystals of *t*-butyl 2,5-dimethyloxazole-4-carboxylate (**2a**) and *t*-butyl 5-ethyl-2-methyloxazole-4-carboxylate (**2b**) or a syrup (**2c**).

*Preparation of **3a**.* A solution of **2a** (0.0177 mol) in dry chloroform (10 ml) was saturated with dry hydrogen chloride with cooling. After standing overnight at room temperature, colorless crystals gradually separated out from the resulting brown solution. The crystalline product was collected and washed with chloroform and then recrystallized from ethanol to give colorless needles (**3a**).

*Preparation of **5a**.* When a solution of **4a** (1.54 g, 0.0043 mol) in ether (10 ml) was saturated with gaseous ammonia with stirring below 10 °C, a colorless crystalline product precipitated immediately. The crystals were identified to be *t*-butyl 2-acetylamino-2-amino-3,3-dibromobutanoate.

In an analogous manner, *t*-butyl 2-acetylamino-2-amino-3,3-dibromopentanoate (**5b**) was obtained from the reaction of **4b** with ammonia.

*Preparation of **6a**.* A solution of **4a** (0.0043 mol) and benzylamine (0.48 g, 0.0045 mol) in ethanol (10 ml) was stirred below 10 °C. A small quantity of water added to the resulting solution and a similar work up gave *t*-butyl 2-acetylamino-2-benzylamino-3,3-dibromobutanoate.

*Preparation of **7a**.* A solution of **4a** (0.0043 mol) and aniline (0.42 g, 0.0045 mol) in ethanol (10 ml) was stirred below 10 °C and worked up similarly to give *t*-butyl 2-acetylamino-2-anilino-3,3-dibromobutanoate.

In an analogous manner, *t*-butyl 2-acetylamino-2-anilino-3,3-dibromopentanoate (**7b**) was obtained from **4b** and aniline.

*Preparation of **8a**.* *t*-Butyl 2-acetylamino-2-(4-ethoxycarbonylanilino)-3,3-dibromobutanoate was prepared from **4a** (0.0043 mol) and ethyl *p*-aminobenzoate (0.75 g, 0.0045 mol) in a manner similar to the preparation of **6a**.

*Preparation of **9a**.* In a similar manner, *t*-butyl 2-acetylamino-2-(2-pyridylamino)-3,3-dibromobutanoate was synthesized from **4a** and 2-aminopyridine (0.0045 mol).

*Preparation of **8b**.* Into a solution of ethyl *p*-aminobenzoate (0.71 g, 0.0043 mol) in benzene (30 ml), **4b** (1.51 g, 0.0041 mol) was added with stirring at room temperature. After stirring for 5 h, the resulting solution was washed successively once with 3M-hydrochloric acid and once with water. The benzene layer was dried over anhydrous magnesium sulfate and then evaporated under reduced pressure to give crystals of *t*-butyl 2-acetylamino-2-(4-ethoxycarbonylanilino)-3,3-dibromopentanoate.

*Preparation of **9b**.* *t*-Butyl 2-acetylamino-2-(2-pyridylamino)-3,3-dibromopentanoate was obtained from **4b** and 2-aminopyridine in the manner described above.

*Preparation of **10a**.* Into a solution of 2-aminothiazole (0.45 g, 0.0045 mol) in benzene (30 ml), **4a** (0.0043 mol) was added with stirring at room temperature. After stirring for 24 h, the crystalline product separated out was collected and washed with ethanol. The crystals were identified to be *t*-butyl 2-acetylamino-2-(2-thiazolylamino)-3,3-dibromobutanoate.

In an analogous manner, *t*-butyl 2-acetylamino-2-(2-thiazolylamino)-3,3-dibromopentanoate (**10b**) was obtained from **4b** and 2-aminothiazole, after stirring for 4 days.

*Preaparation of **11a**.* A solution of **4a** (0.0043 mol) and phenylhydrazine (0.49 g, 0.0045 mol) in ethanol (10 ml) was stirred below 10 °C, and a similar work up gave *t*-butyl 2-acetylamino-2-phenylhydrazino-3,3-dibromobutanoate.

In an analogous manner, *t*-butyl 2-acetylamino-2-phenylhydrazino-3,3-dibromopentanoate (**11b**) was obtained from **4b** and phenylhydrazine.

*Preparation of **14a**.* Into a solution of **4a** (0.0043 mol) in ethanol (10 ml), a solution of hydroxylamine (made from hydroxylamine hydrochloride (0.33 g, 0.0047 mol) and sodium hydrogencarbonate (0.4 g, 0.0047 mol) in water (3 ml)) was added dropwise with stirring below 10 °C. The reaction was immediately completed and a colorless crystalline product was separated out by adding water (10 ml) to the resulting solution. The crystals were collected and washed with a small quantity of petroleum ether, and identified as *t*-butyl 2-acetylamino-3,3-dibromo-2-hydroxyaminobutanoate.

In an analogous manner, *t*-butyl 2-acetylamino-3,3-dibromo-2-hydroxyaminopentanoate (**14b**) was obtained from **4b** and hydroxylamine.

*Preparation of **15a**.* A solution of **4a** (0.0043 mol) and *O*-benzylhydroxylamine (made from *O*-benzylhydroxylamine hydrochloride (0.72 g, 0.0045 mol) and sodium ethoxide (made from sodium (0.1 g, 0.0045 mol) and ethanol (5 ml)) in ethanol (50 ml) was similarly worked up to give a residual yellowish syrup. After adding benzene (50 ml) to the residue, the benzene solution was washed once with water and dried over anhydrous magnesium sulfate, and then evaporated under reduced pressure to give *t*-butyl 2-acetylamino-2-benzyloxyamino-3,3-dibromobutanoate.

In an analogous manner, *t*-butyl 2-acetylamino-2-benzyloxyamino-3,3-dibromopentanoate (**15b**) was obtained from **4b** and *O*-benzylhydroxylamine.

*Preparation of **12a**, **12b**, **16a**, and **16b**.* The acetylation of **5a**, **5b**, **14a**, and **14b** was carried out by the usual procedure using acetic anhydride and pyridine at room temperature, giving the acetoxyamino compounds, **12a**, **12b**, **16a**, and **16b**, respectively.

*Preparation of **13b**.* A solution of **5a** (3 g, 0.008 mol) and benzoyl chloride (1.24 g, 0.0088 mol) in pyridine (20 ml) was stirred below 10 °C for 3 h, and a similar work up gave *t*-butyl 2-acetylamino-2-benzoylamino-3,3-dibromobutanoate.

*Preparation of **17a** and **17b**.* Similarly, **14a** and **14b** were treated with benzoyl chloride below 10 °C in pyridine, giving the benzoyloxyamino compounds, **17a** and **17b**, respectively.

References

1) Part XI: C. Shin, Y. Sato, and J. Yoshimura, *Bull. Chem. Soc. Jpn.*, **49**, 1909 (1976). This work was presented

at the 35th National Meeting of the Chemical Society of Japan, Sapporo, August 1976. Preprint Vol 2, pp. 606.

2) C. Shin, K. Nanjo, T. Nishino, Y. Sato, and J. Yoshimura, *Bull. Chem. Soc. Jpn.*, **48**, 2492 (1975).

3) B. S. Drach and G. N. Mis'kevich, *Zh. Org. Khim.*, **10**, 2315 (1974); *J. Org. Chem., USSR*, **10**, 2329 (1974).

4) K. Matsumura, H. Shimadzu, O. Miyashita, and N. Hashimoto, *Chem. Pharm. Bull.*, **24**, 941 (1976).

5) This work was presented at 30th and 31st National Meetings of the Chemical Society of Japan, Osaka, April, 1974 and Sendai, October 1974.

6) N. Saito and C. Tanabe, *Yakugaku Zasshi*, **76**, 305 (1956).

7) C. Shin, K. Nanjo, E. Ando, and J. Yoshimura, *Bull. Chem. Soc. Jpn.*, **47**, 3109 (1974).

Organic *N*-Halogen Compounds. X.[1] Preparative Studies on *N*-Benzimidoylsulfilimines

Toshio FUCHIGAMI and Keijiro ODO

Department of Electronic Chemistry, The Graduate School, Tokyo Institute of Technology, Ookayama, Meguro-ku, Tokyo 152

(Received December 6, 1976)

N-Chlorobenzamidine (**1**) reacted readily with dimethyl sulfide to form *N*-benzimidoylaminodimethylsulfonium chloride (**2**). Treatment of **2** with sodium hydroxide gave *N*-benzimidoyl-*S*,*S*-dimethylsulfilimine (**3**) quantitatively. The thermolysis of acyl derivatives of **3** gave rise to 1,2,4-oxadiazoles. *N*-Chloro derivative (**6**) prepared by treating **2** with sodium hypochlorite, reacted with potassium thiocyanate to form *N*-(3-phenyl-1,2,4-thiadiazolyl-5-yl)-*S*,*S*-dimethylsulfilimine (**7**).

Sulfilimines, unique in reactivity, are useful for organic synthesis. Many studies on them have been reported, but they deal with the stable *N*-sulfonyl and *N*-acysulfilimines. We wish to report the preparation of a new class of sulfilimines stabilized by an imino group together with some interesting reactions of acyl and *N*-halogen derivatives of *N*-benzimidoyl-*S*,*S*-dimethylsulfilimine, **3**.

Results and Discussion

Preparation of N-*Benzimidoylaminodimethylsulfonium Chloride (2).* *N*-Halogen compounds react readily with sulfides to form sulfonium salts.[2,3] We investigated the possible formation of such a sulfonium salt from *N*-chloroamidine and sulfide in various solvents. *N*-Chlorobenzamidine (**1**) reacted readily with dimethyl sulfide to form sulfonium chloride (**2**). Acetonitrile was found to be the most suitable solvent for the formation of **2**. When the concentration of **1** was high, the yield of **2** increased considerably. Compound **1** did not react with ethyl phenyl sulfide. The results are summarized in Table 1.

TABLE 1. PREPARATION OF SULFONIUM SALT (**2**)

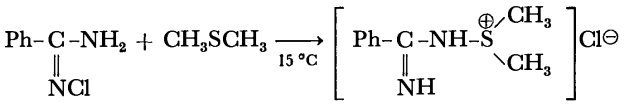

Solvent (ml)	Reaction time (h)[a]	Yield (%)
EtOEt (20)	2.0 (—)[b]	52
CH_2Cl_2 (20)	1.5 (1.0)	62
CH_3CN (20)	1.0 (0.3)	72
CH_3CN (10)	1.0 (0.3)	84

20 mmol scale.
a) Active chlorine disappeared. b) Active chlorine did not disappear.

Preparation of N-*Benzimidoyl*-S,S-*dimethylsulfilimine (3).* Treatment of **2** with aqueous sodium hydroxide gave **3** quantitatively. Treatment of **3** with dry hydrogen chloride afforded the starting material, **2**. The new sulfilimine, **3**, which could be recrystallized from chloroform–ether, melts at 67—68 °C. Sulfilimine **3** is strongly hygroscopic and soluble in common organic solvents except for hydrocarbons. It was found that **3** is quite stable under reflux in tetrahydrofurane for 3 h but decomposes evolving dimethyl sulfide under reflux in xylene for 2 h.

However, the S–N bond of **3** was found to cleave easily on being treated with benzenethiol.

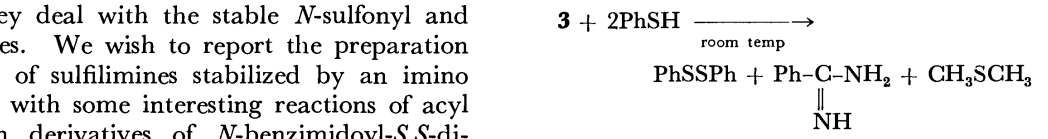

Structure of 3. The structures of **2** and **3** are discussed on the basis of spectral data as follows. In the IR spectra[4] the C=N streching vibration of **2** is at 1650 cm^{-1}, that of **3** at 1510 cm^{-1}. The shift is analogous to that observed in the case of a carbonyl group attached to a ylide carbon or ylide nitrogen atom— (a).

In the UV spectra, **2** and **3** have the same λ_{max} (239 nm) but ε_{max} of **3** (11300) is by 2100 larger than that of **2**— (b).

In the NMR spectra,[5] the resonance of protons to the positively charged sulfur atom and the nitrogen atom shifts upfield by 0.3 and 3.5 ppm, respectively, in going from **2** to **3**— (c).

(a) and (c) suggest that form (**3a**) is a contributor to the sulfilimine structure. (b) and (c) suggest that the S–N bond posesses a partial double bond character due to 2p—3d orbital overlap, (**3b**).

The overall structure can be represented by (A).

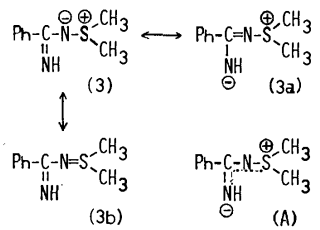

Fig. 1.

These resonance forms can contribute to the stabilization of this new type sulfilimine.

Amidino and Acyl Derivatives of 3. Addition of **3** to diphenylcarbodiimide occurred easily at low temperature to afford amidino derivative (**4**) in a good yield.

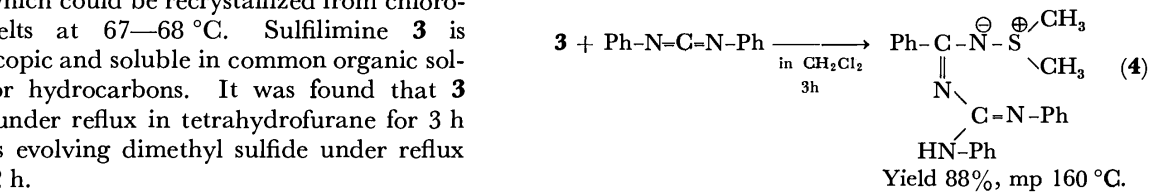

Yield 88%, mp 160 °C.

Cyanamide, which seems to be carbodiimide, did not react with **3** at room temperature, but gave *N*-cyanobenzamidine in 60% yield under reflux in tetrahydrofuran for 30 min.

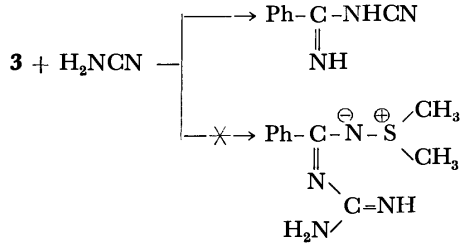

Detailed mechanism has not been clarified yet. The reaction path might be similar to that proposed in the formation of cyanoamidine from amidine and cyanamide.[6]

Acyl derivatives of **3** were easily prepared by the treatment of **2** with acid anhydride.

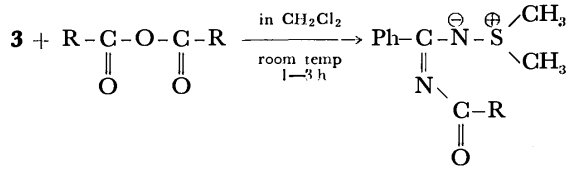

5a: R=Ph
5b: R=*p*-$CH_3C_6H_4$
5c: R=CH_3

The results and physical properties of **5** are given in Table 2.

Table 2. Physical properties of **5**

Compounds	Yield (%)	Mp (°C)	IR (cm^{-1}) $\nu_{C=N}$	IR (cm^{-1}) $\nu_{C=O}$	UV λ_{max} (ε)
5a	66	188—190	1600	1570	245 (11700)
5b	54	172—173	1590	1550	251 (18600)
5c	60	114—116	1620	1600	230 (10800)

These sulfilimines have relatively high melting points and are soluble in common organic solvents except for ether and hydrocarbons.

In the IR spectra, the C=N absorption of **5** is at a shorter wavelength than that of **3**. On the other hand, the C=O absorption is at a longer wavelength than that of normal amide absorption. In view of these shifts in the IR spectra, the structure of **5** can be represented by (B).

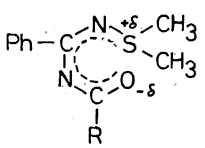

(B)

Fig. 2.

The mass spectrum of **5a** revealed that the primary fragmentation is loss of dimethyl sulfide. Thus, it was expected that 1,2,4-oxadiazole would be formed by elimination of dimethyl sulfide. In fact, heating of **5a** and **5b** without solvent in test tubes at about 200 °C gave rise to 1,2,4-oxadiazoles. However, **5c** gave no corresponding product. The structures of these products were confirmed by elemental analyses and IR spectra. The results are given in Table 3.

Table 3. Formation of 1,2,4-oxadiazoles

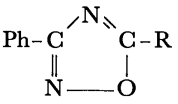

R	Reaction temp (°C)	Reaction time (min)	Yield (%)	Mp (°C)
Ph	200—210	10	70	108 (108)[18]
p-$CH_3C_6H_4$	190—200	20	63	121—122
CH_3	160	5	0	—

Detailed mechanism of this interesting internal ring formation has not been clarified. The thermolysis seems to proceed *via* a nitrene in view of oxadiazole formation from dimethyl diazidomalonate[7] and *N*-benzoyl-*N'*-chloroamidino compounds.[8,9]

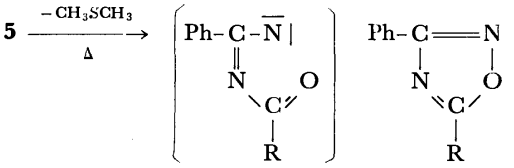

Amidino derivative **4** was also expected to form 1,2,4-triazole by thermolysis. However, no cyclization occurred.

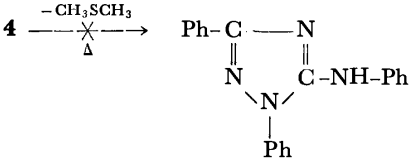

Preparation and Reaction of N-*Chloro Derivative of* **3**. Sulfilimines are stabillized by an electron-withdrawing group attached to the ylide nitrogen atom. Attempts were made to prepare *N*-halogen derivative of **3**. The *N*-chlorosulfilimine (**6**) could easily be prepared quantitatively by treatment of **2** with sodium hypochlorite at low temperature.

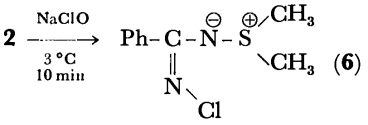

(**6**)

The sulfilimine **6** which can be recrystallized from chloroform–petroleum ether is relatively stable, its melting point being 98—99 °C (with decomposition).

N-Haloamidino compounds readily react with potassium salts of thiocyanic acid and Cyanoiminothiocarbonic acid to give thiadiazoles[10–12] and Δ^4-1,2,4-thiadiazolines[13–16] in good yields. We investigated the reaction of **6** with potassium thiocyanate. The ex-

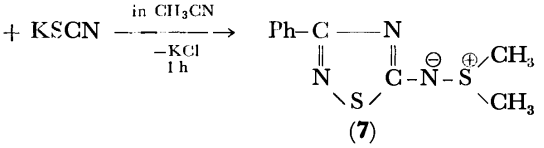

(**7**)

Yield 68%, mp 168—169 °C.

othermic reaction proceeded immediately in acetonitrile to afford *N*-(3-phenyl-1,2,4-thiadiazolyl-5-yl)-*S*,*S*-dimethylsulfilimine (**7**).

The structure of **7** was determined from the following.

(a) No absorption of a thiocyanate group was observed in the IR spectrum.

(b) The analytical values of **7** and its picrate are in good agreement with their theoretical ones.

(c) UV and NMR data.

The formation of **7** might proceed as in the following scheme. The S–N bond was initially formed, internal ring formation being then followed by migration of the dimethylsulfonio group to yield **7**.

No such migration of a sulfonio group in sulfilimine is known.

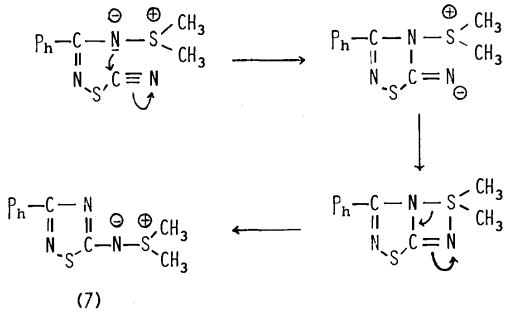

Scheme 1.

Experimental

The melting points are uncorrected. IR spectra were taken with a Hitachi EPI-S2 spectrometer. NMR spectra were recorded at 60 MHz with a Hitachi R-24A spectrometer, and the chemical shifts were given in δ-values, TMS being used as an internal standard. Mass spectra were taken with a JEOL-D100 mass spectrometer. UV spectra were taken in methanol with a Hitachi 624 spectrometer.

N-Chlorobenzamidine (**1**) was prepared by the method[17] described previously.

N-Benzimidoylaminodimethylsulfonium Chloride (2). A solution of **1** (20 mmol) in acetonitrile (5 ml) was added drop by drop to a stirred solution of dimethyl sulfide (24 mmol) in acetonitrile (5 ml). The temperature was maintained below 15 °C during the reaction. After stirring for *ca.* 0.3 h, active chlorine disappeared and sulfonium salt precipitated. The solid was separated by filtration and washed with acetonitrile; yield, 84%; mp 183 °C. Recrystallization from ethanol gave a pure product; mp 183—183.5 °C (Found: C, 49.37; H, 5.76; N, 12.90%. Calcd for $C_9H_{13}N_2SCl$: C, 49.88; H, 6.05; N, 12.93%). Picrate: mp 152—153 °C (from water). (Found: C, 44.15; H, 3.62; N, 17.15%. Calcd for $C_{15}H_{15}N_5SO_7$: C, 44.01; H, 3.69; N, 17.11%).

The reaction when carried out in ether and dichloromethane in a similar way gave **2** in 52 and 62% yields, respectively.

N-Benzimidoyl-S,S-dimethylsulfilimine (3). 2M sodium hydroxide (50 ml) was added to a stirred solution of **2** (70 mmol) in water–chloroform (20—70 ml) at a temperature below 5 °C. After the chloroform layer was separated, residual **3** was extracted twice with 15 ml portions of chloroform. The combined extracts were dried (Na_2SO_4), filtered, and evaporated under reduced pressure. The residual needles were wahsed with ether and separated by filtration under nitrogen atmosphere; yield, quant; mp 65—67 °C. Recrystallization from chloroform–ether gave the pure sulfilimine; mp 67—68 °C. (Found; N, 15.70%. Calcd for $C_9H_{12}N_2S$: N, 15.54 %). *m/e* 180 (M^+).

*Reaction of **3** with Cyanamide.* A mixture of **3** (10 mmol) and cyanamide (10 mmol) in THF (10 ml) was refluxed for 30 min. The reddish reaction mixture was treated with active carbon and was concentrated under reduced pressure. The remaining sirup was dissolved in hot chloroform. Ether was then added. After cooling, the resulting crystals were separated from solution by filtration, and the filtrate was evaporated. The remaining oily material was crystallized from 2 M hydrochloric acid. The total yield of *N*-cyanobenzamidine was 60%; mp 141 °C (from ethanol–water; Ref. 6 mp 141—142 °C).

N-(N-Benzoylbenzimidoyl)-S,S-dimethylsulfilimine (5a). A solution of benzoic anhydride (22 mmol) in dichloromethane (8 ml) was added to a stirred solution of **3** (20 mmol) in dichloromethane (7 ml) at 20—25 °C. After completion of addition, crystals precipitated. After 1 h of continued stirring, the precipitated crystals were separated by filtration and the filtrate was concentrated. The remaining oily material was washed with 2M sodium hydroxide (10 ml) and ether to give crystals of **5a**. The total yield of **5a** was 66%; mp 188—190 °C (from chloroform–ether). (Found; C, 67.36; H, 5.70; N, 9.70%. Calcd for $C_{16}H_{16}N_2OS$: C, 67.58; H, 5.67; N, 9.85%). *m/e* 284 (M^+). NMR (DMSO-d_6): 2.91 (s, CH_3S) and 7.20—8.15 (m, $C_6H_5C{=}O$, $C_6H_5C{=}N$).

N-(N-p-Tolylbenzimidoyl)-S,S-dimethylsulfilimine (5b). This was synthesized by the same procedure. Yield, 54%; mp 172—173 °C (from chloroform–ether). (Found: C, 68.03; H, 6.13; N, 9.10%. Calcd for $C_{17}H_{18}N_2OS$: C, 68.43; H, 6.08; N, 9.39%). *m/e* 298 (M^+). NMR (DMSO-d_6): 2.87 (s, CH_3S), 2.33 (s, $CH_3C_6H_4$), and 7.13—7.96 (m, C_6H_5, $CH_3C_6H_4$).

N-(N-Acetylbenzimidoyl)-S,S-dimethylsulfilimine (5c). Acetic anhydride (17 mmol) and **3** (15 mmol) were stirred in dichloromethane (13 ml) in the presence of sodium carbonate (8.5 mmol) at room temperature for 1 h. After the reaction mixture had been poured into water, the oily layer was separated. The aqueous layer was then extracted twice with 7 ml portions of dichloromethane. After the combined extracts had been dried over sodium sulfate, the solvent was removed by concentration. The remaining oily material was crystallized from ether; yield, 60%; mp 114—116 °C (from dichloromethane–ether). (Found: C, 59.60; H, 6.01; N, 12.51%. Calcd for $C_{11}H_{14}N_2OS$: C, 59.43; H, 6.35; N, 12.60%). NMR (DMSO-d_6): 2.72 (s, CH_3S), 2.02 (s, CH_3-O), and 7.17—7.75 (m, C_6H_5). *m/e* 222 (M^+).

3,5-Diphenyl-1,2,4-oxadiazole. Sulfilimine **5a** was heated in a test tube in an oil-bath at 200—210 °C for 10 min. Evolution of dimethyl sulfide was observed. The contents of the tube were cooled, and the resulting crystals were dissolved in ether. After being treated with active carbon and concentrated to dryness, the remaining crystals were purified by washing with a small amount of aqueous ethanol. Yield, 70%; mp 108 °C (from aqueous ethanol; Ref. 18 mp 108 °C)

3-Phenyl-5-p-tolyl-1,2,4-oxadiazole. After heating **5b** at 190—200 °C for 20 min and then cooling, the contents were dissolved in ether. Treatment of the solution with active carbon and concentration under reduced pressure gave needle-like crystals. Yield, 63%; mp 121—122 °C (from ethanol–water). (Found: C, 76.15; H, 5.08; N, 11.49%. Calcd for $C_{15}H_{12}N_2O$: C, 76.25; H, 5.12; N, 11.86%). *m/e* 236 (M^+).

N-(N-Chlorobenzimidoyl)-S,S-dimethylsulfilimine (6). Sodium hypochlorite (40 mmol) was added to a stirred solution of **2** (36 mmol) in water (20 ml) and dichloromethane

(25 ml) below 3 °C. After stirring for 10 min, the oily layer was separated, and the aqueous layer was extracted with dichloromethane (10 ml). The combined extracts were dried over sodium sulfate, filtered, and concentrated under reduced pressure. The remaining oily substance was crystallized from ether. Yield, 92%; mp 98—99 °C (from chloroform–petroleum ether). (Found: C, 50.05; H, 5.26; N, 13.25%. Calcd for $C_9H_{11}N_2SCl$: C, 50.35; H, 5.16; N, 13.05%). UV: λ_{max} 217 nm (ε: 14000). *m/e* 214 (M^+).

N-*5-(Phenyl-1,2,4-thiadiazoyl)*-S,S-*dimethylsulfilimine (7)*. A solution of **6** (7 mmol) in acetonitrile (4 ml) was added to a stirred suspension of potassium thiocyanate (8 mmol) in acetonitrile (6 ml) with cooling in an ice-bath. A violent exothermic reaction took place, the solution turning yellow. After stirring at room temperature for 1 h, insoluble matter was removed by filtration. A yellowish oily substance was obtained by concentrating the filtrate under reduced pressure. The oil was crystallized from ether and the resulting crystals were collected, yield, 68%. Recrystallization twice from dichloromethane–ether gave pure **7**; mp 168—169 °C. (Found: C, 50.35; H, 4.69; N, 17.88%. Calcd for $C_{10}H_{11}N_3S_2$: C, 50.61; H, 4.67; N, 17.70%). UV: λ_{max} 248 nm (ε: 34000). NMR (DMSO-d_6): 2.88 (s, CH_3S), 7.32—8.15 (m, C$_6H_5$). *m/e* 237 (M^+). Picrate: mp 176 °C (from water). (Found: C, 40.93; H, 2.95; N, 18.06%. Calcd for $C_{16}H_{14}N_6O_7S_2$: C, 41.20; H, 3.03; N, 18.02%).

We thank Dr. E. Ichikawa of Tokyo Institute of Technology and Dr. H. Matsuyama of Tokyo Metropolitan University for their valuable discussions.

References

1) Part IX: T. Fuchigami, T. Nonaka, and K. Iwata, *J. Chem. Soc., Chem. Commun.*, **1976**, 951. Studies of Cyanamide Derivatives. Part 107. Part 106: A. Omura, T. Nonaka, T. Fuchigami, E. Ichikawa, and K. Odo, *Bull. Chem. Soc. Jpn.*, **50**, 914 (1977).

2) H. Kise, G. F. Whitfield, and D, Swern, *Tetrahedron Lett.*, **1971**, 1761; *J. Org. Chem.*, **37**, 1121 (1972).

3) G. F. Whitfield, H. S. Beilan, D. Saika, and D. Swern, *Tetrahedron Lett.*, **1970**, 3543.

4) (**2**): νNH 3250, 3300 cm^{-1}. (**3**): νNH 3300^{-1}.

5) (**2**): δ=3.03 (s, CH_3SCH_3), 9.00 (s, NH), 7.40—7.95 (m, C$_6H_5$). (**3**): δ=2.74 (s, CH_3SCH_3), 5.05 (s, NH), 7.15—7.95 (m, C$_6H_5$).

6) H. R. Huffmann and F. C. Scaefer, *J. Org. Chem.*, **28**, 1812 (1963).

7) R. M. Moriarty, J. M. Kliegman, and C. Shvlin. *J, Am. Chem. Soc.*, **89**, 5958 (1967).

8) T. Fuchigami and K. Odo, *Chem. Lett.*, **1974**, 1139.

9) T. Fuchigami and K. Odo, *Bull. Chem. Soc., Jpn.* **49**, 3607 (1976).

10) J. Goerdeler, *Chem. Ber.*, **87**, 57 (1954).

11) J. Goerdeler and F. Bechlars, *Chem. Ber.*, **88**, 848 (1955).

12) J. Goerdeler and M. Willig, *Chem. Ber.*, **88**, 1071 (1955).

13) T. Fuchigami and K. Odo, *Chem. Lett.*, **1973**, 917.

14) T. Fuchigami and K. Odo, *Bull. Chem. Soc. Jpn.*, **48**, 310 (1975).

15) T. Fuchigami and K. Odo, *Bull. Chem. Soc. Jpn.*, **49**, 3165 (1976).

16) T. Fuchigami, T. Nonaka, and K. Odo, *Bull. Chem. Soc. Jpn.*, **49**, 3170 (1976).

17) T. Fuchigami, E. Ichikawa, and K. Odo, *Bull. Chem. Soc. Jpn.*, **46**, 1765 (1973).

18) E. Beckmann and K. Sandel, *Justus Liebigs Ann. Chem.*, **296**, 285 (1897).

Photochemical Reactions between Dibromomaleic Anhydride and Benzo[*b*]thiophene[1]

Taku MATSUO and Satoru MIHARA

Department of Organic Synthesis, Faculty of Engineering, Kyushu University, Fukuoka 812

(Received December 10, 1976)

On the irradiation of dibromomaleic anhydride in the presence of benzo[*b*]thiophene, both photosubstitution and photocycloaddition are simultaneously induced. The ratio of the substituted product to the cycloadduct increased with solvent polarity, and the same Stern-Volmer plots were obtained with both of the reactions. Kinetic parameters, obtained under various concentrations of benzo[*b*]thiophene, indicate that the reactions proceed *via* a common triplet exciplex. The activation energy for the photosubstitution is higher than that for the cycloaddition by 1—2 kcal/mol, where the former reaction is considered to proceed *via* a more polar transition state than the latter.

Photochemical reaction between maleic anhydride (or maleimide) and benzene (or alkyl-substituted benzene) affords cycloaddition compounds.[2-4] Photosubstitutions are observed, when dibromomaleic anhydride (or dibromomaleimide) is irradiated in the presence of aromatic compounds such as monosubstituted benzenes,[5] phenylpyrrole,[6] and indole.[7] In the case of dibromomaleic anhydride–benzo[*b*]thiophene system, as reported in this paper, both photosubstitution and photocycloaddition proceed simultaneously. The mechanistic detail and the relationship between photosubstitution and photocycloaddition will be discussed below.

Results

Reaction Products. After irradiation of dibromomaleic anhydride (**1**) and benzo[*b*]thiophene (**2**) with a high-pressure mercury lamp, the reaction mixture was treated with silica gel column chromatography, and two crystalline materials were obtained. On the basis of the spectroscopic data, the crystalline materials were suggested to be 1-bromo-2-(3-benzo[*b*]thienyl)-maleic anhydride (**4**) and *anti*-1,2-dibromo-1,2,2a,7b-tetrahydrocyclobuta[*b*]benzo[*d*]thiophene-1,2-dicarboxylic acid (**5**). The compound **5** is a hydrolysis product of *anti*-1,2-dibromo-1,2,2a,7b-tetrahydrocyclobuta[*b*]benzo[*d*]thiophene-1,2-dicarboxylic anhydride (**3**). Thermal decomposition of **3** in acetic anhydride gave **4** (6%) and 1-bromo-2-(2-benzo[*b*]thienyl)maleic anhydride (**6**, 94%).

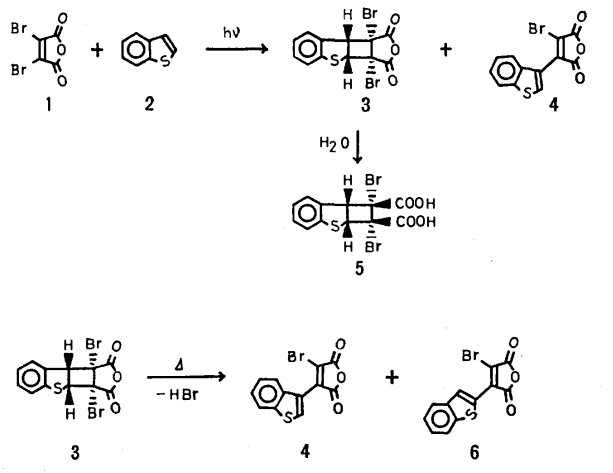

Scheme 1.

Quenching Studies. The variation of the quantum yields for the formation of **3** and **4** in dichloromethane solutions was studied as a function of cyclooctatetraene (COT) concentration (Fig. 1). The amounts of **3** and **4** were evaluated by the visible absorption and GLC, respectively.[8]

The Stern-Volmer plots of both **3** and **4** gave nearly the same straight lines up to Φ_0/Φ-values near 5. The quenching constant (K)[9] was found to depend on the concentration of **2**. Assuming that k_q equals the diffusion-controlled rate parameter, the lifetime of ^{3}**1**(τ_{obsd}) in various concentration of **2** can be estimated from the K-values. The correlation between the concentration of **2** and inverse of the τ_{obsd}-value was linear (Fig. 2). From the intercept, τ^0_{obsd} can be calculated to be 1×10^{-5} s. In addition to benzo[*b*]thiophene, kinetics were also investigated with phenylpyrrole, benzene and chlorobenzene, which gave substituted product by the photo-induced reaction with **1**.[5,6] The results are shown in Fig. 2. Slopes of the straight lines (k_d) in Fig. 2 and the charge transfer bands of TCNE complex for each compound are summarized in Table 1.

Quantum Yields. The reactions were carried out by the use of a modified merry-go-round irradiation apparatus. The light intensity of monochromatic light (313 nm) was monitored by the use of a photochemical reaction between **1** and phenylpyrrole.[6] The quantum yields for the formation of **4** was estimated by the ab-

TABLE 1. THE QUANTUM YIELDS FOR THE FORMATION OF THE SUBSTITUTED PRODUCTS (Φ_S) AND CYCLOADDITION PRODUCTS (Φ_A) AND k_d-VALUES FOR VARIOUS AROMATIC COMPOUNDS[a]

D-H	$h\nu_{CT}$[b] (eV)	Φ_S	Φ_A	k_d ($M^{-1}s^{-1}$)
N-Phenylpyrrole	2.28 (A)[c]	0.67	—	9.1×10^9
Benzo[*b*]thiophene	2.35 (B)[d]	0.17	0.47	6.4×10^9
Benzene	3.23 (B)[d] 3.20 (C)[e]	0.10	—	5.2×10^8
Chlorobenzene	3.27 (C)[e]	0.08	—	7.0×10^7

a) Solvent: CCl_4. [**1**]=[D-H]=10^{-2} M. $h\nu$: 313 nm. b) $h\nu_{CT}$ TCNE complex. Solvent: (A) tetrachloroethane, (B) chloroform, (c) dichloromethane. c) See Ref. 10. d) See Ref. 11. e) See Ref. 12.

Table 2. The quantum yields[a] for photocycloaddition (Φ_A) and photosubstitution (Φ_S), and the difference of activation energies in various solvents under irradiation with 313 nm-light

Solvent	Polarity parameter[b]	Φ_A	Φ_S	Φ_A/Φ_S	ΔE (kcal/mol)
Carbon tetrachloride	32.5	0.23	0.17	1.4	1.4±0.2
Diethyl ether	34.6	0.16	0.14	1.1	—
Dichloromethane	41.1	0.23	0.32	0.72	1.0±0.2
Acetonitrile	46.0	0.045	0.067	0.67	1.1±0.2

a) The values obtained by extrapolation to the infinite concentration of **2**. [**1**]$=10^{-2}$ M. b) Dimroth's E_T-value. See Ref. 13.

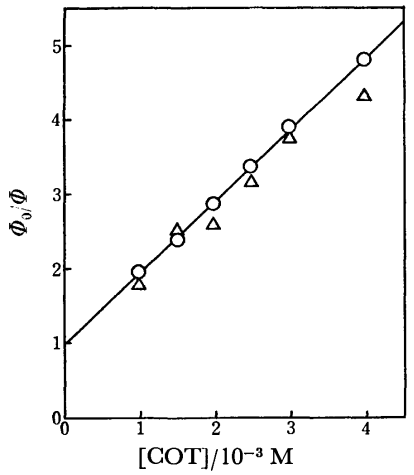

Fig. 1. Stern-Volmer Plots of photosubstitution (—○—) and photocycloaddition (—△—) in dichloromethane solution. [**1**]$=1.5\times10^{-2}$M, [**2**]$=1\times10^{-3}$M.

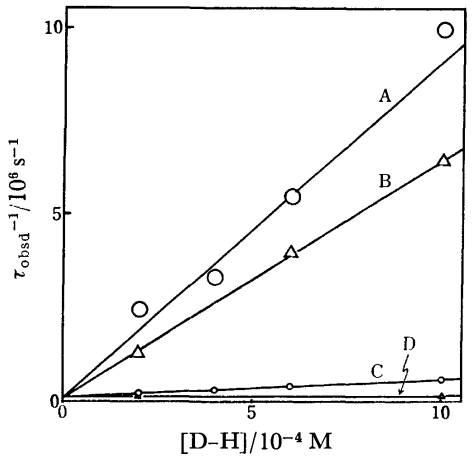

Fig. 2. Relationship between triplet lifetime and concentration of D–H in carbon tetrachloride. [**1**]$=1\times10^{-2}$ M. A: *N*-Phenylpyrrole. B: Benzo[*b*]thiophene. C: Benzene. D: Chlorobenzene.

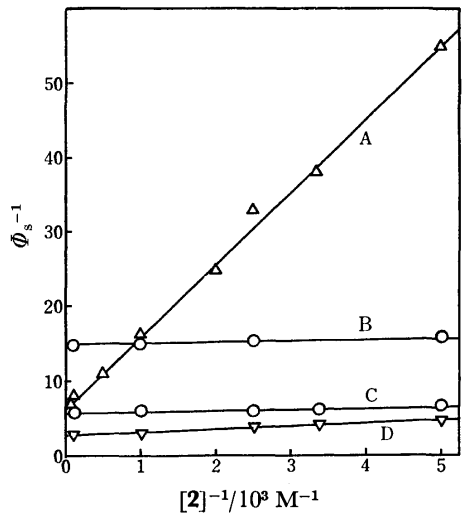

Fig. 3. Relationship between the quantum yield of **4** and the concentration of **2** in various solvents. A: Diethyl ether. B: Acetonitrile. C: Carbon tetrachloride. D: Dichloromethane.

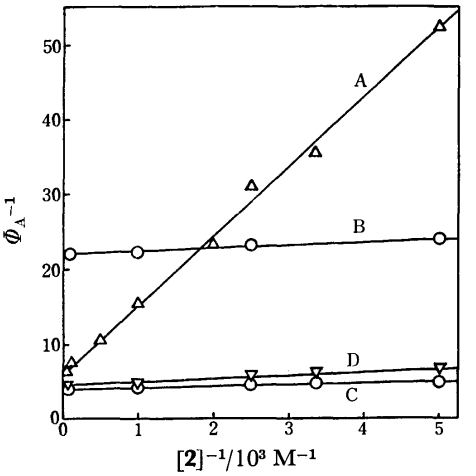

Fig. 4. Relationship between the quantum yield of **3** and the concentration of **2** in various solvents. The notations are the same as those in Fig. 3.

sorption maximum of visible spectrum. Relative yields for the formation of **3** to **4** were evaluated from the GLC peaks area of the pyrolysis products, **4** and **6**. Then the yield for the formation of **3** was calculated from that for **4** and the relative yield, **4**/**3**. The inverses of the quantum yields for the substitution and cycloaddition reactions are plotted *vs.* [**2**]$^{-1}$ in Fig. 3 and Fig. 4, respectively. Linear relationships with different slopes and intercepts were observed with various solvents. The values for Φ_A and Φ_S at the infinite concentration of **2** are given in Table 2.

Temperature Effects. The ratio of quantum yields for formations of **4** to **3** in various solvents was measured at various temperatures. The slope of the Arrhenius

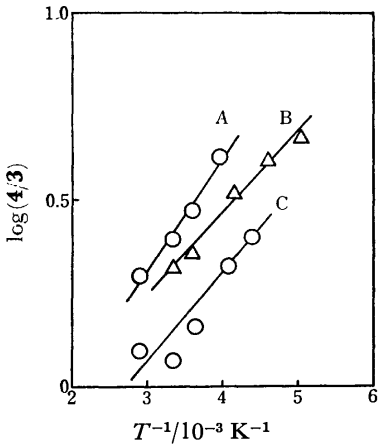

Fig. 5. Arrhenius plots of the product ratio (**4**/**3**) in various solvents. A: Carbon tetrachloride. B: Dichloromethane. C: Acetonitrile.

plots of the ratio, as shown in Fig. 5, corresponds to the difference in activation energies between photosubstitution and photocycloaddition. The difference in activation energies thus obtained also included in Table 2.

Discussion

The above experimental data clearly indicate that the cycloaddition and substitution simultaneously proceed upon the irradiation of **1** and **2**. Thermal decomposition of the cycloadduct **3** at high temperature affords substituted benzo[*b*]thiophene isomers, **4** and **6** (major product), while the formation of **6** was not noticed at all in close examination of the ^{1}H NMR spectra of the irradiated solution. In other words, the photosubstitution takes place exclusively at the 3-position of benzo[*b*]thiophene. The reactions, here investigated, may be summarized by the following scheme:

On the basis of the Stern-Volmer plots (Fig. 1), it is concluded that the triplet species is involved in the formation of both **3** and **4**. The irradiation condition for the quenching experiments is adjusted so that **1** is exculsively excited. Besides, the triplet energy of **1** (E_T=53.5 kcal/mol)[14] is located between those of **2** (E_T=68.9 kcal/mol)[15] and COT ($E_T \leq$39 kcal/mol).[16] Therefore, the active species under discussion must be ^{3}**1**.

The triplet species is quenched by the addition of various aromatic substances as shown in Fig. 2. For a given concentration of the aromatic additive, the apparent lifetime of the triplet (τ_{obsd}) decreases with the increase in the electron-donating property of the additive. Then, the presence of donor-acceptor type interaction in the excited state is indicated. Based on the intercept of the straight lines in Fig. 2, the lifetime of the triplet in the absence of aromatic additive (τ^0_{obsd}) was estimated to be 1×10^{-5} s.

In order to account for the above experimental facts, as well as a linear correlation between $[\mathbf{2}]^{-1}$ and Φ_S^{-1} (or Φ_A^{-1}) in Fig. 3 (or Fig. 4), the following reaction scheme is suggested.

	Rate	
$A \xrightarrow{h\nu} {}^1A$	I_a	(1)
${}^1A \xrightarrow{k_{d-1}} A$	$k_{d-1}[^1A]$	(2)
${}^1A \xrightarrow{k_{isc}} {}^3A$	$k_{isc}[^1A]$	(3)
${}^3A \xrightarrow{k_{d-3}} A$	$k_{d-3}[^3A]$	(4)
${}^3A + Q \xrightarrow{k_q} A + {}^3Q$	$k_q[^3A][Q]$	(5)
${}^3A + D \xrightarrow{k_r} E$	$k_r[^3A][D]$	(6)
$E \xrightarrow{k_{-r}} {}^3A + D$	$k_{-r}[E]$	(7)
$E \xrightarrow{k_{d-e}} A + D$	$k_{d-e}[E]$	(8)
$E \xrightarrow{k_A} P_A$	$k_A[E]$	(9)
$E \xrightarrow{k_S} P_S$	$k_S[E]$	(10)

$$\Phi_{A(\text{or S})}^{-1} = \frac{k_A+k_S+k_{d-e}}{\Phi_{isc}\cdot k_{A(\text{or S})}}\left(1+\frac{k_{d-3}+k_q[Q]}{k_d[D]}\right) \quad (11)$$

$$k_d = \frac{k_A+k_S+k_{d-e}}{k_A+k_S+k_{d-e}+k_{-r}}\cdot k_r \quad (12)$$

$$\frac{(\Phi_{A(\text{or S})})_0}{\Phi_{A(\text{or S})}} = 1+\frac{k_q}{k_d[D]+k_{d-3}}[Q] = 1+k_q\tau_{obsd}[Q] \quad (13)$$

$$\tau_{obsd} = \frac{1}{k_d[D]+k_{d-3}} \quad (14)$$

$$\tau^0_{obsd} = \frac{1}{k_{d-3}} \quad (15)$$

$$\tau^{-1}_{obsd} = (\tau^0_{obsd})^{-1} + k_d[D] \quad (16)$$

The role of donor-acceptor interaction is taken into consideration in the formation of the triplet exciplex (E) between the excited triplet and the aromatic additives. The relevant species **1**, **2** or other aromatic additives used in Fig. 2, the substituted product, the cyclo-

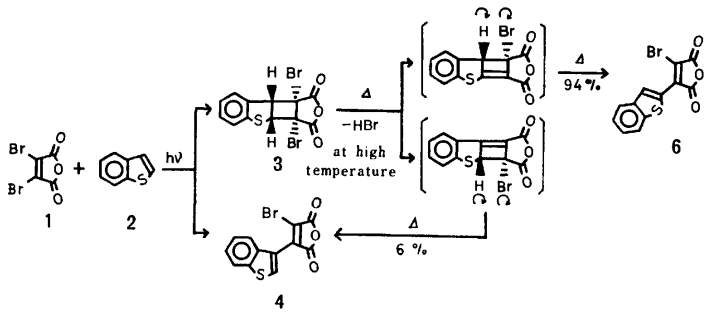

Scheme 2.

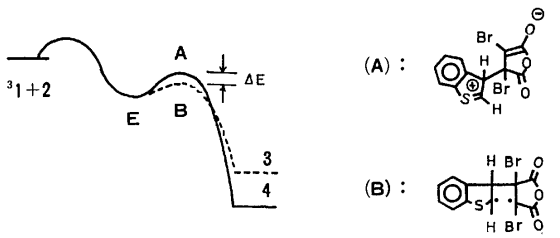

Fig. 6. Reaction diagram.

adduct, and quencher (COT) are denoted by A, D, P_S, P_A, and Q, respectively.

The linear relationships in Fig. 2 are represented by Eq. 16, while those in Figs. 3 and 4 are explained by Eq. 11. By the use of Eq. 11, the $k_d \cdot \tau^0_{obsd}$-value for dibromomaleic anhydride–benzo[*b*]thiophene system in carbon tetrachloride is evaluated to be 3.7×10^4 M^{-1} (Figs. 3 and 4). This value is in good agreement with the product between k_d (6.4×10^9 $M^{-1}\,s^{-1}$) and τ^0_{obsd} (1×10^{-5} s), which were previously obtained by the quenching experiments (Fig. 2, Table 1).

The k_d-value increases with electron-donating ability of D, as summarized in Table 1. In the case of *N*-phenylpyrrole and benzo[*b*]thiophene, the k_d-values are practically the same as k_{diff}. The large k_d-value is associated with high quantum yields ($\Phi_S + \Phi_A$). However, the variation in the k_d-value is approximately ten-times larger than that in the quantum yield. It may be that the deactivation of the triplet exciplex, as represented by Eq. 8 and k_{d-e}, becomes increasingly important as donor-acceptor interaction gets stronger.[17]

Donor-acceptor interactions are favored in polar solvents. Then, the small quantum yields of the photoproducts in acetonitrile is easily understood as due to the increased donor-acceptor interaction in the triplet exciplex in this highly polar solvent. In this connection, the quantum yields in diethyl ether are extraordinary small. Besides the polarity, donor-acceptor interaction between ^{3}A and the solvent itself should be taken into consideration, because ethers have been known to be good electron donors in the study of charge-transfer complex. The donor-acceptor interaction between ^{3}A and diethyl ether may induce quite effective deactivation of the former through radiationless transition.

The ratio of photosubstitution relative to the cycloaddition increases with the temperature and polarity of solvent (Table 2 and Fig. 5). On the basis of the above discussion, it is clear that both reactions proceed *via* the same active species (^{3}A) and the triplet exciplex (E). Since, the photosubstitution is favored in polar solvents, the electronic structure of the transition state may be closer to a polar structure (A). On the other hand, the contribution of a biradical structure (B) may be most important in the transition state of the photocycloaddition, which is at lower energy by approximately 1 kcal/mol than that of the photosubstitution as summarized in Fig. 6.

Experimental

Materials and Equipments. Dibromomaleic anhydride was prepared by the reported procedure.[18] Benzo[*b*]thiophene, COT and solvents of guaranteed grade were purified before use. The photoproducts were isolated either by sublimation or by the use of column chromatography on silica gel (Mallinckrot, silic acid 100 mesh). The IR, NMR, mass, and electronic spectra were recorded on JASCO DS-301, Varian A-60, JEOL JES-01SG, and Shimadzu UV-200 spectrometers, respectively. GLC was obtained by a Shimadzu GC-3BF gas chromatograph.

*Photoreaction between **1** and **2** in Preparative Scale.*

(A) A dioxane solution (250 ml) containing **1** (0.64 g) and **2** (0.34 g) was internally irradiated with a 400 W high-pressure mercury arc lamp (Riko-Sha UVL-400HA) equipped with pyrex jacket in a nitrogen atmosphere for 4.5 h. The pyrex jacket was filled with a filter solution (a layer (1 cm) of an aqueous solutions containing nickel sulfate (0.95 M) and potassium chromic sulfate (0.075 M)). After the solvent was completely removed under reduced pressure, **4** and **6** were isolated from the residue by sublimation (1—2 Torr, 110—150 °C). 1-Bromo-2-(3-benzo[*b*]thienyl)maleic anhydride (**4**): mp 208—209 °C; IR (KBr) 1856, 1823, and 1767 (C=O), 1244 and 1230 (COC) cm^{-1}; UV (Dioxane): λ_{max} 225 (ε 2.83×10^4), 263 (8.45×10^3), and 378 nm (1.82×10^4); Mass, *m/e* 310 (M^+), 308; NMR(Dioxane): δ 8.60 (1H, s, 2-H) and 7.3—8.1 (4H, m, 4-H—7-H); Found: C, 46.58; H, 1.64% Calcd for $C_{12}H_5OBrS$: C, 46.62; H, 1.63%. 1-Bromo-2-(2-benzo[*b*]thienyl)maleic anhydride (**6**): mp 146—147 °C; IR (KBr) 1846, 1816, and 1767 (C=O), 1267, 1252, and 1229 (COC) cm^{-1}; UV (Dioxane): λ_{max} 266 (ε 9.64×10^3) and 383 nm (5.7×10^3); Mass, *m/e* 310 (M^+) and 308; NMR(Dioxane): δ 8.14 (1H, s, 3-H), 7.3—8.1 (4H, m, 4-H—7-H). Found: C, 46.57; H, 1.68%. Calcd for $C_{12}H_5O_3BrS$: C, 46.62; H, 1.63%.

(B) A dichloromethane solution (3 ml) containing **1** (0.39 g) and **2** (0.21 g) was externally irradiated in a nitrogen atmosphere with a 400-W high pressure mercury arc lamp through a pyrex water jacket and window glass filter (2 mm) for 1 h. After the solvent was removed under reduced pressure, the residue was subjected to column chromatography. Elution with a hexane–benzene–ethyl acetate mixture afforded **4** (60 mg) and **5** (143 mg). *anti*-1,2-Dibromo-1,2,2a,7b-tetrahydrocyclobuta[*b*]benzo[*d*]thiophene-1,2-dicarboxylic acid (**5**)[19]: mp 151—153 °C; IR (KBr) 3452 and 3242 (OH), 1760, 1726, and 1712 (C=O) cm^{-1}; Mass, *m/e* 409 (M^+), 408 and 407; NMR (Acetonitrile): δ 4.93 (2H, q, 2-H and 3-H), 7.0—7.3 (4H, m, 4-H—7-H), $J_{2,3}$=8.2 Hz.

*Photoreaction between **1** and Chlorobenzene.* A chlorobenzene solution of **1** (1.3 g/200 ml) was internally irradiated with a 30-W low-pressure mercury arc lamp (Riko-Sha UVL 303-Q) in a nitrogen atmosphere for 15 h. The GLC analysis (column: Silicone DC 430 5% on Chamerite CS 60/80, oven temperature 210 °C) of the crude residue shows the formation of **7** (90% by peak area) accompanied with small amounts of other two products (10% by peak area). After the solvent and **1** were almost removed under reduced pressure, the residue was subjected to column chlomatography. Elution with benzene–hexane mixture afforded **7** (0.25 g). 1-Bromo-2-(*p*-chlorophenyl)maleic anhydride (**7**): mp 85—86 °C; IR (KBr) 1761 and 1839 (C=O), 1250, 1273 and 1293 (COC) cm^{-1}; Mass, *m/e* 290 (M^+), 288 and 286; NMR (CCl_4): δ 7.70(m). UV (CCl_4): λ_{max}, 339 nm ($\varepsilon = 1.40 \times 10^4$). Found: C, 41.84; H, 1.42%. Calcd for $C_{10}H_4O_3BrCl$: C, 41.78; H, 1.40%.

Quenching Experiment. The relative quantum yields (313 nm) in various quencher concentrations were measured by the use of rotating cylinder.[6] After the irradiation, the amount of photoproducts was determined by the use of either

the absorption spectra or GLC analysis (column: silicon OV-17 1.5% on Diasolid L; oven temperature: 215 °C).

Temperature Effects. In the experiments above room temperatures, various solutions containing **1** (1.5×10^{-2}M) and **2**(1.5×10^{-2}M) were placed in a pyrex tube and were immersed in 1 l beaker, whose temperature was controlled by a heater within ±2 °C. In the case of temperatures below 0 °C, the sample tubes were held in a pyrex dewar vessel, filled with methanol. The temperature of dewar vessel was controlled within ±3 °C by adjusting the amount of Dry Ice. Both the dewar vessel and a 400-W high pressure mercury lamp were held in a plastic tube filled with running water. Under these conditions, sample tubes were externally irradiated through the wall of either beaker or pyrex dewar vessel for about 1 h. The amount of photoproducts was evaluated either by the GLC or by the NMR spectra.

References

1) Contribution No. 425 from the Department of Organic Synthesis, Faculty of Engineering, Kyushu University.

2) D. Bryce-Smith, R. R. Deshpande, and A. Gilbert, *Tetrahedron Lett.*, **1975**, 1627.

3) J. S. Brandshaw, *Tetrahedron Lett.*, **1966**, 2039.

4) C. Rivas, M. Vélez, and O. Crescente, *Chem. Commun.*, **1970**, 1474.

5) T. Matsuo, Y. Tanoue, T. Matsunaga, and K. Nagatoshi, *Chem. Lett.*, **1972**, 709.

6) T. Matsuo and S. Mihara, *Bull. Chem. Soc. Jpn.*, **48**, 3660 (1975).

7) T. Matsuo and S. Mihara, *Tetrahedron Lett.*, **1976**, 4581.

8) The amount of **3** was actually calculated from the peaks **4** and **6**, since the pyrolysis of **3** was completed in the GLC tubes.

9) $K=k_q\tau_{obsd}$, see Eq. 13.

10) T. Matsuo and H. Shosenji, *Bull. Chem. Soc. Jpn.*, **41** 1068 (1968).

11) A. R. Cooper, C. W. P. Crowne, and P. G. Farrell, *Trans. Faraday Soc.*, **62**, 18 (1966).

12) E. M. Voigt, *J. Am. Chem. Soc.*, **86**, 3611 (1964).

13) K. Dimroth, C. Reichardt, T. Siepmann, and F. Bohlmann, *Ann. Chem.*, **611**, 1 (1963); K. Dimroth, C. Reichardt, and A. Schweig, *ibid.*, **669**, 95 (1963).

14) H.-D. Scharf, H. Leismann, and H. Lechner, *Chem. Ber.*, **104**, 847 (1971).

15) J. H. Dopper and H. Wynberg, *J. Org. Chem.*, **35**, 1582 (1970).

16) W. I. Ferree Jr. and B. F. Plummer, *J. Am. Chem. Soc.*, **95**, 6709 (1973).

17) F. D. Lewis and C. E. Hoyle, *J. Am. Chem. Soc.*, **98**, 4338 (1976).

18) H. Simonis, *Ber.*, **32**, 2084 (1899); O. Diels and Reinbeck, *ibid.*, **43**, 1271 (1910).

19) This compound slowly decomposed to the substituted product at room temperature.

Photochemical Behavior of 1,2-Diphenylcyclobutene in Protic Solvents. Addition of Secondary Amines

Masako SAKURAGI and Hirochika SAKURAGI*

Research Institute for Polymers and Textiles, 4 Sawatari, Kanagawa-ku, Yokohama 221

**Department of Chemistry, Faculty of Science, The University of Tokyo, Hongo, Bunkyo-ku, Tokyo 113*

(Received December 14, 1976)

Irradiation of 1,2-diphenylcyclobutene (**1**) and diethylamine in hexane with light of longer wavelengths than 300 nm affords *N,N*-diethyl-1,2-diphenylcyclobutanamine (**2a**), 1,2-diphenylcyclobutane (**3**), and 1,1′,2,2′-tetraphenylbicyclobutyl (**4**). Upon similar irradiation, **1** and morpholine afford *N*-(1,2-diphenylcyclobutyl)morpholine **3** and **4**. A mechanism involving a charge-transfer complex is proposed on the basis of the observations that the amines quenched the olefin fluorescence at a rate close to the diffusion limit in hexane, and that when diethylamine-*N*-*d* was used as an additive the deuterium was retained in the methine groups of compounds **2a**, **3**, and **4**.

Amines interact with excited states, singlets and triplets of many molecules, including aromatic hydrocarbons and ketones. This interaction is believed to be of the charge-transfer type, which always results in deactivation of the excited state, and often in photoreactions.[1] In the photoreaction of aromatic hydrocarbons with tertiary amines an α-hydrogen atom of the amines is transferred to hydrocarbon anion radicals, resulting in reduction and addition products.[1] With primary and secondary amines an amino hydrogen atom can be transferred more easily than the α-hydrogen atom, generating a radical pair containing an aminyl radical. Only a few reports have appeared on the amino hydrogen transfer.[1-5] For example, 2-propanamine has been shown to react with 1-phenylcyclohexene, affording a mixture of the C-adduct and the N-adduct in the proportion of 58 : 37.[2] Piperidine and cyclohexanamine react with benzene to afford 1,4-addition products, 2,5-cyclohexadienamine derivatives.[3] Recently, a report was given on the photoinduced exchange of the nuclear hydrogen of benzonitrile with an amino hydrogen of diethylamine and with water in the presence of triethylamine.[4]

In an investigation of the photochemical behavior of 1,2-diphenylcyclobutene (**1**) in protic solvents,[6] it was shown that this cyclobutene is photoprotonated in methanol and acetic acid to give 1,2-diphenyl-1-methoxycyclobutane and 1-(α-methoxybenzyl)-1-phenylcyclopropane, and the corresponding acetates, respectively, and that the polar addition proceeds from the excited singlet state of the cyclobutene on the basis of quenching experiments of the olefin fluorescence.

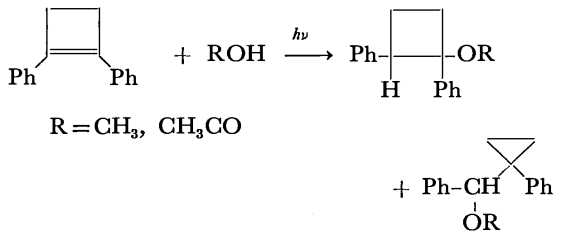

We wish to report on an extended study of the photochemical behavior of the four-membered cyclic olefin with amines. The excited singlet state of the cyclobutene was quenched efficiently by secondary and tertiary amines, among which diethylamine and morpholine gave addition products, the corresponding cyclobutanamine derivatives.

Results and Discussion

Fluorescence quenching experiments of 1,2-diphenylcyclobutene (**1**) by amines were carried out under aerated conditions in hexane. No change was found in the fluorescence maximum and in the shape of fluorescence spectrum of **1** upon the addition of amines in various concentrations. Plots of the reciprocals of the relative fluorescence intensities against the concentrations of the amines are linear, fitting the Stern-Volmer equation,

$$I_0/I = 1 + k_q\tau_0[Q],$$

where I_0 and I denote the intensities of the fluorescence of **1** in the absence and in the presence of the quencher in the concentration [Q], respectively, k_q is the rate constant of the bimolecular quenching process, and τ_0 denotes the average lifetime of the excited singlet state of **1** in the absence of the quencher. The slopes of the Stern-Volmer plots ($k_q\tau_0$) are shown in Table 1 together with ionization potentials of the amines. Since the lifetime of the excited singlet state of **1** (τ_0)

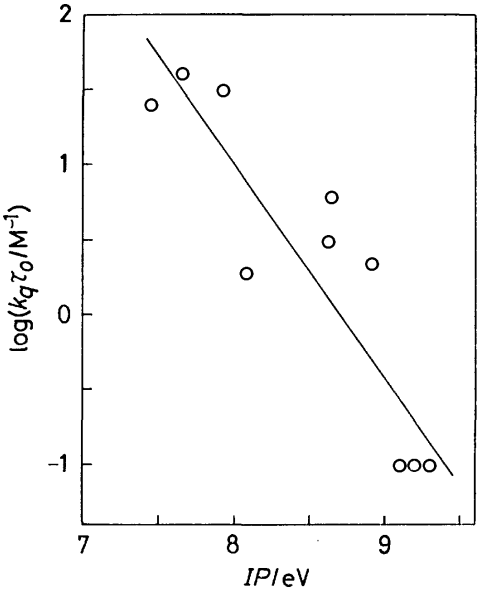

Fig. 1. Correlation of quenching constants of 1,2-diphenylcyclobutene fluorescence by amines with their ionization potentials.

Table 1. Quenching of the fluorescence from 1,2-diphenylcyclobutene by amines in hexane[a]

Amine	Ionization potential (eV)[b]	$k_q\tau_0$ (M^{-1})
n-$BuNH_2$	9.20,[c] 9.40[d]	0.1
s-$BuNH_2$	9.20[c]	0.1
t-$BuNH_2$	9.20[c]	0.1
$PhCH_2NH_2$	9.10[e]	0.1
O NH	8.91[f]	2.2
NH	8.64,[g] 8.66[f,h]	6.2
Et_2NH	8.63[g]	3.1
Et_3N	8.08[i]	1.9
Pr_3N	7.92[i]	32
PhNHMe	7.65[j]	41
$PhNMe_2$	7.45[j]	26

a) Conducted under aerated conditions. b) Vertical ionization potentials obtained from photoelectron spectroscopy. c) H. Ogata, H. Onizuka, Y. Nihei, and H. Kamada, *Bull. Chem. Soc. Jpn.*, **46**, 3036 (1973), and Y. Nihei, private communication. d) S. Katsumata, T. Iwai, and K. Kimura, *ibid.*, **46**, 3391 (1973). e) T. P. Debies and J. W. Rabalais, *Inorg. Chem.*, **13**, 308 (1974). f) F. P. Colonna, G. Distefano, S. Pignataro, G. Pitacco, and E. Valentin, *J. Chem. Soc., Fraday Trans. 2*, **71**, 1572 (1975). g) K. Yoshikawa, M. Hashimoto, and I. Morishima, *J. Am. Chem. Soc.*, **96**, 288 (1974). h) D. H. Aue, H. M. Webb, and M. T. Bowers, *ibid.*, **97**, 4137 (1975). i) D. H. Aue, H. M. Webb, and M. T. Bowers, *ibid.*, **97**, 4136 (1975). j) J. P. Maier and D. W. Turner, *J. Chem. Soc., Faraday Trans. 2*, **69**, 521 (1973).

is reported to be shorter than 5 ns,[7] the quenching rate constants (k_q) of the secondary and tertiary amines can be estimated to be 10^8—10^9 M^{-1} s^{-1}, close to the diffusion limit, whereas the primary amines interact less efficiently with the cyclobutene. Plots of logarithms of the $k_q\tau_0$ values against the ionization potentials of the amines give a linear relationship (Fig. 1). These results suggest that the singlet excited **1** interacts with the ground states of amines, possibly forming exciplex intermediates.[8]

A solution of 1,2-diphenylcyclobutene (**1**, 0.01 M) in a mixture of diethylamine and hexane (1 : 4 by volume) was irradiated with light of longer wavelengths than 300 nm using a 500-W xenon lamp through a filter. The reaction mixture was separated by column chromatography on silica gel into three principal components in addition to the recovered starting material. The products isolated were *N,N*-diethyl-1,2-diphenylcyclobutanamine (**2a**), 1,2-diphenylcyclobutane (**3**), and 1,1′,2,2′-tetraphenylbicyclobutyl (**4**). These were identified mainly on the basis of their elemental analyses and spectral data. The NMR spectrum of the N-adduct, **2a**, of the amine and **1** displayed a six-proton triplet at δ 1.03 (J=7 Hz) and a four-proton quartet at δ 2.55 (J=7 Hz) attributable to the ethyl groups, and a one-proton multiplet at δ 3.7—4.2 attributable to the methine proton. Gas chromatographic analysis showed that **2a** consists of only one isomer. From the NMR spectrum the reduction product, **3**, was found to be a *ca.* 2 : 1 mixture of *cis*- and *trans*-diphenylcyclobutane. The reduction dimer, **4**, was a mixture of more than two isomers, the ratio and configuration of which have not been determined.

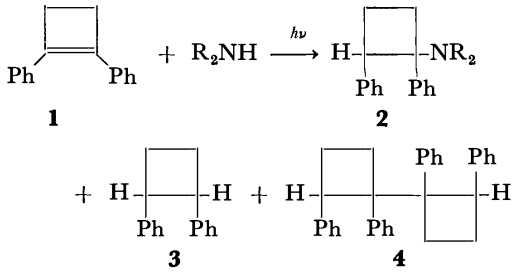

a : R=CH_3CH_2-
b : R_2=-$CH_2CH_2OCH_2CH_2$-

Similar irradiation of a solution of **1** (0.02 M) in a mixture of morpholine and hexane or benzene (1 : 4 by volume) afforded *N*-(1,2-diphenylcyclobutyl)morpholine (**2b**), **3**, and **4**. Small amounts of diphenylacetylene and 1,2,5,6-tetraphenyltricyclo[4.2.0.$0^{2,5}$]octane, the cleavage and dimerization products, respectively, were also obtained on irradiation in hexane.[7,9] The adduct, **2b**, displayed two four-proton triplets (δ 2.37 and 3.59, J=4.5 Hz) attributable to the ethylene groups in the morpholine moiety in the NMR spectrum. The gas chromatographic analysis showed that **2b** also consists of one isomer. The addition products, **2a** and **2b**, as well as aforementioned 1,2-diphenyl-1-methoxycyclobutane and 1,2-diphenylcyclobutyl acetate exhibited a multiplet or a broad

Table 2. Products from the irradiation of 1,2-diphenylcyclobutene and amines[a]

Amine (R_2NH)	Et_2NH	Et_2ND	O NH	
Solvent	Hexane	Hexane	Benzene	Hexane
Product (%)[b]				
Ph Ph R_2N-	26	17[c]	39	41
Ph Ph	25	12[d]	trace	6
Ph Ph Ph Ph	17	5[e]	40	8
PhC≡CPh				5
Ph Ph Ph Ph				6

a) In a mixture of an amine and a solvent (1 : 4 by volume). b) Yield based on the diphenylcyclobutene reacted. c) *N,N*-Diethyl-1,2-diphenylcyclobutanamine-2-*d*. d) 1,2-Diphenylcyclobutane-1-*d*. e) 1,1′,2,2′-Tetraphenylbicyclobutyl-2,2′-d_2.

triplet due to the methine proton at the same region (δ 3.7—4.2) as did *cis*-1,2-diphenylcyclobutane, while *trans*-1,2-diphenylcyclobutane displayed a multiplet at a somewhat higher field (δ 3.2—3.6).[6,10] Taking into account the small effect of the β-substituents on the chemical shift of a methine proton,[11] **2a** and **2b** can be safely assigned to *cis*-configuration. The results are summarized in Table 2. Although the UV spectra of the amines extend to longer wavelengths than 300 nm, their absorbances are very small in this region, more than 99.9% of the incident light being absorbed by **1**.

In order to clarify the origin of hydrogen atoms incorporated in the products, labeling experiments were undertaken using diethylamine-*N*-*d* as the additive. A solution of 1,2-diphenylcyclobutene (**1**) in a mixture of diethylamine-*N*-*d* and hexane (1 : 4 by volume) was irradiated similarly and the products were isolated in a way similar to that described above (Table 2). The NMR spectra of the products showed that a deuterium atom is incorporated in each cyclobutane ring of the product; 1,2-diphenylcyclobutane (**3-d**) undergoes deuteration at C-1, 1,1′,2,2′-tetraphenylbicyclobutyl (**4-d**) at C-2 and C-2′, and *N*,*N*-diethyl-1,2-diphenylcyclobutanamine (**2a-d**) at C-2. From these results it might be concluded that the photoreaction proceeds

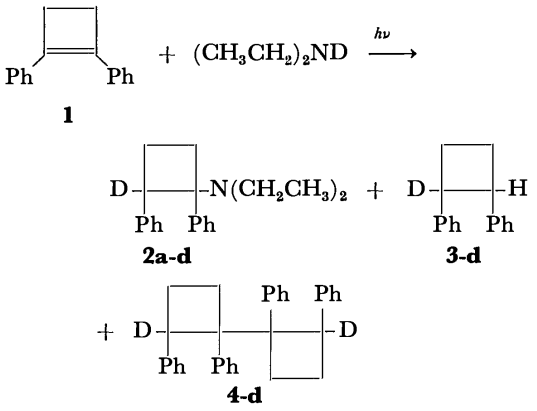

through an initial amino hydrogen transfer with the formation of diphenylcyclobutyl radicals (**7**), which in turn undergo four competing reactions: a) hydrogen atom abstraction from the solvent to afford **3**, b) dimerization affording **4**, c) recombination with the concurrently generated aminyl radicals to afford **2**, and d) disproportionation with the aminyl radicals which regenerates starting materials. The fact that only *cis*-isomer of **2** was produced supports the view that **2** arises from the combination of the diphenylcyclobutyl radical and the aminyl radical within the solvent cage in contrast to the out-of-cage formation of **3** and **4**.

The quantum yields of the reactions of **1** were measured in hexane under aerated conditions in the presence of various amounts of the amines by monitoring the decrease of the starting olefin on irradiation with 330±7-nm light. Although a linear relationship is found between the reciprocal of the quantum yield (Φ) for the decrease of the olefin and the reciprocal of the concentration of the amine, the intercept is not unity but 6.2 and 11 for diethylamine and morpholine, respectively. Since only bimolecular process need be considered upon extraporation to infinitely concentrated amine solution, these results indicate that there should be a bimolecular energy wastage step in the reaction. The following simplest mechanistic scheme accounts for all the above results.

$$\mathbf{1} + h\nu \longrightarrow \mathbf{1}^*$$

$$\mathbf{1}^* \xrightarrow{k_f} \mathbf{1} + h\nu'$$

$$\mathbf{1}^* + O_2 \xrightarrow{k_o} \mathbf{1} + O_2$$

$$\mathbf{1}^* + HNR_2 \xrightarrow{k_q} [\mathbf{1}\cdots HNR_2]^*$$

$$[\mathbf{1}\cdots HNR_2]^* \xrightarrow{k_d} \mathbf{1} + HNR_2$$

$$[\mathbf{1}\cdots HNR_2]^* \xrightarrow{k_r} \mathbf{7} + \cdot NR_2 \longrightarrow \text{products},$$

where **1*** denotes the excited singlet state of **1**, and [**1**···HNR_2]* the exciplex between **1** and the amine. At infinite dilution under degassed conditions the quantum yield for the fluorescence of **1** is unity[7] and therefore intersystem crossing to the triplet state can be neglected. Furthermore, the unimolecular reactions, ring fission giving diphenylacetylene and ethylene, and dimerization, are minor perturbations under the conditions

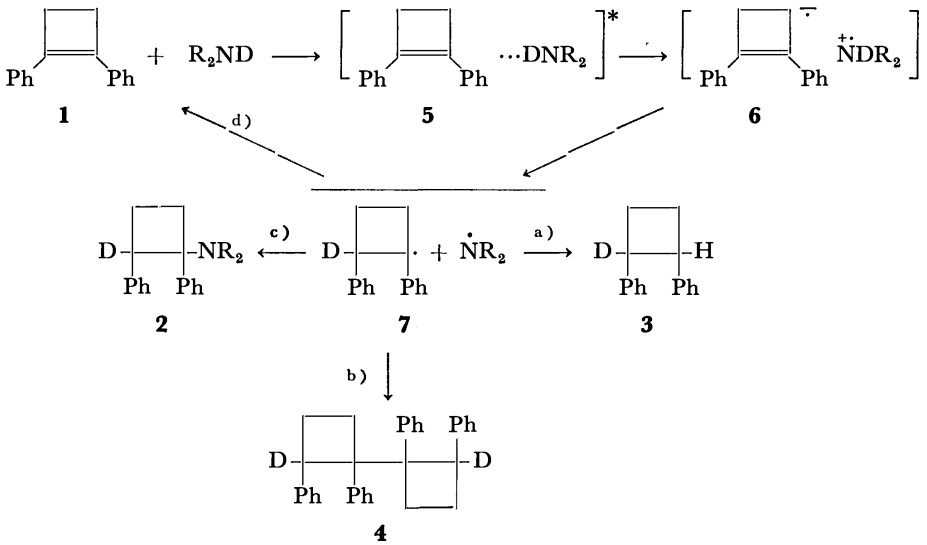

employed, and can be neglected. Thus, by adopting the usual steady-state assumption, the quantum yield for the decrease of **1** is written as follows:

$$1/\Phi = (1+k_d/k_r)(1+1/k_q\tau_0[HNR_2]).$$

The k_d/k_r values, *i.e.*, the ratio of rates for the decay process and the amino hydrogen transfer in the charge-transfer complex, can be estimated to be 5.2 for diethylamine and 10 for morpholine, and the $k_q\tau_0$ values, the quenching constants, are evaluated to be 3.0 M^{-1} for diethylamine and 2.2 M^{-1} for morpholine. These values are in good agreement with those obtained in the fluorescence quenching experiments: 3.1 M^{-1} for diethylamine and 2.2 M^{-1} for morpholine (Table 1). These results substantiate the above mechanism.

The present results together with those reported previously[6,10] show that 1,2-diphenylcyclobutene (**1**) reacts, in its excited singlet state, not only with alcohols and acetic acid by ionic process but with secondary amines by radical process through the charge-transfer complex, to give the addition products, respectively.

Experimental

The IR and UV spectra were recorded on a Hitachi EPI-G3 grating infrared spectrophotometer and a Hitachi EPS-3 recording spectrophotometer, respectively. The NMR spectra were recorded on a JEOL C-60HL NMR spectrometer. GLPC analysis was performed on a Hitachi 163 gas chromatograph equipped with a flame ionization detector. Fluorescence intensities were determined with a Hitachi MPF-2A fluorescence spectrophotometer.

Materials. 1,2-Diphenylcyclobutene was prepared according to the method of Dodson and Zielske.[12] Amines were purified by distillation or recrystallization. Special grade hexane and benzene were distilled prior to use.

Photoreaction of 1,2-Diphenylcyclobutene with Diethylamine. A solution of 1,2-diphenylcyclobutene (400 mg) in a mixture of diethylamine (35 ml) and hexane (140 ml) was irradiated for 50 h using a 500-W xenon lamp through a Corning 0—54 filter. This procedure was repeated five times. The reaction mixtures were combined, concentrated, and subjected to chromatography on silica gel affording four components. The first white solid (trace amounts) was found to be the starting diphenylcyclobutene by GLPC analysis. The second white crystalline solid (500 mg) was deduced to be 1,2-diphenylcyclobutane by comparing its NMR spectrum with that of an authentic specimen of *cis*-1,2-diphenylcyclobutane, prepared by catalytic reduction of 1,2-diphenylcyclobutene,[12] and the reported NMR data of *cis*- and *trans*-1,2-diphenylcyclobutane.[12] The diphenylcyclobutane obtained was found to be a *ca.* 2 : 1 mixture of *cis*- and *trans*-isomers from the NMR and GLPC data. Found: C, 92.28; H, 7.55%. Calcd for $C_{16}H_{16}$: C, 92.26; H, 7.74%.

The third white crystalline solid (340 mg) was 1,1′,2,2′-tetraphenylbicyclobutyl, the structure of which was established by the spectral data and elemental analysis. The NMR spectrum of the solid showed that it consists of more than two isomers. Recrystallization from ethanol gave a single isomer; mp 143—144 °C. NMR($CDCl_3$) δ 1.7—3.0 (m, 8H, CH_2CH_2), 4.54 (t, 2H, methine H), 6.0—7.2 (m, 20H, aromatic H). Mass spectrum (*m/e*) 414 (M^+). Found: C, 92.62; H, 7.37%. Calcd for $C_{32}H_{30}$: C, 92.71; H, 7.29%.

The fourth colorless liquid (700 mg) was *N,N*-diethyl-1,2-diphenylcyclobutanamine, the structure of which was established by the spectral data and elemental analysis. The GLPC analysis showed that it consists of one isomer. NMR($CDCl_3$) δ 1.03 (t, J=7 Hz, 6H, CH_3), 1.7—2.5 (m, 4H, CH_2CH_2), 2.55 (q, J=7 Hz, 4H, CH_2), 3.7—4.2 (m, 1H, methine H), 6.6—7.3 (m, 10H, aromatic H). Mass spectrum (*m/e*) 279 (M^+). Found: C, 85.97; H, 9.24; N, 5.02%. Calcd for $C_{20}H_{25}N$: C, 85.97; H, 9.02; N, 5.01%.

Photoreaction of 1,2-Diphenylcyclobutene with Morpholine. A solution of 1,2-diphenylcyclobutene (1 g) in a mixture of morpholine (40 ml) and benzene (160 ml) was irradiated similarly for 110 h. The reaction mixture was separated similarly, affording the starting olefin (290 mg), 1,2-diphenylcyclobutane (trace amounts), 1,1′,2,2′-tetraphenylbicyclobutyl (280 mg), and *N*-(1,2-diphenylcyclobutyl)morpholine (395 mg). The structure of the last product was established by the spectral data and elemental analysis. The GLPC analysis showed that the adduct consists of one isomer. NMR($CDCl_3$) δ 1.7—2.7 (m, 4H, CH_2CH_2 of cyclobutane), 2.37 (t, J= 4.5 Hz, 4H, NCH_2), 3.59 (t, J=4.5 Hz, 4H, OCH_2), 3.90 (t, J=7.5 Hz, 1H, methine H), 6.5—7.1 (m, 10H, aromatic H). Found: C, 82.01; H, 7.85; N, 4.74%. Calcd for $C_{20}H_{23}NO$: C, 81.87; H, 7.90; N, 4.77%.

A solution of 1,2-diphenylcyclobutene (450 mg) in a mixture of morpholine (40 ml) and hexane (160 ml) was irradiated similarly for 110 h. The products separated similarly on silica gel were *N*-(1,2-diphenylcyclobutyl)morpholine (260 mg), diphenylacetylene (20 mg), 1,2-diphenylcyclobutane (25 mg), 1,1′,2,2′-tetraphenylbicyclobutyl (35 mg), and 1,2,5,6-tetraphenyltricyclo[4.2.0.$0^{2,5}$]octane (25 mg).[7,9]

Photoreaction of 1,2-Diphenylcyclobutene with Diethylamine-N-d. A solution of 1,2-diphenylcyclobutene (1.5 g) in a mixture of diethylamine-*N-d* (40 ml) and hexane (160 ml) was irradiated similarly for 150 h. The chromatographic separation of the reaction mixture gave the starting olefin (190 mg), 1,2-diphenylcyclobutane-1-*d* (160 mg), 1,1′,2,2′-tetraphenylbicyclobutyl-2,2′-d_2 (70 mg), 1,2,5,6-tetraphenyltricyclo[4.2.0.$0^{2,5}$]-octane (160 mg), and *N,N*-diethyl-1,2-diphenylcyclobutanamine-2-*d* (300 mg). The position of deuteration in each product was determined by comparing its NMR spectrum with that for the corresponding non-deuterated product.

Quantum-Yield Measurements. The exciting light for the quantum-yield measurement was furnished by a JASCO CRM-FA spectroirradiator equipped with a 2-kW xenon lamp as the light source and a grating monochromator. The light intensity was measured by potassium ferrioxalate actinometry. Hexane solutions of 1,2-diphenylcyclobutene (10^{-3} M) and amine (0—1 M) were irradiated with 330±7-nm light for 3 min. The reaction mixture was diluted 20 times with the same solvent and its UV spectrum was measured.

References

1) See for example; A. Lablache-Combier, *Bull. Soc. Chim. Fr.*, **1972**, 4791.

2) R. C. Cookson, S. M. de B. Costa, and J. Hudec, *Chem. Commun.*, **1969**, 753.

3) M. Bellas, D. Bryce-Smith, and A. Gilbert, *Chem. Commun.*, **1967**, 862.

4) M. Yoshida, H. Kaneko, A. Kitamura, T. Ito, K. Oohashi, N. Morikawa, H. Sakuragi, and K. Tokumaru, *Bull. Chem. Soc. Jpn.*, **49**, 1697 (1976).

5) P. Grandclaudon and A. Lablache-Combier, *Chem. Commun.*, **1971**, 892.

6) M. Sakuragi and M. Hasegawa, *Chem. Lett.*, **1974**, 29.

7) C. D. DeBoer and R. H. Schlessinger, *J. Am. Chem. Soc.*, **90**, 803 (1968).

8) T. R. Evans, *J. Am. Chem. Soc.*, **93**, 2081 (1971); D. A. Labianca, G. N. Taylor, and G. S. Hammond, *ibid.*, **94**, 3679 (1972).
9) E. H. White and J. P. Anhalt, *Tetrahedron Lett.*, **1965**, 3937.
10) M. Sakuragi, H. Sakuragi, and M. Hasegawa, *Bull. Chem. Soc. Jpn.*, **50**, 1562 (1977).
11) L. M. Jackman and S. Sternhell, "Applications of Nuclear Magnetic Resonance Spectroscopy in Organic Chemistry," 2nd ed, Pergamon Press, London (1969), p. 159; S. L. Murov, "Handbook of Photochemistry," Marcel Dekker, Inc., New York, N. Y. (1973), p. 179.
12) R. M. Dodson and A. G. Zielske, *J. Org. Chem.*, **32**, 28 (1967).

Intrachain Charge-Transfer Complex in Ethanol Solution on a Polysarcosine Chain Having a Terminal Electron Donor and a Terminal Electron Acceptor Groups*

Hiroaki TAKAGI, Masahiko SISIDO,† Yukio IMANISHI, and Toshinobu HIGASHIMURA

Department of Polymer Chemistry, Kyoto University, Kyoto 606

(Received December 16, 1976)

Polysarcosine having a terminal electron donating group (*p*-dimethylaminoanilide group) and a terminal electron accepting group (3,5-dinitrobenzoyl group) was synthesized. An ethanol solution of the polymer showed a distinct charge-transfer absorption band around 435 nm. With use of the extinction coefficient determined for the low-molecular-weight model compounds, the fraction of polymers forming an intrachain complex was evaluated to be about 0.08 for $\bar{n}=6$ ($\bar{n}$ is the degree of polymerization of the polysarcosine chain). The fraction decreased with rise in temperature and increase in chain length. The fraction experimentally observed was considerably larger than that estimated from the Monte Carlo calculation on polysarcosine chain, indicating that the cyclic conformations are greatly stabilized by the intrachain charge-transfer interaction. Thermodynamic parameters were determined for the intrachain complex. The chain length dependence of the parameters in ethanol was the opposite of that obtained previously in a chloroform solution. The difference was explained in terms of the difference of the conformations of polysarcosine chain in chloroform and in ethanol solutions. This was evidenced by the NMR spectra recorded in the solvents.

The intrachain reaction between a pair of terminal groups (X and Y) attached on a polymer chain is affected by the conformational properties of the connecting polymer chain in solution.[1-9] For the reaction with a moderately high activation energy, the intrachain reaction is determined by the equilibrium conformational property, *i.e.*, the probability that a pair of reactive groups approach within a short distance capable of the reaction.[2,5,8,10] The conformational equilibrium would depend not only on external factors such as temperature, solvent, *etc.*, but also on internal factors such as intrachain interactions. If a stabilizing force operates between X and Y, the fraction of cyclic conformations would increase considerably, strongly enhancing the intrachain reaction or intrachain interaction. In this respect, protein molecules are regarded as a limiting case, in which various types of intramolecular interactions operate to stabilize the three-dimensional structures in solution.

The results of a study on the hydrolysis of a *p*-nitrophenoxycarbonyl group catalyzed intramolecularly by a pyridyl group attached to the same polysarcosine chain were found to be in line with the ring-closure probability calculated by the Monte Carlo method taking no intrachain force into account.[2] This indicates that intrachain force virtually does not participate in the above system. On the other hand, when electron-donating and electron-accepting groups are attached to respective ends of a polysarcosine chain, a relatively weak intrachain charge-transfer interaction greatly increases the fraction of cyclic conformations in a chloroform solution.[3] This prompted us to investigate the above system in more detail, the present experiment being carried out with an ethanol solution. Since the conformation of polysarcosine has been found to show a marked solvent dependence,[11-13] it was expected to clarify the effct of polymer conformation upon the intrachain interaction.

* Intrachain Reaction of a Pair Reactive Groups Attached to Polymer Ends. Part IV.

† The author to whom correspondence should be addressed.

Experimental

Polymer samples were synthesized by the polymerization of sarcosine *N*-carboxyanhydride (NCA) with sarcosine *p*-dimethylaminoanilide as an initiator. After complete polymerization, 3,5-dinitrobenzoyl chloride was added to incorporate an electron-accepting group into the other end of the polymer chain. The average degree of polymerization $\bar{n}$ was calculated by Eq. 1,[14] the results agreeing with those determined by vapor pressure osmometry.

$$\bar{n} = [\text{NCA}]/[\text{initiator}] + 1 \qquad (1)$$

A Poisson type distribution of the degree of polymerization was expected.[14] This was confirmed with polysarcosines obtained with use of sarcosine dimethylamide as an initiator.[15] Details of the synthesis of other compounds and the characterization of polymer samples have been reported.[3] Ethanol used for the optical measurement was fractionally distilled from magnesium metal. 220-MHz NMR spectra were obtained with a Varian HR-220 instrument.

Results and Discussion

Intermolecualr Charge-Transfer Complex between Model Compounds. First, the nature of charge-transfer complex in an ethanol solution was examined with model compounds for the terminal electron-donating and electron-accepting groups. The absorption spectrum of the mixture of *N*-acetyl-*N'*,*N'*-dimethyl-*p*-phenylenediamine (I) and *N*-(3,5-dinitrobenzoyl)-sarcosine dimethylamide (II) in ethanol is shown in Fig. 1.

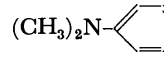

(I)

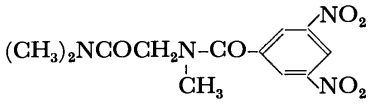

(II)

The spectrum shows a typical charge-transfer band around 430 nm, where virtually no absorption was observed for the component species. No spectral change was detected at least for five days, indicating the chemical stability of the charge-transfer complex in the ethanol solution. The plots of the absorbance

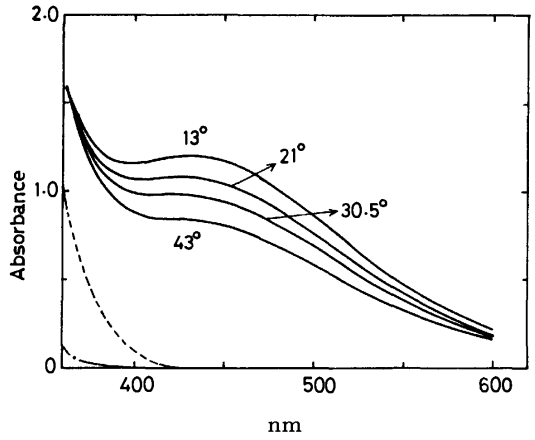

Fig. 1. Absorption spectra of a mixture of the model compounds I and II in ethanol solution at four different temperatures. $[I]=7.3\times10^{-3}$, $[II]=3.7\times10^{-1}$ M. (—·—): The spectrum of I, $[I]=7.3\times10^{-3}$ M, (----): The spectrum of II, $[II]=3.7\times10^{-1}$ M, cell length=1.0 cm.

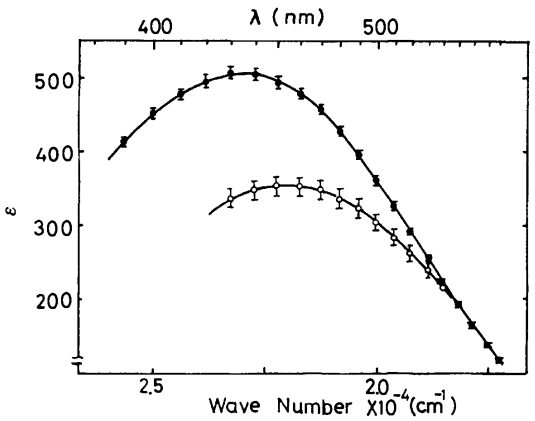

Fig. 2. Extinction coefficient for the charge-transfer complex between I and II in ethanol solution at 13 °C (-●-) and in chloroform solution at 10 °C (-○-) Vertical bars represent the standard errors in non-linear least squares calculation.

at 450, 500, and 550 nm were made as functions of the mole fraction of I, the total concentration of I and II being kept constant. The intensity was strongest at an equimolar concentration of I and II, showing that the composition of the charge-transfer complex was 1 : 1.

The association constant K_2 and the extinction coefficient ε_i at each wavelength for the complex were calculated by the non-linear least squares method.[16] 210 absorption values for 10 different pairs of concentrations and 21 different wavelengths in the range 380—580 nm were used for the calculation. The measurements were made at four temperatures and the least squares calculations were carried out independently at each temperature. The initial set of K_2 and ε_i's for the iterative calculation was obtained from the Benesi-Hildebrand plot.[17] The results are given in Table 1 and the extinction coefficients are plotted in Fig. 2 as a function of the wave number. The extinction coefficient showed virtually no temperature dependence in

TABLE 1. ASSOCIATION CONSTANT AND EXTINCTION COEFFICIENT FOR THE CHARGE-TRANSFER COMPLEX BETWEEN MODEL COMPOUNDS I AND II IN ETHANOL SOLUTION

Temp (°C)	K_2 (M^{-1})	ε_{450}
13.0	1.14±0.01[a]	494±8[a]
21.0	1.01±0.02	494±7
30.5	0.89±0.02	496±6
43.0	0.73±0.04	497±6

$\Delta H_2 = -11.3$ kJ mol^{-1}, $\Delta S_2 = -38.4$ J mol^{-1} K^{-1}

a) Standard errors obtained in non-linear least squares calculation.

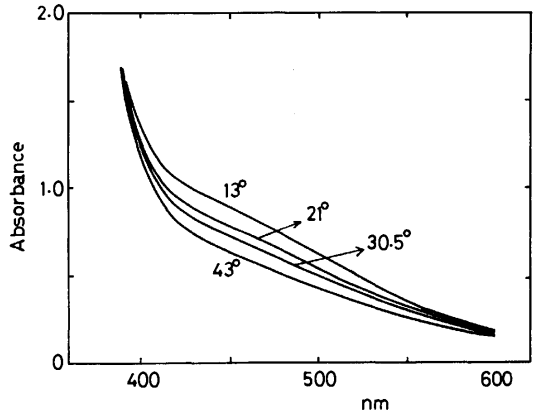

Fig. 3. Absorption spectra of the polymer sample III in ethanol solution at four different temperatures, $c_0=6.5\times1^{-3}$ M, $\bar{n}=16$, Cell length=5.0 cm.

the range 13—43 °C. Figure 2 also shows the extinction coefficients in a chloroform solution. The absorption maximum lies at about 435 nm and at 455 nm in ethanol and chloroform solutions, respectively. The hypsochromic shift of the charge-transfer band caused by a strongly solvating solvent, such as alcohol, has been explained in terms of the specific solvation in the ground state of the component species.[19] The association constant determined in an ethanol solution was nearly equal to that in a chloroform solution.[3]

The plot of log K_2 against $1/T$ gave a straight line. The thermodynamic parameters ΔH_2 and ΔS_2 were evaluated (Table 1). Although the values of K_2 were almost the same in both solvents, the thermodynamic parameters in the ethanol solution were substantially different from those in the chloroform solution ($\Delta H_2 = -5.86$ kJ mol^{-1}, $\Delta S_2 = -20.4$ J mol^{-1}K^{-1}).[3]

Intrachain Charge-Transfer Complex on Polysarcosine Chain. Figure 3 shows the absorption spectrum of polysarcosine having a terminal *p*-dimethylaminoanilide group and a terminal 3,5-dinitrobenzoyl group (III). Although

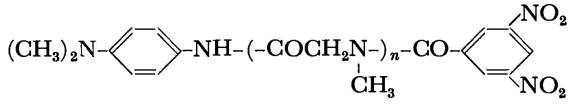

(III)

the polymer concentration is too low to form a measurable amount of *inter*-molecular charge-transfer complex, the spectrum of III shows a considerable intensity

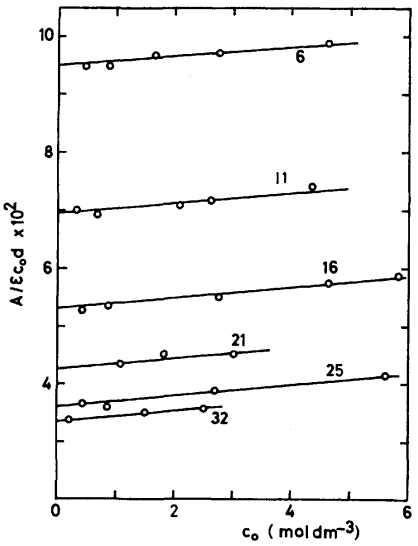

Fig. 4. Plots of $A/\varepsilon c_0 d$ against c_0 for six different degrees of polymerization at 13 °C. Solid lines were drawn with a theoretical slope evaluated according to Eq. 2.

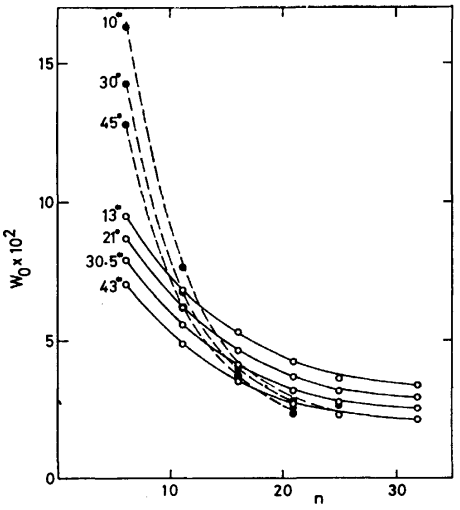

Fig. 5. Dependence of the fraction of polymers forming intraction complex upon the chain length in ethanol solution (—○—), and in chloroform solution (—●—).

around the charge-transfer band. This indicates the formation of an intrachain charge-transfer complex and its predominance over the intermolecular complex. The plot of the absorbance A at 450 nm against the polymer concentration c_0 shows an upward deviation from a straight line, indicating an increased contribution of the intermolecular complex at higher concentrations. In order to separate the contribution of the intrachain complex from that of the intermolecular one, $A/\varepsilon c_0 d$ was plotted against c_0, where ε is the extinction coefficient at 450 nm and d is the cell length (Fig. 4). The intercept gives the fraction of polymers forming intrachain complex at infinite dilution W_0, the slope being proportional to the association constant K_2 for the intermolecular complex between polymer ends (see Appendix).

$$A/\varepsilon c_0 d = W_0 + K_2(1-2W_0)(1-W_0)^2 c_0 + \cdots \quad (2)$$

In Eq. 2 the extinction coefficient for the intrachain complex and that for the intermolecular complex between polymer ends are assumed to be identical with that for the intermolecular complex between the model compounds (Table 1). Figure 4 shows typical plots for different chain lengths at 13 °C, The slope is in good agreement with the calculated value using the association constant between model compounds. This shows that the stability of intermolecular charge-transfer complex between polymer ends is almost the same as that between model compounds, irrespective of the chain length.

The plots was made for six different chain lengths and at four different temperatures, values for W_0 being obtained under various conditions. The results are plotted in Fig. 5 together with the data obtained in a chloroform solution.[3] W_0 increases with decrease in chain length and also temperature. The dependence of W_0 on the chain length is more marked in a chloroform solution, while that on temperature is more marked in an ethanol solution. The values of W_0 in either solution do not differ a great deal. They are 20—100 times as larger as those expected for "unperturbed" chains free from any interachain force. The unperturbed values have been estimated from the rate constants of intramolecularly catalyzed hydrolysis on polysarcosine chain[1] and from the Monte Carlo calculation of randomly coiled polysarcosine chain.[2] The larger values of W_0 indicate that the cyclic conformations are greatly stabilized by the intrachain force based upon the charge-transfer interaction between a pair of terminal groups.

Evaluation of the extent of the stabilization of cyclic conformations made previously[3] was applied to the present case. The free energy of the electronic stabilization in the intramolecular charge-transfer complex ΔG_e was estimated from the thermodynamic parameters of model compounds (Table 1).

$$\begin{aligned} \Delta H_e &= \Delta H_2 = -11.3 \text{ kJ mol}^{-1}, \\ \Delta S_e &= \Delta S_2 - \Delta S_b = -38.4 - (-15.1) \\ &= -23.3 \text{ J mol}^{-1}\text{K}^{-1}, \\ \Delta G_e &= \Delta H_e - T\Delta S_e = -4.23 \text{ kJ mol}^{-1} \ (30.5°\text{C}). \end{aligned} \quad (3)$$

In the second equation the entropy for the bimolecular encounter $S_b = -15.1$ J mol^{-1}K^{-1} was subtracted from the total entropy for the model compounds.[1,3] The association constant for the intrachain complex K_1 is related to W_0 as

$$K_1 = W_0/(1-W_0). \quad (4)$$

K_1 should be related to the association constant K_1^0 for the cyclization of a polymer chain which is free from intrachain interaction, according to the equation

$$K_1 = K_1^0 \exp(-\Delta G_e/RT). \quad (5)$$

The "unperturbed" value of the association constant K_1^0 was evaluated from the rate constant of intramolecularly catalyzed hydrolysis on polysarcosine chain in aqueous solution[1] (Table 2). The value of K_1 calculated by Eq. 5 is compared with that evaluated from the observed value of W_0 (Eq. 4, Table 2). Although the increase in the K_1 value by the electronic stabilization is definite, the calculated value of K_1 is still smaller than the observed one.

TABLE 2. ASSOCIATION CONSTANT FOR THE INTRACHAIN INTERACTION BETWEEN A PAIR OF TERMINAL GROUPS ATTACHED TO POLYSARCOSINE CHAIN

Degree of polymerization	$K_1^0 \times 10^2$ a)	$K_{1,\mathrm{calcd}} \times 10^2$ b)	$K_{1,\mathrm{obsd}} \times 10^2$ c)
5	0.38	2.0	
6			8.6
7	0.37	2.0	
10	0.31	1.7	
11			5.79
12	0.28	1.5	
15	0.23	1.2	
16			4.3
20	0.16	0.86	
21			3.3
25	0.11	0.60	2.9
30	0.098	0.53	
32			2.6
35	0.077	0.41	

a) The "unperturbed" value evaluated from intramolecularly catalyzed hydrolysis on polysarcosine chain in aqueous solution at 35 °C.[1] b) Calculated by mean of Eq. 5 for 30.5 °C. c) Observed with the intrachain charge-transfer complex on polysarcosine chain in an ethanol solution at 30.5 °C.

Thermodynamic Parameters for Intrachain Complex.
The plot of log K_1 against $1/T$ is linear. Thermodynamic parameters ΔH_1 and ΔS_1 were calculated from the slope and the intercept, respectively. They consist of two terms, one associated with the conformational change for the cyclization (ΔH_c or ΔS_c) and the other for the electronic change (ΔH_e or ΔS_e).

$$\Delta H_1 = \Delta H_c + \Delta H_e, \quad \Delta S_1 = \Delta S_c + \Delta S_e. \tag{6}$$

The values of ΔH_e and ΔS_e estimated in the preceding section were used for calculating ΔH_c and $-T\Delta S_c$ (T=298 K). The results are plotted in Fig. 6 as functions of chain length. In an ethanol solution the enthalpy required for the conformational change decreases slightly and the value of $-T\Delta S_c$ increases with increasing chain length. The results are in contrast to those obtained with a chloroform solution where ΔH_c increases with increase in chain length; $-T\Delta S_c$ remaining nearly constant.[3] The latter situation has been observed also in the activation parameters for conformational change accompanied by the intramolecularly catalyzed hydrolysis on polysarcosine chain in aqueous solution.[1] However, the present result is consistent with the result obtained from the Monte Carlo calculation.[2] In the Monte Carlo calculation in which no conformational energy is taken into account, the fraction of cyclic conformations decrease with increase in chain length except for very short chains. This indicates that ΔS_c decreases with increase in chain length whereas ΔH_c is zero irrespective of the chain length.

In view of these results, the experimental finding can be interpreted as follows. In an ethanol solution ΔH_c is nearly zero irrespective of the chain length. In this case, the conformational energy can be neglected in the Monte Carlo calculation. The observed chain length dependence of ΔS_c is in reasonable accordance with the

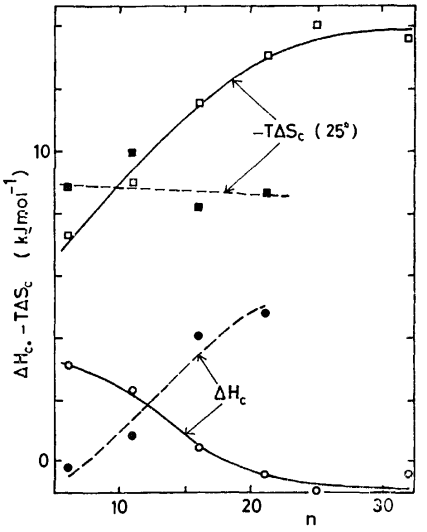

Fig. 6. Dependence of the thermodynamic parameters upon the chain length in ethanol solution (—○—, —□—) and in chloroform solution (--●--, --■--).

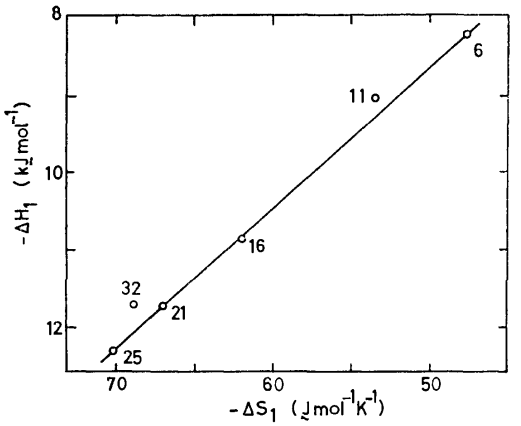

Fig. 7. Correlation between the thermodynamic parameters for the intrachain charge-transfer complex. Numbers in the Figure indicate degree of polymerization.

calculated one. On the other hand, ΔH_c in a chloroform solution or ΔH_c^* in aqueous solution increases considerably with increase in chain length and becomes the dominant factor to determine the chain length dependence of the intrachain association constant or intrachain rate constant. Thus the results of the Monte Carlo calculation, in which no conformational energy has been taken into account, cannot be compared with the experimental data obtained in these solvents. The difference in thermodynamic parameters may be accounted for by the difference in the polymer conformations in the three solvents.

Figure 7 shows the plot of ΔH_1 against ΔS_1 obtained for six different chain lengths. The plot lies on a straight line with a slope of —93 °C. This suggests that the chain length dependence of K_1 vanishes at —93 °C and K_1 increases with increase in chain length below —93 °C. However, this has not been observed because of experimental difficulties.

It is interesting to compare the present result with

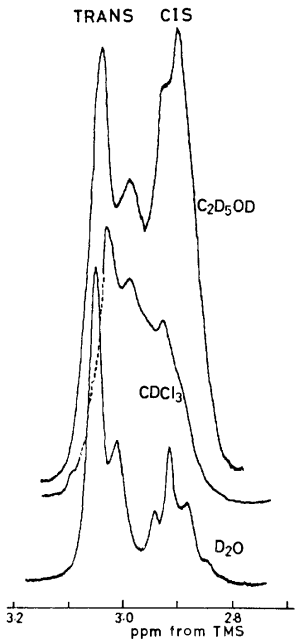

Fig. 8. Partial 220 MHz NMR spectra of polysarcosine in three different solvents. (Only the region of the main chain *N*-methyl protons is shown.) Polymer concentration=*ca.* 10 w/v%.

that obtained in the intramolecularly catalyzed hydrolysis in aqueous solution.[1] In the latter case, the conformational activation enthalpy ΔH_c^* shows a linear relation to the conformational activatioon entropy ΔS_c^*, giving an isokinetic temperature of +93 °C. The temperature should coincide with that in the present experiment (−93 °C), if the conformational properties of polysarcosine chain were the same in both ethanol and aqueous solutions. It should be emphasized that in either case, a mechanism operates to compensate the loss of conformational entropy associated with the cyclization by the decrease in conformational enthalpy, or *vice versa*. If this is the case, the isokinetic or isothermodynamic temperature can be a parameter characterizing a thermodynamic property of polymer conformations in solution. By utilizing the compensation relation, it will be possible to control the intrachain reaction proceeding on a polymer chain by varying the temperature.

Conformation of Polysarcosine Chain in Ethanol, Chloroform, and Aqueous Solution. It was suggested that the conformation of polysarcosine chain in chloroform and aqueous solutions differs a great deal from that in an ethanol solution. The conformation of polysarcosine chains in these solvents was studied by 220-MHz NMR spectroscopy. Figure 8 shows the *N*-methyl region of the NMR spectra. The absorption bands split into several peaks due to the distribution of *trans* and *cis* amide links along the main chain. A peak assignment has been made.[12] The lowest-field peak is ascribed to *trans-trans* and the second lowest to *trans-cis* dyad sequence. These two peaks in lower field correspond to a *trans* conformation. The remaining peaks in higher field correspond to a *cis* conformation. It is evident that the fraction of *cis* conformation in ethanol is considerably larger than that in the other two solvents. This relation holds for other chain lengths except for very short chains.[13]

The NMR data indicate that the conformation of polysarcosine chain in an ethanol solution differs from that in chloroform and aqueous solutions. This is in line with the result of thermodynamic parameters *i.e.*, the dependence of thermodynamic perameters on the chain length in ethanol differs from that in the other two solvents. In an ethanol solution the stability of the *cis* conformation is nearly the same as that of *trans*. Hence, virtually no conformational energy is required to attain the cyclic conformations in which *cis* bond is preferred to *trans* (Fig. 6).[13] For short polysarcosine chains ($\bar{n} \lesssim 10$), the fraction of *cis* conformation has been found to decrease with decrease in chain length.[13] The reduced stability of *cis* conformation may explain the higher conformational enthalpy observed for shorter chains. At present, however, a correspondence between NMR data and thermodynamic parameters is not clear in chloroform and aqueous solutions.

Appendix

In a solution containing X—Y-type polymers a series of linear polymers such as X—Y, X—YX—Y, *etc.* and series of cyclic polymers such as X—Y, X—YX—Y, *etc.* should be relevant to present treatment. The problem is much simplified if participation of the species beyond linear "trimer" and cyclic "dimer" is neglected at a low feed concentration of the linear "monomer" X—Y. If we denote [X—Y]=c, [X—Y]=c_1, [X—YX—Y]=c_2, and the total feed concentration of X—Y=c_0, the association constant for the intrachain complex, K_1 and that for the intermolecular complex, K_2 are expressed as

$$K_1 = c_1/c, \tag{A.1}$$

$$K_2 = c_2/c^2, \tag{A.2}$$

with

$$c_0 = c + c_1 + 2c_2. \tag{A.3}$$

The absorbance at 450 nm is expressed as

$$A = \varepsilon d(c_1 + c_2), \tag{A.4}$$

where ε is the extinction coefficient and d is the cell length. Using the above equations, A is expressed as a function of c_0 as

$$A = \varepsilon d\left\{\left(\frac{K_1}{1+K_1}\right)c_0 + K_2\left[\frac{1}{(1+K_1)^2} - \frac{2K_1}{(1+K_1)^3}\right] + \cdots\right\}, \tag{A.5}$$

where terms up to c_0^2 are retained. Equation 2 is obtained by substituting K_1 for $W_0 = K_1/(1+K_1)$.

References

1) M. Sisido, T. Mitamura, Y. Imanishi, and T. Higashimura, *Macromolecules*, **9**, 316 (1976).
2) M. Sisido, Y. Imanishi, and T. Higashimura, *Macromolecules*, **9**, 320 (1976).
3) M. Sisido, H. Takagi, Y. Imanishi, and T. Higashimura, *Macromolecules*, **10**, 125 (1977).
4) M. Stoll and A. Rouve, *Helv. Chim. Acta*, **18**, 1087 (1935).

5) M. Sisido, *Macromolecules*, **4**, 737 (1971).
6) H. Morawetz and N. Goodman, *Macromolecules*, **3**, 699 (1970).
7) R. Breslow, *Chem. Soc. Rev.*, **1**, 553 (1972).
8) M. A. Winnik, R. E. Trueman, G. Jackowski, D. S. Saunders, and S. G. Whittington, *J. Am. Chem. Soc.*, **96**, 4843 (1974).
9) K. Shimada, Y. Shimozato, and M. Szwarc, *J. Am. Chem. Soc.*, **97**, 5834 (1975) and preceding papers.
10) N. Goodman and H. Morawetz, *J. Polym. Sci., Part C*, **31**, 177 (1970).
11) F. A. Bovey, J. J. Ryan, and F. P. Hood, *Macromolecues*, **1**, 305 (1968).
12) M. Sisido, Y. Imanishi, and T. Higashimura, *Biopolymers*, **11**, 399 (1972).
13) M. Sisido, Y. Imanishi, and T. Higashimura, *Macromolecules*, **9**, 389 (1976).
14) C. H. Bamford, A. Elliott, and W. E. Hanby, "Sythetic Polypeptides," Academic Press, New York (1956), Chap. 3.
15) M. Sisido, Y. Imanishi, and T. Higashimura, Abstr. No. 3P21, 34th National Meeting of the Chemical Society of Japan, Tokyo, April 1976.
16) W. E. Wentworth, W. Hirsch, and E. Chen, *J. Phys. Chem.*, **71**, 218 (1967).
17) H. A. Benesi and J. H. Hildebrand, *J. Am. Chem. Soc.*, **71**, 2703 (1949).
18) R. Foster, "Organic Charge-Transfer Complexes," Academic Press, London (1969), p. 64.

The Structure of Ikarugamycin, an Acyltetramic Acid Antibiotic Possessing a Unique *as*-Hydrindacene Skeleton[1)]

Shosuke Ito and Yoshimasa Hirata

Department of Chemistry, Faculty of Science, Nagoya University, Chikusa-ku, Nagoya 464

(Received December 25, 1976)

The structure and configuration of an antibiotic, ikarugamycin, have been established to be **1e** on the basis of chemical reactions, especially of oxidative degradation. It is suggested that the *as*-hydrindacene skeleton arises biogenetically *via* an intramolecular Diels-Alder reaction.

A new antibiotic, ikarugamycin ($C_{29}H_{38}N_2O_4$), possessing specific antiprotozoal activity has been isolated from the culture broth of *Streptomyces phaeochromogenes var. ikaruganensis* Sakai by Jomom *et al.*[2)] In this paper, we wish to describe evidence for assigning structure **1e** to ikarugamycin. A biogenesis of this antibiotic is also proposed.

Chromophoric Part of Ikarugamycin. On catalytic hydrogenation over PtO_2 for 1 h, ikarugamycin (**1**) absorbed 3 mol of hydrogen giving hexahydroikarugamycin (**2**), $C_{29}H_{44}N_2O_4$. The presence of three disubstituted double bonds in **1** was revealed by PMR spectrometry (Fig. 1). The double bond bearing strongly deshielded H_a and H_b protons (δ 6.96 and 6.64, respectively, in DMSO-d_6) must be trans substituted (J= 15.6 Hz). The other two pairs of olefinic protons (δ 5.6—6.2 in DMSO-d_6) should be attached to cis double bonds; although the H_d proton signal is obscured by those of the H_e and H_f protons, its counterpart, the H_c proton signal appears as a broad doublet with J= 12 Hz,[3)] and the H_e and H_f protons are observed as a broad AB quartet with J=10 Hz. The PMR spectrum of the hexahydro derivative (**2**) exhibited no signals for the olefinic protons.

The presence of an enolized β-tricarbonyl grouping in both **1** and **2** was suggested by an orange-red coloration with ferric chloride and the formation of greenish

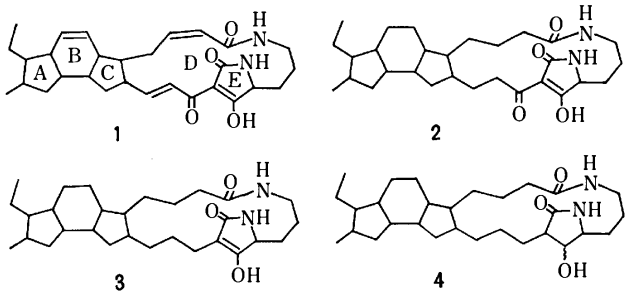

copper complexes, as well as by the formation of an *N*-methylpyrazole derivative upon heating with methylhydrazine. Further catalytic hydrogenation of **2** over PtO_2 for 24 h resulted in conversion of one of the carbonyl groups into a methylene group[4)] giving deoxooctahydroikarugamycin (**3**), $C_{29}H_{46}N_2O_3$. The UV maximum for the compound displayed a bathochromic shift of 33 nm upon the addition of an alkali (Table 1). The PMR spectrum showed a signal at δ 10.32 attributable to an enol proton. These data, coupled with a pK_a value of 7.8 and the formation of an enol ether, as well as of an enol acetate, indicates that an enolized β-dicarbonyl group is present in **3**.

Upon reduction with $LiBH_4$, **3** was readily converted to deoxodecahydroikarugamycin (**4**), $C_{29}H_{48}N_2O_3$ (probably a mixture of epimers) which could also be formed

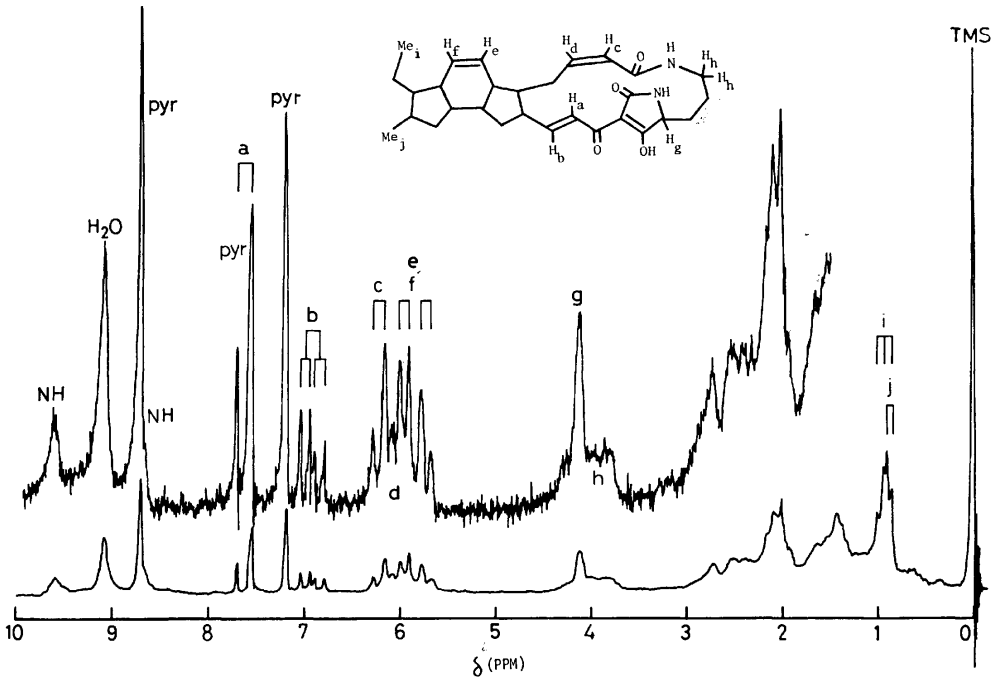

Fig. 1. The 100 MHz PMR spectrum of ikarugamycin (**1**) in pyr-d_5.

Table 1. UV spectra of ikarugamycin, its derivatives and related compounds

	λ_{max} (ε)	Solvent
Ikarugamycin (**1**)	227 (20700), 327 (17300)	MeOH
	243 (21400), 321 (13300)	0.1 M NaOH-MeOH
Hexahydroikarugamycin (**2**)	220 (5000), 280 (12400)	MeOH
	243 (10300), 279 (13600)	0.1 M NaOH-MeOH
Deoxooctahydroikarugamycin (**3**)	220 (6100), 240^{sh} (4600)	MeOH
	222 (3200), 273 (9300)	0.1 M NaOH-MeOH
Deoxodecahydroikarugamycin (**4**)	211 (910)	MeOH
Tenuazoic acid (**10**)[8]	217 (5100), 277 (12900)	EtOH
	239 (9600), 279 (12000)	0.1 M NaOH
Decahydroerythroskyrine[9]	225 (7200), 284 (12900)	EtOH
	246 (14100), 288 (14100)	0.1 M NaOH

directly from **2** under more drastic conditions. That **4** no longer contains the β-dicarbonyl group is evident from its UV spectrum (Table 1) and the formation of an acetate.

In the PMR spectra of **1** to **4**, two 1H broad singlets were always observed in the range of δ 6—9, which disappeared upon the addition of deuterium oxide. This indicates the presence of two secondary amide groups in **1** to **4**, which is further supported by the IR spectrum of **4** showing, in addition to amide NH (3430 cm^{-1}) and amide II (1520 cm^{-1}) bands, two amide carbonyl bands at 1695 and 1655 cm^{-1}. All of the oxygen and nitrogen atoms present in **1** can thus be assigned to a β-tricarbonyl system in which one of the carbonyl groups is involved as an amide carbonyl group, and to an additional amide group.

The relative position of the two amide nitrogen atoms was then established by ozonolysis of **1**. Thus, ether extraction of the oxidation mixture yielded a carboxylic acid which was isolated as bicyclic tetramethyl ester **5**, $C_{14}H_{22}$ $(CO_2Me)_4$, and the water-soluble part gave, after acid hydrolysis, L-ornithine and oxalic acid. These results led to the formulation of the chromophoric part of ikarugamycin as **1a**; in order to account for the formation of **5**, as well as the shift of a UV absorption maximum from 327 nm for **1** to 280 nm for **2** (Table 1), two double bonds should be located at the positions shown in **1a**.

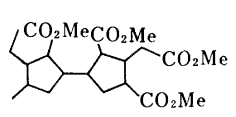

5

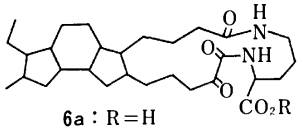

6a : R=H
6b : R=Me

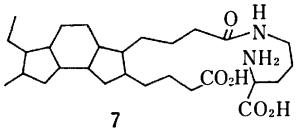

7

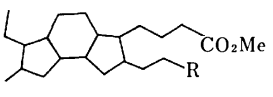

8 : R=CH_2CO_2Me
11 : R=CO_2Me

In principle, an alternative structure **1b** is also consistent with these chemical data. However, such a possibility can be ruled out by the formation of α-DNP-ornithine[5] from **3** *via* **6** and **7**. Chromic acid oxidation of **3** resulted in cleavage of the enolic double bond to give the keto acid **6a**, $C_{29}H_{46}N_2O_5$ and similarly, permanganate oxidation of the enol ether of **3** afforded the corresponding keto ester **6b**, $C_{30}H_{48}N_2O_5$. Treatment of **6a** or **6b** with alkaline hydrogen peroxide cleaved the α-keto amide group, giving an amino acid, **7**, which was characterized as its *N*-acetyl dimethyl ester. Acid hydrolysis of the DNP derivative of **7** gave α-DNP-ornithine and a carboxylic acid isolated as trimethyl dimethyl ester **8**, $C_{21}H_{36}$ $(CO_2Me)_2$. Thus, the partial structure **1a** was established for ikarugamycin. The configurations of the two double bonds were assigned on the following basis. The occurrence of the H_a proton

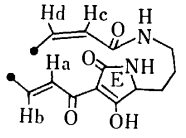

1a

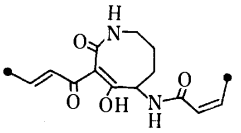

1b

at a lower field than the H_b proton is unusual for olefinic protons in a trans α,β-unsaturated carbonyl system;[6] an example of such a case is found in aspertetronin A (**9**) which gives a PMR spectrum exhibiting H_a' and H_b' protons at δ 7.32 and 7.06, respectively.[7]

Natural products having the acyltetramic acid chromophore are already known and examples include tenuazoic acid (**10**),[8] erythroskyrine,[9] *etc.*[10,11] As expected, the peculiar UV spectral behavior of hexahydroikarugamycin (**2**) closely parallels that of other acyltetramic acids (Table 1). Further chemical evidence for **1a** was provided by alkaline hydrolysis of **2**. The reaction led to cleavage of the tricarbonyl system and the amide bonds to give the carbocyclic part of **2**, a carboxylic acid isolated as dimethyl ester **11**, $C_{20}H_{34}$-$(CO_2Me)_2$.

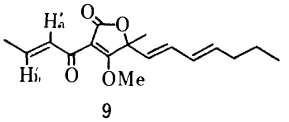

9

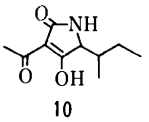

10

Drastic Oxidation of Ikarugamycin, Hexahydroikarugamycin, and Deoxooctahydroikarugamycin. From the molecular formula and the functional groups (three double bonds, a diketo amide, and an amide), ikarugamycin (**1**) is a pentacyclic compound. The formation of the bicyclic tetramethyl ester **5** by ozonolysis of **1** and of the tricyclic dimethyl ester **11** by hydrolysis of **2** indicates that i) **1** possesses three carbocyclic rings, one of which contains the cis double bond not shown in **1a** and ii) two

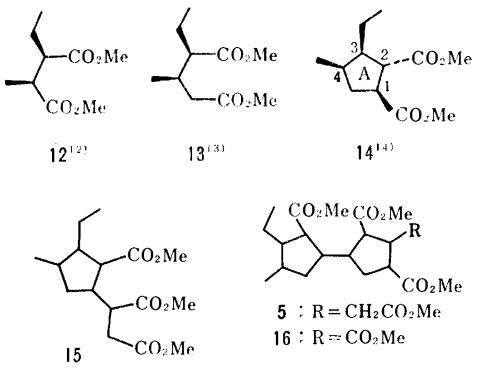

Fig. 2. Permanganate oxidation products of ikarugamycin (**1**).

side chains in the partial structure **1a** are connected with the carbocyclic part, thereby forming a large-membered lactam ring. Although there are 16 carbon atoms in **1** which are not included in **1a**, little information has so far been obtained beyond that revealed by the PMR spectrum of **1** (Fig. 1): the presence of a primary methyl (δ 0.93) and a secondary methyl (δ 0.88) groups. Since the carbon skeleton of **1** appeared to be unique, an attempt was made to obtain information on the structure of the carbocyclic part by oxidative degradations which were vigorous enough to cleave carbon–carbon single bonds. This approach was remarkably successful, as the following results show.

(a) Oxidation of Ikarugamycin (1): Prolonged oxidation of **1** with $KMnO_4$ in pyridine–water at 60 °C yielded, after esterification with diazomethane, a series of esters which was effectively isolated by preparative GLC. The products, including **5** as the major one, are listed in Fig 2 in the order of their GLC retention times. The PMR sepctrum of **14** shows a doublet (J= 7.5 Hz) at δ 0.85 due to a secondary methyl group, a triplet (J=6.7 Hz) at δ 0.89 due to a primary methyl group, a complex multiplet between δ 1.2—2.4 (6H), a triplet (J=8.0 Hz) at δ 2.79 and a multiplet (ddd, J= 8.5, 8.0, and 7.5 Hz) at δ 3.09 attributable to two methine protons on carbons bearing ester groups, and two 3H singlets at δ 3.63 and 3.64 due to two methoxyl groups. Irradiation at δ 3.09 caused the triplet at δ 2.79 to collapse to a doublet (J=8.0 Hz), indicating a vicinal arrangement of the two methoxycarbonyl groups. On the basis of these data, coupled with the concomitant formation of **13**, the diester was formulated to be **14** (not considering stereochemistry). The *r*-1, *t*-2, *c*-3, *c*-4-configuration has been unambiguously established by the synthesis of the four possible 3,4-*cis* diastereomers.[14] The trimethyl ester **15** produced a mass spectrum containing three characteristic peaks at *m/e* 169 due to the $M^+-MeO_2CCH_2\dot{C}HCO_2Me$ ion, at *m/e* 146 due to the $(MeO_2CCH_2CH_2CO_2Me)^+$ ion formed by MacLafferty rearrangement,[15] and at *m/e* 109 due to the $C_8H_{13}^+$ ion from the cyclopentane ring. This, together with the formation of **22** from **2** (see below), suggests the structure **16** for the ester.

Next, chromic acid oxidation in 3 M H_2SO_4–acetic acid at 80 °C was examined. Compared with the permanganate oxidation, the reaction led to more extensive cleavage of carbon bonds as indicated by the products (Fig. 3). The structure for **19** was suggested by the empirical formula $C_6H_8(CO_2Me)_4$ and by the formation of **17** and **18**. The relative configuration of **18** has been established by synthesis.[18]

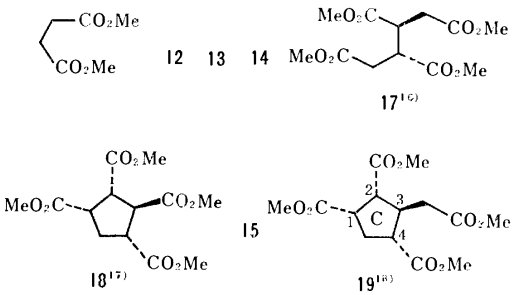

Fig. 3. Chromic acid oxidation products of ikarugamycin (**1**).

(b) Oxidation of Hexahydroikarugamycin (2) and Deoxooctahydroikarugamycin (3): As expected, chromic acid oxidation of **2** under conditions similar to those for **1** gave a completely different series of products (Fig. 4). The structures of **21** and **22** were deduced from their mass and PMR spectra (see Experimental) and were then confirmed by synthesis (of mixtures of diastreomers).[20] The mass spectrum of **23** shows two characteristic peaks at *m/e* 174 and 160 due to the $(MeO_2CCH_2CH_2CH_2CH_2CO_2Me)^+$ and $(MeO_2CCH_2CH_2CH_2CH_2CO_2Me)^+$ ions, respectively, thus indicating the structure. Its *threo* configuration was established by synthesis.[20] Structure of **24** was suggested by its mass spectrum and the formation of **20** and **23**, and was eventually confirmed by synthesis (of a mixture of diastereomers).[20]

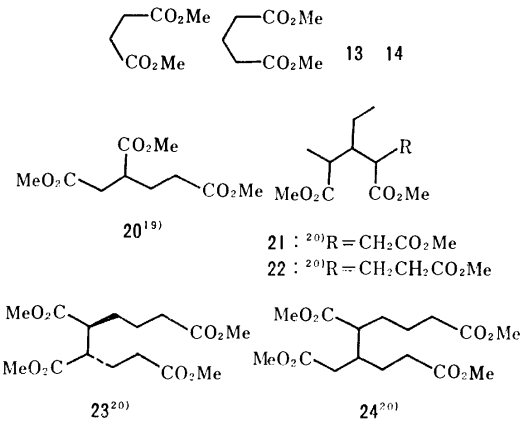

Fig. 4. Chromic acid oxidation products of hexahydroikarugamycin (**2**).

Finally, chromic acid oxidation of **3** was examined, since it should give information concerning the position of the methylene group in **3** which was derived from a carbonyl group in the β-tricarbonyl system of **2**. The oxidation afforded, in addition to all the products from **2**, the trimethyl ester **25** and the tetramethyl esters **26** and **27** (Fig. 5) which are the higher homologs of **20**, **23**, and **24**, respectively. Structure of **27** was suggested by its mass spectrum and the formation of **25** and **26**, and was then confirmed by synthesis.[20]

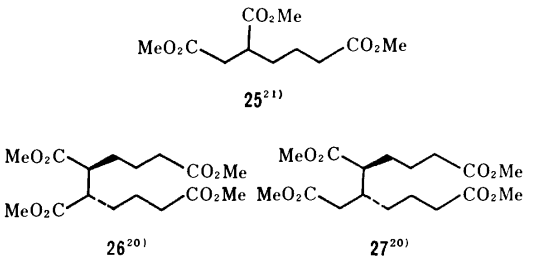

Fig. 5. Chromic acid oxidation products of deoxooctahydroikarugamycin (**3**) (in addition to the compounds shown in Fig. 4).

Structure of Ikarugamycin. The formation of **14** from **1** and of **22** from **2** and **3** but not from **1** can be accounted for by the partial structure **1c** for ikarugamycin. From the structural relationships among **17**, **24**, and **27**, coupled with the formation of **19** from **1**, partial structure **1a** can now be extended to **1d**. The

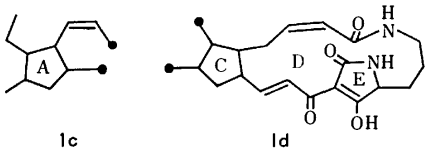

coupling patterns of the H_a–H_d protons in the PMR spectrum of **1** (Fig. 1) are fully consistent with this structure. There then remain two possibilities to explain how these two parts, **1c** and **1d**, could be connected to make up the remaining B ring. This problem was settled by the following experiment. Triester **15** was prepared by the permanganate oxidation of **1** in pyridine–deuterium oxide and was examined by mass spectrometry which showed that the succinyl residue in **15** contained only *ca.* 0.3 deuterium. This indicates that **15** was formed without decarboxylation and therefore, that the C-1 position in **14** should be connected to C-1 (not to C-2) in **19**. Consequently, ikarugamycin can now be represented by structure **1**.

Stereostructure and Biogenesis of Ikarugamycin. In ikarugamycin there are eight consecutive asymmetric centers at the C-2, C-3, C-3a, C-8b, C-5a, C-6, and C-7 positions on rings A, B, and C, and one at the junction of rings D and E. The configuration of the latter is evident from L-ornithine. The relative configurations on rings A and C are also apparent from those of **14** and **19**, respectively. That the latter were formed without epimerization was proved by the oxidation of **1** in deuterium-containing solvents. Thus, the permanganate oxidation in pyridine–deuterium oxide yielded **14** which according to the mass spectrum consisted of d_0 (65%), d_1 (30%), and d_2 (5%) derivatives. Also, the chromic acid oxidation in 3M D_2SO_4–D_2O gave **19** consisting of d_0 (85%) and d_1 (15%) derivatives.

It has already been established that (−)-*erythro*-2-ethyl-3-methylglutarate, $[\alpha]_D$ −14.9°, has the 2*R* : 3*S* (**13a**) configuration.[13b] The natural **13** obtained by the oxidation of **1** has $[\alpha]_D$ −8.6° and, therefore, must have the absolute configuration of **13a**. The absolute configuration of trimethyl (+)-1,2,4-butanetricarboxylate, $[\alpha]_D$ +16.2°, has also been reported to be *R* (**20a**).[19b] Therefore, the absolute configuration of the natural **20** ($[\alpha]_D$ +12.6°) obtained by the oxidation of **2** and hence that of C-7 in ring C was established as shown below. From the combination of these absolute configurations, ikarugamycin can now be assigned the stereostructure **1e**.

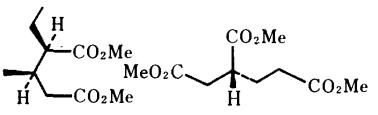

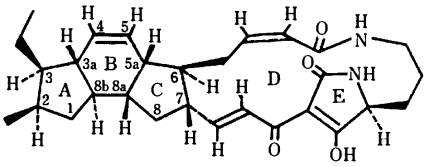

Since, to the best of our knowledge, ikarugamycin is the first example of a natural product with an *as*-hydrindacene skeleton, its biogenesis appears to be of considerable interest. It has been proved that other natural acyltetramic acids, such as tenuazoic acid (**10**), can be biosynthesized from an amino acid (L-isoleucine in case of **10**) and a polyacetate (diacetate in case of **10**).[8b,9b,10b] It appears likely, therefore, that ikarugamycin can also be derived from L-ornithine and two hexaacetate chains as outlined in Scheme **1**. Although exactly how the unique carbon skeleton is formed remains a matter of conjecture, it is suggested that an intramolecular Diels-Alder reaction between the butadiene part and the double bond in a hypothetical intermediate such as **1f** could lead to the formation of the decahydro-*as*-indacene skeleton of ikarugamycin.

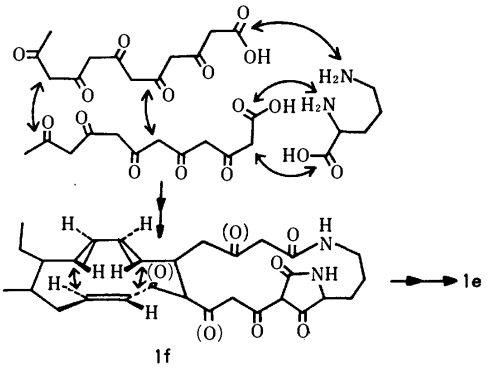

Scheme 1. A biogenesis of ikarugamycin (**1**).

Experimental

The mp values are uncorrected. The IR spectra were recorded with JASCO model IR-S and DS-402G spectrophotometers and for the UV spectra a Perkin-Elmer model 202 spectrophotometer was used. The PMR spectra were recorded on JEOL models JNM-C60H and 4H-100 spectrometers; the chemical shifts are given in ppm relative to internal TMS. The mass spectra were obtained with a Hitachi model RMU-6C mass spectrometer. Optical rotations were determined with a JASCO model ORD/UV-5 spectrophotometer

or a JASCO model DIP-SL polarimeter (for **13** and **20**) and pK_a values were determined from titration curves taken with a Radiometer model TTT1 titrater. For TLC, Merch GF_{254} or PF_{254} silica gel was used and for column chromatography, Mallinckrodt silicic acid. Gas-liguid chromatography (GLC) was carried out with a Varian Aerograph model 1828-4 chromatograph. The column used for preparative GLC was composed of 5% SE-30 on celite 545 (3 m×0.95 cm).

*Properties of Ikarugamycin (**1**).* Repeated recrystallization of crude **1** from MeOH gave colorless needles, mp 228—229 °C (dec), $[\alpha]_D^{25}+390°$ (*c* 0.19, DMF), slightly soluble in DMF, DMSO, THF, EtOH, MeOH, and pyridine. The antibiotic showed pK_a 5.6 (67% EtOH); IR ($CHCl_3$): 3450, 1700, 1665, 1642, 1580, 1510 cm^{-1}; (KBr): 3380, 3220, 1700, 1678, 1645, 1583, 1519 cm^{-1}; PMR (pyr-d_5): δ 0.88 (3H, d, J=7 Hz), 0.93 (3H, t, J=7), 3.6—4.4 (2H, m), 4.1 (1H, narrow m), 5.72 and 5.95 (each 1H, br ABq, J=10), 6.0 (1H, m), 6.20 (1H, br d, J=12), 6.94 (1H, dd, J=15.6 and 9.5), 7.62 (1H, d, J=15.6), 8.7 and 9.6 (each 1H, br s, D_2O exchangeable); (DMSO-d_6): δ 5.6—6.2 (4H, m), 6.64 (1H, dd, J=15.0 and 9.5 Hz), 6.96 (1H, J=15.0), 7.79 and 8.62 (each 1H, br s, D_2O exchangeable). Found: C, 72.67; H, 8.20; N, 5.90%; *m/e* 478.2771. Calcd for $C_{29}H_{38}N_2O_4$: C, 72.77; H, 8.00 N, 5.85%; M, 478.2731.

*Copper Complex of **1**.* A soln of **1** (50 mg) and cupric acetate (12 mg) in EtOH (30 ml) was heated under reflux for 2 h. Crystals deposited after cooling, which were recrystallized from EtOH to give yellow-green needles (21 mg), mp>280 °C. Found: C, 63.50; H, 7.65; N, 5.13%. Calcd for $(C_{29}H_{37}N_2O_4)_2Cu\cdot 4H_2O$: C, 63.86; H, 7.58; N, 5.14%.

*Hexahydroikarugamycin (**2**).* A soln of **1** (600 mg) in EtOH (200 ml) was hydrogenated in the presence of PtO_2 (100 mg) for 1 h at room temp and atmospheric pressure. It was filtered and evaporated to a small volume under reduced pressure. The solid that precipitated was recrystallized from $CHCl_3$ to give 350 mg of **2** as needles, mp 243—244 °C (dec), $[\alpha]_D^{25}+110°$ (*c* 0.44, $CHCl_3$), pK_a 5.1 (67% EtOH), IR ($CHCl_3$): 3450, 1710, 1662, 1610, 1520 cm^{-1}; PMR ($CDCl_3$): δ 5.86 and 6.0 (each 1H, br s, exchangeable with D_2O), no other signals above δ 4.0. Found: C, 71.51; H, 9.27; N, 5.82%; *m/e* 484.3303. Calcd for $C_{29}H_{44}N_2O_4$: C, 71.86; H, 9.15; N, 5.78; M, 484.3301.

*Copper Complex of **2**.* Green crystals, mp>280 °C (from EtOH). Found: C, 65.01; H, 8.74; N, 4.99. Calcd for $(C_{29}H_{43}N_2O_4)_2Cu\cdot 2H_2O$: C, 65.21; H, 8.50; N, 5.25%.

*N-Methylpyrazole Derivative of **2**.* A soln of **2** (48 mg) and *N*-methylhydrazine sulfate (20 mg) in 90% EtOH (5 ml) was heated under reflux for 30 h. The product was subjected to preparative TLC ($CHCl_3$–MeOH, 4 : 1), giving 19 mg of an oil, mass: *m/e* 494 (M^+); IR ($CHCl_3$): 3360, 1680, 1654, 1540 cm^{-1}; UV (MeOH): λ_{max} 226 nm (ε 4900); PMR ($CDCl_3$): δ 3.85 (3H, s), 4.1 (1H, m), 6.8 (1H, br s,) 8.2 (1H, br s).

*Deoxooctahydroikarugamycin (**3**).* A soln of **2** (500 mg) in EtOH (170 ml) was hydrogenated in the presence of PtO_2 (150 mg) for 24 h. It was filtered and evaporated to give an oily residue which was crystallized from MeOH, affording 350 mg of **3** as prisms, mp 155—157.5 °C, pK_a 7.8 (67% EtOH), mass: *m/e* 470 (M^+); IR ($CHCl_3$): 3470, 3250, 1775, 1705, 1665, 1510 cm^{-1}; PMR (DMSO-d_6): δ 7.09, 7.85, and 10.32 (each 1H, br s, D_2O exchangeable). Found: C, 74.12; H, 9.99; N, 6.04%. Calcd for $C_{29}H_{46}N_2O_3$: C, 74.00; H, 9.85: N, 5.95%.

*Enol Ether of **3**.* Treatment of **3** (140 mg) with diazomethane yielded, after preparative TLC, 97 mg of an oil mass: *m/e* 484 (M^+); IR ($CHCl_3$): 3450, 3300, 1677, 1652, 1515 cm^{-1}; UV (MeOH): λ_{max} 224 (ε 5300) and 242^{sh} nm (4600): PMR ($CDCl_3$): δ 3.98 (3H, s).

*Enol Acetate of **3**.* Acetylation of **3** with acetic anhydride–pyridine gave an oily enol acetate, mass: *m/e* 512 (M^+), 470, 452; IR ($CHCl_3$): 3450, 3340, 1781, 1690, 1664, 1515, 1185 cm^{-1}; UV (MeOH): λ_{max} 222 nm (ε 7000); PMR ($CDCl_3$): δ 2.29 (3H, s).

*Deoxodecahydroikarugamycin (**4**).* *(a) From **3**:* A mixture of **3** (100 mg) and $LiBH_4$ (100 mg) in THF (20 ml) was stirred for 24 h at room temp. Water and then 2M HCl were added to the ice-cooled mixture until it became a clear, neutral soln which was then extracted with $CHCl_3$. The extract was washed with water, dried, and evaporated. The residue was crystallized from MeOH to give 68 mg of **4** as needles, mp 220—222 °C, mass: *m/e* 472 (M^+), 454; IR ($CHCl_3$): 3430, 3500—3200, 1695, 1655, 1520 cm^{-1}; PMR (DMSO-d_6): δ 4.4 (1H, m), 5.0, 7.65, 7.88 (each 1H, br, exchangeable with D_2O). Found: C, 71.38; H, 10.18; N, 5.62%. Calcd for $C_{29}H_{48}N_2O_3\cdot H_2O$: C, 70.98: H, 10.27; N, 5.71%.

*(b) From **2**:* A suspension of **2** (150 mg) and $LiBH_4$ (150 mg) in dimethoxyethane (45 ml) was heated under reflux for 6 h with stirring. The work-up described in *(a)* afforded 68 mg of **4**.

*Acetate of **4**.* Acetylation of **4** gave an oily acetate, mass: *m/e* 514 (M^+), 454; IR ($CHCl_3$): 3460, 3400—3200, 1741, 1699, 1662, 1521, 1240 cm^{-1}; PMR ($CDCl_3$): δ 2.18 (3H, s), 5.53 (1H, m).

*Ozonolysis of **1**: Formation of **5**, Oxalic Acid, and* L-*Ornithine.* Through a soln of **1** (100 mg) in MeOH (70 ml) at—70 °C ozonized oxygen was passed until the soln turned pale purple. After the excess of ozone had been expelled by a nitrogen stream, the solvent was removed at room temp and to the residue 98% formic acid (10 ml) and 35% hydrogen peroxide (1 ml) were added. The mixture was stirred for 1 h at 0 °C and then 14 h at room temp. After decomposition of the excess oxidant with $NaHSO_3$ (1 g), the mixture was evaporated to dryness and the residue was dissolved in 0.5 M H_2SO_4 (10 ml) and extracted with ether; the aqueous layer was saved for further experiment (see below). The ether extract was washed with water, dried, and evaporated to leave an oil which was then treated with diazomethane. The crude ester thus obtained was purified by preparative TLC (hexane–ether, 1 : 1), giving 40 mg of the tetramethyl ester **5**, mass: *m/e* 426 (M^+), 366, 334 (base peak), 306, 246; IR (CCl_4): 1740 cm^{-1}; PMR (CCl_4): δ 0.88 (3H, t, J=6.2 Hz), 0.88 (3H, d, J=6.5), 3.57 (3H, s), 3.59 (6H, s), 3.64 (3H, s), Found: *m/e* 426.2254. Calcd for $C_{22}H_{34}O_8$: M, 426.2253.

The aqueous layer (see above) was adjusted to 1 M with respect to H_2SO_4 by the addition of concd H_2SO_4 and heated under reflux for 4 h. Continuous extraction with ether afforded a crude acid which was recrystallized from ether–CCl_4, giving 16 mg of oxalic acid dihydrate (identified by IR) as prisms. The dimethyl ester derivative, mp 51—54 °C, also had an IR spectrum identical with that of dimethyl oxalate. The aqueous layer remaining after the continuous extraction was neutralized with 0.2 M $Ba(OH)_2$ and the $BaSO_4$ precipitated was removed by filtration. The filtrate was concentrated to a small volume under reduced pressure and applied to a column (1×6 cm) of Dowex 50W-X8 (H^+ form). Elution with 1 M NH_4OH (60 ml) afforded an amino acid which was crystallized from dil HCl (pH *ca.* 4)–EtOH to give 15 mg of L-ornithine monohydrochloride (identified by IR) as prisms, mp 224—229 °C (dec), $[\alpha]_D^{25}+40°$ (*c* 0.42, 5 M HCl), lit,[22] $[\alpha]_D^{25}+37.5°$ (*c* 2, 5 M HCl). Found: C, 35.29; H, 7.88; N, 16.60%. Calcd for $C_5H_{12}N_2O_2\cdot HCl$: C, 35.61; H, 7.77; N, 16.61%.

Keto Acid ***6a.*** A suspension of **3** (94 mg) and CrO_3 (80 mg) in 3 M H_2SO_4 (10 ml) was heated at 80 °C for 2 h with stirring. Cooling of the resulting solution caused precipitation of crystals which were filtered, washed well with water, and recrystallized from MeOH–water, yielding 68 mg of microcrystals, mp 222—223 °C, IR (KBr): 3300, 2800—2300, 1745, 1725, 1665, 1617, 1545 cm^{-1}. Found: C, 67.56: H, 9.59; N, 5.32%. Calcd for $C_{29}H_{46}N_2O_5 \cdot MeOH$: C, 67.38; H, 9.43; N, 5.24%.

Keto Ester ***6b.*** To a soln of the enol ether of **3** (145 mg) in a mixture of acetone (20 ml) and water (30 ml) were added KH_2PO_4 (75 mg), $MgSO_4$ (150 mg), and $KMnO_4$ (75 mg). The mixture was stirred for 24 h at room temp and then made clear and neutral by the addition of $NaHSO_3$ powder and 2 M HCl. The soln was extracted with $CHCl_3$ and the extract washed with water, dried, and evaporated to dryness. Crystallization of the residue from MeOH–water afforded 100 mg of **6b**, mp 173—174 °C; mass: *m/e* 516 (M^+), 488; IR (KBr): 3430, 3310, 1760, 1739, 1660, 1639, 1550 cm^{-1}; PMR (pyr-d_5): δ 3.59 (3H, s), 3.63 (3H, s), 4.90 (1H, m), 8.5 and 9.7 (each 1H, br, exchangeable with D_2O). Found: C, 67.51; H, 9.25; N, 5.15%. Calcd for $C_{30}H_{48}N_2O_5 \cdot MeOH$: C, 67.85; H, 9.55; N, 5.11%.

The keto ester was also obtained by esterification (MeOH–HCl) of keto acid **6a**.

Amino Acid ***7.*** To a soln of **6a** (68 mg) in MeOH (10 ml) were added 1 M NaOH (10 ml) and 35% hydrogen peroxide (0.9 ml). After stirring for 64 h at room temp, the mixture was acidified with 6 M HCl, which caused precipitation of an amorphous powder. It weighed 64 mg, was homogeneous (R_f 0.7) on TLC in 1-butanol–acetic acid–water, 4 : 1 : 2, and became pink with ninhydrin.

N-*Acetyl Dimethyl Ester of* ***7.*** To a stirred soln of **7** (18 mg) in 1 M NaOH (1 ml) was added acetic anhydride (0.1 ml) at room temp. After a time, an additional 1 M NaOH (1 ml) was added and the mixture was extracted with $CHCl_3$. The aqueous layer was acidified with 2 M HCl, extracted with $CHCl_3$, and the extract washed with a sat NaCl soln, dried, and evaporated. The residue was then treated with diazomethane and the product was purified by preparative TLC ($CHCl_3$–MeOH, 9 : 1) to give 5 mg of an oil, mass: *m/e* 562 (M^+) ; IR ($CHCl_3$): 3460, 3300, 1739, 1673, 1513 cm^{-1}; PMR ($CDCl_3$): δ 2.04 (3H, s), 3.67 (3H, s), 3.75 (3H, s), 4.5 (1H, m), 6.0 (1H, br s), 6.50 (1H, br d, J=8 Hz).

Hydrolysis of the DNP Derivative of ***7****: Formation of* ***8*** *and 2,4-Dintrophenylornithine.* To a suspension of **7** (40 mg) in EtOH (2 ml) and water (2 ml) were added $NaHCO_3$ (0.2 g) and 2,4-dinitrofluorobenzene (0.1 ml). After stirring at 40 °C for 6 h, the EtOH was removed under reduced pressure and the aqueous residue was extracted with ether. The ether layer was washed with water, and the aqueous layers were combined, acidified with 6 M HCl, and extracted with EtOAc. The extract was washed with water and a sat NaCl aq soln. and dried. Evaporation of the solvent left an oil which was subjected to preparative TLC ($CHCl_3$–MeOH–acetic acid, 90 : 9 : 1), giving 30 mg of the DNP derivative as an amorphous powder. This was dissolved in concd HCl (3 ml) and acetic acid (3 ml) and heated to 110 °C. After 24 h, additional concd HCl (2 ml) was added and heating was continued for another 12 h. The hydrolysate was concentrated to dryness under reduced pressure and the residue, taken up in 50% MeOH, was placed on a column (1.2×2 cm) of Dowex 50W-X8 (H^+ form). Elution with 50% MeOH yielded a crude carboxylic acid which was esterified with diazomethane. Preparative TLC (hexane–ether, 2 : 1) of the crude ester yielded 3 mg of oily **8**, mass *m/e* 406 (M^+), 388 (base peak), 374, 356; IR (CCl_4): 1743 cm^{-1}; PMR (CCl_4): δ 3.61 (6H, s). Found: *m/e* 406.3074. Calcd for $C_{25}H_{42}O_4$: M, 406.3083.

The Dowex column was then eluted with 0.5 M NH_4OH (40 ml) and 1 M NH_4OH (20 ml) to afford an oil which was crystallized from dil HCl. Orange crystals (3 mg) of α-DNP-ornithine were obtained (identified by IR and paper chromatography in comparison with an authenic sample[5]). The R_f values of the α- and δ-DNP-ornithines on paper chromatography in 1-butanol saturated with water were 0.48 and 0.52, respectively.

Alkaline Hydrolysis of ***2****: Formation of* ***11.*** A soln of **2** (25 mg) in ethylene glycol (1 ml) was prepared by heating at 150 °C. To this soln, 40% NaOH (0.3 ml) was added and the mixture heated at 100 °C for 24 h. The ice-cooled mixture was acidified with dil HCl, extracted with EtOAc, and the extract was treated with diazomethanne. After decomposition of the excess diazomethane with acetic acid, the EtOAc soln was washed with water, an aq $NaHCO_3$ soln, and again with water, and then dried. Evaporation of the solvent left an oil which was purified by preparative TLC (hexane–ether, 4 : 1), giving 6 mg of dimethyl ester **11** as an oil, mass: *m/e* 392 (M^+), 374, 361, 360, 343, 319 (base peak); IR (CCl_4): 1743 cm^{-1}; PMR (CCl_4): δ 0.89 (3H, t, J=7 Hz), 0.93 (3H, d, J=7), 3.62 (6H, s). Found: *m/e* 392.2951. Calcd for $C_{24}H_{40}O_4$: M, 392.2926.

Oxidation of ***1*** *with $KMnO_4$ in Pyridine–Water.* A mixture of **1** (478 mg) and $KMnO_4$ (3.5 g) in pyridine (40 ml) and water (40 ml) was stirred at room temp overnight and then at 60 °C for 5 h. The solvents were evaporated under reduced pressure, water was added, and the evaporation repeated. To the residue were added $NaHSO_3$ powder and concd HCl until the mixture became a clear, acidic soln. The latter was continuously extracted with ether for 8 h and the extract was dried and evaporated giving a mixture of carboxylic acids which was then esterified with diazomethane. The esters (260 mg) thus obtained were partially separated by column chromatography on silica gel (5 g); elution with hexane–ether, 4 : 1 and then 1 : 1 gave 35 and 64 mg of oil, respectively. Preparative GLC of the former (column temp: 130—270 °C, 20 °C/min) afforded **12** (1.5 mg), **13** (1.0 mg), **14** (4.2 mg), and **15** (0.3 mg), and that of the latter (column temp: 270 °C) **16** (1.1 mg) and **5** (17 mg).

Dimethyl erythro-*2-Ethyl-3-methylsuccinate* ***(12)***: $[\alpha]_D^{25}$ +2.2° (*c* 0.44, $CHCl_3$); mass: *m/e* 157 (M^+−OMe), 102, 101 (base peak), 88, 87; PMR (CCl_4): δ 0.89 (3H, t, J=7.2 Hz), 1.10 (3H, d, J=7.0), 1.2—1.8 (2H, m), 2.4—2.7 (2H, m), and 3.66 (6H, s). This compound was identified by means of IR, PMR, mass spectrometry, and GLC with an authentic sample of the *erythro* isomer.[12]

Dimethyl erythro-*2-Ethyl-3-methylglutarate* ***(13)***: $[\alpha_D^{25}]$ −8.6° (*c* 0.64, $CHCl_3$), lit[13b] $[\alpha]_D^{25}$ −14.9° (*c* 1.19, $CHCl_3$); mass: *m/e* 171 (M^+−OMe), 142, 129, 102, 101 (base peak), 87, 74; PMR (CCl_4): δ 0.89 (3H, t, J=6.8 Hz), 0.93 (3H, d, J=6.3), 1.1—2.7 (6H, m), 3.61 (3H, s), and 3.62 (3H, s). This ester was identical with an authenic sample of the *erythro* isomer (IR, PMR, mass, and GLC).[13]

Dimethyl c-*3-Ethyl*-c-*4-methyl*-r-*1*,t-*2-cyclopentanedicarboxylate* ***(14)***:[14] $[\alpha]_D^{25}$ +23° (*c* 0.60, $CHCl_3$); mass: *m/e* 228 (M^+), 199, 197, 168, 109 (base peak).

Trimethyl Ester ***15***: Mass: *m/e* 314 (M^+), 169*, 146 (base peak), 109. Found: *m/e* 314.1724. Calcd for $C_{16}H_{26}O_6$: M, 314.1729.

Tetramethyl Ester ***16***: PMR (CCl_4): δ 3.58, 3.59, 3.65,

* The compositions of these peaks were established by high-resolution mass spectrometry.

and 3.67 (each 3H, s). Found: *m/e* 412.2075. Calcd for $C_{21}H_{28}O_8$: M, 412.2097.

Oxidation of **1** *with* CrO_3 *in* H_2SO_4*–Acetic Acid.* A suspension of **1** (500 mg) and CrO_3 (2.5 g) in 3 M H_2SO_4 (25 ml) and acetic acid (25 ml) was heated at 80 °C with stirring. After 16 h, the oxidation mixture was concentrated under reduced pressure, water was added, and the concentration repeated. The residue was taken up in concd NH_4OH (8 ml) and the still strongly acidic soln was continuously extracted with ether for 30 h. The crude acids (108 mg) thus obtained were first esterified with diazomethane and the resultant esters were heated under reflux in MeOH (10 ml) containing concd H_2SO_4 (1 drop) for 1 h to convert some ethyl esters formed during the ether extraction into methyl esters. The MeOH was evaporated, the residue diluted with water, and extracted with ether. The extract was washed with an aq $NaHCO_3$ soln, water, and a sat NaCl soln, and then dried. Evaporation of the solvent left a mixture of methyl esters (110 mg) which was passed through a silica gel (3 g) column. Elution with ether gave 85 mg of an oil which was subjected to preparative GLC (column temp: 200—280 °C, 4 °C/min). The products were (in the order of increasing retention time): dimethyl succinate (4.7 mg), **12** (0.5 mg), **13** (3.8 mg), **14** (1.0 mg), **17** (7.8 mg), **18** (0.2 mg), **15** (0.5 mg), and **19** (1.6 mg).

Tetramethyl meso*-1,2,3,4-Butanetetracarboxylate (17)*: Mp 74—74.5 °C (from ether hexane), lit,[16] mp 75 °C; mass: *m/e* 259 (M^+–OMe), 139 (base peak); PMR (CCl_4): δ 2.1—3.4 (6H, m), 3.66 (6H, s), and 3.69 (6H, s). Found: C, 49.65; H, 6.25%. Calcd for $C_{12}H_{18}O_8$: C, 49.48; H, 6.43%. This compound was identical with an authentic sample of the *meso* isomer (IR, PMR, mass, and GCL).[16]

Tetramethyl r*-1*, c*-2*, t*-3*, c*-4-Cyclopentanetetracarboxylate (18)*: Found: *m/e* 302.0976. Calcd for $C_{13}H_{18}O_8$: M, 302.1001. This ester was identified with an authenic sample having the configuration depicted in **18** (IR, mass, and GLC).[17]

Trimethyl t*-3-(Methoxycarbonylmethyl)-*r*-1,*c*-2,*c*-4-cyclopentanetricarboxylate (19)*:[18] Mass: *m/e* 316 (M^+), 285, 224, 165 (base peak); PMR (CCl_4): δ 2.0—3.4 (8H, m), 3.58 (3H, s), 3.60 (6H, s), and 3.63 (3H. s). Found: *m/e* 316.1160. Calcd for $C_{14}H_{20}O_8$: M, 316.1158.

Oxidation of **2** *with* CrO_3 *in* H_2SO_4. A mixture of **2** (330 mg) and CrO_3 (1.2 g) in 3 M H_2SO_4 (35 ml) was stirred at 80 °C for 8 h. The work-up described for the CrO_3 oxidation of **1** gave 93 mg of methyl esters which were separated by preparative GLC (column temp: 120—280 °C, 10 °C/min). The products were: dimeth l succinate (13.8 mg), dimethyl glutarate (3.2 mg), **13** (1.4 mg), **14** (0.3 mg), **20** (2.2 mg), **21** (0.4 mg), **22** (0.9 mg), **23** (2.9 mg), and **24** (4.2 mg).

Trimethyl 1,2,4-Butanetricarboxylate (20): $[\alpha]_D^{25}$ +12.6° (*c* 0.68, acetone), lit[19b] $[\alpha]_D^{25}$ +16.2° (*c* 13.7, acetone); mass: *m/e* 201 (M^+—OMe); PMR (CCl_4): δ 1.6—2.4 (7H, m), 3.61, 3.62, and 3.64 (each 3H, s). This compound was identified with an authetic sample.[19]

Trimethyl 3-Ethyl-1,2,4-pentanetricarboxylate (21): Mass: *m/e* 243 (M^+—OMe)*, 214 (M^+—HCO_2Me), 187 (fragmentation between C-3 and 4)*, 155 (base peak), 146 [(MeO_2-$CCH_2CH_2CO_2Me$)$^+$]*; PMR (CCl_4): δ 0.88 (3H, t, J= 7.0 Hz), 1.20 (3H, d, J=7.0), 3.69, 3.71, and 3.73 (each 3H, s). This ester exhibited a mass spectrum and GLC behavior identical to a synthetic sample (of a mixture of diastereomers).[20]

Trimethyl 4-Ethyl-1,3,5-hexanetricarboxylate (22): Mass: *m/e* 257 (M^+—OMe)*, 228 (M^+—HCO_2Me)*, 201 (fragmentation between C-4 and 5)*, 169 (base peak), 160 [(MeO_2CCH_2-$CH_2CH_2CO_2Me$)$^+$]*, 129; PMR (CCl_4): δ 0.89 (3H, t, J=7.6 Hz), 1.18 (3H, d, J=7.2), 3.68 (6H, s), 3.70 (3H, s). This ester also exhibited a mass spectrum and GLC behavior identical to a synthetic sample (of a mixture of diastereomers).[20]

Tetramethyl threo*-1,3,4,7-Heptanetetracarboxylate (23)*: Mass: *m/e* 301 (M^+—OMe)*, 174*, 160*, 59 (base peak); PMR (CCl_4): δ 1.2—2.9 (12H, m), 3.63 (6H, s), and 3.67 (6H, s). This compound was identical with a synthetic sample of the *threo* isomer (IR, PMR, mass, and GLC).[20]

Trimethyl 3-(Methoxycarbonylmethyl)-1,4,7-heptanetricarboxylate (24): Mass: *m/e* 315 (M^+–OMe)*, 174 [($MeO_2CCH_2CH_2$-$CH_2CH_2CO_2Me$)$^+$]*, 59 (base peak); PMR (CCl_4): δ 1.1—2.7 (14H, m), 3.62 (9H, s), and 3.66 (3H, s). This ester exhibited a mass spectrum and GLC behavior identical to a synthetic sample (of a mixture of the *threo* and *erythro* isomers).[20]

Oxidation of **3** *with* CrO_3 *in* H_2SO_4*–Acetic Acid.* A mixture of **3** (100 mg) and CrO_3 (600 mg) in 3M H_2SO_4 (5 ml) and acetic acid (5 ml) was stirred for 9 h at 80 °C. Work-up of the oxidation mixture gave 50 mg of a mixture of methyl esters which was separated by preparative GLC (column temp: 140—290 °C, 10 °C/min). The products were: dimethyl succinate (10 mg), dimethyl glutarate (3.2 mg), **13** (0.2 mg), **20** (1.0 mg), **25** (0.3 mg), **21** (0.1 mg), **22** (0.2 mg), **23** (0.9 mg), **24** plus **26** (2.3 mg), and **27** (0.9 mg).

Trimethyl 1,2,5-Pentanetricarboxylate (25): Mass: *m/e* 215 (M^+—OMe), 146; PMR (CCl_4): δ 1.4—1.8 (4H, m), 2.1—2.9 (5H, m), 3.65, 3.66, and 3.69 (each 3H, s), This ester was identical with an authentic sample (IR, PMR, mass, and GLC).[21]

Tetramethyl threo*-1,4,5,8-Octanetetracarboxylate (26)*: The PMR spectrum(CCl_4) of an inseparable mixture of **24** and **26** in the presence of Eu(DPM)[23] gave rise to six methoxyl signals, two of which came from **26** and the others from **24**; the intensities of the former increased upon the addition of a synthetic sample of **26**.[20]

Trimethyl threo*-5-(Methoxycarbonylmethyl)-1,4,8-octanetricarboxylate (27)*: Mass: *m/e* 329 (M^+—OMe)*, 174 [(MeO_2-$CCH_2CH_2CH_2CH_2CO_2Me$)$^+$]*; PMR (CCl_4): δ 1.1—1.9 (8H, m), 1.9—2.6 (8H, m), 3.64 (9H, s), and 3.67 (3H, s). This compound was identical with a synthetic sample of the *threo* isomer (IR, PMR, mass, and GLC).[20]

$KMnO_4$ Oxidation of **1** *in Pyridine–*D_2O. A mixture of **1** (100 mg) and $KMnO_4$ (700 mg) in pyridine (10 ml) and D_2O (10 ml) was heated at 60 °C with stirring. After 5 h, concd HCl and $NaHSO_3$ powder were added to the ice-cooled mixture until it became an acidic, clear soln. This was extracted with ether and the extract was washed with water and a sat NaCl aq soln, and dried. Evaporation of the ether left an oil which was treated with diazomethane. The esters were separated by preparative GLC (column temp: 140—290 °C, 10 °C/min). Esters **14** (0.7 mg) and **15** (0.2 mg) were obtained.

CrO_3 Oxidation of **1** *in 3 M* D_2SO_4. A mixture of **1** (100 mg) and CrO_3 (500 mg) in 3 M D_2SO_4–D_2O (10 ml) was heated at 80 °C for 12 h with stirring. The reaction mixture was then continuously extracted with ether for 10 h and a subsequent work-up gave esters which were separated by preparative GLC giving 1.1 mg of **19**.

The authers are grateful to the Fujisawa Phamaceutical Co., Ltd., for the generous gift of ikarugamycin and for the high-resolution mass spectrometry. They are also indebted to Dr. Tadao Kondo (Nagoya University) for the 100 MHz PMR measurements.

References

1) A preliminary account of this work appeared in: S.

Ito and Y. Hirata, *Tetrahedron Lett.*, **1972**, 1181, 1185, 2557.
2) K. Jomon, Y. Kuroda, M. Ajisaka, and H. Sasaki, *J. Antibiot.*, **25**, 271 (1972).
3) The olefinic protons of *N*-methyl-*cis*-cinnamanilide have $J=12.5$ Hz, while those of the *trans* isomer, 15.5 Hz: R. M. Coates and E. F. Johnson, *J. Am. Chem. Soc.*, **93**, 4016 (1961).
4) For an example of a similar reaction, see H. Smith, *J. Chem. Soc.*, **1953**, 803.
5) F. Sanger, *Biochem. J.*, **40**, 261 (1949).
6) C. Pascual, J. Meiler, and W. Simon. *Helv. Chem. Acta*, **49**, 164 (1966).
7) J. A. Ballantine, V. Ferrito, C. H. Hassal, and V. I. P. Jones, *J. Chem. Soc.*, **1969**, 56. See also Ref. 11 for an example of the occurrence of an α-proton at an unusually low field (δ 7.13) in a dienoyltetramic acid system.
8) a) C. E. Stikings, *Biochem. J.*, **72**, 332 (1959); b) C. E. Stickings and R. J. Townsend, *ibid.*, **78**, 412 (1961).
9) a) J. Shoji, S. Shibata, U. Sankawa, H. Taguchi, and Y. Shibanuma, *Chem. Pharm. Bull.*, **13**, 1240 (1965); b) S. Shibata, "Chemistry of Microbial Products, Preprint of Symposium held on April 1964 at Tokyo," University of Tokyo, Tokyo (1964), pp. 225—227.
10) a) C. W. Holzapfel, *Tetrahedron*, **24**, 2101 (1968); b) C. W. Holzapfel and D. C. Wilkins, *Phytochemistry*, **10**, 351 (1971).
11) F. A. Mackellar, M. F. Grostic, E. C. Olson, R. J. Wnuk, A. R. Branfman, and K. L. Rinehart, Jr., *J. Am. Chem. Soc.*, **93**. 4943 (1971).
12) J. H. Golden and R. P. Linstead, *J. Chem. Soc.*, **1958**, 1732.
13) a) H. R. Snyder and R. E. Putnan, *J. Am. Chem. Soc.*, **76**, 33 (1954); b) S. Ito and Y. Hirata, *Bull. Chem. Soc. Jpn.*, **46**, 672 (1973).
14) S. Ito and Y. Hirata, *Bull. Chem. Soc. Jpn.*, **50**, 227 (1977).
15) H. Budzikiewicz, C. Djerassi, D. H. Williams, "Mass Spectrometry of Organic Compounds," Holden-Day, San Francisco, Cal. (1967), p 155.
16) K. Alder and M. Schumacher, *Justus Liebigs Ann. Chem.*, **564**, 96 (1949).
17) K. Alder, H.-H. Mölls, and R. Reeber, *Justus Liebigs Ann. Chem.*, **611**, 7 (1958).
18) S. Ito and Y. Hirata, *Bull. Chem. Soc. Jpn.*, **46**, 603 (1973).
19) a) F. W. Kay and W. H. Perkin, Jr., *J. Chem. Soc.*, **1906**, 1640; b) K. Freudenberg and J. Geiger, *Justus Liebigs Ann. Chem.*, **575**, 145 (1952).
20) These new compounds were synthesized in unambiguous manners. The syntheses will be reported elsewhere.
21) M. E. Dobson, J. Ferns, and W. H. Perkin, Jr., *J. Chem. Soc.*, **1909**, 2012.
22) S.-C. J. Fu, K. R. Rao. S, M. Birnbaum, and J. P. Greenstein, *J. Biol. Chem.*, **199**, 207 (1952).
23) J. K. M. Sanders and D. H. Williams, *J. Am. Chem. Soc.*, **93**, 641 (1971).

Oxidation of 2,6-Piperazinediones

Tatsuo TANAKA, Hiroaki YAMAZAKI, and Masaki OHTA

Department of Industrial Chemistry, Faculty of Engineering, Ibaraki University, Nakanarusawa-cho, Hitachi-shi, Ibaraki 316

(Received January 6, 1977)

1,4-Disubstituted 2,6-piperazinediones (**1**) are susceptible to oxidation at the methylene group in the piperazine ring, giving piperazinetetrone (**4**) on being treated with selenium dioxide in boiling dioxane. Treatment of 1,4-diphenyl-2,6-piperazinedione (**1a**) with either nitrobenzene or tosyl chloride and triethylamine in benzene gives cyclic dimer (**9**) of dehydrogenated **1a**. Cycloadduct (**10**) is obtained in the presecne of *N*-phenylmaleimide. It seems that both **9** and **10** are formed *via* labile mesoionic intermediate (**8**). Piperazinedione (**1a**) reacted with tosyl chloride, pyridine, and benzoyl chloride to give mesoionic compound (**11**) having 3-benzoyl and 5-(*p*-tolylthio) groups.

Only a few papers have appeared on the oxidation of 2,6-piperazinedione derivatives. Oxidation of piperazinediones by chromium trioxide[1] or nitric acid[2] was reported to afford piperazinetetrones. Honzl *et al.*[3] reported that the reaction of 1,4-disubstituted 2,6-piperazinedione (**1**) with phosphorus pentachloride followed by hydrolysis afforded a piperazinetetrone, while the reaction of 1,4-disubstituted 2,6-piperazinedione with arenesulfonyl chloride in pyridine yielded six-membered mesoionic compound (**2**) by dehydrogenation and substitution at positions 3 and 5. The reaction of 1,4-disubstituted 2,6-piperazinedione with chloranil afforded cycloadducts (**3**) formed by the addition of chloranil to the dehydrogenated 2,6-piperazinedione at positions 3 and 5.[4]

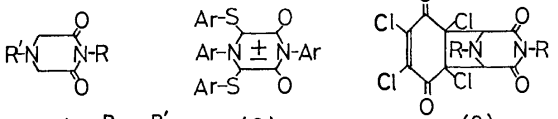

(1) R R′
a: Ph Ph
b: Ph CH_3
c: Ph $PhCH_2$
d: $PhCH_2$ $PhCH_2$

(2) (3)

The peculiar behavior of 2,6-piperazinedione to form a mesoionic intermediate is similar to that of hydrogenated benzenoid aromatics which show a tendency to form aromatic systems by dehydrogenation. These results prompted us to examine the behavior of 2,6-piperazinedione towards various oxidizing reagents. The positions susceptible to oxidation are apparently 3 and 5, the anticipated reactions being the formation of piperazinetetrone (**4**) and a mesoionic intermediate (**8**). The final products of the latter reaction depend on the stability of the mesoionic intermediate and the nature of the oxidizing reagents employed. In the case the intermediate is labile, isolation of its substituted derivative, dimerization product or cycloadduct with a trapping reagent may be anticipated. The present paper deals with the reaction of 1,4-disubstituted 2,6-piperazinediones with several oxidizing reagents other than those so far reported.

Results and Discussion

Oxidation with Selenium Dioxide. Selenium dioxide is usually used for the oxidation of an active methylene or methyl group to a carbonyl group and sometimes

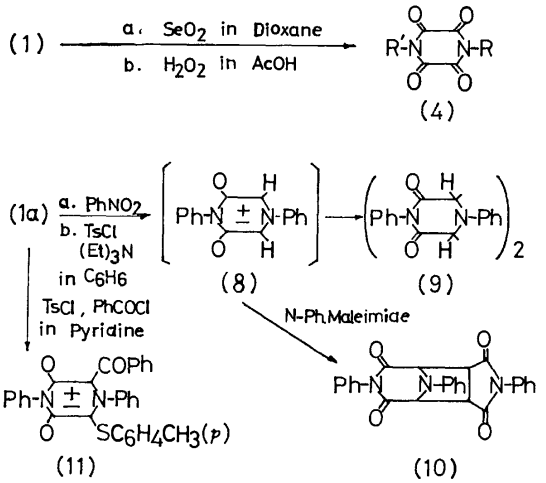

Fig. 1. Reaction scheme of 1,4-disubstituted 2,6-piperazinediones.

for the dehydrogenation of dihydroaromatics to aromatic compounds. We have found that the oxidation of 1,4-disubstituted 2,6-piperazinediones (**1**) with selenium dioxide in dioxane afforded the corresponding piperazinetetrones, (**4a**—**d**) no formation of mesoionic intermediate being observed. The yields, melting points, and IR absorptions of the products are summarized in Table 1.

When some acid anhydrides are used as the cyclization reagent in the synthesis of five-membered mesoionic heterocycles, the products isolated are frequently their stable derivatives formed by acylation of the cyclization products.[5] An attempt to isolate the labile intermediate in the form of its acetyl derivatives by using acetic anhydride instead of dioxane was unsuccessful.

In view of the current mechanism of the selenium dioxide oxidation,[6] the selective oxidation of ring methylene group to carbonyl group can be ascribed to the initial enolization which facilitates the attack of selenium dioxide. When 1,4-diphenyl- or 1-phenyl-4-benzyl-2,6-piperazinedione was oxidized with selenium dioxide in dioxane, a samll amount of the corresponding *N*,*N*′-disubstituted oxamide was isolated along with the tetrone. That these oxamides are formed by hydrolysis of the tetrones was confirmed by a separate experiment wherein the hydrolysis of 1,4-diphenylpiperazinetetrone in boiling dioxane containing a small amount of water in the presence of selenium dioxide

TABLE 1. PRODUCTS FROM THE OXIDATION OF 1,4-DISUBSTITUTED 2,6-PIPERAZINEDIONE WITH SELENIUM DIOXIDE

	Product R	Product R'	Mp (°C) (Recryst. solv.)	IR (cm^{-1})			Yield (%)	By-product (Yield %)
4a	Ph	Ph	290—295 (DMF-EtOH)	1770 1689	1710 1680	1696	34	$(PhNHCO)_2$ (6%)
4b	Ph	CH_3	314—316 (DMF-EtOH)	1767 1704	1744 1688	1712	65	
4c	Ph	$PhCH_2$	268—271 (Acetone-Et_2O)	1770 1688	1713	1704	46	$PhNHCOCONHCH_2Ph$ (3%)
4d	$PhCH_2$	$PhCH_2$	263—265 (CH_2CN)	1760 1686	1705	1696	99	

afforded *N,N'*-diphenyloxamide. The formation of the tetrone derivatives was also observed when 1,4-diphenyl-2,6-piperazinedione was oxidized with hydrogen peroxide in acetic acid.

Reaction with Bromine. Investigation of the behavior of 2,6-piperazinediones towards bromine seems to be of interest in view of the validity of bromine both as an oxidizing and brominating reagent and the polyfunctional structure of 1,4-disubstituted 2,6-piperazinedione. Among the reactions of bromine we have carried out, only one reaction gave an isolable product: the reaction of 1,4-diphenyl-2,6-piperazinedione (**1a**) with an equimolar of bromine in acetic acid at room temperature occurred immediately affording 4-(*p*-bromophenyl)-1-phenyl-2,6-piperazinedione hydrobromide which was readily hydrolyzed by water to give the free base (**5**). This shows that the *p*-position of the 4-phenyl substituent is activated by the amino nitrogen towards electrophilic substitution. Further reaction of the free base with bromine in chloroform immediately gave a precipitation, but work up of the precipitate gave mostly the starting material. From the mother liquor of the reaction, trione (**6**) was isolated in poor yield which was characterized by elemental and spectral analyses. When **5** was reacted with bromine in nitrobenzene at 100 °C, tetrone (**7**) was isolated along with the trione in a poor yield.

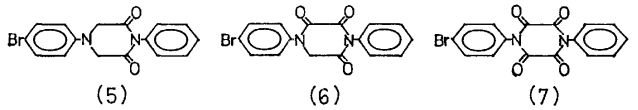

(5) (6) (7)

Oxidation with Nitrobenzene. A well-known reaction in which nitrobenzene plays a role of dehydrogenation to form an aromatic system is the Skraup synthesis of quinoline. The fact that 2,6-piperazinediones are readily dehydrogenated to an aromatic system led us to investigate the reaction of 2,6-piperazinediones with nitrobenzene, the formation of mesoionic intermediates being expected.

When **1a** was heated in nitrobenzene under reflux, a product isolated in poor yield was considered to be a dimer of mesoionic intermediate (**8**) on the basis of elemental and spectral analyses. The formation of this dimer (**9**) was not observed at 170—175 °C and decomposition of **1a** predominated at 210 °C. It was found that the addition of acetic anhydride to the reaction mixture loweres the reaction temperature, improving the yield of the dimer to 23%. However, the role of acetic anhydride in this reaction remains unsettled. The formation of the dimer may be ascribed to the dimerization of the 1,3-dipolar mesoionic intermediate (**8**). The proposed intermediate could successfully trapped by addition of *N*-phenylmaleimide to the reaction mixture and a cycloadduct (**10**) was obtained. **10** was isolated by the reaction of **1a** with chloranil in the presence of *N*-phenylmaleimide.[4]

Reaction of 2,6-Piperazinedione with Tosyl Chloride. Honzl *et al.* obtained mesoionic compounds (**2**) by the reaction of 2,6-piperazinedione with tosyl chloride in pyridine, though the mechanism of this reaction remains unsolved. We tried to improve the yield of the mesoionic product following their procedure[3] by varying the reaction time, reaction temperature, molar ratio of the reactants and using pyridine homologues as the solvent instead of pyridine. However, no improvement was achieved. The reaction of 2,6-piperazinedione with tosyl chloride in benzene in the presence of triethylamine gave the same dimer (**9**) as that obtained by oxidation of 2,6-piperazinedione with nitrobenzene. When the reaction was carried out in the presence of *N*-phenylmaleimide, the cycloadduct (**10**) was obtained. We then performed the reaction of 2,6-piperazinedione with tosyl chloride in pyridine in the presence of benzoyl chloride anticipating the formation of a mesoionic compound having benzoyl groups instead of *p*-tolylthio groups of compound **2**. The reaction gave mesoionic compound (**11**) with a 3-benzoyl-5-(*p*-tolylthio) substituent in 14% yield along with a small quantity of **2**, no 3,5-dibenzoyl derivative being isolated. Compound **11** could be formed neither from **1a** nor **2** by heating with benzoyl chloride in pyridine. This indicates that **11** was formed not *via* **2**, but presumably by benzoylation of mesoionic intermediate having one *p*-tolylthio group.

Experimental

All the melting points are uncorrected. The IR spectra were recorded on a JASCO IRA-2 spectrometer and NMR spectra on a JEOL H-100 spectrometer.

Materials. Commercial selenium dioxide, chloroform, nitrobenzene, triethylamine, benzoyl chloride, pyridine, and *N*-phenylmaleimide were used without further purification. Dioxane was distilled and tosyl chloride was recrystallized from benzene.

General Procedure for Oxidation with Selenium Dioxide. Selenium dioxide (10 mmol) was added to a solution of 1,4-disubstituted 2,6-piperazinedione (5 mmol) in dioxane (20 ml), and the resulting mixture was refluxed for 6 h. After being cooled, solid products were collected by filtration and subjected to continuous extraction with acetone in a Soxhlet apparatus. The extract was evaporated to dryness under reduced pressure and the residue was recrystallized from the solvents given in Table 1.

*1-Methyl-4-phenylpiperazinetetrone (**4b**).* Colorless silky crystals, mp 314—316 °C. Found: C, 56.86; H, 3.38; N, 12.21%. Calcd for $C_{11}H_8N_2O_4$: C, 56.89; H, 3.48: N, 12.07%.

*1-Benzyl-4-phenylpiperazinetetrone (**4c**).* Colorless silky crystals, mp 268—271 °C. Found: C, 66.30; H, 3.96; N, 8.93%. Calcd for $C_{17}H_{12}N_2O_4$: C, 66.22; H, 3.93; N, 9.09 %.

*1,4-Dibenzylpiperazinetetrone (**4d**).* Colorless needles, mp 263—265 °C. Found: C, 67.19; H, 4.38; N, 8.79%. Calcd for $C_{18}H_{14}N_2O_4$: C, 67.07; H, 4.39; N, 8.69%.

*4,9,11,12-Tetraphenyl-4,9,11,12-tetraazatricyclo[5.3.1.1^{2,6}]dodecane-3,5,8,10-tetrone (**9**).* *Method A*: A mixture of **1a** (3 g, 11.3 mmol), acetic anhydride (2.3 g, 22.6 mmol), and nitrobenzene (30 ml) was heated at 170—175 °C for 5 h. The mixture was concentrated under reduced pressure and cooled, and the resulting brown solid was filtered and washed with ethanol. Recrystallization of the solid from DMSO gave 0.8 g (27%) of **9**. Colorless needles, mp 420—423 °C. Found: C, 72.35; H, 4.60; N, 10.58%. Calcd for $C_{32}H_{24}N_4O_4$: C, 72.71; H, 4.58; N, 10.60%. IR (KBr): 1730, 1690 cm^{-1}. MS: *m/e* 528 (M$^+$).

Method B: Triethylamine (3 g, 30 mmol) was added to a solution of **1a** (4 g, 15 mmol) and tosyl chloride (5.7 g, 30 mmol) in benzene (55 ml), and the resulting mixture was refluxed for 27 h. The solvent was evaporated under reduced pressure to give an oil which gradually crystallized by addition of a small amount of benzene under cooling. The crystals were filtered and washed with water to give 0.4 g (10%) of crude **9**.

*4,9,11-Triphenyl-4,9,11-triazatricyclo[5.3.1.0^{2,6}]undecane-3,5,8,-10-tetrone (**10**).* *Method A*: A mixture of **1a** (1 g, 3.3 mmol), *N*-phenylmaleimide (0.65 g, 3.8 mmol), and nitrobenzene (15 ml) was refluxed for 8 h. After cooling, crystals were filtered and washed with diethyl ether. Recrystallization of the product from acetonitrile gave 0.2 g (12%) of **10** as colorless needles, mp 326—327 °C. IR (KBr): 1742, 1708, 1684 cm^{-1}. The product was identified as **10** by comparison of its IR spectrum and mixed melting point measurement with the authentic sample synthesized by the method using chloranil.[4]

Method B: Triethylamine (0.8 g, 8 mmol) was added to a solution of **1a** (1 g, 3.8 mmol), *N*-phenylmaleimide (0.65 g, 3.8 mmol), and tosyl chloride (1,5 g. 7.9 mmol) in benzene (10 ml), and the mixture was refluxed for 20 h. White crystals formed gradually during the course of heating were filtered and washed with water. The crude product was recrystallized from acetonitrile.

*Anhydro-3-benzoyl-2,6-dihydroxy-1,4-diphenyl-5-(p-tolylthio)-pyrazinium dihydroxide (**11**).* A solution of benzoyl chloride (3.2 g, 22.6 mmol) in pyridine (15 ml) was added dropwise to a solution of **1a** (3 g, 11.3 mmol) and tosyl chloride (4.3 g, 22.6 mmol) in pyridine (40 ml) under reflux over a period of 1 h. The resulting mixture was refluxed for 19 h. After cooling, the reaction mixture was poured into ice-water and the resulting dark brown solid was chromatographed on silica gel using chloroform as an eluent. The 4th fraction gave 0.73 g (13.8%) of **11** as yellow needles, mp *ca.* 240 °C. This was recrystallized from 1-propanol to give yellow needles, mp 244—245 °C. Found: C, 73.13; H, 4.58; N, 5.54%. Calcd for $C_{30}H_{22}N_2O_3S$: C, 73.45; H, 4.52; N, 5.71%. IR (KBr): 1675, 1650, 1620 cm^{-1}. NMR (τ): 2.4—3.0 (m, 19, Ar-H), 7.75 (s, 3, CH_3). MS: *m/e* 490 (M$^+$).

Mesoionic 1,4-diphenyl-3,5-di(*p*-tolylthio) derivative (**2**) was isolated from the 3rd fraction of chromatography described above as yellow needles, mp 239—241 °C.

References

1) P. W. Abenius and C. A. Bishoff, *J. Prakt. Chem.*, **40**, 428 (1889).

2) J. V. Dubsky, *Ber.*, **49**, 1037 (1916).

3) J. Honzl, M. Šorm, and V. Hanuš, *Tetrahedron*, **26**, 2305 (1970).

4) T. Tanaka, T. Yokokura, and M. Ohta, *Nippon Kagaku Kaishi*, **1976**, 1450.

5) M. Ohta and H. Kato, "Nonbenzenoid Aromatics," Vol. 1, ed by J. P. Snyder, Academic Press, New York, N. Y. (1969), p. 189, 205.

6) Y. Ogata, "Oxidation and Reduction of Organic Compounds," Nankōdō, Tokyo, Japan (1963), p. 486.

The New Schizandrin-type Lignans, Kadsurin and Kadsurarin

Yuh-Pan CHEN, Rolan LIU, Hon-Yen HSU, Shosuke YAMAMURA,*†
Yoshikazu SHIZURI,** and Yoshimasa HIRATA**

Brion Research Institute of Taiwan, 116 Chung-Ching S. Rd., Sec. 3, Taipei, Taiwan
**Faculty of Pharmacy, Meijo University, Tenpaku-ku, Nagoya 468*
***Chemical Institute, Nagoya University, Chikusa-ku, Nagoya 464*

(Received January 10, 1977)

Two new lignans, kadsurin and kadsurarin, were isolated from *Kadsura japonica* Dunal, and their structures were established. The stereostructures of the schizandrin-type lignans including their conformations were elucidated by measurements of intramolecular nuclear Overhauser effects.[1)]

The decoction of the stems of *Kadsura japonica* Dunal ("Binnan Kadsura" in Japanese) is used in Taiwan as a remedy for snake-bites and also as an antipyretic, antispasmodic and anodyne by the local people.[2)] In the course of our search for physiologically active substances of this plant, we isolated two new schizadrin-type lignans, named kadsurin (**1**) and kadsurarin (**2**). In this paper we wish to describe the isolation and structures of kadsurin and kadsurarin. The conformation of these new lignans with a cyclooctadiene system, which can adopt two possible conformers, is discussed.

The dried stems of *Kadsura japonica* Dunal were pluverized, and then extracted with a large amount of hexane. The extracts were directly chromatographed on silica gel (Kieselgel, E. Merck, Darmstadt) and eluted with hexane–EtOAc (4 : 1) to give colorless needles of kadsurin (**1**), mp 157—158 °C, in a 0.0015% yield. Further elution with hexane–EtOAc (2 : 1) afforded colorless needles of kadsurarin (**2**), mp 255—256 °C, in a 0.005% yield.

Structure of Kadsurin. Kadsurin (**1**) has a molecular formula $C_{25}H_{30}O_8$, and can be regarded as a biphenyl-type compound with two aromatic protons (δ 6.48 and 6.60) on the basis of its spectral data [ν_{max} 1615, 1600, 1585, and 1495 cm^{-1}; λ_{max} 278, 254, and 230 nm (ε, 3500, 11300, and 26300, respectively)]. The UV spectrum of this lignan in particular is almost superimposable on that of schizandrin (**3**),[3)] indicating that kadsurin is a schizandrin-type lignan. From the NMR spectral data (see the Table), kadsurin has four methoxyl groups (δ 3.65, 3.83, 3.89, and 3.92) and one methylenedioxy group (δ 5.99). All of them should be attached to the two aromatic rings, although their accurate positions are still uncertain. The presence of a partial structure [■–CH(OAc)–CH(Me)–CH(Me)–CH_2–■] can be confirmed by analysis of the NMR spectrum of kadsurin with aid of double resonance experiments: irradiation at the center of δ 1.92—2.20 (2H, complex) caused each signal at δ 0.95, 1.08, 2.67, and 5.67 to collapse to a sharp singlet. The presence of the AcO–$\underset{|}{C}$H– grouping is also confirmed by its mass and NMR spectra [*m/e* 398(M^+—AcOH); δ 1.60 and 5.67] together with the following chemical evidence. Reduction of Kadsurin (**1**) with $LiAlH_4$ (room temp, 6 h) readily afforded the corresponding hydroxy compound (**4**) (mp 134—135 °C; $C_{23}H_{28}O_7$; ν_{max} 3560 cm^{-1}) in high yields, although **1** resisted base-catalyzed hydrolysis (0.5 M KOH in MeOH–dioxane) in contrast to kadsurarin (**2**). In the NMR spectrum of **4**, the sharp singlet at δ 1.60 in **1** was not observed, but the signal at δ 5.67 in **1** shifted to δ 4.64 in a higher magnetic field. The structure including the position of each functional group and conformation of kadsurin (**1**) was clarified by measurement of intramolecular nuclear Overhauser effects (NOE), as follows.

Low intensity irradiation at δ 5.67 (AcO–$\underset{|}{C}$H–) caused a 21% increase in the integrated intensity of one of the aromatic protons (H^a), no enhancement of the signal intensity of the remaining proton (H^b) being observed. This indicates that the distance between H^a and the proton, which is attached to the carbon atom bearing the acetoxyl group, is short. It should be noted that the signal intensity of H^a was not increased by irradiation at the frequencies corresponding to the absorbance of each methoxyl group, indicating that none of them

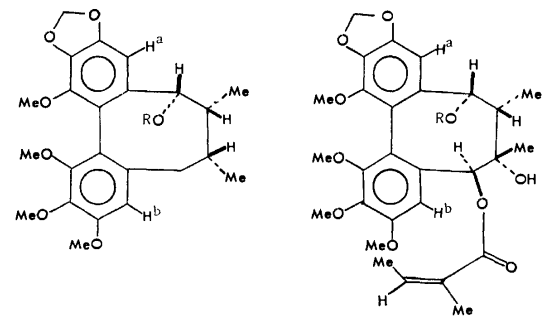

1 R=Ac
4 R=H

2 R=Ac
5 R=H

(a)

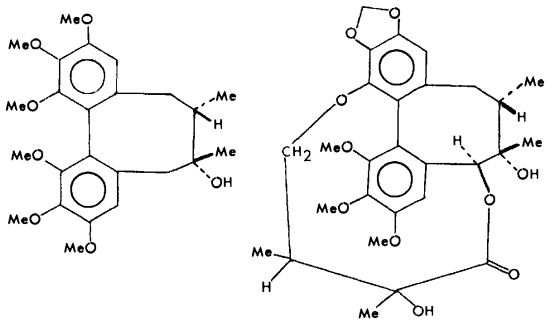

3

6

(b)

Fig. 1.

† To whom inquiries should be addressed.

TABLE. NMR SPECTRA OF KADSURIN (**1**) AND KADSURARIN (**2**)

1	**2**
0.95(3H, d, J=7.0 Hz)	
1.08(3H, d, J=7.0 Hz)	1.23(3H, d, J=6.8 Hz)
	1.36(3H, s)
	1.40(3H, fine spritted s)
1.60(3H, s)	1.60(3H, s)
	1.85(3H, dq, J=7.5, 1.5 Hz)
	2.10(1H, br s, OH)
1.92—2.20(2H, complex)	2.16(1H, q, J=6.8 Hz)
2.67(2H, d, J=4.2 Hz)	
3.65(3H, s)	3.64(3H, s)
3.83(3H, s)	3.75(3H, s)
3.89(3H, s)	3.90(3H, s)
3.92(3H, s)	3.95(3H, s)
5.67(1H, br s)	5.68(2H, br s)
5.99(2H, br s)	5.90(2H, s)
	6.00(1H, br q, J=7.5 Hz)
6.48(1H, s)	6.43(1H, s)
6.60(1H, s)	6.60(1H, s)

can occupy the position adjacent to H^a. Thus, the remaining methylenedioxy group should be located at the position adjacent to H^a, as shown in [A]. In the next step, the measurements of NOE were focused on the signal (δ 6.60) corresponding to the aromatic proton H^b. Low intensity irradiation at δ 3.92, 2.67, and 0.95 caused 11, 13, and 9.6% enhancement, respectively, of the signal intensity of H^b. Therefore, one of four methoxyl groups (δ 3.92) should be located at a position adjacent to H^b, and one of two secondary methyl groups (δ 0.95) and H^b should be close to each other. The configuration of the remaining secondary methyl group was clarified by the following NOE measurements. Low intensity irradiation at δ 1.08 caused a 12% increase of the signal intensity of the proton attached to the carbon atom bearing the acetoxyl group (δ 5.67), no interaction between the secondary methyl group (δ 1.08) and H^a (δ 6.48) being detected. The undetermined secondary methyl group (δ 1.08) should be placed in such a space as depicted in [A]. This is also confirmed by the appearance of the NMR singlet at δ 5.67 with J value ($\approx$0 Hz), indicating that the dihedral angle between the two vicinal methine protons is almost 90°. Thus, the results can be explained only by the conformation [A] for kadsurin (**1**), and not by the other conformation [B].

Structure of Kadsurarin. Kadsurarin (**2**), whose molecular formula is $C_{30}H_{36}O_{11}$, has the same schizandrin-type chromophore as that of kadsurin (**1**) on the basis of its spectral data [ν_{max} 1620, 1585 sh and 1500 cm^{-1}; λ_{max} 280, 255, and 231 nm (ε, 3200, 10600, and 30000, respectively); δ 6.43 and 6.60]. Further analysis of its NMR spectrum indicates that kadsurarin (**2**) has the same carbon skeleton as that of **1** except for some functional groups.

Comparing the NMR spectra of **1** and **2** (see the Table), we see that the former has two secondary methyl groups (δ 0.95 and 1.08) and one methylene group

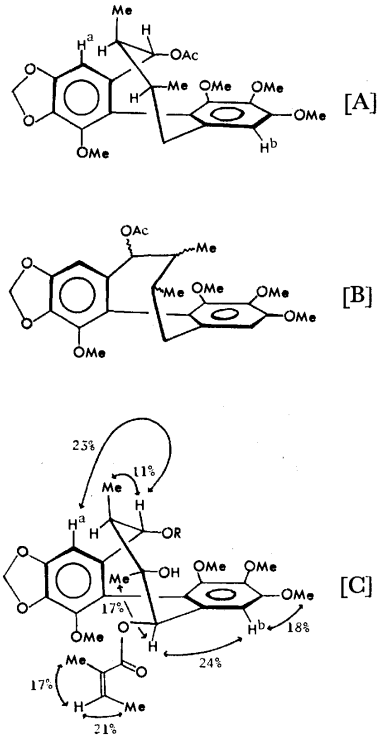

Fig. 2.

(δ 2.67), while **2** has one secondary methyl group (δ 1.27) and no methylene group. However, the latter has a tertiary methyl group (δ 1.36) on the carbon atom having a hydroxyl group, and one proton (δ 5.68)[4] attached to the carbon atom bearing an oxygen atom constituting a part of the angelate (δ 1.40, 1.85, and 6.00).

Kadsurin (**1**) is quite stable under basic conditions. However, when treated with 0.5 M KOH in MeOH–dioxane (room temp, 4.5 h), kadsurarin (**2**) was selectively converted into deacetyl kadsurarin (**5**), mp 227—228 °C ($C_{28}H_{34}O_{10}$), in high yields. In the NMR spectrum of **5**, a new singlet was observed at δ 4.84 (1H) instead of disappearance of the sharp singlet at δ 1.60 (3H) in **2** together with decrease in the integrated intensity at δ 5.68 in **2**. The easy and selective hydrolysis of the acetoxyl group in **2** is attributable to a proximity effect of the tertiary hydroxyl group, whose configuration is based on the NOE measurements of **5**. As shown in [C], the results are essentially similar to those of kadsurin (**1**) except for the following points. No interaction between the tertiary methyl group (δ 1.32) and H^b was detected. However, low intensity irradiation at δ 1.32 caused a 17% enhancement of the integrated intensity of the singlet at δ 5.66. This indicates that the configuration of the tertiary methyl group in **2** clearly differs from that of the corresponding secondary methyl group in **1**. As the first example, the stereostructures of schizandrin-type lignans were established. The stereostructure of schizandrin is still undetermined,[3] but may be similar to that of kadsurarin (**2**), as shown in **3**.

Quite recently, Ikeya *et al.* reported the isolation of gomicin D (**6**), whose stereostructure was also elucidated by means of an X-ray crystallographic analysis of the

corresponding dibromide.[5] The stereostructure of gomicin D is identical with that of kadsurarin (**2**), suggesting that the former can be produced from deacetoxykadsurin in the plant.

Experimental

All the mps are uncorrected. IR spectra were recorded on a JASCO IR-S spectrophotometer. UV spectra were taken on a Perkin-Elmer 202 spectrophotometer using MeOH as a solvent. NMR spectra were recorded on a Varian HA-100 NMR spectrometer using $CDCl_3$ as a solvent. The chemical shifts are given in ppm relative to the internal TMS, only prominent signals being cited (d, doublet; m, multiplet; q, quartet; s, singlet; t, triplet). Mass spectra were obtained on a Hitachi RMU-6D mass spectrometer, operating with an ionization energy of 70 eV. Optical rotations were measured on a JASCO ORD/UV-5 spectrometer using $CHCl_3$ as a solvent.

Isolation of Kadsurin and Kadsurarin. The dried material (2 kg) of the stems of the plant *Kadsura japonica* Dunal was pulverized and extracted with hexane (8 l) by refluxing for 3 h. The hot mixtures were filtered from the undissolved residue which was extracted again in the same way using hexane (8 l). The combined filtrates were evaporated to dryness under reduced pressure. The resulting dark green substance (20 g) was directly chromatographed on silica gel (Kieselgel, E. Merck, Darmstadt) (800 g), and eluted with hexane–EtOAc (4 : 1) to give crude crystals which were repeatedly recrystallized from EtOH to afford colorless needles (30 mg) of kadsurin (**1**); mp 157—158 °C; $[\alpha]_D^{25} = -39°$ ($c=0.13$); ν_{max} (Nujol) 1735, 1615, 1600, 1585, and 1495 cm^{-1}; *m/e* 458 (M^+) and 398 (M^+-60) ($m^*=346$) (Found: C, 65.33; H, 6.66%. Calcd for $C_{25}H_{30}O_8$: C, 65.49; H, 6.60 %). Further elution with hexane–EtOAc (2 : 1) afforded crude crystals, which were recrystallized from EtOAc to give colorless needles (100 mg) of kadsurarin (**2**); mp (dec) 255—256 °C (in a sealed tube); $[\alpha]_D^{25} = -65°$ ($c=0.10$); ν_{max} (Nujol) 3550, 1735, 1720 sh, 1643 sh, 1620 1600 1585 sh, and 1500 cm^{-1}; *m/e* 572 (M^+), 512 (M^+-60) ($m^*=458$), and 412 (Found: C, 63.49; H, 6.28%. Calcd for $C_{30}H_{36}O_{11}$: C, 62.95; H, 6.30%).

Reduction of Kadsurin with $LiAlH_4$. To a solution of kadsurin (20 mg) in tetrahydrofuran (2 ml) was added $LiAlH_4$ (10 mg) at room temperature for 6 h with stirring. After decomposition of excess reagent with ice water, the reaction mixture was diluted with 5% HCl aq solution, and then extracted with EtOAc. The extract was washed with water and then dried over anhydrous Na_2SO_4. Removal of the solvent under reduced pressure gave a white solid (17 mg), which was recrystallized from MeOH to afford colorless needles of deacetylkadsurin (**4**); mp 134—135 °C; ν_{max} (Nujol) 3560, 1620, 1595, 1575, and 1495 cm^{-1}; δ 0.95 (3H, d, $J=$ 7.0 Hz), 1.17(3H, d, $J=7.0$ Hz), 1.45 (1H, br s, OH), 1.95 (1H, q, $J=7.0$ Hz), 2.05(1H, m), 2.65(2H, d, $J=4.5$ Hz), 3.68(3H, s), 3.84 (3H, s), 3.89(3H, s), 3.90(3H, s), 4.64(1H, br.s), 5.98 (2H, s), 6.34(1H, s), and 6.60(1H, s); *m/e* 416 (M^+) and 398 (Found: *m/e* 416.1829. Calcd for $C_{23}H_{28}O_7$: *m/e* 416.1835).

Hydrolysis of Kadsurain with Methanolic KOH. To a solution of kadsurarin (23 mg) in a mixed solvent of dioxane (1 ml) and MeOH (0.5 ml) was added, with stirring, 0.5 M methanolic KOH (1 ml) at room temperature. The resulting solution was stirred at room temperature for 4.5 h, and then diluted with a large amount of water to give crystalline precipitates, which were washed with water and then dried under reduced pressure. Recrystallization from hexane–EtOAc afforded colorless needles (16 mg) of deacetylkadsurarin (**5**); mp 227—228 °C; ν_{max} (Nujol) 3500 br, 1715, 1645 sh, 1620, 1585 sh, and 1500 cm^{-1}; δ 1.32 (3H, s), 1.36 (3H, d, $J=$ 7.2 Hz), 1.39(3H, fine splitted s), 1.73(2H, br s, OH), 1.85 (3H, dq, $J=7.5$, 1.7 Hz), 1.98(1H, q, $J=7.2$ Hz), 3.73(6H, s), 3.87(3H, s), 3.90(3H, s), 4.84(1H, s), 5.66(1H, s), 5.88 (1H, d, $J=1.2$ Hz), 5.92(1H, d, $J=1.2$ Hz), 5.99(1H, qq, $J=7.5$, 1.5 Hz), 6.28(1H, s), and 6.76(1H, s), *m/e* 530 (M^+), 512 and 412 (Found: *m/e* 530.2146. Calcd for $C_{28}H_{34}O_{10}$: *m/e* 530.2152).

The authors wish to thank Drs. Masayasu Kurono and Masaaki Toda, Ono Central Research Laboratories, for measurements of high resolution mass spectra.

References

1) Preliminary communication: Y. Chen, R. Liu, H. Hsu, S. Yamamura, Y. Shizuri, and Y. Hirata, *Tetrahedron Lett.*, **1973**, 4257.

2) S. Sasaki, "Taiwan Minkan Yakuyo Shokubutsu," Kobunkan, Taipei, Taiwan (1924), p. 4; W. S. Kan, "Pharmacetical Botany," National Research Institute of Chinese Medicine, Taipei, Taiwan (1973), p. 242; H. Y. Hsu, "Illustrations of Chinese Herb Medicine of Taiwan," National Health Administration, Taipei, Taiwan (1972), p. 68.

3) N. K. Kochetkov O. S. Chizhov and V. I. Sheichenko, *Tetrahedron Lett.*, **20**, 730 (1961) and references cited therein,

4) The signal at δ 5.68 is due to two protons, one of which is attached to the carbon atom bearing the acetoxyl group.

5) Y. Ikeya, H. Taguchi, and Y. Iitaka, *Tetrahedron Lett.*, **1976**, 1359.

†† The plant was collected at Chiayi, Taiwan.

Studies of Unusual Amino Acids and Their Peptides. VIII. The Syntheses of an Iminohexapeptide as a Model of Bottromycin and Its Related Iminopeptides[1]

Takashi YAMADA, Toshifumi MIYAZAWA, Shigeru KUWATA, and Hiroshi WATANABE

Laboratory of Chemistry, Faculty of Science, Kōnan University, Okamoto, Higashinada-ku, Kobe 658

(Received January 17, 1977)

As a model of bottromycin, the structure of which had been proposed by Nakamura *et al.*, an iminohexapeptide, Z–Val–Val–ImPro–Gly–Phe–Phe–OMe, and its related iminopeptides were synthesized in good yields. These syntheses were achieved by the condensation of the imidates, Z–ImPro–OEt, Z–Val–ImPro–OEt·HCl, or Z–Val–Val–ImPro–OEt·HCl, with the peptide esters, Gly–Phe–OMe·HBr or Gly–Phe–Phe–OMe·HCl, in the presence of triethylamine. All of the resulting iminopeptides were isolated as the hydrobromide or the hydrochloride. The pK_a values of these iminopeptide salts were measured to be 9.75—9.3 in methanol–water; they showed that the pK_a rule of Nakamura *et al.* could not be applied in the cases of these iminopeptides.

In a previous paper,[2] we have reported on some properties and reactions of iminodipeptides and concluded that it is impossible to elongate the *C*-terminal of *N*-benzyloxycarbonyl(Z)-(iminoprolyl)glycine[3] because of the easy formation of an imidazolone derivative. This means that bottromycin (Fig. 1), the structure of which was proposed by Nakamura *et al.*,[1,4] could not be synthesized by the fragment condensation of the three already known dipeptide components; pivaloyl-*t*-leucylvaline,[5] (iminoprolyl)glycine,[2] and *β*-methylphenylalanyl-*β*-(2-thiazolyl)-*β*-alanine methyl ester.[6] Another possible route to build up bottromycin may be through the coupling of the two tripeptide components (pivaloyl-*t*-leucylvalyl(iminoproline) and glycyl-*β*-methylphenylalanyl-*β*-(2-thiazolyl)-*β*-alanine methyl ester) at the iminopeptide bond situated in the middle of this antibiotic molecule, because imidazolone formation could successfully be avoided by locating a carboxyl group (or an alkoxycarbonyl group) sufficiently apart from an imino group in the molecule—*e.g.*, the imidate (I) could be coupled with the dipeptide ester (II), affording the desired iminotripeptide (III)[2] (Scheme 1).

In order to ascertain the possibility of the latter method, as well as to reveal the properties of iminopeptides, we tried to synthesize an iminohexapeptide, Z–Val–Val–ImPro–Gly–Phe–Phe–OMe (XVII), as a model of bottromycin, and its related iminopeptides.

As the *N*-terminal fragments for this purpose, three sorts of imidates were prepared: ethyl *N*-Z-2-pyrrolidinecarboximidate (I),[2] ethyl *N*-(*N*-Z-valyl)-2-pyrrolidinecarboximidate hydrochloride (VII), and ethyl *N*-(*N*-Z-valylvalyl)-2-pyrrolidinecarboximidate hydrochloride (XI). The synthetic routes of these compounds are shown in Scheme 2. The imidates thus obtained were used for the next reaction without further purification.

As the *C*-terminal components, glycylphenylalanine methyl ester hydrobromide (II) and glycylphenylalanylphenylalanine methyl ester hydrochloride (XII) were used. Every coupling reaction was carried out by stirring a methanol solution of a free imidate, prepared from the hydrochloride just before the reaction, or an imidate hydrochloride itself, and a peptide ester salt in the presence of triethylamine at room temperature for 2 days. The products were isolated by chromatography on silica gel.

By the coupling of the imidate (I) with the dipeptide

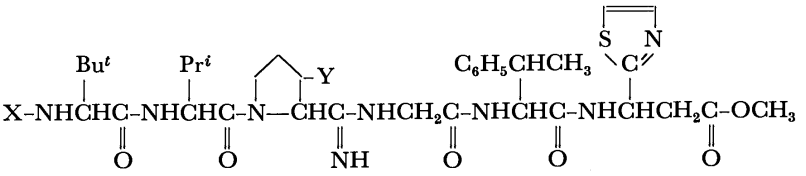

Fig. 1. The structure of bottromycin proposed by Nakamura *et al.*
X=pivaloyl or 4-methyl-2-pentenoyl; Y=H or CH_3;
Bu^t=*t*-butyl; Pr^i=isopropyl

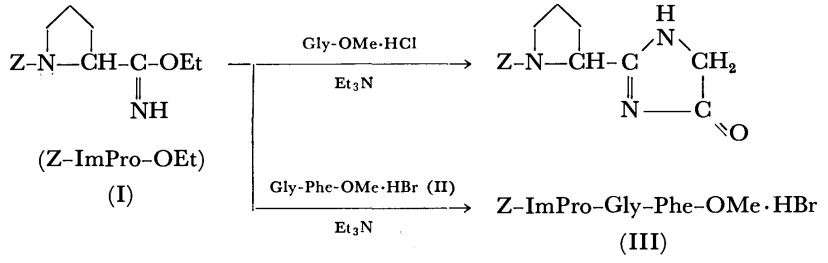

Scheme 1.

TABLE 1. SYNTHESES OF *N*-BENZYLOXYCARBONYL IMINOPEPTIDE HYDROHALIDES

Compd	Iminopeptide hydrohalides	Yield (%)	$[\alpha]_D^{20}$ (c 1, MeOH)	Molecular formula	Found (Calcd) (%) C	H	N
XIII	Z-ImPro-Gly-Phe-Phe-OMe·HCl	60	−17.0°	$C_{34}H_{39}N_5O_6 \cdot HCl \cdot H_2O$	61.26 (61.12)	6.45 (6.34)	10.11 (10.48)
XIV	Z-Val-ImPro-Gly-Phe-OMe·HBr	25[a]	−40.9°	$C_{30}H_{39}N_5O_6 \cdot HBr \cdot 2H_2O$	52.22 (52.79)	6.58 (6.50)	10.13 (10.25)
XV	Z-Val-ImPro-Gly-Phe-OMe·HCl	36[a]	−28.9°	$C_{30}H_{39}N_5O_6 \cdot HCl \cdot H_2O$	58.24 (58.10)	7.10 (6.83)	11.07 (11.29)
XVI	Z-Val-ImPro-Gly-Phe-Phe-OMe·HCl	59	−10.6°	$C_{39}H_{48}N_6O_7 \cdot HCl \cdot H_2O$	60.98 (61.05)	6.54 (6.70)	10.92 (10.95)
XVII	Z-Val-Val-ImPro-Gly-Phe-Phe-OMe·HCl	70	−35.7°	$C_{44}H_{57}N_7O_8 \cdot HCl \cdot H_2O$	61.30 (60.99)	7.35 (6.98)	10.80 (11.32)

a) Both compounds were isolated from the same reaction mixture. See Experimental part.

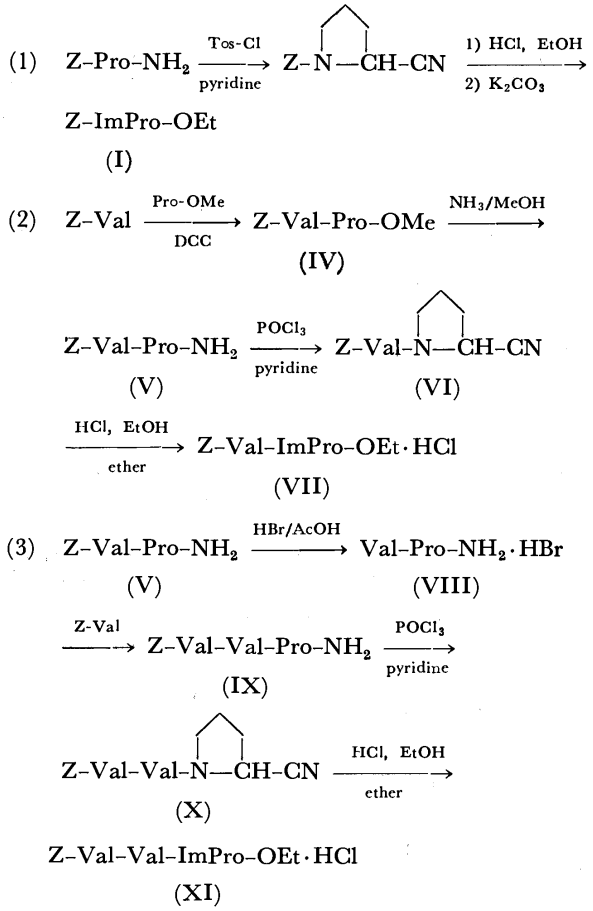

Scheme 2. Synthetic routes of the imidates of *N*-terminal fragments.

ester hydrobromide (II), the desired iminotripeptide derivative was obtained as a foamy solid; however, unexpectedly, it proved to be the hydrobromide instead of the free compound, as described previously.[2] This was also the case for the coupling of the imidate (I) with the tripeptide ester hydrochloride (XII), which yielded the iminotetrapeptide hydrochloride (XIII). In the coupling of the imidate hydrochloride (VII) with the ester hydrobromide (II), the resulting iminotetrapeptide derivative was found to be a mixture of the hydrobromide (XIV) and the hydrochloride (XV), which could be separated chromatographically, though two equivalents of triethylamine were used. The coupling of the dipeptide imidate (VII) with the tripeptide ester (XII) was carried out by using both the hydrochloride in the presence of triethylamine, and the iminopentapeptide derivative was obtained as the hydrochloride (XVI).

Finally, the coupling of the tripeptide imidate hydrochloride (XI) with the tripeptide ester hydrochloride (XII) was attempted under the same conditions as above; the desired model compound (XVII) could be obtained in a 70% yield as the hydrochloride. The synthetic results of these iminopeptides are summarized in Table 1. Supported by this success, we decided to couple the two tripeptide fragments at the iminopeptide bond for the total synthesis of bottromycin. The results will be published later.[7]

TABLE 2. pK_a VALUES OF IMINOPEPTIDES

	Iminopeptides	pK_a	(temp)
III	Z-ImPro-Gly-Phe-OMe·HBr	9.75[a]	(22 °C)
XIII	Z-ImPro-Gly-Phe-Phe-OMe·HCl	9.65[b]	(17 °C)
XIV	Z-Val-ImPro-Gly-Phe-OMe·HBr	9.4[a]	(18 °C)
XVI	Z-Val-ImPro-Gly-Phe-Phe-OMe·HCl	9.45[a]	(18 °C)
XVII	Z-Val-Val-ImPro-Gly-Phe-OMe·HCl	9.3[b]	(18 °C)

a) MeOH–H_2O (1 : 1). b) MeOH–H_2O (3 : 2).

The iminopeptides seemed to be more basic than triethylamine, because all the iminopeptides were isolated as salts in spite of the presence of equimolecular triethylamine, as has been seen above. Therefore, we measured the pK_a values of these iminopeptides, thereby examining the validity of the pK_a rule used by Nakamura *et al.*[4b,8] in order to elucidate the position of the imino group in the bottromycin molucule. The results are shown in Table 2. The basicities of these iminopeptides were unexpectedly found to be less than that of triethylamine (pK_a = 10.4 in MeOH–H_2O (3 : 2)) but the differences were small, so that the unusual isolation of the iminopeptide salts could be explained by also considering the volatility of triethylamine. There also exsists a tendency, though not so marked, that the more inner the iminopeptide bond comes to, the smaller the pK_a value.

It should be pointed out that the pK_a rule of Nakamura *et al.* could not be applied in the cases of our iminopeptides, because the rule predicts that every pK_a value of them is 8.1—8.4. Furthermore, it is noteworthy thet the iminohexapeptide derivative (XVII), prepared here as a model of bottromycin, has a pK_a value of 9.3, in contrast with the 8.1—8.3 value[4b] of the antibiotic.

The antimicrobial activities of these iminopeptides against several microorganisms (gram-positive bacteria containing *Mycobacterium*, a negative one, and some fungi) were examined, but no activities were observed in any.

Experimental

All the melting points are uncorrected. The optical rotations were measured by means of a Yanagimoto polarimeter, OR-10. The pK_a values were measured by means of a Hitachi-Horiba pH meter, F-7. Thin-layer chromatography (TLC) was done on Merck's Kieselgel GF_{254} (Type 60), and circular paper chromatography, on Toyo Roshi No. 2.

Z-Val-Pro-OMe (IV). Into a cold mixture of Z-Val-OH (5.03 g, 20 mmol), H-Pro-OMe·HCl (3.31 g, 20 mmol), and Et_3N (2.02 g, 20 mmol) in CH_2Cl_2 (50 ml) and dioxane (20 ml), a solution of DCC (4.32 g, 21 mmol) in CH_2Cl_2 (10 ml) was stirred below −5 °C. The mixture was stirred at 0 °C for 3 h and then at room temperature overnight. The reaction mixture, treated as usual, gave a crude dipeptide as an oil, which was chromatographed on a silica gel column with benzene–AcOEt (4 : 1) to afford a colorless oil; yield, 5.81 g (80.1%); $[\alpha]_D^{20}$ −87.7° (*c*, 1 MeOH). Found: C, 62.77; H, 7.28; N, 7.64%. Calcd for $C_{19}H_{26}N_2O_5$: C, 62.96; H, 7.23; N, 7.73%.

Z-Val-Pro-NH$_2$ (V). A solution of IV (1.631 g, 4.5 mmol) in a saturated solution of NH_3 in MeOH (21.9%) (20 ml) was allowed to stand at room temperature for 5 days. The solution was then evaporated under reduced pressure to give a syrup, which afforded white crystals when treated with AcOEt; yield, 535 mg (34.2%); mp 131—132.5 °C, $[\alpha]_D^{20}$ −81.6° (*c* 1, MeOH).

When condensed, the filtrate gave a syrup (1.060 g) which was mainly composed of the starting material. The syrup was treated again with a saturated solution of NH_3 in MeOH (20 ml) at room temperature for 15 days, affording white crystals after the treatment described above; yield, 733 mg (46.9 %), mp 131—132 °C, $[\alpha]_D^{20}$ −81.3° (*c* 1, MeOH).

All the crystals obtained were combined and recrystallized from AcOEt–petroleum ether; mp 133—134 °C, $[\alpha]_D^{20}$ −84.3° (*c* 1, MeOH). Found: C, 62.02; H, 7.38; N, 11.92%. Calcd for $C_{18}H_{25}N_3O_4$: C, 62.23; H, 7.25; N, 12.01%.

N-(Z-Val)-2-cyanopyrrolidine (VI). To a stirred solution of V (1.390 g, 4 mmol) in dry pyridine (7 ml), $POCl_3$ (0.48 ml, 5.2 mmol) in CH_2Cl_2 (0.9 ml) was added, drop by drop, below −7 °C. The resulting solution was stirred at about −10 °C for 1 h, and then treated with ice (50 g) and extracted with AcOEt. The organic layer was successively washed with 1M-HCl, water, 1M-$NaHCO_3$ and water, and dried over $MgSO_4$; yield, 1.278 g (97%); slightly yellow oil, $[\alpha]_D^{20}$ −89.0° (*c* 1, MeOH). Found: C, 65.79; H, 7.23; N, 12.64%. Calcd for $C_{18}H_{23}N_3O_3$: C, 65.63; H, 7.04; N, 12.76%.

Z-Val-ImPro-OEt·HCl (VII). This compound was prepared by bubbling dry HCl into a cold solution of VI (658 mg, 2 mmol) and absolute EtOH (120 mg, 2.6 mmol) in dry ether (10 ml) according to our previously described procedures;[2] yield, 820 mg (99.5%); a foamy solid. This imidate hydrochloride was used for the next reaction without purification.

H-Val-Pro-NH$_2$·HBr (VIII). This compound was prepared by the removal of the Z group from V (2.084 g, 6 mmol) with 25% HBr in AcOH (6 g) as usual. A crude product, a yellow syrup, was treated with MeOH–ether to give white crystals; yield, 1.632 g (92.5%); mp 214—217 °C (sublim.), $[\alpha]_D^{20}$ −45.6° (*c* 1, MeOH). Found: C, 40.71; H, 7.26, N, 14.01%. Calcd for $C_{10}H_{19}N_3O_2·HBr$: C, 40.83; H, 6.85; N, 14.28%.

Z-Val-Val-Pro-NH$_2$ (IX). Into a cold solution of Z-Val-OH (754 mg, 3 mmol) and *N*-methylmorpholine (304 mg, 3 mmol) in THF (10 ml), *i*Boc-Cl (410 mg, 3 mmol) was stirred, drop by drop, below −10 °C, after which the turbid mixture was stirred for 15 min at the same temperature. To the mixture we then added a mixture of VIII (883 mg, 3 mmol) and *N*-methylmorpholine (304 mg, 3 mmol) in DMF (10 ml) below −10 °C for 15 min, at about −5 °C for 1 h, and then at room temperature overnight. After the removal of a precipitate, the filtrate was concentrated under reduced pressure. The residual DMF solution was diluted with water (100 ml), extracted with AcOEt, washed with water, 1M-$NaHCO_3$, and water, and dried over $MgSO_4$. The solution was evaporated to a foamy solid; yield, 1.275 g (95.2%); $[\alpha]_D^{20}$ −94.5° (*c* 1, MeOH). Found: C, 61.61; H, 7.72; N, 12.45%. Calcd for $C_{23}H_{34}N_4O_5$: C, 61.86; H, 7.68; N, 12.55%.

N-(Z-Val-Val)-2-cyanopyrrolidine (X). This compound was prepared by the dehydration of IX (1.340 g, 3 mmol) with $POCl_3$ (0.36 ml, 3.9 mmol) in a mixture of dry pyridine (5 ml) and CH_2Cl_2 (0.7 ml) below −10 °C, as has been described above for the preparation of VI; yield, 1.131 g (88%); a foamy solid, $[\alpha]_D^{20}$ −103.0° (*c* 1, MeOH). Found: C, 64.26; H, 7.56; N, 13.19%. Calcd for $C_{23}H_{32}N_4O_4$: C, 64.46; H, 7.53; N, 13.08%.

Z-Val-Val-ImPro-OEt·HCl (XI). This compound was prepared by passing dry HCl into a mixture of X (900 mg, 2.1 mmol) and absolute EtOH (126 mg, 2.73 mmol) in dry ether as has been described above; yield, 1.002 g (93.4%); a foamy solid.

H-Gly-Phe-Phe-OMe·HCl (XII). This compound was prepared by the coupling of Z-Gly-ONp[9] with H-Phe-Phe-OMe in DMF according to the method of Katsoyannis *et al.*,[10] followed by the hydrogenation of the resulting Z-tripeptide ester (5.17 g, 10 mmol) over 5% palladium-carbon (1.5 g) in MeOH (200 ml) containing concentrated hydrochloric acid (0.9 ml); yield, 3.75 g (76.5% based on Z-Gly-ONp); mp 190—192.5 °C (dec), $[\alpha]_D^{20}$ +8.4° (*c* 1, MeOH). Found: C, 59.49; H, 6.28; N, 9.48%. Calcd for $C_{21}H_{25}N_3O_4·HCl$: C, 60.07; H, 6.24; N, 10.01%.

Iminopeptides. a) General Procedure: A solution of an imidate hydrochloride (1.2 mmol), a peptide ester hydrochloride (or hydrobromide) (1.0 mmol), and Et_3N (2.2 mmol) in dry MeOH (5 ml) was stirred at room temperature for 2 days. The solution was then evaporated under reduced pressure, leaving a syrup with some crystals. The syrup was taken up in AcOEt and freed from any insoluble materials by filtration. The filtrate was chromatographed on a silica gel column with MeOH–AcOEt (1 : 4), or on preparative layers of silica gel with MeOH–AcOEt (1 : 4) or $CHCl_3$–MeOH–AcOH (95 : 15 : 3), to give a foamy solid. The results are summarized in Table 1.

b) The Hydrobromide (XIV) and the Hydrochloride (XV) of Z-Val-ImPro-Gly-OMe: A solution of the imidate hydrochloride (VII) (820 mg, 2.0 mmol), the dipeptide ester hydrobromide (II)[2] (634 mg, 2.0 mmol), and Et_3N (404 mg, 4.0 mmol) in MeOH (10 ml) was stirred at room temperature

for 2 days. After the procedure described above, the resulting foamy solid was chromatographed on a silica gel column with MeOH–AcOEt (1 : 9) eluting one compound (A: 336 mg), and then with MeOH eluting the other compound (B: 430 mg); TLC: Compound A, R_f 0.37, Compound B, R_f 0.23 (MeOH–AcOEt (1 : 4)). Circular paper chromatography (1-BuOH–AcOH–H_2O (4 : 1 : 2, upper phase)) of the hydrolysates of these compounds showed both to contain 4 amino acids, and elemental analyses revealed that Compound A is iminotetrapeptide hydrobromide (XIV) and Compound B is the hydrochloride (XV).

The present work was supported by a Grant-in-Aid for Scientific Research from the Ministry of Education (14703, 1976). We are grateful to Dr. Ichiro Chibata and his co-workers, Tanabe Seiyaku Co., Ltd., for the test of the antimicrobial activity.

References

1) This work was presented at the 34th National Meeting of the Chemical Society of Japan, Hiratsuka, April, 1976, Preprint II, p. 699. In the course of the preparation of this paper, a revised study of bottromycin A_2 was published (Y. Takahashi, H. Naganawa, T. Takita, H. Umezawa, and S. Nakamura, *J. Antibiot.*, **29**, 1120 (1976)); it was reported at the 14th Symposium on Peptide Chemistry (Japan), Hiroshima, November, 1976 (Y. Takahashi, H. Naganawa, T. Takita, H. Umezawa, and S. Nakamura, Proceedings of the 14th Symposium on Peptide Chemistry, Japan (1976), p. 117), at the same time with our study.[7])

2) T. Yamada, K. Suegane, S. Kuwata, and H. Watanabe, *Bull. Chem. Soc. Jpn.*, **50**, 1088 (1977).

3) The following nomenclatures and abbreviations are used for iminopeptides and their derivatives. An amino acid containing =NH instead of =O in the carboxyl group is called an imino amino acid and abbreviated as ImAA (AA=amino acid); *e.g.*, 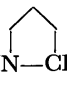 is called iminoproline (ImPro). Therefore, 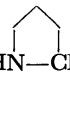 is called (iminoprolyl)glycine (ImPro–Gly), and ethyl *N*-Z-2-pyrrolidinecarboximidate (I) may be abbreviated as Z–ImPro–OEt. Further, an iminopeptide bond means an amidino group (–C(=NH)–NH–) situated between amino acid residues. In addition, abbreviations according to the IUPAC-IUB Commission (*J. Biol. Chem.*, **247**, 977 (1972)) are used throughout. Additional abbreviations: DCC, dicyclohexylcarbodiimide; THF, tetrahydrofuran; DMF, *N*,*N*-dimethylformamide; BuOH, 1-butanol; *i*Boc–Cl, isobutyloxycarbonyl chloride; Tos–Cl, *p*-toluenesulfonyl chloride. The amino acids and their derivatives used here are all of the L-configuration.

4) a) S. Nakamura, T. Chikaike, H. Yonehara, and H. Umezawa, *J. Antibiot.*, **18A**, 60 (1965); S. Nakamura, T. Chikaike, H. Yonehara, and H. Umezawa, *Chem. Pharm. Bull.*, **13**, 599 (1965); b) S. Nakamura, N. Tanaka, and H. Umezawa, *J. Antibiot.*, **19A**, 10 (1966); S. Nakamura, and H. Umezawa, *Chem. Pharm. Bull.*, **14**, 981 (1966); c) S. Nakamura, T. Yajima, Y. C. Lin, and H. Umezawa, *J. Antibiot.*, **20A**, 1 (1967).

5) E. Frauendolfer, W. Steglich, and F. Weygand, *Chem. Ber.*, **106**, 1019 (1973).

6) Y. Kataoka, Y. Seto, M. Yamamoto, T. Yamada, S. Kuwata, and H. Watanabe, *Bull. Chem. Soc. Jpn.*, **49**, 1081 (1976).

7) Our synthetic study of bottromycins B_1 and B_2 was presented at the 14th Symposium on Peptide Chemistry (Japan), Hiroshima, November, 1976; T. Yamada, T. Miyazawa, S. Kuwata, and H. Watanabe, Proceedings of the 14th Symposium on Peptide Chemistry, Japan (1976), p. 113.

8) S. Nakamura, Proceedings of the 2nd Symposium on Peptide Chemistry, Japan (1963), p. 47; S. Nakamura, *Yuki Gosei Kagaku Kyokai Shi*, **24**, 923 (1966).

9) L. Benoiton, *Can. J. Chem.*, **41**, 1718 (1963).

10) P. G. Katsoyannis, J. Gionos, G. P. Schwartz, and A. Cosmatos, *J. Chem. Soc., Perkin Trans. 1*, **1974**, 1311.

Synthesis of Methyl-substituted 1-Cyclopentene-1-carboxylates and Related Compounds*

Akira TAKEDA, Kōichi SHINHAMA, and Sadao TSUBOI
Department of Synthetic Chemistry, School of Engineering, Okayama University, Tsushima, Okayama 700
(Received January 20, 1977)

The treatment of methyl-substituted 1-chloro-2-oxo-1-cyclohexanecarboxylic esters (**7a—e**) with anhydrous Na_2CO_3 in refluxing xylene gave the corresponding methyl-substituted 1-cyclopentene-1-carboxylic esters (**1a—e**). Several intermediates important in the synthesis of natural products, such as 4,4-dimethyl-1-cyclopentene-1-carbaldehyde (**9**), 5-methyl-1-cyclopentene-1-carbaldehyde (**12**), α-(3-methyl-1-cyclopentenyl)propionic acid (**16**), and ethyl 2-methyl-3-oxo-1-cyclopentene-1-carboxylate (**17**), have been prepared starting from esters **1e**, **1d**, **1b**, and **1a**, respectively.

During the course of our work in cyclopentane monoterpene synthesis we required several methyl-substituted 1-cyclopentene-1-carboxylic esters (**1a—d**) and/or the corresponding aldehydes (**2**). The synthetic procedures of **1** as well as **2** so far reported appear to be inconvenient because they yield a mixture of structural isomers.[1,2] Recently Büchi *et al.*[3] have reported the dehydrochlorination-decarbonylation of 2-chloro-2-alkyl-1,3-cyclohexanedione to produce 2-alkyl-2-cyclopentene-1-one. The reaction was then extended to other 2-chloro-1,3-dicarbonyl compounds, such as cyclic α-chloro-β-keto aldehydes and α-chloro-β-keto esters. Thus, the dehydrochlorination-decarbonylation of methyl 1-chloro-2-oxo-1-cyclohexanecarboxylate (**3**) with sodium carbonate in hot xylene afforded methyl 1-cyclopentene-1-carboxylate (**5**).[4] Büchi has suggested that the product originates from the cyclopropanone intermediate (**4**) by thermal, nonconcerted elimination of carbon monooxide.

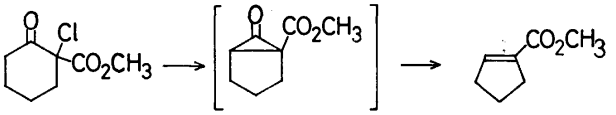

3 **4** **5**

We decided to investigate the dehydrochlorination-decarbonylation of four methyl-substituted 1-chloro-2-oxo-1-cyclohexanecarboxylic esters (**7a—d**) in an attempt to devise a straightforward synthesis of the desired esters **1a—d**.

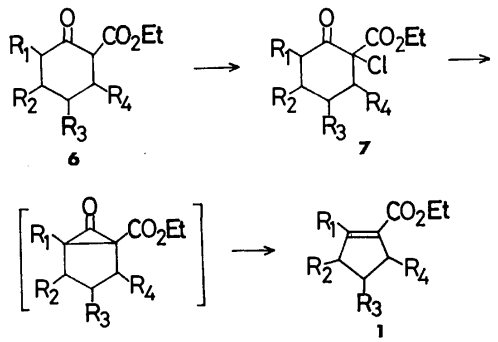

6a, 7a, 1a: $R_1=CH_3$, $R_2=R_3=R_4=H$
6b, 7b, 1b: $R_2=CH_3$, $R_1=R_3=R_4=H$
6c, 7c, 1c: $R_3=CH_3$, $R_1=R_2=R_4=H$
6d, 7d, 1d: $R_4=CH_3$, $R_1=R_2=R_3=H$

Four methyl-substituted 2-oxo-1-cyclohexanecarboxylic esters (**6a—d**) were chlorinated with *t*-butyl hypochlorite (*t*-BuOCl) under conditions similar to those in the literature[4] to give the corresponding α-chloro-β-keto esters (**7a—d**) in good yields (Table 1). The spectral data given in Table 2 support their structure. Both the IR spectra and the NMR spectra of compounds **7a—d** clearly show that they are nonenolizable β-keto esters. The NMR signals of the methyl protons of **7d** shifted to a lower field (δ 1.30) as compared with the other isomers, being affected by the neighboring chlorine atom.

These chlorides were treated with anhydrous Na_2CO_3 in refluxing xylene in the presence of glass powder until their exhaustion to give the corresponding 1-cyclopentene-1-carboxylates (**1a—d**) in 47—82% yields. The results are listed in Tables 3 and 4.

Starting from appropriate cyclopentenecarboxylates, we also prepared several intermediates such as 4,4-dimethyl-1-cyclopentene-1-carbaldehyde (**9**),[10] 5-methyl-1-cyclopentene-1-carbaldehyde (**12**),[12,13] α-(3-methyl-1-cyclopentenyl)propionic acid (**16**),[14] and ethyl 2-methyl-3-oxo-1-cyclopentene-1-carboxylate (**17**), useful for the synthesis of natural products.

The chlorination of ethyl 5,5-dimethyl-2-oxo-1-cyclohexanecarboxylate (**6e**)[11] with *t*-BuOCl gave ethyl 1-chloro-5,5-dimethyl-2-oxo-1-cyclohexanecarboxylate (**7e**) in a 79% yield. The treatment of **7e** with Na_2CO_3 afforded ethyl 4,4-dimethyl-1-cyclopentene-1-carboxylate (**1e**) in a 76% yield. The reduction of **1e** with $LiAlH_4$ gave 4,4-dimethyl-1-cyclopentenylmethanol (**8**) in a 93% yield. This alcohol was oxidized with active manganese dioxide[15] to the aldehyde **9** in a 33%

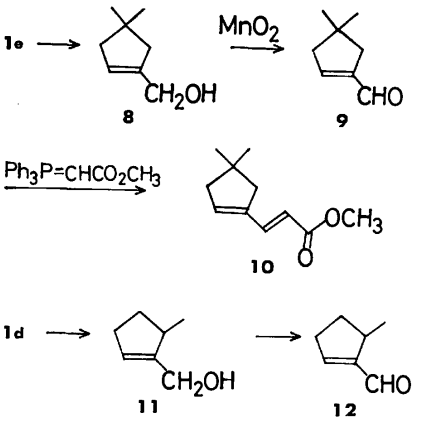

* Presented in part at the 33rd Annual Meeting of the Chemical Society of Japan, Fukuoka, October 1975.

yield. Compound **9** was further converted into methyl *trans*-β-(4,4-dimethyl-1-cyclopentenyl)acrylate (**10**)[10] by the Wittig reaction with $Ph_3P{=}CHCO_2CH_3$.[16] Ethyl 5-methyl-1-cyclopentene-1-carboxylate (**1d**) was also converted into aldehyde **12** *via* 5-methyl-1-cyclopentenylmethanol (**11**) in a 35% overall yield. Ethyl 3-methyl-1-cyclopentene-1-carboxylate (**1b**) can be used as a starting material to prepare the acid **16**. The reaction of 3-methyl-1-cyclopentene-1-carbonyl chloride (**14**) with diazoethane afforded the corresponding diazo ketone (**15**). The thermal decomposition of **15** and the subsequent hydrolysis of the product gave the acid **16**. Compounds **12** and **16** are important intermediates for the synthesis of iridomyrmecin.[12-14] The oxidation of ethyl 2-methyl-1-cyclopentene-1-carboxylate (**1a**) with CrO_3 in glacial acetic acid gave 2-methyl-3-oxo-1-cyclopentene-1-carboxylate (**17**), the ester of the structural isomer of sarcomycine, in a 20% yield.[17]

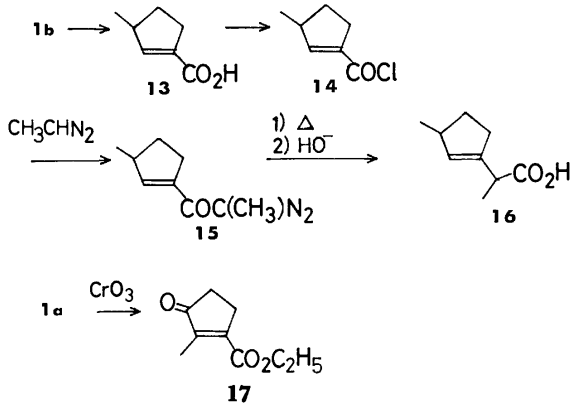

Further synthetic application was carried out by the use of ethyl 3-bromo-2-oxo-1-cyclohexanecarboxylate (**18**),[18,19] 2-chloro-2-acetylcyclohexanone (**19**),[20] 2-chloro-2-acetylcyclopentanone (**22**),[21] propyl 1-chloro-2-oxo-1-cyclopentanecarboxylate (**23**), 2-chloro-2-formylcyclohexanone (**24**), and 2-chloro-2-formyl-4,4-dimethylcyclohexanone (**25**) as substrates. The treatment of the bromide **18** with Na_2CO_3 yielded ethyl 1-cyclopentene-1-carboxylate (**1f**), the same product as that from the 2-halogeno derivative, in a 61% yield. While the IR spectrum of **19** obtained by the

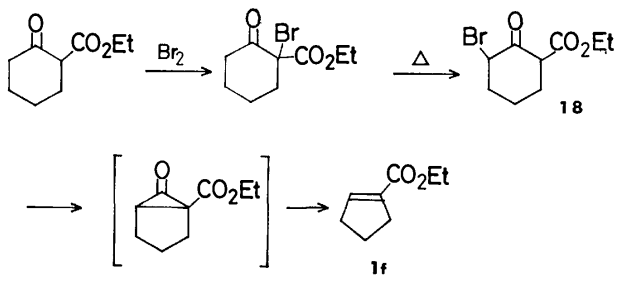

chlorination of 2-acetylcyclohexanone (**31**)[30] with *t*-BuOCl was identical with that of the literature,[20] the TLC analysis as well as the NMR survey indicated the presence of the 6-chloro isomer (**20**) (**19** : **20**=1 : 4). This mixture of isomers **19** and **20** was used for the next step without separation, since the both compounds should give the same Favorskii-type products, as is shown in the case of **18**. Thus, the reaction of the mixture of isomers **19** and **20** afforded 1-acetyl-1-cyclopentene (**26**) in a 23% yield.[22] The reactions of compounds **22**, **23**, **24**, and **25** failed to afford the anticipated products, instead yielding only tarry material.[21]

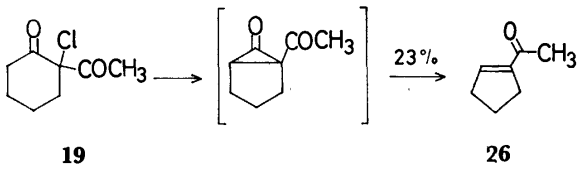

Studies of the synthesis of furopelargone[23] from the ester **1b**, that of photocitral[24] from the aldehyde **12**, and that of nepetalic acid[25] from the ester **1d** are now in progress.

Experimental

The melting points and boiling points are uncorrected. The elemental analyses were carried out by Mr. Eiichiro Amano of our laboratory. The analytical determinations by GLPC were performed on a Hitachi Model K-53 gas chromatograph fitted with the following columns (3 mm o.d. × 1 m) A, 10% Apiezon Grease L on Chromosorb W; B, 10% poly(neopentyl glycol succinate) on Chromosorb W; C, 10% SE-30 on Chromosorb W. The preparative isolations by GLPC were performed on a Yanagimoto Model GCG-550T gas chromatograph (3 mm o.d. ×2.25 m, 10% Apiezon Grease L on Chromosorb W). The mass spectra were obtained with a Hitachi Model RMS-4 mass spectrometer. The NMR spectra (60 MHz) were recorded with a Hitachi Model R-24 apparatus. The thin-layer chromatograms were prepared with Merck Kieselgel 60 PF_{254} (E. Merck AG, Darmstadt). The column chromatograms were prepared with Wakogel B-5F (Wako Junyaku Kogyo Co., Ltd.).

The following compounds were obtained in ways which have been described in the literature: **6a**,[5] **6b**,[6] **6c**,[7] **6d**,[8] **18**,[19] 2-acetylcyclopentanone (**21**),[28] 2-hydroxymethylenecyclohexanone (**30**),[29] and **31**.[30]

The following are typical runs. The reaction of **6b** illustrates the manner in which the chlorination of **6a**—**d** and the dehydrochlorination-decarbonylation of the chlorides **7a**—**d** were carried out.

*Ethyl 1-Chloro-4-methyl-2-oxo-1-cyclohexanecarboxylate (**7b**).* To a stirred solution of 7.4 g (0.04 mol) of ethyl 4-methyl-2-oxo-1-cyclohexanecarboxylate (**6b**)[6] dissolved in 60 ml of methanol was added 4.8 g (0.044 mol) of *t*-BuOCl[31] below 0 °C under nitrogen. After it had been stirred for an additional 1 h at the same temperature, the mixture was kept in a refrigerator for 40 h, and then allowed to stand at room temperature for 4 h. After the evaporation of methanol, the solution was distilled under reduced pressure to give 7.9 g (91%) of **7b**.

*Ethyl 3-Methyl-1-cyclopentene-1-carboxylate (**1b**).* Following the procedure reported by Büchi,[4] a flask was charged with 9.3 g (0.088 mol) of crushed, anhydrous Na_2CO_3 and 36 g of glass powder. After the content of the flask had been dried at 160 °C for 2 h *in vacuo*, it was filled up with nitrogen gas. A solution of 16 g (0.073 mol) of the chloride **7b** in 110 ml of xylene was then added to the flask, and the mixture was refluxed with stirring. The reaction was continued for 40 h until the chloride **7b** had been exhausted, as checked by GLPC. The resulting mixture was cooled and filtered. After evaporation of the solvent, it was fractionally distill-

Table 1. Chlorination of ethyl 2-oxo-1-cyclohexanecarboxylates (**6a—d**)

Product	Yield (%)	Bp (Torr)	Found (%) C	Found (%) H	Calcd (%) for $C_{10}H_{15}ClO_3$ C	Calcd (%) for $C_{10}H_{15}ClO_3$ H
7a[a]	62	80— 83 (0.05)	54.76	6.82	54.93	6.91
7b[a]	91	99—100 (0.07)	54.78	6.93	54.93	6.91
7c[a]	79	80— 81 (0.035)	55.14	6.98	54.93	6.91
7d[b]	70	100—102 (0.05)	55.10	6.84	54.93	6.91

a) *t*-BuOCl 1.1 times as much as **6** in mol was used. b) *t*-BuOCl 1.6 times as much as **6** in mol was used.

Table 2. Spectral data of ethyl 1-chloro-2-oxo-1-cyclohexanecarboxylates

Compound	NMR (CCl_4, δ) CH_3 (ring)	$CO_2CH_2CH_3$	$CO_2CH_2CH_3$	Ring-proton	IR (neat, cm^{-1})
7a	1.04 (d, J=6 Hz, 3H)	1.34 (t, 3H)	4.24 (q, 2H)	1.5—3.0 (m, 7H)	1730
7b	1.05 (d, J=6 Hz, 3H)	1.30 (t, 3H)	4.23 (q, 2H)	1.6—3.0 (m, 7H)	1725, 1750
7c	1.05 (d, J=6 Hz, 3H)	1.31 (t, 3H)	4.25 (q, 2H)	1.6—2.7 (m, 7H)	1725, 1750
7d	1.30 (d, J=6 Hz, 3H)	1.31 (t, 3H)	4.22 (q, 2H)	1.5—3.0 (m, 7H)	1730

Table 3. Dehydrochlorination of 1-chloro-2-oxo-1-cyclohexanecarboxylates (**7a—d**)

Substrate	Product	Yield (%)	Found (%) C	Found (%) H	Calcd (%) for $C_9H_{14}O_2$ C	Calcd (%) for $C_9H_{14}O_2$ H	MS (70 eV) *m/e* (rel intensity)
7a	**1a**	74	69.89	9.17	70.10	9.15	154 (19, M^+), 125 (23), 109 (55), 81 (100)
7b	**1b**	79	69.79	8.79	70.10	9.15	154 (9, M^+), 125 (9), 109 (53), 81 (100)
7c	**1c**	82	69.81	9.15	70.10	9.15	154 (13, M^+), 109 (42), 81 (100)
7d	**1d**	47	70.32	9.15	70.10	9.15	154 (16, M^+), 109 (57), 81 (100)

Table 4. Spectral data of methyl-substituted 1-cyclopentene-1-carboxylates

Compound	NMR (CCl_4, δ) CH_3 (ring)	$CO_2CH_2CH_3$	$CO_2CH_2CH_3$	Ring-proton		IR (neat, cm^{-1}) C=O	C=C
1a	2.08 (s, 3H)	1.28 (t, 3H)	4.13 (q, 2H)	1.6—2.9 (m, 6H)		1705	1642
1b	1.07 (d, 3H)	1.23 (t, 3H)	4.08 (q, 2H)	1.5—2.9 (m, 5H)	6.50 (s, br, 1H)	1710	1625
1c	1.05 (d, 3H)	1.24 (t, 3H)	4.08 (q, 2H)	1.6—3.0 (m, 5H)	6.56 (s, br, 1H)	1710	1625
1d	1.12 (d, 3H)	1.27 (t, 3H)	4.11 (q, 2H)	2.0—3.2 (m, 5H)	6.59 (s, br, 1H)	1710	1623

ed under diminished pressure to give 8.9 g (79%) of the ester **1b**: bp 93—94 °C/22 Torr.

*Ethyl 5,5-Dimethyl-2-oxo-1-cyclohexanecarboxylate (**6e**).*[11] This substance was prepared from 4,4-dimethylcyclohexanone (**29**)[27] in a 24% yield by an adaptation of Snyder's method:[9] bp 90—110 °C/60 Torr [lit,[11] bp 75 °C/1Torr]; IR (neat) 1755, 1720, 1668, and 1627 cm^{-1}; NMR ($CDCl_3$) δ 0.98 (s, 6H), 1.30 (t, 3H), 2.20 (s, 2H), 2.28 (m, 4H), and 4.20 ppm (q, 2H).

*Ethyl 1-Chloro-5,5-dimethyl-2-oxo-1-cyclohexanecarboxylate (**7e**).* The ester **6e** (1.22 g, 62 mmol) was chlorinated in 15 ml of methanol with 0.85 g (7.9 mmol) of *t*-BuOCl in the manner used in the preparation of **7b**. The distillation of the residue obtained after working up as usual gave 1.12 g (79%) of the chloride **7e**: bp 115 °C (0.2 mm); IR (neat) 1730 cm^{-1}; NMR (CCl_4) δ 1.07 (s, 3H), 1.14 (s, 3H), 1.33 (t, 3H), 4.22 (q, 2H), and 1.6—3.0 ppm (m, 6H).

Found: C, 56.99; H, 7.20%. Calcd for $C_{11}H_{17}ClO_3$: C, 56.78; H, 7.36%.

*Ethyl 4,4-Dimethyl-1-cyclopentene-1-carboxylate (**1e**).* The dehydrochlorination-decarbonylation of the chloride **7e** (0.512 g, 2.1 mmol) with anhydrous Na_2CO_3 (0.256 g, 2.4 mmol) was carried out in refluxing xylene (4 ml) in the presence of glass powder (1.5 g). The reaction was continued for 28 h at the refluxing temperature until **7e** was exhausted, as checked by GLPC. The resultant mixture was cooled, filtered, and passed through a column of 10 g of dried silica gel. After the removal of xylene, using hexane as the eluant, a colorless eluate was collected with chloroform. The subsequent evaporation of chloroform afforded 267 mg (76%) of a pure ester (**1e**): IR (neat) 1725, and 1630 cm^{-1}; NMR (CCl_4) δ 1.16 (s, 6H), 1.23 (t, 3H), 2.3 (m, 3H), 2.31 (s, 2H), 4.07 (q, 2H), and 6.51 ppm (br, 1H).

*4,4-Dimethyl-1-cyclopentenylmethanol (**8**).* To a stirred suspension of $LiAlH_4$ (77 mg, 2 mmol) in 3 ml of dry ether was added dropwise the ester **1e** (267 mg, 5 mmol) dissolved in 1 ml of dry ether at −76 °C over a period of 0.5 h. After the addition had been completed, the mixture was stirred for an additional 4.5 h at −50——20 °C. To the mixture which had been allowed to warm up to room temperature was added 132 mg (1.5 mmol) of ethyl acetate to decompose the excess of $LiAlH_4$. The resulting mixture was treated with

0.35 ml of saturated aqueous ammonium chloride. The solid residue was washed with ether. The combined ethereal solution was then dried ($MgSO_4$) and evaporated to yield 175 mg (93%) of crude alcohol (**8**): IR (neat) 3360 cm^{-1}; NMR (CCl_4) δ 1.07 (s, 6H), 2.10 (s, 4H), 3.15 (br, s, 1H), 4.00 (s, 2H), and 5.41 ppm (br, s, 1H).

4,4-Dimethyl-1-cyclopentene-1-carbaldehyde (9). A mixture of 2.0 g of active manganese dioxide,[15] 175 mg (1.39 mmol) of crude alcohol **8**, and 10 ml of petroleum ether (bp 30—44 °C) was stirred for 3.5 h under nitrogen at room temperature, filtered and evaporated to give 168 mg of a crude product. Separation by column chromatography (silica gel) afforded 56 mg (33%) of pure aldehyde (**9**): IR (neat) 1678, and 1617 cm^{-1}; NMR (CCl_4) δ 1.12 (s, 6H), 2.32 (m, 4H), 6.63 (br, s, 1H), and 9.67 ppm (s, 1H).

Methyl trans-*β-(4,4-Dimethyl-1-cyclopentenyl)acrylate (10).* A solution of 56 mg (0.45 mmol) of the aldehyde **9** in 1 ml of benzene was added to 196 mg (0.59 mmol) of $Ph_3P{=}CHCO_2CH_3$,[16] after which the mixture was refluxed for 17 h. After working up,[2] 30 mg (37%) of the ester **10** was obtained. The spectral data (IR and NMR) of this product were identical with those of the literature.[10]

5-Methyl-1-cylopentenylmethanol (11). To a stirred suspension of $LiAlH_4$ (300 mg, 7.9 mmol) in 12 ml of dry ether was added dropwise ethyl 5-methyl-1-cyclopentene-1-carboxylate (**1d**) (937 mg, 6.1 mmol) dissolved in 5 ml of dry ether at −76 °C over a period of 20 minutes. The crude product which was obtained after working up in the manner used in the preparation of the alcohol **8** was subjected to vacuum distillation to yield 257 mg (38%) of pure alcohol (**11**): bp 62—64 °C (10 mm); IR (neat) 3350 cm^{-1}; NMR ($CDCl_3$) δ 1.05 (d, 3H, J=6 Hz), 1.55 (m, 2H), 2.27 (m, 2H), 2.70 (br, m, 1H), 3.60 (br, s, 1H, $-O\underline{H}$), 4.18 (s, 2H, $-C\underline{H}_2OH$), and 5.69 ppm (br, s, 1H).

Found: C, 74.76; H, 10.63%. Calcd for $C_7H_{12}O$: C, 74.95; H, 10.78%.

5-Methyl-1-cyclopentene-1-carbaldehyde (12). A mixture of 3.2 g of active manganese dioxide, 250 mg (2.2 mmol) of the alcohol **11**, and 16 ml of petroleum ether was stirred for 5.5 h under nitrogen at room temperature. The working-up was essentially the same as in the preparation of the aldehyde **9**, yielding 159 mg (65%) of the aldehyde **12**: IR (neat) 1672, and 1610 cm^{-1}; NMR ($CDCl_3$) δ 1.13 (d, 3H, J=6 Hz, $-C\underline{H}_3$), 1.65 (br, m, 2H), 2.50 (br, m, 2H), 3.00 (br, m, 1H), 6.78 (m, 1H, $=C\underline{H}-$), and 9.75 ppm (s, 1H, $-C\underline{H}O$).

3-Methyl-1-cyclopentene-1-carboxylic Acid (13). To a solution of potassium hydroxide (67 g, 1.2 mol) in 500 ml of ethanol was added 57 g (0.37 mol) of ethyl 3-methyl-1-cyclopentene-1-carboxylate (**1b**). The soultion was then refluxed for 20 h. After the evaporation of the solvent, enough dilute hydrochloric acid to acidify the mixture was added. The acidic organic layer was then extracted with ether. After being dried with $MgSO_4$, the ethereal solution was evaporated to dryness to give 47 g (quantitative) of the acid **13**: mp 34 °C (lit,[32] mp 35—36 °C); IR (Nujol) 3600—2100, 1675, and 1625 cm^{-1}; NMR (CCl_4) δ 1.11 (d, 3H, J=7 Hz), 1.3—3.1 (m, 5H), and 6.70 ppm (m, 1H).

3-Methyl-1-cyclopentene-1-carbonyl Chloride (14). This substance was prepared by treating the acid **13** (875 mg, 7 mmol) with $SOCl_2$ (1.05 g, 8.8 mmol) as usual. The subsequent removal of the excess $SOCl_2$ by evaporation gave 838 mg (84%) of the chloride **14**: bp 75—79 °C/31 Torr; IR (neat) 1752, and 1623 cm^{-1}; NMR (CCl_4) δ 1.16 (d, 3H, J=7 Hz), 1.3—3.3 (m, 5H), and 6.96 ppm (m, 1H, $=C\underline{H}-$).

α-(3-Methyl-1-cyclopentenyl)propionic Acid (16). The Arndt-Eistert reaction with diazoethane[33] was employed to prepare this compound. The chloride **14** (793 mg, 5.8 mmol) was allowed to react with 15 mmol of diazoethane in 100 ml of ether to give the diazo ketone (**15**): IR (neat) 3400, 2070, 1718, 1621, and 1550 cm^{-1}. This product was then subjected to thermal decomposition, followed by hydrolysis. The subsequent purification of the crude product with TLC [silica gel, benzene–methanol–AcOH (50 : 1 : 1), R_f=0.3] gave 156 mg of the acid **16** (18% yield from **14**): IR (neat) 3600—2400, 1700, and 1628 cm^{-1}; NMR ($CDCl_3$) δ 1.10 (d, 3H), 2.12 (d, 3H), 1.0—3.0 (br, m, 6H), 6.77 (m, 1H), and 7.44 ppm (br, s, 1H, $CO_2\underline{H}$).

Ethyl 2-Methyl-3-oxo-1-cyclopentene-1-carboxylate (17). To a stirred solution of ethyl 2-methyl-1-cyclopentene-1-carboxylate (**1a**) (1.96 g, 12.7 mmol) in 2.5 ml of glacial acetic acid was added dropwise a solution of chromium trioxide (2.0 g, 20 mmol) in aqueous acetic acid (3.8 ml of AcOH mixed with 1.1 ml of H_2O) over a 1-h period at room temperature. After the completion of the addition, the mixture was stirred for a further 54 h. The resulting mixture was treated with 70 ml of brine and then extracted with ether. The ethereal layer was washed twice with a 5% aqueous sodium hydroxide solution and dried over $MgSO_4$. After the evaporation of the solvent, the residue was subjected to column chromatography (silica gel, hexane : acetone=50 : 1 to 20 : 1), giving 615 mg of the unchanged ester and 418 mg (20%) of the ester **17**: IR (neat) 1712 and 1637 cm^{-1}; NMR (CCl_4) δ 1.33 (t, 3H, $-CO_2-C(=O)-C\underline{H}_3$), 1.99 (t, 3H, $=C(\underline{CH}_3)-$), 2.32 (m, 2H, $=C(\underline{CH}_2^-)-$), 2.65 (m, 2H, $-C(=O)-C\underline{H}_2-$), 4.25 ppm (q, 2H, $-CO_2-C\underline{H}_2-$); MS (70 eV) *m/e* (rel intensity) 168 (M^+, 31), 140 (30), 123 (33), 112 (55), 95 (25), 67 (100).

Ethyl 1-Cyclopentene-1-carboxylate (1f). A mixture of 3.27 g (13.1 mmol) of ethyl 3-bromo-2-oxo-1-cyclohexanecarboxylate (**18**),[19] 2.0 g (19 mmol) of anhydrous Na_2CO_3, and 10 g of glass powder was heated in refluxing xylene (20 ml) under an atmosphere of nitrogen for 29 h. The resulting mixture was filtered and passed through a column packed with 6 g of dry silica gel. After the elution of xylene with hexane, 1.12 g (61%) of the product **1f**, was obtained by washing out with chloroform: IR (neat) 1715 and 1630 cm^{-1} [lit,[34] IR (CCl_4) 1710 and 1620 cm^{-1}]; NMR (CCl_4) δ 1.23 (t, 3H), 1.5—2.7 (m, 6H), 4.09 (q, 2H), and 6.63 ppm (br, s, 1H).

2-Chloro-2-acetylcyclohexanone (19) and 6-Chloro-2-acetylcyclohexanone (20). *t*-BuOCl (2.15 g, 19.8 mmol) was stirred into a solution of 2-acetylcyclohexanone (**31**)[30] (2.31 g, 16.5 mmol) in absolute methanol (20 ml) under nitrogen over a 40 minute period, the temperature being kept below −20 °C. The mixture, which was then worked up as usual, yielded 1.77 g (62%) of a mixture of isomers **19** and **20**: bp 85—105 °C (0.3 Torr) [lit,[20] bp 50—51 °C/0.1 Torr]. The preparative TLC of this product (80 mg) afforded 14 mg of the chloride **19** [R_f=0.38; IR (neat) 1724 cm^{-1}; NMR (CCl_4) δ 2.29 (s, 3H, $-C(=O)-C\underline{H}_3$), 1.5—2.6 ppm (m, 8H, ring proton)], together with 54 mg of the chloride **20** [R_f=0.24; IR(neat) 1720, 1630, and 1585 cm^{-1}; NMR (CCl_4) δ 2.29 (s, 3H, $-C(=O)-C\underline{H}_3$), 1.5—2.3 (m, 7H), 4.1—4.5 (br, m, 0.6H, $-C(=O)-C\underline{H}(-)-C(=O)-$), and 15.02 ppm (s, 0.4H, $-C(-O\underline{H})=C-$)].

2-Chloro-2-acetylcyclopentanone (22). The chlorination of 2-acetylcyclopentanone (**21**)[28] with *t*-BuOCl gave this substance in an 80% yield: bp 75—80 °C (0.1 Torr) [lit,[21] bp

92—94 °C/13 Torr]; IR (neat) 1750, 1715, and 1650 cm^{-1}; NMR (CCl_4) δ 2.40 (s, 3H, $-\overset{\overset{O}{\|}}{C}-CH_3$), and 1.7—2.7 ppm (m, 6H, ring proton).

*Propyl 1-Chloro-2-oxo-1-cyclopentanecarboxylate (**23**).* The chlorination of propyl 2-oxo-1-cyclopentanecarboxylate (**27**) with *t*-BuOCl gave the chloride **23** in an 85% yield: bp 105—110 °C (0.05 Torr); IR (neat) 1755, and 1723 cm^{-1}; NMR (CCl_4) δ 0.77 (t, 3H), 1.72 (m, 2H), 2.0—3.0 (m, 6H), and 4.14 ppm (t, 2H).

*2-Chloro-2-formylcylclohexanone (**24**).* The chlorination of 2-hydroxymethylenecyclohexanone (**30**)[29] with *t*-BuOCl in chloroform gave this substance in a 70% yield: bp 50—60 °C/5 Torr; IR (neat) 1740 and 1720 cm^{-1}; NMR (CCl_4) δ 1.98 (m, 4H), 2.4—3.3 (m, 2H), and 9.55 ppm (s, 1H, $-C\underline{H}O$).

*2-Chloro-2-formyl-4,4-dimethylcyclohexanone (**25**).* The chlorination of 2-hydroxymethylene-4,4-dimethylcyclohexanone (**28**) with *t*-BuOCl in chloroform gave this substance in a 59% yield: bp 74—77 °C/5 Torr; IR (neat) 1740 and 1730 cm^{-1}; NMR (CCl_4) δ 1.08 (s, 3H, $-CH_3$), 1.28 (s, 3H, $-CH_3$), 1.5—3.0 (m, 6H, ring proton), and 9.37 ppm (s, 1H, $-C\underline{H}O$).

*1-Acetyl-1-cyclopentene (**26**). Dehydrochlorination-decarbonylation of the Chloride **19**.* The treatment of the crude chloride **19** (554 mg, 3.2 mmol) with 450 mg of anhydrous Na_2CO_3 in refluxing xylene afforded 267 mg of a crude product, which was subsequently purified by preparative TLC (silica gel, hexane : acetone = 10 : 1) to give 79 mg (23%) of the ketone: IR (neat) 1663 and 1616 cm^{-1}; NMR (CCl_4) δ 2.20 (s, 3H, $-\overset{\overset{O}{\|}}{C}-CH_3$), 1.7—2.8 (m, 6H, ring proton), and 6.52 ppm (br, s, 1H, $=C\underline{H}-$).

*Propyl 2-Oxo-1-cyclopentanecarboxylate (**27**).* This substance was prepared in a 79% yield by the Dieckmann condensation[26] of dipropyl adipate: bp 95—100 °C/7 Torr; IR (neat) 1755, 1720, 1658, and 1620 cm^{-1}; NMR (CCl_4) δ 0.95 (t, 3H), 1.65 (m, 2H), 2.14 (m, 6H), 3.00 (m, 1H), and 4.01 ppm (t, 2H).

*2-Hydroxymethylene-4,4-dimethylcyclohexanone (**28**).* This substance was prepared in a 45% yield by the formylation of 4,4-dimethylcyclohexanone (**29**)[27] in a manner similar to that used in the preparation of 2-hydroxymethylenecyclohexanone (**30**)[29]: bp 63—65 °C/10 Torr; IR (neat) 2900, 1640, and 1600 cm^{-1}: NMR (CCl_4) δ 1.00 (s, 6H), 1.45 (t, 2H), 2.10 (s, 2H), 2.42 (t, 2H), 8.50 (s, 1H, $=C\underline{H}-OH$), and 14 ppm (br, s, 1H, $=CHO\underline{H}$).

References

1) S. J. Rhoads, J. K. Chattopadhyay, and E. E. Waali, *J. Org. Chem.*, **35**, 3352 (1970).

2) S. R. Wilson and R. B. Turner, *J. Org. Chem.*, **38**, 2870 (1973).

3) G. Büchi and B. Egger, *J. Org. Chem.*, **36**, 2021 (1971).

4) G. Büchi, U. Hochstrasser, and W. Pawlak, *J. Org. Chem.*, **38**, 4348 (1973).

5) N. N. Chatterjee and A. Bose, *J. Indian Chem. Soc.*, **18**, 196 (1941); *Chem. Abstr.*, **36**, 762[6] (1942).

6) E. J. Eistenbraun, P. G. Hanel, K. S. Schorno, Sr. St. Francis Diegen, and J. Osiechi, *J. Org. Chem.*, **32**, 3015 (1967).

7) R. Lab, D. S. Organ, and C. Pakistan, *Aust. J. Chem.*, **1969**, 2025; *Chem. Abstr.*, **71**, 112592s (1969).

8) S. Mukherjee, *J. Indian Chem.*, **139**, 347 (1962).

9) H. R. Snyder, L. A. Brooks, and S. H. Shapiro, *Org. Synth.*, Coll. Vol. II, 531 (1943).

10) S. R. Wilson and R. B. Turner, *J. Org. Chem.*, **38**, 2870 (1973). Wilson's route to the marasmic acid system started with the synthesis of the ester **10** *via* the aldehyde **9**. Each of the several routes to **9** herein outlined may afford structural isomers.

11) E. B. Reid and T. E. Gompf, *J. Org. Chem.*, **18**, 661 (1953).

12) F. Korte, J. Falbe, and A. Zschocke, *Tetrahedron*, **6**, 201 (1959).

13) F. Korte, K. H. Büchel, and A. Zschocke, *Chem. Ber.*, **94**, 1952 (1961). Korte *et al.*, prepared this compound by the aldol-type cyclization of 3-methylhexane-1,6-dione, with the formation of 4-methyl-1-cyclopentene-1-carbaldehyde as a by-product.

14) J. Falbe, H. Weitkamp, and F. Forte, *Tetrahedron*, **19**, 1479 (1963). They obtained a mixture of structural isomers and used the mixture for the next step.

15) J. Attenburrow, A. F. B. Cameron, J. H. Chapman, R. M. Evans, B. A. Hems, A. B. A. Jansen, and T. Walker, *J. Chem. Soc.*, **1952**, 1094.

16) O. Isler, H. Gutmann, M. Montavon, R. Riiegg, G. Ryser, and P. Zeller, *Helv. Chim. Acta*, **40**, 1242 (1957).

17) J. Fishman, E. R. H. Jones, G. Lowe, and M. C. Whiting, *J. Chem. Soc.*, **1960**, 3948.

18) J. C. Sheehan and C. E. Mumaw, *J. Am. Chem. Soc.*, **72**, 2127 (1950).

19) M. Utaka, J. Koyama, and A. Takeda, *J. Am. Chem. Soc.*, **98**, 984 (1976).

20) M. E. McEntee and A. R. Pinder, *J. Chem. Soc.*, **1957**, 4419.

21) C. W. T. Hassey and A. R. Pinder, *J. Chem. Soc.*, **1961**, 3525. It is noted by these authors that compound **21** yielded tar, accompanied by unchanged chloro ketone, on treatment with basic reagents.

22) The yield was reduced as a result of the formation of a tarry matter. This compound may also be prepared by the direct acetylation of cyclopentene. *Cf.* N. Jones and H. T. Taylor [*J. Chem. Soc.*, **1959**, 4017], and also S. Dev [*J. Indian Chem. Soc.*, **33**, 703 (1956)].

23) R. E. Wolff, J. C. -N. Ma, and G. Lukas, *C. R. Acad. Sci.*. **257**, 1784 (1963).

24) G. Büchi and H. Wüest, *J. Am. Chem. Soc.*, **87**, 1589 (1965).

25) S. M. McElvain, R. D. Bright, and P. R. Johnson, *J. Am. Chem. Soc.*, **63**, 1558 (1941).

26) P. S. Pinkney, *Org. Synth.*, Coll. Vol. II, 116 (1943).

27) J. -M. Conia and A. Le Craz, *Bull. Soc. Chim. Fr.*, **1960**, 1934; *Chem. Abstr.*, **57**, 3310i (1962).

28) V. Prelog, L. Ruzicka, and O. Metzler, *Helv. Chim. Acta*, **30**, 1883 (1947).

29) S. Hünig, E. Lüche, and W. Brenninger, *Org. Synth.*, **43**, 35 (1963).

30) A. Takeda, S. Tsuboi, F. Sakai, and M. Tanabe, *J. Org. Chem.*, **39**, 3098 (1974).

31) H. M. Teeter and E. W. Bell, *Org. Synth.*, Coll. Vol. IV, 125 (1963).

32) L. Garanti and A. Marchesini, *Ann. Chim. (Rome)*, **53**, (11), 1619 (1963); *Chem. Abstr.*, **60**, 7924h (1964).

33) A. L. Wilds and A. L. Meader, Jr., *J. Org. Chem.*, **13**, 763 (1948).

34) H. D. Scharf and F. Korte, *Chem. Ber.*, **97**, 2425 (1964).

The Daphniphyllum Alkaloids with A New Nitrogen Heterocyclic Skeleton

Shosuke YAMAMURA,† J. A. LAMBERTON,* Hazime IRIKAWA,** Yasuaki OKUMURA,**
Masaaki TODA,*** and Yoshimasa HIRATA***

Faculty of Pharmacy, Meijo University, Tenpaku-ku, Nagoya 468
**Division of Applied Chemistry, C.S.I.R.O., Melbourne, Australia*
***Department of Chemistry, Shizuoka University, Oya, Shizuoka 422*
****Chemical Institute, Nagoya University, Chikusa-ku, Nagoya 464*

(Received January 20, 1977)

The isolation and structures of six new alkaloids [yuzurine, daphnigracine, daphnigraciline, oxodaphnigracine, oxodaphnigraciline, and epioxodaphnigraciline] are described. The structure of yuzurine, which has been elucidated by means of an X-ray crystallographic analysis of the corresponding methiodide, is in full agreement with its spectral data. The structures of the other five alkaloids, all of which were isolated from the plant *Daphniphyllum gracile* Gage collected in New Guinea, were deduced on the basis of an exhaustive comparison of their spectral data coupled with chemical evidences. Finally, a plausible biogenesis of these alkaloids with a new type of nitrogen heterocyclic skeleton is discussed.

The plant *Daphniphyllum macropodium* Miquel ("yuzuriha" in Japanese) contains a great variety of related alkaloids, which can be regarded as a triterpene alkaloid. From a structural point of view, they are divided into five types of nitrogen heterocyclic skeleton represented by daphniphyldine, secodaphniphylline, daphnilactone A, daphnilactone B, and yuzurimine.[1] However, all of them possess in common the 2-azabicyclo[3.3.1]nonane system [A], a part of which constitutes a part of the bicyclo[5.3.0]decane system. Thus, these daphniphyllum alkaloids are reasonably related to one another by bond formation or fission on the basis of our biosynthetic study indicating that they are biosynthesized from six molecules of mevalonic acid *via* a squalene-like intermediate.[2] In particular, the isolation of daphnilactones A and B strongly suggests that such compounds as [B] and [C] must be key intermediates between two main groups represented by daphniphylline and yuzurimine.[3] In connection with the above biogenetic consideration, our considerable efforts have been made to search for the biogenetically important intermediates. In the present paper, we wish to describe the novel structures of six new daphniphyllum alkaloids that have no 2-azabicyclo[3.3.1]nonane system and differ from the other structurally known alkaloids.

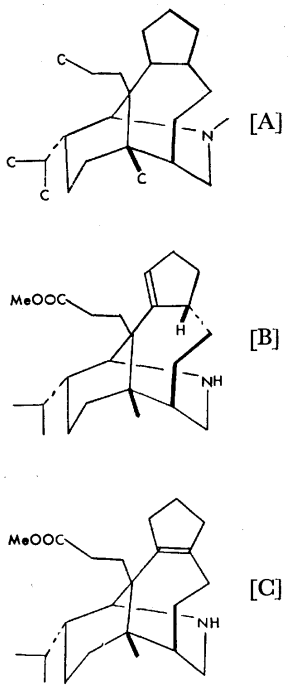

Fig. 1.

The Structure of Yuzurine. Yuzurine (**1**) has been isolated from the bark and leaves of the plant *Daphniphyllum macropodum* M. as one of the minor components, and cited as the alkaloid A_2.[4] This alkaloid is a colorless viscous liquid with a molecular formula [$C_{24}H_{37}O_4N$ (*m/e* 403 (M^+))] and characterized as the corresponding methiodide (**7**); mp 229—230 °C; $C_{25}H_{40}O_4NI$ [*m/e* 403 (M^+-MeI)]. Although this base can be regarded as one of the C_{22}-alkaloids from its molecular formula, the spectral data of **1** and **7** indicate that the carbon skeleton of yuzurine seems to be considerably different from those of the other daphniphyllum alkaloids, whose structures have been already established.

Firstly, yuzurine (**1**) has one ethyl group [δ 0.85 (3H, t, J=7.4 Hz)]. Furthermore, the NMR spectrum of the free base has two methyl singlets at δ 2.17 and 3.21 due to each one of NMe and OMe groups in addition to the presence of a methoxycarbonyl group (ν_{max} 1740 cm^{-1} and δ 3.64) and a $-CH_2-O-$ grouping [δ 3.93 (2H, s)]. In the case of the corresponding methiodide (**7**), the methyl singlet at δ 2.17 in **1** was shifted to lower magnetic field and two singlets were observed at δ 3.57 and 3.63 assignable to two methyl groups attached to the newly formed quaternary nitrogen atom. Secondly, three doublets with a geminal coupling constant (J=12—13.5 Hz) were newly observed at δ 3.35, 4.06, and 4.10 in the NMR spectrum of **7**. In addition, the NMR signal corresponding to the geminal doublet at δ 4.06, is present at δ 3.67—3.85. From these data, the methiodide (**7**) must have a partial structure $(-CH_2-\overset{\overset{Me}{|}}{\overset{+}{N}}-CH_2-)$. Finally, the complex structure of yuzurine (**1**) was elucidated by means of an X-ray crystallographic analysis of the methiodide (**7**),[5] which was subjected to Hofmann degradation to give the

† To whom inquires should be addressed.

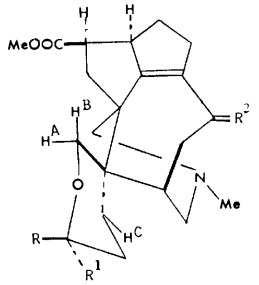

1 R=OMe, R^1=Et, R^2=H_2
2 R=OH, R^1=*i*-Pr, R^2=H_2
3 R=OH, R^1=Et, R^2=H_2
4 R=OH, R^1=*i*-Pr, R^2=O
5 R=OH, R^1=Et, R^2=O
6 R=Et, R^1=OH, R^2=O
12 R=Et, R^1=OMe, R^2=H_2

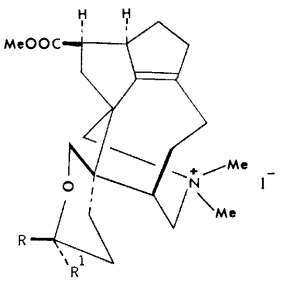

7 R=OMe, R^1=Et
8 R=OH, R^1=*i*-Pr
9 R=OH, R^1=Et
13 R=Et, R^1=OMe

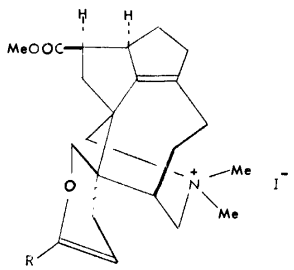

10 R=*i*-Pr
11 R=Et

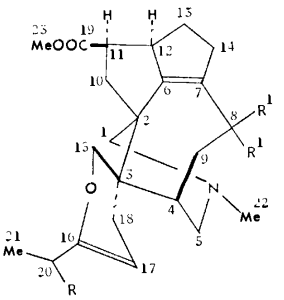

14 R=Me, R^1=H_2
15 R=H, R^1=H_2
16 R=H, R^1·R^1=O

Fig. 2.

original alkaloid (**1**). Further study on this quaternary base[6] has revealed that yuzurine (**1**) has the same absolute configuration as those of daphmacrine[7] and methyl homosecodaphniphyllate.[8] The structure of yuzurine so far obtained is in full agreement with its spectral and chemical data.

As described earlier, many number of alkaloids have been isolated from the plant *Daphniphyllaceae* growing in Japan.[1,3] Recently, an extensive survey was made of the occurrence of alkaloids in New Guinea plants,[9] and according to general procedures (see Experimental) the crude alkaloidal components were obtained from the plant *Daphniphyllum gracile* Gage by one of us (J. A. L). Interestingly, an analytical TLC of the crude oil so far obtained did not show any spots corresponding to daphniphylline and yuzurimine, both of which had been already isolated from the Japanese species as a main product.[10] This crude oil was further separated carefully by repeated preparetive TLC [Kieselgel PF_{254}; hexane–Et_2O–Et_2NH (10 : 10 : 1)] to give five new alkaloids, namely daphnigracine (**2**), daphnigraciline (**3**), oxodaphnigracine (**4**), oxodaphnigraciline (**5**) and in epioxodaphnigraciline (**6**) in 0.0046, 0.023, 0.0041, 0.016, and 0.019% overall yields, respectively.[11]

The Structures of Daphnigracine and Daphnigraciline. Daphnigracine is a colorless viscous liquid [**2**, $C_{24}H_{37}NO_4$; *m/e* 403 (M^+) and 385 (M^+-18)]. This alkaloid has each one of hydroxyl and methoxycarbonyl groups [ν_{max} 3450 cm^{-1}; ν_{max} 1730 cm^{-1} and δ 3.62 (3H, s)], and can be characterized as the corresponding methiodide [**8**, mp (dec) 198—199 °C; $C_{25}H_{40}O_4NI$]. Daphnigraciline [**3**, mp 76—78 °C; $C_{23}H_{35}O_4N$; *m/e* 389 (M^+) and 371 (M^+-18)] has a hydroxyl group (ν_{max} 3500 cm^{-1}) and a methoxycarbonyl group [ν_{max} 1735 cm^{-1} and δ 3.62 (3H, s)]. Similarly, treatment of **3** with MeI in acetone afforded the corresponding methiodide [**9**, mp (dec) 163—165 °C; $C_{24}H_{38}O_4NI$], in an almost quantitative yield. As shown in Tables 1 and 2, the spectral data, particularly NMR spectra, of both alkaloids are quite similar to each other except for the following points: the NMR signal due to an isopropyl group is observed at δ 0.93 in **2**, while daphnigraciline (**3**) has a methyl triplet at δ 0.94. Furthermore, when treated with Ac_2O–AcOH (1 : 1), both of the methiodides (**8** and **9**) were readily converted into the corresponding dehydration products (**10** and **11**) in high yields [**10**; mp (dec) 243—245 °C; $C_{25}H_{38}O_3NI$; *m/e* 385 (M^+—MeI); ν_{max} 1675 cm^{-1}; δ 4.44 (1H, m). **11**; mp (dec) 235—237 °C; $C_{24}H_{36}O_3NI$; *m/e* 371 (M^+—MeI); ν_{max} 1680 cm^{-1}; δ 4.39 (1H, m)]. From these data, clearly, daphnigracine and daphnigraciline must have the same carbon skeleton except for the different alkyl groups. Finally, the structures of these alkaloids were elucidated by conversion of daphnigraciline (**3**) into yuzurine (**1**), as follows.

When treated with MeOH containing one drop of AcOH (room temp, overnight), daphnigraciline (**3**) was converted into yuzurine (**1**), in a high yield, in addition to a small amount of an epimer (**12**) which was characterized as the corresponding methiodide [**13**: mp (dec) 144—146 °C; $C_{25}H_{40}O_4NI$; *m/e* 403 (M^+—MeI); ν_{max} 1730 cm^{-1} and no OH absorption band; δ 3.11 (3H, s)]. On Hofmann degradation, **13** was easily re-

Table 1. NMR spectra of dapiinigracine (**2**) and daphnigraciline (**3**)[a]

2	**3**
0.93(6H, d, J=7.0 Hz)	0.94(3H, t, J=7.0 Hz)
2.15(3H, s)	2.19(3H, s)
3.62(3H, s)	3.62(3H, s)
3.89(1H, dd, J=12.5, 2 Hz)	3.90(1H, dd, J=12.5, 2 Hz)
4.32(1H, d, J=12.5 Hz)	4.35(1H, d, J=12.5 Hz)

a) In $CDCl_3$.

Table 2. NMR spectra of the methiodides (**8** and **9**)[a]

8	**9**
0.95(3H, d, J=7.0 Hz)	0.97(3H, t, J=7.0 Hz)
0.96(3H, d, J=7.0 Hz)	
3.45(3H, s)	3.44(3H, s)
3.50(3H, s)	3.48(3H, s)
3.68(3H, s)	3.70(3H, s)
3.00—3.90(5—6H, complex)	3.00—3.90(5—6H, complex)
4.42(1H, d, J=12.5 Hz)	4.43(1H, d, J=12.5 Hz)

a) In $CDCl_3$–CD_3OD.

converted into the starting base (**12**).

Finally, although the configuration of the hydroxyl group in a acetal moiety is not determined chemically, the NMR spectrum of **2** (or **3**) indicates that this hydroxyl group must be in an axial configuration, as discussed below. In the NMR spectrum of daphnigracine (**2**), as expected, a sharp doublet (δ 4.32) due to the geminal proton (H^A), which is in a 1,3-diaxial relationship to the hydroxyl group, is observed in lower magnetic field than the NMR signal at δ 3.89 assignable to the equatorial geminal proton (H^B) which can couple with a proton (H^C) along the 'W' path.

The Structures of Oxodaphnigracine, Oxodaphnigraciline and Epioxodaphnigraciline. The IR, UV, and NMR spectra of oxodaphnigracine (**4**: mp 116—117 °C; $C_{24}H_{35}O_5N$) and oxodaphnigraciline (**5**: mp 107—109 °C; $C_{23}H_{33}O_5N$) indicate that these two alkaloids must be quite similar to each other except for the alkyl group [δ 0.88 (6H, d, J=7.0 Hz) in **4**; δ 0.94 (3H, t, J=7.0 Hz) in **5**], as seen in the cases of daphnigracine (**2**) and daphnigraciline (**3**). In the UV spectra of **4** and **5**, particularly, the absorption maximum is observed at 253 nm, indicating the presence of an α,β-unsaturated CO group which must be included in the seven-membered ring.[12]

Epioxodaphnigraciline (**6**: mp 102—104 °C; $C_{23}H_{33}O_5N$) has the same molecular formula as that of oxodaphnigraciline (**5**), and their spectral data are also quite similar to each other. However, a remarkable difference is seen in the following points: the NMR spectrum of the former has the sharp doublet (δ 3.88) due to the geminal proton (H^A) at slightly higher magnetic field than that of **5** (δ 4.03). Therefore, the structure of epioxodaphnigraciline must be represented by **6**. Furthermore, these results are supported by the ^{13}C NMR spectra of the dehydration products (**14**, **15**, and **16**), which have been obtained on dehydration of the corresponding alkaloids **2**, **3**, and **5** (or **6**) with Ac_2O–AcOH (1 : 1).

As demonstrated in the previous paper,[13] the methyl, methylene, methine and quaternary carbon signals in the ^{13}C NMR spectra of these dehydro compounds are easily differentiated by measurements of their partially relaxed FT ^{13}C NMR spectra coupled with off-resonance experiments, and the results are summarized in Table 3. In the spectrum of **14**, nine methylene and four methine signals are observed, while ten methylene and three methine signals are found in that of **15**. In the case of **16**, nine methylene and three methine signals are found in addition to one new CO signal (δ 208.9). Furthermore, the olefinic signals at δ 138.6 and 183.3 strongly suggest that this CO group must conjugate with the tetra-substituted double bond (C_6–C_7) in **16**. In the cases of **15** and **16**, the ^{13}C NMR signals of the NMe group [δ 26.6 in **15**; δ 26.5 in **16**] appear at extraordinary high magnetic field. This may be due to complicated steric compression. The other signals of these three dehydration products show the one-to-one correspondence to one another.

From a biogenetic point of view, these new alkaloids may be produced from the plausible intermediate [B] according to a pathway (a) or (b), as shown in Scheme

TABLE 3. ^{13}C CHEMICAL SHIFTS OF **14**, **15**, AND **16**

Functional group	**14**	**15**	**16**	Assignment
CH_3–	20.4 (2 Me)	11.6	11.4	C-21
	32.1	26.6	26.5	C-22
	51.0	51.0	51.5	C-23
–CH_2–	27.2	27.2	21.1	C-9, 13, 14, 20
	27.2	27.2	26.3	
	28.1	27.4	27.7	
		28.0	38.2[a]	
	39.8[a]	39.9[a]	38.6[a]	C-18
	42.6[a]	42.6[a]		C-8
	46.6[a]	46.6[a]	46.1	C-10
	56.5	56.4	56.1	C-5
	62.1	62.2	62.9	C-1
	69.4	69.6	69.1	C-15
–CH–	34.2	34.3	34.4	C-4
	42.6	42.6	42.6	C-12
	54.9	54.9	45.0	C-11
	27.4			C-20
–C–	36.6	36.6	37.1	C-3
	46.5	46.4	50.3	C-2
>C=C<	90.3	92.0	91.8	C-17
	133.6	133.5	138.6	C-7
	159.5	156.0	156.1	C-16
	145.8	145.9	183.3	C-6
>C=O	175.4	175.5	173.7	C-19
			208.9	C-8

a) Assignment of chemical shifts for close-lying peaks may be reversed.

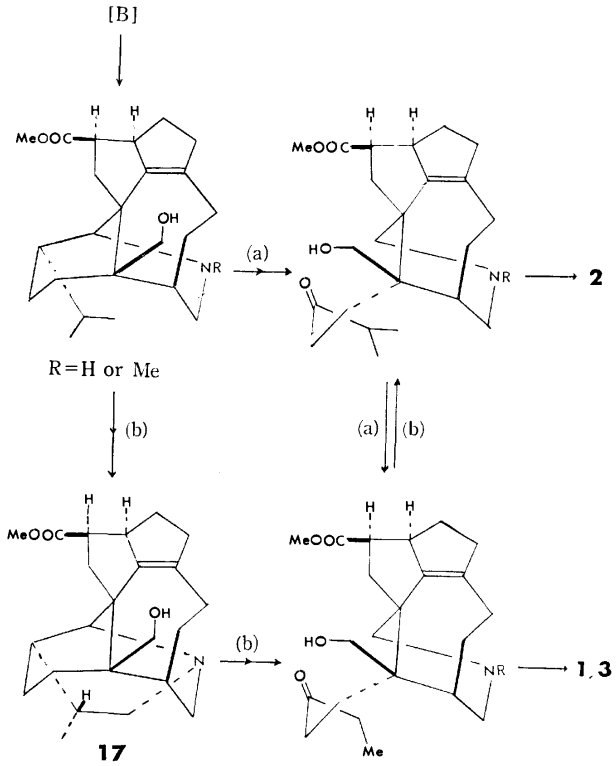

Scheme 1.

1. Of two possibilities, the isolation of daphnigracine (**2**) with an isopropyl group from the plant suggests that yuzurine (**1**) and daphnigraciline (**3**) both are not necessarily derived from yuzurimine B (**17**), but may be produced by oxidative demethylation of daphnigracine (**2**) or its precursor Biosynthetic experiments are further required to solve these problems.

Experimental

All the mps are uncorrected. IR spectra were recorded on a JASCO Model IR-S spectrophotometer. UV spectra were obtained on a Perkin Elmer 202 spectrophotometer, using MeOH as the solvent. NMR spectra were recorded on a Varian Associate AH-100 or A-60, or JEOL JNM-PS 100 NMR spectrometer, using $CDCl_3$ as the solvent, unless otherwise stated. The chemical shifts are given in ppm relative to the internal TMS, and only prominent signals are cited (d, doublet; m, multiplet; q, quartet; s, singlet; t, triplet). Mass spectra were taken on a Hitachi RMU-6C mass spectrometer, operating with an ionization energy of 70 eV.

Column chromatography was carried out on basic alumina (Nakarai Chemical Co., Ltd., *ca.* 300 mesh) or on silicic acid (Mallinckrodt, 100 mesh). Thin layer chromatography was performed on Kieselgel PF_{254} using hexane–Et_2O–Et_2NH (10 : 10 : 1) or Et_2O–Et_2NH (40 : 3), unless otherwise stated.

*Physical Properties of Yuzurine (**1**).* Isolation of this alkaloid was reported in the reference 4. Yuzurine is a colorless viscous liquid (**1**); ν_{max} (film) 1740 cm^{-1}; δ 0.85(3H, t, J=7.4 Hz), 2.17(3H, s), 3.21(3H, s), 3.64(3H, s), and 3.93 (2H, s); *m/e* 403 (M^+ for $C_{24}H_{37}O_4N$), 388, 372, 360, and 344.

*Formation of Yuzurine Methiodide (**7**).* A solution of yuzurine (40 mg) and MeI (1 ml) in acetone (2 ml) was allowed to stand at room temperature overnight, and then concentrated under reduced pressure to give pale yellow crystals (45 mg). Recrystallization from benzene–MeOH afforded pale yellow needles, which were subjected to an X-ray crystallographic analysis.[5] Its physical data are as follows: mp (dec) 229—230 °C; ν_{max} (KBr) 2700 and 1740 cm^{-1}; δ 0.87 (3H, t, J=7.0 Hz), 3.20(3H, s), 3.35(1H, br d, J=13.5 Hz,) 3.57(3H, s), 3.64(3H, s), 3.67(3H, s), 3.67—3.85(1H, superimposed on Me signals), 3.85(2H, br s), 4.06 (1H, d, J=12 Hz), and 4.10(1H, br d, J=13.5 Hz); *m/e* 403 (M^+−MeI) (Found: C, 54.51; H, 7.44; N, 2.51%. Calcd for $C_{25}H_{40}O_4NI$: C, 55.04; H, 7.39; N, 2.57%).

Hofmann Degradation of Yuzurine Methiodide. To a solution of yuzurine methiodide (80 mg) in MeOH–H_2O [(4 : 1) 5 ml] was added excess amounts of Ag_2O (*ca.* 200 mg). The reaction mixture was stirred at room temperature for 1 h, and then filtered. The filtrate was concentrated under reduced pressure to leave a crystalline residue, which was heated *in vacuo* at *ca.* 200 °C for 10 min, and then cooled. The resulting oily residue was purified by preparative TLC, using hexane–Et_2O–Et_2NH (10 : 10 : 1) to afford a colorless oil of yuzurine (47.2 mg) (analytical TLC and IR spectrum).

*Isolation of Daphnigracine (**2**), Daphnigraciline (**3**), Oxodaphnigracine (**4**), Oxodaphnigraciline (**5**), and Epioxodaphnigraciline (**6**).* The leaves of the plant *Daphniphyllum gracile* Gage growing in New Guinea were collected late in January. According to a usual procedure,[9] the air-dried leaves were milled and extracted by continuous percolation with MeOH at 40 °C. The methanolic extracts were concentrated under reduced pressure so that the temperature of the solution did not exceed 40 °C. The concentrate was diluted with water, and then acidified by addition of 1M H_2SO_4. The solution was filtered and made basic by addition of ammonia, and then extracted repeatedly with chloroform. Evaporation of the combined chloroform extracts gave the crude alkaloids as a dark brown residue. This residue was dissolved in chloroform (apart from a small amount of largely nonalkaloidal gum) and the alkaloids were extracted from the solution by repeatedly shaking with successive lots of 1M H_2SO_4. The crude alkaloids as a dark brown oil were recovered from the aqueous acidic solution by basification with ammonia followed by extraction with chloroform. Yield of the crude alkaloids from the air-dried leaves is 0.15% in weight.

The dark brown oil (556 mg) was further separated carefully by repeated preparative TLC using hexane–Et_2O–Et_2NH (10 : 10 : 1) to give five new alkaloids in the following order from the less polar to polar fractions: daphnigracine (**2**) (17.2 mg), daphnigraciline (**3**) (84.3 mg), oxodaphnigracine (**4**) (15 mg), oxodaphnigraciline (**5**) (61.4 mg) and epioxodaphnigraciline (**6**) (70.8 mg). Their physical data are shown below.

*Daphnigracine (**2**)* as a colorless viscous liquid: ν_{max} (film) 3450 and 1730 cm^{-1}: *m/e* 403 (M^+) and 385 (Found: *m/e* 403.27186. Calcd for $C_{24}H_{37}O_4N$: *m/e* 403.27224).

*Daphnigraciline (**3**):* Mp 76—78 °C (from hexane–Et_2O); ν_{max} (Nujol) 3500 and 1735 cm^{-1}; *m/e* 389 (M^+) and 371 [Found: C, 70.70; H, 9.25; N, 3.23% (*m/e* 389.25396). Calcd for $C_{23}H_{35}O_4N$: C, 70.92; H, 9.06; N, 3.60% (*m/e* 389.25659)].

*Oxodaphnigracine (**4**):* Mp 116—117 °C (from hexane–Et_2O); ν_{max} (Nujol) 3400 br, 1730, 1685, and 1650 cm^{-1}; λ_{max} 253 nm (ε, 7500); δ 0.88(6H, d, J=7.0 Hz), 2.10(3H, s), 3.60(1H, dd, J=11, 2 Hz), 3.69(3H, s), and 4.03(1H, d, J=11 Hz); *m/e* 417 (M^+) and 399 (Found: *m/e* 417.25334. Calcd for $C_{24}H_{35}O_5N$: *m/e* 417.25151).

*Oxodaphnigraciline (**5**):* Mp 107—109 °C (from hexane–Et_2O); ν_{max} (Nujol) 3380 br, 1730, 1685, and 1648 cm^{-1}; λ_{max} 253 nm (ε, 8060); δ 0.94(3H, t, J=7.0 Hz), 2.12(3H, s), 3.58(1H, dd, J=11.5, 3 Hz), 3.70(3H, s), and 4.03(1H, d, J=11.5 Hz); *m/e* 403 (M^+) and 385 (Found: *m/e* 403.23692. Calcd for $C_{23}H_{33}O_5N$: *m/e* 403.23585).

*Epioxodaphnigraciline (**6**):* Mp 102—104 °C (from hexane–Et_2O); ν_{max} (Nujol) 3400 br, 1735, 1685, and 1650 cm^{-1}; λ_{max} 252 nm (ε, 7000); δ 0.92 (3H, t, J=7.5 Hz), 2.15(3H, s), 3.61(4H, s)*, and 3.88(1H, d, J=12 Hz); *m/e* 403 (M^+) and 385 (Found: *m/e* 403.23532. Calcd for $C_{23}H_{33}O_5N$: *m/e* 403.23585).

*Formation of Daphnigraciline Methiodide (**9**).* According to the similar procedure as that of yuzurine (**1**), a solution of daphnigraciline (20 mg) in acetone (5 ml) was treated with MeI (1 ml) at room temperature overnight to give pale yellow crystals in quantitative yield:; mp (dec) 163—165 °C (from acetone–Et_2O); ν_{max} (Nujol) 3300 and 1710 cm^{-1}; *m/e* 371 (M^+−MeI−H_2O) (Found: C, 54.17; H, 7.36; N, 2.45%. Calcd for $C_{24}H_{38}O_4NI$: C, 54.23; H, 7.21; N, 2.64%).

*Formation of Daphnigracine Methiodide (**8**).* Under the same conditions as that of daphnigraciline (**3**), daphnigracine methiodide was also produced in an almost quantitative yield; mp (dec) 198—199 °C (from acetone–Et_2O); ν_{max} (Nujol) 3450 br, 3320 and 1710 cm^{-1}; *m/e* 385 (M^+−MeI−H_2O) (Found: C, 53.57; H, 7.15; N, 2.46%. Calcd for $C_{25}H_{40}O_4NI \cdot H_2O$: C, 53.28; H, 7.15; N, 2.64%).

*Dehydration of Daphnigraciline Methiodide (**9**).* A solution of **9** (15 mg) in Ac_2O–AcOH [(1 : 1) 2 ml] was allowed to stand at room temperature overnight, and then concentrated under reduced pressure at 100 °C to leave a crystalline

* One of the geminal protons (H^B) is included.

solid (13 mg). Recrystallization from acetone–Et_2O gave pale yellow needles (**11**): mp (dec) 235—237 °C; ν_{max} (Nujol) 1730 and 1680 cm^{-1}; δ 1.00(3H, t, J=7.2 Hz), 3.29 (1H, d, J=13.5 Hz), 3.54(3H, s), 3.61(3H, s), 3.62(3H, s), 3.73—3.92(2H, br), 4.02(1H, d, J=12 Hz), 4.18(1H, d, J=13.5 Hz), 4.38(1H, d, J=12 Hz), and 4.39(1H, m); *m/e* 371 (M^+—MeI), 356, 343, 340, 328, 314, 312, and 300 (Found: C, 55.99; H, 7.13; N, 2.31%. Calcd for $C_{24}H_{36}O_3NI$: C, 56.14; H, 7.07; N, 2.72%).

Dehydration of Daphnigracine Methiodide (8). Under the similar conditions as that of **9**, daphnigracine methiodide (20 mg) was treated with Ac_2O–AcOH [(1 : 1) 3 ml] to give a crystalline solid (*ca.* 20 mg), which was recrystallized from acetone–Et_2O to give pale yellow needles (**10**): mp (dec) 243—245 °C; ν_{max} (Nujol) 1730 and 1675 cm^{-1}; δ 1.01(6H, d, J=7.0 Hz), 3.30(1H, d, J=13.5 Hz), 3.57(3H, s), 3.63(3H, s), 3.65(3H, s), 3.7—3.90(2H, br), 4.02(1H, d, J=12 Hz), 4.21(1H, d, J=13.5 Hz), 4.44(1H, d, J=12 Hz), and 4.44 (1H, m); *m/e* 385 (M^+—MeI), 370, 357, 354, 342, 326, 314, and 300 (Found: C, 57.45; H, 6.83; N, 2.38%. Calcd for $C_{25}H_{38}O_3NI$: C, 56.92; H, 7.26; N, 2.66%).

Conversion of Daphnigraciline Methiodide (9) into Yuzurine Methiodide (7). Daphnigraciline methiodide (10 mg) was dissolved in MeOH (2 ml) containing one drop of AcOH. The resulting solution was allowed to stand at room temperature overnight, and then concentrated under reduced pressure on a boiling water-bath to give a pale brown solid (*ca.* 10 mg), which was crystallized from MeOH–benzene to afford pale yellow crystals of yuzurine methiodide (**7**) (mp and IR spectrum).

Conversion of the Dehydration Product (11) into Yuzurine Methiodide (7). According to the same procedure as that of daphnigraciline methiodide (**9**), **11** (10 mg) was treated with MeOH (2 ml) containing one drop of AcOH to give a crystalline solid quantitatively, which was recrystallized from MeOH–benzene to give yuzurine methiodide (**7**) (mp and IR spectrum).

Conversion of Daphnigraciline (3) into Yuzurine (1) and Epiyuzurine (12). A solution of **3** (100 mg) in MeOH (5 ml) containing AcOH (*ca.* 0.01 ml) was stirred at room temperature for 4 h, and then concentrated under reduced pressure at 100 °C to leave a slightly brown residue, which was separated by preparative TLC [hexane–Et_2O–Et_2NH (20 : 20 : 3)] to give yuzurine (75 mg) (TLC and IR spectrum) and a colorless viscous liquid of epiyuzurine (*ca.* 7 mg) which was characterized as the corresponding methiodide (**13**), mp (dec) 144—146 °C (from acetone–Et_2O); ν_{max} (Nujol) 1730 cm^{-1}; δ 0.85(3H, t, J=7.0 Hz), 3.11(3H, s), 3.42(2H, br s), 3.55(3H, s), 3.65(3H, s), 3.66 (3H, s), 3.34—3.72(1H, superimposed on Me signals), and 3.84—4.22(3H, complex); *m/e* 403 (M^+—MeI), 388, 371, 343, 340, 328, 314, 312, and 300 (Found: C, 54.59; H, 7.15; N, 2.20%. Calcd for $C_{25}H_{40}O_4NI$: C, 55.04; H, 7.39; N, 2.57%).

Dehydration of Daphnigracine (2). A solution of **2** (20 mg) in Ac_2O–AcOH [(1 : 1) 2 ml] was allowed to stand at room temperature overnight, and then concentrated to dryness under reduced pressure at 100 °C. The resulting pale brown oil was purified by preparative TLC, using hexane–Et_2O–Et_2NH (10 : 10 : 1) to afford a colorless viscous liquid (15 mg) [**14**: ν_{max} (film) 1735 and 1675 cm^{-1} (no OH absorption band) (Found: *m/e* 385.25956. Calcd for $C_{24}H_{35}O_3N$: *m/e* 385.26168) which was characterized as the corresponding methiodide (**10**).

Dehydration of Daphnigraciline (3). According to the same procedure as that of daphnigracine (**2**), treatment of **3** (20 mg) with Ac_2O–AcOH [(1 : 1) 2 ml] afforded the corresponding dehydration product (12 mg) as a colorless viscous liquid [**15**: ν_{max} (film) 1740 and 1678 cm^{-1} (no OH absorption band) (Found: *m/e* 371.24465. Calcd for $C_{23}H_{33}O_3N$: *m/e* 371.24603)]. This product was also characterized as the corresponding methiodide (**11**).

Dehydration of Oxodaphnigraciline (5). According to the same conditions as that of daphnigracine (**2**), **5** (22 mg) was treated with Ac_2O–AcOH [(1 : 1) 2 ml] to give a brown oil, which was purified by preparative TLC using Et_2O–Et_2NH (40 : 3) to afford an almost colorless viscous liquid (10 mg) [**16**: ν_{max} (film) 1735, 1690 br, and 1665 cm^{-1} (no OH absorption band); δ 1.00(3H, t, J=7.5 Hz), 2.16(3H, s), 3.55 (1H, d, J=11.5 Hz), 3.64(3H, s), 4.11(1H, dd, J=11.5, 2 Hz), and 4.36(1H, m) (Found: *m/e* 385.22619. Calcd for $C_{23}H_{31}O_4N$: *m/e* 385.2253)].

The authors wish to thank Dr. Masayasu Kurono (Ono Central Research Laboratories) for measurements of high resolution mass spectra. They are also indebted to Miss. Kikuko Kato (Analytical Center, Meijo University) for elemental analyses. This research has been supported in part by grants from the Ministry of Education, to which greatful acknowledgement is made.

References

1) M. Toda, H. Niwa, H. Irikawa, Y. Hirata, and S. Yamamura, *Tetrahedron*, **30**, 2683 (1974).

2) K. T. Suzuki, S. Okuda, H. Niwa, M. Toda, Y. Hirata, and S. Yamamura, *Tetrahedron Lett.*, **1973**, 799; H. Niwa, Y. Hirata, K. T. Suzuki, and S. Yamamura, *ibid.*, **1973**, 2129.

3) S. Yamamura and Y. Hirata, "The Alkaloids," Vol. XV, ed by R. H. F. Manske, Academic Press, New York (1975), p. 41; see also "International Review of Science," Series 2, Vol. 9, ed by K. Wiesner, Butterworths, London (1976), p. 161.

4) M. Toda, Y. Hirata, and S. Yamamura, *Tetrahedron*, **28**, 1477 (1972).

5) S. Yamamura, K. Sasaki, M. Toda, and Y. Hirata, *Tetrahedron Lett.*, **1974**, 2023.

6) To be published elsewhere.

7) C. S. Gibbons and J. Trotter, *J. Chem. Soc., B*, **1969**, 840.

8) K. Sasaki and Y. Hirata, *J. Chem. Soc., B*, **1971**, 1565.

9) T. G. Hartley, E. A. Dunstone, J. S. Fitzgerald, S. R. Johns, and J. A. Lamberton, *Lloydia*, **36**, 217 (1973).

10) H. Irikawa, N. Sakabe, S. Yamamura, and Y. Hirata, *Tetrahedron*, **24**, 5691 (1968).

11) S. Yamamura, J. A. Lamberton, H. Irikawa, Y. Okumura, and Y. Hirata, *Chem. Lett.*, **1975**, 923.

12) R. H. Silverstein and G. C. Bassler, "Spectrometric Identification of Organic Compounds," John Wiley & Sons Inc., New York (1967), p. 160.

13) S. Yamamura, H. Irikawa, Y. Okumura, and Y. Hirata, *Bull. Chem. Soc. Jpn.*, **48**, 2120 (1975).

Layered Compounds. XLII.[1] Syntheses and Properties of Layered Paracycloheterophanes

Tetsuo OTSUBO, Shigeyoshi MIZOGAMI, Norihisa OSAKA, Yoshiteru SAKATA, and Soichi MISUMI

The Institute of Scientific and Industrial Research, Osaka University, Suita, Osaka 565

(Received January 21, 1977)

A series of multilayered paracyclofuranophanes and paracyclothiophenophanes were synthesized by cross-breeding Hofmann elimination method from mixed quaternary ammonium hydroxides. Their structures and conformations were elucidated by NMR analyses. In electronic spectra, paracyclothiophenophanes exhibited stronger transannular electronic interactions than paracyclofuranophanes whose absorption curves show unexpected resemblance to those of multilayered metaparacyclophanes. Paracyclofuranophanes and [2.2](2,5)furanophane underwent addition reaction with benzyne to give 1 : 1 and 1 : 2 adducts, respectively. Their structures and properties were also studied by spectral measurements.

In recent years, multilayered compounds in which three or more aromatic rings are mutually stratified have been extensively investigated from a viewpoint of transannular π-electronic interaction.[2-4] It has become apparent that such electronic interactions among aromatic rings and the internal strain due to face-to-face benzene ring compression are mainly responsible for a number of anomalous physical and chemical properties of layered compounds, and the interaction increases with an increase of layer number. These results have prompted us to study multilayered cyclophanes containing heteroaromatic ring such as furan and thiophene, **1**—**10**, which might demonstrate much information on the transannular electronic interaction between benzene and heteroaromatic rings and on their chemical properties.

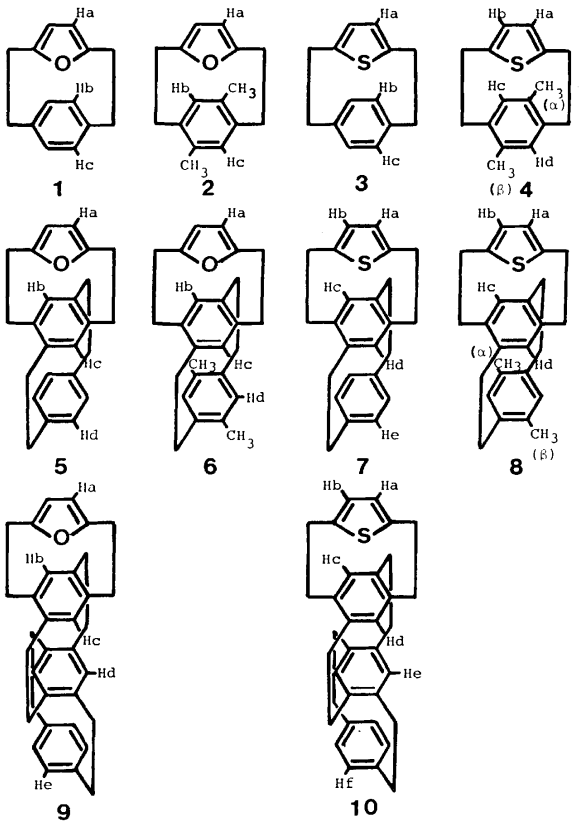

Scheme 1.

Results and Discussion

Syntheses. Although a number of synthetic methods have been recently developed for [2.2]cyclophane,[5] 1,6-Hofmann elimination method presented by Winberg *et al.*[6] is still very convenient and advantageous for the synthesis of multilayered [2.2]paracyclophane because of facile availability of the intermediary compounds.[2,3] In the present work we applied the same method for the syntheses of all paracycloheterophanes **1**—**10**. The syntheses of intermediates, quaternary ammonium salts **11**—**17**, were carried out in the same way as described in literatures.[2,3,6]

Cram and his coworkers first found out the formation of [2.2]paracyclo(2,5)furanophane **1** by the cross-breeding Hofmann degradation of 5-methylfurfuryltrimethylammonium hydroxide **11b** and *p*-methylbenzyltrimethylammonium hydroxide **13b**.[7] Similarly, we prepared [2.2]paracycloheterophanes **2**—**4** by cross-breeding reaction of the corresponding two quaternary ammonium hydroxides. A cross-breeding reaction generally produces a mixture of three main cyclophanes. For example, two intermediates, **18** and **19**, generated from pyrolysis of the corresponding quaternary ammonium hydroxides give cyclophane **20** from a cross coupling and cyclophanes **21**[6] and **22**[2,3,6] from homo-coupling. Besides them, [2.2.2](2,5)thiophenophane **23** was formed from **12** and [2.2.2]paracyclophane **24**[2] from **13** as minor products. Triple- and quadruple-layered paracycloheterophanes **5**—**10** were also synthesized by the same cross-breeding method using the corresponding multilayered quaternary ammonium salts **15**—**17**. In these cases, multilayered [2.2]paracyclophanes such as **25**[2,3] were formed as one of homo-coupling products.

The yields of cross coupling products are fairly low as compared with those of homo-coupling products and decrease with an increasing number of layers because multilayered cyclophanes and layered quinodimethane intermediates are relatively unstable. In the syntheses of layered paracyclophanes, a cross coupling product was easily separated from homo-coupling products by careful column chromatography on silica gel or alumina. However, some paracycloheterophanes were found to be very difficult to purify by means of conventional chromatography. This difficulty could be overcome by

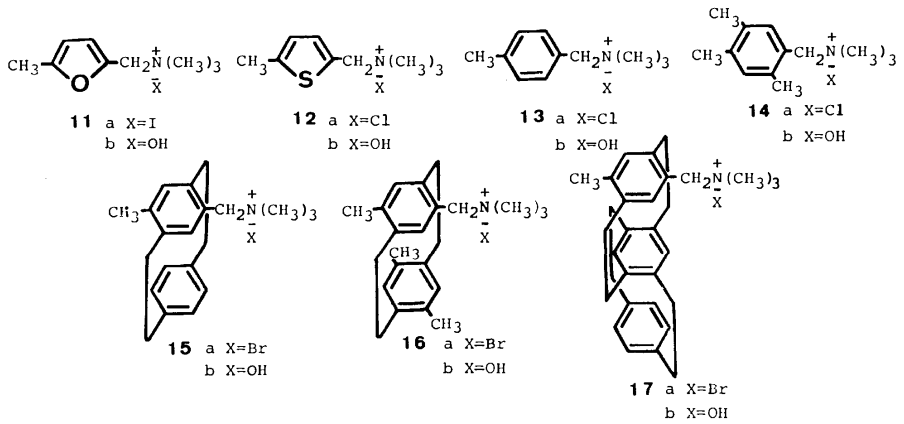

Scheme 2.

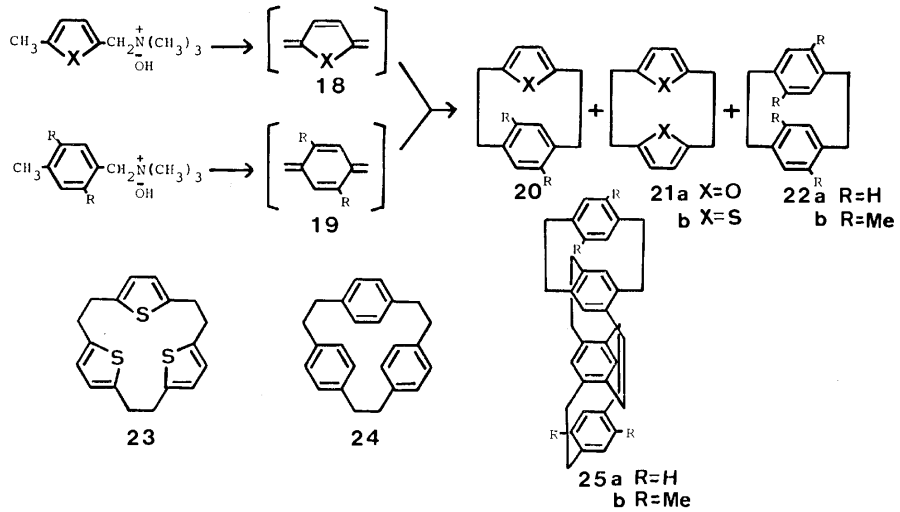

Scheme 3.

use of silica gel coated with silver nitrate, which adsorbed heteroaromatic nucleus more strongly. In addition, use of preparative gel permeation liquid chromatography was found to be advantageous..

Structures and NMR Spectra. The NMR specrtal data of multilayered [2.2]paracycloheterophanes are summarized in Table 1. The most remarkable feature is that the chemical shifts of all the aromatic protons appear at high field as in the case of multilayered [2.2]-paracyclophanes.[8] There has been observed a certain regularity for upfield shifts of the aromatic protons, since each benzene ring is stacked in parallel at regular intervals (mean value 3.06 Å).[9] The upfield shifts of the present paracycloheterophanes are relatively small and rather irregular. This suggests that heteroaromatic rings are not stacked in the same mode as that of benzene rings. Table 1 also shows that two thiophene protons of the paracyclothiophenophanes appear nonequivalently except for **3**. In the case of 4,7-dimethyl-[2.2]paracyclophane **26**, the aromatic protons Ha at pseudo-gem position to methyl group were observed to shift considerably downfield due to the steric compression effect.[8] Similarly the nonequivalence of the thiophene protons is interpreted to arise from a downfield shift of one of the protons, which is sterically compressed by pseudo-*gem* methyl or methylene group. The steric compression effect (−0.32 ppm) of methyl group in **4** is almost same as that (−0.36 ppm) in **26**. The steric compression effect of bridged methylene is generally not observed in a series of paracyclophanes as indicated by equivalence of outer aromatic protons in **25a** or **27**.[8] The appearance of such effect on thiophene proton indicates that the proton is very close to pseudo-*gem* methylene group owing to the bulkiness of sulfur atom. On the other hand, furan series shows no steric compression effect. Thus the NMR signal

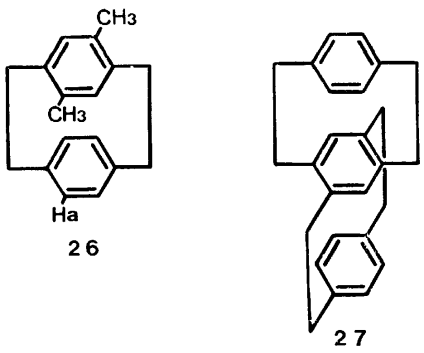

Scheme 4.

Table 1. NMR data of layered paracycloheterophanes in carbon tetrachloride (δ value)

Compound	ArH			CH_2	CH_3
		(Fixed)[a]			
1	Ha	5.52(s, 2H)	5.49(s, 2H)	2.9—2.35(A_2B_2, 8H)	
	Hb	6.68(s, 4H)	6.12(d, 2H)		
	Hc		7.07(d, 2H)		
2	Ha	5.51(s, 2H)	5.62(s, 2H)	3.2—2.3(m, 8H)	2.11(s, 6H)
	Hb	6.37(s, 2H)	6.11(s, 1H)		
	Hc		6.99(s, 1H)		
3	Ha	6.12(s, 2H)		3.4—2.6(m, 8H)	
	Hb	6.08(d, 2H)			
	Hc	6.98(d, 2H)			
4	Ha	6.40(ABd, 3.8 Hz, 1H)		3.5—2.7(m, 8H)	1.77(s, 3H)[b]
	Hb	6.08(ABd, 3.8 Hz, 1H)			2.48(s, 3H)[c]
	Hc	5.68(s, 1H)			
	Hd	6.54(s, 1H)			
5	Ha	5.29(s, 2H)	5.22(s, 2H)	3.4—2.2(m, 16H)	
	Hb	5.75(s, 2H)	5.18(s, 1H)		
	Hc		6.17(s, 1H)		
	Hd	6.15(s, 4H)	6.13(s, 4H)		
6	Ha	5.30(s, 2H)	5.37(s, 2H)	3.4—2.2(m, 16H)	1.99(s, 6H)
	Hb	6.18(s, 2H)	5.72(s, 1H)		
	Hc		6.70(s, 1H)		
	Hd	5.78(s, 2H)	5.89(s, 2H)		
7	Ha, Hb	5.97(ABq, 2.5 Hz, 2H)		3.4—2.2(m, 16H)	
	Hc	5.03(s, 1H)			
	Hd	6.00(s, 1H)			
	He	6.16(s, 4H)			
8	Ha	6.06(ABd, 2.5 Hz, 1H)		3.5—2.2(m, 16H)	1.87(s, 3H)[b]
	Hb	5.97(ABd, 2.5 Hz, 1H)			1.98(s, 3H)[c]
	Hc	5.41(s, 1H)			
	Hd	6.38(s, 1H)			
	He	5.77(s, 2H)			
9	Ha	5.21(s, 2H)	5.15(s, 2H)	3.3—2.0(m, 24H)	
	Hb	5.50(s, 2H)	4.96(s, 1H)		
	Hc		5.84(s, 1H)		
	Hd	5.26(s, 2H)	5.20(s, 2H)		
	He	6.06(s, 4H)	5.99(s, 4H)		
10	Ha, Hb	5.87(ABq, 3 Hz, 2H)		3.4—2.1(m, 24H)	
	Hc	4.80(s, 1H)			
	Hd	5.74(s, 1H)			
	He	5.19(s, 2H)			
	Hf	6.02(s, 4H)			
21a		5.90(s, 4H)		2.65(bs, 8H)	
21b		6.72(s, 4H)		3.5—2.7(A_2B_2, 8H)	
23		6.44(s, 6H)		2.99(s, 12H)	

a) **1**, **5**, and **9** in CS_2; **2** in $CDCl_3$; **6** in 2 : 1 $CDCl_3$-CS_2. b) α-CH_3. c) β-CH_3.

of the furan protons remains to be a singlet even at low temperature which may give rise to fixation of the furan ring. It seems reasonable to assume that the stacking modes of furan and thiophene rings are quite different from each other. In order to elucidate these structural problems, X-ray crystallographic analyses of triple-layered paracycloheterophanes **5** and **8** were very recently carried out by Kasai and his coworkers (Figs. 1 and 2).[10] Thus the furan ring is stacked at some angle on the faced benzene ring just like [2.2]metaparacyclophane.[11] The geometry is consistent with the spectral behavior described above. On the other hand, the thiophene ring is stacked in parallel on the faced benzene ring like [2.2]paracyclophane,[12] but it is slidden in such a way that the thiophene proton comes close to pseudo-*gem* methylene group as predicted by NMR analysis.

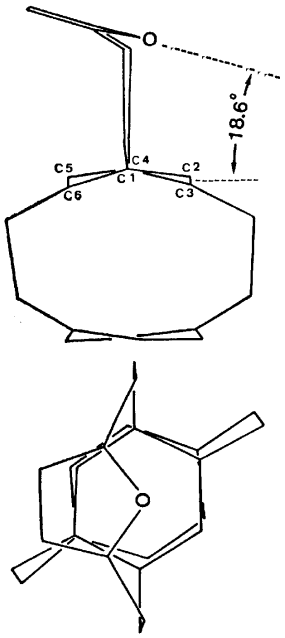

Fig. 1. Profile of triple-layered paracyclofuranophane **5**. Intramolecular non-bonded distances (Å); O···Cl, 2.860; O···C2, 2.927; O···C3, 3.054; O···C4, 2.820; O···C5, 3.011; O···C6, 3.173.

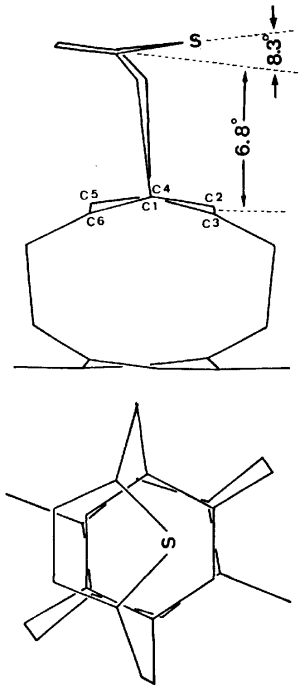

Fig. 2. Profile of dimethyl triple-layered paracyclothiophenophane **8**. Intramolecular non-bonded distances (Å); S···Cl, 3.121; S···C2, 3.049; S···C3, 3.197; S···C4, 3.122; S···C5, 3.436; S···C6, 3.597.

The structural difference between furanophane and thiophenophane is mainly due to larger bulkiness of sulfur atom relative to oxygen atom.

Another striking feature in NMR data is that aromatic protons of benzene ring faced to heteroaromatic ring appear to be nonequivalent in thiophene series and to be equivalent in furan series. These phenomena

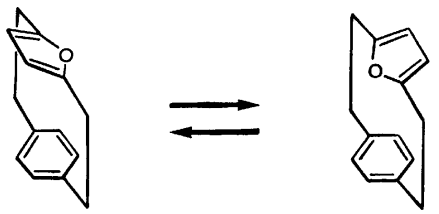

Fig. 3. Ring inversion of [2.2]paracyclofuranophane **1**.

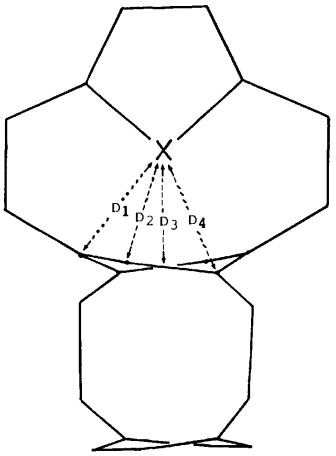

	D_1	D_2	D_3	D_4
X=O	2.91Å	3.01	3.14	3.28
X=S	2.44	2.61	2.63	2.88

Fig. 4. Non-bonded distances between heteroatom and faced benzene in the transition state of the interconversion process.

can be explained to arise from the fixation of thiophene ring in the former series and the rapid interconversion of furan ring in the latter series as shown in Fig. 3.[13] We studied the dynamic behavior of a series of paracyclofuranophanes by variable temperature NMR spectroscopy. When the temperature is lowered, coalescence occurs and the aromatic protons of the faced benzene ring become nonequivalent (Table 1). Activation energy ΔG^* for the interconversion process was calculated by peak separation method according to Gutowsky and Holm[14] (Table 2). The flipping in triple- and quadruple-layered paracyclofuranophanes is appreciably easier than that in double-layered one. This can be explained in terms of the geometry of the faced benzene ring. Molecular model of **1** shows that the benzene ring is deformed into a boat shape like [2.2]paracyclophane.[12] On the other hand, as indicated by X-ray analysis of **5**, the inside benzene ring of multilayered cyclophane is deformed into a twist form which is caused by pulling up and down with two pairs of methylene bridges. Such structural changes of the faced benzene ring are considered to lower the steric barrier for the flipping of the furan ring.

The thiophene ring of paracyclothiophenophanes was, at the beginning, expected to flip at high temperature. However, they showed no change in their NMR spectra up to 150 °C but appreciable decomposition above this temperature. For understanding of the conformational behavior of furan and thiophene, it is advisable to in-

TABLE 2. ACTIVATION ENERGY ΔG_c (kcal/mol), RATE CONSTANT K_c (s^{-1}), LIFE TIME τ_c (s), COALESCENCE TEMPERATURE T_c (°C), AND PEAK SEPARATION $\Delta\nu$ (Hz) OF FACED BENZENE PROTONS FOR THE INVERSION PROCESS OF PARACYCLOFURANOPHANES

Compound	**1**	**2**	**5**	**6**	**9**
ΔG_c	11.4	11.9	10.4	10.2	10.2
K_c	1.26×10^{2}	1.17×10^{2}	1.22×10^{2}	1.28×10^{2}	1.17×10^{2}
τ_c	3.97×10^{-3}	4.25×10^{-3}	4.10×10^{-3}	3.91×10^{-3}	4.26×10^{-3}
T_c	−39	−29	−58	−62	−63
$\Delta\nu$	53.1	53.1	57.0	57.7	52.9

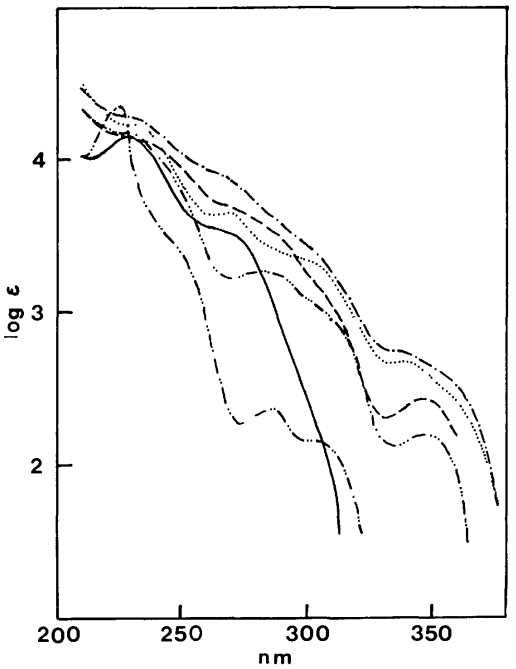

Fig. 5. Electronic spectra of multilayered paracyclothiophenophane **3** (——), **7**(----), and **10** (—·—), together with multilayered paracyclophanes **22a** (—··—), **27** (—···—), and **25a** (·····) in cyclohexane.

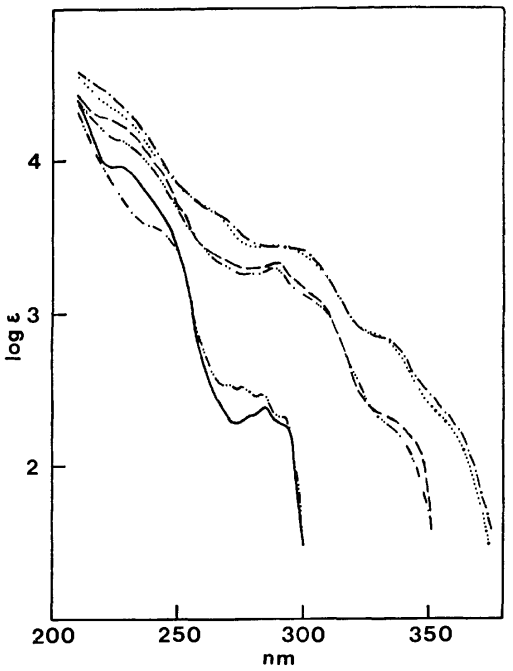

Fig. 6. Electronic spectra of multilayered paracyclofuranophanes **1** (——), **5** (----), and **9** (—·—), together with [2.2]metaparacyclophane (—··—), **28** (—···—), and **29** (·····) in cyclohexane.

quire the non-bonded distances between heteroatom and faced benzene in the transition state where heteroaromatic ring is perpendicular to benzene ring. A minute calculation was performed on a computer using X-ray data of **5** and **8** as shown in Fig. 4.[10] The non-bonded distances for paracyclofuranophane are comparable to van der Waals distance (3.10 Å) of oxygen and benzene, supporting that the ring flipping is feasible according to temperature condition. On the other hand, the non-bonded distances for paracyclothiophenophane are much smaller than van der Waals distance (3.55 Å) of sulfur and benzene. The resulting large steric barrier inhibits the flipping process of thiophene ring.

Electronic Spectra. It is well-known that the transannular electronic interaction between two chromophores which are closely fixed with each other affects strongly the electronic spectra.[15] Multilayered [2.2]-paracyclophanes exhibited strong bathochromic and hyperchromic effects in their spectra with an increasing number of the layers, which were theoretically explained by both exciton and charge-transfer interactions.[16] As shown in Figs. 5 and 6, the present multilayered paracycloheterophanes show an analogous tendency, and the characteristic absorptions of the heteroaromatic rings disappear successively as the number of layer increases. The bathochromic shifts of the thiophene series are more significant than those of the furan series, indicating that thiophene interacts more strongly with benzene than furan. Incidentally, the absorption curves of the former show unexpected resemblance to those of multilayered paracyclophanes **25a** and **27** (Fig. 5) and the spectra of the latter to those of the corresponding multilayered metaparacyclophanes **28** and **29** (Fig. 6).[17] These spectral properties seem to be partly attributable to the stacking modes of paracyclothiophenophane similar to multilayered paracyclophane and paracyclofuranophane to multilayered metaparacyclophane. The transannular electronic interactions are also observed in the cases of [2.2](2,5)thiophenophane **21b**, [2.2.2](2,5)thiophenophane **23**, and [2.2](2,5)furanophane **21a** (Fig. 7). Thiophene or furan itself has no absorption in the ultraviolet region above 230 nm.[18] These cyclophanes clearly show bathochromic shifts or

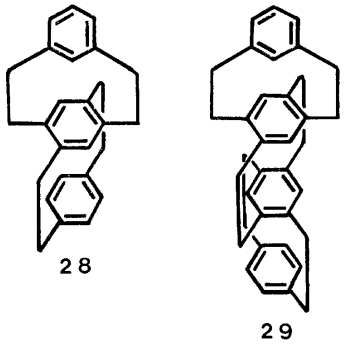

Scheme 5.

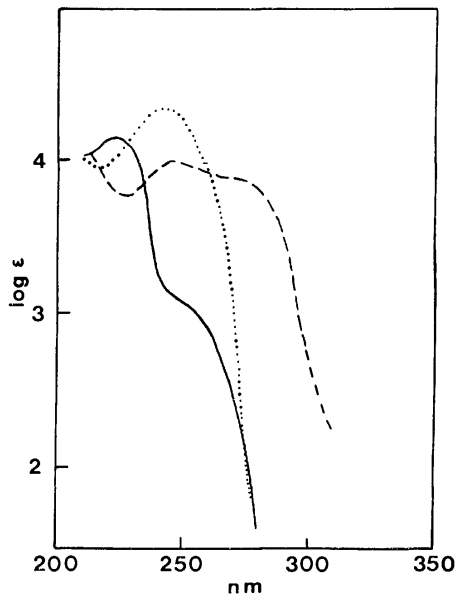

Fig. 7. Electronic spectra of heterophanes **21a** (——), **21b** (----), and **23** (·····) in cyclohexane.

appearance of new peaks in the longer wavelength. The stronger effect in **21b** relative to that in **21a** suggests that d-orbitals of sulfur atom plays significant role in the interaction.

TCNE Complexes. The transannular electronic interaction in cyclophane system is usually reflected in the increase of the π-basicity, in other words, the interaction brings a strong donor character to that system.[2,3,19] The absorption maxima of charge-transfer complexes of the present paracycloheterophanes and tetracyanoethylene (TCNE) are summarized in Table 3. As the number of layers increases, the absorption maxima shift to longer wavelength as seen in the case of multilayered [2.2]paracyclophane.[2,3] Although furan and thiophene have lower ionization potentials (9.00 and 9.10 eV, respectively) than benzene (9.52 eV), the CT bands of multilayered paracycloheterophanes with more than three layers appear at rather shorter wavelength than those of paracyclophane analogues. Evidently the electronic interaction between heteroaromatic and benzene rings is less effective than that between benzene rings. Table 3 also shows that thiophene series has stronger interaction than furan series.

Table 3. Absorption maxima of TCNE complexes (nm) in CH_2Cl_2

2,5-Dimethylfuran	574
2,5-Dimethylthiophene	416, 556
p-Xylene	460
Durene	480
Furanophanes	
1	563
2	563
5	584
6	622
9	570
21a	588
Thiophenophanes	
3	538
4	572
7	626
8	644
10	655
21b	545

Addition Reaction with Benzyne. Layered cyclophanes offer many example of unusual addition reactions.[20] In particular, furanophanes have shown to undergo Diels-Alder reactions to give polycyclic compounds bearing unique skelton.[7,21] However, the present paracyclofuranophanes did not react with ordinary dienophiles such as maleic anhydride, dimethyl acetylenedicarboxylate, and tetracyanoethylene. When benzyne was used as a dienophile, paracyclofuranophanes **1** and **5** gave 1 : 1 adduct respectively. Three types of conformations are possible for these adducts. *e.g.*, **30**, **31**, and **32** from **1**. In the structures **31** and

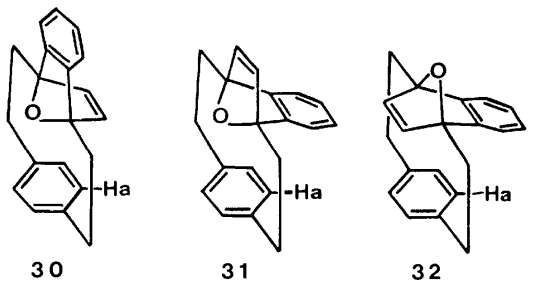

30 **31** **32**

Scheme 6.

32, the NMR signals of Ha protons would shift significantly to high field due to magnetic anisortropy of the fused benzene ring. The NMR spectra of the adducts are consistent with the structures **30** and **33** (Fig. 8). Moreover, examination with molecular model indicates that the structures **31** and **32** are sterically unfavorable because there are considerable repulsion between the fused benzo group and faced benzene rings.

As shown in Fig. 9, the electronic spectra of these adducts exhibit unexpected large bathochromic and hyperchromic shifts. The CT bands of their TCNE complexes also appear at longer wavelength than predicted; **30**, λ_{max} 505 and 570(sh) nm; **33**, λ_{max} 530(sh)

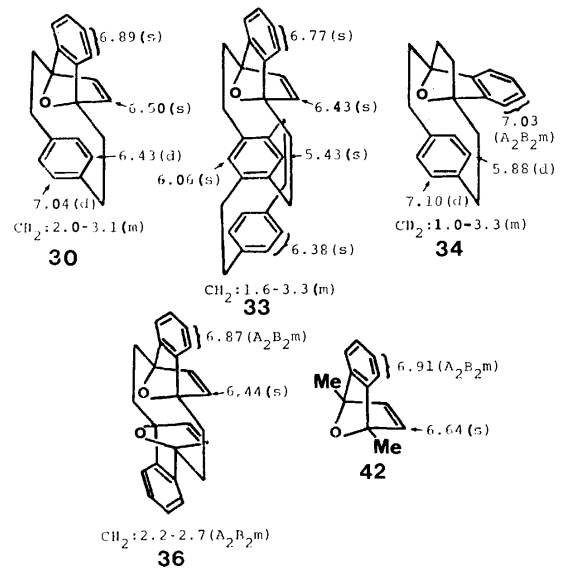

Fig. 8. NMR data of benzyne adducts (δ value in deuteriochloroform).

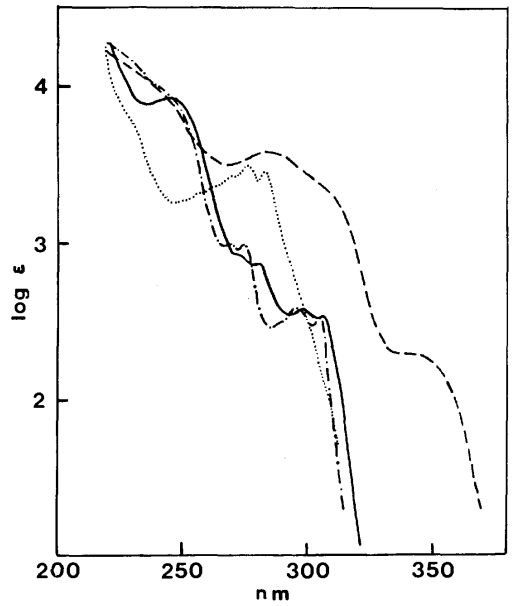

Fig. 9. Electronic spectra of benzyne adducts **30** (——), **33** (----), **34** (—·—), and **36** (·····) in tetrahydrofuran.

and 634 nm in dichloromethane. These data apparently indicate the presence of strong transannular electronic interaction in the adducts. A direct interaction between the two benzene rings does not seem to take place. Therefore, either olefinic group or oxygen atom is predicted to take part in the electronic interaction. In order to obtain further evidence, the olefinic group of **30** was saturated by catalytic reduction using Pd–C. Surprisingly, the hydrogenation gave dihydro compound **34** accompanied by an inversion of the conformation instead of **35** with retention. The structure of **34** is assigned by its NMR spectrum. Thus the Ha proton drastically shifts to high field compared to Ha proton of **30**, which is due to magnetic anisotropy of the fused benzo group. Probably, the conformational change

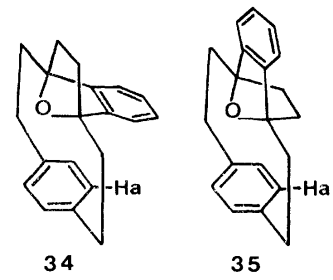

Scheme 7.

arises from an increasing steric hindrance of ethano group with Ha proton in **35**, as compared to that of fused benzo group with Ha proton in **34**. The electronic spectrum of **34** is similar to that of adduct **30** (Fig. 9) and the absorption maxima of its TCNE complex, 490 and 570 nm in CH_2Cl_2, are almost same as those of **30**. These facts suggest that there is no essential difference between the electronic interactions in **30** and **34**, and thereby oxygen atom makes considerable contribution to the interaction in both adducts **30** and **33**.

Battiste and Kapicak[22] reported that [2.2](2,5)furanophane **21a** underwent a Diels-Alder reaction with benzyne to give non-internally cyclized 1 : 1 adduct and 1 : 2 adduct, and that an *anti* structure for the latter bis-adduct would be favored over others on the basis on *anti* structure of **21a** and steric requirement of benzyne approaching. We have carried out the same addition reaction of **21a** with benzyne generated from anthranilic acid and obtained 1 : 2 adduct in 16% yield. Of six possible conformations **36**—**41** for the adduct other than sterically unfavorable structures with outmost oxygen like **32**, the structure **36** is most favorable from NMR data (Fig. 8) which show 0.2 ppm upfield shift for olefinic proton and invariable shift for aromatic proton as compared with a reference compound **42**.[23] The other structures are therefore in conflict with the NMR data. Thus, the structures **40** and **41** would not give any symmetrical NMR pattern. The olefinic proton of **37** would be expected to shift rather to downfield by a deshielding effect of closely placed

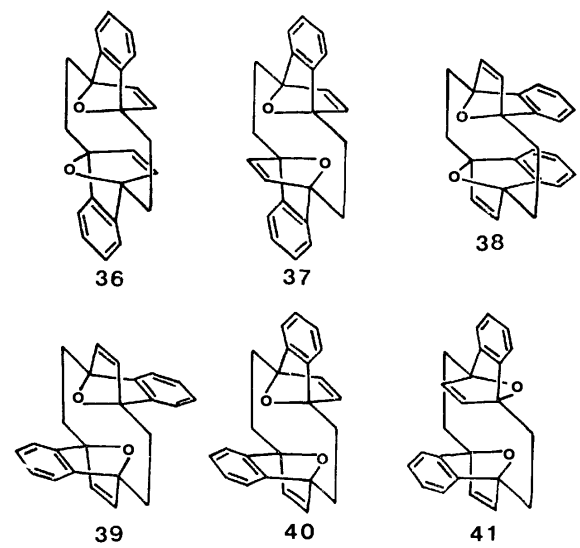

Scheme 8.

oxygen atom. In **38** or **39**, one would predict the olefinic signal to be identical to that of **42** and the aromatic signal to be different from that of **42**. The electronic spectrum of the adduct and the CT spectrum of its TCNE complex (λ_{max}, 410 and 544 nm in CH_2Cl_2) exhibit unusual transannular electronic interaction as in the case of **30** and **33**.

Experimental

Melting points are uncorrected. All solvents are of reagent grade. NMR spectra were taken with a Hitachi Perkin-Elmer R-20 spectrometer (60 MHz) using tetramethylsilane as an internal standard. MS and UV spectra were measured with a Hitachi RMU-7 spectrometer (70 eV) and a Hitachi EPS-3T spectrophotometer, respectively. A general procedure of Hofmann elimination reaction was described in detail in the experimental part of 4,7-dimethyl[2.2]paracyclo-(2,5)furanophane **2**. Chromatography was usually done with silica gel (Merck, activity II—III) of 20 to 100 times of a mixture to be separated. Silica gel coated with silver nitrate was made as follows: silica gel (100 g) was shaken sufficiently with silver nitrate (20 g) in 100 ml of distilled water, and then water was removed using a rotary evaporator. The residual silica gel coated with silver nitrate was activated on standing overnight in an oven at 110 °C and used with care to avoid exposure to light.

4,7-Dimethyl[2.2]paracyclo(2,5)furanophane **2**. 5-Methylfurfuryltrimethylammonium iodide **11a**[6] (15 g, 53 mmol) and duryltrimethylammonium chloride **14a**[3] (10 g, 44 mmol) were dissolved in 500 ml of distilled water and passed through ion exchange column packed with Dowex 1-X8 ion exchange resin which was previously converted to hydroxide form. The eluted aqueous solution of **11b** and **14b** was mixed with xylene (50 ml) and phenothiazine (50 mg). The mixture was heated with stirring in a nitrogen atmosphere, and water was removed by azeotropic distillation using a Dean-Stark type of water separator. After removal of water, reflux was continued for additional 10 h. Insoluble polymer was filtered off and washed with xylene. The filtrate and washing were combined, dried over anhyd magnesium sulfate, and evaporated. The residue was chromatographed on silica gel using petroleum ether as an eluent. There was eluted first a mixture of 4,7-dimethyl[2.2]paracyclo(2,5)furanophane **2** and 4,7,12,15-tetramethyl[2.2]paracyclophane **22b**,[2,3] and then [2.2](2,5)furanophane **21a**[6] (0.6 g). The mixture was rechromatographed on silica gel coated with silver nitrate. Elution with 1 : 1 petroleum ether–ether gave first **2** (884 mg, 9%) and then **22b** (674 mg). Recrystallization of **2** from petroleum ether afforded colorless plates, mp 63.0—64.5 °C.

MS *m/e* 226 (M^+). Found: C, 85.02; H, 8.08%. Calcd for $C_{16}H_{18}O$: C, 84.91; H, 8.01%.

[2.2]Paracyclo(2,5)thiophenophane **3**. In the same way as **2**, the cross-breeding reaction of the quaternary hydroxides derived from 5-methylthenyltrimethylammonium chloride **12a**[6] (4 g, 19 mmol) and *p*-methylbenzyltrimethylammonium chloride **13a** (9.6 g, 48 mmol) gave a mixture of the desired cyclophane **3**, [2.2]paracyclohpane **22a**, [2.2](2,5)thiophenophane **21b**, [2.2.2](2,5)thiophenophane **23**, and [2.2.2]paracyclophane **24**. After usual column chromatography on silica gel and then on silica gel coated with silver nitrate, preparative gel permeation liquid chromatography gave pure **3** (92 mg, 2.3%), colorless prisms from 1 : 1 hexane–benzene, mp 230—231 °C (sealed tube).

MS *m/e* 214 (M^+). Found: C, 78.67; H, 6.36%. Calcd for $C_{14}H_{14}S$: C, 78.48; H, 6.59%.

4,7-Dimethyl[2.2]paracyclo(2,5)thiophenophane **4**. The cross-breeding reaction of the quaternary hydroxides derived from 5-methylthenyltrimethylammonium chloride **12a** (3.0 g, 14.6 mmol) and duryltrimethylammonium chloride **14a** (2.7 g, 11.9 mmol) gave a mixture of **4**, **21b**, and **22b**. The desired cyclophane **4** was separated as in the case of **2**, 50 mg (1.7%), colorless plates from petroleum ether, mp 125.0—126.0 °C.

MS *m/e* 242 (M^+). Found: C, 79.62; H, 7.62; S, 13.06 %. Calcd for $C_{16}H_{18}S$: C, 79.29; H, 7.48; S, 13.23%.

Triple-layered Paracyclofuranophane **5**. The cross-breeding reaction of two quaternary ammonium hydroxides (derived from **11a**, 9.4 g, 33.4 mmol and **15a**, 5.0 g, 13.4 mmol) gave a mixture of **5**, **21a**, and quadruple-layered paracyclophane **25a**. The desired cyclophane **5** was separated by column chromatography on silica gel ,300 mg (6.8%), colorless plates from hexane, mp 117.0—118.0 °C.

MS *m/e* 328 (M^+). Found: C, 87.60; H, 7.16%. Calcd for $C_{24}H_{24}O$: C, 87.76; H, 7.36%.

Dimethyl Triple-layered Paracyclofuranophane **6**. In this case, anion exchange process was carried out by use of silver oxide instead of ion exchange resin. Thus, two quaternary ammonium salts **11a** (0.7 g, 2.5 mmol) and **16a** (1.0 g, 2.5 mmol) were stirred with two equivalents of fresh silver oxide in 30 ml of distilled water for a few hours. After filtration, the aqueous solution was pyrolyzed in the same way as **2**. Column chromatography of the products on silica gel using 1 : 9 benzene–hexane for elution gave first tetramethyl quadruple-layered paracyclophane **25b**, then [2.2](2,5)furanophane **21a** and finally the desired cyclophane **6** (20 mg, 2.2%), colorless prisms from petroleum ether, mp 127.0—128.0 °C.

MS *m/e* 356 (M^+). Found: C, 87.72; H, 7.87%. Calcd for $C_{26}H_{28}O$: C, 87.60; H, 7.91%.

Triple-layered Paracyclothiophenophane **7** *and [2.2.2](2,5)-Thiophenophane* **23**. The cross-breeding reaction of the quaternary hydroxides derived from two ammonium salts **12a** (7 g, 34 mmol) and **15a** (5 g, 13 mmol) and the subsequent column chromatography on silica gel with 1 : 9 benzene–hexane gave first **21b**, and then a mixture of **7** and quadruple-layered paracyclohpane **25a**. From final fraction [2.2.2](2,5)-thiophenophane was obtained as colorless crystals (348 mg, 3.1%), mp 124 °C.

MS *m/e* 330 (M^+). Found: C, 65.45; H, 5.49%. Calcd for $C_{18}H_{18}S_3$: C, 65.44; H, 5.45%.

The desired cyclophane **7** was purified by column chromatography on silica gel coated with silver nitrate, 22 mg (0.5%), colorless prisms from 1 : 3 carbon tetrachloride–acetone, mp 177 °C with dec.

MS *m/e* 344 (M^+). Found: C, 83.50; H, 6.88%. Calcd for $C_{24}H_{24}S$: C, 83.69; H, 7.02%.

Dimethyl Triple-layered Paracyclothiophenophane **8**. As usual, the desired cyclophane **8** was obtained from the cross-breeding reaction of two quaternary ammonium hydroxides (from **12a**, 4 g, 19 mmol and **16a**, 4.6 g, 11 mmol), followed by column chromatography on silica gel and then on silica gel coated with silver nitrate, yield 33 mg (0.8%), colorless plates from petroleum ether, mp 149—151.5 °C with dec.

MS *m/e* 372 (M^+). Found: C, 83.96; H, 7.73%. Calcd for $C_{26}H_{28}S$: C, 83.83; H, 7.58%.

Quadrulpe-layered Paracyclofuranophane **9**. The usual cross-breeding reaction of two quaternary ammonium hydroxides (derived from **11a**, 3.03 g, 10.8 mmol and **17a**, 3.00 g, 6.0 mmol) followed by chromatogrphy on silica gel with 1 : 9 benzene–hexane gave the desired cyclohpane **9** (56 mg, 2%), colorless plates from 1 : 3 carbon tetrachloride–acetone, mp 176—178 °C.

MS *m/e* 458 (M^+). Found: C, 88.94; H, 7.27%. Calcd for $C_{34}H_{34}O$: H, 89.04; H, 7.47%.

Quadruple-layered Paracyclothiophenophane ***10***. The cross-breeding reaction of two quaternary ammonium hydroxides (derived from **12a**, 3.5 g, 17 mmol and **17a**, 3.0 g, 6 mmol) and subsequent purification by column chromatography on silica gel with 1 : 9 benzene–hexane gave the cyclophane **10** (40 mg, 1.4%), colorless prisms from 1 : 3 carbon tetrachloride–acetone, dec 195 °C.

MS *m/e* 474 (M^+). Found: C, 85.30; H, 6.99%. Calcd for $C_{34}H_{34}S$: C, 86.04; H, 7.22%.[24]

Addition Reaction of [2.2]Paracyclo(2,5)furanophane ***1*** *with Benzyne.* Anthranilic acid (525 mg, 3.83 mmol) in 25 ml of 1,2-dimethoxyethane and isopentyl nitrite (672 mg, 5.74 mmol) in 25 ml of 1,2-dimethoxyethane were added dropwise and simultaneouly with stirring for one hour into a refluxed solution of **1** (253 mg, 1.28 mmol) in 25 ml of 1,2-dimethoxyethane. After the addition, reflux was continued for additional 30 min. Sodium hydroxide solution (1.7 M, 300 ml) was added in the cooled mixture, and the mixture was extracted with benzene. The extract was washed with water, dried over anhyd sodium sulfate, and evaporated *in vacuo*. The residue was taken up in carbon tetrachloride and subjected to column chromatography on silica gel or alumina to give the adduct **30** (85 mg, 24%), colorless plates from hexane, mp 84.5—85.5 °C.

MS *m/e* 274 (M^+). Found: C, 87.56; H, 6.43%. Calcd for $C_{20}H_{18}O$: C, 87.56; H, 6.61%.

Addition Reaction of Triple-layered Paracyclofuranophane ***5*** *with Benzyne.* In the same way as **30**, the adduct **33** was obtained from the benzyne reaction of **5** (235 mg, 0.72 mmol), yield 230 mg (79%), colorless columns from toluene, mp 245—252 °C with dec.

MS *m/e* 404 (M^+). Found: C, 89.13; H, 6.84%. Calcd for $C_{30}H_{28}O$: C, 89.07; H, 6.98%.

Addition Reaction of [2.2](2,5)Furanophane ***21a*** *with Benzyne.* [2.2](2,5)Furanophane **21a** (501 mg, 2.66 mmol) was allowed to react with anthranilic acid (1.09 g, 8.0 mmol) and isopentyl nitrite (1.61 ml, 12 mmol) in the same way as **30**. The usual purification of the crude product gave 1 : 2 adduct **36** (142 mg, 16%), colorless plates from toluene, dec 220 °C.

MS *m/e* 340 (M^+). Found: C, 84.85; H, 5.81%. Calcd for $C_{24}H_{20}O_2$: C, 84.68; H, 5.92%.

Hydrogenation of Adduct ***30***. The adduct **30** (85 mg, 0.31 mmol) was hydrogenated in the presence of a 5% Pd–C in 20 ml of tetrahydrofuran until hydrogen absorption was ceased. The mixture was filtered and the filtrate was condensed. Column chromatography of the residue on alumina gave dihydro compound **34** (58 mg, 68%), colorless plates from hexane, mp 95—96 °C.

MS *m/e* 276 (M^+). Found: C, 87.21; H, 6.97%. Calcd for $C_{20}H_{20}O$: C, 86.92; H, 7.26%.

We are grateful to Professor Nobutami Kasai and Dr. Yasushi Kai of Osaka University for their kind information of X-ray crystallographic structures of triple-layered paracycloheterophanes prior to publication and for their helpful discussions. Thanks are also due to Mr. T. Fujino for microanalyses and to Mr. Y. Takai for NMR measurements. This research is partly supported by the Grant-in-Aid of the Ministry of Education.

References

1) Part XLI, H. Ohno, H. Horita, T. Otsubo, Y. Sakata and S. Misumi, *Tetrahedron Lett.*, **1977**, 265.

2) T. Otsubo, S. Mizogami, I. Otsubo, Z. Tozuka, A. Sakagami, Y. Sakata, and S. Misumi, *Bull. Chem. Soc. Jpn.*, **46**, 3519 (1973); T. Otsubo, H. Horita, and S. Misumi, *Synth. Commun.*, **6**, 591 (1976).

3) D. T. Longone and H. S. Chow, *J. Am. Chem. Soc.*, **86**, 3898 (1964).

4) A. J. Hubert, *J. Chem. Soc., C*, **1967**, 13.

5) For review, F. Vögtle and P. Neumann, *Synthesis*, **1973**, 85; S. Misumi, *Mem. Inst. Sci. & Ind. Res., Osaka Univ.*, **33**, 53 (1976); *Kagaku No Ryoiki* (Japanese), **28**, 927 (1974).

6) H. E. Winberg, F. S. Fawcett, W. E. Mochel, and C. W. Theobald, *J. Am. Chem. Soc.*, **82**, 1428 (1960); H. E. Winberg and F. S. Fawcett, *Org. Synth.*, Coll. Vol. V, 883 (1973).

7) D. J. Cram and G. R. Knox, *J. Am. Chem. Soc.*, **83**, 2204 (1961); D. J. Cram, C. S. Montgomery, and G. R. Knox, *ibid.*, **88**, 515 (1966).

8) T. Otsubo, S. Mizogami, Y. Sakata, and S. Misumi, *Bull. Chem. Soc. Jpn.*, **46**, 3831 (1973).

9) H. Mizuno, K. Nishiguchi, T. Otsubo, S. Misumi, and N. Morimoto, *Tetrahedron Lett,*. **1972**, 4981; H. Mizuno, K. Nishiguchi, T. Toyoda, T. Otsubo, S. Misumi, and N. Morimoto, *Acta Crystallogr.*, **B33**, 329 (1977).

10) N. Kasai and Y. Kai, private communication.

11) F. Vögtle and P. Neumann, *Chimia*, **26**, 64 (1972) and references cited therein.

12) C. J. Brown, *J. Chem. Soc.*, **1953**, 3265; D. K. Lonsdale, H. J. Milledge, and K. V. K. Rao, *Proc. R. Soc. London, Ser. A*, **255**, 82 (1960); H. Hope, J. Bernstein, and K. N. Trueblood, *Acta Crystallogr.*, **B28**, 1733 (1972).

13) G. M. Whitesides, B. A. Pawson, and A. C. Cope, *J. Am. Chem. Soc.*, **90**, 639 (1968).

14) H. S. Gutowsky and C. H. Holm, *J. Chem. Phys.*, **25**, 1228 (1956).

15) D. J. Cram, *Rec. Chem. Progr.*, **20**, 71 (1959); S. J. Cristol and D. C. Lewis, *J. Am. Chem. Soc.*, **89**, 1476 (1967).

16) I. H. Hillier, L. Glass, and S. A. Rice, *J. Am. Chem. Soc.*, **88**, 5063 (1966); S. Iwata, K. Fuke, M. Sasaki, S. Nagakura, T. Otsubo, and S. Misumi, *J. Mol. Spcetrosc.*, **46**, 1 (1973).

17) N. Kannen, T. Umemoto, T. Otsubo, and S. Misumi, *Tetrahedron Lett.*, **1973**, 4537; N. Kannen, T. Otsubo, Y. Sakata, and S. Misumi, *Bull. Chem. Soc. Jpn.*, **49**, 3203 (1976); N. Kannen, T. Otsubo, and S. Misumi, *ibid.*, **49**, 3208 (1976).

18) H. H. Jaffé and M. Orchin, "Theory and Applications of Ultraviolet Spectroscopy," John Wiley & Sons, Inc. (1962), p. 345.

19) D. J. Cram and R. H. Bauer, *J. Am. Chem. Soc.*, **81**, 5971 (1959).

20) T. Kaneda, T. Ogawa, and S. Misumi, *Tetrahedron Lett.*, **1973**, 3373; T. Inoue, T. Kaneda, and S. Misumi, *ibid.*, **1974**, 2969; T. Toyoda, A. Iwama, Y. Sakata, and S. Misumi, *ibid.*, **1975**, 3203; T. Toyoda, A. Iwama, T. Otsubo, and S. Misumi, *Bull. Chem. Soc. Jpn.*, **49**, 3300 (1976).

21) H. H. Wasserman and R. Kitzing, *Tetrahedron Lett.*, **1969**, 3343; H. Wynberg and R. Helder, *ibid.*, **1971**, 4317; R. Helder and H. Wynberg, *ibid.*, **1973**, 4321; M. A. Battiste, L. A. Kapicak, M. Mathew, and G. P. Palenik, *Chem. Commun.*, **1971**, 1536.

22) L. A. Kapicak and M. A. Battiste, *J. Chem. Soc., Chem. Commun.*, **1973**, 930.

23) L. F. Fieser and M. J. Haddadin, *Can. J. Chem.*, **43**, 1599 (1965).

24) Satisfactory elemental analysis within 0.3% error was not obtained for **10** due to gradual decomposition during purification.

Total Synthesis of Minosaminomycin[1]

Katsuharu IINUMA, Shinichi KONDO,* Kenji MAEDA, and Hamao UMEZAWA
Institute of Microbial Chemistry, 14-23, Kamiosaki 3-chome, Shinagawa-ku, Tokyo 141
(Received January 21, 1977)

A component of the antibiotic minosaminomycin (**1**), (−)-1D-1-amino-1-deoxy-*myo*-inositol (**4**) was synthesized from D-inositol (**3**) by catalytic oxidation of an axial hydroxyl group followed by reduction of the ketoxime. Minobiosamine, 1D-1-amino-1-deoxy-4-*O*-(α-D-kasugaminyl)-*myo*-inositol (**2**), was synthesized from 2′,4′-di-*N*-acetylkasuganobiosamine (**9**) by a similar method, and separated from the two isomers of **2**. The total synthesis of **1** was accomplished by coupling 2′,4′-di-*N*-benzyloxycarbonylminobiosamine (**14**) and N^{α}-[(*S*)-1-benzyloxycarbonyl-3-methylbutylcarbamoyl]enduracididine (**15**) followed by removal of the protective groups. Compound **14** was derived from 1,2′,4′-tri-*N*-benzyloxycarbonylminobiosamine through the formation of the *cis*-1,2-carbamate. A diastereomer of **1** was also synthesized using alloenduracididine.

Minosaminomycin (**1**), produced by a streptomyces, inhibits the growth of mycobacteria.[2] The mechanism of action of **1** is similar to that of kasugamycin; that is, **1** inhibits the initiation of protein synthesis in a cell free system of *Escherichia coli* and exhibits stronger inhibition than kasugamycin.[3] The structure of **1** and its partial synthesis from natural minobiosamine (**2**) have been reported in a previous communication.[4] In this paper we report the synthesis of (−)-1D-1-amino-1-deoxy-*myo*-inositol (L-*myo*-inosamine-1) (**4**) from D-inositol (**3**), the synthesis of **2** from kasuganobiosamine[5] (**5**) and the total synthesis of **1**.

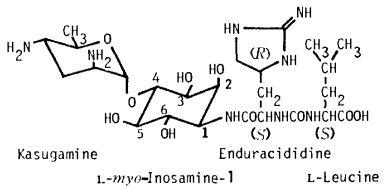

1

The absolute structure of the new aminocyclitol **4** determined by application of the TACu method,[2] was confirmed by the following synthesis. Catalytic oxidation of **3** with platinum black by the method of Post and Anderson[6] gave L-*myo*-inosose-1 (**6**).[7] The inosose **6** was treated with hydroxylamine to give a ketoxime (**7**) and then **7** was reduced with sodium amalgam to afford **4** in 16.5% yield from **3** by the method of Anderson and Lardy.[8] The identity of **4** with the natural material was confirmed in all respects. The synthesis of **4** also yielded the new aminocyclitol, (+)-1L-1-amino-1-deoxy-*chiro*-inositol (D-inosamine-2) (**8**) which was isolated by column chromatography on Amberlite CG-50 resin and silica gel in 12.4% yield. The structure of **8** was confirmed by the NMR spectrum of its *N*,*O*-hexaacetate in chloroform-*d*, which showed signals for an axial *O*-acetyl groups (δ 2.16), an axial *N*-acetyl and four equatorial *O*-acetyl groups (δ 2.05×3, 2.03, and 2.00)[9] and by application of the TACu method ($\Delta[M]_{TACu}$ −800°).[10]

Based on the successful synthesis of **4**, we designed a synthesis of **2** from **5** which had been synthesized in the total synthesis of kasugamycin.[11,12] Catalytic oxidation of 2′,4′-di-*N*-acetylkasuganobiosamine[5] (**9**) with platinum black followed by treatment with hydroxylamine gave a mixture of ketoximes **10** and **11**. Reduction of the mixture with sodium amalgam followed by alkaline hydrolysis with 2 M sodium hydroxide afforded a mixture of **2**, 1L-1-amino-1-deoxy-4-*O*-(α-D-kasugaminyl)-*chiro*-inositol (**12**) and 1D-1-amino-1-deoxy-5-*O*-(α-D-kasugaminyl)-*myo*-inositol (**13**) which were separated by column chromatography on Amberlite CG-50 resin in 7.9, 16.3, and 5.4% yields from **9**, respectively. The synthetic **2** was identical with the natural one in all respects. From the NMR spectra of **12** and **13** in deuterium oxide, the 1-amino group was confirmed to have an axial orientation in **12** (H-1: δ 3.76, multiplet having small coupling constants with two vicinal protons), and an equatorial orientation in **13** (H-1: δ 3.25, multiplet having a large coupling constant with one of vicinal protons). Acid hydrolysis of the *N*,*O*-heptaacetate of **12** gave **8**. The NMR spectra of the tri-*N*-acetyl-di-*O*-isopropylidene derivative (**12a**) of **12** (methyl signals of *trans*-*O*-isopropylidene: δ 1.37 and 1.39, *cis*: δ 1.32 and 1.48)[13] and the tri-*N*-acetyl-mono-*O*-isopropylidene derivative (**13a**) of **13** (methyl singals of *cis*-*O*-isopropylidene: δ 1.36 and 1.52) confirmed the structures of **12** and **13**.

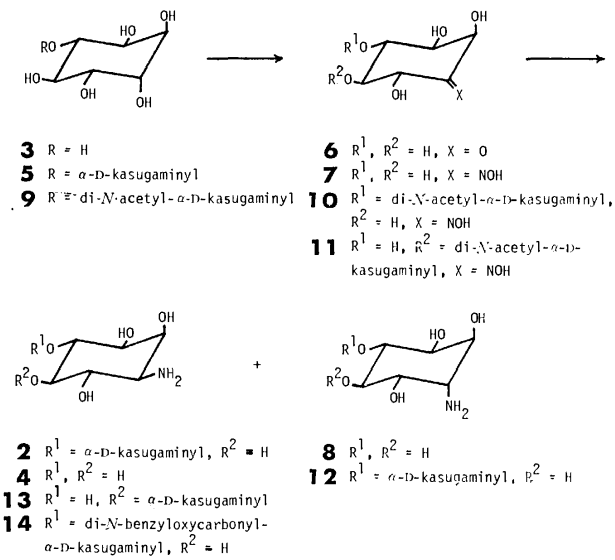

3 R = H
5 R = α-D-kasugaminyl
9 R = di-*N*-acetyl-α-D-kasugaminyl

6 R^1, R^2 = H, X = O
7 R^1, R^2 = H, X = NOH
10 R^1 = di-*N*-acetyl-α-D-kasugaminyl, R^2 = H, X = NOH
11 R^1 = H, R^2 = di-*N*-acetyl-α-D-kasugaminyl, X = NOH

2 R^1 = α-D-kasugaminyl, R^2 = H
4 R^1, R^2 = H
13 R^1 = H, R^2 = α-D-kasugaminyl
14 R^1 = di-*N*-benzyloxycarbonyl-α-D-kasugaminyl, R^2 = H

8 R^1, R^2 = H
12 R^1 = α-D-kasugaminyl, R^2 = H

For the total synthesis of **1**, 2′,4′-di-*N*-benzyloxycarbonylminobiosamine[4] (**14**) was prepared from 1,2′,4′-tri-*N*-benzyloxycarbonylminobiosamine in good yield by fromation of a cyclic carbamate with sodium hydride in *N*,*N*-dimethylformamide followed by hydrolysis with 5% barium hydroxide octahydrate solution in 50%

* To whom correspondence should be addressed.

aqueous dioxane at 80 °C.[14] The structure of the cyclic carbamate was shown to be the *cis*-1,2-carbamate of **14** by the NMR spectrum of its mono-*O*-isopropylidene derivative (**14a**) which showed methyl signals for a *trans*-*O*-isopropylidene group at δ 1.38.

The total synthesis of **1** was accomplished in 21% yield by condensation of **14** with N^{α}-[(*S*)-1-benzyloxycarbonyl-3-methylbutylcarbamoyl]enduracididine (**15**) by the activated ester method using 1-hydroxybenzotriazole and dicyclohexylcarbodiimide in *N*,*N*-dimethylformamide[15] followed by catalytic hydrogenation with 5% palladium on carbon in a mixture of methanol, acetic acid and water, as described in a previous communication.[4] The ureylene compound **15** was prepared from L-leucine benzyl ester hydrochloride in 33% yield by treatment with trichloromethyl chloroformate in toluene followed by coupling with enduracididine.[16] Enduracididine found in the antibiotic enduracidin[17] has recently been synthesized from L-histidine by Shiba and coworkers.[18]

We synthesized also a diastereomer (2*R*-isomer) of **1** from alloenduracididine[16] in place of enduracididine. This isomer showed about 20% of the bacteriostatic activity of **1** by the cylinder plate method using *Mycobacterium smegmatis* ATCC 607 as the test organism.

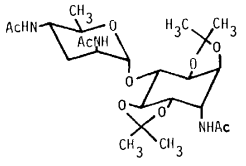

12a

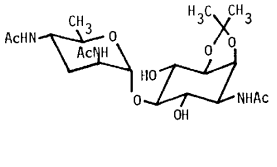

13a

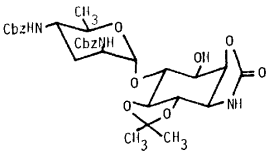

14a

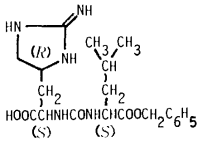

15

Experimental

Melting points were determined in capillary tubes and uncorrected. IR spectra were measured in KBr pellets with a Hitachi EPI-S2 spectrometer. NMR spectra were obtained on either a Varian A60-D, HA-100D, or XL-100 spectrometer. Chemical shifts in D_2O were recorded in ppm using tetramethylsilane as an external reference. All chemical shifts in other solvents were recorded in ppm downfield from internal tetramethylsilane. Optical rotations were measured with a Carl Zeiss LEP A2 polarimeter. Mass spectra were recorded with a Hitachi RMU-6M spectrometer. In all the experiments, TLC was carried out on silica gel plates (Merck, Art. 5721) and the spots on TLC were visualized with ninhydrin, 10% sulfuric acid, Rydon-Smith,[19] and HBr–ninhydrin (sprayed with 48% hydrobromic acid and heated at 105 °C, then with ninhydrin) reagents. High-voltage paper electrophoresis was carried out with a Model LT-48A from Savant Instruments under 3500 V for 15 min using formic acid–acetic acid–water (1 : 3 : 36) as an electrolyte solution.[19]

L-myo-*Inosamine-1* (*4*) *and* D-*Inosamine-2* (*8*) *from* D-*Inositol* (*3*). According to the method of Post and Anderson,[6] an aqueous solution (70 ml) of **3** (700 mg, 3.9 mmol) was mixed with an aqueous suspension (35 ml) of platinum black prepared from 350 mg of platinum dioxide just before the reaction, and then oxygen gas was bubbled through at 45 °C for 3 h with stirring. The catalyst was removed by filtration and the filtrate was concentrated to dyrness under reduced pressure, yielding a crude powder (752 mg) of L-*myo*-inosose-1 (**6**). By the method of Anderson and Lardy,[8] to an aqueous solution (12 ml) of the crude **6** (602 mg) and hydroxylamine hydrochloride (323 mg, 4.65 mmol), an aqueous solution (6 ml) of sodium acetate (318 mg, 3.88 mmol) was added dropwise under stirring, and the ketoxime (**7**) was formed by further stirring for 2.5 h at room temperature. To the reaction mixture diluted with water (5 ml), 5% sodium amalgam (total 25 g) was added at 10-min intervals for 1 h under stirring and cooling to below 25 °C in a water bath. The pH was held between 5.5 and 6.5 by the occasional addition of acetic acid (4 ml) and the reaction mixture was continuously stirred for 2 h, After removal of mercury by decantation, the supernatant was made up to 200 ml with water and charged on a column of Amberlite CG-50 (a mixture of 70% NH_4^+ form and 30% H^+ form, 80 ml). The column was washed with water (320 ml) and the eluate with 0.15 M ammonia (800 ml) was collected in 8-ml fractions. The ninhydrin-positive fractions (Nos. 59—66) were combined and concentrated to dryness yielding a slightly yellow powder (256 mg). An aqueous solution (4 ml) of the powder was adjusted to pH 8.2 by 1 M hydrochloric acid and rechromatographed on a column of Amberlite CG-50 (NH_4^+ form, 50 ml). The column was washed with water (200 ml) and eluted with 0.05 M ammonia (500 ml). The eluate was collected in 5-ml fractions. Evaporation of the ninhydrin-positive fractions (Nos. 12—31) afforded a white crystalline powder of **8** (69 mg, 12.4% from **3**); mp 192—193 °C (dec), $[\alpha]_D^{22}$ +55.2° (*c* 0.78, water) (lit,[20] L-isomer: mp 200—205 °C (dec), $[\alpha]_D^{23}$ −64.3°), $\Delta[M]_{TACu}$ −800°.[10] MS *m/e* 180 $[(M+1)^+]$, NMR (D_2O) δ 3.86 (1H t, J=3 Hz, H-1) and 3.9—4.6 (5H), TLC (chloroform–methanol–28% ammonia–water, 1 : 4 : 2 : 1) R_f 0.41. Found: C, 39.78; H, 7.19; N, 7.59%. Calcd for $C_6H_{13}NO_5$: C, 40.22; H, 7.31; N, 7.82%.

Evaporation of other ninhydrin-positive fractions (Nos. 49—59) from the rechromatography afforded a crude powder (156 mg) of **4**. The crude powder was chromatographed on a column of silica gel (Wakogel C-200, Wako Pure Chemicals, 15 g) developed with methanol–chloroform–17% ammonia (4 : 1 : 1), affording a white crystalline powder of **4** (91 mg, 16.5% from **3**); mp 207—212 °C (dec), $[\alpha]_D^{25}$ −4.2° (*c* 2.86, water). MS *m/e* 180 $[(M+1)^+]$, NMR (D_2O) δ 3.18 (1H m, H-1), 3.6—4.3 (4H) and 4.48 (1H br, H-2), TLC (chloroform–methanol–28% ammonia–water, 1 : 4 : 2 : 1) R_f 0.35. Found: C, 38.94; H, 7.04; N, 7.91%. Calcd for $C_6H_{13}NO_5 \cdot 1/2H_2O$: C, 38.30; H, 7.50; N, 7.44%.

The hydrochloride of **4** was crystallized from a mixrute of water and ethanol as colorless needles; mp 201—203 °C (dec), $[\alpha]_D^{25}$ −8.9° (*c* 1.35, water) (lit,[2] mp 201—203 °C, $[\alpha]_D^{26}$ −9.5°). This compound was identical with natural **4** hydrochloride ($C_6H_{13}NO_5 \cdot HCl \cdot 1/2H_2O$)[2] in all respects.

N,O-*Hexaacetates of* **4** *and* **8**. Treatment of **4** (47 mg) with acetic anhydride (0.25 ml) in pyridine (0.5 ml) at room temperature for 21.5 h gave mono-*N*-acetyl-penta-*O*-acetyl-L-*myo*-inosamine-1. Crystallization from a mixture of methanol and diethyl ether afforded colorless needles (97 mg); mp 212—214 °C (dec), $[\alpha]_D^{22}$ −15° (*c* 2.92, chloroform). MS *m/e* 432 $[(M+1)^+]$, IR (KBr) 1750 and 1230 (ester C=O), 1690, and 1530 cm^{-1} (amide), NMR ($CDCl_3$) δ 1.91 (3H s, eq NAc), 1.97 (3H s, eq OAc), 2.01 (6H s, eq OAc×2), 2.04 (3H

s, eq OAc), 2.21 (3H s, ax OAc), 4.51 (1H m, H-1), 5.52 (1H t, J=3 Hz, H-2), and 5.81 (1H d, J=9 Hz, amide), TLC (chloroform–ethanol, 10 : 1) R_f 0.65. Found: C, 50.31; H, 5.66; N, 3.65%. Calcd for $C_{18}H_{25}NO_{11}$: C, 50.11; H, 5.84; N, 3.25%.

Treatment of **8** (23 mg) with acetic anhydride (0.25 ml) in pyridine (0.5 ml) at room temperature for 18 h gave mono-*N*-acetylpenta-*O*-acetyl-D-inosamine-2. Crystallization from diethyl ether afforded colorless crystals (56 mg); mp 151—152 °C (dec), $[\alpha]_D^{23}$ −1.7° (*c* 0.67, chloroform). MS *m/e* 432 [(M+1)$^+$], IR (KBr) 1755 and 1230 (ester C=O), 1650 and 1550 cm^{-1} (amide), NMR ($CDCl_3$) δ 2.00 (3H s, eq OAc), 2.03 (3H s, eq OAc or ax NAc), 2.05 (9H s, eq OAc or ax NAc×3), 2.16 (3H s, ax OAc), 4.71 (1H m, H-1), and 6.51 (1H d, J=8 Hz, amide), TLC (chloroform–ethanol, 10 : 1) R_f 0.56. Found: C, 49.99; H, 5.62; N, 4.08%. Calcd for $C_{18}H_{25}NO_{11}$: C, 50.11; H, 5.84; N, 3.25%.

*Minobiosamine (**2**) and Its Isomers (**12** and **13**) from Kasuganobiosamine (**5**).* According to the method of Suhara *et al.*[5] 2′,4′-di-*N*-acetylkasuganobiosamine (**9**) was derived from **5**. An aqueous solution (200 ml) of **9** (2.0 g, 5.1 mmol) was mixed with an aqueous suspension (100 ml) of platinum black which was prepared from 1.0 g of platinum dioxide, and then oxygen gas was bubbled through at 45 °C for 2.5 h with stirring.[6] The catalyst was removed by filtration and the filtrate was concentrated to dryness yielding a mixture (1.75 g) of oxo compounds. To an aqueous solution (30 ml) containing the mixture (1.48 g) and hydroxylamine hydrochloride (396 mg, 5.7 mmol), an aqueous solution (15 ml) of sodium acetate (390 mg, 4.75 mmol) was added dropwise under stirring at room temperature, and stirring was continued for 2 h. The reaction mixture was concentrated to dryness yielding a mixture (1.946 g) of ketoximes **10** and **11**. The ketoxime (896 mg) in water (15 ml) was reduced with 25 g of 5% sodium amalgam in the same manner as described for **7**. After removal of mercury by decantation, the supernatant was concentrated to dryness. The residue was dissolved in 2 M sodium hydroxide (40 ml) and refluxed for 15 h in an oil bath at 125 °C to remove the acetyl groups. After neutralization with acetic acid (4.8 ml), the solution was made up to 400 ml with water and charged on a column of Amberlite CG-50 (a mixture of 70% NH_4^+ form and 30% H^+ form, 150 ml). The column was washed with water (600 ml) and the eluate with 900 ml of 0.5 M ammonia was collected in 15-ml fractions. Ninhydrin-positive fractions (Nos. 27—31) were combined and concentrated to dryness yielding a white powder (271 mg). It was dissolved in 5 ml of water and rechromatographed on a column of Amberlite CG-50 (NH_4^+ form, 80 ml). The column was washed with water (160 ml) and products were eluted with 0.1 M ammonia. The eluate was collected in 4-ml fractions which were examined by TLC with chloroform–methanol–28% ammonia–water (1 : 4 : 2 : 1). The fractions (Nos. 40—47) with R_f 0.69 were combined and concentrated to dryness yielding an epimer of **2**, 1L-1-amino-1-deoxy-4-*O*-(α-D-kasugaminyl)-*chiro*-inositol (**12**), as a white powder (81 mg, 16.3% from **9**); mp 104—115 °C (dec), $[\alpha]_D^{27}$ +117° (*c* 0.3, water). MS *m/e* 308 [(M+1)$^+$], NMR (D_2O) δ 1.72 (3H d, J=6 Hz, H-6′), 2.38 (2H m, H-3′), 3.44 (1H m, H-4′), 3.76 (2H, H-1 and -2′), and 5.43 (1H br, H-1′).

The fractions (Nos. 60—79) which contained material with R_f 0.64 were combined and concentrated to dryness yielding a positional isomer of **2**, 1D-1-amino-1-deoxy-5-*O*-(α-D-kasugaminyl)-*myo*-inositol (**13**), as a white powder (27 mg, 5.4% from **9**); mp 112—128 °C (dec), $[\alpha]_D^{27}$ +76° (*c* 0.59, water). MS *m/e* 308 [(M+1)$^+$], NMR (D_2O) δ 1.71 (3H d, J=6 Hz, H-6′), 2.36 (2H m, H-3′), 3.10—3.55 (2H, H-1 and -4′), 3.71 (1H m, H-2′), and 5.46 (1H d, J=2 Hz, H-1′).

The fractions (Nos. 80—102) with R_f 0.66 by TLC were combined and concentrated to dryness affording a white powder (39 mg, 7.9% from **9**) of **2**; mp 126—128 °C (dec), $[\alpha]_D^{32}$ +82.5° (*c* 1.0, water) (lit,[4] mp 126—128 °C (dec), $[\alpha]_D^{29}$ +81°). MS *m/e* 308 [(M+1)$^+$], NMR (D_2O) δ 1.69 (3H d, J=6 Hz, H-6′), 2.24 (2H m, H-3′), 2.95—3.38 (2H m, H-1 and -4′) 3.58 (1H m, H-2′), and 5.37 (1H d, J=2 Hz, H-1′). Found: C, 44.52; H, 8.38; N, 12.45%. Calcd for $C_{12}H_{25}N_3O_6\cdot H_2O$: C, 44.29; H, 8.36; N, 12.93%.

N,O-*Heptaacetate of **2**.* Treatment of **2** (37 mg) with acetic anhydride (0.4 ml) in pyridine (0.8 ml) at room temperature for 18 h afforded the *N,O*-heptaacetate of **2**. Crystallization from a mixture of methanol and diethyl ether gave colorless needles (48 mg); mp 273—274 °C (dec), $[\alpha]_D^{25}$ +4.3° (*c* 2.55, chloroform). MS *m/e* 602 [(M+1)$^+$], IR (KBr) 1755 and 1230 (ester C=O), 1660 and 1550 cm^{-1} (amide), NMR ($CDCl_3$) δ 1.14 (3H d, J=6 Hz, H-6′), 1.75 (2H m, H-3′), 1.89 (3H s, 1-eq NAc), 1.95, 1.98, 2.01, 2.04, 2.15 (each 3H s, eq OAc×3, 2′-NAc and 4′-NAc), 2.18 (3H s, 2-ax OAc), and 6.1—6.8 (3H, amides), TLC (chloroform–ethanol, 10 : 1) R_f 0.26. Found: C, 51.52; H, 6.25; N, 6.56%. Calcd for $C_{26}H_{39}N_3O_{13}$: C, 51.91; H, 6.53; N, 6.99%. It was identical with the *N,O*-heptaacetate derived from natural **2** in all respects.

N,O-*Heptaacetates of **12** and **13**.* Compound **12** (79 mg) was treated with acetic anhydride (0.75 ml) in pyridine (1.6 ml) at room temperature for 18 h and the reaction mixture was concentrated to dryness. The residue was chromatographed on a column of silica gel (Wakogel C-200, 14 g) developed with chloroform–ethanol (10 : 1). Fractions containing the *N,O*-heptaacetate of **12** were combined and concentrated to dryness yielding a white crystalline powder (127 mg); mp 158—160 °C (dec), $[\alpha]_D^{24}$ +29° (*c* 0.74, chloroform). MS *m/e* 602 [(M+1)$^+$], NMR ($CDCl_3$) δ 1.17 (3H d, J=6 Hz, H-6′), 1.80 (2H m, H-3′), 1.97, 2.00, 2.02, 2.04, 2.05, 2.11 (each 3H s, eq OAc ×3, 1-ax NAc, 2′-NAc and 4′-NAc), 2.12 (3H s, 2-ax OAc), and 6.2—7.2 (3H, amides), TLC (chloroform–ethanol, 10 : 1) R_f 0.15.

Treatment of **13** (25 mg) with acetic anhydride (0.25 ml) in pyridine (0.5 ml) at room temperature for 18 h followed by column chromatography on silica gel (Wakogel C-200, 4.5 g) developed with chloroform–ethanol (20 : 1) gave a white crystalline powder of the *N,O*-heptaacetate of **13** (30 mg); mp 172—177 °C (dec). MS *m/e* 602 [(M+1)$^+$], NMR ($CDCl_3$) δ 1.12 (3H d, J=6 Hz, H-6′), 1.75 (2H m, H-3′), 1.89 (3H s, 1-eq NAc), 1.95, 1.97, 1.99, 2.07, 2.11 (each 3H s, eq OAc×3, 2′-NAc and 4′-NAc), 2.20 (3H s, 2-ax OAc), and 6.0—6.7 (3H, amides), TLC (chloroform–ethanol, 10 : 1) R_f 0.20.

Hydrolysis of the N,O-*Heptaacetate of **12**.* The *N,O*-heptaacetate of **12** (45 mg) was hydrolyzed with 6 M hydrochloric acid (2 ml) by refluxing in an oil bath at 100 °C for 5 h and the reaction mixture was concentrated to dryness. The residue was chromatographed on a column of Amberlite CG-50 (NH_4^+ form, 5 ml) eluted with 0.05 M ammonia (50 ml). The eluate containing **8** was concentrated to dryness yielding a white crystalline powder of **8** (11 mg, 82%).

*1L-1-Acetamido-1-deoxy-4-*O*-(di-*N*-acetyl-α-D-kasugaminyl)-2,3 : 5,6-di-*O*-isopropylidene*-chiro*-inositol (**12a**).* Compound **12** (20 mg, 0.067 mmol) was treated with acetic anhydride (0.3 ml) in methanol (0.6 ml) at room temperature for 6.5 h and the reaction mixture was concentrated to dryness yielding a slightly yellow powder (26 mg) of the tri-*N*-acetate of **12**. To a solution of this powder in dry *N,N*-dimethylformamide (0.6 ml) were added 2,2-dimethoxypropane (62 mg, 0.6 mmol) and *p*-toluenesulfonic acid monohydrate (1.4 mg

0.006 mmol). The reaction mixture was heated at 60 °C for 2 h under stirring. After neutralization with triethylamine (1.2 mg), the reaction mixture was concentrated to dryness. Purification by column chromatography on silica gel (Silic AR CC-7, Mallinckrodt, 4 g) developed with chloroform–ethanol (12 : 1) gave a white powder of **12a** (13 mg); mp 177—181 °C (dec), $[\alpha]_D^{23}$ +111° (*c* 0.73, methanol). IR (KBr) 1650 and 1545 cm^{-1} (amide), NMR (CD_3OD) δ 1.15 (3H d, J=6 Hz, H-6′), 1.32, 1.37, 1.39, 1.48 (each 3H s), 1.80 (2H m, H-3′), 1.91 (3H s, NAc), 1.99 (6H s, NAc×2), and 4.97 (1H br, H-1′), TLC (chloroform–ethanol, 1 : 1) R_f 0.81.

1-D-*1-Acetamido-1-deoxy-5-*O-*(di-*N-*acetyl-α-*D-*kasugaminyl)-2,3-*O-*isopropylidene-*myo-*inositol (**13a**).* Treatment of **13** (4.0 mg, 0.013 mmol) with acetic anhydride (0.05 ml) in methanol (0.15 ml) at room temperature for 7 h afforded a slightly yellow powder (5.0 mg) of the tri-*N*-acetate of **13**. Treatment of this powder in dry *N,N*-dimethylformamide (0.2 ml) with 2,2-dimethoxypropane (12 mg, 0.115 mmol) and *p*-toluenesulfonic acid monohydrate (0.2 mg, 0.001 mmol) at 60 °C for 2 h followed by neutralization with triethylamine (0.2 mg) and evaporation gave a crude powder. Purification by column chromatography on silica gel (Silic AR CC-7, 800 mg) developed with chloroform–ethanol (4 : 1) yielded a white crystalline powder of **13a** (2.9 mg); mp 157—162 °C (dec), $[\alpha]_D^{24}$ +64° (*c* 0.43, chloroform–ethanol (4 : 1)). IR (KBr) 1640 and 1540 cm^{-1} (amide), NMR (CD_3OD–$CDCl_3$ (1 : 1)) δ 1.16 (3H d, J=6 Hz, H-6′), 1.36, 1.52 (each 3H s), 1.85 (2H m, H-3′), 1.97, 2.02, 2.06 (each 3H s, NAc×3), and 5.01 (1H br, H-1′), TLC (chloroform–ethanol, 1 : 1) R_f 0.59.

*2′,4′-Di-*N*-benzyloxycarbonylminobiosamine (**14**).* To a solution of **2** (1.03 g, 3.35 mmol) and sodium hydrogencarbonate (1.1 g, 13 mmol) in water (15 ml), benzyloxycarbonyl chloride (1.88 g, 11 mmol) was added dropwise. The mixture was stirred for 1.5 h in an ice bath and then allowed to stand overnight at room temperature. The resulting precipitate was filtered and washed with water (30 ml) and diethyl ether (50 ml) to give a colorless powder of 1,2′,4′-tri-*N*-benzyloxycarbonylminobiosamine (2.02 g, 85%); mp 171—172 °C (dec), $[\alpha]_D^{24}$ +33° (*c* 1.0, *N,N*-dimethylformamide). IR (KBr) 1690 and 1525 cm^{-1} (amide), NMR (CD_3COCD_3) δ 1.15 (3H d, J=6 Hz, H-6′), 2.02 (2H m, H-3′), 5.06 (6H s, CH_2-ar), 5.16 (1H br, H-1′), and 7.34 (15H, ar), TLC (chloroform–methanol, 10 : 1) R_f 0.60. Found: C, 60.25; H, 6.41; N, 5.97%. Calcd for $C_{36}H_{43}N_3O_{12}$: C, 60.92; H, 6.11; N, 5.92%.

To a solution of 1,2′,4′-tri-*N*-benzyloxycarbonylminobiosamine (1.50 g, 2.1 mmol) in dry *N,N*-dimethylformamide (15 ml), 50% sodium hydride (273 mg, 5.7 mmol) was added, and the mixture was stirred for 4.5 h in an ice bath under a stream of nitrogen. After neutralization with acetic acid (0.36 ml), the solution was concentrated to dryness. A solution of the residue in ethyl acetate (50 ml) was washed with water (10 ml), dehydrated with anhydrous sodium sulfate, and evaporated to give a pale yellow oil (2.0 g). The oil was chromatographed on a column of silica gel (Silic AR CC-7, 100 g) developed with chloroform–methanol (10 : 1). Fractions containing 2′,4′-di-*N*-benzyloxycarbonylminobiosamine-1,2-carbamate were combined and concentrated to dryness yielding a white powder (970 mg, 77%); mp 115—118 °C (dec), $[\alpha]_D^{25}$ +45° (*c* 1.0, chloroform). IR (KBr) 1750 (C=O), 1690, and 1525 cm^{-1} (amide), NMR ($CDCl_3$) δ 1.14 (3H br, H-6′), 1.84 (2H m, H-3′), 4.98 (4H s, CH_2-ar ×2), and 7.22 (10H, ar), TLC (1-butanol–ethanol–chloroform–17% ammonia, 4 : 5 : 2 : 1) R_f 0.52. Found: C, 57.50; H, 6.96; N, 6.80%. Calcd for $C_{29}H_{35}N_3O_{11}$: C, 57.90; H, 6.86; N, 6.99%.

A solution containing the carbamate (914 mg, 1.52 mmol) and barium hydroxide octahydrate (765 mg, 2.34 mmol) in 50% aqueous dioxane (29 ml) was heated at 80 °C for 6 h. The reaction mixture was neutralized with carbon dioxide, and the resulting precipitates were removed by filtration. The filtrate was concentrated to give a solid (793 mg), which was chromatographed on a column of silica gel (Silic AR CC-7, 80 g) developed with 1-butanol–ethanol–chloroform–17% ammonia (8 : 10 : 4 : 1). Fractions containing **14** were combined and concentrated to dryness yielding a white powder of **14** (556 mg, 64%); mp 123—126 °C (dec), $[\alpha]_D^{24}$ +43° (*c* 1.0, *N,N*-dimethylformamide). IR (KBr) 1690 and 1520 cm^{-1} (amide), NMR (CD_3OD) δ 1.13 (3H d, J=6 Hz, H-6′), 1.88 (2H m, H-3′), 2.62 (1H m, H-1), 5.04 (5H, H-1′ and CH_2-ar), and 7.30 (10H, ar), TLC (1-butanol–ethanol–chloroform–17% ammonia, 4 : 5 : 2 : 1) R_f 0.24. Found: C, 56.77; H, 6.67; N, 7.12%. Calcd for $C_{28}H_{37}N_3O_{10}\cdot H_2O$: C, 56.65; H, 6.62; N, 7.08%.

*2′,4′-Di-*N*-benzyloxycarbonyl-5,6-*O*-isopropylideneminobiosamine-1,2-carbamate (**14a**).* To a solution of 2′,4′-di-*N*-benzyloxycarbonylminobiosamine-1,2-carbamate (17 mg, 0.029 mmol) in dry *N,N*-dimethylformamide (0.3 ml) were added 2,2-dimethoxypropane (31 mg, 0.3 mmol) and *p*-toluenesulfonic acid monohydrate (0.7 mg, 0.003 mmol). The mixture was heated at 60 °C for 2 h under stirring. After neutralization with triethylamine (0.6 mg), the reaction mixture was concentrated to dryness. Purification by column chromatography on silica gel (Silic AR CC-7, 3 g) developed with chloroform–ethanol (30 : 1) gave a white crystalline powder of **14a** (14.7 mg); mp 121—124 °C (dec), $[\alpha]_D^{23}$ +49.5° (*c* 0.85, methanol). IR (KBr) 1755 (C=O), 1700, and 1520 cm^{-1} (amide), NMR (CD_3OD) δ 1.19 (3H d, J=6 Hz, H-6′), 1.38 (6H s), 1.90 (2H m, H-3′), 4.92 (1H br, H-1′), 5.08 (4H s, CH_2-ar), and 7.32 (10H, ar), TLC (chloroform–ethanol, 10 : 1) R_f 0.50.

*Minosaminomycin (**1**).* To a solution of L-leucine benzyl ester hydrochloride (206 mg, 0.8 mmol) in dry toluene (4 ml), trichloromethyl chloroformate (336 mg, 1.7 mmol) was added. After refluxing for 4.5 h in an oil bath at 130 °C, the reaction mixture was evaporated to give a colorless oil of the isocyanate of L-leucine benzyl ester (189 mg, 95%); $n_D^{25.5}$ 1.4987, $[\alpha]_D^{26}$ −29° (*c* 1.55, toluene). IR (KBr) 2200 (N=C=O) and 1740 cm^{-1} (ester C=O), NMR ($CDCl_3$) δ 0.90 (6H d, J=5 Hz, CH_3×2), 1.4—2.0 (3H m, CH_2–CH), 4.10 (1H dd, J=7, 8 Hz, α-methine), 5.26 (2H s, CH_2-ar), and 7.42 (5H, ar).

A solution containing the isocyanate (189 mg, 0.77 mmol) and enduracididine (73 mg, 0.43 mmol) in dry dimethyl sulfoxide (4.5 ml) was stirred at room temperature for 17.5 h and then freeze dried to give a colorless oil (350 mg). Purification of the oil by column chromatography on silica gel (Silic AR CC-7, 36 g) developed with 1-butanol–ethanol–water (10 : 1 : 1) gave a white powder of N^{α}-[(*S*)-1-benzyloxycarbonyl-3-methylbutylcarbamoyl]enduracididine (**15**) (64 mg, 33% from enduracididine). To a methanolic solution (1 ml) of **15**, 0.5 M hydrochloric acid (0.28 ml) was added, and the solution was concentrated to dryness yielding a white powder (67 mg) of the monohydrochloride of **15**. To a solution containing the monohydrochloride (64 mg, 0.13 mmol) and 1-hydroxybenzotriazole[15] (22 mg, 0.16 mmol) in dry *N,N*-dimethylformamide (1.5 ml) was added a solution of **14** (77 mg, 0.13 mmol) in dry *N,N*-dimethylformamide (2 ml) and then dicyclohexylcarbodiimide (28 mg, 0.13 mmol). The mixture was stirred at 0 °C for 1 h and then at room temperature for 22.5 h. The dicyclohexylurea formed was removed by filtration and the filtrate was concentrated to dryness yielding a solid (202 mg). To remove the *N*-benzyl-

oxycarbonyl and benzyl ester groups, this solid in a mixture of methanol (3 ml), water (1 ml), and acetic acid (1 ml) was hydrogenated with 5% palladium on carbon (126 mg) under atmospheric pressure for 5 h. The catalyst was removed by filtration and the filtrate was concentrated to dryness yielding a white powder. An aqueous solution of the powder was charged on a column of Amberlite CG-50 (a mixture of 70% NH_4^+ form and 30% H^+ form, 5 ml). The column was washed with water (20 ml) and **1** was eluted with 0.15 M ammonia. Fractions containing **1** detected by high-voltage paper electrophoresis were combined and concentrated to dryness yielding a crude powder of **1** (35.8 mg). Purification by rechromatogrphy on a column of Amberlite CG-50 (NH_4^+ form, 5 ml) eluted with 0.05 M ammonia (50 ml) gave a white powder of **1** (17 mg, 21% from **15**); mp 225—260 °C (dec), $[\alpha]_D^{23}$ +28.4° (*c* 0.53, water) (lit,[2]) mp 225—260 °C (dec), $[\alpha]_D^{22}$ +30°). It was identical with natural **1** ($C_{25}H_{46}N_8O_{10}\cdot 2H_2O$) in all respects including biological activity.

2R-Isomer of 1. A diastereomer (2*R*-isomer) of **1** was synthesized using alloenduracididine with the method described for **1**. To a solution of alloenduracididine (51 mg, 0.3 mmol) in dry dimethyl sulfoxide (4 ml) was added the isocyanate of L-leucine benzyl ester (146 mg, 0.6 mmol) in dry dimethyl sulfoxide (1 ml). The mixture was stirred at room temperature for 22.5 h, and freeze-dried to give a slightly yellow oil (280 mg). The oil was chromatographed on a column of silica gel (Wokogel C-200, 28 g) developed with 1-butanol–ethanol–water (10 : 1 : 1) and a white powder (23 mg, 17% from alloenduracididine) of the 2*R*-isomer of **15** was obtained. The monohydrochloride of the 2*R*-isomer of **15** was prepared by addition of 0.5 M hydrochloric acid (0.08 ml) in a methanolic solution (0.5 ml). To a solution of the monohydrochloride in dry *N,N*-dimethylformamide (0.5 ml) was added **14** (33 mg, 0.057 mmol) in dry *N,N*-dimethylformamide (0.5 ml), 1-hydroxybenzotriazole (11.5 mg, 0.085 mmol), and dicyclohexylcarbodiimide (10.7 mg, 0.052 mmol). The mixture was stirred at 0 °C for 1 h and then at room temperature for 26.5 h. The dicyclohexylurea formed was removed by filtration and the filtrate was concentrated to give a solid (83.4 mg). This solid in a mixture (2.5 ml) of methanol, water, and acetic acid (3 : 1 : 1) was hydrogenated with 5% palladium on carbon (50 mg) under atmospheric pressure for 6.5 h. After removal of the catalyst, the solution was concentrated to dryness. The residue was purified by column chromatography with Amberlite CG-50 (a mixture of 70% NH_4^+ form and 30% H^+ form, 5 ml) eluted with 0.15 M ammonia to yield a crude powder (15.6 mg). The crude powder was rechromatographed on a column of Amberlite CG-50 (NH_4^+ form, 5 ml) eluted with 0.05 M ammonia to give a white powder (2.9 mg, 9% from the 2*R*-isomer of **15**) of the pure 2*R*-isomer of **1**; mp 195—220 °C (dec), $[\alpha]_D^{27}$ +42° (*c* 0.95, water). IR (KBr) 1660 and 1570 cm^{-1} (amide), TLC (1-butanol–ethanol–chloroform–17% ammonia, 4 : 5 : 2 : 5) R_f 0.13.

We wish to express our deep gratitude to Emeritus Professor Sumio Umezawa, Keio University, for his encouragement through the course of this work. We also wish to thank Dr. I. R. Hooper, Bristol Laboratories, for critical reading of the manuscript.

References

1) A preliminary report of this work was presented at the 19th Symposium on the Chemistry of Natural Products, Hiroshima, October, 1975.

2) M. Hamada, S. Kondo, T. Yokoyama, K. Miura, K. Iinuma, H. Yamamoto, K. Maeda, T. Takeuchi, and H. Umezawa, *J. Antibiot.*, **27**, 81 (1974).

3) K. Suzukake, M. Hori, Y. Uehara, K. Iinuma, M. Hamada, and H. Umezawa, *J. Antibiot.*, **30**, 132 (1977).

4) K. Iinuma, S. Kondo, K. Maeda, and H. Umezawa, *J. Antibiot.*, **28**, 613 (1975).

5) Y. Suhara, K. Maeda, H. Umezawa, and M. Ohno, "Deoxy Sugars, Advances in Chemistry Series," ed by R. F. Gould, American Chemical Society, Washington, D. C. (1968), p. 15.

6) G. G. Post and L. Anderson, *J. Am. Chem. Soc.*, **84**, 471 (1962).

7) B. Magasanik and E. Chargaff, *J. Biol. Chem.*, **175**, 929 (1948).

8) L. Anderson and H. A. Lardy, *J. Am. Chem. Soc.*, **72**, 3141. (1950).

9) F. W. Lichtenthaler and P. Emig, *Carbohydr. Res.*, **7**, 121 (1968).

10) S. Umezawa, T. Tsuchiya, and K. Tatsuta, *Bull. Chem. Soc. Jpn.*, **39**, 1235 (1966).

11) Y. Suhara, F. Sasaki, K. Maeda, H. Umezawa, and M. Ohno, *J. Am. Chem. Soc.*, **90**, 6559 (1968); Y. Suhara, F. Sasaki, G. Koyama, K. Maeda, H. Umezawa, and M. Ohno, *ibid.*, **94**, 6501 (1972).

12) M. Nakajima, H. Shibata, K. Kitahara, S. Takahashi, and A. Hasegawa, *Tetrahedron Lett.*, **1968**, 2271.

13) F. I. Carroll, *J. Org. Chem.*, **31**, 366 (1966).

14) D. Ikeda, T. Tsuchiya, S. Umezawa, and H. Umezawa, *J. Antibiot.*, **25**, 741 (1972).

15) W. König and R. Geiger, *Chem. Ber.*, **103**, 788 (1970).

16) S. Horii and Y. Kameda, *J. Antibiot.*, **21**, 665 (1968).

17) M. Asai, M. Muroi, N. Sugita, H. Kawashima, K. Mizuno, and A. Miyake, *J. Antibiot.*, **21**, 138 (1968).

18) S. Tsuji, S. Kusumoto, and T. Shiba, *Chem. Lett.*, **1975**, 1281.

19) H. Umezawa and S. Kondo, "Methods in Enzymology, Vol. 43. Antibiotics," ed by J. H. Hash, Academic Press, New York (1975), p. 279.

20) G. G. Post, Ph. D. Thesis, University of Wisconsin, USA, 1959.

ESR Studies of *N*-(Arylthio)-*t*-butylaminyls[1]

Yozo MIURA, Hidetsugu ASADA, and Masayoshi KINOSHITA

Department of Applied Chemistry, Faculty of Engineering, Osaka City University, Sumiyoshi-ku, Osaka 558

(Received January 21, 1977)

It was found that *N*-(arylthio)-*t*-butylaminyls (**2**) are easily generated by the photolysis of *N*-*t*-butylbenzenesulfenamides (**1**). The ESR spectra of **2** were split into a 1 : 1 : 1 triplet by the interaction with the nitrogen nucleus (11.70—11.89 G), and each of the triplet was further split by the ring protons ($a_{o\text{-}H}$: 0.89—1.07 G). The *g*-values of **2** lie in the range from 2.0068—2.0073. The radicals persist in benzene and it appears that they are not sensitive to the atmospheric oxygen.

A number of nitrogen-centered free radicals have so far been prepared and extensive ESR spectroscopic studies of these radicals have been undertaken.[2] In the course of ESR studies on nitrogen-centered free radicals containing sulfur atoms adjacent to the radical center, it was found that *N*-(arylthio)-*t*-butylaminyls (**2**) can easily be generated by the photolysis of *N*-*t*-butylbenzenesulfenamides (**1**). Up to the present time, some structually related radicals have been detected, *e.g.* $2\text{-}NO_2C_6H_4\dot{S}NH$,[3] $Me_3C\dot{N}SN(CMe_3)MR_n$,[4] $Ar\dot{N}S\text{-}Ar'$,[1,5,6] and $4\text{-}ClC_6H_4\dot{S}NR$.[7] The last-mentioned radical, which was detected as an intermediate radical upon the thermal decomposition of *N*-alkenyl-*N*-(2,3-dihydro-2-oxobenzoxazol-3-yl)-*p*-chlorobenzenesulfenamides, is closely related to that examined in the present experiment. However, a detailed ESR spectroscopic investigation of $R\dot{N}SAr$ has not been undertaken. In this report, an ESR spectroscopic investigation of **2** will be described.

$$t\text{-Bu-NH-S-Ar} \xrightarrow{-H\cdot} t\text{-Bu-}\dot{N}\text{-S-Ar}$$

1 **2**

Ar: **a**=C_6H_5, **b**=4-FC_6H_4, **c**=4-ClC_6H_4, **d**=4-BrC_6H_4, **e**=4-$NO_2C_6H_4$

Results and Discussion

Generation of the Radicals. One of the most conventional methods for generating the desired free radicals is hydrogen-abstruction from an appropriate precursor by a *t*-butoxyl radical. This method was first employed for the generation of **2**. In a typical procedure, after a benzene solution of **1c** and di-*t*-butyl peroxide had been degassed, it was irradiated with a high-pressure mercury lamp. From the solution, two paramagnetic species were detected. The ratio drived from the intensities of the respective ESR signals was *ca.* 1 : 2. The stronger signal was present in the form of a 1 : 1 : 1 triplet (11.75 G) with each the triplet further split into a poorly-resolved 1 : 2 : 1 triplet (0.93 G). The *g*-value of the radical was found to be 2.0071. From these results, the radical was assigned to the desired radical, *N*-(4-chlorophenylthio)-*t*-butylaminyl (**2c**). The ESR parameters are close to those reported for $4\text{-}ClC_6H_4\dot{S}NR$ (a_N: 11 G, *g*-value: 2.0073).[7] The other radical resulted in a simple 1 : 1 : 1 triplet (a_N: 14.11 G) and its *g*-value was found to be 2.0051. These ESR parameters are close to those reported for *N*-alkoxyalkylaminyls.[8] Thus, it appears likely that it is an *N*-alkoxyalkylaminyl, *N*-(*t*-butoxy)-*t*-butylaminyl.[9] In the ESR spectrum obtained by this procedure, the two signals partially overlapped. Thus, it was difficult to accurately determine the ESR parameters of **2**. For this reason, another procedure for the generation of **2** was examined. It was found that after a degassed benzene solution containing **1** alone had been irradiated with a high-pressure mercury lamp, only **2** was detected in the solution. In this case, the mechanism for the generation of **2** may be illustrated as follows:

$$\mathbf{1} \xrightarrow{h\nu} t\text{-Bu-}\dot{N}\text{H} + \text{ArS}\cdot$$

$$\downarrow \mathbf{1}$$

$$t\text{-Bu-NH}_2 + \mathbf{2}$$

A typical ESR spectrum of **2** is illustrated in Fig. 1, and the ESR parameters for **2** are listed in Table.

Although the coupling due to the *ortho* and *para* protons could be observed for all the radicals, the values of coupling constant for the ring protons of **2a** could not be accurately determined because of poor resolution. In **2b**, further coupling due to the fluorine nucleus was observed in addition to that due to the ring protons (Fig. 2).

Radical **2** was also generated by oxidation with lead dioxide and potassium carbonate. A benzene solution of **1** was stirred for 5 min in the presence of the oxidizing agents under ambient conditions and, after the oxidizing agents were removed, only **2** was detected in the solution.

On the other hand, the ESR parameters for *t*-butyl arylthio nitroxide radicals (in benzene) are 15.90—

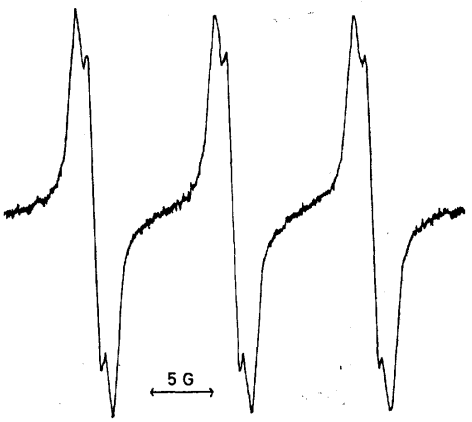

Fig. 1. Experimental ESR spectrum of *N*-(4-chlorophenylthio)-*t*-butylaminyl in benzene at room temperature.

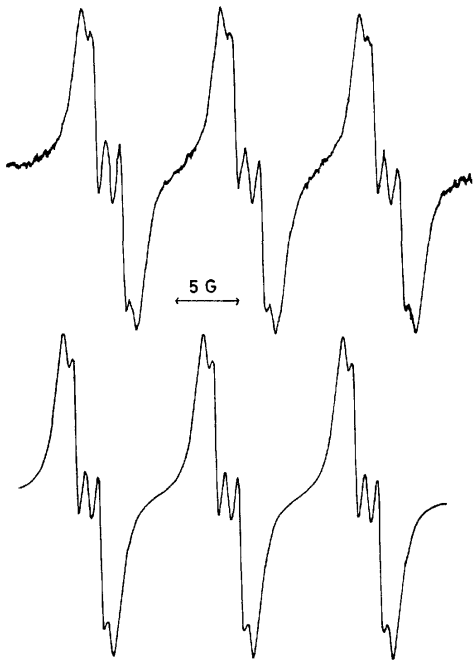

Fig. 2. Experimental ESR spectrum of *N*-(4-fluorophenylthio)-*t*-butylaminyl (**2b**) in benzene at room temperature (upper), and computer simulated, using Lorentzian line shapes and a line width of 0.96 G.

18.03 G (a_N) and 2.0066—2.0067 (*g*-value).[10,11] On the basis of these results, it is obvious that radical **2** is not the corresponding nitroxide radical.

From the ESR parameters shown in the table, it can be safely said that in **2** the unpaired electron is mainly located on the nitrogen ($2p_z$ orbital) because of the large a_N values. Considering the *g*-values, they are rather large for a nitrogen-centered free radical. This indicates that extent of delocalization of the spin onto the adjacent sulfur is not small.[12] In comparing the ESR parameters for **2** with those of the other related radicals described above, the values of a_N for **2** are somewhat smaller than those for $Me_3CNS(Me_3)MR_n$-[$a_N(\alpha)$: 12.0—12.6 G],[5] and are considerably larger than those for ArNSAr′ (8.74—9.59 G).[6] This can be explained in terms of the larger ability of the phenyl rings to delocalize an unpaired electron in comparison with the $-SN(CMe_3)MR_n$ or the *t*-butyl group.

Decay Kinetics of the Radicals. Decay kinetic investigations were performed, and the results are illustrated in Fig. 3. As can be seen from the figure, the radicals are fairly long-lived.[7] This may be explained by a) the protection by the *t*-butyl group of the radical center and b) the absence of hydrogen atoms at the β position. In addition to this explanation, it appears likely that Form II makes an important contribution to the persistence.[6]

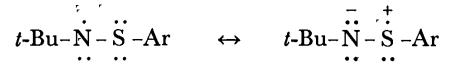

Form I. Form II.

Moreover, decay kinetics were carried out both in the presence and absence of the atmosphere in order to examine whether or not radical **2** reacts with oxygen.

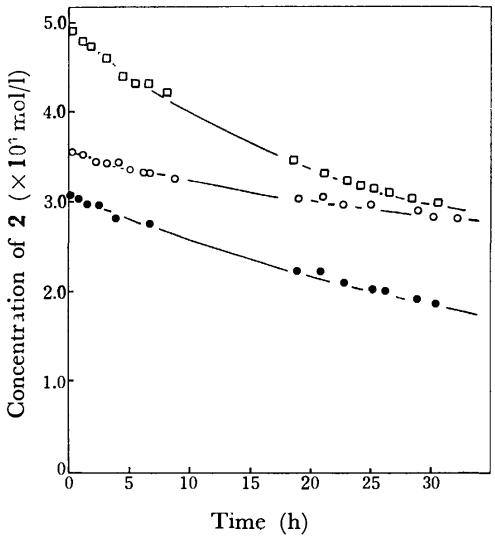

Fig. 3. Decay plots of *N*-(arylthio)-*t*-butylaminyls (**2**) in benzene at 15 °C; (□): **2a** in the absence of oxygen, (○): **2c** in the absence of oxygen, (●): **2c** in the presence of oxygen.

TABLE. ESR PARAMETERS FOR *N*-(ARYLTHIO)-*t*-BUTYLAMINYLS[a]

t-Bu-N-S-Ar	Ar	Coupling constant a_N	$a_{o\text{-H}}$	a_{other}	*g*-Value
2a	C_6H_5	11.70			2.0069
2b[b]	4-FC_6H_4	11.83	0.89	2.22 (a_F)	2.0070
2c	4-ClC_6H_5	11.75	0.93		2.0071
2d	4-BrC_6H_4	11.76	1.00		2.0072
2e	4-$NO_2C_6H_4$	11.89	1.07		2.0068

a) In benzene at room temperature (15 °C). b) The coupling constants were determined by computer simulation.

In both cases, radical **2c** decayed at about the same rate. On the other hand, the *t*-butyl arylthio nitroxide radicals,[11] which were generated by the photolysis of diaryl disulfide in the presence of 2-methyl-2-nitrosopropane, decayed comletely within 20 s after turning off of the mercury lamp used to produce the arylthiyl radicals from the diaryl disulfides. This indicates that the *t*-butyl arylthio nitroxide radicals are extremely short-lived. From these results, it appears that **2** is not sensitive to the atmospheric oxygen.

Experimental

All melting points are uncorrected. The IR spectra were obtained on a Jasco model IR-G Spectrometer. The NMR spectra were recorded on a Hitachi-Perkin-Elmer R-20 Spectrometer using TMS as an internal standard.

Materials. The benzene used for the ESR measurements was purified by the usual method.[13] Benzenethiol, 4-chlorobenzenethiol, and *t*-butylamine were obtained commercially and used without further purification. 4-Fluoro-,[14] 4-bromo-,[15] and 4-nitrobenzenethiol[16] were prepared by the reported methods.

General Procedure for Preparation of N-t-*Butylbenzenesulfen-*

amides (1). Benzenethiol was treated with chlorine gas in dry chloroform at −5 to 0 °C. After removal of chloroform, the residual oil was distilled (56—57 °C/3 Torr for benzenesulfenyl chloride, and other sulfenyl chlorides were used in the following step without distillation).

A solution of *t*-butylamine (0.050 mol) and triethylamine (0.050 mol) in dry diethyl ether (ether, 200 ml) was cooled to 0 °C. To the solution was added dropwise benzenesulfenyl chloride (0.045 mol) in dry ether (30 ml) with stirring. After the addition of the sulfenyl chloride, the reaction mixture was further stirred at 0 °C for 30 min. After the triethylamine hydrochloride had been filtered off, ether was evaporated to give crude **1**. The purification of **1** is described below for each case. The purities of the **1** prepared were examined by TLC [alumina (E. Merck GF_{254})–hexane for **1a**—**d** and benzene–hexane (1 : 1 in vol) for **1e**].

N-t-*Butylbenzenesulfenamide (1a).* After the residue had been distilled (60—62 °C/0.07 Torr), a small amount of hexane (*ca.* 1 ml) was added to the distillate and the solution was cooled to −20 °C, giving colorless prisms. The parent solution was decanted, the residual crystals were then dissolved in hexane and the resulting solution was again cooled to −20 °C. This cycle was repeated several times, and finally, the crystals were dried in a vacuum at 0 °C. Yield 45% (before recrystallization). n_D^{25}: 1.5429 (lit,[17] n_D^{25}: 1.5435)). NMR (CCl_4): δ 1.17 (s, *t*-Bu), 2.65 (bs, NH), and 6.86—7.32 (m, C_6H_5).

N-t-*Butyl-4-fluorobenzenesulfenamide (1b).* After the residue had been distilled (69—71 °C/0.07 Torr), the distillate was treated similarly to the case of **1a**. Yield 63% (based on the amount of 4-fluorobenzenethiol and before recrystallization). n_D^{20}: 1.5227. IR (liquid): 3320 cm^{-1}(NH). NMR (CCl_4): δ 1.15 (s, *t*-Bu), 2.75 (bs, NH), and 6.76—7.73 (m, C_6H_4). Found: C, 60.01; H, 6.91; N, 6.99%. Calcd for $C_{10}H_{14}FNS$: C, 60.27; H, 7.08; N, 7.03%.

N-t-*Butyl-4-chlorobenzenesulfenamide (1c).* After the residue had been distilled (94—95 °C/0.07 Torr), the distillate was recrystallized from hexane (cooled to −20 °C), giving colorless prisms with mp 44—45 °C in a 34% yield (based on the amount of 4-chlorobenzenethiol). IR (KBr): 3320 cm^{-1}(NH). NMR (CCl_4): δ 1.14 (s, *t*-Bu), 2.68 (bs, NH), and 7.02 (s, C_6H_4). Found: C, 55.37; H, 6.31; N, 6.52%. Calcd for $C_{10}H_{14}ClNS$: C, 55.66; H, 6.55; N, 6.49%.

N-t-*Butyl-4-bromobenzenesulfenamide (1d).* After the residue had been distilled (111—113 °C/0.07 Torr), the distillate was recrystallized from hexane (cooled to −20 °C), giving colorless prisms with mp 37—38 °C in a 33% yield (based on the amount of 4-bromobenzenethiol). IR (KBr): 3320 cm^{-1}(NH). NMR (CCl_4): δ 1.14 (s, *t*-Bu), 2.63 (bs, NH), and 7.05 and 7.27 (d, J=8 Hz, C_6H_4). Found: C, 46.27; H, 5.18; N, 5.43%. Calcd for $C_{10}H_{14}BrNS$: C, 46.16; H, 5.42; N, 5.38%.

N-t-*Butyl-4-nitrobenzenesulfenamide (1e).*[18] The residue obtained was recrystallized from hexane, giving yellow needles with mp 78—79 °C in an 18% yield (based on the amount of 4-nitrobenzenethiol). IR (KBr): 3300 cm^{-1}(NH). NMR (CCl_4): δ 1.12 (s, *t*-Bu), 2.34 (bs, NH), and 7.18 and 8.02 (d, J=8 Hz, C_6H_4). Found: C, 53.07; H, 5.95; N, 12.26%. Calcd for $C_{10}H_{14}N_2O_2S$: C, 53.05; H, 6.23; N, 12.38%.

Generation of N-*(Arylthio)*-t-*butylaminyls (2).* *a*) The compound **1** (20 mg) and benzene (0.20 ml) were placed in an ESR tube. The solution was degassed by three freeze-thaw cycles and the tube was then sealed. After the solution had been irradiated for 5 min from a distance of 10 cm with a 100 W high-pressure mercury lamp (JES-UV-1), the tube was set in the ESR cavity; *b*) **1** (0.10 g) in benzene (2 ml) was stirred for 5 min in the presence of lead dioxide (0.50 g) and potassium carbonate (0.50 g). After the oxidizing agents had been filtered off, 0.2 ml of the filtrate was placed in an ESR tube and the soluion was degassed as described above, and the tube was then sealed.

Decay Kinetics. When the kinetics was carried out in degassed benzene, the sample was prepared according to procedure *a*. On the other hand, when the kinetics was carried out in a system containing air, the sample was prepared as follows: after photolysis of a degassed benzene solution of **1**, the solution was exposed to the atmosphere and shaken well, and then the tube was set in the ESR cavity. The decay rates of **2** were measured at 15 °C in the dark by monitoring the intensities of ESR signal. Integration of the ESR signals was achieved using a Model JES-ID-2 Integrator, with a benzene solution of 3,4-dihydro-2,4,6-triphenyl-2*H*-1,2,4,5-tetrazin-1-yl (1,3,5-triphenylverdazyl)[19] as a standard.

The ESR spectra were recorded at 15 °C on a JES-ME-3X Spectrometer equipped with 100 kHz field modulation. Computer simulation of the spectrum was carried out using a FACOM 270-30 Computer equipped with a FACOM 6201B Plotter. The simulation was fitted by trial and error.

References

1) Part V of this series, Y. Miura, Y. Katsura, and M. Kinoshita, *Chem. Lett.*, **1977**, 409.

2) For recent reviews see (a) A. R. Forrester, J. M. Hay, and R. H. Thomson, "Organic Chemistry of Stable Free Radicals," Academic Press, New York, N. Y. (1968); (b) S. F. Nelsen, "Free Radicals," Vol. II ed by J. K. Kochi, John Wiley, New York, N. Y. (1973), p. 527; (c) W. C. Danenand F. A. Neugebauer, *Angew. Chem.*, **87**, 823 (1975).

3) U. Schmidt, K. H. Kabitzke, and K. Markau, *Angew. Chem.*, **76**, 376 (1964).

4) G. Brunton, J. F. Taylor, and K. U. Ingold, *J. Am. Chem. Soc.*, **98**, 4879 (1976).

5) J. Flood and K. E. Russell, *Can. J. Chem.*, **53**, 1123 (1975).

6) Y. Miura and M. Kinoshita, *Bull. Chem. Soc. Jpn.*, **50**, 1142 (1977).

7) R. S. Atkinson, S. B. Awad, E. A. Smith, and M. C. R. Symons, *J. Chem. Soc., Chem. Commun.*, **1976**, 22.

8) (a) W. C. Danen, C. T. West, and T. T. Kensler, *J. Am. Chem. Soc.*, **95**, 5716 (1973); (b) R. A. Kaba and K. U. Ingold, *ibid.*, **98**, 7375 (1976).

9) This is an unidentified radical.

10) I. H. Leaver and G. C. Ramsay, *Tetrahedron*, **25**, 5669 (1969).

11) Unpublished results.

12) The spin-orbit coupling parameter of sulfur is 382 cm^{-1}; D. S. McClure, *J. Chem. Phys.*, **20** 682 (1952).

13) Y. Miura, N. Makita, and M. Kinoshita, *Bull. Chem. Soc. Jpn.*, **50**, 482 (1977).

14) H. Zahn and H. Zuber, *Chem. Ber.*, **86** 172 (1953).

15) H. F. Wilson and D. S. Tarbell, *J. Am. Chem. Soc.*, **72** 5200 (1950).

16) C. C. Price and G. W. Stacy, *J. Am. Chem. Soc.*, **68**, 498 (1946).

17) D. A. Armitage, M. J. Clark, and A. C. Kinsey, *J. Chem. Soc., C*, **1971**, 3867.

18) Brit. Amended 1123506; *Chem. Abstr.*, **76**, 26223u (1972).

19) R. Kuhn and H. Trischmann, *Monatsh. Chem.*, **95**, 457 (1964).

Layered Compounds. XLIII.[1] Syntheses and Properties of [2.2]Naphthaleno- and [2.2]Anthraceno-heterophanes

Tetsuo Otsubo, Shigeyoshi Mizogami, Norihisa Osaka, Yoshiteru Sakata, and Soichi Misumi

The Institute of Scientific and Industrial Research, Osaka University, Suita, Osaka 565

(Received January 24, 1977)

Several [2.2]naphthaleno- and [2.2]anthraceno-heterophanes were synthesized by cross-breeding Hofmann degradation of the corresponding two quaternary ammonium hydroxides. Two isomers, *anti*- and *syn*-forms, were obtained for [2.2](1,4)naphthaleno(2,5)thiophenophane, and one isomer, *anti*-form, for the [2.2](1,4)anthraceno homologue. The structures of the heterophanes were determined by variable temperature NMR analysis. Transannular π-electronic interactions between the condensed aromatic ring and the heteroaromatic ring were examined on the basis of electronic and emission spectra. The thiophene ring interacts more strongly with the condensed aromatic ring than the furan ring. For anthracenophanes, 9,10-bridged system shows more effective interaction than 1,4-bridged one.

The syntheses and properties of a series of multilayered paracycloheterophanes have been reported in the preceding paper.[1] A transannular π-electronic interaction has been observed between the benzene and the heteroaromatic ring in double-layered [2.2]paracycloheterophanes **1** and **2**, increasing with an increase in layer number of multilayered [2.2]paracycloheterophanes. The structures of the paracycloheterophanes, *i.e.*, facile flipping of the furanophane system and tight fixation of the thiophenophane system, and the addition reactions of the former series with benzyne as well as the NMR spectra and CT spectra of TCNE complexes have been reported. The present work was undertaken to study transannular electronic interaction between heteroaromatic and condensed aromatic rings. A series of naphthaleno- and anthraceno-heterophanes **3**—**9** were synthesized with expectation of marked interaction as compared with those of multilayered paracycloheterophanes.

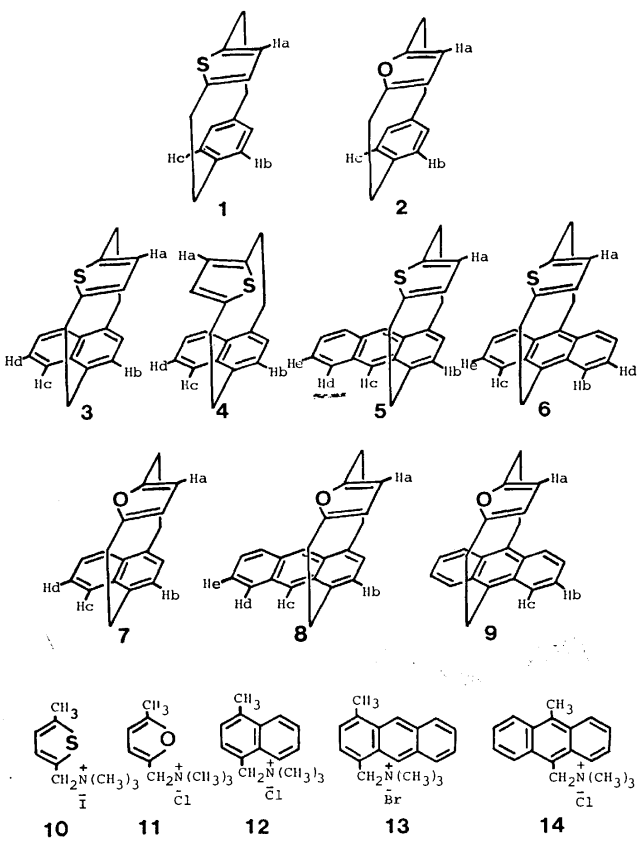

Scheme 1.

Results and Discussion

Syntheses. Five quaternary ammonium salts **10**—**14** were prepared according to the reported methods.[2-5] All the new cyclophanes were obtained by the cross-breeding Hofmann degradation of the corresponding two quaternary ammonium hydroxides in the same method as **1** and **2**. **2** shows the flipping of the furan ring at room temperature. However, **1** exhibits tight fixation of the thiophene ring even at 150 °C due to the bulkiness of sulfur atom.[1] Thus, both conformers, *anti* **3** and *syn* **4**, of [2.2](1,4)naphthaleno(2,5)thiophenophane are expected to be separated as stable ones. Actually the two isomers **3** and **4** were obtained by the pyrolysis of mixed quaternary hydroxides, derived from **10** and **12**, in boiling xylene. The mass spectra of **3** and **4** showed an identical pattern, indicating that both are isomeric with each other. Their structures were assigned on the basis of NMR analyses. The lower yield (0.3%) of *syn*-form **4** than that (4.2%) of *anti*-form **3** is ascribed to π-π repulsion between fused benzo group and thiophene ring in *syn* form. Although *syn*-[2.2](1,4)naphthalenophane and *syn*-[2.2](1,4)anthracenophane were thermally isomerized to *anti*-form, no isomerization of **4** to **3** was observed because of its ready decomposition. In the case of [2.2](1,4)anthraceno(2,5)thiophenophane, however, only one isomer was obtained in 2.8% yield by a cross-breeding reaction of two quaternary ammonium hydroxides derived from **10** and **13** in boiling xylene. Its structure was assigned to *anti*-conformer **5** by NMR spectrum. The *syn*-isomer could not be detected either when the pyrolysis was carried out in boiling toluene (pyrolysis at lower temperature). The *syn*-conformer seems to be very unstable due to both the increasing π-π repulsion and access of the reactive part of the anthracene ring to the thiophene ring. [2.2](9,10)Anthraceno(2,5)thiophenophane **6** and [2.2](1,4)anthraceno(2,5)furanophane **8** were synthesized by similar cross-breeding reactions in 5.5% yield from **10** and **14** and in 0.8% yield from **11** and **13**, respectively. As reference compounds, [2.2](1,4)naphthaleno(2,5)furanophane **7**[6] and [2.2](9,10)-anthraceno(2,5)furanophane **9**[5] were also prepared

Table 1. NMR spectra of [2.2]naphthaleno- and [2.2]anthraceno-heterophanes (δ value in $CDCl_3$)

Compd	Aromatic proton	Calcd shift	Benzylic CH_2
1	Ha 6.34(s, 2H)	+0.11	2.5—3.3(m, 8H)
	Hb 6.20(d, J=2Hz, 2H)	+0.86	
	Hc 7.04(d, J=2Hz, 2H)	+0.02	
2	Ha 5.64(s, 2H), 5.49(s, 2H)[b]	+0.06	2.4—4.1(m, 8H)
	Hb, Hc 6.79(s, 4H) {6.12(bs, 2H)[b], 7.07(bs, 2H)[b]}	+0.27 {+0.78[b], −0.17[b]}	
3	Ha 6.38(s, 2H)	+0.07	3.8—4.1(m, 2H)
	Hb 6.48(s, 2H)	+0.67	2.6—3.3(m, 6H)
	Hc 8.05(A_2B_2dd, J=6.5, 3.5 Hz, 2H)	−0.09	
	Hd 7.50(A_2B_2dd, J=6.5, 3.5 Hz, 2H)	−0.04	
4[a]	Ha 5.17(s, 2H)	+1.28	3.7—4.3(m, 2H)
	Hb 7.09(s, 2H)	−0.08	2.7−3.5(m, 6H)
	Hc 7.55(A_2B_2m, 2H)	+0.27	
	Hd 7.20(A_2B_2m, 2H)	+0.12	
5	Ha 6.38(s, 2H)	+0.07	3.8—4.1(m, 2H)
	Hb 6.42(s, 2H)	+0.77	2.6—3.2(m, 6H)
	Hc 8.44(s, 2H)	+0.07	
	Hd 8.00(A_2B_2dd, J=6.5, 3.5 Hz, 2H)	+0.02	
	He 7.46(A_2B_2dd, J=6.5, 3.5 Hz, 2H)	+0.01	
6	Ha 5.42(s, 2H)	+1.03	3.9—4.3(m, 4H)
	Hb 7.95(A_2B_2dd, J=7, 3.5 Hz, 2H)	+0.37	2.6—3.4(m, 4H)
	Hc 8.25(A_2B_2dd, J=7, 3.5 Hz, 2H)	+0.07	
	Hd, He 7.2—7.6(m, 4H)	−0.1—+0.3	
7	Ha 5.62(s, 2H)	+0.08	3.7—4.1(m, 2H)
	Hb 6.55(s, 2H)	+0.70	2.2—3.1(m, 6H)
	Hc 8.10(A_2B_2dd, J=6, 3 Hz, 2H)	−0.09	
	Hd 7.53(A_2B_2dd, J=6, 3 Hz, 2H)	+0.03	
8	Ha 5.65(s, 2H)	+0.05	3.6—4.1(m, 2H)
	Hb 6.52(s, 2H)	+0.67	2.4—3.1(m, 6H)
	Hc 8.59(s, 2H)	−0.08	
	Hd 8.00(A_2B_2dd, J=7, 3.5 Hz, 2H)	+0.02	
	He 7.47(A_2B_2dd, J=7, 3.5 Hz, 2H)	0	
9	Ha 4.98(s, 2H)	+0.72	3.8—4.2(m, 4H)
	Hb 8.15(A_2B_2dd, J=7, 3.5 Hz, 4H)	+0.17	2.4—2.7(m, 4H)
	Hc 7.35(A_2B_2dd, J=7, 3.5 Hz, 4H)	+0.14	

a) In CCl_4. b) In CS_2 at −60 °C.

according to the reported methods.

Structure and NMR Spectra. The NMR spectral data of all the naphthaleno- and anthraceno-heterophanes **3**—**9** as well as [2.2]paracycloheterophanes **1** and **2** are summarized in Table 1. Heterophanes **3**—**9** show the signals of all the bridged methylene protons to be roughly divided into two groups of multiplets. Of these, the lower field multiplet is associated with the endo proton (see **15**) of methylenes attached to condensed aromatic ring for 1,4-bridged systems (**3**, **4**, **5**, **7**, and **8**) or both protons of methylenes attached to the same ring for 9,10-bridged systems (**6** and **9**). The downfield shift of these protons is explained by the large deshielding effect of the neighbouring condensed aromatic ring. Most aromatic protons show more or less upfield shifts and are reasonably assigned by considering

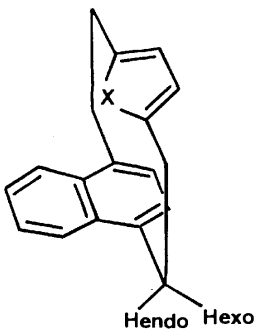

15

Scheme 2.

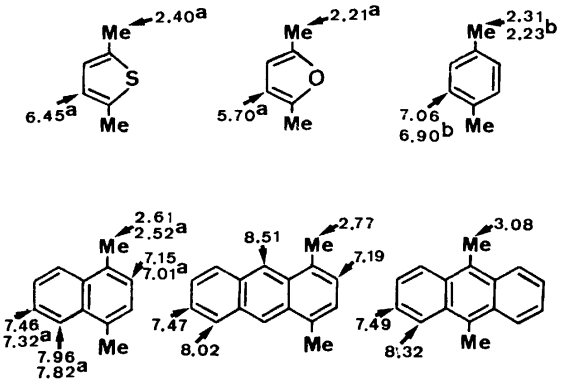

Fig. 1. NMR data of reference compounds, δ value in deuteriochloroform. a) in carbon tetrachloride. b) in carbon disulfide.

diamagnetic anisotropy of the opposite aromatic rings. As shown in Table 1, the magnitudes of the shifts are calculated using the chemical shifts (Fig. 1) of the aromatic protons of 2,5-dimethylfuran, 2,5-dimethylthiophene, *p*-xylene, 1,4-dimethylnaphthalene, 1,4-dimethylanthracene, and 9,10-dimethylanthracene as standards. The structural difference between **3** and **4** is unequivocally realized in the NMR spectra. The upfield shift (1.28 ppm) of thiophene proton Ha of **4** is drastic as compared with that of **1** (0.11 ppm) or **3** (0.07 ppm), suggesting that the proton is situated above the center of the opposite naphthalene ring. The naphthalene protons Hc and Hd show reasonable upfield shifts. However, Hb proton shows absorption at rather lower field. On the other hand, the shifts of Hc and Hd protons in **3** are negligible, the upfield shift (0.67 ppm) of Hb proton being marked and roughly the same as that (0.86 ppm) of Hb proton in **1**. These data are best accommodated by the *anti*-conformation for **3** and *syn*-conformation for **4**. The structure of 1,4-bridged anthracenothiophenophane **5** can be assigned to *anti*-conformation by a comparison of its NMR data with those of **3** and **4**. Thus the upfield shifts of Ha and Hb protons in **5** are identical with those of Ha and Hb in **3**, respectively. Small shielding effects on the Hc, Hd, and He protons are also explained by *anti* structure, but not by *syn* structure. The NMR pattern of 9,10-bridged anthracenothiophenophane **6** is in contrast to that of 1,4-bridged one **5**, and the chemical shifts are explained by considering both shielding effects of *anti*-form **3** and *syn*-form **4**.

A variable temperature NMR analysis of [2.2]paracyclofuranophane **2** exhibited the conformational flipping of the furan ring at room temperature and the fixation at low temperature (T_c, −39 °C).[1,7] Thus, 1,4-bridged naphthalenofuranophane **7** and anthracenofuranophane **8** are expected to show similar behavior, that is, consisting of one isomer at room temperature and two conformers, *syn* and *anti*, at low temperature. However, the NMR spectra exhibited no temperature-dependence, though the temperature was lowered to −100 °C. The upfield shifts of Hb protons of **7** and **8** are much larger than that of benzene proton of **2** at room temperature and close to that at ring fixation temperature. The furan protons Ha show no large

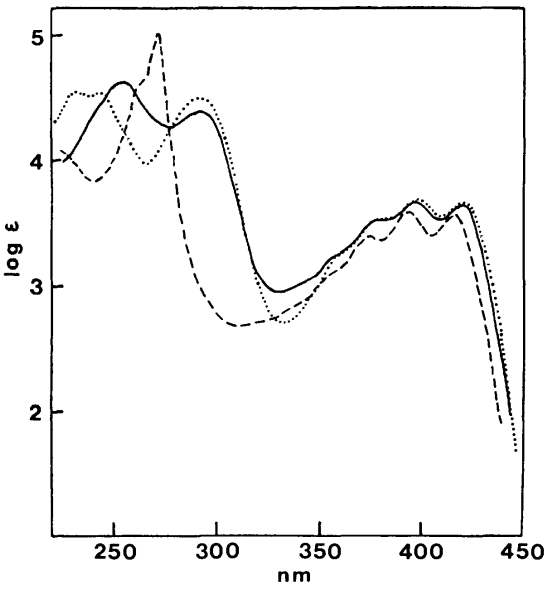

Fig. 2. Electronic spectra of **6** (——), **9** (----), and **18** (·····) in tetrahydrofuran.

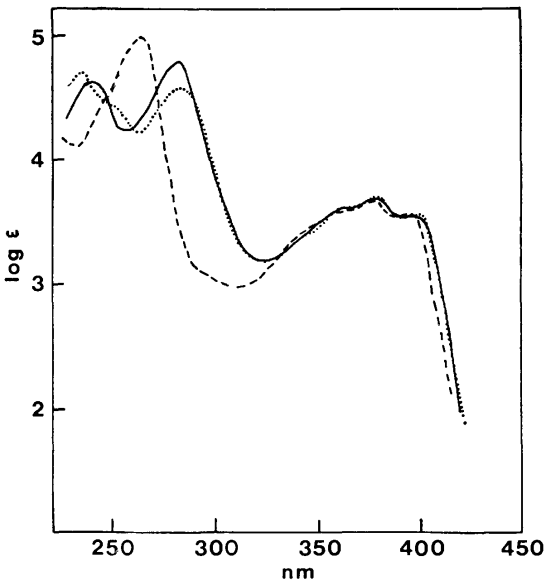

Fig. 3. Electronic spectra of **5** (——), **8** (----), and **17** (·····) in tetrahydrofuran.

shielding effect due to the fused aromatic ring. These data support the view that both **7** and **8** exist exclusively in the *anti*-conformation rather than in the *syn*-conformation owing to a π-π repulsive instabilization in the latter conformation.[8] The NMR spectrum of 9,10-bridged anthracenophane **9** is characterized by a symmetrical pattern, indicating a rapid flipping of the furan ring unlike **7** and **8**.

Electronic Spectra and Emission Spectra. Figures 2, 3, and 4 show the electronic spectra of naphthaleno- and anthraceno-heterophanes together with those of the corresponding paracyclophanes **16**—**18**.[9] All the absorption curves exhibit common features of cyclophanes, *viz.*, broadening, bathochromic and hyperchromic shifts,[10] caused by the transannular electronic interaction. A comparison of Fig. 2 with Fig. 3 shows that

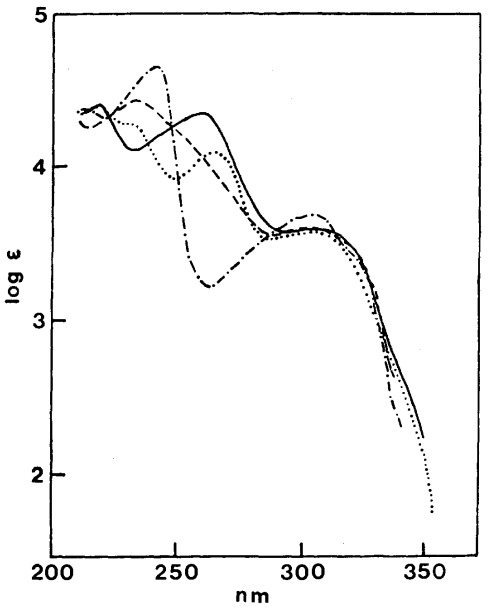

Fig. 4. Electronic spectra of **3** (——), **4** (----), **7** (—·—), and **16** (·····) in cyclohexane.

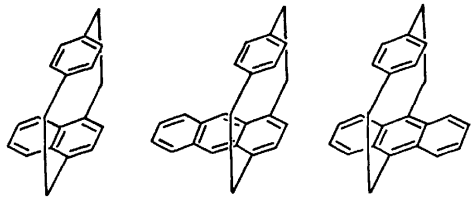

16 **17** **18**

Scheme 3.

the interactions in 9,10-bridged anthracenophanes are more effective than those in 1,4-bridged analogues. The spectra of the thiophenophane are very similar to those of the corresponding paracyclophanes as in the case of multilayered paracyclothiophenophanes,[1] indicating a strong interaction between thiophene and condensed aromatic ring. The broad long wavelength band and the short wavelength band are due to ^1L_a and ^1B_b transitions of naphthalene or anthracene. The single band between them (260 nm for *anti*-form **3**, 281 nm for *anti*-form **5**, and 292 nm for **6**) is considered to be associated with a transition of the thiophene ring, showing a considerable bathochromic shift due to the strong interaction with the condensed aromatic ring, as compared with an absorption band (230 nm) of thiophene itself.[11] On the other hand, absorption of the thiophene ring in *syn*-form **4** exhibits no such large shift, being superposed on ^1B_b band of naphthalene at 233 nm. The difference between the *anti* and *syn* forms suggests that the d-orbitals of sulfur atom play an important role in the interaction, especially for the former.

Furan shows no absorption in the long wavelength region above 220 nm[11] In the present furanophanes, the absorption due to the furan ring is submerged by band ^1B_b of the naphthalene or anthracene ring. The presence of reasonable transannular electronic interaction in the furan series is supported by the broadening and bathochromic shift of the long wavelength band (^1L_a band). However, the shift value is smaller than that of the other cyclophanes. The interaction between furan ring and condensed aromatic ring is relatively weak.

Table 2. Emission spectra of layered heterophanes containing condensed aromatic nuclei at room temperature

Compound	Solvent	Fluorescence maximum
Thiophenophane		
3	EPA	342, 380 nm
5	THF	421,[a] 437
6	THF	445, 460
Furanophane		
7	EPA	345,[a] 357
8	THF	418,[a] 432
9	THF	438, 455
Paracyclophane		
16	THF	418, 435
17	THF	440, 461
Naphthalene	Cyclohexane	322, 335
Anthracene	Cyclohexane	378, 400

a) Shoulder.

In order to obtain further informations on the interaction, emission spectra were measured (Table 2). Since the heteroaromatic ring shows about zero value of fluorescence quantum yield and, in the present cycloheterophanes, energy transfer is expected to take place transannularly from the excited state of the heteroaromatic ring to the lowest excited level of the condensed aromatic ring, only transitions $^1L_a \rightarrow {}^1A$ of the condensed aromatic rings are observed as fluorescence. Their fluorescence maxima show remarkable bathochromic shifts as compared with that of naphthalene or anthracene. The feature of the shifts agrees with that discussed on the electronic absorption spectra; the thiophenophanes and the 9,10-bridged anthracenoheterophanes show more effective interaction than the furanophanes and the 1,4-bridged analogues, respectively.

Experimental

Melting points are uncorrected. All the solvents are of reagent grade. NMR spectra were taken with a Hitachi-Perkin Elmer R-20 spectrometer (60 MHz) using tetramethyl silane as an internal standard. MS spectra were measured with a Hitachi RMU-7 spectrometer and UV spectra with a Hitachi EPS-3T spectrophotometer. Emission spectra were taken on a Hitachi MPF-2A spectrophotometer using 1×10^{-3}M degassed solution in tetrahydrofuran or EPA (5 : 5 : 2 volume ratio of ethyl ether–isopentane–ethanol) at room temperature. Emission spectra are uncorrected.

anti- *and* syn-*[2.2](1,4)Naphthaleno(2,5)thiophenophanes*, ***3*** *and* ***4***. 5-Methylthenyltrimethylammonium iodide **10** (8.2 g, 40 mmol) and (1-methyl-4-naphthylmethyl)trimethylammonium chloride **12** (5 g, 20 mmol) were dissolved in distilled water (*ca.* 300 ml) and passed through a column of strong anion exchange resin (Dowex 1-X8) which had been

converted into hydroxide form with 3M sodium hydroxide solution. The eluted solution (*ca.* 700 ml) was mixed with xylene (150 ml) and phenothiazine (100 mg), water being removed by azeotropic distillation in a nitrogen atmosphere. After complete removal of water, reflux was continued for 7 h. The insoluble polymer was filtered and washed with xylene. The filtrate and the washings were combined and concentrated. The residue was taken up in benzene and subjected to column chromatography on silica gel. Elution with 1 : 9 benzene–hexane gave successively [2.2](2,5)thiophenophane,[2] *syn*-[2.2](1,4)naphthaleno(2,5)thiophenophane **4**, *anti*-[2.2](1,4)naphthaleno(2,5)thiophenophane **3**, and a mixture of *anti*- and *syn*-[2.2](1,4)naphthalenophanes.[3] Recrystallization of **3** from 1 : 1 hexane–benzene gave colorless prisms (222 mg, 4.2%), mp 182—183 °C.

MS *m/e* 264 (M^+). Found: C, 81.90; H, 6.04%. Calcd for $C_{18}H_{16}S$: C, 81.79; H, 6.10%.

Recrystallization of **4** from 1 : 1 hexane–benzene gave colorless plates (16 mg, 0.3%), mp 142—143 °C.

MS *m/e* 264 (M^+). Found: C, 81.59; H, 6.00%. Calcd for $C_{18}H_{16}S$: C, 81.79; H, 6.10%.

[2.2](1,4)Anthraceno(2,5)thiophenophane **5**. The method described above was used for the cross-breeding reaction of the quaternary hydroxides derived from 5-methylthenyltrimethylammonium iodide **10** (6 g, 29 mmol) and (1-methyl-4-anthrylmethyl)trimethylammonium bromide **13** (5 g, 14.5 mmol). The cross coupling product **5** was separated from homo coupling products, [2.2](2,5)thiophenophane,[2] [2.2.2](2,5)-thiophenophane,[1] *anti*-[2.2](1,4)anthracenophane,[4] and *syn*-[2.2](1,4)anthracenophane and its photoisomer[12] by careful column chromatography on silica gel using 1 : 9 benzene–hexane and recrystallized from 1 : 1 benzene–hexane to give pale yellow prisms (130 mg, 2.8%), mp 195 °C with decompn.

MS *m/e* 314 (M^+). Found: C, 84.25; H, 5.59%. Calcd for $C_{22}H_{18}S$: C, 84.05; H, 5.77%.

[2.2](9,10)Anthraceno(2,5)thiophenophane **6**. The method described for **3** and **4** was used for pyrolysis of the quaternary hydroxides derived from a mixture of two ammonium salts **10** (6 g, 29 mmol) and **14** (4.5 g, 15 mmol), giving cross coupling cyclophane **6**, together with homo coupling products, [2.2](2,5)thiophenophane,[2] [2.2.2](2,5)thiophenophane,[1] and [2.2](9,10)anthracenophane.[5,13] Column chromatography on silica gel with 1 : 9 benzene–hexane and recrystallization from pentane–dichloromethane gave pure greenish yellow needles **6** (260 mg, 5.5%), dec>100 °C.

MS *m/e* 314 (M^+). Found: C, 83.80; H, 5.57%. Calcd for $C_{22}H_{18}S$: C, 84.05; H, 5.77%.

[2.2](1,4)Anthraceno(2,5)furanophane **8**. The method described for **3** and **4** was used for the pyrolytic reaction of the quaternary hydroxides derived from a mixture of two ammonium salts **11** (8 g, 28 mmol) and **14** (5 g, 14 mmol), the desired cyclophane **8** being obtained. After removal of homo coupling cyclophanes by column chromatography, recrystallization of **8** from 1 : 1 benzene–hexane gave pale yellow prisms (34 mg, 0.8%), dec>154 °C.

MS *m/e* 298 (M^+). Found: C, 88.32; H, 5.97%. Calcd for $C_{22}H_{18}O$: C, 88.56; H, 6.08%.

This research was partly supported by a Grant-in-Aid of the Ministry of Education.

References

1) Part XLII, T. Otsubo, S. Mizogami, N. Osaka, Y. Sakata, and S. Misumi, *Bull. Chem. Soc. Jpn.*, **50**, 1841 (1977).

2) H. E. Winberg, F. S. Fawcett, W. E. Mochel, and C. W. Theobald, *J. Am. Chem. Soc.*, **82**, 1428 (1960); H. E. Winberg and F. S. Fawcett, *Org. Synth.*, Coll. Vol. V, 883 (1973).

3) D. J. Cram, C. K. Dalton, and G. R. Knox, *J. Am. Chem. Soc.*, **85**, 1088 (1963); H. H. Wasserman and P. M. Keehn, *ibid.*, **91**, 2374 (1969).

4) T. Toyoda, I. Otsubo, T. Otsubo, Y. Sakata, and S. Misumi, *Tetrahedron Lett.*, **1972**, 1731.

5) H. Wynberg and R. Helder, *Tetrahedron Lett.*, **1971**, 4317.

6) H. H. Wasserman and P. M. Keehn, *Tetrahedron Lett.*, **1969**, 3227.

7) G. M. Whitesides, B. A. Pawson, and A. C. Cope, *J. Am. Chem. Soc.*, **90**, 639 (1968).

8 Reference 6 indicates that *anti*-conformation is favorable for [2.2](1,4)naphthaleno(2,5)furanophane.

9) D. J. Cram and R. A. Reeves, *J. Am. Chem. Soc.*, **80**, 3094 (1958); A. Iwama, T. Toyoda, T. Otsubo, and S. Misumi, *Chem. Lett.*, **1973**, 587.

10) D. J. Cram, *Rec. Chem. Progr.*, **20**, 71 (1959).

11) H. H. Jaffé and M. Orchin, "Theory and Applications of Ultraviolet Spectroscopy," John Wiley & Sons (1962), p. 345.

12) *syn*-[2.2](1,4)Anthracenophane was first synthesized by thermal isomerization of its photoisomer.[4] Later it was found to be directly obtainable by the Hofmann elimination reaction in the dark.

13) J. H. Golden, *J. Chem. Soc.*, **1961**, 3741.

New Method for the Preparation of Carboxylic Esters

Kazuhiko SAIGO,[1] Masahiro USUI, Kazunori KIKUCHI,
Eiichiro SHIMADA, and Teruaki MUKAIYAMA
Department of Chemistry, Faculty of Science, The University of Tokyo, Hongo, Bunkyo-ku, Tokyo 113
(Received February 4, 1977)

Various carboxylic esters including functionalized ones are prepared in good yields from equimolar amounts of free carboxylic acids and alcohols under mild conditions by the use of 2-chloro- or 2-bromopyridinium salt, a new and efficient coupling reagent.

The ester formation is one of the most fundamental reactions in organic synthesis and a number of methods have been presented. However, relatively little work has been reported on the successful preparation of carboxylic esters by the equimolar reaction of free carboxylic acids and alcohols except when *p*-toluenesulfonyl chloride,[2] trifluoroacetic anhydride,[3] polyphosphate ester,[4] dicyclohexylcarbodiimide,[5] and graphite hydrogensulfate[6] were employed as coupling reagents.

This prompted us to develop a new and efficient coupling reagent, and 2-chloro- and 2-bromopyridinium salts were found to be efficient for the preparation of carboxylic esters from equimolar amounts of free carboxylic acids and alcohols as briefly reported in the previous communications.[7]

The work was undertaken based on the following considerations; 2-acyloxy-1-methylpyridinium iodide (**2**), an active acylating intermediate, would be produced easily and rapidly by a nucleophilic attack of the carboxylate ion on 2-chloro- or 2-bromo-1-methylpyridinium iodide (**1**) since the halogen atom at 2-position of **1** is facile to be displaced by the attack of nucleophiles. The intermediate, **2**, is in turn converted into stable molecules, *i.e.*, carboxylic esters (**3**), 1-methyl-2-pyridone (**4**) and ammonium salt (**5**) by the nucleophilic attack of alcohol to carbonyl carbon of **2** in the presence of tertiary amine, a hydrogen iodide captor.

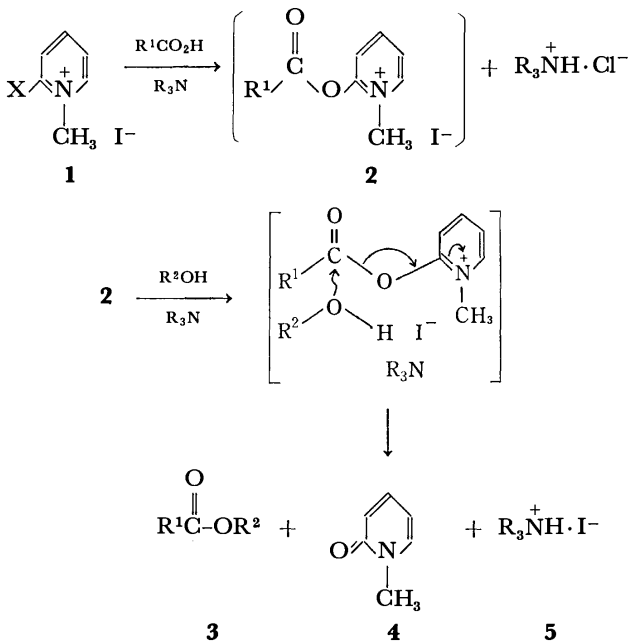

In the first place, the effective hydrogen halide captors in the ester forming reaction were examined using equimolar amounts of phenylacetic acid and benzyl alcohol. Several runs were carried out in the presence of 2.4 molar amounts of tertiary amines, such as triethylamine, tributylamine, 2,6-lutidine, α-picoline, pyridine, and *N*,*N*-diethylaniline, by the use of 2-chloro-1-methylpyridinium iodide. Of the amines employed, triethylamine, tributylamine, and 2,6-lutidine gave good results (see Table 1). These results indicate that the basicity of tertiary amine influences on the yield of benzyl phenylacetate, namely, the yield decreases with lowering basicity of the amine.

Next, the effect of the solvent on the reaction of phenylacetic acid and benzyl alcohol was examined using 2-chloro-1-methylpyridinium iodide in the presence of tributylamine. As listed in Table 1, no remarkable solvent effect was observed, that is, benzyl phenylacetate was obtained in almost quantitative yield in all of the solvents used.

Based on these results, several equimolar reactions of free carboxylic acids and alcohols were carried out in dichloromethane by the use of 2-chloro-1-methyl-

TABLE 1. EFFECTS OF TERTIARY AMINE AND SOLVENT

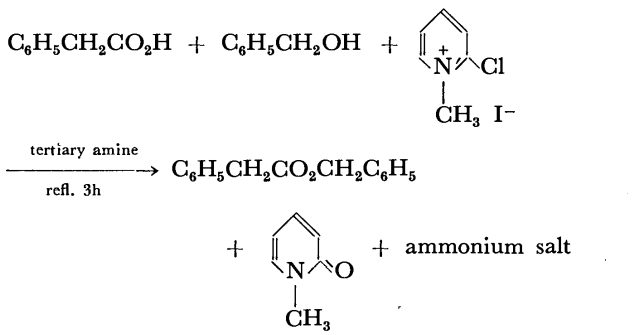

Tertiary amine	Solvent	Temp (°C)	Yield (%)
Triethylamine	CH_2Cl_2	refl.	98
Tributylamine	CH_2Cl_2	refl.	99
2,6-Lutidine	CH_2Cl_2	refl.	97
α-Picoline	CH_2Cl_2	refl.	77
Pyridine	CH_2Cl_2	refl.	62
N,*N*-Diethylaniline	CH_2Cl_2	refl.	43
Tributylamine	$(C_2H_5)_2O$	refl.	97
	CH_2Cl_2	refl.	99
	THF[a]	45—50	97
	CH_3CN	45—50	98
	DME[b]	45—50	98
	C_5H_5N	45—50	98
	CH_3-C_6H_5	45—50	99

a) Tetrahydrofuran. b) 1,2-Dimethoxyethane.

Table 2. Esterification using 2-chloro- or 2-bromo-1-methylpyridinium iodide as a coupling reagent

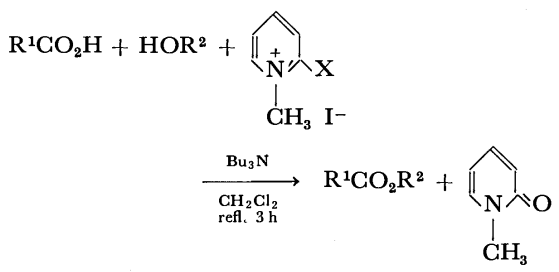

X	R^1	R^2	Yield (%)
Br	C_6H_5	$C_6H_5CH_2$	80
	$C_6H_5CH_2$	CH_3CH_2	92
	$C_6H_5CH_2$	$C_6H_5CH_2$	97
	$C_6H_5CH_2$	$(CH_3)_3C$	70 (82)
	CH_3	$C_6H_5CH_2$	80
	CH_3	$C_6H_5CH{=}CHCH_2$	80
Cl	$C_6H_5CH_2$	C_6H_5	90
	$C_6H_5CH_2$	$C_6H_5CH_2CH_2$	93
	$C_6H_5CH_2$	$(CH_3)_3C$	81 (84)
	$C_6H_5CH_2$	$C_6H_5(CH_3)CH$	85 (88)
	CH_3	$C_6H_5CH_2CH_2$	74
	$(CH_3)_3C$	$C_6H_5CH_2$	31 (62)

Values in parentheses indicate the yields when the esterification was carried out in toluene under refluxing for 3 h.

Table 3. Examination of pyridinium salts

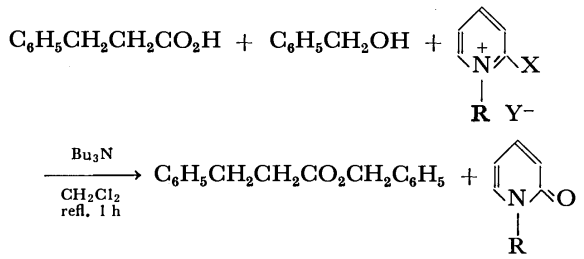

R	X	Y	Yield (%)
CH_3	Cl	I	69
CH_3	Br	I	61
C_2H_5	Cl	BF_4	73
C_2H_5	Br	BF_4	82

pyridinium iodide and tributylamine, and good results were obtained. 2-Bromo-1-methylpyridinium iodide was also found to be as effective as 2-chloro-1-methylpyridinium iodide in the esterification. An improvement in the yields was rarely recognized except for the case of the condensation of pivalic acid, a bulky carboxylic acid, with benzyl alcohol when the esterifications were carried out at an elevated temperature, that is, in refluxing toluene (see Table 2).

The consideration that both the counter ion and halogen atom attached to 2-position of the pyridinium salt would influence on the yield of carboxylic esters urged us to look for more effective pyridinium salt. The equimolar reaction of 3-phenylpropionic acid with benzyl alcohol was undertaken by the use of 2-halo-

Table 4. Esterification employing 2-bromo-1-ethylpyridinium tetrafluoroborate

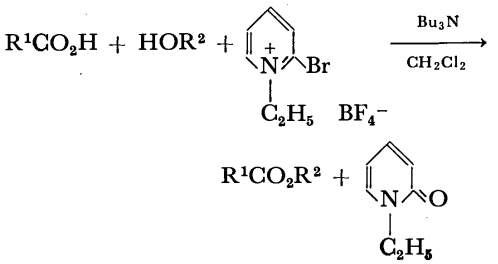

R^1	R^2	Conditions: refl. 3 h Yield (%)	Conditions: r.t. overnight Yield (%)
$C_6H_5CH_2CH_2$	C_2H_5	73 (59)	
$C_6H_5CH_2CH_2$	C_6H_5	57	61
CH_3CH_2	$C_6H_5CH_2$	62 (39)	71
CH_3CH_2	$C_6H_5CH_2CH_2$	60 (48)	
$C_6H_5CH{=}CH$	$C_6H_5CH_2$	71 (62)	
$C_6H_5CH{=}CH$	C_2H_5	43 (27)	78
$(CH_3)_3C$	$(CH_3)_3C$	21[a]	54[a]
$C_6H_5CH_2$	$(CH_3)_3C$		78
Cl_3C	$C_6H_5CH_2$	40	62
$ClCH_2$	$C_6H_5CH_2$	88	
$ClCH_2$	$C_6H_5CH_2CH_2$	80	
	$C_6H_5CH_2$		97
$C_6H_5C{\equiv}C-$	$C_6H_5CH_2$		85
$C_6H_5COCH_2$	$C_6H_5CH_2$		87
$CH_3COCH_2CH_2$	$C_6H_5CH_2$		45[b]
	$C_6H_5CH_2$		62
$CH_3CH{=}CH{-}CH{=}CH$	$C_6H_5CH_2$		59[c]

Values in parentheses indicate the yields when the reactions were carried out in dichloromethane under refluxing for 3 h using 2-chloro-1-methylpyridinium iodide as a coupling reagent.
a) Yields determined by GLC. b) As a by-product, 4-benzyloxy-4-methyl-4-butanolide was obtained in 13% yield. c) Sorbic anhydride was obtained in 21% yield.

pyridinium iodide or tetrafluoroborate to determine the influence on the yield. As shown in Table 3, 2-bromo-1-ethylpyridinium tetrafluoroborate gave the best result.

Based on the above results, the reaction of several free carboxylic acids, including functionalized ones, with equimolar amounts of alcohols was carried out employing 2-bromo-1-ethylpyridinium tetrafluoroborate as the coupling reagent, and favorable results were obtained especially when the esterification was undertaken at room temperature (see Table 4).

In conclusion, it is noted that various carboxylic esters are conveniently prepared in good yields from equimolar amounts of free carboxylic acids and alcohols under mild conditions by the use of 2-chloro- or 2-bromo-1-methylpyridinium iodide or 2-bromo-1-ethylpyridinium tetrafluoroborate, as a coupling reagent, in the presence of tributylamine. The present method is also successfully applied to the carboxylic ester synthesis

Table 5. Physical data of products

Compound	IR $\nu_{C=O}$ (cm^{-1})	NMR (δ)	Elemental analysis (%)
$C_6H_5CH_2COC_2H_5$ (O)	1740	1.15(t, 3H), 3.45(s, 2H), 4.05(q, 2H), 7.20(s, 5H)	—
$C_6H_5CH_2COCH_2C_6H_5$ (O)	1740	3.50(s, 2H), 5.00(s, 2H), 7.15(s, 10H)	—
$C_6H_5CH_2COC(CH_3)_3$ (O)	1735	1.35(s, 9H), 3.40(s, 2H), 7.15(s, 5H)	Calcd for $C_{12}H_{16}O_2$: C, 74.97; H, 8.39. Found: C, 74.77; H, 8.57.
$C_6H_5CH_2COCH(CH_3)C_6H_5$ (O)	1740	1.40(d, 3H), 3.50(s, 2H), 5.85(q, 1H), 7.25(s, 10H)	Calcd for $C_{16}H_{16}O_2$: C, 79.97; H, 6.71. Found: C, 79.85; H, 6.65.
$C_6H_5CH_2COC_6H_5$ (O)	1740	3.45(s, 2H), 7.20(s, 5H), 7.25(s, 5H)	—
$C_6H_5CH_2COCH_2CH_2C_6H_5$ (O)	1740	2.75(t, 2H), 3.40(s, 2H), 4.15(t, 2H), 7.05(s, 5H), 7.15(s, 5H)	—
$CH_3COCH_2C_6H_5$ (O)	1745	1.95(s, 3H), 5.00(s, 2H), 7.25(s, 5H)	—
$CH_3COCH_2CH=CHC_6H_5$ (O)	1745	2.00(s, 3H), 4.65(d, 2H), 6.15(d-t, 1H), 6.60(d, 1H), 7.25(s, 5H)	—
$CH_3COCH_2CH_2C_6H_5$ (O)	1720	1.90(s, 3H), 2.85(t, 2H), 4.20(t, 2H), 7.20(s, 5H)	—
$C_6H_5CH_2CH_2COC_2H_5$ (O)	1735	1.10(t, 3H), 2.4—3.4(m, 4H), 4.05(q, 2H), 7.10(s, 5H)	—
$C_6H_5CH_2CH_2COC_6H_5$ (O)	1740	2.6—3.1(m, 4H), 6.8—7.4(m, 10H)	—
$CH_3CH_2COCH_2CH_2C_5H_5$ (O)	1740	1.05(t, 3H), 2.20(q, 2H), 2.90(t, 2H), 4.25(t, 2H), 7.10(s, 5H)	—
$CH_3CH_2COCH_2C_6H_5$ (O)	1735	1.10(t, 3H), 2.25(q, 2H), 5.00(s, 2H), 7.20(s, 5H)	—
$(CH)_3CCOCH_2C_6H_5$ (O)	1735	1.20(s, 9H), 5.05(s, 2H), 7.25(s, 5H)	Calcd for $C_{12}H_{16}O_2$: C, 74.97; H, 8.39. Found: C, 75.02; H, 8.53.
$(CH_3)_3CCOC(CH_3)_3$ (O)	1710	—	Calcd for $C_9H_{18}O_2$: C, 68.31; H, 11.47. Found: C, 68.45; H, 11.51.
$C_6H_5COCH_2C_6H_5$ (O)	1730	5.30(s, 2H), 7.1—7.5(m, 8H) 8.0—8.3(m, 2H)	—
$C_6H_5CH=CHCOC_2H_5$ (O)	1720	1.30(t, 3H), 4.20(q, 2H), 6.40(d, 1H), 7.40(s, 5H), 7.65(d, 1H),	Calcd for $C_9H_{18}O_2$: C, 74.97; H, 6.86. Found: C, 75.12; H, 7.08.
$C_6H_5CH=CHCOCH_2C_6H_5$ (O)	1720	5.15(s, 2H), 6.40(d, 1H), 7.25(s, 10H), 7.65(d, 1H)	—
$Cl_3CCOCH_2C_6H_5$ (O)	1760	5.30(s, 2H), 7.35(s, 5H)	Calcd for $C_8H_7O_2Cl_3$: C, 42.64; H, 2.79; Cl, 41.95. Found: C, 42.67; H, 2.72; Cl, 41.88.
$ClCH_2COCH_2C_6H_5$ (O)	1730	3.55(s, 2H), 5.20(s, 2H)	—
$ClCH_2COCH_2CH_2C_6H_5$ (O)	1730	2.50(t, 2H), 3.50(s, 2H) 3.90(t, 2H), 6.85(s, 5H)	—
$CH_3CH=CH-CH=CHCOCH_2C_6H_5$ (O)	1705	1.80(d, 3H), 5.10(s, 2H), 5.75(d, 1H), 6.05(m, 2H), 7.25(d-d, 1H), 7.25(s, 5H)	Calcd for $C_{13}H_{14}O_2$: C, 77.20; H, 6.98. Found: C, 77.00; H, 7.06.
$C_6H_5C\equiv CCOCH_2C_6H_5$ (O)	1700 2200 (C≡C)	5.15(s, 2H), 7.1—7.5(m, 10H)	Calcd for $C_{16}H_{12}O_2$: C, 81.34; H, 5.12. Found: C, 81.50; H, 5.41.

Table 5. (Countinued)

Compound	IR $\nu_{C=O}$, (cm^{-1})	NMR (δ)	Element analysis (%)
$C_6H_5CCH_2COCH_2C_6H_5$ (O O)	1760 1680	3.85(s, 4/3H), 5.05(s, 4/3H), 5.15(s, 2/3H), 5.65(s, 2/3H), 7.1—7.9(m, 10H)	Calcd for $C_{16}H_{14}O_3$: C, 75.57; H, 5.55. Found: C, 75.70; H, 5.41.
$CH_3CCH_2CH_2COCH_2C_6H_5$ (O O)	1700	2.00(s, 3H), 2.50(qusi s, 4H), 5.00(s, 2H), 7.25(s, 5H)	Calcd for $C_{12}H_{14}O_3$: C, 69.88; H, 6.84. Found: C, 69.62; H, 6.87.
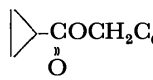	1780	0.8—1.1(m, 4H), 1.3—1.7(m, 1H), 5.00(s, 2H), 7.25(s, 5H)	Calcd for $C_{11}H_{12}O_2$: C, 74.97; H, 6.86. Found: C, 74.67; H, 6.88.
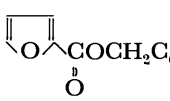	1700	5.20(s, 2H), 6.30(d-d, 1H), 7.05(d, 1H), 7.25(s, 5H), 7.45(d, 1H)	Calcd for $C_{12}H_{10}O_3$: C, 71.28; H, 4.99. Found: C, 71.12; H, 4.90.

starting from free carboxylic acids or alcohols having bulky alkyl group or having functional group sensitive toward acid or base.

Experimental

Spectra. Proton NMR were obtained on Hitachi R-24 spectrometer. Chemical shifts are reported on the δ scale relative to tetramethylsilane as an internal standard. Infrared spectra were taken using Hitachi EPI-G2 spectrophotometer. Products were identified by NMR and IR spectra and elemental analyses.

Materials. All solvents used here were distilled according to the general methods and were stored over molecular sieves or sodium metal as a drying agent. Carboxylic acids and alcohols were recrystallized or distilled before use.

2-Chloro-1-methylpyridinium Iodide. To a solution of 2-chloropyridine (10.0 g, 88 mmol) in acetone (3 ml) was added methyl iodide (15.0 g, 106 mmol) at 0 °C and the mixture was stirred for 3 days at room temperature. Precipitate appeared was filtered and washed with dry ether (50 ml). After drying under reduced pressure, 2-chloro-1-methylpyridinium iodide (18.0 g, 80%) was obtained and used for the esterification without recrystallization.

2-Bromo-1-ethylpyridinium Tetrafluoroborate. A solution of 2-bromopyridine (2.88 g, 18 mmol) was added to triethyloxonium tetrafluoroborate (4.00 g, 21 mmol) at room temperature under an argon atmosphere. The solution became clear in a few minutes and white precipitate appeared gradually. After the suspension was warmed at 50—60 °C for 1 h, the mixture was cooled with ice-water bath. The precipitate was filtered and washed with dry ether (15 ml). Drying under reduced pressure at room temperature gave 2-bromo-1-ethylpyridinium tetrafluoroborate (4.07 g, 83%) which was employed for condensation without recrystallization.

General Procedure for Carboxylic Ester Synthesis by the Use of 2-Chloro- or 2-Bromo-1-methylpyridinium Iodide. To a suspension of 2-chloro-1-methylpyridinium iodide (612 mg, 2.4 mmol) or 2-bromo-1-methylpyridinium iodide (720 mg, 2.4 mmol) in dichloromethane or toluene (2 ml) was added a solution of free carboxylic acid (2.0 mmol), alcohol (2.0 mmol), and tributylamine (888 mg, 4.8 mmol), in the solvent (2 ml) under an argon atmosphere and the mixture was stirred for 3 h under refluxing. The solution became clear in accordance to progress of the reaction. After evaporation of the solvent, the residue was separated by silica gel column chromatography to give carboxylic ester.

General Procedure Utilizing 2-Bromo-1-ethylpyridinium Tetrafluoroborate. To a solution of 2-bromo-1-ethylpyridinium tetrafluoroborate (329 mg, 1.2 mmol) in dichloromethane (2 ml) was added a mixture of free carboxylic acid (1.0 mmol), alcohol (1.0 mmol), and tributylamine (444 mg, 2.4 mmol) at room temperature under an argon atmosphere. After stirring overnight at room temperature, the solvent was evaporated and the residue was chromatographed on silica gel to give carboxylic ester. The NMR and IR spectra and elemental analysis data of products were listed in Table 5.

References

1) Present Address: Department of Applied Chemistry, Faculty of Engineering, Saitama University, Shimo-okubo, Urawa, Saitama, 338.

2) J. H. Brewster and C. J. Ciotti, Jr., *J. Am. Chem. Soc.*, **77**, 6214 (1955).

3) R. C. Parish and L. M. Stock, *Tetrahedron Lett.*, **1964**, 1258; *J. Org. Chem.*, **30**, 927 (1965).

4) Y. Kanaoka, O. Yonemitsu, K. Tanizawa, K. Matsuzaki, and Y. Ban, *Chem. Ind. (London)*, **1964**, 2102.

5) A. Buzas, C. Egnell, and P. Freon, *C. R. Acad. Sci.*, **256**, 1804 (1963); S. Neelakuntan, R. Padmasani, and T. R. Seshadri, *Tetrahedron*, **21**, 3531 (1965).

6) J. Bertin, H. B. Kagan, and J. J. Luche, *J. Am. Chem. Soc.*, **96**, 8113 (1974).

7) T. Mukaiyama, M. Usui, E. Shimada, and K. Saigo, *Chem. Lett.*, **1975**, 1045; T. Mukaiyama, H. Toda, and S. Kobayashi, *Chem. Lett.*, **1976**, 13.

Inositol Derivatives. 10. Isopropylidenation of 1,2-*O*-Cyclohexylidene-*myo*-inositol Derivatives and Preparation of Unaccessible Blocked Inositols

Seiichiro OGAWA, Shuichi OKI, Hideo KUNITOMO, and Tetsuo SUAMI

Department of Applied Chemistry, Faculty of Engineering, Keio University, Hiyoshi, Yokohama 223

(Received February 8, 1977)

Isopropylidenation of 1,2-*O*-cyclohexylidene-*myo*-inositol and its 3-*O*-tosyl- and 3-*O*-benzoyl derivatives with 2,2-dimethoxypropane in *N*,*N*-dimethylformamide in the presence of acid catalyst gave the corresponding 4,5- and 5,6-*O*-isopropylidene derivatives. Selective benzoylation of 1,2-*O*-cyclohexylidene-4,5-*O*-isopropylidene-*myo*-inositol with benzoyl chloride in pyridine gave mainly the 3-*O*-benzoate, whereas with benzoic anhydride the 6-*O*-benzoate. Several unaccessible blocked inositols were prepared by displacement reaction of the protected sulfonyl derivatives with sodium benzoate.

Partially blocked *myo*-inositol is a potential intermediate for the synthesis of various kinds of inositol derivatives. In continuation to the previous paper,[1] isopropylidenation of 1,2-*O*-cyclohexylidene-*myo*-inositol (**1a**),[2] and its 3-*O*-tosyl- and 3-*O*-benzoyl derivatives (**1b**[2] and **1c**[1]) has been studied. Preparation of several unaccessible protected derivatives of *allo*-, *chiro*-, and *muco*-inositols starting from the sulfonates obtained in this studies has also been carried out.

Isopropylidenation. Treatment of **1a** with 2,2-dimethoxypropane in *N*,*N*-dimethylformamide in the presence of *p*-toluenesulfonic acid gave the 4,5-*O*-isopropylidene derivative (**2a**) as crystals in 22% yield, which was further characterized as the ditosylate and diacetate (**2b** and **2c**). The remaining syrupy product consisted mainly of the 5,6-*O*-isopropylidene derivative (**3a**) was directly tosylated or benzoylated to give the crystalline ditosylate (**3b**) or dibenzoate (**3c**) in an isolated yield of 26 or 62% based on **1a**. Positions of the isopropylidene groups in **2a** and **3a** were established by converting **2b** and **3b** into the known 1,4- and 1,6-di-*O*-tosyl-*myo*-inositol,[2] respectively.

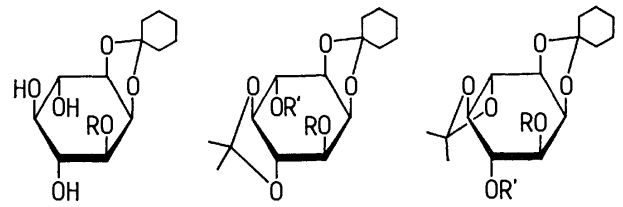

1a~c

a	R=H
b	R=Ts
c	R=Bz

2a~j

	R	R′
a	H	H
b	Ts	Ts
c	Ac	Ac
d	Ts	H
e	Ts	Ac
f	Bz	H
g	Bz	Ac
h	Bz	Me
i	Bz	Bz
j	H	Bz

3a~j

	R	R′
a	H	H
b	Ts	Ts
c	Bz	Bz
d	Ts	H
e	Ts	Ac
f	Bz	H
g	Bz	Ac
h	Bz	Me
i	Me	Bz
j	Me	H

Scheme 1.

Under the identical reaction conditions, 1,2-*O*-cyclohexylidene-3-*O*-tosyl-*myo*-inositol (**1b**) was acetonated to afford the crystalline 4,5- and 5,6-*O*-isopropylidene derivatives (**2d** and **3d**) in 18 and 19% yields, respectively. Their structures were determined by converting them into **2b** and **3b**, respectively.

Similarly, isopropylidenation of 1-*O*-benzoyl-2,3-*O*-cyclohexylidene-*myo*-inositol (**1c**) gave, upon separation by silica gel chromatography, the 5,6-*O*-isopropylidene derivative (**2f**, 20%) as crystals, and the 4,5-*O*-isopropylidene derivative (**3f**, 43%) as a syrup. The assigned structures were confirmed on the basis of the following evidences. Acetylation of **2f** and **3f** afforded the corresponding acetates (**2g** and **3g**). In the NMR spectrum of **2g**, the signals due to two protons which attached to the carbon atoms bearing the acyloxy functions were shown not to be coupled with each other. Methylation of **3f** with methyl iodide and silver oxide in *N*,*N*-dimethylformamide gave two crystalline methyl ethers (**3h** and **3i**) in 75 and 4% yields, respectively.[3] While, the methyl ether (**2h**) derived from **2f** was different from either **3h** or **3i**. On removal of the blocking groups followed by acetylation, **3h** and **3i** were transformed into the known 4-[4] and 1-*O*-methyl-*myo*-inositol pentaacetate,[5] respectively.

Selective Benzoylation and Tosylation. Treatment of **2a** with 1.5 molar equiv of tosyl chloride in pyridine at 0—5 °C for 2 days yielded **2d** almost exclusively in 57% yield. When **2a** was treated with 1.3 molar equiv of benzoyl chloride in pyridine at −5 °C for 1.5 h, **2f** and the dibenzoate (**2i**) were obtained in 33 and 28% yields, respectively. These results indicated that the C-3 hydroxyl group being adjacent to *cis*-arranged cyclohexylidene oxygen atom is more reactive than the less hindered C-6 hydroxyl group.[6]

On the other hand, selective benzoylation of **2a** with 1.3 molar equiv of benzoic anhydride in pyridine at room temperature for 5 days gave rise to the 6-*O*-benzoate (**2j**) in 52% yield, together with **2i** (12%) and a trace of **2f**. Accordingly, in contrast to the case of acid halide, steric factor seemed to play a role in selectivity of *O*-acylation with acid anhydride.

Preparation of Blocked Inositols. Unaccessible partially protected *chiro*-inositol derivatives were obtained by nucleophilic displacement reaction of the tosylates of **2a** with a benzoate ion. Thus, **2d** was treated with an excess of sodium benzoate in boiling *N*,*N*-dimethylformamide for 120 h to give 1-*O*-benzoyl-5,6-*O*-cyclohexylidene-2,3-*O*-isopropylidene-*chiro*-inositol (**4a**) in 52% yield. On de-*O*-benzoylation followed by mild acid treatment, **4a** was converted into 1,2-*O*-cylohexylidene-*chiro*-inositol (**5**) in 95% yield, whose structure was ascertained by conversion to *chiro*-inositol.[7]

Treatment of **2b** with sodium benzoate under the

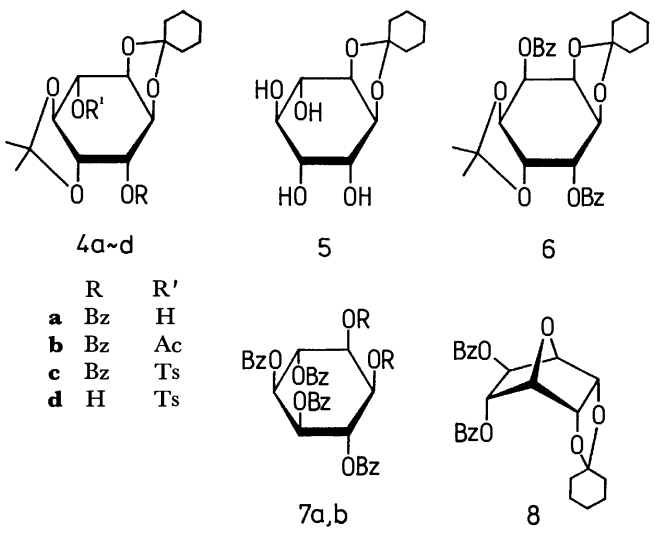

Scheme 2.

similar conditions for 50 h afforded 1-*O*-benzoyl-5,6-*O*-cyclohexylidene-2,3-*O*-isopropylidene-4-*O*-tosyl-*chiro*-inositol (**4c**) in 72% yield. When the reaction time was prolonged to 70 h, the tosyloxy group on C-6 was partially displaced with a benzoate ion giving 2,5-di-*O*-benzoyl-3,4-*O*-cyclohexylidene-1,6-*O*-isopropylidene-*allo*-inositol (**6**) in 10% yield, together with 31% yield of **4c**. The structure of **4c** was tentatively assigned by comparing the NMR spectrum with those of **4a** and its acetate (**4b**).

Additionally, the protected *muco*-inositol was prepared by the following reaction sequence. Reaction of **1b** with potassium carbonate in boiling 80% aqueous 2-methoxyethanol for 30 h followed by benzoylation gave 1,2,3,6-tetra-*O*-benzoyl-4,5-*O*-cyclohexylidene-*muco*-inositol (**7a**) in 51% yield, which was, upon de-*O*-cyclohexylidenation, converted into tetrabenzoyl-*muco*-inositol (**7b**) in 92% yield. The NMR spectrum of **7a** supported the assigned structure. Conversion of **7b** into *muco*-inositol[8] gave the final evidence.

A small amount of crystals (**8**, 1.3%) was isolated from the mother liquor from **7a** after a long storage. The elemental analysis and NMR spectrum suggested that **8** had an 1,4-anhydro ring. On lithium aluminum hydride reduction followed by benzoylation,[9] 1,4-anhydro-5,6-*O*-cyclohexylidene-3-*O*-tosyl-*chiro*-inositol[10] gave 1,4-anhydro-2,3-di-*O*-benzoyl-5,6-*O*-cyclohexylidene-*chiro*-inositol that was shown to be identical with **8**. Mechanistically, **7a** was formed by diaxial opening of the intemediate 3,4-epoxide with OH^- and **8** was obtained by the rear-side attack of the 6-hydroxyl group on C-3.

Experimental[11]

*Isopropylidenation of 1,2-O-Cyclohexylidene-*myo*-inositol (**1a**).* To a slurry of **1a** (20 g) in *N,N*-dimethylformamide (100 ml) was added 2,2-dimethoxypropane (30 ml) and *p*-toluenesulfonic acid (0.2 g), and the mixture was heated at 70—75 °C for 90 min. The cooled reaction mixture was treated with sodium hydrogencarbonate (5 g) and then evaporated to dryness. The crystalline residue was extracted with hot 2-butanone (3×50 ml) and the extracts were evaporated to give crystals that were recrystallized from 2-butanone–toluene to afford 1,2-*O*-cyclohexylidene-4,5-*O*-isopropylidene-*myo*-inositol (**2a**, 5.1 g, 22%) as needles: mp 180.5—181.5 °C.

Found: C, 60.12; H, 7.93%. Calcd for $C_{15}H_{24}O_6$: C, 59.98; H, 8.05%.

Compound **2a** (3 g) was treated with tosyl chloride (7.7 g) in pyridine (30 ml) at room temperature for 2 days. The reaction mixture was poured into ice–water and the resulting crystals were collected. Recrystallization from 2-butanone–toluene gave the ditosyl derivative (**2b**, 5.7 g, 93%): mp 192—195 °C; NMR ($CDCl_3$) δ 2.43 (s, 6, two tosyl CH_3), 3.35 (dd, 1, $J_{4,5}$=9 Hz, $J_{5,6}$=11 Hz, H-5), 4.01 (dd, 1, $J_{3,4}$=11 Hz, H-4), 4.12 (dd, 1, $J_{1,2}$=5 Hz, $J_{1,6}$=6.5 Hz, H-1), 4.41 (dd, 1, $J_{2,3}$=4 Hz, H-2), 4.80 (dd, 1, H-3), 5.38 (dd, 1, H-6).

Found: C, 57.37; H, 5.88; S, 10.47%. Calcd for $C_{29}H_{36}O_{10}S_2$: C, 57.22; H, 5.97; S, 10.53%.

Compound **2b** (0.1 g) was refluxed with 80% aqueous acetic acid (10 ml) for 2 h. After cooling, the resulting crystals were collected by filtration, washed with water, and dried to give 1,4-di-*O*-tosyl-*myo*-inositol (0.07 g, 89%): mp 199—200 °C. This compound was identified with an authentic sample[2] (mp 198—200 °C) by comparison with IR spectra.

Compound **2a** (0.2 g) was treated with acetic anhydride (5 ml) and pyridine (5 ml) at room temperature for 2 h. The mixture was poured into ice–water and the resulting crystals were collected by filtration. Recrystallization from ethanol gave the diacetyl derivative (**2c**, 0.24 g, 95%) as needles: mp 175.5—176.5 °C; NMR ($CDCl_3$)[12] δ 2.16 (s, 3) and 2.20 (s, 3) (OAc), 3.55 (dd, 1, $J_{4,5}$=11 Hz, $J_{5,6}$=9 Hz, H-5), 4.21 (dd, 1, $J_{2,3}$=5 Hz, $J_{3,4}$=6.5 Hz, H-3), 4.21 (dd, 1, $J_{1,6}$=11 Hz, H-6), 4.70 (t, 1, $J_{1,2}$=4.5 Hz, H-2), 5.20 (dd, 1, H-1), 5.38 (dd, 1, H-4).

Found: C, 59.60; H, 7.35%. Calcd for $C_{19}H_{28}O_8$: C, 59.36; H, 7.34%.

The mother liquor obtained from **2a** was concentrated and purified by passing through a short alumina column with 2-butanone as an eluent to give a syrupy product (*ca.* 16 g) consisting mainly of **3a**. A 6-g portion of the syrup was tosylated as described for **2a** to give 1,2-*O*-cyclohexylidene-5,6-*O*-isopropylidene-3,4-di-*O*-tosyl-*myo*-inositol (**3b**, 4.3 g, 25% yield based on **1a** used) as needles, after recrystallization from 2-butanone–toluene: mp 165—167 °C; NMR ($CDCl_3$) δ 2.47 (s, 6, two tosyl CH_3), 3.45 (dd, 1, $J_{4,5}$=8 Hz, $J_{5,6}$=10 Hz, H-5), 4.02 (dd, 1, $J_{1,6}$=7 Hz, H-6), 4.80 (t, 1, $J_{2,3}$=$J_{3,4}$=3 Hz, H-3), 4.99 (dd, 1, H-4).

Found: C, 57.12; H, 5.90; S, 10.92%. Calcd for $C_{29}H_{36}O_{10}S_2$: C, 57.22; H, 5.97; S, 10.53%.

Compound **3b** (50 mg) was treated with boiling 80% aqueous acetic acid followed by acetylation in the usual manner to give 1,6-di-*O*-tosyl-*myo*-inositol tetraacetate (40 mg, 84%) as crystals: mp 195—197 °C, which was identified with an authentic sample[2] (mp 196—197.5 °C) by comparison with IR spectra.

A 10-g portion of crude **3a** was treated with benzoyl chloride (30 ml) in pyridine (70 ml) at room temperature overnight. The reaction mixture was poured into ice–water and the resulting gum was extracted with chloroform (2×50 ml). The extracts were washed with aqueous sodium hydrogencarbonate and water, dried, and concentrated to leave a syrup, which was crystallized from toluene to give the dibenzoyl derivative (**3c**). Recrystallization from 2-butanone gave pure crystals (12.5 g, 62% yield besed on **1a** used): mp 199—202 °C.

Found: C, 68.43; H, 6.27%. Calcd for $C_{29}H_{32}O_8$: C, 68.49; H, 6.34%.

Isopropylidenation of 1,2-O-Cyclohexylidene-3-O-tosyl-myo-inositol (1b). To a solution of **1b**[2] (20 g) in *N,N*-dimethylformamide (100 ml) were added 2,2-dimethoxypropane (40 ml) and *p*-toluenesulfonic acid (0.2 g), and the mixture was heated at 90 °C for 15 min. After cooling, the reaction mixture was neutralized by treating with Amberlite IRA-410 (OH^-) and then concentrated to give a syrup that was crystallized from 2-butanone–toluene to give 1,2-*O*-cyclohexylidene-4,5-*O*-isopropylidene-3-*O*-tosyl-*myo*-inositol (**2d**, 4.3 g, 18%) as needles: mp 167—169 °C; NMR ($CDCl_3$) δ 2.46 (s, 3, tosyl C$\underline{H}_3$), 3.31 (dd, 1, $J_{4,5}$=10 Hz, $J_{5,6}$=10.5 Hz, H-5), 4.45 (t, 1, $J_{1,2}=J_{2,3}$=4.5 Hz, H-2), 4.89 (dd, 1, $J_{3,4}$=10 Hz, H-3).

Found: C, 58.41; H, 6.65; S, 7.19%. Calcd for $C_{22}H_{30}O_8S$: C, 58.13; H, 6.65; S, 7.05%.

Compound **2d** (0.2 g) was acetylated in the usual manner and the crude product was recrystallized from 2-butanone–methanol to give the acetyl derivative (**2e**, 0.2 g, 91%): mp 215—216 °C; NMR ($CDCl_3$) δ 2.14 (s, 3, OAc), 2.48 (s, 3, tosyl C$\underline{H}_3$), 3.40 (dd, 1, $J_{4,5}$=9 Hz, $J_{5,6}$=11 Hz, H-5), 4.12 (dd, 1, $J_{3,4}$=10.5 Hz, H-4), 4.13 (dd, 1, $J_{1,2}$=4.5 Hz, $J_{1,6}$=7 Hz, H-1), 4.46 (t, 1, $J_{2,3}$=4.5 Hz, H-2), 4.90 (dd, 1, H-3), 5.29 (dd, 1, H-6).

Found: C, 58.13; H, 6.46; S, 6.62%. Calcd for $C_{24}H_{32}O_9S$: C, 57.67; H, 6.46; S, 6.23%.

Treatment of **2d** (0.2 g) with tosyl chloride (0.25 g) in pyridine (2 ml) at room temperature for 2 days gave **2b** (0.21 g, 77%), mp 187—189 °C, after recrystallization from chloroform–ethanol, which was identified with the sample obtained before.

The mother liquor from **2d** was concentrated to leave a syrup that was crystallized from toluene giving 1,2-*O*-cyclohexylidene-5,6-*O*-isopropylidene-3-*O*-tosyl-*myo*-inositol (**3d**, 4.1 g, 19%) as crystals. It melted at 163—165 °C, solidified at 168—175 °C, and then remelted at 223—227 °C with decomposition; NMR ($CDCl_3$) δ 2.49 (s, 3, tosyl C$\underline{H}_3$), 3.43 (dd, 1, $J_{4,5}$=9 Hz, $J_{5,6}$=10 Hz, H-5), 4.71 (t, 1, $J_{2,3}=J_{3,4}$=*ca.* 4.5 Hz, H-3).

Found: C, 58.00; H, 6.61; S, 6.84%. Calcd for $C_{22}H_{30}O_8S$: C, 58.13; H, 6.65; S, 7.05%.

Compound **3d** (0.2 g) was acetylated to give, after crystallization from ethanol, the acetyl derivative (**3e**, 0.19 g, 91%) as crystals: mp 151—153 °C; NMR ($CDCl_3$) δ 2.04 (s, 3, OAc), 2.49 (s, 3, tosyl C$\underline{H}_3$), 3.52 (dd, 1, $J_{4,5}$=9 Hz, $J_{5,6}$ 10.5 Hz, H-5), 3.99 (dd, 1, $J_{1,6}$=7 Hz, H-6), 4.86 (dd, 1, $J_{2,3}$=4.5 Hz, $J_{3,4}$=5.5 Hz, H-3), 5.41 (dd, 1, H-4).

Found: C, 58.04; H, 6.51; S, 6.46%. Calcd for $C_{24}H_{32}O_9S$: C, 57.67; H, 6.46; S, 6.23%.

Tosylation of **3d** (0.2 g) in the usual manner gave **3b** (0.16 g, 52%), mp 165—167 °C, which was identical with the compound obtained before.

Isopropylidenation of 1-O-Benzoyl-2,3-O-cyclohexylidene-myo-inositol (1c). To a solution of **1c** (6 g) in *N,N*-dimethylformamide (60 ml) were added 2,2-dimethoxypropane (12 ml) and *p*-toluenesulfonic acid (0.06 g), and the mixture was heated for 5 min at 90 °C. After cooling, the reaction mixture was neutralized with 5% aqueous potassium carbonate and then poured into ice–water(300 ml). The resulting white powder was collected by filtration and dried over phosphorus pentaoxide *in vacuo* giving a gum (*ca.* 6 g). A 4-g portion of this product was chromatographed on silica gel (135 g) with 2-butanone–toluene (1 : 6, v/v) as an eluent. Two fractions were separated according to the results of TLC. The first fractions gave 1-*O*-benzoyl-2,3-*O*-cyclohexylidene-4,5-*O*-isopropylidene-*myo*-inositol (**3f**, 1.9 g, 43%) as a homogeneous syrup. The second fractions gave a syrup (0.9 g) that was crystallized from ethanol to give 1-*O*-benzoyl-2,3-*O*-cyclohexylidene-5,6-*O*-isopropylidene-*myo*-inositol (**2f**, 0.6 g, 13%) as needles: mp 172.5—173 °C; NMR ($CDCl_3$), **2f**: δ 3.57 (dd, 1, $J_{4,5}$=8.5 Hz, $J_{5,6}$=9.5 Hz, H-5), 4.76 (t, 1, $J_{1,2}=J_{2,3}$=4.5 Hz, H-2), 5.41 (dd, 1, $J_{1,6}$=10 Hz, H-3); **3f**: δ 3.57 (dd, 1, $J_{4,5}$=10 Hz, $J_{5,6}$=8.5 Hz, H-5), 4.10 (dd, $J_{1,2}$=4 Hz, $J_{2,3}$=7 Hz, H-3), 5.31 (t, 1, $J_{1,6}$=4 Hz, H-1).

Found for **2f**: C, 65.58; H, 6.89%. Calcd for $C_{22}H_{28}O_7$: C, 65.32; H, 6.99%.

Compound **2f** (0.1 g) was acetylated in the usual manner to give, after crystallization from chloroform–ethanol, the acetyl derivative (**2g**, 0.09 g, 77%): mp 219 °C (sublimation); NMR ($CDCl_3$) δ 2.15 (s, 3, OAc), 3.59 (dd, 1, $J_{4,5}$=11 Hz, $J_{5,6}$=9.5 Hz, H-5), 4.23 (dd, 1, $J_{2,3}$=4.5 Hz, $J_{3,4}$=7 Hz, H-3), 4.34(dd, 1, $J_{1,6}$=10 Hz, H-6), 4.75 (t, 1, $J_{1,2}$=4.5 Hz, H-2), 5.38 (dd, 1, H-4), 5.43 (dd, 1, H-1).

Found: C, 64.40; H, 6.67%. Calcd for $C_{24}H_{30}O_8$: C, 64.55; H, 6.79%.

Compound **3f** (0.1 g) gave the acetyl derivative (**3g**, 0.1 g, 98%) as a homogeneous syrup; NMR ($CDCl_3$) δ 2.10 (s, 3, OAc), 3.71 (dd, 1, $J_{4,5}$=10 Hz, $J_{5,6}$=8.5 Hz, H-5), 4.07 (t, 1, $J_{2,3}=J_{3,4}$=7 Hz, H-3).

Methylation of 3f. To a solution of **3f** (1.9 g) in *N,N*-dimethylformamide (19 ml) were added silver oxide (2.8 g) and methyl iodide (2.8 ml), and the mixture was stirred at room temperature for 24 h under dark. An insoluble matter was filtered off and the filtrate was evaporated to dryness. The residue was extracted with hot ethyl acetate and the extract was passed through a short alumina column. The solution was evaporated and crystallized from ethanol to give the 6-*O*-methyl derivative (**3h**, 1.5 g, 75%) as prisms: mp 129—131 °C; NMR ($CDCl_3$) δ 3.58 (s, 3, OC$\underline{H}_3$).

Found: C, 66.33; H, 7.10%. Calcd for $C_{23}H_{30}O_7$: C, 66.00; H, 7.24%.

The mother liquor from **3h** afforded, after long storage in a refrigerator, crystals that were recrystallized from ethanol to give 4-*O*-benzoyl-1,2-*O*-cyclohexylidene-5,6-*O*-isopropylidene-3-*O*-methyl-*myo*-inositol (**3i**, 0.07 g, 4%) as needles: mp 150.5—151.5 °C; NMR ($CDCl_3$) δ 3.58 (s, 3, OC$\underline{H}_3$), 3.71 (dd, 1, $J_{4,5}$=7.5 Hz, $J_{5,6}$=8.5 Hz, H-5), 5.43 (dd, $J_{3,4}$=2.5 Hz, H-4).

Found: C, 66.16; H, 7.31%. Calcd for $C_{23}H_{30}O_7$: C, 66.00; H, 7.24%.

1-O-Benzoyl-2,3-O-cyclohexylidene-5,6-O-isopropylidene-4-O-methyl-myo-inositol (2h). Methylation of **2f** (0.45 g) with silver oxide (0.45 g) and methyl iodide (0.45 g) in *N,N*-dimethylformamide (5 ml) gave, after crystallization from ethanol, **2h** (0.33 g, 70%) as needles: mp 128—129.5 °C; NMR ($CDCl_3$) δ 3.61 (s, 3, OC$\underline{H}_3$), 4.76 (t 1, $J_{1,2}=J_{2,3}$=4.5 Hz, H-2), 5.37 (dd, 1, $J_{1,6}$=11 Hz, H-1).

Found: C, 66.20; H, 7.33%. Calcd for $C_{23}H_{30}O_7$: C, 66.00; H, 7.24%.

1,2-O-Cyclohexylidene-5,6-O-isopropylidene-3-O-methyl-myo-inositol (3j). To a solution of **3i** (0.19 g) in methanol (5 ml) was added 0.1 M methanolic sodium methoxide (0.1 ml) and the mixture was allowed to stand at room temperature overnight. After having been neutralized with Amberlite IR-120 (H^+), the solution was evaporated and the crystalline residue was recrystallized from ethanol to give **3j** (0.12 g, 86%): mp 169—171 °C.

Found: C, 61.27; H, 8.14%. Calcd for $C_{16}H_{26}O_6$; C, 61.12; H, 8.35%.

Compound **3j** (0.21 g) was hydrolyzed with boiling 80% aqueous acetic acid (10 ml) for 2 h. The reaction mixture was evaporated and the product was crystallized from ethanol to give 1-*O*-methyl-*myo*-inositol (DL-bornesitol) (0.09 g, 71%)

as crystals: mp 197—198 °C (lit,[13] 198—200 °C). Acetylation gave the pentaacetyl derivative: mp 152—154 °C (lit,[4] 154—154.5 °C).

1-O-Acetyl-2,3-O-cyclohexylidene-4,5-O-isopropylidene-6-O-methyl-myo-*inositol (**3k**).* De-*O*-benzoylation of **3h** (5 g) with methanolic sodium methoxide in methanol (100 ml) gave a syrupy product, which was, without furhter purification, acetylated in the usual manner to give, after crystallization from ethanol, **3k** (3.7 g, 89%): mp 140.5—141.5 °C.

Found: C, 60.88; H, 7.75%. Calcd for $C_{18}H_{28}O_7$: C, 60.65; H, 7.93%.

Compound **3k** (0.2 g) was hydrolyzed with boiling 80% aqueous acetic acid (10 ml) and acetylated to give pentaacetyl-4-*O*-methyl-*myo*-inositol (-DL-ononitol) (0.21 g, 84%): mp 131—132 °C (lit,[5] 134—135 °C).

*Selective Tosylation of **2a**.* To a solution of **2a** (10 g) in dry pyridine (100 ml) was added tosyl chloride (9.5 g, 1.5 molar equiv) at −5 °C under stirring, and then the mixture was allowed to stand in a refrigerator for 2 days. The mixture was poured into ice-water and the precipitates were collected by filtration. The crude product (10.5 g) was recrystallized from toluene to give **2d** (8.6 g, 57%) as practically pure crystals: mp 154—155 °C.

*Selective Benzoylation of **2a**.* *a)* To a solution of **2a** (0.5 g) in dry pyridine (5 ml) was added benzoyl chloride (0.25 ml, 1.3 molar equiv) at −5 °C under stirring. After having been stood at room temperature for 1.5 h, the mixture was poured into ice-water to give 0.5 g of crude products. TLC indicated the presence of two components. Fractional crystallization from 2-butanone gave **2f** (0.22 g, 33%) and the dibenzoyl derivative (**2i**, 0.24 g, 28%): mp 230 °C; NMR ($CDCl_3$) δ 5.77 (dd, 1, $J_{4,5}$=11 Hz, $J_{5,6}$=9 Hz, H-5), 4.44 (dd, 1, $J_{2,3}$=4.5 Hz, $J_{3,4}$=6 Hz, H-3), 4.45 (dd, 1, $J_{1,6}$=10 Hz, H-6), 4.85 (t, 1, $J_{1,2}$=4.5 Hz, H-2), 5.51 (dd, 1, H-1), 5.69 (dd, 1, H-4).

Found: C, 68.56; H, 6.43%. Calcd for $C_{29}H_{32}O_8$; C, 68.49; H, 6.34%.

b) To a solution of **2a** (3 g) in dry pyridine (30 ml) was added benzoic anhydride (2.9 g, 1.3 molar equiv) and the mixture was allowed to stand at room temperature for 5 days. TLC indicated one major and one minor spots. The reaction mixture was poured into ice-water and the resulting crystals were recrystallized from 2-butanone to give **2i** (0.6 g, 12%). The mother liquor from **2i** was concentrated and crystallized from toluene to give 6-*O*-benzoyl-1,2-*O*-cyclohexylidene-4,5-*O*-isopropylidene-*myo*-inositol (**2j**, 2.1 g, 52%) as needles: mp 169—174 °C. Recrystallized sample melted at 177—178 °C: NMR ($CDCl_3$) δ 5.63 (dd, 1, $J_{1,6}$=6 Hz, $J_{5,6}$=11 Hz, H-6).

Found: C, 65.47; H, 7.00%. Calcd for $C_{22}H_{28}O_7$: C, 65.32; H, 6.99%.

The presence of a trace of **2f** was detected in crude **2j** by the NMR spectrum.

1-O-Benzoyl-5,6-O-cyclohexylidene-2,3-O-isopropylidene-chiro-*inositol (**4a**).* A mixture of **2d** (4 g) and sodium benzoate (3.8 g, 3 molar equiv) in *N,N*-dimethylformamide (100 ml) was refluxed for 120 h. After cooling, ethyl acetate (80 ml) was added to the reaction mixture and an insoluble matter was removed by filtration. The filtrate was evaporated to dryness and the residue was extracted with hot ethyl acetate (3×50 ml). The extracts were filtered through a short column of alumina and evaporated to give a syrup, which was crystallized from ethanol to give **4a** (1.8 g, 52%) as crystals: mp 176.5—177 °C.

Found: C, 65.46; H, 6.96%. Calcd for $C_{22}H_{28}O_7$: C, 65.32; H, 6.99%.

Compound **4a** (0.2 g) was acetylated in the usual manner to give, after crystallization from ethanol, the acetyl derivative (**4b**, 0.19 g, 86%) as needles: mp 166.5—167 °C; NMR ($CDCl_3$) δ 2.19 (s, 3, OAc), 5.42 (dd, 1, J=5.5 Hz, J=11 Hz, H-3), 6.07 (t, 1, J=1.5 Hz, H-6).

Found: C, 64.28; H, 6.67%. Calcd for $C_{24}H_{30}O_8$: C, 64.55; H, 6.79%.

1,2-O-Cyclohexylidene-chiro-*inositol (**5**).* Compound **4a** (3 g) was dissolved in a mixture of chloroform (60 ml) and ethanol (15 ml), and *p*-toluenesulfonic acid (0.3 g) was added at 0 °C. The mixture was allowed to stand in a refrigerator overnight. Then the mixture was diluted with methanol (60 ml) and 1 M methanolic sodium methoxide (12 ml) was added. After having been stood at room temperature, the resulting crystals were collected to give **5** (1.8 g, 95%): mp 181—183 °C. Recrystallization from ethanol–water gave pure prisms: mp 182—183 °C.

Found: C, 55.64; H, 7.73%. Calcd for $C_{12}H_{20}O_6$: C, 55.36; H, 7.76%.

Hydrolysis of **5** (0.05 g) with boiling 6 M hydrochloric acid (10 ml) for 1 h gave *chiro*-inositol (0.03 g, 81%) as crystals: mp 227—235 °C. Recrystallization from ethanol–water gave a pure sample: mp 245—247 °C (lit,[7] 253 °C).

1-O-Benzoyl-5,6-O-cyclohexylidene-2,3-O-isopropylidene-4-O-tosyl-chiro-*inositol (**4c**).* *a)* A mixture of **2b** (2.5 g) and sodium benzoate (2 g) in *N,N*-dimethylformamide (50 ml) was refluxed for 50 h. The reaction mixture was cooled to room temperature and diluted with 2-butanone (30 ml). An insoluble matter was removed by filtration and the filtrate was filtrated through a short alumina column. Evaporation gave a syrup that was crystallized from methanol to give **4c** (1.7 g, 72%): mp 141.5—144.5 °C. Recrystallization from 2-butanone–methanol gave pure product (1.4 g, 63%): mp 165.5—167 °C; NMR ($CDCl_3$) δ 2.43 (s, 3, tosyl CH_3), 4.70—5.00 (m, 1, H-4), 5.94 (broad d, 1, J=*ca.* 2 Hz, H-1).

Found: C, 62.57; H, 6.19; S, 5.92%. Calcd for $C_{29}H_{34}O_9S$: C, 62.34; H, 6.14; S, 5.74%.

b) A mixture of **2b** (2 g) and sodium benzoate (2 g) in *N,N*-dimethylformamide (70 ml) was refluxed for 70 h. The mixture was processed as described above to give crystalline mixtures. Fractional crystallization from ethanol–ethyl acetate gave **4c** (0.55 g, 31%): mp 162—165 °C, and 2,6-di-*O*-benzoyl-3,4-*O*-cyclohexylidene-1,6-*O*-isopropylidene-*allo*-inositol (**6**, 0.16 g, 10%): mp 210—212 °C; NMR ($CDCl_3$) δ 4.26 (dd, 1, J=10.5 Hz, J=2.5 Hz), 4.70 (dd, 1, J=3 Hz, J=10.5 Hz), 5.95—6.20 (m, 2, H-2 and H-5).

Found: C, 68.47; H, 6.44%. Calcd for $C_{29}H_{32}O_8$: C, 68.49; H, 6.34%.

1,2-O-Cyclohexylidene-4,5-O-isopropylidene-3-O-tosyl-chiro-*inositol (**4d**).* A solution of **4c** (2 g) in 2-butanone (20 ml) was treated with catalytic amount of methanolic sodium methoxide for 40 min at room temperature. The reaction mixture was neutralized with acetic acid and evaporated to give a white solid, which was chromatographed on silica gel (70 g) with 2-butanone–toluene (1 : 4, v/v). The major fractions were collected and crystallized from 2-butanone–toluene to give **4d** (0.5 g, 31%): mp 134—136 °C.

Found: C, 57.97; H, 6.58; S, 7.10%. Calcd for $C_{22}H_{30}O_8S$: C, 58.13; H, 6.65; S, 7.05%.

1,2,3,6-Tetra-O-benzoyl-4,5-O-cyclohexylidene-muco-*inositol (**7a**) and 1,4-Anhydro-2,3-di-O-benzoyl-5,6-O-cyclohexylidene*-chiro-*inositol (**8**).* A mixture of **1b** (10 g), anhydrous potassium carbonate (10 g) and 80% aqueous 2-methoxyethanol (200 ml) was refluxed for 3.5 h, and then evaporated to dryness. After the residue was dried by codistillation with dry toluene, it was treated with benzoyl chloride (23 ml) in pyridine (60 ml) under ice cooling. After overnight at room temperature, the reaction mixture was poured into ice-water (300 ml) and the resulting gum was extracted with chloro-

form (100 ml). The extract was washed successively with 1M hydrochloric acid, 5% aqueous sodium carbonate, and water, dried, and evaporated to give a syrup that was crystallized from chloroform–ethanol giving a mixture of **7a** and **8**. Fractional crystallization from the same solvents gave **7a** (8.3 g, 51%): mp 177—179 °C; NMR ($CDCl_3$) δ 4.58 (broad d, 2, J=4 Hz, H-4 and H-5), 5.86 (broad d, 2, J=6 Hz, H-1 and H-2), 6.14 (broad dd, 2, H-3 and H-6).

Found: C, 71.26; H, 5.39%. Calcd for $C_{40}H_{36}O_{10}$: C, 70.99; H, 5.36%.

From the mother liquor of **7a**, a small amount of **8** (0.14 g, 1.3%) was obtained as hair like needles: mp 155—157 °C; NMR ($CDCl_3$) δ 4.6—5.2 (m, 4, H-1, H-4, H-5, and H-6), 5.37 (broad t, 1, $J_{2,3}$=3.5 Hz, $J_{3,4}$=4.5 Hz, $J_{3,5}$=*ca.* 1 Hz, H-3), 6.05 (d, 1, H-2).

Found: C, 69.55; H, 5.90%. Calcd for $C_{26}H_{26}O_7$: C, 69.32; H, 5.82%.

1,2,3,6-Tetra-O-*benzoyl*-muco-*inositol (**7b**)*. A mixture of **7a** (6 g) and 80% aqueous acetic acid (50 ml) was refluxed for 1 h. After cooling, the resulting crystals were collected by filtration to give **7b** (4.9 g, 92%): mp 252—254 °C. An analytical sample melted at 256—257 °C after recrystallization from pyridine-ethanol.

Found: C, 68.24; H, 4.90%. Calcd for $C_{34}H_{28}O_{10}$: C, 68.47; H, 4.73%.

A solution of **7b** (0.5 g) in 2-methoxyethanol (10 ml) was treated with 1 M methanolic sodium methoxide (0.5 ml) at 90 °C for 10 min. The reaction mixture was diluted with water and treated with Amberlite IRA-120 (H^+) and then evaporated to give a crystalline residue that was pulverized with ethanol and collected to give crude *muco*-inositol (0.15 g, 98%): mp 190—220 °C. Recrystallization from water–ethanol gave a pure sample (0.13 g): mp 285—290 °C (lit,[8] 281—290 °C).

The authors wish to thank Mr. Toru Fukata, Mr. Shukichi Muto, and Mr. Keiji Iwata for assistance in preparative experiments.

References

1) T. Suami, S. Ogawa, K. Ohashi, and S. Oki, *Bull. Chem. Soc. Jpn.*, **45**, 3660 (1972).

2) T. Suami, S. Ogawa, T. Tanaka, and T. Otake, *Bull. Chem. Soc. Jpn.*, **44**, 835 (1971).

3) These results were reasonably accounted for by base-catalyzed acyl group migration often encountered in methylation under the conditions employed in this studies. See, for example, S. J. Angyal and G. J. H. Melrose, *J. Chem. Soc.*, **1965**, 6501 and the references cited therein.

4) S. J. Angyal, P. T. Gilham, and C. G. Macdonald, *J. Chem. Soc.*, **1957**, 1417.

5) M. Nakajima, N. Kurihara, and T. Ogino, *Chem. Ber.*, **96**, 619 (1963).

6) A. H. Haines, *Adv. Carbohydr. Chem. Biochem.*, **33**, 12 (1976).

7) M. Nakajima, I. Tomida, N. Kurihara, and S. Takei, *Chem. Ber.*, **92**, 173 (1959).

8) G. Dangshat and H. O. L. Fischer, *Naturwissenschaften*, **27**, 756 (1939).

9) S. Ogawa, Y. Funaki, and T. Suami, unpublished result.

10) T. Suami, S. Ogawa, S. Oki, and K. Ohashi, *Bull. Chem. Soc. Jpn.*, **45**, 2597 (1972).

11) Melting points were determined in a capillary in a liquid bath and are uncorrected. Solutions were evaporated under diminished pressure at 40—50 °C. NMR spectra were measured at 60 MHz on a Varian A-60D spectrometer in deuteriochloroform ($CDCl_3$) with reference to tetramethylsilane as an internal standard and the peak positions are give in δ-values. Values given for coupling constants are of first-order. TLC was performed on silica gel (Wako gel B-10, Wako Pure Chemical Industries, Ltd.) using a mixture of 2-butanone and toluene as an eluent. Elemental analyses were performed by Mr. Saburo Nakada, to whom our thanks are due.

In this paper, all the compounds except for meso compounds are racemic. All the formulas depict one enantiomer of the respective racemates.

12) Compound **2c** is named 1,4-di-*O*-acetyl-2,3-*O*-cyclohexylidene-5,6-*O*-isopropylidene-*myo*-inositol.

13) E. G. Griffin and J. M. Nelson, *J. Am. Chem. Soc.*, **37**, 1552 (1915).

Proton NMR Spectra and Conformations of *N*-Alkyl-*N*-benzyl- and *N*-Alkyl-*N*-(α-chlorobenzyl)carbamoyl Chlorides

Kinko KOYANO, Hiroshi SUZUKI, and Colin R. MCARTHUR*

Department of Chemistry, College of General Education, The University of Tokyo, Komaba, Meguro-ku, Tokyo 153

**Department of Chemistry, York University, 4700 Keele Street, Toronto, Ontario, Canada*

(Received February 12, 1977)

Rotational isomerization about the amide C–N bond of twelve *N*-alkyl-*N*-benzylcarbamoyl chlorides (C_6H_5-CHX-NR-COCl, **1**: X=H, **2**: X=Cl; R=CH_3, C_2H_5, *n*- and *i*-C_3H_7, *n*- and *t*-C_4H_9) was studied by proton NMR spectroscopy. The values of ΔG^* for the isomerization are 15.8—17.3 kcal/mol for compounds **1** and 13.3—15.9 kcal/mol for compounds **2**. Another kind of slow rotation was observed about the benzyl–nitrogen bond of **1**(R=*t*-C_4H_9) and the α-chlorobenzyl–nitrogen bond of **2**(R=CH_3) at low temperature. The chiral centers of compounds **2** produce large nonequivalences for the geminal protons of the 2-methylene group of **2**(R=*n*-C_3H_7) as well as **2**(R=*n*-C_4H_9) and for the geminal methyl protons of **2**(R=*i*-C_3H_7), reflecting some conformational preference of these compounds.

It is well established that the structure of amides can be represented by the hybrid structure I.

I

Extensive studies by NMR spectroscopy, which have been reviewed,[1,2] substantiate the assignment of a partial double bond character to the C–N bond of the amide group. This double bond character, as pointed out by Stewart and Siddall,[1] leads to the following consequences: A comparatively large barrier to the rotation about the C–N bond of the amide group, which can result in nonequivalent signals for the protons in R^1 and the corresponding ones in R^2 even if $R^1=R^2$; and subsidiary hindered rotations about other bonds as a consequence of a rigid, approximately planar framework of the amide group.

In the case of carbamoyl chlorides (I, R^3=Cl), kinetic studies of their amide C–N bond rotations have been reported, especially on dimethylcarbamoyl chloride[3-6] and also on some other derivatives.[7]

The present study examines the NMR spectra of a series of six *N*-alkyl-*N*-benzylcarbamoyl chlorides [**1**; $C_6H_5CH_2$–NR–COCl, R=CH_3 (**1-a**), C_2H_5 (**1-b**), *n*-C_3H_7 (**1-c**), *i*-C_3H_7 (**1-d**), *n*-C_4H_9 (**1-e**), *t*-C_4H_9 (**1-f**)] and of a series of six correspondingly *N*-alkylated (α-chlorobenzyl)carbamoyl chlorides (**2**; C_6H_5CHCl–NR–COCl). First, results of a kinetic study of the amide C–N bond rotations are presented. Secondly, evidence is presented that the restricted rotations about the amide C–N bond gives rise to another slow rotations about the benzyl–nitrogen bond of **1-f** and also the α-chlorobenzyl–nitrogen bond of **2-a** on NMR time scale as the temperature is lowered further. Thirdly, preference of rotational conformations about single bonds of compounds **2** is discussed in view of the nonequivalences of the 2-methylene geminal protons of **2-c** and the geminal methyl groups of **2-d**.

Experimental

The proton NMR spectra were recorded on a JEOL JNM-MH100 spectrometer operating at 100 MHz in the frequency-sweep and internal TMS-locked mode, using Iwasaki-Tsushin UC-80033 universal counter, for *ca.* 5% (w/v) degassed solution in $CDCl_3$ or in hexachloro-1,3-butadiene at various temperatures. Temperatures were calibrated with the hydroxyl shifts of methanol below room temperature and of 1,3-propanediol above room temperature.

The IR spectra were taken with a Japan Spectroscopic Co., Ltd. JASCO DS-403 grating infrared spectrometer.

N-Alkyl-N-benzylcarbamoyl Chlorides. To a stirred solution of 75 ml of a 12.5% solution of phosgene in benzene (0.15 mol of phosgene), maintained in an ice bath, was added, dropwise, a benzene solution (50 ml) of the appropriate *N*-alkylbenzylamine (0.07 mol). The reaction mixture was stirred at room temperature for an hour, and then filtered to remove amine hydrochloride. Benzene was removed from the solution by distillation to afford crude carbamoyl chloride.

*N-Methyl-N-benzylcarbamoyl Chloride (**1-a**)*:[8] Yield 57.5%; bp 81 °C (6×10^{-3} Torr);[9] mp 23 °C (recrystd from diethyl ether); IR (Nujol): $\nu_{C=O}$ 1751 cm^{-1}.

*N-Ethyl-N-benzylcarbamoyl Chloride (**1-b**)*: Yield 32.7%; bp 84—85 °C (3×10^{-4} Torr); mp 21 °C (recrystd from diethyl ether); IR (Nujol): $\nu_{C=O}$ 1747 cm^{-1}. Found: C, 60.71; H, 5.84; Cl, 18.07; N, 6.98%. Calcd for $C_{10}H_{12}ClNO$: C, 60.76; H, 6.12; Cl, 17.94; N, 7.09%.

*N-Propyl-N-benzylcarbamoyl Chloride (**1-c**)*: Yield 35.7%; bp 83 °C (2×10^{-4} Torr); IR (Nujol): $\nu_{C=O}$ 1747 cm^{-1}. Found: C, 61.97; H, 6.48; Cl, 17.01; N, 6.68%. Calcd for $C_{11}H_{14}ClNO$: C, 62.41; H, 6.67; Cl, 16.75; N, 6.62%.

*N-Isopropyl-N-benzylcarbamoyl Chloride (**1-d**)*: Yield 38%; bp 92 °C (2×10^{-4} Torr); IR (Nujol): $\nu_{C=O}$ 1742 cm^{-1}. Found: C, 62.13; H, 6.55; Cl, 16.48; N, 6.61%. Calcd for $C_{11}H_{14}ClNO$: C, 62.41; H, 6.67; Cl, 16.75; N, 6.62%.

*N-Butyl-N-benzylcarbamoyl Chloride (**1-e**)*: Yield 40%; bp 100 °C (2×10^{-4} Torr); IR (Nujol); $\nu_{C=O}$ 1745 cm^{-1}. Found: C, 64.08; H, 7.16; Cl, 16.01; N, 6.42%. Calcd for $C_{12}H_{16}ClNO$: C, 63.85; H, 7.15; Cl, 15.71; N, 6.21%.

*N-t-Butyl-N-benzylcarbamoyl Chloride (**1-f**)*:[10] Yield 47.1%; mp 86—87 °C (recrystd from heptane); IR (Nujol): $\nu_{C=O}$ 1753 cm^{-1}.

N-Alkyl-N-(α-chlorobenzyl)carbamoyl Chlorides. By a procedure similar to that described for *N*-methyl-*N*-(α-chlorobenzyl)carbamoyl chloride (**2-a**),[11] the appropriate *N*-alkylbenzylideneamine was treated with phosgene to give the corresponding *N*-alkyl-*N*-(α-chlorobenzyl)carbamoyl chloride.

*N-Ethyl-N-(α-chlorobenzyl)carbamoyl Chloride (**2-b**)*: Yield 74.4%; bp 96—98 °C (3×10^{-3} Torr); IR (Nujol): $\nu_{C=O}$ 1749 cm^{-1}. Found: C, 51.77; H, 4.94; Cl, 30.51; N, 6.12%. Calcd for $C_{10}H_{11}Cl_2NO$: C, 51.75; H, 4.78; Cl, 30.55; N,

6.04%.

N-*Propyl*-N-*(α-chlorobenzyl)carbamoyl Chloride (2-c)*: Yield 56.9%; bp 99 °C (3×10^{-3} Torr); IR (Nujol): $\nu_{C=O}$ 1747 cm^{-1}. Found: C, 53.74; H, 5.50; Cl, 28.71; N, 5.66%. Calcd for $C_{11}H_{13}Cl_2NO$: C, 53.68; H, 5.32; Cl, 28.81; N, 5.69%.

N-*Isopropyl*-N-*(α-chlorobenzyl)carbamoyl Chloride (2-d)*: Yield 89%, mp 49—51 °C (recrystd from diethyl ether); IR (Nujol): $\nu_{C=O}$ 1758 cm^{-1}. Found: C, 53.47; H, 5.45; Cl, 28.60; N, 5.54%. Calcd for $C_{11}H_{13}Cl_2NO$: C, 53.68; H, 5.32; Cl, 28.81; N, 5.69%.

N-*Butyl*-N-*(α-chlorobenzyl)carbamoyl Chloride (2-e)*: Yield 51.9%; bp 118 °C (4×10^{-4} Torr); IR (Nujol): $\nu_{C=O}$ 1745 cm^{-1}. Found: C, 55.58; H, 5.92; Cl, 27.11; N, 5.44%. Calcd for $C_{12}H_{15}Cl_2NO$: C, 55.39; H, 5.81; Cl, 27.25; N, 5.38%.

N-t-*Butyl*-N-*(α-chlorobenzyl)carbamoyl Chloride (2-f)*: A sealed tube containing 22.5 g (0.14 mol) of freshly distd *N-t*-butylbenzylideneamine and 150 g of a 12.5% soultion of phosgene in benzene (0.3 mol of phosgene) was heated at about 50 °C for three days. The white precipitate produced (*N-t*-butylbenzylideneamine hydrochloride) was removed by filtration. Removal of benzene from the solution by distillation afforded 30.7 g (84.1% yield) of crude **2-f**; mp 44.5—46.5 °C (recrystd from heptane), dec above 100 °C;[12] IR (Nujol): $\nu_{C=O}$ 1760 cm^{-1}. Found: C, 55.37; H, 5.60; Cl, 27.10; N, 5.27%. Calcd for $C_{12}H_{15}Cl_2NO$: C, 55.39; H, 5.81; Cl, 27.25; N, 5.38%.

Results and Discussion

N-*Alkyl*-N-*benzylcarbamoyl Chlorides (Series 1)*.

Chemical shifts (δ, ppm) of the *N*-alkyl-*N*-benzylcarbamoyl chlorides (**1-a**, **1-b**, **1-c**, **1-d**, **1-e**, and **1-f**) at room temperature are listed in Table 1.

Rotational Isomerism about the Amide C–N Bond: The presence of a pair of singlet signals with unequal intensities for the benzyl α protons of **1-a**, **1-b**, **1-c**, and **1-e** and also a pair of singlet signals for the methyl protons of **1-a** can be interpreted in terms of rotational isomerism between conformers represented as A and B resulting from slow rotation about the amide C–N bond.[1,2]

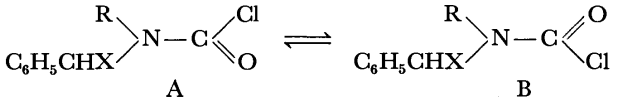

A ⇌ B

X=H (Series **1**); X=Cl (Series **2**)

Isbrandt and Rogers[3c] showed, by the use of a europium shift reagent, that, of the two signals for dimethylcarbamoyl chloride, the lower-field resonance is assignable to the protons of the methyl group that is cis to the chlorine atom. By analogy, the benzyl α proton signals of the present carbamoyl chlorides at δ=4.6—4.9 ppm (the lower-field signals) can be assigned to those of conformer B, while those at δ=4.5—4.6 ppm (the higher-field signals) can be assigned to the benzylic protons of conformer A.

The fractional populations, P_A and P_B, for each pair of these conformers, together with their coalescence temperatures, are shown in Table 2. From these data, the free energies of activation for the rotational conversion from A to B (ΔG^*_A) and the reverse (ΔG^*_B) were calculated. The results are also included in Table 2.

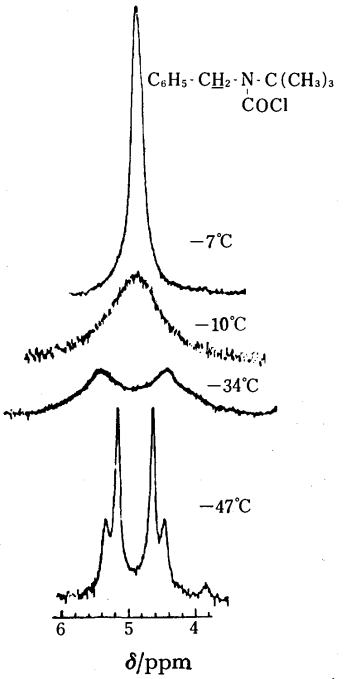

Fig. 1. The temperature dependence of the NMR spectrum of the benzyl protons of *N-t*-butyl-*N*-benzylcarbamoyl chloride, **1-f**, in $CDCl_3$.

For those compounds in which the *N*-alkyl substituent, R, is primary (**1-a**, **1-b**, **1-c**, and **1-e**), conformer A is more stable than conformer B. In those cases in which R is secondary (**1-d**) or tertiary (**1-f**), the reverse occurs. The order of relative populations of conformer A (P_A) is **1-a**≈**1-b**>**1-c**≈**1-e**>**1-d**≫**1-f**. That is, the sterically larger alkyl groups exibit a preference for sites which are further from the chlorine atom (cis to the oxygen atom). For the *N*-methyl derivative (**1-a**), the free energies of activation, ΔG^*_A and ΔG^*_B, are 17.3 and 17.1 kcal/mol, respectively, which are comparable with the value (17 kcal/mol) reported for dimethylcarbamoyl chloride.[3a,3b,4,5,6] With increasing bulkiness of the *N*-alkyl group, the free energy of activation for such rotations decreases. This trend is the same as observed with *N,N*-dialkylamides.[14]

Nonequivalence of the Benzyl α Protons of 1-f: The geminal protons at the benzyl α position of **1-f**, which exists in conformation B exclusively (*cf.* Table 2), resonate nonequivalently at temperatures below −34 °C (AB quartet, ν_{AB}=72.3 Hz, J_{AB}=19.0 Hz), as shown in Fig. 1. Although the benzyl α protons of some *N*-alkyl-*N-t*-butylbenzylamines are nonequivalent because of slow rates of nitrogen inversion,[15] such explanation is unlikely in the present case. The rationale for this conclusion is based on a comparison of the infrared spectrum of **1-f** with that of its α-chlorobenzyl analogue (**2-f**). The carbonyl absorptions are indicative of as much double bond character of the amide C–N bond of **1-f** ($\nu_{C=O}$=1753 cm^{-1}) as that of **2-f** ($\nu_{C=O}$=1760 cm^{-1}). Such double bond character of the amide C–N bond in **2-f** is established by NMR data, which indicates that **2-f** exists in two conformations as a results of restricted rotation about this bond (see the following section). Therefore, the hybridization state of the nitrogen atom of **1-f** is probably sp^2 or nearly so.

Table 1. Proton NMR chemical shifts of *N*-alkyl-*N*-benzylcarbamoyl chlorides at room temperature

Compound[a]		δ/ppm for protons[b]						
		$C_6H_5CH_2$-		H[1]		H[2]	H[3]	H[4]
	R	A	B	A	B			
1-a	CH_3	4.553	4.702	3.050	2.985			
1-b	C_2H_5	4.555	4.671	3.410		1.148		
1-c	*n*-C_3H_7	4.561	4.680	3.314		1.561	0.871	
1-d	*i*-C_3H_7	4.639		4.204		1.172		
1-e	*n*-C_4H_9	4.570	4.688	3.350		1.591	1.331	0.890
1-f	*t*-C_4H_9		4.865			1.430		

a) $C_6H_5CH_2$-NR-COCl. b) Numbering of alkyl protons: *n*-C_3H_7=-CH^1_2-CH^2_2-CH^3_3, *i*-C_3H_7=-CH^1-$(CH^2_3)_2$, *t*-C_4H_9=-$C(CH^2_3)_3$.

Table 2. Chemical shift, population, coalescence temperature and free energy of activation for interconversion of conformers A and B of *N*-alkyl-*N*-benzylcarbamoyl chlorides

Compound[a]		Proton[b]					T_c	ΔG^*_A	ΔG^*_B[c]
	R	observed	δ_A	δ_B	P_A	P_B	°C	kcal/mol	
1-a	CH_3	$\underline{CH_3}$	3.080	3.015	0.567	0.433	47.0	17.3	17.1
		$C_6H_5\underline{CH_2}$	4.596	4.730	0.570	0.430	54.5	17.3	17.1
1-b	C_2H_5	$C_6H_5\underline{CH_2}$	4.568	4.704	0.532	0.468	45.0	16.6	16.5
1-c	*n*-C_3H_7	$C_6H_5\underline{CH_2}$	4.573	4.704	0.524	0.476	47.5	16.8	16.7
1-d	*i*-C_3H_7	$C_6H_5\underline{CH_2}$	4.545	4.661	0.312	0.688	30.5	15.8	16.5
1-e	*n*-C_4H_9	$C_6H_5\underline{CH_2}$	4.580	4.711	0.524	0.476	47.5	16.8	16.7
1-f	*t*-C_4H_9	$C_6H_5\underline{CH_2}$		4.874	0	1			

a) $C_6H_5CH_2$-NR-COCl. b) The protons whose resonances are observed are indicated by underlines. c) Free energy of activation at the coalescence temperature. Throughout this paper 1 cal_{th}=4.184 J. The equations used to calculate the free energies of activation are as follows. $1/\tau=1/\tau_A+1/\tau_B$, when τ_A and τ_B are the lifetimes of species A and B, respectively. Case 1) $P_A=P_B$, $1/2\tau=(\pi/\sqrt{2})\cdot\Delta\nu$, $\Delta G^*=RT_c\ln(2\tau kT_c/h)$. Case 2)[13] $P_A\neq P_B$, $X=2\pi\Delta\nu\tau$, $P_A-P_B=\Delta P=\{(X^2-2)/3\}^{3/2}\cdot 1/X$, $\Delta G^*_A=RT_c\ln\{2\tau kT_c/h(1-\Delta P)\}$, $\Delta G^*_B=RT_c\ln\{2\tau kT_c/h(1+\Delta P\}$.

Table 3. Proton NMR chemical shifts of *N*-alkyl-*N*-(α-chlorobenzyl)carbamoyl chlorides at room temperature

Compound[a]		δ/ppm for protons[b]				
	R	H[1]	H[2]	H[(2)]	H[3]	H[4]
2-a	CH_3	2.940				
2-b	C_2H_5	3.376	0.970			
2-c	*n*-C_3H_7	3.231	1.591 1.165		0.684	
2-d	*i*-C_3H_7	3.663	1.465	1.006		
2-e	*n*-C_4H_9	3.255	1.58 1.06		1.059	0.741
2-f	*t*-C_4H_9		1.515			

a) C_6H_5CHCl-NR-COCl. b) Numbering of alkyl protons: *n*-C_3H_7=-CH^1_2-CH^2_2-CH^3_3, *i*-C_3H_7=-$CH^1(CH^2_3)CH^{(2)}_3$, *t*-C_4H_9=-$C(CH^2_3)_3$.

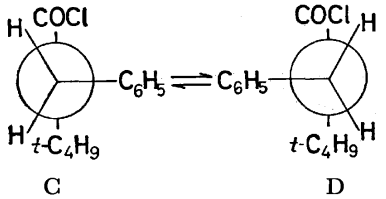

C D

Fig. 2. The Newman projection formulas for staggered conformations of *N*-*t*-butyl-*N*-benzylcarbamoyl chloride, **1-f**, with respect to the rotation about the benzyl–nitrogen bond.

The nonequivalence of the benzyl α protons of **1-f** at temperatures below −34 °C can be explained in terms of the molecular asymmetry produced by slow rotation about the benzyl–nitrogen bond, the rotational barriers of which result from the rigidity of the amide plane and the bulkiness of the *t*-butyl group. The most stable conformations are probably staggered conformations C and D in Fig. 2. When the interconversion is slow, the asymmetric field will be brought about on the benzyl α geminal protons. The mean barrier height between C and D was calculated to be 11.4

TABLE 4. CHEMICAL SHIFT, POPULATION, COALESCENCE TEMPERATURE AND FREE ENERGY OF ACTIVATION FOR INTERCONVERSION OF CONFORMERS A AND B OF *N*-ALKYL-*N*-(α-CHLOROBENZYL)CARBAMOYL CHLORIDES

Compound[a]	R[b]	δ_A	δ_B	P_A	P_B	T_c °C	ΔG^*_A kcal/mol	ΔG^*_B[d] kcal/mol
2-a	$\underline{CH}_3$	2.931	2.831	0.645	0.355	24.5	15.9	15.6
2-b	$\underline{CH}_2CH_3$	3.426	3.325	0.539	0.461	16.0	15.2	15.2
2-c	$\underline{CH}_2C_2H_5$	3.270	3.190	0.5	0.5	6—7	14.7	14.7
2-d	$\underline{CH}(CH_3)_2$	3.654				7—9[c]		
2-e	$\underline{CH}_2C_3H_7$	3.329	3.248	0.5	0.5	14.3	15.2	15.2
2-f	$C(\underline{CH}_3)_3$	1.670	1.400	0.386	0.614	9.0	13.3	13.5

a) C_6H_5CHCl-NR-COCl. b) The protons whose resonances are observed are indicated by underlines. c) The multiplet blurred in the temperature range, and it could not be analyzed at lower temperature. d) Free energies of activation at the coalescence temperature, calculated by the use of the equations in Table 2. note c).

kcal/mol from the values of T_c, $\Delta\nu_{AB}$, and J_{AB}.[16]

Kiefer[17] reported that the geminal protons of the chloromethyl group of *N*-*t*-butyl-*N*-(chloromethyl)carbamoyl chloride are nonequivalent. This can be interpreted in terms of slow rotation about the chloromethyl–nitrogen bond, in view of the present conclusion on the case of **1-f**.

N-Alkyl-N-(α-chlorobenzyl)carbamoyl Chlorides (Series 2). The chemical shifts (δ, ppm) of **2-a**, **2-b**, **2-c**, **2-d**, **2-e**, and **2-f** at room temperature are given in Table 3. The signals of the benzyl α proton were not detectable, hidden by the signals of the aromatic protons.

Rotational Isomerism about the Amide C–N Bond: Calculations pertaining to equilibrium A⇌B were made from the signals of the methyl protons of **2-a** and **2-f**, and of the 1-methylene protons, H^1, of **2-b**, **2-c**, and **2-e**. In these compounds, as in the compounds of series **1**, the protons of the alkyl groups which are cis to the chlorine atom of the chloroformyl group (conformer A) are assumed to resonate at lower-field regions than those which are trans to the chlorine atom (conformer B). Calculated fractional populations (P_A, P_B) and free energies of activation (ΔG^*_A and ΔG^*_B) are shown in Table 4.

The *N*-methyl derivative (**2-a**) prefers conformation A, while the *N*-*t*-butyl derivative (**2-f**) prefers conformation B, which is consistent with that found for **1-a** and **1-f**. The values of P_A/P_B for **2-a**, **2-b**, and **2-f**, which were relatively precisely estimated, are greater than the values for the corresponding compounds of series **1**, **1-a**, **1-b**, and **1-f**, respectively. The free energies of activation for rotation about the C–N bond of the compounds of series **2** are smaller than the corresponding compounds of series **1**. These facts are attributed to the increase in repulsive interactions of the benzyl group with the chloroformyl group, especially its chlorine atom, in stable conformations A and B, by introduction of the α-Cl substituent. The free energies of activation are lowest for **2-f**. This is probably due to destabilization of conformations A and B by steric repulsion of the chloroformyl group with the bulky *t*-butyl group in addition to that with the α-chlorobenzyl group.

The δ value of the signal of the *t*-butyl protons of **2-f** in conformation B is 1.40 ppm, while that in conformation A is 1.67 ppm. Since the δ value of the signal of the *t*-butyl protons of **1-f** is 1.43 ppm, the aforementioned assignment of B to the most preferred conformation of **1-f** is consistent.

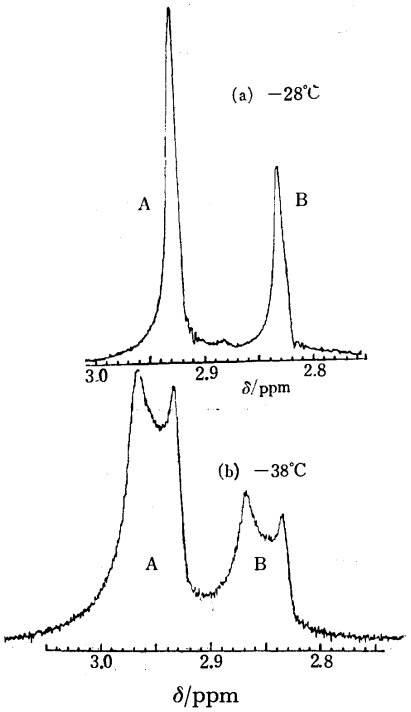

Fig. 3. NMR spectra of the methyl protons of *N*-methyl-*N*-(α-chlorobenzyl)carbamoyl chloride, **2-a**, (a) at −28 °C and, (b) −38 °C.

Rotational Isomerism about the α-Chlorobenzyl–Nitrogen Bond of 2-a: **2-a** shows two kinds of spectral change at low temperatures. The first one is due to the conformational interconversion A⇌B with the signal coalescence temperature at 24.5 °C. The second one is the splitting of each of the methyl signals for conformations A and B into two signals, shown in Fig. 3. The latter spectral change is ascribed to freezing of the interconversion of two relatively stable conformations about the α-chlorobenzyl–nitrogen bond. The values of ΔG^* for this conversion is estimated at about 10 kcal/mol. This comparatively large restriction to the conversion is probably caused by rigidity of the amide plane.

In light of a result of calculation of van der Waals energy by Allinger's modification[18a,b] of Hill's method[19] a qualitative potential energy curve for the rotation about the α-chlorobenzyl–nitrogen bond of **2-a** is

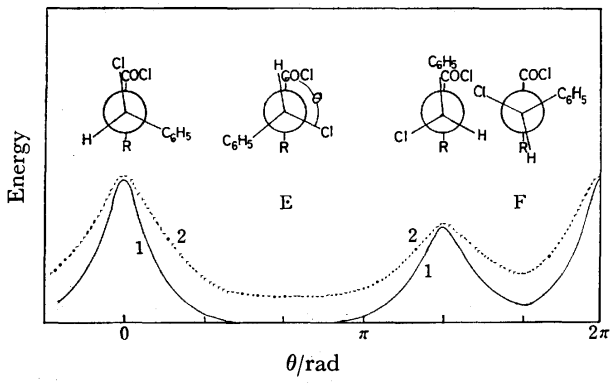

Fig. 4. Schematic potential-energy diagram for the rotation about the benzyl–nitrogen bond of *N*-alkyl-*N*-(α-chlorobenzyl)carbamoyl chlorides. θ represents the dihedral angle between the chlorine–carbon bond of the α-chlorobenzyl group and the chloroformyl–nitrogen bond. Curve 1——: **2-a**; curve 2……: **2-c**.

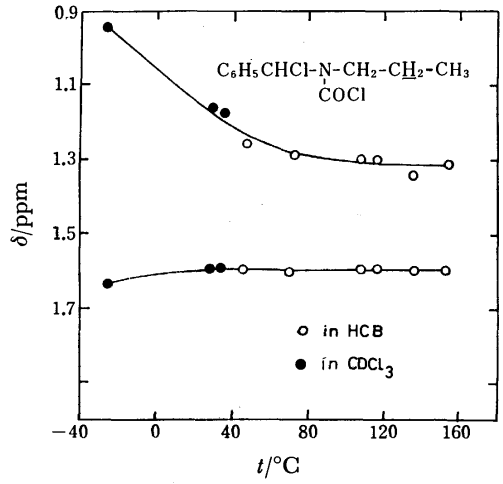

Fig. 5. Temperature-dependence of nonequivalent chemical shifts (from TMS) of the 2-methylene geminal protons of *N*-propyl-*N*-(α-chlorobenzyl)carbamoyl chloride, **2-c**. ●: in $CDCl_3$; ○: in hexachlorobutadiene.

depicted with a solid line (curve 1) in Fig. 4, which shows two stable conformations, E and F, intervened by potential energy barriers at $\theta=0$ and $4\pi/3$ rad. θ is the dihedral angle between the chlorine–carbon bond of the α-chlorobenzyl group and the chloroformyl–nitrogen bond. Of the two peaks of each of the methyl signals for A and B in Fig. 3(b), the more intense one at lower field is assigned to the more stable conformation, E, and the weaker one at higher field to the less stable conformation, F. In conformation E, the phenyl group and the chlorine atom of the α-chlorobenzyl group are close to the methyl group, and hence, must exert a downfield effect on it.

Nonequivalence of the 2-Methylene Protons of ***2-c*** *and* ***2-e***: As is seen in Table 3, even above the coalescence temperature for the interconversion of conformations A and B, the geminal protons of the 2-methylene group, H^2, of **2-c** as well as those of **2-e**, give rise to two signals of equal intensity, that is, are nonequivalent, although the geminal protons of the other methylene groups appear

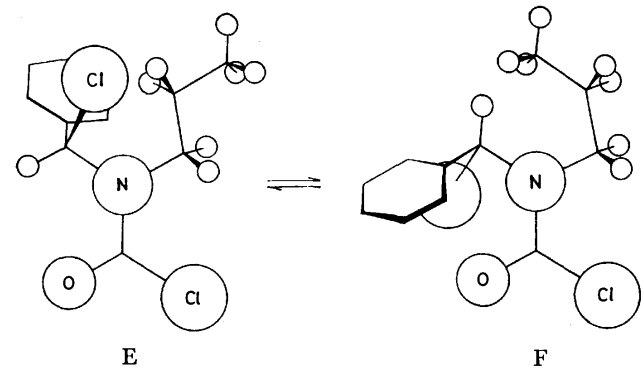

Fig. 6. Molecular model representation for a conversion between conformations E and F of *N*-propyl-*N*-(α-chlorobenzyl)carbamoyl chloride, **2-c**: rotation about the α-chlorobenzyl–nitrogen bond.

as equivalent. It is evident that these nonequivalences are originated from the chirality of the configuration about the α-carbon atom of the α-chlorobenzyl group.

These nonequivalences decrease with rising temperature. In the case of **2-c**, the difference in chemical shift between the two signals is about 80 Hz at −30 °C, and decreases to 40 Hz at 80 °C, as shown in Fig. 5. In spite of the shift, the splitting patterns of the nonequivalent signals do not essentially change. This fact indicates that rotation about any bond other than the amide C–N bond is not frozen even at the lowest temperature measured (−30 °C).

The shift may be elucidated by the change in population of the conformers about the α-chlorobenzyl–nitrogen bond, as follows. The potential energy curve of **2-c** as well as **2-e** about this bond may be similar to that of **2-a**, as a whole, but may be somewhat shallower, as shown with a dotted line (curve 2) in Fig. 4. In the more stable conformation E, the alkyl group is in close proximity of the phenyl group and the chlorine atom, both of which have large magnetic anisotropies and must impart large asymmetric field gradient to the 2-methylene protons. The terminal methyl or ethyl group of the alkyl group of the molecule in conformation E forces the protons of the 2-methylene group to face the chiral center, as a result of avoiding its repulsive interaction with the α-chlorobenzyl group (Fig. 6). When the molecule is in conformation F, the field gradient experienced by the same protons should be small because of the long distance from the chiral center. Therefore, increasing contribution of conformation F with rising temperature reduces the nonequivalence of the 2-methylene protons.

Nonequivalence of the Geminal Methyl Groups of ***2-d***: The protons of the geminal methyl groups, H^2 and $H^{(2)}$, of **2-d** are also nonequivalent. Raising temperature causes a decrease in the separation of the signals accompanied by a gradual movement to higher fields, as shown in Fig. 7. This nonequivalence is not caused by the conformational interconversion A⇌B. The difference in chemical shift of H^1 between conformations A and B is not so large to permit the analysis of multiplets. As to the chemical shift of the methyl groups, there is no difference between conformations A and B of **2-d**, while the corresponding chemical shifts of **2-f**

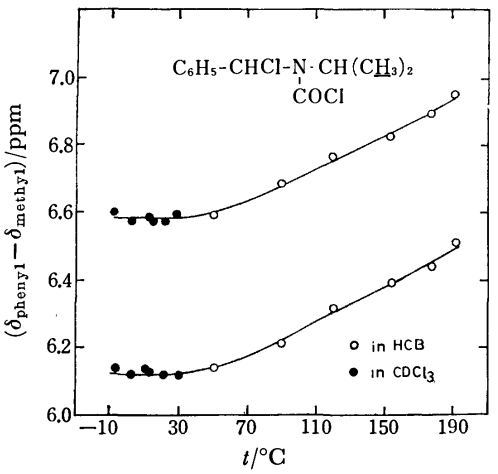

Fig. 7. Temperature-dependence of nonequivalent chemical shifts, $(\delta_{phenyl}-\delta_{methyl})$/ppm, of the geminal methyl protons of *N*-isopropyl-*N*-(α-chlorobenzyl)-carbamoyl chloride, **2-d**. ●: in $CDCl_3$; ○: in hexachlorobutadiene.

are separated 0.27 ppm from each other. This implies that both methyl groups of the isopropyl group can be apart from the chloroformyl group, while, at least, one of the methyl groups of the *t*-butyl group must be in close proximity to the chloroformyl group. The preferable conformation of **2-d** may resemble conformation E of **2-c** shown in Fig. 6. In this conformation, the nonequivalence of the two methyl signals may be largest, because one of the methyl groups approaches the chlorine atom, receiving a downfield effect from it, and the other methyl group comes just above the plane of the phenyl ring, receiving an upfield effect from it.

In the present cases, nonequivalent protons is three bonds removed from the chiral center. In a study of the NMR spectra of a series of compounds, $C_6H_5CH(CH_3)CH(CH_3)_2$, $C_6H_5CH(CH_3)O(CH_2)_nCH(CH_3)_2$ (n=0,1,2) and $C_6H_5CH(CH_3)O(CH_2)_2O(CH_2)_nCH(CH_3)_2$($n$=0,1), Whitesides *et al.*[20] have found that the nonequivalence of the geminal methyl protons does not decrease monotonically as the number of bonds separating the chiral center from the geminal methyl groups increases, and that it is unexpectedly large when these methyl groups are five bonds removed from the chiral center. The difference may originate from a greater flexibility of an ether molecule compared with the present carbamoyl chloride molecules, which bear a rigid amide plane and bulky phenyl and chlorine substituents.

References

1) a) W. E. Stewart and T. H. Siddall, III, *Chem. Rev.*, **70**, 517 (1970); b) T. H. Siddall, III and W. E. Stewart, "Progress in Nuclear Magnetic Resonance Spectroscopy," Vol. 5, ed by J. W. Emsley, J. Feeney, and L. H. Sutcliffe, Pergamon Press, New York (1969), Chap. 2, and the references cited therein.

2) M. B. Robin, F. A. Bovey, and H. Basch, "The Chemistry of Amides," ed by J. Zabicky, Interscince Publishers, New York (1970), Chap. 1.

3) a) M. T. Rogers and J. C. Woodbrey, *J. Phys. Chem.*, **66**, 540 (1962); b) J. C. Woodbrey and M. T. Rogers, *J. Am. Chem. Soc.*, **84**, 13 (1962). c) L. R. Isbrandt and M. T. Rogers, *J. Chem. Soc., Chem. Commun.*, **1971**, 1378.

4) R. C. Neuman, Jr., D. N. Roark, and V. Jonas, *J. Am. Chem. Soc.*, **89**, 3412 (1967).

5) A. Allerhand and H. S. Gutowsky, *J. Chem. Phys.*, **41**, 2115 (1964).

6) K. C. Ramey, D. J. Louick, P. W. Whitehurst, and W. B. Wise, *Org. Magn. Reson.*, **3**, 201 (1971).

7) B. U. Schlottmann, *Tetrahedron Lett.*, **1971**, 1221.

8) a) R. M. Harts and M. A. Whitehead, *Can. J. Chem.*, **49**, 2508 (1971); b) T. Saegusa, T. Tsuda, and Y. Iseyama, *J. Org. Chem.*, **36**, 858 (1971); c) A. Takamizawa, I. Makino, and S. Yonezawa, *Chem. Pharm. Bull.*, **22**, 286 (1974).

9) 1 Torr≈133.322 Pa.

10) J. N. Tilley and A. A. R. Sayigh, *J. Org. Chem.*, **28**, 2076 (1963). mp 85—89 °C.

11) K. Koyano and C. R. McArthur, *Can. J. Chem.*, **51**, 333 (1973).

12) A. Botta, P. Heitkaemper, and H. Krimm, Ger. Patent 2146069 (1973); *Chem. Abstr.*, **78**, 146882w (1973); bp 107—110 °C (0.1 Torr).

13) H. Shanan-Atidi and K. H. Bar-Eli, *J. Phys. Chem.*, **74**, 967 (1970).

14) R. M. Hammaker and B. A. Gugler, *J. Mol. Spectrosc.*, **17**, 356 (1965).

15) C. H. Bushweller, W. G. Anderson, P. E. Stevenson, D. L. Burkey, and J. W. O'Neil, *J. Am. Chem. Soc.*, **96**, 3892 (1974).

16) The calculation was made by the use of the following equations.
$1/2\tau=(\pi/\sqrt{2})\cdot(\Delta\nu_{AB}^2+6J_{AB}^2)^{1/2}$, at T_c.
$\Delta G^*=RT_c\ln(2\tau kT_c/h)$.

17) H. Kiefer, *Synthesis*, **1**, 39 (1972).

18) a) N. L. Allinger and L. A. Freiberg, *J. Am. Chem. Soc.*, **84**, 2201 (1962); b) E. L. Eliel, N. L. Allinger, S. J. Angyal, and G. A. Morrison, "Conformational Analysis," Interscience Publishers, New York (1965), Chap. 7, pp. 449—460.

19) T. L. Hill, *J. Chem. Phys.*, **16**, 399 (1948).

20) G. M. Whitesides, D. Holtz, and J. D. Roberts, *J. Am. Chem. Soc.*, **86**, 2628 (1964).

The σ-Bonded Palladium(II) Complex of 2-Pyridylferrocene

Akira KASAHARA, Taeko IZUMI, and Mitsugi MAEMURA

Department of Applied Chemistry, Faculty of Engineering, Yamagata University, Yonezawa 992

(Received February 22, 1977)

2-Pyridylferrocene reacts with lithium tetrachloropalladate(II) in the presence of sodium acetate to give an *ortho*-palladated binuclear complex (**4**). The σ-bonded structure of **4** was confirmed by studies of the IR and NMR spectra and of the reactions of **4** with thallium(I) acetylacetonate and lithium aluminum deuteride. The reactions of **4** with carbon monoxide, butyllithium, and bromine were also examined.

Following the first report of the intramolecular *ortho*-palladation of azobenzene and *N,N*-dimethylbenzylamine[1] there has been considerable interest in the intramolecular *ortho*-metalation of nitrogen, phosphorus, and sulfur donor ligands by transition metals.[2] With reference to the *ortho*-metalation, Alper[3] reported the first example of the intramolecular *ortho*-palladation of a metallocene by the reaction of thiopivaloylferrocene with sodium tetrachloropalladate(II); Gaunt and Shaw[4] also described the intramolecular *ortho*-palladation of (dimethylaminomethyl)ferrocene. One might, therefore, expect that 2-pyridylferrocene (**1**) would undergo palladation very readily, since it is well known that a ring in ferrocene is much more susceptible to electrophilic attack than a benzene ring.[5] In this report, we wish to report on the intramolecular *ortho*-palladation of **1** and the reaction of the metalation product with various reagents.

Results and Discussion

The treatment of **1** in methanol or dioxane with lithium tetrachloropalladate(II) gave dichlorobis(2-pyridylferrocene)palladium(II) (**2**) containing the unpalladated ligand. The **2** structure was consistent with the results of the elemental analysis and the IR spectrum of the compound. Rosenblum and Howells[6] have previously suggested that the IR spectra may serve to define the structures of homoannularly-disubstituted ferrocene derivatives; the 1,2-isomer possesses one band near 917 cm^{-1}. Compound **2** exhibited no absorption near 917 cm^{-1}. Furthermore, the reaction of **2** with triphenylphosphine in a ligand-replacement reaction gave a quantitative yield of dichlorobis(triphenylphosphine)-palladium(II) (**3**), as identified by comparison with an authentic sample.

On the other hand, when mole equivalents of lithium tetrachloropalladate(II), **1**, and sodium acetate trihydrate were stirred together in methanol, a new complex (**4**) was obtained. On the basis of the microanalytical and spectroscopic data, the molecular weight, and the reactions, **4** was shown to be an intramolecularly *ortho*-palladated complex. It has previously been shown that the acetate ion promoted an internal metalation reaction.[7] The **4** complex shows reactions typical of a chlorine-bridged binuclear complex of palladium; the reactions with thallium(I) acetylacetonate and triphenylphosphine produce the monomeric acetylacetonate (**5**) and triphenylphosphine (**6**) derivatives respectively. The IR spectra of the ferrocene derivatives prepared in this study are recorded in Table 1. Compounds **4**, **5**, and **6** exhibited absorptions near 1100, 1000, and 910 cm^{-1} characteristic of homoannularly 1,2-disubstituted ferrocene derivatives.[6] In addition, in the far-infrared spectrum of **4** there are three bands, assigned to bridged Pd–Cl stretching absorptions at 317, 296, and 255 cm^{-1}. Presumably the band at 296 cm^{-1} is due to a solid-state effect. The lithium aluminum hydride reduction of **4** gave **1**, whose mass spectrum was identical with that of an authentic sample. On the other hand, the lithium aluminum deuteride reduction of **4** gave 1-(2-pyridyl)ferrocene-2-d_1 (**7**). The position of the deuterium and, therefore, the site of the carbon-to-palladium σ-bond were established by a comparison of the NMR spectrum of **7** with that of the undeuterated **1**. The above evidence established that a σ-bond has been formed between the palladium and the ferrocene moiety.

Recently, the reactions of *ortho*-palladation products from numerous α-arylnitrogen derivatives with carbon monoxide,[8,9] chlorine,[10] and alkyllithium or a Grignard reagent[11,12] have been reported. The carbonylation of *ortho*-palladation products of azobenzene, Schiff bases, and tertiary benzylamines usually gives a variety of heterocyclic compounds.[8,9] The attempted carbonylation of the **4** complex in ethanol was unsuccessful, even at 100 °C; however, the triphenylphosphine derivative, **6**, in ethanol was readily carbonylated at 100 °C to produce an uncyclized ester, 2-ethoxycarbonyl-1-(2-pyridyl)ferrocene (**8**), in a 37% yield. The **6** complex was also smoothly brominated in chloroform at room temperature, forming 2-bromo-1-(2-pyridyl)ferrocene (**9**) in a 35% yield. Furthermore, the treatment of **6** with

Table 1. The IR absorption frequencies (cm^{-1}) of 2-pyridylferrocene derivatives

Compound	1100—1000 rule	917 rule	Other bands
1	1102, 1002	absent	
2	1104, 1000	absent	344, 336 (terminal Pd-Cl)
4	1100, 1003	910	332, 296, 255 (bridged Pd-Cl)
5	1100, 1009	921, 910	1580, 1550 (Acac group), 1200 (H-C bending of Acac group)
6	1102, 1000	920, 903	315 (terminal Pd-Cl)
7	1105, 1000	absent	
8	1102, 1000	918	1703 (ester group)
9	1100, 1004	920	
10	1105, 1000	915	
11	1100, 1002	908	

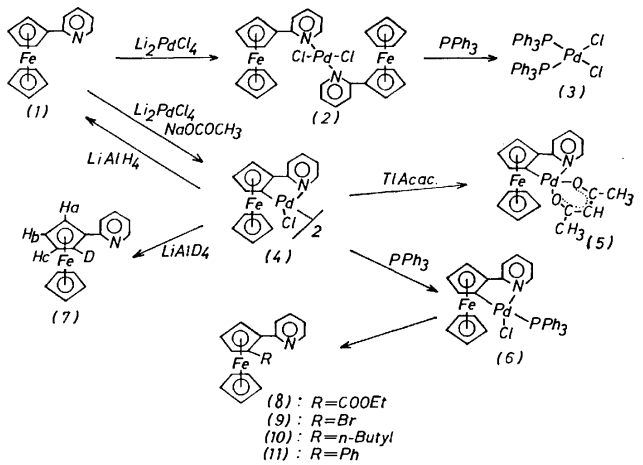

Fig. 1.

butyllithium and phenyllithium gave 2-butyl-1-(2-pyridyl)ferrocene (**10**) (34% yield) and 2-phenyl-1-(2-pyridyl)ferrocene (**11**) (27% yield) respectively. Compounds **8**, **9**, **10**, and **11** exhibit absorptions near 1100, 1000, and 910 cm^{-1} characteristic of homoannularly 1,2-disubstituted ferrocene derivatives.[6] Moreover, the NMR and mass spectra of the compounds were all consistent with the proposed structures.

Experimental

Materials and Analysis. All the melting points are uncorrected. The 2-pyridylferrocene (**1**) was prepared by the method previously reported.[13] The IR spectra were measured on KBr disks (4000—650 cm^{-1}) or in Nujol mulls mounted on thin polythene windows (700—200 cm^{-1}), using Hitachi 215 and EPI-L spectrometers. The NMR spectra were taken in $CDCl_3$ with TMS as the standard and were recorded with a Hitachi R-22 spectrometer at 90 MHz. The mass spectra were obtained with a Hitachi RMU-6M mass spectrometer, using a direct inlet and an ionization energy of 70 eV. The molecular weight was determined in $CHCl_3$, using a Hitachi 115 vapor-pressure osmometer.

Dichlorobis(2-pyridylferrocene)palladium(II) (2). A solution of 1.31 g (5 mmol) of lithium tetrachloropalladate(II) in 30 ml of methanol or 30 ml of a mixture of dioxane and water (1 : 1) was stirred drop by drop at room temperature, into a solution of 1.31 g (5 mmol) of **1** in 20 ml of methanol or dioxane. The brownish precipitate which formed immediately was filtered and washed successively with several portions of water and then ether. The solid (3.4 g, 97% yield) was insoluble in all common solvents; mp 185—190 °C (dec). Found: C, 51.02; H, 3.56; N, 3.77%. Calcd for $C_{30}H_{26}Cl_2Fe_2N_2Pd$: C, 51.21; H, 3.72; N, 3.98%.

*Ligand-replacement Reaction of **2** with Triphenylphosphine.* 0.35 g of **2** and 0.13 g of triphenylphosphine were placed in 15 ml of ethanol, and the mixture was stirred at 80 °C for 24 h. The resultant solid was collected and washed several times with ethanol to give a quantitative yield of dichlorobis(triphenylphosphine)palladium(II) (**3**) (mp 250—260 °C (dec)), whose IR spectrum was identical to that of an authentic sample.[14] The concentration of the filtrate *in vacuo* gave **1** (mp 91—92 °C (lit,[13] mp 92—93 °C)).

Di-μ-chlorobis[2-(2-pyridyl)ferrocenyl]dipalladium(II) (4). A solution of 1.31 g (5 mmol) of **1** in methanol (30 ml) was added to a mixture of lithium tetrachloropalladate(II) (1.31 g, 5 mmol) and sodium acetate trihydrate (0.68 g, 5 mmol) in methanol (50 ml). The new mixture was then stirred for 20 h at room temperature, and the reddish precipitate which formed was filtered off and dried (yield: 4.20 g; 99% yield). A portion was recrystallized from chloroform-cyclohexane; mp 240—244 °C (dec). NMR δ: 4.31 (6H, H_b+unsubstituted ferrocene ring protons, singlet); 5.14 (1H, H_a, multiplet); 5.33 (1H, H_c, multiplet); 7.01—8.64 ppm (4H, pyridyl protons, multiplet). Found: C, 44.46; H, 2.87; N, 3.41%; mol wt 786. Calcd for $C_{30}H_{24}Cl_2Fe_2N_2Pd_2$: C, 44.60; H, 2.99; N, 3.46%; mol wt, 808.

Acetylacetonato[2-(2-pyridyl)ferrocenyl]palladium(II) (5). A solution of thallium(I) acetylacetonate (0.30 g, 1 mmol) and the **4** complex (0.40 g, 0.5 mmol) in benzene (20 ml) was stirred for 24 h at room temperature and then filtered. The filtrate was then evaporated under reduced pressure, giving a red oil. After purification by column chromatography on silica gel (benzene), the product, **5**, was obtained as orange prisms from hexane–benzene; mp 151—152 °C, NMR δ: 2.06 (6H, CH_3 of acac group, singlet); 4.18 (5H, unsubstituted ferrocene ring protons, singlet); 4.40 (1H, H_b, double-doublet); 4.63 (1H, H_a, doublet); 4.76 (1H, H_c, doublet); 5.41 (1H, **H**–C of acac group, singlet); 6.97—8.70 ppm (4H, pyridyl protons, multiplet). Found: C, 51.25; H, 3.97; N, 2.91%; M^+, 467. Calcd for $C_{20}H_{19}FeNO_2Pd$: C, 51.37; H, 4.09; N, 2.99%; M, 467.

Chloro[2-(2-pyridyl)ferrocenyl](triphenylphosphine)palladium(II) (6). Triphenylphosphine (0.26 g, 1 mmol) and the **4** complex (0.40 g, 0.5 mmol) were dissolved in benzene (20 ml), and then the mixture was stirred for 4 h. The solvent was removed under reduced pressure, and the product (0.60 g, 90% yield) was obtained as orange plates from ethanol; mp 136—138 °C (dec). Found: C, 59.25; H, 3.96; N, 2.03 %; mol wt, 654 (in $CHCl_3$). Calcd for $C_{33}H_{27}ClFeNPPd$: C, 59.49; H, 4.07; N, 2.12%; mol wt, 666.

*Reduction of the **4** Complex with Lithium Aluminum Hydride.* Lithium aluminum hydride (0.02 g, 0.5 mmol) in anhydrous ether (50 ml) was slowly added to a solution of the **4** complex (0.4 g, 0.5 mmol) in anhydrous ether (50 ml). The resulting black mixture was stirred at room temperature for 4 h; then water (10 ml) was added with cooling. The ether layer was washed with water and dried over anhydrous magnesium sulfate. After the removal of the solvent, **1** was obtained as reddish plates from benzene-cyclohexane; mp 91—92 °C (lit,[13] mp 92—93 °C). NMR δ: 4.07 (5H, unsubstituted ferrocene ring protons, singlet); 4.42 (2H, H_b, multiplet); 4.94 (2H, H_a, multiplet); 7.01—8.59 ppm (4H, pyridy protons, multiplet). MS: M^+ 263. Calcd for $C_{15}H_{13}FeN$: M, 263.

*Reduction of the **4** Complex with Lithuim Aluminum Deuteride.* The reduction of **4** (0.40 g) in anhydrous ether with lithium aluminum deuteride (0.02 g) was carried out as in the preceding experiment; this gave a product (mp 92—93 °C) which can be identified as 1-(2-pyridyl)ferrocene-2-d_1 (**7**) on the basis of the following evidence: NMR δ: 4.07 (5H, unsubstituted ferrocene ring protons, singlet); 4.42 (2H, H_b, multiplet); 4.92 (1H, H_a, multiplet); 7.00—8.60 ppm (4H, pyridyl protons, multiplet). Found: C, 68.05; H, 5.31; N, 5.19%; M^+, 264. Calcd for $C_{15}H_{12}DFeN$: C, 68.13; H, 5.38; N, 5.30%; M, 264.

*Carbonylation of the **6** Complex in Ethanol.* In ethanol (50 ml), the **6** complex (3.33 g, 5 mmol) was carbonylated at 100 °C under a carbon monoxide pressure of 80 atm for 10 h with shaking. The product was then isolated by filtering to remove a precipitated palladium and distilling under reduced pressure to remove the solvent. The residue was dissolved in chloroform and chromatographed on silica gel to afford red crystals (0.62 g; 37% yield), which can be identified as 2-ethoxycarbonyl-1-(2-pyridyl)ferrocene (8); mp 108

—110 °C. NMR δ: 1.21 (3H, CH_3 of ester group, triplet); 4.29 (5H, unsubstituted ferrocene ring protons, singlet); 4.40 (3H, $\mathbf{H_b}+\mathbf{CH_2}$ of ester group, multiplet); 4.68 (1H, $\mathbf{H_a}$, multiplet); 4.87 (1H, $\mathbf{H_c}$, multiplet); 7.06—8.74 ppm (4H, pyridyl protons, multiplet). Found: C, 64.38; H, 5.06; N, 4.05%; M^+, 335. Calcd for $C_{18}H_{17}FeNO_2$: C, 64.52; H, 5.11; N, 4.17%; M, 335.

Reaction of the ***6*** *Complex with Bromine.* Under a nitrogen atmosphere, bromine (0.90 g, 5 mmol) in chloroform (15 ml) was slowly added in a solution of the **6** complex (3.33 g, 5 mmol) in chloroform (50 ml). After stirring at room temperature for 4 h, the reaction mixture was filtered and the chloroform phase washed several times with water, dried over anhydrous magnesium sulfate, and concentrated. The residue was dissolved in chloroform and chromatographed on silica gel afford reddish crystals (0.60 g; 35% yield), which can be identified as 2-bromo-1-(2-pyridyl)ferrocene (**9**); mp 95—97 °C. NMR δ: 3.70 (5H, unsubstituted ferrocene ring protons); 4.32 (2H, $\mathbf{H_b}+\mathbf{H_c}$, multiplet); 4.85 (1H, $\mathbf{H_a}$, multiplet); 7.16—8.64 ppm (4H, pyridyl protons, multiplet). Found: C, 52.21; H, 4.10; N, 3.89%; M^+, 344. Calcd for $C_{15}H_{12}BrFeN$: C, 52.37; H, 4.01; 4.07%; M, 344.

Reaction of the ***6*** *Complex with Butyllithium.* Under a nitrogen atmosphere, the **6** complex (3.33 g, 5 mmol) in dry benzene (50 ml) was reacted with 10 mmol of butyllithium in ether. After stirring at 50 °C for 8 h, the products were isolated by diluting the cooled reaction mixtures with water and chloroform. The chloroform phase was separated, washed several times with water, dried over anhydrous magnesium sulfate, and concentrated. The residue was dissolved in chloroform and chromatographed on silica gel. The first elution with chloroform afforded red crystals (0.21 g, mp 91—93 °C); they were identified as 2-pyridylferrocene (**1**) by a comparison of the IR and NMR spectra with those of an authentic sample and by a mixed-melting-point determination. The second elution with chloroform afforded a heavy reddish oil (0.54 g, 34% yield) which can be identified as 2-butyl-1-(2-pyridyl)ferrocene (**10**) on the basis of the following evidence: NMR δ: 0.92 (3H, $\mathbf{CH_3}$ of butyl group, triplet), 1.15—1.87 (4H, $\mathbf{CH_2}$ of butyl group, multiplet); 2.80 (2H, ferrocenyl-$\mathbf{CH_2}$–, triplet); 4.11 (5H, unsubstituted ferrocene ring protons, singlet); 4.38 (2H, $\mathbf{H_b}+\mathbf{H_c}$, multiplet); 4.96 (1H, $\mathbf{H_b}$, multiplet); 6.80—8.60 ppm (4H, pyridyl protons, multiplet). Found: C, 71.28; H, 6.55; N, 4.26%; M^+, 319. Calcd for $C_{19}H_{21}FeN$: C, 71.49; H, 6.63; N, 4.38%; M, 319.

Reaction of the ***6*** *Complex with Phenyllithium.* The reaction of **6** (3.33 g, 5 mmol) with 10 mmol of phenyllithium in ether was carried out as in the preceding experiment; it gave a product (0.46 g, yield, 27%) which can be identified as 2-phenyl-1-(2-pyridyl)ferrocene (**11**); mp 235 °C (dec). NMR δ: 3.93 (5H, unsubstituted ferrocene ring protons); 4.12 (1H, $\mathbf{H_b}$, multiplet); 4.77 (2H, $\mathbf{H_a}+\mathbf{H_c}$, multiplet); 7.18—8.49 ppm (9H, phenyl and pyridyl protons, mutiplet). Found: C, 74.25; H, 4.87; N, 4.03; M^+, 339. Calcd for $C_{21}H_{17}FeN$: C, 74.40; H, 5.05; N, 4.13; M, 339.

References

1) A. C. Cope and R. W. Siekman, *J. Am. Chem. Soc.*, **87**, 3272 (1965).
2) a) P. M. Maitlis, "The Organic Chemistry of Palladium," Academic Press, Vol. 1, New York (1971), p. 82; b) J. Tsuji, *Yuki Gosei Kagaku Kyokai Shi*, **35**, 10 (1977).
3) H. Alper, *J. Organomet. Chem.*, **80**, C 29 (1974).
4) J. C. Gaunt and B. L. Shaw, *J. Organomet. Chem.*, **102**, 511 (1975).
5) M. Rosenblum, J. O. Santer, and W. G. Howells, *J. Am. Chem. Soc.*, **85**, 1450 (1963).
6) M. Rosenblum, *J. Am. Chem. Soc.*, **81**, 4530 (1959); M. Rosenblum and W. G. Howells, *ibid.*, **84**, 1167 (1962).
7) a) J. M. Duff and B. L. Shaw, *J. Chem. Soc., Dalton Trans.*, **1972**, 219; b) J. M. Duff, B. E. Mann, B. L. Shaw, and B. Turtle, *ibid.*, **1974**, 139.
8) H. Takahashi and J. Tsuji, *J. Organomet. Chem.*, **10**, 511 (1967).
9) J. M. Thompson and R. F. Heck, *J. Org. Chem.*, **40**, 2667 (1975).
10) D. R. Fahey, *Chem. Commun.*, **1970**, 417; *J. Organomet. Chem.*, **27**, 283 (1971).
11) S.-I. Murahashi, Y. Tanba, M. Yamamura, and I. Moritani, *Tetrahedron Lett.*, **1974**, 3749.
12) M. Yamamura, I. Moritani, and S.-I. Murahashi, *Chem. Lett.*, **1974**, 1423.
13) K. Schogl and M. Fried, *Monatsh. Chem.*, **94**, 537 (1963).
14) L. Malatesta, *J. Chem. Soc.*, **1955**, 1186.

NOTES

BULLETIN OF THE CHEMICAL SOCIETY OF JAPAN, VOL. 50 (7), 1881—1882 (1977)

The Effect of Water Vapor on Contamination of Metallic Oxide Surfaces

Yasukatsu TAMAI, Toshiaki MATSUNAGA, and Kazutomi SUZUKI

Chemical Research Institute of Non-Aqueous Solutions, Tohoku University, Katahira, Sendai 980

(Received February 2, 1977)

Synopsis. The contamination rates of the clean surfaces of metallic oxides by liquid-paraffin vapor are largely reduced by the coexisting water vapor. They are related to the hydrophilicity of oxides evaluated as the water-solid interaction free energy by the two-liquid-contact-angle method.

High energy surfaces such as those of metallic oxides or metals are liable to be contaminated by organic vapor in the air. The sensitive change in the contact angle of water can be utilized for the detection of organic contaminant.[1] As White[2] pointed out, organic contamination should be regarded as adsorption and not the "falling out" of materials onto a surface.

Since oxide surfaces have strong affinity to water, coexisting water vapor would have some effect on the adsorption of organic compounds on a high energy surface. In order to study the effect of coexisting water vapor on organic contamination of several metallic oxides by liquid-paraffin vapor, we have measured the contact angles of water drops. The results are discussed in relation to the affinity of oxide surfaces to water.

Experimental

A quartz glass plate for an optical cell, and five single crystal plates of oxides, rutile (TiO_2)(001), chromia (Cr_2O_3)(0001), α-alumina (Al_2O_3)(0001), nickel oxide (NiO)(100), and strontium titanate ($SrTiO_3$) were examined. The numbers in parentheses indicate the crystal planes investigated. The surface of strontium titanate was not a low index crystal plane. The purity of single crystals was 99.9—99.99%.

All the surfaces were polished up to specular surfaces with emery paper and diamond-powder paste. The surfaces were cleaned before each measurement with an ultrasonic cleaner in a detergent solution, followed by thorough washing with redistilled water. Water could perfectly wet the surfaces.

In order to detect possible impurities originating from the cleaning process, the Auger spectra for alumina samples were measured with a Physical Electronics Instruments, Type CAS 545, apparatus. Only traces of phosphorus and carbon other than aluminum and oxygen were detected. Their coverage was estimated to be smaller than 1% Carbon might have come from the contaminants in the Auger apparatus.

The oxide plate was subjected to contamination in a Petri dish containing two small vessels, one filled with liquid paraffin and the other with water for wet atmosphere and with phosphorus pentoxide for dry atmosphere. The oxide sample was picked out after a certain time and transfered to an optical cell for measurement of contact angles of water drops by means of a goniometer-telescope system at 20±0.5 °C. The points in Figs. 1 and 2 represent the average of ten to twenty advancing contact angles, the accuracy being *ca.* ±2 degrees.

Liquid paraffin (spectroscopic grade) was used as an organic contaminant. Water was redistilled from an alkaline permanganate solution in a Pyrex glass apparatus.

Results and Discussion

Changes in contact angle of water with time in dry atmosphere and in saturated water are shown in Figs. 1 and 2, respectively. The order of contamination rates is: silica<α-alumina<nickel oxide<chromia<strontium titanate<rutile. This order is the same under both conditions, regardless of the coexisting water vapor. However, water vapor supresses organic contamination of all the oxides. The tendency is larger for the surfaces which are more easily contaminated, such as rutile or strontium titanate.

Since surface contamination can be regarded as competitive adsorption of organic and water vapor, the contamination rates would be related to the affinity of

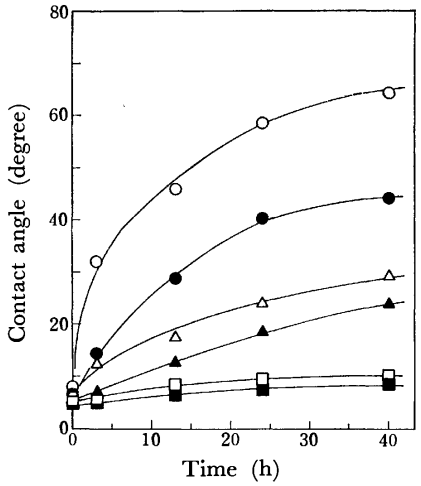

Fig. 1. Variation of contact angles under the dried atmosphere.
○: TiO_2, ●: $SrTiO_3$, △: Cr_2O_3, ▲: NiO, □: Al_2O_3, ■: SiO_2.

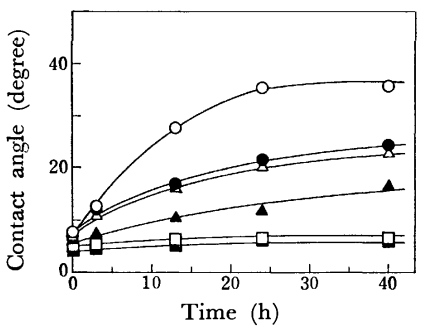

Fig. 2. Variations of contact angles under the wet atmosphere. (Symbols are the same in Fig. 1.)

oxide surface to water. Evaluation of the hydrophilicity of oxides can be carried out by such methods as adsorption of water and the heat of immersion in water, but they are restricted to powder samples.

The interaction free energy due to nondispersive forces (mainly the hydrogen bonding force) at the interface between solid and water, I^n_{sw}, can be obtained from the contact angles of water drops in hydrocarbon liquid. This can be defined in terms of surface tension γ by

$$I^n_{sw} = \gamma^n_s + \gamma^n_w - \gamma^n_{sw},$$

where subscripts s, w, and sw denote solid, water, and solid/water interface, respectively, and n indicates the component due to nondispersive forces. The details of the method[3,4] and the results for the oxides have been reported.[5]

The I^n_{sw} values obtained for the oxides are[5] as follows: TiO_2, 91.4; $SrTiO_3$, 93.2; Cr_2O_3, 93.6; NiO, 94.0; Al_2O_3, 97.6; and SiO_2, 99.2 in mJ m^{-2} at 20 °C. The accuracy is *ca.* ± 0.3 mJ m^{-2}. The order of the I^n_{sw} values corresponds to the reverse order of the contamination rates (Figs. 1 and 2). The oxides which have smaller I^n_{sw} values and are thus less hydrophilic are more easily contaminated by organic vapors. This seems reasonable in view of the competitive adsorption.

It was found that the coexisting water vapor can largely reduce the contamination rates of the clean surfaces, suggesting an appropriate method for keeping the washed oxide surface clean.

The authors wish to express their appreciation to Dr. I. Shiota for the measurement of Auger spectra.

References

1) For example, J. J. Bikerman, "Physical Surfaces," Academic Press, New York (1970), p. 269.

2) M. L. White, in "Clean Surfaces," ed by G. Goldfinger, Marcel Dekker, New York (1970), p. 361.

3) Y. Tamai, K. Makuuchi, and M. Suzuki, *J. Phys. Chem.* **71**, 4176 (1967).

4) Y. Tamai and H. Kobayashi, *J. Colloid Interface Sci.* **32**, 369 (1970).

5) Y. Tamai, T. Matsunaga, and K. Suzuki, Proc. VIIth Int. Cong. Surface Active Substances at Moscow (1976), in press.

BULLETIN OF THE CHEMICAL SOCIETY OF JAPAN, VOL. 50 (7), 1883—1884 (1977)

Catalytic Behavior of Sulfonium Trihalides in the Low-temperature Liquid-phase Oxidation of Tetralin

Katsutoshi OHKUBO, Teruo AOJI, and Kohji YOSHINAGA

Department of Synthetic Chemistry, Faculty of Engineering, Kumamoto University, Kurokami, Kumamoto 860

(Received November 25, 1975)

Synopsis. Homogeneous oxidation of nonpolar tetralin catalyzed by sulfonium trihalides was found to proceed *via* a radical chain mechanism in which the trihalide catalysts promoted the reaction through the activation of molecular oxygen.

Although numerous investigations have hitherto been performed on the bond property of trihalide ions with the conclusion that the trihalide ions can be well explained by their Rundle 3c-4e (three center four-electron) bonds without the participation of d-orbitals to their almost covalent linear bonds,[1] onium trihalides, especially of the sulfonium type, have received only limited attention in terms of their chemical reactivity in solutions. An interesting chemical property of sulfonium trihalides has recently been found in this laboratory: their remarkable catalytic activity in the low-temperature liquid-phase oxidation of hydrocarbons. In this paper, experimental and MO-theoretical studies of the sulfonium trihalides are reported with a view of examining how they accelerate the liquid-phase oxidation of hydrocarbons.

Experimental

Materials and Experimental Procedure. The triphenylsulfonium and tetrabutylammonium compounds used as oxidation catalysts were prepared by the usual methods.[2-4] A portion (10 ml) of the fresh distillate of tetralin was subjected to homogeneous liquid-phase oxidation with a catalyst (0.005 mmol) in the temperature range of 45—85 °C under atmospheric pressure. UV spectroscopic measurements of triphenylsulfonium trihalides were carried out in CH_3OH at 25 °C using Shimadzu 200 and Hitachi 200-10 spectrophotometers.[5]

Results and Discussion

Let us first examine the activities of several triphenylsulfonium trihalides for homogeneous oxidation of tetralin at 65 °C. As can be seen from Table 1, the sulfonium trihalides markedly accelerate the oxidation rate with no induction period (in an autocatalytic fashion) resulting in a monotonic accumulation of tetralin hydroperoxide (HPO) only as an oxidation product, although tetralin autoxidation indicated an induction period of 24 min. Also, the sulfonium trihalides are more active than ammonium salts having the corresponding trihalide anions. It is also noteworthy that the maximum O_2-absorption rate (R_{max}) appearing during the initial short reaction stage (up to 7 min) without appreciable decomposition of HPO showed a first-order dependence on the concentration of the sulfonium trihalide and that more than 85% of the trihalide can be recovered from the reaction mixture after a reaction time of about 15 min.[6] From these observations the following dissociation of sulfonium trihalide ($R_3SX^1X^2X^3$: X^2=middle halogen and X^1=X^3=terminal halogen) into sulfonium monohalide (R_3SX^2) and a halogen molecule (X^1X^3), within a reaction time of up to 10 min, is not believed to be very important:

$$R_3SX^1X^2X^3 \overset{K}{\rightleftharpoons} R_3SX^2 + X^1X^3 \quad (1)$$

where K is an equilibrium constant, and X^2 is assumed to be more electronegative than either X^1 or X^3. The dissociation of $R_3SX^1X^2X^3$ is also not expected in such nonpolar hydrocarbons as tetralin, in view of the fact that the K values are very small even in $CHCl_3$ at 20 °C (about 10^{-5}—10^{-4} mol/l[4]).

Now, we consider how $R_3SX^1X^2X^3$ initiates the present oxidation reaction which was confirmed to proceed *via* the usual radical-chain mechanism. The formation of radical initiators through the decomposition of peroxides (ROOH) by $R_3SX^1X^2X^3$ does not occur during the initial short reaction stage, because ROOH is monotonically accumulated in amount (mol) corresponding almost quantitatively to the oxygen absorbed (mol) and because the addition of ROOH to the reaction system markedly depressed the reaction rate. These results are due to the promotion of the dissociation of $R_3SX^1X^2X^3$ or partly due to the blocking effect by species containing lone-pair electrons against interaction of the oxidation catalyst ($R_3SX^1X^2X^3$ or R_3SX^2) with O_2 (see later).[7] The dissociation products (R_3SX^2 and X^1X^3) in equimolar amounts did not initiate the reaction in spite of the existence of effective oxidation catalysts (R_3SX^2) in the reaction system. This might also be due to the above-mentioned blocking effect of X^1X^3.

The markedly higher activity of $R_3SX^1X^2X^3$ as compared with the ammonium trihalides, despite the nearly identical K values (*ca.* 10^{-4} mol/l[4]) in $CHCl_3$ at 20 °C) of ammonium trihalide as that of $R_3SX^1X^2X^3$ does not support the halide-anion catalysis which is expected in ammonium halides.[8]

The following initial step, in which $R_3SX^1X^2X^3$ accelerates the reaction *via* the activation of O_2, appears to be most reasonable in connection with the catalytic behavior of R_3SX for hydrocarbon oxidation:[5,8,9]

$$R_3SX^1X^2X^3 + O_2 \rightleftharpoons [R_3S(X^1X^2X^3)^{\delta+}\cdots O_2^{\delta-}] \xrightarrow{RH} R\cdot + HO_2\cdot + R_3SX^1X^2X^3 \quad (2)$$

If Reaction 2 is plausible, one can expect direct interaction between $R_3SX^1X^2X^3$ and O_2, and hence, some specific orbitals of the former should play an important role in the activation of the latter. In regard to the interaction molecular oxygen appreciably shifts the

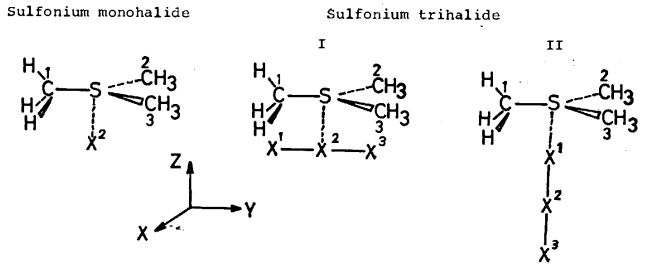

Fig. 1. Molecular structures of $(CH_3)_3SX^1X^2X^3$ and $(CH_3)_3SX^2$ (S-C(fixed bond-length in the calculation)=1.82 Å; $\angle CSC=120°$; $S-X^2$ or $S-X^1$=purely ionic distance; X^1-X^2 or X^2-X^3=purely covalent distance.)

sulfur $(3p)^2\rightarrow(3p)(3d)$ transition (λ_{max}=208—210 nm and $\log\varepsilon$=4.61—4.72 in CH_3OH at 25 °C in an N_2 atmosphere) of the sulfonium cation[10] to longer wavelengths over an energy scale from 0.03 to 0.09 eV. This implies that the lowering of the partially-occupied sulfur d-orbitals (see below), which results from charge transfer from the d-orbitals (especially, the d_{xz} orbital in Fig. 1) to O_2, simplifies the above-mentioned electron excitation mechanism. In this sense, it can be believed that the more the electron density of the d_{xz} orbital increases, the higher becomes the catalytic activity (as reflected in the R_{max} value) of $R_3SX^1X^2X^3$. In fact, as Fig. 2 indicates, the R_{max} values of $R_3SX^1X^2X^3$ (and

Table 1. Catalytic activitities of triphenylsulfonium trihalides (0.005 mmol) in tetralin (10 ml) oxidation at 65 °C

Compound	(O_2)absd[a] (mmol)	HPO[b] (%)	10^4R_{max} (M/s)	Compound	(O_2)absd[a] (mmol)	HPO[b] (%)	10^4R_{max} (M/s)
$(C_6H_5)_3SBrClBr$	0.95	99.4	0.61	$(C_6H_5)_3SClICl$	0.70	99.7	0.42
$(C_6H_5)_3SIClI$	0.93[c]	99.8[a]	0.75[c]	$(C_6H_5)_3SBrIBr$	0.66	99.4	0.35
	0.59	99.5	0.49	$(C_6H_5)_3SI_3$	0.60	99.7	0.35
	0.41[d]	99.7[d]	0.25[d]	$(C_6H_5)_3SI$	0.78	99.0	0.61
	0.26[e]	99.5[e]	0.20[e]	$(C_6H_5)_3SBF_4$	0.18	100	0.17
$(C_6H_5)_3SCl$	1.08	99.2	1.19	$(n\text{-}C_4H_9)_4NBrClBr$	0.26	100	0.17
$(C_6H_5)_3SClBrCl$	0.82	99.8	0.53	$(n\text{-}C_4H_9)_4NBr_3$	0.21	100	0.15
$(C_6H_5)_3SBr_3$	0.76	99.4	0.50	$(n\text{-}C_4H_9)_4NBF_4$	0.05	100	0.05
$(C_6H_5)_3SIBrI$	0.91	99.2	0.52	none	0.01[f]	100[f]	0.01[f]
$(C_6H_5)_3SBr$	0.94	99.5	0.83				

a) After a reaction time of 30 min. b) Based on the O_2 absd (mmol). c) At 85 °C. d) At 55 °C. e) At 45 °C. f) The incubation period was 24 min.

Table 2. UV transition energies and formal charges of $X^1X^2X^3$ ions in $R_3SX^1X^2X^3$

Compound	Transition energy of $X^1X^2X^3$	Formal charge	
		X^2	$X^1=X^3$
	Obsd[a] (Calcd) (eV)	Obsd (Calcd)	Obsd (Calcd)
$(C_6H_5)_3SBrClBr$	4.63 (4.78)	— (0.29)	— (−0.39)
$(C_6H_5)_3SIClI$	4.28 (4.23)	— (0.22)	— (−0.45)
$(C_6H_5)_3SClBrCl$	4.88 (5.20)	— (0.35)	−0.56[b] (−0.46)
$(C_6H_5)_3SBr_3$	4.64 (4.99)	0.06[c] (0.30)	−0.34[c] (−0.41)
$(C_6H_5)_3SIBrI$	4.25 (4.53)	— (0.24)	— (−0.46)
$(C_6H_5)_3SClICl$	5.35 (4.49)	0.29[d] (0.31)	−0.62[d] (−0.51)
$(C_6H_5)_3SBrIBr$	4.64 (4.39)	0.19[e] (0.25)	−0.50[e] (−0.47)
$(C_6H_5)_3SI_3$	4.28 (3.86)	0.05[e] (0.20)	−0.51[e] (−0.49)

a) From $(C_6H_5)_3SX^1X^2X^3$ in CH_3OH at 25 °C. b) E. F. Riedel and R. D. Willett, *J. Am. Chem. Soc.*, **97**, 701 (1975). c) G. L. Breneman and R. D. Willett, *J. Pyhs. Chem.*, **71**, 3084 (1967). d) S. Hagiwara, K. Kato, Y. Abe, and M. Minematsu, *J. Phys. Soc. Jpn.*, **12**, 1166 (1957); J. C. Evans and Y. G. S. Lo, *Inorg. Chem.*, **6**, 836 (1967). e) G. A. Bowmaker and S. Hacobian, *Aust. J. Chem.*, **21**, 551 (1968).
The calculated values were obtained from $(CH_3)_3SX^1X^2X^3$.

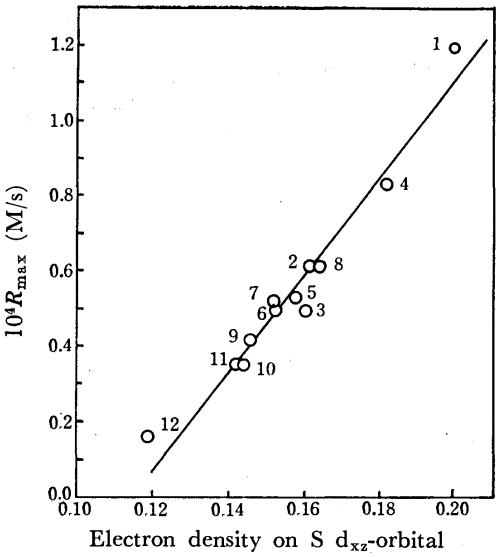

Fig. 2. Correlation between R_{max} values and electron densities on S d_{xz}-orbital.
1: $(C_6H_5)_3SCl$, 2: $(C_6H_5)_3SBrClBr$, 3: $(C_6H_5)_3SIClI$, 4: $(C_6H_5)_3SBr$, 5: $(C_6H_5)_3SClBrCl$, 6: $(C_6H_5)_3SBr_3$, 7: $(C_6H_5)_3SIBrI$, 8: $(C_6H_5)_3SI$, 9: $(C_6H_5)_3SClICl$, 10: $(C_6H_5)_3SBrIBr$, 11: $(C_6H_5)_3SI_3$, 12: $(C_6H_5)_3SBF_4$.

R_3SX) show a correlation with the electron densities of the d_{xz} orbital which is favorably distributed for interaction with the $(1\pi_g)_z$ orbital of O_2.[9]

Finally, it is worthy of notice that the ASMO-SCF calculations[11] of $R_3SX^1X^2X^3$, as $(CH_3)_3SX^1X^2X^3$ for computation simplicity, resulted in reasonable electronic properties for energetically more stable $R_3SX^1X^2X^3$ (I in Fig. 1) in terms of the approximate coincidence between the calculation results and the spectroscopic (UV and NQR) observations (see Table 2).

References

1) R. J. Hach and R. E. Rundle, *J. Am. Chem. Soc.*, **73**, 4321 (1951).
2) W. A. Bonner, *J. Am. Chem. Soc.*, **74**, 5078 (1952).
3) K. Fukui, K. Kanai, and H. Kitano, *Nippon Kagaku Zasshi*, **82**, 178 (1961).
4) K. Kanai, T. Hashimoto, H. Kitano, and K. Fukui, *Nippon Kagaku Zasshi*, **86**, 534 (1965).
5) The detailed procedures are the same as in K. Ohkubo and T. Yamabe, *J. Org. Chem.*, **36**, 3149 (1971).
6) The unrecovered sulfonium trihalide was found by means of UV spectroscopic measurements to be converted into sulfonium monohalide and a halogen molecule.
7) K. Fukui, K. Ohkubo, and T. Yamabe, *Bull. Chem. Soc. Jpn.*, **42**, 312 (1969); K. Ohkubo, T. Yamabe, and K. Fukui, *Bull. Chem. Soc. Jpn.*, **42**, 2220 (1969).
8) H. Bredereck, A. Wagner, and A. Kottenhahn, *Angew. Chem.*, **70**, 503 (1958).
9) The mode of interaction between R_3SX and O_2 can be found in K. Ohkubo, *Tetrahedron Lett.*, **1971**, 2571 and K. Ohkubo and H. Kanaeda, *J. Chem. Soc., Fraday Trans. 2*, **68**, 1164 (1972).
10) A detailed discussion can be found in Ref. 5.
11) The calculation method has been described in H. Kato, H. Konishi, and T. Yonezawa, *Bull. Chem. Soc. Jpn.*, **40**, 1017 (1967), and the parametrizations were the same as those given in Ref. 9.

BULLETIN OF THE CHEMICAL SOCIETY OF JAPAN, VOL. 50 (7), 1885—1886 (1977)

The Titanium Trichloride-catalyzed Oxidation of Triphenylphosphine with Oxygen in Acetonitrile

Yasuo CHIMURA and Kimio TARAMA

Department of Hydrocarbon Chemistry, Faculty of Engineering, Kyoto University, Sakyo-ku, Kyoto 606

(Received October 29, 1976)

Synopsis. Titanium trichloride catalyzed very rapidly the oxidation of triphenylphosphine with oxygen in acetonitrile, yielding triphenylphosphine oxide and a yellow precipitate. The main catalytic cycle did not contain Cl_3Ti–O–$TiCl_3$ which was produced in the oxidation of $TiCl_3$ alone, but the precursors of Cl_3Ti–O–$TiCl_3$ as intermediates. The yellow precipitate was a titanium(IV) complex with a discrete TiO group.

Titanium(III) complexes are oxidized by molecular oxygen in anhydrous organic solvents to give a μ-peroxo dimeric complex,[1] μ-oxo dimeric complexes,[2,3] or monomeric complexes containing TiO groups.[4] The oxidations of organic compounds with oxygen using titanium complexes as catalysts, however, are unknown. This paper will describe briefly the $TiCl_3$-catalyzed oxidation of triphenylphosphine (PPh_3) with oxygen in acetonitrile as a continuation of previous studies[5] of dioxygen complexes of transition metals.

Experimental

Materials. The acetonitrile was distilled from diphosphorus pentaoxide and again from calcium hydride and then stored under nitrogen. The titanium trichloride was converted to trichlorotris(acetonitrile)titanium(III),[6] which was then dissolved in acetonitrile to yield a 0.130 M solution (M=mol/dm^3). The triphenylphosphine was recrystallized from methanol and stored under nitrogen. Commercial oxygen gas was used without further purification.

Apparatus and Procedure. A 200-cm^3, three-necked, flat-bottomed flask containing a Teflon-coated magnetic stirrer was fitted with a thermometer and a serum cap at each of the two necks, while through the other neck it was connected to a vacuum system with a manometer, a gas buret, *etc.* The flask was then immersed in a constant-temperature bath operated at 20 °C. The system was filled with atmospheric oxygen after the introduction of PPh_3 (1.00—8.93 mmol) and acetonitrile (35.0 cm^3). Then, the acetonitrile solution of $TiCl_3$ (5.0 cm^3) was injected as soon as possible by means of a syringe through the serum cap, with vigorous stirring. The uptake of oxygen was followed at the constant pressure of 1 atm. After 2 days, the resulting yellow precipitate was filtered, washed with acetonitrile, and dried under a vacuum. The filtrate was hydrolyzed with dilute hydrochloric acid and extracted with ether. The ether layer was evaporated under a vacuum, leaving a pale yellow residue, which was then chromatographed over silica gel to give PPh_3 and triphenylphosphine oxide ($OPPh_3$).

Spectra. The IR spectra of the yellow precipitate and the reaction solution were measured by means of a JASCO IRA-2 spectrophotometer as Nujol mulls and using a solution cell respectively. The visible spectra of mixtures of $TiCl_3$ and PPh_3 in acetonitrile were recorded under nitrogen with a JASCO UVIDEC-1 spectrophotometer. The ESR spectrum of the precipitate was recorded on a JEOL-JES-3BS-X spectrometer.

Analysis. Carbon, hydrogen, phosphorus, and chlorine analyses of the yellow precipitate were carried out by specialists. The titanium was chelatometrically back-titrated at pH 5.5 with a 0.05 M zinc(II) nitrate solution in 50% aqueous ethanol using Xylenol Orange as an indicator.

Results and Discussion

In the absence of PPh_3, the blue color of an injected $TiCl_3$ solution immediately turned yellow. The uptake of oxygen was very rapid and ceased within a minute. The amount of oxygen taken up was about a fourth of the $TiCl_3$ concentration (Table 1). The IR spectrum of the yellow solution showed a peak at 788 cm^{-1} and a shoulder at 749 cm^{-1}. They were assigned to the stretching vibrations of a Ti–O–Ti group, since Cl_3Ti–O–$TiCl_3(CH_3CN)_4$[7] showed a strong peak and a shoulder at 800 and 740 cm^{-1} respectively. Thus, $TiCl_3$ seems to be oxidized to the same Cl_3Ti–O–$TiCl_3$ complex (**1**) in acetonitrile as in pyridine.[3]

In the presence of PPh_3, an injected $TiCl_3$ solution immediately turned brown, and after several minutes a yellow powder was precipitated. The rate of oxygen uptake was initially very fast, and then it fell rapidly. The amounts of oxygen uptake and of the products formed are shown in Table 1. The ratio of oxygen taken up after 1 min to that after 2 days changed from 0.51 to 0.93 as the amount of PPh_3 decreased. At every stage of the reaction, the amount of oxygen uptake increased with an increase in the amount of PPh_3 and exceeded the amount of $TiCl_3$; that is, the oxidation proceeded catalytically, and the turnover number increased with the increasing amounts of PPh_3. The PPh_3 introduced was recovered almost quantitatively as $OPPh_3$ and unreacted PPh_3. The oxygen taken up was also found almost quantitatively in $OPPh_3$ and in the oxidized catalyst, assuming that the oxidized catalyst bound oxygen in a Ti : O atomic ratio of 2 : 1.

The precipitated yellow complex was air-stable and was hardly soluble in acetonitrile at room temperature. The yield was 33—60%. The complex when recovered from different runs showed the same IR spectra, which contained a strong band at 1146 cm^{-1} and very strong bands at 726 and 1121 cm^{-1} due to the P=O stretching vibration and the X-sensitive vibrations[8] of the coordinating $OPPh_3$ respectively. The spectra also showed a sharp and very strong band at 1060 cm^{-1}, which was assigned to a Ti=O stretching vibration.[4,9] The lack of any absorption between 2000 and 2600 cm^{-1} and between 770 and 960 cm^{-1} indicates the absence of acetonitrile and of a Ti–O–Ti group respectively. The absence of an ESR signal of the complex either at room temperature or at 77 K indicates that the titanium ion is not trivalent but tetravalent. The results of the

Table 1. The amounts of oxygen uptake and products[a]

Introduced PPh_3 mmol	O_2 Uptake mmol			$2\times O_2$ Uptake mmol (2 day)	Recovered from solution mmol		$OPPh_3$[b] contained in ppt mmol	Total $OPPh_3$ mmol	Total $OPPh_3$ + PPh_3 mmol	Total[c] O atom in products mmol
	1 min	30 min	2 day		PPh_3	$OPPh_3$				
0	0.17	0.17	—	0.34	—	—	—	—	—	—
1.00	0.62	0.65	0.67	1.34	—[d]	—[d]	0.694	—	—	—
2.00	0.80	0.87	1.02	2.04	0.33	0.94	0.666	1.61	1.94	1.94
5.00	0.95	1.30	1.58	3.16	1.93	2.34	0.574	2.91	4.84	3.24
8.93	1.10	1.71	2.16	4.32	4.80	3.60	0.406	4.01	8.81	4.34
3.00[e]	0.03	0.13	0.66	1.32	1.70	0.65	0.597	1.25	2.95	1.25

a) The amount of $TiCl_3$ was 0.650 mmol. b) Value calculated assuming that $OPPh_3$ is the sole organic component in ppt. c) The Ti : O ratio in an oxidized catalyst was assumed to be 2 : 1. d) They were lost in handling. e) An oxidized $TiCl_3$ solution ($TiCl_3$, 0.650 mmol) was employed as the catalyst.

Table 2. Elemental analyses of the yellow complex

Introduced PPh_3 mmol	%H	%C	%P	%Cl	%Ti	Atomic ratio		
						H/C/P[a]	Cl/Ti	P/Ti
1.00	3.82	57.58	7.80	17.66	7.09	14.2/18/0.946	3.37/1	1.70/1
8.93	4.24	58.59	7.83	16.38	6.66	15.5/18/0.933	3.32/1	1.82/1
3.00[b]	3.98	55.89	7.93	16.53	7.47	15.3/18/0.990	2.99/1	1.64/1

a) The calculated ratio is 15/18/1 for $OPPh_3$. b) An oxidized $TiCl_3$ solution was used as the catalyst.

elemental analysis of the complex are shown in Table 2. The composition depended a little upon the reaction conditions. However, the H/C/P and Cl/Ti ratios were nearly equal to 15/18/1 and 3/1. This shows that a PPh_3 moiety is the sole organic component, and that anionic ligands other than a chloride anion must be present, with a negative charge per titanium ion, since the titanium ion is tetravalent. Thus, the complex must have the following structural features: (1) The titanium ion is tetravalent, (2) a discrete TiO group is present, and (3) the other ligands are chloride anions and $OPPh_3$. Oxotitanium(IV) complexes are apt to have polymeric chain-type structures, *i.e.*, –Ti–O–Ti–O–; complexes such as this complex with discrete titanyl groups (TiO^{2+}) are rare.

There have been no reports on the isolation of the complex formed between $TiCl_3$ and PPh_3. The two d-d transition bands of $TiCl_3$ in acetonitrile under nitrogen, however, were changed a little by the addition of PPh_3; that is, the two bands which were at 585 nm (ε, 25.6) and 680 nm (ε, 15.4) for a triphenylphosphine-free acetonitrile solution of $TiCl_3$ (0.025 M) appeared at 588 nm (ε, 24.3) and 680 nm (ε, 17.7), and at 590 nm (ε, 24.7) and 680 nm (ε, 19.0), when the concentrations of added PPh_3 were 0.104 and 0.203 M respectively. This indicates the presence of a weak interaction between $TiCl_3$ and PPh_3 in an acetonitrile solution.

The oxidation mechanism of $TiCl_3$ with oxygen in acetonitrile seems to be similar to that in pyridine,[3] involving $Cl_3Ti–O_2$ (**2**), $Cl_3Ti–O_2–TiCl_3$ (**3**), and $Cl_3–Ti–O$ (**4**) as intermediates. Species like **2**,[5b,10,11] **3**,[11] and **4**[10] have been reported.

The oxidation of PPh_3 catalyzed by **1** had a much slower rate than that catalyzed by $TiCl_3$ (Table 1). Therefore, **1** is not contained in the main catalytic cycle of the $TiCl_3$-catalyzed oxidation, but seems to play a large part in the slow oxygen uptake in the later stage of the oxidation. The **2**, **3**, and/or **4** species reacting with PPh_3 would yield $OPPh_3$ and $TiCl_3$, and also $TiCl_3$ coordinated by PPh_3 would react with oxygen to give **2** coordinated by PPh_3, which would then decompose to $TiCl_3$ and $OPPh_3$. Thus, the main catalytic cycle seems to be composed. Since the oxidation of $TiCl_3$ to **1** was very rapid, the reactions of **2**, **3**, and/or **4** with PPh_3 and the decomposition must also be very rapid.

The authors are grateful to Dr. Toshimitsu Suzuki of this department for his gift of $TiCl_3$.

References

1) D. P. Bauer and R. S. Macomber, *Inorg. Chem.*, **15**, 1985 (1976).

2) S. A. Giddings, *Inorg. Chem.*, **3**, 684 (1964); H. Noeth and R. H. Hartwimmer, *Chem. Ber.*, **93**, 2246 (1960); R. Coutts and R. C. Wailes, *Inorg. Nucl. Chem. Lett.*, **3**, 1 (1967).

3) C. D. Schmulbach, C. C. Hinckley, C. Kolich, T. A. Ballintine, and P. J. Nassiff, *Inorg. Chem.*, **13**, 2026 (1974).

4) IR 1087 cm^{-1} (TiO) for $TiO(acac)_2$: M, Cox. J. Lewis, and R. S. Nyholm, *J. Chem. Soc.*, **1965**, 2840.

5) a) Y. Chimura, H. Kanai, S. Yoshida, and K. Tarama, *Chem. Lett.*, **1973**, 1217; b) Y. Chimura, *ibid.*, **1974**, 393; c) Y. Chimura, M. Beppu, S. Yoshida, and K. Tarama, *ibid.*, **1976**, 375.

6) R. J. H. Clark, J. Lewis, D. J. Machin, and R. S. Nyholm, *J. Chem. Soc.*, **1963**, 379.

7) This complex was prepared by the partial hydrolysis of $TiCl_4(CH_3CN)_2$: A. Feltz, *Z. Anorg. Allg. Chem.*, **332**, 35 (1964).

8) G. B. Deacon and J. H. S. Green, *Chem. Ind. (London)*, **1965**, 1031.

9) IR 975 cm^{-1} (TiO) for $[N(C_2H_5)_4]_2[TiOCl_4]$: A. Feltz, *Z. Anorg. Allg. Chem.*, **334**, 242 (1965).

10) J. H. Lunsford, *Catal. Rev.*, **8**, 135 (1973).

11) B. R. McGarvey and E. L. Tepper, *Inorg. Chem.*, **8**, 498 (1969).

BULLETIN OF THE CHEMICAL SOCIETY OF JAPAN, VOL. 50 (7), 1887—1888 (1977)

Purification of Xylenol Orange by the High-Speed Liquid Chromatography

Shoji NAKADA, Mutsuo YAMADA, Tasuku ITO, and Masatoshi FUJIMOTO
Department of Chemistry, Faculty of Science, Hokkaido University, Sapporo 060

(Received January 8, 1977)

Synopsis. A relatively large amount of 3,3′-bis[*N*, *N*-bis(carboxymethyl)aminomethyl]-*o*-cresolsulfonphthalein (Xylenol Orange, XO) is purified easily by the high-speed liquid chromatography (HSLC).

Despite of many interesting problems concerning the solution chemistry of metal complexes of a multidentate ligand XO, serious discrepancies have often been noted among the data reported by different authors. The discrepancies are primarily caused by the use of commercial or incompletely purified XO, which usually contains iminodiacetic acid (IDA), Semi-Xylenol Orange (SXO), and/or *o*-Cresol Red (*o*-CR) as the starting materials or a by-product of the synthesis of XO.[1-4] Since SXO and IDA also form metal complexes, the use of XO free from these impurities is essential for the quantitative studies of metal complex formation. Among the impurities *o*-CR is easy to remove, but the separation of IDA and SXO from XO is quite difficult.[3] Recently, a new method was established for the sharp separation of SXO and XO by the preparative thin-layer chromatography.[3] However, the method for easy separation of XO and IDA on a preparative scale has not been reported so far. In the present study we applied a technique of preparative HSLC and obtained easily a relatively large amount of pure XO.

The sample for HSLC was preliminarily purified by the cellulose column chromatography using an eluent, 1-butanol saturated with 10 or 25% aqueous acetic acid.[2,5] The paper partition chromatography (PPC) of the pretreated sample gave no spots of SXO and *o*-CR, but IDA still remained unremoved.

Figure 1 shows a typical elution curve of the preparative HSLC for the pre-purified sample. One gram of the sample was dissolved in 5 ml of water. Six hundred microliters of the solution were injected for each run. For the elution 5% aqueous acetic acid–methanol (80/20, v/v) was used as a solvent at a flow rate of 6.0 ml min^{-1} (pressure: 2400 psi). XO was clearly separated from the impurities on a preparative scale. The retention time assigned for IDA, XO, and SXO was measured beforehand with corresponding pure substances. Even a trace amount of SXO undetected by PPC was sharply discriminated as a peak of the preparative HSLC. The peak of *o*-CR, if any, is expected to appear at a retention time longer than 2 h under this condition.* The component for a peak at the retention time of 10 min was yellow and unidentified. After the elution of SXO the column was regenerated by washing with methanol for 20 min. This procedure flushed out the unknown yellow material. The column thus regenerated was used repeatedly.

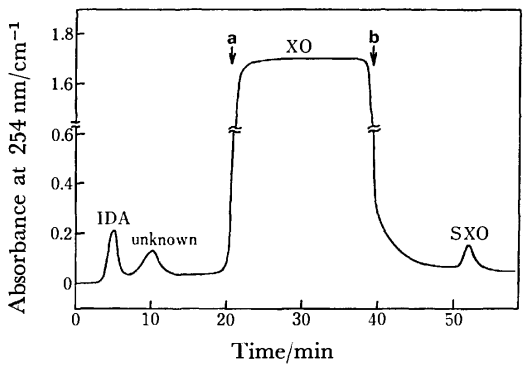

Fig. 1. Elution curve of the crude sample of XO.

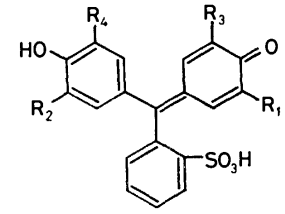

XO: $R_1=R_2=CH_2N(CH_2COOH)_2$, $R_3=R_4=CH_3$
SXO: $R_1=CH_2N(CH_2COOH)_2$, $R_2=H$, $R_3=R_4=CH_3$

The effluent between **a** and **b** as shown in Fig. 1 was collected as a portion of pure XO for each run. Each effluent was combined and concentrated in a rotary evaporator at 60—65 °C and dried in a vacuum desiccator. About 560 mg of the sodium salt of pure XO were obtained on eight runs from 960 mg of the pre-purified sample. From the elution curve and the amount of the isolated XO, the injected sample was found to consist of more than 58% XO, at most 19% IDA, 0.01% SXO, and other unknown materials.

Increasing methanol content in the developing solvent accelerated the elution of XO and SXO, but did not affect the retention time of IDA. The solvent composed of 5% aqueous acetic acid and methanol in the ratio 80/20 (v/v) gave the best separation of XO from IDA and SXO. This solvent is volatile and is more suitable for the subsequent treatment than the 1-butanol–acetic acid–water system used for the ordinary chromatographic method.

The pre-purification is not essential for the purification of XO by HSLC. By lowering the methanol content of the eluent, the present technique of HSLC is applicable to the sample obtained directly from the synthesis. *o*-CR, which is present in the synthetic mixture and is removable in the step of pre-purification, is

* A preliminary work of HSLC with a small column Microbondapak C_{18}, 4 mm × 300 mm, and a solvent of higher methanol content as 5% aqueous acetic acid–methanol (60/40, v/v) revealed that the retention time of *o*-CR was 17 min and much longer than that of IDA, XO, and SXO, 1.8, 3.5, and 8 min, respectively.

easily eliminated by the HSLC. However, since a crude XO obtained directly from the synthesis contains usually a fairly large amount of SXO, the unavoidable cross-contamination of SXO and XO might occur. In the present study, therefore, the pre-purification was carried out for the sake of the better yield and efficiency.

It is interesting to note that the sodium salt of the XO purified by the HSLC was not retained at all on a column of Dowex 50W-X8, a strongly acidic cation-exchange resin of medium cross-linking and in the hydrogen-form, whereas the sodium salt of the XO purified by the ordinary cellulose column chromatography was always partly and strongly retained on the exchanger.

Experimental

Materials. Acetic acid of analytical grade and an HSLC grade methanol were used for the elution chromatography. Water was deionized. A crude XO was synthesized according to the literature.[2)]

Instruments. All separations were carried out with a Waters Model ALC/GPC 244 chromatographic instrument equipped with two 7 mm×610 mm columns in series and a spectrophotometric detector (λ=254 nm). The columns were packed with Bondapak C_{18}/Porasil.

The Free Acid of the XO. An aqueous solution of the sodium salt of the purified XO was passed through a column of Dowex 50W-X8 in the hydrogen-form. The effluent was concentrated at *ca.* 60 °C in a rotary evaporator and dried in a vacuum desiccator. Mp *ca.* 286 °C (dec). Found: C, 53.33; H, 4.94; N, 4.14; S, 4.67%; S/N =1.13. Calcd for $C_{31}H_{32}O_{13}N_2S\cdot H_2O$: C, 53.91; H, 4.96; N, 4.06; S, 4.64%; S/N=1.14.

The authors wish to thank Messrs. C. Nakayama and M. Sato, Nihon Waters Ltd., for the kindness in the use of the HSLC instrument.

References

1) J. Körbl and R. Přibil, *Chem. Ind. (London)*, **1957**, 233.
2) M. Murakami, T. Yoshino, and S. Harasawa, *Talanta*, **14**, 1293 (1967).
3) M. Yamada and M. Fujimoto, *Bull. Chem. Soc. Jpn.*, **49**, 693 (1976).
4) B. Buděšínský, *Z. Anal. Chem.*, **206**, 262 (1964).
5) S. Nakada and M. Fujimoto, unpublished result.

BULLETIN OF THE CHEMICAL SOCIETY OF JAPAN, VOL. 50 (7), 1889—1890 (1977)

Polarographic Catalytic Currents Observed in Mixtures of Pb(II) and H_2O_2 in Neutral Solutions

Sadayuki HIMENO

Department of Chemistry, College of General Education, Kobe University, Nada-ku, Kobe 657

(Received January 13, 1977)

Synopsis. Normal pulse polarography has shown that the catalytic wave observed in neutral mixtures of Pb(II) and H_2O_2 is caused by $Pb(OH)^+$ at the electrode surface, and that OH^- ions are liberated in the vicinity of the electrode due to the catalytic reaction.

It was first noticed by Strnad that traces of Pb(II) ions in neutral air-saturated solutions greatly increased the first oxygen wave.[1] This effect of Pb(II) ions was explained as being due to the reduction of H_2O_2 arising from the reduction of oxygen.

This paper will describe the results of a polarographic investigation of the Pb(II)–H_2O_2 system.

Apparatus and Reagents

Apparatus. The polarograms were obtained with a PAR (Princeton Applied Research) Polarograph, Model 174. The polarograms were recorded on a Riken Denshi X-Y Recorder, Model D-8C. The dropping mercury electrode (DME) used had a $m^{2/3} t^{1/6}$ of 1.45 $mg^{2/3} s^{-1/2}$ in 0.1 M KNO_3 in an open circuit. The drop time of the DME was controlled at 1.0 s by means of a Mechanical Drop Time Controller, Model 172-A. The pH values of the test solutions were measured with a Hitachi-Horiba pH Meter, Model M-7. A saturated calomel electrode (SCE) was used as the reference electrode. The solutions were deoxygenated by bubbling nitrogen gas through them. All the experiments were carried out at (25±0.1)°C.

Reagents. All the chemicals were of a reagent grade and were used without further purification.

Results and Discussion

Figure 1(A) shows the effect of the pH on the DC polarogram of 1.0 mM Pb(II) in 0.1 M $NaNO_3$ without dissolved oxygen. When pH <5, a single wave was observed with a half-wave potential of −0.38 V. As the pH was increased, the wave split into two waves, the relative heights being pH-dependent. When pH >8.5, the first wave disappeared and only the second one remained.

Figure 1(B) shows the percentage distribution curves calculated from the data[2] for the four possible species present in Pb(II) solutions. The observed dependence of the relative wave heights on the pH corresponds to the changing ratio of the aquated Pb(II) ion to the hydroxide species. Therefore, the first wave is ascribed to the reduction of the aquated Pb(II) ion, and the second, to the reduction of $Pb(OH)^+$.

Figure 2 illustrates DC polarograms of 0.4 mM Pb(II) in 0.1 M $NaNO_3$ (pH 4.6) containing 5 mM H_2O_2. The catalytic wave was observed in unbuffered solutions in the pH range of 4—8 (Curve a).

The polarographic behavior of the Pb(II) ion in buffered solutions of various pH values was also investigated. When the pH was adjusted with either an acetate or barbital buffer to lie in the range of 4—5, where $Pb(OH)^+$ did not exist to any appreciable extent in the solution, no catalytic wave appeared (Curve b in Fig. 2). However, in either a borate or barbital buffer with a pH of about 7.5 (in the pH region where $Pb(OH)^+$ exists), the catalytic wave appeared.

Normal pulse polarography was applied to elucidate a catalytically active Pb(II) species. Figure 3 shows normal pulse polarograms of 1.0 mM Pb(II) in 0.1 M $NaNO_3$ (pH 4.8) containing various concentrations of H_2O_2. With the H_2O_2 concentration of 2 mM, the initial single wave split into three waves. Above this

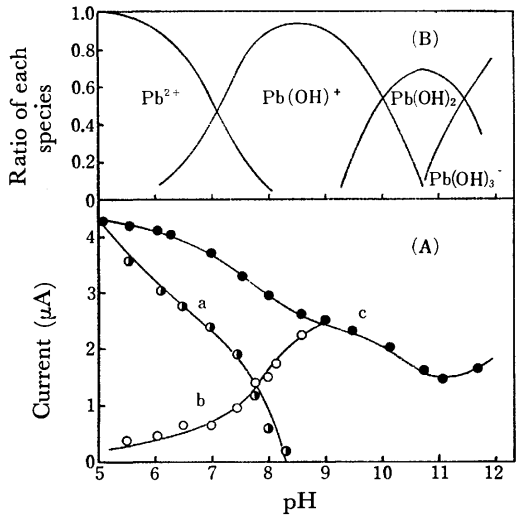

Fig. 1(A). Effect of pH on DC polarographic wave of 1.0 mM Pb(II) in 0.1 M $NaNO_3$ without dissolved oxygen.
a) lst wave. b) 2nd wave. c) Total wave.
Fig. 1(B). Effect of pH on the ratio of four Pb(II) species.

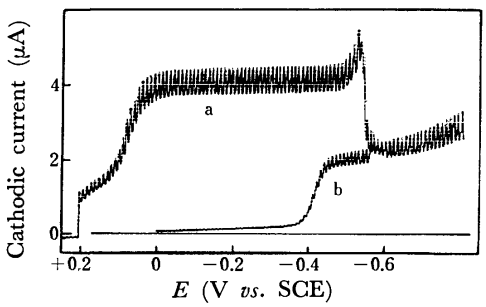

Fig. 2. Catalytic wave.
a) 0.4 mM Pb(II) in 0.1 M $NaNO_3$ (pH 4.6) containing 5 mM H_2O_2.
b) Solution (a) with acetate buffer (pH 4.6).

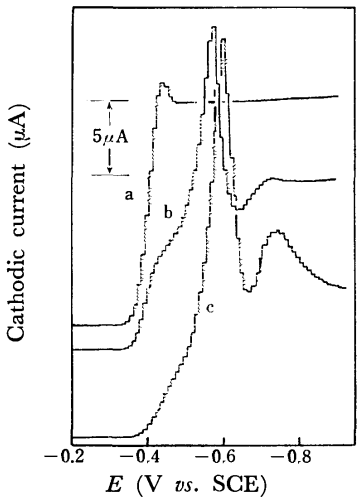

Fig. 3. Normal pulse polarograms of 1.0 mM Pb(II) in 0.1 M $NaNO_3$ (pH 4.8) containing various concentrations of H_2O_2. H_2O_2 concentration (mM) a) 0. b) 2.0. c) 3.0. $E_1 = -0.2$ V.

H_2O_2 concentration, the first wave disappeared with an increase in the height of either the second or the third one.

To identify the Pb(II) species responsible for each wave, normal pulse polarograms in unbuffered solutions containing 1 mM Pb(II) and dissolved oxygen were also recorded. When the initial potential was set at +0.3 V, which was more anodic than the reduction potential of the first oxygen wave, the normal pulse polarogram of Pb(II) had two reduction waves. The first wave was interpreted as being due to the reduction of the aquated Pb(II) ion, and the second, to the reduction of $Pb(OH)^+$, the behavior of which was analogous to that observed in DC polarography. When the initial potential was set at −0.2 V, where the reduction of oxygen took place, the normal pulse polarogram consisted of three waves similar to Curve (b) of Fig. 3. Under these conditions, the concentration of OH^- ions increases in the vicinity of the electrode at the initial potential because of the reduction of the oxygen.

By buffering the solution, either the second or the third wave disappeared completely and the first wave became well defined.

As has been reported previously,[3,4] $Ni(OH)_2$ and $Fe(OH)_2$ produced similar waves on a normal pulse polarogram under the same conditions. Similarly, the third wave reflects the reduction of the $Pb(OH)_2$ formed at the electrode surface.

By analogy with the system composed of Pb(II) and dissolved oxygen, it is conculded that the first wave of Fig. 3(b) corresponds to the reduction of the aquated Pb(II) ion, and that the two remaining waves are due to the reduction of $Pb(OH)^+$ and $Pb(OH)_2$. This means that the catalytic reaction between Pb(II) and H_2O_2 proceeds with the formation of OH^- ions in the vicinity of the electrode.

Figure 4 shows the effect of the pH on the normal pulse polarogram of 1.0 mM Pb(II) in 0.1 M $NaNO_3$ containing 5 mM H_2O_2. Clearly, under the conditions where the catalytic reaction occurs, the aquated Pb(II) ion does not exist in the solution, and the region where $Pb(OH)^+$ is present is about from pH 4 to 8, this range agreeing with that where the catalytic wave appears in DC polarography.

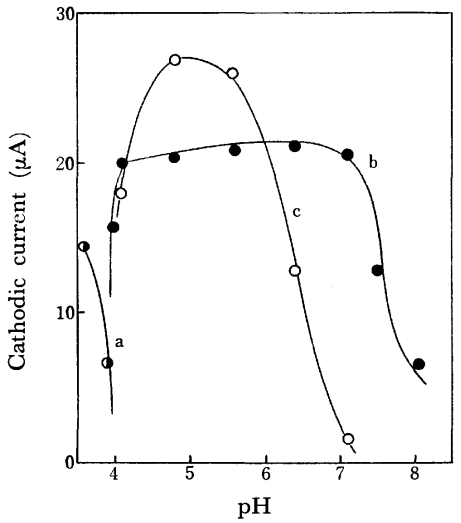

Fig. 4. Effect of pH on normal pulse polarographic wave of 1.0 mM Pb(II) in 0.1 M $NaNO_3$ containing 5 mM H_2O_2.
a) lst wave. b) 2nd wave. c) 3rd wave.
$E_1 = -0.2$ V.

As is shown in Fig. 2, the catalytic current drops at −0.55 V, which is about 0.17 V more negative than the reduction potential of the aquated Pb(II) ion. This result also indicates that the aquated Pb(II) ion is converted to $Pb(OH)^+$ as a result of the catalytic reaction. This is inconsistent with the work of Strnad, who explained the current drop in terms of the direct reduction of the aquated Pb(II) ion to Pb(0).

The most likely mechanism for the catalytic reaction is that $Pb(OH)^+$ is oxidized by H_2O_2 to the Pb(IV) ion, which is then rapidly reduced at DME to produce a catalytic wave. Traces of $Pb(OH)^+$ may cause the catalytic reaction in unbuffered solutions in the pH range of 4—5. An increase in $Pb(OH)^+$ at the electrode surface is necessary for the catalytic reaction to proceed under these conditions.

The author wishes to thank Professor Atsuyoshi Saito for his valuable advice and for his helpful discussions throughout this study.

References

1) F. Strnad, *Collect. Czech. Chem. Commun.*, **11**, 391 (1939).
2) A. Martell and L. G. Sillén, "Stability Constants of Metal-ion Complexes," The Chemical Society, London (1964), p. 69.
3) A. Saito and S. Himeno, *Nippon Kagaku Kaishi*, **1975**, 1751.
4) S. Himeno, *Bull. Chem. Soc. Jpn.*, **49**, 2451 (1976).

BULLETIN OF THE CHEMICAL SOCIETY OF JAPAN, VOL. 50 (7), 1891—1892 (1977)

Preparation and Resolution of (4-Aminobutanoic acidato)bis-(ethylenediamine)cobalt(III) Ion

Masaaki KOJIMA, Hiromichi TAKAYANAGI, and Junnosuke FUJITA

Department of Chemistry, Faculty of Science, Nagoya University, Chikusa, Nagoya 464

(Received January 31, 1977)

Synopsis. A new complex containing a seven-membered chelate ring, $[Co(amb)(en)_2]^{2+}$ (amb=4-aminobutanoato ion) was prepared and resolved. The complex is decomposed in 1.0 M $HClO_4$ at room temperature to give $[Co(H_2O)(Hamb)(en)_2]^{3+}$ in which the Hamb acts as a unidentate ligand with a free carboxyl group.

Although complexes of the type, $[Co(am)(en)_2]^{2+}$ (am=amino acidate ion) have been prepared and resolved for a variety of amino acids, no complex has been reported for 4-aminobutanoato ion (amb) which forms a seven-membered chelate ring. This Note will describe the preparation and resolution of $[Co(amb)(en)_2]^{2+}$ and compare the absorption and circular dichoism(CD) spectra with those of the corresponding glycinato and β-alaninato complexes. Koine *et al.*[1] prepared a complex containing amb, *trans*(*N*)-K[Co(nta)(amb)]·$3H_2O$(nta =nitrilotriacetate ion). However, no evidence was given for the formation of a seven-membered chelate ring. Such large chelate ligands as amb tend to coordinate to a metal ion as a unidentate ligand or to two metal ions as a bridging ligand.[2,3]

Experimental

Ligands. Guaranteed reagent grade 4-aminobutanoic acid, β-alanine, and glycine were obtained from Wako Pure Chemical Industries Co. and used without further purification.

$[Co(amb)(en)_2]Cl_2\cdot 2.5H_2O$. A solution of sodium methoxide (0.16 g, 3.0 mmol) and 4-aminobutanoic acid (0.31 g, 3.0 mmol) in methanol (7 cm^3) was added to a solution of *trans*-$[CoCl_2(en)_2]ClO_4$ (0.9 g, 3.0 mmol) in DMSO(250 cm^3). The solution was stirred for 20 h at 40 °C, and then diluted with 3 dm^3 of water. This was passed through an SP-Sephadex column ($\phi 4.5\times 30$ cm), and the adsorbed complexes were chromatographed with a 0.2 M Na_2SO_4 solution. The column showed seven separate bands. The effluent of the first red band was diluted with 3 dm^3 of water and poured again on an SP-Sephadex column ($\phi 2.7\times 3$ cm). The adsorbed complex was eluted with a 1.0 M $CaCl_2$ solution, and the effluent was concentrated to a syrup in a vacuum desiccator over P_2O_5. The excess $CaCl_2$ was extracted repeatedly with a small amount of isopropyl alcohol until the complex began to crystallize. The complex was dissolved in a small amount of water, and isopropyl alcohol was added to the solution. Purplish red crystals which formed on cooling the mixing solution in a refrigerator were filtered off and washed with isopropyl alcohol. The complex was recrystallized from water by the addition of isopropyl alcohol. Found: C, 24.24; H, 7.38; N, 18.10%. Calcd for $CoC_8H_{29}N_5O_{4.5}Cl_2$=[Co(amb)$(en)_2]Cl_2\cdot 2.5H_2O$: C, 24.19; H, 7.36; N, 17.63%.

$[Co(gly)(en)_2](ClO_4)_2$ and $[Co(\beta\text{-ala})(en)_2](ClO_4)_2\cdot H_2O$. $[Co(gly)(en)_2](ClO_4)_2$ was prepared by the method of Shimura and Tsuchida.[4] $[Co(\beta\text{-ala})(en)_2](ClO_4)_2\cdot H_2O$ was obtained from the corresponding chloride.[5] The complex chloride adsorbed on SP-Sephadex was eluted with a 1.0 M $NaClO_4$ solution, and the effluent was concentrated to a small volume in a vacuum desiccator over P_2O_5. The concentrate was mixed with ethanol, and cooled. Red crystals were filtered off, washed with ethanol, and recrystallized from water by the addition of ethanol. Found: C, 17.40; H, 4.99; N, 14.46%. Calcd for $CoC_7N_5H_{24}O_{11}Cl_2$=$[Co(\beta\text{-ala})(en)_2](ClO_4)_2\cdot H_2O$: C, 17.36; H, 5.00; N, 14.46%.

Chromatographic Resolution of the Complexes. A solution containing about 0.1 mmol of the amb complex (or the β-ala or the gly complex) was poured on an SP-Sephadex column ($\phi 2.7\times 120$ cm) and the adsorbed band was eluted with a 0.1 M sodium $(+)_{589}$-tartrate or a 0.08 M sodium $(+)_{589}$-tartratoantimonate(III) solution. Two bands, the $(+)_{589}$- and $(-)_{589}$-isomers, were eluted in this order. Each eluate was passed through an SP-Sephadex column ($\phi 1.5\times 3$ cm) after dilution with water and the adsorbed complex was eluted with a 1.5 M $NaClO_4$ solution.

Measurements. Absorption and CD spectra were obtained on a Hitachi 323 spectrophotometer and a JASCO J-20 spectropolarimeter, respectively.

Results and Discussion

$[Co(gly)(en)_2]^{2+}$ and $[Co(\beta\text{-ala})(en)_2]^{2+}$ can easily be prepared by the reactions of *trans*-$[CoCl_2(en)_2]^+$ with gly or β-ala, respectively in water at fairly high concentration of the reactants. A reaction with amb under a similar condition is not expected to give the desired complex, since such large chelate ligands as amb or tmd(tetramethylenediamine) tend to act as a bridging

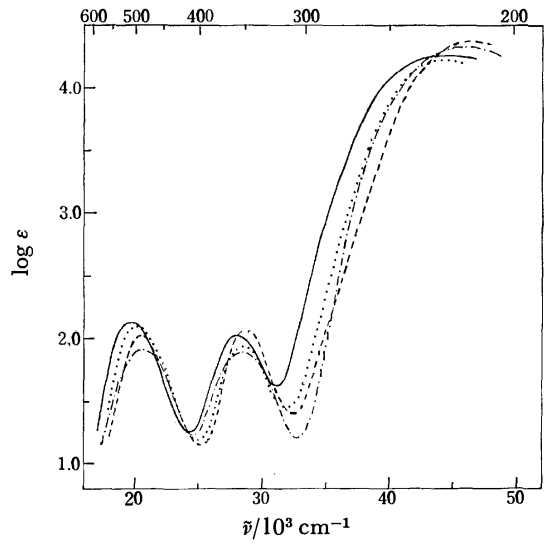

Fig. 1. Absorption spectra of $[Co(gly)(en)_2]^{2+}$(----), $[Co(\beta\text{-ala})(en)_2]^{2+}$(·····), and $[Co(amb)(en)_2]^{2+}$(——) in water, and $[Co(H_2O)(Hamb)(en)_2]^{3+}$(—·—) in 1.0 M $HClO_4$.

Table 1. Absorption and CD spectral data

Complex	Absorption[a]		CD[b]	
	$\bar{\nu}$/cm^{-1}	log ε	$\bar{\nu}$/cm^{-1}	$\Delta\varepsilon$
$(+)_{589}$[Co(gly)(en)$_2$]$^{2+}$	20450	2.00	19690	+2.26
	28800	2.03	27000	+0.09
			30300	+0.15
	45900	4.15	46700	−27
$(+)_{589}$[Co(β-ala)(en)$_2$]$^{2+}$	20160	2.09	19270	+1.28
			21800	−0.52
	28400	1.93	27300	+0.21
	44100	4.22	44100	−12
$(+)_{589}$[Co(amb)(en)$_2$]$^{2+}$	19800	2.11	18690	+1.27
			21470	−0.71
	27900	2.03	27400	+0.20
	44100	4.27	47200	−17
$(+)_{589}$[Co(H_2O)(Hamb)-(en)$_2$]$^{3+}$	20530	1.90	20620	+0.31
	28500	1.89	26400	+0.10
			30300	+0.03
	45500	4.32	45700	−8.5

a) In water except for $(+)_{589}$[Co(H_2O)(Hamb)(en)$_2$]$^{3+}$ which was measured in 1.0 M $HClO_4$. b) In 1.5 M $NaClO_4$ except for $(+)_{589}$[Co(H_2O)(Hamb)(en)$_2$]$^{3+}$ which was measured in 1.0 M $HClO_4$.

ligand to yield polymeric complexes.[3] Thus, we have carried out the reaction in a highly dilute solution as described in the Experimental part. The use of organic solvent, DMSO is known to be useful for preparing complexes containing large chelate rings.[6]

The formation of the amb chelate ring is evidenced by the following observations. The absorption spectrum of the amb complex in a 1.0 M $HClO_4$ solution changes with isosbestic points(416, 458 nm), the change at room temperature(25 °C) being completed in a day. Since the first absorption band (487 nm) of the final spectrum is nearly the same as that (485 nm) of *cis*-[Co(H_2O)(NH_3)(en)$_2$]$^{3+}$,[7] the spectral change may correspond to a ring-opening reaction of the amb chelate to give *cis*-[Co(H_2O)(Hamb)(en)$_2$]$^{3+}$ (Fig. 1). The absorption spectra of the gly and β-ala complexes in 1.0 M $HClO_4$ remained unchanged over a prolonged heating. Further, the amb complex adsorpbed on SP-Sephadex is eluted with a 0.2 M Na_2SO_4 solution with a similar R_f value to those of the gly and β-ala complexes.

As Fig. 1 and Table 1 show, the d-d absorption bands of the present series of complexes, [Co(am)(en)$_2$]$^{2+}$ shift to longer wavelengths as the number of ring members of the amino acidate ligands increases. A similar shift was observed for complexes of the type, [Co(en)$_2$(diamine)]$^{3+}$; the first absorption bands of [Co(en)$_3$]$^{3+}$, [Co(en)$_2$(tn)]$^{3+}$(tn=trimethylenediamine), and [Co(en)$_2$(tmd)]$^{3+}$ are at 21.3, 21.0, and 20.9×10^3 cm^{-1}, respectively.[3]

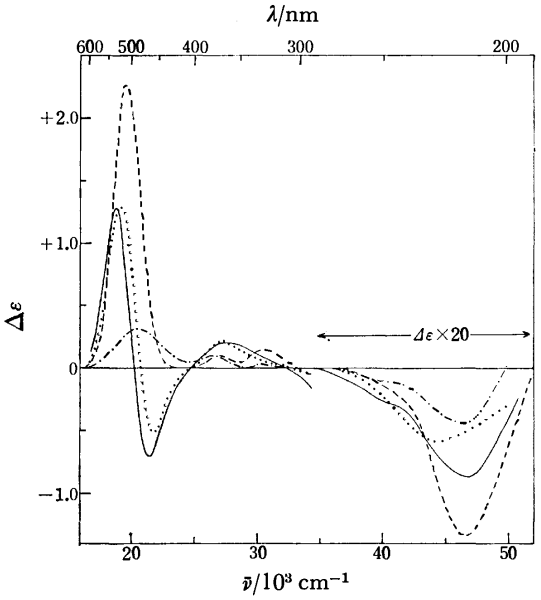

Fig. 2. CD spectra of $(+)_{589}$[Co(gly)(en)$_2$]$^{2+}$(----), $(+)_{589}$[Co(β-ala)(en)$_2$]$^{2+}$(·····), and $(+)_{589}$[Co(amb)-(en)$_2$]$^{2+}$(——) in 1.5 M $NaClO_4$, and $(+)_{589}$ [Co(H_2O)-(Hamb)(en)$_2$]$^{3+}$(—·—) in 1.0 M $HClO_4$.

All the complexes have been completely resolved by SP-Sephadex column chromatography. Figure 2 shows the CD spectra of the $(+)_{589}$-isomers. The CD spectrum of the gly complex agrees well with that reported previously.[8] All the $(+)_{589}$-isomers give a main positive and a strong negative CD band in the first absorption and the charge transfer region, respectively. Therefore, it can be concluded that these isomers have the same absolute configuration, *Λ*. The β-ala and the amb complexes exhibit negative CD components at a shorter wavelength side of the first absorption band. Although no such a component is observed for the gly complex, these negative components seem to increase the strength as the number of ring member of the amino acidate ligand increases.

References

1) N. Koine, N. Sakota, J. Hidaka, and Y. Shimura, *Bull. Chem. Soc. Jpn.*, **42**, 1583 (1969).
2) A. Takenaka, E. Oshima, S. Yamada, and T. Watanabe, *Acta Crystallogr., Sect. B*, **29**, 503 (1973).
3) H. Ogino and J. Fujita, *Bull. Chem. Soc. Jpn.* **48**, 1836 (1975).
4) Y. Shimura and R. Tsuchida, *Bull. Chem. Soc. Jpn.*, **29**, 311 (1956).
5) M. Ogawa, Y. Shimura, and R. Tsuchida, *Nippon Kagaku Zasshi*, **81**, 72 (1959).
6) H. Ogino and J. Fujita, *Chem. Lett.*, **1973**, 517.
7) F. Basolo, *J. Am. Chem. Soc.*, **72**, 4393 (1950).
8) C. T. Liu and B. E. Douglas, *Inorg. Chem.*, **3**, 1356 (1964).

BULLETIN OF THE CHEMICAL SOCIETY OF JAPAN, VOL. 50 (7), 1893—1894 (1977)

An X-Ray Diffraction Study on the Structure of the Aqua Indium(III) Ion in the Perchlorate Solution

Masunobu MAEDA[1] and Hitoshi OHTAKI

Laboratory of Solution Chemistry, Tokyo Institute of Technology, O-okayama, Meguro-ku, Tokyo 152

(Received March 4, 1977)

Synopsis. The structure of the aqua indium(III) ion has been studied in a 3 mol dm^{-3} $In(ClO_4)_3$ solution at 25 °C by an X-ray diffraction method. The result showed that the indium(III) ion has six nearest water molecules and the In–OH_2 bond distance is 2.15±0.03 Å.

Only a few investigations have been carried out on the structure of indium(III) ion in aqueous solution. Fratiello *et al.*[2] reported from NMR measurements that the indium(III) ion is coordinated by six water molecules in aqueous acetone mixtures. Celeda and Tuck[3] found the $In(OH_2)_6^{3+}$ complex in an aqueous perchlorate solution by densitometry. However, no X-ray analysis has been carried out both for crystal hydrates and solutions, and no datum for the bond length between the indium(III) ion and the coordinated water molecules is available. In the present work, we aimed at determining the bond distance within the aqua indium(III) complex as well as the coordination number of the indium(III) ion in solution.

Experimental Procedure and Treatment of Data

Indium(III) perchlorate was prepared by dissolving indium oxide (99.99% purity) in perchloric acid and recrystallized twice from water. Crystals were dissolved in dilute perchloric acid in order to suppress hydrolysis of the indium(III) ions. The concentration of indium(III) ions in the sample solution was determined gravimetrically by using 8-quinolinol.[4] The concentrations of hydrogen and perchlorate ions were determined as described previously.[5] The atomic composition of the sample solution is listed in Table 1.

TABLE 1. ATOMIC COMPOSITIONS OF THE INDIUM(III) PERCHLORATE SOLUTION (in g-atom dm^{-3})

In	3.023
Cl	9.388
O	71.61
H	68.44

X-Ray scattering data were obtained at 25 °C on a θ-θ diffractometer (JEOL Co., Tokyo) equipped with a Philips Mo-X-ray tube (wavelength λ=0.7107 Å). The measured scattering angles (2θ) ranged from 2 to 140°. Details of measurements and treatments of data are described elsewhere.[5]

Results and Discussion

The radical distribution curve $D(r)$ calculated from the scattered intensities is shown in Fig. 1. Two distinct peaks are seen at around 1.4 and 2.3 Å. The first peak is readily identified to be due to the Cl–O bond within the ClO_4^- ion.[5] The second peak may be ascribed to the In^{3+}–OH_2 bond within the aqua indium(III) ion, because the peak appears at the position as is expected from the sum of the ionic radius of In^{3+} (0.81 Å[6]) and the size of a water molecule ({O–O in water}/2=1.4 Å[7]). This peak contains the contribution from the O–O contact within the tetrahedral ClO_4^- ion (1.4 Å×$\sqrt{8/3}$=2.3 Å). The contribution of the Cl–O and O–O contacts within the perchlorate ion (curve b) was subtracted from the radial distribution curve. The bond distances r, temperature factors b, and frequency factors n of the atom pairs are quoted from Ref. 5. The rest is depicted as curve c in Fig. 1.

The bond distance between In^{3+} and the water molecules in the first hydration shell and the number of hydrated water molecules were determined from curve c by the trial-and-error method. The assumption of r=2.15 Å, b=0.004 $Å^2$, and n=6 led to a smooth background curve (curve e) without an indication of other atom pairs having bond distances less than 2.5 Å. The theoretical peak calculated by using these parameters is drawn as curve d in the same figure. The uncertainty in r is estimated approximately to be ±0.03 Å by the trial-and-error method. We could not find a clear indication for the octahedral structure of the $In(OH_2)_6^{3+}$

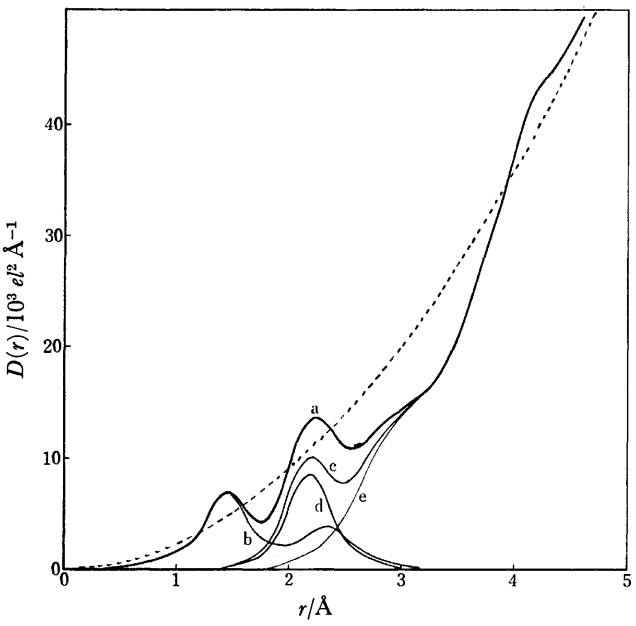

Fig. 1. a: $D(r)$ curve, b: theoretical peak shapes for the Cl–O and O–O contacts within ClO_4^-, c: residual curve ($D(r)$ − curve b), d: theoretical peak shape for the In–OH_2 bond within $In(OH_2)_6^{3+}$, e: background curve (curve c − curve d). The broken curve denotes $4\pi r^2\rho_0$.

complex, because the radial distribution curve did not give distinct peaks (although humps are observed) at about 3.04 Å ($=2.15\ Å \times \sqrt{2}$) and about 4.30 Å ($=2.15\ Å \times 2$) for the *cis*-O–O and *trans*-O–O contacts, respectively, within the $In(OH_2)_6^{3+}$ ion.

The present work is financially supported in part by the Japan Society for Promotion of Science.

References

1) Present address: Department of Applied Chemistry, Nagoya Institute of Technology, Gokiso, Showa, Nagoya 466.
2) A. Fratiello, R. E. Lee, V. M. Nishida, and R. E. Schuster, *J. Chem. Phys.*, **48**, 3705 (1968).
3) J. Celeda and D. G. Tuck, *J. Inorg. Nucl. Chem.*, **36**, 373 (1974).
4) G. L. Royer, *Ind. Eng. Chem. Anal. Ed.*, **12**, 439 (1940).
5) H. Ohtaki, M. Maeda, and S. Ito, *Bull. Chem. Soc. Jpn.*, **47**, 2217 (1974).
6) L. Pauling, "The Nature of the Chemical Bond", Cornell University Press (1960).
7) A. H. Narten, ORLN-4578 (1970).

BULLETIN OF THE CHEMICAL SOCIETY OF JAPAN, VOL. 50 (7), 1895—1896 (1977)

The Reactions of Several Anilides with Phosphoryl Chloride

Masahiro FUKUDA, Yoshiki OKAMOTO, and Hiroshi SAKURAI

The Institute of Scientific and Industrial Research, Osaka University, Yamada-kami, Suita-shi, Osaka 565

(Received July 8, 1976)

Synopsis. Chloroacetanilide and *p*-methylchloroacetanilide reacted with phosphoryl chloride to give 2-chloromethyl-3-chloro-4-anilinoquinoline and 2-chloromethyl-3-chloro-4-(*p*-toluidino)-6-methylquinoline respectively. In the case of propionanilide, 2-ethyl-3-methyl-4-anilinoquinoline was obtained when the reaction was carried out at 20—30 °C. On the other hand, when the reaction temperature was raised to 80—100 °C, *N*-(1-chloro-1-propenyl)-*N*,*N*′-diphenylacetamidine was obtained.

It is well known that a Vilsmeier reagent can be prepared from an *N*,*N*-disubstituted amide, such as *N*,*N*-dimethylformamide or *N*,*N*-dimethylbenzamide, with phosphoryl chloride.[1] *N*,*N*-Unsubstituted amides, such as acetamide and benzamide, are also known to be converted into the corresponding nitrile in good yields by treatment with phosphoryl chloride.[2] In this paper, we wish to report the reaction of anilides with phosphoryl chloride.

Results

Propionanilide was allowed to react with phosphoryl chloride at 80—100 °C for 3 h, thus giving *N*-(1-chloro-1-propenyl)-*N*,*N*′-diphenylpropionamidine(I). When the reaction was carried out in the temperature range between 20 and 30 °C for 24 h, 2-ethyl-3-methyl-4-anilinoquinoline(II) and *N*,*N*′-diphenylpropionamidine (III) were obtained.

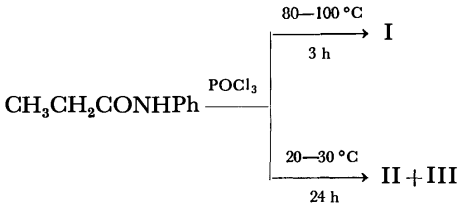

(1)

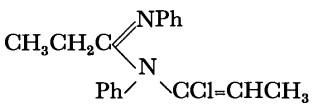

(I)

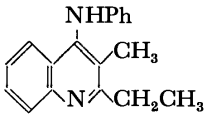

(II)

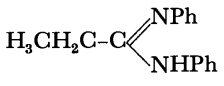

(III)

When chloroacetanilide(IVa) and *p*-methylchloroacetanilide(IVb) were used in place of propionanilide, 2-chloromethyl-3-chloro-4-anilinoquinoline(Va) and 2-chloromethyl-3-chloro-4-(*p*-toluidino)-6-methylquinoline(Vb) were isolated in 50—60 and 26% yields respectively. Amidine derivatives were not detected, regardless of the reaction temperature.

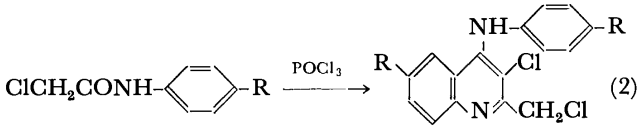

(2)

(IVa, R=H; IVb, R=Me) (Va, R=H; Vb, R=Me)

On the other hand, when the reaction of acetanilide with phosphoryl chloride was run at 80 °C for 3 h, *N*,*N*-diphenylacetamidine(VI) and *N*-(1-chlorovinyl)-*N*,*N*′-diphenylacetamidine(VII) were yielded in an equimolar ratio. When the reaction conditions were controlled at 20—30 °C for 24 h, the distribution of products VI and VII was changed to the molar ratio of 74 : 26.

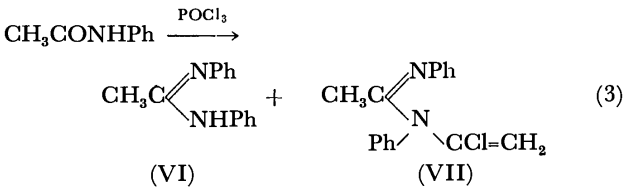

(3)

(VI) (VII)

In the case of formanilide with phosphoryl chloride, *N*,*N*′-diphenylformamidine(VIII) was obtained in a 10% yield.

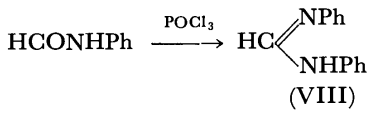

(VIII)

The results of these experiments are summarized in Table 1.

Experimental

All the melting and boiling points are uncorrected. The NMR spectra were measured at 100 MHz on a JNM-TS-100 spectrometer, with TMS as the internal reference in deuteriochloroform. The mass spectra were recorded on a Hitachi RMU-6 or RMU-7 spectrometer.

Materials. Commercial first-grade acetanilide and formanilide were used after recrystallization. Chloroacetanilide (mp 138 °C), *p*-methylchloroacetanilide (mp 163 °C), and propionanilide (mp 104 °C) were prepared in the usual way.

Reaction of Anilides with Phosphoryl Chloride. General Procedure: In a 150-ml flask fitted with a reflux condenser we placed 50 mmol of anilide and 55 mmol of phosphoryl chloride. The mixture was then magnetically stirred, and the temperature was maintained at 20—30 or 80—100 °C for an appropriate period. After cooling, the mixture was poured into 150 ml of ice water, the solution was then allowed to stand for an additional 24 h. The HCl salt of the quinoline derivative(II, V, and VIII) was precipitated if quinoline was present, and easily separated by filtration. The filtrate was extracted twice with ether to remove the unreacted anilide. The aqueous layer was neutrallized with a 1 M NaOH aq solution to pH 7. The crude amidine derivative (I or VII) was extracted with ether. The aqueous layer was treated

Table 1. The reaction of several anilides with phosphoryl chloride

Anilide	Temp (°C)	Time (h)	Product, isolated yield (%)	
			Quinoline derivative	Amidine derivative(s)
$HCONHC_6H_5$	20—30	1	0	10
$CH_3CONHC_6H_5$	20—30	24	0	78
	80—100	3	0	50
$CH_3CH_2CONHC_6H_5$	20—30	24	23	trace
	80—100	3	0	8
$ClCH_2CONHC_6H_5$	20—30	24	59	0
	80—100	3	50	0
$ClCH_2CONHC_6H_4 \cdot CH_3$-*p*	80	2	26	0

with a large amount of a 1 M NaOH solution. The amidines (III, VI, and VIII) were precipitated.

Physical Properties and Analytical Data of the Products. *Product I*: Bp 100 °C/10^{-4} Torr. NMR ($CDCl_3$): δ 1.00 (t, 3H, $-CH_2\underline{CH_3}$) 1.80 (d, 3H, $=CH\underline{CH_3}$) 2.45 (q, 2H, $-\underline{CH_2}CH_3$) 5.82 (q, 1H, $=\underline{CH}CH_3$) 6.7—7.6 (m, 10H, aromatic protons). MS: *m/e* (rel intensity) 298 (M^+ Cl^{35}, 2) 283 (11) 167 (15) 132 (100) 103 (18) 93 (69) 77(92). Found: Cl, 11.54%. Calcd for $C_{18}H_{19}N_2Cl$: Cl, 11.74%.

Product II: Mp 183 °C. NMR: δ 1.38 (t, 3H, $-CH_2\underline{CH_3}$) 2.30 (s, 3H, $-CH_3$) 3.05 (q, 2H, $-\underline{CH_2}CH_3$) 5.85 (br, 1H, NH) 6.5—8.1 (m, 9H, aromatic protons). MS: *m/e* 262 (M^+, 100) 245 (18) 234 (13). Found: Cl, 11.65%. Calcd for $C_{18}H_{18}N_2 \cdot HCl$: Cl, 11.89%. The product(II) had NMR and mass spectra identical with those of an authentic sample.[3]

Product III: Mp 100—102 °C. NMR: δ 1.10 (t, 3H, $-CH_2\underline{CH_3}$) 2.26 (q, 2H, $-\underline{CH_2}CH_3$) 5.8 (br, 1H, NH) 6.9—7.3 (m, 10 H, aromatic protons). MS: *m/e* 224 (M^+, 17) 132 (100) 104 (9) 77 (43). The product(III) had NMR and mass spectra identical with those of an authentic sample, which had been prepared from propionanilide and aniline by the method of Partridge and Smith.[4]

Product Va: Mp 133—133.5 °C. NMR: δ 4.96 (s, 2H, $-CH_2Cl$) 6.5—8.1 (m, 10 H, aromatic protons and NH). MS: *m/e* 302 (M^+ Cl^{35} Cl^{35}, 100) 267 (29) 231 (97) 115 (16) 102 (13) 77 (26). Found: C, 63.02; H, 3.87; N, 9.16%. Calcd for $C_{16}H_{12}N_2Cl_2$: C, 63.37; H, 3.96; N, 9.24%.

Product Vb: Mp 130—132 °C. NMR: δ 2.28 (s, 6H, two methyl groups) 4.88 (s, 2H, $-CH_2Cl$) 6.5—8.0 (m, 8H, aromatic protons and NH). MS: *m/e* 332 (Cl^{36} Cl^{36}, 75) 330 (M^+ Cl^{35} Cl^{35}, 100) 296 (30) 259 (75).

Product VI: Mp 131—132 °C. NMR: δ 2.00 (s, 3H, $-CH_3$) 6.15 (s, 1H, NH) 7.0—7.5 (m, 10 H, aromatic protons). MS: *m/e* 210 (M^+, 21) 118 (100) 93 (9) 77 (32). Found: C, 79.87; H, 6.66; N, 13.16%. Calcd for $C_{14}H_{14}N_2$: C, 79.96; H, 6.71; N, 13.32%.

Product VII: Mp 117.5—118.5 °C. NMR: δ 1.90 (s, 3H, $-CH_3$) 5.37 (d, $1H_a$, $=CH_aH_b$ J_{ab} 4Hz) 5.45 (d, $1H_b$) 6.7—7.4 (m, 10 H, aromatic protons). MS: *m/e* 270 (M^+ Cl^{35}, 16) 118 (100) 77 (76). Found: C, 70.93; H, 5.35; N, 10.21; Cl 13.60%. Calcd for $C_{16}H_{15}N_2Cl$: C, 71.11; H, 5.55; N, 10.37; Cl, 13.15%.

Product VIII: Mp 136—136.6 °C. NMR: δ 7.0—7.5 (m, 10 H, aromatic protons) 8.22 (br, 1H, NH) 8.55 (s, 1H, CH). MS: *m/e* 196 (M^+, 26) 104 (11) 93 (100) 77(26). Found: C, 79.40; H, 6.02; N, 14.22%. Calcd for $C_{13}H_{12}N_2$: C, 79.56; H, 6.16; N, 14.28%.

References

1) H. H. Bosshard and H. Zollinger, *Helv. Chim. Acta*, **42**, 1659 (1959).
2) R. B. Wagner and H. D. Zook, "Synthetic Organic Chemistry," John Wiley & Sons, New York (1953), p. 596.
3) J. von Braum and A. Heymons, *Ber.*, **63**, 3191 (1930).
4) M. W. Partridge and A. Smith, *J. Chem. Soc., Perkin Trans. 1*, **5**, 453 (1973).

BULLETIN OF THE CHEMICAL SOCIETY OF JAPAN, VOL. 50 (7), 1897—1898 (1977)

Reaction of Camphene with Chloroacetic Acid and the Synthesis of 2-(8-Camphenyl)ethanol[1,2]

Takao KISHIMOTO, Hiroshi ISHIHARA, and Yoshiharu MATSUBARA

Department of Applied Chemistry, Faculty of Science and Technology, Kinki University, Kowakae, Higashiosaka 577

(Received October 14, 1976)

Synopsis. Camphene (**1**) reacts with chloroacetic acid (**2**) or its polymer, polyacetoxamer; α-chloro, ω-carboxy in the presence of potassium bromide at reflux temperature to give the 2,2-dimethyl-*exo*-3-hydroxynorbornane-*endo*-3-propanoic acid lactone and the 2,2-dimethyl-*endo*-3-hydroxynorbornane-*exo*-3-propanoic acid lactone in a 50% yield. The synthesis of 2-(8-camphenyl)ethanol from **1** was simplified by utilizing this reaction.

There are no reports on the reactions of terpenes with halocarboxylic acids and also few reports on the reactions of olefins with halocarboxylic acids. These are reports on the carboxymethylation of olefins making use of iodo- and bromoacetic acids.[3] Specifically, the carboxymethylation of naphthalene[4] in the presence of potassium bromide was carried out using chloroacetic acid or its polymer, polyacetoxamer; α-chloro, ω-carboxy in the title reaction. However, it is of interest to note that the reaction of manganese(III) acetate with olefins in cyanoacetic acid was recently reported by Heiba *et al.*[5] and therefore, γ-lactones can be obtained in a single step.

As a part of the study of the reactions of olefins with halocarboxylic acids, the reaction of camphene (**1**) with chloroacetic acid (**2**) or its polymer, polyacetoxamer; α-chloro, ω-carboxy (**3**) was first investigated in the presence of potassium bromide. As a result, it was found that **1** reacts with **2** or **3** to give γ-lactones, which are useful in the synthesis of 2-(8-camphenyl)ethanol (**7**). Therefore, the structure of the γ-lactones and a simple method for synthesizing **7** from **1** are reported here.

Results and Discussion

The results of the experiments are shown in Table 1. In the presence of potassium bromide (KBr), the treatment of camphene (**1**) with chloroacetic acid (**2**) at reflux temperature gave, after distillation, the maximum yield (50%) of the γ-lactones which was composed of two components, **4A** and **4B**, in a gas chromatogram. These components (**4A** and **4B**) were isolated by redistillation and gas chromatography. Their structures were confirmed by IR and NMR spectroscopy or by a comparison of their physical constants with those reported in the literature. Table 2 shows the properties of **4A** and **4B**. The IR and NMR spectra showed the characteristic absorptions of γ-lactones and the *gem*-dimethyl group. These data indicate a configurational isomer **4A** or **4B** in Fig. 1. Of the two γ-lactones obtained, the melting point for the **4B** isomer agreed precisely with that reported by Bhati.[6] Therefore, the **4B** isomer can be assigned to the 2,2-dimethyl-*endo*-3-hydroxynorbornane-*exo*-3-propanoic acid lactone (**4B**) in Fig. 1. Consequently, the **4A** isomer supported the structure of the 2,2-dimethyl-*exo*-3-hydroxynorbornane-*endo*-3-propanoic acid lactone (**4A**) in Fig. 1. The structure of **4A** was confirmed, moreover, by deriving 2-(8-camphenyl)ethanol (**7**) from a mixture of **4A** and **4B**. The γ-lactone **4A** has not as yet been synthesized.

On the other hand, when **1** was treated with **2** in the absence of KBr, the γ-lactone fraction was afforded in only an 8% yield (Table 1). A gas chromatogram of the γ-lactone fraction also showed the two components, **4A** and **4B**. Their structures were confirmed by IR and NMR spectroscopy. In contrast with the reaction in the presence of KBr, the yield of γ-lactones was much lower. This behavior shows that in the presence of KBr, bromoacetic acid may initially be formed. The decomposition of bromoacetic acid can result in the formation of the carbonium ion ($^{+}CH_2C$-OOH),[4] which might account for an attack upon the

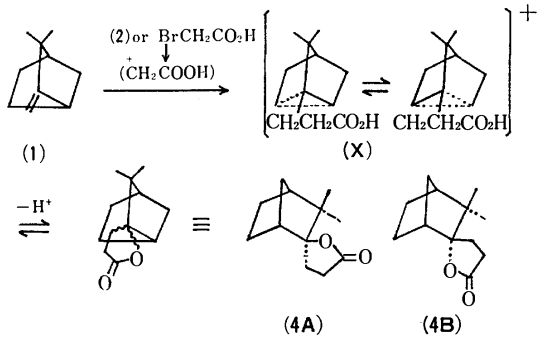

Fig. 1. Lactonization of **1**.

TABLE 1. THE RESULTS OF EXPERIMENT

Expt No.	Conditions (1) g(mol)	(2) g(mol)	(3) g	KBr g	Temp[a] °C	Time h	Lactones Yield[b] %	Formation (4A)	Ratio[c] (4B)
1	35.8(0.25)	24.9(0.32)	—	3.0	187	20	20	41	59
2	35.8(0.25)	24.9(0.32)	—	3.0	189	30	38	35	65
3	35.8(0.25)	24.9(0.32)	—	3.0	180	40	50	39	61
4	35.8(0.25)	24.9(0.32)	—	—	178	20	8	42	58
5	10.0(0.07)	— (—)	10.0	1.0	172	20	17	35	65

a) Shows the temperature of the refluxing liquid after completion of stirring. b) Based on **1** used. c) Shows the relative ratio of the γ-lactone from gas chromatographic analysis.

TABLE 2. PROPERTIES OF γ-LACTONES

γ-Lactone	Rt.[a] (min)	Mp (°C)	IR(cm⁻¹)[b] OCO		C(CH₃)₂		NMR(ppm)[c] C(CH₃)₂	(CH₂)₂CO
(**4A**)	58.0	99—100	1780, (sh)	1760 (vs)	1385, (w)	1365 (m)	1.01 (br s)	2.13—2.48 (M)
(**4B**)	64.5	103—104[d]	1780, (sh)	1760 (vs)	1386, (w)	1366 (m)	0.99, (s)	1.04 (s) 2.10—2.47 (M)

a) Retention time in gas chromatogram, PEG-20M, 4m, 180 °C. b) vs: very strong, sh: shoulder, w: weak, m: medium. c) s: singlet, br: broad, M: multiplet. d) Value from the literature (mp 103—104 °C[6]).

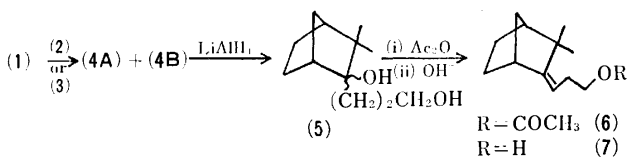

Fig. 2. Synthesis of **7**.

methylene group of **1** to give the γ-lactones (**4A** and **4B**) by lactonization of an intermidiate (**X**), as is shown in Fig. 1.

Next, polyacetoxamer; α-chloro, ω-carboxy (**3**) in the presence of KBr was also allowed to react with **1** to give the γ-lactones which comprised the two components, **4A** and **4B**. However, the γ-lactone yield was only about 17% (Table 1). These components were isolated using gas chromatography and their structures were confirmed by comparisons of their IR and NMR spectra with those of authentic samples. From this method, the lactonization could be explained by assuming the formation of carbonium ions of the type $^{+}CH_2CO_2(CH_2CO_2)_pCH_2CO_2H$.[4]

Lactone **4B** has in general been prepared by the hydration of tricycloekasantalic acid, which was obtained by the oxidation of the higher boiling fraction of East Indian sandalwood oil or α-santalene, as well as by the hydration of bicycloekasantalic acid or isobicycloekasantalic acid.[6-8] However, no simple synthesis of the γ-lactones (**4A** and **4B**) from **1** has yet been established. Bhati[6] has reported only that **4B** was synthesized *via* a multi-step process starting from **1**, in order to determine whether **4A** or **4B** is the hydration product (70 % yield) of tricycloekasantalic acid. The method described by Bhati is the only route for synthesizing **4B** from **1**, but it is not a method applicable to the synthesis of **7** from **1**. Using the present method, the γ-lactones (**4A** and **4B**) were prepared in a 50% yield in a single step from **1**, which is readily available. The synthesis of **7** was carried out according to known procedures,[7] as shown in Fig. 2. The γ-lactones (**4A**/**4B**=39/61) upon reduction with lithium aluminium hydride afforded a crystalline diol (**5**) which was converted to the corresponding unsaturated alcohol **7** by treatment with acetic anhydride, followed by saponification of the resultant acetate (**6**).

Experimental

Material. Camphene (**1**): bp 157—159 °C/760 Torr, mp 51—53.5 °C, purity 95% (in gas chromatogram, contains 5% tricyclene). Potassium bromide: commercial material (Wako Pure Chemical Industries) was used without purification. Polyacetoxamer; α-chloro, ω-carboxy (**3**): this polymer was prepared by the method of Southwick *et al.*[4] The resulting black powder was dried under reduced pressure for one day. Mp 115—158 °C (lit,[4] mp 118—138 °C)

Measurements. The NMR spectra were recorded on a Hitachi Perkin-Elmer R-24 (60 MHz) instrument. The IR spectra were obtained on a Yanagimoto ISG-25 spectrometer.

*Reaction of **1** with **2**.* *In the Presence of KBr*: In a flask fitted with a thermometer, stirrer and reflux condenser were placed 24.9 g (0.32 mol) of **2** and 3.0 g of KBr. The mixture was stirred vigorously in a sand bath for one hour at reflux temperature and 35.8 g (0.25 mol) of **1** was added to the solution dropwise for 30 min. The stirring was then continued for 30 h at the reflux temperature. At the end of the heating period, the temperature of the refluxing liquid was 189 °C. After cooling and benzene extraction, the extract was washed with a 10% aqueous solution of sodium carbonate and then water. The benzene extracts were dried over magnesium sulfate. Evaporation of the dried benzene layer followed by distillation gave the γ-lactone fraction (bp 122—125 °C/1 Torr, 18 g, 50% yield based on the amount of **1** used), which was composed of two components, **4A** and **4B**, in a 35 : 65 ratio based on gas chromatographic analysis. The γ-lactone fraction was crystallized from hexane: mp 98—99.5 °C; IR(KBr): 1780, 1760, 1386, and 1365 cm^{-1}.

In the Absence of KBr: A mixture of 24.9 g (0.32 mol) of **2** and 35.8 g (0.25 mol) of **1** was heated with stirring for 20 h at reflux temperature. At the end of the heating period, the temperature of the refluxing liquid was 178 °C. The conventional working-up described above and distillation afforded a mixture of 2.85 g (an 8% yield) of **4A** and **4B** in a 42 : 58 ratio.

*Reaction of **1** with **3** in the Presence of KBr.* The reaction was carried out with the same apparatus as used in the reaction of **1** with **2**. A mixture of 10 g of **3** and 1.0 g of KBr were heated with stirring for one hour at 160±2 °C and then 10.0 g (0.07 mol) of melted **1** was added to the solution dropwise for 30 min. Stirring was then continued for 20 h at reflux temperature. At the end of the heating period, the temperature of the refluxing liquid was 172 °C. The conventional work-up and distillation afforded 1.7 g (17% yield) of a mixture of **4A** and **4B** in a 35 : 65 ratio.

*Synthesis of **7**.* The alcohol was prepared according to the method of Ramaswami *et al.*[7] The diol (**5**): yield 85%, mp 99—107 °C, (lit,[7] mp 112 °C); IR: 3350, 1380, 1365, 1062, and 1040 cm^{-1}, NMR ($CDCl_3$) δ=0.91, 0.98 (two s, 6, CMe_2), 2.05 (br s, 2, OH, disappeared with D_2O), 3.90—3.75 ppm (m, 2, CH_2O), 2-(8-camphenyl)ethyl acetate (**6**): yield 90%, bp 107—109 °C/1 Torr, d_4^{25}=0.9915, n_D^{25}=1.4775, IR: 1740, 1666, 1380, 1365, and 842 cm^{-1}, NMR ($CDCl_3$) δ=0.98, 1.00 (two s, 6, CMe_2), 2.01 (s, 3, OAc), 3.88—4.11 (t, 2, CH_2O), and 4.69—4.98 ppm (t, 1, =CH–), (lit,[8] bp 105—110 °C/0.5 Torr, n_D^{28}=1.4749). 2-(8-Camphenyl)ethanol (**7**): yield 82%, bp 95—97.5 °C/2 Torr, n_D^{25}=1.4970, IR: 3300, 1666, 1383, 1366, and 842 cm^{-1}, NMR ($CDCl_3$) δ=1.02 (br s, 6, CMe_2), 1.86 (br s, 1, OH, disappeared with D_2O), 3.46—3.68 (t, 2, CH_2O), and 4.72—4.68 ppm (m, 1, =CH–), (lit,[8] bp 96—98 °C/2 Torr, n_D^{25}=1.4963).

References

1) Studies on the Reaction of Olefins with Halocarboxylic Acids. Part I.

2) Presented at the 35th National Meeting of the Chemical Society of Japan, Sapporo, August 1976.

3) N. Kharasch, P. L. Lewis, and R. K. Sharma, *Chem. Commun.*, 1967, 435.

4) P. L. Southwick, L. A. Pursglove, B. M. Pursglov, and W. L. Walsh, *J. Am. Chem. Soc.*, **76**, 754 (1954).

5) E. I. Heiba, R. M. Dessau, and P. G. Rodewald, *J. Am. Chem. Soc.*, **96**, 7977 (1974).

6) A. Bhati, *J. Org. Chem.*, **27**, 2135 (1962).

7) S. Ramaswami, S. K. Ramaswami, and S. C. Bhattacharyya, *J. Org. Chem.*, **27**, 2791 (1962).

8) P. R. Bai, S. Y. Kamat, B. B. Ghatge, K. K. Chakravarti, and S. C. Battacharyya, *Tetrahedron*, **21**, 629 (1965).

BULLETIN OF THE CHEMICAL SOCIETY OF JAPAN, VOL. 50 (7), 1899—1900 (1977)

The Intramolecular Cyclization Reaction of Unsaturated Acid with Palladium(II) Salt

Akira KASAHARA, Taeko IZUMI, Kazuhiro SATO, Mitsugi MAEMURA, and Tomohide HAYASAKA

Department of Applied Chemistry, Faculty of Engineering, Yamagata University, Yonezawa 992

(Received January 13, 1977)

Synopsis. The stoichiometric reaction of sodium salts of 3-butenoic acid, 3-pentenoic acid, 4-pentenoic acid, and 4-hexenoic acid with lithium tetrachloropalladate(II) affords 2-buten-4-olide, 4-methyl-2-buten-4-olide (**2b**), **2b**, and 4-ethyl-2-buten-4-olide respectively. Similarly, the reaction of 2-styrylbenzoic acid with palladium(II) salt leads to the formation of 3-phenylisocoumarin.

It is well known that most of the 2-buten-4-olides can be synthesized by the dehydrohalogenation of α-halobutyrolactones,[1] by the lactonization of γ-keto-acids,[2] or by the oxidation of α,β-unsaturated esters with selenium dioxide.[2,3] Recently, an intramolecular cyclization of olefinic compounds *via* oxypalladation[4-6] has received wide attention. In relation to these reactions, we wish to report herein the palladium-induced intramolecular cyclization of both 3-butenoic acids and 4-pentenoic acids to 2-buten-4-olides.

The sodium salts of 3-butenoic acid (**1a**) and 3-pentenoic acid (**1b**) were treated with lithium tetrachloropalladate(II) in water to produce 2-buten-4-olide (**2a**) and 4-methyl-2-buten-4-olide (β-angelica lactone) (**2b**) in 38 and 32% yields respectively. In the reactions of both **1a** and **1b** with palladium(II) salt, no formation of 3-buten-4-olide derivatives was observed. Henry and Ward[7] have reported that the reaction of cyclohexene with palladium(II) acetate gave products which were consistent with a *trans* acetoxypalladation, followed by Pd(II)-hydride elimination and readdition. In the reaction of **1a** and **1b** with palladium(II) salt, the formation of **2a** and **2b** can be explained by the Scheme 1, involving intramolecualr oxypalladation to give the intermediate (**3**), followed by the β-elimination of the HPdCl species.

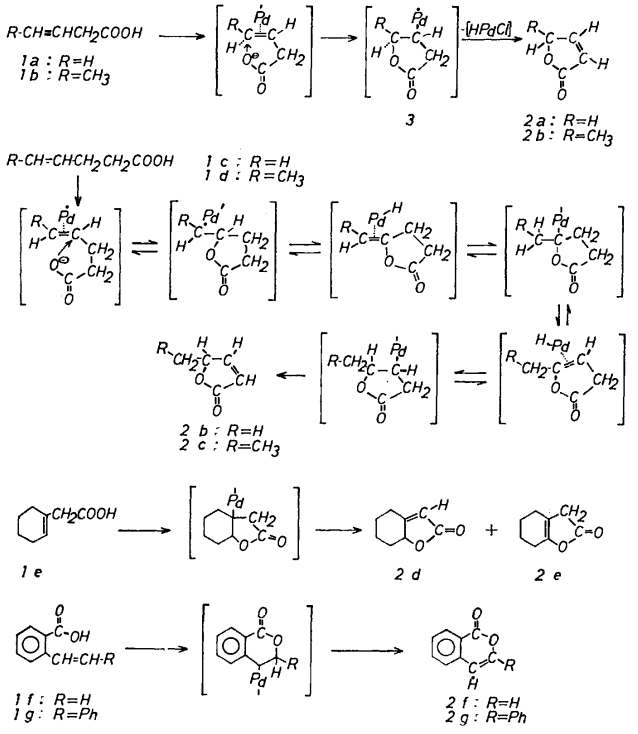

Fig. 1.

Furthermore, under the same conditions, 4-pentenoic acid (**1c**) and 4-hexenoic acid (**1d**) afforded **2b** and 4-ethyl-2-buten-4-olide (**2c**) in 38 and 30% yields respectively. In the reactions of both **1c** and **1d** with palladium(II) salt, no formation of the six-membered ring products was observed. The results are summarized in Table 1.

Hosokawa *et al.*[4f] have recently reported the regioselectivity of the palladium(II)-induced intramolecular cyclization of 2-(3-methyl-2-butenyl)phenol. However, in the reaction of **1c** and **1d** with palladium(II) salt, the formation of the five-membered ring products indicated that the cyclization of **1c** and **1d** involves a preferential attack of the oxygen atom of the carboxyl group on the 4-position of unsaturated acid (**1c** or **1d**), followed by a Pd(II)-hydride elimination-readdition process (see Scheme 1).

On the other hand, the reaction of 1-cyclohexenylacetic acid (**1e**) with palladium(II) salt led to the formation of a mixture of 5,6,7,7a-tetrahydro-2(4*H*)-benzofuranone (**2d**) and 4,5,6,7-tetrahydro-2(3*H*)-benzofuranone (**2e**). Similarly, the reaction of 2-vinylbenzoic acid (**1f**) and 2-styrylbenzoic acid (**1g**)

Table 1. Reaction of unsaturated acid (**1**) with lithium tetrachloropalladate(II)

Substrate	Solvent	Product (yield, %)
1a	H_2O	**2a** (R=H)[a] (38%)
1b	H_2O	**2b** (R=CH_3)[b] (32%)
1c	H_2O	**2b** (R=H) (38%)
1d	H_2O	**2c** (R=CH_3)[c] (30%)
1e	H_2O	**2d**[d] (28%) + **2e**[e] (10%)
1f	H_2O-dioxane	**2f** (R=H)[f] (46%)
1g	H_2O-dioxane	**2g** (R=Ph)[g] (42%)

a) Bp 90—92 °C/16 Torr, (lit,[h] bp 107—109 °C/24 Torr). b) Bp 78—80 °C/5 Torr, (lit,[i] bp 208 °C). c) Bp 85—86 °C/5 Torr, (lit,[i] bp 72 °C/1.5 Torr). d) Bp 115—117 °C/5 Torr, (lit,[i] bp 108—108.5 °C/1 Torr). e) Bp 92—95 °C/3 Torr, (lit,[i] bp 88—93 °C/1 Torr). f) Mp 47 °C, (lit,[j] mp 45—46 °C). g) 88—90 °C, (lit,[k] mp 89—90 °C). h) C. C. Price and J. M. Judge, *Org. Synth.*, **45**, 22 (1965). i) F. A. Kuehl, Jr., R. P. Linstead, and B. A. Orkin, *J. Chem. Soc.*, **1950**, 2213. j) C. Schöpf and R. Kühne, *Chem. Ber.*, **83**, 390 (1950). k) S. Siegel, S. K. Coburn, and D. R. Levering, *J. Am. Chem. Soc.*, **73**, 3163 (1951).

with palladium(II) salt afforded isocoumarin (**2f**) and 3-phenylisocoumarin (**2g**) respectively. The palladium-promoted reaction of **1e**, **1f**, and **1g** also proceeds *via* a intramolecular oxypalladation, followed by an elimination of HPdCl.

Experimental

Materials. The following compounds were synthesized by the methods described in the literature: 3-butenoic acid (**1a**),[8] 3-pentenoic acid (**1b**),[9] 4-pentenoic acid (**1c**),[10] 4-hexenoic acid (**1d**),[11] 1-cyclohexenylacetic acid (**1e**),[12] 2-vinylbenzoic acid (**1f**),[13] and 2-styrylbenzoic acid (**1g**).[14]

General Procedure for The Reaction of Unsaturated Acid with Palladium(II) Salt. A solution of 10 mmol of unsaturated acid and 5 mmol of sodium carbonate in water (50 ml) or dioxane–water (1 : 1, 50 ml) was stirred with 10 mmol of lithium tetrachloropalladate(II) at room temperature. After stirring for 24 h, the reaction mixture was then extracted with ether. The ether extract was washed with aqueous sodium hydrogencarbonate and dried over anhydrous magnesium sulfate. After the evaporation of the solvent, the product was isolated by distillation or by column chromatography on silica gel. The structures of the products were confirmed by a mixed-melting-point determination, by comparing the retention times on gas chromatograms, and by the observation of the IR and NMR spectra.

References

1) C. C. Price and J. M. Judge, *Org. Synth.*, **45**, 22 (1965).
2) F. A. Kuehl, Jr., R. P. Linstead, and B. A. Orkin, *J. Chem. Soc.*, **1950**, 2213.
3) N. Danielli, Y. Mazur, and F. Sondheimer, *J. Am. Chem. Soc.*, **84**, 875 (1962).
4) a) T. Hosokawa, K. Maeda, K. Koga, and I. Moritani, *Tetrahedron Lett.*, **1973**, 739; b) K. Maeda, T. Hosokawa, S.-I. Murahashi, and I. Moritani, *ibid.*, **1973**, 5075; c) T. Hosokawa, H. Ohkata, and I. Moritani, *Bull. Chem. Soc. Jpn.*, **48**, 1533 (1975); d) T. Hosokawa, N. Shimo, K. Maeda, A. Sonoda, and S.-I. Murahashi, *Tetrahedron Lett.*, **1976**, 383; e) T. Hosokawa, M. Hirata, S.-I. Murahashi, and A. Sonoda, *ibid.*, **1976**, 1821; f) T. Hosokawa, S. Yamashita, S.-I. Murahashi, and A. Sonoda, *Bull. Chem. Soc. Jpn.*, **49**, 3662 (1976).
5) a) A. Kasahara, T. Izumi, and M. Ooshima, *Bull. Chem. Soc. Jpn.*, **47**, 2526 (1974); b) T. Izumi and A. Kasahara, *ibid.*, **48**, 1673 (1975); c) A. Kasahara and T. Saito, *Chem. Ind. (London)*, **1975**, 745; d) A. Kasahara and N. Fukuda, *ibid.*, **1976**, 485; e) A. Kasahara, *ibid.*, **1976**, 1032.
6) L. S. Hegedus, G. F. Allen, and E. L. Waterman, *J. Am. Chem. Soc.*, **98**, 2674 (1976).
7) P. M. Henry and G. A. Ward, *J. Am. Chem. Soc.*, **93**, 1494 (1971).
8) E. Rietz, *Org. Synth.*, Coll. Vol. 3, 851 (1965).
9) J. F. Lane, J. Fentress, and L. T. Sherwood, Jr., *J. Am. Chem. Soc.*, **66**, 545 (1944).
10) R. P. Linstead and H. N. Rydon, *J. Chem. Soc.*, **1933**, 580.
11) E. N. Eccott and R. P. Linstead, *J. Chem. Soc.*, **1929**, 2153.
12) J. Klein, *J. Am. Cnem. Soc.*, **81**, 3611 (1959).
13) G. M. Pogosyan, T. G. Karapetyan, and S. G. Matsoya, *Zh. Org. Khim.*, **6**, 139 (1970).
14) S. Gabriel and T. Posner, *Ber.*, **27**, 2506 (1894).

BULLETIN OF THE CHEMICAL SOCIETY OF JAPAN, VOL. 50 (7), 1901—1902 (1977)

Synthesis of Manninotriose Undecaacetate

Ryoichi ADACHI and Tetsuo SUAMI*

Department of Applied Chemistry, Faculty of Engineering, Keio University, Hiyoshi, Yokohama 223

(Received January 17, 1977)

Synopsis. Manninotriose undecaacetate has been prepared from melibiose. Tritylation of melibiose, followed by acetylation gave 6′-*O*-trityl-*β*-melibiose heptaacetate. Detritylation of the compound gave hepta-*O*-acetyl-*β*-melibiose, which was condensed with tetra-*O*-benzyl-D-galactopyranosyl chloride. Deacetylation of the condensation product, followed by hydrogenolysis and acetylation afforded the title compound.

Manninotriose, *O*-α-D-galactopyranosyl-(1→6)-*O*-α-D-galactopyranosyl-(1→6)-D-glucose, has been found in a free form in an ash manna from *Fraxinus ornus* and *F. rotundifolia*, and it has been well known that this trisaccharide is a component of a tetrasaccharide: stachyose.[1] The enzymic synthesis of manninotriose from melibiose has been reported in a literature,[2] but a chemical synthesis has never been described.

In connection with the preceding papers,[3,4] we have attempted to synthesize manninotriose undecaacetate (**6**) from melibiose (**1**) chemically. When **1** was treated with trityl chloride in pyridine and the product was subsequently acetylated, 6′-*O*-trityl-*β*-melibiose heptaacetate (**2**) was obtained as crystals in 65% yield.

Detritylation of **2** with hydrogen bromide in glacial acetic acid afforded 1,2,2′,3,3′,4,4′-hepta-*O*-acetyl-*β*-melibiose (**3**). Condensation between **3** and 2,3,4,6-tetra-*O*-benzyl-D-galactopyranosyl chloride[5] (**4**) gave 1,2,2′,3,3′,4,4′-hepta-*O*-acetyl-2″,3″,4″,6″-tetra-*O*-benzyl-*β*-manninotriose (**5**) as a chromatographically homogeneous solid. Deacetylation of **5**, followed by catalytic hydrogenolysis and subsequent acetylation afforded **6** as crystals in 30% yield. Compound **6** was identified by direct comparison with an authentic sample prepared by hydrolysis of stachyose.[6]

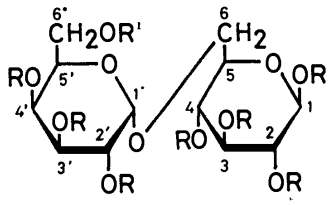

1: R=R′=H
2: R=Ac, R′=Tr
3: R=Ac, R′=H
5: R=Ac, R′=2,3,4,6-tetra-*O*-benzyl-α-D-galactopyranosyl
6: R=Ac, R′=2,3,4,6-tetra-*O*-acetyl-α-D-galactopyranosyl

Experimental

General. Melibiose and stachyose were purchased from a commercial source. Melting points were determined in capillary tubes, and are uncorrected. Solutions were evaporated under diminished pressure. IR spectra were determined for potassium bromide discs with a Hitachi 225 spectrophotometer. Optical rotations were recorded on a Japan Spectroscopic DIP-SL polarimeter. ^{1}H NMR spectra were determined at 60 MHz with a Varian A-60D spectrometer in deuteriochloroform with tetramethylsilane as an internal standard, and the peak positions are given in δ-values. TLC was performed on a silica gel (Wakogel B-10) plate, and silica gel (Wakogel C-200) was used for a column chromatography.

1,2,2′,3,3′,4,4′-Hepta-O-acetyl-6′-O-trityl-β-melibiose (2). To a solution of melibiose (**1**, 200 mg, 0.58 mmol) in dry pyridine (10 ml), trityl chloride (976 mg, 3.50 mmol) was added, and the mixture was agitated for 97 h at ambient temperature. Then, acetic anhydride (5 ml) was added to the reaction mixture. After 15 h, the mixture was poured into ice cold water (200 ml) and triphenylmethanol was removed by filtration. The filtrate was evaporated, and the residue was purified by a column chromatography using 1 : 5 (v/v) 2-butanone–toluene as eluent to give 424 mg of a chromatographically homogeneous product (R_f 0.43 on TLC in 1 : 4 (v/v) 2-butanone–toluene). Recrystallization from 80% aqueous ethanol gave 332 mg (65%) of **2**, mp 108—112 °C, $[\alpha]_D^{22}$+79.1° (*c* 1.05, chloroform), ^{1}H NMR: δ 1.88 (s, 3, OAc), 1.98 (s, 6, 2×OAc), 2.02 (s, 12, 4×OAc), 5.74 (d, 1, *J*=8.0 Hz, H-1), 6.35 (d, 1, *J*=3.5 Hz, H-1′).

Found: C, 61.22; H, 5.71%. Calcd for $C_{45}H_{50}O_{18}$: C, 61.50; H, 5.73%.

1,2,2′,3,3′,4,4′-Hepta-O-acetyl-β-melibiose (3). To a solution of **2** (318 mg) in glacial acetic acid (2.0 ml), glacial acetic acid (0.2 ml) saturated with hydrogen bromide was added under ice cooling. After stirring for 2 min, the precipitated bromotriphenylmethane was filtered off and the filtrate was quenched into ice cold water (60 ml). The solution was extracted with chloroform repeatedly and the combined chloroform layer was washed with dilute sodium hydrogencarbonate solution and water. After drying over sodium sulfate, the extract was evaporated. The residue was purified by a column chromatography using 1 : 2 (v/v) 2-butanone–toluene as eluent to give 181 mg (79%) of **3** as a chromatographically homogeneous solid (R_f 0.39 on TLC in 20 : 1 (v/v) chloroform–ethanol), $[\alpha]_D^{21}$+132.9° (*c* 0.82, chloroform). ^{1}H NMR: δ 1.98 (s, 6, 2×OAc), 2.04 (s, 3, OAc), 2.09 (s, 6, 2×OAc), 2.12 (s, 3, OAc), 2.13 (s, 3, OAc), 5.67 (d, 1, *J*=8.0 Hz, H-1), 6.27 (d, 1, *J*=4.0 Hz, H-1′).

Found: C, 49.07; H, 5.56%. Calcd for $C_{26}H_{36}O_{18}$: C, 49.06; H, 5.70%.

2,3,4,6-Tetra-O-benzyl-D-galactopyranosyl Chloride (4). The compound was prepared by the method of Austin *et al.*[5]

1,2,2′,2″,3,3′,3″,4,4′,4″,6″-Undeca-O-acetyl-β-manninotriose (6). To a solution of **3** (1.10 g, 1.73 mmol) and **4** (3.14 g, 5.62 mmol) in dry benzene (30 ml), mercury(II) cyanide (1.5 g) and "Drierite" (3.0 g) were added. The mixture was heated under reflux for 17 h, and an insoluble matter was removed by a centrifugal separator. The supernatant solution was washed with sodium hydrogencarbonate solution and water. The benzene solution was dried over sodium sulfate and evaporated. The residue was purified by a column chromatography using 1 : 5 (v/v) 2-butanone–toluene as eluent to give

* To whom correspondence should be addressed.

1.78 g (89%) of 1,2,2′,3,3′,4,4′-hepta-*O*-acetyl-2″,3″,4″,6″-tetra-*O*-benzyl-β-manninotriose (**5**) as a chromatographically homogeneous solid (R_f 0.52 on TLC in 1 : 3 (v/v) 2-butanone–toluene).

Compound **5** (1.70 g) was deacetylated in 0.1 M methanolic sodium methoxide (30 ml) overnight. The solution was neutralized with Amberlite IR-120 (H^+) resin and evaporated. The residue was hydrogenated in methanol (35 ml) in the presence of palladium black under a hydrogen atmosphere (3.4 kg/cm²) for 20 h in a Parr apparatus. The catalyst was filtered off and the filtrate was evaporated. The residue was acetylated with acetic anhydride (3 ml) and sodium acetate (0.3 g). The product was purified by a column chromatography using 1 : 5 (v/v) acetone–benzene to give 409 mg of a product which showed a single spot at R_f 0.38 on TLC in the same solvent. Recrystallization from ethanol afforded 268 mg (30%) of **6**, mp 106—107.5 °C, $[\alpha]_D^{21}$+132.7 °C (*c* 0.98, chloroform). ^{1}H NMR: δ 1.96 (s, 6, 2×OAc), 2.00 (s, 6, 2×OAc), 2.01 (s, 3, OAc), 2.05 (s, 9, 3×OAc), 2.09 (s, 6, 2×OAc), 2.11 (s, 3, OAc), 5.70 (d, 1, J=8.0 Hz, H-1). The IR and ^{1}H NMR spectra were superimposable on those of an authentic sample.

Found: C, 49.46; H, 5.51%. Calcd for $C_{40}H_{54}O_{27}$: C, 49.69; H, 5.63%.

*Compound **6** from Stachyose.* Manninotriose was prepared from stachyose by the method of Tanret.[6] The product was acetylated to give **6** in 47% yield, mp 106—107.5 °C, $[\alpha]_D^{21}$+137° (*c* 1.27, chloroform). (Found: C, 49.48; H, 5.56%).

References

1) D. French, *Adv. Carbohydr. Chem.*, **9**, 170 (1954).
2) D. French, *Adv. Carbohydr. Chem.*, **9**, 157 (1954).
3) T. Suami, T. Otake, T. Nishimura, and T. Ikeda, *Carbohydr. Res.*, **26**, 234 (1973).
4) T. Suami, T. Otake, T. Nishimura, and T. Ikeda, *Bull. Chem. Soc. Jpn.*, **46**, 1014 (1973).
5) P. W. Austin, F. E. Hardy, J. G. Buchanan, and J. Baddiley, *J. Chem. Soc.*, **1965**, 1419.
6) C, Tanret, *C. R. Acad. Sci.*, **134**, 1586 (1902).

BULLETIN OF THE CHEMICAL SOCIETY OF JAPAN, VOL. 50 (7), 1903—1904 (1977)

Syntheses with 2-Furylmagnesium Bromides. I. Synthesis of Rosefuran and Sesquirosefuran*

Akira TAKEDA, Kōichi SHINHAMA, and Sadao TSUBOI

Department of Synthetic Chemistry, School of Engineering, Okayama University, Tsushima, Okayama 700

(Received February 2, 1977)

Synopsis. The preparation and reactions of 2-furylmagnesium bromide and 3-methyl-2-furylmagnesium bromide (**4b**) have been studied. Activated 90% magnesium–copper alloy was used to prepare the Grignard reagents. The reaction of 1-bromo-3-methyl-2-butene with **4b** gave rosefuran in a 40% yield; that of geranyl bromide with **4b** gave sesquirosefuran in a 26% yield.

Furylmetal compounds such as 2-furyllithium[1,2] and di-2-furylmercury(II)[1–3] are widely used for introducing 2-furyl moiety of natural products, *i.e.* rosefuran (**1b**), a trace component of Bulgarian rose oil (*Rosa damascene* Mill.),[1] and sesquirosefuran (**2b**), a constituent isolated from the oil of the leaves of *Actinodaphne longifolia* (Blume) Nakai.[4] The scheme of synthesis with 2-furylmagnesium derivatives has not been studied before. It seems worth while to devise a synthetic route leading to these natural products in which innoxious Grignard reagents are used in place of organomercury compounds. We have studied the preparation and reaction of 2-furylmagnesium bromides, and wish to report a new synthesis of compounds **1b** and **2b** by the reaction of 3-methyl-2-furylmagnesium bromide (**4b**) with 1-bromo-3-methyl-2-butene (**5**)[6] for the former, and geranyl bromide (**6**)[2] for the latter.

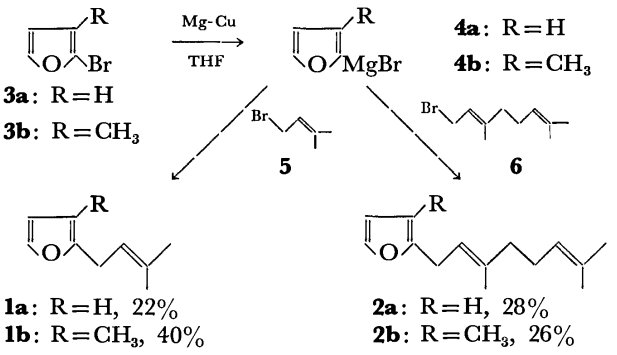

Few studies have been carried out on the reaction of 2-furylmagnesium compounds, except for the first work on the preparation of 2-furylmagnesium bromide (**4a**),[5] which was transformed into furoic acid by the action of carbon dioxide solely for the sake of confirming its formation. We have thus carried out the synthesis of 2-(3-methyl-2-butenyl)furan (**1a**)[7] and 2-geranylfuran (**2a**). The solution of 2-furylmagnesium bromide was prepared by reacting 2-bromofuran (**3a**)[8] with an activated magnesium–copper alloy (90 : 10) in THF, at room temperature for 3.5 h. Conversion of **3a** into the Grignard reagent was confirmed by a test with Michler's ketone.[9] Since the 12.75% Cu–Mg alloy recommended by Shepard *et al.*[5] was not available, we used the powder alloy obtained from a mixture of 90 parts of magnesium powder and 10 parts of copper powder by heating to red-hot under nitrogen. For each reaction, the alloy was reactivated by heating with half its weight of iodine at 50 °C. The reaction of the Grignard reagent **4a** with the bromide **5** gave furan **1a** in a 22% yield and that with bromide **6** gave furan **2a** in a 28% yield. The structures of these products were confirmed by spectral data (IR, NMR, and MS).

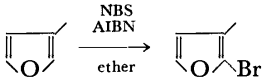

3b

The solution of Grignard reagent **4b** was prepared from 2-bromo-3-methylfuran (**3b**) in a way similar to that for the formation of **4a**. Bromofuran **3b** was obtained in a 56% yield by the action of *N*-bromosuccinimide (NBS) on 3-methylfuran by means of the procedure of Prugh *et al.*[8] The reaction of **4b** with compound **5**, gave furan **1b** in a 40% yield and that with compound **6** gave furan **2b** in a 26% yield. The spectral data (IR, NMR, and MS) of these synthetic furans were identical with those reported.[1,4] Although the yields are small as compared with those of the Friedel-Crafts-type alkenylation of furan,[7] the present route has a merit for the synthesis of 2,3-disubstituted furans, since it affords no other disubstituted isomers.

Experimental

Elemental analysis was carried out by Mr. Eiichiro Amano. Analytical determinations by GLPC were performed on a Hitachi Model K-53 gas chromatograph fitted with the following columns (3 mm o.d. × 1 m): A, 10% Apiezon Grease L on Chromosorb W; B, 10% poly(neopentyl succinate) on Chromosorb W; C, 10% SE-30 on Chromosorb W. Mass spectra were obtained with a Hitachi Model RMS-4 mass spectrometer. ^{1}H NMR spectra were taken at 60 MHz on a Hitachi Model R-24 apparatus. ^{13}C NMR spectra were obtained with a JEOL Model JNM-FX-100 spectrometer. Thin layer chromatograms were prepared with Merck Kieselgel 60 PF_{254} (E. Merck AG, Darmstadt). Compounds **3a**,[8] **5**,[6] **6**,[2] and 3-methylfuran[10] were prepared according to reported methods.

Preparation of a 90% Mg–Cu Alloy. A small glass tube (15 mm i.d. × 15 cm) was charged with a mixture consisting of 1.8 g of magnesium powder and 0.2 g of copper powder. After the air in the tube was sufficiently replaced by nitrogen, the mixed metal powder was heated to red-hot with a colorless flame for 20 min under nitrogen. After being cooled, the lump of alloy was crushed in a mortar, and stored in a small rubber-stoppered bottle.

*2-(3-Methyl-2-butenyl)furan (**1a**).*[7] A mixture of 0.21 g of 90% Mg–Cu alloy and 0.1 g of iodine was heated for 1 h at 50 °C under nitrogen. To the resulting mixture was added

* Presented at the 36th Annual Meeting of the Chemical Society of Japan, Higashiōsaka, April 1977.

slowly a solution of 2-bromofuran (0.73 g, 5.0 mmol) in 2 ml of THF, over a period of 20 min. Stirring was continued for 3 h at room temperature. After the formation of the Grignard reagent **4a** in the solution had been confirmed by a test with Michler's ketone,[9] it was added dropwise to a boiling solution of 1-bromo-3-methyl-2-butene (**5**) (0.74 g, 5.0 mmol) in 2 ml of THF over a period of 1 h under nitrogen. The mixture was refluxed for 1 h, and then allowed to stand at room temperature for 12 h. It was neutralized with dilute H_2SO_4, extracted with ether, and dried over $MgSO_4$. Distillation of the residue obtained after removal of the solvent gave 147 mg (22%) of **1a**: IR (neat) 1670, 1595, 1563, 1508, 1093, 1012, and 736 cm^{-1}; NMR ($CDCl_3$) δ 1.64 (s, 6H, $=\langle^{CH_3}_{CH_3}$), 3.29 (d, J=7 Hz, 2H, $-CH_2-$), 5.28 (t, J=7 Hz, 1H, $\rangle=\langle H$), 5.90 (m, 1H, β'-H of furan), 6.20 (m, 1H, β-H of furan), and 7.24 ppm (m, 1H, α-H of furan).

*2-Geranylfuran (**2a**).* A solution of **4a** prepared from 1.1 g (7.5 mmol) of **3a** in 3 ml of THF and 0.33 g of Mg–Cu alloy was reacted with a solution of geranyl bromide (**6**) (1.63 g, 7.5 mmol) in the same way as in the foregoing experiment of **1a**. A crude product (700 mg, 28%) with a 62% purity by GLPC was obtained by distillation: bp (bath temperature) 100—120 °C (2 Torr). It was purified by preparative TLC (silica gel, hexane, R_f=0.3) and analyzed: IR (neat) 1596, 1503, 1007, 798, and 728 cm^{-1}; NMR (CCl_4) δ 1.59 (s, 3H, $\diagup=\langle CH_3$), 1.67 (s, 6H, $=\langle^{CH_3}_{CH_3}$), 2.0 (br, s, 4H, H_2 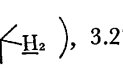 H_2), 3.27 (d, J=8 Hz, 2H, $-CH_2-$), 5.04 (br, m, 1H, $H\rangle=\langle^{CH_3}_{CH_3}$), 5.29 (t, J=8 Hz, 1H, $H\rangle=\langle CH_3$), 5.80 (m, 1H, β'-H of furan), 6.12 (t, 1H, β-H of furan), and 7.18 ppm (m, 1H, α-H of furan); MS (70 eV) *m/e* (rel intensity) 204 (1, M^+), 162 (3), 123 (18), 81 (47), 67 (100).

Found: C, 82.14; H, 9.76%. Calcd for $C_{14}H_{20}O$: C, 82.30; H, 9.87%.

*2-Bromo-3-methylfuran (**3b**).* A 50 ml flask was charged with 5.4 g (34 mmol) of NBS and 0.26 g of AIBN. To the mixture was added a solution of 3-methylfuran[10] in 25 ml of dry ether under nitrogen. The resulting mixture was stirred for 3 h under reflux. It was then filtered, washed with 1% aqueous $NaHCO_3$, and dried over anhydrous $MgSO_4$ containing 20 mg of hydroquinone and 0.1 g of $CaCO_3$. After removal of the solvent and subsequent addition of 5 ml of quinoline, the mixture was subjected to fractional distillation under diminished pressure to yield 3.1 g (56%) of **3b**: bp 56—57 °C (60 Torr) [lit,[8] bp 28—30 °C (12 Torr)]; IR (neat) 1495, 1160, 1075, 892, and 736 cm^{-1}; NMR (CCl_4) δ 1.97 (s, 3H, $-CH_3$), 6.18 (d, J=2 Hz, 1H, β-H of furan), and 7.29 ppm (d, J=2 Hz, 1H, α-H of furan).

*2-(3-Methyl-2-butenyl)-3-methylfuran (**1b**). Synthesis of Rosefuran*: A solution of the Grignard reagent **4b** was prepared from 1.21 g (7.5 mmol) of 2-bromo-3-methylfuran (**3b**) dissolved in 4 ml of THF and 0.33 g of 90% Mg–Cu alloy, which was reactivated as usual. It was then added to a boiling solution of **5** (1.11 g, 7.5 mmol) in 3 ml of THF under nitrogen in the course of 45 min. Refluxing was continued for 3 h. It was then cooled and acidified with dilute H_2SO_4. The organic layer was extracted with ether and the ethereal extract was dried over anhydrous $MgSO_4$. After removal of the solvent the residue was distilled to give 512 mg of **1b** (87% purity by GLPC), yield 40%: bp (bath temperature) 80—100 °C (18 Torr) [lit,[1] bp 39—40 °C (1 Torr)]; IR (neat) 1670, 1628, 1512, 1450, 1380, 1158, 1088, 899, 857, and 733cm^{-1}; NMR ($CDCl_3$) δ 1.70 (d, J=1 Hz, 6H, $=\langle^{CH_3}_{CH_3}$), 1.94 (s, 3H, ring $-CH_3$), 3.26 (d, J=7 Hz, 2H, $-CH_2-$), 5.23 (t, J=7 Hz, 1H, $H\rangle=\langle$), 6.10 (d, J=2 Hz, 1H, β-H of furan), 7.16 (d, J=2 Hz, α-H of furan); MS (70 eV) *m/e* (rel intensity) 150 (79, M^+), 135 (100).

The natural abundance ^{13}C NMR spectrum of **1b** is summarized in the following structure. Off-resonance decoupling was used to support the assignment.

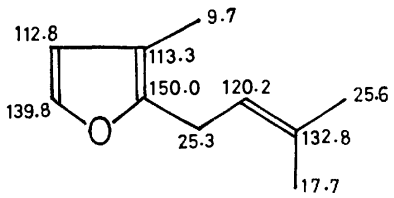

*2-Geranyl-2-methylfuran (**2b**). Synthesis of Sesquirosefuran*: A solution of **4b** prepared from 1.45 g (9.0 mmol) of **3b** and 0.4 g of 90% Mg–Cu alloy was reacted with a solution of **6** (1.96 g, 9.0 mmol) in the same way as in the foregoing experiments. A crude product (909 mg, 26%) with a 56% purity by GLPC was obtained by distillation: bp (bath temperature) 100—120 °C (0.3 Torr). A pure sample was obtained by preparative TLC (silica gel, hexane, R_f=0.3): IR (neat) 1623, 1560, 1507, 1148, 1079, 886, and 720 cm^{-1}; NMR (CCl_4) δ 1.58 (s, 3H, $\diagup=\langle CH_3$), 1.68 (d, J=1 Hz, 6H, $=\langle^{CH_3}_{CH_3}$), 1.93 (s, 3H, ring $-CH_3$), 2.0 (br, s, 4H, H_2 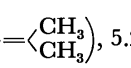 H_2), 3.21 (d, J=8 Hz, 2H, $-CH_2-$), 5.07 (br, m, 1H, $H\rangle=\langle^{CH_3}_{CH_3}$), 5.19 (t, J=8 Hz, 1H, $H\rangle=\langle CH_3$), 6.10 (d, J=2 Hz, 1H, β-H of furan), and 7.07 ppm (d, J=2 Hz, 1H, α-H of furan).

References

1) G. Büchi, E. Sz. Kovats, P. Enggist, and G. Uhde, *J. Org. Chem.*, **33**, 1227 (1968),

2) Y. Gopichand, R. S. Prasad, and K. K. Chakravarti, *Tetrahedron Lett.*, **1973**, 5177.

3) S. Kumazawa, K. Nishihara, T. Kato, Y. Kitahara, H. Komae, and N. Hayashi, *Bull. Chem. Soc. Jpn.*, **47**, 1530 (1974).

4) N. Hayashi, H. Komae, S. Eguchi, M. Nakayama, S. Hayashi, and T. Sakao, *Chem. Ind. (London)*, **1972**, 572.

5) A. F. Shepard, N. R. Winslow, and J. R. Johnson, *J. Am. Chem. Soc.*, **52**, 2083 (1930).

6) H. Staudinger, W. Kreis, and W. Schilt, *Helv. Chim. Acta*, **5**, 750 (1922).

7) Yu. I. Tarnopol'skii and V. N. Belov, *Zh. Org. Khim.*, **1**, 595 (1965); *Chem. Abstr.*, **81**, 1761d (1965). The alkenylation of furan with 1-chloro-3-methyl-2-butene catalyzed by $ZnCl_2$ in ether gave 50% 2-(3-methyl-2-butenyl)furan.

8) J. D. Prugh, A. C. Huitric, and W. C. McCarthy, *J. Org. Chem.*, **29**, 1991 (1964). We used ether as a solvent in place of benzene, since it was difficult to separate benzene from the product by distillation.

9) H. Gilman and F. Schulze, *J. Am. Chem. Soc.*, **47**, 2002 (1925).

10) J. W. Cornforth, *J. Chem. Soc.*, **1958**, 1310.

Emission Spectra of CH($A^2\Delta$) Produced from CH_3CN in the Argon Flowing-Afterglow Reaction

Kaoru SUZUKI and Kozo KUCHITSU

Department of Chemistry, Faculty of Science, The University of Tokyo, Hongo, Bunkyo-ku, Tokyo 113

(Received January 7, 1977)

Emission spectra from CH($A^2\Delta$) formed in the reaction of positive ionic species of argon with CH_3CN were studied by the flowing-afterglow method. The rotational distributions for the $v'=0$, 1, and 2 of CH($A^2\Delta$) are characterized by effective rotational temperatures of *ca.* 5000, 2000, and 1500 K, respectively, whereas the distributions in lower levels ($N' \lesssim 11$), especially for $v'=0$, are characterized by that of *ca.* 700 K. The average vibrational and rotational energies distributed in the CH radicals produced initially are estimated to be 0.32 ± 0.04 and 0.34 ± 0.06 eV, respectively.

When a rare gas is subjected to microwave discharge, metastable atoms and ions are generated. The active species can react with molecules and produce fragments in electronically excited states. Photoemissions of such fragments formed in reactions of metastable argon atoms have been studied in detail.[1,2] On the other hand, emissions followed by dissociative reactions with active ionic species of thermal kinetic energy have scarcely been reported.

When the flowing afterglow method was applied to the reaction of metastable argon atoms with CH_3CN, it was suggested that the formation of CH($A^2\Delta$) was caused by a different mechanism from that of CN($B^2\Sigma^+$), because the dependence of CH $A^2\Delta$-$X^2\Pi$ and CN $B^2\Sigma^+$-$X^2\Sigma^+$ emission intensities on the argon pressure was different.[3,4] The present article reports that the active species of argon mainly contributing to the production of CH($A^2\Delta$) radicals in the reaction with CH_3CN are ionic. The vibrational and rotational structures of the visible emission spectrum from CH($A^2\Delta$) have been analyzed to obtain information about the energy distributed to the vibrational and rotational motions of the CH($A^2\Delta$) radical.

Experimental

The experimental apparatus is essentially the same as that described in previous reports.[3-5] The flow tube was evacuated by a 500 l/s mechanical booster pump. The argon gas of 99.99% nominal purity was purified by passage through a trap at 77 K before it was introduced into the discharge section. Positive ions and metastable atoms, $Ar(^3P_{2,0})$, were produced by a 2450 MHz microwave discharge. An output power of about 450 W from a magnetron was fed into the discharge section. The reactant gas was introduced into the flow through a nozzle (0.4 mm in diameter) placed 15 cm downstream from the discharge section. The acetonitrile sample was of extra pure grade.

The gas pressure was measured in the reaction zone by a Pirani gauge calibrated against a McLeod gauge. The argon pressure was varied from 0.3 to 1.7 Torr. The pressure of CH_3CN was about 0.01 Torr.

Emission spectra were observed through a quartz window by using a 1-m Spex 1704 scanning monochromator with a 1200 grooves/mm grating blazed at 500 nm, an HTV R585 photomultiplier, and a photon counting system.

The CH($A^2\Delta$-$X^2\Pi$, 0-0, 1-1, and 2-2) emission was observed in the 420—440 nm region at an argon pressure above about 0.3 Torr. The spectrum shown in Fig. 1 was obtained at an argon pressure of about 0.7 Torr with a spectral resolution of about 0.05 nm FWHM. The R-branch lines of the 0-0 band were resolved from those of the 1-1 band for $N' \gtrsim 6$ (except for $N'=12$). The CH $B^2\Sigma^-$-$X^2\Pi$ band was also observed in the 385—405 nm region, where the R-branch was overlapped by the CN violet band.

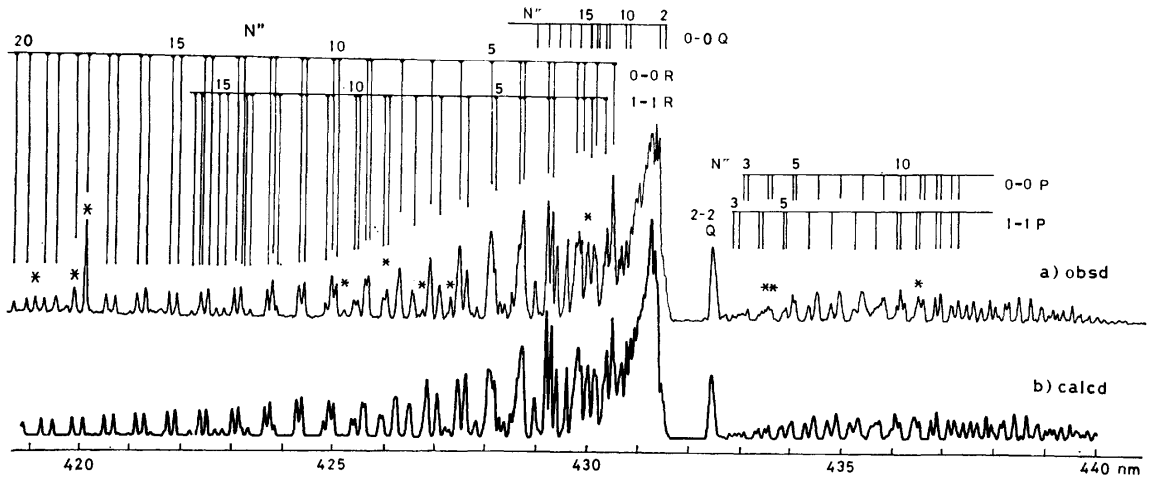

Fig. 1. Observed (a) and simulated (b) spectra of CH $A^2\Delta$-$X^2\Pi$. Lines marked * are overlapped by stray argon lines.

Estimation of Active Ionic Species

In order to remove the ionic species reaching the reaction zone, grids (stainless steel mesh, transparency *ca.* 0.74) were placed between the discharge section and the reaction zone, and an electrostatic potential was applied. The collected ion currents and the emission intensities of CH $A^2\Delta$-$X^2\Pi$ and CN $B^2\Sigma^+$-$X^2\Sigma^+$ are plotted against the potential applied to the grid in

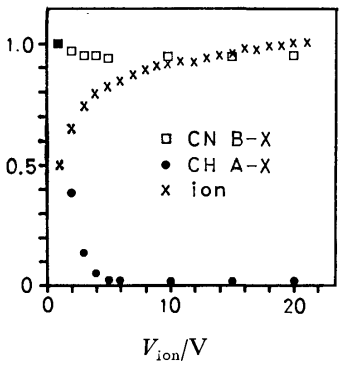

Fig. 2. The relative emission intensities of CN $B^2\Sigma^+$-$X^2\Sigma^+$ (□) and CH $A^2\Delta$-$X^2\Pi$ (●) formed from CH_3-CN in the flowing afterglow reaction of argon, and the relative ion currents (×) collected with an ion-collector grid are plotted against a potential applied to the ion-collector grid, V_{ion}, at an argon pressure of 0.4 Torr. The relative currents due to the ions reaching the reaction zone is proportional to the difference from the saturated ion current at $V_{ion}>20$ V.

Fig. 2. The CH $A^2\Delta$-$X^2\Pi$ emission intensity was monitored at 431 and 424 nm, which correspond to the 0-0 head and the R(12) line of the 0-0 band, respectively, with a band pass of about 1.6 Å. These emission intensities had essentially the same dependence on the potential applied to the grid. Therefore, the trend for CH $A^2\Delta$-$X^2\Pi$ shown in Fig. 2 is regarded as representing that of the total emission from $CH(A^2\Delta)$, *i.e.*, the dependence of the density of $CH(A^2\Delta)$ produced in the reaction on the potential. The CN $B^2\Sigma^+$-$X^2\Sigma^+$ emission monitored at 385 and 386 nm had only slight dependence on the potential. It is therefore evident that ionic species are mainly responsible for the $CH(A^2\Delta)$ formation, whereas $CN(B^2\Sigma^+)$ is mainly produced by neutral atoms.

Attempts have been made to identify the ionic species. If a single collision of active species produces $CH(A^2\Delta)$, there are energetically possible channels in which singly charged argon ions in the metastable states, $Ar^{+M}(^4D_{7/2}$, $^4F_{9/2,7/2}$, $^2F_{2/7}$, $^2G_{9/2,7/2})$,[6] and multiply charged ions, especially doubly charged ions, are involved. In the present experiment, Ar^{+M} seems to have a lifetime long enough to reach the reaction zone and take part in the dissociative excitation. The radiative lifetime of Ar^{+M} has not been measured, but it is estimated to be longer than 1 s[7] if multiple-quantum transitions do not contribute significantly. The lifetime for collisional relaxation is also estimated to be longer than the time of flight under the present experimental conditions. Hence, Ar^{+M} seems to be a plausible candidate. On the other hand, argon ions in the ground electronic state, $Ar^+(^2P_{3/2,1/2})$, or argon molecular ions, Ar_2^+, can be excluded by energetic considerations: Their available energies are 15.76[6] and 14.4 eV,[8] respectively, whereas the minimum energy to produce $CH(A^2\Delta)$ by charge exchange and dissociation is 25.3 eV.[9]

However, the possibility that $CH(A^2\Delta)$ is produced by successive collisions of ionic and neutral species (Ar^+, Ar_2^+, $Ar(^3P_{2,0})$, *etc.*) cannot be excluded. In order to specify the reaction channels involved in the $CH(A^2\Delta)$ formation, it is necessary to identify and monitor the positive ions present in the flow at the reaction zone.

Analysis of Rotational and Vibrational Distributions

The relative intensities of the emission spectrum was analyzed to estimate the vibrational and rotational populations of $CH(A^2\Delta)$ formed in the reaction with active species discussed above. In the following procedure, production of the $CH(A^2\Delta)$ state by cascading from higher states is ignored for the following reasons: a) The CH $B^2\Sigma^-$-$A^2\Delta$ and CH $C^2\Sigma^+$-$A^2\Delta$ transitions are forbidden. b) The allowed CH $D^2\Pi$-$A^2\Delta$ emission (near 280 nm) was not observed in the present experiment. c) No cascading effect from higher states (D, E, F, *etc.*) has been reported in the lifetime measurement of $CH(A^2\Delta)$[10,11] produced by electron impact on CH_4 and C_2H_2.

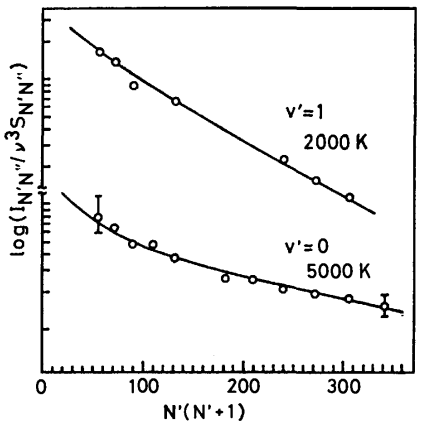

Fig. 3. Estimation of effective rotational temperatures from the slopes of $\log(I_{N'N''}/\nu^3 S_{N'N''})$ *vs.* $N'(N'+1)$. Solid lines represent a two-temperature distribution estimated by Eq. 2, with $n_L/n_H=0.27$, $T_L=700$ K, and $T_H=5000$ K for the $v'=0$ state and $T_H=2000$ K for the $v'=1$ state. Typical uncertainties are indicated by error bars.

Relative rotational populations are estimated by using the intensities of the R-branch. In Fig. 3, $I_{N'N''}/\nu^3 S_{N'N''}$ is plotted against $N'(N'+1)$, where $I_{N'N''}$ is the relative transition intensity, ν is the transition frequency, and $S_{N'N''}$ is the rotational line-strength calculated by the Hönl-London formula.[12]

An approximately linear relationship, *i.e.*, approximately a Boltzmann distribution, is obtained for the $v'=1$ state. From the slope, $-hcB_{v'}/kT_{rot}$, where $B_{v'}$ is the rotational constant,[13] the effective rotational

temperature, T_{rot}, is estimated to be 2000 ± 500 K. For the $v'=0$ state, however, the populations at lower ($N'\lesssim11$) levels appear to deviate from the linear relationship, their effective rotational temperature being an order of magnitude lower. A similar remark was made by Brennen and Carrington,[14] who observed a two-temperature distribution in the CH($A^2\Delta$) spectrum produced in the $O+C_2H_2$ reaction. Though they seem to have disregarded the overlapping of the R-branch by the Q-branch near 430 nm, as remarked by Beenakker *et al.*,[15] their observations indicate that the distribution characterized by a lower effective rotational temperature was produced by rotational relaxation to the equilibrium distribution corresponding to the ambient temperature. They also observed that the distribution corresponding to the higher temperature was unaffected by the rotational relaxation.

The observed rotational distribution is analyzed on the assumption that the distribution is represented by a superposition of two Boltzmann distributions. It is called a two-level model;[14,16] *i.e.*, CH radicals initially produced in a distribution with a higher rotational temperature, T_H, are relaxed by collisions to another distribution with a lower temperature, T_L (see Appendix). In this model the ratio of the number of CH radicals in the "relaxed" low-temperature distribution, n_L, to that in the "initial" high-temperature distribution, n_H, is given by

$$n_L/n_H = \tau k_e[\mathrm{Ar}], \tag{1}$$

where τ is the radiative lifetime of the CH($A^2\Delta$) state, k_e is the effective rate constant for the rotational relaxation of CH($A^2\Delta$, $v'=0$), and [Ar] is the number density of the argon atoms. The observed values of τ and k_e are 460 ns[17] and 2.6×10^{-11} cm^3 molecule^{-1} s^{-1}, respectively. (The k_e value reported in Ref. 14 has been modified slightly in accordance with the τ taken from Ref. 17.) The ratio, n_L/n_H, is thus estimated to be 0.27 when the argon pressure is 0.7 Torr. The relative intensity, $I_{N'N''}/\nu^3S_{N'N''}$, is expressed as

$$I_{N'N''}/\nu^3S_{N'N''} \propto (n_H/T_H)\exp[-hcB_{v'}N'(N'+1)/kT_H] + (n_L/T_L)\exp[-hcB_{v'}N'(N'+1)/kT_L]. \tag{2}$$

By adjustment of the T_H and T_L in Eq. 2 to reproduce the observed relative intensity, as shown in Fig. 3, the temperatures are estimated to be $T_H=5000\pm1000$ K and $T_L=700\pm200$ K. These T_H and T_L values are essentially independent of the argon pressure between 0.4 and 0.7 Torr.

It is shown in Fig. 3 that the observed relative intensities are well represented by Boltzmann distributions with two different effective rotational temperatures, T_H and T_L. This implies that the two-level model adopted in our analysis holds good for accounting for the observed relative intensities phenomenologically.

The distribution for the $v'=1$ state is also consistent with a two-temperature distribution with $T_H=2000\pm500$ K and $T_L=700\pm200$ K, although the contribution from the low-temperature component is less conspicuous, as shown in Fig. 3.

Relative vibrational populations for $v'=0$, 1, and 2 and the effective rotational temperature for $v'=2$ are estimated by simulation of the spectrum. A computer program was written following Baas and Beenakker[18] for the MELCOM 7700 computer at the Educational Computer Center of the University of Tokyo. Transition frequencies, line intensities, and the band envelope were calculated using the molecular constants reported in the literature.[12,13,19,20]

The ratio of the vibrational populations, $P_{vib}(1)/P_{vib}(0)=0.5\pm0.1$, is obtained by simulation of the R-branch 0-0 and 1-1 transitions for $N'\gtrsim11$. For the $v'=2$ level, the effective rotational temperature, $T_{rot}=1500\pm500$ K, and the vibrational population, $P_{vib}(2)/P_{vib}(0)=0.07\pm0.02$, are obtained by simulation of the Q-branch of the 2-2 transition. The calculated spectrum based on the estimated values reproduces the overall feature of the observed spectrum, as shown in Fig. 1.

Distributions of mean internal energies listed in Table 1 are estimated in the following way.[5] The mean rotational energy possessed by the CH($A^2\Delta$) radicals produced "initially" is approximated by

$$\langle E_{rot}\rangle = [\sum_{N'=2} hcB_{v'}\{N'(N'+1)-4\}R_{N'}]/(\sum_{N'=2} R_{N'}), \tag{3}$$

where $R_{N'}$ is the rotational distribution,

$$R_{N'} = (2N'+1)\exp[-hcB_{v'}N'(N'+1)/kT_H]. \tag{4}$$

The mean vibrational energy is calculated from the vibrational energies, $E_{vib}(v)$, and the relative vibrational population, $P_{vib}(v)$, by

$$\langle E_{vib}\rangle = \sum_v E_{vib}(v)P_{vib}(v). \tag{5}$$

As shown in Table 1, approximately equal energies, *ca.* 0.3 eV, are distributed to the vibrational and rotational motions of the CH radicals formed in the reaction of CH_3CN with active ionic species of argon.

Table 1. Relative vibrational populations, effective rotational temperatures, and average vibrational and rotational energies for CH($A^2\Delta$) produced in the argon afterglow reaction with CH_3CN

v	P_{vib}	E_{vib}/eV[a]	T_{rot}/K
0	0.63 ± 0.05	0.179	5000 ± 1000[b]
1	0.32 ± 0.10	0.518	2000 ± 500[b]
2	0.05 ± 0.02	0.834	1500 ± 500
		$\langle E_{vib}\rangle$/eV	$\langle E_{rot}\rangle$/eV
		0.32 ± 0.04	0.34 ± 0.06

a) Calculated from the ω_e and $\omega_e x_e$ values given in Ref. 13. b) Effective rotational temperatures derived from higher rotational levels, $N'\gtrsim11$.

The authors are grateful to Drs. T. Kondow, T. Fukuyama, T. Urisu, I. Tokue, and W. Shearer-Izumi for their critical reading of the manuscript.

Appendix. Two-level Model.

The two-level model for rotational relaxation is a phenomenological treatment, in which microscopic level-to-level transitions among the rotational levels are overlooked. Its main idea[14,16] is to represent the whole rotational distribution by two distributions characterized by different parameters. In the present case an effective Boltzmann temperature was chosen as one of the parameters. A sophisticated treatment was

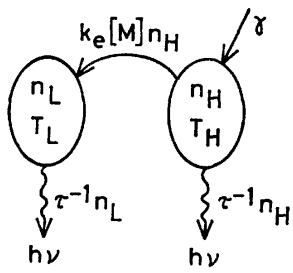

Fig. 4. Schematic diagram of the two-level model for rotational relaxation by collisions.

carried out by Sokabe[16] for the $OH(A^2\Sigma^+)$ rotational distributions formed from H_2O in the reaction with metastable argon atoms, but in the present study a simpler model shown in Fig. 4 was used. Photoemitting species are formed in the distribution characterized by an effective rotational temperature, T_H, at a rate, γ. These species, then, suffer collisional relaxation with surrounding particles to the other distribution characterized by a lower temperature, T_L, at an effective rate constant, k_e. The populations in these "levels" are denoted by n_H and n_L. Photoemissions are observed from these levels with a radiative lifetime, τ.

Rate equations for the two states are written as

$$dn_H/dt = \gamma - k_e[M]n_H - n_H/\tau, \quad (6)$$

$$dn_L/dt = k_e[M]n_H - n_L/\tau. \quad (7)$$

When the steady-state condition, *i.e.*, $dn_H/dt = dn_L/dt = 0$, is assumed, the following relation is obtained from Eq. 7:

$$n_L/n_H = \tau k_e[M]. \quad (8)$$

References

1) D. H. Stedman and D. W. Setser, *Prog. React. Kinet.*, **6**, 193 (1971).
2) D. L. King and D. W. Setser, *Ann. Rev. Phys. Chem.*, **27**, 407 (1976).
3) T. Urisu and K. Kuchitsu, *Chem. Lett.*, **1972**, 813.
4) T. Urisu and K. Kuchitsu, *J. Photochem.*, **2**, 409 (1974).
5) T. Urisu and K. Kuchitsu, *Chem. Phys. Lett.*, **18**, 337 (1973).
6) C. E. Moore, "Atomic Energy Levels," Vol. I, NBS Circular 467, U. S. Government Printing Office, Washington, D. C. (1949); G. Norlén, *Phys. Scr.*, **8**, 249 (1973).
7) H. D. Hagstrum, *Phys. Rev.*, **104**, 309 (1956).
8) The dissociation energy of Ar_2^+ was taken from R. S. Mulliken, *J. Chem. Phys.*, **52**, 5170 (1970).
9) The final products are: $CH(A^2\Delta)+H^++HCN$ or $CH(A^2\Delta)+H+HCN^+$. Ionization potentials were taken from J. L. Franklin, J. G. Dillard, H. M. Rosenstock, J. T. Herron, K. Draxl, and F. H. Field, "Ionization Potentials, Appearance Potentials, and Heats of Formation of Gaseous Positive Ions," NSRDS-NBS 26, U. S. Government Printing Office, Washington, D. C. (1969). Dissociation energies were taken from B. deB. Darwent, "Bond Dissociation Energies in Simple Molecules," NSRDS-NBS 31, U. S. Government Printing Office, Washington, D. C. (1970). The electronic energy for $CH(A^2\Delta)$ was taken from Ref. 12.
10) E. H. Fink and K. H. Welge, *J. Chem. Phys.*, **46**, 4315 (1967).
11) J. E. Hesser and B. L. Lutz, *Astrophys. J.*, **159**, 703 (1970).
12) G. Herzberg, "Molecular Spectra and Molecular Structure, I. Spectra of Diatomic Molecules," 2nd ed., van Nostrand Reinhold, New York (1950).
13) I. Botterud, A. Lofthus, and L. Veseth, *Phys. Scr.*, **8**, 218 (1973).
14) W. Brennen and T. Carrington, *J. Chem. Phys.*, **46**, 7 (1967).
15) C. I. M. Beenakker, P. J. F. Verbeek, G. R. Möhlmann, and F. J. de Heer, *J. Quant. Spectrosc. Radiat. Transfer*, **15**, 333 (1975).
16) N. Sokabe, *J. Phys. Soc. Jpn.*, **33**, 473 (1972).
17) S. W. Jørgensen and G. Sørensen, *J. Chem. Phys.*, **62**, 2550 (1975).
18) R. Ch. Baas and C. I. M. Beenakker, *Computer Phys. Commun.*, **8**, 236 (1974).
19) R. S. Mulliken, *Rev. Mod. Phys.*, **3**, 89 (1931).
20) R. H. Garstang, *Proc. Phys. Soc.*, **83**, 545 (1963).

Spectroscopic and Kinetic Studies of the Photochromism of *N*-Salicylideneanilines and Related Compounds

Ryoichi NAKAGAKI, Takayoshi KOBAYASHI,* Junko NAKAMURA,* and Saburo NAGAKURA

Institute for Solid State Physics, The University of Tokyo, Minato, Tokyo 106

**Institute of Physical and Chemical Research, Wako, Saitama 351*

(Received January 10, 1977)

Photochromism of *N*-salicylideneanilines and related compounds was studied by measuring the electronic and vibrational spectra of the transient species. The rise time of the transient electronic spectra of the photochromic colored species was measured by picosecond time-resolved spectroscopy and was found to be dependent upon solvent viscosity. FT IR spectra showed that the photochromic colored species took the keto amine form. Picosecond kinetic analysis demonstrated that an intermediate existed in the transfer process from *cis*-keto amine to the photochromic species. These facts led us to the conclusion that the photochromic phenomenon of *N*-salicylideneanilines occurred through enol imine$\xrightarrow{h\nu}$enol imine*→*cis*-keto amine*→the intermediate→*trans*-keto amine(photochromic species).

A number of *N*-salicylideneanilines have been reported to be photochromic both in crystal and in rigid and fluid solutions.[1-5] Cohen and his co-workers showed that the hydroxyl group is essential for the photochromic effect: The effect vanishes when the *o*-hydroxyl group is methylated or the Schiff's bases are derived from benzaldehyde or *p*-hydroxybenzaldehyde.[2a]

Several studies have indicated that photochromic change occurs through hydrogen transfer followed by a geometrical rearrangement of the molecule.[1a,2a,3b,4a,5] Ottolenghi and his co-workers first proposed that the rearrangement is the cis-trans isomerization due to rotation about the C_1–C_7 bond,[5b] and later proposed mainly on the basis of theoretical consideration that the rotation takes place both about the C_1–C_7 bond and about the C_7–N bond, resulting in two non-planar photochromic colored species.[5c]

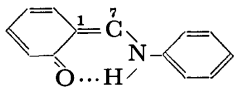

In the present investigation we attempted to elucidate the primary process of photochromism of *N*-salicylideneanilines and related compounds by using the time-resolved spectroscopy techniques in the time range of millisecond to picosecond and to clarify the molecular structure of the photochromic colored species by means of FT(Fourier transform) IR spectroscopy.

Experimental

The compounds employed in the present work are *N*-salicylidene-*p*-toluidine (**1**), *N*-salicylidene-*o*-toluidine (**2**), 2-chloro-*N*-salicylideneaniline (**3**), *N*-salicylidene-*m*-toluidine (**4**), *N*-salicylidene-*m*-toluidine[hydroxy-*d*] (**5**), *N*-3-methoxysalicylidene-4-nitroaniline (**6**), *N*-[1-(*o*-hydroxyphenyl)ethylidene]-aniline (**7**), *N,N'*-disalicylideneethylenediamine (**8**), and 2-(*o*-hydroxyphenyl)benzothiazole (**9**).

Compounds **1**—**4** and **6**—**8** were synthesized by direct condensation of the appropriate carbonyl compounds with corresponding amines in ethanol, and were purified by recrystallization and vacuum sublimation. **5** was prepared by treating **4** in excess CH_3OD for 8 h, the isotopic purity being determined to be about 90% by means of NMR spectroscopy. Commercially available **9** was chromatographed from benzene on activated alumina. Spectrograde diethyl ether, methylcyclohexane, and toluene, GR grade cyclohexanol and liquid paraffin were used without further purification. The other solvents used were purified according to the usual method.[6]

A flash photolysis apparatus constructed by Kira and Nishi[7] was used for measurements of time-resolved absorption spectra in the time range longer than microsecond. A Blumlein type N_2 laser with a pulse-width of 3.6 ns (FWHM) and with a peak power of 500 kW was constructed to be used as an exciting light source for photolysis in the nanosecond time range and for determination of the fluorescence decay time. For the nanosecond time-resolved spectroscopy, a pulsed Xe flash with about 3 μs half-duration was used as an analyzing light source. The light intensity was detected with an HTV 1P28 photomultiplier through a 0.25 m Jarrel-Ash grating monochromator (JE 25). A TRW Model 32A decay time computer was used for determination of the fluorescence lifetime.

An amplified single pulse selected from a pulse train of a mode-locked ruby laser (JEOL JLS-R10) was used for the picosecond time-resolved spectroscopy experiment. The pulse width was *ca.* 20 ps. The exciting light pulse at 347.2 nm was obtained by the frequency-doubling of 694.3 nm fundamental through an ADP crystal. Details of the apparatus were published elsewhere.[8]

FT IR spectra were measured with a JEOL FT IR spectrophotometer JIR-03F at the Department of Chemistry, The University of Tokyo.

Results and Discussion

Photochromic Colored Species of N-*Salicylideneanilines.* Transient absorption spectra of **1**—**3** and **7**—**9** were measured in PM (a mixed solvent of isopentane and methylcyclohexane with 1 : 1 volume ratio) at room temperature. Photochromic effect was examined for **4** and **5** in crystalline state. Since **6** is scarcely soluble in PM, the mixed solvent of diethyl ether and toluene (1 : 1 volume ratio) was used for the measurement of the transient absorption spectrum of **6**. Some of the transient absorption spectra are shown in Figs. 1 and 2. The observed spectra and their decay kinetics are not affected by dissolved O_2. This result is consistent with the previous result.[3] The fact that compounds **1**—**9** commonly having the enol imine structure show the photochromic effect leads us to the conclusion that the structure is essential to formation of the photochromic species.

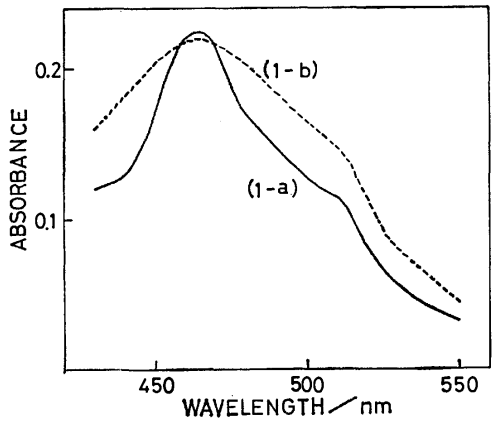

Fig. 1. The photochromic transient absorption spectrum of **1** in PM at 293 K: 1-a, 10 ns after triggering (the 1.4×10^{-3} M solution, 10 mm cell length); 1-b, 35 μs after triggering (the 1.4×10^{-4} M solution, 100 mm cell length).

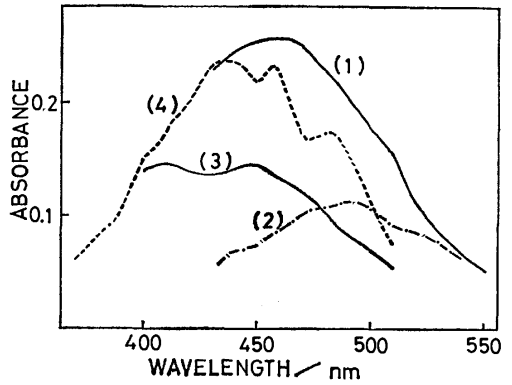

Fig. 2. The photochromic transient absorption spectra of **3**, **6**, **7**, and **8** at 293 K: (1), **3** in PM, 35 μs after triggering (1.7×10^{-4} M); (2), **6** in diethyl ether–toluene (1: 1), 90 μs after triggering (8.4×10^{-5} M); (3), **7** in PM (1.0×10^{-3} M), 10 ns after triggering; (4), **8** in PM (1.8×10^{-4} M), 35 μs after triggering.

Fading of the photochromic colored species of **3** and **6** follows first-order kinetics within the limitations of experimental error, and their decay times were derived to be 55 and 440 μs, respectively, while that of **1**, **2**, **8**, and **9** follows neither first-order nor second-order kinetics. Kinetic analysis at every 10 nm in the measured wavelength region for **1**, **2**, **8**, and **9** shows that there are two different kinds of contributions to the fading: a large but narrowly-distributed contribution from the short-lived component and a small but widely-distributed contribution from the long-lived component. This can explain the observation that the transient absorption bands of **1** becomes blurred with increasing time.

The decay curves observed with **1**, **2**, **8**, and **9** were analyzed by resolving into the long- and short-lived components. The results are given in Table 1 together with those for **3** and **6**. We can see that the decay time of the photochromic colored species is dependent on the solvent viscosity. This is important in connection with the mechanism of the photochromic phenomenon.

The Structure of the Photochromic Colored Species. On the basis of indirect evidence there have been several proposals that the photochromic colored species is formed by hydrogen transfer in the excited state followed by a molecular rearrangement.[1-5] We obtained for the first time the direct evidence that the photochromic colored species take the keto amine form in the crystalline state. IR difference spectra recording transmittance ratios ($T=I_1/I_2$) *vs.* wave numbers were measured with **4** and **5** in KBr disk at room temperature. Here I_1 and I_2 represent transmitted light intensity before and after irradiation with UV light (Hg 365 nm line), respectively. Crystal of **4** was taken as a sample since it gave a long-lived photochromic colored species at room temperature. For the convenience of assignment of the vibrational bands deuterated anil **5** was examined at the same time. The result of **4** is shown in Fig. 3. The frequencies of the characteristic bands observed with **4** and **5** are given in Table 2. Bands with $T>1$ and $T<1$ are attributed to the parent compounds (**4** and **5**) and the photochromic colored species, respectively.

From the characteristic bands with $T>1$ such as C=N stretching at 1616 cm^{-1}, the skeletal streching of a benzene ring at 1597 and 1570 cm^{-1}, and the OH out-of-plane angle bending at 837 cm^{-1}, we can see that the parent compounds **4** and **5** take the enol imine form in the crystalline state. This is consistent with the

Table 1. Decay times of the photochromic colored species

No.				
3	55 μs (in PM)			
6	440 μs (in diethyl ether–toluene)			
	S	L	S	L
	in PM		in LP	
1	30±10 μs	70±20 μs	0.9±0.3 ms	3±1 ms
2	30±10 μs	70±20 μs		
8	30±10 μs	130±30 μs		
9	30±10 μs	80±30 μs	2±1 ms	7±2 ms

S: Short-lived component, L: Long-lived component, LP: Liquid paraffin.

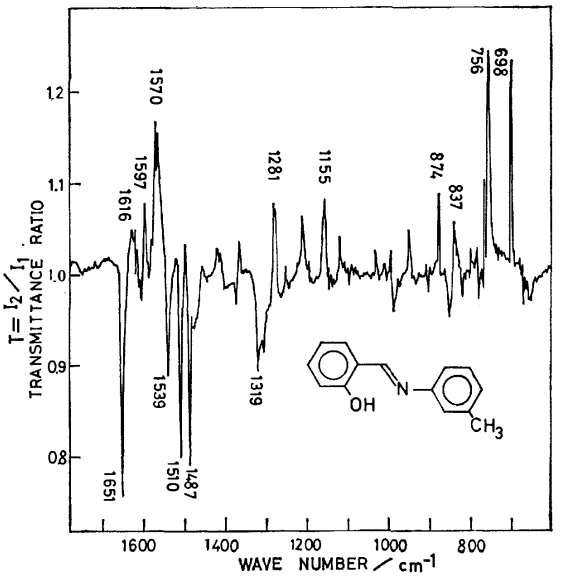

Fig. 3. IR difference spectrum of the photochromic colored species of **4** in KBr disk at 298 K.

Table 2. Characteristic IR bands of the enol imine and keto amine forms of *N*-salicylideneanilines

	Vibrations	4	5
$T>1$	$\nu_{C=N}$	1616	1620
	Ring skeletal stretching	1597	1597
		1570	1570
	γ_{OH}	837	
	γ_{OD}		613
	γ_{CH} [a)]	756	756
$T<1$	$\nu_{C=O}$	1651	1644
	Amide vinylog and ring skeletal stretching	1539	1529
		1510	1505
		1487	1487
	ν_{C-N}	1319	1319

All frequencies are given in cm^{-1}. (KBr disk at 298 K.) a) *o*-Disubstituted benzenes.

results obtained by X-ray crystal analysis.[9] Concerning the bands with $T<1$, strong absorption bands at 1651 cm^{-1} for **4** and 1644 cm^{-1} for **5** show that the photochromic colored species has the carbonyl group. Furthermore, the species show the skeletal stretching of a quinoid ring and the amide vinylog NHC=CC=O vibration at 1539, 1510, and 1487 cm^{-1}, and the C–N stretching at 1319 cm^{-1} for **4**. These results clearly demonstrate that the photochromism is caused by photoisomerization of the enol imine to the keto amine:

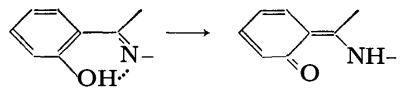

enol imine keto amine

Photochromic Schiff's bases are known to exhibit similar transient electronic absorption spectra in crystalline state and in rigid and fluid solutions.[1-5,10] This means that the photochromic colored species has the same structure, the keto amine form, both in crystalline phase and in rigid and fluid solutions.

Picosecond Photolysis and the Mechanism of Photochromism. We determined for the first time the rise times of the photochromic transient absorption for **1** and **9**, and clarified the existence of the precursor of the photochromic colored species by using the picosecond time-resolved spectroscopy technique. In the PM solution of **1** with viscosity of 0.40 cP at 25 °C, absorbance at 465 nm was saturated 200 ps after photoexcitation and the rise time was determined to be 84 ps (Fig. 4-A). On the other hand, in the cyclohexanol solution with viscosity of 47 cP at 27 °C, the absorbance of **1** at 475 nm continued to increase 200 ps after photoexcitation and its rise time was estimated to be longer than 180 ps (Fig. 4-B). This means that the enol imine in the excited singlet state passes over an energy barrier sensitive to viscosity in the course of transformation into the photochromic colored species; in other words, that in the photochromic phenomenon the hydrogen transfer in the excited state is followed by a geometrical change in the molecular framework which is sensitive to viscosity. The occurrence of the geometrical change in the photochromic process is also supported by the fact that the electronic absorption spectrum of the photochromic

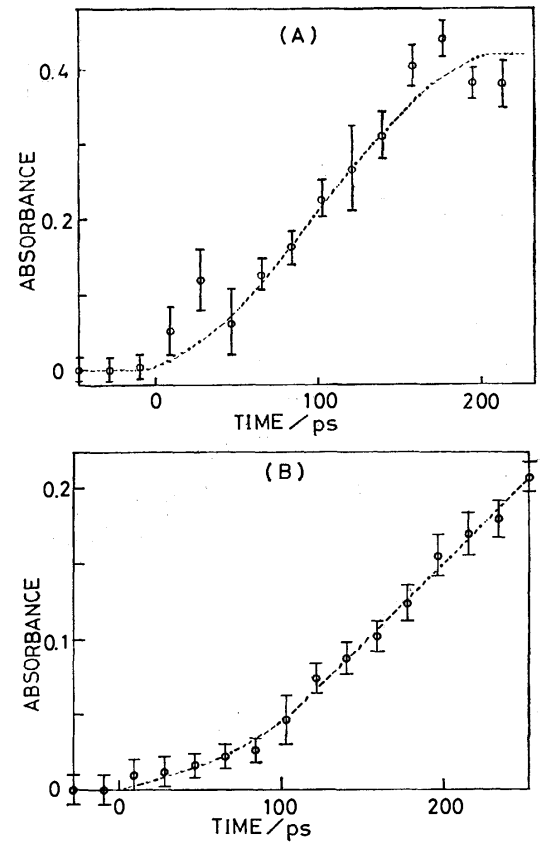

Fig. 4. Formation of the photochromic colored species of **1**. (A) Absorbance at 460 nm plotted as a function of time at 298 K (1.1×10^{-3} M in PM). (B) Absorbance at 475 nm plotted as a function of time at 300 K (1.7×10^{-3} M in cyclohexanol).

colored species is different from that of the *cis*-keto amine formed simply by the hydrogen transfer in the ground state.[5c]

Since the keto amine can take *cis*- and *trans*-forms, it is reasonable to consider that the photochromic colored species is the *trans*-keto amine, and that the photochromic process involves the transformation of the *cis*-keto amine in the excited state into the *trans*-keto amine in the ground state.

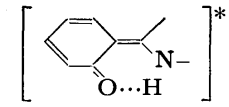

cis-keto amine in the excited state

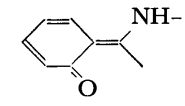

trans-keto amine

According to this mechanism, the thermal bleaching of the photochromic colored species is conversion of the *trans*-keto amine to the enol imine and involves the rearrangement of the molecular framework besides the intramolecular hydrogen transfer. This scheme for the thermal bleaching gives a reasonable explanation to the following findings:

(1) The half-life of the photochromic colored species of **4** in crystalline phase is 1300 and 200 min at 16 and 27 °C, respectively.[11]

(2) The fading kinetics of the photochromic colored species in fluid solution is dependent on viscosity of the solvent.

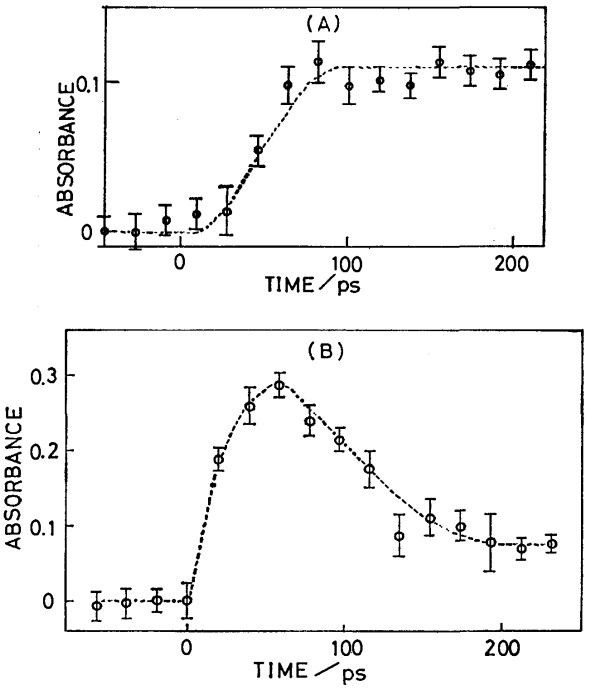

Fig. 5. (A) Formation of the photochromic colored species of **9** at 293 K (1.3×10^{-3} M in PM). Absorbance at 470 nm plotted as a function of time. (B) Decay of the intermediate X* of **9** at 293 K (8.8×10^{-4} M in PM).

The rise time of the photochromic colored species was measured with **9** in PM at 20 °C to be 56 ps (Fig. 5-A). In addition, the transient absorption with very short lifetime was observed with **9** in PM at 20 °C. Absorbance at 385 nm was plotted as a function of time in Fig. 5-B. There are two kinds of contributions to absorbance at 385 nm; the short-lived and the long-lived components. The decay time of the short-lived component was determined to be 53 ps[12] in agreement with the rise time of the long-lived component (the photochromic colored species). Therefore, the short-lived component is considered to be the precursor of the photochromic colored species. On the other hand, the decay time of the fluorescent state of the *cis*-keto amine was determined to be 0.7 ns. These observations clearly show that the molecular rearrangement of the *cis*-keto amine to the photochromic colored species does not occur from the fluorescent state, but originates from the precursor with the lifetime of 53 ps, which may be considered to be the higher vibrationally excited state of the *cis*-keto amine. Rosenfeld *et al.* derived a similar conclusion for *N*-salicylideneaniline from the exciting wavelength dependence of the quantum yields of the photochromic colored species and the fluorescence of the *cis*-keto amine.[5c] We have concluded directly and definitely the existence of the precursor.

A scheme for formation of the photochromic colored species by photoexcitation of the enol imine in the ground state, E, is represented in Fig. 6. The excited singlet state E* of the enol imine produced by photoexcitation of E results in formation of the photochromic colored species in the ground state, P, through the hydrogen transfer and the molecular rearrangement (cis-trans isomerization). The intermediate X* is an excited singlet state from which the photochromic colored species and the fluorescent state of the *cis*-keto amine, K_f*, originate.

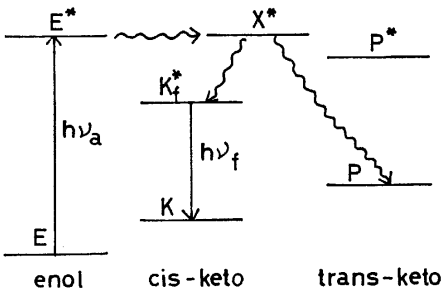

Fig. 6. Schematic explanation of the photochromic species formation.

The authors wish to thank Professor Kenji Tamaru and Professor Takaharu Onishi, The University of Tokyo, for their kind help in measuring the IR difference spectra, and Dr. Akira Kira, Institute of Physical and Chemical Research, for the kindness in putting the flash photolysis apparatus at their disposal and valuable discussion.

References

1) (a) M. D. Cohen and G. M. J. Schmidt, *J. Phys. Chem.*, **66**, 2442 (1962); (b) M. D. Cohen, G. M. J. Schmidt, and S. Flavian, *J. Chem. Soc.*, **1964**, 2041; (c) M. D. Cohen and S. Flavian, *J. Chem.. Soc. B*, **1967**, 329, 334.

2) (a) M. D. Cohen, Y. Hirshberg, and G. M. J. Schmidt, *J. Chem. Soc.*, **1964**, 2051; (b) M. D. Cohen and S. Flavian, *J. Chem. Soc. B*, **1967**, 316, 321.

3) (a) G. Wettermark and L. Dogliotti, *J. Chem. Phys.*, **40**, 1486 (1964); (b) D. G. Anderson and Wettermark, *J. Am. Chem. Soc.*, **87**, 1433 (1965).

4) (a) R. S. Becker and W. F. Richey, *J. Am. Chem. Soc.*, **89**, 1298 (1967); (b) W. F. Richey and R. S. Becker, *J. Chem. Phys.*, **49**, 2092 (1968).

5) (a) M. Ottolenghi and D. S. McClure, *J. Chem. Phys.*, **46**, 4613, 4620 (1967); (b) R. Potashnik and M. Ottolenghi, *ibid.*, **51**, 3671 (1969); (c) T. Rosenfeld, M. Ottolenghi, and A. Y. Meyer, *Mol. Photochem.*, **5**, 39 (1973).

6) A. Weissberger, E. S. Proskauer, J. A. Riddick, and F. E. Toops, "Technique of Organic Chemistry," Vol. II, Organic Solvents, 2nd ed, Interscience, New York (1966), Chap. V.

7) A. Kira and K. Nishi, *Rikagakukenkyusho Hokoku*, **44**, 56 (1968).

8) T. Kobayashi and S. Nagakura, *Chem. Phys. Lett.*, **43**, 429 (1976).

9) (a) J. Bregman, L. Leiserowitz, and G. M. J. Schmidt, *J. Chem. Soc.*, **1964**, 2068; (b) J. Bregman, L. Leiserowitz, and K. Osaki, *ibid.*, **1964**, 2086.

10) D. Lexa, M-M. Duval, and R. Viovy, *J. Chim. Phys. Phys.-Chim. Biol.*, **65**, 292 (1968).

11) A. A. Burr, E. J. Llewellyn, and G. F. Lothian, *Trans. Faraday Soc.*, **60**, 2177 (1964).

12) We defined the following quantities:
$A(t)$=absorbance t ps after photoexcitation,
$A(\infty)$=the final value of absorbance,
$D(t)=A(t)-A(\infty)$.
From the plot of log $D(t)$ *vs.* time, t, the decay time of the short-lived component was determined to be 53 ps.

Reactivity of Excited Triplet Alkyl Ketones in Solution. I. Quenching and Hydrogen Abstraction of Triplet Acetone

Masakazu ANPO and Yutaka KUBOKAWA

Department of Applied Chemistry, College of Engineering, University of Osaka Prefecture, Mozu-Umemachi, Sakai, Osaka 591

(Received January 18, 1977)

The photolysis of acetone in various solutions has been investigated by analysis of reaction products as well as absorption spectroscopy. The rate of photolysis of acetone in aqueous solution decreases on addition of methanol or with increasing concentration of acetone, being much higher than that in methanol and heptane solutions. The results suggest that intermolecular hydrogen abstraction plays a significant role in quenching of triplet acetone. This is supported by spectroscopic studies which reveal formation of the enol form of acetone as an intermediate in the decay process of triplet acetone.

The photolysis of acetone in the liquid as well as in the gas phase has been studied by many workers.[1] The quantum yields for the photolysis were found to be much lower in neat acetone than in aqueous solution, the nature of such a difference being discussed. Porter *et al.*[2] investigated the lifetime of the excited triplet state of acetone in various solutions, and suggested that intermolecular hydrogen abstraction plays a significant role in quenching of triplet acetone, *i.e.*, photolysis and triplet self-quenching by intermolecular hydrogen abstraction may be competitive processes.

Although information on the intermolecular hydrogen abstraction of the excited triplet state of alkyl ketones is important for understanding its reactivity in solution, there is relatively little work along this line. Intermolecular and intramolecular hydrogen abstraction of the excited carbonyl compounds appears to be of interest from a theoretical point of view.[3] We have investigated the photolysis of alkyl ketones in various solutions in order to obtain more detailed information on the relationship between the quenching and the intermolecular hydrogen abstraction in the photolysis of alkyl ketones.

Experimental

Materials. All the compounds (Tokyo Kasei Kogyo Co., Ltd., Grade SG) were purified by fractional distillation. Deionized double-distilled water was degassed by alternate freezing and thawing *in vacuo*. Acetone-d_6 of 99.5 mol% and deuterium oxide of 99.9 mol% isotopic purity (E. Merck, Darmstadt) were used without further purification. Particular care was taken to remove water and oxygen completely from the solvents and reactants.

Apparatus and Procedure. Details of the apparatus and procedure were described previously.[4] A conventional vacuum system was used in conjunction with a rectangular quartz cell (4.0×1.0 cm) of path length 0.5 cm, having two outlets. One was sealed off after admission and degassing of the sample solution. Another had a breakable seal which made it possible to attach the cell to a conventional analytical system after irradiation. Photolysis was carried out at 25±2 °C with light of 270±2.5 nm using a monochromator equipped with a 500 W xenon lamp. The intensity of incident light was determined by means of potassium ferrioxalate actinometry. Intensity in the range 6.4—6.7×10^{13} quanta/s was used. The analytical system consists of three traps and a modified Ward still. The gaseous products were separated by fractional distillation and analyzed by gas chromatography. The absorption spectra before and after irradiation were measured with a Hitachi EPS 3T spectrophotometer. Details of the isotopic analysis of the deuterated methane and acetone were described previously.[5] The CD_2HCOCD_3/CD_3COCD_3 ratio was determined by measurement of the parent peaks at $m/e=63$ [$CD_2HCOCD_3^+$] and $m/e=64$ [$CD_3COCD_3^+$].

Results and Discussion

Table 1 shows the effect of solvents upon the quantum yield of methane formation in the photolysis of acetone. The corresponding results with 2-butanone and 2-pentanone are also included. It should be noted that the quantum yield for the photolysis of acetone is much lower than that for other alkyl ketones, especially in heptane and methanol.

TABLE 1. QUANTUM YIELDS FOR DISAPPEARANCE OF ALKYL KETONES IN THE PHOTOLYSIS IN VARIOUS SOLVENTS AT 25 °C

	Heptane	Methanol	Water
Acetone[a]	0.003	0.004	0.061
Acetone-d_6[b]	—	0.004	0.064
2-Butanone[c]	0.217	0.297	0.306
2-Pentanone[d]	0.237	0.319	0.337

The concentration of alkyl ketones was a) 0.085—0.091 mol/l, b) 0.085 mol/l, c) 0.048 mol/l, and d) 0.051 mol/l. a, b) As seen in Table 3, in view of much lower yield of ethane (less than 2% of methane formation) the value can be regarded as the quantum yield for disappearance of acetone. c, d) The values are obtained from the quantum yields of major products (larger than 95% of total products) such as ethane for 2-butanone and propane (type I) as well as ethylene (type II) for 2-pentanone.

TABLE 2. CD_3H CONTENT OF THE METHANE FORMED FROM THE PHOTOLYSIS OF ACETONE-d_6 AT 25 °C

	Heptane	Methanol	Water
CD_3H content (%)[a]	97.9	97.5	8.80
$\frac{CD_2HCOCD_3}{CD_3COCD_3}$ (%)	—	—	7.01

The concentration of acetone-d_6, 0.090 mol/l. Irradiation time, 60 min. a) The methane consists of only CD_4 and CD_3H, other species being negligible.

The contents of CD_3H in methane formed from the photolysis of acetone-d_6 in various solvents are given in Table 2. Very large contents observed with heptane and methanol solutions show that methyl radicals formed from the primary processes abstract hydrogen atoms only from the solvent molecules. Table 2 also suggests that in aqueous solution most part of CD_3H in methane arises from the H-D exchange reaction between acetone-d_6 and water molecules. It is therefore concluded that methyl radicals scarcely abstract hydrogen atoms from water molecules. Although the conclusion has already been suggested by Pieck and Steacie,[6] the above results offer an unambiguous evidence for it.

Table 3. Effect of added methanol upon the photolysis of acetone in aqueous solution at 25 °C

Concentration of added methanol mol/l	Yield of methane 10^{-4} ml/h	Yield of ethane 10^{-6} ml/h
0	6.67	8.01
0.901	3.63	3.51
1.61	2.69	1.02
2.49	2.02	0.50
2.90	1.85	0
4.40	1.32	0

The concentration of acetone, 0.102 mol/l.
Irradiation time, 60 min.

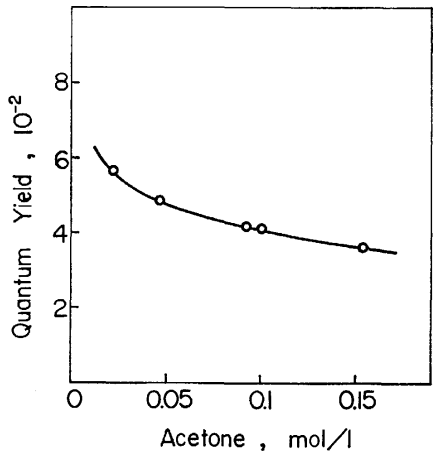

Fig. 1. The effect of the concentration of acetone upon the quantum yields for methane formation from the photolysis of acetone in aqueous solution at 25 °C. Irradiation time, 60 min.

Table 3 shows the effect of added methanol upon the photolysis of acetone in aqueous solution. The rates of methane and ethane formation decrease with increasing concentration of methanol. A similar decrease in the quantum yields for the photolysis of acetone in aqueous solution was obtained when the concentration of acetone increased (Fig. 1). Considering that acetone besides methanol is an efficient hydrogen donor, the results suggest that quenching of the excited acetone molecule is closely associated with hydrogen abstraction reactions. It is well-known that in the condensed phase efficiency of the intersystem crossing from the excited singlet state to the triplet state of acetone is unity.[7] In fact, it was found in the present work that the rate of photolysis is reduced to zero on addition of oxygen. Thus, there is no doubt that the photolysis of acetone in solution proceeds *via* the excited triplet state. Porter *et al.*[2] found that the lifetime of the triplet acetone molecule is much shorter in neat acetone than in aqueous solution and suggested that self-quenching of triplet acetone molecules occurs by intermolecular hydrogen abstraction and may compete its α-cleavage. Thus, the decrease in the rate of photolysis of acetone in aqueous solution caused by addition of methanol or with increasing concentration of acetone would be explicable on the basis of quenching of triplet acetone due to such intermolecular hydrogen abstraction. Furthermore, markedly higher quantum yields of the photolysis in aqueous solution as compared with those in heptane and methanol solutions could be attributed to an unefficient hydrogen abstraction in aqueous solution.

For quenching by methanol of radical products formation from acetone photolysis in aqueous solution, the following Stern-Volmer quenching equation holds:

$$Q_0/Q = 1 + \tau k_q[\text{Methanol}],$$

where Q_0 and Q are the rates of formation in the absence and presence of methanol, respectively; τ and k_q are the lifetime of excited triplet acetone and the quenching rate constant, respectively. The value of τ under our conditions (0.09 mol/l) can be determined to be 17.5×10^{-6} s by using the τ value at 0.05 mol/l, 20×10^{-6} s reported by Porter *et al.*,[8] together with its dependence upon the concentration of acetone (Fig. 2). The value of k_q thus determined is 0.54×10^5 l/mol s, being smaller than the corresponding value for acetonitrile solution, *i.e.*, 1×10^5 l/mol s reported by Porter *et al.*[2] Such a difference would be attributed to the fact that hydrogen bond strength is larger between acetone and water than between acetone and acetonitrile.

Information on the mechanism of quenching of excited

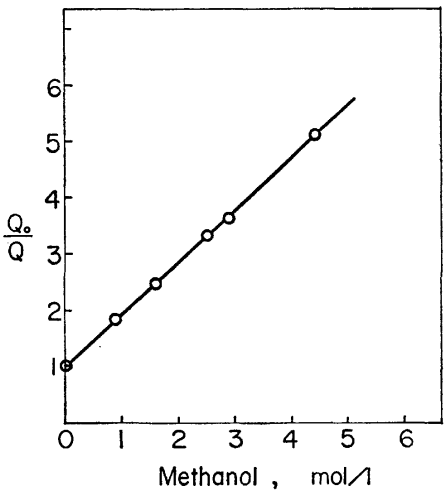

Fig. 2. Stern-Volmer quenching plots for the effect of added methanol upon the yields of methane formed from the photolysis of acetone in aqueous solution at 25 °C. The concentration of acetone, 0.120 mol/l. Irradiation time, 60 min.

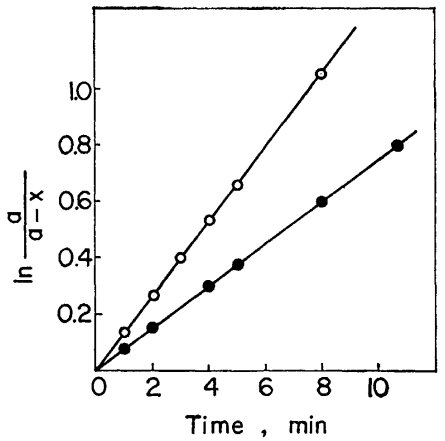

Fig. 3. The recovery of the (n, π^*) band of acetone as a function of time at 25 °C. x represents the recovery of the absorbance at λ_{max} (271 nm). The concentration of acetone, 0.120 mol/l. Irradiation time, 60 min. ○: Acetone, ●: acetone-d_6.

triplet acetone molecules by hydrogen abstraction was obtained from the following results. In methanol and heptane, except in aqueous solution, the UV irradiation led to a much larger decrease in the intensity of the (n, π^*) band of acetone than what would be expected from the extent of its photolysis. As soon as the irradiation ceased, the reduced intensity of the (n, π^*) band began to increase, an almost original intensity being recovered. Such a recovering process was found to obey the first order rate law as shown in Fig. 3. The half-lives obtained from the plots were 5.2 min for acetone and 8.9 min for acetone-d_6. Such a phenomenon was not observed with the photolysis of 2-pentanone or 2-butanone, where the rate of photolysis was unaffected by addition of methanol.

It has been found by ESR and UV studies that ketyl radicals are formed by hydrogen abstraction of excited triplet acetone from 2-propanol.[8,9] Henne and Fischer[9c] found by NMR studies that disproportionation of ketyl radical pairs leads to formation of the enol form of acetone and 2-propanol, and proposed that by ketonization of the former the ground state of acetone is reformed. A similar situation would be expected for the photolysis of acetone in methanol solution. The following mechanism is proposed:

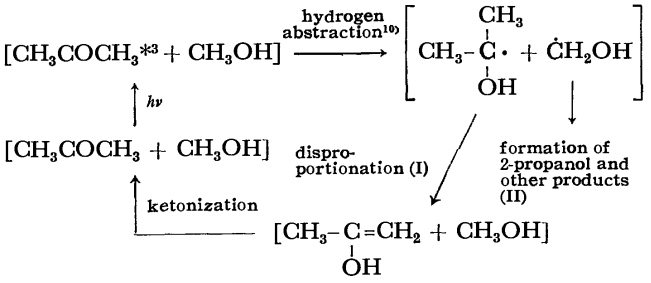

According to the above mechanism, such a recovering process of the reduced intensity of the (n, π^*) band (Fig. 3) would be explicable by the occurrence of ketonization of the enol form of acetone formed by irradiation.

McMillan *et al.*[11] found that in the gas phase photolysis of 2-pentanone enol acetone formed by Norrish type II reaction rearranges to the keto form with a half-life of 4.7±0.3 min, in approximate agreement with that of ketonization determined from Fig. 3. The rate of reactions within the solvent cage such as the disproportionation reaction seems to be greater than that of reaction (II) such as formation of pinacol as well as 2-propanol as has been found by Singh.[12] As regards the disproportionation path, the reaction resulting in formation of enol acetone will be predominant by taking into consideration the fact that $\dot{C}H_2OH$ radicals are more reactive than ketyl radicals toward hydrogen abstraction. Thus, the rate of reaction (II) is expected to be negligibly small as compared with that of reaction (I). In fact, the products of reaction (II) such as 2-propanol and others were found to be negligible.[13]

The absence of such a recovery of the reduced intensity of the (n, π^*) band observed with 2-butanone as well as 2-pentanone would be attributable to a much lower efficiency of hydrogen abstraction of its excited triplet state than that of acetone triplet. In contrast with the case of acetone, a small difference between the rate of photolysis in water and that in heptane or methanol solution was observed for the cases of 2-butanone as well as 2-pentanone. Such behavior would be explained on a similar basis.

We would like to express our thanks to Messrs. K. Yamamoto and T. Shimatani for carrying out some parts of the experiments.

References

1) D. H. Volman and L. W. Swanson, *J. Am. Chem. Soc.*, **82**, 4141 (1960). J. G. Calvert and J. N. Pitts, Jr., "Photochemistry," Wiley, New York (1965), p. 366. J. C. Dalton and N. J. Turro, *Ann. Rev. Phys. Chem.*, **21**, 499 (1970). C. H. Bamford and C. F. H. Tripper, "Comprehensive Chemical Kinetics," Vol. 5, Elservier, New York (1972), p. 309.

2) G. Porter, S. K. Dogra, R. O. Loutfly, S. E. Sugamori, and R. W. Yip, *J. Chem. Soc., Faraday Trans. 1*, **69**, 1462 (1973).

3) J. C. Scaiano, *J. Photochem.*, **2**, 81 (1973/4). S. J. Formosinho, *J. Chem. Soc., Faraday Trans. 2*, **72**, 1313 (1976).

4) M. Anpo and Y. Kubokawa, *Bull. Chem. Soc. Jpn.*, **48**, 3085 (1975).

5) M. Anpo, S. Hirohashi, and Y. Kubokawa, *Bull. Chem. Soc. Jpn.*, **48**, 985 (1975).

6) R. Pieck and E. W. R. Steacie, *Can. J. Chem.*, **33**, 1304 (1955).

7) R. F. Borkman and D. R. Kearns, *J. Chem. Phys.*, **44**, 945 (1966).

8) G. Porter, R. W. Yip, J. M. Dunston, A. J. Cessna, and S. E. Sugamori, *J. Chem. Soc., Faraday Trans. 1*, **67**, 3149(1971).

9) a) R. Livingston and H. Zeldes, *J. Chem. Phys.*, **44**, 1245 (1966); b) G. P. Laroff and H. Fischer, *Helv. Chim. Acta*, **56**, 2011 (1973); c) A. Henne and H. Fischer, *ibid.*, **58**, 1598 (1975).

10) $\dot{R} + CH_3OH \xrightarrow{k_o} CH_3\dot{O} + RH$
$\dot{R} + CH_3OH \xrightarrow{k_c} \dot{C}H_2OH + RH$
The k_c/k_o ratio is 0.06 at 30 °C in the gas phase,[14] and 5.0 at the same temperature in the liquid phase.[15]

11) G. R. McMillan, J. G. Calvert, and J. N. Pitts, Jr., *J. Am. Chem. Soc.*, **86**, 3602 (1964).
12) P. Singh, *J. Chem. Soc., C*, **1971** 714.
13) Even if reaction (II) should occur, its products such as 2-propanol and others will disappear owing to their reactions with excited triplet acetone molecules, since their hydrogen atom-donating ability is higher than that of methanol.[16]
14) T. W. Shannon and A. G. Harrison, *Can. J. Chem.*, **41**, 2455 (1963).
15) M. Cher, *J. Phys. Chem.*, **67**, 605 (1963).
16) G. S. Hammond, W. P. Baker, and W. H. Moore, *J. Am. Chem. Soc.*, **83**, 2795 (1961).

Electronic Structures of Meso-ionic Azapentalenes Studied by X-Ray Photoelectron Spectroscopy

Toshiaki OHTA, Masayuki YOSHIDA, and Haruo KURODA

Department of Chemistry, Faculty of Science, The University of Tokyo, Hongo, Tokyo 113

(Received January 28, 1977)

X-Ray photoelectron spectra of meso-ionic azapentalenes were observed in the solid phase. The charge distributions in these molecules were investigated by using the observed chemical shifts of core-electron levels, employing Siegbahn's electrostatic potential model and the results of CNDO/2 calculations.

Pentalene is very unstable because of 8π electron system, and pentalene itself has not yet been synthesized.[1] If a carbon atom in the five-membered ring is replaced by a hetero atom with 2π electrons, the resulted molecule has aromaticity and would be stabilized. As shown in Fig. 1, a series of hetero aza-pentalenes, namely, 2,5-diphenyl[1,2,3]triazolo[4,5-*d*][1,2,3]triazole (I), and 5-phenyl-5*H*-[1,2,3]triazolo[4,5-*c*][1,2,5]-oxadiazole (II), -thiadiazole (III), and -selenadiazole (IV) are expected to be stable compounds since the introduction of a hetero atom at position 2 and a nitrogen atom at position 5, provides 2π electrons to the pentalene skeleton so as to form 10π electron system. In effect, they have recently been synthesized by one of the authors (M.Y.) and his coworkers, and turned to be very stable solid. Syntheses and some properties of these compounds were published elsewhere.[2,3] As readily guessed from Fig. 1, these compounds have meso-ionicity and are expected to have large electronic polarization. It is therefore of great interest to investigate to what extent electronic charges are polarized in these molecules.

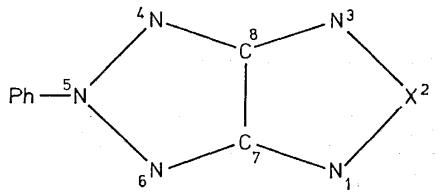

(I) X=N–Ph, (II) X=O, (III) X=S, (IV) X=Se

Fig. 1. Molecular structure of azapentalenes.

Recently, X-ray photoelectron spectroscopy (XPS) has proved to be a powerful means for the study of charge distribution in a molecule, having been successfully applied to a number of organic molecules.[4,5] The purpose of this paper is to elucidate charge distributions in the above-described compounds by the measurement and analyses of the chemical shifts of core electron levels with the aid of Siegbahn's electrostatic potential model and CNDO/2 calculation. In addition, a geometry optimization technique in the framework of the CNDO/2 method was used to predict the molecular geometries of these compounds, since they have not yet been determined experimentally.

X-Ray photoelectron spectra of the compounds studied were measured with a McPherson ESCA 36 electron spectrometer, by employing Al $K\alpha$ radiation. Each sample, purified by recrystallization in advance, was coated on an aluminium plate. Core electron binding energies were calibrated by using the Au $4f_{7/2}$ (84.0 eV) peak of a thin gold film deposited onto the sample surface.

TABLE 1. CORE ELECTRON BINDING ENERGIES OF HETEROAZAPENTALENES (eV)

	C 1s	N 1s	$\Delta E_{splitting}$ (N 1s)	O 1s	S $2p_{3/2}$	Se $3p_{3/2}$
I	(287.1) 284.2	(402.0) 399.3	2.7			
II	(286.1) 284.2	(402.0) 399.2	2.8	532.2		
III	(286.1) 284.2	(401.8) 398.9	2.9		164.0	
IV	(287.1) 284.2	(401.9) 398.7	3.2			160.5

A shoulder and/or a weaker peak is listed in the parenthesis.

Determined core electron binding energies are listed in Table 1. All of C 1s spectra have a small shoulder in the higher binding energy side of the main peak. The C 1s binding energy of the main peak is consistently the same for all compounds, so that it can be assigned to the phenyl carbons. The small shoulder is possibly associated with carbons in the pentalene ring. Figure 2 shows N 1s spectra of these compounds. We can see well-resolved two peaks except for compound (II), in which case the main peak is a little broader than the others. The intensity ratio of the two peaks in compound (I) is 1 : 1.9, so that the stronger peak at the lower binding energy side is easily assigned to the nitrogen atoms at the positions 1, 3, 4, 6 and the weaker peak is to the nitrogen atoms at positions 2 and 5. On the other hand, in compounds (II), (III), and (IV), intensity ratios of two peaks are nearly 1 : 4, so that the stronger peak has the same origin as compound (I), and the weaker peak is due to the nitrogen atom at position 5. These spectra show clearly that the nitrogen atom at position 5 has a less negative charge than the nitrogen atoms at positions 1, 3, 4, and 6. It is to be noted that the splitting of N 1s peaks is larger as the atomic number of the substituent atom is higher, as listed in the fourth column of Table 1.

XPS chemical shift is influenced not only by the charge density of the ionizing atom, but also by those of atoms surrounding it. Siegbahn and his coworkers have proposed the following equation for interpreting chemical shifts:[6]

$$\Delta E_A = kq_A + \sum_{B \neq A}^{\text{molecule}} \frac{e^2 q_B}{R_{AB}}, \quad (1)$$

where k is a constant characteristic of atom, q_A and q_B

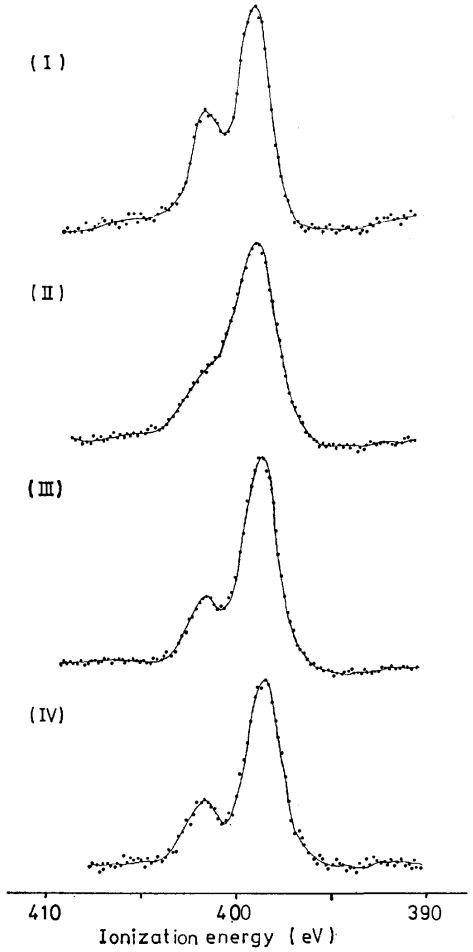

Fig. 2. N 1s spectra of azapentalenes.

are charge densities of atom A and B, respectively, and R_{AB} is the distance between them. For a variety of molecules containing carbon, nitrogen, and oxygen, the chemical shifts of core-electron levels have been successfully interpreted with Eq. 1, by use of CNDO/2 charge densities.

In the present compounds, molecular geometries have not yet been determined experimentally, so that it is difficult to obtain reliable charge densities by MO calculation since they would be influenced more or less by the molecular geometry. Accordingly, geometry optimization has been carried out for these molecules within the scheme of CNDO/2 formulation. The geometry for the CNDO/2 total-energy minimum was searched by using the differentiation of two-center integral terms. Since molecule (I) or (II) is too complex to be calculated with CNDO/2, the simplified model, in which the phenyl group is replaced by a hydrogen atom, was used for the geometry optimization. Such simplification would not affect the interpretation of N 1s chemical shifts. The model compounds are denoted as (I') and (II'), and so on. A regular pentagon structure with a bond length of 1.35 Å was used as the initial geometry for each molecule. Furthermore, the molecular symmetry, D_{2h} for (I') and C_{2v} for (II') and (III'), was retained throughout the geometry optimization. Determined geometries of (I') and (II') are shown in Fig. 3. The N–N or N–O bond length is smaller than the C–N

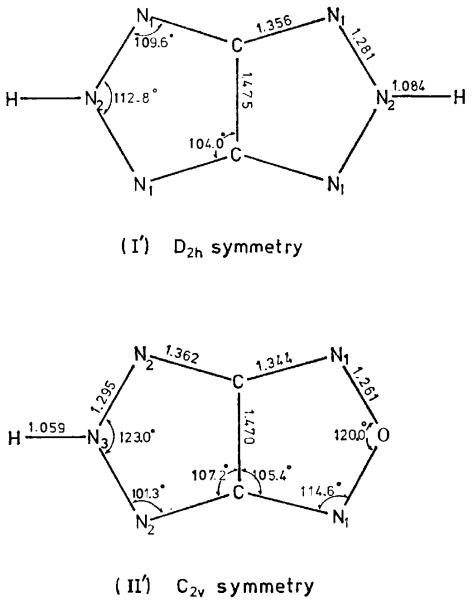

Fig. 3. Optimized geometries of molecules (I') and (II').

TABLE 2. TOTAL CHARGE AND π ELECTRON DENSITIES OF MOLECULES (I') AND (II')

	(I') D_{2h} symmetry			(II') C_{2v} symmetry	
Atom[a]	Total charge density	π electron density	Atom[a]	Total charge density	π electron density
C	0.086	−0.043	C	0.090	−0.016
N_1	−0.161	−0.275	N_1	−0.085	−0.233
N_2	0.149	0.592	N_2	−0.163	−0.295
H	0.088		N_3	0.190	0.677
			O	0.032	0.409
			H	0.095	

a) Refer to Fig. 3 about atomic species.

bond length. The C–C bond is much longer than that in benzene and has a character of single bond to large extent. These results seem to be plausible from the comparison with geometries of the related compounds whose structures have already been determined.[7] CNDO/2 charge densities in molecules (I') and (II') are listed in Table 2. In molecule (I'), the total charge density of N_1 atom is negative and that of N_2 is positive. This is in accord with the conclusion derived from the N 1s chemical shift. This tendency is much stronger in the π electron charge distribution as indicated in Table 2. By using calculated charge densities and a k value of 21.5 eV/unit charge as proposed by Siegbahn *et al.*,[6] we obtained 2.9 eV for the N 1s splitting in molecule (I'), which is very close to the observed spliting, 2.7 eV. This would mean that the calculated charge distribution in this molecule is reliable. Similar results are obtained for molecule (II'), in which there are three kinds of nitrogen atom. Calculated shifts are −0.96 eV, −0.92 eV, and 2.41 eV for N_1, N_2, and N_3, respectively. ΔE *fwhm* of the N 1s main peak of compound (II) is 2.5 eV, which is broader than the N 1s peaks of other compounds by about 0.5 eV. The main N 1s peak of compound (II) is composed of the two components,

which are due to N_1 and N_2, respectively. Consequently, its broadening can be understood as that arising from the splitting of the two components by chemical shift. The chemical shift of the N 1s level of N_3 is a little overestimated by MO calculations as compared with the observed result. We tried to carry out the geometry optimization also for molecule (III'), which contains a sulfur atom. In general, CNDO/2 method gives less reliable results for molecules containing second row atoms. In fact, the optimized geometry of molecule (III') shows an unusually long N–S bondlength, 1.8 Å. The charge densities calculated for this geometry could not explain the observed N 1s chemical shifts of compound (III).

We tried to estimate the charge distribution in molecule (III') from the observed N 1s binding energies for compound (III), using the procedure called "ACHARGE" analysis.[5,8] Since the number of obtained experimental values is too limited to give the whole charge distribution, the following assumptions were adopted to carry out the ACHARGE analysis; first, the geometry of molecule (III') was assumed to be the same as molecules (II'), and, second, the charge densities on C and H atoms were assumed to be the same as those in (II'), since they are likely to be small and relatively independent of the substitution of a hetero atom. Resulted charge densities are $-0.17e(N_1)$, $-0.16e(N_2)$, $0.15e(N_3)$, and 0.23e(S). They are almost the same as those in molecules (I') and (II'). From the above-described analyses of XPS chemical shifts, it can be concluded that in these molecules the nitrogen at position 5 and the hetero atom at position 2 have positive charges, while the nitrogen atoms at positions 1, 3, 4, and 6 have negative charges, and that the degree of charge polarization in these molecules is not so large, although they have been regarded as meso-ionic compounds.

References

1) See for example, S. A. R. Knox and F. G. A. Stone, *Acc. Chem. Res.*, **7**, 321 (1974).
2) M. Yoshida, A. Matsumoto, and O. Simamura, *Bull. Chem. Soc. Jpn.*, **43**, 3587 (1970).
3) A. Matsumoto, M. Yoshida, and O. Simamura, *Bull. Chem. Soc. Jpn.*, **47**, 1493 (1974).
4) T. Ohta, M. Yamada, and H. Kuroda, *Bull. Chem. Soc. Jpn.*, **47**, 1158 (1974).
5) T. Ohta, T. Fujikawa, and H. Kuroda, *Bull. Chem. Soc. Jpn.*, **48**, 2017 (1975).
6) K. Siegbahn, C. Nordling, G. Johanson, J. Hedman, P. F. Hedén, K. Hamrin, U. Gelius, T.Bergmark, L. Q. Werme, R.Manne, and Y. Baer, "ESCA Applied Free Molecules," North-Holland, Amsterdam (1969).
7) For example, molecular structures of 1,2,4,5-tetrazine, 5-amino-2-methyltetrazole, and adenine hydrochloride hemihydrate have been determined. (See "Tables of Interatomic Distances and Configuration in Molecules and Ions" compiled by H. J. M. Bowen *et al.*, The Chemical Society, London (1958)).
8) T. D. Thomas, *J. Chem. Phys.*, **52**, 1373 (1970).

On the Phase Transition of Ammonium Hexafluoroferrate(III)

Keiichi MORIYA, Takasuke MATSUO, Hiroshi SUGA, and Syûzô SEKI
Department of Chemistry, Faculty of Science, Osaka University, Osaka 560
(Received January 31, 1977)

The heat capacities of $(NH_4)_3[FeF_6]$ crystal have been measured from 15 to 350 K with an adiabatic calorimeter. A heat capacity anomaly was observed at 267.02 ± 0.05 K. The enthalpy and entropy changes of the transition are 6490 ± 500 J mol^{-1} and 24.8 ± 1.9 J K^{-1} mol^{-1}, respectively. This value of entropy was discussed in terms of a model involving orientational disorder of the ammonium as well as hexafluoroferrate(III) ions. Based on the assumption of the average fcc symmetry of the crystal and internal rigidity of the ions, the proposed model predicts the transition entropy equal to R ln $16=23.05$ J K^{-1} mol^{-1} which is in close agreement with the experimental value. Temperature dependent splitting of the Raman band due to the internal vibration of the anion was found to be consistent with the model. The excess heat capacity follows the prediction of the Landau theory of phase transitions of the second kind. Properties of the present and the similar crystals including ammonium and alkali salts of hexafluoro-complex ions were discussed in terms of the ionic orientational disorder.

An early X-ray diffraction work by Pauling[1] showed that ammonium hexafluoroferrate(III) has a face-centered cubic lattice at room temperature. This was confirmed later by Steward and Rooksby[2] who studied the crystal by X-ray powder method at room temperature and at 93 K. They found a tetragonal lattice at the lower temperature, a phase transition being suspected at some intermediate temperature. The phase transition was found at 263 K by Mørup and Thrane[3] in a Mössbauer line-width study of the compound. The mechanism of the phase transition has not been understood well, since the only available data are those concerned with the Bravais lattice change and Mössbauer spectrum narrowing. The latter was interpreted as indicating that the symmetry of the iron site becomes lower in the low temperature phase.[4]

There are a number of factors in the $(NH_4)_3[FeF_6]$ crystal that can lead to the phase transition. The ammonium ion is, of course, well-known for its tendency toward disordering in a number of crystals, the most notable example being ammonium chloride in which the ammonium ion takes at random one of the two allowed orientations. The ammonium ions in the present crystal are not all equivalent, but are grouped into two sets.[5] Those which belong to one set occupy the octahedral sites (the 4b positions)[6] in the fcc lattice, while those belonging to the other set are in the tetrahedral sites (the 8c positions). Consequently, the role played by the ammonium ions in this phase transition may be more complicated than in the ammonium halides. The hexafluoroferrate(III) ion, $[FeF_6]^{3-}$, has the octahedral ionic symmetry and occupies the octahedral 4a position. One might hence expect that the hexafluoroferrate(III) ions are in a uniquely determined orientation in the crystal and, as such, would play a rather passive role in the phase transition. However, consideration based on the lattice dimension and empirical radii of Fe^{3+}, F^- and NH_4^+ ions[7] shows that coincidence of the ionic and crystalline tetrad axes might not be taken for granted: the ions are too bulky to lie simultaneously on the tetrad axis. Instead, the high crystal symmetry might be a result of the orientational disorder of the $[FeF_6]^{3-}$ ions. Therefore, the orientational degree of freedom of the anion has also to be taken into account in a satisfactory description of the mechanism of the phase transition. This type of ionic disorder is an interesting possibility which the heat capacity measurement can prove or refute.

Another motivation for studying the present substance is that it belongs to a large family of crystals which contain fluorine octahedra as their major constituent and for which a vast amount of structural information has been accumulated.[5] Specifically, three closely related ammonium salts are of particular interest: $NH_4[PF_6]$,[8] $(NH_4)_2[SiF_6]$,[9] and $(NH_4)_3[AlF_6]$.[2] The structural relation among these fcc crystals are briefly as follows. The NH_4^+ ion in $NH_4[PF_6]$ crystal occupies the site corresponding to the octahedral position (4b) of the $(NH_4)_3[FeF_6]$ structure, with the 8c tetrahedral positions unoccupied. This is the rock-salt structure with the sodium and chloride ions replaced by the ammonium and the hexafluorophosphate(V) ions, respectively. In the cubic $(NH_4)_2[SiF_6]$ crystal, the occupations is just reversed, *i.e.*, the tetrahedral 8c sites are occupied by the ammonium ions while the octahedral 4b sites are vacant. In $(NH_4)_3[AlF_6]$ both the 4b and 8c positions are occupied. This last crystal is isomorphous with ammonium hexafluoroferrate(III) crystal. The heat capacities of the fluorophosphate,[10] fluorosilicate,[11] and fluoroaluminate[12] have been measured. It will be shown below that comparison of the properties of these compounds leads to an insight into the molecular mechanism of the phase transitions in these ammonium salts.

Finally a peculiar property of the present crystal is noticed in Table 1 which summarizes the room temperature crystal systems and the molar volumes of $A_3[FeF_6]$ type crystals (A; alkali or ammonium ions). The

TABLE 1. ROOM-TEMPERATURE CRYSTAL PROPERTIES OF SOME CRYOLITE-TYPE COMPOUNDS $A(I)_3[FeF_6]$

A(I)	Crystal system	Molar volume/cm^3 mol^{-1}
Li	(complex)	—
Na	monoclinic	76.0
K	tetragonal	96.2
Rb	tetragonal	106.6
Cs	tetragonal	122.3
NH_4	cubic	111.3

structure of the lithium compound is complicated and is not successfully analysed, but the symmetry of the crystal is certainly the lowest.[13] The sodium compound is monoclinic, while the potassium, rubidium and cesium compounds are tetragonal. A gradual trend toward the higher symmetry with increasing cationic size is evident. The ammonium compound, whose molar volume lies between those of the rubidium and cesium compounds (this fact is itself somewhat anomalous because the apparent ionic volume of the ammonium ion is usually between those of potassium and rubidium) has the highest cubic symmetry in the series of the crystals. It should be noted that the enhancement of the crystal symmetry is caused by substitution of the less symmetric ammonium ion for spherical alkali ions. This unusual property of the ammonium salt will be explained below as an entropy effect. This paper reports on the heat capacity measurement of $(NH_4)_3[FeF_6]$ crystal and the interpretation of the experimental results in terms of the above general consideration.

Experimental

Sample Preparation. Extra-pure grade reagent of $Fe(NO_3)_3 \cdot 9H_2O$ crystal (Wako Pure Chemical Industries, Ltd.) was dissolved in distilled water. This solution was added dropwise to a concentrated aqueous solution of extra-pure grade reagent of NH_4F (Wako Pure Chemical Industries, Ltd.). $(NH_4)_3[FeF_6]$ crystal precipitated rapidly as finely divided powder. The crystal was separated from the mother liquor and dried at 70 °C. Contamination of the sample with the fluorosilicate was avoided by using polyethylene ware throughout the sample preparation. Elemental analysis gave F, 50.9±0.4%; Fe, 24.94±0.04%; H, 5.39±0.2% (Fe by EDTA gravimetric method, F by thorium nitrate titration, and H by gravimetric method). The calculated values for $(NH_4)_3[FeF_6]$ are F, 50.90%; Fe, 24.94%; H, 5.40%. It was important to use an excess amount of ammonium fluoride solution slightly acidified with hydrofluoric acid. Otherwise, the hydrated crystal appeared to precipitate as noted by Cox and Sharpe.[14] Several other attempts were made until the above preparation was found to be successful. These other attempts gave less than ideal elemental analysis. As an additional guide for the preparation, the differetial thermal analysis (DTA) was employed. The crystal used for the heat capacity measurement gave a sharp endothermic peak on heating through 266±1K. Table 2 summarized the chemical analyses and the DTA results for five different preparations. It should be emphasized that, contrary to Cox and Sharpe's statement,[14] the stoichiometric $(NH_4)_3[FeF_6]$ crystal was prepared by the wet method.

Calorimetry. The heat capacities of $(NH_4)_3[FeF_6]$ crystal were measured from 15 to 350 K with an adiabatic calorimeter. The apparatus is described elsewhere.[15-18] The calorimetric sample crystal, 32.4949 g (0.14510 mol) in weight, was put in the calorimeter cell together with helium heat-exchange gas. The procedure of the measurement was standard one, *i.e.*, intermittent heating method with the temperature increment of 1 K at 20 K and 2 K above 80 K. Smaller steps were employed near the phase transition. The total enthalpy change of the transition was determined by introducing electric energy to the specimen from approximately 4 K below the transition temperature to 4 K above under the adiabatic condition.

Raman Spectrum. Temperature dependence of Raman spectra were recorded with a laser-excited Raman apparatus. The high symmetry of $[FeF_6]^{3-}$ ion is particularly suitable for the vibrational-spectroscopic study because changes in its ionic environment affect the degenerate internal vibration, causing well-resolved splitting of the spectral band. The same situation was exploited in a study of the phase transition in $[Co(NH_3)_6]Cl_2$,[19] in which the hexaamminecobalt(II) ion has a similar high ionic symmetry. The sample crystal was sealed in a thin wall glass ampule and attached to the cold finger in a cryostat. The sample temperature was controlled by adjusting the amount of liquid nitrogen introduced into the coolant chamber and monitored with a copper-constantan thermocouple fixed to the glass ampule.

Table 2. Elemental analysis and DTA of $(NH_4)_3[FeF_6]$ crystals prepared by different methods

	Chemical composition		DTA peak
	Fe	F	
(1)	24.87%	50.0%	sharp[a]
(2)	24.95	50.2	sharp
(3)	24.61	50.5	broad
(4)	25.06	50.7	broad
(5)	24.94	50.9	sharp
Calcd	24.94	50.9	

a) A small peak was found at 257 K besides the main peak at 267 K. The crystals were prepared as follows. (1) From aqueous solutions of $Fe(NO_3)_3 \cdot 9H_2O$ and $NH_4F \cdot HF$. (2) From aqueous solutions of $FeCl_3 \cdot 6H_2O$ and NH_4F. (3) Direct reaction of $Fe(NO_3)_3 \cdot 9H_2O$ crystal with NH_4F solution. (4) The same as described in the text but without addition of hydrofluoric acid. (5) As described in the text.

Results

The experimental values of the molar heat capacity of $(NH_4)_3[FeF_6]$ crystal are given in Table 3 and also shown in Fig. 1. Graphically smoothed heat capacities and derived thermodynamic functions are given in Table 4. The heat capacity changes smoothly with temperature except in the transition region which spans approximately from 180 to 270 K. The highest value of the heat capacity reaching 20000 J K^{-1} mol^{-1} was observed at 267.02±0.05 K. This temperature is 4 K higher than the line width transition temperature 263 K reported by

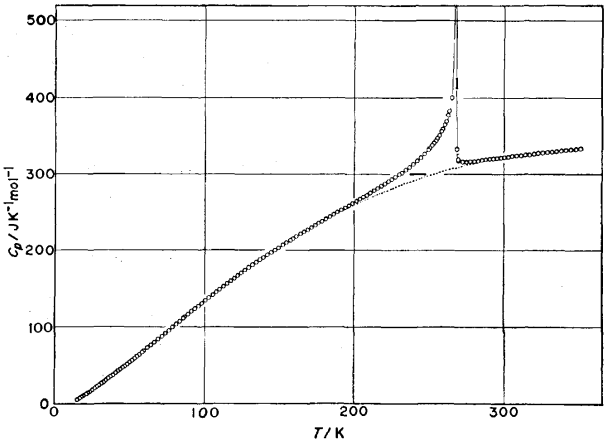

Fig. 1. Molar heat capacity of $(NH_4)_3[FeF_6]$.

Table 3. Heat capacity of $(NH_4)_3[FeF_6]$

T_{av}/K	C_p/J K^{-1} mol^{-1}	T_{av}/K	C_p/J K^{-1} mol^{-1}	T_{av}/K	C_p/J K^{-1} mol^{-1}	T_{av}/K	C_p/J K^{-1} mol^{-1}	T_{av}/K	C_p/J K^{-1} mol^{-1}
		78.39	100.2	163.96	223.2	239.62	315.2	332.34	331.1
1 st series		80.87	104.3	166.43	225.6	242.20	319.5	335.38	331.9
		83.26	108.0	168.88	228.8	244.74	323.6	338.48	332.6
15.06	6.23	85.58	112.0	171.33	231.7	247.26	328.8	341.62	333.7
15.81	7.05			173.75	234.5	249.75	333.8	344.85	334.0
16.89	8.34	3 rd series		176.13	237.5	252.22	339.5	348.16	334.6
18.13	9.75			178.50	239.9	254.65	345.5	351.47	335.3
19.20	11.08	81.43	106.4	181.02	243.0	257.05	352.7		
20.15	12.25	84.22	109.7	183.68	246.0	259.41	361.1	9 th series	
21.14	13.48	86.49	113.4	186.29	249.0	261.73	371.2		
22.25	14.88	88.85	117.2	188.88	251.9	264.01	384.9	233.06	305.3
23.58	16.46	91.14	121.4	191.45	254.8	266.10	545.6	235.72	309.1
25.01	18.52	93.38	124.4	193.99	257.9	266.94	15270	238.36	313.0
26.65	20.70	95.62	128.0	196.51	260.6	267.01	26580	240.98	317.3
28.10	22.62	97.87	131.5	199.01	263.6	267.07	20030	243.57	321.6
29.61	24.66	100.23	135.2	201.49	266.4	267.96	623.2	246.12	326.6
31.18	26.83	102.68	139.0	203.94	269.3	270.15	319.7	248.65	331.6
32.61	28.85	105.08	142.7	206.38	271.9	272.79	318.1	250.57	335.9
34.04	30.86	107.42	146.2			275.39	318.1	251.93	338.9
35.63	33.11	109.83	149.9	5 th series		277.96	318.7	253.29	342.4
37.27	35.50	112.31	153.5			280.58	318.8	254.64	345.9
38.92	37.75	114.75	157.2	201.15	266.0	283.27	319.6	255.89	349.0
40.60	40.28	117.15	160.8	203.63	269.1	285.78	320.6	257.21	353.2
42.16	42.60	119.50	164.1	206.10	271.7	288.29	321.0	258.51	358.3
43.62	44.85	121.80	167.4	208.54	274.0	290.80	321.9	259.40	360.9
45.11	47.16	124.23	170.8	210.96	277.2	293.32	322.6	260.69	366.6
46.65	49.20	126.78	174.5	213.42	280.3	295.83	322.7	261.96	372.8
48.23	51.95	129.27	178.0	215.91	283.3	298.32	323.6	263.21	379.8
49.87	54.36	131.78	181.8	218.38	286.2	300.80	324.2	264.45	388.6
51.42	56.92	134.25	184.7	220.80	289.3	303.28	324.8	265.66	402.9
53.03	59.25	136.64	188.1	223.23	292.4	305.75	325.2	266.58	892.9
54.70	62.21	139.12	191.2					266.93	11690
56.40	64.55	141.70	194.8	6 th series		8 th series		266.98	20520
58.16	67.57	144.25	198.1					267.01	24700
		146.76	201.4	222.96	291.8	301.04	324.4	267.04	23880
2 nd series		149.24	204.6	225.42	295.4	303.60	324.8	267.07	21650
		149.71	205.2	227.86	298.2	306.16	325.5	267.11	11550
56.51	64.82	152.03	208.1	230.29	301.8	308.89	326.2	267.52	733.6
59.33	69.39	154.43	211.2	232.71	304.9	311.72	326.8	268.58	334.9
61.54	73.63	157.01	214.6			314.49	327.5	269.95	321.3
64.02	76.95	159.56	217.4	7 th series		317.36	327.5	271.34	319.0
66.33	80.69					320.30	329.0	272.73	318.3
68.83	84.70	4 th series		232.14	303.9	323.23	329.5	274.41	318.1
71.21	88.62			234.67	307.8	326.23	330.0	276.37	318.4
73.57	92.51	158.96	216.8	237.11	311.0	329.31	330.7	278.32	318.7
75.96	96.18	161.12	220.0						

Mørup and Thrane in the Mössbauer study. The difference between these two temperatures is well beyond the claimed accuracies of the temperature measurements. The origin of the discrepancy is not clear at present. The time required for thermal equilibration in the calorimeter increased near the phase transition to about an hour compared with ten minutes normally required. Such a behavior is often observed in first order transitions.

In order to evaluate the enthalpy and the entropy of transition, the "normal" heat capacity has to be estimated. However, the spectroscopic data on which the estimation of the vibrational heat capacity should be based are insufficient at present, because not only the long wavelength optical vibrations but also the normal modes of the every branch from the entire Brillouin zone contribute to the heat capacity. Thermal motion of the ammonium ions adds further difficulty since their torsional lattice vibration is certainly highly anharmonic. One of the practicable resorts is to interpolate the low and high temperature heat capacities smoothly into the transition region and to make the

Table 4. Thermodynamic functions of $(NH_4)_3[FeF_6]$

T / K	C_p° / J K^{-1} mol^{-1}	S° / J K^{-1} mol^{-1}	$[H^\circ-H_0^\circ]/T$ / J K^{-1} mol^{-1}	$-[G^\circ-H_0^\circ]/T$ / J K^{-1} mol^{-1}
10	(1.93)	(0.66)	(0.49)	(0.17)
20	12.10	4.60	3.38	1.22
30	25.16	11.91	8.41	3.50
40	39.48	21.09	14.36	6.73
50	54.57	31.49	20.88	10.61
60	70.37	42.82	27.80	15.02
70	86.54	54.89	35.04	19.85
80	102.8	67.51	42.50	25.01
90	119.0	80.56	50.10	30.46
100	134.9	93.96	57.79	36.17
110	150.2	107.5	65.50	42.04
120	164.8	121.2	73.17	48.07
130	178.9	135.0	80.76	54.23
140	192.4	148.7	88.26	60.49
150	205.6	162.5	95.65	66.83
160	218.3	176.2	102.9	73.23
170	230.2	189.7	110.1	79.69
180	241.8	203.2	117.1	86.18
190	253.2	216.6	123.9	92.69
200	264.6	229.9	130.7	99.22
210	276.2	243.1	137.3	105.8
220	288.2	256.2	143.9	112.3
230	301.2	269.3	150.5	118.8
240	315.7	282.4	157.0	125.4
250	334.4	295.7	163.7	132.0
260	363.7	309.3	170.8	138.5
270	321.4	340.7	195.2	145.5
280	319.0	352.3	199.6	152.6
290	321.7	363.5	203.8	159.7
300	324.1	374.4	207.8	166.7
310	326.3	385.1	211.6	173.5
320	328.6	395.5	215.2	180.3
330	330.8	405.6	218.7	187.0
340	332.9	415.6	222.0	193.6
350	335.0	425.2	225.2	200.1

Table 5. Normal heat capacity of $(NH_4)_3[FeF_6]$

T / K	C_p / J K^{-1} mol^{-1}	T / K	C_p / J K^{-1} mol^{-1}
160	217.8	260	306.5
170	229.5	270	311.2
180	240.8	280	315.5
190	251.3	290	319.3
200	261.3	300	322.6
210	270.8	310	325.5
220	279.5	320	328.2
230	287.5	330	330.6
240	294.6	340	340.8
250	301.0	350	350.9

"normal" heat capacity thus estimated available to the reader, as is done here (Table 5). The dotted curve in Fig. 1 represents the assumed normal heat capacity. The enthalpy and entropy of the phase transition based on this normal heat capacity are 6490 ± 500 J mol^{-1} and 24.8 ± 1.9 J K^{-1} mol^{-1}, respectively.

The Raman spectra are shown in Fig. 2. The

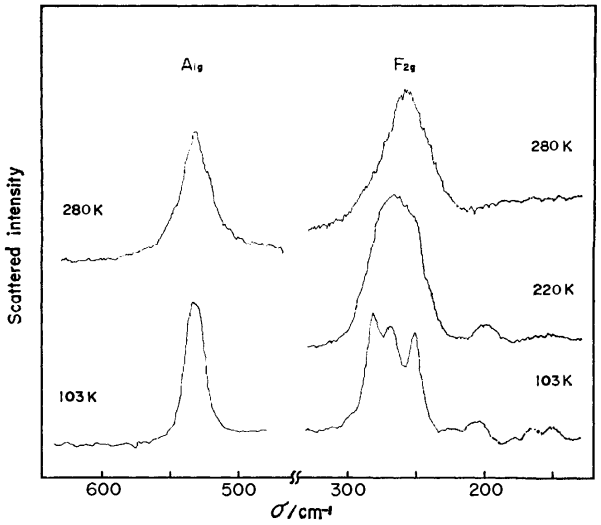

Fig. 2. Temperature dependence of the Raman scattering from the $\nu_1(A_{1g})$ and $\nu_5(F_{2g})$ modes of $[FeF_6]^{3-}$ ion.

frequency of the $\nu_1(A_{1g})$ mode of the $[FeF_6]^{3-}$ ion is 535 cm^{-1} at 280 K, which is compared favorably with 538 cm^{-1} reported by Wieghardt and Eysel.[20] The $\nu_5(F_{2g})$ vibration was observed at 256 cm^{-1} compared with Wieghardt and Eysel's value at 253 cm^{-1}.[20] The weak band at 374 cm^{-1} was assigned to the $\nu_2(E_g)$ mode. Raman bands of the ammonium ion were not informative because of their low intensity. They are not discussed in the following. Effect of the phase transition on the Raman spectra is most explicitly shown in the temperature dependence of the A_{1g} and F_{2g} modes. On cooling to 103 K, the A_{1g} band narrows appreciably but does not show any splitting. On the other hand, the triply degenerate F_{2g} mode, which is relatively broad at 280 K, broadens further on cooling through the transition temperature with a gradually emerging structure resulting in a well-resolved triplet at 103 K. In view of the relatively large separation between the component frequencies, this splitting is a site group splitting of the threefold degenerate vibration rather than a Davydov splitting. Another explanation that assumes presence of three distinct sets of octahedral sites for the $[FeF_6]^{3-}$ ions may be a least probable possibility and will not be considered further. We conclude, therefore, that the site symmetry of $[FeF_6]^{3-}$ ion is lower than axial. This low site symmetry is rather surprising, because structural and spectroscopic investigations of the related compounds containing octahedral hexafluoride complex have shown that the site symmetry is trigonal or higher if the counter-cation is potassium or a larger ion.[5,21]

The Mössbauer spectra of the present compound have also been interpreted on the assumption of the tetragonal axial symmetry.[3,4] The present Raman data seem to require revision of the interpretation of the Mössbauer results.

Discussion

In the present section we will be concerned with interpretation of the experimental transition entropy, $\Delta S_{tr}=24.8\pm1.9$ J K^{-1} mol^{-1}, by assuming that it is

related to the ionic configurations by the expression

$$\Delta S_{tr} = R \ln (W_h/W_l).$$

Here, R is the gas constant, W_h and W_l the numbers of accessible ionic configurations in the high and low temperature phases, respectively. We assume that W_l is equal to unity, *i.e.*, the ionic configuration is uniquely determined in the low temperature phase. The ionic disorder in the high temperature phase is assumed to be orientational rather than positional in the sense that the dositions of the nitrogen and iron atoms are fixed. We assume further that the $[FeF_6]^{3-}$ and NH_4^+ ions themselves are rigid so that they retain the O_h and T_d symmetries, respectively, in the crystal. Our problem is then to enumerate the allowed ionic orientations compatible with the average face-centered cubic symmetry. The ammonium ion in the 8c position is surrounded by twelve fluorine atoms. At first sight, this seems to offer large number of orientations to the ammonium ion. However, a closer examination of the ionic environment shows that this is not the case. The twelve fluorine atoms are grouped into four sets, each belonging to one of the four iron atoms that form a tetrahedron around the ammonium ion. The other four corners, which, together with the four iron atoms, form the cube around the ammonium ion, are occupied by the other set (4b) of the ammonium ions. Therefore, the environment of the 8c ammonium ion is predominantly tetrahedral. The ammonium ion will settle snugly into this tetrahedral environment without disorder. We assign zero configurational entropy to the 8c ammonium ions.

The ammonium ion in the 4b position is surrounded octahedrally by six fluorine atoms. We associate two distinct orientations with this ammonium ion, assuming that the stable orientation of the ion is such that each of the N–H bonds is directed to the unoccupied corner of the cube surrounding the ammonium ion. Evidently, there are two equivalent orientations of this type for each of the 4b ammonium ions. These orientations would be the most favorable, because it avoids too close a contact between the hydrogen and fluorine atoms. Thus far, we have treated the fluorine atoms as situated on the 24e position on the tetrad axis of the crystal. We consider next the possibility of the orientational disorder of the $[FeF_6]^{3-}$ ion. There are in general twelve types of positions (one general and eleven special) in the fcc lattice. Of these positions, only 192a and 24e are acceptable as the fluorine site. The other special positions are incompatible with the rigid $[FeF_6]^{3-}$ ion. These statements are derived algebraically as follows. We express the position of the fluorine atom by $(u\ v\ w)$, where the first, second and third positions in the parentheses designate, respectively, the x, y, and z coordinates of the atom. The coordinate axes are so chosen as to coincide with the cubic axes, the Fe atom being on the origin. Without loss of generality we may put

$$u \geqq v \geqq |w|.$$

Here, u, v, and w are related to the Fe–F bond length r by the following expression:

$$u^2 + v^2 + w^2 = r^2.$$

The rigidity assumption requires that the coordinates of the six fluorine atoms belonging to the iron atom should be

$$\begin{array}{llll} (u & v & w), & (\bar{u} \ \bar{v} \ \bar{w}), \\ (w & u & v), & (\bar{w} \ \bar{u} \ \bar{v}), \\ (v & w & u), & (\bar{v} \ \bar{w} \ \bar{u}). \end{array} \quad (1)$$

The three fluorine atoms on the left column in (1) are related to the three on the right through the inversion about the origin. The orthogonality condition of the first three Fe–F bonds are expressed by

$$vw + wu + uv = 0. \quad (2)$$

One solution of this equation is

$$\begin{aligned} u &= r \\ v &= 0 \\ w &= 0. \end{aligned} \quad (3)$$

The six fluorine coordinates corresponding to this solution are

$$\begin{array}{llll} (r & 0 & 0), & (\bar{r} \ 0 \ 0), \\ (0 & r & 0), & (0 \ \bar{r} \ 0), \\ (0 & 0 & r), & (0 \ 0 \ \bar{r}). \end{array}$$

These are the 24e positions mentioned above and corresponds to the ordered orientation of the fluorine octahedron. It should be noted that application of the O_h site symmetry operations to this arrangement does not produce any different orientations. Another solution, which is of more interest, is given by

$$u > v > 0, \quad w < 0.$$

This solution corresponds to the disordered orientation of the $[FeF_6]^{3-}$ ion. There are eight distinct orientations of this type. The other seven are derived from the general expression (1) by successive application of the operations of the site symmetry O_h as follows:

$$(u\ v\ \bar{w})\ (w\ u\ \bar{v})\ (\bar{v}\ \bar{w}\ u), \quad (4)$$
$$(u\ \bar{w}\ v)\ (\bar{v}\ u\ \bar{w})\ (w\ \bar{v}\ u), \quad (5)$$
$$(u\ w\ v)\ (v\ u\ w)\ (w\ v\ u), \quad (6)$$
$$(u\ \bar{v}\ \bar{w})\ (\bar{w}\ u\ v)\ (\bar{v}\ w\ u), \quad (7)$$
$$(u\ \bar{v}\ w)\ (\bar{w}\ u\ \bar{v})\ (v\ \bar{w}\ u), \quad (8)$$
$$(u\ w\ \bar{v})\ (v\ u\ \bar{w})\ (\bar{w}\ \bar{v}\ u), \quad (9)$$
$$(u\ \bar{w}\ \bar{v})\ (\bar{v}\ u\ w)\ (\bar{w}\ v\ u). \quad (10)$$

Here, we have given only the coordinates of three fluorine atoms corresponding to the three on the left column of the expression (1). Other three are easily derived from them by the inversion operation. Figure 3 illustrates the above argument. The eight orientations given by the expressions (1), (4), (5), ···, (10) correspond to the fluorine positions numbered as 1, 2, 3, ···, 8 in the Fig. 3. We conclude that the orientational entropy of the fluorine octahedra is either zero or R ln 8. Intermediate values of R ln N (N=2, 3, 4, or 6) often encountered in various models or orientational disorder are incompatible with the rigidity of the ion or the equivalence of the fluorine atoms in the ion in the present crystal.

Morfee *et al.*[22] considered a similar situation in connection with a phase transition in $K_2[SnCl_6]$, but seem to have failed to take into account the restrictive nature of the fcc symmetry. The transition entropy ($\simeq R$ ln 2) of $K_2[SnCl_6]$ is too small to support this

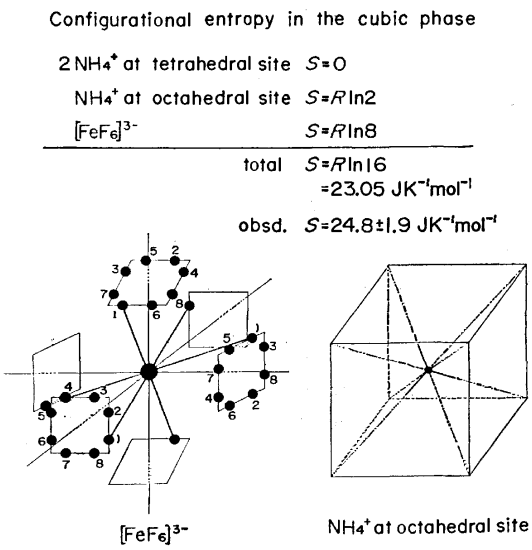

Fig. 3. Orientational disorder of $[FeF_6]^{3-}$ and NH_4^+ ions in the cubic phase of $(NH_4)_3[FeF_6]$.

mechanism in this crystal. The total entropy ΔS of the ionic orientation is given by the sum of the contributions from the ammonium and hexafluoroferrate(III) ions:

$$\Delta S = R \ln 2 + R \ln 8$$
$$= 23.05 \text{ J K}^{-1} \text{ mol}^{-1}$$

The experimental value of the transition entropy 24.8 ± 1.9 J K^{-1} mol^{-1} is in close agreement with this value, giving a support to the disorder mechanism considered above. In recent papers Heyns and Pistorius[23,24] considered a closely related structural disorders in $K[PF_6]$ and $K[AsF_6]$. From an entropy argument they concluded that the location of the fluorine atom may be smeared into a torus-like distribution instead of the eight distinct positions considered here. Precise determination of the electron distribution in these disordered crystals will be rewarding in this respect.

Next we compare the behavior of the present crystal with those of $NH_4[PF_6]$ and $(NH_4)_2[SiF_6]$ crystals. $NH_4[PF_6]$ has the NaCl structure at room temperature and undergoes phase transitions at 131.3 and 191.8 K. The total entropy change of the transitions is 19.7 J K^{-1} mol^{-1}.[10] The cubic modification of $(NH_4)_2[SiF_6]$, on the other hand, has no phase transitions down to 25 K,[11] although a disordering of ammonium ion with quite different nature has been suspected.[9] These observations, in conjunction with the structural information outlined in the introduction, lead to a conjecture that presence of ammonium ion at the 4b site causes lattice instability which is restored at the higher temperatures by increased orientational entropy pertaining both to the ammonium and hexafluoro-complex ions. If the ammonium ions are absent from the 4b positions, the cubic symmetry is maintained without invoking the ionic disorder. Consequently the crystal is expected to remain cubic down to the lowest temperature as does ammonium hexafluorosilicate.

The concept of the ionic disorder is useful also for rationalizing the structural relation of $(NH_4)_3[FeF_6]$ with other alkali hexafluoroferrates(III). As pointed out earlier, replacement of the spherical ion by the tetrahedral ammonium ion enhances the symmetry of the crystal (Table 1). This observation is understood if the orientational disorder is taken into account as follows. As is well known, the relative stability of phases of a substance is determined by the enthalpy and entropy of the phases involved. In the ammonium salt, the highly symmetric environment of the ammonium ion is stabilized relative to the less symmetric ordered arrangement by the increased entropy due to the increased ionic disorder at the higher temperatures even if the disordered arrangement may be enthalpically less favorable. In contrast, such a stabilization due to the entropy effect is not available for the alkali salts because the alkali ions do not possess orientational degree of freedom. This explains the apparent paradox that less symmetric ammonium ion enhances the crystal symmetry in the $A_3[FeF_6]$ type crystals. Other effects may also be responsible for the stabilization of the cubic phase of the ammonium salts. For instance, change in the ionic radius of the alkali ion will change the (tetragonal) axial ratio of the crystal. The axial ratio might happen to be unity with the ammonium ion. This would augment the tendency toward ionic disorder, and hence toward stabilization of the cubic phase.

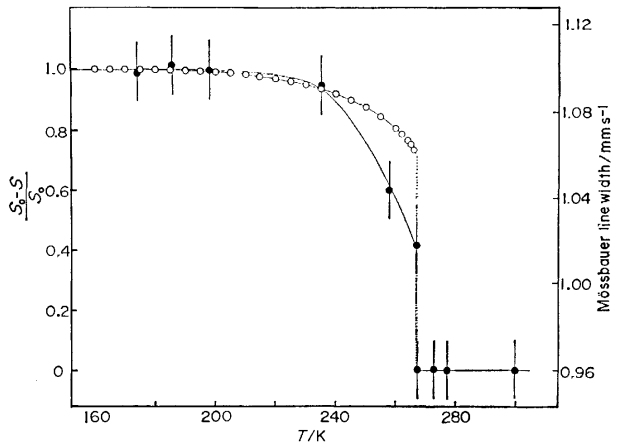

Fig. 4. Temperature dependence of the reduced anomalous entropy $(S_0-S(T))/S_0$ (-○-○-, present data) and the Mössbauer line width (-●-●-●-, from Ref. 3).

Finally we discuss briefly the temperature dependence of the anomalous heat capacity of $(NH_4)_3[FeF_6]$ crystal. In Fig. 4, the quantity $(S_0-S(T))/S_0$ is plotted against the temperature, together with the temperature dependence of the Fe Mössbauer line width.[3] Here, $S(T)$ is the anomalous part of the entropy at the temperature T and S_0 is the high temperature limit of the entropy. This quantity is equivalent to the square of the order parameter in the Landau theory of phase transitions of the second kind.[25] These two quantities change similarly with the temperature, implying that there is a close relation between the ionic ordering and the relaxation mechanism of the iron nuclear spin. In the Mössbauer study,[3] the nuclear quadrupole effect is *a priori* neglected in the cubic phase. Although the iron environment is certainly cubic on the average, our model proposed

above for the ionic disorder implies that it deviates from the cubic symmetry if observed in a short duration of time.[26] The Mössbauer data[3] seem to set an upper limit for the time during which the proposed local non-cubic ionic arrangement persists: it is less than the electronic relaxation time 10^{-9}—10^{-11}. It may be noted that the averaging to the octahedral symmetry is effected by random jumping of the $[FeF_6]^{3-}$ ion over the eight configurations illustrated in Fig. 3. It is not necessary for the anion to reorient by 90°. The former smaller-scale reorientation would involve a smaller barrier to be overcome, and thus would be consistent with the small value of the orientational life time. In passing, Fig. 4 indicates clearly that the phase transition is of the first order. The total entropy change, 24.8 ± 1.9 J K^{-1} mol^{-1} is absorbed gradually up to 6.3 J K^{-1} mol^{-1} and the remaining part is absorbed isothermally at the transition point.

Landau's thermodynamic theory predicts that the anomalous heat capacity C_{an} follows the temperature dependence:

$$\frac{C_{an}}{T} = A(T_k - T)^{-1/2},$$

provided that the temperature is not too close to the critical value. Figure 5 illustrates an attempt to fit the expression to the experimental anomalous heat capacity. The parameter T_k was so chosen as to yield the widest linear portion in the plot. Actually, the experimental points fit closely to the linear plot up to the onset of the first order effect. This means that we are not in the critical region even at the transition temperature. The large value of the isothermally absorbed entropy is in line with this observation. A conclusion drawn from the favorable comparison with the Landau theory as shown in Fig. 5 is that a restriction is placed on the crystal symmetry of the low temperature phase: the space group of the low temperature phase is a subgroup of the space group of the cubic phase. This is not particularly informative for the present crystal because the high temperature phase involved has the highest symmetry Fm3m.

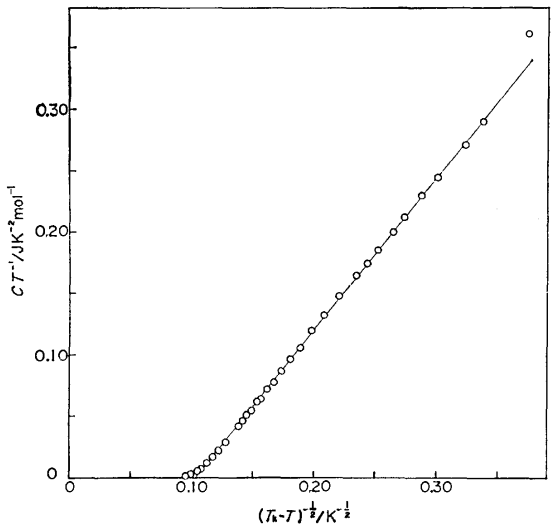

Fig. 5. C_p/T plotted against $(T_k - T)^{-1/2}$ with T_k= 272.8 K. Linearity of the plot implies conformity of the anomalous heat capacity to the Landau theory.

We are grateful to Mr. Mitsuo Ohama for the measurements of the Raman spectra and to Messrs. Masakazu Okuniya and Hiroshi Minari for the chemical analyses.

References

1) L. Pauling, *J. Am. Chem. Soc.*, **46**, 2738 (1924).
2) E. G. Steward and H. P. Rooksby, *Acta Crystallogr.*, **6**, 49 (1953).
3) S. Mørup and N. Thrane, *Solid State Commun.*, **11**, 1319 (1972).
4) S. Mørup and N. Thrane, *Phys. Rev. B*, **8**, 1020 (1973).
5) D. Babel, *Structure and Bonding*, **3**, 23 (1967).
6) "International Table for X-Ray Crystallography," Vol. I Kynoch Press, Birmingham, England (1952), p. 338.
7) H. Bode and E. Voss, *Z. Anorg. Allg. Chem.*, **290**, 1 (1957).
8) H. Bode and H. Clausen, *Z. Anorg. Allg. Chem.*, **265**, 229 (1951).
9) E. O. Schlemper, W. C. Hamilton, and J. J. Rush, *J. Chem. Phys.*, **44**, 2499 (1966).
10) L. A. K. Staveley, N. R. Gray, and M. J. Layzell, *Z. Naturforsch., Teil A*, **18**, 148 (1963).
11) C. C. Stephenson, C. A. Wulff, and O. R. Lundell, *J. Chem. Phys.*, **40**, 967 (1964).
12) K. Moriya, T. Matsuo, H. Suga, and S. Seki, to be published.
13) A. Tressaud, J. Portier, S. Shearer-Turrell, J. L. Dupin, and P. Hagenmuller, *J. Inorg. Nucl. Chem.*, **32**, 2179 (1970).
14) B. Cox and A. G. Sharpe, *J. Chem. Soc.*, **1954**, 1798.
15) H. Suga and S. Seki, *Bull. Chem. Soc. Jpn.*, **38**, 1000 (1965).
16) T. Matsuo, H. Suga, and S. Seki, *J. Phys. Soc. Jpn.*, **30**, 785 (1971).
17) M. Oguni, T. Matsuo, H. Suga, and S. Seki, *Bull. Chem. Soc. Jpn.*, **48**, 379 (1975).
18) T. Matsuo, Y. Kume, H. Suga, and S. Seki, *J. Phys. Chem. Solids*, **37**, 499 (1976).
19) T. Matsuo, M. Tatsumi, H. Suga, and S. Seki, *J. Phys. Chem. Solids*, **34**, 136 (1973).
20) K. Wieghardt and H. H. Eysel, *Z. Naturforsch., Teil B*, **25**, 105 (1970).
21) S. F. A. Kettle, *Proc. IUPAC Conf. Coordination Chem. (Warsaw)*, **1970**, 113.
22) R. G. S. Morfee, L. A. K. Staveley, S. T. Walters, and D. L. Wiegley, *J. Phys. Chem. Solids*, **13**, 132 (1960).
23) A. M. Heyns and C. W. F. T. Pistorius, *Spectrochim. Acta, Part A*, **30**, 99 (1974).
24) A. M. Heyns and C. W. F. T. Pistorius, *Spectrochim. Acta, Part A*, **31**, 1293 (1975).
25) L. Landau, *Phys. Z. Sowjun.*, **8**, 113 (1935).
26) Recently, W. von der Ohe (*J. Chem. Phys.*, **65**, 3575 (1976)) reported a Raman study of the trigonal $(NH_4)_2[TiF_6]$ single crystal in which the $[TiF_6]^{2-}$ ion has a similar octahedral configuration but is situated at a trigonal site. The $\nu_5(F_{2g})$ mode of the complex ion is site-group-split by 1 cm^{-1} at the room temperature. The overall width of the ν_5 spectrum is reported to be 20 cm^{-1}. This is considerably smaller than the width ($\approx$38 cm^{-1}) of the corresponding mode of the $[FeF_6]^{3-}$ ion in the cubic phase of the $(NH_4)_3[FeF]_6$ crystal, suggesting that the latter is composed of overlapping modes. This, in turn, implies that local environment of the $[FeF_6]^{3-}$ ion has a trigonal or lower symmetry when observed in such a short time as is relevant to the Raman scattering, even though the diffraction symmetry of the site is O_h. The orientational disorder model considered in the text is thus consistent with the spectroscopic observation.

The Nuclear Quadrupole Spin-Lattice Relaxation of ^{35}Cl in Methylammonium Hexachlorostannate(IV) and Hexachloroplatinate(IV)

Yoshihiro FURUKAWA, Hideko KIRIYAMA, and Ryuichi IKEDA*

The Institute of Scientific and Industrial Research, Osaka University, Yamadakami, Suita 565

**Department of Chemistry, Nagoya University, Chikusa, Nagoya 464*

(Received February 17, 1977)

The ^{35}Cl nuclear quadrupole spin-lattice relaxation time, T_1, in $(CH_3NH_3)_2MCl_6$ (M=Sn and Pt) was measured from 4.2 to 434 K in order to clarify the dynamic aspect of the phase transitions at 156 and 125 K respectively. The relaxation process in both low-temperature phases is dominated by the rotational vibration of the octahedral $[MCl_6]^{2-}$ ions. Far above the transition point, T_{tr}, the T_1 decreases very rapidly with an increase in the temperature. This indicates that each octahedron reorients about its threefold axis, with the activation energies of 77 ± 3 for $[SnCl_6]^{2-}$ ions and 95 ± 10 kJ mol^{-1} for $[PtCl_6]^{2-}$ ions. At T_{tr}, the $\log(T_1/s)$ *vs.* kK/T curve shows a distinct minimum, as in some K_2PtCl_6-type compounds. This anomalous behavior can be explained in terms of a soft rotary mode of the $[MCl_6]^{2-}$ ions. The softening is estimated to be about 60%, according to Armstrong's approach.

Most hexahalogenometallates(IV) with cubic antifluorite structures of the K_2PtCl_6 type are known to undergo structural transitions to low-temperature phases of less symmetric structures. Recent studies of the nuclear quadrupole resonance (NQR) in these crystals have shown that their NQR frequencies and relaxation times near the transition points are greatly affected by the condensation of rotary lattice modes.[1]

On the other hand, methylammonium hexachlorometallates (IV) form rhombohedral $R\bar{3}m$ crystals with a slightly deformed antifluorite structure.[2,3] Very recently, Kume *et al.* have, from ^{35}Cl NQR measurements, found phase transitions in $(CH_3NH_3)_2SnCl_6$ and $(CH_3NH_3)_2PtCl_6$ at 156 and 125 K respectively.[4] In interpreting the unusual behavior of the NQR frequency at the transition point, they suggested the existence of a soft mode involving the libration of the complex anions. On the other hand, the results of proton second moments and spin-lattice relaxation times showed that the methylammonium ion is reorienting as a whole about its three-fold symmetry axis in the low-temperature phase, giving rise to a deep minimum of T_1 at about 53 K for 60 MHz.[5] As the temperature increases toward the phase-transition point, the correlation times of the individual motions of CH_3 and NH_3 groups become very different. Consequently, another shallow minimum of T_1 appears on the high-temperature side of the deep minimum, but a few tens of degrees below T_{tr}. This second minimum may be ascribed to the dipole-dipole interaction between the CH_3 and NH_3 groups in the cation. Just at T_{tr}, however, the proton T_1 *vs.* $1/T$ curve showed no appreciable discontinuity, suggesting that the motion of the cation may play a rather indirect role in the phase transition.[5]

In general, spin-lattice relaxation times for quadru polar nuclei are very sensitive to EFG (electric field gradient) fluctuations associated with the phase transition. The present study of the ^{35}Cl nuclear quadrupole relaxation has been undertaken in order to clarify the motion of the $[MCl_6]^{2-}$ anion in $(CH_3NH_3)_2MCl_6$(M= Sn, Pt), and also in order to ascertain whether or not it is responsible for the phase transition, as was suggested in previous papers.[4,5]

Experimental

The spin-lattice relaxation time of ^{35}Cl were measured with a Bruker pulsed NMR spectrometer (B-KR 322s 4—62 MHz). A boxcar integrator or a NIC 1074 signal averager was set up after the spectrometer in order to increase the SN ratio. The T_1 was determined by a 90°-t-90°-t'-180° pulse sequence and by fitting the echo amplitude to the $A(t)=A_0[1-\exp(-t/T_1)]$ equation for a fixed t'. In the temperature range studied, the recovery of the nuclear magnetization was well described by a single exponential function. The error of each T_1 value is within about 5%. The T_2 was measured by means of a 90°-t/2-180° spin echo pulse sequence and by fitting the echo amplitude to $A(t)=A_0\exp[-(t/T_2)^2]$. For both compounds, the T_2 values were temperature-independent at 550 μs, except above 330 K.

The powdered samples of methylammonium hexachlorostannate(IV) and its platinum analogue were the same as those used in the earlier NQR and proton NMR experiments.[4,5]

The sample temperature was measured with a copper *vs.* constantan thermocouple and was controlled with an estimated accuracy of ±0.5 K below and ±1 K above room temperature. Temperatures lower than 77 K were obtained by allowing the sample to warm from the temperature of liquid helium and measured with a gold-cobalt *vs.* copper thermocouple.

Results and Discussion

The nuclear quadrupole interaction Hamiltonian is given by

$$\mathcal{H}_Q = \Sigma_\mu Q_\mu V_\mu, \quad \mu = 0, \pm1, \pm2, \tag{1}$$

where the Q_μ's are the quadrupole operators and the V_μ's, the electric-field-gradient components. Each V_μ can be expanded as a power series in the relative displacements or fluctuations of the nuclei from their equilibrium positions. Thus, the time-independent terms are responsible for the NQR frequency, ν_Q, while the time-dependent ones are responsible for the spin-lattice relaxation.[6]

The compounds studied gave one NQR line in both the low- and high-temperature phases,[4] consistent with the crystal structure proposed by an X-ray diffraction study.[3] It was confirmed that the ν_Q-T curve exhibits a

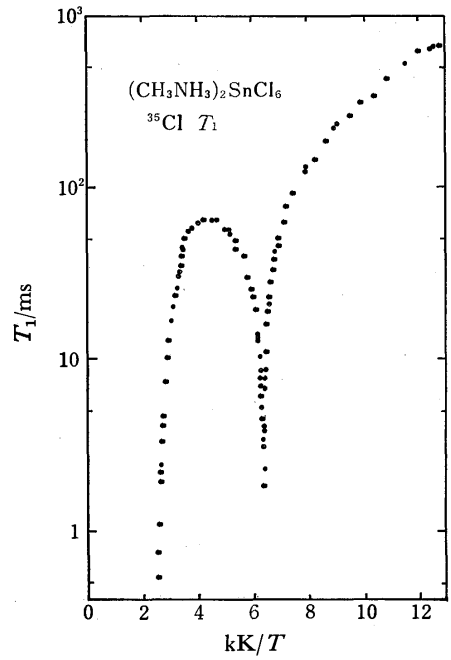

Fig. 1. A plot of the ^{35}Cl spin-lattice relaxation time in $(CH_3NH_3)_2SnCl_6$ as a function of $1/T$.

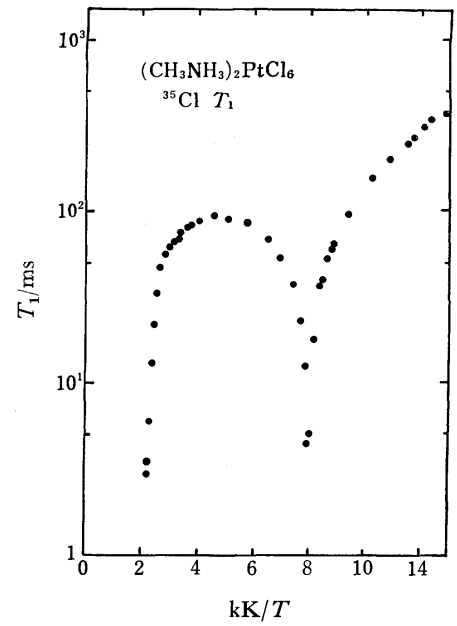

Fig. 2. A plot of the ^{35}Cl spin-lattice relaxation time in $(CH_3NH_3)_2PtCl_6$ as a function of $1/T$.

small, but distinct cusp-shaped reduction in a narrow temperature range about the T_{tr}. This cusp may be due to certain fluctuations enhanced as the transition point is approached, probably caused by soft librational modes of the octahedron, in analogy with K_2PtBr_6.[1]

The ^{35}Cl spin-lattice relaxation times in $(CH_3NH_3)_2SnCl_6$ are shown in Fig. 1 as a function of the inverse temperature. A distinct minimum was found at T_{tr}, in contrast to the proton spin-lattice relaxation time, which does not show such an anomaly.[5] The temperature dependences of the ^{35}Cl T_1, as well as of the NQR frequency, of $(CH_3NH_3)_2PtCl_6$ are very similar to those of $(CH_3NH_3)_2SnCl_6$ (Fig. 2). This indicates that the relaxation process and the mechanism of the phase transition can be interpreted from the same standpoint for both compounds.

Low-temperature Region. Armstrong *et al.* have extensively studied the lattice dynamics and phase transitions in cubic antifluorite-type crystals, R_2MX_6, and in cubic perovskite-type $CsPbCl_3$ by means of NQR spectroscopy.[1] They have derived theoretical equations for the quadrupole relaxation time and have pointed out that the most dominant relaxation process for the X nuclei is the anharmonic Raman process, with a rotary lattice mode of the $[MX_6]^{2-}$ octahedron. On the other hand, the internal vibration is less important than the former process, and so its contribution is negligible. According to them,

$$T_1^{-1} = CT^2/\bar{\omega}^5, \tag{2}$$

where C is a constant depending on the crystal structure, and $\bar{\omega}$, the zone-averaged rotary mode frequency. Then, T_1^{-1} would be proportional to T^2 in a stable lattice such as Cs_2PtCl_6.[1] The C coefficient is much too complicated to estimate for the rhombohedral lattice, although it was estimated for the cubic K_2PtCl_6-type structure.[1]

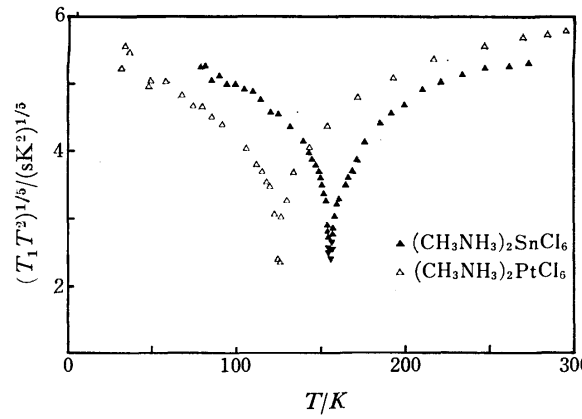

Fig. 3. Temperature dependences of $(T_1\ T^2)^{1/5}$ in $(CH_3NH_3)_2SnCl_6$ and in $(CH_3NH_3)_2PtCl_6$.

In Fig. 3 the $(T_1T^2)^{1/5}$ value is plotted against the temperature in order to see whether or not Eq. 2 holds even in the vicinity of T_{tr}.[1] Far below or above T_{tr}, the $(T_1T^2)^{1/5}$ is nearly constant, indicating that $T_1^{-1} \propto T^2$. The T_1 measurement was further extended to the region from 77 to 4.2 K only on the platinate complex, as Fig. 4 shows. The T_1^{-1} data in this temperature region show no T^2 dependence, because the high-temperature approximation breaks down in Eq. 2. In such a case, the T_1^{-1} is expressed by:

$$T_1^{-1} = C' \sinh^{-2}(\hbar\bar{\omega}/2kT). \tag{3}$$

The temperature dependence of T_1 (Eq. 3) is shown in Fig. 4 by a full line with parameters of $C'=2.69\ s^{-1}$ and $\hbar\bar{\omega}/k=137$ K. The agreement between the calculated and observed values below 80 K indicates that the relaxation of the ^{35}Cl nuclei is associated with the harmonic rotational vibration of the octahedron in this temperature region.

Phase-transition Region. The anomalous behavior

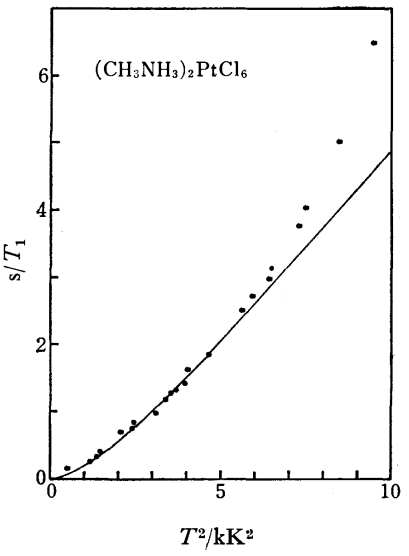

Fig. 4. The ^{35}Cl spin-lattice relaxation rate as a function of T^2 in $(CH_3NH_3)_2PtCl_6$. The full line was calculated by Eq. 3.

of T_1 around T_{tr} is very similar to that of R_2MX_6, which has the antifluorite structure.[1] This deep, distinct T_1 minimum in $(CH_3NH_3)_2MCl_6$ suggests that the phase transition is ascribable to a softening of a rotary lattice mode of the octahedron. If this is the case, then, according to Eq. 2, the temperature dependence of $(T_1T^2)^{1/5}$ reflects the variation in the average rotary mode frequency. The value of $(T_1T^2)^{1/5}$ was reduced by about 60% as the T_{tr} was approached from above for both compounds (Fig. 3). Referring to Armstrong *et al.*, this reduction denotes a 60% apparent softening of a rotary mode frequency, which is comparable to the 40 and 58% softening of zone-center phonons in K_2PtBr_6 and $(NH_4)_2PtBr_6$ respectively obtained from the Br T_1 measurements.[1]

Such softening of some rotary mode of the $[SnCl_6]^{2-}$ or $[PtCl_6]^{2-}$ octahedron suggests the possibility of a lowering of the crystal symmetry in the low-temperature phase, as is found in cubic R_2MX_6. An X-ray study was, therefore, performed on the tin complex in our laboratory.[3] It revealed that the space group ($R\bar{3}m$) and crystal structure are unchanged on passing through T_{tr}. Moreover, the X-ray results suggested that a $\boldsymbol{k}=0$ acoustic mode softens to make a bulk deformation without any structural change. This mode, however, could not explain the T_1 anomaly occuring at T_{tr}.[1] It is, therefore, conceivable that the tilting of the octahedra is too small to be detected by X-ray diffraction.

High-temperature Region. At high temperatures (above 300 K), a rapid decrease in T_1 occurs exponentially with a decrease in $1/T$, showing that another relaxation mechanism is dominant. This process is attributable to the hindered rotation of the $[MCl_6]^{2-}$ octahedron, probably around its three-fold axis, which coincides with the triad axis of the rhombohedral cell. The relaxation time is given as

$$T_1 = C \cdot \tau_0 \exp(E_a/RT) \quad (4)$$

where C is a constant, equal to 2/3 for the C_3 rotation of octahedra.[7] By fitting the data in Figs. 1 and 2 to Eq. 4, the activation energies (E_a) of the hindered rotation were determined to be 77 ± 3 for the $[SnCl_6]^{2-}$ ion and 95 ± 10 k J mol^{-1} for the $[PtCl_6]^{2-}$ ion. These values are comparable to 78.7 and 76.6 k J mol^{-1} for the C_4 rotation in cubic K_2PtCl_6 and K_2IrCl_6 respectively.[1,8]

The authors wish to express their thanks to Professor Ryôiti Kiriyama for his continuous encouragement and to Dr. Katsuki Kitahama for his helpful comments.

References

1) R. L. Armstrong, *J. Magn. Reson.*, **20**, 214 (1975), and also the references cited therein.
2) R. W. G. Wyckoff, *Am. J. Sci.*, **16**, 349 (1928).
3) K. Kitahama, Y. Baba, H. Kiriyama, and R. Kiriyama, unpublished data.
4) Y. Kume, R. Ikeda, and D. Nakamura, *J. Magn. Reson.*, **20**, 276 (1975).
5) R. Ikeda, Y. Kume, D. Nakamura, Y. Furukawa, and H. Kiriyama, *J. Magn. Reson.*, **24**, 9 (1976).
6) F. Borsa and A. Rigamonti, *J. Magn. Reson.*, **20**, 232 (1975).
7) M. Goldman, "Spin Temperature and Nuclear Magnetic Resonance in Solids," Oxford Univ. Press, England (1970), p. 67.
8) K. R. Jeffrey, R. L. Armstrong, and K. E. Kisman, *Phys. Rev.*, *B*, **1**, 3770 (1970).

Multielement Analysis of Deep-Sea Sediments by Photon Activation

Toyoaki KATO,† Nobuyoshi SATO,* and Nobuo SUZUKI

Department of Chemistry, Faculty of Science, Tohoku University, Sendai 980

**College of General Education, Iwate University, Morioka 020*

(Received November 26, 1976)

A nondestructive photon activation with 30 MeV bremsstrahlung has been applied to the multielement determination in the pelagic sediments in a region of the Pacific Ocean. The abundances for 6 major and 10 trace elements were measured in several deep-sea floors and the core samples, discussion being given on the results. Determination of trace elements such as Cr, Co, Ni, and Sr is valuable because of their geochemical significance.

The essential problem involved in the geochemistry of deep-sea sediments is to establish the distribution and original source of a number of their elements. Although research has been performed for this purpose, it seems to be insufficient. It is desirable to develop a method by which it is possible to analyze samples for wide spectra of elements.

The importance of photon activation, mainly with 30 MeV bremsstrahlung, as a nondestructive multielement analytical technique has been stressed for several years. A number of papers have been presented describing methods and application, ranging from the measurements of a number of the elements in round-robin materials[1-3] to the environmental pollution research.[4-7] The availability of a comprehensive body of basic reference data in the form of photonuclear reaction yields,[8-10] sensitivities,[9,10] and gamma rays emitted from numerous products[11] pertaining to 30 MeV bremsstrahlung activation with a linear electron accelerator (Tohoku University) has made the method feasible for further application to a wide variety of materials. This paper deals with the nondestructive determination for several major and trace elements present in oceanographic samples, including several pelagic deep-sea floor sediments and selected core samples of the Pacific Ocean, obtained by the Geophysical and Geological Research Project planned and carried out under the auspices of the Ocean Research Institute, the University of Tokyo (1973). The methodology of photon activation analysis in geochemical application has been reported.[1,2,10] We will descibe some additional comments in individual determinations and discuss the results.

TABLE 1. DEEP-SEA SEDIMENTS ANALYZED

Floor samples

Sample	Location	Depth (m)
F-1	North Philippine Basin Lat. 21°55.8′N Long. 133°02.8′E— Lat. 21°51.5′N Long. 133°00.9′E	5618—5622
F-2	North Fiji Basin Lat. 08°00.3′S Long. 172°49.4′E— Lat. 07°58.3′S Long. 172°44.9′E	5350—5375
F-3	Central Basin fault in Philippine Basin Lat. 16°09.1′N Long. 130°33.4′E— Lat. 16°15.0′N Long. 130°36.6′E	6500—6200
F-4	Mariana Basin Lat. 13°44.0′N Long. 151°30.5′E	5600
F-5	Mariana Basin Lat. 11°01.6′N Long. 149°53.6′E	6030
F-6	Mariana Basin Lat. 10°11.7′N Long. 149°16.7′E	6000
F-7	North Fiji Basin Lat. 15°00.0′S Long. 172°22.5′E	4150

Core samples

Sample	Location	Depth (m)	Core length (cm)
C-1	Mariana Basin Lat. 12°37.8′N Long. 151°30.5′E	5920	668
C-2	Melanesia Basin Lat. 02°41.3′N Long. 164°50.2′E	4170	1115
C-3	Melanesia Basin Lat. 01°33.2′S Long. 167°38.6′E	4000	1163

Experimental

Materials. The study was carried out on the pelagic sediments collected in a region of the Western Equatorial Pacific. The sampling sites, depths and core lengths are given in Table 1. The deep-sea floor sediments which were dredged were dark brown and fairly homogeneous. The core samples consist of piston cores, about 10 m long. The core column was cut into segments each 1 cm thick along its entire length, and selected specimens were subjected to analyses. Age was determined on the basis of calcareous organisms and found to be *ca.* 2 million years at the bottom of the 10-m core.[12] Each sample was dried at 70 °C for 24 h, crushed and mixed in an agate mortar to attain homogeneity. 300 mg of the dried sample was wrapped in a small piece of aluminum foil and then compacted into a disc, diam. 9 mm, height 4 mm. The JB-1 basalt was used as a multielement comparative standard, because of the well-characterized nature of the matrix and the known elemental composition. The abundances of the elements of interest were taken from the data compiled by Ando *et al.*[13] An amount weighing 300 mg was wrapped in a small piece of aluminum foil and made into a diam. 9 mm disc. To assess the magnitude of interference, foils of iron with diam. 9 mm were made from a thin sheet of pure iron, about 10 μm thick, with a chemical purity of 99.99%. A unit of materials to be irradiated consists of a sample disc, two standard discs and four iron foils. They were stacked in a silica tube with the standard discs placed on both sides of the sample and the iron foils between them and at the front and back of the unit for simultaneous irradiation. The

† Present address; College of General Education, Tohoku University, Kawauchi, Sendai 980.

photon flux gradient along the length of this unit was about 10%.

Irradiation. Bremsstrahlung irradiation was carried out with a linear electron accelerator. Typically, a 70 μA beam of 30-MeV electrons was made to impinge on a 2 mm thick platinum converter. Details involving irradiation assembly and converter-sample configuration have been reported.[8-10] After irradiation for 4—5 h, the wrapping foil was rejected and the content of each sample was again wrapped in fresh aluminum foil for gamma-counting.

Counting and Abundance Determination. The counting equipment consists of a 68 cm^3 Ge(Li) detector, Canberra Model 7200-7600-1423. Its output was coupled to a 4096-channel pulse height analyzer (Toshiba Electric Co., Ltd.). Details involving counting, characterization of gamma rays and quantitative treatment of the spectrum data were essentially the same as reported.[10] A mean specific activity for any specified gamma ray in terms of the peak areas from the standard discs on both sides was used for calculating the abundance of the element in question. Because of the adverse nuclear properties, aluminum was determined separately by means of spectrophotometric measurement followed by solvent extraction with 8-hydroxyquinoline.[14]

Results and Discussion

As in the multielement analysis of standard rocks,[1,2] 6 major and 10 trace elements were subjected to determination. Pertinent nuclear data for the reaction products are given in Table 2 together with the optimal time intervals for measurement after irradiation and practical detection limits. The practical detection limits were estimated from the spectral data of the JB-1 rocks. They are the amounts of the elements giving a full-energy peak area corresponding to three times the standard deviation of the area under the peak of interest, with 5 h irradiation time with a 70 μA beam of 30 MeV electrons, counting at optimal time intervals given in Table 2. We see that major elements (Ca—Ti) in crustal materials can not be highly activated. This turns out to be advantageous over competing methods when simultaneous multielement determination is the goal. In thermal neutron activation analysis, the full capability of the method might be restricted by high levels of interference, such as that from ^{24}Na. Such difficulty is not inherent in the present method. Nondestructive analysis of several specific elements such as Nb, Y, and Zr, not readily determined by thermal neutron activation analysis, is significant in geochemical substances. Comments are given on the individual determinations in the following.

The results for calcium are the average values obtained for each of the 374 and 617 keV peaks of ^{43}K, and the 1298 keV peak of ^{47}Ca. When the values obtained from these three different peaks were averaged, the relative deviations from the means were within ±2% for all of the samples studied. The samples were relatively high in titanium. For titanium, therefore, the 1121 keV peak of 83.9 d ^{46}Sc was given prior consideration, because of the favorable peak-to-background ratios obtained at longer decay times. For the sake of confirmation, the gamma rays from ^{47}Sc and ^{48}Sc were used.

The inter-element interference problems can be found in Table 3 in which major competing reactions yielding nuclides identical to those used for abundance determinations are given. In some cases, neutron-induced reactions other than the photonuclear processes are the major sources of interferences. Degrees of their contribution were determined from relative probability of forming pertinent nuclide through different reaction

Table 2. Pertinent nuclear data and detectability of the products

Element	Process	Product nuclide	Half-life	γ-Ray used for determination (keV)	Other γ-rays observed	Suitable decay time for measurement	Detection limit (μg)
Ca	(γ,p)	^{43}K	22.4 h	374	219, 394, 593,	1—2 d	123
				617	990, 1021, 1524 (^{42}K)	1—2 d	200
	(γ,n)	^{47}Ca	4.53 d	1298	160 (^{47}Sc), 488, 808	10—15 d	470
Fe	(γ,p)	^{56}Mn	2.576 h	847	1811, 2110	2—5 h	400
Mg	(γ,p)	^{24}Na	15.0 h	1368	1732 (DE), 2243 (SE), 2754	1—2 d	37
Mn	(γ,n)	^{54}Mn	303 d	835		>10 d	5.2
Na	(γ,n)	^{22}Na	2.60 y	1275	1786 (sum)	>10 d	82
Ti	(γ,p)	^{46}Sc	83.9 d	1121	889, 160 (^{47}Sc), 893, 1040, 1314 (^{48}Sc)	>10 d	32
Ba	(γ,n)+(γ,γ′)	^{135m}Ba	28.7 h	268		1—2 d	37
Ce	(γ,n)	^{139}Ce	140 d	166	145 (^{141}Ce)	30—40 d	1.0
Co	(γ,n)	^{58}Co	71.3 d	811		30—40 d	2.1
Cr	(γ,n)	^{51}Cr	27.8 d	319		10—15 d	13
Nb	(γ,n)	^{92m}Nb	10.16 d	934		10—15 d	0.5
Ni	(γ,n)	^{57}Ni	36.0 h	1378	1757, 1918	1—2 d	19
Rb	(γ,n)	^{84}Rb	33.0 d	881	1076, 1897	10—15 d	2.6
Sr	(γ,n)	^{87m}Sr	2.83 h	388		2—5 h	3.9
Y	(γ,n)	^{88}Y	108 d	1836	898	>10 d	1.0
Zr	(γ,n)	^{89}Zr	78.4 h	910		2—3 d	1.1

TABLE 3. MAJOR INTERFERENCES IN MULTIELEMENT PHOTON ACTIVATION ANALYSIS

Element to be detected	Competing reaction	Effect of interference	Interfering contribution (%)		
			JB-1	Sediment	Earth's crust
Ca	$^{45}Sc(\gamma, 2p)^{43}K$	Sc/Ca=7.2×10^{1}	6.0×10^{-4}	neg.	7.3×10^{-4}
	$^{49}Ti(\gamma, 2p)^{47}Ca$	(Ti/Ca=4×10^{1})	(0.3)	neg.	(0.3)
Fe	$^{55}Mn(n,\gamma)^{56}Mn$	Mn/Fe=2.8	0.66	1.6—8.3	0.60
Mg	$^{27}Al(n,\alpha)^{24}Na$	Al/Mg=206	0.79	0.7—1.7	2.0
	$^{23}Na(n,\gamma)^{24}Na$	Na/Mg=225	0.20	0.4—1.4	0.53
Mn	$^{56}Fe(\gamma,pn)^{54}Mn$	Fe/Mn=1.2×10^{2}	31	3—17	33
Na	$^{24}Mg(\gamma,pn)^{22}Na$	Mg/Na=7.7×10^{1}	2.8	0.4—1.5	1.1
	$^{27}Al(\gamma,\alpha n)^{22}Na$	Al/Na=1.3×10^{3}	0.28	0.06—0.2	0.26
Ti	$^{51}V(\gamma,\alpha n)^{46}Sc$	V/Ti=5.7×10^{2}	4.6×10^{-3}	neg.	0.004
Ba	$^{140}Ce(\gamma,\alpha n)^{135m}Ba$	(Ce/Ba=9×10^{2})	(<0.02)	neg.	(<0.02)
Ce	$^{141}Pr(\gamma,pn)^{139}Ce$	(Pr/Ce=2×10^{3})	—	neg.	(0.007)
Co	$^{60}Ni(\gamma,pn)^{58}Co$	Ni/Co=7.2×10^{1}	4.6	1.3—8.4	4.0
Cr	$^{56}Fe(\gamma,\alpha n)^{51}Cr$	Fe/Cr=1.6×10^{4}	0.96	2.2—10.2	3.4
Nb	$^{94}Mo(\gamma,pn)^{92m}Nb$	Mo/Nb=1.7×10^{3}	0.07	neg.	4.4×10^{-3}
Ni	None				
Rb	$^{86}Sr(\gamma,pn)^{84}Rb$	Sr/Rb=1.1×10^{4}	0.10	0.005—0.9	0.038
Sr	$^{89}Y(\gamma,pn)^{87m}Sr$	Y/Sr=5.9×10^{2}	0.01	0.002—0.08	0.015
Y	$^{90}Zr(\gamma,pn)^{88}Y$	Zr/Y=4.3×10^{2}	1.4	0.2—1.2	1.2
Zr	$^{94}Mo(\gamma,\alpha n)^{89}Zr$	Mo/Zr=2.3×10^{4}	7×10^{-4}	neg.	4×10^{-5}

paths. The effects of interferences were expressed as a ratio of the weights of the elements to produce same amounts of nuclide under consideration. To evaluate the effects, the yield data for the reactions of various types obtained on irradiating a series of individual elements under comparable conditions to those used for samples[9] were used. The values in parentheses are not experimentally obtained, but estimated from the yield data as a function of atomic number.[9] Interfering contributions thus evaluated are for several matrices. Values for the sediments are interfering contributions for the samples used in this work. In order to provide information on geochemical application of this method, corrections necessary for the average composition of the earth's crust were also calculated in Table 3. For this purpose, the abundance data compiled by Turekian and Wedepohl[15] were used.

A severe interference problem is the $^{56}Fe(\gamma,pn)^{54}Mn$ contribution to the total ^{54}Mn activity in the manganese determination. Corrections required for the samples were made by using the production rate ratio, $^{54}Mn/^{56}Mn$, found in the irradiated iron foils.[1,2] However, it was found that the ratio varies depending on the converter-material configuration in an irradiation system. An increase of 3% of the ratio obtained in the front foil was found in the back foil in the material unit. In such cases where the interfering contributions turn out to be very large, careful corrections should be made by using monitor foils irradiated under identical conditions to those used for samples. The $^{27}Al(n,\alpha)^{24}Na$ contribution to the total ^{24}Na activity was estimated from the aluminum values determined spectrophotometrically. Corrections required for the samples studied were less than 2%. Thus this source of interference may not be serious.

All elemental abundances are given in Tables 4 and 5. Reproducibility and reliability of the method have been demonstrated by analyzing a series of standard rocks of various types.[1,2] The abundance values obtained were reproducible: The average relative deviations for all the elements determined, based on the duplicate samples, were within 4%. Agreement of the results with published data was excellent. Although no replicate analyses were made on each of the samples, we estimate that the overall uncertainties associated with individual determinations for all of the elements studied are within ±10%.

The sodium values will be high to some extent because of sea water which was trapped within the accumulating sediments. The floor samples F-6 and F-7 are very high in calcium. The marked difference coincides with a

TABLE 4. ELEMETAL ABUNDANCES OF DEEP-SEA FLOOR SEDIMENTS

Sample	Major element (%)						
	Ca	Fe	Mg	Mn	Na	Ti	Al
F-1	1.04	4.97	1.74	0.98	3.27	0.34	6.30
F-2	1.80	7.12	2.14	1.35	4.96	0.46	5.47
F-3	1.03	7.26	2.04	1.85	3.01	0.50	7.16
F-4	1.17	5.89	1.92	0.55	3.02	0.52	6.86
F-5	1.25	5.60	2.02	0.56	3.74	0.53	6.29
F-6	21.2	3.56	2.18	0.31	1.89	0.42	3.20
F-7	27.6	3.53	1.04	0.36	2.26	0.17	1.83

Sample	Trace element (ppm)									
	Ba	Ce	Co	Cr	Nb	Ni	Rb	Sr	Y	Zr
F-1	425	79	56	60	6.4	85	273	182	31	166
F-2	626	64	88	39	5.2	188	58	243	78	125
F-3	223	99	146	86	8.9	178	180	198	44	143
F-4	410	102	106	87	9.2	176	359	178	76	175
F-5	376	90	91	73	8.0	166	245	185	72	167
F-6	220	40	47	75	5.4	121	114	699	49	108
F-7	314	17	18	29	1.5	17	58	1218	28	29

Table 5. Elemental abundances of core samples

Sample	Depth in core (cm)	Major element (%)						Trace element (ppm)									
		Ca	Fe	Mg	Mn	Na	Ti	Ba	Ce	Co	Cr	Nb	Ni	Rb	Sr	Y	Zr
C-1	Top of core	0.87	7.15	2.08	1.54	3.04	0.58	332	109	115	84	6.4	181	208	197	80	195
	Bottom of core (668)	0.86	7.03	2.15	1.91	3.37	0.61	479	87	129	70	8.4	306	125	210	101	193
C-2	9—10	34.3	0.92	0.44	0.06_3	1.19	0.09_6	347	7.6	12	26	1.2	31	14	884	18	21
	205—206	35.4	1.04	0.40	0.14	1.08	0.12	225	7.3	11	22	0.8	41	11	1000	17	20
	405—406	33.2	1.20	0.50	0.07_1	1.19	0.12	623	11	8.5	26	1.1	27	16	1600	23	29
	605—606	21.8	2.43	0.84	0.10	1.60	0.20	611	23	24	50	2.2	64	26	1880	42	56
	805—806	27.4	1.84	0.72	0.08_9	1.57	0.15	547	16	19	29	1.8	46	22	1490	35	41
	1005—1006	26.3	1.35	0.50	0.08_0	1.42	0.12	432	12	8.8	20	1.2	25	17	1340	29	31
	1105—1106	29.4	1.59	0.60	0.15	1.60	0.12	501	8.5	22	27	1.4	45	20	1390	34	38
C-3	105—106	35.3	0.77	0.35	0.16	1.17	0.04_1	328	4.4	7.4	11	0.7	49	6	1380	18	14
	205—206	29.8	1.08	0.38	0.07_8	1.12	0.08_5	330	7.6	7.4	14	0.4	17	8	1580	22	20
	305—306	33.4	1.22	0.50	0.13	1.32	0.10	751	8.8	12	19	0.4	39	12	1520	31	27
	405—406	33.0	0.82	0.34	0.06_1	0.98	0.06_5	371	6.7	6.8	9.1	0.6	18	8	2040	20	17
	605—606	34.2	1.12	0.44	0.06_9	1.12	0.10	399	7.8	7.5	17	0.8	23	9	1970	24	22
	805—806	34.1	0.90	0.41	0.07_0	1.17	0.08_1	419	7.1	9.1	11	0.8	18	6	1560	27	19
	905—906	34.1	0.87	0.38	0.08_5	1.08	0.05_7	505	7.1	11	9.5	0.2	19	5	1470	25	16
	1055—1056	32.0	1.24	0.46	0.12	1.27	0.06_9	739	8.3	13	21	0.7	33	10	1310	31	20
	Bottom of core (1163)	31.8	1.02	0.45	0.09_9	1.26	0.13	712	7.8	14	8.0	0.9	29	11	1380	20	23

considerable amount of calcareous shell materials found in them (Table 4).[12] These two samples were the carbonate type sediments and could be distinguished visually from the other clay type sediments. The carbonate compensation depth occurs at 3500 m in the Pacific Ocean.[16] Since the samples were collected at depths below it, the high contents of calcium can not be attributed to descent from the overlying water. Major parts of calcium in these samples may thus be due to calcareous organisms originating in the seamount which is located near the sampling sites. The deep-sea sediment of the carbonate type has only a relatively low content of most of trace elements, while the clays are generally rich in trace elements as compared to the carbonates.[16] The results in Table 4 show a typical pattern of this sort in the elemental composition. Strontium is an exception to this category. A similar exception has also been reported.[15] Samples F-3, F-4, and F-5 seem to be high in some trace elements such as Co, Cr, and Ni.

Of the core samples tested, C-1 sample contained less calcium at both the top and bottom of the core column. The elemental composition of this core can be related to the clay type sediments. In contrast, the other two core samples are highly calcareous and are characterized by their low contents of other major and trace elements except strontium. Each core sample is homogeneous in the elemental composition along the core column. No direct evidence of the early diagenesis or post-depositional migration of the elements has been obtained.

In conclusion, photon activation analysis with 30 MeV bremsstrahlung provides useful information on the elemental distribution in deep-sea sediments. The technique is nondestructive and can provide reliable abundance data for at least 6 major and 10 trace elements of geochemical significance.

We would like to express our appreciation to members of the linac machine and radioisotope groups, the Institute of Nuclear Science, Tohoku University, for their kind cooperation in the irradiation. We also thank Prof. Yokichi Takayanagi, the Institute of Geology and Palaeontology, Tohoku University, and Dr. Michio Kato, Department of Geology, Faculty of Integrated Arts and Science, Hiroshima University, for the supply of deep-sea sediments and valuable suggestions.

References

1) T. Kato, I. Morita, and N. Sato, *J. Radioanal. Chem.*, **18**, 97 (1973).
2) N. Sato, T. Kato, and N. Suzuki, *Radiochim. Acta*, **21**, 63 (1974).
3) T. Kato, N. Sato, and N. Suzuki, *Anal. Chim. Acta*, **81**, 337 (1976).
4) J. S. Hislop and D. R. Williams, *J. Radioanal. Chem.*, **16**, 329 (1973).
5) N. K. Aras, W. H. Zoller, G. E. Gordon, and G. J. Lutz, *Anal. Chem.*, **45**, 1481 (1973).
6) A. Chattopadhyay and R. E. Jervis, *Anal. Chem.*, **46**, 1630 (1974).
7) T. Kato, N. Sato, and N. Suzuki, *Talanta*, **23**, 517 (1976).
8) T. Kato and Y. Oka, *Talanta*, **19**, 515 (1972).
9) T. Kato, *J. Radioanal. Chem.*, **16**, 307 (1973).
10) T. Kato, K. Masumoto, N. Sato, and N. Suzuki, *J. Radioanal. Chem.*, **32**, 51 (1976).
11) T. Kato, *Res. Rept. Lab. Nucl. Sci., Tohoku Univ.*, **5**, 137 (1972).
12) Y. Takayanagi, T. Takayama, T. Sakai, M. Oda, and M. Kato, "Late Cenozoic Micropaleontologic Events in the Equatorial Pacific Sediments," to be published.
13) A. Ando, H. Kurasawa, T. Ohmori, and E. Takeda, *Geochem. J.*, **8**, 175 (1974).
14) H. Hashitani and K. Motojima, *Bunseki Kagaku*, **7**, 478 (1958).
15) K. K. Turekian and L. H. Wedepohl, *Bull. Geol. Soc. Am.*, **72**, 175 (1961).
16) J. P. Riley and R. Chester, "Introduction to Marine Chemistry," Academic Press, London (1971), Chap. 13.

Polarographic Behavior of Chloramine-T in an Acidic Solution at a Rotating Platinum Electrode

Toshio MATSUDA

Department of Chemistry, Ritsumeikan University, Kyoto 603

(Received December 6, 1976)

The polarographic behavior of chloramine-T at a rotating platinum electrode has been investigated in an acidic solution. Chloramine-T gives a well-defined reduction wave at a relatively positive potential. This is found to be due to the reduction of the non-ionized species of *N*-chloro-*p*-toluenesulfonamide and of dichloramine-T produced by disproportionation reaction of chloramine-T. The chemical process attributed to the disproportionation reaction is involved in the electrode process. The shape of the wave which varies with the recording procedure is correlated with the change of surface conditions. At pH lower than 4, a small prewave of hypochlorous acid produced by hydrolysis is observed at a more positive side. The diffusion current of the total wave, very stable and proportional to the concentration, is due to a two-electron reduction.

Chloramine-T (sodium salt of *N*-chloro-*p*-toluenesulfonamide, CAT) is known to be a stable oxidizing reagent for titrimetric analysis.[1] The purpose of this work is to investigate the electrochemical characteristics of CAT and to develop the end point detection techniques for a redox titration using CAT.

Recent studies[2,3] on the polarographic behavior at a dropping mercury electrode have shown that the over-all reaction of CAT involves two electrons over the pH range 2—13. However, it was impossible to measure the reduction potential of CAT since the reduction occurs at a more positive potential than that of the mercury dissolution. In an acidic solution, the limiting current tends to decrease with time by the reaction with mercury. On the other hand, well-defined reduction waves were observed at considerable positive potential at a rotating platinum electrode (RPE).

The polarographic behavior of CAT at a RPE was investigated in an acidic solution in order to elucidate the nature of the electrode process, the results of which are given in this report.

The free acid of CAT predominates in an acidic solution, producing *N,N*-dichloro-*p*-toluenesulfonamide (dichloramine-T, DCT) by disproportionation.[4,5] Discussion is given on the disproportionation and the effect of the electrode surface conditions on the reduction process.

Experimental

Apparatus and Reagent Used. The apparatus for the measurements of d.c. and a.c. polarograms was essentially the same as that described previously.[3] A Shimadzu synchronous rotator, RE-3, was used with a vertical platinum wire microelectrode (5.0 mm long, 0.5 mm in diameter) at r.p.m., 600. The sensitivity of electrode was 9.28 μA/mM in an electrolyte solution of hexacyanoferrate(III) ion containing 0.1 M KNO_3 and Britton-Robinson buffer at pH 5.0. An electrolytic cell of glass cylinder (50 mm in height and 45 mm in diameter) was used in a thermostat maintained at 25±0.2 °C. N_2 gas was used to deoxygenate the solution, flowing over the surface of the solution during the recording of the polarogram. The potentials are referred to a SCE connected to the solution with a KNO_3-agar salt bridge.

The preparation of the stock solutions of chloramine-T, *p*-toluenesulfonamide and other chemicals has been reported.[3] A satutated solution of *N,N*-dichloro-*p*-toluenesulfonamide (dichloramine-T) was prepared from the reagent grade salt and standardized against an arsenite standard solution. Water was used after distillation of deionized water in the presence of small amounts of $KMnO_4$ and NaOH solutions in a glass apparatus.

Measurement of Polarogram. Before each run for a polarogram of CAT, the polarograms of hexacyanoferrate(III) ion were recorded by use of the electrode which had been pretreated in a 0.1 M $HClO_4$ solution.[6] The values obtained for the diffusion current and the half-wave potential of hexacyanoferrate(III) ion were used to normalize the conditions for the preoxidation and rotation of the electrode, *etc.* An electrolyte solution was prepared by adding an adequate amount of the standard solution of CAT to the base solution, *i.e.*, 0.1 M KNO_3 and Britton-Robinson (B.R.) buffer solution. An aliquot of the solution was deoxygenated in an electrolytic cell. Polarograms were recorded by forward or backward scan. By forward scan, the electrode potential was shifted from positive to negative potentials. By backward scan, the situation was reversed. The rate of the potential scan was 200 mV per minute. A damping condenser of 5 μF was used.

Results and Discussion

Polarograms of Chloramine-T at Various pH Values. Figure 1 shows typical polarographic waves of 0.4 mM chloramine-T (CAT) in a supporting electrolyte solution containing 0.1 M KNO_3 and B.R. buffer at various pH values. The reduction waves in an acidic solution appeared at more positive potential than the reduction potential of platinum oxide. A maximum current on the plateau of the forward curves is due to the cathodic dissolution pattern of platinum oxide film. With the electrode covered with the oxide film, the waves shifted to negative potential and became drawn out, as shown on the forward curves, the results thus becoming less reproducible. This indicates that the electrode reaction is strongly inhibited by the oxide film. On the other hand, when the potential was scanned backward with the electrode reduced at an adequate negative potential after preoxidation, well-defined waves were observed at more positive side, the results being reproducible. On these curves, the main wave was two-stepped at pH lower than 7, a small prewave being observed at the more positive side at pH lower than 4 and a single wave at pH about 8.

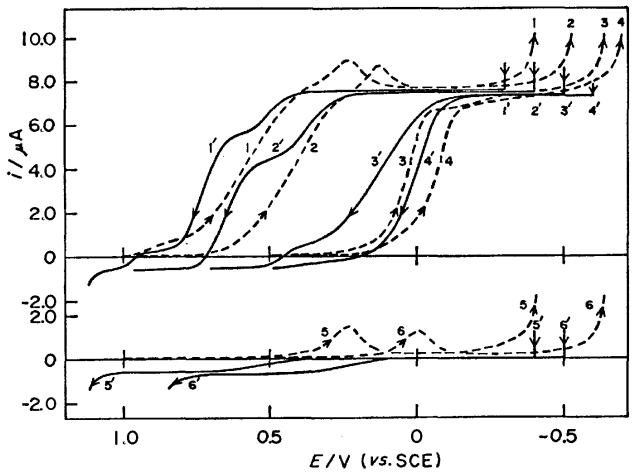

Fig. 1. Polarograms of 0.4 mM CAT in a solution containing 0.1 M KNO_3 and B.R. buffer at various pH values. (1,1') pH 3.40; (2,2') pH 5.05; (3,3') pH 7.10; (4,4') pH 8.10. Lower polarograms are residual current curves at various pH values. (5,5') pH 3.40; (6,6') pH 7.10. Dotted lines are forward curves recorded from +1.0 or +0.5 V after preoxidation at an adequate positive potential. Solid lines are backward curves recorded from between −0.3 and −0.6 V after the preoxidation.

The relations between pH and limiting current and between pH and half-wave potential of the backward wave are given in Figs. 2 and 3, respectively. The values of limiting current have been corrected for the residual current. On the main wave, the value of $\Delta E_{1/2}/\Delta$pH for the first step was −65 mV per unit pH, except at pH *ca.* 2. For the second step, the value was −80 mV per unit pH in the pH range 2—6. The limiting current of the first step varied with pH in the above pH range, giving a maximum value at pH 4—5. On the second step at pH higher than 6, the slope became remarkably drawn out, the half-wave potential shifting to negative potential. The results suggest that the reduction wave in an acidic solution can be characterized with the two-stepped wave at pH lower than 6 and that its electrode reaction differs from that at pH about 8. The half-wave potential shifts slightly to negative potential

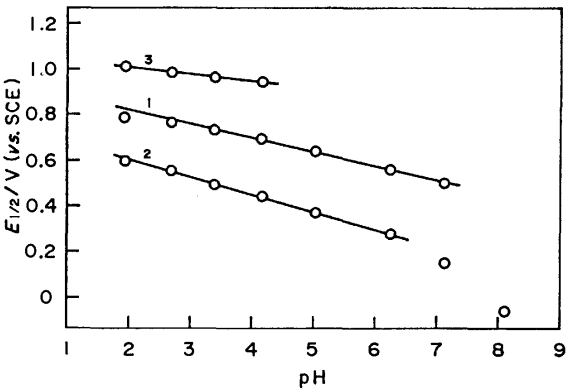

Fig. 3. Relation between the half-wave potential of the backward wave and pH for 0.4 mM CAT. (1) First wave; (2) second step; (3) prewave.

at pH *ca.* 2, which is considered to be attributable to the deactivation of the electrode surface. This tendency for the electrode surface to be rapidly deactivated, especially in an acidic solution, was also observed for the reduction of *N*-bromosuccinimide.[7]

The limiting current of the total wave was independent of the recording procedure, provided that the correction for the residual current in each case was applied. Its value remained constant within deviation of ±2.0% in the pH range 2—8, being proportional to the concentration from 0.05 to 0.6 mM CAT (Table 1). The plot of log $^{T}i_d$ *vs.* log *N* (*N* is r.p.m. of the electrode, which varied from 600 to 1200) gave a straight line, the slope of which was determined to be 1/3 (Fig. 4). A similar result was obtained for the diffusion current of hexacyanoferrate(III) ion. The temperature coefficient of $^{T}i_d$ measured in the temperature range 15—40 °C was 1.8% per degree. The limiting current can be concluded to be controlled by diffusion.

The value of $^{T}i_d/C$ for the total wave found to be 18.18±0.32 μA/mM in the above pH range. It can be seen that this value corresponds to a two-electron reduction on the basis of a similar calculation.[6] The values of diffusion coefficient used for this calculation were 0.79×10^{-5} $cm^2\,s^{-1}$ and 0.85×10^{-5} $cm^2\,s^{-1}$ for CAT[5] and hexacyanoferrate(III) ion,[5] respectively. The resut with respect to the limiting current of the

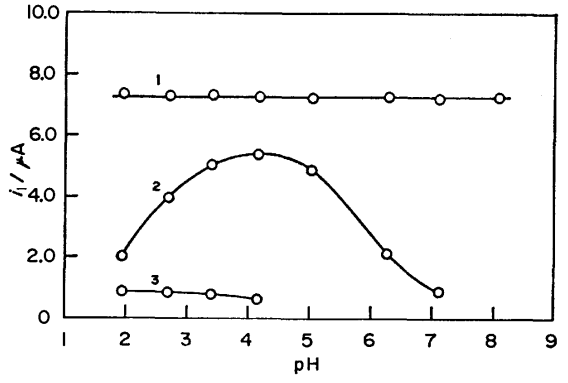

Fig. 2. Relation between the limiting current of the backward wave and pH for 0.4 mM CAT. (1) Total wave; (2) first step; (3) prewave.

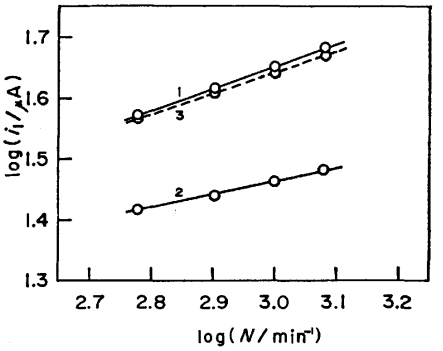

Fig. 4. Plots of log i_l *vs.* log *N* for (1) total wave, (2) first wave on the backward wave of 0.4 mM CAT and (3) reduction wave of 0.8 mM $K_3Fe(CN)_6$ in 0.1 M KNO_3 and B.R. buffer at pH 5.05.

TABLE 1. POLAROGRAPHIC DATA FOR THE REDUCTION WAVE OF CAT[a)]

pH	C/mM	Total wave		First step			Second step	Prewave		
		${}^{T}i_d/\mu A$	${}^{T}i_dC^{-1}$ $\mu A\ mM^{-1}$	${}^{I}i_l/\mu A$	${}^{I}i_lC^{-1}/$ $\mu A\ mM^{-1}$	${}^{I}E_{1/2}/V$ (*vs.* SCE)	${}^{II}E_{1/2}/V$ (*vs.* SCE)	${}^{P}i_d/\mu A$	${}^{P}i_dC^{-1}/$ $\mu A\ mM^{-1}$	${}^{P}E_{1/2}/V$ (*vs.* SCE)
5.05	0.600	10.71	17.85	6.88	11.47	+0.641	+0.380	b)		
	0.500	8.93	17.86	5.82	11.64	+0.640	+0.380	b)		
	0.400	7.22	18.05	4.90	12.25	+0.643	+0.376	b)		
	0.200	3.59	17.95	2.54	12.70	+0.642	+0.390	b)		
	0.100	1.790	17.90	1.300	13.00	+0.642	c)	b)		
	0.0500	0.910	18.20	0.743	14.68	+0.645	c)	b)		
3.40	0.600	10.84	18.07	7.16	11.93	+0.725	+0.505	1.16	1.93	+0.960
	0.500	8.99	17.98	6.36	12.72	+0.725	+0.510	0.94	1.88	+0.960
	0.400	7.36	18.40	5.11	12.77	+0.730	+0.505	0.76	1.91	+0.965
	0.200	3.64	18.20	2.83	14.15	+0.728	+0.510	0.38	1.90	+0.965
	0.100	1.790	17.90	1.442	14.42	+0.730	c)	b)		
	0.0500	0.920	18.40	0.742	14.84	+0.733	c)	b)		

a) Values were obtained from backward waves in a supporting electrolyte solution containing 0.1 M KNO_3 and Britton-Robinson buffer at various pH values. b) No prewave. c) No second step.

total wave was identical with that obtained at a dropping mercury electrode.[3)] It could be assumed, therefore, that the non-ionized species of *N*-chloro-*p*-toluenesulfonamide is mainly reduced in an acidic solution. However, the fact that the limiting current of the first step varies with pH as shown in Fig. 2 and that it has a kinetic character suggest that the electrode process of the main wave can not be accounted for by the reduction process of the non-ionized species only.

The limiting current of the first step was not proportional to the concentration (Table 1). The plot of $\log {}^{I}i_l$ *vs.* $\log N$ gave a straight line, the slope of which was determined to be 1/5. The temperature coefficient of ${}^{I}i_l$ determined in the temperature range 15—40 °C was 2.8% per degree, indicating that the limiting current has a kinetic character.

Effect of Surface Conditions of Electrode. In order to clarify the nature of the two-stepped wave, the effect of surface conditions of the electrode was investigated around pH 5.

With the reduced electrode, current-time curves were recorded in 0.4 mM CAT solution at pH 5.10 at +0.6 and +0.5 V, on the rising portion and the plateau of the first step, respectively, and at +0.4 V on the rising portion of the second step. As seen in Fig. 5, currents

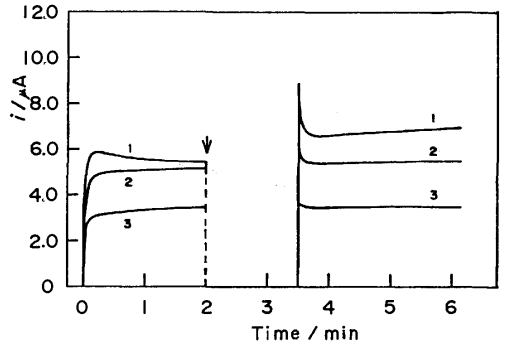

Fig. 5. Current-time curves of the reduction wave of 0.4 mM CAT at pH 5.10. (1) At +0.4 V; (2) at +0.5 V; (3) at +0.6 V. The point of open-circuit is denoted by arrow on the time-axis.

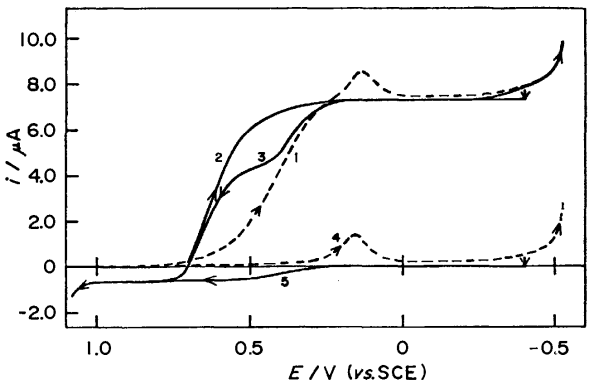

Fig. 6. Effect of the recording procedures on the polarogram of 0.4 mM CAT at pH 5.10.
(1) Forward scan from +1.0 V after preoxidation at +1.5 V; (2) forward scan from +0.7 V after preoxidation at +1.5 V followed by polarization at −0.4 V for a few minutes; (3) backward scan from −0.4 V after preoxidation at +1.5 V; (4) same as in curve (1) (residual current), (5) same as in curve (3) (residual current).

increased at these potentials, except at +0.6 V, after the electrode had been allowed to stand for 90 seconds at a natural electrode potential in an open-circuit condition. The natural electrode potential in this solution was found to be +0.8 V *vs.* SCE. At this potential, the platinum electrode would be oxidized (Fig. 6, curve 5). The increase of current is thus considered to be attributable to the formation of the oxide film. It is assumed that the current might not increase at +0.6 V, since the thin oxide film was produced at an earlier stage of the curve.

The height of the first step decreased due to the addition of *p*-toluenesulfonamide (TSA), a reduction product. The decrease was not detected in the presence of potassium chloride. A.c. base-current was recorded in both the presence and absence of TSA by the conventional a.c. polarographic method[3)] with the reduced electrode. It decreased in the presence of TSA at the potential region in which the platinum electrode is

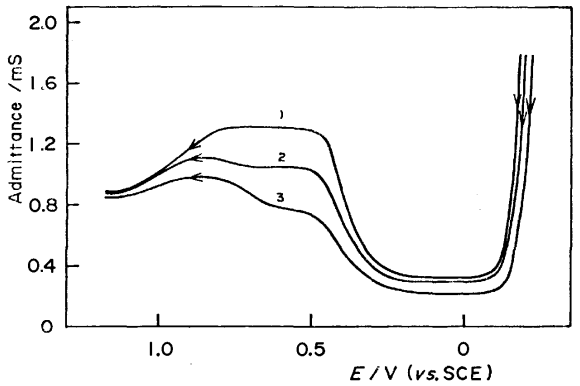

Fig. 7. Effect of TSA on the a.c. base-current curve in a solution containing 0.1 M KNO_3 and B.R. buffer at pH 5.10. (1) TSA was not added; (2) TSA was added in 0.1 mM; (3) TSA was added in 0.4 mM.

reduced (Fig. 7), which indicates that TSA is adsorbed on the surface of the reduced electrode.

It can be seen that TSA is adsorbed on the oxide-free surface and is desorbed partly by the formation of the oxide film. Thus, the two-stepped wave would be correlated with the adsorption of TSA. In fact, the curve recorded by the forward scan with an electrode covered thinly with the oxide film showed a single wave (Fig. 6, curve 2). This result is in line with the fact that the current increases as a result of the formation of the oxide film (Fig. 5).

Comparison with Reduction Wave of Dichloramine-T. Non-ionized species of CAT undergoes disproportionation in an acidic solution into dichloramine-T (DCT) and *p*-toluenesulfonamide (TSA)[4,5] according to

$$2RSO_2NHCl \rightleftharpoons RSO_2NCl_2 + RSO_2NH_2, \quad (1)$$

where $R=CH_3C_6H_4$. DCT as well as CAT act as a relatively strong oxidizing reagent in an acidic solution.[8] It can be expected, therefore, that a reduction wave of DCT is involved in the reduction wave of the CAT. A comparison with the reduction wave of DCT was made.

The value of the equilibrium constant (K_d) of the disproportionation is reported[4,5] to be 6.1×10^{-2} at 25 °C. DCT hydrolyzes to hypochlorous acid, the hydrolysis constant being 8×10^{-7}. If we assume that the amount of hydrochlorous acid is negligibly small and the non-ionized species predominates in the bulk solution, the equilibrium concentration of DCT can be calculated to be approximately 0.02 mM in the solution of 0.4 mM CAT.

DCT in an acidic solution gave a reduction wave (Fig. 8). The shape of the wave was very similar to that of CAT. The values of the half-wave potential and $\Delta E_{1/2}/\Delta pH$ for the first step were idential with those for the first step of CAT (Fig. 3). Although the slope of the second step became slightly drawn out, the value of $\Delta E_{1/2}/\Delta pH$ was close to that of CAT. At pH lower than 5, the height of the total wave remained constant. The wave obtained by the same recording procedure (Fig. 6, curve 2) became a single wave. Consequently, the behavior was identical with that of the reduction wave of CAT. The value of the diffusion current of the total wave at pH lower than 5 was found to correspond to a four-electron reduction.

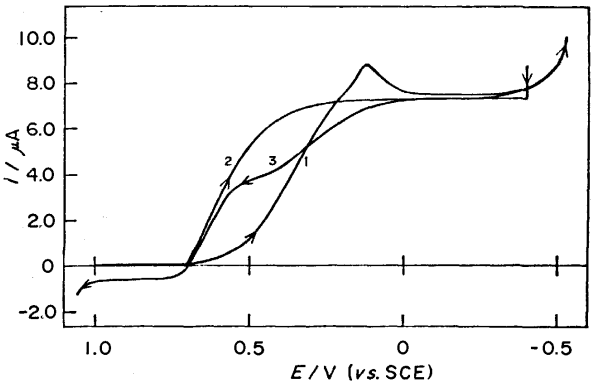

Fig. 8. Polarograms of 0.2 mM DCT in a solution containing 0.1 M KNO_3 and B.R. buffer at pH 5.20. (1) Forward scan from +1.0 V after preoxidation at +1.5 V; (2) forward scan from +0.7 V after preoxidation at +1.5 V followed by polarization at −0.4 V for a few minutes; (3) backward scan from −0.4 V after preoxidation at +1.5 V.

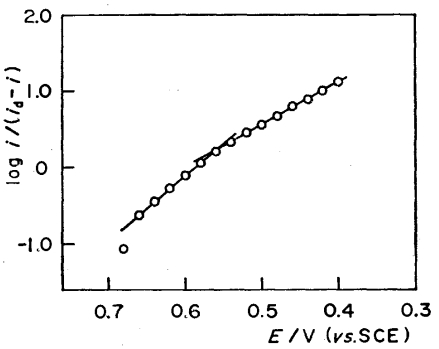

Fig. 9. Plot of log $[i/(i_d-i)]$ *vs.* E for the reduction wave of 0.4 mM CAT at pH 5.10, which was obtained by recording procedure as in curve 2 of Fig. 6.

The results suggest that the electrode process of the reduction wave in the CAT solution is essentially the same as that of DCT.

Electrode Process of the Reduction Wave of Chloramine-T. On the single wave (Fig. 6, curve 2), the plot of log-$[i/(i_d-i)]$ *vs.* E consists of two straight lines (Fig. 9). The potential at the point of intersection corresponds to that on the plateau of the first of the two-stepped wave. A similar result was obtained on the single wave in the DCT solution (Fig. 8).

The electrode process of the reduction wave in the CAT solution at pH lower than 6 can be explained as follows.

The reduction wave is made up of the following reactions:

$$RSO_2NCl_2 + H^+ + 2e^- \longrightarrow RSO_2NHCl + Cl^- \quad (2)$$

$$RSO_2NHCl + H^+ + 2e^- \longrightarrow RSO_2NH_2 + Cl^- \quad (3)$$

Reaction 2 occurs fast and is followed by Reaction 3. With the electrode from which TSA is desorbed, the two reactions occur continuously and the resulting wave becomes a single wave. With the electrode surface adsorbed with TSA, Reaction 3 is inhibited and the resulting wave becomes a two-stepped wave. It seems that, on the two straight lines of the log-plot, the left-

side branch from the point of intersection corresponds to Reaction 2 and the right-side branch to Reaction 3, *viz.*, the two-stepped wave; the first step is due to Reaction 2 and the second step to Reaction 3. According to Higuchi *et al.*,[9] the rate of disproportionation given by Reaction 1 is relatively great. We might thus expect that, over the potential region where only Reaction 2 occurs, DCT undergoes transformation on the surface by the chemical process attributed to Reaction 1. The limiting current of the first step is greater than that corresponding to the equilibrium concentration of DCT, which can be accounted for by this chemical process. This consideration is supported by the fact that the limiting current of the first step has a kinetic character and that its pH-dependence (Fig. 2, curve 2) is the same as that of the forward rate constant for Reaction 1.[9]

As regards the behavior at pH higher than 7, the reduction of ionized species might be considered.

Behavior of Prewave. The value of $\Delta E_{1/2}/\Delta$pH was determined to be -33 mV per unit pH on the small prewave obtained by backward scan with the reduced electrode at pH lower than 4. The limiting current was proportional to the concentration of CAT (Table 1) and found to be controlled by diffusion.

Hypochlorous acid gives a reduction wave at a relative positive potential on a platinum electrode,[10,11] giving a reduction wave at the same potential as that of the prewave under the same experimental conditions as in this study. The behavior was the same as that of the prewave. Thus, it is concluded that the prewave results from the reduction of hypochlorous acid produced by hydrolysis in the CAT solution.[4,5]

The value of i_d/C for the reduction wave of hypochlorous acid was determined separately to be 26.9 μA/mM in the same electrolyte solution. By use of this value and the value of the prewave (Table 1), the amount of hypochlorous acid in the solution of 0.4 mM CAT is calculated to be *ca.* 0.03 mM at pH 3. This is in line with the interpretation that the fraction of hypochlorous acid present in the CAT solution is much less than 10%.[3]

Analytical Aspect. When current-time curves were recorded at several potentials on the plateau of the total wave, no detectable variations of current were observed over a period of 10 min at pH lower than 6. This indicates that the limiting current of the total wave is remarkably stable and reproducible over the pH range studied. This behavior is advantageous for analysis as compared with that of a dropping mercury electrode,[3] in which the limiting current decrease is due to the reaction with mercury or maximum suppressor.

It can be concluded that the limiting current in an acidic solution is useful for amperometric titration in the short-circuit method.

The author wishes to express his hearty thanks to Prof. Taitiro Fujinaga, Kyoto University, for his encouragement, and to Prof. Toyoshi Nagai, Ritsumeikan University, for his helpful suggestions and discussions.

References

1) A. Berka, J. Vulterin, and J. Zýka, "Newer Redox Titrants," Pergamon Press, London, New York (1965), p. 37.
2) T. Nagai, T. Matsuda, and N. Sugii, *Nippon Kagaku Zasshi*, **90**, 790 (1969).
3) T. Matsuda, *J. Electroanal. Chem.*, **69**, 251 (1976).
4) J. C. Morries, J. A. Salazar, and M. A. Wineman, *J. Am. Chem. Soc.*, **70**, 2036 (1948).
5) E. Bishop and V. J. Jennings, *Talanta*, **1**, 197 (1958).
6) T. Nagai and T. Matsuda, *Rev. Polarog. (Kyoto)*, **16**, 16 (1969).
7) T. Nagai and T. Matsuda, *Rev. Polarog. (Kyoto)*, **17**, 133 (1971).
8) D. S. Mahadevappa and N. M. Made Gowda, *Talanta*, **22**, 771 (1975).
9) T. Higuchi, K. Ikeda, and A. Huddain, *J. Chem. Soc., B*, **1967**, 546.
10) H. C. Marks and G. L. Bannister, *Anal. Chem.*, **3**, 200 (1947).
11) O. Schwarzer and R. Landsberg, *J. Electroanal. Chem.*, **19**, 391 (1968).

Kinetics of the Oxidation of Ethylenediaminetetraacetato and Aqua Complex of Dimeric Molybdenum(V) by the μ-Hyperoxo-bis[pentaamminecobalt(III)] Ion in Aqueous Perchloric Acid Solution

Yoichi SASAKI

Chemistry Department, Faculty of Science, Tohoku University, Aoba, Aramaki, Sendai 980

(Received December 21, 1976)

Kinetics of the oxidation of double-bridged Mo(V) complexes, $[Mo_2O_4(edta)]^{2-}$ (H_4edta=ethylenediaminetetraacetic acid) and $[Mo_2O_4(aq)]^{2+}$ with $[(NH_3)_5CoO_2{}^{(-)}Co(NH_3)_5]^{5+}$ has been studied in aqueous perchloric acid solution at 25—50 °C. The oxidation of $[Mo_2O_4(edta)]^{2-}$ is characterized by the electron transfer within the ion-pair formed between the two reactants. The first order rate constants for the electron transfer process (k_e) are independent of $[H^+]$ ($[H^+]=0.05$—0.1 M; $I=0.1$—2.0 M) (M=mol dm^{-3}). At 40 °C and $I=0.1$ M, k_e is equal to $(1.34\pm0.08)\times10^{-3}$ s^{-1} and the corresponding activation parameters are $\Delta H^{\ddagger}=28\pm4$ kcal mol^{-1} and $\Delta S^{\ddagger}=18\pm11$ cal K^{-1} mol^{-1}. The rate of oxidation of $[Mo_2O_4(aq)]^{2+}$ is independent of the oxidant concentration and accelerated by halide ions and Mo(VI). The rate-determining step is the formation of a single-bridged Mo(V) dimer (A) prior to electron transfer. The first order rate constants for the formation of A (k_1) are reciprocally dependent on $[H^+]$ ($[H^+]=0.5$—2.0 M; $I=2.0$ M). k_1 is $(4.3\pm0.3)\times10^{-6}$ s^{-1} at 25 °C and for $[H^+]=1.0$ M. The difference in the oxidation mechanism of the two complexes has been discussed in terms of the charge of the complex, stabilization of the Mo_2O_4-unit by the ligands, and the role of coordinated water.

The redox and substitution properties of molybdenum ions in various oxidation states are of current interest[1,2] in view of the involvement of molybdenum ions in biological systems.[3] The redox properties of simple molybdenum(V) complexes have been studied by many workers.[1,4-11]

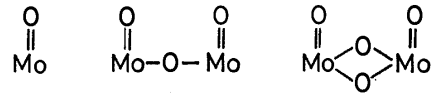

Fig. 1. Basic units of three types of structure of molybdenum(V) complexes.

Most of the molybdenum(V) complexes can be classified into three types (Fig. 1). Recent studies on the oxidation of some type I complexes by nitrate[6,10,11] and nitrite[7] ions revealed that they are much more readily oxidized than dimeric complexes. The oxidation of dimeric Mo(V) complex (structure not clearly described) by nitrate ions is considered to involve a small amount of monomeric Mo(V) which is in equilibrium with the Mo(V) dimer.[12] For the oxidation of the Mo(V) dimer with I_3^- and O_2, Mo(IV) was proposed as a redox active intermediate.[13] On the other hand, for the oxidation of $[Mo_2O_4(edta)]^{2-}$ with $[IrCl_6]^{2-}$ or $[Fe(phen)_3]^{3+}$ (phen=1,10-phenanthroline), it is not necessary to consider an intermediate formation prior to the electron transfer process.[8]

The purpose of this work is to get further information on the oxidation mechanism of the molybdenum(V) complexes of type III, by comparing the behavior of two complexes, $[Mo_2O_4(edta)]^{2-}$ [14] and $[Mo_2O_4(aq)]^{2+}$.[15,16] Coordinated water molecules in the latter are labile to substitution,[17] whereas $[Mo_2O_4(edta)]^{2-}$ is inert unless acid concentration is sufficiently high ($[H^+]>0.5$ M; M=mol dm^{-3}).[14] The μ-hyperoxo dicobalt(III) ion, $[(NH_3)_5CoO_2{}^{(-)}Co(NH_3)_5]^{5+}$ was used as an oxidizing reagent which is known to be reduced through an outer-sphere mechanism to the corresponding μ-peroxo ion by one electron transfer process.[18,19]

Experimental

Materials. *Disodium μ(N,N′)-Ethylenediaminetetraacetato-di-μ-oxo-bis[oxomolybdate(V)] Dihydrate, $Na_2[Mo_2O_4(edta)]\cdot2H_2O$*: The complex was prepared by a method similar to that described previously;[14] dipyridinium pentachlorooxomolybdate(V) ($(pyH)_2[MoOCl_5]$)[20] was used instead of the corresponding ammonium salt.

A Solution of the Aqua Complex of Di-μ-oxo-bis[oxomolybdenum(V)], $[Mo_2O_4(aq)]^{2+}$: Ten grams of $(pyH)_2[MoOCl_5]$ was dissolved in 500 cm^3 of 0.1 M perchloric acid ($HClO_4$). An orange solution was obtained, containing $[Mo_2O_4(aq)]^{2+}$ as the main species. In order to remove impurities, the solution was treated with an ion-exchange column, Dowex 50W-X8 resin (H^+-form). An orange band remained on the column. The column was washed with 100 cm^3 each of 0.1, 0.2, and 0.5 M $HClO_4$ and 50 cm^3 of 1 M $HClO_4$ successively. $[Mo_2O_4(aq)]^{2+}$ was eluted with 2 M $HClO_4$. About 0.05 M (as dimer) solution of $[Mo_2O_4(aq)]^{2+}$ was obtained (*ca.* 150 cm^3). All the preparative and the ion-exchange work was carried out under nitrogen atmosphere to avoid air oxidation of $[Mo_2O_4(aq)]^{2+}$.[14] This procedure is important since Mo(VI)[21] did not seem to have been completely removed by ion-exchange purification. The concentration of $[Mo_2O_4(aq)]^{2+}$ in the eluate was determined spectroscopically from the optical density at 384 nm ($\varepsilon=103$ per dimer[14]).

Other Materials: μ-Hyperoxo-bis[pentaamminecobalt(III)] perchlorate dihydrate, $[(NH_3)_5CoO_2{}^{(-)}Co(NH_3)_5](ClO_4)_5\cdot2H_2O$, was prepared from the chloride salt[23] according to the method of Linhard and Weigel.[24] Sodium perchlorate (special grade) was used for the adjustment of ionic strength without further purification. Lithium perchlorate, used for the adjustment of ionic strength, was prepared from lithium carbonate and perchloric acid, and recrystallized twice. The concentration of the solution of lithium perchlorate (*ca.* 3 M) was determined by exchanging the lithium ion for proton with an ion-exchange regin of H^+-type (Amberlite IR-120), and titration with a standard sodium hydroxide solution.

Measurements. A Hitachi 124 spectrophotometer with

a Hitachi recorder QPD-34 was used for the measurement of visible and ultraviolet absorption spectra and for kinetic studies.

Kinetic Runs. Solutions of $[(NH_3)_5CoO_2{}^{(-)}Co(NH_3)_5](ClO_4)_5 \cdot 2H_2O$ and $Na_2[Mo_2O_4(edta)] \cdot 2H_2O$ were prepared every day, whereas that of $[Mo_2O_4(aq)]^{2+}$ was kept in a refrigerator for *ca.* a week under nitrogen atmosphere. Each solution was kept in a thermostat at the desired temperature for at least 30 min, and mixed to start kinetic runs. The rate of decrease in concentration of the μ-hyperoxo ion was followed at 670 nm, where it has a strong absorption peak (ε= 832 per dimer[25]), and no other compounds involved in the reaction have significant absorption. The reaction cell was shaken quickly at appropriate time intervals in order to remove the bubbles of oxygen gas on the cell walls formed during the course of reaction. For the reaction of $[Mo_2O_4(aq)]^{2+}$, all the procedures were carried out under nitrogen atmosphere with use of syringes, needles and rubber caps. Without such a precaution, it was difficult to get reproducible results. A strong catalytic effect of Mo(VI) on the rate of the reaction seems to be responsible. It was difficult to get the solution of $[Mo_2O_4(aq)]^{2+}$ free from pyridinium ion by the ion-exchange separation. $[Mo_2O_4(aq)]^{2+}$ seems to be eluted easily for dipositive ion. It was found that pyridinium ion does not affect the rate of the reaction up to the concentration 0.01 M.

Results

Kinetics of the Oxidation of $[Mo_2O_4(edta)]^{2-}$ with $[(NH_3)_5CoO_2{}^{(-)}Co(NH_3)_5]^{5+}$. $[Mo_2O_4(edta)]^{2-}$ undergoes acid hydrolysis in aqueous perchloric acid solution ($[H^+]>0.5$ M).[14] In this work, $[H^+]$ was adjusted to 0.1 M or lower so that it was not necessary to consider the effect of acid hydrolysis. When an aqueous solution of $[Mo_2O_4(edta)]^{2-}$ was mixed with that of the μ-hyperoxo dicobalt(III) ion in 0.1 M $HClO_4$, the light absorption of these two ions in the visible region decreased slowly, no rapid change in absorption spectra preceding. No rapid reaction between these two ions other than weak interaction such as ion-pair formation is feasible.

The stoichiometry of the reaction corresponding to the slow change was determined as follows. 0.1 M perchloric acid solutions containing the μ-hyperoxo ions more than twice $[Mo_2O_4(edta)]^{2-}$ in molar concentration were kept at 40 °C for a day, and the amount of remaining μ-hyperoxo ions was estimated from the intensity of the absorption peak at 670 nm. Two moles of the μ-hyperoxo ions were consumed per one mol of $[Mo_2O_4(edta)]^{2-}$. Thus each molybdenum(V) ion in the complex was oxidized to Mo(VI) by one μ-hyperoxo ion. The μ-peroxo ion, $[(NH_3)_5CoO_2{}^{(2-)}Co(NH_3)_5]^{4+}$, the initial product of the electron transfer reaction should have decomposed rapidly in acid solutions to give Co(II), O_2, and ammonium ions.[26] Mo(VI) is in dimer-monomer equilibrium.[22] The coordination of the edta-ligand is unlikely under the given acid concentration.[27] The entire reaction can be written as follows.

$$[Mo_2O_4(edta)]^{2-} + 2[(NH_3)_5CoO_2{}^{(-)}Co(NH_3)_5]^{5+} + (20+n)H^+ \longrightarrow 2Mo(VI) + H_nedta^{(4-n)-} + 4Co(II) + 2O_2 + 20NH_4^+ \quad (1)$$

Kinetics of the reaction was studied at 35—50 °C and ionic strength 0.1—2.0 M (adjusted with $NaClO_4$). The molybdenum(V) complex was used in at least 10 fold excess to the μ-hyperoxo ion. The first-order plots log (OD_t) against time t are linear to over 90% of the course of reaction (OD_∞ was approximated to zero), where OD_t stands for the absorbance at 670 nm at time t. The first-order rate constant k_{obsd} is independent of $[H^+]$ in the range 0.05—0.1 M. The dependence of k_{obsd} on the concentration of $[Mo_2O_4(edta)]^{2-}$ at various ionic strengths is shown in Fig. 2. The rate constant increases with decrease in the ionic strength, tending to be saturated at higher concentrations of $[Mo_2O_4(edta)]^{2-}$. The plots $k_{obsd}{}^{-1}$ against $[Mo_2O_4(edta)^{2-}]^{-1}$ are linear (Fig. 3). Intercepts of the straight

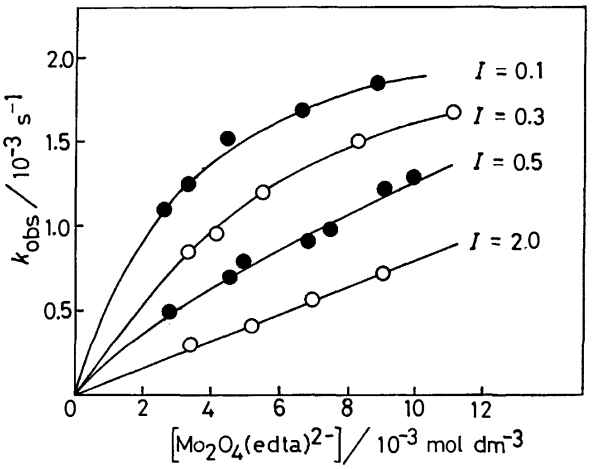

Fig. 2. The dependence of k_{obsd} on $[Mo_2O_4(edta)^{2-}]$ for the oxidation of $[Mo_2O_4(edta)]^{2-}$ with $[(NH_3)_5CoO_2{}^{(-)}Co(NH_3)_5]^{5+}$ in 0.1 M perchloric acid, with $[Mo_2O_4(edta)]^{2-}$ in large excess at various ionic strengths (adjusted with $NaClO_4$), at 40 °C and $[\mu\text{-}O_2{}^{(-)}] = (2—5) \times 10^{-4}$ mol dm^{-3}.

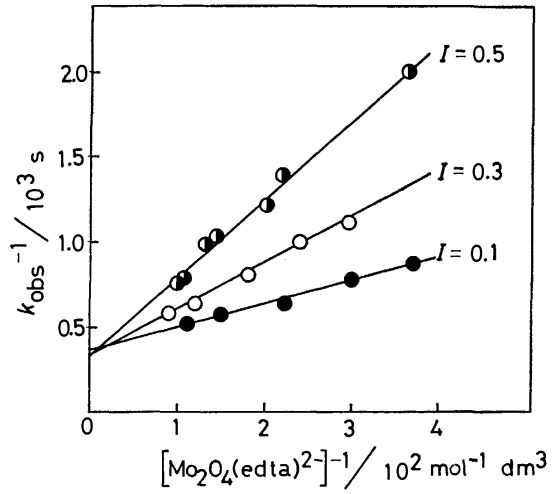

Fig. 3. The dependence of $k_{obsd}{}^{-1}$ on $[Mo_2O_4(edta)^{2-}]^{-1}$ for the oxidation of $[Mo_2O_4(edta)]^{2-}$ with $[(NH_3)_5CoO_2{}^{(-)}Co(NH_3)_5]^{5+}$ in 0.1 M perchloric acid, with $[Mo_2O_4(edta)]^{2-}$ in large excess at various ionic strength (adjusted with $NaClO_4$), at 40 °C and $[\mu\text{-}O_2{}^{(-)}] = (2—5) \times 10^{-4}$ mol dm^{-3}.

lines at three different ionic strengths coincide with each other within experimental error. The rate of Reaction 1 does not change in the presence of Cl^- up to 0.1 M.

Kinetics of the Oxidation of $[Mo_2O_4(aq)]^{2+}$ *with* $[(NH_3)_5CoO_2^{(-)}Co(NH_3)_5]^{5+}$. Similar to the case of the oxidation of $[Mo_2O_4(edta)]^{2-}$, the reaction of $[Mo_2O_4(aq)]^{2+}$ with the μ-hyperoxo ion is expressed as follows from the change of absorption spectra and stoichiometric studies in 2 M $HClO_4$:

$$[Mo_2O_4(aq)]^{2+} + 2[(NH_3)_5CoO_2^{(-)}Co(NH_3)_5]^{5+} + 20H^+ \longrightarrow 2Mo(VI) + 4Co(II) + 2O_2 + 20NH_4^+. \quad (2)$$

Kinetics of the reaction was studied at 25—40 °C for $[H^+]=0.5$—2.0 M. It was difficult at lower $[H^+]$ to get the concentration of $[Mo_2O_4(aq)]^{2+}$ high enough for the kinetic studies. $[Mo_2O_4(aq)]^{2+}$ undergoes structural change for $[H^+]<0.1$ M.[14,17] The molybdenum complex was used in large excess as compared to the μ-hyperoxo ion. The concentration ranges of the reactants are $(8—35)\times10^{-3}$ M for $[Mo_2O_4(aq)]^{2+}$ and $(2.5—5)\times10^{-4}$ M for the μ-hyperoxo ion.

The decrease of absorbance (OD) at 670 nm did not obey the first order rate law. The OD decreased linearly with time at the initial stage of the reaction (until the concentration of the μ-hyperoxo ion reached *ca.* 1.5×10^{-4} M), and subsequently more slowly. The slope of the plots, OD_t against t, did not change when the concentration of the μ-hyperoxo ion changed from 3×10^{-4} to 5×10^{-4} M at a constant concentration of $[Mo_2O_4(aq)]^{2+}$.

The OD change per second was converted into the molar consumption of the μ-hyperoxo ion per second (denoted by k_i) by using the ε value (832)[25] at 670 nm. The dependence of k_i on the concentration of $[Mo_2O_4(aq)]^{2+}$ at $[H^+]=2.0$ M (Fig. 4) suggests that k_i is of first-order with respect to $[Mo_2O_4(aq)^{2+}]$.

The effect of $[H^+]$ on k_i was studied with a fixed concentration of the reactants and at $I=2.0$ M ($LiClO_4$). The k_i values seem to be inversely proportional to $[H^+]$.

The effect of anions added was studied for Cl^- and Br^-. Significant acceleration of the rate by both ions was observed. The rate of disappearance of the μ-hyperoxo ion turned out to be of first-order. Under the conditions $[H^+]=2.0$ M, $[Mo_2O_4(aq)^{2+}]=8.55\times10^{-3}$ M, $[\mu\text{-}O_2^{(-)}]=3.50\times10^{-4}$ M, and $[Cl^-]=0.12$ M and at 35 °C, $\tau_{1/2}$ is about 4 min, whereas under similar conditions in the absence of Cl^-, it took more than 8 h for the reaction to complete. The effect of Br^- is of similar magnitude to that of Cl^-. Mo(VI) also accelerates the rate. The rate of disappearance of the μ-hyperoxo ion remained in zero-order for a much longer part of the reaction. Under the conditions $[H^+]=2.0$ M, $[Mo_2O_4(aq)^{2+}]=8.55\times10^{-3}$ M, $[\mu\text{-}O_2^{(-)}]=3.50\times10^{-4}$ M and [Mo(VI)] (as sodium molybdate) $=0.015$ M, the rate was *ca.* 4 times greater than that without Mo(VI). The extent of enhancement depends approximately linearly on the concentration of the Mo(VI) ($[Mo(VI)]=(0.5—3)\times10^{-2}$ M). The effect was more remarkable at lower acid concentrations. Apparently the effect depends on the time after mixing of $[Mo_2O_4(aq)]^{2+}$ and Mo(VI).

It must be considered whether the Mo(VI) which is built up during the kinetic runs is catalytic to Reaction 2. The Mo(VI) concentrations are equal to the initial concentrations of the μ-hyperoxo ion at the end of the runs: $(2.5—5)\times10^{-4}$ M. It is therefore concluded that the Mo(VI) produced does not have a significant effect upon the rate of the reaction, at least at the initial part of the reaction which is important in this study.

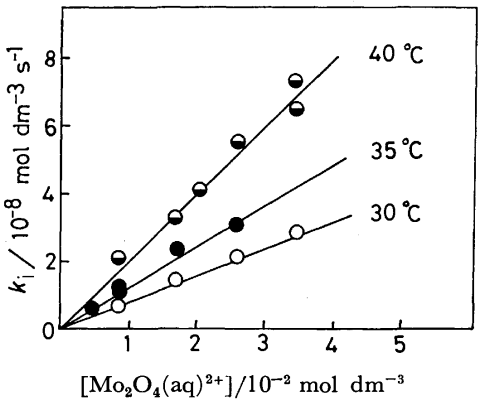

Fig. 4. The dependence of k_i on $[Mo_2O_4(aq)^{2+}]$ for the oxidation of $[Mo_2O_4(aq)]^{2+}$ with $[(NH_3)_5CoO_2^{(-)}Co(NH_3)_5]^{5+}$ in 2 M perchloric acid, with $[Mo_2O_4(aq)]^{2+}$ in large excess, at various temperatures and $[\mu\text{-}O_2^{(-)}]=(2.5—5)\times10^{-4}$ mol dm^{-3}.

Discussion

Mechanism of the Oxidation of $[Mo_2O_4(edta)]^{2-}$ *by* $[(NH_3)_5CoO_2^{(-)}Co(NH_3)_5]^{5+}$. The results shown in Figs. 1 and 2 can be interpreted in terms of an ion-pair formation between the two reactants, the formation constant being expected to be large since they have high opposite charges (+5 and −2).

Since the μ-hyperoxo ion is one electron oxidizing reagent, oxidation of dimeric $[Mo_2O_4(edta)]^{2-}$ should proceed in two steps, and an immediate product of the first electron transfer process should be a mixed valence dimer, "$Mo^{V}Mo^{VI}$," the structure of which is not known. Wharton *et al.*[8] studied the oxidation of $[Mo_2O_4(edta)]^{2-}$ with $[IrCl_6]^{2-}$ and $[Fe(phen)_3]^{3+}$, and found that the following reactions are reversible:

$$[Mo_2O_4(edta)]^{2-} + \underset{([Fe(phen)_3]^{3+})}{[IrCl_6]^{2-}} \rightleftharpoons \underset{([Fe(phen)_3]^{2+})}{\text{“}Mo^{V}Mo^{VI}\text{”} + [IrCl_6]^{3-}}. \quad (3)$$

They suggested that the mixed valence dimer most likely decomposes into two monomers Mo(V) and Mo(VI), the former being rapidly oxidized by the oxidant. In the present case, the process corresponding to Reaction 3 is not reversible since the reduced form of the oxidant decomposes rapidly under the experimental conditions.[26] The oxidation of "$Mo^{V}Mo^{VI}$" by the second μ-hyperoxo ion should be rapid possibly through the decomposition into the monomers. There was no intermediate (corresponding to "$Mo^{V}Mo^{VI}$") detectable from the change of absorption spectra during the course of reaction and from the kinetic treatment.

The following mechanism (4—7) is proposed for

Reaction 1, where μ-$O_2^{(-)}$ and μ-$O_2^{(2-)}$ stand for $[(NH_3)_5CoO_2^{(-)}Co(NH_3)_5]^{5+}$ and $[(NH_3)_5CoO_2^{(2-)}Co(NH_3)_5]^{4+}$, respectively:

$$[Mo_2O_4(edta)]^{2-} + \mu\text{-}O_2^{(-)} \overset{K_{IP}}{\rightleftharpoons} \text{ion-pair}, \quad (4)$$

$$\text{ion-pair} \xrightarrow{k_e} \text{“}Mo^{V}Mo^{VI}\text{”} + \mu\text{-}O_2^{(2-)}, \quad (5)$$

$$\text{“}Mo^{V}Mo^{VI}\text{”} + \mu\text{-}O_2^{(-)} \xrightarrow{\text{fast}} 2Mo(VI) + \mu\text{-}O_2^{(2-)}, \quad (6)$$

$$\mu\text{-}O_2^{(2-)} \xrightarrow[H^+]{\text{fast}} 2Co(II) + O_2 + 10NH_4^+. \quad (7)$$

From this, we obtain

$$-\frac{d[\mu\text{-}O_2^{(-)}]}{dt} = \frac{2k_eK_{IP}[Mo_2O_4(edta)^{2-}][\mu\text{-}O_2^{(-)}]}{1+K_{IP}[Mo_2O_4(edta)^{2-}]}, \quad (8)$$

which is in line with the experimental results. k_{obsd} can be expressed by

$$k_{obsd} = \frac{2k_eK_{IP}[Mo_2O_4(edta)^{2-}]}{1+K_{IP}[Mo_2O_4(edta)^{2-}]}, \quad (9)$$

which can be rearranged to

$$\frac{1}{k_{obsd}} = \frac{1}{2k_eK_{IP}[Mo_2O_4(edta)^{2-}]} + \frac{1}{2k_e}. \quad (10)$$

For I=2.0, where the ion-pair formation is less favorable due to the presence of higher concentration of the electrolyte, $NaClO_4$, the assumption $1 \gg K_{IP}[Mo_2O_4(edta)^{2-}]$ would be useful for interpretation of the experimental results. The values of k_e, K_{IP}, and k_eK_{IP} are calculated from the data for various ionic strengths (Table 1). The k_e values are almost constant regardless of ionic strength, suggesting that the rate of electron transfer process within the ion-pair is not affected by ionic strength. The results provide an excellent example of electron transfer within an ion-pair.

Table 1. Rate constants and ion-pair formation constants for the oxidation of $[Mo_2O_4(edta)]^{2-}$ with $[(NH_3)_5CoO_2^{(-)}Co(NH_3)_5]^{5+}$ in 0.1 M perchloric acid[a]
(Ionic strengths were adjusted with $NaClO_4$)

Ionic strength (I)	Temperature (°C)	k_e (10^{-3} s^{-1})	K_{IP} (mol dm^{-3})	k_eK_{IP} (10^{-1} s^{-1} mol dm^{-3})
0.1	35.4	0.64±0.01	320±10	2.02±0.05
0.1	40.0	1.34±0.08	270±40	3.62±0.05
0.1	45.0	2.5 ±0.2	350±70	8.9 ±1.3
0.3	40.0	1.5 ±0.1	120±20	1.8 ±0.1
0.5	40.0	1.5 ±0.2	70±20	1.07±0.05
2.0	40.0			0.40±0.02
2.0	45.0			0.78±0.04
2.0	51.2			1.8 ±0.2

a) Errors were determined by the least-square treatment with no weighing (confidence level, 0.7).

The activation parameters were compared with those of oxidation of $[Mo_2O_4(edta)]^{2-}$ with other oxidants (Table 2). The parameters vary remarkably with the charge of the oxidant. This suggests the important role of electrostatic interactions on the reaction mechanism.

Table 2. Comparison of the activation parameters for the oxidation of $[Mo_2O_4(edta)]^{2-}$ with various oxidants

Oxidant	Term	I (M)	$\Delta H^{\ddagger}$ (kcal mol^{-1})	$\Delta S^{\ddagger}$ (cal K^{-1} mol^{-1})
$[(NH_3)_5CoO_2^{(-)}Co(NH_3)_5]^{5+}$	k_e	0.1	28 ±4	18 ±11
$[(NH_3)_5CoO_2^{(-)}Co(NH_3)_5]^{5+}$	k_eK_{IP}	2.0	26.5±0.8	21 ± 3
$[Fe(phen)_3]^{3+}$ [a]	k_eK_{IP} [b]	1.0	16.6±0.4	12.3±1.3
$[IrCl_6]^{2-}$ [a]	k_e [b]	1.0	13.3±0.3	−10.0±1.0

a) From Ref. 8. b) The term was assumed from the charge of the reactants.

Kinetics of the Oxidation of $[Mo_2O_4(aq)]^{2+}$ with $[(NH_3)_5CoO_2^{(-)}Co(NH_3)_5]^{5+}$. The following mechanism is proposed to explain the experimental results: It involves the conversion of $[Mo_2O_4(aq)]^{2+}$ into an intermediate A which is then oxidized by the μ-hyperoxo ion;

$$[Mo_2O_4(aq)]^{2+} \overset{k_1}{\underset{k_{-1}}{\rightleftharpoons}} A, \quad (11)$$

$$A + \mu\text{-}O_2^{(-)} \xrightarrow{k_2} \text{“}Mo^{V}Mo^{VI}\text{”} + \mu\text{-}O_2^{(2-)}. \quad (12)$$

Reaction 12 is followed by similar steps to those of Reactions 6 and 7. By applying stationary state approximation to A, we obtain

$$-\frac{d[\mu\text{-}O_2^{(-)}]}{dt} = \frac{2k_1k_2[\mu\text{-}O_2^{(-)}][Mo_2O_4(aq)^{2+}]}{k_{-1}+k_2[\mu\text{-}O_2^{(-)}]}. \quad (13)$$

If $k_{-1} \ll k_2[\mu\text{-}O_2^{(-)}]$, this can be simplified to

$$-\frac{d[\mu\text{-}O_2^{(-)}]}{dt} = 2k_1[Mo_2O_4(aq)^{2+}], \quad (14)$$

which is consistent with the observed zero-order dependence of the rate on $[\mu\text{-}O_2^{(-)}]$ at the initial part of the reaction.

For most of the runs, only k_i (equal to $2k_1$) was estimated from the initial part of the absorbance change. No other rate constants were estimated since the reaction was too slow to be followed until completion. Attempts to work with a large excess of the μ-hyperoxo ion as compared to the molybdenum complex, which may be more useful for checking Eq. 13, were not successful. No appropriate wavelength was found at which absorbance change was sufficiently big.

The reciprocal dependence of k_i on $[H^+]$ can best be explained by assuming a conjugate base of the aqua ion, $[Mo_2O_4(OH)(aq)]^+$. As the $[H^+]$-independent path is negligible, intermediate A should be formed almost exclusively from this conjugate base. k_i is then expressed by

$$k_i = 2k_1 = 2k_{OH}K_a[H^+], \quad (15)$$

where k_{OH} is the rate constant for the formation of A from $[Mo_2O_4(OH)(aq)]^+$. K_a is the acid dissociation constant of $[Mo_2O_4(aq)]^{2+}$. It is assumed to be negligibly small as compared with $[H^+]$. The K_a value was not obtained, and the only relevant datum is the pK_a value (3.02) of the aqua ligand of $[Mo_2O_4(hedta)(H_2O)]^-$ (H_3hedta = *N*-(2-hydroxyethyl)ethylenediamine-*N*,*N*′,*N*′-triacetic acid).[28] At 25 °C, $k_{OH}K_a = (4.3 \pm 0.3) \times 10^{-6}$

mol dm^{-3} s^{-1} and the corresponding activation parameters (25—40 °C) are $\Delta H^{\ddagger}=18.5\pm1.4$ kcal mol^{-1} and $\Delta S^{\ddagger}=-21\pm5$ cal K^{-1} mol^{-1}.

Structure of the Intermediate of the Oxidation of $[Mo_2O_4(aq)]^{2+}$. Intermediate A is considered to have a structure similar to that of the type II species (Fig. 1), a single bridged Mo(V) species.

The conversion of type III complexes into type II is known. The structure of Mo(V) was studied in hydrochloric and sulfuric acid solutions of various acid concentrations.[29] Equilibrium 17 exists in these acid solutions, and shifts in a rightward direction as the concentation of acid becomes higher.

$$\underset{\text{(type III)}}{Mo_2O_4^{2+}} \rightleftharpoons \underset{\text{(type II)}}{Mo_2O_3^{4+}} \rightleftharpoons \underset{\text{(type I)}}{2MoO^{3+}} \qquad (16)$$

Our preliminary observation suggests that the rate of interconversion is very great, the interconversion finishing within several seconds at 25 °C in *ca.* 5 M HCl solution. Type II species is known to be predominant in 5 M HCl, and type III in 5 M $HClO_4$.[14] Thus the formation of type II (and possibly type I) complexes seems to be mainly due to the presence of Cl^- or HSO_4^- and not that of proton.

Also the color change of $[Mo_2O_4(L\text{-cys})_2]^{2-}$ (L-cys= L-cysteinate dianion) from orange to blue in basic solution (pH=*ca.* 10) was claimed to be due to slow formation of a single-bridged species.[30,31] Such a change was not observed in a solution of lower pH (<7). The resulting single-bridged species was far more easily oxidized by flavines[32] and cytochrome c[9] than was the parent complex.

Guymon and Spence studied the oxidation of dimeric Mo(V) with NO_3^-,[12] I_3^-,[13] and O_2[13] in tartrate and phosphate buffer solutions, but did not discuss the detailed structure of the Mo(V) dimer they were dealing with. It is now possible to assume reasonably that the complex had type III structure with some buffer anions coordinated.[1] From the EPR measurement and half-order dependence of the rate on the Mo(V) dimer concentration, they proposed monomeric Mo(V) species as an intermediate of the reaction with NO_3^-. For the reaction with I_3^- and O_2, they observed zero-order dependence of the rate on the dimer concentration, and proposed Mo(IV)[33] as a redox active intermediate, assuming the disproportionation of Mo(V) dimer to Mo(IV) and Mo(VI). Reports have recently been given on the disproportionation of some dimeric Mo(V) complexes,[34,35] but they are of only type II complexes with sulfur-donor ligands. No disproportionation of type III complex is yet known. Both Mo(IV) and monomeric Mo(V) species would be regarded as secondary products of type III complexes through type II species. The results of Guymon and Spence on the reactions with I_3^- and O_2 might be explained also in terms of a single-bridged intermediate.

It should be noted that we cannot deny the existence of Mo(IV) and monomeric Mo(V) as a real reacting species for our reaction, if the postulated single-bridged species formed Mo(IV) or monomeric Mo(V) very rapidly (*viz.*, the rate-determining step is still the formation of the single-bridged species). However, the positive catalytic effect of Mo(VI) would not support the involvement of Mo(IV), since the addition of Mo(VI) would be expected to suppress the disproportionation of Mo(V) dimer.[34]

We thus concluded that A is a single-bridged Mo(V) dimer rather than the Mo(V) monomer or the Mo(IV) species.

Influence of Halide Ions and Mo(VI) on the Oxidation of $[Mo_2O_4(aq)]^{2+}$. The presence of Cl^- and HSO_4^- makes a single-bridged Mo(V) dimer predominant over a double-bridged dimer in aqueous acid solutions. The positive catalytic effect of Cl^- and Br^- on Reaction 2 can be explained by this fact. Since the aqua ligands in $[Mo_2O_4(aq)]^{2+}$ are labile,[17] Cl^- and Br^- would readily substitute for the water and might facilitate bridge cleavage. The halide ions and OH^- in $[Mo_2O_4(OH)(aq)]^+$ may exert a similar electronic effect on the bridge cleavage.

We have no explanation for the catalytic effect of Mo(VI) on the rate of Reaction 2. It is possible that a similar interaction to that in molybdenum blue would reduce the stability of Mo_2O_4-moiety, increasing the sensitivity to oxidative attack. The effect depends on the time after mixing Mo(VI) with $[Mo_2O_4(aq)]^{2+}$.

Comparison of the Oxidation Mechanism of the Two Mo(V) Complexes. The most interesting feature of the present results is the difference in the kinetic behavior of the two complexes $[Mo_2O_4(edta)]^{2-}$ and $[Mo_2O_4(aq)]^{2+}$ towards their oxidation by $[(NH_3)_5CoO_2^{(-)}Co(NH_3)_5]^{5+}$. The ion-pair formation was important for the oxidation of $[Mo_2O_4(edta)]^{2-}$ but not favorable for that of positively charged $[Mo_2O_4(aq)]^{2+}$, which gave the zero-order dependence on $[\mu\text{-}O_2^{(-)}]$. In the latter case, formation of a more easily oxidizable intermediate was proposed.

Recently Cayley *et al.*[36] examined the oxidation of $[Mo_2O_4(aq)]^{2+}$ by $[Fe(phen)_3]^{3+}$ or $[IrCl_6]^{2-}$ and found two term rate laws, one term independent of the oxidant concentration and the other linearly dependent on it. Their oxidants ($E_0=1.06$ V and 1.017 V respectively)[37] are marginally better than the μ-hyperoxo ion ($E_0=ca.$ 1.0 V)[38] in terms of redox potentials, and the 5+ charge and inaccessibility of the μ-hyperoxo group are presumably responsible for exclusion of the direct bimolecular route.

Oxidation of $[Mo_2O_4(edta)]^{2-}$ by these three oxidants gave no oxidant independent path. Multidentate edta-ligand would stabilize the Mo_2O_4-moiety through firm coordination, making the cleavage of the oxo bridge more difficult. Also the lack of coordinated water may be an important factor to determine the reaction pattern, since the water ligands of $[Mo_2O_4(aq)]^{2+}$ play important roles for the formation of intermediate. The absence of the effect of Cl^- and the independence of $[H^+]$ for the rate of the reaction of $[Mo_2O_4(edta)]^{2-}$ are explained also by the lack of water ligand.

The author thanks Professor Kazuo Saito for his valuable discussions. He also thanks Dr. A. G. Sykes, The University of Leeds, England, for making his results available prior to publication and also for helpful comments.

References

1) R. A. D. Wentworth, *Coord. Chem. Rev.*, **18**, 1 (1976).
2) K. Saito and Y. Sasaki, *Kagaku (Kyoto)*, **29**, 769 (1974).
3) R. C. Bray and J. C. Swann, *Structure and Bonding*, **11**, 107 (1972).
4) J. T. Spence, *Coord. Chem. Rev.*, **4**, 475 (1969), and references cited therein.
5) J. T. Spence and P. Kroneck, "Proceeding of the First International Conference on the Chemistry and Uses of Molybdenum," ed by P. C. H. Mitchell (1973), p. 243, and references cited therein.
6) C. D. Garner, M. R. Hyde, F. E. Mabbs, and V. I. Routledge, *J. Chem. Soc., Dalton Trans.*, **1975**, 1180.
7) M. R. Hyde and C. D. Garner, *J. Chem. Soc., Dalton Trans.*, **1975**, 1186.
8) R. K. Wharton, J. F. Ojo, and A. G. Sykes, *J. Chem. Soc., Dalton Trans.*, **1975**, 1526.
9) G. D. Lawrence and J. T. Spence, *Biochemistry*, **14**, 3626 (1975).
10) R. D. Taylor and J. T. Spence, *Inorg. Chem.*, **14**, 2815 (1975).
11) C. D. Garner, M. R. Hyde, and F. E. Mabbs, *Inorg. Chem.*, **15**, 2327 (1976).
12) E. P. Guymon and J. T. Spence, *J. Phys. Chem.*, **70**, 1964 (1966).
13) E. P. Guymon and J. T. Spence, *J. Phys. Chem.*, **71**, 1616 (1967).
14) Y. Sasaki and A. G. Sykes, *J. Chem. Soc., Dalton Trans.*, **1974**, 1468.
15) The aqua ion of molybdenum(V) was originally formulated as $[Mo_2O_4(H_2O)_6]^{2+}$.[16] However, as no conclusive evidence was presented for the number of water molecules coordinated, we use the formula $[Mo_2O_4(aq)]^{2+}$ for this species.
16) M. Ardon and A. Pernick, *Inorg. Chem.*, **12**, 2484 (1973).
17) Y. Sasaki, R. S. Taylor, and A. G. Sykes, *J. Chem. Soc., Dalton Trans.*, **1975**, 356.
18) A. G. Sykes, *Chem. Britain*, **10**, 170 (1974), and references cited therein.
19) T. D. Hand, M. R. Hyde, and A. G. Sykes, *Inorg. Chem.*, **14**, 1720 (1975).
20) H. Sabat, M. F. Rudolf, and B. Jezowska-Trzebiatowska, *Inorg. Chim. Acta*, **7**, 365 (1973).
21) Hexavalent molybdenum is in monomer-dimer equilibrium in the $[H^+]$-range 0.2—3.0 M.[22] In this paper, 'Mo(VI)' represents the hexavalent molybdenum in the equilibrium state.
22) J. F. Ojo, R. S. Taylor, and A. G. Sykes, *J. Chem. Soc., Dalton Trans.*, **1975**, 500.
23) R. Davies, M. Mori, A. G. Sykes, and J. A. Weil, *Inorg. Synth.*, **12**, 197 (1970).
24) M. Linhard and M. Weigel, *Z. Anorg. Allg. Chem.*, **308**, 254 (1961).
25) Y. Sasaki, J. Fujita, and K. Saito, *Bull. Chem. Soc. Jpn.*, **42**, 146 (1969).
26) A. G. Sykes, *Trans. Faraday Soc.*, **59**, 1325 (1963).
27) M. Naarova, J. Podlahova, and J. Podlaha, *Collect. Czech. Chem. Commun.*, **33**, 1991 (1968).
28) Y. Sasaki and T. S. Morita, *Bull. Chem. Soc. Jpn.*, **50**, 1637 (1977).
29) M. F. Rudolf and A. Wolniak, *Z. Anorg. Allg. Chem.*, **408**, 214 (1974), and references cited therein.
30) P. Kroneck and J. T. Spence, *J. Inorg. Nucl. Chem.*, **35**, 3391 (1973).
31) R. F. Stephenson and F. A. Shultz, *Inorg. Chem.*, **12**, 1762 (1973).
32) P. Kroneck and J. T. Spence, *Biochemistry*, **12**, 5020 (1973).
33) Mo(IV) has most likely a monomeric structure. J. F. Ojo, Y. Sasaki, R. S. Taylor, and A. G. Sykes, *Inorg. Chem.*, **15**, 1006 (1976).
34) G. J.-J. Chen, J. W. McDonald, and W. E. Newton, *Inorg. Nucl. Chem. Lett.*, **12**, 697 (1976), and references cited therein.
35) L. J. De Hayes, H. C. Faulkner, W. H. Doub, Jr., and D. T. Sawyer, *Inorg. Chem.*, **14**, 2110 (1975).
36) G. R. Cayley, R. S. Taylor, R. K. Wharton, and A. G. Sykes, Private Communication from A. G. Sykes.
37) W. M. Latimer, "Oxidation States of the Elements and Their Potentials in Aqueous Solutions," 2nd ed, Prentice-Hall, Engelwood Cliffs, N. J. (1952).
38) A. G. Sykes and J. A. Weil, *Prog. Inorg. Chem.*, **13**, 47 (1970).

Potentiometric and Polarographic Studies on Complex Formation of Cadmium(II) Ion with Ethylenediaminemonoacetic Acid

Noboru OYAMA, Masashi HORIE, Hiroaki MATSUDA, and Hitoshi OHTAKI

Department of Electronic Chemistry, Tokyo Institute of Technology, O-okayama, Meguro-ku, Tokyo 152

(Received January 13, 1977)

The complex formation equilibria between Cd(II) ion and ethylenediaminemonoacetic acid (EDMA) were examined by potentiometry in a 1.0 mol dm^{-3} $NaClO_4$ solution at (25.00±0.02) °C, and it was found that neither protonated nor hydrolyzed complex was formed in the range of pH from 2 to 10. The formation constants of Cd(II)–EDMA complexes as well as the protonation constants of EDMA anion determined were as follows: log-β_{101}=6.86, log β_{102}=12.32; log β_{011}=9.97, log β_{021}=16.71, log β_{031}=18.76, where $\beta_{pqr}=[M_pH_qL_r]/[M]^p[H]^q[L]^r$. The formation constants were also examined polarographically.

In the previous works[1,2] we examined the complex formation equilibria of Cd(II) ion with *N*-(2-hydroxyethyl)ethylenediamine-*N,N',N'*-triacetate (L=hedta^{3-}) and ethylendiamine-*N,N,N',N'*-tetraacetate (L=edta^{4-}) by potentiometric titrations over a wide range of pH, and found that a number of protonated complexes of the type MH_qL (q=1, 2 for the HEDTA complex and q=1, 2, 3 for the EDTA complex) are formed in the acidic region (pH<*ca.* 3.5). Furthermore, from comparison of the successive protonation constants of the complexes with those of the corresponding ligands, we derived the conclusion that the protons of the protonated complexes are located at the acetate groups of the ligands. It can be deduced therefrom that the chelate formation between Cd(II) ion and the ligands occurs through the two nitrogen atoms and at least one acetate group of the ligands and thus when all the acetate groups of the ligands are protonated, such ligands do not form any complex with Cd(II) ion. Then, a question may arise: if the ethylenediamine skeleton has only one acetate group, does such a ligand form a protonated complex with Cd(II) ion ? The present work thus aims at examining the possibility of the formation of protonated complexes between Cd(II) and ethylenediaminemonoacetate (L=edma$^-$) ions. Although the complex formation of Cd(II) ion with edma$^-$ anion was already studied by Fujii *et al.*[3] by polarography, their measurements were done only in a neutral solution (pH 6.0—7.0) of ionic strength of 0.2 mol dm^{-3}. Thus, in the present work we shall reexamine the equilibria between Cd(II) and edma$^-$ ions by potentiometric titrations over a wide range of pH, especially noting the acidic region, in which protonated complexes might be formed. Furthermore, for comparison, we shall describe the results of polarographic measurements performed under the same experimental conditions as for the potentiometric titrations.

Symbols

h	Concentration of hydrogen ion at equilibrium
m	Concentration of metal ion at equilibrium
H	Analytical excess of hydrogen ion in a test solution
c_{Cd}	Total concentration of Cd(II)
L	Ethylenediaminemonoacetate anion (edma$^-$)
c_L	Total concentration of L
l	Concentration of free L
X	Degree of neutralization of HL: $(-H+h-K_w/h)/c_L$
K_w	Autoprotolysis constant of water in 1 mol dm^{-3} $NaClO_4$ solution ($10^{-13.95}$ mol^2 dm^{-6}).[4]
$\bar{n}$	Average number of protons bound to one L
$\bar{Z}$	Average number of edma anions bound to one Cd(II)
p	Number of cadmium ions bound to complex species
q	Number of protons bound to complex species
r	Number of edma anions bound to complex species
s	Number of chloride anions bound to complex species
β_{pqrs}	Equilibrium constant for the reaction $pCd + qH + rL + sCl = Cd_pH_qL_rCl_s$
[ ]	Concentration
[ ]$_t$	Total concentration
D_{Cd}	Diffusion coefficient of aqua cadmium(II) ion
D_c	Average diffusion coefficient of Cd(II)–EDMA complexes
$(E^r_{1/2})_{Cd}$	Reversible half-wave potential of aqua Cd(II) ion
$(E_{1/2})_{rev}$	Reversible half-wave potential of the Cd(II)–EDMA system

All ionic charges are omitted for the sake of convenience.

Experimental

Reagents. *Ethylenediaminemonoacetic acid bis(hydrogen chloride) dihydrate* (Hedma·2HCl·2H_2O) was prepared and purified by the method described by Fujii *et al.*[5] Though we first attempted to obtain crystals of diperchlorate of ethylenediaminemonoacetic acid (EDMA), it was not successful because of their large solubility. The replacement of chloride ions of Hedma·2HCl with perchlorate ions was not attempted, because the stock solution of the ligand may not be accurately standardized with any standard metal solution and the replacement procedure may introduce impurities. Thus, the EDMA solutions used in the present work necessarily contained chloride ions exactly twice as much as edma$^-$ anions. The result of the elemental analysis of the EDMA crystals obtained was as follows: Calcd for $C_4H_{10}N_2O_2$·2HCl·2H_2O: C, 21.26; H, 7.10; N, 12.34%. Found: C, 21.65; H, 7.12; N, 12.29%.

All other chemicals were prepared and purified by the methods described previously.[1,2]

Potentiometric Measurements. The apparatus and the experimental procedures used for potentiometric titrations have been described in the previous paper.[1] The measurements were carried out in a paraffin oil thermostat at (25.00±0.02) °C

by using glass and cadmium-amalgam electrodes. Sodium perchlorate was used as an indifferent salt to keep the perchlorate concentration at 1.0 mol dm^{-3} in all runs.

Polarographic Measurements. The polarographic appratus and the experimental procedures have been described previously.[6]

Results and Discussion

Evaluation of Protonation Constants of EDMA. Overall protonation constants of the edma base, β_{0n1}, were determined from the formation function, $\bar{n}$ and $\bar{n}_{\mathrm{calcd}}$, by using the generalized least squares method;[1]

$$\bar{n}_{\mathrm{calcd}} = (\sum_{n=1}^{3} n\beta_{0n1}h^n)/(1+\sum_{n=1}^{3}\beta_{0n1}h^n), \quad (1)$$

$$\bar{n} = \frac{c_{\mathrm{L}}+H-h+(K_{\mathrm{w}}/h)}{c_{\mathrm{L}}}. \quad (2)$$

The protonation constants obtained were $\log \beta_{011}=9.97$, $\log \beta_{021}=16.71$, and $\log \beta_{031}=18.76$. Fujii *et al.*[7] reported the values of $\log \beta_{011}=10.15$, $\log \beta_{021}=16.80$, and $\log \beta_{031}=18.95$ at an ionic strength 0.2 at 25.0 °C.

Determination of the Composition and the Formation Constants of Complexes by Potentiometric Titrations. Titration curves of the Cd(II)–EDMA solution were shown in Fig. 1. The experiments were carried out under the conditions that the ratios of $c_{\mathrm{Cd}}/c_{\mathrm{L}}$ were 1/1, 1/2, and 1/5, where c_{Cd} and c_{L} were changed from 1 mmol dm^{-3} to 5 mmol dm^{-3} and from 5 mmol dm^{-3} to 25 mmol dm^{-3}, respectively. For each run, c_{Cd} and c_{L} were kept practically constant. As can be seen in Fig. 1, the values of X were independent of c_{Cd} and c_{L} over the pH range 2—5. This result showed that no proton was released from the ligand by the complex formation.

Since a stock solution of the ligand EDMA contains chloride ions, the equilibria of the Cd(II)–EDMA system may be described by the general formula including chloride ions;

$$p\mathrm{Cd}^{2+} + q\mathrm{H}^{+} + r\mathrm{L}^{-} + s\mathrm{Cl}^{-} = \mathrm{Cd}_p\mathrm{H}_q\mathrm{L}_r\mathrm{Cl}_s^{(2p+q-r-s)}, \quad (3)$$

with the equilibrium constant, β_{pqrs}. From the material balance for Cd(II) ion, we obtain

$$c_{\mathrm{Cd}} = [\mathrm{Cd}] + \sum_p\sum_q\sum_r\sum_s p[\mathrm{Cd}_p\mathrm{H}_q\mathrm{L}_r\mathrm{Cl}_s]$$
$$= m + \sum_p\sum_q\sum_r\sum_s p\beta_{pqrs}m^p h^q l^r[\mathrm{Cl}]^s. \quad (4)$$

Rearrangement of Eq. 4 leads to

$$\xi = \log\{(c_{\mathrm{Cd}}-m)/m\}$$
$$= \log\{\sum_p\sum_q\sum_r\sum_s p\beta_{pqrs}m^{p-1}h^q l^r[\mathrm{Cl}]^s\}. \quad (5)$$

As a first approach for analyzing data, we assume that only one complex is formed; then Eq. 5 is reduced to

$$\xi = \log p\beta_{pqrs} + (p-1)\log m + q\log h + r\log l + s\log[\mathrm{Cl}]. \quad (6)$$

The plots of ξ *vs.* $-\log h$ are shown in Fig. 2. From this figure, we can see the following facts in the pH range 2—5. (1) Although ξ seemed to depend on c_{L}, it was independent of $-\log h$, and therefore, ξ can not be a

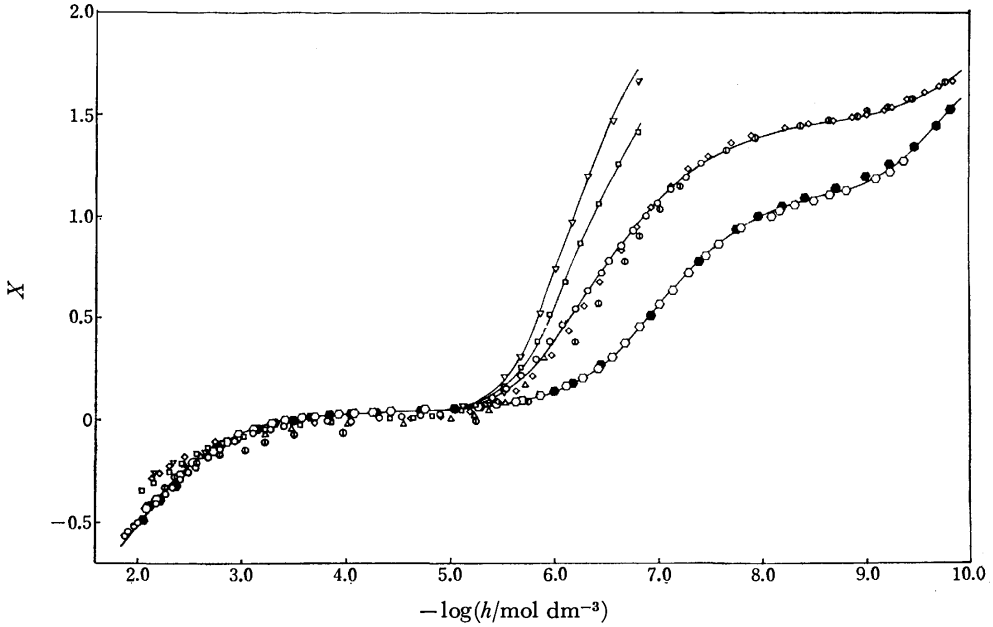

Fig. 1. Degree of neutralization, X, of ethylenediaminemonoacetic acid (EDMA) solutions for the Cd(II)–EDMA systems.
(○): $c_{\mathrm{Cd}}=0.0$ mol dm^{-3}, $c_{\mathrm{L}}=0.005013$ mol dm^{-3};
(●): $c_{\mathrm{Cd}}=0.0$ mol dm^{-3}, $c_{\mathrm{L}}=0.01003$ mol dm^{-3};
(◑): $c_{\mathrm{Cd}}=0.001016$ mol dm^{-3}, $c_{\mathrm{L}}=0.005018$ mol dm^{-3};
(△): $c_{\mathrm{Cd}}=0.002611$ mol dm^{-3}, $c_{\mathrm{L}}=0.005057$ mol dm^{-3};
(◇): $c_{\mathrm{Cd}}=0.002650$ mol dm^{-3}, $c_{\mathrm{L}}=0.01263$ mol dm^{-3};
(▽): $c_{\mathrm{Cd}}=0.005074$ mol dm^{-3}, $c_{\mathrm{L}}=0.005183$ mol dm^{-3};
(□): $c_{\mathrm{Cd}}=0.005045$ mol dm^{-3}, $c_{\mathrm{L}}=0.01007$ mol dm^{-3};
(○): $c_{\mathrm{Cd}}=0.005055$ mol dm^{-3}, $c_{\mathrm{L}}=0.02514$ mol dm^{-3}.
Solid lines are the values of X calculated by the use of the formation constants in Table 1.

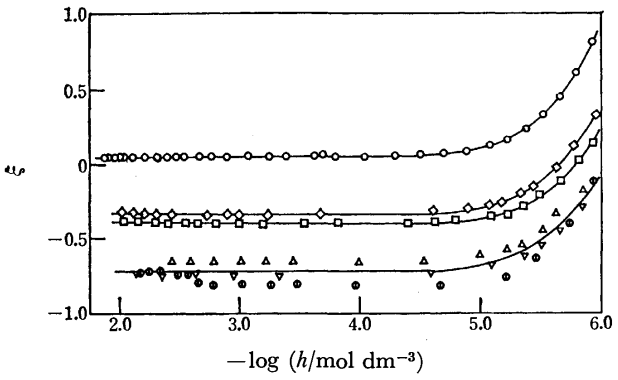

Fig. 2. Relationships between $\bar{\xi}$ and $-\log h$. Symbols are the same as those in Fig. 1. Solid lines are the values calculated by the use of the formation constants in Table 1 and of the formation constant of the $CdCl^+$ complex, $10^{1.35}$.

function of l, which may be approximately calculated by the following equation:

$$l \simeq c_L / \sum_{n=1}^{3} \beta_{0n10} h^n. \quad (7)$$

(2) The dependence of $\bar{\xi}$ on c_L should be explained in terms of the contribution of chloride ions, instead of EDMA anion, in the complex formation. The concentration of chloride ion was $2c_L$ in the present experiment. (3) $\bar{\xi}$ was independent of c_{Cd} at constant c_L (0.005 mol dm^{-3}) within experimental errors. From these results, we can conclude that no Cd–edma complex but a mononuclear $CdCl_s^{(2-s)+}$ complex formed in the pH range of 2—5.

Since $c_{Cd} < c_{Cl}$ in all cases and the degree of complexation of Cd(II) ion with chloride ion is rather small, we can assume that the concentration of free chloride ion ($[Cl]_f$) is almost equal to that of total chloride ion ($[Cl]_t$). When $\bar{\xi}$ is plotted against log $[Cl]_t$ calculated as $\log(2 \times c_L)$, a linear relation of the unit slope resulted (see Fig. 3). Thus, the complex formation, $Cd^{2+} + Cl^- = CdCl^+$, ($p=1$, $q=0$, $r=0$, and $s=1$), took place, and the formation constant was determined as $\log \beta_{1001} = 1.35$ by application of a successive approximation to Eq. 6.

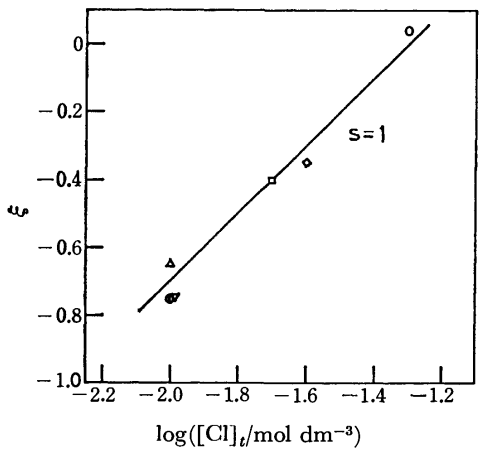

Fig. 3. Plot of $\bar{\xi}$ against log $[Cl]_t$ at $-\log(h/\text{mol dm}^{-3}) = 2.4$. $[Cl]_t$ denotes the total concentration of choride ion.

The constant coincides with the value of 1.35 reported by Vanderzee and Dawson in a 1 mol dm^{-3} $NaClO_4$ solution at 25 °C.[8]

Above pH 5.5, the titration curves of solutions containing Cd(II) ions deviated from that of the solution containing only the ligand, as shown in Fig. 1. In the cases of $c_{Cd}/c_L = 1/1$ and 1/2, white precipitates were separated out in an alkaline region and stable emf's could not be recorded. On the other hand, the titration curves for the case of $c_{Cd}/c_L = 1/5$ converged on a single curve over the pH range 5.5—10.0. Since the titration curves at $c_{Cd}/c_L = 1/5$ were independent of the total concentration of Cd(II) ion (0.001—0.005 mol dm^{-3}), it is seen that no polynuclear complex species was formed. Then, the concentration of free edma is expressed as follows:

$$l = \{c_L + H - h + (K_w/h)\}/(\sum_{n=1}^{3} n\beta_{0n10} h^n), \quad (8)$$

and the formation function $\bar{Z}$ is expressed by

$$\bar{Z} = (c_L - \sum_{n=1}^{3} \beta_{0n10} l h^n)/c_{Cd} \quad (\beta_{0010} = 1), \quad (9)$$

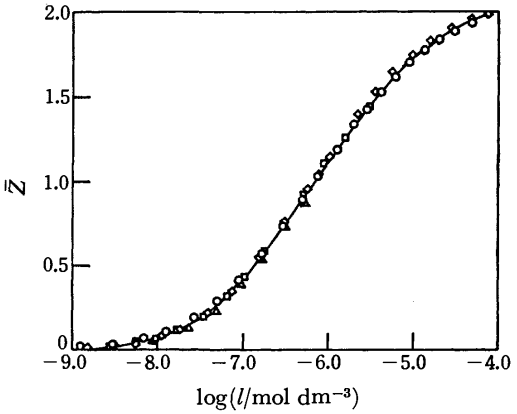

Fig. 4. Relationships between the formation function $\bar{Z}$ and log l. Solid line is the best fit curve calculated by Eq. 11. Symbols are the same as those in Fig. 1.

where c_{Cd} is the total concentration of Cd(II) ion. Figure 4 demonstrates the plots of $\bar{Z}$ *vs.* log l. As can be seen in this figure, a single curve was obtained regardless of the variations of c_{Cd}, c_L, and $[Cl]_t$. Therefore, no mixed complexes of Cd(II) ion with chloride and $edma^-$ ions were formed. Furthermore, the values of $\bar{Z}$ approached 2.0 as the values of log l increased. The formation curve thus obtained could be overlapped with a normalized curve

$$\bar{Z}_{calcd} = (pv + 2v^2)/(1 + pv + v^2), \quad (10)$$

with $p = \beta_{1010}/\sqrt{\beta_{1020}}$, and $\log v = \log l + 1/2 \log \beta_{1020}$,[9] and thus the formation of the CdL^+ and CdL_2^0 complexes was concluded. The formation constants of these complexes were evaluated from the best fit curve with the experimental one. By using the values, $\log \beta_{1010} = 6.9$ and $\log \beta_{1020} = 12.3$, thus determined as the initial values, the formation constants were refined by means of a generalized least squares method in which the minimum error square sum $U = \Sigma(\bar{Z}_{calcd} - \bar{Z})^2$ was

Table 1. Formation constants of Cd(II)-EDMA complexes (log β_{pqrs}) in 1.0 mol dm^{-3} $NaClO_4$ solution at 25.0 °C

$\beta_{pqrs}=[M_pH_qL_rCl_s^{(2p+q-r-s)+}]/[M^{2+}]^p[H^+]^q[L^-]^r[Cl^-]^s$

log $\beta_{0110}=9.97\pm0.02$, log $\beta_{0210}=16.71\pm0.02$, log $\beta_{0310}=18.76\pm0.02$.

	log β_{1010}	log β_{1020}
Potentiometry	6.86±0.02	12.32±0.02
Polarography	7.20±0.05	13.13±0.05
	(8.48)	(13.23)

( ): Ref. 3.

searched, where $\bar{Z}_{calcd}$ is given by

$$\bar{Z}_{calcd} = (\beta_{1010}l+2\beta_{1020}l^2)/(1+\beta_{1010}l+\beta_{1020}l^2). \quad (11)$$

The results were shown in Table 1. The solid curve in Fig. 4 represents the calculated one by using the final values.

Determination of the Formation Constants by Polarography. As described in the section of potentiometric measurements, the CdL^+ and CdL_2 complexes were formed at pH>6.0. In order to examine the polarographic behavior of these complexes, the change of the half-wave potential with l was measured over the pH range 6.0—7.5. No buffer reagent was used, because the test solutions have a sufficient buffer capacity due to the ligand itself which is present in a large excess in comparison with Cd(II) ion. Single waves with the diffusion-controlled limiting current were observed and the conventional log-plots of the current-potential curves yielded straight lines with the reciprocal slopes of (30±1) mV, in accord with the fact that the reversible two-electron reduction occurred. Since the half-wave potential shifted to the negative side with the increase of pH, the formation constants of the complexes can be determined from this shift by the method developed by DeFord and Hume.[10,11]

DeFord and Hume's function F_0 is defined as follows:

$$F_0 = \sum_{r=0}^{N}\beta_{10r0}l^r$$

$$= (D_{Cd}/D_c)^{1/2}\exp\left(\frac{nF}{RT}\right)\{(E_{1/2}^r)_{Cd}-(E_{1/2})_{rev}\}. \quad (12)$$

The factor $(D_{Cd}/D_c)^{1/2}$ was obtained from the ratio of the diffusion current of Cd(II) ion to that of the complexes. The measured value of −0.575 V *vs.* SCE was used for $(E_{1/2}^r)_{Cd}$. A new function $F_1=(F_0-1)/l$ is defined and extrapolation of the F_1 curve toward $l=0$ gives an intercept corresponding to β_{1010}. The procedure was repeated until a horizontal line was obtained. The sets of the plots analyzed to obtain β_{10r0} are shown in Fig. 5. The formation constants β_{1010} and β_{1020} thus found are given in Table 1. In these procedures, the complex formation of Cd(II) ion or Cd–edma complex with chloride ion was neglected.

As can be seen from Table 1, the values of the formation constants of 1 : 1 and 1 : 2 Cd(II)–edma complexes obtained by polarography were larger than the values

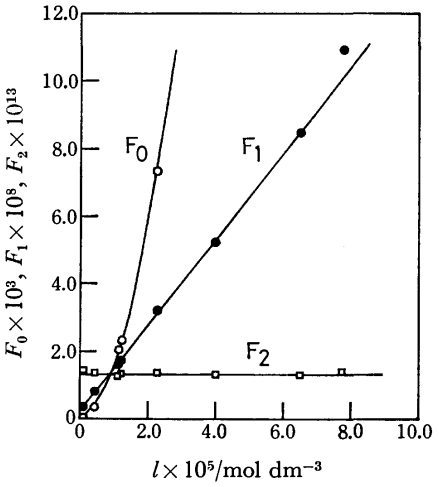

Fig. 5. Dependence of F_p (p=0, 1, 2) on l at total EDMA concn=0.0100 mol dm^{-3}.

obtained by potentiometry. Such discrepancies have sometimes been observed for the complex formation of Cd(II) ion with other multidentate ligands. The value of log β_2 of the Cd(II)–diethylenetriamine complex obtained by potentiometry[12,13] is 13.9, whereas the value determined by polarography[14] is 14.8. Log β_1 of the Cd(II)–triethylenetetramine complex is estimated to be 10.8 by potentiometry,[15] whereas the value for this complex obtained by polarography[14] is 13.9. Thus the values obtained by polarography are often larger than those obtained by potentiometry. The difference in these values may be attributed to the difference in the methods employed, but the reason is not clear yet.

The ethylenediaminemonoacetate ligand formed no protonated complex with Cd(II) ion. In combination with the results obtained in the previous works for the Cd(II)–edta[2] and –hedta[1] complexes, we concluded that the two nitrogen atoms and at least one acetate group are indispensable for the chelate formation of a diaminepolyacetate ligand with Cd(II) ion.

The authors thank Dr. Yuki Fujii, Department of Chemistry, Ibaraki Univ., for his suggestion for preparing and purifying ethylenediaminemonoacetic acid.

References

1) N. Oyama, T. Shirato, H. Matsuda, and H. Ohtaki, *Bull. Chem. Soc. Jpn.*, **49**, 3047 (1976).
2) N. Oyama, H. Matsuda, and H. Ohtaki, *Bull. Chem. Soc. Jpn.*, **50**, 406 (1977).
3) Y. Fujii, T. Ueda, and M. Kodama, *Bull. Chem. Soc. Jpn.*, **43**, 409 (1970).
4) G. Anderegg, *Helv. Chim. Acta*, **50**, 2333 (1967).
5) Y. Fujii, E. Kyuno, and R. Tsuchiya, *Bull. Chem. Soc. Jpn.*, **43**, 786 (1970).
6) N. Oyama and H. Matsuda, *J. Electroanal. Chem. Interfacial Electrochem.*, **78**, 89 (1977).
7) Y. Fujii and M. Kodama, *Bull. Chem. Soc. Jpn.*, **42**, 3172 (1969).
8) C. E. Vanderzee and H. J. Dawson, Jr., *J. Am. Chem. Soc.*, **75**, 5659 (1953).

9) L. G. Sillén, *Acta Chem. Scand.*, **10**, 186 (1956).
10) D. D. DeFord and D. N. Hume, *J. Chem. Soc.*, **73**, 5321 (1951).
11) D. N. Hume, D. D. DeFord, and G. C. Cava, *J. Am. Chem. Soc.*, **73**, 5323 (1951).
12) J. E. Prue and G. Schwarzenbach, *Helv. Chim. Acta.*, **33**, 985 (1950).
13) J. P. Scharf and M. R. Paris, *C. R. Acad. Sci., Ser. C*, **265**, 488 (1967).
14) B. E. Douglas, H. A. Laitinen, and J. C. Bailar, *J. Am. Chem. Soc.*, **72**, 2484 (1950).
15) C. N. Reilley and R. W. Schmid, *J. Elisha Mitchell Sci. Soc.*, **73**, 279 (1957); *Chem. Abstr.* 7001i (1958).

Semiintegral Electroanalysis in the Absence of Supporting Electrolyte

Masashi GOTO,* Morten GRENNESS,** and Keith B. OLDHAM
Department of Chemistry, Trent University, Peterborough, Ontario, Canada
(Received January 24, 1977)

The limiting semiintegral of the current which flows when a stationary electrode is progressively polarized in the presence of electroactive species has been investigated under the condition of no supporting electrolyte present in the solution. The semiintegral, $m(t)$, of the current, $i(t)$, is defined by

$$m(t) = \frac{d^{-1/2}}{dt^{-1/2}} i(t) = \frac{1}{\pi^{1/2}} \int_0^t \frac{i(\lambda)}{(t-\lambda)^{1/2}} d\lambda.$$

The electroreduction of a number of heavy metal ions has been studied at a mercury drop electrode and it was found that the limiting semiintegral is larger than that observed with excess supporting electrolyte present. The finding is in agreement with a simple theory which considers both diffusion and migration mass transfer processes. The factor by which the limiting semiintegral increases has been shown to depend on the diffusion coefficients and charge numbers of the cation and anion.

Basic theory of the new electroanalytical method "semiintegral electroanalysis" has been presented and experimentally verified in previous papers.[1,2] It has been also demonstrated[1,3] that semiintegral electroanalysis has the merit of being completely independent of the signal under typical electroanalytical conditions. The independence of the limiting semiintegral of current, $m(\tau)$, from the form of the applied potential signal permits a large resistance to be present in the solution without impairment of the analysis, so that semiintegral electroanalysis can tolerate very low or even zero supporting electrolyte concentrations. Existing theory,[1] however, is based on the assumption that the mass transport is by diffusion only, whereas migration must also be admitted if the supporting electrolyte concentration is not in excess. In this article we show both theoretically and experimentally that the proportionality between $m(\tau)$ and the electroactive concentration is maintained even in the total absence of supporting electrolyte. The constant of proportionality is, however, different from the excess supporting electrolyte case. The implication of these findings for semiintegral electroanalysis in such fresh waters as lakes and rivers is clear.

Theory

The exact treatment of any electroanalytical experiment under conditions in which both migration and diffusion are important is inordinately difficult. Nevertheless, there have been numerous attempts to overcome this difficulty,[4-10] especially in the context of chronopotentiometry. Some of these treatments have been very sophisticated and, in comparison, our present treatment is naive.

Consider a plane indicator electrode immersed in an unstirred solution containing only two ions: those of species O (cation) and P (anion), without any supporting electrolyte. Only the species O is reduced by the z_O electron reaction,

$$O(soln) + z_O e^- \longrightarrow R(solid\ or\ amalgam) \quad (1)$$

to the initially-absent species R, which is uncharged. The solution is assumed to extend to infinity in the direction perpendicular to the electrode. According to the established theories,[11-13] the rate of change in concentration of O at a distance x from the electrode surface at a time t is presented by

$$\frac{\partial C_O(x,t)}{\partial t} = -\frac{\partial J_O(x,t)}{\partial x} = \frac{D_O D_P[z_O - z_P]}{[z_O D_O - z_P D_P]} \frac{\partial^2 C_O(x,t)}{\partial x^2}, \quad (2)$$

where C is the concentration, J is the flux, D is the diffusion coefficient, z is the charge number, and the subscripts represent the species concerned. The flux of O is given by the following equation:

$$J_O(x,t) = -\frac{1}{[z_O D_O - z_P D_P]} \times \left\{ D_O D_P [z_O - z_P] \frac{\partial C_O(x,t)}{\partial x} + \frac{D_O i(t)}{AF} \right\}, \quad (3)$$

where $i(t)$ is the faradaic current at a time t, A is the electrode area, and F is the Faraday constant.

Equation 2 is identical with Fick's second law except that the diffusion coefficient is replaced by the composite constant $D_O D_P (z_O - z_P) / (z_O D_O - z_P D_P)$. Accordingly, when combined with the initial condition,

$$C_O(x, 0) = C_O = \text{constant}, \quad (4)$$

corresponding to a uniform O concentration before electrolysis, and the boundary condition,

$$C_O(\infty, t) = C_O, \quad (5)$$

appropriate to semiinfinite conditions, the equation

$$\frac{\partial^{1/2}}{\partial t^{1/2}} [C_O(x,t) - C_O] = -\sqrt{\frac{D_O D_P (z_O - z_P)}{z_O D_O - z_P D_P}} \frac{\partial C_O(x,t)}{\partial x} \quad (6)$$

may be derived in a strictly analogous way to that used[14] in establishing the theory of semiintegral electroanalysis with excess supporting electrolyte. $\partial^{1/2}/\partial t^{1/2}$ is the partial semidifferentiation operator with respect to t and the semidifferentiation operator, $d^{1/2}/dt^{1/2}$, is defined by

$$\frac{d^{1/2}}{dt^{1/2}} f(t) = \frac{d}{dt} \left[\frac{1}{\pi^{1/2}} \int_0^t \frac{f(\lambda)}{(t-\lambda)^{1/2}} d\lambda \right].$$

Since only the species O reacts at the electrode, the

* Present address: Department of Applied Chemistry, Faculty of Engineering, Nagoya University, Chikusa-ku, Nagoya 464.
** Present address: Chloride Technical Limited, Swinton, Manchester, England.

fluxes of each species at the electrode surface are given by

$$J_O(0,t) = \frac{-i(t)}{z_O AF}, \quad (7)$$

and

$$J_P(0,t) = 0. \quad (8)$$

The combination of Eqs. 3, 6, and 7 produces

$$\frac{\partial^{1/2}}{\partial t^{1/2}}[C_O(0,t) - C_O] = \frac{z_P\sqrt{D_P}\,i(t)}{z_O AF\sqrt{D_O}\sqrt{z_O - z_P}\sqrt{z_O D_O - z_P D_P}}. \quad (9)$$

Semiintegrating Eq. 9 and rearranging terms, we obtain

$$m(t) = z_O AF\sqrt{D_O}[C_O(0,t) - C_O]\frac{\sqrt{z_O - z_P}\sqrt{z_O D_O - z_P D_P}}{z_P\sqrt{D_P}}. \quad (10)$$

The limiting semiintegral of current at the time τ, when the concentration of O at the electrode surface is equal to zero, is

$$m(\tau) = z_O AF\sqrt{D_O}C_O\left[\frac{\sqrt{z_O - z_P}\sqrt{z_O D_O - z_P D_P}}{-z_P\sqrt{D_P}}\right] \quad (11)$$

$$= m(\tau)_{xse}\sqrt{\frac{D_O}{D_{OC}}}\sqrt{1 - \frac{z_O}{z_P}}\sqrt{1 - \frac{z_O D_O}{z_P D_P}}, \quad (12)$$

where $m(\tau)_{xse}$ and D_{OC} are the semiintegral of current at the time τ and the diffusion coefficient of O respectively in the solution containing excess supporting electrolyte. Equation 11 is the basic relationship between the limiting semiintegral and concentration for this method in the absence of supporting electrolyte. Equation 11 will be verified by testing experimentally Eq. 12 in the remainder of this paper.

Experimental

The salts $Cd(NO_3)_2$, $CdCl_2$, $CdSO_4$, $Ni(NO_3)_2$, $NiCl_2$ $NiSO_4$, $Cu(NO_3)_2$, $CuSO_4$, $Cu(CH_3COO)_2$, $Zn(NO_3)_2$, $ZnSO_4$, $Pb(NO_3)_2$, $TlNO_3$, and $InCl_3$ were used as solutes. The concentration of solutions for the present study was 1.00 mmol/l or 5.00 mmol/l. In order to measure limiting semiintegral in excess supporting electrolyte, 100 mmol/l or 200 mmol/l KNO_3 was used as a supporting electrolyte. The electrolytic solutions were deoxygenated by bubbling argon gas. The reagents were generally of laboratory grade or in some cases analytical grade. The distilled water for solutions and cleaning of glassware was further deionized by ion exchange resin, the conductivity corresponding to less than 0.02 ppm NaCl.

Three electrodes, cell and instrumentation were substantially the same as previously reported.[1,2] Simple or capped ramp signals were applied to a hanging mercury drop electrode *vs.* a saturated calomel electrode by using a mercury pool as a counter electrode. All the experimental work was carried out at room temperature (≈22°C).

In polarography, difficulties frequently arise from the presence of polarographic maxima. Similar difficulties have been experienced in the present study. The maxima were suppressed, whenever possible, by prepolarizing the hanging mercury drop electrode at the initial (equilibrium) potential for a few minutes. In more severe cases the addition of small quantities of methyl red or a freshly prepared solution of gelatin (0.2%) was required. In general it was found that the maxima were more pronounced in solutions without supporting electrolyte, possibly because the current density is less uniform.

Results and Discussion

As typical examples of investigated species, Figs. 1 and 2 show the neopolarograms of 1.00 mmol/l $Cd(NO_3)_2$ and $TlNO_3$, respectively, in the absence of supporting electrolyte together with those in excess supporting electrolyte. The "neopolarograms" are the graphs *vs.* potential, E, of the semiintegral of current, m. The value m is measurable in the unit[1] of A $s^{1/2}$ or C $s^{-1/2}$. The shape of neopolarograms in the absence of supporting electrolyte is apparently deformed by the potential drop resulting from a large resistance present in solution, however the semiintegral levels off at a plateau. The upward slope of the plateau is more pronounced than in the presence of supporting electrolyte.[15] The limiting semiintegral values were determined by the empirical procedure illustrated by the dashed lines in curve I of Fig. 1.

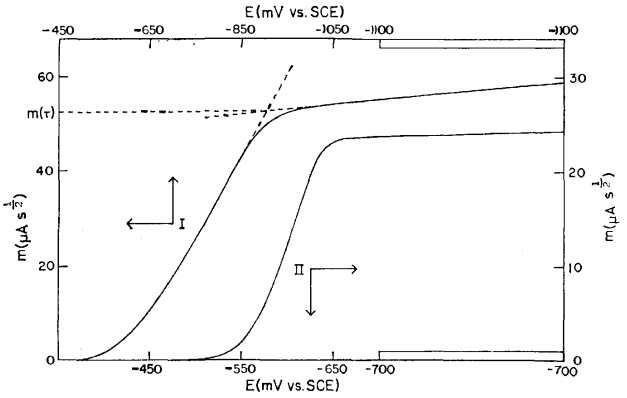

Fig. 1. Neopolarograms of 1.00 mmol/l $Cd(NO_3)_2$ in the absence and presence of supporting electrolyte. Electrode area: 4.69×10^{-2} cm^2, Scan rate: 100 mV/s, supporting electrolyte: I none, II 100 mmol/l KNO_3.

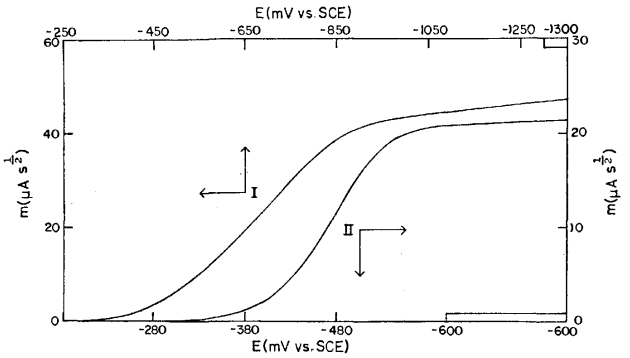

Fig. 2. Neopolarograms of 1.00 mmol/l $TlNO_3$ in the absence and presence of supporting electrolyte. Conditions as in Fig. 1.

In order to verify Eq. 12 the limiting semiintegrals in both the absence of supporting electrolyte and the presence of excess supporting electrolyte were measured for various salts of uni-, bi-, and ter-valent cations, and their ratios are listed in Table 1. The limiting semi-

Table 1. $m(\tau)/m(\tau)_{xse}$ ratios for various salts
Salt concentration: 1.00 mmol/l, electrode area: 4.69×10^{-2} cm^2.

Salt	Concn of KNO_3 (mmol/l)	$m(\tau)$ ($\mu A\ s^{1/2}$)	$m(\tau)/m(\tau)_{xse}$ Exptl	Theor.
$Cd(NO_3)_2$	0	57.2	2.49	2.34
	100	23.0		
$CdCl_2$	0	46.3	2.20	2.31
	100	21.0		
$CdSO_4$	0	39.2	1.74	1.87
	100	22.5		
$Ni(NO_3)_2$	0	57.0	2.33	2.28
	100	24.5		
$NiCl_2$	0	54.5	2.36	2.25
	100	23.1		
$NiSO_4$	0	42.8	1.83	1.82
	100	23.4		
$Cu(NO_3)_2$	0	49.1	2.00	2.33
	100	24.6		
$CuSO_4$	0	35.0	1.50	1.86
	200	23.4		
$Cu(CH_3COO)_2$	0	58.3	2.48	2.69
	200	23.5		
$Zn(NO_3)_2$	0	51.5	2.17	2.43
	200	23.7		
$ZnSO_4$	0	38.7	1.65	1.94
	200	23.5		
$TlNO_3$	0	42.0	2.06	2.12
	100	20.4		
$Pb(NO_3)_2$	0	66.7	2.56	2.68
	100	26.1		
$InCl_3$	0	61.1	1.97	2.80
	100	31.0		

integral in the absence of supporting electrolyte was, in general, about twice larger than that observed in the excess supporting electrolyte, the ratio $m(\tau)/m(\tau)_{xse}$ being the largest for $Pb(NO_3)_2$ and the smallest for $CuSO_4$.

Table 2. Diffusion coefficients at infinite dilution at 25 °C[16]

Cation	$D\times10^6$ (cm^2/s)	Anion	$D\times10^6$ (cm^2/s)
K^+	19.8	Cl^-	20.3
Tl^+	20.0	NO_3^-	19.2
Pb^{2+}	9.8	CH_3COO^-	10.9
Cd^{2+}	7.2	SO_4^{2-}	10.8
Zn^{2+}	7.2		
Cu^{2+}	7.2		
Ni^{2+}	6.9		
In^{3+}	5.6		

Table 2 shows literature values[16] of diffusion coefficients (except the case of In^{3+}) for various ions under the condition of infinite dilution at 25 °C. For the case of In^{3+}, the known limiting equivalent conductances of ions λ°,[17] of ter-valent lanthanide cations were plotted against the crystal ionic radii, r.[18] There is a linear relationship between the two quantities as shown in

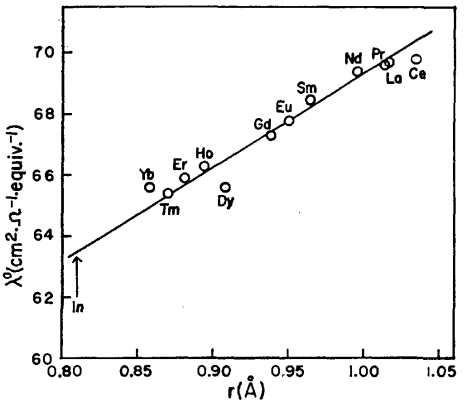

Fig. 3. Relationship between limiting equivalent ionic conductances and crystal ionic radii for ter-valent cations at 25 °C.

Table 3. Diffusion coefficients in excess supporting electrolyte at 25 °C[19]

Ion	Supporting electrolyte		$D\times10^6$ (cm^2/s)
Tl^+	0.1 mol/l	KNO_3	18.2
Pb^{2+}	0.1 mol/l	KNO_3	8.28
Cd^{2+}	0.1 mol/l	KNO_3	6.90
Zn^{2+}	0.1 mol/l	KNO_3	6.38
Cu^{2+}	0.1—0.2 mol/l	KNO_3	6.94[a]
Ni^{2+}	0.1 mol/l	KNO_3	6.86[a]
In^{3+}	0.1 mol/l	KNO_3	5.23[a]

a) Value evaluated by semiintegral electroanalysis.

Fig. 3. The limiting equivalent conductance of 1/3 In^{3+} was estimated to be 63.5 cm^2 Ω^{-1} equiv^{-1} from the line of Fig. 3 and the ionic radius 0.81 Å,[18] whence the diffusion coefficient at infinite dilution of In^{3+} was calculated from the Nernst-Einstein equation. Table 3 shows the diffusion coefficients of metal ions in excess supporting electrolyte from the literature[19] together with the values of Cu^{2+}, Ni^{2+}, and In^{3+} evaluated by semiintegral electroanalysis. The theoretical $m(\tau)/m(\tau)_{xse}$ ratios were calculated from Eq. 12 by using the diffusion coefficients in Tables 2 and 3, and are listed in Table 1. Apart from $InCl_3$, the theoretical ratios generally compare well with the values obtained by experiment, though the theoretical ratios are usually slightly larger than the experimental values. This tendency possibly suggests some existence of hydrolysis reaction such as

$$Cu^{2+} + H_2O \rightleftharpoons CuOH^+ + H^+,$$

$$CuOH^+ + 2e^- \rightleftharpoons Cu(amalgam) + OH^-.$$

In the case of $InCl_3$, the experimental ratio is much smaller than the theoretical value. We believe this result to be due to a hydrolysis reaction of In^{3+}, because 10 mmol/l aqueous solutions of $InCl_3$ began to produce white suspensions in the originally clear solutions a few hours after preparing at a room temperature. The formation rate was accelerated on heating, but the suspension disappeared on adding acid. Another possible cause is the presence of complex ions such as $[InCl]^{2+}$ and $[InCl_2]^+$ formed with chloride ion, but this explanation is unlikely because a similar $m(\tau)/m(\tau)_{xse}$

ratio was observed in the case of $In(NO_3)_3$ solute.

Table 1 shows that Eq. 12 applies whether the reduction product is solid or amalgam, because most metals among investigated species are soluble in a mercury electrode but the metallic nickel does not form an amalgam.

In the classical polarography using a dropping mercury electrode, Lingane and Kolthoff[20] obtain the following relation between the initial limiting current, i_l, without supporting electrolyte present and the diffusion current, i_d, in an excess of indifferent electrolyte

$$\frac{i_l}{i_d} = \sqrt{\frac{D_O D_P [z_O - z_P]}{D_{OC}[z_O D_O - z_P D_P]}} \left[\frac{1}{1-T_O}\right] \qquad (13)$$

for cation reductions, where T_O is the transference number of O. It should be realized by the comparison between Eqs. 12 and 13 that $m(\tau)/m(\tau)_{xse}$ ratio observed in this semiintegral electroanalysis at higher scan rate of potential is identical with i_l/i_d ratio in classical polarography.

TABLE 4. $m(\tau)/m(\tau)_{xse}$ RATIOS AT DIFFERENT SCAN RATES OF POTENTIAL

Conditions: Electroactive species: 1.00 mmol/l $CdCl_2$, electrode area: 4.69×10^{-2} cm².

		$m(\tau)$ (μA s$^{1/2}$) Scan rate (mV/s)				
		50	100	200	500	
Concn of KNO_3 (mmol/l)	100	20.8	21.1	21.0	21.1	
	0	46.6	45.8	46.5	46.2	
$\frac{m(\tau)}{m(\tau)_{xse}}$ Exptl		2.23	2.17	2.22	2.19	2.21(av.)
Theor.		2.31	2.31	2.31	2.31	

TABLE 5. $m(\tau)/m(\tau)_{xse}$ RATIOS AT DIFFERENT CONCENTRATIONS OF ELECTROACTIVE SPECIES

Condition: Electrode area: 4.69×10^{-2} cm².

		$m(\tau)$ (μA s$^{1/2}$)			
Species		$Cd(NO_3)_2$		$TlNO_3$	
Concn of species (mmol/l)		1.00	5.00	1.00	5.00
Concn of KNO_3 (mmol/l)	100	23.0	120	20.4	95.7
	0	57.2	273	42.0	210
$\frac{m(\tau)}{m(\tau)_{xse}}$ Exptl		2.49	2.28	2.06	2.19
Theor.		2.34	2.34	2.12	2.12

The dependencies of $m(\tau)/m(\tau)_{xse}$ ratio on the scan rate for $CdCl_2$ and on concentration for $Cd(NO_3)_2$ and $TlNO_3$ are tested in Tables 4 and 5, respectively. The ratio is independent of scan rate and concentration as the theory predicts.

Thus the applicability of semiintegral electroanalysis in the absence of supporting electrolyte has been demonstrated. It is found that the sensitivity of detection is about twice as great as that with excess supporting electrolyte, but is dependent on the nature of the counter ion.

The financial support of the National Research Council of Canada is gratefully acknowledged.

References

1) M. Grenness and K. B. Oldham, *Anal. Chem.*, **44**, 1121 (1972).
2) M. Goto and K. B. Oldham, *Anal. Chem.*, **45**, 2043 (1973).
3) K. B. Oldham, *Anal. Chem.*, **44**, 196 (1972).
4) P. Delahay, C. C. Mattax, and T. Bertins, *J. Am. Chem. Soc.*, **76**, 5319 (1954).
5) M. D. Morris and J. J. Lingane, *J. Electroanal. Chem.*, **6**, 300 (1963).
6) M. D. Morris, *J. Electroanal. Chem.*, **8**, 1 (1964).
7) P. Bro, *J. Electrochem. Soc.*, **111**, 1104 (1964).
8) J. Broadhead and G. J. Hills, *J. Electroanal. Chem.*, **13**, 354 (1967).
9) J. Newman, *J. Phys. Chem.*, **73**, 1843 (1969).
10) E. Levart and D. Schuhmann, *J. Electroanal. Chem.*, **24**, 41 (1970).
11) I. M. Kolthoff and J. J. Lingane, "Polarography," 2nd ed, Interscience Publishers, New York (1965), p. 53.
12) I. Tachi and M. Senda, *Denki Kagaku*, **21**, 575 (1953).
13) Z. Zembura, A. Fulinski, and M. Bierowski, *Z. Elektrochem.*, **65**, 887 (1961).
14) K. B. Oldham and J. Spanier, *J. Mathem. Anal. Appl.*, **39**, 655 (1972).
15) M. Goto and K. B. Oldham, *Anal. Chem.*, **46**, 1522 (1974).
16) M. Shinagawa, "Polarography," Kyoritsu Shupan, Tokyo (1965), p. 215.
17) R. A. Robinson and R. H. Stokes, "Electrolyte Solutions," 2nd ed, Butterworths, London (1959), p. 463.
18) "Handbook of Chemistry and Physics," 52nd ed, The Chemical Rubber, Cleveland (1971—1972), p. F171.
19) J. Heyrovsky and J. Kuta, "Principles of Polarography," Academic Press, New York (1965), p. 106.
20) I. M. Kolthoff and J. J. Lingane, "Polarography," 2nd ed, Interscience Publishers, New York (1965), p. 122.

Structure and Characterization of Copper(II) and Nickel(II) Complexes with 3-Acetyl-5,6-dimethylpyridazine Hydrazone, the Condensation Product of Biacetyl and Hydrazine

Hisashi OKAWA, Naohide MATSUMOTO, and Sigeo KIDA

Department of Chemistry, Faculty of Science, Kyushu University 33, Hakozaki, Higashi-ku, Fukuoka 812

(Received February 21, 1977)

Copper(II) and nickel(II) complexes, $MLX_2 \cdot nH_2O$ (L=$C_{16}H_{24}N_8$; X=Cl^-, Br^-, NO_3^-, ClO_4^-, BF_4^-; n=0, 2), were obtained by reacting diacetyl with hydrazine in the presence of a metal ion and characterized. The condensation product L was found to be 3-acetyl-5,6-dimethylpyridazine hydrazone. The molecular structure of $NiL(ClO_4)_2 \cdot 2H_2O$ has been determined, the configuration around the nickel(II) ion being a distorted octahedron.

Metal complexes of 1,5,9,13-tetraaza[16]annulene (Fig. 1, a), which is the inner-ring system of porphyrins, are of interest in connection with the study on metalloenzymes such as peroxidases and cytochromes. Busch *et al.*[1-4] obtained tetrabenzo[*b*,*f*,*j*,*n*][1,5,9,13]tetraaza[16]annulene complexes by condensing 2-aminobenzaldehyde in the presence of a metal ion. Step-wise oxidation of metal complexes with tetraazamacrocycles of lower unsaturation seems a promising method for synthesizing tetraazaannulene metal complexes. By this method 5,7,12,14-tetramethyl-1,4,8,11-tetraaza[14]annulene has been prepared.[5] Tang and Holm[6] oxidized 15- and 16-membered tetraazamacrocyclic complexes and synthesized corrin-like macrocyclic complexes. However, 1,5,9,13-tetraaza[16]annulene and its homologues with simple substituents are not known.

In order to prepare 3,4,7,8,11,12,15,16-octamethyl-1,2,5,6,9,10,13,14-octaaza[16]annulene complexes (Fig. 1, b), we treated biacetyl and hydrazine in the presence of copper(II) or nickel(II) ion and obtained metal complexes of the type $MLX_2 \cdot nH_2O$ (M=Cu(II), Ni(II): X=Cl^-, Br^-, NO_3^-, ClO_4^-, BF_4^-; n=0, 2) where L denotes the condensation product with the composition $C_{16}H_{24}N_8$. The composition is the same as that of the desired compound 3,4,7,8,11,12,15,16-octamethyl-1,2,5,6,9,10,13,14-octaaza[16]annulene. However, L can not be the annulene, since the infrared spectrum of each complex clearly indicates the presence of an amino group. The purpose of this study is to characterize the condensation product and the metal complexes.

Experimental

Syntheses. *$CuL(ClO_4)_2$*: A methanol solution (50 ml) of biacetyl (4.3 g) and hydrazinium chloride (3.5 g) was refluxed for 10 min. To this was added copper(II) acetate monohydrate (2.5 g) and the mixture was heated under reflux for 3 h. A yellow precipitate formed was separated from the solution by filtration, and an aqueous solution of sodium perchlorate was added to the filtrate to give yellow-brown prisms. These were recrystallized from water. The yield was 0.7 g.

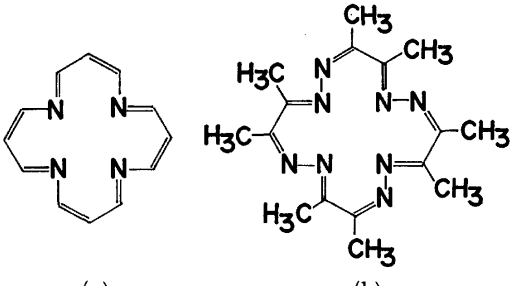

(a) (b)

Fig. 1.

Found: C, 32.43; H, 3.98; N, 19.03; Cu, 10.85%. Calcd for $C_{16}H_{24}N_8O_8Cl_2Cu$: C, 32.52; H, 4.09; N, 18.96; Cu, 10.75%.

$CuLBr_2$: Biacetyl (4.3 g) and hydrazinium bromide (5.7 g) were dissolved in methanol (70 ml) and the mixture was refluxed for 10 min. To this was added copper(II) acetate monohydrate (2.5 g) and the mixture was heated under reflux for 3 h. The reaction mixture was filtered while it was hot and the filtrate wes allowed to stand overnight to give greenish brown prisms. The yield was 0.2 g.

Found: C, 34.70; H, 4.35; N, 20.22; Cu, 11.79%. Calcd for $C_{16}H_{24}N_8Br_2Cu$: C, 34.83; H, 4.38; N, 20.31; Cu, 11.52%.

$NiL(ClO_4)_2 \cdot 2H_2O$: This complex was obtained in the same way as that for $CuL(ClO_4)_2$ from biacetyl (4.3 g), hydrazine hydrochloride (3.5 g) and nickel(II) chloride hexahydrate (3.0 g). A yellow precipitate formed was separated from the reaction mixture. To the filtrate was added an aqueous solution of sodium perchlorate (3.0 g) to give yellow prisms. A small amount of the product was recovered from the solid part of the reaction mixture by extraction with hot water and treatment with an aqueous solution of sodium perchlorate. The product was recrystallized from water to give yellow brown prisms (3.9 g).

Found: C, 30.76; H, 4.71; N, 17.84%. Calcd for $C_{16}H_{28}N_8N_8O_{10}Cl_2Ni$: C, 30.89; H, 4.54; N, 18.01%.

$NiL(BF_4)_2 \cdot 2H_2O$: The complex was obtained as golden yellow needle by addition of an aqueous solution of sodium tetrafluoroborate to an aqueous solution of $NiL(ClO_4)_2 \cdot 2H_2O$.

Found: C, 32.13; H, 4.73; N, 18.50%. Calcd for $C_{16}H_{28}N_8O_2B_2F_8Ni$: C, 32.20; H, 4.73; N, 18.78%.

$NiLCl_2$: The complex was obtained as red-orange prisms, when an aqueous solution of excess sodium chloride was added to an aqueous solution of $NiL(ClO_4)_2 \cdot 2H_2O$.

Found: C, 41.44; H, 5.32; N, 24.33%. Calcd for $C_{16}H_{24}N_8Cl_2Ni$: C, 41.96; H, 5.28; N, 24.46%.

$NiL(NO_3)_2$: The complex was obtained as yellow-brown prisms by mixing an aqueous solution of $NiL(ClO_4)_2 \cdot 2H_2O$ and an aqueous solution of excess sodium nitrate.

Found: C, 37.36; H, 4.77; N, 27.41%. Calcd for $C_{16}H_{24}N_{10}O_6Ni$: C, 37.60; H, 4.73; N, 27.40%.

Isolation of the Condensation Product. To an aqueous solution (200 ml) containing $Na_2H_2edta \cdot 2H_2O$ (4.0 g) and NaOH (4.0 g) was added $NiL(ClO_4)_2 \cdot 2H_2O$ (3.0 g), and the mixture was heated under reflux for 5 h. Pale yellow needles which separated were collected and recrystallized from metha-

nol. The yield was 1.3 g; mp 185 °C.

Found: C, 64.81; H, 6.75; N, 28.53%; MS: *m/e*, 296 and 297. Calcd for $C_{16}H_{20}N_6$: C, 64.86; H, 6.80; N, 28.38%; mol wt, 296.38.

Measurements. Infrared spectra were measured with a Hitachi Infrared Spectrophotometer Model 215 on a KBr disk, electronic spectra with a Shimadzu Multipurpose Spectrophotometer Model MSP-5000, and NMR spectra with a Hitachi NMR Spectrophotometer Model R-20B in CD_3CN using tetramethylsilane as the internal standard.

Table 1. Crystal data

$NiCl_2O_{10}N_8C_{16}H_{28}$, Mol wt=622.07
Monoclinic, $P2_1/c$
$a=7.095(2)$Å
$b=11.578(3)$
$c=16.515(7)$
$\beta=102.7(3)°$
$V=1323.6$Å^3
$\mu(MoK\alpha)=18.58$ cm^{-1}
$D_m=1.56$ g cm^{-3}, $D=1.56$ g cm^{-3} (for $Z=2$)

Structure Determination of $NiL(ClO_4)_2\cdot 2H_2O$. The crystal is yellow-brown rhombic prisms elongated along the c-axis. Unit cell dimensions were determined by the least-squares method from high-angle fifteen reflections measured on a Syntex $P\bar{1}$ four-cycle automatic diffractometer. The crystal data are givin in Table 1. Three-dimensional intensity data were collected by the 2θ-θ scan technique on a Syntex $P\bar{1}$ diffractometer using Mo$K\alpha$ radiation made monochromatic by means of graphite plate. Of 2345 independent reflections collected in $2\theta \lesssim 48°$, 1636 reflections greater than $2.33\sigma(F)$ were used in the analysis. They were corrected for the Lorentz and polarization effects, no corrections being made for absorption.

Solution and Refinement of the Structure

The structure was solved by the heavy atom method. For two molecules in a unit cell of space group $P2_1/c$, the nickel atom is required to be in a special position. The chlorine atom was easily deduced from the three dimensional Patterson synthesis and the minimum function. All the remaining non-hydrogen atoms were revealed by the Fourier syntheses. The positional and anisotropic thermal parameters were refined by the block diagonal least-squares method, the final disagreement factor being 11.2% for the observed reflections. The final positional and thermal parameters and their standard deviations are given in Table 2. In the least-squares procedure, weight ω is taken to be equal to unity for $|F_0| \geqq 5.0$ reflections and zero for $|F_0| < 5.0$ reflections. The F_o-F_c table is kept at the office of the Chem. Soc. Japan (Document No. 7712). The scattering factors for all the atoms were taken from the International Table for X-ray Crystallography.[7] All calculations were carried out by the UNICS program system using a Facom 230-75 Computer in the Computer Center of Kyushu University.

Description of the Structure

The molecule has a center of symmetry, the nickel atom being required to be in its position. Two molecules of 3-acetyl-5,6-dimethylpyridazine hydrazone are coordinated to nickel(II) ion with two water molecules in apical positions. The molecular structure of $NiL(ClO_4)_2\cdot 2H_2O$ with the numbering systems utilized for description of the molecule is shown in Fig. 2. Bond distances and bond angles with their standard deviations are given in Table 3. Two organic moieties and nickel(II) ion are almost coplanar. The deviation of each atom from the least-squares plane formed by N2, N3, and Ni atoms is given in Table 4.

Discussion

As is seen in Fig. 2, the organic moiety is demonstrated

Table 2. The final positional and thermal parameters with their standard deviations ($\times 10^4$)
The anisotoropic thermal parameters are in the form of $\exp[-(B_{11}h^2+B_{22}k^2+B_{33}l^2+B_{12}hk+B_{13}hl+B_{23}kl)]$.

Atom	x/a	y/b	z/c	B_{11}	B_{22}	B_{33}	B_{12}	B_{13}	B_{23}
Ni	0	0	0	130(3)	397(1)	57(1)	41(4)	−60(3)	−22(2)
Cl	1569(4)	1518(3)	3405(2)	195(7)	66(2)	91(2)	−20(7)	38(6)	−38(4)
O	−778(9)	−387(6)	1126(6)	209(20)	63(6)	79(5)	69(19)	−14(17)	−34(10)
N1	−3908(10)	1061(8)	−724(7)	136(20)	73(9)	82(7)	58(23)	−107(20)	−26(13)
N2	−2129(10)	1260(6)	−231(6)	147(19)	45(6)	56(5)	44(19)	−52(17)	−9(10)
N3	1415(10)	1422(6)	596(6)	143(19)	41(6)	55(5)	35(19)	−28(17)	−12(10)
N4	3239(10)	1397(7)	981(6)	139(19)	49(7)	60(5)	15(20)	−62(17)	−8(10)
C1	−2945(12)	3311(9)	−137(7)	198(27)	45(8)	67(7)	101(26)	−65(23)	−1(13)
C2	−1658(12)	2278(9)	58(7)	149(24)	48(8)	55(6)	45(23)	−26(20)	−2(12)
C3	311(11)	2369(9)	557(7)	134(22)	42(7)	55(6)	41(22)	−57(20)	−14(12)
C4	1032(12)	3363(9)	985(7)	188(25)	40(7)	43(6)	15(24)	−23(20)	−13(11)
C5	2928(12)	3346(9)	1424(7)	195(26)	45(8)	46(6)	−27(24)	−14(20)	−2(12)
C6	3997(12)	2340(9)	1410(7)	160(23)	46(8)	43(6)	−3(23)	−16(19)	4(11)
C7	6076(12)	2212(9)	1861(8)	144(24)	70(10)	64(7)	−22(27)	−47(22)	0(14)
C8	3799(13)	4371(10)	1948(8)	301(36)	48(9)	71(8)	−63(31)	−75(29)	−36(14)
O1	930(17)	722(14)	2770(10)	712(60)	232(20)	125(10)	−45(56)	41(39)	−136(23)
O2	3040(14)	2195(13)	3281(9)	407(39)	222(19)	133(11)	−186(45)	−66(33)	124(24)
O3	−162(16)	1947(13)	3345(9)	313(33)	269(22)	145(11)	134(46)	18(32)	−135(28)
O4	2047(14)	697(13)	3965(10)	667(57)	196(18)	110(9)	−147(51)	−21(37)	128(22)

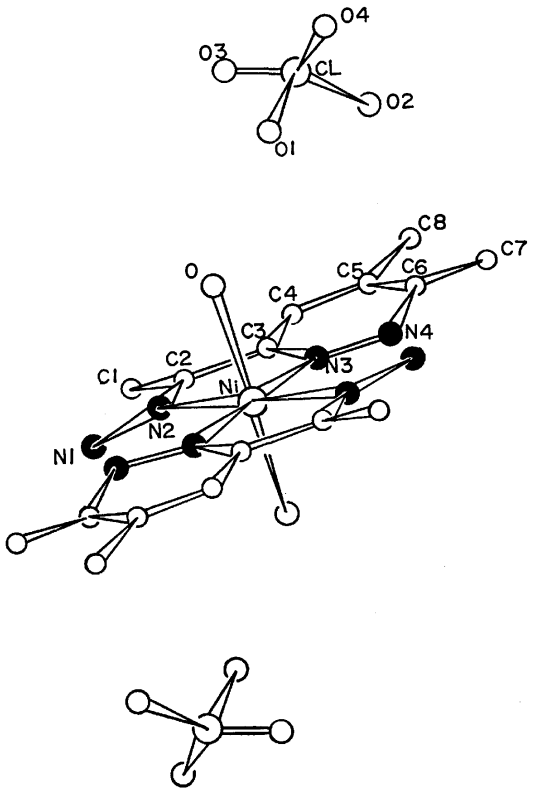

Fig. 2. Molecular structure of $NiL(ClO_4)_2 \cdot 2H_2O$.

Table 3. Bond distances and bond angles

Bond distances (Å) with their standard deviations.			
Ni–O	2.102(10)	C4–C5	1.382(18)
Ni–N2	2.075(11)	C3–C4	1.389(18)
Ni–N3	2.047(10)	C1–C2	1.496(20)
N1–N2	1.363(17)	C5–C8	1.518(20)
N2–C2	1.288(17)	C6–C7	1.507(19)
C2–C3	1.462(19)	C1–C1	1.372(20)
C3–N3	1.345(17)	C1–O2	1.380(19)
N3–N4	1.323(15)	C1–O3	1.343(20)
N4–C6	1.347(17)	C1–O4	1.339(20)
C5–C6	1.393(18)		
N2···N3′	3.215(17)	N1···N4′	2.93 (17)

Bond angles (°). Each of the standard deviations is blow 1.1°.			
O–Ni–N2	90.5	N2–C2–C3	114.3
O–Ni–N3	87.9	C1–C2–C3	121.7
N2–Ni–N3	77.4	N3–C3–C2	115.5
N2–Ni–N3′	102.5	N3–C3–C4	121.3
Ni–N2–N1	122.1	C2–C3–C4	123.1
Ni–N2–C2	117.1	C3–C4–C5	117.5
N1–N2–C2	120.4	C4–C5–C6	118.2
Ni–N3–N4	122.9	C4–C5–C8	121.0
Ni–N3–C3	115.0	C6–C5–C8	120.6
N4–N3–C3	121.7	N4–C6–C5	122.0
N3–N4–C6	118.9	N4–C6–C7	114.5
N2–C2–C1	123.7	C5–C6–C7	123.4

to be 3-acetyl-5,6-dimethylpyridazine hydrazone. This acts as a bidentate chelating agent, in which the ring nitrogen adjacent to the acetyl and the imino-nitrogen of hydrazone coordinate to nickel(II) ion to form a five-membered chelate ring. Two 3-acetyl-5,6-dimethylpyridazine hydrazone and nickel(II) ion are almost coplanar, although C8 (methyl carbon at the 6-position of pyridazine) slightly deviates from the least-squares plane formed by N2, N3, and Ni atoms. The distance between the nickel(II) ion and the water oxygen is 2.102 Å, the direction being nearly at right angles to the least-squares plane. Thus, the molecule has a twofold axis, the symmetry around the nickel(II) ion being approximately D_{2h}.

Table 4. Deviation of atoms from the least squeares plane (Å)

N1	−0.10	C4	0.21
N4	0.03	C5	0.26
C1	−0.10	C6	0.17
C2	0.00	C7	0.20
C3	0.08	C8	0.48

The least squares plane is defined by Ni, N2, and N3.

One of the characteristics of this molecule is a distorted configuration around the metal ion. Equatorial nitrogens form a rectangle; the distance between N2 and N3 is 2.58 Å, while the distance between N2 and N3′ is 3.215 Å. Thus, the N2–Ni–N3 angle is only 77.4°, while the N2–Ni–N3′ angle is 102.5°. These interatomic distances and bond angles are comparable with those in the nickel(II) complex with 2-pyridinecarboxamide anion.[8] The marked distortion around the metal ion can be attributed to the strain inherent in the ligand, which forms a five-membered chelate ring with conjugated double bonds.

In general, hydrazines condense with carbonyl compounds to form heterocyclic compounds.[9] However, the condensation between hydrazine and biacetyl has not yet been fully elucidated. Biacetyl hydrazone, the initial condensation product between diacetyl and hydrazine, has an active methyl group in addition to amino and carbonyl groups. Accordingly, under acidic and alkaline conditions the Aldol type condensation reaction as well as Schiff base formation are possible It is likely that 3-acetyl-5,6-dimethylpyridazine hydrazone was formed by the scheme shown in Fig. 3.

In order to separate and characterize the hydrazone, $NiL(ClO_4)_2 \cdot 2H_2O$ was decomposed with ethylenediaminetetraacetic acid in an alkaline solution. The isolated product, however, differs in composition from that of 3-acetyl-5,6-dimethylpyridazine hydrazone.

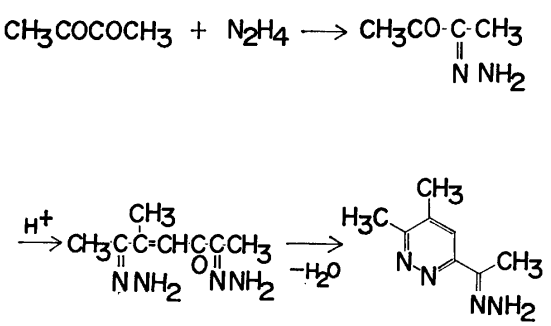

Fig. 3. The possible reaction scheme for 3-acetyl-5,6-dimethylpyridazine hydrazone formation.

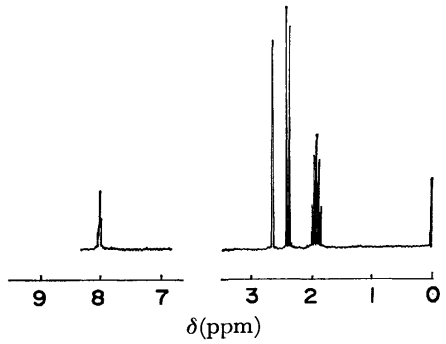

Fig. 4. NMR spectrum of 3-acetyl-5,6-dimethylpyridazine azine.

Judging from elemental analyses and the molecular weight determined from mass spectroscopy (m/e=296 and 297), the compound is likely to be 3-acetyl-5,6-dimethylpyridazine azine. This is supported by its NMR spectrum (Fig. 4) in which only four singlet signals are observed at 2.36, 2.42, 2.64, and 8.01 ppm with the intensity of 3, 3, 3, and 1 in ratio, respectively. The quintet around 1.9 ppm is due to CHD_2CN. The signals at 2.65 and 8.01 ppm are assigned to the α-methyl and the hydrogen on the ring, respectively. The signals at 2.36 and 2.42 ppm are ascribed to the methyl on the pyridazine ring. Infrared spectrum of 3-acetyl-5,6-dimethylpyridazine azine displays the C=N stretching vibration at 1670 cm^{-1} and the skeletal vibrations at 1595 and 1445 cm^{-1}. Thus, it is evident that 3-acetyl-5,6-dimethylpyridazine hydrazone in the complex was transformed into to 3-acetyl-5,6-dimethypyridazine azine by demetallation. Since azines are more stable than hydrazones, it is likely that a relatively severe reaction conditions (reflux around 100 °C in an alkaline solution) caused the azine formation.

Selected infrared absorption bands, molar conductivities and magnetic moments of the complexes are given in Table 5. Antisymmetric and symmetric N–H stretching vibrations of the amino group were found around ≈3340 and ≈3180 cm^{-1}, respectively. The C=N stretching vibration and the skeletal vibrations in the complexes were observed at 1640 cm^{-1} and at ≈1580 and ≈1440 cm^{-1}, respectively. Each band is lower in frequency as compared with that in the free ligand. The skeletal vibrations for 3-acetyl-5,6-dimethylpyridazine hydrazone should be practically the same in frequency as 3-acetyl-5,6-dimethylpyridazine azine because of the similarity in structure, while the C=N band in the hydrazone may be slightly higher than that in the azine because of the lower conjugation in the former. This is attributable to the coordination of the hydrazone nitrogen and the pyridazine nitrogen to the metal ion. Effective magnetic moment of each complex is comparable to the value for common copper(II) or high-spin nickel(II) complexes.

Electronic spectra of the complexes are given in Figs. 5 and 6. Reflectance spectra of $CuL(ClO_4)_2$ and $CuBr_2$ differ a great deal from each other, indicating the different structures in solid state. However, their solution spectra in methanol are nearly the same. Since the powder spectrum of $CuL(ClO_4)_2$ is similar to the solution spectrum, the configuration around the metal is nearly the same in solid and in solution. The fact

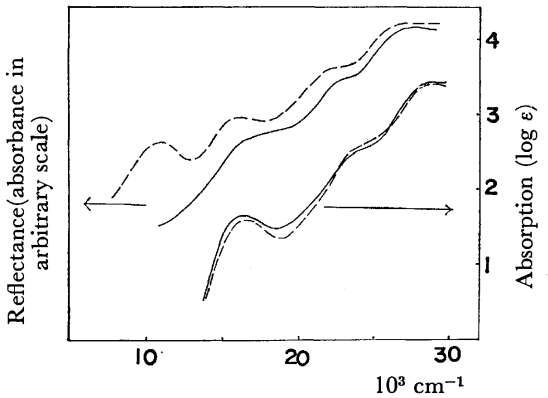

Fig. 5. Electronic spectra of $CuL(ClO_4)_2$ (——) and $CuLBr_2$ (– – –).

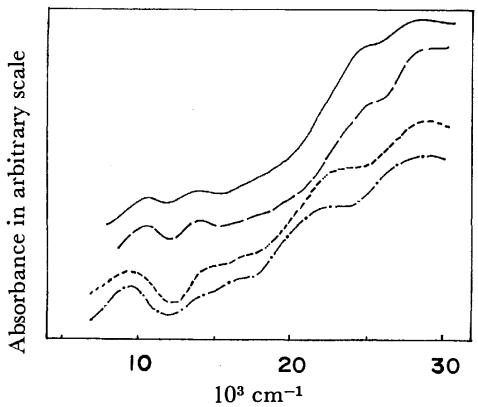

Fig. 6. Reflectance spectra of $NiL(ClO_4)_2 \cdot 2H_2O$ (——), $NiL(BF_4)_2 \cdot 2H_2O$ (– – –), $NiLCl_2$ (- - - - -), and $NiL(NO_3)_2$ (- · - · -).

Table 5. Selected IR bands (cm^{-1}), molar conductivity Λ (Ω^{-1} cm^2 mol^{-1}), and effective magnetic moment μ_{eff} (Bohr magneton) of complexes

	IR									Λ	μ_{eff}
	N–H		C=N	Skeletal		X–					
$CuL(ClO_4)_2$	3350	3150	1640	1580	1445	1105	1050			182 (MeOH)	1.75
$CuBr_2$	3280	3125	1640	1580	1440					171 (MeOH)	1.76
$NiL(ClO_4)_2 \cdot 2H_2O$	3340	3180	1640	1585	1440	1120—1080				165 (MeOH)	2.96
$NiL(BF_4)_2 \cdot 2H_2O$	3330	3180	1640	1583	1440	1080—1020				178 (MeOH)	3.00
$NiLCl_2$	3340	3190	1640	1585	1440					257 (H_2O)	3.06
$NiL(NO_3)_2$	3350	3190	1640	1587	1440	1420	1305	825		235 (H_2O)	3.04

that the infrared spectral band due to perchlorate ion splits considerably (1105 and 1050 cm^{-1}) implies that perchlorate oxygen coordinates weakly to the copper(II) ion at the apical positions.[10]

The d-d band of $CuLBr_2$ in solid state splits into two bands, the lower band being very low in frequency (11100 cm^{-1}). The splitting of the ligand field bands in the low energy region is generally caused by the fifth coordination to copper(II) ion.[11] Since the spectrum of $CuLBr_2$ resembles spectra[12] of [Cu(trien)SCN]SCN, $[Cu(NH_3)_5](BF_4)_2$, and $[Cu(en)_2NH_3]X_2$ whose configuration is supposed to be tetragonal-pyramidal, it is likely that $CuLBr_2$ has a distorted five-coordinate structure with a bromide ion at the apical position. Molar conductivity of the copper(II) complexes indicates that they are 2: 1 electrolyte in methanol.

The nickel(II) complexes are also 2: 1 electrolyte in methanol or water. Because of relatively low solubility in most solvents the electronic spectra of the nickel(II) complexes were measured on a solid sample. The spectra of $NiL(ClO_4)_2 \cdot 2H_2O$ and $NiL(BF_4)_2 \cdot 2H_2O$ are similar to each other, where there are some d-d bands in the region 16000—22000 cm^{-1} in addition to the well resolved bands at $\approx$10500 and $\approx$14000 cm^{-1}. Since the symmetry around the metal in $NiL(ClO_4)_2 \cdot 2H_2O$ is approximately D_{2h} (or lower symmetry), the transitions $^3T_{2g} \leftarrow {}^3A_{2g}$ and $^3T_{1g} \leftarrow {}^3A_{2g}$ for nickel(II) under O_h-symmetry split into two (or three) components respectively in $NiL(ClO_4)_2 \cdot 2H_2O$ and $NiL(BF_4)_2 \cdot 2H_2O$, hence producing a complicated spectrum.

Spectra of $NiLCl_2$ and $NiL(NO_3)_2$ are similar to each other, but differ from those of $NiL(ClO_4)_2 \cdot 2H_2O$ and $NiL(BF_4)_2 \cdot 2H_2O$. Since these spectra also show complicated d-d bands in the region 14000—23000 cm^{-1}, the configuration around the metal may be a distorted octahedron, where it is presumed the apical ligands are chloride or nitrate ion. In fact the infrared spectrum of $NiL(NO_3)_2$ indicates characteristic bands of nitrate ion at 1420, 1305, and 825 cm^{-1} indicating that the nitrate ion acts as a unidentate ligand.[13]

The authors are grateful to Assoc. Prof. T. Inazu, Kyushu Univesity, for measuring NMR spectra, and to Prof. M. Yamaguchi and Dr. T. Katsuki, Kyushu University, for measuring mass spectra. Thanks are also due to Prof. T. Komori for allowing us to use the Syntex Pī automatic diffractometer.

References

1) L. T. Taylor, F. L. Urbach, and D. H. Busch, *J. Am. Chem. Soc.*, **91**, 1072 (1969).
2) V. Katovic, L. T. Taylor, and D. H. Busch, *J. Am. Chem. Soc.*, **91**, 2172 (1969).
3) V. Katovic, L. T. Taylor, and D. H. Busch, *Inorg. Chem.*, **10**, 4581 (1971).
4) Sue C. Cummings and D. H. Busch, *Inorg. Chem.*, **10**, 1220 (1971).
5) T. J. Truex and R. H. Holm, *J. Am. Chem. Soc.*, **94**, 4529 (1972).
6) S. C. Tang and R. H. Holm, *J. Am. Chem. Soc.*, **97**, 3359 (1975).
7) "Internal Tables for X-Ray Crystallography," Vol. III, Kynoch Press, Birmingham (1962).
8) Y. Nawata, H. Iwasaki, and Y. Saito, *Bull. Chem. Soc. Jpn.*, **40**, 515 (1967).
9) *E.g.* a) R. H. Wiley and P. E. Hexner, *Org. Synth.*, Coll. Vol. IV, 351 (1963); b) C. L. Habraken and J. A. Moore, *J. Org. Chem.*, **30**, 1892 (1965); c) J. Levisailles, *Bull. Soc. Chim. Fr.*, **1957**, 1004; d) G. O. Schenk, *Chem. Ber.*, **80**, 289 (1947); e) W. R. Vaughan and S. L. Baird, Jr., *J. Am. Chem. Soc.*, **68**, 1314 (1946).
10) K. Nakamoto, "Infrared Spectra of Inorganic and Coordination Compounds," 2nd ed, John-Wiley & Sons, Inc., New York (1970), p. 175.
11) M. Ciampolini, *Struct. Bond.*, **6**, 52 (1969).
12) A. A. G. Tomlinson and B. Hathaway, *J. Chem. Soc.*, *A*, **1968**, 1685, 1905.
13) K. Nakamoto, "Infrared Spectra of Inorganic and Coordination Compounds," 2nd ed, John-Wiley & Sons, Inc., New York (1970), p. 171.

Photoreaction of 4-Substituted Quinoline *N*-Oxide and 2(1*H*)-Quinolinone in Propionic Acid[1)]

Akio IDE, Yukinori MORI, Kunihiko MATSUMORI, and Hiroyasu WATANABE
Department of Agricultural Chemistry, Faculty of Agriculture, Ehime University, Tarumi, Matsuyama 790
(Received September 1, 1976)

4-Substituted *cis*-3-ethyl-2-oxo-1,2,3,4-tetrahydro-2-quinoline was formed as a major product, by irradiation of quinoline *N*-oxide and 2(1*H*)-quinolinone substituted with an electron-withdrawing group at the C-4 position in propionic acid. Also, the products were confirmed by direct comparison with synthesized compounds.

Recently, photoalkylation reactions of aza aromatic compounds have been reported by several authors.[2)] Concerning this reaction, Ide *et al.* have also described the photoalkylation of quinolinecarbonitriles and isoquinolinecarbonitriles in propionic acid.[3)] The reaction products were found to be ethylated in the aza aromatic rings of quinoline and isoquinoline. Moreover, the position of alkylation was explained well by the reaction indices of nucleophilic or radical superdelocalizability in a simple HMO calculation.[3)] The present paper is concerned with photoinduced reactions of quinoline *N*-oxide and 2(1*H*)-quinolinone (carbostyril) having an electron-withdrawing group at the C-4 position in propionic acid.

Results and Discussion

It is well known that azanaphthalene *N*-oxide are predominantly transformed into lactams, as a result of ultraviolet irradiation in hydroxylic solvents.[4,5)] As seen from Table 1, a simple HMO calculation indicates that the C-3 position of the lactam, 2-oxo-1,2-dihydro-4-quinolinecarbonitrile, is the most reactive site in the molecule. Accordingly, irradiation of 4-quinolinecarbonitrile *N*-oxide (**1a**) in propionic acid may give the lactam (**2a**) which then undergoes photoalkylation at the C-3 position. An experimental proof of these assumptions is of interest with respect to the mechanism of the photoalkylation of aza aromatic compounds. Therefore, the present authors carried out the irradiation of **1** and **2** in propionic acid using a high-pressure mercury lamp and a quartz filter.

Table 1. Reaction indices for 2-oxo-1,2-dihydro-4-quinolinecarbonitrile

No[a)]	Superdelocalizability[b)]		
	Electrophilic	Nucleophilic	Radical
1	1.570	0.348	0.959
2	0.314	0.711	0.513
3	1.275	1.363	1.319
4	0.705	1.101	0.903
5	0.905	1.004	0.854
6	1.053	0.747	0.900
7	0.844	0.943	0.894
8	1.116	0.810	0.963
9	0.743	0.843	0.793
10	0.959	0.654	0.806
11	0.460	0.996	0.728
12	0.833	1.035	0.934
13	0.987	0.423	0.705

a) Numbered as follows.

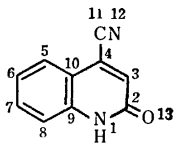

b) Calculated according to the method of Fukui.[6)] The following parameters were adopted from the textbook of Pullmann[7)] and were used in the simple HMO calculation. Coulomb integral: $\alpha_N^{CN}=\alpha+1.1\beta$, $\alpha_C^{C=O}=\alpha$, $\alpha_O^{C=O}=\alpha+1.2\beta$, $\alpha_N^{CON}=\alpha+\beta$. Resonance integral: $\beta_{C-N}^{C\equiv N}=1.4\beta$, $\beta_{C-N}^{CON}=0.9\beta$, $\beta_{C-O}^{C=O}=2\beta$.

Both compounds **1** and **2** gave the same products in the yields given in Table 2. The products were determined to be 4-substituted 3-ethyl-2-oxo-1,2,3,4-tetrahydroquinoline on the basis of the spectral data listed in Tables 3 and 4. It is difficult to assign either a *cis* or a *trans* configuration on the basis of the coupling costant between C^3–H and C^4–H. Accordingly, synthesis of the two isomers was attempted accordingly to the scheme shown in Chart 2.

Following the synthesizing method for (*Z*)-2-(2-oxo-3-indolinylidene)propionic acid of Julian *et al.*,[8)] (*Z*)-2-(2-oxo-3-indolinylidene)butyric acid (**6**) was prepared from oxindole (**5**) and 2-oxobutyric acid. Heating of **6** in hydrochloric acid gave 3-ethyl-2-oxo-1,2-dihydro-4-quinolinecarboxylic acid (**7**) which was identical with the compound obtained by Mulert[9)] from *N*-butylisatin, with respect to the chemical and physical data. Compound (**7**) was catalytically reduced, giving colorless needles. The needles were determined from their infrared spectrum to be *cis*-3-ethyl-2-oxo-1,2,3,4-tetra-

Table 2. Photochemical reaction yields

Starting compound	Product	Yield[a)] (%)	Product	Yield[a)] (%)
1a	**3a**	41 (26)	**4a**	8
2a		53 (40)		9
1b	**3b**	28 (8.7)	**4b**	5
2b		15 (7.0)		8
1c	**3c**[b)]	50 (37)	**4c**[b)]	12
2c		64 (46)		15

a) The amount of the product present in the reaction mixture, and determined by gas chromatography. The numbers in parenthesis are the yields for isolated pure products after treatment of the reaction mixtures. The retention times are 35.4 and 40.6 min for **3a** and **4a**, and 140 and 149 min for **3b** and **4b**. b) Obtained from a reaction mixture treated with diazomethane.

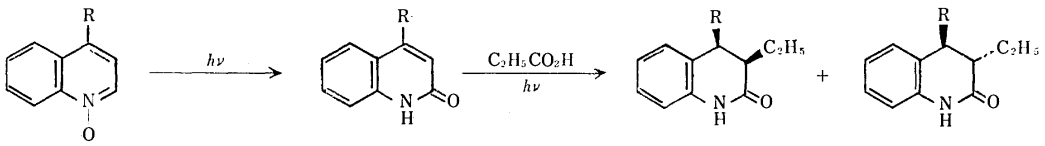

1 2 3 4

a: R=CN, b: R=CO_2CH_3, c: R=CO_2H

Chart 1.

TABLE 3. PHYSICAL PROPERTIES OF THE COMPOUNDS

Compound	mp (°C)	IR (ν_{max}^{KBr}, cm^{-1})	MS (*m/e*, %)
3a	187—188	2280(ν_{CN}, carbonitrile), 1681($\nu_{C=O}$, lactam)	200(85, M^+), 172(67, $M^+-(CH_2=CH_2)$), 171(96, $M^+-(CH_2=CH_2, H)$), 146(100, $M^+-(CH_2=CH_2, CN)$), 145(20, $M^+-(CH_2=CH_2, HCN)$)
3b	166—167	1737($\nu_{C=O}$, ester), 1690($\nu_{C=O}$, lactam)	233(77, M^+), 174(99, $M^+-(CH_2=CH_2, OCH_3)$), 146(100, $M^+-(CH_2=CH_2, CO_2CH_3)$)
3c	221—222	1720($\nu_{C=O}$, acid), 1662($\nu_{C=O}$, lactam)	219(63, M^+), 191 (58, $M^+-(CH_2=CH_2)$), 174 (99, $M^+-(OH, CH_2=CH_2)$), 146(100, $M^+-(CH_2=CH_2, CO_2H)$)
4a	194—195	2300(ν_{CN}, carbonitrile), 1685($\nu_{C=O}$, lactam)	200(78, M^+), 172 (72, $M^+-(CH_2=CH_2)$), 171 (100, $M^+-C_2H_5$), 146(70, $M^+-(CH_2=CH_2, CN)$)
4b	121—122	1726($\nu_{C=O}$, ester), 1674($\nu_{C=O}$, lactam)	233(54, M^+), 174(100, $M^+-(CO_2CH_3)$), 146(91, $M^+-(CO_2CH_3, CH_2=CH_2)$), 132(68, $M^+-(CO_2CH_3, CH_2=CH_2, CH_2)$)
4c	127—128	1720($\nu_{C=O}$, acid), 1670($\nu_{C=O}$, lactam)	219(50, M^+), 174(100, $M^+-(CO_2H)$), 146(71, $M^+-(CO_2H, CH_2=CH_2)$), 132(65, $M^+-(CO_2H, CH_2=CH_2, CH_2)$)
6	203—204	1756($\nu_{C=O}$, lactam(5 membered)), 1720($\nu_{C=O}$, acid), 1644($\nu_{C=C}$, exo)	217(48, M^+), 199(61, M^+-H_2O), 171(100, $M^+-(C=O, H_2O)$), 143(61, $M^+-(C, C_2H_5, CO_2H)$)
8	246—247	1700(amide I), 1680($\nu_{C=O}$, lactam)	218(50, M^+), 174(100, $M^+-(CONH_2)$), 146(78, $M^+-(CONH_2, CH_2=CH_2)$), 132 (67, $M^+-(CONH_2, CH_2=CH_2, CH_2)$)
10	205—206	1700(amide I), 1670($\nu_{C=O}$, lactam)	218(51, M^+), 174(100, $M^+-(CONH_2)$), 146(80, $M^+-(CONH_2, CH_2=CH_2)$), 132(85, $M^+-(CONH_2, CH_2=CH_2, CH_2)$)

TABLE 4. NMR DATA OF PHOTOLYSATES AND RELATED COMPOUNDS (from internal TMS, δ value (ppm))[a]

Compound	$-CH_2CH_3$ (3H)	$-CH-CH_2-CH_3$ (2H)	$-CH-CH-CH_2-$ (1H)	$-CH-CH$ (1H)	Others
3a[b]	1.10 (t, J=7 Hz)	1.6—2.5 (m)	2.7—3.0 (m)	4.6 (d, J=6 Hz)	7.0—7.5(4H, m, Ar-**H**), 9.5(1H, bs, N-**H**)
3b[b]	1.10 (t, J=7 Hz)	1.7—2.5 (m)	2.6—3.0 (m)	4.10 (d, J=6 Hz)	6.9—7.5(4H, m, Ar-**H**), 9.25(1H, bs, N-**H**), 3.65(3H, s, CO_2CH_3)
3c	1.21 (t, J=7 Hz)	1.8—2.1 (m)	2.6—2.9 (m)	4.28 (d, J=5 Hz)	
4a	1.11 (t, J=7 Hz)	1.91 (d×q, J=7 and 7 Hz)	3.00 (d×t, J=8 and 7 Hz)	4.59 (d, J=8 Hz)	
4b	1.02 (t, J=7 Hz)	1.67 (d×q, J=7 and 7 Hz)	3.11 (d×t, J=4 and 7 Hz)	4.02 (d, J=4 Hz)	3.56(3H, s, CO_2CH_3)
4c[b]	1.08 (t, J=7 Hz)	1.69 (d×q, J=7 and 7 Hz)	3.28 (d×t, J=3 and 7 Hz)	4.08 (d, J=3 Hz)	
8	1.21 (t, J=8 Hz)	1.8—2.4 (m)	2.6—2.9 (m)	4.32 (d, J=6 Hz)	
10	1.14 (t, J=7 Hz)	1.82 (d×q, J=7 and 7 Hz)	3.45 (d×t, J=4 and 7 Hz)	4.23 (d, J=4 Hz)	
6	1.36(3H, t, J=7 Hz, $-CH_2CH_3$), 2.94(2H, q, J=7 Hz, $-CH_2CH_3$), 6.9—7.7(4H, m, Ar-**H**)				

a) Measured in pyridine, except for b). S, di t, q, m, and bs stand for singlet, doublet, triplet, quartet, multiplet, and broad singlet, respectively. b) Measured in acetone-d_6.

hydro-4-quinolinecarboxylic acid (**3c**) with bands at 1720 (ν C=O, acid) and 1662 cm^{-1} (ν C=O, lactam), and by the *cis*-addition mechanism for catalytic hydrogenation. Compound (**6**) was catalytically reduced, giving an oily product which was presumed to have the structure of **9** shown in Chart 2. The crude oily product was refluxed in hydrochloric acid yielding colorless prisms, mp 127 °C. The prisms were determined to be *trans*-3-ethyl-2-oxo-1,2,3,4-tetrahydro-4-quinolinecarboxylic acid (**4c**), since the physical properties of

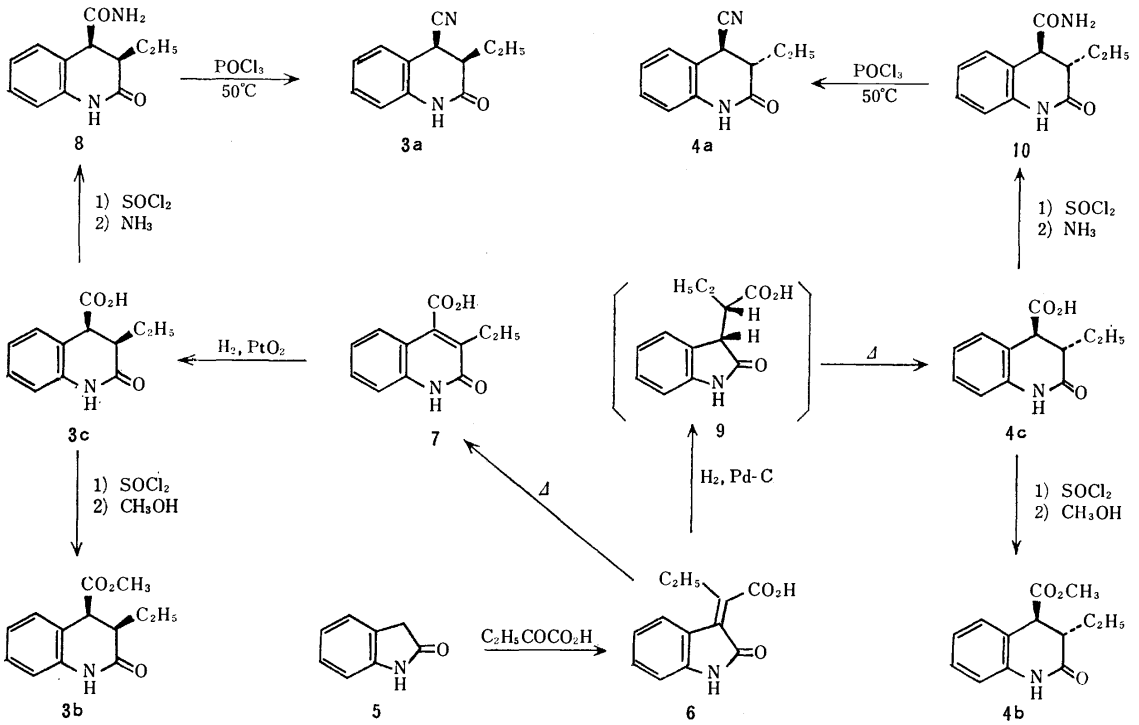

Chart 2.

4c were similar but not identical to those of **3c**. *cis*-(**3a**) and *trans*-3-ethyl-2-oxo-1,2,3,4-tetrahydro-4-quinolinecarbonitrile (**4a**) were synthesized from **3c** and **4c** *via cis*-(**8**) and *trans*-3-ethyl-2-oxo-1,2,3,4-tetrahydro-4-quinolinecarboxamide (**10**), respectively. The main product isolated from the mixture of the photoreactions of **1** and **2** coincided with compound **3**, the *cis* isomer obtained above. However, a small amount of the *trans* isomer, although difficult to isolate, was detected in the mixture by means of gas chromatography, as indicated in Table 2.

The fact that the *cis* isomer was obtained as a major product indicates that the *trans*-addition of ethyl and hydrogen groups occurs at the C-3 double bond of 2(1*H*)-quinolinone. This also indicates that the alkylated position in the present alkylation reaction is easily explained by the reaction indices in the simple HMO calculation. These results are important to an understanding of the mechanism of photoalkylation of aza aromatic compounds.

Experimental

All melting points were determined using a YANACO micromelting point apparatus and are uncorrected. Infrared spectra were recorded on a JASCO IR-S infrared spectrometer. Ultraviolet spectra were determined with a Hitachi 124 spectrophotometer. Nuclear magnetic resonance spectra were measured with a JEOL JNM-100H spectrometer at 100 MHz using TMS as an internal standard. Mass spectra were obtained with a JEOL JMS-OlSG-2 mass spectrometer, using a direct inlet and an electron energy of 75 eV.

Irradiation was carried out using a high-pressure mercury arc (USHIO UM-102) surrounded by a quartz water jacket at 30 °C.

The yield of the reaction products was determined by analysis on a SHIMADZU GC-5A gas chromatograph using a column (3 mm×2 m) packed with OV-225 (1.5%) on chromosorb-W (DMSC-A/W). The oven temperature was 186 °C for **3a** and **4a**, and 155 °C for **3b** and **4b**. The flow rate of the carrier gas (N_2) was 60 ml/min.

Materials. 2-Oxo-1,2-dihydro-4-quinolinecarboxylic acid, 2-oxo-1,2-dihydro-4-quinolinecarbonitrile, methyl 2-oxo-1,2-dihydro-4-quinolinecarboxylate and 4-quinolinecarbonitrile *N*-oxide were prepared according to the methods of Jacobs *et al.*,[10] Daeniker *et al.*,[11] Mayer,[12] and Daeniker,[11] respectively.

4-Substituted quinoline *N*-oxide were synthesized by the method of Ochiai.[14]

Methyl 4-Quinolinecarboxylate N-*Oxide* (**1b**). Colorless needles (from methanol), mp 149—150 °C. IR(KBr): 1701 (*ν* C=O), 1250 (*ν* N–O) cm^{-1}, Found: C, 70.72; H, 4.81; N, 7.36%. Calcd for $C_{11}H_9NO_2$: C, 70.58; H, 4.86; N, 7.48%.

4-Quinolinecarboxylic Acid N-*Oxide* (**1c**). Colorless prisms (from acetic acid), mp 256 °C (dec). IR (KBr): 2400—2900 (b, *ν* OH), 1714 (*ν* C=O), 1170 (*ν* N–O) cm^{-1}. Found: 63.53; H, 3.65; N, 7.49%. Calcd for $C_{10}H_7NO_3$: C, 63.49; H, 3.37; N, 7.41%.

(Z)-*2-(2-Oxo-3-indolinylidene)butyric Acid* (**6**). Metallic sodium (2.1 g) was added to absolute ethanol (70 ml). To this solution was added a solution of oxindol (**5**, 3.9 g) in absolute ethanol (30 ml) with stirring and then a solution of 2-oxobutyric acid (3.0 g) in absolute ethanol (30 ml). The mixture was refluxed for 3 h with stirring. The solid formed upon cooling was collected by filtration and dissolved in water (50 ml). The solution was acidified with 2M-hydrochloric acid. The resulting solid was dried and recrystallized from ethyl acetate to give yellow prisms, mp 203—204 °C, in 3.7 g (58.1%) yield. UV (λ_{max}^{EtOH} nm (ε)): 346(1600), 293 (7200), 258 (31300), 252(28000). Found: C, 66.52; H, 5.12; N, 6.43%. Calcd for $C_{12}H_{11}NO_3$: C, 66.35; H, 5.11; N, 6.45%.

3-Ethyl-2-oxo-1,2-dihydro-4-quinolinecarboxylic Acid (**7**).
A suspension of **6** (2.2 g) in hydrochloric acid (6%, 200 ml) was refluxed for 20 h and the mixture was concentrated under

reduced pressure. The residue was recrystallized from 50% ethanol to give colorless needles (1.1 g, 50%), mp 308—310 °C (lit,[9] 289 °C). IR (KBr): 1705 (ν C=O, acid), 1655 (ν C=O, lactam)cm^{-1}. MS (*m/e* (%)): 217 (M^+, 98), 172 (M^+ −COOH, 100).

cis-*3-Ethyl-2-oxo-1,2,3,4-tetrahydro-4-quinolinecarboxylic Acid (3c).* *(a) By Photochemical Reaction Involving* **1c**: A solution of **1c** (1.0 g) in propionic acid (500 ml) was irradiated for 3 h. The mixture was concentrated to dryness *in vacuo*. The residue was shaken in a sodium hydrogencarbonate solution (2%, 20 ml). The aqueous solution was washed three times with ethyl acetate, acidified with concentrated hydrochloric acid, and extracted with ethyl acetate (20 ml×3). The combined extract was washed with a saturated sodium chloride solution, dried over sodium sulfate, and evaporated. The syrupy residue was purified through a silica gel column (120 g, 3×40 cm) with a mixed solvent of dichloromethane–methanol (9: 1, v/v). The purified **3c** was recrystallized twice from water to afford colorless needles (0.43 g, 37%), mp 221—222 °C. Found: C, 65.93; H, 5.82; N, 6.41%. Calcd for $C_{12}H_{13}NO_3$: C, 65.74; H, 5.98; N, 6.31%.

(b) By Photochemical Reaction Involving **2c**: Photolysis of **2c** (0.5 g) in propionic acid (400 ml) was performed in a manner similar to that described in *(a)*, and **3c** was obtained (0.27 g, 46%).

(c) By Catalytic Reduction of 3-Ethyl-2-oxo-1,2-dihydro-4-quinolinecarboxylic Acid (7) in the Presence of Platinum Oxide: A mixture of **7** (217 mg), methanol (40 ml) and platinum oxide (0.1 g) prepared according to the method of Bruce[13] was shaken in an atmosphere of hydrogen for 4 h. The mixture was filtered and the filtrate was concentrated to dryness. The residue was taken up with methanol and subjected to chromatography on a preparative silicagel thin layer with dichloromethane–methanol (4: 1, v/v). The product was recrystallized from water. Mp 211—212 °C. Yield 156 mg (71%).

trans-*3-Ethyl-2-oxo-1,2,3,4-tetrahydro-4-quinolinecarboxylic Acid (4c).* *(Z)*-2-(2-Oxo-3-indolinylidene)butyric acid (2.17 g) and palladium on charcoal (10%, 0.5 g) were stirred in ethanol (30 ml) in a hydrogen atmosphere at room temperature and normal pressure. After 30 min, the catalyst was removed by filtration, and then the filtrate was evaporated. The residue was distilled at 0.08 Torr to give 2.17 g of colorless oils, bp 210 °C (bath temp). The oily product was refluxed in hydrochloric acid (6%, 200 ml) for 20 h. The reaction mixture was concentrated to dryness. The residue was recrystallized from water to give colorless prisms (1.56 g, 71.2%), mp 127 °C. Found: C, 60.88; H, 6.45; N, 5.97%. Calcd for $C_{12}H_{13}NO_3 \cdot H_2O$: C, 60.75; H, 6.37; N, 5.90%.

cis-*3-Ethyl-2-oxo-1,2,3,4-tetrahydro-4-quinolinecarboxamide(8).* **3c** (380 mg) was refluxed in thionyl chloride (5 ml) for 3 h. The reaction mixture was concentrated to dryness and the residue was suspended in absolute ether. Through this suspension, dry ammonia gas was passed with stirring. The precipitate was collected, washed with and recrystallized from ethanol to give colorless needles (212 mg, 56%), mp 246—247 °C. Found: C, 66.17; H, 6.58: N, 12.81%. Calcd for $C_{12}H_{14}N_2O_2$: C, 66.04; H, 6.47; N, 12.83%.

trans-*3-Ethyl-2-oxo-1,2,3,4-tetrahydro-4-quinolinecarboxamide (10).* **4c** (474 mg) was allowed to react in a manner similar to that described for the preparation of **8** to give 240 mg (55%) of colorless flakes, mp 205 °C. Found: C, 66.12; H, 6.51; N, 12.86%. Calcd for $C_{12}H_{14}N_2O_2$: C, 66.04; H, 6.47; N, 12.83%.

cis-*3-Ethyl-2-oxo-1,2,3,4-tetrahydro-4-quinolinecarbonitrile (3a)* *(a) By Photochemical Reaction Involving* **1a**: A solution of **1a** (5 g) in propionic acid (500 ml) was irradiated for 28 h. The mixture was concentrated and the residue was taken up with ethyl acetate. The ethyl acetate layer was successively washed with 2M-hydrochloric acid, an aqueous 2M-ammonia solution and a saturated sodium chloride solution, dried over sodium sulfate, and evaporated. The residue was recrystallized from methanol and then from ethanol to give colorless needles (1.5 g, 26%), mp 191—192 °C. Found: C, 72.09; H, 6.12; N, 14.10%. Calcd for $C_{12}H_{12}N_2O$: C, 71.98; H, 6.04; N, 13.99%.

(b) By Photochemical Reaction Involving **2a**: A solution of **2a** (1.5 g) in propionic acid (500 ml) was irradiated for 20 h. The mixture was treated in a manner similar to that for *(a)*, giving 0.7 g (40%) of **3a**, mp 191—192 °C.

(c) By Synthesis: A mixture of **8** (108 mg) and phosphoryl chloride (3 ml) was stirred at 50 °C for 2.5 h. The mixture was concentrated under reduced pressure (5 Torr). The residue was taken up with ethyl acetate. The ethyl acetate solution was washed sodium hydrogen carbonate and saturated sodium chloride solutions, dried over sodium sulfate and evaporated. The residue was recrystallized twice from ethanol to give colorless needles (50 mg, 50%), mp 192—193 °C.

trans-*3-Ethyl-2-oxo-1,2,3,4-tetrahydro-4-quinolinecarbonitrile(4a).* A mixture of **10** (109 mg) and phosphorylchloride (5 ml) was treated in a manner similar to that for *(c)* to give colorless prisms (53 mg, 53%), mp 194—195 °C. Found: C, 72.13; H, 5.93; N, 14.04%. Calcd for $C_{12}H_{12}N_2O$: C, 71.98; H, 6.04; N, 13.99%.

Methyl cis-*3-Ethyl-2-oxo-1,2,3,4-tetrahydro-4-quinolinecarboxylate (3b).* *(a) By Photochemical Reaction Involving Methyl 4-Quinolincarboxylate* N-*Oxide*: A solution of **1b** (5.0 g) in propionic acid (500 ml) was irradiated for 22 h. The mixture was concentrated under reduced pressure. The residue was fractionally distilled *in vacuo*. The distillate having a boiling point from 190 to 200 °C at 0.02 Torr was collected and crystallized by the addition of a mixture of hexane and ethyl acetate (1: 1, v/v). The crystals were recrystallized from ethanol to give colorless needles (0.5 g, 8.7%), mp 166—167 °C. Found: C, 67.02; H, 6.53; N, 5.94%. Calcd for $C_{13}H_{15}NO_3$: C, 66.94; H, 6.84; N, 6.00%.

(b) By photochemical Reaction Involving **2b**: A solution of **2b** (0.50 g) in propionic acid (100 ml) was irradiated for 4 h. The mixture was concentrated to dryness under reduced pressure. The residue was taken up with ethyl acetate (100 ml). The ethyl acetate solution was washed with sodium hydrogencarbonate (5%) and saturated sodium chloride solutions, dried over sodium sulfate, and evaporated. The residue was treated with methanol (20 ml) and filtered. The filtrate was concentrated. The syrupy residue was purified on a column (1×30 cm) of silica gel (30 g) with a mixed solvent of benzene and ethyl acetate (9: 1, v/v). The resultant crystals were recrystallized twice from ethanol to give colorless needles (0.04 g, 7.0%).

(c) By Esterification of **3c**: A mixture of **3c** (119 mg) in thionyl chloride (5 ml) was refluxed for 2 h. After evaporation of the excess thionyl chloride, the residue was refluxed in absolute methanol (10 ml) for 1 h. The mixture was concentrated under reduced pressure. The residue was recrystallized from ethanol to give colorless needles (85 mg 67.1%), mp 165—166 °C.

Methyl trans-*3-Ethyl-2-oxo-1,2,3,4-tetrahydro-4-quinolinecarboxylate (4b).* A mixture of **4c** (226 mg) in thionyl chloride (3 ml) was refluxed for 2 h. A procedure was carried out similar to that described of the preparation of **3b**. The crops were recrystallized from diisopropyl ether to give colorless prisms (107 mg, 42%), mp 121—122 °C. Found: C, 66.98; H, 6.51; N, 5.91%. Calcd for $C_{13}H_{15}NO_3$: C, 66.94;

H, 6.48; N, 6.00%.

The authors are indebted to the members of the Laboratory of Organic Analysis, Tanabe Pharmaceutical Co., Ltd., for the elemental analysis and also to Miss M. Maeda of the Faculty of Engineering, Ehime University, for the NMR measurements.

References

1) (a) Synthesis of Quinoline and Isoquinoline Derivatives VIII. Part VII of this series: A. Ide, H. Watanabe, and H. Watanabe, *Nippon Nogei Kagaku Kaishi*, **47**, 29 (1973); (b) Presented at the Annual Meeting of the Agricultural Chemical Society of Japan, Sapporo, 1975.

2) N. Hata, I. Ono, S. Matono, and H. Hirose, *Bull. Chem. Soc. Jpn.*, **46**, 942 (1973); F. R. Stermitz, C. C. Wei, and C. M. O'Donnel, *J. Am. Chem. Soc.*, **92**, 2745 (1970); R. Noyori, M. Kato, M. Kawanishi, and H. Nozaki, *Tetrahedron*, **25**, 1125 (1969); E. F. Ullmann, *Acc. Chem. Res.*, **1**, 353 (1968); F. R. Stermitz, R. P. Seiber, and D. E. Nicodem, *J. Org. Chem.*, **33**, 1136 (1968).

3) A. Ide, H. Watanabe, and H. Watanabe, *Nippon Nogei Kagaku Kaishi*, **47**, 29 (1973).

4) I. Ono and N. Hata, *Bull. Chem. Soc. Jpn.*, **46**, 3658 (1973).

5) C. Kaneko, I. Yokoe, S. Yamada, and M. Ishikawa, *Chem. Pharm. Bull.*, **17**, 1290 (1969).

6) K. Fukui, T. Yonezawa, C. Nagata, and H. Shingu, *J. Chem. Phys.*, **22**, 1433 (1954).

7) B. Pullmann and A. Pullmann, "Quantum Biochemistry," Interscience Publishers, John Willy & Sons, N. Y. (1963), p 108.

8) P. L. Julian, H. C. Printy, R. Ketcham, and R. Doone, *J. Am. Chem. Soc.*, **75**, 5305 (1953).

9) B. Mulert, *Ber.*, **39**, 1907 (1906).

10) T. L. Jacobs, S. Winstein, G. B. Linden, J. H. Robson, E. F. Levy, and D. Seymour, *Org. Synth.*, Coll. Vol. III, 456 (1965).

11) H. U. Daeniker and J. Druey, *Helv. Chim. Acta*, **41**, 2148 (1958).

12) H. Mayer, *Monatsh. Chem.*, **26**, 1321 (1905).

13) W. F. Bruce, *J. Am. Chem. Soc.*, **58**, 687 (1936).

14) E. Ochiai, "Aromatic Amine Oxides," Elsevier Publishing Company, Amsterdam (1967), Chap. 3.

The Chemistry of Phenalenium Systems. XXIII.[1] Syntheses and Properties of Cyclohepta[*cd*]phenalen-6-one and the Cyclohepta[*cd*]phenalenium Ion[2]

Kagetoshi YAMAMOTO, Yutaka KAYANE, and Ichiro MURATA

Department of Chemistry, Faculty of Science, Osaka University, Toyonaka, Osaka 560

(Received August 5, 1976)

The syntheses of cyclohepta[*cd*]phenalen-6-one (**8**) and the cyclohepta[*cd*]phenalenium tetrafluoroborate (**1**) are reported. As expected, it is apparent that in the transition from 10,11-dihydrocyclohepta[*cd*]phenalen-6-one to the fully conjugated ketone **8**, all the vinyl protons move downfield by 0.22 to 0.53 ppm. The plausible explanation suggests that these shifts arise from deshielding due to the existence of a diamagnetic ring current induced in the 14π periphery of **8**. In accord with theoretical prediction, the cation **1** is extremely stable. The substantial thermodynamic stability of **1** is reflected to its pK_{R^+} of 8.4. The ion **1** can be regarded as a perturbed [15]annulenium ion weakly coupled with a localized central vinyl crosslink.

Although there has been considerable interest in the neutral nonalternant isomers of pyrene such as cyclohept[*fg*]acenaphthylene (acepleiadiene),[3] cyclohepta[*def*]fluorene,[4] cyclohept[*bc*]acenaphthylene,[5] cyclohepta[*klm*]benz[*e*]indene,[6] dicyclopenta[*ef,kl*]heptalene (azupyrene),[7] pentaleno[6,6a,1,2-*def*]heptalene,[8] and dicyclohepta[*cd,gh*]pentalene,[9] the ionic 14π perimeter species which are isoelectronic with pyrene have received little attention. The ionic 14π perimeter species so far known have been confined to the anions, *e.g.* cyclopenta[*cd*]phenalenide ion,[10] pyracylene dianion,[11] dibenzo[*cd,gh*]pentalenyl dianion,[12] and cyclopenta[*def*]-phenanthrenide ion,[13] no cationic species have been reported to date. According to theoretical (HMO) prediction by Zahradnik *et al.*[14] the cyclohepta[*cd*]-phenalenium ion (**1**) ought to be quite stable and might be reasonably accessible.

On the other hand, cyclohepta[*cd*]phenalen-6-one (**8**), a key intermediate for the synthesis of **1**, is of interest in connection with current studies on the peripheral conjugation in peri-condensed polyarenes. We have recently reported the synthesis and properties of cyclopenta[*cd*]phenalen-4-one,[15] cyclopenta[*cd*]phenalen-5-one,[16] cyclohepta[*cd*]phenalen-1-one,[17] and cyclohepta[*cd*]phenalen-4-one,[18] wherein the structural phenalenone moiety is incorporated into the molecule. In these cases, we have proposed that these compounds can be regarded as [13]- and [15]annulenone perturbed by internal vinyl crosslink. Here we describe the synthesis of **1** as the first example of a 14π perimeter cationic system along with **8** as an adequate model compound for perturbed [15]annulenone.

Results and Discussion

Synthesis and Properties of Cyclohepta[cd]*phenalen-6-one (8).* Reduction of the hydroxy ester, which was obtained by the Reformatsky reaction of 2,3-dihydrophenalenone (**2**)[19] with methyl 4-bromocrotonate, over palladium hydroxide on charcoal proceeds accompanying with hydrogenolysis of the benzylic hydroxyl group. The butylate thus obtained was hydrolyzed with potassium hydroxide in ethanol to give the carboxylic acid (**3**) in 48% yield. Cyclization of **3** with polyphosphoric acid at 90 °C for 1 h afforded the tetracyclic ketone (**4**) in 75% yield. The ketone (**4**) was converted into the α,α-dibromo ketone (**5**) in quantitative yield by treatment with bromine in dry carbon tetrachloride. Dehydrobromination of **5** to give 10,11-dihydrocyclohepta[*cd*]phenalen-6-one (**6**) was accomplished by heating in hexamethylphosphoric triamide with lithium chloride for 1 h at 95—100 °C. The structure of **6** was

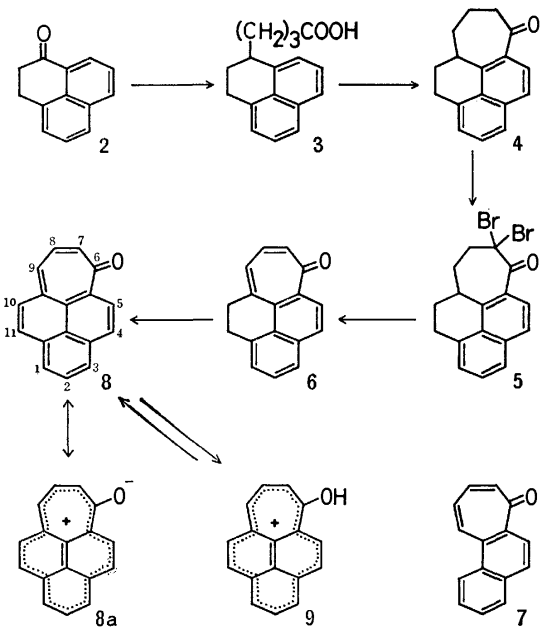

confirmed on the basis of its spectroscopic properties. The mass spectrum of **6** showed intense peaks at *m/e* 232 (M^+, 64%), 204 (M^+-CO, 100%), 203 (93%) and 202 (pyrene ion, 82%). The IR spectrum exhibited characteristic absorption of tropone skeleton at 1625, 1590, and 1580 cm^{-1}.[20] The absorption bands of the UV spectrum of **6**, 243 nm (log ε, 4.38), 287 (4.33), and 344 (3.91), are in good agreement with those of cyclohepta[*a*]-naphthalen-7-one (**7**).[21] The conversion of **6** into the desired fully conjugated ketone (**8**) was effected by treatment with 2,3-dichloro-5,6-dicyano-1,4-benzoquinone in benzene in a sealed tube at 120 °C for 20 h in 21% yield. However, it was found that the compound (**8**) could be more readily obtained in a higher yield (33%) on treatment of **6** with triphenylmethyl tetrafluoroborate in refluxing acetic acid under nitrogen

Table 1. Comparison of NMR data for **6** and **8**[a)]

	in $CDCl_3$			in CF_3COOH			**6**	**8**
	6	**8**	$\Delta\delta$(**8**—**6**)	**6**	**8**	$\Delta\delta$(**8**—**6**)	$\delta_{CF_3COOH}-\delta_{CDCl_3}$	$\delta_{CF_3COOH}-\delta_{CDCl_3}$
H-1, 2, 3	7.30—7.78	7.68—8.02	0.38—0.24	7.82—8.21	8.63—9.16	0.81—0.95	0.52—0.43	0.95—1.14
H-7, 8, 9	6.73—7.10	7.20—7.56	0.41—0.46	8.24—8.62		0.39—0.54	1.90—2.06	1.43—1.60
H-10, 11	2.88—3.35			3.43—3.82			0.55—0.47	
H-4	7.96	8.18	0.22	8.62	9.23	0.61	0.66	1.05
H-5	8.24	8.77	0.53	9.05	9.74	0.69	0.81	0.97
$J_{4,5}$	9.0	9.0		9.2	9.2			

a) Chemical shifts are given in δ-values with respect to TMS as an internal standard and coupling constants are given in Hz.

atmosphere for 2 h. The identity of **8** was established in the following manner. Mass spectrometry gave a parent peak at *m/e* 230. As would be expected for a compound containing tropone moiety, the base peak in the mass spectrum was found to be M^+-CO (*m/e* 202).[22)] The UV spectrum of **8** showed maxima at 249 nm (log ε, 4.48), 311 (4.07), 321 (4.08), 430 (4.23) indicating an extend conjugation. Further evidence was also provided by ^{1}H-NMR spectrum.

The NMR chemical shifts and coupling constants of **8** compared with those of the reference compound **6** are summarized in Table 1. Although complete assignments of the proton chemical shifts could not be made except H-4 and H-5 due to their complex spectral pattern, it is apparent that (i) in the transition from the dihydro ketone (**6**) to the fully conjugated ketone (**8**), all the vinyl protons move downfield by 0.2—0.5 ppm (ii) the downfield shift is enhanced (0.4—0.95 ppm) when **8** is protonated in trifluoroacetic acid (iii) in the case of **6**, only protons of seven-membered ring (H-7, 8, and 9) move downfield in trifluoroacetic acid compared with those of the neutral form whereas the full conjugated ketone (**8**) exhibited marked downfield shifts of all the vinyl protons. These findings suggest the existence of a diamagnetic ring current induced in the 14π periphery (**8a**) of **8**. The diatropic effect is enhanced in trifluoroacetic acid owing to the formation of the 6-hydroxycyclohepta[*cd*]phenalenium ion (**9**). Furthermore, supportive evidence for the formation of **9** in an acidic media was provided by the UV-visible spectrum of **8** in concentrated sulfuric acid which was closely similar to that of the parent cation (**1**) [*vide infra*] in acetonitrile both in absorption maxima and in band shape [see Fig. 1].

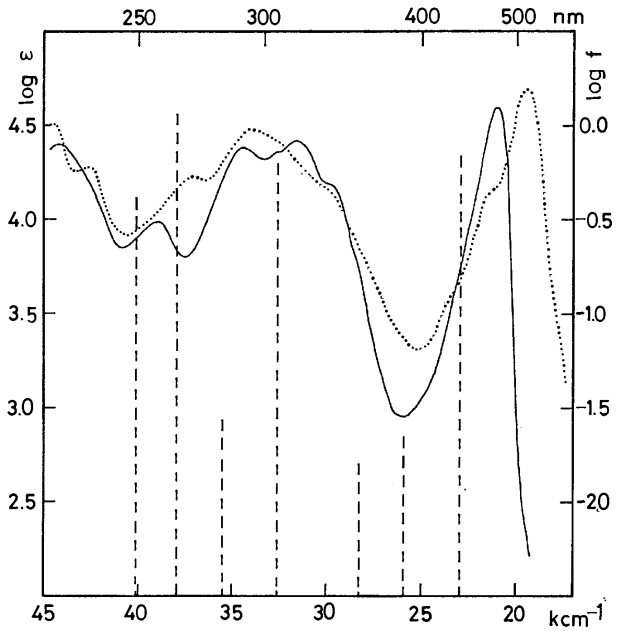

Fig. 1. Electronic spectra of the cyclohepta[*cd*]phenalenium tetrafluoroborate (**1**) in CH_3CN and cyclohepta-[*cd*]phenalen-6-one (**8**) in concd H_2SO_4.
——: (**1**), ……: (**8**).
Vertical dashed lines denote calculated transitions for (**1**).

Synthesis and Properties of Cyclohepta[cd]*phenalenium Tetrafluoroborate (1).* Reduction of **8** with lithium aluminum hydride–aluminum chloride complex in ether at −50 °C for 2 h led to a mixture of isomeric hydrocarbons, 6*H*-cyclohepta[*cd*]phenalene (**10**) and 7*H*-cyclohepta[*cd*]phenalene (**11**) in a ratio of about 9: 13. The mixture was isolated in 56% yield after chromatography on alumina deactivated with 10% water. Owing to their highly unstable nature, compounds **10** and **11** have to be handled under nitrogen atmosphere throughout reaction and isolation. Although **10** and **11** could

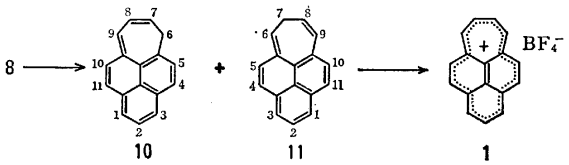

not be separated due to their pronounced sensitivity toward air and heat, their structural assignments were readily borne out by 100 MHz ^{1}H-NMR and NMDR experiments. The mixture of **10** and **11** showed signals assignable to **10** at δ 2.71 (H-6,6′, d, $J_{6,7}$=6.7 Hz), 5.51 (H-7, dt, $J_{7,6}$=6.7, $J_{7,8}$=9.2 Hz), 6.33 (H-8, dd, $J_{8,7}$=9.2, $J_{8,9}$=6.5 Hz), 6.84 (H-9, d, $J_{9,8}$=6.5 Hz), and **11** at 1.66 (H-7,7′, dd, $J_{7,6}$=7.3, $J_{7,8}$=6.5 Hz), 4.82 (H-8, dtd, $J_{8,7}$=6.5, $J_{8,9}$=8.5, $J_{8,6}$=2.4 Hz), 5.27 (H-6, td, $J_{6,7}$=7.3, $J_{6,8}$=2.4 Hz), and 6.66(H-9,d, $J_{9,8}$=8.5 Hz) along with multiplet of the aromatic protons at 7.02—8.07. Irradiation at δ 2.71 (H-6,6′ of **10**) converted the doublets of triplet at δ 5.51 attributed to H-7 of **10** into a clean doublet with J=9.2 Hz. Another irradiation at δ 1.66 assigned to H-7,7′ of **11** changed the triplets of doublet at δ 5.27 and the doublets of triplets of doublet at δ 4.82 into a broad singlet and a broad doublet, respectively. Additional evidence in favor

of the assigned structures is the mass spectrum of the mixture which showed peaks at *m/e* 216 (M^+, 100%), 215 (M^+—H, 73%), and 202 (pyrene ion, 21%).

Hydride abstraction from the freshly prepared mixture of **10** and **11** with triphenylmethyl tetrafluoroborate in chloroform at room temperature immediately gave the desired cation (**1**).

In conformity with the theoretical prediction by Zahradnik *et al.*[14] the cyclohepta[*cd*]phenalenium tetrafluoroborate (**1**) is extremely stable reddish brown crystals which sinter at 199—201 °C and show no definite melting point. **1** can be stored without any change under atmospheric condition. The electronic spectrum of **1** is reproduced in Fig. 1. At least three major bands can be discerned. In either acetonitrile or water **1** shows essentially the same spectrum. The analysis of the electronic spectrum was kindly carried out by Zahradnik and Slanina[23] and was summarized in Table 2 and displayed in Fig. 1. The 100 MHz ^{1}H-NMR spectrum of **1** in deuteriotrifluoroacetic acid (see Fig. 2) consists of superimposed signals of AA'XX',[24] 2×AB, and A_2B spin systems at δ 9.08 (H-7, 8 or H-6, 9), 9.66 (H-6, 9 or H-7, 8), 9.16 (H-5, 10),[25] 9.50 (H-4, 11),[25] 9.40 (H-1, 3), and 9.00 (H-2) with coupling constants of $J_{6,7}=J_{8,9}=10.9$, $J_{7,8}=9.0$, $J_{6,8}=J_{7,9}=1.4$, $J_{6,9}=0$, $J_{4,5}=J_{10,11}=8.9$, and $J_{1,2}=J_{2,3}=7.7$ Hz. The observed vicinal coupling constants in the six-membered ring are in good agreement with those predicted by the empirical correlation against SCF bond orders.[26] Thus using SCF bond orders,[23] we obtain 8.5 Hz for $J_{4,5}$ and $J_{10,11}$ and 7.6 Hz for $J_{1,2}$ and $J_{2,3}$. The comparative uniformity of the coupling constants indicates no appreciable bond fixation exists in the periphery of **1**. Both the substantial downfield chemical shifts with rather narrow range (δ 9.00—9.66 ppm) and the symmetrical pattern of the signals show the cation **1** to have fully delocalized structure with C_{2v}-symmetry.

Despite the fact that an unit positive charge resides over the fifteen peripheral carbon atoms, the ^{1}H-NMR signals of **1** are comparable to those of the tropylium ion (δ 9.20 in acetonitrile)[27] and the phenalenium ion (δ 9.30 and 8.48 in arsenic trichloride).[28] This provides evidence of the existence of a strong induced diamagnetic ring current associated with the 14π perimeter of **1**. These evidences support the idea that the cation **1** is best thought of as a perturbed [15]annulenium ion weakly coupled with a localized central vinyl cross-link.[29]

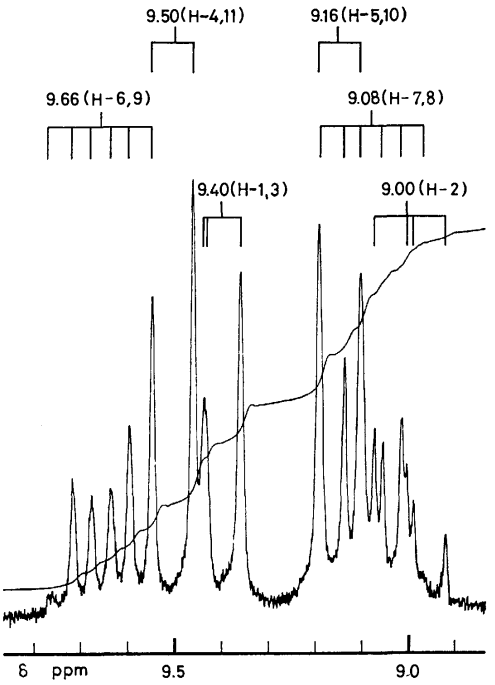

Fig. 2. 100 MHz ^{1}H-NMR spectrum of the cyclohepta-[*cd*]phenalenium tetrafluoroborate (**1**) in CF_3COOD.

The thermodynamic stability of **1** is clearly reflected in its pK_R^+ value. Standard spectrophotometric method was used for the pK_R^+ determination in 20% aqueous acetonitrile solution. The pK_R^+ value of 8.4 thus obtained is the lower limit, since the intensity of absorbancy decreases with elapse of time in the pH range near pK_R^+. Thus the measurement at 180 s after preparation of the solution yields a somewhat small value of 8.1. In any way, pK_R^+ value of **1** is about 1 pK unit larger than that of the 8-cycloheptatrienyl-heptafulvenyl cation ($pK_R^+=7.1$,[30] 7.49[31]). To our knowledge, **1** is the most stable hydrocarbon cation so far reported.

TABLE 2. ELECTRONIC SPECTRA OF **1**

No.	Calcd[a]						Obsd[b]	
	E (eV)	10^{-3} ν(cm^{-1})	λ (nm)	Polarization[c]	log f	Configuration	λ	log ε
1	2.86	23.1	433	y	−0.17	8—9	475	4.49
2	3.21	25.9	386	x	−1.64	8—10 7—9	344	4.18 s
3	3.49	28.2	355	x	−1.79	6—9	316	4.40
4	4.05	32.7	306	x	−0.21	7—9	307	4.37 s
5	4.42	35.6	281	y	−0.56	6—10	291	4.37
6	4.70	37.9	264	y	0.03	7—10	257	3.99
7	4.98	40.2	249	x	−0.51	8—12	224	4.40
8	4.99	40.2	249	y	−0.38	5—9		

a) The calculations are based upon the LCI-SCF (PPP-type) method. Parameters used are: I_c= 11.42 eV, A_c=0.58 eV, β_{cc}^{core}= −2.318 eV. Singly excited configurations were formed by promotions of electrons between the four highest occupied and the four lowest unoccupied MO's. b) The values are obtained in acetonitrile solution. c) x and y denote polarization along short and long axes of **1**, respectively.

Experimental

All melting points are uncorrected. The IR spectra were obtained on a Hitachi EPI G21 spectrometer. The electronic spectra were taken with a Hitachi 124 double beam spectrophotometer and were recorded in nm and the log ε values were given in parentheses. The mass spectra were obtained on a Hitachi RM-50 spectrometer at 70 eV. The ^{1}H-NMR spectra measured on a Varian T-60 and a Varian XL-100-15 spectrometers were given in δ-values with respect to tetramethylsilane as an internal standard, and the coupling constants (*J*) are given in Hz.

γ-(2,3-Dihydrophenalenyl)butyric Acid (3). A soln of 2,3-dihydrophenalenone (**2**) (9.1 g, 50 mmol) in a 1:1 mixture of anhyd benzene and ether (100 ml), zinc amalgam (10 g), and a small amount of iodine were placed in a three-necked flask. To this mixture methyl 4-bromocrotonate (2.2 g, 20 mmol) was added. The mixture was heated to 60 °C to start the reaction. After exothermic reaction occur additional methyl 4-bromocrotonate (8.8 g, 40 mmol) was added dropwise. After refluxing for 24 h the mixture was cooled and treated with dil hydrochloric acid. The organic layer was separated and washed successively with water, saturated sodium hydrogencarbonate soln, and water, dried (Na_2SO_4) and the solvent was removed to give methyl γ-(2,3-dihydro-1-hydroxyphenalenyl)crotonate as a viscous oil. IR (neat): 3450 (OH), 1700 cm^{-1} (C=O); NMR ($CDCl_3$): 1.8—2.1 (m, 2H), 2.4 (d, J=7, 2H), 2.8—3.1 (m, 2H), 2.9 (s, 1H), 3.6 (s, 3H), 5.6 (d, J=15, 1H), and 6.7—7.6 (m, 7H).

The crude ester thus obtained, palladium hydroxide charcoal (2 g), and 100 ml of ethanol were placed in a flask. The mixture was stirred under hydrogen atmosphere in an usual manner. After filtration of the catalyst, resulting soln was concd and the residue was dist under reduced pressure to give methyl γ-(2,3-dihydrophenalenyl)butylate as yellow oil, bp 170—174 °C/2 Torr, 8.4 g; IR (neat): 1730 cm^{-1} (C=O); NMR (CCl_4): 1.5—2.4 (m, 8H), 2.9—3.3 (m, 3H), 3.6 (s, 3H), and 7.0—7.7 (m, 6H).

Found: C, 80.34; H, 7.52%. Calcd for $C_{18}H_{20}O_2$: C, 80.56; H, 7.51%.

A mixture of the ester (8.4 g), 50% aq potassium hydroxide (10 ml), and ethanol (50 ml) was stirred for overnight at room temp. Most of the ethanol was removed and replaced by water. The aq layer was then washed with ether and acidified with 3M hydrochloric acid. The mixture was extracted with ether and the extract was washed with water and dried (Na_2SO_4). Evaporation of the solvent gave crude **3**. Recrystallization of the crude **3** from benzene–hexane yielded pure **3** as colorless plates, mp 90.0—90.5 °C; 6.11 g (48% yield based on **2**). IR(KBr): 3500—2500 (OH), 1700 cm^{-1} (C=O); NMR($CDCl_3$): 1.6—2.5(m, 8H), 2.9—3.3(m, 3H), 7.0—7.7(m, 6H), 10.7(bs, 1H).

Found: C, 80.42; H, 7.13%. Calcd for $C_{17}H_{18}O_2$: C, 80.28; H, 7.13%.

6H-7,8,9,9a,10,11-Hexahydrocyclohepta[cd]*phenalen-6-one (4).* To polyphosphoric acid prepared from 130 ml of phosphoric acid and 260 g of phosphorus pentaoxide was added 6.11 g of **3** at 90 °C by portion with care. The resultant soln was stirred at this temp for 1 h, then poured onto ice. Extraction with ether and the extract was washed successively with water, saturated aq soln of sodium hydrogencarbonate, and water, and dried (Na_2SO_4). Evaporation of the solvent gave crude **4** which on recrystallization from benzene–hexane afforded **4** as colorless plates, mp 97.5—98 °C; 4.7 g (75%); IR(KBr): 1665 cm^{-1} (C=O); NMR(CCl_4): 1.6—2.2(m, 6H), 2.5—2.7(m, 2H), 2.9—3.5(m, 3H), 7.0—7.7(m, 5H); MS: *m/e* 236(M^+, 100%), 208(M^+—CO, 27%).

Found: C, 86.65; H, 6.85%. Calcd for $C_{17}H_{16}O$: C, 86.40; H, 6.83%.

7,7-Dibromo-6H-7,8,9,9a,10,11-hexahydrocyclohepta[cd]*phenalen-6-one (5).* To a soln of **4** (1.0 g, 4.2 mmol) in carbon tetrachloride (30 ml) was added a soln of bromine (1.5 g, 9 mmol) in carbon tetrachloride (8 ml). The resultant soln was stirred for overnight at room temp and then washed with saturated aq soln of sodium hydrogensulfate and water, and dried (Na_2SO_4). Evaporation of the solvent under reduced pressure at 0 °C gave crude dibromide **5** as viscous oil in quantitative yield. IR(neat): 1695 cm^{-1} (C=O); NMR(CCl_4): 1.5—2.7(m, 6H), 2.8—3.3(m, 3H), 7.0—7.7(m, 5H). The crude **5** was used for subsequent reaction without further purification.

6H-10,11-Dihydrocyclohepta[cd]*phenalen-6-one (6).* Anhyd lithium chloride (0.55 g, 13 mmol) was added at once to a soln of **5**, prepared from 10 g of **4** described as above, in hexamethylphosphoric triamide (40 ml). The stirred mixture was heated at 95—100 °C for 1 h under nitrogen. After cooling the mixture was poured into 300 ml of water and the product, which was isolated by ether extraction, was chromatographed on 10 g of alumina eluted with benzene to give the tetracyclic ketone **6** (650 mg, 66.7%). Further elution with ether gave the full conjugated ketone **8** (110 mg, 10%). **6**: pale yellow plates, mp 90.0—90.5 °C, MS: *m/e* 232(M^+, 64%), 204(M^+—CO, 100%), 202(82%); IR (KBr): 1625, 1590, 1580 cm^{-1}; UV(ethanol): 243(4.38), 287 (4.33), 344(3.91); (cyclohexane): 240(4.39), 283(4.31), 337 (3.98); (concd H_2SO_4): 249(4.51), 299(4.57), 418(3.90); NMR: see text.

Found: C, 87.73; H, 5.28%. Calcd for $C_{17}H_{12}O$: C, 87.90; H, 5.21%.

Cyclohepta[cd]*phenalen-6-one (8).* (i) To a dry Pyrex tube were added 100 mg of **6** (0.43 mmol), 120 mg of 2,3-dichloro-5,6-dicyano-1,4-benzoquinone (0.53 mmol) and anhyd benzene (20 ml). The tube was evacuated and sealed and placed in a 120 °C oil bath for 20 h. Upon cooling, a small amount of ppt's was removed by filtration and the solvent was evaporated. Chromatography on alumina with benzene gave 41 mg of the starting material. Successive elution with ether afforded **5** (13 mg, 22%).

(ii) To a soln containing **6** (1.2 g, 5.2 mmol) in 30 ml of glacial acetic acid was added 1.8 g of triphenylmethyl tetrafluoroborate (5.5 mmol). The soln was refluxed under a nitrogen atmosphere for 1.5 h. After cooling, the mixture was poured into 200 ml of water and extracted with ether. The ethereal extracts were washed successively with a saturated soln of sodium hydrogencarbonate and water, dried (Na_2SO_4) and concentrated. The residue was purified by column chromatography on alumina with ether gave 500 mg of **5** (42%): orange scales, mp 144—146 °C, MS: *m/e* 230 (M^+, 27%), 202(M^+—CO, 100%); IR(KBr): 1600, 1590, 1560 cm^{-1}; UV(ethanol): 249(4.48), 311(4.07), 321(4.08), 430 (4.23); cyclohexane): 246(4.47), 311(4.10), 430(4.19); (concd H_2SO_4): 235(4.29), 269(4.27, sh), 294(4.45), 469(4.16, sh), 494 (4.58); NMR: see text.

Found: C, 88.41; H, 4.41%. Calcd for $C_{17}H_{10}O$: C, 88.67; H, 4.38%.

6H-(10) and 7H-Cyclohepta[cd]*phenalene (11).* Lithium aluminum hydride–aluminum chloride complex was prepared from 1.2 g (31.6 mmol) of $LiAlH_4$, 4.2 g (31.5 mmol) of $AlCl_3$ and 100 ml of ether under reflux. The clear supernatant (40 ml) was transferred into dry flask precooled to −55 °C by syringe. To this soln was added dropwise a soln of 120 mg of **7** (0.52 mmol) in 25 ml of dry THF over a period of 1 h at −55 °C. After stirring for 2 more h at −50 °C the mixture was stand for overnight maintained at −80 °C. To this soln was added a moist THF to prevent the reaction. The resultant yellow supernatant was transferred under nitrogen into a flask containing anhyd sodium sulfate by decantation and filtered. The solvent was concd at 0 °C under reduced pressure and replaced by hexane. The hexane soluble portion was chromatographed on a column of alumina deactivated with 10% water with light pet. ether afforded a 9:13 mixture of **10** and **11** (63 mg, 56%) as a yellow oil. MS: *m/e* 216(M^+, 100%), 215(M^+—H, 73%), 202(21%); NMR: see text. All manipulations have to be carried out under a nitrogen atmosphere to avoid decomposition.

Cyclohepta[cd]*phenalenium Tetrafluoroborate (1).* A suspen-

sion of 70 mg (0.21 mmol) of triphenylmethyl tetrafluoroborate in 2 ml of chloroform was stirred under a nitrogen atmosphere and a soln of a mixture of **10** and **11** in 2 ml of chloroform was added *via* syringe. The resultant reddish brown ppt's of **1** were filtered and washed thoroughly with chloroform followed by carbon tetrachloride. Reddish crystals, 50 mg (79%), mp sinter at 199—201 °C and show no definite melting point. IR(KBr): 1040 cm^{-1} (BF_4^-); UV(acetonitrile): 224(4.40), 257(3.99), 291(4.37), 307(4.37, sh), 316(4.40), 334 (4.18, sh), 475(4.49); NMR: see text.

Found: C, 67.96; H, 3.59%. Calcd for $C_{17}H_{11}BF_4$: C, 67.59; H, 3.67%.

*p*K *Determinations.* The cation **1** (1.968 mg) was dissolved in 50 ml of acetonitrile. Each 2 ml of the soln was then made up to 10 ml with the buffer soln. The region between pH 4.3 to 8.0 was covered with buffers made up from mixtures of 0.1 M citric acid and 0.2 M Na_2HPO_4. The pH's greater than 8.0 were obtained with a buffer containing 0.1 M ammonium chloride and 0.1 M ammonia water.

The standard procedure was adopted of examining the electronic spectrum of **1** in thirteen soln's of buffer spaced through a pH range of about 5.4 to 9.5. The absorbancy at a wavelength characteristic of the cation was plotted against pH and the mid-point of the resulting titration curve was taken as the pK_R^+. The wavelength used was 475 nm. The pH's were read on a Beckman model G pH meter. Because after long periods the absorbancy was irreversibly changed on the basic side (pH>7), all spectra were taken just after 90 s of mixing the soln of the cation with that of the buffer. The pK_R^+ value thus obtained was found to be 8.4. When the spectra were taken after 180 s of mixing, the pK_R^+ was found to be 8.1.

The authors wish to thank Prof. R. Zahradnik and Dr. Z. Slanina, Czechoslovak Academy of Sciences, for their PPP-LCI-SCF calculations on **1** and for their generous permission to quote the results in this paper.

References

1) Part XXII of this series, see K. Nakasuji and I.Murata, *Tetrahedron Lett.*, **1976**, 2155.

2) Preliminary communications of the present paper appeared: (a) I. Murata, K. Yamamoto, and Y. Kayane, *Angew. Chem.*, **86**, 861 (1974); *Angew. Chem. Int. Ed. Engl.*, **13**, 807 (1974); (b) I. Murata, K. Yamamoto, and Y. Kayane, *Angew. Chem.*, **86**, 862 (1974); *Angew. Chem. Int. Ed. Engl.*, **13**, 808 (1974).

3) V. Boekelheide, W. E. Langeland, and C.-T. Liu, *J. Am. Chem. Soc.*, **73**, 2432 (1951); V. Boekelheide and G. K. Vick, *ibid.*, **78**, 653 (1956); H. Prinzbach, L. Knothe, and H.-W. Schneider, *Angew. Chem.*, **85**, 1113 (1973); *Angew. Chem. Int. Ed. Engl.*, **12**, 1009 (1973).

4) R. Munday and I. O. Sutherland, *J. Chem. Soc.*, **1969**, 1427, and references cited therein.

5) D. H. Reid, W. H. Stafford, and G. P. Ward, *J. Chem. Soc.*, **1955**, 1193.

6) P. D. Gardner, C. E. Wulman, and C. L. Osborn, *J. Am. Chem. Soc.*, **80**, 143(1958).

7) A. G. Anderson, Jr., A. A. MacDonald, and A. F. Montana, *J. Am. Chem. Soc.*, **90**, 2993 (1968); A. G. Anderson, Jr., G. M. Masada, and A. F. Montana, *J. Org. Chem.*, **38**, 1439 (1973); A. G. Anderson, Jr., A. F. MacDonald, and G. M. Masada, *ibid.*, **38**, 1445(1973); Ch. Jutz and E. Schweiger, *Angew. Chem.*, **83**, 886 (1971); *Angew. Chem. Int. Ed. Engl.*, **10**, 808 (1971); Ch. Jutz and E. Schweiger, *Synthesis*, **1974**, 193.

8) K. Hafner, R. Fleischer, and K. Fritz, *Angew. Chem.*, **77**, 42 (1965); *Angew. Chem. Int. Ed. Engl.*, **4**, 69 (1965).

9) H. Reel and E. Vogel, *Angew. Chem.*, **84**, 1074 (1972); *Angew. Chem. Int. Ed. Engl.*, **11**, 1013 (1972).

10) I. Murata, K. Yamamoto, M. Morioka, M. Tamura, and T. Hirotsu, *Tetrahedron Lett.*, **1975**, 2287.

11) B. M. Trost, D. Buhner, and G. M. Bright, *Tetrahedron Lett.*, **1973**, 2787.

12) B. M. Trost and P. L. Kinson, *J. Am. Chem. Soc.*, **92**, 2591 (1970); **97**, 2438 (1975).

13) (a) R. H. Cox, E. G. Janzen, and J. L. Gerlock, *J. Am. Chem. Soc.*, **90**, 5906 (1968); (b) I. Willner and M. Rabinovitz, *Tetrahedron Lett.*, **1976**, 1223.

14) R. Zahradnik, J. Michl, and J. Pancir, *Tetrahedron*, **22**, 1355 (1966).

15) I. Murata and K. Yamamoto, *Chem. Lett.*, **1973**, 413.

16) I. Murata, K. Yamamoto, T. Hirotsu, and M. Morioka, *Tetrahedron Lett.*, **1972**, 331.

17) I. Murata, K. Yamamoto, and T. Hirotsu, *Tetrahedron Lett.*, **1972**, 3389.

18) I. Murata and K. Yamamoto, unpublished results.

19) L. F. Fieser and M. D. Gates, *J. Am. Chem. Soc.*, **62**, 2335 (1940); V. Boekelheide and C. E. Larrabee, *ibid.*, **72**, 1240 (1950); D. M. Reid and R. G. Sutherland, *J. Chem. Soc.*, **1963**, 3295.

20) E. Kloster-Jensen, N. Tarkoy, A. Eschenmoser, and E. Heilbronner, *Helv. Chim. Acta*, **39**, 786 (1956); N. J. Leonard, L. A. Miller, and J. W. Berry, *J. Am. Chem. Soc.*, **79**, 1485 (1957); H. H. Rennhard, G. DiModica, J. Simon, A. Eschenmoser, and E. Heilbronner, *Helv. Chim. Acta*, **40**, 957 (1957).

21) S. Julia and Y. Bonnet, *Bull. Soc. Chim. Fr.*, **1957**, 1340.

22) J. D. McCollum and S. Meyerson, *J. Am. Chem. Soc.*, **85**, 1739 (1963); J. M. Wilson, M. Ohashi, H. Budzikiewicz, C. Djerassi, S. Ito, and T. Nozoe, *Tetrahedron*, **19**, 2247 (1963).

23) Private communication (June 28, 1974) from Prof. R. Zahradnik. Calculated bond orders ($p_{1,j}$) and charge densities (q_1) of **1** are: $p_{1,2}=0.669$, $p_{3,3a}=0.589$, $p_{3a,4}=0.493$, $p_{4,5}=0.764$, $p_{5,5a}=0.529$, $p_{5a,6}=0.535$, $p_{6,7}=0.716$, $p_{7,8}=0.574$, $p_{3a,3b}=0.526$, $p_{5a,5b}=0.512$, $p_{3b,5b}=0.534$, and $q_1=0.907$, $q_2=0.962$, $q_{3a}=1.002$, $q_4=0.894$, $q_5=1.003$, $q_{5a}=0.916$, $q_6=0.911$, $q_7=0.900$, $q_{3b}=1.009$, $q_{5b}=0.964$.

24) The analysis of AA'XX' spectrum was performed according to the following literature: H. Gunther, *Angew. Chem.*, **84**, 907(1972); *Angew. Chem. Int. Ed. Engl.*, **11**, 861 (1972).

25) The assignment of H-5,10 and H-4,11 was made according to the calculated π-electron density at their respective carbon atoms.[23]

26) H. Günther, A. Shyoukh, D. Cremer, and K. H. Frisch, *Tetrahedron Lett.*, **1974**, 781.

27) G. Fraenkel, R. E. Carter, A. McLachlan, and J. H. Richards, *J. Am. Chem. Soc.*, **82**, 5846 (1960); T. Schaeffer and W. G. Schneider, *Can. J. Chem.*, **41**, 966 (1963); J. R. Leto, F. A. Cotton, and J. S. Waugh, *Nature (London)*, **180**, 978 (1957).

28) H. Prinzbach, V. Freudenberger, and U. Scheidegger, *Helv. Chim. Acta*, **50**, 1087(1967).

29) Recent ESR studies have revealed that the neutral radical derived from **1** by an electrolytic reduction in DMF at −40°C can be well characterized by the phenalenyl radical coupled to the *cis*-1,3-butadiene π-system. F. Gerson, J. Jachimowicz, I. Murata, K. Nakasuji, and K. Yamamoto, *Helv. Chim. Acta*, **58**, 2473(1975).

30) I. Fleming, *J. Chem. Soc., Perkin Trans. 1*, **1973**, 1019.

31) Y. Kayama, M. Oda, and Y. Kitahara, *Chem. Lett.*, **1973**, 1169.

Reaction between 2,2-Diphenyl-1-picrylhydrazyl and Phenols. Substituent and Solvent Effects

Norio NISHIMURA, Toshimichi MORIYA, Yoshiko OKINO, Kazue TANABE, Kimio KAWABATA, and Toshihiko WATANABE

Department of Chemistry, Faculty of Science, Okayama University, Tsushima, Okayama 700

(Received December 22, 1975)

A kinetic study has been made of the reaction between 2,2-diphenyl-1-picrylhydrazyl and phenols in various solvents. Polar effects in the rate-determining transition state are discussed in terms of the Hammett type relationship. Remarkable solvation effects were observed. For *p*-methoxyphenol the reaction rate is the greatest in the solvents which do not form strong H-bond with phenols, and the smallest in aprotic H-accepting solvents. For *o*-methoxyphenol the rate is the greatest in protic solvents. The results are interpreted in terms of the difference in the mode of hydrogen bondings. The rate for the reaction of the radical with α-naphthol was followed in dioxane–2,2,4-trimethylpentane mixtures. The results are explained by the theory of Kondo and Tokura, indicating that the free energy depression in the ground state takes place mainly through hydrogen bonding.

The oxidation of phenols is known to be complicated from the fact that different products are obtained from the same phenols by use of different oxidants.[1] The stable free radical 2,2-diphenyl-1-picrylhydrazyl (DPPH) has been used not only as a radical scavenger but also as a hydrogen acceptor. The strong H-accepting property of DPPH has been demonstrated by a number of reactions between the radical and compounds containing C–H, N–H, O–H, and S–H bonds.[2-7]

The hydrogen abstraction reactions of DPPH from phenols have been a subject of interest. Hogg *et al.*[6] found that the rate is first-order with respect to DPPH and phenols; about two moles of DPPH is consumed by one mol of the phenols; retardation by the major product, 2,2-diphenyl-1-picrylhydrazine ($DPPH_2$), is generally observed; the rates are roughly correlated with the Hammett σ in the range $-0.4<\sigma<0.2$ ($\rho=-6$), but not beyond the entire range, the *o*-substitution lowering the rate remarkably. They suggested that the H-abstraction is involved in the rate-determining step. McGowan *et al.*[4] suggested that the rate-determining step involves the removal of a hydride ion to give a cation, since the substituent effect is very similar to the solvolysis of α,α-dimethylbenzyl chlorides.

Among the factors that influence the rate, the solvent effect is considered to be one of the most important. However, information is scanty. If we select closely related phenols and carry out the reaction in a variety of selected solvents, the effect of individual factors could be observed. Bivalent phenols, *o*- and *p*-methoxyphenols, and α-naphthol were chosen and the reaction was carried out in various solvents and their binary mixtures.

Experimental

Materials. $DPPH_2$ was prepared according to the method given by Goldschmidt and Renn,[8] or Poirier *et al.*[9] Recrystallization was carried out from a chloroform–ethanol mixture. DPPH was prepared by oxidizing $DPPH_2$ in benzene with lead dioxide, and purified by repeated crystallization from a benzene–ligroin mixture, and then from carbon disulfide. Solid phenols of reagent grade were purified by means of sublimation. The reagents were stored in the dark and sublimed again just before use. *o*-Methoxyphenol was distilled twice under reduced pressure. Solvents were dried and purified in the usual way.

Procedures. DPPH exhibits a strong absorption around 520 nm. The absorbance at this wavelength was followed by means of a Hitachi 101 or 124 Spectrophotometer. The solutions of these phenols(10^{-3}—10^{-5} M) and DPPH(*ca.* 10^{-5} M) of desired concentrations were prepared separately and allowed to stand for about 30 min in a thermostat. The mixture of the two solutions was transferred quickly into a 3 cm optical cell equipped with a jacket through which thermostated water is circulated. The reaction temperature was controlled within ±0.2 °C. The absorbance at 520 nm was recorded at appropriate time intervals. In transforming the absorbance into concentration, a small correction due to the production of $DPPH_2$ was made. The rate constants were checked by duplicate runs.

Results

Effects of Oxygen, $DPPH_2$, and Picryl Chloride. It is possible that oxygen exerts some effect on the rate and nature of products. In order to examine this, the reaction was carried out in aerated and deaerated solutions. No appreciable difference in rates was observed for hydroquinone and catechol. Thus all the reactions involving them were carried out in the presence of air. No retardation was observed even when a great excess of $DPPH_2$ was added with respect to DPPH. For resorcinol, the rate was somewhat greater in aerated solutions than in deaerated ones (Table 1). Retardation occurred for phenols other than hydroquinone and

TABLE 1. RATE CONSTANTS FOR THE REACTION BETWEEN DPPH AND BIVALENT PHENOLS IN BENZENE

Temp (°C)	$k(M^{-1} s^{-1})$			
	Resorcinol		Hydroquinone ($\times 10^2$)	Catechol ($\times 10^2$)
	in N_2	in Air		
15	—	—	0.91	1.5_0
20	0.15_4	0.16_9	1.0_8	1.7_0
25	0.19_6	0.24_4	1.2_7	1.9_5
30	0.29_4	0.30_9	1.4_8	2.2_0
35	0.36_4	0.46_5	—	—
40	0.49_3	0.54_3	—	—
E_a(kcal/mol)	$10._5$	$10._3$	5.6_6	4.0_2
ΔS^*(gibbs/mol)	$-28._4$	$-28._9$	$-31._9$	$-36._6$

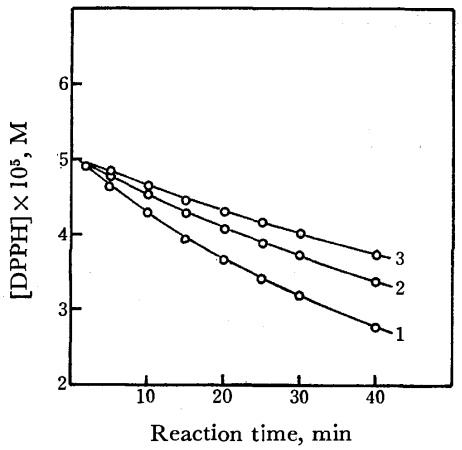

Fig. 1. Retardation effect by added $DPPH_2$ for the reaction between DPPH and resorcinol in deaerated benzene at 30 °C; $[DPPH]_0=5\times10^{-5}$ M, $[Res]_0=10^{-3}$ M, $[DPPH_2]_0$: 1, 0; 2, 2×10^{-5} M, 3, 4×10^{-5} M.

catechol in the presence of $DPPH_2$. An example is shown in Fig. 1. Picryl chloride was added to the system, since substances having a picryl group often form picrates with many compounds and this might exert a specific effect on the rate. However, no appreciable change in rate was observed.

Stoichiometry and Reaction Products. Aliquots of the DPPH and phenol solutions were mixed and allowed to stand. After the reaction had ceased, the concentrations of the remaining DPPH were determined and plotted against $[DPPH]_0/[Phenol]_0$. We see that the molar ratios of DPPH to both hydroquinone and catechol reacted are 2: 1 (Fig. 2). The same holds for α-naphthol. For resorcinol the reaction was too slow to determine the ratio exactly, more than two moles of DPPH being consumed per mole of resorcinol after a long time. More than 75% of consumed DPPH was converted into $DPPH_2$, the isolation of which from a reaction mixture being made by alumina column chromatography. The quantities of the produced quinones were estimated by iodometry recommended by Mahoney and DaRooge.[10] It was found that 90 and 93% of hydroquinone and catechol were converted into the corresponding quinones, respectively. Isolation and identification of the products from other phenols were unsuccessful.

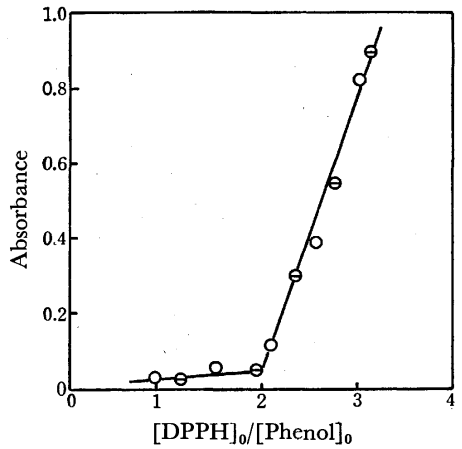

Fig. 2. Stoichiometry for the reaction between DPPH and bivalent phenols. ○: Catechol, ⊖: hydroquinone.

Order of Reaction. The reaction between DPPH and hydroquinone (and catechol) was found to follow strictly the second-order kinetics over almost the entire course of reaction. The apparent rate constants were estimated on the basis of the integrated second-order rate equation in which the above stoichiometry was taken into account. For other phenols, the conventional initial-rate method was applied to determine the order. The reaction was found to be first-order with respect to both DPPH and the phenols.

Reaction Rates. The values of the rate constants in benzene at various temperatures are given in Table 1 together with the Arrhenius parameters. The rate constants in various solvents are given in Tables 2 and 3. The activation parameters in benzene are $E_a=9.4$ kcal/mol. $\Delta S^*(300\text{ K})=-25$ gibbs/mol for *o*-methoxyphenol, and $E_a=4.7$ kcal/mol, $\Delta S^*(300\text{ K})=-22$ gibbs/mol for *p*-methoxyphenol. The values for the latter are in good agreement with those reported.[6] The difference in the activation energies (4.7 kcal/mol) in benzene can be ascribed to the energy of intramolecular H-bonding for the *o*-isomer. The rate constants for α-naphthol in the binary dioxane-2,2,4-trimethylpentane(isooctane) mixtures are given in Table 4 together with the activation parameters.

Table 2. Rate constants for the reaction of DPPH with hydroquinone and catechol in various solvents

Solvent	Temp (°C)	$k(M^{-1}s^{-1})$ Hydroquinone	$k(M^{-1}s^{-1})$ Catechol
Benzene	30	$1.4_8\times10^2$	$2.2_0\times10^2$
Carbon tetrachloride	28.8	—[a]	$1.8_1\times10^2$
Dioxane	25	6.3_0	2.1_2
Acetone	30	5.4_5	1.8_7
Diethyl ether	28.8	2.3_0	1.5_5
Ethanol[b]	28.8	≈5	≈20
Methanol[b]	28.8	≈20	—

a) Insoluble. b) Reproducibility poor. Contamination by a trace of water possibly responsible.[11]

Table 3. Rate constants for the reaction of DPPH with methoxyphenols at 20 °C

Solvent	$k(M^{-1}s^{-1})$ *p*-Isomer	$k(M^{-1}s^{-1})$ *o*-Isomer
Carbon tetrachloride	120	0.67
Benzene	40	0.47
Methanol[a]	≈16	≈5
2-Propanol[a]	≈9	≈3
Diethyl ether	1.23	0.087
Dioxane	0.60	0.039

a) Reproducibility poor as compared with that in the other solvents.

TABLE 4. RATE CONSTANTS FOR THE REACTION OF DPPH WITH α-NAPHTHOL IN ISOOCTANE–DIOXANE MIXTURES

Mole fraction of isooctane	k_{mix}, (M^{-1} s^{-1}) 15 °C	20 °C	25 °C	E_a kcal/mol	log A s^{-1}
0.000	0.42 (14.5 °)	0.61	0.75	9.9	7.1
0.049	0.53	0.65	0.88	8.5	6.2
0.121	0.60	0.74	1.0	8.2	6.0
0.194	0.68	0.91	1.2	9.6	7.1
0.340	1.1	1.4	1.9	9.6	7.3
0.608	2.7	3.4	4.6	9.4	7.6
0.699	4.1	5.3	7.1	9.8	8.0
0.823	9.4	12	16	9.6	8.3
0.954	42	51	61	6.6	6.5
1.000[a]	15 (−60 °)	110 (0 °)	350 (30 °)	4.6	5.8

a) Rate measured at temperatures as indicated in parentheses, because of a great reaction rate and low activation energy in pure isooctane.

Discussion

Reaction Sequence. A possible main reaction sequence for the reaction of DPPH with bivalent phenols can be given by

$$QH_2 + DPPH \underset{k_{-1}}{\overset{k_1}{\rightleftharpoons}} QH\cdot + DPPH_2$$

(1) (foward reaction), (1′) (reverse reaction)

$$QH\cdot + DPPH \xrightarrow{k_2} Q + DPPH_2 \quad (2)$$

$$2QH\cdot \xrightarrow{k_3} \text{Combination, Disproportionation}^{12-15)} \quad (3)$$

$$QH\cdot + O_2 \xrightarrow{k_4} \text{Peroxide}^{16)} \quad (4)$$

where QH_2 and Q denote the bivalent phenols and the corresponding quinones, respectively, and QH· the phenoxy radical.

For hydroquinone and catechol, Reactions 1′ and 4 can be neglected on the basis of experimental evidence. In order to be consistent with the rate equation and the reaction products, Reaction 3 could also be neglected as compared with Reaction 2. This may be rationalized by the following consideration: The termination constants for unhindered phenoxy radicals have been measured by flash photolysis[14,15] and ESR[12] techniques. The reported values are 10^6—10^9 M^{-1} s^{-1} depending on substituent and solvent. If we assume that $k_3 \approx 10^9$ M^{-1} s^{-1} (diffusion-controlled rate constant), then it can be shown that Reaction 3 can be neglected only when k_2 is approximately larger than 10^7 M^{-1} s^{-1}. Since DPPH has been used as a radical scavenger, a value as large as $\approx 10^7$ M^{-1} s^{-1} is not surprising.

The free energy of activation for Reaction 2 would be favored by the resonance contribution such as

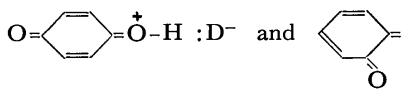

in the transition states for hydroquinone and catechol, where D denotes DPPH. Using the data given by Ayscough and Russell[13] and Mahoney *et al.*,[17] the heat of reaction of DPPH with hydroquinone was calculated to be $\Delta H = -12.3$ kcal/2 mol of DPPH. Since the heat of reaction of 1 can be estimated to be *ca.* 26 kcal/mol from the difference in the dissociation energy of N–H and O–H bonds, the driving forces of Reaction 2 must be the large exothermicity ($\Delta H = -38.3$ kcal/mol) and probably a low activation energy of this step. It can thus be concluded that the rate-determining step is involved in Reaction 1.

The rates for hydroquinone and catechol are of the same order of magnitude.* This indicates that the first abstracted hydrogen atom for catechol is the one which is not intramolecularly H-bonded. For resorcinol, the phenoxy radicals may be consumed *via* competition reactions (1′, 2, 3, and 4) making kinetic analysis difficult. The existence of opposing reaction (Reaction 1′) might be responsible for the upward deviation from the pseudo first-order plot and the retardation by $DPPH_2$ (Fig. 1), as suggested for other phenols.[6] The fact that a small increase in rates in aerated solutions was observed for resorcinol (Table 1) seems to suggest the importance of Reaction 1′.

An alternative explanation for the retardation effect of $DPPH_2$ is to assume complex formation between DPPH and $DPPH_2$; it was introduced to explain the kinetics of the reaction of DPPH with amines and solvents.[2,18] It cannot be excluded since we found that the absorbance of DPPH–$DPPH_2$ mixture at 520 nm is slightly smaller than that expected from the additivity rule. However, if any complex formation were to occur, it would not exert remarkable effect on the reaction rate, since no retardation was observed for hydroquinone and catechol.

Substituent Effects. The reaction between DPPH and resorcinol proceeds much more slowly, the activation energy being *ca.* 5 kcal/mol higher than that for other bivalent phenols. Since the activation energies of univalent phenols are between 4.8 and 16.1 kcal/mol,[6] the difference in the rate is considered to be due to the substituent effects rather than the change in mechanism. Hogg *et al.*[6] studied the dependence of the rate on substituents and obtained a linear relation with a break point at σ nearly equal to 0.2 in the normal Hammett plot. On the other hand, McGowan *et al.*[4] found that the relative rates of the reactions in carbon tetrachloride are very close to those for the solvolysis of α,α-dimethylbenzyl chlorides, and suggested an ionic mechanism involving the abstraction of a hydride ion from phenols.

The polar effect arguments[19-21] in hydrogen abstraction reactions by radicals have been introduced to rationalize the substituent effects in the radical reactions. It was found that the correlation is better when log (relative-reactivity) is plotted against σ^+-values than against σ-values.[22-26] The contribution of polar mesomeric structures for the interpretation of radical reactions has been recognized to be useful.[19,27] It may

* The apparent rate constant for hydroquinone in Table 1 should be divided by two for comparison with other univalent phenols and catechol. Catechol reacts about three times faster than hydroquinone.

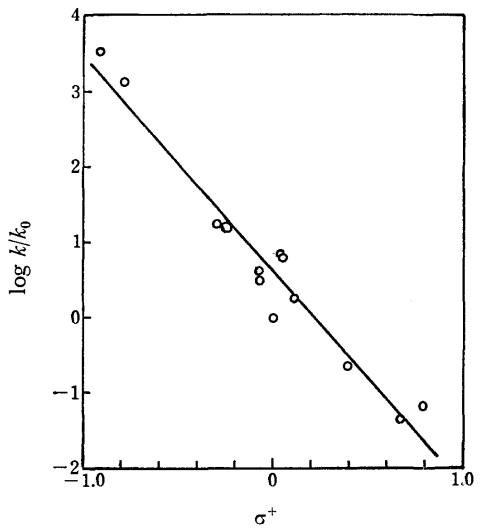

Fig. 3. Corelation of the rate constants for the reaction between DPPH and phenols with σ^+-values; in benzene at 30 °C.

be worthwhile to reexamine the polar effect in this reaction series. Using the data of Hogg *et al.*[6] and those in the present study, log k/k_0 is plotted against σ^+ (Fig. 3). ρ is calculated to be -2.8 by the least-squares method. The correlation coefficient $r=-0.970$ of the σ^+-plot is much better than for the normal Hammett σ-plot ($r=-0.883$). It is noted that ρ has a very large negative value as compared with that for other H-abstraction reactions with more reactive radicals than DPPH.[22-26] Mahoney and DaRooge[10] reported that $\rho=-2.8$($\rho\sigma^+$-plot) for the reaction of 2,4,6-tri-*t*-butylphenoxyl with substituted phenols. We also found that $\rho=-3.1$($\rho\sigma^+$-plot, $r=-0.993$) for the reaction of 2,6-di-*t*-butyl-α-(3,5-di-*t*-butyl-4-oxo-2,5-cyclohexadiene-1-ylidene)-*p*-tolyloxyl(galvinoxyl) with substituted phenols.[28] Such high selectivity would be caused by the extremely stable and electrophilic nature of these radicals. Thus the large ρ-value in this reaction series is not regarded as exceptional. The existence of a better correlation with σ^+-substituent constants and the very large negative value indicate that the contribution of the resonance structures such as II, III, and IV virtually plays an important role in stabilizing the transition state. Hence DPPH acts as an electrophile as in the case of aromatic amines.[4]

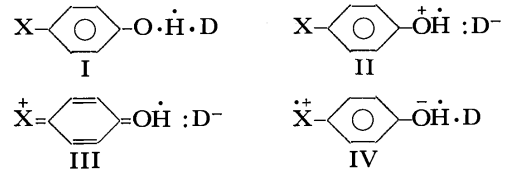

Zavitsas[29,30] suggested that σ merely reflects the difference in the bond dissociation energies. However, since the reaction rates are not always directly related to the bond dissociation energies, his suggestion is questionable.[20,21]

In order to interpret the large substituent effect, we might assume the formation of a CT-complex between the phenols and DPPH, followed by a slow proton transfer. However, we have no spectroscopic evidence. Addition of picryl chloride has no effect on the rate. The kinetic data are not in line with the assumption. Thus such a CT-complex may exist, if any, only as a transient species.

Solvent Effects. Although bulk properties such as the dielectric constant of medium are important in radical reactions, specific solvation effect such as H-bonding would be more important. We see from Table 2 that the rate is the greatest in solvents which do not usually form H-bond, and the slowest in aprotic H-accepting solvents. Acetone, dioxane, and diethyl ether act as H-acceptors. Since the reaction involves the abstraction of the H-bonded hydrogen, extra energy is required for desolvation in the transition state. The rates in protic solvents seem to suggest that the solvents act as a proton-donor as well as a proton-acceptor. There is a marked difference between *o*- and *p*-methoxyphenols in reactivity (Table 3). It seems that the difference is too large to be ascribed to the steric and/or electronic effects since the reactivity ratios depend strongly on the nature of solvent. It is reasonable to ascribe the slower rate for *o*-methoxyphenol to the intramolecular H-bonding. In diethyl ether and dioxane, there should be an intermolecular H-bond formation between the *p*-isomer and these solvents. This may be responsible for the pronounced decrease in rates. It is noted that the rates are of the same order as those for the *o*-isomer in benzene and carbon tetrachloride. On the other hand, since the *o*-isomer is already intramolecularly H-bonded, no serious solvent effect is expected for this compound. However, the rates decreased one order of magnitude in dioxane and diethyl ether as compared with benzene and carbon tetrachloride (Table 3). This could be interpreted in terms of the masking effect through partial H-bonding with the solvents. For the *o*-isomer the rates are greater in methanol and 2-propanol than in other solvents. The alcohols would behave as a proton donor as well as a proton acceptor. The hydroxyl group of the solvents would help push out the hydrogen atom being abstracted. The fact that the rate is greater for catechol than for hydroquinone supports this idea. Judging from the experimental results, the pushing effect overwhelms the masking effect for the *o*-isomer. Since the hydroxyl group of this compound is fixed by the neighboring methoxy group, the pushing effect may become predominant. On the other hand, the masking effect is operative for the *p*-isomer. The rate can be determined by a compromise between the two effects.

An alternative interpretation is that a rapid proton exchange in protic solvents results in only a small difference in the rates of the two isomers. In this respect, the comparatively poor reproducibility in the protic solvents (Tables 2 and 3) deserves attention.

Reaction in Binary Mixtures. If the thermodynamic quantities for solvation are known, they can be correlated with the rate factors. If we examine the dependency of the reaction rate on the composition of mixed solvents, with one of which the reactant is solvated, the result would be of interest. Kondo *et al.*[31] have developed a theory of the reaction rates in binary mixed solvents.

They derived rate equations

$$A + B \longrightarrow M^* \longrightarrow X + Y \cdots$$

for a general second-order reaction in mixed solvents which consist of two components denoted by 1 and 4. If only one of the reactants, say B, is solvated in the solvent 4 to form an addition product, the simplified rate equation is given by

$$\ln k_{mix} = x_1 \ln k_1 + x_4 \ln k_4 + x_4 \ln (K_x + 1) - \ln (x_4 K_x + 1), \quad (5)$$

where K_x denotes the association constant expressed in terms of mole fractions for the formation of the addition product; x_1 and x_4 are the mole fractions of 1 and 4, respectively. The expression for the activation energy is given by differentiating Eq. 5 with respect to temperature;

$$E_{mix} = x_1 E_1 + x_4 E_4 - \frac{x_1 x_4 \Delta H^\circ}{(1 + 1/K_x)(x_4 + 1/K_x)}, \quad (6)$$

where ΔH° denotes the heat of formation of the adduct.

In acetone–cyclohexane mixtures, the rate deviates considerably from that expected from an ideal solution (Figs. 4 and 5). Although the deviation is as expected from Eq. 5, the rate in pure cyclohexane and the K_x-value could not be obtained in this system.

For examination of Eqs. 5 and 6, we carried out the reaction of DPPH with α-naphthol in isooctane–dioxane mixtures; the results are given in Table 4. The system was chosen since Baba and Suzuki[32] reported that the association constant for the reaction

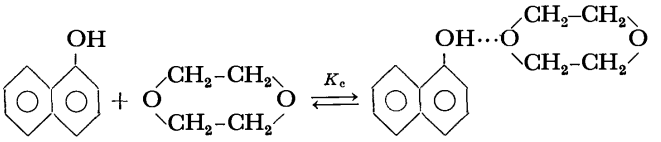

is K_c(20 °C)=20.9 M^{-1} and the heat of formation is ΔH° = −5.4 kcal/mol. The heat of formation of the adduct agrees with the difference in activation energy for the reaction in pure dioxane and isooctane (Table 4). In the

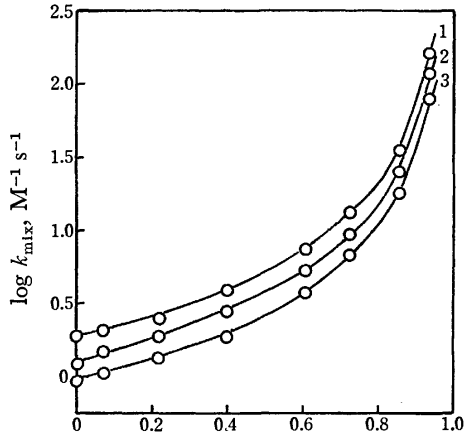

Fig. 4. Plots of log k_{mix} *vs.* the mole fraction of cyclohexane (x_1) for the reaction between DPPH and catechol in cyclohexane–acetone mixed solvent. Temperatures: 1, 30 °C; 2, 25 °C; 3, 20 °C.

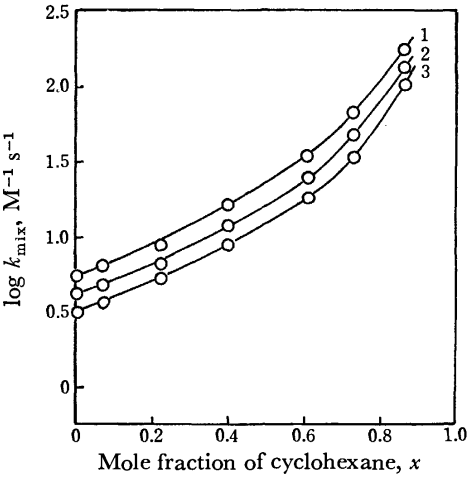

Fig. 5. Plots of log k_{mix} as a function of x_1 for DPPH–hydroquinone system. Temperatures: 1, 30 °C; 2, 25 °C; 3, 20 °C.

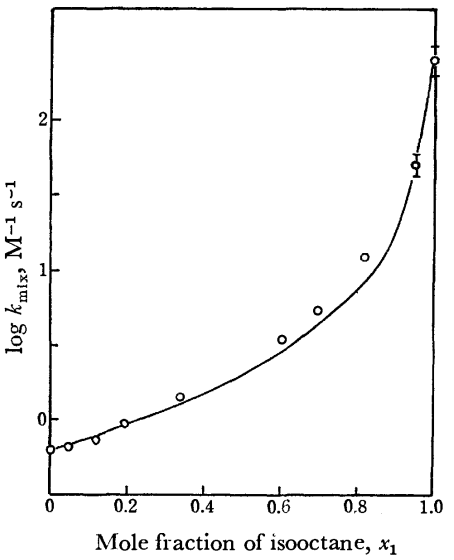

Fig. 6. Dependence of log k_{mix} on the mole fraction of isooctane for the reaction between DPPH and α-naphthol in dioxane–isooctane mixtures at 20 °C.

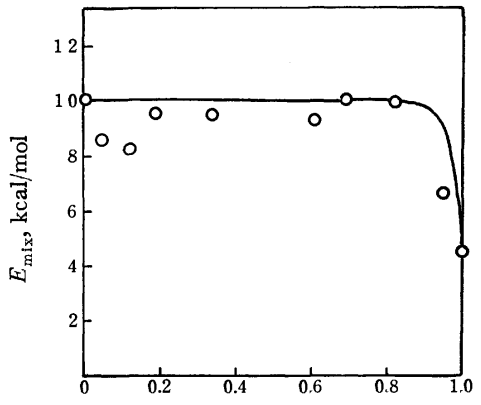

Fig. 7. Dependence of the activation energy on the mole fraction of isooctane.

papers of Kondo *et al.*[31] K_x-values were tacitly assumed to be independent of the solvent composition. However, this is not the case generally. In the present case the K_x-value varies from 245 in pure dioxane to 126 in pure isooctane when $K_c=20.9\ M^{-1}$ is used. By means of Eq. 5, the rate constant k_{mix} at any composition can be calculated using the values for k_1 and k_4 (Table 4) and the K_x-values estimated from the K_c-values obtained by Baba and Suzuki. The predicted k_{mix}-values are plotted in Fig. 6 as a function of the mole fraction of isooctane (solid line), together with the experimental points (open circles). It can be seen that the behavior of the specific solvation interaction in the binary dioxane–isooctane system is expressed by this theory. A similar treatment has been carried out for the energy of activation (Fig. 7). As a results of the specific solvation, the energy of activation decreases sharply as the mole fraction of isooctane approaches unity, as predicted by the theory.

It is concluded that in the hydrogen abstraction reaction in this system, the most important factors which govern the reaction rate are the polar mesomeric and H-bonding effects which affect greatly the free energies in the transition and ground states, respectively.

The authors wish to thank Proffessor S. Hasegawa, Dr. M. Kimura, and Dr. S. Yamamoto for their valuable discussions and suggestions.

References

1) W. A. Waters, *J. Chem. Soc., B*, **1971**, 2026.
2) E. A. Braude, A. G. Brook, and R. P. Linstead, *J. Chem. Soc.*, **1954**, 3574.
3) K. E. Russell, *J. Phys. Chem.*, **58**, 437 (1954).
4) J. C. McGowan, T. Powell, and R. Raw, *J. Chem. Soc.*, **1959**, 3103.
5) J. C. McGowan and T. Powell, *J. Chem. Soc.*, **1961**, 2160.
6) J. S. Hogg, D. H. Lohmann, and K. E. Russell, *Can. J. Chem.*, **39**, 1588 (1961).
7) H. Watanabe and K. Kido, *Kogyo Kagaku Zasshi*, **60**, 1476 (1957).
8) S. Goldschmidt and K. Renn, *Ber.*, **55**, 628 (1922).
9) R. H. Poirier, E. J. Kahler, and F. Benington, *J. Org. Chem.*, **17**, 1437 (1952).
10) L. R. Mahoney and M. A. DaRooge, *J. Am. Chem. Soc.*, **92**, 890 (1970).
11) G. H. Schenk and D. J. Brown, *Talanta*, **14**, 257 (1967).
12) L. R. Mahoney and S. A. Weiner, *J. Am. Chem. Soc.*, **94**, 585 (1972).
13) P. B. Ayscough and K. E. Russell, *Can. J. Chem.*, **45**, 2020 (1967).
14) E. J. Land and G. Porter, *Trans. Faraday Soc.*, **59**, 2016 (1963).
15) G. Dobson and L. I. Grossweiner, *Trans Faraday Soc.*, **61**, 708 (1965).
16) C. D. Cook, R. C. Woodworth, and P. Fianu, *J. Am. Chem. Soc.*, **78**, 4159 (1956).
17) L. R. Mahoney, F. C. Ferris, and M. A. DaRooge, *J. Am. Chem. Soc.*, **91**, 3883 (1969).
18) P. J. Proll and L. H. Sutcliffe, *Trans. Faraday Soc.*, **59**, 2090 (1963).
19) W. A. Pryor, "Free Radicals," McGraw-Hill, New York, N. Y. (1966), p. 170.
20) R. W. Henderson, *J. Am. Chem. Soc.*, **95**, 6993 (1973).
21) W. A. Pryor, W. H. Davis, Jr., and J. P. Stanley, *J. Am. Chem. Soc.*, **95**, 4754 (1973).
22) R. E. Pearson and J. C. Martin, *J. Am. Chem. Soc.*, **85**, 3142 (1963).
23) G. A. Russell and R. C. Williamson, Jr., *J. Am. Chem. Soc.*, **86**, 2357 (1964).
24) R. Kennedy and K. U. Ingold, *Can. J. Chem.*, **44**, 2381 (1966).
25) H. Sakurai and A. Hosomi, *J. Am. Chem. Soc.*, **89**, 458 (1967).
26) C. Walling and J. A. McGuinness, *J. Am. Chem. Soc.*, **91**, 2053 (1969).
27) J. E. Leffler and E. Grunwald, "Rates and Equilibria of Organic Reactions," John Wiley & Sons, Inc., New York (1963), p. 177.
28) N. Nishimura, K. Okahashi, T. Yukutomi, unpublished results.
29) A. A. Zavitsas, *J. Am. Chem. Soc.*, **94**, 2779 (1972).
30) A. A. Zavitsas and J. A. Pinto, *J. Am. Chem. Soc.*, **94**, 7390 (1972).
31) Y. Kondo, K. Uosaki, and N. Tokura, *Bull. Chem. Soc. Jpn.*, **44**, 2548 (1971), and references cited therein.
32) H. Baba and S. Suzuki, *J. Chem. Phys.*, **35**, 1118 (1961).

Syntheses of 4-Phenylcoumarins Containing a Dimethylpyran Ring

Takanao MATSUI,* Shinji NISHIMURA, Mitsuru NAKAYAMA, Shûichi HAYASHI, and Kenji FUKUI

**Department of Industrial Chemistry, Faculty of Engineering, Miyazaki University, Miyazaki 880*
Department of Chemistry, Faculty of Science, Hiroshima University, Higashisenda-machi, Hiroshima 730

(Received January 26, 1977)

Three isomers of 2*H*,8*H*-benzo[1,2-*b*: 3,4-*b*']dipyran and 2*H*,8*H*-benzo[1,2-*b*: 5,4-*b*']dipyran, were synthesized by dehydrogenation of the dihydrobenzodipyran derivatives using DDQ or NBS and by dehydration of the secondary alcohol prepared by reduction of 4-phenylcoumarin derivatives bearing dihydropyranone ring with sodium borohydride.

A number of coumarins containing a dimethylpyran ring have been found in nature, *e.g.* calophyllolide,[1] inophyllolide,[1,2] ponnalide,[3] tomentolide A[4] as 4-phenylcoumarins. Total syntheses of these compounds and several synthetic routes of a dimethylpyran ring or dimethylchromene ring have been reported.[5-9] In the case of these 4-phenylcoumarins, it is known that the chemical shifts of dimethyl groups in fused dimethylpyran ring at 5,6-position and of the other substituents situated in the proximity of 4-phenyl ring show marked shifts from their normal values in NMR spectra.[4,10]

We have synthesized three isomers of 2*H*,8*H*-benzo[1,2-*b*: 3,4-*b*']dipyran and 2*H*,8*H*-benzo[1,2-*b*: 5,4-*b*']dipyran, (**1**—**7**), by dehydrogenation of the dihydropyran ring using 2,3-dichloro-5,6-dicyano-*p*-benzoquinone (DDQ) or *N*-bromosuccinimide (NBS) and by reduction of the dihydropyranone ring with sodium borohydride, followed by dehydration of the corresponding alcohol. The chemical shifts of methyl protons (*gem*-dimethyl, acetoxyl, and methoxyl groups) of 4-phenylcoumarin derivatives bearing dimethylpyran, dimethyldihydropyran, or dimethyldihydropyranone ring were investigated with respect to a shielding effect of 4-phenyl ring in NMR spectra.

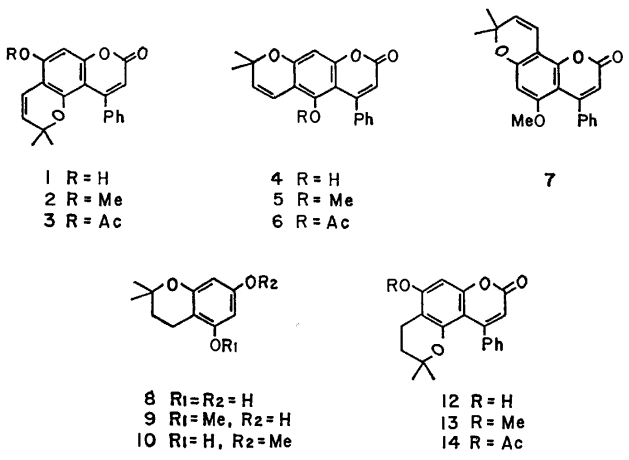

Scheme 1.

Dimethylchromans (**8**—**10**) and dimethylchromanone (**11**) were used as the starting material for an approach to syntheses of the isomeric 2*H*,8*H*-benzodipyran derivatives (**1**—**7**). The Pechmann reaction of **8** with ethyl benzoylacetate in the presence of sulfuric acid in acetic acid afforded hydroxy-4-phenylcoumarin (**12**), whose structure was proved on the basis of the accompanying evidences. The methyl ether (**13**) of **12** could be synthesized from **9** by a method similar to that for **8**. Bromination of the acetate (**14**) of **12** with NBS in benzene, followed by treatment with zinc dust gave the desired dehydro compound (**1**). The IR spectrum of **1** exhibited absorption due to the hydroxyl group at 3240 cm^{-1} and the double bond at 1647 cm^{-1}. In its NMR spectrum, the signals at δ 0.94 ppm (6H, s) and 5.42, 6.45 ppm (each 1H, d, J=10.0 Hz) showed the presence of a dimethylpyran ring. Therefore, the structure of **1** was established as 5-hydroxy-2,2-dimethyl-10-phenyl-2*H*,8*H*-benzo[1,2-*b*: 3,4-*b*']dipyran-8-one. On the other hand, the dehydrogenation of **13** with DDQ afforded the corresponding dehydro compound (**2**), which was identical with the methyl ether of **1** by a mixed-melting-point determination and by IR and NMR spectral comparison.

The linear isomers (**4**), (**5**), and (**6**) bearing dimethylpyran ring on 6,7-position of coumarin nucleus were prepared by the following procedure. Treatment of **11** with ethyl benzoylacetate in the presence of polyphosphoric acid (PPA) gave two products, 6,7-dihydro-5-hydroxy-4-phenyl-2*H*,8*H*-benzo[1,2-*b*: 5,4-*b*']dipyran-2,6-dione (**15**) and 3,4-dihydro-5-hydroxy-10-phenyl-2*H*,8*H*-benzo[1,2-*b*: 3,4-*b*']dipyran-4,8-dione (**18**), as expected, both of which could be separated by column chromatography. The IR spectrum of **15** exhibited absorption bands due to the α-pyrone at 1740 and 1623 cm^{-1}. The NMR spectrum indicated the presence of a phenolic proton at δ 13.00 ppm (1H, s) having an intramolecular hydrogen bonding. Reduction of the methyl ether (**16**) of **15** with sodium borohydride, followed by dehydration of the resulting secondary alcohol (**21**) with pyridine–acetic anhydride gave the corresponding dehydro compound (**5**). The NMR spectrum of **5** showed signals at δ 1.46 ppm (6H, s) and 5.63, 6.43 ppm (each 1H, d, J=10.0 Hz) due to *gem*-dimethyl protons and vinyl protons of the dimethylpyran ring. By a similar method, the dehydro compound (**2**) was obtained from the methyl ether (**19**) of **18** *via* secondary alcohol (**25**). However, reaction of the acetate (**17**) or (**20**) with sodium borohydride converted the carbonyl function of the pyranone ring into the methylene function to give **22** or **12** as the main product, respectively. The structures of **12** and **22** were assigned by IR and NMR spectral comparisons. The acetate (**24**) of **22** was treated with NBS. Subsequent dehydrobromination of the resulting brominated product with zinc dust yielded the dehydro compound (**6**). After hydrolysis of **6** with hydrochloric acid in methanol, the

Table 1. NMR spectral data of acetoxy and methoxy compounds of 4-phenylcoumarins

Compound	$(CH_3)_2C$[a]	$C_{3'}$–H and/or $C_{4'}$–H[b]	C_3–H[c]	C_6–H or C_8–H[c]	OAc[d]	OMe[d]
2	0.91(s)	5.30, 6.48(each d, J=10.0 Hz)	5.91(s)	6.39(s)		3.82(s)
3	0.92(s)	5.41, 6.22(each d, J=10.0 Hz)	6.07(s)	6.62(s)	2.30(s)	
5	1.46(s)	5.63, 6.43(each d, J=10.0 Hz)	6.00(s)	6.61(s)		3.00(s)
6	1.46(s)	5.66, 6.11(each d, J=10.0 Hz)	6.00(s)	6.75(s)	1.34(s)	
7	1.48(s)	5.90, 6.90(each d, J=10.0 Hz)	5.98(s)	6.18(s)		3.38(s)
13	0.84(s)	1.58, 2.58(each t, J=6.7 Hz)	5.98(s)	6.50(s)		3.89(s)
14	0.87(s)	1.62, 2.55(each t, J=6.7 Hz)	6.04(s)	6.68(s)	2.37(s)	
16	1.42(s)	2.64(s)	6.01(s)	6.66(s)		3.06(s)
17	1.46(s)	2.66(s)	6.05(s)	6.85(s)	1.46(s)	
19	0.95(s)	2.50(s)	6.00(s)	6.47(s)		3.93(s)
20	0.98(s)	2.50(s)	6.17(s)	6.70(s)	2.39(s)	
23	1.35(s)	1.78, 2.70(each t, J=6.7 Hz)	6.00(s)	6.63(s)		2.97(s)
24	1.33(s)	1.76, 2.43(each t, J=6.7 Hz)	5.95(s)	6.73(s)	1.33(s)	
29	1.38(s)	1.86, 2.88(each t, J=6.7 Hz)	5.97(s)	6.15(s)		3.37(s)
31	1.38(s)	1.87, 2.91(each t, J=6.7 Hz)	5.94(s)	6.29(s)	1.32(s)	

a) Each 6H. b) Each 1H or 2H. c) Each 1H. d) Each 3H.

resulting hydroxy derivative (**4**) was methylated with methyl iodide in the presence of anhydrous potassium carbonate to give a methyl ether, which was shown to be identical with **5**.

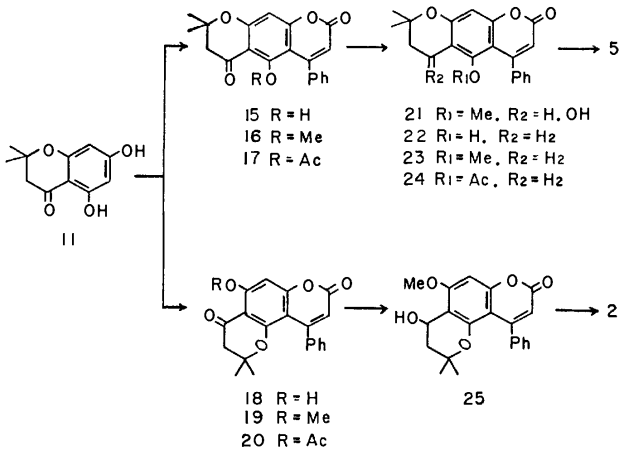

Scheme 2.

The synthesis of another isomer (**7**) bearing dimethylpyran ring on 7,8-position was carried out as follows. The Hoesch reaction of **10** with benzonitrile using zinc chloride as a catalyst afforded 8-benzoyl-5-hydroxy-7-methoxy-2,2-dimethylchroman (**26**) in higher yield than that of 6-benzoyl isomer (**27**). **26** was readily transformed into **27** in the presence of an acidic catalyst such as sulfuric acid or aluminium chloride.[11] Confirmation of the structures was performed by spectral data and an alcoholic ferric chloride reaction. The acetate (**28**) of **27** was then converted into the coumarin derivative (**29**) by dehydration in the presence of a mixture of acetic anhydride and sodium acetate. **29** was also obtained together with **12** and **30** by the Pechmann reaction of **10** with ethyl benzoylacetate. **29**, **30**, and **31** have been derived from natural mammeisin, and their IR, UV spectra and melting points are compatible with those of authentic samples.[12] Dehydrogenation of **29** with DDQ gave the expected dehydro compound (**7**), which showed signals at δ 1.48 ppm (6H, s) and 5.90, 6.90 ppm (each 1H, d, J=10.0 Hz) due to methyl protons and vinyl protons of the dimethylpyran ring in the NMR spectrum.

It is significant to compare the NMR spectral data of some synthetic samples. The chemical shifts of dimethyl protons of **2**, **3**, **13**, **14**, **19**, and **20** (δ 0.84—0.98 ppm) containing dimethylpyran, dimethyldihydropyran, or dimethyldihydropyranone ring at 5,6-position, appeared in a higher magnetic field than those of **5**, **6**, **7**, **16**, **17**, **23**, **24**, **29**, and **31** (δ 1.33—1.48 ppm) containing a pyran ring at 6,7- or 7,8-position in coumarin nucleus (Table 1). The methyl protons of acetoxyl or methoxyl group substituted at 5-position showed chemical shifts in a higher magnetic field than those at 7-position. These characteristic shifts are though to be due to the anisotropic shielding effect of the phenyl ring at 4-position,[13] as has been found to be the case[2,4,10] in calophyllolide and inophyllolide. Thus, NMR spectral analysis might be useful for the structural confirmation of 4-phenylcoumarin derivatives.

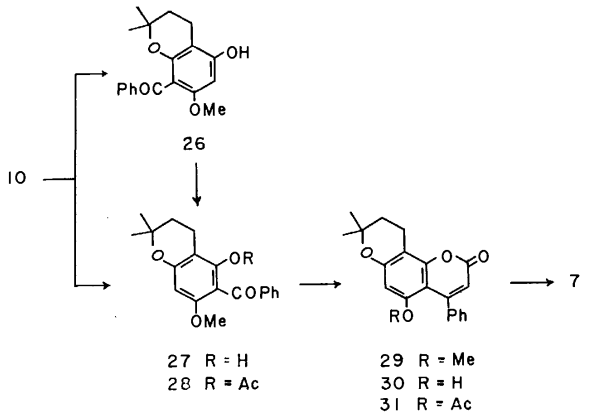

Scheme 3.

Experimental

All the melting points are uncorrected. Unless otherwise stated, the NMR spectra were taken in deuteriochloroform using tetramethylsilane as an internal standard on a Hitachi

Model R-20 NMR spectrometer (60 MHz) or a JEOL JNM-MH-100 spectrometer (100 MHz). The chemical shifts are expressed in δ values; s: singlet; br: broad; d: doublet; t: triplet. The data of the UV spectra are described in terms of λ_{max}^{EtOH} nm (log ε). The column chromatography was carried out using Merck silica gel (0.063 or 0.08 mm). PPA was prepared by stirring a mixture of phosphoric acid and phosphorus pentoxide (wt ratio of 1: 1) at 85—90 °C for 3 h.

2,2-Dimethyl-5-methoxy-7-hydroxychroman (9). 2,2-Dimethyl-5-methoxy-7-hydroxychromanone (1 g), which had been prepared by hydrolysis of 2,2-dimethyl-5-methoxy-7-(*p*-tolylsulfonyloxy)chromanone[14] with 7% aq potassium carbonate, was refluxed with zinc amalgam (prepared from zinc dust (12.7 g), mercuric chloride (0.68 g), concentrated hydrochloric acid (0.7 ml), and water (18 ml)), in 10% aq ethanol (100 ml) for 15 h, 1 ml of hydrochloric acid being added at 1 h intervals. After removal of an inorganic material, the solution was concentrated under reduced pressure. The concentrated solution was extracted with ether and the ether layer was washed with water, dried and evaporated. The residue was recrystallized from ethanol to give **9** as colorless needles; mp 107—108°C; yield, 0.4 g, IR (KBr) cm^{-1}: 3330, 1605; Found: C, 69.32; H, 8.01%. Calcd for $C_{12}H_{16}O_3$: C, 69.21; H, 7.74%.

The Pechmann Reaction of 8. 75% sulfuric acid (4 ml) was added to a mixture of **8**[15] (0.8 g) and ethyl benzoylacetate (0.8 g) in acetic acid (6 ml) at room temp and the mixture was allowed to stand for 2 day. After the mixture had been poured into ice–water, the resulting solid was collected, washed, dried and then recrystallized from ethanol to give **12** as colorless prisms, mp 320 °C (lit,[16] 315—320 °C); yield, 0.7 g; IR (Nujol) cm^{-1}: 3245, 1680, 1640, 1590, 1565; UV: sh 253 (3.98), 260 (3.99), 338 (4.16); Found: C, 74.48; H, 5.59%. Calcd for $C_{20}H_{18}O_4$: C, 74.52; H, 5.63%.

Acetate (14): Acetic anhydride–pyridine method; mp 144—145 °C (from methanol) (lit,[16] 140—141 °C), colorless needles; IR (Nujol) cm^{-1}: 1775, 1725, 1605, 1560; UV: 255 (3.95), 310 (4.11); Found: C, 72.45; 5.55%. Calcd for $C_{22}H_{20}O_5$: C, 72.51; H, 5.53%.

Methyl Ether (13): Methyl iodide–potassium carbonate method; mp 202—203 °C (from ethanol) (lit,[16] 200—202 °C), colorless prisms; IR (Nujol) cm^{-1}: 1720, 1605, 1570, 1550; UV: 259 (3.90), 331.5 (4.00); Found: C, 74.80; 6.05%. Calcd for $C_{21}H_{20}O_4$: C, 74.98; H, 5.99%.

The mother liquor of the recrystallization was concentrated to give a small amount of the isomer (**30**) as colorless plates; mp 292—294 °C (lit,[12] 273—276 °C); IR (KBr) cm^{-1}: 3256, 1678, 1628, 1600, 1560; UV: 266 (4.20), 338 (4.10); Found: C, 74.46; H, 5.64%. Calcd for $C_{20}H_{18}O_4$: C, 74.52; H, 5.63%.

Acetate (31): Acetic anhydride–pyridine method; mp 155—156 °C (from aq ethanol) (lit,[12] 161—163 °C), colorless prisms; IR (Nujol) cm^{-1}: 1773, 1730, 1618, 1588; UV: 251 (4.03), 260 (4.00), 334 (4.12); Found: C, 72.60; H, 5.60%. Calcd for $C_{22}H_{20}O_5$: C, 72.51; H, 5.53%.

Methyl Ether (29): Methyl iodide–potassium carbonate method; mp 133—134 °C (from aq ethanol) (lit,[12] 130—132 °C), colorless needles; IR (Nujol) cm^{-1}: 1715, 1615, 1590; UV: 263 (4.16), 286 (3.72), 337 (4.10); Found: C, 74.68; H, 6.01%. Calcd for $C_{21}H_{20}O_4$: C, 74.98; H, 5.99%.

The Pechmann Reaction of 9. A mixture of **9** (0.3 g), ethyl benzoylacetate (0.3 g), and 75% sulfuric acid (4 ml) in acetic acid (7 ml) was allowed to stand at room temp for 2 day. By a treatment to that described above, the crude solid was recrystallized from ethanol to give **13** (0.4 g), which showed superimposable IR and NMR spectra and non-depression of mixed-melting-point with the sample prepared from **12**.

The Pechmann Reaction of 10. A mixture of **10**[17] (2 g), ethyl benzoylacetate (1.8 g), and 75% sulfuric acid (17 ml) in acetic acid (20 ml) was allowed to stand at room temp for 2 day. After the usual work-up, the crude product was purified by a fractional crystallization from aq ethanol to give **12** (1.2 g), **29** (0.2 g), and a small amount of **30**. **12**, **29**, and **30** were identical with the above samples.

*5-Hydroxy-2,2-dimethyl-10-phenyl-2*H, *8*H-*benzo*[*1*, *2*-b : *3*, *4*-b′]-*dipyran-8-one (1).* A mixture of **14** (0.6 g), NBS (0.3 g), and a trace of benzoyl peroxide in dry carbon tetrachloride (30 ml) was refluxed for 1.5 h. The cooled mixture was filtered and the filtrate was evaporated to dryness under reduced pressure. The residue was dissolved in a mixture of acetic acid (15 ml) and sodium acetate (2 g) and gently refluxed for 1 h. The mixture was poured into ice–water and the resulting material was collected, washed and dried. The crude material was refluxed with fresh zinc dust (0.3 g) in acetic acid (15 ml) for 8 h. The mixture was filtered and the filtrate was poured into water. The resulting solid was collected, washed, dried and recrystallized from methanol to give **1**, as colorless prisms; mp 281—283 °C (lit,[8c] 260—263 °C); yield 0.2 g; IR (Nujol) cm^{-1}: 3240, 1695, 1647, 1585; UV: 233 (4.33), 283 (4.32), 337 (4.12); NMR (DMSO): 0.94 (6H, s, $(CH_3)_2\dot{C}$–), 5.45, 6.45 (each 1H, d, and J=10.0 Hz, –CH=CH–), 5.77 (1H, s, C_3–H), 6.36 (1H, s, C_8–H); Found: C, 74.85; H, 5.21%. Calcd for $C_{20}H_{16}O_4$: C, 74.99; H, 5.03%.

Acetate (3): Acetic anhydride–pyridine method; mp 171—173 °C (from aq methanol), colorless plates; IR (Nujol) cm^{-1}: 1758, 1722, 1635, 1610; UV: 231 (4.29), 261.5 (4.14), 270 (4.17), 295 (4.23); Found: C, 72.68; H, 5.03%. Calcd for $C_{22}H_{18}O_5$: C, 72.92; H, 5.01%.

*5-Methoxy-2, 2-dimethyl-10-phenyl-2*H, *8*H-*benzo*[*1*, *2*-b : *3*, *4*-b′]-*dipyran-8-one (2).* A mixture of **13** (0.17 g) and DDQ (0.5 g) in dry benzene (60 ml) was refluxed under a stream of nitrogen for 25 h until the hydroquinone separated out. While the mixture was hot, it was filtered and the filtrate was evaporated to a solid which was purified by means of column chromatography on silica gel (20 g), using chloroform–petroleum ether (1: 1) as the eluent, to give **2**; mp 183—185 °C, colorless prisms (lit,[19] 184—185 °C; lit,[3b] 192—194 °C); yield, 0.15 g, IR (Nujol) cm^{-1}: 1722, 1640, 1598, 1553; UV: sh 276 (4.28), 283 (4.31), 329 (4.11); Found: C, 75.68; H, 5.39%. Calcd for $C_{21}H_{18}O_4$: C, 75.43; H, 5.43%. **2** was also derived by methylation of **1** with diazomethane.

The Pechmann Reaction of 11. A mixture of **11**[18] (1 g), ethyl benzoylacetate (1 g), and PPA (16 g) was stirred at 75—80 °C for 1 h. After cooling, ice–water was added to the mixture in order to decompose PPA. The resulting solid was collected, washed, dried and then was chromatographed on silica gel (20 g), with chloroform as the eluent. The faster effluent yielded a solid, which was recrystallized from ethanol to give **15** as colorless needles; mp 235—237 °C; yield, 0.15 g. This is shown by the deep violet coloration with ferric chloride in ethanol. IR (Nujol) cm^{-1}: 1740, 1648, 1623, 1603, 1564; UV: 283 (4.49), 328 (4.08); NMR: 1.42 (6H, s, $(CH_3)_2\dot{C}$–), 2.68 (2H, s, $-COCH_2-$), 5.94 (1H, s, C_3–H), 6.33 (1H, s, C_8–H), 7.40 (5H, br, $-C_6H_5$), 13.00 (1H, s, OH); Found: C, 71.30; H, 4.64%. Calcd for $C_{20}H_{16}O_5$: C, 71.42; H, 4.80%.

Acetate (17): Acetic anhydride–sodium acetate method; mp 196—198 °C (from aq ethanol), colorless prisms; IR (Nujol) cm^{-1}: 1767, 1738, 1693, 1613, 1595; Found: C, 69.54; H, 4.79%. Calcd for $C_{22}H_{18}O_6$: C, 69.83; H, 4.80%.

Methyl Ether (16): Dimethyl sulfate–potassium carbonate method; mp 218.5—219.5 °C (from ethanol), colorless prisms; IR (Nujol) cm^{-1}: 1743, 1708, 1613, 1598; Found: C, 71.99; H, 5.12%. Calcd for $C_{21}H_{18}O_5$: C, 71.99; H, 5.18%.

The slower effluent was recrystallized from ethanol to give

18 (0.3 g) as colorless prisms; mp 246—247 °C; this is shown by the deep violet coloration with ferric chloride in ethanol; IR (Nujol) cm^{-1}: 1733, 1650, 1624, 1586; UV: 282 (4.47), 329 (4.08); NMR: 0.97 (6H, s, $(CH_3)_2\dot{C}$–), 2.56 (2H, s, –CO-CH_2–), 5.94 (1H, s, C_3–H), 6.44 (1H, s, C_8–H), 7.38 (5H, br, $-C_6H_5$), 12.27 (1H, s, OH); Found: C, 71.55; H, 4.94%. Calcd for $C_{20}H_{16}O_5$: C, 71.42; H, 4.80%.

*Acetate (**20**)*: Acetic anhydride–sodium acetate method; mp 187—189 °C (from ethanol), colorless flocks; IR (Nujol) cm^{-1}: 1765, 1738, 1688, 1610, 1600, 1587; Found: C, 69.97; H, 4.91%. Calcd for $C_{22}H_{18}O_6$: C, 69.83; H, 4.80%.

*Methyl Ether (**19**)*: Dimethyl sulfate–potassium carbonate method; mp 225—226.5 °C (from ethanol) (lit,[16] 216—218 °C), colorless prisms; IR (Nujol) cm^{-1}: 1746, 1690, 1604, 1598; Found: C, 71.99; H, 5.08%. Calcd for $C_{21}H_{18}O_5$: C, 71.99; H, 5.18%.

*Reduction of **16** and **19**. From **16***: A mixture of **16** (150 mg) and sodium borohydride (30 mg) in ethanol (40 ml) was stirred at 20—25 °C for 4 h. The mixture was made slightly acidic with acetic acid–water to decompose an excess sodium borohydride and concentrated to a solid under reduced pressure. The solid was collected, washed, dried and then chromatographed on silica gel, with chloroform as the eluent, to give **21**. This was further recrystallized from benzene; mp 181.5—182.5 °C, colorless prisms; yield, 63 mg; IR ($CHCl_3$) cm^{-1}: 3540, 1720, 1605, 1550; NMR: 1.39, 1.48 (each 3H and s, $(CH_3)_2\dot{C}$–), 2.08 (2H, d, J=6 Hz, $(CH_3)_2$-$\dot{C}CH_2$–), 3.06 (3H, s, OMe), 3.31 (1H, s, OH), 4.95 (1H, t, J=6 Hz, –$\dot{C}$HOH), 6.05 (1H, s, C_3–H), 6.65 (1H, s, C_8–H), 7.40 (5H, s, $-C_6H_5$); Found: C, 71.81; H, 5.71%. Calcd for $C_{21}H_{20}O_5$: C, 71.58; H, 5.72%.

*From **19***: A mixture of **19** (200 mg) and sodium borohydride (42 mg) in ethanol (40 ml) was stirred at 20—23 °C for 4.5 h. The mixture was treated in a similar way to that described above. The crude product was recrystallized from ethanol to give **25** as colorless needles; mp 205—207 °C; yield, 164 mg; IR ($CHCl_3$) cm^{-1}: 3580, 1720, 1605, 1560; NMR: 0.82, 1.04 (each 3H and s, $(CH_3)_2\dot{C}$–), 1.84 (2H, d, J=6 Hz, $(CH_3)_2$-$\dot{C}CH_2$–), 3.04 (1H, s, OH), 3.96 (3H, s, OMe), 4.92 (1H, t, J=6 Hz, –$\dot{C}$HOH), 5.96 (1H, s, C_3–H), 6.49 (1H, s, C_8–H), 7.30 (5H, br, $-C_6H_5$); Found: C, 71.45; H, 5.82%. Calcd for $C_{21}H_{20}O_5$: C, 71.58; H, 5.72%.

*Reduction of **17** and **20**. From **17***: A mixture of **17** (200 mg) and sodium borohydride (40 mg) in ethanol (50 ml) was stirred at 23—26 °C for 5 h. After the usual work-up, the resulting solid was chromatographed on silica gel, with benzene as the eluent, to give **22**, which was further recrystallized from benzene; mp 233—234 °C, colorless prisms; yield, 110 mg; IR ($CHCl_3$) cm^{-1}: 3510, 1720, 1620, 1560; NMR: 1.32 (6H, s, $(CH_3)_2\dot{C}$–), 1.76, 2.52 (each 2H, t, and J=6.7 Hz, $-CH_2CH_2$–), 5.38 (1H, s, OH), 5.87 (1H, s, C_3–H), 6.44 (1H, s, C_8–H), 7.51 (5H, br, $-C_6H_5$); Found: C, 74.60; H, 5.64%. Calcd for $C_{20}H_{18}O_4$: C, 74.52; H, 5.63%.

*Acetate (**24**)*: Acetic anhydride–pyridine method; mp 195—196 °C (from ethanol), colorless prisms; IR ($CHCl_3$) cm^{-1}: 1765, 1720, 1618, 1552; Found: C, 72.25; H, 5.45%. Calcd for $C_{22}H_{20}O_5$: C, 72.51; H, 5.53%.

*Methyl Ether (**23**)*: Methyl iodide–potassium carbonate method; mp 179—180 °C (from aq ethanol), colorless plates; IR ($CHCl_3$) cm^{-1}: 1710, 1610, 1550; Found: C, 74.95; H, 6.03%. Calcd for $C_{21}H_{20}O_4$: C, 74.98; H, 5.99%.

*From **20***: A mixture of **20** (200 mg) and sodium borohydride (40 mg) in ethanol (70 ml) was stirred at 24—27 °C for 5 h. After the usual work-up, the crude product was recrystallized from ethanol to give **12** (70 mg), which was identical with the sample described above.

*Dehydration of **21** and **25**. From **21***: **21** (160 mg) was refluxed in a mixture of acetic anhydride (5 ml) and pyridine (2—3 drops) for 5.5 h. After cooling, the mixture was poured into ice–water and acidified with dilute hydrochloric acid. The resulting solid was collected, washed, dried and then chromatographed on silica gel (5 g), with chloroform as the eluent, to give **5** (60 mg), which was further recrystallized from ethanol; mp 211—212 °C, colorless prisms; IR ($CHCl_3$) cm^{-1}: 1715, 1640, 1605; Found: C, 75.29; H, 5.45%. Calcd for $C_{21}H_{18}O_4$: C, 75.43; H, 5.43%.

*From **25***: **25** (160 mg) was dehydrated to give **2** (110 mg), which was identical with the above mentioned sample.

*5-Acetoxy-8,8-dimethyl-4-phenyl-2H,8H-benzo[1,2-b:5,4'-b]dipyran-2-one (**6**)*. A mixture of acetate (**24**: 225 mg), NBS (210 mg), and a trace of benzoyl peroxide in dry carbon tetrachloride (20 ml) was refluxed for 3 h. The resulting succinimide was then filtered off and the solvent was removed. The residue was successively treated according to the usual work-up. The crude product was chromatographed on silica gel (7 g), with benzene as the eluent, to give **6**, which was further recrystallized from methanol; mp 227.5—228.5 °C, colorless prisms; yield, 140 mg, IR ($CHCl_3$) cm^{-1}: 1773, 1720, 1640, 1620; Found: C, 72.87; H, 4.99%. Calcd for $C_{22}H_{18}O_5$: C, 72.92; H, 5.01%.

*5-Hydroxy-8,8-dimetyl-4-phenyl-2H,8H-benzo[1,2-b:5,4-b']dipyran-2-one (**4**)*. **6** (95 mg) was hydrolyzed with a mixture of concentrated hydrochloric acid (1 ml) and methanol (24 ml), refluxing for 4 h. After removal of the solvent, the resulting solid was collected, washed and dried. This was recrystallized from benzene to give **4** (24 mg) as colorless needles; mp 197—198 °C; IR ($CHCl_3$), cm^{-1}: 3510, 1720, 1640, 1617; NMR: 1.45 (6H, s, $(CH_3)_2\dot{C}$–), 5.53, 6.46 (each 1H, d, and J=10.0 Hz, –CH=CH–), 5.29 (1H, s, OH), 5.90 (1H, s, C_3–H), 6.44 (1H, s, C_8–H), 7.55 (5H, br, $-C_6H_5$); Found: C, 74.25; H, 5.05%. Calcd for $C_{20}H_{16}O_4$: C, 74.99; H, 5.03%.

*6-Benzoyl-5-hydroxy-7-methoxy-2,2-dimethylchroman (**27**) and 8-Benzoyl Isomer (**26**)*. A mixture of **10** (4.7 g), benzonitrile (4.0 g), and anhydrous zinc chloride (3.5 g) in dry ether (80 ml) was saturated with dry hydrogen chloride under ice-cooling and the mixture was allowed to stand at room temp overnight. After removal of the upper ethereal layer by decantation, the residue was heated with 1% hydrochloric acid (100 ml) on a water bath for 3 h. The resulting solid was collected, washed and dried and then recrystallized from ethanol to give **27** as pale yellow needles; this is shown by the violet brown coloration with ferric chloride in ethanol; mp 122—123 °C; yield, 0.9 g; IR (Nujol) cm^{-1}: 1620, 1600, 1585; UV: 253 (3.68), 312 (4.09); Found: C, 73.08; H, 6.60%. Calcd for $C_{19}H_{20}O_4$: C, 73.06; H, 6.45%.

*Acetate (**28**)*: Acetic anhydride–sodium acetate method; mp 126—127 °C (from ethanol), colorless prisms; IR (Nujol) cm^{-1}: 1769, 1669, 1619, 1593, 1580; UV: 251 (4.19), 283 (3.65); NMR: 1.35 (6H, s, $(CH_3)_2\dot{C}$–), 2.02 (3H, s, OAc), 1.78, 2.52 (each 2H, t, and J=6.7 Hz, $-CH_2CH_2$–), 3.60 (3H, s, OMe), 6.35 (1H, s, C_8–H), 7.65 (5H, br, $-C_6H_5$); Found: C, 71.02; H, 6.27%. Calcd for $C_{21}H_{22}O_5$: C, 71.17; H, 6.26%.

The mother liquor of the recrystallization was concentrated to give **26** as pale yellow prisms, which showed a negative ferric chloride reaction in ethanol; mp 213—215 °C; yield, 1.7 g; IR (Nujol) cm^{-1}: 3280, 1645, 1605, 1515; UV: 247 (4.17), 292 (3.41), 308 (3.41); Found: C, 73.23; H, 6.71%. Calcd for $C_{19}H_{20}O_4$: C, 73.06; H, 6.45%.

*Conversion of **26** to **27**. a) Aluminium Chloride Method*: A mixture of **26** (1 g) and anhydrous aluminium chloride in dry ether (125 ml) was refluxed for 12 h. After removal of the solvent, ice–water was added to the residue which was then acidified with dilute hydrochloric acid. The resulting

solid was collected, washed, dried and recrystallized from methanol to give **27** (0.7 g); mp 123—124 °C, pale yellow needles. The compound was identical with the sample prepared above.

b) Sulfuric Acid Method: Concentrated sulfuric acid (0.5 ml) was added to a solution of **26** (100 mg) in acetic acid (5 ml) and heated at 65—67 °C for 5 h. After cooling, ice–water was added to the mixture and the resulting solid was collected, washed, dried and recrystallized from methanol to give **27** (50 mg).

*Preparation of **29** from **28**.* A mixture of **28** (200 mg), acetic anhydride (1 ml), and anhydrous sodium acetate (500 mg) was heated at *ca.* 130 °C for 2 min. After cooling, ice–water was added to the mixture and the resulting solid was collected, washed and recrystallized from aq ethanol to give **29** (30 mg); mp 133—134 °C. This was shown to be identical with the above mentioned samples.

*5-Methoxy-8,8-dimethyl-4-phenyl-2*H,*8*H-benzo[*1,2*-b:*3,4*-b′]-*dipyran-2-one (7).* A mixture of **29** (150 mg) and DDQ (150 mg) in dry benzene (25 ml) was treated in a similar way to that described above. The crude product was recrystallized from ethanol to give **7** (70 mg) as colorless plates; mp 143—144 °C. IR (Nujol) cm^{-1}: 1718, 1648, 1618, 1587, 1578; UV: 234 (4.56), 284 (4.25), 330 (4.02); Found: C, 75.67; H, 5.52%. Calcd for $C_{21}H_{18}O_4$: C, 75.43; H, 5.43%.

References

1) J. Polonsky, *Bull. Soc. Chim. Fr.*, **1957**, 1079.

2) K. Kawazu, H. Ohigashi, and T. Mitsui, *Tetrahedron Lett.*, **1968**, 2383.

3) a) D. Adinayana and T. R. Seshadri, *Bull. Nat. Inst. Sci. India*, **31**, 91 (1965); The revised structure of ponnalide; b) V. V. S. Murti, P. S. Sampath Kumar, and T. R. Seshadri, *Indian. J. Chem.*, **10**, 255 (1972).

4) S. K. Nigam, C. R. Mitra, G. Kunesch, B. C. Das, and J. Polonsky, *Tetrahedron Lett.*, **1967**, 2633.

5) E. Spath and R. Hiller, *Ber.*, **72**, 963 (1939); S. K. Mukerjee, S. C. Sarkar, and T. R. Seshadri, *Tetrahedron*, **25**, 1063 (1969).

6) A. K. Ganguly, B. S. Joshi, V. N. Kamat, and A. H. Manmade, *Tetrahedron*, **23**, 4777 (1967).

7) J. Hlubucek, E. Ritchie, and W. C. Taylor, *Tetrahedron Lett.*, **1969**, 1369; S. K. Mukerjee, S. C. Sarkar, and T. R. Seshadri, *Indian. J. Chem.*, **8**, 861 (1970).

8) a) W. M. Bandaranayake, L. Crombie, and D. A. Whiting, *Chem. Commun.*, **1969**, 970; b) J. R. Lewis and J. B. Reary, *J. Chem. Soc., C*, **1970**, 1662; c) D. E. Games and N. J. Haskins, *Chem. Commun.*, **1971**, 1005.

9) A. C. Jain, V. K. Khanna, P. Lal, and T. R. Seshadri, *Indian J. Chem.*, **8**, 480 (1970).

10) G. D. Breck and G. H. Stout, *J. Org. Chem.*, **34**, 4203 (1969).

11) A similar isomerization took place between 8-acetyl-5-hydroxy-7-methoxy-2,2-dimethylchroman and 6-acetyl isomer as reported in a previous paper: M. Nakayama, S. Nishimura, T. Matsui, S. Hayashi, and K. Fukui, *Nippon Kagaku Zasshi*, **91**, 1092 (1970).

12) R. A. Finnegan, M. P. Morris, and C. Djerassi, *J. Org. Chem.*, **26**, 1180 (1961).

13) This effect can be further observed by comparison of the NMR spectra of 4-phenyl and 4-methylcoumarin derivatives; unpublished results.

14) M. L. Wolfrom, E. W. Koos, and H. B. Bhat, *J. Org. Chem.*, **32**, 1058 (1967).

15) W. Wridge, R. G. Heysand, and A. Robertson, *J. Chem. Soc.*, **1937**, 284; H. B. Bhat and K. Venkataraman, *Tetrahedron*, **19**, 77 (1963).

16) J. Polonsky, *Bull. Soc. Chim. Fr.*, **1956**, 914.

17) A. P. Johnson and A. Pelter, *J. Chem. Soc., C*, **1966**, 606.

18) M. Miyano and M. Matsui, *Bull. Chem. Soc. Jpn.*, **31**, 397 (1958); T. Matsui, K. Kaneko, and J. Tsukamoto, *Bull. Fac. Eng. Miyazaki Univ.*, **19**, 19 (1973).

19) J. Polonsky, *Bull. Soc. Chim. Fr.*, **1958**, 929.

Synthesis and ^{13}C NMR Spectra of *endo*-5-(4-Imidazolyl)bicyclo-[2.2.2]oct-*endo*- and *exo*-2-yl *trans*-Cinnamates

Masanori UTAKA, Mamoru AKIYAMA,* and Akira TAKEDA

Department of Synthetics Chemistry, School of Engineering, Okayama University, Tsushima, Okayama 700

(Received February 4, 1977)

The Synthesis of *endo*-5-(4-imidazolyl)bicyclo[2.2.2]oct-*endo*- and *exo*-2-yl *trans*-cinnamates was carried out starting from 2-butyn-1,4-diol. The key intermediate, *endo*-5-(4-imidazolyl)bicyclo[2.2.2]octan-2-one, was obtained by oxidation of *endo*-5-(4-imidazolyl)bicyclo[2.2.2]oct-2-ene with palladium chloride, the oxidation being stereo- and regiospecific. The mode of 2,5 disubstitution and endo, exo stereochemistry were determined by means of ^{13}C chemical shifts of the bicyclo[2.2.2]octane framework.

In a previous paper[1] a report was given on the synthesis and separation of *endo*- and *exo*-5-(4-imidazolyl)bicyclo[2.2.1]hept-*endo*-2-yl *trans*-cinnamates *via* 5-(1-oxo-2-hydroxyethyl)bicyclo[2.2.2]hept-2-enes. These cinnamates were synthesized as a model for acyl-α-chymotrypsin since the bicyclo[2.2.1]heptane ring system possesses a rigid framework which can bear the imidazolyl and acyloxy groups with correct spatial alignment as in the acyl enzyme.

In this report we describe the synthesis of the title compounds which also simulate the acyl enzyme and have a less rigid framework of bicyclo[2.2.2]octane as compared to that of bicyclo[2.2.1]heptane. It seems of interest to investigate the difference in reactivity caused by the less rigid framework.[2,3] The endo, endo compound has a correct stereochemistry, but not the endo, exo compound. Properties of the former can be compared with those of the latter.

The synthesis was carried out following the scheme for the bicyclo[2.2.1]heptane derivatives, several key steps being found to be quite different. For elucidation of the structures of the title compounds ^{13}C NMR spectroscopy was indispensable, although ^1H NMR spectra were used effectively for the corresponding bicyclo-[2.2.1]heptane derivatives.

Results and Discussion

Synthesis. The synthetic route is shown in Scheme 1. The starting ketone **1** was obtained in 12% yield from 2-butyn-1,4-diol. The yield is lower than the 20% yield for the corresponding bicyclo[2.2.1]-heptenyl ketone which can be attributed to the low reactivity of 1,3-cyclohexadiene as a Diels-Alder diene. The endo: exo ratio of the ketone **1** was determined to be 9: 1 referring to the relative intensity of the ^1H NMR signals of the alcoholic methylene protons at δ 4.30 (exo) and 4.26 (endo). The signals of the olefinic protons were useless for the determination unlike the case of the corresponding bicyclo[2.2.1]heptenyl ketone.

Formation of the imidazolyl derivative **2** was achieved in a similar way to that for the corresponding bicyclo-[2.2.1]heptane derivative. The yield was 60—70%, comparable to that of the latter. The endo: exo ratio was 3: 1 as determined by the ^1H NMR signals of the imidazolyl C-4 proton at δ 6.87 (exo) and 6.65 (endo).

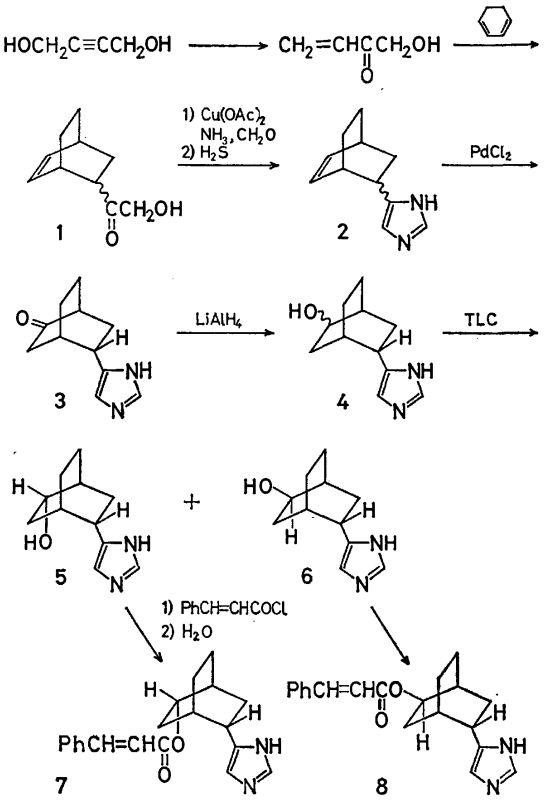

Scheme 1.

These values are similar to those (6.83 and 6.63) for 5-(4-imidazolyl)bicyclo[2.2.1]hept-2-enes.

Introduction of an oxo group to the olefinic bond of **2** was attained effectively using palladium chloride in dilute hydrochloric acid. The crude oxidation product obtained from the endo, exo mixture of **2** was chromatographed over basic alumina to give the endo ketone **3** in 30% yield (40% based on the *endo*-imidazolyl derivative of **2**). Neither exo ketone nor the isomeric 2,6-disubstituted product was detected. The reaction conditions such as temperature, time, speed of addition of the substrate, acidity of the solution, and mole ratios of the substrate to the oxidant were varied without any appreciable increase in the yield. The *exo*-imidazolyl derivative of **2** was recovered only in part by chromatography, being lost mostly as unidentified products.

The oxidation was stereo- and regiospecific. It seems to proceed *via* a palladium complex intermediate which requires both the ethylenic double bond and the *endo*-

* Present address: Nippon Goseikagaku Kogyo Co., Ltd., Mizushima, Kurashiki 712.

imidazolyl ring as a bidentate ligand. So far, no such palladium complex seems to have been reported.[4,5]

The mode of 2,5 disubstitution and the endo stereochemistry of **3** were determined by the ^{13}C chemical shift.

In order to obtain the desired compounds **7** and **8**, the endo ketone **3** was reduced to the hydroxy derivative **4** followed by acylation and partial hydrolysis after separation of the endo, endo derivative **5** and the endo, exo derivative **6**. The procedure is similar to that for the corresponding bicyclo[2.2.1]heptane derivatives.

An alternative method of introducing an oxo group to the olefinic double bond was the use of 98—100% formic acid which was utilized for the corresponding bicyclo[2.2.1]heptene. An addition reaction of formic acid to the olefinic double bond of **2** proceeded slowly at 160 °C over a period of 50 h to give the expected formate and its corresponding alcohol in a combined yield of 50—60% and these reaction products afforded the oxo derivative by oxidation with chromium trioxide. However, the total yield from **2** was not improved. The presence of both the *endo*- and *exo*-imidazolyl derivatives in the oxidation product complicated the isolation of the isomers. The situation became more serious when the oxo derivative were reduced to the hydroxy derivatives since almost equimolecular amounts of the *endo*- and *exo*-hydroxy derivatives were produced. Thus the use of formic acid was abandoned.

Hydrogenation of **2** with 10% Pd–C gave a hygroscopic glassy solid of 2-(4-imidazolyl)bicyclo[2.2.2]-octane (**9**), which could be distilled but not crystallized. The ^{13}C chemical shifts are indispensable for elucidation of the stereochemistry of **3**, **7**, and **8** as shown in Tables 1 and 2.

^{13}C Chemical Shifts. The ^{13}C chemical shifts for a number of bicyclo[2.2.2]octanes substituted in the 2 and 2,5 positions have been reported by Garratt and Riguera.[3] They derived substitution parameters from the 2-substituted compounds and utilized them for the determination of the relative stereochemistry of substituents at C-2 and C-5. Their parameters for the hydroxyl and oxo groups are given in Table 1. The down field shifts for the α-, β-, and γ-carbon atoms were obtained by comparing the chemical shifts in the 2-substituted bicyclo[2.2.2]octanes with those in the parent hydrocarbon, where the α-carbon atom is C-2 and the γ-carbon atom is C-6 or C-7. The parameters for the 4-imidazolyl and *trans*-cinnamoyloxy groups (Table 1) were derived from the present work.

Table 1. Substituent effects on ^{13}C chemical shifts for 2-substituted bicyclo[2.2.2]octanes[a]

Substituent	α	β(C-1)	β(C-3)	γ-syn	γ-anti
4-Imidazolyl	8.3	5.7	5.8	−5.2	−0.9
trans-Cinnamoyloxy	46.5	6.3	8.8	−7.0	−3.0
Hydroxy[b]	43.3	7.5	11.3	−7.5	−2.3
Oxo[b]	190.7	18.3	18.6	−2.7	−2.7

a) The values show downfield shifts in ppm. Values for the 4-imidazolyl group were derived from the chemical shifts of 5-(4-imidazolyl) bicyclo[2.2.2]-octane (Table 2) by comparison with the shifts (24.14 for C-1 and 26.16 for C-2) for bicyclo[2.2.2]-octane. For the *trans*-cinnamoyloxy group an average value has been taken from the endo and exo cinnamates (Table 2). b) Values taken from Ref. 3.

The ^{13}C chemical shifts for various 2-substituted 5-(4-imidazolyl)bicyclo[2.2.2]octanes are given in Table 2. The agreement between the observed and the calculated values is good within $\pm$0.6 ppm. Deviations as large as 0.8—1.2 ppm are seen for C-2 and C-3 of the oxo derivative and C-4 and C-5 of the *exo*-cinnamoyloxy derivative, but no ambiguity in their assignment results from these deviations.

In order to obtain the substitution parameters for the 4-imidazolyl group, the ^{13}C NMR spectrum of 5-(4-imidazolyl)bicyclo[2.2.2]octane (**9**)[6] was assigned as follows. The tertiary carbons C-1, C-4, and C-5 were shown to be doublets by an off-resonance experiment and the chemical shift of 24.44 ppm was attributed to C-1 since it shifts least from the value of 24.14 ppm[3] for the C-1 of the parent hydrocarbon. The largest and the moderate downfield shifts from the value of 26.16 ppm[3] for the C-2 of the parent hydrocarbon are ascribed to the carbons C-5 and C-4, respectively. The

Table 2. ^{13}C Chemical shifts for 2-substituted *endo*-5-(4-imidazolyl)bicyclo[2.2.2]octanes[a]

2-Substituent (Compound)	C-1	C-2	C-3	C-4	C-5	C-6	C-7	C-8	Imidazolyl carbons
Unsubstituted (**9**)	24.44	26.55*	20.95	29.80	34.43	31.91	25.82*	25.25	140.83
									134.57
									117.92
Oxo (**3**)	42.98	218.11	40.40	33.74	33.91	29.35	22.92	25.61	142.85
	(42.4)	(216.9)	(39.6)	(29.8)	(34.5)	(29.1)	(23.5)	(25.3)	135.25
				(33.8)[b]					114.38
endo-trans-Cinnamoyloxy (**7**)	30.40	72.90	29.49	29.49	34.30	25.46	22.87	25.46	140.99
	(30.4)	(72.7)	(29.8)	(29.8)	(34.5)	(25.0)	(23.2)	(25.3)	134.49
									117.21
exo-trans-Cinnamoyloxy (**8**)	30.37	72.45	30.07	28.71	33.54	29.39	18.79	25.97	142.42
	(30.4)	(72.7)	(29.8)	(29.8)	(34.5)	(29.0)	(19.2)	(25.3)	134.90
									115.62

a) The chemical shifts are in ppm downfield from internal tetramethylsilane in chloroform-*d*. The values in parentheses are those calculated with use of parameters in Table 1. The chemical shifts for the *trans*-cinnamoyloxy group were found to be essentially the same as those for ethyl *trans*-cinnamate. The asterisks designate a reversible pair of shifts. b) Corrected for the downfield shift (4.0 ppm) of C-4 in bicyclo[2.2.2]octan-2-one (Ref. 3).

remaining five carbons showed triplets by an off-resonance experiment. The carbons C-2 and C-7 are expected to show chemical shifts nearest to 26.16 ppm The largest downfield shift of 31.91 ppm was assigned to C-6 and the largest upfield shift of 20.95 ppm to C-3 which is γ-syn to C-5. The remaining shift of 25.25 ppm corresponds to the carbon C-8 which is γ-anti to C-5.

The parameters for the *trans*-cinnamoyloxy group were calculated from the *endo*- and *exo-trans*-cinnamoyloxy derivatives **7** and **8** by subtracting the shifts due to the imidazolyl group. An average was taken from the values for **7** and **8**. As expected, the parameters for the imidazolyl and *trans*-cinnamoyloxy groups show a similar trend in their magnitudes as compared with that for the hydroxyl group.

Physical Properties and endo, exo Stereochemistry. Using ^{13}C chemical shifts as described above, we determined the mode of 2,5 disubstitution and the endo, exo stereochemistry of the oxo, hydroxy, and cinnamoyloxy derivatives. In conformity with the determination, the *exo*-hydroxy-*endo*-imidazolyl derivative **6** and the hydrochloride of the *exo*-cinnamoyloxy-*endo*-imidazolyl derivative **8** were observed to have higher melting points than their corresponding *endo*-hydroxy-*endo*-imidazolyl derivative **5** and hydrochloride of the *endo*-cinnamoyloxy-*endo*-imidazolyl derivative **7**, respectively. The exo, endo derivative **6** was also found to have a smaller R_f value than the corresponding endo, endo derivative **5**. These observations are understandable on the basis of the relative spatial alignment of the two functional groups, the same situation being observed for the bicyclo[2.2.1]heptane system previously.[1)]

Another means for differentiating the endo or exo stereochemistry is the ^1H chemical shift for the proton attached to the C-4 carbon of the imidazolyl group. The chemical shifts for the endo, endo derivatives **5** and **7** were found to be 0.08 ppm downfield from those of the corresponding exo, endo derivatives **6** and **8**. Although it cannot be explained clearly, a similar downfield shift of 0.06—0.15 ppm is also observed for the bicyclo-[2.2.1]heptane system.[1)]

Thus the physical properties so far observed are consistent with the endo, exo stereochemistry determined by the ^{13}C chemical shift.

Experimental

All melting points and boiling points are uncorrected. ^1H NMR spectra were obtained on a Hitachi Model R-24 spectrometer at 60 MHz. Tetramethylsilane was used as an internal standard unless otherwise noted. ^{13}C NMR spectra were recorded with a JEOL JNM FX-100 spectrometer at 25.05 MHz equipped with Fourier transform facilities. Mass spectra were obtained with a Hitachi Model RMS-4 mass spectrometer at 70 eV. Elemental analyses were carried out by Mr. E. Amano of our laboratory.

endo- *and* exo-*5-(1-Oxo-2-hydroxyethyl)bicyclo[2.2.2]oct-2-enes* (*1*). In order to obtain a Diels-Alder dienophile, 26.8 g (0.313 mol) of 2-butyn-1,4-diol was isomerized to hydroxymethyl vinyl ketone.[1)] The crude ketone was heated with 5.0 g (0.063 mol) of 1,3-cyclohexadiene at 100—120 °C for 13 h. The resulting viscous reddish oil was distilled to give 6.1 g (0.037 mol) of crude **1**: bp 110—125 °C (12 Torr); IR (neat) 3650—3200 (OH), 3030 (=C–H), 1710 (C=O), 1615 (C=C), and 1065 cm^{-1} (C–O); ^1H NMR ($CDCl_3$) δ 6.4—5.9 (m, 2, CH=CH), 4.30 (s, *ca.* 0.2, *exo*-CH_2–O), 4.26 (s, *ca.* 1.8, *endo*-CH_2–O), 3.3 (s, 1, OH), 3.0—2.3 (m, 3), and 2.0—1.0 ppm (m, 6).

endo- *and* exo-*5-(4-Imidazolyl)bicyclo[2.2.2]oct-2-enes* (*2*). The hydroxymethyl ketone **1** was treated with 28% aq ammonia, copper(II) acetate, and 37% aq formaldehyde,[1)] giving a very viscous, transparent, and reddish oil of crude **2** in 60—70% yield: IR (neat) 3500—2200 (NH), 1615 (CH=CH), and 1580—1560 cm^{-1} (imidazole ring); ^1H NMR ($CDCl_3$) δ 9.1 (s, 1, NH), 7.58, 7.48 (two s, 1, N=CH–N), 6.87 (s, 0.25, N–CH=C), 6.65 (s, 0.75, N–CH=C), 6.5—5.95 (m, 2, CH=CH), 3.0 (m, 1, H_5), 2.85—2.4 (m, 2, H_1 and H_4), and 2.3—1.0 ppm (m, 6).

In order to obtain the picrate of **2**, an equimolar amount of picric acid in chloroform was added to a solution of **2** in chloroform. The picrate precipitated by cooling was collected and recrystallized: mp 151—152 °C; ^1H NMR (DMSO-d_6) δ (solvent peak, δ 2.50 as internal standard) 8.98 (d, 0.15, N–CH=N), 8.88 (d, 0.85, N–CH=N), 8.55 (s, 2, picrate anion), 7.57 (d, 0.15, N–CH=C), 7.18 (d, 0.85, N–CH=C), 6.5—5.85 (m, 2, CH=CH), 3.04 (m, 1, H_5), 2.9—2.4 (m, 2, H_1 and H_4), and 2.3—1.0 ppm (m, 6). Found: C, 50.99; H, 4.18; N, 17.19%. Calcd for $C_{17}H_{16}N_5O_7$: C, 50.75; H, 4.01; N, 17.46%.

endo-*5-(4-Imidazolyl)bicyclo[2.2.2]octan-2-one* (*3*). In a solution of 2.85 ml of 1 M hydrochloric acid and 25 ml of water, 560 mg (3.16 mmol) of palladium chloride was dissolved by heating at 80 °C for 30 min. To this solution was added dropwise 500 mg (2.87 mmol) of **2** in 2.85 ml of 1 M hydrochloric acid and 8 ml of water over a period of 10 min with stirring. The mixture was then heated at 95 °C for 30 min and filtered. The filtrate was concentrated to half the original volume and extracted with chloroform after the pH of solution had been adjusted to 9 with 28% aq ammonia. After being dried over magnesium sulfate, the solvent was removed to give 320 mg of a viscous yellow oil. This oil was developed three times over basic alumina (Merck, HF_{254} Type E) using dichloromethane–methanol (50/1 vol/vol), to give 170 mg (31%) of the ketone **3** (R_f value 0.1—0.4). This was recrystallized from chloroform–carbon tetrachloride: mp 147—148 °C; IR (KBr) 3500—2200 (NH), 1720 (C=O), and 1580—1560 cm^{-1} (imidazole ring); ^1H NMR ($CDCl_3$) δ 9.15 (s, 1, NH), 7.55 (s, 1, N–CH=N), 6.75 (s, 1, N–CH=C), 3.18 (m, 1, H_5), and 2.6—1.5 ppm (m, 10); MS *m/e* 190 (M^+). Found: C, 69.60; H, 7.42; N, 14.68%. Calcd for $C_{11}H_{14}N_2O$: C, 69.45; H, 7.42; N, 14.72%.

Twenty mg of **2** was recovered (R_f value 0.5).

endo-*5-(4-Imidazolyl)bicyclo[2.2.2]octan*-endo- *and* exo-*2-ols* (*4*). With lithium aluminum hydride in THF 1.48 g of the crude oil of **3** was reduced to give 1.23 g of a crude solid of **4**.[1)]

endo-*5-(4-Imidazolyl)bicyclo[2.2.2]octan*-endo-*2-ol* (*5*). Isolation of **5** from **4** was achieved by preparative TLC. About 240 g of basic alumina (Merck, HF_{254} Type E) was coated on ten glass plates (20×20 cm) and activated. After application of 1.23 g of the crude **4** in methanol, the plates were developed four times with use of dichloromethane–methanol (15/1 vol/vol). The endo alcohol **5** obtained (R_f value 0.4—0.65) amounted to 450 mg. This gave white crystals from methanol by adding carbon tetrachloride: mp 144—146 °C; IR (KBr) 3550 (OH), 3400—2200 (NH), and 1580—1560 cm^{-1} (imidazole ring); ^1H NMR ($CDCl_3$) δ 7.48 (s, 1, N–CH=N), 6.82 (s, 1, N–CH=C), 3.82 (m, 1, H_2), 2.89 (m, 1, H_5), and 2.3—1.2 ppm (m, 10).

endo-5-(4-Imidazolyl)bicyclo[2.2.2]octan-exo-*2-ol (6)*. The exo alcohol **6** obtained (R_f value 0.1—0.4) amounted to 420 mg. This gave white crystals from methanol–carbon tetrachloride: mp 219—220 °C; IR (KBr) 3550 (OH), 3400 2200 (NH), and 1580—1560 cm^{-1} (imidazole ring); ^1H NMR ($CDCl_3$) δ 7.51 (s, 1, N–CH=N), 6.74 (s, 1, N–CH=C), 3.88 (m, 1, H_2), 2.90 (m, 1, H_5), and 2.4—1.0 ppm (m, 10). Found: C, 68.59; H, 8.11; N, 14.28%. Calcd for $C_{11}H_{16}N_2O$: C, 68.72; H, 8.39; N, 14.57%.

endo-5-(4-Imidazolyl)bicyclo[2.2.2]octan-endo-*2-yl* trans-*Cinnamate (7)*. In 5 ml of freshly distilled ethanol-free chloroform 230 mg (1.2 mmol) of **5** was heated with 720 mg (4.3 mmol) of *trans*-cinnamoyl chloride at 85 °C for 2 h. The clear, light yellow solution was evaporated to dryness and the residual solid was dissolved in THF–methanol–water. The pH of the solution was then adjusted to 9 with aqueous sodium carbonate and allowed to stand for 6 h at room temperature. Removal of the organic solvents by a rotary evaporator gave a heterogeneous aqueous solution, which was extracted with chloroform twice. The extract was washed with water and dried over magnesium sulfate. Removal of the solvent gave 390 mg (100%) of crude **7**. This was passed through a column of basic alumina using dichloromethane–methanol to give 220 mg of a colorless brittle solid of **7**: IR (KBr) 3400—2200 (NH), 1700 (C=O), 1635 (C=C), 1575 (imidazole ring), and 1170 cm^{-1} (C–O); ^1H NMR ($CDCl_3$) δ 8.3 (s, 1, NH), 7.59 (d, 1, J=16 Hz, C*H*=CH), 7.53 (s, 1, N–CH=N), 7.65—7.15 (m, 5, phenyl), 6.87 (s, 1, N–CH=C), 6.33 (d, 1, J=16 Hz, CH=C*H*), 4.98 (m, 1, H_2), 2.94 (m, 1, H_5), and 2.4—1.2 ppm (m, 10).

To crystallize **7** as hydrochloride, 93 mg of **7** was dissolved in 0.1 M hydrochloric acid and the solution was evaporated to dryness. The residual solid was crystallized from a minimum quantity of chloroform by dilution with warm carbon tetrachloride and cooling in a refrigerator, giving 91 mg of the colorless hydrochloride of **7**: mp 167.5—170 °C (dec). Found: C, 66.61; H, 6.49; N, 8.17%. Calcd for $C_{20}H_{23}N_2O_2Cl$: 66.93; H, 6.46; N, 7.81%.

endo-5-(4-Imidazolyl)bicyclo[2.2.2]octan-exo-*2-yl* trans-*Cinnamate (8)*. In a similar way to that for **5**, 200 mg of **6** was converted into 109 mg of a colorless brittle solid of **8**: IR (KBr) 3400—2200 (NH), 1700 (C=O), 1635 (CH=CH), 1575 (imidazole ring), and 1170 cm^{-1} (C–O); ^1H NMR ($CDCl_3$) δ 9.4 (s, 1, NH), 7.63 (d, 1, J=16 Hz, C*H*=CH), 7.55 (s, 1, N–CH=N), 7.6—7.15 (m, 5, phenyl), 6.79 (s, 1, N–CH=C), 6.37 (d, 1, J=16 Hz, CH=C*H*), 5.00 (m, 1, H_2), 3.00 (m, 1, H_5), and 2.4—1.1 ppm (m, 10).

In a similar way to that for **7**, 47 mg of **8** gave 44 mg of the hydrochloride: mp 208 °C (dec). Found: C, 66.72; H, 6.56; N, 8.09%. Calcd for $C_{20}H_{23}N_2O_2Cl$: C, 66.93; H, 6.46; N, 7.81%.

2-(4-Imidazolyl)bicyclo[2.2.2]octane (9). To 200 mg of crude **2** in 10 ml of methanol was added 50 mg of 10% Pd–C[7] and the mixture was shaken under a hydrogen atmosphere (1 atm) for 3 h until the theoretical volume of hydrogen was absorbed. The mixture was filtered and the catalyst was washed with methanol. The combined filtrate and washings were evaporated to give 173 mg (87%) of a slightly yellow, brittle solid. This was distilled in a glass tube at 160 °C (0.15 mmHg) to give a colorless viscous oil, which solidified on cooling. The hygroscopic solid obtained could not be crystallized: IR (neat) 3400—2200 (NH) and 1590—1560 cm^{-1} (imidazole ring); ^1H NMR ($CDCl_3$) δ 9.3 (s, 1, NH), 7.56 (s, 1, N–CH=N), 6.83 (s, 1, N–CH=C), 2.97 (m, 1, H_2), and 2.3—1.1 ppm (m, 12); MS *m/e* (rel intensity), 176 (M^+, 50), 175 (14), 147 (16), 146 (10), 145 (13), 119 (10), 110 (8), 109 (8), 96 (25), 95 (100), 94 (25), 82 (18), 81 (25), 80 (13), and 79 (10).

The present work was supported partially by a Grant-in-Aid for Scientific Research from the Ministry of Education.

References

1) M. Utaka, A. Takeda, and M. L. Bender, *J. Org. Chem.*, **39**, 3772 (1974).

2) A. H. Beckett, A. A. Al-Badr, and A. Q. Khakhar, *Tetrahedron*, **31**, 3103 (1975).

3) P. J. Garratt and R. Riguera, *J. Org. Chem.*, **41**, 465 (1976).

4) P. M. Maitlis, "The Organic Chemistry of Palladium," Vols. 1 and 2, Academic Press, New York (1971); G. N. Schrauzer, Ed., "Transition Metals in Homogeneous Catalysis," Marcel Dekker, New York (1971).

5) Oxidation of *endo*-5-(2-imidazolyl)bicyclo[2.2.2]oct-2-ene with palladium chloride was reported by A. F. Wagner, P. E. Wittreich, B. H. Arison, and L. H. Sarett, *J. Org. Chem.*, **36**, 2609 (1971), to give the 2-oxo derivative in 60% yield. However, no result implicated the possibility of the 2-imidazolyl group as a key ligand.

6) The carbon atom bearing the imidazolyl group is denoted by C-5 for consistency in the numbering.

7) R. Mozingo, *Org. Synth.*, Coll. Vol. III, 687 (1955).

Chemical Studies on Tuberactinomycin. XI.[1] Semisyntheses of Tuberactinomycin Analogs with Various Amino Acids in Branched Part[2]

Tateaki WAKAMIYA, Tadashi TESHIMA, Hideo SAKAKIBARA,*
Kiyoshi FUKUKAWA,* and Tetsuo SHIBA

Department of Chemistry, Faculty of Science, Osaka University Toyonaka, Osaka 560
**The Research Laboratories, Toyo Jozo Co., Ltd., Ohito, Shizuoka 410-23*

(Received February 7, 1977)

Thirty two semisynthetic tuberactinomycins were prepared by introduction of various amino acids to amino group of tuberactinamine N, a cyclic peptide moiety of tuberactinomycin N and O, which was isolated from natural tuberactinomycin N by acid treatment with liberation of γ-hydroxy-β-lysine of the branched part. Among introduced amino acids, β-amino acids were synthesized from corresponding α-amino acids by modified Arndt-Eistert reaction. After couplings of N-protected amino acids with tuberactinamine N, deprotections were carried out to give semisynthetic tuberactinomycins. From their minimum inhibitory concentrations against many bacteria, it was suggested that a branched part effects significantly to the strength of antimicrobial activities though most important active site must locate in the cyclic peptide moiety, and basicity and/or hydrophobicity of the branched part seemed to strengthen the antibacterial activity especially.

In our recent studies on the antibiotics tuberactinomycins,[3] tuberactinamine N, the cyclic peptide moiety of tuberactinomycin N as well as O, could be isolated as fine crystals by acid treatment of tuberactinomycin N with liberation of γ-hydroxy-β-lysine of the branched part[4] (Fig. 1). Tuberactinamine N thus obtained showed a comparable antituberculous activity to that of original tuberactinomycin N, maintaining the intramolecular hydrogen bond between α-amide proton of capreomycidine residue and carbonyl group of serine[3] residue as in all of tuberactinomycins.[5] From these facts, tuberactinamine N seemed to be a very promising key-intermediate for preparation of novel semisynthetic tuberactinomycins, which have more favorable properties, *e.g.*, high biological activities, less toxicities, and different antibacterial spectra. Such study may also afford very valuable informations concerning relationships between structure and antibacterial activity in tuberactinomycins. Although the cyclic peptide part, *i.e.*, tuberactinamine N, may be the most important site for exhibition of biological activities in tuberactinomycins, its activity is weakened as compared with tuberactinomycin N. This may indicate that the branched amino acid as β-lysine or γ-hydroxy-β-lysine in original tuberactinomycins is required to strengthen the microbial activities.

Along this line, various amino acids were attempted to be linked to the free α-amino group of α,β-diaminopropionic acid residue in tuberactinamine N in this investigation. A number of protected amino acids with benzyloxycarbonyl or *t*-butoxycarbonyl group[6] were coupled with tuberactinamine N by active ester method and then the protecting groups were removed by catalytic hydrogenation or acid treatment respectively (Fig. 2). The second functional groups of α-amino acids like aspartic acid, glutamic acid, serine, histidine, and arginine were protected with *t*-butyl, benzyl, *t*-butyl, tosyl, and nitro groups, respectively, which were removed later together with α-amino-protecting groups. β-Amino acids as materials were prepared from the corresponding α-amino acids by the modified Arndt-Eistert reaction.[7] Furthermore, in this study, we introduced a new convenient way for direct preparation of β-(acylamino) acid *N*-hydroxysuccinimide active

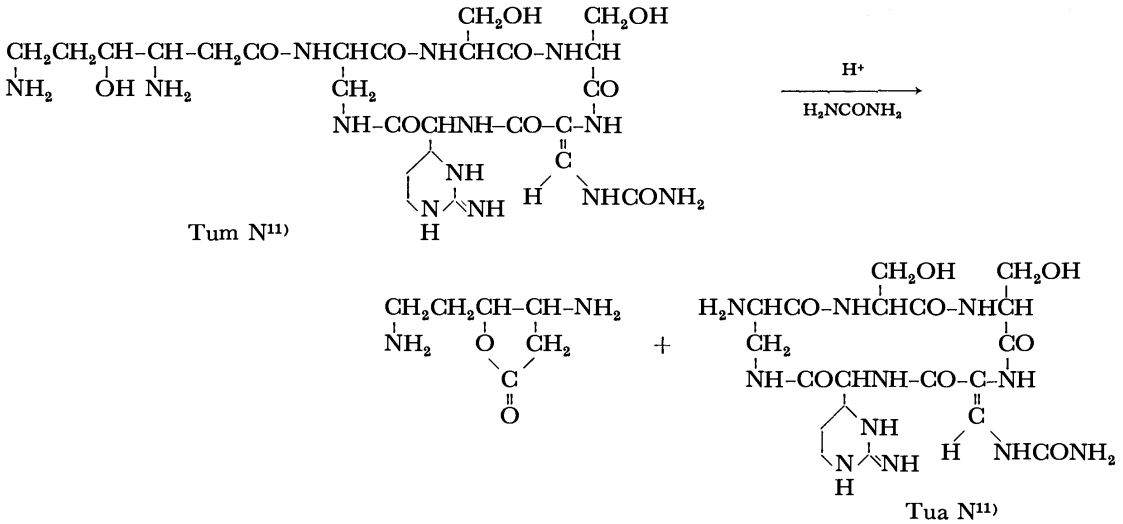

Fig. 1.

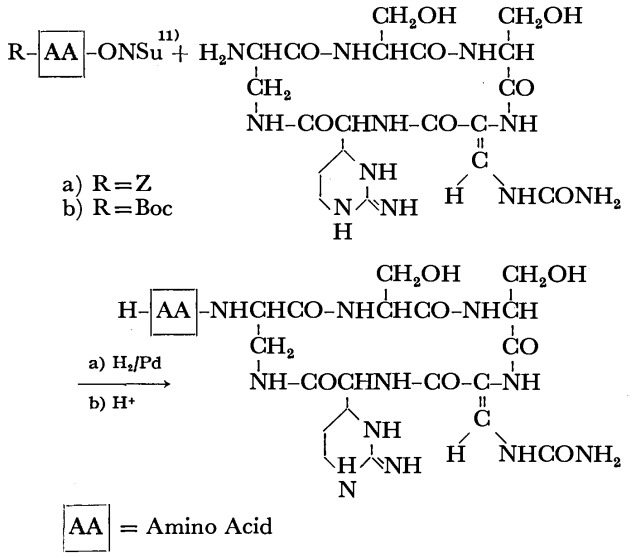

Fig. 2.

ester from diazo ketone derivative of α-(acylamino) acid by use of *N*-hydroxysuccinimide instead of methanol at the step of Wolff rearrangement (Fig. 3).

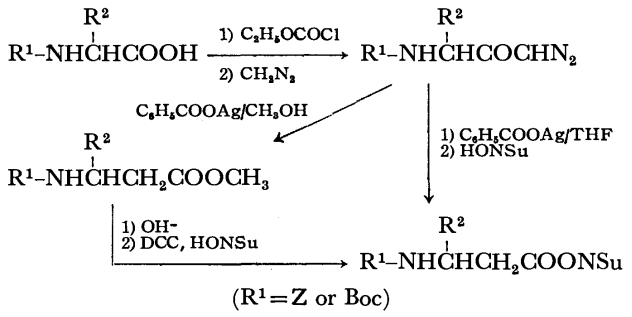

Fig. 3.

Many semisynthetic tuberactinomycins thus prepared were measured their minimum inhibitory concentration (MIC) to various bacilli and studied their ORD and CD spectra.

Experimental

All melting points are uncorrected. The specific rotations were obtained with a Perkin-Elmer 141 Polarimeter. ORD and CD spectra were obtained with a JASCO Model ORD/UV-5 in water. Thin-layer chromatography was carried out by the ascending method on silica gel G using a developing solvent of butanol-acetic acid-water (4: 1: 2).

Z-L-A_2pr(Z)-ONSu.[11] To a solution of Z-L-A_2pr(Z)-OH (372 mg, 1.0 mmol) in 5 ml of THF, DCC (227 mg, 1.1 mmol) and HONSu (127 mg, 1.1 mmol) were added with stirring at 0 °C. Stirring was continued at this temperature for 1 h and then at room temperature for 6 h. *N,N'*-Dicyclohexylurea was filtered off and filtrate was concentrated *in vacuo*. When crystalline residue was dissolved in ethyl acetate and stored in refrigerator, *N,N'*-dicyclohexylurea was again precipitated. After removal of the precipitate by filtration, hexane was added to the filtrate to obtain fine needles, yield 390 mg (83%), mp 113—116 °C, $[\alpha]_D^{24}$ −36.2° (*c* 1.00, DMF).

Found: C, 58.93; H, 4.99; N, 8.96%. Calcd for $C_{23}H_{23}O_8N_3$: C, 58.84; H, 4.94; N, 8.95%.

Boc-L-A_2bu(Boc)-ONSu. Boc-L-A_2bu(Boc)-OH (oily; 3.18 g, 10.0 mmol), DCC (2.06 g, 10.0 mmol) and HONSu (1.15 g, 10.0 mmol) were treated as described in the preparation of Z-L-A_2pr(Z)-ONSu. The product was recrystallized from dioxane and hexane, yield 3.50 g (84%), mp 141—142 °C, $[\alpha]_D^{26}$ −34.4 ° (*c* 1.00, DMF).

Found: C, 52.04; H, 7.03; N, 10.13%. Calcd for $C_{18}H_{29}O_8N_3$: C, 52.04; H, 7.04; N, 10.12%.

Preparation of β-(Acylamino) Acids N-*Hydroxysuccinimide Active Ester. Method A (Preparation of Boc-L-β-Lys(Z)-ONSu)*: To a solution of Boc-L-Orn(Z)-OH (3.66 g, 10.0 mmol) in 30 ml of ethyl acetate, *N*-methylmorpholine (1.01 g, 10.0 mmol) and then ethyl chloroformate (1.08 g, 10.0 mmol) were added under cooling in an ice-salt bath and then diazomethane in ether was added. The reaction mixture was stirred for 2 h and allowed to stand at room temperature overnight. A small amount of precipitate was filtered off and filtrate was concentrated *in vacuo*. The yellowish crystalline residue was dissolved in 50 ml of methanol and silver benzoate (100 mg, 0.436 mmol) in 1 ml of triethylamine was added. The reaction mixture was stirred at room temperature for 4 h in the dark, and then concentrated *in vacuo*. Insoluble material of the residue in ethyl acetate was filtered off. Filtrate was washed with 1M hydrochloric acid or 10% citric acid, water, saturated sodium hydrogencarbonate solution, and water to neutral successively. Organic layer was dried over anhydrous sodium sulfate and concentrated *in vacuo*. Crystalline residue (3.20 g, 81%) was recrystallized from ethyl acetate and hexane to give a fine Boc-L-β-Lys(Z)-OMe, yield 2.38 g (60%), mp 69—71 °C, $[\alpha]_D^{14}$ −5.1 ° (*c* 1.00, DMF).

Found: C, 60.86; H, 7.74; N, 7.12%. Calcd for $C_{20}H_{30}O_6N_2$: C, 60.89; H, 7.67; N, 7.10%.

To a solution of Boc-L-β-Lys(Z)-OMe (960 mg, 2.43 mmol) in 5 ml of dioxane, 2.43 ml of 1 M sodium hydroxide was added with stirring at 0 °C. Stirring was continued at this temperature for 30 min, and then at room temperature for additional 2 h. The reaction mixture was acidified with 10% citric acid and extracted with ethyl acetate. Organic layer was washed with water to neutral, and was dried over anhydrous sodium sulfate and concentrated *in vacuo*. Crystalline residue thus obtained was recrystallized from ethyl acetate and hexane to give Boc-β-L-Lys(Z)-OH, yield 740 mg (80%), mp 89—91 °C, $[\alpha]_{365}^{14}$ +4.5 ° (*c* 1.01, DMF).

Found: C, 59.98; H, 7.45; N, 7.30%. Calcd for $C_{19}H_{28}O_6N_2$: C, 59.98; H, 7.42; N, 7.36%.

Boc-L-β-Lys(Z)-OH (1.90 g, 5.00 mmol), DCC (1.24 g, 6.00 mmol) and HONSu (690 mg, 6.00 mmol) were allowed to react as described in the preparation of Z-L-A_2pr(Z)-ONSu. The product was recrystallized from ethyl acetate and hexane, yield 1.70 g (71%), mp 73 (sintered)—80 °C, $[\alpha]_D^{14}$ −6.1 ° (*c* 1.00, DMF).

Found: C, 57.74; H, 6.56; N, 8.82%. Calcd for $C_{21}H_{31}O_8N_3$: C, 57.85; H, 6.54; N, 8.80%.

Method B (Preparation of Boc-L-β-Orn(Boc)-ONSu): To a solution of Boc-L-A_2bu(Boc)-OH (1.59 g, 5.0 mmol) in 25 ml of ethyl acetate, *N*-methylmorpholine (506 mg, 5.0 mmol) and then ethyl chloroformate (543 mg, 5.0 mmol) were added with stirring in an ice-salt bath and stirring was continued for 3 h. *N*-Methylmorpholine hydrochloride was filtered off. A large excess of diazomethane in ether was added to the cold filtrate. A solution was stirred in the cold for 1 h and then at room temperature overnight. Oily residue obtained after vacuum concentration was dissolved in 10 ml of THF. To the solution, HONSu (2.30 g, 20 mmol) and silver benzoate (100 mg, 0.44 mmol) in 1 ml of triethylamine were added. The mixture was stirred at room temperature in the dark for

TABLE 1. PHYSICOCHEMICAL PROPERTIES OF β-(ACYLAMINO) ACID *N*-HYDROXYSUCCINIMIDE ACTIVE ESTERS

R^1-NHCHCH$_2$COONSu (R^2)	Method	Yield (%)[a]	Mp (°C)	$[\alpha]_D^{23}$ (*c* 1, DMF)
R^1=Z, R^2=CH(CH$_3$)$_2$ (β-Leu)	B	79	74—76	+28.5°
R^1=Z, R^2=CH$_2$CH(CH$_3$)$_2$ (β-Hle)	B	80	83—84	−4.9°
R^1=Z, R^2=CH(CH$_3$)CH$_2$CH$_3$ (β-Hil)	B	74	78—80	+25.6°
R^1=Z, R^2=CH$_2$C$_6$H$_5$ (β-Hph)	B	84	127—128	−12.4°
R^1=Z, R^2=CH$_2$CH$_2$CH$_3$ (β-Ahx)[b]	B	91	oil	—
R^1=Z, R^2=CH$_2$NH–Z (β, γ-A$_2$bu)	A	70	80[c]	+5.1°
R^1=Boc, R^2=CH$_2$CH$_2$NH–Boc (β-Orn)	B	71	130—132	−13.8°
R^1=Boc, R^2=CH$_2$CH$_2$CH$_2$NH–Z (β-Lys)	A	72	101—103	−6.6°

a) Overall yield from α-(acylamino) acids. b) Only in this case, DL-form of the starting α-amino acid was used while the other starting amino acids were all of L-forms. c) Sintered at 73 °C.

4 h and then concentrated *in vacuo*. After the residue was triturated with ethyl acetate, insoluble inorganic material was filtered off. Filtrate was washed with 10% citric acid, water, saturated sodium hydrogencarbonate solution, and finally water to neutral. Ethyl acetate layer was dried over anhydrous sodium sulfate and concentrated *in vacuo*. Oily residue was treated with hexane to be crystallized, yield 1.52 g (71%). Recrystallization from ethyl acetate and hexane afforded pure substance, yield 1.26 g (59%), mp 130—132 °C, $[\alpha]_D^{23}$ −13.8° (*c* 0.99, DMF).

Found: C, 52.76; H, 7.27; N, 9.65%. Calcd for $C_{19}H_{13}O_8N_3$: C, 53.13; H, 7.28; N, 9.79%.

β-(Acylamino) acid active esters were mainly prepared by method B and their physicochemical properties were listed in Table 1.

Preparation of New Tuberactinomycin Analogs. [L-*Lys*[1]]-*Tum N·3HCl*: To a suspension of Tua N·2HCl[4] (300 mg, 0.49 mmol) in 10 ml of DMF, Boc-L-Lys(Boc)-ONSu (324 mg, 0.73 mmol) and triethylamine (51 mg, 0.50 mmol) were added, and stirred at room temperature overnight. Disappearance of Tua N was checked by TLC. A clear solution was concentrated *in vacuo* and the residue was triturated with dioxane or THF.[8] Gelatinous precipitate was filtered or collected by centrifugation. For a complete removal of unreacted active ester, an aqueous solution of the product is better extracted with ethyl acetate. Concentration of the aqueous layer *in vacuo* gave a pure coupling product in a quantitative yield as hygroscopic powder. It was immediately dissolved in 3 ml of 3 M hydrochloric acid and allowed to stand for 45 min at room temperature. Additions of ethanol and ether gave precipitate, yield 340 mg (89%). It was recrystallized from water and ethanol to give fine needles 307 mg, 81%), mp 236—237 °C (dec), $[\alpha]_D^{24}$ −9.8° (*c* 1.00, H_2O).

Found: C, 38.36; H, 6.13; N, 23.01; Cl, 13.36%. Calcd for $C_{25}H_{43}O_9N_{13}\cdot 3HCl\cdot 1/2H_2O$: C, 38.10; H, 6.01; N, 23.11; Cl, 13.50%.

[L-β-*Leu*[1]]-*Tum N*: To a suspension of Tua N·2HCl[4] (307 mg, 0.50 mmol) in 10 ml of DMF, Z-L-β-Leu-ONSu (217 mg, 0.60 mmol) and triethylamine (61 mg, 0.60 mmol) were added. After Tua N was consumed, a clear solution was concentrated *in vacuo*. The residue was triturated with THF and gelatinous product was collected by centrifugation. Powder obtained quantitatively was dissolved in water containing 0.1 ml of concentrated hydrochloric acid and extracted with ethyl acetate several times. The aqueous layer was subjected to hydrogenation by use of palladium black catalyst. The reaction was followed by TLC and catalyst was filtered off after completion of debenzyloxycarbonylation. Filtrate was concentrated *in vacuo* and the residue was treated with ethanol to make it powder, yield 350 mg (96%). It was recrystallized from water and ethanol, yield 300 mg (82%), mp 238 °C (dec), $[\alpha]_D^{24}$ −22.7° (*c* 1.00, H_2O).

Found: C, 40.07; H, 6.16; N, 22.23; Cl, 9.25%. Calcd for $C_{25}H_{42}O_9N_{12}\cdot 2HCl\cdot H_2O$: C, 40.27; H, 6.22; N, 22.54; Cl, 9.51%.

All of the other acids applied were coupled to the Tua N *via* *N*-hydroxysuccinimide ester, in similar manners, by

TABLE 2. PHYSICOCHEMICAL PROPERTIES OF SEMISYNTHETIC TUBERACTINOMYCIN ANALOGS (R-Tua N)

R	Mp (dec) (°C)	$[\alpha]_D^6$ (*c* 1.0, H_2O)	Yield (%)	Protecting group of amino group
Asp	245	−17.2°	94	Z
Glu[f]	246	−19.2°	91	Boc
Gly	232—234	−20.7°	63	Boc
Ala	248—249	−13.5°	75	Z
Ser	235—236	−16.5°	66	Boc
Val	253—254	−13.6°	88	Z
Leu	>250	−15.3°	88	Z
Ile	247—248	−14.9°	86	Z
Phe	233—235	−7.6°	87	Z
Tyr	236—238	−3.8°	32	Boc
Trp	248—249	+3.5°	53	Boc
Pgl[f],[11]	247—249	−9.2°	48	Z
Pro	235	−37.4°	73	Z
β-Ala	232—234	−23.2°[a]	91	Z
β-Leu	238	−22.7°	82	Z
β-Hle	239—240	−19.6°	83	Z
β-Hil	240—241	−14.8°	78	Z
β-Hph	241	−19.0°	88	Z
β-Ahx	244—245	−20.1°	69	Z
ε-Ahx	233—234	−25.6°	90	Boc
Lys	236—237	−9.8°[c]	81	Boc
Lys[f]	236—238	−28.8°	30	Boc
Orn	241—243	−9.0°[a]	83	Boc
α, γ-A$_2$bu	234—235	−2.0°	79	Boc
α, β-A$_2$pr	>250	−4.3°	77	Z
β-Orn	241—243	−14.0°	83	Boc
β, γ-A$_2$bu	249	−14.1°	85	Z
Arg	>250	−8.7°[b]	53	Nps
His	229—231	−3.9°	53	Boc
Ac-β-Lys	239	−34.0°[e]	55	Z
β-Lys(Ac)	236	−24.2°[e]	65	Boc
Ac-β-Lys(Ac)	215	−34.6°[d]	68	—

a) at 11 °C. b) at 16 °C. c) at 24 °C. d) at 25 °C. f) D-from.

either procedure mentioned above depending on the protecting group used except in the case of arginine. All protecting groups in the products were finally removed with acid or by hydrogenation in the presence of acid. However N^{im}-tosyl group of histidine was readily removed with HOBt after coupling reaction.[9] Physicochemical data for all other semisynthetic tuberactinomycins are listed in Table 2.

[L-Arg¹]-Tum N·3HCl. To a solution of Tua N·2HCl[4] (300 mg, 0.49 mmol), Nps–Arg(NO_2)–OH (181 mg, 0.54 mmol), and HOBt (72 mg, 0.54 mmol) in a mixture of 5 ml of DMF and 4 ml of water, 1-ethyl-3-(3-dimethylaminopropyl)carbodiimide (78 mg, 0.54 mmol) was added with stirring in an ice bath. It was stirred in an ice bath for 3 h and then at room temperature overnight. The solution thus obtained was concentrated *in vacuo* and the residue was triturated with ethyl acetate. Precipitate was filtered and then suspended in 10 ml of 1 M hydrochloric acid and 10 ml of ether. The mixture was stirred at room temperature for 30 min. Aqueous layer separated was washed with ether three times. The aqueous solution was concentrated *in vacuo* and the residue was reprecipitated from water and ethanol to remove sulfur-containing compound completely. Precipitate was again dissolved in 20 ml of water containing 0.5 ml of concd hydrochloric acid and hydrogenated in the presence of palladium black. After completion of deprotection, the catalyst was removed by filtration. Filtrate was concentrated *in vacuo* and the residue was treated with ethanol to give powder, yield 355 mg (90%). For purification, it was applied to Amberlite IRC 50 (CG 50 Type 1 1.5×23 cm) column and eluted gradiently with pH 3.1 to pH 5.0 buffer (0.2—2 M pyridine–acetate). Eluates containing [L-Arg¹]-Tum N were collected and concentrated *in vacuo*. To a solution of the residue in 6 M hydrochloric acid, ethanol was added to precipitate the product, yield 208 mg (53%), mp >250 °C, $[\alpha]_D^{16}$ −8.7 ° (*c* 1.01, H_2O).

Found: C, 37.05; H, 5.84; N, 24.86; Cl, 12.76%. Calcd for $C_{25}H_{43}O_9N_{15}\cdot 3HCl\cdot H_2O\cdot 1/2C_2H_5OH$: C, 36.82; H, 6.06; N, 24.77; Cl, 12.54%.

[Ac–L-β-Lys¹]-Tum N (Nᵝ-Ac–Tum O)·2HCl. To a suspension of Tua N·2HCl[4] (1.50 g, 2.44 mmol) in 50 ml of DMF, Boc–L-β-Lys(Z)–ONSu (1.28 g, 2.69 mmol) and triethylamine (245 mg, 2.44 mmol) were added. After completion of reaction, a clear solution was concentrated *in vacuo* and oily residue was triturated with THF to make gelatinous precipitate of diacyl peptide, which was collected by centrifugation, yield 1.94 g (89%).

For removal of Boc group, an aliquot of the product (200 mg, 0.22 mmol) was dissolved in a mixture of 50% acetic acid (1 ml) and concd hydrochloric acid (0.5 ml), and then stirred at room temperature for 1.5 h. Addition of ethanol and ether to the solution gave white precipitate, yield 179 mg (92%). To a solution of the product (179 mg, 0.20 mmol) in 10 ml of DMF, AcONSu (35 mg, 0.22 mmol) and triethylamine (23 mg, 0.22 mmol) were added. The mixture was stirred at room temperature overnight and then concentrated *in vacuo*. When oily residue was triturated with THF, gelatinous precipitate was formed which was immediately hydrogenated in aqueous solution containing 0.5 ml of 1 M hydrochloric acid by use of palladium black catalyst. After completion of hydrogenolysis, catalyst was filtered off and filtrate was concentrated *in vacuo*. The residue was treated with ethanol to make it powder, yield 113 mg (71%), which was reprecipitated from water and ethanol to give pure desired material, yield 89 mg (55%), mp 239 °C (dec), $[\alpha]_D^{26}$ −34.0 ° (*c* 1.00, H_2O).

Found: C, 40.79; H, 6.12; N, 22.76; Cl, 8.99%. Calcd for $C_{27}H_{47}O_{10}N_3\cdot 2HCl\cdot 1/2H_2O$: C, 40.86; H, 6.10; N, 22.93; Cl, 8.93%.

[L-β-Lys(Ac)¹]-Tum N (Nᵋ-Ac–Tum O)·2HCl. [Boc–L-β-Lys(Z)¹]-Tum N (*N*ᵝ-Boc–*N*ᵋ-Z–Tum O)·2HCl (200 mg, 0.22 mmol) obtained during the above procedure was dissolved in DMF and hydrogen was bubbled with stirring in the presence of palladium black. Debenzyloxycarbonylation was completed in 30 h and thereafter catalyst was filtered off. After addition of AcONSu (35 mg, 0.22 mmol) to filtrate, the reaction mixture was stirred at room temperature for 15 h and concentrated *in vacuo*. The residue was treated with THF to give a single product of solid which was then dissolved in 4 M hydrochloric acid to remove Boc group. After 1 h, ethanol was added to the solution precipitating a product. Addition of ether completed the precipitation, yield 143 mg (82%). Product was reprecipitated from water and ethanol to obtain a pure compound, yield 114 mg (65%), mp 236 °C (dec), $[\alpha]_D^{26}$ −24.2 ° (*c* 1.01, H_2O).

Found: C, 40.70; H, 6.14; N, 22.66; Cl, 9.00%. Calcd for $C_{27}H_{45}O_{10}N_3\cdot 2HCl\cdot 1/2H_2O$: C, 40.86; H, 6.10; N, 22.93; Cl, 8.93%.

[Ac-β-Lys(Ac)¹]-Tum N (Nᵝ,Nᵋ-(Ac)₂-Tum O)·HCl. AcONSu (88 mg, 0.56 mmol) and triethyl amine (53 mg, 0.52 mmol) were added to a suspension of Tum O·3HCl (200 mg, 0.26 mmol) in 10 ml of DMF. The mixture was stirred for 20 h. Gelatinous residue obtained after vacuum concentration was treated with THF to give powder in a quantitative yield. Recrystallization from water and ethanol gave a pure product, yield 139 mg (68%), mp 215 °C (dec), $[\alpha]_D^{25}$ −34.6 ° (*c* 1.02, H_2O).

Found: C, 43.28; H, 6.23; N, 22.55; Cl, 4.32%. Calcd for $C_{29}H_{47}O_{11}N_{13}\cdot HCl\cdot H_2O$: C, 43.09; H, 6.24; N, 22.53; Cl, 4.39%.

Results and Discussions

Minimum inhibitory concentrations of semisynthetic tuberactinomycins preparated in this study to many bacteria were listed in Table 3. Several noticeable features were summarized as follows: 1) Although most of the synthetic compounds showed more or less antimicrobial activity against *Mycobacterium* and *Corynebacterium*, the coupling of basic amino acids gave favorable results in general. 2) Acidic amino acids as branch part extinguish the activity at all. 3) Coupling of neutral amino acids with bulky or hydrophobic side chain was relatively effective particularly against *Mycobacterium* as well as in the case of basic amino acids. 4) Remarkable relationship between methylene lengths in diamino acids and their activities against *Mycobacterium* (Table 4) was recognized. 5) Among semisynthetic tuberactinomycins prepared in this study only [L-β-Orn¹]-Tum N showed a similar antimicrobial spectrum and comparable activity to that of natural Tum N. From above results, it can be inferred that a fairly strict structure is required at a branch amino acid part to maintain a full antimicrobial activity of natural compounds, *i.e.*, presence of β-amino group and of longer chain than three carbons between two amino groups in diamino acid are necessary.

In connection with the last assumption, the role of both amino groups of β-lysine in natural tuberactinomycins was next investigated by the preparation of five following derivatives, *i.e.*, [β-Ahx¹]-Tum N, [ε-Ahx¹]-

TABLE 3. MINIMUM INHIBITORY CONCENTRATIONS[a] OF SEMISYNTHETIC TUBERACTINOMYCIN ANALOGS (R-Tua N)

Test Organisms[b]	Asp	Glu[c]	Gly	Ala	Ser	Val	Leu	Ile	Phe	Tyr	Trp
Corynebacterium diphtheriae P.W. 8	>100	>100	>100	>100	>100	>100	25	>100	50	100	25
Bacillus subtilis ATCC 6633	>100	>100	>100	>100	>100	>100	>100	>100	>100	>100	>100
Escherichia coli NIHJ	>100	>100	>100	>100	>100	>100	100	>100	>100	>100	>100
Escherichia coli B	>100	>100	>100	>100	>100	>100	>100	>100	>100	>100	>100
Salmonella typhosa H 901	>100	>100	>100	>100	>100	>100	>100	>100	>100	>100	>100
Shigella sonnei E33	>100	>100	>100	>100	>100	>100	>100	>100	>100	>100	>100
Klebsiella pneumonia ATCC 10031	>100	>100	>100	>100	>100	>100	>100	>100	>100	>100	>100
Mycobacterium ATCC 607	>100	>100	50	25	100	25	6.3	25	50	12.5	6.3

Test Organisms[b]	Pgl[c]	Pro	β-Ala	β-Leu	β-Hle	β-Hil	β-Hph	β-Ahx[d]	ε-Ahx	Lys	Lys[c]
Corynebacterium diphtheriae P.W. 8	100	100	100	50	50	50	50	100	100	12.5	50
Bacillus subtilis ATCC 6633	>100	>100	>100	>100	>100	>100	>100	>100	>100	100	100
Escherichia coli NIHJ	>100	>100	>100	>100	>100	>100	>100	>100	>100	>100	>100
Escherichia coli B	>100	>100	>100	>100	>100	>100	>100	>100	>100	>100	>100
Salmonella typhosa H 901	>100	>100	>100	>100	>100	>100	>100	>100	>100	100	>100
Shigella sonnei E33	>100	>100	>100	>100	>100	>100	>100	>100	>100	>100	>100
Klebsiella pneumonia ATCC 10031	>100	>100	>100	>100	>100	>100	>100	>100	>100	>100	>100
Mycobacterium ATCC 607	25	>100	100	50	100	100	100	100	>100	6.3	12.5

Test Organisms[b]	Orn	A_2bu	A_2pr	β-Orn	β,γ-A_2bu	Arg	His	Ac–β-Lys	Ac β-Lys	Ac–β-Lys	Tum N
Corynebacterium diphtheriae P.W. 8	50	100	100	12.5	100	—	—	>100	100	>100	6.3
Bacillus subtilis ATCC 6633	100	>100	>100	25	>100	>100	>100	>100	>100	>100	25
Escherichia coli NIHJ	>100	>100	>100	50	>100	>100	>100	>100	>100	>100	50
Escherichia coli B	>100	>100	>100	50	>100	>100	>100	>100	>100	>100	50
Salmonella typhosa H 901	>100	>100	>100	50	>100	>100	>100	>100	>100	>100	50
Shigella sonnei E33	>100	>100	>100	50	>100	>100	>100	>100	>100	>100	50
Klebsiella pneumonia ATCC 10031	>100	>100	>100	25	>100	>100	>100	>100	>100	>100	50
Mycobacterium ATCC 607	25	50	100	12.5	50	25	>100	>100	100	>100	6.3

a) μg/ml. b) All of semisynthetic Tum analogs were inactive to the following organisms: *Staphylococcus aureus* ATCC 6538p, *Staphylococcus epidermidis* sp-al-1, *Streptococcus pyogenes* N.Y.5, *Sarcina lutea* ATCC 9341, *Micrococcus flavus* ATCC 10240, *Salmonella paratyphi* PA 41-N-22, *Salmonella enteritidis* Gaertner, *Shigella flexineri* type 3a, *Proteus vulgaris* OX 19, *Serratia marcescens*, *Pseudomonas aeruginosa* IAM 1095. c) D-form. d) DL-form. The other amino acids were of L-form.

TABLE 4. RELATIONSHIP BETWEEN METHYLENE LENGTHS IN DIAMINO ACIDS AND ACTIVITIES AGAINST MYCOBACTERIUM ATCC 607

α,ω-Diamino acids	MIC (μg/ml)[a]
$\underset{NH_2}{CH_2}CH_2CH_2CH_2\underset{NH_2}{CH}$-CO-	6.3 (D=12.5)
$\underset{NH_2}{CH_2}CH_2CH_2\underset{NH_2}{CH}$-CO-	25
$\underset{NH_2}{CH_2}CH_2\underset{NH_2}{CH}$-CO-	50
$\underset{H_2N}{CH_2}\underset{NH_2}{CH}$-CO-	100

β,ω-Diamino acids	MIC(μg/ml)[a]
$\underset{NH_2}{CH_2}CH_2CH_2\underset{NH_2}{CH}$-$CH_2$CO-[b]	6.3
$\underset{NH_2}{CH_2}CH_2\underset{NH_2}{CH}$-$CH_2$CO-	12.5
$\underset{H_2N}{CH_2}\underset{NH_2}{CH}$-$CH_2$CO-	50

a) MIC: Minimum inhibitory concentration.
b) Tum O.

Tum N, N^{β}-Ac–Tum O, N^{ε}-Ac–Tum O, and $N^{\beta}.N^{\varepsilon}$-$(Ac)_2$–Tum O.[11] Antimicrobial activities of them were markedly affected by such modifications as can be seen in Table 3. Disappearance of the activities in all derivatives indicated the indispensability of both free amino groups, being consistent with the results mentioned before. From observation that weak activities remain in [β-Ahx[1]]-Tum N and N^{ε}-Ac–Tum O compared to three other derivatives, β-amino group seems to be slightly rather effective than ω-one. Recently, Kitagawa and his collaborators also pointed out the significance of both amino groups in β-lysine residue from their study on viomycin.[10]

In order to elucidate a relationship between the structure and biological activity of those semisynthetic antibiotics prepared here, ORD and CD of several synthetic as well as natural tuberactinomycins were measured. Their spectra were depicted in Fig. 4, in which extreme similarities in patterns are noticed. Thus we could understand that molecules of semisynthetic tuberactinomycins are forced to a definite conformation fixed by an intramolecular hydrogen bond[5] in cyclic peptide moiety despite of large difference in branched

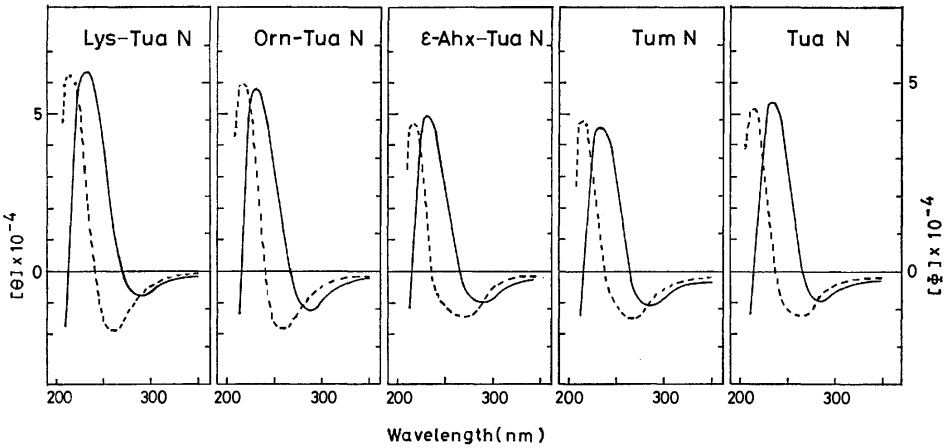

Fig. 4. ORD and CD curves of Tum analogs. ——: ORD, ------: CD, solvent: water.

part structure. Most important conclusion is that such conformation of whole molecule is not necessarily related to the biological activity, since inactive [ε-Ahx[1]]-Tum N showed quite similar pattern of ORD and CD spectra to natural antibiotics.

Activities against human tubercule bacilli, either sensitive or resistant to tuberactinomycin B, were also measured for some of the semisynthetic tuberactinomycins which are active to *Mycobacterium* ATCC 607, as shown in Table 5. While they showed significant antibacterial activity to sensitive human tubercule bacillus, none of them showed antibacterial activity to human tubercule bacillus resistant to tuberactinomycin B. Therefore any changes of the branched amino acid could not effect on cancellation of drug-resistancy of human tubercule bacilli so far.

In conclusion, all the results obtained in the present study can be summarized as follows. Most important active site in antibiotics of tuberactinomycin family must be in the cyclic peptide moiety, though its presence does not assure an exhibition of full biological activity, and basicity and/or hydrophobicity of the molecule seems to be the second important requisite for antimicrobial activity. At present time, there are found no semisynthetic compounds with stronger activity or more favorable quality than natural ones. However this study could explore a new way to modify natural tuberactinomycins by different kinds of acylation for the purpose of searching more desirable analogs.

Table 5. Minimum inhibitory concentrations[a] of semisynthetic tuberactinomycin analogs against mycobacterium and human tubercule bacilli

	Mycobacterium ATCC 607	*Human tubercule bacillus*	*Human tubercule bacillus* (200μg-Resistance to Tum B)
Leu-Tua N	6.3	25	>200
Ile-Tua N	12.5	25	>200
Tyr-Tua N	12.5	25	>200
β-Orn-Tua N	12.5	25	>200
Trp-Tua N	6.3	25	>200
Tum N	6.3	25	>200

a) μg/ml.

Authors are deeply indebted to Dr. Masayasu Yamazaki, National Sanatorium, Toneyama Hospital for measurements of activities against human tubercule bacilli.

References

1) Part X. T. Teshima, S. Nomoto, T. Wakamiya, and T. Shiba, *Tetrahedron Lett.*, **1976**, 2343.

2) A part was presented at the 32th Annual Meeting of the Chemical Society of Japan, Tokyo, April, 1975; p. 1699.

3) a) A. Nagata, T. Ando, R. Izumi, H. Sakakibara, T. Take, K. Hayano, and J. Abe, *J. Antibiot.*, **21**, 681 (1968); b) T. Ando, K. Matsuura, R. Izumi, T. Noda, T. Take, A. Nagata, and J. Abe, *ibid.*, **24**, 680 (1971); c) R. Izumi, T. Noda, T. Ando, T. Take, and A. Nagata, *ibid.*, **25**, 201 (1972).

4) T. Wakamiya and T. Shiba, *J. Antibiot.*, **28**, 292 (1975).

5) T. Wakamiya and T. Shiba, *Bull. Chem. Soc. Jpn.*, **48**, 2502 (1975).

6) Nps group was used only in the case of arginine.

7) T. Wakamiya, H. Uratani, T. Teshima, and T. Shiba, *Bull. Chem. Soc. Jpn.*, **48**, 2401 (1975).

8) In the case of a small scale experiment, dioxane or THF was poured into a solution to obtain the product as precipitate.

9) T. Fujii and S. Sakakibara, *Bull. Chem. Soc. Jpn.*, **47**, 3146 (1974).

10) a) T. Kitagawa, T. Miura, S. Tanaka, and H. Taniyama, *J. Antibiot.*, **25**, 429 (1972); b) T. Kitagawa, T. Miura, M. Takaishi, and H. Taniyama, *Chem. Pharm. Bull.*, **23**, 2123 (1975).

11) Abbreviations according to IUPAC-IUB commission, *J. Biol. Chem.*, **247**, 977 (1972), are used. Tum: tuberactinomycin, Tua: tuberactinamine, DCC: dicyclohexylcarbodiimide, HONSu: *N*-hydroxysuccinimide, HOBt: 1-hydroxybenzotriazole, Nps: *o*-nitrophenylsulphenyl, Z: benzyloxycarbonyl, Boc: *t*-butoxycarbonyl, DMF: *N,N*-dimethylformamide, THF: tetrahydrofuran, Pgl: phenylglycine, Hle: homoleucine, Hil: homoisoleucine, Hph: homophenylalanine, Ahx: aminohexanoic acid, A_2bu: α,γ-diaminobutyric acid, β,γ-A_2bu: β,γ-diaminobutyric acid, A_2pr: α,β-diaminopropionic acid.

Synthesis of 3(2*H*)-Furanones by the Iron Carbonyl-promoted Cyclocoupling Reaction of α,α'-Dibromo Ketones and Carboxamides. A Convenient Route to Muscarines[1,2]

Yoshihiro HAYAKAWA, Hidemasa TAKAYA, Shinji MAKINO, Norihiro HAYAKAWA, and Ryoji NOYORI

Department of Chemistry, Nagoya University, Chikusa, Nagoya 464

(Received February 21, 1977)

Reaction of α,α'-dibromo ketones and *N,N*-dimethylcarboxamides with the aid of $Fe_2(CO)_9$ affords the corresponding reductive cyclocoupling products, 5-(dimethylamino)tetrahydro-3-furanones. In usual, the adducts derived from di-*s*-alkyl ketone dibromides easily eliminated dimethylamine to afford 3(2*H*)-furanones. *N,N*-Dimethylformamide (DMF), *N,N*-dimethylacetamide, *N,N*-dimethylbenzamide, and *N*-methylpyrrolidone have been used as dibromo ketone receptors. Thus, this general method provides a new, singleflask procedure for the preparation of the oxygen-containing five-membered ketones. The iron carbonyl-promoted 3+2 cyclocoupling reaction is interpreted as proceeding *via* a stepwise cycloaddition of a reactive 2-oxyallyl–Fe(II) intermediate and carboxamide. A facile conversion of such furanones to muscarine alkaloids is described.

We have developed the iron carbonyl-assisted cyclocoupling reaction between α,α'-dibromo ketones and olefins[3] or dienes,[4] which provides a new tool for making various carbocyclic frameworks. Our recent work has shown that this reaction can be extended to the preparation of a heterocyclic system, 3(2*H*)-furanones, when carboxamides are employed as the unsaturated substrate.[2] The furanones are an important class of compounds in connection with the chemistry of various natural products; particularly, they may be expected to serve as versatile precursors of muscarine alkaloids. These unsaturated five-membered compounds are also followed with great theoretical interest as significant substances for the examination of possible keto-enol tautomerization of heterocycles.[5] Consequently, a variety of preparative methods have been reported.[5] However, most of them can form the derivatives of only certain paticular types and are not generally useful. The approaches that have a general usefulness are, we feel: (1) The preparation of 5-alkyl derivatives by the hydrogenolysis of 3-alkylisoxazoles, followed by acid-catalyzed cyclization;[6] (2) the acid-catalyzed rearrangement of 4-alkylidene-1,3-dioxolanes to alkylated 3(2*H*)-furanones;[7,8] (3) the synthesis of 2-acyl-3-alkyl derivatives by the pyrolytic reaction of dimethylsulfonium acyl-(3-alkylpropionyl)methylide,[9] and (4) the formation of the 2,2-dialkyl compounds *via* the reaction of 2-lithio-2-(2,2-dimethoxyethyl)-1,3-dithiane and ketones, followed by hydrolysis.[10] This paper will describe a general, expeditious route to 2,4-dialkyl-3(2*H*)-furanones *via* the iron carbonyl aided 3+2 cyclocoupling of α,α'-dibromo ketones and carboxamides, and its application to the synthesis of muscarines.

Results and Discussion

Cyclocoupling Reaction between α,α'-Dibromo Ketones and Carboxamides. A. Reaction with Tertiary Dibromoketones: Reduction of 2,4-dibromo-2,4-dimethyl-3-pentanone (**1**) with $Fe_2(CO)_9$ (1 : 1 mol ratio) was carried out in dry DMF solvent containing disodium dihydrogen ethylenediaminetetraacetate (Na_2H_2edta) under nitrogen atmosphere. The reaction proceeded smoothly at room temperature to give, after usual extractive work-up, the cyclic product **2** and the enone **3** in 3 and 80% yields, respectively. The minor compound **2** gave, in its IR spectrum, the carbonyl absorption at 1756 cm^{-1} characteristic of five-membered ketones, and NMR data identical with those previously reported.[7]

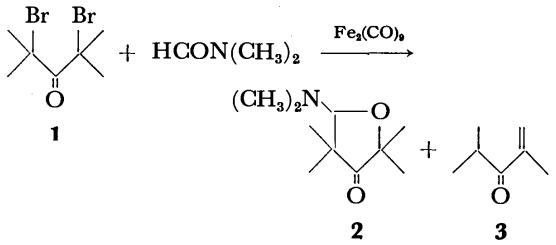

1 **2** **3**

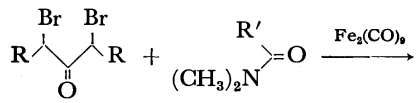

4: R = CH_3
5: R = C_2H_5
6: R = $CH(CH_3)_2$
16: R = $C(CH_3)_3$

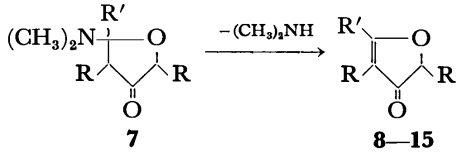

7 **8—15**

Scheme 1.

B. Reaction with Secondary Dibromo Ketones: As is outlined in Scheme 1, the reaction of secondary dibromo ketones and *N,N*-dimethylated carboxamides with the aid of $Fe_2(CO)_9$ first led to labile 2,4-dialkyl-5-(dimethylamino)tetrahydro-3-furanones of type **7**, which in turn underwent the facile elimination of dimethylamine to produce 3(2*H*)-furanone derivatives **8**—**15**. The overall transformation can be viewed formally as the construction of a carbon-oxygen bridge between the α and α' positions of the parent dialkyl ketones.

For example, stirring of a mixture of the dibromide **4** and $Fe_2(CO)_9$ (1 : 1.2 mol ratio) in DMF in the presence of Na_2H_2edta at room temperature for 22 h gave, after extractive work-up and distillation, the 3(2*H*)-

furanone **8** in 53% yield. Here, the absence of Na_2H_2-edta in the reaction system resulted in a drastic decrease in yield of this coupling product. Structure determination of **8** was based on the spectral analysis. This product showed strong IR stretching bands at 1704 (C=O) and 1624 cm^{-1} (C=C),[11] and a UV maximum at 270 nm (log ε 3.89) characteristic of 3(2*H*)-furanones.[5-10,12] The NMR spectrum also supported the assigned structure. The presence of an $OCH(CH_3)$-C=O linkage was deduced from a methyl doublet appearing at δ 1.39 with J=7.5 Hz and a one-proton quartet with the same coupling constant at a rather low field, δ 4.31. The vinylic methyl group exhibited a doublet signal at δ 1.67, indicating that the splitting (J=2 Hz) is due to a long-range coupling with the vinylic proton, giving a quartet at δ 7.90.[7] The mass spectrum exhibited a molecular-ion peak confirming the the formula of $C_6H_8O_2$. Notably, this product exists solely in a keto form and did not give a positive $FeCl_3$ test.

This cyclocoupling reaction is operationally quite simple and has a wide application. In place of DMF, *N*,*N*-dimethylacetamide and *N*,*N*-dimethylbenzamide can be employed as well. Furanones obtained by the cyclocoupling reaction of the secondary dibromides and carboxamides are summarized in Table 1. The product

Table 1. Iron carbonyl-promoted furanone synthesis

Dibromo ketone	Carboxamide	Furanone product	Yield, %	IR absorptions of neat film, cm^{-1} $\nu_{C=O}$ and $\nu_{C=C}$	UV absorption in C_2H_5OH, nm (log ε)
4	DMF	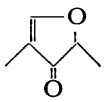 **8**	53[b,c]	1695 and 1621 1704 and 1624[d]	270(3.89)
4	$CH_3CON(CH_3)_2$	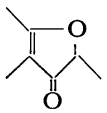 **9**	21[c]	1703 and 1636	273(4.06)
4	$C_6H_5CON(CH_3)_2$	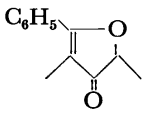 **10**	25[c]	1697 and 1620[d]	225(3.77), 232(3.97) 242(3.79), 306(4.04)
5	DMF	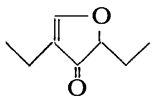 **11**	78, 64[b]	1700 and 1617	272(3.68)
5	$CH_3CON(CH_3)_2$	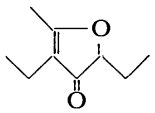 **12**	51[c]	1696 and 1633	272(4.00)
5	$C_6H_5CON(CH_3)_2$	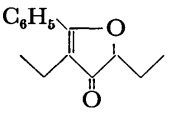 **13**	42[b,c]	1696 and 1623[d]	237(3.73), 306(3.91)
6	DMF	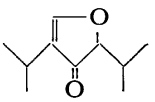 **14**	89[e]	1699 and 1618	269(3.89)
6	$CH_3CON(CH_3)_2$	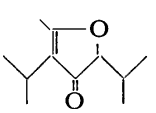 **15**	87[c,e]	1691 and 1631	273(3.98)

a) Determined by an NMR analysis of the crude reaction mixture. b) Isolated yield. c) Na_2H_2edta (three equiv of the dibromide) was added to the reaction system. d) In CCl_4 solution. e) Result obtained after heating the initial product at 110 °C for 10 min.

yield is usually moderate to high. When the dibromide bears bulky alkyl substituents, the initial adduct **7** can be isolated in a stable form after usual work-up. In such a case, in order to attain complete deamination, brief heating at an elevated temperature is required. Thus, the highly sterically crowded adduct **17** produced from the dibromo ketone **16** and DMF was quite stable and remained unchanged even after heating at 110 °C

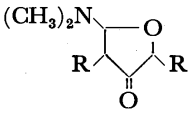

17: R=C(CH$_3$)$_3$
21: R=CH(CH$_3$)$_2$

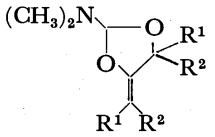

20: R^1=alkyl; R^2=H
29: R^1=R^2=CH$_3$

for 20 min. Certain lactams can also be used as dibromo ketone receptors. For instance, the reaction of the dibromo ketone **6** and *N*-methylpyrrolidone at room temperature gave rise to the amino furanone **19** in 26% yield. Apparently the formation of **19** resulted from intramolecular deamination of the initial spiro-fused intermediate **18**. Unfortunately, methyl ketone dibromides gave no or little cyclocoupling products. For example, the reaction of α,α′-dibromoacetone and DMF under ordinary reaction conditions failed to afford the coupling product. The use of $Fe(CO)_5$ in place of

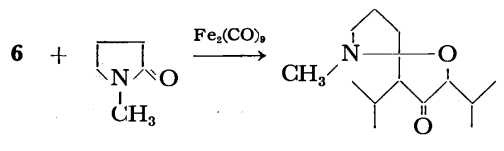

18

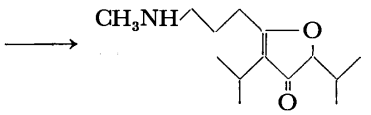

19

$Fe_2(CO)_9$ did not reduce dibromo ketones under comparable thermal conditions; in this case, irradiation by visible light was necessary to achieve the reaction. As has been reported previously,[13] the use of Zn–Cu couple as the reducing agent forms another type of 1 : 1 coupling product, 1,3-dioxolane **20**, in a fair to good yield; the product can be converted to the furanones by acid treatment.

Reaction Mechanism of the 3+2 Cyclocoupling Reaction. A. The Reactive Species: In the absence of $Fe_2(CO)_9$, no reaction took place between dibromo ketones and carboxamides. By contrast, when a reducing agent was added to such a mixture, the cyclocoupling reaction proceeded smoothly. When the reaction of **6** and $Fe_2(CO)_9$ was carried out in a 1 : 1 DMF–furan mixture, both the DMF adduct **21** (65%) and the furan adduct **22**[4a,c] (27%) were produced. These observations strongly indicate that reactive 2-oxyallyl–Fe(II) intermediates of type **23**[14] are generated under the present reaction conditions. The occurrence of such species in DMF has also been suggested by the reductive rearrangement of 2,4-dibromo-6,6-diphenylbicyclo[3.1.0]-hexan-3-one[14] and nucleophilic trapping experiments.[14] This view is also consistent with the formation of the enone **3** as a major product in the reaction of **1**. Thus, carboxamides serve as extremely efficient trapping agents of the oxyallyl intermediate and even compete well with furan. It is also worthwhile to note that the oxyallyl–Fe(II) species **24**, which smoothly undergoes a neopentyl-type rearrangement in benzene,[14] affords the DMF adduct **17** prior to the skeletal change.

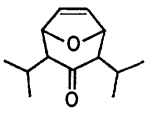

22

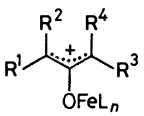

23, R^1—R^4=alkyl or H
24, R^1=R^4=C(CH$_3$)$_3$; R^2=R^3=H
L=CO, Br, solvent, *etc.*

B. Reaction Course of Cycloaddition of the Oxyallyl Species and Carboxamides: The cycloaddition is best accounted for by the path outlined in Scheme 2, where, for the sake of simplicity, the reaction of unsubstituted oxyallyl **25** and DMF is taken up. First, there occurs the electrophilic attack of **25** on the oxygen atom of DMF, producing the highly stable ionic intermediate **26**. Subsequent cyclization through bonding between the cationic and enolate carbons results in the adduct **27**. The zwitterionic intermediate **26** may also undergo the C–O cyclization, thus giving the dioxolane product **28**;[13] the reverse process, if possible, could lead ultimately to the more stable product **27**. Indeed, treatment of **29** with $FeBr_2$ in DMF gave **2** in a moderate (20—30%) yield. However, there has not yet been any direct evidence for the presence of the equilibrium, **26**⇄**28**. When the reaction course was monitored, the dioxolane

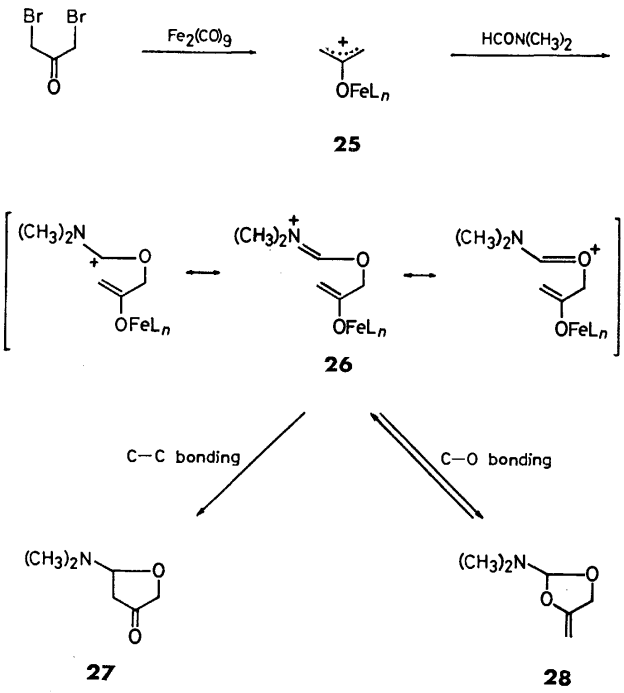

Scheme 2.

product **28** could not be detected at any stage of the reaction.

In any events, the intermediacy of the resonance-stabilized ionic intermediate **26** appears to be crucial for the cyclization to proceed. Thus, the overall process can be envisaged as a stepwise [$_\pi$2+$_\pi$2] cycloaddition. A related stepwise mechanism has been claimed for the reaction forming certain carbocyclic five-membered skeletons.[3] The dioxolane **28**, even if formed, cannot be derived through a concerted [$_\pi$2+$_\pi$4]-type cycloaddition of an electron-accepting oxyallyl, **23**, and an electron-donating carboxamide, because, in the lowest unoccupied molecular orbital of **23**, the orbital does not develop over the oxygen atom to any great extent.[15]

Application to Muscarine Synthesis. In the natural field, there are many compounds with the furanone or related skeletons. Muscarine (**30**) isolated from fly agaric [*Amantia muscaria* (L. ex Fr.) Quel.] is a representative compound. This alkaloid has long attracted the attention of pharmacologists and chemists because of its marked and peculiar actions on the autonomic nervous system. This product, however, exists in such small amounts in natural plants that a satisfactory supply of the alkaloids is difficult to obtain only by extraction; hence, an efficient method of preparing muscarine

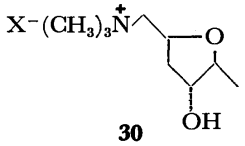

30

chemically has been sought for a long period. The synthetic methods thus far developed can be broadly divided, in terms of the construction mode of the heterocyclic system, into the following four types:[16] (1) the diazotization of β,γ-dihydroxy α-amino acids such as glucosamine[17] and 2-amino-4,5-dihydroxyhexanoic acid,[18] affording 3-hydroxytetrahydrofuran rings; (2) the condensation of iodopropionic ester and malic ester[19] or, more conveniently, of α-hydroxypropionic ester and maleic or fumaric ester[20] to form 4,5-bis-(ethoxycarbonyl)-2-methyltetrahydro-3-furanone; (3) the condensation of epichlorohydrin and sodioacetoacetic ester, giving α-acetyl-δ-chloro-γ-valerolacetone;[21] and (4) the condensation of glucose or mannose and β-keto carboxylic ester to produce 2-methyl-5-tetrahydroxybutylfuran-2-carboxylic ester.[22] We will describe here a new general entry into muscarine analogs[23] starting from the 2,4-dialkyl-3(2*H*)-furanones obtained by the iron carbonyl-promoted cyclocoupling reaction of dibromo ketones and DMF. The method is based on the introduction of a dimethylaminomethyl group to the C_5 position of the furanones.

The route to 4-methylmuscarine iodide (**36**) is shown in Scheme 3. First, treatment of **8** with acetyl chloride in 1,2-dimethoxyethane afforded the acetoxy furan **31** in 68% yield. The IR absorption at 1760 cm^{-1} was instructive in determining the enol acetate structure. Further, in the NMR spectrum, a sharp three-proton singlet appeared at δ 2.21, confirming the presence of an acetyl group. The furan-ring structure was supported

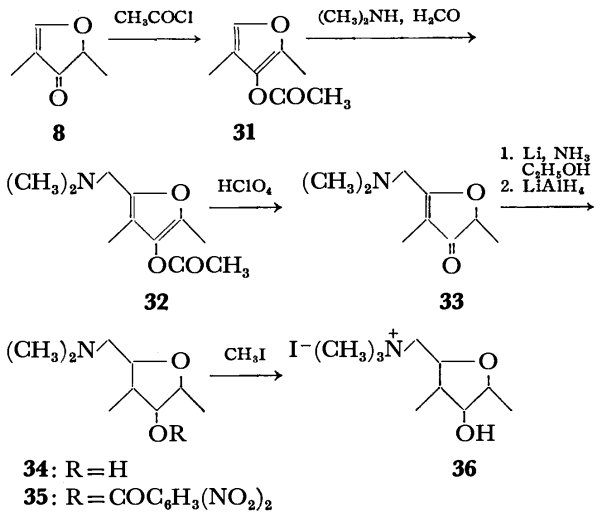

Scheme 3.

by a finely splitting quartet at δ 6.92. The Mannich aminomethylation of **31** was performed with 40% aq dimethylamine and 37% aq formaldehyde in acetic acid[24] at 70 °C, producing the amino furan **32** in 80% yield. The IR spectrum showed absorptions of the $N(CH_3)_2$ group at 2840, 2795, and 2745 cm^{-1}. In addition, the introduction of the dimethylaminomethyl function to C_5 was confirmed by the NMR characteristics, *viz.*, the appearance of two singlets at δ 2.28 and 3.42 (3: 1 ratio), and the disappearance of a low-field signal due to the vinyl proton. Hydrolysis of **32** by heating with 70% $HClO_4$ gave the furanone **33** in >95% yield. The occurrence of 3(2*H*)-furanone skeleton was confirmed by strong IR bands at 1698 (C=O) and 1623 cm^{-1} (C=C) as well as by a UV maximum at 274 nm (log ε 4.01).[12] In the NMR spectrum, there appeared a coupled three-proton doublet and a one-proton quartet at δ 1.37 and 4.24 (J=7.0 Hz), respectively, indicating the presence of an $OCH(CH_3)C{=}O$ moiety. The Birch reduction of **33** using Li–ethanol, followed by $LiAlH_4$ treatment,[25] formed desired 4-methylnormuscarine (**34**, two stereoisomers) in 61% yield. The presence of the OH function was confirmed by a broad IR absorption at 3400—3200 cm^{-1}, and the NMR spectrum confirmed the existence of two secondary methyls. Finally, treatment of **34** with methyl iodide in benzene produced 4-methylmuscarine iodide (**36**) quantitatively. The quaternization was monitored by appearance of the NMR signal at δ 3.21 due to $\overset{+}{N}(CH_3)_3$.[26] 4-Methylmuscarine iodide (**36**) thus obtained displayed the physiological activities characteristic of muscarine alkaloids; the smooth muscle of the intestinal tract was stimulated, increasing tone and mobility, while atropine inhibited these actions.

Experimental

General. All melting and boiling points are uncorrected. The IR spectra were measured on a JASCO IR-A-I or JASCO DS-402G spectrometer in the noted phase. The UV spectra were taken on a Perkin-Elmer Model 202 or a Hitachi Model 323 spectrometer in ethanol solution. The IR and UV spectral data of 3(2*H*)-furanones **8**—**15** are listed in Table 1.

The NMR spectra were recorded on a JEOL C-60H instrument in CCl_4 solution unless otherwise stated; the chemical shifts are given in ppm downfield from internal tetramethylsilane. 1,1,2,2-Tetrachloroethane or tetralin was used as the standard for the quantitative analysis. The mass spectra (MS) were obtained on a Hitachi RMU-6C mass spectrometer, operating with an ionization energy of 70 eV. The exact MS were performed at the Faculty of Agriculture, Nagoya University, and at the Hitachi Naka Works. Elemental analyses were carried out at the Analytical Centers of Kyoto University and Meijo University. All $Fe_2(CO)_9$-assisted cyclocoupling reactions were performed under nitrogen atmosphere. Drying of organic extracts was done over anhyd Na_2SO_4. For concentration of organic solvents, a vacuum (60—90 Torr) rotary evaporator was used. Products on TLC plates were detected by irradiation of UV-light (254 nm), by a spray of $Ce(SO_4)_2$ in 65% H_2SO_4 or molybdophosphoric acid in 10% ethanol, followed by heating, or by exposure to I_2 vapor.

Chromatography. GLPC analysis and separation were performed on a Yanagimoto Model G-8, Yanagimoto Model GCG-3D, or Varian 1700 instrument. Columns used were: A, 3 mm×2 m 5% poly(ethylene glycol succinate) on Chromosorb W AW; B, 3 mm×2 m 5% poly(ethylene glycol) on Celite 545; C, 4 mm×4 m 10% LAC on Chromosorb W AW; D, 3 mm×2 m 5% Silicone OV-1 on Chromosorb W AW; E, 4 mm×2 m 12% diisodecyl phthalate on Neopak 1A; F, 3 mm×2 m 5% Apiezon grease L on Diasolid M; G, 5 mm×2 m 33% Apiezon grease L on Neopak 1A. Analytical and preparative TLC were done on E. Merck alumina GF_{254} plates. For column chromatography, Woelm basic alumina (Activity I) was employed.

Solvents and Materials. α,α′-Dibromo ketones **1**, **4**—**6**, and **16** were prepared by the procedures in the literature.[27,28] Oily dibromides were purified by passing them through a short alumina column immediately before use. Photolytic preparation of $Fe_2(CO)_9$ from $Fe(CO)_5$ was carried out according to the method of King.[29] The carbonyl complex was used after drying over KOH in a vacuum desiccator. 2-Dimethylamino-4-isopropylidene-5,5-dimethyl-1,3-dioxolane (**29**) solution in DMF (*ca.* 0.3 M) was obtained by the procedure of Hoffmann.[13] Dry DMF was produced by refluxing over CaH_2 at 60 °C under reduced pressure (20 mm) for 4 h, followed by distillation *in vacuo*; it was stored over molecular sieves 3A under nitrogen. Other carboxamides were used after a simple distillation of the commercially supplied ones. Benzene, tetrahydrofuran (THF), and 1,2-dimethoxyethane (DME) were distilled from $LiAlH_4$. Furan was distilled from CaH_2. Disodium dihydrogen ethylenediaminetetraacetate (Na_2H_2edta) dihydrate was dehydrated by heating it at 120 °C (0.01 mm) for 12 h.

Reaction of 2,4-Dibromo-2,4-dimethyl-3-pentanone (1) with $Fe_2(CO)_9$ in DMF. A mixture of the dibromo ketone **1** (833 mg, 3.06 mmol), $Fe_2(CO)_9$ (1.31 g, 3.60 mmol), and octane (32.5 mg, 0.29 mmol, an internal standard for GLPC analysis) in DMF (10.5 ml) was stirred at room temperature for 18 h. GLPC analysis of the reaction aliquots taken up at appropriate intervals showed the formation of three products. These products were identified, by comparison with authentic samples, as 5-(dimethylamino)tetrahydro-2,2,4,4-tetramethyl-3-furanone (**2**) [retention time (t_r) 9.8 min, column F, 130 °C, 3% yield], 2,4-dimethyl-1-penten-3-one (**3**) (t_r 7.8 min, column E, 90 °C, 80% yield), and 2,4-dimethyl-3-pentanone (t_r 6.5 min, column E, 90 °C, 9% yield). An analytical sample of **2** was obtained by GLPC separation (column G, 123 °C). Its spectral (IR, NMR, and mass) data were identical with the reported ones[9] (Found: C, 65.00; H, 10.47%).

2,4-Dimethyl-3(2H)-furanone (8). A mixture of 2,4-dibromo-3-pentanone (**4**) (8.70 g, 35.6 mmol), $Fe_2(CO)_9$ (15.6 g, 42.8 mmol), and Na_2H_2edta (18.0 g, 53.3 mmol) in DMF (80 ml) was stirred at room temperature for 12 h. After addition of benzene (80 ml), the reaction mixture was left at room temperature for 10 h and then poured into water (400 ml). The aq mixture was extracted with 1:1 ether-petroleum ether (160 ml×5). The combined organic extracts were washed with water (120 ml×3) and dried. The solvent was removed to give a dark brown oil (4.06 g). Upon addition of petroleum ether (80 ml), dark brown precipitates appeared immediately, which were then removed by filtration. Concentration of the filtrate gave a yellow oil (2.46 g), which was distilled at room temperature—70 °C (0.2 Torr) to afford the furanone **8** (2.11 g, 53% yield) as a colorless oil. NMR δ 1.39 (d, 3, J=7.5 Hz, $CHC\underline{H}_3$), 1.67 (d, 3, J=2 Hz, $=CC\underline{H}_3$), 4.31 (q, 1, J=7.5 Hz, $C\underline{H}CH_3$), and 7.90 (q, 1, J=2 Hz, =CH); MS *m/e* 112 (M^+). Found: *m/e* 112.0519. Calcd for $C_6H_8O_2$: M, 112.0523.

2,4,5-Trimethyl-3(2H)-furanone (9). A mixture of the dibromide **4** (488 mg, 2.00 mmol), $Fe_2(CO)_9$ (876 mg, 2.40 mmol), and Na_2H_2edta (2.03 g, 6.00 mmol) in *N,N*-dimethylacetamide (7.0 ml) was magnetically stirred at room temperature for 19 h. The reaction mixture was quenched by addition of saturated KNO_3 solution (20 ml) and extracted with ethyl acetate (5 ml×6). The combined organic extracts were washed with water (5 ml×3), dried, and concentrated, thus giving a red oil (168 mg). The NMR analysis showed that the furanone **9** was produced in 21% yield. An analytical sample (R_f 0.70) was obtained by TLC separation (CH_2Cl_2), followed by distillation. NMR δ 1.35 (d, 3, J=7.5 Hz, $CHC\underline{H}_3$), 1.62 (s, 3, $=CC\underline{H}_3$), 2.15 (s, 3, $=CC\underline{H}_3$), and 4.25 (q, 1, J=7.5 Hz, $C\underline{H}CH_3$); MS *m/e* 126 (M^+). Found: *m/e* 126.0690. Calcd for $C_7H_{10}O_2$: M, 126.0680.

2,4-Dimethyl-5-phenyl-3(2H)-furanone (10). To a suspension of $Fe_2(CO)_9$ (876 mg, 2.40 mmol) and Na_2H_2edta (2.03 g, 6.00 mmol) in benzene (5.0 ml) were added *N,N*-dimethylbenzamide (7.0 ml) and then the dibromo ketone **4** (488 mg, 2.00 mmol). The resulting mixture was stirred at room temperature for 19 h. The mixture was added to saturated KNO_3 solution (10 ml), and the aq mixture was extracted with 1:2 benzene–hexane (6 ml×6). The organic layers were collected, washed with water (6 ml×6), and dried. Evaporation of the solvent afforded a pale yellow oil, NMR analysis of which indicated the formation of the furanone **10** in 25% yield. TLC (1:10 ether–hexane, R_f 0.70), followed by short-path distillation, formed an analytical specimen of **10**. NMR δ 1.48 (d, 3, J=7.5 Hz, $CHC\underline{H}_3$), 1.95 (s, 3, $=CC\underline{H}_3$), 4.46 (q, 1, J=7.5 Hz, $C\underline{H}CH_3$), and 7.45 (m, 3) and 7.74 (m, 2) (C_6H_5); MS *m/e* 188 (M^+). Found: *m/e* 188.0854. Calcd for $C_{12}H_{12}O_2$: M, 188.0836.

2,4-Diethyl-3(2H)-furanone (11). A mixture of 3,5-dibromo-4-heptanone (**5**) (462 mg, 1.70 mmol) and $Fe_2(CO)_9$ (876 mg, 2.40 mmol) in DMF (7.0 ml) was stirred at room temperature for 12 h. The reaction mixture was treated with saturated aq Na_2H_2edta solution (40 ml) and extracted with 1:1 ethyl acetate–hexane (8 ml×5). The collected organic extracts were washed with water (8 ml×3) and dried. The solvent was removed under reduced pressure at room temperature to afford a residual oil (273 mg). Its NMR spectrum indicated that the furanone **11** was produced in 92% yield. This oil was dissolved in ethyl acetate (5 ml) and passed through a short column packed with alumina using ethyl acetate as eluent. Concentration of the filtrate gave the

furanone **11** (152 mg, 64% yield) as a pale yellow oil. An analytical sample was obtained by preparative GLPC (column A, 120 °C). NMR δ 0.97 (t, 3, J=7.0 Hz, CH_3), 1.08 (t, 3, J=7.0 Hz, CH_3), 1.5—2.4 (m, 4, 2 CH_2), 4.21 (dd, 1, J=4.5 and 7.0 Hz, OCHCO), and 7.90 (br s, 1, =CH); MS *m/e* 140 (M^+). Found: C, 68.38; H, 8.87%. Calcd for $C_8H_{12}O_2$: C, 68.54; H, 8.63%.

*2,4-Diethyl-5-methyl-3(2H)-furanone (**12**).* To a mixture of $Fe_2(CO)_9$ (876 mg, 2.40 mmol) and Na_2H_2edta (2.03 g, 6.00 mmol) was added *N,N*-dimethylacetamide (7.0 ml), followed by the dibromo ketone **5** (462 mg, 1.70 mmol). The resulting mixture was stirred at room temperature. After 19 h, saturated KNO_3 solution (20 ml) was added to the reaction mixture, and the aq layer was extracted with ethyl acetate (6 ml×5). The combined organic extracts were washed with water (40 ml×3) and dried. On removal of the solvent there was obtained a pale yellow oil. Addition of benzene (2 ml) yielded insoluble brown solides. The precipitates were removed by filtration through a short column of alumina and evaporation of the solvent afforded a colorless oil (130 mg). Yield of the furanone **12**, as estimated by NMR analysis, was 51%. Preparative TLC (1: 1 benzene–hexane) gave **12** as an oil. An analytical sample was obtained by preparative GLPC (column A, 120 °C). NMR δ 0.96 (t, 3, J=7.0 Hz, $CH_2C\underline{H}_3$), 1.01 (t, 3, J=7.5 Hz, $CH_2C\underline{H}_3$), 2.15 (s, 3, $=CCH_3$), 1.4—2.4 (m, 4, 2 CH_2), and 4.12 (dd, 1, J= 6.0 and 7.0 Hz, OCH); MS *m/e* 154 (M^+). Found: C, 70.32; H, 9.57%. Calcd for $C_9H_{14}O_2$: C, 70.01; H, 9.15%.

*2,4-Diethyl-5-phenyl-3(2H)-furanone (**13**).* To a mixture of $Fe_2(CO)_9$ (876 mg, 2.40 mmol) and Na_2H_2edta (2.03 g, 6.00 mmol) in benzene (5.0 ml) was added *N,N*-dimethylbenzamide (7.0 ml) and the dibromide **5** (462 mg, 1.70 mmol). The resulting mixture was kept, with stirring at room temperature for 14 h and then quenched with saturated KNO_3 solution. The aq layer was extracted with ethyl acetate (6 ml×5), and the combined organic extracts were washed with water (6 ml ×2) and dried. Removal of the solvent gave a feebly yellow oil (6.0 g), which without solvent, was heated at 110 °C for 15 min under nitrogen. After dilution with 1: 2 benzene–hexane (10 ml), the product was washed with water (4 ml×4) and dried. The organic solvent was evaporated to afford a pale yellow oil (873 mg). Purification by preparative TLC (benzene) yielded the furanone **13** (R_f 0.38, 175 mg, 42% yield) as a colorless oil. NMR δ 1.00 (t, 3, J=7.0 Hz, CH_3), 1.13 (t, 3, J=7.0 Hz, CH_3), 1.6—2.2 (m, 2, $CHC\underline{H}_2$), 2.41 (q, 2, J=7.0 Hz, $=CCH_2$), 4.32 (dd, 1, J=5.0 and 6.5 Hz, OCH), and 7.40 (m, 3) and 7.72 (m, 2) (C_6H_5); MS *m/e* 216 (M^+). Found: *m/e* 216.1119. Calcd for $C_{14}H_{16}O_2$: M, 216.1149.

*2,4-Diisopropyl-3(2H)-furanone (**14**).* A mixture of 3,5-dibromo-2,6-dimethyl-4-heptanone (**6**) (300 mg, 1.00 mmol) and $Fe_2(CO)_9$ (437 mg, 1.20 mmol) in DMF (3.5 ml) was stirred at room temperature for 12 h. The reaction mixture was poured into saturated aq $NaHCO_3$/KNO_3 solution (10 ml) and extracted with ethyl acetate (4 ml×5). The collected organic extracts were washed with water (4 ml×3) and dried sufficiently. The solvent was removed under reduced pressure to give a crude yellow oil (192 mg) containing mainly 5-(dimethylamino)-2,4-diisopropyltetrahydro-3-furanone (**21**). IR (neat film) 1753 cm^{-1} (C=O); NMR δ 0.8—1.3 (m, 12, 2 $CH(C\underline{H}_3)_2$), 1.8—2.4 (m, 3, 2 $C\underline{H}(CH_3)_2$ and $CHC\underline{H}CO$), 2.47 (s, 6, $N(CH_3)_2$), 3.40 (d, 1, J=4.5 Hz, OCHCO), and 4.57 (d, 1, J=9.0 Hz, OCHN); MS *m/e* 213 (M^+). The neat oil was heated at 140 °C for 15 min under nitrogen, followed by distillation *in vacuo* (60 °C, 1 Torr), to afford the furanone **14** (149 mg, 89% yield). NMR δ 0.83 (d, 3, J= 7.0 Hz, $CHCH(C\underline{H}_3)_2$), 1.12 (d, 3, J=6.5 Hz, $CHCH(C\underline{H}_3)_2$), 1.15 (d, 6, J=7.0 Hz, $=CCH(C\underline{H}_3)_2$), 2.0—2.8 (m, 2, 2 $C\underline{H}(CH_3)_2$), 4.10 (d, 1, J=3.8 Hz, OCHCO), and 7.89 (br s, 1, =CH); MS *m/e* 168 (M^+). Its structure was further confirmed by converting it through hydrogenation, into 2,4-diisopropyltetrahydro-3-furanone. A suspension of 10% Pd–C (500 mg) in ethanol (4 ml) was stirred at room temperature for 24 h under 1-atm hydrogen. To this was added a solution of **14** (1.00 g, 5.95 mmol) in ethanol (4 ml), and the resulting mixture was stirred at room temperature for 24 h under an atmospheric pressure of hydrogen. The mixture was passed through a Celite 545 column, and the filtrate was concentrated, giving the tetrahydro-3-furanone (*ca.* 1 g) as a single isomer (stereochemistry unconfirmed). An analytical sample of the product was collected by GLPC separation (column B, 100 °C). IR (neat film) 1750 cm^{-1} (C=O); NMR δ 0.8—1.1 (m, 12, 4 CH_3), 1.5—2.4 (m, 3, 2 $C\underline{H}(CH_3)_2$ and $C\underline{H}CH_3$), 3.40 (d, 1, J=5.5 Hz, OCH), and 3.9—4.2 (m, 2, OCH_2); MS *m/e* 170 (M^+). Found: C, 70.30; H, 10.75%. Calcd for $C_{10}H_{18}O_2$: C, 70.54; H, 10.66%.

*2,4-Diisopropyl-5-methyl-3(2H)-furanone (**15**).* To a mixture of $Fe_2(CO)_9$ (874 mg, 2.40 mmol) and Na_2H_2edta (2.03 g, 6.00 mmol) was added a solution of the dibromo ketone **6** (600 mg, 2.00 mmol) and tetralin (26.4 mg, 0.20 mmol) in *N,N*-dimethylacetamide (7.0 ml). The resulting mixture was stirred at room temperature for 12 h. The reaction mixture was poured into saturated $NaHCO_3$/KNO_3 solution (20 ml) and extracted with ethyl acetate (8 ml×5). The combined organic extracts were washed with water (8 ml ×3) and dried. After evaporation of the solvent, an oil was obtained. The NMR spectrum of this residue showed two doublets at δ 3.95 (J=3.8 Hz) and 3.38 (J=4.5 Hz) due to the C_2 methine proton of **15** and 5-(dimethylamino)-2,4-diisopropyl-5-methyltetrahydro-3-furanone (**7**, R=$CH(CH_3)_2$; R′=CH_3), respectively. The intensity of signals, as compared with that of a singlet due to the aromatic protons of tetralin internal standard, indicated that **15** and the amino tetrahydro-3-furanone were produced in 49 and 39% yields, respectively. When the crude oil was heated at 110 °C for 15 min under nitrogen, **15** was obtained as an oily product (316 mg, 87% yield). Distillation (90 °C, 3 mm), followed by preparative GLPC (column C, 108 °C), afforded an analytical sample. NMR δ 0.79 (d, 3, J=6.5 Hz, $CHCH(C\underline{H}_3)_2$), 1.05 (d, 3, J=6.5 Hz, $CHCH(C\underline{H}_3)_2$), 1.15 (d, 6, J=7.0 Hz, $=CCH(C\underline{H}_3)_2$), 2.15 (s, 3, $=CCH_3$), 2.0—2.8 (m, 2, 2 $C\underline{H}(CH_3)_2$), and 3.95 (d, 1, J=3.8 Hz, OCH); MS *m/e* 182 (M^+). Found: *m/e* 182.1295. Calcd for $C_{11}H_{18}O_2$: M, 182.1305.

*2,4-Di-t-butyl-5-(dimethylanmio)tetrahydro-3-furanone (**17**).* To a mixture of 3,5-dibromo-2,2,6,6-tetramethyl-4-heptanone (**16**) (110 mg, 0.34 mmol) and $Fe_2(CO)_9$ (146 mg, 0.40 mmol) was added DMF(1.0 ml). The resulting suspension was stirred at room temperature for 17 h. The reaction mixture was diluted with 1:1 ethyl acetate–hexane (5 ml) and then quenched by saturated aq $NaHCO_3$ solution (5 ml). The organic layer was washed with water and dried. After removal of the solvent, the residue was purified TLC (ethyl acetate) to give **17** (79 mg, 98% yield) as a slightly yellow oil. IR (CCl_4) 1746 cm^{-1} (C=O); NMR δ 0.97 (s, 9, $C(CH_3)_3$), 1.02 (s, 9, $C(CH_3)_3$), 1.93 (d, 1, J=9.0 Hz, $CHC\underline{H}C(CH_3)_3$), 2.48 (s, 6, $N(CH_3)_2$), 3.18 (s, 1, OCHCO), and 4.59 (d, 1, J=9.0 Hz, OCHN); MS *m/e* 241 (M^+). Found: *m/e* 241.2017. Calcd for $C_{14}H_{27}NO_2$: M, 241.2042.

Quaternization of **17** with CH_3I(excess) in benzene at 50 °C for 14 h afforded colorless plates; mp 152—156 °C (from 1: 1 acetone–hexane).

*2,4-Diisopropyl-5-(3-methylaminopropyl)-3(2H)-furanone (**19**).* Dry *N*-methylpyrrolidone (25 ml) and the dibromide **6** (0.90 g, 3.00 mmol) were added sequentially to $Fe_2(CO)_9$ (1.30 g, 3.60

mmol), and the resulting mixture was stirred at room temperature for 48 h, during which period a characteristic dark red color developed. The reaction mixture was quenched by saturated NaCl solution and extracted with ethyl acetate. The organic layer was washed with brine and dried. Evaporation of the solvent at room temperature *in vacuo* left a deepred oil (644 mg). This residue was distilled under reduced pressure to give a yellow oil; bp 140 °C (0.05 Torr). Purification by TLC (1 : 1 ether–hexane) afforded the amino furanone **19** (187 mg, 26% yield) as a pale yellow oil. IR (CCl_4) 1690 (C=O) and 1620 cm^{-1} (C=C); UV 274 nm (log ε 4.04); NMR δ 0.83 (d, 3, J= 6.5 Hz, $CHCH(C\underline{H}_3)_2$), 1.09 (d, 3, J=6.5 Hz, $CHCH(C\underline{H}_3)_2$), 1.17 (d, 3, J=7.0 Hz, $=CCH(C\underline{H}_3)_2$), 1.20 (d, 3, J=7.0 Hz, $=CCH(C\underline{H}_3)_2$), 1.4—2.5 (m, 9, 2 $C\underline{H}(CH_3)_2$, 3 CH_2, and NH), 2.39 (s, 3, NCH_3), and 3.97 (d, 1, J=3.5 Hz, OCH); MS *m/e* 239 (M^+). Found: *m/e* 239.1877. Calcd for $C_{14}H_{25}NO_2$: M, 239.1885.

*Reduction of the Dibromo Ketone **6** with $Fe_2(CO)_9$ in a Mixture of Furan and DMF.* A mixture of the dibromide **6** (300 mg, 1.00 mmol) and $Fe_2(CO)_9$ (437 mg, 1.20 mmol) in freshly distilled furan (2.00 ml, 1.87 g, 27.5 mmol) and DMF (2.13 ml, 2.01 g, 27.5 mmol) was stirred at room temperature for 22 h. The reaction mixture was poured into aq $NaHCO_3$ solution and extracted with 1 : 1 ethyl acetate–hexane (10 ml×4). The organic layer was washed with water (10 ml) and dried. Concentration *in vacuo* gave a yellow oil (213 mg), the NMR spectrum of which indicated the formation of **21** (49% yield) and 2,4-diisopropyl-8-oxabicyclo[3.2.1]oct-6-en-3-one (**22**) (only the *cis* isomer, 20% yield), and the recovery of the starting dibromide **6** (25%). Yields of **21** and **22** based on **6** consumed were 65 and 27%, respectively.

Reaction of 1,3-Dibromo-2-propanone with $Fe_2(CO)_9$ in DMF. 1,3-Dibromo-2-propanone (216 mg, 1.00 mmol) was added to $Fe_2(CO)_9$ (437 mg, 1.20 mmol) in DMF (3.5 ml), and the resulting mixture was stirred at room temperature for 12 h. The complex mixture was obtained after usual work-up, but no coupling product with an appropriate GLPC retention time was detected (column A, 70 °C).

*Reaction of the Dibromide **5** with $Fe(CO)_5$ in* N,N-*Dimethylacetamide. A. Under Thermal Conditions*: To a mixture of $Fe(CO)_5$ (470 mg, 2.40 mmol) and Na_2H_2edta (1.01 g, 3.00 mmol) in *N,N*-dimethylacetamide (3.5 ml) was added the dibromo ketone **5** (230 mg, 0.85 mmol). The mixture was then magnetically stirred at room temperature for 45 h. After quenching by saturated KNO_3 solution (10 ml), the reaction mixture was extracted with ethyl acetate (6 ml×5). The combined organic layers were washed with water (6 ml×2 and 4 ml×5) and dried. Removal of the solvent gave a pale yellow oil (181 mg). The NMR spectrum indicated the recovery of most of the starting dibromide and the absence of any cyclocoupling reaction.

B. Under Photo-irradiation Conditions: A mixture of the dibromide **5** (230 mg, 0.85 mmol), $Fe(CO)_5$ (470 mg, 2.40 mmol), and Na_2H_2edta (1.01 g, 3.00 mmol) in *N,N*-dimethylacetamide (3.5 ml) was stirred at room temperature with irradiation by >350 nm-light with a 200 W high-pressure Hg arc through 5% aq $CuSO_4$ solution. After 24 h the reaction mixture was quenched by the addition of saturated KNO_3 solution (15 ml) and extracted with ethyl acetate (6 ml×5). The collected organic extracts were washed with water (6 ml×4), dried, and concentrated, producing a viscous red oil (125 mg). The residue was dissolved in benzene (2 ml) and passed through a short alumina column. Evaporation of the filtrate gave a pale yellow oil (65 mg). NMR analysis of the oil indicated that the furanone **12** was formed in 41% yield.

*Reaction of the Dibromide **6** and DMF in the Absence of Reducing Agent.* A solution of the dibromide **6** (30.0 mg, 0.10 mmol) and hexadecane (10.0 mg, 0.05 mmol, an internal standard for GLPC analysis) in DMF (0.5 ml) was allowed to stand at room temperature for 12 h. GLPC (column D, 150 °C) of the mixture showed that **6** (t_r 6.8 min) remained unchanged.

*Treatment of 2-(Dimethylamino)-4-isopropylidene-5,5-dimethyl-1,3-dioxolane (**29**) with $FeBr_2$ in DMF.* A solution of $FeBr_2$ in DMF was prepared according to the following known method.[30] Into a solution of $Fe(CO)_5$ (20.0 mg, 0.01 mmol) in DMF (0.5 ml) was added bromine (16.0 mg, 0.01 mmol) with stirring. The color of bromine immedately disappeared, and vigorous gas evolution was observed. To the resulting deep red mixture was added a solution of the dioxolane **29** (26.8 mg, 0.15 mmol) in DMF (0.5 ml), and the mixture was stirred at room temperature for 24 h. The reaction aliquot was passed through a short column packed with alumina–Celite 545 under nitrogen and immediately subjected to NMR analysis, which showed the formation of the amino tetrahydro-3-furanone **2** in 24% yield.

*3-Acetoxy-2,4-dimethylfuran (**31**).* A mixture of the furanone **8** (1.60 g, 14.3 mmol), acetyl chloride (11.3 g, 143 mmol), and DME (20 ml) was heated at 55 °C for 14 h. The reaction mixture was added to ethyl acetate (10 ml), washed with saturated $NaHCO_3$ solution (10 ml×2) and KNO_3 solution (5 ml), and dried. Evaporation of the solvent gave a pale yellow oil (2.0 g), which was distilled with a bulb-to-bulb apparatus (bath temperature 70—110 °C, 20 Torr) to afford the acetate **31** (154 mg, >97% pure, 68% yield). IR (CCl_4) 1760 cm^{-1} (C=O); NMR δ 1.82 (d, 3, J=1.3 Hz, $CH{=}CCH_3$), 2.12 (s, 3, $C{=}CCH_3$), 2.21 (s, 3, $COCH_3$), and 6.92 (q, 1, J=1.3 Hz, =CH); MS *m/e* 154 (M^+). The acetate thus obtained was highly volatile and hydrolyzable (especially in the presence of acids); hence, the structure was assigned on the basis only of the spectral characteristics. Its immediate use, without purification, was required for obtaining a high yield in the next step.

*3-Acetoxy-5-(dimethylaminomethyl)-2,4-dimethylfuran (**32**).* To cooled (0—5 °C) acetic acid (0.19 ml) were added 40% aq dimethylamine (0.13 ml; 47.3 mg, 1.05 mmol as dimethylamine), 37% aq formaldehyde (0.08 ml; 32.3 mg, 1.08 mmol as formaldehyde), and the acetate **31** (120 mg, 0.78 mmol). The heterogeneous mixture was allowed to stand at room temperature for 5 min and then heated at 70 °C for 40 min with stirring. The resulting homogeneous solution was diluted with ethyl acetate (5 ml) and washed with saturated $NaHCO_3$/KNO_3 solution (5 ml). After drying, the organic layer was concentrated to leave a pale yellow oil (150 mg) consisting mainly of the amino furan **32**. This product was homogeneous on TLC (ethyl acetate, R_f 0.61), but the NMR analysis showed it to be only 85—90% pure. Yield of the amine was estimated as *ca.* 80%. Bulb-to-bulb distillation of this crude oil (bath temperature 100 °C, 0.2 Torr) gave analytically pure amine (115 mg, 70% yield) as a pale yellow oil. IR (CCl_4) 2840, 2795, and 2745 ($N(CH_3)_2$), and 1760 cm^{-1} (C=O); NMR δ 1.85 (s, 3, $=CCH_3$), 2.15 (s, 3, $=CCH_3$), 2.28 (s, 9, $COCH_3$ and $N(CH_3)_2$), and 3.42 (s, 2, CH_2); MS *m/e* 211 (M^+), 167 ($M^+-N(CH_3)_2$), and 125. Its picrate melted at 170—171 °C. Found: C, 46.23; H, 4.44; N, 12.63%. Calcd for $C_{17}H_{20}N_4O_{10}$: C, 46.36; H, 4.58; N, 12.72%. This amino furan is sensitive to air, turning brown, and so its immediate use is recommended.

*5-(Dimethylaminomethyl)-2,4-dimethyl-3(2H)-furanone (**33**).* A mixture of the amino furan **32** (70 mg, 0.33 mmol), 70% $HClO_4$ (0.5 ml), and DME (1.25 ml) was heated at 50 °C for 30 min. The mixture was then diluted with ethyl acetate (5 ml) and chilled at 0 °C by an ice bath. To the cooled mixture was added saturated $NaHCO_3$ solution until the separated aq layer changed to basic (pH *ca.* 8). The aq layer was extracted with ethyl acetate (5 ml×4). The combined organic extracts were washed with cold saturated KNO_3 solution (5 ml), dried,

and concentrated, affording a colorless oil (66 mg) which contained the amino furanone **33** as a major component [R_f 0.61 (ethyl acetate), >80% pure based on NMR]. Yield of **33** was >95%. IR (CCl_4) 2840, 2795, and 2745 ($N(CH_3)_2$), 1698 (C=O), and 1623 cm^{-1} (C=C); UV 274 nm (log ε 4.01); NMR δ 1.37 (d, 3, J=7.0 Hz, $CHC\underline{H}_3$), 1.66 (s, 3, $=CCH_3$), 2.25 (s, 6, $N(CH_3)_2$), 3.25 (s, 2, CH_2), and 4.24 (q, 1, J=7.0 Hz, OCH); MS *m/e* 169 (M^+). Found: *m/e* 169.1080. Calcd for $C_9H_{15}NO_2$: M, 169.1103.

*5-(Dimethylaminomethyl)-3-hydroxy-2,4-dimethyltetrahydrofuran (4-Methylnormuscarine) (**34**).* Into a 30-ml, two-necked flask equipped with a rubber septum and a Dry Ice condenser connected at its top with a bubbler was charged liquid NH_3 (*ca.* 15 ml). To this, ethanol (4.0 ml) and a solution of **33** (66 mg, 0.39 mmol) in DME (1.0 ml) were added through the septum by means of a syringe. After a few minutes, the septum was removed and small-cut Li (540 mg, 90.0 mg-atom) was added quickly. The resulting bronze-colored mixture was magnetically stirred for 1.5 h, quenched by the addition of solid NH_4Cl (2 g) with cooling by a Dry Ice–methanol bath, and warmed up to room temperature. To the voluminous gel was added ice water (20 ml), and the aq mixture was extracted with ethyl acetate (10 ml×4). The combined organic extracts were dried and concentrated to yield an oil (70 mg). The oil was dissolved in benzene, passed through an Na_2SO_4 column, and concentrated, giving a viscous oil. To a solution of the residue in THF (3.0 ml) was added $LiAlH_4$ (100 mg, 2.63 mmol) at −50 °C, after which the mixture was stirred at the same temperature for 1.5 h. The mixture was quenched with ethyl acetate at −78 °C, warmed up, and treated water. The aq layer was extracted with ethyl acetate (20 ml×2 and 10 ml×2), and the organic extracts were collected. Removal of the solvent produced viscous, oily material (60 mg), which was then subjected to preparative TLC (ethyl acetate) to afford the alcohol **34** (R_f 0.3—0.4, 41 mg, 61% yield). IR (CCl_4) 3400—3200 cm^{-1} (OH); NMR δ 1.18 (d, 3, J=7.0 Hz, $CHC\underline{H}_3$), 1.25 (d, 3, J=6.0 Hz, $CHC\underline{H}_3$), 2.45 (s, 6, $N(CH_3)_2$), 1.8—3.0 (complex, 4, $C\underline{H}CH_3$, CH_2, and OH), and 3.3—4.0 (m, 3, 2 OCH and $C\underline{H}OH$); MS *m/e* 173 (M^+) and 155 (M^+-H_2O). The structure of **34** was further confirmed through its quantitative transformation to 5-(dimethylaminomethyl)-3-(3,5-dinitrobenzoyloxy)-2,4-dimethyltetrahydrofuran (**35**).

A solution of **34** (15.0 mg, 0.09 mmol) in 1: 5 DME–benzene (0.8 ml) was mixed with 3,5-dinitrobenzoyl chloride (38 mg, 0.15 mmol) and pyridine (0.03 ml) and then left at room temperature for 20 h. The reaction mixture was diluted with ethyl acetate (4 ml) and washed with water (2 ml×2), saturated $NaHCO_3$ solution (2 ml×2), and KNO_3 solutiom (1 ml). The organic layer was dried and concentrated, affording an oil. TLC separation (1: 5 ether–hexane) of this crude product yielded the 3,5-dinitrobenzoate **35** (R_f 0.4, 31 mg, 97% yield). The NMR spectrum showed two kinds of singlets due to $N(CH_3)_2$ protons at δ 2.25 and 2.49 (*ca.* 9: 1 ratio), suggesting that **35** was a mixture of two difficult-to-separate diastereomers. NMR (major isomer) δ 1.25 (d, 6, J=6.5 Hz, 2 $CHC\underline{H}_3$), 2.0—2.4 (m, 1, $CHC\underline{H}CH_2$), 2.25 (s, 6, $(NCH_3)_2$, 2.4—2.6 (m, 2, CH_2), 3.50 (q-like m, 1, OCH), 3.97 (m, 1, OCH), 5.03 (m, 1, $C\underline{H}OCOC_6H_3(NO_2)_2$), and 8.8—9.0 (m, 3, $C_6H_3(NO_2)_2$). The signals of minor isomer could not be observed for certain. Other spectral data of the diastereomeric mixture were: IR (CCl_4) 1730 cm^{-1} (C=O); MS *m/e* 367 (M^+), 195, and 172 ($M^+-COC_6H_3(NO_2)_2$). Found: *m/e* 367.1392. Calcd for $C_{16}H_{21}N_3O_7$: M, 367.1379.

*4-Methylmuscarine Iodide (**36**).* A solution of the alcohol **34** (12 mg, 0.07 mmol) in benzene (0.5 ml) was mixed with methyl iodide (0.01 ml, 22.8 mg, 0.19 mmol) at room temperature. After 1 min, a yellow oil was separated. The heterogeneous mixture was left at room temperature for 5 min and then at 50 °C for 5 min. Most of the organic solvents were evaporated by bubbling in nitrogen gas. The heterogeneous residue, contaminated with a small amount of benzene, was mixed with methanol, and the solvents were removed azeotropically, affording viscous, oily material **36** (20 mg, 100% yield) as a mixture of difficult-to-separate diastereomers. NMR (CD_3OD) [major isomer (*ca.* 90%)] δ 1.07 (d, 3, J= 6.5 Hz, $CHC\underline{H}_3$), 1.11 (d, 3, J=6.5 Hz, $CHC\underline{H}_3$), 1.6—2.4 (m, 1, $C\underline{H}CHCH_2$), 3.21 (s, 9, $\overset{+}{N}(CH_3)_3$), and 3.25—4.25 (m, 5, 2 OCH, $C\underline{H}OH$, and CH_2). The ammonium salt **36** increased the tone and mobility of the smooth muscle of the intestinal tract.

We are grateful to the Ministry of Education, Japanese Government (Grant-in-Aid for Scientific Research, Nos. 743005 and 147022, and Grant-in-Aid for Developmental Scientific Research, No. 984014) for partial financial support. We also wish to thank Mr. Osamu Asano of the Sanwa Kagaku Kenkyusho Co. for testing the physiological effects of 4-methylmuscarine iodide.

References

1) Carbon–Carbon Bond Formations Promoted by Transition Metal Carbonyls. XXIII. Part XXII; R. Noyori, Annals of the New York Academy of Sciences (The Place of Transition Metals in Organic Synthesis) (in press).

2) For a preliminary communication on this work, see R. Noyori, Y. Hayakawa, S. Makino, N. Hayakawa, and H. Takaya, *J. Am. Chem. Soc.*, **95**, 4103 (1973).

3) Five-membered ring formation by the 3+2→5 cyclocoupling reaction. a) With enamines: Y. Hayakawa, K. Yokoyama, and R. Noyori, to be published; R. Noyori, K. Yokoyama, S. Makino, and Y. Hayakawa, *J. Am. Chem. Soc.*, **94**, 1772 (1972); b) with aromatic olefins: Y. Hayakawa, K. Yokoyama, and R. Noyori, to be published; R. Noyori, K. Yokoyama, and Y. Hayakawa, *J. Am. Chem. Soc.*, **95** 2722 (1973); Y. Hayakawa, K. Yokoyama, and R. Noyori, *Tetrahedron Lett.*, **1976**, 4347.

4) Seven-membered ring formation by the 3+4→7 cyclocoupling reaction. a) In general: H. Takaya, S. Makino, Y. Hayakawa, and R. Noyori, to be published; b) with open-chain 1,3-dienes: R. Noyori, S. Makino, and H. Takaya, *J. Am. Chem. Soc.*, **93**, 1272 (1971); c) with cyclopentadiene and furans: R. Noyori, S. Makino, Y. Baba, and H. Takaya, *Tetrahedron Lett.*, **1973**, 1743; R. Noyori, S. Makino, and H. Takaya, *ibid.*, **1973**, 1745; R. Noyori, S. Makino, T. Okita, and Y. Hayakawa, *J. Org. Chem.*, **40**, 806 (1975); R. Noyori, T. Souchi, and Y. Hayakawa, *ibid.*, **40**, 2681 (1975); Y. Hayakawa, M. Sakai, and R. Noyori, *Chem. Lett.*, **1975**, 509; d) with pyrroles: Y. Hayakawa, Y. Baba, S. Makino, and R. Noyori, to be published; R. Noyori, Y. Baba, and Y. Hayakawa, *J. Am. Chem. Soc.*, **96**, 3336 (1974); R. Noyori, S. Makino, Y. Baba, and Y. Hayakawa, *Tetrahedron Lett.*, **1974**, 1049.

5) A. R. Katritzky and J. M. Lagowski, "Advances in Heterocyclic Chemistry," Vol. 2, ed by A. R. Katritzky, Academic Press, New York, N.Y. (1963), pp. 5—8; P. Bosshard and C. H. Eugster, "Advances in Heterocyclic Chemistry," Vol. 7, ed by A. R. Katritzky and A. J. Boulton, Academic Press, New York, N. Y. (1966), pp. 462—468; N. Bodor, M. J. S. Dewar, and A. J. Harget, *J. Am. Chem. Soc.*, **92**, 2929 (1970).

6) G. Casnati and A. Ricca, *Tetrahedron Lett.*, **1967**, 327.
7) B. K. Carpenter, K. E. Clemens, E. A. Schmidt, and H. M. R. Hoffmann, *J. Am. Chem. Soc.*, **94**, 6213 (1972).
8) H. Meister, *Justus Liebigs Ann. Chem.*, **752**, 163 (1971).
9) M. Yamamoto, *J. Chem. Soc., Perkin Trans. 1*, **1976**, 1688.
10) F. Sher, J. L. Isidor, H. R. Taneja, and R. M. Carlson, *Tetrahedron Lett.*, **1973**, 577.
11) There are some discrepancies between the reported and present data. Hoffmann, *et al.*, reported that **8** showed IR absorption at 1760 and 1700 cm^{-1}, without any assignment.[7] However, the adduct obtained here did not exhibit a band around 1760 cm^{-1}.
12) J. V. Greehill, P. H. B. Ingle, and M. Ramli, *J. Chem. Soc., Perkin Trans. 1*, **1972**, 1667.
13) H. M. R. Hoffmann, K. E. Clemens, E. A. Schmidt, and R. H. Smithers, *J. Am. Chem. Soc.*, **94**, 3201 (1972).
14) R. Noyori, Y. Hayakawa, H. Takaya, S. Murai, R. Kobayashi, and N. Sonoda, to be published; R. Noyori, Y. Hayakawa, M. Funakura, H. Takaya, S. Murai, R. Kobayashi, and S. Tsutsumi, *J. Am. Chem. Soc.*, **94**, 7202 (1972).
15) Unpublished result obtained by Mr. Masashi Yamakawa in these laboratories.
16) Reviews: C. H. Eugster, *Adv. Org. Chem.*, **2**, 427 (1960); S. Wilkinson, *Quart. Rev., Chem. Soc.*, **15**, 153 (1961).
17) E. Hardegger and F. Lohse, *Helv. Chim. Acta*, **40**, 2383 (1957); H. C. Cox, E. Hardegger, F. Kögl, P. Liechti, F. Lohse, and C. A. Salemink, *ibid.*, **41**, 229 (1958); E. Hardegger, H. Furter, and J. Kiss, *ibid.*, **41**, 2401 (1958).
18) J. Whiting, Y.-K. Au-Young, and B. Belleau, *Can. J. Chem.*, **50**, 3322 (1972).
19) H. Corrodi, E. Hardegger, F. Kögl, and P. Zeller, *Experientia*, **13**, 138 (1957).
20) H. Corrodi, E. Hardegger, and F. Kögl, *Helv. Chim. Acta*, **40**, 2454 (1957).
21) F. Kögl, H. C. Cox, and C. A. Salemink, *Justus Liebigs Ann. Chem.*, **608**, 81 (1957); F. Kögl, H. C. Cox, and C. A. Salemink, *Experientia*, **13**, 137 (1957).
22) C. H. Eugster, *Helv. Chim. Acta*, **40**, 2462 (1957); C. H. Eugster, F. Häfliger, R. Denss, and E. Griod, *ibid.*, **41**, 205, 583, 705 (1968).
23) The syntheses of several artificial derivatives of muscarine have been reported: 2-Desmethylmuscarine: G. Zwicky, P. G. Waser, and C. H. Eugster, *Helv. Chim. Acta*, **42**, 1177 (1959); cyclopentyl analog: G. S. Givens, D. R. Rademacher, J. Kongs, and J. Dikerson, *Tetrahedron Lett.*, **1974**, 3211; open-chain analog: J. G. Cannon, P. J. Mulligan, J. P. Long, and S. Heintz, *J. Pharm. Sci.*, **62**, 830 (1973).
24) E. L. Eliel and M. T. Fisk, *Org. Synth.*, Coll. Vol. IV, 626 (1963).
25) Without $LiAlH_4$ reduction, a small amount of 5-(dimethylaminomethyl)-2,4-dimethyltetrahydro-3-furanone [IR 1750 cm^{-1} (C=O)] remained.
26) For the chemical shift of $\overset{+}{N}(CH_3)_3$ protons, see T. M. Moynehan, K. Schofield, R. A. Y. Jones, and A. R. Katritzky, *J. Chem. Soc.*, **1962**, 2637; F. Bovey, "NMR Data Tables for Organic Compounds," Vol. I, Interscience, New York, N. Y. (1967).
27) C. Rappe, *Acta Chem. Scand.*, **16**, 2467 (1962).
28) J. Ciabattoni and E. C. Nathan, III, *J. Am. Chem. Soc.*, **91**, 4766 (1969).
29) R. B. king, *Organomet. Synth.*, **1**, 93 (1965).
30) J. Dewar and H. O. Jones, *Proc. R. Soc. London, Ser. A*, **76**, 558 (1905); F. Calderazzo, R. Ercoli, and G. Natta, "Organic Syntheses *via* Metal Carbonyls," Vol. 1, ed by I. Wender and P. Pino, Interscience, New York, N. Y. (1968), p. 99.

Studies of Peptide Antibiotics. XXXV.[1] Synthesis of Gramicidin S by a Fragment Solid-Phase Method

Kazuki SATO, Hayao ABE,* Tetsuo KATO, and Nobuo IZUMIYA

Laboratory of Biochemistry, Faculty of Science 33, Kyushu University, Higashi-ku, Fukuoka 812

(Received March 18, 1977)

In order to examine the usefulness of a fragment condensation procedure in solid-phase peptide synthesis, gramicidin S (GS) was synthesized by three different procedures such as stepwise elongation, fragment condensation with dipeptide fragments, and fragment condensation with tripeptide fragments. The two fragment condensation procedures gave intermediate peptide derivatives in high yields and in high purity. Such differences in the purity of the intermediate peptides disappeared in the final product, GS dihydrochloride. The GS synthesized by the three procedures exhibited the same antibacterial activities as those of natural GS.

A large number of peptides have been synthesized by a solid-phase method.[2] This technique has obvious merits to simplify and accelerate peptide synthesis.[3] However, a crucial defect in this method is unavoidable accumulation of contaminating by-products, and this makes purification of desired products very difficult.[4] Application of a fragment condensation procedure to the solid-phase synthesis is undoubtedly an attractive approach for the improvement in this solid-phase synthesis.[5] Although several biologically active peptides have been prepared by the solid-phase fragment condensation procedure,[6] various aspects of this procedure remain insufficiently explored. Furthermore, there is scarcely any experiment on the comparison between the stepwise elongation procedure and the fragment condensation procedure in the solid-phase synthesis of a biologically active peptide as a target compound.

This paper deals with the solid-phase synthesis of gramicidin S (GS) by various procedures and compares the properties of the synthesized peptides. The solid-phase synthesis of the open-chain linear decapeptide corresponding to the sequence of GS was carried out with three procedures as follows: procedure **a**, stepwise elongation using Boc-amino acids;[7] procedure **b**, fragment condensation with Boc-dipeptide fragments except for Boc-D-phenylalanine at N-terminus; and procedure **c**, fragment condensation with Boc-tripeptide fragments. The syntheses of the peptide fragments are outlined in Fig. 1.

The peptide fragments were prepared by the active ester method with HONSu[8] in order to prevent racemization and to simplify synthetic procedures. Each coupling reaction proceeded quickly in a good yield, unreacted active ester being removed as a water-soluble amide by the addition of 1-(2-aminoethyl)piperazine.[9] Each peptide fragment obtained was carefully recrys-

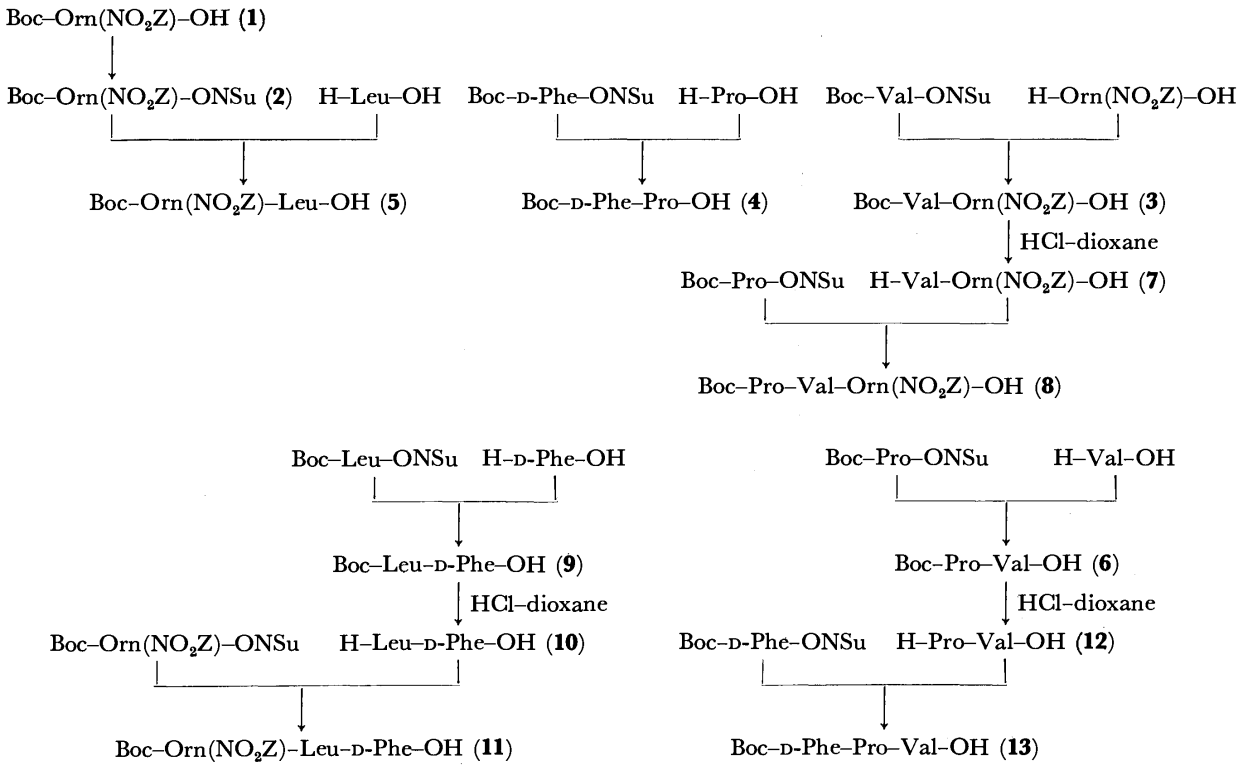

Fig. 1. Synthesis of peptide fragments.

* Present address: Institute of Biological Science, Mitsui-Toatsu Chemicals, Inc., Mobara 297.

tallized to remove the possible contamination of Boc-amino acid derived from the hydrolysis of the active ester during the coupling reaction in an aqueous solution. The δ-amino group of ornithine was protected by NO_2Z group.[10] Since this group showed extremely intense absorption at 268 nm, the purity of the synthetic intermediate peptides was ascertained spectrophotometrically by measuring the absorption of the group.[11]

Boc-Leu-resin
↓ 1. 1 M HCl–AcOH
↓ 2. 10% TEA–DMF
↓ 3. procedure **a**; Boc-amino acid and DCC
procedure **b**; Boc-dipeptide, HOBt, and DCC
procedure **c**; Boc-tripeptide, HOBt, and DCC
↓
Boc-(D-Phe-Pro-Val-Orn(NO_2Z)-Leu)$_2$-resin (**14a—c**)
↓ $N_2H_4 \cdot H_2O$–DMF
Boc-(D-Phe-Pro-Val-Orn(NO_2Z)-Leu)$_2$-N_2H_3 (**16a—c**)
↓ 0.1 M HCl–HCOOH
H-(D-Phe-Pro-Val-Orn(NO_2Z)-Leu)$_2$-$N_2H_3 \cdot 2HCl$ (**17a—c**)
↓ $NaNO_2$, HCl
(H-(D-Phe-Pro-Val-Orn(NO_2Z)-Leu)$_2$-$N_3 \cdot HCl$)
↓ pyridine
cyclo(-(D-Phe-Pro-Val-Orn(NO_2Z)-Leu)$_2$-) (**18a—c**)
↓ H_2/Pd, HCl
cyclo(-(D-Phe-Pro-Val-Orn-Leu)$_2$-)$\cdot 2HCl$ (**19a—c**)

Fig. 2. Synthesis of GS by three procedures.

TABLE 1. SCHEDULE FOR SOLID-PHASE SYNTHESIS[a]

Step	Reagent	Volume (ml)	Times of repetition	Time (min)
1	AcOH wash	20	3	5
2	1 M HCl in AcOH	20	1	30
3	AcOH wash	20	3	5
4	EtOH wash	20	3	5
5	DMF wash	13	3	5
6	10% TEA in DMF	13	1	10
7	DMF wash	13	3	5
8	CH_2Cl_2 wash	12	3	5
9	Boc-amino acid in CH_2Cl_2	7	1	10
10	DCC in CH_2Cl_2	5	1	240[b]
11	CH_2Cl_2 wash	12	3	5
12	EtOH wash	20	3	5

a) Schedule in procedure **a** is described. b) 480 min for Val and Pro.

The solid-phase synthesis of GS is outlined in Fig. 2. The schedule for each coupling reaction is shown in Table 1. As a coupling reagent, DCC (four equivalents) was used in procedure **a**, and DCC and HOBt[12] (four equivalents, each) were used in procedures **b** and in **c**. The progress of each coupling reaction was followed by chloride titration[13] and by the Kaiser test.[14] The results of the chloride titration were shown in Fig. 3. An aliquot of the peptidyl resin was withdrawn, hydrolyzed, and subjected to amino acid analysis after fourth, fifth, and ninth coupling steps in

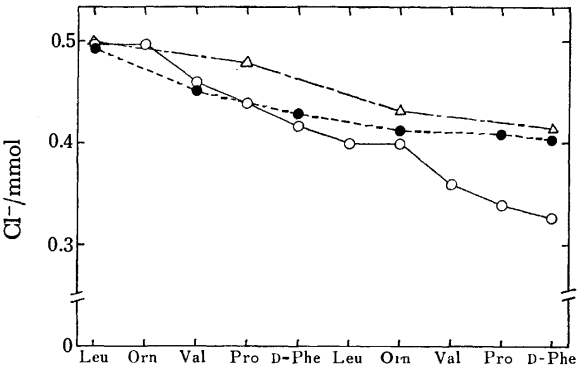

Fig. 3. Titration pattern of chloride ion in the course of synthesis of protected decapeptidyl-resin (**14**) by precedure **a** (○——○), by procedure **b** (●——●), and by procedure **c** (△·····△). Final value was determined by a portion of the peptidyl-resin.

procedure **a** and after each coupling step in procedure **b** and **c**. The yield of each coupling reaction was calculated on the basis of the results of amino acid analysis as shown in Fig. 4.

NO_2Z NO_2Z
Boc-D-Phe-Pro-Val-Orn-Leu-D-Phe-Pro-Val-Orn-Leu-resin

Procedure a	98	97	87	100	96	94	96	95	100
Procedure b	98	97		100		92		95	
Procedure c	95			94			96		

Fig. 4. Coupling yield in each coupling step.

In procedure **a**, the coupling reaction of Boc-valine gave the unsatisfactory yield of 87%. In procedure **b**, the coupling of Boc-D-Phe-Pro-OH (**4**) with the tripeptidyl resin resulted in the low yield of 92%. The low yield in this step may be due to steric hindrance caused by the bulky side chain of the valine residue in the tripeptidly resin. The coupling reactions of the other three peptide fragments (**3**, **5**, **6**) and of the final Boc-D-phenylalanine gave good yields. In procedure **c**, all the coupling reactions gave excellent yields. Repetition of the coupling reaction was avoided in order to compare the reactivity of each reactant under the same reaction conditions. As shown in Fig. 4, the yield of each coupling reaction in procedure **a** was good except for valine; however, the nine consecutive coupling reactions caused lowering of the over-all coupling yield. The over-all yields calculated from the results of the amino acid analyses were 68, 83, and 86% in procedure **a**, **b**, and **c**, respectively.

After completion of the final coupling cycle, peptidyl resin (**14**) was dried under a reduced pressure and weighed. The yield estimated from the weight increase in procedure **a** agreed with those estimated from amino acid analysis and chloride titration. In procedures **b** and **c**, however, the yields estimated from the weight increases were lower than those estimated from the other methods. A possible reasoning of this disagreement

TABLE 2. AMINO ACID RATIOS OF SYNTHETIC INTERMEDIATES AND SYNTHETIC GRAMICIDIN S

Compound	Procedure **a**					Procedure **b**					Procedure **c**				
	D-Phe	Pro	Val	Orn	Leu	D-Phe	Pro	Val	Orn	Leu	D-Phe	Pro	Val	Orn	Leu
14	0.85	0.88	0.92	1.00	1.00	0.91	0.92	0.93	0.95	1.00	0.92	0.94	0.95	0.98	1.00
15	0.86	0.85	0.97	1.14	1.00	0.96	1.00	0.97	1.01	1.00	0.96	1.02	0.95	0.98	1.00
16	0.93	1.01	1.07	1.16	1.00	1.03	1.00	1.01	1.00	1.00	0.97	1.00	0.98	1.00	1.00
18	0.97	1.01	0.95	0.99	1.00	1.01	1.01	1.02	1.01	1.00	1.01	1.00	0.99	1.02	1.00
19	0.90	0.90	0.98	0.95	1.00	1.02	0.98	0.97	1.04	1.00	0.96	0.99	1.00	1.00	1.00

is that frequent withdrawals of the peptidyl resin in the latter procedures caused much more loss of the resin than expected.

Hydrazinolysis of **14** was carried out as described previously,[11] and yielded a crude protected decapeptide hydrazide (**15**), this hydrazide being purified with recrystallization. The properties of **15** and purified hydrazide (**16**) were compared. Crude hydrazides **15a**, **15b**, and **15c** showed similar physical constants and chromatographic behavior. However, after recrystallization, purified hydrazides **16b** and **16c** showed some improvements in physical constants such as melting points and optical rotations and also in the results in amino acid analyses as shown in Table 2. The properties of **16a** were not changed significantly. Partially protected decapeptide hydrazide (**17**) was obtained quantitatively by the deprotection of Boc-group in **16** with hydrogen chloride in formic acid.[15] Thin-layer chromatography and paper electrophoresis of each of **17a—c** showed a main spot and another faint spot. All three hydrazides **17a**, **17b**, and **17c** revealed similar chromatographic behavior and similar results in measurements of the melting points and UV absorptions.

Cyclization of **17** by an azide method gave a protected cyclic decapeptide (**18**). Properties of **18a**, **18b**, and **18c** were compared, an acylated derivative (**18n**) of natural GS being used as a reference compound. There was no distinct differences in the patterns in thin-layer and Sephadex LH-20 column chromatography. However, products **18b** and **18c** showed better results in amino acid analyses and the optical rotations.

Hydrogenation of **18** gave synthetic GS·2HCl (**19**) as fine needles similar to the crystals of natural GS·2HCl. The synthetic and natural GS·2HCl showed the same results in thin-layer, paper, and carboxymethylcellulose column chromatography, paper electrophoresis, and measurements of the optical rotations and the melting points. The antibacterial activities of **19** also were the same as those of natural GS·2HCl.

The purities of the compounds obtained from the three different procedures turned to nearly the same in the final stage of the synthesis. A small amount of impurities seemed to be removed in the course of repeated chemical reactions and recrystallizations. Minute differences in purity, observed in **15** and **16**, were disappeared in **19**. Thus, the results of this solid-phase synthesis of GS indicated that the fragment condensation procedure had advantage of the ease of purification, the advantage being shown in the purification of **15**. In the usual fragment condensation, peptide fragments which placed glycine or proline at C-terminus have been employed to avoid racemization.[16] The results in this synthesis revealed that the use of DCC–HOBt as coupling reagents gave satisfactory results in coupling yield and in prevention of racemization, when applied to the solid-phase fragment condensation.

Experimental

All the melting points are uncorrected. The ratio in parentheses after a solvent system was indicated by vol. TLC was carried out on silica gel G (Merck) with the following solvent systems: R_f^1, $CHCl_3$–MeOH (5:1); R_f^2, 1-BuOH–AcOH–pyridine–H_2O (4:1:1:2). Paper chromatography was carried out on Toyo Roshi No. 52 paper; R_f^3, the same solvent as R_f^2 for TLC. PEP was carried out on the same paper under conditions of 500 V/30 cm with the solvent system; HCOOH–AcOH–MeOH–H_2O (1:3:6:10) at pH 1.8, the mobilities of samples being reported as the ratio to that of lysine (R_{Lys}). UV spectra were determined on a Hitachi-Perkin-Elmer spectrophotometer, Model 139. Optical rotations were measured on a Yanagimoto polarimeter, OR-20. Amino acid analyses were performed on a Hitachi amino acid analyzer, KLA-3B, after hydrolysis in a mixture of 6 M HCl and propionic acid (1:1) at 110 °C for 24 h.[17] Molecular weight was determined with a Hitachi Osmometer, Model 115, DMF being used as a solvent.

*Boc–Orn(NO_2Z)–OH·DCHA (**1**·DCHA).* To a solution of δ-NO_2Z-ornithine[11] (12.4 g, 40 mmol) and TEA (16.8 ml, 120 mmol) in water (40 ml) was added Boc-N_3 (8.22 g, 60 mmol) in dioxane (50 ml). The reaction mixture was treated according to the procedure of Sakakibara *et al.*,[18] and the product was recrystallized from MeOH–ether–petroleum ether; yield, 20.24 g (85%); mp 89—90 °C; $[\alpha]_D^{20}+13.6°$ (*c* 1, MeOH); UV_{max} (EtOH) 268 nm (ε 1.01×10^4).

Found: C, 60.76; H, 8.53; N, 9.16%. Calcd for $C_{30}H_{48}O_8N_4$: C, 60.79; H, 8.16; N, 9.45%.

*Boc–Orn(NO_2Z)–ONSu (**2**).* Compound **1** (8.23 g, 20 mmol) which was derived from **1·DCHA** by the usual procedure was converted to the corresponding HONSu ester according to the procedure of Anderson *et al.*[19] The product was recrystallized from EtOAc–ether; yield, 5.56 g (55%); mp 87—88 °C; $[\alpha]_D^{20}-4.4°$ (*c* 1, $CHCl_3$).

Found: C, 51.80; H, 5.78; N, 10.87%. Calcd for $C_{22}H_{28}O_{10}N_4$: C, 51.96; H, 5.55; N, 11.02%.

*Boc–Val–Orn(NO_2Z)–OH (**3**).* To a solution of δ-NO_2Z-ornithine (3.74 g, 12 mmol) and TEA (1.68 ml, 12 mmol) in water (25 ml) was added a solution of Boc–Val–ONSu (3.50 g, 10 mmol) in dioxane (25 ml) at room temperature. The reaction mixture was stirred overnight, and a few drops of 1-(2-aminoethyl)piperazine was added to the solution. After being stirred for 30 min, dioxane was evaporated *in vacuo* and the solution was acidified with 10% citric acid under cooling. Separated oil was extracted with EtOAc, and the organic layer was washed with water and dried (Na_2SO_4). The solution was evaporated to leave an oil, which was crystallized by the addition of ether. The product was recrystallized from

MeOH–ether; yield, 4.89 g (96%); mp 86—88°C; $[\alpha]_D^{20}$ −9.3° (*c* 1, MeOH); R_f^1 0.52.

Found: C, 54.55; H, 6.92; N, 10.72%. Calcd for $C_{23}H_{34}O_9N_4$: C, 54.11; H, 6.71; N, 10.98%.

Other protected peptide fragments (**4**—**6**, **8**, **9**, **11**, **13**), were prepared by a manner similar to that described for **3**.

Boc-D-Phe-Pro-OH (**4**). Yield, 81%; mp 171—173 °C; $[\alpha]_D^{20}$ −46.9° (*c* 1, MeOH); R_f^1 0.54.

Found: C, 62.90; H, 7.30; N, 7.75%. Calcd for $C_{19}H_{26}O_5N_2$: C, 62.96; H, 7.23; N, 7.73%.

Boc-Orn(NO$_2$Z)-Leu-OH (**5**). Yield, 82%; mp 73—75 °C; $[\alpha]_D^{20}$ −10.2° (*c* 1, MeOH); R_f^1 0.66.

Found: C, 55.10; H, 7.12; N, 10.42%. Calcd for $C_{24}H_{36}O_9N_4$: C, 54.95; H, 7.12; N, 10.42%.

Boc-Pro-Val-OH·DCHA (**6·DCHA**). Yield, 63%; mp 126—127 °C; $[\alpha]_D^{20}$ −40.4° (*c* 1, MeOH); R_f^1 0.61.

Found: C, 65.39; H, 10.08; N, 8.35%. Calcd for $C_{27}H_{49}O_5N_3$: C, 65.43; H, 9.98; N, 8.84%.

Boc-Pro-Val-Orn(NO$_2$Z)-OH (**8**). Yield, 69%; mp 159—161 °C; $[\alpha]_D^{20}$ −48.2° (*c* 1, MeOH); R_f^1 0.51.

Found: C, 54.96; H, 6.72; N, 11.58%. Calcd for $C_{28}H_{41}O_{10}N_5$: C, 55.34; H, 6.80; N, 11.53%.

Boc-Leu-D-Phe-OH·DCHA (**9·DCHA**). Yield, 82%; mp 115—116 °C; $[\alpha]_D^{20}$ −46.3° (*c* 1, MeOH); R_f^1 0.67.

Found: C, 68.73; H, 9.73; N, 7.46%. Calcd for $C_{32}H_{53}O_5N_3$: C, 68.66; H, 9.54; N, 7.51%.

Boc-Orn(NO$_2$Z)-Leu-D-Phe-OH (**11**). Yield, 80%; mp 90—91 °C; $[\alpha]_D^{20}$ −24.1° (*c* 1, MeOH); R_f^1 0.58.

Found: C, 58.91; H, 6.88; N, 10.23%. Calcd for $C_{33}H_{45}O_{10}N_5$: C, 59.00; H, 6.75; N, 10.43%.

Boc-D-Phe-Pro-Val-OH (**13**). Yield, 54%; mp 172—173 °C; $[\alpha]_D^{20}$ −78.8° (*c* 1, MeOH); R_f^1 0.61.

Found: C, 62.37; H, 7.69; N, 9.14%. Calcd for $C_{24}H_{35}O_6N_3$: C, 62.45; H, 7.64; N, 9.11%.

H-Val-Orn(NO$_2$Z)-OH·HCl (**7·HCl**). Compound **3** (2.55 g, 5 mmol) was dissolved in 2.6 M hydrogen chloride in dioxane (39 ml). The solution was allowed to stand for 1 h at room temperature and then evaporated. Resulting oil was solidified by the addition of ether. The product was recrystallized from EtOH–ether; yield, 1.93 g (86%); mp 159—161 °C; $[\alpha]_D^{20}$ +10.3° (*c* 1, 6 M HCl); R_f^2 0.80.

Found: C, 48.98; H, 6.53; N, 11.79%. Calcd for $C_{18}H_{27}O_7N_4Cl$: C, 48.37; H, 6.09; N, 12.54%.

H-Leu-D-Phe-OH·HCl (**10·HCl**). Compound **9** was treated as described for **7**; yield, 83%; mp 200—202 °C; $[\alpha]_D^{20}$ +37.0° (c 1, 6 M HCl); R_f^2 0.78.

H-Pro-Val-OH (**12**). Compound **6** (1.57 g, 5 mmol) was treated as described for **7**. The oily residue (**12·HCl**) was dissolved in water (50 ml) and the solution was neutrallized with TEA (0.7 ml, 5 mmol). The addition of EtOH (50 ml) gave crystals, which were recrystallized from water–EtOH; yield, 0.88 g (82%); mp 242—243 °C (dec); $[\alpha]_D^{20}$ −70.2° (*c* 1, 6 M HCl); R_f^2 0.56.

Found: C, 55.80; H, 8.62; N, 12.98%. Calcd for $C_{10}H_{18}O_3N_2$: C, 56.05: H, 8.47; N, 13.08%.

Boc-(D-Phe-Pro-Val-Orn(NO$_2$Z)-Leu)$_2$-resin (**14a—c**).

14a: Boc-Leu-resin[20] (1.88 g, containing 0.5 mmol of Boc-leucine), which was prepared from chloromethylated copolystyrene divinylbenzene (2%) resin (0.65 mmol of Cl/g), was placed in a reaction vessel and swollen with AcOH (15 ml) overnight; this starting material was prepared similarly for **14b** and **14c**. Elongation of peptide chain was carried out according to the schedule shown in Table 1. The coupling time was generally 4 h and exceptionally 8 h for Boc-valine and for Boc-proline. After completion of the final coupling cycle, the resin was washed with DMF, EtOH, AcOH, and CH_2Cl_2 successively, and dried *in vacuo*. Weight increase, 473 mg (68%).

14b: Instead of Boc-amino acid in procedure **a**, the Boc-dipeptide fragment and HOBt (four equivalents, each) were added. After the addition of DCC (four equivalents), the vessel was shaken for 24 h. Weight increase, 542 mg (78%).

14c: The Boc-tripeptide fragment, HOBt, and DCC (four equivalents, each) were added, and the reaction time was 48 h. Weight increase, 508 mg (73%).

Boc-(D-Phe-Pro-Val-Orn(NO$_2$Z)-Leu)$_2$-N$_2$H$_3$ (**16a—c**).

16a: To a suspension of **14a** (1.19 g, 0.18 mmol) in DMF (13 ml) was added 100% hydrazine hydrate (0.35 ml, 7.2 mmol). The mixture was shaken for 3 days at room temperature, the resin was removed by filtration and washed with DMF (13 ml×3), and the combined filtrate was evaporated *in vacuo*. The residue was treated with water (100 ml) to give yellowish powder; yield of crude hydrazide (**15a**), 273 mg (94%); mp 141—148 °C; $[\alpha]_D^{20}$ −103° (*c* 0.5, MeOH); purity estimated from absorption at 268 nm, 98%; R_f^1 0.76 with a faint tailing strip; R_f^2 0.93. Compound **15a** (200 mg) was dissolved in hot MeOH (20 ml), an insoluble material in a small amount being filtered off. The filtrate was evaporated to 4 ml and white precipitate of purified hydrazide (**16a**) was obtained by the addition of ether; yield, 178 mg (89%); mp 150—151 °C; $[\alpha]_D^{20}$ −119° (*c* 0.5, MeOH); purity at 268 nm, 96%.

Found: C, 58.98; H, 7.12; N, 13.82%. Calcd for $C_{79}H_{110}O_{20}N_{16}\cdot H_2O$: C, 58.50; H, 6.96; N, 13.82%.

16b: Compound **14b** (1.06 g, 0.18 mmol) was treated as described for **15a**; yield of crude hydrazide (**15b**), 286 mg (98%); mp 136—143 °C; $[\alpha]_D^{20}$ −117° (*c* 0.5, MeOH); purity at 268 nm, 96%; R_f^1 0.76 with a faint tailing strip; R_f^2 0.93. Compound **15b** (200 mg) was treated as described for **16a**; yield of **16b**, 188 mg (94%); mp 152 °C; $[\alpha]_D^{20}$ −145° (*c* 0.5, MeOH); purity at 168 nm, 98% (Found: C, 58.06; H, 6.96; N, 13.62%).

16c: Compound **14c** (1.14 g, 0.18 mmol) was treated as described for **15a**; yield of crude hydrazide (**15c**), 285 mg (98%); mp 134—140 °C; $[\alpha]_D^{20}$ −125° (*c* 0.5, MeOH); purity at 268 nm, 95%; R_f^1 0.76 with a faint tailing strip; R_f^2 0.93. Compound **15c** (200 mg) was treated as described for **16a**; yield **16c**, 184 mg (92%); mp 153 °C; $[\alpha]_D^{20}$ −135° (*c* 0.5, MeOH); purity at 268 nm, 97% (Found: C, 58.29; H, 6.96; N, 14.37 %).

H-(D-Phe-Pro-Val-Orn(NO$_2$Z)-Leu)$_2$-N$_2$H$_3$·2HCl (**17a—c**).

17a: A solution of **16a** (164 mg, 0.1 mmol) in 0.1 M hydrogen chloride in formic acid (2.2 ml) was allowed to stand for 8 h at room temperature and then evaporated. The oily residue was solidified by the addition of ether; yield, 160 mg (99%); mp 168—171 °C; R_f^1 0.49 with a faint tailing strip; R_f^2 0.79; R_{Lys} 0.53 with a faint tailing strip; purity at 268 nm, 96%.

17b: This was prepared from **16b** (164 mg, 0.1 mmol) as described for **17a**; yield, 161 mg (100%); mp 175 °C; R_f^1 0.49 with a faint tailing strip; R_f^2 0.79; R_{Lys} 0.53 with a faint tailing strip; purity at 268 nm, 95%.

17c: This was prepared from **16c** (164 mg, 0.1 mmol) as described for **17a**; yield, 157 mg (97%); mp 175 °C; R_f^1 0.49 with a faint tailing strip; R_f^2 0.79; R_{Lys} 0.53 with a faint tailing strip; purity at 268 nm, 94%.

cyclo(-(D-*Phe-Pro-Val-Orn(NO$_2$Z)-Leu)$_2$-*) (**18a—c**).

18a: To a solution of **17a** (144 mg, 0.09 mmol) in a mixture of AcOH (0.45 ml) and DMF (1.8 ml) were added 1 M HCl (0.1 ml) and 1 M $NaNO_2$ (0.1 ml) at −30 °C. After being left for 30 min, the reaction mixture was added into pyridine (37 ml) at 0 °C. After being stirred for 3 days at 5 °C, the

solution was evaporated and the residue was dissolved in a mixture (12 ml) of MeOH and water (10: 1). The solution was applied on columns (1.9×20 cm, each) of Dowex 1 (OH^- form) and Dowex 50 (H^+ form). The columns were washed with the same solvent (200 ml) and the combined effluent was evaporated to leave an oily residue, which was crystallized by the addition of ether. The product was recrystallized from MeOH–ether; yield, 63 mg (46%); mp 218—223 °C; $[\alpha]_D^{20}$ −230° (*c* 0.3, MeOH); purity at 268 nm, 96%; R_f^1 0.71; R_f^2 0.94.

Found: C, 59.67; H, 6.95; N, 12.64%; mol wt, 1509. Calcd for $C_{76}H_{102}O_{18}N_{14}\cdot 2H_2O$: C, 59.38; H, 6.90; N, 12.76%; mol wt, 1500.

18b: This was prepared from **17b** (144 mg, 0.09 mmol) as described for **18a**; yield, 64 mg (47%); mp 225—230 °C;$[\alpha]_D^{20}$ −242° (*c* 0.3, MeOH); purity at 268 nm, 101%; R_f^1 0.71; R_f^2 0.94; mol wt, 1504 (Found: C, 60.16; H, 6.94; N, 12.74 %).

18c: This was prepared from **17c** (144 mg, 0.09 mmol) as described for **18a**; yield, 48 mg (35%); mp 225—230 °C; $[\alpha]_D^{20}$ −243° (*c* 0.3, MeOH); purity at 268 nm, 101%; R_f^1 0.71; R_f^2 0.94; mol wt, 1507 (Found: C, 60.30; H, 6.97; N, 12.71%).

*Preparation of **18n** from Natural GS.* To a solution of natural GS (21 mg, 0.017 mmol) in pyridine (1.7 ml) was added *p*-nitrobenzyloxycarbonyl chloride[10] (0.36 g, 1.7 mmol) at −10 °C. After being stirred for 7 h at 0 °C, the solution was evaporated. The resulting residue afforded a yellowish precipitate (0.25 g) by the addition of water. The precipitate was dissolved in MeOH (5 ml), and the solution was applied on a column of Sephadex LH-20 (1.8×110 cm) and developed with MeOH. The fractions with the desired product were collected and evaporated, the resulting oily residue being crystalized by the addition of ether; yield, 23 mg (75 %); mp 245—247 °C; $[\alpha]_D^{20}$ −248° (*c* 0.3, MeOH); purity at 268 nm, 100%; R_f^1 0.71; R_f^2 0.94 (Found: C, 59.54; H, 6.96; N, 12.61%).

*Sephadex LH-20 Column Chromatography of **15a—c** and **18a—c**.*
15a: A portion (10 mg) of **15a** was applied on a column of Sephadex LH-20 (1.8×110 cm) using MeOH as an eluate. The chromatogram showed a single peak at 145 ml.

15b** and **15c: The chromatograms of **15b** and **15c** in the same conditions also showed the same patterns as that of **15a**.

18a: A portion (5 mg) of **18a** was applied on the same column as described for **15a**. The chromatogram showed the same single peak at 149 ml as that of the reference compound (**18n**).

18b** and **18c: The chromatograms of **18b** and **18c** in the same conditions also showed the same patterns as that of **18n**.

cyclo*(-(D-Phe-Pro-Val-Orn-Leu)$_2$-)·2HCl (**19a—c**).*

19a: Compound **18a** (30 mg, 0.02 mmol) dissolved in 0.01 M hydrogen chloride in MeOH (6 ml) was hydrogenated using palladium black as a catalyst. The filtrate was evaporated and the residual solid was recrystallized from EtOH–1 M HCl; yield, 18 mg (76%); mp 269—275 °C; $[\alpha]_D^{20}$ −260° (*c* 0.4, EtOH); R_f^2 0.83, R_f^3 0.80.

Found: C, 56.53; H, 7.79; N, 12.41%. Calcd for $C_{60}H_{92}O_{10}N_{12}\cdot 2HCl\cdot 4H_2O$: C, 56.01; H, 7.94; N, 13.07%.

19b: This was prepared from **18b** (30 mg, 0.02 mmol) as described for **19a**; yield, 15 mg (60%); mp 274—279 °C;$[\alpha]_D^{20}$ −252° (*c* 0.4, EtOH); R_f^2 0.83; R_f^3 0.80 (Found: C, 55.85; H, 7.63; N, 12.46%).

19c: This was prepared from **18c** (30mg, 0.02 mmol) as described for **19a**; yield, 16 mg (65%); mp 274—279 °C; $[\alpha]_D^{20}$ −253° (*c* 0.4, EtOH); R_f^2 0.83; R_f^3 0.80 (Found: C, 56.12; H, 7.65; N, 12.64%).

*Comparison of Synthetic GS·2HCl (**19a—c**) with Natural GS·2HCl.* Physical constants and R_f values of **19a—c** were shown above. Physical constants and R_f values of natural GS·2HCl; mp, 274—276 °C; $[\alpha]_D^{20}$ −258° (*c* 0.6, EtOH); R_f^2 0.83 R_f^3; 0.80. In addition to showing the same R_f values in paper and thin-layer chromatography, the natural and all three synthetic GS·2HCl revealed indistinguishable paper electrophoretic patterns and identical behavior in the carboxymethylcellulose column chromatography in the conditions described previously.[21]

Microbiological Assays. The minimum amount of the synthetic and natural GS·2HCl necessary for the complete inhibition of growth of several microorganisms was determined by a dilution method using a nutrient agar. All three synthetic GS·2HCl exhibited the same antibacterial activities as those of natural GS·2HCl. The minimum inhibitory concentration of the compounds were 2—4 μg/ml on *Staphylococcus aureus*, 4—7 μg/ml on *Bacillus subtilis*, and 50—100 μg/ml on *Escherichia coli*.

The authors wish to express their thanks to the staff of Institute of Biological Science, Mitsui-Toatsu Chemicals, Inc., Mobara, for the biological assays. They also thank to Meiji Seika Kaisha, Ltd. for the donation of natural GS.

References

1) Part XXXIV of this series: K. Okamoto, K. Nonaka, and N. Izumiya, *Bull. Chem. Soc. Jpn.*, **50**, 231 (1977).

2) A. Marglin and R. B. Merrifield, *Ann. Rev. Biochem.*, **39**, 841 (1970); G. R. Marchall and R. B. Merrifield, "Biochemical Aspects of Reactions on Solid Supports," Academic Press, New York, N. Y. (1971), pp. 111—169.

3) R. B. Merrifield, *Fed. Proc.*, **21**, 412 (1962); R. B. Merrifield, *J. Am. Chem. Soc.*, **85**, 2149 (1963).

4) E. Bayer, H. Eckstein, K. Hagel, W. A. König, W. Brüning, H. Hagenmaier, and W. Parr, *J. Am. Chem. Soc.*, **92**, 1735 (1970).

5) F. Weygand and U. Ragnarsson, *Z. Naturforsch.*, **21b**, 1141 (1966).

6) B. F. Gisin, R. B. Merrifield, and D. C. Tosteson, *J. Am. Chem. Soc.*, **91**, 2691 (1969); H. Yajima and Y. Kiso, *Chem. Pharm. Bull.*, **22**, 1087 (1974); U. Ragnarsson, S. M. Karlsson, and U. Hamberg, *Int. J. Pept. Protein Res.*, **7**, 307 (1975); Protein Synthesis Group, Shanghai Institute of Biochemistry, Academia Sinica, *Scientia Sinica*, **18**, 745 (1975); R. E. Larsson, P. Melin, and U. Ragnarsson, *Int. J. Pept. Protein Res.*, **8**, 39 (1976).

7) Abbreviations according to IUPAC-IUB Commission, *J. Biol. Chem.*, **247**, 977 (1972), are used throughout. Additional abbreviations: DCC, dicyclohexylcarbodiimide: DMF, *N,N*-dimethylformamide; HOBt, 1-hydroxybenzotriazol; HONSu, *N*-hydroxysuccinimide; TEA, triethylamine; Boc, *t*-butyloxycarbonyl; NO_2Z, *p*-nitrobenzyloxycarbonyl; PEP, paper electrophoresis. Amino acid symbols except D-Phe denote the L-configuration.

8) G. W. Anderson, J. E. Zimmerman, and F. M. Callahan, *J. Am. Chem. Soc.*, **86**, 1839 (1964).

9) E. Wünsch, G. Wendlberger, and A. Högel, *Chem. Ber.*, **104**, 2430 (1971).

10) F. H. Carpenter and D. T. Gish, *J. Am. Chem. Soc.*, **74**, 3818 (1952).

11) M. Ohno, K. Kuromizu, H. Ogawa, and N. Izumiya, *J. Am. Chem. Soc.*, **93**, 5251 (1971).

12) F. Weygand, D. Hoffmann, and E. Wünsch, *Z. Natur-*

forsch., **21b**, 426 (1966).
13) J. M. Stewart and J. D. Young, "Solid Phase Peptide Synthesis," Freeman & Co., San Francisco (1969), p. 55.
14) E. Kaiser, R. L. Colescott, C. D. Bossinger, and P. I. Cook, *Anal. Biochem.*, **34**, 595 (1970).
15) W. Troll and R. K. Cannan, *J. Biol. Chem.*, **200**, 803 (1953).
16) H. Yajima, H. Kawatani, and H. Watanabe, *Chem. Pharm. Bull.*, **18**, 1333 (1970).
17) J. Scotchler, R. Lozier, and A. B. Robinson, *J. Org. Chem.*, **35**, 3151 (1970).
18) S. Sakakibara, H. Honda, K. Takeda, M. Miyoshi, T. Ohnishi, and K. Okumura, *Bull. Chem. Soc. Jpn.*, **42**, 809 (1969).
19) G. W. Anderson and A. C. McGregor, *J. Am. Chem. Soc.*, **79**, 6180 (1957).
20) J. M. Stewart and J. D. Young, "Solid Phase Peptide Synthesis," Freeman & Co., San Francisco (1969), p. 32.
21) H. Aoyagi, T. Kato, M. Waki, O. Abe, R. Okawa, S. Makisumi, and N. Izumiya, *Bull. Chem. Soc. Jpn.*, **42**, 782 (1969).

The Isolation and Structure of Toxic Principles, Milliamines A, B, and C, from *Euphorbia Millii*

Daisuke UEMURA and Yoshimasa HIRATA

Department of Chemistry, Faculty of Science, Nagoya University, Chikusa, Nagoya 464

(Received November 30, 1976)

Toxic compounds were isolated from *Euphorbia Millii* Ch. des Moulins (*Euphorbiaceae*). The structure of the milliamines was established from chemical and spectral evidence. Furthermore, the acute toxicity of milliamine A was examined.

Although *Euphorbia Millii* Ch. des Moulins (Japanese name, Hanakirin) is widely cultivated for decorative purposes, its toxicity is also known. The toxic compound of this plant is of interest. A detailed survey of methanol extracts gave three alkaloidal toxic compounds, namely, milliamines A (**1**),[1] B (**2**),[1] C (**3**).[2] Particularly milliamine A hydrochloride possesses high toxicity (LD_{50}=0.64 mg/kg).

Isolation of Milliamines. Dried roots were extracted with methanol over a period of a few days. The evaporation of methanol under reduced pressure gave a moist oily material, which was extracted with ether several times. The organic layers were concentrated and the residual oily material was subjected to chromatography on silicic acid. The toxic material responded positively to the Dragendorff test. A fraction (responding positively to the Dragendorff test) afforded milliamine A, which was purified as a hydrochloride. Milliamine A hydrochloride was recrystallized from acetone. Milliamines B and C were purified by preparative thin-layer chromatography. Milliamine B hydrochloride was obtained as a powder. Milliamine C was unstable in acidic media, and was purified by repetitive preparative thin-layer chromatography. The physical and spectral data of these new compounds are summarized in Table 1.

The Structure of Milliamine A. Milliamine A (**1**) possesses the molecular formula, $C_{45}H_{49}N_3O_{10}$. Strong hydrogen bonding was present in **1** judging from the absorption in the region of 2800—3600 cm^{-1} in the IR spectrum. Also, the IR spectrum showed the presence of carbonyl groups (1725, 1690, 1670, and 1645 cm^{-1}) including an ester group, which is cleavable by methanolysis. In practice, treatment of milliamine A (**1**) with sodium methoxide afforded an alkaloidal part, compound **4**, and an alcohol (**5**).

Compounds **4** was purified by recrystallization from methanol and possesses the molecular formula $C_{24}H_{23}N_3O_5$: mp 160—161 °C; IR (KBr) 3400, 3250, 2400—3000, 1690, 1670, 1630, 1590, 1510, and 1300 cm^{-1}; NMR (60 MHz, acetone-d_6) δ 2.73 [6H, s, $-N(CH_3)_2$], 3.77 (3H, s, $-COOCH_3$), 6.8—7.6 (8H, m), 7.7—8.1 (2H, m), 8.60 (1H, d of d, J=1.0 and 10 Hz), 9.26, 11.3, and 12.9 (1H each, br s, exchangeable with D_2O). The IR spectrum of compound **4** indicates the presence of α,β-unsaturated ester group (1690 cm^{-1}), and reduction with lithium aluminum hydride of **4** afforded an alcohol (**6**). Furthermore, the presence of two amide

TABLE 1. PHYSICAL CONSTNATS AND SPECTRAL DATA OF MILLIAMINES

	Milliamine A (**1**) $C_{45}H_{49}N_3O_{10}$	Milliamine B (**2**) $C_{43}H_{47}N_3O_9$	Milliamine C (**3**) $C_{43}H_{47}N_3O_9$
Mp	167—170 °C (hydrochloride)	140 °C (dec) (hydrochloride)	amorphous powder
$[\alpha]_D^{25}$	+6 (c 1.4, $CHCl_3$) (hydrochloride)	−14 (c 1.4, $CHCl_3$) (hydrochloride)	+11 (c 1.0, $CHCl_3$)
UV (MeOH)	232 (ε 37300), 260 (21900) 315 (14100), and 342 nm (4800) (hydrochloride)	227 (ε 43800), 260 (18800), 315 (14600), and 342 nm (5000) (hydrochloride)	227 (ε 43500), 262 (18800), 315 (14500), and 342 nm (4900)
IR	2800—3600, 1725, 1690, 1670, 1645, 1610, 1585, 1530, and 1310 cm^{-1} (KBr, hydrochloride)	2800—3600, 1710, 1685, 1670, 1650, 1610, 1580, 1520, and 1300 cm^{-1} (KBr, hydrochloride)	2800—3600, 1715, 1695, 1680, 1630, 1610, 1580, 1520, and 1300 cm^{-1} ($CHCl_3$)
NMR (60 MHz, $CDCl_3$)	δ 0.5—1.4 (11H, complex pattern), 1.83 (3H, d, J=1.0 Hz, H-19), 2.05 (3H, s), 2.83 (6H, s), 3.64 (1H, s, OH), 3.95 (1H, m, H-5), 4.15 (1H, m, H-8), 4.10 (1H, br s, OH), 4.43, 4.80 (2H, AB q, J=13 Hz, H-20), 5.80 (1H, s, H-3), 6.15 (2H, m, H-1 and H-7), 7.1—7.8 (8H, complex pattern), 7.9—8.3 (2H, m), 8.85 (1H, d of d, J=1.0 and 10 Hz), 9.3—9.8, 11.6, and 13.3 (1H each, br s, OH) ppm	δ 0.93 (3H, d, J=6.0 Hz, H-18), 1.05 (3H, s), 1.09 (3H, s), 0.5—1.2 (2H, m), 1.76 (3H, d, J=1.0 Hz, H-19), 2.78 (6H, s), 3.65 (1H, m, H-5), 3.6—3.7 (1H, br s, OH), 4.10 (1H, m, H-8), 4.0—4.2 (2H, br s, OH), 4.35 (1H, s, H-3), 4.34, 4.83 (2H, AB q, J=13 Hz, H-20), 5.85 (1H, q, J=1.0 Hz, H-1), 6.12 (1H, m, H-7), 6.9—7.8 (8H, complex pattern), 7.9—8.2 (2H, m), 8.79 (1H, d, of d, J=1.0 and 10 Hz), 9.50, 11.7, and 13.4 (1H each, br s, OH) ppm	δ 1.02 (3H, d, J=6.0 Hz, H-18), 1.03 (6H, s, H-16 and H-17), 1.80 (3H, d, J=1.0 Hz, H-19), 2.80 (6H, s), 3.65 (1H, s, OH), 3.8—4.5 (6H, m, H-5, H-8, H-20, and 2 OH), 5.75 (1H, s, H-3), 6.0—6.2 (2H, m, H-1 and H-7), 7.0—7.8 (8H, complex pattern), 7.9—8.3 (2H, m), 8.80 (1H, m), 9.5, 11.5, and 13.2 (1H each, br s, OH) ppm

groups was indicated by the IR spectrum (1670, 1630, 1510, and 1300 cm^{-1}). The remaining nitrogen atom was deduced to be present in a dimethylamino group, judging from the signal in the NMR spectrum of compound **4** [δ 2.73 (6H, s)]. Also, the remaining oxygen atom was suggested to be in a hydroxyl group forming strong a hydrogen bond, which was assigned to the signal at δ 12.9 in the NMR spectrum. This data suggests that compound **4** possesses aromatic rings. A high-resolution mass spectrum showed the presence of three fragment ions, $C_9H_{10}NO^{+\cdot}$, $C_7H_5NO_3^{+\cdot}$, and $C_8H_9NO_2^{+\cdot}$. This indicates that these fragments are dimethylanthraniloyl, hydroxyanthraniloyl, and methyl anthranilate groups, respectively. In particular, the dimethylanthraniloyl group was confirmed by the fact that oxidation of **4** with $KMnO_4$ afforded a quinazolone (**7**), which was identified with a naturally-occurring alkaloid (**7**), glycomicine,[3] from spectral data[4] and physical constants. This compound (**7**) was produced by the oxidation of one methyl group in the dimethylanthraniloyl group and the aromatic ring in the hydroxyanthraniloyl group, followed by cyclization. The hydrolysis of **4** with an aqueous NaOH solution afforded a carboxylic acid (**8**), but with 6 M HCl–MeOH gave methyl *N*-(dimethylanthraniloyl)-3-hydroxyanthranilate (**9**) and methyl anthranilate. Compound **9** was deduced to possess a dimethylanthraniloyl group and a hydroxyanthraniloyl from its fragmentation of mass spectrum. The fragment peak resulting from dehydration, in this spectrum, was much stronger than that of the usual phenolic compounds. This observation is explained by the next reaction: **9** was readily dehydrated to a benzoxazole (**10**) in a gas-liquid chromatograph. That the hydroxyanthraniloyl group is 3-hydroxyanthraniloyl, but not 6-hydroxyanthraniloyl (*i.e.* a 3-aminosalicyloyl group), was supported by a comparison of the NMR spectra of compound **9** and a 3-aminosalicyloyl derivative. The structure of compound **9** was confirmed by synthesis. Dimethylanthranilic acid was converted to the imidazolide by the action of *N,N'*-carbonyldiimidazole with no solvent. To a THF solution of this imidazolide was added 3-hydroxyanthranilic acid, and the subsequent addition of CH_2N_2 gave methyl *N*-(dimethylanthraniloyl)-3-hydroxyanthranilate, which exhibits IR, NMR, and mass spectra and a melting point identical with compound **9**.

On the other hand, alcohol **5** was converted to a triacetate (**11**), which was identical with ingenol triacetate. The structure of ingenol triacetate was unambiguously established using X-ray analysis by Hecker *et al.*[5]

Milliamine A is an ingenol derivative esterified by acid **8**, as described above, and by acetic acid, the presence of the latter acid being apparent in the NMR spectrum (see Table 1). Although the esterified position of ingenol remains to be defined, this problem was solved by the following chemical and spectral evidence. Treatment of the hydrochloride of milliamine A with methanol–aqueous $NaHCO_3$ gave ingenol monoacetate (**12**), whose NMR spectrum showed that the signal due to two protons at C-20, which appeared at δ 4.10 in ingenol (**5**), was observed as an AB quartet at δ 4.25 and 4.80 (J=10 Hz), indicating that a primary acetoxyl group is present in milliamine A (**1**). Furthermore, in the 100 MHz NMR spectrum of milliamine A, the singlet observed at δ 5.80 (δ 4.32 in ingenol) was converted into a sharp singlet upon irradiation of the doublet attributed to three protons at C-19 [δ 1.83 (J=1.0 Hz)]. This phenomenon can be understood as long-range coupling through the sp^2 carbon atom. In addition, the fact that this signal, appearing at δ 5.80, can be attributed to the proton at C-3 was clarified by the following chemical evidence. Ingenol (**5**) was converted to a monocarbonate (**13**) by a reaction with *N,N'*-carbonyldiimidazole, which possesses a six-membered carbonate ring (IR 1745 cm^{-1}). The monocarbonate, **13**, gave a dicarbonate (**14**) using the same procedure at elevated temperatures, in which six-membered (1780 cm^{-1}) and five-membered (1830 cm^{-1}) carbonate rings were present. A comparison of the NMR spectra of carbonates **13** and **14** showed that only for the formation of the five-membered carbonate ring can the signal assigned to H-3 (δ 5.3) undergo a downfield shift. Moreover, cleavage of the bond between C-3 and C-4 in the monocarbonate (**13**) by $NaIO_4$ was attempted giving compound **15**: IR ($CHCl_3$) 3400, 1820, and 1725 cm^{-1}; MS *m/e* 372 (M^+); NMR (100 MHz, $CDCl_3$) δ 0.97 (3H, s), 1.08 (3H, s), 1.11 (3H, d, J=6.0 Hz, H-18), 1.90 (3H, br s, H-19), 2.80 (1H, m, H-11), 3.13 (1H, br d, J=10 Hz, H-8), 4.18, 4.50 (2H, AB q, J=13 Hz, H-20), 5.53 (1H, s, H-3), 5.82 (1H, br s, H-1), and 6.40 (1H, d, J=4.5 Hz, H-7). In the NMR spectrum of the urethane (**16**) of this compound **15**, the signal due to the protons at C-20 appears at δ 4.80 as a singlet. It is believed that this compound **15** was formed by aldol condensation of the desired keto-aldehyde intermediate (**17**) and subsequent migration of the carbonate group.

On the basis of these results, it is concluded that the

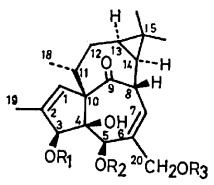

1 R_1=X, R_2=H, R_3=Ac
2 R_1=R_2=H, R_3=X
3 R_1=X, R_2=R_3=H
5 R_1=R_2=R_3=H
11 R_1=R_2=R_3=Ac
12 R_1=R_2=H, R_3=Ac

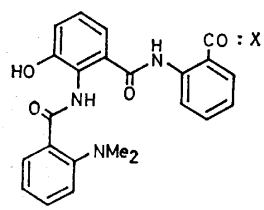

4 X=OCH_3
8 X=OH

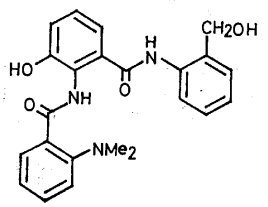

6

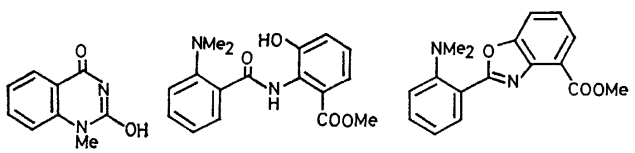

7 9 10

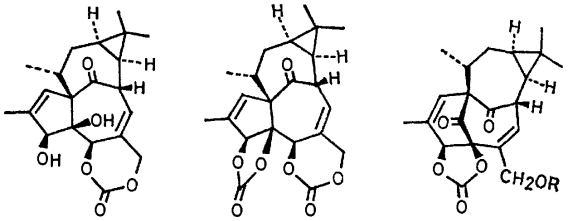

13 14 15 R=H 16 R=CONHPh

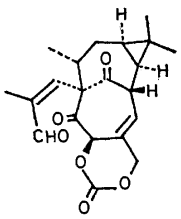

17

structure of milliamine A is **1**.

Examination of the Acute Toxicity of Milliamine A. The acute toxicity of milliamine A was examined using 30 male ICR-SLC strain mice. The mode of administration was intraperitoneal injection. For one week after njection, LD_{50} was determined from the mortality rate of the mice according to Weil's method.[6] The LD_{50} of milliamine A was 0.642 mg/kg. The symptoms observed 2—3 h after the injection were slight ptosis, diarrhea, decreased respiration, decreased body temperature, tremors, *etc.*, and occasionally, dyspnoe and clonic-tonic convulsion. From autopsies of the mice, hemorrhaging and lung and spleen congestion were observed. It is assumed that the cause of death was respiratory arrest derived from injuries to the circulatory system. In a control experiment, 20% ethanol was used as a solvent, but no deaths were observed. These results are summarized in Table 2.

Table 2. Toxicity of milliamine A

Dose injected intraperitoneally (μg/kg)	Mortality	LD_{50} (μg/kg)
270	0/5	
400	1/5	
600	1/5	642
900	5/5	
1350	4/5	
2025	5/5	

The Structure of Milliamine B. In milliamine B (**2**) an acetoxyl group is present. The structure of milliamine B is suggested from the result that methanolysis of milliamine B afforded a compound (**4**) and an ingenol (**5**), which was identified as ingenol triacetate (**7**). The position esterified by the alkaloidal moiety was at C-20, on the basis of the NMR spectrum in which the signals attributed to two protons appeared at δ 4.43 and 4.83 as an AB quartet.

Thus, the structure of milliamine B is represented by **2**.

The Structure of Milliamine C. Milliamine C (**3**) afforded a compound **4** and ingenol (**5**) upon methanolysis with NaOMe in MeOH. The ingenol (**5**) was converted to triacetate **7** for identification with an authentic sample. In the NMR spectrum of **3**, the acetoxyl group observed in the NMR spectrum of milliamine A, was absent and the signal assigned to the proton at C-3 appeared at δ 5.75 as a singlet. Consequently, the structure of milliamine C was determined to be **3**.

Although the relationship between the toxicity and the structure is complex, the following facts are suggested. Ingenol and the triacetate are non-toxic, but ingenol derivative, in which the hydroxyl group at C-3 was esterified with fatty acids[2,7] or an alkaloidal moiety, indicate toxicity. However, according to our results, it appears that at least the acetylation of the hydroxyl group at C-20 has no relation to the toxicity of these derivatives because milliamines A and C are toxic. On the other hand, the presence of a 3-hydroxyanthraniloyl derivative is rare[8] and its carcinogenic properties may influence the cocarcinogenic characteristics of ingenol derivatives reported by Hecker.[7] During this work, experiments concerning the carcinogenic activity of milliamine A were undertaken, but no results were obtained due to interference of the strong toxicity.

Experimental

All melting points are uncorrected. The UV spectra were measured in MeOH on a Perkin-Elmer Model 202 spectrophotometer. The IR spectra were recorded with a Jasco Model IRS spectrometer. The NMR spectra were determined on JNMC-60H, JNM4H-100, and Varian HA-100 spectrometers; Chemical shifts (δ) are given in ppm relative to the internal TMS. The mass spectra were determined on a Hitachi RMU-6C mass spectrometer equipped with a direct inlet system, and the high-resolution mass spectra on a JEOLCO GMS-O1SG mass spectrometer. A Hitachi K-53 gas chromatograph was employed for analytical GLC. A Varian 1820-4 gas chromatograph was used for preparative GLC. For TLC, silica gel GF_{254}, PF_{254} (E. Merck, A. G., Germany) and alumina PF_{254}-Type T (E. Merck, A. G., Germany) were used; the thickness employed were 0.25 mm for analytical purposes, and 1.00 mm for preparative purposes. For column chromatography, silica gel (100 mesh, Mallinckrodt, U.S.A.) was used. The organic solutions were dried over Na_2SO_4 and evaporated in a vacuum evaporator.

Extraction of Milliamines A (1), B (2), and C (3). Roots (7.7 kg) of *Euphorbia Millii* Ch. des Moulins (45 kg) were dried and cut into small pieces. 20 l of methanol was added to the roots. The mixture was left for a few days at room temp and was filtered with suction. This methanol-extraction procedure was repeated twice. The combined methanol extracts were concentrated below 60 °C, to afford a green solution (50 ml) which was diluted with ether (500 ml). The ether layer was separated from a water layer which was extracted with ether three times. The combined ether

solutions were washed with saturated NaCl aq solution, dried, and concentrated, giving an oily mixture (41 g). The resulting material was subjected to chromatography on silicic acid (500 g) with $CHCl_3$. The eluates of $CHCl_3$ afforded some triterpene compounds. After changing the solvent to $CHCl_3$–MeOH (V/V=20/1), the early fraction gave an oily material (7 g) containing milliamine A. To an ethereal solution (100 ml) of this mixture was added 15 ml of ether saturated with HCl gas. Filtration with suction afforded a green powder of hydrochloride (1.2 g), which was dissolved in acetone (5 ml) and the solution was allowed to stand, giving crude crystals (691 mg). Recrystallization from acetone afforded 480 mg of milliamine A hydrochloride. The next eluate gave a mixture of milliamines B and C, which were purified by repeated TLC. Milliamine B (67 mg) was obtained as a hydrochloride following the same procedure as for milliamine A. The unstable properties of milliamine C in acidic conditions did not permit further purification *via* hydrochloride formation. After repeated TLC, 30 mg of milliamine C was obtained. The physical and spectral data are recorded in Table 1. **1**, (Found: C, 64.80; H, 5.99; N, 4.84; Cl, 4.30%. Calcd for $C_{45}H_{50}N_3O_{10}Cl$: C, 64.76; H, 6.10; N, 5.07; Cl, 4.28%). **2**, (Found: C, 64.53; H, 6.04; N, 5.19%. Calcd for $C_{43}H_{48}N_3O_9Cl$: C, 64.50; H, 6.09; N, 5.32%).

*Methanolysis of Milliamine A (**1**).* To a solution of milliamines A hydrochloride (30 mg) in anhydrous MeOH (2 ml) was added a solution (0.5 ml) of NaOMe in MeOH (prepared from 100 mg of Na and 20 ml of anhydrous MeOH) at room temp. The solution was stirred at room temp for 1 h. Neutralization through a column of Amberlite IRC-50 (H-form) (4 ml) was performed. This eluate and a methanol washing solution were combined and concentrated. The resulting yellow oily material was subjected to chromatography on silicic acid. The $CHCl_3$ eluate afforded compound **4** (17 mg), which was recrystallized from MeOH, and the 10% MeOH–$CHCl_3$ eluate gave glassy **5** (15 mg). **4**, Found: *m/e* 433.1638. Calcd for $C_{24}H_{23}N_3O_7$: *m/e* 433.1631. Found: *m/e* 151.0614. Calcd for $C_8H_9NO_2$: *m/e* 151.0633. Found: *m/e* 148.0747. Calcd for $C_9H_{10}NO$: *m/e* 148.0762. Found: *m/e* 135.0304. Calcd for $C_7H_5NO_2$: *m/e* 135.0304. **5**, IR ($CHCl_3$) 3410, 1705, and 1635 cm^{-1}; NMR (60 MHz, $CDCl_3$) 0.6—1.2 (2H, m, H-13 and H-14), 0.94 (3H, d, J=6.0 Hz, H-18), 1.12 (3H, s), 1.52 (3H, s), 1.82 (3H, d, J=1.0 Hz, H-19), 3.77 (1H, br s, H-5), 4.10 (2H, br s, H-20), 4.32 (1H, s, H-3), 4.0—4.4 (1H, m, H-8), 3.0—4.0 (4H, br s, OH), 5.84 (1H, q, J=1.0 Hz, H-1), and 6.02 (1H, br d, J=3.0 Hz, H-7); MS 348 (M^+).

*Alcohol (**6**).* A mixture of **4** (5 mg) and LAH (3 mg) in anhydrous ether (2 ml) was stirred at 0 °C for 1 h, and diluted with 5 ml of water. The mixture was extracted with three 5 ml portions of $CHCl_3$. The combined $CHCl_3$ layers were washed with saturated NaCl aq solution, dried, and concentrated to afford an oily product. The product was purified by preparative TLC. **6**, IR ($CHCl_3$) 3600, 3550, 1655, 1630, 1595, 1515, and 1315 cm^{-1}; NMR (60 MHz, acetone-d_6) 2.72 (6H, s), 4.70 (2H, br s,) 4.70 (1H, s, OH), 7.0—7.5 (10H, m), 8.00 (1H, m), 9.42, 9.80, and 13.2 (1H each, br s, OH); MS 405 (M^+).

*Quinazolone (**7**).* A mixture of **4** (37 mg) and $KMnO_4$ (40 mg) in a 6% aq NaOH solution was stirred at room temp for 15 min. After the addition of water (5 ml), the aq solution was repeatedly extracted with $CHCl_3$. The $CHCl_3$ layer were dried over Na_2SO_4, and concentrated giving an oily material (10 mg). The water layer was neutralized with HCl and extracted with $CHCl_3$ (5 ml). The extracts were dried over Na_2SO_4 and concentrated to give compound **7**. Recrystallization from ether afforded crystalline **7** (3 mg); mp 269—270 °C (lit, 269—270 °C);[3] IR (KBr) 3410, 1708, 1690, 1660, and 1605 cm^{-1}; MS 176 (M^+) (Found: *m/e* 176.0585. Calcd for $C_9H_8N_2O_2$: *m/e* 176.0587).

*Hydrolysis of **4**.* Compound **4** (5 mg) was dissolved in MeOH (2 ml). After the addition of a 5% aq NaOH solution (2 ml) to the solution, the mixture was stirred at room temp for 2 h. After acidification (to *ca.* pH 2) with an aq HCl solution, a cloudy solution was extracted with three 3-ml portions of $CHCl_3$. The $CHCl_3$ layers were combined, dried over Na_2SO_4, and concentrated to give an oily compound **8** (3 mg); IR ($CHCl_3$) 2800—3500, 1690, 1670, 1625, and 1590 cm^{-1}; NMR (60 MHz, $CDCl_3$) 2.90 (6H, s), 7.1—7.6 (8H, m), 8.0—8.3 (3H, m), and 9.5—10.0 (4H, br s, OH) (Found: *m/e* 419.1500. Calcd for $C_{23}H_{21}N_3O_5$: *m/e* 419.1506).

*Methyl N-(Dimethylanthraniloyl)anthranilate (**9**).* A solution of compound **4** in MeOH (2 ml)–6 M HCl (2 ml) was stirred at 60 °C for 18 h. After dilution with 10 ml of water, the mixture was extracted with five 5-ml potions of $CHCl_3$. The extracts were dried over Na_2SO_4 and concentrated to give an oily product (15 mg). Purification by preparative TLC on alumina with benzene yielded **9** (7 mg) and methyl anthranilate (2 mg), **9**, mp 89—90 °C (recrystallized from methanol); IR ($CHCl_3$) 2800—3450, 1705, 1630, 1595, and 1300 cm^{-1}; NMR (60 MHz, acetone-d_6) 2.84 (6H, s), 3.88 (3H, s), 7.0—7.7 (6H, m), 8.10 (1H, m), 9.43, and 13.1 (1H each, br s,); MS 314 (M^+), 296 (Found: *m/e* 314.1266. Calcd for $C_{17}H_{18}N_2O_4$: *m/e* 314.1283).

*Benzoxazole **10**.* Injection of compound **9** (10 mg) into a column (5% SE-30 on chromosorb W, 1′/4×10 ft) for GLC (270 °C, 60 ml/h flow of He carrier gas) afforded **10** after a period of 4.2 min. **10**, IR ($CHCl_3$) 1715, 1600, 1570, 1540, 1490, and 1300 cm^{-1}; NMR (60 MHz, acetone-d_6) 2.76 (6H, s), 3.90 (3H, s), and 6.8—8.0 (7H, m) (Found: *m/e* 296.1199. Calcd for $C_{17}H_{16}H_2O_3$: *m/e* 296.1190).

*The Synthesis of Methyl N-(Dimethylanthraniloyl)anthranilate (**9**).* A mixture of methyl dimethylanthranilate (50 mg) and *N,N′*-carbonyldiimidazole (50 mg) was heated to 90 °C for 2 min and maintained at room temp for 30 min. To the mixture, 50 mg of 3-hydroxyanthranilic acid was added. This oily mixture was maintained at 90 °C for 10 min, and was dissolved in a 30-ml solution of THF and stirred at 90 °C for 2 h. After dilution with water (10 ml), the solution was extracted with five 10-ml portions of $CHCl_3$. The extracts were dried over Na_2SO_4 and concentrated to afforded an oily mixture. The oily product was methylated in ether with CH_2N_2, giving crude **9**. The mixture was separated by preparative TLC on alumina with benzene. The eluate from alumina with $CHCl_3$–AcOEt (1: 1) which was then evaporated afforded **9** (72 mg), which was recrystallized from methanol to give **9** (55 mg); mp 89—90 °C.

*Ingenol Triacetate (**11**).* A solution of ingenol (**5**) (32 mg) in Ac_2O (0.06 ml) and dried pyridine (2 ml) was maintained at room temp overnight, to which 10 ml of water was added. The solution was extracted with five 10-ml portions of $CHCl_3$. The $CHCl_3$ layers were combined, washed with an aq HCl solution, an aq $NaHCO_3$ solution, and saturated NaCl aq solution dried over Na_2SO_4, and concentrated to give an oily compound. This oily product was recrystallized from MeOH to afford crystalline ingenol triacetate (**11**) (25 mg); mp 197—198 °C (lit, 196—197 °C);[5] IR ($CHCl_3$) 3440, 1740, 1710, and 1635 cm^{-1}; NMR (60 MHz, $CDCl_3$) 0.6—1.0 (2H, m), 1.00 (3H, d, J=6.0 Hz), 1.07 (3H, s), 1.11 (3H, s), 1.78 (3H, d, J=1.5 Hz), 2.03 (3H, s), 2.15 (3H, s), 2.23 (3H, s), 3.25 (1H, s, OH), 4.0—4.3 (1H, m), 4.18, 4.62 (2H, AB q, J=12 Hz), 5.00 (1H, s), 5.41 (1H, br s), 6.10 (1H, q, J=1.0 Hz), and 6.25 (1H, br d, J=4.5 Hz) (Found: *m/e*

474.2259. Calcd for $C_{26}H_{34}O_8$: *m/e* 474.2253).

Ingenol Monoacetate (12). Milliamine A hydrochloride (52 mg) was dissolved in an aq solution (10 ml) of $NaHCO_3$ (300 mg) and 20 ml of MeOH. This mixture was stirred for 1 h at room temp. Water was added to this solution, which was extracted with five 10-ml portions of $CHCl_3$. The $CHCl_3$ layers were combined, washed with a saturated NaCl solution, dried over Na_2SO_4, and concentrated to give an oily product (55 mg). This product was purified by preparative TLC to give ingenol monoacetate (**12**) (15 mg); IR ($CHCl_3$) 3480, 1725, and 1645 cm^{-1}; NMR (60 MHz, $CDCl_3$) 0.95 (3H, d, J=6.0 Hz), 1.03 (3H, s), 1.07 (3H, s), 1.80 (3H, d, J=1.0 Hz), 2.01 (3H, s), 3.60 (1H, br s), 3.8—4.2 (1H, m), 4.40 (1H, s), 4.25, 4.80 (2H, AB q, J=10 Hz), 5.90 (1H, q, J=1.0 Hz), and 6.05 (1H, m) (Found: *m/e* 390.2014. Calcd for $C_{22}H_{30}O_6$: *m/e* 390.2041).

Ingenol Monocarbonate (13). A mixture of ingenol (**5**) (20 mg) and *N,N'*-carbonyldiimidazole (15 mg) was dissolved into THF (2 ml), stirred for 2 h at room temp and monitered by TLC on silicic acid. Evaporation of THF at 40 °C afforded an oily product, which was dissolved into a 1% aq HCl solution (5 ml) and $CHCl_3$ (5 ml) by shaking. The $CHCl_3$ was separated and purified by preparative TLC to give monocarbonate **13** (13 mg) and ingenol (5 mg) **13**, IR ($CHCl_3$) 3450, 1745, 1725, and 1665 cm^{-1}; NMR (60 MHz, $CDCl_3$) 0.90 (3H, d, J=6.0 Hz), 1.05 (3H, s), 1.10 (3H, s), 1.83 (3H, d, J=1.0 Hz), 4.0—5.0 (7H, m), 5.80 (1H, q, J=1.0 Hz), and 6.20 (1H, m); MS 374 (M^+).

Ingenol Dicarbonate (14). A THF solution (1 ml) of monocarbonate (**13**) (10 mg) and *N,N'*-carbonyldiimidazole (10 mg) was stirred at 40 °C for 2 h and concentrated to give a mixture. After preparative TLC, an oily product was recrystallized from ether to afford crystalline **14**; mp 204—206 °C; IR ($CHCl_3$) 1830, 1780, 1740, and 1660 cm^{-1}; NMR (60 MHz, $CDCl_3$) 0.9 (3H, d, J=6.0 Hz), 1.1 (3H, s), 1.2 (3H, s), 2.1 (3H, d, J=1.0 Hz), 3.7 (1H, br. d, J=12 Hz), 4.5—4.8 (2H, AB q, J=13.5 Hz), 4.7 (1H, m), 5.3 (1H, s), 5.9 (1H, q, J=1.0 Hz), and 6.2 (1H, m) (Found: *m/e* 400.1510. Calcd for $C_{22}H_{24}O_7$: *m/e* 400.1521).

Compound 15. A mixture of monocarbonate **13** and an aq $NaIO_4$ solution (100 mg/5 ml H_2O) in THF was stirred for 7 h at 40 °C. After the addition of water (5 ml), the mixture was extracted with four 5-ml portions of $CHCl_3$. The extracts were washed with saturated NaCl aq solution, dried, and concentrated to give oily **15** (13 mg) (Found: *m/e* 372.1518. Calcd for $C_{21}H_{24}O_6$: *m/e* 372.1571).

Urethane 16. A mixture of compound 15 (10 mg) and phenyl isocyanate (30 mg) in THF containing a trace of pyridine was stirred at 80 °C for 3 h. After dilution with water, the aq solution was extracted with three 5-ml portions of $CHCl_3$. The extracted layers were combined, dried over Na_2SO_4, and concentrated to yield a product. Separation and purification by preparative TLC on silicic acid afforded glassy **16**; IR ($CHCl_3$) 3430, 1830, 1730, 1605, and 1525 cm^{-1}; NMR (60 MHz, $CDCl_3$) 4.80 (2H, s), 5.50 (1H, q, J=1.0 Hz), 5.95 (1H, m), 6.50 (1H, br d, J=4.5 Hz), 6.90 (1H, s, NH), and 7.00 (5H, m); MS 491 (M^+).

Methanolysis of Milliamine B (2). To a solution of **2** (29 mg) and anhydrous MeOH (2 ml) was added a solution (0.3 ml) of NaOMe in MeOH (prepared from 374 mg of Na and 40 ml of anhydrous MeOH). The solution was maintained at room temp for 1 h and was added the Amberlite IRC-50 (H-form) required for neutralization of the NaOMe. The resin was filtered with suction and the filtrate was concentrated, affording an oily mixture (32 mg), which was separated by preparative TLC on silica gel. Two eluates of AcOEt were concentrated, affording **4** and **5**. Compound **4** was recrystallized from methanol to give crystalline **4** (7 mg); mp 160—162 °C. Ingenol (**5**) was acetylated with Ac_2O and pyridine (2 ml) to give ingenol triacetate (**11**). **11**, mp 196—198 °C (recrystallized from MeOH).

Methanolysis of Milliamine C (3). To a solution of milliamine C (22 mg) in anhydrous MeOH (2 ml) was added a solution (0.1 ml) of NaOMe in MeOH (prepared from 200 mg of Na and 40 ml of anhydrous MeOH). The solution was maintained at room temp for 1 h and the Amberlite IRC-50 (H-form) required for neutralization of the NaOMe. The resin was filtered with suction and the filtrate was concentrated, affording an oily mixture (18 mg). The mixture was separated by preparative TLC on silica gel. Two eluates of AcOEt were concentrated to yield **4** and **5**. Compound **4** was recrystallized from MeOH to afford crystalline **4** (2 mg); mp 159—161 °C. Alcohol **5** was treated with Ac_2O (0.1 ml) and pyridine (2 ml), followed repeated by evaporation of the Ac_2O and pyridine under reduced pressure after addition of benzene. The residue was recrystallized from MeOH to give crystalline **11**, mp 195—198 °C.

References

1) D. Uemura and Y. Hirata, *Tetrahedron Lett.*, **1971**, 3673.
2) D. Uemura and Y. Hirata, *Tetrahedron Lett.*, **1973**, 881.
3) S. C. Pakrashi and H. Budzikiewicz, *Tetrahedron*, **19**, 1011 (1963).
4) H. Budzikiewicz, C. Djerassi, and D. H. Williams, "Structure Elucidation of Natural Products of Mass Spectrometry," Vol. I, Holden-Day, Inc., San Francisco (1964), p. 212.
5) K. Zechmeister, F. Brandl, W. Hoppe, E. Hecker, H. J. Opferkuch, and W. Adolf, *Tetrahedron Lett.*, **1970**, 4075.
6) C. S. Weil, *Biometrics*, **8**, 249 (1952).
7) E. Hecker, *Cancer Res.*, **28**, 2338 (1968).
8) A. J. Evans, *J. Chem. Soc.*, **101**, 544 (1912).

Aromatic Sextets and Aromaticity in Benzenoid Hydrocarbons

Jun-ichi AIHARA

Department of Chemistry, Faculty of Science, Hokkaido University, Sapporo 060

(Received December 27, 1976)

The aromatic sextet theory of Clar was used to estimate the degree of aromaticity in benzenoid hydrocarbons. The resonance energies obtained correlate well with the Dewar-type resonance energies calculated in a previous paper.

An aromatic sextet is defined as a benzene unit (six sp^2 carbon atoms arranged in a hexagon) which can be chosen from a benzenoid hydrocarbon, on condition that when the benzene unit and all the adjacent π bonds are removed from the π system, one or more Kekulé structures can be written for the residual π system.[1] One or more aromatic sextets may further be chosen from the residual π system. Clar long ago stressed the importance of writing the structural formula of a benzenoid hydrocarbon with a maximum number of aromatic sextets.[1] These aromatic sextets, isolated from each other in the same π system, are considered to be the main origin of aromatic stabilization.[1-7] A structural formula thus defined is termed a sextet formula.[4] In this paper, the degree of aromaticity in a benzenoid hydrocarbon is examined on the basis of the Clar aromatic sextet theory.[1]

Theoretical

First, a new polynomial $A(X)$ characterizing the aromaticity of a benzenoid hydrocarbon is proposed in the form

$$A(X) = \sum_{k=0}^{m}(-1)^k r(k) X^{2m-2k}, \tag{1}$$

where $r(k)$ denotes the number of ways in which k disconnected aromatic sextets can be chosen from the π system. Each coefficient of this polynomial has exactly the same meaning as the corresponding coefficient of a sextet polynomial $B(X)$ defined by Hosoya and Yamaguchi.[5] By definition $r(0)$ is equal to unity. Therefore, k is less than, or equal to, the number of aromatic sextets m in the sextet formula. This type of polynomial is termed a resonance polynomial. For example, the resonance polynomial for triphenylene is

$$A(X) = X^6 - 4X^4 + 3X^2 - 1. \tag{2}$$

Furthermore, the sextet polynomial[5] for this compound is

$$B(X) = 1 + 4X + 3X^2 + X^3. \tag{3}$$

Next, the roots of the equation, $A(X)=0$, are arranged in decreasing order,

$$X = X_1, X_2, \cdots, X_m, X_{m+1}, \cdots, X_{2m-1}, X_{2m}. \tag{4}$$

We then define a new quantity, RE^*, as

$$RE^* = K\sum_{k=1}^{m} X_k, \tag{5}$$

where the proportionality constant, K, is equal to the resonance energy of benzene (*i.e.*, of a single aromatic sextet).

Let us consider the physical meaning of this equation. We remember that, for an acyclic polyene, the HMO characteristic polynomial $P(X)$ can be written as[8]

$$P(X) = \sum_{k=0}^{n}(-1)^k p(k) X^{2n-2k}, \tag{6}$$

where $p(k)$ is the number of ways in which k disconnected π bonds are chosen from the π system, and n is the number of formal double bonds in the canonical structure. The roots of the secular equation $P(X)=0$ can be related to the π energy of the formal double bonds plus the additional π energy associated with a migration of this double bond character throughout the π system. By close analogy in form with this secular equation, the roots of the equation $A(X)=0$ can be formally expected to give some energetic quantity related to the aromatic sextets and their migration throughout the π system. To be more concrete, RE^* in Eq. 5 can be interpreted as the resonance energy induced by the aromatic sextets in a benzenoid hydrocarbon. This quantity refers to the resonance energy in Dewar's sense.[9-12]

Discussion

The following considerations help one to interpret RE^* as the resonance energy. The resonance energy for a π system composed of aromatic fragments, connected by essentially single bonds, should be additive. This requirement is fulfilled by the definition of RE^*. For example, a resonance polynomial for a polyphenyl (*p*-polyphenyl) composed of m phenyl groups is written in the form

$$A(X) = \sum_{k=0}^{m}\frac{m!}{k!(m-k)!}X^{2m-2k} = (X^2-1)^m. \tag{7}$$

Therefore, for the polyphenyl,

$$RE^* = mK. \tag{8}$$

This result is consistent with the two resonance theoretical approaches proposed by Herndon and others.[2,3,13,14]

Further support for RE^* is given by the close relationship found between the resonance energy and the Kekulé structure count for benzenoid hydrocarbons. As mentioned in a previous paper,[12] the following approximation holds fairly well for any polynomial $Q(X)$, if all the roots of equation $Q(X)=0$ lie in the interval between -3.0 and 3.0;

$$\sum_{k=1}^{2m}|X_k| \approx 6.0846 \log |Q(i)|, \tag{9}$$

where $2m$ indicates the degree of the equation and $i=\sqrt{-1}$. For most benzenoid hydrocarbons, the resonance polynomial $A(X)$ fulfils the prerequisite for

this approximation. Accordingly,

$$RE^* \approx 3.0423K \log |A(i)|. \quad (10)$$

Here, the fact was used that if X' is a root of the equation $A(X)=0$, $-X'$ is also a root. By comparing $A(X)$ with the corresponding sextet polynomial $B(X)$ defined by Hosoya and Yamaguchi,[5] $|A(i)|$ is evaluated as

$$|A(i)| = B(1) = SC, \quad (11)$$

where SC is the Kekulé structure count. We then arrive at the interesting expression

$$RE^* \approx 3.0423K \log SC. \quad (12)$$

This is none other than one of the expressions previously proposed by Herndon *et al.*[13,14] The confluence of their resonance theory and the present approach obviously provides mutual support for arguing the essential correctness of both approaches.

Extensive numerical analysis gives definite support to the view that RE^* represents the resonance energy of a benzenoid hydrocarbon. For this purpose, the equation $A(X)=0$ were solved for 30 typical benzenoid hydrocarbons. The RE^* values obtained were compared with the Dewar-type resonance energies, RE, analytically obtained by Aihara[11] (see Table 1 and Fig. 1). A refined definition of RE is given in the Appendix. Figure 1 shows fairly good correlation between the values for RE and RE^*/K. As indicated by Eq. 5, RE^*/K signifies the sum of the first m roots of equation $A(X)=0$. On the basis of this figure, the coefficient K actually appears close to the resonance energy of benzene ($0.2726\,\beta$).[11] These facts firmly establish the above view of RE^*, namely,

$$RE \approx RE^*. \quad (13)$$

However, if Fig. 1 is examined in detail, it is found that the benzenoid hydrocarbons investigated must be classified into groups, depending on the number of aromatic sextets, m, in the sextet formula. First, compounds with $m=1$ (polyacenes) form the first group. The resonance polynomial for a polyacene with n hexagons is

$$A(X) = X^2 - n. \quad (14)$$

RE^* can be expressed as

$$RE^* = \sqrt{n}K. \quad (15)$$

The solid line in Fig. 1 indicates that the resonance energies of the polyacenes fit Eq. 15 well if the resonance energy of benzene is assigned to K. This suggests that the aromatic character of benzene is fully retained in the aromatic sextet of all polyacenes.

Moreover, the present interpretation of Clar's aromatic sextets shows that the migration of a single aromatic sextet in a polyacene considerably increases the overall resonance energy. This is in marked contrast to the structure-resonance theory of Herndon,[2,3] which predicts the limiting resonance energy of a polyacene to be 2.8 times the resonance energy of benzene. Equation 15 strongly suggests that such a small value for the resonance energy of an infinitely large polyacene is rather doubtful.

Compounds with $m=2$ form the second group of benzenoid hydrocarbons, in the sense that the RE^* values correlate differently with the RE values. In this case, if the coefficient K in Eq. 5 is slightly decreased, good linear correlation is maintained. As indicated by

Table 1. Resonance energies of benzenoid hydrocarbons

Compound	m	RE^*/K	Resonance energy (β)	
			RE^*	RE
Benzene	1	1.000	0.273[a]	0.273
Naphthalene	1	1.414	0.385[a]	0.389
Anthracene	1	1.732	0.472[a]	0.475
Naphthacene	1	2.000	0.545[a]	0.553
Pentacene	1	2.236	0.610[a]	0.626
Hexacene	1	2.449	0.668[a]	0.706
Phenanthrene	2	2.236	0.560[b]	0.546
Pyrene	2	2.449	0.613[b]	0.598
Benz[*a*]anthracene	2	2.613	0.654[b]	0.643
Benzo[*c*]phenanthrene	2	2.732	0.684[b]	0.687
Chrysene	2	2.732	0.684[b]	0.688
Perylene	2	2.828	0.708[b]	0.740
Benzo[*a*]naphthacene	2	2.909	0.728[b]	0.725
Benzo[*a*]pyrene	2	2.909	0.728[b]	0.725
Pentaphene	2	3.000	0.751[b]	0.746
Dibenzo[*def,mno*]chrysene	2	3.076	0.770[b]	0.766
Benzo[*b*]chrysene	2	3.078	0.770[b]	0.781
Triphenylene	3	3.181	0.745[b]	0.739
Benzo[*e*]pyrene	3	3.402	0.797[c]	0.791
Dibenzo[*a,j*]anthracene	3	3.449	0.808[c]	0.806
Dibenzo[*a,h*]anthracene	3	3.449	0.808[c]	0.807
Dibenzo[*c,g*]-phenanthrene	3	3.494	0.819[c]	0.832
Picene	3	3.494	0.819[c]	0.835
Benzo[*b*]triphenylene	3	3.574	0.837[c]	0.845
Benzo[*ghi*]perylene	3	3.646	0.854[c]	0.853
Dibenzo[*a,c*]naphthacene	3	3.878	0.909[c]	0.929
Benzo[*c*]picene	3	4.078	0.955[c]	0.980
Coronene	3	4.135	0.969[c]	0.947
Dibenzo[*fg,op*]-naphthacene	4	4.351	1.019[c]	0.983
Dibenzo[*g,p*]chrysene	4	4.449	1.042[c]	1.041

a) $K=0.2726\beta$. b) $K=0.2503\beta$. c) $K=0.2343\beta$.

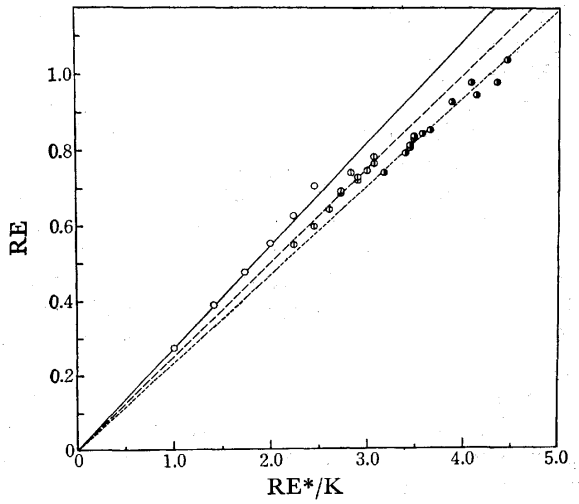

Fig. 1. Plot of *RE versus* RE^*/K for benzenoid hydrocarbons. Compounds with $m=1$ are marked by ○, those with $m=2$ by ①, and those with $m\geq 3$ by ◑.

the slope of long dashes in Fig. 1, the best K value is $0.2503\,\beta$ for compounds with $m=2$.

In this context, there is some evidence showing that each aromatic sextet in a polycyclic π system should rather be considered as a kind of substituted benzene. The resonance energy of any substituted benzene is somewhat smaller than that of benzene itself.[11] This effect can readily be understood by comparing the resonance energies of benzene and biphenyl. The resonance energy of biphenyl ($0.5017\,\beta$) is somewhat smaller than twice the resonance energy of benzene ($0.2726\,\beta$).[11] Accordingly, the effective resonance energy assignable to each aromatic sextet in a polycyclic π system should be somewhat smaller than that of benzene. This may be the reason why the K-value for compounds with $m\geq 2$ becomes somewhat smaller than the resonance energy of benzene.

Compounds with $m\geq 3$ constitute the third group of benzenoid hydrocarbons. For these compounds, the good linear relationship between the values for RE and RE^* is characterized by a K-value of $0.2343\,\beta$. The short-segmented broken line in Fig. 1 represents this situation. Here, it is noteworthy that 86% of the resonance energy of benzene is still retained in the K for such large benzenoid systems.

Concluding Remarks

As seen above, an analysis of Clar's aromatic sextet theory[1] appears to form the important basis for a resonance-theoretical consideration of conjugated hydrocarbons. It is interesting to note that some energetic quantities can be derived from such polynomials as Eqs. 1 and 6. Finally, one minor difficulty must be admitted in the present approach. This is caused by the fact that some roots of the equation $A(X)=0$ for certain compounds have a small imaginary part. Considering that the value of RE^* is always real and is a good approximation to the exact resonance energy RE, this aspect of the approach need not be a cause for concern.

Appendix

The definition of resonance energy previously given by Aihara[11] can be refined within the HMO theory as follows. Let the characteristic polynomial for a conjugated compound $P(X)$ and the corresponding reference polynomial $R(X)$ be written, respectively, as

$$P(X) = X^N + \sum_{k=1}^{N} a_k X^{N-k}, \tag{A1}$$

and

$$R(X) = X^N + \sum_{k=1}^{N} b_k X^{N-k}, \tag{A2}$$

where N is the number of atoms in the π system. The roots of the secular equation $P(X)=0$, arranged in decreasing order, are

$$X = X_1, X_2, \cdots, X_{N-1}, X_N. \tag{A3}$$

Each root, X_t, can be considered to be a function of N coefficients of $P(X)$, *i.e.*,

$$X_t = X_t(a_1, a_2, \cdots, a_{N-1}, a_N). \tag{A4}$$

If each variable a_k in the function X_t takes the value for a corresponding coefficient b_k of $R(X)$, X_t becomes the energy of the reference orbital related to the t-th molecular orbital in an actual π system. The resonance energy of the compound, RE, is then defined as

$$RE = \sum_{t}^{\text{occ}} g_t\{X_t(a_1, a_2, \cdots, a_{N-1}, a_N) - X_t(b_1, b_2, \cdots, b_{N-1}, b_N)\}, \tag{A5}$$

where t extends over all occupied π-molecular orbitals, and g_t is the number of electrons which occupy the t-th orbital. The resonance energies given in Table 1 are, of course, in agreement with this definition.

References

1) E. Clar, "Polycyclic Hydrocarbons," Vol. I, Academic Press, London (1964), Chaps. 5—8; "The Aromatic Sextet," Wiley, London (1972).

2) W. C. Herndon, *J. Am. Chem. Soc.*, **95**, 2404 (1973); W. C. Herndon and M. L. Ellzey, Jr., *ibid.*, **96**, 6631 (1974); W. C. Herndon, *J. Chem. Educ.*, **51**, 10 (1974).

3) Randić, *Tetrahedron*, **31**, 1477 (1975); *Chem. Phys. Lett.*, **38**, 68 (1976).

4) J. Aihara, *Bull. Chem. Coc. Jpn.*, **49**, 1429 (1976).

5) H. Hosoya and T. Yamaguchi, *Tetrahedron Lett.*, **1975**, 4659.

6) O. E. Polansky and G. Derflinger, *Int. J. Quantum Chem.*, **1**, 379 (1967); J. Kruszewski, *Soc. Sci. Lodz., Acta Chim.*, **16**, 77 (1971); M. Randić, *Tetrahedron*, **30**, 2067 (1975).

7) H. Hosoya, K. Hosoi, and I. Gutman, *Theor. Chim. Acta*, **38**, 37 (1975).

8) H. Hosoya, *Theor. Chim. Acta*, **25**, 215 (1972); A. Graovac, I. Gutman, N. Trinajstić, and T. Živković, *ibid.*, **26**, 67 (1972); I. Gutman and N. Trinajatić, *Top. Curr. Chem.*, **42**, 49 (1973).

9) M. J. S. Dewar and G. J. Gleicher, *J. Am. Chem. Soc.*, **87**, 685, 692 (1965); M. J. S. Dewar and C. de Llano, *ibid.*, **91**, 789 (1969); M. J. S. Dewar, "The Molecular Orbital Theory of Organic Chemistry," McGraw-Hill, New York, N. Y. (1969), Chap. 5; J. Aihara, *Kagaku No Ryoiki*, **30**, 269 (1976).

10) N. C. Baird, *Can. J. Chem.*, **47**, 3535 (1969); H. P. Figeys, *Tetrahedron*, **26**, 5225 (1970); B. A. Hess, Jr., and L. J. Schaad, *J. Am. Chem. Soc.*, **93**, 305, 2413 (1971); L. J. Schaad and B. A. Hess, Jr., *ibid.*, **94**, 3068 (1972); *J. Chem. Educ.*, **51**, 640 (1974); J. Aihara, *Bull. Chem. Soc. Jpn.*, **48**, 517, 1501 (1975).

11) Aihara, *J. Am. Chem. Soc.*, **98**, 2750 (1976); *ibid.*, **99**, 2048 (1977); *Kagaku No Ryoiki*, **30**, 379 (1976).

12) J. Aihara, *J. Org, Chem.*, **41**, 2488 (1976); *J. Am. Chem. Soc.*, **98**, 6840 (1976); *Kagaku No Ryoiki*, **30**, 812 (1976).

13) R. Swinborne-Sheldrake, W. C. Herndon, and I. Gutman, *Tetrahedron Lett*,. **1975**, 755; W. C. Herndon, *J. Org. Chem.*, **40**, 3583 (1975); *J. Am. Chem. Soc.*, **98**, 887 (1976).

14) C. F. Wilcox, Jr., I. Gutman, and N. Trinajstić, *Tetrahedron*, **31**, 147 (1975); C. F. Wilcox, Jr., *Croat. Chem. Acta*, **47**, 87 (1975); I. Gutman and N. Trinajstić, *ibid.*, **48**, 297 (1976).

Deoxygenation of Nitrobenzene by Tributylphosphine in the Presence of Alcohols. Synthesis of 2-Alkoxy-3*H*-azepines

Mitsuo MASAKI, Kiyoshi FUKUI, and Junichirō KITA

Polymer Research Laboratory, Ube Industries, Ltd., Minami-kaigan, Goi, Ichihara, Chiba 290

(Received January 5, 1977)

Deoxygenative reduction of nitrobenzene by tributylphosphine in the presence of primary or secondary alcohols gave 2-alkoxy-3*H*-azepines in good yields. The use of acidic hydroxylic compounds, such as phenol or acetylacetone, in place of the alcohols did not lead to ring enlargement. Triphenylphosphine could be used as a reducing agent, but the yields of the azepines were relatively low. 2-Alkoxy-3*H*-azepines were converted into 2-amino-3*H*-azepine in good yields by the reaction with ammonium carbonate. 2,3-Dihydro-1*H*-azepin-2-one was prepared by the hydrolysis of 2-butoxy-3*H*-azepine or 2-amino-3*H*-azepine.

Deoxygenation of nitro- and nitrosobenzene by tervalent phosphorus reagents in the presence of primary or secondary alkylamines results in the ring enlargement giving 2-alkylamino-3*H*-azepines.[1] Phenylnitrene is postulated as an intermediate for this reaction. It is accepted that nucleophilic attack of amines on 7-azabicyclo[4.1.0]heptatriene, assumed to be in equilibrium with phenylnitrene, leads to ring enlargement.[2] Such a ring enlargement is also observed in the thermolysis[3] or photolysis[4] of phenyl azide and in the photolysis of oxaziridines[5] or anthranils.[6] Although the formation of 2-methoxy-3*H*-azepines by photolysis of phenyl azide[7,8] or anthranils[6] in methanol is known, no report has appeared on the ring enlargement of nitro- and nitrosobenzene in the presence of alcohols as the nucleophile. Sundberg and Smith, Jr. observed the formation of alkoxyanilines in the deoxygenation of nitrosobenzene by triethyl phosphite in the presence of alcohols.[7,9]

This paper deals with the deoxygenation of nitrobenzene by tertiary phosphines in the presence of alcohols, providing a convenient method for the preparation of 2-alkoxy-3*H*-azepine, 2,3-dihydro-1*H*-azepin-2-one and several other azepine derivatives in good yields.

Results and Discussion

Tervalent phosphorus reagents for the deoxygenation of nitrobenzene include phosphorus triamide, trialkyl phosphite and phosphonite. Cadogan and Todd studied the order of reactivity of the reagents in the deoxygenation of 2-nitrobiaryl, and observed that tributyl- and triphenylphosphine are not reactive as phosphorus triamide or diethyl methylphosphonite,[1b] while Odum and Brenner reported the deoxygenative ring enlargement of nitrosobenzene by means of triphenylphosphine in the presence of alkylamines.[1a] We have confirmed that tributylphosphine and tripiperidinophosphine are most reactive for the deoxygenation of nitrobenzene in piperidine giving 2-piperidino-3*H*-azepine.

When nitrobenzene was treated with tributylphosphine in refluxing 1-butanol for 1 h, 2-butoxy-3*H*-azepine (**1d**) was formed in 89% yield. The structure of **1d** was determined by IR, NMR, and mass spectra as well as elemental analysis. The IR spectrum exhibited a strong intensity band at 1615 cm^{-1} and a medium band at 1515 cm^{-1}, both of which are due to C=C and C=N stretching vibration. The NMR spectrum shows peaks at τ 7.43 (d, 2H), 4.85 (q, 1H), 4.20 (m, 1H), 3.88 (m, 1H), and 3.21 (d, 1H) other than peaks due to protons of butyl group. The peak pattern indicates 3*H*-azepine skelton since it is very close to that reported for 2-diethylamino-3*H*-azepine.[4a] The mass spectrum of **1d** shows the molecular ion (*m/e* 165) as the highest mass feature, which corresponds to the parent peak of the expected structure.

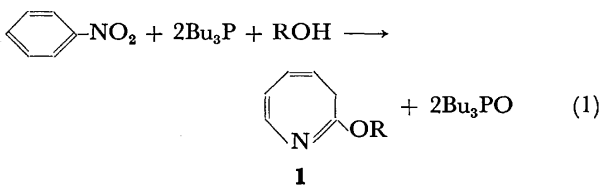

$$\text{ArNO}_2 + 2\text{Bu}_3\text{P} + \text{ROH} \longrightarrow \text{1} + 2\text{Bu}_3\text{PO} \qquad (1)$$

	a	b	c	d	e	f
R:	Me	Et	*i*-Pr	*n*-Bu	*n*-C_6H_{13}	cyclo-C_6H_{11}

	g	h	i
R:	*n*-C_7H_{15}	$PhCH_2$	CF_3CH_2

The deoxygenative ring enlargement of nitrobenzene by tributylphosphine was then studied in the presence of various hydroxylic compounds. The results are summarized in Table 1.

Deoxygenation in the presence of primary or secondary alcohols led to ring enlargement to give the corresponding 2-alkoxy-3*H*-azepines (**1**) in moderate or good yields (Eq. 1). Attempted reactions in the presence of tertiary alcohols (2-methyl-2-propanol and 2-phenyl-2-propanol) failed to give the azepine, probably owing to the bulkiness of the nucleophiles. The use of 2,2,2-trifluoroethanol (pK_a 12.3) results in a formation of 2-(2,2,2-trifluoroethoxy)-3*H*-azepine (**1i**) but only in 19% yield.[9] Phenol (pK_a 9.98) and acetylacetone (pK_a 8.24) were also examined as a nucleophile in the deoxygenation, but no ring enlargement product was obtained.

The results show that hydroxylic compounds whose pK_a value is greater than *ca.* 12 are available as the nucleophiles for the ring enlargement.[10]

Solvent and temperature effects on the ring enlargement reaction were examined by means of deoxygenation in the presence of benzyl alcohol as a nucleophile. The solvent effect was hardly observed, since the reactions in dioxane, pyridine, 4-methyl-2-pentanone and toluene at the same temperature led to the formation of 2-benzyloxy-3*H*-azepine (**1h**) in nearly equal yields. On the other hand, temperature effect was remarkable. The results of the reactions in xylene at various tempera-

Table 1. Deoxygenation of nitrobenzene by tributylphosphine in the presence of hydroxylic compounds (ROH)

	Reactants, mmol			Reaction conditions				3*H*-Azepine (Yield, %)	$PhNO_2$ recovered, %
	ROH	$PhNO_2$	Bu_3P	Solvent (ml)	Temp, °C	Time, h	Method[b]		
MeOH	624	75	172		110	25	A	**1a** (60)	0
EtOH	890	25	55		110	30	A	**1b** (71)	0
i-PrOH	400	50	125		120	25	A	**1c** (62)	0
n-BuOH	720	120	240		127—139	4	B	**1d** (89)	6
	150	25	50[a]		120	6.5	B	**1d** (22)	62
t-BuOH	318	50	125		120	25	A	(0)	0
n-$C_6H_{13}OH$	150	25	55	Pyridine (50)	124	10	C	**1e** (66)	—
cyclo-$C_6H_{11}OH$	950	50	105		165	6	B	**1f** (65)	4
n-$C_7H_{15}OH$	705	50	110		160	2	B	**1g** (69)	0
$PhCH_2OH$	600	100	250	Pyridine (200)	120	6	C	**1h** (84)	0
	485	25	62[a]		160	6	B	**1h** (28)	38
$PhC(Me)_2OH$	150	25	55	Xylene (50)	150	5	C	(0)	0
CF_3CH_2OH	150	25	55	Benzene (50)	110	24	A	**1i** (19)	0
PhOH	150	25	55	Pyridine (50)	125	7	C	(0)	0
Acetylacetone	487	25	63		110	7.5	B	(0)	0

a) Triphenylphosphine was used in place of tributylphosphine. b) See Experimental.

Table 2. Temperature effect on the formation of 2-benzyloxy-3*H*-azepine (**1h**) in xylene

Reaction conditions		Yield of **1h**, %	$PhNO_2$ recovered, %
Temp, °C	Time, h		
80	20	51	33
100	20	70	16
120	7	76	12
150	3	93	4
180	1	94	5

tures are summarized in Table 2. **1h** was obtained in 99% yield based on nitrobenzene consumed at 180 °C, and in 76% yield at 80 °C. Lowering the reaction temperature decreases the yield of **1h** based on nitrobenzene consumed. This might be related to the fact that the deoxygenation of nitrosobenzene in the presence of methanol at 0 °C gives *o*- and *p*-anisidine.[7]

Triphenylphosphine could also be used in place of tributylphosphine for the deoxygenation of nitrobenzene in the presence of 1-butanol or benzyl alcohol, but the

Table 3. Analytical and spectral data of 2-alkoxy-3*H*-azepine (**1**)

	Bp °C/Torr	Found %	Calcd %	IR cm^{-1}	NMR[a] τ	MS *m/e*
a	74—6/32	C, 68.00 H, 7.12 N, 11.40	68.27 7.37 11.37	1620, 1525, 1320, 1250, 1160	7.41(d, 2H), 4.81(q, 1H), 4.14(m, 1H), 3.85(m, 1H), 3.14(d, 1H)	123(M^+), 108(M−Me)
b	105/78	C, 69.98 H, 8.11 N, 10.10	70.04 8.08 10.21	1610, 1525, 1310, 1245, 1205, 1160	7.45(d, 2H), 4.86(q, 1H), 4.20(m, 1H), 3.90(m, 1H), 3.20(d, 1H)	137(M^+), 122(M−Me), 109(M−CH_2=CH_2), 108(M−Et)
c	89/31	C, 71.64 H, 8.65 N, 9.56	71.49 8.67 9.26	1610, 1515, 1310, 1245, 1205, 1160	7.44(d, 2H), 4.81(m, 1H), 4.15(m, 1H), 3.83(m, 1H), 3.15(d, 1H)	151(M^+), 109(M−CH_3CH=CH_2)
d	126/49	C, 72.69 H, 9.16 N, 8.62	72.69 9.15 8.48	1615, 1515, 1325, 1250, 1210, 1165	7.43(d, 2H), 4.85(q, 1H), 4.20(m, 1H), 3.88(m, 1H), 3.21(d, 1H)	165(M^+), 150(M−Me), 136(M−Et), 109(M−CH_2=CHEt)
e	98/3.5	C, 74.56 H, 10.06 N, 7.21	74.57 9.91 7.25	1610, 1525, 1310, 1245, 1205, 1160	7.43(d, 2H), 4.85(m, 1H), 4.19(m, 1H), 3.89(m, 1H), 3.20(d, 1H)	193(M^+), 164(M−Et), 150(M−Pr), 109(M−CH_2=CHBu)
f	104—6/5.5	C, 75.53 H, 10.40 N, 6.70	75.32 10.21 6.76	1610, 1525, 1320, 1245, 1205, 1160	7.42(d, 2H), 4.83(q, 1H), 4.19(m, 1H), 3.88(m, 1H), 3.19(d, 1H)	207(M^+), 109(M−CH_2=CHPe)
g	86/1	C, 75.49 H, 9.18 N, 7.43	75.35 8.96 7.32	1605, 1525, 1325, 1245, 1205, 1160	7.47(d, 2H), 4.90(q, 1H), 4.21(m, 1H), 3.90(m, 1H), 3.21(d, 1H)	
h	173/27	C, 78.10 H, 6.86 N, 7.02	78.36 6.58 7.03	1610, 1525, 1315, 1245, 1205, 1160	7.38(d, 2H), 4.84(q, 1H), 4.16(m, 1H), 3.88(m, 1H), 3.15(d, 1H)	199(M^+), 108(M−$PhCH_2$)
i	69/27	C, 50.57 H, 4.44 N, 7.48	50.27 4.22 7.33	1615, 1415, 1330, 1245, 1205, 1160,	7.34(d, 2H), 4.78(q, 1H), 4.08(m, 1H), 3.85(m, 1H), 3.18(d, 1H),	191(M^+), 172(M−F), 108(M−CF_3CH_2)

a) The peaks due to alkoxy group in 2-position are omitted.

yield of the azepine (**1d** or **1h**) was relatively low.

Deoxygenation of 4- and 2-nitrotoluene was also carried out in the presence of 1-hexanol, 5-methyl- (58%), and 7-methyl-2-hexyloxy-3*H*-azepine (**5**, 30%), respectively, being isolated. The position of the methyl group was determined by NMR spectroscopic examination. Although two isomeric products were possible in the deoxygenation of 2-nitrotoluene, no formation of 2-hexyloxy-3-methyl-3*H*-azepine took place. The deoxygenation of 2-nitrotoluene in the presence of diethylamine has been reported to give 2-diethylamino-3-methyl-3*H*-azepine (**4**, 36%) by de Boer *et al.*,[2] who explained the predominant formation of 3-methyl isomer by an attack of a relatively small nucleophile, diethylamine, on 5-methyl-7-azabicyclo[4.1.0]hepta-2,4,6-triene (**2**) which is expected to predominate in the equilibrium with 1-methyl isomer (**3**) of the azabicycle on steric grounds. The formation of **5** is due to the nucleophilic attack of 1-hexanol on the 1-methyl azabicyclic intermediate **3** (Scheme 1) as in the case where the nucleophile is triethyl phosphite.[11]

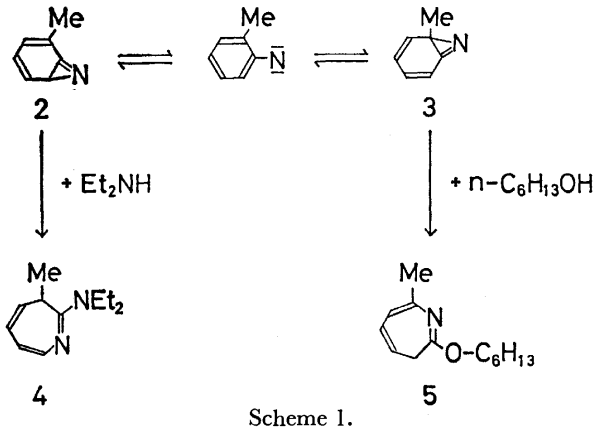

Scheme 1.

Transformation of 2-alkoxy-3*H*-azepines into some azepine derivatives was examined (Scheme 2).

Hydrogenation of 2-butoxy-3*H*-azepine (**1d**) on palladium-carbon gave 7-butoxy-3,4,5,6-tetrahydro-2*H*-azepine in 80% yield, and the hydrogenation of 2-benzyloxy-3*H*-azepine (**1h**) on the same catalyst gave hexahydro-2*H*-azepin-2-one in 77% yield. 2-Amino-3*H*-azepine was obtained in 90 and 75% yields by the reactions of 2-butoxy (**1d**) and 2-cyclohexyloxy-3*H*-azepine (**1f**), respectively, with ammonium carbonate in methanol, while the reactions of 2-cyclohexyloxy-3*H*-azepine (**1f**) with ammonium acetate and ammonium chloride[12] gave 2-amino-3*H*-azepine in 55 and 5% yields, respectively. Hydrolysis of 2-amino-3*H*-azepine afforded 2,3-dihydro-1*H*-azepin-2-one in 97% yield, which was alternatively obtained in 83% yield by the hydrolysis of 2-butoxy-3*H*-azepine (**1d**) under neutral conditions at 150 °C. The hydrolysis of 2-butoxy-3*H*-azepine hardly proceeds below 100 °C under neutral or alkaline conditions. Mineral acids promote the hydrolysis remarkably but subsequent hydrolysis of the product takes place. Paquette observed that 3,7-dimethyl- or 3,5,7-trimethyl-2,3-dihydro-1*H*-azepin-2-one is readily hydrolyzed under acidic conditions to give dihydro-2(3*H*)-furanones.[13]

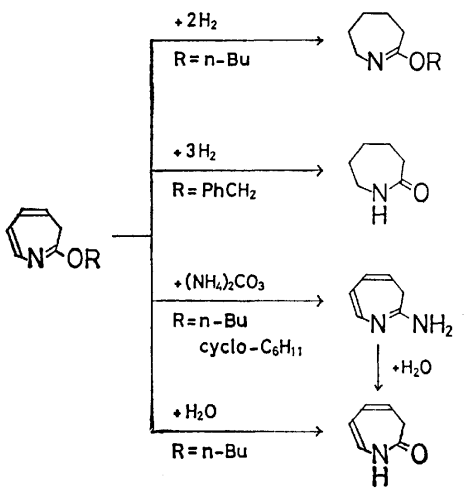

Scheme 2.

Experimental

All the organic reagents and solvents were purified by distillation or recrystallization before use, while commercial inorganic materials were used without further purification. All the melting and boiling points were uncorrected. The GLPC analyses were carried out on a Shimadzu GC-4APT instrument with a thermal conductivity detector, using a 20% PEG 20 M on Celite 545 column (2 m; Temp: 180 °C; Carrier gas: He 30 ml/min; Internal standard: biphenyl). IR spectra were measured on a Hitachi G-2 instrument, NMR spectra on a JEOL C-60HL instrument in CCl_4 solution using TMS as an internal standard, and mass spectra on a Hitachi RMU-6E instrument.

Deoxygenation of Nitrobenzene by Tervalent Phosphorus Reagents in the Presence of Piperidine. A solution of nitrobenzene (3.08 g, 25 mmol) in piperidine (10 ml) was added drop by drop to a solution of tripiperidinophosphine[14] (bp 125 °C/0.5 Torr, 14.17 g, 50 mmol) and biphenyl (3.86 g, 25 mmol) in piperidine (40 ml) under reflux in nitrogen atmosphere. After being refluxed for 30 h, the mixture was analyzed by GLPC. 2-Piperidino-3*H*-azepine[1d] was formed in 88% yield.

When tributylphosphine (10.2 g, 50 mmol), triphenylphosphine (13.2 g, 50 mmol), and triethyl phosphite (8.35 g, 50 mmol) were used in place of tripiperidinophosphine, the yields of 2-piperidino-3*H*-azepine were 94, 16, and 24%, respectively.

Deoxygenation of Nitrobenzene by Tervalent Phosphorus Reagents in the Presence of Hydroxylic Compounds. The following three typical procedures are employed depending on the kind of hydroxylic compound or the reaction temperature. The results are summarized in Table 1, the analytical and spectral data of 2-alkoxy-3*H*-azepines (**1**) being given in Table 3.

Method A. A mixture of nitrobenzene (9.23 g. 75 mmol), tributylphosphine (34.89 g, 172 mmol), and methanol (20 g, 624 mmol) was heated in a sealed tube at 110 °C for 25 h and then evaporated by using a rotary evaporator under reduced pressure. Distillation of the residue afforded 2-methoxy-3*H*-azepine (**1a**, 5.5 g, 60%).

Method B. A mixture of nitrobenzene (14.77 g, 120 mmol), tributylphosphine (48.56 g, 240 mmol), and 1-butanol (57 g, 720 mmol) was heated under reflux (127—139 °C) for 4 h. The resulting mixture was stripped of 1-butanol and the product was distilled under reduced pressure. 2-Butoxy-3*H*-azepine (**1d**) was obtained 17.69 g (89%).

Method C. A solution of nitrobenzene (3.08 g, 25 mmol), tributylphosphine (11.13 g, 55 mmol), and 1-hexanol (15.33 g, 150 mmol) in pyridine (50 ml) was refluxed for 7 h. The

mixture was fractionated under reduced pressure and the fraction (bp 65.5—146 °C/3.5 Torr, 7.32 g) was subjected to redistillation to yield 2-hexyloxy-3*H*-azepine (**1e**, 3.19 g, 66%).

*2-Hexyloxy-7-methyl-3*H*-azepine (**5**).* A mixture of 2-nitrotoluene (6.86 g, 50 mmol), tributylphosphine (22.26 g, 110 mmol) and 1-hexanol (100 ml) was heated under reflux for 3.5 h. The resulting mixture was fractionated under reduced pressure and the fraction (bp 53—141.5 °C/4.5 Torr, 21.4 g) was subjected to redistillation to give **5** (3.13 g, 30%): bp 81.5—82.5 °C/1.5 Torr; IR 1610, 1545, 1310, 1260, 1195, and 1150 cm^{-1}; NMR[16] τ=7.94 (s, 3H), 7.45 (d, 2H), 4.95 (m, 1H), 4.31 (d, 1H), and 3.98 (q, 1H). Found: C, 74.71; H, 10.28; N, 6.97%. Calcd for $C_{13}H_{21}NO$: C, 75.36; H, 10.14; N, 6.76%.

*2-Hexyloxy-5-methyl-3*H*-azepine.* A solution of 4-nitrotoluene (6.86 g, 50 mmol) and tributylphosphine (22.35 g. 60 mmol) in hexanol (100 ml) was heated under reflux for 6.5 h. The resulting mixture was distilled and the fraction (bp 117.5—148.5 °C/4.5 Torr, 7.92 g) was subjected to redistillation to give 2-hexyloxy-5-methyl-3*H*-azepine (6.05 g, 58%): bp 97—100 °C/3 Torr; IR 1610, 1535, 1325, 1250, 1195, and 1160 cm^{-1}; NMR[16] τ=8.13 (s, 3H), 7.51 (d, 2H), 5.05 (q, 1H), 4.29 (d, 1H), and 3.28 (d, 1H). Found: C, 75.62; H, 10.40; N, 6.80%. Calcd for $C_{13}H_{21}NO$: C, 75.32; H, 10.41; N, 6.76%.

*Hydrogenation of 2-Butoxy-3*H*-azepine (**1d**).* 2-Butoxy-3*H*-azepine (**1d**, 6.73 g, 41 mmol) was hydrogenated at room temperature in 1-butanol (40 ml) with palladium catalyst (10% on carbon, 1.6 g) at an initial hydrogen pressure of 65 kg/cm^2. Hydrogenation was completed in 15 min. The catalyst and solvent were removed and the product was distilled to give 7-butoxy-3,4,5,6-tetrahydro-2*H*-azepine (3.8 g, 80%): bp 128—128.5 °C/48 Torr (lit, 214—216 °C;[15a] 80 °C/3.5 Torr,[15b] Found: C, 71.19; H, 11.25; N, 8.31%).

*Hydrogenation of 2-Benzyloxy-3*H*-azepine (**1h**).* Hydrogenation of **1h** (4.96 g, 25 mmol) was performed in toluene (40 ml) with palladium catalyst (10% on carbon, 1.33 g) at 80 °C for 2.5 h, the initial hydrogen pressure being 70 kg/cm^2. Removal of the catalyst and solvent gave crude hexahydro-2*H*-azepin-2-one (2.61 g, 92%). The crude substance was dissolved in diisopropyl ether (60 ml) and extracted with water (50 ml×10). The combined extracts were concentrated to *ca.* 45 ml and extracted with chloroform (40 ml×7). The combined extracts were dried over anhydrous sodium sulfate and evaporated to give hexahydro-2*H*-azepin-2-one (mp 67—69.5 °C, 2.18 g, 77%), which was identified by comparing its retention time in GLPC and its IR spectrum with those of an authentic sample.

*6-Amino-3*H*-azepine.* A solution of 2-butoxy-3*H*-azepine (**1d**, 3.3 g, 20 mmol) and commercial ammonium carbonate (2.3 g) in methanol (50 ml) was kept at 40 °C for 3 days. The mixture was concentrated under reduced pressure and the residue was treated with benzene (100 ml) and the precipitate was removed by filtration. The filtrate was evaporated to give crude 2-amino-3*H*-azepine (1.94 g, 90%). Sublimation at 90 °C and 1 Torr yielded 1.74 g (81%) of 2-amino-3*H*-azepine: mp 90—91 °C (lit,[4a] 90—91 °C, Found: C, 66.40; H, 7.25; N, 25.69%).

2-Amino-3*H*-azepine was isolated by treatment of 2-cyclohexyloxy-3*H*-azepine (**1f**, 3.3 g, 17 mmol) with commercial ammonium carbonate (1.95 g) in methanol (50 ml) at room temperature for 4 days, treatment of **1f** (3.83 g, 20 mmol) with ammonium acetate (3.09 g, 40 mmol) in methanol (50 ml) at room temperature for 6 days, and treatment of **1f** (2.92 g, 15 mmol) with ammonium chloride (1.63 g, 30 mmol) in methanol (50 ml) at room temperature for 9 days in 75, 55, and 5% yields, respectively.

*2,3-Dihydro-1*H*-azepin-2-one. a) Hydrolysis of 2-Amino-3*H*-azepine*: A solution of 2-amino-3*H*-azepine (1.5 g, 14 mmol) in water (40 ml) was refluxed for 5 h, treated with aqueous hydrochloric acid (3 drops of a 3M solution), and extracted with chloroform (30 ml×10). The combined extracts were concentrated to give 2,3-dihydro-1*H*-azepin-2-one (1.47 g, 97%): mp 48—49 °C. Recrystallization from hexane afforded colorless crystals: mp 49—50 °C (lit, 48—50 °C;[17] 47.5—48.5 °C,[4a] Found: C, 66.06; H, 6.38; N, 12.91%).

*b) Hydrolysis of 2-Butoxy-3*H*-azepine (**1d**)*: A mixture of **1d** (4.6 g, 28 mmol), ethanol (36 ml), and water (10 ml) was heated at 150 °C in a stainless steel autoclave for 3.5 h. The mixture was stripped of ethanol, water, and 1-butanol and the oily residue was dissolved in diethyl ether (50 ml). The solution was extracted with water (40 ml×7) and the combined extracts were concentrated to give crude 2,3-dihydro-1*H*-azepin-2-one (2.52 g, 83%). Recrystallization from cyclohexane afforded colorless crystals of mp 48—50 °C, which showed no depression on admixture with the sample obtained above.

References

1) a) R. A. Odum and M. Brenner, *J. Am. Chem. Soc.*, **88**, 2074 (1966); b) J. I. G. Cadogan and M. J. Todd, *J. Chem. Soc., C*, **1969**, 2808; c) R. J. Sundberg, B. P. Das, and R. H. Smith, Jr., *J. Am. Chem. Soc.*, **91**, 658 (1969); d) F. R. Atherton and R. W. Lambert, *J. Chem. Soc., Perkin Trans. 1*, **1973**, 1079.

2) T. de Boer, J. I. G. Cadogan, H. M. McWilliam, and A. G. Rowley, *J. Chem. Soc., Perkin Trans. 2*, **1975**, 554.

3) a) R. Huisgen, D. Vossius, and M. Appl, *Chem. Ber.*, **91**, 1 (1958); b) M. Appl and R. Huisgen, *ibid.*, **92**, 2961 (1959).

4) a) W. von E. Doering and R. A. Odum, *Tetrahedron*, **22**, 81 (1966); b) R. K. Smalley and H. Suschitzky, *J. Chem. Soc., Suppl.*, **1964**, 5922.

5) a) E. Mayer and G. W. Griffin, *Angew. Chem.*, **79**, 648 (1967); b) H. Shindo and B. Umezawa, *J. Pharm. Soc. Jpn.*, **1**, 492 (1962).

6) M. Ogata, H. Kano, and H. Matsumoto, *J. Chem. Soc., Chem. Commun.*, **1968**, 397; M. Ogata and H. Matsumoto, *Tetrahedron*, **25**, 5205 (1969).

7) R. J. Sundberg and R. H. Smith, Jr., *J. Org. Chem.*, **36**, 295 (1971).

8) A. C. Mair and M. F. G. Stevens, *J. Chem. Soc., C*, **1971**, 2317.

9) Deoxygenation of nitrosobenzene with triethylphosphite in the presence of trifluoroethanol gives 2′,2′,2′-trifluoro-*p*-phenethidine (21%) and 1-phenyl-1*H*-azepine (34%); R. J. Sundberg and R. H. Smith, Jr., *Tetrahedron Lett.*, **1971**, 267.

10) Deoxygenation of nitrobenzene with triphenylphosphine in hydrogen fluoride gives *p*-fluoroaniline; P. H. Scott, C. P. Smith, E. Kober, and J. W. Churchill, *Tetrahedron Lett.*, **1970**, 1153.

11) a) J. I. G. Cadogan, R. K. Mackie and M. J. Todd, *Chem. Commun.*, **1968**, 736; b) J. I. G. Cadogan, D. J. Sears, D. M. Smith, and M. J. Todd, *J. Chem. Soc., C*, **1969**, 2813.

12) Ammonium chloride is an effective reagent for the amination of 7-methoxy-3,4,5,6-tetrahydro-2*H*-azepine; R. E. Benson and T. L. Cairns, *J. Am. Chem. Soc.*, **70**, 2115 (1948).

13) L. A. Paquette, *J. Am. Chem. Soc.*, **85**, 3288 (1963).

14) M. Luyembourg, *Ber.*, **28**, 2207 (1895).

15) a) Ger. Patent 488447 (1926); *Chem. Abstr.*, **27**, 994[1] (1933); b) U. S. Patent 2516293 (1950); *Chem. Abstr.*, **45**, 640 g, (1951).

16) The peaks due to alkoxy group in 2-position are omitted.

17) E. Vogel and R. Erb, *Angew. Chem. Int. Ed. Engl.*, **1**, 53 (1962).

Photochemical Reaction of Diphenylcyclobutenedione Derivatives. Formation and Reaction of Conjugated Bisketene and Its *N*-Analog*

Naruyoshi OBATA and Takeo TAKIZAWA

Faculty of Pharmaceutical Sciences, The University of Tokyo, Hongo, Bunkyo-ku, Tokyo 113

(Received January 12, 1977)

The photolysis of diphenylcyclobutenedione derivatives (Va, b) under N_2 and that in the presence of substrate, O_2 or isocyanide, have been studied. The former resulted in the recovery of a large amount of V and the fragmentation; the latter gave the insertion products into V, diphenylmaleic anhydrides and iminocyclopentenones in good yield. The intermediates, bisketene and ketene-ketenimine as primary photo products were confirmed by the photolysis of Va in methanol to give succinates and by low-temperature IR-technique. Structural aspects of bisketene intermediate were discussed.

In a previous paper,[1] we reported facile ring-enlargement reactions of diphenylcyclopentenone (I) with 2,6-xylyl isocyanide to give cyclopentenetrione (III) together with a small amount of isomaleimide (IV), and cyclobutenedione (Va) in the presence of catalytic amount of triphenylphosphine. Since Va did not react further with the isocyanide in the dark, we proposed a tentative mechanism *via* ketene-ketenimine intermediate (II) rather than that of stepwise insertion of isocyanide into carbon-carbon bond of I *via* Va.

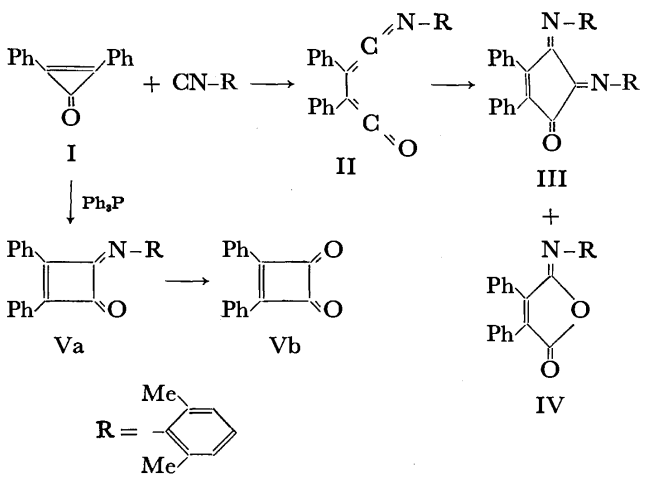

Scheme 1.

We found that diphenylcyclobutenedione (Vb) obtained from the hydrolysis of Va readily undergoes photochemical reaction to give a yellow solid on exposure to direct sunlight in the air. The same phenomenon to give a tan solid was observed by Blomquist and LaLancette[2b] who assumed it was a dimer of Vb. However, details of the photochemical reaction and the structure of the products have remained unsolved. A few photochemical reactions of cyclobutenedione derivatives were reported,[2,3] in which bisketene derivatives were only postulated as an intermediate. In view of the possible isolation of bisketenes under certain photochemical reactions, the photolysis of cyclobutenediones Va and Vb with and without O_2 or isocyanide were investigated.

Result and Discussion

Vb in benzene was irradiated with a high-pressure mercury lamp for 6 h under a slow stream of O_2 at room temperature. The reaction products were chromatographed on silica gel. 9,10-Phenanthrenedicarboxylic anhydride (VI, in 52% yield), diphenylmaleic anhydride (VII, in 4% yield), and diphenylacetylene (VIII, in 4% yield), were obtained together with the recovery of Vb in 30% yield. These compounds could not be obtained without light under O_2. Photolysis of VII under the same conditions as above gave VI in good yield *via* oxidative cyclization.[4]

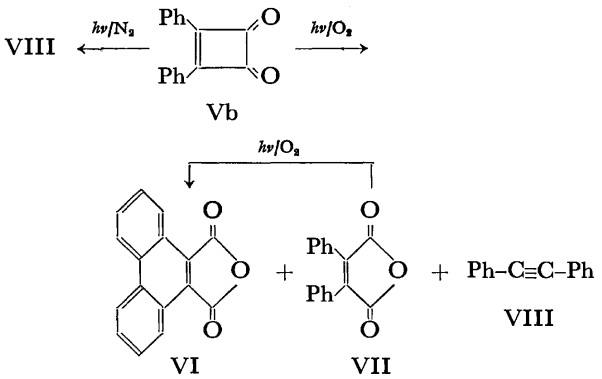

Scheme 2.

The structures of VI, VII, and VIII were confirmed by elemental analysis, molecular weight determination, spectroscopic data, and direct comparison with the samples prepared by the authentic route.[5,6] The mp and IR spectrum of VI agreed with those of the compound assumed to be a dimer of Vb.[2b]

Irradiation of Vb in benzene under N_2 stream for 6 h at room temperature gave VIII in 28% yield as the sole product accompanied by the recovery of Vb in 69% yield.

Photolysis of Va under O_2 stream gave *N*-(2,6-dimethylphenyl)diphenylisomaleimide (IV, in 25% yield), 4,5-bis(2,6-dimethylphenylimino)-2,3-diphenylcyclopenten-1-one (III, in 5% yield), and VIII in 8% yield.

* A part of this work has been published: N. Obata and T. Takizawa, *Chem. Commun.*, **1971**, 587. It was also presented at the 23rd National Meeting of the Chemical Society of Japan, Tokyo, April 1970.

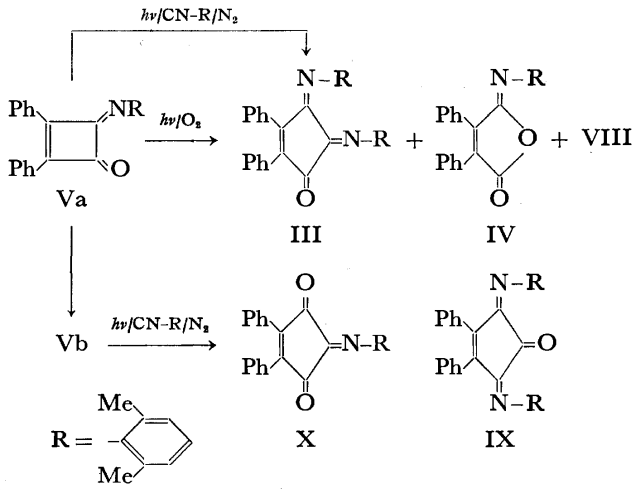

Scheme 3.

The molecular formula for III was found to be $C_{33}H_{28}ON_2$ on the basis of elemental analysis and molecular weight. In the IR spectrum, III showed characteristic two peaks at 1640 and 1710 cm^{-1} due to νC=N and νC=O on cyclopentene skeleton. In the NMR spectrum, III showed multiplets at 2.40—2.90 τ(10H) and 3.10—3.40 τ(6H), and two singlets at 7.95 τ(6H) and 8.25 τ(6H) due to 2,6-disubstituted methyl group on phenyl ring, suggesting that III is not symmetrical 2,5-bis(2,6-dimethylphenylimino)-3,4-diphenylcyclopenten-1-one (IX).

IV, the molecular formula $C_{24}H_{19}O_2N$, showed characteristic IR bands at 1710 and 1800 cm^{-1} due to νC=N and νC=O on cyclopentene ring, and UV spectrum in ethanol at 230 nm (log ε 4.26), 253 nm (4.12) and 330 nm (3.98). All these data were similar to those of *N*-substituted isomaleimide reported.[7] Treatment of IV with dil. HCl in methanol gave *N*-substituted diphenylmaleimide, which was prepared by a modification of the reaction by Reimer[6] and characterized.

The structures of III and IV were further confirmed by comparison with those obtained from the reaction of I with 2,6-xylyl isocyanide.[8] In contrast to the photolysis of VII in O_2, IV was not further photooxidized to phenanthrene derivatives upon prolonged irradiation.

III might be produced by the insertion of 2,6-xylyl isocyanide eliminated from Va with concomitant formation of VIII and CO during the course of photolysis. The isocyanide eliminated so far was also detected by thin-layer chromatography on silica gel and UV spectrum. Photolysis of Va in the presence of the isocyanide under N_2 gave III in 80% yield. However, no reaction of Va with the isocyanide in benzene at 80 °C was observed in the dark.

The photolysis of Vb in the presence of the isocyanide gave 5-(2,6-dimethylphenylimino)-2,3-diphenylcyclopenten-1,4-dione (X, in 86% yield). The structure of X was established by elemental analysis, molecular weight determination and spectral data. IV as well as VI and VII could be formed as a result of the insertion of O_2[9] into Va and Vb in a similar way to that for III.

In order to trap the intermediate in the photochemical reactions of Va, Vb with O_2 and isocyanide to give their insertion products, photolysis of Va and Vb in methanol at room temperature was carried out.[10] When Vb in methanol was irradiated at room temperature, dimethyl *meso*-diphenylsuccinate (XIa, in 67% yield) and dimethyl *dl*-isomer (XIb, in 17% yield) were obtained.

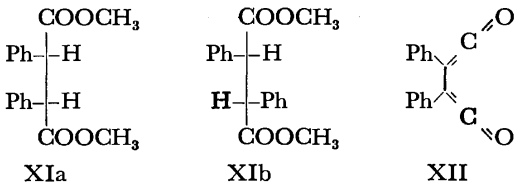

Scheme 4.

The photolysis of Vb in THF–methanol at −78 °C gave the same products in about the same ratio. The structures of XIa and XIb were confirmed by direct comparison with samples prepared by an authentic route.[11]

A solution of Va or Vb in THF was irradiated under N_2 at −78 °C (10 h for Va: 2 h for Vb). Addition of 2,6-xylyl isocyanide to both solution at −78 °C in the dark gave III and X in 78 and 82% yield, respectively. When O_2 was bubbled into the solution obtained from the photolysis of Vb at −78 °C in the dark, VII was obtained in 42% yield. Addition of cold methanol to the solution gave succinate XIa (39%) and XIb (14%) along with a trace amount of VIII. All these results indicate that the primary intermediacy of the photolysis of Va and Vb would be bisketene (XII) and keteneketenimine (II) which are stable at −78 °C.

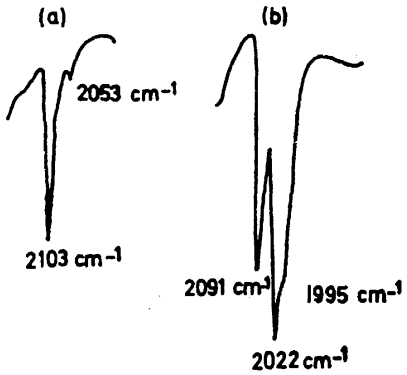

Fig. 1. IR spectra (tetrahydrofuran solution) of (a) XII at −50°C and (b) II at −46°C.

For direct observation of the intermediates II and XII, IR spectra of the solution irradiated at low temperature (−46 °C for II: −50 °C for XII) were determined using a Nihon-Bunko DS-403G IR spectrophotometer equipped with a low-temperature solution cell.[12] The results are shown in Fig. 1. The band at 2103 cm^{-1} for XII is readily assigned to the νC=O of the ketene. It follows that the 2091 and 2022 cm^{-1} bands of II are attributable to ketene νC=O and ketenimine νC=N, respectively.

II and XII in THF are stable in the dark for several days at −78 °C, but on warming slowly the THF solution of XII to above 0 °C, the characteristic peak at

2103 cm^{-1} disappears completely. When methanol was added to the THF solution of XII after the solution had been warmed to room temperature, no more succinate was obtained. However, Vb was recovered in 15% yield together with a small amount of VIII and a large amount of glassy material, while no Vb was recovered on addition of methanol to the solution at −78 °C following the work-up at room temperature.

These results seems to indicate that by photolysis at room temperature under N_2, primary photo products II and XII come to equilibrium with Va and Vb, which is responsible for the retardation of the photochemical fragmentation *via* II and XII to give VIII, CO and/or isocyanide. This is in marked contrast to the photolysis at low temperature which is very effective in the transformation of Va and Vb into II and XII.

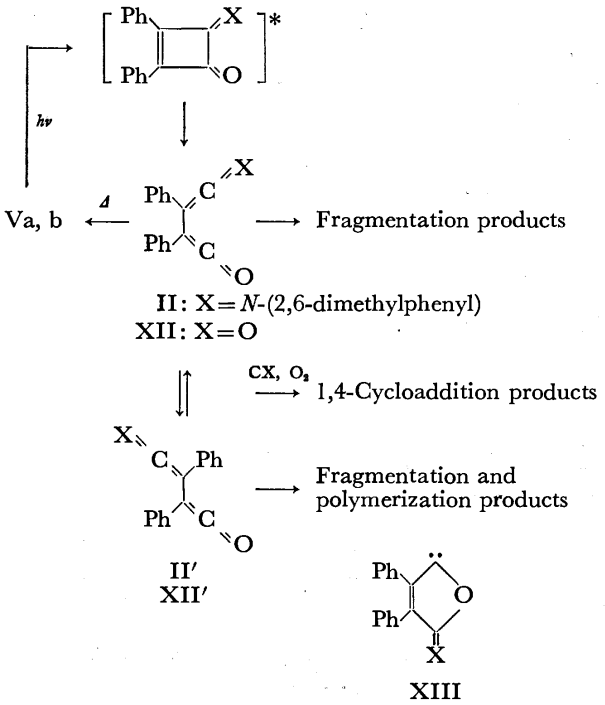

Scheme 5.

On the other hand, the ratio (4: 1) of XIa and XIb isolated on the direct photolysis of Vb in methanol at room temperature and in THF–methanol at −78 °C differs a great deal from that (3: 2) on addition of cold methanol to a THF solution at −78 °C after photolysis. This indicates that II and XII in high concentration at low temperature might be equilibrated with geometrical isomers II′ and XII′, warming of which to room temperature might favor the formation of polymeric glassy materials for reverting to the starting ketones.

In conclusion, the superficial insertion of the substrate CX (*e.g.*, isocyanide) or O_2 into V in the present photolysis might take a route of 1,4-cycloaddition reaction of the substrate with primary photo products II and XII which might be equilibrated with starting ketones Va, Vb and their geometrical isomers II′, XII′, although some other mechanism, *e.g.*, *via* carbene (XIII)[2b,13] cannot be excluded completely.

Experimental

All the melting points were uncorrected. IR spectra were determined using a Nihon-Bunko DS-402G infrared spectrophotometer. UV spectra were obtained with a Carry 11 recording spectrophotometer. NMR spectra were obtained with a Varian A-60 spectrometer, using tetramethylsilane as an internal standard. The molecular weight was determined by use of a Hitachi 105 vapor pressure osmometer.

Photolysis of Diphenylcyclobutenedione (Vb) under O_2 Stream. A solution of Vb (0.4 g, 1.7 mmol) in dry benzene (40 ml) was irradiated with a high-pressure mercury lamp for 6 h under O_2 stream at 15 °C. Yellow crystals precipitated gradually. Recrystallization from THF gave 9,10-phenanthrenedicarboxylic anhydride (VI, 0.16 g, 52%), mp 320—322 °C (lit,[5] 321—322 °C). The mother liquor was concentrated and the residue was chromatographed on silica gel. Diphenylacetylene (VII, 0.03 g, 14%) was obtained from the eluent with hexane. Elution with hexane–benzene (1: 1) gave diphenylmaleic anhydride (VII, 0.01 g, 4%), mp 156—158 °C (lit,[6] 155—156 °C). The structures of VI and VII were established by direct comparison of the melting point and spectral data with those of the authentic samples.[5,6] The starting ketone Vb (0.21 g, 30%) was recovered from the eluent with benzene.

Photolysis of VII under O_2 Stream. A solution of VI (0.1 g, 0.4 mmol) in dry benzene (10 ml) was irradiated under similar conditions to those given above. Chromatography on silica gel gave VI (0.08 g, 78%).

Photolysis of Vb under N_2 Stream. Vb (0.3 g, 1.3 mmol) was dissolved in dry benzene (30 ml) and irradiated with a 500 W high-pressure mercury lamp for 6 h under N_2 stream at 15 °C. After removal of the solvent, the residue was subjected to silica gel chromatography. Elution with hexane gave VIII (0.066 g, 28%) and elution with benzene resulted in the recovery of Vb (0.21 g, 69%).

Photolysis of Iminocyclobutenone (Va) under O_2 Stream. A solution of Va (0.5 g, 1.5 mmol) in dry benzene (40 ml) was irradiated with a high-pressure mercury lamp for 15 h under O_2 stream at 15 °C. After removal of the solvent under reduced pressure, the residue was subjected to silica gel chromatography. Elution with hexane gave VIII (0.022 g, 8%) and from the eluent with hexane–benzene (7: 3), *N*-(2,6-dimethylphenyl)diphenylisomaleimide (IV, 0.13 g, 25%), mp 172—173 °C was obtained.

Found: C, 81.57; H, 5.42; N, 4.31%; mol wt: 353 (by MS). Calcd for $C_{24}H_{19}O_2N$: C, 81.56; H, 5.42; N, 3.96%; mol wt: 353.4. IR (KBr): 1710 (νC=N) and 1800 cm^{-1} (νC=O). NMR (CCl_4): 2.65 (m, 10H), 3.10 (m, 3H), and 7.85τ (s, 6H). UV (Ethanol) max: 230^{sh} (log ε 4.26), 253 (4.12), and 330 nm (3.98).

Further elution with benzene gave a small amount of 4,5-bis(2,6-dimethylphenylimino)-2,3-diphenylcyclopenten-1-one (III, 0.005 g, 5%), mp 184 °C and unidentified substances.

Found: C, 84.62; H, 5.98; N, 6.06%; mol wt: 468 (by MS). Calcd for $C_{33}H_{26}ON_2$: C, 84.58; H, 6.02; N, 5.98%; mol wt: 468.7. IR (KBr): 1640 (νC=N) and 1710 cm^{-1} (νC=O). NMR (CCl_4): 2.4—2.9 (m, 10H), 3.1—3.4 (m, 6H), 7.95 (s, 6H), and 8.25 τ (s, 6H), UV (Ethanol) max: 240 (log ε 4.4) and 330 nm (4.18).

Hydrolysis of IV. IV (0.05 g, 0.14 mmol) in methanol containing a catalytic amount of HCl was refluxed for 2 h. Recrystallization from methanol gave *N*-(2,6-dimethylphenyl)-diphenylmaleimide (0.035 g, 72%), mp 191—192 °C. The compound was rigorously characterized by comparison with

a sample prepared by the reaction of diphenylmaleic anhydride with 2,6-dimethylaniline, a modification of reported reaction.[6]

Found: C, 81.66; H, 5.55; N, 4.24%; mol wt: 340 (by osmometer). Calcd for $C_{24}H_{19}O_2N$: C, 81.56; H, 5.42; N, 3.96%; mol wt: 353.4. IR (KBr): 1770 and 1710 cm^{-1} (νC=O). NMR ($CDCl_3$): 2.60 (m, 10H), 2.8 (m, 3H), and 7.75 τ (s, 6H).

Photolysis of Va in the Presence of 2,6-Xylyl Isocyanide. A solution of Va (0.3 g, 0.9 mmol) and 2,6-xylyl isocyanide (0.13 g, 1 mmol) in dry benzene (30 ml) was irradiated with a high-pressure mercury lamp under N_2 at 15 °C. After removal of the solvent, recrystallization of the residue from hexane–benzene gave III (0.34 g, 80%).

Photolysis of Vb in Methanol. A solution of Vb (0.3 g, 1.3 mmol) in dry methanol (30 ml) was irradiated with a high-pressure mercury lamp at 15 °C. While crystals precipitated within 10 min and yellow solution was completely decolorized in 40 min. Filtration and repeated recrystallization from hexane–CH_2Cl_2 gave dimethyl *meso*-diphenylsuccinate (XIa, 0.26 g, 67%), mp 220—221 °C (lit,[11] 219—220 °C). The mother liquor was concentrated. Repeated recrystallization from hexane gave dimethyl *dl*-diphenylsuccinate (XIb, 0.065 g, 17%), mp 171—172 °C (lit,[11] 173.5—174 °C). NMR ($CDCl_3$) for XIa: 2.70 (m, 10H) and 6.6 (s, 6H); for XIb: 3.0 (m, 10H) and 6.35 τ (s, 6H).

Photolysis of Va at Low Temperature (−78 °C) Followed by Addition of Methanol. A solution of Vb (0.30 g, 1.3 mmol) in dry THF (30 ml) was irradiated with a high-pressure mercury lamp at −78 °C under N_2 stream. After irradiation for 1.5 h, the lamp was turned off and cold methanol was added to the solution at −78 °C in the dark. The solution was then warmed slowly to room temperature. After removal of the solvent, recrystallization of the residue from hexane–CH_2Cl_2 gave XIa (0.11 g, 29%). The mother liquor was concentrated and the residue was subjected to silica gel chromatography. Elution with hexane gave a trace amount of VIII. Elution with benzene gave additional XIa (0.03 g, 8%). XIb (0.05 g, 13%) and a small amount of unidentified high-melting compound were obtained from the eluent with benzene–CH_2Cl_2 (1: 1). When the irradiated solution was allowed to warm slowly to room temperature, starting Vb was recovered in 15% yield and a large amount of glassy material was obtained by chromatography on silica gel.

Photolysis of Vb at Low Temperature (−78 °C) Followed by the Reaction with O_2. A solution of Vb (0.2 g, 0.86 mmol) in dry THF (20 ml) was irradiated for 1.5 h under N_2 stream at −78 °C. The lamp was turned off and O_2 gas was bubbled into the solution in the dark to warm it to room temperature. After removal of the solvent under reduced pressure, the residue was chromatographed on silica gel. Elution with hexane gave VIII (0.01 g, 7%) and elution with hexane–benzene gave VII (0.09 g, 42%). Elution with benzene–CH_2Cl_2 gave unidentified glassy materials.

Photolysis of Vb in the Presence of 2,6-Xylyl Isocyanide. A solution of Vb (0.3 g, 1.3 mmol) and 2,6-xylyl isocyanide (0.17 g, 1.3 mmol) in dry benzene (10 ml) was irradiated with a high-pressure mercury lamp under N_2 at room temperature for 1.5 h. After removal of the solvent, the residue was recrystallized from hexane–benzene to give 5-(2,6-dimethylphenylimino)-2,3-diphenylcyclopenten-1,4-dione (X, 0.41 g, 86%), mp 142—143 °C.

Found: C, 81.88; H, 5.35; N, 3.94%; mol wt: 362 (by osmometer). Calcd for $C_{25}H_{19}O_2N$: C, 82.17; H, 5.24; N, 3.83%; mol wt: 365.4. IR (KBr): 1780, 1770, 1745, and 1700 cm^{-1} (νC=O and νC=N). UV (Ethanol) max: 230^{sh} (log ε 4.39), 280^{sh} (4.00), 332 (4.23), and 535 nm (2.84). NMR (CCl_4): 2.70 (broad s, 10H), 3.20 (broad s, 3H), and 8.00 τ (s, 6H).

References

1) N. Obata and T. Takizawa, *Tetrahedron Lett.*, **1970**, 2231.

2) a) A. T. Blomquist and R. A. Vierling *Tetrahedron Lett.*, **1961**, 655; b) A. T. Blomquist and E. A. LaLancette, *J. Am. Chem. Soc.*, **84**, 220 (1962).

3) a) F. B. Mallory and J. D. Roberts, *J. Am. Chem. Soc.*, **83**, 393 (1961). b) H. A. Staab and J. Ipaktschi, *Tetrahedron Lett.*, **1966**, 583. c) F. A. Beringer, R. E. K. Winter, and J. A. Castellano, *Tetrahedron Lett.*, **1968**, 6183.

4) W. M. Moore, D. D. Morgen, and F. R. Stermitz, *J. Am. Chem. Soc.*, **85**, 829 (1963); A. Padwa and R. Hartman, *ibid.*, **88**, 3759 (1966).

5) A. Jeanes and R. Adams, *J. Am. Chem. Soc.*, **59**, 2608 (1937).

6) C. L. Reimer, *Ber.*, **13**, 741 (1880).

7) R. J. Cotler, C. K. Snares, and J. M. Whelan, *J. Org. Chem.*, **26**, 10 (1961).

8) N. Obata and T. Takizawa, *Tetrahedron Lett.*, **1969**, 3403.

9) The incorporation of atomic oxygen from O_2 into substrate is interesting but the mechanism is not clear.

10) An ethanol solution of Vb allowed to stand for two weeks at room temperature was reported to give a mixture of the *meso* and *dl*-diethyldiphenylsuccinate. A. T. Blomquist and E. A. LaLancette, *J. Am. Chem. Soc.*, **83**, 1387 (1961). When a solution of Vb in methanol was refluxed for 16 h under N_2 in the dark, however, no succinate was obtained and Vb was recorvered completely.

11) C. Wren and C. J. Still, *J. Chem. Soc.*, **107**, 444, 1453 (1915).

12) N. Obata and T. Takizawa, *Chem. Commun.*, **1971**, 587.

13) N. Obata, H. Mizuno, T. Koitabashi, and T. Takizawa, *Bull. Chem. Soc. Jpn.*, **48**, 2287 (1975).

Reaction of Coordinated Phosphines. III. Reaction of Phenyl Compounds of Typical Groups V and VI Elements with Palladium(II) Salts in the Presence of Olefinic Compounds[1]

Teruo KAWAMURA, Kiyoshi KIKUKAWA, Makoto TAKAGI, and Tsutomu MATSUDA

Department of Organic Synthesis, Faculty of Engineering, Kyushu University, Hakozaki, Higashi-ku, Fukuoka 812

(Received January 18, 1977)

The reaction of phenyl compounds of typical groups V and VI elements, Ph_nA and Ph_nAX_2 (n=2, 3; A=P, As, Sb, Bi, S, Se, Te; X=Cl or X_2=O), with Pd(II) salts was studied in the presence of olefinic compounds (1-octene and ethyl acrylate) in acetonitrile. The phenyl migration from A to Pd to produce phenylpalladium species, which lead to the phenylation of olefin, was observed for all Ph_nA and Ph_nAX_2 (except for A=S and Ph_3PX_2) when $Pd(OAc)_2$ was utilized. The reaction, however, was inhibited or greatly suppressed for the compounds of P and As when $PdCl_2$ was used in place of $Pd(OAc)_2$. The compounds of Sb and Bi readily react with $PdCl_2$. Mechanistic discussion was given in terms of the extent of nucleophilic assistance by acetate ion when Pd(II) attacks the aromatic nucleus electrophilically at the carbon atom bonded to A.

Previous observations on the migration of the aryl group from Ar_3P (coordinated to $Pd(OAc)_2$) to Pd under mild conditions,[2] prompted us to examine other typical groups V and VI elements for similar reaction. Since the resulting phenylpalladium species is expected to show a similar reactivity to that derived from Ph_3P or phenylmercury(II) salts, the rate and extent of phenyl migration were assessed by the phenylation of added olefin. Asano *et al.* found that Ph_3As, Ph_3Sb and Ph_3Bi give *trans*-stilbine and biphenyl on reaction with $Pd(OAc)_2$ and styrene in refluxing dioxane–acetic acid.[3] The present study deals with a more detailed aspect of the reactions under milder conditions with the aim of obtaining a general mechanistic insight into this type of phenyl migration.

Results

The reaction of Ph_nA with $Pd(OAc)_2$ in the presence of 1-octene or ethyl acrylate in acetonitrile is summarized in Table 1, and given in the following. The reaction was nearly complete within 5 h. It is seen that all the phenyl groups in Ph_3Sb, Ph_3Bi, and Ph_2Te can be mobilized under suitable conditions. Only one phenyl group of Ph_3As was mobilized in the 5 h reaction, but

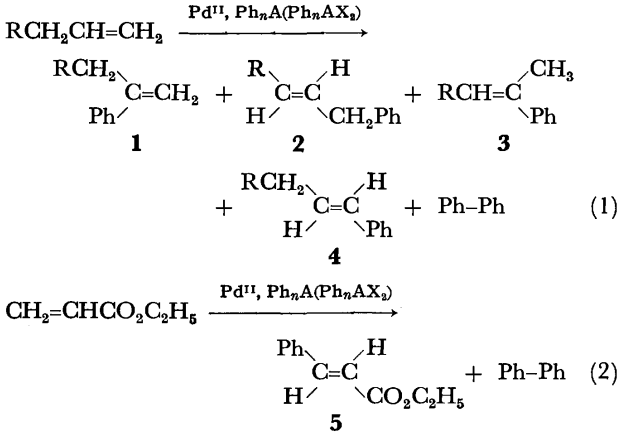

the final yield (24 h reaction) of the phenylated olefins and biphenyl indicates that two phenyl groups out of three could migrate from As to Pd. No phenyl of Ph_2S was mobilized in 5 h. However, a trace of phenylated olefins could be detected on GLC after 25 h. The time dependence of the reaction shows that the phenyl migration was especially rapid for Ph_3Sb, Ph_3Bi, and Ph_2Te as compared with Ph_3As or Ph_2Se. The variation

TABLE 1. REACTION OF Ph_nA WITH $Pd(OAc)_2$ AND OLEFINS IN ACETONITRILE (50 °C, 5 h)

Ph_nA. Molar ratio, A/Pd	Olefin[a]	Yield of phenylated olefin, %[b] (composition)[c]	Yield of biphenyl, %[d]	Total phenyl mobilized, %[e]
Ph_3As				
0.5	O	33(17, 32, 2, 49)	23	79
2	O	13(32, 28, 1, 39)	2	17
0.5	E	21	10	41
1	E	48	21	90
2	E	8	4	16
Ph_3Sb				
1[f]	O	113(16, 12, 15, 57)	70	253
0.5	E	120	15	150
1	E	203	20	243
2	E	208	30	268
3	E	195	60	315
Ph_3Bi				
1[f]	O	48(11, 29, 8, 52)	120	288
0.5	E	43	43	129
1	E	80	100	280
2	E	73	240	553
3	E	47	260	567
Ph_2Se				
1	O	27(26, 29, 4, 41)	g)	(>27)
1	E	23	g)	(>23)
2	E	22	g)	(>22)
Ph_2Te				
0.5	E	90	h)	(>90)
1	E	147	h)	(>147)
2	E	194	h)	(>194)

a) O: 1-Octene; E: ethyl acrylate. b) (Mol of phenylated olefin/mol of $Pd(OAc)_2$) × 100. c) % Composition of the phenylated octenes, **1**, **2**, **3**, and **4**, in this order. d) (Mol of biphenyl/mol of $Pd(OAc)_2$) × 100. e) (Mol of phenyl group released from A/mol of $Pd(OAc)_2$) × 100, calculated from (% value from b)) plus (% value from d)) × 2. f) Reaction at 25°C. g) Not determined, less than the phenylated olefin. h) Not determined.

in A/Pd ratio did not cause much difference in the reaction rate for the compounds of Bi, Sb, Te, and Se. However, the increase in As/Pd ratio over 1 considerably decreased the rate of phenyl migration. A similar observation was made for the reaction of Ph_3P.[2a] It is probable that as in the case of Ph_3P, the coordination of the second molecule of Ph_3As to Pd exercises some unfavorable effect on the phenyl migration process.

Some reaction systems show a marked tendency to form biphenyl rather than phenylated olefins. This is especially true for the system where the formation of the phenylpalladium species is rapid (*e.g.*, Ph_3Sb and Ph_3Bi). This is at least partially due to the fact that without sufficient supply of olefin the phenylpalladium species decompose to form biphenyl. A slight modification was made in experimental procedure for the reaction of Ph_3Sb and Ph_3Bi (Table 1). A mixture of the olefin and Ph_nA (A=Sb, Bi) was added to a solution of $Pd(OAc)_2$ in acetonitrile. When they were subjected to reaction by the standard procedure (prior reaction of $Pd(OAc)_2$ and Ph_3A in acetonitrile, see Experimental), most of the organic products were biphenyl. The reaction of PhHgOAc studied under comparative conditions indicates that the formation of biphenyl is unimportant (1—2% yield). The marked tendency of Ph_3Bi to form biphenyl seems to reflect a certain inherent nature of the compound.

The time-yield profiles for various Ph_nA are given in Fig. 1 to show the phenylation of ethyl acrylate under the same reaction conditions. Solid Ph_3A (0.50 mmol) was added to a solution of $Pd(OAc)_2$ (0.50 mmol) in a mixture of ethyl acrylate (5.0 mmol) and acetonitrile (3.0 g) at 50 °C. Some discrepancy in yields (at 5 h of reaction) from those in Table 1 reflects a subtle difference in the experimental procedure.[4]

Phenylation of olefins with Ph_3P–$Pd(OAc)_2$ under nitrogen proceeds much more slowly than that under ordinary atmosphere.[1] The aerobic reaction might remove excess phosphine ligand from the coordination sphere of Pd through oxidation. Thus, the reaction of Ph_3As is greatly suppressed under nitrogen, while no major effect is observed with the compounds of Sb, Bi, Te, and Se. The reaction of PhHgOAc with olefin under nitrogen was also shown not to differ from that under aerobic conditions.

Ph_3P–$PdCl_2$ does not phenylate olefins in the absence of added sodium acetate.[2a] A similar study indicates that the compounds of P, As, and Se are completely or almost inactive without acetate ion. The compounds of Sb, Bi, and Te, on the other hand, exhibit somewhat decreased reactivity, but still phenylate ethyl acrylate effectively. Phenylmercury(II) chloride coupled with $PdCl_2$ has been utilized as an effective phenylating agent for olefin.[6] Hg requires no assistance by acetate ion in the migration of phenyl group from Hg to Pd. These observations indicate an essential difference in the mechanism of phenyl migration according to the nature of elements. If the nucleophilic attack by acetate ion on the coordinated A atom[2a] is important for the reaction of Ph_3P, Ph_3As, and Ph_2Se with bivalent Pd, we might expect that the reaction is suppressed for quinquevalent P and As (or with quadrivalent Se), since the coordination through A atom is impossible. The reactions of Ph_3PO or Ph_3PCl_2 were completely inhibited, those of Ph_3AsO or Ph_3AsCl_2 being suppressed a great deal. The reactions of Ph_2SeCl_2 were slightly suppressed. On the other hand, no major influence on the phenyl transfer activity was observed for Ph_3SbCl_2 and Ph_3BiCl_2. These observations are in line with the idea that the mechanism of phenyl migration can vary among elements A.

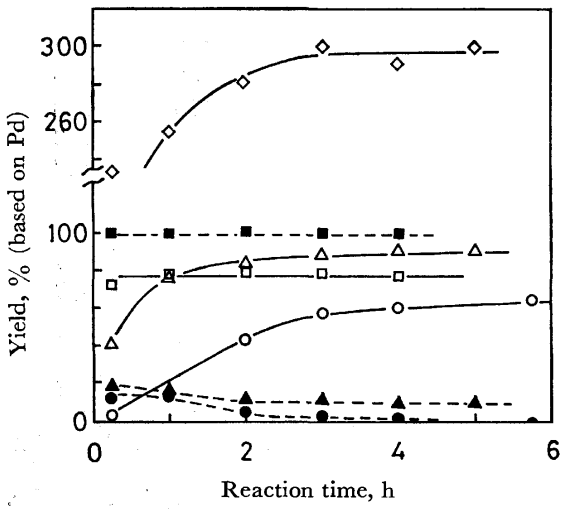

Fig. 1. The reaction of Ph_3A with $Pd(OAc)_2$ in the presence of ethyl acrylate (50 °C). Ph_3A, 0.50 mmol; $Pd(OAc)_2$, 0.50 mmol; ethyl acrylate, 5.0 mmol; acetonitrile, 3.0 g. ——, **5**; ——, biphenyl. A: P(○,●), As(△,▲), Sb(◇), Bi(□,■).

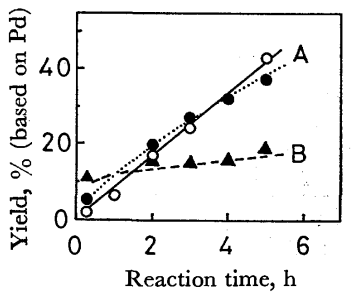

Fig. 2. The phenyl transfer from P to Pd as assessed by quenching with bromine (A) and by phenylation of ethyl acrylate (B) (25 °C).
A: Ph_3P, 2.0 mmol; $Pd(OAc)_2$, 2.0 mmol; acetonitrile, 30 g; ○, ●, duplicate runs.
B: Ph_3P, 0.50 mmol; $Pd(OAc)_2$, 0.50 mmol; ethyl acrylate, 5.0 mmol; acetonitrile, 3 g.
yield: (mol of bromobenzene or **5**/mol of $Pd(OAc)_2$) × 100.

The formation of phenylpalladium species has hitherto been studied by the phenylation of olefins. As a more direct method for characterizing the unstable intermediate, the quenching experiments with bromine were attempted for the reaction of Ph_3P and $Pd(OAc)_2$ at 25 °C (Fig. 2). The aliquots withdrawn at appropriate time intervals were allowed to react with excess bromine in carbon tetrachloride. Bromobenzene which seems to be formed by the "bromodepalladation reaction"[7] of the phenylpalladium salts increased approxi-

mately linearly with the reaction time, supporting the formation of the chemical species containing the phenylpalladium bond. Phenylation of ethyl acrylate under similar conditions was obviously slow as compared to the formation of phenylpalladium species. A problem remains in the quenching practice as to a satisfactory way for standardizing the analytical method. In the reaction of $PhPd(Ph_3P)_2I$ with excess bromine, 67% of bromobenzene was obtained along with 4% of iodobenzene, indicating that the bromodepalladation of the complex is not quantitative.

Discussion

The results could be rationalized by two extreme reaction mechanisms for the phenyl transfer from A to Pd. The first is represented by Ph_3P given in Scheme 3 where only the relevant ligands on Pd are shown. PPh_3 coordinated to bivalent Pd is in effect phosphonium ion, which is attacked by acetate ion on P, and concurrently, the phenyl group on P migrates to the vacant coordination site on Pd. Thus, the mechanism is an electrophilic aromatic substitution of P by Pd (or a 1,2-shift of phenyl group from P to Pd) promoted by nucleophilic assistance by acetate ion. It is not at all certain, however, whether the acetate ion which attacks P requires a prior coordination to Pd (Scheme 3). The process of phenyl migration

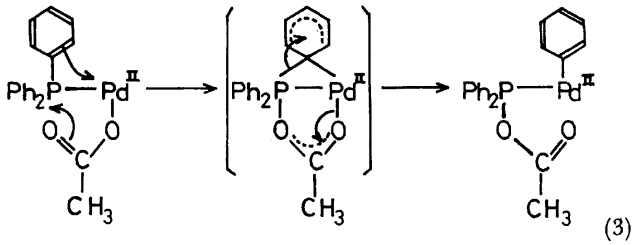

(3)

from an electron rich to electron deficient center (1, 2-shift of aryl group[8]) and the ability of acetoxyl group for anchimeric assistance[9] are familiar in organic chemistry. On the other hand, the reaction of the compounds of Bi seems neither to require the prior coordination of A to Pd nor necessitate the nucleophilic assistance by acetate ion. Thus, a simple electrophilic aromatic substitution by bivalent Pd would be enough to describe the reaction (Scheme 4). Phenylmercury (II) salts might react with bivalent Pd in a similar way.

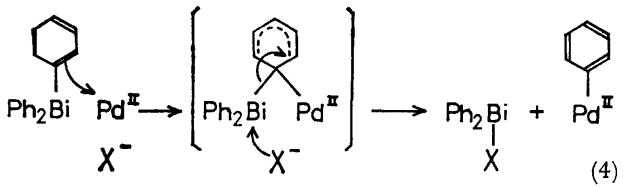

(4)

For the elements other than P and Bi, the entity of the reaction would be somewhere between the two extremes, and no discontinuous change in mechanism seems to be involved. The reactions of As are more related to those of P, while the reactivity of Sb and Te seems to be close to that of Bi or Hg. The factors responsible for these varying reactivities of Ph_3A would be the decreasing A–C bond energy in the order Bi< Sb<As<P[3] coupled with the decreasing electronegativity Bi<Sb<P<As,[10] both facilitating the electrophilic aromatic substitution on the carbon atom bonded to Bi or Sb. In order to cleave the more stable P–C bond *via* electrophilic process on carbon, a prior coordination of phosphorus to palladium is required, which not only brings the reactants into close proximity but also enables the nucleophilic assistance by acetate ion on the coordinated P atom. The donor ability of Ph_3A increases in the order P>As>Sb≫Bi.[11]

Experimental

Materials. $Pd(OAc)_2$ was prepared by the method of Stephenson *et al.*[12] Commercial transition metal salts were used. The following phenyl derivatives of groups V and VI typical elements were synthesized according to the reported procedures and identified by elemental analyses as well as by comparison of IR and melting points; Ph_3Sb,[13] Ph_3Bi,[14] Ph_2Se,[15] Ph_2Te,[16] Ph_3PCl_2,[17] Ph_3AsCl_2,[17,18] Ph_3AsO,[19] Ph_3SbCl_2,[14] Ph_3BiCl_2,[20] Ph_2SO,[21] Ph_2SeCl_2.[22] Commercial Ph_3P and Ph_3As were used with or without further purification. Phenylpalladium complex, $PhPd(Ph_3P)_2I$, was prepared[23] and identified by elemental analysis.

Reaction of Ph_nA with Pd(II) Salt in the Presence of Olefinic Compounds. The reaction was carried out in the following way with slight modifications. In a reaction cell fitted with a constant-temperature water jacket were placed 0.50 mmol of Ph_nA (or Ph_nAX_2), desired amount (0.25—1.0 mmol) of Pd(II) salt and 3.0 g of acetonitrile. After the mixture had been stirred for 5 min, 5.0 mmol of olefin (1-octene or ethyl acrylate) and an internal standard (diethylene glycol dibutyl ether or 1,2-diphenylethane) were added. The reaction was monitored by analyzing the phenylated olefins and biphenyl, until the precipitation of palladium black was complete (usually 24 h). Identification of the reaction products was reported.[2]

Reaction of Ph_3P with $Pd(OAc)_2$, Quenching with Bromine. $Pd(OAc)_2$ (0.50 mmol) was dissolved in acetonitrile (3.0 g, with chlorobenzene as an internal standard) in a thermostatted cell at 25 °C. Ph_3P (0.50 mmol) was then added. Samples were withdrawn from the reaction mixture and added to the excess bromine (≈2 mmol) dissolved in carbon tetrachloride. The mixture was shaken with 10% aq $Na_2S_2O_3$, and the organic layer was separated. The latter solution was analyzed by GLC after being dried with $MgSO_4$. The use of iodine in place of bromine proved inadequate, since the reaction of Ph_3P with iodine did not reach completion and the phenyl transfer reaction continued to take place. The reaction of $PhPd(Ph_3P)_2I$ with bromine was carried out in a similar way. The complex was dissolved in acetonitrile or in a mixture of acetonitrile and dichloromethane and treated with 4—5 folds molar excess bromine in carbon tetrachloride.

References

1) Presented at 21st (Sendai, 1973) and 22nd (Kyoto, 1974) Symposium on Organometallic Chemistry. The lectures 205 and 205B, respectively, in the Abstract.

2) a) T. Yamane, K. Kikukawa, M. Takagi, and T. Matsuda, *Tetrahedron*, **29**, 955 (1973); b) K. Kikukawa, T. Yamane, M. Takagi, and T. Matsuda, *Chem. Commun.*, **1972**, 695.

3) R. Asano, I. Moritani, Y. Fujiwara, and S. Teranishi, *Bull. Chem. Soc. Jpn.*, **46**, 2910 (1973).

4) The yield of biphenyl decreases with time (Fig. 1). Control experiments showed that most of the biphenyl detected at the early stage of the reaction is an artifact induced by direct GLC analysis.

5) R. F. Heck, *J. Am. Chem. Soc.*, **93**, 6896 (1971) and Refs. cited therein.

6) R. F. Heck, *J. Am. Chem. Soc.*, **90**, 5518 (1968).

7) The halodemetallation reaction of various arylmetal compounds is summarized in R.O.C. Norman and R. Taylor, "Electrophilic Substitution in Benzenoid Compounds," Elsevier, New York, N.Y. (1965), Chap. 10.

8) R. Muneyuki and H. Tanida, "Theoretical Organic Chemistry, Structural Part," (in Japanese), ed by M. Nakagawa, Kagaku-dojin, Kyoto (1974), p. 50.

9) "Molecular Rearrangements, Part One, ed by P. de Mayo, Interscience Publishers, New York, N.Y. (1963), p. 1244.

10) F. A. Cotton and G. Wilkinson, "Advanced Inorganic Chemistry, A Comprehensive Text," 2nd ed, Interscience Publishers, New York, N.Y. (1966), p. 486.

11) S. Murahashi, "Yukikinzoku Handobukku," Asakura Shoten, Tokyo (1967), p. 706.

12) T. A. Stephenson, S. M. Morehouse, A. R. Powell, T. P. Heffer, and G. Wilkinson, *J. Chem. Soc.*, **1965**, 3632.

13) G. S. Hiers, *Org. Synth.*, Coll. Vol. I, 550 (1956).

14) W. J. Lile and R. C. Menzies, *J. Chem. Soc.*, **1950**, 617.

15) H. M. Leicester, *Org. Synth.*, Coll. Vol. II, 238 (1950).

16) a) O. Steiner, *Ber.*, **34**, 570 (1901); b) K. Lederer, *ibid.*, **48**, 1345 (1915).

17) L. Horner, H. Oediger, and H. Hoffmann, *Justus Liebigs Ann. Chem.*, **626**, 26 (1959).

18) A. Michaelis, *Justus Liebigs Ann. Chem.*, **321**, 162 (1902).

19) A. W. Johnson, *J. Org. Chem.*, **25**, 183 (1960).

20) G. Wittig and K. Clauss, *Justus Liebigs Ann. Chem.*, **578**, 136 (1952).

21) C. E. Colby and C. S. McLoughlin, *Ber.*, **20**, 195 (1887).

22) H. M. Leicester, *Org. Synth.*, Coll. Vol. II, 240 (1950).

23) P. Fitton, M. P. Johnson, and J. E. McKeon, *Chem. Commun.*, **1968**, 6.

Synthesis of Amino Compounds under Phase Transfer Conditions

Yosuke NAKAJIMA, Ryo-ichi KINISHI, Jun'ichi ODA, and Yuzo INOUYE

Institute for Chemical Research, Kyoto University, Uji, Kyoto 611

(Received January 20, 1977)

The phase transfer process was applied to the reaction of organic bromides with azide anion. The reduction of intermediary azide derivatives gave the corresponding amino compounds, benzylamine, glycine, alanine, butyrine, and serine in fairly good yields. Effective catalytic activity was demonstrated by the difference in chemical yields in the case of methyl bromoacetate and ethyl α-bromopropionate. In order to examine the role of phase transfer catalyst, two bromohydrins (methyl β-hydroxy-α-bromopropionate and styrene bromohydrin) were subjected to the present reaction. Methyl β-hydroxy-α-bromopropionate afforded serine exclusively in the presence of 18-crown-6 and tetrabutylammonium bromide, but in the absence of the catalyst a mixture of serine and isoserine was obtained. A different regioselectivity was observed in the case of styrene bromohydrin.

Use of quaternary ammonium and phosphonium salts and crown ethers as a phase transfer catalyst is epochal in synthetic organic chemistry. Many synthetic routes are now being developed, giving products in good yields under simple and mild conditions.[1]

The mechanism proposed by Starks[2] was verified[3] in accord with the reactivity of 2-bromooctane toward aqueous alkali solution. Herriott and Picker[3] concluded that the catalyst functions so as to solubilize the anionic reagents into the organic phase in their system, but not rigorously applicable to others.[1,4]

We describe herewith the substitution reaction of organic halides with sodium azide under phase transfer-catalyzed conditions, which permit easy access to amino compounds. The probable mechanism for the present systems in connection with the reactivity of bromohydrins is discussed.

Experimental

IR spectra were recorded on a Hitachi 215 grating spectrophotometer and PMR spectra on a Varian model EM-360 spectrometer.

The general procedure for nucleophilic substitution of organic bromide with azide anion is exemplified by a typical run (run 1, Table 1). The reactions were repeated with the reaction parameters modified.

Benzyl bromide (10 mmol; 1.71 g) and sodium azide (15 mmol; 0.98 g) were stirred in a mixture of water (4 ml) and tetrabutylammonium bromide (0.5 mmol; 161 mg) at room temperature for 6 h, after which the solution was extracted 3 times with dichloromethane. The dried dichloromethane solution was evaporated and the residue was reduced with LAH. Benzylamine was obtained in the usual way. Yield, 936 mg (87.4%). IR and PMR spectra were identical with those of an authentic specimen. Identification of other products was also confirmed in satisfactory agreement with respective data in literature.

Determination of the ratio of isomeric serines, and amino alcohols (I and II) was made by a comparison of integral values of β-methylene and α-methin protons. The chemical shift of β-methylene proton of isomeric serines in D_2O–NaOH and TMDS as an internal standard: δ 3.80 for serine; 3.08 for isoserine. The chemical shift of α-methin proton in $CDCl_3$ and TMS of I and II: δ 4.58 for I; 3.97 for II.

Results and Discussion

Organic bromides reacted with sodium azide in a two-phase (liquid–liquid or solid–liquid) system in the presence of a phase transfer catalyst such as tetrabutylammonium bromide and 18-crown-6,[5] to give the corresponding azides in good yields, which were easily converted into the amines. For example, benzyl bromide underwent nucleophilic substitution at room temperature. The end product, benzylamine, was obtained by the LAH reduction of intermediate azide (Table 1). Benzene was found to be superior to ether in the solid–liquid system.

TABLE 1. NUCLEOPHILIC DISPLACEMENT OF BENZYL BROMIDE BY SODIUM AZIDE

$$PhCH_2Br \xrightarrow[\text{PTC (5 mol\%) at room temp}]{NaN_3} PhCH_2N_3 \xrightarrow{LAH} PhCH_2NH_2$$

Run	PTC[a)]	Solvent	Reaction period (h)	% Yield
1	NX[b)]	H_2O	6	87.4
2	CE[c)]	Benzene	6	48.3
3	CE	Ether	6	27.1

a) PTC : phase transfer catalyst.
b) NX : tetrabutylammonium bromide.
c) CE : 18-crown-6.

Amination of α-halogenated esters is a conventional method for synthesis of α-amino acids, so that we duly applied the phase transfer technique to the reaction. Glycine, alanine, and butyrine were obtained in good

TABLE 2. NUCLEOPHILIC DISPLACEMENT OF α-BROMO ESTERS BY SODIUM AZIDE

$$RCHCOOR' \xrightarrow[\text{PTC (5 mol\%) at room temp}]{NaN_3} RCHCOOR' \quad (Br \rightarrow N_3)$$

$$RCHCOOR' \xrightarrow[Pd/C]{H_2} RCHCOOH \quad (NH_2) \qquad (H_3O^+)$$

Run	PTC	R	R′	Solvent	Reaction period (h)	% Yield
1	NX	H	Me	H_2O	12	79.0
2	CE	H	Me	Benzene	6	97.1
3	—	H	Me	Benzene	6	trace
4	NX	Me	Et	H_2O	1	82.3
5	NX	Me	Et	H_2O	6	94.4
6	—	Me	Et	H_2O	1	3.5
7	NX	Et	Et	H_2O	6	90.3

Table 3. Reaction of β-methoxy- or β-hydroxy-α-bromopropionates with sodium azide

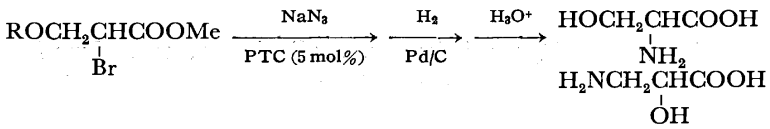

Run	PTC	R	Solvent	Reaction period (h)	Reaction temperature	% Yield	Serine : Isoserine	
1	NX	Me	H_2O	6	room temp	84.0	only	
2	NX	H	H_2O	24	40 °C	63.2	only	
3	CE	H	CH_3CN	24	50 °C	60.0	only	
4	—	H	MeOH–H_2O	12	reflux	30.5	60	40

yields. Effectiveness of the phase transfer catalyst was reflected in the distinct difference in chemical yield (runs 2, 3 and 4, 5, 6 in Table 2).

The data obtained for the amination of methyl β-methoxy-[6] and β-hydroxy-α-bromopropionate[7] to give serine in moderate yields by phase transfer catalysis are summarized in Table 3.

Levene and Schormüller[8] reported the formation of β-azido-α-hydroxypropionate as the sole product of the reaction of methyl β-hydroxy-α-bromopropionate with sodium azide in methanol–water medium. In contrast, we obtained a mixture of serine and isoserine (60: 40) as the end product of the same reaction under exactly the same conditions in the absence of catalyst (run 4, Table 3).[9] With ammonium halide and crown ether as a phase transfer catalyst, the reaction gave serine as the sole product in improved yields.

The present reaction would proceed through intermediate formation of methyl glycidate from bromohydrin followed by the nucleophilic attack of azide anion to give isomeric serines depending on whether it takes on α- or β-carbon of the glycidate. In order to confirm the mechanism, we subjected ethyl glycidate[10] as the substrate to the same reaction under the same conditions. We see from Table 4 that isoserine was the sole product in all cases, regardless of the presence or absence of catalyst and difference in medium. The intervention of glycidate is thus excluded. Consequently, in the phase transfer-catalyzed reactions, the nucleophilic attack of azide anion took place directly on the α-carbon of methyl β-hydroxy-α-bromopropionate to displace bromine.

Table 4. Reaction of ethyl glycidate with sodium azide

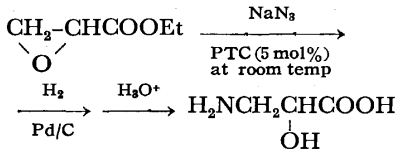

PTC	Solvent	Reaction period (h)	% Yield of isoserine
NX	Buffer(pH 7)	12	60.6
—	Buffer(pH 7)	12	59.1
NX	H_2O	15	62.8
—	H_2O	15	64.4
CE	CH_3CN[a)]	21	22.9

a) Heated under reflux.

The complete regiospecificity as well as improved chemical yields found for the present reaction systems can be utilized in synthetic organic chemistry.

In order to elucidate the function of phase transfer catalyst in the present systems, it seemed of interest to examine the reactivity of other substrates capable of easy rearrangement. For this purpose, styrene bromohydrin[11] seems to be suitable since it is prone to rearrangement. Upon nucleophilic substitution, styrene bromohydrin may give rise to the substitution product I and/or the rearrangement product II (Scheme 1).

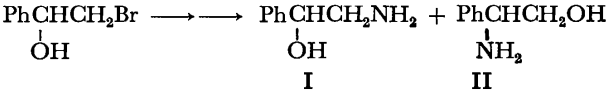

Scheme 1.

The experimental results are given in Table 5. In the system of styrene bromohydrin also, styrene oxide is considered to be the probable intermediate. However, the results with styrene oxide used as a substrate suggest that the contribution of oxiran intermediate is negligible (Table 6).

Styrene bromohydrin reacted with sodium azide in benzene in the presence of crown ether to give exclusively the substitution product I (run 1, Table 5). In polar protic environment (run 3, Table 5), only the rearrangement product II was obtained from the same substrate. The difference might be attributed to the ability of medium to solvate anion species; the reduced solvation of azide anion in crown ether–benzene system suppresses intramolecular hydroxyl rearrangement, whereas in polar protic medium, the neighboring

Table 5. Reaction of styrene bromohydrin with sodium azide

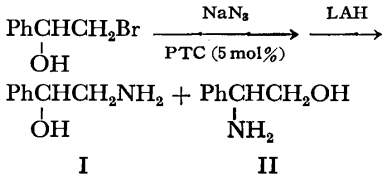

Run	PTC	Solvent	Reaction period (h)	Reaction temperature	% Yield	I : II	
1	CE	Benzene	23	50 °C	28.5	100	
2	NX	H_2O	23	40 °C	58.4	44	56
3	—	MeOH–H_2O	14	reflux	63.0		100

Table 6. Reaction of styrene oxide with sodium azide

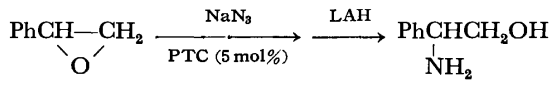

II

PTC	Solvent	Reaction period (h)	Reaction temperature	% Yield of II
CE	CH_3CN	4	reflux	trace
NX	H_2O	8	room temp	8
NX	Buffer(pH 7)	7	room temp	72
CE	H_2O	8.5	room temp	53
CE	Buffer(pH 7)	6	room temp	50

hydroxyl participation has preference to the attack of solvated azide anion.

In the liquid–liquid system with tetrabutylammonium bromide used as phase transfer catalyst (run 2, Table 5), however, no clear-cut selectivity was observed.

For the purpose of clarifying the function of quaternary ammonium salt, we examined to what extent the product distribution is affected by the change in dosage of catalyst and by the addition of organic solvent such as chloroform and benzene to the organic phase. Since the solubility of azide anion in organic phase would be greatly increased under these circumstances, we could predict the preferential formation of the substitution product I due to the enhanced reactivity of azide anion. In accordance with expectation, the product ratio I: II increased with increase in the amount of catalyst and by addition of organic solvent (Table 7).

Table 7. Influence of the reaction parameters on the product distribution of isomeric amino alcohols

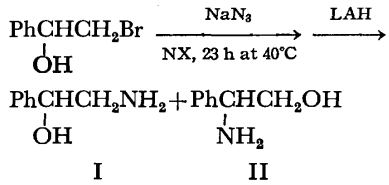

I II

Run	Mol % of NX	Solvent	% Yield	I	:	II
1	5	H_2O	58.4	44		56
2	20	H_2O	75.3	65		35
3	60	H_2O	77.9	77		23
4	0	H_2O	10.6			100
5	5	C_6H_6–H_2O	36.2	77		23
6	5	$CHCl_3$–H_2O	48.6	85		15

The experimental results in the present systems (Tables 5, 6, and 7) show that the reaction takes place in rather aprotic environment as indicated by the high product ratio (runs 3, 5, and 6, Table 7). The mechanism proposed by Starks and Herriott seems to be operative under these conditions. However, in the reaction system which involves the substrate alone as organic phase (run 1, Table 7), the predominant formation of rearrangement product II is observed in spite of the presence of quaternary ammonium salt. This might result from the sparing solubility of ammonium azide ion-pair in organic phase. Under such conditions as employed in run 1 (Table 7), therefore, the function of a co-sphere outside the interface between organic and aqueous phases to furnish a possible reaction site could not be entirely neglected. As another likelihood, the protic character of styrene bromohydrin constituting an organic phase may be responsible for the observed preferential formation of II, despite the fact that the reaction occurs in organic phase.

References

1) G. W. Gokel and H. D. Durst, *Synthesis*, **1976**, 168; J. Dockx, *ibid.*, **1973**, 441; E. V. Dehmlow, *Angew. Chem. Int. Ed. Engl.*, **13**, 170 (1974); M. Makosza, *Pure Appl. Chem.*, **43**, 439 (1976).

2) C. M. Starks, *J. Am. Chem. Soc.*, **93**, 195 (1971); C. M. Starks and R. M. Owens, *ibid.*, **95**, 3613 (1973).

3) A. W. Herriott and D. Picker, *Tetrahedron Lett.*, **1972**, 4521; *J. Am. Chem. Soc.*, **97**, 2345 (1975).

4) J. H. Fendler and E. J. Fendler, "Catalysis in Micellar and Macromolecular Systems," Academic Press, New York (1975), pp. 387—389.

5) G. W. Gokel, D. J. Cram, C. L. Liotta, H. P. Harris, and F. L. Cook, *J. Org. Chem.*, **39**, 2445 (1974).

6) J. L. Wood and V. du Vigneaud, *J. Biol. Chem.*, **134**, 413 (1940).

7) K. C. Leibman and S. K. Fellner, *J. Org. Chem.*, **27**, 438 (1962).

8) P. A. Levene and A. Schormüller, *J. Biol. Chem.*, **105**, 547 (1934).

9) Levene and Schormüller reported the isolation of isoserine alone by the catalytic hydrogenolysis of distilled azide ester. This might be due to the probable fractionation during the procedure for obtaining the end product.

10) W. D. Emmons and A. S. Pagano, *J. Am. Chem. Soc.*, **77**, 89 (1955).

11) J. Read and W. G. Reid, *J. Chem. Soc.*, **1928**, 1487.

Hydration of Aza-aromatic Aldehydes. I. Isolation of the Solid Hydrates and the Thermodynamic Properties in Dimethyl Sulfoxide

Kazuhisa ABE, Minoru HIROTA,* Isao TAKEUCHI,** and Yoshiki HAMADA**

Department of Applied Chemistry, Faculty of Engineering, Yokohama National University Minami-ku, Yokohama 233

***Faculty of Pharmacy, Meijo University, Tempaku-cho, Tempaku-ku, Nagoya 468*

(Received February 14, 1977)

The covalent hydration forming geminal diol is shown to be general in six-membered aza-aromatic aldehydes substituted by a formyl group at ortho or para-position to the nitrogen atom, and the equilibrium constants and thermodynamic quantities of the reaction are determined by NMR spectroscopic measurements. The results are compared with those of their hemiacetal formation. In several cases, solid monohydrates are isolated and identified.

In contrast to easy formation of hemiacetals,[1] hydration of carbonyl compounds is much less predominant, and only a few examples have been reported.[2,3] Trichloroacetaldehyde crystallizes as monohydrate, and its geminal diol structure is confirmed by ultraviolet spectroscopy.[2] Formaldehyde also exists to some extent as methanediol in aqueous solution. Some aliphatic aldehydes were also found to exist as equilibrium mixtures between the carbonyl and geminal diol forms in aqueous solutions.[4-6] However, the hydrate forms of most complex aldehydes are rather unstable, aldehydes behaving as normal carbonyl compounds even in aqueous or alcoholic solutions. The $n\rightarrow\pi^*$ absorption of many aldehydes including formaldehyde, acetaldehyde, and other simple aldehydes have been measure in these solutions, and their intensities were shown to be in the same order as those in aprotic solvents.[7]

Since the hydration and hemiacetal formation of carbonyl compounds both proceed *via* nucleophilic attack of water and alcohol molecules towards the carbonyl carbon atom, electron-withdrawing moieties attached to the carbonyl group should favor the formation of these addition products. The hydration of aza-aromatic aldehydes carrying so-called electron deficient rings was investigated. The position of the carbonyl function relative to the intra-ring nitrogen atoms affects the equilibrium of the hydration remarkably. The difference in equilibrium constants was interpreted in terms of the electronic effect and hydrogen bonding.

Experimental

Preparation of Materials. Most of the quinoline- and naphthyridinecarbaldehydes were prepared by the methods reported.[8] The samples of pyridinecarbaldehydes were obtained by distilling twice the commercial materials.

3-Quinolinecarbaldehyde (**5**) was perpared from 3-aminoquinoline by a modified method.[11] The starting material(3.6 g) was dissolved in diluted hydrochloric acid(3.5 M, 23 ml), aqueos sodium nitrite solution(1.75 g in 2.5 ml water) being added gradually to the solution. The pH of the diazonium salt solution thus prepared was adjusted to be *ca.* 5 by addition of sodium carbonate, and 10% aqueous formaldehyde oxime was added to the diazotized solution with efficient stirring during 30 min, the temperature of the reaction mixture being kept at 5—10 °C. The mixture was acidified with diluted hydrochloric acid (to pH=3). A ferric chloride solution(15 g in 15 ml water) was added, and the solution was digested at 100 °C for about 1 h. Neutralization by sodium carbonate, extraction by ether, and evaporation of the solvent gave the crude 3-quinolinecarbaldehyde. Colorless needles(recrystd from pentane). Mp 68—70 °C(lit, 70 °C). MS, m/e=157(M^+).

Their hydrates were prepared by crystallization from aqueous or aqueous-dimethyl sulfoxide solutions. Dimethyl sulfoxide seems to accelerate and to favor formation of the hydrates. 4-Pyridinecarbaldehyde monohydrate. Mp 65—80 °C (dec). Found: C, 57.80; H, 5.58; N, 11.32%. Calcd for $C_6H_7O_2N$: C, 57.59; H, 5.64; N, 11.20%. 1,8-Naphthyridine-4-carbaldehyde monohydrate. Mp 129—130 °C (dec). Found: C, 61.57; H, 4.39; N, 15.65%. Calcd for $C_9H_8O_2N_2$: C, 61.36; H, 4.58; N, 15.90%.

Measurement of the Spectra. The IR spectra were recorded with a Hitachi Model 225 grating infrared spectrophotometer and the UV spectra with a Hitachi EPS-3T spectrophotometer. Proton NMR spectra were measured with a JMN C-60H spectrometer equipped with a JES-VT-3 apparatus for variable temperature measurements. Chemical shifts are given in terms of part per million (ppm) downfield from TMS, and temperatures were calibrated by measuring the chemical shifts of 1,3-propanediol before and after scan of the spectrum.

Results and Discussion

Isolation of Crystalline Monohydrates of Aza-aromatic Aldehydes. In the course of synthetic and pharmaceutical investigations on naphthyridines and related heterocycles,[8-10] a series of aza-aromatic aldehydes were prepared and their infrared spectra were measured. Among these aldehydes, 1,8-naphthyridine-4-carbaldehyde (**8**), prepared by the oxidation of 4-methyl-1,8-naphthyridine, crystallizes to form monohydrate, and shows no carbonyl absorption in the frequency range 1750—1650 cm^{-1} when the spectrum is obtained in the solid state (as a potassium bromide pellet). Some absorption bands of the aldehyde under discussion are given in Table 1. The broad and intense absorption of 1,8-naphthyridine-4-carbaldehyde hydrate at *ca.* 3200 cm^{-1} can be assigned to the associated (or chelated) hydroxyl group. The broad bands at the lower frequencies might originate from the OH bending and CO stretching modes of vibration of geminal diol group. Mass spectrum of the hydrate shows no molecular ion peak but M−18 (m/e: 158) peak which corresponds to the parent peak of the anhydrous aldehyde. Further studies on its infrared spectrum in solution reveal the existence of the carbonyl form in aprotic solvents. The

* To whom correspondence should be addressed.

Table 1. Infrared spectra of several aza-aromatic aldehydes

Aldehyde		State	ν_{max}/cm^{-1} a)	C=O Bond order
2-Pyridinecarbaldehyde (anhydrous)	**1**	liquid	1714(s)	0.8659
3-Pyridinecarbaldehyde (anhydrous)	**2**	liquid	1707(s)	0.8618
4-Pyridinecarbaldehyde (anhydrous)	**3**	liquid	1712(s)	0.8707
(hydrate)		solid	3270(s,b)	
			1560(s)	
2-Quinolinecarbaldehyde (anhydrous)	**4**	solid	1706(s)	0.8685
3-Quinolinecarbaldehyde (anhydrous)	**5**	solid	1690(s)	0.8599
4-Quinolinecarbaldehyde (anhydrous)	**6**	liquid	1703(s)	0.8669
1,5-Naphthyridine-4-carbaldehyde (anhydrous)	**7**	solid	1697(s)	0.8630
1,8-Naphthyridine-2-carbaldehyde (anhydrous)	**8**	solid	1707(s)	0.8692
1,8-Naphthyridine-4-carbaldehyde[b] (hydrate)	**9**	solid	3200(s,b)	0.8696
			1510(b)	
			1310(s,b)	
(hydrate)		$CHCl_3$ soln	1711(s)[c]	
(hydrate)		CH_3CN soln	1706(s)[c]	

a) s: strong, b : broad. b) Anhydrous substance was not obtained by recrystallization from aqueous ethanol.
c) Carbonyl stretching absorption of the free carbonyl group (see text).

acetonitrile solution of the hydrate shows the carbonyl stretching absorption at 1706 cm^{-1} with ε_{max}=595. In aprotic solvents, the hydrated molecule seems to dissociate into the free aldehyde as follows.

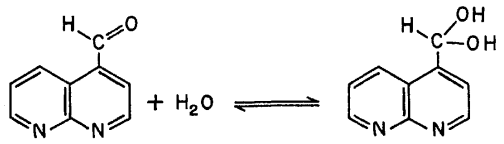

(I) (II)

Since the carbonyl chromophore is destroyed to form the saturated dihydroxymethyl group in the course of hydration, the process of hydration is best pursued by means of ultraviolet spectrometry. The spectra of 1,8-naphthyridine-4-carbaldehyde (**9**) were measured in various solvents. The results are illustrated in Fig. 1. For the sake of comparison, the spectrum of the parent 1,8-naphthyridine is also shown. The spectrum of **9** in water resembles remarkably that of 1,8-naphthyridine. The similarity is reasonanble since the hydrated form of **9** has a 1,8-naphthyridine chromophore slightly perturbed by the dihydroxymethyl moiety. Similar

Table 2. Ultraviolet spectra of several aza-aromatic aldehydes

Aldehyde	λ_{max}/nm (ε_{max}/l mol^{-1} cm^{-1})		
	in H_2O	in CH_3CN	in CH_3OH
4-Pyridinecarbaldehyde (**3**)	225 (11200)	223 (6760)	251 (1820)
	259 (2000)	284 (1780)	258 (2340)
	264sh (1700)		265sh (1860)
	286 (1260)		
4-Quinolinecarbaldehyde (**6**)	248 (11300)	224 (35900)	250 (2140)
	316 (7050)	250 (14700)	285b (3880)
	330b (4910)	325b (7660)	303 (3660)
			316 (3530)
1,5-Naphthyridine-4-carbaldehyde (**7**)	263 (9490)	320 (8080)	263 (7480)
	273 (8420)	275 (7260)	272 (5920)
	306 (10500)		290 (4550)
	312 (10600)		299 (6980)
	330sh (3070)		309 (8240)
1,8-Naphthyridine-2-carbaldehyde (**8**)	242sh (7960)	274b (8230)	258 (6340)
	302 (7660)	320b (5630)	299 (9390)
	311 (8640)		303 (10300)
	330sh (1910)		311 (10600)
1,8-Naphthyridine-4-carbaldehyde (**9**)	268b (7880)	278 (4910)	265 (10700)
	303 (9410)	322 (4910)	296 (9440)
	311 (9700)		303 (11500)
	330sh (2350)		311 (11200)

sh: shoulder, b : broad.

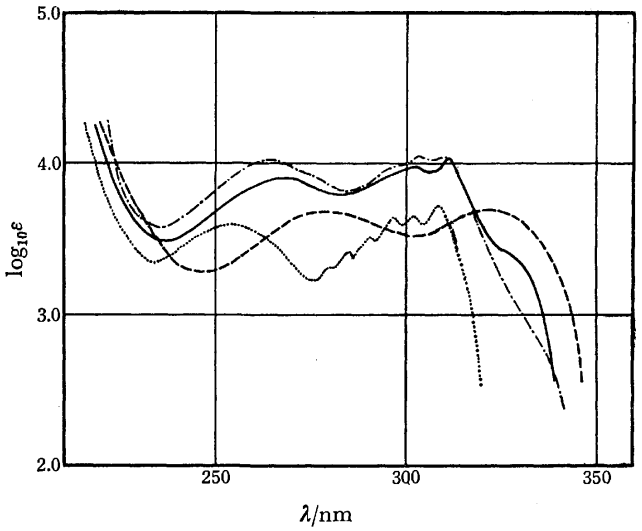

Fig. 1. Ultraviolet spectra of 1,8-naphthyridine-4-carbaldehyde. [—— in water, —— in acetonitrile, -·-·- in methanol (hemiacetal), and ····· 1,8-naphthyridine (as reference) in acetonitrile].

changes in spectra have been observed during the course of acetal formation of some heteroaromatic aldehydes.[3] The hypsochromic shifts of the bands caused by acetal formation are also explained to be due to the saturation of the carbonyl chromophore to form the geminal dialkoxy-compound.

Crystalline hydrates can also be obtained in several cases (*e.g.* 1,8-naphthyridine-2-carbaldehyde (**8**), 4-pyridinecarbaldehyde (**3**)) as solids which deposit spontaneously on the wall of the sample tube when their NMR spectra were measured in aqueous organic solvents (especially in D_2O–DMSO solvent system). Their geminal diol structures were proved by observing the presence of the two OD stretching bands (2438 and 2322 cm^{-1} in the case of **3**) and the absence of the C=O stretching band in their infrared spectra. In the case of **3**, the solid hydrate ($C_6H_5NO \cdot H_2O$) obtained from aqueous solution is identified by the NMR spectrum in DMSO-d_6 [δ=6.58 (d, 2, J=7.5 Hz, OH's of *gem*-diol) and 5.77 ppm (α-CH) and also by elementary analysis (see Experimental). The ultraviolet spectra of the aldehydes in water are also compared with those in aprotic solvents, hypsochromic shifts attributable to the covalent hydration being again observed (Table 2).

Determination of the Equilibrium Constants and Thermodynamic Quantities of the Hydration and Hemiacetalization of the Aza-aromatic Aldehydes. Further investigation on their NMR spectra shows that hydration of the heteroaromatic aldehydes of this class occurs generally, and proceeds reversibly in various solvents.[12] Thus, the measurement provides a suitable means to study the reaction quantitatively. An example of the NMR spectra of 4-pyridinecarbaldehyde–D_2O-dimethyl sulfoxide-d_6 ternary system is given in Fig. 2. The rate of the hydration is sufficiently small to make it possible to observe the proton signals of the free and the hydrate species of the aldehyde separately, the CHO and the $CH(OD)_2$ protons resonating at about 10.1 and 6.0 ppm, respectively. The relative intensities of these

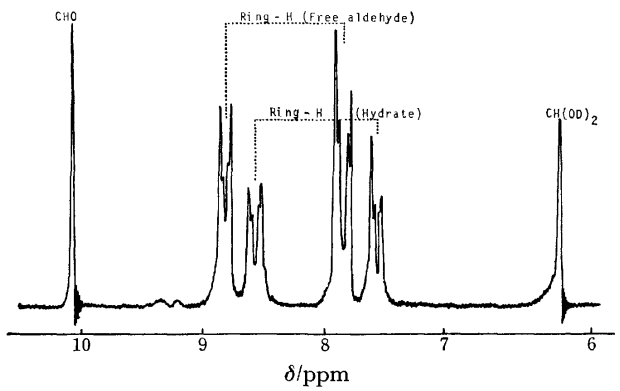

Fig. 2. The proton NMR specrum of 4-pyridinecarbaldehyde in deuterium oxide–dimethyl sulfoxide-d_6.

signals vary with the displacement of the equilibrium between the free and hydrate species. The relative intensities of the signals were determined as the average of integrated intensities recorded by the scan of the integrator. The scan was repeated at least three times to obtain a reliable equilibrium constant, the data with larger deviations being omitted. When the proton NMR signals of the ring are relatively simple (as in the spectrum of 4-pyridinecarbaldehyde in Fig. 2), the intensity measurement on these signals gives a more reliable equilibrium constant. The equilibrium constants thus obtained are given in Table 3. The temperature dependence measurements gave the enthalpies and

Table 3. Equilibrium constants at various temperatures for the hydration of aza-aromatic aldehydes in D_2O–DMSO-d_6

2-Pyridinecarbaldehyde (**1**)					
T/K	281	287	298	307.5	316
$K\times10^2$/1 mol^{-1}	1.64	1.32	1.10	0.861	0.673
4-Pyridinecarbaldehyde (**3**)					
T/K	291.5	303	307.5	315	325.5
$K\times10^2$/1 mol^{-1}	5.24	3.65	3.16	2.57	2.08
2-Quinolinecarbaldehyde (**4**)					
T/K	297	303	307.5	316	325.5
$K\times10^2$/1 mol^{-1}	3.33	2.65	2.27	1.71	1.07
4-Quinolinecarbaldehyde (**6**)					
T/K	307.5	316.5	328	338	
$K\times10^2$/1 mol^{-1}	5.10	3.93	3.33	2.14	
1,5-Naphthyridine-4-carbaldehyde (**7**)					
T/K	307.5	316	331	338	
$K\times10^2$/1 mol^{-1}	9.83	6.70	3.96	2.69	
1,8-Naphthyridine-2-carbaldehyde (**8**)					
T/K	307.5	314.5	325.5	335.5	
$K\times10^2$/1 mol^{-1}	8.43	5.00	3.76	2.66	
1,8-Naphthyridine-4-carbaldehyde (**9**)					
T/K	307.5	315.5	325	334.5	347.5
$K\times10^2$/1 mol^{-1}	12.9	9.86	6.25	3.67	3.12

Table 4. Thermodynamic quantities for the hydration of aza-aromatic aldehydes in D_2O–DMSO-d_6

Aldehyde	K(34.5°C)/1 mol^{-1}	ΔH/kJ mol^{-1}	ΔS/mol^{-1} K^{-1}
2-Pyridinecarbaldehyde (**1**)	8.61×10^{-3}	−16.3	−92
3-Pyridinecarbaldehyde (**2**)	3.6×10^{-3} a)	—	—
4-Pyridinecarbaldehyde (**3**)	3.16×10^{-2}	−21.7	−99
2-Quinolinecarbaldehyde (**4**)	2.27×10^{-2}	−26.7	−110
3-Quinolinecarbaldehyde (**5**)	b)	—	—
4-Quinolinecarbaldehyde (**6**)	5.10×10^{-2}	−21.8	−95
1,5-Naphthyridine-4-carbaldehyde (**7**)	8.43×10^{-2}	−32.1	−126
1,8-Naphthyridine-2-carbaldehyde (**8**)	1.29×10^{-1}	−34.8	−130
1,8-Naphthyridine-4-carbaldehyde (**9**)	9.83×10^{-2}	−35.2	−134
4-Nitrobenzaldehyde (**10**)	1.51×10^{-2}	—	—

a) The reaction proceeds slowly taking several days to attain equilibrium.
b) No signals of the hydrate from were observed even after standing for two weeks.

entropies of hydration as shown in Table 4. Since 3-pyridine- and 3-quinoline-carbaldehydes show by far less inclination to form hydrates than the rest of the aza-aromatic aldehydes (Table 3), the hydration would be strikingly favored by the mesomeric effect of the ring nitrogen atoms. The electonegative nitrogen atom in the six-membered heteroaromatic ring attracts the π-electrons on the ring, producing positive charges on ortho- and para-carbon atoms. The charges, in turn induce the positive charges on the carbonyl carbon atoms by displacement of the σ-bonding electrons, facilitating the nucleophilic attack of water and the alcohol molecules.

Bond orders have often been used as reactivity indices for the addition reactions,[13–16] a higher C=O bond order being expected to favor the addition reaction of the water molecule. The PPP[17] bond orders for aldehydes **1**—**9** were calculated and tabulated together with their C=O frequencies (Table 1). Since the stretching force constant of the bond increases with increase in the bond order, the C=O stretching frequency can be a measure for its bond order. Trichloroacetaldehyde, which forms a very stable hydrate, has its C=O absorption band at a remarkably higher frequency (1764 cm^{-1}) than those of simple aliphatic aldehydes. When compared with isomers of the above aza-aromatic aldehydes, the C=O stretching absorption of the "meta"-aldehydes (**2** and **5**) are considerably lower than those of the other aldehydes capable of forming the hydrate to a larger extent. This is in line with the above discussion. The bond order as well as the amount of the positive charge on carbon atom predicts the tendency of covalent hydration.

When the equilibrium constants and other thermodynamic properties are compared, the hydration of the para-isomer is more favorable than that of the ortho-isomer in the three series of the aldehydes, *i.e.* pyridinecarbaldehydes (**1** and **3**), quinolinecarbaldehydes (**4** and **6**), and 1,8-naphthyridinecarbaldehydes (**8** and **9**). The mechanism of this ortho-effect has not been clarified as yet. However, the effect can be interpreted in the following way. The dihydroxymethyl group generated in the course of hydration is bulkier than the formyl group and might cause the desolvation of the water molecule originally hydrogen-bonded to the ring

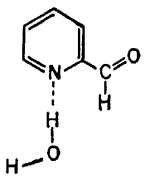

(III)

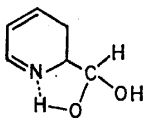

(IV)

nitrogen atom ortho to the carbonyl group (at least partially) by the steric hindrance. As a result, an energetically more favorable OH···N intermolecular hydrogen bond in III is replaced by a weaker intramolecular hydrogen bond in IV during the course of hydration. Thus, a somewhat unfavorable effect is expected with the hydration of "ortho"-aldehydes **1**, **4**, and **8**. The hydration of the naphthyridinecarbaldehydes seems a little more favorable than in the cases of other monoaza-aromatic aldehydes.

Table 5. Thermodynamic quantities for the hemiacetal formation of 4-pyridinecarbaldehyde

Alcohol	Solvent	K(34.5 °C) / 1 mol^{-1}	ΔH / kJ mol^{-1}	ΔS / J mol^{-1} K^{-1}
Methanol	DMSO-d_6	5.77×10^{-1}	−27.7	95
	Acetone-d_6	4.72×10^{-1}	—	—
Ethanol	DMSO-d_6	2.85×10^{-1}	−33.3	118
Isopropyl alcohol	DMSO-d_6	8.79×10^{-2}	−25.8	105
t-Butyl alcohol	DMSO-d_6	4.3×10^{-3}	—	—
Methanol with aldehyde **10**	DMSO-d_6	2.35×10^{-1}	−33.1	−119

In order to compare the hydration reactions with hemiacetal formation of these aldehydes, similar measurements were carried out on the ternary system of the aldehyde–alcohol–solvent (mostly dimethyl sulfoxide-d_6). The results are given in Table 5. In general, hemiacetal formation is more predominant than hydration, due probably to the stronger nucleophilicity of alcohols. However, the equilibria tend to be less favorable as the alkyl groups of the alcohols become bulkier,[4,5] and the acetal formation is remarkably hindered in *t*-butyl alcohol. The equilibrium constant for the hydration

is comparable with that of ethyl or isopropyl alcohol.

The experiments on *p*-nitrobenzaldehyde (**10**) reveal the fact that hemiacetalization is again more favorable than hydration in benzaldehydes carrying electron-withdrawing substituents, and the hydration of benzaldehydes without electron-attracting groups is practically negligible even in aqueous solutions. The hydration of **10** is considerably less favorable than those of 4-pyridinecarbaldehyde (**3**) and its analogs but more favorable than those of 3-pyridine- and 3-quinoline-carbaldehydes. This indicates that the electron-withdrawing power of intra-ring nitrogen atom is more predominant than that of nitro group attached to the aromatic ring. The hydration reactions are sensitive to the nature of the solvents, and the hydrogen accepting power of the solvent in hydrogen bond formation seems to favor the reaction remarkably.[12]

The authors are grateful to Miss Hiroko Endo for her technical assistance in the measurements of the spectra.

References

1) E. P. Crowell, W. A. Powell, and C. J. Varsel, *Anal. Chem.*, **35**, 184 (1963)

2) E. S. Stern and C. J. Timmons, "Electronic Absorption Spectroscopy in Organic Chemistry," 3rd ed, Edward Arnold Ltd., London (1970) p. 221

3) E. Laviron and J. Tirouflet, *C. R. Acad. Sci.*, **248**, 826 (1959).

4) P. Greenzaid, Z. Luz, and D. Samuel, *J. Am. Chem. Soc.*, **89**, 756 (1967).

5) Y. Fujiwara and S. Fujiwara, *Bull. Chem. Soc. Jpn.*, **36**, 574, 1106 (1963).

6) M. L. Ahrens and H. Strehlow, *Discuss. Faraday Soc.*, **39**, 112 (1965).

7) K. Hirayama, "Jikken-Kagaku-Koza," I, Maruzen Ltd., Tokyo (1957) p. 53.

8) Y. Hamada, I. Takeuchi, and M. Hirota, *Chem. Pharm. Bull.*, **19**, 1751 (1971).

9) Y. Hamada, I. Takeuchi, and M. Hirota, *Chem. Pharm. Bull.*, **22**, 485 (1974).

10) Y. Hamada, I. Takeuchi, and M. Hirota, *Tetrahedron Lett.*, **1974**, 495.

11) A. H. Cook, I. M. Heilbron, and L. Steger, *J. Chem. Soc.*, **1943**, 412.

12) K. Abe and M. Hirota, unpublished data (presented to the 36 th National Meeting of the Chemical Society of Japan, Osaka, 1977).

13) G. M. Badger, *J. Chem. Soc.*, **1949**, 456; *ibid.*, **1950**, 1809.

14) R. D. Brown, *Aust. J. Sci. Res.*, **A2**, 564 (1949); *J. Chem. Soc.*, **1950**, 3249; *ibid.*, **1951**, 1950.

15) C. A. Coulson, *J. Chem. Soc.*, **1950**, 2252.

16) V. Gold, *Trans. Faraday Soc.*, **45**, 191 (1949).

17) The PPP-MO calculations were carried out by employing the parameters proposed in the following literatures: a) R. Pariser and G. Parr, *J. Chem. Phys.*, **21**, 767 (1953); b) J. Hinze and H. H. Jaffé, *J. Am. Chem. Soc.*, **84**, 540 (1962); c) M. J. S. Dewar and T. Morita, *ibid.*, **91**, 796 (1969).

Synthesis and Absolute Stereochemistry of (+)-6,15-Dihydro-6,15-ethanonaphtho[2,3-*c*]pentaphene as Determined by Exciton Chirality and X-Ray Bijvoet Methods[1)]

Nobuyuki HARADA, Yuki TAKUMA, and Hisashi UDA

Chemical Research Institute of Nonaqueous Solutions, Tohoku University, Katahira, Sendai 980

(Received February 18, 1977)

(6*R*,15*R*)-(+)-6,15-Dihydro-6,15-ethanonaphtho[2,3-*c*]pentaphene (**1**) was synthesized from (9*R*,10*R*)-(+)-dimethyl 9,10-dihydro-9,10-ethanoanthracene-1,5-dicarboxylate, the absolute configuration of which has been established by the X-ray Bijvoet method and chemical correlations. The CD spectrum of **1** clearly exhibits very strong positive first and negative second Cotton effects due to coupling of the ^1B_b transitions ($\Delta\varepsilon_{268.0}=+931.3$ and $\Delta\varepsilon_{249.7}=-720.8$; $A(=\Delta\varepsilon_1-\Delta\varepsilon_2)=+1652.1$), the positive sign of the A value being in accord with the positive exciton chirality between the two long axes of the anthracene moieties in **1**. The results demonstrate an ideal case of chiral exciton coupling in CD spectra, and provide evidence of the consistency between nonempirical CD exciton chirality and X-ray Bijvoet methods.

The circular dichroic Cotton effects due to a chiral exciton coupling between two or more chromophores enable one to determine the absolute stereochemistry in a nonempirical manner, as does the X-ray crystallographic Bijvoet method. The present circular dichroic method has been extensively studied in the fields of biopolymers,[2)] inorganic complexes,[3)] physical chemistry,[4,5)] synthetic organic compounds,[6)] as well as in natural products.[7)] In the cases of steroidal glycol dibenzoates and several natural products, we have quantitatively calculated the coupled Cotton effects on the basis of the molecular exciton theory, obtaining excellent agreement between observed and calculated Cotton effects. Not only the sign of a Cotton effect but also its amplitude, location, and shape were satisfactorily reproduced based on the quantum mechanical calculation.[8)]

Although the optical circular dichroic exciton chirality and X-ray crystallographic Bijvoet methods are independent of each other, the two nonempirical methods should give the same absolute stereochemistry. The X-ray Bijvoet method utilizes the anomalous dispersion effect by heavy atoms, and is therefore applicable to all compounds containing a heavy atom. Actually, the X-ray Bijvoet method has been employed for various chemical compounds, since the first determination of the absolute configuration of (+)-tartaric acid was reported by Bijvoet *et al.* in 1951.[9)]

On the other hand, the circular dichroic exciton chirality method is based on the Cotton effects due to the chiral exciton coupling between two or more chromophores. The assignment of Cotton effects should be unambiguous and reliable in view of a nonempirical quantum mechanical calculation. Thus for the determination of the absolute stereochemistry by the application of the present optical method, it is important to choose a proper electronic transition of proper chromophores which satisfy the following requirements of a chiral exciton coupling: (i) Large extinction coefficient values in UV spectra; (ii) isolation of the band in question from other strong absorptions; (iii) established direction of the electric transition moment in the geometry of the chromophore; (iv) unambiguous determination of the exciton chirality in space, inclusive of configuration and conformation; (v) negligible molecular orbital overlapping between the chromophores.

The syntheses and chiroptical properties of optically active triptycene derivatives and 1,5-disubstituted 9,10-dihydro-9,10-ethanoanthracenes have been extensively studied by Nakagawa *et al.*[10)] They determined the absolute configurations of two key compounds, (1*R*,6*S*)-(+)-2,5-dimethoxy-7-aminotriptycene hydrobromide (**2**) and (9*S*,10*S*)-(−)-9,10-dihydro-9,10-ethanoanthracene-1,5-diamine dihydrobromide (**3**) by the X-ray Bijvoet method (Fig. 1).[11)] The absolute stereochemistry of other compounds has been established by the chemical correlations to these key compounds.[10,12)] For example, (+)-dimethyl 9,10-dihydro-9,10-ethanoanthracene-1,5-dicarboxylate (**6**) was converted into the antipode of (−)-diamino derivative (**3**), which corroborated the

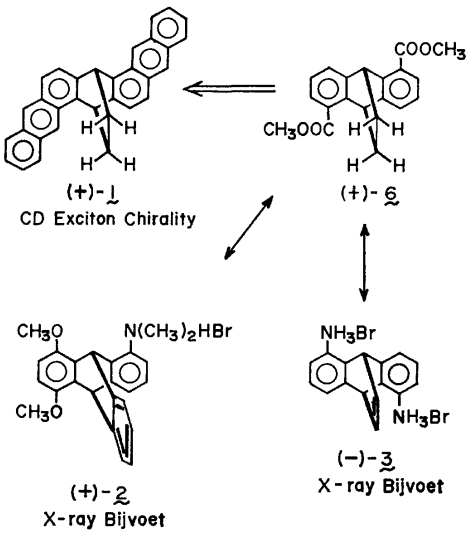

Fig. 1. Correlations between absolute stereochemistries of 9,10-dihydro-9,10-ethanoanthracene derivatives; absolute configurations of (+)-**2** and (−)-**3** have been determined by Tanaka, *et al.*,[11)] using the X-ray Bijvoet method. The arrow (↔) indicates the chemical correlations made by Nakagawa, *et al.*[10,11b)] The synthesis indicated by the arrow (⇐) and the absolute stereochemistry of (+)-**1** as determined by the CD exciton chirality method are described in this paper.

(9*R*,10*R*) absolute configuration of diester (+)-**6**.

Theoretical determination of the absolute stereochemistry of these compounds in view of the chiral exciton coupling mechanism was attempted by Tanaka *et al.*[11b,13] Their analyses of circular dichroic spectra led to the antipodal absolute configurations, contradictory with X-ray Bijvoet data. On the other hand, the absolute stereochemistry calculated by Hagishita and Kuriyama,[14] and others[15–17] is consistent with the X-ray Bijvoet data. Therefore, it is necessary to determine the absolute configurations of these cage compounds on the basis of reliable and unambiguous assignment of exciton coupled Cotton effects. It is also of significance to clarify the applicability of the present optical method.

This paper reports the synthesis and the (6*R*,15*R*) absolute stereochemistry of (+)-6,15-dihydro-6,15-ethanonaphtho[2,3-*c*]pentaphene (**1**) as determined by both circular dichroic exciton chirality and X-ray Bijvoet methods (Fig. 1). Hydrocarbon **1** was found to be the ideal compound satisfying the requirements of a chiral exciton coupling. It should be emphasized that the results obtained by the exciton chirality method are consistent with those by the X-ray Bijvoet method.

Results and Discussions

*Synthesis of (6*R*,15*R*)-(+)-6,15-Dihydro-6,15-ethanonaphtho[2,3-*c*]pentaphene (**1**).* The hydrocarbon (+)-**1** was synthesized from (9*R*,10*R*)-(+)-dimethyl 9,10-dihydro-9,10-ethanoanthracene-1,5-dicarboxylate (**6**), the absolute configuration of which has been established by the X-ray Bijvoet method and chemical correlations (Scheme 1).[10–12]

The diester (+)-**6**, mp 120.0—120.5 °C, $[\alpha]_D$ +359.2°, was quantitatively reduced to 9,10-dihydro-9,10-ethanoanthracene-1,5-dimethanol (**7**) with sodium bis(2-methoxyethoxy)aluminumhydride (SMEAH), followed by oxidation with activated manganese (IV) oxide under nitrogen giving (+)-9,10-dihydro-9,10-ethanoanthracene-1,5-dicarbaldehyde (**8**), mp 128.0—129.5 °C, $[\alpha]_D$ +487.3°. Since dialdehyde **8** was air-sensitive the crude product was immediately used for the subsequent Grignard reaction. Dialdehyde **8** was treated with excess *o*-tolylmagnesium bromide at room temperature to afford an epimeric mixture of 9,10-dihydro-α,α′-bis(*o*-tolyl)-9,10-ethanoanthracene-1,5-dimethanol (**9**). Since the additional chiralities of the secondary alcoholic moiety collapse at the next stage, the epimeric mixture of glycol **9** was used without separation. The Jones oxidation of glycol **9** afforded (+)-9,10-dihydro-9,10-ethanoanthracene-1,5-diylbis(*o*-tolyl)methanone (**10**), mp 151.0—152.5 °C, $[\alpha]_D^{20}$ +177°, (56% yield from (+)-dialdehyde **8**).

The selective oxidation of two aromatic methyl groups of diketone (+)-**10** was achieved by refluxing with $KMnO_4$ in aqueous NaOH–pyridine to give 2,2′-(9,10-dihydro-9,10-ethanoanthracene-1,5-diyldicarbonyl)dibenzoic acid (**11a**) contaminated with a small amount of monocarboxylic acid. The oxidation occurred exclusively on the aromatic methyl groups, the bridge head hydrogens remaining unchanged. The stability of the bridgehead hydrogens to oxidation can be accounted for by the fact that the carbon-hydrogen bond is perpendicular to the π-orbitals of the aromatic moiety and the rigidity of the molecular frame prevents the enolization of the bridgehead hydrogens. The structure of dibenzoic acid **11a** was characterized by the physical data of diester **11b**, and also by those of monoester **11c** derived from the intermediate monocarboxylic acid.

Cyclization of dibenzoic acid **11a** in polyphosphoric acid yielded (+)-6,15-dihydro-6,15-ethanonaphtho[2,3-*c*]pentaphene-5,9,14,18-tetrone (**12**), mp 268.0—268.5 °C, $[\alpha]_D^{20}$ +1000°, as the sole product (64% from diketone (+)-**10**). Finally, reduction of quinone (+)-**12** with zinc powder and successive dehydration catalyzed with acetic acid gave a very strong fluorescent hydrocarbon, (+)-6,15-dihydro-6,15-ethanonaphtho[2,3-*c*]-pentaphene (**1**), $[\alpha]_D$ +1157°, in solid masses.

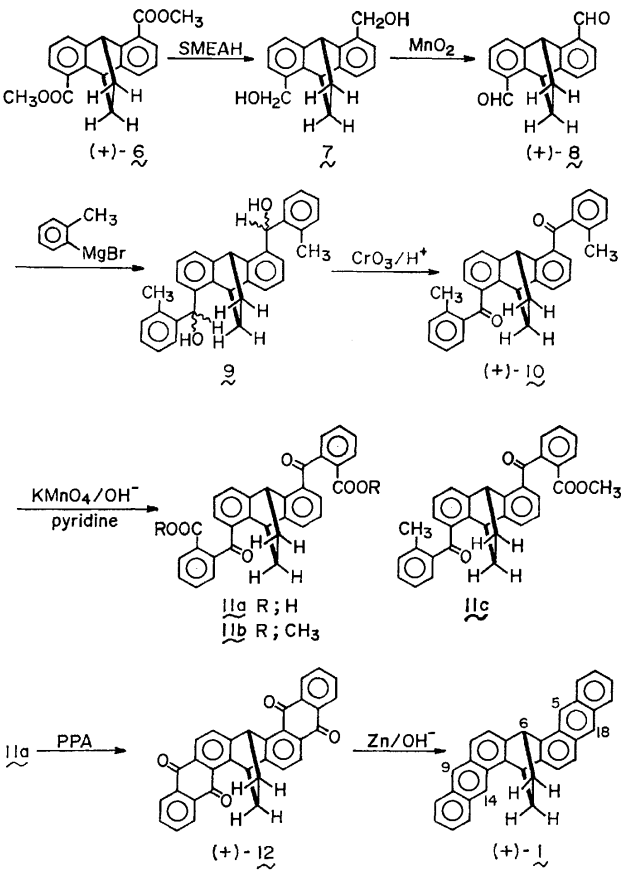

Scheme 1.

Since the configuration of the ethano-bridge remains unchanged throughout all the reactions, it is concluded that the (6*R*,15*R*) absolute stereochemistry of hydrocarbon (+)-**1** has been established by the X-ray Bijvoet method and chemical correlations.

Circular Dichroic Spectra and Absolute Stereochemistries. The characterization of the electronic spectra of polyacene chromophores has been established by theoretical and experimental studies since the discovery of quantum mechanics. For example, anthracene exhibits at least four absorptions above 200 nm wavelength: the ^1L_a transition of medium-intensity around 380—300 nm

(ε 7600) with vibrational structures, the weak ^1L_b transition buried under the ^1L_a band, the intense ^1B_b transition at 251.9 nm (ε 204000), and the ^1C_b transition around 200 nm. Among these transitions, the allowed ^1B_b transition has been well established to have the electric transition moment along the long axis of the chromophore, while the ^1L_a transition has been assigned to be polarized parallel to the short axis, as illustrated in Fig. 2.[18]

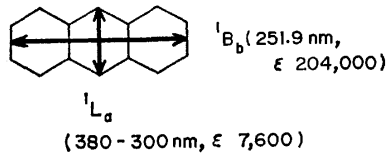

Fig. 2. Polarizations of the electric transition moments of anthracene.

The electronic spectrum of (+)-**1** resembles that of anthracene; it exhibits the ^1L_a transition around 410—300 nm (ε 11200) with five peaks, the very strong ^1B_b transition at 267.2 nm (ε 268600) with an inflection around 250 nm, and the broad ^1C_b transition around 220 nm (ε 34200) (Fig. 3).

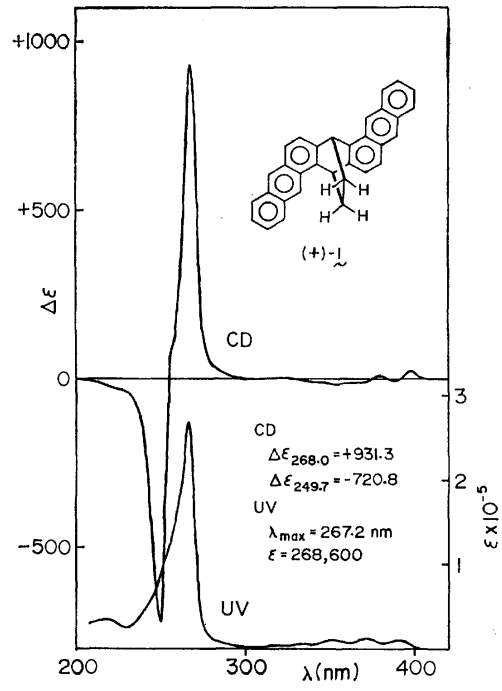

Fig. 3. CD and UV spectra of (6*R*,15*R*)-(+)-6,15-dihydro-6,15-ethanonaphtho[2,3-*c*]pentaphene (**1**) (see text for the solvent systems).

From these electronic properties and the rigidity of the molecular frame, it is obvious that the hydrocarbon **1** meets the requirements of the exciton chirality method: Namely, (i) the allowed ^1B_b transition of the component chromophore of **1**, *i.e.*, anthracene, exhibits a very strong ε value of the order of 10^5, (ii) the location of the present band around 260 nm is sufficiently separated from the weak ^1L_a and ^1L_b transitions around 400—300 nm and also from the ^1C_b transition so that the contribution of the weak absorption bands can be neglected, (iii) the polarization of the ^1B_b transition in anthracene is well established, (iv) because of the rigidity of the present cage compound **1**, the positive exciton chirality in space can be definitely determined, and (v) there is no direct conjugation between the two component chromophores, and the contribution of homoconjugation if any, is negligible[19] because of the large exciton dipole-dipole coupling term.

As expected, the circular dichroic spectrum of (+)-**1** clearly exhibits very strong positive first and negative second Cotton effects due to the coupling of the ^1B_b transitions ($\Delta\varepsilon_{268.0}=+931.3$, and $\Delta\varepsilon_{249.7}=-720.8$; $A(\Delta\varepsilon_1-\Delta\varepsilon_2)=+1652.1$) (Fig. 3). These Cotton effects are about one hundred times larger than those of common organic compounds.

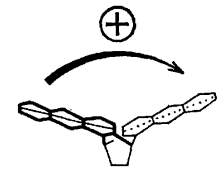

Fig. 4. Positive exciton chirality between the two axes of the anthracene moieties in hydrocarbon (+)-**1**.

Since the sign of the *A* value is positive, it is concluded that the hydrocarbon (+)-**1** has a positive exciton chirality, *i.e.*, a clockwise screwness, between the two long axes of the anthracene moieties, which corresponds to the (6*R*,15*R*) absolute stereochemistry in consistency with the X-ray data (Fig. 4). The present data thus not only determine the absolute configuration of (+)-**1** in a nonempirical manner, but also provide *definite evidence of the consistency between nonempirical circular dichroic and X-ray Bijvoet methods.*

In contrast to the case of intense absorption, the simple exciton coupling mechanism is not always applicable to the Cotton effects due to a weak absorption. For example, the ^1L_a transition of (+)-**1** exhibits weak and complicated Cotton effects around 400—300 nm, which are of positive sign at longer wavelength side and of negative sign at shorter wavelength side, in conflict with the signs expected from the negative exciton chirality between the two short axes of anthracene moieties (Fig. 3). It seems that the homoconjugation effect between the two chromophores and/or the mixing of the ^1L_a transition with the intense ^1B_b transition[20] make a dominant contribution to these weak Cotton effects.

A similar situation was observed for dialdehyde (+)-**8**; both the ^1L_b transition at 307.5 nm and the intramolecular charge transfer band at 252.5 nm exhibit only weak positive Cotton effects instead of split ones (Fig. 5). The circular dichroism of (+)-**10** also shows a simple pattern; two weak positive Cotton effects of the ^1L_b and intramolecular charge transfer bands and a negative one at 228 nm (Fig. 6). The small amplitude ($\Delta\varepsilon\simeq 10$) of these Cotton effects can be ascribed to the complicated polarization spectra of benzophenone chromophore[21] and to the conformational flexibility of the *o*-toluoyl group.

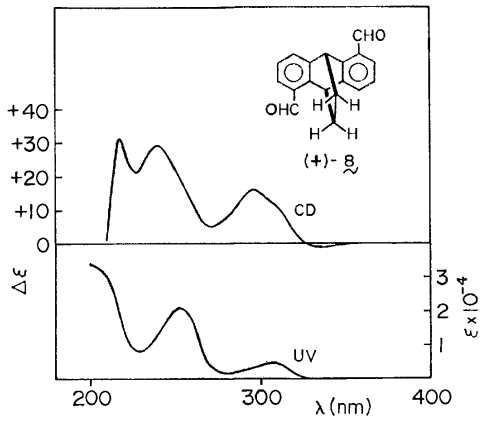

Fig. 5. CD and UV spectra of (+)-9,10-dihydro-9,10-ethanoanthracene-1,5-dicarbaldehyde (**8**)(see text for the solvent systems).

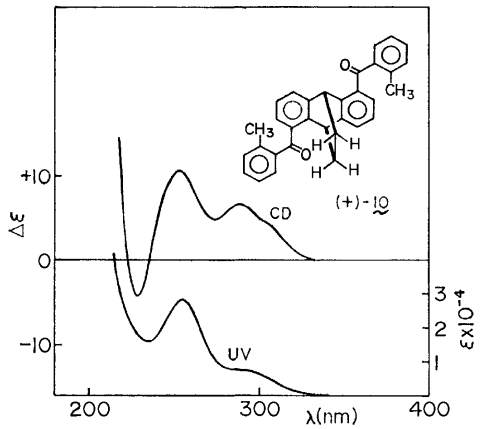

Fig. 6. CD and UV spectra of (+)-9,10-dihydro-9,10-ethanoanthracene-1,5-diylbis(*o*-tolyl)methanone (**10**) (see text for the solvent systems).

In contrast to (+)-**8** and (+)-**10**, quinone (+)-**12** exhibits relatively strong Cotton effects over 400—200 nm ($\Delta\varepsilon$ −44—+133) (Fig. 7). The polarization of the electronic transitions of 9,10-anthraquinone is established on the basis of the polarized phosphorescence spectrum;[22] the π-π^* transition (I) at 360—300 nm, the transition (II) at 300—260 nm, and the transition (III) at 260—240 nm are polarized along long, short, and long axes, respectively, of the chromophores. On the basis of the present polarization spectra, we have tentatively assigned the CD spectrum of (+)-**12** as follows: The positive Cotton effect at 360 nm and the negative one at 324 nm are attributable to the coupling of transition I, corresponding to the positive exciton chirality. In a similar way, the negative exciton coupling of transition II and the positive one of transition III give rise to the negative/positive and positive/negative Cotton effects, respectively, in which the two positive Cotton effects overlap each other at 260 nm. The present assignment is not definite because of the proximity of the two intense transitions II and III, and the weak intensity of transition I. It is difficult to determine the absolute stereochemistry of (+)-**10** based on the circular dichroic data.

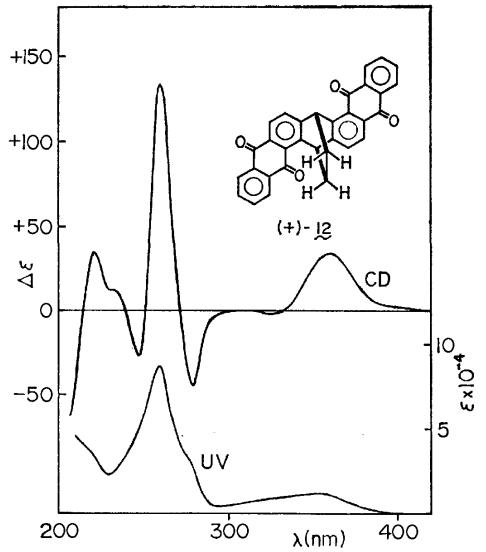

Fig. 7. CD and UV spectra of (+)-6,15-dihydro-6,15-ethanonaphtho[2,3-*c*]pentaphene-5,9,14,18-tetrone (**12**) (see text for the solvent systems).

As in the case of hydrocarbon (+)-**1**, the ^1B_b transition of polyacenes is ideal for the nonempirical determination of absolute stereochemistry on the basis of a chiral exciton coupling. On the other hand, the use of chromophores which exhibit weak transitions and/or complicated polarization spectra is undesirable for the present purpose. Therefore *one should choose a proper electronic transition of proper chromophores which satisfy the requirements of the exciton chirality method*, if one wish to determine absolute stereochemistry on sound grounds.

Experimental

General Procedures. Melting points are uncorrected. Spectral data were recorded on the following instruments: NMR, Jeol C-60HL, PMX60, and JNMPS-100 spectrometers; IR, Hitachi EPI-G2 infrared spectrophotometer; MS, Jeol JMS-01SG-2 mass spectrometer; UV, Hitachi EPS-3T spectrophotometer; CD, Jasco J-20 spectropolarimeter;optical rotations, Jasco DIP-4 and ORD/UV-5 spectropolarimeters.

The following CD data are those of the extrema and zero line interactions.

Elemental analyses were carried out in the microanalytical laboratories of our institute.

Both (+)- and (−)-dimethyl 9,10-dihydro-9,10-ethanoanthracene-1,5-dicarboxylate (6) were prepared according to the reported procedure;[10e] 9,10-dihydro-9,10-ethenoanthracene-1,5-dicarboxylic acid (**4**) was optically resolved with (−)-strychnine. The crystalline salt of (−)-**4** and (−)-strychnine was recrystallized four times from ethanol to afford a salt of constant rotation, $[\alpha]_D$ −305.1° (*c* 0.20059, pyridine). The optically pure salt was treated with 50% acetic acid to give (−)-diacid **4**, which was esterified by refluxing in methanol containing concd H_2SO_4, followed by recrystallization three times from methanol giving (−)-dimethyl 9,10-dihydro-9,10-ethenoanthracene-1,5-dicarboxylate (**5**) of constant rotation: mp 149.5—150.0°C; $[\alpha]_D$ −350.0° (*c* 0.30048, methanol), $[\alpha]_{405}$ −1016° (*c* 0.03100, methanol) (lit,[10e] mp 151.5—151.8 °C; $[\alpha]_{405}$ −1160° (*c* 0.00546, methanol)).

Catalytic hydrogenation of (−)-**5** over PtO_2 in tetrahydrofuran and recrystallization three times from methanol yielded

optically pure diester (−)-**6**: mp 121.0—121.5 °C; $[\alpha]_D$ −360.4° (*c* 0.30032, methanol), $[\alpha]_{405}$ −1064° (*c* 0.03055, methanol) (lit,[10e] mp 121.8—122.4 °C; $[\alpha]_{405}$ −1170° (*c* 0.00600, methanol)).

The mother liquor obtained after the first recrystallization of the strychnine salt of (±)-diacid **4** was evaporated to dryness. The residual crystalline salt was acidified and esterified in the same way as described for the (−)-diacid **4**, giving diester (+)-**5**: mp 147.5—148.0 °C from methanol; $[\alpha]_{405}$ +1000.1° (*c* 0.006344, methanol), optical purity 98.4% based on the rotation.

Catalytic hydrogenation of (+)-**5** and recrystallization four times from methanol afforded optically pure diester (+)-**6**: mp 120.0—120.5 °C; $[\alpha]_D$ +359.2° (*c* 0.30037, methanol).

Found: C, 74.59; H, 5.80%. Calcd for $C_{20}H_{18}O_4$: C, 74.52; H, 5.63%.

9,10-Dihydro-9,10-ethanoanthracene-1,5-dimethanol (7). A 7.0 % solution of sodium bis(2-methoxyethoxy)aluminumhydride in toluene (30.6 ml, 11.0 mmol) was added dropwise to a solution of 1.0 g (3.1 mmol) of diester (+)-**6** in 20 ml of dried benzene under ice-cooling. The ice bath was removed and the solution was stirred at room temp for 2.5 h. The reaction mixture was quenched with a minimum amount of water to precipitate hydroxides. After decantation of the supernatant, the precipitate was washed with ether, and the combined organic solution was dried over anhyd Na_2SO_4. Evaporation of the solvent gave a syrup of dimethanol **7** in a quantitative yield: IR($CHCl_3$) ν_{max} 3580, 3550—3090, 2990, 2940, 2850, 1460, 1435, 1380, 1140, 1000 cm^{-1}; NMR(100 MHz, $CDCl_3$) δ 1.64 (br s, 4H, ethane bridge), 2.60 (br s, 2H, hydroxy), 4.64 (br s, 6H, $-CH_2O-$ and bridgehead), 6.93—7.30 ppm (m, 6H, aromatic).

(+)-9,10-Dihydro-9,10-ethanoanthracene-1,5-dicarbaldehyde (8). A solution of 830 mg of dimethanol **7** in 150 ml of acetone was stirred overnight with 10.0 g of activated MnO_2 at room temp under nitrogen. The reaction mixture was filtered through celite, and MnO_2 was washed with acetone. The filtrate was evaporated to give 791 mg (97%) of crude crystalline dialdehyde (+)-**8**. Since dialdehyde **8** is air sensitive, the crude product was used for the next reaction without purification.

An analytical sample was obtained by recrystallization from ethanol, mp 128.0—129.5 °C; IR(KBr) ν_{max} 2960, 2925, 2850, 1670, 1580, 1460, 1440, 1405, 1240, 1140, 1060, 1030, 790, 770, 750, 730 cm^{-1}; NMR (100 MHz, $CDCl_3$) δ 1.79 (br s, 4H, ethane bridge), 5.75 (s, 2H, bridge head), 7.28 (t, J=7.5 Hz, 2H, aromatic meta to formyl), 7.57 (dd, J= 7.5, 2.0 Hz, 2H, aromatic para to formyl), 7.59 (dd, J= 7.5, 2.0 Hz, 2H, aromatic ortho to formyl), 10.28 ppm (s, 2H, formyl); $[\alpha]_D$ +487.3° (*c* 0.01026, $CHCl_3$); UV(EtOH) λ_{max} 307.5 (ε 4400), 252.5 nm (ε 20200); CD(EtOH) $\Delta\varepsilon_{335.0}=-1.1$, $\Delta\varepsilon_{328.0}=0.0$, $\Delta\varepsilon_{296.5}=+16.0$, $\Delta\varepsilon_{240.0}=+29.4$, $\Delta\varepsilon_{218.5}=+31.2$.

Found: C, 81.97; H, 5.46%. Calcd for $C_{18}H_{14}O_2$: C, 82.42; H, 5.38%.

9,10-Dihydro-α,α′-bis(o-tolyl)-9,10-ethanoanthracene-1,5-dimethanol (9). A solution of 4.245 g (24.8 mmol) of *o*-bromotoluene in 150 ml of ether was stirred overnight with 603 mg (24.8 mmol) of magnesium filings at room temp under nitrogen. To the greenish black solution of the Grignard reagent of *o*-tolylmagnesium bromide was added dropwise, over a period of 20 min, a solution of 781 mg (3.1 mmol) of dialdehyde (+)-**8** in 50 ml of abs ether. The reaction mixture was stirred for 4 h at room temp, then quenched by addition of wet ether. After addition of water to precipitate hydroxides and decantation of the supernatant, the precipitate was washed with ether and the combined ethereal solution was dried over anhyd Na_2SO_4. Evaporation of the solvent afforded 1.360 g (*ca.* 100%) of crude solid glycol **9**.

Thin layer chromatography of **9** on silica gel ($CHCl_3$–methanol 10: 1) showed partially overlapping three spots, which indicates that glycol **9** is a mixture of epimers (theoretically three epimers are possible). Product **9** was used for the next oxidation reaction, without separation of epimers.

(+)-9,10-Dihydro-9,10-ethanoanthracene-1,5-diylbis(o-tolyl)-methanone (10). To a cold solution of 1.360 g (6.1 mmol of hydroxyl group) of an epimeric mixture of **9** in 40 ml of acetone was added dropwise over 2 min, under ice-cooling, 1.52 ml of Jones reagent (6.1 mmol of oxygen equivalent; a standard solution made by dissolving 26.72 g of CrO_3 in 23 ml of concd H_2SO_4 diluted with water to a volume of 100 ml). The reaction mixture was stirred for 3 min. Addition of ethanol and water, extraction with ether, washing with water and brine, and evaporation of solvent gave 1.193 g of crystalline material, which was recrystallized from ethanol to yield 746 mg (56% from dialdehyde **8**) of diketone (+)-**10**: mp 151.0—152.5 °C from ethanol; IR(KBr) ν_{max} 1662, 1640, 1270, 758, 752, 740 cm^{-1}; NMR(60 MHz, $CDCl_3$) δ 1.72 (br s, 4H, ethane bridge), 2.46 (s, 6H, aromatic methyl), 4.95 (br s, 2H, bridgehead), 6.91—7.56 ppm (m, 14H, aromatic); $[\alpha]_D^{20}$ +177° (*c* 0.02032, ethanol); UV (EtOH) λ_{infl} 298 (ε 6800), λ_{max} 255.1 nm (ε 28200); CD (EtOH) $\Delta\varepsilon_{289.0}=+6.6$, $\Delta\varepsilon_{254.0}=+10.6$, $\Delta\varepsilon_{236.0}=0.0$, $\Delta\varepsilon_{228.0}=-4.1$, $\Delta\varepsilon_{222.5}=0.0$.

2,2′-(9,10-Dihydro-9,10-ethanoanthracene-1,5-diyldicarbonyl)-dibenzoic Acid (11a). A mixture of 231 mg (0.52 mmol) of diketone (+)-**10**, 30 ml of pyridine, 20 ml of 4% aq NaOH, and 4.0 g of $KMnO_4$ was gently refluxed for 2 h. Additional 20 ml of 4% aq NaOH and 4.0 g of $KMnO_4$ were added and the reaction mixture was refluxed for 3 h, during which the reaction was monitored by TLC on silica gel ($CHCl_3$–methanol 10: 1). After cooling to room temp, the reaction mixture was acidified with 6 M HCl, followed by addition of aq satd Na_2SO_3 solution in order to dissolve the brown precipitate of MnO_2. Extraction with ether, washing with brine, and evaporation of solvent afforded 253 mg (96%) of syrup, which was predominantly dibenzoic acid **11a**, contaminated with a small amount of monocarboxylic acid.

Dimethyl 2,2′-(9,10-Dihydro-9,10-ethanoanthracene-1,5-diyldicarbonyl)dibenzoate (11b). The crude dibenzoic acid **11a** (70 mg) was treated with ethereal diazomethane solution under ice-cooling and the reaction mixture was allowed to stand for 30 min. Evaporation of solvent gave 66 mg of syrup, which was subjected to preparative TLC (petroleum ether–ethyl acetate 10: 3) to yield 27 mg (56%) of pure dibenzoate **11b**: IR($CHCl_3$) ν_{max} 1724, 1663, 1282, 1138 cm^{-1}; NMR (100 MHz, $CDCl_3$) δ 1.81 (br s, 4H, ethane bridge), 3.53 (s, 6H, ester methyl), 5.43 (s, 2H, bridgehead), 6.95—7.13 (m, 4H, aromatic), 7.34—7.66 (m, 8H, aromatic), 7.85—8.02 ppm (m, 2H, aromatic).

By preparative TLC, a monoester product, methyl 2-(9,10-dihydro-5-*o*-toluoyl-9,10-ethanoanthracene-1-ylcarbonyl)-benzoate (**11c**) was isolated as a minor product: NMR (60 MHz, $CDCl_3$) δ 1.75 (br s, 4H, ethane bridge), 2.43 (s, 3H, aromatic methyl), 3.49 (s, 3H, ester methyl), 4.90 (br s, 1H, bridgehead 9-H), 5.40 (br s, 1H, bridgehead 10-H), 6.88—7.66 (m, 13H, aromatic), 7.76—7.97 ppm (m, 1H, aromatic).

(+)-6,15-Dihydro-6,15-ethanonaphtho[2,3-c]pentaphene-5,9,14,18-tetrone (12). A mixture of 253 mg of dibenzoic acid **11a** in 26 ml of polyphosphoric acid (prepared by dissolving 100 g of P_2O_5 in 100 ml of 85% H_3PO_4) was heated at 90 °C for 1.5 h under stirring. At the end of the reaction period, TLC on silica gel ($CHCl_3$–acetone 50: 1) revealed only one yellow spot with strong UV absorption. After cooling to room temp, the reaction mixture was poured into ice-water and extracted with ether. The ethereal solution was dried over anhyd

Na_2SO_4; evaporation of the solvent yielded 191 mg of crystals, which were purified by short column chromatography on silica gel giving 157 mg (64% yield from **10**) of quinone (+)-**12**: mp 268.0—268.5 °C from benzene–ether; IR(KBr) ν_{max} 1662, 1588, 1567, 1348, 1325, 1280, 1137, 988, 717 cm^{-1}; NMR (60 MHz, $CDCl_3$) δ 1.85 (br s, 4H, ethane bridge), 6.43 (br s, 2H, bridgehead), 7.53—7.76 (m, 6H, aromatic meta to carbonyl), 7.95—8.22 ppm (m, 6H, aromatic ortho to carbonyl); $[\alpha]_D^{20}$ +1000° (*c* 0.01009, 10% dioxane in ethanol); UV(0.47% dioxane in ethanol) λ_{max} 350.0 (ε 11100), λ_{infl} 278 (ε 30300), λ_{max} 259.2 nm (ε 86500); CD(1.0% dioxane in ethanol) $\Delta\varepsilon_{360}=+33.6$, $\Delta\varepsilon_{332}=0.0$, $\Delta\varepsilon_{324}=-2.1$, $\Delta\varepsilon_{308}=0.0$, $\Delta\varepsilon_{278.5}=-44.1$, $\Delta\varepsilon_{271}=0.0$, $\Delta\varepsilon_{260}=+133.4$, $\Delta\varepsilon_{251}=0.0$, $\Delta\varepsilon_{247}=-26.3$, $\Delta\varepsilon_{239}=0.0$, $\Delta\varepsilon_{232}=+12.3$, $\Delta\varepsilon_{221}=+34.2$, $\Delta\varepsilon_{214.5}=0.0$.

*(+)-6,15-Dihydro-6,15-ethanonaphtho[2,3-c]pentaphene (**1**).* To a solution of 76 mg of quinone (+)-**12** in 20 ml of benzene were added 4.0 g of activated zinc powder, 20 ml of 10% aq NaOH, and 0.5 ml of aq satd $CuSO_4$. The reaction mixture of a deep red color was refluxed under vigorous stirring for 10 h, during which the red color faded.

The reaction was monitored by TLC on silica gel ($CHCl_3$–acetic acid 5: 0.03). In this case, acetic acid in a developing solvent is important for catalyzing the dehydration of hydroxy intermediates which are more polar than the starting material **10**.

After cooling to room temp, zinc metal was filtered and washed with water and benzene. The combined filtrate was neutralized with acetic acid, followed by extraction with ether and evaporation of solvent to give 70 mg of a syrup. The remaining material was dissolved in 30 ml of chloroform containing 0.04 ml of acetic acid and gently refluxed for 3 h to complete the dehydration. The solvent was evaporated *in vacuo*, and the residual matter was subjected to preparative TLC on silica gel (petroleum ether–benzene 10: 3), giving 52 mg (78%) of a strong fluorecent hydrocarbon (+)-**1**. Attempts to carry out recrystallization from various solvents were unsuccessful. Instead, yellow solid masses were obtained from benzene–ethanol. Hydrocarbon **1** was characterized by the following spectral data: IR(KBr) ν_{max} 3040, 2955, 1615, 1150, 874, 740, 467 cm^{-1}; NMR(60 MHz, $CDCl_3$) δ 1.79 (br s, 4H, ethane bridge), 5.41 (br s, 2H, bridgehead), 6.89—8.07 (m, 12H, aromatic), 8.22 (s, 2H, 9-H and 18-H), 8.75 ppm (s, 2H, 5-H and 14-H); $[\alpha]_D$ +1157° (*c* 0.034, dioxane); UV 0.08% dioxane in ethanol) λ_{max} 391.0 (ε 9130), λ_{max} 371.2 (ε 11170), λ_{max} 352.7 (ε 8950), λ_{max} 267.2 (ε 268600), λ_{max} 219.5 nm (ε 34200); CD(0.18% dioxane in ethanol) $\Delta\varepsilon_{397.2}=+26.4$, $\Delta\varepsilon_{390.6}=0.0$, $\Delta\varepsilon_{388.1}=-2.3$, $\Delta\varepsilon_{384.9}=0.0$, $\Delta\varepsilon_{378.0}=+6.3$, $\Delta\varepsilon_{374.5}=0.0$, $\Delta\varepsilon_{370.0}=-9.7$, $\Delta\varepsilon_{362.9}=-9.7$, $\Delta\varepsilon_{352.8}=-14.5$, $\Delta\varepsilon_{330.5}=0.0$, $\Delta\varepsilon_{268.0}=+931.3$, $\Delta\varepsilon_{256.0}=0.0$, $\Delta\varepsilon_{249.7}=-720.8$; MS *m/e* (relative intensity), 406 (39, M^+), 378 (100, $M-C_2H_4$), 188 (29).

Found: *m/e* 406.1718. Calcd for $C_{32}H_{22}$: M, 406.1720.

The authors thank Dr. Hiroshi Hayashi, Asahi Chemicals Industry, Co., for measurements of the mass spectra. The present work was partially supported by a Grant-in-Aid for Scientific Research from the Ministry of Education.

References

1) A part of the present studies has appeared in a preliminary communication: N. Harada, Y. Takuma, and H. Uda, *J. Am. Chem. Soc.*, **98**, 5408 (1976).

2) I. Tinoco, Jr., *Adv. Chem. Phys.*, **4**, 113 (1962); I. Tinoco, Jr. and C. A. Bush, *Biopolym. Symp.*, **1**, 235 (1964); I. Tinoco, Jr., *Radiat. Res.*, **20**, 133 (1963).

3) B. Bosnich, *Acc. Chem. Res.*, **2**, 266 (1969).

4) J. A. Schellman, *Acc. Chem. Res.*, **1**, 144 (1968).

5) A D. Buckingham and P. J. Stiles, *Acc. Chem. Res.*, **7**, 258 (1974).

6) The theoretical determination of absolute stereochemistries of 1,1′-bianthryl derivatives: R. Grinter and S. F. Mason, *Trans. Faraday Soc.*, **60**, 274 (1964); S. F. Mason, R. H. Seal, and D. R. Roberts, *Tetrahedron*, **30**, 1671 (1974); see also X-ray and chemical correlation data, H. Akimoto and Y. Iitaka, *Acta Crystallogr., Sect. B*, **25**, 1491 (1969); H. Akimoto and S. Yamada, *Tetrahedron*, **27**, 5999 (1971).

7) N. Harada and K. Nakanishi, *Acc. Chem. Res.*, **5**, 257 (1972) and references cited therein.

8) N. Harada, S. L. Chen, and K. Nakanishi, *J. Am. Chem. Soc.*, **97**, 5345 (1975) and references cited therein.

9) J. M. Bijvoet, A. F. Peerdeman, and A. J. van Bommel, *Nature*, **168**, 271 (1951).

10) (a) F. Ogura, Y. Sakata, and M. Nakagawa, *Bull. Chem. Soc. Jpn.*, **45**, 3646 (1972); (b) M. Kuritani, Y. Sakata, F. Ogura, and M. Nakagawa, *Bull. Chem. Soc. Jpn.*, **46**, 605 (1973); (c) Y. Sakata, F. Ogura, and M. Nakagawa, *Bull. Chem. Soc. Jpn.*, **46**, 611 (1973); (d) F. Ogura and M. Nakagawa, *Bull. Chem. Soc. Jpn.*, **46** 651 (1973); (e) H. Tatemitsu, F. Ogura, and M. Nakagawa, *Bull. Chem. Soc. Jpn.*, **46**, 915 (1973); (f) Y. Shimizu, T. Naito, F. Ogura, and M. Nakagawa, *Bull. Chem. Soc. Jpn.*, **46**, 1520 (1973); (g) M. Hashimoto, Y. Simizu, F. Ogura, and M. Nakagawa, *Bull. Chem. Soc. Jpn.*, **47**, 1761 (1974).

11) (a) N. Sakabe, K. Sakabe, K. Ozeki-Minakata, and J. Tanaka, *Acta Crystallogr., Sect. B*, **28**, 3441 (1972); (b) J. Tanaka, C. Katayama, F. Ogura, H. Tatemitsu, and M. Nakagawa, *J. Chem. Soc. Chem. Commun.*, **1973**, 21.

12) Y. Shimizu, H. Tatemitsu, F. Ogura, and M. Nakagawa, *J. Chem. Soc. Chem. Commun.*, **1973**, 22.

13) (a) J. Tanaka, F. Ogura, M. Kuritani, and M. Nakagawa, *Chimia*, **26**, 471 (1972); (b) J. Tanaka, K. Ozeki-Minakata, F. Ogura, and M. Nakagawa, *Nature(London), Phy. Sci.*, **241**, 22 (1973); (c) J. Tanaka, K. Ozeki-Minakata, F. Ogura, and M. Nakagawa, *Spectrochim. Acta, Part A*, **29**, 897 (1973).

14) S. Hagishita and K. Kuriyama, *Tetrahedron*, **28**, 1435 (1972).

15) S. F. Mason, *J. Chem. Soc., Chem. Commun.*, **1973**, 239.

16) A. M. F. Hezemans and M. P. Groenewege, *Tetrahedron*, **29**, 1223 (1973).

17) A. Kaito, A. Tajiri, M. Hatano, F. Ogura, and M. Nakagawa, *J. Am. Chem. Soc.*, **98**, 7932 (1976).

18) A paper on the polarization spectra of anthracene and its derivatives: J. Michl, E. W. Thulstrup, and J. H. Eggers, *Ber. Bunsenges. Phys. Chem.*, **78**, 575 (1974). See also other theoretical and experimental investigations cited therein.

19) In contrast to the case of the anthracene compound **1**, the homoconjugation effect is important in the CD spectra of benzene compounds, *e.g.*, 9,10-dihydro-9,10-ethanoanthracene derivatives.[14]

20) Even in anthracene itself, the vibronic mixing of the ^1L_a transition with the ^1B_b band has been observed at 360—300 nm.[18]

21) R. Shimada and L. Goodman, *J. Chem. Phys.*, **43**, 2027 (1965).

22) (a) H. R. Drott and H. H. Dearman, *J. Chem. Phys.*, **47**, 1896 (1967); (b) J. D. Scott and W. H. Watson, *J. Chem. Phys.*, **49**, 4246 (1968).

The Cycloaddition of Dispiro[2.2.2.2]deca-4,9-diene with the Styrene Derivatives. The Syntheses and Spectral Properties of the [4.2]Paracyclophane Derivatives

Tohru SHIBATA, Takashi TSUJI, and Shinya NISHIDA

Department of Chemistry, Faculty of Science, Hokkaido University, Sapporo 060

(Received March 8, 1977)

The thermal cycloaddition of dispiro[2.2.2.2]deca-4,9-diene **1** with the styrene derivatives has afforded [4.2]paracyclophane derivatives, **3**. A reaction mechanism by way of the biradical intermediates, involving the initial homolytic cleavage of the cyclopropane ring in **1** followed by the addition to the styrene molecule, is proposed. In the reaction of **1** with styrene, and methyl α-phenylacrylate, the yields of **3** were improved with the dilution of the reactants, while in the reaction with *trans*-stilbene, no appreciable dependence on the reactant concentration was observed. The mass spectra of the substituted [4.2]paracyclophanes show a predominant fragmentation to the substituted *p*-xylene-α,α'-diyl (or elements thereof) ion radical. [4.2]Paracyclophane exhibited a temperature-dependent NMR spectrum which could be ascribed to the rapid equilibration between two structurally equivalent conformers. Bulky substituents on C-1 and C-2 shifted the equilibrium to one side.

We have previously reported the thermal cycloaddition of dispiro[2.2.2.2]deca-4,9-diene **1**[1] with 1,3-butadiene derivatives, which afforded [8]paracycloph-4-enes by way of the biradical intermediate formed through the homolytic cleavage of the cyclopropane ring in **1**.[2] In the course of our continuing study of the cycloaddition reaction of **1**, we found that the thermal cycloaddition of the styrene derivatives, **2**, to **1** gave [4.2]paracyclophanes, **3**, in fair to good yields.[3] Although the chemistry of cyclophanes is currently a subject of considerable interest,[4] relatively few preparation methods of [4.2]-paracyclophanes are known.[5] The present reaction is experimentally simple and provides a convenient route to [4.2]paracyclophanes functionalized at C-1 and C-2. In this report we will describe the preparation and the spectral properties of [4.2]paracyclophane derivatives and will discuss the probable mechanism of this novel cycloaddition reaction.

Results and Discussion

Reaction of Dispiro[2.2.2.2]deca-4,9-diene 1 with the Styrene Derivatives, 2. A solution of **1** (0.16 M) and 1,1-diphenylethylene **2g** (0.37 M) in *t*-butyl alcohol was heated at 150—155 °C for 12 h under argon in a sealed glass ampoule. The subsequent separation of the reaction product by column and preparative gas chromatographies afforded 1-phenyl[4.2]paracyclophane **3g** as colorless crystals in a 67% yield. Analogously, the reaction of **1** with some related styrene derivatives, **2a—2f**, gave **3a—3f** respectively. The results are summarized in Table 1. Proof of the structures of those products was provided by the elemental analysis and their spectral properties. In the NMR spectra, the signals of the aromatic ring protons appeared at an unusually high field, δ 6.2—6.6, reflecting the shielding effect by the facing aromatic ring,[5b] and in the UV spectra, a bathochromic shift of λ_{max} to 282—283 nm and the disappearance of the fine structure were noted.[5a] The mass spectra of **3** showed prominent peaks which could be explained in terms of the predominant fragmentation to the *p*-xylene-α,α'-diyl (or methylenetropylium) ion radicals. These characteristics clearly show

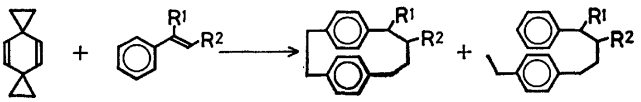

1 2 3 4

a, $R^1=R^2=H$; b, $R^1=CH_3, R^2=H$; c, $R^1=OSi(CH_3)_3$, $R^2=H$
d, $R^1=H$, $R^2=CO_2CH_3$; e, $R^1=CO_2CH_3$, $R^2=H$
f, $R^1=H$, $R^2=C_6H_5$; g, $R^1=C_6H_5$, $R^2=H$; h, $R^1=OH$, $R^2=H$

Table 1. Products from the reaction of dispiro[2.2.2.2]deca-4,9-diene **1** with **2** styrenes[a]

	Styrene		Reactant concentrations		Products (% Yield)[b]		
	R^1	R^2	**1** (mol/l)	**2** (mol/l)	**3**	**4**	Others[c]
a	H	H	0.010	0.038	7.6	0.7	**5**, 3.4
b	CH_3	H	0.05	0.15	46	5.7	
c[d]	$OSi(CH_3)_3$	H	0.10	0.22	4.4		**6**, 7.2
d	H	$COOCH_3$	0.08	0.20	28		
e	$COOCH_3$	H	0.017	0.033	78[e]		
f	H	C_6H_5	0.16	0.40	34[e]	7.0[e]	
g	C_6H_5	H	0.16	0.37	67		

a) The reactions were carried out in *t*-butyl alcohol unless otherwise noted. b) The yields are from the weight of the isolated product unless otherwise noted. c) Besides the characterized products, the formation of a few unidentified minor products was invariably observed. The major part of the residue, however, was an intractable, tarry material. d) Reaction in hexane. e) The yields were determined by GLC.

TABLE 2. MELTING POINTS AND SPECTRAL PROPERTIES OF [4.2]PARACYCLOPHANES

Compd	Mp (°C)	UV Spectrum[a] λ_{max} in nm($\varepsilon \times 10^{-2}$)	Mass spectrum[b] *m/e* (Relative intensity)
3a	71.0—72.0[c]	271(4.7), 283(2.7)	236(M^+, 35), 208(18), 145(16), 132(10), 131(20), 130(23), 129(13), 117(32), 116(33), 115(19), 105(18), 104(100), 103(13), 91(21), 78(19), 77(13),
3b	58.1—58.8	271(3.0), 283(1.9)	251(13), 250(M^+, 53), 145(22), 133(51), 132(27), 131(21), 119(14), 118(100), 117(66), 115(11), 105(27), 104(19), 91(17)
3c	82.0—82.8		325(24), 324(M^+, 59), 297(15), 296(49), 252(10), 193(23), 192(100), 178(50), 147(30), 117(13), 73(27)
3d	85.2—86.9	271(4.5), 283(3.1)	294(M^+, 40), 208(29), 189(25), 131(11), 130(11), 129(19), 119(12), 118(9), 117(42), 115(11), 105(30), 104(100), 91(16), 71(10)
3e	70.6—71.7	251(3.9), 271(3.9) 282(sh, 2.7) 292(sh, 0.8)	295(16), 294($M,^+$ 66), 235(21), 189(18), 175(10), 163(28), 162(16), 143(17), 132(14), 131(51), 129(18), 120(10), 119(100), 118(12), 117(40), 115(20), 105(30), 104(82), 103(12), 91(29), 77(12)
3f	148.0—148.5	255(4.0), 262(5.8), 265(6.1), 268(6.8), 283(3.1)	312(M^+, 16), 208(16), 207(22), 118(10), 117(12), 105(15), 104(100), 103(13), 77(15)
3g	70.8—71.8	254(5.3), 263(6.6), 270(7.0), 283(3.6)	313(10), 312(M^+, 30), 194(13), 181(18), 180(100), 179(16), 178(16), 167(19), 165(30), 145(13), 131(11), 117(10),115(13), 104(12), 91(13)
3h	116.3—116.8	271(3.6), 283(2.3)	252(M^+, 3.4), 234(32), 143(17), 131(11), 130(100), 129(58), 128(18), 118(30), 117(10), 115(40)
6	107.3—108.0	250(57)[d]	251(22), 250(M^+, 93), 133(72), 118(32), 117(100), 80(11)
7	102.6—103.0[e]	227(105), 268(53)	234(M^+, 34), 143(16), 131(11), 130(100), 129(55), 128(18), 118(30), 115(45)

a) The spectra were taken in hexane unless otherwise noted. The shoulder was denoted as sh.
b) The ions of each spectrum were normalized to the spectrum's most intense ion set equal to 100. The spectra were taken at an ionizing voltage of 80 eV. c) Reported to be 74.4—75.0°C.[5b] d) The spectrum was taken in 95% ethanol. e) Reported to be 100—101°C.[5d]

that the products, **3**, have a paracyclophane structure. The spectra and melting point of **3a** also agreed very well with those previously reported.[5a,b]

In the reaction of **1** with **2a**, besides the 1:1 cycloadduct, **3a**, an open-chain addition product, **4a** (0.7%), and a 1:2 cycloadduct, **5** (3.4%), were isolated from the reaction mixture. Open-chain adducts were also produced in the reactions of **2b** and **2f**. The reaction with **2c** proceeded rather anomalously and afforded [4.2]paracyclophan-1-one **6** as the most abundant product, together with **3c**. The alcohol obtained by the $NaBH_4$ reduction of **6** was identical in all respects with the hydrolysis product of **3c**. The application of the present reaction to the acetylenic compound was also examined. The reaction of **1** (0.20 M) with ethynylbenzene (0.40 M) in *t*-butyl alcohol at 160 °C, however, gave [4.2]paracycloph-1-ene, **7**, in only a low yield (2.3%) and was accompanied by the formation of a dispiro[2.2.4.2]dodecane derivative, **8** (13%).

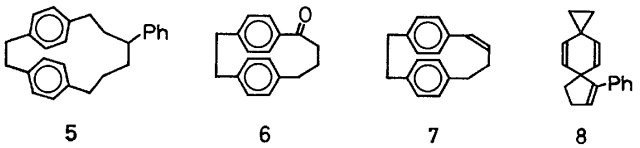

5 6 7 8

Mechanism. The present reaction may be explained by the pathway outlined in Scheme 1. We have previously demonstrated that the cyclopropane ring in **1** cleaves homolytically at an appreciable rate above 150 °C.[1,6] The biradical, **9**, thus generated reversibly from **1** adds to **2** to give **10**. The intramolecular coupling of the biradical, **10**, at the *p*-position of the benzylic radical moiety leads to the formation of **11** which subsequently rearranges to **3** under the present reaction conditions. Hydrogen abstraction by **9** and/or **10** would result in the formation of *p*-diethylbenzene and the open-chain adduct **4**. The addition of **10a** to another molecule of

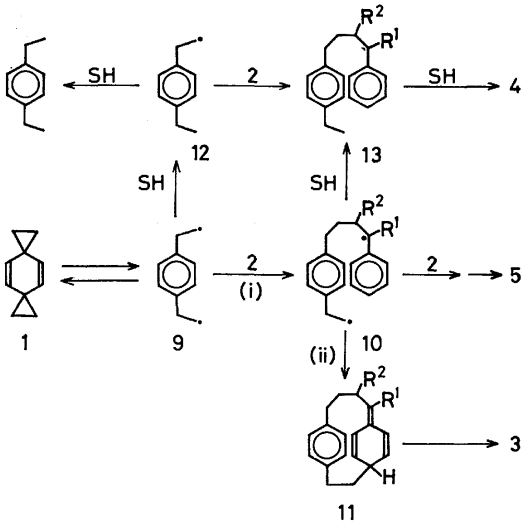

Scheme 1.

2a, followed by the ring closure, afforded **5**. The isomerization of 1-methylene-2,5-cyclohexadiene to toluene, which corresponds to the rearrangement of **11** to **3**, has been known to take place at the boiling point of diethyl ether.[7] Interestingly, the reaction of **1** with **2b** did not afford the intramolecular (formally at least) disproportionation product of the biradical intermediate, **10b**, in a detectable yield (<0.5%); this is in contrast to the reaction with isobutene, which gave **15** as the major product, probably *via* **14**.[8] These results imply that the cyclization of **10** at the *p*-position of the benzylic radical moiety is not hampered in the presence of such a potential hydrogen donor in the molecule.

The reaction of **1** with ethynylbenzene resulted in the formation of the dispiro compound, **8**, and the yield of the cyclophane, **7**, was low. In the reaction of **1** with **2**, no adducts with the dispiro[2.2.4.2]dodecane structure were isolated. The different behavior of the biradical, **16**, from that of **10** may be accounted for by the higher structural barrier imposed on the approach of the reaction sites in **16** to give **17** than in **10** to give **11** and/or a higher strain in the cyclized intermediate **17** than in **11**.

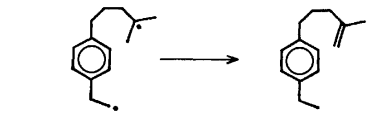

14 15

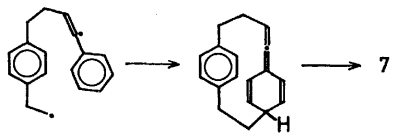

16 17

In the reaction of **1** with dimethyl *trans,trans*-2,4-hexadienoate, CIDNP has been observed in the cycloaddition product.[2b] Therefore, one may expect CIDNP in the reaction of **1** with **2** as well. The NMR spectrum recorded during the reaction of **1** and **2g** in biphenyl at 190 °C indeed showed CIDNP, and the characteristic signal of the aromatic protons in **3g**, shifted up-field, appeared as a weak emission substantiating the radical pathway of the reaction. The attempts to detect a signal which could be ascribed to the probable intermediate **11g** have, however, been fruitless thus far.

The addition of the biradical intermediate **9** to **2** is in competition with side reactions including the hydrogen abstraction to **12**, and, to give **3**, the resulting biradical **10** must collapse before side reactions including the addition to another molecule of **2** can take place. Therefore, the concentration of **2** should exert opposite effects on the yield of **3** at Steps (i) and (ii). with a few of the styrene derivatives, the effect of dilution on the yield of **3** was examined. In the reaction of **1** with **2e**, the yield of **3e** increased with the dilution of the reactants, and a similar trend was noted with **2a**. In the reaction with **2f**, however, no clear relationship between the yield of **3f** and the reactant concentration was observed. Since **2e** has a high reactivity toward the alkyl radical,[9] and since the addition of **9** would proceed efficiently even in a dilute solution, the dilution of the reactants might act favorably for the intramolecular cyclization of **10e**. In the case of **2f**, which has a relatively low reactivity, the opposite effects of the olefin concentration at Steps (i) and (ii) might balance. The reaction with **2a**, which very rapidly polymerizes, resulted in a low yield of **3a** probably because the addition of **10a** to another molecule of **2a** rather than the collapse to **11a** might predominate even in a dilute solution.

Although the reaction could be carried out in other solvents, such as benzene and hexane, *t*-butyl alcohol was used simply because of its low reactivity toward hydrogen abstraction. In benzene, the addition of **9** took place and 1-phenyl-2-*p*-tolylethane was formed, though in a small amount.

Mass Spectra of Substituted [4.2]Paracyclophanes. The mass spectra of [4.2]paracyclophane and its derivatives showed a fair generality in the fragmentation pattern and are in good accord with the assigned structures. In the spectrum of **3a**, the most intense peak occurred at *m/e* 104; its origin could be reasonably formulated by the cleavage at the benzylic positions to the *p*-xylene-α,α′-diyl (or methylenetropylium) ion radical, **19**.[10] The above fragmentation appeared common to the [4.2]paracyclophane derivatives. Thus, in the spectra of **3d** and **3f**, the most intense peak occurred at the same *m/e*, and, in those of 1-substituted derivatives, **3b**, **3c**, and **3g**, the fragment corresponding to the substituted *p*-xylene-α,α′-diyl[10] appeared as the base peak. In that of **3e**, the *p*-xylene-α,α′-diyl fragment ion peak was not the most intense, but it was still prominent. The appearance of the most intense peak at *m/e* 130 in the spectrum of **7**, which might be ascribed to **21**,[10] was also in line with the above fragmentation pattern.[11] The spectrum of **6** was distinct from the others and showed two dominant peaks, at *m/e* 117 (base peak) and 133, which could be explained by the cleavage at the ethano-bridge, followed by the McLafferty rearrangement.[12] Besides the above fragments characteristic peaks, though not intense, were observed at *m/e* corresponding to **20**[10] which demonstrated unambiguously the position of the substituent.

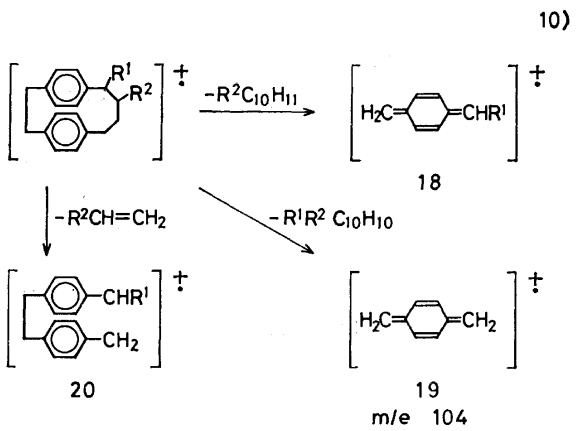

Thus, the mass spectrum provides a convenient tool for the structural analysis of [4.2]paracyclophane derivatives.

Temperature Dependence of NMR Spectrum and Conformation of 3. An examination of the NMR spectra of **3** provided information regarding the conformation. The parent [4.2]paracyclophane **3a** shows four peaks in the NMR spectrum at room temperature: two singlets at δ 6.45 (8H, aromatic protons) and 2.96 (4H, H-5, and H-6), and two relatively narrow multiplets at δ 2.22 (4H, H-1, and H-4) and 1.40 (4H, H-2, and H-3). Upon cooling, all the signals broadened from about −40 °C and resharpened again by −110 °C, accompanying the splitting of those signals into two sets of signals equal in intensity: the singlet at δ 6.45 into an AB quartet (J=8 Hz) centered at δ 6.55 and a singlet at δ 6.22, the singlet at δ 2.96 into an AA'BB' multiplet, the multiplet at δ 2.22 into a doublet of doublets (J=4 and 12 Hz) centered at δ 2.54 and a triplet (J=13 Hz) at δ 1.82, and the multiplet at δ 1.40 into two complex multiplets centered at δ 1.89 and 0.67. These observations may be explained in terms of the equilibration between two equally numerous conformers, **25a** and **26a**. A similar conformational equilibration has been invoked by Cram *et al.* to explain the temperature-dependent NMR spectrum of *cis*-2,3-diacetoxy[4.2]paracyclophane.[13] The signals observed at low temperatures can reasonably be assigned as is shown in Fig. 2, which indicates the shielding of Ha and Hd by 0.8 and 0.9 ppm respectively and the deshielding of Hc by 0.3 ppm, while there is no apparent shift of Hb compared with the corresponding protons in propylbenzene. An examination of the molecular models supports the above explanation and also reveals that R^1 in the **25** conformer is less sterically hindered than in **26** and that for R^2 the situation is the same.[14] The NMR spectrum of the 1-methyl derivative, **3b**, exhibited a similar temperature dependence and the characteristic doublet signal of the methyl protons split into two sets of doublets, 3: 1 in intensity, at δ 1.20 and 1.03 upon cooling; these sets of doublets might be ascribed to the conformers, **25b** and **26b**, respectively. More bulky substituents on C-1 and C-2 would displace the equilibrium to one side, and the chemical shifts of protons in the NMR spectra of **3d**—**g** can be explained reasonably on the basis of the **25d**—**g** conformers respectively. The coupling constants in **3d** and **3g** which have been determined thus far are also consistent with the above conformations.

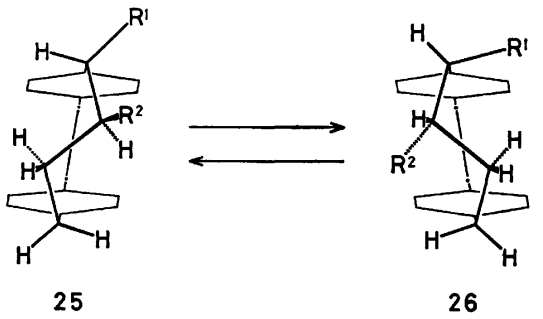

25 26

Fig. 1. Conformational equilibration in [4.2]paracyclophane derivatives.

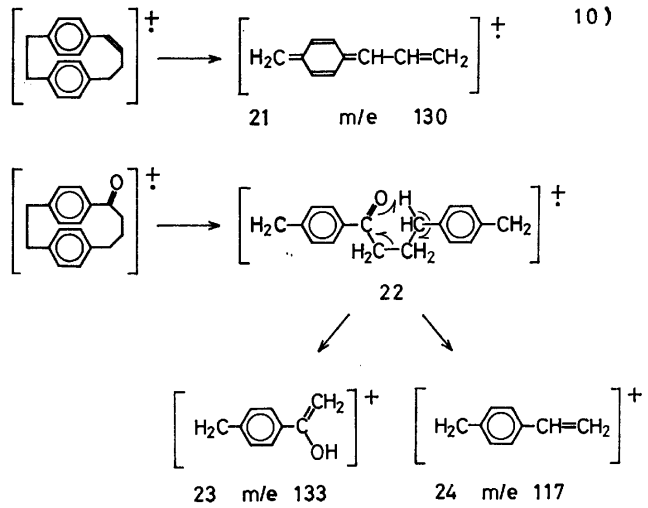

Experimental

General. Melting points are corrected. NMR spectra were obtained with JEOL PS-100 and Hitachi R-24 spectrometers at 100 and 60 MHz respectively; chemical shifts are given in ppm from $Si(CH_3)_4$. IR spectra were taken on a Hitachi Model 215 grating spectrometer and are given in cm^{-1}. Mass spectra were recorded on a Hitachi Model RMU-6E spectrometer at an ionizing voltage of 80 eV; ions of each spectrum were normalized to the spectrum's most intense ion set equal to 100. UV spectra were taken on a

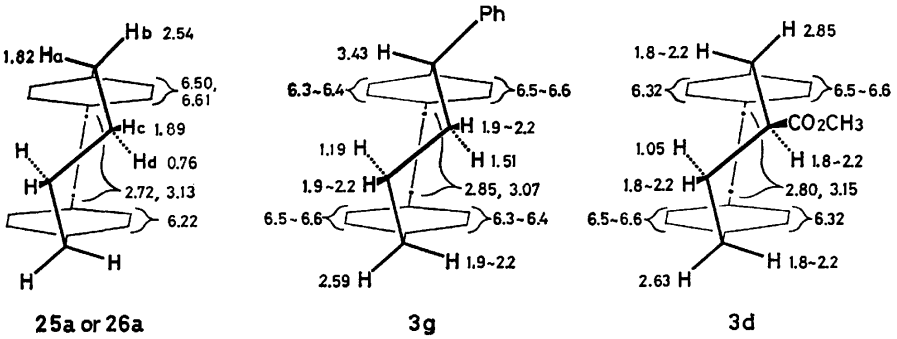

25a or 26a 3g 3d

Fig. 2. Chemical shifts in [4.2]paracyclophane derivatives. Chemical shifts in **25a** were obtained from the spectrum taken at *ca.* −115°C in CS_2 and those in **3d** and **3g** were obtained from the spectra at 23°C in CCl_4.

Cary Model 17 spectrophotometer and are given in nm. GLC work was done on a Hitachi Type 063 gas chromatograph with a thermal conductivity detector, using helium as a carrier gas. The following glass columns were used: A, 3% Apiezon Grease L on Celite 545, 3 mm×70 cm; B, 15% Apiezon Grease L on Celite 545, 3 mm×1 m; C, 20% Apiezon Grease L on Celite 545, 3 mm×1 m; D, 20% PEG phthalate on Celite 545, 4 mm×2 m; E, 20% Silicon DC-550 on Celite 545, 4 mm×1.5 m. Yields were calculated on the basis of **1** used in the reaction.

Materials. The preparation of dispiro[2.2.2.2]deca-4,9-diene **1** was carried out as has been described previously.[1] Styrene, α-methylstyrene, 1,1-diphenylethylene, and methyl cinnamate were obtained from commercial sources and were purified by fractional distillations. α-Trimethylsiloxystyrene was prepared by the method of House *et al.*[15] Methyl α-phenylacrylate was prepared following the procedure of Saquet and Thuillier.[16] *trans*-Stibene was obtained by the $NaBH_4$ reduction of desyl chloride.[17] Ethynylbenzene was prepared through the bromination and dehydrobromination of styrene.[18] *t*-Butyl alcohol was purified by fractional distillation from sodium.

*Reaction of **1** with Styrene **2a**.* A solution of 108 mg of **1** (0.82 mmol) and 345 μl of **2a** (3.0 mmol) in 80 ml of *t*-butyl alcohol was distributed among glass ampoules, bubbled with argon for 10 min, and heated at 160 °C for 10.5 h under argon (50 atm) in an autoclave. After the reaction, only a trace amount of **1** and *ca.* one fifth of the starting **2a** remained. The solvent was then removed and the residue was chromatographed on silica gel. Elution with a petroleum ether–benzene 5: 1 mixture produced an oil which was shown by GLC analysis to consist of one major and three minor components. Separation by preparative GLC (column C, 210 °C) geve 14.7 mg of [4.2]paracyclophane **3a** (7.6%) which when recrystallized from methanol had a mp of 71.0—72.0 °C (lit, 74.4—75.0 °C),[5b] 1.4 mg of **4a** (0.7%) and 3.3 mg of a mixture of two uncharacterized products. Elution with a petroleum ether–benzene 1: 1 mixture and separation by preparative GLC (column A, 210—230 °C) yielded three products in comparable amounts: 8.6, 9.4, and 4.1 mg . The second component was cheracterized as 3-phenyl[6.2]paracyclophane **5** (3.4%) on the basis of its physical properties. Further elutions with benzene and benzene–methanol produced only a polymeric, intractable material. **3a**, NMR (CS_2, 100 MHz): 1.40 (m, 4H), 2.22 (m, 4H), 2.96 (s, 4H), 6.45 (s, 8H). **4a**, NMR (CCl_4, 60 MHz): 1.17 (t, J=7.5 Hz, 3H), 1.4—1.7 (complex m, 4H), 2.2—2.7 (complex m, 8H), 6.90 (s, 4H), 7.02 (br s, 5H); mass: *m/e* 238 (M^+, 34), 131 (32), 120 (17), 119 (100), 117 (19), 115 (12), 105 (21), 104 (21), 92 (12), 91 (84), 78 (13), 77 (16), 65 (16), 41 (17). **5**,[19] NMR (CCl_4, 100 MHz): 0.9—2.6 (complex m, 11H), 3.00 (s, 4H), 6.2—6.7 (m, 8H), 6.9—7.3 (m, 5H); UV (hexane): λ_{max} (ε), 268 (1160), 282 (sh, 400); mass: *m/e* 341 (31), 340 (M^+, 100), 235 (15), 208 (30), 207 (99), 149 (15), 145 (10), 131 (45), 129 (13), 128 (11), 118 (16), 117 (85), 116 (14), 115 (34), 105 (21), 104 (47), 103 (15), 91 (88), 79 (10), 78 (14), 77 (14), 65 (19).

*Reaction of **1** with α-Methylstyrene **2b**.* From a reaction mixture of 133 mg of **1** (1.00 mmol) and 390 μl of **2b** (3.0 mmol) in 20 ml of *t*-butyl alcohol, the solvent was removed after heating at 155 °C for 12 h. Chromatography of the residue on silica gel, with petroleum ether–benzene (4: 1) elution, gave 183 mg of a mixture of four components, two of which were found by GLC analysis to be very minor (less than one hundredth of the major component in the peak area). The isolation of the two major products by preparative GLC (column D, 200 °C) afforded 115 mg of colorless crystals, **3b** (46%), which when recrystallized from methanol had a mp of 58.1—58.8 °C and 14.3 mg of **4b** (5.7%). Further elution with a petroleum ether–benzene 1: 1 mixture and benzene produced 65 mg of a viscous oil whose NMR spectrum indicated it to be a mixture of 1: 1 and 1: 2 adducts which have not yet been separated. **3b**, NMR (CS_2, 100 MHz): 0.9—1.7 (complex m containing d at 1.14, J=7 Hz, 7H), 1.9—2.5 (complex m, 3H), 2.96 (m, 4H), 6.37 (s, 4H), 6.47 (s, 2H), 6.56 (s, 2H). Found: C, 91.15; H, 8.78%. Calcd for $C_{19}H_{22}$: C, 91.14; H, 8.86%. **4b**, NMR (CCl_4, 100 MHz): 1.1—1.3 (t at 1.20, J=7.5 Hz, and d at 1.21, J=7 Hz, 6H), 1.3—1.7 (m, 4H), 2.4—2.8 (complex m, 5H), 6.93 (s, 4H), 6.9—7.3 (m, 5H);mass: *m/e* 252 (M^+,24), 119 (34), 117 (16), 115 (10), 106 (11), 105 (100), 104 (18), 103 (14), 91 (37), 79 (17), 78 (11), 77 (20). Found: C, 90.54; H, 9.58%. Calcd for $C_{19}H_{24}$: C, 90.41; H, 9.58%.

*Reaction of **1** with α-Trimethylsiloxystyrene **2c**.* A solution of 132 mg of **1** (1.00 mmol) and 416 mg of **2c** (2.0 mmol) in 10 ml of hexane was heated at 155 °C for 12 h under argon. The solvent was then removed and the residue was chromatographed on silica gel which had been dried at 150 °C under 1—2 Torr. Elution with dry benzene produced 183 mg of an oily complex mixture which has not been characterized. Further elution with dry benzene produced 21 mg of crystals which, when recrystallized from petroleum ether, gave 15 mg of analytically pure **3c** (4.4%), mp 82.0—82.8 °C. Elution with a chloroform–ethyl acetate 3: 1 mixture produced 70 mg of an oil which contained **6** and acetophenone. Dry air was bubbled in at 100 °C under 1—2 Torr to remove the acetophenone. The subsequent recrystallization of 33 mg of the crystalline residue from petroleum ether gave 18 mg of **6** (7.2 %, mp 104.4—106.8 °C) which, when recrystallized again from petroleum ether, had a mp of 107.3—108.0 °C. **3c**, NMR (CCl_4, 100 MHz): 0.04 (s, 9H), 1.0—1.8 (br s, 4H), 2.27 (br s, 2H), 3.01 (s, 4H), 4.44 (br s, 1H), 6.46 (m, 7H), 6.81 (d, J=8 Hz, 1H). **6**, NMR (CCl_4, 100 MHz): 2.04 (m, 2H), 2.60 (m, 4H), 2.97 (m, 4H), 6.27 (d, J=8 Hz, 2H), 6.45 (d, J=8 Hz, 2H), 6.52 (d, J=8 Hz, 2H), 6.96 (d, J=8 Hz, 2H); IR (KBr): 1665 (C=O). Found: C, 86.21; H, 7.20%. Calcd for $C_{18}H_{18}O$: C, 86.36; H, 7.25%.

*Reaction of **1** with Methyl Cinnamate **2d**.* A mixture of 64 mg of **1** (0.48 mmol) and 191 mg of **2d** (1.18 mmol) in 5.9 ml of *t*-butyl alcohol was placed in a glass ampoule and bubbled with argon. The ampoule was then sealed off and kept at 150 °C for 14 h. After concentration, the residual mixture was chromatographed on silica gel and eluted with benzene. The preparative GLC separation (column B, 220 °C) of the eluted mixture afforded 39.5 mg of **3d** (28%) which when recrystallized from methanol had a mp of 85.2—86.9 °C, besides 68 mg of unreacted **2d**. **3d**, NMR (CCl_4, 100MHz): 1.05 (t, J=13 Hz, 1H), 1.7—3.4 (complex m, 10H), 3.73 (s, 3H), 6.2—6.7 (m, 8H); IR (KBr): 1731 (C=O). Found: C, 81.62; H, 7.55%. Calcd for $C_{20}H_{22}O_2$: C, 81.60; H, 7.53%.

*Reaction of **1** with Methyl α-Phenylacrylate **2e**.* Following the procedure described for the reaction of **1** with **2d**, 103 mg of **3e** (43%) was obtained from the reaction of 108 mg of **1** (0.82 mmol) with 306 mg of **2e** (1.89 mmol) in 5 ml of *t*-butyl alcohol. **3e**, mp 70.6—71.7 °C; NMR (CCl_4, 100 MHz): 0.8—3.2 (complex m, 11H), 3.59 (s, 3H), 6.4—6.8 (m, 8H); IR (KBr): 1743 (C=O). Found: C, 81.57; H, 7.54%. Calcd for $C_{20}H_{22}O_2$: C, 81.60; H, 7.53%.

*Reaction of **1** with* trans-*Stilbene **2f**.* A mixture of 108 mg of **1** (0.82 mmol) and 336 mg of **2f** (1.87 mmol) in 10 ml of *t*-butyl alcohol was heated in a sealed glass ampoule at 150 °C for 14 h under argon. The solvent was then removed *in vacuo* and the partially crystallized, unreacted **2f** was filtered off from the residue. The oily residue was chromatographed on silica gel and eluted with a petroleum ether–benzene 4: 1 mixture to separate the reaction product from **2f**. The con-

centration of the fraction containing the reaction product afforded 48 mg of crystalline **3f** and an oily mixture, which was subjected to preparative GLC (column A, 220 °C) to yield 15.5 mg of **3f** (combined yield, 25%) and 10 mg of **4f** (3.9%). **3f**, mp 148.0—148.5 °C; NMR (CCl_4, 100 MHz): 1.40 (t, J= 12 Hz, 1H), 1.8—3.4 (m, 10H), 6.3—6.8 (m, 8H), 7.24 (s, 5H). Found: C, 92.12; H, 7.72%. Calcd for $C_{24}H_{24}$: C, 92.26; H, 7.74%. **4f**, NMR (CCl_4, 100 MHz): 1.23 (t, J= 7.5 Hz, 3H), 1.98 (m, 2H), 2.40 (m, 2H), 2.55 (quart, J=7.5 Hz, 2H), 2.7—3.0 (complex m, 3H), 6.8—7.3 (complex m, 14H); mass: *m/e* 314 (M^+, 9), 145 (15), 119 (100), 117 (13), 104 (24), 91 (43), 77 (10), 65 (10). Found: C, 91.61; H, 8.44%. Calcd for $C_{24}H_{26}$: C, 91.67; H, 8.33%.

Reaction of **1** *with 1,1-Diphenylethylene* **2g**. A mixture of 108 mg of **1** (0.82 mmol) and 330 μl of **2g** (1.87 mmol) in 5 ml of *t*-butyl alcohol was heated at 150—155 °C for 12 h as has been described above. The subsequent removal of the solvent and chromatography on silica gel with petroleum ether–benzene (4: 1) elution gave 138 mg of unreacted **2g** and then 176 mg of oil. A part of the latter, which was found on the GLC analysis to consist of one major and two minor components was subjected to preparative GLC (column A, 210 °C) and the major component was collected. The viscous oil thus obtained crystallized slowly on standing. The residual oil was seeded with the crystals obtained above to give 172 mg of **3g** (67%) which when recrystallized from ethanol had a mp of 70.8—71.8 °C. Further elution with benzene produced only a polymeric material (115 mg). **3g**, NMR (CCl_4, 100 MHz): 0.9—3.2 (complex m, 10H), 3.43 (d, J=10 Hz, 1H), 6.2—6.6 (m, 8H), 7.18 (s, 5H). Found: C, 92.36; H, 7.71%. Calcd for $C_{24}H_{24}$: C, 92.26; H, 7.74%.

1-Hydroxy[4.2]paracyclophane **3h**. The treatment of **3c** with methanol containing a trace amount of potassium hydroxide produced **3h** which when recrystallized from petroleum ether had a mp of 116.3—116.8 °C. The reduction of **6** with $NaBH_4$ in 2-propanol as usual gave **3h** (mp 115.5—117.0 °C), which showed no depression of the melting point on a mixed-melting-point measurement with the **3h** obtained above. **3h**, IR (KBr): 3340 (O–H), 1089 (C–O). Found: C, 85.58; H, 8.07%. Calcd for $C_{18}H_{20}O$: C, 85.67; H, 7.99%.

Reaction of **1** *with Ethynylbenzene*. A solution of 132 mg of **1** (1.00 mmol) and 220 μl of ethynylbenzene (*ca.* 2 mmol) in 5 ml of *t*-butyl alcohol was heated at 160 °C for 11 h. A GLC analysis of the reaction mixture showed that 71% of the ethynylbenzene was consumed. The solvent was removed and the residue was chromatographed on silica gel. Elution with petroleum ether produced unreacted ethynylbenzene. Further elution with petroleum ether–benzene 5: 1 and 3: 1 mixtures produced 81 mg of the product mixture. Preparative GLC (column B, 200 °C) afforded 29.9 mg of **8** (13%), 6.0 mg of an unidentified product, and 15.3 mg of a mixture which was again subjected to preparative GLC (column D, 210 °C) to give 5.4 mg of **7** (2.3%) which when recrystallized from methanol had a mp of 102.6—103.0 °C (lit, 100—101 °C).[5d] Further elution with benzene produced only a highly viscous polymeric oil (176 mg). **7**, NMR (CCl_4, 100 MHz): 2.2—3.1 (m, 8H), 5.3—5.8 (m, 1H), 6.0—6.8, (m, 9H).[5d] **8**, NMR (CCl_4, 100 MHz): 0.80 (s, 4H), 2.02 (t, J=7 Hz, 2H), 2.45 (t of d, J=2.5 and 7 Hz, 2H), 5.00 (d, J=10 Hz, 2H), 5.33 (d, J=10 Hz, 2H), 5.97 (t, J=2.5 Hz, 1H), 7.06 (m, 3H), 7.38 (m, 2H).

Effect of the Reactant Concentration on the Yield of **3e**. A solution of *ca.* 7 mg of **1** (0.05 mmol) and 16 μl of **2e** (each accurately weighed) in a specified volume of *t*-butyl alcohol was heated at 155 °C for 14 h in a sealed glass ampoule under argon. The solvent was then removed *in vacuo* and the residue was dissolved in 0.50 ml of benzene. The yield of **3e** was determined on GLC using triphenylethylene as the internal standard.

Run	**1** (mg)	*t*-BuOH (ml)	**1** (mol/l)	**2e** (mol/l)	Yield of **3e**(%)
1	6.6	3.0	0.017	0.033	78
2	6.9	1.0	0.052	0.10	61
3	6.6	0.33	0.15	0.30	59
4	7.4	0.11	0.51	0.90	35

Effect of the Reactant Concentration on the Yield of **3f**. A solution of *ca.* 10 mg of **1** and *ca.* 36 mg of **2f** in a specified volume of *t*-butyl alcohol was heated at 160 °C for 13.3 h as has been described above. The solvent was then removed *in vacuo* and the residue was dissolved in 1.00 ml of benzene. The yield of **3f** was calculated from the ratio of the peak area on GLC to that of the standard solution of **3f**.

Run	**1** (mg)	*t*-BuOH (ml)	**1** (mol/l)	**2f** (mol/l)	Yield of **3f**(%)
1	10.1	4.0	0.019	0.050	25
2	9.9	2.0	0.038	0.10	27
3	11.1	1.0	0.084	0.20	31
4	10.3	0.50	0.16	0.40	34
5	10.1	0.25	0.31	0.79	32

References

1) T. Tsuji, S. Nishida, and H. Tsubomura, *J. Chem. Soc., Chem. Commun.*, **1972**, 284.

2) a) T. Tsuji and S. Nishida, *J. Am. Chem. Soc.*, **95**, 7519 (1973); b) T. Tsuji and S. Nishida, *Chem. Lett.*, **1973**, 1335.

3) For a preliminary report, see T. Shibata, T. Tsuji, and S. Nishida, *Tetrahedron Lett.*, **1976**, 4095.

4) a) D. J. Cram and J. M. Cram, *Acc. Chem. Res.*, **4**, 204 (1971); b) F. Vögtle and P. Neumann, *Angew. Chem. Int. Ed. Engl.*, **11**, 73 (1972); c) H. Irngartinger, R.-D. Acker, W. Rebafka, and H. A. Staab, *ibid.*, **14**, 674 (1975); d) R. Gray and V. Boekelheide, *ibid.*, **14**, 107 (1975); e) H. Horita, N, Kannen, T. Otsubo, and S. Misumi, *Tetrahedron Lett.*, **1974**, 501; f) R. C. Helgeson, J. M. Timko, and D. J. Cram, *J. Am. Chem. Soc.*, **96**, 7381 (1974).

5) a) D. J. Cram and H. Steinberg, *J. Am. Chem. Soc.*, **73**, 5691 (1951); b) D. J. Cram and R. C. Helgeson, *ibid.*, **88**, 3515 (1966); c) H. J. Reich and D. J. Cram, *ibid.*, **91**, 3517 (1969); d) M. H. Delton and D. J. Cram, *ibid.*, **94**, 1669 (1972); e) S. E. Potter and I. O. Sutherland, *J. Chem. Soc., Chem. Commun.*, **1973**, 520; f) F. Vögtle and J. Grutze, *Angew. Chem. Int. Ed. Engl.*, **14**, 559 (1975).

6) T. Tsuji and S. Nishida, *J. Am. Chem. Soc.*, **96**, 3649 (1974).

7) H. Plieninger and W. Maier-Bost, *Chem. Ber.*, **98**, 2504 (1965).

8) T. Shibata, T. Tsuji, and S. Nishida, unpublished results.

9) K. U. Ingold, "Free Radicals," ed by J. K. Kochi, John Wiley & Sons, Vol. I, New York, N. Y. (1973), p. 92.

10) The actual structures of the fragments **18**—**24** are not certain. It is probable that those fragments have the corresponding tropylium ion structures.

11) The mass spectra of **3h** is very similar to that of **7** in the region up to *m/e* 234. Thermal or electron-bombardment-induced dehydration may have occurred.

12) F. W. McLafferty, "Interpretation of Mass Spectra," 2nd ed, W. A. Benjamin, Reading, Mass. (1973), pp. 57—63.

13) a) D. J. Cram, R. B. Hornby, E. A. Truesdale, H. J. Reich, M. H. Delton, and J. M. Cram, *Tetrahedron*, **30**, 1757 (1974); b) N. Kato, T. Kondo, K. Endo, and S. Ito, 7th Symposium on Structural Organic Chemistry, Tokyo, October, 1974.

14) R^1 and the aromatic ring are more eclipsed in the **26** conformer than in **25** and R^1 is *gauche* to C-3 in **26**, while in **25** R^1 is *anti* to C-3. R^2 and the aromatic ring, in the **26** conformer, are *gauche* to each other and R^2 and C-4 are nearly eclipsed.

15) H. O. House, L. J. Czuba, M. Gall, and H. D. Olmstead, *J. Org. Chem.*, **34**, 2324 (1969).

16) M. Saquet and A. Thuillier, *Bull. Soc. Chim. Fr.*, **12**, 3972 (1966).

17) L. F. Fieser, "Organic Experiments," D. C. Heath and Co., Boston, Mass. (1964), p. 219.

18) W. Franke, W. Ziegenbein, and H. Meister, "Newer Methods of Preparative Organic Chemistry," ed by W. Foerst, Academic Press, Vol. III, New York, N. Y. (1964), p. 444.

19) L. G. Kaufman and D. T. Longone, *Tetrahedron Lett.*, **1974**, 3229.

Ion-Molecule Reactions in the Binary Mixture of Ethylene Oxide and Trioxane. I. Hydrogen Atom and Proton Transfer Reactions

Minoru KUMAKURA and Toshio SUGIURA*

Takasaki Radiation Chemistry Research Establishment, Japan Atomic Energy Research Institute, Takasaki, Gunma 370-12

**Japan Atomic Energy Research Institute, Shinbashi, Minato-ku, Tokyo 105*

(Received December 13, 1976)

The formation mechanism of protonated molecular ions by cross-reactions in ethylene oxide–trioxane mixtures has been studied with use of a modified time-of-flight mass spectrometer. The precursors of the product ions were determined by analysis of the fine structure of their ionization efficiency curves using deuterated ethylene oxide. Protonated ethylene oxide is formed by the hydrogen atom transfer reaction of ethylene oxide molecular ion with trioxane, and protonated trioxane by the proton transfer reaction of CHO^+ (from ethylene oxide) with trioxane. In the ion-molecule reactions of ethylene-d_4 oxide–trioxane mixtures, appreciable isotope effect was observed. The CHO^+ from ethylene oxide is an important reactant ion as compared with that from trioxane in the proton transfer reaction, and CHO^+ from ethylene oxide was suggested as a thermal reactive ion. The order of proton affinity could be estimated from the proton transfer reactions involving CHO^+. It was found that the proton affinity of trioxane is smaller than that of ethylene oxide.

The ion-molecule reactions in trioxane (1,3,5-trioxane) and ethylene oxide have been studied in connection with an elementary process in radiation and ion chemistry.[1,2] In trioxane, consecutive-association reactions of protonated ions with trioxane were observed, but the reactions were not carried out in ethylene oxide. The results of the ion-molecule reactions could be correlated with the behavior of observed radiation-induced polymerization in which trioxane was easily polymerized,[3,4] appreciable polymerization taking place less easily in ethylene oxide.[5] On the other hand, protonated ethylene oxide was mainly formed by the proton transfer reaction from CHO^+ in ethylene oxide, CHO^+ from trioxane not playing an important role for the formation reaction of protonated trioxane.[1] It seems that the reactivity of CHO^+ in proton transfer reaction is attributed to the molecular source producing CHO^+. The proton transfer reaction due to CHO^+ would be affected by the property of neutral molecule. Futrell *et al.*[6] studied the effect of the kinetic energy of CHO^+ in proton transfer reactions with a tandem mass spectrometer, and stated that the reactivity of CHO^+ is affected by its energy state. Various oxygenated fragment ions are produced by electron impact from compounds containing oxygen. Since oxygenated ions giving the same structure are produced from various cyclic ether, it is of interest to examine the reactivity of these ions. The formation reaction of protonated molecular ions has been studied for alcohols,[7–9] ketones,[10–12] aldehydes,[11–13] and dimethyl ether,[11,12] but not for cyclic compounds containing oxygen. The ion-molecule reactions in pure system of ethylene oxide and trioxane have been studied.[1,2] The present work deals with the formation mechanism of the protonated molecular ions by cross-reactions (reactions between ions of one molecule and the molecules of the other) in ethylene oxide (or ethylene-d_4 oxide)–trioxane mixtures. The reactivity of the CHO^+ ions from both ethylene oxide and trioxane was examined by means of proton transfer reactions.

Experimental

A Bendix Model 12-101 time-of-flight mass spectrometer was used. A part of the spectrometer was modified in order to study ion-molecule reactions.[2] Some pulse electronic circuits of the apparatus were modified. A Hewlett Packard 214A pulse generator and a pulse generator (Sanwa Denshi Production Co., Ltd.) were used for suppling the ionizing and ion withdrawal pulses. A variable delay time circuit permitted a variation of the time between the end of the ionizing pulse and the onset of the ion withdrawal pulse.[2] During the delay time, the entire ionization chamber is field-free, so that ion-molecule reactions occurring during the time interval are under purely thermal conditions.

The retarding potential differential technique (RPD) was adopted for appearance potential and ionization efficiency curve measurement. A report has been given on the technique.[14] The measurement of the ionization efficiency curves of two ions was simultaneously performed by the two-channel ion detection method. The ion currents of two different ions were recorded with a Rikadenki R-34 three-pen recorder.

The gas-sample inlet-system consisting of a dual-leak and dual-reservoir was used. Two kinds of samples are introduced individually into the ionization chamber through two separate leaks from separate reservoirs (5L). The partial pressure of the two samples was indirectly measured with an MKS Baratron 90-X RP-2 capacitance manometer and the pressure was calibrated by known rate constant (1.11×10^{-9} cm^3 molecule^{-1} s^{-1}) of CH_5^+ in the ion-molecule reaction of methane.[15]

The following reagents were used: trioxane (Celanese Chemical), ethylene oxide (Nisso Yuka Industly Co., Ltd.), and ethylene-d_4 oxide (Merck Sharp and Dohme of Canada, deuterium atom purity, least 98%). The samples were used after being subjected to vacuum distillation several times.

Results and Discussion

Delay Time Dependence. The delay time dependence plots of fragment ions in a 1 : 1 mixture of ethylene oxide and trioxane are shown in Fig. 1. The plots were obtained as a function of delay time at ionization chamber pressure of 1.70×10^{13} molecules cm^{-3}. The *m/e* 44 ($C_2H_4O^+$), 43 ($C_2H_3O^+$), and 29 (CHO^+) are

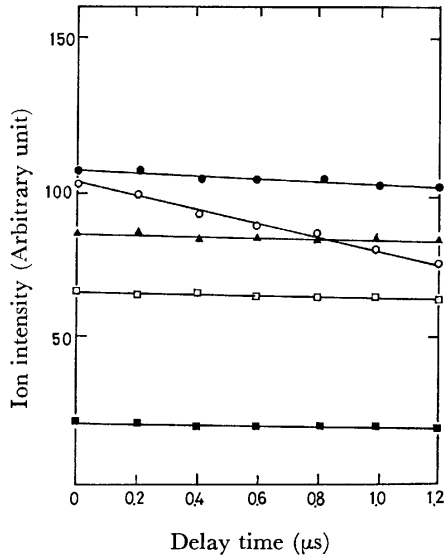

Fig. 1. Delay time dependence of fragment ions in ethylene oxide–trioxane mixtures.
●: $C_2H_5O_2^+$, ▲: $C_2H_4O^+$, ●: CHO^+ (×1/2),
□: $C_3H_5O_3^+$, ■: $C_2H_3O^+$.

major fragment ions from ethylene oxide, while *m/e* 89 ($C_3H_5O_3^+$), 61 ($C_2H_5O_2^+$), and a part of *m/e* 29 are those from trioxane.

The delay time dependence plots of product ions are shown in Fig. 2. The formation of protonated ethylene oxide (*m/e* 45, $C_2H_5O^+$) is remarkable as compared with protonated trioxane (*m/e* 91, $C_3H_7O_3^+$), the ion intensity ratio of $C_2H_5O^+$ to $C_3H_7O_3^+$ being *ca.* 5.5 at delay time of 1.0 μs.

The ion-molecule reactions in ethylene-d_4 oxide–trioxane mixtures were studied in order to clarify the formation mechanism of product ions under the same conditions as for ethylene oxide–trioxane mixtures. The plots of delay time dependence for fragment and isotopic product ions are shown in Figs. 3 and 4, respectively.

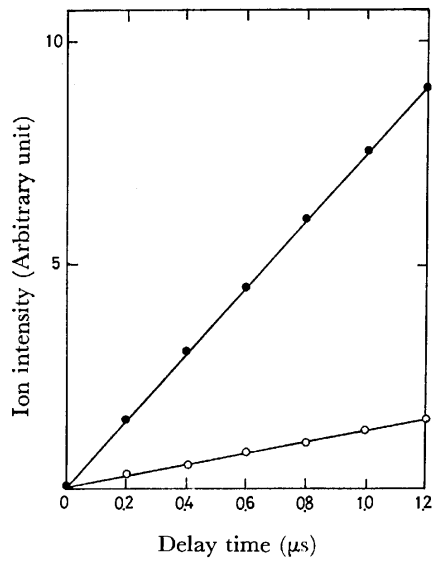

Fig. 2. Delay time dependence of protonated molecular ions in ethylene oxide–trioxane mixtures.
●: $C_2H_5O^+$, ○: $C_3H_7O_3^+$.

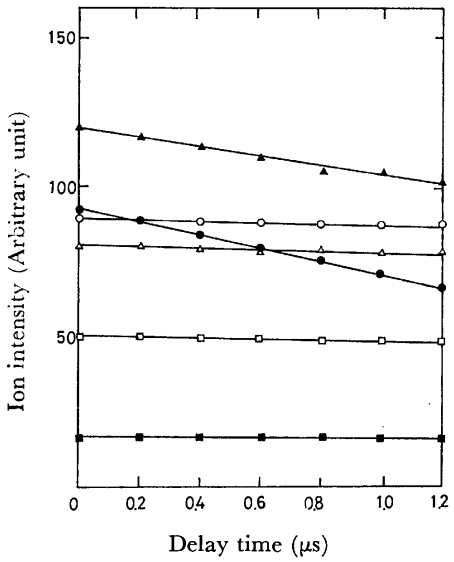

Fig. 3. Delay time dependence of fragment ions in ethylene-d_4 oxide–trioxane mixtures.
▲: CDO^+ (×1/2), ○: $C_2H_5O_2^+$, △: $C_2D_4O^+$,
□: $C_3H_5O_3^+$, ●: CHO^+ (×1/2), ■: $C_2H_3O^+$.

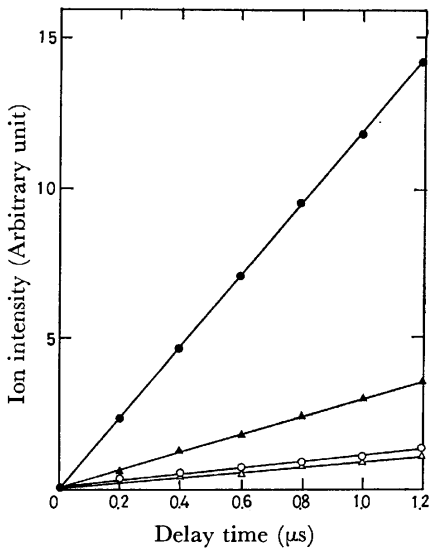

Fig. 4. Delay time dependence of protonated and deuteronated molecular ions in ethylene-d_4 oxide–trioxane mixtures.
●: $C_2D_4HO^+$ (×2), ▲: $C_2D_5O^+$ (×2), ○: $C_3H_7O_3^+$,
△: $C_3H_6DO_3^+$ (×5).

The CHO^+ ions from both molecules are separated into CHO^+ and CDO^+. The ions markedly decreased with increasing delay time as compared with other fragment ions of high mass number (Fig. 3). The cause of decrease is mainly due to a mass discrimination effect though there is a contribution of these ions to ion-molecule reactions. The isotopic distribution of product ions is given in Fig. 4. The *m/e* 49 ($C_2D_4HO^+$) and 50 ($C_2D_5O^+$) are protonated and deuteronated trioxane, respectively. The $C_2D_4HO^+$ and $C_3H_6DO_3^+$ ions are formed by cross-reactions and the $C_2D_5O^+$ and $C_3H_7O_3^+$ ions by homo-reactions. The ion intensity ratios of $C_2D_4HO^+$ to $C_2D_5O^+$, and $C_3H_6DO_3^+$ to C_3H_7-

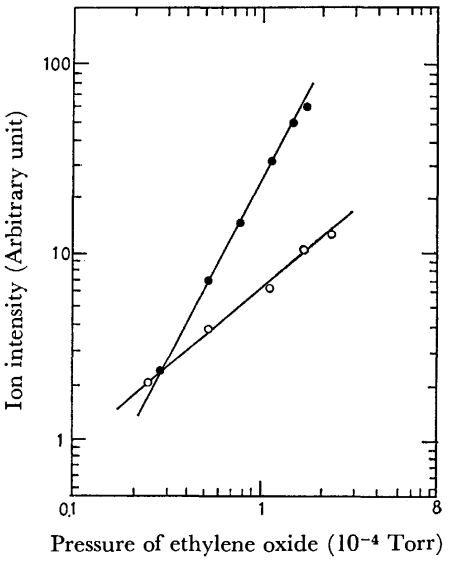

Fig. 5. Pressure dependence of protonated molecular ions to ethylene oxide at delay time of 1.0 μs.
●: $C_2H_5O^+$, ○: $C_3H_7O_3^+$.

O_3^+ are *ca.* 5 and 0.2 at delay time of 1.0 μs, suggesting that a drastic reaction occurs in the mixture system.

Pressure Dependence. The pressure dependence of the product ions on each molecule was examined in order to clarify the contribution of molecules of ethylene oxide and trioxane. The pressure dependence plots of the protonated molecular ions on the pressure of ethylene oxide, shown in Fig. 5, were obtained by the pressure variation of ethylene oxide at fixed pressure (8.5×10^{12} molecules cm^{-3}) of trioxane and delay time of 1.0 μs. Protonated ethylene oxide shows a dependence of *ca.* second order on the pressure of ethylene oxide, while protonated trioxane shows one of *ca.* first order. This suggests that the formation of protonated trioxane is correlated with ethylene oxide.

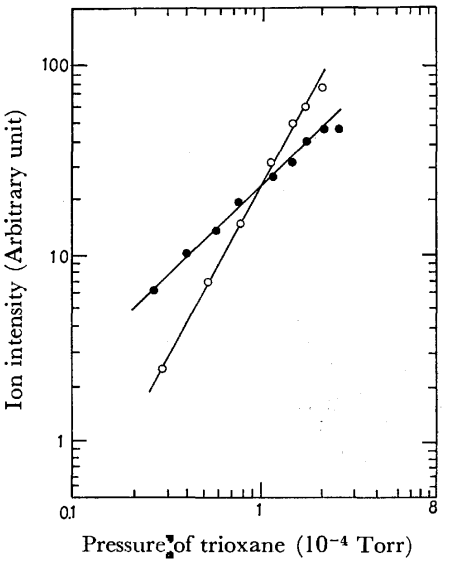

Fig. 6. Pressure dependence of protonated molecular ions to trioxane at delay time of 1.0 μs.
●: $C_2H_5O^+$, ○: $C_3H_7O_3^+$.

The pressure dependence plots of protonated molecular ions to trioxane at fixed pressure (8.5×10^{12} molecules cm^{-3}) of ethylene oxide are shown in Fig. 6. Protonated trioxane shows the dependence of second order on trioxane pressure and protonated ethylene oxide that of the first order on trioxane one. These results suggest that protonated ethylene oxide and trioxane are formed by means of proton or hydrogen atom transfer reactions.

Ionization Efficiency Curves. The ionization efficiency curves of fragment and product ions in ethylene-d_4 oxide–trioxane mixtures were measured at delay time of 1.0 μs. The ionization efficiency curves of $C_2D_4HO^+$, $C_2D_4O^+$, and $C_3H_5O_3^+$ are shown in Fig. 7, and those of $C_3H_6DO_3^+$, $C_2D_5O^+$, and CDO^+ in Fig. 8. The precursors of the product ions can be identified by comparison of the onset and fine structures of the curves of these product ions with those of fragment ions.

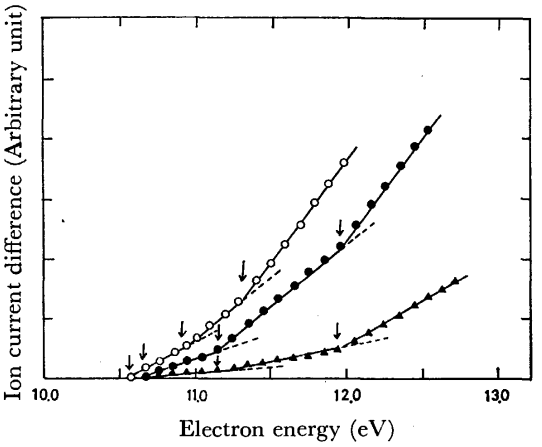

Fig. 7. Ionization efficiency curves of $C_2D_4O^+$(●), $C_2D_4HO^+$(▲), and $C_3H_5O_3^+$(○) in ethylene-d_4 oxide–trioxane mixtures.

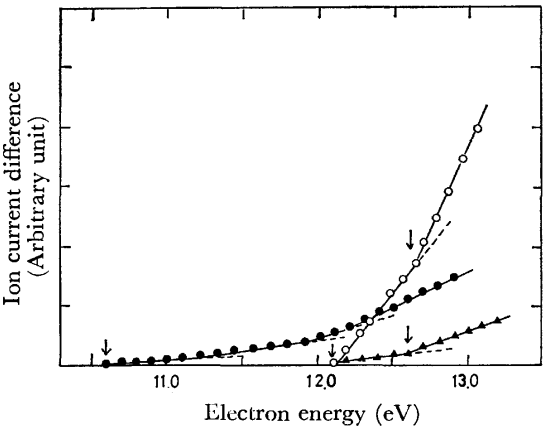

Fig. 8. Ionization efficiency curves of CDO^+(○), $C_2D_5O^+$(●), and $C_3H_6DO_3^+$(▲) in ethylene-d_4 oxide–trioxane mixtures.

The ionization potential of ethylene oxide and the appearance potential of $C_3H_5O_3^+$ from trioxane were 10.64 ± 0.1 and 10.59 ± 0.05 eV, respectively.[2,14] The onset and break points in the ionization efficiency curves of both $C_2D_4HO^+$ and $C_2D_4O^+$ agree. The onset of

$C_2D_4HO^+$ approached that of $C_3H_5O_3^+$; however, the fine structures of both curves differ from each other. The appearance potential of other fragment ions from trioxane is higher than that of $C_2D_4HO^+$.[14] The break points of the curve of $C_2D_4HO^+$ does not agree with the appearance potentials of these fragment ions. It is concluded that the precursor of $C_2D_4HO^+$ is $C_2D_4O^+$ and fragment ions from trioxane does not correlate as a precursor.

The onset of $C_3H_6DO_3^+$ agrees with that of CDO^+ and is higher than the ionization potential of $C_2D_4O^+$ by *ca.* 1.5 eV. The fine structures of the ionization efficiency curves of $C_3H_6DO_3^+$ and $C_2D_4O^+$ differ from each other. The appearance potentials of other fragment ions from ethylene oxide deviate from that of $C_3H_6DO_3^+$, and thus these ions do not contribute to the formation of $C_3H_6DO_3^+$. From the results, we see that the precursor of $C_3H_6DO_3^+$ is CDO^+ from ethylene-d_4 oxide.

Reaction Mechanism. It is found that a part of $C_2H_5O^+$ and $C_2D_5O^+$ is formed by the following reactions in ethylene oxide (or ethylene-d_4 oxide)–trioxane mixtures, as observed in the ion-molecule reactions in pure ethylene oxide.[2]

$$\underset{\backslash O /}{CH_2\text{–}CH_2^+} + \underset{\backslash O /}{CH_2\text{–}CH_2} \longrightarrow \underset{\backslash OH /}{CH_2\text{–}CH_2^+} + C_2H_3O, \quad (1)$$

$$CHO^+ + \underset{\backslash O /}{CH_2\text{–}CH_2} \longrightarrow \underset{\backslash OH /}{CH_2\text{–}CH_2^+} + CO, \quad (2)$$

$$\underset{\backslash O /}{CD_2\text{–}CD_2^+} + \underset{\backslash O /}{CD_2\text{–}CD_2} \longrightarrow \underset{\backslash OD /}{CD_2\text{–}CD_2^+} + C_2D_3O, \quad (3)$$

$$CDO^+ + \underset{\backslash O /}{CD_2\text{–}CD_2} \longrightarrow \underset{\backslash OD /}{CD_2\text{–}CD_2^+} + CO. \quad (4)$$

The ion intensity of $C_2D_4HO^+$ increases with increasing delay time (Fig. 4), and the appearance potential of this ion agrees with the ionization potential of ethylene-d_4 oxide (Fig. 7). Thus, it is suggested that $C_2D_4HO^+$ is formed by hydrogen atom transfer reaction as follows.

$$\underset{\backslash O /}{CD_2\text{–}CD_2^+} + \begin{array}{c} CH_2 \\ /\quad\backslash \\ O \quad O \\ | \quad | \\ CH_2 \quad CH_2 \\ \backslash\quad/ \\ O \end{array} \longrightarrow \underset{\backslash OH /}{CD_2\text{–}CD_2^+} + C_3H_5O_3. \quad (5)$$

This shows that predominant formation of $C_2H_5O^+$ in ethylene oxide–trioxane mixtures is due to Reaction 6 rather than Reactions 1 and 2.

$$\underset{\backslash O /}{CH_2\text{–}CH_2^+} + \begin{array}{c} CH_2 \\ /\quad\backslash \\ O \quad O \\ | \quad | \\ CH_2 \quad CH_2 \\ \backslash\quad/ \\ O \end{array} \longrightarrow \underset{\backslash OH /}{CH_2\text{–}CH_2^+} + C_3H_5O_3. \quad (6)$$

$C_3H_7O_3^+$ was formed by Reaction 7 in ion-molecule reactions of trioxane.[1]

$$C_3H_5O_3^+ + \begin{array}{c} CH_2 \\ /\quad\backslash \\ O \quad O \\ | \quad | \\ CH_2 \quad CH_2 \\ \backslash\quad/ \\ O \end{array} \longrightarrow \begin{array}{c} CH_2 \\ /\quad\backslash \\ O \quad OH^+ \\ | \quad | \\ CH_2 \quad CH_2 \\ \backslash\quad/ \\ O \end{array} + C_3H_4O_3. \quad (7)$$

It was observed that the ion intensity of $C_3H_6DO_3^+$ increases slightly with increasing delay time in ethylene-d_4 oxide–trioxane mixtures (Fig. 4). From the ionization efficiency curves (Figs. 7 and 8), it is concluded that $C_3H_6DO_3^+$ in ethylene-d_4 oxide–trioxane mixtures is formed by deuteron transfer from CDO^+ to trioxane molecule.

$$CDO^+ + \begin{array}{c} CH_2 \\ /\quad\backslash \\ O \quad O \\ | \quad | \\ CH_2 \quad CH_2 \\ \backslash\quad/ \\ O \end{array} \longrightarrow \begin{array}{c} CH_2 \\ /\quad\backslash \\ O \quad OD^+ \\ | \quad | \\ CH_2 \quad CH_2 \\ \backslash\quad/ \\ O \end{array} + CO. \quad (8)$$

In the ion-molecule reactions of ethylene oxide, CHO^+ was an important reactant ion in the formation reaction of protonated ethylene oxide.[2] CHO^+ is a proton donor ion. It follows that Reaction 8 predominates in the formation of $C_3H_6DO_3^+$. Similarly, Reaction 9 would participate in the formation of $C_3H_7O_3^+$ in ethylene oxide–trioxane mixtures.

$$CHO^+ + \begin{array}{c} CH_2 \\ /\quad\backslash \\ O \quad O \\ | \quad | \\ CH_2 \quad CH_2 \\ \backslash\quad/ \\ O \end{array} \longrightarrow \begin{array}{c} CH_2 \\ /\quad\backslash \\ O \quad OH^+ \\ | \quad | \\ CH_2 \quad CH_2 \\ \backslash\quad/ \\ O \end{array} + CO. \quad (9)$$

Rate Constants. In the calculation of the rate constant for $C_2H_5O^+$ formed in the mixture system, the ion intensities of $C_2H_4O^+$ and $C_2H_5O^+$ are corrected. The equation of rate constant (k_6) for Reaction 6 can be expressed as follows:

$$\frac{I_{C_2H_5O^+(M)} - I_{C_2H_5O^+(E)}}{I_{C_2H_4O^+(M)}} = k_6[C_3H_6O_3]t + C, \quad (10)$$

where $I_{C_2H_5O^+(M)}$ and $I_{C_2H_4O^+(M)}$ are the ion intensities of $C_2H_5O^+$ and $C_2H_4O^+$ in ethylene oxide–trioxane mixtures, respectively; $I_{C_2H_5O^+(E)}$ is the ion intensity of $C_2H_5O^+$ formed in the ion-molecule reactions of pure ethylene oxide;[2] $[C_3H_6O_3]$ is the concentration of trioxane in the ionization chamber, and t is delay time. The rate constants obtained are given in Table 1. The rate constants of the formation reactions of protonated and deuteronated molecular ions in ethylene oxide (or ethylene-d_4 oxide)–trioxane mixtures are summarized in Table 1.

Table 1. Rate constants

Ethylene oxide–trioxane		Ethylene-d_4 oxide–trioxane	
Reaction	$k \times 10^9$ cm^3 molecule^{-1} s^{-1}	Reaction	$k \times 10^9$ cm^3 molecule^{-1} s^{-1}
(1)	0.145[a]	(3)	0.130
(2)	2.09[a]	(4)	1.81
(6)	4.00	(5)	4.18
(7)	1.15[a]	(7)	1.10
(9)	0.121	(8)	0.101

a) Ref. 2.

Reactivity. The molecular ion from trioxane is unstable. Its ion intensity is relatively low, while that from ethylene oxide is high (Fig. 1). Thus, the reactivity of molecular ion from trioxane can not be discussed in comparison with that from ethylene oxide. On the other hand, it is of interest to examine the reactivity of the CHO^+ ions from both molecules. The CHO^+ from ethylene oxide participates preferentially for

proton transfer reaction as compared with that from trioxane in the mixture system. No contribution of CHO^+ for protonated trioxane has been observed in the ion-molecule reactions of trioxane.[1] A proton transfer reaction involving CHO^+ seems to be affected by its energy state. It was demonstrated that the energy of CHO^+ from trioxane is considerably higher than that of ethylene oxide in the measurement of the translational enrgies of the CHO^+ ions from oxygen-containing organic compounds.[16] It is suggested that CHO^+ from ethylene oxide is a thermal reactive ion as compared with that from trioxane.

Proton Affinity. The proton affinity of ethylene oxide has been reported to be 183 kcal mol^{-1}.[17,18] The proton affinity of trioxane is not known but the basicities for trioxane and ethylene oxide which correlate with their proton affinities have been found to be 10 and 7.3 respectively.[19] In this mixture system, the reactant, ions in Reactions 2 and 9 are CHO^+ from ethylene oxide, the rate constant ratio (k_2/k_9) being 17.3. This indicates that the proton affinity of ethylene oxide is larger than that of trioxane. The proton affinity of a molecule is defined as the enthalpy change for proton transfer reactions. A number of determinations of absolute proton affinity have been undertaken by the appearance potential method and an empirical correlation of excess energies in ion-molecule reactions.[18] The relative proton affinity was also studied from observation of ion-molecule reactions.[20-22] It is found that the order of relative proton affinity can be estimated using rate constant in proton transfer reaction involving CHO^+. The general scheme is as follows:

$$MH^+ + M_1 \longrightarrow M_1H^+ + M, \quad (11)$$

$$MH^+ + M_2 \longrightarrow M_2H^+ + M, \quad (12)$$

where the order of proton affinity (PA) for neutral molecule (M_1, M_2) is $PA(M_1) > PA(M_2)$, when the rate constant in both reactions is $k_{11} > k_{12}$. A proton donor ion such as CHO^+ which is a thermal energy ion is desirable for reactant ion (MH^+).

Isotope Effects. The difference of the rate constant in the proton and deuteron transfer reactions was observed (Table 1). The ratios k_1/k_3, k_2/k_4, and k_9/k_8 were 1.12, 1.15, and 1.20, respectively. The values of k_5 and k_6 were almost equal. Gupta *et al.*[23] studied the isotope effects in the ion-molecule reactions of water and methane. They reported that the ratio of the rate constant for proton (from OH^+) and deuteron transfer (from OD^+) is 2.10, and the ratio of the rate constant for the formation of CH_5^+ and CD_5^+ 1.49. Chong and Franklin[24] observed that the rate constants for the transfer of an H or a D atom are the same, but the rate constant of the transfer of D^+ is only *ca.* 0.62 times as great as that for an H^+ in ion-molecule reactions of methane–methane-d_4 mixtures. The isotope effect we observed is smaller than theirs.

The authors wish to express appreciation to Prof. K. Hayashi, Osaka University, and Dr. A. Ito and Mr. K. Arakawa of our Establishment for interesting and stimulating discussions.

References

1) M. Kumakura and T. Sugiura, in "Recent Developments in Mass Spectroscopy," ed by K. Ogata and T. Hayakawa, Univ. of Tokyo Press, Tokyo (1970), p. 988.
2) M. Kumakura, A. Ito, and T. Sugiura, *Mass Spectroscopy*, **22**, 61 (1974).
3) K. Hayashi, H. Ochi, and S. Okamura, *J. Polym. Sci., Part A-2*, **1964**, 2929.
4) M. Sakamoto, I. Ishigaki, M. Kumakura, H. Yamashina, T. Iwai, A. Ito, and K. Hayashi, *J. Macromol. Chem.*, **1**, 639 (1966).
5) D. Cordischi, A. Mele, and A. Somogyi, "Proceedings of the Second Tihany Symposium on Radiation Chemistry," ed by J. Dobo and P. Hedvig, Akad. Kiado, Budapest (1967), p. 483.
6) J. H. Futrell, F. P. Abramson, A. K. Bhattacharya, and T. O. Tiernan, *J. Chem. Phys.*, **52**, 3655 (1970).
7) J. M. S. Henis, *J. Am. Chem. Soc.*, **90**, 1477 (1970).
8) K. R. Ryan, L. W. Sieck, and J. H. Futrell, *J. Chem. Phys.*, **41**, 111 (1964).
9) S. K. Gupta, E. G. Jones, A. G. Harrison, and J. J. Myher, *Can. J. Chem.*, **45**, 3107 (1967).
10) K. A. G. Macneil and J. H. Futrell, *J. Phys. Chem.*, **76**, 409 (1972).
11) H. Prichard and A. G. Harrison, *J. Chem. Phys.*, **48**, 5623 (1968).
12) A. S. Blair and A. G. Harrison, *Can. J. Chem.*, **51**, 703 (1973).
13) S. Okada, A. Matsumoto, T. Dohmaru, S. Taniguchi, and T. Hayakawa, *Mass Spectrosc.*, **20**, 311 (1972).
14) M. Kumakura, T. Sugiura, and S. Okamura, *Mass Spectrosc.*, **16**, 16 (1968).
15) C. W. Hand and H. Weyssenhoff, *Can. J. Chem.*, **42**. 195 (1964).
16) M. Kumakura, K. Arakawa, and T. Sugiura, to be published.
17) J. L. Beauchamp and R. C. Dunbar, *J. Am. Chem. Soc.*, **92**, 1477 (1970).
18) B. H. A. Haney and J. L. Franklin, *Trans. Faraday Soc.*, **65**, 1794 (1968).
19) E. Z. Utyanskaya, *Polym. Sci. USSR*, **13**, 595 (1971).
20) V. L. Talroze and E. L. Frankevich, *Dokl. Akad. Nauk SSSR*, **111**, 376 (1956).
21) J. L. Beauchamp and S. E. Butrill, *J. Chem. Phys.*, **48**, 1783 (1968).
22) D. Holtz and J. L. Beauchamp, *J. Am. Chem. Soc.*, **91**, 5913 (1969).
23) S. K. Gupta, E. G. Jones, A. G. Harrison, and J. J. Myher, *Can. J. Chem.*, **45**, 3107 (1967).
24) S. L. Chong and J. L. Franklin, *J. Chem. Phys.*, **55**, 641 (1971).

Shock Tube Study on the Mechanism of Hydrogenation and Pyrolysis of Acetylene

Hiroo OGURA

Institute of Space and Aeronautical Science, The University of Tokyo, Komaba, Meguro-ku, Tokyo 153

(Received January 27, 1977)

Mixtures of acetylene and deuterium have been subjected to shock heating in a single-pulse shock tube in the temperature range 1000—1600 K. The reaction products were quite the same as those obtained from the pyrolysis of acetylene alone, with a considerable increase in the yields of the minor products. The predominance of 1-buten-3-yne formation and no appreciable dependence of its rate on the concentration of deuterium suggest that the initiation step is the same as that proposed in the pyrolysis of acetylene by itself, *viz.* $2C_2H_2 \rightarrow C_4H_3+H$, the initiation step of the bimolecular reaction of C_2H_2 with D_2 not being important. A complementary analysis of the isotopic distributions of 1-buten-3-yne, ethylene, and acetylene shows that hydrogenation also occurs by a free-radical chain mechanism, and the C_4H_3 radical and H atom generated by the initiation step are mainly responsible for the formation of1-buten-3-yne and ethylene, respectively. The ethylene formation was of first-order in both acetylene and deuterium, and the second-order rate constant was obtained as

$$k(\mathrm{cm^3\ mol^{-1}\ s^{-1}}) = (4.9\pm1.3)\times10^{11}\exp((-34900\pm600)/RT).$$

The hydrogenation of acetylene has been studied by several investigators.[1-6] Skinner and co-workers aimed at clarifying the pyrolysis of ethylene.[2,3] Benson and Haugen, in an attempt to estimate the elementary reaction rate constants of radical reactions which might participate in the pyrolysis of the unsaturated hydrocarbons,[4] made a kinetic analysis of the hydrogenation of acetylene, and concluded that a free-radical chain mechanism should predominate. Skinner *et al.* showed that C_2H_3D is the most abundant among the ethylene isomers produced in the shock heated mixture of acetylene and deuterium. The result is in line with the prediction from the free-radical chain mechanism proposed by Benson and Haugen. In their scheme the chain propagation is initiated by the bimolecular reaction of acetylene and deuterium, $C_2H_2+D_2 \rightarrow C_2H_2D+D$.

On the other hand, the effects of added hydrogen on the yields of the pyrolysis products were extensively examined in static and flow systems.[7-10] It was shown that the addition of hydrogen has little influence on the yields of the major products of the pyrolysis.

The pyrolysis of acetylene proceeds *via* the free-radical chain mechanism initiated by the bimolecular reaction of acetylene,[11] $2C_2H_2 \rightarrow C_4H_3+H$. The H atom produced by the initiation step can lead to the formation of ethylene as well as 1-buten-3-yne in the presence of hydrogen. When deuterium instead of hydrogen is added, the product distribution and isotopic distribution can be utilized for clarifying the mechanisms of the pyrolysis and hydrogenation of acetylene.

Experimental

Apparatus and Procedure. The hydrogenation and pyrolysis of acetylene in the presence of deuterium was studied in a 4-cm single-pulse shock tube, the length of the driven section being 277 cm long, and that of the driver section adjustable but fixed at 157 cm. The design and operation of the shock tube were reported previously.[11,12]

The driver section was isolated from the pump when the vacuum of the tube reached below 10^{-3} Torr, and then filled with the driver gas at about 2 atm of pressure in order to optimize the rupture of the diaphragms by the needle. The driven section was further pumped to a vacuum better than 10^{-4} Torr before each run. The leak plus outgassing rate was measured by a cathode ionization gauge immediately after the isolation of the tube from the pump, 6×10^{-5} Torr per minute being obtained. Helium was used as the driver gas. The shocks were fired within 5 min after the driven section had been filled with test gases.

Materials. Three different mixtures with the composition of $C_2H_2/D_2/Ar = 10/10/80$; 5/10/85; and 10/5/85 were prepared in a 5-l glass vessel and allowed to stand for at least one day before use.

Acetylene(Matheson Co.) was washed with concd sulforic acid and dried through a soda lime tower and then purified by bulb-to-bulb vacuum distillation. Deuterium (Showa Denko Co., 99.5% D atom) and argon (Nippon Sanso Co., nominal purity of 99.9995%) were used without further purification.

A variety of pure gas mixtures with the desired concentrations were prepared for the calibration of the gas chromatography. Argon was also used as the diluent.

1-Buten-3-yne and 1,3-butadiyne synthesized in a pyrolysis experiment were used. The other pure gases (Takachiho Shoji Co., research grade) were used as received.

Analytical. The shock heated sample was introduced into 60-ml volume bulb, and analyzed by gas chromatography. Details of the gas chromatographic analysis were reported.[11]

The isotopic distributions of acetylene, 1-buten-3-yne, and ethylene were determined with a Hitachi Model RM-50 mass spectrometer. Acetylene and ethylene were separated on a 3 mm×2 m Porapak T column at 50 °C with helium as the carrier. Each gas component was collected in a trap cooled by liquid nitrogen. The cooled trap was then evacuated for several minutes to remove the carrier gas and contaminants, especially nitrogen and oxygen.

For the measurement of mass spectra of ethylene isomers, the ionization potential was maintained at *ca.* 12 eV to simplify the fragmentation patterns, in which only the parent peaks of the isomers appeared in the mass spectra. The influence of nitrogen and oxygen on $m/e=28$ and 32 in the mass spectra, respectively, can be neglected at a low ionization potential. The mass spectra of 1-buten-3-yne and acetylene isomers were measured at an ionization potential of 50 eV. The method of mass spectral analyses for acetylene and 1-buten-3-yne isomers was described elsewhere.

Results

Three mixtures were heated behind the reflected shock waves in the temperature range 1000—1600 K. The total densities behind the reflected shock waves were maintained within $(2.35\pm0.11)\times10^{-5}$ mol/cm^3, which were the same as those in the pyrolysis experiment in the absence of deuterium.

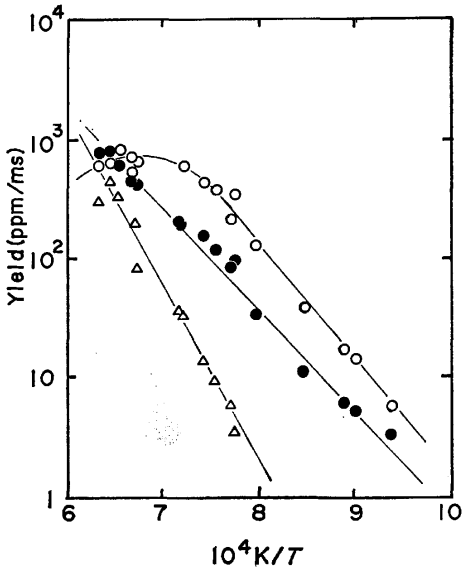

Fig. 1. Major product distribution as a function of temperature($C_2H_2/D_2/Ar=5/10/85$).
○; 1-Buten-3-yne, ●; ethylene, △; 1,3-butadiyne.

Major Products. The shock heated gas samples were analyzed by gas chromatography. The analytical results in the case of the mixture with the ratio of $C_2H_2/D_2/Ar$ equal to 5/10/85 are shown in Fig. 1. The major products were 1-buten-3-yne, ethylene, and 1,3-butadiyne in the decreasing order of amount, 1-buten-3-yne and 1,3-butadiyne being the major products of the pyrolysis of acetylene by itself. This indicates that under the present experimental conditions the hydrogenation of acetylene occurs simultaneously with the pyrolysis of acetylene, and in the temperature range up to 1400 K the formation of 1-buten-3-yne dominates that of ethylene.

1-Buten-3-yne and 1,3-Butadiyne: As shown in Fig. 1, the yields of 1-buten-3-yne and 1,3-butadiyne as a function of temperature are similar to those of the pyrolysis in the absence of deuterium. The concentration of 1-buten-3-yne also reaches maximum at *ca.* 1500 K.

The effects of added deuterium on the production of 1-buten-3-yne and 1,3-butadiyne for the three mixtures are shown in Figs. 2 and 3, respectively. We see that the yields of 1-buten-3-yne and 1,3-butadiyne seem to be entirely dependent on the initial acetylene concentration, and are little affected by that of deuterium. The rate (yield expressed in ppm/ms) of 1-buten-3-yne formation is approximately of second-order with respect to acetylene, which is the same as that in the C_2H_2–Ar system. The second-order rate expression fits the

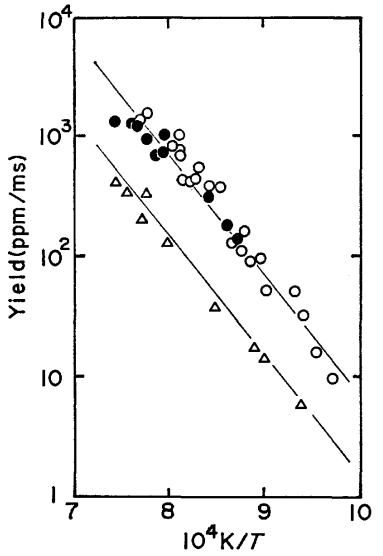

Fig. 2. Effect of deuterium on the 1-buten-3-yne formation.
○; $C_2H_2/D_2/Ar=10/10/80$, △; $C_2H_2/D_2/Ar=5/10/85$, ●; $C_2H_2/D_2/Ar=10/5/85$.

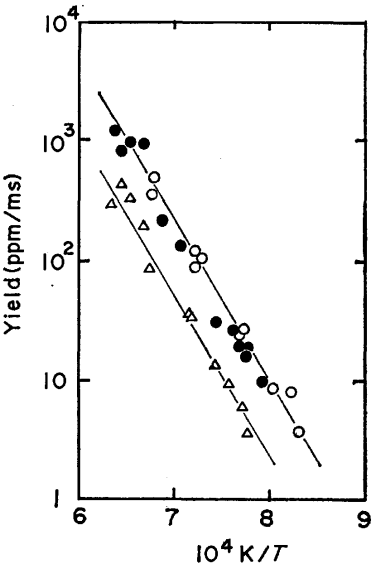

Fig. 3. Effect of deuterium on the 1,3-butadiyne formation.
○; $C_2H_2/D_2/Ar=10/10/80$, △; $C_2H_2/D_2/Ar=5/10/85$, ●; $C_2H_2/D_2/Ar=10/5/85$.

data obtained below 1350 K (41 points) by the least-squares method:

$$k_1(\mathrm{cm^3\ mol^{-1}\ s^{-1}}) = (14.8\pm1.8)\times10^{13} \times\exp((-44200\pm1500)/RT), \quad (1)$$

where the activation energy is expressed in cal*/mol, the errors denoting the standard deviation of the least-squares method.

In order to confirm the effects of deuterium added, the isotopic distribution of 1-buten-3-yne was determined by mass spectrometry. The mass spectral

* 1 cal_{th}=4.184 J.

Table 1. Isotopic distributions of 1-buten-3-yne and acetylene

T_5/K[a]	1205	1245	1296	1371	1312[h]	1290	1322
C_4H_4[b]	1.000	0.994	0.938	0.720	1.000	0.812	0.734
C_4H_3D	—[g]	0.006	0.054	0.255	—	0.188	0.239
$C_4H_2D_2$	—	—	0.008	0.018	—	—	0.019
C_4HD_3	—	—	—	0.007	—	—	0.008
C_4D_4	—	—	—	—	—	—	—
C_2H_2[c]	0.996	0.981	0.959	0.896	0.979	0.933	0.912
C_2HD	0.004	0.014	0.034	0.093	0.019	0.053	0.078
C_2D_2	—	0.005	0.007	0.011	0.002	0.014	0.010
$[C_4H_4]$[d]	447	834	1582	2165	1281	348	365
τ/μs[e]	650	710	690	780	690	820	840
C_2H_2/D_2[f]	10/10	10/10	10/10	10/10	10/5	5/10	5/10

a) T_5 is the temperature behind the reflected shock wave. b), c) The total amounts of 1-buten-3-yne and acetylene are taken to be equal to 1.000. d) Total yield of 1-buten-3-yne isomers expressed in ppm/ms. e) τ is the dwell time. f) Composition of the mixture. g) Undetectable. h) Deuterated 1-buten-3-ynes are not detected at 1290 and 1340 K in the mixture of $C_2H_2/D_2=10/5$.

analyses of the 1-buten-3-ynes together with the acetylenes were carried out for several samples taken out of the three mixtures. The results are summarized in Table 1. No appreciable amount of deuterium-substituted 1-buten-3-ynes is formed at lower temperatures. No detectable amount of deuterated 1-buten-3-ynes is observed in the case of the mixture with the composition $C_2H_2/D_2/Ar=10/5/85$. The effect of added deuterium (hydrogen) on the formation of 1-buten-3-yne is small.

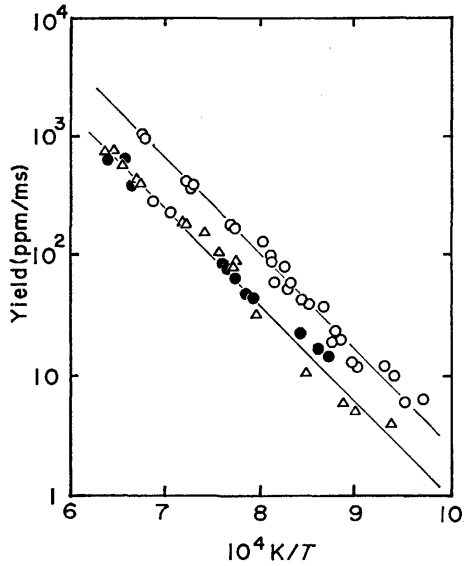

Fig. 4. Concentration dependence of the ethylene formation.
○; $C_2H_2/D_2/Ar=10/10/80$, △; $C_2H_2/D_2/Ar=5/10/85$, ●; $C_2H_2/D_2/Ar=10/5/85$.

Ethylene: Although the formation of ethylene was not the predominant reaction under the present experimental conditions, the yield of ethylene remarkably increased in the presence of deuterium.

The yield of ethylene is plotted against the reciprocal of the reaction temperature in Fig. 4. The dependence of the rate on the concentrations of acetylene and deuterium is approximately equal, being approximately of first-order with respect to acetylene and deuterium. Assuming that the rate equation has the form $d[\text{total ethylene}]/dt=k_2[C_2H_2][D_2]$, the second-order rate constant was obtained by the least-squares method:

$$k_2(\text{cm}^3\ \text{mol}^{-1}\ \text{s}^{-1}) = (4.9\pm1.3)\times10^{11} \times \exp((-34900\pm600)/RT). \quad (2)$$

The isotopic distribution of ethylene was determined by mass spectrometry for several samples out of the shock heated mixture of 10% C_2H_2 and 10% D_2 in argon. The results of the mass spectral analyses are given in Table 2. We see that C_2H_3D is the most abundant species among the ethylene isomers. Considerable amounts of $C_2H_2D_2$ and C_2H_4 are produced.

Table 2. Isotopic distribution of ethylene

T_5/K[a]	1271	1313	1388	1407	1480
C_2H_4[b]	0.158	0.111	0.149	0.141	0.187
C_2H_3D	0.709	0.744	0.653	0.661	0.487
$C_2H_2D_2$	0.121	0.131	0.169	0.176	0.258
C_2HD_3	0.008	0.011	0.019	0.016	0.060
C_2D_4	0.004	0.003	0.010	0.006	0.008
τ/μs[c]	920	940	930	800	780
C_2H_2/D_2[d]	10/10	10/10	10/10	10/10	10/10

a) T_5 is the temperature behind the reflected shock wave. b) The total amount of ethylene isomers is taken to be equal to 1.000. c) τ is the dwell time. d) Composition of the mixture.

Minor Products. Methane, ethane, allene, propyne, and 1,3-butadiene were detected as minor products. Although all of them are observed in the pyrolysis of acetylene alone, their yields as a function of temperature differ from those in the case of the C_2H_2–Ar system. The yields, especially that of 1,3-butadiene, considerably increased in the presence of deuterium.

The influence of the addition of deuterium to acetylene system on the yields of 1,3-butadiene and methane is shown in Figs. 5 and 6, respectively. The yields of 1,3-butadiene and methane are dependent on both acetylene and deuterium concentrations, those of allene and propyne showing a similar dependence on concentration. This distinct dependence of the minor product yields on the deuterium concentration suggests that they are

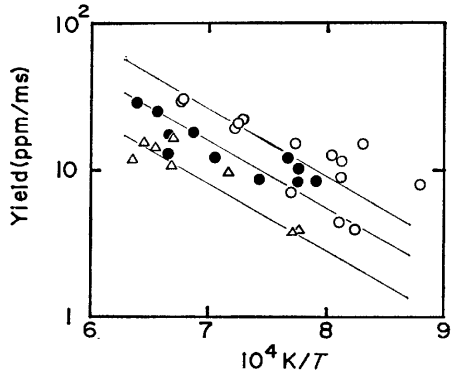

Fig. 5. Effect of deuterium on the 1,3-butadiene formation.
○; $C_2H_2/D_2/Ar=10/10/80$, △; $C_2H_2/D_2/Ar=5/10/85$, ■ ●; $C_2H_2/D_2/Ar=10/5/85$.

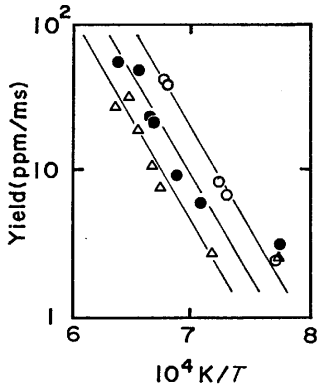

Fig. 6. Effect of deuterium on the methane formation.
○; $C_2H_2/D_2/Ar=10/10/80$, △; $C_2H_2/D_2/Ar=5/10/85$, ●; $C_2H_2/D_2/Ar=10/5/85$.

formed by different paths from those in the C_2H_2–Ar system. Thus the direct participation of deuterium in their formation reactions appears evident.

Discussion

Mechanism of Ethylene and 1-Buten-3-yne Formation. The formation of 1-buten-3-yne was the predominant reaction, the shape of the yield-temperature plots for 1-buten-3-yne not being affected by the addition of deuterium. The dependence of rate on the concentration of acetylene was the same as that observed in the pyrolysis of acetylene by itself, deuterium being a negligible effect on the production rate of 1-buten-3-yne. This suggests that the mechanism of 1-buten-3-yne formation is the same as that proposed for the pyrolysis of acetylene in the C_2H_2–Ar system. The scheme is represented as follows:[11]

$$2C_2H_2 \longrightarrow C_4H_3 + H, \quad (3)$$

$$H + C_2H_2 \longrightarrow C_2H_3, \quad (4)$$

$$C_2H_3 + C_2H_2 \longrightarrow C_4H_4 + H, \quad (5)$$

$$C_4H_3 + C_2H_2 \longrightarrow C_6H_5, \quad (6)$$

$$C_6H_5 + C_2H_2 \longrightarrow C_4H_4 + C_4H_3. \quad (7)$$

The yield of ethylene increases markedly in the presence of deuterium. If the addition of deuterium to acetylene occurred by a molecular mechanism, $C_2H_2D_2$ would be expected primarily among the ethylene isomers. However, actually C_2H_3D was produced in a large amount. The isotopic distribution obtained in the present analysis is in line with that obtained by Skinner *et al.*,[3] who supported a free-radical chain mechanism for the formation of ethylene.

In the temperature range up to 1400 K, the formation of 1-buten-3-yne is predominant. The initiation step for the formation of ethylene is expected to be the same as that for the production of 1-buten-3-yne. In the above mechanism, Reactions 3 and 4 should be responsible for the formation of ethylene. The scheme of ethylene production is thus completed by the following reactions:

$$C_2H_3 + H_2 \longrightarrow C_2H_4 + H, \quad (8)$$

$$2C_2H_3 \longrightarrow C_4H_6, \quad (9)$$

$$H + C_2H_3 \longrightarrow C_2H_4. \quad (10)$$

The recombination of H atoms with argon as a third body is a relatively slow process and could be neglected. For the sake of simplicity, hydrogen, instead of deuterium, is considered, only bimolecular recombination reactions being taken into account in Reactions 9 and10.

Against the initiation Reaction 3, an alternative initiation step was proposed for the hydrogenation of acetylene:[4]

$$C_2H_2 + H_2 \longrightarrow C_2H_3 + H. \quad (11)$$

Reactions 3 and 11 would compete with each other. When Reaction 11 becomes predominant in the C_2H_2–H_2 system, 1-buten-3-yne should be formed by the subsequent Reactions 4 and 5. Assuming steady-state concentrations of H atom and C_2H_3 radical in the above mechanism with the termination of Reaction 9, the steady-state rate of 1-buten-3-yne formation is given by

$$d[C_4H_4]/dt = k_5(k_{11}/k_9)^{1/2}[C_2H_2]^{3/2}[H_2]^{1/2}. \quad (12)$$

The same concentration dependence of the rate of 1-buten-3-yne generation is also derived in the case of the termination of Reaction 10. Equation 12 shows that the yield of 1-buten-3-yne in the C_2H_2–H_2 system should be dependent on the concentration of hydrogen, which is in conflict with the observed dependence on the concentration of deuterium.

Another support for the insignificance of Reaction 11 may be presented by the estimation of the rate constants of Reactions 3 and 11. The adopted rate constant[13] was $k_{-3}=k_{-11}(\mathrm{cm^3\ mol^{-1}\ s^{-1}})=2\times10^{13}$. The approximate rate constant of the forward Reaction 3 was estimated to be[11]

$$k_3(\mathrm{cm^3\ mol^{-1}\ s^{-1}}) = 3.5\times10^{13}\exp(-47400/RT). \quad (13)$$

In the estimation of the equilibrium constant of Reaction 11, the heat of formation of 59.6 kcal/mol[14] is used for C_2H_3 radical, the enthalpy and entropy being the same as those evaluated by Benson.[15] The approximate rate constant of forward Reaction 11 is given by

$$k_{11}(\mathrm{cm^3\ mol^{-1}\ s^{-1}}) = 8\times10^{13}\exp(-56400/RT). \quad (14)$$

The estimated k_{11} is about two and one order of magnitude smaller than k_3 at 1000 and 1600 K, respectively.

Reaction 11 is not likely to occur as the primary initiation step for the pyrolysis and hydrogenation of acetylene in the C_2H_2–$H_2(D_2)$ system.

As regards the role of C_4H_3 radical and H atom in the pyrolysis, previously we could not determine the relative importance of C_4H_3 radical and H atom, since the kinetic behavior of the propagation steps initiated by C_4H_3 radical and H atom was expected to be similar, but we have obtained more data which may be useful to determine the relative importance of the above two radicals in the pyrolysis of acetylene.

Although the total yield of 1-buten-3-yne was little affected by the addition of deuterium, appreciable amounts of deuterated 1-buten-3-ynes were produced in the C_2H_2–D_2 system. Thus the isotopic distribution of 1-buten-3-yne together with those of ethylene and acetylene could be utilized for testing formation reactions of deuterated 1-buten-3-ynes, especially 1-buten-3-yne-d_1, the most abundant species among the deuterated isomers. The formation of 1-buten-3-yne and ethylene isomers in the C_2H_2–D_2 system seems complicated, a schematic reaction diagram being shown in Fig. 7.

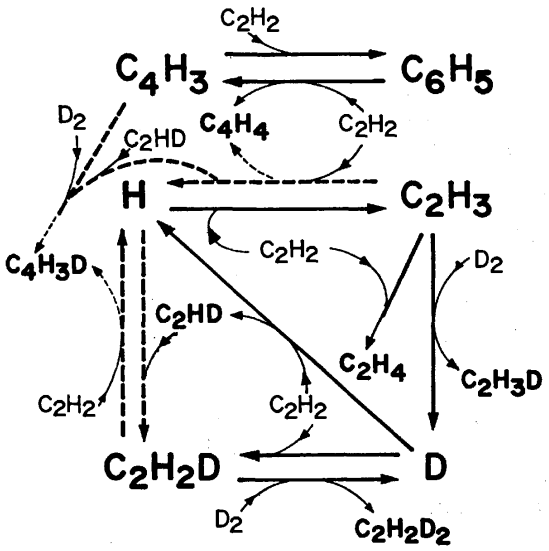

Fig. 7. Schematic reaction diagram for the major product formation in the C_2H_2–D_2 system. Solid line represents the reaction which is responsible for the formation of the relevant product, and broken line denotes ineffective reaction.

First the chain propagation step initiated by H atom, Reactions 4 and 5, will be considered. A considerable amount of C_2HD is produced, which may result from the H–D exchange reaction between C_2H_2 and D_2 (Table 1). The C_2HD in a considerable amount as well as C_2H_2 might participate in the formation of 1-buten-3-yne-d_1. If C_4H_3D were mainly formed by the reaction of C_2HD with the radicals, as an example, with C_2H_3 radical;

$$C_2H_3 + C_2HD \longrightarrow C_4H_3D + H, \quad (15)$$

the ratio of $[C_4H_3D]/[C_4H_4]$ would be given by

$$[C_4H_3D]/[C_4H_4] = (k_{15}/k_5)([C_2HD]/[C_2H_2]). \quad (16)$$

Since k_5 and k_{15} (kinetic isotope effect) are expected to be approximately equal at high temperatures, the ratios of $[C_4H_3D]/[C_4H_4]$ and $[C_2HD]/[C_2H_2]$ as a function of temperature should be nearly same. However, this is not the case. Thus the paths of this type to form deuterated 1-buten-3-ynes are insignificant.

In the C_2H_2–D_2 system, C_2H_3D, instead of C_2H_4, is formed by the following reaction:

$$C_2H_3 + D_2 \longrightarrow C_2H_3D + D. \quad (17)$$

In order to be compatible with the observed isotopic distribution of ethylene, the D atom thus generated is quickly converted into H atom by

$$C_2H_2 + D \longrightarrow C_2HD + H. \quad (18)$$

Simultaneously a reaction analogous to Reaction 4 would occur as follows:

$$C_2H_2 + D \longrightarrow C_2H_2D. \quad (19)$$

The concentration of the C_2H_3 radical present in the system should be greater than that of the C_2H_2D radical, since C_2H_3D is the predominant species among the ethylene isomers. C_2H_2D radical reacts with D_2 in a similar way:

$$C_2H_2D + D_2 \longrightarrow C_2H_2D_2 + D. \quad (20)$$

Reactions 17 and 20 are competitive with each other, the relative abundance of C_2H_3D and $C_2H_2D_2$ being given by

$$[C_2H_2D_2]/[C_2H_3D] = (k_{20}/k_{17})([C_2H_2D]/[C_2H_3]). \quad (21)$$

On the other hand, the C_2H_2D radical present in the system could lead to the formation of C_4H_3D by a reaction with C_2H_2 analogous to Reaction 5:

$$C_2H_2D + C_2H_2 \longrightarrow C_4H_3D + H. \quad (22)$$

Similarly, the ratio of $[C_4H_3D]/[C_4H_4]$ is givn by

$$[C_4H_3D]/[C_4H_4] = (k_{22}/k_5)([C_2H_2D]/[C_2H_3]). \quad (23)$$

As in Eq. 16, $k_{17}=k_{20}$ and $k_5=k_{22}$ can be expected at the present temperatures. Then Eqs. 21 and 22 show that the relative abundance of C_4H_3D and C_4H_4 would be comparable with that of $C_2H_2D_2$ and C_2H_3D. The observed ratios of $[C_4H_3D]/[C_4H_4]$ and $[C_2H_2D_2]/[C_2H_3D]$ as a function of temperature are summarized in Table 3. The above two ratios as a function of temperature differ from each other. Thus H atom may be an insignificant radical in the pyrolysis, but is primarily responsible for the formation of ethylene. It is concluded that C_4H_3 radical plays an important role in the formation of 1-buten-3-yne.

Table 3. Observed ratios of $[C_4H_3D]/[C_4H_4]$ and $[C_2H_2D_2]/[C_2H_3D]$ as a function of temperature

T_5/K[a]	1205	1245	1296	1371	
$[C_4H_3D]/[C_4H_4]$[b]	—[c]	0.006	0.058	0.354	
T_5/K[a]	1271	1313	1388	1407	1480
$[C_2H_2D_2]/[C_2H_3D]$[b]	0.171	0.176	0.258	0.266	0.538

a) T_5 is the temperature behind the reflected shock wave. b) The values are calculated from Tables 1 and 2 for the case of the mixture of $C_2H_2/D_2/Ar$= 10/10/80. c) Value not determined.

C_4H_3D could not be formed by the reaction of C_4H_3 radical with D_2, since the concentration of C_4H_3 radical is a function of acetylene alone, and about half the

amount of C_4H_3D produced in the mixture of $C_2H_2/D_2/Ar=10/10/80$ at around 1300 K could have been detected in the mixture of $C_2H_2/D_2/Ar=10/5/85$.

The ineffectiveness of the reaction of C_4H_3 radical with $H_2(D_2)$ may be understood in view of the heat of the reaction:[16]

$$C_4H_3 + H_2 \longrightarrow C_4H_4 + H, \quad \Delta H^\circ = 24.9. \quad (24)$$

The heat is greater than the activation energy of Reaction 7, which was estimated to be 17.9—22.6 kcal/mol.[11] The chain propagation process of Reactions 6 and 7 is more effective for the formation of 1-buten-3-yne than Reaction 24.

The occurrence of ethylene in a considerable amount is also in accordance with the prediction from the viewpoint of

$$C_2H_3 + H_2 \longrightarrow C_2H_4 + H, \quad \Delta H^\circ = 5.0. \quad (8)$$

The formation of C_2H_4 in a considerable amount in the C_2H_2–D_2 system cannot be accounted for by the reactions of the vinyl radicals with D_2. C_2H_4 thus can be formed by the hydrogen atom abstraction reaction of C_2H_3 radical from C_2H_2 molecule in the same way as in the pyrolysis of acetylene alone:

$$C_2H_3 + C_2H_2 \longrightarrow C_2H_4 + C_2H, \quad \Delta H^\circ = 12.7. \quad (25)$$

In a previous work the main primary C_4 product in the early stage of the pyrolysis of acetylene was concluded to be 1-buten-3-yne. If 1,3-butadiyne were formed at first and then reacted with D_2 to produce 1-buten-3-yne behind reflected shock wave and/or in the cooling process[17]

$$C_4H_2 + D_2 \longrightarrow C_4H_2D_2, \quad (26)$$

a significant amount of $C_4H_2D_2$ would be generated. This is inconsistent with the present isotopic distribution of 1-buten-3-yne.

Formation Reaction for the Minor Products. The secondary products of the pyrolysis were considerably affected by the addition of deuterium. The dependence of their yields on the deuterium concentration suggests that the minor products are produced by the reactions of the relevant radicals in the pyrolysis of acetylene by itself with deuterium.

In the present analysis, however, only the total yield of each minor product is obtained, and the C_2H_2–H_2 system will be considered in the following discussion. In the C_2H_2–Ar system the formation of CH_4 and C_3H_4 was interpreted in terms of the reactions of CH_3 and C_3H_3 radicals with acetylene molecule, respectively. In the C_2H_2–H_2 system, however, the radicals would react with H_2 rather than C_2H_2 molecule. In the case of the CH_4 formation the following two reactions would be competitive:

$$CH_3 + H_2 \longrightarrow CH_4 + H \quad \Delta H^\circ = -0.6, \quad (27)$$

$$CH_3 + C_2H_2 \longrightarrow CH_4 + C_2H \quad \Delta H^\circ = 7.1. \quad (28)$$

The heat of Reaction 27 is *ca.* 8 kcal/mol lower than that of Reaction 28. Reaction 27 is expected to have lower activation energy than that of Reaction 28.

A remarkable increase in the 1,3-butadiene yield in the C_2H_2–H_2 system can be ascribed to the reaction of C_4H_5 radical with hydrogen in a similar way:

$$C_2H_3 + C_2H_2 \longrightarrow C_4H_5, \quad \Delta H^\circ = -18.7, \quad (29)$$

$$C_4H_5 + H_2 \longrightarrow C_4H_6 + H, \quad \Delta H^\circ = 11.0. \quad (30)$$

All the minor products observed in the C_2H_2–H_2 system were also found in the pyrolysis of acetylene by itself at temperatures above 1300 K. On the other hand, in the presence of hydrogen (deuterium) they were produced at temperatures above 1100 K. This may be accounted for by the reactions stated above. Thus the addition of hydrogen to acetylene system appreciably increases the consumption of acetylene.

Rate of Ethylene Formation. The H atom generated by the initiation step is responsible for the formation of ethylene. The kinetic isotope effect is neglected and the C_2H_2–H_2 system is considered, since the total yield of ethylene was obtained for all runs. The rate of ethylene formation will be derived from the proposed mechanism.

In our mechanism the steady-state treatment is applicable in the same way as in the 1-buten-3-yne formation.[11] The recombination reaction of H atom with C_2H_3 radical is not important, since C_2H_3 radical is predominant. Neglecting the backward reactions, the steady-state assumption is applied to the scheme of Reactions 3, 4, 8, and 9. The steady-state rate of the ethylene formation is given by

$$d[C_2H_4]/dt = k_8(k_3/2k_9)^{1/2}[C_2H_2][H_2]. \quad (31)$$

k_8 is calculated from k_{-8} evaluated by Schofield[18] by the combination of the equilibrium constant of Reaction 8 at 1300 K, and k_9 is taken equal to k_t in Ref. 11:

$$k_8(\mathrm{cm^3\ mol^{-1}\ s^{-1}}) = 5.39\times10^{11}\exp(-12900/RT), \quad (32)$$

$$k_9(\mathrm{cm^3\ mol^{-1}\ s^{-1}}) = 2.9\times10^{12}. \quad (33)$$

Substituting these values in Eq. 30, the second-order rate constant is given by

$$k_8(k_3/2k_9)^{1/2}(\mathrm{cm^3\ mol^{-1}\ s^{-1}}) = 1.6\times10^{12}\exp(-36600/RT). \quad (34)$$

The steady-state rate constant agrees with the observed (Eq. 2) within a factor of 2 in the temperature range studied.

When a large excess of hydrogen present relative to acetylene, the initiation step of Reaction 11 may become more important. Taylor and Van Hook[1] reported the higher activation energy of 42 kcal/mol for the mixtures of $C_2H_2/H_2=1$—$1/32$ in the temperature range 770—810 K. This might be related to the change of the initiation step from Reaction 3 to 11, the activation energy of which is estimated to be higher than that of Reaction 3.

The author wishes to express his gratitude to Professor Kenji Kuratani, The University of Tokyo, for his helpful discussions and suggestions throughout this work.

References

1) H. A. Taylor and A. Van Hook, *J. Phys. Chem.*, **39**, 811 (1935).

2) G. B. Skinner and E. M. Sokoloski, *J. Phys. Chem.*, **64**, 1028 (1960).

3) G. B. Skinner, R. C. Sweet, and S. K. Davis, *J. Phys. Chem.*, **75**, 1 (1971).

4) S. W. Benson and G. R. Haugen, *J. Phys. Chem.*, **71**, 1735 (1967); *ibid.*, **71**, 4404 (1967).

5) S. H. Bauer, *Int. Symp. Combust.*, **11**, 105 (1967).
6) T. Asaba, Y. Yoneda, and T. Hikita, *Kogyo Kagaku Zasshi*, **64**, 47 (1957).
7) E. A. Westbrook, K. Hellwig, and R. C. Anderson, *Int. Symp. Combust.*, **5**, 631 (1955).
8) G. J. Minkoff, D. M. Newitt, and P. Rutledge, *J. Appl. Chem.*, **7**, 406 (1957).
9) K. C. Hou and R. C. Anderson, *J. Phys. Chem.*, **67**, 1579 (1963).
10) C. F. Cullis and N. H. Franklin, *Proc. R. Soc. London, Ser. A*, **280**, 139 (1964).
11) H. Ogura, *Bull. Chem. Soc. Jpn.*, **50**, 1044 (1977).
12) M. Tsuda and K. Kuratani, *Bull. Chem. Soc. Jpn.*, **41**, 53 (1968).
13) "Kinetic Data on Gas Phase Unimolecular Reactions," S. W. Benson and H. E. O'Neal, National Bureau of Standards NSRDS-NBS 21, U. S. Government Printing Office Washington D. C. (1970), p. 26.
14) F. P. Lossing, *Can. J. Chem.*, **49**, 357 (1971).
15) S. W. Benson, "Thermochemical Kinetics," Wiley, New York (1968).
16) In the calculation of the heats of the reactions, ΔH° (kcal/mol) at 298 K, the same values as in a previous work[11] are used for the heats of formation.
17) E. F. Greene, R. L. Taylor, and W. L. Patterson, Jr., *J. Phys. Chem.*, **62**, 238 (1958).
18) K. Schofield, *Planet. Space Sci.*, **15**, 643 (1967).

Determination of Micropore Volumes of Active Carbon Using Dubinin-Radushkevich Plots

Ryoichi TSUNODA

Industrial Research Institute of Kanagawa Prefecture, Showa-machi, Kanazawa-ku, Yokohama 236

(Received January 27, 1977)

The adsorption of methanol on active carbons at 30 °C was carried out and a new method for determining the micropore volume in the Dubinin-Radushkevich plot is presented. From this method, it was found that the adsorption volume (V) corresponding to the adsorption potential ($A=RT\ln P_0/P$), at which the plot of $dV/d(-A)$ *vs.* A has its minimum value, is the value of the micropore volume in cases where extrapolation of the Dubinin-Radushkevich plot cannot be applied because of non-linearity of the Dubinin-Radushkevich plot.

The Dubinin-Radushkevich equation has been extensively used in studies of gas adsorption on microporous carbons. Its application has been reported in the determination of the micropore volume of heat-treated and activated carbons. For this application, the Dubinin-Radushkevich equation[1] is written as

$$V = V_0 \exp[-k(A/\beta)^2], \quad (1)$$

where V is the volume adsorbed at relative pressure P/P_0, $A=RT\ln P_0/P$, and k and β are constants. Equation 1 is converted to its linear form

$$\log V = \log V_0 - D\log^2 P_0/P, \quad (2)$$

where $D=2.303\,k\,R^2T^2/\beta^2$, and the micropore volume (V_0) is obtained by extrapolation.

However, deviations from linearity can be observed at low values of $\log^2 P_0/P$ and great care must be taken in the extrapolation for the determination of the micropore volume.

Furthermore, the pore structure of carbon is customarily classified into three types, micropores (radii< 15—16 Å), transitional pores (15—16 Å<radii<1000—2000 Å), and macropores (radii>1000—2000 Å).[1]

Generally speaking, the lower limit of pore size for which the Kelvin equation is applicable is about 15 Å in radius.[1] The pore-volume distribution in the transitional pore range (15 Å<radii<≈100 Å) can usually be obtained by application of the Kelvin equation on the adsorption isotherm, and that in the transitional and macropore range (≈100 Å<radii) using a mercury porosimeter. However, there is no satisfactory method for estimating the pore-volume distribution in the micropore range, although the micropore volume can be obtained by subtracting the cumulative pore volume (15 Å≦radii≦100 Å) from the volume adsorbed at the relative pressure corresponding to a radius of 100 Å in the Kelvin equation.

In this paper, the applicability of the proposed method for determining micropore volumes is discussed.

Experimental

Active Carbons. Commercially available Pittsburgh SGL- and PCB-type activated carbons were used. PCB-type activated carbons were treated with steam at 600 and 800 °C, respectively, for 6 h with supply of *ca.* 1.4 g-H_2O/g-carbon h. The percentages of burn-off of these treated PCB carbons were 5.3 and 33.3%, respectively, and can be described as PCB (5.3% burn-off) and PCB (33.3% burn-off).

Methanol Adsorption. The adsorption of methanol on active carbons at 30 °C was measured gravimetrically by means of a conventional quartz spring balance. Prior to the adsorption measurement, the active carbon dried overnight at 110 °C was outgassed at a pressure of 10^{-6} Torr at 30 °C for 14 h. In all cases, the time required for adsorption equilibrium was rapid and was established within 45 min.

Pore-volume Distribution. From the adsorption isotherms, the pore-volume distribution, lying in the radius range between 15 and 100 Å, was calculated employing the Kelvin equation.[2]

In transitional pores, there occur monomolecular and multimolecular adsorption and filling of the free space between the adsorption layers by the capillary condensation mechanism. The Kelvin equation is applicable to the space of the capillary condensate.

In the desorption step, the volume, ΔV, of the capillary condensate is lost between the beginning and the end of a step between two relative pressures P_1/P_0 and P_2/P_0. When the capillary condensate is lost, monolayers and multilayers remain on the pore walls and, thus, the radius of the meniscus of the capillary condensate is less than the actual radius of the pores by the adsorption thickness t. Thus, the quantity ΔV must be multiplied by the factor $[\bar{r}/(\bar{r}-\bar{t})]^2$, where $\bar{r}=(r_1+r_2)/2$ and $\bar{t}=(t_1+t_2)/2$. Multiplication by $[\bar{r}/(\bar{r}-\bar{t})]^2$ is also used in the calculation for the adsorption side of the adsorption isotherm.

The Kelvin equation, giving the relationship between the relative pressure P/P_0 and the pore radius r(Å), can be expressed as follows:

$$\ln P/P_0 = -2\gamma v\cos\theta/RT(r-t), \quad (3)$$

$$\log P/P_0 = -2\times 21.7\times 41.0\times 1/2.303\times 8.31\times 10^7 \times 303.2\times(r-t)\times 10^{-8} = -3.07/(r-t), \quad (4)$$

and

$$t = 4.6\times(-\ln P/P_0)^{-1/6}, \quad (5)$$

where γ is the methanol surface tension, v the molar volume of methanol, θ the contact angle between the methanol and the carbon (=0), R the gas constant, and t the thickness of the adsorbed methanol layer.[3]

Discussion

In his early work, Dubinin[1,4] demonstrated the linearity of the Dubinin-Radushkevich plots for gas adsorption on active carbon, however, afterward many investigators[5-7] frequently observed deviations from linearity.

Marsh and Siemieniewska[8] have suggested that the linearity of the Dubinin-Radushkevich plots occurs

because the distribution of the adsorption potential with adsorption volume follows the Rayleigh distribution. On the other hand, Gregg and Sing[9] and Sutherland[10] have considered that the apparent wide applicability of the Dubinin-Radushkevich equation arises because the log V *vs.* $\log^2 P_0/P$ plot is inherently insensitive and that the distribution of adsorption potential with adsorption volume need not be of the Rayleigh-distribution type.

Since, there have been many discussions of the determination of micropore volumes using Dubinin-Radushkevich plots.

Dubinin[1] suggested that upward deviations from linearity for low values of $\log^2 P_0/P$ can be attributed to the filling of transitional pores and that extrapolation in the Dubinin-Radushkevich plots of the linear section for high values of $\log^2 P_0/P$ can be used to predict the micropore volume. Chiche, Marsh, and Prégermain[5] have adopted extrapolation in the second section of the Dubinin-Radushkevich plots for estimations of the micropore volume when the Dubinin-Radushkevich plot is composed of two linear sections with downward deviations for low values of $\log^2 P_0/P$. In a recent paper, Rand[7] has applied the more generalized Dubinin-Astakhov equation

$$V = V_0 \exp\left[-k(A/E)^n\right], \qquad (6)$$

with E being a constant, in order to linearize the data. In this case, the micropore volume was obtained by the extrapolation of the linearized Dubinin-Astakhov equation.

If the Dubinin-Radushkevich plot can be shown to be strictly linear in form, a plot of $dV/d(-A)$ must be of the Rayleigh-distribution type. Thus, the plot of $dV/d(-A)$ *vs.* A can be considered to give more important information about the micropore volume using the Dubinin-Radushkevich plot.

Assuming the micropore volume to be equivalent to the V_0 obtained by extrapolating the Dubinin-Radushkevich plot only in cases when the Dubinin-Radushkevich plot is strictly linear and when the plot of $dV/d(-A)$ *vs.* A follows the Rayleigh distribution, upward deviations of $dV/d(-A)$ *vs.* A from the Rayleigh distribution for low values of A can be considered to indicate filling of the transitional pores. The adsorption volume corresponding to the adsorption potential A at the point of the upward deviation from the Rayleigh distribution, which is really of Rayleigh-like distribution, can be evaluated as the micropore volume.

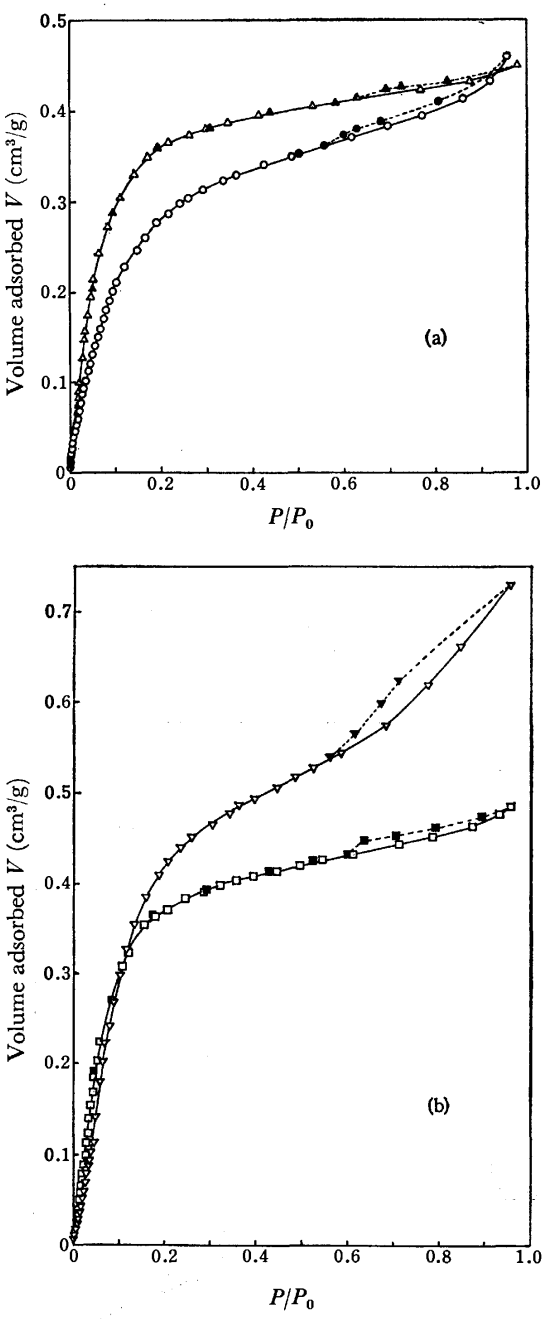

Fig. 1. Adsorption isotherms of active carbons.
(a) △ PCB, ○ SGL.
(b) ▽ PCB(33.3% Burn-off), □ PCB(5.3% Burn-off).
Filled symbols indicate desorption.

Results

The adsorption isotherms, Dubinin-Radushkevich plots, characteristic curves, distribution curves of the adsorption potential, and pore volume distributions of the activated carbons are shown in Figs. 1—5.

The Dubinin-Radushkevich plot of SGL-type activated carbon is linear for low values of $\log^2 P_0/P$, as is shown in Fig. 2. If the plot is extrapolated, the micropore volume is evaluated to be 0.370 cm³/g, which is considerably higher than that calculated using the Kelvin equation (Table 1). This means that the Dubinin-Radushkevich plot is insensitive and great care must be taken in extrapolation. However, as shown in Figs. 4(a) and 5 and in Table 1, the value of the adsorption volume corresponding to the adsorption potential at which the plots of $dV/d(-A)$ *vs.* A deviate upward, *i.e.*, at the minimum value of $dV/d(-A)$, occur coincides with that of the micropore volume obtained using the Kelvin equation.

In the cases of PCB, PCB (5.3% burn-off) and PCB (33.3% burn-off), the Dubinin-Radushkevich plots are curved and the conventional method of extrapolation cannot be applied (see Figs. 2(a)—(b)). However, the

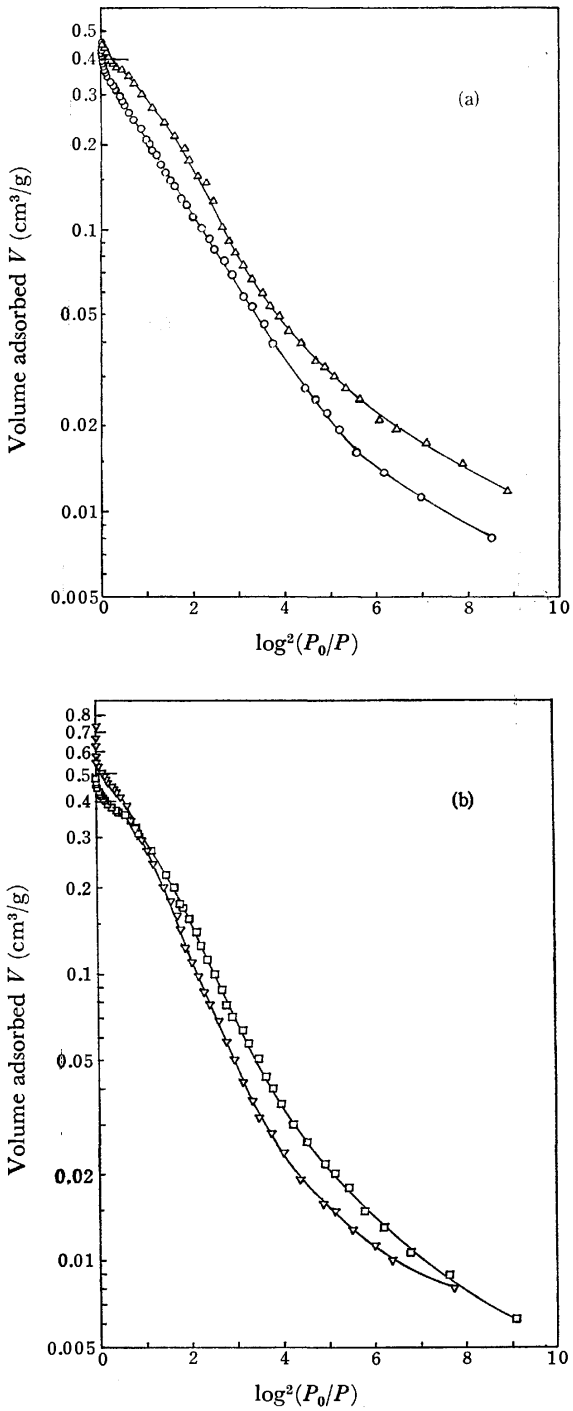

Fig. 2. Dubinin-Radushkevich plots of active carbons.
(a) △ PCB, ○ SGL.
(b) ▽ PCB(33.34% Burn-off), □ PCB(5.3% Burn-off).

distribution curves of the adsorption potential clearly show upward deviations for low values of A. As in the case of SGL-type activated carbon, the values of the adsorption volume corresponding to the adsorption potential at which the upward deviations occur in the distribution curves coincide with those of the micropore volume calculated using the Kelvin equation, as shown in Figs. 4(a)—(b) and 5 and in Table 1.

There are three points to be discussed concerning the applicability of the new method proposed for deter-

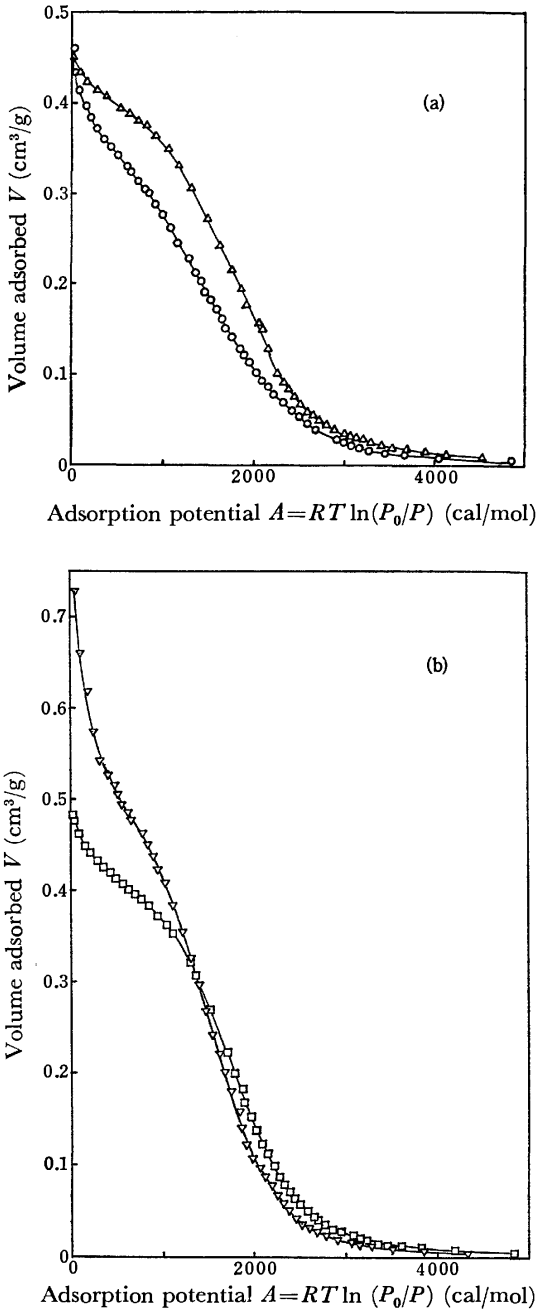

Fig. 3. Characteristic curves of active carbons.
(a) △ PCB, ○ SGL.
(b) ▽ PCB(33.3% Burn-off), □ PCB(5.3% Burn-off).

TABLE 1. MICROPORE VOLUMES OF ACTIVE CARBONS

Active carbon	Methods of determination		
	Kelvin equation		Adsorption volume at $dV/d(-A)=$ mininum (cm³/g)
	Adsorption side (cm³/g)	Desorption side (cm³/g)	
SGL	0.313	0.305	0.315
PCB	0.384	0.381	0.390
PCB (5.3% burn-off)	0.393	0.386	0.405
PCB (33.3% burn-off)	0.417	0.411	0.480

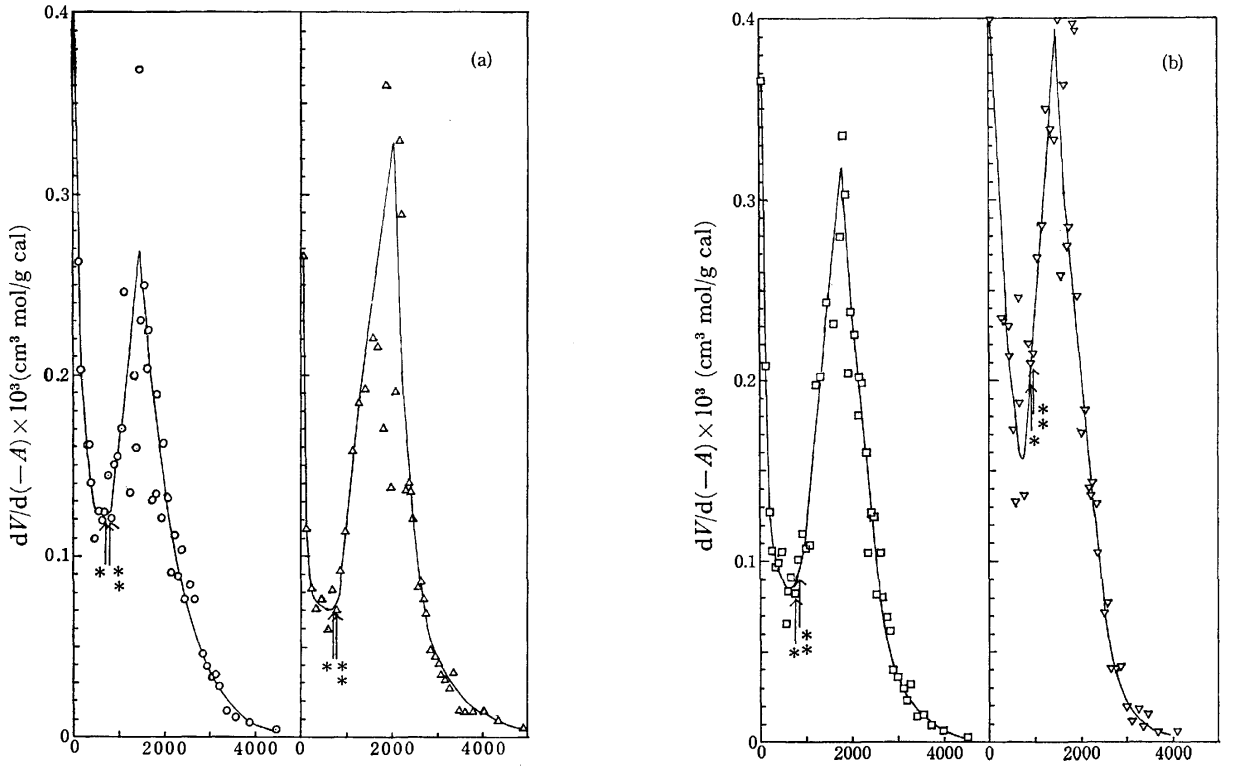

Fig. 4. Distribution curves of adsorption potential of active carbons.
(a) ○ SGL, △ PCB.
(b) □ PCB(5.3% Burn-off), ▽ PCB(33.3% Burn-off).
Marks, * and ⁑, indicate the points of the adsorption potential which correspond to the adsorption volume, the values of which are equal to the micropore volume (radii≦15.5 Å) calculated by the Kelvin equation from the adsorption and desorption sides of the isotherms, respectively.

mining micropore volumes.

1) The effective radius at the beginning of hysteresis loop is considered to be 15 Å and the hysteresis is attributed to the filling of transitional pores by the mechanism of capillary condensation.[1)]

However, in both the adsorption and desorption steps, monolayers and multilayers exist on the walls of pores larger than those filled due to capillary condensation. The adsorption volume, V_h, at the beginning of hysteresis loop is considered to be the sum of the adsorption volume in the micropore and that of monolayers and multilayers on the walls of transitional pores. The values of the adsorption volume, V_h, for SGL, PCB, PCB (5.3% burn-off), and PCB (33.3% burn-off) activated carbons are 0.360, 0.415, 0.430, and 0.535 cm³/g, respectively, as shown in Figs. 1(a) and (b). These are somewhat higher than the micropore volume determined by the method proposed in this paper, as shown in Table 1.

2) Concerning the calculation of the pore-volume distribution, there are two assumptions.

a) The shapes of the pores are assumed to be cylindrical, although the true shapes are complicated and not necessarily cylindrical.

b) The walls of active carbon pores are heterogeneous surfaces and it is impossible to observe the actual thickness, t, of the adsorption layers on active carbons. The thickness, t, observed for substances with nonporous and homogeneous surfaces is assumed to be equal to the actual thickness on active carbon.

Due to these assumptions, discrepancies between the actual micropore volume and the volume calculated using the Kelvin equation will occur.

3) According to the theory of Dubinin,[1)] if the Dubinin-Radushkevich plot is strictly linear, V_0 in Equation 1 is the micropore volume. In this case, the potential-distribution curve $dV/d(-A)$ *vs.* A is really a type of Rayleigh distribution.

The shape of the Rayleigh distribution is shown in Ref. 6 with a maximum value at $A=\beta/\sqrt{2k}$ below which $dV/d(-A)$ decreases to zero.

If active carbons were ideally composed only of micropores, the shape of the plot of $dV/d(-A)$ *vs.* A would have the form of a Rayleigh distribution. However real active carbons have transitional pores, in addition to micropores. Due to the filling of the transitional pores, the Dubinin-Radushkevich plot deviates upward from linearity, and at the same time the plot of $dV/d(-A)$ *vs.* A also deviates upward from the Rayleigh distribution. It can be assumed that the point of deviation, *i.e.*, the point of the $dV/d(-A)$ minimum represents the end of micropore filling and, at the same time, the beginning of transitional-pore filling by capillary condensates and, strictly speaking, the beginning of the adsorption of mono- and multilayers on

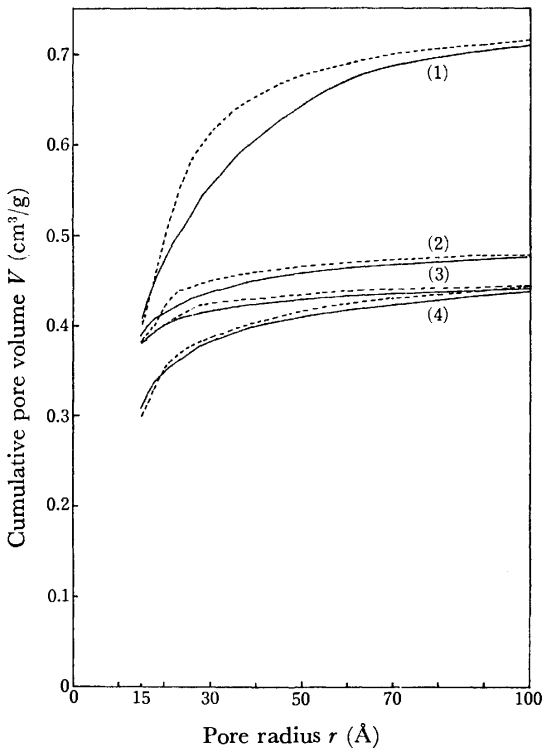

Fig. 5. Pore volume distributions of active carbons.
(1) PCB(33.3% Burn-off), (2) PCB(5.3% Burn-off), (3) PCB, (4) SCL.
—— Calculated from the desorption side of the isotherms.
—— Calculated from the adsorption side of the isotherms.

the transitional pores. The present experimental results show that the proposed method is applicable to the determination of micropore volumes.

From these results, the micropore volume can be estimated by plotting the values of $dV/d(-A)$ *vs.* A and by finding the adsorption volume corresponding to the adsorption potential at which the plots of $dV/d(-A)$ *vs.* A show a minimum value, in cases where extrapolation of the Dubinin-Radushkevich plot cannot be applied because of non-linearity of the Dubinin-Radushkevich plot.

References

1) M. M. Dubinin, "Chemistry and Physics of Carbon," ed by P. L. Walker, Jr., Vol. 2, Marcell Dekker, Inc., N. Y. (1966), p. 51.
2) K. Urano, H. Mizusawa, and R. Kiyoura, *Kogyo Kagaku Zasshi*, **73**, 1911 (1970).
3) M. Daimon and R. Kondo, *Nippon Kagaku Kaishi*, **1972**, 238.
4) M. M. Dubinin, *Chem. Rev.*, **60**, 235 (1960).
5) P. Chiche, H. Marsh, and S. Prégermain, *Fuel*, **46**, 341 (1967).
6) H. Marsh and B. Rand, *J. Colloid Interface Sci.*, **33**, 101 (1970).
7) B. Rand, *J. Colloid Interface Sci.*, **56**, 337 (1976).
8) H. Marsh and T. Siemieniewska, *Fuel*, **46**, 441 (1967).
9) S. J. Gregg and K. S. W. Sing, "Adsorption, Surface Area and Porosity," Academic Press, London (1967), p. 5.
10) J. W. Sutherland, "Porous Carbon Solids," ed by R. L. Bond, Academic Press, London (1967), Chap. 1.

Formation of a Charge-Transfer Complex between the 1-Methyl-1-phenylethylperoxyl Radical and Pyridine during Decomposition of 1-Methyl-1-phenylethyl Hydroperoxide

Shun-ichi FUKUZUMI and Yoshio ONO

Department of Chemical Engineering, Tokyo Institute of Technology, Ookayama, Meguro-ku, Tokyo 152

(Received February 4, 1977)

The apparent rate constant for the self-reaction of 1-methyl-1-phenylethylperoxyl radicals ($RO_2^{\cdot}$) in the presence of pyridine was determined from simultaneous measurements of the rate of oxygen generation and the concentration of the peroxyl radical during the decomposition of 1-methyl-1-phenylethyl hydroperoxide with lead dioxide. The apparent rate constant decreased markedly with an increase in the concentration of pyridine, which clearly demonstrates the low reactivity of $RO_2^{\cdot}$ in the presence of pyridine. This behavior is taken as evidence that the charge-transfer complex between the peroxyl radical and pyridine is formed and that the reactivity of complexed peroxyl radicals is much lower than that of uncomplexed peroxyl radicals. The equilibrium constant for the formation of the charge-transfer complex has been determined to be 0.55 M^{-1} at 293 K and the values of $-\Delta H$ and $-\Delta S$ were found to be 31 kJ mol^{-1} and 109 J mol^{-1} K^{-1}, respectively.

The effects of solvents on the reactivity of free radicals due to complex formation between the radicals and the solvents have been investigated by several authors.[1-10] Porter and Smith[1] have explained the influence of chaperon molecules on the recombination rate of iodine atoms in terms of a charge-transfer complex intermediate between the two species, spectroscopic support of which has also been reported.[2-4] Russell[5] has shown that the pronounced solvent effects on chlorine atom-substrate complexes of similar nature. Boozer and Hammond[6,7] have postulated the formation of charge-transfer complexes between alkylperoxyl radicals and inhibitors (aromatic amines and phenols) in the autoxidation of hydrocarbons. Thomas[8] has also examined the possibility of complex formation between the 1-methyl-1-phenylethylperoxyl radical and pyridine in a study on the autoxidation of cumene at 330 and 347 K, but no clear evidence was obtained. Thus, an inhibition mechanism involving charge-transfer between a chain propagating radical and the antioxidant has often been suggested,[6-8] but has rarely been identified with any certainty.

Previously, the present authors postulated the following complex formation between the 1-methyl-1-phenylethylperoxyl radical and 1-methyl-1-phenylethyl hydroperoxide as the result of electron spin resonance and kinetic studies of hydroperoxide decomposition with lead dioxide.[9]

$$RO_2^{\cdot} + n\,ROOH \rightleftharpoons (RO_2^{\cdot} \cdots n\,ROOH).$$

The value $n=2$ was obtained from the change in the ESR line width of the peroxyl radical, as well as from kinetic results of the hydroperoxide decomposition. The reactivity of the complexed radicals was found to be much lower than that of uncomplexed radicals. Similar results indicating that complex formation between radicals and solvents leads to a decrease in the apparent reactivity of the radicals has been obtained in the case of the autoxidation of ethyl methyl ketone in aqueous solutions.[10] It was shown that equilibrium in the reaction

$$RO_2^{\cdot} + m\,H_2O \rightleftharpoons (RO_2^{\cdot} \cdots m\,H_2O)$$

is rapidly established in the system. In this case, the value, $m=1$, was obtained. Thus, there are cases in which the apparent reactivity of radicals decreases markedly as the results of complex formation between radicals and solvents, although these processes remain some of the least understood of all inhibition mechanism.[11]

Pyridine is known to form strong charge-transfer complexes with acceptors such as iodine.[12] Therefore, in the present study, the change in apparent reactivity of the 1-methyl-1-phenylethylperoxyl radical for the self-reaction in the presence of pyridine was investigated by electron spin resonance and kinetic methods, and evidence of the formation of charge-transfer complexes between the peroxyl radical and pyridine is presented. The equilibrium constant, K, and the values of ΔH and ΔS for complex formation are reported.

Experimental

The apparatus has been described in detail elsewhere.[9,13] The decomposition of 1-methyl-1-phenylethyl hydroperoxide in CCl_4 and pyridine in the presence of lead dioxide powder was carried out in a 50- or 100-cm^3 flask immersed in a temperature-controlled bath, stirred magnetically and attached to a wet-gasometer. In order to determine the concentration of the peroxyl radical as well as the rate of oxygen generation under the same conditions, simultaneous measurements of the radical concentration and the rate of oxygen generation were performed as follows. While the rate of oxygen generation was measured with a wet-gasometer, the part of the solution involving the catalyst powder was circulated, using a roller pump, through the ESR cavity where the ESR measurements were carried out. The intensity of the ESR signal was confirmed to be independent of the feed rate of the roller pump over the range from 50—200 cm^3/min. A JEOL-X-band spectrometer (JES-PE-1X) with 100-kHz magnetic modulation was used to detect the radicals. The radical concentration was determined by comparing the absorption area of the radical with that of 1,1-diphenyl-2-picrylhydrazyl in benzene. The change in sensitivity of the spectrometer due to the decrease in the Q factor caused by introducing a polar solvent such as pyridine was calibrated using an ESR marker in the ESR cavity.

Results and Discussion

When lead dioxide powder is added to the hydroperoxide solution, the ESR spectrum of the 1-methyl-1-phenylethylperoxyl radical is observed and oxygen gas evolves. The ESR spectrum consists of a single symmetrical line with no detectable hyperfine structure and an isotropic g-factor of 2.0148 ± 0.0004, which is in good agreement with the values reported previously.[9,13-15] No ESR signal was obtained and no oxygen gas evolved unless lead dioxide powder was added. Simultaneous measurements of the radical concentration and the rate of oxygen generation were carried out both in the absence of and in the presence of pyridine. All the experiments were performed in hydroperoxide concentrations below 0.3 M, for which complex formation between the peroxyl radical and the hydroperoxide is negligible.[9]

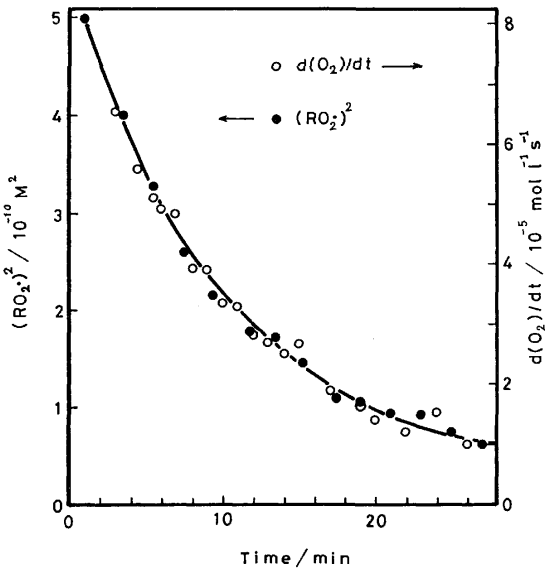

Fig. 1. The square of the 1-methyl-1-phenylethylperoxyl radical concentration and the rate of oxygen generation are plotted against time for the decomposition of 1-methyl-1-phenylethyl hydroperoxide with lead dioxide in the presence of pyridine at 303 K.
Initial concentration of the hydroperoxide: 0.254 M, initial ratio of PbO_2 weight to liquid volume: 40.5 g/l, pyridine concentration: 1.70 M, solvent: CCl_4.

A typical example of the change in the rate of oxygen generation and the peroxyl radical concentration with reaction time is shown in Fig. 1, in which the ordinates are the square of the radical concentration and the rate of oxygen generation. The initial concentrations of the hydroperoxide and pyridine were 0.254 and 1.70 M, respectively, and the ratio of catalyst weight to liquid volume was 40.5 g/l. As shown in Fig. 1, by selecting appropriate ordinate scales, the square of the radical concentration and the rate of oxygen generation behave in exactly the same manner, that is, the rate of oxygen generation is proportional to the square of the radical concentration, thus

$$\frac{d[O_2]}{dt} = k_6^{exp}[RO_2\cdot]^2, \quad (1)$$

where k_6^{exp} is a constant. It is well accepted that 1-methyl-1-phenylethyl hydroperoxide undergoes induced decomposition as follows:[16-18]

$$RO_2\cdot + RO_2\cdot \xrightarrow{k_6} 2RO\cdot + O_2, \quad (2)$$

$$RO\cdot + ROOH \xrightarrow{k_5} ROH + RO_2\cdot. \quad (3)$$

Equation 1 clearly indicates that the oxygen generation reaction involves a bimolecular reaction of $RO_2\cdot$ (2) and that most $RO\cdot$ radicals react with ROOH and thus regenerate $RO_2\cdot$; the fraction of $RO\cdot$ radicals which do not react with ROOH (*e.g.*, due to β-sission resulting in the absorption of O_2) is negligible.[9] In fact, the main product, ROH (90%), and only a small amount of acetophenone (7%) were obtained by decomposition of the hydroperoxide with lead dioxide. Furthermore, it was confirmed that the molar ratio of the ROH produced to the oxygen evolved was very close to 2.[9] Then, it should be obvious that the proportionality constant, k_6^{exp}, gives the rate constant of the bimolecular reaction for the peroxyl radicals, Reaction 2.

In the same manner for the case shown in Fig. 1, the proportionality constant, k_6^{exp}, was determined for various pyridine concentrations. Figure 2 shows the relation between k_6^{exp} and the pyridine concentration at various reaction temperatures from 293—313 K. As is shown in Fig. 2, k_6^{exp} decreases with increasing pyridine concentration. This clearly demonstrates the decrease in the $RO_2\cdot$ reactivity for the $RO_2\cdot$ self-reaction, Reaction 2, with increasing pyridine concentration. It should be noted that complex formation between the hydroperoxide and pyridine, if occurs, cannot have any influence on k_6^{exp} since the rate-determining step for chain propagation is Reaction 2 and relation 1 is valid.

Solvent effects on the rate constants for reactions involving polar solvents have frequently been described using Kirkwood's equation:[19]

$$\log k_6 = \log k_6^0 - \frac{1}{kT}\frac{\varepsilon-1}{2\varepsilon+1}\left(\frac{\mu_1^2}{r_1^3}+\frac{\mu_2^2}{r_2^3}+\frac{\mu_3^2}{r_3^3}\right), \quad (4)$$

where k_6^0 is the rate constant at $\varepsilon=1$, k is the Boltzmann constant, μ_1, μ_2, r_1, and r_2 are the dipole moments and effective radii of the reactants, and μ_3 and r_3 refer to those of the activated complex. According to Kirkwood's equation, the rate constant should increase with increasing polarity of the solvent. This has been reported to be the case for the oxidation of ethyl methyl ketone in benzene solutions.[10] In the present case, however, the apparent rate constant, k_6^{exp}, decreases with the pyridine concentration even though the polarity of the medium increases. Then, the following complex formation between the peroxyl radical and pyridine is postulated in order to explain the experimental observations in Fig. 2;

$$RO_2\cdot + n\,Py \overset{K}{\rightleftharpoons} (RO_2\cdot\cdots n\,Py). \quad (5)$$

Two types of peroxyl radicals, uncomplexed ($RO_2\cdot$) and complexed ($RO_2\cdot\cdots nPy$), are in equilibrium in the system. The peroxyl radical concentration $(RO_2\cdot)_t$ measured using ESR is equal to the sum of the concentration of the two species, thus

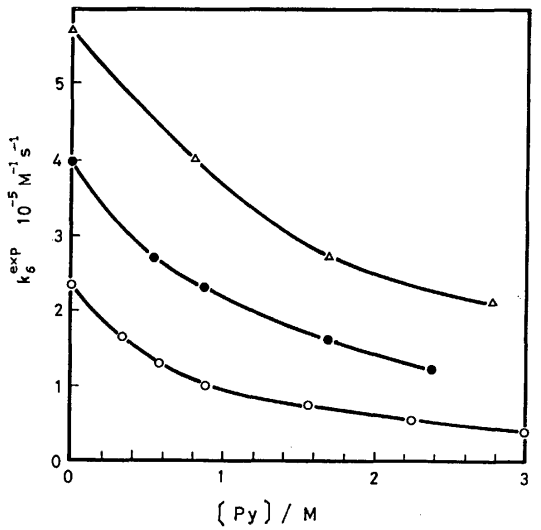

Fig. 2. k_6^{exp} as a function of the pyridine concentration for different temperatures.
○ 293 K, ● 303 K, △ 313 K.

$$[RO_2^\cdot]_t = [RO_2^\cdot] + [RO_2^\cdot \cdots n\,Py]. \quad (6)$$

The peroxyl radical self-reactions may be represented as

$$RO_2^\cdot + RO_2^\cdot \xrightarrow{k_6} O_2 + 2RO\cdot, \quad (7)$$

$$RO_2^\cdot + (RO_2^\cdot \cdots n\,Py) \xrightarrow{k_6'} O_2 + 2RO\cdot + n\,Py, \quad (8)$$

$$(RO_2^\cdot \cdots n\,Py) + (RO_2^\cdot \cdots n\,Py) \xrightarrow{k_6''} O_2 + 2RO\cdot + 2n\,Py. \quad (9)$$

From Eqs. 5—9, the rate of oxygen generation is given by

$$\frac{d[O_2]}{dt} = \frac{k_6 + k_6'K[Py]^n + k_6''K^2[Py]^{2n}}{(1+K[Py]^n)^2}[RO_2^\cdot]_t^2. \quad (10)$$

Thus, the experimental rate constant, k_6^{exp}, is expressed as

$$k_6^{exp} = \frac{k_6 + k_6'K[Py]^n + k_6''K^2[Py]^{2n}}{(1+K[Py]^n)^2} \quad (11)$$

If one assumes that the reactivity of the complexed peroxyl radical is much lower than that of the uncomplexed radical, that is, that k_6' and $k_6'' \ll k_6$, then, Eq. 11 reduces to

$$k_6^{exp} = \frac{k_6}{(1+K[Py]^n)^2}. \quad (12)$$

Equation 12 can be rewritten as

$$\log\left(\left(\frac{k_6}{k_6^{exp}}\right)^{1/2} - 1\right) = n \log [Py] + \log K. \quad (13)$$

In Fig. 3, the plot of log $((k_6/k_6^{exp})^{1/2}-1)$ as a function of log [Py] is a straight line for each temperature, which indicates the validity of the above mechanism. The value $n=1$ is obtained from the slopes of these lines. This indicates the association of one pyridine molecule with a single peroxyl radical.

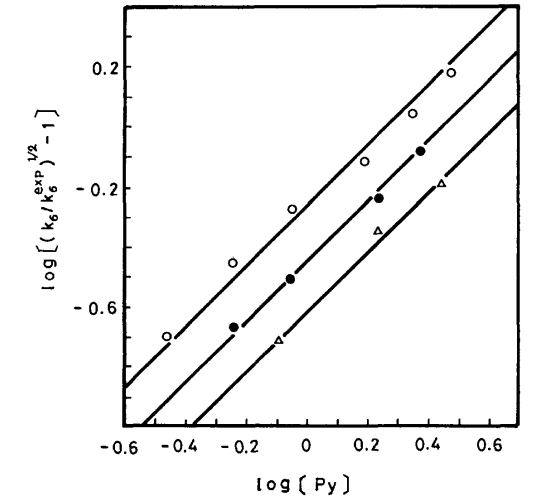

Fig. 3. log $[(k_6/k_6^{exp})^{1/2}-1]$ as a function of log [Py] for different temperatures.
○ 293 K, ● 303 K, △ 313 K.

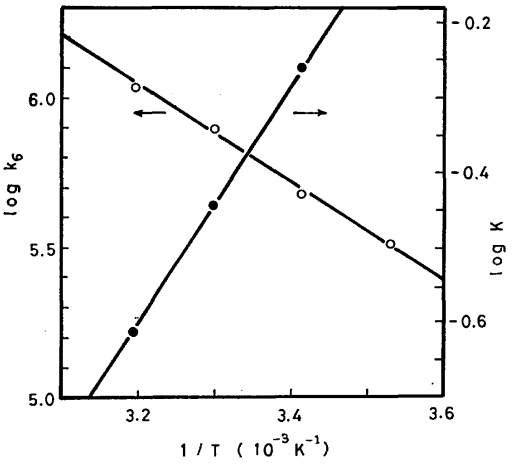

Fig. 4. The dependence of log K and log k_6 on $1/T$.

Table 1. Activation parameters for the self-reaction of 1-methyl-1-phenylethylperoxyl radicals and complex formation between the 1-methyl-1-phenylperoxyl radical and pyridine

Log A_6/M^{-1} s^{-1}	E_6 kJ mol^{-1}	$-\Delta H$ kJ mol^{-1}	$-\Delta S$ J mol^{-1} K^{-1}	Ref.
11.2	31	31	109	This study
10.9[a]	30[a]			13
		33[b]	65[b]	12

a) Obtained for the autoxidation of cumene with lead dioxide. b) Activation parameters for the charge-transfer complex between pyridine and iodine.

The temperature dependence of k_6 and K obtained from Fig. 3 is shown in Fig. 4. The values of the activation parameters for the radical self-reaction, A_6 and E_6, as well as ΔH and ΔS for the complex formation derived from Fig. 4, are summarized in Table 1 together with the activation parameters, A_6 and E_6, obtained from the autoxidation of cumene with lead dioxide.[13] The Arrhenius parameters of the peroxyl radical self-reaction in hydroperoxide decomposition are in good agreement with those obtained for the autoxidation of cumene. The high ΔH value, 31 kJ mol^{-1}, explains why Thomas[8] was unable to estimate the equilibrium constant K

for the $RO_2^{\cdot}$–pyridine complex in the autoxidation of cumene; his experiments were carried out at higher temperatures (330 and 347 K) since he used the thermal initiator AIBN. The equilibrium constant K has the small values 0.14 M^{-1} at 330 K and 0.08 M^{-1} at 347 K, as estimated from the ΔH and ΔS values given in Table 1. These K values are consistent with the estimation of Thomas that K cannot have a value in excess of 0.4 M^{-1}. Since pyridine is known to form strong charge-transfer complexes with acceptors such as iodine,[12] the values of ΔH and ΔS for the formation of the charge-transfer complex between pyridine and iodine are compared with those for the present case in Table 1. The ΔH value for the $RO_2^{\cdot}$–pyridine complex is in good agreement with that for the charge-transfer complex between pyridine and iodine. Hence, the complex formation between 1-methyl-1-phenylethylperoxyl radical and pyridine can be considered to follow a charge-transfer process analogous to the pyridine–iodine complex, *i.e.*,

$$RO_2^{\cdot} + Py \rightleftarrows (RO_2^{\delta-}\ Py^{\delta+}). \qquad (14)$$

Thus, the 1-methyl-1-phenylethylperoxyl radical is an electron acceptor in complex formation with pyridine.

The authors thank Professor T. Keii for helpful discussions.

References

1) G. Porter and J. A. Smith, *Proc. R. Soc. London, Ser. A*, **261**, 28 (1961).
2) T. A. Grover and G. Porter, *Proc. R. Soc. London, Ser. A*, **262**, 476 (1961).
3) S. J. Rand and R. L. Strong, *J. Am. Chem. Soc.*, **82**, 5 (1960).
4) R. L. Strong, S. J. Rand, and J. A. Britt, *J. Am. Chem. Soc.*, **82**, 5053 (1960).
5) G. A. Russell, *J. Am. Chem. Soc.*, **80**, 4987 (1958).
6) C. E. Boozer and G. S. Hammond, *J. Am. Chem. Soc.*, **76**, 3861 (1954).
7) C. E. Boozer, G. S. Hammond, C. E. Hamilton, and J. N. Sen, *J. Am. Chem. Soc.*, **77**, 3233 (1955).
8) J. R. Thomas, *J. Am. Chem. Soc.*, **85**, 591 (1963).
9) S. Fukuzumi and Y. Ono, *J. Chem. Soc., Perkin Trans. 2*, **1977**, 625.
10) G. E. Zaikov and Z. K. Maizus, *Adv. Chem. Ser.*, **75**, 150 (1968).
11) K. U. Ingold, *Adv. Chem. Ser.*, **75**, 296 (1968).
12) R. S. Mulliken and W. B. Berson, "Molecular Complex," Wiley-Interscience (1969).
13) S. Fukuzumi and Y. Ono, *J. Chem. Soc., Perkin Trans. 2*, **1977**, 784.
14) M. Bersohn and J. R. Thomas, *J. Am. Chem. Soc.*, **86**, 959 (1964).
15) J. J. Zwolenik, *J. Phys. Chem.*, **71**, 2464 (1967).
16) T. G. Traylor and P. D. Bartlett, *Tetrahedron Lett.*, **24**, 30 (1960).
17) D. B. Denney and J. D. Rosen, *Tetrahedron*, **20**, 271 (1964).
18) R. Hiatt, T. Mill, and F. R. Mayo, *J. Org. Chem.*, **33**, 1464 (1968).
19) S. Glasstone, K. Laidler, and G. Eyring, "Theory of Rate Processes," Princeton University Press, New York-London (1941), p. 400.

Mechanism of the Photochemical Ring Expansion of *N*-Vinyl-2-pyrrolidone. Estimation of the Recombination-Time of Biradical

Haruo SHIZUKA, Toshio OGIWARA, and Toshifumi MORITA
Department of Chemistry, Gunma University, Kiryu, Gunma 376
(Received February 15, 1977)

The photochemical ring expansion of *N*-vinyl-2-pyrrolidone (NVP) has been carried out at 254 nm. The reaction quantum yield depends a great deal on the solvnet viscosity and temperature. The recombination time of the biradical of RP produced by Norrish type I fission was estimated to be $\approx 10^{-10}$ s by application of the Einstein and Smoluchowski-Debye equations. The spin inversion of the biradical in a solvent cage is also discussed according to Kaptein's theory of the radical-pair mechanism.

Geminate recombinations[1] of primary products (radicals or free ions) produced in a solvent cage by irradiation have been studied experimentally and theoretically.[2-8] Since the processes involved in cage effect reactions[9] are in a range beyond the scope of conventional dynamic methods, the geminate recombination was monitored indirectly *via* the dependence of the products on the concentration of added scavengers.[10] A more powerful experimental technique involves the application of pulsed excitation. Eisenthal *et al.*[5] have carried out direct measurements of the geminate recombination of a radical-pair (iodine atoms) with picosecond pulses at 5300 Å, the recombination time τ being 70 and 140 ps in hexadecane and carbon tetrachloride, respectively. The fast reactions can be explained by a theory similar to that of the radical-pair mechanism for CIDNP and CIDEP.[11]

According to the mechanism developed by Kaptein,[12] the radical-pair model can be divided into two types depending upon the distance r between radicals in a solvent cage.

1) Closed Radical-pair $\overline{\mathrm{A}\cdot\cdot\mathrm{B}}$. The distance of r in this pair is shorter than that of r_0 ($\approx$6Å)[13] which is roughly given by the condition that the exchange integral J is of the order of the nuclear hyperfine interactions. In the region $r<r_0$, no Zeeman effects in CIDNP and CIDEP experiments can be detected from the pair except very high fields; no singlet-triplet mixing in the pair exists appreciably since the S-T energy gap ($2J$) is very large. The geminate recombination of the triplet closed radical-pair $\overline{{}^3\mathrm{A}\cdot\cdot\mathrm{B}}$ would therefore occur *via* a triplet separated radical-pair $\overline{{}^3\mathrm{A}\cdot|\cdot\mathrm{B}}$. In contrast, the geminate recombination of the singlet pair $\overline{{}^1\mathrm{A}\cdot\cdot\mathrm{B}}$ is very fast ($\approx 10^{-11}$ s).[6]

2) Separated Radical-pair $\overline{\mathrm{A}\cdot|\cdot\mathrm{B}}$. The radicals in this pair are separated by solvent molecules[14] to give the distance r ($\geq r_0$), but they are enclosed within a solvent cage. The $\overline{\mathrm{A}\cdot|\cdot\mathrm{B}}$ is produced from $\overline{\mathrm{A}\cdot\cdot\mathrm{B}}$ or diffusing radicals. The exchange term J becomes small[15] in the region $r\geq r_0$, and the singlet-triplet mixing takes place due to the nuclear hyperfine and the spin-orbit interactions, resulting in the recombination of $\overline{{}^3\mathrm{A}\cdot|\cdot\mathrm{B}}$. In the presence of the external magnetic field, Zeeman terms also contribute to the S-T mixing in the pair, and CIDNP and CIDEP phenomena would be observed from $\overline{\mathrm{A}\cdot|\cdot\mathrm{B}}$ as has been proposed by Kaptein.[12] As for the recombination of $\overline{{}^1\mathrm{A}\cdot|\cdot\mathrm{B}}$, its recombination probability may decrease with increasing S-T mixing.

Brocklehurst[2] applied the radical-pair model to the rate of loss of spin correlation in geminate pairs of radical ions produced by radiolysis. Schulten *et al.*[16] have recently studied the fast intersystem crossing in an exciplex due to the radical-pair mechanism.

In contrast to the cases of pair radicals and radical ions, the lack of recombination time of a biradical was pointed out.[17] It seems that the behavior of the biradical in a solvent cage is similar to that of the radical-pair. However, the radical site of the biradical is always combined with a molecular chain: the structure allows a reversible change similar to $\overline{\mathrm{A}\cdot\cdot\mathrm{B}}\leftrightarrow\overline{\mathrm{A}\cdot|\cdot\mathrm{B}}$ without escape of the radicals from solvent cage. Thus, an appreciable S-T mixing may be expected, effecting the recombination of biradical. The kinetic behavior of a biradical has been studied from these viewpoints.

N-Vinyl-2-pyrrolidone (NVP) yields photochemically the ring expansion product (P) of 4-azacyclohepten-1-one in alcohols[18] as follows:

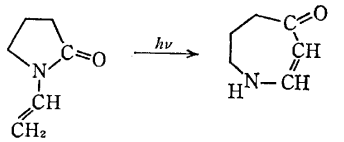

NVP P (1)

In this ring expansion, α-cleavage (the Norrish type I fission) to give the biradical RP (Eq. 2) may be involved as considered from the other photochemical ring expansion.[19] In the present work, the compound NVP was chosen in order to estimate the recombination time of biradical. We have measured the quantum yields for the intramolecular ring expansion of NVP at 254 nm as a function of η/T, where η and T denote viscosity and absolute temperature of solutions, respectively.

Experimental

N-Vinyl-2-pyrrolidone (E.P-grade, Tokyo Kasei Co., Ltd.) was purified by distillation before use. Ethanol (G.R.-grade, Tokyo Kasei Co., Ltd.) and spectrograde glycerol were used without further purification. The viscosity of sample solutions was adjusted with a mixed solvent (ethanol–glycerol system).[20]

A low-pressure mercury lamp with a Vycor glass filter was

used as the 254 nm radiation source. Actinometry was carried out using a ferric oxalate solution.[21] The quantum yields for the product formation were measured by spectrophotometry. For the measurement of temperature effect on the quantum yield, a quartz Dewar flask designed for spectrometry was used as a reaction cell, the temperature being controlled to within ±2 °C. In the measrements of degassed samples, the solutions were thoroughly degassed on a high-vacuum line by the freeze-pump-thaw method. Absorption and fluorescence spectra were measured with Hitachi 139 and 124 spectrophotometers and with a Hitachi MPF-2A fluorimeter, respectively.

Results

The spectrum of the degassed ethanol solution of *N*-vinyl-2-pyrrolidone (NVP) changed markedly upon irradiation with the 254 nm light at 293 K as shown in

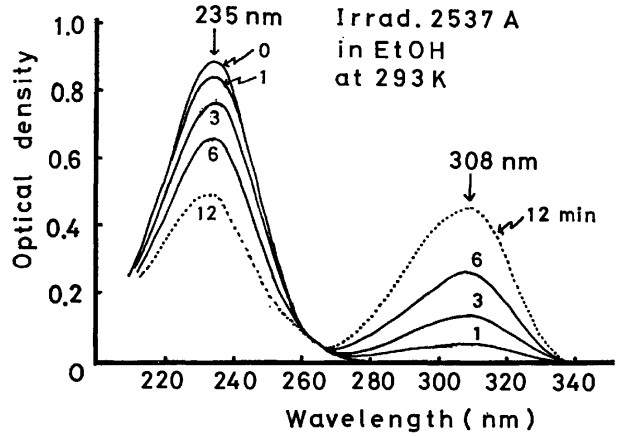

Fig. 1. The spectral change of ethanol solution of NVP with lapse of time at 254 nm. Numbers refer to time of measurement in minutes.

Fig. 1. The 235 nm band of NVP (ε: 1.68×10^4 M^{-1} cm^{-1}) and a new band with maximum at 308 nm (ε: 1.96×10^4 M^{-1} cm^{-1}) appeared. The spectral change shows the formation of ring expansion product of 4-aza-cyclohepten-1-one. The photochemical conversion from NVP into the photoproduct P in the initial stages of the reaction was very efficient (>90%). The photoproduct was separated by column chromatography and confirmed by UV, IR, and NMR, and comparison of its mp with that in the literature.[18]

The quantum yields for the product formation Φ_R in ethanol [Φ_R=5.4 ($\pm$0.2)$\times10^{-2}$ at 293 K, η=12.2 mp] did not change with variations of irradiation time (2—15 min), initial concentration of NVP (0.5×10^{-4}—1×10^{-2} M) and the addition of piperylene ($\leq2.2\times10^{-2}$ M). There was no dissolved oxygen effect on Φ_R. The results are shown in Fig. 2. However, significant effects of viscosity (η) and temperature (T) on Φ_R at 254 nm were observed (Table 1). The Φ_R values decreased with increase in η and decreased with fall in temperature. The dependence of Φ_R on η at 254 nm in ethanol or an ethanol–glycerol mixture is shown in Fig. 3. The difference between the two curves is due to the temperature effect on Φ_R.

No photochemical ring expansion of NVP was

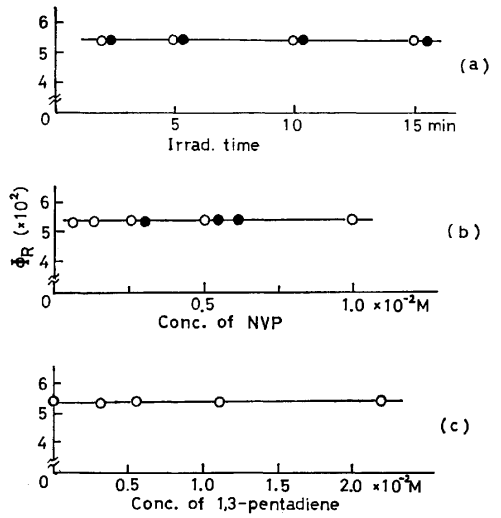

Fig. 2. Dependence of quantum yields for the product formation in ethanol at 254 nm and 293K.
(a) On irradiation time with initial concentration of 5×10^{-3}M.
(b) On concentration of NVP.
(c) On addition of 1,3-pentadiene.
○: In aerated ethanol.
●: In degassed ethanol.

Table 1. Viscosity and temperature effects on Φ_R at 254 nm

Solvent	T/K	η mpoise	$\Phi_R\times10^2$
EtOH[a]	303	10.0	5.5(±0.2)
	293	12.2	5.4(±0.2)
	273	17.7	4.6(±0.2)
	263	22	4.3(±0.2)
	253	28	3.9(±0.2)
	233	48	3.0(±0.2)
	203	120	2.1(±0.2)
Gly Vol %[b]			
0	293	12.2	5.4(±0.2)
5	293	16.7	5.0(±0.2)
10	293	22.3	4.5(±0.2)
20	293	41.1	3.9(±0.2)
30	293	63.3	3.6(±0.2)

a) The data of viscosity of ethanol were taken from "Handbook of Chemistry and Physics," ed by R. C. Weast, The Chemical Rubber Co, Ohio (1969).
b) Taken from Ref. 20. Gly Vol % denotes the glycerol volume percent in ethanol.

observed in a rigid EPA matrix at 77 K. Neither fluorescence (at 77 and 293 K) nor phosphorescence (at 77 K) could be observed. The emission quantum yields should be less than 10^{-4}. The photochemical ring expansion took place even in the gas phase. No quantitative work has been made.

Discussion

The Norrish Type I Dissociation. The Norrish type I fission (α-cleavage) of organic carbonyl compounds

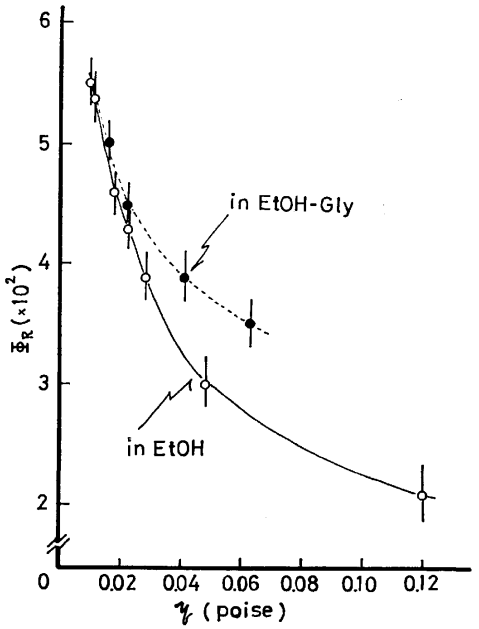

Fig. 3. The quantum yield for the product formation Φ_R as a function of viscosity η.

can be divided into three typical classes as follows:[22]

1) Photochemical fission of alkyl ketones occurs *via* both $^1(n, \pi^*)$ and $^3(n, \pi^*)$ states.[23,24]

2) Photochemical dissociation of aryl ketones[25] and some cyclohexanones[24] takes place *via* $^3(n, \pi^*)$, which might be due to the rapid intersystem crossing in the excited molecules.

3) Photochemical cleavages of aryl esters originate from $^1(\pi, \pi^*)$ $^1B_2$ states.[26]

The rate constants for the fissions are estimated to be 10^7—10^8 s^{-1} in case 1,[23,24] $\approx 10^{10}$ s^{-1} or more in case 2[25] and $\approx 10^9$ s^{-1} in case 3.[26] However, little is known about the reactive state responsible for photochemical ring expansions. The photochemical reaction of spiro[2.4]-heptan-4-one in methanol is an exception; the triplet state of the ketone ($\tau_T \simeq 2\times10^{-9}$ s) seems to be the reactive state from the result of the quenching experiment by 3 M 1,3-pentadiene.[27] The presence of triplet quenchers [1,3-pentadiene$\leq 2.2\times10^{-2}$ M[28a] and dissolved oxygen $\simeq 2.1\times10^{-3}$ M[29]] do not affect the Φ_R values. The results indicate that the photochemical ring expansion of NVP proceeds *via* a singlet precursor and/or very short-lived triplet state. The reactive state of $^3(n, \pi^*)$ is more likely than that of $^1(n, \pi^*)$, if we consider the allowed transition of $^1(\pi, \pi^*)\rightarrow{}^3(n, \pi^*)$ according to the El-Sayed rule.[30] The $^1(n, \pi^*)$ state in NVP lies energetically under the $^1(\pi, \pi^*)$ state, which was calculated by the CNDO/2 method.[28b] The $^1(n, \pi^*)$ band should be masked by the $^1(\pi, \pi^*)$ band at 235 nm.[31] The lack of emission from NVP shows that the excited state of NVP decays *via* rapid radiationless transitions [intersystem crossing, internal conversion, and the photochemical channel in part ($\leq 6.7\times10^{-2}$)]. Recent studies deal with the rapid radiationless processes in the excited molecules.[22,23]

Kinetics of Photochemical Ring Expansion of NVP. Viscosity and temperature dependence upon the reaction quantum yields Φ_R can be accounted for by the scheme shown in Fig. 4, which is simplified with respect to the processes of internal conversion and intersystem crossing, where NVP and NVP* are the ground and the electronically excited states of the staring material, respectively: RP the radical-pair (biradical) formed by the Norrish type I fission of NVP* (Eq. 2); and RP′ the biradical produced by rotational diffusion of RP resulting in the ring expansion product P (Eq. 3).

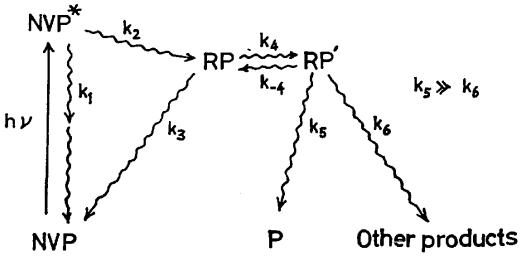

Fig. 4. A schematic energy state diagram for the photochemical ring expansion of NVP.

RP: 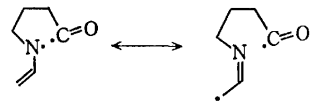 (2)

RP′: 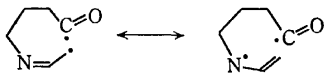 (3)

By use of the usual steady-state approximation, the quantum yield for the product formation Φ_R is given by

$$\Phi_R = \left(\frac{k_2}{k_1+k_2}\right)\left\{\frac{k_4}{k_4+k_3\left(1+\frac{k_{-4}}{k_5+k_6}\right)}\right\}\left(\frac{k_5}{k_5+k_6}\right). \quad (4)$$

From the result of high efficiency (>90%) for the photochemical conversion NVP→P, the following should hold:

$$k_5 \gg k_6. \quad (5)$$

Using this we obtain

$$\Phi_R = \Phi_{RP}\left\{\frac{k_4}{k_4+k_3\left(1+\frac{k_{-4}}{k_5}\right)}\right\}, \quad (4')$$

where Φ_{RP} is the efficiency for the RP formation from NVP*. From Eq. 4′, we obtain

$$\frac{1}{\Phi_R} = \frac{1}{\Phi_{RP}}\left(1+\frac{k_{-4}k_3}{k_4k_5}\right) + \frac{1}{\Phi_{RP}}\cdot\frac{k_3}{k_4}. \quad (6)$$

The rate constants k_4 and k_{-4} in the structural change between RP and RP′ seem to be diffusion-controlled, and should be proportional to $T\eta^{-1}$. Thus, Eq. 6 can be further simplified to

$$\frac{1}{\Phi_R} = a + b\frac{\eta}{T} \quad (7)$$

where a denotes the first term in Eq. 6 and b the term $\alpha k_3 \Phi_{RP}^{-1}$ (α: constant). The plot of Φ_R^{-1} *vs.* ηT^{-1} obtained experimentally, which agrees with Eq. 7, is shown in Fig. 5. The values of a and b are taken from the plot.

$$a = 15, \quad (8)$$

and

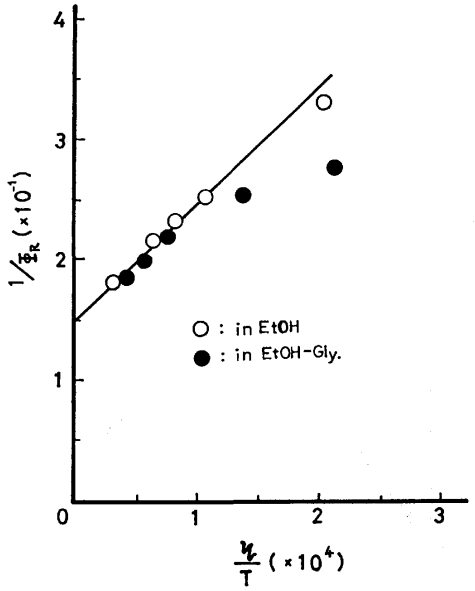

Fig. 5. Plot of Φ_R^{-1} as a function of ηT^{-1}.

$$b = 8.3\times10^{4}(\mathrm{dyn^{-1}\,s^{-1}\,cm^{2}\,deg}). \quad (9)$$

Deviations at high viscosity in the ethanol-glycerol system (Fig. 5) might be caused by inhomogeneity in the solvent.

Estimation of the Recombination Time of RP. Noyes's treatment[33] based on a random flight model is not applicable to the recombination of a biradical, since the radical sites of the biradical are combined with a molecular chain. Let us consider the recombination of the biradical of RP (or RP') using the following approximations (Cases A, B, and C).

Case A: If we assume that the reversible process RP←RP' is negligible, *i.e.* $k_{-4}\ll k_5$, Eq. 6 can be simplified to

$$\frac{1}{\Phi_R} = \frac{1}{\Phi_{RP}}\left(1+\frac{k_3}{k_4}\right) \quad (6')$$

Using the experimental values a and Φ_R^{-1}, a linear plot of k_3/k_4 *vs.* η/T is obtained, showing that k_3/k_4 is less than unity in the range $\eta\ T^{-1}<1.5\times10^{-4}$ poise deg^{-1}. This indicates that the diffusion rate constant k_4 (or k_{-4}) is greater than that of the recombination k_3 (or k_5). Thus, the assumption is not adequate.

Case B: If we assume that k_4 is approximately equal to k_{-4}, since both k_4 and k_{-4} are diffusion-controlled, we obtain from Eq. 6

$$\frac{1}{\Phi_R} = \frac{1}{\Phi_{RP}}\left(1+\frac{k_3}{k_5}+\frac{k_3}{k_4}\right). \quad (6'')$$

The value of k_4 (or k_{-4}) is related to the Debye rotational correlation time τ_0:[34]

$$\tau_0(\simeq k_4^{-1}) = \frac{4\pi a_0^3\eta}{3\kappa T}, \quad (10)$$

where a_0 is the radius of rotating particle and κ the Boltzmann constant. We thus get

$$k_4 = \frac{RT}{V\eta} \quad (11)$$

(*e.g.* $k_4\simeq4.0\times10^{10}\ \mathrm{s^{-1}}$ in EtOH at 293K),

where R is the gas constant and V the specific volume of rotating sphere (the specific volume of rotating part (C–N–CH=CH$_2$) in RP is assumed to be about 50 ml).

Substituting Eq. 11 into Eq. 6'', we get

$$\frac{1}{\Phi_R} = \frac{1}{\Phi_{RP}}\left(1+\frac{k_3}{k_5}\right) + \frac{k_3V}{\Phi_{RP}R}\cdot\frac{\eta}{T}, \quad (12)$$

where

$$\frac{1}{\Phi_{RP}}\left(1+\frac{k_3}{k_5}\right) = a, \quad \text{and} \quad \frac{k_3V}{\Phi_{RP}R} = b.$$

The reaction quantum yield Φ_R at $\eta\ T^{-1}\to0$ is found to be 6.7×10^{-2} (Fig. 5); *viz.*, $\Phi_{RP}\geq6.7\times10^{-2}$ by means of Eq. 12. Thus, we can estimate the value of k_3 from Eqs. 8, 9, and 12 as follows:

$$k_3 \geq 9.2\times10^{9}\ \mathrm{s^{-1}}. \quad (13)$$

If we assume that the rate constants k_3 and k_5 are approximately the same, the value of $(\Phi_{RP})^{-1}$ is equal to 7.5 from Eq. 12. We then obtain

$$k_3 \simeq 1.8\times10^{10}\ \mathrm{s^{-1}}. \quad (14)$$

However, there are some problems in the approximations.

(1) The assumption $k_4\simeq k_{-4}$ holds under the conditions that the potential energy and the frequency factor in the process k_4 are equal to those in the process k_{-4}. Strictly speaking, such conditions are unlikely, since there may be a difference in the steric hindrance between RP and RP'. Similarly, both k_3 and k_5 values may not be the same.

(2) The Debye equation is applicable to an entire molecule; the rotational diffusion in the present case is a restricted rotation.

Case C: We assume that the structural change of biradical (RP→RP') occurs due to the Brownian movement of solvent molecules surrounding it. Einstein's theory of the Brownian movement can be applied to the diffusion of a molecule to an adjacent site.[35] When a solvent molecule adjacent to RP moves into a solvent hole with the rate constant τ_D^{-1}, an empty space may be

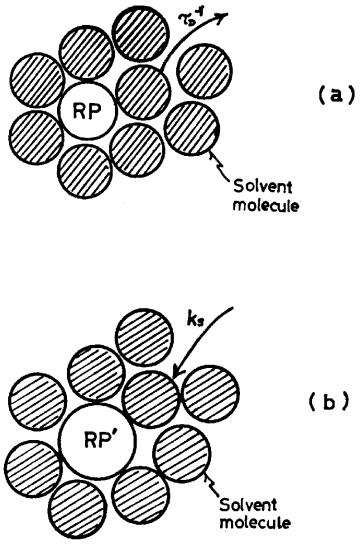

Fig. 6. Schematic models (a) for the Brownian movement of the proper solvent molecule with the rate constant τ_D^{-1} and (b) for the translational diffusion of a solvent molecule into the site adjacent to RP' with the rate constant k_s. See the text.

produced as shown in Fig. 6(a). This makes the conformational change RP→RP′ possible. The value of k_4 may be equal to that of τ_D^{-1}. From the Einstein's equation for the Brownian movement, we have

$$k_4 \simeq \tau_D^{-1} = \frac{6(D_1+D_2)}{\bar{r}^2}, \quad (15)$$

where D_1 and D_2 are the diffusion constants of EtOH and RP respectively, and $\bar{r}$ is the average distance of the movement of the proper ethanol molecule ($\bar{r}=2\,a_1$, where a_1 denotes the radius of an ethanol molecule). The values of D_1 and D_2 can be determined by Stoke's formula for the translational diffusion:

$$D = \frac{\kappa T}{6\pi a_i \eta}, \quad (16)$$

where a_i is the radius of the corresponding species ($a_1\simeq$ 2.85 Å for EtOH; $a_2\simeq$3.48 Å for RP). From Eqs. 15 and 16, the value of k_4 can be estimated as a function of $T\eta^{-1}$:

$$k_4 = 8.6\times10^5\, T\eta^{-1} \quad (17)$$

(*e.g.* $k_4\simeq 2\times10^{10}\,s^{-1}$ in EtOH at 293K).

On the other hand, the rate constant k_{-4} can be evaluated by applying the Smoluchowski-Debye equation.[35,36] We assume that the conformational change RP′→RP is accomplished by the diffusion of a solvent molecule to an adjacent site with the rate constant k_s (Fig. 6(b)). The value of k_{-4} seems to be close to that of k_s:

$$k_{-4} \simeq k_s = \frac{4\pi PN\sigma(D_1+D_2)[\mathrm{solv}]}{1000}, \quad (18)$$

where D_1 and D_2 are diffusion coefficients in $cm^2\,s^{-1}$; σ is the effective collision diameter in cm ($\sigma\simeq a_1+a_2=6.33\times10^{-8}$ cm); N is Avogadro's number; P the steric factor (assumed to be unity); [solv] the concentration of neat EtOH (17.1 M). Thus, the value of k_{-4} is estimated from Eq. 18 to be

$$k_{-4} \simeq 5.4\times10^{10}\,s^{-1} \text{ at } 293K. \quad (19)$$

From Eqs. 6 and 17, we get

$$\frac{k_3}{\Phi_{RP}} \geq 7.1\times10^{10}\,s^{-1}, \quad (20)$$

where $\Phi_{RP}\geq6.7\times10^{-2}$. Thus

$$k_3 \geq 4.8\times10^9\,s^{-1}. \quad (21)$$

However, the value of k_3 should not exceed that of diffusion-controlled k_4 (*e.g.* $2\times10^{10}\,s^{-1}$ at 293 K). Thus, we can estimate the recombination time τ of RP as follows:

$$50\text{ ps} < \tau \leq 200\text{ ps}. \quad (22)$$

The τ value of the biradical RP is the order of $\approx10^{-10}$ s, which is the same order of magnitude of the geminate recombination times between iodine atoms measured with picosecond pulses (70 ps in hexadecane and 140 ps in CCl_4).[5] The approximation in Case C seems to be the best.

Multiplicity and Spin Inversion of RP. The question arises as to the multiplicity of the biradical RP. If the singlet RP is produced *via* $^1(n,\pi^*)$, the direct back reaction $^1RP\rightarrow NVP$ is faster than the recombination of ^3RP, since the recombination should occur after the spin inversion of $^3RP\rightarrow{}^1RP$. The time for the direct back reaction is the same as that ($\approx10^{-11}$ s) of $\overline{^1A\cdot\cdot B}$. The processes $^1(n,\pi^*)\rightarrow{}^1RP\rightarrow NVP$ can not be observed in the present experiment, even if they are involved in the radiationless processes of NVP*. Judging from the recombination time of RP ($\approx10^{-10}$ s) and the reactive state of NVP $^3(n,\pi^*)$, it is probable that the multiplicity of RP is triplet. The spin inversion time of ^3RP can be evaluated to be $\approx10^{-10}$ s, since spin inversion is the rate-determining step in the recombination of ^3RP. The spin inversion of ^3RP needs time of $\approx10^{-10}$ s to cause appreciable enhancement due to the radical-pair mechanism. Several re-encounters between the radical sites of ^3RP would occur before recombination. This supports Adrian's model[37] for the radical-pair mechanism.

The structure of biradical RP allows a reversible change similar to $\overline{A\cdot\cdot B}\leftrightarrow\overline{A\cdot|\cdot B}$ without further complete separation between radical sites, since the molecular chain joints them. The possibility for the formation of the $\overline{^3A\cdot|\cdot B}$ type of ^3RP is greater than that of freely diffusing radicals. The J value of a reorienting biradical fluctuates depending upon the distance between the radical sites [the correlation time of reorientation k_4^{-1} (or k_{-4}^{-1}) is $\approx10^{-11}$ s in EtOH at room temperature], which decreases exponentially with increasing distance.[15] A small S-T energy gap ($2J$) of the triplet biradical gives rise to an efficient S-T mixing due to the nuclear hf and the spin-orbit interactions. The rapid spin inversion of ^3RP might be caused by the appreciable S-T mixing.

A similar fast spin inversion has been studied by Eisenthal *et al.*[5] using a picosecond laser at 5300 Å. At this frequency I_2 molecules are excited to the $^3\Pi_{o^+u}$ ($v'\simeq33$) state. Only a small fraction of I_2 molecules are excited to the $^1\Pi_u$ state, dissociating directly. The I_2 molecules excited to the $^3\Pi_{o^+u}$ state undergo a predissociation induced by collision *via* the $^3\Pi_{1u}$ state leading to a pair of ground state, $^2P_{3/2}$, iodine atoms. According to the spin conservation rule, the radical-pair of iodine atoms in a solvent cage should be triplet. However, the geminate recombination time τ is very short (70—140 ps),[38] indicating that spin inversion takes place within τ. The fast geminate recombination of iodine atoms can be understood by the radical-pair mechanism resulting in the S-T mixing. The large spin-orbit coupling due to the heavy atom and the nuclear hf interactions may be involved in the system.

Conclusion

The mechanism of the photochemical ring expansion of NVP involving the Norrish type I dissociation at 254 nm in EtOH is shown in Fig. 4. The recombination time τ of the biradical RP was estimated to be $\approx10^{-10}$ s. The spin inversion of the triplet biradical requires a time of about 10^{-10} s to cause efficient enhancement due to the radical-pair mechanism.

The authors are grateful to Professor I. Tanaka, Tokyo Institute of Technology, for his valuable discussions. They would also like to thank Professor S.

Nagakura, the University of Tokyo, and Dr. H. Hayashi, the Institute of Physical and Chemical Research, for their interest and helpful discussions.

Appendix

The behavior of primary geminate and secondary recombination between radicals in fluid media schematically is shown as follows:

1) Radical-pair.

a) Singlet radical-pair:

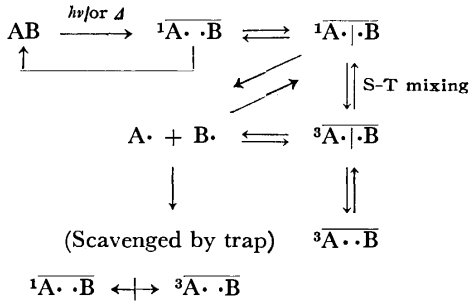

(A1)

b) Triplet radical-pair.

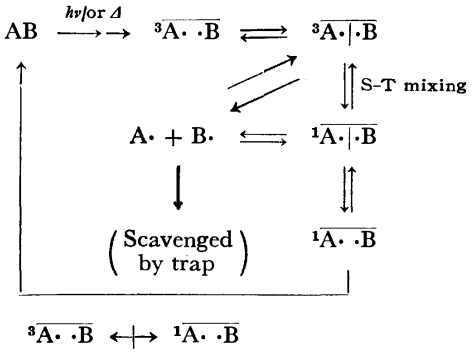

(A2)

2) Biradical.

a) Singlet biradical:

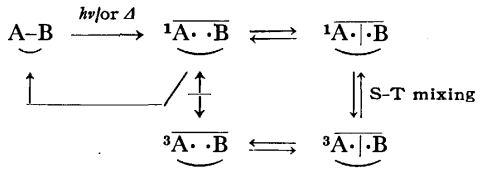

(A3)

b) Triplet biradical:

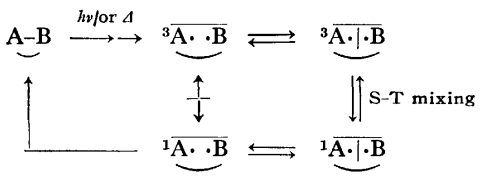

(A4)

References

1) R. M. Noyes, *J. Am. Chem. Soc.*, **77**, 2042 (1955).

2) B. Broklehurst, *Chem. Phys.*, **2**, 6 (1973); *Chem. Phys. Lett.*, **28**, 357, 361 (1974).

3) F. Dainton, M. B. Ledyer, R. May, and C. A. Salmon, *J. Phys. Chem.*, **77**, 45 (1973).

4) D. M. Goodall, N. Orbach, and M. Ottolenghi, *Chem. Phys. Lett.*, **26**, 365 (1974).

5) K. B. Eisenthal, *Acc. Chem. Res.*, **8**, 118 (1975); T. J. Chuang, G. W. Hoffmann, and K. B. Eisenthal, *Chem. Phys. Lett.*, **25**, 201 (1974).

6) J. F. Garst, *J. Am. Chem. Soc.*, **97**, 5062 (1975).

7) K. Hayashi, D. Lindenan, W. Schnabel, and M. Irie, *J. Phys. Chem.*, **80**, 2807 (1976).

8) Y. Tanimoto, H. Hayashi, S. Nagakura, H. Sakuragi, and K. Tokumaru, *Chem. Phys. Lett.*, **41**, 267 (1976).

9) J. Franck and E. Rabinowitch, *Trans. Faraday Soc.*, **30**, 120 (1934).

10) F. W. Lampe and R. M. Noyes, *J. Am. Chem. Soc.*, **76**, 2140 (1954).

11) A number of excellent reviews on CIDNP and CIDEP have been reported. For CIDNP: a) H. R. Ward, *Acc. Chem. Res.*, **5**, 18 (1972); b) R. G. Lawler, *ibid.*, **5**, 25 (1972); c) J. Potenza, *Adv. Mol. Relaxation Proc.*, **4**, 229 (1972); d) H. D. Roth, *Mol. Photochem.*, **5**, 91 (1973). e) G. L. Closs in "Chemically Induced Magnetic Polarization," ed by A. R. Lepley and G. L. Closs, Wiley, New York (1973), Chap. 2; f) R. Kaptein in Ref. 11e, Chap. 4. For CIDEP: a) J. K. S. Wan, S.-K. Wong, and D. A. Huchison, *Acc. Chem. Res.*, **7**, 58 (1974); b) P. W. Atkins and K. A. McLauchlan, in Ref. 11e, Chap. 2.

12) R. Kaptein, *J. Am. Chem. Soc.*, **94**, 6251 (1972).

13) A number of r_0 have been reported : a) C. Herring and M. Flicker, *Phys. Rev.*, **134**, A362 (1964), $r_0 \approx 6$Å for H-atom 1st orbitals; b) J. N. Murrell and J. J. C. Teixeira-Dias, *Mol. Phys.*, **19**, 521 (1970), $r_0 \approx 10$Å for 2p and 2s orbitals; c) H. Hirota and S. I. Weissmann, *J. Am. Chem. Soc.*, **86**, 2538 (1964), $r_0 \approx 5$—6Å in ion pair; d) K. Itoh, H. Hayashi, and S. Nagakura, *Mol. Phys.*, **17**, 561 (1969), $r_0 \approx 7$Å for nitroxide biradical; e) $r_0 = 6$Å quoted by Ferruti *et al.*, P. Ferruti, D. Gill, M. P. Klein, H. H. Wang, G. Entine, and M. Calvin, *J. Am. Chem. Soc.*, **92**, 3704 (1970).

14) The number of solvent molecules seems to be 1—3, judging from the r_0 value (6Å).

15) J decreases exponentially with distance [see Ref. 13-(a)].

16) K. Schulten, H. Staerk, A. Weller, H.-J. Werner, and D. Nickel, *Z. Phys. Chem. (Frankfurt am Main)*, **101**, 371 (1976).

17) R. G. Bergman, in "Free Radicals," Vol. 1, ed by J. K. Kochi, Wiley, New York (1973), Chap. 5.

18) G. Buhr, German Offen., 2013761 (1971); *Chem. Abstr.*, **76**, 14376h (1972).

19) P. Yates and R. O. Loutfy, *Acc. Chem. Res.*, **8**, 209 (1975).

20) H. Shizuka, K. Kubota, and T. Morita, *Mol. Photochem.*, **3**, 335 (1972).

21) C. G. Hatchard and C. A. Parker, *Proc. R. Soc. London, Ser. A*, **235**, 518 (1956).

22) K. Tsutsumi, K. Matsui, and H. Shizuka, *Mol. Photochem.*, **7**, 325 (1976).

23) N. C. Yang and E. D. Feit, *J. Am. Chem. Soc.*, **90**, 504 (1968); N. C. Yang, E. D. Feit, M. H. Hui, N. J. Turro, and J. C. Dalton, *ibid.*, **92**, 6974 (1970).

24) J. C. Dalton, D. M. Pond, D. S. Weiss, F. D. Lewis, and N. J. Turro, *J. Am. Chem. Soc.*, **92**, 2566 (1970); P. J. Wagner and R. W. Spoerke, *ibid.*, **91**, 4437 (1969).

25) F. D. Lewis, R. T. Lauterbach, H.-G. Heine, W. Hartmann, and R. Rudolph, *ibid.*, **97**, 1519 (1975); H.-G. Heine, W. Hartmann, D. R. Kory, J. G. Magyar, C. E. Hoyle, J. K. McVey, and F. D. Lewis, *J. Org. Chem.*, **39**, 691 (1974).

26) H. Shizuka and I. Tanaka, *Bull. Chem. Soc. Jpn.*, **41**, 2343 (1968); **42**, 909 (1969); H. Shizuka, *ibid.*, **42**, 52, 57 (1969).

27) N. J. Turro and D. R. Morton, *J. Am. Chem. Soc.*, **93**, 2569 (1971); D. R. Morton and N. J. Turro, *ibid.*, **95**, 3947 (1973).

28) a) The addition of 1,3-pentadiene was up to about 2×

10^{-2} M, since 1,3-pentadiene has a weak absorption at 254 nm; b) Unpublished results.

29) S. L. Murov, "Handbook of Photochemistry", Marcel Dekker, New York (1973), p. 89.

30) S. K. Lower and M. A. El-Sayed, *Chem. Rev.*, **66**, 199 (1966).

31) No. $^1(n, \pi^*)$ band could be observed even in cyclohexane.

32) H. Shizuka, K. Matsui, T. Okamura, and I. Tanaka *J. Phys. Chem.*, **79**, 2731 (1975); H. Shizuka, K. Matsui, Y. Hirata, and I. Tanaka, *ibid.*, **80**, 2070 (1976); H. Shizuka, Y. Ishii, M. Hoshino, and T. Morita, *ibid.*, **80**, 30 (1976); K. Sorimachi, T. Morita, and H. Shizuka, *Bull. Chem. Soc. Jpn.*, **47**, 987 (1974); H. Shizuka, T. Ogiwara, and T. Morita, *ibid.*, 3385 (1975); H. Shizuka, T. Ogiwara, S. Cho, and T. Morita, *Chem. Phys. Lett.*, **42**, 311 (1976).

33) R. M. Noyes, *J. Chem. Phys.*, **22**, 1349 (1954); *J. Am. Chem. Soc.*, **78**., 5486 (1965).

34) P. Debye, "Polar Molecules," Dover, New York (1974); N. Bloembergen, E. M. Purcell, and P. V. Pound, *Phys. Rev.*, **73**, 679 (1948).

35) A similar treatment has been carried out by Emerson *et al.*: *cf.* M. T. Emerson, E. Grunwald, and R. A. Kromhout, *J. Chem. Phys.*, **33**, 547 (1960).

36) M. V. Smoluchowski, *Phys. Z.*, **17**, 557, 585 (1916).

37) J. Adrian, *J. Chem. Phys.*, **54**, 3918 (1971); **57**, 1004 (1972).

38) Eisenthal *et al.*[5] have also shown that the iodine atoms which have escaped will recombine at a much later time ($\approx 10^{-8}$ s). It seems that, except for very high fields, the CIDNP and CIDEP phenomena can be observed in slow recombination [*i.e.* secondary recombination, with time longer than $\approx 10^{-9}$ s (probably 10^{-6}—10^{-8} s)], but not in rapid geminate recombination.

ESR and ENDOR Studies of the Ion Pairs of Double-, Triple-, and Quadruple-layered [2.2]Paracyclophane Radical Anions and Alkali Metal Cations

Masamoto Iwaizumi, Shouichi Kita, Taro Isobe, Masahiro Kohno,* Takamitsu Yamamoto,* Hisanori Horita,** Tetsuo Otsubo,** and Soichi Misumi**

Chemical Research Institute of Non-Aqueous Solutions, Tohoku University, Katahira, Sendai 980
**Analytical Instrument Division, JEOL, Ltd., Akishima, Tokyo 196*
***The Institute of Scientific and Industrial Research, Osaka University, Suita, Osaka 565*

(Received February 28, 1977)

The radical anions of double-, triple-, and two kinds of quadruple-layered [2.2]paracyclophane $XX^{\cdot-}$, $XDX^{\cdot-}$, $XDDX(C_{2h})^{\cdot-}$ and $XDDX(D_2)^{\cdot-}$, were examined by means of ESR and ENDOR spectroscopy. The spin distributions in these radical anions are largely polarized by interaction with counter ions. An MO calculation has been attempted to account for the observed ion-pairing effects. It is shown by the calculations that the observed ion-pairing effects can be explained by the ion-pair models where the cation is located above the center of the outermost benzene ring. It is also shown that the potassium ion migrates from one side of the radical molecule to the other in a loosely bound ion pair of $XDX^{\cdot-}$ in a 1,2-dimethoxyethane(DME)–tetrahydrofuran(THF) 1 : 1 mixed solvent, as in the ion pair of $XX^{\cdot-}$ with the potassium ion in DME–THF (2 : 1) which has been previously reported by Gerson *et al.* Such migration of cations in ion pairs was not observed for the quadruple-layered [2.2]paracyclophane radical anions.

Several ESR investigations of the radical anion of double-layered [2.2]paracyclophane, $XX^{\cdot-}$, and its related compounds have been reported.[1-6] The use of ENDOR spectroscopy has also been tried in an attempt to confirm the analysis by the ESR method.[7] Of prime interest in these investigations in the electron transfer between the two aromatic rings and the effects of counter ions on the spin distributions in the radical anions. It has been shown[3,7] that, in $XX^{\cdot-}$, the unpaired electrons are distributed equally on both benzene rings when the radical anion is free from interaction with alkali metal cations. Ion pairing with alkali metal cations remarkably affects the spin distribution in the radical molecules. Gerson *et al.* have shown[6] that the alkali ion resides above the one benzene ring in the ion pair of $XX^{\cdot-}$. The present work was undertaken in order to investigate the distribution of unpaired electrons in the multilayered-paracyclophane radical anions and the interaction of these multilayered paracyclophane radical anions with counter ions in solutions. The radical anions of triple- and two kinds of quadruple-layered [2.2]paracyclophane, XDX, $XDDX(C_{2h})$, and $XDDX(D_2)$, were examined by the ESR and ENDOR methods. Though the observation of the spectra for the free anions was unsuccessful, ESR and ENDOR data concerning ion pairs of the radical anions could be obtained. In this paper we will discuss the ion-pair structures of $XDX^{\cdot-}$, $XDDX(C_{2h})^{\cdot-}$, and $XDDX(D_2)^{\cdot-}$ on the basis of the observed ion-pairing effects on the hfs constants and theoretical calculations about the effects. Though the ion pairs of $XX^{\cdot-}$ have been extensively examined by Gerson *et al.*,[3,6,7] the ESR spectra of $XX^{\cdot-}$ have also been measured in order to obtain wider information about the ion-pairing effects on the hfs constants, and the theoretical calculations used above are used to confirm that the calculations predict well the observed results and the ion-pair structures.

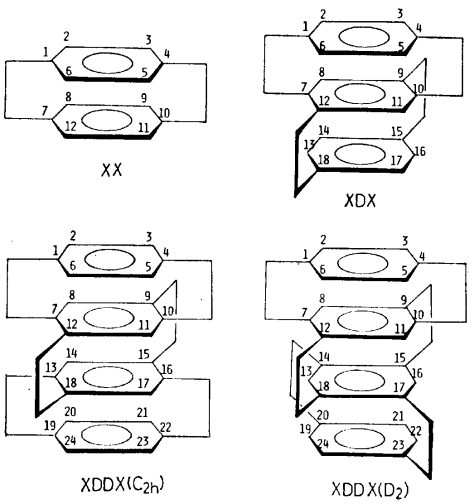

Experimental

The XX, XDX, $XDDX(C_{2h})$, and $XDDX(D_2)$ were synthesized according to the procedure described previously.[8] These substances were purified by column chromatography on silica gel or by preparative gel permeation liquid chromatography and then repeated recrystallizations (XX from chloroform, mp 285 °C; XDX from toluene, 231.5—232.5 °C dec; $XDDX(C_{2h})$ from toluene, 250 °C dec; $XDDX(D_2)$ from carbon tetrachloride–acetone (1 : 3), 240 °C dec).

The radical anions were prepared by reduction with potassium or a potassium/sodium alloy, and in a few cases, by reduction with caesium in ethereal solvents. Reduction with sodium was attempted, but no formation of the radical anions was observed. 1,2-dimethoxyethane (DME), tetrahydrofuran (THF), 2-methyltetrahydrofuran (MTHF), diethyl ether (DEE), mixtures of DME and THF, and DME containing a low percentage of hexamethylphosphoric triamide (HMPA), were tried as solvents. When DME and DME–HMPA were used for XDX, $XDDX(C_{2h})$, and $XDDX(D_2)$, the observed radicals were attributable to secondary production, and no ESR spectra due to the radical anions of XDX, $XDDX(C_{2h})$, and $XDDX(D_2)$ could be observed.[9] For experiments with $XDX^{\cdot-}$, $XDDX(C_{2h})^{\cdot-}$, and $XDDX(D_2)^{\cdot-}$, it was necessary to keep the solutions below −90 °C, but $XX^{\cdot-}$

was more stable than the above and the ESR measurements for XX^{τ} could be carried out at temperatures up to −50 °C.

The glass apparatus used for the alkali-metal reduction of ordinary aromatic compounds was modified for the preparation of XDX^{τ}, $XDDX(C_{2h})^{\tau}$, and $XDDX(D_2)^{\tau}$ by coating alkali-metal mirror inside the side arm for ESR or ENDOR measurements so that the reduction could proceed in the side arm. Thus, the radicals were prepared in an ESR or ENDOR cavity cooled to the desired temperatures; ESR and ENDOR measurements could thus be carried out immediately after the completion of the reduction reaction. This was accomplished without any movement of the sample tube which may accompany the decomposition of the radical anions, while increasing the solution temperature. Such a modification of the apparatus was very effective for the preparation of XDX^{τ}, $XDDX(C_{2h})^{\tau}$, and $XDDX(D_2)^{\tau}$.

The ESR and ENDOR spectra were recorded with a Hitachi 771 X-band ESR spectrometer and a JEOL ES-EDX-1 ENDOR spectrometer respectively.

Results

ESR Spectra for XX^{τ}. The ESR spectra have been reported[3] for XX^{τ} reduced with potassium in several ethereal solvents. The same ESR spectra for these systems were reproduced in the present work. In addition, the temperature dependencies of the hfs constants in THF and MTHF were measured. The results are shown in Fig. 1, together with the values obtained from the DME–HMPA solutions at −90 °C.

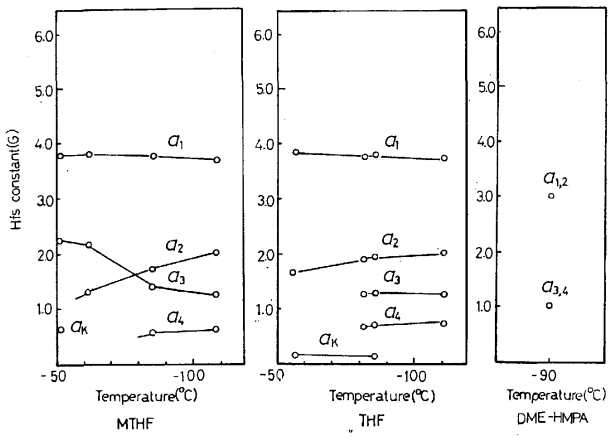

Fig. 1. Temperature dependence of the hfs constants for XX^{τ}. The subscripts of a are given in order of magnitude of the hfs constants. The counter ion is the potassium ion.

ESR Spectra for XDX^{τ}. The ESR spectrum observed for XDX^{τ} in DME–THF (1 : 1), with the potassium ion as a cation, consists of seven groups with a separation of 5.68 G. Moreover, each group shows further resolution. When XDX^{τ} is prepared with caesium in DME–THF (1 : 1) or with potassium in MTHF or DEE, the ESR spectra change to broad triplet patterns with splittings of 5.95, 6.13, and 6.48 G. On the other hand, XDX^{τ} in THF, with the potassium ion, shows an ESR spectrum which appears to be a superposition of the two hyperfine patterns of septet and triplet splittings. The ESR spectra observed for XDX^{τ}, with the potassium ion as a cation, are shown in Fig. 2.

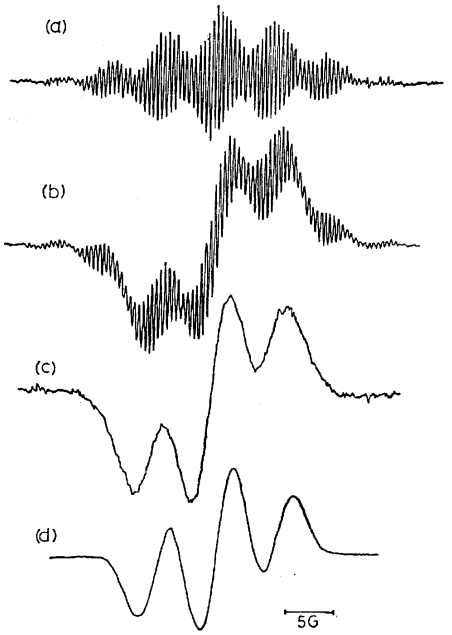

Fig. 2. ESR spectra for XDX^{τ}, with the potassium ion as a cation in (a) DME–THF(1 : 1), (b) THF, (c) MTHF, and (d) DEE at −100 °C.

ESR Spectra for $XDDX(C_{2h})^{\tau}$ and $XDDX(D_2)^{\tau}$. $XDDX(C_{2h})^{\tau}$ and $XDDX(D_2)^{\tau}$, with the potassium ion as a cation, show ESR spectra with a triplet pattern similar to those observed for XDX^{τ} in MTHF and DEE, regardless of the solvent used. Slight changes of the triplet splittings with solvents were observed; those for $XDDX(C_{2h})^{\tau}$ increase in this order of the solutions: DME–THF (1 : 1) (6.28 G), THF (6.40 G), MTHF (6.54 G), and DEE (6.62 G), while those for $XDDX(D_2)^{\tau}$ increase in another order: DME–THF (1 : 1) (6.20 G) and THF (6.30 G). Some typical ESR spectra for these radicals are shown in Figs. 3 and 4.

ENDOR Spectra for XDX^{τ}. As has been seen above, most of the systems of XDX^{τ}, $XDDX(C_{2h})^{\tau}$ and $XDDX(D_2)^{\tau}$ showed the broad triplet ESR pattern; hence, it is impossible to obtain detailed information about the hyperfine interaction of radicals from the ESR spectra only. Thus, ENDOR spectroscopic analysis was attempted for XDX^{τ}, $XDDX(C_{2h})^{\tau}$, and $XDDX(D_2)^{\tau}$. Figure 5 shows the ENDOR spectra observed for XDX^{τ} in MTHF. No ENDOR spectra

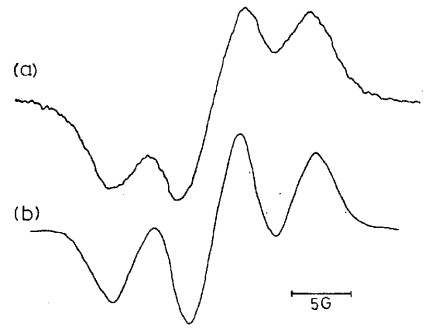

Fig. 3. ESR spectra for $XDDX(C_{2h})^{\tau}$, with the potassium ion as a counter ion in (a) DME–THF(1 : 1) and (b) MTHF at −100 °C.

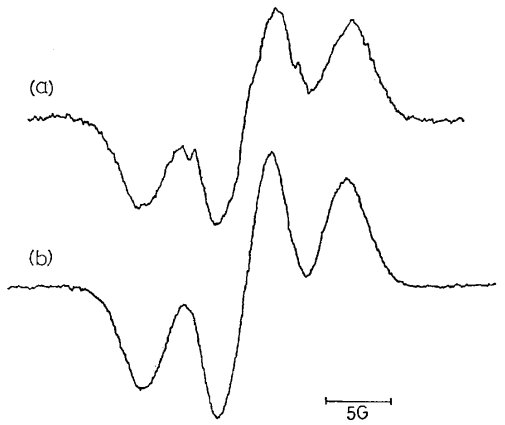

Fig. 4. ESR spectra for XDDX$(D_2)^{\cdot-}$, with the potassium ion as a counter ion in (a) DME-THF(1:1) and (b) THF at −100 °C.

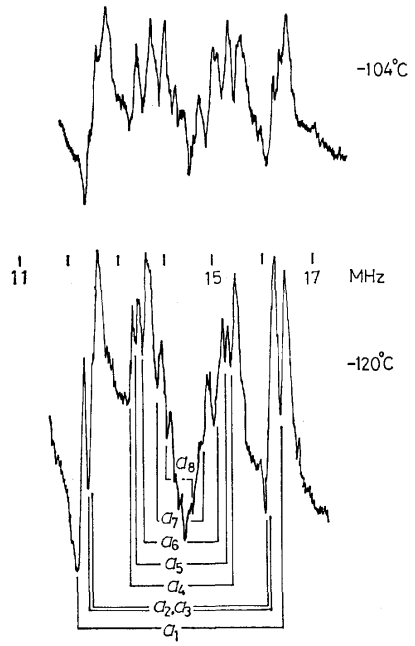

Fig. 5. ENDOR spectra for $XDX^{\cdot-}$ in MTHF, with the potassium ion at different temperatures.

Table 1. Hfs constants of $XDX^{\cdot-}$ observed by means of ENDOR at −117 °C

Numbering of hfs consts. in the ENDOR spectra	Hfs constants (G) Solvent, Cation		Assignments
	MTHF, K^+	THF, Cs^+	
a_1	1.47	1.83	8, 11
a_2	1.34	1.40	3, 6
a_3	1.23	0.97	
a_4	0.75	0.77	
a_5	0.64	0.54	
a_6	0.52	0.29	
a_7	0.32	—	
a_8	0.20	—	

were obtained from $XDX^{\cdot-}$ in DME-THF mixed solvents or in THF with the potassium cation. It is interesting that the ENDOR spectra were successfully observed only for systems showing the ESR spectra with the broad triplet pattern. However, it should be noted that even in systems where the ENDOR spectra were successfully observed, ENDOR signals due to the protons responsible for the triplet splittings in ESR spectra could not be detected. These protons may have different optimum temperature conditions for ENDOR observation from those of the other protons.

As Fig. 5 shows, the ENDOR spectra vary appreciably with the temperature. Changes with different solvents

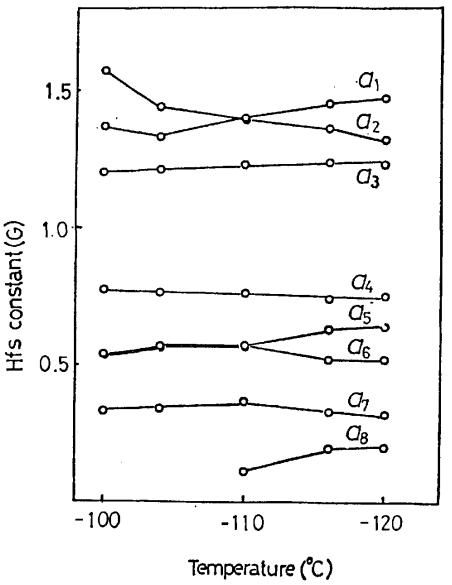

Fig. 6. Changes of the hfs constants with temperature, for $XDX^{\cdot-}$ in MTHF with the potassium ion.

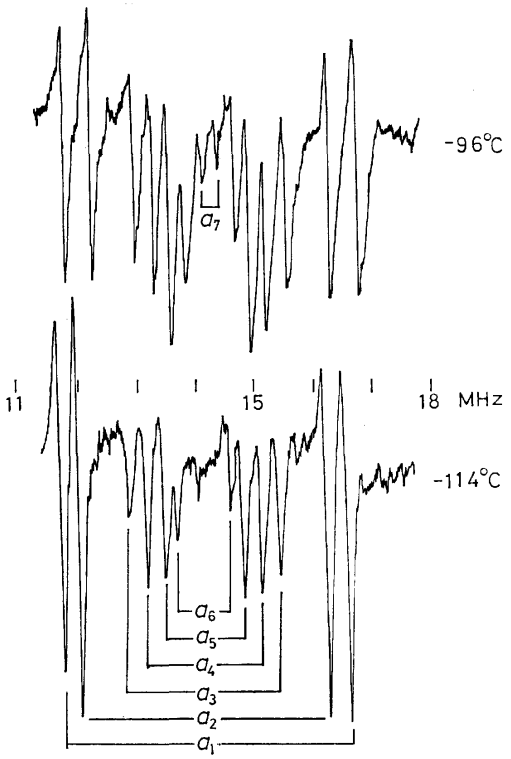

Fig. 7. ENDOR spectra for XDDX$(C_{2h})^{\cdot-}$ in THF, with the potassium ion at different temperatures.

and cations were also observed (Table 1). The hfs constants observed from the MTHF solution with the potassium cation are shown as a function of the temperature in Fig. 6.

ENDOR Spectra for XDDX(C_{2h})$^-$ and XDDX(D_2)$^-$. The ENDOR spectra for XDDX(C_{2h})$^-$ and XDDX(D_2)$^-$ were obtained from all the systems treated here, but, as is the case for XDX$^-$, the ENDOR signals due to the protons which caused the triplet splittings in the ESR spectra could not be detected. Some typical ENDOR spectra for XDDX(C_{2h})$^-$ and XDDX(D_2)$^-$ are given in Figs. 7—9. Although there are no appreciable differences between the ESR spectra for the XDDX(C_{2h})$^-$ and XDDX(D_2)$^-$ radical anions, their ENDOR spectra clearly show different hyperfine

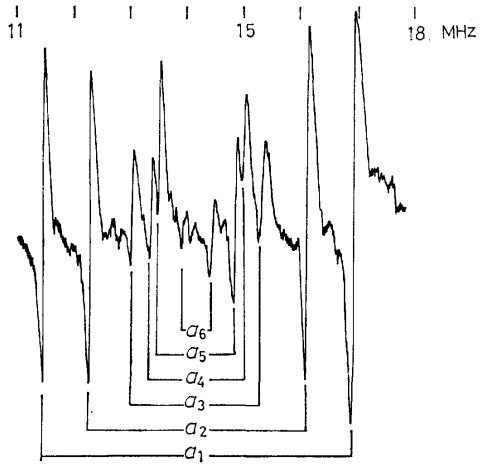

Fig. 8. ENDOR spectrum for XDDX(C_{2h})$^-$ in MTHF, with the potassium ion at −124 °C.

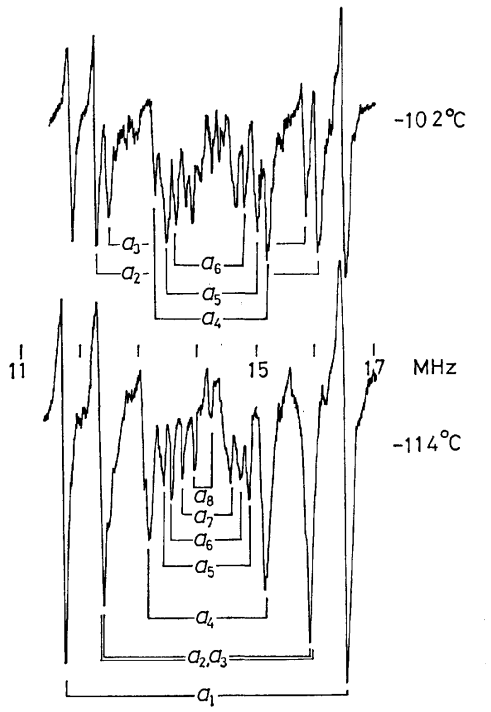

Fig. 9. ENDOR spectra for XDDX(D_2)$^-$ in THF, with the potassium ion at different temperatures.

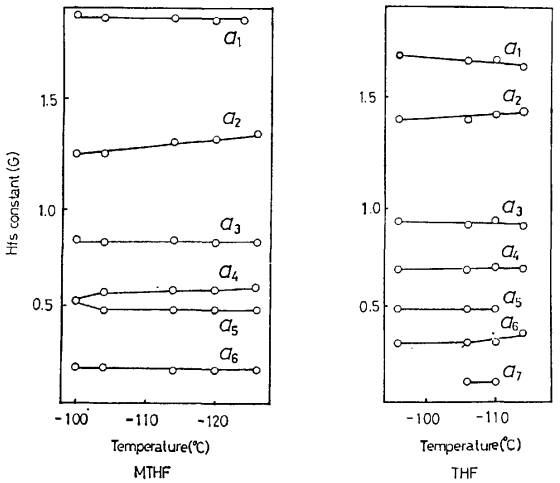

Fig. 10. Changes of the hfs constants with temperature, for XDDX(C_{2h})$^-$ in MTHF and in THF with the potassium ion.

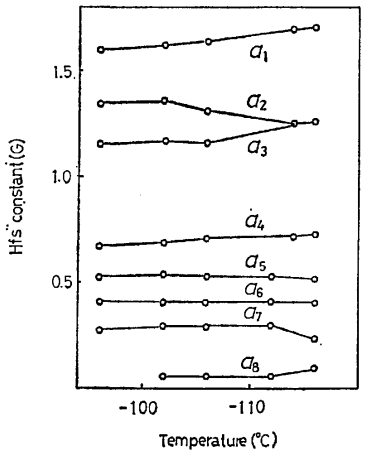

Fig. 11. Changes of the hfs constants with temperature, for XDDX(D_2)$^-$ in MTHF with the potassium ion.

Table 2. Hfs constants of XDDX(C_{2h})$^-$ and XDDX (D_2)$^-$ observed by means of ENDOR at −114°C

Numbering of hfs consts. in the ENDOR spectra	XDDX(C_{2h})$^-$ Hfs consts.(G) Solvent, Cation		Assignments	XDDX(D_2)$^-$ Hfs consts.(G) Solvent, Cation	Assignments
	THF, K^+	MTHF, K^+		THF, K^+	
a_1	1.74	1.99	3, 6	1.70	8, 11
a_2	1.50	1.34	8, 11	1.26	3, 6
a_3	0.91	0.84	9, 12	1.26	9, 12
a_4	0.69	0.59		0.72	
a_5	0.48	0.49		0.52	
a_6	0.33	0.17		0.41	
a_7	—	—		0.29	
a_8	—	—		0.09	

interactions corresponding to their different molecular structures. The variation in the hfs constants with the solvent and the temperature is shown in Figs. 10 and 11. The values of the hfs constants obtained at −114 °C are summarized in Table 2.

Analysis of ESR Spectra by Means of Fourier Transform

As has been described above, although the ESR spectrum of $XDX^{\cdot}$ in DME–THF (1 : 1) with the potassium ion gave a better resolution than the spectra in other systems, a direct analysis of the ESR spectrum was impossible and an ENDOR spectrum could not be obtained. For the purpose of ESR-spectrum analysis, we employed the Fourier transform of the ESR spectrum. The method used here is nearly the same as that used by Silsbee[11] and by Gubanov *et al.*[12]

We expressed the observed ESR spectra $F(x)$ by the Fourier transform

$$F(x) = \frac{1}{2\pi}\int_{-\infty}^{+\infty} G(y)e^{-ixyx}dx, \tag{1}$$

with an inverse transform

$$G(y) = \int_{-\infty}^{+\infty} F(x)e^{-ixxy}dx. \tag{2}$$

Here,

$$G(y)^2 = G_a(y)^2 + G_b(y)^2, \tag{3}$$

where $G_a(y)$ and $G_b(y)$ are the cosine and sine coefficients of the Fourier transform, expressed by

$$G_a(y) = \frac{1}{N}\sum_{x=-N}^{N} F(x)\cos\left(\frac{\pi}{N}yx\right), \tag{4}$$

$$G_b(y) = \frac{1}{N}\sum_{x=-N}^{N} F(x)\sin\left(\frac{\pi}{N}yx\right). \tag{5}$$

If the observed ESR spectra are expressed as an odd function of x (as in the case of the ordinary isotropic 1st derivative ESR spectra), $G(y)$ is expressed in terms of $G_b(y)$, and $G_a(y)$ need not be taken into account. Since the ESR spectrum including hyperfine interactions with n nuclei is the n-fold convolution of the spectrum including a hyperfine interaction with a single nucleus, its Fourier transform can be expressed as the product of the transforms of $f_i(x)$:

$$G(y) = \prod_{i=0}^{n} g_i(y), \tag{6}$$

where

$$g_i(y) = \int_{-\infty}^{+\infty} f_i(x)e^{-ixxy}dx.$$

Hence, the Fourier transform of the observed 1st derivative ESR spectra can be simulated by this equation

$$G(y) = Kg_0(y)\prod_{i=1}^{KA}\left[\cos\left(\frac{a_i}{2}y\right)\right]^{Na_i} \times \prod_{j=1}^{KB}[1+2\cos(a_jy)]^{Na_j} \times \prod_{k=1}^{KC}\left[\cos\left(\frac{3}{2}a_ky\right)+\cos\left(\frac{1}{2}a_ky\right)\right]^{Na_k}, \tag{7}$$

where a_i, a_j, and a_k are the hfs constants of the i, j, and k nuclei, with spin $I=1/2$, 1, and 3/2 respectively. Na_i, Na_j, and Na_k are the numbers of protons with hfs constants of a_i, a_j, and a_k. KA, KB, and KC are the numbers of different kinds of nuclei with spins of 1/2, 1, and 3/2 respectively, and where $g_0(y)$ is a function expressed as

$$g_0(y) = \exp(-3\pi\Delta H|y|), \tag{8}$$

when the ESR lines are Lorentzian, and as

$$g_0(y) = \exp(-\pi^2\Delta H^2y^2/2), \tag{9}$$

when the ESR lines are Gaussian. Here, $\Delta H=2/T_2$.

The ESR charts recorded by a Hitachi 771 X-band ESR spectrometer were converted to the digital form with a JEC-CR-114 chart reader and a JEC-6 spectrum computer. The inverse Fourier transforms and the simulation of the transformed spectra were done by means of the NEAC 700 computer at the Tohoku University Computer Center. Figure 12 shows the Fourier transform of the observed ESR spectrum, its computer simulation, and the simulation of the observed

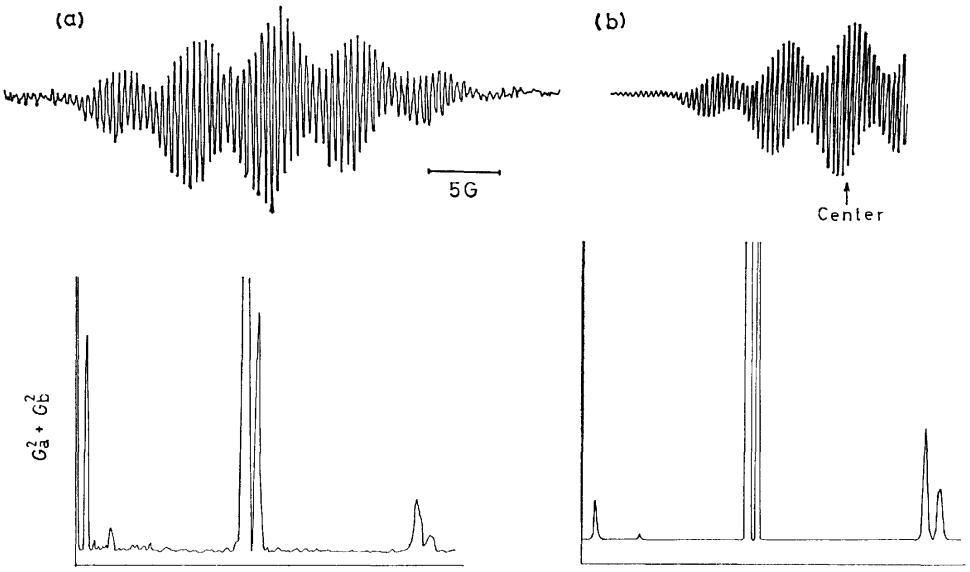

Fig. 12. Observed and theoretical ESR spectra and corresponding Fourier transform, for $XDX^{\cdot}$ in DME–THF(1 : 1) with the potassium ion.

Table 3. Hfs constants obtained by fourier transform and computer simulation of the ESR spectrum for $XDX^{\cdot-}$ in DME–THF (1:1) with the potassium ion

Hfs constants(G)	Nuclear spins	Numbers of nuclei
5.83	1/2	6
1.37	1/2	4
0.92	1/2	8
0.46	1/2	8

ESR spectrum. The hfs constants thus obtained are listed in Table 3.

Calculations of the Spin Densities, the Hfs Constants, and the Effects of Counter Ions

The spin distributions in $XX^{\cdot-}$, $XDX^{\cdot-}$, $XDDX(C_{2h})^{\cdot-}$ and $XDDX(D_2)^{\cdot-}$ were calculated by the McLachlan method.[13] In this calculation the resonance integrals are taken to be proportional to the overlap integrals.[14] The interatomic distances required for the calculation of the overlap integrals were taken from the X-ray data for the compounds XX[15] and $XDDX(C_{2h})$.[16] For the other compounds, estimates were made with reference to $XDDX(C_{2h})$ because of the absence of X-ray data. The hyperconjugation of the ethylene bridges was ignored in the MO calculation, but induction effects were taken into account for atoms directly bonded to the alkylbridges; therefore, $\alpha_C=\alpha_C^\circ-0.1\beta_{CC}$. The λ coefficient in the McLachlan calculation was taken to be 1.1. The proton hfs constants were calculated by using the obtained spin densities and McConnell's equation. The Q values used in the equation were 20.5 and 25.1 for the ring and the alkyl protons respectively; this gives consistent hfs constants for $XX^{\cdot-}$ in the free anion state.

On the other hand, the effects of the counter ions were calculated by combining the McClelland treatment of the counterion effect[17] with the McLachlan MO calculation by means of the following effective Hamiltonian:

$$\mathcal{H}_{eff} = \mathcal{H}^\circ - \frac{e^2}{e(r)\cdot r}, \qquad (10)$$

where $\mathcal{H}^\circ$ is the usual Hückel Hamiltonian; the second term is the electrostatic attraction of the radical anions and the counter ion. The $e(r)$ in the second term are the dielectric constants in a microscopic meaning; they may be referred to as screening constants and vary with the solvent and with the position in the radical anions. In the present case, however, for convenience $e(r)$ is taken to be 1.5 throughout the calculations. The oscillational motion of the cation around the potential minimum point in the ion pairs is also ignored in the calculation. Because of the approximation of $e(r)$ and the cation motion in the ion pair, the distances between the anion and the cation in the calculation do not have any quantitative meaning, but these distances can be regarded as a qualitative measure of either the strength of the cation-anion interaction or the cation-anion distances. The hfs constants of the ion pairs were calculated as functions of the cation-anion distances. The results will be shown later.

The cation-anion interaction energies were also calculated by means of this equation:

$$E = \sum_x \nu_x(E_x - E_x^\circ) - \sum_t \frac{e^2}{r_t} \qquad (11)$$

where E_x° and E_x are the energies of the Hückel MO Ψ_x° of the free anion and the modified Hückel MO Ψ_x of the ion pair respecively, and where ν_x is the occupation number of the relevant MOs. The last term represents the Coulomb repulsion between the cation and the effective positive charge of the carbon cores. Calculations have been done for the radical anions of the layered compounds and for some ordinary aromatic hydrocarbons. The result shown below is for the case where the cation moves along the axis connecting the 1 and 4 positions (x axis) for the layered compounds, or along the long molecular axis (x axis) for the other aromatic compounds, at a distance of 0.38 nm from the (outermost) nuclear plane of the radical anions.

Discussion

Ion-pair Structure of $XX^{\cdot-}$. It is known that $XX^{\cdot-}$ in DME–HMPA exists as a free anion, but when $XX^{\cdot-}$ is prepared by means of potassium in DME–THF, THF, or MTHF, the radical anion forms ion pairs with the counter ion.[3,7] This ion-pair formation can be concluded on the basis of the observation of the hyperfine splitting due to the potassium nucleus and the appreciable polarization in the spin distributions due to the cation. Ion pairing divides both the ring and alkyl protons into two groups with equal numbers of protons and different hfs constants. Three ion-pair models

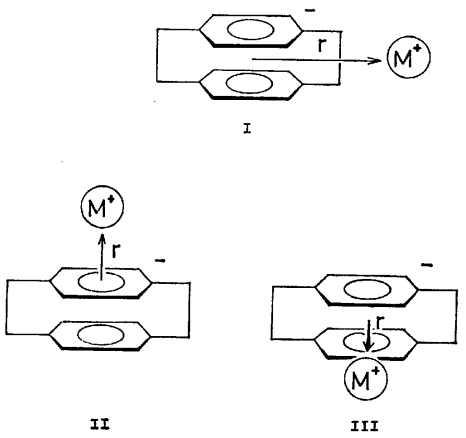

Fig. 13. Ion pair models of $XX^{\cdot-}$.

(Fig. 13) were first considered,[3] but a recent paper by Gerson *et al.*[6] has concluded, based on experiments with deuterio compounds, that the ion pair takes the structure of Model II where the cation is situated above the center of the one benzene ring. Before proceeding to discuss the ion pairs of the triple- and quadruple-layered radical anions, let us examine the ion-pair structure of $XX^{\cdot-}$ by means of the theoretical calculation of the cation effects on the hfs constants. The calculated

results will be compared with the experimental results shown in Fig. 1.

Calculations have been done for the three ion-pair models. In Model I the unpaired electron comes to occupy the MO level which gives the alkyl proton hfs constants larger than those of the ring protons when the cation-anion interaction becomes appreciable. This model is apparently improper, because the experimental results indicate that the larger hfs constant is due to the ring protons.[3,6]

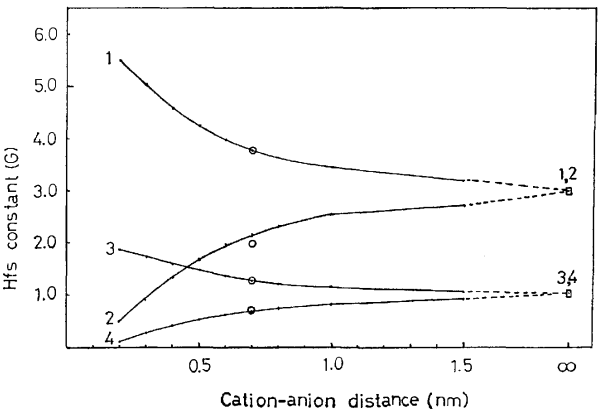

Fig. 14. Effects of the counter ion on the hfs constants of XX^- calculated for ion pair model II in Fig. 13 as a function of anion-cation distance r. □ and ○ are the plots of the experimental hfs constants for XX^- in the free anion state and thos observed in THF with the potassium ion. The numbers given to the curves are the carbon positions to which the corresponding ring proton or methylene group is bonded.

The observed trend of the ion-pairing effects on the hfs constants is predicted by calculations based on Models II and III, though in the calculation of Model III our approximation can not give different hfs constants for the two protons within one CH_2 group; the calculations for both models indicate that the hfs constant for ring protons at the cation side increases by the ion pairing, while the hfs constant for the opposite side decreases. Figure 14 shows the results for Model II. In view of the well-known facts that ion pairing is more favored at higher temperatures and in MTHF than in THF,[18] the changes observed in hfs constants with the temperature and the solvents (Fig. 1) can be surprisingly well predicted by calculations based on Model II. Both the theoretical and empirical results indicate that, as the cation-anion interaction increases, the hfs constants of the ring and methylene protons on the cation side increase, while those on the opposite side decrease. When the cation-anion interaction becomes more marked, the hfs constant of the methylene protons on the cation side becomes larger than that for the ring protons on the opposite side.

Though the calculation for Model III predicts the observed trend of the ion-pairing effects, the polarization effect due to the cation is less than 1/3 of that in Model II, and it seems to be too small to explain the observed magnitude of the effects. Apparently the calculations for Model II show the best fit with the observed changes in the hfs constants; the results indicate that the calculations used here can well predict the correct ion-pair structure.

XDX^- in DME–THF. As in the case of XX^-, the remarkable changes in ESR spectra for XDX^- can be attributed to the ion-pairing effect. In view of the general features of the solvent effects on ion pairing, the interaction of the radical anion in DME–THF is considered to be the weakest among the systems treated here. According to the MO calculation (*vide infra*), the largest hyperfine interaction of XDX^- in the free anion state should arise from protons at the 8 and 11 positions, which show triplet splitting in the ESR spectrum. The septet splitting observed for the DME–THF solution (Fig. 2(a)) suggests that there may still be some appreciable interaction with the cation in the solution.

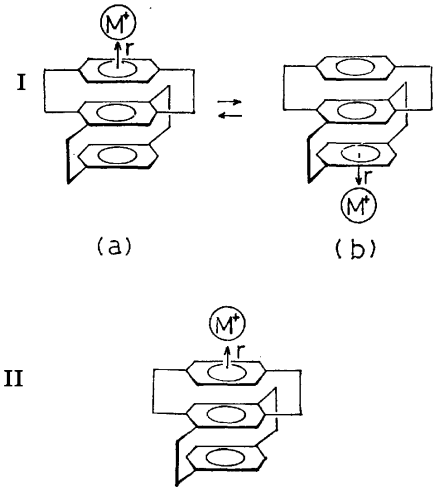

Fig. 15. Ion pair models for XDX^-.

To explain the ESR pattern observed, the ion-pairing effect on the hfs constants was calculated for both ion-pair models in Fig. 15. In these models, the cation is assumed to favor a location above the plane of the outermost benzene rings of the molecule, as in the case of XX^-. However, in Model I the cation rapidly changes position from one side of the molecule to the other. In this case the observed hfs constants are given by the average of ion-pair states, (a) and (b). In Model II it is assumed that XDX^- forms a tighter ion pair where the cation is positioned on one side of the molecule.

The calculated results (Fig. 16) show that the septet splitting in the ESR spectrum seems due to the ion pair corresponding to the area marked by Arrow A, where the six protons at the 2, 5, 8, 11, 14, and 17 positions have hyperfine interactions of the same magnitude so as to give the septet hyperfine splitting in the ESR spectrum. The calculated result also indicates that the other protons have hyperfine interactions much smaller than the septet splitting. These results are in accord with the results of the Fourier transform analysis of the ESR spectrum. Since the other ion-pair models can not explain the observed septet ESR pattern, it can be concluded that XDX^- in DME–THF (1:1) has the ion-pair state predicted by Model I (Fig. 15).

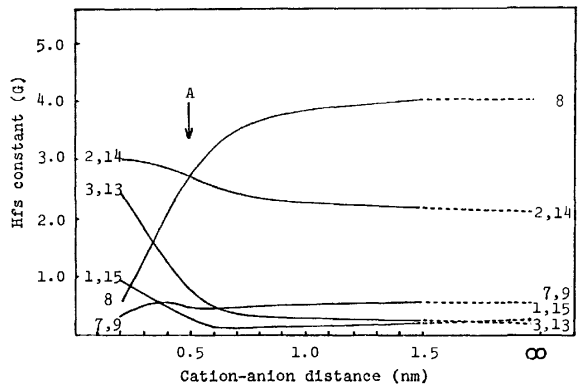

Fig. 16. Effects of the counter ion on the hfs constants of XDX^- calculated for ion pair model I in Fig. 15. The numbers given to the curves have the same meaning as in Fig. 14. Mark A: see text.

XDX^- in THF, MTHF, and DEE. As has been mentioned above, the ESR spectra observed from XDX^- in THF with the caesium ion, and in MTHF and DEE with the potassium ion, show broad triplet splitting. Considering that these systems are in a more favorable condition for ion pairing than is the DME–THF mixed solvent system, the triplet splitting can be attributed to their ion pairs being bound more tightly than in the DME–THF mixed solvent. The calculation shown in Fig. 17 predicts well this triplet splitting; *i.e.*, it indicates that the unpaired electron is redistributed on the benzene ring on the cation side (especially at the 2 and 5 positions) by the formation of strong ion pairs of the Model II type. The hyperfine interaction of the 2 and 5 protons gives the triplet splitting observed in the ESR spectrum. In the ENDOR spectra for XDX^- in MTHF, the presence of eight kinds of protons was observed (Figs. 5 and 6). However, the ENDOR signal corresponding to the triplet splitting in the ESR spectrum could not be detected. Taking into account this triplet splitting in the ESR spectrum, the observed ENDOR spectra indicate that there are nine types of protons in the radical anion; this finding is in agreement with the expectation from the ion-pair model being considered here.

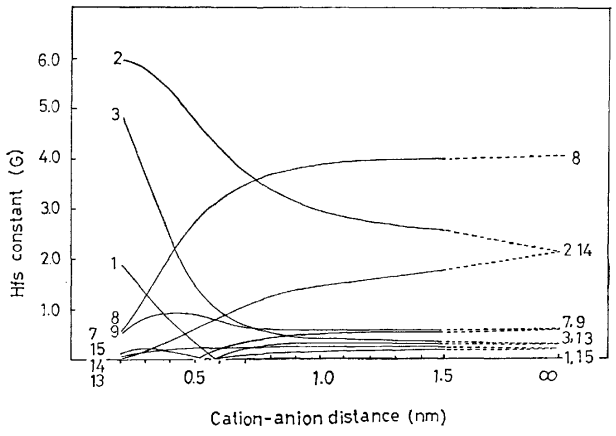

Fig. 17. Effects of the counter ion on the hfs constants of XDX^- calculated for ion pair model II in Fig. 15. The numbers given to the curves have the same meaning as in Fig. 14.

The changes observed in the hfs constants with the temperature and the solvent can be explained by this ion-pair model. It has already been noted that the triplet splitting observed in the ESR spectra increases from 6.13G to 6.48G when the solvent is changed from MTHF to DEE. This indicates that the largest hyperfine interaction in the XDX^- ion pair will increase with an increase in the cation-anion interaction. It may also be seen from Fig. 6 that the hfs constant, a_1, observed in the ENDOR spectra increases with an elevation of the temperature, while a_2 decreases; as the cation-anion interaction increases, a_1 increases, but a_2 decreases. These experimental results correspond well to the behavior of the hfs constants calculated for the ion-pair state with a cation-anion distance of about 0.4 nm (Fig. 17).

Thus, it seems reasonable to conclude that, in these cases, XDX^- exists as a relatively tight ion pair with the structure shown in Fig. 15 II. The change in the cation position from one side of the molecule to the other is slow. From a comparison with the calculated results, the triplet splitting observed in the ESR spectra may be attributed to the hyperfine interaction of protons at the 2 and 5 positions, while the a_1 and a_2 observed in the ENDOR spectra may be attributed to protons at the 8 and 11, and 3 and 6 positions, respectively. The reliable assignment of the other hyperfine interactions is difficult.

For XDX^- in THF with the potassium ion, the ESR spectrum appeared to be a superposition of two types of spectra, a triplet pattern and a septet pattern. This indicates that there is an equilibrium between the two types of ion pairs, loosely bound and tightly bound.

Ion Pairs of $XDDX(C_{2h})^-$ and $XDDX(D_2)^-$. The triplet hyperfine pattern observed in the ESR spectra strongly suggests, as in the case of XDX^-, that $XDDX(C_{2h})^-$ and $XDDX(D_2)^-$ are the ion pairs where the alkali metal ion is situated above either of the outermost benzene rings of the molecules. The unpaired electron is mainly distributed on the benzene ring at the cation side, producing the large triplet splittings due to the two ring protons. However, because of the complex molecular structure, it was difficult to find perfect correlations between the observed and the calculated effects of the cation on the hfs constants. Considering only the largest three or four hfs constants, however, some correlation can be seen, as will be discussed below.

For $XDDX(C_{2h})^-$, the triplet splitting in the ESR spectra increases with the change in solvent from THF to MTHF and DEE (*vide ante*). In other words, the splitting increases with an increase in the cation-anion interaction. Taking into account the general effects of the solvent and temperature on ion pairing, it may be seen from Fig. 10 that the hfs constant, a_1, observed in the ENDOR spectra increases with an increase in the cation-anion interaction, while a_2 and a_3 decrease. These changes correspond to the changes in the hfs constants with a cation-anion distance of about 0.4 nm (Fig. 18), as with the ion pair model in Fig. 19. That is, the triplet splitting in the ESR spectra corresponds to

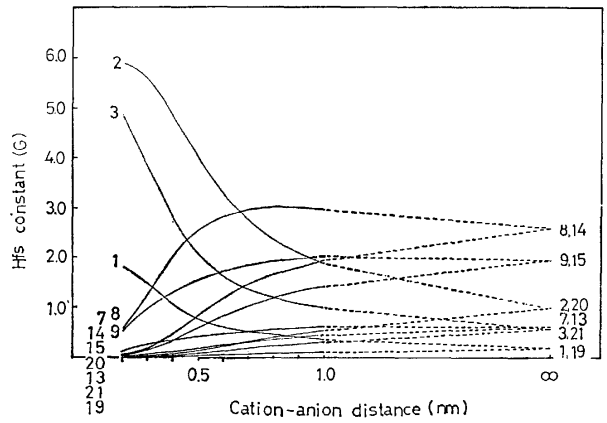

Fig. 18. Effects of the counter ion on the hfs constants of $XDDX(C_{2h})^-$ calculated for the ion pair model in Fig. 19. The numbers given to the curves have the same meaning as in Fig. 14.

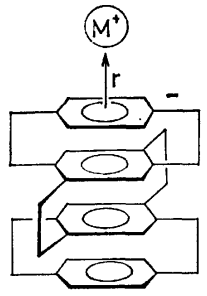

Fig. 19. Ion pair model for $XDDX(C_{2h})^-$.

the hfs constant at the 2 and 5 positions, while a_1, a_2, and a_3 in the ENDOR spectra correspond to those at 3 and 6, 8 and 11, and 9 and 12, respectively.

In a similar way, the hyperfine interactions observed in the ESR and ENDOR spectra for $XDDX(D_2)^-$ correspond to the results calculated in the region of about 0.5 nm in Fig. 20; the interactions are calculated for a similar ion-pair model in Fig. 19. Though the quantitative fit is not necessarily sufficient, the ion-pair model where the alkali metal cation is placed above the benzene ring at the outermost side of the molecules

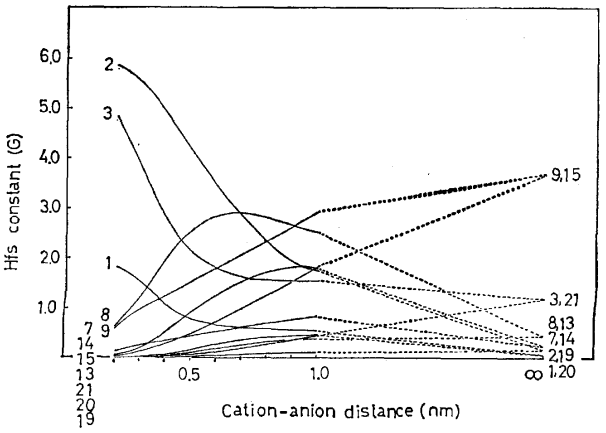

Fig. 20. Effects of the counter ion on the constants of $XDDX(D_2)^-$ calculated for the ion pair model in Fig. 19. The numbers given to the curves have the same meaning as in Fig. 14.

seems reasonably to account for the experimental results.

It may be notable that the cation-anion distances at which the behavior of the predicted hfs constants correspond well to the observed ones are different for $XDDX(C_{2h})^-$ and $XDDX(D_2)^-$. Since the distance for $XDDX(C_{2h})^-$ is smaller, this may imply that $XDDX(C_{2h})^-$ has a more tightly bound ion pair than does $XDDX(D_2)^-$. On the contrary, the results calculated for the cation-anion interaction enrgies (Fig. 21) suggest that $XDDX(D_2)^-$ may form a stronger ion pair than $XDDX(C_{2h})^-$. The difference in the ion pairing between the isomers is very interesting, but a reliable conclusion regarding this problem must await further investigation.

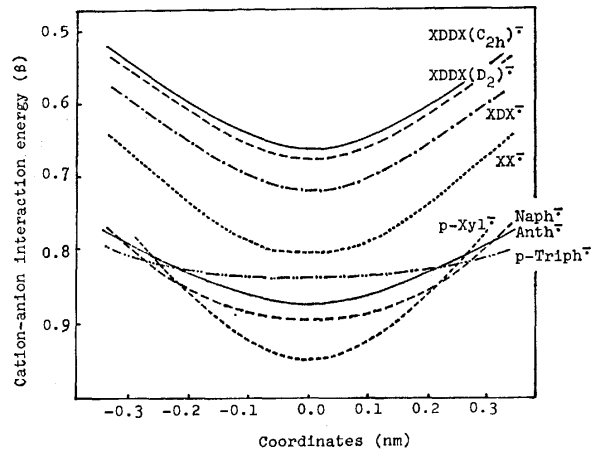

Fig. 21. Cation-anion interaction energies calculated for the radical anions of the layered compounds and for some aromatic hydrocarbons.

Motion of the Alkali Metal Ion in the Ion Pairs. Gerson *et al.*[3] reported that the ESR spectrum of XX^- in DME–THF (2: 1) shows a line-width alternation effect; they explained this as arising from the motion of the alkali ion between the two symmetrical positions. In this paper we also found that the potassium ion in the ion pair of XDX^- in DME–THF (1: 1) changes its position from one side of the anion molecule to the other. Whether such alkali metal motion is an intramolecular or an intermolecular effect (Eqs. 12 and 13) is an interesting problem.

$$XDX^-M^+ \rightleftharpoons M^+XDX^-, \quad (12)$$

$$M^{*+} + XDX^-M^+ \rightleftharpoons M^{*+}XDX^- + M^+. \quad (13)$$

The motion of the cation in the XX^- ion pair can be concluded to be intramolecular in nature by the observation of the distinct hyperfine splitting due to the potassium nucleus in the ESR spectrum showing the linewidth-alternation effect. In the case of XDX^- however, no such potassium hyperfine splitting could be found in the ESR spectrum. However, an intramolecular exchange mechanism is suggested by the fact that the quadruple-layered compounds, which tend to form looser ion pairs than XDX^- (see Fig. 21), are in the ion pairs having a long enough lifetime in the ESR time scale and by the fact that no effects due to the dissociation of the ion pair are observed, not even

in the DME–THF solution.

In the case of $XDDX(C_{2h})^{\cdot-}$ and $XDDX(D_2)^{\cdot-}$, the intramolecular migration of the alkali ions in the ion pairs is considered to be much slower than for $XDX^{\cdot-}$, even though the alkali ions are bound more loosely to the radical anions, because of the long distance between the two potential minimum sites in the ion pairs.

Polarization by Ion Pairing. The radical anions of the layered compounds reveal marked effects of ion pairing in the ESR and ENDOR spectra. However, this large effect does not necessarily mean that the radical anions form strong ion pairs. Figure 21 shows that the cation-anion interaction energies in the radical anions of the layered compounds are smaller than those of ordinary aromatic hydrocarbon radical anions. The most remarkable feature of these radical anions is that they show a large redistribution of unpaired electrons by the counter ions. In $XDX^{\cdot-}$, for example, when the radical is in the free anion state, a large portion of the unpaired electrons will be distributed on the inside benzene ring; hence, a large hfs constant at the 8 and 11 positions is expected (Fig. 17). Because of the ion pairing, the unpaired electron distribution is polarized towards the cation side and the hfs constants of the protons in the benzene ring on the cation side increase significantly. In the ordinary aromatic hydrocarbon radical anions, the redistribution of the unpaired electrons is usually very small. In the case of the naphthalene radical anion, the changes in the hfs constants by ion pairing are only about 0.12G or less.[19] Aside from such layered compounds, only a few examples are known which show such a large redistribution of the unpaired electrons upon interaction with the counter ion.[20,21] The 9,10-dihydroanthracene radical anion is one example.[21]

We hoped to obtain the ESR or ENDOR spectra for the triple-, and quadruple-layered [2.2]paracyclophane radical anions in the free anion state. However, such attempts have been unsuccessful. It should be noted that the unpaired electrons in free $XDX^{\cdot-}$, $XDDX(C_{2h})^{\cdot-}$, and $XDDX(D_2)^{\cdot-}$ can be expected, according to theoretical calculations, to be distributed more on the inside benzene rings. In the present calculation, the unpaired electron densities on the inside benzene ring in free $XDX^{\cdot-}$ amount to about 50%. Further efforts to observe free $XDX^{\cdot-}$, $XDDX(C_{2h})^{\cdot-}$, and $XDDX(D_2)^{\cdot-}$ are in progress.

The authors wish to express their hearty thanks to Dr. Hiroshi Sugiyama, Chemical Research Institute of Non-Aqueous Solutions, Tohoku University, for his valuable advice.

References

1) S. I. Weissman, *J. Am. Chem. Soc.*, **80**, 6462 (1958).
2) A. Ishitani and S. Nagakura, *Mol. Phys.*, **12**, 1 (1967).
3) F. Gerson and W. B. Martin, Jr., *J. Am. Chem. Soc.*, **91**, 1883 (1969).
4) D. J. Williams, J. M. Pearson, and M. Levy, *J. Am. Chem. Soc.*, **93**, 5483 (1971).
5) T. Hayashi, N. Mataga, Y. Sakata, and S. Misumi, *Bull. Chem. Soc. Jpn.*, **48**, 416 (1975).
6) F. Gerson, W. B. Martin, Jr., and C. Wydler, *Helv. Chim. Acta*, **59**, 1365 (1976).
7) F. Gerson, W. B. Martin, Jr., and C. Wydler, *J. Am. Chem. Soc.*, **98**, 1318 (1976).
8) a) T. Otsubo, S. Mizogami, Y. Sakata, and S. Misumi, *Tetrahedron Lett.*, **1971**, 4803; b) T. Otsubo, S. Mizogami, I. Otsubo, Z. Tozuka, A. Sakagami, Y. Sakata, and S. Misumi, *Bull. Chem. Soc. Jpn.*, **46**, 3519 (1973); c) T. Otsubo, H. Hirota, and S. Misumi, *Synth. Commun.*, **6**, 591 (1976).
9) The observed ESR spectra were not reproducible, and the reaction seemed to be sensitive to several factors.
10) The values were obtained from the ESR spectra at −100 °C.
11) R. H. Silsbee, *J. Chem. Phys.*, **45**, 1710 (1966).
12) V. A. Gubanov, V. I. Koryakov, and A. K. Chirkov, *J. Magn. Reson.*, **11**, 326 (1973).
13) A. D. McLachlan, *Mol. Phys.*, **3**, 233 (1960).
14) The proportional constant for the integrals between layers was taken to be 1.5 times larger than that of the integrals within layers. Such a modification was required to obtain reasonable results for the calculation of the counter-ion effects on the spin distributions.
15) a) C. J. Brown, *J. Chem. Soc.*, **1953**, 3265; b) D. K. Londsdale, F. R. S., H. J. Milledge, and K. V. K. Rao, *Proc. R. Soc. London, Ser. A*, **255**, 82 (1960); c) H. Hope, J. Bernstein, and K. N. Trueblood, *Acta Crystallogr., Sect. B*, **28**, 1733 (1972); d) D. J. Cram and J. M. Cram, *Acc. Chem. Res.*, **4**, 204 (1971).
16) a) H. Mizuno, K. Nishiguchi, T. Otsubo, S. Misumi, and N. Morimoto, *Tetrahedron Lett.*, **1972**, 4981; b) H. Mizuno, K. Nishiguchi, T. Toyoda, T. Otsubo, S. Misumi, and N. Morimoto, *Acta Crystallogr., Sect. B*, **33**, 329 (1977).
17) B. J. McClelland, *Trans. Faraday Soc.*, **57**, 1458 (1961).
18) M. Szwarc, ed, "Ions and Ion Pairs in Organic Reactions," Wiley, Vol. 1, New York, N. Y. (1971).
19) M. Iwaizumi, M. Suzuki, T. Isobe, and H. Azumi, *Bull. Chem. Soc. Jpn.*, **41**, 732 (1968).
20) a) F. Gerson, B. Kowert, and B. M. Peake, *J. Am. Chem. Soc.*, **96**, 118 (1974); b) F. Gerson, R. Gleiter, G. Moshuk, and A. S. Dreiding, *ibid.*, **94**, 2919 (1972).
21) M. Iwaizumi and J. R. Bolton, *J. Magn. Reson.*, **2**, 278 (1970).

Fluorescence and Laser Photolysis Studies on the Intramolecular Exciplex Systems in Micellar Solutions

Hiroshi MASUHARA, Katsumi KAJI, and Noboru MATAGA

Department of Chemistry, Faculty of Engineering Science, Osaka University, Toyonaka, Osaka 560

(Received March 2, 1977)

The behavior of intramolecular exciplex systems consisting of pyrene and *N,N*-dimethylaniline was studied in cationic, anionic and neutral micellar solutions. These systems are favorable for the study of photoinduced CT interaction in micellar systems, since (i) a pair of donor-acceptor is always solubilized in the micelle and (ii) the complicated effect of the intermolecular interaction can be prevented. No exciplex emission was detected and relative quantum yields as well as lifetimes were measured on the monomer fluorescence. The results are interpreted by assuming two solubilized forms in the micelle-water interface. Efficient quenching occurs in the dodecyltrimethylammonium chloride solution irrespective of the length of the methylene chain, suggesting a different solubilization from the cases of other detergents. The efficient quenching is ascribed to the rapid ion-pair formation in the micelle-water interface, which was directly demonstrated by the ns laser photolysis method.

Studies on the photoprimary processes of the excited electron donor-acceptor (EDA) systems are indispensable for the interpretation of photooxidation-reduction reactions. They are closely related to mechanistic organic photochemistry.[1-4] We have investigated the electronic structure and dynamic behavior of these systems, and shown that the dependence upon the molecular interaction between donor-acceptor pairs and upon the environment is essential.[1-3] Studies on the excited EDA systems in micellar solution are of interest from the view that (i) basic aspects of the EDA interaction in inhomogeneous systems of biological importance will be clarified, and (ii) new information might be obtained on the structure and function of the micelle, not obtained by means of fluorescence polarization and photoionization (electron ejection). So far the following two exciplex-micelle systems have been reported. The quaternary ammonium groups of the *N*-dodecyl-*N,N*-dimethylbetaine quenches the excited pyrene and forms an exciplex showing a fluorescence band with maximum at 480 nm and the lifetime of 70 ns.[5] A similar exciplex emission was also obtained in the case of pyrene solubilized in the mixed micelle of sodium dodecyl sulphate and dodecylamine.[6] However, since the distance and relative orientation between pyrene and the amines, and the environmental conditions of the solubilized probe molecule were not made clear, the quenching mechanism including an exciplex formation is unknown. Thus we have studied the typical intramolecular exciplex compounds (pyrene)-$(CH_2)_n$-(*N,N*-dimethylaniline) (abbreviated as P_n).

Experimental

Sodium dodecyl sulphate (SDS) and α-dodecyl-ω-hydroxypoly(oxyethylene) (Brij) (special grade, Nakarai), and dodecyltrimethylammonium chloride (DTAC), (pure grade, Tokyo Kasei), were used. Brij and SDS were recrystallized twice from ethanol; DTAC was recrystallized from benzene. They were dried under reduced pressure for a few days. The concentration of Brij was adjusted to 0.065 M, while, 0.1 M solutions were prepared in the case of ionic surfactants. The concentrations lead to $\approx 1.6 \times 10^{-3}$ M micelle concentration.[7] Deionized water was distilled, refluxed over potassium permanganate and redistilled. A 50 μl acetone solution of 10^{-3} M P_n was poured into a 5 ml measuring flask and dried. The prepared micellar solution was then added and treated with the ultrasonic cleaner for ten minutes. This gave the same solution as that prepared by stirring the solution for 3 h at 50 °C. The concentration of 10^{-5} M solubilizate was checked by optical density measurements. These solutions were flushed with nitrogen gas for 25 min.

Absorption spectra were measured with a Shimadzu MPS-50 L UV spectrophotometer. The fluorescence and excitation spectra were obtained with an Aminco-Bowman spectrophotofluorometer. The fluorescence rise and decay curves were observed with a pulsed nitrogen laser and Tektronix 585A oscilloscope.[8] Transient absorption spectra were obtained by the usual nanosecond laser photolysis method.[3]

Results and Discussion

1. Fluorescence Studies and the Solubilized Site of the P_n Compounds in Micellar Solutions. The effects of surrounding environments upon the exciplex have been revealed by the analysis of spectra, quantum yields and lifetimes of monomer as well as exciplex fluorescence. In the case of organic solvents,[1,2] the red shift of the fluorescence maxima and the decrease in the yield as well as lifetime is observed with the increase of solvent polarity. Exciplex emission is no longer detected, ionic dissociation being observed in polar solvents such as acetonitrile. On the other hand, exciplex formation is retarded with increase in the viscosity of the solvent. In the rigid solvents the molecular motion is completely suppressed and only the monomer fluorescence can be measured. The present P_n compounds in micellar solution have been investigated in view of the above tendencies.

The experimental conditions of the present probe molecules are suitable for studying the interaction between the donor-acceptor groups in micellar solutions for the following reasons. (i) A donor-acceptor pair is always solubilized in the micelle; (ii) the appropriate concentration of P_n for the laser photolysis, given that the absorbance at 337 and 347 nm is larger than 0.3, is *ca.* 10^{-5} M, one-hundredth of the micelle concentration, which indicates that the intermolecular interaction between the P_n molecules in the same micelle is completely neglected; (iii) without detergents the concentration of the aromatics in question is so low that the

contribution of the molecules dissolved in water phase is neglected. The problem is to find a standard compound which is not quenched by the *N,N*-dimethylaniline moiety. Ethylpyrene (EP) is appropriate since (i) the absorption bands in the 300—360 nm region are almost identical with those of P_n compounds within 2 nm, although detailed information on the 380 nm band could not be obtained because of low concentration, and (ii) the absolute fluorescence yield of EP in cyclohexane (0.5) is almost equal to the value of P_1 in hexane (0.6), where no exciplex emission is observed.[9]

Table 1. Relative quantum yields of pyrene monomer fluorescence of P_n compounds in N_2-bubbled micellar solutions

	EP	P_1	P_2	P_3
Brij	1.0[a]	0.5_0	0.4_7	0.4_2
SDS	1.0[a]	0.4_8	0.3_0	0.2_0
DTAC	1.0[a]	0.0_1	0.0_3	0.0_3

a) Normalized to unity.

Table 2. Lifetimes of pyrene monomer fluorescence of P_n compounds in N_2-bubbled micellar solutions (nanoseconds)[a]

	EP	P_1	P_2	P_3
Brij	150	150	140	110
SDS	225	270	260	240
DTAC	170	short,[b] 130[c]	short,[b] 130[c]	short,[b] 180[c]

a) All values averaged, fluctuations being within 10 ns. b) Rise and decay curves determined with our time constant, *ca.* 5 ns with a Tektronix 475 oscilloscope. c) Errors large due to low intensity.

As regards the experimental results in micellar solutions, relative quantum yields and lifetimes of pyrene monomer fluorescence of EP and P_n are given in Tables 1 and 2, respectively. Although fluorescence quenching occurs in the case of P_n as compared to the results of EP, no new exciplex emission was detected. The monomer fluorescence intensity decreases with increase in the number of methylene (abbreviated as *n*) observed in the Brij and SDS solutions. The lifetime of P_1 is larger than that of EP in SDS solution, which may be due to the different solubilized sites of their molecules. Efficient quenching was observed independent upon *n* in the case of DTAC surfactant. As shown in Fig. 1, the decay in DTAC solution shows rapid and slow components. The latter seems to be single exponential, while the former is too short to be analysed. In the cases of Brij and SDS, no rapid component was observed, the values of the slow component decreasing with the increase of *n*. This might suggest dynamic quenching by the DMA group. In the case of DTAC solution the experimental error of the lifetimes is rather large because of their low intensity. No detailed discussion on the slow component can be given.

The micellar effect on the exciplex systems will be discussed on the basis of the present results. One problem of the micellar systems is the location of the probe molecule. Large aromatic molecules such as pyrene are often considered to be in the interior of the micelle. In fact a recent NMR study of pyrene in hexadecyltrimethylammonium bromide supports this view.[10] If the present P_n compound is also dissolved in the interior of the micelle, an exciplex emission can be expected because of the analogy between the aliphatic part of micelle and the viscous aliphatic solvents. We have observed no exciplex emission in the present system, although it is observed in viscous decaline.[9] If the large viscosity of the interior prohibits a molecular motion for exciplex formation, the fluorescence yield and lifetimes should remain unchanged when *n* is changed. Thus, the simple solubilization model is inconsistent with the present results.

We see from Tables 1 and 2, that yield and lifetime show different dependence upon *n*. The yield decreases with *n*, while the change of lifetime with *n* is rather small. This can be interpreted by assuming two solubilized forms of P_n in micellar systems. In one form the fluorescence quenching occurs quite rapidly, while in the other the molecular motion for the interaction between the two moieties is prohibited. The probability of taking the latter form decreases with the increase of *n*. The interpretation is also in line with the two-component decay of pyrene monomer fluorescence in DTAC solution. The solubilized forms are considered

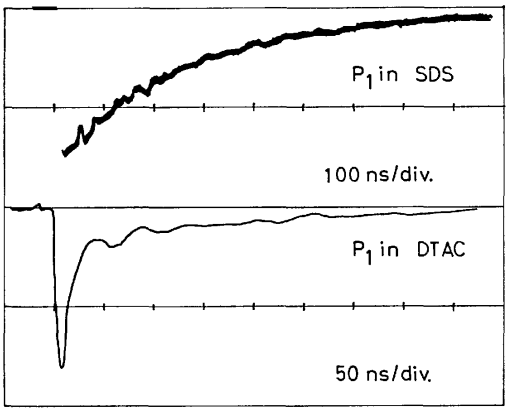

Fig. 1. Oscillograms observed at 400 nm, showing the pyrene monomer fluorescence decay of P_1 in SDS and DTAC solutions.

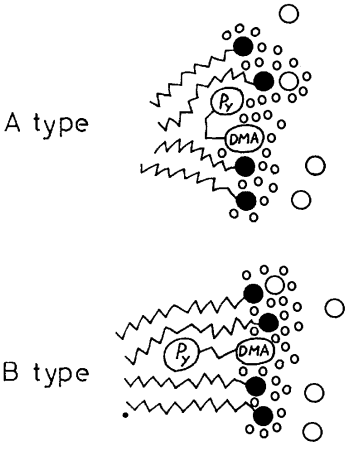

Fig. 2. Schematic representation of the solubilized form of intramolecular exciplex systems in micellar solution. ●: Head groups; ○: counter ion; ○: H_2O molecule.

to be as follows. (i) Pyrene seems to be dissolved in the interior of the micelle, while DMA in hexadecyltrimethylammonium bromide indicates the predominating solubilization mechanism to be absorption close to the α-CH_2 groups.[11] The other data show the existence of DMA in the water-micelle interface.[6] The results suggest that both the solubilized sites are in the vicinity of the water phase. (ii) The fluorescence quantum yields of EP and P_1 in hexane are almost equal to each other, no exciplex emission of the latter being observed. This implies that the quenching by the DMA group of the P_1 system is impossible in nonpolar aliphatic environments such as the interior of the micelle. The yield of P_1 is about a half of that of EP even in Brij and SDS solutions, while no exciplex emission was observed. This is also ascribed to the more polar character of environments, in which the probe molecule is dissolved.

The above considerations are schematically given in Fig. 2. In the solubilization form of A, pyrene and DMA groups are in contact with water molecules and the excited states are easily quenched immediately after excitation. On the other hand, in the case of B the interaction between the pyrene and DMA groups hardly arises during the lifetime of the excited pyrene. The P_n compound may thrust the DMA moiety into the head groups of the surfactant, leaving the pyrene moiety in the interior. This form might be too rigid to undergo quenching interaction. The probability of form A being taken may increase from P_1 to P_3 as the freedom of the molecular motion increases. In the DTAC solution particularly, almost all the probe molecules take the A configuration, which might be ascribed to a different solubilization mechanism of DTAC from that of anionic and neutral detergents.

2. Quenching Mechanism of P_n in the DTAC Solution. Quenching is very efficient in the DTAC solution, irrespective of *n*. An oscillogram showing the short-lived transient is given in Fig. 3. The transient absorption spectra of P_1 obtained immediately after the excitation is shown in Fig. 4(a). These spectra are reproduced by a superposition of the bands of the pyrene anion and the DMA cation and easily assigned to the ion-pair of the acceptor anion and the donor cation. This is supported by the fact that the present spectra are similar to those of P_3 in acetonitrile,[12] shown in Fig. 4(b). Similar spectra were observed also in the cases of P_2 and P_3, while no such ionic species with short lifetime was detected in the Brij solution of P_2. Thus it is concluded that the rapid ion-pair formation leading to the quenching occurs easily in the DTAC solution. In general the

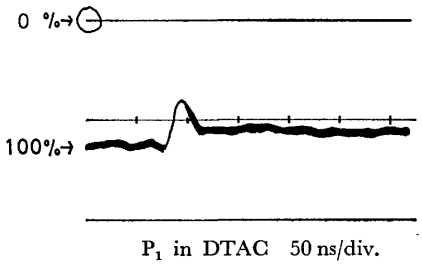

Fig. 3. Oscillogram observed at 500 nm, showing the transient absorption of P_1 in DTAC solution.

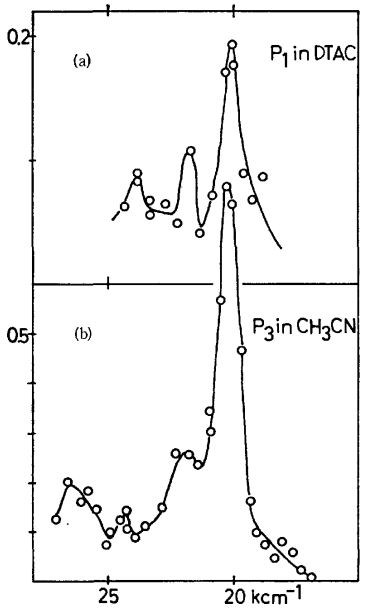

Fig. 4. (a) Transient absorption spectra of P_1 in DTAC solution obtained immediately after laser excitation. (b) Reference spectra of P_3 in acetonitrile.[12]

formation of ionic species is possible when the molecular pair are set in the polar environment, as confirmed by the systems in organic solvents. The P_n compounds in the DTAC systems seem to be dissolved near the water-micelle interface and influenced by the polar water molecules, which is consistent with the result of the fluorescence studies. The ionic species of the exciplex systems are also formed in the micellar solution, as in the polar organic solvents. Confirmation by nanosecond photolysis indicates that the ionic dissociation processes play an important role in the photoprimary processes of aromatic molecules in water and micellar solutions.

The authors wish to express their sincere thanks to Profs. S. Misumi and Y. Sakata of this University for supplying the intramolecular exciplex systems.

References

1) N. Mataga, in "Exciplex," ed by M. Gordon and W. R. Ware, Academic Press, New York (1975), p. 113; N. Orbach and M. Ottolenghi, *ibid.*, p. 75; M. Ottolenghi, *Acc. Chem. Res.*, **6**, 153 (1973); H. Masuhara and N. Mataga, *Chem. Phys. Lett.*, **22**, 305 (1973).

2) M. Shimada, H. Masuhara, and N. Mataga, *Bull. Chem. Soc. Jpn.*, **46**, 1903 (1973); H. Masuhara and N. Mataga, *Chem. Phys. Lett.*, **22**, 305 (1973); H. Masuhara, T. Hino, and N. Mataga, *J. Phys. Chem.*, **79**, 994 (1975); T. Hino, H. Akazawa, H. Masuhara, and N. Mataga, *ibid.*, **80**, 33 (1976); S. Masaki, T. Okada, N. Mataga, Y. Sakata, and S. Misumi, *Bull. Chem. Soc. Jpn.*, **49**, 1277 (1976).

3) H. Masuhara, M. Shimada, N. Tsujino, and N. Mataga, *Bull. Chem. Soc. Jpn.*, **44**, 3310 (1971).

4) R. S. Davidson, in "Molecular Association," Vol. 1, ed by R. Foster, Academic Press, N. Y. (1975), p. 215; A. Lablache-Combier, *Bull. Chim. Soc. Fr.*, **1972**, 4792.

5) M. Chen, M. Graetzel, and J. K. Thomas, *Chem. Phys. Lett.*, **24**, 65 (1974).

6) M. Graetzel and J. K. Thomas, *J. Am. Chem. Soc.*, **95**, 6885 (1973).
7) E. J. Fendler and J. H. Fendler, *Adv. Phys. Org. Chem.*, **8**, 276 (1970).
8) T. Hayashi, Thesis, Osaka University (1976).
9) T. Okada, T. Saito, N. Mataga, Y. Sakata, and S. Misumi, *Bull. Chem. Soc. Jpn.*, **50**, 331 (1977).
10) M. Graetzel, K. Kalyanasundaram, and J. K. Thomas, *J. Am. Chem. Soc.*, **96**, 7869 (1974).
11) P. H. Elworthy, A. T. Florence, and C. B. Macfarlane, "Solubilization by Surface-active Agents," Chapman and Hall Ltd. (1968), p. 78.
12) N. Mataga, T. Okada, H. Masuhara, N. Nakashima, Y. Sakata, and S. Misumi, *J. Luminescence*, **12/13**, 159 (1976).

The Structural Role of the Aluminum Ion in Alkali Aluminophosphate Glass Containing Less Than 50 mol% of P_2O_5

Akira KISHIOKA

Department of Chemistry, Faculty of Science and Technology, Sophia University, Kioicho, Chiyoda-ku, Tokyo 102

(Received December 10, 1976)

Several series of alkali (Na and K) aluminophosphate glasses with a constant P_2O_5 content of less than 50 mol % were prepared. From the infrared absorption spectra of these glasses, and also from the paper chromatograms of aqueous solutions of these glasses, we obtained the following results: The PO_4^{3-} ion increased with an increase in the amount of Al_2O_3 when the P_2O_5 content was kept constant. The PO_4^{3-}/P_2O_5 ratio in the glass increased with an increase in the Al_2O_3 content, whereas it decreased with an increase in the P_2O_5 content. In the composition of 32.5 mol % of P_2O_5, the glass containing exclusively PO_4^{3-}-type ions as a phosphate species was found. The PO_4^{3-}/Al^{3+} ratio was smaller than unity in the case of a lower Al_2O_3 content and larger than unity in the case of a higher Al_2O_3 content. From these results, the structural role of the Al^{3+} ion can be revealed as follows: In the glass with a lower Al_2O_3 content, two kinds of Al^{3+} ions exist—(1) the Al^{3+} ion, which forms the P–O–Al linkage by the substitution of the P^{5+} ion in the P–O–P linkage, and (2) the Al^{3+} ion, which does not form such a linkage, whereas in the glass with a higher Al_2O_3 content all the Al^{3+} ions substitute the P^{5+} ion to form the P–O–Al linkage.

It is well known that Al_2O_3 stabilizes the structure of phosphate glass and increases the chemical durability. It has been considered that this effect of the Al_2O_3 in the phosphate glass is due to the formation of an ($AlPO_4$) group in the glass structure.[1] The detailed structural role of Al^{3+} ion in aluminophosphate glass, however, has not yet been clarified. The coordination number of the Al^{3+} ion in phosphate glass is particularly interesting in connection with the role of this ion in the glass structure. Sakka[2] has reported that most of the Al^{3+} ions in the glass with a higher P_2O_5 content were 6-fold coordinated, while those with a lower P_2O_5 content were 4-fold coordinated; the present authors[3] have also reported a similar change in the glass-forming regions in the Na_2O–Al_2O_3–P_2O_5 and K_2O–Al_2O_3–P_2O_5 systems.

In this investigation, several series of sodium and potassium aluminophosphate glasses with the same P_2O_5 content of less than 50 mol % (polyphosphate composition) were prepared, and the infrared absorption spectra of these glasses were examined and the aqueous solutions of these glasses were subjected to paper chromatography in order to separate the orthophosphate from the other polyphosphate ion species. The contents of the Al_2O_3, P_2O_5, and PO_4^{3-} ion were gravimetrically determined. The structural role of the Al^{3+} ion was discussed in terms of the Al_2O_3 and P_2O_5 contents as well as the PO_4^{3-}/P_2O_5 and PO_4^{3-}/Al^{3+} ratios obtained by these analyses.

Experimental

Preparation of Glass. Twenty-two kinds of glasses with the compositions represented in Tables 1 and 2 were prepared. Most of these compositions are selected inside the glass-forming regions of less than 50 mol % of P_2O_5 in the Na_2O–Al_2O_3–P_2O_5 and K_2O–Al_2O_3–P_2O_5 systems.[3]

The materials used were sodium dihydrogenphosphate, anhydrous sodium carbonate, potassium dihydrogenphosphate, anhydrous potassium carbonate, aluminum oxide, and orthophosphoric acid (85%). They were all of a reagent grade. About a 40-g portion of a mixture obtained by mixing the necessary amounts of the above compounds was used for each batch. The samples were placed in platinum dishes and heated in a electric furnace. After the samples had been dehydrated by gradually heating them up to 500 °C over about a 5-h period, they were kept at this temperature for 2 h. Then, the temperature was raised further to 1350 °C over a 2-h period and kept at this temperature for 1 h. The melt of each batch was poured out and quenched by pressing it with copper plates cooled with water. All the quenched melts were obtained as transparent colorless glasses except for the sample with the initial composition of $30K_2O \cdot 30Al_2O_3 \cdot 40P_2O_5$ which was obtained as a mixture of glass and crystal, the glassy part being used for the experiment.

Determination of Al_2O_3. Glass powder containing about 0.1 g of Al_2O_3 was dissolved in 150 ml of 1 M (1 mol dm^{-3}) HCl by boiling, after which the polyphosphate ion species in the sample were hydrolyzed to orthophosphate ions by prolonged boiling for 30 min. The Al^{3+} ion in this solution was gravimetrically determined as $AlPO_4$.[4]

Determination of Total Phosphate as P_2O_5. Glass powder containing about 0.1 g of P_2O_5 was dissolved in 80 ml of 1 M HCl. The experimental procedure after the hydrolysis of the polyphosphate ions to orthophosphate ions was the same as in the determination of the PO_4^{3-} ion.[5]

Determination of the Orthophosphate Ion. After 0.25—1.5 g of the pulverized glass had been dissolved in 40 ml of a 0.5 M (0.5 mol dm^{-3}) NaOH solution at room temperature, the PO_4^{3-} ion was gravimetrically determined as $Mg_2P_2O_7$ by the method described in a previous paper.[5]

Paper Chromatography. One-dimensional paper chromatography was used for the separation of orthophosphate from other polyphosphates.[6] The solvent was prepared by mixing 25 ml of a 20% trichloroacetic acid solution, 7 ml of water, and 68 ml of acetone. This solvent is a modification of the Solvent A reported by Bernhart and Chess.[7] Pulverized glass containing about 0.1 g of phosphorus was dissolved in 50 ml of a 0.5 M NaOH solution at room temperature. A spot of about 5 μl of this solution was developed on a strip of filter paper of No. 51A (2 cm × 50 cm) for about 3 h at room temperature. After a perchloric acid–molybdate solution had been sprayed on the paper, the paper was exposed to day light until blue spots appeared. The phosphate species on the chromatogram was identified by comparing it with the spots of a reference solution containing known phosphates.

Infrared Spectra. The infrared absorption spectra of the glasses were obtained by means of a Hitachi EPI-2G

Table 1. Composition of Na_2O–Al_2O_3–P_2O_5 glass

Batch composition	Na_2O (wt %)		Al_2O_3 (wt %)		P_2O_5 (wt %)	
	Calcd[a]	Obsd	Calcd[a]	Obsd	Calcd[a]	Obsd
$52.5Na_2O \cdot 5Al_2O_3 \cdot 42.5P_2O_5$	33.22	(33.41)	5.20	5.39	61.58	61.20
$47.5Na_2O \cdot 10Al_2O_3 \cdot 42.5P_2O_5$	29.45	(29.42)	10.20	10.63	60.35	59.95
$42.5Na_2O \cdot 15Al_2O_3 \cdot 42.5P_2O_5$	25.83	(25.70)	15.00	15.78	59.17	58.52
$57.5Na_2O \cdot 5Al_2O_3 \cdot 37.5P_2O_5$	37.92	(38.65)	5.43	5.46	56.65	55.89
$52.5Na_2O \cdot 10Al_2O_3 \cdot 37.5P_2O_5$	33.91	(34.63)	10.62	10.68	55.47	54.69
$47.5Na_2O \cdot 15Al_2O_3 \cdot 37.5P_2O_5$	30.05	(30.59)	15.61	15.63	54.34	53.78
$42.5Na_2O \cdot 20Al_2O_3 \cdot 37.5P_2O_5$	26.35	(26.86)	20.40	20.34	53.25	52.80
$37.5Na_2O \cdot 25Al_2O_3 \cdot 37.5P_2O_5$	22.79	(23.74)	25.00	24.22	52.21	52.04
$52.5Na_2O \cdot 15Al_2O_3 \cdot 32.5P_2O_5$	34.63	(35.03)	16.28	16.23	49.09	48.74
$47.5Na_2O \cdot 20Al_2O_3 \cdot 32.5P_2O_5$	30.68	(31.10)	21.25	21.35	48.07	47.55
$42.5Na_2O \cdot 25Al_2O_3 \cdot 32.5P_2O_5$	26.89	(27.77)	26.02	25.83	47.09	46.40
$37.5Na_2O \cdot 30Al_2O_3 \cdot 32.5P_2O_5$	23.25	(23.79)	30.60	30.16	46.15	46.05

a) Calculated from the batch composition.

Table 2. Composition of K_2O–Al_2O_3–P_2O_5 glass

Batch composition	K_2O (wt %)		Al_2O_3 (wt %)		P_2O_5 (wt %)	
	Calcd[a]	Obsd	Calcd[a]	Obsd	Calcd[a]	Obsd
$50K_2O \cdot 5Al_2O_3 \cdot 45P_2O_5$	40.58	(40.83)	4.39	4.62	55.03	54.55
$45K_2O \cdot 10Al_2O_3 \cdot 45P_2O_5$	36.40	(36.61)	8.75	9.33	54.85	54.06
$40K_2O \cdot 15Al_2O_3 \cdot 45P_2O_5$	32.25	(32.24)	13.09	13.45	54.66	54.31
$35K_2O \cdot 20Al_2O_3 \cdot 45P_2O_5$	28.13	(28.95)	17.39	17.09	54.48	53.96
$55K_2O \cdot 5Al_2O_3 \cdot 40P_2O_5$	45.58	(46.07)	4.48	4.59	49.94	49.34
$50K_2O \cdot 10Al_2O_3 \cdot 40P_2O_5$	41.29	(42.13)	8.94	8.66	49.77	49.21
$45K_2O \cdot 15Al_2O_3 \cdot 40P_2O_5$	37.04	(37.78)	13.36	13.25	49.60	48.97
$40K_2O \cdot 20Al_2O_3 \cdot 40P_2O_5$	32.80	(33.65)	17.76	17.70	49.44	48.65
$35K_2O \cdot 25Al_2O_3 \cdot 40P_2O_5$	28.61	(29.42)	22.12	21.69	49.27	48.89
$30K_2O \cdot 30Al_2O_3 \cdot 40P_2O_5$	24.45	(25.81)	26.45	25.61	49.10	48.58

a) Calculated from the batch composition.

spectrophotometer, using the KBr pellet technique.

Results and Discussion

Composition of Glass. The composition of the glasses determined from the analyses is shown in Tables 1 and 2. The Na_2O or K_2O content given in parentheses is the value obtained by subtracting the Al_2O_3 and P_2O_5 contents from the weight of the sample. Since the phosphate glass usually contains a small amount of water in its structure,[8,9] the Na_2O or K_2O content shown in parentheses is actually the (Na_2O+H_2O) or (K_2O+H_2O) content in the glass. As is shown in Tables 1 and 2, in each series of the glasses with a constant P_2O_5 content, the heating loss of P_2O_5 was less than 0.8 wt %. Therefore, it can be said that the contents of P_2O_5 in these glasses are practically constant.

Papaer Chromatography. The paper chromatography was carried out for each sample of 37.5 mol % of P_2O_5 in the Na_2O–Al_2O_3–P_2O_5 system and of 40 mol % of P_2O_5 in the K_2O–Al_2O_3–P_2O_5 system. As is shown in the chromatograms in Figs. 1 and 2, the amount of the PO_4^{3-} ion increased with an increase in the Al_2O_3 content. When a two-component sample of 62.5 $Na_2O \cdot$ 37.5 P_2O_5 was heated for 1 h at 1350 °C, converted to an aqueous solution, and examined by paper chromatography, the P O $^{4-}$ and $P_3O_{10}^{5-}$ ions were found, while

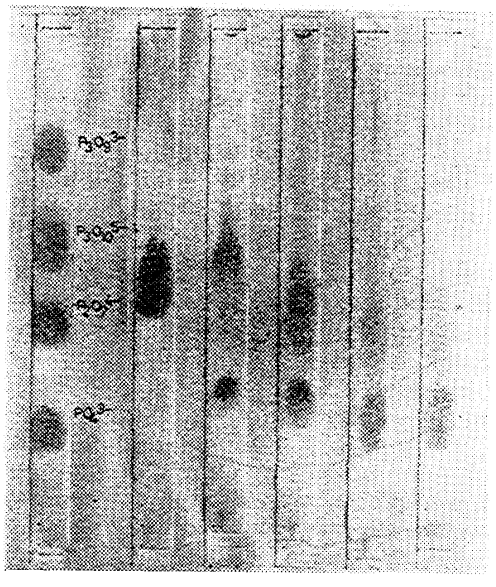

Fig. 1. Paper chromatograms of $(62.5-x)Na_2O \cdot xAl_2O_3 \cdot 37.5P_2O_5$ glass.
(1) Reference sample, (2)$x=5$, (3)$x=10$, (4)$x=15$, (5) $x=20$, (6)$x=25$.

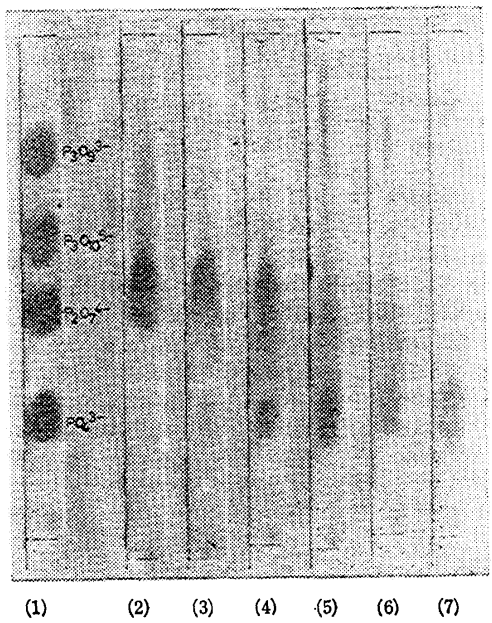

Fig. 2. Paper chromatograms of $(60-x)K_2O \cdot xAl_2O_3 \cdot 40P_2O_5$ glass.
(1) Reference sample, (2)$x=5$, (3)$x=10$, (4)$x=15$, (5) $x=20$, (6)$x=25$, (7)$x=30$.

the PO_4^{3-} ion was not found. Thus, it seems that the above PO_4^{3-} ion was given by the substitution of the P^{5+} ion in P–O–P linkage by the Al^{3+} ion, and the increase in the amount of this PO_4^{3-} ion may be due to the increase in the P–O–Al linkage in the glass. The phosphate species in the glasses with the highest Al_2O_3 content ($x=25$ in Fig. 1 and $x=30$ in Fig. 2) were substantially composed of the PO_4^{3-} ion. It is natural to consider that a large number of the chains in these

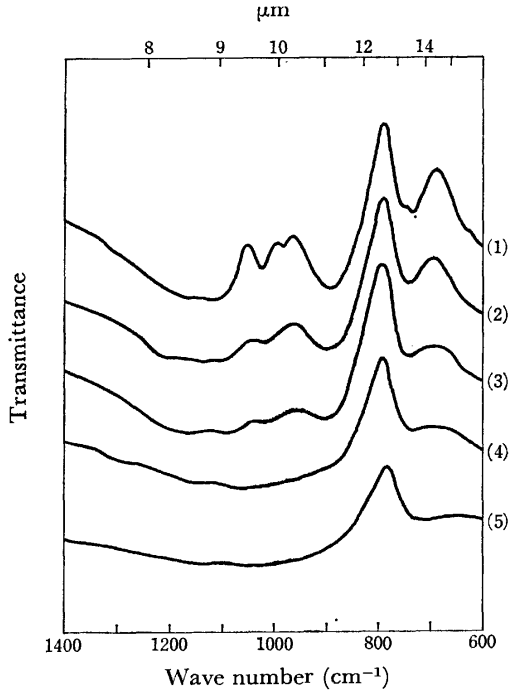

Fig. 3. Infrared spectra of $(62.5-x)Na_2O \cdot xAl_2O_3 \cdot 37.5-P_2O_5$ glass.
(1)$x=5$, (2)$x=10$, (3)$x=15$, (4)$x=20$, (5)$x=25$.

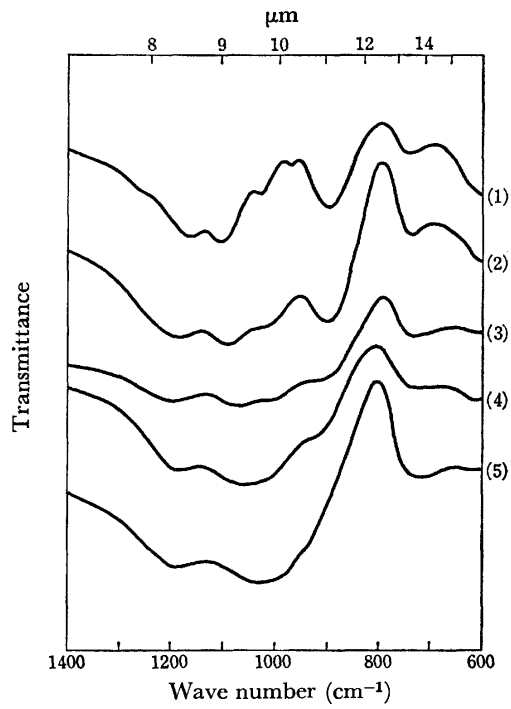

Fig. 4. Infrared spectra of $(60-x)K_2O \cdot xAl_2O_3 \cdot 40P_2O_5$ glass.
(1)$x=10$, (2)$x=15$, (3)$x=20$, (4)$x=25$, (5)$x=30$.

glasses are in the form of an alternate arrangement of the PO_4 tetrahedron and the AlO_4 tetrahedron.

Infrared Spectra. The infrared absorption spectra of the same series of glasses as those examined by paper chromatography are shown in Figs. 3 and 4. Between the glasses with a lower Al_2O_3 content ($x=5$ and 10) and those with a higher Al_2O_3 content ($x=20$, 25, and 30), marked differences are found in the absorption spectra in the range from 1100 to 900 cm^{-1}. With the increase in the Al_2O_3 content, the absorptions in the above-noted range increased and the absorption bands became broad. According to Corbridge and Lowe,[10,11] the absorption band in the range from 1100—900 cm^{-1} is to be assigned to ionic P–O stretching, $-P\langle^{O}_{O}{}^{(2-)}_{O}$ group, P–O–P stretching, and P–O–H bending vibrations; especially, the absorption of the $-P\langle^{O}_{O}{}^{(2-)}_{O}$ group appears at about 1030—960 cm^{-1}. Therefore, the change in the infrared spectra with the increase in the Al_2O_3 content can be considered to be concordant with the results of the paper chromatography. It can also be mentioned that the broad absorption in the glasses with a higher Al_2O_3 content is due to the increase in the disorder derived from the formation of P–O–Al linkage in the glass structure.

Orthophosphate Ion in the Glass. The contents of the PO_4^{3-} ion in all the glasses were determined gravimetrically. In Figs. 5 and 6 these results are given by plotting the change in the PO_4^{3-}/P_2O_5 ratio (the ratio of the amount of PO_4^{3-} ion, expressed as P_2O_5 against the total P_2O_5 content) with the Al_2O_3 content in the glass. In all the series of glasses with a constant P_2O_5

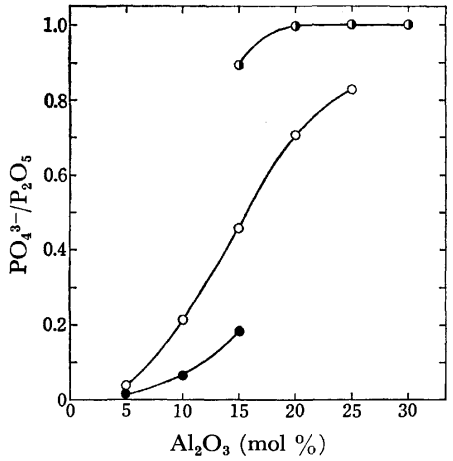

Fig. 5. Relation between PO_4^{3-}/P_2O_5 ratio and Al_2O_3 content in Na_2O–Al_2O_3–P_2O_5 glass.
◑: 32.5 mol % P_2O_5, ○: 37.5 mol % P_2O_5,
●: 42.5 mol % P_2O_5.

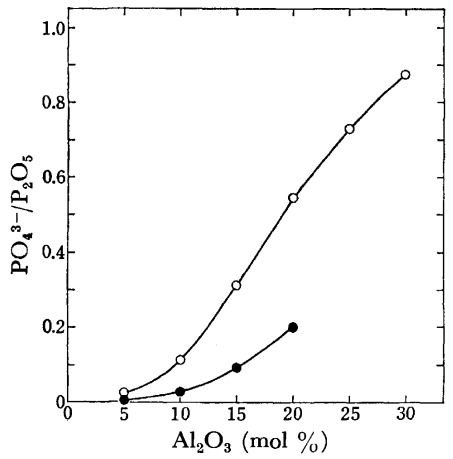

Fig. 6. Relation between PO_4^{3-}/P_2O_5 ratio and Al_2O_3 content in K_2O–Al_2O_3–P_2O_5 glass.
○: 40 mol % P_2O_5, ●: 45 mol % P_2O_5.

content in both the Na_2O–Al_2O_3–P_2O_5 and K_2O–Al_2O_3–P_2O_5 systems, the PO_4^{3-}/P_2O_5 ratio increases with an increase in the Al_2O_3 content, while this ratio decreases with an increase in the P_2O_5 content. In the glass with 32.5 mol % of P_2O_5, the PO_4^{3-}/P_2O_5 ratio rises to unity when the Al_2O_3 content approaches 25 mol % or more, as is shown in Fig. 5.

In Figs. 7 and 8, the PO_4^{3-}/Al^{3+} ratios are plotted *vs.* the Al_2O_3 content. The ratio increases with an increase in the Al_2O_3 content except for the Na_2O–Al_2O_3–P_2O_5 glass with 32.5 mol % of P_2O_5 (Fig. 7), whereas the ratio decreases with an increase in the P_2O_5 content in all the glasses. The PO_4^{3-}/Al^{3+} ratio can be regarded as showing the degree of the substitution of the P^{5+} ion in P–O–P linkage by the Al^{3+} ion. Therefore, the above-mentioned change in this value can be explained as follows. When the PO_4^{3-}/Al^{3+} ratio is smaller than unity, there exist two sorts of Al^{3+} ions, the Al^{3+} ion forming the P–O–Al linkage and the Al^{3+} ion not forming such a linkage. When this ratio is equal to or larger than unity, however, all the Al^{3+} ions are in the form

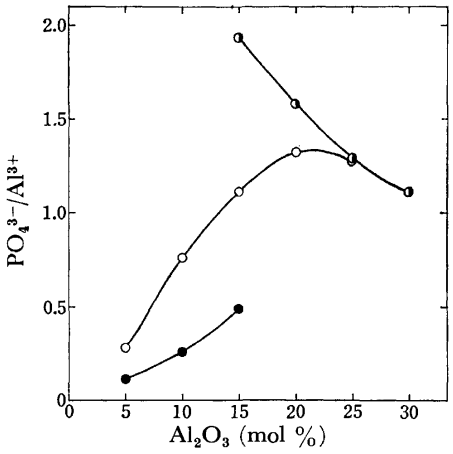

Fig. 7. Relation between PO_4^{3-}/Al^{3+} ratio and Al_2O_3 content in Na_2O–Al_2O_3–P_2O_5 glass.
◑: 32.5 mol % P_2O_5, ○: 37.5 mol % P_2O_5,
●: 42.5 mol % P_2O_5.

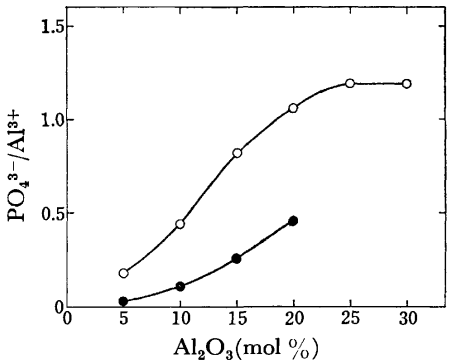

Fig. 8. Relation between PO_4^{3-}/Al^{3+} ratio and Al_2O_3 content in K_2O–Al_2O_3–P_2O_5 glass.
○: 40 mol % P_2O_5, ●: 45 mol % P_2O_5.

of P–O–Al linkage. Since the PO_4^{3-}/Al^{3+} ratios of the glasses with a lower Al_2O_3 content are smaller than 0.5, it can be considered that more than half of the Al^{3+} ions do not form the P–O–Al linkage. In the glass with 32.5 mol % of P_2O_5, when the value of PO_4^{3-}/Al^{3+} is larger than 1.5, it is possible that the "cluster" may be formed by the linkage between more than two PO_4 tetrahedra and one AlO_4 tetrahedron.

From the results of the determination of the PO_4^{3-} ion in the glasses, it can also be presumed that, in metaphosphate (50 mol % of P_2O_5) and ultraphosphate (more than 50 mol % of P_2O_5) compositions, no substitution of the P^{5+} ion by the Al^{3+} ion occurs; hence, the P–O–Al linkage described above is not formed in these compositions of glasses.

The author wishes to thank Associate Professor Makio Kinoshita of Sophia University for his interest and encouragement, and also Mr. Samon Isogai for his assistance in the experimental work.

References

1) N. J. Kreidl and W. A. Weyl, *J. Am. Ceram. Soc.*, **24**, 372 (1941).
2) S. Sakka, *Bull. Inst. Chem. Res., Kyoto Univ.*, **49**, 349

(1971).
3) A. Kishioka, M. Hayashi, and M. Kinoshita, *Bull. Chem. Soc. Jpn.*, **49**, 3032 (1976).
4) E. P. Treadwell and W. T. Hall, "Analytical Chemistry," 9th English ed, Vol. 2 (1951), pp. 150—151.
5) A. Kishioka and M. Kinoshita, *Nippon Kagaku Kaishi*, **1976**, 608.
6) A. Kishioka, M. Hayashi, S. Isogai, and K. Suzuki, Abstr. No. 2G13, 31th National Meeting of the Chemical Society of Japan, Sendai, October 1974.
7) D. N. Bernhart and W. B. Chess, *Anal. Chem.*, **31**, 1026 (1959).
8) H. Namikawa and M. Munakata, *Yogyo Kyokai Shi*, **73**, 86 (1965).
9) A. Naruse, Y. Abe, and H. Inoue, *Yogyo Kyokai Shi*, **76**, 36 (1968).
10) D. E. C. Corbridge and E. J. Lowe, *J. Chem. Soc.*, **1954**, 493.
11) D. E. C. Corbridge and E. J. Lowe, *J. Chem. Soc.*, **1954**, 4555.

Induced Circular Dichroism Spectra of Cobalt(III) Complexes in a Chiral Medium Containing $(+)_{589}$-Diethyl Tartrate

Yutaka TANIGUCHI, Jinsai HIDAKA,* and Yoichi SHIMURA

Department of Chemistry, Faculty of Science, Osaka University, Toyonaka, Osaka 560

(Received January 20, 1977)

The induced circular dichroism (CD) spectra of 21 achiral or racemic cobalt(III) complexes have been measured in a chiral medium containing $(+)_{589}$-diethyl tartrate in the region of the first d-d transition bands. The absolute value of the molar circular dichroism ($\Delta\varepsilon$) observed for these complexes is in the range of about 0.04—0.3 cm^{-1} mol^{-1} dm^3. The induced CD spectra of the racemic complexes show a different pattern from the natural CD spectra of their resolved enantiomers. The observed induced CD spectra have been discussed in relation to the stereochemistry of the complexes.

Circular dichroism (CD) is induced for some achiral or racemic compounds when they are dissolved in a chiral medium. Since Mason and Norman[1] observed this phenomenon, several workers have reported the CD induced for organic[2-6] and inorganic[2,7-10] compounds. The mechanism of this phenomenon has been discussed generally in terms of the following effects; (1) the CD may be induced by a direct interaction between a symmetric chromophore and a chiral field produced by chiral solvents, (2) a symmetric chromophore may be solvated by chiral solvents forming a chiral configuration, and (3) one enantiomer in a racemate may be associated with chiral solvents preferentially. It was initially suggested that the hydrogen bonding was the main origin of the phenomenon,[1-4] but later it was found that such hydrogen bonding was not a prerequisite.[5,6] Thus the precise mechanism of the phenomenon is still unknown.

In the works on cobalt(III) complexes, so far as we know, the induced CD has been observed for only four chromophores: $[Co(NH_3)_6]^{3+}$,[1] $[Co(en)_3]^{3+}$,[9] *trans*-$[CoCl_2(en)_2]^+$,[2] and *trans-meso*-$[CoCl_2(2,3,2\text{-tet})]^+$.[8] In the present paper, it will be shown that twenty-one achiral or racemic cobalt(III) complexes also exhibit the induced CD in the region of their first d-d transition bands when the complexes are dissolved in a chiral medium containing $(+)_{589}$-diethyl tartrate, and that the spectral feature of those induced CD is dependent on the properties of ligands.

Experimental

Materials. $(+)_{589}$-Diethyl tartrate was prepared by the method of Sugasawa[11] and distilled *in vacuo*, bp 123.5—124.5 °C at 2 Torr, $[\alpha]_D$ +7.71 ° (neat). Found: C, 46.57; H, 6.82%. Calcd for $C_8H_{14}O_6$: C, 46.60; H, 6.84%.

All the cobalt(III) complexes were prepared by well-known methods and identified spectrophotometrically. Many of the complexes were converted into their tetraphenylborate salts by adding the equivalent amount of sodium tetraphenylborate in water to an aqueous solution of the complex ion. Found: C, 70.58; H, 7.32; N, 6.91%. Calcd for $[Co(NH_3)_6](BPh_4)_3\cdot 6H_2O$: C, 70.48; H, 7.39; N, 6.85%. Found: C, 71.87; H, 7.34; N, 7.01%. Calcd for $[Co(NH_3)_4(en)](BPh_4)_3\cdot 5H_2O$: C, 72.03; H, 7.35; N, 6.81%. Found: C, 74.55; H, 7.30; N, 6.51%. Calcd for *cis*-$[Co(NH_3)_2(en)_2](BPh_4)_3\cdot 4H_2O$: C, 73.44; H, 7.30; N, 6.76%. Found: C, 73.52; H, 7.33; N, 6.83%. Calcd for *trans*-$[Co(NH_3)_2(en)_2](BPh_4)_3\cdot 4H_2O$: C, 73.44; H, 7.30; N, 6.76%. Found: C, 71.84; H, 7.34; N, 6.44%. Calcd for $[Co(en)_3](BPh_4)_3\cdot 6H_2O$: C, 71.79; H, 7.42; N, 6.44%. Found: C, 67.01; H, 6.86; N, 9.68%. Calcd for $[Co(NO_2)(NH_3)_5](BPh_4)_2\cdot 2H_2O$: C, 66.68; H, 6.88; N, 9.72%. Found: C, 49.49; H, 6.38; N, 14.33%. Calcd for *cis*-$[Co(NO_2)_2(NH_3)_4](BPh_4)\cdot 2H_2O$: C, 50.19; H, 6.32; N, 14.63%. Found: C, 50.49; H, 6.23; N, 14.76%. Calcd for *trans*-$[Co(NO_2)_2(NH_3)_4](BPh_4)\cdot 2H_2O$: C, 50.19; H, 6.32; N, 14.63%. Found: C, 67.03; H, 6.89; N, 8.16%. Calcd for $[CoF(NH_3)_5[(BPh_4)_2\cdot 2H_2O$: C, 68.83; H, 7.10; N, 8.36%. Found: C, 67.45; H, 6.96; N, 8.17%. Calcd for $[CoCl(NH_3)_5](BPh_4)_2\cdot 2H_2O$: C, 67.50; H, 6.96; N, 8.20%. Found: C, 65.88; H, 6.59; N, 8.05%. Calcd for $[CoBr(NH_3)_5](BPh_4)_2\cdot H_2O$: C, 65.48; H, 6.53; N, 7.95%. Found: C, 55.57; H, 6.22; N, 10.76%. Calcd for *trans*-$[CoCl_2(NH_3)_4](BPh_4)$: C, 55.73; H, 6.24; N, 10.83%. Found: C, 57.38; H, 6.36; N, 10.30%. Calcd for *trans*-$[CoCl_2(NH_3)_2(en)](BPh_4)$: C, 57.49; H, 6.31; N, 10.31%. Found: C, 58.83; H, 6.39; N, 9.78%. Calcd for *trans*-$[CoCl_2(en)_2](BPh_4)$: C, 59.07; H, 6.37; N, 9.84%. Found: C, 67.90; H, 6.98; N, 7.70%. Calcd for $[Co(CH_3COO)(NH_3)_5](BPh_4)_2\cdot 2.5H_2O$: C, 67.73; H, 7.16; N, 7.90%. Found: C, 59.86; H, 6.86; N, 9.48%. Calcd for *cis*-$[Co(CH_3COO)_2(NH_3)_4](BPh_4)\cdot 0.5H_2O$: C, 58.65; H, 6.86; N, 9.77%. Found: C, 59.81; H, 6.87; N, 9.88%. Calcd for *trans*-$[Co(CH_3COO)_2(NH_3)_4](BPh_4)$: C, 59.59; H, 6.79; N, 9.93%. Found: C, 17.57; H, 7.61; N, 20.47%. Calcd for $[Co(en)_3]Cl_3\cdot 3.5H_2O$: C, 17.64; H, 7.65; N, 20.57%. Found: C, 9.32; H, 5.01; N, 22.01%. Calcd for $[Co(ox)(NH_3)_4]Cl\cdot 0.5H_2O$: C, 9.26; H, 5.05; N, 21.59%. Found: C, 22.42; H, 5.67; N, 17.32%. Calcd for $[Co(ox)(en)_2]Cl\cdot H_2O$: C, 22.48; H, 5.66; N, 17.47%. Found: C, 21.33; H, 2.89; N, 8.25%. Calcd for $Na[Co(ox)_2(en)]\cdot H_2O$: C, 21.44; H, 3.00; N, 8.33%. Found: C, 25.90; H, 3.71; N, 7.15%. Calcd for $K[Co(mal)_2(en)]\cdot H_2O$: C, 25.27; H, 3.71; N, 7.37%.

Measurements. The electronic absorption spectra were measured by a Shimadzu spectrophotometer UV-200. The CD spectra were recorded with a Jasco Model J-20 spectropolarimeter with the CD attachment. All measurements were made at room temperature in chiral media in a constant concentration of the complex ion, 0.002 mol dm^{-3}. The chiral media were prepared by mixing $(+)_{589}$-diethyl tartrate (17 cm^3) with water (3 cm^3) for the oxalato and malonato complexes, and with acetone (3 cm^3) for the other complex tetraphenylborates. The concentration of $(+)_{589}$-diethyl tartrate in the chiral media was approximately 4.96 mol dm^{-3}. The CD measurements were confined in the region of the first d-d transition band, because the chiral media showed very strong absorption in the ultraviolet region.

* Present address: Department of Chemistry, The University of Tsukuba, Ibaraki 300-31.

Results and Discussion

Each of the complexes reported here has an identical electronic absorption spectrum of the first d-d transition band in the chiral media containing diethyl tartrate and in the aqueous solution. This shows that the inner coordination sphere remains unchanged in the chiral media. For the induced CD intensity of the $[Co(NH_3)_6]^{3+}$ complex dissolved in a mixture of acetone and $(+)_{589}$-diethyl tartrate (4.96 mol dm^{-3}), Beer's law holds good over the concentration range $0—7\times10^{-3}$ mol dm^{-3} of the complex. For the same chromophore, the induced CD intensity increases with an increase in the concentration of $(+)_{589}$-diethyl tartrate, steeply in the range of 0—0.1 in its mole fraction, and reaches to a saturation at the mole fraction *ca.* 0.3. The saturated intensity is dependent on the solvent mixed with $(+)_{589}$-diethyl tartrate; the increasing order of intensity is water<methanol<acetone. This suggests that the association of the complex ion with diethyl tartrate by hydrogen bonding has an important contribution to the induced CD.

Ammine–Ethylenediamine Mixed Complexes (Fig. 1). These $[Co(N)_6]^{3+}$ type complexes show a single negative CD band at or near the position of their first absorption band with an exception of *trans*-diammine complex, which has a small positive CD band at the lower energy side of the dominant negative one. The absolute CD intensity decreases in the following order: $[Co(NH_3)_6]^{3+} > [Co(NH_3)_4(en)]^{3+} > [Co(en)_3]^{3+} > cis$-$[Co(NH_3)_2(en)_2]^{3+} > trans$-$[Co(NH_3)_2(en)_2]^{3+}$. The sequence shows that the ammonia ligand is more effective to the induction of CD than ethylenediamine. This is consistent with the fact that the former ligand has more N–H groups available for hydrogen bonding than the latter. Moreover the N–H groups of the ethylenediamine ligand cannot interact so freely with the chiral solvent molecules as those of ammonia. The tris(ethylenediamine) complex gives somewhat larger induced CD than the diamminebis(ethylenediamine) complexes, and both the racemic tris- and *cis*-bis(ethylenediamine) complexes have a different type of CD pattern from the natural CD of their resolved enantiomers. Such racemic complexes cannot be discussed equally with the achiral complexes. Since the chiral solvent molecules interact with a chiral complex ion in a different way from its enantiomer, the observed induced CD of a racemate comes from the overall effect, and differs from the individual induced CD of the enantiomers. The *trans*-bis(ethylenediamine) complex shows an induced CD pattern analogous to the natural CD of the *trans*-$[Co(NH_3)_2(S\text{-pn})_2\delta\delta]^{3+}$ complex which also has a small positive band at the lower energy side of a dominant negative band.[12] Thus the positive band of the bis(ethylenediamine) complex may be attributed to the ethylenediamine chelate rings which take preferentially the δ-conformation on the interaction with the chiral slovent.

Ammine–Nitro Mixed Complexes (Fig. 2). These

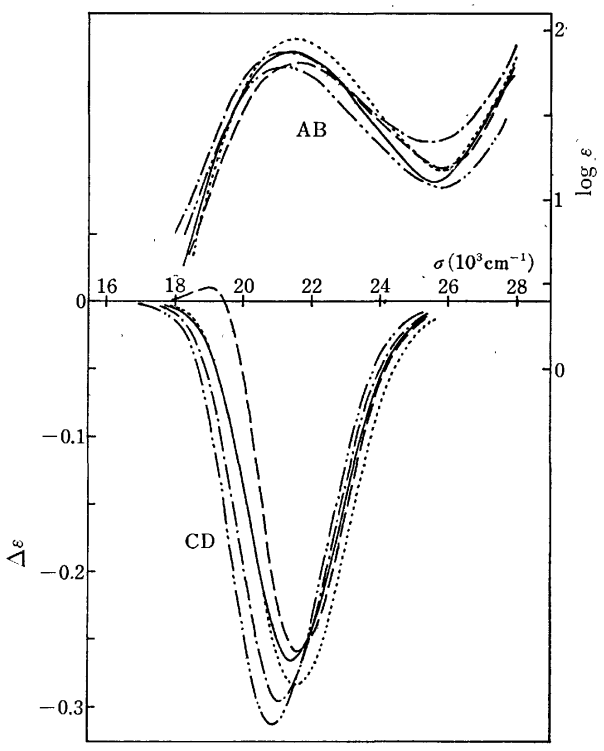

Fig. 1. Absorption (AB) and induced CD spectra of ammine–ethylenediamine mixed complexes in a chiral medium $(+)_{589}$-diethyl tartrate–acetone. $[Co(NH_3)_6]^{3+}$ (–···–), $[Co(NH_3)_4(en)]^{3+}$ (– · –), *rac-cis*-$[Co(NH_3)_2(en)_2]^{3+}$ (——), *trans*-$[Co(NH_3)_2(en)_2]^{3+}$ (– – – –), *rac*-$[Co(en)_3]^{3+}$ (·····).

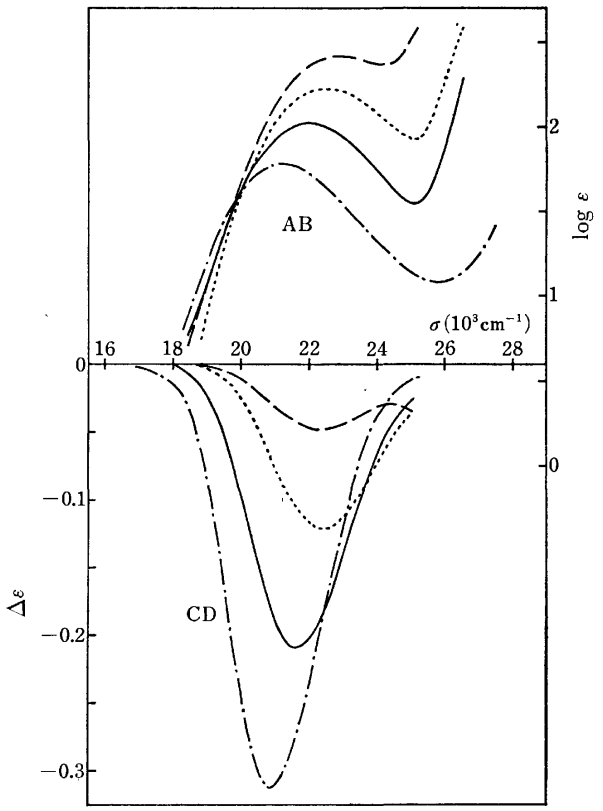

Fig. 2. Absorption (AB) and induced CD spectra of ammine–nitro mixed complexes in a chiral medium $(+)_{589}$-diethyl tartrate–acetone. $[Co(NH_3)_6]^{3+}$ (– · –), $[Co(NO_2)(NH_3)_5]^{2+}$ (——), *cis*-$[Co(NO_2)_2(NH_3)_4]^{+}$ (·····), *trans*-$[Co(NO_2)_2(NH_3)_4]^{+}$ (– – – –).

complexes also show a single negative CD band. The position of the CD peak shifts regularly to the higher energy side by replacing ammine ligands with nitro ones, as in the case of the absorption peak. The CD intensity decreased stepwise with the same replacement, in contrast to absorption. In the dinitro complexes, there is a marked difference between the geometrical isomers, that is, the induced CD of the *trans* isomer is about a half of that of the *cis* isomer.

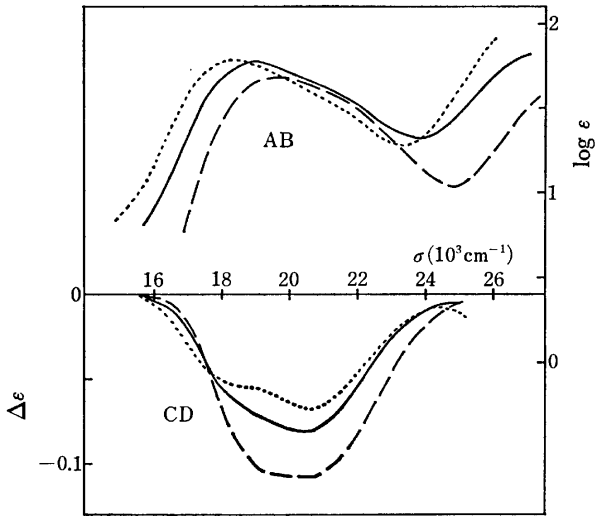

Fig. 3. Absorption (AB) and induced CD spectra of three pentaamminehalogeno complexes in a chiral medium $(+)_{589}$-diethyl tartrate–acetone. $[CoF(NH_3)_5]^{2+}$ (——), $[CoCl(NH_3)_5]^{2+}$ (——), $[CoBr(NH_3)_5]^{2+}$(·····).

Pentaamminehalogeno Complexes (Fig. 3). The first absorption band of these complexes splits clearly into the A_2 and E components of C_{4v} symmetry. The induced CD spectra also show splitting into the two components with a negative sign. The A_2 non-degenerate component is dominant contrary to the absorption spectrum, and as expected from Yamatera's rule,[13] the A_2 component with higher energy remains at about the same position as that of the T_{1g} transition of the $[Co(NH_3)_6]^{3+}$ chromophore, irrespective of the kinds of halogens. On the other hand, the E component, which appears as a shoulder at the lower energy side of the dominant A_2 component, shifts according to the spectrochemical series of halogens. As for the CD intensity, the smaller the atomic number of halogens, the stronger the CD intensity. It is evident that the halogeno ligands have an important contribution to the induced CD.

trans-*Tetraamminedichloro Type Complexes (Fig. 4).* The induced CD of the *trans*-$[CoCl_2(N)_4]^+$ chromophores also shows a marked splitting for the first absorption band region. If we adopt the representation of D_{4h} symmetry for these complexes, their CD peaks correspond to the A_{2g} (higher energy) and E_g (lower energy) components. The induced CD of the E_g component increases proportionally with the number of ethylenediamine rings, but that of the A_{2g} component shows a tendency to decrease. The induced CD of the tetraamminedichloro complex does not contain any contribution from the chiral ring conformation, whereas the induced CD of the other two complexes having one or

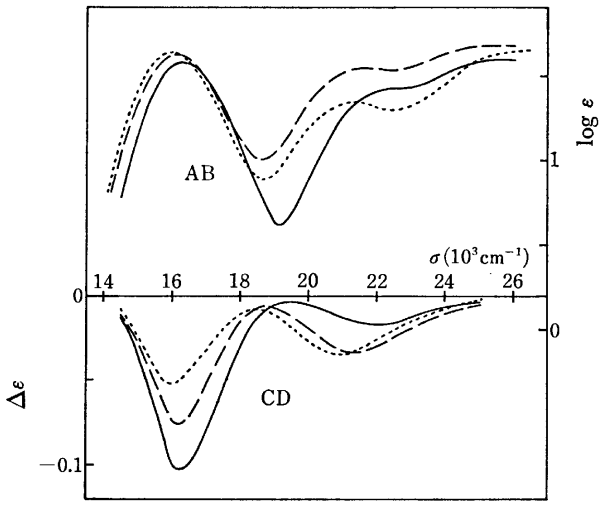

Fig. 4. Absorption (AB) and induced CD spectra of *trans*-tetraamminedichloro type complexes in a chiral medium $(+)_{589}$-diethyl tartrate–acetone. *trans*-$[CoCl_2(NH_3)_4]^+$ (·····), *trans*-$[CoCl_2(NH_3)_2(en)]^+$(——), *trans*-$[CoCl_2(en)_2]^+$ (——).

two puckered ethylenediamine rings would contain some contribution from the chelate ring conformation. The conformational contribution in these two complexes would be approximated by the CD difference from the tetraamminedichloro complex. On the E_g component, it is really found that the ratio of the differences is about 1:2 for the mono(ethylenediamine) to the bis(ethylenediamine) complex. Hawkins and his coworkers[14] reported that the natural CD spectra of the analogous chromophore having one or two (*R*)-propylenediamine chelate rings of λ-conformation instead of ethylenediamine rings showed a positive sign for the E_g component, and that the rotational strength of the bis(propylenediamine) complex was approximately twice that of the mono(propylenediamine) complex. From the analogy with this, it is suggested that the ethylenediamine chelate rings of the present complexes are partially fixed to a preferable δ-conformation because of the interaction with the chiral solvent. In the A_{2g} region, the propylenediamine complexes gave a negative natural CD band, whose sign is opposite to the induced CD of the present ethylenediamine complexes. This result, however, is not in conflict with the above discussion, because Bosnich and Harrowfield[15] showed that the natural CD displayed in such a region for several *trans*-$[CoCl_2(N)_4]^+$ chromophores is markedly dependent on solvents.

Acetato–Ammine Mixed Complexes (Fig. 5). Three complexes in this group show induced CD spectra quite different from each other. The monoacetato complex exhibits a single negative CD band in its A_2 region, *i.e.* in the region of T_{1g} band of the $[Co(N)_6]^{3+}$ chromophore. The *trans* diacetato complex shows a positive and a negative CD band of comparable intensities which correspond to the E_g (lower energy) and A_{2g} (higher energy) components, respectively. The *cis* diacetato complex shows a dominant positive and a small negative CD band in the order of increasing energy; the former corresponds to the B_1 component and the latter to the

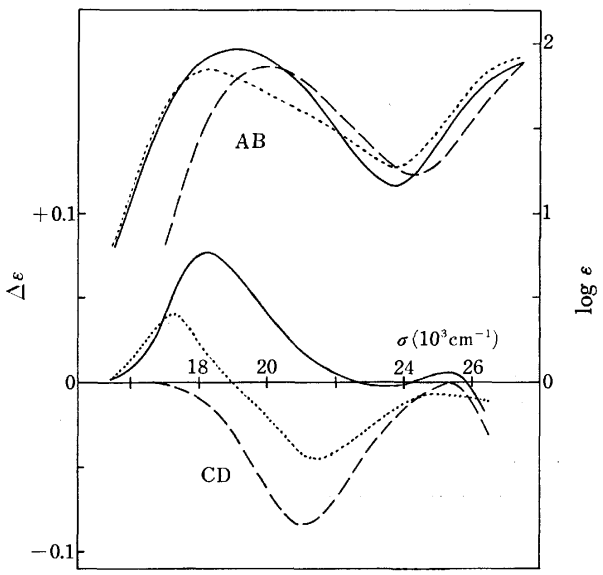

Fig. 5. Absorption (AB) and induced CD spectra of acetato–ammine mixed complexes in a chiral medium $(+)_{589}$-diethyl tartrate–acetone. $[Co(CH_3COO)(NH_3)_5]^{2+}$ (----), *cis*-$[Co(CH_3COO)_2(NH_3)_4]^+$ (——), *trans*-$[Co(CH_3COO)_2(NH_3)_4]^+$ (·····).

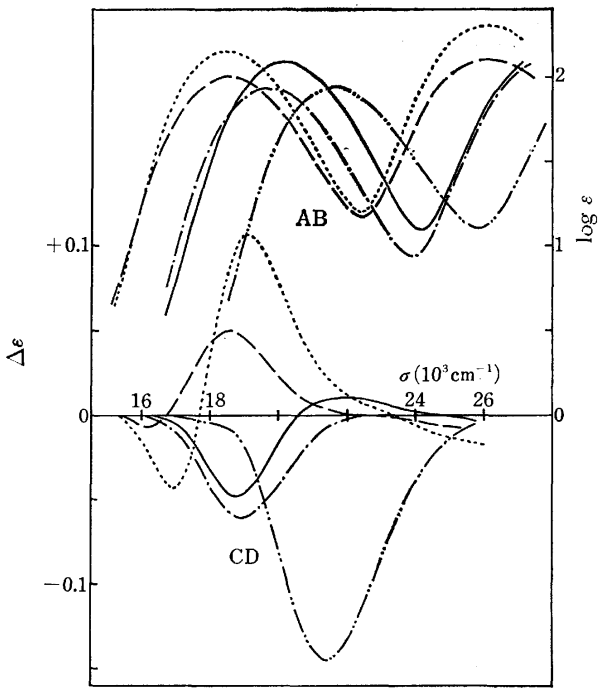

Fig. 6. Absorption (AB) and induced CD spectra of oxalato and malonato complexes in a chiral medium $(+)_{589}$-diethyl tartrate–water. *rac*-$[Co(en)_3]^{3+}$ (-·-·-), $[Co(ox)(NH_3)_4]^+$ (- · -), *rac*-$[Co(ox)(en)_2]^+$ (——), *rac*-$[Co(ox)_2(en)]^-$ (·····), *rac*-$[Co(mal)_2(en)]^-$ (----).

A_2+B_2 component. The monoacetato complex has the induced CD intensity of the same order as the natural CD intensity of the (α-amino carboxylato)-pentaamminecobalt(III) complexes,[16] which also belong to the chromophore $[Co(O)(N)_5]^{2+}$, its natural CD being contributed by the so-called vicinal effect of the coordinated chiral amino carboxylate ligand. In this respect, the induced CD of these three acetato–ammine complexes may be recognized as a kind of vicinal effect of the chiral solvent molecules.

Oxalato and Malonato Complexes (Fig. 6). Figure 6 shows the absorption and induced CD spectra of these four complexes measured in a chiral medium $(+)_{589}$-diethyl tartrate–water. The induced CD spectra of the $[Co(en)_3]^{3+}$ and $[Co(ox)(en)_2]^+$ complexes in this medium showed essentially the same pattern as in the $(+)_{589}$-diethyl tartrate–acetone medium, except that the intensity in the aqueous medium is reduced to about one-half of that in the acetone medium.

The $[Co(ox)(en)_2]^+$ complex has a dominant negative and a small positive induced CD band in the order of increasing energy. The $[Co(ox)(NH_3)_4]^+$ complex gives a single negative band at the position of the dominant band of the bis(ethylenediamine) complex. The tetraammine complex has a slightly more intense induced CD than the ethylenediamine complex. The $[Co(ox)_2(en)]^-$ and $[Co(mal)_2(en)]^-$ complexes of the *cis*-$[Co(O)_4(N)_2]^-$ chromophore also show a negative and a positive induced CD band in the order of increasing energy. The band at the higher energy side is dominant in contrast to the above *cis*-$[Co(O)_2(N)_4]^+$ chromophore; thus it is common to both kinds of chromophores that the dominant band appears in the region of the non-degenerate component. Although the induced CD patterns are alike in the oxalato and malonato complex anions, the intensity for the latter complex is about one-half of that for the former. As has been noted in one of the preceding sections, the induced CD spectra of the racemic complexes of this group have quite a different pattern from the natural CD spectra of their enantiomers.[17,18]

References

1) S. F. Mason and B. J. Norman, *Chem. Commun.*, **1965**, 335.
2) B. Bosnich, *J. Am. Chem. Soc.*, **89**, 6143 (1967).
3) K. Noack, *Helv. Chim. Acta*, **52**, 2501 (1969).
4) J. Bolard, *J. Chem. Phys.*, **66**, 389 (1969).
5) E. Axelrod, G. Barth, and E. Bunnenberg, *Tetrahedron Lett.*, **1969**, 5031.
6) L. D. Hayward and R. N. Totty, *Can. J. Chem.*, **49**, 624 (1971).
7) B. Bosnich, *J. Am. Chem. Soc.*, **88**, 2606 (1966).
8) B. Bosnich and J. MacB. Harrowfield, *J. Am. Chem. Soc.*, **93**, 4086 (1971).
9) B. Nordén, *Acta Chem. Scand.*, **26**, 111 (1972).
10) I. Jonáš and B. Nordén, *Acta Chem. Scand.*, **A28**, 289 (1974).
11) S. Sugasawa, *J. Pharm. Soc. Jpn.*, **1927**, 1050.
12) S. F. Mason, "Fundamental Aspects and Recent Developments in Optical Rotatory Dispersion and Circular Dichroism," ed by F. Ciardelli and P. Salvadori, Heyden & Son (1973), p. 213.
13) H. Yamatera, *Bull. Chem. Soc. Jpn.*, **31**, 95 (1958).
14) C. J. Hawkins, E. Larsen, and I. Olsen, *Acta Chem. Scand.*, **19**, 1915 (1965).
15) B. Bosnich and J. MacB. Harrowfield, *J. Am. Chem. Soc.*, **94**, 3425 (1972).
16) C. J. Hawkins and P. J. Lawson, *Inorg. Chem.*, **9**, 6 (1970).
17) A. J. McCaffery, S. F. Mason, and B. J. Norman, *J. Chem. Soc.*, **1965**, 5094.
18) B. E. Douglas, R. A. Haines, and J. G. Brushmiller, *Inorg. Chem.*, **2**, 1194 (1963).

Evaluation of PAC, TAC, 2-IAC as Metallochromic Indicators in the EDTA Titrations of Nickel

Hiroko WADA, Osamu NAKAZAWA, and Hajime TAKADA

Laboratory of Analytical Chemistry, Nagoya Institute of Technology, Gokiso-cho, Showa-ku, Nagoya 466

(Received March 29, 1977)

The rates of color change of 2-(2-pyridylazo)-4-methylphenol (PAC), 2-(2-thiazolylazo)-4-methylphenol (TAC) and 2-(2-imidazolylazo)-4-methylphenol (2-IAC) during EDTA–nickel titration have been determined. The rate is a thousand times greater for TAC and 2-IAC than for PAC. From equilibrium considerations, the rate of color change and the color contrast change, an evaluation of PAC, TAC, and 2-IAC as metallochromic indicators for nickel is given. The optimum pH ranges with TAC and 2-IAC are from 6 to 7 and from 5 to 7, respectively, at 80 °C. With PAC, the titration should be conducted with boiling at pH 4—5. 2-IAC is the best indicator due to the good visual color contrast and the wide pH range over which it is applicable.

In EDTA titrations, the sharpness of the color change of metallochromic indicators is governed by the reaction rate for substitution of the metal-indicator chelate with EDTA, as well as the equilibrium conditions involved. Usually, the reaction rate for substitution of nickel-indicator chelates with EDTA being slow, the rate of indicator color change is important. The PAC[2-(2-pyridylazo)-4-methylphenol],[1] TAC[2-(2-thiazolylazo)-4-methylphenol],[2] and 2-IAC[2-(2-imidazolylazo)-4-methylphenol][3] synthesized previously can be used as indicators for nickel–EDTA titrations. In a previous paper,[4] the reaction rate for substitution of nickel–TAC chelates with EDTA was determined and the mechanism of the color change was proposed. Since PAC, TAC, and 2-IAC have different heterocyclic rings, differences in the rate of color change is expected.

In the present paper, the substitution reaction rate for PAC and 2-IAC are presented and PAC, TAC, and 2-IAC are evaluated as metallochromic indicators for nickel–EDTA titration.

Experimental

Reagents. PAC, TAC, and 2-IAC, which had been previously synthesized and purified, were dissolved in dioxane and 10^{-3} M solutions were prepared.

A nickel(II) solution was prepared from reagent grade nickel nitrate and standardized with dimethylglyoxime by gravimetry.

EDTA·2Na was recrystallized from water and standardized against zinc metal(99.99% pure).

An MES[2-morpholino-1-ethanesulfonic acid]–potassium hydroxide solution was used as a buffer.

All other reagents used were of reagent grade.

Apparatus. A Union Giken RA-401 Stopped-Flow Spectrophotometer, a Union Giken SM-401 High-Sensitivity Spectrophotometer, and a Radiometer PHM 26c pH meter were used.

All experiments were carried out in 20% dioxane solutions at μ=0.1 (KNO_3) and at 25±1 °C.

Results

The Reaction for Substitution of Ni–PAC or Ni–2-IAC with EDTA. In the presence of a large excess of PAC or 2-IAC, nickel forms a 1 : 2 chelate (NiL_2) over the pH range from 5 to 7, as well as in the case of TAC. When EDTA is added to the nickel chelate solution in highly excessive amounts, the following substitution reaction proceeds to completion:

$$NiL_2 + edta' \longrightarrow Ni(edta)^{2-} + 2L', \quad (1)$$

where L is an anion of the PAC or 2-IAC. The rate law can be expressed as

$$-\frac{d[NiL_2]}{dt} = k_{0(L,EDTA,H)}[NiL_2], \quad (2)$$

where $k_{0(L,EDTA,H)}$ is the conditional rate constant involving the indicator, EDTA, and hydrogen ion concentrations. By representing the absorbances at reaction times 0, t, and ∞ by A_0, A_t, and A_∞, we obtain

$$\log (A_t - A_\infty) = -\frac{k_{0(L,EDTA,H)}}{2.303}t + \log (A_0 - A_\infty). \quad (3)$$

A solution containing nickel, an indicator and a buffer was vigorously mixed with a solution containing

Table 1. First-order rate constants $k_{0(L,EDTA,H)}$ for PAC under various conditions

C_{Ni}=1.86×10^{-5} M, 25 °C, μ=0.1, dioxane 20%v/v.

C_{EDTA} (×10^{-3} M)	C_{PAC} (×10^{-4} M)	pH	$k_{0(L,EDTA,H)}$ (×10^{-3} s^{-1})
7.00	1.00	5.56	1.61
		5.65	1.52
		5.75	1.20
		6.02	0.833
	1.13	5.55	1.42
	1.25	5.55	1.22
		5.75	1.05
	1.50	5.52	1.12
	2.00	5.37	0.993
		5.43	0.917
		5.46	0.907
		5.50	0.889
		5.57	0.872
		5.74	0.604
		5.92	0.600
	3.00	5.74	0.412
	4.00	5.52	0.417
		5.75	0.333
	5.00	5.52	0.333
9.05	1.00	5.49	2.19
	2.00	5.47	1.27
13.00	2.00	5.41	1.76

TABLE 2. FIRST-ORDER RATE CONSTANTS $k_{0(L,EDTA,H)}$ FOR 2-IAC UNDER VARIOUS CONDITIONS
$C_{Ni}=5.00\times10^{-6}$ M, 25 °C, $\mu=0.1$, dioxane 20%v/v.

C_{EDTA} ($\times10^{-4}$ M)	$C_{2\text{-IAC}}$ ($\times10^{-4}$ M)	pH	$k_{0(L,EDTA,H)}$ ($\times10^{-2}$ s^{-1})
2.00	1.00	5.82	6.25
		5.90	5.53
		5.95	5.30
		6.05	4.60
		6.10	4.55
		6.25	3.98
		6.33	3.45
	1.20	5.95	4.37
		6.33	2.95
	1.40	5.89	4.48
		5.95	3.78
		6.33	2.54
3.00	1.00	5.95	7.65
		6.22	5.59
		6.34	5.07
4.00	1.00	5.95	10.3
		6.22	7.25
		6.34	6.95

EDTA and a buffer, and the absorbance at 570 nm for PAC or at 555 nm for 2-IAC was recorded as a function of the reaction time. From plots of $\log(A_t-A_\infty)$ *vs.* the reaction time (t), Reaction 1 was recognized to be of pseudo first-order with respect to NiL_2 in both cases. The conditional rate constants, $k_{0(L,EDTA,H)}$, obtained are shown in Tables 1 and 2.

These results indicate that the values of $k_{0(L,EDTA,H)}$ are proportional to the EDTA concentration and to the reciprocal of the indicator concentration in both cases, as for the case of TAC. Plots of $k_{0(H)}$ *vs.* $[H^+]$ give straight lines (Fig. 1).

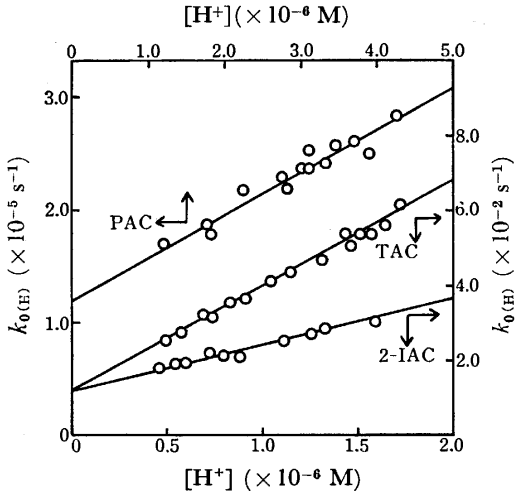

Fig. 1. Plots of $k_{0(H)}$ *vs.* $[H^+]$.

Therefore, the rate law can be expressed as

$$-\frac{d[NiL_2]}{dt}=k_{0(H)}\frac{[NiL_2][edta']}{[HL]}=(k_1'[H^+]+k_2')\frac{[NiL_2][edta']}{[HL]}, \quad (4)$$

where [edta'] is the total concentration of the EDTA not combined with nickel ions. The reaction mechanism is the same as that in the case of TAC:

$$\begin{cases} NiL_2 + H^+ \rightleftharpoons NiL^+ + HL, & (5) \\ NiL^+ + edta' \xrightarrow{k_1} Ni(edta)^{2-} + HL, & (6) \end{cases}$$

$$\begin{cases} NiL_2 + H_2O \rightleftharpoons NiL(OH) + HL, & (7) \\ NiL(OH) + edta' \xrightarrow{k_2} Ni(edta)^{2-} + HL + OH^-. & (8) \end{cases}$$

Reactions 5 and 7 precede Reactions 6 and 8, and the reactions of NiL^+ and NiL(OH) with EDTA are the rate-determining steps. Equation 4 can be rewritten as

$$-\frac{d[NiL_2]}{dt}=k_1[NiL^+][edta']+k_2[NiL(OH)][edta'], \quad (9)$$

where $k_1=k_1'K^L_{NiL_2}/K^H_{HL}$ and $k_2=k_2'K^L_{NiL_2}/K^H_{HL}K^{OH}_{NiL(OH)}K_W$. The values of k_1' and k_2' are obtained from the slopes and y-intercepts, respectively, of the straight lines in Fig. 1. For PAC and 2-IAC, the values of $K^{OH}_{NiL(OH)}$ could not be estimated. The rate constants are summarized in Table 3.

TABLE 3. RATE CONSTANTS
25 °C, $\mu=0.1$, dioxane 20%v/v.

	PAC	TAC	2-IAC
k_1'(M^{-1} s^{-1})	3.7	2.7×10^4	1.3×10^4
k_1(M^{-1} s^{-1})	6.9×10	2.1×10^3	3.9×10^3
k_2'(s^{-1})	1.2×10^{-5}	1.3×10^{-2}	1.2×10^{-2}
k_2(M^{-1} s^{-1})	—	7.9×10^6	—

Discussion

As shown in Table 4, the basicities of donor atoms of TAC are less than those of PAC, and the rate constants for TAC are smaller than those for PAC. In the substitution reactions of copper(II)–PAC and TAC chelates with EDTA, the same results were observed.[5] On the other hand, although the basicity of 2-IAC is larger than that of PAC, the rate constants for 2-IAC are much greater than those for PAC and are almost equal to those for TAC. This is in good agreement with the correlation between the reagent basicities and the nickel chelates stabilities, *i.e.*, in spite of the larger 2-IAC basicity, the formation constants for nickel chelates are smaller than those for nickel–PAC chelates. The coordination bond of the nitrogen atom in the imidazole ring of 2-IAC should be weaker than that in the pyridine ring of PAC. The characteristics of the nitrogen in the imidazole ring may be somewhat different from those of the nitrogen in the pyridine ring due to the resonance between pyridine-like and pyrrole-like nitrogens.

TABLE 4. EQUILIBRIUM CONSTANTS
25 °C, $\mu=0.1$, dioxane 20%v/v.

	PAC	TAC	2-IAC
pk_1	2.22	<0.5	3.68
pk_2	9.58	8.34	9.22
log K_{NiL}	11.18	8.00	8.95
log K_{NiL_2}	10.85	7.24	8.70

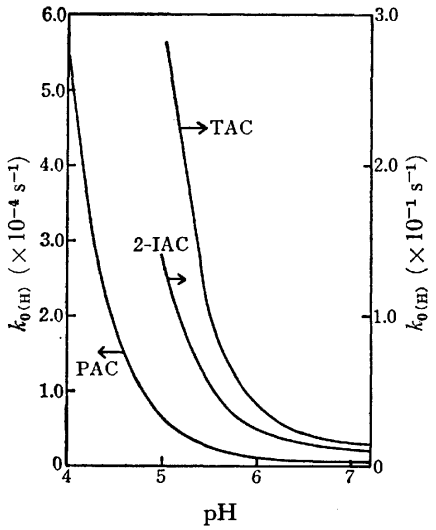

Fig. 2. Dependence of the rate of color change on pH.

TABLE 5. AMOUNTS OF NICKEL TITRATION IN AN ACETATE BUFFER AT 80 °C

pH	Ni taken (mg)	Ni found (mg)		
		PAC	TAC	2-IAC
4	5.78	5.88		
	11.55	11.61		11.44
4.5	5.78	5.89	5.50	5.77
5	5.78	6.21	5.64	5.78
	11.55	11.70	11.31	11.54
5.5	2.89		2.87	2.88
	5.78		5.75	5.78
	11.55		11.48	11.56
6	5.78		5.78	5.78
	11.55		11.56	11.56
6.5	2.89		2.90	2.90
	5.78		5.78	5.78
	11.55		11.57	11.56
7	5.78		5.78	5.83

The rate constants, $k_{0(H)}$, are plotted against the pH in Fig. 2. In the titration of nickel, the rate of indicator color change decreases with increasing pH, so that titration at lower pH results in a higher rate of indicator color change. However, the equilibrium conditions and the color contrast between the free indicator and the nickel chelate restrict the pH range for titration to pH 6—8 (PAC), pH 6—7 (TAC), and pH 6—8 (2-IAC). Within these pH ranges, free PAC, TAC, and 2-IAC are yellow and the nickel chelates are red-violet for PAC and 2-IAC, and blue for TAC. At higher pH values, the free indicators are red-orange due to dissociation of the phenolic proton, and visual detection of end point is difficult due to the poor color contrast. The results of nickel titrations using PAC, TAC, and 2-IAC are shown in Table 5. When titration using PAC was carried out at pH 4 and at 80 °C, the end point was overshot. Thus, titration should be performed slowly with boiling. Since the conditional formation constant for the nickel–TAC chelate is too small for pH values less than 6, using TAC the end point appeared too soon. If the nickel concentration is large, even at pH values higher than 6, a negative error often occured because of the poor visibility of the color change from blue to yellow-green. In the case of 2-IAC, although the conditional formation constant for the nickel–2-IAC chelate is of the same order as that of the nickel–TAC chelate, the end point was correctly detected, even at pH 5, because it is easy for the human eye to detect the color change from red-violet to yellow or yellow-green. At pH values higher than 7, a positive error occured due to the slow rate of indicator transition. From these results, the optimum pH ranges for nickel titrations are pH 4—5 with PAC, 6—7 with TAC, and 5—7 with 2-IAC. Thus, of these three, 2-IAC is the best indicator for nickel from the standpoints of good visibility of the color change and a wide optimum pH range.

By the addition of a small amount of 1,10-phenanthroline, titrations can be carried out at 50 °C using TAC[4] or 2-IAC,[3] while in the case of PAC, the rate of color change is not sufficiently enhanced.

We thank Dr. Genkichi Nakagawa for his valuable advice and the Ministry of Education of Japan for financial support.

References

1) G. Nakagawa and H. Wada, *Nippon Kagaku Zasshi*, **83**, 1098 (1962).
2) G. Nakagawa and H. Wada, *Nippon Kagaku Zasshi*, **85**, 202 (1964).
3) H. Wada and G. Nakagawa, *Bunseki Kagaku*, **24**, 239 (1975).
4) G. Nakagawa, H. Wada, and O. Nakazawa, *Talanta*, **23**, 155 (1976).
5) G. Nakagawa, H. Wada, and O. Nakazawa, to be published.

The Effect of 1,10-Phenanthroline on the Rate of Xylenol Orange Indicator Color Change

Hiroko WADA, Tomosuke ISHIZUKI, and Genkichi NAKAGAWA

Laboratory of Analytical Chemistry, Nagoya Institute of Technology, Gokiso-cho, Showa-ku, Nagoya 466

(Received January 29, 1977)

1,10-Phenanthroline(phen) accelerates the rate of the color change of Xylenol Orange(XO) in the copper(II)–EDTA titrations due to the formation of a mixed-ligand complex, $(Cuphen)_2xo$. The rate of the substitution reaction of Cu_2xo with 1,10-phenanthroline or with EDTA in the presence of 1,10-phenanthroline has been determined by the stopped-flow method over the pH range of 6.9—7.6 at $\mu=0.1$ (KNO_3) and 25 ± 1 °C. At 6.2×10^{-5}—1.2×10^{-3}M 1,10-phenanthroline, the rate-law is expressed as $-d[(Cu_2xo)']/dt=k_1[H][(Cu_2xo)']$. The reaction mechanism proposed is $Cu_2xo \xrightarrow{2phen} (Cuphen)_2xo \rightleftarrows (Cuphen)_2xo\cdots H \xrightarrow[r.d.s.]{H^+} Cuphen+(Cuphen)Hxo \xrightarrow{fast} 2Cuphen+xo'$, and $k_1=5.5\times10^7$ M^{-1} s^{-1}. By the addition of 2.5×10^{-6}—10^{-5} M 1,10-phenanthroline, copper(II) can be titrated with EDTA at room temperature with XO as an indicator.

In the copper(II)–EDTA titrations with Xylenol Orange (XO) as an indicator, hexamine slows down the rate of the color change of XO. The mechanism of the color change was reported in our previous paper.[1] On the other hand, 1,10-phenanthroline accelerates the rate of color change of the XO indicator remarkably.[2,3] This may be due to the mixed-ligand complex formation of the Cu_2xo chelate with 1,10-phenanthroline, and it may contribute to the color change as in the case of PAN.[4]

In this paper the composition of the mixed-ligand complexes of Cu–XO–phen and the rate of the substitution reaction of Cu–XO–phen with EDTA are determined, and the acceleration mechanism of the color change of XO by 1,10-phenanthroline is discussed.

Experimental

Reagents. XO was synthesized by the published method.[5,6] The solvent of the reaction product was distilled off under reduced pressure, and crude XO was obtained. The fractional precipitation of XO from the reaction mixture with ethanol[5,6] gives a lower yield of XO because of decomposition. The pure XO was completely separated on a cellulose column(prepared with Toyo-Roshi cellulose powder) by elution with butyl alcohol saturated with 10% acetic acid. The free-acid form(H_6xo) was obtained by passing the solution of the sodium salt through a column of Dowex 50W-X8(H^+) cation-exchange resin(100—200 mesh). The purity of H_6xo was estimated to be almost 100% by means of paper chromatography, pH-titration with a standard sodium hydroxide solution, and spectrophotometric titration with a standard copper(II) solution.

The 1,10-phenanthroline was recrystallized from an ethanol–water solution.

The other reagents employed were the same as those reported previously.[1]

The following buffers were used for adjusting the pH: pH 6.8—7.6: 0.02 M 3-morpholino-1-propanesulfonic acid(MOPS)–NaOH; pH<6.8: 0.02 M 2-morpholino-1-ethanesulfonic acid(MES)–NaOH. MOPS and MES were obtained from Dojindo Laboratories, Kumamoto, Japan.

The ionic strength was kept at 0.1 with KNO_3.

All the experiments were carried out at 25 ± 1 °C.

Apparatus. A Union Giken Stopped-Flow Spectrophotometer, Type RA-401, a Union Giken High Sensitivity Spectrophotometer, Type SM-401, a Hitachi Spectrophotometer, Type 124, and a Radiometer pH Meter, Type PHM 26c, were used.

Results

Mixed-Ligand Complexes of Cu_2xo with 1,10-Phenanthroline. In the presence of more than a 2-fold excess of copper(II), XO forms the Cu_2xo chelate above pH 5.5; the absorption maximum appears at 574 nm. When 1,10-phenanthroline (phen) was added to the Cu_2xo solution, the absorption maximum shifted to a longer wavelength (585 nm) and the molar absorp-

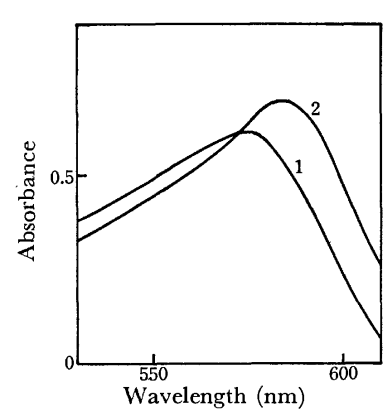

Fig. 1. Absorption spectra of Cu_2xo and $(Cuphen)_2xo$. $C_{xo}=1.32\times10^{-5}$ M, $C_{Cu}=2.58\times10^{-5}$ M. (1) Cu_2xo, pH 6.04; (2) $(Cuphen)_2xo$, $C_{phen}=3.29\times10^{-5}$ M, pH 7.00.

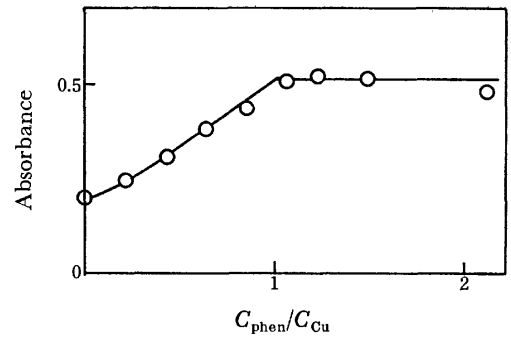

Fig. 2. Molar-ratio method of the mixed-ligand complex. $C_{xo}=1.32\times10^{-5}$ M, $C_{Cu}=2.58\times10^{-5}$ M, pH 6.93.

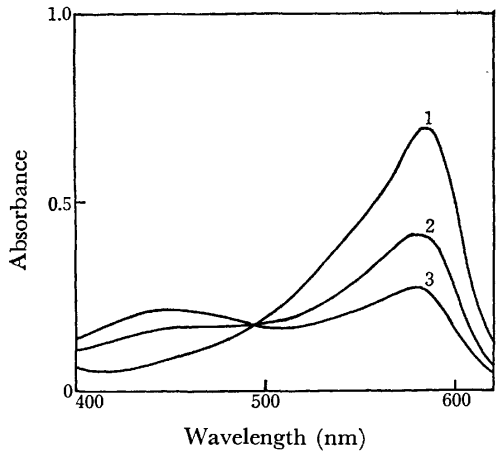

Fig. 3. Absorption spectra of the mixed-ligand complexes at different pH.
$C_{XO}=1.32\times10^{-5}$ M, $C_{Cu}=2.58\times10^{-5}$ M, $C_{phen}=3.29\times10^{-5}$ M, pH: (1) 7.00; (2) 5.98; (3) 5.50.

tivity increased by about 20% compared to that of Cu_2xo (Fig. 1). By the molar-ratio method it was found that $(Cuphen)_2xo$ was formed (Fig. 2).

The absorption spectra of a copper–XO chelate solution containing a 2.5-fold amount of 1,10-phenanthroline at different pH values are shown in Fig. 3. The absorption maximum shifts from 440 to 585 nm with an increase in the pH, an isosbestic point appears at 492 nm. Since copper(II) forms the Cu_2Hxo chelate with an absorption maximum at 444 nm at pH values lower than 4.5 in the absence of 1,10-phenanthroline, it is clear that $(Cuphen)_2Hxo$ is formed at lower pH values and that a proton may dissociate with an increase in pH. Thus, the following equilibrium exists in the pH range between 4.5 and 7.0:

$$(Cuphen)_2Hxo^- \rightleftarrows (Cuphen)_2xo^{2-} + H^+. \quad (1)$$

The equilibrium constant,

$$K^H_{(Cuphen)_2Hxo} = \frac{[(Cuphen)_2Hxo]}{[(Cuphen)_2xo][H]},$$

was evaluated to be $10^{5.7}$ from the change in the absorbance at 585 nm with the pH. The dissociation of the proton in $(Cuphen)_2Hxo$ is more difficult than that in Cu_2Hxo ($K^H_{Cu_2Hxo}=10^{4.55}$).[1]

The Substitution Reaction of Cu_2xo with 1,10-Phenanthroline. The rate of the substitution reaction of Cu_2xo with a large excess of 1,10-phenanthroline was measured by the stopped-flow method. Figure 4 shows a plot of the absorbance at 580 nm against the reaction time. The rapid increase in the absorbance at beginning indicates the formation of the mixed-ligand complex $(Cuphen)_2xo$. Then the reaction proceeds as

$$Cu_2xo^{2-} + 2phen \longrightarrow (Cuphen)_2xo^{2-}, \quad (2)$$

$$(Cuphen)_2xo^{2-} + 4phen \longrightarrow 2Cu(phen)_3^{2+} + xo'. \quad (3)$$

Under the present experimental conditions, the substitution reaction proceeds to completion and the reverse reaction can be neglected. The rate law may be expressed as:

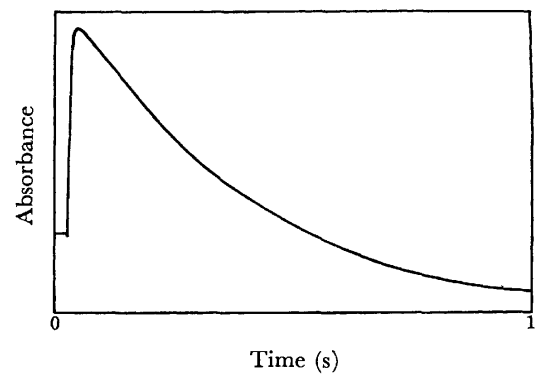

Fig. 4. Substitution reaction of Cu_2xo with 1,10-phenanthroline.
$C_{XO}=1.22\times10^{-5}$ M, $C_{Cu}=2.27\times10^{-5}$ M, $C_{phen}=8.67\times10^{-4}$ M, pH 7.43, 580 nm.

$$-\frac{d[(Cu_2xo)']}{dt} = k_{0(H,phen)}[(Cu_2xo)'], \quad (4)$$

where $[(Cu_2xo)']$ is the total concentration of copper–XO complexes and $k_{0(H,phen)}$ is the conditional rate constant involving the concentrations of the hydrogen ion and 1,10-phenanthroline. Representing the absorbances at the reaction times of 0, t, and ∞ as A_0, A_t, and A_∞ respectively, we obtain from Eq. 4

$$\log(A_t-A_\infty) = -\frac{k_{0(H,phen)}}{2.303}t + \log(A_0-A_\infty). \quad (5)$$

The experiments were carried out under the conditions where $C_{XO}=1.22\times10^{-5}$ M, $C_{Cu}=2.27\times10^{-5}$ M, and $C_{phen}=(6.19\text{—}12.4)\times10^{-4}$ M, pH 6.89—7.60. The rate plots of $\log(A_t-A_\infty)$ *vs.* t were linear for at least 90% of the reactions. The data in Table 1 indicate that the values of $k_{0(H,phen)}$ are proportional to the hydrogen-ion concentration, but independent of the 1,10-phenanthroline concentration; *i.e.*,

Table 1. First-order conditional rate constants $k_{0(H,phen)}$
$C_{XO}=1.22\times10^{-5}$ M, $C_{Cu}=2.27\times10^{-5}$ M, 25 °C, $\mu=0.1$.

pH	$C_{phen}(\times10^{-4}$ M)	$k_{0(H,phen)}(s^{-1})$
6.89	6.19	7.48
	7.43	7.48
	8.67	7.48
	9.90	7.36
	11.1	7.48
	12.4	7.48
6.94	6.19	6.10
	7.43	6.18
	8.67	6.13
	9.90	6.13
7.04	6.19	5.06
	8.67	5.18
7.19	7.43	3.33
	8.67	3.33
7.43	6.19	2.42
	8.67	2.50
7.60	6.19	1.80
	7.43	1.80
	8.67	1.78

$$k_{0(H,phen)} = k_1[H]. \quad (6)$$

This result indicates that the equilibrium (Eq. 2) shifts to the right completely and that the following reaction is the rate-determining step:

$$(Cuphen)_2xo^{2-} + H^+ \rightleftarrows H \cdots xo(Cuphen)_2 \xrightarrow{r.d.s.} (Cuphen)Hxo^{3-} + Cuphen^{2+}. \quad (7)$$

The resulting (Cuphen)Hxo may undergo rapid substitution with 1,10-phenanthroline. The rate constant, k_1, was evaluated as 5.5×10^7 M^{-1} s^{-1}.

The Substitution Reaction of Cu_2xo with EDTA in the Presence of 1,10-Phenanthroline. When a large excess of 1,10-phenanthroline is added to a Cu_2xo solution the substitution proceeds and the absorbance of Cu–XO complex decreases. The substitution of Cu_2xo with a solution containing a large excess of EDTA and (6.0—24.8)$\times10^{-5}$ M phenanthroline was, then, carried out.

The rate expression is given as

$$-\frac{d[(Cu_2xo)']}{dt} = k_{0(EDTA,H,phen)}[(Cu_2xo)']. \quad (8)$$

Table 2. First-order conditional rate constants $k_{0(EDTA,H,phen)}$
$C_{XO}=1.22\times10^{-5}$ M, $C_{Cu}=2.27\times10^{-5}$ M, 25 °C, $\mu=0.1$.

C_{EDTA} ($\times10^{-4}$ M)	C_{phen} ($\times10^{-5}$ M)	pH	$k_{0(EDTA,H,phen)}$ (s^{-1})
4.48	6.20	6.92	6.49
	12.4		6.90
	18.4		6.96
	24.8		6.77
	3.71	7.00	5.46
	4.21		5.46
	6.20	7.28	3.07
	12.4		2.88
	18.4		3.02
	24.8		2.90
	6.20	7.48	1.87
	12.4		1.84
6.73			2.01
8.97			2.01
11.2			1.96

In this case, the values of $k_{0(EDTA,H,phen)}$ in Table 2 were proportional to only the concentration of the hydrogen ion, just as in the case of the substitution with 1,10-phenanthroline. Therefore, the mechanism of the substitution reaction of Cu_2xo is the same as that in the case of phenanthroline, and (Cuphen)Hxo may undergo rapid substitution with EDTA. The rate constant was obtained as 5.5×10^7 M^{-1} s^{-1}, which is in good agreement with the value obtained in the preceding section.

The substitution under conditions which are very close to those in practical titrations was examined; *i.e.*, a solution containing Cu_2xo and a 2.1—3-fold excess of phenanthroline was replaced with a large excess of EDTA. The values of $k_{0(EDTA,H,phen)}$ are shown in Table 3. We observed no dependence of $k_{0(EDTA,H,phen)}$ on the concentration of EDTA, but a linear relation to the hydrogen ion with the zero intercept and the 1,10-phenanthroline with an intercept were observed (Fig. 5). From these results the following equation is deduced:

Table 3. First-order conditional rate constants $k_{0(EDTA,H,phen)}$
$C_{XO}=1.32\times10^{-5}$ M, $C_{Cu}=2.58\times10^{-5}$ M, 25 °C, $\mu=0.1$.

C_{EDTA} ($\times10^{-4}$ M)	C_{phen} ($\times10^{-5}$ M)	pH	$k_{0(EDTA,H,phen)}$ (s^{-1})
5.61	2.74	6.89	4.02
		7.05	2.96
		7.25	1.92
	3.29	6.89	4.68
		7.05	3.26
		7.25	2.11
	3.84	6.89	4.76
		7.05	3.35
		7.25	2.30
6.73	3.29	7.05	3.22
7.85			3.22
8.97			3.22

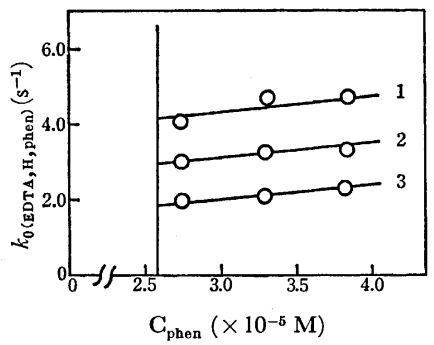

Fig. 5. Plots of $k_{0(EDTA,\ H,\ phen)}$ *vs.* C_{phen}.
$C_{XO}=1.32\times10^{-5}$ M, $C_{Cu}=2.58\times10^{-5}$ M, $C_{EDTA}=5.61\times10^{-4}$M, pH: (1) 6.89; (2) 7.05; (3) 7.25.

$$k_{0(EDTA,H,phen)} = (k_1+k_2[phen])[H]. \quad (9)$$

Under those experimental conditions the mixed-ligand complex $(Cuphen)_2xo$ may not be formed completely and a small amount of $(Cu_2phen)xo$ exists, so the second term in Eq. 9 is due to the following equilibrium preceding the rate-determining step (Eq. 7):

$$(Cu_2phen)xo^{2-} + phen \rightleftarrows (Cuphen)_2xo^{2-}. \quad (10)$$

Consequently, the substitution mechanism is virtually the same as that with 1,10-phenanthroline.

Discussion

As has been reported previously,[1] for the substitution reaction of Cu_2xo with EDTA the rate-law is expressed by

$$-\frac{d[Cu_2xo]}{dt} = k[Cu_2xo][edta'], \quad (11)$$

and the reaction mechanism is as follows:

$$Cu_2xo^{2-} + edta' \rightleftarrows edta \cdots Cu(xo)Cu \xrightarrow{r.d.s.} Cu(edta)^{2-} + CuHxo^{3-}, \quad (12)$$

$$CuHxo^{3-} + edta' \xrightarrow{fast} Cu(edta)^{2-} + xo'. \quad (13)$$

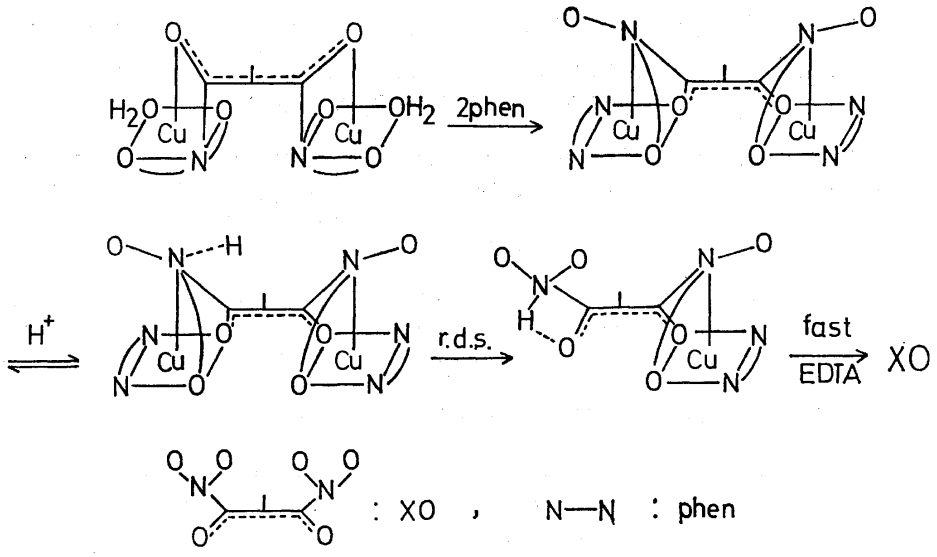

Fig. 6. Proposed reaction mechanism for substitution of $(Cuphen)_2xo$ with EDTA.

EDTA coordinates with one of the two coppers in the Cu_2xo chelate, and the release of the first copper ion from the intermediate edta···Cu(xo)Cu may be the rate-determining step, while the resulting CuHxo undergoes a rapid substitution with EDTA.

When 1,10-phenanthroline is present, the copper–XO chelate forms a mixed-ligand complex with 1,10-phenanthroline, and it may have a distorted octahedron structure, just as in the case of the copper–PAN–phen mixed-ligand complex.[4] Therefore, the release of the first copper from the $(Cuphen)_2xo$ chelate by the attack of a hydrogen ion on one of the nitrogen atoms in the iminodiacetic acid groups may be the rate-determining step (Fig. 6).

In practical titrations of copper(II) with EDTA, the rate of the color change of the XO indicator depends on the concentration of 1,10-phenanthroline and the titration pH. The rates of color change in the presence and in the absence of 1,10-phenanthroline were compared at pH 6.1 (MES buffer) using the stopped-flow spectrophotometer. A solution of copper (1.03×10^{-3} M) containing XO (1.22×10^{-5} M) and 1,10-phenanthroline and a solution containing EDTA (1.04×10^{-3} M, *i.e.* a 1% excess) were rapidly mixed. Usually in a visual titration 90% of the indicator transition is recognized as a complete color change; therefore, the time required for a 90% color transition was measured (Table 4). In the presence of 2.7×10^{-6} M 1,10-phenanthroline the rate of color change is 20-times as much as that in the absence, and with 1.2×10^{-5} M the rate increases by 50-times. Thus, 2.5×10^{-6}—10^{-5} M of 1,10-phenanthroline is sufficient for titration at room temperature. The addition of a larger amount of 1,10-phenanthroline may cause an underconsumption of EDTA.

Table 4. Effect of 1,10-phenanthroline on the rate of color change

	Concentration of 1,10-phenanthroline (M)				
	0	2.7×10^{-6}	6.2×10^{-6}	1.2×10^{-5}	2.4×10^{-5}
Time for 90% color change (s)	63	3.3	1.6	1.2	0.7

XO=1.22×10^{-5} M, Cu=1.03×10^{-3} M, EDTA=1.04×10^{-3} M, pH 6.1 (MES buffer), λ=580 nm, μ=0.1, 25 °C.

The financial support of the Ministry of Education of Japan is gratefully acknowledged.

References

1) H. Wada, T. Ishizuki, and G. Nakagawa, *Talanta*, **23**, 669 (1976).
2) R. Přibil, *Talanta*, **3**, 91 (1959).
3) G. Nakagawa and H. Wada, *Talanta*, **20**, 829 (1973).
4) G. Nakagawa and H. Wada, *Talanta*, **22**, 563 (1975).
5) J. Körbl and R. Přibil, *Chem. Ind. (London)*, **1957**, 233.
6) M. Murakami, T. Yoshino, and S. Harasawa, *Talanta*, **14**, 1293 (1967).

Preparation of Optically Active 1,3-Diphenyl-1,3-propanediamine (dppn) and the Circular Dichroism of *trans*-[$CoCl_2$-(*S,S*-dppn)$_2$]$^+$ and [Co(*S,S*-dppn)$_3$]$^{3+}$ *

Sumio Arakawa, Kazuo Kashiwabara,** Junnosuke Fujita,** and Kazuo Saito

Department of Chemistry, Faculty of Science, Tohoku University, Aramaki, Sendai 980

***Department of Chemistry, Faculty of Science, Nagoya University, Chikusa-ku, Nagoya 464*

(Received March 14, 1977)

1,3-Diphenyl-1,3-propanediamine (dppn) was prepared from 1,3-diphenyl-2-propen-1-one. The meso and racemic isomers were isolated. The racemate was resolved into enantiomers with (+)$_D$-di-*O*-benzoyltartrate. The absolute configuration of the free diamine was determined by comparing the circular dichroism (CD) spectrum of *trans*-[$CoCl_2$(*S,S*- or *R,R*-dppn)$_2$]$^+$ with that of *trans*-[$CoCl_2$(*R,R*-2,4-pentanediamine)$_2$]$^+$. The absolute configurations of Δ- and Λ-[Co(*S,S*-dppn)$_3$]$^{3+}$ were also assigned on the basis of the CD spectra.

Recently, several groups have reported the stereochemistry and circular dichroism (CD) of cobalt(III) complexes containing 2,4-pentanediamine (ptn) which forms a six-membered chelate ring upon coordination.[1-4] Among possible conformations of coordinated ptn, the chair and skew forms are energetically preferred as indicated by conformational energy calculation.[5] X-Ray crystallographic studies confirm the skew form of coordinated (*R,R*)-ptn in $(-)_{546}$- and $(+)_{546}$-[Co(*R,R*-ptn)$_3$]$^{3+}$ and the chair form of (*R,S*)-ptn in $(+)_{510}$-[Co(ox)(*R,S*-ptn)$_2$]$ClO_4 \cdot H_2O$(ox=oxalate).[7] The chair form of coordinated trimethylenediamine (tn) was found in $(-)_{589}$-[Co(tn)$_3$]$^{3+}$.[8] These results indicate that chelated 1,3-diamines can take a variety of conformations in the solid state.

An equilibrium among these conformations of 1,3-diamines will be expected in solution. We have pointed out in a previous paper that the CD spectra of Δ-[Co(*R,R*-ptn)$_3$]$^{3+}$ and *cis*-Δ-[$Co(NH_3)_2$(*R,R*-ptn)$_2$]$^{3+}$ in the first absorption band region show a remarkable variation on the addition of electrolytes such as chloride and sulfate, and that the variation is accounted for the conformational change of the flexible (*R,R*)-ptn ligands.[9] Such a conformational stability of coordinated 1,3-diamines will differ depending on the kind of substituent on the six-membered chelate ring. In order to investigate the effect of substituent on the conformation of a chelate ring, we have prepared optically active 1,3-diphenyl-1,3-propanediamine (dppn) which forms a six-membered chelate ring with two phenyl groups on the asymmetric carbons. This paper will report the preparation and the absolute configuration of optically active dppn as well as the CD spectra of *trans*-[$CoCl_2$(*S,S*-dppn)$_2$]$^+$ and Δ- and Λ-[Co(*S,S*-dppn)$_3$]$^{3+}$.

Experimental

Preparation of Ligand. (1) Racemic and meso-*1,3-Diphenyl-1,3-propanediamine*: The dioxime of 1,3-diphenyl-1,3-propanedione was prepared by modifying slightly the method of Auwers and Müller.[10] An ethanol solution(95%, 1.2 dm^3) of 1,3-diphenyl-2-propen-1-one(208 g) was mixed dropwise with hydroxylamine hydrochloride(183 g) in water(200 cm^3), and then with potassium hydroxide(240 g) in water(200 cm^3) at 50 °C. The solution was refluxed for 20 min, cooled in ice water, and filtered to remove potassium chloride. The ethanol was removed under reduced pressure in a rotary evaporator. Enough water was added to the concentrate to give white precipitate. After a day the precipitate was filtered off and dried at 70 °C and then over P_2O_5 *in vacuo*. Recrystallization from hot ethanol gave white needle-like crystals of the dioxime (160 g). Mp 207 °C (dec). Found: C; 71.12, H; 5.53, N; 11.02%. Calcd for the dioxime($C_{15}H_{14}N_2O_2$): C; 70.87, H; 5.51, N; 11.02%. Recrystallization from hot benzene gave the hydroxyamino oxime. Mp 145 °C. Found: C; 70.77, H; 6.41, N; 11.27%. Calcd for the hydroxyamino oxime($C_{15}H_{16}N_2O_2$): C; 70.31, H; 6.25, N; 10.94%. These compounds were identified by IR spectra.

The dioxime was reduced with metallic sodium in ethanol according to the method used for preparing 2,4-pentanediamine.[11,12] The dioxime(80 g) was suspended in absolute ethanol(1.5 dm^3) in a three necked round bottom flask(3 dm^3) equipped with a large reflux condenser. Small pieces (5—8 cm^3) of metallic sodium (300 g) were added in portions to the suspension, to which was added additional amount of absolute ethanol from time to time. The mixture was allowed to stand for 30 min. Aqueous ethanol was added carefully to hydrolyze excess of sodium in the mixture and then 1 dm^3 of water was added. Ethanol was removed by evaporation. The aqueous solution was shaken with diethyl ether and ether layer was washed with water several times. Hydrogen chloride was bubbled into the ether solution to give white precipitate, which was filtered off and dried in air. Yield 70 g. Found: C; 56.78, H; 6.99, N; 8.83%. Calcd for 1,3-diphenyl-1,3-propanediamine dihydrochloride monohydrate($C_{15}H_{22}N_2OCl_2$): C; 57.00, H; 6.70, N; 8.49%. This diamine is a mixture of meso(*R,S*) and racemic(*R,R* and *S,S*) isomers.

(2) Separation of the meso- *and* dl-*1,3-Diphenyl-1,3-propanediamine Dihydrochloride: Method 1)*. The purified mixture of meso and racemic dihydrochloride(140 g) was suspended in boiling ethanol(400 cm^3) containing concd hydrochloric acid (20 cm^3). The suspension was stirred for 30 min and filtered in hot to remove a small amount of residue. White crystals were obtained on cooling the filtrate to room temperature. Both the products (residue and crystals) are the pure meso dihydrochloride. The PMR spectrum is shown in Fig. 1.

The filtrate was concentrated to 100 cm^3 and cooled to room temperature. White crystals(28 g) of the recemic dihydrochloride, contaminated by a small amount of the meso isomer, were filtered off. They were dissolved again in boiling ethanol(400 cm^3) and mixed with concd hydrochloric acid (10 cm^3). The solution was concentrated to 100 cm^3 to yield white crystals(9 g), which were filtered off. The pure racemic dihydrochloride(18 g) was obtained by evaporating the fil-

* A part of the Ph.D. thesis submitted by S. Arakawa to Tohoku University, 1976.

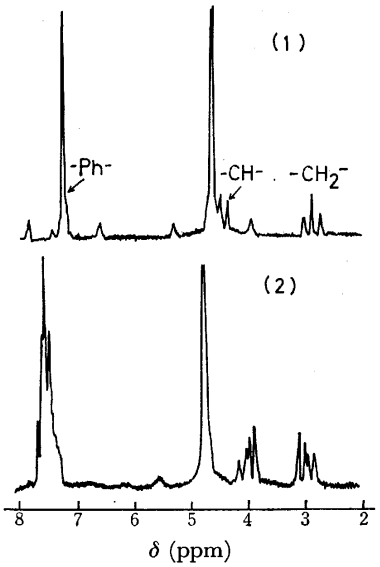

Fig. 1. PMR spectra of (1) *meso*-dppn·2HCl and (2) *dl*-dppn·2HCl in D_2O (60 MHz).

trate to almost dryness and by the addition of acetone. The PMR spectrum is shown in Fig. 1. The two isomers, meso and racemic, can be distinguished by the PMR spectra. Found for the meso isomer: C; 60.08, H; 6.99, N; 9.31%. Found for the racemic isomer: C; 59.58, H; 6.93, N; 9.22%. Calcd for 1,3-diphenyl-1,3-propanediamine dihydrochloride($C_{15}H_{20}N_2Cl_2$): C; 60.21, H; 6.74, N; 9.36%.

Method 2). Sodium hydroxide(30 g) in water(50 cm³) was added dropwise to a mixture of *meso*- and *dl*-dppn dihydrochloride(8.3 g) in cold water(50 cm³). The released dppn, insoluble in water, was extracted with chloroform(100 cm³). After removal of chloroform under reduced pressure, the oily residue was dissolved in ethanol(100 cm³). To the ethanol solution was added dropwise $(+)_D$-tartaric acid (8.3 g) in water(100 cm³). White crystals were obtained on cooling the solution in a refrigerator overnight. The crystals are *meso*-dppn $(+)_D$-tartrate. No crystal was obtained from the concentrated filtrate. The oily residue is *dl*-dppn $(+)_D$-tartrate. These isomers were identified by comparison with those prepared by method 1.

(3) Resolution of dl-*1,3-Diphenyl-1,3-propanediamine*: Potassium hydroxide (20 g) in water(20 cm³) was added dropwise to a cold aqueous solution (50 cm³) of *dl*-dppn dihydrochloride(9.2 g). The released dppn was extracted with chloroform(100 cm³), which was evaporated off and the oily residue was dissolved in methanol (40 cm³). The methanol solution was mixed with a methanol solution(40 cm³) of $(+)_D$-di-*O*-benzoyltartaric acid (10.7 g), and then with diethyl ether. The solution was allowed to stand overnight at room temperature. The precipitated white crystals were filtered off and washed with a mixture of methanol and diethyl ether (1: 1) and then with diethyl ether. Recrystallization from methanol by the addition of diethyl ether gave white crystals (7.8 g), $[\alpha]_D=-52.1°$ (*c*: 0.0048 g in 100 cm³ of a mixture of ethanol and water (1: 1)). This rotation did not change with further recrystallization. The absolute configuration of dppn in the less soluble diastereomer was assigned to the *(S,S)* configuration as described later.

Preparation of the Complexes. (1) trans-[*CoCl₂*(S,S-*dppn*)₂]-*Cl·HCl·H₂O*: Sodium hydroxide (15 g) in water(20 cm³) was added dropwise to a suspension of $(-)_D$-dppn-di-*O*-benzoyltartrate(6 g) in cold water(50 cm³). The released dppn was extracted with chloroform(100 cm³). The chloroform was removed under reduced pressure, and methanol(25 cm³) was added to the residue. The methanol solution was added dropwise with stirring to a mixture(60 cm³) of water and ethanol (2: 1) containing $Na_3[Co(NO_2)_6]$ (2 g). The total volume of the solution was adjusted to 200 cm³ with methanol. The solution was allowed to stand at 50 °C for 5 h. Hydrogen chloride was bubbled into the solution for 30 min until the color changed from orange to brown. The solution was kept in an evaporating dish at 50 °C with the addition of concd hydrochloric acid and methanol from time to time. The precipitated green solid was filtered off. Recrystallization from ethanol containing a small amount of concd hydrochloric acid gave green crystals(2 g). Found: C; 54.01, H; 5.68, N; 8.61 %. Calcd for $[CoCl_2(S,S\text{-dppn})_2]Cl\cdot HCl\cdot H_2O$ ($C_{30}H_{39}N_4OCl_4Co$): C; 53.59, H; 5.85, N; 8.33%. The perchlorate was obtained by adding sodium perchlorate to a methanol solution of the chloride.

(2) trans-[*CoCl₂*(R,S-*dppn*)₂]*Cl·H₂O*: To an aqueous solution (35 cm³) of $Na_3[Co(NO_2)_6]$(2.7 g) was added dropwise *(R,S)*-dppn(3 g) in ethanol(20 cm³). Yellow brown precipitate formed immediately. The suspension was stirred at 50 °C for 5 h and the yellow brown precipitate was filtered off(5.6 g), which was dissolved in methanol(1 dm³). When hydrogen chloride was bubbled for 10 min, the color changed from yellow to violet. The violet solution was concentrated in an evaporating dish to yield green precipitate, which was filtered off and washed with 4 M hydrochloric acid, then cold ethanol and diethyl ether. Yield 4 g. Found: C; 56.19, H; 6.09, N; 8.75%. Calcd for $[CoCl_2(R,S\text{-dppn})_2]Cl\cdot H_2O$ ($C_{30}H_{38}N_4OCl_3Co$): C; 56.66, H; 6.02, N; 8.81%.

(3) [*Co*(S,S-*dppn*)₃]*Cl₃*: A dimethyl sulfoxide (DMSO) solution (25 cm³) of dppn obtained from $(-)_D$-dppn-di-*O*-benzoyltartrate(2.4 g) was added dropwise to a DMSO solution(25 cm³) of *trans*-$[CoCl_2(S,S\text{-dppn})_2]Cl\cdot HCl\cdot H_2O$(1.8 g). The solution was allowed to stand at 25 °C for 7 h and then passed through a column (5×30 cm) of SE-Cellulose. The adsorbed band was eluted with a mixture of ethanol and water (1: 1). Orange yellow eluates were cooled in a refrigerator overnight to yield orange crystals (1.2 g), which were recrystallized from warm methanol(50 cm³, 60 °C). Found: C; 57.35, H; 6.73, N; 8.39%. Calcd for $[Co(S,S\text{-dppn})_3]Cl_3\cdot 5.5H_2O(C_{45}H_{65}N_6O_{5.5}Cl_3Co)$: C; 57.29, H; 6.94, N; 8.91 %. This complex has the *Δ* configuration as described later.

The unmoved band on the column was eluted with 0.5 M sodium perchlorate in a mixture of ethanol and water (1: 1). The orange eluates were concentrated to give red orange solid, which was dissolved in a mixture of water and methanol (4: 1). The solution was passed through a column(2×20 cm) of an SP-Sephadex C-25 ion exchanger. After washing with water, the adsorbed band was eluted with 1 M hydrochloric acid. The orange eluates were concentrated under reduced pressure to give orange crystals, which were filtered off and dried *in vacuo*. Yield 20 mg. Found: C; 57.62, H; 6.80, N; 8.42%. Calcd for $[Co(S,S\text{-dppn})_3]Cl_3\cdot 5.5H_2O(C_{45}H_{65}N_6O_{5.5}Cl_3Co)$: C; 57.29, H; 6.94, N; 8.91%. This complex has the *Λ* configuration as described later.

Measurements. Visible and ultraviolet absorption spectra were recorded on a Hitachi 323 spectrophotometer. CD spectra were obtained with JASCO J-20 and J-40 spectropolarimeters. PMR spectra were recorded on Varian A-60 and HA-100 spectrometers in deuterated solvents using sodium 2,2-dimethyl-2-silapentane-5-sulfonate (DSS) as the internal standard. All the solvents for optical measurements are of spectroscopic grade and used without further purification.

Results and Discussion

1,3-Diphenyl-1,3-propanediamine (dppn) is a six-membered chelate ligand, an analogue of 1,2-diphenyl-1,2-ethanediamine (stien) which forms a five-membered chelate ring. The skeleton is the same as that of 2,4-pentanediamine (ptn) in which the substituents on the asymmetric carbons are methyl groups. Therefore, there are two aspects for the cobalt(III) complexes of dppn: the first is the comparison with the ptn complexes and the second with the stien complexes.

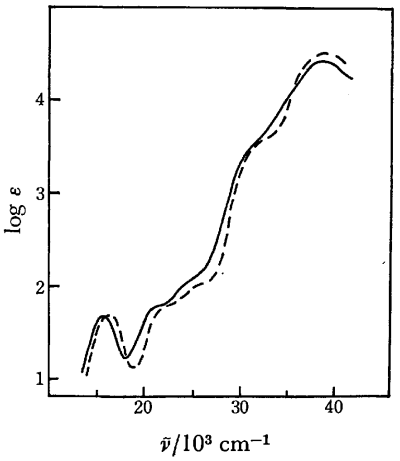

Fig. 2. Absorption spectra of *trans*-$[CoCl_2L_2]^+$ in methanol, L=(*S*,*S*)-dppn (——) and (*S*,*S*)-stien (– – –).

Table 1. Absorption data in the first absorption band region

	$\bar{\nu}/10^3$ cm^{-1} (ε)	
Λ-$[Co(S,S\text{-dppn})_3]Cl_3\cdot 5.5H_2O$	19.76(115.5)*2)	
Δ-$[Co(S,S\text{-dppn})_3]Cl_3\cdot 5.5H_2O$	20.28(84.2)*2)	
Λ-$[Co(R,R\text{-ptn})_3]Cl_3\cdot 2H_2O$[a]	20.58(97.7)*1)	
Δ-$[Co(R,R\text{-ptn})_3](ClO_4)_3\cdot H_2O$[a]	20.75(75.9)*1)	
trans-$[CoCl_2(S,S\text{-dppn})_2]Cl\cdot HCl\cdot H_2O$	15.63(45.7)*3)	22(sh)[d]
trans-$[CoCl_2(R,S\text{-dppn})_2]Cl\cdot H_2O$	15.63(49.5)*3)	22(sh)
trans-$[CoCl_2(R,R\text{-ptn})_2]ClO_4$[a]	15.75(42.7)*4)	21(sh)
trans-$[CoCl_2(R,S\text{-ptn})_2]Cl$[a]	15.75(39.0)*4)	21(sh)
trans-$[CoCl_2(S,S\text{-stien})_2]Cl\cdot 2H_2O$[b]	16.50(50.1)*3)	23(sh)
$[Co(NH_3)_4(S,S\text{-dppn})]Br_3\cdot H_2O$[c]	20.83(85.4)*2)	
	20.88(79.0)*1)	
$[Co(NH_3)_4(R,S\text{-dppn})]Br_3\cdot H_2O$[c]	20.79(88.6)*1)	
$[Co(NH_3)_4(R,R\text{-ptn})](ClO_4)_3$[a]	20.96(69.2)*1)	
$[Co(NH_3)_4(S,S\text{-stien})](ClO_4)_3\cdot 4H_2O$[c]	21.19(91.1)*2)	
	21.28(83.3)*1)	

*Solvent: 1) water, 2) DMSO, 3) methanol, 4) ethanol. a) Ref. 1. b) Ref. 19. c) The preparation for these complexes will be reported elsewhere. d) sh=shoulder.

Absorption Spectra. In Fig. 2, the absorption spectra of *trans*-$[CoCl_2(S,S\text{-dppn})_2]^+$ and *trans*-$[CoCl_2(S,S\text{-stien})_2]^+$ are compared in methanol. The absorption data are summarized in Table 1. We should point out some features of six-membered chelate rings from these data. (1) Red shift is observed for the complexes with six-membered chelate rings as compared with those containing five-membered chelate rings. This is commonly expected for complexes containing large chelate rings.[13] (2) The diastereomers, *Λ*- and *Δ*-$[Co(S,S\text{-dppn})_3]^{3+}$ as well as *Λ*- and *Δ*-$[Co(R,R\text{-ptn})_3]^{3+}$, give different absorption energies from each other in the first absorption band region. Such a difference is very small for the *Λ*- and *Δ*-$[Co((R)\text{-propylenediamine})_3]^{3+}$ complexes.[14] (3) The absorption peaks of the (*S*,*S*)-dppn complexes lie at lower energies than those of the corresponding (*R*,*R*)-ptn complexes. Hence, the ligand field strength may be (*R*,*R*)-ptn>(*S*,*S*)-dppn.

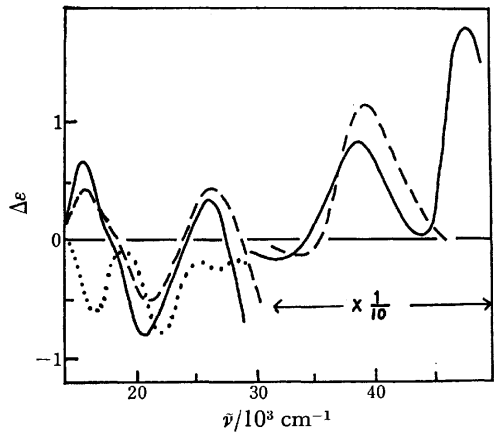

Fig. 3. CD spectra of *trans*-$[CoCl_2L_2]^+$ in methanol, L=(*S*,*S*)-dppn (——), (*R*,*R*)-ptn (– – –), and (*S*,*S*)-stien (·····).

Assignment of Absolute Configuration of dppn. The CD spectra of the complexes, *trans*-$[CoCl_2L_2]^+$ in methanol are shown in Fig. 3, where L represents (*S*,*S*)-dppn, (*R*,*R*)-ptn or (*S*,*S*)-stien. The absolute configuration of (*S*,*S*)-dppn can be assigned by comparing the CD spectrum of the (*S*,*S*)-dppn complex with that of the (*R*,*R*)-ptn complex. Both spectral patterns are similar to each other in the region of 14 to 45×10^3 cm^{-1}. It has been recognized that the optical activity of *trans*-$[CoCl_2(diamine)_2]^+$ complexes is affected strongly by the conformational contribution of the diamine and weakly by the vicinal effect of asymmetric carbons.[15] Hence, the conformation of the dppn seems to be the same

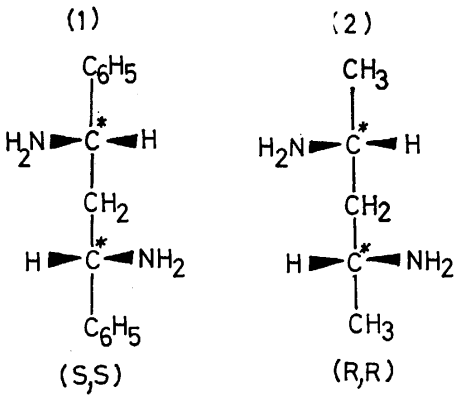

Fig. 4. Absolute configurations of (*S*,*S*)-dppn (1) and (*R*,*R*)-ptn (2).

λ-skew form as that of the ptn ligand, in which the two substituent groups on the asymmetric carbons adopt equatorial orientation. The λ-skew form of (*R,R*)-ptn chelate has been confirmed on $(+)_{546}$-[Co(*R,R*-ptn)$_3$]Cl$_3$·H$_2$O by an X-ray diffraction method.[6] According to the sequence rule,[16] the designation (*S,S*) of the dppn is opposite to that of the ptn to form the same λ-skew form (Fig. 4).

Circular Dichroism Spectra. Yano *et al.*[15] studied the CD spectra of various complexes of the type, *trans*-[CoCl$_2$(1,2-diamine)$_2$]$^+$ in methanol. In the Ib($^1A_{2g} \leftarrow {}^1A_{1g}$, D_{4h}) region, cobalt(III) complexes of (*R*)-1-phenyl-1,2-ethanediamine and (*R,R*)-stien which form five-membered λ-gauche chelate rings gave a CD peak with the opposite sign to that of the corresponding (*R*)-1-alkyl- or (*R,R*)-1,2-dialkyl-1,2-diamine complexes. However, all these complexes show similar CD patterns in the charge transfer region. They ascribed the difference to the vicinal effect of the phenyl groups on the chelate. Such a discussion is not applicable to the dppn complex. The pattern of the CD spectrum of *trans*-[CoCl$_2$(*S,S*-dppn)$_2$]$^+$ differs from that of the corresponding (*S,S*)-stien complex, while it resembles that of the corresponding (*R,R*)-ptn complex. The CD spectra of cobalt(III) complexes containing six-membered chelate diamines may not be appreciably affected by the presence of phenyl groups on the asymmetric carbons.

Figure 5 shows the absorption and CD spectra of the two diastereomers (named I and II) of [Co(*S,S*-dppn)$_3$]Cl$_3$ in DMSO. The CD spectrum of the isomer II which is eluted later from an SE-Cellulose column gives a weak minus peak at 18.2×10^3 cm^{-1} ($\Delta\varepsilon=-0.58$) and a strong plus peak at 20.2×10^3 cm^{-1} ($\Delta\varepsilon=+2.75$) in the first absorption band region. This pattern is similar to that of Λ-[Co(*R,R*-ptn)$_3$](ClO$_4$)$_3$ in DMSO (Fig. 6).[9] The CD spectrum of the isomer I which is eluted earlier from an SE-Cellulose column is similar to that of Δ-[Co(*R,R*-ptn)$_3$](ClO$_4$)$_3$ in water. Thus, we assigned

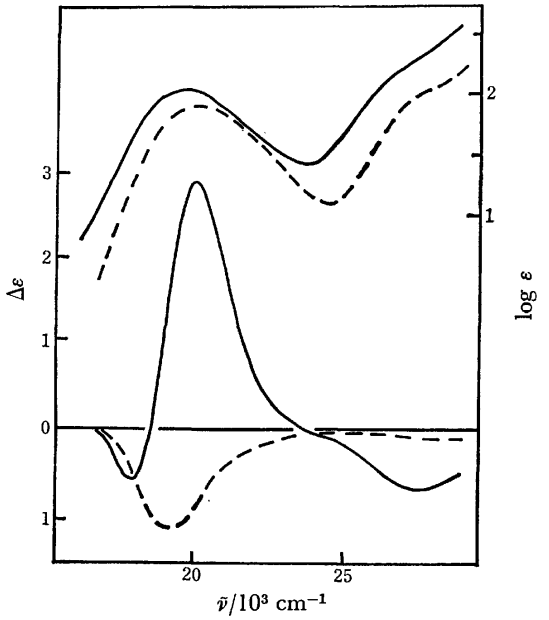

Fig. 5. Absorption and CD spectra of the diastereomers of [Co(*S,S*-dppn)$_3$]Cl$_3$ in DMSO, I(——) and II(——).

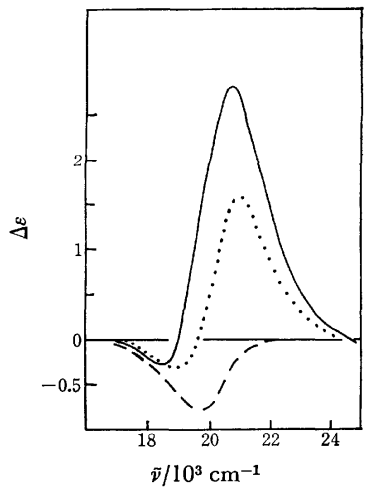

Fig. 6. CD spectra of Λ-[Co(*R,R*-ptn)$_3$](ClO$_4$)$_3$ in DMSO (——), Δ-[Co(*R,R*-ptn)$_3$](ClO$_4$)$_3$·3H$_2$O in water(– – –) and Δ-[Co(*R,R*-ptn)$_3$]Br$_3$ in DMSO (·····).[9]

II to Λ and I to Δ isomer. However, the spectrum of I is very different from that of Δ-[Co(*R,R*-ptn)$_3$]Br$_3$ in DMSO (Fig. 6). In a previous paper,[9] we have shown that the CD spectrum of Δ-[Co(*R,R*-ptn)$_3$]$^{3+}$ shows a remarkable variation in the first absorption band region in the presence of various electrolytes and in various solvents. There must be similar variations for the corresponding dppn complexes because of the flexible six-membered chelate rings. Detailed discussion for this system cannot be made unless the solvent effect is investigated. However, the solubility restriction of [Co(*S,S*-dppn)$_3$]Cl$_3$ makes us difficult to investigate the solvent effect.

The assignment of the absolute configuration of the [Co(*S,S*-dppn)$_3$]Cl$_3$ complex will be also supported by the formation ratio of the diastereomers. When the (*S,S*)-dppn takes a λ-skew form upon coordination, a tris complex can give two diastereomers, $\Lambda(\lambda\lambda\lambda)$ and $\Delta(\lambda\lambda\lambda)$. It has been known that the former complex in which the two asymmetric carbons of (*S,S*)-dppn lie oblique to the C_3 axis of the complex ion is less stable than the latter. The reason is believed to be due to large steric interactions among chelate rings in the former complex.[5,17] In fact, the formation ratio of the *lel*$_3$-$\Delta(\lambda\lambda\lambda)$ isomer to the *ob*$_3$-$\Lambda(\lambda\lambda\lambda)$ isomer is *ca.* 10 for tris(*R,R*-ptn)cobalt(III) complexes.[1] The tris(*S,S*-dppn)cobalt(III) complex gives always a large amount of the $\Delta(\lambda\lambda\lambda)$ isomer as described in the Experimental section.

Figure 7 shows the cofigurational and the vicinal effect curves derived from the CD spectra of Δ- and Λ-[Co(*S,S*-dppn)$_3$]Cl$_3$ in DMSO. The CD spectrum of [Co(NH$_3$)$_4$(*S,S*-dppn)]Br$_3$[18] in water is also shown. Although the additivity on CD curves is only an empirical rule, it may be useful to compare the difference between six-membered and five-membered chelate ligands. The additivity of the vicinal (conformational) contribution holds satisfactorily for a variety of five-membered chelate ring systems.[14,19] This is not the case for the present dppn system. The spectral pattern of the calculated vicinal effect curve of (*S,S*)-dppn in

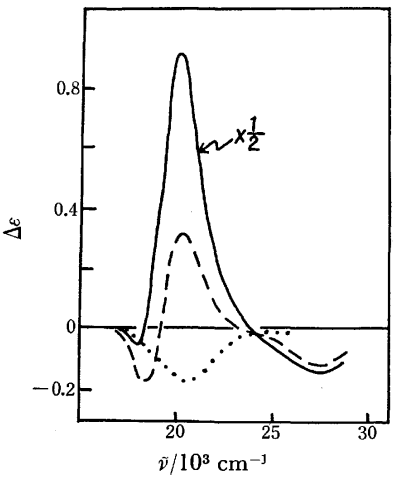

Fig. 7. The configurational (——) and the vicinal(– – –) contribution in the CD calculated from the spectra of the two diastereomers of $[Co(S,S\text{-dppn})_3]Cl_3$ in DMSO, and the CD spectra of $[Co(NH_3)_4(S,S\text{-dppn})]Br_3$ in water(·····).

$[Co(S,S,\text{-dppn})_3]^{3+}$ resembles that derived from the two diastereomers of $[Co(S,S\text{-dppn})(en)_2]^{3+}$ in water,[18] but differs completely from that of $[Co(NH_3)_4(S,S\text{-dppn})]^{3+}$ in water. Interligand steric interactions in $[Co(S,S\text{-dppn})_3]^{3+}$ must be larger than those in the tetraammine complex of dppn. The most stable conformation of each bulky and flexible six-membered chelate ring in these complexes might be somewhat different from each other.

References

1) F. Mizukami, H. Ito, J. Fujita, and K. Saito, *Bull. Chem. Soc. Jpn.*, **45**, 2129 (1972); *ibid.*, **46**, 2410 (1973).
2) M. Kojima and J. Fujita, *Chem. Lett.*, **1976**, 429.
3) R. Kuroda, J. Fujita, and Y. Saito, *Chem. Lett.*, **1975**, 225.
4) H. Boucher and B. Bosnich, *Inorg. Chem.*, **15**, 1471, 2364 (1976).
5) S. R. Niketic and F. Woldbye, *Acta Chem. Scand.*, **27**, 621, 3811 (1973).
6) A. Kobayashi, F. Marumo, and Y. Saito, *Acta Crystallogr., Sect. B*, **28**, 3591 (1972); *ibid.*, **29**, 2443 (1973).
7) I. Oonishi, S. Sato, and Y. Saito, *Acta Crystallogr., Sect. B*, **30**, 2256 (1974).
8) T. Nomura, F. Marumo, and Y. Saito, *Bull. Chem. Soc. Jpn.*, **42**, 1016 (1969); R. Nagao, F. Marumo, and Y. Saito, *Acta Crystallogr., Sect. B*, **29**, 2438 (1973).
9) M. Kojima, M. Fujita, and J. Fujita, *Bull. Chem. Soc. Jpn.*, **50**, 898 (1977).
10) K. Auwers and H. Müller, *J. Prakt. Chem.*, **137**, 57 (1933).
11) C. Harries and T. Haga, *Ber.*, **32**, 1191 (1893).
12) C. J. Dippel, *Recl. Trav. Chim. Pays-Bas*, **50**, 525 (1931).
13) H. Ogino and J. Fujita, *Bull. Chem. Soc. Jpn.*, **48**, 1836 (1975).
14) K. Ogino, K. Murano, and J. Fujita, *Inorg. Nucl. Chem. Lett.*, **4**, 351 (1968).
15) S. Yano, M. Saburi, S. Yoshikawa, and J. Fujita, *Bull. Chem. Soc. Jpn.*, **49**, 101 (1976).
16) R. S. Cahn, C. K. Ingold, and V. Prelog, *Angew. Chem., Int. Ed. Engl.*, **5**, 385 (1966).
17) J. Corey and J. C. Bailar, Jr., *J. Am. Chem. Soc.*, **81**, 2620 (1959).
18) S. Arakawa, K. Kashiwabara, J. Fujita, and K. Saito, *Chem. Lett.*, **1976**, 105. In this communication, $[Co(NH_3)_4(S,S\text{-dppn})]^{3+}$ in Fig. 2 should be replaced by $[Co(NH_3)_4(R,R\text{-dppn})]^{3+}$.
19) B. E. Douglas, *Inorg. Chem.*, **4**, 1813(1965); S.F. Mason, A. M. Sargeson, R. Larsson, B. J. Norman, A. J. McCaffery, and G. M. Searl, *Inorg. Nucl. Chem. Lett.*, **2**, 333 (1966); *J. Chem. Soc.*, **1968**, 1304, 1310; N. Matsuoka, J. Hidaka, and Y. Shimura, *Inorg. Chem.*, **9**, 719 (1970); *Bull. Chem. Soc. Jpn.*, **48**, 458 (1975).

INDO-UHF-CI Calculations of the Electronic Structure of Formaldehyde-Hydrogen Systems*

Kimiko MIZUTANI, Toyoo IZUMI,** and Shiro MATSUMOTO

Department of Chemistry, College of Science and Engineering, Aoyama Gakuin University, Chitosedai, Setagaya-ku, Tokyo 157

(Received October 29, 1976)

The electronic structures were calculated for the ground and several excited states of systems composed of a formaldehyde molecule and a hydrogen atom at various relative positions by means of an INDO-UHF-CI method, in order to elucidate the hydrogen-abstracting process of excited carbonyl compounds. The results were presented and discussed by means of the adiabatic potential energy curves, by means of configuration analysis using the various states of the non-interacting component species as reference, and by means of electron-density maps. The results showed in a concrete way that the process may proceed through an intermediate charge-transfer state, and the electron-density maps had features suggesting an attractive force acting on the positively charged hydrogen atom.

There have been increasing efforts to understand the mechanisms of chemical reactions in terms of the electronic structures of the molecular systems concerned.[1] The analyses have mostly been restricted to reactions between molecules in their ground states, although the principle may be the same for the cases when one or both of the partners are in excited states.

In the present work, electronic structures were calculated for systems composed of a formaldehyde molecule and a hydrogen atom at various relative positions in an attempt to get some insight into the nature of the hydrogen abstraction reaction of excited ketone molecules, as that reaction is one of the most clear-cut and best investigated chemical processes of excited states.[2] The process has, though, been described and discussed based only on the qualitative features of the electronic structures of the excited ketone molecules.[2,14c,15] For a more detailed understanding of the process, it seemed essential to compute the electronic structures of the combined system for a series of relative positions of the reactants. Since the calculation seemed, unfortunately, to be beyond the power of moderate computational facilities for real systems investigated experimentally, a model calculation was undertaken.

Ground and excited states of formaldehyde have been the subject of semiempirical calculations[3] of various precisions as well as of *ab initio* calculations.[4] The electronic states of the HCHO–H_2O system were calculated by Iwata and Morokuma.[5] In the case of the HCHO–H system, open shell or shells are involved in all the states, including the ground state. One way of treating the system would be a configuration interaction (CI) calculation using the configuration state functions (CSF's) constructed by the molecular orbitals (MO's) calculated for isolated HCHO plus an MO localized on the additional H atom. However, another method was attempted in this work; that is, the whole system was treated as a quasi-molecule by an SCF procedure. The method takes into account all the interactions between the components in a direct way at any internuclear distance. The resulting wavefunctions may be too complicated to be interpreted directly, but their expansions with the CSF's of the components (configuration analysis)[6] would help to grasp the characteristics of the states pictorially. As the RHF treatment will encounter the problem of orbital orthogonalization,[7] and as the wavefunction must be computed for a variety of geometries, the calculation was done by the INDO-UHF procedure[9] in order to obtain approximate wavefunctions without using too much computer time. Similar procedures have been used by several authors for similar purposes.[1d,1e] A fairly limited configuration interaction has been taken to improve the qualities of the excited states as well as of the ground state and to secure correct dissociation behavior[10b] of each state. In such a limited CI procedure, the SCF orbitals may be superior to the isolated HCHO and H orbitals for the state mainly composed of the ground-state configuration, as Brillouin's theorem[10c] states. For excited states, the situation was more subtle, but again the SCF orbitals seemed to be a better choice, as many terms cancelled each other out in the CI matrix element calculations. To visualize the results further, electron-density maps were drawn for some typical geometries. The conclusions obtained therefrom were in general agreement with those obtained by other methods of analysis; one interesting feature was that the maps were indicative of the direction of the force exerted on the approaching H atom.

Method of Calculation

The geometry of HCHO was taken to be planar (Fig. 1), and the dimensions were those given by the microwave analysis by Takagi.[8] They were fixed throughout this calculation. The position of the additional H atom will be defined below using the coordinate system given in Fig. 1. The method of INDO-UHF calculation was the same as that given in Ref. 9. The configuration interaction was confined to the 18 doublet CSF's*** resulting from the excitation of the π, n, and

* A part of this work was presented at the Symposium on Molecular Structure, Osaka, November 1975.

** Present address: Kyōei Keisan Center Co., Ltd., Setagaya-ku, Tokyo.

*** Quartet states resulting from ^{3}(HCHO)+H were not considered here, as they seemed to be of little importance in the photochemical process.

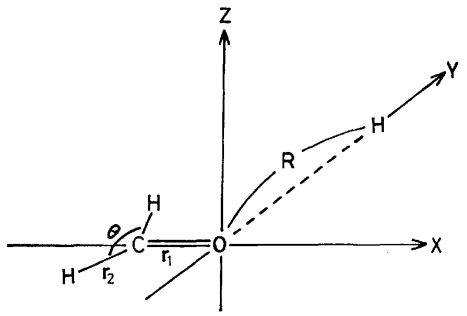

Fig. 1. Geometry of HCHO–H.
r_1=1.2078 Å, r_2=1.1161 Å, θ=116°31′.

TABLE 1. LIST OF CONFIGURATION STATE FUNCTIONS

ψ_1		$(\pi)^2(n)^2(h)$
ψ_2		$(\pi)^2(n)(h)(\pi^*)$ [a]
ψ_3		$(\pi)^2(n)(h)(\pi^*)$ [a]
ψ_4		$(\pi)(n)^2(h)(\pi^*)$ [c]
ψ_5		$(\pi)^2(h)(\pi^*)^2$
ψ_6		$(\pi)(n)^2(h)(\pi^*)$ [c]
ψ_7	(BCT_1)	$(\pi)^2(n)(h)^2$
ψ_8		$(\pi)(n)(h)(\pi^*)^2$ [b]
ψ_9		$(\pi)(n)(h)(\pi^*)^2$ [b]
ψ_{10}	(BCT_2)	$(\pi)(n)^2(h)^2$
ψ_{11}	(CT_1)	$(\pi)^2(n)^2(\pi^*)$
ψ_{12}	(BCT_3)	$(\pi)^2(h)^2(\pi^*)$
ψ_{13}	(BCT_4)	$(\pi)(n)(h)^2(\pi^*)$ [d]
ψ_{14}		$(n)^2(h)(\pi^*)^2$
ψ_{15}	(CT_2)	$(\pi)^2(n)(\pi^*)^2$
ψ_{16}	(BCT_5)	$(\pi)(n)(h)^2(\pi^*)$ [d]
ψ_{17}	(CT_3)	$(\pi)(n)^2(\pi^*)^2$
ψ_{18}	(BCT_6)	$(n)^2(h)^2(\pi^*)$

a), b), c), d) These configuration state functions are independent-spin-state pairs.

h orbitals to the π^* virtual orbital. Here, the π, π^*, and n orbitals were named by analogy with the orbitals of isolated HCHO, and h denotes the orbital with its main component on the approaching H atom. These CSF's are summarized in Table 1, together with the numbering used below. The primitive UHF determinantal wavefunctions are not exact spin eigenfunctions, and the generation of exact state functions therefrom requires complicated procedures.[10] In view of the rather semi-quantitative nature of this work and various approximations already done in INDO calculation, no effort was made to spin-project the UHF determinantal wavefunctions; when their linear combinations were essential, as when three singly occupied orbitals existed, the following simple approximation was

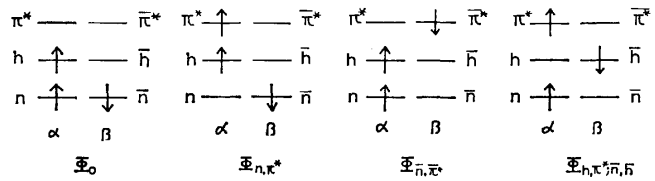

Fig. 2. Three independent arrangements of electrons resulting from $n\pi^*$ excitation.

taken tentatively for the doublet wavefunctions. First, let it be assumed that the orbital functions for the α- and β-spins coincide as in RHF calculations. Corresponding to the excitation of an n electron in the ground configuration, Φ_0, to the π^* orbital, for example, there may result three independent determinantal wavefunctions: Φ_{n,π^*}, $\Phi_{\bar{\pi},\bar{n}^*}$, and $\Phi_{h,\pi^*;\bar{n},\bar{h}}$ (Fig. 2). Two independent combinations of these determinants, which are exact doublets,[11] may be taken as

$$\Psi_a = (\Phi_{n,\pi^*}+\Phi_{\bar{n},\bar{\pi}^*})/\sqrt{2}, \quad (1)$$

$$\Psi_b = (-\Phi_{n,\pi^*}+\Phi_{\bar{n},\bar{\pi}^*}+2\Phi_{h,\pi^*;\bar{n},\bar{h}})/\sqrt{6}. \quad (2)$$

In the UHF case, orbital forms for α- and β-spins generally differ; however, if the differences are not too serious, Ψ_a and Ψ_b can be taken as representing approximately two doublet CSF's. For the estimation of the matrix elements of interaction between these CSF's, Slater's rule[12] was invoked, and the one- and two-electron integrals therein were again evaluated according to the prescription of the INDO method.

Configuration analysis was done in essentially the same way as the original paper[6] with necessary adaptations to doublets. The reference states were those of a hypothetical system composed of non-interacting component species. Here, two combinations,

$$\Psi_a^\circ = (\Phi_{n,\pi^*}^\circ+\Phi_{\bar{n},\bar{\pi}^*}^\circ)/\sqrt{2}, \quad (1')$$

$$\Psi_b^\circ = (-\Phi_{n,\pi^*}^\circ+\Phi_{\bar{n},\bar{\pi}^*}^\circ+2\Phi_{h,\pi^*;\bar{n},\bar{h}}^\circ)/\sqrt{6}. \quad (2')$$

represent exact doublets, as the orbital functions for α- and β-spins coincide in this case. The superscript, o, on Φ means the reference state. On the other hand, the CSF's assumed above for the real system are contaminated by the quartet character. A third linear combination,

$$\Psi_c^\circ = (-\Phi_{n,\pi^*}^\circ+\Phi_{\bar{n},\bar{\pi}^*}^\circ-\Phi_{h,\pi^*;\bar{n},\bar{h}}^\circ)/\sqrt{3},$$

is orthogonal to both Ψ_a° and Ψ_b° and represents a CSF quartet.[11] Thus, it would be appropriate to expand any state function, Ψ, in terms of this type of trio,

$$\Psi = \cdots + C_1(\Phi_{n,\pi^*}^\circ+\Phi_{\bar{n},\bar{\pi}^*}^\circ)/\sqrt{2} + C_2(-\Phi_{n,\pi^*}^\circ+\Phi_{\bar{n},\bar{\pi}^*}^\circ+2\Phi_{h,\pi^*;\bar{n},\bar{h}}^\circ)/\sqrt{6} + C_3(-\Phi_{n,\pi^*}^\circ+\Phi_{\bar{n},\bar{\pi}^*}^\circ-\Phi_{h,\pi^*;\bar{n},\bar{h}}^\circ)/\sqrt{3} + \cdots. \quad (3)$$

Equation 3 may be rewritten as:

$$\Psi = \cdots + f_1\Phi_{n,\pi^*}^\circ + f_2\Phi_{\bar{n},\bar{\pi}^*}^\circ + f_3\Phi_{h,\pi^*;\bar{n},\bar{h}}^\circ + \cdots, \quad (4)$$

with

$$f_1 = C_1/\sqrt{2} - C_2/\sqrt{6} - C_3/\sqrt{3},$$
$$f_2 = C_1/\sqrt{2} + C_2/\sqrt{6} + C_3/\sqrt{3}, \quad (5)$$
$$f_3 = 2C_2/\sqrt{6} - C_3/\sqrt{3}.$$

The coefficients, f_1, f_2, and f_3 are determined by means of the Ψ function, Φ_{n,π^*}°, $\Phi_{\bar{n},\bar{\pi}^*}^\circ$, and $\Phi_{h,\pi^*;\bar{n},\bar{h}}^\circ$ functions by the use of equations similar to those given in Ref. 6. The three Eqs. 5 are then solved to give

$$C_1 = (f_1+f_2)/\sqrt{2},$$
$$C_2 = (-f_1+f_2+2f_3)/\sqrt{6},$$
$$C_3 = (-f_1+f_2-f_3)/\sqrt{3}.$$

The C_3 coefficients are measures of the spin-contamination of the Ψ function.

Results and Discussion

Potential Curves and Configuration Analysis. The adiabatic potential curves obtained for several low-lying states are given in Figs. 3—5 for three modes of approach of the H atom. The results of configuration analysis along these curves are shown in Tables 2—6. In these figures, potential curves correlating to Ψ_5°, Ψ_7°, Ψ_8°, Ψ_9°, Ψ_{10}°, Ψ_{12}°, *etc.* for $R=\infty$ are not shown in order to avoid confusion. Each state, except for the one denoted as CT_1 in the figures, was found to dissociate rationally to an H atom and an HCHO molecule in its ground or in some of its excited states, which are shown beside each potential curve. The irreducible representation of each state is also indicated there. The CT symbol (charge transfer) is used here to denote states in which an electron in the h orbital is transferred to one of the empty orbitals of the HCHO component. As several different CT states arise, they are distinguished by subscripts, 1, 2, ···. They were found to dissociate to an H^+ and an $HCHO^-$ in its ground or various excited states. In the CT_1 state, the transferred electron occupies the LUMO π^* and has been found to play an important role in the chemical process under consideration. The BCT symbol (back charge transfer) indicates the states in which two electrons occupy the h orbital.

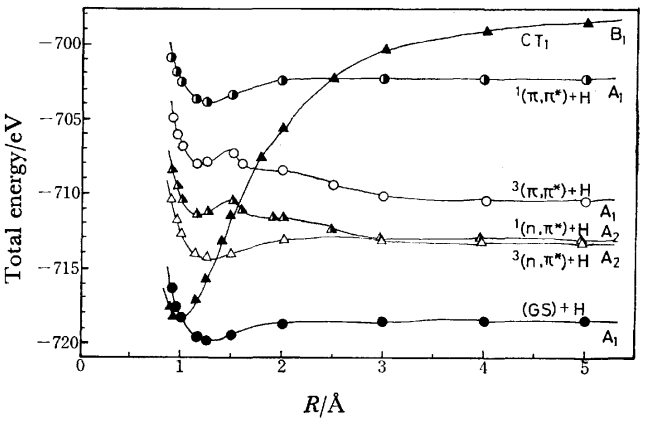

Fig. 3. Potential energy curves of ground and lower excited states of HCHO–H system; approaching H on X-axis. Beside each curve are given the states of components to which the state dissociates and the irreducible representation in C_{2v} point group.

When the H atom approaches along the X-axis (Fig. 3), the CT_1 curve drops sharply as R is reduced, but it merely crosses the lower potential curves. Even finite speed motions of the H atom will not cause transitions between these states. As a consequence, the H atom will not be attracted strongly by an $n\pi^*$ or $\pi\pi^*$ excited HCHO molecule in these geometries. A shallow minimum found in each potential curve at an R value of $\approx$1.2 Å is also seen in the ground-state potential curve; it might represent an attraction which is the cause of a stable ketyl radical formation from an H atom and an HCHO in the ground state. Another notable point in this nuclear configuration is that the potential curves of the $[^3(n\pi^*)+H]$ and $[^1(n\pi^*)+H]$ states closely approach at an R value of 2.84 Å, where the two states exchange characters rather abruptly, but continuously (Fig. 3 and Table 2). This is a case of pseudo-crossing,[13] and the transition between these adiabatic states may become possible by finite-speed motions of the H atom relative to the HCHO molecule. This observation is interesting because it seems to represent a mechanism by which singlet-triplet transitions of molecules are promoted through the formation of charge-transfer complexes with other species having odd electrons.

Table 2. Configuration analysis of $[^3(n\pi^*)+H]$ (H on X-axis)

R(Å)	ψ_2°	ψ_3°	ψ_8°	Total (%)
4.0	1.0	—	—	100
3.0	0.993	0.007	−0.003	98.7
2.848	0.896	0.420	−0.005	98.0
2.846	0.734	0.634	−0.004	98.5
2.844	0.536	0.840	−0.003	99.2
2.0	0.019	0.992	−0.003	98.4
1.5	0.022	0.958	−0.008	90.5
1.25	0.028	0.898	−0.016	80.7
1.15	0.039	0.866	−0.020	75.1
1.0	0.046	0.796	−0.021	63.1
0.95	0.046	0.751	−0.019	56.8
0.9	0.042	0.687	−0.014	47.6

$\psi_2^\circ = [^3(n\pi^*)+H]^\circ$, $\psi_3^\circ = [^1(n\pi^*)+H]^\circ$, $\psi_8^\circ = [^3(n\pi, \pi^*\pi^*)+H]^\circ$.

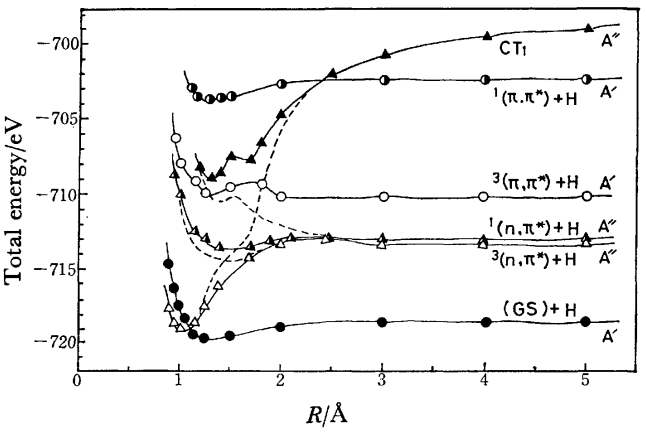

Fig. 4. Potential energy curves of ground and lower excited states of HCHO–H system; approaching H on Y-axis. Beside each curve are given the states of components to which the state dissociates and the irreducible representation in C_s point group.

When the H approaches along the Y-axis to the HCHO in the $^1(n\pi^*)$ or $^3(n\pi^*)$ excited state, the energy of the system decreases remarkably as a result of the strong configurational mixing with the CT_1 state (Fig. 4 and Table 3). The broken lines in Fig. 4 are intended to express these facts schematically. The transition to the ground state is, however, impossible in this mode of approach.

When the H atom is on the Z-axis, it is the $[^3(\pi\pi^*)+H]$ state which shows a marked decrease in energy as a result of the configurational mixing. The situation is

Table 3. Configuration analysis of $[^3(n\pi^*)+H]$ (H on Y-axis)

R(Å)	ϕ_2°	ϕ_3°	ϕ_{11}°	ϕ_{12}°	ϕ_{17}°	Total (%)
4.0	0.999	—	−0.005	−0.014	0.001	100
3.0	0.997	0.008	−0.012	−0.024	0.003	99.4
2.4	0.785	0.600	−0.022	−0.055	0.005	97.9
2.0	0.004	0.967	−0.214	−0.033	0.028	93.8
1.7	0.242	−0.353	0.622	0.440	−0.151	79.0
1.5	0.099	−0.194	0.739	0.325	−0.191	73.7
1.25	−0.245	−0.162	0.704	0.244	−0.197	68.2
1.15	−0.176	−0.172	0.707	0.194	−0.202	64.1
1.0	−0.176	−0.189	0.678	0.185	−0.201	60.5
0.95	−0.151	−0.197	0.671	0.171	−0.191	58.7

$\phi_2^\circ = [^3(n\pi^*)+H]^\circ$, $\phi_3^\circ = [^1(n\pi^*)+H]^\circ$, $\phi_{11}^\circ = CT_1^\circ$, $\phi_{12}^\circ = BCT_3^\circ$, $\phi_{17}^\circ = CT_3^\circ$.

complicated here because of the abundance of states involved, but the results of configuration analysis may be summarized schematically as follows. The CT_1 state first interacts with $[^1(\pi\pi^*)+H]$ in the region of R= 2.5—3.0 Å, and its character is transferred to the latter. The second state then interacts with $[^3(\pi\pi^*)+H]$ in the region of R=2.2−1.3 Å; the lower state acquires a CT_1 character, and its energy drops remarkably as R becomes smaller, until it reaches near that of the ground state, where a third pseudo-crossing to the latter state occurs. The lowest adiabatic state is seen to have a CT_1 character as the main one for $R \lesssim 1.0$ Å. Another feature of these geometries is that the BCT_6 character seems to be an important cause of the energy decrease of the $[^3(\pi\pi^*)+H]$ state in the region of R=3.0−2.2 Å.

The importance of the charge-transfer type of intermediate states has frequently been suggested for quench-

Table 4. Configuration analysis of $[^3(\pi\pi^*)+H]$ (H on Z-axis)

R(Å)	ϕ_1°	ϕ_4°	ϕ_6°	ϕ_{10}°	ϕ_{11}°	ϕ_{14}°	ϕ_{17}°	ϕ_{18}°	Total (%)
4.0	—	0.996	0.002	−0.011	−0.048	0.001	0.002	−0.080	100
3.0	−0.001	0.857	0.063	−0.063	−0.269	0.021	0.014	−0.428	99.8
2.2	−0.004	0.510	0.266	−0.080	−0.508	0.081	0.048	−0.618	98.7
1.7	0.027	0.069	0.344	−0.050	−0.635	0.089	0.059	−0.298	63.0
1.5	0.121	0.200	0.384	−0.049	−0.711	0.064	0.048	−0.303	81.0
1.3	0.312	0.229	0.395	−0.004	−0.656	0.174	0.103	−0.323	88.3
1.15	0.521	0.259	0.337	0.121	−0.494	0.227	−0.071	−0.306	86.4
1.0	0.628	0.196	0.229	0.265	−0.319	0.269	−0.039	−0.156	75.5
0.95	0.675	0.244	0.232	0.287	−0.303	0.319	−0.076	−0.182	88.5

$\phi_1^\circ = [(GS)+H]^\circ$, $\phi_4^\circ = [^3(\pi\pi^*)+H]^\circ$, $\phi_6^\circ = [^1(\pi\pi^*)+H]^\circ$, $\phi_{10}^\circ = BCT_2^\circ$, $\phi_{11}^\circ = CT_1^\circ$, $\phi_{14}^\circ = [(\pi\pi, \pi^*\pi^*)+H]^\circ$, $\phi_{17}^\circ = CT_3^\circ$, $\phi_{18}^\circ = BCT_6^\circ$.

Table 5. Configuration analysis of [(GS)+H] (H on Z-axis)

R(Å)	ϕ_1°	ϕ_4°	ϕ_6°	ϕ_{10}°	ϕ_{11}°	ϕ_{14}°	ϕ_{17}°	ϕ_{18}°	Total (%)
4.0	1.0	—	—	—	—	—	—	—	100
3.0	0.994	0.002	−0.010	0.022	0.003	0.029	−0.099	−0.002	100
2.0	0.969	0.004	−0.040	0.132	0.009	0.109	−0.159	−0.026	99.5
1.5	0.925	0.008	−0.043	0.270	0.057	0.132	−0.123	−0.028	96.8
1.25	0.817	0.054	−0.064	0.331	0.243	0.076	−0.064	0.078	86.1
1.15	0.691	−0.016	−0.118	0.331	0.399	0.027	0.044	0.095	77.2
1.0	0.475	−0.010	−0.171	0.304	0.545	0.021	0.070	0.152	68.4
0.95	0.436	−0.137	−0.189	0.266	0.555	−0.019	0.097	0.145	65.6
0.9	0.377	−0.218	−0.340	0.253	0.552	−0.079	0.158	0.149	73.1

$\phi_1^\circ = [(GS)+H]^\circ$, $\phi_4^\circ = [^3(\pi\pi^*)+H]^\circ$, $\phi_6^\circ = [^1(\pi\pi^*)+H]^\circ$, $\phi_{10}^\circ = BCT_2^\circ$, $\phi_{11}^\circ = CT_1^\circ$, $\phi_{14}^\circ = [(\pi\pi,\pi^*\pi^*)+H]^\circ$, $\phi_{17}^\circ = CT_3^\circ$, $\phi_{18}^\circ = BCT_6^\circ$.

Table 6. Configuration analysis of $[CT_1]$ (H on Z-axis)

R(Å)	ϕ_4°	ϕ_6°	ϕ_{10}°	ϕ_{11}°	ϕ_{12}°	ϕ_{14}°	ϕ_{17}°	ϕ_{18}°	Total (%)
5.0	—	—	—	1.00	—	—	—	—	100
4.0	0.048	−0.082	0.005	0.995	0.001	−0.023	−0.006	−0.003	99.9
3.4	0.146	−0.263	0.044	0.945	0.006	−0.068	−0.003	−0.025	98.2
3.0	0.250	−0.513	0.144	0.776	0.144	−0.120	0.021	−0.081	97.2
2.5	0.262	−0.865	0.077	0.231	0.231	−0.173	0.140	−0.157	95.2
2.0	−0.229	0.799	−0.210	0.140	−0.365	0.164	0.185	−0.085	96.3
1.8	−0.198	0.573	−0.333	0.144	−0.570	0.118	−0.089	0.238	90.7
1.7	−0.381	0.633	−0.219	−0.024	−0.123	0.256	−0.292	0.496	99.1
1.6	−0.400	0.652	−0.035	−0.026	0.058	0.286	−0.344	0.520	99.9
1.5	−0.495	0.385	−0.017	−0.155	0.022	0.409	−0.466	0.252	88.5

$\phi_4^\circ = [^3(\pi\pi^*)+H]^\circ$, $\phi_6^\circ = [^1(\pi\pi^*)+H]^\circ$, $\phi_{10}^\circ = BCT_2^\circ$, $\phi_{11}^\circ = CT_1^\circ$, $\phi_{12}^\circ = BCT_3^\circ$, $\phi_{14}^\circ = [(\pi\pi,\pi^*\pi^*)+H]^\circ$, $\phi_{17}^\circ = CT_3^\circ$, $\phi_{18}^\circ = BCT_6^\circ$.

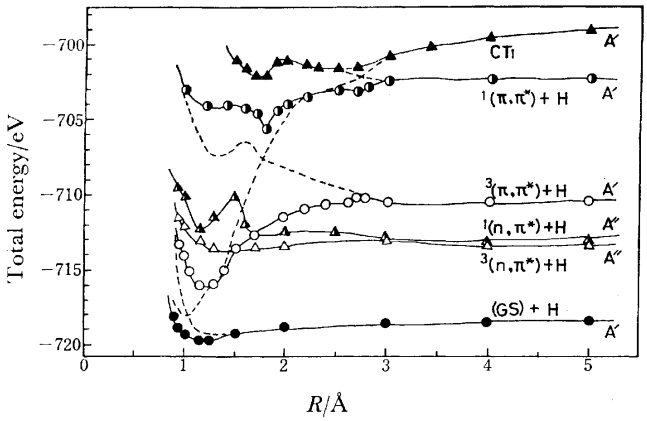

Fig. 5. Potential energy curves of ground and lower excited states of HCHO–H system; approaching H on Z-axis. Beside each curve are given the states of components to which the state dissociates and the irreducible representation in C_s point group.

Table 7. Quartet expansion coefficients of some state functions

a) [³(nπ*)+H] (H on X-axis)

R(Å)	2.845	2.4	2.0	1.5	1.25
C_3	0.0056	−0.0003	0.0009	0.0024	0.0011
C_3'	−0.00007	0.0005	−0.0021	−0.011	−0.019

b) [³(nπ*)+H] (H on Y-axis)

R(Å)	2.5	2.0	1.5	1.25
C_3	−0.0075	−0.012	−0.32	−0.32

c) [³(ππ*)+H] (H on Z-axis)

R(Å)	2.5	2.0	1.5	1.25
C_3''	0.025	0.059	0.32	0.25

C_3, C_3', and C_3'' are the coefficients in Eq. 3 for the $(\pi)^2(n)(h)(\pi^*)$, $(\pi)(n)(h)(\pi^*)^2$, and $(\pi)(n)^2(h)(\pi^*)$ configurations of the reference system respectively.

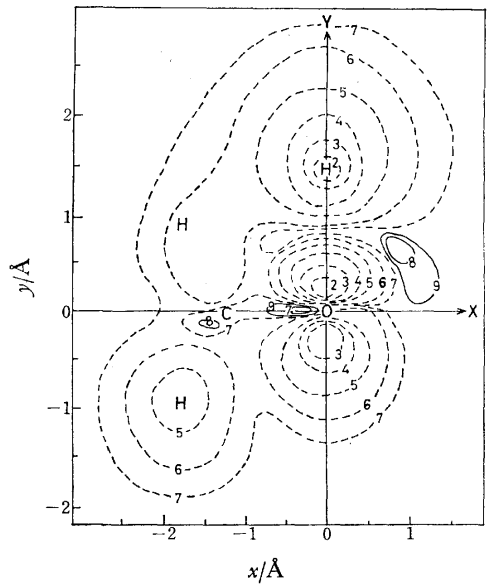

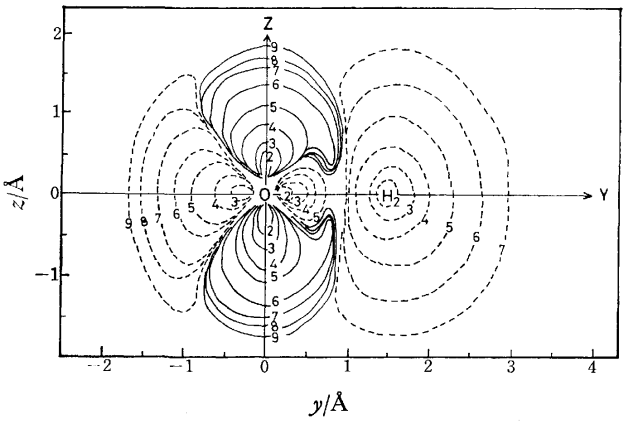

Fig. 6. Change in electron density upon ³(nπ*) excitation; approaching H on Y-axis. Full lines indicate increase and broken lines decrease in electron density. The numbers 1, 2, ···, 9 beside the contours indicate electron density change of 2.0, 1.0, 0.5, 0.2, 0.05, 0.01, 0.002, 0.0005, and 0.0001 electrons/Å³, respectively. a) XY-plane, b) YZ-plane.

ing and photochemical redox processes,[14] and potential curves have been deduced[14a] to describe them in a general but semi-quantitative way. The present straightforward calculation yielded a more concrete picture of the process. One point of criticism that might affect the quantitative aspects of the results was, however, the spin-contaminations of the wavefunctions used. The C_3 coefficients were moderate for the X-approach, but took appreciable values at certain geometries for the Y- and Z-approaches (Table 7). This will considerably obscure the quantitative aspects of the C_1 and C_2 coefficients of the same configuration at those geometries. An inspection showed that the main contribution to the large values in Tables 7b and 7c came from the expansion of CT_1 CSF, and showed the necessity of at least a partial spin-projection in a more quantitative work.

Electron-density Maps. The chemical process could be perceived more visually through inspections of the electron-density maps. The electron-density distributions of the total valence electrons for the system of an HCHO in the ground state and of an H atom on the X-axis were not much different from that of an isolated HCHO, except for a slight electron density in the regions between the two components. This may be the cause of a shallow minimum seen in the [(GS)+H] curve of Fig. 3. The same was found to be true for the system of the ³(nπ*) HCHO and the H atom on the X-axis, in which case charge-transfer cannot occur because of symmetry reasons.

The electron density was also not much different from that of the isolated system with the H on the Y-axis when the HCHO component was in the ground state, but an essential change was seen when the HCHO was excited to the ³(nπ*) state. The difference in the electron densities between the two states is shown in Fig. 6a. In most of the XY-plane, the electron densities are taken off perpendicularly to both sides of the plane upon excitation, whereas small regions of increased electron density appear near the O atom on the CO-axis and in the first quadrant. As there is only a weak attraction exerted on the H atom in the ground state, the separated charge upon excitation may be responsible

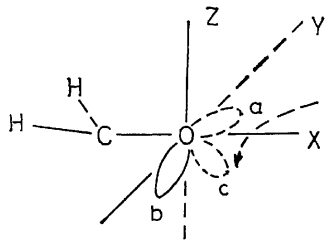

Fig. 7. Inferred path of H toward ($n\pi^*$) excited HCHO in a quasi-static approach. a, b: Leaves of n orbital. c indicates O–H bond orbital in ketyl radical.

for determining the remarkable attraction exerted on the H in this nuclear configuration. One may see that the projection of the vector of the attraction force on the XY-plane is not toward the carbonyl oxygen, but toward a region which is an extension of the CO-axis, as may be seen in Fig. 6a. A similar contour map on the YZ-plane is given in Fig. 6b. The positively charged H atom is seen to be attracted by the negative charge generated on both sides of the XY-plane upon $n\pi^*$ excitation.

By reference to the results obtained above, one may guess the way the H atom is abstracted from a hydrogen donor by $n\pi^*$ excited HCHO. The excited state of HCHO is known to be bent. Let the two H atom of HCHO be above the XY-plane (Fig. 7). When the H being abstracted approaches along a path on the XZ-plane, no charge-transfer contribution may be expected to lower the potential energy of the system, just as in the cases shown in Figs. 3 and 5. The most favorable path of statical approach seems again to be nearly along a leaf (a in Fig. 7) of the n orbital at first, then gradually curving to the final place in the ketyl radical (at an end of c in Fig. 7). The electron-density increase may be more pronounced in the negative Z-direction than in the positive Z-direction, as compared with the pattern in Fig. 6b, as a result of the bent structure of HCHO. The attraction force on the positively charged H may be directed toward the region of the outweighted negative charge. In this case, a less symmetric nuclear arrangement will allow the transition from the CT_1 mixed state to the ground state at a potential curve crossing point similar to the one seen in Fig. 4.

From Fig. 5 it may seem that the $^3(\pi\pi^*)$ excited HCHO could also abstract hydrogen from a hydrogen donor approaching from the Z-direction if a non-adiabatic transition occurred between the potential curves of $[^3(\pi\pi^*)+H]$ and $[(GS)+H]$ around a geometry of $R\approx 1.1$ Å.

The present calculation does not seem to account for the fact[15] that carbonyl compounds with $^3(\pi\pi^*)$ as the lowest triplet have, in general, less reactivities toward hydrogen abstraction than those with $^3(n\pi^*)$ as the lowest triplet. One explanation seems to be as follows. According to Slater's rule, the CI matrix element between two CSF's is calculated, if they are different in one spin-orbital pair, as the energy of the overlap density of the pair orbitals in the field generated by the nuclei and the electrons in the orbitals other than this pair. The CI matrix element between $[(\pi\pi^*)+H]$ and CT_1 is, then, mainly determined by the overlap density between the π and the h orbital, whereas the matrix element between $[(n\pi^*)+H]$ and CT_1 is determined by that between the n and the h orbitals. The carbonyl compounds commonly used in the hydrogen abstraction reaction contain large conjugated π systems, and the overlap between π and h orbitals may be comparatively smaller than in the present case. The orbital overlap between n and h may be affected only slightly by the conjugation due to the local nature of the n orbital. In the carbonyl compounds with the lowest CT-triplet,[15] this effect may even become prominent.

References

1) a) H. Nakatsuji, *J. Am. Chem. Soc.*, **96**, 30 (1974); b) A. Igawa and H. Fukutome, *Prog. Theor. Phys.*, **52**, 115 (1974); c) K. Fukui, S. Kato, and H. Fujimoto, *J. Am. Chem. Soc.*, **97**, 1 (1975); d) K. Ohta, K. Yamaguchi, and T. Fueno, 2L20, 34th National Meeting of the Chemical Society of Japan, Hiratsuka, April (1976); e) S. Nagase and T. Fueno, *Bull. Chem. Soc. Jpn.*, **49**, 2920 (1976).

2) a) J. C. Dalton and J. N. Turro, *Ann. Rev. Phys. Chem.*, **21**, 499 (1970); b) G. Porter, "Reactivity, Radiationless Conversion and Electron Distribution in the Excited States," and N. C. Yang, "Photochemical Reactions of Ketones in Solution, the Hydrogen Transfer Reaction," in "Reactivity of the Photoexcited Organic Molecules," Interscience Publishers, New York (1967), p. 79, 145.

3) J. W. Sidman, *J. Chem. Phys.*, **27**, 429 (1957); F. L. Pilar, *ibid.*, **47**, 884 (1967).

4) J. L. Whitten and M. Hackmeyer, *J. Chem. Phys.*, **51**, 5584 (1969); R. J. Buenker and S. D. Peyerimhoff, *ibid.*, **53**, 1368 (1970); J. L. Whitten, *ibid.*, **56**, 5458 (1972); K. Tanaka, *Int. J. Quantum Chem.*, **8**, 981 (1974).

5) S. Iwata and K. Morokuma, *J. Am. Chem. Soc.*, **95**, 7563 (1973).

6) H. Baba, S. Suzuki, and T. Takemura, *J. Chem. Phys.*, **50**, 2078 (1969).

7) C. C. J. Roothaan, *Rev. Mod. Phys.*, **32**, 179 (1960); W. J. Hunt, T. H. Dunning, Jr., and W. A. Goddard III, *Chem. Phys. Lett.*, **3**, 606 (1969).

8) K. Takagi and T. Oka, *J. Phys. Soc. Jpn.*, **18**, 1174 (1963).

9) J. A. Pople and D. L. Beveridge, "Approximate Molecular Orbital Theory," McGraw-Hill Book Company, New York (1967).

10) H. F. Schaefer, III, "The Electronic Structure of Atoms and Molecules," Addison-Wesley Pub. Co., Reading (1972); a) p. 24, b) p. 148, c) p. 10.

11) R. Pauncz, "Alternant Molecular Orbital Method," W. B. Saunders Co., Philadelphia, Pa. (1967).

12) R. McWeeny and B. T. Sutcliff, "Method of Molecular Quantum Mechanics," Academic Press, New York (1969), p. 48.

13) D. R. Bates, "Atomic and Molecular Processes," Acad. Press, New York (1962), p. 608.

14) a) Y. Mori, *Bull. Chem. Soc. Jpn.*, **35**, 1584 (1962); b) H. Leonhardt and A. Weller, *Ber. Bunsenges. Phys. Chem.*, **67**, 791 (1963); c) G. Porter and P. Suppan, *Trans. Faraday Soc.*, **62**, 3375 (1966); d) A. Bjerre and E. E. Nikitin, *Chem. Phys. Lett.*, **1**, 179 (1967); e) G. Karl, P. Krauss, J. C. Polanyi, and I. W. M. Smith, *J. Chem. Phys.*, **46**, 244 (1967); f) E. Bauer, E. R. Fischer, and F. R. Gilmore, *J. Chem. Phys.*, **51**, 4173 (1969); g) G. H. Parsons, Jr. and S. G. Cohen, *J. Am. Chem. Soc.*, **96**, 2948 (1974).

15) G. Porter and P. Suppan, *Trans. Faraday Soc.*, **61**, 1664 (1965).

Infrared Spectra of 1,3-Butadiene Adsorbed on Alumina-supported Metal Catalysts at Various Temperatures

Yuko SOMA

College of General Education, University of Tokyo, Komaba, Tokyo 153

(Received November 22, 1976)

The infrared spectra of 1,3-butadiene adsorbed on Pd, Ni, and Co catalysts were measured while changing the adsorption temperature. These catalysts behaved differently in butadiene adsorption, and π-adsorbed butadiene was the major adsorbed species below 0 °C on Pd and Ni. This π-species was easily hydrogenated to produce butene at the same temperature.

There have been many infrared spectroscopic studies of hydrocarbons, especially olefins, adsorbed on transition metals.[1-3] The spectra of chemisorbed olefins have been measured mostly using supported metals at room temperature, and have been demonstrated to be of a complex nature caused by the existence of various dissociatively adsorbed hydrocarbons on the metal surface. Although π-bonded olefins on metal catalysts have been considered to be the intermediates of such reactions as hydrogenation, there has been no definite evidence from infrared spectroscopic measurements of the species on the metal surface. Recently π-adsorbed ethylene on Pd was observed from the difference in the spectra of the adsorbed species before and after hydrogenation[4] or in a low-temperature measurement.[5]

The hydrogenation reaction of 1,3-butadiene on transition metals has been studied in detail by Bond, Wells, and their co-workers.[6] According to their investigations, the reaction rate is proportional to the first order of the hydrogen pressure, while it is nearly proportional to the zero order of the butadiene pressure, like other olefin hydrogenation reactions. The composition of hydrogenated products (1-butene, *trans*- and *cis*-2-butene) varies depending on the metals and on the method of preparing the catalysts; this suggests the importance of the configurations of the adsorbed butadienes on the surface in deciding the compositions of hydrogenated products, kinds of butene. They considered three types of adsorbed butadiene: mono-π-bonded species, and *trans*- and *cis*-di-π-bonded species. Therefore, the direct measurement of the infrared spectra of adsorbed species will be helpful in understanding the mechanism and selectivity of the reaction.

The infrared spectra of butadiene adsorbed on Ni at room temperature were investigated by Erkelens,[3] and only methylene-rich polymeric species were observed. On Pd metal, no absorption band for adsorbed species appeared at room temperature, but that of polymerized species was observed after hydrogen addition.[2]

In this paper the infrared spectra of butadiene adsorbed on alumina-supported Ni, Pd, and Co catalysts will be reported in the temperature range between room temperature and −80 °C. At low temperatures, the side reactions were supressed and the spectra of π-bonded butadiene were clearly observed. The differences between the three metal catalysts in the adsorption of 1,3-butadiene were demonstrated to be of interest in connection with their catalytic properties in the hydrogenation reaction.

Experimental

Nickel or cobalt catalyst was prepared from a suspension of alumina in an aqueous solution of each metal nitrate, which was decomposed in air at 450 °C. Palladium particles were deposited on alumina in a $PdCl_2$ solution with the addition of formaldehyde and sodium hydroxide. Each of these catalysts contains about 9 wt % metal.

These catalysts were used in the shape of discs for the infrared measurements. For room-temperature measurements, the disc was evacuated at 420 °C for 2 h in an infrared cell and then reduced in hydrogen for 3 h at the same temperature. About 60 Torr of gaseous butadiene was placed in contact with the Ni catalyst for 15 min, but with Co catalyst for 20 h, and the spectra were measured after the cell was evacuated to 10^{-3} Torr. The cryogenic cell for low-temperature measurements was similar to that used by Avery.[2] As the highest temperature which could be attained with this cell was about 300 °C, the disc was evacuated and reduced at 400 °C in an glass vessel; the disc was then transferred to the cryogenic cell and was reduced again at 300 °C. The catalyst was placed in contact with gaseous butadiene for about 30 min; the butadiene was then removed by trapping and evacuation to 10^{-3} Torr. The adsorption of butadiene on an alumina support is negligible under these experimental conditions.

The 1,3-butadiene(*h*-butadiene) (Tokyo-Kasei Co.) and 1,3-butadiene-1,1,4,4-d_4(CD_2=CH−CH=CD_2) (MSD Co.) were purified by passing it through a heated palladium thimble.

Gas chromatography with a DMF–alumina column was used for the analysis of gaseous hydrocarbons.

Results

Palladium. Figure 1 shows a spectrum of $\Delta^{1,3}$-C_4H_6 chemisorbed on Pd-Al_2O_3 at −32 °C, together with the band frequencies of Fe–butadiene complexes and free butadiene. It is evident that the spectrum is quite different from that of gaseous butadiene, but corresponds to that of Fe–butadiene complexes except for a broad band at 1653 cm^{-1}. The assignment of the bands of chemisorbed $\Delta^{1,3}$-C_4H_6 can be made on the basis of the results for the Fe–C_4H_6 complex reported by Davidson *et al*:[7] 1433 for $\nu_{C=C}$, 1224 cm^{-1} for ν_{C-C}, and 1473 and 1376 cm^{-1} for CH_2 scissors vibrations. (π_d)* The existence of the band at 1653 cm^{-1} shows that a part of the chemisorbed butadiene has a

* π_s and π_d show two adsorbed species of butadiene on Pd below 0 °C. These structures will be shown in the 'Discussion' section.

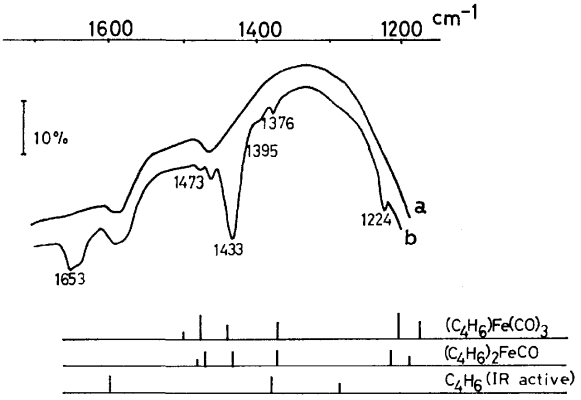

Fig. 1. IR spectrum of $\Delta^{1,3}$-C_4H_6 adsorbed on Pd–Al_2O_3 at −32°C(b), (a) Pd-Al_2O_3 background. The lines under the spectra show the positions and band intensities of Fe–C_4H_6 complexes and gaseous C_4H_6.

free C=C double bond and has another C=C bond interacting with the surface Pd. (π_s)*

The existence of two kinds of adsorbed species (π_d, π_s) is consistent with the fact that the band intensity at 1653 cm^{-1} relative to that at 1433 cm^{-1} varies with the butadiene coverage and the temperature. The ratio of these peak intensities was about 0.34 when a small amount of butadiene was adsorbed at −80 °C, while the value reached 0.60 when adsorption was saturated at −25 °C. If it is assumed that the band at 1433 cm^{-1} is due to both π_s and π_d species, while the band at 1653 cm^{-1} is due only to the π_s species, the relative amount of the π_s species can be estimated to be small at a low butadiene coverage, but to increase with a rise in the adsorption temperature. The rate of the decrease of the absorbance at 1653 cm^{-1} upon D_2 addition is 1.2 times faster than that of the absorbance at 1433 cm^{-1} on both Pd and Ni at −50 °C. These observations indicate that the π_s species is less stable than the π_d species.

When hydrogen was introduced on butadiene chemisorbed over a Pd catalyst at −50 °C, new bands attributable to the formation of a methyl group and a co-ordinated C=C double bond appeared, as is shown in Fig. 2. These bands which appeared upon hydrogen addition (indicated by arrows in Fig. 2c) are closely related to the bands of butene in K[$PtCl_3$(*trans*-C_4H_8)],[9] except for a part of the band at 1650 cm^{-1} which disappeared easily upon evacuation and the band at 1580 cm^{-1}. The only gaseous products were butenes and *n*-butane, and the butenes adsorbed on Al_2O_3 showed a band at 1580 cm^{-1}, so the above two bands may be attributed to gaseous butene and to butene adsorbed on Al_2O_3 respectively. It may be concluded that the π-species of chemisorbed butadiene was hydrogenated to form chemisorbed butene, a part of which was liberated into the gas phase or adsorbed on Al_2O_3.

At room temperature, no spectrum of butadiene adsorbed on Pd was observed, in agreement with the result by Avery,[2] whereas weak bands due to the formation of a methyl group were observed after hydrogen addition.

Nickel. The spectrum of $\Delta^{1,3}$-C_4H_6 chemisorbed on Ni at low temperatures (−78—0 °C) is almost

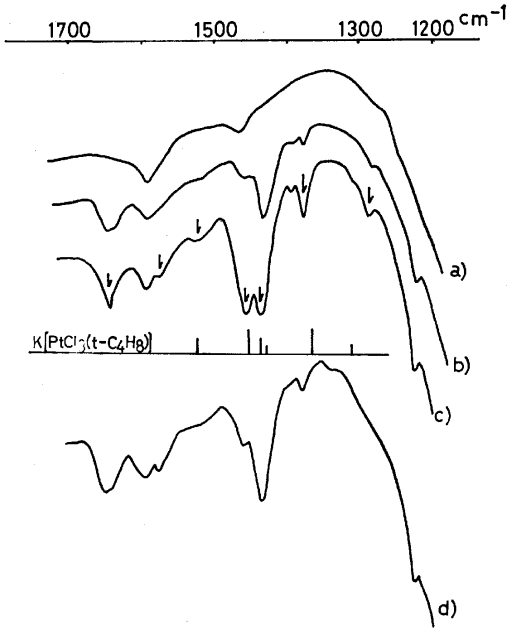

Fig. 2. IR spectra of $\Delta^{1,3}$-C_4H_6 adsorbed on Pd–Al_2O_3 at −50°C and spectral changes with addition of H_2. a) Background. b) Chemisorbed $\Delta^{1,3}$-C_4H_6 at −50°C. c) After introduction of 25 Torr H_2. Arrows show the bands which appeared by H_2 addition. d) Evacuated to 10^{-3} Torr. The inserted lines show the band positions and strengths of Pt–C_4H_8 complex.

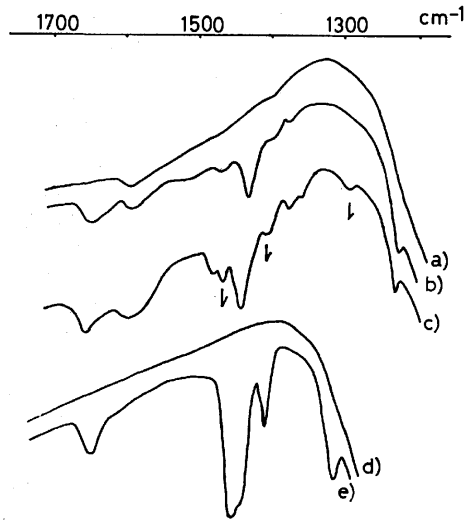

Fig. 3. IR spectra of $\Delta^{1,3}$-C_4H_6 adsorbed on Ni–Al_2O_3 at various temperatures.
a) Background of the spectra b and c. b) −35°C. c) 15°C. d) Background of the spectrum e. e) Room temperature. Arrows show the bands increased in intensity at higher temperatures.

identical to that chemisorbed on Pd. The spectrum changed, however, as is shown in Fig. 3, when the temperature was raised, and new bands appeared which could not be removed by room-temperature evacuation. The spectra at room temperature are shown in Fig. 4, while the observed frequencies and their assignments are listed in Table 1. The two adsorbed species can be distinguished from each other on the basis of their behavior

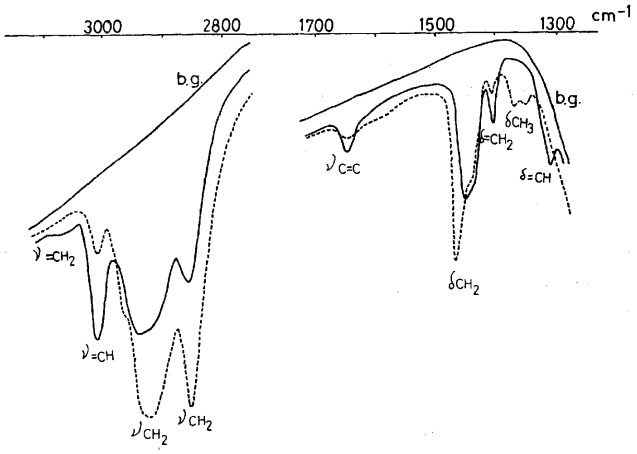

Fig. 4. IR spectrum of $\Delta^{1,3}$-C_4H_6 adsorbed on Ni-Al_2O_3 at room temperature(——) and that after hydrogen was introduced (-----). b. g.; Ni-Al_2O_3 background.

Table 1. Observed frequencies of 1,3-butadiene chemisorbed on Ni-Al_2O_3 at room temperature, the intensity changes of these bands upon hydrogen addition, and the band assignments

CH_2=CH-CH=CH_2 cm^{-1}	New bands appearing after H_2 addition cm^{-1}	Intensity changes after H_2 addition	Assignments
3075		decreased	$\nu_{=CH_2}$
3010		decreased	$\nu_{=CH}$
	2960 sh		ν_{CH_3}
2925		increased	ν_{CH_2}
2854		increased	ν_{CH_2}
1650		decreased	$\nu_{C=C\ free}$
	1467		δ_{CH_2}
1440		decreased	$\delta_{=CH_2}$ or $\nu_{C=C\ ads.}$
1407		decreased	$\delta_{=CH}$
	1370		δ_{CH_3}
1308		decreased	$\delta_{=CH_2}$

CD_2=CH-CH=CD_2 cm^{-1}	New bands appearing after D_2 addition cm^{-1}	Intensity changes after D_2 addition	Assignments
3006		decreased	$\nu_{=CH}$
2955		decreased	ν_{-CHM-}
2910		increased and shifted to 2897cm^{-1}	ν_{CH}
	2860 sh		
2300		decreased	$\nu_{=CD_2}$
2210		increased and shifted to 2202 cm^{-1}	ν_{CD_2}
2125		decreased	ν_{-CD_2M}
2100		increased and shifted to 2106 cm^{-1}	ν_{CD_2}
1645		decreased	$\nu_{C=C\ free}$
1403		decreased	$\delta_{=CH}$
	1308		δ_{CHD}

upon hydrogen addition; the intensity of one increases, while that of the other decreases. The former bands can be assigned to the CH_2 stretching (2925, 2854) and CH_2 scissors (1467 cm^{-1}) of polyethylene. The latter bands are located at 3010, 1650, 1440, 1407, and 1308 cm^{-1} and may be assigned as is shown in Table 1. The weak band at 1370 cm^{-1} and the shoulder at about 2960 cm^{-1} may be due to the methyl group. In the case of butadiene-d_4, the bands at 3006, 2955, 2300, 2125, 1645, and 1403 cm^{-1} decreased in intensity upon hydrogen addition.

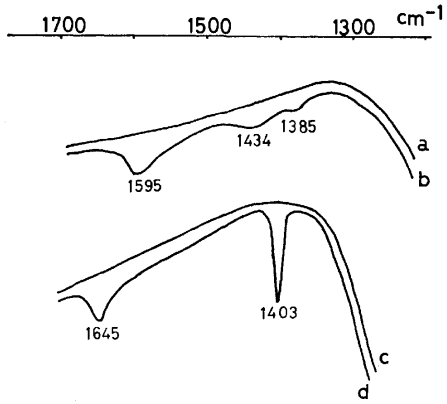

Fig. 5. IR spectra of CD_2=CH-CH=CD_2 adsorbed on Ni-Al_2O_3.
a, c) Background. b) Adsorption at −29°C. d) Adsorption at room temperature.

The adsorbed species, the amount of which decreased upon hydrogen addition at room temperature, can be considered to be different from those (π_d, π_s) observed below 0 °C, because the former species shows sharp bands at 1407 and 1308 cm^{-1} which were not observed in the π_d and π_s species of *h*-butadiene. Furthermore, the spectra of butadiene-d_4 changed remarkably with a change in the adsorption temperature, as is shown in Fig. 5. The free C=C double bond stretching band was observed at 1595 and 1645 cm^{-1} in low-temperature and room-temperature spectra respectively. This fact supports the above-mentioned deduction, since the adsorption of butadiene-d_4 produces, probably, the same species as *h*-butadiene adsorption.

The rate of butadiene hydrogenation to butene was zero-order to the butadiene pressure, and proportional to the hydrogen pressure, on the Pd and Ni catalysts in the low-temperature range (−60—10 °C) and on Co between 0 and 100 °C. The number of active sites of butadiene hydrogenation can be estimated from the amount of the C_4 species ($C_4H_8+C_4H_{10}$) formed by the addition of hydrogen to chemisorbed butadiene. As is shown in Table 2, the amount of C_4 species desorbed from the Ni catalyst by hydrogen decreases with an increase in the adsorption temperature, though the amount of butadiene adsorbed has a tendency to increase because of polymerization on the surface. At −31.5 °C almost all of the Ni atoms on the surface are active in hydrogenation, but at higher temperatures, polymerization on the surface destroys the active sites

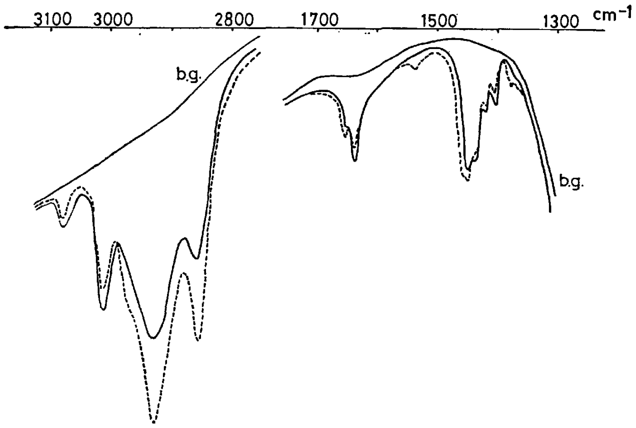

Fig. 6. IR spectrum of $\Delta^{1,3}$-C_4H_6 adsorbed on Co–Al_2O_3 at room temperature(——) and that after hydrogen was introduced(----). b. g.; Co–Al_2O_3 background.

for hydrogenation to butene. The number of active sites at room temperature is less than 10% of the surface Ni atoms.

Cobalt. Figure 6 shows the spectrum of butadiene chemisorbed on Co–Al_2O_3 at room temperature and that after hydrogen addition. The adsorption at room temperature was very slow, and the catalyst had to be in contact with butadiene for 20 h to obtain a sufficient intensity of the spectrum of the adsorbed species. When butadiene was in contact for 20 h, several weak bands appeared at 2960, 2920, 2860, 1460, and 1370 cm^{-1} on Al_2O_3 without metal. Though the spectra of chemisorbed species on Co–Al_2O_3 resemble, as a whole, those on Ni at room-temperature adsorption, some significant differences can be noted. The difference between Ni and Co spectra can be clearly seen in Fig. 7.

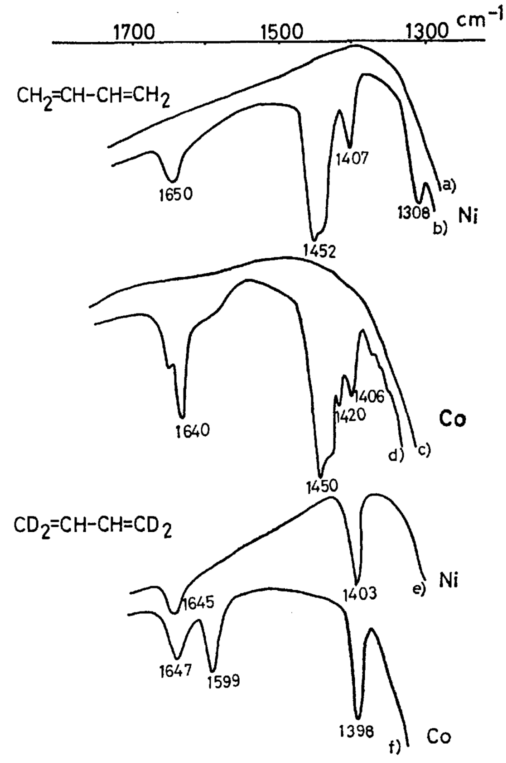

Fig. 7. IR spectra of 1,3-butadiene adsorbed on Ni– and Co–Al_2O_3 at room temperature.
a, c) Background. b, d) C_4H_6 adsorption on Ni and Co resp. e, f) $C_4H_2D_4$ adsorption on Ni and Co resp.

Discussion

Palladium. When pre-adsorbed butadiene on Pd was removed by introducing hydrogen below 0 °C, the gaseous products were butadiene, butene, and butane. Thus, butadiene may be considered to be non-dissociatively adsorbed on Pd in this temperature range. The observed similarity between the spectrum of butadiene chemisorbed on the Pd surface and that of the Fe complex may indicate that one type of adsorbed butadiene on Pd has the following structure, as butadiene in the Fe complex has a *cis* configuration with the two C=C bonds π-bonded to Fe:[7)]

π_d; 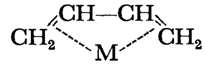

It may be considered there exists another species which has a free C=C stretching band at 1653 cm^{-1}. The only band which were distinct to this species was the band at 1653 cm^{-1}, so it is reasonable to consider this species to have a structure similar to that of the above species, π_d. Thus, the following structure may be considered:

$$\pi_s;\quad CH_2{=}CH{-}CH{=}CH_2 \text{ (M coordinated below the terminal C=C)}$$

It has been reported that the butadiene in the $[PdCl_2(C_4H_6)]_2$ complex is monodentate at −40 °C and that it gives the free C=C stretching band at 1660 cm^{-1} and a strong band around 1440 cm^{-1}.[8)] Because the C=C stretching band is presumed to exhibit the largest shift with the change in the nature of π-bonding between butadiene and a metal atom, it is not unreasonable that the remaining bands of this π_s butadiene could not be observed from π_d butadiene.

Nickel. Butadiene chemisorbed on Ni below 0 °C must have structures similar to those chemisorbed on Pd, judging from the agreement of the spectrum; those were π_s and π_d.

However, the spectrum at room temperature is different from that below 0 °C. The former spectrum is explained as showing the co-existence of two adsorbed species; one is polyethylene, whose intensity increased upon hydrogen addition:

$$\text{polymer: } -(CH_2)_n-$$

From the spectra it was deduced that the other species had C=C, CH_2=, and CH= groups in *h*-butadiene and C=C, CD_2=, =CH, –CHM–, and –CD_2M groups in butadiene-d_4. Although the stretching bands due to –CHM– and –CH_2M groups in *h*-butadiene could not be observed, those bands were considered to overlap with the strong bands of polyethylene. The species with these bands most probably has the structure:

$$\sigma:\ CH_2{=}CH{-}\underset{\mid}{\overset{}{CH}}{-}\underset{\mid}{CH_2}$$
$$\qquad\qquad\ \ M\quad\ M$$

Cobalt. There are one σ-type species and one

polymeric species on Ni, whereas on Co there is still another adsorbed species which decreased in intensity upon hydrogen addition at room temperature, as is shown in Fig. 7. The third species has the bands at 1640 and 1420 cm^{-1} for C_4H_6 and at 1599 cm^{-1} for butadiene-d_4. As the bands of the species on Co agree with those on Pd or Ni in the low-temperature range, and are assigned to π-adsorbed species (π_s, π_d), the two kinds of π-adsorbed species remain stable at room temperature on Co, though they are unstable on Pd and Ni.

The observed species of 1,3-butadiene chemisorbed on alumina-suported Pd, Ni, and Co catalysts can be summarized as follows:

	Low temperatures (−50—0 °C)	Room temperature
Pd	$\pi_s+\pi_d$	—
Ni	$\pi_s+\pi_d$	polymer+σ
Co	—	polymer+σ+π_s+π_d

The σ-type species was easily hydrogenated at room temperature and can be considered to be a precursor of polyethylene and/or 1-butene.

The π-species which were observed on Pd and Ni at low temperatures and on Co at room temperature were composed of two species (π_s, π_d), and the π_s species was less stable than the π_d species. These π-adsorbed species covered almost all of the Ni surface atoms at low temperatures (−35 °C), as is shown in Table 2, and were easily hydrogenated by hydrogen to form adsorbed butene at the same temperature (Fig. 2).

Table 2. Desorption products of adsorbed C_4H_6 on Ni-Al_2O_3, which were removed by the addition of H_2[a)]

T °C	Amounts of desorbed species ($C_4H_8+C_4H_{10}$) mol/g-cat	(C_4H_6) mol/g-cat	Amounts of surface Ni atoms[b)] mol/g-cat
−31.5	8.37×10^{-5}	0.77×10^{-5}	9.78×10^{-5}
2	3.69	0.62	
29.8	0.71	0.54	

a) 75 Torr of C_4H_6 was adsorbed for 30 min at the above temperature and evacuated to 0.03 Torr, and then 25 Torr of hydrogen was introduced to hydrogenise and remove the adsorbed species. The gaseous desorption products were C_4H_6, C_4H_8, and C_4H_{10}. b) The Ni surface area was estimated from the amount of H_2 adsorbed at 0 °C.

The π_s species may be considered to be a precursor of 1-butene, and the π_d species, to be that of 2-butene in butadiene hydrogenation.

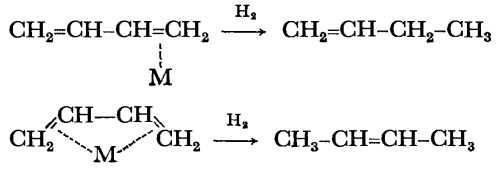

$CH_2=CH-CH=CH_2 \xrightarrow{H_2} CH_2=CH-CH_2-CH_3$

$CH_2=CH-CH=CH_2 \xrightarrow{H_2} CH_3-CH=CH-CH_3$

π-Bonded ethylene was observed by IR measurement on Al_2O_3-supported Pd or Pt catalysts at low temperatures (−86 °C) as the main adsorbed species on the surface,[5)] whereas the main adsorbed species were σ-bonded or dissociatively adsorbed species at room temperature.[1,4)] In the butadiene adsorption, also σ-type and polymerized species were shown to be formed on Ni only above room temperature, while π-bonded species were observed at low temperatures. These facts indicate that π-bonded species of olefins which are considered to be precursors of hydrogenation reaction, become predominant on transition metals at low temperatures, where the reactivity of the metal catalysts is lowered. It is interesting that Pd, Ni, and Co behave differently from each other in butadiene adsorption; the difference in the stability of π-adsorbed species on Pd and Ni from that on Co, and the existence of polymerized species on Ni and Co, which decreases the active sites for hydrogenation reaction.

Wells and his co-workers discriminate various Ni or Co catalysts as Type A or Type B for butadiene hydrogenation.[6)] According to them, the 1,2-addition of hydrogen is preferred on a Type A catalyst, while on a Type B catalyst 1,4-addition occurs mainly. All the catalysts used here (Ni, Co, and Pd) showed Type A behavior; more than 50% of the butene produced was 1-butene, although the *trans*: *cis* ratio was high on Pd (7—8), but low on Ni and Co, (2—3). Type B behavior could not be observed even when the reduction temperature was raised above 400 °C; this might be because of the small metal particle size of these catalysts (less than 60 Å).

The author is grateful to Professor T. Onishi and Professor M. Nishikawa for their helpful discussions.

References

1) B. A. Morrow and N. Sheppard, *Proc. R. Soc. London, Ser. A*, **311**, 391, 415 (1969); A. Ravi and N. Sheppard, *J. Phys. Chem.*, **76**, 2699 (1972); G. Blyholder and W. V. Wyatt, *J. Phys. Chrm.*, **78**, 618 (1974).
2) N. R. Avery, *J. Catal.*, **19**, 15 (1970).
3) J. Erkelens, *J. Catal.*, **37**, 332 (1975).
4) J. D. Prentice, A. Lesiunas, and N. Sheppard, *J. Chem. Soc. Chem. Commun.*, **1976**, 76.
5) Y. Soma, *J. Chem. Soc. Chem. Commun.*, **1976**, 1004.
6) G. C. Bond, G. Webb, P. B. Wells, and J. M. Winterbottom, *J. Chem. Soc.*, **1965**, 3218; J. J. Phillipson, P. B. Wells, and G. R. Wilson, *J. Chem. Soc., A*, **1969**, 1351; A. J. Bates, Z. K. Leszczyński, J. J. Phillipson, P. B. Wells, and G. R. Wilson, *ibid.*, **1970**, 2435; R. G. Oliver and P. B. Wells, "Proceedings of the 5th International Congress on Catalysis, 1972," North-Holland Publishing Co., Amsterdam (1973), Paper 44, p. 659.
7) G. Davidson and D. A. Duce, *J. Organomet. Chem.*, **44**, 365 (1972).
8) M. Donati and F. Conti, *Tetrahedron Lett.*, **1966**, 1219.
9) J. Hiraishi, D. Finseth, and F. A. Miller, *Spectrochim. Acta, Part A*, **25**, 1657 (1969).

Determination of Magnetic Susceptibilities of Diamagnetic Liquids by an Improved Viscometer Method

Kazuo SUEOKA and Toshio IKEDA*

Department of Chemistry, Johsai University, Sakado, Saitama 350-02
**Department of Chemistry, Shizuoka University, Shizuoka 420*

(Received December 25, 1976)

An improved viscometer method is presented for the determination of the magnetic susceptibility of a liquid with a complete exclusion of the oxygen effect. The method was found to be excellent even in determining the magnetic susceptibilities of diamagnetic liquids, giving results accurate to within ±0.05%. The influence of air (or oxygen) was also discussed.

Previously, one of the present authors reported a viscometer method[1] for the determination of the magnetic susceptibilities of paramagnetic liquids by measuring the rate of flow of liquid through the capillary of a viscometer of the Ostwald type under the action of an external magnetic field. In the present study, the measuring device was improved using a modified Ubbelohde viscometer so that one may determine accurately the diamagnetic susceptibilities of liquids as well even by using an electromagnet of a comparatively small size. The diamagnetic susceptibilities of some organic liquids measured with the use of the improved cell under nitrogen were found to be in good agreement with those values reported in the literature within a range of deviation such as was pointed out by Eggleston *et al.*[2]

Theoretical

A modified capillary viscometer of the Ubbelohde type (Fig. 1) is placed in a magnetic field so that the lower end of the capillary is in the center of a gap between the pole pieces of an electromagnet, while its capillary part extends vertically, through the inhomogeneous region, outside of the field. Then, a liquid in the capillary of the cell is forced to flow down by the action of gravity downwards and by that of the magnetic force upwards (or downwards, as the case may be), both acting simultaneously on the liquid when it passes through the inhomogeneous region of the field.

The Hagen-Poiseuille expression for the flow of a liquid may be written as

$$\frac{1}{t_H} = \frac{\pi r^4}{8lv\eta}\left(\rho g\tilde{h} + \frac{1}{2}\kappa H^2\right), \tag{1}$$

where t_H is the time required by the liquid of a certain volume, v, to flow down in the presence of the field through a capillary with a certain radius, r, and a certain length, l; g is the acceleration of gravity; h is the mean effective head of the liquid; the ρ, η, and κ symbols represent the density, the viscosity coefficient, and the volume magnetic susceptibility of the liquid respectively; H denotes the local magnetic field strength near the center of the pole-pieces gap of the magnet. Denoting by t_0 the time of flow of the liquid in the absence of an external magnetic field, one may write $1/t_0 = \pi r^4 \rho g\tilde{h}/8lv\eta$. Since η is practically independent of the field of such an order of strength as is used here, we obtain from Eq. 1 the following relation:

$$\frac{t_0 - t_H}{t_H} = \frac{\kappa H^2}{2\rho g\tilde{h}} = \frac{\chi H^2}{2g\tilde{h}}, \tag{2}$$

where χ represents the mass magnetic susceptibility of the liquid. Equation 2 is the basic equation for determining the magnetic susceptibility in the present method. As is clear in Eq. 2, the time, t_H, should be longer than t_0 for diamagnetic liquids, while it is shorter for paramagnetic liquids. Upon taking into consideration the fact that the present type of viscometer is so made that the mean effective head, h, is controlled automatically to an exactly fixed value in every measurement, one may always be allowed to write

$$\frac{t_0 - t_H}{t_H\chi} = K, \tag{3}$$

so long as t_H is measured under the same field strength, H, where K is a constant characteristic of the cell used and is dependent on H, but entirely independent of the nature of the liquid. If once the constant, K, is determined for a certain standard liquid substance, such as water, whose magnetic susceptibility is known accurately, the susceptibilities of all the other liquid substances can be determined by merely measuring the two corresponding quantities, t_0 and t_H, of the sample to be studied.

Experimental

Materials. Commercial nitrogen with a purity of more than 99.9% was dried by passing silica gel and phosphorus pentaoxide through. The water was purified by sub-boiling distillation from a pure quartz still after deionization. The benzene, carbon tetrachloride, methanol, 2,2,4-trimethylpentane, and cyclohexane were Dotite Primasol solvents, while the toluene, dioxane, ethyl acetate, heptane, hexane, 2-propanol, and acetone were Dotite Spectrosol solvents obtained from the Dojindo Co. The other solvents, such as, acetic acid, ethanol, and nitrobenzene, were of the Wakō Guaranteed Reagent grade. These organic solvents were used without further purification.

Capillary Cell. A capillary viscometer cell of a modified Ubbelohde type, equipped with a thermostat jacket, was fixed in the pole gap of a magnet so that the lower end of its capillary part was located at the center of the pole gap of the magnet, while its upper part extended vertically out of the magnetic field through the inhomogeneous region of the field. Figure 1 shows the experimental equipment, where a capillary cell made of Pyrex glass is fixed upright in duplicated water jacket cabinets made of poly(vinyl chloride). The cabinets are covered with foam polystylene to which a glass window, W,

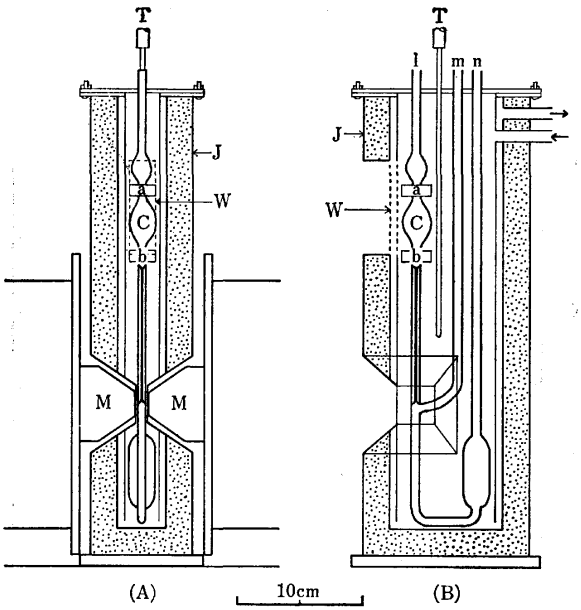

Fig. 1. Experimental setup, A, Front view, and B, side view. C, Capillary cell; a and b, detectors of viscometer; W, glass window; M, magnet; J, cabinet made of poly(vinyl chloride) covered with foam polystylene; T, thermistor. The openings, l, m, and n, connected to the operation tube (Fig. 2).

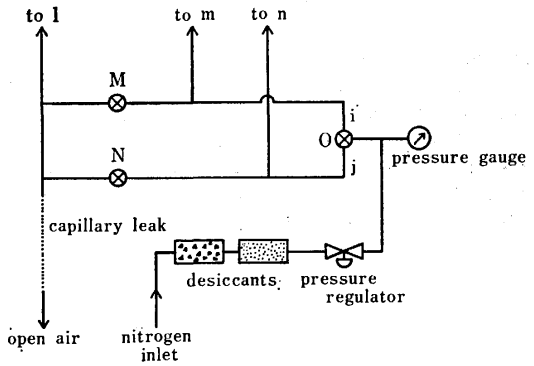

Fig. 2. Connection diagram of the operation tube.

is attached at the level of the upper globular part, C, of the cell.

Magnet. A Weiss-type 100-kg electromagnet manufactured by Nihon Kohmitsu Kenkyusho was used. The magnet pole pieces, about 20 mm in tip diameter, were set at a separation of 8 mm. The magnetic field was controlled using a stabilized dc source (±0.01%) up to 4 A, corresponding to a maximum field of 18800 Oe. The magnetic-field strength was calibrated with a Yokogawa gauss meter, type 3251, at the center of the pole gap.

Measuring. Prior to measuring, the liquid sample which was to be put in the cell was saturated with nitrogen by passing nitrogen through the liquid for about 10 min, and the residual inside space of the cell was fully filled with nitrogen by the aid of an operation tube (Fig. 2) connected to the cell. After this, until the measurement came to an end, nitrogen was continually allowed to flow through the operation tube so that the liquid in the cell was never exposed to air again. When it was necessary to shift the liquid sample up to the globular part, C, of the cell, a moderate pressure slightly higher than the exterior was applied by introducing nitrogen through the operation tube during the measurements,

Table 1. Operation of M, N, and O valves

	M	N	O
Removing air	close	open	i
Shifting up liquid	close	close	j
Measuring	open	open	j

while the inside pressure was kept constant. The direction of the flow of nitrogen was controlled, as occasion called for, by operating three magnetic valves made of Teflon in the way indicated in Table 1. The time of flow of the liquid was measured to an accuracy of ±0.01 s using a viscometer of the Shibayama Scientific Co. provided with an electric detector connected to an electronic clock for monitoring the passage of the meniscus of the liquid. The temperature around the cell was controlled at 20±0.01 °C by circulating thermostated water. The measurement of the flow time was repeated alternately in the presence or in the absence of the magnetic field, and the value of $(t_0-t_H)/t_H$ was calculated for each step. The observed values were found to become closely reproducible after several repetitions of measurements in the beginning. Twenty or fifty measurements were averaged to calculate the magnetic susceptibility.

Results and Discussion

The results are shown in Fig. 3. In all cases a perfect linear relation may be seen passing through the point of origin. These results can be expressed by the following experimental formula:

$$\frac{t_0-t_H}{t_H} = \alpha H^2, \tag{4}$$

where α should, in comparison with Eq. 2, be proportional to the mass susceptibility, χ, of the liquid in such a way that $\alpha=\chi/2gh$; this has proved to be true experimentally as well, as may be seen in Table 2. Thus, Eq. 3 was well confirmed.

The susceptibilities were calculated by the aid of Eq. 3 for some liquids, taking water as a standard reference. The results are shown in Fig. 4 and Table 3. The observed values of χ are found to be reproducible within ±0.05% and are in good agreement with the

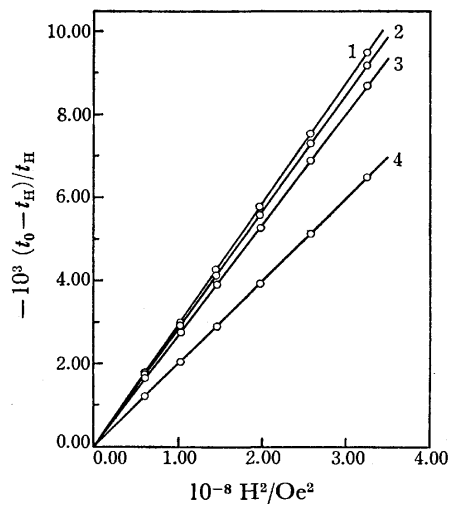

Fig. 3. Relationship between the time of flow of diamagnetic liquids and the external magnetic field strength: 1, ethanol; 2, water; 3, methanol; 4, nitrobenzene.

Table 2. Comparison of α values with magnetic susceptibilities of liquids at 20 °C

Materials	$-10^{11}\alpha$[a] dyn^{-1} cm^2	$-10^6\chi_{lit}$[b] e.m.u.	$-10^5\alpha/\chi_{lit}$ dyn^{-1} cm^2 e.m.u.$^{-1}$
Water	2.82	0.719	3.92
Methanol	2.67	0.660—0.669	4.05—3.99
Ethanol	2.91	0.717—0.736	4.06—3.95
Benzene	2.76	0.675—0.707	4.09—3.90
Nitrobenzene	2.00	0.500—0.505	4.00—3.96
Toluene	2.82	0.711—0.722	3.97—3.91

a) Mean of 10 measurements.
b) Obtained by the conversion of the molar magnetic susceptibilities, χ_M, Landolt-Börnstein, "Zahlenwerte und Funktionen aus Physik, Chemie, Astronomie, Geophysik und Technik," II Band, 10 Teil, Springer Verlag, Berlin (1967).

literature values. However, strictly speaking, most of them are slightly larger than the literature values, except for acetone and cyclohexane.

As is shown in Fig. 5 for benzene, the observed value of $(t_0-t_H)/t_H$ was practically attained within about 2 min after nitrogen was passed through; this is its final steady state value, observed after the complete removal of air from the cell. Since, in the present work, the passage of nitrogen was carried out for a sufficiently long time (more than 10 min), the influence of air that was found in the cell in the beginning, including the liquid sample, could be assumed to be reduced to the limits of accuracy of this method, *i.e.*, within $\pm 0.05\%$.

Eggleston *et al.*[2] pointed out experimentally that most of the diamagnetic susceptibilities reported in the past are in error by an amount corresponding to the effect due to dissolved air. The magnetic susceptibility of a liquid dissolving air may be expressed in the following relationship:

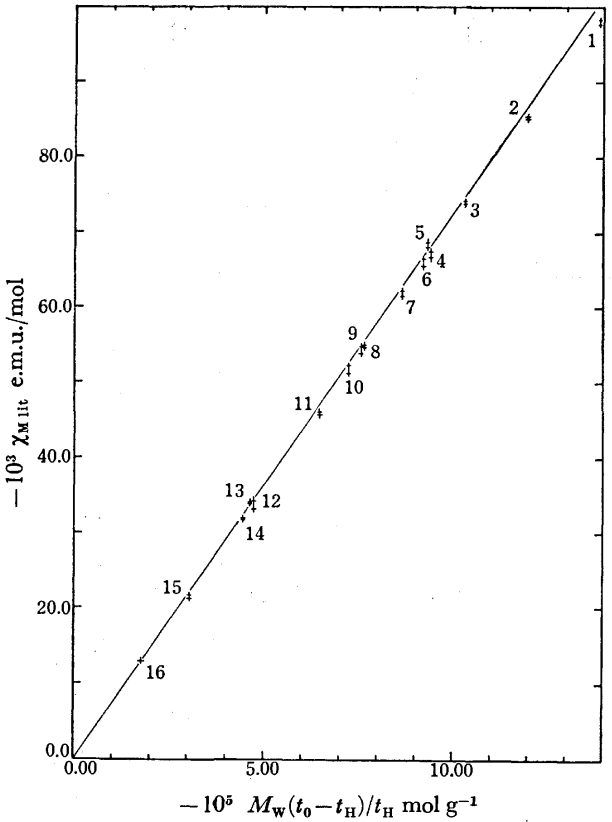

Fig. 4. Relationship between the $(t_0-t_H)/t_H$ value found at a fixed magnetic-field strength of 18800 Oe and the literature values of the magnetic susceptibility of the liquids. M_w, molecular weight. 1,2,2,4-trimethylpentane; 2, heptane; 3, hexane; 4, carbon tetrachloride; 5, cyclohexane; 6, toluene; 7, nitrobenzene; 8, benzene; 9, ethyl acetate; 10, dioxane; 11, 2-propanol; 12, ethanol; 13, acetone; 14, acetic acid; 15, methanol; 16, water.

Table 3. Diamagnetic susceptibilities of liquids in 10^{-6} e.m.u. at 20 °C

Liquids	t_0[a] s	t_H[a,b] s	$-10^3\cdot(t_0-t_H)/t_H$	This work $-\chi$	This work $-\chi_M$	Literature[c] $-\chi_M$
Water	397.54_0	401.51_8	9.90_7	0.7192*[c]	12.96[c]	12.96
Methanol	297.57_8	300.41_1	9.43_0	0.684_6	21.9_3	21.15—21.60
Ethanol	616.89_2	623.27_4	10.23_9	0.743_3	34.2_4	33.05—34.18
2-Propanol	1259.46_0	1273.10_9	10.72_1	0.778_3	46.7_8	45.68—46.02
Acetic acid	478.49_1	482.06_8	7.42_0	0.538_7	32.3_5	31.6 —31.9
Acetone	163.65_0	164.96_2	7.95_3	0.577_3	33.5_3	33.64—33.99
Carbon tetrachloride	248.04_6	249.57_1	6.11_0	0.443_6	68.2_3	66.6 —67.45
Hexane	200.06_9	202.49_0	11.95_6	0.867_9	74.8_0	73.80—74.42
Heptane	243.12_2	246.06_3	11.95_2	0.867_7	86.9_5	85.20—85.5
2,2,4-Trimethylpentane	295.12_8	298.76_3	12.16_7	0.883_3	100.9_0	97.58—98.34
Ethyl acetate	203.85_0	205.61_4	8.57_9	0.622_8	54.8_7	53.9 —54.28
Dioxane	507.16_0	511.34_8	8.19_0	0.594_6	52.3_9	51.1 —52.16
Cyclohexane	509.00_5	514.69_6	11.05_7	0.802_7	67.5_6	68.04—68.7
Benzene	297.19_8	300.13_5	9.78_6	0.710_4	55.4_9	54.7 —55.00
Nitrobenzene	676.28_1	681.05_3	7.00_7	0.508_7	62.6_3	61.53—62.15
Toluene	272.55_2	275.30_1	9.98_5	0.724_9	66.7_9	65.54—66.52

χ_M: molar susceptibility. *: Taken as the standard. a) Mean of 20—50 measurements. b) Measured in 18800 Oe. c) Landolt-Börnstein, "Zahlenwerte und Funktionen aus Physik, Chemie, Astronomie, Geophysik und Technik," II Band, 10 Teil, Springer Verlag, Berlin (1967).

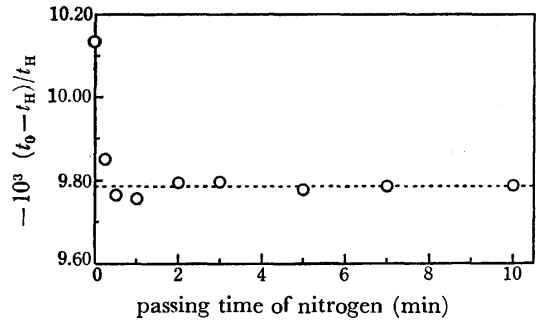

Fig. 5. Effect of atmospheric air in the cell on the flow time of benzene. (The broken line shows the level to be observed under ideal conditions when the air in the cell is completely removed. Such ideal conditions might be nearly attained, for example, by means of the freeze-pump technique and finally by saturation with nitrogen using the operation tube.)

$$\chi = \chi^\circ + \frac{\rho_{air}}{\rho}\beta\chi_{air}, \qquad (5)$$

where χ° and χ_{air} are the mass magnetic susceptibilities of a deaerated pure liquid and of air respectively, β is the solubility of air in the liquid, and ρ and ρ_{air} are the densities of the liquids and of air respectively. Since χ and χ° for diamagnetic liquids are opposite in sign to χ_{air}, and since the last term of Eq. 5 is of an order of magnitude of about 10^{-8} e.m.u., χ should be observed to be less than χ° by a fraction as small as 1.0—1.4% in most of the organic liquids studied here. This estimate is in nice agreement with the deviation found from the data reported in the past with regard to the susceptibilities of liquids of the same kinds as studied here. On the other hand, the influence of the dissolved air upon the χ value of water, which was adopted as the standard reference here, is only 0.14%. Thus, it seems certain that most literature values for organic liquids are spoiled by the dissolved air, except those given by Eggleston *et al.*,[2] who were unique in making measurements of the susceptibility with sufficient care to deaerate the sample. The values of the present work (Table 3) are found to be very close to those χ values, -0.7081 and -0.8665×10^{-6} e.m.u., given by Eggleston *et al.*[2] for benzene and heptane respectively, though there still remaining deviations of about 0.2—0.3%.

In order to get reliable results, it is preferable to make measurements in as strong a magnetic field as possible, not to speak of the necessity of a severe regulation of the temperature, because even a slight change in the temperature may cause a considerable change in the viscosity and, consequently, in the flow time. The advantages of the present method are: (1) The extensively homogeneous region of the magnetic field is not needed, because the meniscus of the liquid at the lower end of capillary does never shift throughout the measurement of the flow time; (2) the outside diameter of the cell near the lower end of the capillary part in the pole gap is so small that there is no need to use an electromagnet of a large scale; a small size magnet such as used here is sufficient; (3) the influence of air (or oxygen) that spoils the measurement of the diamagnetic susceptibility can be eliminated almost completely; and (4) it has been confirmed experimentally that an occasional slight shock or vibration in the table on which the magnet is mounted has practically no appreciable effect on the observed values.

References

1) T. Ikeda and H. Yoshioka, *J. Phys. Chem.*, **72**, 4392 (1968).

2) B. C. Eggleston, D. F. Evans, and R. E. Richards, *J. Chem. Soc.*, **1954**, 941.

Effect of the Third Virial Coefficient on the Intensity of Light Scattered by Mixed Aqueous Solution of Poly(vinylpyrrolidone) and Sodium Dodecyl Sulfate

Masayuki NAKAGAKI and Saburo SHIMABAYASHI

Faculty of Pharmaceutical Sciences, Kyoto University, Sakyo-ku, Kyoto 606

(Received January 10, 1977)

It was found that the reduced intensity of scattered light, R_θ, increases and then decreases with polymer concentration, becoming maximum for a certain concentration of the polymer, when the third virial coefficient, A_3, is positive. The theoretical concentration of polymer for the maximum R_θ is $(3A_3M_2)^{-1/2}$, where M_2 is the molecular weight of the polymer. This was observed in the case of the aqueous solution of poly(vinylpyrrolidone) (PVP) mixed with sodium dodecyl sulfate (SDS). In the mixed solution, PVP and SDS form a complex which behaves like a polyelectrolyte with or without a simple salt of low concentration. Such a solution often has higher-order virials. The value of the polymer concentration for the maximum scattered light intensity agreed with the theoretical value.

Turbidity or intensity of scattered light increases, for the first approximation, in proportion to the concentration of colloidal or macromolecular solutes. This is utilized as a method of chemical analysis such as nephelometry of turbidimetry. According to the fluctuation theory, however, the intensity of scattered light does not necessarily increase but sometimes decreases with the solute concentration under certain conditions. The possibility of decrease of turbidity with increase of polymer concentration is of particular interest in relation to physiological problems such as the transparency of eye lenses. The lens of a human eye is transparent in the normal condition of water content (62%), but the lens becomes turbid when the content of water increases to 80—90%. Thus the lens of high content of macromolecules (protein) is less turbid than that of low content of the protein.

In this paper, the effect of solute concentration on the reduced intensity of the scattered light is discussed theoretically and the results are compared with those obtained by using the mixed system of poly (vinylpyrrolidone) (PVP) and sodium dodecyl sulfate (SDS) in aqueous solution.

Theoretical

The reduced scattering intensity, R_θ, for unpolarized incident beam is defined as follows:

$$R_\theta = \left(\frac{r^2 I_\theta}{I_0}\right) \Big/ (1+\cos^2\theta), \tag{1}$$

where r is the photometric distance, and I_0 and I_θ are the intensity of the incident light and scattered light, respectively, per unit volume at the scattering angle of θ. The term $(r^2 I_\theta / I_0)$ is the Rayleigh ratio.

According to fluctuation theory, the intensity of the scattered light depends on the fluctuation both of the density of solvent and of the concentration of solute. The former component is assumed to be constant regardless of solute concentration when solute concentration is sufficiently low. The latter component of the reduced intensity of the scattered light, R_θ, is proportional both to $(\partial\pi/\partial c_2)^{-1}$ and to $(\partial n_{12}/\partial c_2)^2$, where π is the osmotic pressure, n_{12} the refractive index of the solution, and c_2 the concentration of the solute. Thus,

$$\frac{Kc_2}{R_\theta} = \frac{1}{RT}\cdot\frac{\partial\pi}{\partial c_2}, \tag{2}$$

where R and T are the gas constant and the absolute temperature, respectively, of the solution. K is a constant defined as follows:

$$K = 2\pi^2 n_1^2 \left(\frac{\partial \bar{n}_{12}}{\partial c_2}\right)^2 \Big/ N_A \cdot \lambda_0^4, \tag{2-a}$$

where N_A is the Avogadro number, n_1 the refractive index of the solvent, and λ_0 the wavelength of the incident beam *in vacuo*. The left-hand side of Eq. 2 is, therefore, a quantity which can be determined as a function of θ and c_2.

The interference factor, $P(\theta)$, should be introduced into the equation of R_θ when the light scattering by large particle is considered. By expanding both terms $(\partial\pi/\partial c_2)$ and $P(\theta)$ in power series, we obtain the following equation which is used to analyse the data of the light scattering in a polymer solution:[1]

$$\frac{Kc_2}{R_\theta} = \frac{1}{M_2}\left(1+\frac{16\pi^2 n_1^2}{3\lambda_0^2}\langle R_G^2\rangle \sin^2(\theta/2)\right) + 2A_2c_2, \tag{3}$$

where M_2 is the molecular weight of the solute (polymer), $\langle R_G^2\rangle$ the mean-square value of the radius of gyration of polymer coil in the solution, and A_2 the second virial coefficient.

When the scattering angle, θ, is zero, the interference factor is equal to unity. In order to consider the effect of polymer concentration, the term $(\partial\pi/\partial c_2)$ in Eq. 2 is expanded to the third virial, and we obtain[2,3]

$$Kc_2/R_0 = \frac{1}{M_2} + 2A_2c_2 + 3A_3c_2^2, \tag{3-a}$$

where A_3 is the third virial coefficient. From this, the reduced intensity, R_0, of the scattered light at $\theta=0°$ is given by

$$R_0 = Kc_2 \Big/ \left(\frac{1}{M_2}+2A_2c_2+3A_3c_2^2\right), \tag{4}$$

and the differential of R_0 by c_2 by

$$\frac{\partial R_0}{\partial c_2} = \frac{K\left(\frac{1}{M_2}-3A_3c_2^2\right)}{\left(\frac{1}{M_2}+2A_2c_2+3A_3c_2^2\right)^2}. \tag{5}$$

Case 1: When $A_2=0$ and $A_3=0$, Eqs. 4 and 5

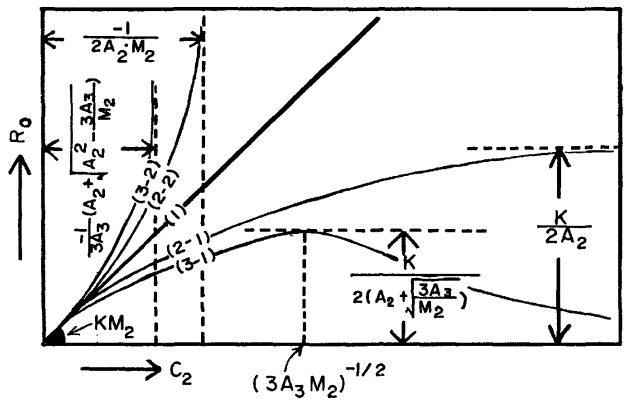

Fig. 1. Schematic diagram for the relationship between the reduced intensity of the scattered light, R_0, and solute concentration, c_2.
curve(1): $A_2=0$ and $A_3=0$, (2-1): $A_2>0$ and $A_3=0$,
(2-2): $A_2<0$ and $A_3=0$, (3-1): $A_2\geqq 0$ and $A_3>0$
(3-2): $A_2\leqq 0$ and $A_3<0$:

become as follows:

$$R_0 = KM_2c_2, \tag{6}$$

$$\frac{\partial R_0}{\partial c_2} = KM_2. \tag{7}$$

The relationship between R_0 and c_2 is shown in Fig. 1 as straight line (1), the slope of which is KM_2 as shown by Eq. 7.

Case 2: When $A_2\neq 0$ and $A_3=0$, Eqs. 4 and 5 become as follows:

$$R_0 = Kc_2\Big/\left(\frac{1}{M_2}+2A_2c_2\right), \tag{8}$$

$$\frac{\partial R_0}{\partial c_2} = \left(\frac{K}{M_2}\right)\Big/\left(\frac{1}{M_2}+2A_2c_2\right)^2. \tag{9}$$

In this case, R_0 increases monotonically with c_2. The initial slope (slope at $c_2\to 0$) is KM_2 as in case 1. If A_2 is positive, R_0 and $\partial R_0/\partial c_2$ approach $K/(2A_2)$ and zero, respectively, with increasing c_2. On the other hand, if A_2 is negative, both R_0 and $\partial R_0/\partial c_2$ diverge to infinity when c_2 approaches $-1/(2A_2M_2)$. These relationships are shown in Fig. 1 by curves (2-1) and (2-2) for $A_2>0$ and <0, respectively.

Case 3: When $A_3\neq 0$, the initial slope for the relationship between R_0 and c_2 is KM_2 as in cases 1 and 2. If $A_3>0$ and $A_2\geqq 0$, R_0 has a maximum value, according to Eq. 5, where

$$c_{2,\max} = (3A_3M_2)^{-1/2}, \tag{10}$$

and

$$R_{0,\max} = \frac{K}{2\left(A_2+\sqrt{\frac{3A_3}{M_2}}\right)}. \tag{11}$$

This relation is shown by curve (3-1) in Fig. 1. Thus, the reduced intensity of the scattered light, R_0, decreases in spite of the increase in the concentration of polymer, c_2, when c_2 is larger than $c_{2,\max}$. This is in contrast to the case $A_3=0$ in cases 1 and 2. If $A_3<0$ and $A_2\leqq 0$, both R_0 and $\partial R_0/\partial c_2$ tend to infinity at

$$c_2 = -\frac{1}{3A_3}\left(A_2+\sqrt{A_2^2-\frac{3A_3}{M_2}}\right). \tag{12}$$

This relation is also shown by curve (3-2) in Fig. 1.

From Eq. 4, the specific reduced intensity of the scattered light R_0/c_2 is given by

$$\frac{R_0}{c_2} = K\Big/\left(\frac{1}{M_2}+2A_2c_2+3A_3c_2^2\right), \tag{13}$$

and its differential by the solute concentration $\partial(R_0/c_2)/\partial c_2$ by

$$\frac{\partial}{\partial c_2}\left(\frac{R_0}{c_2}\right) = \frac{-2K(A_2+3A_3c_2)}{\left(\frac{1}{M_2}+2A_2c_2+3A_3c_2^2\right)^2}. \tag{14}$$

According to Eq. 13, R_0/c_2 becomes KM_2 irrespective of the values of A_2 and A_3 when c_2 approaches zero. As for the inclination of the (R_0/c_2) *vs.* c_2 curves given by Eq. 14,

$$\frac{\partial}{\partial c_2}(R_0/c_2) = 0, \tag{15}$$

for $A_2=0$ and $A_3=0$, and R_0/c_2 is constant regardless of the value of c_2. When $A_2>0$ and $A_3\geqq 0$, we have

$$\frac{\partial}{\partial c_2}(R_0/c_2) < 0, \tag{16}$$

and R_0/c_2 decreases monotonically with c_2, while for $A_2<0$ and $A_3\leqq 0$,

$$\frac{\partial}{\partial c_2}(R_0/c_2) > 0, \tag{17}$$

and R_0/c_2 increases monotonically with c_2.

Straight line (1) shows the proportionality of the scattering intensity R_0 to the polymer concentration c_2. Thus, R_0/c_2 becomes constant. This is in the case of a solution with θ-solvent.

Curves (2-1) and (3-1) show the dependence of the scattering intensity, R_0, on the polymer concentration, c_2, in a good solvent. In these cases, the polymer coil expands enough and the degree of fluctuation of concentration is relatively small, because of positive A_2 and A_3 in a good solvent. R_0, shown by curve (2-1) or (3-1), therefore, deviates negatively from the straight line (1) in Fig. 1, R_0/c_2 decreasing with c_2. Particularly in the case of curve (3-1) where A_3 is not equal to zero but positive, the repulsion between expanded polymer coils suppresses the concentration fluctuation so that the scattering intensity decreases with the increase of the polymer concentration at high concentration region.

Curves (2-2) and (3-2), on the other hand, show the dependency of R_0 on c_2 in a poor solvent. R_0 deviates positively from the straight line (1) and R_0/c_2 increases with c_2 because of the negative values of A_2 and A_3 and the large fluctuation in a poor solvent. Both the reduced intensity and the specific reduced intensity of the scattered light tend to infinity at a critical polymer concentration. This is the critical opalescence due to the two-phase separation of the polymer solution at the polymer concentration higher than the critical value.

So far, only typical conditions for the real solution have been considered. From a mathematical viewpoint, other conditions such as $A_2>0$ and $A_3<0$, or $A_2<0$ and $A_3>0$, should be considered, but discussion was not made.

Experimental

Material and Solution. Poly(vinylpyrrolidone) (hereafter called PVP) and sodium dodecyl sulfate(SDS) are the same as those reported.[4] The materials were dissolved in twice distilled water. The molecular weight of PVP, M_P, was kept constant throughout the experiment, but that of complex, $M_{complex}$, changed with the concentration of SDS; the relation is given by Eq.19-a.

The membrane equilibrium should be attained before the measurement since PVP and SDS form a complex in aqueous solution, the complex behaving like a polyelectrolyte.[5] Visking Cellulose Tubing was used with an initial inner solution of PVP mixed with SDS, and initial outer solution of SDS. The method of the membrane equilibrium is the same as that reported.[4]

After the membrane equilibrium has been attained, a solution of concentration of PVP–SDS complex, $c_{complex}$, at a given concentration of free SDS, c_s^f, can be prepared, if the outer solution is used as a solvent or as a diluting agent for the inner solution of PVP–SDS complex, since chemical potential of SDS in the inner solution is equal to that in the outer solution at the membrane equilibrium. The amount of SDS bound to PVP of unit weight can also be kept constant when c_s^f is kept constant through the dilution process. A solution, in which the amount of SDS is bound to PVP at the membrane equilibrium, can be prepared by adjusting the concentration of SDS of both sides of the membrane before the membrane equilibrium is attained. The dependence of the scattering intensity, R_θ, both on the scattering angle, θ, and on the concentration of complex, $c_{complex}$, was measured under the conditions of a constant concentration of free SDS, c_s^f. This system will be called the dialysed system.

The same measurement was carried out under the conditions of a constant concentrations of total SDS, c_s^t, in order to compare the results with those of the dialysed system. Concentration c_s^t indicates the sum of concentrations of free SDS and of bound SDS in a solution of PVP mixed with SDS. This system will be called the undialysed system.

Measurements of the Reduced Intensity of Scattered Light and the Increment of Refractive Index. Methods of measurement of refractive index increment are the same as those reported.[4] In order to measure the scattering intensity, a Shimadzu Electrophotometric Light Scattering Photometer PG-21 was used at 436 nm and at 25 °C. The reduced intensity of the scattered light, R_θ, is experimentally given as follows.

$$R_\theta = \phi_\theta \frac{G_\theta}{G_0} \tag{18}$$

where G_θ and G_0 are intensity of electric current in a phototube at scattering angle of θ and of zero degree, respectively. ϕ_θ is an empirical coefficient depending both on a scattering angle, θ, and the refractive index of the solvent, n_1.[6]

Results

Dependence of the Reduced Intensity of Scattered Light on Polymer Concentration. The concentrations of PVP and the PVP–SDS complex are denoted by c_P and $c_{complex}$, respectively, in order to distinguish them from the concentration of "polymer," c_2. The relationship between c_P and $c_{complex}$ is given by

$$c_{complex} = (1+y)c_p, \tag{19}$$

where y is the weight of SDS bound per unit weight of PVP. The relationship between the molecular weight of PVP, M_P, and that of the complex, $M_{complex}$, is given by

$$M_{complex} = (1+y)M_p \tag{19-a}$$

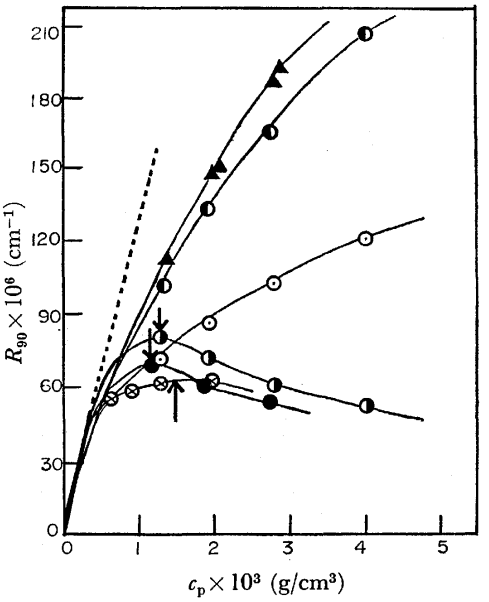

Fig. 2. Relationship between concentration of PVP, c_p and reduced intensity of scattered light at 90°, R_{90}. These are undialysed systems, and each concentration of total SDS, c_s^t, is kept constant through the measurement. Concentration of total SDS, c_s^t(mM): ▲ 0.0, ◐ 2.0, ⊙ 4.0, ⊗ 6.0, ● 8.0, ◑ 10.0.

Empirical relationship between PVP concentration, c_P, and the reduced intensity of the scattered light measured at 90°, R_{90}, are given in Fig. 2, where total concentration of SDS, c_s^t, is kept constant. This is the result obtained by the undialysed system. When c_s^t is small, *viz.*, in the case of 0 mM(▲), 2 mM(◐), and 4 mM(⊙), R_{90} increases with c_P, but when c_s^t is large, *viz.*, in the case of 6 mM(⊗), 8 mM(●) and 10 mM(◑), R_{90} decreases in spite of the increase in c_P. In the case of the undialysed system in which c_s^t is kept constant throughout the measurement (Fig. 2), it should be noted that PVP and SDS form a complex with each other, so that $M_{complex}$ as well as the amount of SDS bound per unit weight of PVP, y, decrease with c_p. It is thus difficult to analyse the effect of c_s^t, $c_{complex}$, and $M_{complex}$ on the reduced scattering intensity, R_{90}, and to explain the results. However it may be emphasized that the anomalous decrease of the scattered light intensity with the increase in the polymer concentration is observed even under simple experimental conditions.

On the other hand, it is easy in the case of the dialysed system to analyse the change of R_{90} with the concentration of PVP, c_P, since the free concentration of SDS, c_s^f, the amount of bound SDS, y, and the molecular weight of the complex, $M_{complex}$, can be kept constant throughout the measurement of R_{90}.

Since the value of y as a function of c_s^f is known,[4,5] the relationship between R_{90} and $c_{complex}$ can be obtained (Fig. 3). Each symbol indicates the experimental value. When c_s^f is large, R_{90} decreases in spite

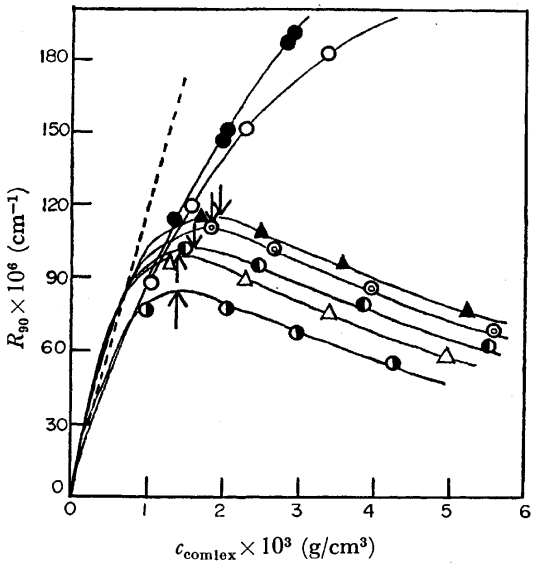

Fig. 3. Relationship between complex concentration, c_{comlex}, and reduced intensity of scattered light at 90°, R_{90}. These results are of the dialysed system, and concentration of free SDS, c_s^f, is kept constant through the measurement. Each arrow mark shows the maximum point of each curve, which is calculated by Eq. 10 as same as in the case of Fig. 2. The dotted line shows the initial slope for the aqueous solution of PVP without SDS.
Concentration of free SDS, c_s^f(mM): ● 0.00, ○ 2.00, ◑ 5.37, △ 6.82, ◐ 8.68, ◎ 15.58, ▲ 19.16.

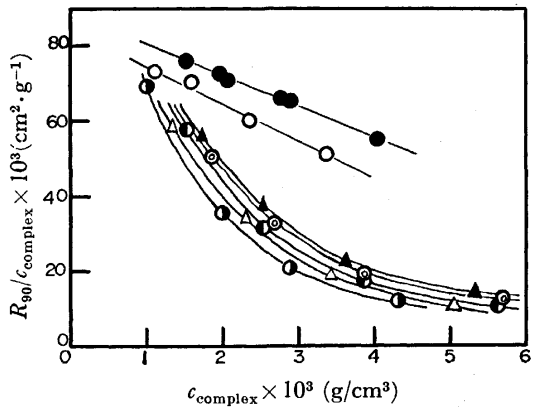

Fig. 4. Relationship between concentration of complex, $c_{complex}$, and specific reduced intensity of scattered light, $R_{90}/c_{complex}$. These results are of the dialysed system.
Concentration of free SDS, c_s^f(mM): ● 0.00, ○ 2.00, ◑ 5.37, △ 6.82, ◐ 8.68, ◎ 15.58, ▲ 19.16.

of the increase in the concentration of the complex, $c_{complex}$, in the region of high concentration of $c_{complex}$ as in the case of the undialysed system (Fig. 2). The anomalous behavior can thus be observed in both the dialysed and undialysed systems.

The relationship between the specific reduced intensity of the scattered light, $R_{90}/c_{complex}$, and $c_{complex}$ is shown in Fig. 4 on the basis of the data of Fig. 3 for the dialysed system. In the case of low concentration of free SDS, c_s^f, such as 0 mM(●) and 2 mM(○), $R_{90}/c_{complex}$ decreases linearly with $c_{complex}$, but in the case of high concentration of free SDS, such as 5.37 mM(◑) and higher, $R_{90}/c_{complex}$ decreases rapidly even in the region of low concentration of the complex, $c_{complex}$. Neither a maximum nor a minimum like that shown in Fig. 3 can be observed. The theoretical deduction has been verified experimentally.

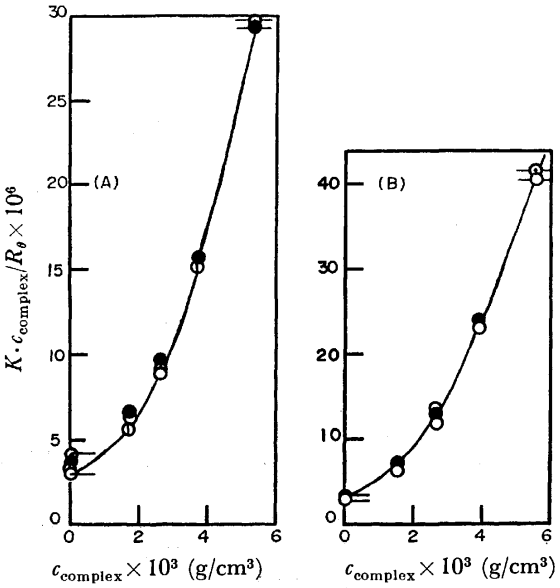

Fig. 5. Relationship between concentration of complex, $c_{complex}$, and $Kc_{complex}/R_\theta$. Different angles of the scattering, θ, are shown by different symbols. The solid line is the theretical curves calculated by Eq. 3-a.
Curve: (A)c_s^f=19.16mM, (B)c_s^f=8.68mM. Scattering angle: ○ 0°, ⦶ 45°, ● 90°, ⊙ 135°.

Dependence of Kc_2/R_θ on c_2 at Various θ. Dependence of Kc_2/R_θ on c_2 is shown in Fig. 5 for the dialysed system, for given θ-values as θ=0°(○), 45°(⦶), 90°(●) and 135°(⊙), where the data at θ=0° is quoted from the Zimm Plot for the solution of PVP-SDS complex.[7] The pairs of short bars in Fig. 5, drawn at both the lowest and highest concentration of the complex, show the range of $Kc_{complex}/R_\theta$ from θ=0° through θ=135° at the respective complex concentrations. We see that the effect of θ is relatively small, the dependence of $Kc_{complex}/R_\theta$ on $c_{complex}$ being approximately independent of θ. The conclusion is also applicable to the other data of both the dialysed and undialysed systems not shown in Fig. 5. The shapes of the curves show that the virial coefficients A_2 and A_3 of Eq. 3-a are both positive.

Discussion

Determination of Virial Coefficients, A_2 and A_3. Eq. 3-a can be rewritten as follows for the experimental determination of A_2 and A_3:

$$\frac{1}{c_2}\left(\frac{Kc_2}{R_0}-\frac{1}{M_2}\right)=2A_2+3A_3c_2. \qquad (20)$$

Virial coefficients, A_2 and A_3, can thus be determined from a linear relationship between $(Kc_2/R_0-1/M_2)/c_2$ and c_2.

In the case of the dialysed system such as shown in Fig. 6, the subscript "2" in Eq. 20 should be read as

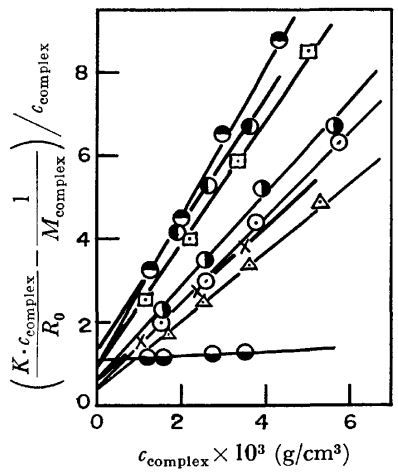

Fig. 6. The relationship between $c_{complex}$ and $(Kc_{complex}/R_0-1/M_{complex})/c_{complex}$. Both A_2 and A_3 can be estimated from the intercept and the slope of each straight line, as shown in Eq. 20. These results are for the dialysed system.
Concentration of free SDS(mM): ◒ 2.00, ◐ 3.73, ◓ 5.37, ⊡ 6.82, ◑ 8.68, ⊙ 10.64, × 13.40, △ 19.16.

the subscript "complex." The free concentration of SDS, c_s^f, is kept constant for each line, all lines in Fig. 6 being straight. The virial coefficients, A_2 and A_3, are thus obtained for each concentration of free SDS, c_s^f, for each molecular weight of the complex. A_2 and A_3 are of the PVP–SDS complex in aqueous solution of free SDS.

On the other hand, in the case of the undialysed system, subscript "2" in Eq. 20 should be assumed to be "p". The relationship between $(Kc_P/R_0-1/M_P)/c_P$ *vs.* c_P at constant c_s^t becomes a straight line as in the case of the dialysed system (Fig. 6), in spite of the variation in the molecular weight of the complex when c_P changes at constant c_s^t. Apparent values of A_2 and A_3 are determined from these straight lines.

The dependence of A_2 and A_3 on c_s^f for the dialysed system(●) and that of the apparent A_2 and A_3 on c_s^t for the undialysed system(⊙) are shown in Fig. 7. In the region of low concentration of SDS, c_s^f or c_s^t, the

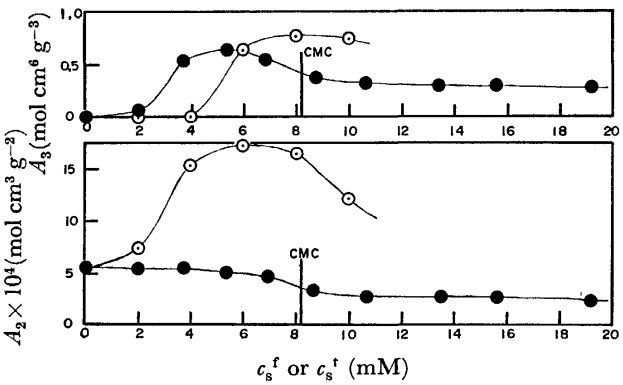

Fig. 7. The relationship between virial coefficients, A_2 or A_3, and concentration of SDS, c_s^f or c_s^t, for dialysed and undialysed system, respectively.
⊙ Undialysed system *versus* c_s^t, ● dialysed system *versus* c_s^f.

third virial coefficient, A_3, is negligible, increasing with SDS concentration (Fig. 7). This is of particular interest, since the positive third virial coefficient is responsible for the anomalous decrease in R_0 or R_θ with the increase in c_2.

Comparison of Observed R_{90} with Calculated R_0.
A comparison between experimental R_{90}-values and theoretical R_0-values is made herewith on the basis of the results where the effect of θ on R_θ is small (Fig. 5).

Solid curves in Figs. 2, 3, and 5 indicate the theoretical value of R_0 calculated by means of Eq. 4 using the values of A_2 and A_3 given in Fig. 7. Arrows (↑) in Figs. 2 and 3 show the maximum value of the reduced scattering intensity calculated by Eqs. 10 and 11. Agreement of the experimental R_{90}-values with the theoretical R_0-curves, and of the experimental maximum values with the theoretical ones (arrows) is good. It can therefore be concluded that the anomalous behaviour in Figs. 2 and 3 can be explained as the contribution of the third virial coefficient to the reduced scattering intensity.

The maximum point of the curve for $c_s^f=2$ mM of the dialysed system is not shown in Fig. 3, since the concentration of the complex at the maximum point is higher because of the smallness of A_3. In the case of 0 mM of c_s^f, that is an aqueous solution of PVP without SDS, R_{90} or R_0 increases with the polymer concentration ($c_{complex}$ on the abscissa should read c_P in this case) and does not have a maximum point since A_3 is zero and the curve corresponds to curve (2-1) in Fig. 1. Broken lines in Figs. 2 and 3 indicate initial slopes for the curve of 0 mM of SDS (*i.e.* aqueous solution of PVP without SDS). Even when A_3 is zero, deviation from the broken line increases with the polymer concentration because of the contribution of the effect of the second virial coefficient, A_2. The initial slope, KM_2, is constant for all the curves in Figs. 1 and 2, since the molecular weight is assumed to be constant (M_2 or M_p). However, the initial slopes for the curves in Fig. 3, $KM_{complex}$, are variable and not constant since the molecular weight of the complex, $M_{complex}$, depends on the amount of SDS bound to PVP, y, which also depends on the concentration of free SDS, c_s^f, as shown by Eqs. 19 and 19-a. Thus, the initial slope, $KM_{complex}$, depends on y or c_s^f. The initial slope for the respective curves are not shown in Fig. 3 in order to avoid confusion.

Estimation of the Effect of the Interference Factor.
In a rigorous sence it is wrong to compare R_{90} with R_0, since R_{90} is not equal to R_0 due to the interference factor, $P(\theta)^{-1}$. The effect of $P(\theta)^{-1}$, given by the following equation or the term in parenthesis on the right-hand

$$P(\theta)^{-1}=1+\frac{16\pi^2 n_1^2}{3\lambda_0^2}\langle R_G^2\rangle \sin^2(\theta/2), \qquad (21)$$

side of Eq. 3, should be evaluated at $\theta=90°$ of the present experimental conditions in order to check the difference between R_{90} and R_0.

Assuming that θ is equal to 90° and a radius of gyration of PVP, $\langle R_G^2\rangle^{1/2}$, in water is 210 Å,[6,7] Eq. 21 is evaluated to be 1.12. The maximum value of $\langle R_G^2\rangle^{1/2}$ of the complex of PVP–SDS is *ca.* 1.5 times

that of PVP in water, since the intrinsic viscosity of the complex at the highest amount of SDS bound to PVP is 3.5 times that of PVP in water.[5] Assuming that $\theta=90°$ and $\langle R_G^2\rangle^{1/2}=315$ Å, the value of Eq. 21 is found to be 1.27. Thus, $1.12 \leqq P(90°)^{-1} \leqq 1.27$.

The relative difference of $Kc_{complex}/R_{90}$ against $Kc_{complex}/R_0$ is, therefore, assumed to be greater than 12% and less than 27% in the region of very low concentration of the polymer. However, in the region of high concentration of the polymer, the relative difference decreases with polymer concentration, because of the contribution of higher order virials such as $2A_2c_{complex}$ and $3A_3c_{complex}^2$ as shown by Eqs. 3 and 3-a. All the data of θ (Fig. 5) lie nearly on the theoretical curve for $\theta=0°$ calculated by means of A_2 and A_3 and Eq. 3-a. We might compare the experimental results obtained for $\theta=90°$ with the theoretical ones deduced for $\theta=0°$.

Comparison of the Theory of Debye and Bueche with Ours. Debye and Bueche[8] showed that R_θ increases and then decreases with c_2, and the concentration of polymer at the maximum value of R_θ is proportional to $M_2^{-1/2}$, not depending on the virial coefficients. However, the second and third virial coefficients are important for expressing the concentration, $c_{2,max}$, of the maximum value, $R_{0,max}$, of the reduced scattering intensity, as shown by means of Eqs. 10 and 11.

References

1) M. Nakagaki and H. Inagaki, "Experiments in Light Scattering (Kosanran Zikkenho)," Chaps. 1 and 2, Nankodo, Tokyo (1965).

2) C. Tanford, "Physical Chemistry of Macromolecules," John-Wiley, New York (1967), p. 287, 307.

3) Japan Chemical Society, "Shin Zikken Kagaku Koza, Light, part II," Maruzen, Vol. 4, Tokyo (1976), p. 737.

4) M. Nakagaki and S. Shimabayashi, *Nippon Kagaku Kaishi*, **1976**, 757.

5) M. Nakagaki and S. Shimabayashi, *Nippon Kagaku Kaishi*, **1972**, 1496.

6) M. Nakagaki, S. Shimabayashi, S. Yoshida, and M. Saito, *Yakugaku Zasshi*, **96**, 757 (1976).

7) M. Nakagaki and S. Shimabayashi, *Nippon Kagaku Kaishi*, to be published.

8) P. Debye and A. M. Bueche, *J. Chem. Phys.*, **18**, 1423 (1950).

Hydrogen Isotope Effect on the Radical Addition of the Hydrogensulfite Ion to Allyl Alcohol in Aqueous Solutions

Teijiro MIYATA, Akihisa SAKUMOTO, and Masamitsu WASHINO
Japan Atomic Energy Research Institute, Takasaki, Gunma 370-12
(Received September 6, 1976)

A study of the radiation-induced addition of HSO_3^- to allyl alcohol was carried out in D_2O–H_2O mixtures. It was found that a linear relationship held between the apparent rate constant of $NaHSO_3$ consumption and the atom fraction of deuterium in the mixture, and that the hydrogen atom abstraction from HSO_3^- by $HOCH_2\dot{C}H$-$CH_2SO_3^-$ was the rate-determining step. The kinetic isotope effect of this abstraction was 4.38.

In a previous paper,[1] we proposed the following mechanism for the radiation-induced addition of the hydrogensulfite ion (HSO_3^-) to allyl alcohol in aqueous solutions:

Initiation,

$$A + HSO_3^- \longrightarrow AH + \dot{S}O_3^-, \quad (1)$$

Propagation

$$\dot{S}O_3^- + CH_2{=}CHCH_2OH \longrightarrow HOCH_2\dot{C}HCH_2SO_3^-, \quad (2)$$

$$HOCH_2\dot{C}HCH_2SO_3^- + HSO_3^- \longrightarrow HOCH_2CH_2CH_2SO_3^- + \dot{S}O_3^-, \quad (3)$$

Termination

$$HOCH_2\dot{C}HCH_2SO_3^- + CH_2{=}CHCH_2OH \longrightarrow HOCH_2CH_2CH_2SO_3^- + CH_2{=}CH\dot{C}HOH, \quad (4)$$

where A represents the active species which contribute to the initiation. This addition reaction involves the hydrogen abstraction from HSO_3^- represented by Eq. 3. It follows, then, that a hydrogen isotope effect may be found if this abstraction reaction is the rate-determining step.[2]

The present study was undertaken to get direct evidence for the rate-determining step by means of the determination of the hydrogen isotope effect of the addition reaction. The reaction system employed was radiation-induced addition in D_2O–H_2O mixtures of various D_2O concentrations. The determination was made possible by finding the relationship between the atom fraction of deuterium in the mixture and the over-all rate constant of sodium hydrogensulfite consumption.

Experimental

The D_2O (Shōwa Denkō, 99.75 mol% D_2O) used was distilled twice under an atomosphere of nitrogen: first in the presence of a trace of potassium permanganate acidified with sulfuric acid and then in the absence of additives. The H_2O used was redistilled before use. The other reagents used were similar to those described previously.[1]

Solutions were prepared by dissolving 0.25 mol/l of Na_2SO_3, 0.50 mol/l of $NaHSO_3$, and 1.47 mol/l of allyl alcohol in D_2O–H_2O mixtures containing up to 100% of D_2O.

The irradiation vessel and analytical procedure used in this work were analogous to those described previously.[1] The pH measurements were carried out using a Tōa Denpa Model HM-5A pH meter with ordinary glass electrodes. The standardization of the pH meter in water solutions was made with conventional buffer solutions of an appropriate acidity. A 3450-curie Co-60 γ-source was used, and the dose rate was determined by the Fricke dosimeter in light water, taking $G(Fe^{3+})=15.6$.

Results and Discussion

Rate-determining Step. In aqueous solutions, $NaHSO_3$ dissociates into Na^+ and HSO_3^-, which is in equilibrium with the hydrogen ion, in the following two ways:

$$HSO_3^- \rightleftharpoons H^+ + SO_3^{2-}, \quad (5)$$

$$HSO_3^- + H^+ \rightleftharpoons H_2SO_3. \quad (6)$$

Accordingly, DSO_3^- is formed in D_2O instead of HSO_3^- being formed in H_2O. In the D_2O–H_2O mixture, a part of the HSO_3^- is assumed to be displaced with DSO_3^- in proportion to the D_2O concentration in the mixture.

The total G-value of the active species, A, produced from the radiolysis of D_2O is reported to be slightly higher than that from H_2O.[3] The concentration of DSO_3^- in D_2O can be estimated to be higher than that of HSO_3^- in H_2O since weak acids are less dissociated in D_2O than in H_2O.[4] These facts lead to the assumption that the rate of $NaHSO_3$ consumption may be greater in the D_2O–H_2O mixtures than in H_2O.

In order to evaluate the effects of D_2O on the addition reaction, the solutions were irradiated by Co-60 γ-rays at a dose rate of 8.45×10^{15} eV/cm^3 s and at room temperature. The conversion of $NaHSO_3$ decreased with the increase in the atom fraction of deuterium in the mixture, as is shown in Fig. 1. This result disagrees with the above assumption.

The addition reaction involves DSO_3^- as well as HSO_3^- in the D_2O–H_2O mixtures, as is represented in

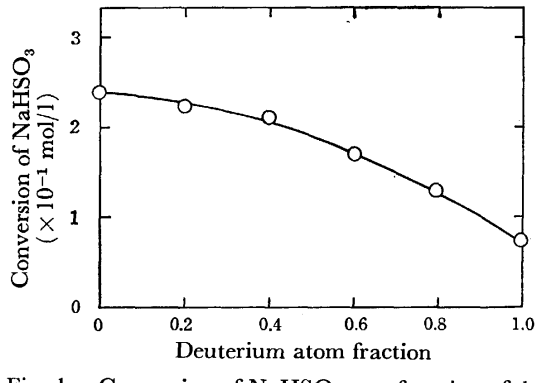

Fig. 1. Conversion of $NaHSO_3$ as a function of deuterium atom fraction in the mixture.

Eqs. 1 and 3, where the hydrogen-atom abstraction from these ions takes place. The hydrogen-atom abstraction causes an appreciable isotope effect.[2] On the basis of these findings, it is reasonable to assume that the above disagreement results from the isotope effect of these hydrogen-atom abstractions.

Reaction 1 plays a minor role in the isotope effect because most of the species formed in other reactions which involve A can initiate the addition reaction.[1] On the other hand, Reaction 3 involves $HOCH_2\dot{C}HCH_2SO_3^-$, which takes part both in the propagation shown by Reactions 2 and 3 and in the termination shown by Reaction 4. In addition, the chain length of the addition reaction is as large as 344,[1] and it is susceptible to small changes in the rate of Reaction 3 provided this reaction is the rate-determining step of the propagation. Consequently, it can be assumed that Reaction 3 is the rate-determining step of the propagation and mainly causes the isotope effect.

Total Concentration of HSO_3^- and DSO_3^- in D_2O–H_2O Mixtures. The concentration of HSO_3^- in an aqueous $NaHSO_3$ solution containing Na_2SO_3 at pH 5—7 is given by[1]

$$[HSO_3^-] = \frac{[NaHSO_3]+[Na_2SO_3]}{1+(K_5/a_H)(f_{HSO_3^-}/f_{SO_3^{2-}})}, \quad (7)$$

where $[NaHSO_3]$ and $[Na_2SO_3]$ are the initial concentrations of $NaHSO_3$ and Na_2SO_3; K_5, the dissociation constant of HSO_3^-; a_H, the activity of the hydrogen ion; and $f_{HSO_3^-}$ and $f_{SO_3^{2-}}$, the activity coefficients of HSO_3^- and SO_3^{2-}.

The dissociation constant of a weak acid in a D_2O–H_2O mixture is expressed by[5] Eq. 8:

$$K_N = K_H \frac{0.302n^3+1.37n^2(1-n)+2.04n(1-n)^2+(1-n)^3}{(1-n)+0.302(K_H/K_D)n}, \quad (8)$$

where K_N, K_H, and K_D refer to the dissociation constants of the weak acid in the D_2O–H_2O mixture, H_2O, and D_2O respectively, and where n is the atom fraction of deuterium in the mixture. In the case of HSO_3^- as the weak acid, K_H/K_D in Eq. 8 can be estimated to be 3.68 from the relationship[4] between K_H/K_D and $-\log K_H$, in which the K_H for HSO_3^- is 1.02×10^{-7}.[6] Substituting these values into Eq. 8, we obtain the K_N values shown in Table 1.

Table 1. Dissociation constants of HSO_3^-[a] in D_2O–H_2O mixtures

n[b]	0	0.2	0.4	0.6	0.8	1.0
$K_N\times10^8$	10.2	8.18	6.46	5.00	3.78	2.77

a) HSO_3^- at n=0, DSO_3^- at n=1, and the mixture of HSO_3^- and DSO_3^- at n 0.2 to 0.8. b) The atom fraction of deuterium in the mixture.

Using electrodes standardized for H_2O solutions, the pL, the generalized equivalent of pH (where L includes all the isotopically different hydrogen ions), in a mixture of the deuterium atom fraction of n is given by pL=(meter reading)+0.40n.[7] In addition, since the dielectric constant of D_2O is very close to that of H_2O,[8] it may be assumed that $f_{HSO_3^-}/f_{SO_3^{2-}}$ ratio is equal to that of $f_{DSO_3^-}/f_{SO_3^{2-}}$ and that these ratios are independent of the atom fraction of deuterium in the mixture. Hence, the value of 1.468[1] can be used as $f_{HSO_3^-}/f_{SO_3^{2-}}$ in Eq. 7 at the concentrations of 0.25 mol/l of Na_2SO_3 and 0.50 mol/l of $NaHSO_3$ in the D_2O–H_2O mixtures. Substituting these values into Eq. 7, we obtain the total concentration of HSO_3^- and DSO_3^-, $[\mathbf{HSO_3^-}]$, in the D_2O–H_2O mixtures (Table 2). As can be seen in Table 2, the total concentration increased slightly with the increase in the atom fraction of deuterium in the mixture.

Table 2. Total concentrations of HSO_3^- and DSO_3^-, $[\mathbf{HSO_3^-}]$, in D_2O–H_2O mixtures

n[a]	pH_{obs}	pH_{corr}	$[\mathbf{HSO_3^-}]$ (mol/l)	$\frac{[\mathbf{HSO_3^-}]}{[NaHSO_3]}$[b]
0	6.48	6.48	0.516	1.03
0.2	6.40	6.48	0.550	1.10
0.4	6.41	6.57	0.555	1.11
0.6	6.40	6.64	0.568	1.14
0.8	6.46	6.78	0.562	1.12
1.0	6.50	6.90	0.567	1.13

a) The atom fraction of deuterium in the mixture. b) The concentration ratio between $\mathbf{HSO_3^-}$ and the initial $NaHSO_3$.

Rate Constant in D_2O–H_2O Mixtures. The rate equation for the addition of HSO_3^- to allyl alcohol in an aqueous solution is expressed by[1]

$$-\frac{d[NaHSO_3]}{dt} = \frac{gIk_3[HSO_3^-]}{100k_4[\text{Allyl Alcohol}]}, \quad (9)$$

where g is the G-value of A; I, dose rate (eV/cm^3 s); k_3 and k_4, the rate constants for Reactions 3 and 4 respectively; and [Allyl Alcohol], the concentration of allyl alcohol. Equation 9 can be rewritten as

$$-\frac{d[NaHSO_3]}{dt} = \frac{gIk_3}{100k_4}\cdot\frac{[HSO_3^-][NaHSO_3]}{[NaHSO_3][\text{Ally Alcohol}]}. \quad (10)$$

Since the $[HSO_3^-]/[NaHSO_3]$ ratio is independent of the concentration of $NaHSO_3$ in H_2O,[1] the $[\mathbf{HSO_3^-}]/[NaHSO_3]$ ratio may also be assumed to be independent of the concentration of $NaHSO_3$ in the D_2O–H_2O mixtures. However, this ratio depends on the atom fraction of deuterium in the mixture, as is apparent from Table 2. The conversion of $NaHSO_3$ is equal to that of allyl alcohol.[1] Hence, the rate equation in the D_2O–H_2O mixtures is derived as:

$$\frac{dx}{dt} = \alpha k_n\cdot\frac{(a-x)}{(b-x)}, \quad (11)$$

where

$$k_n = \frac{gIk_3}{100k_4}, \quad (12)$$

$\alpha=[\mathbf{HSO_3^-}]/[NaHSO_3]$ at a concentration of D_2O given by the n of the atom fraction of deuterium, a and b are the initial concentrations of $NaHSO_3$ and allyl alcohol respectively, and x is the concentration of $NaHSO_3$ that reacts in time t. The integration of Eq. 11 yields

$$k_n = \frac{1}{\alpha t}\left\{(b-a)\ln\left(\frac{a}{a-x}\right)+x\right\}, \quad (13)$$

from which k_n can be obtained by substituting the values presented in Fig. 1 and Table 2. Table 3 presents the k_n values thus obtained.

Kinetic Hydrogen Isotope Effect. Taking the ratio

Table 3. Over-all rate constants for the addition of HSO^-_3 to allyl alcohol in D_2O–H_2O mixtures

n[a]	0	0.2	0.4	0.6	0.8	1.0
$k_n \times 10^4$ (mol/l s)	2.30	1.99	1.88	1.38	1.05	0.554

a) The atom fraction of deuterium in the mixture.

of k_n given by Eq. 12 for H_2O to that for the D_2O–H_2O mixture leads to the following equation:

$$\frac{k_H}{k_n} = \frac{g_H I_H k_{3H} k_{4n}}{g_n I_n k_{3n} k_{4H}}, \quad (14)$$

where the subscripts H and n refer to the values for H_2O and those for the D_2O–H_2O mixture respectively. Equation 14 can be simplified as

$$\frac{k_H}{k_n} = \frac{g_H k_{3H}}{g_n k_{3n}}, \quad (15)$$

since it can be assumed that I_H/I_n is nearly unity, because the electron density is nearly equal in both H_2O and D_2O, and since there are no solvent effects on Reaction 4.

The radiation-induced addition of HSO_3^- to allyl alcohol in aqueous solutions is initiated by the active species, the hydrogen atom, the hydroxyl radical, and the hydrated electron, produced from the radiolysis of water.[1] Hence, g in Eq. 12 is assumed to be equal to the sum of the G-values of these three active species. At pH about 6, g_H is 5.20 and the g for D_2O, g_D, is 5.48,[3] while no precise value of g_n is known. Since the formation of ions and excited molecules will occur in the same pattern in both H_2O and D_2O,[9] it is reasonable to assume that g_n is $g_H+(g_D-g_H)n$. Using these values and the k_n values given in Table 3, we can obtain $k_n(g_H/g_n)$.

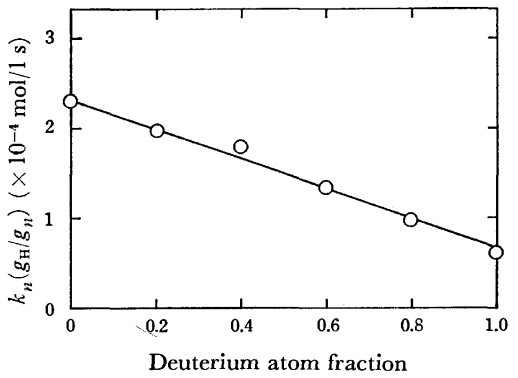

Fig. 2. k_n (g_H/g_n) as a function of deuterium atom fraction in the mixture.

Figure 2 shows the plot of $k_n(g_H/g_n)$ against n. It is apparent from this figure that a good linear relationship holds between these terms. This means that the magnitude of the kinetic isotope effect of Reaction 3 is equal to k_{3H}/k_{3D}, which can be calculated from the k_H, k_D, g_H, and g_D values. According to Eq. 15, k_{3H}/k_{3D} is 4.38 at the dose rate of 8.45×10^{15} eV/cm^3 s since $k_H=2.30\times10^{-4}$ mol/l s, $k_D=0.554\times10^{-4}$ mol/l s, $g_H=5.20$, and $g_D=5.48$. Similar values of 4.46 and 4.41 were obtained at the dose rate of 1.35×10^{16} eV/cm^3 s and 1.69×10^{16} eV/cm^3 s. Thus, the kinetic isotope effect is independent of the dose rate.

It has been reported[10] that there are two isomeric forms of HSO_3^-, (I) and (II), in aqueous solutions:

(I) (II)

This means that two types of hydrogen-atom abstraction should be taken into account; one is the abstraction from the O–H bond, and the other is that from the S–H bond.

Since the stretching vibration of O–H is higher than that of S–H, it seems reasonable to predict that a greater isotope effect is found in the former case than in the latter case. In fact, a value of about 8 for the isotope effect has been reported at 30 °C in the hydrogen-atom abstraction by 2,2-diphenyl-1-picrylhydrazyl (DPPH) from the O–H bond in such phenols as 2,6-di-*t*-butyl phenol and 4-bromophenol,[11] while the value of 5.4 has been reported for a similar abstraction by the same radical from the S–H bond in benzenethiol at 25 °C.[12] The kinetic isotope effect found in the hydrogen-atom abstraction from HSO_3^- is closer to that for benzenethiol than for phenols.

The simplest interpretation of the kinetic isotope effects[2] is based on the assumption that, on passing from the reactants to the transition state, the zero-point energy associated with the stretching vibration of the bond which is concerned in the abstraction is lost. It is thus predicted that

$$k_H/k_D = \exp(\Delta E_0/RT), \quad (16)$$

where ΔE_0 is the difference between the zero-point energy of the bond attached to deuterium and that attached to hydrogen.

The S–H stretching vibration of $HS_2O_5^-$ in an aqueous $K_2S_2O_5$ solution is 2532 cm^{-1}, while the S–D stretching vibration of $DS_2O_5^-$ in the D_2O solution of $K_2S_2O_5$ is 1843 cm^{-1}.[10] Hence, Eq. 16 becomes

$$k_H/k_D = \exp(985/RT). \quad (17)$$

At 25 °C, according to Eq. 17, k_H/k_D is 5.3, which is comparable with the kinetic isotope effect ($k_H/k_D=5.4$) for the hydrogen-atom abstraction from benzenethiol described above.

According to the theory of a three-center transition-state model,[13] the magnitude of the primary isotope effect in a hydrogen-transfer reaction varies with the symmetry of the transition state, which depends on the nature of the substrate and that of the acceptor of the hydrogen. For the determination of the hydrogen-abstraction reaction in the rate-determining step, more work is clearly needed.

The authors wish to thank Dr. Nobutake Suzuki for his valuable discussions.

References

1) T. Miyata, A. Sakumoto, M. Washino, and T. Abe, *Nippon Kagaku Kaishi*, **1976**, 15.

2) L. Melander, "Isotope Effects on Reaction Rates," Ronald Press, New York, N. Y. (1960), p. 20.

3) Z. D. Draganić, O. I. Mićić, and M. T. Nenadović, *J. Phys. Chem.*, **72**, 511 (1968).
4) C. K. Rule and V. K. LaMer, *J. Am. Chem. Soc.*, **60**, 1974 (1938).
5) E. L. Purlee, *J. Am. Chem. Soc.*, **81**, 263 (1959).
6) Landolt-Börnstein, "Zahlenwerte und Funktionen," IIB., 7 teil, Springer (1960), p. 842.
7) P. Salomaa, L. L. Schaleger, and F. A. Long, *J. Am. Chem. Soc.*, **86**, 1 (1964).
8) Ref. 6, p. 615.
9) T. J. Hardwick, *J. Chem. Phys.*, **31**, 226 (1959).
10) A. Simon and K. Waldmann, *Z. Anorg. Chem.*, **281**, 113 (1955).
11) R. A. Bird, G. A. Harpell, and K. E. Russel, *Can. J. Chem.*, **40**, 701 (1962).
12) W. A. Pryor and K. G. Kneipp, *J. Am. Chem. Soc.*, **93**, 5584 (1971).
13) Ref. 12, and references cited therein.

Formose Reactions. IV. The Formose Reaction in Homogeneous Systems and the Catalytic Functions of Calcium Ion Species

Yoshihiro SHIGEMASA, Masayuki SHIMAO, Chikahiro SAKAZAWA, and Teruo MATSUURA*

Department of Industrial Chemistry, Faculty of Engineering, Tottori University, Tottori 680

**Department of Synthetic Chemistry, Faculty of Engineering, Kyoto University, Kyoto 606*

(Received November 10, 1976)

By using the previously developed analytical method of oxidation-reduction potential measurement, the formose reaction homogeneously-catalyzed by calcium formate-potassium hydroxide at pH 10.5—12.0 was found to proceed as effectively as that heterogeneously-catalyzed by calcium hydroxide. Other calcium salts, including chloride, bromide, acetate, and propionate, could be used in place of calcium formate. Kinetic studies with the calcium formate–KOH system showed a linear dependence of the concentration of the dissolved calcium ion species on the induction period (T_{min}) and the formose-forming period ($T_{max}-T_{min}$) at a given pH. From the results, the relationships, $T_{min}=a[CaOH^+]+c$ and $T_{max}-T_{min}=a[CaOH^+]+b[Ca(OH)_2]+c$, were obtained, suggesting that $CaOH^+$ is the principal catalytic species in the induction step, while both $CaOH^+$ and $Ca(OH)_2$ (or OH^-) are present in the formose-forming step. The effects of various factors on both steps and the sugar yield were also examined.

In a preceding paper,[1] which dealt with an examination of various factors affecting the formose reaction carried out with solid $Ca(OH)_2$ in a batch-reactor, it was suggested that the dissolved calcium ion is an essential catalyst for either the induction and the sugar-forming step, and that the hydroxide anion plays a significant role as a catalyst for the latter step. In order to obtain more information on the nature of catalysis in the formose reaction, it appeared necessary to investigate the reaction with a simpler system, such as a homogeneous one, which can excluded the complexity caused by the undissolved $Ca(OH)_2$.

Although Weiss *et al.*, in their studies of the formose reaction using a continuously stirred tank-reactor (CSTR), regarded the reaction as a homogeneously-catalyzed one,[2-4] both the undissolved and dissolved $Ca(OH)_2$ coexist in the reaction mixture. The homogeneously-catalyzed formose reaction has been briefly investigated using alkali-metal hydroxides, organic bases, and other catalysts.[5-12] These reactions, however, usually need a longer period and a higher temperature than the $Ca(OH)_2$-catalyzed formose reaction, and with alkali hydroxides the Cannizzaro reaction of formaldehyde occurs to a large extent. Among those investigations, only a report by Fujino *et al.*[12] concerns the calcium salt-catalyzed formose reaction in a homogeneous system, for which a glucose-calcium complex is used as a catalyst.

On the basis of kinetic studies using CSTR and on the basis of the fact that the reaction rate decreases dramatically when the pH is either too low or too high, Weiss and John have reported that $CaOH^+$ is the principal catalyst.[4] They have also proposed a simplified metathesis mechanism involving $CaOH^+$; it is shown by Scheme 1, where B^+ denotes $CaOH^+$. However, a question arises whether the $CaOH^+$ species is an effective catalyst in both induction and formose-forming steps, because these authors did not perform separate analyses of the two steps.

The purpose of this paper is to explore the standard experimental conditions for the formose reaction catalyzed homogeneously by calcium salts and to obtain evidence for the active catalytic species participating in

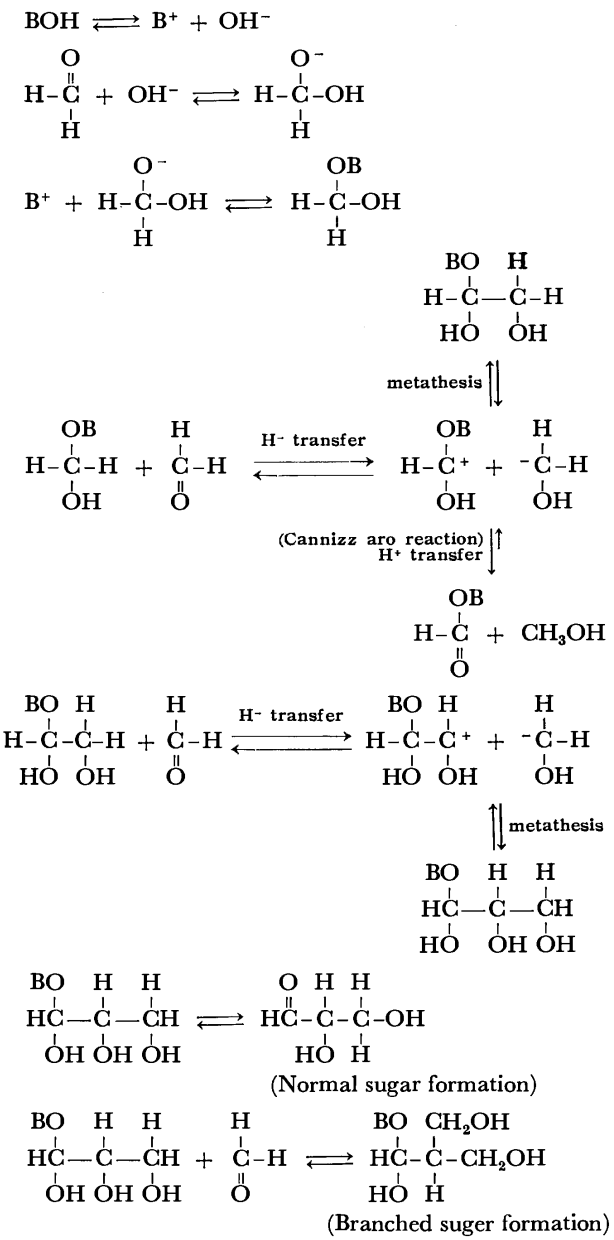

Scheme 1.

the induction and the formose-forming steps. The oxidation-reduction potential (ORP) measurement of the reaction system is applied to the analysis of the reaction. The method has been proved to be useful for the separate analysis of each step by observing an ORP minimum at the end of the induction period and a maximum at the end of the formose-forming step.[1,13,14]

Experimental

Procedure. The apparatus and the experimental procedure are virtually the same as those described previously.[14] Formaldehyde solutions were prepared from paraformaldehyde by refluxing for 4 h, followed by the filtration of the insoluble substances. The pH of the reaction was maintained by adding concentrated aqueous potassium hydroxide or formic acid. The reactor was flushed with nitrogen which had been bubbled through saturated aqueous barium hydroxide. The temperature was controled by means of a cooler dipped in a water bath to avoid the significant temperature rise which would otherwise occur in the formose-forming step. The formaldehyde consumption, the sugar yield, the concentration of the dissolved calcium ion species, and the ORP were measured by the method described in the previous paper.[14] The calcium salts and other reagents were of an analytical grade.

To examine the effect of the pH on the concentration of the calcium ion, an aqueous formaldehyde solution prepared at a desired concentration was maintained at 60 °C in a three-necked flask and nitrogen was passed through the solution. After the pH of the solution had been adjusted by carbonate-free concentrated KOH, calcium formate was added and stirred until precipitates appeared. A turbid supernatant was filtered through asbestos, and the filtrate was analyzed for the calcium ion by the EDTA method, using NN-reagent as an indicator.[15] The results are shown in Fig. 1.

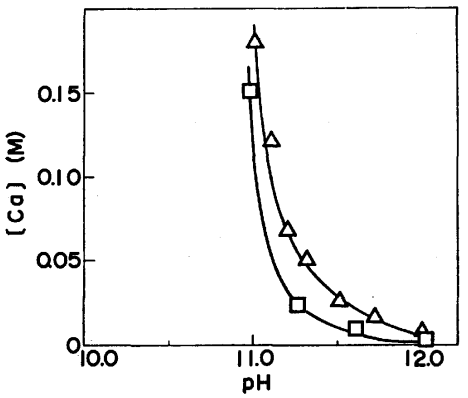

Fig. 1. Relationship between [Ca] and pH.
Temperature, 60 °C; Under N_2; [HCHO]: □, 0 M; △, 1 M; $Ca(HCOO)_2$ was used as the source of Ca^{2+} (See Experimental).

Results and Discussion

The following terms are adopted in this paper: [HCHO], [$Ca(HCOO)_2$], and [Ca], the concentrations of formaldehyde, calcium formate, and the dissolved calcium ion species respectively; T_{min}, the length of the induction step, namely, the time from the start to the ORP minimum; T_{max}, the time from the start to the ORP maximum, and $T_{max}-T_{min}$, the length of the formose-forming step (see the preceding paper[1]).

The Formose Reaction Homogeneously Catalyzed by the Calcium Ion. The reactant solution was prepared by dissolving a given amount of calcium formate into an aqueous formaldehyde solution and by adjusting the pH by the addition of concentrated aqueous KOH. After the reaction had been started at 60 °C, the pH of the mixture was maintained by adding concentrated aqueous KOH; the subsequent reaction was followed by ORP measurement and analyzed as usual. We have previously shown that the ORP of the reaction mixture increases from the minimum at the beginning of the formose-forming period up to the maximum at its end in the pH-uncontrolled reaction.[13,14] In the experiments at a constant pH, however, the increase in ORP in this period was found to be very small.

As is shown in Table 1, in a certain range of pH and [Ca] the formose reaction did occur. At pH 10.5 (Runs 1—3), T_{min} and $T_{max}-T_{min}$ were reduced with an increased [Ca], indicating that the rates of both the induction and formose-forming processes are dependent on the amount of the dissolved calcium ion species. At higher pHs, the situation became considerably different. At pH 11.0 (Run 4), even though [Ca] was the same as that of Run 1, in which the reaction was very slow, T_{min} and $T_{max}-T_{min}$ were as fast as Run 2, in which [Ca] was three times higher. At pH 11.5 (Run 5), although part of the calcium ion separated out as solid $Ca(OH)_2$, the rate was comparable to that of Run 3,

Table 1. Formose reaction at a constant pH
Temp, 60 °C; [HCHO]=1.0 M.

Run No.	[Ca-(HCOO)$_2$] (M)	pH	HCHO consumption (%) at		[Ca] (mM) at			T_{min} (min)	T_{min} (min)	$T_{max}-T_{min}$ (min)	Sugar yield (%) at	
			T_{min}	T_{max}	T_s	T_{min}	T_{max}				T_{max}	T_3[a]
1	0.1	10.5	$(11.2)_{60}$		100	$(90)_{60}$		—[b]	—[b]	—	$(0.3)_{60}$	
2	0.3	10.5	20.0	97.9	290	290	290	58.0	68.0	10.0	46.8	33.1
3	0.55	10.5	18.7	98.3	530	540	540	8.5	14.5	6.0	53.7	35.4
4	0.1	11.0	31.6	97.8	100	90	100	61.0	69.0	8.0	53.3	34.6
5[c]	0.1	11.5	29.2	97.0	70	80	80	12.5	14.5	2.5	52.5	26.3
6[c]	0.1	12.0	$(29.9)_{60}$		20	$(10)_{60}$		—[b]	—[b]	—	$(0.7)_{60}$	

a) T_3=3 min after T_{max}. b) No minimum ORP or maximum ORP is observed. The subscript number is the reaction time, in min. c) Heterogeneous system.

TABLE 2. EFFECTS OF VARIOUS CALCIUM SALTS ON THE FORMOSE REACTION

Cat.	T_{min} (min)	T_{max} (min)	$T_{max}-T_{min}$ (min)	HCHO consumption (%) at T_{min}	HCHO consumption (%) at T_{max}	Sugar yield (%) at T_{max}	Sugar yield (%) at T_3[b]
$CaCl_2$	14.0	16.0	2.0	29.4	94.2	55.2	28.0
$CaBr_2$	17.0	21.0	4.0	26.2	97.3	42.6	32.4
$Ca(HCOO)_2$	22.0	25.5	3.5	33.7	99.8	45.3	34.6
$Ca(CH_3COO)_2$	26.0	30.0	4.0	28.0	98.1	52.3	36.1
$Ca(C_2H_5COO)_2$	30.5	34.0	3.5	38.9	98.1	44.7	36.7

a) [HCHO]=1.0 M; [Ca]=0.15 M; Temp, 60 °C; pH=11.0. b) T_3=3 min after T_{max}.

in which [Ca] was about seven times higher. The results suggest that the catalytic function of the dissolved calcium ion species increases with an increased pH. As will be discussed later, the active species catalyzing the formose reaction is believed to be $CaOH^+$.

At pH 12.0, most of the dissolved calcium ion species separated out as the solid $Ca(OH)_2$ and the reaction rate became very slow. As is shown in Fig. 1, when calcium formate was used as the source of the calcium ion, [Ca] decreased sharply above pH 11.0 in both the presence and absence of formaldehyde with an increased pH. The slow-down of the $Ca(OH)_2$-catalyzed formose reaction at a high pH[1,4] can now be ascribed to the deficiency of the dissolved calcium ion species. It follows that a high concentration of the catalyst cannot be employed for the homogeneously-catalyzed formose reaction carried out at an elevated pH. However, we found that the formose reaction took place smoothly even at pHs above 12, with the appearance of both an ORP minimum and a maximum, when an ion-exchange resin, Amberlite IR 120 (Ca^{2+}), was used as the catalyst in place of $Ca(OH)_2$ or a calcium salt-KOH system. The pH dependence of T_{min} and T_{max} in the formose reaction with the resin had a relation parallel to that of the $CaOH^+$ distribution in an aqueous $Ca(OH)_2$ solution shown in Fig. 4.

Next, a homogeneous formose reaction using other calcium salts was examined. If the formose reaction is mainly dependent on the dissolved calcium ion concentration and on the pH, it will not be much affected by the nature of the counter anion of calcium salts. The results summarized in Table 2 indicate that this is indeed the case. So far as the sugar formation is concerned, the formose reaction with these calcium salts was virtually the same as that with calcium formate-KOH or with calcium hydroxide. However, the reaction rate estimated by T_{min} and T_{max} showed a tendecy to decrease with a decrease in the dissociation ability of the calcium salts.

Effects of pH in a Homogeneously Catalyzed Formose Reaction. As is shown in Table 1 (Runs 1, 4, and 5), the induction period is shortened with an increase in the pH in the range from pH 10.5 to 11.5 in the homogeneous system. The pH dependence of the formose-forming period and the sugar yield was examined, after the homogeneous formose reaction using calcium formate had been started at pH 11.0, by varying the pH at T_{min} and by determining $T_{max}-T_{min}$ and the sugar yield. The results are shown in Figs. 2 and 3. The formose-forming step was shortened at

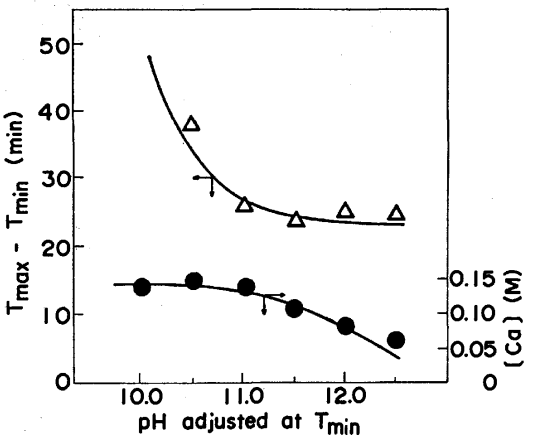

Fig. 2. Effect of pH variation at T_{min} on $T_{max}-T_{min}$ and [Ca].
[HCHO]=1.0 M; [$Ca(HCOO)_2$]=0.15 M; Starting pH=11.0 (Under these conditions, T_{min} was *ca.* 22 min).

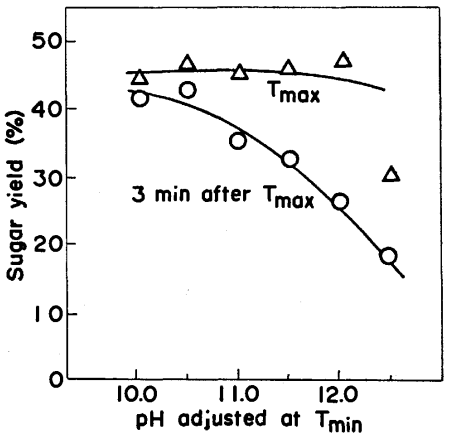

Fig. 3. Effect of pH variation at T_{min} on the sugar yield.
Reaction conditions; same as those in Fig. 2.

higher pHs, although [Ca] came to decrease at pHs above 11.5 as a result of the precipitation of the solid $Ca(OH)_2$. On the other hand, the sugar yield practically remained unchanged upon pH variation except for at pH 12.5, but the decomposition of the sugars occurring after T_{max} became more significant with an increased pH. The results indicate that the hydroxide ion may be as an effective catalyst in the formose-forming step as the dissolved calcium ion species.

Active Catalytic Species in the Formose Reaction Homogeneously Catalyzed by Calcium Ions. In view of the

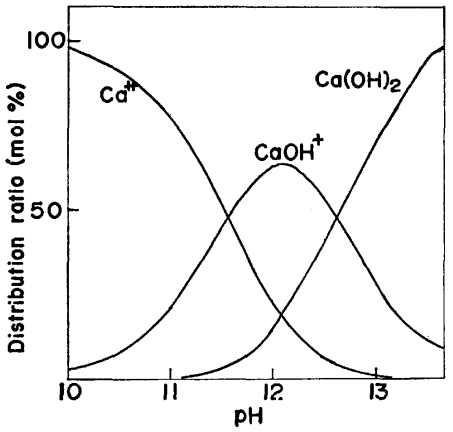

Fig. 4. Calculated distribution of dissolved Ca^{2+}, $CaOH^+$, and $Ca(OH)_2$ at different pHs.

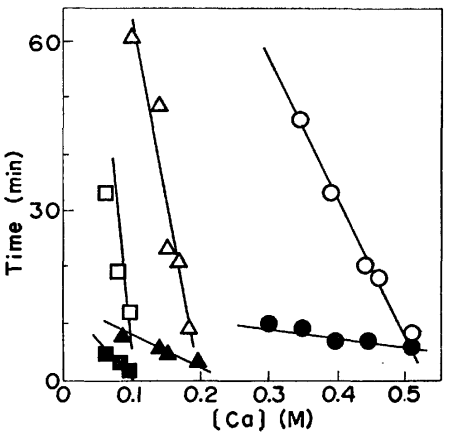

Fig. 5. Relationship between T_{min} or $T_{max}-T_{min}$ and [Ca] at different pHs.
[HCHO]=1.0 M; Catalyst, $Ca(HCOO)_2$; Temp, 60°C; T_{min}: ○,△ and □, pH 10.5, 11.0 and 11.5, respectively; $T_{max}-T_{min}$: ●,▲, and ■, pH 10.5, 11.0, and 11.5, respectively.

importance of the dissolved calcium ion species and the pH in the formose reaction, the distribution of $Ca(OH)_2$, $CaOH^+$, and Ca^{2+} in solution at different pHs was calculated (Fig. 4) on the basis of the acid-base equilibria of $Ca(OH)_2$:[17]

$$Ca^{2+} + H_2O \rightleftarrows CaOH^+ + H^+ \quad (pK_{a_1}=11.57),$$

$$CaOH^+ + H_2O \rightleftarrows Ca(OH)_2 + H^+ \quad (pK_{a_2}=12.63).$$

The Weiss proposal that $CaOH^+$ might be the active catalyst in the formose reaction catalyzed by calcium hydroxide now becomes very plausible. The calculated distribution of $CaOH^+$ at different pHs could not be applied exactly to our experimental data because of the differences of the conditions employed. However, the distribution was proved to be very useful for interpreting the experimental facts thus far obtained, provided that the pH of the maximum distribution of $CaOH^+$ under either heterogeneously- or homogeneously-catalyzed formose reaction conditions is shifted to *ca.* 11.5 from the calculated pH of 12. An example is given by a comparison of Runs 3 and 5 in Table 1. Although the initial concentration of the dissolved calcium ion species in Run 5 is considerably lower than that in Run 3, the rate of the induction and the formose-forming steps are comparable in both cases. This can be qualitatively explained by assuming that the concentrations of the active catalytic species, namely, $CaOH^+$, are almost equal in both runs.

(1) $CaOH^+$ as the Catalyst in the Induction Step: More quantitative experiments became necessary for proving the role of $CaOH^+$ as the catalyst. Figure 5 shows plots of T_{min} as a function of [Ca] at different pHs (10.5, 11.0, and 11.5) in a homogeneously-catalyzed formose reaction using $Ca(HCOO)_2$–KOH. An approximate linear relation was obtained at each pH. This relation led us to express T_{min} by

$$T_{min} = af_i[Ca] + c, \qquad (1)$$

where a and c are constants, and where f_i is the molar fraction of $CaOH^+$ in the dissolved calcium ion species at pH=i. The values of af_i and c are obtained from the slope and the interception of each line respectively. The same plots were made for the formose reaction catalyzed by $CaCl_2$–KOH, and a linear relation was again obtained at each pH. The c value was 130 min for the $Ca(HCOO)_2$–KOH system (105 for the $CaCl_2$–KOH system). When $a=-2000$ min M^{-1} (-2056), f_i is 0.12 (0.10), 0.33 (0.30), and 0.67 (0.69) at pH 10.5, 11.0, and 11.5 respectively. These f_i values are in fairly good agreement with the calculated values of Fig. 4. The constants, a and c, would depend on the reaction conditions, such as [HCHO] and the reaction temperature. Thus, Eq. 1 can be simplified to

$$T_{min} = a[CaOH^+] + c. \qquad (2)$$

Equation 2 means that the induction period is shortened linearly with an increase in the concentration of $CaOH^+$ at the same [HCHO] and pH in a certain range of [Ca].

(2) Effective Catalytic Species in the Formose-forming Step: We have suggested in the preceding paper and this paper that the OH^- as well as $CaOH^+$ participates in the catalysis in the formose-forming step in either a heterogeneous or homogeneous formose reaction.[1] Weiss and John have concluded, from their experiments using CSTR, that the rate of the formose reaction at the intermediate conversion level of formaldehyde, which is regarded as the actual formose-forming step, is first-order for calcium hydroxide ($r_F=k_F[Ca(OH)_2]$).[4] However, since their reaction system was heterogeneous, both dissolved and undissolved calcium hydroxide must contribute to the reaction rate. In order to clarify the role of the dissolved calcium ion species in the formose-forimng step, $T_{max}-T_{min}$ was plotted as a function of [Ca] at different pHs (10.5, 11.0, and 11.5) in the homogeneously catalyzed formose reaction.

The results, shown in Fig. 5, indicate that $T_{max}-T_{min}$ and [Ca] have a linear relation at different pHs. Similar relations were obtained with the $CaCl_2$–KOH system. These relations, however, are not simple as in Eq. 1, but can be expressed by

$$T_{max} - T_{min} = af_i^a[Ca] + bf_i^b[Ca] + c, \qquad (3)$$

where af_i^a, bf_i^b, and c are constants and where f_i^a and f_i^b are the molar fractions of $CaOH^+$ and $Ca(OH)_2$ respectively in the dissolved calcium ion species at pH=i. The experimental data eventually gave the following values:

a, -133 min M^{-1} for the $Ca(HCOO)_2$–KOH system (-67 for the $CaCl_2$–KOH system); b, -537 min M^{-1} (-33); c, 14.1 min (3.7); $f^a_{10.5}$, 0.12 (0.10); $f^a_{11.0}$, 0.33 (0.30); $f^a_{11.5}$, 0.67 (0.69); $f^b_{10.5}$, 0 (0); $f^b_{11.0}$, 0.03 (0.03); $f^b_{11.5}$, 0.07 (0.09). The f_i^a and f_i^b values are in fairly good agreement with the values calculated from Fig. 3. Thus, Eq. 3 can be simplified to

$$T_{max} - T_{min} = a[CaOH^+] + b[Ca(OH)_2] + c, \quad (4)$$

which means that, under these conditions, both dissolved $CaOH^+$ and $Ca(OH)_2$ act as effective catalytic species in the formose-forming step.

Equation 4 implies that the formose-forming step may occur when either $CaOH^+$ or $Ca(OH)_2$ is present in solution. For example, the reaction occurs at pH 10.5, where, practically, $[Ca(OH)_2]=0$. Furthermore, $Ca(OH)_2$ can be replaced merely by the OH^- ion. In fact, as was shown in Fig. 2, the formose-forming step still occurs even at pH values above 12, where [Ca] becomes very small due to the precipitation of the solid $Ca(OH)_2$. However, for such a case and for the formose reaction heterogeneously-catalyzed by $Ca(OH)_2$, one cannot neglect the possibility that the solid $Ca(OH)_2$ also participates in the catalysis in the formose-forming step, as has been proposed by Weiss *et al.*[2-4]

Equations 1—4, on the other hand, can be extrapolated to limiting values of c when [Ca] or $[CaOH^+]=0$. Since the reaction does not, of course, occur without a dissolution of the calcium ion species, it can be said that the c values have no significant physical meaning, but merely imply the feasibility of the induction and the formose-forming steps under the conditions employed.

Sugar Yield in the Homogeneously-Catalyzed Formose Reaction. The effects of [Ca] on the sugar yield at T_{max} and at 3 min after T_{max} at different pHs are illustrated in Fig. 6. The sugar yield at T_{max}, where sugars formed are most accumulated,[1] has a tendency to increase with an increase in [Ca], but the decomposition of the sugars is more accelerated with an increase in [Ca] at the same pH. The latter finding

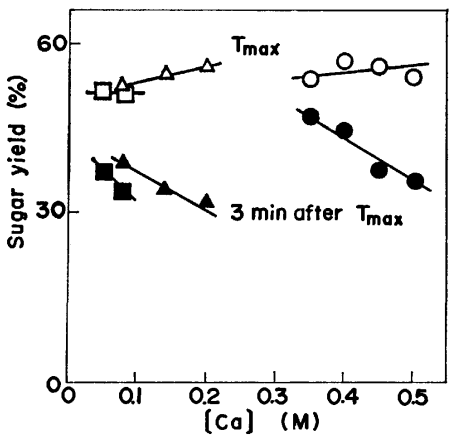

Fig. 6. Effect of [Ca] on the sugar yield.
[HCHO]=1.0 M; Catalyst, $Ca(HCOO)_2$; Temp, 60 °C; pH: ○,●, 10.5; △,▲, 11.0; □,■, 11.5.

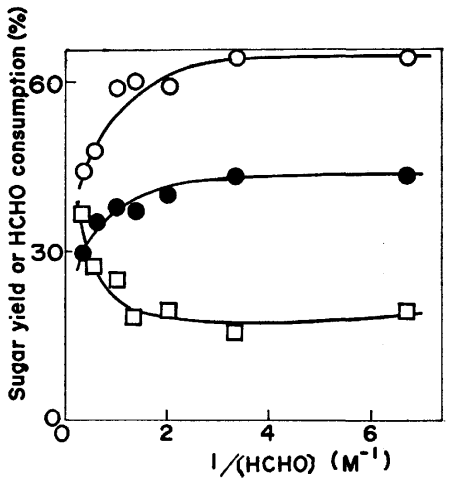

Fig. 7. Effect of the formaldehyde concentration on the sugar yield.
[$Ca(HCOO)_2$]=0.15 M; pH=11.0; Temp, 60 °C; ○, sugar yield at T_{max}; ●, sugar yield at 3 min after T_{max}; □, HCHO consumption at T_{min}.

suggests that the dissolved calcium ion species participate in the sugar decomposition like the hydroxide anion, which may take less part.

The sugar yield was found to be strongly affected by the initial [HCHO] in the present homogeneous system. This is shown in Fig. 7. At a constant [Ca], the sugar yield decreases with an increase in [HCHO] at relatively high [HCHO] values. As may be seen from Fig. 7, the decrease in the sugar yield is due to the increased consumption of formaldehyde by the Cannizzaro reaction in the induction step.

References

1) Y. Shigemasa, T. Fujitani, C. Sakazawa, and T. Matsuura, *Bull. Chem. Soc. Jpn.*, **50**, 1527 (1977).
2) A. H. Weiss, R. B. La Pierre, and J. Shapira, *J. Catal.*, **16**, 332 (1970).
3) H. Tambawala and A. H. Weiss, *J. Catal.*, **26**, 388 (1972).
4) A. H. Weiss and T. John, *J. Catal.*, **32**, 216 (1974).
5) O. Loew, *Ber.*, **21**, 270 (1888).
6) H. Schmalfuss, *Biochem. Z.*, **185**, 70 (1927).
7) S. Malinowski and J. Kehl, *Rocz. Chem.*, **34**, 391 (1960); *Chem. Abstr.*, **55**, 374h (1961).
8) E. Pfeil and G. Schroth, *Ber.*, **85**, 293 (1952).
9) K. Runge and R. Mayer, *Ann.*, **707**, 161 (1967).
10) R. Mayer and L. Jäschke, *Ann.*, **635**, 145 (1960).
11) T. Mizuno, T. Mori, N. Shiomi, and H. Nakatsuji, *Nippon Nogei Kagaku Kaishi*, **44**, 324 (1970).
12) K. Fujino, J. Kobayashi, and I. Higuchi, *Nippon Kagaku Kaishi*, **1972**, 2287, 2292.
13) T. Matsuura, Y. Shigemasa, and C. Sakazawa, *Chem. Lett.*, **1974**, 13.
14) Y. Shigemasa, M. Shimao, C. Sakazawa, and T. Matsuura, *Bull. Chem. Soc. Jpn.*, **48**, 2099 (1975).
15) J. Patton and W. Reeder, *Anal. Chem.*, **28**, 1026 (1956).
16) G. Schwarzenbach and H. Ackermann, *Helv. Chim. Acta*, **30**, 1798 (1947).
17) "Kagaku Binran," Kiso Hen 2, ed by Nippon Kagaku Kai, Maruzen, Tokyo (1975), p. 994.

Syntheses of Gramicidin S Analogs Containing δ-Aminovaleric Acid.[1] [5-1′-δ-Aminovaleric Acid]-Gramicidin S and [5-1′, 5′-1-Bis-(δ-Aminovaleric Acid)]-Gramicidin S

Shōsuke Sōfuku, Akio Yoshida, Hiroki Baba, and Ichiro Muramatsu

Department of Chemistry, College of Science, Rikkyo (St. Paul's) University, Nishi-Ikebukuro, Tokyo 171

(Received December 7, 1976)

Gramicidin S (GS) analogs, [5-1′-δ-aminovaleric acid]-GS dihydrochloride (XIII) and [5-1′, 5′-1-bis(δ-aminovaleric acid)]-GS dihydrochloride (XIX), were synthesized. Both peptides are the analogs in which one or two L-prolyl-L-valyl residues of GS are replaced with one or two δ-aminovaleric acid residues. The spectra of optical rotatory dispersion (ORD) and circular dichroism (CD) of XIII and XIX were measured. The molar optical rotation of XIII is smaller than that of GS, but its ORD spectrum resembles that of GS. Analog XIII shows some antimicrobial activity, but not the analog XIX.

Analogs of gramicidin S (GS) containing δ-aminovaleric acid (δAva) residue have been synthesized in order to investigate the role of amide bond in the three-dimensional structure and antibiotic activity of GS. When one or two dipeptide residues of the antibiotic are replaced by δAva, one or two amide groups turn into ethylene groups, the chain length and ring size remaining unaltered. However, if the replaced amide group of GS participates in the hydrogen bond essential to the proper secondary structure of the original molecule, the replacement would lead to the impracticability of hydrogen bond formation, giving rise to the deformation of the ring structure and the loss of the biological activity.

In previous papers,[1,2] the syntheses and properties of [δAva$^{4-5,4'-5'}$]-GS and [δAva$^{4-5}$]-GS were reported. It has been deduced that the stabilization of the ring structure of GS needs the existence of D-phenylalanyl-L-prolyl residue, although it does not take part in intramolecular hydrogen bond formation. The NH groups of L-valyl residues seem to participate in the intramolecular hydrogen bonds, stabilizing the pleated sheet structure of GS.[3,4]

In this paper, we describe the syntheses of [δAva$^{5-1'}$]-GS and [δAva$^{5-1',5'-1}$]-GS, giving the results of antimicrobial assays and optical rotatory dispersion (ORD) and circular dichroism (CD) measurements. Both peptides are the analogs in which one or two L-prolyl-L-valyl residues participating in the hydrogen bonds in GS are replaced by δAva. The analogs are devoid of one or two amide groups in the corresponding residues of GS. The modification would be of use for a study of the conformation of GS.

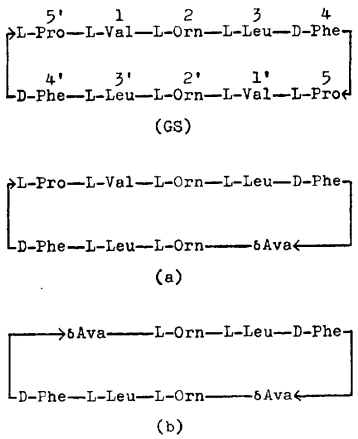

Fig. 1. Structures of gramicidin S (GS), [δAva$^{5-1'}$]-GS (a), and [δAva$^{5-1'}$, $^{5'-1}$]-GS (b).

The analogs were synthesized according to Schemes 1 and 2. The cyclization reactions were carried out by using the *p*-nitrophenyl esters of liner peptides XI and XVII. The reaction procedures were the same as in the cyclization.[2] The cyclic peptides XII and XVIII were obtained in 61 and 14% yields, respectively. In analogy with the yields of cyclization in the syntheses of [δAva$^{4-5}$]-GS (71%)[2] and [δAva$^{4-5,4'-5'}$]-GS

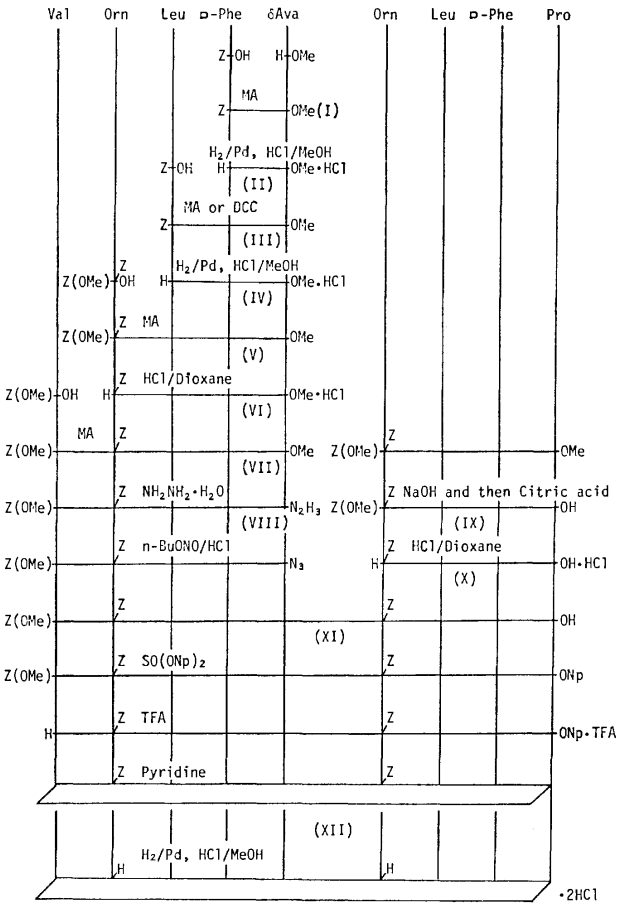

Scheme 1.

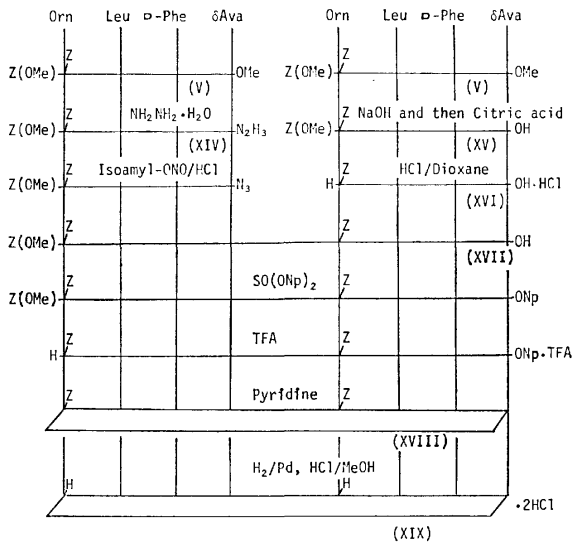

Scheme 2.

(32%),[1] the results might reflect the relative stability of the conformation favorable for cyclization of each active ester. [δAva$^{5-1'}$]-GS dihydrochloride (XIII) and [δAva$^{5-1',5'-1}$]-GS dihydrochloride (XIX) were obtained by hydrogenolysis of the benzyloxycarbonyl groups on the ornithyl residues of XII and XVIII. The purity of the synthetic analogs was confirmed by means of dansyl chloride (1-dimethylamino-5-naphthalenesulfonyl chloride) procedure,[2] paper electrophoresis, and amino acid analysis.

Table 1. Antimicrobial activity of GS and its analogs

Test organisms	Minimum inhibitory concentration[a] (μg/ml)		
	GS·2HCl	XIII[b]	XIX[c]
Staphylococcus aureus ATCC 6538p	6.3	50	>100
Streptococcus pyogenes N. Y. 5	6.3	25	>100
Sarcina lutea ATCC 9341	6.3	>100	100
Corynebacterium diphtheriae P. W. 8	1.6	3.2	>100
Bacillus subtilis ATCC 6633	6.3	25	>100
Escherichia coli B	>100	>100	>100
Proteus vulgaris OX 19	>100	>100	>100

a) Agar dilution method. b) [δAva$^{5-1'}$]-GS·2HCl.
c) [δAva$^{5-1',5'-1}$]-GS·2HCl.

Results of the antimicrobial assay of these analogs for several microorganisms are given in Table 1. ORD and CD spectra are shown in Figs. 2 and 3. The minimum value in ORD spectrum of XIII (1.4×10^{-4} M) is observed at 232 nm. Although the molar optical rotation of XIII is smaller than that of GS, its ORD spectrum shape resembles that of GS. The analog XIII exhibits some antimicrobial activity against several microorganisms. CD spectrum of XIII has two troughs near 200 nm. The trough at 203 nm corresponds to that

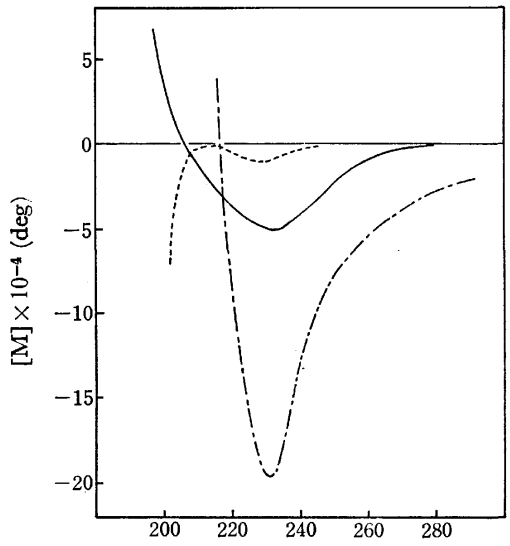

Fig. 2. ORD spectra of [δAva$^{5-1'}$]-GS·2HCl (XIII), [δAva$^{5-1',5'-1}$]-GS·2HCl (XIX), and gramicidin S 2HCl (GS) in water; XIII (——), XIX (----), and GS (- · -). Measurements were made using a 1 mm quartz cell at room temperature.

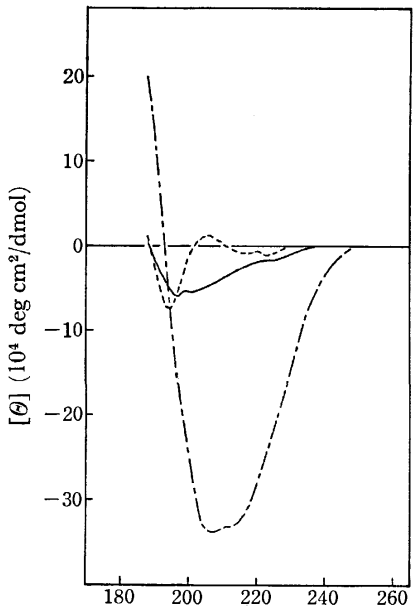

Fig. 3. CD spectra of [δAva$^{5-1'}$]-GS·2HCl (XIII), [δAva$^{5-1',5'-1}$]-GS·2HCl (XIX), and gramicidin S 2HCl (GS) in water; XIII(——), XIX(----), and GS(- · -). Measurements were made using 0.5 mm and 0.1 mm (XIX) quartz cells at room temperature.

of CD spectrum of [δAva$^{4-5}$]-GS,[2] which has a GS-like conformation. The trough in shorter wave length region is not observed in the spectrum of GS; it might arise from the partially flexible structure of XIII. The ORD and CD spectra of XIX (9.5×10^{-4} M) differ from both those of GS (1.3×10^{-4} M) and those of other GS analogs containing δAva.[1,2] Analog XIX shows no antimicrobial activity.

[MeVal^{1}]-GS and [MeVal$^{1,1'}$]-GS[5] were synthesized by Abe *et al.*[6] From the lack of amide hydrogen between L-prolyl and L-valyl residues, these analogs are comparable with analogs XIII and XIX. XIII shows antimicrobial activity and ORD spectrum similar to those of [MeVal^{1}]-GS.[6] If the part of ornithyl-leucyl-D-phenylalanyl-prolyl-valyl-ornithyl-leucyl[7] in the primary structure of XIII has a fixed secondary structure containing two hydrogen bonds and β-turn (D-phenylalanyl-prolyl),[4] analog XIII possibly exists in a GS-like conformation which can be illustrated by use of CPK model.

Experimental[5]

The purity of the synthetic compounds was confirmed by thin-layer chromatography (TLC) on silica gel plates using the following solvent systems (v/v): Solv. 1, $CHCl_3$–MeOH–AcOH–pyridine (95: 5: 3: 4); Solv. 2, $CHCl_3$–MeOH–AcOH (95: 5: 3); Solv. 3, $CHCl_3$–MeOH (9: 1); Solv. 4, *n*-BuOH–AcOH–pyridine–H_2O (4: 1: 1: 2); Solv. 5, *n*-BuOH–AcOH–H_2O (4: 1: 1). The molecular weight was determined with a Hitachi molecular weight apparatus model 115, using methanol. Amino acid analyses were performed with a JEOL automatic amino acid analyzer, after hydrolyzing samples with 6 M HCl in evacuated sealed ampoules for 20 h at 110 °C. ORD and CD spectra were measured with a JASCO model J-20 spectrometer and are represented in terms of molar optical rotation and molar ellipticity, respectively.

Z-D-Phe-δAva-OMe (I). The peptide was synthesized according to the method of Anderson *et al.*[8] Et_3N (1.39 ml, 10 mmol) was added to a solution of isobutyl chloroformate (1.44 ml, 11 mmol) in THF (20 ml) at −10 °C. After 3 min, a solution of Z-D-Phe-OH (2.99 g, 10 mmol) in THF was added dropwise to the above solution at −15 °C. After the reaction mixture had been stirred for 15 min, a mixture of H-δAva-OMe·HCl[2] (1.68 g, 10 mmol) and Et_3N (1.39 ml) in $CHCl_3$ (20 ml) was added. The reaction mixture was further stirred at −15 °C for 1 h and at room temperature overnight. After filtration, the filtrate was concentrated *in vacuo*. The residue was dissolved in ethyl acetate, and the solution was washed successively with 0.5 M HCl, water, 5% $NaHCO_3$, and water, and then dried over Na_2SO_4. After removal of the drying agent, the solution was concentrated *in vacuo* and the residue was recrystallized from ethyl acetate and petroleum ether. Yield, 3.38 g (81.9%); mp 103—104 °C; $[\alpha]_D^{20}$ +3.2° (*c* 4, MeOH).

Found: C, 67.14; H, 6.87; N, 6.99%. Calcd for $C_{23}H_{28}N_2O_5$: C, 66.97; H, 6.84; N, 6.79%.

H-D-Phe-δAva-OMe·HCl (II). I (4.13 g, 10 mmol) in MeOH (30 ml) containing methanolic 1.2 M HCl (10 ml) was hydrogenolyzed in the presence of Pd black (0.5 g) for 2 h. After removal of the catalyst and concentration of the filtrate *in vacuo*, white precipitate was obtained by trituration of the oily residue with diethyl ether in a theoretical yield.

Z-Leu-D-Phe-δAva-OMe (III). *a*) DCC (2.06 g, 10 mmol) was added to a mixture of II (3.15 g, 10 mmol) and Z-Leu-OH·DCHA[9] (4.48 g, 10 mmol) in $CHCl_3$ (50 ml) at 2—3 °C in an ice-salt bath.[10] The reaction mixture was stirred at this temperature for 3 h and then at room temperature overnight. After evaporation of the solvent *in vacuo* and addition of ethyl acetate to the residue, insoluble substance was removed by filtration. The filtrate was treated in a way similar to that for the synthesis of I. The pure product was obtained by recrystallization from ethyl acetate, EtOH and hexane. Yield, 3.7 g (70.3%); mp 145.5 °C; $[\alpha]_D^{20}$ +10.5° (*c* 2, MeOH). *b*) Z-Leu-OH obtained from the corresponding DCHA salt (14.73 g, 33 mmol) was combined with 30 mmol of II by a method similar to that for the synthesis of I. The product was recrystallized from ethyl acetate and petroleum ether. Yield, 12.42 g (77.8%); mp 144—145 °C; $[\alpha]_D^{22}$ +11.6° (*c* 2, MeOH).

Found: C, 66.46; H, 7.39; N, 8.01%. Calcd for $C_{29}H_{39}N_3O_6$: C, 66.26; H, 7.48; N, 7.99%.

H-Leu-D-Phe-δAva-OMe-HCl (IV). III (10.51 g, 20 mmol) was hydrogenolyzed by the method for II. The product was obtained in a theoretical yield.

Z(OMe)-Orn(Z)-Leu-D-Phe-δAva-OMe (V). This was prepared from IV (20 mmol) and Z(OMe)-Orn(Z)-OH obtained from the corresponding DCHA salt[11] (13.47 g, 22 mmol). The coupling method was similar to that for the preparation of I. The reaction mixture was concentrated *in vacuo*. The residue was dissolved in $CHCl_3$, and the solution was washed successively with water, 5% citric acid, water, 5% $NaHCO_3$, and water, and then dried over Na_2SO_4. After removal of the drying agent, the filtrate was concentrated *in vacuo*, and the residue was recrystallized from MeOH (600 ml). Yield, 12.52 g (77.9%); mp 182—183 °C; $[\alpha]_D^{22}$ +5.5° (*c* 1, DMF); TLC: R_f 0.64 (Solv. 3).

Found: C, 64.30; H, 7.10; N, 8.79%. Calcd for $C_{43}H_{57}N_5O_{10}$: C, 64.24; H, 7.15; N, 8.71%.

H-Orn(Z)-Leu-D-Phe-δAva-OMe·HCl (VI). V (1.85 g, 2.3 mmol) was added to 2 M HCl–dioxane (25 ml) containing anisole (0.6 ml). The solution was stirred at room temperature for 3 h and then evaporated *in vacuo*. The oily residue was triturated with diethyl ether and the resulting white precipitate was collected by filtration. After drying, the product weighed 1.42 g (89.1%).

Z(OMe)-Val-Orn(Z)-Leu-D-Phe-δAva-OMe (VII). Z(OMe)-Val-OH obtained from the corresponding DCHA salt[11] (1.16 g, 2.5 mmol) was introduced to a mixed anhydride in a way similar to that for the preparation of I. To this THF solution (19 ml) was added a solution of VI (1.42 g, 2.1 mmol) and Et_3N (0.29 ml) in DMF (15 ml) at −15 °C. The reaction mixture was stirred at this temperature for 1 h and at room temperature overnight and then filtered. The filtrate was concentrated to dryness *in vacuo*. The residue was washed on a filter funnel with water, 5% citric acid, water, 5% $NaHCO_3$, and water. The dried crude product was recrystallized from MeOH and diethyl ether. Yield, 1.2 g (63.2%); mp 193.5—195 °C; $[\alpha]_D^{18}$ +6.5° (*c* 1, DMF).

Found: C, 63.97; H, 7.41; N, 9.46%. Calcd for $C_{48}H_{66}N_6O_{11}$: C, 63.84; H, 7.36; N, 9.31%.

Z(OMe)-Val-Orn(Z)-Leu-D-Phe-δAva-NHNH$_2$ (VIII). $NH_2NH_2·H_2O$ (80%, 12.5 g) was added to a solution of VII (2.72 g, 3.0 mmol) in DMF (50 ml) and the resulting solution was stirred at room temperature for 4.5 d. The hydrazide precipitated by addition of water (400 ml) was filtered, washed with water, and dried. Yield, 2.68 g (98.9%); mp 213.5—215 °C; $[\alpha]_D^{20}$ +7.0° (*c* 1, HMPA).

Found: C, 62.05; H, 7.28; N, 12.07%. Calcd for $C_{47}H_{66}N_8O_{10}$: C, 62.51; H, 7.36; N, 12.41%.

Z(OMe)-Orn(Z)-Leu-D-Phe-Pro-OH (IX). Z(OMe)-Orn(Z)-Leu-D-Phe-Pro-OEt[2] (1.63 g, 2.0 mmol) was saponified in a mixture of MeOH (10 ml), dioxane (10 ml), and 1 M NaOH (4 ml) at room temperature for 3 h. After filtration of the reaction mixture, an oily product resulting by the addition of 5% citric acid (25 ml) in an ice bath was separated from the aqueous layer by decantation. The product was reprecipitated from MeOH, 5% citric acid, and excess water, washed with water, and dried. Yield, 1.46 g (92.5%); TLC: R_f 0.64 (Solv. 1).

H-Orn(Z)-Leu-D-Phe-Pro-OH·HCl (X). HCl–dioxane (8.6 M, 5 ml) was added to a solution of IX (1.46 g, 1.85 mmol) in dioxane (10 ml) containing anisole (0.22 ml). The solution was stirred at room temperature for 1 h. After the solvent had been evaporated *in vacuo*, the product was obtained by trituration with diethyl ether and decantation; yield, 1.19 g (97.5%).

Z(OMe)-Val-Orn(Z)-Leu-D-Phe-δAva-Orn(Z)-Leu-D-Phe-Pro-OH (XI). VIII (1.63 g, 1.8 mmol) was suspended in DMF (20 ml), followed by addition of 8.16 M HCl–dioxane (0.88 ml) and butyl nitrite (0.25 ml, 2.2 mmol) at −40 °C.[12] After the reaction mixture had been stirred at −20——30 °C for 15 min, Et_3N (1 ml) was added at −60 °C, followed by the addition of a mixture of X (1.19 g, 1.8 mmol) and Et_3N (0.5 ml) in DMF (15.5 ml) at −20——30 °C. The reaction mixture was stirred at this temperature for 1 h and at 0 °C for 66 h and then poured into cold water (500 ml). The resulting precipitate was collected by filtration, and washed with water, 5% citric acid, and water. The dried crude product (2.61 g) was recrystallized from DMF and diethyl ether. Yield, 1.53 g (56.7%); mp 226—227 °C; $[\alpha]_D^{24}$ −21.6° (*c* 0.5, DMF); TLC: R_f 0.52 (Solv. 1).

Found: C, 63.00; H, 7.25; N, 10.23%. Calcd for $C_{80}H_{107}N_{11}O_{17}\cdot 2H_2O$: C, 62.77; H, 7.31; N, 10.06%.

cyclo(-Val-Orn(Z)-Leu-D-Phe-δAva-Orn(Z)-Leu-D-Phe-Pro-) (XII). The cyclic peptide was prepared in the same way as described.[2] The reaction of XI (1.05 g, 0.7 mmol) with bis(*p*-nitrophenyl)sulfite (1.59 g) in a mixture of DMF (18 ml) and pyridine (8 ml) at room temperature for 43 h gave the *p*-nitrophenyl ester of XI. After the removal of Z(OMe)-group of this ester with TFA (7 ml) containing anisole (1.12 ml), cyclization of the resulting peptide ester was carried out in pyridine (467 ml) at 58—60 °C. The solution was concentrated *in vacuo*. The residue was dissolved in aq MeOH and passed through Dowex-1 (OH^- form) and Dowex-50 (H^+ form). After evaporation of the effluent, the product (628 mg) was recrystallized from aq MeOH. Yield, 561 mg (61.1%); mp 126—130 °C; $[\alpha]_D^{24}$ −158.0° (*c* 0.3, EtOH); TLC: R_f 0.5 (Solv. 2); mol wt, found: 1331 (calcd for $C_{71}H_{97}N_{11}O_{13}$: 1313).

Found: C, 64.09; H, 7.56; N, 11.03%. Calcd for $C_{71}H_{97}N_{11}O_{13}\cdot CH_3OH$: C, 64.31; H, 7.57; N, 11.46%.

cyclo(-Val-Orn-Leu-D-Phe-δAva-Orn-Leu-D-Phe-Pro-)·2HCl (XIII). Benzyloxycarbonyl groups of XII (394 mg, 0.3 mmol) were hydrogenolyzed in MeOH (10 ml) containing 1 M HCl (0.9 ml) in the presence of Pd-black (100 mg) for 7.5 h. After removal of the catalyst, the filtrate was concentrated *in vacuo*. The residue was washed with diethyl ether by decantation and then dissolved in water. The solution was filtered through active charcoal and the filtrate was lyophilized. Yield, 293 mg (77.4%); mp 228—231 °C (dec); $[\alpha]_D^{24}$ −157.0° (*c* 1, EtOH); TLC: R_f 0.82 (Solv. 4). Paper electrophoresis: migration distance −12 cm, *cf.* −12 cm for GS [HCOOH: AcOH: H_2O=4: 15: 180 v/v (pH 1.9), 600 V, 12—14.5 mA, 2 h, Toyo no. 50 (15×40 cm)]. Amino acid ratios: Val, 0.95; Orn, 2.00; Leu, 2.07; Phe, 2.00; Pro, 1.05; δAva, 0.96 (recovery 90%).

Found: C, 52.57; H, 7.15; N, 11.90%. Calcd for $C_{55}H_{87}N_{11}O_9Cl_2\cdot 6H_2O\cdot HCl$: C, 52.35; H, 7.99; N, 12.21%.

Z(OMe)-Orn(Z)-Leu-D-Phe-δAva-NHNH₂ (XIV). A solution of V (2.01 g, 2.5 mmol) and 80% $NH_2NH_2\cdot H_2O$ (4.7 g) in DMF (15 ml) was stirred at room temperature for 3 d. The solution was concentrated *in vacuo* to a volume of *ca.* 10 ml. White precipitate was obtained by the addition of excess water to the concentrate. The filtered and dried product weighed 1.94 g (96.5%). Mp 203.5—205.5 °C. A sample for analysis was obtained by crystallization from MeOH–ethyl acetate–diethyl ether. Mp 205.5—207.5 °C; $[\alpha]_D^{21}$ +8.4° (*c* 1, DMF).

Found: C, 62.47; H, 7.25; N, 12.46%. Calcd for $C_{42}H_{57}N_7O_9$: C, 62.75; H, 7.15; N, 12.19%.

Z(OMe)-Orn(Z)-Leu-D-Phe-δAva-OH (XV). A solution of V (2.41 g, 3 mmol) in a mixture of dioxane (50 ml) and MeOH (30 ml) containing 1 M NaOH (9 ml) was stirred at room temperature for 2.5 h. To this was added 1 M NaOH (3 ml) and the stirring was continued. Another portion (3 ml) of the alkali solution was added 1 h later. Four h after the last addition, the solution was acidified with citric acid (3.15 g) and concentrated *in vacuo*. On the addition of water to the residue, precipitate appeared immediately. After filtration and drying, the precipitate was recrystallized from MeOH. Yield, 1.80 g (75.9%); mp 165—167 °C; $[\alpha]_D^{21}$ +5.0° (*c* 1, DMF); TLC: R_f 0.18 (Solv. 3).

Found: C, 64.03; H, 7.19; N, 9.18%. Calcd for $C_{42}H_{55}N_5O_{10}$: C, 63.86; H, 7.02; N, 8.87%.

H-Orn(Z)-Leu-D-Phe-δAva-OH·HCl (XVI). XV (1.58 g, 2 mmol) was treated with a solution of 2.2 M HCl–dioxane (20 ml) containing anisole (0.65 ml) at room temperature for 2 h. The product was obtained in a theoretical yield following the procedure in the preparation of X.

Z(OMe)-Orn(Z)-Leu-D-Phe-δAva-Orn(Z)-Leu-D-Phe-δAva-OH (XVII). XIV (1.61 g, 2 mmol) and XVI (1.32 g, 2 mmol) were subjected to the same treatment as that for XI, except for the use of isopentyl nitrite (0.42 ml) instead of butyl nitrite. The reaction mixture was stirred at 0 °C for 70 h and filtered. The precipitate and the residue obtained from the filtrate after concentration *in vacuo* were combined, and washed with 5% citric acid and water. Recrystallization of the dried crude product from DMF and MeOH gave 1.65 g (59.0%) of the pure product. Mp 218—220 °C; $[\alpha]_D^{24}$ +3.4° (*c* 0.6, DMF).

Found: C, 64.10; H, 7.48; N, 9.79%. Calcd for $C_{75}H_{100}N_{10}O_{16}$: C, 64.45; H, 7.21; N, 10.02%.

cyclo(-Orn(Z)-Leu-D-Phe-δAva-Orn(Z)-Leu-D-Phe-δAva-) (XVIII). This cyclic peptide was synthesized following the same procedure as described for the prepararion of XII. From XVII (1.40 g, 1 mmol), 194 mg of crude product was obtained. Upon recrystallization from aq MeOH, 174 mg (14.3%) of the pure product was obtained. Mp 274—275 °C; $[\alpha]_D^{24}$ −20.7° (*c* 0.1, EtOH); TLC: R_f 0.46 (Solv. 3); mol wt, found: 1142 (calcd for $C_{66}H_{90}N_{10}O_{12}$: 1216).
Found: C, 64.71; H, 7.33; N, 11.60%. Calcd for $C_{66}H_{90}N_{10}O_{12}$: C, 65.22; H, 7.46; N, 11.52%.

cyclo(-Orn-Leu-D-Phe-δAva-Orn-Leu-D-Phe-δAva-)·2HCl (XIX). XVIII (146 mg, 0.12 mmol) was hydrogenolyzed in MeOH containing 1 M HCl (0.4 ml) in the presence of Pd-black (50 mg) for 6 h. After removal of the catalyst, the filtrate was concentrated *in vacuo*. After trituration of the residue with diethyl ether and decantation, it was dissolved in water. The solution was filtered through active charcoal. By lyophilization of the filtrate the product was obtained in a 71.2% yield (94.4 mg). Mp 199—202 °C (dec); $[\alpha]_D^{25}$ −20.7° (*c* 0.1, H_2O); TLC: R_f 0.59 (Solv. 4) and 0.69 (Solv. 5). Paper electrophoresis: migration distance −10 cm, *cf.* −10.5 cm for GS [HCOOH: AcOH: H_2O=4: 15: 180 v/v (pH 1.9), 600 V, 11.8—14.8 mA, 2 h, Toyo no. 50 (15×40 cm)]. Amino acid ratios: Orn, 0.96; Leu, 1.00; Phe, 0.90; δAva, 1.06 (recovery 96%).

Found: C, 52.88; H, 7.34; N, 12.03%. Calcd for $C_{50}H_{80}N_{10}O_8Cl_2\cdot 4H_2O\cdot HCl$: C, 53.21; H, 7.95; N, 12.41%.

The authors are indebted to the members of the

Research Laboratories of Toyo Jozo Co. for their elemental analyses and microbiological assays. They also wish to thank Mr. Yoshiaki Motoki for the amino acid analyses.

References

1) Part II of this series: S. Sōfuku, I. Muramatsu, K. Okada, and A. Hagitani, *Bull. Chem. Soc. Jpn.*, **48**, 2888 (1975).
2) S. Sōfuku, *Bull. Chem. Soc. Jpn.*, **46**, 968 (1973).
3) A. Stern, W. A. Gibbons, and L. C. Craig, *Proc. Natl. Acad. Sci. U. S. A.*, **61**, 734 (1968).
4) M. Ohnishi and D. W. Urry, *Biochem. Biophys. Res. Commun.*, **36**, 194 (1969).
5) Abbreviations: MeVal, *N*-methylvaline; Z–, benzyloxycarbonyl; Z(OMe)–, *p*-methoxybenzyloxycarbonyl; –ONp, *p*-nitrophenoxy; –OMe, methoxy; –OEt, ethoxy; DMF, *N,N*-dimethylformamide; THF, tetrahydrofuran; Et_3N, triethylamine; DCHA, dicyclohexylamine; DCC, dicyclohexylcarbodiimide; TFA, trifluoroacetic acid; HMPA, hexamethylphosphoramide; MA, mixed anhydride method.
6) H. Abe, T. Kato, and N. Izumiya, Abstr. 1F30, 32nd National Meeting of the Chemical Society of Japan, Tokyo, April 1975; N. Izumiya, Tampakushitsu Kakusan Koso, Extra number **1976** (5), 166.
7) Amino acid symbols with no prefix denote the L-configuration.
8) G. W. Anderson, J. E. Zimmerman, and F. M. Callahan, *J. Am. Chem. Soc.*, **89**, 5012 (1967).
9) E. Klieger, E. Schröder, and H. Gibian, *Ann. Chem.*, **640**, 157 (1961).
10) K. Kuromizu and N. Izumiya, *Bull. Chem. Soc. Jpn.*, **28**, 1874 (1963).
11) S. Sōfuku, M. Mizumura, and A. Hagitani, *Bull. Chem. Soc. Jpn.*, **43**, 177 (1970).
12) J. Honzl and J. Rudingr, *Collect. Czech. Chem. Commun.*, **26**, 2333 (1961).

Rhodium Complex Catalyzed Hydrogenation of α,β-Unsaturated Aldehydes to Unsaturated Alcohols

Tsutomu MIZOROKI, Katsumi SEKI, Shun-ichi MEGURO, and Atsumu OZAKI

Research Laboratory of Resources Utilization, Tokyo Institute of Technology, Ohokayama Meguro-ku, Tokyo 152

(Received January 14, 1977)

Rhodium complexes were found to be effective in catalyzing selective hydrogenation of cinnamaldehyde to cinnamyl alcohol in the presence of strongly basic amine such as triethylamine or *N*-methylpyrrolidine under oxo reaction conditions. The selectivity of analogous hydrogenation of aliphatic unsaturated aldehyde was poorer than that of aromatic aldehyde. When a catalytic amount of triphenylphosphine was added, the selectivity was drastically changed to exclusive formation of hydrocinnamaldehyde. In order to elucidate the nature of rhodium-amine interaction, $Rh_2Cl_2(CO_4)$ was immobilized on a cross-linked chloromethylated polystyrene which was functionalized with pyrrolidine, the polymer amine acting as a tertiary amine. The polymer–rhodium complex was found to be stable and to effect the selective hydrogenation of cinnamaldehyde, while addition of triphenylphosphine seemed to liberate the rhodium complex from the polymer. It is concluded that a rhodium–amine–carbonyl complex is responsible for the selective hydrogenation of α,β-unsaturated aldehyde to the unsaturated alcohol.

Hindered unsaturated aldehydes having highly substituted carbon-carbon double bonds can be hydrogenated to the corresponding unsaturated alcoholes.[1] For unhindered α,β-unsaturated aldehydes such as cinnamaldehyde and crotonaldehyde, however, a very limited number of catalysts are known to be effective, *i.e.* platinum and palladium supported on carbon combined with zinc and iron(II) chlorides,[2] although no mechanistic study has been reported. On the other hand, a number of transition metal complexes have been reported to catalyze hydrogenation of olefin and aldehyde under mild reaction conditions.[3] No efficient homogeneous catalyst is known for preferential hydrogenation of these unsaturated aldehydes to the unsaturated alcohols using molecular hydrogen. In the presence of a tertiary amine, rhodium complex catalysts are much more active than cobalt carbonyls for oxo-alcohol syntheses without accompanying hydrogenation of olefin.[4,5] This suggested that rhodium complexes would be effective in the presence of carbon monoxide and tertiary amine for the selective hydrogenation of α,β-unsaturated aldehyde. Kogami *et al.* examined cobalt carbonyl catalyst in the presence of amine for hydrogenation of cinnamaldehyde and its derivatives under oxo reaction conditions, no preferential hydrogenation to the unsaturated alcohols being found.[6]

This work was undertaken to elucidate the necessary conditions for selective hydrogenation of cinnamaldehyde and croton aldehyde to the unsaturated alcohols with rhodium complex catalyst in the presence of tertiary amine under oxo reaction conditions, and to study the interaction of amine with rhodium atom in its coordination sphere by immobilizing $Rh_2Cl_2(CO)_4$ on an aminated polystyrene.

Experimental

Materials. Tetracarbonyldichlorodirhodium (I), $Rh_2Cl_2(CO)_4$, was prepared from $RhCl_3 \cdot 3H_2O$ and carbon monoxide[7] (Found: C, 11.2; Cl, 18.8%. Calcd for: C, 12.4; Cl, 18.2%). Commercial $RhCl_3 \cdot 3H_2O$, carbon monoxide (98%) and all the α,β-unsaturated aldehydes and amines (Tables 2 and 3) were used without purification. Benzene of extra pure grade guaranteed for UV spectrometry (Wako Pure Chemicals Industry Ltd.) was used as a solvent to avoid the effect of contaminants such as thiophene.

Aminated polystyrene was prepared by an appropriate modification of the method used for the amination of chloromethylated polymers.[8] A cross-linked chloromethylated polystyrene (divinylbenzene 3%. Mitsubishi Chemical Industry Ltd.) was washed with dioxane and water under nitrogen atmosphere, and dried at 50—60 °C in a vacuum (Found: H, 6.9; C, 75.2; Cl, 15.6%. Total 97.7%). The chloromethylated polystyrene (50 g) were aminated with pyrrolidine (100 g) in dioxane (150 ml) under nitrogen atmosphere at room temperature for 48 h. The resulting polymer was washed three times with a water–dioxane solution of hydrogen chloride to remove the excess pyrrolidine and then three times with an aqueous sodium carbonate solution to liberate the amine chemically linked to the polymer. Subsequently the aminated polystyrene was washed thoroughly with water and methanol and dried at 20 °C in a vacuum (Found: H, 9.1; C, 84.3; N, 5.4; Cl, 1.1%. Total 99.9%).

Reaction Procedure. All the reactions were carried out with use of a stainless steel autoclave (100 ml) equipped with a magnetic stirrer. A benzene solution (20 ml) of a tertiary amine (2.5—40 mmol) and one of α,β-unsaturated aldehydes (20—23 mmol) and $RhCl_3 \cdot 3H_2O$ (0.13 mmol) or $Rh_2Cl_2(CO)_4$ (0.065 mmol) were placed in the autoclave under nitrogen atmosphere, followed by introduction of carbon monoxide and hydrogen at room temperature. The autoclave was then heated up to the desired temperature within 10—15 min, and the temperature was kept constant. After a given period of run, the autoclave was rapidly cooled with water to room temperature, and gaseous materials were purged out. The products were quantitatively analyzed by a gas chromatograph equipped with a 4 meter column of DC-550, polyethylene glycol, or ethylene glycol succinate polyester using an appropriate substance as internal standard. The hydrogenation products were isolated by a preparative gas chromatograph, and identified by NMR, IR, or mass spectroscopy, when necessary.

Results and Discussion

General Features of Reaction. The results for cinnamaldehyde using $RhCl_3 \cdot 3H_2O$ as a catalyst are shown in Table 1. In the absence of carbon monoxide

Table 1. Hydrogenation of cinnamaldehyde catalyzed by rhodium complex

PhCH=CHCHO 20 mmol, C_6H_6 20 ml, P_{H_2} 40 kg/cm² at r.t., Temp 90 °C, React time 60 min.

Catalyst (mmol)	P_{CO} (kg/cm²)	NEt_3 (mmol)	Temp (°C)	Conv. (%)	Selectivity (%) II[a]	III[a]	IV[a]
$RhCl_3 \cdot 3H_2O$ 0.13	40	0	90	35	≈0	≈0	≈0
	0	20	90	18	96	0	≈0
	40	20	90	93	7.9	63	22
	40	20 +PPh_3 1.0	90	100	95	0	≈0
	40	20 +$AsPh_3$ 1.0	90	7.5	95	0	0.9
	40	20 +NPh_3 1.0	90	86	10	51	22
$RhCl(PPh_3)_3$ 0.10	40	0	90	0	—	—	—
	0	20	90	44	81	0	3.1
	40	20	90	100	100	0	≈0
$RhCl_3 \cdot 3H_2O$ 0.13	40	20	70	10	—	—	—
	40	20	60[b]	72	5	61	8
$Rh_2Cl_2(CO)_4$ 0.065	40	20	60	94	2	85	11

a) II Hydrocinnamaldehyde, III Cinnamyl alcohol, IV Hydrocinnamyl alcohol.
b) Pretreatment with CO (40—50 kg/cm²) at 90 °C for 60 min.

or triethylamine, small amounts of hydrogenated products are obtained, no cinnamyl alcohol being detected. Addition of triethylamine, however, significantly increases not only the catalytic activity but the selectivity to cinnamyl alcohol under the oxo reaction conditions, giving no hydroformylation products. Addition of primary or secondary amine in place of tertiary amine was ineffective in giving hydrogenation products. This is presumably caused by the formation of highly stable Rh(III)–amine complexes.[9] On the other hand, the addition of a catalytic amount of triphenylphosphine strikingly increases the selectivity for the hydrogenation of the carbon-carbon double bond to give hydrocinnamaldehyde. Triphenylamine has little effect, while triphenylarsine decreases the catalytic activity. $RhCl(PPh_3)_3$ is a highly active catalyst for preferential hydrogenation of the carbon-carbon double bond under the same conditions. The results indicate that both carbon monoxide and tertiary amine play important roles for the selective hydrogenation to cinnamyl alcohol with rhodium complex catalyst.

Although $RhCl_3 \cdot 3H_2O$ exhibits only a low activity at lower temperatures, it can be activated by treatment with carbon monoxide (30—50 kg/cm²) at 90 °C for 60 min before introduction of hydrogen, so that cinnamaldehyde can be hydrogenated even at 60 °C. When $Rh_2Cl_2(CO)_4$ is used as the catalyst, the selective hydrogenation takes place more readily without pretreatment, suggesting that $RhCl_3$ is reduced during the course of hydrogenation.

Effect of Tertiary Amine. The effect of tertiary amine in the hydrogenation of cinnamaldehyde is given in Table 2. Two features of amine effect are observed. Firstly, highly basic amines such as triethylamine (pK_b= 3.3), *N*-methylpyrrolidine (pK_b=3.8) and *N*-methylpiperidine (pK_b=2.8) are effective not only for catalytic activity but also for preferential hydrogenation to cinnamyl alcohol. *N,N*-Dimethylbenzylamine (pK_b= 5.1) is not effective, and less basic amines such as *N,N*-dimethylaniline (pK_b=8.9) and pyridine (pK_b=8.9) give no cinnamyl alcohol at all. Such a trend in the effectiveness of tertiary amines was also reported for oxo-alcohol synthesis from hexene or octene catalyzed by rhodium catalysts combined with tertiary amine and water.[4] Secondly, both catalytic activity and selectivity to cinnamyl alcohol substantially depend on the amount of amine, this being pronounced in the presence of large excess of triethylamine or *N*-methylpyrrolidine (amine/Rh=100—200 in mol). It is interesting to see the effect of diamines, since the interaction between rhodium atom and diamines could be strengthened by their chelate effect. The diamines (Table 2) are clearly effective for selective hydrogenation, but they are required in a large amount to increase the yield of cinnamyl alcohol, and no chelate effect is observed. *p,p'*-Bis(dimethylamino)diphenylmethane as well as *N,N*-dimethylaniline give no cinnamyl alcohol. The interaction between rhodium complex and amine will be discussed on the basis of the hydrogenation using $Rh_2Cl_2(CO)_4$ catalyst immobilized on an aminated polystyrene.

Effects of Carbon Monoxide and Hydrogen. Effects of carbon monoxide and hydrogen on the conversion of cinnamaldehyde and selectivity of hydrogenation are shown in Figs. 1 and 2. Under the conditions specified in Fig. 1, the highest conversion of cinnamaldehyde is obtained at 20 kg/cm² of carbon monoxide, where the selectivity to hydrocinnamyl alcohol is also the highest. The selectivity to cinnamyl alcohol increases with increase in the pressure of carbon monoxide, the formation of hydrocinnamaldehyde being significantly retarded by carbon monoxide. The increase in hydrogen pressure under a constant pressure of carbon monoxide (40 kg/cm²) increases the conversion of cinnamaldehyde,

Table 2. Effect of tertiary amine on hydrogenation of cinnamaldehyde

PhCH=CHCHO 20 mmol, C_6H_6 20 ml, $RhCl_3 \cdot 3H_2O$ 0.13 mmol, Press. 80 kg/cm² ($CO/H_2=1$) at r.t., Temp 90 °C, Time 60 min.

Amine (mmol)	Conv. (%)	Selectivity (%) II[b]	III[b]	IV[b]
NEt_3(10)	88	56	28	14
NEt_3(20)	93	7.9	63	22
N-Methylpyrrolidine(20)	100	≈0	83	10
N-Methylpyrrolidine(5)[a]	30	9.0	59	≈0
N-Methylpyrrolidine(10)[a]	67	3.7	83	11
N-Methylpyrrolidine(20)[a]	88	2.2	75	14
N-Methylpyrrolidine(30)[a]	99	0	69	11
N-Methylpiperidine(20)	100	0	83	13
$N(CH_3)_2CH_2Ph$(20)	55	28	39	16
$N(CH_3)_2Ph$(20)	7.7	0	0	0
NC_5H_5(20)	≈0	—	—	—
$(CH_3)_2N-(CH_2)_2-N(CH_3)_2$(2.5)	21	51	50	~0
$(CH_3)_2N-(CH_2)_2-N(CH_3)_2$(5)	53	21	52	12
$(CH_3)_2N-(CH_2)_2-N(CH_3)_2$(10)	96	6.5	58	35
$(CH_3)_2N-(CH_2)_2-N(CH_3)_2$(15)	99	1.3	65	34
$(CH_3)_2N-(CH_2)_2-N(CH_3)_2$(20)	63	12	77	9.1
$(CH_3)_2N-(CH_2)_3-N(CH_3)_2$(10)	77	14	73	17
$(CH_3)_2N-(CH_2)_6-N(CH_3)_2$(10)	72	14	59	17
$(CH_3)_2N-C_6H_4-CH_2-C_6H_4-N(CH_3)_2$(10)	13	—	—	—

a) Pretreatment with CO (30—40 kg/cm²) at 90 °C for 60 min. b) II Hydrocinnamaldehyde, III Cinnamyl alcohol, IV Hydrocinnamyl alcohol.

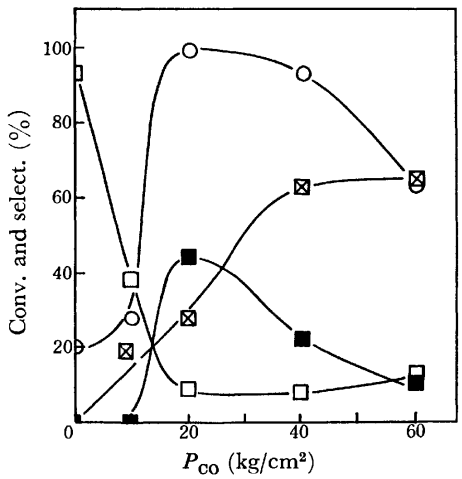

Fig. 1. Effect of the pressure of carbon monoxide on hydrogenation of cinnamaldehyde.
PhCH=CHCHO 20 mmol, NEt_3 20 mmol, C_6H_6 20 ml, $RhCl_3 \cdot 3H_2O$ 0.13 mmol, P_{H_2} 40 kg/cm² at r.t., Temp 90 °C, Time 60 min. ○ Conversion, □ hydrocinnamaldehyde, ⊠ cinnamyl alcohol, ■ hydrocinnamyl alcohol.

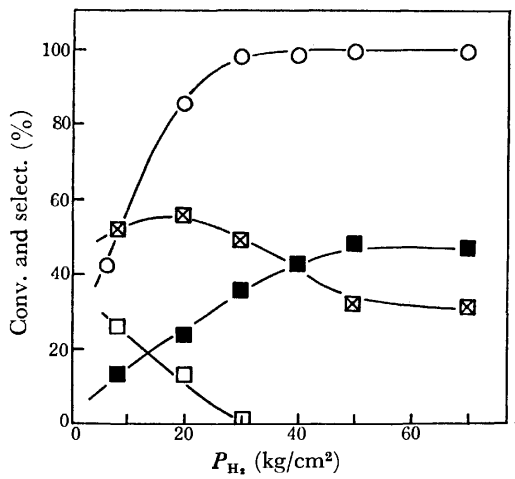

Fig. 2. Effect of the pressure of hydrogen on hydrogenation of cinnamaldehyde.[a]
PhCH=CHCHO 20 mmol, NEt_3 20 mmol, C_6H_6 20 ml, $RhCl_3 \cdot 3H_2O$ 0.13 mmol, P_{CO} 40 kg/cm² at r.t., Temp 90 °C, Time 60 min. ○ Conversion, □ hydrocinnamaldehyde, ⊠ cinnamyl alcohol, □ hydrocinnamyl alcohol.
a) Under low hydrogen pressure, it was supplied during the reaction to keep the pressure constant.

while the consecutive hydrogenation of cinnamyl alcohol produced is much slower than that of cinnamaldehyde. (Fig. 2). Thus, in the presence of carbon monoxide, the hydrogenation of the CHO group can be preferentially enhanced. This was verified by separate runs of hydrogenation of hydrocinnamaldehyde and cinnamyl alcohol under the same conditions specified in Fig. 1. Under 30—50 kg/cm² of carbon monoxide, hydrocinnamaldehyde was almost quantitatively hydrogenated to hydrocinnamyl alcohol (90%), while the extent of hydrogenation of cinnamyl alcohol was less than 25% in the same period.

The highest conversion to hydrocinnamyl alcohol is obtained at 20 kg/cm² of carbon monoxide (Fig. 1), considerable amounts of hydrocinnamaldehyde being formed under lower pressures of hydrogen (10, 20 kg/cm²) (Fig. 2). Strohmeier and Weigelt reported that 2-methyl-2-propanol is rapidly isomerized to

Table 3. Hydrogenation of other α,β-unsaturated aldehydes

C_6H_6 20 ml, P_{H_2} 40 kg/cm, Time 60 min.

Aldehyde (mmol)	$CH_3NC_4H_8$ (mmol)	P_{CO} kg/cm²	Temp °C	Conv. (%)	Selectivity (%) II[e]	III[e]	IV[e]
$PhCH{=}C(CH_3)CHO$	(20)[a]	20	40	60	99[d]	0	87[d]	13[d]
PhCH=CHCHO	(20)[a]	20	40	60	100	0	83	9.8
$C_3H_7CH{=}C(C_2H_5)CHO$	(20)[a]	20	40	60	47	18	34	48
C_3H_7CH=CHCHO	(20)[a]	20	40	60	100	0	47	53
CH_3CH=CHCHO[c]	(23)[a]	30	40	40	99	4.6	41	53
CH_3CH=CHCHO[c]	(23)[b]	20	20	40	99	0	52	48
CH_3CH=CHCHO[c]	(23)[b]	10	20	40	74	14	50	33
CH_3CH=CHCHO[c]	(23)[b]	5	20	40	50	25	49	22
CH_3CH=CHCHO[c]	(23)[b]	5	0	40	99	99	0	1.3
CH_3CH=CHCHO[c]	(23)[c]	5	10	40	80	13	47	34

a) $RhCl_3 \cdot 3H_2O$ 0.13 mmol. Pretreatment with CO (40—50 kg/cm²) at 60—90 °C for 60 min.
b) $Rh_2Cl_2(CO)_4$ 0.065 mmol. Without pretreatment. c) Water (12—14 wt%) was contained.
d) Calculated from peak areas on the gas chromatograph.
e) II Saturated aldehyde, III Unsaturated alcohol, IV Saturated alcohol.

isobutyraldehyde with $RhH(CO)(PPh_3)_3$ as a homogeneous catalyst in trifluoroethanol at 70 °C[10] (CH_2=$C(CH_3)CH_2OH \longrightarrow [(CH_3)_2C$=$CHOH] \longrightarrow (CH_3)_2CHCHO$). Thus, the isomerization of cinnamyl alcohol to hydrocinnamaldehyde should be taken into account for the formation of hydrocinnamyl alcohol. With the present catalyst system, it seems likely that carbon monoxide retards the isomerization of cinnamyl alcohol as well as hydrogenation of the carbon-carbon double bond, since the selectivity of hydrocinnamyl alcohol is considerablely low under higher pressures (40—60 kg/cm²) of carbon monoxide (Fig. 1), gradually increasing even under high pressures of hydrogen (Fig. 2). However, we have no evidence for the course of formation of hydrocinnamyl alcohol.

Hydrogenation of Other α,β-Unsaturated Aldehydes. The results for other α,β-unsaturated aldehydes are given in Table 3. *N*-Methylpyrrolidine was used as the modifier, and the catalyst solutions were treated with carbon monoxide (40—50 kg/cm²) at 90 °C for 60 min before the hydrogenation at 40—60 °C by introduction of hydrogen. α-Methyl cinnamaldehyde as well as cinnamaldehyde are hydrogenated to the unsaturated alcohol selectively, while in the case of aliphatic unsaturated aldehydes such as croton aldehyde, 2-hexenal, or 2-ethyl-2-hexenal, the unsaturated alcohols produced are further hydrogenated to the saturated alcohols. All attempts to increase the selectivity to *trans*-2-buten-1-ol by over 50% using $Rh_2Cl_2(CO)_4$ as the catalysts were unsuccessful. Acrylaldehyde, presumably oligomerized before hydrogenation, gave only a trace amount of propionaldehyde.

Immobilization of Rhodium Complex. Since a large amount of tertiary amine is required for the selective hydrogenation of cinnamaldehyde, and little evidence on the nature of interaction of amine with rhodium atom in its coordination sphere is available, attempts to isolate a rhodium–amine complex from the product solution being unsuccessful, we attempted to immobilize $Rh_2Cl_2(CO)_4$ on a cross-linked chloromethylated polystyrene functionarized with pyrrolidine, *i.e.* $\{\text{-}C_6H_4\text{-}CH_2\text{–}NC_4H_8$. When a deep red benzene solution of $Rh_2Cl_2(CO)_4$ is added to the pale yellow polymer swollen in benzene at room temperature under nitrogen atmosphere, the complex is rapidly adsorbed on the polymer, the deep red colour disappearing within a few minutes. A pale dark brown polymer was separated by filtration. The immobilized rhodium complex was used as a catalyst for the hydrogenation of cinnamaldehyde without addition of any other amine. The results are summarized in Table 4, the amounts of the polymer used for immobilizing $Rh_2Cl_2(CO)_4$ (0.065 mmol) being 0.65—5.2 g (2.5—20 mmol equivalents of N). After the runs, the immobilized rhodium complex suspended in a colourless product solution was washed twice with benzene and separated by filtration in the air before

Table 4. Hydrogenation of cinnamaldehyde with immobilized rhodium complex catalyst

PhCH=CHCHO 20 mmol, C_6H_6 20 ml, $Rh_2Cl_2(CO)_4$ 0.065 mmol, Press. 80 kg/cm² (CO/H_2=1), Temp 60 °C, Time 60 min.

No.	Aminated polystyrene (N-mmol)	Conv. (%)	Selectivity (%) II	III	IV
1	2.5	69 (66)	11 (9.3)	73 (72)	13 (6.6)
2	5.0	84 (95)	7.1 (2.4)	76 (87)	16 (12)
3	10	77 (100)	8.6 (≈0)	62 (90)	14 (9.8)
4	20	65 (99)	13 (≈0)	58 (75)	13 (11)
5	Recycle (run 3)	77	9.2	60	14
6	Recycle (run 5)	67	12	65	11
7	Recycle (run 4)	69	13	63	14
8	5.0, $+PPh_3$ 0.13	79	78	0	4.6
9	Recycle (run 8)	63	16	54	10
10	5.0, $+PPh_3$ 0.195	92	78	0	1.3
11	Recycle (run 10)	13	—	—	—

Table 5. IR absorptions of rhodium carbonyl complexes

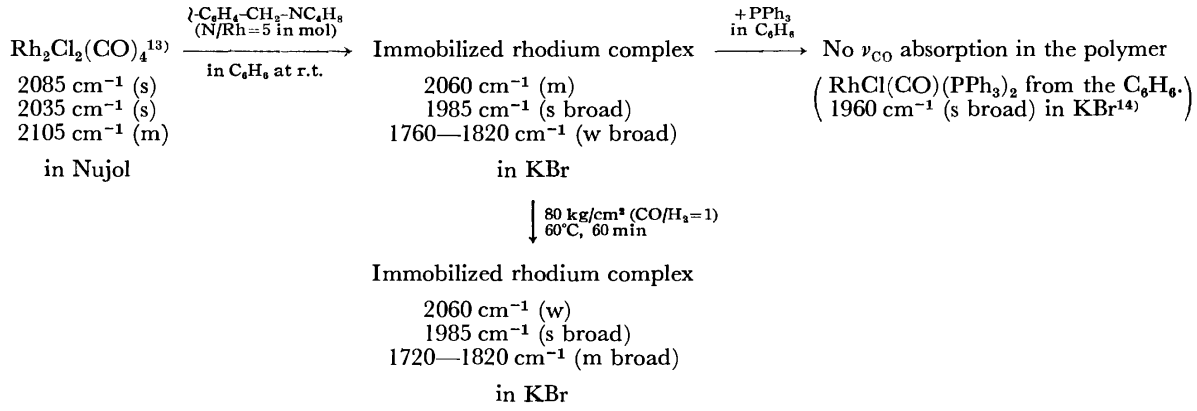

analysis of hydrogenation products of cinnamaldehyde, since some of them were adsorbed on the polymer. The results obtained from the corresponding homogeneous catalyst system using *N*-methylpyrrolidine under the same conditions are given in parentheses in Table 4. Selective hydrogenation is again observed in heterogeneous catalyst system, although its catalytic activity and selectivity are slightly lower than those in homogeneous one. The polymer catalysts recovered in the air from runs 3, 5, and 4 reproduce almost the same activity and selectivity (runs 5, 6, and 7 respectively), indicating that the rhodium complexes are fairly air-stable, retaining original linkage to the aminated polystyrene after the runs. Addition of catalytic amounts of triphenylphosphine ($PPh_3/Rh=2$—3), however, gave exclusively hydrocinnamaldehyde and no cinnamyl alcohol at all (comparison of run 1 with runs 8 and 10) as observed in homogeneous catalyst system (Table 1). Since the product solutions were pale yellow in the runs with triphenylphosphine, some part of the rhodium complex seem to have been eluted from the polymer. In fact, the polymer catalyst recovered from run 10 was almost inactive for hydrogenation, although the one recovered from run 8 had some activity for selective hydrogenation (comparison of run 9 with run 2).

The interaction of $Rh_2Cl_2(CO)_4$ with the polymer was investigated by IR. The immobilized complex ($N/Rh=5$)[11] showed three absorptions, 2060(m), 1985(s broad), and 1720—1820 (w broad) cm^{-1}, in carbonyl stretching region. The last broad absorption, which was not observed in the parent rhodium complex, $Rh_2Cl_2(CO)_4$ (2105(m), 2085(s), and 2035(s) cm^{-1}), could be assigned to bridged carbonyls, suggesting the formation of a polynuclear rhodium carbonyl.[12] After treatment of the immobilized rhodium complex with $CO-H_2$ mixture ($CO/H_2=1$) in benzene under 80 kg/cm^2 at 60 °C for 60 min, the first absorption became weaker and the last one (1720—1820 cm^{-1}) relatively increased. On the other hand, all these absorptions disappeared after the treatment with triphenylphosphine ($PPh_3/Rh=3$) in benzene either in the presence or absence of the $CO-H_2$ mixture. From the benzene solution, $RhCl(CO)(PPh_3)_2$ (Found: C, 63.0; H, 4.25%. Calcd for: C, 64.3; H, 4.38%. $\nu_{CO}=1960$ (s broad) cm^{-1}), was isolated and recrystalized from benzene–methanol, indicating that triphenylphosphine coordinates to rhodium atom much more strongly than the amine. The IR absorptions of carbonyls are summarized in Table 5.

From a comparison of these IR absorptions of immobilized complexes with the effects of amine and triphenylphosphine shown in Table 4, it is evident that under oxo reaction conditions the rhodium–amine–carbonyl complex catalyzes the selective hydrogenation of α,β-unsaturated aldehyde to the unsaturated alcohol, while $RhCl(CO)(PPh_3)_2$ is effective only for the preferential hydrogenation of the carbon-carbon double bond to give the saturated aldehyde.

Referensec

1) R. Adams and B. S. Garvey, *J. Am. Chem. Soc.*, **48**, 477 (1926); D. Burn, G. Cooley, M. T. Davis, J. W. Ducker, B. Ellis, P. Feather, A. K. Hiscock, D. N. Kirk, A. P. Leftwick, V. Petrow, and D. M. Williamson, *Tetrahedron*, **20**, 597 (1964).

2) P. N. Rylander, "Catalytic Hydrogenation over Platinum Metals," Academic Press, New York and London (1967), pp. 249—256.

3) B. R. James, "Homogeneous Hydrogenation," John Wiley & Sons, New York (1973).

4) B. Fell and A. Geurts, *Chem.-Ing.-Teh.*, **44**, 708 (1972).

5) A. T. Jurewicz, L. D. Rollmann, and D. D. Whitehurst, Preprints of the conference on Prospects in Organotransition-metal Chem., Japan-US Cooperative Science Program, Honolulu, Hawai, April 30-May 4 (1947), p. 113.

6) K. Kogami, O. Takahashi, and J. Kumanotani, *Bull. Chem. Soc. Jpn.*, **45**, 604 (1972); *ibid.*, **46**, 3562 (1973).

7) *Inorg. Synth.*, Vol. 8, McGrow-Hill Book Company (1966), p. 211.

8) K. W. Pepper, H. M. Paisley, and M. S. Young, *J. Chem. Soc.*, **1953**, 4097.

9) K. Mori, T. Mizoroki, and A. Ozaki, *Bull. Chem. Soc. Jpn.*, **49**, 748 (1976).

10) W. Strohmeier and L. Weigelt, *J. Organomet. Chem.*, **86**, C17 (1975).

11) Even at this low ratio of N/Rh, all $Rh_2Cl_2(CO)_4$ seems to be linked to the polymer, since the colour of the benzene solution disappeared completely during the preparation within 10 min.

12) $Rh_6(CO)_{16}$ catalyzes hydrogenation of activated carbon-carbon double bonds of various vinyl compounds in the presence of amine with carbon monoxide and water: T. Kitamura, N. Sakamoto, and T. Joh, *Chem. Lett.*, **1973**, 379.

13) Ref. p. 213.

14) Ref. p. 216.

Preparation of 5,5-Bis(ethoxycarbonyl)-5,6-dihydro-3,7-diaryl-4*H*-1,2-diazepines and Their Halogenations[1)]

Otohiko Tsuge,* Kichinosuke Kamata,** and Seiichi Yogi***

Research Institute of Industrial Science, Kyushu University 86, Hakozaki, Higashiku, Fukuoka 812

***Department of Industrial Chemistry, Kurume Technical College, Kurume 830*

****Department of Chemistry, Faculty of Science and Engineering, Ryukyu University, Naha 903*

(Received January 18, 1977)

5,5-Bis(ethoxycarbonyl)-5,6-dihydro-3,7-diaryl-4*H*-1,2-diazepines (**4**) were prepared by the condensation of α-bromoacetophenone azines with diethyl malonate in the presence of sodium ethoxide. Halogenation of **4** afforded 7,7-bis(ethoxycarbonyl)-2,5-diaryl-3,4-diazanorcaradiene, 4,6-dihalodihydrodiazepines, 1-halodiazanorcaradienes, and/or 4,4,6,6-tetrachlorodihydrodiazepine, whose relative yields depended upon the reaction conditions. Dehalogenation of the halogenated products was also investigated.

It has been reported that the treatment of 3,7-diphenyl-5,6-dihydro-4*H*-1,2-diazepines (**1**) with halogenation-reagents resulted in ring contraction to pyridazines. The isolation of 3,4-diazanorcaradienes (**2**, R=H,[2)] Ph[3)]) has been cited as evidence for their intermediacy in the contraction reaction which presumably proceeds by a halogenation-dehydrohalogenation process. However, halogenated intermediates have not been isolated (Scheme 1).

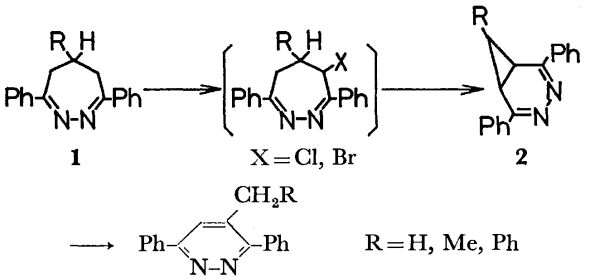

Scheme 1.

This paper is concerned with the preparation of 5,5-bis(ethoxycarbonyl)-5,6-dihydro-3,7-diaryl-4*H*-1,2-diazepines, and with their halogenations which afforded halogenated intermediates and diazanorcaradienes in good yields.

Results and Discussion

Preparation of 5,5-Bis(ethoxycarbonyl)-5,6-dihydro-3,7-diaryl-4H-1,2-diazepines (4). 5,5-Disubstituted 5,6-dihydro-4*H*-1,2-diazepines have not been reported in literature. α-Bromoacetophenone azine (**3a**)[4)] which was prepared by the bromination of acetophenone azine, would be expected to react with active methylene compounds, affording the corresponding 5,6-dihydro-4*H*-1,2-diazepines. In fact, **3a** reacted with diethyl malonate in the presence of sodium ethoxide to give the expected 5,5-bis(ethoxycarbonyl)-5,6-dihydro-3,7-diphenyl-4*H*-1,2-diazepine (**4a**). Similarly, 3,7-di(*p*-tolyl) and 3,7-bis(*p*-chlorophenyl) derivatives, **4b** and **4c**, were prepared from the corresponding azines, **3b** and **3c**, respectively.

Structural elucidation of **4** was accomplished on the basis of spectral data and the results of microanalyses,

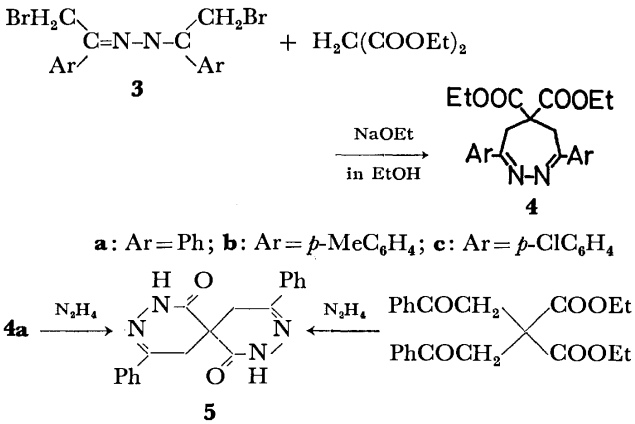

Scheme 2.

Table 1. 5,5-Bis(ethoxycarbonyl)-5,6-dihydro-3,7-diaryl-4*H*-diazepines **4**[a)]

	Yield %	Mp, °C	IR, $\nu_{C=O}$ cm^{-1}	NMR ($CDCl_3$) δ ppm	Found (Calcd) % C	H	N
4a	77	124—125	1760, 1740	1.15 (6H, t, CH_2CH_3), 3.30 (4H, s, CH_2) 4.13 (4H, q, CH_2Me), 7.3—8.0 (10H, m, ArH)	70.44 (70.39)	6.12 (6.16)	7.13 (7.14)
4b	45	103—104	1760, 1740	1.18 (6H, t, CH_2CH_3), 2.36 (6H, s, CH_3) 3.23 (4H, s, CH_2), 4.15 (4H, q, CH_2Me) 7.1—7.8 (8H, m, ArH)	71.40 (71.41)	6.73 (6.71)	6.65 (6.66)
4c	58	129—130	1750, 1730	1.17 (6H, t, CH_2CH_3), 3.21 (4H, s, CH_2) 4.11 (4H, q, CH_2Me), 7.2—7.9 (8H, m, ArH)	59.90 (59.87)	4.82 (4.80)	6.09 (6.07)

a) All **4** are colorless prisms.

* To whom correspondence should be addressed.

which are given with the yields and melting points in Table 1.

Treatment of **4a** with hydrazine hydrate in acetic acid afforded 5,5′-spirobi(1*H*-3-phenyl-4,5-dihydropyridazin-6-one) (**5**), which was identical with an authentic sample prepared from diethyl diphenacylmalonate and hydrazine hydrate (Scheme 2).

Bromination. When **4a** was treated with an equimolar amount of bromine in methanol at room temperature, 7,7-bis(ethoxycarbonyl)-2,5-diphenyl-3,4-diazanorcaradiene (**7a**), mp 120—121 °C, was obtained in excellent yield. The reaction of **4a** with two molar amounts of bromine in methanol gave 5,5-bis(ethoxycarbonyl)-4,6-dibromo-5,6-dihydro-3,7-diphenyl-4*H*-1,2-diazepine (**8a**) and/or 1-bromo-7,7-bis(ethoxycarbonyl)-2,5-diphenyl-3,4-diazanorcaradiene (**9**); whose relative yields greatly depended upon the reaction time. That is, the reaction for 10 min gave **8a** and **9** in 83 and 16% yields respectively, whereas the reaction for 2 h exclusively produced **9**. On the other hand, the reactions of **4a** with two molar amounts of bromine in methylene dichloride, chloroform, and acetic acid, and with excess *N*-bromosuccinimide (NBS) in carbon tetrachloride did not give **8a** and **9**, but instead **7a** was only formed.

Similarly, the reaction of 3,7-di(*p*-tolyl)- **4b** and 3,7-bis(*p*-chlorophenyl)dihydrodiazepine **4c** with two molar amounts of bromine in methanol for 5 min afforded the corresponding dibromides **8b** and **8c** respectively. In these cases, the corresponding 1-bromodiazanorcaradines were not obtained.

Hydrolysis of **7a** with ethanolic potassium hydroxide afforded the half ester **10**, which on heating in ethanol or ethanol-d_1 underwent decarboxylation to give 7-*exo*-ethoxycarbonyl-2,5-diphenyl-3,4-diazanorcaradiene (**11**) or its 7-deuterio derivative **11**-d_1 respectively. When **10** was heated at 130—140 °C without solvent, ring opening occurred to yield 4-ethoxycarbonylmethyl-3,6-diphenylpyridazine (**12**) (Scheme 3).

The structures of all products, **7**—**12**, were confirmed on the basis of their spectral data.

Although the monobromide **6** has not been isolated, it is clear that the diazanorcaradienes **7a** and **9** are formed *via* internal nucleophilic displacement of the monobromide **6** and dibromide **8** respectively as delineated in Scheme 3.

Chlorination. The treatment of **4a** with an equimolar amount of sulfuryl chloride in methylene dichloride at room temperature afforded traces of an unidentified compound, together with recovery of **4a**. However, **4a** reacted with two molar amounts of sulfuryl chloride to give 5,5-bis(ethoxycarbonyl)-4,6-dichloro-5,6-dihydro-3,7-diphenyl-4*H*-1,2-diazepine (**13**) and/or 7,7-bis(ethoxycarbonyl)-1-chloro-2,5-diphenyl-3,4-diazanorcaradiene (**14**); whose relative yields depended upon the reaction time again. Further chlorination of the dichloride **13** with sulfuryl chloride afforded the 4,4,6,6-tetrachlorodihydrodiazepine **15** in good yield. The tetrachloride **15** was formed directly from chlorination of **4a** with excess sulfuryl chloride or chlorine gas. Structural elucidation of **13**—**15** was accomplished on the basis of their spectral data.

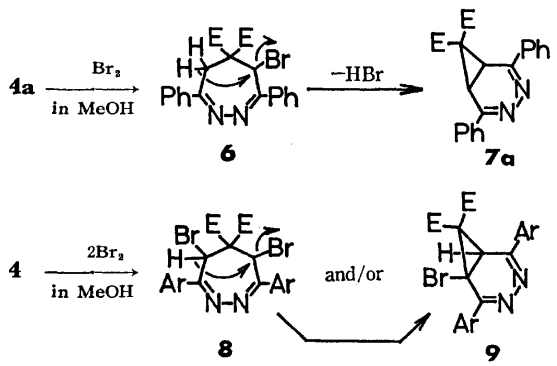

a: Ar=Ph; **b**: Ar=*p*-MeC$_6$H$_4$; **c**: Ar=*p*-ClC$_6$H$_4$

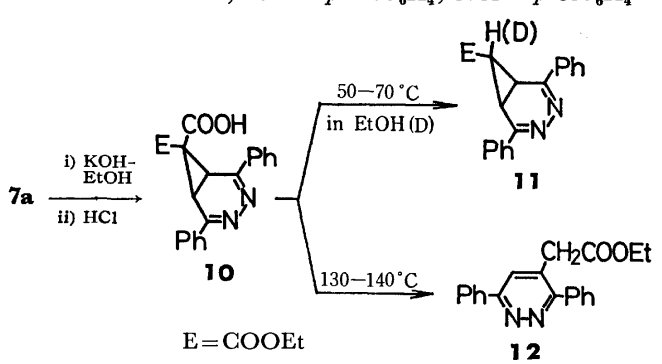

Scheme 3.

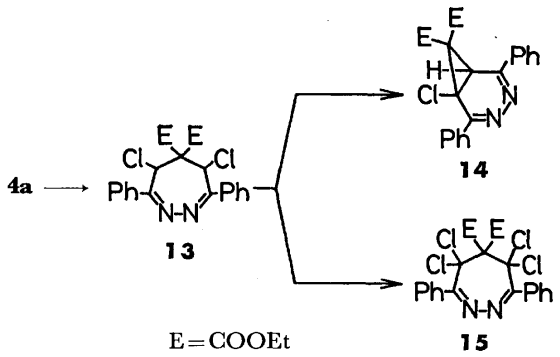

Scheme 4.

It is considered that activation of the methylene groups at positions 4 and 6 in **4** to halogenation is attributable to the electron-withdrawing azine and ethoxycarbonyl groups. As shown above. 7,7-bis(ethoxycarbonyl)diazanorcaradienes, **7**, **9**, and **14**, were isolated in good yields respectively; this fact suggests that the diazanorcaradienes are stabilized by the extended π-electron conjugation.

Dehalogenations of the Halogenated Products. When dibromides, **8a**—**8c**, were treated with sodium iodide in boiling acetone for 2 h, the corresponding diazanorcaradienes, **7a**—**7c**, were obtained in good yields. Although the dichloride **13** was unchanged under similar conditions, **13** was also converted to **7a** on prolonged heating with sodium iodide in ethanol. Similarly, treatment of the tetrachloride **15** with sodium iodide in boiling acetone afforded the 1,6-dichlorodiazanorcaradiene **16** quantitatively (Scheme 5).

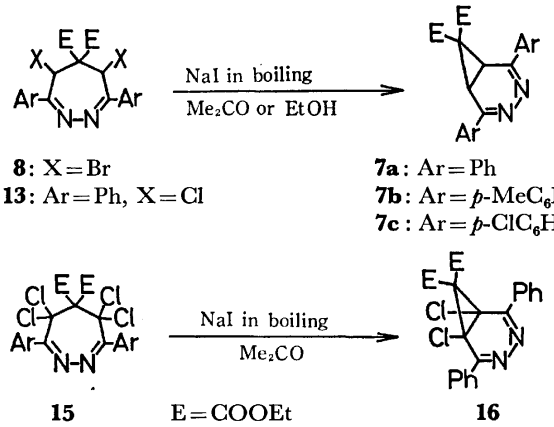

8: X=Br
13: Ar=Ph, X=Cl

7a: Ar=Ph
7b: Ar=*p*-MeC$_6$H$_4$
7c: Ar=*p*-ClC$_6$H$_4$

15 E=COOEt **16**

Scheme 5.

Next, we have investigated the dehalogenation with zinc dust in boiling ethanol. In contrast to the above dehalogenation using sodium iodide, the dihalides, **8a** and **13**, did not give the diazanorcaradines **7a**, but instead the dihydrodiazepine **4a**, 3,6-diphenylpyridazine (**17**), and diethyl malonate were formed in the respective yields shown in Scheme 6. As illustrated in Scheme 6, these reactions proceed through two different pathways from the organozinc halide; one is direct decomposition by ethanol to give **4a**, and the other is ring contraction, followed by decomposition to afford **17** and diethyl malonate.

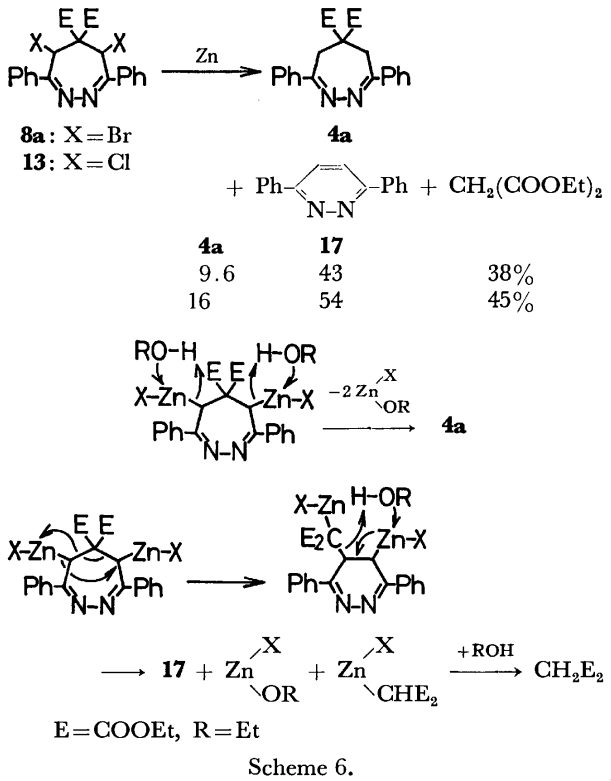

8a: X=Br
13: X=Cl

4a **17**

9.6	43	38%
16	54	45%

E=COOEt, R=Et

Scheme 6.

On the other hand, similar treatments of halogenated diazanorcaradienes, **9**, **14**, and **16**, afforded 4-[bis(ethoxycarbonyl)methyl]-3,6-diphenylpyridazine (**18**) in 47, 51, and 13% yields respectively. The pyridazine **18** was also obtained in 16% yield from the tetrachloride

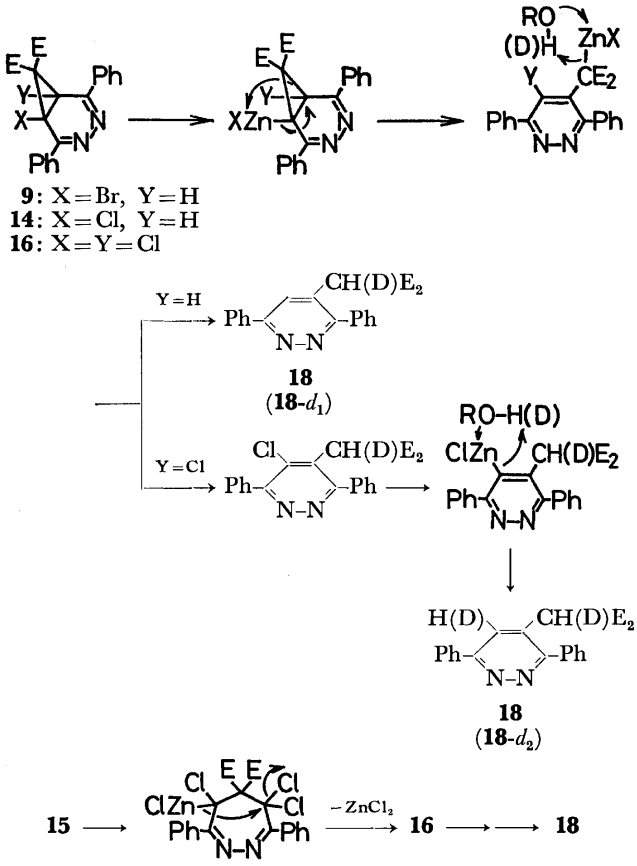

9: X=Br, Y=H
14: X=Cl, Y=H
16: X=Y=Cl

18 (**18**-d_1)

18 (**18**-d_2)

15 → **16** → → **18**

E=COOEt, R=Et

Scheme 7.

15. The dehalogenation of **14** and **15** with zinc dust in boiling ethanol-d_1 afforded the pyridazines, **18**-d_1 and **18**-d_2, respectively.

On the basis of the above results, the pathways for the formation of **18** from **9** and **14**—**16** are interpreted as depicted in Scheme 7.

Experimental

All the melting points are uncorrected. The NMR spectra were determined with a Hitachi R-20 Model spectrometer, with TMS as the internal standard. The IR spectra were measured as KBr disks, and the MS were obtained on a Hitachi RMS-4 mass spectrometer with a direct inlet and an ionization energy of 70 eV.

α-Bromoacetophenone Azines (3). α-Bromoacetophenone azine (**3a**), mp 151—152 °C (lit,[4] mp 151—152 °C), was prepared by the bromination of acetophenone azine. Similarly, α-bromo-*p*-methylacetophenone azine (**3b**) and α-bromo-*p*-chloroacetophenone azine (**3c**) were prepared from the corresponding acetophenone azine.

3b: mp 182—183 °C; IR 1590 cm^{-1} (C=N). Found: C, 51.23; H, 4.15; N, 6.75%. Calcd for $C_{18}H_{18}N_2Br_2$: C, 51.19; H, 4.27; N, 6.63%.

3c: mp 186—187 °C; IR 1597 cm^{-1} (C=N). Found: C, 41.14; H, 2.67; N, 6.31%. Calcd for $C_{16}H_{12}N_2Br_2Cl_2$: C, 41.47; H, 2.60; N, 6.05%.

5,5-Bis(ethoxycarbonyl)-5,6-dihydro-3,7-diaryl-4H-1,2-diazepines (4). A solution of the azine **3a** (3.94 g, 0.01 mol) in benzene (50 ml) was added to a solution of diethyl malonate (3.2 g, 0.02 mol) and sodium ethoxide (1.4 g, 0.02 mol) in

ethanol (20 ml), and then the reaction mixture was refluxed for 1 h. The mixture was poured into water (100 ml) and the benzene layer was separated and evaporated *in vacuo* to leave crystals. Recrystallization from ethanol gave 3.0 g (77%) of the dihydrodiazepine **4a**.

Similarly, 3,7-di(*p*-tolyl) and 3,7-bis(*p*-chlorophenyl) derivatives, **4b** and **4c**, were prepared from the corresponding azines, **3b** and **3c**, respectively. The yields, physical data, and results of microanalyses of **4** are given in Table 1.

5,5'-Spirobi(1H-3-phenyl-4,5-dihydropyridazine-6-one) (5). A solution of the dihydrodiazepine **4a** (3.92 g, 0.01 mol) and hydrazine hydrate (1.0 g, 0.02 mol) in acetic acid (50 ml) was heated at 60—70 °C for 2 h. The mixture was poured into water (10 ml) and was allowed to stand at room temperature to give crystals. Recrystallization from ethanol gave 0.66 g (20%) of **5**, mp 315 °C (dec), as colorless prisms. NMR (pyridine-d_5) δ 3.19, 3.90 (each 2H, C**H**$_2$, J=17.4 Hz), 7.2—8.1 (10H, m, aromatic protons), 12.86 ppm (2H, br, N**H**).

Found: C, 68.78; H, 4.88; N, 17.02%. Calcd for $C_{19}H_{16}N_4O_2$: C, 68.66; H, 4.85; N, 16.86%.

The spirobipyridazinone **5** was identical with an authentic sample prepared by the following manner. A solution of diethyl diphenacylmalonate (1.33 g) and hydrazine hydrate (0.5 g) in acetic acid (10 ml) was heated at 60—70 °C for 2 h, and a similar work-up gave 0.65 g (59%) of **5**.

Bromination of the Dihydrodiazepines 4. *i*) A solution of bromine (0.8 g, 5 mmol) in methanol (40 ml) was added, drop by drop, over a period of 1 h to a suspension of the dihydrodiazepine **4a** (1.96 g, 5 mmol) in methanol (20 ml), and then the reaction mixture was stirred at room temperature for 2 h. The mixture was added to water (200 ml), and was extracted with benzene (40 ml×2). The benzene extract was washed with water, dried over sodium sulfate, and then evaporated *in vacuo* to leave crystals, which on recrystallization from petroleum ether (bp 60—80 °C) afforded 1.91 g (98%) of 7,7-bis(ethoxycarbonyl)-2,5-diphenyl-3,4-diaza-2,4-norcaradiene (**7a**), mp 120—121 °C, as yellow prisms. IR 1725, 1735 cm^{-1} (C=O); NMR ($CDCl_3$) δ 0.82, 1.35 (each 3H, t, CH_2CH_3), 3.38 (2H, s, ≥C**H**), 3.89, 4.40 (each 2H, q, C**H**$_2$Me), 7.3—7.7 (6H, m), 7.9—8.3 ppm (4H, m); MS *m/e* 390 (M^+).

Found: C, 70.79; H, 5.69; N, 7.18%. Calcd for $C_{23}H_{22}N_2O_4$: C, 70.75; H, 5.68; N, 7.18%.

Bromination of **4a** in acetic acid, chloroform, and carbon tetrachloride under similar conditions afforded **7a** in excellent yields respectively.

ii) Bromine (3.2 g, 0.02 mol) was added to a suspension of the dihydrodiazepine **4a** (3.92 g, 0.01 mol) in methanol (60 ml), and the reaction mixture was stirred at room temperature. The mixture changed to a solution and then yellow crystals separated out after about 5 min. Filtration gave crystals which were washed with methanol (30 ml). Recrystallization from ethanol afforded 4.5 g (83%) of 5,5-bis(ethoxycarbonyl)-4,6-dibromo-5,6-dihydro-3,7-diphenyl-4*H*-1,2-diazepine (**8a**), mp 150—151 °C, as yellow prisms. NMR ($CDCl_3$) δ 1.15 (6H, t, CH_2CH_3), 4.18 (4H, q, C**H**$_2$Me), 5.73 (2H, s, ≥C**H**), 7.3—7.7 (6H, m), 7.9—8.3 ppm (4H, m); MS *m/e* 548, 550, 552, 554 (M^+).

Found: C, 50.22; H, 4.04; N, 5.15%. Calcd for $C_{23}H_{22}N_2O_4Br_2$: C, 50.20; H, 4.04; N, 5.09%.

The filtrate and methanol washing were combined, poured into water (300 ml), and extracted with benzene (80 ml×2). The benzene extract was washed with water, dried over sodium sulfate, and then evaporated *in vacuo* to leave 0.74 g (16%) of crystals. Recrystallization from petroleum ether (bp 60—80 °C) afforded 1-bromo-7,7-bis(ethoxycarbonyl)-2,5-diphenyl-3,4-diazanorcaradiene (**9**), mp 133—134 °C, as yellow prisms. NMR ($CDCl_3$) δ 0.87, 1.44 (each 3H, t, CH_2CH_3), 3.88 (1H, s, ≥C**H**), 3.95, 4.54 (each 2H, q, C**H**$_2$Me), 7.3—7.7 (6H, m), 7.9—8.3 ppm (4H, m); MS *m/e* 468, 470 (M^+).

Found: C, 59.01; H, 4.52; N, 5.94%. Calcd for $C_{23}H_{21}N_2O_4Br$: C, 58.86; H, 4.51; N, 5.97%.

Similar reactions of the dihydrodiazepines **4b** and **4c** with bromine in methanol for 5 min afforded the corresponding dibromodihydrodiazepines **8b** and **8c** in 75 and 86% yields respectively.

8b: Mp 151—152 °C, yellow prisms. NMR ($CDCl_3$) δ 1.21 (6H, t, CH_2CH_3), 2.41 (6H, s, C**H**$_3$), 4.20 (4H, q, C**H**$_2$Me), 5.70 (2H, s, ≥C**H**), 7.2—8.1 ppm (8H, m).

Found: C, 51.89; H, 4.52; N, 4.85%. Calcd for $C_{25}H_{26}N_2O_4Br_2$: C, 51.92; H, 4.53; N, 4.84%.

8c: Mp 149—150 °C, yellow prisms. NMR ($CDCl_3$) δ 1.17 (6H, t, CH_2CH_3), 4.07 (4H, q, C**H**$_2$Me), 5.60 (2H, s, ≥C**H**), 7.3—8.1 ppm (8H, m).

Found: C, 44.63; H, 3.28; N, 4.50%. Calcd for $C_{23}H_{20}N_2O_4Br_2Cl_2$: C, 44.61; H, 3.26; N, 4.52%.

iii) When a mixture of **4a** (1.96 g, 5 mmol) and bromine (1.6 g, 10 mmol) in methanol (30 ml) was stirred at room temperature for 1 h, the precipitated dibromide **8a** dissolved. After the reaction mixture was stirred for another 1 h, it was evaporated *in vacuo* to leave crystals which on recrystallization from petroleum ether gave 2.31 g (98.5%) of the 1-bromodiazanorcaradiene **9**.

7-exo-Ethoxycarbonyl-2,5-diphenyl-3,4-diphenyl-3,4-diazanorcaradine (11). After a solution of the 7,7-bis(ethoxycarbonyl)-diazanorcaradiene **7a** (3.9 g) in ethanol (50 ml) was stirred with potassium hydroxide (4.0 g) at room temperature for 3 h, the mixture was acidified with dil. hydrochloric acid to give 2.5 g (70%) of the half ester **10**. A solution of the half ester **10** (1.0 g) in ethanol (5 ml) was warmed at 50—70 °C for 15 min, and then allowed to stand at room temperature, giving 0.47 g (54%) of the mono(ethoxycarbonyl)diazanorcaradiene **11**, mp 233—234 °C, as yellow needles. NMR ($CDCl_3$) δ 1.35 (3H, t, CH_2CH_3), 1.41 (1H, t, ≥C**H**, J=4.2 Hz), 3.25 (2H, d, 2×≥C**H**, J=4.2 Hz), 4.34 (2H, q, C**H**$_2$Me), 7.3—7.7 (6H, m), 7.9—8.3 ppm (4H, m); MS *m/e* 318 (M^+).

Found: C, 75.35; H, 5.61; N, 8.92%. Calcd for $C_{20}H_{18}N_2O_2$: C, 75.45; H, 5.70; N, 8.80%.

A similar treatment of **10** with ethanol-d_1 gave the 7-deuterio derivative **11**-d_1, mp 233—234 °C, in 60% yield. NMR ($CDCl_3$) δ 1.35 (3H, t, CH_2CH_3), 3.22 (2H, s, ≥C**H**), 4.43 (2H, q, C**H**$_2$Me), 7.3—7.7 (6H, m), 7.9—8.3 ppm (4H, m); MS *m/e* (rel. intensity %) 319 (M^+, 88), 318 (15), 246 (M^+−COOEt, 12).

4-Ethoxycarbonylmethyl-3,6-diphenylpyridazine (12). The half ester **10** (1.0 g) was heated at 130—140 °C (bath temperature) for 5 min, and then the residue was recrystallized from ethanol to give 0.54 g (63%) of the pyridazine **12**, mp 139—140 °C, as colorless prisms. NMR ($CDCl_3$) δ 1.20 (3H, t, CH_2CH_3), 3.72 (2H, s, C**H**$_2$), 4.15 (2H, q, C**H**$_2$Me), 7.85 (1H, s, pyridazine ring proton), 7.4—8.3 ppm (10H, m); MS *m/e* 318 (M^+).

Found: C, 75.31; H, 5.68; N, 8.72%. Calcd for $C_{20}H_{18}N_2O_2$: C, 75.45; H, 5.70; N, 8.80%.

Chlorination of the Dihydrodiazepine 4a. A solution of **4a** (1.96 g, 5 mmol) and sulfuryl chloride (1.35 g, 10 mmol) in methylene dichloride (40 ml) was stirred at room temperature for 5 min, and then the solvent was removed *in vacuo*. The residue was triturated with methanol (10 ml) and filtration gave crystals which on recrystallization from petroleum ether (bp 60—80 °C) afforded 2.97 g (64%) of 5,5-bis(ethoxycarbonyl)-4,6-dichloro-5,6-dihydro-3,7-diphenyl-4*H*-1,2-di-

azepine (**13**), mp 112—113 °C, as colorless prisms. NMR ($CDCl_3$) δ 1.15 (6H, t, CH_2CH_3), 4.18 (4H, q, CH_2Me), 5.73 (2H, s, $\geq CH$), 7.3—7.7 (6H, m), 7.8—8.3 ppm (4H, m); MS *m/e* 460, 462, 464 (M^+).

Found: C, 59.70; H, 4.78; N, 6.05%. Calcd for $C_{23}H_{22}N_2O_4Cl_2$: C, 59.88; H, 4.81; N, 6.07%.

The methanol filtrate was poured into water and extracted with benzene (40 ml×2). The benzene extract was washed with water, dried over sodium sulfate, and then evaporated *in vacuo* to give crystals. Recrystallization from petroleum ether (bp 60—80 °C) afforded 1.27 g (30%) of 7,7-bis(ethoxycarbonyl)-1-chloro-2,5-diphenyl-3,4-diazanorcaradiene (**14**), mp 130—131 °C, as yellow prisms. NMR ($CDCl_3$) δ 0.86, 1.41 (each 3H, t, CH_2CH_3), 3.88 (1H, s, $\geq CH$), 3.94, 4.50 (each 2H, q, CH_2Me), 7.3—7.7 (6H, m), 7.9—8.3 ppm (4H, m); MS *m/e* 424, 426 (M^+).

Found: C, 64.77; H, 4.92; N, 6.57%. Calcd for $C_{23}H_{21}N_2O_4Cl$: C, 65.02; H, 4.98; N, 6.59%.

The same reaction for 2 h afforded 1.87 g (88%) of **14**.

*5,5-Bis(ethoxycarbonyl)-5,6-dihydro-3,7-diphenyl-4,4,6,6-tetrachloro-4H-1,2-diazepine (**15**).* A solution of the dichloride **13** (0.46 g, 1 mmol) and sulfuryl chloride (0.27 g, 2 mmol) in methylene dichloride (10 ml) was stirred at room temperature for 2 h. The reaction mixture was evaporated *in vacuo* to leave crystals which on recrystallization from ethanol afforded 0.45 g (85%) of the tetrachloride **15**, mp 143—144 °C, as colorless prisms. NMR ($CDCl_3$) δ 1.21 (6H, t, CH_2CH_3), 4.35 (4H, q, CH_2Me), 7.3—7.7 (6H, m), 7.8—8.1 ppm(4H, m); MS *m/e* 528, 530, 532, 534, 536 (M^+).

Found: C, 51.82; H, 3.72; N, 5.22%. Calcd for $C_{23}H_{20}N_2O_4Cl_4$: C, 52.09; H, 3.81; N, 5.28%.

The tetrachloride **15** was directly obtained from chlorination of the dihydrodiazepine **4a** with excess sulfuryl chloride or chlorine gas. A solution of **4a** (1.96 g, 5 mmol) and sulfuryl chloride (2.7 g, 20 mmol) in methylene dichloride (40 ml) was stirred at room temperature for 2 h. A similar work-up of the reaction mixture as above gave 1.68 g (63%) of the tetrachloride **15**.

Chlorination of **4a** with excess chlorine gas in methanol, acetic acid, carbon tetrachloride, chloroform, and methylene dichloride afforded **15** in 45, 79, 79, 87, and 47% yields respectively.

Dehalogenation of the Dihalodihydrodiazepines with Sodium Iodide. *i*) A solution of the dibromide **8a** (1.1 g, 2 mmol) and sodium iodide (0.75 g, 5 mmol) in acetone (20 ml) was refluxed for 2 h. The reaction mixture was poured into water (100 ml) and extracted with benzene (40 ml×2). The benzene extract was washed with sodium thiosulfate aqueous solution, water, and dried over sodium sulfate, and then evaporated *in vacuo* to leave 0.76 g (97%) of the diazanorcaradiene **7a**.

Similarly, treatment of the dibromides **8b** and **8c** with sodium iodide in boiling acetone afforded 7,7-bis(ethoxycarbonyl)-2,5-di(*p*-tolyl)- (**7b**) and 7,7-bis(ethoxycarbonyl)-2,5-bis(*p*-chlorophenyl)-3,4-diaza-2,4-norcaradiene (**7c**) in 83 and 90% yields respectively.

7b: Mp 128—129 °C, yellow prisms. NMR ($CDCl_3$) δ 0.86, 1.36 (each 3H, t, CH_2CH_3), 2.45 (6H, s, CH_3), 3.35 (2H, s, $\geq CH$), 3.88 4.41 (each 2H, q, CH_2Me), 7.2—8.1 ppm (8H, m).

Found: C, 71.71; H, 6.20; N, 6.67%. Calcd for $C_{25}H_{26}N_2O_4$: C, 71.75; H, 6.26; N, 6.69%.

7c: Mp 165—166 °C, yellow prisms. NMR ($CDCl_3$) δ 0.85, 1.35 (each 3H, t, CH_2CH_3), 3.25 (2H, s, $\geq CH$), 3.85, 4.36 (each 2H, q, CH_2Me), 7.3—8.1 ppm (8H, m).

Found: C, 60.10; H, 4.36; N, 6.08%. Calcd for $C_{23}H_{20}N_2O_4Cl_2$: C, 60.14; H, 4.38; N, 6.09%.

ii) A solution of the dichloride **13** (0.92 g, 2 mmol) and sodium iodide (0.75 g, 5 mmol) in ethanol (20 ml) was refluxed for 24 h. A similar work-up as above afforded 0.75 g (96%) of the diazanorcaradiene **7a**.

*7,7-Bis(ethoxycarbonyl)-1,6-dichloro-2,5-diphenyl-3,4-diaza-2,4-norcaradiene (**16**).* A solution of the tetrachloride **15** (1.06 g, 2 mmol) and sodium iodide (0.75 g, 5 mmol) in acetone (20 ml) was refluxed for 2 h. A similar work-up as above and recrystallization of the product from petroleum ether (bp 60—80 °C) gave 0.88 g (97%) of the 1,6-dichlorodiazanorcaradiene **16**, mp 118—119 °C, as yellow prisms. NMR ($CDCl_3$) δ 0.89, 1.45 (each 3H, t, CH_2CH_3), 4.0, 4.5 (each 2H, q, CH_2Me), 7.3—7.7 (6H, m), 7.9—8.3 ppm (4H, m); MS *m/e* 458, 460, 462 (M^+).

Found: C, 60.09; H, 4.38; N, 6.15%. Calcd for $C_{23}H_{20}N_2O_4Cl_2$: C, 60.15; H, 4.38; N, 6.10%.

Dehalogenation of the Dibromide 8a with Zinc Dust. A solution of **8a** (1.1 g) in ethanol (40 ml) was refluxed with zinc dust (1.0 g) for 2 h. The reaction mixture was filtered and the residue was washed with hot ethanol (30 ml). The ethanol filtrate and washing were combined, concentrated to about 30 ml, and allowed to stand at room temperature. Filtration gave 0.2 g (43%) of 3,6-diphenylpyridazine (**17**), mp 223 °C (lit,[5] mp 222 °C), as colorless prisms. The filtrate was further concentrated to about 5 ml to give 75 mg (9.6%) of the dihydrodiazepine **4a**. The solution which was removed **4a** was chromatographed on silica gel to give 0.12 g (38%) of diethyl malonate.

A similar treatment of the dichloride **13** with zinc dust afforded the dihydrodiazepine **4a**, pyridazine **17**, and diethyl malonate; the yields are shown in Scheme 6.

*Dehalogenation of the 1-Bromodiazanorcaradiene **9** with Zinc Dust.* A solution of **9** (0.94 g) in ethanol (30 ml) was refluxed with zinc dust (1.0 g) for 2 h. A similar work-up as above afforded 0.38 g (47%) of 4-bis(ethoxycarbonyl)methyl-3,6-diphenylpyridazine (**18**), mp 131—132 °C, as colorless needles. IR 1740, 1760 cm^{-1} (C=O); NMR ($CDCl_3$) δ 1.23 (6H, t, CH_2CH_3), 4.25 (4H, q, CH_2Me), 4.93 (1H, s, $\geq CH$), 7.4—7.8 (6H, m), 8.0—8.4 (4H, m), 8.23 ppm (1H, s, pyridazine ring-H); MS *m/e* 390 (M^+).

Found: C, 70.82; H, 5.69; N, 7.21%. Calcd for $C_{23}H_{22}N_2O_4$: C, 70.75; H, 5.68; N, 7.18%.

Similarly, the chlorodiazanorcaradiene **14**, tetrachloride **15**, and dichlorodiazanorcaradiene **16** afforded the pyridazine **18** in 51, 16, and 13% yields respectively. Treatments of **14** and **15** with zinc dust in ethanol-d_1 under similar conditions afforded the pyridazines **18**-d_1 and **18**-d_2 in 54 and 13% yields respectively. **18**-d_1: NMR (DMSO-d_6) δ 1.20 (6H, t, CH_2CH_3), 4.20 (4H, q, CH_2Me), 7.4—7.8 (6H, m), 8.25 ppm (1H, s, pyridazine ring-H); MS *m/e* 391 (M^+). **18**-d_2: NMR (DMSO-d_6) δ 1.20 (6H, t, CH_2CH_3), 4.20 (4H, q, CH_2Me), 7.4—7.8 (6H, m), 8.0—8.4 ppm (4H, m); MS *m/e* 392 (M^+).

References

1) Studies of Medium-membered Heterocyclic Compounds. III. Part II of this series: O. Tsuge and K. Kamata, *Heterocycles*, **3**, 547 (1975).

2) O. Tsuge and K. Kamata, *Heterocycles*, **3**, 15 (1975).

3) G. G. Amiet, R. B. Johns, and K. R. Markham, *Chem. Commun.*, **1965**, 128.

4) O. Tsuge, M. Tashiro, K. Kamata, and K. Hokama, *Org. Prep. & Proced. Int.*, **3**, 289 (1971).

5) J. D. Loudon and L. B. Young, *J. Chem. Soc.*, **1963**, 5496.

Substitution on Carbenoid Carbon of α-Halocyclopropyllithium. A Novel Stereoselective Synthesis of Geminally Substituted Cyclopropanes

Katuzi KITATANI, Hajime YAMAMOTO, Tamejiro HIYAMA, and Hitosi NOZAKI

Department of Industrial Chemistry, Kyoto University, Yoshida, Kyoto 606

(Received January 27, 1977)

The halogen atom of the title carbenoids is susceptible to displacement by butyllithium. 1-Butyl-1-lithiocyclopropanes are formed, in which the butyl group occupies the less hindered site (*trans* or *exo* position). The new reaction provides a means for the preparation of geminally disubstituted cyclopropanes with high degree of stereoselectivity.

In contrast to the view that the halogen atom on cyclopropane carbon is not easily displaced by nucleophiles,[1] it was found that the halogen atom of α-halocyclopropyllithium undergoes a displacement reaction, the process being applicable to the synthesis of *gem*-disubstituted cyclopropanes.

Addition of 1,1-dibromo-2-phenylcyclopropane (**1a**) to excess butyllithium at −95 °C, followed by aqueous work-up, afforded 1-butyl-2-phenylcyclopropane (**2a** and **3a**, 90: 10). The product distribution changes with reaction time, as shown in Fig. 1, according to Scheme 1. Apparently the decrease of the initially predominant *trans*-lithiocarbenoid **4**[2,3] is accompained by an increase of the *trans*-alkylated cyclopropyllithium **6**, whereas the concentration of the thermodynamically favored carbenoid **5** remains almost constant. The bulky phenyl substituent probably prevents the conversion of **5** into **7**. When the temperature is raised, however, the conversion occurs along with partial isomerization to **4** which would account for **6** to some extent.

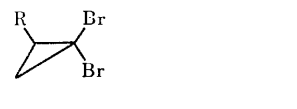

1a: R=Ph
1b: R=$PhCH_2OCH_2$

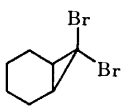

1c

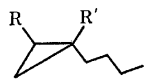

2a: R=Ph, R′=H
2b: R=Ph, R′=D
2c: R=Ph, R′=Me_3Si
2d: R=Ph, R′=PhCO
2e: R=Ph, R′=MeS
2f: R=Ph, R′=I
2g: R=Ph, R′=Me
2h: R=$PhCH_2OCH_2$, R′=Me

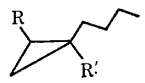

3a: R=Ph, R′=H
3b: R=Ph, R′=D
3c: R=Ph, R′=Me_3Si
3d: R=Ph, R′=PhCO
3e: R=Ph, R′=MeS
3f: R=Ph, R′=I
3g: R=Ph, R′=Me
3h: R=$PhCH_2OCH_2$, R′=Me

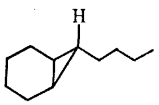

2i

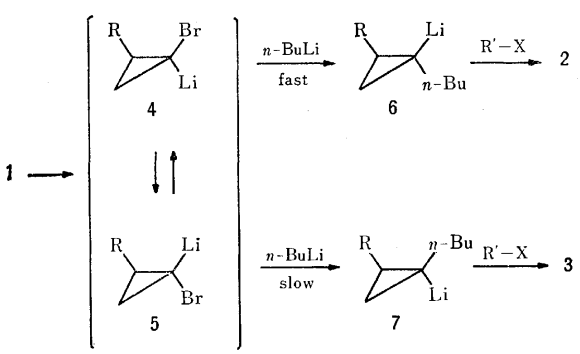

Scheme 1.

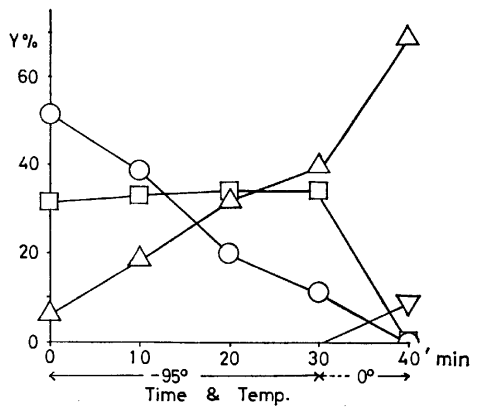

Fig. 1. Products distribution *vs.* reaction time in the reaction of **1a** with 3.3 molar eq of *n*-BuLi (as determined by GLC after methanol quenching). The reaction time was counted after completion of the addition of **1a** which required 5 min. ○: *cis*-1-Bromo-2-phenylcyclopropane corresponding to **4a**; □: *trans*-1-Bromo-2-phenylcyclopropane corresponding to **5a**; △: **2a** which corresponds to **6a**; ▽; **3a** which corresponds to **7a**.

Synthetic utility of cyclopropyllithium (**6**) and (**7**) was subsequently found in the reaction with several electrophiles. The results are summarized in Table 1. Stereoselectivity (91—100%) was excellent as compared with that (86%) obtained in the dibutylcuprate reaction.[1d] The reaction of the cyclopropyllithium with methyl iodide resulted in the formation of an iodocyclopropane **2f** in sharp contrast to the reaction of cyclopropylcopper species[1d] which afforded methylated cyclopropanes **2g** and **3g**. They were obtained by the reaction of **6** and **7** with dimethyl sulfate. Similarly **1b** afforded **2h** as the sole product.

More hindered 7,7-dibromonorcarane (**1c**) gave a mixture of *exo*-7-butylnorcarane (**2i**) and *exo*-7-bromo-

Table 1. Preparation of *gem*-disubstituted cyclopropanes

Dihalocyclopropane	R′–X	Products	Yield (%) of **2** and **3**	**2**:**3**
1a	H_2O	**2a** and **3a**	80	90:10
1a	D_2O	**2b** and **3b**	76	91:9
1a	Me_3SiCl	**2c**	46	100:0[a]
1a	PhCOCl	**2d**	45	100:0[a]
1a	MeSSMe	**2e** and **3e**	55	94:6
1a	I_2	**2f**	59	100:0[b]
1a	MeI	**2f**	58	100:0[b]
1a	$(MeO)_2SO_2$	**2g** and **3g**	53	96:4
1b	$(MeO)_2SO_2$	**2h**	40	100:0
1c	MeOH	**2i**	24	100:0[c]

a) By-products **2a** and **3a** were obtained (see Experimental). Complete absence of **3c** isomer is attributed to the preferential protonolysis of **7** to **3a**. The proton source is still obscure. b) 1,1-Dibutyl-2-phenylcyclopropane (**8**) was also obtained. c) *exo*-7-Bromonorcarane formed as a by-product.

norcarane. The stereochemical outcome strongly suggests the large steric hindrance of the tetramethylene chain prohibiting the attack of butyl anion to the carbenoid of type **5** and the large barrier in the configurational isomerization of carbenoid **5** to **4**.

Extension of the reaction of **4** and **5** with anionic species other than butyl anion was not successful with the exception of that of lithium phenylthiolate complexed with tetramethylethylenediamine which afforded *trans*-1-phenyl-2-phenylthiocyclopropane (**9**) in 25% yield.

Experimental

All the temperatures are uncorrected. The IR spectra were obtained on a Shimadzu spectrometer 27-G, MS on a Hitachi RMU-6L, and PMR on JEOL JNM-PMX 60, Varian EM-360, or Varian HA-100D spectrometer. Butyllithium from Aldrich Chemical Co. Ltd. was used. Tetrahydrofuran (THF) was dried on benzophenone ketyl and freshly distilled before use. Tetramethylethylenediamine was dried on KOH and distilled. All the reactions were performed under nitrogen atmosphere. The cold bath was prepared by mixing liquid nitrogen with a solvent (−95 °C: toluene; −126 °C: methylcyclohexane).

1-Butyl-2-phenylcyclopropanes (2a and 3a).[3] *A Standard Procedure*: A solution of **1a** (0.40 g, 1.5 mmol) in THF (3 ml) was cooled to −78 °C and added to a stirred solution of *n*-BuLi (3.7 ml of 1.33 M in hexane, 5.0 mmol) in THF (30 ml) at −95 °C during 5 min. After 30 min the cold bath was removed and the reaction mixture was rapidly warmed to 0 °C in 10 min. This procedure is pertinent to the preparation of **2a**—**g** and their isomers if any. Work-up followed by preparative TLC (silica gel, hexane, R_f 0.7—0.8) afforded a mixture of **2a** and **3a** (0.20 g, 80% yield). Each isomer was identified by comparison of spectral data with those of authentic sample.

1-Butyl-1-deuterio-2-phenylcyclopropanes (2b and 3b). Addition of deuterium oxide (0.1 ml) to cyclopropyllithium (**6**) and (**7**) followed by work-up and preparative TLC (silica gel, hexane, R_f 0.7—0.8) afforded a mixture of **2b** and **3b** (0.20 g, 76% yield, 73% deuterium content). Bp 65—68 °C (bath temp)/15 Torr; IR (neat): 1605, 1495, 1455, 1370, 1025, 745, 695 cm^{-1}; MS: *m/e* (%), 175 (M^+, 16), 174 (M^+−1, 8), 119 (68), 117 (100), 104 (93), 91 (38); PMR (CCl_4): δ 0.5—2.0 (m, 12H), 6.7—7.5 (m, 5H, Ph).

1-Butyl-r-1-trimethylsilyl-c-2-phenylcyclopropane (2c). Addition of Me_3SiCl (0.24 g, 2.3 mmol) to the reaction mixture obtained from **1a** (0.42 g, 1.5 mmol) and 5.0 mmol of *n*-BuLi, followed by work-up and preparative TLC (silica gel, hexane, R_f 0.7—0.8), afforded **2c** (0.17 g, 46%). Bp 106—111 °C (bath temp)/3 Torr; IR (neat): 1600, 1490, 1245, 1030, 835, 780, 755, 730, 700 cm^{-1}; MS: *m/e* (%), 246 (M^+, 5), 172 (49), 129 (35), 117 (60), 104 (69), 73 (100); PMR (CCl_4): δ −0.30 (s, 9H, Me_3Si), 0.5—1.8 (m, 11H), 1.97 (dd, J=6, 8 Hz, 1H, PhC<u>H</u>), 7.1—7.3 (m, 5H, Ph). Found: C, 78.1; H, 10.9%. Calcd for $C_{16}H_{26}Si$: C, 78.0; H, 10.6%. By-products **2a** (7%) and **3a** (7%) were also obtained.

r-*1-Benzoyl-1-butyl-c-2-phenylcyclopropane (2d).* Dibromocyclopropane (**1a**) (0.41 g, 1.5 mmol) was subjected to the reaction with *n*-BuLi as above. Benzoyl chloride (0.35 g, 2.5 mmol) was then added. Work-up and preparative TLC (silica gel, hexane–ether 20:3, R_f 0.5—0.6) afforded **2d** (0.19 g, 45%). Mp 69.5—70.5 °C (hexane); IR (Nujol): 1660, 1455, 1064, 785, 770, 715, 690 cm^{-1}; MS: *m/e* (%), 278 (M^+, 17), 235 (36), 105 (100), 91 (18), 77 (47); PMR (CCl_4): δ 0.5—2.6 (m, 12H), 6.7—7.7 (m, 10H). Found: C, 86.6; H, 8.2%. Calcd for $C_{20}H_{22}O$: C, 86.3; H, 8.0%. By-products were **2a** (7%) and **3a** (6%).

1-Butyl-r-1-methylthio-c-2-phenylcyclopropane (2e). Quenching the cyclopropyllithium (**6** and **7**) with dimethyl disulfide (0.21 g, 2.3 mmol) and work-up afforded **2e** (0.18 g, 55% yield). A small amount of its stereoisomer **3e** was detected by GLC and identified by MS. Physical properties of **2e**: bp 120—124 °C (bath temp)/3 Torr; IR (neat): 1600, 1495, 1030, 770, 700 cm^{-1}; MS: *m/e* (%), 222 (M^++2, 1.5), 220 (M^+, 21), 205 (30), 173 (100), 129 (71), 115 (79); PMR (CCl_4): δ 0.7—1.7 (m, 11H), 1.66 (s, 3H, SMe), 2.13 (dd, J=6, 7 Hz, 1H, PhC<u>H</u>), 7.0—7.3 (m, 5H, Ph). Found: C, 75.7; H, 9.4%. Calcd for $C_{14}H_{20}S$: C, 76.0; H, 9.6%.

1-Butyl-r-1-iodo-c-2-phenylcyclopropane (2f).[3] Iodine (0.46 g, 1.8 mmol) in THF (2 ml) was added to the cyclopropyllithium prepared as above, and the resulting mixture was stirred at 0 °C for 1 h and subjected to work-up. Preparative TLC (silica gel, hexane, R_f 0.5—0.6) of the crude product afforded **2f** (0.26 g, 59% yield) besides 2,2-dibutyl-1-phenylcyclopropane (**8**) (38 mg, 10%).

Treatment of the cyclopropyllithium with excess methyl iodide (1 ml) at 0 °C gave **2f** (58%) and **8** (14%).

1-Butyl-1-methyl-2-phenylcyclopropanes (2g and 3g).[3] Dibromocyclopropane **1a** (0.28 g, 1.0 mmol) was treated with 3.3 mmol of *n*-BuLi and then dimethyl sulfate (0.20 g, 1.5 mmol). Work-up and preparative TLC (silica gel, hexane, R_f 0.7—0.8) afforded an oil (0.15 g). The ratio of **2g** to **3g** was estimated by GLC assay (10% HVSG on Celite 545, 122 °C, 0.8 kg/cm^2, naphthalene as an internal standard).

c-*2-Benzyloxymethyl-r-1-butyl-1-methylcyclopropane (2h).*[3] To *n*-BuLi (2.5 ml of 1.98 M hexane solution, 5.0 mmol) in THF (20 ml) was added a cooled solution of **1b** (0.48 g, 1.5 mmol) in THF (2 ml) at −95 °C. After 30 min the reaction mixture was warmed rapidly to 0 °C. Dimethyl sulfate (0.21 ml, 2.3 mmol) was then added. Work-up and preparative TLC afforded **2h** (0.14 g, 40%).

exo-*7-Butylnorcarane (2i).*[4] A cooled solution (−78 °C) of **1c** (0.25 g, 0.99 mmol) in a mixture[5] of THF–ether–hexane (50:5:18, 3 ml) was added to a solution of *n*-BuLi (1.7 ml, of 1.92 M in hexane, 3.2 mmol) in the same solvent mixture (22 ml) at −126 °C. After 7 h the reaction mixture was quenched with methanol and subjected to work-up affording

2i (24% yield by GLC, R_f (hexane) 0.8—0.9); bp 90—100 °C (bath temp)/20 Torr; IR (neat): 1450, 1370, 1112, 1064 cm^{-1}; MS: *m/e* (%), 152 (M^+, 12), 109 (24), 95 (51), 81 (65), 67 (100), 55 (46), 41 (51); PMR (CCl_4): δ 0.4—0.6 (m, 3H), 0.6—2.1 (m, 17H). By-product, *exo*-7-bromonorcarane,[6] was also obtained (53% yield by GLC, R_f (hexane) on silica gel TLC 0.7—0.8).

trans-*1-Phenyl-2-phenylthiocyclopropane (9)*. The dibromocyclopropane **1a** (0.41 g, 1.5 mmol) in THF (3 ml) was added to a THF (15 ml) solution of *n*-BuLi (0.82 ml of 1.95 M hexane solution, 1.6 mmol) and tetramethylethylenediamine (0.19 g, 1.6 mmol) cooled to *ca.* −95 °C Subsequently a THF (10 ml) solution of PhSLi (3.3 mmol, prepared from thiophenol and *n*-BuLi)[7] and tetramethylethylenediamine (0.42 g, 3.6 mmol) which had been cooled to −78 °C was added dropwise in a period of 8 min. After 30 min the whole was allowed to warm to 0 °C and then worked up. Preparative TLC (silica gel, hexane, R_f 0.3—0.4) of the crude product afforded **9** (85 mg, 25%). Bp 100—105 °C (bath temp)/1 Torr; IR (neat): 1603, 1582, 1493, 1480, 1085, 1020, 733, 685 cm^{-1}; MS: *m/e* (%), 228 (M^++2, 1.8), 226 (M^+, 30), 115 (100), 109 (8), 91 (49), 77 (98); PMR (CCl_4): δ 1.1—1.6 (m, 2H), 2.0—2.4 (m, 2H,) 6.9—7.3 (m, 10H). Found: C, 79.4; H, 6.2%. Calcd for $C_{15}H_{14}S$: C, 79.6; H, 6.2%.

Financial support (Grant-in-Aid No. 185188) by the Ministry of Education, Japanese Govenment, is acknowledged.

References

1) Intramolecular substitution takes place readily: a) B. M. Trost, *Acc. Chem. Res.*, **7**, 85 (1974); b) M. Brown, R, Dammann, and D. Seebach, *Chem. Ber.*, **108**, 2368 (1975); c) T. Hiyama, S. Takehara, K. Kitatani, and H. Nozaki. *Tetrahedron Lett.*, **1974**, 3295; d) K. Kitatani, T. Hiyama, and H. Nozaki, *J. Am. Chem. Soc.*, **98**, 2362 (1976).

2) It is remarkable that the kinetically produced carbenoid **4** is predominant under the reaction conditions in contrast to the result given by K. Kitatani, T. Hiyama, and H. Nozaki, *J. Am. Chem. Soc.*, **97**, 949 (1975).

3) K. Kitatani, T. Hiyama, and H. Nozaki, *Bull. Chem. Soc. Jpn.*, **50**, 1600 (1977).

4) G. Köbrich and W. Goyert, *Tetrahedron*, **24**, 4327 (1968); D. Seyferth and R. L. Lambert, Jr., *J. Organomet. Chem.*, **88**, 287 (1975).

5) Trapp-solvent mixture: G. Köbrich and H. Trapp, *Chem. Ber.*, **99**, 680 (1966).

6) D. Seyferth, H. Yamazaki, and D. L. Alleston, *J. Org. Chem.*, **28**, 703 (1963).

7) G. H. Posner, C. E. Whitten, and J. J. Sterling, *J. Am. Chem. Soc.*, **95**, 7788 (1973).

Substituent Effects on Dissociation Constants of *trans*-3-Hydroxy-6-styryl-4-pyrones

Hiromichi Besso,* Kimiaki Imafuku, and Hisashi Matsumura

Department of Chemistry, Faculty of Science, Kumamoto University, Kurokami, Kumamoto 860

(Received February 18, 1977)

The dissociation constants of 6-substituted 3-hydroxy-4-pyrones and *trans*-6-(substituted styryl)-3-hydroxy-4-pyrones were measured spectrophotometrically in 50% aqueous methanol at 25 °C. The results are correlated to the substituent constants σ, the following equations being obtained: $pK_a = 8.57 - 1.53\sigma$ and $pK_a = 8.54 - 0.23\sigma$. The transmission coefficient through the styryl group was found to be 0.150 for the 3-hydroxy-6-styryl-4-pyrone system.

Choux and Benoit[1] measured the dissociation contants of 6-substituted 3-hydroxy-4-pyrones in water at 25 °C, and obtained the following Hammett equation:

$$pK_a = 8.01 - 1.63\sigma \quad (r=0.978). \qquad (1)$$

However, little is known about the substituent effects for 3- or 5-hydroxy-4-pyrones. We report herewith on the substituent effects of 3-hydroxy-4-pyrones having styryl groups in the 6-position.

Studies were made on the substituent effects on dissociation constants of 4- and 5-styryltropolones.[2,3] The transmission of electronic effects from one aromatic ring to another through the ethylene linkage between them has been investigated in detail. It is of interest to compare the reaction constants of 4- and 5-styryltropolones with that of 3-hydroxy-6-styryl-4-pyrones. We found that the electronic effects of substituents in the benzene ring are transmitted through the ethylene linkage to 4-pyrone nucleus, the effects being comparable to those of 4-hydroxystilbenes.

Results and Discussion

Dissociation Constants. The dissociation constants of 6-substituted 3-hydroxy-4-pyrones (I) and 6-(substituted styryl)-3-hydroxy-4-pyrones (II) were determined spectrophotometrically in 50% aqueous methanol at 25 °C. The results are summarized in Tables 1 and 2.

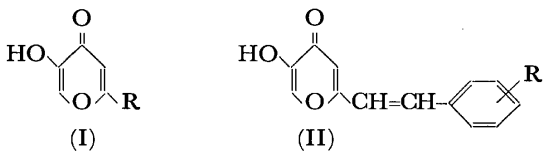

(I) (II)

Ia R=H IIa R=H IIe R=*p*-Cl
Ib R=CH_3 IIb R=*p*-OCH_3 IIf R=*m*-NO_2
Ic R=COOH IIc R=*p*-CH_3 IIg R=*p*-NO_2
Id R=CH_2Cl IId R=3′,4′-$(OCH_3)_2$

Table 1. Dissociation constants of 6-substituted 3-hydroxy-4-pyrones

R	σ	pK_a
CH_3	−0.17[a]	8.84
H	0.00	8.55
COO^-	0.13[b]	8.38
CH_2Cl	0.18[a]	8.29

a) Ref. 5. b) Ref. 6.

Table 2. Dissociation constants of 6-(substituted styryl)-3-hydroxy-4-pyrones

No.[a]	R	σ[b]	pK_a
1	*p*-OCH_3	−0.27	8.60
2	*p*-CH_3	−0.17	8.58
3	3′,4′-$(OCH_3)_2$	−0.15	8.57
4	H	0.00	8.55
5	*p*-Cl	0.23	8.52
6	*m*-NO_2	0.71	8.37
7	*p*-NO_2	0.78 (1.27)[c]	8.26

a) Numbers correspond to those in Fig. 1.
b) Ref. 5. c) σ^- Value.

The pK_a values of these 4-pyrones are smaller than those of phenols ($pK_a = 10.02$ for phenol),[4] since the carbonyl group of 4-pyrones causes a decrease in the pK_a values by its electron withdrawing effect.

Substituent Effects. The pK_a values of 6-substituted 3-hydroxy-4-pyrones (I) and 6-(substituted styryl)-3-hydroxy-4-pyrones (II) were plotted against the Hammett substituent constants σ.[5,6] As an example, the Hammett plot of the latter is shown in Fig. 1. The following Eqs. 2 and 3 were obtained by the least squares method for systems (I) and (II), respectively (except for the *p*-nitro group in Eq. 3).

$$pK_a = 8.57 - 1.53\sigma \quad (r=0.998), \qquad (2)$$

$$pK_a = 8.54 - 0.23\sigma \quad (r=0.983). \qquad (3)$$

The plot of the *p*-nitro group deviates from the straight line given by Eq. 3 (Fig. 1). The deviation might be

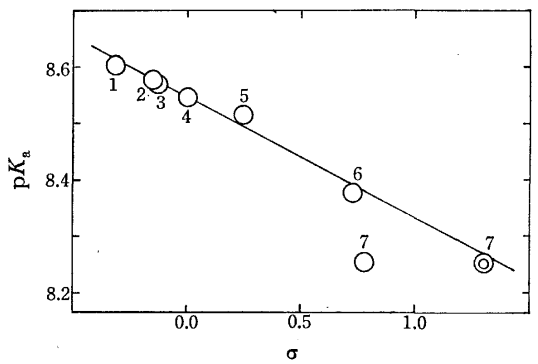

Fig. 1. The Hammett plot of pK_a's of 3-hydroxy-6-styryl-4-pyrones.
◎; Plotted against σ^- (1.27).

* Present address: Wakunaga Pharmaceutical Co., Ltd., Koda-machi, Takata-gun, Hiroshima 729-64.

attributed to the resonance interaction between the *p*-nitro group and the hydroxyl group in the 3-hydroxy-4-pyrone. Application of the σ^--value (1.27)[6] for the *p*-nitro group gives good linearity (Fig. 1). A similar resonance effect was also observed in the dissociation of *trans-p*-nitro-4-hydroxystilbene.[7] In 4- and 5-styryltropolones, the resonance effect might be present only in 5-styryltropolones, but this was not confirmed since 5-(*p*-nitrostyryl)tropolone was not available.

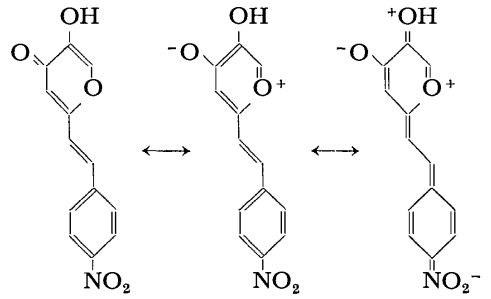

Reaction Constants. The reaction constants of 6-substituted 3-hydroxy-4-pyrones (I) and 6-(substituted styryl)-3-hydroxy-4-pyrones (II) are 1.53 and 0.23, respectively. These values are comparable to those of phenols (2.55)[8] and 4-hydroxystilbenes (0.37),[7] respectively. The reaction constant of 3-hydroxy-6-styryl-4-pyrones lies between 0.13 and 0.60 constants of 4- and 5-styryltropolones, respectively. The difference can be attributed to the tautomerism of tropolones.

Transmission Coefficients. When the reaction constants for the same reaction of two series of aromatic compounds, which are parents, and styryl-substituted compounds are denoted by ρ_M and ρ_S, respectively, the transmission coefficient π of the styryl group can be defined as follows:

$$\pi = \rho_S/\rho_M.$$

The transmission coefficients π for several systems are given in Table 3. The π-value of 3-hydroxy-6-styryl-4-pyrone system is 0.150, and comparable to that of 4-hydroxystilbenes. We found that the electronic effects of the substituents in the benzene ring are transmitted through the styryl group in the order, 4-styryltropolones <4-hydroxystilbenes≒3-hydroxy-6-styryl-4-pyrones< 5-styryltropolones.

Table 3. Reaction constants and transmission coefficienis

System	Solvent	Temp (°C)	ρ	π
Phenols	49% EtOH	20—22	2.55[a]	
4-Hydroxystilbenes	50% EtOH	20	0.37[b]	0.145
Tropolones	H_2O	25	2.68[c]	
4-Styryltropolones	50% MeOH	20	0.13[d]	0.049
5-Styryltropolones	50% MeOH	20	0.60[e]	0.224
3-Hydroxy-4-pyrones	50% MeOH	25	1.53[f]	
3-Hydroxy-6-styryl-4-pyrones	50% MeOH	25	0.23[f]	0.150

a) Ref. 8. b) Ref. 7. c) N. Yui, *Sci. Repts. Tohoku Univ., I*, **40**, 102, 114 (1956). d) Ref. 2. e) Ref. 3. f) Results in this work.

Experimental

All the melting points were measured on a Yanagimoto micromelting point apparatus and are uncorrected. The IR spectra were taken on a JASCO IRA-1 spectrophotometer, and the NMR spectra on a Hitachi-Perkin-Elmer R-24 spectrometer (60 MHz).

The pK_a values of 4-pyrones were measured spectrophotometrically in 50% aqueous methanol at 25 °C by the method of Albert and Serjeant.[9] The UV spectra were taken on a Hitachi EPS-3T spectrophotometer, while the pH values were measured with a Hitachi-Horiba F-7 pH meter.

Materials. All 6-substituted 3-hydroxy-4-pyrones were prepared according to the method given in references: Ia, mp 117—118 °C (lit,[10] 118 °C); Ib, mp 152 °C (lit,[11] 152—153 °C); Ic, mp 270 °C (lit,[12] 273—274 °C); Id, mp 166—167 °C (lit,[13] 166—167 °C).

6-(Substituted styryl)-3-hydroxy-4-pyrones were obtained by the Wittig reaction. Phosphonium salt was prepared by the reaction of 5-hydroxy-2-chloromethyl-4-pyrone[13] with triphenylphosphine in benzene, 58% yield. Phosphonium salt (1.1 mmol) and benzaldehyde (1 mmol) were added to a sodium ethoxide (2 mmol) solution, and the resulting mixture was stirred for 2 h at room temperature under nitrogen atmosphere. After 2 M hydrochloric acid had been poured into the reaction mixture, the products were extracted with chloroform. Chloroform was evaporated off and the residue was chromatographed on silica gel column [Wakogel C-100 (60 g) and B-10 (10 g)] with chloroform to afford 3-hydroxy-6-styryl-4-pyrones, which were recrystallized from benzene. The yields, mp's spectral and analytical data are as follows: IIa; Yield, 34%; mp 183—185 °C; IR (KBr) 3180, 1660, 970 cm^{-1}; NMR ($CDCl_3$) δ: 7.85 (s, 1H), 7.7—7.2 (m, 6H), 6.66 (d, 1H, J=17.3 Hz), 6.45 (s, 1H), 8.3—7.6 (br, 1H). Found: C, 73.18; H, 4.77%. Calcd for $C_{13}H_{10}O_3$: C, 72.89; H, 4.71%. IIb: Yield, 32%; mp 187.5—189 °C; IR (KBr) 3100, 1655, 975 cm^{-1}; NMR ($CDCl_3$) δ: 7.79 (s, 1H), 7.35 (d, 1H, J=15.3 Hz), 7.5—6.8 (m, 4H), 6.49 (d, 1H, J=15.3 Hz), 6.36 (s, 1H), 3.82 (s, 3H), 8.0—7.5 (br, 1H). Found: C, 68.98; H, 4.95%. Calcd for $C_{14}H_{12}O_4$: C, 68.84; H, 4.95%. IIc: Yield, 25%; mp 216.5—217.5 °C; IR (KBr) 3200, 1660, 965 cm^{-1}; NMR ($CDCl_3$) δ: 7.31 (s, 1H), 7.5—7.0 (m, 5H), 6.58 (d, 1H, J=15.6 Hz), 6.38 (s, 1H), 2.36 (s, 3H), 8.0—7.5 (br, 1H). Found: C, 73.54; H, 5.32%. Calcd for $C_{14}H_{12}O_3$: C, 73.67; H, 5.30%. IId, Yield; 21%; mp 175—175.5 °C; IR (KBr) 3230, 1655, 955 cm^{-1}; NMR ($CDCl_3$) δ: 7.79 (s, 1H), 7.5—6.4 (m, 5H), 6.42 (s, 1H), 3.91 (s, 3H), 3.89 (s, 3H), 6.7—6.0 (br, 1H). Found: C, 65.52; H, 5.07%. Calcd for $C_{15}H_{14}O_5$: C, 65.69; H, 5.15%. IIe; Yield; 31%; mp 232 °C (dec); IR (KBr) 3250, 1660, 960 cm^{-1}; NMR (CF_3COOH) δ: 8.65 (s, 1H), 7.95 (d, 1H, J=15.7 Hz), 7.7—7.4 (m, 4H), 7.63 (s, 1H), 7.10 (d, 1H, J=15.7 Hz). Found: C, 62.87; H, 3.74%. Calcd for $C_{13}H_9O_3Cl$: C, 62.79; H, 3.65%. IIf: Yield, 20%; mp 250 °C (dec); IR (KBr) 3230, 1665, 965 cm^{-1}; NMR (CF_3COOH) δ: 8.78 (s, 1H), 8.7—7.2 (m, 6H), 7.56 (s, 1H), Found: C, 59.73; H, 3.63; N, 5.16%. Calcd for $C_{13}H_9NO_5$: C, 60.23; H, 3.50; N, 5.40%. IIg; Yield, 11%; mp 245—247 °C (dec); IR (KBr) 3200, 1655, 970 cm^{-1}; NMR (CF_3COOH) δ: 8.63 (s, 1H), 8.5—7.7 (m, 5H), 7.46 (s, 1H), 7.21 (d, 1H, J=16.7 Hz). Found: C, 60.36; H, 3.50; N, 5.32%. Calcd for $C_{13}H_9NO_5$: C, 60.23; H, 3.50; N, 5.40%.

References

1) G. Choux and R. L. Benoit, *J. Org. Chem.*, **32**, 3974

(1967).
2) K. Imafuku, S. Nakama, and H. Matsumura, *Tetrahedron*, **26**, 1821 (1970).
3) K. Hamada, S. Nakama, K. Imafuku, K. Kurosawa, and H. Matsumura, *Tetrahedron*, **27**, 337 (1971).
4) W. Bartok, P. J. Lucchesi, and N. S. Snider, *J. Am. Chem. Soc.*, **84**, 1842 (1962).
5) H. H. Jaffé, *Chem. Rev.*, **53**, 191 (1953).
6) D. H. McDaniel and H. C. Brown, *J. Org. Chem.*, **23**, 420 (1958).
7) H. Veshambre, G. Dauphin, and A. Kergomard, *Bull. Soc. Chim. Fr.*, **1967**, 2846.
8) S. Shcwarzenbach and E. Rudin, *Helv. Chim. Acta*, **22**, 360 (1939).
9) A. Albert and E. P. Serjeant, "Ionization Constants of Acids and Bases," 1st ed, Methuen & Co., London (1962), Chap. 4.
10) F. M. Dean, "Naturally Occurring Oxygen Ring Compounds," Butterworth & Co., London (1963), p. 82.
11) M. G. Brown, *J. Chem. Soc.*, **1956**, 2558.
15) G. A. Garkusha, *Zh. Obshch. Khim.*, **23**, 1578 (1953); *Chem. Abstr.*, **48**, 11400 (1954).
13) T. Yabuta, *J. Chem. Soc.*, **125**, 575 (1924).

Preparation of Perfluoroalkylated Benzoheterocyclic Compounds Using Hexafluoro-1,2-epoxypropane

Nobuo Ishikawa and Shigekuni Sasaki

Department of Chemical Technology, Tokyo Institute of Technology, Ookayama, Meguro-ku, Tokyo 152

(Received March 22, 1977)

Utilizing the high reactivity of hexafluoro-1,2-epoxypropane (HFPO, hexafluoropropylene oxide), several new benzoheterocyclic compounds containing CF_3 and C_2F_5 were prepared as follows: (1) 2-(pentafluoroethyl)benzoxazoles by treating 2-aminophenols with HFPO/Et_3N, followed by dehydrating cyclization, (2) 3-(trifluoromethyl)-2*H*-1,4-benzoxazin-2-ones, 3-(trifluoromethyl)-2(1*H*)-quinoxalinone and 2-fluoro-2-(trifluoromethyl)-2,3-dihydro-1,4-benzothiazin-3-one by reactions of ortho-bifunctional benzenes with HFPO, and (3) 2-(pentafluoroethyl)-4*H*-3,1-benzoxazin-4-one by treating anthranilic acid with HFPO/Et_3N.

A number of heterocyclic compounds containing a perfluoroalkyl group, especially CF_3, are known pharmaceutically and agrochemically.[1] However, knowledge of the structure of this kind of compound is limited, because the introduction of a perfluoroalkyl group into a heterocyclic ring is usually not easy.[2,3]

On the other hand, it is well known that nucleophiles readily attack the central carbon atom of HFPO, resulting in the formation of α-substituted tetrafluoropropionyl fluoride, which further reacts with an additional molecule of the nucleophile, forming an ester or an amide,[4-6] thus

$$CF_3\text{-}\underset{\diagdown O \diagup}{CF}\text{-}CF_2 \xrightarrow[(-F^-)]{Nu^-} CF_3\text{-}\underset{Nu}{CF}\text{-}CF{=}O \xrightarrow[(-F^-)]{Nu^-} CF_3\text{-}\underset{Nu}{CF}\text{-}\overset{O}{\overset{\diagup}{C}}\diagdown Nu,$$

where NuH=ROH, RSH, or RNH_2.

HFPO is also known to isomerize to pentafluoropropionyl fluoride under the action of a base.[7] The present authors have reported a convenient preparative method for esters and amides of pentafluoropropionic acid by reactions of HFPO and alcohols, thiols or amines in acetonitrile in the presence of triethylamine,[8] thus

$$HFPO \xrightarrow{Base} CF_3CF_2CF{=}O$$

$$HFPO + R\text{-}XH \xrightarrow{Et_3N} CF_3CF_2\text{-}\underset{O}{\overset{\|}{C}}\text{-}XR,$$

where X=O, S, NH. They have also reported that non-fluorinated carboxylic acids are readily converted into their fluorides by treating them in a HFPO-triethylamine system,[9] thus

$$HFPO + \underset{O}{\overset{\|}{R}}COH \xrightarrow{Et_3N} C_2F_5CO_2H + \underset{O}{\overset{\|}{R}}CF.$$

The reactivities of HFPO described above were applied to the preparation of benzoheterocyclic compounds and several kinds of new heterocyclic compounds which contain a trifluoromethyl or a pentafluoroethyl group were obtained.

Results and Discussion

Preparation of 2-(Pentafluoroethyl)benzoxazoles. According to the method of preparation for pentafluoropropionyl amides,[8] 2-(pentafluoropropionylamino)phenol (**1**) was obtained in a good yield by the reaction between *o*-aminophenol and HFPO–triethylamine in acetonitrile. The structure of **1** was evident from its IR and ^{19}F NMR data. In the IR spectrum, a broad band due to an OH group, and a characteristic band due to the C=O of an amide group were observed at 3320 and 1695 cm^{-1}, respectively. In the ^{19}F NMR spectrum two signals due to CF_3 and CF_2 groups appeared at 6.0 and 45.3 ppm.*

The dehydrating ring closure of **1** was carried out by heating in diphosphorus pentaoxide at 200—230 °C, affording 2-(pentafluoroethyl)benzoxazole (**2**) in an 84% yield. In the IR spectrum of this compounds, the characteristic absorption bands for **1** due to OH and C=O disappeared, and a new band due to C=N appeared at 1615 cm^{-1}.

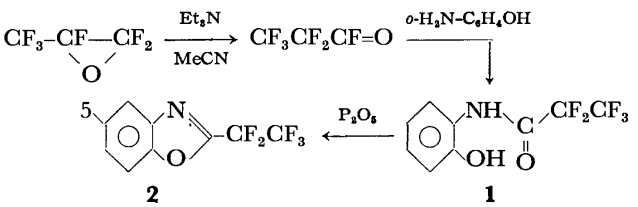

2-Amino-4-methyl- and 2-amino-4-chlorophenols, containing an electron donor or attractive group on the benzene ring, also gave 5-substituted 2-(pentafluoroethyl)benzoxazoles by a similar procedure. Although a number of 2-trifluoromethylbenzoxazoles are known,[10] no 2-pentafluoroethyl derivatives have been reported in the literature, The synthetic route described here appears to be a useful method for preparing this kind of compound.

Preparation of 3-(Trifluoromethyl)-2H-1,4-benzoxazin-2-ones, 3-(Trifluoromethyl)-2(1H)-quinoxalinone and 2-Fluoro-2-(trifluoromethyl)-2,3-dihydro-1,4-benzothiazin-3-one. When 2-aminophenol was allowed to react with HFPO in dioxane, without any base, it readily gave 3-(trifluoromethyl)-2*H*-1,4-benzoxazin-2-one (**3**) in an 85% yield, together with a small amount (7%) of 2-(pentafluoropropionylamino)phenol (**1**).** The reaction must be as follows:

* All the ^{19}F-chemical shifts throughout this article are given in δ ppm upfield from external trifluoroacetic acid.

** These yields are based on the ^{19}F-NMR signal intensities.

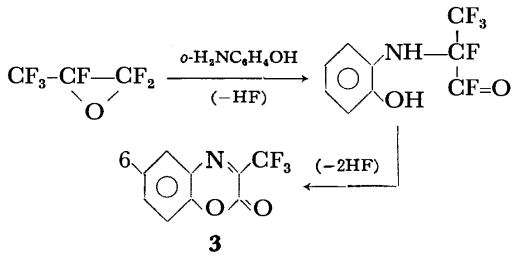

3

Thus, the amino group of *o*-aminophenol first attacks the central carbon atom of HFPO, as usual, and the resulting fluoroformyl group condensed with the ortho hydroxy group forming an oxazine ring. On the other hand, pentafluoropropionyl fluoride, formed by the isomerization of HFPO, pentafluoropropionated 2-aminophenol giving a small amount of **1**. When acetonitrile was used as the solvent, **3** and **1** were formed in yields of 45 and 22%, respectively. This probably means that the ionic isomerization of HFPO is accelerated by the polar solvent.

The structure of **3** was established from its spectral data. In the ^{19}F NMR spectrum, only one singlet signal was observed at −6.9 ppm, which means that there are no hydrogen or fluorine atoms around the CF_3 group. The IR spectrum indicates a characteristic band at 1765 cm^{-1} due to ester bonding, and the mass spectrum showed the expected parent peak at *m/e* 215.

6-Methyl- and 6-chloro-3-(trifluoromethyl)-2*H*-1,4-benzoxazin-2-ones were also obtained in good yields from 2-amino-4-methyl- and 2-amino-4-chlorophenols, respectively.

Like 2-aminophenol, *o*-phenylenediamine with HFPO gave another heterocyclic compound. In this case, however, more isomerization of HFPO to pentafluoropropionyl fluoride occurred becauseof the higher basicity of phenylenediamine compared to 2-aminonophenol. Thus, the reaction between *o*-phenylenediamine and HFPO in dioxane gave only a 30% yield of 3-(trifluoromethyl)-2(1*H*)-quinoxalinone (**4**). Then using diethyl ether as a solvent, together with sodium hydrogencarbonate to remove the hydrogen fluoride formed, the yield was increased to 84%. Bases stronger than sodium hydrogencarbonate were not used because they accelerate the isomerization of HFPO, and lower the yield of **4**.

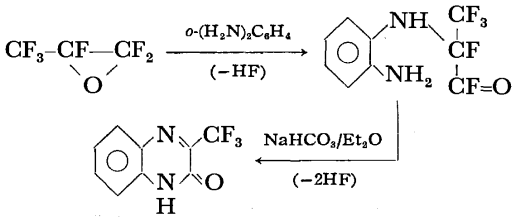

4

The structure of **4** was also elucidated from spectral data (Table 1).

o-Aminobenzenethiol and HFPO in *N,N*-dimethylacetamide provided another heterocyclic compound, 2-fluoro-2-(trifluoromethyl)-2,3-dihydro-1,4-benzothiazin-3-one (**5**). The mercapto group, which is more nucleophilic than the amino group, first attacked the central carbon atom of HFPO, and an intramolecular

Table 1. Physical properties of **1**—**7**

Product	Mp °C or (Bp)	Yield (%)	IR (cm^{-1})	^{19}F NMR (ppm)[a]	MS (*m/e*)	Found (Calcd) % C	H	N
1	117—118	79	3320(OH), 1695(C=O)	6.0(CF_3), 45.3(CF_2)		42.26 (42.38)	2.43 (2.37)	5.40 (5.49)
4-Me-**1**	125	90	3330(OH), 1705(C=O)	5.5(CF_3), 44.7(CF_2)		44.98 (44.62)	2.91 (3.00)	5.30 (5.20)
4-Cl-**1**	151—152	63	3350(OH), 1695(C=O)	5.2(CF_3), 44.5(CF_2)		37.21 (37.33)	1.73 (1.74)	4.87 (4.84)
2	(166—167)	84	1615(C=N)	6.5t (CF_3), 38.1q(CF_2)	237(M^+), 168(M^+-CF_3)	45.17 (45.59)	1.85 (1.70)	5.70 (5.91)
5-Me-**2**	(182—183)	70	1615(C=N)	6.4t (CF_3), 38.4q(CF_2)		47.96 (47.82)	2.51 (2.41)	5.53 (5.58)
5-Cl-**2**	(194—195)	82	1610(C=N)	6.2t (CF_3), 38.4q(CF_2)		40.16 (39.80)	1.26 (1.11)	5.10 (5.16)
3	77—78	66	1765(C=O)	−6.9s(CF_3)	215(M^+), 187(M^+-CO)	49.55 (50.25)	1.94 (1.87)	6.48 (6.51)
6-Me-**3**	119—120.5	76	1760(C=O)	−7.0s(CF_3)		52.31 (52.41)	2.59 (2.64)	6.08 (6.11)
6-Cl-**3**	88—89	83	1750(C=O)	−6.9s(CF_3)		42.96 (43.31)	1.24 (1.21)	5.51 (5.61)
4	233—234.5	84	3330(NH), 1675(C=O)	−7.5s(CF_3)	214(M^+), 186(M^+-CO)	50.09 (50.48)	2.35 (2.35)	13.08 (13.08)
5	182—183	26	3370(NH), 1695(C=O)	−2.3d(CF_3), 70.2q(CF)	251(M^+), 182(M^+-CF_3)	43.03 (43.03)	2.02 (2.01)	5.37 (5.58)
6	48—49	89	1770(C=O)	5.6(CF_3), 42.8(CF_2)	265(M^+)	44.63 (45.30)	1.56 (1.52)	5.24 (5.28)
7	168—169	70	3500—2400(OH) 3250(NH) 1715, 1670(C=O)	5.8(CF_3), 45.8(CF_2)		42.47 (42.42)	2.17 (2.14)	4.75 (4.95)

a) Upfield from external CF_3CO_2H.

amide linkage was subsequently formed.

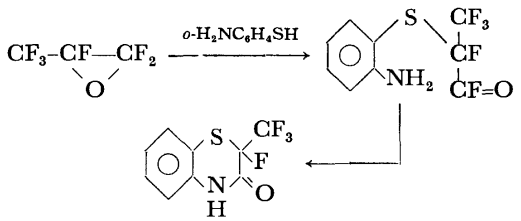

5

When dioxane or acetonitrile was used instead of *N,N*-dimethylacetamide, the formation of another product, which appeared to contain only a CF_3 group, was observed in the ^{19}F NMR spectrum. This compound was not isolated for identification.

In the ^{19}F NMR spectrum for **5**, two signals, a doublet and a quartet were observed, the mutual coupling constant being $J=10.2$ Hz. This indicates that a fluorine atom and a trifluoromethyl group are geminally attached to one carbon atom.

Preparation of 2-(Pentafluoroethyl)-4H-3,1-benzoxazin-4-one. The reaction of anthranilic acid with two molar amounts of HFPO in acetonitrile, in the presence of triethylamine, afforded 2-(pentafluoroethyl)-4*H*-3,1-benzoxazin-4-one (**6**) in a good yield. The reaction proceeded as follows:

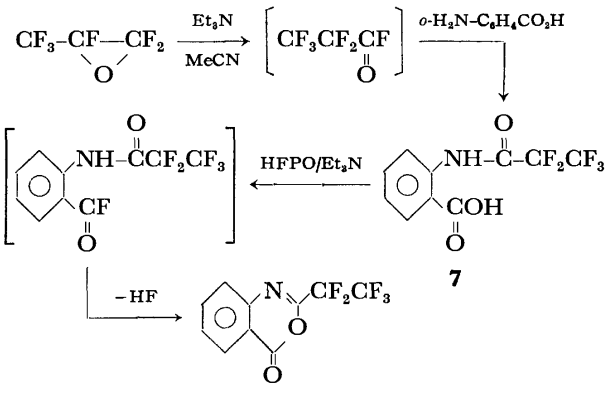

7

6

When an equimolar amount of HFPO was used in this reaction, 2-(pentafluoropropionylamino)benzoic acid (**7**) was obtained.

The structures of these products were obvious from their spectra (Table 1). In particular, in the IR spectrum of **7**, the characteristic bands due to OH and NH groups appeared over 2400—3500 and at 3250 cm^{-1}, respectively, which were not observed in the spectrum of **6**.

Experimental

2-(Pentafluoropropionylamino)phenol (1). 2-Aminophenol (2.18 g, 20 mmol), triethylamine (2.02 g, 20 mmol) and acetonitrile (20 ml) were placed in a glass pressure vessel, which was then cooled to −75 °C in a Dry Ice–acetone bath. Liquefied HFPO (3.32 g, 20 mmol) was introduced into the vessel, and the whole system was brought to room temperature. After stirring for 30 min at that temperature, the reaction mixture was poured into water (200 ml) and the precipitated material was collected by filtration. By treating the precipitate with dilute aqueous hydrochloric acid to remove any basic material, crude 2-(pentafluoropropionylamino)phenol, (mp 113—116 °C, 4.02 g, 79%) was obtained. Recrystallization from benzene gave a pure product, mp 116.5—118 °C. When 2-amino-4-methyl- and 2-amino-4-chlorophenol was used instead of unsubstituted 2-aminophenol, 4-methyl- and 4-chloro-2-(pentafluoropropionylamino)phenols were obtained (Table 1), respectively.

2-(Pentafluoroethyl)benzoxazole (2). A mixture of 2-(pentafluoropropionylamino)phenol (2.55 g, 10 mmol) and diphosphorus pentaoxide (2.84 g, 20 mmol) in a distilling flask was heated gently to 220 °C. An oily product having a boiling point of 166—167 °C was distilled out, and an additional amount of the product was obtained by vacuum distillation of the residue. Almost pure 2-(pentafluoroethyl)benzoxazole (2.00 g, 84%) was thus obtained.

Following a similar procedure, 5-methyl and 5-chloro derivatives of **2** were obtained from 2-(pentafluoropropionylamino)-4-methyl- and -4-chlorophenols, respectively (Table 1).

3-(Trifluoromethyl)-2H-1,4-benzoxazin-2-one (3). Into a pressure vessel containing 2-aminophenol (1.09 g, 10 mmol) and dioxane (20 ml), liquefied HFPO (1.91 g, 11.5 mmol) was introduced as described above. After 3 h of stirring at room temperature, the reaction mixture was thrown into water, and the precipitated product was collected by filtration. An additional amount of the product was obtained from the filtrate by extraction with diethyl ether. Crystallization of the combined material from hexane gave a crude product (1.42 g, 66%), which was purified by recrystallization, mp 77—78 °C.

From 4-methyl- and 4-chloro-2-aminophenols, 6-substituted derivatives of **3** were obtained by the same procedure (Table 1).

3-(Trifluoromethyl)-2(1H)-quinoxalinone (4). A mixture of *o*-phenylenediamine (1.08 g, 10 mmol) and sodium hydrogen carbonate (2.54 g, 30 mmol) in diethyl ether (30 ml) was allowed to react with HFPO (2.09 g, 12.6 mmol) for 3 h at room temperature. A solid product was separated by filtration, washed with water, and dried to give crude benzodiazinone (1.27 g), mp 230—232 °C. Concentration of the parent solution yielded an additional product (0.53 g), mp 232—233.5 °C. The combined material (1.80 g, 84%) was recrystallized from benzene to give pure **4**, mp 233—234.5 °C.

2-Fluoro-2-(trifluoromethyl)-2,3-dihydro-1,4-benzothiazin-3-one (5). 2-Aminophenol (2.50 g, 20 mmol) in *N,N*-dimethyl acetamide (20 ml) was allowed to react with HFPO (3.82 g, 2.3 mmol) for 3 h at room temperature. The reaction mixture was poured into water and extracted with diethyl ether. The extract was washed with water, dried over magnesium sulfate and concentrated. The residue was recrystallized from benzene, yielding crude crystals of **5** (1.29 g, 26%), mp 177—178 °C. Further crystallization gave pure material, mp 181.5—182.5 °C.

2-(Pentafluoropropionylamino)benzoic Acid (7). Anthranilic acid (2.74 g, 20 mmol) and triethylamine (2.02 g, 20 mmol) in acetonitrile (20 ml) were allowed to react with HFPO (3.03 g, 18.3 mmol) in the usual manner. After 15 min of stirring at room temperature, the reaction mixture was poured into water and the precipitate formed was separated by filtration. By washing the precipitate with dilute aqueous hydrochloric acid, a crude product (2.53 g) was obtained. An additional amount of the product (1.13 g) was obtained by extraction of acidified aqueous layer with diethyl ether. The combined material was recrystallized from benzene, providing **7** (3.62 g, 70%), mp 166—169 °C. Further crystallization gave a pure product, mp 168—169 °C.

*2-(Pentafluoroethyl)-4*H*-3,1-benzoxazin-4-one* (**6**). (*a*): Anthranilic acid (1.37 g, 10 mmol) and triethylamine (3.03 g, 30 mmol) in acetonitrile (20 ml) were allowed to react with HFPO (3.40 g, 20.5 mmol) for 30 min at room temperature. The reaction mixture was worked up as usual. The residue from an ether extract was treated with pentane, and the insoluble material was removed by filtration. Evaporation of the solvent yielded a crude product (2.37 g, 89%), which was recrystallized to give pure material, mp 48—49 °C. (*b*): 2-(Pentafluoropropionylamino)benzoic acid (2.83 g, 10 mmol) and triethylamine (2.02 g, 20 mmol) in acetonitrile (15 ml) were allowed to react with HFPO (1.84 g, 11.1 mmol) as usual. The reaction mixture was worked up to give crude 2-(pentafluoroethyl)-4*H*-3,1-benzoxazin-4-one (2.45 g, 92%), mp 46—48 °C.

References

1) See, for example, R. Filler, "Adv. in Fluorine Chemistry," Vol. 6 (1970), p. 1; R. Filler, *Chemtech.*, **4**, 752 (1974).
2) Y. Kobayashi and A. Kumadaki, *Yuki Gosei Kagaku Kyokai Shi*, **29**, 126 (1971).
3) Y. Kobayashi, A. Kumadaki, and A. Osawa, *Yuki Gosei Kagaku Kyokai Shi*, **31**, 477 (1973).
4) D. Sianesi, A. Rasetti, and F. Tarli, *J. Org. Chem.*, **31**, 2312 (1966).
5) A. Pasetti, F. Tarli, and D. Sianesi, *Gazz. Chim. Ital.*, **98**, 277, 290 (1968).
6) I. L. Knunyants, V. V. Shokina, and I. V. Galakhov, *Khim. Geterotsikl. Soedin.*, **1966**, 873.
7) Du Pont, Brit. Patent, 1019788 (1966).
8) N. Ishikawa and S. Sasaki, *Nippon Kagaku Kaishi*, **1976**, 1954.
9) N. Ishikawa and S. Sasaki, *Chem. Lett.*, **1976**, 1407.
10) T. Tanabe, M. Komiya, and N. Ishikawa, The 3rd Symposium on Fluorine Chemistry, Japan, Oct. 18, 1975.

The Absolute Configuration of Sepiapterin

Sadao MATSUURA, Takashi SUGIMOTO, and Motoo TSUSUE*

Department of Chemistry, College of General Education, Nagoya University, Chikusa-ku, Nagoya 464
**Biological Laboratory, Kitasato University, Sagamihara City 228*

(Received March 31, 1977)

The absolute configuration of sepiapterin was determined to be 2-amino-7,8-dihydro-6-(*S*)-lactoyl-4(3*H*)-pteridinone from an analysis of the L-lactic acid produced from sepiapterin by oxidation cleavage in a sodium borate solution.

Sepiapterin, the yellow pigment contained in the eye of *Drosophila melanogaster*, was first isolated in 1954 by Forrest and Mitchel[1] and later by Viscontini and Möhlman[2] from a *sepia* mutant of the insect. Structural elucidation by Nawa[3] revealed the pigment to be 2-amino-7,8-dihydro-6-lactoyl-4(3*H*)-pteridinone (I). Sepiapterin possesses a chiral carbon at the 2-position of the side chain and has been found to be optically active,[2,4] as expected. Although no optically-active sepiapterin has been synthesized (with the exception of the recent work of Pfleiderer, see below), its racemate was produced by an unusual method starting from 2-amino-7,8-dihydro-4(3*H*)-pteridinone and 3-hydroxy-2-oxobutanoic acid.[5] It has been found that, of the

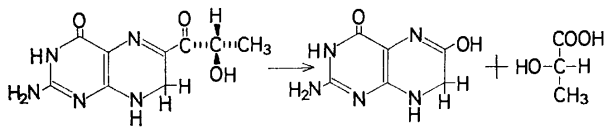

I

racemic sepiapterin isomers, only the enantiomer with the same configuration as naturally occurring sepiapterin is reduced by sepiapterin reductase.[5] However, from these results, it was not possible to reach a final determination of the configuration. Recently, Pfleiderer reported that the oxidation of 5,6,7,8-tetrahydrobiopterin yielded sepiapterin, which was found to be identical with natural sepiapterin in every respect, and thus, the configuration of the chiral carbon of sepiapterin was determined to be the (*S*)-configuration, the same as for biopterin.[7]

In this paper, an alternative approach for determining the absolute structure of sepiaterin is reported, which involves cleavage of the lactoyl group to lactic acid. Sepiapterin is known to undergo oxidative degradation to give lactic acid and 7,8-dihydroxanthopterin in a 4% sodium borate solution under aerobic conditions.[3] Since the 2-position of the side chain is not involved in the degradation reaction, its configuration is maintained throughout the reaction. Thus, it is possible to determine the absolute configuration of sepiapterin by examining the configuration of the lactic acid produced.

First, the oxidative degradation reaction was reinvestigated under a variety of conditions. It was found that sepiapterin remained practically unchanged in a phosphate buffer at pH 10.0. However, it was converted to 7,8-dihydroxanthopterin fairly slowly in a 4% sodium borate solution, as has been reported.[3] This reaction was found to be markedly enhanced by the addition

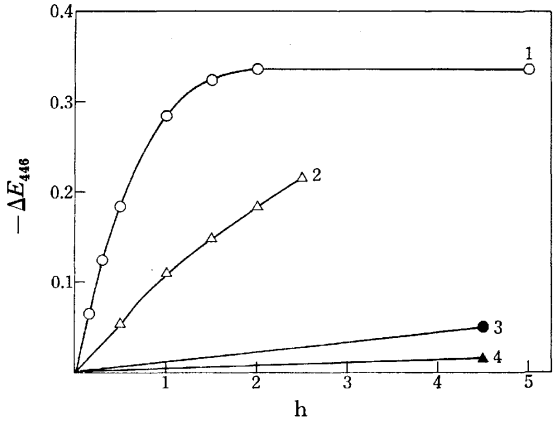

Fig. 1. Oxidative degradation of sepiapterin at 25 °C under aerobic conditions in the dark place. The initial concentration of sepiapterin was 50 μM and the reaction was monitored by reading the absorbance at 446 nm.
1: In 4% sodium borate containing cupric sulfate (25 μM).
2: In 4% sodium borate containing sodium hydroxide (0.1 M).
3: In 4% sodium borate.
4: In a 0.05M phosphate buffer at pH 10.0.

of sodium hydroxide or more effectively by a trace amount of copper(II) sulfate. This reaction was conveniently monitored spectroscopically (see Fig. 1).

Both L- and D-lactic acids can be assayed using an enzymatic method with L- and D-lactic acid dehydrogenases (LDH and D-LDH), respectively.[8] Therefore, the experimental conditions were examined using the enzymatic method in order to determine the lactic acid produced during the degradation reaction. This method employs NAD (nicotinamide-adenine dinucleotide) as a hydrogen acceptor; the amount of lactic acid can be calculated from the increment of the absorbance at 340 nm (ΔE_{340}). It was observed that the LDH activities were hindered by borate ions present in the solution (see Fig. 2), probably because the cofactor NAD is masked by borate ions due to the formation of a complex at the ribosyl moiety. However, the hindrance effects disappear upon the addition of an excess amount of D-ribose to the solution prior to the addition of NAD and the enzyme (Fig. 2).

Using the present method, a 1.03 ± 0.01 molar amount of L-lactic acid and no D-lactic acid were detected from the degradation solution of sepiapterin.

From these data, it is evident that the configuration at the chiral 2-position of the side chain of sepiapterin is

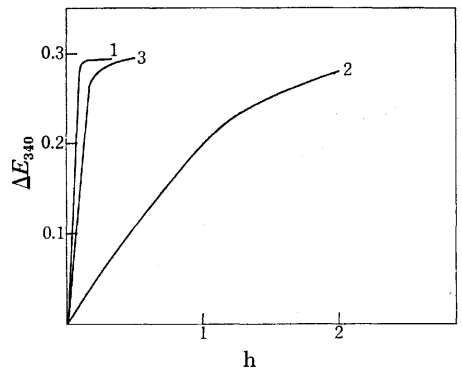

Fig. 2. Effects from borate ions and D-ribose on the dehydrogenation of L-lactic acid by a LDH–NAD system. The reaction was carried out at 25 °C in an assay solution composed of a glycine–hydrazine buffer (800 μl), 50 mM NAD (50 μl), 1 mM DL-lactic acid (100 μl), LDH (5 mg/ml; 10 μl), and distilled water (50 μl) or 4% sodium borate (50 μl).
1: In the absence of sodium borate and D-ribose.
2: In the presence of sodium borate (4%; 50 μl).
3: In the presence of sodium borate (4%; 50 μl) and D-ribose (10 mg).

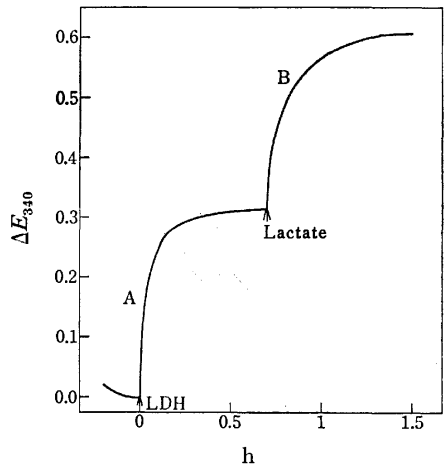

Fig. 3. Determination of L-lactic acid by a LDH–NAD system. First, the acid contained in 50 μl of the oxidative degradation solution (equivalent to 50 μmol of sepiapterin) was dehydrogenated by the system (curve A). When the reaction was complete (40 min), 50 μmole of lithium L-lactate was added (curve B) (for details, see experimental).

the (*S*)- or L-configuration as shown in the formula (I). The present conclusion is consistent with that of Pfleiderer.[7]

Experimental

Sepiapterin was obtained from *D. melanogaster sepia* by a method previously described.[4] NAD, LDH (EC.1.1.1.27; from rabbit muscle; 5 mg/ml, 550 U/mg), and D-LDH (EC. 1.1.1.28; from *Lactobacillus leichmanni*; 1 mg/ml, 300 U/mg) were purchased from Boehringer Mannheim.

Oxidation Degradation of Sepiapterin. A solution of sepiapterin (0.290 mg) in 4% sodium borate (1.22 ml; the concentration of sepiapterin was 1.00 mM) was stirred in air in the dark at 25 °C for 48 h. The sepiapterin degradated to 7,8-dihydroxanthopterin which was further oxidized to xanthopterin by air during the reaction. After completion of the reaction, the solution was adjusted to exactly 1.22 ml with water and used directly for the analysis of lactic acid.

Determination of L-Lactic Acid. The assay solution was composed of a glycine–hydrazine buffer (100 ml contains 7.5 g of glycine, 5.2 g of hydrazine sulfate, 0.2 g of EDTA $Na_2H_2 \cdot 2H_2O$, 51 ml of 2M-NaOH, and water to make the solution 100 ml; 840 μl), D-ribose (10%; 100 μl), NAD (50 mM; 50 μl), and 50 μl of the above reaction solution (equivalent to 50.0 μmol of sepiapterin). The assay solution was placed in both the sample and reference quartz cells which were maintained at 25 °C by a thermostatically-controlled cell holder. Then, to the sample cell was added 10 μl of LDH (5 mg/ml, 550 U/mg), and the increment of the absorbance at 340 nm (ΔE_{340}) was recorded. Within 40 min, the reaction was complete and the ΔE_{340} was found to be 0.305 (ΔE^1). Then, 50 μl of a lithium L-lactate solution (1.00 mM; equivalent to 50.0 μmol) was added to the sample cell. In about the same time as above, an additional ΔE_{340} of 0.296 (ΔE^2) was observed (Fig. 3). The amount of L-lactic acid contained in 50 μl of the oxidative degradation solution (equivalent to 50.0 μmol of sepiapterin) was determined using the following calculation:

$$\frac{0.305(\Delta E^1)}{0.296(\Delta E^2)} \times 50.0\ \mu\text{mol} = 51.5\ \mu\text{mol}.$$

By repeating the same procedures several times, it was concluded that 1.03 ± 0.01 mol of L-lactic acid was produced from sepiapterin. When D-LDH was used in place of LDH in the above procedures, no appreciable increase in absorbance at 340 nm was observed.

References

1) H. S. Forrest and H. K. Mitchel, *J. Am. Chem. Soc.*, **76**, 5656 (1954).
2) M. Viscontini and E. Möhlmann, *Helv. Chim. Acta*, **42**, 836 (1959).
3) S. Nawa, *Bull. Chem. Soc. Jpn.*, **33**, 1555 (1960).
4) M. Tsusue and M. Akino, *Zool. Mag.*, **74**, 91 (1965).
5) K. Sugiura and M. Goto, *Nippon Kagaku Kaishi*, **1972**, 206.
6) M. Matsubara, K. Katoh, M. Akino, and S. Kaufman, *Biochem. Biophys., Acta*, **122**, 202 (1966).
7) W. Pfleiderer, "Chemistry and Biology of Pteridines," ed by W. Pfleiderer, Walter de Gruyter, Berlin (1975), p. 941.
8) H. J. Hohorst, "Methods of Enzymatic Analysis," ed by H. U. Bergmeyer, Academic Press, New York (1963), p. 266.

The Intramolecular Hydrogen Abstraction Reaction in the Photolysis of Aminated 1,4-Naphthoquinones

Kazuhiro MARUYAMA, Tadashi KOZUKA, and Tetsuo OTSUKI

Department of Chemistry, Faculty of Science, Kyoto University, Kyoto 606

(Received February 14, 1977)

Photolysis of aminated 1,4-naphthoquinones **1a**—**c** in liquid phase was investigated. After photolysis and successive autoxidation, 2-(3-pyrrolin-1-yl)-1,4-naphthoquinone **1a** gave 2-(1-pyrrolyl)-1,4-naphthoquinone **3** quantitatively. However, in the reaction, 2-(1-pyrrolydinyl)-1,4-naphthoquinone **1b** and 2-(2-methoxycarbonyl-1-pyrrolidinyl)-1,4-naphthoquinone **1c** afforded the corresponding hetero-ring opened products; 2-(4-oxobutylamino)-1,4-naphthoquinone **5** and 2-(4-methoxycarbonyl-4-oxobutylamino)-1,4-naphthoquinone **8** in good yields. Possible mechanisms for the formation of **3**, **5**, and **8** are presented.

The photochemistry of aminoquinones having a β-aminoenone grouping (–N–C=C–C=O) in the molecule is of interest from the synthetic viewpoint of antibiotics such as mytomycin and streptrigrin, but only a few investigations have been made.[1-3]

We describe herewith the synthesis and photochemistry of quinones **1**.

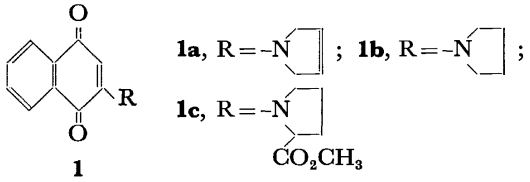

Results and Discussion

Compounds **1a**—**c** were prepared from the corresponding amines and 1,4-naphthoquinone by standing overnight in methanol. After purification by column chromatography and recrystallization, the spectral data of all the aminated 1,4-naphthoquinones were found to be consistent with the assigned structures.

Photolysis of 2-Aminated 1,4-Naphthoquinones ***1a—c.*** Irradiation of a solution of the quinone **1a** (8.88×10^{-3} M) in benzene for 1 h and bubbling the resulting solution with air for several minutes gave quinone **3** quantitatively. The ^{1}H-NMR spectrum ($CDCl_3$) of **3** showed two characteristic triplets, centered at 7.31(2H) and 6.42(2H) ppm. The quinone vinyl singlet, 6.84(1H) ppm, shifted to the lower field, suggesting the presence of 1-substituted pyrrole ring. Compound **3** was identified by comparison with the authentic sample prepared by dehydrogenation of **1a** with Pd–C.

The photochemical process was followed by measuring the UV spectrum of degassed benzene solution of **1a** during the course of irradiation. As the reaction proceeds the absorbance of the peak at 276 and 460 nm diminishes and the peak at 318 and 332 nm increases, exhibiting isosbestic points at 302 and 342 nm (Fig. 1). On the other hand, we examined the same reaction by ^{1}H-NMR spectrometry irradiating of a degassed C_6D_6 solution of **1a**. The examination revealed that the reaction proceeded quite smoothly. As the methylene and olefinic protons of 3-pyrroline ring diminish, two characteristic triplets due to the pyrrole ring protons and phenolic hydroxy protons (2H) grow. This indicates that an unstable compound **2** is produced in the reaction. Unstable **2** was trapped as its diacetate **4** by treatment with acetic anhydride in pyridine under degassed conditions. It was confirmed that the change in concentration of reactant **1a** (<0.2 M) gave no essential change on the course of reaction. Thus, the reaction of **1a** to **2** can be explained by a mechanism involving initial intramolecular hydrogen abstraction by carbonyl, followed by subsequent free rotation of C–N bond and secondary intramolecular hydrogen transfer as shown by Eq. 1.

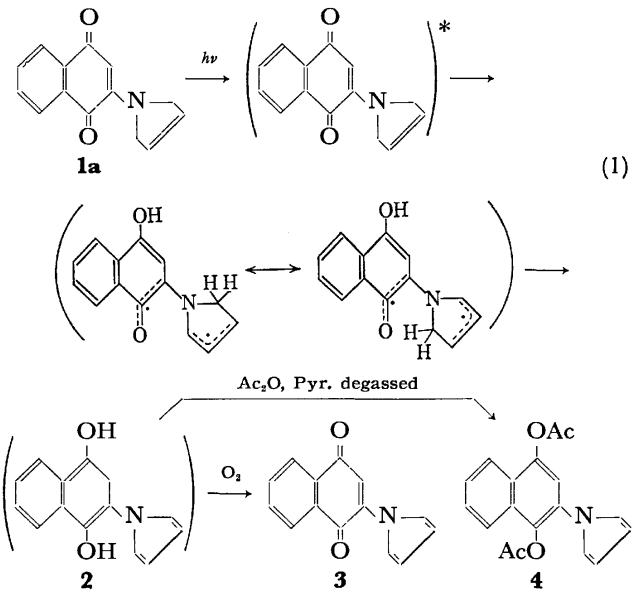

(1)

Aminated quinone **1b** dissolved in benzene (2.20×10^{-3} M, for 1.5 h) is also highly photosensitive. After the usual work-up **1c** gave **5** (78%), together with small amount of **3** (2%) and **6** (3%). The structure of **5** was compatible with its spectral data; ν_{NH}: 3340, ν_{CO}: 1720 cm^{-1}; ^{1}H-NMR: 6.00 (br s, 1H, NH), 9.77 (s, 1H, CHO) ppm. Treatment of **5** with methanolic hydrogen chloride yielded acetal **7**. Structure **3** was confirmed by the spectral data and comparison with the authentic sample. The structure **6** was assigned on the basis of the spectral data, but compound **6** is unstable against light in solution. When the solution, after UV irradiation of **6** in chloroform, was left to stand overnight under contact with air, the color of solutions turned light yellow from purple red, the absorption spectrum of **6**

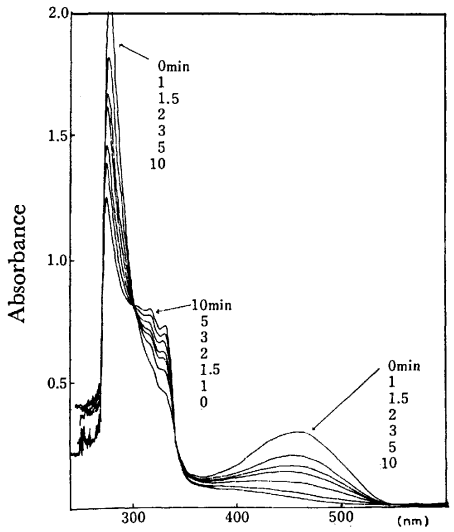

Fig. 1.

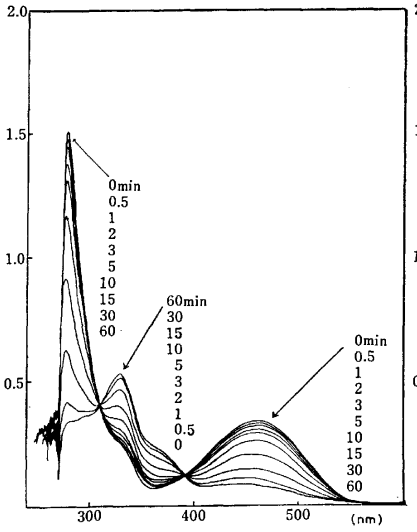

Fig. 2.

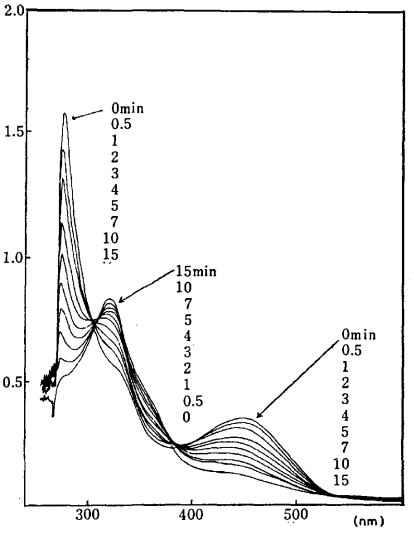

Fig. 3.

UV spectra of **1a**—**c**(benzene), before irradiation and during irradiation. A strictly degassed solution of **1a**—**c** was irradiated in a UV cell (1 cm×1 cm) by high pressure Hg arc lamp (300 W) through VY-42 glass filters (1 cm×3). In this experiment a glass filter was employed to eliminate the light of wavelength shorter than 400 nm.

(λ_{max}: 520 nm) disappearing, and new peaks corresponding to **3** and **5** appearing at 256, 270, and 441 nm. Presumably compound **6** changes to **3** and **5** by photolysis followed by air oxidation.

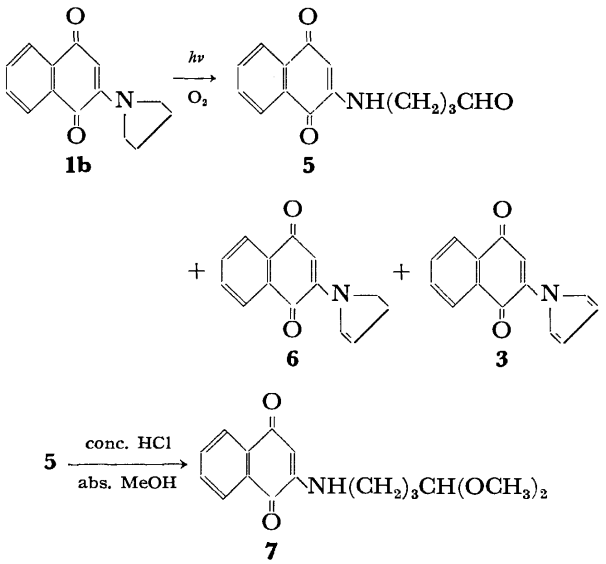

Photolysis of **1b** in degassed benzene was followed by UV spectroscopy. The orange yellow solution finally became colorless. Two isosbestic points at 309 and 392 nm appeared, indicating that the reaction is simple and clean (Fig. 2). The first order kinetic plot of the reaction showed a straight line (Fig. 4). When the reaction vessel was opened and aerated with bubbling of air, the solution turned yellow. The UV spectrum of the resulting solution was essentially the same as that of the benzene solution of **5**, λ_{max} (benzene): 278 and 440 nm (log ε: 4.24 and 3.52). Apparent maximum absorption of UV spectrum of the final solution is at

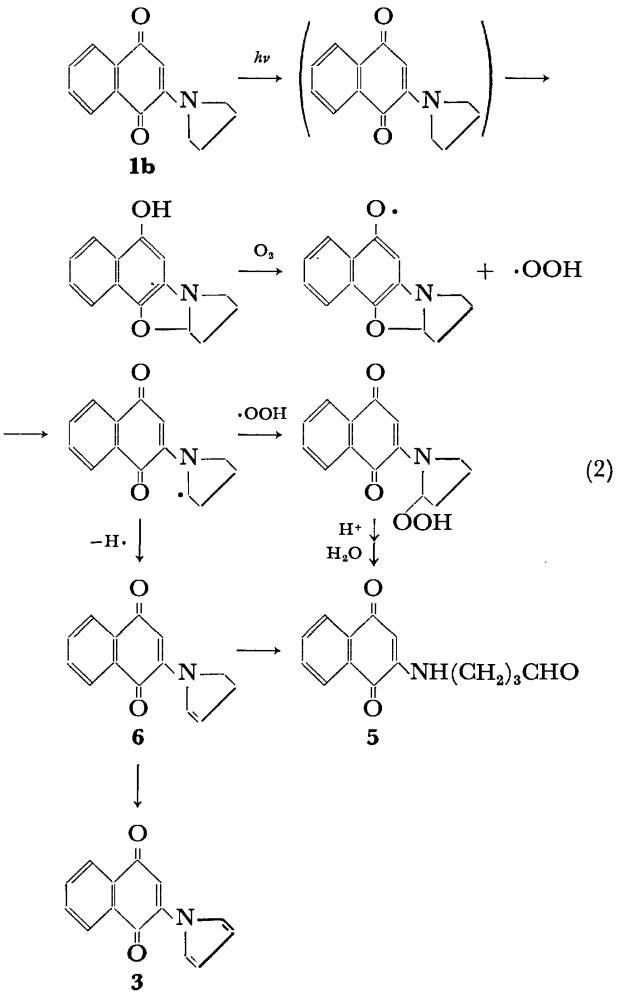

(2)

λ_{max} (benzene): 330 nm (log ε: *ca.* 3.8). From the results the photolysis of **1b** and successive air-oxidation

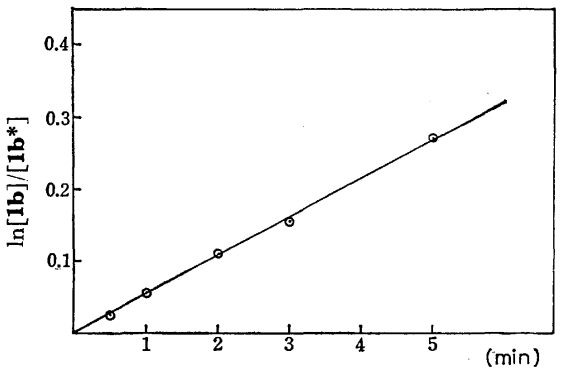

Fig. 4. First order kinetic plot in the photolysis of **1b** (solvent: benzene).
[**1b**]; absorbance(at 460 nm) before irradiation of **1b**.
[**1b***]; absorbance(at 460 nm) during irradiation of **1b**.

can be formulated as shown in Eq. 2. However, the detailed mechanism for the hetero-ring opening still remains unclarified.

Compounds **8** and **9** were obtained in 30 and 6%, respectively, after irradiation of **1c** (2.50×10^{-3} M) in benzene for 3 h and subsequent aeration. Structures **8** and **9** were assigned on the basis of their spectral data. Compound **8** was reduced to **10** by treatment with sodium borohydride in methanol.

Photolysis of **1c** in deaerated benzene was also followed by UV spectroscopy. No isosbestic point was observed during the course of reaction, suggesting that the reaction is complex (Fig. 3). This is in line with the lower yield of the identified products.

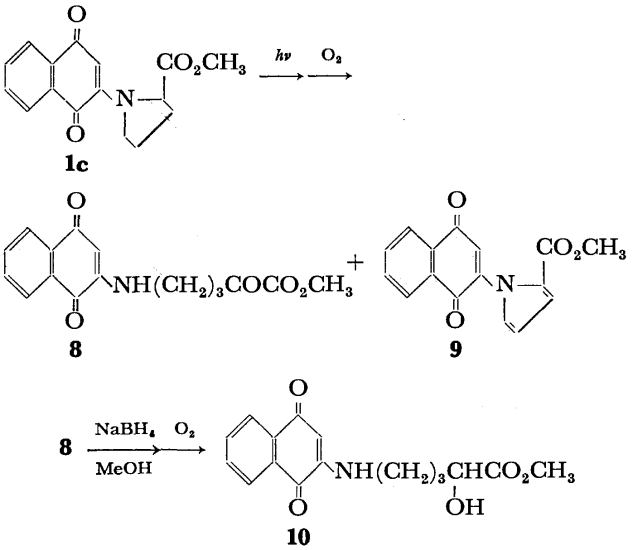

Experimental

Photolysis of 1a. A benzene solution of 2-(2-pyrrolin-1-yl)-1,4-naphthoquinone **1a**[4] (8.88×10^{-3} M) was irradiated without degassing with a high pressure Hg arc lamp through water layer. Aeration of the solution after 1 h gave 2-(1-pyrrolyl)-1,4-naphthoquinone **3** quantitatively; mp 164.5—164.7 °C. IR (KBr); 1670 cm^{-1}. Mass: *m/e*=223 (M^+). ^{1}H-NMR ($CDCl_3$); 6.43 (t, 2H), 6.84 (s, 1H), 7.31 (t, 2H), 7.71, 8.08 (m, 4H) ppm. UV max ($CHCl_3$); 256, 305, 395 nm (log ε: 4.31, 3.95, 3.54). Found: C, 75.03; H, 3.87; N, 6.09%. Calcd for $C_{14}H_9O_2N$: C, 75.32; H, 4.06; N, 6.28%.

During the course of irradiation the ^{1}H-NMR spectra of **1a** in degassed C_6D_6 indicated the formation of single product; *i.e.*, highly oxygen-sensitive compound **2**, which was identified by the subsequent acetylation with acetic anhydride–pyridine under degassed conditions as diacetate **4** (86%); mp 138—139 °C. IR (KBr); 1755 cm^{-1}. Mass: *m/e*=309 (M^+). ^{1}H-NMR ($CDCl_3$): 2.30 (s, 3H), 2.46 (s, 3H), 6.32 (t, 2H), 6.95 (t, 2H), 7.37, 7.57, 7.91 (m, 5H) ppm. Found: C, 69.61; H, 4.94; N, 4.68%. Calcd for $C_{18}H_{15}O_4N$: C, 69.89; H, 4.89; N, 4.53%.

Photolysis of 1b. By irradiating (1.5 h) of dry benzene solution of 2-(1-pyrrolidinyl)-1,4-naphthoquinone **1b**[5] (2.20×10^{-3} M) with a high pressure Hg arc lamp through a filter solution of 5,7-dimethyl-2*H*-3,6-dihydro-1,4-diazepine perchlorate, three products **5**, **6**, and **3** were isolated: 2-(4-oxobutylamino)-1,4-naphthoquinone **5** (78%): mp 146—147 °C. IR (KBr); 3340, 2825, 2725, 1680 cm^{-1}. Mass: *m/e*=243 (M^+). ^{1}H-NMR ($CDCl_3$); 2.04 (m, 2H), 2.63 (t, 2H), 3.23 (m, 2H), 5.69 (s, 1H), 6.00 (br s, 1H), 7.64, 8.02 (m, 4H), 9.77 (s, 1H) ppm. UV max ($CHCl_3$); 243, 270, 337, 441 nm (log ε: 4.07, 4.33, 3.50, 3.51). Found: C, 68.60; H, 5.33; N, 5.30%. Calcd for $C_{14}H_{13}O_3N$: C, 69.12; H, 5.39; N, 5.76%. 2-(2-Pyrrolin-1-yl)-1,4-naphthoquinone **6** (3%); mp 141—143 °C. IR (KBr); 1660, 1613, 1586, 1550 cm^{-1}. Mass: *m/e*=225 (M^+). ^{1}H-NMR ($CDCl_3$); 2.72 (tdd, 2H), 3.79 (t, 2H), 5.46 (m, 1H), 5.73 (s, 1H), 7.88 (m, 1H), 7.68, 8.01 (m, 4H) ppm. UV max ($CHCl_3$); 243, 250, 273, 520 nm (log ε: 4.08, 4.09, 4.29, 3.67). 2-(1-Pyrrolyl)-1,4-naphthoquinone **3** (2%): *vide supra.*

Acetalization of **5** gave 2-(4,4-dimethoxybutylamino)-1,4-naphthoquinone **7** (75%): mp 91—93 °C. IR (KBr); 3330, 1685 cm^{-1}. ^{1}H-NMR ($CDCl_3$); 1.74 (m, 4H), 3.22 (m, 2H), 3.35 (s, 6H), 4.38 (t, 1H), 5.71 (s, 1H), 6.06 (br s, 1H), 7.66, 8.05 (m, 4H) ppm. UV max ($CHCl_3$); 242, 271, 330, 440 nm (log ε 3.79, 4.06, 3.23, 3.20).

Photolysis of 1c. A chloroform solution of 2-(2-methoxycarbonyl-1-pyrrolydinyl)-1,4-naphthoquinone **1c**[6] (2.50×10^{-3} M) was irradiated with a high pressure Hg arc lamp through a filter solution of copper(II) sulfate. After irradiation for 3 h, two products, **8** and **9**, were isolated: 2-(4-Methoxy carbonyl-4-oxobutylamino)-1,4-naphthoquinone **8** (30%) mp 181—183 °C. IR (KBr); 3330, 1730, 1676 cm^{-1}. Mass: *m/e*=301 (M^+). ^{1}H-NMR ($CDCl_3$); 2.01 (m, 2H), 3.04 (t, 2H), 3.30 (q, 2H), 3.92 (s, 3H), 5.78 (s, 1H), 6.00 (br s, 1H), 7.07, 8.08 (m, 4H) ppm. UV max ($CHCl_3$); 242, 270, 331, 444 nm (log ε: 4.11, 4.35, 3.53, 3.49). Found: C, 63.91; H, 4.87; N, 4.69%. Calcd for $C_{16}H_{15}O_2N$: C, 63.78; H, 5.02; N, 4.65%. 2-(2-Methoxycarbonyl-1-pyrrolyl)-1,4-naphthoquinone **9** (6%): mp 116—120 °C. IR (KBr); 1708, 1687 cm^{-1}. Mass: *m/e*=281 (M^+). ^{1}H-NMR ($CDCl_3$); 3.74 (s, 3H), 6.40 (m, 1H), 6.90 (m, 1H), 7.12 (m, 1H), 6.86 (s, 1H), 7.79, 8.14 (m, 4H) ppm. UV max ($CHCl_3$); 248, 254, 298 (log ε: 4.20, 4.20, 3.63).

The reduction of **8** with sodium borohydride gave 2-(4-hydroxy-4-methoxycarbonylbutylamino)-1,4-naphthoquinone **10** (74%): mp 126—127 °C. IR (KBr); 3515, 3345, 1735, 1725, 1680 cm^{-1}. Mass: *m/e*=303 (M^+). ^{1}H-NMR ($CDCl_3$); 1.86 (m, 4H), 3.26 (q, 2H), 3.81 (s, 3H), 4.24 (br s, 1H), 5.72 (s, 1H), 6.06 (br s, 1H), 3.05 (br s, 1H), 7.65, 8.04 (m 4H) ppm. UV max ($CHCl_3$); 242, 271, 330, 445 (log ε: 4.19, 4.42, 3.69, 3.63).

References

1) E. P. Fokin and E. P. Prudchenko, *Izv. Sib. Otd. Akad.*

Nauk. SSSR, Ser. Khim. Nauk, **1966**, (2), 98; *Chem. Abstr.*, **66**, 37809 (1967). E. P. Fokin and A. M. Detsina, *ibid.*, **1969**, (3), 95; *Chem. Abstr.*, **72**, 12500n (1970).

2) D. W. Cameron and R. G. F. Giles, *J. Chem. Soc., C*, **1968**, 1461.

3) R. G. F. Giles, *Tetrahedron Lett.*, **1972**, 2253.

4) Mp 180.5—181.5 °C.

5) Mp 164—165 °C.

6) Mp 149.5—150.0 °C.

Intramolecular Catalytic Substitution Reaction of *N*-(ω-Bromoalkyl)-pyridinium Bromide with Potassium Cyanide

Masahide YAMADA, Tohru SAKAKIBARA, Tetsuyoshi TAKAMOTO, and Rokuro SUDOH

Department of Chemistry, Faculty of Science, Tokyo Institute of Technology, Ookayama, Meguro-ku, Tokyo 152

(Received December 24, 1976)

It was found by means of NMR spectrometric and potentiometric titration technique that the intramolecular catalytic substitution of *N*-(ω-bromoalkyl)pyridinium bromide with KCN proceeds in the range $n=2$—6 of methylene chain on the pyridinium salt and the intermolecular substitution in $n=7$ and 9, and the addition of cyanide anion to the pyridine ring takes place only for $n=1$.

Our recent interest has been focused on the reaction selectivity resulting from the conversion of a bimolecular into an intramolecular reaction in view of entropy point. In the enzymatic reaction involving a typical intramolecular catalytic process, the formation of an adsorptive complex of enzymes with an appropriate substrate results in high reaction selectivity through a favorable orientation of reaction site on the catalytic center. Thus a substrate severely constrained in the complex should be a good model of the activated key-intermediates for our study.

The counter-anion of quaternary ammonium and phosphonium salts has been shown to behave as a nucleophile in phase-transfer catalyzed reaction.[1] When a reaction site and a nucleophile are involved in a quaternary salt at the same time, an intramolecular substitution might take place smoothly at the reaction site with significant interactions to the quaternary center.[2] In this paper we wish to report the reaction of pyridinium salts having a general formula $Py^+(CH_2)_n$-$CH_2Br \cdot Br^-$ ($n=1$—9) with potassium cyanide in aqueous solution.

The key-intermediary pyridinium salts (**1a**—**1h**) were prepared by the direct quaternization of pyridine with a series of the corresponding α,ω-dibromoalkanes. Successful induction of reactions of these salts with potassium cyanide, sodium acetate, and sodium azide was proved by IR and/or NMR spectroscopy. Since NMR spectroscopic studies have shown that methylene protons bearing a cyano group can be clearly recognized at higher field, potassium cyanide was used as a nucleophile for examining details of the substitution. The reaction of pyridinium salts (0.5 mol/l) with potassium cyanide (0.55 mol/l) in deuterium oxide at 64.5 °C was monitored by NMR spectroscopy with regard to the changing intensities at δ 3.2—3.4 (CH_2Br) and 2.6—2.8 (CH_2CN). Since the series of the substitution product, *N*-(ω-cyanoalkyl)pyridinium bromide, is too hygroscopic for isolation and characterization, one of them (**3b**) was immediately treated with sodium borohydride[3] to give *N*-(3-cyanopropyl)-1,2,3,6-tetrahydropyridine.

In order to let an intramolecular reaction take place, a very dilute solution is used. With respect to the amount of cyanide anion left during the course of reactions, potentiometric titration was employed for tracing in the 0.02 mol/l concentration scale since it has much sharper responses than in NMR spectrometry. As shown in Fig. 1, the rate of the substitution reaction decreases along with the sequence **1e**≈**1f**≥**1h**≈**1g**≥**1d**≈**1c**≈**1b** as in the NMR study. In the case of **1a** ($n=1$), however, addition of cyanide anion to the pyridine ring took place, since the unstable product[4] obtained in chloroform–water system only was no longer a quaternary salt as confirmed on the basis of the absorption band of cyano group and C–C double bond in the IR spectrum. Such a difference between **1a** and **1b**—**1h** can be explained as follows. It is very hard for a four-membered cyclic intermediate to form on **1a** for the intramolecular catalytic substitution; in addition quaternary pyridinium salts are liable to undergo nucleophilic additions.[4] Thus the intramolecular catalytic substitution proceeds primarily if the cyclic intermediate is available, whereas addition takes place if not. Thus the case of $n=5$ or 6 (**1e** or **1f**)

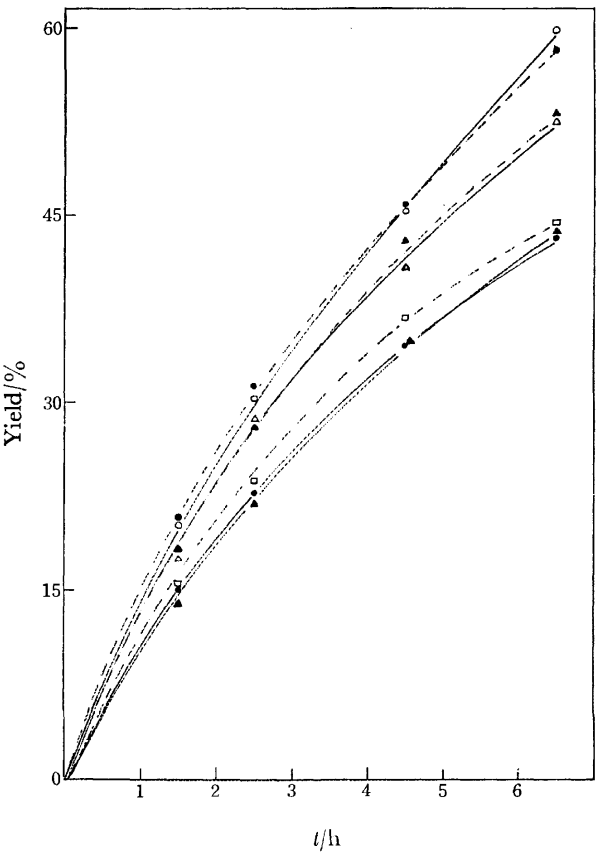

Fig. 1. Relationship between the yield and reaction time; **1** (0.020 mol/l) and potassium cyanide (0.021 mol/l) —●— **1b**; —▲— **1c**; ---□--- **1d**; —○— **1e**; ---●--- **1f**; —△— **1g**; ---▲--- **1h**.

showed the highest reaction rate through the maximum interaction between the catalytic center and the reaction site (Fig. 1). However, no first order reaction rate constant could be obtained from the results, since an ion-exchange equilibrium might take place between cyanide and bromide anions giving rise to the dependence of the reaction rate on the concentration of *N*-(ω-bromoalkyl)pyridinium cyanide (**2**). The reaction rate of **1b** and **1e**, in fact, were accelerated by addition of potassium cyanide and fairly retarded with potassium bromide as expected from the above assumption (Table 1).

Table 1. Effect of the added salts to the yield[a] of *N*-(ω-cyanoalkyl)pyridinium salts

Concn. of salts mol/l	Starting material[b]	Reaction time (h) 0.5	1.5	2.5	3.5	4.5
KCN 0.021	**1b**	5.8	15.2	23.2	—	34.9
	1e	7.8	20.3	30.2	—	45.4
	1h	6.3	18.6	28.0	—	43.3
KCN 0.091	**1b**	17.0	43.0	60.7	69.4	78.6
	1e	29.1	55.1	70.1	78.2	86.6
	1h	20.7	48.6	67.1	74.2	79.1
KCN 0.181	**1b**	23.1	53.0	71.2	83.5	—
	1e	40.8	77.3	92.0	97.1	—
	1h	24.3	52.7	70.9	79.9	—
KCN 0.021 KBr 0.20	**1b**	4.1	11.0	—	—	—
	1e	4.8	15.0	—	—	—
	1h	6.0	18.7	—	—	—

a) Determined by the potentiometric titration. b) 0.020 mol/l was used in all cases.

Although there is no such effect of potassium bromide on **1h**, the reaction rate approached that of **1b** when potassium cyanide was added up to 0.19 mol/l. The reason for **1h** being more reactive than **1b** might be the term of the positive micellar effect[5] (cmc of **1h**: *ca.* 0.019 mol/l at 25 °C).[6]

The results show that the quaternary nitrogen atom plays a considerable catalytic role with favorable interactions to an appropriate reaction site even in aqueous solution. Such an idea might thus be applied to regio-specific substitutions in view of the intramolecular catalysts.

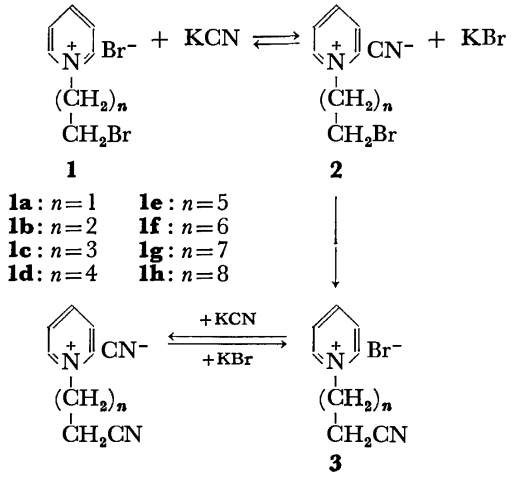

Experimental

Instruments. NMR and IR spectra were recorded with a Varian T-60 and Hitachi EPI-S2 spectrometers, respectively. The potentiometric titration was carried out with a Toa HM-5A potentiometer.

N-(ω-Bromoalkyl)pyridinium Bromide (1). After a mixture of pyridine (3.16 g, 0.05 mol) and α,ω-dibromoalkane (0.10 mol) had been refluxed in ethanol (50 ml) for 5 h, the solvent and excess α,ω-dibromoalkane were removed by means of evaporation, decantation, and extraction with ethyl acetate. The α,ω-bispyridinium salts was crystallized from 2-propanol (60 ml) (in the case of **1a**—**1e**) and from acetone (**1f**—**1h**) crystalline **1** deposited in an icebox after the solvent was concentrated to half. Recrystallization from ethanol (**1a**, **1b**, and **1c**) or 2-propanol (**1d** and **1e**) or acetone (**1f**, **1g**, and **1h**) gave pure salts. All these did not show clear melting points because of being too hygroscopic. Analytical data, **1a**; Found: C, 31.85; H, 3.58; N, 5.30%. Calcd for $C_7H_9NBr_2$: C,31.49; H, 3.40; N, 5.25%. **1b**; Found: C, 34.22; H, 3.58; N, 5.30%. Calcd for $C_8H_{11}NBr_2$: C, 34.19; H, 3.98; N, 4.99%. **1c**; Found: C, 36.96; H, 4.84; N, 5.01%. Calcd for $C_9H_{13}NBr_2$: C, 36.64; H, 4.44; N, 4.75%. **1d**; Found: C, 38.12; H, 4.93; N, 4.21%. Calcd for $C_{10}H_{15}NBr_2$: C, 38.86; H, 4.89; N, 4.53%. **1e**; Found: C, 41.14; H, 5.22; N, 4.23%. Calcd for $C_{11}H_{17}NBr_2$: C, 40.89; H, 5.30; N, 4.34%. **1f**; Found: C, 42.82; H, 5.13, N, 3.95%. Calcd for $C_{12}H_{19}NBr_2$: C, 42.75; H, 5.68; N, 4.16%. **1g**; Found: C, 44.76; H, 6.45; N, 4.10%. Calcd for $C_{13}H_{21}NBr_2$: C, 44.46; H, 6.03; N, 3.99%. **1h**; Found: C, 46.36; H, 6.41; N, 3.91%. Calcd for $C_{14}H_{23}NBr_2$: C, 46.05; H, 6.35; N, 3.84%.

Reduction of N-(3-Cyanopropyl)pyridinium Bromide (3c). A solution of *N*-(3-bromopropyl)pyridinium bromide (**1c**) (1.12 g, 4 mmol) and potassium cyanide (0.286 g, 4.4 mmol) in water (30 ml) was heated in a water bath for 6 h. After evaporation of water, the residue was dissolved in methanol (30 ml) and treated with sodium borohydride (1.52 g, 40 mmol) below 5 °C. After being stirred for 1 h, the reaction product obtained by evaporation was dissolved in water and then extracted with ether several times. The extracts were evaporated to give syrup which was chromatographed with silica gel (Wako C300) using a solvent system ethyl acetate–acetone 10: 1 (500 ml) and then 5: 1 (500 ml). The fractions eluted by the system 5: 1 were combined and distilled in a Ball Tube Oven at 150 °C/26 Torr. The compound was very unstable in the air. Found: C, 72.29; H, 9.34: N, 18.71%. Calcd for $C_9H_{14}N_2$: C, 71.95; H, 9.39; N, 18.65%. IR(KBr) 2250 (CN) and 1610 cm^{-1} (C=C); NMR ($CDCl_3$) δ 5.67 (m, 2H, $J_{CH=CH}$=1 Hz, CH=CH) and 2.99 (s, 2H, NCH_2–CH=).

Reaction of 1 with Potassium Cyanide. NMR Study: A deuterium oxide solution of **1** (1.0 mol/l) and a potassium cyanide solution (1.1 mol/l) were prepared and then 0.2 ml of each was mixed in NMR tube at 5 °C. The mixture was kept at 64.5±2 °C in a Kugelrohr Oven and the intensities at δ 3.2—3.4 (CH_2Br) and 2.6—2.8 (CH_2CN) were measured at every 0.5 h.

Potentiometric Titration: An aqueous solution of **1** (0.2 mol/l) and that of potassium cyanide (0.21 mol/l) were prepared, and 10 ml of each was mixed and made up to 100 ml with water in a measuring flask. The solution was kept at 64.5 ±0.5 °C in a water bath. Two 5 ml portions of the solution were taken at regular time intervals, cooled immediately in ice–methanol bath and then titrated with silver electrode.

References

1) C. M. Starks, *J. Am. Chem. Soc.*, **93**, 195 (1971).

2) E. L. Colichman, W. R. Vanderzanden, and S. K. Liv, *J. Am. Chem. Soc.*, **74**, 1953 (1952).
3) R. E. Lyle, E. F. Perlowski, H. J. Troscianiec, and G. G. Lyle, *J. Org. Chem.*, **20**, 1761 (1952).
4) R. H. Reuss, N. G. Smith, and L. J. Winters, *J. Org. Chem.*, **39**, 2027 (1974), and see refs. cited therein.
5) E. J. Fendler and J. H. Fendler, "Advances in Physical Chemistry," ed by V. Gold, Academic Press, Vol. 8, New York (1970), pp. 271—406.
6) Determined from the electromotive force value of **1h**; K. M. Kolthoff and W. F. Hohnson, *J. Phys. Chem.*, **52**, 22 (1948).

NOTES

BULLETIN OF THE CHEMICAL SOCIETY OF JAPAN, VOL. 50 (8), 2177—2178 (1977)

An ESR Study of Photo-Induced Electron Transfer Reaction between Zinc(II)-Tetraphenylporphyrin and *p*-Benzoquinone in Solutions

Masayuki SHIOZAWA, Haruhiko YAMAMOTO, and Yuzaburo FUJITA*

Faculty of Pharmaceutical Sciences, The University of Tokyo, Hongo, Bunkyo-ku, Tokyo 113

(Received November 24, 1976)

Synopsis. The titled reaction was studied, by means of the ESR technique at room temperature, as a model reaction of the primary process in the photosynthesis. Two kinds of radicals were observed in dichloromethane upon illumination with light of the porphyrin excitation; the zinc-tetraphenylporphyrin cation radical and the semiquinone neutral radical.

Since Tollin and Green[1] first observed the ESR signal of the semiqunone anion radical, Q^-, upon the illumination of ethanolic solutions containing chlorophyl (Chl) and *p*-benzoquinone (Q) at room temperature, both rise and decay processes of intermediates have been investigated in order to clarify the primary process of the photo-induced one-electron transfer from Chl to Q by using either ESR or the flash-photolysis technique. However, now there is a large discrepancy in the intermediates observed by two groups of workers using the former and latter techniques;[2] the latter group[3] has observed both Chl^+ and Q^- radicals, while the former group[4] has not yet succeeded in detecting Chl^+ at room temperature. Accordingly, the following proposals for the electron-transfer mechanism in the systems have been advocated:

1) Both Chl^+ and Q^- are in reality produced by the direct electron transfer from Chl to Q, but the lifetime of Chl^+ is shortened by a fast decay process with either ethanol[3] or an unknown material, X.[2]

2) Q^- and solvent radicals are formed by the electron transfer within a ternary complex among Chl, Q, and ethanol in which Chl acts as a photosensitizer.[4]

The identification of Chl^+ by flash photolysis is complicated by the overlap of the spectra of other species, such as Chl^T and Q^-; therefore, the unambiguous identification of Chl^+ by ESR at room temperature seems to be desirable. It is considered that the use of an appropriate solvent, in which the Chl^+ formed can exist with a longer lifetime, will lead to the easy detection of Chl^+ by ESR. Moreover, in this study zinc(II)-tetraphenylporphyrin, ZnTPP, was used as a model compound for chlorophyl, because the ESR spectrum of the $ZnTPP^+$ cation radical had been reported to reveal a well-defined hyperfine structure.[5]

ZnTPP and its π-cation radical, $ZnTPP^+$, were prepared by the method of Fajer *et al.*[5] *p*-Benzoquinone was purified by sublimation. The ethanol and dichloromethane used as solvents were purified by distillation. Unless otherwise specified, the concentrations of ZnTPP and Q were 10^{-4} and 10^{-1} M respectively. All the samples were thoroughly degassed by repeated freeze-degas-thaw cycles on a vacuum line prior to the measurements. The ESR spectra were recorded on a JEOL PE-1X spectrometer at room temperature. In most of the measurements, the sample in the cavity of ESR spectrometer was illuminated with light of wavelengths longer than 520 nm from a 650 W tungsten filament lamp, using a colored glass filter (Toshiba V-052).

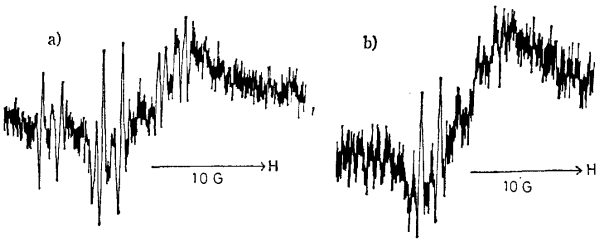

Fig. 1. ESR spectrum of the solution of ZnTPP and Q in dichloromethane upon illumination (>520 nm).
Modulation amplitude 0.63 G.
Microwave power: a) 4 mW, b) 20 mW.

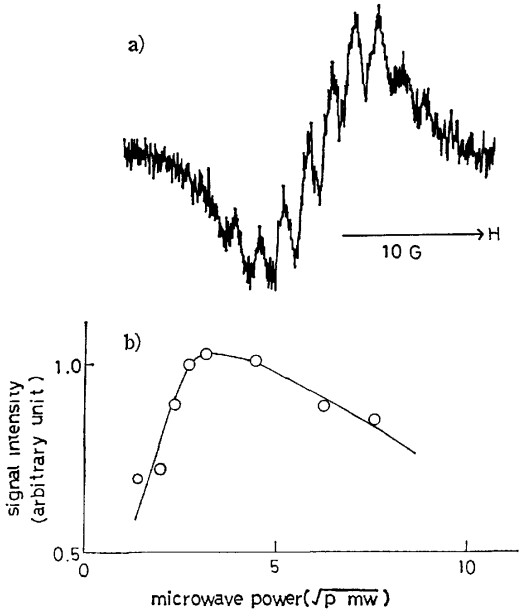

Fig. 2. a) Signal I with partially resolved hyperfine structure.
Modulation amplitude 1.0 G.
Microwave power 8 mW.
b) Saturation behavior of signal I.

* To whom correspondence should be addressed: Faculty of Pharmaceutical Sciences, Okayama University, Tsushima-naka, Okayama 700.

When the solution of ZnTPP and Q in ethanol was illuminated with yellow light (>520 nm), only an ESR signal of the semiquinone anion radical, Q^-, was observed; this is in agreement with Quinlan's results.[6]

On the other hand, upon the illumination (>520 nm) of the solution of ZnTPP and Q in dichloromethane, the ESR spectrum shown in Fig. 1a was obtained. It was composed of two overlapped signals—one with a broad singlet (Signal I, g=2.0027) on the high-field side on the spectrum, and another with a rather well-resolved hyperfine structure (Signal II, g=2.0046) on the low-field side. The existence of the two kinds of radicals was confirmed by the method of microwave-power saturation; at higher microwave power levels, the intensity of Signal I increased, whereas that of Signal II decreased and its hyperfine structure became obscure (Fig. 1b). Both signals decayed completely within a second after light-off. In the dark, none of the signals were detected. Also, no signals were observed in either solvent with either ZnTPP or Q alone upon illumination with yellow light. More than a threefold increase in the porphyrin concentration resulted in a change in the spectrum of Fig. 1 to that in Fig. 2a, in which Signal I appeared as a partially resolved spectrum. Signal I did not saturate until moderately high microwave power levels (20 mW) as is shown in Fig. 2b. This saturation behavior clearly differs from that of the semiquinone radical saturable at higher levels than 4 mW, and rather resembles that of $ZnTPP^+$. The hyperfine coupling constant, which is inaccurate because of the poor S/N ratio, was estimated to be 1.7 G and compared with that of $ZnTPP^+$ (g=2.0025, a= 1.6 G) prepared by electrochemical oxidation in dichloromethane. In a preliminary experiment by flash photolysis, an intermediate species with a lifetime of a few milli seconds was detected; its absorption spectrum was not inconsistent with that of $ZnTPP^+$ reported previously.[5] Thus, Signal I was reasonably assigned to $ZnTPP^+$.

On the other hand, p-benzoquinone alone in dichloromethane showed an ESR signal assignable to the neutral semiquinone radical, QH (g=2.0046, 18-line signal), upon illumination with light longer than 420 nm. This signal showed a well-resolved 15-line hyperfine structure at the modulation amplitude of 0.63 G, as is shown in Fig. 3, and its ESR parameters were in good agreement with those of Signal II.

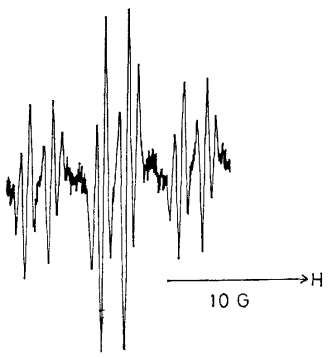

Fig. 3. ESR spectrum of the solution of Q in dichloromethane upon illumination (>420 nm).
Modulation amplitude 0.63 G.
Microwave power 4 mW.

As has been described above, on the illumination (>520 nm) of the solution of ZnTPP and Q in dichloromethane, the $ZnTPP^+$ and QH radicals are produced, whereas in ethanolic solutions only the p-benzoquinone anion radical is observed. These facts imply that there is a great difference in the lifetimes of the $ZnTPP^+$ produced in the two solvents, *i.e.*, a difference in the decay processes of $ZnTPP^+$. Barashkov and Chibisov[3] have proposed the following decay processes of Chl^+ and Q^- in ethanol on the basis of the kinetic results obtained by flash photolysis:

$$Chl^+ + Q^- \longrightarrow Chl + Q, \quad k = 2.0\times10^9\ M^{-1}\ s^{-1}, \tag{1}$$

$$2Q^- \longrightarrow Q + Q^{2-}, \quad k = 2\times10^7\ M^{-1}\ s^{-1}, \tag{2}$$

$$Chl^+ + Q^{2-} \longrightarrow Chl + Q^-, \quad k = 5.5\times10^5\ M^{-1}\ s^{-1}, \tag{3}$$

$$Chl^+ + C_2H_5OH \longrightarrow Chl + C_2H_5OH^+, \quad k = 8.6\times10^2\ M^{-1}\ s^{-1}. \tag{4}$$

Therefore, we examined the reactivity of $ZnTPP^+$, prepared by electrochemical oxidation in dichloromethane, toward both ethanol and hydroquinone in view of the similarity of Chl and ZnTPP. On the addition of hydroquinone to the solution, $ZnTPP^+$ was quickly reduced to reproduce ZnTPP stoichiometrically. Therefore, a decay process similar to (3) seems to be operative in our system, also. However, in the case of ethanol, only a trace amount of $ZnTPP^+$ decreased rapidly to reproduce ZnTPP. This fact indicates that a decay process similar to (4) is not important, but some decay process other than (4), such as a reaction with an unknown material, X, proposed by Hales and Bolton[2] may play a role in an ethanolic solution:

$$Chl^+ + X \longrightarrow Chl + X^+, \quad k > 10^3\ s^{-1}\ \text{(with X in excess)}. \tag{5}$$

The lifetime of $ZnTPP^+$ in ethanol may be shortened by a process similar to (5), but in dichloromethane the absence of decay processes similar to (4) and (5) may explain why $ZnTPP^+$ is not detected in an ethanolic solution.

Our present results indicate that the decay processes differ greatly in the solvents used; that is, they depend on the environment of the primarily produced radicals. A similar investigation using micellar systems in which ZnTPP is incorporated is now in progress.

References

1) G. Tollin and G. Green, *Biochim. Biophys. Acta*, **60**, 524 (1962).
2) B. J. Hales and J. R. Bolton, *J. Am. Chem. Soc.*, **94**, 3314 (1972).
3) B. I. Barashkov and A. K. Chibisov, *Biofizika*, **17**, 775 (1972).
4) J. R. Harbour and G. Tollin, *Photochem. Photobiol.*, **19**, 147 (1974).
5) J. Fajer, D. C. Borg, A. Forman, D. Dolphin, and R. H. Felton, *J. Am. Chem. Soc.*, **92**, 3451 (1968).
6) K. P. Quinlan, *J. Phys. Chem.*, **72**, 1797 (1968).

BULLETIN OF THE CHEMICAL SOCIETY OF JAPAN, VOL. 50 (8), 2179—2180 (1977)

A Semi-empirical NDDO Method for All-valence-electron Systems. II. Extension to Compounds Containing Nitrogen and/or Oxygen

Osamu KIKUCHI and Akira MAEDA

Department of Chemistry, The University of Tsukuba, Sakura-mura, Ibaraki 300-31

(Received December 2, 1976)

Synopsis. A semi-empirical NDDO method is extended to compounds containing nitrogen and/or oxygen, and is applied to the evaluation of the molecular geometries and excitation energies of the compounds and of the heats of reactions relating to them. The agreement between the calculated and observed values is comparable with that previously attained for hydrocarbons except for the conformations of NH_3 and CH_3NH_2.

In the previous paper,[1] a semi-empirical NDDO method was applied to the evaluation of the molecular geometries and excitation energies of a variety of hydrocarbons, and of the heats of reactions among them. It was shown that the NDDO method gave at the same time well-balanced values of the above three quantities. Here, the method will be extended to compounds containing nitrogen and/or oxygen. In the NDDO procedure, the off-diagonal core matrix element between AO's, μ and ν, on the different atoms,

$$H_{\mu\nu} = \frac{1}{2}S_{\mu\nu}(\beta_\mu+\beta_\nu),$$

and the core repulsion energies between atoms A and B,

$$E_{\text{core}}^{\text{AB}} = Z_A Z_B\left\{\frac{b}{R_{AB}^a}+c\right\} \qquad (R_{AB}<R_0),$$

are estimated empirically. The empirical parameters in these formulae were determined in the same way as in the previous paper.[1] The parameters obtained are listed in Tables 1 and 2. The equilibrium geometries, heats of reactions, and excitation energies of compounds containing nitrogen and/or oxygen were calculated using the parameters listed in Tables 1 and 2. They are

Table 1. Values of β_μ (eV)

	1s(H)	2s(C)	2p(C)	2s(N)	2p(N)	2s(O)	2p(O)
β_μ	−7.5	−13.2	−9.3	−22.0	−18.6	−30.0	−27.0

Table 2. Parameters in core-core repulsion formula[a)]

	a	b	R_0
H–H	10.45	0.7436	2.642
H–C	14.00	0.5034	2.779
H–N	14.58	0.5334	2.291
H–O	21.97	0.3346	2.015
C–C	13.16	0.4899	3.621
C–N	13.22	0.5432	3.327
C–O	18.09	0.3811	2.147
N–N	17.65	0.3897	2.332
N–O	15.73	0.4676	2.192
O–O	17.18	0.4429	1.902

a) The core-core repulsion energies calculated from the parameters are in eV.

Table 3. Calculated equilibrium geometries of compounds containing nitrogen and/or oxygen[a)]

Compound	Type	Calcd	Obsd[2,3)]
Water	O–H	0.953	0.957
	HOH	119.8	104.5
Methanol[b)]	O–H	0.960	0.967
	C–O	1.378	1.428
	COH	121.2	107.3
Formaldehyde	C=O	1.204	1.210
	C–H	1.102	1.102
	HCH	114.4	121.1
Formic acid	C–O	1.369	1.343
	C=O	1.213	1.202
	C–H	1.078	1.097
	HCO_1	129.2	124.1
	OCO	118.0	124.9
	COH	106.7	106.3
Dimethyl ether[b)]	C–O	1.391	1.42
	COC	125.4	111.0
Ammonia	N–H	1.048	1.014
	HNH	120.0	106.9
Methylamine[b)]	C–N	1.515	1.474
	HNH	117.0	105.8
Hydrazine	N–H	1.077	1.04
	N–N	1.439	1.47
	HNN	117.2	108
Hydrogen cyanide	H–C	1.086	1.066
	C≡N	1.147	1.153
Azomethane[b)]	C–N	1.552	1.482
	N=N	1.219	1.247
	NNC	125.1	112.3
Diazomethane	C–N	1.362	1.34
	N=N	1.121	1.13
	C–H	1.101	
	HCH	111.8	
Acetonitrile	C–C	1.487	1.465
	C≡N	1.166	1.155
Hydroxylamine	N–O	1.412	1.46
	HNH	115.0	107
	NOH	118.5	103
Formamide	C–N	1.360	1.300
	C=O	1.234	1.255
	HNH	114.2	
	NCO	118.1	121.5
Nitromethane[b)]	C–N	1.550	1.47
	N–O	1.236	1.22
	ONO	126.2	135
Ethylene oxide	C–C	1.536	1.472
	C–O	1.438	1.436
	C–H	1.086	1.082
	HCH	114.0	121.7

a) Bond lengths in Å; bond angles in degrees.
b) The geometry of the CH_3 group was assumed to be the same as that of ethane.

Table 4. Calculated heats of reactions (kcal/mol)[a)]

Reaction	Heats of reaction	
	Calcd	Obsd[4)]
$1/2N_2+3/2H_2\rightarrow NH_3$	9.4	11.0
$N_2H_4\rightarrow N_2+2H_2$	17.6	22.7
$HCN+2H_2\rightarrow CH_3NH_2$	49.0	37.9
$CH_2O+H_2\rightarrow CH_3OH$	39.1	20.4
$CH_3CHO+H_2\rightarrow C_2H_5OH$	30.1	16.5
$CH_2CO+H_2\rightarrow CH_3CHO$	30.0	25.2
$CH_2N_2+H_2\rightarrow CH_4+N_2$	69.8	69.2
$CH_3NH_2+O_2\rightarrow CH_3NO_2$	13.7	5.5
$H_2+1/2O_2\rightarrow H_2O$	56.2	57.8
$H_2+O_2\rightarrow H_2O_2$	54.9	32.5
$CH_4+1/2O_2\rightarrow CH_3OH$	51.0	30.2
$CH_2O+1/2O_2\rightarrow HCOOH$	63.3	62.8
$CH_3CHO+1/2O_2\rightarrow CH_3COOH$	69.6	64.0
Ethylene$+1/2O_2\rightarrow$Ethylene oxide	36.0	24.7
$CH_2CO+H_2O\rightarrow CH_3COOH$	43.4	31.4
$CH_3NNCH_3\rightarrow C_2H_6+N_2$	60.2	71.4

a) The energy of the ground state of O_2(triplet) was calculated by means of the CI method.

Table 5. Calculated excitation energies (eV)

Compound	Nature of excitation	Calcd	Obsd[3,5)]
Formaldehyde	$n\rightarrow\pi^*$	3.05	4.2
	$n\rightarrow\sigma^*$	5.80	7.1
	$\pi\rightarrow\pi^*$	7.53	8.0
Acetaldehyde	$n\rightarrow\pi^*$	3.22	3.56
	$\pi\rightarrow\pi^*$	7.63	6.82
Ketene	$n\rightarrow\pi^*$	2.62	3.84
	$\pi\rightarrow\pi^*$	5.69	5.82
Diazomethane	$n\rightarrow\pi^*$	2.14	3.14
	$\pi\rightarrow\pi^*$	5.03	5.70
Nitromethane	$n\rightarrow\pi^*$	3.38	4.59
	$\pi\rightarrow\pi^*$	6.75	6.12

listed in Tables 3—5. All the bond lengths except the CN-type ones agree with the observed values within 0.05 A. The XOY types of bond angles are larger than the observed values by about 15°. The method fails to give the correct conformations of NH_3 and CH_3NH_2; it predicts the planar conformations. These defects were also found in the NINDO/2 method, which is at the same level of parametrization as the present method; the XOY types of bond angles were estimated to be 180° by MINDO/2.[6)] The agreement between the calculated and observed heats of reactions (average error, 9 kcal/mol) is comparable with that previously attained for hydrocarbons. The singlet excitation energies of several compounds were calculated by the CI method, in which only singly excited configurations were included. The calculated energies for the $n\rightarrow\pi^*$ types of excitations are smaller than the observed values about by 1 eV, while those for the $\pi\rightarrow\pi^*$ types differ from the observed values by about 0.5 eV. This somewhat large discrepancy comes from the empirical parameters which were chosen so as to give, at the same time, well-balanced values for the above three quantities. Better excitation energies can be obtained by the use of other sets of parameters which would simultaneously give poor molecular geometries and heats of reactions.[1)] The present NDDO results in Table 5 are felt to be satisfactory in comparison with the excitation energies[7)] estimated by the CNDO and MINDO/2 methods which are currently used in the theoretical studies of chemical reaction processes.

The authors wish to express their thanks to Professor Keizo Suzuki for his helpful suggestions.

References

1) O. Kikuchi, *Bull. Chem. Soc. Jpn.*, **50**, 593 (1977).
2) E. Sutton, "Tables of Interatomic Distances," Special Publications No. 11, The Chemical Society, London (1958); N. Gailar and K. Plyler, *J. Chem. Phys.*, **24**, 1139 (1956); A. Almenninger, I. M. Anfinsen, and A. Haaland, *Acta Chem. Scand.*, **24**, 1230 (1970).
3) G. Herzberg, "Electronic Spectra and Molecular Structure III," Van Nostland, New York (1967).
4) "Selected Values of Chemical Thermodynamic Properties," National Bureau of Standards Circular 500, US, Government Printing Office, Washington, D.C. (1952); L. H. S. Green, *Quart. Rev. (London)*, **15**, 125 (1961); G. Chilty, C. F. Aten, Jr., and J. Bauer, *J. Phys., Chem.*, **66**, 1426 (1962); A. H. Laufer and H. Okabe, *J. Am. Chem. Soc.*, **93**, 4137 (1971); R. A. Back and J. Betts, *Can. J. Chem.*, **43**, 2157 (1965).
5) J. W. Rabalais, J. M. McDonald, V. Scherr, and S. P. McGlynn, *Chem. Revs.*, **71**, 73 (1971); H. Sponer and E. Teller, *Rev. Mod. Phys.*, **13**, 75 (1941).
6) N. C. Baird and M. J. S. Dewar, *J. Chem. Phys.*, **50**, 1262 (1969); N. Boder, M. J. S. Dewar, A. Harget, and E. Haselbach. *J. Am. Chem. Soc.*, **92**, 3854 (1970). The MINDO/3 version, in which a large number of parameters are introduced, gives satisfactorily the XOY angles and conformation of NH_3: R. C. Bingham, M. J. S. Dewar, and D. H. Lo, *J. Am. Chem. Soc.*, **97**, 1285, 1294, 1307 (1975).
7) The $n\rightarrow\pi^*$ excitation energy of formaldehyde, for example, calculated by the MINDO/2 was 2.19 eV. See also: O. Kikuchi, *Bull. Chem. Soc. Jpn.*, **42**, 47 (1969).

BULLETIN OF THE CHEMICAL SOCIETY OF JAPAN, VOL. 50 (8), 2181—2182 (1977)

Active Sites of MoO_3 and MoO_3-SiO_2 Catalysts for Isomerizaiton of Butenes. Characterization by Tracer Study

Hideshi HATTORI, Kazumasa MARUYAMA, and Kozo TANABE
Department of Chemistry, Faculty of Science, Hokkaido University, Sapporo 060

(Received January 12, 1977)

Synopsis. Deuterium atom distribution of butenes in the coisomerization of *cis*-2-butene d_0/d_8 over MoO_3 and MoO_3–SiO_2 indicates that the reaction involves intermolecular hydrogen transfer for both catalysts. Butenvs produced over deuterium-exchanged MoO_3–SiO_2 contain deuterium atoms, those produced over deuterium-exchanged MoO_3 none.

Catalytic properties of MoO_3–SiO_2 and MoO_3 were investigated in view of surface acidity and basicity.[1] For the isomerization of butenes, it was suggested from the correlation of activity with acidity or basicity that the active sites on MoO_3–SiO_2 are acidic, while those on MoO_3 are basic. If the isomerization proceeds on the acidic sites, a hydrogen atom of butene is exchanged during the course of reaction. If the active sites are of Brönsted type, surface hydrogen atoms would be incorporated into the products. In the mechanism proposed for basic sites, the isomerization is initiated by the abstraction of a proton from butene to form the carbanion. In this case hydrogen atoms are not exchanged between butenes unless hydrogen atoms rapidly migrate over the surface.

Hightower and Hall investigated the isomerization of butene over Al_2O_3 and SiO_2–Al_2O_3 by means of a "tracer study" using deuterium as a tracer.[2] They developed a coisomerization technique, in which a mixture of nondeuterated and perdeuterated butene was used as a reactant. If the isomerization involves intermolecular hydrogen transfer, the product should contain both non-exchanged isotopic species d_0 and d_8, and mono-exchanged isotopic species d_1 and d_7. In the case of intramolecular hydrogen transfer, only non-exchanged isotopic species should be produced. The relative ratio of product from nondeuterated reactant to that from perdeuterated reactant shows an isotope effect when extraporated to zero conversion.

In the present work the coisomerization of butene over MoO_3–SiO_2 and MoO_3, and the reaction over the deuterium exchanged catalysts were carried out, the reaction mechanism and the nature of active sites being investigated.

Experimental

Molybdenum trioxide (MoO_3) was prepared by the precipitation from an aqueous solution of ammonium molybdate with nitric acid. MoO_3–SiO_2 was prepared by precipitation from a mixture of ammonium molybdate and tetraethyl orthosilicate with nitric acid. Precipitates were dried at 100 °C and finally calcined at 500 °C for 3 h in air. Details were described previously.[1]

A microcatalytic pulse reactor was used for the reaction. A catalyst (0.25 g) was evacuated at 500 °C prior to reaction. For the reaction over deuterium exchanged catalyst, surface hydrogen atoms were exchanged with deuterium atoms by exposing the catalyst evacuated to *ca.* 10 Torr of D_2O at 250 °C, the catalyst being evacuated at 500 °C for 1 h.

ca. 40 μmol of butene was passed over the catalyst in a helium carrier, and products were trapped by liquid nitrogen before being flash evaporated into a gaschromatographic column (Propylene carbonate on Uniport C in 10-m length, 8-mm o.d. Cu-tubing) operated at 0 °C. The separated products were collected in liquid nitrogen traps and subjected to mass spectroscopic analysis.

For the coisomerization, a mixture containing about equal amounts of nondeuterated and perdeuterated *cis*-2-butene was used as a reactant. The isotopic purity of the perdeuterated *cis*-2-butene was higher than 99.6%.

Results and Discussion

The isotopic profiles of butenes in the coisomerization and the reactions over deuterium exchanged catalysts are given in Table 1. The number of H (or D) atoms exchanged per molecule (AEM) was calculated by

$$\sum_{i=0}^{4} i \cdot N_i + \sum_{5}^{8} (8-i) N_i,$$

where N_i is a mole fraction of each isotopic species containing i deuterium atoms. An isotope effect (IE) was obtained by the relative reactivity of nondeuterated species to that of perdeuterated species, which was calculated by

$$\left(\sum_{0}^{3} N_i + \frac{1}{2} N_4\right) \Big/ \left(\sum_{5}^{8} N_i + \frac{1}{2} N_4\right),$$

where d_4 species in the product was assumed to be produced equally from d_0 and d_8 reactant.

Over both MoO_3 and MoO_3–SiO_2, the products in the coisomerization contained a considerable fraction of mono-exchanged d_1 and d_7 isotopic species. If there were no isotope effect, the AEM value at zero conversion would be 0.5 for the intermolecular hydrogen transfer, and would decrease when isotope effect becomes larger. AEM values of 1-butene close to 0.5 for both catalysts indicate that the isomerization to 1-butene involves intermolecular hydrogen transfer over both catalysts.

Considerable amounts of d_1 species were produced over deuterium exchanged MoO_3–SiO_2, (Table 2). This in addition to the existence of acidic sites on the surface[1] and the occurrence of intermolecular hydrogen transfer, strongly suggest that the active sites are of a Brönsted type and the isomerization to 1-butene proceeds *via* a carbenium ion intermediate. The number of H (or D) atoms exchanged per molecule in *trans*-2-butene was smaller than that in 1-butene. If the carbenium ions are weakly bonded to the surface, *trans*-2-butene may be produced from the carbenium ion by release of either the hydrogen atom that came from the surface or the hydrogen atom that was originally the vinyllic

Table 1. Isomerization of *cis*-2-butene and coisomerization of *cis*-2-butene d_0/d_8 over MoO_3–SiO_2 and MoO_3 at 250 °C

Catalyst	Pulse number	Reactant	Product	Each product (%)	Isotopic distributions (%) d_0	d_1	d_2	d_3	d_4	d_5	d_6	d_7	d_8	AEM	IE
MoO_3–SiO_2	1	d_0	1	5.5											
			t	9.2											
			c	85.3											
	3	d_0	1	4.6											
			t	7.5											
			c	87.9											
	4	d_0, d_8	1	2.9	42.5	17.6	0.4	0	0	0	1.0	23.3	15.2	0.437	1.53
			t	5.7	39.5	10.6	0	0	0	0	0.7	18.3	30.8	0.303	1.00
			c	91.4	50.3	0.4	0	0	0	0	0	2.2	46.7	0.026	1.03
	5	d_0	1	4.2											
			t	6.9											
			c	88.9											
MoO_3	1	d_0	1	10.8											
			t	19.3											
			c	68.9											
	3	d_0	1	3.5											
			t	5.5											
			c	91.0											
	5	d_0	1	2.3											
			t	3.5											
			c	94.2											
	6	d_0, d_8	1	1.4	42.9	20.7	0.1	0	0	0	0.7	19.6	16.0	0.419	1.75
			t	2.9	39.1	11.3	0	0	0	0	0.3	14.0	35.4	0.259	1.01
			c	95.7	50.0	0.8	0	0	0	0	0	2.1	47.1	0.029	1.03
	7	d_0	1	7.1											
			t	10.9											
			c	82.0											

Table 2. Isomerization of *cis*-2-butene over deuterium exchanged MoO_3–SiO_2 and MoO_3 at 250 °C

Catalyst	Product	Each product (%)	Isotopic distributions (%) d_0	d_1	d_2	d_3	d_4—d_8	ϕ value
MoO_3–SiO_2	1	16.9	72.3	24.8	3.0	0.1	0	0.311
	t	36.2	81.1	17.9	1.0	0	0	0.199
	c	46.9	86.3	13.0	0.7	0	0	0.144
MoO_3	1	7.2	100	0	0	0	0	0
	t	11.5	100	0	0	0	0	0
	c	81.3	100	0	0	0	0	0

hydrogen of *cis*-2-butene. This might result in a smaller number of exchanged hydrogen atoms in *trans*-2-butene.

On the other hand, no deuterium was incorporated into the products over deuterium exchanged MoO_3. Surface H (or D) atoms should not participate in the reaction. The active sites on MoO_3 were poisoned not by ammonia but by carbon dioxide, suggesting that MoO_3 is of a basic type of catalyst.[1] The reaction could be initiated by the abstraction of the allylic proton in *cis*-2-butene by basic sites. If the proton migrates over the surface very rapidly, intermolecular hydrogen transfer would occur.

On introducing an oxygen pulse to MoO_3 after the six pulses of butene, the activity was restored to the level of the second butene pulse. The activity was also recovered almost completely by allowing the catalyst to stand in the reactor overnight at room temperature with no carrier gas flowing. The results suggest that surface Mo^{6+} ions rather than Mo^{5+} ions participate in the reaction, though the amplitude of Mo^{5+} signal in the ESR spectrum decreases only slightly by exposure to oxygen at 250 °C. The Mo^{5+} ions may be produced by a loss of oxygen atoms attached to Mo^{6+} ions. By allowing the catalyst to stand overnight, oxygen atoms seem to diffuse from the bulk to the surface and Mo^{6+} ions are reproduced. The abstraction of protons from butene molecules seems to be performed much more easily by oxygen ions than by metal cations. Thus, it is suggested that the active sites on MoO_3 consist of pairs of oxygen ions and Mo^{6+} on the surface, at least in the initial stage of the reaction.

References

1) K. Maruyama, H. Hattori, and K. Tanabe, *Bull. Chem. Soc. Jpn.*, **50**, 86 (1977).

2) J. W. Hightower and K. Hall, *Chem. Eng. Prog. Symp. Ser.*, **63**, 122 (1967).

BULLETIN OF THE CHEMICAL SOCIETY OF JAPAN, VOL. 50 (8), 2183—2184 (1977)

Radical Reaction in a Silent Electric Discharge of Ethylene

Junichi Itoh, Kazuto Takimoto, and Satoru Tsuda

Department of Chemistry, Faculty of Engineering, Hiroshima University, Senda-machi, Hiroshima 730

(Received February 24, 1977)

Synopsis. In the silent electric discharge of ethylene, it was revealed, by studying the effects of various scavengers on the formation of gaseous products, that the radical reaction plays an important role, unlike as in the reaction in radiolysis. Furthermore, the existence of several intermediates was directly or indirectly demonstrated by using an ESR technique and by adding iodine as a radical scavenger.

In a silent electric discharge as well as radiolysis, various active species, that is, cations, anions, excited molecules, and dissociated atoms (or free radicals), are produced by the collision of electrons with molecules. Paal and Foldiak[1] have reported that a gaseous-discharge reaction at 0.5—1.0 mA under 10 kV in a discharge tube of the Giemens-ozonizer type corresponds to the radiolysis at 10^7—10^8 rad/h.

The present authors have studied the discharge reaction of aqueous solutions.[2] This investigation is further extended to a gas phase to reveal the correlation between the discharge reaction and radiolysis. Ethylene was selected as the objective gas since the radiolysis of the gas has been studied in detail and the reaction mechanism has been relatively well clarified.[3,4] In the radiolysis of ethylene, only ethane is formed through the radical reaction, whereas hydrogen, acetylene, and butane are produced through the molecular dissociation and the ionic reaction.[3,4] Our purpose in this work is to reveal the molecular dissociation and the subsequent radical reaction and also to confirm the intermediate in the silent electric discharge of ethylene.

Experimental

The research-grade ethylene was used after several distillations. Purified nitrogen monoxide and iodine were used as radical scavengers. On the other hand, ethanol was employed as a positive ion scavenger. The identification and the determination of the gaseous products were performed by using a Hitachi RMU-6D mass spectrometer and a Hitachi 730 type gas chromatograph respectively.

In the discharge of ethylene below an atmospheric pressure, a linear relationship was confirmed between the applied potential and the current over 0.3 mA. Every experiment was, therefore, performed under the following conditions: a duration of 20 s at 0.5 mA and an ethylene pressure of 100 Torr. The energy (W) dissipated electrically by the discharge was estimated from the equation by Fuji and Takemura.[5]

The intermediates formed by the discharge of ethylene were trapped on the silica gel in a discharge tube of an ozonizer type as is shown in Fig. 1. The silica gel was prepared by the hydrolysis of sodium silicate, which had been baked at 600 °C for 6 h in air. Their intermediates were identified by the ESR technique.[6]

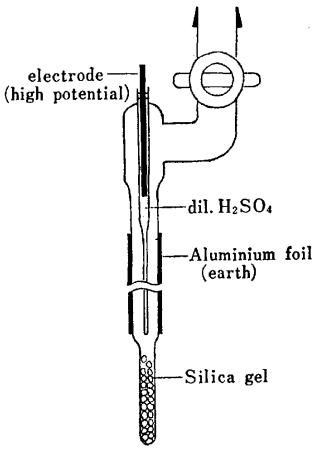

Fig. 1. Schematic diagram of discharge tube.

Results and Discussion

The major gas products formed by the silent electric discharge of ethylene were C_2H_2, H_2, n-C_4H_{10}, C_3H_8, CH_4, C_2H_6, C_3H_6, and $CH_2{=}CHC_2H_5$. The trace gas products were i-C_4H_8, *trans*-2-C_4H_8, *cis*-2-C_4H_8, $CH_3CH{=}C(CH_3)_2$, n-C_5H_{12}, i-C_5H_{12}, $CH_3C(CH_3)_2C_2H_5$, $CH_3CH(CH_3)_2$, $C_2H_5CH(CH_3)C_2H_5$, n-C_6H_{14}, and C_6H_6.

When ethanol was added as a positive ion scavenger, the yield of methane decreased with an increase in the additive amount of ethanol (0—8 mol %), whereas the formation of the other products was scarcely affected within the range of experimental error.

Figure 2 shows the effect of nitrogen monoxide on the

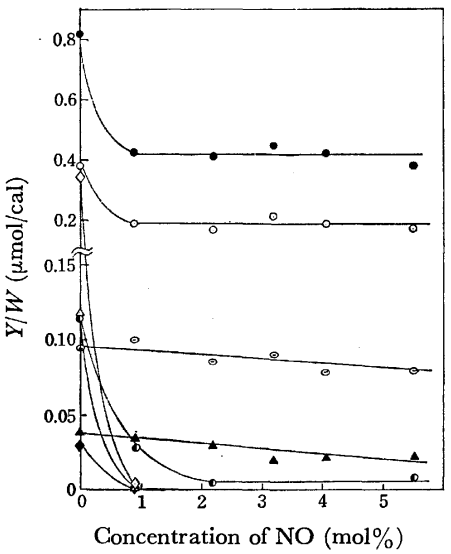

Fig. 2. Effect of nitrogen monoxide on the formation of each product.
●: Acetylene, ○: hydrogen, ◇: butane,
△: propane, ◐: ethane, ⊖: methane,
▲: propylene, ◆: 1-butene.

formation of each product. This suggests that all of the ethane, propane, butane, and 1-butene and a part of the hydrogen and acetylene is formed by the radical reaction.

The decompositions of ethylene excited by the discharge can be represented as follows:

$$C_2H_4^* \longrightarrow C_2H_2 + H_2, \quad (1)$$

$$\longrightarrow C_2H_2 + 2H, \quad (2)$$

$$\longrightarrow C_2H_3 + H. \quad (3)$$

The dissociation probabilities of Reactions 1 and 2 were calculated from the yields of the hydrogen and acetylene formed by the electric discharge of the ethylene–nitrogen monoxide system:

$$(1):(2) = 0.44:0.56 \text{ at } 100 \text{ Torr } C_2H_4,$$

$$0.38:0.62 \text{ at } 355 \text{ Torr } C_2H_4.$$

Meisels and his co-worker[4] estimated the relative probability of Reaction 3 by assuming the $(C_2H_3)/(1\text{-}C_4H_8)=3.3$ ratio. By using this ratio tentatively, the dissociation probabilities of the three reactions could be calculated:

$$(1):(2):(3) = 0.36:0.45:0.19 \text{ at } 100 \text{ Torr } C_2H_4,$$

$$(1):(2):(3) = 0.26:0.42:0.32 \text{ at } 355 \text{ Torr } C_2H_4.$$

On the other hand, Meisels and his co-worker[4] have reported that the relative dissociation probabilities for ethylene excited by slow electrons at $E/P=26.9$ V/cm Torr and at the ethylene pressure of 50 Torr were as follows:

$$(1):(2):(3) = 0.38:0.46:0.16.$$

The relative probabilities for ethylene discharged at 100 Torr happened to agree closely with those for ethylene irradiated by slow electrons at $E/P=26.9$ V/cm Torr and at the ethylene pressure of 50 Torr. This seems to support our previous conclusion[7] that the silent electric-discharge reaction corresponds to that by slow electrons.

Janzen and others have detected some radicals produced in a microwave discharge by using a technique called "spin trapping."[8] So far as we know, the detection technique of radicals by using a discharge tube of the ozonizer type such as is shown in Fig. 1, has hardly even been used. However, we succeeded in detecting hydrogen and the ethyl radical directly by using this technique.

When the silica gel evacuated at 300 °C for 10 h was discharged at 8 kV in the presence of argon gas, only a broad singlet centered at about $g=2.0036$ was observed, as is shown in Fig. 3(a). On the other hand, silica gel discharged under an ethylene pressure of about 20 Torr

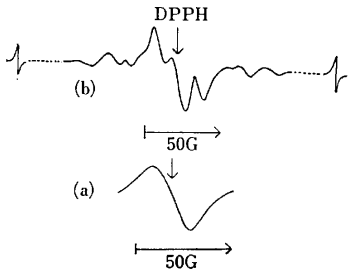

Fig. 3. ESR spectra of ethylene discharged at 77 K on the silica gel.
(a) Argon–silica gel, (b) ethylene–silica gel.

showed the ESR spectrum shown in Fig. 3(b). A hydrogen atom with a coupling constant of about 500 G and an ethyl radical which are superimposed on the broad singlet described above could be detected.

Furthermore, the existence of some radicals participating in the radical reaction was evidenced by the results of an analysis of the iodides resulting from the radical scavenging by iodine: $C_2H_5I=0.160$, $C_2H_3I=0.029$, $n\text{-}C_4H_9I=0.011$, $CH_3I=0.004$, and $n\text{-}C_3H_7I=0.001$, where each unit is μmol/cal. However, HI and CH_2I could not be detected.

In conclusion, if the discharge reaction of ethylene is compared with the radiolysis reaction, the final products in both reactions are similar to each other. However, the dominant reactions in the radiolysis are the ionic reaction and the molecular decomposition.[3] On the contrary, in the discharge reaction the radical reaction and the molecular decomposition play important roles.

References

1) Z. Paal and O. Foldiak, Radiation Chemistry, Proceedings of the 1962 Symposium, p. 445.

2) A. Yokohata and S. Tsuda, *Bull. Chem. Soc. Jpn.*, **40**. 2507 (1976); **41**, 2292 (1967).

3) M. C. Sauer, Jr., and L. M. Dorfman, *J. Phys. Chem.*, **66**, 322 (1962).

4) G. G. Meisels and T. J. Sworski, *J. Phys. Chem.*, **69**, 2867 (1965).

5) S. Fuji and N. Takemura, *Denki Shikensho Iho*, **14**, 283 (1950).

6) A. Hasegawa and M. Miura, *Bull. Chem. Soc. Jpn.* **40**, 2553 (1967).

7) A. Yokohata and S. Tsuda, *Bull. Chem. Soc. Jpn.*, **39**, 46 (1966).

8) E. G. Janzen, T. Kasai, and K. Kuwata, *Bull. Chem. Soc. Jpn.*, **46**, 2061 (1973).

BULLETIN OF THE CHEMICAL SOCIETY OF JAPAN, VOL. 50 (8), 2185—2186 (1977)

Ligand-Substitution Reaction of Bis(acetylacetonato)copper(II) and Bis(acetylacetonato)zinc(II) with 2-(2-Pyridyl)benzimidazole

Michio KONDO

Central Research Laboratories, Sankyo Co., Ltd., Hiromachi 1-2-58, Shinagawa-ku, Tokyo 140

(Received November 16, 1976)

Synopsis. The reaction of bis(acetylacetonato)-copper(II) with 2-(2-pyridyl)benzimidazole (**1**) in ethanol was studied by means of absorption, fluorescence, and ^{1}H NMR spectroscopies, and it was found that one of the acetylacetonate anions in the complex is replaced by the anion of **1**. Bis-(acetylacetonato)zinc(II) reacts with **1** in a similar manner. Neither acetylacetonate reacts with 2-(3-pyridyl)- or 2-(4-pyridyl)benzimidazole.

It is well known that bis(β-diketonato)copper(II) complexes behave as Lewis acid and form addition compounds with nitrogen bases.[1] Several five-coordinate addition compounds of square planar bis(β-diketonato)copper(II) complexes with heterocyclic nitrogen bases have been isolated.[2] A stable 2,2'-bipyridine adduct of bis(hexafluoroacetylacetonato)-copper(II)[3] and a reaction product of bis(acetylacetonato)copper(II) with ethylenediamine[4] have been isolated, and their structures were determined by means of X-ray analysis. It has been reported that bis(acetylacetonato)zinc(II) forms stable addition compounds with 4,4'-bipyridine and pyrazine.[5] In all these cases no ligand-substitution occurs. This paper describes a new mixed ligand copper(II) complex formed by ligand-substitution between bis(acetylacetonato)copper-(II) and 2-(2-pyridyl)benzimidazole.

Experimental

Three 2-pyridylbenzimidazoles 2-(2-pyridyl)- (**1**), 2-(3-pyridyl)- (**2**), and 2-(4-pyridyl)benzimidazole (**3**), were prepared according to the literature.[6] Commercial bis(acetylacetonato)copper(II) and -zinc(II) (**4** and **5**) were purified by recrystallization from chloroform and ethanol, respectively. To a hot ethanol solution (50 ml) of **1** (0.98 g, 1/200 mol), was added a hot ethanol solution (500 ml) of **4** (1.31 g, 1/200 mol). The resulting green solution was concentrated to about 200 ml in a water bath, giving almost black crystals upon cooling. Found: C, 57.19; H, 4.09; N, 11.78%. Calcd for substitution product, $CuC_{17}H_{15}N_3O_2$: C, 57.19; H, 4.21; N, 11.77%. Calcd for adduct, $CuC_{22}H_{23}N_3O_4$: C, 57.82; H, 5.07; N, 9.20%.

The absorption, fluorescence, and ^{1}H NMR spectra were recorded with Hitachi spectrophotometers, Model 356, and MPF-2, at 25 °C and a Varian XL-100 spectrometer at 28 °C, respectively.

Results and Discussion

Figure 1 shows the absorption spectra of ethanol solutions of **1** in the presence of various amounts of **4**. Two isosbestic points are observed at 327 and 304 nm, indicating the existence of a stoichiometric complex-forming equilibrium. A new absorption band at about 350 nm can be ascribed to the complex formed, because neither **1** nor **4** has an absorption band in this region.

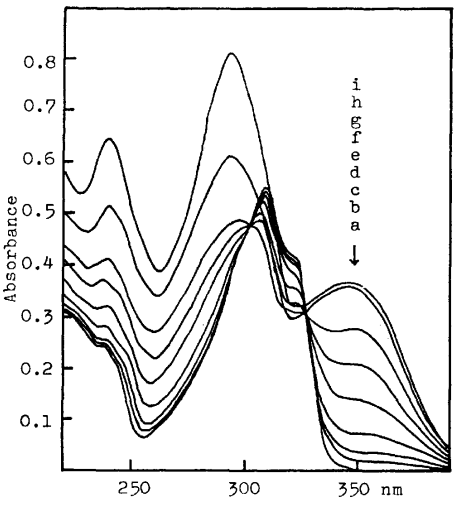

Fig. 1. The absorption spectral change of **1** (2.43×10^{-5} M) in ethanol in the presence of various amounts of **4**. The values of molar ratio, **4**/**1**, are: a, 0; b, 0.044; c, 0.088; d, 0.176; e, 0.352; f, 0.528; g, 0.704; h, 1.056; i, 1.408.

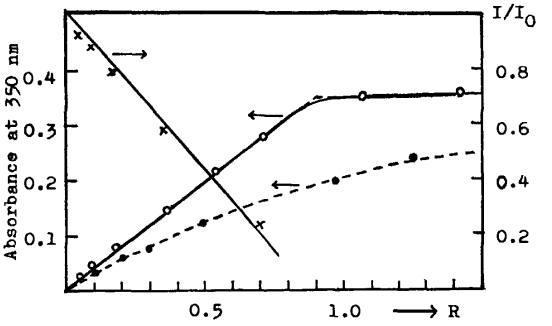

Fig. 2. Plots of absorbance at 350 nm and of relative fluorescence intensity (I/I_0; I_0 is the intensity observed in the absence of **4**), against the molar ratio, **4**/**1**:——, **1**—**4**;----, **1**—**5**.

In Fig. 2, the increments in the absorbance at 350 nm are plotted *versus* the molar ratio (R). The absorbance increases linearly with R until it ceases to increase at $R=1$. It can be concluded, therefore, that 1 : 1 complex with a large stability constant is formed. The high stability of this complex and the result of elemental analysis of the almost black crystals obtained from an ethanol solution of the 1 : 1 mixture of **1** and **4**, indicate that it is not merely an addition product of **1** and **4**, but a mixed ligand complex in which **1** coordinates to the Cu(II) ion as a bidentate ligand replacing an acetylacetonate anion in **4**. Consistent with this conclusion, the absorption spectrum of an ethanol solution of the almost black crystals was very similar to that

of the 1 : 1 mixture of **1** and **4**, though the latter shows stronger absorbance at shorter wavelengths, $\lambda<300$ nm, because of the contribution from acetylacetone molecules liberated by the ligand-substitution.

The fluorescence spectra of these solutions showed a marked decrease in intensity without any sign of the appearance of a new band in the presence of **4**. A plot of the observed intensities at 358 nm *versus* R yielded a straight line which crosses the abscissa at about $R=1$. This observation indicates that the complex formed is nonfluorescent and that the fluorescence emission originates only from the free molecules of **1**.

The ^{1}H NMR spectrum of **1** in $CDCl_3$ gave a broad signal due to the imidazolic proton at δ 11.3 and complex signals with fine structures due to the aromatic protons over the range of δ 7.2—8.7. The addition of a few drops of a dark blue chloroform solution of **4** to this solution gave a green color and, at the same time, a broadening of the aromatic proton signals, accompanied by the appearance of new weak signals at δ 2.04, 2.22, 3.57, and 5.52. These new signals can be ascribed to acetylacetone molecules liberated by the ligand-substitution, because these δ values are very close to those assigned to acetylacetone.[7]

For the system of **1** and bis(acetylacetonato)zinc(II) (**5**) in ethanol, a very similar absorption spectral behavior was observed, a smaller complex formation constant being inferred from the plot of the absorbance increase at 350 nm *versus* R (Fig. 2). This system showed a quite different fluorescence spectral change. The zinc-complex is strongly fluorescent; the new fluorescence band at about 420 nm can be ascribed to the zinc-complex because its intensity increases linearly as the absorbance at 350 nm increases.

The nonfluorescent property of the copper-complex can be interpreted in terms of the paramagnetism of the copper(II) ion, which may induce intersystem crossing in the excited state. The zinc-complex, on the other hand, is diamagnetic and fluorescent. In this connection, Bark and Rixon have studied the application of the zinc complex of **1** to the fluorimetric determination of zinc.[8]

The corresponding mixed complexes did not appear to be formed between **4** and **2** (or **3**) in ethanol, because the absorption spectra of the mixtures are almost the same as the sums of those of their components and because the fluorescence quenching of **2** and **3** in the presence of **4** was negligible.

The acetylacetonate anion in **4** is replaced only by the anion of **1** but not by those of **2** and **3**. This fact indicates the necessity of appropriate positioning of the imidazolic NH group and the pyridine nitrogen atom in order to function as a bidentate ligand. It can also be said that the ionizable property of the imidazolic proton in **1** is very important in the ligand-substitution reaction, because such substitution reactions did not occur between **4** and ethylenediamine or between bis(hexafluoroacetylacetonato)copper(II) and 2,2′-bipyridine.[3,4]

A mixed ligand copper(II) complex, Cu(acac)-(OCH_3), was prepared directly by treating **4** with sodium hydroxide in methanol. The methoxo ligand can be replaced by a pyrazolate anion and the resultant copper(II) complex has been proposed to have a dimeric structure on the basis of its antiferromagnetic properties.[9] This fact suggests that the possibility of a dimeric structure of the present mixed ligand complex cannot be discounted.

No double coordination of the anion of **1** to the copper(II) ion was observed. This indicates the relative instability of $Cu(\mathbf{1}^-)_2$ compared with $Cu(acac)(\mathbf{1}^-)$ from an energy point of view, probably because of the van der Waals' interaction between two anions of **1**, which is bulkier than the acetylacetnate anion.

The apparently smaller stability constant inferred for the zinc-complex may be ascribed to the smaller difference between the affinities of the two ligands in question to the zinc(II) ion.

References

1) D. P. Graddon, *Coord. Chem. Rev.*, **4**, 1 (1969).
2) A. F. Garito and B. B. Wayland, *J. Am. Chem. Soc.*, **91**, 866 (1969).
3) M. V. Veidis, G. H. Schreiber, T. E. Gough, and G. J. Palenik, *J. Am. Chem. Soc.*, **91**, 1859 (1969).
4) T. Kurauchi, M. Matsui, Y. Nakamura, S. Ooi, S. Kawaguchi, and H. Kuroya, *Bull. Chem. Soc. Jpn.*, **47**, 3049 (1974).
5) S. Ambe and F. Ambe, *J. Inorg. Nucl. Chem.*, **35**, 1109 (1973).
6) *Cf.* a) T. Hisano and M. Ichikawa, *Chem. Pharm. Bull.* **22**, 1923, (1974); b) Y. Sasaki and T. Shigematsu, *Bull. Chem. Soc. Jpn.*, **46**, 3438 (1973); References cited in these.
7) J. L. Burdett and M. T. Rogers, *J. Am. Chem. Soc.*, **86**, 2105 (1964).
8) L.S. Bark and A. Rixon, *Anal. Chim. Acta*, **45**, 425 (1969).
9) C. G. Barraclough, R. W. Brookes, and R. L. Martin, *Aust. J. Chem.*, **27**, 1843 (1974).

BULLETIN OF THE CHEMICAL SOCIETY OF JAPAN, VOL. 50 (8), 2187—2188 (1977)

1,3-Dithian-2-one Tosylhydrazone. Synthesis and Carbenoid Decomposition

Naruyoshi OBATA

Faculty of Pharmaceutical Sciences, The University of Tokyo, Bunkyo-ku, Tokyo 113

(Received January 12, 1977)

Synopsis. 1,3-Dithian-2-one tosylhydrazone was prepared by the reaction of potassium 3-tosyldithiocarbazate and 1,3-dibromopropane. Carbenoid reactions of the tosylhydrazone were investigated.

Much attention has been paid on the synthesis of 1,3-dithiane derivatives and their application in organic synthesis as a nucleophile of acyl anion equivalent.[1] In the carbene analog, however, only a few acyclic dithiocarbenes[2-4] and ethylenedithiocarbene[2] to give fragmentation products have been reported. As compared with these carbenes, trimethylenedithiocarbene is of great interest both in its reactivity and as synthetic tool. In this paper I present a convenient synthesis of 1,3-dithian-2-one tosylhydrazone (II) and its carbenoid decomposition under several conditions.

Potassium 3-tosyldithiocarbazate (I) prepared[3] from tosylhydrazine and carbon disulfide in the presence of KOH in methanol was alkylated with 1,3-dibromopropane. After chromatography on silica gel were obtained tosylhydrazone (II) and 3-(tosylamino)tetrahydro-1,3-thiazine-2-thione (III) in 36 and 28% yields, respectively, along with 11% recovery of tosylhydrazine. The structures of II and III were established by the elemental analysis and spectroscopic data. The structure of III was confirmed by reduction with zinc in acetic acid to give tetrahydro-1,3-thiazine-2-thione (IV) in 74% yield, the structure of which was determined by direct comparison with a sample prepared by the authentic route.[5]

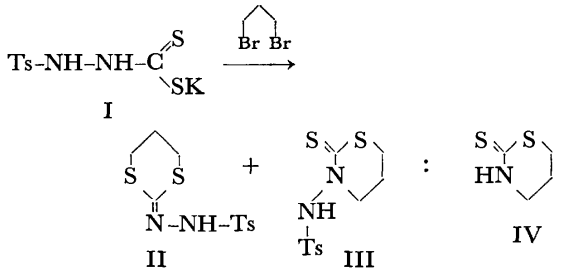

Sodium salt (V) was prepared from II and NaH in hexane and was subjected to carbenoid decomposition, the Bamford-Stevens reaction.[6] Thermal decomposition of V in pyridine and in DMF at 90—95 °C for 2 h gave 2,2'-bi(1,3-dithianylidene) (VII) in 36 and 29% yields, respectively. Similarly, irradiation of V in DMF with 500 W high-pressure mercury lamp yielded VII in 23% yield along with unknown products. The structure of VII was established by elemental analysis and mass and NMR spectra.

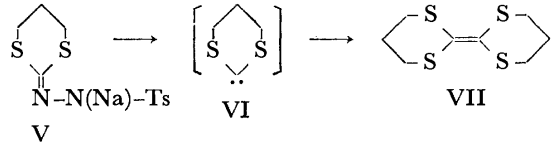

The formation of the dimer VII seems to be a good indication that trimethylenedithiocarbene (VI) is a real intermediate[7] in both thermal and photochemical reactions of V. This carbene is in marked contrast to ethylenedithiocarbene[2] in reactivity, which gave no dimerization product but only fragmentation products, ethylene and carbon disulfide.

Experimental

Reaction of Potassium 3-Tosyldithiocarbazate (I) with 1,3-Dibromopropane. A solution of KOH (1.74 g, 0.031 mol) in methanol (10 ml) was added to I (9.32 g, 0.031 mol) prepared by the method of Schöllkopf and Wiscott[3] and the mixture was stirred at 50 °C for 10 mim. To this solution was added dropwise 1,3-dibromopropane (8.08 g, 0.04 mol) in methanol (10 ml) during a period of 1 h under stirring and the mixture was stirred for 2 h at room temperature. Removal of the solvent and addition of benzene caused precipitation. After filtration, the filtrate was concentrated and the residue was chromatographed on silica gel. Elution with benzene gave 1,3-dithian-2-one tosylhydrazone (II) (3.28 g, 36%), mp 172—173 °C from hexane–CH_2Cl_2.

Found: C, 43.72; H, 4.64; N, 9.48%; mol wt: 302 (mass). Calcd for $C_{11}H_{14}O_2N_2S_3$: C, 43.71; H, 4.67; N, 9.72%, mol wt: 302.4. IR(KBr): 3160 (νN–H) and 1520 cm^{-1} (νC=N). NMR($CDCl_3$): δ 2.16 (m, 2H), 2.42 (s, 3H), 3.04 (m, 4H), 7.50 (s, 1H), and 7.80 (d, 2H). Elution with benzene–CH_2Cl_2 (2: 1) gave 3-(tosylamino)tetrahydro-1,3-thiazine-2-thione (III) (2.65 g, 28%), mp 100—101 °C from hexane–CH_2Cl_2.

Found: C, 43.79; H, 4.72; N, 9.78%; mol wt: 302 (mass). Calcd for $C_{11}H_{14}O_2N_2S_3$: C, 43.71; H, 4.67; N, 9.27%; mol wt: 302.4. IR(KBr): 3140 (νN–H) and 1540 cm^{-1} (νC=S). NMR($CDCl_3$): δ 2.42 (s+t, 5H), 3.00 (t, 2H), 4.10 (t, 2H), 7.28 (d, 2H), 7.70 (d, 2H), and 9.46 (d, 2H). Further elution with CH_2Cl_2 gave tosylhydrazine (0.66 g, 11%).

Redution of III with Zinc in Acetic Acid. 1.0 g Zn was added to a solution of III (0.40 g, 1.3 mmol) in AcOH (15 ml) and the resulting mixture was refluxed for 3 h. After filtration, the filtrate was concentrated and dried under reduced pressure. The residue was chromatographed on silica gel. Elution with CH_2Cl_2 gave tetrahydro-1,3-thiazine-2-thione (IV) (0.13 g, 74%), mp 132—133 °C from hexane–CH_2Cl_2 (lit,[5] mp 132 °C).

Thermal Decomposition of Sodium Salt of Tosylhydrazone (V) in Pyridine. A solution of V (1.0 g, 3.3 mmol) in pyridine (20 ml) was heated at 90—95 °C for 2 h with stirring under argon. After evaporation of the solvent under reduced pressure, CH_2Cl_2 solution of the residue was washed with water and dried with $MgSO_4$. After eveporation of CH_2Cl_2, the residue was chromatographed on silica gel. Elution with benzene gave 2,2'-bi(1,3-dithianylidene) (VII) (0.28 g, 36%), mp 140—141 °C from CH_2Cl_2–hexane (lit,[8] mp 140.8—141.6 °C).

Found: C, 40.43; H, 5.12%; mol wt: 236 (mass). Calcd for $C_8H_{12}S_4$: C, 40.68; H, 5.12%; mol wt: 236.4. NMR($CDCl_3$): δ 2.16 (m, 4H) and 2.94 (t, 8H).

Photochemical Decomposition of V in DMF. A solution of

V (1.0 g, 3.3 mmol) in DMF (20 ml) was irradiated with 500 W highpressure mercury lamp for 5 h at room temperature under argon. After a similar work-up to that mentioned above, chromatographing on silica gel of the mixture gave VII (0.18 g, 23%).

References

1) See, for example, D. Seebach, *Synthesis*, **1969**, 17; L. Field, *ibid.*, **1972**, 101.
2) D. M. Lemal and E. H. Banitt, *Tetrahedron Lett.*, **1964**, 245.
3) U. Schöllkopf and E. Wiskott, *Justus Liebigs Ann. Chem.*, **694**, 44 (1966).
4) D. Seebach, *Angew. Chem.*, **79**, 469 (1967).
5) F. M. Hamer and R. J. Rathbone, *J. Chem. Soc.*, **1943**, 243.
6) W. R. Bamford and T. S. Stevens, *J. Chem. Soc.*, **1952**, 4735.
7) See, for example, "Carbene," ed by M. Jones and R. A. Moss, John Wiley & Sons, New York (1973).
8) D. Seebach, *Angew. Chem.*, **79**, 468 (1967).

BULLETIN OF THE CHEMICAL SOCIETY OF JAPAN, VOL. 50 (8), 2189—2190 (1977)

Vilsmeier Reaction of Phenols. I. Synthesis of Aryl Formates[1)]

Syoji MORIMURA, Hideo HORIUCHI, and Keisuke MURAYAMA

Central Research Laboratories, Sankyo Co., Ltd., Shinagawa-ku, Tokyo 140

(Received January 27, 1977)

Synopsis The reaction of phenol and *o*-*t*-butylphenols with *N*,*N*-dimethylformamide–phosphoryl chloride complex in dimethylformamide afforded the corresponding formates in fairly good yields. The scope and limitation of *o*-formylation of highly sterically hindered phenols with the complex were also examined.

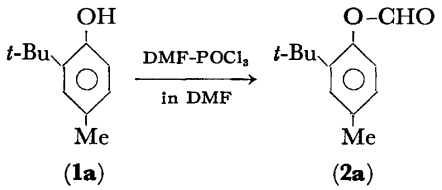

(**1a**) (**2a**)

Vilsmeier reagents have been shown to be effective in formylating the benzene nuclei of phenol derivatives. For example, the preparation of vanillin by the formylation of guaiacol with *N*-methylformanilide–phosphoryl chloride complex has been disclosed in an early patent.[2)] Furthermore, it has been shown that the hydroxyl group of picric acid is replaced by a chlorine atom when treated with (chloromethylene)dimethylammonium chloride.[3)] However, examples of formylation of the phenolic hydroxyl group by Vilsmeier reagent have not yet been reported. During the course of our study on the hindered phenol-type antioxidants, we have found that dimethylformamide–phosphoryl chloride (DMF–$POCl_3$) complex reacts with phenol derivatives to afford the formates in fairly good yields.

When 2-*t*-butyl-*p*-cresol (**1a**) was treated with DMF–$POCl_3$ complex in DMF at 80 °C for 5 h, the formate (**2a**) was obtained in 78% yield after hydrolysis of the reaction mixture. No product arising from the formylation of the benzene nucleus was isolated. The structure of **2a** was confirmed by the satisfactory analytical values and the following spectral data. The IR spectrum did not show OH absorption but exhibited the characteristic absorption at 1750 cm^{-1} for the ester carbonyl group. The NMR spectrum indicated the presence of three aromatic protons.

o-*t*-Butylphenols, **1b**—**g**, listed in the Table 1 also gave the corresponding formates, **2b**—**g**, when treated with DMF–$POCl_3$ complex. In the case of 6-*t*-butyl-*m*-cresol (**1d**), formation of the formate (**2d**) accompanied the production of 6-*t*-butyl-4-formyl-*m*-cresol (**3d**) as the minor product. The aldehyde **3d** showed carbonyl and hydroxyl absorptions at 1667 and 3320 cm^{-1} respectively in the IR spectrum, and the NMR spectrum exhibited two singlets at 7.50 and 7.28 ppm due to the isolated aromatic protons. Bis(5-*t*-butyl-4-hydroxy-2-methylphenyl sulfide (**1f**) is less reactive toward the complex, and a considerable amount of monoformate (**3f**) was obtained together with the diformate (**2f**) even when the reaction period was extended up to 24 h.

Further reactions with *o*,*o*′-disubstituted phenols such as 6-*t*-butyl-2,4-xylenol (**1h**) and 2,6-di-*t*-butyl-*p*-cresol (**1i**) were investigated in order to examine the limitation of the present method of formylation. The former phenol (**1h**) gave the formate (**2h**) in a low yield, whereas the latter (**1i**) was recovered after being treated with DMF–$POCl_3$ complex for 20 h at 85—95 °C. Employment of drastic reaction conditions (25 h at 120—125 °C) on the above reaction of **1i** resulted in the elimination of the *t*-butyl group, giving 2-*t*-butyl-4-methylphenyl formate (**2a**) in 76% yield.

6-*t*-Butyl-4-formyl-*m*-cresol (**3d**) was not formylated by DMF–$POCl_3$ complex. The inertness of this phenol is probably based on the deactivation due to the electron-

TABLE 1. REACTION OF DMF–$POCl_3$ COMPLEX WITH PHENOLS

Phenol	Reactant ratio (phenol: complex) (molar ratio)	React. temp (°C)	React. time (h)	Product	Yield (%)
2-*t*-Butyl-*p*-cresol (**1a**)	1:1.5	78—80	5	Formate (**2a**)	78
4,6-Di-*t*-butyl-*m*-cresol (**1b**)	1:1.5	80—90	3	Formate (**2b**)	82
2,4-Di-*t*-butylphenol (**1c**)	1:1.5	90—95	9	Formate (**2c**)	58
6-*t*-Butyl-*m*-cresol (**1d**)	1:1.5	70—80	3	Formate (**2d**)	83
				6-*t*-Butyl-4-formyl-*m*-cresol (**3d**)	10
1,1-Bis(5-*t*-butyl-4-hydroxy-2-methylphenyl)butane (**1e**)	1:3.0	95—100	8	Diformate (**2e**)	68
Bis(5-*t*-butyl-4-hydroxy-2-methylphenyl)sulfide (**1f**)	1:3.0	95—100	24	Diformate (**2f**)	38
				Monoformate (**3f**)	45
1,1,3-Tris(5-*t*-butyl-4-hydroxy-2-methylphenyl)butane (**1g**)	1:5.0	85—90	8	Triformate (2**g**)	71
6-*t*-Butyl-2,4-xylenol (**1h**)	1:1.5	85—90	20	Formate (**2h**)	10
2,6-Di-*t*-butyl-*p*-cresol (**1i**)	1:1.5	120—125	25	**2a**	76
Phenol (**1j**)	1:1.5	75—80	4	Formate (**2j**)	59

Table 2. Physical constants and analytical data of formates

Compd	Mp (°C) [Bp (°C/Torr)]	Molecular formula	Found (Calcd) C%	H%
2a	39.5—40.5	$C_{12}H_{16}O_2$	75.04 (74.97)	8.42 (8.39)
2b	78—79	$C_{16}H_{24}O_2$	77.28 (77.37)	9.66 (9.74)
2c	[112—115/3.5]	$C_{15}H_{22}O_2$	76.79 (76.88)	9.40 (9.46)
2d	[93—94/3.5]	$C_{12}H_{16}O_2$	74.91 (74.97)	8.43 (8.39)
3d	168—169	$C_{12}H_{16}O_2$	75.11 (74.97)	8.36 (8.39)
2e	77—78	$C_{28}H_{38}O_4$	76.66 (76.67)	8.67 (8.73)
2f	90—91	$C_{24}H_{30}O_4S$	69.48 (69.54)	7.36 (7.30)
3f	144—165	$C_{23}H_{30}O_3S$	71.38 (71.48)	7.89 (7.82)
2g	153.5—154.5	$C_{40}H_{52}O_6$	76.52 (76.40)	8.30 (8.34)
2h	[103.5—104.5/3.5]	$C_{13}H_{18}O_2$	75.72 (75.69)	8.74 (8.80)
2j	[87—88/24]	$C_7H_6O_2$	68.70 (68.84)	4.87 (4.95)

withdrawing formyl function.

In connection with the formation of the formates from the hindered phenols, the formylation of phenol (**1j**) was also investigated. It had previously been reported that *p*-hydroxybenzaldehyde (**3j**) was obtained in a low yield when **1j** was heated with an equimolar mixture of DMF and $POCl_3$.[4] In the present work, the reaction was carried out using excess DMF as the solvent, and phenyl formate (**2j**) was obtained in 59% yield. The aldehyde, **3j**, was not isolated.

The formates of hindered phenols prepared in this work were shown to be useful for preventing the degradation of several synthetic polymers.[5]

Experimental

*Reaction of DMF–$POCl_3$ Complex with Phenols (**1a—1i**).* An example is cited for the reaction with 2-*t*-butyl-*p*-cresol (**1a**). Similar procedures were used in the reactions with other phenols. The products, **2b**, **3d**, and **2f**, were purified by recrystallization from ethanol, and **2e**, **3f**, and **2g** from benzene. Purification of the oily products, **2c**, **2d**, and **2i** was effected by distillation under reduced pressure. Results of elemental analyses of the products are given in Table 2. To a stirred solution of 16.4 g (0.1 mol) of **1a** in 40 ml of DMF, 22.6 g (0.15 mol) of $POCl_3$ added dropwise at 0—5 °C. After being stirred for 1 h at room temp, the mixture was heated slowly to 80 °C and kept at 78—80 °C for 5 h. To this reaction mixture were added 300 ml of hexane and then 240 ml of 10% aqueous sodium acetate at 0—5 °C with stirring. The hexane solution was separated, washed successively with clod aqueous $NaHCO_3$ and ice-water, and dried over Na_2SO_4. The solvent was removed under reduced pressure at temp below 50 °C, and the residue was recrystallized from ether to give 14.4 g (78%) of the formate, **2a**, mp 39.5—40.5 °C. IR (Nujol) 1750 cm^{-1} (C=O). NMR (CCl_4) δ 1.35 (s, 9H, -C-($C\underline{H}_3$)$_3$), 2.32 (s, 3H, -$C\underline{H}_3$), 6.84 (d, J=8.0 Hz, 1H, C_6-$\underline{H}$), 7.06 (d-d, J=8.0 and 2.0 Hz, 1H, C_5-$\underline{H}$), 7.22 (d, J=2.0 Hz, 1H, C_3-$\underline{H}$), 8.29 (s, 1H, -C$\underline{H}$O).

The authors are grateful to Dr. Ko Arima, Director of this Laboratories, for his encouragement throughout this study. They are also indebted to the members of the Analytical Section of this Laboratories for the elemental analyses and the spectral data.

References

1) Presented at the 21st National Meeting of the Chemical Society of Japan, April, 1968.

2) G. Kalischer, H. Scheyer, and K. Keller, Ger. Patent 514415 (1927).

3) H. Eilingsfeld, M. Seefelder, and H. Weidinger, *Angew. Chem.* **72**, 836 (1960).

4) N. P. Buu-Hoi, N, D. Xuong, M. Sy, G. Lejeune, and N. B. Tien, *Bull. Soc. Chim. Fr.*, **1955**, 1954.

5) K. Murayama, S. Morimura, T. Yoshioka, H. Horiuchi, S. Akagi, T. Kurumada, and I. Watanabe, Jpn. Patent 543832 (1968); U. S. Patent 3437633 (1969).

BULLETIN OF THE CHEMICAL SOCIETY OF JAPAN, VOL. 50 (8), 2191—2192 (1977)

A New Synthesis of 4-Methoxy-6-valeryl-5,6-dihydro-2-pyrone*

Akira TAKEDA, Eiichiro AMANO, and Sadao TSUBOI

Department of Synthetic Chemistry, School of Engineering, Okayama University, Tsushima, Okayama 700

(Received February 2, 1977)

Synopsis. The reaction of ethyl 2-acetoxy-3-oxoheptanoate with γ-bromo-β-methoxy-*cis*-crotonate in the presence of sodium ethoxide afforded diethyl 3-methoxy-5-hydroxy-5-valeryl-2-hexenedioate (**7**) in 65% yield. Treatment of **7** with a dilute aqueous NaOH in acetone gave (±)-4-methoxy-6-valeryl-5,6-dihydro-2-pyrone, a key intermediate leading to pestalotin, in 41% yield.

Several reports have appeared on the synthesis of the pestalotin (**1**),[1-7] a gibberellin synergist isolated by Kimura and Tamura from the culture broth of *Pestalotia cryptomeriaecola* Sawada. First total synthesis of optically active pestalotin was accomplished by Seebach and Meyer[6] by the asymmetric reduction of (±)-4-methoxy-6-valeryl-5,6-dihydro-2-pyrone (**2**) in *ca.* 10% optical yield. They obtained dihydropyrone **2** *via* its 1,3-dithiane derivative. This paper deals with a convenient, alternative synthesis of dihydropyrone **2**.

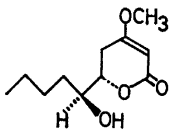

1

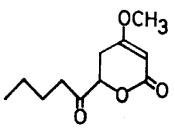

2

Chlorination of ethyl 3-oxoheptanoate (**3**) with sulfuryl chloride gave ethyl 2-chloro-3-oxoheptanoate (**4**) in 88% yield. This was converted into ethyl 2-acetoxy-3-oxoheptanoate (**5**)[9] by the action of potassium acetate in 61% yield. Reaction of the ester **5** with ethyl γ-bromo-β-methoxy-*cis*-crotonate (**6**) in the presence of sodium ethoxide afforded diester **7** in 65% yield. Treatment of **7** with a weak aqueous NaOH in acetone gave the desired dihydropyrone **2** in 41% yield. The spectral data (IR, NMR) of this product support its structure. Reduction of **2** with sodium borohydride in aqueous dioxane gave a mixture of (±)-pestalotin and (±)-epipestalotin in 90% yield.

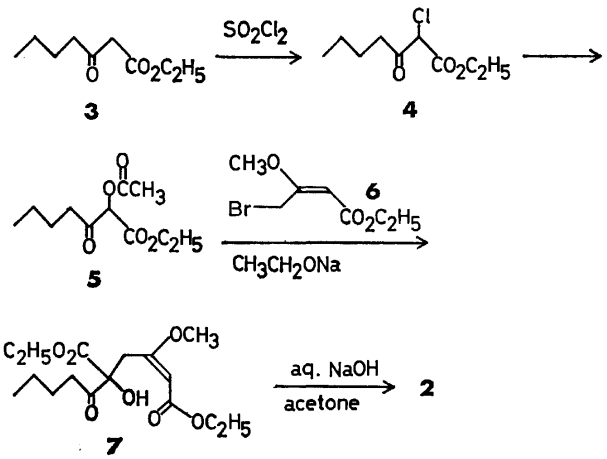

* Presented at the 32nd National Meeting of the Chemical Society of Japan, Tokyo, April 1975.

Experimental

Melting points and boiling points are uncorrected. UV spectra were taken with a Hitachi Model EPS-3T recording spectrophotometer, IR spectra with a Hitachi Model EPI-S2 spectrometer, NMR spectra (60 MHz) with a Hitachi Model R-24 spectrometer, and MS spectra with a Hitachi Model RMS-4 mass spectrometer (70 eV). Analytical and preparative TLC were carried out on silica gel PF_{254} (E. Merck AG, Darmstadt) with layers of 0.25 mm and 1.0 mm thickness, respectively. Compounds **3** and **6** were prepared according to the methods of Anderson *et al.*[10] and Ellestad *et al.*,[3] respectively.

Ethyl 2-Chloro-3-oxoheptanoate (4). To a solution of ethyl 3-oxoheptanoate (**3**) (80 g, 0.47 mol) in 90 ml of dichloromethane was added slowly 63.5 g (0.47 mol) of sulfuryl chloride at a temperature below 45 °C. After the addition was over the mixture was refluxed for 2 h. Removal of the solvent left a clean oil which, on distillation, gave 84.5 g (88%) of **4**; bp 130—135 °C/30 Torr; IR (neat) 1750—1710 (C=O), 1630 (C=C), and 1600 cm^{-1} (enolic C=O); NMR ($CDCl_3$) δ 0.90 (t, 3H, J=6 Hz, $C\underline{H}_3(CH_2)_3$–), 1.0—1.7 (m, 4H, $CH_3(C\underline{H}_2)_2CH_2$–), 1.30 (t, 3H, J=7.5 Hz, $CO_2CH_2C\underline{H}_3$), 2.61 (t, 2H, J=6 Hz, –$C\underline{H}_2CO$–), 4.25 (q, 2H, J=7.5 Hz, $CO_2C\underline{H}_2CH_3$), and 4.72 ppm (s, 1H, –C<u>H</u>Cl–).

Ethyl 2-Acetoxy-3-oxoheptanoate (5). This compound was prepared according to the procedure given by Henecka.[8] To a mixture of potassium acetate (106 g, 1.08 mol), acetic acid (300 ml) and acetic anhydride (20 ml) was added 81.8 g (0.4 mol) of **4** at 110 °C. The mixture was stirred at 135 °C for 6 h. The solvent was removed *in vacuo*, and the residue was neutralized with dilute aqueous $NaHCO_3$. The organic layer was extracted with ether, washed with water, and dried over $MgSO_4$. After removal of the solvent the residue was distilled to give 56.3 g (61%) of **5**: bp 129—135 °C/8 Torr (lit,[9] bp 138—140 °C/17 Torr); IR (neat) 1750—1715 (C=O); NMR ($CDCl_3$) δ 0.91 (t, 3H, J=6 Hz, $C\underline{H}_3(CH_2)_3$–), 1.28 (t, 3H, J=7.5 Hz, $CO_2CH_2C\underline{H}_3$), 1.0—1.8 (m, 4H, $CH_3(C\underline{H}_2)_2CH_2$–), 2.14 (s, 3H, –$OCOC\underline{H}_3$), 2.56 (br, t, 2H, J=6.5 Hz, $CH_3(CH_2)_2C\underline{H}_2$–), 4.18 (q, 2H, J=7.5 Hz, $CO_2C\underline{H}_2CH_3$), and 5.29 ppm (s, 1H, –C<u>H</u>$CO_2C_2H_5$); MS (70 eV) *m/e* (rel intensity) 188 (4), 185 (4), 146 (39), 104 (83), 85 (100), 76 (26), 57 (98).

Diethyl 3-Methoxy-5-hydroxy-5-valeryl-2-hexenedioate (7). Sodium (1.15 g, 0.05 mol) was dissolved in 75 ml of absolute ethanol, 11.5 g (0.05 mol) of the ester **5** being added dropwise at 0—5 °C. The mixture was stirred for 2.5 h at room temperature, and to this was added dropwise 11.2 g (0.05 mol) of ethyl γ-bromo-β-methoxy-*cis*-crotonate (**6**) at 5 °C. The resulting mixture was brought to room temperature, and then stirred for 1 h. After it was made weakly acidic, the solvent was removed. The residue was extracted with ether, and the ethereal layer was washded with water and dried over $MgSO_4$. Removal of the solvent left a clean oil which, on

distillation, gave 10.2 g (65%) of **7**: bp 168—170 °C/0.06 Torr: IR (neat) 3455 (OH), 1740 (ester C=O), 1720 (ketone C=O), 1680 (conjugated ester C=O), and 1630 cm^{-1} (C=C); NMR ($CDCl_3$) δ 0.90 (t, 3H, J=6 Hz, $C\underline{H}_3(CH_2)_3CO$–), 1.25 (t, 6H, J=7.5 Hz, 2 $CO_2CH_2C\underline{H}_3$), 1.00—1.90 (m, 4H, $CH_3(C\underline{H}_2)_2CH_2CO$–), 2.3—2.8 (m, 4H, $-C\underline{H}_2C(OCH_3)$=CH– and $CH_3(CH_2)_2C\underline{H}_2CO$–), 3.56 (s, 3H, $C\underline{H}_3O$–), 4.18 (q, 4H, 2 $CO_2C\underline{H}_2CH_3$), 4.90 (s, 1H, O<u>H</u>), and 5.19 ppm (s, –C<u>H</u>=C〈).

Found: C, 57.90; H, 7.92%. Calcd for $C_{16}H_{26}O_7$: C, 58.17; H, 7.93%.

4-Methoxy-6-valeryl-5,6-dihydro-2-pyrone (2). To a solution of 1.0 g, (3 mmol) of **7** in 90 ml of acetone was added 60 ml of 0.2 M aqueous NaOH at room temperature during a period of 3 min. After being stirred for 2 h, the mixture was poured into a large amount of water. Acetone was removed *in vacuo*. The residue was extracted with ether, washed with water, and then dried over $MgSO_4$. Removal of the solvent left 0.27 g (41%) of **2**: mp 82—83 °C (from hexane) (lit,[6] mp 83 °C): IR (KBr) 1705 (C=O), 1690 (shoulder, conjugate C=O), and 1620 cm^{-1} (C=C); NMR ($CDCl_3$) δ 0.90 [t, 3H, $C\underline{H}_3(CH_2)_3$–), 1.10—1.90 (m, 4H, $CH_3(C\underline{H}_2)_2$-CH_2CO–), 2.50—3.00 (m, 4H, $-C\underline{H}_2C(OCH_3)$=CH– and $CH_3(CH_2)_2C\underline{H}_2CO$–), 3.72 (s, 3H, $C\underline{H}_3O$–), 4.70 (t, 1H, –COC<u>H</u>–O–), and 5.13 ppm (s, 1H, –C<u>H</u>=C〈).

Reduction of **2** *with Sodium Borohydride.* To a solution of dihydro-2-pyrone **2** (88 mg, 0.42 mmol) in 0.3 ml of 75% aqueous dioxane was added dropwise a solution of $NaBH_4$ (17 mg, 0.42 mmol) in 0.3 ml of 75% aqueous dioxane with stirring at 25 °C. After being stirred for 3 h the mixture was acidified with dilute H_2SO_4, and extracted with chloroform. The chloroform extract was dried over $MgSO_4$, and evaporated to yield 80 mg (90%) of an oil which showed one spot at TLC (benzene: ethyl acetate=1: 1, R_f=0.35). This was subjected to preparative TLC for analysis and spectral determinations: IR (neat) 3430, 1710—1670, and 1630 cm^{-1}; NMR ($CDCl_3$) δ 0.9 (t, br, 3H), 1.1—1.7 (m, br, 6H,) 1.95—2.2 (s, br, 1H, OH), 2.20 (m, 1H, ring methylene), 2.81 (m, 1H, ring methylene), 3.72 (m, br, 1H, –C<u>H</u>(OH)–), 3.74 (s, 3H, CH_3O–), 4.28 (m, 1H, ring >H<u>C</u>–O–), and 5.14 ppm (d, 1H, =C<u>H</u>); MS (70 eV) *m/e* (rel intensity) 214 (M^+), 127 (base peak); UV λ_{max} 233 nm (ε=12000, 95% EtOH).

Found: C, 61.86; H, 8.22%. Calcd for $C_{11}H_{18}O_4$: C, 61.66; H, 8.47%.

The authors wish to express their gratitude to Dr. Yasuo Kimura, The University of Tokyo, for the supply of IR and NMR spectra of pestalotin.

The present work was partially supported by a Grant-in-Aid for Scientific Research from the Ministry of Education (Grant No. 647079).

References

1) Y. Kimura, K. Katagiri, T. Inoue, and S. Tamura, *Agric. Biol. Chem.*, **35**, 1313 (1971).

2) Y. Kimura, K. Katagiri, and S. Tamura, *Tetrahedron Lett.*, **1971**, 3137.

3) G. A. Ellestad, W. J. McGahren, and M. P. Kunstmann *J. Org. Chem.*, **37**, 2045 (1972).

4) K. Kimura and S. Tamura, *Agric. Biol. Chem.*, **36**, 1925 (1972).

5) R. M. Carlson and A. R. Oyler, *Tetrahedron Lett.*, **1974**, 2615.

6) D. Seebach and H. Meyer, *Angew. Chem.*, **86**, 40 (1974).

7) K. Mori, M. Oda, and M. Matsui, *Tetrahedron Lett.*, **1976**, 3173.

8) H. Henecka, *Chem. Ber.*, **81**, 188 (1948).

9) N. Sugiyama, M. Yamamoto, T. Takano, and C, Kashima, *Bull. Chem. Soc. Jpn.*, **40**, 2909 (1967).

10) G. W. Anderson, I. F. Halverstadt, W. H. Miller, and R. O. Roblin, Jr., *J. Am. Chem. Soc.*, **67**, 2197 (1945).

BULLETIN OF THE CHEMICAL SOCIETY OF JAPAN, VOL. 50 (8), 2193—2194 (1977)

Mono *S*-Acylated 1,8-Naphthalenedithiol. Isolation and Characterization of Tetrahedral Intermediate in the Intramolecular Acyl Transfer Reaction

Makoto TAKAGI, Ryoji ISHIHARA, and Tsutomu MATSUDA

Department of Organic Synthesis, Faculty of Engineering, Kyushu University, Hakozaki, Higashi-ku, Fukuoka 812

(Received February 8, 1977)

Synopsis. The tetrahedral intermediate in the intramolecular acyl transfer reaction of mono-*S*-acylated 1,8-naphthalenedithiol was found to be sufficiently stable to allow isolation or direct characterization by spectroscopy. Formation of carbenium ion from the intermediate is suggested in sulfuric acid.

Mono-*S*-benzoylation of 1,8-naphthalenedithiol with benzoyl chloride in pyridine under nitrogen afforded the compound with correct data of elemental analysis after purification by column chromatography on silica gel or by simple recrystallization (60—75% yield as monobenzoate). Its IR spectra (Nujol mull), however, show a strong ν_{O-H} band around 3300 cm^{-1} but no absorption for $\nu_{C=O}$ or ν_{S-H}. The crystals obtained from carbon tetrachloride or benzene–petroleum ether gave a slightly yellowish coloration and mp 121—123 °C. Recrystallization from methanol or ethanol afforded white crystals with 1/4 molecule of the solvent (mp of the methanol adduct, 80—81.5 °C), which on evacuation at 70 °C over P_2O_5 turned to the same yellowish material. Mass spectra showed M^+ at *m/e* 296 (relative intensity, 19%) and $C_7H_5CO^+$ at *m/e* 105 (100%). In contrast to the IR spectra in solid state, the solution spectra in chloroform show a strong carbonyl band at 1675 cm^{-1} indicating the presence of normal functional group for ArSCOPh. In the ^1H NMR spectra in $CDCl_3$, only a sharp singlet for S–H (1H, δ 3.97 from TMS) was present besides the complex multiplets for aromatic protons (11H, δ 7.05—8.15). The sample recrystallized from methanol and ethanol showed additional broad singlets for O–H protons centered at δ 2.60 and δ 3.05, respectively, as well as the normal proton signals for methyl and ethyl groups. The signal for S–H was not affected appreciably by the presence of alcohol when the measurements were made at relatively low sample concentrations (5%). The results indicate that monobenzoylated 1,8-naphthalenedithiol can exist in two isomeric forms, 8-benzoylthio-1-naphthalenethiol (**1**) and 2-phenylnaphtho[1,8-*de*][1,3]dithian-2-ol (**2**). The latter is isolable as solid only by a fortuitous stabilization in the crystal lattice, the former structure being energetically favorable in solution.

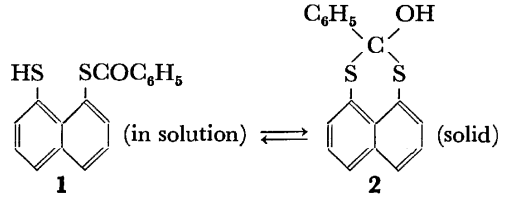

A similar attempt for the preparation of the monoacetyl derivative by the reaction with acetic anhydride yielded a viscous oil after purification on silica gel (25% yield as monoacetate).[1] This preparation gave the exact result in elemental analysis for the expected thioester. However, the IR spectra (neat) showed only a weak carbonyl band at 1690 cm^{-1} and strong ν_{O-H} band at 3300 cm^{-1}, indicating the presence of substantial amount of O–H containing species. Thus, the NMR spectra in $CDCl_3$ consist of two sets of signals, which most probably arise from the two structural isomers **3** and **4** (Fig. 1), analogous to those for the monobenzoate derivative. In contrast to the benzoyl

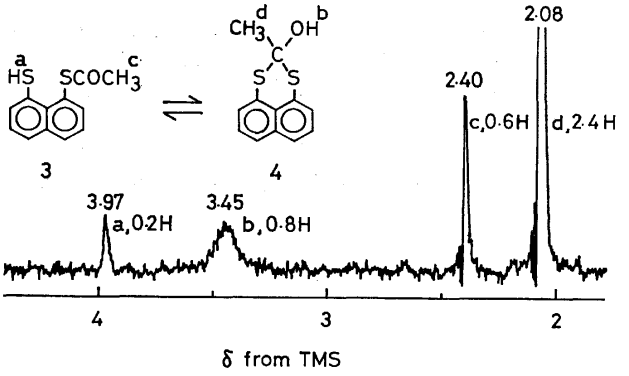

Fig. 1. NMR spectrum of monoacetylated 1,8-naphthalenedithiol ($CDCl_3$).

derivative, the cyclic isomer **4** is more favored as compared to **3** in the ratio *ca.* 4: 1. This is understandable if we recall the fact that the resonance stabilization associated with the conjugation between carbonyl and phenyl groups is eliminated on going from **1** to **2**. The equilibrium is also dependent on the nature of the solvent. In deuteriated methanol only one species, probably **4**, was observed in the NMR spectrum (one methyl signal in the high-field side, δ 2.03; however, the possibility that the two isomers are in rapid equilibrium in NMR time scale can not be excluded), and the carbonyl band at 1670 cm^{-1} was very weak in intensity. It is reasonable that the hydroxylic medium favors the formation of **4**, since the latter would be more stabilized than **3** in virtue of hydrogen bonding interaction with the solvent.

Another property related to the stability of the cyclic structure is the behavior in a strong acid. As an example, **3** (**4**) dissolves in 96% sulfuric acid with intense bluish-violet coloration, showing a single methyl signal at δ 2.75 (ppm from external TMS) and multiplet at δ 7.0—8.0. The former is featured by a considerable down-field shift as compared to that of **3** or **4**. Dilution of the solution with cold water gave only a trace of

recovered **3** (**4**), affording **5** as white crystalline solid. Compound **5** (mp 130—131 °C; $\nu_{C=O}$, 1690 cm^{-1}; NMR in $CDCl_3$, δ 1.78 (s, 3H), 2.23 (s, 3H), 7.1—8.0 (m, 12H), confirmed also by EA and molecular weight measurement by osmometer) was isolable as a by-product by monoacetylation in 20% yield. This is presumably formed by acid catalysed bimolecular condensation of **3** and **4** during the course of isolation. The solution of **5** in H_2SO_4 gave identical NMR signals to those of **3** (**4**). Though the evidences are preliminary, they seem to indicate the formation of carbenium ion **6**[2] in sulfuric acid solution.

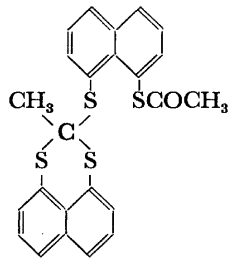

5

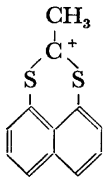

6

It is interesting that the structures of **2** and **4** embody the tetrahedral addition intermediate from the ester (RCOSR') and the nucleophile (R'SH) of interest in acyl transfer mechanism, whose isolation and characterization have only recently been successfully carried out for a specifically designed polyfunctional compound directed to the study of enzyme-like catalysis for acyl transfer processes.[3] The facile formation of the tetrahedral intermediate for the present compounds is undoubtedly related to the unique spatial disposition of the two aromatic thiyl groups around the hemiacylal carbon. For the monoacylated analogues derived from aliphatic 1,3-dithiols,[4] no such intermediates were detected.[5]

References

1) A photochemical method has been described for the preparation of monoacyl derivative of 1,8-naphthalenedithiol (Ref. 4), but the ordinary acylation practice proved to be more convenient for large scale synthesis.

2) **6** seems to be the first example of dithiyl-substituted carbenium ion from 1,8-naphthalenedithiol.

3) G. A. Rogers and T. C. Bruice, *J. Am. Chem. Soc.*, **96**, 2481 (1974).

4) M. Takagi, S. Goto, and T. Matsuda, *J. Chem. Soc., Chem. Commun.*, **1976**, 92.

5) In sulfuric acid, however, the aliphatic analogues were found to behave somewhat similarly. 1,3-Dithiol is a structural unit of coenzyme dihydrolipoic acid which functions as an acetyl carrier in pyruvate dehydrogenase. In this connection, thermodynamic stability of the tetrahedral addition intermediate exhibited by mono-*S*-acetylated 1,8-naphthalenedithiol should not be overlooked. However, implications based on a simple structural analogy between the aromatic and aliphatic 1,3-dithiols should not be made.

BULLETIN OF THE CHEMICAL SOCIETY OF JAPAN, VOL. 50 (8), 2195—2196 (1977)

Light Induced Tritiation of Methyl Benzoate with Diethylamine-*N*-*t* and Triethylamine-Tritiated Water Mixture

Akihide KITAMURA, Hiroyuki KANEKO,* Naotake MORIKAWA,** Kunio OOHASHI,**
Hirochika SAKURAGI,* Katsumi TOKUMARU, Mamoru UMEDA,* and Masayuki YOSHIDA*

Institute of Chemistry, The University of Tsukuba, Sakura-mura, Ibaraki 300-31
**Department of Chemistry, Faculty of Science, The University of Tokyo, Bunkyo-ku, Tokyo 113*
***Radioisotope Centre, The University of Tokyo, Bunkyo-ku, Tokyo 113*

(Received February 18, 1977)

Synopsis. Methyl benzoate was tritiated at both nuclear and methyl positions on irradiation with diethylamine-*N*-*t* in benzene and with triethylamine–tritiated water in acetonitrile.

In a previous paper we demonstrated that irradiation of benzonitrile with diethylamine-*N*-*t* or a triethylamine–tritiated water mixture causes tritium uptake in the nucleus of benzonitrile, and proposed a mechanism involving the exciplex between benzonitrile and the amines.[1] In this paper we wish to report on our studies of methyl benzoate: irradiation of methyl benzoate with diethylamine-*N*-*t* and a triethylamine–tritiated water mixture, as well as 1-propanethiol-*S*-*t*,[2] brings about the incorporation of tritium not only in the nucleus but also in the methyl group of the ester.

Results and Discussion

A mixture of methyl benzoate, benzene, and diethylamine-*N*-*t* was irradiated with a 1 kW high pressure mercury arc lamp for 30 h. The aromatic compounds were separated by fractional distillation and submitted to tritium assay. Methyl benzoate was degraded by the known procedures[3] in order to determine the tritium distribution. Light induced tritiation of methyl benzoate was also carried out with triethylamine and tritiated water in acetonitrile. Methyl benzoate was recovered and degraded in a similar way.

The rates of nuclear tritiation of methyl benzoate relative to benzene (k_N/k_B) and relative to the methyl group of the ester (k_N/k_M) and the tritium distribution in the nucleus of the ester are shown in Table 1. The relative rate, k_N/k_B, is high and the order of reactivity among the nuclear positions is *para*≫*ortho*>*meta* in the tritiation with both diethylamine-*N*-*t* and the mixture of triethylamine and tritiated water. These results are similar to those obtained for benzonitrile,[1] suggesting the following mechanism for the tritiation of methyl benzoate with diethylamine-*N*-*t*:

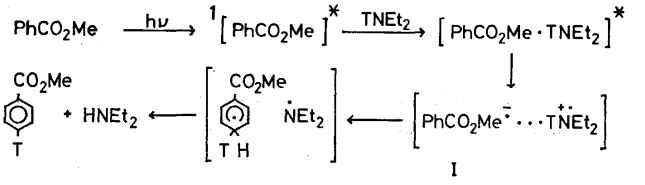

The singlet excited methyl benzoate forms an exciplex with the amine, which collapses to a radical cation and a radical anion (I). Triton transfer from the former to the latter produces a radical pair of a cyclohexadienyl radical and a diethylaminyl radical, which in turn disproportionates, leading to the tritiation of methyl benzoate. In the tritiation with triethylamine triton is transferred to the radical anion, I, from tritiated water.

In order to estimate the nature of the postulated radical anion, its charge density was calculated by the molecular orbital method using the CNDO/2 approximation.[4] The geometry of I was assumed to be planar with the benzene ring and the methyl group apart and was constructed by using the standard bond lengths and angles.[5] The results show that the charge on the *meta* carbons is slightly positive ($C_{meta}=+0.006$), while those on the *ortho* and *para* carbons are greatly negative ($C_{ortho}=-0.057$ and $C_{para}=-0.119$). Although the geometry used for the calculation was not optimized, the charge distribution pattern itself did not change seriously for small variant in the geometry. The similarity between the charge density and the tritium distribution pattern may be taken as indicating the intermediacy of the methyl benzoate radical anion, I, in the tritiation.

More remarkable is the methyl tritiation, of which specific mention must be made. The finding that no tritiation occurred at both methyl and nuclear positions on irradiation of methyl benzoate with tritiated water in the absence of triethylamine suggests that the methyl tritiation proceeds through the radical anion, I, or at least through the exciplex between methyl benzoate and the amines. The radical anion, I, might take intramolecularly a proton from the methyl group, producing a carbanion (II), which then undergoes a set of triton capture and protium loss, leading to methyl

TABLE 1. LIGHT INDUCED TRITIATION OF METHYL BENZOATE

Triton donor	Tritium distribution (%)[a]			k_N/k_B[b]	k_N/k_M[c]
	ortho	*meta*	*para*		
Diethylamine-*N*-*t*	17	1	82	183	12
Triethylamine and tritiated water	8	trace	92		4
1-Propanethiol-*S*-*t*	17[d]	1[d]	82[d]	421[d]	8[e]

a) Average values of data obtained by duplicate runs. b) Rate (per C–H bond) of nuclear tritiation of methyl benzoate relative to benzene. c) Rate (per C–H bond) of nuclear tritiation relative to the methyl group. d) Data taken from Ref. 1. e) Unpublished data.

tritiation. If these reaction pathways were operating,

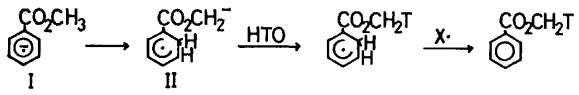

the use of methyl-*t* benzoate as the starting ester would lead to the incorporation of tritium in the nucleus. Thus, a mixture of methyl-*t* benzoate, triethylamine, water, and acetonitrile was exposed to light from the 1 kW lamp for 30 h. For the recovered methyl benzoate, no incorporation was observed in the nucleus and the mechanism involving the proton (triton) transfer from the methyl group to the nucleus is improbable.

Under illumination the radical anion, I, might be excited to a higher electronic state represented by structure III. The excited radical anion, III, could intramolecularly abstract a hydrogen atom from the methyl group to afford another radical anion (IV), in which the proton on the hydroxy group would be exchangeable with tritons in the system. The resulting radical anion-*O*-*t* would decay to the starting radical anion, I, containing a triton at the methyl group.

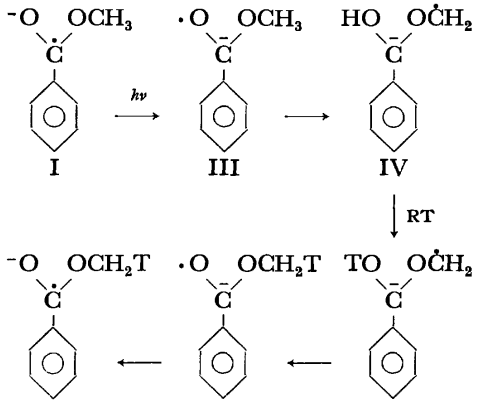

Although no direct evidence was obtained for this mechanism, it is rationalized by the aforementioned circumstantial evidence; the tritiation with tritiated water proceeds only in the presence of triethylamine and the extent of the tritiation of the methyl group relative to that of the nucleus is not much affected by varying the triton donors. Accordingly, we suppose the above mechanism most probable.

Experimental

Materials. Benzene, triethylamine, and methyl benzoate were purified by distillation or vacuum distillation. Diethylamine-*N*-*t* was prepared by the method reported.[1] Methyl-*t* benzoate was prepared in the usual way from the reaction of methanol-*t* (1.72 g, 53.8 mmol, 51.5 mCi/mol) with benzoyl chloride (7.19 g, 51.2 mmol) in hexane (20 ml) in the presence of pyridine (4.5 ml), and distilled *in vacuo* (6.08 g, 87%, 43.5 mCi/mol, radiochemical yield: 71%).

Tritiation of Methyl Benzoate with Diethylamine-N-t. A mixture of diethylamine-*N*-*t* (1.18 g, 16.2 mmol, 2.19 Ci/mol), methyl benzoate (10.6 g, 77.7 mmol), and benzene (6.06 g, 77.7 mmol) was irradiated in a Pyrex tube under nitrogen for 30 h with a 1 kW high pressure mercury arc lamp. The reaction mixture was washed with 1 M sulfuric acid and water to remove the amine, and the aromatic compounds were separated by distillation. Benzene and methyl benzoate were further purified by fractional distillation and submitted to tritium assay (benzene, 3.64×10^{-3} mCi/mol; methyl benzoate, 0.581 mCi/mol). Methyl benzoate was hydrolyzed with a sodium hydroxide solution. Benzoic acid, isolated and purified by recrystallization, was submitted to tritium assay (0.554 mCi/mol).

Tritiation with Triethylamine and Tritiated Water. A solution of methyl benzoate (2.64 g, 19.4 mmol), triethylamine (1.46 g, 14.4 mmol), and tritiated water (2 ml, 111 mmol, 335 mCi/mol) in acetonitrile (10 ml) was irradiated in a Pyrex tube under argon for 30 h with a 1 kw lamp. Triethylamine, acetonitrile, and water were removed by distillation, and the residual methyl benzoate was washed with watre and fractionally distilled. Methyl benzoate purified and benzoic acid obtained by hydrolysis of the ester were submitted to tritium assay (methyl benzoate, 0.541 mCi/mol; benzoic acid, 0.477 mCi/mol).

Irradiation of Methyl Benzoate with Tritiated Water. A solution of methyl benzoate (5.28 g, 38.8 mmol) and tritiated water (4 ml, 222 mmol, 123 mCi/mol) in acetonitrile (20 ml) was irradiated for 30 h with a 1 kW lamp and treated in a similar way to that above mentioned. No tritium was found to be incorporated in methyl benzoate.

*Irradiation of Methyl-*t *Benzoate in the Presence of Triethylamine and Water.* A solution of methyl-*t* benzoate (7.92 g, 58.2 mmol, 3.63 mCi/mol), triethylamine (4.37 g, 43.2 mmol), and water (6 ml, 333 mmol) in acetonitrile (30 ml) was irradiated with a 1 kW lamp. No tritium was found to be incorporated in benzoic acid obtained after the usual work-up.

Degradation of benzoic acid for the determination of tritium distribution and tritium activity measurements were carried out as reported.[1]

References

1) M. Yoshida, H. Kaneko, A. Kitamura, T. Ito, K. Oohashi, N. Morikawa, H. Sakuragi, and K. Tokumaru, *Bull. Chem. Soc., Jpn.*, **49**, 1697 (1976).

2) H. Takiguchi, K. G. Yoshida, H. Ouchi, M. Yoshida, N. Morikawa, and O. Simamura, *Chem. Lett.*, **1974**, 593.

3) W. A. Bonner, *J. Am. Chem. Soc.*, **79**, 2469 (1957); R. M. White and F. S. Rowland, *ibid.*, **82**, 4713 (1960).

4) J. A. Pople and G. A. Segal, *J. Chem. Phys.*, **44**, 3289 (1966).

5) J. A. Pople and D. L. Beveridge, "Approximate Molecular Orbital Theory," McGraw-Hill, New York (1970), p. 110.

BULLETIN OF THE CHEMICAL SOCIETY OF JAPAN, VOL. 50 (8), 2197—2198 (1977)

5-Fluorouracil Derivatives. II.[1] A Convenient Synthesis of 5-Fluoro-2′-deoxyuridine

Shoichiro OZAKI, Tsutomu KATAKAMI, and Mineo SANEYOSHI*

Research Center, Mitsui Toatsu Chemicals, Inc., 1190 Kasama-cho, Totsuka-ku, Yokohama 247

**Faculty of Pharmaceutical Sciences, Hokkaido University, Sapporo 060*

(Received February 21, 1977)

Synopsis. The reaction of 5-fluorouridine with propionyl bromide in acetonitrile afforded 3′,5′-di-*O*-propionyl-2′-bromo-5-fluoro-2′-deoxyuridine (**2**). Compound **2** was then hydrogenated, using Pd–C as the catalyst, to afford 3′,5′-di-*O*-propionyl-5-fluoro-2′-deoxyuridine (**3**). Compound **3** was deacylated with methanolic ammonia to give 5-fluoro-2′-deoxyuridine (FUDR). In this way, FUDR, a good antitumor agent, can easily be prepared from 5-fluorouridine by three steps in a 48.9% total yield.

5-Fluoro-2′-deoxyuridine (FUDR, **4**) was first prepared by enzymic procedures[2] and then by the chemical condensation method using a mercury-process.[3] In the latter process, methyl 2-deoxy-D-ribofuranoside was converted to the 3,5-di-*O*-*p*-toluoyl derivative, which was treated with HCl to give 3,5-di-*O*-*p*-toluoyl-2-deoxy-D-ribosyl chloride. 5-Fluorouracil-mercury was synthesized from 5-fluorouracil and mercury(II) acetate. The condensation of 3,5-di-*O*-*p*-toluoyl-2-deoxy-D-ribosyl chloride with 5-fluorouracil-mercury and the subsequent deacylation of the condensation product yielded **4** in a 30.8% total yield. Autitumor activities of **4** were demonstrated in several experimental tumors[4,5] and by clinical studies.[6]

Compound **4**, an approved drug for clinical use, has a remarkable anti-tumor activity with low toxicity. Unfortunately, this material was too expensive, because an industrial synthetic method had not yet been found.

In this paper, we wish to report a convenient and industrial method for the synthesis of **4** starting from 5-fluorouridine (**1**), which can be prepared[7,8] easily from trimethylsilylated 5-fluorouracil and 1-acetyl-2,3,5-tribenzoylribose.

2′-Deoxyuridine was synthesized by Marumoto *et al.*[9] from uridine. When this synthetic procedure was applied to 5-fluorouridine (**1**), **4** was obtained from **1** *via* three steps in a 48.9% total yield. The synthetic route is illustrated in Scheme 1.

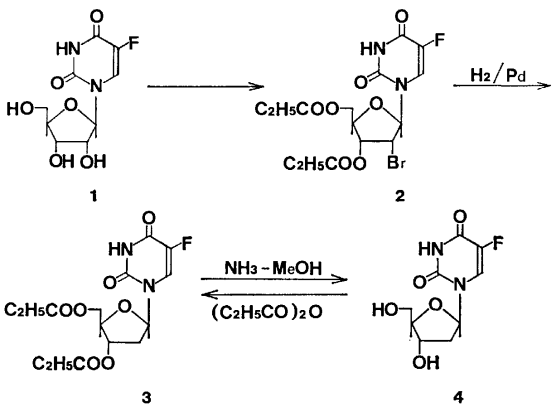

Scheme 1.

5-Fluorouridine (**1**) was suspended in acetonitrile, and the mixture was heated. Propionyl bromide was then added to the mixture at reflux to afford, after the usual work-up, 3′,5′-di-*O*-propionyl-2′-bromo-5-fluoro-2′-deoxyuridine (**2**) with a mp of 160—162 °C. This reaction may take place by means of the following mechanism,[9] even though no intermediate was isolated.

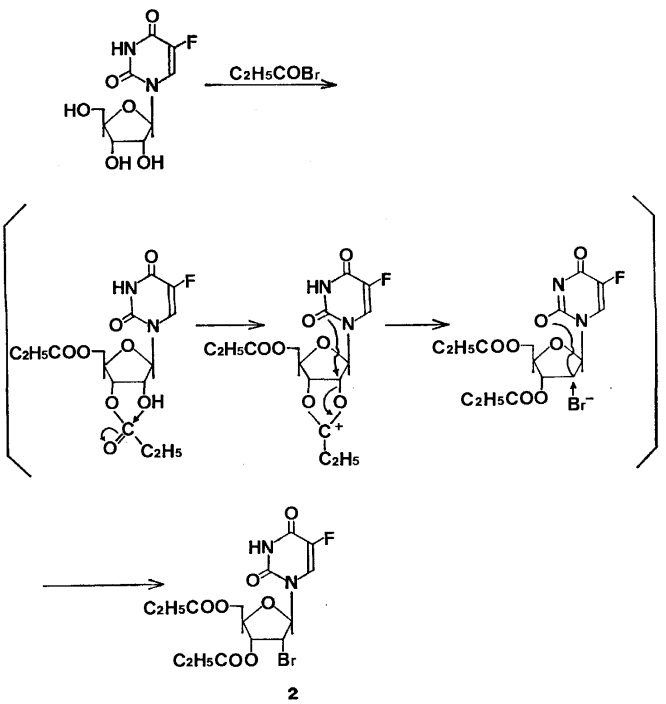

2

Compound **2** was hydrogenated on Pd–$BaSO_4$ as a catalyst at 1 atm 20 °C for 4 h to afford 3′,5′-di-*O*-propionyl-5-fluoro-2′-deoxyuridine (**3**) in a crystalline form in a 85.9% yield.

Compound **3** was also obtained by the reaction of authentic **4** with propionic anhydride, which was identical with the above sample. Compound **3** was deacylated with methanolic ammonia at 5 °C for 14 h to afford **4**. The structures of **2**, **3**, and **4** were confirmed by elemental analysis, IR, and NMR. The properties of the synthesized **4** were in good accord in all respects with those of an authentic **4** (obtained from PCR Inc. Gainesville, Florida, USA) and showed no depression in mixed mp. It may be concluded that this synthetic method is a convenient and inexpensive method to produce **4**.

Experimental

3′,5′-Di-O-propionyl-2′-bromo-5-fluoro-2′-deoxyuridine (2).

Into a boiling suspension of 5-fluorouridine (1310 mg, 5 mmol) in acetonitrile (60 ml), was added propionyl bromide (3 ml, 30 mmol) over a 30-min period. The stirring was then continued for a further 3 h. After the reaction mixture had been cooled, the solvent was evaporated, the residue was dissolved in methanol, and the solution was again evaporated to dryness. The residue was purified by column chromatography on silica gel using a benzene–methanol (4: 1) solvent. The crude product was crystallized from methanol to afford **2** (1764 mg, 80.8%): mp 160—161 °C. R_f=0.43 (benzene 4: methanol 1); IR (KBr) 3220, 3000, 1737 (s), 1710, 1475, 1392, 1357, 1289, 1270, 1212, 1180, 1162, 1098, 1068, 1040, 875, 812, cm^{-1}; NMR (60 MHz, CD_3OD) 1.12 (6H, t, J=7 Hz, CH_3), 2.44 (4H, q, J=7 Hz, CH_2), 4.36 (3H, m, OCH_2 and C_4'-H), 4.75 (CH_3O in CD_3OD+C_3'-H), 5.20 (1H, m, C_2'-H). Found: C, 40.96; H, 4.15; Br, 18.65; F, 4.25%. Calcd for $C_{15}H_{18}BrFN_2O_7$: C, 41.21; H, 4.15; Br, 18.28; F, 4.35%.

3',5'-Di-O-propionyl-5-fluoro-2'-deoxyuridine (3). *a*): To a suspension of a 5% Pd–$BaSO_4$ catalyst (40 mg) in water (10 ml), was added a solution of **2** (169 mg, 0.364 mmol) and sodium acetate (89 mg, 1.09 mmol) in methanol (20 ml). The mixture was shaken in a hydrogen atmosphere at 1 atm and 23 °C for 4 h. The catalyst was then removed by filtration, and the filtrate was concentrated. The resulting sirup was mixed with water (10 ml) and extracted with chloroform. The chloroform layer was dried (Na_2SO_4) and evaporated. The residue was crystallized from ethanol to afford **3** (123 mg, 85.9%): mp 122—123 °C. TLC R_f=0.46 (benzene 4: methanol 1); IR (KBr) 3240, 3100, 3020, 1730 (s), 1685, 1470, 1372, 1290, 1280, 1260, 1200, 1180, 1142, 1076, 1012, 968, 927, 892, 866, 810, 789, 765 cm^{-1}. Found: C, 50.33; H, 5.38; F, 5.25; N, 7.71%. Calcd for $C_{15}H_{19}FN_2O_7$: C, 50.28; H, 5.34; F, 5.30; N, 7.82%.

b): A mixture of **4** (246 mg, 1 mmol), propionic anhydride (0.5 ml, 4 mmol), and anhydrous pyridine (20 ml) was heated at 110 °C for 2 h. The solvent was then evaporated *in vacuo*, and the residue was purified by column chromatography on silica gel (using 4: 1 benzene–methanol as the eluting solvent). Crude **3** was crystallized from ethanol to give pure **3** (277 mg, 77%): mp 122—123 °C.

5-Fluoro-2'-deoxyuridine (4). 3',5'-Di-*O*-propionyl-5-fluoro-2'-deoxyuridine (218.6 mg, 0.61 mmol) in 20% methanolic ammonia (20 ml) was kept overnight at 5 °C. The reaction mixture was then concentrated to afford an oily substance. The oil was crystallized from methanol to afford **4** (177 mg, 70.5%); mp 150 °C. The sample was confirmed by IR, elemental analysis, and a mixed mp determination (150 °C) to be the same as the authentic **4**.

References

1) Part 1: S. Ozaki, Y. Ike, H. Mizuno, K. Ishikawa, and H. Mori, *Bull. Chem. Soc. Jpn.*, in press.

2) R. Duschinsky, E. Pleven, J. Malbica, and C. Heidelberger, Abst. Am. Chem. Soc. Meeting, Sept, 8, 1957, p. 19C.

3) M. Hoffer, R. Duschinsky, J. J. Fox, and N. Yung, *J. Am. Chem. Soc.*, **81**, 4112 (1959).

4) C. Heidelberger, L. Griesbach, O. Crug, R. J. Schnitzer, and E. Grunberg, *Proc. Soc. Exp. Biol. Med.*, **97**, 470 (1958).

5) J. H. Burchenal, E. A. D. Holmberg, J. J. Fox, S. C. Hemphill, and J. A. Reppert, *Cancer Res.*, **19**, 494 (1959).

6) A. R. Curreri and F. Ansfield, *Cancer Chemother. Rep.*, **2**, 8 (1959); M. L. Murphy, R. R. Elison, F. S. Aquila, R. Sullivan, M. C. Li, and J. H. Burchenal, *ibid.*, **2**, 12 (1959); J. A. Montgomery, *Prog. Drug Res.*, **8**, 431 (1965).

7) Mitsui Pharmaceutical, Inc., Japan Patent, Open 50-93983 (1975).

8) M. Saneyoshi, *Chem. Pharm. Bull.*, submitted for publication.

9) R. Marumoto and M. Honjo, *Chem. Pharm. Bull.*, **22**, 128 (1974).

BULLETIN OF THE CHEMICAL SOCIETY OF JAPAN, VOL. 50 (8), 2199—2200 (1977)

The Reaction of Copper(I) Methyltrialkylborates with Allylic Halides or 2-Propynylic Halides

Norio MIYAURA, (the late) Mitsuomi ITOH, and Akira SUZUKI*
Faculty of Engineering, Hokkaido University, Sapporo 060
(Received March 7, 1977)

Synopsis. The reactions between copper(I) methyltrialkylborates (readily obtainable from organoboranes) and allylic halides or 2-propynylic halides were found to give corresponding alkylation products. These reactions provide novel synthetic routes to 1-alkenes or 1,2-alkadienes from organoboranes.

Recently we have reported that lithium methyltrialkylborate readily undergoes a cation exchange reaction by copper(I) halide to give copper(I) methyltrialkylborate (**1**), which successfully reacts with acrylonitrile, ethyl acrylate, 1-acyl-2-vinylcyclopropane,[1] benzylic bromides,[2] and aroyl chlorides.[3]

In an attempt to develop reaction of such borate complexes, we examined the possibility of alkylation reactions of 2-propenylic halides and 2-propynylic halides. No reaction occurs between allyl bromide and lithium methyltrialkylborates at room temperature, whereas when copper(I) borates (**1**) are used instead of lithium borates, the reaction proceeds smoothly to give corresponding products as shown in Eqs. 1. and 2.

$$R_3B + MeLi \longrightarrow [R_3BMe]Li \xrightarrow{CuX} \underset{\mathbf{1}}{[R_3BMe]Cu} + LiX \quad (1)$$

$$\mathbf{1} + CH_2{=}CHCH_2X' \longrightarrow RCH_2CH{=}CH_2 + R_2BMe + CuX' \quad (2)$$

The yields of alkylation products are dependent upon the copper(I) halides and allyl halides employed, as revealed in the case of copper(I) methyltrihexylborate in Table 1. In general, allyl chloride gives good yields of products. This reaction is applicable to representative organoboranes and 2-propenylic chlorides. The reaction appears to proceed through an allylic rearrangement as the main path, judging from the results obtained in the reaction of copper(I) methyltripropylborate with cinnamyl chloride, and it was noted that the attack of the methyl group in the borate complex may not be involved.

In the same way, copper(I) methyltrialkylborates react with 2-propynylic halides to give corresponding 1,2-alkadienes (Eq. 3). Some of the representative results are summarized in Table 1. Although the latter

$$\mathbf{1} + R'{-}C{\equiv}C{-}CH_2Br \longrightarrow \underset{\mathbf{2}}{\overset{R}{\underset{R'}{\diagdown\!\!\diagup}}C{=}C{=}CH_2} + \underset{\mathbf{3}}{\overset{Me}{\underset{R'}{\diagdown\!\!\diagup}}C{=}C{=}CH_2} \quad (3)$$

reaction provides a convenient synthetic procedure of 1,2-alkadienes from organoboranes, the formation of undesirable products (**3**) by the attack of methyl groups in borates reduces yields of desired products (**2**).

It is becoming increasingly evident that copper(I) methyltrialkylborates have a considerably high utility in organic synthesis. The applicability of this new alkylating agent to coupling and addition reactions is under further investigation.

Experimental

Materials. All copper(I) halides, allylic halides, and

TABLE 1. REACTION OF COPPER(I) METHYLTRIALKYLBORATES WITH ALLYLIC HALIDES AND 2-PROPYNYLIC HALIDES[a]

R_3B	CuX	Allylic or 2-propynylic halide	Product	Yield[b] %
Hexyl	CuI	$CH_2{=}CHCH_2Br$	1-Nonene	53
	CuBr			42
	CuCl			47
	CuCN			49
	CuBr	$CH_2{=}CHCH_2Cl$		82
Octyl	CuBr		1-Undecene	87
5-Chloropentyl	CuBr		8-Chloro-1-octene	91
Propyl	CuBr	$PhCH{=}CHCH_2Cl$	$PhCH(Pr){-}CH{=}CH_2$	96
			$PhCH{=}CHCH_2Pr$	trace
Pentyl	CuBr	$HC{\equiv}CCH_2Cl$	1,2-Octadiene	32
		$HC{\equiv}CCH_2Br$		54
Octyl			1,2-Undecadiene	53
Butyl		$PhC{\equiv}CCH_2Br$	3-Phenyl-1,2-heptadiene	31
			3-Phenyl-1,2-butadiene	59

a) Reactions were carried out for 2 h by using a 20% excess of borate complexes at room temperature. b) Based on 2-propenylic or 2-propynylic halides employed.

* To whom all correspondences should be addressed.

2-propynylic halides are commercially available. The organic compounds used in the experiments were purified by distillation before use. Trialkylboranes were prepared by the usual procedure.[5]

The IR and NMR spectra were taken on a Hitachi-Perkin-Elmer Model 125 spectrophotometer and a Hitachi R-22 spectrometer at 90 MHz using tetramethylsilane as the internal standard, respectively.

General Procedure. The following procedure for the preparation of 8-chloro-1-octene is representative. A dry 50 ml-flask was charged under dry nitrogen atmosphere with 1.72 g (12 mmol) of copper(I) bromide and 6 ml of dry tetrahydrofuran. To this mixture was added lithium methyltris(5-chloropentyl)borate[2,4] (12 mmol in THF) at 0 °C, and the mixture was stirred for 5 min. Then allyl chloride (0.815 ml, 10 mmol) was gradually added and the mixture was stirred for further 2 h at room temperature. The residual organoborane was oxidized with 5.4 ml of 3 M NaOH and 5.4 ml of 30% H_2O_2 at room temperature for 2 h. The product was extracted with ether. The combined extract was washed with water and then dried over anhydrous sodium sulfate. The ether solution thus obtained was analyzed by VPC, revealing the formation of 8-chloro-1-octene (9.1 mmol, 91%). An analytically pure sample was obtained by preparative VPC with Varian autoprep Model-2800.

Identification of the Products. 1-Nonene and 1-undecene were identified by direct comparison with authentic samples which were commercially available from Tokyo Kasei Kogyo Co., Ltd. 1,2-Octadiene and 1,2-undecadiene were characterized by comparison with samples prepared by the methods reported by Meisters[6] and Moore,[7] respectively.

8-Chloro-1-octene: n_D^{24} 1.4508. Found: C, 65.31; H, 10.15%. Calcd for $C_8H_{15}Cl$: C, 65.52; H, 10.31%. Mass; m/e=146, 148 (M^+). IR (neat): 3055, 1630, 910 cm^{-1}. NMR (CCl_4); τ, 8.6 (8H, s), 7.99 (2H, t, J=7.0 Hz), 6.51 (2H, t, J=6.5 Hz), 4.85—5.15 (2H, m), 4.0—4.45 (1H, m).

3-Phenyl-1-hexene: n_D^{24} 1.4999. Found: C, 89.75; H, 9.91%. Calcd for $C_{12}H_{16}$: C, 89.94; H, 10.06%. Mass: m/e=158 (M^+). IR (neat): 1630, 1600, 915 cm^{-1}. NMR (CCl_4); τ, 9.10 (3H, t, J=6.3 Hz), 8.50—8.95 (2H, m), 8.15—8.45 (2H, m), 6.78 (1H, q), 4.90—5.15 (2H, m), 3.85—4.25 (1H, m), 2.82 (5H, s).

3-Phenyl-1,2-heptadiene: n_D^{24} 1.5637. Found: C, 90.77; H, 9.42%. Calcd for $C_{13}H_{16}$: C, 90.64; H, 9.36%. Mass: m/e=172 (M^+). IR (neat): 1945, 1600, 1496, 695 cm^{-1}. NMR (CCl_4): τ, 9.05 (3H, t, J=6.5 Hz), 8.3—8.8 (4H, m), 7.40—7.70 (2H, m), 4.96 (2H, m). 2.5—2.9 (5H, m).

3-Phenyl-1,2-butadiene: n_D^{24} 1.5612. Found: C, 92.35; H, 7.68%. Calcd for $C_{10}H_{10}$: C, 92.26; H, 7.74%. Mass; m/e=130 (M^+). IR (neat): 1945; 1600, 1500, 965, 695 cm^{-1}. NMR (CCl_4): τ, 7.93 (3H, t, J=2.6 Hz), 4.90—5.50 (2H, m), 2.55—2.90 (5H, m).

References

1) N. Miyaura, M. Itoh, and A. Suzuki, *Tetrahedron Lett.*, **1976**, 255.

2) N. Miyaura, M. Itoh, and A. Suzuki, *Synthesis*, **1976**, 655.

3) N. Miyaura, M. Sasaki, M. Itoh, and A. Suzuki, *Tetrahedron Lett.*, **1977**, 173.

4) H. C. Brown and K. A. Keblys, *J. Am. Chem. Soc.*, **86**, 1791 (1964); G. W. Kabalka, *Tetrahedron*, **29**, 1159 (1973).

5) H. C. Brown, "Organic Syntheses *via* Boranes," John-Wiley, New York (1975).

6) A. Meisters and J. M. Swan, *Aust. J. Chem.*, **18**, 155 (1963).

7) R. Moore and H. R. Ward, *J. Org. Chem.*, **27**, 4179 (1962).

BULLETIN OF THE CHEMICAL SOCIETY OF JAPAN, VOL. 50 (8), 2201—2202 (1977)

Photo-induced Cycloaddition of 1-Nitrocyclooctene and Cyclopentadiene

Keiichi YOKOYAMA, Masao KATÔ, and Ryoji NOYORI

Department of Chemistry, Nagoya University, Chikusa, Nagoya 464

(Received April 4, 1977)

Synopsis. Irradiation of 1-nitrocyclooctene produces first the strained *trans* isomer, which in turn undergoes thermal Diels-Alder reaction with cyclopentadiene affording the tricyclic adduct.

As a part of our investigation of the photochemical behavior of medium-sized cycloalkene derivatives,[1] a reaction of 1-nitrocyclooctene (**1**) has been examined.[2]

In the dark and below room temperature, no appreciable reaction took place between the nitro olefin **1** and cyclopentadiene. However, when the mixture immersed in a Dry Ice bath was irradiated by a high-pressure mercury arc through a Pyrex filter (n-π^* excitation), smooth reaction occurred and after 4 h the 1:1 cycloadduct **3** was obtained in *ca.* 40% yield. The norbornene type structure as well as the endo stereochemistry of the nitro group was deduced from the NMR signals of the vinylic protons;[3] both proton

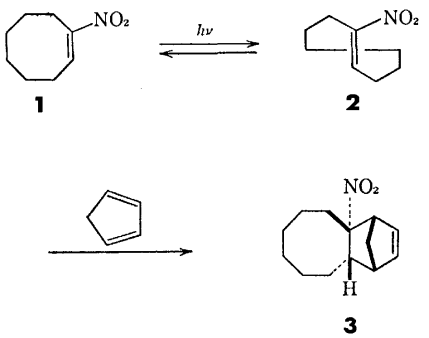

signals appeared as a doublet of doublets with J=6 and 3 Hz with a rather great chemical shift difference, $\Delta\delta$ 0.42 ppm, due to the presence of anisotropic influence of the neighboring nitro group.[4] Unlike photoreaction of 1-acetylcyclooctene[1f,g] or 1-carbomethoxycyclooctene,[5] no double-bond migration was observed with this eight-membered olefin.

Apparently the cycloaddition forming **3** involves the initial photo-induced *cis* to *trans* isomerization of the nitro olefin, **1**→**2**,[6] followed by thermal Diels-Alder reaction with cyclopentadiene.[7] The evidence for the intermediacy of the strained ground-state molecule **2** was obtained by a standard technique. Thus a solution of **1** in methylcyclohexane was first irradiated at −78 °C for 3 h. After the light source was removed, an excess of cold cyclopentadiene was added and the mixture was allowed to warm up to ambient temperature, which produced the cycloadduct **3**. The product to recovered **1** ratio indicated that the *trans* olefin **2** exists in rather high concentration (at least 28%) in the photo-equilibrium mixture produced by the photolysis of **1**.

Experimental

Photolysis of 1-Nitrocyclooctene (1) in Cyclopentadiene. The nitro olefin **1** was prepared by the known procedure,[8] bp 87—88 °C (3 Torr). The UV spectrum in hexane solution exhibited absorption maxima at 257 (ε 8470) and 345 nm (weak). A solution of **1** (550 mg, 3.54 mmol) in freshly distilled cyclopentadiene (50 ml) was placed in three Pyrex tubes (15×180 mm), flushed with nitrogen, and immersed in a Dry Ice–CH_3OH bath. Then irradiation was effected externally with a 200 W hign-pressure mercury arc for 4 h. The photolysate was concentrated at room temperature under reduced pressure and the residue was chromatographed on a silica gel plate (Merck Kieselgel GF_{254}, 10:1 hexane–ether). The fraction slightly less polar than **1** was extracted to give 2α-nitro-(1β, 2α,9β,10β)-tricyclo[8.2.1.$0^{2,9}$]tridec-11-ene (**3**) (236 mg; 32%). The yield based on the unrecovered starting olefin was *ca.* 40%. In addition, several unidentified products were produced.[2] A sample of **3** for analysis was obtained by recrystallization from hexane, mp 76.0—76.5 °C (uncorrected). IR (CCl_4) 1610 (C=C), 1534, 1354, 1335 cm^{-1} (NO_2); NMR (CCl_4 containing tetramethylsilane as internal standard) δ 1.2—3.2 (broad signal with four envelopes), 5.88 (dd, J=6 and 3 Hz, vinylic proton at C_{11}), and 6.30 (dd, J=6 and 3 Hz, vinylic proton at C_{12}); MS (70 eV) *m/e* 221 (M^+), 190, 175, 147, 91, and 66 ($M^+ - C_5H_6$, *retro*-Diels-Alder process).

Found: C, 70.45; H, 8.74; N, 6.24%. Calcd for $C_{13}H_{19}O_2N$: C, 70.55; N, 8.65; N, 6.33%.

Dark Reaction of the Trans *Isomer of 1 and Cyclopentadiene.* A methylcyclohexane solution (25 ml) of **1** (256.6 mg, 1.66 mmol) in Pyrex tubes was cooled in a Dry Ice–CH_3OH bath and irradiated under nitrogen for 3 h. After the lamp had been turned off, to the photolysate was added cyclopentadiene (*ca.* 20 ml) and the mixture was warmed up spontaneously to room temperature with stirring. The volatile substances were removed by evaporation. TLC separation of the residual mixture afforded **3** (77 mg; 22% yield) and unchanged **1** (141 mg; 55% recovery).

References

1) a) H. Nozaki, M. Kurita, and R. Noyori, *Tetrahedron Lett.*, **1968**, 2025; b) H. Nozaki, M. Kurita, and R. Noyori, *ibid.*, **1968**, 3635; c) R. Noyori, A. Watanabe, and M. Katô, *ibid.*, **1968**, 5443; d) R. Noyori, H. Inoue, and M. Katô, *Chem. Commun.*, **1970**, 1965; e) R. Noyori and M. Katô, *Bull. Chem. Soc. Jpn.*, **47**, 1460 (1974); f) R. Noyori, H. Inoue, and M. Katô, *J. Am. Chem. Soc.*, **92**, 6699 (1970); g) R. Noyori H. Inoue, and M. Katô, *Bull. Chem. Soc. Jpn.*, **49**, 3673 (1976); h) R. Noyori, Y. Ohnishi, and M. Katô, *J. Am. Chem. Soc.*, **97**, 928 (1975).

2) Review on photochemistry of nitro compounds: H. A. Morrison, "The Chemistry of the Nitro and Nitroso Groups," Part I, H. H. Feuer, ed., Interscience, New York, N. Y. (1969), Chap. 4. For photochemistry of nitroalkenes and related subjects, see H. E. Zimmerman, L. C. Roberts, and R. Arnold, *J. Org. Chem.*, **42**, 621 (1977), and references cited therein.

3) P. Laszlo and P. v. R. Schleyer, *J. Am. Chem. Soc.*, **86**,

1171 (1964); R. R. Fraser, *Can. J. Chem.*, **40**, 78 (1962).
4) R. J. Ouellette and G. E. Booth, *J. Org. Chem.*, **30,** 423 (1965).
5) T. W. Gibson, S. Majeti, and B. L. Barnett, *Tetrahedron Lett.*, **1976**, 4801.
6) A. L. Bluhm and J. Weinstein, *J. Am. Chem. Soc.*, **87,** 5511 (1965).
7) Diels-Alder trapping of strained *trans*-cycloalkenes: E. J. Corey, M. Tada, R. LeMahieu, and L. Libit, *J. Am. Chem. Soc.*, **87,** 2051 (1965); P. E. Eaton, *Acc. Chem. Res.*, **1,** 50 (1968); H. Shingaki, S. Arai, and M. Tada, *Bull. Chem. Soc. Jpn.*, **49,** 821 (1976).
8) W. K. Seifert, *J. Org Chem.*, **28,** 125 (1963).

BULLETIN OF THE CHEMICAL SOCIETY OF JAPAN, VOL. 50 (8), 2203—2204 (1977)

Utilizing Emulsification in the Synthesis of Dihydro-*exo*-dicyclopentadienyl Ethers and Their Esters

Akira HATANO and Yoshiyuki IWASE

Mitsui Petrochemical Industries, Ltd., Waki-cho, Kuga-gun, Yamaguchi 740

(Received December 17, 1976)

Synopsis. Alcohols and carboxylic acids were subjected to an addition reaction with dicyclopentadiene, using dodecylbenzenesulfonic acid both as the emulsifying agent and the acid catalyst. Dihydro-*exo*-dicyclopentadienyl ethers and their esters were syntheized in good yields and found to be free of undesirable side reactions.

It is important to investigate the method of synthesizing dicyclopentadienyl ethers and their esters because of the usefulness of these compounds as plasticizers and drying oils. There are two known methods for preparing these compounds. One involves the reaction of a carboxylic acid with hydroxy-dihydro-*exo*-dicyclopentadiene and an alkaline metal alcoholate with dihydro-*exo*-dicyclopentadienyl halide.[1] The other method consists of an electrophilic addition reaction[2] of dicyclopentadiene with an alcohol or a carboxylic acid by using the difference in the reactivities[3] of the two double bonds in dicyclopentadiene in the presence of an acid catalyst, although the yields for this method are generally low.

The present paper describes an alternative method of preparing these compounds with a view to obtaining satisfactory yields. The necessary procedures are also dealt with.

Results and Discussion

Bruson *et al.* have reported on the preparation of dihydro-*exo*-dicyclopentadienyl ether[4] by the electrophilic reaction of an alcohol with dicyclopentadiene, and of dihydro-*exo*-dicyclopentadienyl ester by a similar reaction involving a carboxylic acid with dicyclopentadiene.[5]

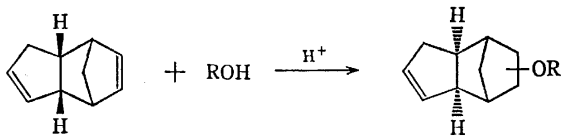

Table shows the results of this experiment. It is noted that the amount of acid catalyst required in the reaction of dicyclopentadiene with a carboxylic acid is rather small in comparison with that in the reaction of dicyclopentadiene with an alcohol, since in the former case it is needed only as a co-catalyst. As can be readily seen, both alcohols charaterized by poor or no solubility in dicyclopentadiene, as well as carboxylic acids, gave the addition products in very low yields. It is assumed that the most important cause of the limited yields in the heterogeneous system is due to the poor or no solubility of these compounds in dicyclopentadiene. In particular, the heterogeneous system causes side reactions *i.e.*, partial cationic polymerization[6] of dicyclopentadiene or a dehydratic condensation reaction[7] of alcohol in the presence of concentrated sulfuric acid.

To avoid this and to increase the yield, it was thought that a compound that would homogenize the heterogeneous system and at the same time act as a catalyst for the reaction would be worth testing. The refore, use was made of dodecylbenzenesulfonic acid, a strong acid capable of emulsifying action. The results show that the emulsifying action homogenized the heterogeneous system and restrained side reactions at the same time, thus increasing the yield and permitting the use of

TABLE 1. RESULTS OF THE PREPARATION OF DIHYDRO-*exo*-DICYCLOPENTADIENYL ETHERS AND THEIR ESTERS

	R	Solubility of ROH in dicyclopentadiene	Run A (98% H_2SO_4) Run B ($C_{12}H_{25}C_6H_5SO_3H$) Amount of catalyst[a] (mol)	Yield[b] (%)	Bp (°C/Torr)	Found (Calcd %) C	H	O	IR (cm^{-1})	NMR[8-10] (ppm)	Mass (*m/e*)$^+$
1a	CH_3	poor (hetero)[c]	A 0.25	31	96—98/12—13	80.71	9.80	9.49	1610	3.1 (3H, CH_3)	164
			B 0.05	81		(80.44)	(9.83)	(9.74)	1100	3.15(1H, H_3)	15
1b	CH_2CH_2OH	insoluble (hetero)	A 0.3	16	105—106/0.5	74.05	9.23	16.72	1615	2.72(1H, OH)	194
			B 0.05	76		(74.19)	(9.34)	(16.47)	1100	3.4 (1H, H_3) 3.45, 3.65 (4H, $-CH_2-$)	45
1c	C_6H_5	good (homo)[d]	A 0.3	20	121—122/1	85.12	8.15	6.73	1610	4.1 (1H, H_3)	226
			B 0.05	79		(84.19)	(8.02)	(7.07)	1600 1500 1250	6.6—7.2 (5H, C_6H_5)	77
2a	$OCCH_3$	good (homo)	A 0.05	61	96—97/5	74.83	8.21	16.96	1730	1.9 (3H, CH_3)	192
			B 0.04	82		(74.97)	(8.39)	(16.64)	1620 1250	4.6 (1H, H_3)	43
2b	$OCCH=CH_2$	good (homo)	A 0.05	62	131—132/7	76.32	7.81	15.87	1725	4.65(1H, H_3)	204
			B 0.04	85		(76.44)	(7.90)	(15.67)	1630 1600 1200	5.8—6.3 (3H, $CH=CH_2$)	55
2c	OCC_6H_5	poor (hetero)	A 0.2[e]	19	158—159/1	80.10	7.02	12.88	1720	4.9 (1H, H_3)	254
			B 0.04	63		(80.28)	(7.13)	(12.58)	1610 1600 1500 1280	7.4, 8.0 (5H, C_6H_5)	105

a) The amount of the catalyst was calculated on the basis of one mol of dicyclopentadiene. b) Given in the ratio of the percentage of the amount obtained from GLPC (without **1c** and **2c** isolated) to that calculated from the mol of dicyclopentadiene used. c) Heterogeneous system in the reaction. d) Homogeneous system in the reaction. e) BF_3OEt_2 was used.

smaller amounts of the acid catalyst. From the above data, it was concluded that an acid with emulsifying action and capable of catalyzing the reaction, such as dodecylbenzenesulfonic acid, gives the addition product in better yields for carboxylic acids, as well as for alcohols, even when these are poorly soluble or insoluble in dicyclopentadiene.

Experimental

The NMR spectra were recorded on a Nippon Denshi Kogaku Model JNM-4H-100 spectrometer in parts per million (ppm) from internal tetramethylsilane. The IR spectra were obtained on a Nippon Bunko Model DS-701 D spectrometer using neat liqids between KBr disks. The mass spectra were measured on a Nippon Denshi Model D-100 spectrometer with an electron bombarding energy of 75 eV.

*Preparation of Ethylene Glycol Mono(dihydro-*exo*-dicyclopentadienyl) Ether.* Dodecylbenzenesulfonic acid (8.15 g, 0.025 mol) was added dropwise to the stirred ethylene glycol (31 g, 0.5 mol) at room temperature. The dicyclopentadiene (66 g, 0.5 mol) was added dropwise and the mixture was rapidly stirred until it was emulsified. The emulsified mixture was then heated to 100 °C and the reaction proceeded for 4 h. The reaction mixture was cooled to room temperature and benzene (100 g) was added to the stirred mixture. The mixture was poured into 3% aqueous sodium chloride (500 g) containing sodium hydroxide (1.4 g, 0.035 mol) to neutralize the acid, and left standing to separate out the oil layer. The layer was washed four times with a portion of 3% aqueous sodium chloride (500 g), dried over sodium sulfate, and distilled *in vacuo*. Bp 105—106 °C/0.5 Torr, Yield: 76% (from GLPC).

*Preparation of Dihydro-*exo*-dicyclopentadienyl Acetate.* Dodecylbenzenesulfonic acid (6.5 g, 0.02 mol) was added slowly to acetic acid (30 g, 0.5 mol), and cooled to 10 °C, followed by dropwise addition of dicyclopentadiene (66 g, 0.5 mol). The stirred mixture was heated to 100 °C and allowed to react for 5 h. The reaction mixture was cooled to room temperature, ethyl ether (100 g) was added and the mixture was poured into water (500 g) to separate out the oil layer. The oil layer was neutralized with sodium carbonate, washed a few times with a portion of water (500 g), dried over sodium sulfate, and vacuum distilled. Bp 96—97 °C/5 Torr, Yield: 82% (from GLPC.).

Preparation of the addition products using other alcohols or carboxylic acids was similar in principle to the procedure described above.

References

1) G. T. Youngblood and P. Wilder, *J. Org. Chem. Soc.*, **21**, 1436 (1956); J. K. Stille and S. C. Stinson, *Tetrahedron*, **20**, 1387 (1964).

2) G. L. Nelson and C. L. Kuo, *Synthesis*, **2**, 105 (1975); H. A. Bruson and T. W. Riener, *J. Am. Chem. Soc.*, **67**, 723 (1945).

3) P. v. Schleyer, J. E. Williams, and K. R. Blanchard, *J. Am. Chem. Soc.*, **92**, 2377 (1970).

4) H. A. Bruson and T. W. Riener, *J. Am. Chem. Soc.*, **68**, 8 (1946).

5) H. A. Bruson and T. W. Riener, *J. Am. Chem. Soc.*, **67**, 1178 (1945).

6) T. Corner, R. G. Foster, and P. Hepworth, *Polymer*, **10**, 393 (1969).

7) S. Sugasawa and K. Huziwara, *J. Pharm. Soc. Jpn.*, **71**, 365 (1951).

8) The chemical shifts of the protons of dihydro-*exo*-dicyclopentadienyl derivatives are more complicated at high fields (1.2—2.7 ppm). However, these chemical shifts were assigned from the data based on Refs. 9 and 10. Each proton of the dihydro-*exo*-dicyclopentadienyl group is numbered as follows:

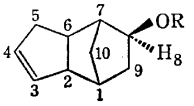

(or OR at C_9) R=Alkyl or acyl group

9) R. R. Fraster, *Can. J. Chem.*, **40**, 78 (1962); K. Tori, Y. Hata, R. Muneyuki, Y. Takano, H. Tanida, and T. Tsuzi, *Can .J. Chem.*, **42**, 926 (1964); E. W. C. Wong and C. C. Lee, *Can. J. Chem.*, **42**, 1245 (1964).

10) R. G. Foster and M. C. Mclvor, *J. Chem. Soc., B*, **1969**, 188; K. C. Ramey and D. C. Lini, *J. Magn. Reson.*, **3** (1), 94 (1970).

BULLETIN OF THE CHEMICAL SOCIETY OFJ APAN, VOL. 50 (8), 2205—2206 (1977)

Photolysis of Benzenesulfonic Acid[1)]

Yoshiro OGATA,* Katsuhiko TAKAGI, and Shin YAMADA
Department of Applied Chemistry, Faculty of Engineering, Nagoya University, Nagoya 464
(Received August 2, 1976)

Synopsis. Photolysis of benzenesulfonic acid(**1**) in an aqueous solution gave sulfurous acid, SO_2, and/or sulfuric acid as inorganic products in a total yield of 38.6% based on the consumed **1** along with organic products. The organic products are mainly acidic tarry material containing sulfur(8.7%) together with a small amount of biphenyl (1%). Photolysis of an alkaline solution of **1** afforded a considerable amount of benzene (16%) and biphenyl(<1%). The photolysis is started by the C–S bond fission of **1** to give Ph· and $\cdot SO_3H$ radicals. The quantum yield for decomposition of **1** in acidic conditions is 0.26.

Sodium alkylbenzenesulfonate is known to be an environmental pollutant. The studies on the photochemical decomposition of the sulfonate have recently been increasing,[2)] but little is known about the mechanism and intermediates of the photolysis except for photolysis of sulfonate ester[3)] and sulfonanilide.[4)] The present paper deals with the attempts to obtain on the subject, in particular, the mechanism for photolysis of benzene sulfonic acid as a model of the surfactant.

Results and Discussion

Irradiation of Alkaline Aqueous Sodium Benzenesulfonate. The photolysis of an aqueous mixture of benzenesulfonic acid (**1**) and two equivalents of NaOH was carried out by bubbling N_2 gas in order to introduce volatile materials into a trapping tube containing ethyl ether cooled at −50 °C. After irradiation for 24 h, GLC analysis of the ether solution showed formation of benzene in a 16% yield on the basis of starting **1**. The irradiated reaction mixture was found to contain a trace amount of biphenyl (<1%) by GLC up to 250 °C.

Irradiation of Aqueous Benzenesulfonic Acid (1). Aqueous benzenesulfonic acid (**1**) was irradiated with a high-pressure mercury lamp under N_2. Evolved gas was identified to be SO_2 by the fuchsine test. The photolysis of **1** was carried out by bubbling N_2 in order to introduce the evolved gas into a trapping tube containing 10% H_2O_2. The evolved SO_2 was converted into H_2SO_4 by aqueous H_2O_2 and titrated with standard aqueous alkali. The yield of resulting SO_2 was 9.6% based on the consumed **1**. The irradiated solution was extracted with ether. The aqueous layer, containing unreacted **1** and other acidic materials, was concentrated *in vacuo*, esterified by CH_2N_2, and then analyzed by GLC. Only a peak of methyl benzenesulfonate was observed (35% recovery). The aqueous layer contains H_2SO_3 and/or H_2SO_4 in a total yield of 29.0%.

On the other hand, the organic layer of the ether extract contains biphenyl (1%, mp and mixture mp 69—70 °C). No formation of benzene was observed even under conditions similar to those for sodium benzenesulfonate. In contrast to sodium benzenesulfonate, the resulting phenyl radical formed by homolysis of the C–S bond may form complex products; the H_2SO_3 (and probably H_2SO_4) may attack the phenyl radical, inhibiting the formation of benzene.

Addition of 6-fold excess H_2O_2 to the system markedly increased the consumption of **1**. About 97% of **1** disappeared after 11 h to afford CO_2 (8%), H_2SO_4 (34%), phenol (<1%) *etc.*

No reaction occurred in the dark with the same system. Hence the acceleration by H_2O_2 may be due to the oxidation induced by ·OH radical from H_2O_2. The quantum yield for decomposition of **1** in water was 0.26 with 254 nm light.

Attempt to Characterize Tarry Material. Irradiation of **1** under acidic conditions yielded only a small amount of volatile product, biphenyl (1%), most part of the product being a black tarry material (95 wt % based on the consumed **1**). The structure of the substance is still obscure on account of its contaminant and experimental difficulties. After elimination of **1** and H_2SO_4, the tarry substance was found to contain 8.7 wt % of sulfur atom, the total amount of sulfur in recovered and isolated materials reaching 91%.

Attempts were made to isolate organic substance from the residue. Chromatography of the tarry material with a SiO_2 column yielded an yellow oil (5 wt %), giving two GLC peaks. However, the two components were too small in quantity for further purification. They were thus analyzed by GLC-MS, the results of which indicated their molecular weight to exceed 300 with no aromatic fragment ions (*e.g.*, *m/e* 77 and 91). The structure has not been identified yet. A remaining solid was obtained by the column chromatography.

Mechanism. The photoproducts, *e.g.*, benzene and biphenyl, indicate that the primary process may be the fission of C–S bond. The sum of yields of fission products ($SO_2+H_2SO_4$) in Eq. 1 reaches 38.6% based on the consumed **1**; thus Eq. 1 should be the main primary path for the decomposition. The fate of the resulting Ph· and $\cdot SO_3H$ radicals may be as follows:

$$PhSO_3H\ (\mathbf{1}) \xrightarrow{h\nu} Ph\cdot + \cdot SO_3H \quad (1)$$

$$Ph\cdot + \mathbf{1} \longrightarrow Ph_2 + \cdot SO_3H \quad (2)$$

$$Ph\cdot + RH \longrightarrow PhH + \cdot R \quad (3)$$

$$\cdot SO_3H \longrightarrow SO_2 + \cdot OH \quad (4)$$

$$\cdot OH + \mathbf{1} \longrightarrow \text{(OH, H, } -SO_3H\text{ (2))} \quad (5)$$

$$\mathbf{2} \longrightarrow Ph\cdot + H_2SO_4 \quad (6)$$

$$\mathbf{2} \longrightarrow \text{further reaction (tarry materials)} \quad (7)$$

$$2\cdot OH \longrightarrow H_2O_2 \quad (8)$$

$$H_2O_2 + SO_2 \longrightarrow H_2SO_4 \quad (9)$$

(RH: Hydrogen sources)

It may be concluded that the homolysis of excited **1** to (Ph· + ·SO_3H) is more plausible than the heterolysis into phenyl cation because of the formation of biphenyl but not phenol in both acidic and basic media. Water cannot be a hydrogen source for phenyl radical to benzene in Eq. 3, since the bond energy of C–H for benzene (112 kcal/mol) is lower than that of O–H for H_2O (120 kcal/mol).[5] Intermediary products such as **2** may play the role of hydrogen donor in Eq. 3.

It is of interest to note that the formation of benzene is favored in alkaline media. A plausible reason is as follows. In acidic media, ·SO_3H collapses into SO_2 and ·OH which subsequently oxidizes **1**, whereas in alkaline media, ·SO_3H exists as metastable ·SO_3^- species[6] which expels only slowly ·OH radical. The anion radical ·SO_3^- is known to add to unsaturated bonds, *e.g.*, aromatic ring according to Eq. 10.[7] Species **3** in Eq. 10 as well as **2** in Eq. 5 can be H· source for benzene formation.

$$\cdot SO_3^- + \diagdown C{=}C \diagup \longrightarrow \underset{\text{(3)}}{-\overset{\cdot}{C}-\overset{|}{C}-SO_3^-} \qquad (10)$$

Intermediacy of phenyl radical was also confirmed by the formation of benzene in the photolysis of **1** in the presence of a hydrogen donor such as 2-PrOH even under acidic conditions. The observed biphenyl may be formed either by the coupling of two Ph· or by an attack of Ph· on a phenyl ring of the starting **1** followed by a collapse to biphenyl and ·SO_3H radical (Eq. 2).

Another fragment, ·SO_3H, can be succesively decomposed to SO_2 and hydroxyl radical (Eq. 4). Hydration of SO_2 gives H_2SO_3, which is easily converted by H_2O_2 into H_2SO_4. Formation of H_2SO_4 from SO_2 and H_2O_2 was actually observed (Eq. 9). The resulting ·OH radical may couple to form H_2O_2 and also may attack **1** and other materials to give derivatives of **2** and oxidized tarry materials.[8]

It is less probable that $PhSO_3H$ is cleaved to ·OH and $PhSO_2$·, and then collapses to Ph· and SO_2, since the fission of $PhSO_2$· to Ph· and SO_2 is endothermic.[9]

The following results suggest that the reactive state is a singlet: (i) No quenching by a triplet quencher, *i.e.*, molecular oxygen, and (ii) no heavy atom effect by *n*-BuBr as a solvent.

Experimental

Melting points were measured on a hot plate with a Ynagimoto micro melting point apparatus and were corrected. IR spectra were measured with a Perkin-Elmer Model 337 spectrophotometer. A Yanagimoto GCG 550F gas chromatograph was used with two 2 m×2.5 mm columns, one packed with 2.5% PEG 20 M on a Chamelite CS and the other with Bentone 34+DIDP on a Chromosorb. A Shimadzu GC-MS 7000 was used for GLC-MS spectra.

A Typical Photolysis of Sodium Benzenesulfonate in Alkali. An aqueous solution (500 ml, 2.2×10^{-2} M) of **1**(2 g) with two equivalents of NaOH was irradiated with a 300 w Halos high pressure Hg lamp. Volatile materials evolved were introduced with N_2 gas as a carrier into a trapping tube containing ethyl ether at −50 °C. After irradiation for 24 h, GLC analysis of the ether solution indicated the formation of benzene (16% based on the starting **1** used). Biphenyl(<1%) was detected by GLC of the irradiated aqueous solution.

A Typical Photolysis of Benzenesulfonic Acid(1). An aqueous solution (200 ml, 5×10^{-2} M) of **1**(1.65 g) was irradiated under N_2 for 16 h using a 100 w Halos high pressure Hg lamp. Evolved SO_2 was identified by the color change of a fuchsine solution. The yield of evolved SO_2 was 9.6% based on the consumed **1** using titrimetry with a 0.01 M NaOH after its conversion into H_2SO_4 with aqueous H_2O_2. After the completion of irradiation, the solution was extracted with ether (200 ml). Biphenyl was obtained after evaporation of ether (20 mg, mp and mixture mp 69—70 °C).

The aqueous layer was subdivided into three equal portions. The first portion was used for the measurement of the conversion of **1**. After concentration under reduced pressure, it was esterified with CH_2N_2. The conversion of **1** was found to be 65% by GLC. The data were checked by a blank experiment in the dark.

The yield of H_2SO_3 and/or H_2SO_4 in the second portion (29.0%) was determined as $BaSO_4$ (0.13 g) by addition of $BaCl_2$ after treatment of excess H_2O_2.

The third portion was condensed *in vacuo* to give a black tarry material (0.5 g) contamintated with **1** (0.17 g). The yield of this was 95 wt % based on the consumed **1**.

Column Chromatography. The tarry material (0.5 g) was passed through a column of 50 cm×2.0 cm packed with SiO_2. A mixture of benzene and methanol was used as an eluant. The eluate, a mixture of two components not separable, showed the following spectra: IR(cm^{-1}) 1725(C=O); NMR(CCl_4) δ 0.7—1.8, 4.0—4.3, and 7.2—7.6; *m/e* 362, 265, 247, 176, 149, 121, 99, 70, 69, and 43. The elemental analysis of the black solid. Found; C, 59.00; H, 3.83; O, 27.68; S, 9.49%.

Quantum Yield. An aqueous 5×10^{-6} M solution of **1** in a 10 mm thick quartz cell(10 ml) was irradiated with a 30 w low-pressure Hg lamp (254 nm). A ferrioxalate actinometer was used.[10]

Quenching Study. A 4.6×10^{-2} M solution of **1** saturated with a quencher, molecular oxygen, was irradiated with a 300 w high-pressure Hg lamp for 8 h. The conversion of **1** was 54%, which was similar to that(50% for 8 h) in the experiment in the absence of the quencher.

References

1) Contribution No. 223.

2) a) Y. Kojima, *PPM*, 42(1973); b) T. Kobayashi, *Kogyo Yosui*, **103**, 38 (1967); c) K. E. Conroe, *Water and Sewage Works*, **113**, 237 (1966).

3) Y. Izawa and N. Kuromiya, *Bull. Chem. Soc. Jpn.*, **48**, 3197 (1975).

4) H. Nozaki, T. Okada, R. Noyori, and M. Kawanishi, *Tetrahedron*, **22**, 2177 (1966).

5) R. T. Sanderson, "Chemical Bonds and Bond Energy," Second Edit., Academic Press, New York(1976), p. 169, 170.

6) H. N. Alyear and H. L. J. Bäckström, *J. Am. Chem. Soc.*, **51**, 90 (1929).

7) a) C. J. Norton, N. F. Seppi, and M. J. Reuter, *J. Org. Chem.*, **33**, 4158 (1968); b) R. O. C. Norman and P. M. Storey, *J. Chem. Soc., B*, **1971**, 1009.

8) a) C. R. E. Jafcoate, J. R. Lindsay- Smith, and R. O. C. Norman, *J. Chem. Soc., B*, **1967**, 530; b) P. Neta, M. Z. Hoffman, and M. Simic, *J. Phys. Chem.*, **76**, 847 (1971).

9) J. M. Squire and W. A. Waters, *J. Chem. Soc.*, 2068 (1962).

10) C. A. Parker, *Proc. R. Soc. London., Ser. A*, **220**, 104 (1973).

BULLETIN OF THE CHEMICAL SOCIETY OF JAPAN, VOL. 50 (8), 2270 (1977)

Synthesis of 4′-Vinylbenzo-15-crown-5 from Benzo-15-crown-5

Kiyoshi KIKUKAWA, Kazuhiko NAGIRA, and Tsutomu MATSUDA

Department of Organic Synthesis, Faculty of Engineering, Kyushu University, Hakozaki, Higashi-ku, Fukuoka 812

(Received March 22, 1977)

Synopsis. 4′-Vinylbenzo-15-crown-5 was conveniently synthesized in 30% yield by the reaction of diazotized 4′-aminobenzo-15-crown-5 with ethylene (6—10 kg/cm²) in the presence of zerovalent palladium at room temperature.

Vinylbenzocrown ethers are useful monomers for the preparation of the polymers attached with crown ethers.[1] 4′-Vinylbenzocrown ethers have been synthesized using 4-acetyl- or 4-formylcatechol as a starting material.[1,2]

We recently reported a novel catalytic arylation of olefins with arenediazonium salts in the presence of zerovalent palladium.[3] In view of the higher reactivity of ethylene with arylpalladium reagents, the reaction can be expected to be a convenient method to replace an amino group in primary aromatic amines with a vinyl group. It is interesting to apply this method to the vinylation of benzocrowns, since nitrobenzocrowns and thus aminobenzocrowns are readily available from the parent crown ethers.[4]

4′-Vinylmonobenzo-15-crown-5 (**1**) was synthesized using monobenzo-15-crown-5 as a starting material in the overall yield of 20—25% (Scheme 1). 4′-Aminobenzo-15-crown-5 (**4**) which is labile to air oxidation, and its diazonium salt (**5**) were used without isolation for the subsequent reactions.

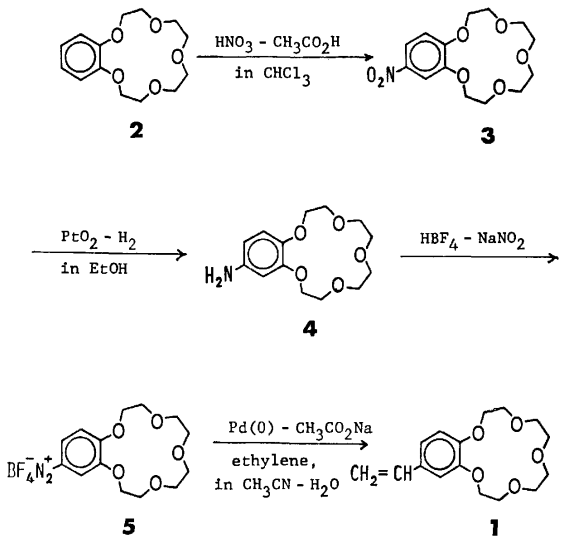

Scheme 1.

Experimental

4′-Nitrobenzo-15-crown-5 (3). This compound was prepared in 70—80% yields according to the procedure described by Smid *et al.*[4] with some modifications. Thus, the reaction mixture was neutralized with aq NaOH and the crude product was recrystd from methanol.

4′-Aminobenzo-15-crown-5 (4) and the Diazonium Salt (5). In a glass autoclave, 7.79 g of **3** in 200 ml ethanol was hydrogenated to **4** at 30—40 °C for 8 h in the presence of 0.1 g of platinum oxide under hydrogen pressure of 8—10 kg/cm². After the reaction, the catalyst was filtered off under nitrogen and the ethanol was evaporated under reduced pressure. To the residue were added 30 ml of 42% HBF_4 and 140 ml of water to give a suspension of the less soluble salts. The mixture was cooled to 0 °C in an ice bath and then 1.7 g of $NaNO_2$ in 20 ml water was added dropwise at 0—5 °C under efficient stirring. The diazonium salt was soluble in water.

4′-Vinylbenzo-15-crown-5 (1). The diazotized soln was placed in a glass autoclave (500 ml), and then 100 ml of acetonitrile, 10.3 g of sodium acetate and 3.0 g of bis(dibenzylideneacetone)palladium(0) were added to the soln. After ethylene was introduced to a pressure of 6—10 kg/cm², the soln was stirred at room temp for 2 days. The reaction mixture was extracted with ether, and the extract was washed with satd aq $NaHCO_3$ soln followed by satd aq NaCl soln, and dried over anhyd $MgSO_4$ with the addition of 4-*t*-butylcatechol as an inhibitor. The mixture was filtered, and the filtrate was evaporated under reduced pressure. The residue was extracted several times with hot hexane, and after removal of a small amount of less soluble dibenzylideneacetone, concentration of the hexane soln gave **1** as white crystals. Yield 30% from **3**, mp 40—45 °C. Recrystallization from hexane gave pure **1**, mp 43.5—44.2 °C, which did not exhibit any depression of the mp on admixture with the authentic specimen prepared *via* 4′-acetylbenzo-15-crown-5.[1] NMR ($CDCl_3$) δ=4.0 (16H, m, $-CH_2-$), 5.3 (2H, m, vinyl $=CH_2$), 6.6 (1H, m, vinyl $-CH-$), 6.9 (3H, m, aromatic H).

References

1) S. Kopolow, T. E. Hogen Esch, and J. Smid, *Macromolecules*, **6**, 133 (1973).

2) J. Smid, B. El Haj, T. Majewicz, A. Nonni, and R. Sinta, *Org. Prep. Proced. Int.*, **8**, 193 (1976).

3) K. Kikukawa and T. Matsuda, *Chem. Lett.*, **1977**, 159.

4) R. Ungaro, B. El Haj, and J. Smid, *J. Am. Chem. Soc.*, **98**, 5198 (1976).

Isolated Molecule Approach to the Orbital Study of Chemical Reactions. I. Bimolecular Nucleophilic Substitution

Hiroshi FUJIMOTO and Nobuhiro KOSUGI

Faculty of Engineering, Kyoto University, Sakyo-ku, Kyoto 606

(Received December 22, 1976)

A method of analyzing chemical interactions between two systems is presented and applied to the bimolecular nucleophilic substitution of methylfluoride by fluoride ion. In order to get a clear insight into the mechanisms of chemical interactions, the interacting system has been represented by a combination of various electron configurations of the reactants involved. The matrix elements necessary for the configuration interaction have been obtained by transforming the MO's of the isolated reactants into a set of orthogonalized functions. The change in the energy and the redistribution of the electrons due to the interaction in the reaction have been calculated by the use of the *ab initio* (STO-3G) MO's and have been divided into the Coulomb, exchange, delocalization, and polarization interactions. A comparison of the results with the results of the SCF CI calculations of the composite system has shown the utility of the method in studying weak and moderately strong interactions between two systems.

The bimolecular nucleophilic substitution (S_N2) reaction of aliphatic systems is one of the most extensively investigated reactions in organic chemistry.[1] Since Hughes and Ingold,[2] numerous experiments have attempted to study the mechanism of the reactions. It is now well-established that the attacking base approaches the substrate from the back, displacing the leaving group. Thus, the Walden inversion is characteristic of S_N2 reactions. It has been suggested that the carbon atom of a substrate under attack will take a nearly sp^2 planar structure at the transition state, although no stable intermediate has ever been trapped.

Recent developments in quantum mechanical methods of calculating the electronic structure of sizable molecules have led us to consider the detailed molecular mechanisms of organic reactions. In particular, *ab initio* MO methods have been accepted as a way of studying the basic nature of chemical reactions in recent years. Although it is unlikely, at present, that such methods can supply us with quantitatively reliable results on the magnitude of the activation energy and the geometry of transition state complex for systems with many degrees of freedom, an extensive configuration interaction with a large set of basis functions will lead to an improvement of the calculations.[3] In this respect, MO approaches to chemical reactions seem to be promising.

The perturbation theory is a convenient tool to deal with weakly interacting systems. The energy and the electron density are separated into several interaction terms and are interpreted in relation to chemical and physical concepts of molecular interaction.[4] In this paper, we will present the result of our calculation of the electron reorganization in a model S_N2 reaction. A direct evaluation of the interaction integrals and configuration energies is attempted. Our primary aim is to develop a theoretical method of studying molecular interactions, furnished both with the accuracy of *ab initio* calculations and with the accessibility of perturbation theories to the nature of chemical reactions.

Description of Chemical Interactions

In order to study the molecular mechanism of S_N2 reactions, we have chosen methylfluoride and fluoride ion as the substrate and the attacking base respectively.[5] The geometry of the reacting system was taken to be as is given in Fig. 1, after Veillard.[5c] In an early stage of the reaction, the electronic structure of the composite system can be represented by a wave function which is a linear combination of various electron configurations of the reactants involved:[4]

$$\Psi = \sum_p C_p \Psi_p . \qquad (1)$$

Some of the most important configurations are illustrated in Fig. 2. The wave functions of these electron configurations are given by the Slater determinants, as usual. The original configuration contains only the occupied MO's of the isolated reactants:

$$\Psi_0 = |a_1 \cdots a_i \cdots a_m b_1 \cdots b_k \cdots b_n \bar{a}_1 \cdots \bar{a}_i \cdots \bar{a}_m \bar{b}_1 \cdots \bar{b}_k \cdots \bar{b}_n| ,$$

where a and $\bar{a}$ are the spinorbitals of methylfluoride ($m=9$) with spin α and spin β respectively, and where

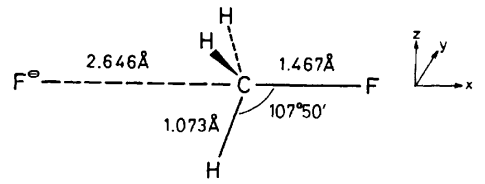

Fig. 1. A sketch of reaction model after Veillard.[5c]

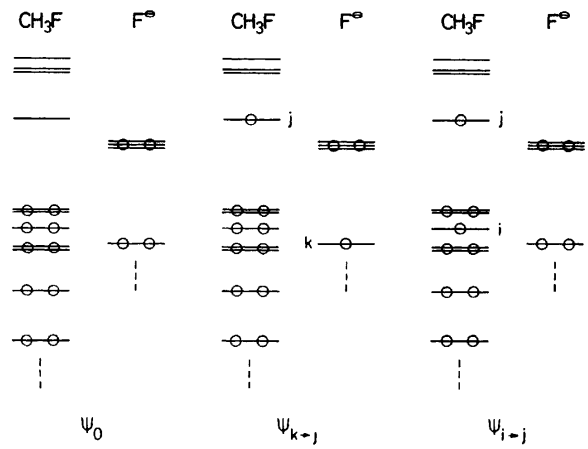

Fig. 2. An illustration of some electron configurations.

b and $\bar{b}$ are the spinorbitals of the fluoride ion ($n=5$). Similarly, we have:

$$\Psi_{k\to j} = 1/\sqrt{2}\,(|a_1\cdots a_m b_1\cdots a_j\cdots b_n\bar{a}_1\cdots\bar{a}_m\bar{b}_1\cdots\bar{b}_k\cdots\bar{b}_n| + |a_1\cdots a_m b_1\cdots b_k\cdots b_n\bar{a}_1\cdots\bar{a}_m\bar{b}_1\cdots\bar{a}_j\cdots\bar{b}_n|),$$

$$\Psi_{i\to j,i\to j} = |a_1\cdots a_j\cdots a_m b_1\cdots b_n\bar{a}_1\cdots\bar{a}_j\cdots\bar{a}_m\bar{b}_1\cdots\bar{b}_n|.$$

It should be noted here that, in general, the MO's a_i and b_k are not mutually orthogonal.

Among the various electron configurations appearing in Eq. 1, Ψ_0 is the dominant term, and the expansion coefficients, C_p, can be obtained as the solution of the simultaneous equations:

$$(\boldsymbol{H}-E\boldsymbol{S})\boldsymbol{C} = 0, \tag{2}$$

in which:

$$H_{p,q} = \int \Psi_p^* H \Psi_q \mathrm{d}\tau,$$

$$S_{p,q} = \int \Psi_p^* \Psi_q \mathrm{d}\tau.$$

The Hamiltonian operator for the interacting system is given by:

$$H = \sum_i -1/2\Delta_i + \sum_i\sum_\alpha -Z_\alpha/r_{i\alpha} + \sum_{i<j}\sum 1/r_{ij} + \sum_{\alpha<\beta}\sum Z_\alpha Z_\beta/R_{\alpha\beta}, \tag{3}$$

where the familiar notations are used.[4b] In obtaining the matrix elements in Eq. 2, it is convenient to carry out a certain transformation of the basis MO's into a set of orthogonalized orbitals and/or corresponding orbitals.[6,7] Thus, all the integrals can be calculated exactly in the framework of the method of the MO calculation employed. In the present calculation, we used an SCF LCAO MO approximation, all the necessary atomic integrals being evaluated by expanding the basis Slater atomic orbiatls in three-term Gaussian functions (STO-3G).[8,9] No polarization function was adopted.

Calculation of Matrix Elements

Here we may mention briefly the method of calculating the integrals appearing in the secular equations. First, we consider overlap integrals. A wave function, $\boldsymbol{\phi}$, is a subset of the MO's chosen from the occupied and unoccupied MO's of methylfluoride and the fluoride ion:

$$\boldsymbol{\phi} = (\phi_1\phi_2\cdots\cdots\phi_N) \qquad (N=m+n=14)$$

where the one-electron function, ϕ_i, corresponds to one of the a's or b's of the isolated reactants. In a similar manner, $\boldsymbol{\phi}'$, $\boldsymbol{\varphi}$, and $\boldsymbol{\varphi}'$ span other subsets:

$$\boldsymbol{\phi}' = (\phi_1'\phi_2'\cdots\cdots\phi_N'),$$
$$\boldsymbol{\varphi} = (\varphi_1\varphi_2\cdots\cdots\varphi_N),$$
$$\boldsymbol{\varphi}' = (\varphi_1'\varphi_2'\cdots\cdots\varphi_N').$$

Now the overlap integral between two configurations, p and q, is given by:

$$\Psi_p = |\phi_1\cdots\cdots\phi_N\bar{\phi}_1'\cdots\cdots\bar{\phi}_N'| = A(\boldsymbol{\phi}\cdot\bar{\boldsymbol{\phi}}')/N_p,$$
$$\Psi_q = |\varphi_1\cdots\cdots\varphi_N\bar{\varphi}_1'\cdots\cdots\bar{\varphi}_N'| = A(\boldsymbol{\varphi}\cdot\bar{\boldsymbol{\varphi}}')/N_q,$$
$$S_{p,q} = 1/(N_p\cdot N_q)\cdot|\boldsymbol{S}_{\phi,\varphi}|\cdot|\boldsymbol{S}_{\bar{\phi}',\bar{\varphi}'}|, \tag{4}$$

where $\boldsymbol{S}$ is an MO overlap matrix:

$$\boldsymbol{S}_{\phi,\varphi} = \int {}^+\boldsymbol{\phi}\cdot\boldsymbol{\varphi}\mathrm{d}\tau = (s_{i,j}), \tag{5}$$

$$s_{i,j} = \int \phi_i\varphi_j \mathrm{d}v.$$

When the wave functions, Ψ_p and Ψ_q are given by the linear combinations of Slater determinants, $S_{p,q}$ is the sum of the overlap integrals between the determinantal wave functions. The normalization factors, N_p, for the wave functions due to the intermolecular MO overlap are immediately derived from Eq. 4,[10]

$$\Psi_0 = 1/\sqrt{(2N)!}\cdot 1/|\boldsymbol{S}_{0,0}|\cdot A(\boldsymbol{\phi}_0\cdot\bar{\boldsymbol{\phi}}_0), \tag{6}$$

$$\Psi_{k\to j} = 1/\sqrt{(2N)!}\cdot 1/(2|\boldsymbol{S}_{0,0}|\cdot|\boldsymbol{S}_{k\to j,k\to j}| + 2|\boldsymbol{S}_{0,k\to j}|^2)^{1/2}\cdot\{A(\boldsymbol{\phi}_0\cdot\bar{\boldsymbol{\phi}}_{k\to j}) + A(\boldsymbol{\phi}_{k\to j}\cdot\bar{\boldsymbol{\phi}}_0)\}, \tag{7}$$

$$\Psi_{i\to j,i\to j} = 1/\sqrt{(2N)!}\cdot 1/|\boldsymbol{S}_{i\to j,i\to j}|\cdot A(\boldsymbol{\phi}_{i\to j}\cdot\bar{\boldsymbol{\phi}}_{i\to j}), \tag{8}$$

where:

$$\boldsymbol{S}_{0,0} = \int {}^+\boldsymbol{\phi}_0\cdot\boldsymbol{\phi}_0\mathrm{d}\tau,$$

$$\boldsymbol{S}_{0,k\to j} = \int {}^+\boldsymbol{\phi}_0\cdot\boldsymbol{\phi}_{k\to j}\mathrm{d}\tau,$$

$$\boldsymbol{S}_{i\to j,i\to j} = \int {}^+\boldsymbol{\phi}_{i\to j}\cdot\boldsymbol{\phi}_{i\to j}\mathrm{d}\tau,$$

$$\boldsymbol{\phi}_0 = (a_1\cdots a_i\cdots a_m b_1\cdots b_k\cdots b_n),$$
$$\boldsymbol{\phi}_{k\to j} = (a_1\cdots a_m b_1\cdots a_j\cdots b_n),$$
$$\boldsymbol{\phi}_{i\to j} = (a_1\cdots a_j\cdots a_m b_1\cdots b_n).$$

The corresponding electron density can be calculated by means of the following equation:

$$\rho_{p,q} = 1/(N_p\cdot N_q)\{|\boldsymbol{S}_{\bar{\phi}',\bar{\varphi}'}|\cdot(\boldsymbol{\varphi}\hat{\boldsymbol{S}}_{\phi,\varphi}{}^+\boldsymbol{\phi}) + |\boldsymbol{S}_{\phi,\varphi}|\cdot(\bar{\boldsymbol{\varphi}}'\hat{\boldsymbol{S}}_{\bar{\phi}',\bar{\varphi}'}{}^+\bar{\boldsymbol{\phi}}')\}, \tag{9}$$

where $\hat{\boldsymbol{S}}_{\phi,\varphi}$ is the minor of $\boldsymbol{S}_{\phi,\varphi}$ with respect to the particular MO's concerned, ϕ and φ.

Next let us consider the energy matrix between various electron configurations. As has been mentioned above, $\boldsymbol{\varphi}$ is not generally orthogonal to $\boldsymbol{\phi}$. Now, let us assume that $\boldsymbol{\varphi}$ can be converted into a set of orbitals, $\boldsymbol{\lambda}$, by a certain transformation, $\boldsymbol{X}$, to give rise to:

$$\boldsymbol{\lambda} = \boldsymbol{\varphi}\boldsymbol{X}, \tag{10}$$

which satisfies the condition that:

$$\boldsymbol{1} = \int {}^+\boldsymbol{\phi}\cdot\boldsymbol{\lambda}\mathrm{d}\tau. \tag{11}$$

Therefore, we obtain:

$$\boldsymbol{X} = \boldsymbol{S}_{\phi,\varphi}{}^{-1}. \tag{12}$$

The matrix element between two configurations is given by:

$$H_{p,q} = \int|\phi_1\cdots\phi_N\bar{\phi}_1'\cdots\bar{\phi}_N'|H|\varphi_1\cdots\varphi_N\bar{\varphi}_1'\cdots\bar{\varphi}_N'|\mathrm{d}\tau$$
$$= \int|\phi_1\cdots\phi_N\bar{\phi}_1'\cdots\bar{\phi}_N'|H|\lambda_1\cdots\lambda_N\bar{\lambda}_1'\cdots\bar{\lambda}_N'|\mathrm{d}\tau/|\boldsymbol{S}_{\phi,\varphi}{}^{-1}|\cdot|\boldsymbol{S}_{\bar{\phi}',\bar{\varphi}'}{}^{-1}|$$
$$= \int|\phi_1\cdots\phi_N\bar{\phi}_1'\cdots\bar{\phi}_N'|H|\lambda_1\cdots\lambda_N\bar{\lambda}_1'\cdots\bar{\lambda}_N'|\mathrm{d}\tau\cdot|\boldsymbol{S}_{\phi,\varphi}|\cdot|\boldsymbol{S}_{\bar{\phi}',\bar{\varphi}'}|. \tag{13}$$

We can define here the bond order matrix, $\boldsymbol{P}^{\alpha}$ for electrons with the α spin and $\boldsymbol{P}^{\beta}$ for electrons with the β spin:

$$\boldsymbol{P}^{\alpha}_{p,q} = (\boldsymbol{c}_{\varphi}\boldsymbol{X})^{+}\boldsymbol{c}_{\phi} = \boldsymbol{c}_{\varphi}\boldsymbol{S}_{\phi,\varphi}{}^{-1+}\boldsymbol{c}_{\phi}, \tag{14}$$

$$\boldsymbol{P}^{\beta}_{p,q} = \boldsymbol{c}_{\bar{\varphi}}\boldsymbol{S}_{\bar{\phi}',\bar{\varphi}'}{}^{-1+}\boldsymbol{c}_{\bar{\phi}'}, \tag{15}$$

where $\boldsymbol{c}$ is the LCAO coefficient matrix of the basis AO's $\boldsymbol{\chi}$:

$$\boldsymbol{\phi} = \boldsymbol{\chi}\boldsymbol{c}_{\phi}, \tag{16}$$

$$\boldsymbol{\varphi} = \boldsymbol{\chi}\boldsymbol{c}_{\varphi}. \tag{17}$$

By the use of the partial bond order, P_{rs}, between the AO's χ_r and χ_s defined as the (r,s) element of the matrix $\boldsymbol{P}$, we obtain:

$$\begin{aligned} H_{p,q} = {} & [\sum_{r}\sum_{s}(P^{\alpha}_{rs}+P^{\beta}_{rs})(t_{rs}+v_{rs}) \\ & + \sum_{r}\sum_{s}\sum_{t}\sum_{u}(P^{\alpha}_{rs}P^{\alpha}_{tu}+P^{\beta}_{rs}P^{\beta}_{tu})/2 \\ & \cdot\{(rs|tu)-(rt|su)\} + \sum_{r}\sum_{s}\sum_{t}\sum_{u}P^{\alpha}_{rs}P^{\beta}_{tu}(rs|tu) \\ & + \sum_{\alpha<\beta}\sum Z_{\alpha}Z_{\beta}/R_{\alpha\beta}]\cdot\boldsymbol{S}_{p,q}, \end{aligned} \tag{18}$$

where:

$$t_{rs} = \int \chi_r(1)(-1/2\Delta_1)\chi_s(1)\mathrm{d}v_1,$$

$$v_{rs} = \int \chi_r(1)(\sum_{\alpha} -Z_{\alpha}/r_{1\alpha})\chi_s(1)\mathrm{d}v_1,$$

and:

$$(rs|tu) = \iint \chi_r(1)\chi_t(2)(1/r_{12})\chi_s(1)\chi_u(2)\mathrm{d}v_1\mathrm{d}v_2.$$

When the wave functions Ψ_p and Ψ_q are represented by linear combinations of the Slater determinants, the matrix element, $H_{p,q}$, is given by the sum of the integrals obtained in a similar manner.[11]

Results of Calculation

Figure 3 shows the relative spacings of the MO's of methylfluoride and the fluoride ion in an isolated state.

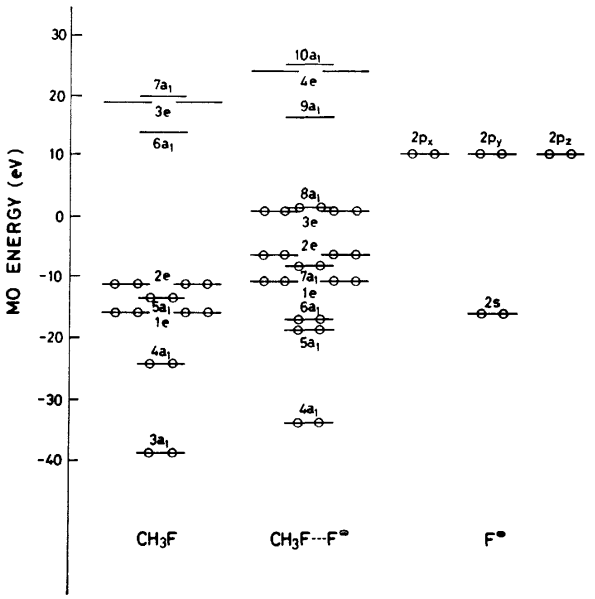

Fig. 3. Orbital diagram of interaction between methylfluoride and fluoride ion. Orbital exponents were taken after Hehre *et al.*[20]

The SCF MO levels of the composite system are also given in Fig. 3, although they are not necessary for our isolated-molecule approach to chemical interactions. They are used later in order to compare our results with the usual supermolecule calculation of the interacting system by the aid of configuration analysis. The matrix elements of Eq. 2 are given in Tables 1 and 2 with regard to some mono- and diexcited and electron-transferred configurations. It may be seen that the transferred configuration in which an electron is moved from the $2p_x$ of the fluoride ion to the LUMO of methylfluoride is located low only 4.02 eV above Ψ_0 and has a large off-diagonal element 0.80 eV. The pi-type interaction between the $2p_y$ or $2p_z$ of the fluoride ion and the $3e$ MO's of methylfluoride is found to be weaker than the sigma-type interaction. Ditransferred configurations can scarcely contribute to the stabilization of the system.

Table 1. The energies $(H_{p,p}-H_{0,0})$ of monoexcited and monotransferred configurations (upper) and diexcited and ditransferred configurations (lower) above Ψ_0 (in eV)

		j[a]		
		$6a_1$	$3e$	$7a_1$
i[a]	$5a_1$	21.474	—	26.105
		35.320	—	61.207
	$2e$	—	24.420	—
		—	63.667	—
k[a]	2s	30.880	—	36.510
		94.747	—	99.948
	$2p_x$	4.015	—	9.661
		43.448	—	48.667
	$2p_{y,z}$	—	9.215	—
		—	49.958	—

a) i and j stand for the occupied and unoccupied MO's of methylfluoride respectively, and k denotes the occupied MO's of the fluoride ion.

Table 2. The interaction integrals $(H_{0,p}-S_{0,p}H_{0,0})$ of monoexcited and monotransferred configurations (upper) and diexcited and ditransferred configurations (lower) (in eV) (The values in parentheses indicate the intramolecular portions.)

		j[a]		
		$6a_1$	$3e$	$7a_1$
i[a]	$5a_1$	1.258	—	0.035
		4.874(4.873)	—	0.759(0.758)
	$2e$	—	0.307	—
		—	0.852(0.852)	—
k[a]	2s	0.336	—	0.193
		0.003	—	0.001
	$2p_x$	0.803	—	0.239
		0.013	—	0.000
	$2p_{y,z}$	—	0.351	—
		—	0.003	—

a) The same as in Table 1.

The locally diexcited configurations in methylfluoride possess large off-diagonal matrix elements with Ψ_0, although they lie very high. These integrals originate, however, principally from intramolecular electron repulsions and, hence, should be further partitioned into several terms in evaluating the intermolecular interaction energy. The values in parentheses indicate the intramolecular parts. One may see that the enhancement of diexcited configurations due to the intermolecular interaction is negligibly small in this case.[12] The large matrix element, 1.26 eV, for the monoexcited configuration, $\Psi_{5a\to 6a}$, signifies a strong polarization of methylfluoride under the influence of the electrostatic field of the fluoride ion.

The coefficients of the ground-state wave function are given approximately by:

$$C_0 = 1 - \sum_{p\neq 0} (H_{0,p}-S_{0,p}H_{0,0})S_{0,p}/(H_{0,0}-H_{p,p}) - 1/2\sum_{p\neq 0}(H_{0,p}-S_{0,p}H_{0,0})^2/(H_{0,0}-H_{p,p})^2, \quad (19)$$

$$C_p = (H_{0,p}-S_{0,p}H_{0,0})/(H_{0,0}-H_{p,p}) + \sum_{q\neq 0,p}(H_{p,q}-S_{p,q}H_{0,0}) \cdot (H_{0,q}-S_{0,q}H_{0,0})/\{(H_{0,0}-H_{p,p})\cdot(H_{0,0}-H_{q,q})\}. \quad (20)$$

They are listed in Table 3. The monotransferred configuration in which an electron is shifted from the $2p_x$ of the fluoride ion to the $6a_1$ MO of methylfluoride is found to be dominant among the various electron configurations except for Ψ_0. The electron transfer from the $2p_y$ and $2p_z$ of the fluoride ion to the $3e$ MO's of methylfluoride is not effective. The present calculation indicates that the reaction is initiated by the attack of the 2p orbitals of the anion. The participation of the 2s orbital is found to be minor at the beginning of the reaction.

The electron density of the composite system can be divided into several terms:

$$\rho = \rho(CH_3F) + \rho(F^-) + \rho_K + \rho_\Pi + \rho_D + \cdots, \quad (21)$$

where $\rho(CH_3F)$ and $\rho(F^-)$ mean the electron densities of the isolated methylfluoride and fluoride ion respectively, and where ρ_K, ρ_Π, and ρ_D represent the exchange, polarization, and delocalization interactions respectively. The polarization density covers the locally excited electron configurations, while the delocalization density consists of the electron-transferred configurations involved in Table 3. The exchange density is defined by:

$$\rho_K = \rho_{0,0} - \rho(CH_3F) - \rho(F^-). \quad (22)$$

The exchange, polarization, and delocalization densities are illustrated in Fig. 4. The exchange interaction brings about a negative difference density between the attacking anion and the substrate, since both of the reactants possess closed-shells. On the other hand, the electron delocalization from the anion to methylfluoride produces a positive density in the intermolecular region. The competition between the exchange interaction and the delocalization interaction seems to govern the appearance of the new chemical bond to be formed between the reagent and the reactant. The polarization of methylfluoride induced by the electrostatic field of the fluoride ion causes a drift of electrons from carbon to fluorine to increase the polarity of the bond to be broken.

The energy of the interacting system is divided in a similar manner[4b] for the ground-state of the interacting

Table 3. The expansion coefficients of the ground-state wave function of the interacting system obtained by perturbation calculations[b]

$C_0=0.966$		j[a]		
		$6a_1$	$3e$	$7a_1$
i[a]	$5a_1$	0.059	—	0.001
		0.138	—	0.012
	$2e$	—	0.013	—
		—	0.013	—
k[a]	2s	0.011	—	0.005
		0.000	—	0.000
	$2p_x$	0.200	—	0.025
		0.000	—	0.000
	$2p_{y,z}$	—	0.038	—
		—	0.000	—

a) The same as in Table 1. b) Absolute values are given. The upper numbers correspond to monoexcited and monotransferred configurations, and the lower ones, to diexcited and ditransferred configurations.

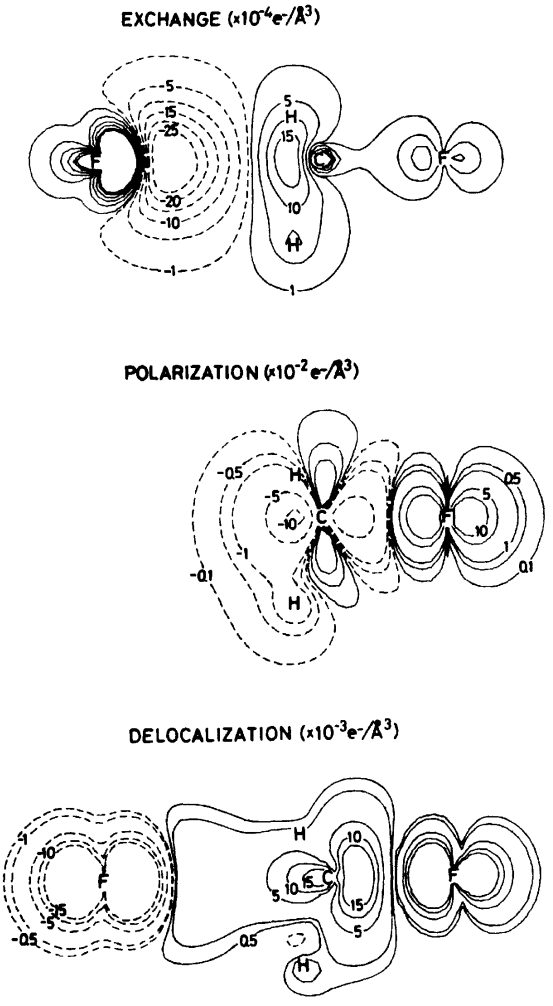

Fig. 4. Contour maps for the exchange, polarization, and delocalization densities in x-z plane at y=0.

system:

$$E_g = E(CH_3F) + E(F^-) + \varepsilon_Q + \varepsilon_K + \varepsilon_{II} + \varepsilon_D + \cdots, \quad (23)$$

where $E(CH_3F)$ and $E(F^-)$ are the energies of the isolated reactants and where ε_Q, ε_K, ε_{II}, and ε_D mean the Coulomb, exchange, polarization, and delocalization energies respectively. We have $\varepsilon_Q = -0.271$ eV, $\varepsilon_K = 0.110$ eV, $\varepsilon_{II} = -0.081$ eV, and $\varepsilon_D = -0.198$ eV for this system.

Configuration Analysis

An alternative way of calculating the coefficients in Eq. 1 is the configuration analysis of the SCF MO wave function of the interacting systems.[10,13] The given SCF wave function, Ψ, of the composite system can be expanded in terms of the various electron configurations, Ψ_p, of the reactants. Table 4 presents the result of the analysis of the wave function without CI. A comparison of the results given in Table 4 with those in Table 3 indicates that a single determinantal wave function describes the basic feature of the interaction pretty well in this case.[14] The inclusion of CI with the diexcited configurations of the composite system in which a pair of electrons are removed from an occupied MO and placed in an unoccupied MO improves the wave function appreciably, as is shown in Table 5. That is, the diexcited configurations in methylfluoride are recovered. The changes in the occupation numbers of the MO's of methylfluoride and the fluoride ion due to the interaction are given in Table 6.[15] The results confirm our conclusion that the electron delocalization from the $2p_x$ orbital of the fluoride ion to the $6a_1$ MO of methylfluoride plays the key role in the early stage of the S_N2 reaction.[16]

Table 4. The expansion coefficients of the ground-state wave function of the interacting system without CI obtained by configuration analysis[b]

$C_0=0.981$		j[a]		
		$6a_1$	$3e$	$7a_1$
i[a]	$5a_1$	0.049	0	0.000
		0.001	0	0.000
	$2e$	0	0.006	0
		0	0.000	0
k[a]	2s	0.012	0	0.005
		0.000	0	0.000
	$2p_x$	0.159	0	0.021
		0.013	0	0.000
	$2p_{y,z}$	0	0.035	0
		0	0.001	0

a) The same as in Table 1. b) The same as in Table 3.

Table 5. The expansion coefficients of the ground-state wave function of the interacting system with CI obtained by configuration analysis[b]

$C_0=0.968$		j[a]		
		$6a_1$	$3e$	$7a_1$
i[a]	$5a_1$	0.054	0	0.001
		0.119	0.004	0.009
	$2e$	0	0.006	0
		0.014	0.012	0.005
k[a]	2s	0.012	0	0.005
		0.002	0.000	0.002
	$2p_x$	0.159	0	0.020
		0.001	0.001	0.000
	$2p_{y,z}$	0	0.034	0
		0.000	0.000	0.000

a) The same as in Table 1. b) The same as in Table 3.

Table 6. The changes in the occupation numbers of the MO's due to the interaction

	MO	Isolated state	Interacting state
CH_3F	$4a_1$	1.997	1.997
	$1e$	1.995	1.996
	$5a_1$	1.966	1.968
	$2e$	1.999	1.999
	$6a_1$	0.036	0.064
	$3e$	0.005	0.006
	$7a_1$	0.003	0.003
F^-	2s	2.000	1.999
	$2p_x$	2.000	1.970
	$2p_{y,z}$	2.000	1.998

Discussion

As the first attempt to test the validity of our analysis, we carried out a preliminary evaluation of the expansion coefficients by the use of a perturbation formalism. The breakdown of the energy and the electron density was made tentatively by utilizing the coefficients. It may be unnecessary to say that they can be replaced by those derived from a configuration analysis of an SCF wave function of the interacting system. In this respect, the present method retains the flexibility of adapting to any degree of sophistication in the MO methods. Attempts to get information about the aspects of complicated chemical reactions by means of elaborate MO calculations seem to be getting more and more frequent in organic chemistry with the progress of computing facilities. On the other hand, the concept of orbital interaction based on rather simplified reaction models has provided us with some governing principles of chemical reactions.[17] Though qualitative in nature, the approach offers a promise of uncovering new insights into chemical reactions. In this study, we preferred a configuration interaction approach[4b] to the one-electron-orbital interaction approach,[17] because the former is expected to be capable of elucidating the characteristics of chemical interactions in a more acceptable manner both chemically and physically.

We have focused our attention mainly on the development of a method of relating the qualitative but lucid theory of molecular interactions to up-to-date computations of chemically interacting systems in a quantitative way. The numerical results presented here with regard to an S_N2 reaction do not necessarily give us novel information about the nature of the reaction. One may recognize, however, that further applications and possible refinements to fit for various kinds of reactions, involving open-shells, external perturbations,[18]

and so on, will verify the utility of our method for studying the molecular mechanisms of chemical reactions.

It has been demonstrated in this calculation that our isolated-molecule approach gives us a wave function which is comparable to the one obtained by the SCF CI calculation of the composite system. The usual SCF MO method possesses a serious drawback in that it fails to give a stable solution for weakly interacting systems. Therefore, it is necessary to employ the multiconfiguration SCF MO method in place of the single configuration SCF MO method to study weak interactions. On the contrary, our present method is quite useful in dealing with loosely bound systems, such as the early stages of chemical reactions and dissociation processes. Applications to strongly interacting systems by enlarging the basis electron configurations are in progress.

Finally, it should be noted that the destabilization of an interacting system due to the necessary distortion of the reactants in the course of the reaction must be an important source of activation energy, though the distortion is likely to take place in such a way as to promote further electron delocalization.[19] Accodingly, in order to obtain a reasonable activation energy from an MO calculation, it seems to be important to employ a basis set which is able to reproduce the energy change for a wide range of molecular deformations of the reactants.

This work was supported in part by a Grant-in-Aid from the Ministry of Education. The computation was carried out on a FACOM 230-75 of the Data Processing Center, Kyoto University. We are grateful to Mr. Tsutomu Minato for his assistance in our STO-3G MO calculations.

References

1) a) C. K. Ingold, "Structure and Mechanism in Organic Chemistry," 2nd ed, Cornell University Press, Ithaca (1969), pp. 418—610; b) E. S. Gould, "Mechanism and Structure in Organic Chemistry," Holt, Rinehart and Winston, New York (1959), pp. 250—313.

2) a) L. C. Bateman, E. D. Hughes, and C. K. Ingold, *J. Chem. Soc.*, **1940**, 979; b) I. Dostrousky, E. D. Hughes, and C. K. Ingold, *ibid.*, **1946**, 173.

3) See, for instance, H. F. Schaefer, III, *Chem. Br.*, **11**, 227 (1975).

4) a) J. N. Murrel, M. Randić, and D. R. Williams, *Proc. R. Soc. London, Ser. A*, **284**, 566 (1965); b) K. Fukui and H. Fujimoto, *Bull. Chem. Soc. Jpn.*, **41**, 1989 (1968); c) H. Fujimoto and K. Fukui, "Chemical Reactivity and Reaction Paths," ed by G. Klopman, Wiley-Interscience, New York (1974), pp. 23—54; d) G. Klopman, *J. Am. Chem. Soc.*, **90**, 223 (1968); e) L. Salem, *ibid.*, **90**, 543, 553 (1968); f) R. Sustmann and G. Binsch, *Mol. Phys.*, **20**, 1, 9 (1971); g) L. Libit and R. Hoffmann, *J. Am. Chem. Soc.*, **96**, 1370 (1974); h) T. Fueno, S. Nagase, K. Tatsumi, and K. Yamaguchi, *Theor. Chim. Acta*, **26**, 43 (1972).

5) a) G. Berthier, D.-J. David, and A. Veillard, *Theor. Chim. Acta*, **14**, 329 (1965); b) A. Dedieu and A. Veillard, *Chem. Phys. Lett.*, **5**, 328 (1970); c) A. Dedieu and A. Veillard, *J. Am. Chem. Soc.*, **94**, 6730 (1972); d) H. Kato, K. Morokuma, T. Yonezawa, and K. Fukui, *Bull. Chem. Soc. Jpn.*, **38**, 1749 (1965); e) A. J. Duke and R. F. W. Bader, *Chem. Phys. Lett.*, **10**, 631 (1971); f) P. Cremaschi, A. Gamba, and M. Simonetta, *Theor. Chim. Acta*, **25**, 237 (1972); g) F. Keil and R. Ahlrichs, *J. Am. Chem. Soc.*, **98**, 4787 (1976). The substitution of methylfluoride by fluoride ion is not realistic. We adopted the system in this study only to investigate the common feature of the S_N2 reactions. The geometry obtained by Veillard contains some arbitrariness in the procedure of the optimization. Duke and Bader pointed out that the activation energy could not be obtained in calculations with the small basis set. In actual reactions, solvation and desolvation might play a significant role in determining the height of the barrier.

6) P.-O. Löwdin, *J. Chem. Phys.*, **18**, 365 (1950). See also A. H. Pakiari and J. W. Linnet, *J. Chem. Soc., Faraday Trans. 2*, **72**, 641 (1976).

7) A. T. Amos and G. G. Hall, *Proc. R. Soc. London, Ser. A*, **263**, 483 (1961).

8) a) K. O-ohata, H. Taketa, and S. Huzinaga, *J. Phys. Soc. Jpn.*, **21**, 2306 (1966); b) H. Taketa, S. Huzinaga, and K. O-ohata, *ibid.*, **21**, 2313 (1966).

9) R. F. Stewart, *J. Chem. Phys.*, **52**, 431 (1970).

10) a) H. Fujimoto, S. Kato, S. Yamabe, and K. Fukui, *J. Chem. Phys.*, **60**, 572 (1974); b) S. Kato, H. Fujimoto, S. Yamabe, and K. Fukui, *J. Am. Chem. Soc.*, **96**, 2024 (1974).

11) When the overlap integral between two wave functions, ϕ and φ, happens to be zero, the inverse matrix, $S_{\phi,\varphi}^{-1}$, is indefinable. In this case, the matrix element can be calculated by expanding the density matrix as Eq. 9.

12) In symmetry-forbidden reactions, the mixing in of diexcited electron configurations plays a crucial role along non-least-motion reaction paths.

13) H. Baba, S. Suzuki, and T. Takemura, *J. Chem. Phys.*, **50**, 2078 (1969).

14) The present system is a typical ionic reaction. It seems to be unlikely, therefore, that CI brings about a drastic change in the calculated results as to the nature of the reaction. In relation to the biradical character of chemical reactions, the consequence of CI was reviewed by Salem and Rowland. See L. Salem and C. Rowland, *Angew. Chem., Int. Ed. Engl.*, **11**, 92 (1972).

15) Non-integer values in an isolated state come from the CI for the isolated reactant.

16) K. Fukui, H. Fujimoto, and S. Yamabe, *J. Phys. Chem.*, **76**, 232 (1972). Our previous semiempirical calculation gave qualitatively the same conclusion as the present work.

17) J. P. Lowe, *J. Am. Chem. Soc.*, **93**, 301 (1971).

18) H. Fujimoto and R. Hoffmann, *J. Phys. Chem.*, **78**, 1874 (1974).

19) K. Fukui and H. Fujimoto, *Bull. Chem. Soc. Jpn.*, **42**, 3399 (1969).

20) W. J. Hehre, R. F. Stewart, and J. A. Pople, *J. Chem. Phys.*, **51**, 2657 (1969).

^{14}N Nuclear Quadrupole Resonances of the Molecular Complexes of Urea

Hisao NEGITA, Tsuneo KUBO, and Michio MAEKAWA

Department of Chemistry, Faculty of Science, Hiroshima University, Hiroshima 730

(Received February 9, 1977)

The ^{14}N nuclear quadrupole resonance (NQR) was studied on three kinds of molecular complexes of urea, such as the urea-hydrogen peroxide complex (H_2O_2 complex), the urea-sodium chloride-water complex (NaCl complex), and the urea-sodium bromide-water complex (NaBr complex). The ^{14}N quadrupole coupling constants and asymmetry parameters are as follows: $|e^2Qq/h|=3493.8$ kHz and $\eta=0.3456$ for the H_2O_2 complex; $|e^2Qq/h|=3597$ kHz and $\eta=0.293$ for the NaCl complex, and $|e^2Qq/h|=3636.7$ kHz and $\eta=0.2778$ for the NaBr complex. From the temperature dependence of the resonance frequencies, it is considered that the hydrogen bonds in the H_2O_2 complex are stronger than those in the NaCl complex. The electron densities at nitrogen atoms in these complexes were derived from the corresponding NQR parameters, and were compared with those in urea.

The molecular complexes of urea have been investigated by various spectroscopic methods.[1,2] The NQR method is particularly useful for investigating the charge distributions in these complexes. However, only a few ^{14}N NQR data on molecular complexes have been reported thus far. Therefore, we planned to examine ^{14}N NQR in molecular complexes of urea, such as the urea–hydrogen peroxide complex (H_2O_2 complex), the urea–sodium chloride–water complex (NaCl complex), and the urea–sodium bromide–water complex (NaBr complex). On the basis of the ^{14}N NQR in these complexes, the strength of the hydrogen bonds and the charge distributions at the nitrogen atoms were compared with those in urea itself.

Experimental

The ^{14}N NQR spectra of the H_2O_2 complex, the NaCl complex, and the NaBr complex were obtained by the use of a frequency-modulated spectrometer described previously.[3] The resonance frequencies were measured by means of a heterodyne-type frequency meter, the frequency of which was checked by means of a frequency counter, TR-5104, from the Takeda Riken Co. Measurements were carried out at several temperatures between the temperature of liquid nitrogen and room temperature. The temperatures were measured by the use of a copper-constantan thermocouple.

Preparation of Samples. The sample of the H_2O_2 complex was obtained by cooling a solution of urea in 30% hydrogen peroxide, in a molar ratio of 2 : 3, the solution had been heated for a few minutes at a temperature of about 60 °C.[4] Found: C, 12.96; H, 6.39; N, 30.02; H_2O_2, 34.6%. Calcd for the H_2O_2 complex: C, 12.77; H, 6.43; N, 29.78; H_2O_2, 36.2%.

The sample of the NaCl complex was prepared by slowly evaporating an equimolar solution of urea and sodium chloride.[5] Found: C, 9.48; H, 4.39; N, 21.81; Cl, 25.4%. Calcd for the NaCl complex: C, 8.80; H, 4.43; N, 20.52; Cl, 26.0%.

The sample of the NaBr complex was obtained from an equimolar solution of urea and sodium bromide. Found: C, 6.62; H, 3.24; N, 15.66; Br, 43.4%. Calcd for the NaBr complex: C, 6.64; H, 3.34; N, 15.48; Br, 44.2%. All the samples were ground into powder after drying, and about a 20-g portion of the samples was used for the measurement.

Results and Discussion

Generally a pair of ^{14}N NQR frequencies, ν_- and ν_+, are observed for a species of nitrogen atoms:

$$\nu_\pm = \frac{|e^2Qq|}{4h}(3\pm\eta), \tag{1}$$

where $|e^2Qq/h|$ and η are the quadrupole coupling constant and the asymmetry parameter respectively. In the H_2O_2 complex and the NaBr complex, a pair of resonance lines was found, as is shown in Fig. 1. The quadrupole coupling constants and asymmetry parameters derived from these frequencies are listed in Table 1. In the case of the NaCl complex, four resonance lines were found, as is shown in Fig. 1. However, these lines could not be paired because both higher and lower lines of the two pairs were closely spaced. Accordingly, the quadrupole coupling constant and the asymmetry parameter were derived from the average values of ν_- and ν_+; they are listed in Table 1.

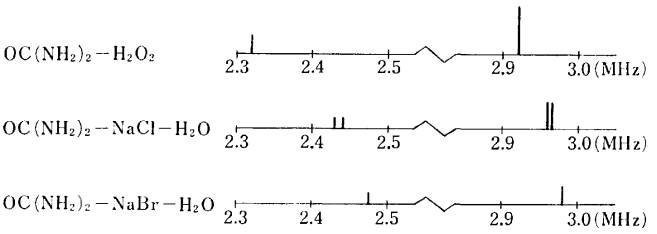

Fig. 1. NQR absorption lines in urea complexes at liquid nitrogen temperature.

TABLE 1. NQR PARAMETERS IN UREA COMPLEXES

Complex	ν_-/kHz	ν_+/kHz	$\lvert e^2Qq/h\rvert$/kHz	η
$OC(NH_2)_2$-H_2O_2	2318.4	2922.3	3493.8	0.3456
$OC(NH_2)_2$-NaCl-H_2O	2428.7 2439.1	2958.8 2964.5	3597	0.293
$OC(NH_2)_2$-NaBr-H_2O	2474.8	2980.1	3636.7	0.2778

Figure 2 shows the temperature dependence of the resonance frequencies of the ν_+ lines in the H_2O_2 complex, the NaCl complex, and urea.[6] In the case of the NaCl complex, the intensities of the ν_+ lines decrease gradually as the temperature rises, and become too weak to be observed at 181 K. The temperature dependence in the H_2O_2 complex is slightly smaller than that in urea, as is shown in Fig. 2. In the case of the H_2O_2 complex, each nitrogen atom of the urea molecule makes two hydrogen bonds, N–H···O, with lengths of 2.94 Å and 3.04 Å,[4] as is shown in Fig. 3,

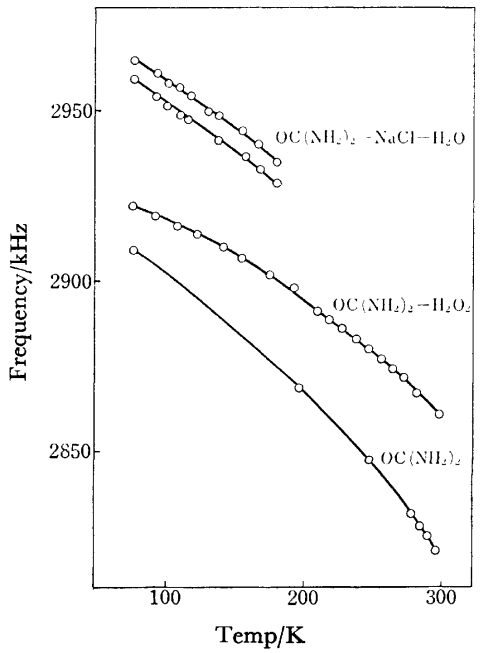

Fig. 2. The temperature dependence of the resonance line, ν_+, in urea-sodium chloride-water, urea-hydrogen peroxide, and urea.

whereas those in urea are 2.99 and 3.04 Å.[7] The smaller temperature dependence in the H_2O_2 complex can be explained by the difference in the hydrogen-bond distance between the H_2O_2 complex and urea. That is, the hydrogen bonds in the H_2O_2 complex are slightly stronger than in urea. On the other hand, Fig. 2 shows that the temperature dependence in the NaCl complex is nearly equal to that in urea. This suggests that the hydrogen bonds in the NaCl complex are nearly equal to those in urea and are weaker than in the H_2O_2 complex.

In the H_2O_2 complex, the hydrogen bonds are not very strong, as is shown in Fig. 3. Therefore, the electronic state of nitrogen in the NH_2 group may be considered to be nearly equal to that in urea, and we assumed the nitrogen σ-bond orbitals to be sp^2-hybrids. In the case of the NaCl complex, there are two crystallographically nonequivalent nitrogen atoms, and each nitrogen atom forms only one hydrogen bond with a chloride ion of sodium chloride, the length of which is 3.05 or 3.22 Å.[5] However, the electronic state of nitrogen in the NH_2 groups may be considered not

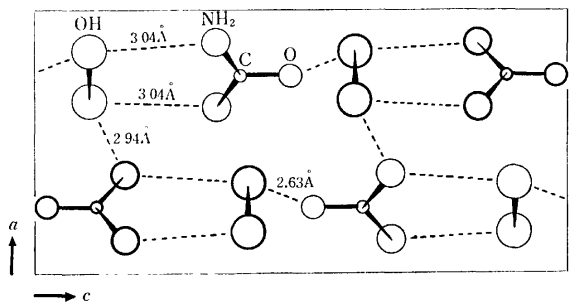

Fig. 3. The crystal structure of urea-hydrogen peroxide (b-axis projection).

to be largely different from that in urea, and we assumed that the nitrogen σ-bond orbitals are sp^2-hybrids. As is shown in Table 1, the quadrupole coupling constant and the asymmetry parameter in the NaBr complex are nearly equal to those in the NaCl complex. Therefore, we assumed sp^2-hybridization for nitrogen, as above.

The electron densities of the nitrogen atoms in these complexes can be calculated by means of the following equations derived by Lucken:[8]

$$2\eta \cdot |e^2Qq/e^2Qq_p| = 3(c-b)(1-\cot^2\gamma), \quad (2)$$

$$(1-\eta/3) \cdot |e^2Qq/e^2Qq_p| = a - c, \quad (3)$$

where a is the electron density in the lone-pair orbital; b and c are the σ-electron densities in the N–C and N–H bonds respectively; 2γ is the $\angle$HNH bond angle, approximately 120°, and $|e^2Qq_p/h|$ is the quadrupole coupling constant due to one 2p-electron of a nitrogen atom. In the case of the H_2O_2 complex, the NaCl complex, and the NaBr complex, it is assumed that $|e^2Qq_p/h|$ is 9 MHz and that the σ-electron density for the N–C bond is the same as that for the N–C bond in urea (1.206);[8] therefore, the values of the a and c parameters can be evaluated. Table 2 lists the values thus obtained. The σ_{NH} values in these complexes decrease in the order of the H_2O_2 complex, the NaCl complex, and the NaBr complex, showing that the strength of the hydrogen bond decreases in this order.

TABLE 2. ELECTRON DENSITIES IN UREA AND ITS MOLECULAR COMPLEXES

Compound	σ_{NH}	Lone-pair
$OC(NH_2)_2$	1.331	1.679
$OC(NH_2)_2$–H_2O_2	1.340	1.684
$OC(NH_2)_2$–NaCl–H_2O	1.323	1.684
$OC(NH_2)_2$–NaBr–H_2O	1.318	1.685

On the other hand, the σ_{NH} value in the H_2O_2 complex is larger than that in urea. This suggests that the hydrogen bonds in this complex are stronger than those in urea, which is parallel to the conclusion from the temperature dependence of the resonance frequencies.

References

1) T. Ichikawa and M. Iwasaki, *J. Chem. Phys.*, **44**, 2979 (1966).
2) K. Aida, *J. Inorg. Nucl. Chem.*, **25**, 165 (1963).
3) H. Negita, M. Hayashi, and T. Okada, *J. Sci. Hiroshima Univ., Ser. A*, **35**, 85 (1971).
4) Chia-S. Lu, E. W. Hughes, and P. A. Giguère, *J. Am. Chem. Soc.*, **63**, 1507 (1941).
5) J. H. Palm and C. H. MacGillavry, *Acta Crystallogr.*, **16**, 963 (1963).
6) T. Chiba, M. Toyama, and Y. Morino, *J. Phys. Soc. Jpn.*, **14**, 379 (1959).
7) P. Vaughan and J. Donohue, *Acta Crystallogr.*, **5**, 530 (1952).
8) E. A. C. Lucken, "Nuclear Quadrupole Coupling Constants," Academic Press, London and New York (1969), p. 225.

Statistical Thermodynamics of Liquid Mixtures

Kazuo TOKIWANO* and Kiyoshi ARAKAWA
Research Institute of Applied Electricity, Hokkaido University, Sapporo 060
**Faculty of Engineering, Hokkaido University, Sapporo 060*
(Received February 10, 1977)

A statistical thermodynamic theory of binary liquid mixtures has been worked out on the basis of the equivalent free volume defined without use of lattice model. A liquid mixture is regarded as a mixture of hard spheres immersed in a uniform background potential. The total free energy is expressed as the sum of terms given by the analytical solution of the generalized Percus-Yevick equation for the hard sphere mixture and the term resulting from the uniform background potential. Thermodynamic functions are in a simple form convenient for practical applications. The nature of the equivalent free volume for the mixture which consists of molecules differing in size is elucidated. The energy interaction parameters and excess thermodynamic functions for eight binary mixtures composed of nonpolar molecules are calculated, and the results are discussed.

Since the designation of "regular solution" by Hildebrand and Scott[1] attempts have been made to develop a statistical theory of liquid mixtures. The most remarkable theories are those presented by Prigogine and co-workers,[2] and Flory.[3] Prigogine *et al.* presented the theories based on the average potential model, and Flory introduced the interactions between surface-sites of molecules, using the corresponding state theorem. These theories have been used by many workers during the last two decades.[4] However, the basic assumptions underlying the theories seem to require further examination.

The most important problem in the statistical theories of liquid mixtures is to estimate the "entropy of mixing" for the mixtures composed of molecules differing in size. A cell or lattice model has been used for estimation, but no rigorous treatment has been given so far. The solution for mixtures of hard spheres was first given by Lebowitz,[5] who succeeded in obtaining an analytical and explicit solution of the generalized Percus-Yevick equation.

Snider and Herrington[6] made a direct application of the Lebowitz solution to binary mixtures on the basis of the Longuet-Higgins and Widom model[7] which was proposed first for pure fluids. For the excess thermodynamic functions of binary mixtures of nonpolar molecules, they obtained good agreement between the calculated and experimental values. Marsh and others tested Snider and Herrington's treatment for several binary mixtures[8] and Kreglewski *et al.* carried out a statistical thermodynamic treatment along the same line.[9] However, the physical nature of those theories remains unclarified.

The equivalent free volume for mixtures of hard spheres has been defined on the basis of the Lebowitz solution without assuming any specified lattice.[10] We indicate in the present work that all molecules constituting a liquid mixture hold the same magnitude of the "equivalent free volume" in spite of their different sizes. A simple and convenient formulation of thermodynamic functions for liquid mixtures is attempted in terms of equivalent free volume.

For calculation, molecular parameters for each component are usually determined from the thermodynamical data for pure species. However, the energy interaction parameter between different species, which is necessary for the calculation of various excess thermodynamic functions, can not be obtained directly. The data for one of excess functions are used to determine the parameter. Excess enthalpy or excess Gibbs free energy has been used so far for the determination of the parameter. Snider and Herrington[6] calculated the energy interaction parameter for binary mixtures from the experimental values of excess Gibbs free energy. We have determined it from the observed values of excess volume obtained more easily than for the other thermodynamic functions such as excess heat *etc.* The results are satisfactory. Their significance is discussed in this paper.

Theory

The Liquid Model. For the formulation of the theory, the liquid mixture consisting of various species of molecules is regarded as a mixture of hard spheres immersed in a uniform background potential resulting from the attractive forces between molecules. Longuet-Higgins and Widom[7] applied the model to liquid Argon. The model has later been applied to pure liquid and solutions by several workers[6,9-11] including the present authors.

The Free Energy and Entropy. In the liquid model, the translational part of the total partition function for the mixture becomes identical with the partition function for the mixture of hard spheres with no attraction between themselves. In a previous paper,[10] an analytical expression was given on the translational partition function for mixtures of hard spheres on the basis of the Lebowitz solution for the Percus-Yevick equation. A partition function Z_0 at a given volume V and temperature T for an assembly of r components is expressed as

$$Z_0 = \frac{N!}{\prod_{i=1}^{r} N_i!} \prod_{i=1}^{r} \left[\left(\frac{2\pi m_i kT}{h^2} \right)^{3/2} \left(e \frac{Vf_m}{N} \right) \right]^{N_i}. \quad (1)$$

The Helmholtz free energy F_0 becomes

$$F_0 = -kT \sum_{i=1}^{r} N_i \ln \left(\frac{2\pi m_i kT}{h^2} \right)^{3/2} - NkT \ln \left(e \frac{Vf_m}{N} \right) - T\Delta S_{\text{id.mix.}}. \quad (2)$$

The equivalent free volume fraction f_m is given by

$$f_m = (1-\xi) \exp \left[-\frac{9}{\pi} \frac{V}{N} \frac{1}{(1-\xi)^2} (2XY - 2XY\xi + X^3) \right], \quad (3)$$

and the packing fraction for the mixture, ξ, by

$$\xi = \sum_{i=1}^{r} \frac{\pi}{6} \frac{N_i}{V} R_i^3, \tag{4}$$

where N_i is the number of molecules, m_i the mass, R_i the diameter of hard spheres for i-th species, $N(=\sum_{i=1}^{r} N_i)$ the total number of molecules, and

$$X = \sum_{i=1}^{r} \frac{\pi}{6} \frac{N_i}{V} R_i^2, \quad Y = \sum_{i=1}^{r} \frac{\pi}{6} \frac{N_i}{V} R_i. \tag{5}$$

The ideal entropy of mixing $\Delta S_{\text{id. mix.}}$ is

$$\Delta S_{\text{id.mix.}} = k \ln[N!/\prod_{i=1}^{r} N_i!]. \tag{6}$$

Equation 2 (or Eq.1) is seen to have a form which is identical with that given in the usual free volume theories. Thus we have the "equivalent free volume,"

$$v_f = V f_m / N. \tag{7}$$

Hence, f_m has been defined as the "equivalent free volume fraction,"[10] which is an extension of the case of a one-component fluid[11] to mixtures. No cell or lattice model is presupposed in the definition of the equivalent free volume.

Equation 2 indicates that the equivalent free volume v_f is the same for all the species in the mixture, in spite of their different sizes. The physical meaning of this remarkable fact will be discussed, in comparison with the interpretation of "free volume" made in the usual free volume theories of solutions.[12]

Let us assume that the attractive forces give rise to a uniform background potential, taking the liquid model proposed by Longuet-Higgins and Widom[7] into consideration. A uniform background potential is given by $U_{\text{BG}} = -N^2(\sum_{i=1}^{r}\sum_{j=1}^{r} x_i x_j a_{ij})/V$, where $x_i(=N_i/N)$ is the mole fraction of i-th species, a_{ii} the energy constant for the pure component, and $a_{ij}(i \neq j)$ the additional one for the mixture.[13] Thus, the free energy is written as

$$F = F_0 - \frac{N^2}{V}(\sum_i \sum_j x_i x_j a_{ij})$$

$$= F_{\text{id,m}} - NkT \ln(f_m) - \frac{N^2}{V}(\sum_i \sum_j x_i x_j a_{ij}), \tag{8}$$

where $F_{\text{id, m}}$ is the free energy of the mixture of ideal gases which is given by[14]

$$F(V, T, N_1 \cdots N_r)_{\text{id,m}} = -NkT \sum_i x_i \ln\left(\frac{2\pi m_i kT}{h^2}\right)^{3/2} - NkT \ln\left(e\frac{V}{N}\right) - T\Delta S_{\text{id.mix.}}. \tag{9}$$

The first term $F_{\text{id, m}}$ in the right-hand side of Eq. 8 is the ideal term, the second one $-NkT \ln(f_m)$ is the contribution from the repulsive interaction between molecules in the fluctuational thermal motions, and the third one is that from the uniform background potential in which the molecules constituting the mixture are immersed.

The entropy S is expressed as

$$S = S_{\text{id,m}} + Nk \ln(f_m), \tag{10}$$

where $S_{\text{id, m}}$ is given by

$$S(V, T, N_1 \cdots N_r)_{\text{id,m}} = Nk \sum_i x_i \ln\left(\frac{2\pi m_i kT}{h^2}\right)^{3/2} + \frac{3}{2}Nk + Nk \ln\left(e\frac{V}{N}\right) + \Delta S_{\text{id.mix.}}. \tag{11}$$

The Equation of State. Differentiating Eq. 8 with respect to V at constant T, we have

$$pV = NkT + NkT\frac{V}{f_m}\left(\frac{\partial f_m}{\partial V}\right)_{T,N} - \frac{N^2}{V}(\sum_i \sum_j x_i x_j a_{ij}) \tag{12}$$

$$= NkT\chi_m(\xi) - \frac{N^2}{V}(\sum_i \sum_j x_i x_j a_{ij}), \tag{13}$$

where

$$\chi_m(\xi) = \frac{1}{(1-\xi)^3}\left[(1-\xi)^2 + \frac{18}{\pi}\frac{V}{N}(XY - XY\xi + X^3)\right]. \tag{14}$$

$\chi_m(\xi)$ is the compressibility factor given by Lebowitz.[5]

Excess Thermodynamic Functions. Various excess molar quantities are given in the following. The excess volume V^E is given by

$$V^E = V - \sum_i x_i V_i, \tag{15}$$

where V_i and V are the molar volume for the pure fluid of i-th species and that for the mixture, respectively.

The excess free energy F^E is given by

$$F^E = F - \sum_i x_i F_i + T\Delta S_{\text{id.mix.}}, \tag{16}$$

where F_i is the free energy for the pure fluid of i-th species. Thus F^E is derived as follows by means of Eq. 8.

$$F^E = -N_A kT \sum_i x_i \ln\left(\frac{f_m V}{f_i V_i}\right) - \left[\frac{N_A^2}{V}\sum_i \sum_j x_i x_j a_{ij} - \sum_i x_i \frac{N_A^2}{V_i} a_{ii}\right], \tag{17}$$

where f_i is the equivalent free volume fraction for the pure fluid of i-th species and N_A Avogadro's number.

For the excess entropy, using Eq. 10 we obtain

$$S^E = S - \sum_i x_i S_i - \Delta S_{\text{id.mix.}}$$

$$= N_A k \sum_i x_i \ln\left(\frac{f_m V}{f_i V_i}\right). \tag{18}$$

Ignoring the difference between the energy and enthalpy of a liquid at ordinary pressure, we obtain the excess enthalpy H^E from Eqs. 17 and 18.

$$H^E = F^E + TS^E = -\left[\frac{N_A^2}{V}\sum_i \sum_j x_i x_j a_{ij} - \sum_i x_i \frac{N_A^2}{V_i} a_{ii}\right]. \tag{19}$$

Eqs. 17 and 19 can be expressed in terms of ξ, using the equation of state at vanishing pressure.[11,15] Equating the right-hand side of Eq. 13 to zero, we obtain

$$(N_A^2/V)\sum_i \sum_j x_i x_j a_{ij} = N_A kT\chi_m(\xi) \quad \text{(for a mixture)}, \tag{20}$$

$$(N_A^2/V)a_{ii} = N_A kT\chi(\xi_i) \quad \text{(for a pure fluid)}, \tag{21}$$

where ξ_i is the packing fraction for the pure fluid of

species i. $\chi(\xi_i)$ is the compressibility factor for a one-component fluid of hard spheres.[16] Eqs. 17 and 19 are rewritten as follows:

$$F^E = -N_A kT \sum_i x_i \ln\left(\frac{f_m V}{f_i V_i}\right) - N_A kT[\chi_m(\xi) - \sum_i x_i \chi(\xi_i)], \quad (22)$$

and

$$H^E = -N_A kT[\chi_m(\xi) - \sum_i x_i \chi(\xi_i)]. \quad (23)$$

The f_i[11] and $\chi(\xi_i)$[16] are given as

$$f_i = (1-\xi_i)\exp\left[-\frac{3\xi_i(2-\xi_i)}{2(1-\xi_i)^2}\right] \quad (24)$$

and

$$\chi(\xi_i) = \frac{(1+\xi_i+\xi_i^2)}{(1-\xi_i)^3}, \quad (25)$$

respectively, where

$$\xi_i = \frac{\pi}{6}\frac{N_A}{V_i}R_i^3. \quad (26)$$

It is confirmed that the free energy of a pure fluid of species i is derived from Eq. 8 for the mixture when $x_i=1$ and all $x_j=0$ for $i\neq j$. For the case of a one-component fluid, we see that f_m (Eq. 3) is reduced to f_i (Eq. 24) and that U_{BG} for the mixture becomes $U_{BG}=-N_A^2 a_{ii}/V_i$, which is the uniform background potential for a pure fluid.[7]

Calculation and Results

The binary liquid mixtures chosen in this work consist of nonpolar molecules which are regarded as approximately spherical. Calculations have been made for equimolar mixtures.

Determination of a_{ii} for a Pure Component. The energy parameter a_{ii} for a pure fluid is determined from the observed values of molar volume V_i and those of the heat of vaporization $\Delta H_{vap.}$ at a given temperature, using the relation

$$a_{ii} = (V_i/N_A^2)(\Delta H_{vap.} - N_A kT). \quad (27)$$

The values of $\chi(\xi_i)$, ξ_i, and f_i are calculated by means of Eqs. 21, 26, and 24, respectively.

For the determination of a_{ii}, we have used the observed values of $\Delta H_{vap.}$ and of V_i at 25 °C, except for the case of neopentane for which boiling-point data have been used. Experimental data of V_i and $\Delta H_{vap.}$, and the calculated values of a_{ii} are given in Table 1, where a_{ii} is expressed in kcal cm³/mol². All the experimental data refer to ordinary pressure.

Calculation of the Energy Interaction Parameter between Different Species, a_{12}, and Excess Thermodynamic Functions. Experimental data and calculated values are given in Table 2. For a binary mixture we have

$$\xi = (x_1\xi_1 V_1 + x_2\xi_2 V_2)/V, \quad (28)$$

and

$$a_{12} = \left[N_A kT\chi_m(\xi)\frac{V}{N_A^2} - (x_1^2 a_{11} + x_2^2 a_{22})\right]\frac{1}{2x_1x_2}. \quad (29)$$

By means of Eq. 28, ξ is calculated from the observed value of excess volume V^E at 25 °C (at 0°C for the systems including neopentane). a_{12} is then obtained by means of Eqs. 29, 14, and 5.

Table 1. Energy parameter a_{ii} for pure components

	T (°C)	$V_{i,obsd}$ (cm³/mol)	$\Delta H_{vap.}$ (kcal/mol)	a_{ii} (kcal cm³/mol²)
CCl_4	25	97.09[a]	7.83[b]	702.7
C_6H_6	25	89.41[a]	8.09[a]	670.4
c-C_6H_{12}	25	108.75[a]	7.89[a]	794.3
$C_6H_5CH_3$	25	106.85[a]	9.08[a]	906.9
$C(CH_3)_4$	9.5	119.67[a]	5.44[c]	583.8

a) J. Timmermans, "Physico-Chemical Constants of Pure Organic Compounds," Elsevier Publ. Co., Amsterdam (1950, 1965). b) See Ref. 1. c) N. A. Lange, "Lange's Handbook of Chemistry," McGraw-Hill, New York (1973).

The calculated values of H^E are obtained by Eqs. 23, 14, and 21, those of TS^E being obtained by Eqs. 18, 3, and 24. The agreement between the calculated and observed values is good.

The values of a_{12} calculated from the observed values of excess enthalpy H^E are also given in Table 2 for a comparison with those obtained from the excess volume. In calculating ξ from H^E_{obsd}, Eq. 23 has been used replacing V by $(x_1\xi_1V_1+x_2\xi_2V_2)/\xi$. The agreement between the values of a_{12} from V^E_{obsd} and those from H^E_{obsd} is very good.

Other excess functions V^E_{calcd} and TS^E_{calcd} obtained from H^E_{obsd} are also given.

Equivalent Free Volume Fraction. We have calculated the values of equivalent free volume fraction f_i and f_m using Eqs. 24 and 3. The values of f_i (the free volume fraction for the pure liquid i), packing fraction ξ_i and equivalent free volume are given in Table 3. A free volume refers to $V_i f_i (=Nv_f(\text{cm}^3/\text{mol}))$. The values of f_m which are identical for all components constituting the mixture, ξ and Vf_m are given in Table 4.

Discussion

Equivalent Free Volume Fraction for Mixtures. The concept of the equivalent free volume fraction was investigated for the case of a one-component hard-sphere fluid.[11] The same argument is applied to the case of mixtures.

As shown in Eqs. 1, 2, and 8, the free volume available for the molecule within the liquid mixture is Vf_m. The equivalent free volume fraction f_m given by Eq. 3 consists of a factor $(1-\xi)$ and an exponential factor. The former is equal to the fraction of void space for the total volume V, and the latter is supposed to come from the volume exclusion effect of hard sphere molecules in their thermal motions, similar to the case of a one-component fluid.[11]

The further problem is associated with the fact that the molecules constituting a mixture differ in size. We see from Eq. 2 that Vf_m is identical for all species of molecules included in the mixture, where f_m is determined from the diameters and number densities of all the constituents (Eq. 3). In other words, the same magnitude of the equivalent free volume, $v_f=Vf_m/N$, is as-

Table 2. Energy interaction parameter a_{12} and excess thermodynamic functions for equimolar mixtures at 25°C (at 0 °C for $CCl_4+C(CH_3)_4$ and $C_6H_6+C(CH_3)_4$)
a_{12} is in kcal cm³/mol², V^E in cm³/mol, and H^E and TS^E in cal/mol.

	Observed			Calculated from V^E_{obsd}			Calculated from H^E_{obsd}		
	V^E_{obsd}	H^E_{obsd}	TS^E_{obsd} [a]	a_{12}	H^E_{calcd}	TS^E_{calcd}	a_{12}	V^E_{calcd}	TS^E_{calcd}
$CCl_4+C_6H_6$	0.01 [b]	27 (±1) [c,d,e]	6 [b]	685.5	12	4	683.5	0.07	9
CCl_4+c-C_6H_{12}	0.16 [f]	40 [c,g]	23 [h]	741.9	41	14	742.1	0.15	13
C_6H_6+c-C_6H_{12}	0.65 [i]	192 [j]	118 [k]	706.9	185	59	706.0	0.68	62
$CCl_4+C_6H_5CH_3$	−0.04 [l]	10 [l]		798.2	−1	−2	796.6	0.00	1
$C_6H_6+C_6H_5CH_3$	0.06 [l]	15 (±1) [l,m,n]		778.3	14	7	778.1	0.07	7
c-$C_6H_{12}+C_6H_5CH_3$	0.56 (±0.01) [j,m,o]	146 (±4) [j,m,n,p]		823.1	172	46	827.1	0.45	39
$CCl_4+C(CH_3)_4$	−0.53 [q]	75 [r]	−3 [q]	623.6	202	42	641.8	−1.22	2
$C_6H_6+C(CH_3)_4$*	−0.5 [q]	(135) [q,r]		601.0	(236)	73	621.4	−1.27	27

a) Estimated from the observed values of excess Gibbs free energy and H^E_{obsd}. b) G. Scatchard, S. E. Wood, and J. M. Mochel, *J. Am. Chem. Soc.*, **62**, 712 (1940). c) J. R. Goates, R. J. Sullivan, and J. Bevan, *J. Phys. Chem.*, **63**, 589 (1959). d) J. A. Larkin and M. L. McGlashan, *J, Chem. Soc.*, **1961**, 3425. e) C. G. Savini, D. R. Winterhalter, L. H. Kovack, and H. C. van Ness, *J. Chem. Eng. Data*, **11**, 40 (1966). f) S. E. Wood and J. A. Gray, *J. Am. Chem. Soc.*, **74**, 3729 (1952); M. D. Peña and M. L. McGlashan, *Trans. Faraday Soc.*, **57**, 1511 (1961). g) H. Kehlen and H. Sackmann, *Z. Physik. Chem. (Frankfiurt)*, **50**, 135, 144 (1966). h) G. Scatchard, S. E. Wood, and J. M. Mochel, *J. Am. Chem. Soc.*, **61**, 3206 (1939). i) S. E. Wood and A. E. Austin, *J. Am. Chem. Soc.*, **67**, 480 (1945). j) A. E. P. Watson, I. A. Mclure, J. E. Bennett, and G. C. Benson, *J. Phys. Chem.*, **69**, 2753 (1965). k) G. Scatchard, S. E. Wood, and J. M. Mochel, *J. Phys. Chem.*, **43**, 119 (1939). l) R. P. Rastogi, J. Nath, and J. Misra, *J. Phys. Chem.*, **71**, 1277 (1967). m) A. R. Mathieson and J. C. J. Thynne, *J. Chem. Soc.*, **1956**, 3708. n) Kuei-Yen Hsu and H. L. Clever, *J. Chem. Thermodyn.*, **7**, 435 (1975). o) S. A. Sanni, C. J. D. Fell, and H. P. Hutchison, *J. Chem. Eng. Data*, **16**, 424 (1971). p) G. W. Lundberg, *J. Chem. Eng. Data*, **9**, 193 (1964). q) V. Mathot and A. Desmyter, *J. Chem. Phys.*, **21**, 782 (1953). r) A. Englert-Chwoles, *J. Chem. Phys.*, **23**, 1168 (1955).
* For $C_6H_6+C(CH_3)_4$ system, the values in bracket are those of excess Gibbs free energy, and the values given in columns 8—10 are calculated from excess Gibbs free energy.

Table 3. Equivalent free volume fraction f_i, free volume V_f (cm³/mol) and packing fraction ξ_i for pure liquids at 25 °C

	$f_i\times10^3$	V_f	ξ_i
CCl_4	8.96	0.87	0.48_1
C_6H_6	7.94	0.71	0.48_6
c-C_6H_{12}	8.69	0.94	0.48_2
$C_6H_5CH_3$	5.11	0.55	0.50_3
$C(CH_3)_4$ [a]	22.23	2.62	0.43_7

a) Calculated for 0 °C.

Table 4. Equivalent free volume fraction f_m, free volume $V_{f,m}$ (cm³/mol) and packing fraction ξ for mixtures at 25 °C

	$f_m\times10^3$	$V_{f,m}$	ξ
$CCl_4+C_6H_6$	8.48	0.79	0.48_3
CCl_4+c-C_6H_{12}	9.00	0.93	0.48_1
C_6H_6+c-C_6H_{12}	9.07	0.90	0.48_1
$CCl_4+C_6H_5CH_3$	6.74	0.69	0.49_3
$C_6H_6+C_6H_5CH_3$	6.41	0.63	0.49_5
c-$C_6H_{12}+C_6H_5CH_3$	7.17	0.78	0.49_0
$CCl_4+C(CH_3)_4$ [a]	12.42	0.69	0.46_6
$C_6H_6+C(CH_3)_4$ [a]	12.26	0.66	0.46_7

a) Calculated for 0 °C.

signed to all the molecules included in a liquid mixture in spite of the difference in their diameters.

In the usual free volume theories of solutions, it is important to know how the available total free volume is shared between molecules differing in size. However, the determination whether the free volume is shared equally between the molecules or shared unequally between them is made with some *ad hoc* assumptions.[2,12,17] The present treatment starting from Eqs. 2 and 8, considered to be equivalent to the free volume theory of fluids, suggests that the available total free volume for a fluid mixture is shared equally between the molecules.

We see from Tables 3 and 4 that the values of the equivalent free volume fraction are in the range 5—9×10^{-3} in most cases of pure fluids and mixtures, and that the values of free volume are in the range 0.55—0.93 cm³/mol. We obtain $f_1<f_m<f_2$ in most cases, where subscripts 1 and 2 refer to pure components constituting the mixture. The values of packing fraction ξ are in the range 0.48—0.50 and we have $\xi_1<\xi<\xi_2$. The values for the systems including neopentane differ considerably from those shown above. This might be attributed to the fact that the temperature of measurement is near the boiling point of $C(CH_3)_4$.

The Generalized van der Waals Equation of State and the Longuet-Higgins and Widom Model. Longuet-Higgins and Widom[7] proposed the following equation of state for pure fluids.

$$pV = p_0V - aN^2/V, \tag{30}$$

where p_0 is the pressure exerted by hard cores taken to be the true 3-dimentional hard-sphere pressure rather than the value $NkT/(V-b)$ as in the original van der Waals theory.

The equation of state Eq.13, which was presented for binary mixtures by Snider and Herrington,[6] is an extention of the generalized van der Waals equation of state Eq. 30 to mixtures.

The liquid model of Longuet-Higgins and Widom rests on the following view for fluid. The repulsive forces between molecules play the most important role in determining the short range behavior of molecules in a liquid, the attractive forces merely maintaining the liquid density. This view seems to be essentially correct, as stated also by Leland, Rowlinson and Sather[13]. The Lebowitz solution is an analytical solution of the generalized Percus-Yevick equation for hard sphere mixtures, giving the "entropy of mixing" for mixtures on the theoretically more sound ground than the lattice theories of fluids.[18] Snider and Herrington used the equation of state of hard spheres obtained from the Lebowitz solution, but they did not elucidate the nature of the Lebowitz solution, giving very lengthy expressions untractable for practical use.[20]

Energy Parameters and Excess Functions. The values of a_{12} from V^E_{obsd} are in extremely good agreement with those from H^E_{obsd} (fifth and eighth columns, Table 2). The values do not differ from each other by more than about 0.5%, except in the case of the systems including neopentane. The energy interaction parameter a_{12} between different species has been introduced for extending a uniform background potential for pure fluids to mixtures ($U_{BG} = -N_A^2 \sum_i \sum_j x_i x_j a_{ij}/V$). The striking agreement between the values of a_{12} from V^E_{obsd} and those from H^E_{obsd} shows the reality of that parameter and the effectiveness of the present treatment.

In order to determine a_{12}, data for one of excess thermodynamic functions must be used. Usually, the experimental data of H^E or that of the excess Gibbs free energy is used. The results shown in Table 2 permit us to calculate the values of a_{12} from the measured values of V^E (or density). This is very useful in practical applications since the density can be measured more easily than other thermodynamic quantities such as excess heat.

The agreement between the values of H^E calculated from V^E_{obsd} and the experimental values is fairly good. This is ascribed to the good agreement between the values of a_{12} from V^E_{obsd} and those from H^E_{obsd}. Reasonable values of H^E and S^E as well as a_{12} can be obtained from V^E_{obsd}.

In the present treatment, a_{ii} has been regarded as unchanged with the variation of temperature. In order to determine the values, the observed values of $\Delta H_{vap.}$ and V_i at 25 °C were used. The values of a_{ii} for C_6H_6 calculated from the data of $\Delta H_{vap.}$ and V_i at various temperatures are given in Table 5. The standard deviation of errors in the values of a_{ii} is about 7 kcal cm³/mol² (about 1.1% to the mean values) in the range 10—50 °C. The values of a_{ii} can be regarded to be constant in this range. In the range, 0—80.1 °C (boiling point), it is about 14.4 kcal cm³/mol² (about 2.2%).

Temperature Dependence of Excess Functions and Energy Parameters. The calculation of excess functions for the binary mixtures of CCl_4, C_6H_6 and *c*-C_6H_{12} at 20—

Table 5. Values of a_{ii} at various temperatures for C_6H_6

T (°C)	$V_{i,obsd}$ (cm³/mol)	$\Delta H_{vap.}$ (kcal/mol)	a_{ii} (kcal cm³/mol²)
0	86.78[a]	8.35_8[b]	$678._2$
10	87.82[c]	8.21_7[c]	$672._2$
25	89.41[c]	8.09_0[c]	$670._4$
50	92.26[c]	7.75_6[c]	$656._3$
80.1	95.90[c]	7.35_3[c]	$638._0$

a) S. E. Wood and J. P. Brusie, *J. Am. Chem. Soc.*, **65**, 1891 (1943). The value was estimated by extrapolation. b) See Table 1, footnote b. c) See Table 1, footnote a.

Table 6. Excess thermodynamic functions for equimolar mixtures and energy interaction parameter a_{12} at 20, 30, and 40 °C

V^E is in cm³/mol, H^E and TS^E in cal/mol, and a_{12} in kcal cm³/mol².

T (°C)	Observed			Calculated from V^E_{obsd}			Calculated from H^E_{obsd}		
	V^E_{obsd}	H^E_{obsd}	TS^E_{obsd}[a]	a_{12}	H^E_{calcd}	TS^E_{calcd}	a_{12}	V^E_{calcd}	TS^E_{calcd}
$CCl_4+C_6H_6$									
20	0[b]	24[c]	4[d]	$685._8$	9	3	$684._1$	0.05	8
30	0.02[b]	28[c]	9[d]	$685._2$	14	5	$683._5$	0.07	9
40	0.04[b]	31[c]	12[d]	$684._7$	19	6	$683._1$	0.09	10
CCl_4+c-C_6H_{12}									
20	0.16[e]	40[c,e]	23[f]	$741._6$	42	14	$742._1$	0.15	13
30	0.16[e]	40[c,e]	23[f]	$742._0$	40	13	$742._2$	0.16	14
40	0.16[e]	40[c,e]	23[f]	$742._3$	39	14	$742._0$	0.17	14
C_6H_6+c-C_6H_{12}									
20	0.65[g]	197[h]	121[i]	$706._4$	189	59	$705._5$	0.68	62
30	0.66[g]	190[h]	116[i]	$707._1$	183	59	$705._9$	0.70	61
40	0.66[g]	180[h]	109[i]	$708._3$	175	58	$707._5$	0.68	60

a) See Table 2, footnote a. b) See Table 5, footnote a. c) See Table 2, footnote c. d) See Table 2, footnote b. e) See Table 2, footnote g. f) See Table 2, footnote h. g) See Table 2, footnote i. h) Estimated from the heats of mixing as reported in the following works: G. Scatchard, L. B. Ticknor, J. R. Goates, and E. R. McCartney, *J. Am. Chem. Soc.*, **74**, 3721 (1952); R. Thacker and J. S. Rowlinson, *Trans. Faraday Soc.*, **50**, 1036 (1954); W. R. Moore and G. E. Styan, *Trans. Faraday Soc.*, **52**, 1556 (1956); see also Table 2, footnote j. i) See Table 2, footnote k.

40 °C has been carried out (Table 6). For the values of V_i and V^E we used the observed ones at each temperature. Concerning the values of a_{ii}, we used those given in the fifth column of Table 1 regarding as unchanged with the variation in temperature. The results obtained from the data of H^E_{obsd} are also included in Table 6.

We see that the calculated values for the various excess functions reproduce the trend of the temperature dependence in the observed values, but not necessarily the absolute magnitude. The values of the energy parameter a_{12}, which has been treated as a constant, are practically constant in the range 20—40 °C.

Concluding Remarks

A statistical thermodynamic theory of binary liquid mixtures has been worked out using the notion of the equivalent free volume fraction.

(a) The total free energy is expressed as the sum of three terms: the translational term of an ideal-gas mixture, the term resulting from the equivalent free volume fraction, and the energy term resulting from the uniform background potential.

(b) The equivalent free volume fraction is found to be identical for all species of molecules constituting the mixture, *viz.*, the same magnitude of equivalent free volume is assigned to all the molecules in spite of their different sizes, which is in sharp contrast to the cases in usual free volume theories.

(c) Concerning the energy parameter of mixtures, the form of a quadratic sum of a_{ij} has been used. The values of the energy interaction parameter a_{12} calculated from the values of V^E_{obsd} are found to be in good agreement with those from H^E_{obsd}. This result shows the reality of a_{12} and permits us to calculate the values of a_{12} from V^E_{obsd}.

(d) The agreement between the experimental and calculated values of various excess thermodynamic functions is found to be good on the whole, except for the case of the systems including neopentane.

References

1) J. H. Hildebrand and R. L. Scott, "The Solubility of Nonelectrolytes," 3rd ed, Reinhold, New York (1950).

2) I. Prigogine, A. Bellemans, and V. Mathot, "The Molecular Theory of Solutions," North-Holland Pub. Co. (1957).

3) P. J. Flory, *J. Am. Chem. Soc.*, **87**, 1833 (1965); A. Abe and P. J. Flory, *ibid.*, **87**, 1838 (1965).

4) K. Arakawa, *Kobunshi*, **22**, 285 (1973); *Kagaku Sosetsu*, No. 11, "Ions and Solvents," (1976), p. 13.

5) J. L. Lebowitz, *Phys. Rev. A*, **133**, 895 (1964); J. L. Lebowitz and J. S. Rowlinson, *J. Chem. Phys.*, **41**, 133 (1964).

6) N. S. Snider and T. M. Herrington, *J. Chem. Phys.*, **47**, 2248 (1967).

7) H. C. Longuet-Higgins and B. Widom, *Mol. Phys.*, **8**, 549 (1964).

8) K. N. Marsh, *J. Chem. Thermodyn.*, **3**, 355 (1971); K. N. Marsh, M. L. McGlashan, and C. Warr, *Trans. Faraday Soc.*, **66**, 2453 (1970).

9) A. Kreglewski, R. C. Wilhoit, and B. J. Zwolinski, *J. Phys. Chem.*, **77**, 2212 (1973).

10) K. Arakawa, K. Tokiwano, and K. Kojima, *Bull. Chem. Soc. Jpn.*, **50**, 65 (1977), Appendix I.

11) K. Arakawa and K. Kojima, *Bull. Chem. Soc. Jpn.*, **48**, 26 (1975).

12) A. Münster, "Statistical Thermodynamics," Vol. 2, First English ed, Springer-Verlag, Berlin (1974), Chap. XVII, pp. 641, 672.

13) T. W. Leland, J. S. Rowlinson, and G. A. Sather, *Trans. Faraday Soc.*, **64**, 1447 (1968).

14) T. L. Hill, "Statistical Mechanics," McGraw-Hill, New York (1956), p. 399.

15) K. Arakawa and O. Kiyohara, *Bull. Chem. Soc. Jpn.*, **43**, 975 (1970).

16) M. Wertheim, *Phys. Rev. Lett.*, **10**, 321 (1963); E. Thiele, *J. Chem. Phys.*, **39**, 474 (1963).

17) A. Bellemans, V. Mathot, and M. Simon, *Adv. Chem. Phys.*, **11**, 117 (1967).

18) Estimation of the "entropy of mixing" has been the most important problem in the lattice theories of fluid mixtures consisting of molecules differing in size. A f.c.c. lattice is presupposed usually for each component fluid before mixing and the lattice is assumed to remain unchanged in the solution. However, it is unreasonable to assume that a mixture of the molecules can be packed in the same way as in each component fluid when the difference in diameter of the molecules is fairly large.[15,19]

19) I. Prigogine and A. Bellemans, *Discuss. Faraday Soc.*, **15**, 80 (1953).

20) I. R. McDonald, A Specialist Periodical Report, "Statistical Mechanics," Vol. 1, ed by K. Singer, The Chemical Society, London (1973), Chap. 3.

Switching in Copper-Phthalocyanine Films

Yoshihiko SADAOKA and Yoshiro SAKAI

Department of Industrial Chemistry, Faculty of Engineering, Ehime University, Matsuyama 790

(Received February 10, 1977)

Bistable switching between two impedance states was observed in copper-phthalocyanine films. The *turn-on* can be interpreted in terms of the steady thermal breakdown model. The stable high conductivity in the *on-state* is attributed to the partly carbonized copper-phthalocyanine which was formed by Joule heating along the filamentary paths. The *J-V* characteristic in the *off-state* and the threshold-field strength were found to be expressed as $J \propto V^6/d^{3.8}$ and $E_{th} \propto 1/d^{0.46}$ respectively.

The memory- and threshold-switching phenomena have recently received considerable attention as a practical application of organic semiconductors.[1,2] Although similar phenomena have been reported in thin films of inorganic semiconductors,[3-5] our understanding of switching is still incomplete, particularly in organic semiconductors.

In the present work the preswitching conduction and the memory-switching characteristics have been investigated in thin films of α-copper-phthalocyanine (CuPc).

Experimental

Pure copper-phthalocyanine was prepared by repeated sublimations *in vacuo* at 380 °C, followed by washing with acetone to remove any thermal decomposition products.

The geometry of the cell was of a sandwich type, where copper-phthalocyanine was deposited from a Pyrex crucible on a cleaned glass substrate with a silver electrode which had been evaporated through an etched stainless steel mask. The upper electrodes (Al) were deposited by vacuum evaporation through the mask. The vacuum evaporation was performed at pressures below 10^{-6} Torr. The film of CuPc was confirmed to be α-type crystalline by the methods described in a preceding paper.[6]

The film thickness of the copper-phthalocyanine, as measured with the aid of an interferometer, varied over the range of 10^{-6}—10^{-4} cm. The current-voltage characteristics were obtained by applying step voltages using a high-voltage dc power supply (John-Fluke, model 412 B), an electrometer, and a picoammeter (Takeda Riken, models TR8651 and TR8641 respectively). A series resistor ($10^6\Omega$) was used to limit the current flow in the circuit. The measurements were performed at a pressure of *ca.* 10^{-3} Torr.

The states of the film before and after the switching were observed using a scanning electron microscope (Hitachi and Akashi, model MSM-4).

Results and Discussion

In the Al–CuPc–Ag cell, the current with the forward-bias voltage (Ag(+), Al(−)) was much higher than that with the backward-bias voltage in the high-field region (Fig. 1). Its marked asymmetry can be explained by a pin-structure at the CuPc–Al junction, a detailed discussion of which has been given by Tantzscher and Hamann.[7] In the present paper the results with the backward-bias voltages will not be discussed.

Initially the film has a very high resistance (*off-state*), and the non-linear current-voltage characteristic is observed, as is shown in Fig. 1, as long as the applied voltage is lower than a certain value (threshold voltage;

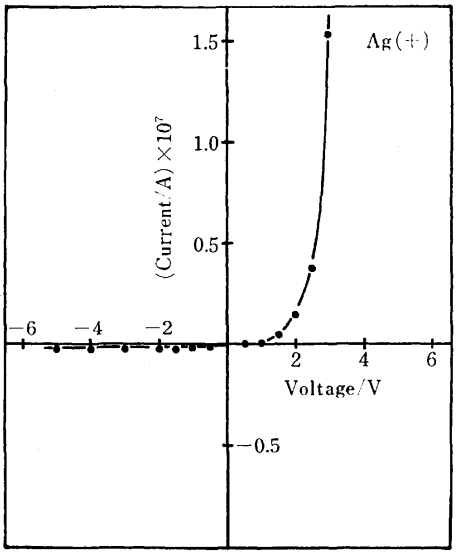

Fig. 1. A typical *V-I* characteristic in the Ag–CuPc–Al cell. Film thickness 1.7×10^{-5} cm.

V_{th}). When the applied voltage exceeds V_{th}, the current abruptly increases, and simultaneously the field drops, so that a new low-resistance state (*on-state*) with a memory effect appears. This new state can be easily quenched by applying a short current pulse (pulse width, 10 μs, maximum voltage, 180 V) from a capacitor of 0.047 μF. The scanning electron microscopic inspection of the film in the *on-state* shows that this state is accompanied by the formation of conducting channels (Fig. 2). The upper electrode (Al) was partly molten (A), and the region of CuPc (B) transformed by the localized Joule heating was confirmed in this figure, so

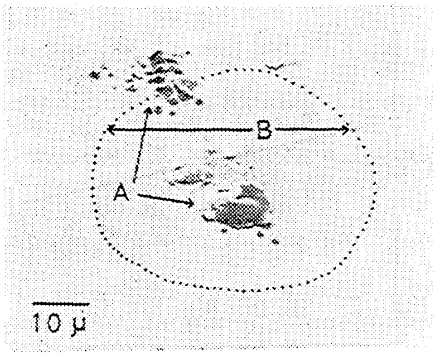

Fig. 2. Scanning electron microscope picture of damaged region. A) Partly molten electrode (Al), B) transformed region.

that it may be presumed that a temperature higher than 660 °C (the melting point of aluminium) has been temporarily attained in this region.

Souma[8] has reported that, when CuPc was heated at 625 °C, the carbonization and/or the condensation occurred and the conductivity increased rapidly. It has also been reported that poly-CuPc has a conductivity about 10^6 times larger than that of the monomer, and the activation energy (E) in $\sigma=\sigma_0 \exp(-E/kT)$ was estimated to be 0.06 eV[9] in a sample previously heated to 450 °C. In the present work, the activation energy in the high-conductivity state was estimated to be 0.05 eV from the temperature dependence of the current obtained in the range of 15—70 °C. Since this value is in fair agreement with the value for poly-CuPc, the conducting channels may be made up of the poly-CuPc.

Although many authors[10-12] have reported that the stable *on-state* in some organic compounds arises from the formation of metallic filaments or carbonized paths, the exact mechanism for the formation of such filaments is not clear.

The various models proposed to explain the memory-switching process for chalcogenide glass, *etc.* can be classified into two categories: (1) the electronic effect and (2) the thermal effect. In the former case, the *on-state* without a memory effect is formed first, and the *lock-on* occurs after a certain time by the excessive current flow in this state, while in the latter case, the switching occurs by means of the local Joule heating in the *off-state*.

The measurement of the thickness dependence of the threshold-field strength, E_{th}, which equals V_{th}/d, is a very powerful method of distinguishing between the thermal effect and the electronic effect.[13] If the switching is caused by the electronic mechanism, as explained by the space-charge-overlap model[14] or the one-carrier space-charge limited-current (SCLC) model,[15] in which the concentrations of the injected carriers are sufficient to exceed the critical concentration, the threshold-field strength can be expressed as $E_{th} \propto$ (thickness). Since Fig. 3 shows that E_{th} is not proportional to the thickness, the electronic model can be excluded.

On the other hand, according to the steady-state thermal-breakdown model,[16] the *turn-on* occurs when the temperature derivative of the power input exceeds that of heat loss. Below the critical point, Eq. 1 holds:

$$J \cdot V = \lambda(T - T_0), \tag{1}$$

where J is the current density; V, the applied voltage; λ, a constant external thermal conductivity, and T_0, the ambient temperature. At the critical point where thermal breakdown commences, the following equations are given:

$$\partial(J_c \cdot V_c)/\partial T = \lambda, \tag{2}$$

$$J_c \cdot V_c = \lambda(T_c - T_0), \tag{3}$$

where J_c and V_c are the critical current density and the voltage for breakdown respectively, and where T_c is the critical temperature.

To resolve these relations, the voltage and the thickness dependence of the current density in the preswitching state were observed (Figs. 4 and 5). The results are experimentally expressed as $J \propto V^{6.0}$ and $J \propto 1/d^{3.8}$ respectively in the high-field region, while the relation

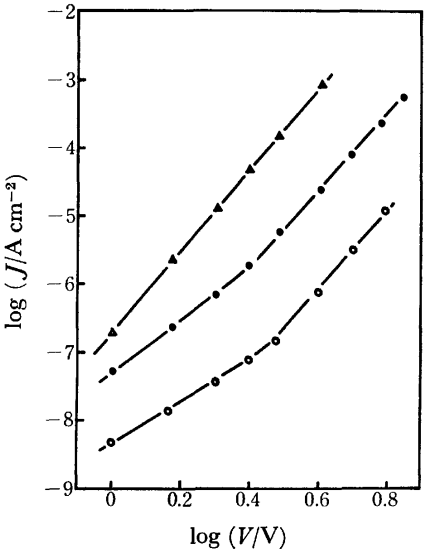

Fig. 4. The voltage dependence of the current. △) 0.18 μm, ●) 0.48 μm, ○) 1.2 μm.

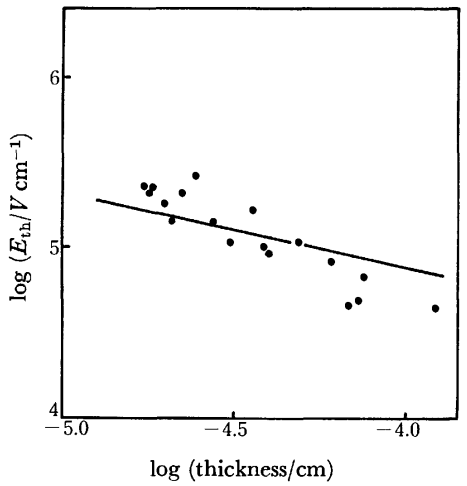

Fig. 3. The relation between log(E_{th}) and log(thickness).

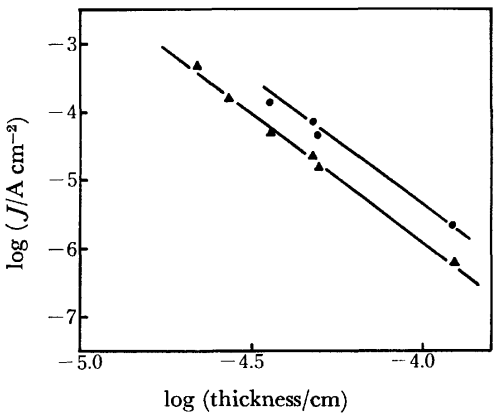

Fig. 5. The thickness dependence of the current. ▲) 4 V, ●) 5 V.

between the current density and the applied voltage expected from the scaling law[17] ($J \propto V^{l+1}/d^{2l+1}$) was confirmed in the low-field region for thicker films. Since the observed J-V characteristics were reversible with an increase and then a decrease in the voltage, the possibility of a thermal effect may be excluded. The high value of l in the high-field region may be attributed to the other conduction components, such as the emission limited current (ELC). A quantitative analysis of the J-V characteristics for ELC under the conditions of SCLC flow was reported by the Frank and Simmons.[18] According to this analysis, the transition from SCLC to ELC for the M–I–M junction can be expected to occur when a negative charge begins to appear on the cathode as well as inside the insulator, and the contact changes from an Ohmic to a blocking one with an increase in the voltage. As is shown in Fig. 6, the straight line in the plot of log J *vs.* $(V/d)^{1/2}$ indicates that the high-field conduction is predominantly governed by ELC in the preswitching state.

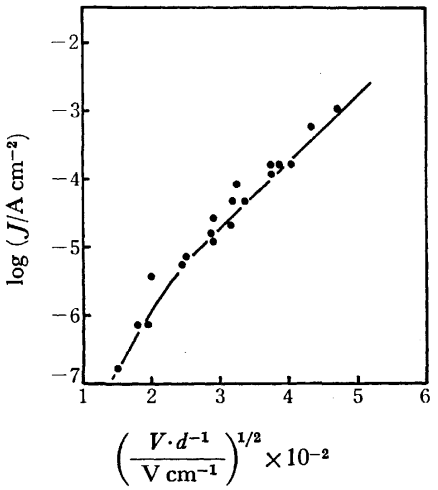

Fig. 6. The plots of log J *vs.* $(V/d)^{1/2}$.

If it is assumed that the I-V characteristic is expressed as Eq. 4* and that the *on-state* is formed filamentarily as is shown in Fig. 2, the critical current density in the area of the filamental paths is proportional to the current density geometrically obtained (J_G):

$$J_G = C \cdot \frac{V^{6.0}}{d^{3.8}} \exp(-\phi/kT), \tag{4}$$

$$J_c \propto J_G \tag{5}$$

where C is a constant; ϕ, the activation energy, and k, the Boltzmann constant.

The substitution of Eqs. 4 and 5 into Eqs. 1, 2, and 3 gives:

$$V_c^{7.0}/d^{3.8} \propto \frac{T_c^2}{\phi} \exp(\phi/kT_0) = \text{constant}. \tag{6}$$

Thus,

$$(V_c/d)^{7.0} = K \cdot d^{-3.2}, \tag{7}$$

where K is a constant.

* If the ELC relation ($J_G \propto \exp(V/d)^{1/2}$) is used, the relation between E_{th} and d is expressed as $\log E_{th} = -0.5 \log d + \text{constant}$ instead of by Eq. 8.

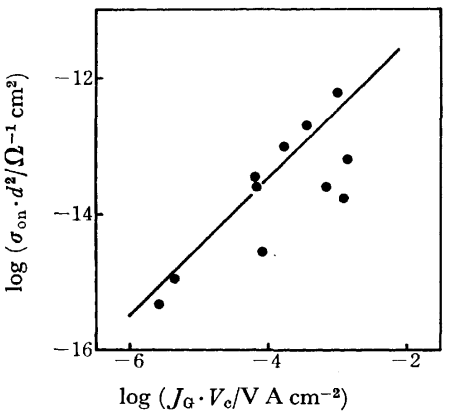

Fig. 7. The plots of $\log(\sigma_{on} \cdot d^2)$ *vs.* $\log(J_G \cdot V_c)$.

Since V_c/d is equal to E_{th}, Eq. 8 is obtained:

$$\log E_{th} = -0.46 \log d + \text{constant}. \tag{8}$$

The solid line in Fig. 3, drawn with a slope of −0.46, is in fair agreement with the experimental data. In addition, Fig. 7 shows that $\sigma_{on} \cdot d^2$ is proportional to $J_G \cdot V_c$, where σ_{on} is the conductance of the sample in the *on-state*. Since $\sigma_{on} \cdot d^2$ is proportional to the volume of the conducting paths and $J_G \cdot V_c$ is the heat evolved by the current, this result is also evidence in support of the thermal-breakdown mechanism.

One of us (Y. Sadaoka) thanks the Sakkokai Foundation for a grant.

References

1) L. F. Pender and R. J. Fleming, *J. Appl. Phys.*, **46**, 3426 (1975).
2) H. Kasica, W. Wtodarski, H. Kurczewska, and A. Szymanski, *Thin Solid Films*, **30**, 325 (1975).
3) P. J. Walsh, R. Vogel, and E. J. Evans, *Phys. Rev.*, **178**, 1274 (1969).
4) S. R. Ovshinsky and H. Fritzsche, *IEEE Trans. Electr. Dev.*, **20**, 91 (1973).
5) A. C. Warren, *IEEE Trans. Electr. Dev.*, **20**, 123 (1973).
6) Y. Sakai, Y. Sadaoka, and H. Yokouchi, *Bull. Chem. Soc. Jpn.*, **47**, 1886 (1974).
7) C. Tantzscher and C. Hamann, *Phys. Status Solidi A*, **26**, 443 (1974).
8) I. Souma, *Nippon Kagaku Kaishi*, **1972**, 1059.
9) A. Epstein and B. S. Wildi, *J. Chem. Phys.*, **32**, 324 (1960).
10) J. Kucirka, D. C. Larson, and M. M. Labes, *Bull. Am. Phys. Soc.*, **18**, 132 (1973).
11) H. Carchano, R. Lacoste, and Y. Segui, *Appl. Phys. Lett.*, **19**, 414 (1971).
12) J. Kevorkian, M. M. Labes, D. C. Larson, and D. C. Wu, *Discuss. Faraday Soc.*, **51**, 139 (1971).
13) B. T. Kolomiets, E. A. Lebedev, and I. A. Taksami, *Soviet Phys.-Semiconductors*, **3**, 267 (1969).
14) H. Iida, *Bussei*, **15**, 295 (1974).
15) T. Shiraishi, T. Kurosu, and M. Iida, *Oyo Butsuri*, **46**, 36 (1977).
16) J. J. O'Dwyer, "The Theory of Electrical Conduction and Breakdown in Solid Dielectrics," Clarendon Press, Oxford (1973), p. 182.
17) P. Mark and W. Helfrich, *J. Appl. Phys.*, **33**, 205 (1962).
18) R. I. Frank and J. G. Simmons, *J. Appl. Phys.*, **38**, 832 (1967).

Proton Transfer between Styrene Molecular Anion and Ethanol in Rigid Organic Matrices

Shoji Noda, Yasumi Fujii, and Hiroshi Yoshida

Faculty of Engineering, Hokkaido University, Kita-ku, Sapporo 060

(Received February 18, 1977)

The proton transfer from ethanol to styrene molecular anion was studied by examining the yield of the anion and α-methylbenzyl radical generated in γ-irradiated 2-methyltetrahydrofuran–ethanol mixed matrix at 77 K by means of optical absorption measurements. The radical yield was found to increase in proportion to the ethanol fraction at the expense of the anion yield. The maximum radical yield, 2.2, was identical with the yield of scavengeable electron in ethanol matrix where no anion was observed. Upon photobleaching the anion was transformed into the radical in the matrix. The transformation efficiency was constant, *ca.* 0.6, for the ethanol fraction 0.3—0.9. It is concluded that the radical arises from the anion through the proton transfer from ethanol to the β-carbon of vinyl group of the styrene anion. The proton transfer occurs readily only when a specific solvent site around the anion is populated by ethanol molecules. Otherwise, the proton transfer does not occur at all because of the restricted translational motion in the rigid matrix.

The proton transfer to aromatic radical anions in alcoholic solutions has been studied by means of pulse radiolysis technique[1] and its rate constant has been found to depend on the nature of the anion as well as the solvent. The proton transfer generally proceeds slowly because of a small pre-exponential factor in the rate constant. It has been observed to occur also in rigid alcoholic matrices at 77 K.[2–4] A steric factor is expected to affect significantly the rate of the proton transfer in the rigid matrices, since the translational motion of reactants are highly restricted. Styrene molecular anion (styrene anion) is transformed into α-methylbenzyl radical *via* proton transfer in γ-irradiated alcoholic matrices,[2–4] whereas it is stably trapped in aprotic rigid matrix of 2-methyltetrahydrofuran (MTHF) at 77 K.[2] In order to elucidate microscopically the mechanism of the proton transfer to an anion radical we have studied the transformation of the styrene anion into the α-methylbenzyl radical in the rigid matrices of MTHF–ethanol mixtures. The anion and the radical give distinct optical absorption spectra distinguishable from each other, so that the transformation can advantageously be followed by the optical spectrophotometric method.

Experimental

MTHF was distilled several times and treated with Na–K alloy. GR grade ethanol (Tokyo Kasei Chemical Ind., Ltd.) was used without further purification. Styrene was washed with aqueous solution of NaOH, distilled, dried with CaH_2, dehydrated with baked BaO and stored. It was distilled in a vacuum immediately before use. Sample solutions were degassed by a freeze-pump-thaw technique, transferred to an optical absorption cell of quartz or an ESR sample tube of quartz and sealed off in a vacuum of 10^{-5} Torr. γ-Irradiation was carried out at 77 K at a dose rate of 2 Mrad/h or 1 Mrad/h mostly to a dose of 0.2 Mrad. Optical absorption spectra were recorded with a conventional recording spectrophotometer (Hitachi, ESP-3A or Shimadzu, MPS-50L) and electron spin resonance (ESR) spectra with a conventional X-band spectrometer (JEOL, JES-3M) both at 77 K. The samples were annealed, when necessary, above 77 K with a controlled flow of cold nitrogen gas.

Results and Discussion

Yield of Styrene Anion and α-Methylbenzyl Radical. When an MTHF matrix containing styrene is irradiated at 77 K with γ-rays, the styrene anion is generated through the electron attachment to styrene, giving optical absorption bands at 415 and 600 nm.[2,3,5] Shida and Hamill reported that when a matrix of ethanol dissolving styrene is irradiated, α-methylbenzyl radical is exclusively detected by its absorption band with a maximum at 320 nm. Formation of the α-methylbenzyl radical in the ethanol matrix was evidenced by means of the fluorescence spectrophotometric method: the observed emission spectrum with the 0-0 band at 470 nm and the excitation spectra in visible and UV regions are essentially the same as those for the α-methylbenzyl radical generated by dissociative electron attachment to (1-chloroethyl)benzene in γ-irradiated organic matrices.[6] Williams and his co-workers[2] demonstrated by ESR studies a two-step mechanism for the formation of the α-methylbenzyl radical from styrene in the ethanol matrix, an electron attachment to styrene followed by proton transfer from a solvent molecule. Based on this mechanism, the stable trapping of the styrene anion in the MTHF matrix is attributed to the nature of MTHF solvent which cannot act as a proton donor.

A typical optical absorption spectrum recorded for the irradiated matrix of MTHF–ethanol mixtures con-

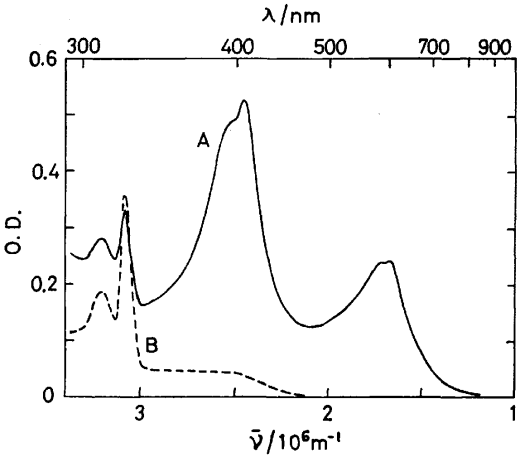

Fig. 1. Optical absorption spectra of a MTHF–ethanol mixed matrix (50 : 50 in mole) containing 50 mmol dm^{-3} styrene irradiated by γ-rays to 200 krad at 77 K (A) before and (B) after photobleaching with white light. Optical path-length: 0.2 cm.

taining styrene, for a solvent composition 50 : 50 in mole, is shown in Fig. 1A. The formation of trapped electron was completely depressed by 30 mmol dm^{-3} of styrene, the observed spectrum consisting of the band with the maximum at 320 nm due to α-methylbenzyl radical and the bands at 415 and 600 nm both due to the styrene anion. Figure 2 shows the relative yields of the radical and the anion monitored at 320 and 415 nm, respectively, as a function of the mole fraction of ethanol, X_{EtOH}, in the mixed matrix. The radical yield increases in proportion to X_{EtOH}, while the yield of the anion decreases linearly. This indicates, in accord with the two-step mechanism, that the radical is generated at the expense of the anion.

No transformation was observed from the anion into the radical after the irradiation as long as the matrix was kept at 77 K in the dark. This indicates that the proton transfer occurs so rapidly that it is completed during the course of γ-irradiation.

Proton Transfer in Rigid Matrix. The proton transfer reaction in a fluid solution is expected to follow the rate equation, $d[Radical]/dt = k[Anion][C_2H_5OH]$. If we ignore subsidiary reactions such as ion recombination, the ethanol concentration would affect not the ultimate yield of the α-methylbenzyl radical but the rate of the radical formation. However, the proton transfer in the rigid matrix showed a different feature. The change in X_{EtOH} caused the change in the radical yield as shown in Fig. 2.

The translational motion of molecules is highly restricted in the rigid matrix. Only the anion with an ethanol molecule (or molecules) located properly around it might undergo the proton transfer, but not the anion having no ethanol molecule in a proper location. Assuming that at the maximum the solvent site can be adequately populated by n ethanol molecules for the reaction, the probability is given by $(1-X_{EtOH})^n$ for the site being all populated by MTHF molecules, or for an anion not undergoing the proton transfer reaction.

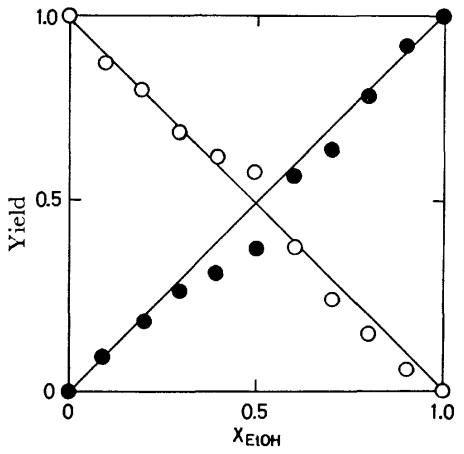

Fig. 2. Dependence of the yield of (○) styrene anion and (●) α-methylbenzyl radical upon the ethanol fraction in the MTHF-ethanol mixed matrix. The yields were corrected, so that their maximum value is 1.0. Straight lines indicate the dependence expected from Eq. 1 for $n=1$. Styrene concentration: 50 mmol dm^{-3}. γ-Irradiation: 200 krad.

Thus, the radical yield is given by $[Radical]=[Anion]_0 \cdot \{1-(1-X_{EtOH})^n\}$, where $[Anion]_0$ denotes the anion yield in the MTHF matrix or $X_{EtOH}=0$. Since the G-value of scavengeable electrons is almost the same in the MTHF and ethanol matrices,[7] the dependence of the radical yield on X_{EtOH} is given by

$$\frac{[Radical]}{[Radical]_{max}} = 1 - \frac{[Anion]}{[Anion]_0} = 1 - (1-X_{EtOH})^n \quad (1)$$

where $[Radical]_{max}$ denotes the radical yield for $X_{EtOH}=1$.

If $n>1$, the radical yield *vs.* X_{EtOH} curve should be convex upward. For instance, $[Radical]/[Radical]_{max}$ is calculated to be 7/8 for $n=3$ and $X_{EtOH}=1/2$. The reaction in a fluid solution is an extreme case: an anion has a chance to encounter all the ethanol molecules present in the solution suitably for the proton transfer, so that n is effectively infinite, and that $[Radical]/[Radical]_{max}=1$ except for $X_{EtOH}=0$. The result shown in Fig. 2 can be interpreted by n of unity, indicating that the proton transfer to the styrene anion occurs from an ethanol molecule located very close to and specifically with respect to a reactive site of the anion. This is consistent with the pulse radiolysis result in fluid solution which shows that the slow proton transfer is associated with a small pre-exponential factor of the rate constant.[1] It is also indicated that the linear decrease in the anion yield with X_{EtOH} is entirely due to the transformation of the anion into the radical and not to the recombination between the anion and a cation.

Site of Proton Attachment. The attachment of a proton to the β-carbon of the vinyl group in the styrene anion directly results in the formation of α-methylbenzyl radical. Alternatively, the α-methylbenzyl radical could be generated, when the intramolecular hydrogen transfer occurs in the phenethyl radical primarily formed by the proton attachment to the α-carbon of the vinyl group. Such an intramolecular hydrogen transfer was suggested from the observation of α-methylbenzyl radical when dissociative electron attachment to (2-chloroethyl)benzene occurred in γ-irradiated rigid matrices.[6,8]

In order to confirm the possibility of the latter mode of α-methylbenzyl radical formation, the stability of the phenethyl radical was examined in the MTHF matrix by the ESR method. Upon photolyzing (2-bromoethyl)benzene in the matrix at 77 K with UV light, a seven-line spectrum extending over 15 mT was observed, distinctly differing from the spectrum assigned to α-methylbenzyl radical,[2] and probably due to the phenethyl radical. It was found to decay with no change in its spectral shape when warmed to 100 K.

When the MTHF matrix containing (2-bromoethyl)benzene was irradiated with γ-rays at 77 K, the observed spectral shape consisted of the superposition of the well-known spectrum of MTHF radical,[9] and that attributable to the phenethyl radical. The change in the spectral shape upon warming to 100 K was found to be due to the decay of only the latter spectrum by examining the difference in spectral shape before and

after the warming. In this case the phenethyl radical seems to be formed by dissociative electron attachment to (2-bromoethyl)benzene.

From these photolysis and radiolysis studies it is obvious that the radical is too stable for the intramolecular hydrogen transfer to occur. Thus, the α-methylbenzyl radical is concluded to be generated exclusively by the direct mode of formation, the proton attachment to the α-carbon, the indirect mode being excluded. It is inferred that the proton transfer to the styrene anion in the mixed matrix occurs when an ethanol molecule happens to be properly located close to the β-carbon of the anion. Based on MO calculations, electron density is the highest as this carbon atom in the anion, so that it is expected to be the most reactive toward the proton attachment.

According to the present optical absorption study, the *G*-value of the α-methylbenzyl radical in the γ-irradiated ethanol matrix was determined to be 2.2 by using the extinction coefficient, 1.5×10^4 mol^{-1} dm^3 cm^{-1} at the absorption maximum for benzyl radical.[10] It is almost identical to the *G*-value of scavengeable electron in the ethanol matrix.[7] This coincidence of the *G*-values supports the view that the α-methylbenzyl radical arises from the styrene anion generated by the electron attachment to styrene, and that the proton transfer to the anion occurs almost exclusively to the β-carbon.

Photobleaching of Styrene Anion. Upon photobleaching with white light from an incandescent lamp ($\lambda>400$ nm), the styrene anion in the mixed matrix could be completely eliminated, being transformed partially into the α-methylbenzyl radical (Fig. 1B). The efficiency of this photoinduced transformation (the ratio of the increment of the radical yield to the yield of the photobleached anion) increases with increasing X_{EtOH} to reach a plateau value of *ca.* 0.6 (Fig. 3). The plateau could be determined by the competition for electrons photoreleased from the styrene anions between the dissociative electron scavenge reaction of ethanol[11,12] and the non-dissociative electron scavenge reaction of styrene associated with an ethanol molecule suitable for the proton transfer. Both the dissociative and non-dissociative scavenge reactions proceed at a rate proportional to the ethanol concentration in the mixed matrix, so that the transformation efficiency is independent of the ethanol concentration. The rate of non-dissociative scavenge reaction proportional to the ethanol concentration implies that only one ethanol molecule can be located in the solvent site adequate for the proton transfer, consistent with $n=1$ in Eq. 1.

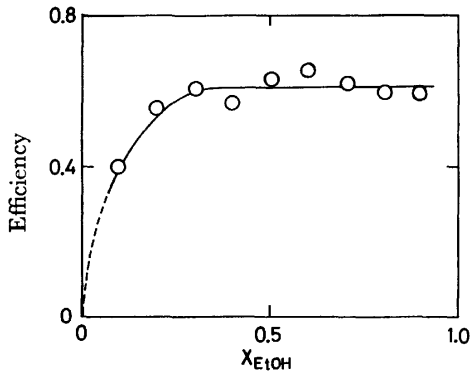

Fig. 3. Efficiency of photoinduced transformation of styrene anion into α-methylbenzyl radical as a function of the ethanol fraction in the MTHF–ethanol mixed matrix. Photobleaching was carried out with white light at 77 K after irradiating the matrices containing 50 mmol dm^{-3} styrene to the dose of 200 krad.

The fall of efficiency at low values of X_{EtOH} can be attributed to an increasing contribution of charge recombination reaction between the photoreleased electrons and positive ions, since the rate becomes low for both scavenge reactions.

So far the discussion has been given on the assumption that ethanol is perfectly missible in MTHF and *vice versa*, so that the mixed matrix is microscopically homogeneous. Sawai and Hamill studied the optical absorption spectra of trapped electrons in γ-irradiated MTHF–methanol mixed matrix and interpreted the spectral feature in terms of the microscopically homogeneous mixing of the two solvent components.[13]

References

1) L. M. Dorfman, *Acc. Chem. Res.*, **3**, 224 (1970).
2) J. Lin, K. Tsuji, and F. Williams, *Trans. Faraday Soc.*, **64**, 2896 (1968).
3) T. Iwamoto, K. Hayashi, S. Okamura, Ka. Hayashi, and H. Yoshida, *Int. J. Radiat. Phys. Chem.*, **1**, 1 (1969).
4) T. Shida and W. H. Hamill, *J. Am. Chem. Soc.*, **88**, 3689 (1966).
5) T. Shida and W. H. Hamill, *J. Chem. Phys.*, **44**, 4372 (1966).
6) T. Saito and H. Yoshida, *Bull. Chem. Soc. Jpn.*, **47**, 3167 (1974).
7) L. Kevan, "Advences in Radiation Chemistry," Vol. 4, ed by M. Burton and J. L. Magee, Wiley-Interscience, New York (1973), p. 210.
8) Dissociative electron attachment to (2-chloroethyl)-benzene leads to the formation of phenethyl radical. The observed α-methylbenzyl radical was therefore suggested to arise from the phenethyl radical.[6] However, the α-methylbenzyl radical was detected by the sensitive fluorescence spectrophotometric method, the formation of the phenethyl radical not being examined. It seems to us that the main product from (2-chloroethyl)benzene is the phenethyl radical and that the α-methylbenzyl radical is generated by a subsidiary reaction in the γ-irradiated matrices.
9) See for example, D. R. Smith and J. J. Pieroni, *Can. J. Chem.*, **43**, 876 (1965); T. Shida, T. Warashina, H. Yoshida, and S. Okamura, *Ann. Repts. Research Reactor Inst. Kyoto Univ.*, **3**, 19 (1970).
10) J. B. Gallivan and W. H. Hamill, *Trans. Faraday Soc.*, **61**, 1960 (1965).
11) T. Shida and M. Imamura, *J. Phys. Chem.*, **78**, 232 (1974).
12) T. Ichikawa, T. Moriya, and H. Yoshida, *J. Phys. Chem.*, **80**, 1278 (1976).
13) T. Sawai and W. H. Hamill, *J. Phys. Chem.*, **78**, 3452 (1969).

Ultrasonic and Volumetric Investigation of Aqueous Solutions of Amides

Fumio KAWAIZUMI, Makoto OHNO, and Yutaka MIYAHARA

Department of Chemical Engineering, Faculty of Engineering, Nagoya University, Chikusa-ku, Nagoya 464

(Received February 21, 1977)

The ultrasonic velocity and density of aqueous solutions of *N*-methylformamide, *N*,*N*-dimethylformamide, and *N*,*N*-dimethylacetamide have been measured at 25 and 35 °C over the entire concentration range. The compressibility, excess compressibility, partial molar compressibility, partial molar volume, and pressure dependence of the partial molar volume have been calculated. The concentration dependences of the velocity and density are highly nonlinear, and the velocity maxima are observed in all the amide solutions at *ca.* 20 mol%. Minima in the partial molar volume exist in solutions of DMF and DMAA, but not in that of MFA. On taking account of the results for viscosity, the velocity maxima are ascribed to the complex formation, and the minima in the partial molar volume, to the competition between the volume increase due to the complex formation and the volume decrease due to the breaking-down of the water structure. The pressure dependence of the partial molar volume shows that amides and water have strong interactions, even in the low-mole-fraction regions for each component.

Numerous investigators have studied solute-solvent interaction in nonelectrolytic aqueous solutions from the point of view of their ultrasonic and volumetric behavior. In binary liquid mixtures, the nonlinear variation in the ultrasonic velocity with the concentration has been frequently observed, but the systems showing a velocity maximum are limited to aqueous solutions, except for the very rare case of the liquid paraffin–carbon tetrachloride system.

From among the many nonelectrolytes known to form aqueous solutions with a velocity maximum at a certain concentration, the present authors chose amides. The ultrasonic velocities and densities of aqueous solutions of *N*-methylformamide(MFA), *N*,*N*-dimethylformamide (DMF), and *N*,*N*-dimethylacetamide (DMAA) will be reported.

The aqueous solutions of amides have the following characteristic features concerning their ultrasonic and volumetric properties. First, the ultrasonic velocity and the density of pure amides have values similar to those of water. Secondly, in a solution of DMF, the maximum has been observed in the concentration dependence of the velocity as well as in that of the density. Nonelectrolytes showing a similar solution behavior include some kinds of amines (ethylenediamine and benzylamine[1]), acetic acid, dioxane,[2] and pyridine.[3]

The ultrasonic velocities in aqueous solutions of DMF[4] and DMAA[5] have been reported by Endo, and the densities of the aqueous solutions of DMF[6] and DMAA,[7] by Arakawa *et al.* and Assarsson and Eirich. We have undertaken the re-determination of the velocities and densities of these three aqueous solutions of amides in order to obtain consistent data. For instance, the density of DMAA given by Assarsson and Eirich[7] is 0.9350 g/ml at 25 °C. This value is not compatible with our result (0.9367_0 g/cm^3) nor with the value of 0.9366 g/cm^3 found in the literature.[8] The data by Assarsson and Eirich[7] are, as they themselves say, not accurate enough to establish whether or not a small minimum in the partial molar volume exists, as in alcohol–water systems, at a very low mole fraction of the amides.

Experimental

Materials. The MFA(guaranteed grade) and DMF (spectral grade), obtained respectively from the Tokyo Kasei Co., Ltd., and Nakarai Chemicals were used without further purification. The DMAA (guaranteed grade) was purified by distillation under reduced pressure.

Apparatus and Procedures. Measurements of the sound velocity were carried out at a fixed frequency of 4 MHz by means of an improved ultrasonic interferometer. This interferometer has the great advantage that a good parallelism between the reflector and the quartz surface can be attained by the aid of the screws and the springs, while in the interferometer used hitherto in our laboratory, the parallelism was mechanically determined. The parallelism is established by the application of the pulse-echo method. The measurement of the sound velocity was reproducible within 0.4 m/s. Further accuracy has been obtained by finely polishing the surface of the reflector. The density has been measured by using a 20-ml pycnometer. The density data are accurate to ±3 units in the fifth decimal place. Measurements were done at 25 and 35 °C.

Results and Discussion

Density and Velocity. The experimental results of the density and the ultrasonic velocity as a function of the composition are summarized in Tables 1—3. In all three aqueous solutions of amides studied in this work, the density as well as the ultrasonic velocity shows a high nonlinear dependence on the concentration. In the MFA system, the density maximum exists in the vicinity of 20 mol% of MFA. In the DMF and DMAA systems, sinuous but slight variations of the density have been observed in the low-concentration region of amide. After passing this region, the concentration dependence of the density is marked, but in a linear fashion. The aqueous solutions of alcohols, which exhibit a marked nonlinear dependence on the concentration in many physical properties, do not show such a clearly sinuous variation or a maximum point in relation to the concentration dependence of the density. All three amide systems show velocity maxima in the concentration range of 15—20 mol%, this range corresponds to the region where the decreases of density begin. The concentration dependence of the ultrasonic velocity in general, and also the position of the maximum, correspond well with the viscosity results of many kinds of aqueous solutions of amides.[7] Assarsson and Eirich, considering phase diagrams and heat of mixing in amide–water systems,[9] have related the observed maximum of viscosity to the formation of the complex. The veloc-

TABLE 1. DENSITY AND ULTRASONIC VELOCITY *vs.* COMPOSITION FOR THE *N*-METHYLFORMAMIDE (MFA)-WATER SYSTEM

	MFA (mol%)	Density (g/cm³)	Velocity (m/s)
At 25 °C	0.0	0.9970_4	$1496._3$
	2.265	1.000_0	$1527._5$
	5.958	1.004_7	$1563._2$
	12.12	1.010_7	$1595._4$
	19.57	1.014_3	$1606._7$
	24.02	1.015_7	$1602._7$
	35.19	1.015_7	$1577._7$
	48.38	1.012_7	$1536._3$
	66.97	1.007_0	$1487._7$
	79.79	1.003_4	$1460._9$
	100.00	0.9985_4	$1431._5$
At 35 °C	0.0	0.9940_3	$1519._5$
	6.258	1.000_6	$1570._6$
	11.90	1.004_9	$1590._5$
	17.36	1.007_5	$1594._2$
	24.42	1.009_1	$1586._0$
	35.10	1.008_4	$1556._2$
	50.66	1.004_4	$1507._9$
	67.64	0.9988_5	$1459._3$
	83.09	0.9943_6	$1431._0$
	100.00	0.9898_0	$1401._6$

TABLE 2. DENSITY AND ULTRASONIC VELOCITY *vs.* COMPOSITION FOR THE *N*,*N*-DIMETHYLFORMAMIDE (DMF)-WATER SYSTEM

	DMF (mol%)	Density (g/cm³)	Velocity (m/s)
At 25 °C	0.0	0.9970_4	$1496._3$
	1.724	0.9961_1	$1536._7$
	2.919	0.9960_4	$1560._6$
	7.072	0.9964_7	$1621._8$
	9.002	0.9965_8	$1642._5$
	14.51	0.9972_5	$1676._3$
	19.28	0.9964_0	$1688._3$
	24.01	0.9948_4	$1684._5$
	34.27	0.9876_3	$1661._3$
	49.77	0.9766_4	$1602._1$
	64.63	0.9651_3	$1548._8$
	79.21	0.9549_2	$1507._8$
	86.38	0.9506_5	$1487._5$
	100.00	0.9442_0	$1458._5$
At 35 °C	0.0	0.9940_3	$1519._5$
	1.724	0.9929_6	$1551._1$
	2.919	0.9923_2	$1569._7$
	6.179	0.9915_1	$1607._8$
	9.002	0.9910_2	$1631._3$
	15.82	0.9896_0	$1657._3$
	20.06	0.9881_6	$1659._9$
	23.98	0.9862_6	$1653._6$
	33.82	0.9797_5	$1626._3$
	49.13	0.9678_2	$1567._8$
	65.25	0.9552_3	$1509._9$
	80.01	0.9454_3	$1466._1$
	86.38	0.9414_2	$1448._5$
	100.00	0.9347_7	$1422._2$

TABLE 3. DENSITY AND ULTRASONIC VELOCITY *vs.* COMPOSITION FOR THE *N*,*N*-DIMETHYLACETAMIDE (DMAA)-WATER SYSTEM

	DMAA (mol%)	Density (g/cm³)	Velocity (m/s)
At 25 °C	0.0	0.9970_4	$1496._3$
	1.616	0.9956_4	$1546._3$
	3.060	0.9955_0	$1584._1$
	5.897	0.9965_7	$1641._8$
	8.229	0.9972_2	$1678._8$
	11.50	0.9985_1	$1711._3$
	18.14	0.9985_0	$1737._4$
	24.39	0.9959_2	$1730._9$
	36.81	0.9858_6	$1682._1$
	49.63	0.9739_1	$1626._1$
	66.25	0.9591_7	$1557._9$
	77.76	0.9502_6	$1517._7$
	85.58	0.9446_1	$1493._2$
	100.00	0.9367_0	$1462._6$
At 35 °C	0.0	0.9940_3	$1519._5$
	1.353	0.9926_0	$1554._1$
	2.541	0.9918_5	$1580._6$
	5.879	0.9914_0	$1636._8$
	7.762	0.9914_1	$1660._2$
	11.62	0.9915_6	$1690._6$
	16.76	0.9907_9	$1704._7$
	24.52	0.9869_1	$1693._6$
	35.69	0.9774_5	$1647._4$
	48.01	0.9657_6	$1591._4$
	68.38	0.9482_0	$1510._8$
	75.64	0.9426_9	$1485._7$
	89.92	0.9336_5	$1442._1$
	100.00	0.9274_3	$1418._9$

ity maximum has been reported in the aqueous solutions of tetrahydrofran, 1,4-dioxane, and *t*-butyl alcohol in the concentration range of 3—8 mol%.[10] These compounds form solid clathrates of 17 hydrates. In these cases, there is no doubt of the relationship between the occurrence of the velocity maximum and the formation of a "compound" (hydrate or other).

Generally speaking, the velocity maximum in solutions do not always necessiate the formation of a "compound." However, in the aqueous solutions of amides concerned in this work, the resemblance between the concentration dependence of the ultrasonic velocity and that of the viscosity indicates that the velocity maximum arises from the formation of the complex, therefore, the position of the velocity maximum indicate its composition. However, the structure of the complex formed in amide–water systems may not be similar to those in an ordinary clathrate like 17 hydrate or $8X \cdot 136H_2O$.

Compressibility. From the values of the velocity and density, the adiabatic comprssibility, κ_s has been calculated. The concentration dependence of κ_s is shown in Fig. 1. DMAA gives a similar dependence of the compressibility. Concerning Fig. 1 two facts should be mentioned: the appearance of the minimum and the temperature-independent point. The former

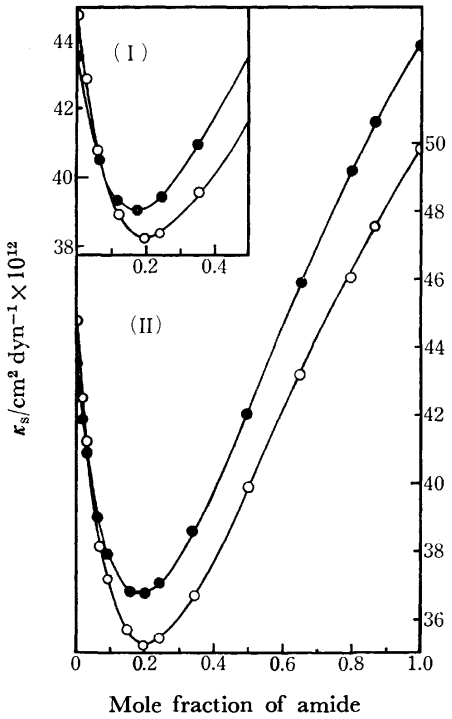

Fig. 1. Concentration dependence of adiabatic compressibility of the aqueous solutions of MFA (I) and DMF (II).
○: 25 °C, ●: 35 °C.

corresponds to the occurrence of the maximum in the velocity (and also in the density for the MFA system). The latter corresponds to the appearance of the common intersection in the relation of the temperature dependence of the velocity in solution. The phenomenon of the common intersection in the velocity has often been observed in many nonelectrolytic aqueous solutions.[4,5,11,12] Endo[4,5] has argued that this phenomenon is due to the clathrate formation and that the concentration of the common intersection should give the composition of the clathrate. The measurements of the ultrasonic velocity of Endo are quite extensive in terms of materials and the temperature range. However, his discussion of the common intersection has the crucial defect that comparisons with other properties which have intimate relations to the ultrasonic velocity, such as the density and the ultrasonic absorption coefficients, are disregarded. The relation between the common intersection and the partial molar volume will be discussed below.

The excess adiabatic compressibility, κ_S^E has been calculated from κ_S, and the molar volumes, V, of the mixtures and the pure components, A and B by means of this equation:

$$\kappa_S^E = \kappa_S - \frac{1}{V}(X_A V_A \kappa_{S,A} + X_B V_B \kappa_{S,B}).$$

The results are shown in the Fig. 2. κ_S^E's are always negative, and the values decrease as the $-CH_2-$ group increases. The temperature coefficients change their sign at a certain concentration in all systems.

Partial Molar Volume and Partial Molar Compressibility. From the density data given in Tables 1—3, the characteristic behavior of the partial molar volume of amides in solutions represented in Fig. 3 is obtained. The relation of the partial molar volume to the composition at 35 °C falls on the curves shown in Fig. 3. Similarly, as for κ_S^E, the curves become steeper as the number of the $-CH_2-$ group increases. The behavior of the aqueous solutions of amides shown in Fig. 3 closely resembles that of aqueous solutions of alcohols[13] and amines.[14] Sometimes the position of the minimum in the partial molar volume *vs.* composition relation roughly coincides with the common intersection of the ultrasonic velocity (therefore, the compressibility), for example, in aqueous solutions of tetramethylurea[11] and ethers.[12] The comparison of Fig. 1 with Fig. 3 shows that, for

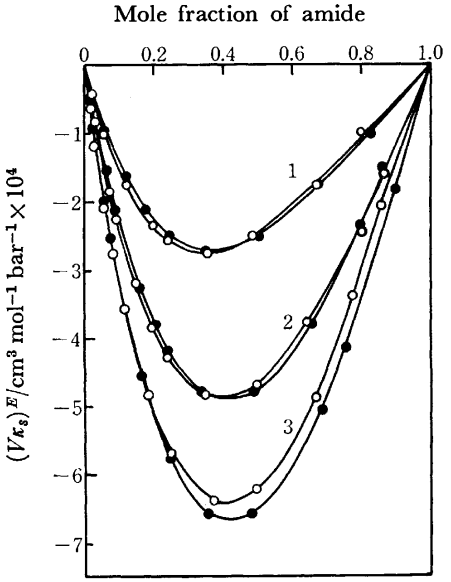

Fig. 2. Concentration dependence of excess compressibility of the amides solutions.
1: MFA–water system, 2: DMF–water system,
3: DMAA–water system.
○: 25 °C, ●: 35 °C.

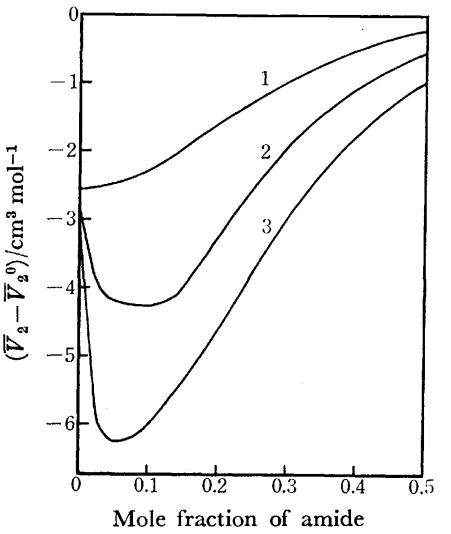

Fig. 3. Partial molar volume of amides in aqueous solution at 25 °C.
1: MFA, 2: DMF, 3: DMAA.

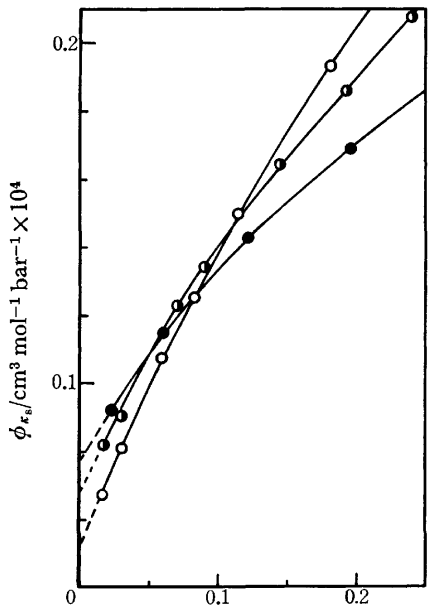

Fig. 4. Apparent molar compressibility of dilute aqueous solutions of amides at 25 °C.
●: MFA, ◑: DMF, ○: DMAA.

DMA and DMAA, this coincidence holds, but for MFA this is not the case.

Figure 4 shows the apparent molar compressibility, ϕ_{κ_s}, at 25 °C as calculated by means of this equation:

$$\phi_{\kappa_s} = \frac{1000(\kappa_s - \kappa_{s,1})}{c} + \kappa_{s,1}\phi_v,$$

where the subscript 1 refers to the solvent, c is the concentration in molarity, and ϕ_v is the apparent molar volume. According to Fig. 4, at an infinite dilution the ϕ_{κ_s} values are in this order: MFA, DMF, DMAA: that is to say, as a molecule has more $-CH_2-$ groups, the more rigid it becomes. The order of the rigidity, however, is inverted in the concentration range above *ca.* 10 mol%.

As an inversion of the order of the values of ϕ_{κ_s}, the common intersection in the ultrasonic velocity, and the minimum in the partial molar volume, occur in a similar region of the concentration, these phenomena may have some interrelations. However, any interpretations of these phenomena must be consistent with the appearances of the velocity maximum and the viscosity maximum observed in the concentration range beyond 20 mol%.

As has been mentioned above, the maximum in ultrasonic velocity has been ascribed to the complex formation. The following is a tentative interpretation of the partial molar volume as a function of the concentration. The complex formed by the hydrogen-bonding between amide and water has a rigid, but bulky structure. Therefore, the complex formation gives rise to an increase in the apparent volume of amide. The minimum in the partial molar volume may, then, be attributed to the competition between the volume increase due to the complex formation and the volume decrease due to the breaking-down of the water structure.

The relationship of the common intersection in the ultrasonic velocity with the other phenomena is not clear at present. The coincidence of the minimum position in the partial molar volume with the common intersection in the ultrasonic velocity is part of the complicated nature of the aqueous solutions. However, with regard to the aqueous solutions of amides studied in this work, the composition of the common intersection of the ultrasonic velocity can not be considered to indicate that of the "compound" formed in solution.

Pressure Dependence of the Partial Molar Volume.
For the partial molar volume of a solute, its pressure dependence can be calculated from the following equation:[16]

$$\frac{\partial \overline{V}_2}{\partial p} = -\kappa \overline{V}_2 - (1-X)V\frac{\partial \kappa}{\partial X}.$$

The results of calculation are given in Fig. 5. In a dilute solution of amides, the three curves in Fig. 5 intersect with one another, and this intersection corresponds to the inversion of the order of ϕ_{κ_s} in Fig. 4. In a dilute region, $\partial\overline{V}_2/\partial p$ is very large. As the concentration of a solute increases, the variation in $\partial\overline{V}_2/\partial p$ gradually decreases. For small molecules, the variation in $\partial\overline{V}_2/\partial p$ with the concentration ceases in more dilute solutions than in case of large molecules, and in the pure state of amide, the order of $\partial\overline{V}_2/\partial p$ for the three systems is, as it should be, MFA, DMF, DMAA. The strong dependence of $\partial\overline{V}_2/\partial p$ on the concentration in a dilute aqueous solution of amides indicates the strong solute-solvent interaction in solution. Calculations using the data at 35 °C have given, for all three systems, more negative values than those shown in Fig. 5. The negative values of $\partial\overline{V}_2/\partial p$ are equivalent to the negative values of K_x, where K_x is the relative partial specific compression of the solute,[15] and where the amide is taken as a solute. A negative K_x value signifies the non-existence of an incompressible region in the solution. However, this does not contradict with the complex formation between amides and water, because the hydrogen-bonding interactions are not so strong as to

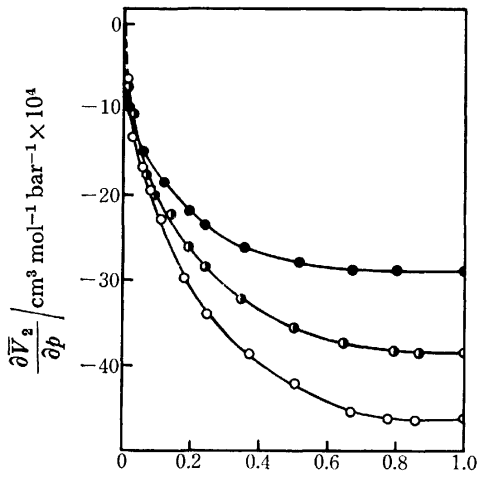

Fig. 5. Concentration dependence of $\partial\overline{V}_2/\partial p$ at 25 °C.
●: MFA–water system, ◑: DMF–water system,
○: DMAA–water system.

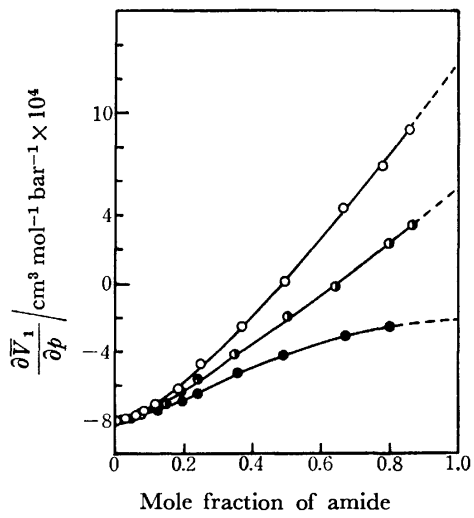

Fig. 6. Concentration dependence of $\partial \overline{V}_1/\partial p$ at 25 °C.
●: MFA–water system, ◑: DMF–water system,
○: DMAA–water system.

the coulombic ones typically observed in the form of ionic hydration.

The pressure dependence of the partial molar volume of the solvent can be obtained in a similar way; the results are shown in Fig. 6. The values of $\partial \overline{V}_1/\partial p$ and its concentration dependence are in the order of DMAA, DMF, and MFA. For solutions of DMAA and DMF, $\partial \overline{V}_1/\partial p$ are positive in the water-rich region. The marked dependence of $\partial \overline{V}_1/\partial p$ on the concentration in the water-rich region shows that, when a small amount of water is dissolved in amides, water molecules interact very strongly with amide molecules.

In summing up the results of Figs. 5 and 6, it is evident that strong interactions exist between water and amides, even in low-mole-fractions for each component.

References

1) M. V. Kaulgud and K. J. Patil, *Acustica*, **28**, 130 (1973).
2) Density data; 2a) V. S. Griffiths, *J. Chem. Soc.*, **1952**, 1326; velocity data; 2b) K. Arakawa, N. Takenaka, and K. Sasaki, *Bull. Chem. Soc. Jpn.*, **43**, 636 (1970).
3) Density data in 2a), velocity data in "Cho-onpa Gijyutu Binran," Nikkan Kogyo Shinbunsha, Tokyo (1966).
4) H. Endo, *Bull. Chem. Soc. Jpn.*, **46**, 1106 (1973).
5) H. Endo, *Bull. Chem. Soc. Jpn.*, **46**, 1586 (1973).
6) H. Arakawa, N. Takenaka, and K. Sasaki, 18th Meeting of Ultrasound Physics and Chemistry of Japan, Osaka, November, 1973, p. 7.
7) P. Assarsson and F. R. Eirich, *J. Phys. Chem.*, **72**, 2710 (1968).
8) A. Weissberger, ed, "Techniques of Chemistry," Vol. 7; "Organic Solvents," 2nd ed, Interscience, New York (1971).
9) P. Assarsson and F. R. Eirich, *Adv. Chem. Ser.*, **84**, 1 (1968).
10) E. K. Baumgarter and G. Atkinson, *J. Phys. Chem.*, **75**, 2336 (1971).
11) K. Sasaki and K. Arakawa, *Bull. Chem. Soc. Jpn.*, **46**, 2738 (1973).
12) N. Takenaka and K. Arakawa, *Bull. Chem. Soc. Jpn.*, **47**, 566 (1974).
13) K. Nakanishi, *Bull. Chem. Soc. Jpn.*, **33**, 793 (1960).
14) M. V. Kaulgud and K. J. Patil, *J. Phys. Chem.*, **80**, 138 (1976).
15) For a discussion of the quantity K_x, see, for example, H. Nomura and Y. Miyahara, *J. Appl. Polym. Sci.*, **3**, 1643 (1964).
16) For the derivation of the equation, see Y. Miyahara, "Yo-ekiron," Kodansha, Tokyo (1976).

The Dimorphism and Electronic and Vibrational Spectra of 2-Anilino-1,4-naphthoquinones

Yoshio MATSUNAGA, Nobuhiko MIYAJIMA, and Atushi TOGASHI
Department of Chemistry, Faculty of Science, Hokkaido University, Sapporo 060
(Received February 23, 1977)

Dimorphic forms were isolated for over ten derivatives of 2-anilino-1,4-naphthoquinone, 2-anilino-3-chloro-1,4-naphthoquinone, and 2-anilino-3-bromo-1,4-naphthoquinone carrying substituents on the phenyl ring. One of the two forms exhibits a relatively sharp vibrational band near 3300 cm^{-1}, the other, a relatively broad band at a lower wave number. The spectra in the region from 700 to 1700 cm^{-1} are often markedly different from each other. In several instances, the two forms are differently colored. This difference is attributed to the appearance of, or a change in the intensity of, an intermolecular charge-transfer absorption band. Not only the dimorphic forms, but also most of the derivatives examined, could be classified into two groups on the basis of the location and the sharpness of the vibrational band appearing in the region from 3150 to 3350 cm^{-1}.

A large number of the condensation products of 1,4-naphthoquinone and its 2,3-dihalo derivatives with various anilines have been synthesized and examined for possible use as vat dyestuffs and as bactericides.[1-9] Among them, 2-(*p*-carboxyanilino)-1,4-naphthoquinone was isolated as yellow and red crystals by Hauschka.[7] The tautomerism involving *p*-quinonoid and *o*-quinonoid forms:

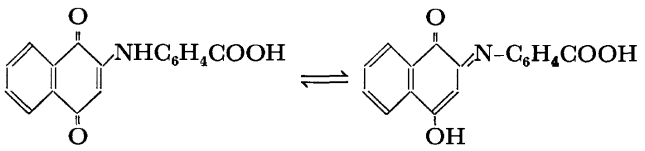

was pointed out as a possible cause of the marked difference in color. However, he added that the spectroscopic study failed to provide concrete evidence in support of this assumption. Because of the recent work on a related compound by Bloom and Dudek, a further study of the suggested tautomerism seemed to be desirable. These authors found that the electronic absorption spectrum of 4,8-dianilino-1,5-naphthoquinone is solvent-dependent.[10] In polar, associating solvents, the lowest-energy absorption appearing at 661 nm is of maximum intensity and decreases with a decrease in the solvent-associating ability. Further evidence for the existence of a tautomeric equilibrium in solution has been provided by their work on the proton magnetic resonance of the ^{15}N-substituted compound.

As we have reported for the dimorphic forms of *o*- and *p*-anisyl-*p*-benzoquinones,[11] there is another possible explanation for the difference in color. The molecule consists of an electron-donating and an accepting moieties; therefore, the color of the crystal may depend upon the intermolecular charge-transfer absorption, the location and the intensity of which can be modified, to some extent, by the mode of molecular stacking. No matter which is the cause, the dimorphism is certainly influenced by the kind and the position of substituent, and one may isolate more dimorphic forms by examining closely related compounds. Spectroscopic studies of many pairs of such modifications may be fruitful in deciding the origin of this phenomenon. Accordingly, a careful examination of various 2-anilino-1,4-naphthoquinones and its 3-chloro and 3-bromo derivatives was set up.

Experimental

Materials. The naphthoquinone and its 2,3-dichloro derivative were obtained commercially. The 2,3-dibromo-1,4-naphthoquinone was prepared following the method reported by Miller.[12] The condensation reaction between the naphthoquinones and anilines was carried out in boiling ethanol unless otherwise stated. The isolation of dimorphic forms was attempted by sublimation in a vacuum and by recrystallization from appropriate solvents, and under various conditions. Hereafter, X denotes the substituent on the phenyl group, and Y, the atom attached to the 3 position of the quinone.

Measurements. The vibrational spectra in the rock-salt region were recorded on a Jasco IR-G infrared spectrophotometer as Nujol mineral oil or hexachlorobutadiene mulls.

The diffuse reflectance of solid samples was measured using a Beckman DK-2A spectroreflectometer in the range from 325 to 700 nm. The anilinoquinone crystals were pulverized with sodium chloride in a concentration of the order of one weight percent. The spectra were recorded as the difference between the mixture and pure sodium chloride and were plotted using the Kubelka-Munk function, $f(R)=(1-R)^2/2R$, where R is the reflectance. In all the figures in this paper, the electronic spectra are plotted taking the maxima of the lowest-energy absorption arbitrarily as 1.00.

Results

2-(Carboxyanilino)-1,4-naphthoquinones (X=COOH, Y=H). The vibrational spectra of the yellow form and the red form of the *p*-derivative obtained by vacuum sublimation are presented in Fig. 1. There is a marked difference in the region from 3150 to 3350 cm^{-1}. The yellow form exhibits a sharp absorption band at 3310 cm^{-1}, and the red form, a rather broad one at 3220 cm^{-1}. They may be assigned to the N–H or O–H stretching vibration. As their locations are known to be strongly affected by hydrogen bonding, it is difficult to decide whether or not the shift is an indication of the tautomerism. For example, 2-hydroxy-1,4-naphthoquinone, which is isomeric with 4-hydroxy-1,2-naphthoquinone, shows a very broad O–H stretching band at 3150 cm^{-1}, suggesting the presence of strong hydrogen bonding. On the other hand, 2-amino-3-hydroxy-1,4-naphthoquinone gives a sharp band at 3450 cm^{-1} and a broad one at 3300 cm^{-1}. As is shown in Fig. 1, the dimorphic forms significantly differ from

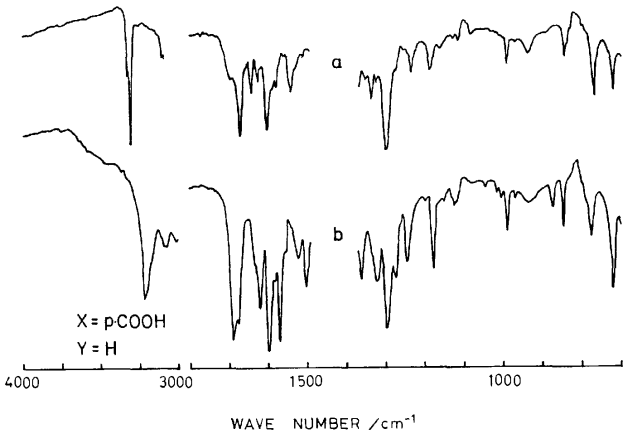

Fig. 1. Vibrational spectra of 2-(*p*-carboxyanilino)-1,4-naphthoquinone: (a) the yellow form and (b) the red form.

each other also in the pattern of the region from 1000 to 1700 cm^{-1}.

The electronic spectra of the yellow and red forms are given in Fig. 2. The absorption maximum is located at 435 nm in the yellow form and at 510 nm in the red form. As the location of the shoulder appearing in the former spectrum coincides exactly with the maximum in the latter, our yellow sample may be contaminated with a small amount of the red form. The maximum in the yellow form is close to the one observed in an acetone solution, 450 nm. No appreciable change was detected either in the location or in the intensity when methanol, ethyl acetate, chloroform, and pyridine were employed as the solvents. The temperature-dependence measured in the last mentioned solvent revealed that the absorption maximum decreases and shifts a little bit to the short wavelength side when the temperature is elevated, *e.g.*, 464 nm at 18 °C and 457 nm at 66 °C. The isosbestic points appearing at 360 and 422 nm probably arise from this shift. The present molecule is flexible, and the electronic transition considered is of the charge-transfer type; therefore, the temperature-dependence may be interpreted in terms of the thermal excitation of the distortion modes, as has been suggested by Kordes *et al.*[13]

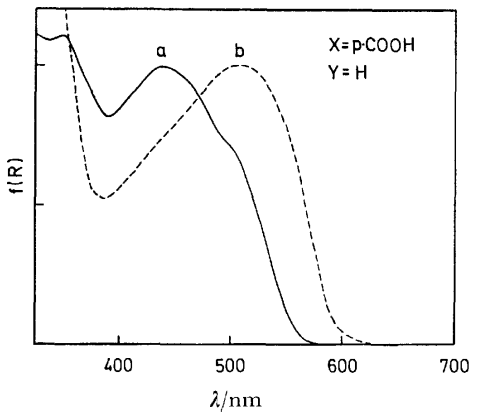

Fig. 2. Electronic spectra of 2-(*p*-carboxyanilino)-1,4-naphthoquinone: (a) the yellow form and (b) the red form.

In accordance with the observation by Hauschka, the *o*-derivative is obtainable as orange-red crystals, and the *m*-derivative, as red crystals. In the region near 3300 cm^{-1}, no vibrational band is found for the former compound, but a sharp band at 3280 cm^{-1} is found for the latter. The electronic spectrum of the *o*-derivative has a maximum at 475 nm, and the *m*-derivative, one at 520 nm.

Other 2-Anilino-1,4-naphthoquinones (Y=H). Among the sixteen compounds examined, only the *p*-methoxy and *m*-ethoxy derivatives were found to be dimorphic. When the condensation reaction between the quinone and *p*-anisidine was carried out in boiling ethanol, reddish violet crystals were deposited. The same form could be obtained by recrystallization under various conditions and also by sublimation in a vacuum. This stable form gives a broad vibrational band at 3215 cm^{-1}. Because of the reasoning to be presented later, the preparation was repeated in cold media with the hope of isolating the unstable form. A bluish violet product of the condensation in ethanol at room temperature showed a sharp band at 3325 cm^{-1} in addition to the above-mentioned broad one. The whole vibrational pattern, which is more complicated than that of the reddish violet form, suggested the coexistence of two forms. Since the transformation was suspected to be accelerated by the solvent, the reaction in cold water, in which the product is hardly soluble, was also attempted. This time, the product gave no broad band near 3200 cm^{-1}; however, the purity did not seem to be high, as the spectrum consists of rather broad bands. Thus, the unstable form could not be isolated. The *m*-ethoxy derivative prepared in boiling ethanol was reddish brown and showed a band at 3320 cm^{-1}. Upon sublimation in a vacuum the color turned dark red, and the vibrational spectrum was considerably modified. The above-mentioned sharp band was replaced by a broad one at 3255 cm^{-1}. The difference in the electronic spectrum is not large for this compound; the maximum is at 500 nm in both forms. These two compounds were initially prepared by Grossmann, but he did not note the dimorphism.[8]

For all the other derivatives, we saw no indication of dimorphism. On the basis of the vibrational band in the region from 3150 to 3350 cm^{-1}, they can be classified into two groups. The first group consists of the following derivatives, exhibiting a sharp band near 3300 cm^{-1}: X=H (3310 cm^{-1}), *m*-Me (3305), *p*-Me (3325), *o*-MeO (3300), *m*-MeO (3320), *o*-EtO (3330), *p*-EtO (3320), and 3,4-Me_2 (3315). On the other hand, a broad band was observed near 3200 cm^{-1} only with the halo derivatives—namely, *m*-Cl (3180 cm^{-1}), *p*-Cl (3185), *m*-Br (3180), *p*-Br (3200), and *p*-I (3200). The *p*-ethyl and *m*-carboxy derivatives are exceptional. A band with an intermediate breadth was found at 3280 cm^{-1}. Grossmann noted that the color of the *m*-methoxy derivative appreciably varies with the kind of solvent; that is, the pyridine solution is light yellow, the benzene solution is orange red, and the ethanolic solution is bluish red.[8] Nevertheless, we found that the absorption spectrum in pyridine is identical with that in ethanol. The maximum at room temperature is at 470 nm in both solvents.

2-Anilino-3-chloro-1,4-naphthoquinones (Y=Cl). Dimorphic forms could be isolated with the *m*-methyl, *p*-ethyl, 2,4-dimethyl, *m*-ethoxy, and *m*-carboxy derivatives. In the case of the *m*-methyl derivative, the form deposited from the reaction mixture gives a sharp vibrational band at 3300 cm^{-1}, while the other form, obtained by recrystallization from ethanol, gives a broad band at 3245 cm^{-1}. A mixture of the two forms was obtained by sublimation in a vacuum. The difference in the other region is less significant compared with the case shown in Fig. 1 (X=*p*-COOH, Y=H). The former form is dark reddish violet and gives an absorption maximum at 485 nm and a shoulder at 515 nm. The latter is bright reddish violet, and its maximum is located at 510 nm.

The crystals of the *p*-ethyl derivative, separated from the reaction mixture and also purified by vacuum sublimation, are reddish violet and give a sharp vibrational band at 3270 cm^{-1}, while the crystals deposited from acetone are similarly colored, but give a broader band at 3235 cm^{-1}. In both the dimorphs, the absorption maxima are located at 515 nm.

The 2,4-dimethyl derivative, as prepared in boiling ethanol, was found to be a mixture of two forms. The reddish brown form isolated by recrystallization from ethanol shows a sharp vibrational band at 3305 cm^{-1}. The color turns reddish violet upon vacuum sublimation, and the sharp band is replaced by a broad one appearing at 3250 cm^{-1}. The splitting of the carbonyl stretching vibrational band is observed only in the former form. The electronic absorption maximum is at 495 nm in the form obtained by recrystallization and at 505 nm in the form obtained by sublimation.

The *m*-ethoxy derivative is dimorphic; that is, the vibrational spectrum of the crystals as prepared in ethanol differs from that of the crystals obtained by vacuum sublimation or by recrystallization from ethanol. The former form gives a sharp band at 3325 cm^{-1}, and the latter, a broad one at 3240 cm^{-1}. The electronic spectra are essentially the same, both having a maximum at 500 nm.

Two forms distinctly differnt in color were isolated for the *m*-carboxy derivative. The crystals deposited from the reaction mixture are yellow or yellowish orange. Upon vacuum sublimation the color turned scarlet.

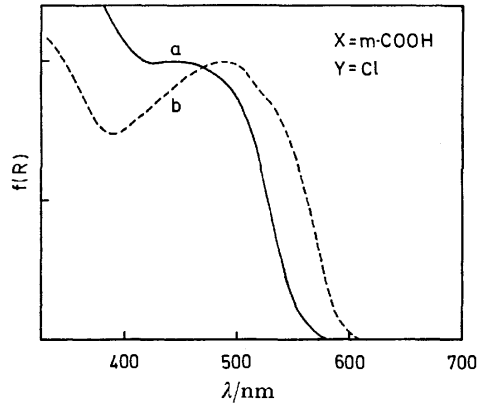

Fig. 3. Electronic spectra of 2-(*m*-carboxyanilino)-3-chloro-1,4-naphthoquinone: (a) the yellow form and (b) the scarlet form.

Although Buu-Hoi carried out his preparation in the same solvent, the color he described seems to be in agreement with the latter.[9] The former form shows a sharp vibrational band at 3340 cm^{-1}, and the latter, a broad one at 3275 cm^{-1}. The electronic spectra of these dimorphs are presented in Fig. 3. The maxima are located at 450 and 490 nm respectively. In addition, the scarlet form gives a shoulder at 525 nm. Both a sharp vibrational band at 3325 cm^{-1} and a broad one at 3225 cm^{-1} were observed with the *p*-propyl derivative, suggesting the existence of two forms. Unfortunately, we could not separate them.

Only one form each was obtained for the seventeen other derivatives examined. Among them, the following six derivatives give sharp vibrational bands near 3300 cm^{-1}: X=2,3-Me_2 (3295 cm^{-1}), 2,4,5-Me_3 (3290), *o*-MeO (3340), *o*-EtO (3320), *o*-COOH (3300), and *p*-COOH (3300). Broad bands are observable with the following eleven, including the unsubstituted compound: X=H (3245 cm^{-1}), *o*-Me (3240), *p*-Me (3220), 2,4-Me_2 (3225), 3,4-Me_2 (3250), *m*-MeO (3220), *p*-MeO (3245), *p*-EtO (3235), *m*-Cl (3225), *p*-Cl (3230), and *p*-I (3260). In this series, not only the halo derivatives, but also some alkyl and alkoxy derivatives, are classified into the second group. Therefore, it is apparent that the form with a broad vibrational band near 3200 cm^{-1} favors the substitution with the chlorine atom at the 3 position of the naphthoquinone. When the X derivative with Y=H belongs to the first group and the corresponding derivative with Y=Cl belongs to the second group, it is likely that the effect of the X substituent is nearly matched by the effect of the Y substituent. Assuming that the chance of finding dimorphs is high with these two derivatives, they were particularly carefully examined.

2-Anilino-3-bromo-1,4-naphthoquinones (Y=Br). With the *p*-ethyl, 2,3-dimethyl, 3,4-dimethyl, and *o*-ethoxy derivatives, dimorphic forms could be isolated. A broad vibrational band appearing at 3240 cm^{-1} was observed with the crystals of the *p*-ethyl derivative as prepared in boiling ethanol and also with those recrys-

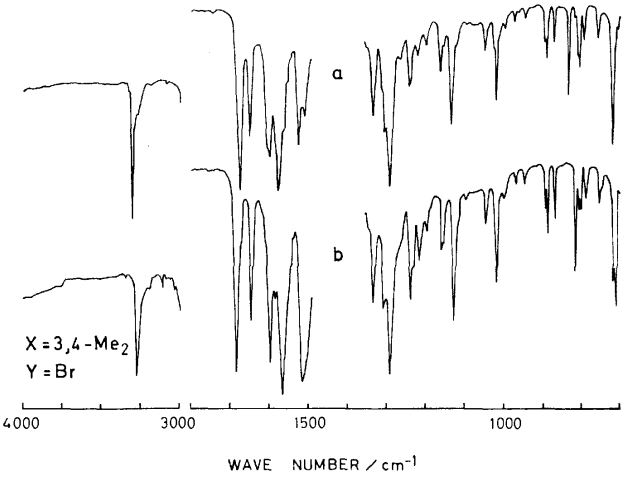

Fig. 4. Vibrational spectra of 2-(3,4-dimethylanilino)-3-bromo-1,4-naphthoquinone: (a) the form deposited from the reaction mixture and (b) the form isolated by recrystallization from aqueous ethanol.

tallized from the same solvent. By adding water to the cold solution and then letting stand the mixture overnight, crystals showing a sharper band at 3275 cm^{-1} were deposited. In the electronic spectra, the maximum is at 510 nm in the former form and shifts to 495 nm in the latter.

The difference in the vibrational spectrum is small in the dimorphic forms of the dimethyl derivatives, as is exemplified by the 3,4-derivative shown in Fig. 4. The reaction products show a band at 3280 cm^{-1} in both cases. A sharp band appears at 3305 cm^{-1} upon the vacuum sublimation of the 2,3-derivative. The crystals deposited from the reaction mixture show an electronic absorption maximum at 505 nm, while the crystals obtained by sublimation show a maximum at 485 nm. On the other hand, the form showing a sharp band at 3310 cm^{-1} was isolated by recrystallization from aqueous ethanol in the case of the 3,4-derivative. The maximum in the electronic spectrum is at 505 nm for both of the dimorphs.

The two forms for the *o*-ethoxy derivative do not differ much from each other in the vibrational spectrum; that is, the crystals deposited from the reaction mixture exhibit a sharp band at 3340 cm^{-1}, while the crystals obtained by sublimation in a vacuum or by recrystallization from benzene show a sharp band at 3325 cm^{-1}. The absorption maximum in the electronic spectrum is at 515 nm in the former form and at 530 nm in the latter. Nevertheless, the two spectra can be almost superposed on each other.

The presence of dimorphic forms was noted for the *m*- and *p*-methyl derivatives, but they could not be separated. A sharp band was observed at 3325 cm^{-1} with the crystals of the former compound deposited from the reaction mixture, and also with those recrystallized from ethanol. Upon vacuum sublimation, an additional band appeared at 3225 cm^{-1}. On the other hand, the synthesis, recrystallization, and vacuum sublimation yielded the form showing a broad band at 3225 cm^{-1} for the latter. However, the appearance of an additional sharp band at 3335 cm^{-1} was noted when the crystals were deposited from a cold aqueous ethanolic solution.

The following six derivatives of the anilinobromonaphthoquinone are classified into the first group: X= *p*-Pr (3280 cm^{-1}), *o*-MeO (3355), *m*-EtO (3330), *m*-COOH (3280), *p*-COOH (3320), and 2,4,5-Me_3 (3295). The second group consists of X=H (3245 cm^{-1}), *o*-Me (3255), *m*-MeO (3225), *p*-MeO (3255), *p*-EtO (3250) 2,4-Me_2 (3265), and 2,5-Me_2 (3225). The halo derivatives expected to be members of this group were not included in this study, as the observation of dimorphism with them seemed to be very unlikely. It may be added that the locations are generally at higher wave numbers compared with those of the corresponding derivatives in the chloronaphthoquinone series.

To supplement the above results, we carried out spectral measurements of the condensation product between two moles of 2,3-dichloro-1,4-naphthoquinone and one mole of 3,3′-dimethoxybenzidine. The color of this particular compound has been reported to be red in hot xylene and to turn reddish violet upon cooling.[14] However, we could record no unusual temperature dependence with this system.

Discussion

In order to examine the relative stabilities of the possible tautomeric forms within the framework of the HMO method, we compared the bonding energies of the two forms of the unsubstituted anilinonaphthoquinone. This approach has been employed by Kuder as a criterion of the tautomeric stability of hydroxyarylazo compounds.[15] The bonding energy is given by the difference between the total π-electron energy and the energy of the π-electrons localized on atomic *p*-orbitals. The latter is defined by $\sum_{i=1}^{n} s_i\alpha_i$, where n is the number of atomic centers, s_i is the number of electrons contributed by the i atom to the π-electron system, and α_i is the Coulomb integral for the i atom. The tautomeric form with the larger bonding energy or bonding energy per electron may be considered to be more stable. The heteroatom parameters, h_x and k_{xy}, in the Coulomb and resonance integrals, $\alpha_x=\alpha+h_x\beta$ and $\beta_{xy}=k_{xy}\beta$, were the same as those used by Kuder, namely, $h_{NH}=1.50$, $h_O=1.00$, k_{C-N}(the bond to naphthoquinone)$=0.90$, k_{C-N}(the bond to phenyl group)$=0.70$, and $k_{C=O}=1.00$ for the *p*-quinonoid form and $h_N=0.50$, $h_O=1.00$, $h_{OH}=2.00$, $k_{C=N}=1.10$, $k_{C-N}=0.90$, $k_{C=O}=1.00$, and $k_{C-O}=0.80$ for the *o*-quinonoid form. The effect of an intramolecular hydrogen bond, O···H–N, was also considered by taking the following parameters: $\alpha'_{NH}=\alpha_{NH}-0.20\beta$, $\alpha'_{O-H}=\alpha_O+0.20\beta$, $\beta_{O-H-N}=0.20\beta$. The bonding energies computed in terms of the carbon-carbon resonance integral, β, are shown below:

	p-Quinonoid	*o*-Quinonoid
No hydrogen bond	24.851	24.823
With a hydrogen bond	24.967	—

Consequently, the *p*-quinonoid form appears to be more stable than the *o*-quinonoid form, regardless of the hydrogen bond. It has been argued by Kuder that a difference in bonding energy per electron in excess of 0.002β leads to the presence of only one tautomer. This criterion suggests that only the *p*-quinonoid form of the anilinonaphthoquinone will be seen if the hydrogen bond is formed.

The above-mentioned situation may be affected, to some extent, by the introduction of a substituent on the phenyl group. However, our observations cannot be correlated with the nature of the substituents. Not only the derivative with an electron-withdrawing group, but also the one with an electron-donating group on the same position were found to be dimorphic: *e.g.*, X= *p*-COOH and *p*-MeO with Y=H and X=*m*-COOH, *m*-EtO, and *m*-Me with Y=Cl. Furthermore, the electronic spectrum not being sensitive to the nature of solvents and its small temperature-dependence seem to be inconsistent with the presence of a tautomeric equilibrium in solutions. The molar absorption coefficient of the band in the visible region is in the range from 2600 to 5400, depending mainly upon the kind and position of the X substituent. This absorption may be attributed to an intramolecular charge-transfer transi-

tion. The difference in vibrational spectrum must, then, be due to a change in the molecular configuration. The change appears to be large in the case shown in Fig. 1 (X=*p*-COOH, Y=H) and small in the case shown in Fig. 4 (X=3,4-Me_2, Y=Br). In other cases, the difference varies between these extremes. The band appearing in the region from 3150 to 3350 cm^{-1} can now be definitely assigned to the N–H stretching vibration. The shift implies that the strength of the hydrogen bond varies with the configuration. As the mode of stacking is governed by the molecular configuration, the difference in color between dimorphic forms may be attributed largely to changes in the location and the intensity of the intermolecular charge-transfer absorption between the electron-donating moiety of a molecule and the accepting moiety of the neighboring molecule.

References

1) T. Zincke, *Ber.*, **12**, 1641 (1879).
2) R. T. Plimpton, *J. Chem. Soc.*, **37**, 633 (1880).
3) C. Baltzer, *Ber.*, **14**, 1899 (1881).
4) A. Plagemann, *Ber.*, **15**, 484 (1882).
5) L. Elsbach, *Ber*, **15**, 685 (1882).
6) R. Pummerer and K. Brass, *Ber*,. **44**, 1647 (1911).
7) R. Hauschka, *J. Prakt. Chem.* (*2*), **90**, 447 (1914).
8) E. Grossmann, *J. Prakt. Chem.* (*2*), **92**, 370 (1915).
9) N. P. Buu-Hoi, *Bull. Soc. Chim. Fr.*, **11**, 578 (1944).
10) S. M. Bloom and G. O. Dudek, *J. Org. Chem.*, **36**, 235 (1971).
11) J. Aihara, G. Kushibiki, and Y. Matsunaga, *Bull. Chem. Soc. Jpn.*, **46**, 3584 (1973).
12) O. Miller, *Ber.*, **17**, 356 (1884).
13) J. Kordes, P. Avouris, and M. A. El-Bayoumi, *J. Phys. Chem.*, **79**, 2420 (1975).
14) K. Brass and O. Papp, *Ber.*, **53**, 446 (1920).
15) J. E. Kuder, *Tetrahedron*, **28**, 1973 (1972).

Threshold Switching in Anthracene Thin Films

Yoshihiko SADAOKA, Yoshiro SAKAI, and Kohhei KISHI

Department of Industrial Chemistry, Faculty of Engineering, Ehime University, Matsuyama 790

(Received February 23, 1977)

Threshold switching was observed in anthracene thin films (<3 μm) using a circuit with a high protective resistance. On the other hand, when the protective resistance was small, the switching was erratic and irreproducible. In the latter case, the switching was occasionally accompanied by filamentary damages caused by the excess current focused at the electrically weak spots, and the threshold voltage was poorly dependent on the protective resistance. The threshold-switching characteristics for thin films are interpretable in terms of the transition from the trap-limited SCLC to the trap-filled SCLC. The thermal breakdown model is not adaptable.

In general, switching phenomena may be classified into two categories: memory and threshold switching. The threshold switching has no memory effect, and a *turn-off* can be achieved below the critical voltage, called the holding voltage. This type of switching has been observed in several organic thin films.[1,2] On the other hand, many authors[3-5] have reported memory-switching characteristics which arise from the formation of a metallic filament or a carbonized conducting channel. However, our understanding is still incomplete.

The purpose of this study is to report that a non-destructive switching in anthracence can be observed by means of circuit with an appropriate protective resistor and to discuss the mechanism of the switching.

Experimental

Pure anthracene was prepared by a method similar to that described by Nakada[6] and was then further purified by zone melting. The geometry of the cell was of the sandwich type, where anthracene was deposited on a glass substrate with an evaporated silver electrode through an etched stainless steel mask. The temperature of the substrate was controlled in the range from −70 to −50 °C.

The film thickness of anthracene was varied in the range of 5×10^{-6}—1.0×10^{-3} cm. The thickness was measured with the aid of an interferometer when the films were thin, while for the thicker films an ac bridge was used. Silver was deposited as the upper electrode by vacuum evaporation through the mask. The area of the electrode was *ca.* 0.01 cm².

The *I-V* characteristics were observed by means of the circuit described in a previous paper.[7] The protective resistor in the circuit can be varied in the range of 10^3—10^8 Ω in order to control the current which flows in the sample.

The states of the sample before and after the switching were observed using a scanning-electron microscope and an optical microscope.

Results and Discussion

Initially the anthracene film has a very high resistance, but when a certain value of voltage (threshold voltage, V_{th}) is applied, the current increases drastically; simultaneously, the voltage applied to the sample descreases and a new high conductivity state is formed. Figure 1 shows the relationship between the protective resistance, R_p, and the resistance, R_A, at the high conductivity state formed by applying the threshold voltage. It may be observed that the value of R_A increases with the protective resistance; consequently, non-linear current-voltage characteristics can be predicted in the high conductivity state.

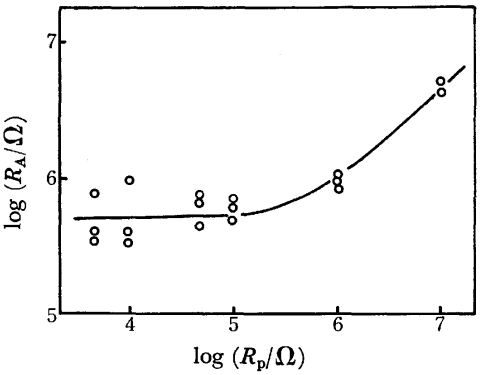

Fig. 1. Relationship between R_p and R_A.

More than 500 thin films were used for the current-voltage-characteristic measurements. When N_s and N represent respectively the total number of cells used in the measurements for a given protective resistor and the number of the cells with which the threshold switching without any structural changes were observed, the ratio of N/N_s increases with the value of the protective resistor, while the value of V_{th} is poorly dependent on the value of the protective resistor. Erratic and irreproducible switching characteristics, accompanied by structural changes, were occasionally observed. In these cases a stable high conductivity state with a memory effect was observed. The results of a scanning-electron-microscopic inspection of the cell after the erratic memory switching are shown in Fig. 2. The transformed area may be formed by the localized excessive current flow at the weak spots in the film.

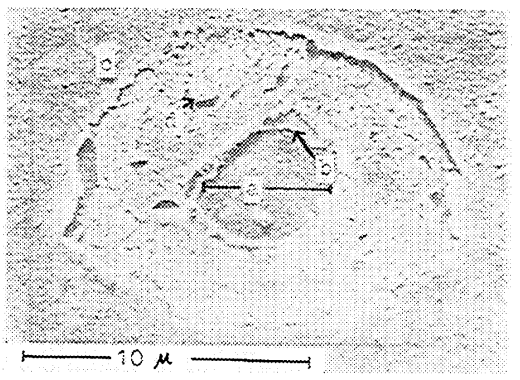

Fig. 2. Scanning electron microscopic view of the film.
a) Center void, b) lower electrode, c) upper electrode, d) anthracene.

The current-voltage relation in single crystals of anthracene, expressed as $I \propto V^n$, where $n>2$ in the high-field region, has been explained on the assumption that current carriers are trapped by the local states exponentially distributed within an energy region; the reduction of the value of n with the density of the trapping centers has previously been reported by Thomas *et al.*[8] On the other hand, Williams *et al.*[9] interpreted the precipitous transition from the ohmic region to the cubic region for the carbon fiber diode in terms of the trap-filled-limit.

Since, in this work, it is confirmed that the current obeys the scaling law in the preswitching state (Figs. 3 and 4), the current-voltage relation obtained in the high-field region may be expressed as:

$$J_{off} \propto \frac{V^{l+1}}{d^{2l+1}} \exp(-\phi/kT), \quad (1)$$

where J_{off} is the current density in the preswitching state; d the film thickness: ϕ, the activation energy; k, the Boltzmann constant, T, the temperature, and l, the constant. The averaged value of l was, from the results shown in Figs. 3 and 4, estimated to be 1. This behavior can be interpreted in terms of the space-charge-limited current in an insulator with a single type of traps.

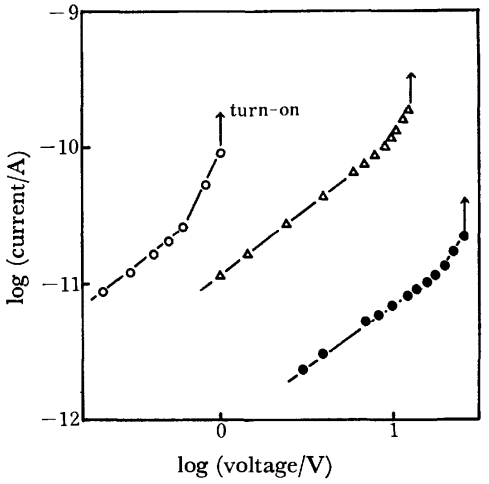

Fig. 3. Current-voltage characteristics in the *off state* for three different thickness.
○) 0.34 μm, △) 0.64 μm, ●) 0.99 μm.

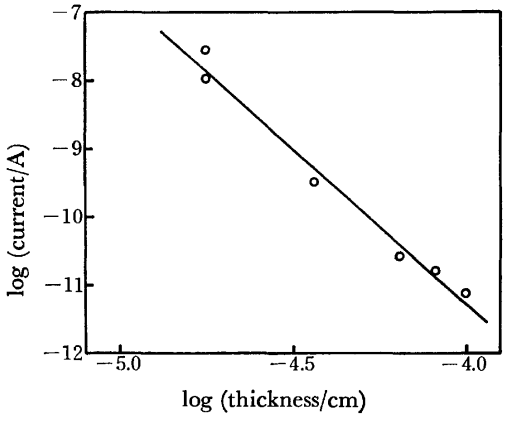

Fig. 4. Relation between the current and the film thickness in the *off state*.

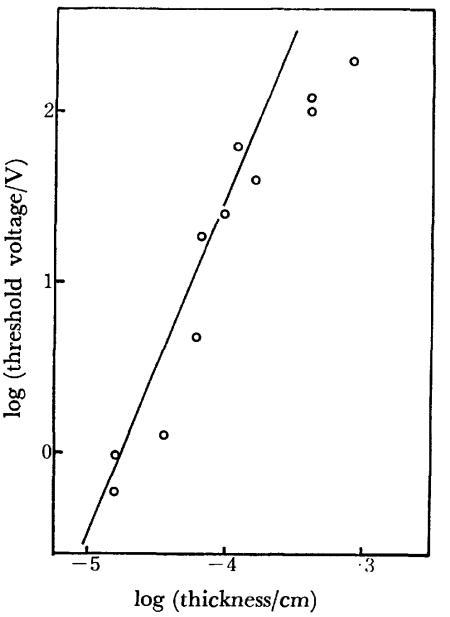

Fig. 5. Relation between the threshold voltage and the film thickness.
Solid line; $V_{th} \propto d^2$.

It is well known that the causes of switching and/or breakdown proposed by many authors can be classified into two categories; (1) the thermal effect and (2) the electronic effect. In order to determine which of these effects is the cause of the switching in the case of anthracene, the relation between the threshold voltage, V_{th}, and the film thickness, d, was observed. The results are plotted in Fig. 5. This figure shows that V_{th} is proportional to d^2.

In the thermal-breakdown model, the temperature of the film may be expected to be uniform for a thin film, so the switching conditions can be determined by the use of Eqs. 2, 3 and 4. These equations are induced by assuming that the thermal breakdown occurs when the temperature derivative of the power input exceeds that of the heat loss:[10]

$$J \cdot V = \lambda(T - T_0), \quad (2)$$

$$\partial(J \cdot V)/\partial T = \lambda, \quad (3)$$

$$J_c \cdot V_c = \lambda(T_c - T_0), \quad (4)$$

where λ is a constant external thermal conductivity; T_0, the ambient temperature; J_c, the current density at the critical temperature (T_0), and V_c, the breakdown voltage. The substitution of the current density in Eq. 1 into Eqs. 2, 3, 4 and subsequent rearrangement give:

$$V_c^{l+1} \propto d^{2l+1}. \quad (5)$$

However, the experimental results shown in Fig. 5 do not agree with this equation, unless $l=\infty$. Therefore, the possibility of the thermal breakdown was excluded.

On the other hand, the space-charge-limited-current (SCLC) in the preswitching state has been taken into consideration in some electronic models.[11,12] In these models, the *turn-on* can be achieved when the space-charge density in the film reaches a critical value. In this case, the relationship between the threshold voltage

and the film thickness is given by:

$$V_{th} \propto d^2. \quad (6)$$

The experimental results agree well with this expected relation deduced from the electronic model. Furthermore, the trap density, N_t, was estimated to be 10^{15}—10^{16} cm^{-3} by assuming that the *turn-on* condition is equivalent to the transition condition from the trap limited space-charge-limited current (SCLC) to the trap-filled SCLC. In this case, V_{th} is expressed as:

$$V_{th} = ed^2N_t/2\varepsilon\varepsilon_0. \quad (7)$$

The trap density thus obtained is comparable to the value, $(3-7)\times10^{13}$ cm^{-3}, obtained by Garrett *et al.*,[13] and to that 10^{13}—10^{19} cm^{-3}, obtained by Thomas *et al.*[8]

On other hand, a typical current-voltage relationship in the high-conductivity state is shown in Fig. 6. The square law holds in the high-field region, while in the low-field region the current is lower than the value estimated by extrapolation from the high-field region on the assumptions that the current obeys the square law and that this deviation from the square law increases with a decrease in the applied voltage. The *turn-off* can be achieved when the applied voltage decreases below *ca.* 1 volt. In the square law region, it was found that the current is proportional to d^{-3}. Therefore, the current density, J_{on}, in the high-conductivity state is expressed by the scaling law, l being 1:

$$J_{on} = \alpha \cdot V^2/d^3, \quad (8)$$

where α is a constant. It was confirmed by the analysis* of an equivalent circuit that the observed R_A is proportional to $R_p^{1/2}$ when a high protective resistance is used in the measurement circuit, whereas R_A is poorly dependent on R_p when a low protective resistance is used. These analytical results are in good agreement with the observed data plotted in Fig. 2.

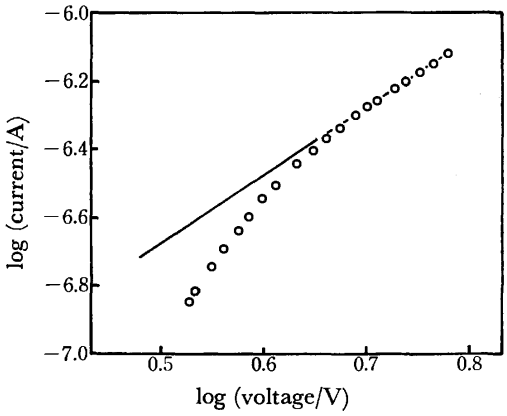

Fig. 6. Current-voltage characteristic in the *on state* solid line; $I \propto V^2$.

* Since the resistance in the preswitching state is much larger than that of the protective resistance, V_{th} is approximately equal to the total applied voltage. When the *turn-on* occurs, the voltage applied to the cell is equal to $V_{th}\cdot R_A/(R_A+R_P)$.

From the results thus obtained, it may be concluded that the threshold switching observed in thinner films is based on the transition from the trap-limited SCLC to the trap-filled SCLC, without any structural changes.

For thicker films (>3 μm), no reproducible threshold switching was observed. In these films, an instantaneous increase of current was observed when measurements were carried out using a circuit with a high protective resistor (10^8 Ω). On the other hand, a high-conductivity state with a memory effect was observed when a lower protective resistor was used. In this case, the relationship between V_{th} and the thickness is expressed as $V_{th} \propto d^n$, $0.5<n<1$; this relation can be introduced by the thermal-breakdown model (Eq. 5), while the current-voltage characteristics in the pre-breakdown region are expressed as $I \propto V^m$, ranging in value of m from 1 to 2 for these thicker samples.

It is well known[14,15] that the thickness dependence of V_{th} for the thick films is different from that for the thin films and that the thermal breakdown occurs in thicker films, while in thinner films the switching caused by the electronic mechanism is predominant, especially for amorphous semiconductors. The results for thicker anthracene films reported in this paper are consistent with those obtained by Garrett *et al.*[13]

One of us (Y. Sadaoka) thanks the Sakkokai Foundation for a grant.

References

1) C. H. Culp, D. E. Echels, and P. H. Sidles, *J. Appl. Phys.*, **46**, 3658 (1975).
2) Y. Sadaoka and Y. Sakai, *Bull. Chem. Soc. Jpn.*, **49**, 325 (1976).
3) J. Kevorkian, M. M. Labes, D. C. Larson, and D. C. Wu, *Discuss. Faraday Soc.*, **51**, 139 (1971).
4) L. F. Pender and R. J. Fleming, *J. Appl. Phys.*, **46**, 3426 (1975).
5) W. P. Ballard and R. W. Christy, *J. Non-Cryst. Solids*, **17**, 81 (1975).
6) I. Nakada, *Kogyo Kagaku Zasshi*, **64**, 1218 (1961).
7) Y. Sadaoka and Y. Sakai, *J. Chem. Soc., Faraday Trans. 2*, **72**, 1911 (1976).
8) J. M. Thomas, J. O. Williams, and L. M. Turton, *Trans. Faraday Soc.*, **64**, 2405 (1968).
9) W. G. Williams, P. L. Spong, and D. J. Gibbons, *J. Phys. Chem. Solids*, **33**, 1879 (1972).
10) J. J. O'Dwyer, "Theory of Electrical Conduction and Breakdown in Solid Dielectrics," Clarendon Press, Oxford (1973), p. 182.
11) H. K. Henish, E. A. Fagen, and S. R. Ovshinsky, *J. Non-Cryst. Solids*, **4**, 538 (1970).
12) T. Shiraishi, T. Kurosu, and M. Iida, *Oyo Butsuri*, **46**, 36 (1977).
13) S. G. E. Garrett, R. Pethig, and V. Soni, *J. Chem. Soc., Faraday Trans. 2*, **70**, 1732 (1974).
14) H. Fritzsche, "Amorphous and Liquid Semiconductors," ed by J. Tauc, Plenum Press, London and New York (1974), p. 313.
15) B. T. Kolomiets, E. A. Lebedev, and I. A. Taksami, *Soviet Phys.-Semicond.*, **3**, 267 (1969).

Shock Tube Study of the H–D Exchange Reaction between Acetylene and Deuterium

Hiroo OGURA

Institute of Space and Aeronautical Science, Tokyo University, Komaba, Meguro-ku, Tokyo 153

(Received March 5, 1977)

H–D exchange reaction between acetylene and deuterium has been investigated in a single-pulse shock tube in the temperature range 1200—1500 K. Empirically, in the C_2HD appearance the order with respect to acetylene was 0.25 ± 0.09, and that with respect to deuterium 1.14 ± 0.15. The rate constant of 1.39 th order for the C_2HD increase was obtained as; $k(\mathrm{cm^{1.17}\ mol^{-0.39}\ s^{-1}})=(24.4\pm7.5)\times10^{11}\exp((-51200\pm2400)/RT)$. The isotopic distributions of acetylene and hydrogen as determined by mass spectrometry suggest that C_2D_2 and H_2 are formed by the subsequent reactions of C_2HD and HD, respectively. A free-radical chain mechanism initiated by the same bimolecular reaction of acetylene, *viz.* $2C_2H_2\rightarrow C_4H_3+H$, as in the pyrolysis and hydrogenation of acetylene was proposed. A steady-state treatment of the proposed mechanism shows that the empirical rate and concentration dependence of the C_2HD increase are in line with those of the steady-state rate.

The H–D exchange reaction between acetylene and deuterium has been studied by several investigators. Shock tube techniques were employed in all the experimental studies.

Kuratani and Bauer[1] derived empirical power rate formulas by the analysis of the infrared emission profiles of C_2H_2 and C_2HD, and proposed that C_2HD and C_2D_2 were produced from the same molecular complex $C_2H_2D_2$*. Besides, Bauer *et al.*[2–4] discussed the structure and thermodynamic property of $C_2H_2D_2$*.

Gay *et al.*[5] studied the pyrolysis of acetylene combining a shock tube with a TOF mass spectrometer and found C_4H_3 radical. They proposed a radical mechanism for the isotopic exchange reaction between C_2H_2 and C_2D_2, suggesting that this might be the case for the H–D exchange reaction between C_2H_2 and D_2.

Benson and Haugen[6] proposed a free-radical chain mechanism by the analysis of both kinetic and thermodynamic data available. By a single-pulse shock tube Skinner *et al.*[7] studied the reaction of the C_2H_2–D_2 system in the temperature range 1069—1280 K. They found that the amount of C_2D_2 was less than one half of C_2HD amount, C_2H_3D being the most abundant among ethylene isomers. From these observations, they supported the radical chain mechanism postulated by Benson and Haugen, but did not execute the quantitative analysis of kinetic date obtained.

The pyrolysis and hydrogenation of acetylene proceed *via* the free-radical chain mechanism initiated by the same bimolecular reaction of acetylene; $2C_2H_2\rightarrow C_4H_3+H$, C_4H_3 radical being responsible for the formation of 1-buten-3-yne and H atom for the production of ethylene.[8] On the other hand, the H atom could also lead to the H–D exchange reaction between acetylene and deuterium in the C_2H_2–D_2 system. As in the pyrolysis and hydrogenation of acetylene, the H–D exchange between acetylene and deuterium would occur by a free-radical chain mechanism. The study of the H–D exchange reaction in the C_2H_2–D_2 system could provide another test for the mechanism of hydrogenation of acetylene.

Experimental

Apparatus and Procedure. The H–D exchange reaction between acetylene and deuterium was investigated in a 4-cm single-pulse shock tube. A full description of the shock tube and the details of operation have been given previously.[8,9]

Shock tube was evacuated to below 1×10^{-4} Torr before each run, leak and outgassing rate being *ca.* 6×10^{-5} Torr/min. Prior to the opening of the tube for the renewal of the diaphram, the entire tube was pressurized with helium above the atmospheric pressure to avoid the exposure of the tube to the air. The shocks were fired within five minutes after the introduction of sample gases. Helium was used as the driver gas.

Materials. Three mixtures with the composition of $C_2H_2/D_2/Ar=10/10/80$; 5/10/85; and 10/5/85 were prepared in a 5-l glass vessel. The mixed gases were allowed to stand at a room temperature for about one day and analyzed by gas chromatography to check trace amount of oxygen prior to shock heating. All analyses showed that the oxygen in the sample mixtures was less than 10 ppm. The procedure of purification of acetylene, deuterium, and argon was identical with that in the pyrolysis and hydrogenation experiments.

Analytical. The isotopic distribution of acetylene was determined with a Hitachi Model RM-50 mass spectrometer. Details of the mass spectral analyses were described elsewhere. In some runs the isotopic distribution of hydrogen was determined at the same time. For this purpose, the bulb containing sample gas was condensed by liquid nitrogen, while the uncondensables were transferred into another evacuated bulb, which served for the measurement of the isotopic distribution of hydrogen. The removal of hydrocarbons by the procedure mentioned above could minimize the interference in the hydrogen peaks due to the fragmentation of the hydrocarbons. The relative intensity among the hydrogen isotopes was determined using an equilibrium mixture of hydrogen isotopes, which was prepared by platinum-black catalyzed reaction between H_2 and D_2.

Results

Three mixtures were subjected to shock heating in the temperature range 1000—1600 K, and then analyzed by mass spectrometry. The total densities behind the reflected shock waves were $(2.35\pm0.11)\times10^{-5}$ mol/cm^3, the average reaction time(dwell time) being *ca.* 800 μs in all runs.

Isotopic Distributions. Several shocks were fired with the mixture of 10% C_2H_2 and 10% D_2 in argon. The isotopic distribution of hydrogen together with that of acetylene was determined by mass spectrometry. The ionization potential was maintained at 50 eV for the

Table 1. Isotopic distributions of acetylene and hydrogen

T_5/K[a]	C_2H_2[b]	C_2HD	C_2D_2	D_2[b]	HD	H_2	τ/μs[c]
1271	0.946	0.051	0.003	0.954	0.044	0.002	920
1313	0.932	0.067	0.001	0.934	0.060	0.006	940
1388	0.894	0.102	0.004	0.888	0.095	0.017	930
1395	0.908	0.087	0.005	0.904	0.093	0.003	850
1396	0.886	0.110	0.004	0.882	0.111	0.006	890
1480	0.763	0.214	0.023	0.743	0.231	0.026	780

a) T_5 is the temperature behind the reflected shock wave. b) The total amounts of acetylene and hydrogen isomers are taken equal to 1.000 respectively. c) τ is the dwell time.

measurement of hydrogen isotope mass spectra, while at *ca.* 12 eV for that of acetylene isomers. The results of mass spectral analyses are summarized in Table 1.

As shown in Table 1, approximately equal amounts of C_2HD and HD, and those of C_2D_2 and H_2 are produced, the yields of the latter being much less than one half of the former.

Rate of H–D Exchange Reaction. The relative amounts of acetylene isomers were determined throughout all runs. In this case the ionization potential was kept at 50 eV. The rates of C_2HD and C_2D_2 appearance were derived from the relative amounts of acetylene isomers, neglecting the decrease of the total acetylene concentrations due to the pyrolysis and hydrogenation of acetylene occurring simultaneously with the H–D exchange reaction. The rates were defined as $[C_2HD]/\tau$ and $[C_2D_2]/\tau$, where τ is the dwell time. The rates at temperatures below 1200 K were too slow to allow a quantitative analysis and were ruled out The rates of the H–D exchange reaction of acetylene are shown in Fig. 1 in the case of the mixture of $C_2H_2/D_2/Ar=5/10/85$. The rates of C_2HD appearance increase linearly with temperature at temperatures below 1400 K, while they deviate from a linear line at temperatures above 1400 K. The ratio of $[C_2D_2]/[C_2HD]$ is dependent on temperature. This indicates that the formation of C_2D_2 by the subsequent reaction of C_2HD and the reverse reaction of C_2HD to reform C_2H_2 cannot be neglected at temperatures above 1400 K for the mixture of $C_2H_2/D_2/Ar=5/10/85$.

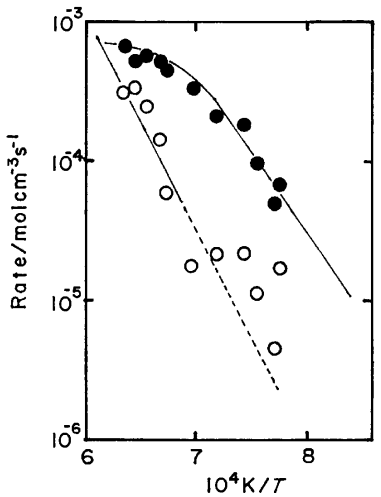

Fig. 1. Rates of the C_2HD and C_2D_2 increase in the case of the mixture of $C_2H_2/D_2/Ar=5/10/85$.
●; C_2HD increase, ○; C_2D_2 increase.

Table 2. Isotopic distribution of acetylene as determined with ionization potential of 50 eV

T_5/K[a]	C_2H_2[b]	C_2HD	C_2D_2	τ/μs[c]	$C_2H_2/D_2/Ar$[d]
1371	0.896	0.093	0.011	780	10/10/80
1380	0.900	0.091	0.009	810	10/10/80
1386	0.854	0.133	0.013	910	10/10/80
1473	0.701	0.259	0.040	770	10/10/80
1480	0.690	0.274	0.036	700	10/10/80

a) T_5 is the temperature behind the reflected shock wave. b) The total amount of acetylene is normalized to be 1.000. c) τ is the dwell time. d) The composition of the mixture.

The rates of C_2D_2 increase scatter considerably at lower temperatures. Some of the results of the relative yields of acetylene isomers for the mixture of $C_2H_2/D_2/Ar=10/10/80$, as determined at an ionization potential of 50 eV, are presented in Table 2. Apparent greater C_2D_2 abundance in Table 2 may result from the contamination of nitrogen, since at the lower ionization potential of 12 eV the fragmentation of nitrogen can be neglected(Table 1). However, the relative yields of C_2HD seem little affected by the ionization potential employed. Thus the kinetic analysis of the data obtained was made only for the rates of C_2HD increase.

The rates of C_2HD appearance obtained from the three shock heated mixtures are shown in Fig. 2. We see that the rates of C_2HD formation are strongly dependent on deuterium and slightly dependent on acetylene concentration.

In the above definition of rate, the rates of C_2HD increase are well defined only when the successive exchange of C_2HD to C_2D_2 (alternatively C_2H_2) is negligibly slow. The rates of C_2D_2 formation were less than one tenth of those of C_2HD increase in the temperature range up to 1500 K in the mixtures of $C_2H_2/D_2/Ar=10/10/80$ and $10/5/85$ and up to 1400 K for the mixture of $C_2H_2/D_2/Ar=5/10/85$.

An empirical power rate formula was derived by the least-squares method in the temperature range mentioned above, where the rates of C_2HD formation increase monotonically with temperature and successive exchange of C_2HD is negligibly slow:

$$d[C_2HD]/dt = k_1[C_2H_2]^{0.25\pm0.09}[D_2]^{1.14\pm0.15}, \quad (1)$$

$$k_1 = (24.4\pm7.5)\times10^{11}\exp((-51200\pm2400)/RT), \quad (2)$$

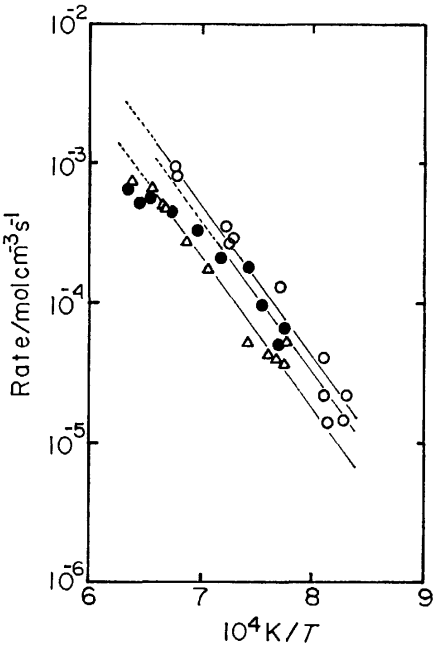

Fig. 2. Concentration dependence of the C_2HD increase.
○; $C_2H_2/D_2/Ar=10/10/80$, ●; $C_2H_2/D_2/Ar=5/10/85$,
△; $C_2H_2/D_2/Ar=10/5/85$.

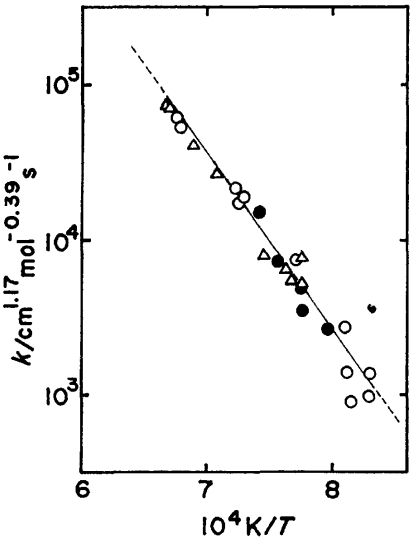

Fig. 3. Arrhenius plot of 1.39th order rate constants for the C_2HD appearance.
○; $C_2H_2/D_2/Ar=10/10/80$, ●; $C_2H_2/D_2/Ar=5/10/85$,
△; $C_2H_2/D_2/Ar=10/5/85$.

where $d[C_2HD]/dt$ and k_1 are expressed in mol cm^{-3} s^{-1} and cm$^{1.17}$ mol$^{-0.39}$ s^{-1}, respectively, the activation energy being given in cal/mol. The errors denote the standard deviation of the least-squares method. The Arrhenius plots of the 1.39 th order rate constants are shown in Fig. 3.

Discussion

Mechanism of H–D Exchange Reaction. The isotopic distributions of acetylene and hydrogen(Table 1) are in line with those obtained by Skinner *et al.*,[7] who supported a free-radical chain mechanism. The very low ratios of $[C_2D_2]/[C_2HD]$ and $[H_2]/[HD]$, and the dependence of the former on temperature suggest that C_2D_2 and H_2 are produced successively by the reactions of C_2HD and HD, respectively.

Under the present experimental conditions, the H–D exchange reaction occurs simultaneously with the pyrolysis and hydrogenation of acetylene, the pyrolysis being predominant. The initiation step of the pyrolysis becomes an important source of radicals. The most probable free-radical chain mechanism for the H–D exchange reaction is outlined as follows:

$$2C_2H_2 \longrightarrow C_4H_3 + H, \quad (3)$$
$$H + D_2 \longrightarrow HD + D, \quad (4)$$
$$D + C_2H_2 \longrightarrow C_2HD + H, \quad (5)$$
$$H + HD \longrightarrow H_2 + D, \quad (6)$$
$$D + C_2HD \longrightarrow C_2D_2 + H. \quad (7)$$

The H and D atoms present in the system concurrently participate in the formation of ethylenes:

$$H + C_2H_2 \longrightarrow C_2H_3, \quad (8)$$
$$D + C_2H_2 \longrightarrow C_2H_2D, \quad (9)$$
$$C_2H_3 + D_2 \longrightarrow C_2H_3D + D, \quad (10)$$
$$C_2H_2D + D_2 \longrightarrow C_2H_2D_2 + D. \quad (11)$$

The termination occurs by the recombination or disproportionation reactions of the two vinyl radicals or by those of vinyl radicals with H or D atom.

A molecular complex mechanism was proposed by Kuratani and Bauer, which was essentially expressed as;

$$C_2H_2 + D_2 \longrightarrow C_2H_2 : D_2 \longrightarrow C_2H_2D_2^*, \quad (12)$$

where $C_2H_2 : D_2$ and $C_2H_2D_2^*$ were suggested to be the carbene and excited ethylene with V_d symmetry, respectively. In their scheme the $C_2H_2D_2^*$ rotates around the C=C bond to $C_2HD : HD$ or $C_2D_2 : H_2$ (alternatively $C_2H_2 : D_2$), and then decompose to C_2HD or C_2D_2. Accordingly, the ratios of $[C_2D_2]/[C_2HD]$ and $[H_2]/[HD]$ would be *ca.* 0.5 and would be substantially independent of temperature. These predictions from the molecular complex mechanism disagree with the observed isotopic distributions.[10]

Steady-state Rate. In the proposed mechanism the successive exchange reactions of C_2HD and HD and the backward reactions except for Reactions 8 and 9 can be neglected in the early stage of the exchange reaction, since the reaction times were extremely short, the yields of C_2D_2 and H_2 being far less than those of C_2HD and HD in the temperature range defined above. Reactions 9 and 11 can be also neglected, since C_2H_3D was the most predominant species among ethylene isomers.[8]

It is well known that the addition of H atom to acetylene yields vibrationally excited vinyl radical with subsequent dissociation to initial reactants or collisional stabilization to form thermal vinyl radical;[11–14]

$$H + C_2H_2 \longrightarrow C_2H_3^*, \quad (13)$$
$$C_2H_3^* \longrightarrow H + C_2H_2, \quad (14)$$
$$C_2H_3^* \xrightarrow{(+M)} C_2H_3, \quad (15)$$

where $C_2H_3^*$ and M are vibrationally excited vinyl

radical and a third body, respectively. Reactions 13—15 overall reduce to

$$H + C_2H_2 \rightleftharpoons C_2H_3, \quad (8')$$

where the reverse reaction is included, since C_2H_3D was formed in a considerable amount. In the case of the addition of D atom to C_2H_2, the above processes become as follows:[12,14]

$$D + C_2H_2 \longrightarrow C_2H_2D^*, \quad (16)$$

$$C_2H_2D^* \longrightarrow D + C_2H_2, \quad (17)$$

$$C_2H_2D^* \longrightarrow H + C_2HD, \quad (18)$$

$$C_2H_2D^* \xrightarrow{(+M)} C_2H_2D. \quad (19)$$

Practically, these steps reduce to Reactions 5 and 9. The reverse Reaction 9 can be neglected, for the yield of $C_2H_2D_2$ was small relative to C_2H_3D yield. Reactions 8 and 9 involve thermalized vinyl radicals, while in Reaction 5 the dissociation of the "hot" vinyl radical is significant. The formation of thermal vinyl radical from "hot" vinyl radical under our experimental conditions is estimated to be slow compared with exchange.[6]

As in the hydrogenation of acetylene, the termination reaction of H atom with C_2H_3 radical is insignificant, since the concentration of H atom is much lower than that of C_2H_3 radical. The simplified free-radical chain mechanism for the C_2HD(HD) appearance is thus represented as:

$$2C_2H_2 \longrightarrow C_4H_3 + H, \quad (3)$$

$$H + D_2 \longrightarrow HD + D, \quad (4)$$

$$D + C_2H_2 \longrightarrow C_2HD + H, \quad (5)$$

$$H + C_2H_2 \rightleftharpoons C_2H_3, \quad (8')$$

$$C_2H_3 + D_2 \longrightarrow C_2H_3D + D, \quad (10)$$

$$2C_2H_3 \longrightarrow C_4H_6. \quad (20)$$

For the termination, only the recombination reaction of two vinyl radicals is taken into account.

The steady-state assumption is applied to the simplified mechanism. The steady-state concentrations of H, D, and C_2H_3 radical are given by the following equations;

$$[C_2H_3]_{ss} = (k_3/2k_{20})^{1/2}[C_2H_2] = k_{21}[C_2H_2], \quad (21)$$

$$[H]_{ss} = (1/k_{8'})(k_3[C_2H_2] + k_{-8'}k_{21} + k_{10}k_{21}[D_2]), \quad (22)$$

$$[D]_{ss} = (1/k_5[C_2H_2])(k_4[H]_{ss}[D_2] + k_{10}[C_2H_3]_{ss}[D_2]), \quad (23)$$

where $k_{21}=(k_3/2k_{20})^{1/2}$. Rearranging Eq. 23, the following relation is derived:

$$d[C_2HD]/dt = d[HD]/dt + d[C_2H_3D]/dt \quad (23')$$

The rate of C_2H_3D formation is slower than that of HD increase. The rate of HD increase is approximately equal to that of C_2HD appearance, which is consistant with the observed isotopic distributions (Table 1). Thus the steady-state rate for C_2HD increase is given by

$$d[C_2HD]/dt = d[HD]/dt = k_4[H]_{ss}[D_2]. \quad (23'')$$

Equation 23″, if reduced to a power dependence on concentrations, predicts order with respect to acetylene and deuterium of 0 to 1 and 1 to 2, respectively.

The rate constants used in the derivation of an apparent power rate formula for the C_2HD increase are listed in Table 3. The pressure dependent bimolecular rate constant of Reaction 8′ is uncertain. The rate constant is assumed to have the same activation energy as that in high pressure limit with a correction in frequency factor.[13] Assuming the same activation energy as that of the observed rate (Eq. 2), an apparent power rate formula for the C_2HD increase is given by

$$d[C_2HD]/dt(\text{mol cm}^{-3}\text{ s}^{-1}) = k_{24}[C_2H_2]^{0.31}[D_2]^{1.39}, \quad (24)$$

$$k_{24}(\text{cm}^{2.10}\text{ mol}^{-0.70}\text{ s}^{-1}) = 1.16\times10^{14}\exp(-51200/RT). \quad (25)$$

The absolute values of the steady-state rate agree with those of the empirical power rate (Eqs. 1 and 2) within the error limit of 40%, and the power dependence of the steady-state rate is in good agreement with the observed rate within the present experimental errors.

The empirical power rate expression for the increase of C_2HD obtained by Kuratani and Bauer in the temperature range 1300—1600 K is given by

$$d[C_2HD]/dt = ((k_\alpha+k_\beta)/2.64)[C_2H_2]^{0.24}[D_2]^{1.0}, \quad (26)$$

where,

$$k_\alpha(\text{cm}^{0.72}\text{ mol}^{-0.24}\text{ s}^{-1}) = 4.2\times10^8\exp(-33800/RT)$$

and

$$k_\beta(\text{cm}^{0.72}\text{ mol}^{-0.24}\text{ s}^{-1}) = 1.6\times10^8\exp(-29300/RT).$$

The dependence of the rates on the concentrations seems essentially the same between the two power rate expressions (Eqs. 1 and 26), in spite of the different definition of rate, that is, their rates are the initial rates, on the other hand, our rates are the mean rates during the reaction times. The absolute rates obtained by them and those of the present agree within a factor of 2.

The steady-state rate of C_2H_3D production is directly derived from Eq. 21;

$$d[C_2H_3D]/dt(\text{mol cm}^{-3}\text{ s}^{-1}) = k_{10}k_{21}[C_2H_2][D_2], \quad (27)$$

where,

$$k_{10}k_{21}(\text{cm}^3\text{ mol}^{-1}\text{ s}^{-1}) = 1.3\times10^{12}\exp(-36600/RT). \quad (28)$$

Table 3. The rate constants relating to the H-D exchange reaction and the formation reaction of ethylene

Reaction	Rate constant (s^{-1} or $cm^3\,mol^{-1}\,s^{-1}$)	Ref.	λ[a]
3	$3.5\times10^{13}\exp(-47400/RT)$	9	1.0
4	$6.5\times10^{13}\exp(-8560/RT)$	15	2.0
5	$3.1\times10^{13}\exp(-3700/RT)$	12	1.0
8′	$7.53\times10^{11}\exp(-2410/RT)$	13	1/7.2
−8′	$8.19\times10^{11}\exp(-50210/RT)$	b)	1/7.2
10	$5.39\times10^{11}\exp(-12900/RT)$	8	1.0
20	4.45×10^{12}	c)	1.0

a) λ is the correction factor for the frequency factor with the same activation energy as that given in the reference. b) This rate constant was calculated by the combination of the rate constant of Reaction 8′ with the equilibrium constant at 1300 K. c) The activation energy was assumed to be zero, and the frequency factor was calculated at 1300 K, taking the collision diameter of C_2H_3 radical as 4.23 Å.

Equation 27 indicates that as far as the rate of Reaction 8′ is fast enough to reach a steady-state concentration of C_2H_3 radical during the reaction time, the rates of Reactions 8′ and −8′ do not produce any change in the rate of ethylene formation together with the steady-state concentration of C_2H_3 radical (Eq. 21). However, the steady-state concentration of H(D) atom is affected by the rates of Reactions 8′ and by the rates of Reaction 8′ and its reverse reaction (Eq. 22). This indicates that the H–D exchange reaction is closely related to the C_2H_3 radical formation and ethylene formation. The following relation may hold well:[8]

$$[C_2H_3D]/[C_2H_2D_2] = (k_{10}/k_{11})([C_2H_3]/[C_2H_2D]) = (k_{8'}/k_9)([H]/[D]) = (k_5/k_4)([C_2H_2]/[D_2]). \quad (29)$$

In the above derivation, $k_{8'}=k_9$ and $d[HD]/dt \gg d[C_2H_3D]/dt$ are assumed. The ratios of $[C_2H_3D]/[C_2H_2D_2]$, observed and calculated from Eq. 29, are summarized in Table 4. The agreement between the observed and calculated appears considerably good. Therefore, the inclusion of H–D exchange propagation process into the ethylene formation scheme provides a reasonable explanation of the rate and isotopic distribution of ethylene.

TABLE 4. THE COMPARISON OF THE OBSERVED RATIO OF $[C_2H_3D]/[C_2H_2D_2]$ WITH THE CALCULATED VALUE

T_5/K[a]	$[C_2H_3D]/[C_2H_2D_2]$		γ[c]	$C_2H_2/D_2/Ar$[d]
	Obsd[b]	Calcd		
1271	5.86	2.90	2.02	10/10/80
1313	5.68	2.74	2.08	10/10/80
1388	3.86	2.49	1.55	10/10/80
1407	3.76	2.44	1.54	10/10/80
1480	1.89	2.25	0.84	10/10/80

a) T_5 is the temperature behind the reflected shock wave. b) Calculated value from Table 2 in Ref. 8. c) γ is the ratio of the observed value to the calculated one from Eq. 29. d) The composition of the mixture.

At temperatures above 1500 K, the formation of 1,3-butadiyne becomes comparable to that of ethylene or predominant. The butadiyne formation cannot be neglected in the H–D exchange reaction, since H atom is responsible simultaneously for the butadiyne formation:[9]

$$H + C_2H_2 \longrightarrow C_2H + H_2, \quad (30)$$

$$C_2H + C_2H_2 \longrightarrow C_4H_2 + H. \quad (31)$$

D atom present in the system can abstract H atom from acetylene molecule:

$$D + C_2H_2 \longrightarrow HD + C_2H, \quad (32)$$

$$C_2H + D_2 \longrightarrow C_2HD + D. \quad (33)$$

Reactions 32 and 33 construct a chain for the H–D exchange reaction between acetylene and deuterium. Furthermore, the yield of 1-buten-3-yne begins to decrease at temperatures around 1500 K, H atom being supposed to participate in the 1-buten-3-yne decrease. The validity of our mechanism should be limited to the temperature range where the formation of 1-buten-3-yne and ethylene is dominant and that of butadiyne is negligibly slow.

The author wishes to thank Professor Kenji Kuratani, Tokyo University, for his valuable advice and helpful discussions during the course of this study.

References

1) K. Kuratani and S. H. Bauer, *J. Am. Chem. Soc.*, **87**, 150 (1965).
2) S. H. Bauer and P. Jeffers, *J. Am. Chem. Soc.*, **87**, 3278 (1965).
3) S. H. Bauer, *Int. Symp. Combust.*, **11**, 759 (1966).
4) S. H. Bauer, P. Jeffers, and N. Zevos, *J. Phys. Chem.*, **71**, 4412 (1967).
5) I. D. Gay, R. D. Kern, G. B. Kistiakowsky, and H. Niki, *J. Chem. Phys.*, **45**, 2371 (1966).
6) S. W. Benson and G. R. Haugen, *J. Phys. Chem.*, **71**, 4404 (1967).
7) G. B. Skinner, R. C. Sweet, and S. K. Davis, *J. Phys. Chem.*, **75**, 1 (1971).
8) H. Ogura, *Bull. Chem. Soc. Jpn.*, **50**, 2051 (1977).
9) H. Ogura, *Bull. Chem. Soc. Jpn.*, **50**, 1044 (1977).
10) Bauer *et al.*[4] explained the observed low ratio of $[C_2D_2]/[C_2HD]$ by the accompanied self-exchange reaction between C_2H_2 and C_2D_2 such as; $C_2H_2+C_2D_2 \rightarrow 2C_2HD$. In our pyrolysis experiments of 5% equimolar mixture of C_2H_2 and C_2D_2, however, the mass spectrometric analysis of acetylene isomers showed that the amount converted into C_2HD was at most 10% of the initial acetylene concentration.[9]
11) K. Hoyermann, H. Gg. Wagner, and J. Wolfrum, *Ber. Bunsenges. Phys. Chem.*, **72**, 1004 (1968).
12) K. Hoyermann, H. Gg. Wagner, J. Wolfrum, and R. Zellner, *Ber. Bunsenges. Phys. Chem.*, **75**, 22 (1971).
13) W. A. Payne and L. J. Stief, *J. Chem. Phys.*, **64**, 1150 (1976). They obtained the high pressure limit of the rate constant for the $H+C_2H_2$ over the range 193 to 400 K, showing that with increasing temperature, the pressure effect becomes pronounced and the high pressure limit is reached at increasingly higher pressures. Therefore, over our extended temperatures the high pressure limit could not be reached at the present pressures. The correction factor is the average value by which the reduced power rate for the C_2HD appearance is compatible with the observed power dependence on the concentrations at 1350 K (the mean temperature studied).
14) D. G. Keil, K. P. Lynch, J. A. Cowfer, and L. V. Michael, *Int. J. Chem. Kinet.*, **8**, 825 (1976).
15) K. Schofield, *Planet. Space Sci.*, **15**, 643 (1967).

The Transition to Detonation from Deflagration in Ethylene–Oxygen Systems

Tadaaki INOMATA and Momotaro SUZUKI

Department of Chemistry, Faculty of Science and Technology, Sophia University, Chiyoda-ku, Tokyo 102

(Received March 8, 1977)

The flames of ethylene and oxygen mixtures (initial pressure, 50—500 mmHg, and ethylene content, 20—40%) were studied, especially for the transition to detonation from deflagration. The flames may roughly be divided into four groups: **A**, a flame without any shock wave generation; **B**, a flame with a shock wave generation; **C**, a flame with many shock waves and much turbulence of the flame, and finally **D**, the detonation produced by the collision of a flame and a reflected shock wave at the bottom of the tube. The flame transit to detonation from deflagration is a linear relation between the velocities of the flames at the point of detonation and DID, or the distance from the point of ignition to the detonation for all the sorts of flames given above, in spite of several apparent differences.

Since Berthelot and Vieille, and Le Chatelier and Mallard observed the propagation of detonation waves in 1881,[1] numerous works on the velocities of detonation waves, the theory of the transition to detonation, *etc.* have been published.[2] In the investigation of the transition to detonation, Payman and Titman observed the process using a streak schlieren photograph and discussed the mechanism of the onset of detonation.[3] Later, Bone *et al.* and White and Martin[4] investigated this process, while Oppenheim and his co-workers studied the transition processes in especial detail.[5] They used the stroboscopic schlieren system with a laser light and observed the mechanism of the transition to detonation in hydrogen–oxygen systems, classifying the process into the following four sections: 1) the explosion in the vicinity of a flame front, 2) the action of a shock wave formed at the lip of a flame, 3) the ignition at a shock front, and 4) the shock merging ahead of a flame.

In the present investigation, the processes of the transition to detonation in ethylene–oxygen systems were studied and the factors involved in this transition were fully discussed.

Experimental

The experiments were performed with C_2H_4–O_2 mixtures, at an initial pressure of 50—500 mmHg, in a square, 4×4 cm cross section and a 162 cm-long detonation tube, fitted on both sides with optically flat 4×30 cm glass windows.

The optical observations have been made by means of stroboscopic schlieren photographs. This observation was accomplished using 30 cm mirrors Z-type schlieren system, an argon stroboflash lamp, and a drum camera. The ignition was effected by means of a hot-wire glow coil.

Results and Discussion

In several mechanisms of the transition to detonation in flames, a detonation is generally produced by an explosion of the flame itself or is effected by means of a shock wave. In this study, four cases of transition to detonation were observed: **A**, without any shock wave generation; **B**, with a shock wave generation and a little distortion of a flame; **C**, with many shock waves, with much production of flame turbulences, and **D**, by the collision of a flame and a reflected shock wave at the bottom of the tube.

Figure 1 shows diagrams of the concentrations of the ethylene *versus* the pressures of the total gas mixture in a 162 cm-long tube. The regions between curves are the ranges where flames of Type **A**, **B**, **C**, and **D** are found; Type **A** is generated very exceptionally.

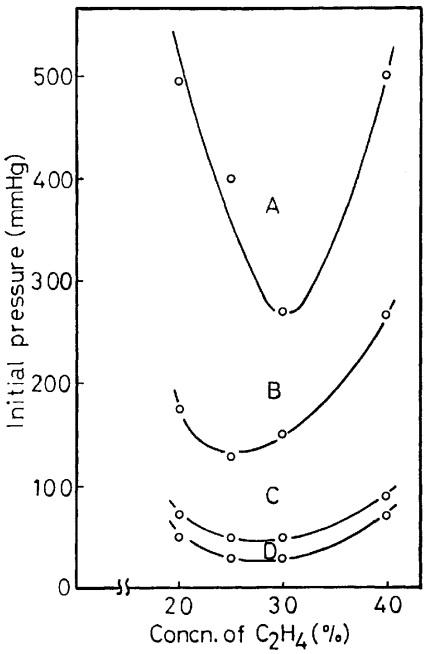

Fig. 1. Classification of propagation of flames.

In Fig. 2, a schlieren photograph of Type **A** is given. The flame has a dome shaped flame front until the region of the transition to detonation, without any sign of turbulence ahead of the flame. The surfaces of the flame are not uniform, but are blurred before the onset

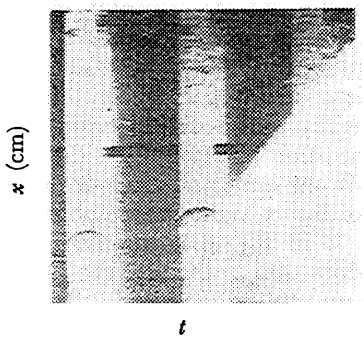

Fig. 2. Schlieren photograph of flame, type A.
x: Distance from ignition point, t: 25 μs/frame.

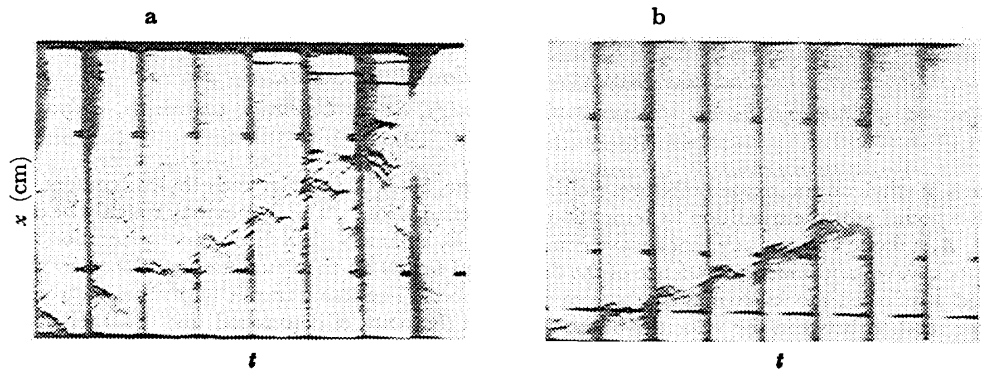

Fig. 3. Schlieren photograph of flame, type C.
x: Distance from ignition point, t: 25 μs/frame.

of detonation; this may be attributed to the cellular structure, or the local explosion started at a flame front with a high temperature and a high pressure conveyed from the reaction part. The only difference between the **A** and **B** types is the generation of shock waves. If shock wave is generated in Type **B**, the shock wave is very weak and cannot generate the detonation. Therefore, the transition to detonation occurs in a similar way in Types **A** and **B**.

Type **C**, depicted in Fig. 3, is most frequently observed. The four mechanisms reported by Oppenheim *et al.*[5] and mentioned above are also of this type. A detonation wave starts at a flame front or immediately ahead of a flame, as is shown in Fig. 3. In this type, the state of a flame front and the unburned mixture ahead of a flame change every time. Two forms of the onset of detonation are observed, one at the shock wave generated at the lip of a flame front (Fig. 3-a), and the other, in the vicinity of a flame front (Fig. 3-b).

The transition to detonation is essentially connected with the initial pressure of the gas mixture and the mixing ratio of the composition. Besides these, the detonation induction distance, DID, or the distances from the ignition of a flame to the point of detonation *versus* the initial gas pressures of mixture are shown in Fig. 4. The curves decrease against the pressures of the initial gas mixtures and approach constant values over 300 mmHg. These values seem rather small compares with the values which has been cited for hydrogen–oxygen,[6] methane–oxygen, and acetylene–oxygen[7] by other investigators, who have all reported constant values of a few atmospheres.

As DID change its value according to the values of the tube diameters and the condition of the tube wall, one can hardly expect constant values to be determined by, for example, initial pressures. Therefore, the absolute numerical values of these constants have not so much meaning as they seem to have.

For the generation of detonation, the turbulences of a wave front or the onsets of shock waves which make the velocities of flames higher are responsible; therefore, Types **B** and **C** in Fig. 4 correspond in these cases, but Type **A** does not. Actually, the DID of Type **A** does not concern initial pressures in higher region than a certain value, and consequently there is no effect on the state after the flame begins to move and there is still detonation. Therefore, the phenomena, such as

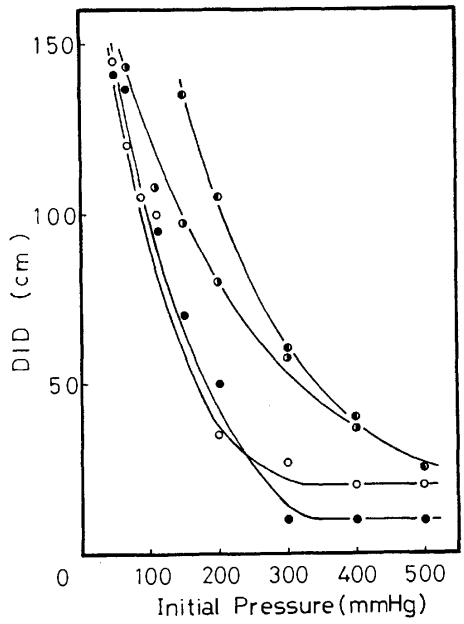

Fig. 4. Detonation induction distance of ethylene-oxygen mixture.
◑: 20% C_2H_4-80% O_2, ○: 25% C_2H_4-75% O_2,
●: 30% C_2H_4-70% O_2, ◐: 40% C_2H_4-60% O_2.

the turbulence of a flame or a shock wave after a flame begin to propagate, may not necessarilly always be responsible for the onset of detonation. Presumably an ignition energy of Type **A**, which maintains the system at the beginning, may be enough for the detonation.

Now the definite conditions, other than shock waves and turbulence, for which the detonation is responsible, can be considered. Figure 5 shows the relation of DID *versus* flame velocities immediately before the onset of detonation. The graph is linear for all sorts of flames at pressures of 70—500 mmHg and at compositions of the gas mixture of 20—40% ethylene, independent of the generation of shock waves or the turbulence of the flame. The flame which transits to detonation must have, at the very point of detonation, a definite value of a flame velocity. The flame in Type **A** which has enough flame velocity without any support of turbulence, transits to detonation by itself, while Types **B** and **C**, the velocities of which are insufficient to reach detonation, must get the support of turbulence of a flame to

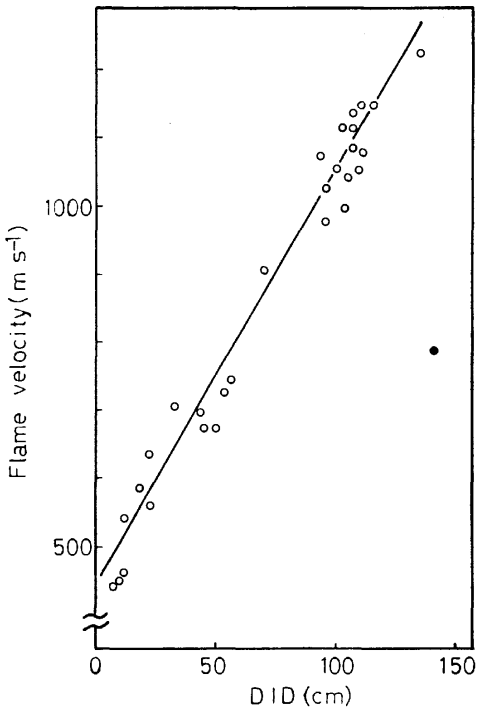

Fig. 5. Flame velocity at the detonation point.
○: Without the collision of reflected shock waves,
●: with the collision.

make the velocities higher. Thus, the velocity of the flame at the point of detonation is the largest factor in the detonation.

In Fig. 5 there is one point (the dot on the right of the diagram) which is outside the curves and which belongs to Type **D**. Figure 6 shows a typical example of this type. In Type **D** the detonation wave is generated after the collision of a flame and a reflected shock wave. The point outside the diagram in Fig. 5 does not contradict the theory. After the collision, the flame propagates in the region of higher pressures and higher temperatures, and the particle velocity becomes nil. If the tube is longer or the collision of a flame and a reflected shock wave does not occur, the dot in Fig. 5 will shift and find itself on the elongation of the straight line. In Type **D**, just before the detonation the turbulences in both the unburnt gas and the flame are less and the velocity of flame is slower than in Type **C**. Therefore, in Type **D** the detonation will be aroused through the collision of a flame and a reflected shock wave. After the collision, the flame propagates through the region of higher pressures. The value of this pressure, according to the theory, is 420 mmHg (observed 460 mmHg), and the velocity of flame at the point of the collision is 760 m s^{-1}. In Fig. 5, if the initial pressure is 460 mmHg, then the flame of 550 m s^{-1} is detonated and in Fig. 6 the actual flame velocity of 760 m s^{-1} will have enough energy for the detonation. Thus, the point of the dot in Fig. 5 elucidates the generation of detonation.

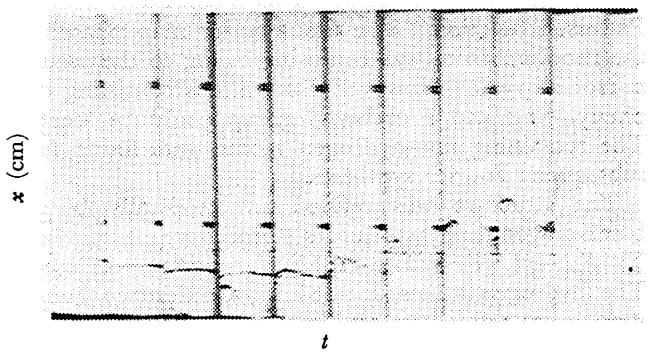

Fig. 6. Schlieren photograph of flame, type D.
x: Distance from ignition point, t: 25 μs/frame.

Another example is the initial gas flame of the pressure of 30 mmHg, which cannot be detonated by the collision of a flame and a reflected shock wave. The observed pressure of the reflected shock wave is 230 mmHg, the observed velocity of the flame is 510 m s^{-1} and the acceleration of the flame and the velocity of the shock wave are very similar to the flame of 50 mmHg. The flame with the initial pressure of 230 mmHg will be detonated with the flame velocity of 650 m s^{-1}, which can also be concluded from the theory. Therefore, if the flame is accelerated for some 10 m s^{-1} before the collision on the bottom plate, then the flame will detonated, but the flame collides with the plate, before that and will not be detonated with enough energy. Thus, in Type **D** the transition from the deflagration depends on a flame velocity which gains from the collision of the flame and the reflected shock wave.

At any rate, the velocity of the flame at the point of detonation and the DID are the predominating factors for the phenomena of the transition to detonation from deflagration, with or without any collision of a flame and a reflected shock wave.

References

1) M. Berthelot and P. Vieille, *C. R. Acad. Sci.*, **93**, 18 (1881); E. Mallard and H. Le Chatelier, *ibid.*, **93**, 145 (1881).
2) D. L. Chapman, *Philos. Mag.*, **47**, 90 (1899); E. Jouguet, *J. Mathem.*, **6**, 5 (1904); Ya. B. Zeldovich, *JETP*, **10**, 542 (1904); J. Neuman, *Office of Scientific Research and Development*, No. 549, (1943); W. Döring, *Ann. Phys. (N. Y.)*, **43**, 421 (1943).
3) W. Payman and H. Titman, *Proc. R. Soc. London, Ser. A*, **120**, 90 (1928).
4) N. A. Bone, R. P. Fraser, and W. H. Weeler, *Philos. Trans.*, **A235**, 29 (1935); F. J. Martin and D. R. White, Seventh Symposium (International) on Combustion, 856 (1956).
5) A. K. Oppenheim and P. A. Urtiew, *Proc. R. Soc. London, Ser. A*, **295**, 13 (1966); A. K. Oppenheim and R. A. Stern, Seventh Symposium (International) on Combustion, 837 (1959).
6) L. E. Bollinger, M. C. Fraser, and R. Edse, *J. Am. Rocket Soc.*, **31**, 588 (1961).
7) A. Egerton and S. Gates, *Proc. R. Soc. London, Ser. A*, **114**, 137 (1927).

The Molecular Structure of μ-Carbonyl-di-μ-diphenylmethylene-bis(π-cyclopentadienylrhodium), $[(\pi\text{-}C_5H_5)_2Rh_2\{C(C_6H_5)_2\}_2(CO)]$

Hiroshi UEDA, Yasushi KAI, Noritake YASUOKA, and Nobutami KASAI*

Department of Applied Chemistry, Faculty of Engineering, Osaka University, Yamadakami, Suita, Osaka 565

(Received March 26, 1977)

The molecular structure of $[(\pi\text{-}C_5H_5)_2Rh_2\{C(C_6H_5)_2\}_2(CO)]$ has been determined from three-dimensional X-ray diffraction data ($R=0.040$ for 2394 reflections). The crystal belongs to the monoclinic system, space group A2/a, with four formula units in a cell of dimensions: $a=19.967(5)$, $b=10.343(1)$, $c=16.526(4)$ Å, and $\beta=123.05(2)°$. The molecule has C_2 symmetry: the two-fold axis passes through the bridge carbonyl group, being perpendicular to the Rh–Rh bond (Rh—Rh=2.548(1) Å). The diphenylcarbene moieties bridge between rhodium atoms. The planar cyclopentadienyl rings lie 1.94 Å from the nearest rhodium atom and exihibit the usual π-bonded geometry.

In recent years many transition metal-carbene complexes have been reported[1-4], in which the carbene ligands are stabilized by an adjacent oxygen or nitrogen atom. Recently, P. Hong and co-workers[5] have prepared some stable diphenyl-carbene complexes, which have no hetero atom adjacent to the carbene ligand.

The reaction between $[Rh(CO)_2Cl]_2$ (**1**) and diphenyl-ketene gives an insoluble, brick red complex $[Rh(CO)\{C(C_6H_5)\}_2Cl]_n$ (**2**). The reaction of **2** with cyclopentadienyl sodium in THF gives air stable, green, needle-like crystals **3**. The complex **3** in solution slowly loses the bridging carbonyl on heating, and finally changes into **4**. The reaction from **3** to **4** is reversible.

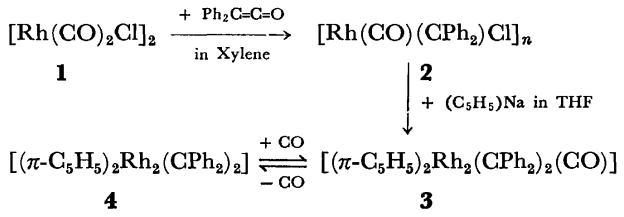

X-Ray molecular structures of **3** and **4** have been determined. This paper describes the crystal and molecular structure determination of **3**.

Experimental

The crystals used in this study were supplied by Professor N. Hagihara and co-workers. After preliminary X-ray work which showed that the crystal belongs to the monoclinic system, the unit-cell dimensions were determined by a least-squares fit using 2θ-values of 20 strong reflections measured on a G. E. single crystal orienter equipped on a Rigaku SG-2 goniometer.

Crystal Data. $C_{37}H_{30}ORh_2$, F. W. 696.5, $a=19.967(5)$, $b=10.343(1)$, $c=16.526(4)$ Å, $\beta=123.05(2)°$, $U=2860.0(9)$ Å^3, $D_m=1.60$ g cm^{-3}, $Z=4$, $D_c=1.62$ g cm^{-3}, μ(Mo)=11.2 cm^{-1}.

The systematic absences of reflections, hkl: $k+l=2n+1$ and $h0l$: $h=2n+1$, suggested the probable space group as A2/a (No. 16) or Aa (No. 9). Besides these diffraction aspects, the intensities of $h=2n+1$ layers were generally much weaker than those of $h=2n$ layers.

A single crystal with dimensions *ca.* $0.18\times0.21\times0.24$ mm was used to collect intensity data. Three-dimensional data were measured by means of the θ-2θ scan technique on a Rigaku automated, four-circle diffractometer using zirconium-filtered Mo $K\alpha$ radiation. The integrated intensity was determined by scanning over a peak at a rate of 4°min^{-1}, and subtracting the background by averaging the two values measured for 5 s at both ends of a scan. The scan width $\Delta(2\theta)$ of each reflection was computed by the equation: $\Delta(2\theta)=(2.0+0.70\tan\theta_c)°$, where θ_c is the calculated value of the Bragg angle for Mo $K\alpha_1$($\lambda=0.70926$ Å). The intensities of three standard reflections were measured after every 50 reflections. There was no evidence of crystal decomposition. After reflections up to $\sin\theta/\lambda=0.481$ were measured, reflections with $h=2n$ in the range $0.47\leqq\sin\theta/\lambda\leqq0.66$ were also collected since the intensities of high angle reflections with $h=2n+1$ were too weak to be measured. A total of 2394 independent reflections was obtained. Lorentz and polarization corrections were made in the usual manner, but no absorption correction was applied.

Structure Solution and Refinement

The structure was solved by using a three-dimensional Patterson function. A clue for the solution of the structure was obtained from the characteristic intensity distribution of the reflections mentioned above, from which it could be assumed that the space group A2/a was preferable and the y parameter of the rhodium atom nearly equal to zero. This is consistent with the Patterson function. The first Fourier map phased by the rhodium atom was confusing owing to the pseudo-mirror at $y=0$. However, light atoms consisting of a phenyl ring and a carbonyl group could be located. The remaining non-hydrogen atoms were found from subsequent Fourier syntheses.

The structure was refined anisotropically by the block-diagonal least-squares procedure minimizing $\Sigma(|F_o|-k|F_c|)^2$. The HBLS V program was used.[6] The hydrogen atoms, located by a difference Fourier map, were refined isotropically. The final R value is 0.040 for non-zero reflections. Atomic scattering factors used were those of Hanson, Herman, Lea and Skillman.[7] The positional and thermal parameters are given in Table 1.**

* To whom any correspondence should be addressed.

** The table of structure factors is kept as Document No. 7714 at the Chemical Society of Japan.

TABLE 1. ATOMIC POSITIONAL AND THERMAL PARAMETERS

Estimated standard deviations in parentheses. Anisotropic thermal parameters are expressed in the form $\exp\{-(\beta_{11}h^2+\beta_{22}k^2+\beta_{33}l^2+\beta_{12}hk+\beta_{13}hl+\beta_{23}kl)\}$ and isotropic thermal parameters $\exp\{-B\sin^2\theta/\lambda^2\}$.

Atom	x	y	z	B or β_{11}	β_{22}	β_{33}	β_{12}	β_{13}	β_{23}
Rh	0.19361(2)	0.00744(5)	0.01464(3)	0.00222(1)	0.00631(4)	0.00379(2)	−0.00147(5)	0.00300(3)	−0.00044(7)
O	0.25000	−0.2523(6)	0.0	0.0055(4)	0.0037(6)	0.0099(6)	0.0	0.0038(8)	0.0
C(1)	0.3075(3)	0.0893(5)	0.1015(4)	0.0018(2)	0.0049(5)	0.0035(3)	−0.0006(5)	0.0028(4)	−0.0002(6)
C(2)	0.25000	−0.1409(8)	0.0	0.0023(3)	0.0064(8)	0.0048(5)	0.0	0.0020(7)	0.0
C(11)	0.3200(4)	0.2333(5)	0.1135(4)	0.0020(2)	0.0056(5)	0.0036(3)	−0.0009(5)	0.0022(4)	−0.0004(6)
C(12)	0.3947(4)	0.2822(6)	0.1448(5)	0.0027(2)	0.0065(6)	0.0058(4)	−0.0006(6)	0.0032(6)	0.0003(6)
C(13)	0.4116(4)	0.4123(7)	0.1605(6)	0.0034(3)	0.0092(8)	0.0074(5)	−0.0046(8)	0.0026(6)	−0.0006(10)
C(14)	0.3538(5)	0.4965(7)	0.1468(5)	0.0053(3)	0.0061(6)	0.0063(4)	−0.0027(10)	0.0032(6)	−0.0032(11)
C(15)	0.2810(4)	0.4513(7)	0.1197(5)	0.0046(3)	0.0072(6)	0.0055(4)	0.0034(8)	0.0041(6)	−0.0011(9)
C(16)	0.2632(4)	0.3204(6)	0.1029(5)	0.0027(2)	0.0063(6)	0.0047(4)	0.0001(6)	0.0026(5)	−0.0012(7)
C(21)	0.3531(4)	0.0222(6)	0.1969(4)	0.0020(2)	0.0069(7)	0.0038(3)	−0.0024(5)	0.0024(5)	−0.0005(6)
C(22)	0.3637(4)	0.0834(7)	0.2788(6)	0.0032(3)	0.0113(8)	0.0044(4)	−0.0003(7)	0.0034(6)	−0.0016(9)
C(23)	0.4015(5)	0.0235(8)	0.3671(5)	0.0048(3)	0.0146(11)	0.0040(4)	−0.0019(9)	0.0038(6)	−0.0007(10)
C(24)	0.4316(5)	−0.0986(8)	0.3800(5)	0.0042(3)	0.0152(10)	0.0043(4)	−0.0052(10)	0.0015(6)	0.0064(11)
C(25)	0.4245(5)	−0.1608(7)	0.3022(5)	0.0044(3)	0.0088(8)	0.0055(4)	−0.0021(10)	0.0012(6)	0.0040(10)
C(26)	0.3852(4)	−0.1010(6)	0.2121(5)	0.0038(3)	0.0071(6)	0.0043(4)	−0.0018(7)	0.0024(5)	−0.0000(8)
C(31)	0.0911(5)	0.0931(9)	0.0189(6)	0.0037(3)	0.0163(11)	0.0089(6)	−0.0029(10)	0.0092(7)	−0.0036(13)
C(32)	0.1489(5)	0.0428(10)	0.1119(6)	0.0041(3)	0.0278(13)	0.0060(5)	−0.0074(7)	0.0074(7)	−0.0066(14)
C(33)	0.1533(6)	−0.0927(10)	0.1063(7)	0.0059(4)	0.0192(13)	0.0085(6)	−0.0029(12)	0.0096(9)	0.0064(15)
C(34)	0.1000(5)	−0.1318(9)	0.0098(7)	0.0054(4)	0.0146(11)	0.0104(7)	−0.0092(11)	0.0094(8)	−0.0026(14)
C(35)	0.0612(4)	−0.0180(10)	−0.0452(6)	0.0024(2)	0.0218(13)	0.0075(5)	−0.0066(10)	0.0065(6)	−0.0069(14)
H(12)	0.436(3)	0.225(5)	0.156(4)	0.1(10)					
H(13)	0.452(4)	0.431(7)	0.177(4)	3.6(18)					
H(14)	0.362(4)	0.577(6)	0.158(4)	1.8(14)					
H(15)	0.246(4)	0.504(6)	0.103(4)	1.4(12)					
H(16)	0.211(3)	0.287(5)	0.080(4)	0.8(11)					
H(22)	0.341(4)	0.168(7)	0.270(4)	2.5(16)					
H(23)	0.410(4)	0.075(7)	0.425(5)	2.8(17)					
H(24)	0.461(4)	−0.141(6)	0.446(4)	1.9(14)					
H(25)	0.449(4)	−0.242(7)	0.306(5)	3.4(18)					
H(26)	0.384(4)	−0.139(6)	0.166(4)	1.5(14)					
H(31)	0.079(3)	0.208(8)	0.001(5)	3.9(19)					
H(32)	0.179(5)	0.115(8)	0.169(6)	5.0(21)					
H(33)	0.186(5)	−0.161(8)	0.159(6)	4.6(21)					
H(34)	0.088(5)	−0.230(9)	−0.021(6)	5.5(23)					
H(35)	0.020(4)	−0.019(7)	−0.115(5)	3.7(18)					

Results and Discussion

The molecular structure and the numbering scheme of atoms are shown in Fig. 1. A stereoscopic drawing of the molecule is given in Fig. 2. Bond lengths and bond angles are listed in Table 2. Table 3 shows the equations of several least-squares planes.

The remarkable feature of the molecule is that it has C_2 symmetry; a crystallographic two fold axis passes through the bridging carbonyl groups, being perpendicular to the Rh–Rh bond. The diphenylmethylene moieties bridge between rhodium atoms instead of bonding to single rhodium atom. Each of the cyclopentadienyl group is π-bonded to a rhodium atom, and the two cyclopentadienyl rings are staggered about the Rh–Rh bond (Fig. 1).

The Rh–Rh single bond length 2.548(1) Å is significantly shorter than those in other π-cyclopentadienyl rhodium carbonyl complexes: 2.681(2) Å in $[(\pi\text{-}C_5H_5)_2Rh_2(CO)_3]$,[9] 2.62 Å in $[(\pi\text{-}C_5H_5)_3Rh_3(CO)_3]$,[10] 2.776(1) Å in $Rh_6(CO)_{16}$[11] and 2.690 Å in rhodium metal.[12]

The cyclopentadienyl rings are planar: the maximum deviation from the plane is ±0.001 Å. The C–C bond lengths and C–C–C bond angles are 1.411(16)—1.453 (14) (av. 1.425) Å, and 105.5(9)—109.7(9) (av. 108.0)°, respectively. Each ring makes an angle of 83° to the Rh–Rh bond and lies 1.94 Å away from the rhodium atom. The average Rh–C(C_5H_5) distance is 2.290(12) Å, which is comparable to the values of 2.24 Å in $[(\pi\text{-}C_5H_5)_3Rh_3(CO)_3]$, 2.26 Å in $[(\pi\text{-}C_5H_5)_2Rh_2(CO)_3]$, and 2.25 Å in $[(\pi\text{-}C_5H_5)Rh(CO)(C_2F_5)I]$.[13]

The Rh–C(1) bond lengths are 2.094(6) and 2.088 (6) (av. 2.091) Å, which are close to the Rh(III)–C-

Table 2. Bond lengths and bond angles

Bond lengths [l/Å]

Rh-Rh′	2.548(1)	Rh-C(2)	1.995(9)	C(26)-C(21)	1.386(10)	C(31)-C(32)	1.421(15)
Rh-C(1)	2.094(6)	Rh′-C(1)	2.088(6)	C(32)-C(33)	1.412(15)	C(33)-C(34)	1.411(16)
Rh-C(31)	2.266(10)	Rh-C(32)	2.271(11)	C(34)-C(35)	1.430(10)	C(35)-C(31)	1.453(14)
Rh-C(33)	2.312(11)	Rh-C(34)	2.325(11)				
Rh-C(35)	2.276(10)	C(1)-C(1)	2.851(12)	C(12)-H(12)	0.95(7)	C(13)-H(13)	0.72(9)
C(1)-C(11)	1.505(9)	C(1)-C(21)	1.493(9)	C(14)-H(14)	0.85(8)	C(15)-H(15)	0.83(7)
C(2)-O	1.152(10)	C(11)-C(12)	1.381(10)	C(16)-H(16)	0.96(7)	C(22)-H(22)	0.96(8)
C(12)-C(13)	1.377(12)	C(13)-C(14)	1.363(13)	C(23)-H(23)	1.02(9)	C(24)-H(24)	1.01(8)
C(14)-C(15)	1.349(13)	C(15)-C(16)	1.388(11)	C(25)-H(25)	0.96(9)	C(26)-H(26)	0.85(8)
C(16)-C(11)	1.384(10)	C(21)-C(22)	1.402(10)	C(31)-H(31)	1.22(9)	C(32)-H(32)	1.08(10)
C(22)-C(23)	1.372(12)	C(23)-C(24)	1.364(13)	C(33)-H(33)	1.03(10)	C(34)-H(34)	1.10(11)
C(24)-C(25)	1.375(13)	C(25)-C(26)	1.393(12)	C(35)-H(35)	0.99(9)		

Bond angles [φ/°]

Rh′-Rh-C(2)	50.3(2)	Rh′-Rh-C(1)	52.4(2)	H(26)-C(26)-C(21)	118(5)
Rh-Rh′-C(1)	52.6(2)	C(2)-Rh-C(1)	85.5(3)	H(31)-C(31)-C(32)	124(4)
C(2)-Rh′-C(1)	85.6(3)	C(1)-Rh-C(1)′	86.0(2)	H(32)-C(32)-C(33)	136(5)
Rh-C(2)-Rh′	79.4(3)	Rh-C(2)-O	140.3(7)	H(33)-C(33)-C(34)	120(5)
Rh-C(1)-Rh′	75.1(2)	Rh-C(1)-C(11)	122.1(4)	H(34)-C(34)-C(35)	124(5)
Rh′-C(1)-C(11)	116.1(4)	Rh-C(1)-C(21)	110.2(4)	H(35)-C(35)-C(31)	128(5)
Rh-C(1)-C(21)	118.4(4)	C(11)-C(1)-C(21)	111.1(5)	C(11)-C(12)-H(12)	120(4)
C(16)-C(11)-C(12)	116.9(6)	C(11)-C(12)-C(13)	122.2(7)	C(12)-C(13)-H(13)	116(7)
C(12)-C(13)-C(14)	119.7(8)	C(13)-C(14)-C(15)	119.6(9)	C(13)-C(14)-H(14)	124(5)
C(14)-C(15)-C(16)	121.2(8)	C(15)-C(16)-C(11)	120.4(7)	C(14)-C(15)-H(15)	118(5)
C(26)-C(21)-C(22)	115.4(6)	C(21)-C(22)-C(23)	121.9(7)	C(15)-C(16)-H(16)	123(4)
C(22)-C(23)-C(24)	121.6(8)	C(23)-C(24)-C(25)	118.4(8)	C(21)-C(22)-H(22)	117(5)
C(24)-C(25)-C(26)	120.2(8)	C(25)-C(26)-C(21)	122.5(7)	C(22)-C(23)-H(23)	118(5)
C(35)-C(31)-C(32)	105.5(9)	C(31)-C(32)-C(33)	109.7(9)	C(23)-C(24)-H(24)	121(4)
C(32)-C(33)-C(34)	108.8(10)	C(33)-C(34)-C(35)	107.2(9)	C(24)-C(25)-H(25)	124(5)
C(34)-C(35)-C(31)	108.8(9)			C(25)-C(26)-H(26)	119(5)
		H(16)-C(16)-C(11)	117(4)	C(35)-C(31)-H(31)	131(4)
H(12)-C(12)-C(13)	118(4)	H(22)-C(22)-C(23)	121(5)	C(31)-C(32)-H(32)	115(5)
H(13)-C(13)-C(14)	124(7)	H(23)-C(23)-C(24)	120(5)	C(32)-C(33)-H(33)	131(5)
H(14)-C(14)-C(15)	117(5)	H(24)-C(24)-C(25)	120(4)	C(33)-C(34)-H(34)	129(5)
H(15)-C(15)-C(16)	120(5)	H(25)-C(25)-C(26)	115(5)	C(34)-C(35)-H(35)	123(5)

(sp^3) distances of 2.08(3) in $[(\pi\text{-}C_5H_5)Rh(CO)(C_2F_5)I]$ and 2.08 Å in $[Rh_2I_2(SMe_2)_3Me_4]$.[14]

In the diphenylmethylene moiety, bond angles around the C(1) atom deviate from the tetrahedral angle: Rh–C(1)–Rh′ 75.1(2), Rh–C(1)–C(11) 122.1(4), Rh–C(1)–C(21) 110.2(4), Rh′–C(1)–C(11) 116.1(4), Rh′–C(1)–C(21) 118.4(4), C(11)–C(1)–C(21) 111.1(5)°. Bond lengths and bond angles in phenyl rings have normal values [C–C(av.)=1.38 Å and C–C–C(av.)=120.0°]. The two phenyl rings are roughly perpendicular to each other, the dihedral angle being 85.3°.

The Rh–C(2) bond length 1.995(9) Å is shorter than that of Rh–C(1). However, this distance is close to the values of 2.01 Å in $[(\pi\text{-}C_5H_5)_2Rh_2(CO)_3]$ and 2.00 Å in $[(\pi\text{-}C_5H_5)_3Rh_3(CO)_3]$. The bridging Rh–C(2)–Rh′ angle is 79.4(3)°, which is smaller than the corresponding angles of 84.0° in $[Rh_2(C_5H_5)_2(CO)_3]$, 81.9° in $[(\pi\text{-}C_5H_5)_3(CO)_3]$ and 82° in $[\{(PPh_3)_2Rh(CO)\}_2,2CH_2Cl_2]$.[15] The C–O length of the bridged carbonyl group, C(2)–O=1.152(10) Å, is comparable to the values of 1.15(4) and 1.18(4) Å in $[(\pi\text{-}C_5H_5)_3Rh_3(CO)_3]$ and 1.17 Å in $[\{(PPh_3)Rh(CO)\}_2,2CH_2Cl_2]$.

The overall molecular geometry of the present complex, except for the bridging carbonyl group, is similar to that of the diamagnetic complex $[(C_6H_5)_2PCo(C_5H_5)]_2$.[16] The molecular structure of the cobalt complex was described by the formation of a so-called "bent" metal-metal bond. However, this is not the case for the present complex because the bridging carbonyl group prevents the formation of the "bent" metal-metal bond. The $(CPh_2)_2$ bridging system is not planar: the dihedral angle between the two planes formed by Rh, Rh′, and C(1) and Rh, Rh′, and C(1)′ being decreased from 180 to 121° (Fig. 1(b)). The intra- and inter-molecular atomic contacts indicate that the magnitude of twisting of the phenyl rings is primarily determined by non-bonding intra-molecular interactions. The dihedral angles formed by the plane defined by C(1), C(1)′ and C(2) with phenyl rings 1 and 2 are 61.1, 31.8°, respectively. Because of the short C(1)···

TABLE 3. LEAST-SQUARES PLANES AND ATOM DEVIATIONS

Plane equations are of the form $AX+BY+CZ+D=0$, where X, Y, Z and D are measured in Å units: $X=ax+cz\cos\beta$, $Y=by$ and $Z=cz\sin\beta$.

(a) Plane through Rh, C(2) and Rh'
$-0.1592X-0.9873Z+0.7945=0$
C(1)* 1.426 C(1)'* −1.426

(b) Plane through Rh, C(1)' and Rh'
$-0.0813X+0.8598Y-0.5041Z+0.3395=0$

(b') Plane through Rh, C(1) and Rh'
$-0.0813X-0.8598Y-0.5041Z+0.4719=0$

(c) Plane through C(1), C(1)' and C(2)
$-0.9867X+0.1627Z+4.9253=0$

(d) Phenyl ring 1 (C(11)-C(16))
$-0.2694X-0.1258Y+0.9548Z+0.2350=0$
C(11) −0.014 C(13) −0.003 C(15) 0.009
C(12) 0.012 C(14) −0.016 C(16) 0.014

(d') Phenyl ring 1' (C(11)'-C(16)')
$-0.2664X+0.1236Y+0.9559Z+2.4525=0$
C(11)' 0.018 C(13)' −0.002 C(15)' −0.008
C(12)' −0.013 C(14)' 0.012 C(16)' −0.008

(e) Phenyl ring 2 (C(21)-C(26))
$-0.8973X-0.3838Y-0.2182Z+5.4261=0$
C(21) 0.009 C(23) −0.001 C(25) −0.010
C(22) −0.009 C(24) 0.010 C(26) 0.000

(e') Phenyl ring 2' (C(21)'-C(26)')
$-0.8973X+0.3838Y-0.2181Z+3.5325=0$
C(21)' −0.009 C(23)' 0.000 C(25)' 0.010
C(22)' 0.009 C(24)' −0.010 C(26)' −0.000

(f) Cyclopentadienyl ring (C(31)-C(35))
$0.9771X-0.1198Y+0.1757Z+1.6801=0$
C(31) −0.000 C(33) −0.001 C(35) −0.001
C(32) 0.001 C(34) 0.001 Rh* −1.942

(f') Cyclopentadienyl ring (C(31)'-C(35)')
$-0.9771X+0.1198Y+0.1757Z+8.0751=0$
C(31)' 0.000 C(33)' 0.001 C(35)' 0.001
C(32)' −0.001 C(34)' −0.001 Rh'* 1.942

* Not included in the least-squares plane calculation.

DIHEDRAL ANGLES [φ/°]

Between planes	Dihedral angles
a, b	120.7
b, b'	118.6
c, d	61.1
c, e	31.8
d, d'	14.3
d, e	85.3
d, e'	90.8
e, f	45.1
f, f'	13.8

ANGLE BETWEEN INTERATOMIC VECTOR AND PLANE [φ/°]

Rh-Rh' bond·····C_5H_5 plane	83.1

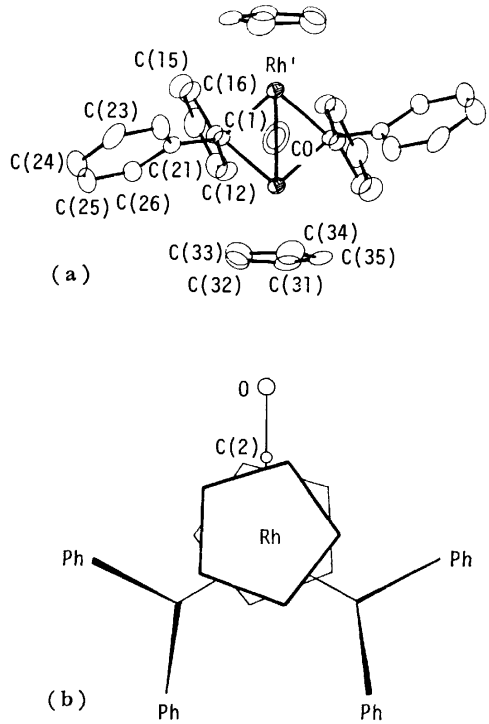

Fig. 1. The molecular structure of $[(\pi\text{-}C_6H_5)_2Rh_2(CO)(CPh_2)_2]$ and the numbering scheme of atoms.
(a) Projected along the C–O bond.
(b) Projected along the Rh-Rh bond. Rh atoms are omitted.

TABLE 4. SHORT INTERMOLECULAR ATOMIC CONTACTS LESS THAN 3.1 Å [l/Å]

H(14)···O[a]	2.92(8)	H(15)···O[a]	3.07(7)
H(26)···H(14)[b]	2.97(11)	H(22)···H(33)[c]	2.34(13)
H(15)···H(23)[c]	2.96(11)	H(23)···H(34)[c]	2.56(15)
H(24)···H(31)[d]	2.14(12)		

key a x, $1+y$, z; b x, $-1+y$, z; c $0.5-x$, $0.5+y$, $0.5-z$; d $0.5-x$, $-0.5+y$, $0.5+z$.

C(1)' distance of 2.851(12) Å, the phenyl rings 1 and 1' related by the crystallographic two-fold axis are not parallel to each other: C(11)···C(11)'=3.232(13) Å, C(12)···C(16)'=3.578(11) Å and C(14)···C(15)'=3.733(13) Å, and the dihedral angle between the phenyl rings 1 and 1' is 14.3°.

A stereoscopic drawing of the crystal structure is shown in Fig. 3. Short intermolecular atomic contacts (less than 3.1 Å) are given in Table 4.

Computations throughout the present study were carried out on a NEAC 2200-700 computer at Osaka University.

The authors express their deep thanks to Professor Nobue Hagihara and Professor Kenkichi Sonogashira and their co-workers of Osaka University, and to Dr. Donald Mullen who read the manuscript.

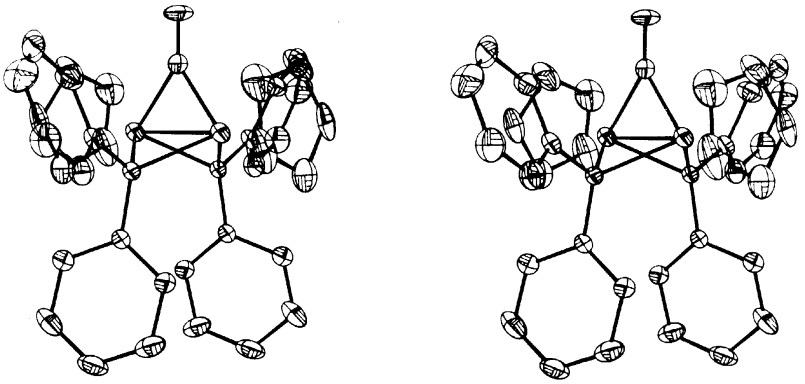

Fig. 2. A stereoscopic ORTEP drawing[8] of the molecule

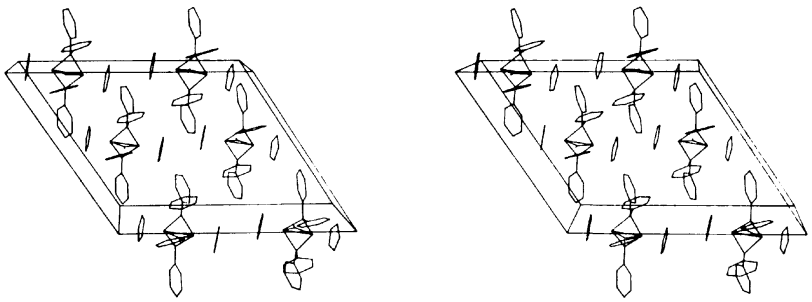

Fig. 3. A stereoscopic drawing[8] of the crystal structure projected along the b axis.

References

1) E. O. Fischer and A. Maasbol, *Angew. Chem.*, **76**, 645 (1964).

2) F. Bonati, G. Minghetti, T. Boschi, and B. Crociani, *J. Organomet. Chem.*, **25**, 255 (1970).

3) D. J. Cardin, B. Cetinkaya, M. Lappert, Lj. Manojlovic-Muir, and K. W. Muir, *Chem. Commun.*, **1971**, 400.

4) M. H. Chisholm and H. C. Clark, *Chem. Commun.*, **1970**, 763.

5) P. Hong, N. Nishii, K. Sonogashira, and N. Hagihara, *J. Chem. Soc., Chem. Commun.*, **1972**, 993.

6) T. Ashida, The Universal Crystallographic Computing System-Osaka, The Computation Center, Osaka University (1973), p. 55.

7) H. P. Hanson, F. Herman, J. D. Lea and S. S. Skillman, *Acta Crystallogr.*, **17**, 1040 (1964).

8) C. K. Johnson, ORTEP, Report ORNL-3794, Oak Ridge National Laboratory, Tennessee, 1965.

9) O. S. Mills and J. P. Nice, *J. Organomet. Chem.*, **10**, 337 (1967).

10) O. S. Mills and E. F. Paulus, *J. Organomet. Chem.*, **10**, 331 (1967).

11) E. R. Corey, L. F. Dahl, and W. Beck, *J. Am. Chem. Soc.*, **85**, 1202 (1963).

12) H. J. Goldschmidt and T. Land, *J. Iron Steel Inst.*, **155**, 221 (1947).

13) M. R. Churchill, *Inorg. Chem.*, **4**, 1734 (1965).

14) E. F. Paulus, H. P. Fritz, and K. E. Schwarzhaus, *J. Organomet. Chem.*, **11**, 647 (1968).

15) P. Singh, C. B. Dammann, and D. J. Hodgson, *Inorg. Chem.*, **12**, 1335 (1973).

16) J. M. Coleman and L. F. Dahl, *J. Am. Chem. Soc.*, **89**, 542 (1967).

Electronic Structures and Spectra of the Keto and Enol Forms of Acetylacetone

Hiroshi NAKANISHI, Hiroshi MORITA, and Saburo NAGAKURA

The Institute for Solid State Physics, The University of Tokyo, Roppongi, Minato, Tokyo 106

(Received March 30, 1977)

Near and vacuum UV absorption spectra of acetylacetone were measured in the vapor phase and in several organic solvents at various temperatures. From the temperature dependence of the spectra, the equilibrium constant and enthalpy change between the keto and enol forms of acetylacetone were determined to be 25 at 20 °C and −4.3 kcal/mol, respectively, in the vapor phase. Rydberg excitation bands were observed at 47170 and 53300 cm^{-1} for the enol form, and $\approx$52000 cm^{-1} for the keto form. The estimated values of the quantum defect indicate that the Rydberg orbitals are 3s and 3p. A modified CNDO-CI method was applied to the valence-shell transitions. A weak band observed at $\approx$34000 cm^{-1} for the keto form was assigned to the first n-π^* transition, and relatively strong bands observed at 38020 and 56800 cm^{-1} for the enol form, to the first and second π-π^* transitions, respectively. Special attention was paid to the charge-transfer (CT) character pertinent to the intramolecular hydrogen bond in the excited states of the enol form. Configuration analysis of the wave functions revealed us that the first π-π^* band observed at 38020 cm^{-1} has the CT character.

Acetylacetone and its congeners in the enol form have a strong intramolecular hydrogen bond with the O···O distance of 2.38—2.55 Å as revealed from the X-ray diffraction[1] and gas-phase electron diffraction studies.[2,3] The electronic structures of the molecules in the ground states have been studied by the nonempirical[4-6] and semiempirical[6-8] calculations. The electronic absorption spectra of acetylacetone and its congeners in the near ultraviolet (UV) region have been measured by several authors[9-13] and have been compared with the spectra of their metal chelates.[12] The spectroscopic results so far obtained, however, are restricted only to the first allowed band and no spectral information is available for discussing the higher excitation bands of acetylacetone.

The charge-transfer (CT) mechanism of hydrogen bond between a proton donor and a proton acceptor is important.[14] Electronic structure of the symmetrical intramolecular hydrogen bond of the hydrogen maleate anion was investigated in previous papers[15,16] and the CT character pertinent to the hydrogen bond was discussed in detail for the ground and excited states from theoretical and experimental points of view.[16] For intermolecular hydrogen-bonded systems between acetic acid and some aliphatic amines, the CT band pertinent to the hydrogen bond was observed successfully in the vacuum ultraviolet (VUV) region by the present authors.[17]

In the present paper, in order to investigate the electronic structures of the keto and enol forms of acetylacetone, electronic absorption spectra in the near and vacuum UV (30000—61000 cm^{-1}) region have been measured with acetylacetone in the vapor phase and also in various solvents. The observed valence-shell transition and Rydberg excitation bands have been interpreted on the basis of theoretical results by a modified CNDO-CI method[18] and the configuration analysis[19] of the ground and excited states.

Experimental

Acetylacetone (Wako G. R. Grade) was distilled three times under reduced pressure immediately before use. Methanol (Kanto G. R. Grade) used as a solvent was purified by fractional distillation. Acetonitrile and heptane (Wako Spectro Grade) were fractionally distilled over diphosphorus pentaoxide and sodium metal wire, respectively. Perfluorohexane (Kishida G. R. Grade) was purified by vacuum distillation through a column filled with silica gel.

Near and vacuum UV absorption spectra were measured with a Cary recording spectrophotometer model 14, with a vacuum UV spectrophotometer constructed in our laboratory,[20] and in part with a JASCO VUV-3 recording spectrophotometer,[21] the cells of 0.1 mm—10 cm light path length being used. In the vapor phase measurement between 18—300 °C, temperature of the sample cell was regulated within ±0.5 °C by a thermoregulator.

Theoretical

The electronic structures of the keto and enol forms of acetylacetone and of its anion were calculated by the modified CNDO-CI method[18] to investigate the characters of the valence-shell transitions. The following one-center Coulomb repulsion integral (γ) and bonding parameter (β^0) were commonly used for all the 2s and 2p atomic orbitals (AO) of the methyl carbon atom of the enol form and the anion, and of all the carbon atoms of the keto form (molecular skeleton of which is not planar); γ(C)=12.78 eV and β^0(C)=−15.4 eV. The other semiempirical parameters used in the calculations were the same as reported previously,[16] the effect of excess formal charge in the anion being considered by the parametrization.[16] In the configuration interaction (CI) treatment, 80 singly excited π-π^* and σ-σ^* configurations and 70 singly excited π-σ^* and σ-π^* configurations were taken into account for the enol form and the anion, and 80 singly excited configurations, for the keto form.

Geometrical structures were taken for the keto form from the gas-phase electron diffraction study[2] and for the enol form from the X-ray diffraction study of tetraacetylethane[1,22] (hydrogen-bonded O···O distance, 2.424 Å), a linear symmetrical hydrogen bond being assumed. The molecular geometry of the anion was assumed to be the same as that of the enol form, except for the fact that the hydrogen-bonded hydrogen atom was removed.

The configuration analysis[19] was applied to the ground and two excited (B_1 symmetry) states of the enol

form. In order to elucidate the electronic structures of the symmetrical intramolecular hydrogen bond, the 35 molecular orbitals (MO) of the anion and the 1s orbital of the hydrogen-bonded hydrogen atom were adopted as the reference MO's, as for the case of the symmetrical hydrogen bond of the hydrogen maleate anion.[16] The ground state of the enol form was analyzed by the ground and 101 singly excited π-π^* and σ-σ^* reference configurations (with A_1 symmetry) and by all the doubly excited reference configurations derived from the above configurations, and the excited states of the enol form were analyzed by 99 singly excited π-π^* and σ-σ^* reference configurations (with B_1 symmetry) and 99×101 doubly excited reference configurations.

Results and Discussion

Electronic Absorption Spectra of Acetylacetone. Figure 1 shows near and vacuum UV absorption spectra in the 30000—61000 cm^{-1} region measured with acetylacetone in the vapor phase and in perfluorohexane at room temperature. As pointed out by the NMR[23] and IR[24,25] spectroscopic studies, acetylacetone predominantly exists as the enol form in the vapor phase and in nonpolar solvents at room temperature. Therefore, both spectra shown in Fig. 1 are due to the enol form. The difference between them in the frequency region higher than 45000 cm^{-1} can be explained by the fact that Rydberg transition bands in the vapor phase disappear in the condensed phase, *i.e.*, in perfluorohexane.[26] From this point of view, a weak band at 47170 cm^{-1} and a moderately strong band at 53300 cm^{-1} are assigned to the Rydberg transitions of the enol form.

The Rydberg excitation energy is expected to satisfy the following formula;[26]

$$h\nu = I_p - 109737/(n-\delta)^2, \quad (1)$$

where $h\nu$ is the excitation energy (cm^{-1}), I_p is the ionization potential (cm^{-1}), n is the principal quantum number, and δ is the quantum defect. The equation was applied to the 47170 cm^{-1} (5.85 eV) and 53300 cm^{-1} (6.61 eV) bands of the enol form by the use of the first I_p value (9.00 eV) obtained by photoelectron spectroscopy.[27] δ was determined to be 0.92 for the former band, and 0.62 for the latter band, corresponding to $n=3$. This strongly suggests that the 47170 cm^{-1} and 53300 cm^{-1} bands are due to the transitions to the 3s and 3p Rydberg orbitals, respectively, from the highest occupied π orbital.

In addition to the Rydberg transition bands, the enol form has valence-shell transition bands at 38020 cm^{-1} (4.72 eV) in the vapor phase or at 36770 cm^{-1} (4.56 eV) in perfluorohexane and at 56800 cm^{-1} (7.04 eV) in perfluorohexane. From Table 1 which shows the observed and theoretical values of the transition energies and oscillator strengths of the valence-shell transition bands, we can see that the bands at 4.72 and 7.04 eV are assigned to the first and second π-π^* transitions of the enol form, respectively.

In such polar solvents as acetonitrile and water, the amount of the keto form increases and the intensity of the 4.72 eV band pertinent to the enol form decreases with an approximate linear correlation with the dielectric constants of solvents. Figure 2 shows the intensity change of the band in several solvents.

Figure 3 shows the vapor phase absorption spectra of acetylacetone measured at various temperatures (20—204 °C) in the 30000—54000 cm^{-1} region. We can see that in the vapor phase the fraction of the keto form increases at higher temperatures. From the temperature dependence of the spectra in the 30000—35000 cm^{-1} region in Fig. 3, a weak band due to the keto form was found at $\approx$34000 cm^{-1} ($\approx$4.2 eV) in the vapor phase. The observed transition energy and oscillator strength are compared with the theoretical values in Table 1. We can see that the band is safely assigned to the first n-π^* transition of the keto form (calculated at 3.97 eV).

Let us turn to the Rydberg transition band of the keto form. In the region of 50000—54000 cm^{-1} in which the Rydberg transition bands of acetylacetone appear, spectral intensity increases at $\approx$52000 cm^{-1} with increasing temperature, whereas the bands at 47170 and 53300 cm^{-1} pertinent to the enol form decrease in intensity (see Fig. 3). This indicates that the band at $\approx$52000 cm^{-1} is ascribed to the keto form. By the aid of the equilibrium constant mentioned later, the 50000

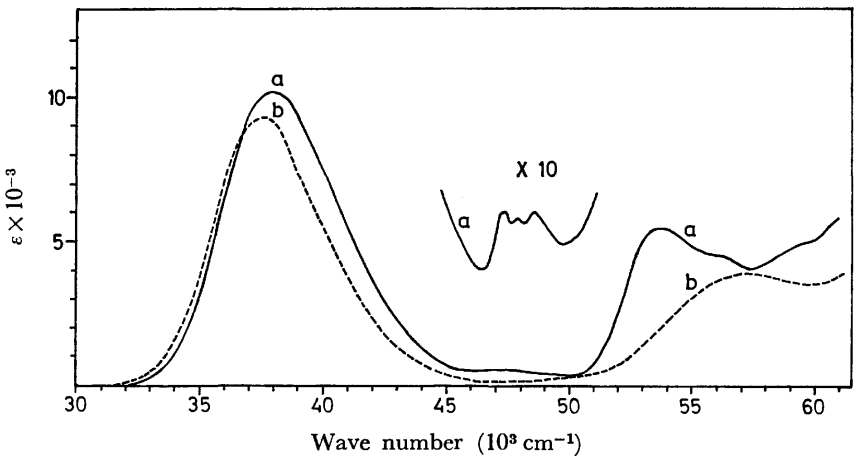

Fig. 1. Near and vacuum UV absorption spectra of acetylacetone measured (a) in the vapor phase and (b) in perfluorohexane at room temperature.

TABLE 1. TRANSITION ENERGIES ($^1\Delta E$(eV)) AND OSCILLATOR STRENGTHS (f) OBSERVED AND CALCULATED FOR THE ENOL AND KETO FORMS OF ACETYLACETONE

Assignment	Enol form					Keto form			
	Obsd		Calcd		Main[a] config.	Obsd		Calcd	
	$^1\Delta E$	f	$^1\Delta E$	f[b]		$^1\Delta E$	f	$^1\Delta E$	f[c]
σ-π^*			2.85	0.000_2 (z)	20-21	≈4.2[d]	≈0.007[d]	3.97	0.000_2 (z)
π-π^*	4.72[d]	0.24[d]	4.47	0.120 (x)	19-21			4.00	0.000 (y)
σ-π^*			5.31	0	20-22			7.30	0.207 (x)
σ-π^*			6.89	0	18-21			7.99	0.002 (y)
π-π^*	7.04[e]	≈0.13[e]	7.20	0.216 (y)	19-22			8.02	0.014 (z)
σ-π^*			7.61	0.017 (z)	(16, 13)-21			8.22	0.000_3 (y)
					18-22				
π-σ^*			8.00	0.025 (z)	19-(23, 25)			8.81	0.031 (z)
σ-σ^*			8.38	0.002 (x)	20-23			8.97	0.106 (y)
π-π^*			8.46	0.120 (y)	17-21			9.15	0.024 (xz)[f]
σ-π^*			8.58	0.004 (z)	(16, 13)-21			9.16	0.042 (y)
π-σ^*			8.60	0.009 (z)	19-26			9.35	0.013 (y)
σ-σ^*			8.93	0.022 (y)	20-(27, 24)			9.52	0.018 (z (x))[g]
π-σ^*			9.00	0	19-(27, 24)			9.54	0.023 (z)
σ-σ^*+π-π^*			9.02	0.685 (x)	20-26			9.94	0.008 (y)
					14-21				
σ-π^*			9.06	0	15-21				
π-σ^*			9.78	0.019 (z)	19-(28, 23, 25)				
σ-σ^*			9.94	0.045 (x)	20-(25, 23)				

a) Main electron configurations of the respective excited states are shown. (i,j)-k denotes the singly excited configurations, i-k and j-k, and i-(k,l), the singly excited configurations, i-k and i-l. b) The direction of the transition moment is shown in the parentheses, the x-axis being taken to be parallel to the O···H···O bond within the molecular (x-y) plane. c) The main component of the transition moment is shown in the parentheses, the x-axis being taken to be parallel to the C_2–C_4 line within the C_2–C_3–C_4 (x-y) plane (see Fig. 6(a)). d) Estimated from the observed intensity measured at 20 °C in the vapor phase by the aid of the equilibrium constant, K. e) Observed value in perfluorohexane. f) x- and z-components of the transition moment contribute comparably with the same sign to each other. g) x-Component of the transition moment contributes appreciably with the opposite sign to z-component.

—54000 cm^{-1} band can be resolved into the Rydberg bands of the keto form (≈52000 cm^{-1}) and the enol form (53300 cm^{-1}); the resolved spectra are also shown in Fig. 3. Equation 1 was applied to the ≈52000 cm^{-1} band of the keto form. From the first I_p value (9.60 eV) of the keto form,[27] δ was determined to be 0.92 corresponding to n=3, suggesting that the ≈52000 cm^{-1} band is due to the transition to the 3s Rydberg orbital from the highest occupied n orbital.

The UV absorption spectrum of the acetylacetonate anion[28] was also measured in 0.1 M NaOH aqueous solution; the result is shown in Fig. 2. Theoretical result tabulated in Table 2 clearly shows that the 34190 cm^{-1} (4.24 eV) band of the anion can be assigned to the first π-π^* transition calculated at 4.60 eV.

Electronic Structure of the Intramolecular Hydrogen Bond. Figure 4 shows the energy levels calculated by the modified CNDO-CI method for some low-lying π-π^* and σ-σ^* excited states of the enol form. In the figure, i–j represents a singly excited configuration caused by the one-electron excitation from the i-th occupied MO to the j-th vacant MO. The shapes of the MO's of the enol form are schematically shown in Fig. 5. The CT band characteristic of the intramolecular hydrogen bond, O···H···O corresponds to the transition from the nonbonding orbital to the antibonding orbital in the hydrogen bond. The 20–26 configuration corresponds to this transition. As is illustrated in Fig. 4, the 20–26 CT configuration interacts significantly with the 19–21 and 14–21 π-π^* configurations, and contributes to the first (calculated at 4.47 eV) and sixth (calculated at 9.02 eV) excited states. The 4.47 eV band is mainly composed of the 19–21 π-π^* (83.3%) and 20–26 CT (9.8%) configurations. The main configurations in other excited states of the enol form are also given in Table 1.

The character of the intramolecular hydrogen bond of acetylacetone can be clarified quantitatively by the configuration analysis; the results for the ground and the first π-π^* excited (calculated at 4.47 eV) states are tabulated in Table 3, together with the result for the first σ-σ^* excited (predicted at 8.38 eV) state. In the ground state, the hydrogen bond is composed of the symmetric covalent structure III (≈45.1%), the ionic structure V (≈42.9%), and the symmetric ionic structure I (≈11.0%). As is shown in a previous paper,[16] the CT structure corresponds to the antisymmetric covalent structure IV and antisymmetric ionic structure II. The antisymmetric covalent and ionic structures contribute fairly (≈9.7%) to the first π-π^* excited state, but contribute only little (≈1.4%) to the first σ-σ^* excited state predicted at 8.38 eV.

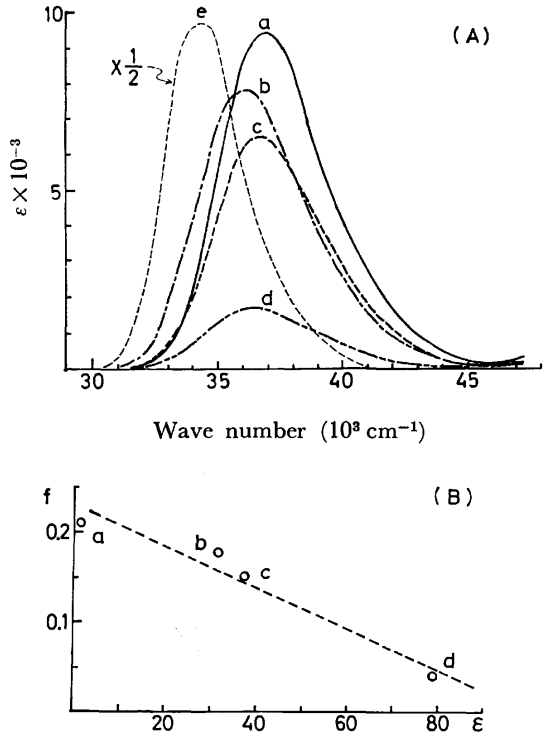

Fig. 2. (A) UV absorption spectra of acetylacetone measured at room temperature in (a) heptane, (b) methanol, (c) acetonitrile, (d) water, and (e) 0.1 M NaOH aqueous solution.
(B) Dependence of the oscillator strength (f) observed with the 36000—37000 cm^{-1} band in (a) heptane, (b) methanol, (c) acetonitrile, and (d) water upon the dielectric constant (ε) of the solvent used.

Electron Densities. Figure 6 shows electron densities for the ground states of the keto and enol forms of acetylacetone, and of its anion. The carbon and oxygen atoms in the five membered ring of the enol form are more polarized than the corresponding atoms in the keto form. By the removal of the hydrogen-bonded proton, electron densities in the anion increase in the whole region of the molecule compared to the corresponding ones in the enol form. Dipole moments of the keto and enol forms of acetylacetone were calculated to be 4.93 and 3.18 Debye, respectively, being in good agreement with the observed value for the enol form in the vapor phase (3.0 Debye).[29]

TABLE 2. TRANSITION ENERGIES ($^1\Delta E$(eV)) AND OSCILLATOR STRENGTHS (f) OBSERVED AND CALCULATED FOR THE ACETYLACETONATE ANION

Assignment[a]	Obsd		Calcd[a]	
	$^1\Delta E$	f	$^1\Delta E$	f[b]
σ-π^*			2.92	0.000_2 (z)
σ-π^*			3.60	0
π-π^*	4.24	0.37	4.60	0.234 (x)
σ-π^*			6.01	0
π-π^*			6.27	0.249 (y)
σ-π^*			6.46	0.027 (z)
π-σ^*			6.83	0.024 (z)
π-π^*			7.30	0.042 (y)
σ-σ^*			7.40	0.001 (x)
π-σ^*			7.51	0
σ-σ^*			7.65	0.015 (y)
σ-π^*			7.98	0
π-σ^*			8.26	0.009 (z)
σ-π^*			8.53	0.001 (z)
σ-σ^*			8.67	0.011 (x)
π-π^*+ σ-σ^*			8.84	0.276 (x)

a) The molecular structure was assumed to be the same to the one of the enol form of acetylacetone except for the fact that the hydrogen-bonded proton was removed.
b) The direction of the transition moment is shown in the parentheses, the x-axis being taken to be parallel to the O···O line within the molecular (x-y) plane.

Equilibrium Constant Between Keto and Enol Forms of Acetylacetone. The equilibrium constant (K) between the keto and enol forms of acetylacetone;

$$K = [\text{enol}]/[\text{keto}] \qquad (2)$$

was determined in the vapor phase from the temperature dependence of the absorption spectrum shown in Fig. 3. As already mentioned, gaseous acetylacetone

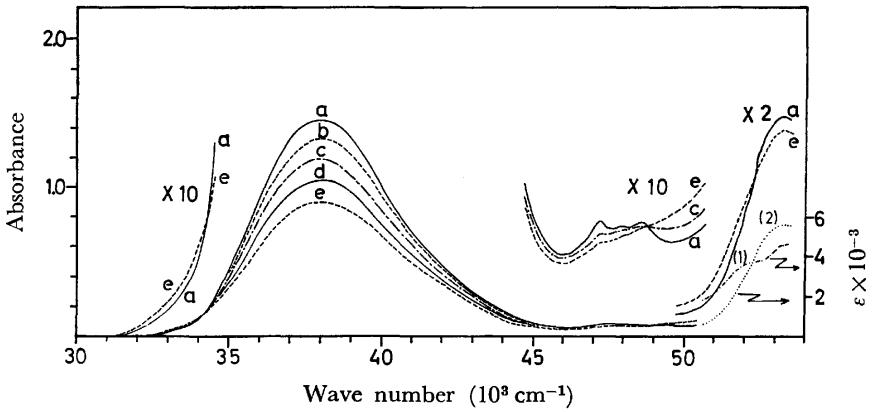

Fig. 3. Absorption spectra of acetylacetone in the vapor phase measured at (a) 20°, (b) 98°, (c) 120°, (d) 169°, and (e) 204 °C. From the mole fraction of the enol form, absorption spectrum in the 50000—54000 cm^{-1} region was resolved into two spectra ascribed to (1) the keto form and (2) the enol form of acetylacetone.

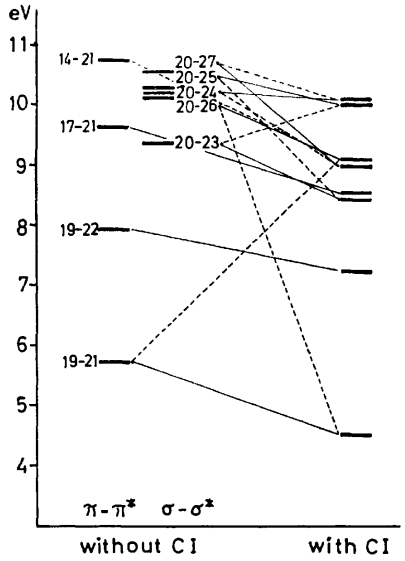

Fig. 4. Energy levels calculated with and without CI treatment for some lower π-π^* and σ-σ^* excited states of the enol form of acetylacetone.

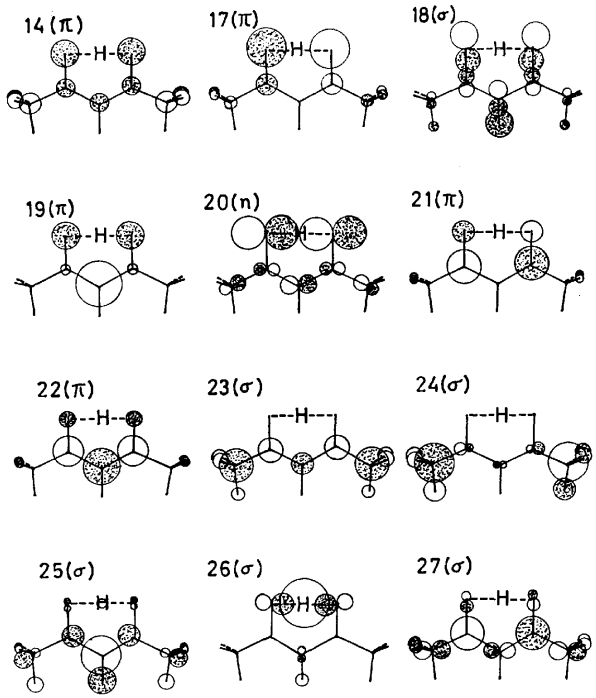

Fig. 5. Schematic shapes of some occupied and vacant MO's of the enol form of acetylacetone. The 20th MO is the highest occupied one.

at room temperature exists almost completely as the enol form. Strictly speaking, however, it may contain slightly the keto form. In view of this, we tried to determine accurately the mole fraction of the enol form and the K value from a linear relationship between $\ln K$ and $1/T$. In actuality, we evaluated K at 68, 120, 169, and 204 °C by combining the observed absorption intensity (at each temperature) at 38020 cm^{-1} and the molar extinction coefficients at the same wave number derived from several appropriate mole fraction values of the enol form at 20 °C, 90.0, 95.0, 96.2, 97.0, and 100%. The values of $\ln K$ obtained thus at 20—204 °C are plotted against $1/T$ (Fig. 7). We can see that the linear relationship is most satisfactorily held for the mole fraction of 96.2%. The K values for this case

Table 3. Results of the configuration analysis (weights) for the ground and the first π-π^* and σ-σ^* excited states of the enol form of acetylacetone

	Structure	Reference configuration[a,b]	State		
			Ground	1st π-π^*	1st σ-σ^*
I	$(OH^-O^+)+(O^+H^-O)$[c]	i,j-36, 36	0.1101	—	—
II	$(OH^-O^+)-(O^+H^-O)$	i,j-36, 36	—	0.0320	0.0045
III	(O-H···O)+(O···H-O)	i-36	0.4166	—	—
		i-36+π-π^*[d]	0.0194	0.3627	0.0386
		i-36+σ-σ^*[d]	0.0153	0.0081	0.3628
		(Total for sym. covalent structure)	(0.4513)	(0.3708)	(0.4014)
IV	(O-H···O)−(O···H-O)	i-36	—	0.0605	0.0085
		i-36+π-π^*[d]	—	0.0028	0.0004
		i-36+σ-σ^*[d]	—	0.0019	0.0003
		(Total for antisym. covalent structure)		(0.0652)	(0.0092)
V	$O^{-1/2}H^+O^{-1/2}$	G^0 [e]	0.3942	—	—
		π-π^*[f]	0.0184	0.3433	0.0365
		σ-σ^*[f]	0.0153	0.0082	0.3460
		i,j-k,l	0.0013	0.0232	0.0297
		(Total for $O^{-1/2}H^+O^{-1/2}$ structure)	(0.4292)	(0.3747)	(0.4122)
		Total	0.9906	0.8427	0.8273

a) i and j denote the 20 occupied MO's of the anion, and k and l, the 15 vacant MO's of the anion. The 1s orbital of the hydrogen-bonded hydrogen is numbered as the 36th vacant orbital. b) i-k and i,j-k,l denote the singly and doubly excited reference configurations, respectively. c) The ionic structure, $((O^+H^-O)+(OH^-O^+))$, is also involved. d) Doubly excited configurations, i,j-k,36. e) The ground reference configuration coincides with the ground state of the anion. f) Singly excited configurations, i-k.

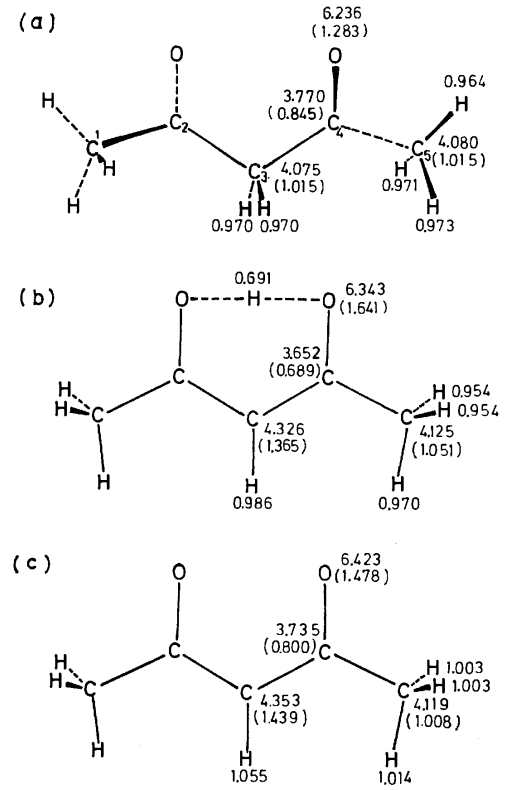

Fig. 6. Total and π-(in parentheses) electron densities calculated for the ground states of (a) the keto form, (b) the enol form, and (c) the anion of acetylacetone.

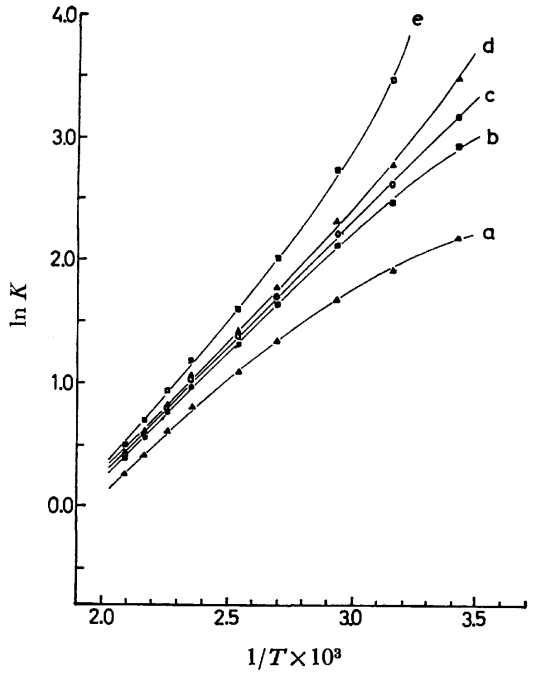

Fig. 7. Plots of $\ln K$ *versus* $1/T$ for acetylacetone in the vapor phase. The assumed mole fraction of the enol form at 20 °C is (a) 90.0%, (b) 95.0%, (c) 96.2%, (d) 97.0%, and (e) 100%.

are 25 at 20 °C, 9.5 at 68 °C, 4.03 at 120 °C, 2.25 at 169 °C, and 1.51 at 204 °C. From the slope of the straight line (c) in Fig. 7, the enthalpy change ($\Delta H°$) between the keto and enol forms in the vapor phase was evaluated to be −4.3 kcal/mol, being in good agreement with the result by an IR study in the vapor phase ($\Delta H° = -3.9$ kcal/mole) by Mecke and Funck.[30] From the mole fraction of the enol form, the ε_{max} and f values of the 38020 cm^{-1} band were calculated to be 10600 and 0.24, respectively.

The authors are indebted to Dr. Akira Kuboyama, National Chemical Laboratory for Industry, for the use of a JASCO VUV-3 recording spectrophotometer at an early stage of the research. This work was partially supported by a Grant-in-Aid for Scientific Research from the Ministry of Education, Science and Culture.

References

1) J. P. Schaefer and P. J. Wheatley, *J. Chem. Soc., A*, **1966**, 528.
2) A. H. Lowrey, C. George, P. D'Antonio, and J. Karle, *J. Am. Chem. Soc.*, **93**, 6399 (1971).
3) A. L. Andreassen, D. Zebelman, and S. H. Bauer, *J. Am. Chem. Soc.*, **93**, 1148 (1971); A. L. Andreassen and S. H. Bauer, *J. Mol. Struct.*, **12**, 381 (1972).
4) J. E. Del Bene and W. L. Kochenour, *J. Am. Chem. Soc.*, **98**, 2041 (1976).
5) G. Karlström, H. Wennerström, B. Jönsson, S. Forsén, J. Almlöf, and B. Roos, *J. Am. Chem. Soc.*, **97**, 4188 (1975); G. Karlström, B. Jönsson, B. Roos, and H. Wennerström, *ibid.*, **98**, 6851 (1976).
6) A. D. Isaacson and K. Morokuma, *J. Am. Chem. Soc.*, **97**, 4453 (1975).
7) P. Schuster, *Chem. Phys. Lett.*, **3**, 433 (1969).
8) M. S. Gordon and R. D. Koob, *J. Am. Chem. Soc.*, **95**, 5863 (1973).
9) P. Grossman, *Z. Phys. Chem.*, **109**, 305 (1924).
10) R. S. Rasmussen, D. D. Tunnicliff, and R. R. Brattain, *J. Am. Chem. Soc.*, **71**, 1068 (1949).
11) B. Eistert and W. Reiss, *Chem. Ber.*, **87**, 108 (1954); B. Eistert, E. Merkel, and W. Reiss, *ibid.*, **87**, 1513 (1954).
12) R. H. Holm and F. A. Cotton, *J. Am. Chem. Soc.*, **80**, 5658 (1958).
13) G. S. Hammond, W. G. Borduin, and G. A. Guter, *J. Am. Chem. Soc.*, **81**, 4682 (1959).
14) For the discussion about the CT mechanism of the hydrogen bond, see for example, C. A. Coulson, *Research*, **10**, 149 (1957); S. Bratož, "Advances in Quantum Chemistry," Vol. 3, ed by P. O. Löwdin, Academic Press, New York (1967), p. 209; R. S. Mulliken and W. B. Person, "Molecular Complexes," Wiley-Interscience, New York (1969).
15) S. Nagakura, *J. Chim. Phys.*, **61**, 217 (1964).
16) H. Morita, K. Fuke, and S. Nagakura, *Bull. Chem. Soc. Jpn.*, **50**, 645 (1977).
17) H. Nakanishi, H. Morita, and S. Nagakura, *J. Mol. Spectrosc.*, **65**, 295 (1977).
18) H. Morita, K. Fuke, and S. Nagakura, *Bull. Chem. Soc. Jpn.*, **49**, 922 (1976).
19) H. Baba, S. Suzuki, and T. Takemura, *J. Chem. Phys.*, **50**, 2078 (1968).
20) K. Kaya and S. Nagakura, *J. Mol. Spectrosc.*, **44**, 279 (1972).
21) A. Kuboyama, S. Matsuzaki, H. Takagi, and H. Arano, *Bull. Chem. Soc. Jpn.*, **47**, 1604 (1974).
22) The molecular geometries of acetylacetone determined by vapor-phase electron diffraction studies by different authors[2,3] differ appreciably to each other. The result of

tetraacetylethane by X-ray diffraction study[1] is intermediate between the above two results.

23) L. W. Reeves, *Can. J. Chem.*, **35**, 1351 (1957).

24) J. Powling and H. J. Bernstein, *J. Am. Chem. Soc.*, **73**, 4553 (1951).

25) R. Mecke and E. Funck, *Z. Electrochem.*, **60**, 1124 (1956).

26) M. B. Robin, "Higher Excited States of Polyatomic Molecules," Vol. 1, Academic Press, New York (1974).

27) A. Schweig, H. Vermeer, and U. Weidner, *Chem. Phys. Lett.*, **26**, 229 (1974).

28) F. Hashimoto, J. Tanaka, and S. Nagakura, *J. Mol. Spectrosc.*, **10**, 401 (1963).

29) C. T. Zahn, *Physik. Z.*, **34**, 461 (1933); A. L. McClellan, "Tables of Experimental Dipole Moments," W. H. Freeman, San Francisco (1963), p. 143.

30) R. Mecke and E. Funck, "Hydrogen Bonding," ed by D. Hadži, Pergamon Press, London (1959), p. 433.

Surface Oxidation of the Thin Films of Polycyclic Aromatic Hydrocarbons Studied by X-Ray Photoelectron Spectroscopy

Masamichi YAMADA, Isao IKEMOTO, and Haruo KURODA

Department of Chemistry, Faculty of Science, The University of Tokyo, Hongo, Tokyo 113

(Received March 22, 1977)

The oxidation of the surfaces of thin films of perylene, pentacene, violanthrene, and mesonaphthodianthrene on exposure to oxygen or to the air was studied by means of X-ray photoelectron spectroscopy. A perylene film was found to be the least reactive toward oxygen among the above four hydrocarbons. In the cases of pentacene and violanthrene films, a single, broad O 1s peak grew up with time over the period of a few months as the exposure to the air was prolonged. On exposure to oxygen, a mesonaphthodianthrene film exhibited the O 1s spectrum which apparently consisted of two peaks located at the binding energies, 531.0 and 532.9 eV respectively, and the peak at 532.9 eV reduced its intensity irreversibly on heating the film in a high vacuum, suggesting that it was the one associated with a loosely bound oxygen.

Semiconductive and photoconductive behavior of organic solids are often influenced considerably by the oxygen adsorption on the surface.[1] It is well known that the photoconductivity of anthracene crystal is significantly affected by oxygen.[2,3] In the cases of large polycyclic aromatic hydrocarbons such as mesonaphthodianthrene[4] and quaterrylene,[5]* their evaporated films were reported to exhibit quite different semiconductive behavior in the ordinary atmosphere as compared with those measured in a high vacuum. Generally, the surfaces of organic molecular crystals are rather unreactive to oxygen, so that one could consider that the oxygen species formed on their surfaces by the interaction with ambient oxygen would be primarily the oxygen molecules loosely bound on the crystal surface by physical adsorption. In effect, most of the observed oxygen effects on electrical properties of organic solids were found to vary reversibly depending on the ambient oxygen pressure. However, in some cases, the effects were not entirely reversible,[5] suggesting the formation of strongly-bound oxygen species or surface oxides.

Although a considerable amount of experimental results have been accumulated on the phenomena related to the influence of ambient oxygen on the electrical properties of organic solids,[1] little is known about the actual reactivities of the surfaces of organic crystals toward oxygen. In the present study, we have investigated the oxygen adsorption, or the surface oxidation of the thin films of polycyclic aromatic hydrocarbons by means of X-ray photoelectron spectroscopy.

Experimental

X-Ray photoelectron spectra were measured with McPherson ESCA 36 electron spectrometer employing Al K_α (1486.6 eV). The sample films were prepared by sublimation onto aluminum plates set inside the sample chamber of the spectrometer, which was kept at a vacuum of about 10^{-7} Torr by using a turbomolecular pump and a cryogenic pump. On each sample, the experiments were carried out according to the following steps. First, the C 1s and O 1s regions of Al K_α photoelectron spectrum were recorded immediately after the preparation of the sample film. A wide-scan spectrum was also recorded in order to see if the film was free from any impurity, and if the film was thick enough to prevent the appearance of any spectrum due to the substrate. After the above measurements, the cryogenic pump was switched off prior to the introduction of oxygen into the sample chamber. This inevitably caused a release of gases, including oxygen, from the cryopanel in the sample chamber. Thus, the C 1s and O 1s spectra were recorded again after this operation to examine the effects of the released gases. Then, the oxygen gas of a few hundred Torr was introduced into the sample chamber. After the sample film having been kept in this oxygen gas for 30 min, the oxygen gas was pumped out from the sample chamber to measure Al K_α photoelectron spectrum. In some cases, oxygen was again introduced into the sample chamber, and the film was continuously kept in the oxygen atmosphere for a night before the next measurement of the spectrum. After those experiments, the sample film was taken out of the spectrometer, and kept at a dark place in the ordinary atmosphere to examine the effect of prolonged exposure to the air. The C 1s and O 1s spectra of the sample film were observed occasionally over the period of a few months. Finally, a small amount of gold was deposited onto the sample surface for calibration of binding energies by use of Au $4f_{7/2}$ (84.0 eV) peak as the standard.

Experiments were done on four polycyclic aromatic hydrocarbons; pentacene(**1**), violanthrene(**2**),** perylene(**3**), and mesonaphthodianthrene(**4**).***

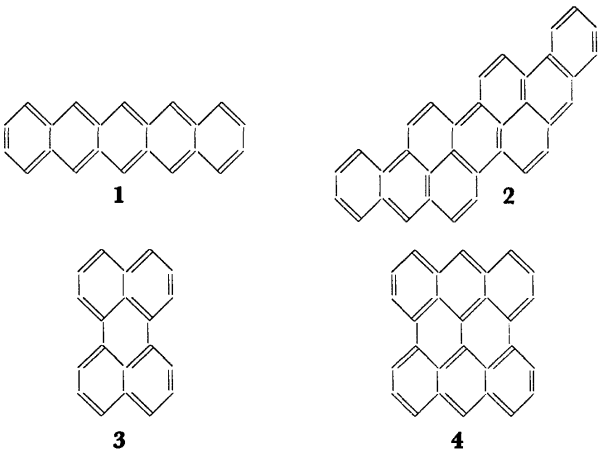

Results and Discussion

It is well known that pentacene, $C_{22}H_{14}$, is quickly oxidized in the solution by the interaction with the oxygen dissolved in the solvent, particularly under the

* Benzo[1,2,3-*cd*: 4,5,6-*c'd'*]diperylene.

** Dinaphtho[1,2,3-*cd*: 3',2',1'-*lm*]perylene.

*** Phenanthro[1,10,9,8-*opqra*]perylene.

action of visible light, to form a transannular peroxide.[6] However, it is quite stable in the crystalline state, so that the crystalline powder of pentacene can be kept in the ordinary atmosphere without significantly suffering the oxidation. The oxygen effect on the photoconductivity of a pentacene film was studied some years ago by one of the present authors.[7] It was observed that, when a pentacene film was exposed to an oxygen gas, the photocurrent through the film under a fixed light intensity gradually increased with time to the stationary-state value which was dependent on the pressure of the ambient oxygen. This oxygen effect was found to be almost reversible, suggesting that it was primarily associated with the oxygen molecules loosely bound on the surface.

The Al K_α photoelectron spectrum of a pentacene film before being exposed to the oxygen gas, did not exhibit any O 1s peak, showing only a strong and sharp C 1s peak (with the FWHM of about 1.7 eV) accompanied by weak satellite bands. When the film was exposed to the oxygen gas for about 30 min, a weak O 1s peak appeared in the photoelectron spectrum, and the intensity of this peak did not decrease at all even by keeping the film in a high vacuum (about 10^{-7} Torr) for a night. This fact indicates that, although the oxygen effect on photoconductivity is mostly reversible,[7] there are some oxygen species which can not be removed by a prolonged pumping from the surface of the pentacene film which has been once exposed to the oxygen gas.

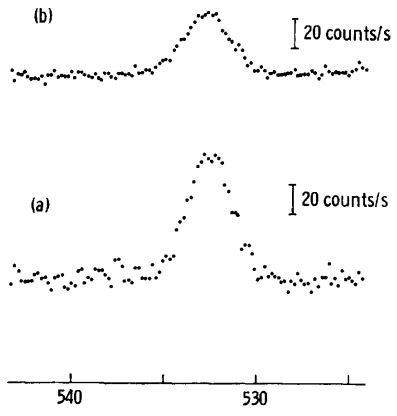

Fig. 1. (a): O 1s spectrum of the pentacene film after exposure to the air for 12 days, (b): O 1s spectrum of the violanthrene film after exposure to the air for 10 days.

On keeping the pentacene film in the air, the O 1s peak further grew up slowly with time. As shown in Fig. 1(a), the FWHM of this O 1s peak was 2.9 eV while a sample containing only a single kind of oxygen would give an O 1s peak with the FWHM of less than 2.0 eV under the same experimental conditions.[8] Thus the broadness of the observed O 1s peak is likely to indicate that there are more than one chemical states of oxygen atoms in the surface region of the pentacene film. In the photoelectron spectrum taken after 38 days' exposure to the air, the ratio of integrated intensity of the O 1s peak to that of the C 1s peak was found to be 0.099, which corresponds to the atom ratio, one oxygen atom per 22 carbon atoms,[9] in other words, one oxygen atom per one pentacene molecule. Since the escape depth of photoelectrons is of the order of two or three molecular layers of pentacene, the above results would possibly mean that every pentacene molecule on the surface is in the state bound with one oxygen molecule. The intensity ratios, O 1s/C 1s, obtained for the pentacene film at different stages of oxygen exposure are summarized in Table 1 together with the data concerned with other hydrocarbon films.

In the case of violanthrene, $C_{34}H_{18}$, the observed behaviors were a little different from those of a pentacene film. When a violanthrene film was exposed to the gases evolved from the cryopanel on turning off the cryogenic pump, there appeared a weak O 1s peak in the photoelectron spectrum of the film, but thereafter its intensity did not detectably increase on keeping the film in the oxygen gas for a night. The growth of the O 1s peak was so slow that we had to keep the film in the air for several days in order to attain an appreciable increase of its intensity. After the 38 days' exposure to the air, the intensity of O 1s peak relative to that of C 1s peak became 0.047, which corresponds to 0.7 oxygen atom per one violanthrene molecule. As in the case of a pentacene film, the observed O 1s peak was broad with the FWHM of about 3 eV as shown in Fig. 1(b).

The film of perylene, $C_{20}H_{12}$, was found to be the least reactive toward oxygen. Any O 1s peak did not appear in the photoelectron spectrum after the 10 min

Table 1. Variation of the intensity ratio, O 1s/C 1s

	Pentacene I_O/I_C[a]	Violanthrene I_O/I_C[a]	Mesonaphthodianthrene I_O/I_C[a]
(Fresh film)			(0.026)
After the cryogenic pump was switched off	0.006	0.013	0.030
After exposure to O_2 for 30 min	0.015	0.014	0.038
After exposure to O_2 for a night	not tried	0.017	0.055
After exposure to the air	12 days 0.062	10 days 0.035	17 days 0.090
	38 days 0.099	38 days 0.047	67 days 0.101

a) Ratio of the integrated intensity of the O 1s peak to that of the C 1s peak.

exposure to the oxygen gas. Even after having been kept in the air for six months, only a very weak O 1s peak appeared in the spectrum, its intensity relative to that of the C 1s peak being only 0.017.

The results described above demonstrate that the films of pentacene, violanthrene, and perylene are markedly different from each other as regards the reactivity toward oxygen. This difference seems to be closely related to the reactivity of the free molecule of each hydrocarbon. As it has been already mentioned, a pentacene molecule in the solution easily forms a transannular peroxide by the interaction with an oxygen molecule.[6] But a transannular peroxide will not be so easily formed in the bulk of a pentacene crystal since its formation requires a large distortion of crystal lattice. This is likely to be the reason why the pentacene crystal can be stably kept in the ordinary atmosphere. However, the situation can be different for the crystal surface, where the change of molecular arrangement can occur more easily than in the bulk. Thus one could consider that the oxygen-containing species formed on the surface of the film on exposing to the oxygen gas is the transannular peroxide of pentacene. One could also consider the formation of other oxides of pentacene such as a quinone or hydroxy compounds. But the observed O 1s peak is too broad to be attributed to any one of these oxides. Possibly, several different kinds of oxides coexist on the surface. In the case of violanthrene, a model like the transannular peroxide is hard to be considered because of the molecular geometry. Possibly, a quinone and/or hydroxy compounds would be the chemical species formed on the surface of the violanthrene film.

An interesting behavior was observed in the case of mesonaphthodianthrene, $C_{28}H_{14}$, which is also known to be very reactive to oxygen.[10] In the photoelectron spectrum of a fresh film, which was measured immediately after the preparation without breaking the vacuum, there appeared a weak O 1s peak at the binding energy of 531.0 eV (see the spectrum(a) of Fig. 2). This must be due to some impurity that originally existed in the powder of mesonaphthodianthrene. The above impurity is likely to be some stable oxide of mesonaphthodianthrene such as mesonaphthodianthrone.**** On exposure to oxygen, a new peak appeared on the higher binding-energy side (at 532.9 eV) of the first peak, as shown in the spectrum(b) of Fig. 2. This new O 1s peak can be attributed to the oxygen-containing species formed on the surface. The intensity of this new peak increased as the film was further exposed to the oxygen gas. However, at the same time, the intensity of the 531.0 eV peak increased by a larger extent, so that, after the 17 days' exposure to the air, the film showed the O 1s spectrum consisting of a strong peak at 531.0 eV and a shoulder at 532.9 eV (see the spectrum(d) of Fig. 2). After the 67 days' exposure to the air, the integrated intensity of the O 1s peak relative to that of the C 1s peak became 0.101 which corresponds to 1.3 oxygen atoms per one mesonaphthodianthrene molecule.

The O 1s spectrum of a mesonaphthodianthrene film once exposed to oxygen was found to vary with time. This behavior is illustrated by the spectra shown in Fig. 3. The spectrum(a) was obtained just after the exposure to oxygen for a night. The intensity of the 532.9 eV peak decreased when the film was kept in a high vacuum for 90 min, while that of the 531.0 eV

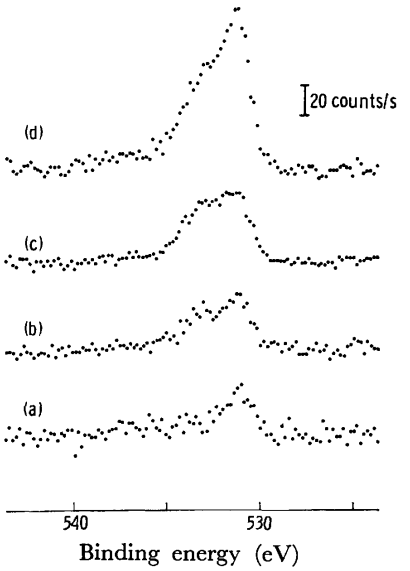

Fig. 2. Variation of the O 1s spectrum of the mesonaphthodianthrene film as exposures to oxygen or to the air were repeated.
(a): Immediately after preparation.
(b): After exposure to oxygen for 30 min.
(c): After exposure of (b) to oxygen for a night.
(d): After exposure of (c) to the air for 17 days.

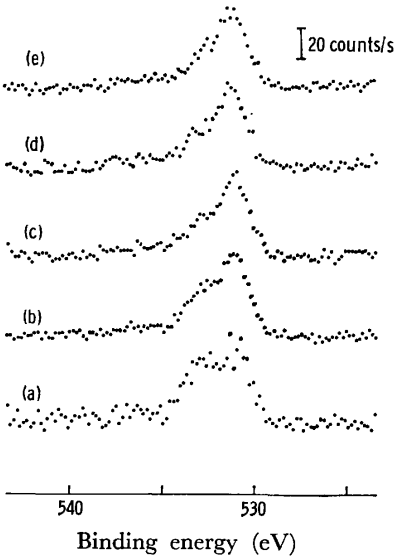

Fig. 3. Variation of the O 1s spectrum of the mesonaphthodianthrene film by heating it in the high vacuum of the sample chamber.
(a): The first recording at room temperature after exposure to oxygen for a night.
(b): Recorded at room temperature after standing (a) for 90 min.
(c): Recorded at about 60 °C.
(d): Recorded at about 100 °C.
(e): Reocrded again at room temperature.

**** Phenanthro[1,10,9,8-*opqra*]perylene-7,14-dione.

peak remained almost the same. This change became faster on elevating the temperature of the film to 60 °C and settled in the state which gave the spectrum(c). Thereafter, the O 1s spectrum did not further change on heating the film to 100 °C (the spectrum(d)), nor on cooling down it to room temperature (the spectrum (e)).

From the observation described above, we can conclude that there are at least two different kinds of oxides; the first is the species responsible for the O 1s peak at the binding energy of 532.9 eV, and the second is the one responsible for the 531.0 eV peak. Possibly the former is a metastable surface oxide where an oxygen molecule is rather loosely bound to a mesonaphthodianthrene molecule, and the latter is a stable oxide of mesonaphthodianthrene. The semiconductivity of a mesonaphthodianthrene film is known to be influenced by the oxygen adsorption.[4] It was observed that the electrical conductivity gradually increased with time in the oxygen gas, and decreased when the ambient oxygen gas was removed. These changes were found to be very slow at room temperature. Matsunaga reported that a sharp ESR signal appeared as the mesonaphthodianthrene powder was exposed to the air, and the intensity of this ESR signal increased slowly with time over the period of a few days.[11] It is most likely that the metastable surface oxide detected by X-ray photoelectron spectroscopy has some connection with the phenomena mentioned above. But, at present, it is hard to derive a definite conclusion as regards the true nature of this oxide.

References

1) F. Gutmann and L. E. Lyons, "Organic Semiconductors," Wiley, New York (1966), pp. 197—214.
2) A. G. Chynoweth, *J. Chem. Phys.*, **22**, 1029 (1954).
3) A. Bree and L. E. Lyons, *J. Chem. Soc.*, **1960**, 5179.
4) H. Kuroda and E. A. Flood, *Can. J. Chem.*, **39**, 1475 (1961).
5) Y. Maruyama and H. Inokuchi, *Bull. Chem. Soc. Jpn.*, **39**, 1418 (1966).
6) E. Clar, "Polycyclic Hydrocarbons," Academic Press, Vol. 1, London (1964), p. 425.
7) H. Kuroda and E. A. Flood, *Can. J. Chem.*, **39**, 1981 (1961).
8) The evaporated film of hydroquinone (cooled to about −50 °C) exhibited an O 1s peak with the FWHM of 1.9 eV under the same experimental conditions.
9) The relative sensitivity of detection for carbon and oxygen is taken as 0.46 : 1.00. This value was derived from gas-phase measurements of nitromethane, acetone, and phenol with the same instrument.
10) H. Kuroda, *J. Chem. Phys.*, **33**, 1586 (1960).
11) Y. Matsunaga, *Can. J. Chem.*, **38**, 323 (1960).

Factor Group Splitting and the Lowest Triplet State of Tetrachlorophthalic Anhydride Crystals

Mizuka SANO, Takatoshi NARISAWA, Mitsunobu MATSUKA, and Yasumasa J. I'HAYA

Department of Materials Science, The University of Electro-Communications, Chofu, Tokyo 182

(Received April 22, 1977)

The electronic configuration of the lowest triplet state for tetrachlorophthalic anhydride (TCPA) was determined to be $B_2(\pi\pi^*)$ by means of Zeeman spectroscopy. The electronic origin for the singlet-triplet absorption of a TCPA single crystal was found in the region of 421.3 nm at 1.7 K. The first peak in the absorption spectrum was found to possess two components; the one observed at 23726.1 cm^{-1} corresponds to the transition to the B_u, and the other observed at 23728.5 cm^{-1} to that to the A_u triplet factor group state. The splitting between the two states is 2.4 cm^{-1}.

The lower excited triplet $n\pi^*$ and $\pi\pi^*$ states of aromatic carbonyls are closely spaced and change their energies differently under the influence of environments (solvents and/or host molecules) or substituent effects. The properties of these nearby triplet states have been the subject of numerous spectroscopic and related studies in recent years.[1] In previous papers we attempted to explain the excited triplet states of aromatic quinones.[2] As an extension of these studies, we take up tetrachlorophthalic anhydride (abbreviated to TCPA hereafter). TCPA is a typical electron acceptor and forms stable charge-transfer complexes with a number of aromatic compounds. Although much effort has been made in understanding spectroscopic properties of TCPA charge-transfer complexes, the excited triplet states of TCPA in a single crystal appear to be less understood.

The present study was undertaken in order to clarify the electronic configuration of the lowest triplet state of TCPA by means of Zeeman spectroscopy. In principle, the electronic configuration of a triplet state can be assigned by determining both the polarization in absorption and an effective route in the spin-orbit interaction. This is because the transition from the ground state to the triplet state in question is assumed to gain its intensity from the transition from the ground state to a perturbing singlet state through the spin-orbit coupling between the triplet state and the perturbing singlet state in the first-order spin-orbit interaction mechanism. In case that a perturbing triplet state is located closely to the triplet state in question, the intensity stealing from the transition between these triplet states must also be taken into consideration. In this work both the direction of polarization in the singlet-triplet absorption transition and the Zeeman intensity pattern were observed for thick TCPA single crystals.

Experimental

The experimental procedures were the same as described in the previous papers.[2] TCPA (Tokyo Kasei Organic Chemicals) was purified by zone-refining for 40 passes with additional 40 passes, and then grown into a single crystal from the melt. Crystal samples with suitable size, about 5×5 mm^2 in area and 3—18.4 mm in thickness, were taken from the crystal, and their faces were identified by the X-ray diffraction method. The reciprocal dispersion of an NLM-E2M spectrometer used for absorption measurements was 0.053 nm mm^{-1} at 420 nm in the 13th order of an Echelles grating. Phosphorescence of a crystal immersed in liquid helium was excited by 365 nm radiation from an ORC 1 kW superhigh-pressure mercury arc.

Results and Discussion

Figures 1 and 2 show the singlet-triplet absorption and the phosphorescence spectra of a TCPA single crystal at 1.7 K, respectively. The first peak in the absorption spectrum was found in the region of 421.3 nm and that in the phosphorescence spectrum at 422.2 nm (23677 cm^{-1}). The intensity of the first absorption peak was measured for the light polarized along each crystallographic axis. The polarization ratio I_a^*/I_c was found

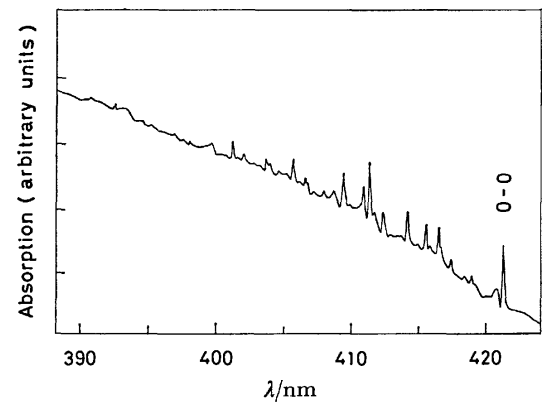

Fig. 1. The c-polarized singlet-triplet absorption spectrum of a TCPA crystal at 1.7 K; broad background due to a xenon arc light source.

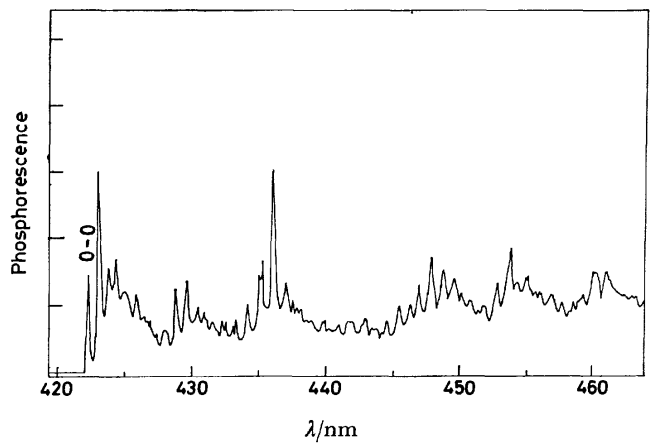

Fig. 2. The phosphorescence spectrum of a TCAP crystal at 1.7 K.

to be 0.53 and the ratio I_c/I_b to be 1.6. This peak was found to split into sublines upon the application of a magnetic field. From these results, the first peak is assigned to the origin of the lowest singlet-triplet transition for crystalline TCPA. Other intense, sharp absorption peaks were found at 24010.3, 24061.5, 24139.1, 24246.7, 24308.3, 24333.8, 24425.9, and 24641.5 cm^{-1} in the spectral region to 400 nm. No absorption peak was observed in the region between 400 and 380 nm, but a broad absorption band with polarization different from the first peak was found at 370 nm (27000 cm^{-1}).

Figure 3a shows the high-resolution absorption spectrum of the first peak for a 18.4 nm oriented crystal with the light propagating along the b axis and polarized along the c axis. The peak was found to possess two components, O_1 at 23726.1 cm^{-1} and O_2 at 23728.5 cm^{-1}. The intensity ratio of the O_1 to the O_2 components, $(I_1/I_2)_c$, was found to be 0.14. The intensity ratio obtained through the light propagating along the c axis, however, depended on the direction of polarization of light. The ratios were found to be 0.07 for the light polarized along the a* axis and 1/0.13 for the light polarized along the b axis.

Upon the application of a magnetic field of 50 kOe along the b axis, the O_2 component observed through the c-polarized light was found to split into two sublines with a separation of about 9.5 cm^{-1}, and the O_1 component remained unchanged, as shown in Fig. 3b. Upon the application of a magnetic field along the a* axis, there appeared five sublines in total, originating from both components, and their intensities were dependent on the polarization of light used for the observation (Fig. 4a).

All the experimental results mentioned above can be reasonably explained in terms of the scheme that the spatial symmetry of the lowest triplet state for TCPA belongs to $B_2(\pi\pi^*)$, and the O_1 and O_2 components in the absorption spectrum correspond to the transitions to

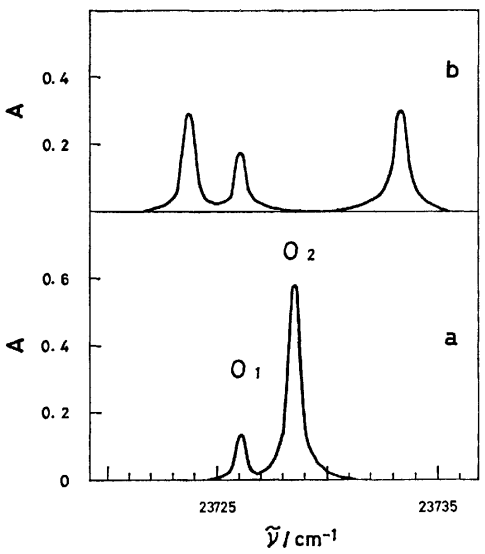

Fig. 3. The electronic origin of the c-polarized singlet-triplet absorption spectrum of a TCAP crystal at 4.2 K. (a) $H=0$, (b) $H=50$ kOe, H//b.

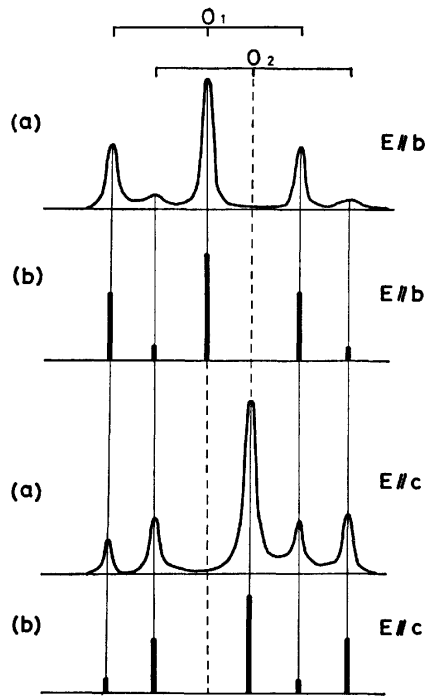

Fig. 4. Zeeman absorption patterns of a TCAP crystal. A magnetic field of 50 kOe was applied along the a* axis.
(a) The observed spectra, (b) the calculated intensities for the scheme of the x-polarized transition with the z-route in the spin-orbit coupling.

the B_u and A_u triplet factor group states, respectively.

The crystal structure of TCPA gives the space group symmetry C_{2h}^5 with four molecules per unit cell. The molecule in a crystal can be regarded as planar, belonging to the C_{2v} point group.[3] The molecular framework z-axis is taken as the molecular twofold axis, and the z,y-plane as the plane of the molecule. If we assume that only one route is active in mixing molecular singlet and triplet states through the spin-orbit coupling, the transition to the A_u state is expected to split into two wing sublines $I_{\pm 1}$, while that to the B_u state to remain unchanged, showing only the central subline I_0, when a magnetic field is applied along the b axis and the absorption is observed through the c-polarized light. The intensity ratio of I_0 to $I_{\pm 1}$ is expressed by

$$\left(\frac{I_0}{I_{\pm 1}}\right)_c = \frac{2m_u^2}{1-m_u^2}, \tag{1}$$

where m_u consists of the direction cosines of the molecular axes x, y, and z with respect to the b axis.[4] This ratio is just twice the absorption intensity ratio between the two factor group splitting components observed through the c-polarized light $(I_1/I_2)_c$. The absorption intensity ratios between the components obtained through the light polarized along each crystallographic axis are related to one another by the equation,

$$\left(\frac{I_1}{I_2}\right)_c = \left(\frac{I_1}{I_2}\right)_{a^*} = 1\Big/\left(\frac{I_1}{I_2}\right)_b. \tag{2}$$

This is just what we have observed for the TCPA crystals. The values of the ratio in Eq. 1 were calculated from the direction consines to be 1.1, 2.8, and

0.13 for x, y, and z routes in the spin-orbit coupling, respectively. The experimental finding is consistent only with the z route involved in the spin-orbit coupling (an A_2 representation in the C_{2v} point group).

The polarization ratio for the first peak, that is, the sum of the O_1 and O_2 components, can be explained in terms of the transition which is primarily out-of-plane polarized (a B_1 representation in the C_{2v} point group). Furthermore, the Zeeman absorption pattern obtained for the light polarized along the c axis or the b axis under the magnetic field directed along the a* axis can be most satisfactorily represented by the scheme that the absorption intensity is taken from the x-polarized transition and the effective route in the spin-orbit coupling is z, as shown in Fig. 4b. Therefore, it is concluded that the lowest triplet state for TCPA belongs to $B_2(\pi\pi^*)$.

The lowest singlet-singlet absorption band of TCPA in the region from 30000 to 32500 cm^{-1} has been assigned theoretically to the transition of $\pi\pi^*$ character. The next band in the region from 35000 to 38000 cm^{-1}, however, has not been explained in terms of a $\pi\pi^*$ transition.[5] The broad absorption band observed at 27000 cm^{-1} in the present study was found to be stronger than the lowest singlet-triplet absorption, but weaker than the singlet-singlet absoption in oscillator strength. Considering the intensity, the broadness, the direction of polarization (mainly z-polarized), and the location of the band in the spectrum, the absorption is tentatively ascribed to the transition to a triplet state of $n\pi^*$ character.

The triplet factor group splitting was observed only for the first absorption peak, which was the strongest in intensity among the peaks in the transition to the lowest triplet state. This result shows that the coupling between molecules in the TCPA crystals is interpreted on the basis of a weak coupling model, where the magnitude of each splitting is roughly proportional to the intensity of a peak.[6]

References

1) E. T. Harrigan and N. Hirota, *Mol. Phys.*, **31**, 663 (1976) and references cited therein.

2) M. Sano, T. Narisawa, and Y. J. I'Haya, *Bull. Chem. Soc. Jpn.*, **48**, 3469 (1975); T. Narisawa, M. Sano, and Y. J. I'Haya, *Chem. Lett.*, **1975**, 1289.

3) R. Rudman, *Acta Crystallogr., Sect. B*, **27**, 262 (1971).

4) R. M. Hochstrasser, *J. Chem. Phys.*, **47**, 1015 (1967); "Molecular Aspects of Symmetry," W. S. Benjamin, Inc., New York (1966), Chap. 10.

5) I. Deperasinka and J. S. Kwiatkowski, *Bull. Acad. Pol. Sci., Ser. Sci. Math. Astron. Phys.*, **19**, 655 (1971).

6) W. T. Simpson and D. L. Peterson, *J. Chem. Phys.*, **26**, 588 (1957).

ENDOR Studies on Low-Symmetry Triphenylmethyl with *ortho*- or *para*-Methoxy Substituents

Kazuhiko Ishizu, Kazuo Mukai, Atsuko Shibayama, and Kyoko Kondo

Department of Chemistry, Faculty of Science, Ehime University, Bunkyo-cho, Matsuyama 790

(Received January 21, 1977)

ENDOR observations were carried out for several triphenylmethyl derivatives with *ortho*- or *para*-methoxy substituents. The alteration of the spin-density distribution caused by steric hindrance, in particular, due to the low symmetrical substitution, was investigated. Using a revised MO parameter proposed by Kulkarni, McLachlan MO calculations were carried out and the twisting angles of the hindered phenyl groups are estimated.

Triphenylmethyl is one of the typical neutral radicals on which a number of ESR studies have been made. In the case of methoxy derivatives, however, the observed ESR hyperfine structures are often complicated by overlapping due to the small methoxy proton splitting, and, sometimes, by modulation of hindered rotation of the substituents.

To the authors' knowledge, the derivatives which have already been studied are chiefly those of higher molecular symmetry such as 4,4′,4″-trimethoxytriphenylmethyl[1] and 2,2′,2″,6,6′,6″-hexamethoxytriphenylmethyl.[2] In the present work, ENDOR studies of several methoxy derivatives of triphenylmethyl with low-symmetrical substitution, as shown in Fig. 1, are reported.

Perturbation of the spin density due to steric hindrance was measured in detail, and the conformation of the hindered phenyls was investigated in terms of McLachlan MO calculations including a correction for the Coulomb integral of the central methyl carbon due to Kulkarni.

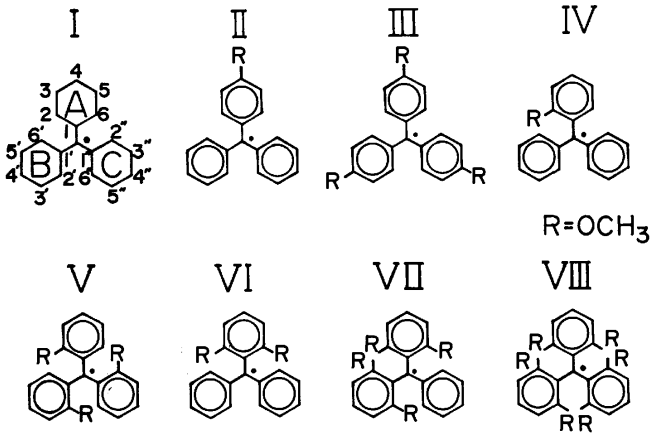

Fig. 1.

Experimental

Triphenylmethanols I, II, III, IV, and V, were synthesized by the Gomberg method,[3] and VI, VII, and VIII were prepared by reactions of 2,6-dimethoxyphenyllithium with benzophenone, ethyl benzoate and ethyl carbonate, respectively. The crude materials produced were purified by recrystallization in a hexane–benzene mixture; [I] mp 165 °C, [II] mp 61 °C, Found: C, 83.21; H, 6.34%. Calcd: C, 82.73; H, 6.25%. [III] Mp 85 °C, Found: C, 75.48; H, 6.31%. Calcd: C, 75.41; H, 6.33%. [IV] Mp 132 °C. Found: C, 83.92; H, 6.19%. Calcd: C, 82.73; H, 6.25%. [V] Mp 188 °C, Found: C, 75.64; H, 6.33%. Calcd: C, 75.41; H, 6.33%. [VI] Mp 137 °C, Found: C, 78.75; H, 6.11%. Calcd: C, 78.73; H, 6.29%. [VII] Mp 107 °C, Found: C, 72.53; H, 6.35%. Calcd: C, 72.61, H, 6.36%. [VIII] Mp 166 °C, Found: C, 67.91; H, 6.44%. Calcd: C, 68.17, H, 6.41%. Radicals VII and VIII were prepared by reduction of the corresponding carbonium ions, which are easily produced by dissolving the alcohols in 10% aqueous sulfuric acid.[2] Radicals I, II, III, IV, V, and VI were obtained by the Gomberg procedure applied to the corresponding chlorides, which were synthesized by treating the alcohols with thionyl chloride in dichloromethane.[4] ENDOR measurements were carried out in a toluene solution of the free radicals according to the procedure described previously.[5]

Results and Discussion

ENDOR Spectrum and the Hyperfine Splittings. A typical example of the ENDOR spectrum observed for 2-methoxytriphenylmethyl [IV] is shown in Fig. 2. Eight sets of the ENDOR signals seen in the figure (a—h) can be assigned with reference to the ENDOR spectrum of the parent triphenylmethyl as follows: signals (d), (g), and (h) are ascribed to the meta-, ortho- and para-ring protons of non-substituted phenyls (B, C) and (a), (b, c), (e), and (f) to the methoxyl protons and the meta-, ortho- and para-ring protons

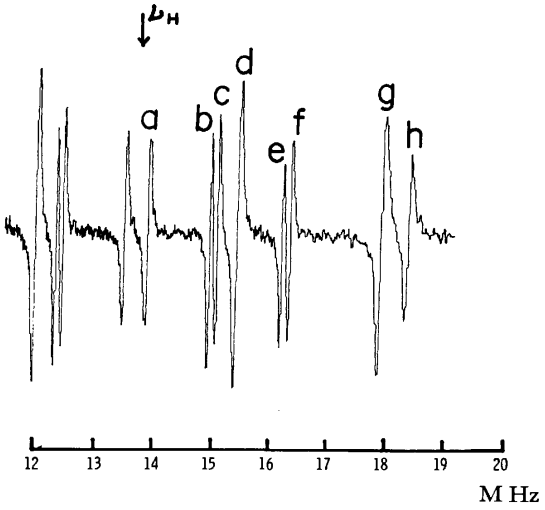

Fig. 2. ENDOR spectrum of 2-methoxytriphenmethyl [IV] recorded at −70 °C.

Table 1. Proton hyperfine coupling constants for triphenylmethyl (in G)

	A					B					C					$-OCH_3$
	2	3	4	5	6	2'	3'	4'	5'	6'	2''	3''	4''	5''	6''	
I	2.56	1.16	2.81			2.56	1.16	2.81			2.56	1.16	2.81			
II	2.59	1.03				2.59	1.14	2.86			2.59	1.14	2.86			0.34
III	2.57	1.03				2.57	1.03				2.57	1.03				0.33
IV		0.89	1.83	0.98	1.74	2.93	1.22	3.26			2.93	1.22	3.26			0.13
V		1.01	2.57	1.13	2.57		1.01	2.57	1.13	2.57		1.01	2.57	1.13	2.57	0.18
VI		0.66	0.84			3.22	1.27	3.58			3.22	1.27	3.58			0.08
VII		0.91	1.17				0.91	1.17			4.09	1.51	4.67			0.11
VIII		1.07	2.35				1.07	2.35				1.07	2.35			0.16

of the substituted phenyl (A), respectively. The larger splitting of either (b) or (c) is assigned to position 5, since the methoxyl substitution causes a small reduction in the spin density at position next to the carbon atom, to which the methoxyl group is bonded. The coupling constants for the ring and the methoxyl protons under the same assumptions are summarized in Table 1, where splittings' assignments, in particular, those for the hindered triphenylmethyls IV and VIII are based on the prediction of the McLachlan MO calculation.

MO Calculation and the Steric Hindrance. In the HMO or McLachlan calculations for triphenylmethyls previously described, the value of the Coulomb integral for the central methyl carbon atom was taken to be equal to that of the aromatic ring carbon atom. This leads to equal spin densities at the ortho- and para-positions, which is contrary to experimental observations.

An improved choice of the parameter was proposed by Kulkarni, who employed the less electronegative value, $\alpha_{Me}=\alpha-1.2\beta$,[6] for the Coulomb integral of the methyl carbon atom. The resonance inhibition between the central methyl and the twisted phenyl $2p_\pi$ orbitals is represented by $\beta\cos\theta$ in which θ is the twisting angle.

In the present work, the inductive effect of the methoxyl group was ignored everywhere, and the hindrance of the phenyl group due to the ortho-substitution was taken into account. As an example, the dependence of the spin densities on the twisting angle (θ) calculated for VII suggested that the spin-density distribution on the substituted phenyls (A) and (B) decreases, but that on the non-substituted phenyl (C) increases, as the degree of steric hindrance in (A) and (B), θ, increases. The MO spin densities are in excellent agreement with the observed values obtained from the McConnel relation ($a^H=Q^H\rho^\pi$, $Q^H=-27$ G), under the assumption that each phenyl, A, B, and C, of VII is twisted outward by 65, 65, and 30°, respectively. The twisting angles of other hindered methyls shown in Table 2, give a satisfactory linear relation between the observed ring proton splitting and the MO spin densities calculated in the same manner, as is shown in Fig. 3. From the slope of the plot, the average value $|Q^H|$ was estimated to be 27.4 G, where the average value $|Q^{OCH_3}|$ is found to be 3.17 G, assuming $a^{OCH_3}=Q^{OCH_3}\cdot\rho_C^\pi$.

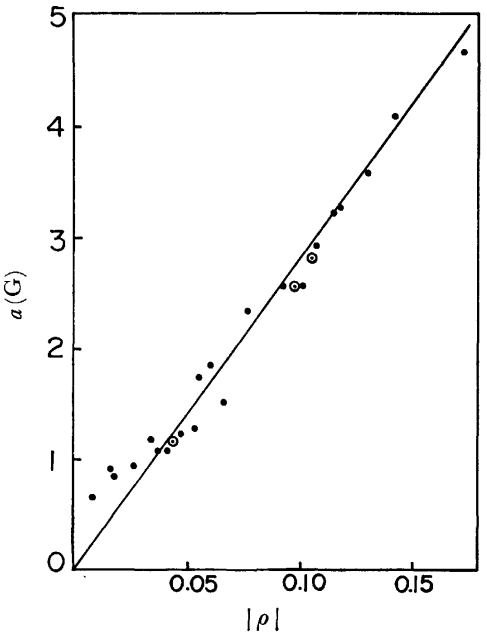

Fig. 3. Relation between the observed proton hyperfine coupling constants and the MO spin densities.
⊙ denotes the plots for mother triphenylmethyl.

Table 2. Twisting angles and MO π-bond orders for triphenylmethyl

	Twisting angle (θ)			Bond order		
	A	B	C	1-7	1'-7	1''-7
I	30°	30°	30°	0.333	0.333	0.333
IV	50°	30°	30°	0.249	0.338	0.338
V	35°	35°	35°	0.317	0.317	0.317
VI	70°	30°	30°	0.134	0.342	0.342
VII	65°	65°	30°	0.168	0.168	0.348
VIII	45°	45°	45°	0.278	0.278	0.278

Of interest is the fact that the twisting angle of the substituted phenyls of high symmetry [VIII] is much smaller than those seen for low symmetrical substitutions, such as VI and VII. This supports the hypothesis that an intramolecular odd-π-electron delocalization does affect the degree of steric hindrance in these molecules. In fact, the HMO bond order cited in Table 2 justifies the fact that the lowest value is predicted between the central methyl and the adjacent ring carbon of the substituted phenyl in derivative VI. On the other hand, the bond order for the non-substituted phenyl is increased by asymmetrical ortho-substitution. This means that the non-substituted phenyl of

derivatives VI and VII may have a more planar conformation compared with that of the parent triphenylmethyl in the true situation. Although the Kulkarni parameter predicts adequate spin densities, a rigorous explanation for the assumption of such a high electronegativity for the central methyl carbon still requires further investigation.[7,8] Other improved calculations for the triphenylmethyl were recently reported,[9,10] in which the resonance integral was chosen by taking into account the bond length of the triphenylmethyl perchlorate determined by X-ray analysis.[11] A tentative calculation for the present derivatives gave a qualitative explanation, but the agreement between the theoretical and experimental spin densities was not sufficient in comparison with the calculation of Kulkarni.

References

1) J. Sinclair and D. Kivelson, *J. Am. Chem. Soc.*, **90**, 5074 (1968).

2) M. J. Sabacky, C. S. Johnson, Jr., R. G. Smith, H. S. Gutowsky, and J. C. Martin, *J. Am. Chem. Soc.*, **89**, 2054 (1967).

3) M. Gomberg, *J. Am. Chem. Soc.*, **22**, 757 (1900).

4) E. A. Chandross and Curtis. F. Sheley, Jr., *J. Am. Chem. Soc.*, **90**, 4345 (1968).

5) T. Yamamoto, K. Sato, and T. Miyamae, *J. Appl. Phys.*, **11**, 1508 (1972).

6) S. V. Kulkarni and C. Trapp, *J. Am. Chem. Soc.*, **92**, 4801 (1970).

7) W. J. Van Der Hart, *Mol. Phys.*, **19**, 75 (1970).

8) A. Hudson and J. W. E. Lewis, *Mol. Phys.*, **19**, 241 (1970).

9) H. G. Benson and A. Hudson, *Mol. Phys.*, **20**, 185 (1971).

10) R. D. Allendoerfer and A. S. Pollock, *Mol. Phys.*, **22**, 661 (1971).

11) A. H. Gomes De Mesquita, C. H. MacGillavry, and K. Eriks, *Acta Crystallogr.*, **18**, 437 (1965).

Vibration Spectra and Rotational Isomerism of Chain Molecules. VI.[1] 2-Chloro-, 2-Bromo-, and 2-Iodoethyl Methyl Ethers

Hiroatsu MATSUURA,* Motomichi KONO, Hiroshi IIZUKA, Yoshiki OGAWA, Issei HARADA, and Takehiko SHIMANOUCHI

Department of Chemistry, Faculty of Science, University of Tokyo, Hongo, Bunkyo-ku, Tokyo 113

(Received April 13, 1977)

The Raman and infrared spectra of 2-chloro-, 2-bromo-, and 2-iodoethyl methyl ethers, $CH_3OCH_2CH_2X$ (X=Cl, Br, and I), were measured for the liquid, glassy, and crystalline states. The gaseous-state spectra of the chloride were also measured. The vibrational frequencies of these molecules were calculated by the use of the force constants transferred directly from unbranched ethers and alkyl halides. The rotational isomerism was studied and the following conclusions were obtained. (1) In the crystalline state, the molecule takes the form having the *trans* conformation about the CO–CC axis and the *gauche* conformation about the OC–CX axis. (2) In addition to this form (TG), three other forms (GG, TT, and GT) exist in the gaseous, liquid, and glassy states. (3) In the liquid state, the TG form is the most stable and the GT form is the least stable. (4) The less polar TT and GT forms are more favored and the more polar TG and GG forms are less favored in the gaseous state than in the liquid state.

In a series of previous papers, we reported the vibration spectra and rotational isomerism of chain molecules which include ethers,[1,2] paraffins,[3] sulfides,[1,4,5] and alkyl halides.[6] These studies gave us knowledge on the stable conformations of the chain molecules. For consistent elucidation of the conformational stabilities, it is important to examine rotational isomerism of molecules which contain two or more different kinds of chemical groups. Such studies are also important for confirming reliability and transferability of the force constants determined from observed vibrational frequencies.

In the present study, therefore, we deal with the rotational isomerism of 2-halogenoethyl methyl ethers, $CH_3OCH_2CH_2X$ (X=Cl, Br, and I), which contain oxygen and halogen atoms in a molecule. The study on these molecules also gives information on the effect of the two polar groups on the conformational stability. The vibrational spectra of 2-chloroethyl methyl ether have been measured by Hayashi[7] and the rotational isomerism has been discussed.

Experimental

2-Chloroethyl methyl ether was synthesized by treating ethylene glycol monomethyl ether with thionyl chloride, and 2-bromoethyl methyl ether by treating 2-bromoethanol with dimethyl sulfoxide. 2-Iodoethyl methyl ether was prepared from 2-chloroethyl methyl ether by treating with sodium iodide in acetone. The samples were distilled prior to the measurements.

The measurements of Raman spectra were made on a JEOL JRS-400D spectrophotometer with a Coherent Radiation CR-3 argon ion laser in the region below 1600 cm^{-1}. The Raman spectra of the chloride were measured for the gaseous, liquid, glassy, and crystalline states and those of the bromide and the iodide for the liquid, glassy, and crystalline states. A multireflection accessory and a gas cell with a heater were used for the measurements of the spectra in the gaseous state. The Raman spectra of the liquid state were recorded at various temperatures to examine the temperature dependence of Raman intensities. The glassy state was obtained by putting into liquid nitrogen the sample enclosed in an ampoule and cooling it rapidly, and the crystalline state by cooling the sample slowly or annealing it repeatedly.

The measurements of infrared spectra were made on a JASCO DS-402G grating spectrometer and a Hitachi EPI-G2 grating spectrometer in the region 1600—400 cm^{-1} and a Hitachi EPI-L grating spectrometer in the region 700—200 cm^{-1}. The infrared spectra of the chloride were measured for the gaseous, liquid, glassy, and crystalline states and those of the bromide and the iodide for the liquid, glassy, and crystalline states. For the measurements in the region below 700 cm^{-1}, the spectrometer was flushed with dry air to get rid of water vapor absorptions. The glassy state was obtained by depositing the sample onto a cooled window of KBr or KRS-5, and the crystalline state by annealing it repeatedly.

Normal Coordinate Treatment

The normal coordinate treatment of 2-halogenoethyl methyl ethers was carried out with a computer program NCTB2[8] and a HITAC 8700/8800 computing system at the Computer Center of the University of Tokyo. The force constants associated with the oxygen and halogen parts were transferred from the unbranched ethers[1,2,8] and alkyl halides.[6,8] The force constants for the C–C stretching and the methylene-methylene interactions were transferred from the corresponding alkyl halides. No further adjustment of the force constants was made. The transferred values were found to be accurate enough for determining the rotational isomerism of the molecules not only in the crystalline state but also in the glassy and liquid states.

Structural parameters and symmetry coordinates used in the calculation and the detailed results of the calculation are reported in a separate paper.[8]

Results

The Raman and infrared spectra of 2-halogenoethyl methyl ethers in various states are shown in Figs. 1—10 and the vibrational assignments based on the calculated potential-energy distributions are listed in Tables 1—3. Each of the molecules has five possible rotational isomers, TT, TG, GT, GG, and GG′, as given in Table 1 of Part I of this series,[2] where the first and second

* Present address: Department of Chemistry, Faculty of Science, Hiroshima University, Higashisenda-machi, Hiroshima 730.

TABLE 1. OBSERVED FREQUENCIES AND VIBRATIONAL ASSIGNMENTS OF 2-CHLOROETHYL METHYL ETHER

Observed frequency (cm^{-1})[a]								Assignment[b]
Gas		Liquid		Glass		Crystal		
R	IR	R	IR	R	IR	R	IR	
				1479 M	1479 M, sh	1486 M		
	1470 M	1470 W	1474 M, sh	1472 M	1473 M		1475 M	(O)CH_2 scis,
		1465 W, sh	1465 M, sh		1463 M, sh	1459 VW	1460 M	CH_3 ip-d-deform,
1458 M		1457 W, sh	1457 M					CH_3 s-deform,
	1448 M, sh	1451 M		1450 M, sh	1453 M	1451 W		CH_3 op-d-deform,
		1443 M		1441 M		1443 VW	1440 M	CH_2(Cl) scis
		1433 W	1433 M	1431 W, sh	1433 M	1437 M		
1390 VW	1390 W	1388 VW	1390 M	1388 VW	1391 M	1392 W	1395 M	(O)CH_2 wag
1305 VW, sh	1313 W, 1303 W	1300 VW	1302 M	1299 VW	1300 M	1299 VW	1301 M	(O)CH_2 twist
		1270 VW, sh						CH_2(Cl) wag (GG)
1261 W	1260 W	1255 W	1258 W	1255 M	1256 W	1258 M	1261 M	CH_2(Cl) wag (TG, TT, GT)
	1230 M	1218 VW	1221 M	1219 W	1221 M	1222 W	1223 S	CH_2(Cl) twist
	1209 S	1207 VW, sh						CH_3 ip-rock (TT)
	1199 S	1197 VW, sh	1198 M		1196 VW			CH_3 ip-rock (GG, GT)
1176 VW, sh	1186 M, sh	1173 VW	1176 M	1174 VW	1178 M	1179 VW	1179 S	CH_3 ip-rock (TG)
1155 VW, sh		1154 VW	1155 W, sh	1159 VW	1159 VW	1162 W	1160 W	CH_3 op-rock
		1146 VW		1143 VW		1145 VW		Origin unknown
1134 W	1139 VS	1126 W	1130 VS	1124 W	1127 VS	1125 M	1130 VS	CO stretch (TG, TT)
	1115 M, sh	1104 VW	1105 S		1102 W			CO stretch (GT, GG)
1063 W	1070 W, 1061 W	1058 VW	1058 M	1059 W	1060 S	1055 W	1056 S	CC stretch (TG, GG, TT)
1045 VW, sh		1043 VW						CC stretch (GT), (O)CH_2 rock (TT, GT)
1009 W	1011 W	1004 W	1005 M	1005 W	1006 S	1004 M	1006 S	CH_2(Cl) rock (TG)
970 M	967 W	963 M	964 M	963 M	962 M	964 M	962 M	(O)CH_2 rock (TG, GG), CO stretch (GG, TT)
935 W	941 W, sh	923 W	923 VW					CO stretch (GT)
835 VW, sh		835 VW						CH_2(Cl) rock (GG)
820 W	820 VW	816 S	816 M	818 M	817 M	833 VW, 823 M	824 M	CO stretch (TG)
765 S	773 M, 765 M	751 M	752 M	748 W	746 VW			CCl stretch (TT, GT)
684 S	691 M, 680 M	666 VS	666 S	661 VS	660 S	665 S, 658 VS	663 S, sh, 658 S	CCl stretch (TG, GG)
508 VW		507 W	506 W	510 W	510 W	515 W, 505 W	512 W, 505 W	OCC deform (TG)
			493 VW, sh					OCC deform (GG)
			463 VW					COC bend (GT)
439 W		438 VW	438 VW					COC bend (TT)
412 VW		421 VW, sh	418 VW, sh					COC bend (GG)
349 S		348 M	345 VW	346 VW, sh				OCC deform (TT, GT)
328 W		329 W	330 VW	327 W	327 W	338 M	332 VW	COC bend (TG)
		282 W, sh						CCCl deform (GT)
		273 W, sh	272 W	285 W	279 W	295 W	293 W	CCCl deform (TG)
252 W		261 W	257 W	264 VW	266 VW, sh			CCCl deform (GG)
				229 VW		228 W	230 W	CH_3 torsion
162 W		≈180 VW, sh						CCCl deform (TT)

Table 1. (Continued)

Observed frequency (cm^{-1})[a]								Assignment[b]
Gas		Liquid		Glass		Crystal		
R	IR	R	IR	R	IR	R	IR	
						150 W		Torsions and lattice vibrations
				130 W, b		140 M		
						113 VW		
						89 M		
						76 S		
						66 S		
						55 W		

a) VS: very strong, S: strong, M: medium, W: weak, VW: very weak, b: broad, sh: shoulder. The broadness of the band shapes in the gaseous state does not always allow us to correlate the individual bands in the liquid state to those in the gaseous state. Only approximate correlations are made in such cases and in other cases of similar situations. b) For the notation and definition of the local symmetry coordinates, see Ref. 16.

conformation symbols in each isomer designation are those for the CO–CC and OC–CX axes, respectively.

The following spectral features are observed for the three halogenoethers studied in this work. (1) The spectra have combined features of ethers and alkyl halides. (2) The number of the bands observed in the crystalline state is the smallest among the various states and corresponds to what is expected for one molecular form. (3) In the glassy and liquid states, additional bands appear in the spectra. The relative band intensities in the two states are considerably different. (4) Systematic variations of frequencies and intensities are observed with the change of the halogen atom.

In the following subsections, the rotational isomerism of the individual molecules is described. The results are summarized in Table 4.

2-Chloroethyl Methyl Ether. The Raman and infrared spectra are shown in Figs. 1 and 2 and the com-

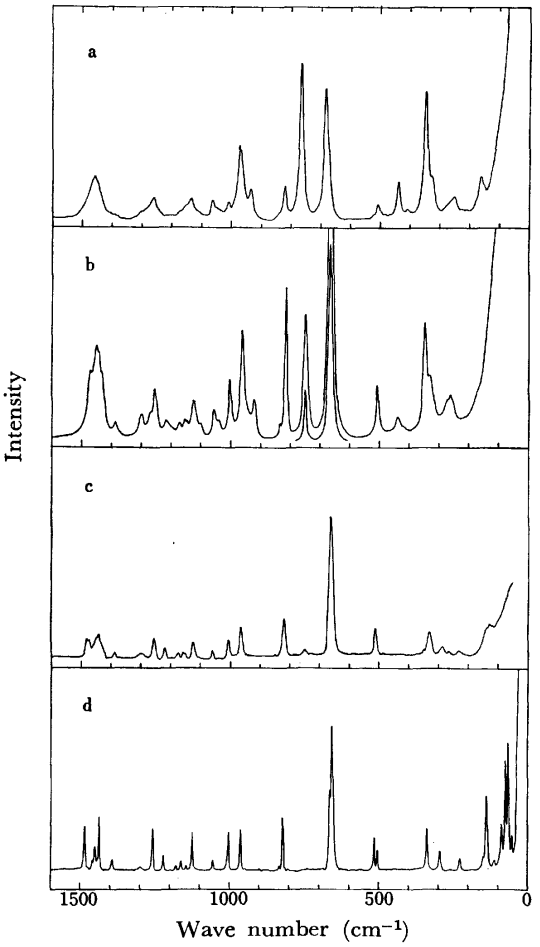

Fig. 1. Raman spectra of 2-chloroethyl methyl ether. a: Gas, b: liquid, c: glass, d: crystal.

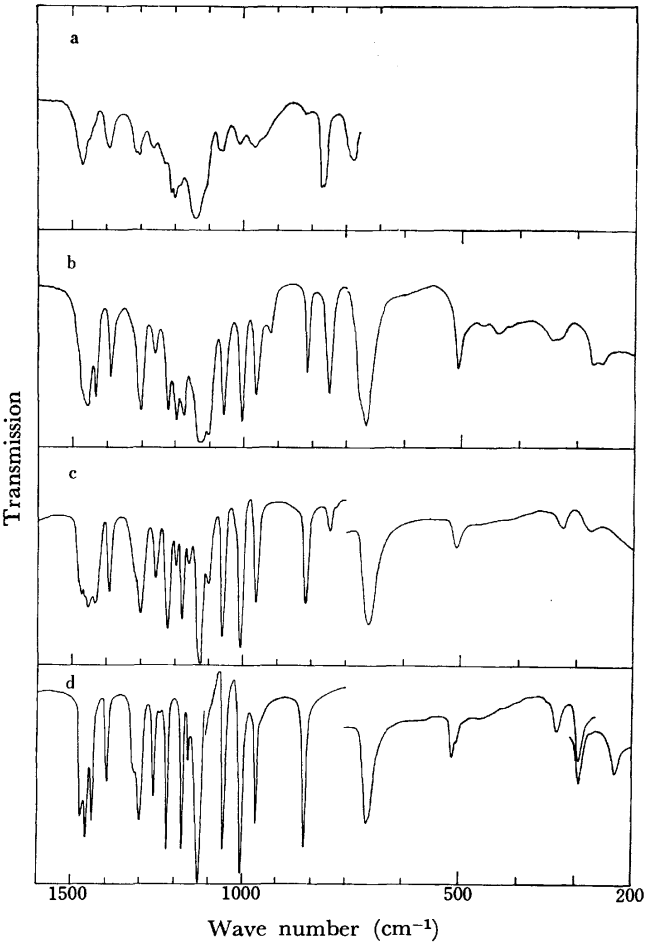

Fig. 2. Infrared spectra of 2-chloroethyl methyl ether. a: Gas, b: liquid, c: glass, d: crystal.

TABLE 2. OBSERVED FREQUENCIES AND VIBRATIONAL ASSIGNMENTS OF 2-BROMOETHYL METHYL ETHER

Observed frequency (cm^{-1})[a]						Assignment[b]
Liquid		Glass		Crystal		
R	IR	R	IR	R	IR	
				1479 M	1480 M	(O)CH_2 scis, CH_3 ip-d-deform, CH_3 s-deform, CH_3 op-d-deform, CH_2(Br) scis
		1471 M	1472 M	1477 M		
1467 W	1468 M, sh		1464 M	1464 VW	1468 W	
1457 W, sh	1458 M		1456 M		1456 M	
1449 M	1450 M, sh		1447 M	1448 W	1451 M	
1442 M	1442 M, sh	1439 M	1435 W	1438 W		
			1428 M	1431 M		
1424 W	1423 M	1424 W	1423 M	1427 M	1428 M	
1382 VW	1385 M	1382 W	1386 M	1387 W	1389 M	(O)CH_2 wag (TG, GG)
1372 VW, sh						(O)CH_2 wag (TT, GT)
			1348 VW			Impurity
1298 VW	1299 M	1301 VW	1301 VW			(O)CH_2 twist (GG, GT)
1276 W	1279 S	1276 M	1279 S	1276 M	1278 S	(O)CH_2 twist (TG, TT)
1235 W	1236 M	1236 W	1237 W	1240 M	1243 M	CH_2(Br) wag (TG, GG)
1224 W						CH_2(Br) wag (TT, GT), CH_2(Br) twist (GT)
1218 W, sh						CH_2(Br) twist (GG)
1212 VW, sh	1212 M	1211 W	1212 M	1214 VW 1208 VW	1214 M	CH_3 ip-rock (TG), CH_2(Br) twist (TT)
1189 VW	1190 S		1189 W			CH_3 ip-rock (TT, GT)
	1174 M					CH_3 ip-rock (GG)
1163 VW	1164 M	1165 VW	1166 M	1166 VW	1169 M	CH_2(Br) twist (TG), CH_3 op-rock (GG, GT)
1154 VW	1154 W	1153 VW	1154 W	1153 VW 1150 VW	1154 W	CH_3 op-rock (TG, TT)
1127 VW	1128 VS	1121 W	1124 VS	1117 W	1122 VS	CO stretch (TG)
1095 VW	1096 S	1092 VW	1095 W			CO stretch (TT)
1056 VW	1056 W	1059 VW				CO stretch (GG, GT)
1045 VW, sh	1044 S	1044 W	1046 S	1045 W	1046 S	CC stretch (TG, GG, TT)
1037 VW	1036 W, sh					CC stretch (GT)
1002 VW	1003 VW	1015 VW			1004 VW	Overtone of OCC deform (TG)
987 W	988 S	988 M	990 S	983 M	987 S	(O)CH_2 rock (TG, TT, GT)
952 M	951 M	948 M	948 M	948 M 942 M	949 M 945 M	CO stretch (TG, GG, TT), (O)CH_2 rock (GG)
918 W	917 W	914 VW	915 VW			CO stretch (GT)
					905 VW	Impurity
	889 VW		889 VW			Impurity
	875 VW		873 VW		870 VW	Impurity
836 VW		833 VW				Origin unknown
802 M	801 W	803 M	803 W	803 M	806 M, sh 802 M	CH_2(Br) rock (TG, GG)
	778 VW					CH_2(Br) rock (TT, GT)
668 S	668 M	669 W				CBr stretch (GT)
		658 W	661 W			CBr stretch (TT)
			608 VW			Impurity
571 VS	570 M	566 VS	565 M	567 VS	565 M	CBr stretch (TG, GG)
500 W	499 W	500 M	499 W	500 M	499 W	OCC deform (TG)
482 VW, sh	483 VW, sh	482 VW, sh				OCC deform (GG)
	445 VW					COC bend (GT)
433 VW	434 VW	427 VW	423 VW			COC bend (TT)
315 W, sh	316 VW					OCC deform (GT)
307 W, sh	307 VW, sh	310 M	308 W	306 M	305 W	COC bend (TG)
295 M		292 W				OCC deform (TT)
262 W	260 VW	275 M	271 W	287 M	284 W	CCBr deform (TG)

Table 2. (Continued)

Observed frequency (cm^{-1})[a]						Assignment[b]
Liquid		Glass		Crystal		
R	IR	R	IR	R	IR	
223 W	218 VW	226 W		220 VW		CCBr deform (GG), CH_3 torsion
189 VW		189 VW				CH_3 torsion
≈160 VW, sh						CCBr deform (TT)
				135 S		Torsions and lattice vibrations
		112 M		104 M		
				82 W		
				72 M		
				62 M		
				45 M		
				34 W		

a), b) See a) and b), respectively, of Table 1.

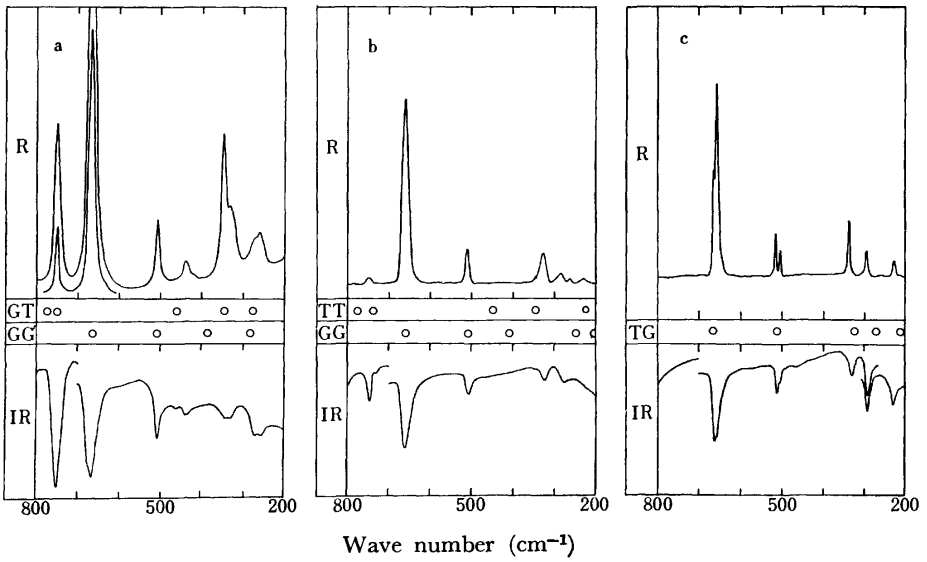

Fig. 3. Comparison of the observed and calculated frequencies of 2-chloroethyl methyl ether.
a: Liquid, b: glass, c: crystal.

parison of the observed and calculated frequencies are shown in Fig. 3.

In the crystalline state, the bands due to the CCl stretching vibration are observed at 658 and 665 cm^{-1} in the Raman spectrum and at 658 and 663 cm^{-1} in the infrared spectrum, the doublet being ascribed to the crystal field splitting. These frequencies indicate clearly that the OC–CCl axis is in the *gauche* conformation.[9] Figure 3 shows that the observed frequencies in the skeletal deformation region are explained only by the TG form. This conclusion agrees with the result of the previous study by Hayashi.[7]

In the glassy state, the bands due to the CCl stretching vibration of the *trans* OC–CCl axis appear at 748 cm^{-1} in the Raman spectrum and at 746 cm^{-1} in the infrared spectrum. The Raman band observed as a shoulder at 346 cm^{-1} is assigned to either one or both of the TT and GT forms. However, the bands assignable only to the TT or GT form are not observed definitely in the spectra. The Raman band at 264 cm^{-1} and the infrared band at 266 cm^{-1} are assigned only to the GG form. Thus, in the glassy state, the TG and GG forms and either one or both of the TT and GT forms exist. The TG form is dominant as seen from the relative band intensities.

The liquid-state spectra exhibit more bands than the glassy-state spectra. In the region below 550 cm^{-1}, the skeletal deformation bands of the individual rotational isomers are clearly observed; the bands at 507, 329, and 273 cm^{-1} are assigned to the TG form,** those at 493, 421, and 261 cm^{-1} to the GG form, those at 463, 348, and 282 cm^{-1} to the GT form, and those at 438 and 348 cm^{-1} to the TT form.

** The band at 273 cm^{-1} shifts to 285 cm^{-1} in the glassy state and to 295 cm^{-1} in the crystalline state. The result of the normal coordinate treatment indicates that the CH_2–CH_2 torsion contributes to this vibration to some extent, making the frequency shift upward on solidification. Similar frequency shifts are observed for the bromide (262 cm^{-1} in the liquid state and 287 cm^{-1} in the crystalline state) and the iodide (248 cm^{-1} in the liquid state and 276 cm^{-1} in the crystalline state).

TABLE 3. OBSERVED FREQUENCIES AND VIBRATIONAL ASSIGNMENTS OF 2-IODOETHYL METHYL ETHER

Observed frequency (cm^{-1})[a]						Assignment[b]
Liquid		Glass		Crystal		
R	IR	R	IR	R	IR	
				1482 W		
1468 W	1468 M	1472 W	1471 M	1476 M	1477 M	
1457 W	1458 M		1464 M		1463 M	(O)CH_2 scis, CH_3 ip-d-deform,
1450 W	1450 M	1455 VW	1455 M	1447 VW, sh	1455 M	CH_3 s-deform, CH_3 op-d-deform,
1441 W	1432 W	1440 W	1446 M	1437 VW	1444 M	CH_2(I) scis
		1422 VW	1423 M, sh	1425 W		
1415 W	1416 M	1414 VW	1415 M		1417 M	
1377 VW	1381 M	1378 W	1381 M	1382 VW	1384 M	(O)CH_2 wag (TG, GG)
1365 VW	1365 W, sh					(O)CH_2 wag (TT, GT)
1291 VW	1293 W		1293 W			(O)CH_2 twist (GG, GT)
1263 W	1265 M	1262 W	1263 S	1263 M	1264 S	(O)CH_2 twist (TG, TT)
					1239 VW	Impurity
1216 W	1220 M	1219 W	1220 S	1221 W	1222 W	CH_3 ip-rock (TG), CH_2(I) wag (GG)
1200 W, sh		1202 VW, sh				CH_3 ip-rock (GG, TT, GT)
1189 M	1188 M	1191 M	1189 M	1192 M	1194 M	CH_2(I) wag (TG, TT, GT)
1162 M	1161 M	1162 W	1159 M	1160 VW	1159 M	CH_3 op-rock (TG, GG, GT), CH_2(I) twist (TT, GT)
	1148 M, sh	1150 VW	1148 M	1146 VW	1148 W	CH_2(I) twist (GG), CH_3 op-rock (TT), origin unknown (crystal)
1123 VW	1124 S	1120 W	1119 VS	1113 W	1115 S	CO stretch (TG), CH_2(I) twist (TG)
1112 VW	1108 S	1105 VW	1107 S			CO stretch (TT)
1089 VW	1088 S		1083 M			CO stretch (GT)
1052 VW		1057 VW	1056 VW			CC stretch (GG)
1038 VW, sh	1037 M	1040 W	1039 S	1042 VW	1040 M	CC stretch (TG)
1030 VW	1030 M, sh	1030 VW, sh	1030 W, sh	1029 VW	1027 W	CO stretch (GG), CC stretch (TT), overtone of CI stretch (TG)
1017 VW	1019 W, sh					CC stretch (GT)
			1005 VW		1003 VW	Combination tone of CI stretch and COC bend (TG)
966 W	967 M	968 M	968 S	966 M	966 S	(O)CH_2 rock (TG, TT, GT)
949 M	950 M	950 W	949 W			CO stretch (TT)
933 W	933 M	933 M	932 M	935 M 932 M	932 M	CO stretch (TG, GG), (O)CH_2 rock (GG)
909 W	909 M	907 VW	906 VW			CO stretch (GT)
		896 VW	895 VW			Impurity
			871 VW			Impurity
			815 VW			Impurity
775 W	777 VW	777 W	777 W	779 W	778 M	CH_2(I) rock (TG, GG)
753 VW	752 VW		757 VW			CH_2(I) rock (TT, GT)
	723 VW		712 VW		714 VW	Impurity
619 S	615 S	620 M	618 W			CI stretch (TT, GT)
516 VS	514 W	517 VS	515 M	518 VS 506 VW	518 W	CI stretch (TG, GG)
489 M	486 W	488 S	487 M	490 S	489 W	COC bend (TG)
468 M	463 VW	469 W	468 VW			OCC deform (GG)
	440 VW		441 VW			COC bend (GT)
427 W	425 VW	420 VW	420 VW			COC bend (TT)
≈390 VW, sh	393 VW		397 VW			COC bend (GG)
304 M	304 W	304 M	303 M	302 M	301 W	OCC deform (TG, GT)
266 M	260 VW					OCC deform (TT)
248 W, sh	250 VW	266 M	264 W	276 S	273 W	CCI deform (TG)
		223 VW	223 W			CCI deform (GT)
200 M		212 VW	210 W	200 W		CCI deform (GG), CH_3 torsion
≈140 W, sh						CCI deform (TT)
				123 M		
				114 M		
				95 M		
				72 M		Torsions and lattice vibrations
				60 M		
				46 S		

a), b) See a) and b), respectively, of Table 1.

Table 4. Rotational isomers of 2-halogenoethyl methyl ethers

	$CH_3OCH_2CH_2Cl$	$CH_3OCH_2CH_2Br$	$CH_3OCH_2CH_2I$
Gas	TG GG TT GT	—	—
Liquid	TG GG TT GT	TG GG TT GT	TG GG TT GT
Glass	TG GG TT[a] GT[a]	TG GG TT GT	TG GG TT GT
Crystal	TG	TG	TG

a) Either one or both of the TT and GT forms exist.

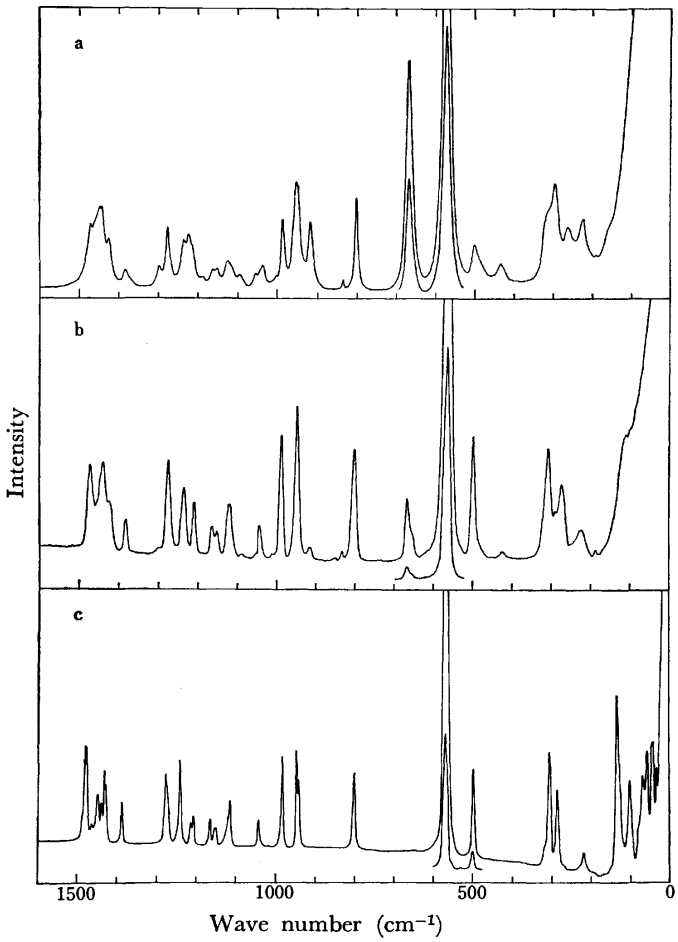

Fig. 4. Raman spectra of 2-bromoethyl methyl ether.
a: Liquid, b: glass, c: crystal.

In the gaseous state, the number of the observed bands is essentially the same as that in the liquid state, indicating the coexistence of the four forms of TG, GG, TT, and GT. However, the relative intensities of several bands are remarkably different between the two states. It is evident from Figs. 1 and 2 that the bands of the TT and GT forms become relatively stronger than those of the TG and GG forms in going from the liquid to the gas. This intensity alteration will be discussed later.

The existence of the GG′ form is unlikely. The result of the normal coordinate treatment for the GG′ form shows that a band due to the vibration of 385 cm^{-1} would be detectable in the Raman spectrum, if this form existed, since the mode of this vibration is a quasi-totally symmetrical deformation of the molecular skeleton. However, no Raman band is actually observed in the region 360—400 cm^{-1} in the liquid or gaseous state.

2-Bromoethyl Methyl Ether. The Raman and infrared spectra are shown in Figs. 4—6. A comparison of the observed and calculated frequencies shows that the spectra in the crystalline state can be explained only by the TG form. In the glassy-state spectra, there appear the bands which are assigned only to the GT form (914 and 669 cm^{-1}), TT form (658, 427, and 292 cm^{-1}), and GG form (482 cm^{-1}). The liquid-state spectra exhibit a similar spectral pattern but considerably different relative intensities. Thus, the four forms of TG, GG, TT, and GT are found to coexist in the glassy and liquid states.

2-Iodoethyl Methyl Ether. The Raman and infrared spectra are shown in Figs. 7—9. A comparison of the observed and calculated frequencies shows that the spectra in the crystalline state are explained only by the TG form, similarly to the cases of the chloride and the bromide. In the glassy- and liquid-state spectra, additional bands appear which are assigned only to the GT form (907 and 441 cm^{-1}), TT form (420 cm^{-1}) and GG form (469 and 397 cm^{-1}). Accordingly, the four forms of TG, GG, TT, and GT are found to coexist in the glassy and liquid states.

Temperature Dependence of the Raman Spectra in the Liquid State. The liquid-state Raman spectra measured at high and low temperatures are shown in Fig. 10. For the chloride, the relative intensities of the bands at 507, 329, and 273 cm^{-1} which are assigned to the TG form are strikingly stronger at the lower temperature. On the other hand, the band at 923 cm^{-1} assigned to the GT form loses its intensity as temperature is lowered. Similar spectral changes are observed for the bromide and the iodide; the bands assigned to the TG form of the bromide at 500, 307, and 262 cm^{-1} and that of the iodide at 489 cm^{-1} become stronger and the band assigned to the GT form of the bromide at 918 cm^{-1} and that of the iodide at 909 cm^{-1} become weaker as temperature is lowered. These spectral observations indicate that for the three molecules in common the TG form is the most stable and the GT form is the least stable in the liquid state.

In the glassy state, the bands of the TG form is dominant and those of the GT form are further weaker than in the cooled-liquid state. This spectral feature is consistent with the conformational stability obtained for the liquid state.

Discussion

The following results were obtained for the three halogenoethers studied in this work. (1) Only the TG form exists in the crystalline state. (2) In the glassy

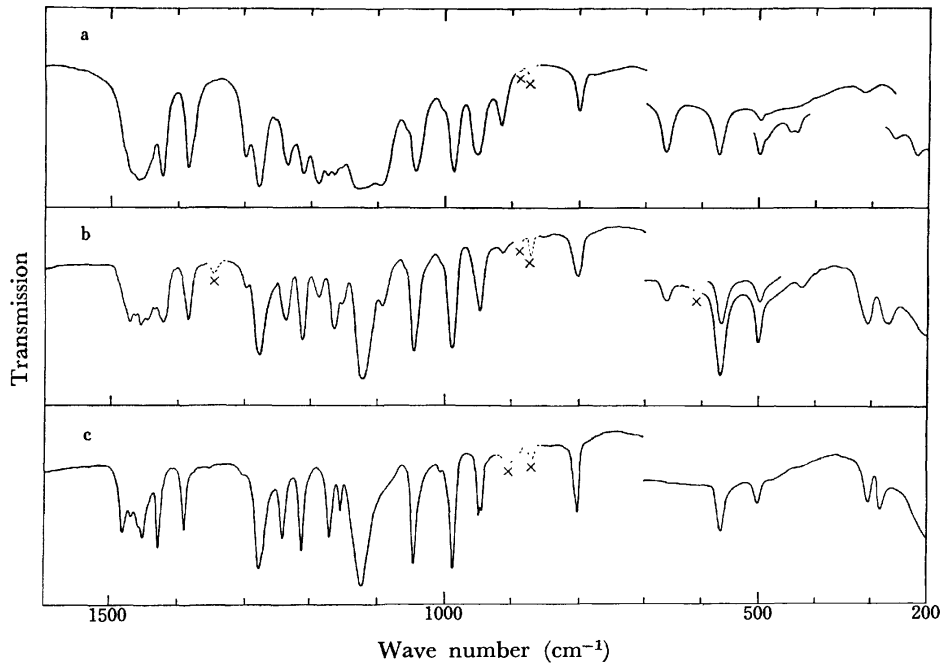

Fig. 5. Infrared spectra of 2-bromoethyl methyl ether.
a: Liquid, b: glass, c: crystal. ×: Bands due to impurities.

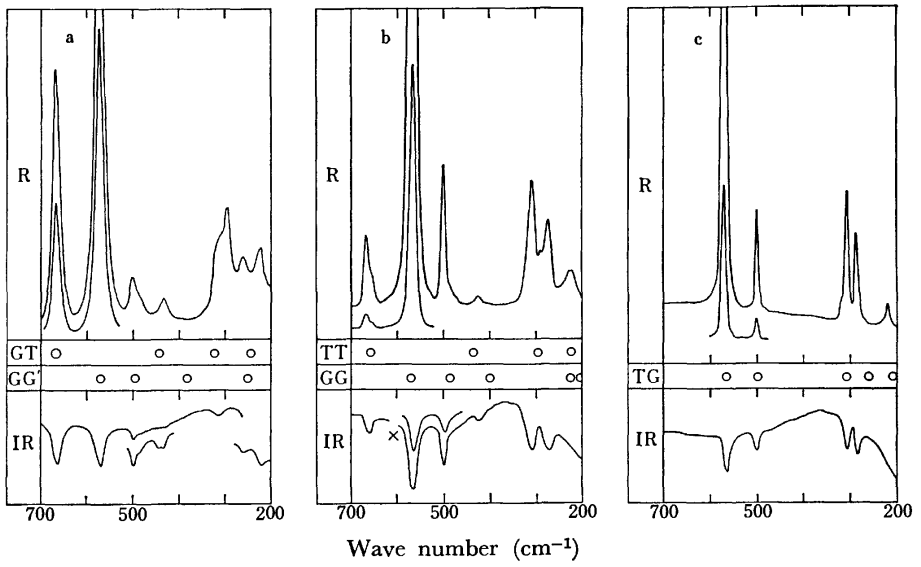

Fig. 6. Comparison of the observed and calculated frequencies of 2-bromoethyl methyl ether.
a: Liquid, b: glass, c: crystal. ×: Band due to impurity.

and liquid states, the GG, TT, and GT forms coexist in addition to the TG form. (3) The TG form is the most stable and the GT form is the least stable in the liquid state.

The stability of the *trans* conformation about the CO–CC axis over the *gauche* conformation is consistent with the results obtained for ethyl methyl ether,[10–12] diethyl ether,[13,14] and longer ethers.[1,2] The enthalpy difference between the *trans* and *gauche* conformations has been obtained as 1.1—1.5 kcal/mol for the former two ethers.

The OC–CX axis was found to be in the *gauche* conformation in the most stable isomer in the liquid state. This result may be compared with the previous findings that the *gauche* conformation about the CC–CX axis in butyl halides is more stable than the *trans* conformation in the liquid state[6] and that the *gauche* conformation about the OC–CC axis in longer chain ethers is as stable as the *trans* conformation in the liquid state.[2]

A comparison of the liquid-state Raman spectra of the three halogenoethers (Figs. 1, 4, and 7) indicates the systematic variation of the intensity ratio of the CX stretching band assigned to the *trans* OC–CX conformation to that assigned to the *gauche* OC–CX conformation. Namely, the intensity ratio, *I(trans)/I(gauche)*, is the smallest for the chloride and is the largest for the iodide. This observation suggests that the stability of the *trans* OC–CX conformation relative to that of the

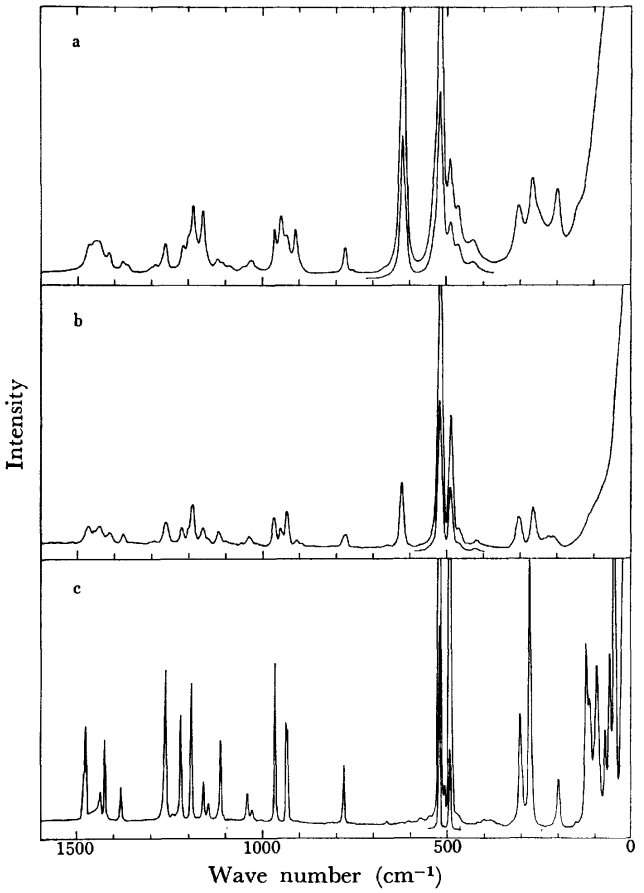

Fig. 7. Raman spectra of 2-iodoethyl methyl ether.
a: Liquid, b: glass, c: crystal.

gauche OC–CX conformation is larger in a molecule with a heavier halogen atom. The steric hindrance between the methylene group and the halogen atom accounts, at least in part, for the difference in conformational stability.

Each of the three halogenoethers contains two polar groups, the oxygen and halogen atoms, in a molecule. The five possible molecular forms are classified into two types on the basis of the polarity of the molecule. By assuming a simple vector summation, the dipole moment μ of the molecule is given by

$$\mu^2 = \mu_{CX}^2 + \mu_{COC}^2 - (2/\sqrt{3})\mu_{CX}\mu_{COC}$$

for the TT, GT, and GG′ forms and

$$\mu^2 = \mu_{CX}^2 + \mu_{COC}^2 + (2/\sqrt{3})\mu_{CX}\mu_{COC}$$

for the TG and GG forms, where μ_{CX} and μ_{COC} are the dipole moments of the CX and COC groups, respectively, and the all bond angles are assumed to be tetrahedral. Accordingly, the TT, GT, and GG′ forms are less polar and the TG and GG forms are more polar. For the chloride, as seen from Figs. 1 and 2, the bands assigned to the TT and GT forms (less polar) become relatively stronger than those of the TG and GG forms (more polar) in going from the liquid to the gas. The intensity ratio of the 751 cm^{-1} band to the 666 cm^{-1} band is reversed between the two states. These observations are consistent with the theoretical expectation that less polar conformations are better stabilized in less polar solvents or gas and that more polar conformations are better stabilized in more polar media.[15] It is thus clear that the *trans* OC–CX conformation of the halogenoethers is more favored in the gaseous state than in the liquid state. Similar intensity variations are observed in the spectra of the cyclohexane solution and the acetone solution.

In conclusion, the rotational isomerism of 2-halogenoethyl methyl ethers was determined from the vibrational s ectra. The satisfactory transferability of the force

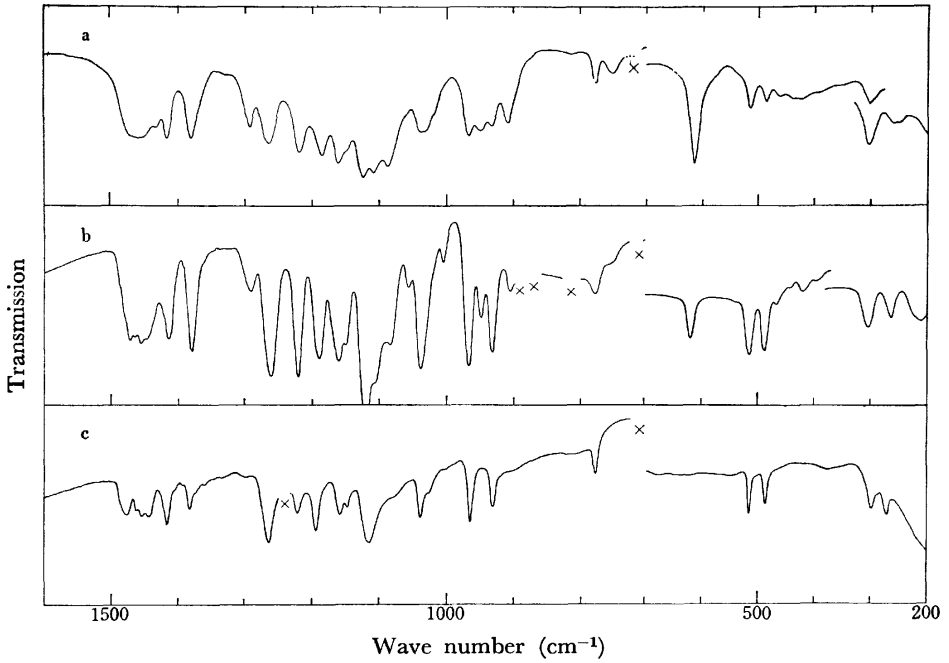

Fig. 8. Infrared spectra of 2-iodoethyl methyl ether.
a: Liquid, b: glass, c: crystal. ×: Bands due to impurities.

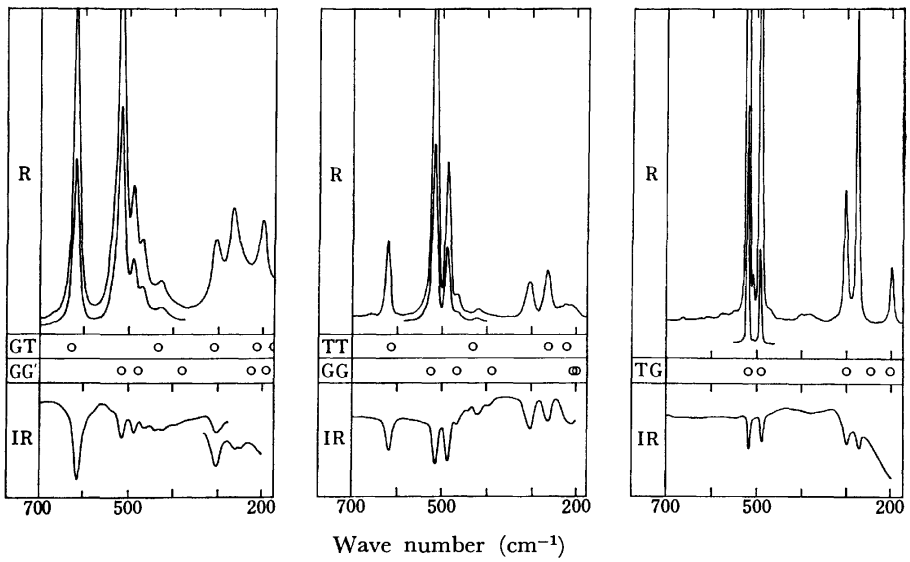

Fig. 9. Comparison of the observed and calculated frequencies of 2-iodoethyl methyl ether.
a: Liquid, b: glass, c: crystal.

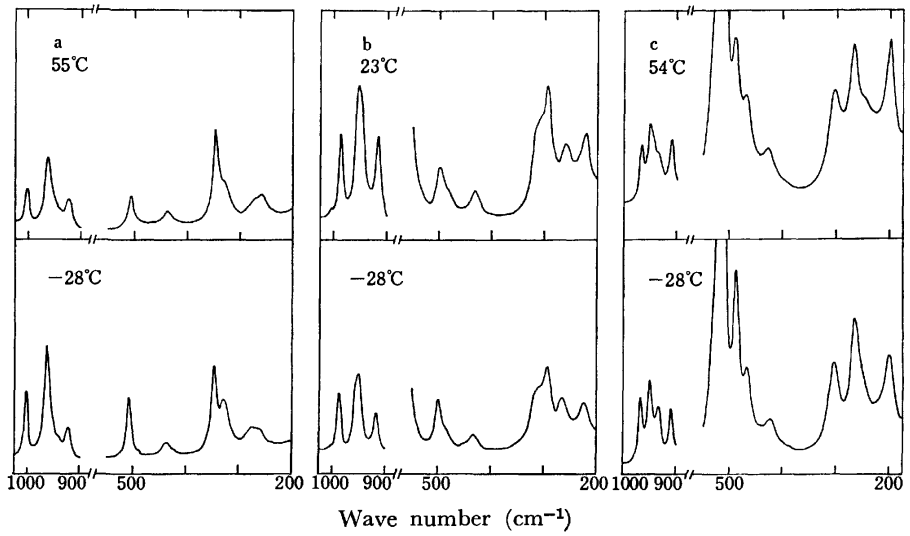

Fig. 10. Raman spectra in the liquid state at high and low temperatures.
a: 2-Chloroethyl methyl ether, b: 2-bromoethyl methyl ether, c: 2-iodoethyl methyl ether.

constants from the ethers and the alkyl halides to the halogenoethers was also shown. These conclusions confirm that the combination of the systematic measurements of vibrational spectra and the systematic calculations of normal vibrations is a reliable method for studying the rotational isomerism of chain molecules. Theoretical studies on the stabilities of rotational isomers should be made on the basis of accumulated experimental data, by taking account of intramolecular and intermolecular interactions.

Erratum

Erratum in Table 2 of Part V.[1] For 764 M,sh listed in the column of R of Crystal read 764 M.

References

1) Part V: Y. Ogawa, M. Ohta, M. Sakakibara, H. Matsuura, I. Harada, and T. Shimanouchi, *Bull. Chem. Soc. Jpn.*, **50**, 650 (1977).
2) Part I: T. Shimanouchi, Y. Ogawa, M. Ohta, H. Matsuura, and I. Harada, *Bull. Chem. Soc. Jpn.*, **49**, 2999 (1976).
3) Part II: I. Harada, H. Takeuchi, M. Sakakibara, H. Matsuura, and T. Shimanouchi, *Bull. Chem. Soc. Jpn.*, **50**, 102 (1977).
4) Part III: M. Sakakibara, H. Matsuura, I. Harada, and T. Shimanouchi, *Bull. Chem. Soc. Jpn.*, **50**, 111 (1977).
5) Part IV: M. Ohta, Y. Ogawa, H. Matsuura, I. Harada, and T. Shimanouchi, *Bull. Chem. Soc. Jpn.*, **50**, 380 (1977).
6) S. Imazeki, Master Thesis, University of Tokyo (1977).
7) M. Hayashi, *Nippon Kagaku Zasshi*, **80**, 1084 (1959).
8) T. Shimanouchi, H. Matsuura, Y. Ogawa, and I. Harada, *J. Phys. Chem. Ref. Data*, to be published.
9) S. Mizushima, T. Shimanouchi, K. Nakamura, M. Hayashi, and S. Tsuchiya, *J. Chem. Phys.*, **26**, 970 (1957).

10) T. Kitagawa and T. Miyazawa, *Bull. Chem. Soc. Jpn.*, **41**, 1976 (1968).
11) J. P. Perchard, *Spectrochim. Acta, Part A*, **26**, 707 (1970).
12) T. Kitagawa, K. Kusaki, and T. Miyazawa, *Bull. Chem. Soc. Jpn.*, **46**, 3685 (1973).
13) H. Wieser, W. G. Laidlaw, P. J. Krueger, and H. Fuhrer, *Spectrochim. Acta, Part A*, **24**, 1055 (1968).
14) J. P. Perchard, J. C. Monier, and P. Dizabo, *Spectrochim. Acta, Part A*, **27**, 447 (1971).
15) S. Mizushima, "Structure of Molecules and Internal Rotation," Academic Press, New York (1954).
16) T. Shimanouchi, "Tables of Molecular Vibrational Frequencies," Consolidated Vol. I, U.S. Govt. Printing Office, No. C13.48:39 (1972).

The Isotope Effect on the Quenching of the Cadmium Triplet State by Methanol

Shigeru TSUNASHIMA, Kuniko MORITA, and Shin SATO

Department of Applied Physics, Tokyo Institute of Technology, Ookayama, Meguro-ku, Tokyo 152

(Received November 15, 1976)

The isotope effect on the Cd-photosensitized emission of methanol has been investigated using CH_3OH, CH_3OD, CD_3OH, and CD_3OD. The relative quenching efficiencies for the 326.1 nm resonance line were 1 : 0.3 : 0.9 : 0.3 in the order of CH_3OH, CH_3OD, CD_3OH, and CD_3OD. The emission intensities from the intermediate complex between an excited cadmium and methanol were also measured. The band-shape was not affected by the substitution of D atoms. The intensity ratio was 1 : 3.1 : 1.1 : 3.1 in the order of CH_3OH, CH_3OD, CD_3OH, and CD_3OD, when the incomplete quenching was corrected. These results were explained by the following quenching processes:

$$Cd^* + CH_3OH \rightarrow Cd\cdots H\cdots O\,CH_3$$
$$\rightarrow Cd\cdots O\langle^{H}_{CH_3}$$

where Cd* represents $Cd(^3P_1)$ and/or $Cd(^3P_0)$. The D/H kinetic isotope effect on the former process was estimated to be 0.3

Recently, Luther *et al.* found a large isotope effect on the quenching of $Hg(^3P_0)$ atoms by methanol using CH_3OH, CH_3OD, CD_3OH, and CD_3OD; for example, the quenching efficiency of CH_3OH is about ten times that of CD_3OD.[1] They also found a HgH formation from CH_3OD, suggesting that the cleavage of the C–H bond in methanol is an important process, as is the cleavage of the O–H bond.[1] This observation, however, contradicts the reaction mechanism widely belived in which almost all the cleavage occurs at the O–H bond in the reaction of methanol photosensitized by triplet mercury, although the bond strength of the C–H is smaller than that of the O–H in methanol.[2]

In the case of the Cd-photosensitized reaction, the isotope effect was also found, as was briefly reported in a previous short communication; for example, the quenching efficiency of CH_3OH for the 326.1 nm resonance line was three times that of CD_3OD and CH_3OD.[3] Based on several assumptions, a reaction mechanism was proposed which explains the observed isotope effect on the quenching of the 326.1 nm resonance line and on the band emission at 395 nm.[3] This mechanism, however, was not consistent with the mechanism proposed by Luther *et al.* for the mercury photosensitization.

The present paper will report the details of the previous short communication, together with new results obtained with CD_3OH. The use of CD_3OH was expected to confirm some of the assumptions made previously.

Experimental

The apparatus and the procedure were essentially the same as those previously described.[4,5] The reaction cell and the cadmium lamp were kept in a furnace at 220±1 °C. Since Pyrex glass is known to be reactive to methanol vapor,[6] the use of Pyrex glass was avoided in constructing the vacuum lines which come in contact with methanol vapor. In order to minimize the effect of the possible D/H exchange reaction on the wall, the reaction system was treated with the same isotopic methanol before every run. All the experiments were carried out in the presence of an excess amount of argon. In order to minimize the pressure dependence of the absorption of the 326.1 nm resonance line, the total pressure in the reaction cell was kept constant.[4,5] The pressure of methanol was changed between 4 and 15% of the total pressure.

The isotopic methanols, CH_3OD, CD_3OH, and CD_3OD, were purchased from Merck Sharp and Dohme of Canada, Ltd. The nominal isotopic purities were more than 99%. All of the methanols were used after being degassed at −80 °C. High purity argon (Jonan Kyodo Sanso) was used after having been passed through a trap containing a molecular sieve, 4A, kept at −120 °C and a reduced copper furnace at 300 °C.

Results

In order to estimate the quenching efficiency for the $5^3P_1 \rightarrow 5^1S_0$ resonance line, the emission intensities at 326.1 nm were measured as a function of the pressure of methanol. The Stern-Volmer plots are shown in Fig. 1, where $I^\circ_{326.1}$ and $I_{326.1}$ are the emission intensities at 326.1 nm in the absence and in the presence of methanol respectively. Since the emission intensities were dependent on the irradiation time because of the accumulation of the reaction products, the $I_{326.1}$ values were obtained by extrapolation to zero irradiation time.

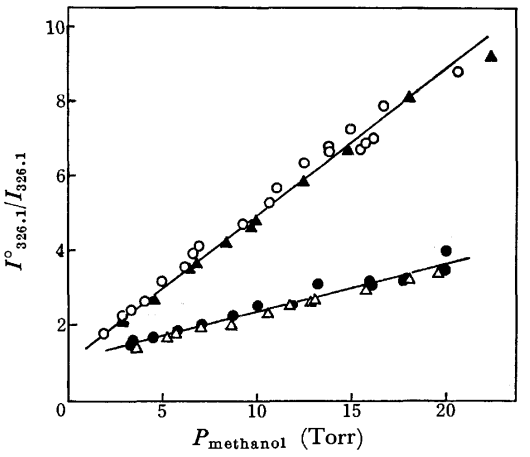

Fig. 1. Stern-Volmer plots for the quenching of the 326.1 nm resonance line by CH_3OH(○), CH_3OD(●), CD_3OH(▲), and CD_3OD(△).

Table 1. Observed isotope effect in the quenching of the 326.1 nm resonance line and the emission intensity at 395 nm

	CH_3OH	CH_3OD	CD_3OH	CD_3OD
H. Q. P. (Torr)[a]	2.4±0.2	7.6±0.7	2.7±0.1	8.0±0.3
Intercept (Torr)[b]	7.4±0.4	8.0±0.4	8.1±0.5	8.1±0.4
Slope (×100)[b]	3.9±0.4	4.3±0.5	4.6±0.4	4.5±0.4
Intensity[c]	1	3.1±0.3	1.1±0.1	3.1±0.3

a) Half-quenching pressure. b) Intercepts and slopes of the straight lines in Fig. 3. c) Total emission intensity at 395 nm, corrected for the incomplete quenching; see Text.

The effect of the argon pressure on the value of $I^{\circ}_{326.1}/I_{326.1}$ was negligibly small. The plots for the $I^{\circ}_{326.1}/I_{326.1}$ ratios *vs.* the methanol pressure lie on a straight line for each methanol. The half-quenching pressures were obtained from the slopes of the straight lines in Fig. 1 and are listed in Table 1.

As was stated in a previous paper,[5] a new band emission at 395 nm was obtained when the Cd–methanol mixture was irradiated with the 326.1 nm resonance line. The emission profile was not affected by the substitution of D atoms. The emission intensities, however, depended on the total pressure and the pressure of methanol. Figure 2 shows the results obtained with CD_3OD. Similar plots were also obtained with CH_3OH, CH_3OD, and CD_3OH. The values of $I_{326.1}[Me]/I_{395}$ were nearly independent of the methanol pressure, but depended on the total pressure, as is shown in Fig. 3. Here, I_{395} is the emission intensity at 395 nm and [Me] is the pressure of methanol. The values of the intercepts and the slopes of the straight lines in Fig. 3 are listed in Table 1.

The areas of the emission band at 395 nm were compared with that obtained with CH_3OH at the same total pressure and the pressure of methanol. When the incomplete quenching of the resonance line was corrected, the ratios of the total emission intensity at 395 nm were nearly independent of the total pressures (35—120 Torr) and also of the pressures of methanol (5—20 Torr). The ratios thus obtained are listed in Table 1.

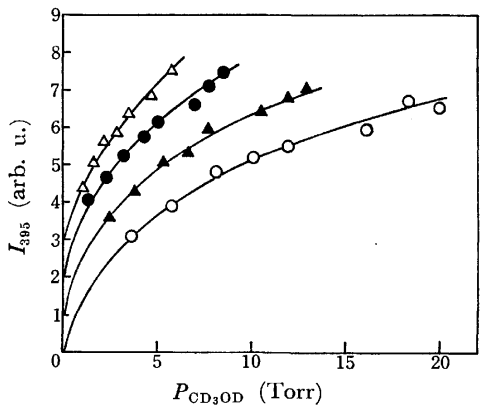

Fig. 2. The intensity of emission at 395 nm from the Cd-CD_3OD system as a function of the pressure of CD_3OD. The total pressures are 121(○), 80(▲), 53(●), and 35(△) in Torr. The plots are displaced upwards by one unit of I_{395} for clarity in the above order of the total pressure.

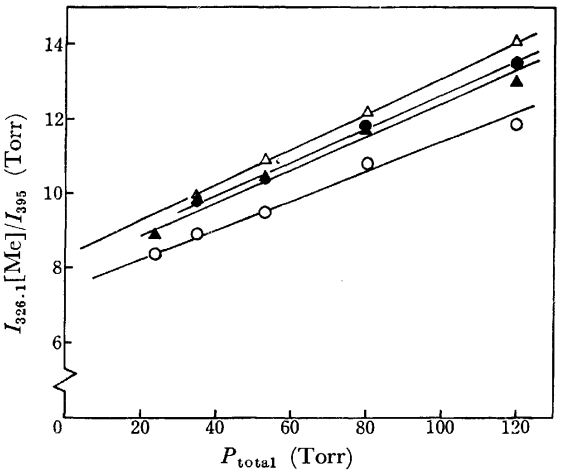

Fig. 3. Plots of $I_{326.1}$ [Me]/I_{395} as a function of the total pressure for CH_3OH(○), CH_3OD(●), CD_3OH(▲), and CD_3OD(△).

Discussion

Reaction Mechanism. As was shown in a previous paper,[4] the Stern-Volmer plots for the quenching of the Cd resonance line at 326.1 nm by ammonia were not linear at a low pressure of ammonia. In the cases of methanol, however, the Stern-Volmer plots give straight lines, as is shown in Fig. 1. This suggests that the reaction mechanism for the 326.1 nm and the 395 nm emissions is simpler than that considered in the case of ammonia.[4] Consequently, the following simplified reaction mechanism may be considered to explain the results obtained here:

$$Cd + h\nu(326.1) \longrightarrow Cd(^3P_1), \quad 1$$

$$Cd(^3P_1) \longrightarrow Cd + h\nu(326.1), \quad 2$$

$$Cd(^3P_1) + M \rightleftharpoons Cd(^3P_0) + M, \quad 3$$

$$Cd^* + Me \longrightarrow Products, \quad 4$$

$$Cd^* + Me \longrightarrow CdMe^*, \quad 5$$

$$CdMe^* \longrightarrow Cd + Me + h\nu(395), \quad 6$$

$$CdMe^* + Me \longrightarrow Cd + 2Me, \quad 7$$

$$CdMe^* + Ar \longrightarrow Cd + Me + Ar. \quad 8$$

Here, Cd* represents $Cd(^3P_1)$ or $Cd(^3P_0)$. Because the equilibrium between $Cd(^3P_1)$ and $Cd(^3P_0)$ is easily established under the present experimental conditions,[7] we cannot discriminate the reactions of these two states. The stationary concentration of $Cd(^3P_0)$ may be approximated as $(k_3/k_{-3})[Cd(^3P_1)]$.[4] CdMe* is a complex between Cd* and methanol(Me), which can emit

the band emission at 395 nm. In the case of ammonia, the formation of an "unstabilized" complex has been assumed; this complex dissociates into the triplet cadmium and methanol or is deactivated to an emissible complex through collision.[4] In the case of methanol, however, it is not necessary to assume the formation of the "unstabilized" complex, since the Stern-Volmer plots give a straight line. If the "unstabilized" complex is formed even in the case of methanol, the lifetime of the "unstabilized" complex must be long enough to be stabilized through collision under the present experimental conditions.

The steady-state treatment of the above mechanism gives the following relation for the quenching of the 326.1 nm resonance line:

$$I^{\circ}_{326.1}/I_{326.1} = 1 + k_q[\mathrm{Me}]/k_2. \quad (1)$$

Here, $I^{\circ}_{326.1}$ and $I_{326.1}$ represent the emission intensities observed at 326.1 nm in the absence and in the presence of methanol respectively. k_q is the sum of the quenching rate constants and is k_4+k_5 in the case of Cd*= Cd($^3P_1$). When Cd* represents a mixture of Cd($^3P_1$) and Cd($^3P_0$), k_4 and k_5 should be replaced by $k_4^1+(k_3/k_{-3})k_4^0$ and $k_5^1+(k_3/k_{-3})k_5^0$ respectively. Here, the superscripts 1 and 0 stand for the reactions of Cd($^3P_1$) and Cd($^3P_0$) respectively.

From the values of the half-quenching pressure listed in Table 1, the relative values of k_q can be estimated; they are listed in Table 2. The isotope effect on the efficiency of methanol has been observed for the quenching of Hg($^3P_0$) by Luther *et al.*[1] The relative values obtained by them are compared in Table 2 with those obtained in this study. In contrast with the case of Hg($^3P_0$)-photosensitization, the quenching efficiency of CD_3OD is 0.3 times that of CH_3OH and is close to that of CH_3OD.

Table 2. Isotope effects in the reaction of methanol[a]

	CH_3OH	CH_3OD	CD_3OH	CD_3OD
k_q(Cd)	1	0.31±0.04	0.88±0.10	0.30±0.03
k_q(Hg)[b]	1	0.31	0.093	0.088
k_5	1	0.93±0.09	0.91±0.09	0.91±0.09
k_8/k_6	1	1.0 ±0.1	1.1 ±0.1	1.1 ±0.1

a) Relative to the values obtained with CH_3OH. b) From Ref. 1.

The imprisonment lifetime of Cd($^3P_1$) is not known under the present experimental conditions. Breckenridge *et al.* have estimated the ratio of the imprisonment lifetime to the natural lifetime of Cd($^3P_1$) in the presence of argon.[8] According to their estimation, the ratio is 1.09 at 260 °C and increases with an increase in the vapor pressure of cadmium. In the present experiment, a smaller imprisonment lifetime may be expected, since the vapor pressure of cadmium in this study is lower than that in their studies.[8] When the lifetime of Cd($^3P_1$) in the present study is assumed to be equal to the natural lifetime, *i.e.*, 2.3×10^{-6} s, the quenching efficiency of CH_3OH can be estimated to be 0.4 Å^2. Because of the rough estimation, this value should be accepted as un upper limit. The cross section of methanol for quenching triplet cadmium is about twenty times smaller than that for quenching triplet mercury.[9]

For the intensity of the emission at 395 nm, I_{395}, the following equation can be derived from the above reaction mechanism:

$$I_{326.1}[\mathrm{Me}]/I_{395} = \alpha(k_2/k_5)(1+k_8[\mathrm{Ar}]/k_6+k_7[\mathrm{Me}]/k_6). \quad (2)$$

The factor, α, depends on the experimental conditions; the geometry of the apparatus, the slitwidth, the efficiency of the monochromator, and the sensitivity of the photomultiplier used. Substituting [Ar]=[M]−[Me] into Eq. 2, where [M] represents the total pressure, we can obtain Eq. 2′:

$$I_{326.1}[\mathrm{Me}]/I_{395} = \alpha(k_2/k_5)(1+k_8[\mathrm{M}]/k_6+(k_7-k_8)[\mathrm{Me}]/k_6). \quad (2')$$

As was stated in the Results section, the observed values of $I_{326.1}[\mathrm{Me}]/I_{395}$ are independent of the change in the pressure of methanol under the same total pressure. Therefore, the third term in the right-hand side of Eq. 2′ may be ignored. From the intercepts and the slopes of the straight lines in Fig. 3, the relative values of k_5 and k_8/k_6 can be estimated; they are listed in Table 2. As is shown in Table 2, the isotope effects on k_5 and k_8/k_6 are negligibly small.

Let us define quantum efficiency of the band emission at 395 nm as the number of photons emitted from the intermediate complex, CdMe*, per quenched Cd($^3P_1$) atom. Then this efficiency, Φ_{em}, may be expressed as follows:

$$\Phi_{em} = (k_5/k_q)/(1+k_8[\mathrm{M}]/k_6). \quad (3)$$

The quantum efficiency of the emission thus defined should be proportional to the emission intensity at 395 nm. Since the isotope effects on k_5 and k_8/k_6 were negligibly small, as is shown in Table 2, the total emission intensity should be inversely proportional to the quenching efficiency. This is indeed the case, as is shown in Tables 1 and 2. Thus, it may be said that the isotope effects observed in the Cd-photosensitized reaction of methanol are mainly due to the isotope effect on the quenching process.

Isotope Effect on the Quenching Process. In a previous short communication, the following three quenching processes were considered in an attempt to explain the results obtained with CH_3OH, CH_3OD, and CD_3OD:[3]

$$\mathrm{Cd}^* + \mathrm{CH_3OH} \rightarrow \mathrm{Cd\cdots H\cdots OCH_3} \quad (a)$$

$$\rightarrow \mathrm{Cd\cdots H\cdots CH_2OH} \quad (b)$$

$$\rightarrow \mathrm{Cd\cdots O\langle^{H}_{CH_3}} \quad (c)$$

The D/H kinetic isotope effects on the (a) and (b) processes are expected to be large. On the other hand, the effect on the (c) process is expected to be small because of the secondary effect. The band emissions have been observed at about 390 nm in the Cd-photosensitized reactions of water and ethers.[5] This fact suggests that the (c) process corresponds to Reaction 5, *i.e.*, the formation of a radiative intermediate complex. In fact, a very small isotope effect on k_5 was observed, as is shown in Table 2.

The observed quenching efficiency, k_q, may be set as equal to the sum of k_a, k_b, and k_c. If the secondary isotope effect can be neglected, we should obtain the following relation between the quenching efficiencies for the isotopic methanol:

$$k_{q,CH_3OH} + k_{q,CD_3OD} = k_{q,CH_3OD} + k_{q,CD_3OH}. \quad (4)$$

As is shown in Table 2, Eq. 4 is satisfied within the limits of experimental error. Since $k_{q,CH_3OH} \simeq k_{q,CD_3OH}$ and $k_{q,CH_3OD} \simeq k_{q,CD_3OD}$, the (b) process may not be important compared with the (a) and (c) processes. Moreover, the quantum yield of the emission at 395 nm has been estimated to be 0.0032.[5] The smallness of the quantum yield of the emission suggests that the (c) process cannot be the main process. Consequently, it may be said that the observed isotope effect on k_q is mainly due to the isotope effect on k_a. The D/H kinetic isotope effect on k_a can be estimated to be about 0.3.

Theoretical Estimation of D/H Kinetic Isotope Effect. The D/H kinetic isotope effect on the (a) process can be estimated by the use of the theory of the kinetic isotope effect:[10]

$$k_D/k_H = \exp\left[-(hc/2kT)\left\{\sum^{3n^\dagger-7}(\nu_i^\dagger(D)-\nu_i^\dagger(H)) - \sum^{3n-6}(\nu_i(D)-\nu_i(H))\right\}\right]. \quad (5)$$

Here, $\nu_i(D)$ and $\nu_i(H)$ are vibrational frequencies in cm^{-1}. The superscript † indicates the transition state. The h, c, k, and T symbols have their conventional significance. Equation 5 has been derived under a heavy-molecule approximation; *i.e.*, the changes in the molecular mass and moment of inertia have no significant influence upon the isotopic rate ratio.[10] The term of the symmetry-number ratio can be set as equal to unity in this reaction system, and so it is omitted in Eq. 5. An approximation, $1-\exp(-hc\nu/kT) \simeq 1$, has already been applied in Eq. 5. When the vibrational frequency is less than 1000 cm^{-1}, however, it is necessary to include the factor of $1-\exp(-hc\nu/kT)$. When the secondary isotope effect can be neglected, the contribution of all the vibrations except for the O–H stretching and two bending frequencies disappear in the reactant part of Eq. 5. Similarly, only a Cd–H–R stretching and two bending frequencies can contribute in the transition state. Here, R denotes the CH_3O radical.

In order to estimate the vibrational frequencies in the transition state, the following three models are considered:

Model a: The Cd atom is located apart from the methanol molecule and has no effect on the vibrational frequencies in the transition state. The reacting hydrogen atom is located in the neighborhood of the R radical. Thus, the two bending frequencies in the transition state may be set as equal to those in the reactant.

Model b: Much as in Model a, the Cd atom is located far from the methanol molecule, but the R–H bond is stretched so that the two bending frequencies in the transition state can be approximated as zero.

Model c: The R–H bond is stretched further, and the reacting hydrogen atom is located in the neighborhood of the Cd atom. The stretching frequency in the transition state is approximated by the Cd–H stretching. The two bending frequencies are also approximated as zero. In Models b and c the term which contains the two bending frequencies in the transition state may be approximated by m_D/m_H.[10] Here, m_D and m_H are the masses of the D and H atoms respectively.

Table 3. Frequencies used in the calculation of Eq. 5[a]

Atom transferred		H	D
O–H	Stretching	3682	2720
	Bending	1340	869
	Twisting	270[b]	191[c]
C–H	Stretching	2977	2227
	Bending	1430	1055
Cd–H	Stretching	1430[d]	1011[c]

a) In cm^{-1} unit. From H. D. Noether, *J. Chem. Phys.*, **10**, 693 (1942) unless otherwise cited. b) G. Herzberg, "Molecular Spectra and Molecular Structure II, Infrared and Raman Spectra of Polyatomic Molecules," D. Van Nostrand Co., Princeton (1945). c) Calculated using $\nu(D) = (1/\sqrt{2})\nu(H)$. d) G. Herzberg, "Molecular Spectra and Molecular Structure I, Spectra of Diatomic Molecules," D. Van Nostrand Co., Princeton (1950).

Table 4. Calculated D/H kinetic isotope effect

	Process (a)	Process (b)
Model a	0.25	0.33
Model b	0.16	0.22
Model c	0.29	0.41
Observed	0.31±0.04	

On the base of the above assumptions, the D/H kinetic isotope effect on the (a) process was calculated using the frequency assignments shown in Table 3. The results are listed in Table 4. For comparison, Table 4 also contains the results of a similar calculation of the (b) process. As is shown in Table 4, the observed D/H isotope effect on the (a) process is close to the case of Model c; *i. e.*, the reacting hydrogen atom is located in the neighborhood of the Cd atom in the transition state.

The present study suggested that the (a) process is the predominant process compared with the (b) and (c) processes in the Cd-photosensitized reaction of methanol. This coincides with the results obtained by Knight *et al.* and Pottie *et al.* in the case of mercury photosensitization.[2] However, it is different from the results obtained by Luther *et al.*[1]

References

1) K. Luther, H. E. Hunziker, and H. R. Wendt, "11th Informal Conference on Photochemistry," Nashville, Tennessee, June 1974.

2) R. F. Pottie, A. G. Harrison, and F. P. Lossing, *Can. J. Chem.*, **39**, 102 (1961); A. R. Knight and H. E. Gunning, *Can. J. Chem.*, **39**, 1231, 2251 (1961).

3) S. Tsunashima, K. Morita, and S. Sato, *Chem. Lett.*,

1976, 453.
4) S. Yamamoto, S. Tsunashima, and S. Sato, *Bull. Chem. Soc. Jpn.*, **48**, 1172 (1975).
5) S. Yamamoto, K. Tanaka, and S. Sato, *Bull. Chem. Soc. Jpn.*, **48**, 2172 (1975).
6) R. P. Porter, *J. Phys. Chem.*, **61**, 1260 (1957).
7) S. Yamamoto, M. Takaoka, S. Tsunashima, and S. Sato, *Bull. Chem. Soc. Jpn.*, **48**, 130 (1975).
8) W. H. Breckenridge, T. W. Broadbent, and D. S. Moore, *J. Phys. Chem.*, **79**, 1233 (1975).
9) R. J. Cvetanović, *Prog. React. Kinet.*, **2**, 39 (1964).
10) L. Melander, "Isotope Effects on Reaction Rates," Ronald Press Co., New York (1960).

Chromium(III) Complexes with Amino Acids. III. Chromium(III) Complexes with Acidic, Basic and Carbamoyl Amino Acids

Hisaya Oki and Yasuko Takahashi

Department of Chemistry, Faculty of Education, Fukui University, Fukui 910

(Received December 6, 1976)

Syntheses by both the isothermal matrix in a solid state and by the usual solution method have been tried for chromium(III) complexes with L- and DL-asparagine, L- and DL-aspartic acid, L- and DL-glutamine, L- and DL-glutamic acid, L- and DL-lysine, and L-ornithine. $[Cr(L\text{-}aspNH_2)_3]\cdot 2H_2O$, $[Cr(DL\text{-}aspNH_2)_3]\cdot 3H_2O$, $(NH_4)_2[Cr(L\text{-}asp)_2][Cr(D\text{-}asp)_2]\cdot 4H_2O$, and $(+)[Cr(L\text{-}lys)_2(NH_3)(H_2O)]Cl\cdot 4H_2O$ were obtained by the matrix method in the solid state, while $[Cr(L\text{-}aspNH_2)_3]\cdot 2H_2O$, $[Cr(DL\text{-}aspNH_2)_3]\cdot 2H_2O$, and $(+)[Cr(L\text{-}lys)_2(NH_3)(H_2O)]Cl\cdot 4H_2O$ were prepared by the usual solution method. The preparation of chromium(III) complexes with other amino acids was not successful. A new type of complex of chromium(III) containing terdentate DL-aspartic acid and a new mixed chromium(III) complex containing three different ligands (L-lysine, ammine, and aqua) were prepared.

Chromium(III) complexes containing terdentate amino acids have not yet been isolated. Amino acids which act as terdentate ligands are classified into amino dicarboxylic (acidic), diamino carboxylic (basic), and carbamoyl amino carboxylic acids (carbamoyl amino acid). In the chromium(III) complexes with L-asparagine,[1] L-aspartic acid,[2] L-glutamine, or L-lysine,[3] all the amino acids work as bidentate ligands. In the present work, attempts were made to prepare chromium(III) complexes with α-amino acids (L- and DL-aspartic acid, L- and DL-glutamic acid, L-ornithine, L- and DL-lysine, L- and DL-asparagine, and L- and DL-glutamine) by applying the methods described in Ref. 4, and to study the difference in complexation among neutral amino acids,[4,5] acidic, basic, and carbamoyl amino acids.

Experimental

Preparation of Chromium(III) Complexes. The methods of preparation are essentially the same as those reported in our previous papers.[4,5]

a) Preparation by Means of Solid State Reaction: The reaction temperature, the mole ratios of amino acids to the starting complex, $[Cr(NH_3)_6](NO_3)_3$, and the reaction time are listed in Table 1.

The reaction products with L- and DL-asparagine were dissolved in water, after which the solutions were kept standing at room temperature for one or two days. Tris(L-asparaginato) and tris(DL-asparaginato)chromium(III) were obtained as pink powder. By the same method, a complex with DL-aspartic acid was obtained as ammonium bis(DL-aspartato)chromate(III) after the solution had stood for two weeks. When the reaction product with L-lysine monohydrochloride was kept standing at room temperature for one or two days, bis(L-lysinato)ammineaquachromium(III) chloride was obtained as pink crystals. In the case of DL-lysine, a mixture of pink powder and free amino acid was obtained. However, the desired complexes could not be separated from the mixture. From the reaction products with L-aspartic acid, L- and DL-glutamine, and L-ornithine, oily substances were obtained, and crystallizations were not successful. In the case of the L- and DL-glutamic acid, the reaction products dissolved in water were kept standing at room temperature for four or five days to give purple crystals. However, the results of the elementary analysis of these crystals were coincident with the composition of neither a tris-type nor a dihydro-bridged dimer complex.

Table 1. Mole ratios of amino acids to the starting complex, the reaction temperature, and the reaction time

Amino acid	Mole ratio	Reaction temperature (°C)	Reaction time (min)
L-Asparagine	2.5	135	60
DL-Asparagine	2.5	135	60
DL-Aspartic acid	2.5	125	120
L-Lysine	5	135	35

b) Preparation by the Reaction in Solution: Hexaamminechromium(III) nitrate (3.4 g), and L-asparagine (4.0 g) were dissolved in water (50 ml), and the mixture was heated on a water-bath until pink crystals began to appear. The pink crystals were tris(L-asparaginato)chromium(III). By the same method, a complex with DL-asparagine was precipitated as a tris-type one. Hexaamminechromium(III) nitrate (3.4 g) and L-lysine monohydrochloride (5.4 g) were dissolved in water (50 ml), and the mixture was concentrated on a water-bath to one-fifth of its orginal volume. When the resulting solution was kept standing at room temperature for one or two weeks, bis(L-lysinato)ammineaquachromium(III) chloride were gradually deposited as pink crystals. In the case of DL-lysine or L-ornithine, a mixture of pink crystals and amino acid was obtained but the pink crystals could not be separated from the mixture.

Attempts to prepare of chromium(III) complexes with other amino acids were not successful, only oily substances were obtained in those cases.

The analytical data of these complexes are given in Table 2.

Apparatus. The absorption spectra were measured with a Hitachi 139 spectrophotometer. The IR spectra were measured with a Hitachi EPI-G3 infrared spectrophotometer in Nujol mull. The CD spectra were recorded on a JASCO Model ORD/UV-5 spectrophotometer with a CD attachment.

Results and Discussion

The absorption spectra of $[Cr(L\text{-}aspNH_2)_3]$ were measured in the solid state and in a perchloric acid solution. The spectrum of $[Cr(DL\text{-}aspNH_2)_3]$ was measured in the solid state, while those of $NH_4[Cr(DL\text{-}asp)_2]$ and $[Cr(L\text{-}lys)_2(NH_3)(H_2O)]Cl$ were measured in aqueous solutions. The numerical data of their maxima are summarized in Table 3. The values of the absorption maxima of $[Cr(L\text{-}aspNH_2)_3]$ in 20%$HClO_4$ and in

Table 2. Analytical data

	C (%)		H (%)		N (%)	
	Calcd	Found	Calcd	Found	Calcd	Found
$[Cr(L\text{-}aspNH_2)_3]\cdot 2H_2O$[a]	29.94	29.97	5.25	4.93	17.46	17.69
$[Cr(DL\text{-}aspNH_2)_3\cdot 3H_2O$[a]	28.86	28.74	5.46	4.88	16.83	16.72
$NH_4[Cr(DL\text{-}asp)_2]\cdot 2H_2O$[a]	25.17	25.09	4.94	4.89	11.44	11.41
$[Cr(L\text{-}lys)_2(NH_3)(H_2O)]Cl\cdot 4H_2O$[a]	29.70	29.26	8.12	7.56	14.44	14.22
$[Cr(L\text{-}aspNH_2)_3]\cdot 2H_2O$[b]	29.94	30.60	5.25	4.85	17.46	17.83
$[Cr(DL\text{-}aspNH_2)_3]\cdot 2H_2O$[b]	29.94	29.69	5.25	4.86	17.46	17.93
$[Cr(L\text{-}lys)_2(NH_3)(H_2O)]Cl\cdot 4H_2O$[b]	29.70	29.47	8.12	7.28	14.44	14.78

a) By the solid state reaction. b) By the reaction in solution.

Table 3. Absorption maxima of chromium(III) complexes

	$\nu_1/10^3$ cm^{-1}	(log ε)	$\nu_2/10^3$ cm^{-1}	(log ε)	
$[Cr(L\text{-}aspNH_2)_3]$[a]	19.3		26.1		Reflactance
$[Cr(L\text{-}aspNH_2)_3]$[a]	18.7	(1.82)	25.1	(1.64)	20%$HClO_4$
$[Cr(DL\text{-}aspNH_2)_3]$[a]	19.8		26.2		Reflactance
$NH_4[Cr(DL\text{-}asp)_2]$[a]	19.5	(1.98)	26.0	(1.56)	H_2O
$[Cr(L\text{-}lys)_2(NH_3)(H_2O)]Cl$[a]	19.5	(1.66)	26.5	(1.68)	H_2O
$[Cr(L\text{-}aspNH_2)_3]$[b]	19.3		26.2		Reflactance
$[Cr(DL\text{-}aspNH_2)_3]$[b]	19.9		26.2		Reflactance
$[Cr(L\text{-}lys)_2(NH_3)(H_2O)]Cl$[b]	19.5	(1.68)	26.5	(1.69)	H_2O

a) By the solid state reaction. b) By the reaction in solution.

the solid state differ from each other. The data suggest that this complex undergoes acid hydrolysis or some other chemical reaction in perchloric acid and that the behavior is similar to that of complexes with L- and DL-alanine.[4,5] The absorption maxima of $[Cr(L\text{-}aspNH_2)_3]$ and $[Cr(DL\text{-}aspNH_2)_3]$ in the solid state are nearly the same as those for chromium(III) complexes with neutral amino acids with the *fac*-structure. Thus, the present complexes of the tris-type have the *fac*-structure.

The spectrum of $NH_4[Cr(DL\text{-}asp)_2]$ is shown in Fig. 1. It may be seen that the second absorption band gives a lower molar extinction coefficient than does the first band and that the absorption curve of this complex is nearly the same as that of the corresponding *cis*(N)-*trans*(O_5) cobalt(III) complex.[6] The complex was adsorbed on an anion exchanger (Dowex 1X8, Cl-form). When a 0.01M NaCl solution was passed through a column of the exchanger, a pink solution was eluted. The spectrum of the eluted solution agreed with that of the original complex. Further, Nessler's reaction for this complex was positive. These results indicate that an ammonia molecule was not coordinated in this complex. In the complex of DL-aspartic acid, there are two possibilities whether both L- and D-aspartic acid are contained, or either. Concerning the geometrical isomers, the former type has one *trans*- and two *cis*-forms, while the latter has one *trans*- and one *cis*-form. The possible geometrical isomers are all shown in Fig. 2.

The reaction product in the solid state with L-aspartic acid was dissolved in water, and the solution was adsorbed on an anion exchanger (Dowex 1 X8, Cl-form). Upon elution with water, one violet band was seen. By eluting with 0.01M NaCl, two pink bands were completely separated. However, the isolation of compounds from these fractions was not carried out. The violet band described above was not adsorbed on a cation exchanger (Dowex 50W X2, H-form). Therefore, this

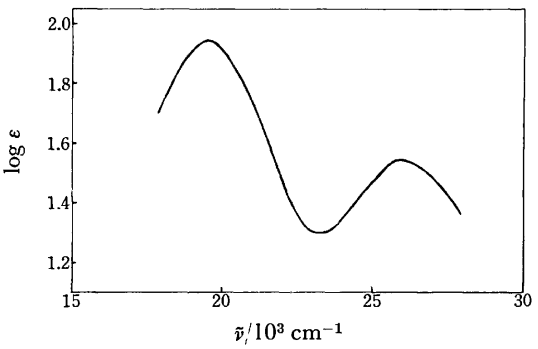

Fig. 1. The absorption spectrum of $(NH_4)_2[Cr(L\text{-}asp)_2]$-$[Cr(D\text{-}asp)_2]$.

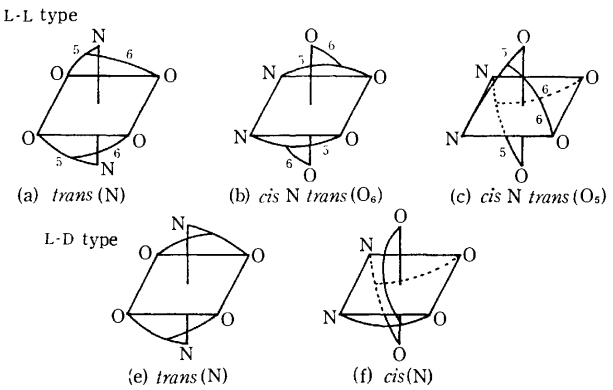

Fig. 2. The possible structures of bis(aspartato)chromate(III) ion.

band is considered to contain a noncharge species. The isolation of the compound from this fraction was also not carried out. By applying the method described above, the reaction product with DL-aspartic acid in the solid state was separated by chromatography. The results were similar to those for the complex with L-aspartic acid. Therefore, the chromium(III) ion was coordinated with two ions of either L- or D-aspartic acid in the bis(DL-aspartato)chromate(III) complex. The spectrum for the ammonium bis(DL-aspartato)-chromate(III) which had been eluted from the ion exchanger agreed with that of the first eluted band of the complex with L-aspartic acid. This complex shows no CD. Therefore, the bis(DL-aspartato)chromate(III) complex was concluded to consist of a racemic structure of $NH_4[Cr(L\text{-}asp)_2]$ and $NH_4[Cr(D\text{-}asp)_2]$. The geometrical structure of the first eluted band of the *cis*-type in the bis(L-aspartato)cobaltate(III) ion has been assigned to *cis*(N)-*trans*(O_5) [Fig. 2 (c)];[6] therefore, the structure of the bis(L-aspartato)chromate(III) ion is assigned to (c) in Fig. 2.

The absorption and CD spectra of $[Cr(L\text{-}lys)_2(NH_3)(H_2O)]Cl$ are shown in Fig. 3. In this complex, six geometrical isomers are possible; they are given in Fig. 4. It is obvious from Fig. 3 that the molar extinction coefficent of the first absorption band is nearly equal to that of the second absorption band, both showing no splitting. The maximum of the first absorption band of this complex is at a frequency nearly equal to those of *fac*-(amino acidato)chromium(III) complexes. The CD spectrum of this complex is shown in Fig. 3. Mizuochi *et al.*[3] reported that the bis(L-lysinato)diaquachromium(III) complex has a *cis* structure with respect to the nitrogen or the oxygen atoms of lysine. These facts lead to presume that the structure of $[Cr(L\text{-}lys)_2(NH_3)(H_2O)]^+$ has a *cis-cis* structure with respect to the nitrogen or the oxygen atoms, (f) in Fig. 4.

The CD spectra for $[Cr(L\text{-}aspNH_2)_3]$ and $[Cr(DL\text{-}aspNH_2)_3]$ were not measured, because these substances were not soluble in common solvents (H_2O, MeOH, EtOH, DMF and DMSO).

The chromium(III) complexes with acidic, basic, or

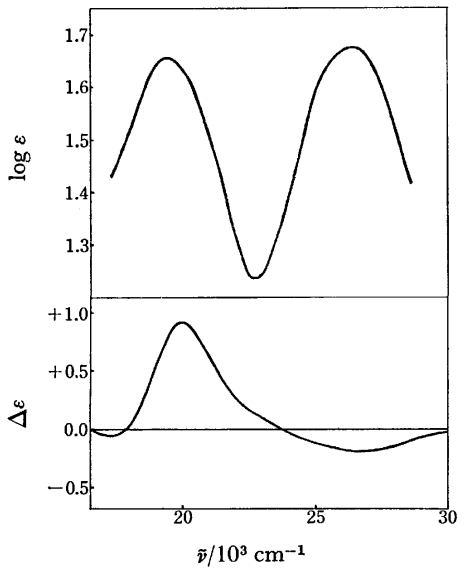

Fig. 3. The absorption and CD spectra of $[Cr(L\text{-}lys)_2(NH_3)(H_2O)]Cl$.

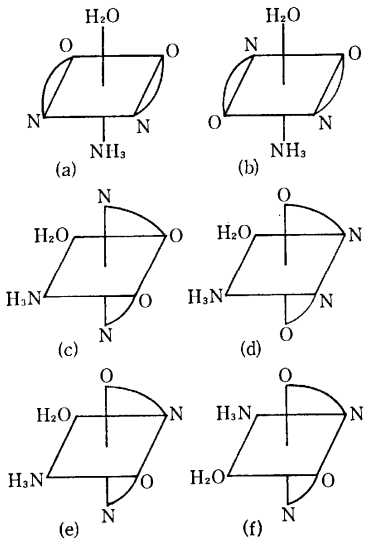

Fig. 4. The possible structures of $[Cr(L\text{-}lys)_2(NH_3)(H_2O)]^+$ ion.

Table 4. Chromium(III) complexes with acidic, basic, and carbamoyl amino acids

Starting material	$[Cr(NH_3)_6](NO_3)_3$		$Cr(OH)_3$	$CrCl_3$
Amino acid	Solid	Solution		
L-Asp	—	—		$[Cr(L)_3]$[2]
DL-Asp	$[Cr(L)_2]$	—		
L-Glu	—	—		
DL-Glu	—	—		
L-Lys	$[Cr(L)_2AB]$	$[Cr(L)_2AB]$		$[Cr(L)_2B_2]$[3]
DL-Lys	mixture	mixture		
L-Orn	—	mixture		
L-$AspNH_2$	$[Cr(L)_3]$	$[Cr(L)_3]$	$[Cr(L)_3]$[1]	$[Cr(L)_3]$[3]
DL-$AspNH_2$	$[Cr(L)_3]$	$[Cr(L)_3]$		
L-$GluNH_2$	purple	—	$[Cr(L)_3]$[3]	$[Cr(OH)(L)_2B]$[3]
DL-$GluNH_2$	purple	—		

L: amino acid, A: NH_3, B, H_2O, —: not crystallized.
Mixture: pink crystal and amino acid. Purple: no pure purple compound.

carbamoyl amino acids were synthesized both in the solid state and in solution. These synthesized complexes are given in Table 4, together with a description of the preparation by the solution method when chromium(III) hydroxide and chromium(III) chloride are used as the starting materials as reported by Volshtein[1,2] and Mizuochi.[3] Only $(NH_4)_2[Cr(L\text{-asp})_2][Cr(D\text{-asp})_2]$ contained terdentate amino acids. Bis(L-aspartato)chromate(III) was not crystallized. Volshtein obtained $Ag_3[Cr(L\text{-asp})_3]$,[2] but the tris-asp complex was not isolated in the present work. When silver nitrate was added to solution eluted by chromatography, the tris-asp complex was not precipitated. The reason for this is not clear.

When a mixture of bis(L-lysinato)ammineaquachromium(III) chloride and L-lysine·HCl in water was heated on a water-bath, a tris-type complex was not prepared and only the starting substances were recovered. Mizuochi *et al.*[3] reported the method of preparing $[Cr(L\text{-lys})_2(H_2O)]Cl$, but not for $[Cr(L\text{-lys})_3]$. The absorption curves of crude pink complexes with DL-lysine and L-ornithine were similar to that of $[Cr(L\text{-lys})_2(NH_3)(H_2O)]Cl$; and therefore, those complexes may be bis-type complexes. Thus, the synthesis of a tris-type complex of basic amino acid seems to be difficult.

In the present work, tris(L- or DL-asparaginato)chromium(III) complexes were prepared by both methods, solid state and solution. These carbamoyl amino acids are regarded as neutral amino acids. In a previous paper, we reported that the solution containing hexaamminechromium(III) nitrate and neutral amino acid naturally neutralized during the course of reaction.[4] In the case of asparagine, the reacting solution is also expected to be naturally neutralized to yield a tris-type complex. However, tris-type complexes with L- and DL-glutamine, as well as asparagine, were not obtained. The reason for this is not clear.

No terdentate bis-type chromium(III) complex could be obtained, except for those with DL-aspartic acid. This might be due to the instability of seven- or eight-membered ring in a bis-type complex, except for the complexes of aspartic acid and asparagine.

In a previous paper,[5] we reported that the preponderance of the formation of one optical isomer is changed depending upon the kind of solvent dissolving the product of the solid state reaction; when reaction products were dissolved in methanol (+) isomers were obtained, while (−) isomers were obtained in ethanol. However, in the present work, the reaction products with amino acids used in the solid state reaction were all insoluble in ethanol. L- and DL-aspartic acid, L- and DL-lysine, L-ornithine and L-glutamine are soluble, but the other amino acids are insoluble in methanol. The complexes with L- and DL-aspartic acid, L-ornithine, and L-glutamine were prepared as oily substances. The complexes with L- and DL-lysine were obtained as pink crystals. However, the results of the elemental analysis of these complexes show a mixture of $[Cr(lys)_2(NH_3)(H_2O)]Cl$ and $[Cr(lys)_2(NH_3)_2]Cl$. These complexes could not be separated, and the relation between the formation of optical isomers and the solvent was not investigated.

The authors wish to thank Professor Muraji Shibata and his co-workers of Kanazawa University for the CD measurement. The authors also wish to thank Professor Ryokichi Tsuchiya of Kanazawa University for valuable discussions and suggestions. This work was financially supported by a Grant-in-Aid from the Ministry of Education.

References

1) L. M. Volshtein and V. P. Molosnova, *Zh. Neorg. Khim.*, **4**, 1995 (1959).
2) L. M. Volshtein, *Zh. Neorg. Khim.*, **1**, 2378 (1956).
3) H. Mizuochi, A. Uehara, E. Kyuno, and R. Tsuchiya, *Bull. Chem. Soc. Jpn.*, **44**, 1555 (1971).
4) H. Oki and K. Otuka, *Bull. Chem. Soc. Jpn.*, **49**, 1841 (1976).
5) H. Oki, *Bull. Chem. Soc. Jpn.*, **50**, 680 (1977).
6) J. I. Legg and J. A. Neal, *Inorg. Chem.*, **12**, 1805 (1973).

Simultaneous Determination of the Atomic Ratio between C, H, O, and N by the Pyrolytic Sulfurization Method

Katsuya Tsuji, Kaoru Fujinaga, and Tadashi Hara

Department of Applied Chemistry, Faculty of Engineering, Doshisha University, Karasuma Imadegawa, Kamigyo-ku, Kyoto 602

(Received January 12, 1977)

From a sample subjected to pyrolytic sulfurization in a sealed quartz tube, the evolved gases, carbon disulfide, carbon monoxide, carbon dioxide, carbonyl sulfide, hydrogen sulfide, and a nitrogen molecule were simultaneously estimated. Determination of the atomic ratio between C, H, O, and N was carried out by means of three calibration curves obtained by use of glycine, L-glutamic acid, L-citrulline, and fumaric acid. They are applicable to carboxylic acids and the other compounds, but not to compounds including nitro and/or sulfo groups.

Various carboxylic acids were subjected to pyrolysis in sulfur(S) vapor and the reaction products such as hydrogen sulfide(H_2S), carbon dioxide(CO_2), and carbon disulfide(CS_2) were analyzed gas chromatographically, followed by determination of the chemical composition and functional group.[1] However, complete sulfurization of carboxylic acids apparently was not accomplished, since the amount of evolved CS_2 was much smaller than the expected one and a black carbonaceous residue remained. The method could not be applied to compounds other than carboxylic acids since the reaction products except for CO_2 were given in terms of the amount of CO_2 and the reaction in addition did not go to completion.

The present study was undertaken to establish an improved method in which a sample is subjected to pyrolytic sulfurization in a sealed quartz tube containing S, and the evolved gases such as H_2S, carbonyl sulfide (COS), CS_2, and a nitrogen molecule(N_2) are simultaneously estimated, followed by determination of the atomic ratio between C, H, O, and N. The calibration curves obtained from four compounds were applicable to carboxylic acids and other compounds, but not to the compounds including nitro and/or sulfo groups. Sulfurization seemed to be complete since no black carbonaceous residue remained. The present method gives more accurate results, no weighing being necessary during the procedure.

Experimental

Apparatus. A sampler, a displacement apparatus and an electric furnace were used. Gas chromatograms were taken on a Yanagimoto GCG-5DH and a Shimadzu GC-4B.

Reagents. Various purification methods including (1) vacuum sublimation, (2) contact with sulfuric acid, (3) nitric acid oxidation of sodium sulfide, (4) decomposition of sodium thiosulfate with hydrochloric acid, and (5) refluxing with magnesium oxide(MgO)[2] were examined, the last one being found the best. The procedure is as follows: 500 g S was gradually heated in a 500 ml four-holed flask with a reflux condenser, with an electric furnace, MgO being added after cessation of gas evolution. The temperature was held at *ca.* 450 °C, S being refluxed for 24 h. The melts were filtered at 120—150 °C through a sintered glass filter protected by a ribbon heater. About 450 g S was obtained as a filtrate to

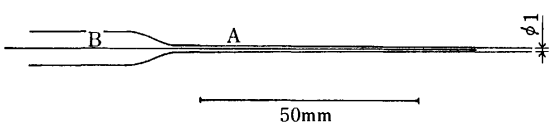

Fig. 1. Sampler.
(A) Quartz capillary, (B) plunger(nickel-chromium alloy).

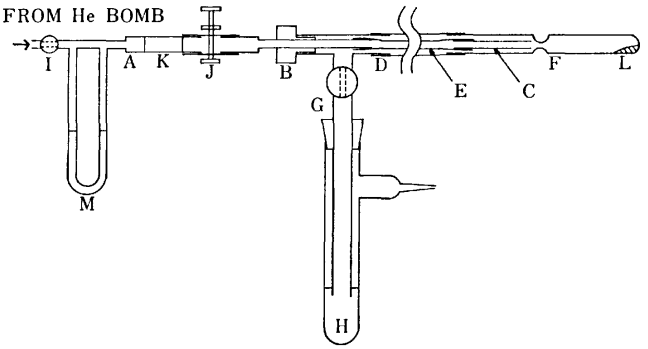

Fig. 2. Displacement apparatus.
A: Joint, B: silicone rubber packing, C: stainless steel tube, D: poly(vinyl chloride) tube, E: silicone rubber tube, F: reaction tube, G: two-way cock, H: water, I: needle valve, J: pinch cock, K: silica gel packing, L: sulfur and sample, M: flow meter.

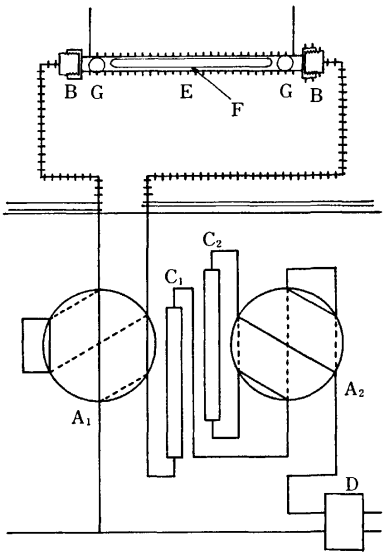

Fig. 3. Schematic diagram of the flow system.
A_1, A_2: Six-way cocks, B: joint, C_1: silica gel column, C_2: molecular sieve 5A column, D: thermal conductivity detector, E: Teflon tube, F: reaction tube, G: quartz wool.

which was added 4.5 g (1%) MgO, the contents being refluxed for 24 h. The operation was repeated six times, *ca.* 150 g S being finally obtained. The S obtained was dried at 150 °C for 3 h. A blank test was carried out using the sealed tube containing 20 mg S. Though slight peaks of air, COS and CS_2 were confirmed at the highest sensitivity of the Shimadzu GC-4B gas chromatograph, they were negligible in the present study.

The other reagents were of analytical grade. Helium was of commercial grade.

Materials. A transparent quartz tube was found suitable as the reaction tube, since an opaque tube gives a large peak owing to the N_2 present in foams. The maximal strength of the quartz tube was estimated to be *ca.* 390 atm at 950 °C from the relationship between the amount of S and the explosion temperature during the course of heating, and on the assumption that S is present as a diatomic molecule[3] at 950 °C. The internal pressure being *ca.* 20 atm, the operation was safely carried out.

The gas sampler E shown in Fig. 2 should be heat-resistant, strong and elastic. A silicone rubber tube is heat-resistant but mechanically weak, a poly(vinyl chloride) tube less heat-resistant, giving a number of impurity peaks. A Teflon tube meets all requirements and can be used more than 100 times at 55 °C, not giving any impurity peaks even at 120 °C.

Procedure. A transparent quartz tube, 3.8 mm i.d., 5.6 mm o.d. and 110 mm long, was treated for 5 h in a Bransonic-52 ultrasonic cleaner, washed, dried, and closed at one end by use of a town gas-oxygen flame, followed by being made narrow at *ca.* 50 mm from the closed end and being heated at 850 °C for 10 min.

Five mg of S was placed in the quartz tube and a definite volume of powdered sample was added to it with the sampler (Fig. 1), a definite length of capillary sample thus being prepared. The reaction tube was connected with the displacement apparatus (Fig. 2). A stream of helium regulated at a flow rate of 100 ml/min by a manometer M and valve I was passed through it to displace the air. Cock G and pinch cock J were closed. The internal pressure of the reaction tube (*ca.* 890 Torr) was balanced with the atmospheric pressure by operating cock G just before glass blowing, followed by sealing. The time required for sealing was *ca.* 15 s. The sealed tube was placed in a quartz case 11 mm i.d. × 90 mm and heated in an electric furnace for 10 min at 600 °C and for 30 min at 950 °C. The sealed tube was held at 90 °C for 5 min in an oven and inserted into a Teflon sampler E (Fig. 3) maintained at 55 °C. E was connected with the gas chromatograph by operating the cock A_1. The sealed tube was broken into pieces by driving a jack across the Teflon sampler and evolved gas was introduced into the gas chromatograph, the column temperature being raised immediately to the programmed one at a rate of 8 °C/min. The molecular sieve 5A column C_2 was separated from the flowing system in *ca.* 5 min after the introduction of evolved gas, and the constituents of relative higher boiling point, which come out of the silica gel column C_1, were analyzed with a thermal conductivity detector after passing through cock A_2.

The gas chromatograph was operated under the following conditions: A 1.5 m stainless steel column C_1 was charged with silica gel (80—100 mesh) and a 0.6 m stainless steel column C_2 with molecular sieve 5A (80—100 mesh), column temperature being programmed between 40 and 185 °C at a rate of 8 °C/min. The flow rate of helium was 30 ml/min at 185 °C. Davison grade 08 silica gel[4] was used instead of Deactigel.[5] The latter is known to be effective for the separation of S-containing compounds. In order to separate the individual constituents in the evolved gas, a combination

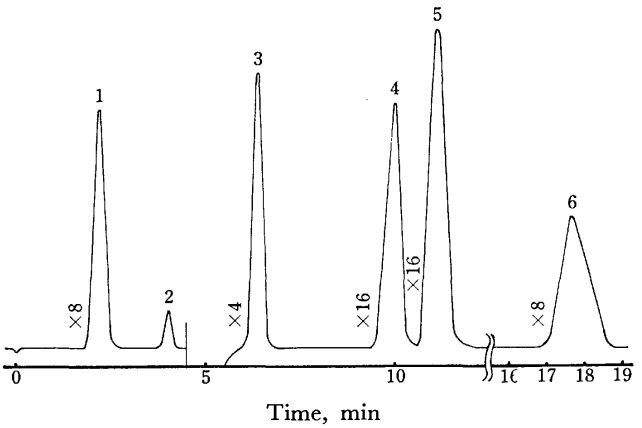

Fig. 4. Typical chromatogram of reaction products. 1: N_2, 2: CO, 3: CO_2, 4: COS, 5: H_2S, 6: CS_2.

of the silica gel column and the molecular sieve 5A column was utilized, by which N_2 was completely separated from carbon monoxide(CO). Glycine was chosen as an example and analyzed. Its chromatogram is shown in Fig. 4. All the peaks were identified by use of an authentic sample and their peak areas were estimated by the half-width method.

Results

Reaction Temperature and Reaction Time. The relationship between reaction products and reaction temperature (Fig. 5) or reaction time (Fig. 6) was examined using glycine. The composition of the reaction products was almost definite at a temperature in the range 750—1050 °C and in more than 20 min after the start of the reaction.

Pyrolytic Sulfurization. The sealed tube containing S and glycine was processed by five separate procedures (Table 1). The coefficients of variation in the values of (N/H), (C/H), and (O/H) were smaller in procedures C and E than in any other, and were thus re-examined using 5 mg S and 0.1—2.0 mg glycine. The results are given in Fig. 7 and Table 2. Procedure C was chosen since it gave a better result.

Amounts of Sample and S. Since the values of (N/H), (C/H) and (O/H) were approximately definite

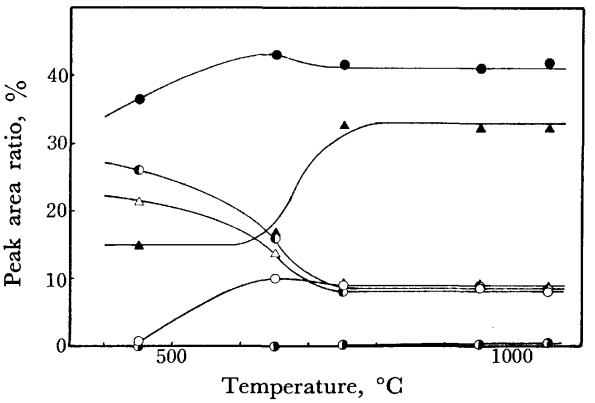

Fig. 5. Effect of reaction temperature on products. 20 mg S and 0.1—1.0 mg glycine made to react for 30 min. ○: N_2, ◑: CO, ◐: CO_2, ▲: COS, ●: H_2S, △: CS_2.

Table 1. Comparison of individual pyrolytic sulfurization procedures[a)]

Procedure	Coefficient of variation (%)[b)]								
	Individual peak area ratio[c)]						Observed atomic ratio[d)]		
	N_2	CO	CO_2	COS	H_2S	CS_2	$(N/H)_f$	$(C/H)_f$	$(O/H)_f$
A	4.0	24.5	3.6	2.9	1.9	8.2	4.7	2.8	4.5
B	4.5	9.1	4.9	2.5	4.9	4.3	9.5	7.8	7.4
C	2.1	20.0	2.4	3.3	1.8	11.1	2.7	3.5	4.2
D	6.1	0	6.6	2.0	4.0	10.9	9.5	6.9	6.9
E	6.8	5.6	6.9	2.0	1.8	10.9	8.5	2.3	2.8

a) 20 mg S and 0.3—1.0 mg glycine used. b) Calculated from five runs for each procedure. c) Ratio to the sum of all peaks. d) Estimated by Eqs. 6, 7, and 8, respectively. A: Heated at 950 °C for 40 min in a quartz case and held in an oven at 90 °C for 5 min, B: Heated at 950 °C for 40 min in a quartz case and held in water for 1 min, C: Heated at 600 °C for 10 min, at 950 °C for 30 min in a quartz case and held in an oven at 90 °C for 5 min, D: Heated at 950 °C for 40 min and held in an oven at 90 °C for 5 min, and E: Heated at 950 °C for 40 min and held in water for 1 min.

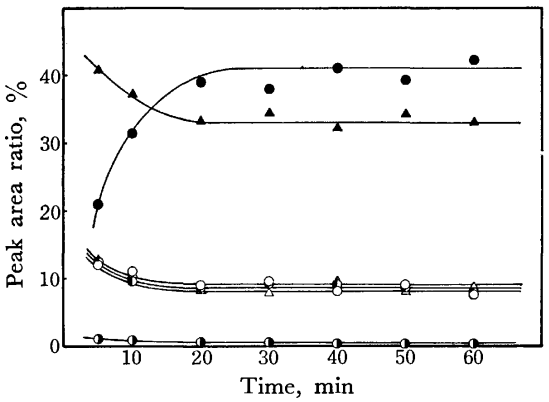

Fig. 6. Effect of reaction time on products.
20 mg S and 0.1—1.0 mg glycine made to react at 950 °C. ○: N_2, ◑: CO, ◐: CO_2, ▲: COS, ●: H_2S, △: CS_2.

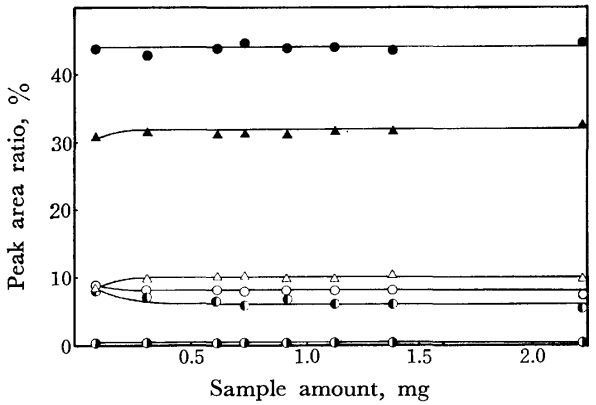

Fig. 7. Effect of the amount of sample on peak area ratios. 5 mg S and glycine made to react by procedure C. ○: N_2, ◑: CO, ◐: CO_2, ▲: COS, ●: H_2S, △: CS_2.

in the reaction between a definite amount of S and 0.3—2.0 mg glycine, the compounds other than glycine were also sampled by the sampler (Fig. 1) so that their amounts would be in the range 0.3—2.0 mg. From the relation between the weight of sample and the peak area in the gas chromatogram, the amount of samples taken

Table 2. Re-examination of the pyroltic sulfurization procedures[a)]

Procedure	Coefficient of variation (%)[b)]		
	$(N/H)_f$	$(C/H)_f$	$(O/H)_f$
C	3.9	1.4	2.4
E	5.0	1.9	2.1

a) Five mg S and 0.3—2.0 mg glycine used. b) Calculated from five runs for each procedure.

was 0.3—1.0 mg. The relation between the amount of sample and the amounts of S was examined. The contents of N_2, CO, and CO_2 in the evolved gas were constant for the weight ratio of S to sample greater than 20. The contents of H_2S and COS decreased with an increase in the amount of S. Five mg of S was used.

Temperature of Gas Sampler. The effect of the internal temperature of the gas sampler E on the peak area of the reaction products was examined (Fig. 8). The peak area ratios of reaction products to N_2 were approximately constant at temperatures 50—120 °C. Thus the internal temperature of the gas sampler E

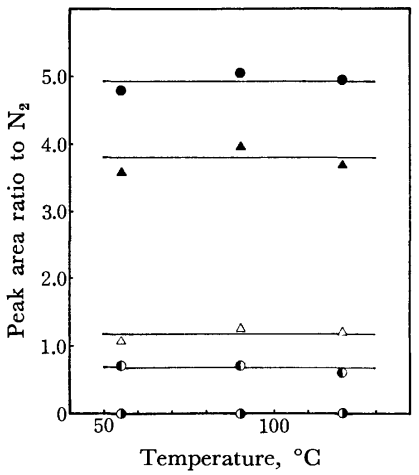

Fig. 8. Effect of the internal temperature of a Teflon tube on peak area ratios.
5 mg S and glycine made to react. ◑: CO/N_2, ◐: CO_2/N_2, ▲: COS/N_2, ●: H_2S/N_2, △: CS_2/N_2.

Table 3. Correction factors

Run number	Peak area ratio[a]				Correction factor[b]		
	CO	CO_2	COS	CS_2	$K(CO_2)$	$K(COS)$	$K(CS_2)$
1	0.8	13.6	65.0	20.6	1.00	1.26	1.51
2	0.6	13.4	65.3	20.4	1.00	1.26	1.52
Average	0.7	13.5	65.2	20.5	1.00	1.26	1.52

a) Individual peak area divided by the sum of all peaks. b) Estimated by Eqs. 4 and 5, respectively.

was held at 55 °C.

Correction Factors for the Relative Peak Area of CO_2, COS, and CS_2. The compound containing C, H, O, and N was subjected to pyrolytic sulfurization to form the following products: CO, CO_2, COS, and CS_2 from carbon atom, H_2S from hydrogen atom, CO, CO_2, and COS from oxygen atom and N_2 from nitrogen atom. In order to determine the composition of the compound, each peak area of N_2, C- and O-containing compounds was divided by the peak area of H_2S, and the atomic ratios between H and C or O or N were estimated from the calibration curves. The relationship between the peak areas of CO, CO_2, COS, and CS_2 and their mole numbers was used to estimate the sum of individual peak areas. Since the peak area of CO was negligibly small in comparison with that of CO_2, COS, and CS_2, no care was taken of the correction factor of CO. CO was sealed into a quartz tube containing S by use of the displacement apparatus (Fig. 2), and the gases evolved by the reaction were analyzed (Table 3). The major products were CO_2, COS, and CS_2, only a minute amount of CO remaining as an unreacted component. The reaction between CO and a diatomic S molecule[3] at 950 °C was assumed to proceed according to the following equations.

$$2CO + S_2 = 2COS, \quad (1)$$

$$2COS = CO_2 + CS_2. \quad (2)$$

CO_2 and CS_2 were formed in equimolecular amounts. On the basis of $K(CO_2)=1.00$, the correction factors were estimated by Eqs. 4 and 5, where $A'(CO)$, $A'(CO_2)$, $A'(COS)$ and $A'(CS_2)$ refer to percent peak area ratios of CO, CO_2, COS, and CS_2 to the sum of all peaks.

$$K(CO_2) = 1.00, \quad (3)$$

$$\frac{K(COS)}{K(CO_2)} = K(COS) = \frac{\{100-[A'(CO)+A'(COS)]\}}{2A'(CO_2)}, \quad (4)$$

$$\frac{K(CS_2)}{K(CO_2)} = K(CS_2) = \frac{A'(CS_2)}{A'(CO_2)}. \quad (5)$$

The value of $100-[A'(CO)+A'(COS)]$ corresponds to the amount of COS consumed. Thus the value of $A'(CO_2)$, $A'(COS)$, and $A'(CS_2)$ divided by $K(CO_2)$, $K(COS)$, and $K(CS_2)$ in that order imply their mole ratios. The correction factors thus obtained were used.

Calibration Curves. Glycine, L-glutamic acid, L-citrulline, and fumaric acid in high purity were analyzed and the numerical ratios of each atom were calculated as follows.

$$\left(\frac{C}{H}\right)_f = \frac{[A(CO)+A(CO_2)+A(COS)/1.26+A(CS_2)/1.52]}{2A(H_2S)}, \quad (6)$$

$$\left(\frac{O}{H}\right)_f = \frac{[A(CO)+2A(CO_2)+A(COS)/1.26]}{2A(H_2S)}, \quad (7)$$

$$\left(\frac{N}{H}\right)_f = \frac{A(N_2)}{A(H_2S)}. \quad (8)$$

Here, $A(CO)$, $A(CO_2)$, $A(COS)$, $A(CS_2)$, $A(H_2S)$, and $A(N_2)$ are referred to the individual peak areas in mm^2 at the chart speed of 5 mm/min. Simultaneous determination of the atomic ratio among C, H, O, and N was made by use of the calibration curves. Experimental values (f) are plotted against theoretical values (t) in Fig. 9.

Analysis of Various Compounds. Amino acids (Table 4) and other carboxylic acids (Table 5) were

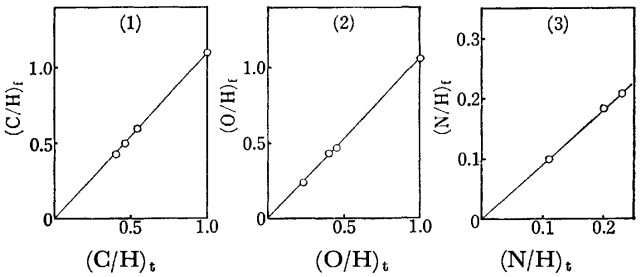

Fig. 9. (1) Calibration curve for (C/H). (2) Calibration curve for (O/H). (3) Calibration curve for (N/H).

Table 4. Analytical results of amino acids

Compound	Formula	
	Theoretical	Found[a]
γ-Aminobutyric acid	$N_1C_4O_2H_9$	$N_{1.0}C_{3.9}O_{2.0}H_9$
L-Phenylalanine	$N_1C_9O_2H_{11}$	$N_{1.0}C_{8.6}O_{2.2}H_{11}$
Tryptophan	$N_2C_{11}O_2H_{12}$	$N_{2.1}C_{10.6}O_{2.2}H_{12}$
L-Methionine	$N_1C_5O_2S_1H_{11}$	$N_{1.0}C_{5.0}O_{2.1}H_{11}$
L-Aspartic acid	$N_1C_4O_4H_7$	$N_{1.0}C_{4.1}O_{4.1}H_7$
L-Threonine	$N_1C_4O_3H_9$	$N_{1.0}C_{3.9}O_{3.0}H_9$
L-Homoserine	$N_1C_4O_3H_9$	$N_{1.0}C_{3.9}O_{2.9}H_9$

a) Calculated from two runs for each sample.

Table 5. Analytical results of carboxylic acids

Compound	Formula	
	Theoretical	Found[a]
Malonic acid	$C_3O_4H_4$	$C_{3.1}O_{4.1}H_4$
Succinic acid	$C_4O_4H_6$	$C_{3.9}O_{3.9}H_6$
Lauric acid	$C_{12}O_2H_{24}$	$C_{12.3}O_{2.2}H_{24}$
Myristic acid	$C_{14}O_2H_{28}$	$C_{13.6}O_{2.3}H_{28}$
Terephthalic acid	$C_8O_4H_6$	$C_{7.9}O_{4.1}H_6$

a) Calculated from two runs for each sample.

Table 6. Analytical results of other compounds

Compound	Formula	
	Theoretical	Found[a)]
2,2′,3,3′,4,4′,5,5′,6-Nonamethyldiphenylmethane	$C_{22}H_{30}$	$C_{22.1}H_{30}$
2,2′-Bipyridine	$N_2C_{10}H_8$	$N_{1.9}C_{10.1}H_8$
Cyanoguanidine	$N_4C_2H_4$	$N_{4.0}C_{1.9}H_4$
Benzil	$C_{14}O_2H_{10}$	$C_{14.1}O_{2.2}H_{10}$
Benzophenone	$C_{13}O_1H_{10}$	$C_{13.0}O_{1.2}H_{10}$
meso-Erythritol	$C_4O_4H_{10}$	$C_{4.0}O_{3.9}H_{10}$
p-Dimethylaminobenzaldehyde	$N_1C_9O_1H_{11}$	$N_{0.9}C_{8.8}O_{1.1}H_{11}$
Dimethylglyoxime	$N_2C_4O_2H_8$	$N_{1.9}C_{4.0}O_{2.1}H_8$
Diphenylglyoxime	$N_2C_{14}O_2H_{12}$	$N_{2.1}C_{14.0}O_{2.3}H_{12}$

a) Calculated from two runs for each sample.

analyzed. No difference between threonine and homoserine was found irrespective of their structural isomerism. Since S atom could not be determined, it was neglected in the composition of methionine. The method was applied to the compounds consisting of C and H as well as C, H, and N, satisfactory results being obtained (Table 6).

Discussion

Relative Correction Factors of CO_2, COS, and CS_2. Eqs. 1 and 2 for the reaction between CO and S were supported by Stock *et al.*[6,7] We found CO_2, COS, and CS_2 as the reaction products. The relative correction factors of CO_2, COS, and CS_2 were determined on the assumption that the reaction between CO and S proceeds in accordance with Eqs. 1 and 2, which were confirmed as follows: The N_2 gas containing 30—100 vol % CO was prepared by use of a N_2 bomb and a CO bomb equipped with a needle-valve and a flow-meter, respectively, and the mixed gas was sealed into a reaction tube containing 20 mg S, followed by heating at 950 °C and analysis of the gases produced (Fig. 10). The peak area ratios of CO, COS, and CS_2 to CO_2

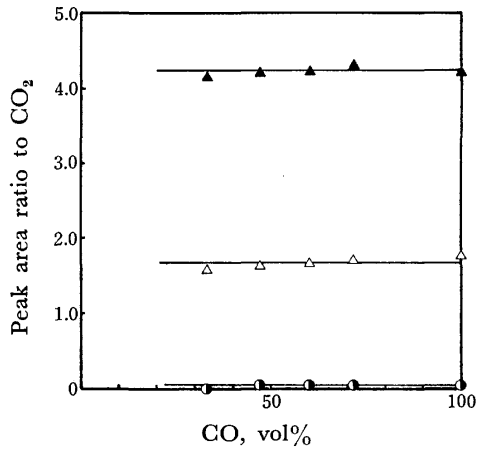

Fig. 10. Relationship between the amount of CO and the peak area ratios using a Yanagimoto GCG-5DH gas chromatograph. ◑: CO/CO_2, ▲: COS/CO_2, △: CS_2/CO_2.

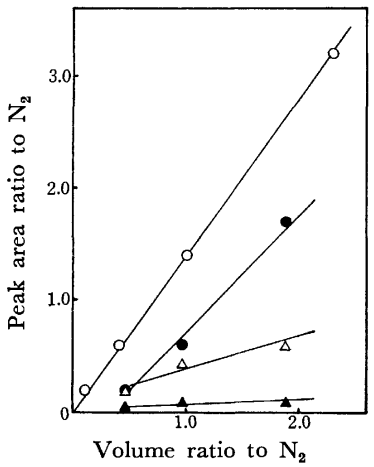

Fig. 11. Effect of CS_2* on the peak area ratios. * CS_2 added by the quartz capillary. (○) Mixture of N_2 and SO_2, (●) mixture of N_2, SO_2 and CS_2, (△) produced CO_2, (▲) produced COS.

were found to be constant irrespective of change of vol% CO. By taking it for granted that the reaction products are restricted to CO_2, COS, and CS_2, Eqs. 1 and 2 are concluded to hold for the reaction between CO, and S under the above conditions. Since CO_2 was produced as shown in Eq. 2, the reaction between CO_2 and S was examined, and the reaction mixture was found to contain the following: CO_2, COS, and sulfur dioxide(SO_2) as the major component, and CO and CS_2 as a trace component. Thus the reaction between CO_2 and S is supposed to proceed primarily as follows.

$$2CO_2 + \frac{3}{2}S_2 = 2COS + SO_2. \quad (9)$$

If we take Eqs. 2 and 9 into consideration, the formation of SO_2 is expected for the reaction between CO and S. However, no SO_2 was found. This is understandable if we accept the equation which was experimentally confirmed (Fig. 11).

$$CS_2 + SO_2 = CO_2 + \frac{3}{2}S_2. \quad (10)$$

The amount of SO_2 decreases by addition of CS_2 to SO_2, CO_2 and COS being simultaneously formed. Though the equation was also

$$3CS_2 + 2SO_2 = 2COS + CO_2 + S_2, \quad (11)$$

described for the formation of CO_2 and COS from CS_2 and SO_2, it was not acceptable since the amount of COS was confirmed experimentally to be about one-fifth that of CO_2, irrespective of the mole ratio of COS: CO_2=2 : 1. Assuming the conversions in Eqs. 2, 9, and 10 to be α, β, and γ, we have equilibrium fractions of each component based on a unit mass of COS as follows:

$$\underset{1-\alpha}{2COS} = \underset{0.5\alpha}{CO_2} + \underset{0.5\alpha}{CS_2}, \quad (2)'$$

$$\underset{0.5\alpha(1-\beta)}{2CO_2} + \frac{3}{2}S_2 = \underset{0.5\alpha\beta}{2COS} + \underset{0.25\alpha\beta}{SO_2}, \quad (9)'$$

$$\underset{0.5\alpha-0.25\alpha\beta\gamma}{CS_2} + \underset{0.25\alpha\beta(1-\gamma)}{SO_2} = \underset{0.25\alpha\beta\gamma}{CO_2} + \frac{3}{2}S_2. \quad (10)'$$

From the values $K_{eq}=2.67\times10^4$ at 1200 K and $K_{eq}=2.24\times10^4$ at 1300 K for Eq. 10,[8] the value of γ becomes approximately equal to 1. The fraction of CS_2 is equal to $0.5\alpha-0.25\alpha\beta\gamma=0.5\alpha-0.25\alpha\beta$ and that of CO_2 to $0.5\alpha(1-\beta)+0.25\alpha\beta\gamma=0.5\alpha-0.25\alpha\beta$. This implies that Eq. 2 holds even in the introduction of Eqs. 9 and 10.

Adaptability of Calibration Curves. The space velocity of a reactant gas was very large in the high temperature range, and the reaction between a sample gas and S could not go to completion.[1] Pyridine derivatives in particular were less decomposable and much carbonaceous residue remained after the reaction. By the present method, pyridine and quinoline derivatives were easily decomposed, no carbonaceous residue remaining. The reaction seems to proceed completely and stoichiometrically (Tables 4, 5, and 6).

The calibration curves obtained from four compounds were applicable to various compounds. However, they cannot be applied to aromatic sulfonic acids and nitro compounds. SO_2 was formed in a batchwise apparatus and a flow-type apparatus,[9] but not by the present method. This seems to be due to the difference in the reaction conditions. SO_2 formed in the former case moves quickly to the low temperature zone with other gases, remaining unreacted, while that in the present case is made to react with CS_2 at 950 °C according to Eq. 10. This is reasonable if we take the relationship between ΔG° and TK into consideration (Fig. 12). Compounds deviated from the calibration curves are given in Table 7. Since the amounts of CO_2 and COS formed according to Eqs. 9 and 10 were considered in Eqs. 6 and 7, the deviation seems to arise from other reasons. The amount of H_2S formed was unexpectedly small and the formation of water(H_2O) was always observed in a sample for which analytical data deviated markedly from the calibration curves. Detection of H_2O was carried out under the following conditions: A 2.2 m Porapak-Q (80—100 mesh) column, initial temperature 60 °C, operated at the rate of 5 °C/min. H_2O was assumed to be formed by the reactions (Eqs. 12, 13, and 14) between SO_2 and H_2S or H_2 from the results of the following experiment. The reaction between SO_2 and H_2 in the presence of S was examined in a similar manner to that given before. The amount of SO_2 decreased with an increase in the amount of H_2 while that of H_2O increased in the opposite way.

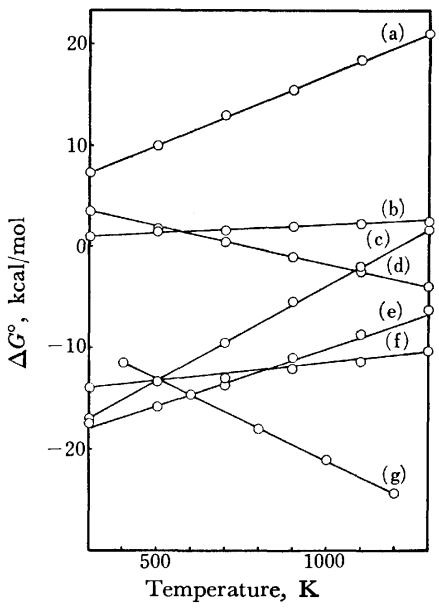

Fig. 12. Relationship between ΔG° and temperature. a: Eq. 9, b: Eq. 2, c: Eq. 1, d: Eq. 12, e: Eq. 13, f: Eq. 14, g: Eq. 10.

Table 7. Compounds deviated from the calibration curves

Compound	Formula	
	Theoretical	Found[a]
2,6-Dimethylphenol	$C_8O_1H_{10}$	$C_{8.5}O_{1.2}H_{10}$
8-Quinolinol	$N_1C_9O_1H_7$	$N_{1.3}C_{9.6}O_{1.1}H_7$
m-Nitroaniline	$N_2C_6O_2H_6$	$N_{2.8}C_{6.4}O_{2.4}H_6$
Sodium 1-naphthalenesulfonate	$C_{10}O_3S_1Na_1H_7$	$C_{9.0}O_{5.3}H_7$

a) Calculated from two runs for each sample.

$$H_2 + \frac{1}{2}S_2 = H_2S, \quad (12)$$

$$H_2S + \frac{1}{2}SO_2 = H_2O + \frac{3}{4}S_2, \quad (13)$$

$$H_2 + \frac{1}{2}SO_2 = H_2O + \frac{1}{4}S_2. \quad (14)$$

Since no correction was made for the formation of H_2O in the present method, the erroneous data of H and O in Eqs. 6, 7, and 8 seem to bring about the deviation from the calibration curves. Some phenols also produced H_2O, causing deviation from calibration curves. Two paths for the formation of H_2O were expected, one leading to Eq. 13 or 14 by way of Eq. 9 and the other based on a direct dehydration reaction instead of a decarbonylation reaction in the thermal decomposition of the sample. Since the conversion of Eq. 9 was found to be fairly low, the path involving Eq. 9 is less expected than that involving a dehydration reaction.

Comparison of the Present Method with Previous One. From a comparison with the method described previously, the characteristics of the present method are summarized as follows: 1) No carbonaceous residue was observed, 2) A large amount of COS was found, 3) No SO_2 was detected, 4) Weighing is unnecessary, 5) No information was obtained on the functional group. 1) and 5) indicate that the reaction is complete. All the compounds containing oxygen atom gave CO, CO_2, and COS, making the determination of atomic ratio complicated. We examined the catalytic disproportionation of COS[10] in the presence of a quartz powder with the intention of obtaining simple products, but no satisfactory results were obtained.

References

1) T. Hara and S. Ito, *Bull. Chem. Soc. Jpn.*, **44**, 2427 (1971).

2) R. F. Bacon and R. Fanelli, *Ind. Eng. Chem.*, **34**, 1043 (1942).

3) J. Berkowitz and J. R. Marquart, *J. Chem. Phys.*, **39**, 275 (1963).
4) W. L. Thornsberry, Jr., *Anal. Chem.*, **43**, 452 (1971).
5) C. T. Hodges and R. F. Matson, *Anal. Chem.*, **37**, 1065 (1965).
6) A. Stock and P. Seeling, *Ber.*, **52**, 681 (1919).
7) A. Stock, W. Sieke, and E. Pohland, *Ber.*, **57**, 719 (1924).
8) I. Barin and O. Knacke, "Thermochemical Properties of Inorganic Substances," Springer-Verlag, Berlin (1973), p. 162.
9) T. Hara and K. Fujinaga, unpublished.
10) J. R. Partington and H. H. Neville, *J. Chem. Soc.*, **1951**, 1230.

Stereochemistry of Cobalt(III) Complexes with Thioethers. I. Circular Dichroism Spectra of Complexes with Bi- or Terdentate Thioethers

Kazuaki YAMANARI, Jinsai HIDAKA,* and Yoichi SHIMURA

Department of Chemistry, Faculty of Science, Osaka University, Toyonaka, Osaka 560

(Received February 21, 1977)

Five (bidentate-*N,S* or *-O,S*)bis(ethylenediamine)cobalt(III) complexes have been optically resolved and their absolute configurations deduced from their circular dichroism (CD) spectra, where bidentate-*N,S* or *-O,S* are $NH_2(CH_2)_2S^-$, $NH_2(CH_2)_2SR$ (R=CH_3 and C_2H_5), and $CH_3S(CH_2)_nCO_2^-$ (n=1 and 2). The chromatographic, CD, and NMR behaviors suggest that the thioether donor atoms are coordinated stereoselectively producing the *Δ*-(*S*) or *Λ*-(*R*) complexes. Three (terdentate-*N,S,O*)[1,1,1-tris(aminomethyl)ethane]cobalt(III) complexes of $NH_2(CH_2)_2SCH_2CO_2^-$, $NH_2(CH_2)_2S(CH_2)_2CO_2^-$, and L-$CH_3SCH_2CH(NH_2)CO_2^-$ have been prepared and the complexes of the former two ligands optically resolved; the absolute configurations have been discussed on the basis of the CD spectra.

Some bis(ethylenediamine)cobalt(III) complexes with a bidentate ligand containing a sulfur donor atom, such as 2-aminoethanethiol, mercaptoacetic acid, and the related thioethers, have been prepared and the absorption spectra have been discussed.[1-5] The contribution of the coordinated sulfur atom of the thioether ligands to CD spectra would be an interesting study. However, no report seems to have appeared on the circular dichroism (CD) spectra of these complexes.

Two series of mixed cobalt(III) complexes with a bi- or a terdentate ligand containing a thioether donor atom, [Co(bidentate-*N,S* or *-O,S*)$(en)_2$]$^{n+}$ and [Co(terdentate-*N,S,O*)(tame)]$^{2+}$ have been prepared and resolved into optical antipodes, and their absorption and CD spectra are discussed in relation to the absolute configurations. Abbreviations used for the ligands are as follows: Haet, 2-aminoethanethiol $NH_2(CH_2)_2SH$; mea, 2-(methylthio)ethylamine $NH_2(CH_2)_2SCH_3$; eea, 2-(ethylthio)ethylamine $NH_2(CH_2)_2SC_2H_5$; Hmta, (methylthio)acetic acid $CH_3SCH_2CO_2H$; Hmtp, 3-(methylthio)propionic acid $CH_3S(CH_2)_2CO_2H$; Haeta, (2-aminoethylthio)acetic acid $NH_2(CH_2)_2SCH_2CO_2H$; Haetp, 3-(2-aminoethylthio)propionic acid $NH_2(CH_2)_2S(CH_2)_2CO_2H$; L-Hsmc, *S*-methyl-L-cysteine $CH_3SCH_2CH(NH_2)CO_2H$; en, ethylenediamine $NH_2(CH_2)_2NH_2$; tame, 1,1,1-tris(aminomethyl)ethane $CH_3C(CH_2NH_2)_3$; *d*-H_4tart, *d*-tartaric acid $C_4O_6H_6$.

Experimental

Preparation of Ligands. 1,1,1-Tris(aminomethyl)ethane: This ligand was prepared by the method of Fleischer *et al.*[6] Found: C, 26.61; H, 8.19; N, 18.34%. Calcd for $C_5H_{15}N_3\cdot 3HCl$: C, 26.51; H, 8.01; N, 18.55%.

(2-Aminoethylthio)acetic Acid: A solution of 77.2 g of 2-aminoethanethiol in 250 cm^3 of water was mixed with a solution of 94.5 g of monochloroacetic acid and 56.1 g of potassium hydroxide in 200 cm^3 of water with vigorous stirring at 80—85 °C on a water bath. The mixed solution was stirred for *ca.* 1 h and cooled in an ice bath. 185 cm^3 of 60% perchloric acid was then added and the resulting deposit, $KClO_4$, was filtered off. The filtrate was concentrated in a vacuum evaporator until it became oily and the deposit, $KClO_4$, was again filtered off. This filtrate was cooled in a refrigerator overnight. The white needles precipitated were recrystallized from a small amount of ethanol and dried in a vacuum desiccator over $CaCl_2$. The second crop was obtained by standing the above filtrate in a refrigerator for several weeks. The total yield: 70%. Found: C, 30.71; H, 6.28; N, 9.09; S, 20.41; Cl, 11.55%. Calcd for $C_4H_9NSO_2\cdot 0.5HCl$: C, 30.52; H, 6.08; N, 8.90; S, 20.37; Cl, 11.26%.

3-(2-Aminoethylthio)propionic Acid. This was prepared as described above, except that 3-bromopropionic acid was used instead of monochloroacetic acid. The yield: 75%. Found: C, 25.52; H, 5.39; N, 5.87; S, 13.07; Br, 33.84%. Calcd for $C_5H_{11}NSO_2\cdot HBr\cdot 0.5H_2O$: C, 25.11; H, 5.48; N, 5.86; S, 13.41; Br, 33.41%.

Preparation and Resolution of Complexes. (2-Aminoethanethiolato)bis(ethylenediamine)cobalt(III) Complexes, [Co(aet)$(en)_2$]$Cl_2\cdot H_2O$: The chloride salt was prepared by the method of Hori.[1]

(+)$_{589}$-[Co(aet)$(en)_2$]$(ClO_4)_2$: The racemic chloride monohydrate (1 g) and the resolving agent $K_2[Sb_2(d\text{-tart})_2]\cdot 3H_2O$ (0.99 g) were dissolved in 10 cm^3 of water at 60 °C. On scratching the side of the flask with a glass rod, the brown diastereomer (+)$_{589}$-[Co(aet)$(en)_2$]$[Sb_2(d\text{-tart})_2]\cdot 2H_2O$ appeared. The mixture was cooled in an ice bath for *ca.* 10 min and then filtered off. The precipitate was washed with ice cold water, ethanol and acetone. Found: C, 20.05; H, 3.71; N, 8.66%. Calcd for (+)$_{589}$-[Co(aet)$(en)_2$]$[Sb_2(d\text{-tart})_2]\cdot 2H_2O=C_{14}H_{26}N_5SO_{12}CoSb_2$: C, 20.34; H, 3.66; N, 8.47%. The diastereomer (0.8 g) was ground in a mortar; water (60 cm^3) was added and then excess sodium perchlorate (5 g), and the mixture was stirred for 10 min. After filtration, the solution was evaporated to 10 cm^3 and cooled in an ice bath. The needle-shaped crystals were removed by filtration and washed with 50% ethanol and acetone. The yield was 0.3 g. Found: C, 15.96; H, 4.91; N, 15.31%. Calcd for (+)$_{589}$-[Co(aet)$(en)_2$]$(ClO_4)_2=C_6H_{22}N_5SO_8Cl_2Co$: C, 15.87; H, 4.88; N, 15.42%.

[2-(Methythio)ethylamine]bis(ethylenediamine)cobalt(III) Complexes, [Co(mea)$(en)_2$]$Cl_3\cdot H_2O$: The racemic complex was derived from the reaction of [Co(aet)$(en)_2$]$Cl_2\cdot H_2O$ and methyl iodide according to the method of Hori.[1]

(+)$_{589}$-[Co(mea)$(en)_2$]$Cl_3\cdot H_2O$: The racemic chloride monohydrate (1.91 g) and the resolving agent $Na_2[Sb_2(d\text{-tart})_2]\cdot 2H_2O$ (1.54 g) were dissolved in 10 cm^3 of water at 50 °C. After being cooled to room temperature, the mixed solution was allowed to stand overnight in a refrigerator. The less soluble diastereomer deposited as orange precipitate was recrystallized from a small amount of hot water. Found: C, 20.40; H, 3.83; N, 8.06%. Calcd for (+)$_{589}$-[Co(mea)$(en)_2$]$Cl[Sb_2(d\text{-tart})_2]\cdot 2H_2O=C_{15}H_{33}N_5SO_{14}ClCoSb_2$: C, 20.53; H, 3.79; N, 7.98%. The diastereomer was converted into the optically active chloride salt by use of

* Present address: Department of Chemistry, The University of Tsukuba, Ibaraki, 300-31.

an anion exchange resin (Dowex 1X8, Cl^- form). Found: C, 22.47; H, 7.24; N, 17.20%. Calcd for $(+)_{589}$-$[Co(mea)(en)_2]Cl_3 \cdot H_2O \cdot 1/3C_2H_5OH = C_6H_{27}N_5SOCl_3Co \cdot 1/3C_2H_5OH$: C, 22.46; H, 7.13; N, 17.08%.

[2-(Ethylthio)ethylamine]bis(ethylenediamine)cobalt(III) Complexes, $[Co(eea)(en)_2]Cl_3 \cdot 2H_2O$: This complex was obtained according to the above procedure, with use of ethyl iodide instead of methyl iodide.

$(+)_{589}$-$[Co(eea)(en)_2]^{3+}$: The resolution procedure was similar to that for $[Co(mea)(en)_2]Cl_3 \cdot H_2O$. Found: C, 20.54; H, 4.33; N, 7.28%. Calcd for $(+)_{589}$-$[Co(eea)(en)_2]Cl[Sb_2(d\text{-tart})_2] \cdot 4.5H_2O = C_{16}H_{40}N_5SO_{16.5}ClCoSb_2$: C, 20.52; H, 4.31; N, 7.48%. The optically active chloride salt was obtained by use of an anion exchange resin (Dowex 1X8, Cl^- form). The CD spectrum of this complex was measured with the eluate, the concentration being calculated from the CD intensity referring to that of the diastereomer.

[(Methylthio)acetato]bis(ethylenediamine)cobalt(III) Complexes, $[Co(mta)(en)_2]Cl_2$: This complex was prepared by the reaction of methyl iodide and $[Co(SCH_2CO_2)(en)_2]Cl$, the latter being prepared according to the literature.[2]

$(+)_{589}$-$[Co(mta)(en)_2]Cl_2 \cdot 1.5H_2O$: The racemic chloride (0.71 g) was dissolved in 2 cm^3 of water at 40 °C. Freshly precipitated silver tartrate, $Ag_2(d\text{-}H_2tart)$ (0.27 g), was added and the mixture was stirred for 10 min. The silver chloride was filtered off, washed with water (1 cm^3). Then *d*-tartaric acid (0.15 g) was added to the filtrate and washing. The mixed solution was cooled in an ice bath. The red diastereomer thus precipitated was recrystallized from 2 cm^3 of hot water by addition of ethanol. Found: C, 29.45; H, 5.76; N, 9.02%. Calcd for $(+)_{589}$-$[Co(mta)(en)_2](d\text{-}H_3tart)_2 \cdot 2H_2O = C_{15}H_{35}N_4SO_{16}Co$: C, 29.13; H, 5.70; N, 9.06%. The diastereomer was converted into the optically active chloride salt by use of an anion exchange resin (Dowex 1X8, Cl^- form). Found: C, 21.93; H, 6.25; N, 14.85%. Calcd for $(+)_{589}$-$[Co(mta)(en)_2]Cl_2 \cdot 1.5H_2O = C_7H_{24}N_4SO_{3.5}Cl_2Co$: C, 22.00; H, 6.33; N, 14.66%.

[3-(Methylthio)propionato]bis(ethylenediamine)cobalt(III) Complexes, $[Co(mtp)(en)_2]Cl_2$: This complex was prepared according to the method described above, except that $[Co(SCH_2CH_2CO_2)(en)_2]Cl$ was used instead of $[Co(SCH_2CO_2)(en)_2]Cl$.

$(-)_{589}$-$[Co(mtp)(en)_2]Cl_2 \cdot 0.5H_2O$: The racemic chloride (1.16 g) and the resolving agent $Na_2[Sb_2(d\text{-tart})_2] \cdot 2H_2O$ (0.93 g) were dissolved in 4 cm^3 water at 50 °C. After the solution had been cooled to room temperature, the diastereomer deposited was filtered and recrystallized from a small amount of hot water by addition of ethanol. Found: C, 20.48; H, 4.03; N, 6.29%. Calcd for $(-)_{589}$-$[Co(mtp)(en)_2][Sb_2(d\text{-tart})_2] \cdot 5H_2O = C_{16}H_{37}N_4SO_{19}CoSb_2$: C, 20.80; H, 4.04; N, 6.05%. The optically active chloride salt was obtained by use of an anion exchange resin (Dowex 1X8, Cl^- form). Found: C, 25.33; H, 6.44; N, 14.92%. Calcd for $(-)_{589}$-$[Co(mtp)(en)_2]Cl_2 \cdot 0.5H_2O = C_8H_{24}N_4SO_{2.5}Cl_2Co$: C, 25.41; H, 6.40; N, 14.81%.

[(2-Aminoethylthio)acetato][1,1,1-tris(aminomethyl)ethane]cobalt(III) Complexes, $[Co(aeta)(tame)]Cl_2 \cdot 0.5H_2O$: 1,1,1-Tris(aminomethyl)ethane (3.4 g) and sodium hydroxide (1.8 g) were added at 0°C to a green solution of tricarbonatocobaltate(III) prepared by the method of Shibata[7] in a 3.6 g scale of $CoCl_2 \cdot 6H_2O$. The mixture was then heated to 40 °C and stirred for 1.5 h. After addition of 3 g of (2-aminoethylthio)acetic acid hemihydrochloride, the solution was stirred at *ca.* 60 °C for 3 h, whereupon the solution turned from violet to red. 6 M acetic acid was then added until gas evolution ceased and the stirring was continued for 2 h at 80 °C. The resulting red solution was evaporated *in vacuo* and then cooled. The chloride salt thus precipitated was recrystallized from a small volume of water by addition of ethanol. Found: C, 27.52; H, 6.25; N, 14.77%. Calcd for $[Co(aeta)(tame)]Cl_2 \cdot 0.5H_2O = C_9H_{24}N_4SO_{2.5}Cl_2Co$: C, 27.70; H, 6.20; N, 14.35%.

$(+)_{589}$-$[Co(aeta)(tame)]Cl_2 \cdot 1.5H_2O$: The racemic chloride (0.39 g) was dissolved in 5 cm^3 of water at 40 °C. Potassium tris(L-cysteinesulfinato-*N*,*S*)cobaltate(III) 6-hydrate, $K_3[Co(L\text{-}cysu)_3] \cdot 6H_2O$[8] (0.22 g) dissolved in 5 cm^3 of water was added with stirring. The mixed solution was kept in a refrigerator for *ca.* 1 h. The orange yellow diastereomer precipitated was filtered and then recrystallized from a large amount of water. Found: C, 23.73; H, 5.59; N, 11.28%. Calcd for $(+)_{589}$-$[Co(aeta)(tame)]_3[Co(L\text{-}cysu)_3]_2 \cdot 14H_2O \cdot 2KCl = C_{45}H_{127}N_{18}S_9O_{44}Cl_2Co_5K_2$: C, 23.91; H, 5.66; N, 11.15%. The optically active chloride salt was obtained by use of an anion exchange resin (Dowex 1X8, Cl^- form). Found: C, 24.97; H, 6.20; N, 13.18%. Calcd for $(+)_{589}$-$[Co(aeta)(tame)]Cl_2 \cdot 1.5H_2O \cdot 1/4KCl = C_9H_{26}N_4SO_{3.5}Cl_2Co \cdot 1/4KCl$: C, 25.32; H, 6.14; N, 13.13%.

[3-(2-Aminoethylthio)propionato][1,1,1-tris(aminomethyl)ethane]cobalt(III) Complexes, $[Co(aetp)(tame)]Br_2 \cdot 1.5H_2O$: This complex was prepared according to the method described above, with use of 3-(2-aminoethylthio)propionic acid monohydrobromide instead of (2-aminoethylthio)acetic acid hemihydrochloride. Found: C, 23.45; H, 5.90; N, 11.35%. Calcd for $[Co(aetp)(tame)]Br_2 \cdot 1.5H_2O = C_{10}H_{28}N_4SO_{3.5}Br_2Co$: C, 23.48; H, 5.52; N, 10.96%.

$(-)_{589}$-$[Co(aetp)(tame)]^{2+}$: The racemic bromide was optically resolved by the same method as that for $[Co(aeta)(tame)]Cl_2$. The CD spectrum of this complex was measured with the eluate and the concentration was calculated from the optical density referring to that of the racemic complex.

Trinitro[1,1,1-tris(aminomethyl)ethane]cobalt(III), $[Co(NO_2)_3(tame)]$: 1,1,1-Tris(aminomethyl)ethane trihydrochloride (4.5 g) and sodium hydroxide (2.4 g) were dissolved in 15 cm^3 of water and the mixture was transferred to a separatory funnel. The solution was added dropwise to a solution of $Na_3[Co(NO_2)_6]$[9] (8.1 g) in 20 cm^3 of water at 70 °C. A yellow precipitate was formed readily and removed by filtration. The crude product was recrystallized from a small amount of hot water. The yield was 2 g. Found: C, 19.05; H, 4.92; N, 26.78%. Calcd for $[Co(NO_2)_3(tame)] = C_5H_{15}N_6O_6Co$: C, 19.12; H, 4.81; N, 26.75%.

Trichloro[1,1,1-tris(aminomethyl)ethane]cobalt(III), $[CoCl_3(tame)] \cdot 0.75H_2O$: Trinitro[1,1,1-tris(aminomethyl)ethane]cobalt(III) (2.5 g) was added to 80 cm^3 of ethanol saturated with hydrogen chloride and gently stirred until the evolution of nitrogen oxide ceased. The solution was kept standing overnight at room temperature. The deep blue precipitate was filtered off and washed with ethanol and ether repeatedly until the washings became colorless. The reaction proceeded almost quantitatively; the yield was 1.9 g. Found: C, 20.13; H, 5.43; N, 14.25%. Calcd for $[CoCl_3(tame)] \cdot 0.75H_2O = C_5H_{16.5}N_3O_{0.75}Cl_3Co$: C, 20.29; H, 5.62; N, 14.20%.

(S-Methyl-L-cysteinato)[1,1,1-tris(aminomethyl)ethane]cobalt(III) Chloride, $[Co(L\text{-}smc)(tame)]Cl_2$: Trichloro[1,1,1-tris(aminomethyl)ethane]cobalt(III) (0.9 g) was suspended in water (10 cm^3); silver perchlorate (1.98 g) was added and the mixture was shaken for 10 min. The resulting solution was filtered in order to remove the silver chloride. The solution obtained by dissolving *S*-methyl-L-cysteine (0.41 g) and sodium hydroxide (0.13 g) in 10 cm^3 of water was then added. The mixed solution was heated to 70 °C and stirred for 3 h. The reaction mixture was poured into a column of SP-Sephadex C-25 (3×40 cm, Na^+ form). The adsorbed band was eluted with 0.15 M NaCl solution at the rate of *ca.* 0.5 cm^3/min. The second orange-red eluate was evaporat-

ed and the deposit, NaCl, was filtered off. To the filtrate was added a large amount of ethanol. The crude product thus obtained was recrystallized from a minimum quantity of water by addition of ethanol, and washed with ethanol and then acetone, and dried in a vacuum desiccator. Found: C, 21.09; H, 4.65; N, 11.31%. Calcd for [Co(L-smc)(tame)]-$Cl_2 \cdot 2NaCl = C_9H_{23}N_4SO_2Cl_2Co \cdot 2NaCl$: C, 21.70; H, 4.65; N, 11.25%.

Measurements. The electronic absorption spectra were measured on a Shimadzu UV-200 spectrophotometer in aqueous solution. The CD spectra were recorded with a Jasco MOE-1 spectropolarimeter, with a cell of 1 cm path-length. A Jasco DIP-4 digital polarimeter was used to check the optical rotations. The proton magnetic resonance spectra were recorded in deuterium oxide on a Varian XL-100-15 NMR spectrometer with DSS as an internal reference. All measurements were carried out at room temperature.

Results and Discussion

Absorption Spectra. The first absorption maximum of $[Co(aet)(en)_2]^{2+}$, which belongs to $[Co(N)_5(S)]$ type having a thiolato group, appears at 20800 cm^{-1} with a shoulder on the low energy side (Fig. 1 and Table 1). The spectrum is very similar to the spectra of [Co(L-cyst)(en)$_2$]I, [Co(L-Hcyst)(en)$_2$]ICl, and [Co(L-cystee)(en)$_2$]I_2[4] (L-H_2cyst=L-cysteine and L-Hcystee=L-cysteine ethyl ester), in which the sulfur containing ligands are coordinated through the amino and thiolato groups. Based on the approximate C_{4v} symmetry, the lower energy band is assigned to the transition $^1A_1 \rightarrow {}^1E$, and the higher band to $^1A_1 \rightarrow {}^1A_2$. The ligand field strength of the thiolato group is very weak and falls close to iodide in the spectrochemical series.

On the other hand, the complexes $[Co(mea)(en)_2]^{3+}$ and $[Co(eea)(en)_2]^{3+}$ which belong to $[Co(N)_5(S)]$ type having a thioether donor atom, show a single band at 20500 cm^{-1} (Fig. 2 and Table 1). The energy corresponds to that for the $[Co(N)_5(O)]$ type complexes, $[Co(gly)(en)_2]^{2+}$, $[Co(L\text{-}ala)(en)_2]^{2+}$, and [Co(sar)-$(en)_2]^{2+}$ (gly=glycinate, L-ala=L-alaninate, and sar=*N*-methyl glycinate). As seen in Fig. 3, the first absorption maxima of the thioether complexes [Co(mta)-$(en)_2]^{2+}$ and [Co (mtp)$(en)_2]^{2+}$, which belong to [Co-$(N)_4(O)(S)$] type, appear at 20000 and 20100 cm^{-1},

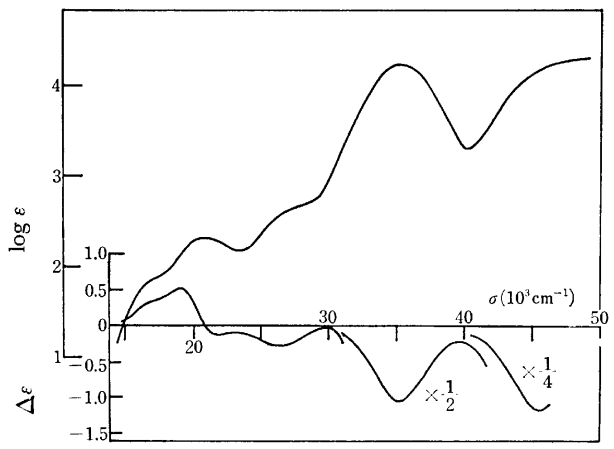

Fig. 1. Absorption and CD spectra of $(+)_{589}$-[Co(aet)-$(en)_2](ClO_4)_2$.

Table 1. Absorption and CD data of bis(ethylenediamine) complexes

Complex	σ_{max}[a] (log ε)	σ_{ext}[a] (Δε)
$(+)_{589}$-[Co(aet)(en)$_2$]-$(ClO_4)_2$	17 (1.85)[c]	17 (+0.36)[c]
	20.8(2.31)	19.1(+0.54)
		21.8(−0.12)
	27 (2.62)[c]	26.5(−0.28)
	35.4(4.24)	35.1(−2.12)
		45.7(−4.70)
$(+)_{589}$-[Co(mea)-(en)$_2$]Cl_3	20.5(2.25)	20.1(+3.22)
	28 (2.35)[c]	26.0(+0.06)
		28.1(−0.13)
	35.5(3.92)	35.5(+5.09)
	45.8(4.21)	47.2(−11.2)
$(+)_{589}$-[Co(eea)-(en)$_2$]$^{3+}$	20.5(2.25)[b]	20.0(+2.84)
	28 (2.37)[b,c]	26.0(−0.05)
		28.0(−0.08)
	35.5(3.94)[b]	35.4(+6.73)
	45.3(4.22)[b]	46.4(−22.2)
$(+)_{589}$-[Co(mta)(en)$_2$]Cl_2	20.0(2.20)	18.9(+2.28)
		21.1(+2.43)
	28 (2.35)[c]	27.5(−0.77)
	35.7(3.85)	33.9(−1.59)
		38.0(+4.44)
	43.7(4.14)	43.9(−23.4)
$(-)_{589}$-[Co(mtp)(en)$_2$]Cl_2	20.1(2.27)	19 (−0.65)[c]
		21.2(−2.15)
	27 (2.36)[c]	27.2(+0.99)
	34.6(3.93)	33.7(+2.93)
	44.5(4.15)	44 (+7.38)[c]

a) The wave numbers are given in 10^3 cm^{-1} unit. b) The racemate. c) A shoulder.

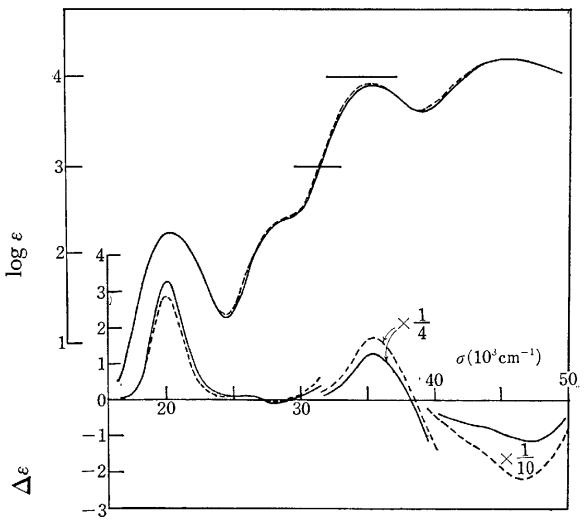

Fig. 2. Absorption and CD spectra of $(+)_{589}$-[Co-(mea)(en)$_2$]Cl_3 (——) and $(+)_{589}$-[Co(eea)(en)$_2$]Cl_3 (----).

respectively, in line with that of $[Co(ox)(en)_2]^+$ which belongs to a $[Co(N)_4(O)_2]$ type. Thus, the thioether R–S–R seems to lie close to the COO^- group in the spectrochemical series. The three tame complexes also belong to the $[Co(N)_4(O)(S)]$ type having the first absorption maxima at 20300—20400 cm^{-1} (Fig. 4 and

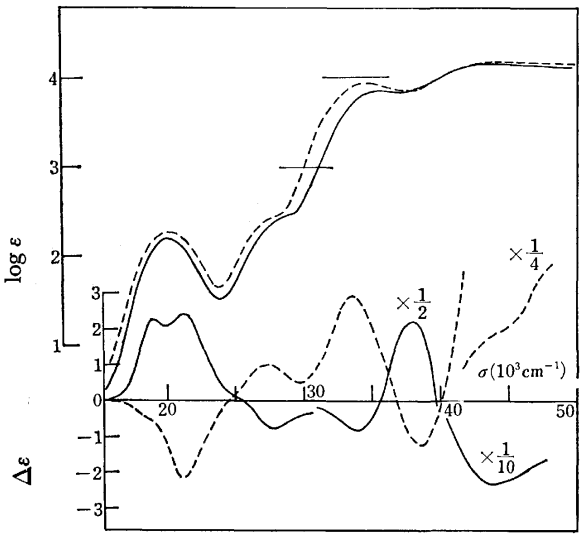

Fig. 3. Absorption and CD spectra of $(+)_{589}$-[Co(mta)(en)$_2$]Cl$_2$ (——) and $(-)_{589}$-[Co(mtp)(en)$_2$]Cl$_2$ (----).

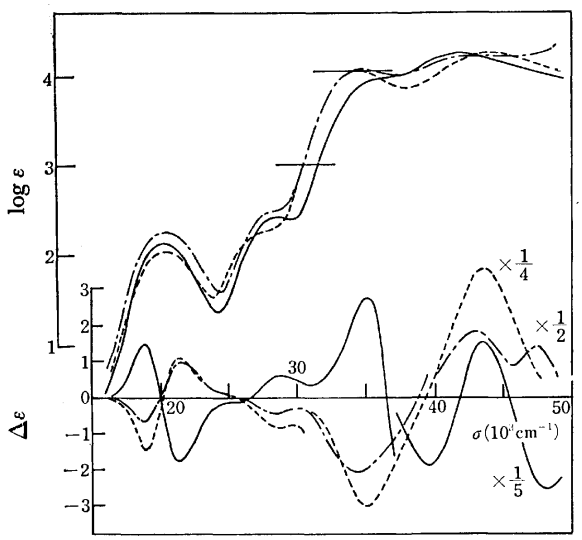

Fig. 4. Absorption and CD spectra of $(+)_{589}$-[Co(aeta)(tame)]$^{2+}$ (——), $(-)_{589}$-[Co(actp)(tame)]$^{2+}$ (------), and $(-)_{589}$-[Co(L-smc)(tame)]$^{2+}$ (----).

Table 2). These maxima are somewhat shifted to higher energy than those of the bis(ethylenediamine) complexes.

In the near-ultraviolet region, the complexes show intense bands ($\log \varepsilon \approx 4.0$). Such bands appear always for the cobalt(III) complexes containing sulfur donor atoms,[10-12] and are considered to be the charge transfer bands due to the lone-pair electrons on the sulfur donor.

CD Spectra of the Bis(ethylenediamine) Complexes. The optical isomer of the complex containing a thiolato group, $(+)_{589}$-[Co(aet)(en)$_2$](ClO$_4$)$_2$ which has only a chirality due to the skew pair of chelate rings, exhibits three weak CD bands in the first absorption band region (Fig. 1). Based on the assignment of the absorption components, two low energy positive bands can be assigned to be the split components of $^1A_1 \rightarrow {}^1E$ and a higher energy negative one $^1A_1 \rightarrow {}^1A_2$. This complex can be assigned to Λ configuration on the basis of the sign of $^1A_1 \rightarrow {}^1E$ components.

Table 2. Absorption and CD data of [Co(terdentate-*N,S,O*)(tame)]$^{2+}$ complexes

Complex	σ_{max}[a] ($\log \varepsilon$)	σ_{ext}[a] ($\Delta\varepsilon$)
$(+)_{589}$-[Co(aeta)-(tame)]Cl$_2$	20.3 (2.12) [b]	18.8 (+1.46)
		21.3 (−1.75)
	28.6 (2.41) [b]	28.8 (+0.61)
	35.7 (3.93) [b,c]	35.1 (+2.79)
	42.4 (4.22) [b]	39.6 (−9.08)
		43.7 (+7.89)
		48.1 (−12.7)
$(-)_{589}$-[Co(aetp)-(tame)]$^{2+}$	20.3 (2.24) [b]	18.7 (−0.66)
		21.4 (+0.99)
	28 (2.43) [b,c]	28.3 (−0.40)
	35.0 (4.03) [b]	34.7 (−2.03)
	44.0 (4.18) [b]	42.9 (+3.76)
		47.5 (+3.14)
$(-)_{589}$-[Co(L-smc)-(tame)]Cl$_2$	20.4 (2.05)	18.7 (−1.39)
		21.2 (+1.08)
	28 (2.25) [c]	28.4 (−0.79)
	34.7 (4.02)	34.8 (−11.9)
	44.4 (4.21)	43.5 (+14.3)

a) The wavenumbers are given in 10^3 cm^{-1} unit. b) The racemate. c) A shoulder.

For each of the four complexes containing a thioether donor atom, four optical isomers, Λ-(*R*), Λ-(*S*), Λ-(*R*), and Λ-(*S*), are possible; both chiralities due to the skew pair of chelate rings (Λ and Λ) and due to the coordinated sulfur atom ((*R*) and (*S*)) contribute to the CD spectra. The optical isomers of the [Co(N)$_5$(S)] type, $(+)_{589}$-[Co(mea)(en)$_2$]$^{3+}$, and $(+)_{589}$-[Co(eea)(en)$_2$]$^{3+}$ which were obtained from the less soluble diastereomers, show one strong positive CD band in the first absorption band region and two weak CD bands of positive and negative signs in the second d-d absorption band region (Fig. 2). The CD spectra are strikingly similar to each other, indicating that the *S*-alkyl groups of both the complexes are in analogous environments. A similar trend has been found for some *N,N'*-dialkylethylenediaminediacetato complexes[13] which have two asymmetric nitrogen donor atoms. The complexes belonging to the [Co(N)$_4$(O)(S)] type, $(+)_{589}$-[Co(mta)-(en)$_2$]$^{2+}$ and $(-)_{589}$-[Co(mtp)(en)$_2$]$^{2+}$, show two CD bands of the same sign in the first absorption band region (Fig. 3). The chiralities arising from the skew pair of chelate rings can be assigned to the present four complexes on the basis of the CD sign in the first absorption band region;[14] namely, Λ,Λ,Λ, and Λ configurations for $(+)_{589}$-[Co(mea)(en)$_2$]$^{3+}$, $(+)_{589}$-[Co(eea)(en)$_2$]$^{3+}$, $(+)_{589}$-[Co(mta)(en)$_2$]$^{2+}$, and $(-)_{589}$-[Co(mtp)(en)$_2$]$^{2+}$, respectively.

The NMR spectra of the resolved complexes show a single peak in the *S*-methyl proton region (Fig. 5). In the chromatographic separation of isomers of each resolved complex, all the fractions had the same CD spectra. The results and molecular model examination suggest that the thioether ligands are coordinated stereoselectively. The *S*-alkyl group in the configuration Λ-(*R*) or Λ-(*S*) has appreciable nonbonded atomic

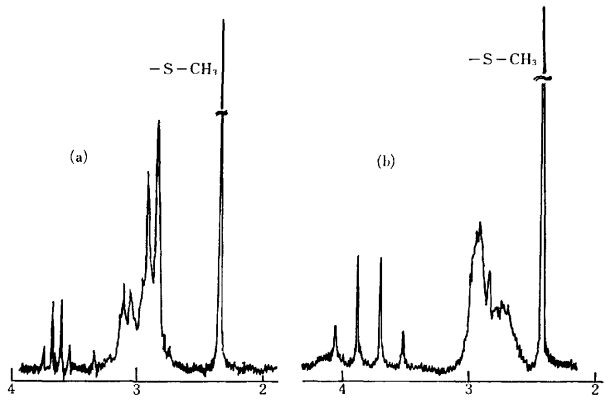

Fig. 5. The NMR spectra of $(+)_{589}$-$[Co(mea)(en)_2]Cl_3$ (a) and $(+)_{589}$-$[Co(mta)(en)_2]Cl_2$ (b) in D_2O.

interactions with the adjacent en chelate ring in contrast to that in the configuration Δ-(*S*) or Λ-(*R*). Thus, it is concluded that the configurations of the resolved complexes are Δ-(*S*) or Λ-(*R*).

In the region of the lower energy thioether charge transfer band, the mea and eea complexes show only one CD band; on the other hand, the mta and mtp complexes show two CD bands of opposite signs. Namely, for the $[Co(N)_5(S)]$ type, the Λ-(*R*) and Δ-(*S*) complexes show (+) and (−) bands, respectively. The Λ-(*R*) complex of the $[Co(N)_4O(S)]$ type shows (−) and (+) CD bands from low energy side, and Δ-(*S*) one (+) and (−).

CD Spectra of the tame Complexes. 1,1,1-Tris-(aminomethyl)ethane is a typical tripod-like ligand and coordinates facially to a Co(III) ion. When three remaining coordination sites are occupied by the three non-equivalent ligating atoms, a kind of chirality due to the arrangement of these donor atoms is expected;[15,16] this kind of chirality contributes dominantly to the CD spectra of $[Co(NH_2CHRCO_2)NH_3(tame)]^{2+}$.[15] In the present system, the terdentate-*N,S,O* ligands occupy the three remaining coordination sites but there is no chirality arising from the skew pair of chelate rings. These complexes have a chirality due to the arrangement of three different donor atoms and another due to the central donor sulfur atom, though both chiralities are associated with each other.

Three tame complexes, $(+)_{589}$-$[Co(aeta)(tame)]^{2+}$, $(-)_{589}$-$[Co(aetp)(tame)]^{2+}$, and $(-)_{589}$-$[Co(L\text{-}smc)(tame)]^{2+}$, exhibit two CD bands of opposite signs in the first absorption band region (Fig. 4): L-smc and aetp $(-)_{589}$-complexes show (−) and (+) bands in the order of increasing energy, but aeta $(-)_{589}$-one shows the reverse CD pattern. As is shown in Fig. 6, the optical isomers of the aeta and aetp complexes have the structure (a) or (b), while the L-smc complex takes the structure (c) because of the complete stereoselectivity due to the L-smc ligand. The arrangement chirality of (b) and (c) are the same but that of (a) is the opposite. Accordingly, by analogy of the CD patterns absolute configurations are assigned as (a) for $(+)_{589}$-$[Co(aeta)(tame)]^{2+}$ and (b) for $(-)_{589}$-$[Co(aetp)(tame)]^{2+}$.

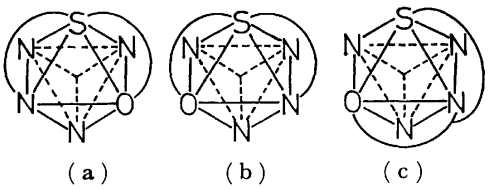

Fig. 6. Optical isomers of [Co(terdentate-*N,S,O*)-(tame)]$^{2+}$, (a) and (b), and the structure of $(-)_{589}$-$[Co(L\text{-}smc)(tame)]^{2+}$ (c).

In the lower energy thioether charge transfer band region, the aeta $(+)_{589}$- and aetp $(-)_{589}$-complexes show a positive and a negative band, respectively, which corresponds to the fact that the two complexes have the opposite absolute configurations.

References

1) K. Hori, *Nippon Kagaku Zasshi*, **90**, 561 (1969).
2) K. Hori, *Bull. Chem. Soc. Jpn.*, **48**, 2209 (1975).
3) K. Hori, *Nippon Kagaku Zasshi*, **92**, 322 (1971).
4) V. M. Kothari and D. H. Busch, *Inorg. Chem.*, **11**, 2276 (1969).
5) K. Hori, *Bull. Yamagata Univ. (Nat. Sci.)*, **8**, 403 (1974).
6) E. B. Fleischer, A. E. Gebala, A. Lever, and P. A. Tasker, *J. Org. Chem.*, **36**, 3042 (1971).
7) M. Shibata, *Nippon Kagaku Zasshi*, **87**, 771 (1966).
8) L. S. Dollimore and R. D. Gillard, *J. Chem. Soc., Dalton Trans.*, **1973**, 933.
9) E. Billmann, *Z. Anal. Chem.*, **39**, 284 (1900).
10) C. K. Jørgensen, *J. Inorg. Nucl. Chem.*, **24**, 1571 (1962).
11) S. E. Livingstone, *Quart. Rev. London*, **19**, 387 (1965).
12) M. Akbal and S. E. Livingstone, *Coord. Chem. Rev.*, **13**, 101 (1974).
13) W. T. Jordan and B. E. Douglas, *Inorg. Chem.*, **12**, 403 (1973).
14) C. J. Hawkins, "Absolute Configuration of Metal Compounds," John Wiley & Sons, Inc., New York (1971), Chap. 5.
15) K. Yamanari, J. Hidaka, and Y. Shimura, *Bull. Chem. Soc. Jpn.*, **48**, 1653 (1975).
16) Y. Hosokawa, J. Hidaka, and Y. Shimura, *Bull. Chem. Soc. Jpn.*, **48**, 3175 (1975).

The Absolute Configuration and Circular Dichroism of the $(-)_{260}$-Diammine((*S*)-1-*N*-methyl-1,2-propanediamine)platinum(II) Ion, $(-)_{260}$-$[Pt(NH_3)_2(N^1\text{-Me-}(S)\text{-pn})]^{2+}$

Yasuji NAKAYAMA, Keiji MATSUMOTO, Shun'ichiro OOI, and Hisao KUROYA

Department of Chemistry, Faculty of Science, Osaka City University, Sumiyoshi-ku, Osaka 558

(Received March 12, 1977)

The optical resolution of $[Pt(NH_3)_2(N^1\text{-Me-}(S)\text{-pn})]Cl_2$ is effected by using silver di-μ-(+)-tartrato(4−)-bis(antimonate(III)) ($Ag_2[Sb_2(+)\text{-tart}_2]$) as the resolving agent. X-Ray structure analysis of the less soluble diastereoisomeric salt, $(+)_{350}$-$[Pt(NH_3)_2(N^1\text{-Me-}(S)\text{-pn})][Sb_2(+)\text{-tart}_2]\cdot H_2O$, revealed that the asymmetric secondary nitrogen is of the *R* configuration. The crystal is orthorhombic, with a $P2_12_12_1$ space group, $a=19.302(7)$ Å, $b=14.791(4)$ Å, $c=7.925(2)$ Å, and $Z=4$. The structure was determined from counter intensity data and refined to *R* 0.049 using the least-squares method for 1955 independent non-zero reflections. The Pt atom has a square-planar coordination with 4 N atoms and both the N–CH_3 and C–CH_3 groups are equatorial with respect to the chelate ring. The circular dichroism spectrum of *R*-$[Pt(NH_3)_2(N^1\text{-Me-}(S)\text{-pn})](ClO_4)_2$, which was obtained from the less soluble di-μ-(+)-tartrato(4−)-bis(antimonate(III)) salt, is presented and discussed on the basis of the distribution of the possible conformers, the relative abundances of which were infered from ^{13}C NMR data.

Since Ito *et al.* studied the circular dichroism (CD) of a number of Pt(II) and Pd(II) complexes,[1] few studies have been made on this subject. Recently, Bosnich and Sullivan have reported the CD and stereochemistries of several Pt(II) chelates of *N*-substituted diamines,[2] and the absolute configuration of $(-)_{280}$-dichloro-((*S*)-1-*N*-methyl-1,2-propanediamine)platinum(II) has been determined by Ball *et al.*[3] Yokoho *et al.* and Matsumoto *et al.* attempted the resolution of dissymmetric Pt(II) complexes into enantiomeric forms in order to work out the CD-structure relationship for these complexes.[4,5] In the course of the present study, the optical resolution of the *N*-racemic $[Pt(NH_3)_2(N^1\text{-Me-}(S)\text{-pn})]Cl_2$ was successful with the final result being the isolation of the $(-)_{260}$-enantiomer in perchlorate form. This paper deals with the absolute configuration and the CD spectrum of the title complex.

Experimental

Preparations of Compounds. (*S*)-1-*N*-methyl-1,2-propanediamine (N^1-Me-(*S*)-pn) was prepared following the method of Saburi *et al.*[6] $[Pt(NH_3)_2(rac\text{-pn})](ClO_4)_2$ and $[Pt(NH_3)_2(rac\text{-chxn})]Cl_2$ were obtained using similar methods to those described in Ref. 1 (pn=1,2-propanediamine; chxn=1,2-cyclohexanediamine).

$(-)_{260}$-$[Pt(NH_3)_2(Meen)](ClO_4)_2$ (Meen=*N*-methylethylenediamine): $(-)_{260}$-$[Pt(NH_3)_2(Meen)]Cl_2$ was obtained following the method of Goddard and Basolo.[7] This chloride was then converted to a perchlorate using $AgClO_4$ in a perchloric acid solution. The resulting perchlorate was washed with methanol and recrystallized from acetone–ethanol acidified slightly with perchloric acid.

Found: C, 7.20; H, 3.14; N, 11.07%. Calcd for $[Pt(NH_3)_2(CH_3NH(CH_2)_2NH_2)](ClO_4)_2$: C, 7.18; H, 3.21; N, 11.16%.

$(+)_{350}$-$[Pt(NH_3)_2(N^1\text{-Me-}(S)\text{-pn})]\,[Sb_2(+)\text{-tart}_2]\cdot H_2O$ ($[Sb_2(+)\text{-tart}_2]^{2-}$=di-$\mu$-(+)-tartrato(4−)-bis(antimonate(III))ion): $[Pt(NH_3)_2(N^1\text{-Me-}(S)\text{-pn})]Cl_2$ was prepared using a method similar to that reported by Bosnich and Sullivan.[2] A solution of $[Pt(NH_3)_2(N^1\text{-Me-}(S)\text{-pn})]Cl_2$ (1.15 g in 20 ml of water) was added dropwise to the solution of $Ag_2[Sb_2(+)\text{-tart}_2]$ (2.12 g in 500 ml of water) and the mixture was stirred at 60 °C for 2 h in the dark. AgCl was then filtered off and the filtrate was rotary evaporated to *ca.* 50 ml. Colorless crystals were separated out and they were then recrystallized from hot water containing a drop of perchloric acid.

Found: C, 16.50; H, 2.84; N, 6.29%. Calcd for $[Pt(NH_3)_2(CH_3NHCH_2CH(CH_3)NH_2)]\,[Sb_2(C_4H_2O_6)_2]\,H_2O$: C, 16.54; H, 2.76; N, 6.43%.

$(-)_{260}$-$[Pt(NH_3)_2(N^1\text{-Me-}(S)\text{-pn})](ClO_4)_2$: Conversion of the preceding salt to the perchlorate was carefully carried out in acidic media, since the rate of racemization of the assymmetric secondary nitrogen is known to be very slow at low pH values.[8] The di-μ-(+)-tartrato(4−)-bis(antimonate(III)) salt (0.40 g) was dissolved in 100 ml of water acidified with a drop of perchloric acid. This solution was passed through an anion-exchange column in the perchlorate form (Dowex 1-X8, 50—100 mesh) at a speed of one drop every 5 s. The effluent was rotary evaporated to near dryness. The residue was dissolved in a minimum amount of acetone and then *ca.* 15 ml of 1-propanol was added. Colorless plate-like crystals were obtained and these were recrystallized three times from acetone acidified slightly with perchloric acid.

Found: C, 9.53; H, 3.52; N, 10.92%. Calcd for $[Pt(NH_3)_2(CH_3NHCH_2CH(CH_3)NH_2)](ClO_4)_2$: C, 9.30; H, 3.49; N, 10.85%.

Spectral Measurements. The FT ^{13}C NMR spectra were recorded at 15.04 MHz with broad-band proton decoupling on a JEOL JNM-FX60 Spectrometer, dioxane being used as an internal reference (the values of chemical shifts given in the text have been converted to the TMS scale). The signal from the solvent, D_2O, was used as an internal lock. Usually, 4096 data points were taken over a 1-kHz spectral width. Electronic spectra were obtained with a Hitachi EPS-3T Recording Spectrometer. A JASCO J-20 Automatic Recording Spectrometer was employed for the CD spectra. All measurements were performed at room temperature. In the case of $(-)_{260}$-$[Pt(NH_3)_2(N^1\text{Me-}(S)\text{-pn})](ClO_4)_2$, the solutions were acidified slightly with DCl (NMR) or with $HClO_4$ (CD) in order to prevent the active complex ion from racemizing.

X-Ray Data Measurement. The crystallographic data for $(+)_{350}$-$[Pt(NH_3)_2(N^1\text{-Me-}(S)\text{-pn})][Sb_2(+)\text{-tart}_2]\cdot H_2O$ are as follows: $M=870.6$, orthorhombic, space group $P2_12_12_1$, $a=19.302(7)$ Å, $b=14.791(4)$ Å, $c=7.925(2)$ Å, $Z=4$, $D_m=2.55$ g cm^{-3}, $D_c=2.56$ g cm^{-3}, $\mu(MoK\alpha)=87.6$ cm^{-1}. The space group was determined from oscillation and Weissenberg photographs. The unit cell dimensions were obtained by a least-squares analysis of 29 θ values measured on a Phillips diffractometer using $MoK\alpha$ radiation.

The intensities were measured using the ω-2θ scan method on a Phillips PW1100 four-circle diffractometer employing a

graphite monochromator and Mo$K\alpha$ radiation (λ=0.71069 Å) with a crystal of dimensions 0.14×0.16×0.18 mm³. A scan speed of 0.017° s⁻¹, a scan width of (0.8+0.2 tan θ)°, and two 20 s background counts were employed. Three standard reflections (800, 060, 004) monitored every 4 h throughout the period of data collection, showed no significant intensity variations. A total of 1955 intensity peaks with $I_t-2\sqrt{I_t}>I_b$ were measured in the $6°\leq 2\theta \leq 55°$ range (I_t is the intensity (counts/s) measured at the top of the peak, and I_b is the mean background intensity (counts/s) obtained from preliminary background measurements for 5 s on each side of the peak). A spherical absorption correction (r=0.08 mm) was applied.

Structure Determination and Refinement. The crystal structure was solved by the heavy-atom technique, and the positional and thermal parameters were refined by the least-squares method, the function minimized being $\sum w\Delta F^2$. In the final stage of refinement, the weighting scheme, w=0.8 for $F_o<32.3$, w=1 for $32.3\leq F_o\leq 161.3$, and $w=(161.3/F_o)^2$ for $F_o>161.3$, was used to render $\sum w\Delta F^2$ approximately constant over the entire ranges of F_o and (sin θ/λ). All parameter shifts in the final cycle refinement were $<0.2\sigma$. The final R value was 0.049. The atomic scattering factors for neutral Pt, Sb, O, N, and C were taken from Ref. 9. The real and imaginary parts of the anomalous dispersion corrections were applied for Pt and Sb atoms.

The atomic coordinates given in Table 1 correspond to the absolute crystal structure which was determined on the basis of the known configuration of the $[Sb_2(+)$-$tart_2]^{2-}$ ion. The observed and calculated structure factors are available at the Chemical Society of Japan (Document No. 7713). The computer programs used are as follows: RSSFR-4, HBLS-4, and DAPH, all of which were adapted to the FACOM 270-30 computer of Osaka City University.

Results and Discussion

X-Ray Structure. The absolute configuration of $(-)_{260}$-$[Pt(NH_3)_2(N^1$-Me-(*S*)-pn)$]^{2+}$ is shown in Fig. 1. The bond lengths and angles are given in Table 2 along with selected interatomic distances. The Pt atom has a square-planar coordination of four nitrogen atoms. The secondary nitrogen atom has *R* absolute configuration and the N–CH_3 group is equatorial. The C–CH_3 group is also disposed equatorially, imposing a δ conformation on the chelate ring. The Pt–N bond lengths range from 2.03 to 2.07 Å with an average value of 2.05 Å, wheras the N–Pt–N bond angle in the chelate ring is 84.1°. These values are comparable to those found in $(+)_{350}$-$[Pt(NH_3)_2(Me_3en)][Sb_2(+)$-$tart_2]\cdot H_2O$ (2.07 Å, 84.4°),[4] $(+)_{350}$-$[Pt(R$-pn)$(Me_2en)][Sb_2(+)$-$tart_2]\cdot 2H_2O$ (2.06 Å, 84.2°),[5] and $[Pt(en)_2][(+)$-

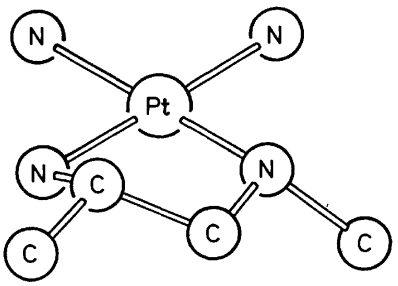

Fig. 1. The absolute configuration of $(-)_{260}$-$[Pt(NH_3)_2(N^1$-Me-(*S*)-pn)$]^{2+}$.

Table 1. Positional and thermal parameters with their e. s. d. values in parenthesis

	x	*y*	*z*	B/Å²		*x*	*y*	*z*	B/Å²
Pt	0.21359(4)	0.19812(5)	0.23194(10)	a)	C(10)	0.430(1)	0.227(2)	−0.027(3)	2.4(4)
N(1)	0.197(1)	0.263(1)	0.009(2)	2.3(3)	C(11)	0.427(1)	0.180(1)	−0.198(3)	2.4(4)
N(2)	0.182(1)	0.318(1)	0.337(2)	2.3(3)	C(12)	0.353(1)	0.148(1)	−0.227(3)	2.7(4)
N(3)	0.251(1)	0.086(1)	0.111(2)	2.3(3)	O(1)	0.536(1)	−0.059(1)	−0.133(2)	3.5(3)
N(4)	0.231(1)	0.131(1)	0.457(2)	2.3(3)	O(2)	0.577(1)	−0.132(1)	0.095(2)	3.6(4)
C(1)	0.179(2)	0.423(2)	−0.103(4)	4.8(6)	O(3)	0.408(1)	−0.050(1)	−0.019(2)	2.6(3)
C(2)	0.203(1)	0.366(2)	0.044(3)	2.8(4)	O(4)	0.494(1)	0.040(1)	0.253(3)	2.7(3)
C(3)	0.160(1)	0.382(2)	0.205(3)	3.4(5)	O(5)	0.367(1)	0.055(1)	0.353(2)	3.0(3)
C(4)	0.123(1)	0.311(2)	0.465(4)	4.0(5)	O(6)	0.342(1)	−0.088(1)	0.320(2)	3.4(3)
Sb(1)	0.44149(8)	−0.01609(10)	−0.24774(20)	a)	O(7)	0.529(1)	0.214(1)	0.159(2)	3.3(3)
Sb(2)	0.45037(9)	0.15363(12)	0.30975(20)	a)	O(8)	0.544(1)	0.284(1)	−0.091(3)	4.1(4)
C(5)	0.528(1)	−0.094(2)	0.016(3)	2.7(4)	O(9)	0.398(1)	0.174(1)	0.098(2)	2.7(3)
C(6)	0.455(1)	−0.092(2)	0.089(3)	2.4(4)	O(10)	0.474(1)	0.108(1)	−0.203(2)	2.9(3)
C(7)	0.458(1)	−0.043(1)	0.264(3)	2.6(4)	O(11)	0.345(1)	0.062(1)	−0.241(2)	2.6(3)
C(8)	0.383(1)	−0.023(2)	0.317(3)	2.7(4)	O(12)	0.306(1)	0.203(1)	−0.237(2)	2.7(3)
C(9)	0.508(1)	0.244(2)	0.012(4)	3.1(4)	O_w(13)	0.297(1)	0.356(1)	0.553(2)	3.8(4)

a) Anisotropic temperature factors (×10⁵) of the form $\exp[-(B_{11}h^2+B_{22}k^2+B_{33}l^2+B_{12}hk+B_{13}hl+B_{23}kl)]$, for the parameters:

	B_{11}	B_{22}	B_{33}	B_{12}	B_{13}	B_{23}
Pt	80(1)	268(3)	755(9)	12(5)	23(9)	−56(13)
Sb(1)	192(4)	328(6)	842(21)	26(8)	34(19)	−120(26)
Sb(2)	195(4)	436(8)	1031(25)	108(11)	−252(17)	−345(25)

TABLE 2. INTERATOMIC DISTANCES (l/Å) AND BOND ANGLES (ϕ/°)

Pt-N(1)	2.03(2)	N(1)-Pt-N(2)	84.1(8)
Pt-N(2)	2.05(2)	N(1)-Pt-N(3)	91.7(8)
Pt-N(3)	2.04(2)	N(2)-Pt-N(4)	96.4(7)
Pt-N(4)	2.07(2)	N(3)-Pt-N(4)	87.7(8)
N(1)-C(2)	1.56(3)	Pt-N(1)-C(2)	107(1)
N(2)-C(3)	1.47(3)	Pt-N(2)-C(3)	111(1)
N(2)-C(4)	1.54(4)	Pt-N(2)-C(4)	115(2)
C(1)-C(2)	1.52(4)	C(3)-N(2)-C(4)	107(2)
C(2)-C(3)	1.55(4)	N(1)-C(2)-C(1)	113(2)
		N(1)-C(2)-C(3)	105(2)
		C(1)-C(2)-C(3)	112(2)
		N(2)-C(3)-C(2)	109(2)

Interatomic distances (l/Å) concerning possible hydrogen bonds

Atom		l/Å of	Position[a] of	
A	B	A···B	A	B
N(2)	O_w(13)	2.85(3)	1	1
O_w(13)	O(2)	2.71(3)	1	2
O_w(13)	O(12)	2.81(3)	1	3

a) The numbers refer to the following equivalent positions: 1; x, y, z, 2; $1-x$, $(1/2)+y$, $(1/2)-z$, 3; x, y, $1+z$.

tart] (2.043 Å, 83.2°),[10] but the Pt–N bond length appears to be slightly longer than that in $(-)_{280}$-[Pt-Cl_2(N^1-Me-(S)-pn)] (2.021 Å, 83.1°).[3] The torsional angle in the N(1)–C(2)–C(3)–N(2) fragment is 52°. The equation for the plane defined by the four nitrogen atoms is

$$-0.936X - 0.350Y - 0.020Z = -4.961,$$

and the deviations of the atoms from this plane are as follows: 0.04 for Pt, 0.04 for N(1), −0.04 for N(2), −0.04 for N(3), 0.04 for N(4), −0.45 for C(1), −0.62 for C(2), 0.05 for C(3), and 1.06 Å for C(4). (The X, Y, and Z coordinates in Å refer to the crystallographic axes.)

Every complex cation is surrounded tetrahedrally by four $[Sb_2(+)\text{-tart}_2]^{2-}$ anions at (x,y,z), $((1/2)-x, -y, (1/2)+z)$, $(-(1/2)+x, (1/2)-y, -z)$, and $(1-x, (1/2)+y, (1/2)-z)$. The $[Sb_2(+)\text{-tart}_2]^{2-}$ anion selects the N(S) and N(S), N′(S)–C(R) isomers yielding the least soluble diasteroisomeric salts $(+)_{350}$-[Pt$(NH_3)_2$(Me_3-en)][$Sb_2(+)$-tart$_2$]·H_2O[4] and $(+)_{350}$-[Pt(R-pn)(Me_2-en)][$Sb_2(+)$-tart$_2$]·$2H_2O$,[5] respectively. In the present case, however, the N(R)–C(S) isomer is preferred by the same anion as the counter ion for the less soluble diastereoisomeric salt, $(+)_{350}$-[Pt$(NH_3)_2$(N^1-Me-(S)-pn)][$Sb_2(+)$-tart$_2$]·H_2O. The geometry and dimensions of the $[Sb_2(+)\text{-tart}_2]^{2-}$ anion agree well with those for $K_2[Sb_2(+)\text{-tart}_2]\cdot 3H_2O$.[11]

CD Spectrum. The absorption and CD spectra of R-[Pt$(NH_3)_2$(N^1-Me-(S)-pn)]$(ClO_4)_2$ are shown in Fig. 3, in which the CD spectrum of the racemic compound is also given. The N(R) isomer is stable with respect to racemization in a 0.01 M perchloric acid solution; actually no appreciable change in the CD curve was observed over a period of 24 h. The electronic spectrum of this complex bears a close resemblance to that of [Pt(R-pn)$_2$]Cl_2, and accordingly, the peak at 35000 cm^{-1}, on the basis of D_{4h} symmetry, can

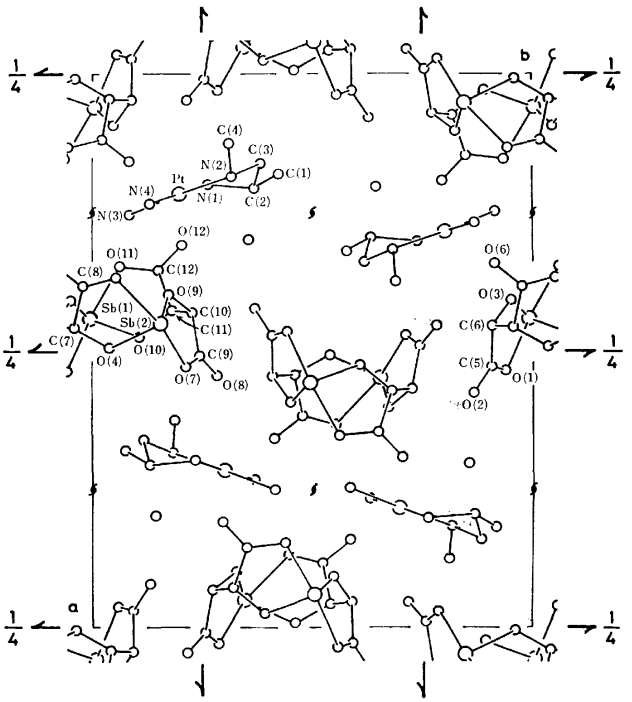

Fig. 2. The crystal structure of $(+)_{350}$-[Pt$(NH_3)_2$(N^1-Me-(S)-pn)]·[$Sb_2(+)$-tart$_2$]·H_2O viewed down the c axis. The atoms denoted as O(1), O(2), O(3), O(6), C(5), and C(6) are related with the corresponding ones in Table 1 by a unit translation in y.

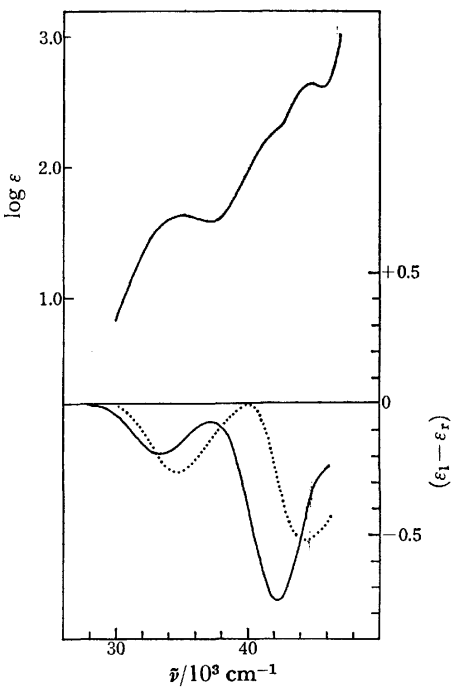

Fig. 3. The absorption (top) and CD (bottom) spectra of $(-)_{260}$-[Pt$(NH_3)_2$(N^1-Me-(S)-pn)]$(ClO_4)_2$: ——, and the CD spectrum of *rac*-[Pt$(NH_3)_2$(N^1-Me-(S)-pn)]Cl_2: ·····.

be assigned to $^1A_{1g} \rightarrow {}^3A_{2g}$, ^3E_g and those at 41500 (shoulder) and 44500 cm^{-1} to $^1A_{2g}$ and ^1E_g transitions.[1] The CD spectra are different from each other, showing marked influence of the vicinal effect of the asymmetric nitrogen.

The optical activity due to the chelate ring of N^1-Me-(*S*)-pn may arise from (i) the vicinal effect of the chiral secondary nitrogen, (ii) the conformational effect of the chelate ring, and (iii) the vicinal effect of the asymmetric carbon. Bosnich and Sullivan have shown that the first and the resultant of the remaining two effects are additive in the rotational strength for *R*- and/or *S*-$[PtCl_2(N^1\text{-Me-}(S)\text{-pn})]$.[2] Such additivity can be anticipated to be valid in the CD of the *R*-$[Pt(NH_3)_2(N^1\text{-Me-}(S)\text{-pn})]^{2+}$ considered here. The CD curve of the racemic N^1-Me-(*S*)-pn complex was subtracted from that of the N(*R*) isomer. The resulting curve (the dotted line in Fig. 4) should be regarded as representing the CD due to the vicinal effect of the *R* asymmetric nitrogen. It is noteworthy that this curve agrees well with the CD of $(-)_{260}$-$[Pt(NH_3)_2(Meen)](ClO_4)_2$ (Fig. 4). The CD band at 31000 cm^{-1} may be assigned to the $^3A_{2g}$ transition.[1]

According to the ^{13}C NMR studies of Bagger[12] and Erickson *et al.*,[13] rapid ring inversion ($\delta \leftrightarrow \lambda$) occurs in the 5-membered chelate ring composed of the Pt(II) and *N*-substituted 1,2-diaminopropane. The present ^{13}C NMR data for *C*-methyl carbons in some relevant complexes are given in Table 3. The β-carbon resonances in $[Pt(NH_3)_2(\text{rac-chxn})]Cl_2$ and the *C*-methyl carbon resonances in $[Pt(NH_3)_2(N^1\text{-Me-}(S)\text{-pn})]X_2$ and $[Pt(NH_3)_2(\text{rac-pn})]Cl_2$ were readily identified by comparison with the corresponding resonances in complexes of the $[Pt(bipy)(diamine)]Cl_2$ type.[13] Each of these signals is accompanied by two ^{195}Pt satellites. The $^3J_{Pt-C}$ value obtained from the spacing of the satellites is the weighted average of the coupling constants of the conformer with the equatorial C–CH_3 group and that with the axial group; ring inversion changes the equatorial C–CH_3 into an axial one or *vise versa*. Following Erickson *et al.*, the coupling constants $^3J_{Pt-C}$ of 0 and 50 Hz were assigned to the axial and equatorial conformers, respectively.[13] The mol fractions of the equatorial conformer calculated from the observed $^3J_{Pt-C}$ values are listed in the last column of Table 3.

The four possible conformers (I—IV) in $[Pt(NH_3)_2(N^1\text{-Me-}(S)\text{-pn})]^{2+}$ are illustrated in Fig. 5. The resonances at 16.3 and 16.7 ppm in the racemic N^1-Me-(*S*)-pn complex are attributable to the N(*R*) and the N(*S*) isomer, respectively. The relative abundances of the equatorial and axial C–CH_3 conformers for each of the N(*R*) and N(*S*) isomers indicate that the equatorial conformer is more stable than the axial. The I : II abundance ratio (86 : 14) is greater than that of III : IV (70 : 30), which reflects a greater conformational energy difference between I and II than between III and IV.

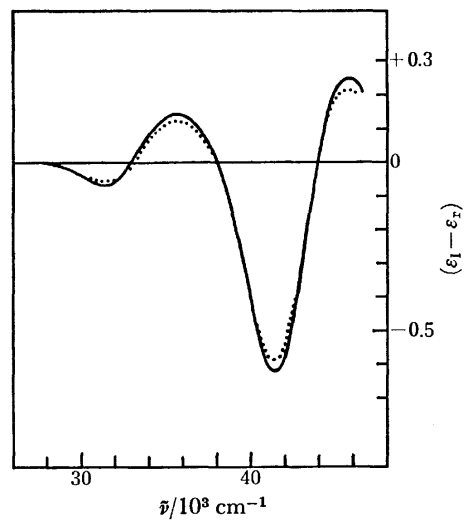

Fig. 4. The calculated curve of $[\Delta\varepsilon(R\text{-}[Pt(NH_3)_2(N^1\text{-Me-}(S)\text{-pn})](ClO_4)_2) - \Delta\varepsilon(rac[Pt(NH_3)_2(N^1\text{-Me-}(S)\text{-pn})]Cl_2)]$: ·····, and the CD spectrum of $(-)_{260}$-$[Pt(NH_3)_2(\text{Me-en})](ClO_4)_2$: ——.

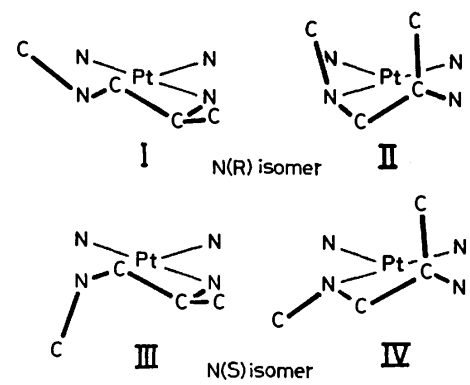

Fig. 5. The four possible conformers in *R*- and *S*-$[Pt(NH_3)_2(N^1\text{-Me-}(S)\text{-pn})]^{2+}$.

Table 3. ^{13}C Chemical shifts and coupling constants ($^3J_{Pt-C}$) of *C*-methyl carbons

	^{13}C chemical shift (δ/ppm)	$^3J_{Pt-C}$ (J/Hz)	n_{eq}[a]
R-$[Pt(NH_3)_2(N^1\text{-Me-}(S)\text{-pn})](ClO_4)_2$	16.3	43	0.86
rac-$[Pt(NH_3)_2(N^1\text{-Me-}(S)\text{-pn})]Cl_2$	16.3 16.7	43 35	0.86 0.70
$[Pt(NH_3)_2(\text{rac-pn})](ClO_4)_2$	16.8	38	0.76[b]
$[Pt(NH_3)_2(\text{rac-chxn})]Cl_2$	33.3	52[d]	1
$[Pt(NH_3)_2(R,R\text{-bn})]Cl_2$[c]		50[d]	1

a) The mol fraction of the equatorial C–CH_3 conformer. b) Making use of the CD data presented in Ref. 1, Hawkins predicted that the ratio of n_{eq} to n_{ax} is of the order of 3 : 1 (Ref. 14, p. 204). c) Ref. 12; *R*,*R*-bn: (2*R*,3*R*)-2,3-butanediamine. d) These were utilized to check the appropriateness of the $^3J_{Pt-C}$ values assigned to the equatorial C–CH_3 conformer.

The chelate ring of the pn or its derivative has been thought to preferentially assume the conformation with equatorial C–CH_3 even for the planar complex.[14] However, in case there is a significant amount of axial conformers in the system, the CD of the Pt(II) chelate of the pn or its analogue must be reconsidered with the relative populations of the δ and λ conformers being taken into account.

As described above, the additivity found by Bosnich and Sullivan for the CD of *R*- and *S*-[$PtCl_2$(*N*¹-Me-(*S*)-pn)] is probably applicable to the case of *R*-[Pt-$(NH_3)_2$(*N*¹-Me-(*S*)-pn)]$^{2+}$. Thus, the CD curves for the conformers I and II can be represented by $x\Delta\varepsilon$-$[V_N(R)]+x\Delta\varepsilon[eq]$ and $(1-x)\Delta\varepsilon[V_N(R)]+(1-x)\Delta\varepsilon$-[ax] respectively, where $\Delta\varepsilon[V_N(R)]$ is the CD arising from the vicinal effect of N(*R*)–CH_3, $\Delta\varepsilon[eq]$ and $\Delta\varepsilon[ax]$ denote, respectively, the CD due to the (*S*)-pn ring with equatorial C–CH_3 and that with axial C–CH_3, and x is the mol fraction of conformer I. A calculation gives $(1/2)(x+y)\Delta\varepsilon[eq]+[1-(1/2)(x+y)]\Delta\varepsilon[ax]$ for the CD of the racemic compound and $\Delta\varepsilon[V_N(R)]+(1/2)(x-y)\cdot(\Delta\varepsilon[eq]-\Delta\varepsilon[ax])$ for that of the calculated curve in Fig. 4 (y=the mol fraction of conformer III). The chelate ring of the (*S*)-pn has two asymmetry factors: the chirality of the chelate ring conformation and the asymmetric carbon atom. For the Co(III) complex in which one bidentate ligand has two asymmetric centers, it has been demonstrated that the two centers act additively for the CD of the complex.[15] Although the situation is somewhat different, the conformational and vicinal effects are expected to be nearly additive for the rotational strength induced by the (*S*)-pn ring. Then $\Delta\varepsilon[eq]$ and $\Delta\varepsilon[ax]$ may be written as $\Delta\varepsilon[eq]\simeq\Delta\varepsilon[\delta]+\Delta\varepsilon[V_C(S)_{eq}]$ and $\Delta\varepsilon[ax]\simeq\Delta\varepsilon[\lambda]+\Delta\varepsilon[V_C(S)_{ax}]$, where $\Delta\varepsilon[\delta$(or $\lambda)]$ is the CD due to the conformational effect of the δ(or λ) chelate ring and $\Delta\varepsilon[V_C(S)_{eq}]$ or $\Delta\varepsilon[V_C$-$(S)_{ax}]$ is the CD ascribed to the vicinal effect of the equatorial or axial C(*S*)–CH_3.[16] However, $\Delta\varepsilon[V_C(S)_{eq}]$ is known to be small[17] and hence, $\Delta\varepsilon[eq]\simeq\Delta\varepsilon[\delta]$. Thus, the calculated curve can be approximated by

$$\Delta\varepsilon[V_N(R)]+(x-y)\Delta\varepsilon[\delta]-(1/2)(x-y)\Delta\varepsilon[V_C(S)_{ax}].$$

Since x=0.86 and y=0.70 (Table 3), this formula becomes

$$\Delta\varepsilon[V_N(R)]+0.16\Delta\varepsilon[\delta]-0.08\Delta\varepsilon[V_C(S)_{ax}].$$

The CD of [$Pt(NH_3)_2$(*S*,*S*-chxn)]Cl_2 shows two negative bands with intensities $\Delta\varepsilon(^3E_g)=-0.40$ (35000 cm^{-1}) and $\Delta\varepsilon(^1E_g)=-0.86$ (45000 cm^{-1}), and that of [$Pt(NH_3)_2$(*S*-pn)]Cl_2 has two minima with $\Delta\varepsilon(^3E_g)=-0.22$ (35200 cm^{-1}) and $\Delta\varepsilon(^1E_g)=-0.51$ (44800 cm^{-1}).[1,18] The CD curve of the former compound can be considered to display an approximate δ conformational effect, $\Delta\varepsilon[\delta](\simeq\Delta\varepsilon[\delta]+2\Delta\varepsilon[V_C(S)_{eq}])$, whereas that of the latter compound may be approximated by $(2x-1)\Delta\varepsilon[\delta]+(1-x)\Delta\varepsilon[V_C(S)_{ax}]$ which becomes $0.52\,\Delta\varepsilon[\delta]+0.24\Delta\varepsilon[V_C(S)_{ax}]$ upon the substitution of 0.76 for x (Table 3; x=the mol fraction of the equatorial conformer). If the $\Delta\varepsilon$ value of the latter CD curve is divided by 0.52, we obtain $\Delta\varepsilon[\delta]+0.46\Delta\varepsilon[V_C(S)_{ax}]$, which gives a curve with two extrema of $\Delta\varepsilon(^3E_g)=-0.42$ (35200 cm^{-1}) and $\Delta\varepsilon(^1E_g)=-0.98$ (44800 cm^{-1}). These $\Delta\varepsilon$ value are in agreement with the corresponding ones for the *S*,*S*-chxn complex. This indicates that the vicinal effect is small compared with the conformational effect: $0.46|\Delta\varepsilon[V_C(S)_{ax}]|\simeq(1/2)|\Delta\varepsilon[V_C(S)_{ax}]|\ll|\Delta\varepsilon[\delta]|$. Therefore, the calculated curve can be taken as representing

$$\Delta\varepsilon[V_N(R)]+0.16\Delta\varepsilon[\delta].$$

The secondary nitrogen in $(-)_{260}$-[$Pt(NH_3)_2$(Me-en)]$^{2+}$ is sure to be of *R* configuration from a comparison of the Cotton effect for this complex with that for $(+)_{260}$-[$Pt(NH_3)_2(Me_3en)$]$SbCl_5$, the absolute configuration of which was determined by the X-ray method[19] (Me_3en= *N*,*N*,*N*′-trimethylethylenediamine). The N–CH_3 group in the *R*-Meen complex is considered to favor the equatorial disposition in view of the steric interaction with solvent molecules (and/or with some anions in the solution) which may be located at the axial positions of the complex cation. This disposition of the N–CH_3 imposes a δ conformation on the chelate ring in contrast to the λ conformation induced by the axial N–CH_3. Accordingly, the CD curve of the *R*-Meen complex is presumably represented by the formula

$$\Delta\varepsilon[V_N(R)]+z\Delta\varepsilon[\delta]$$

(z=the difference between the mol fraction for the equatorial N–CH_3 conformer and that of the axial conformer, which is greater than zero in this case). Although the good agreement between the calculated curve and the CD spectrum of the *R*-Meen complex is accidental, this agreement supports the fact that the δ conformational effect is partly responsible for the calculated curve,[20] and moreover, this curve receives little contribution from the vicinal effect of the asymmetric carbon.

As mentioned above, $\Delta\varepsilon[\delta]$ may be very similar to the CD of [$Pt(NH_3)_2$(*S*,*S*-chxn)]$^{2+}$ and, hence, may have relatively intense ^3E_g and ^1E_g CD bands. If the curves shown in Fig. 4 are corrected for the δ conformational contribution, the intensities of the ^3E_g and ^1E_g components due to the N(*R*) vicinal effect will have some, not insignificant, enhancement. However, the signs of the Cotton effects are taken to be those characteristic of the N(*R*)–CH_3 group.

This research was supported by a Grant-in-Aid for Scientific Research from the Ministry of Education. The authors wish to express their thanks to Drs. Kousuke Kusuda and Sabu Kasai of Osaka City University for the ^{13}C NMR measurements.

References

1) H. Ito, J. Fujita, and K. Saito, *Bull. Chem. Soc. Jpn.*, **40**, 2584 (1967).
2) B. Bosnich and E. A. Sullivan, *Inorg. Chem.*, **14**, 2768 (1975).
3) R. G. Ball, N. J. Bowman, and N. C. Payne, *Inorg. Chem.*, **15**, 1704 (1976).
4) K. Yokoho, K. Matsumoto, S. Ooi, and H. Kuroya, *Bull. Chem. Soc. Jpn.*, **49**, 1864 (1976).
5) K. Matsumoto, S. Ooi, M. Sakuma, and H. Kuroya, *Bull. Chem. Soc. Jpn.*, **49**, 2129 (1976).
6) M. Saburi, Y. Tsujito, and S. Yoshikawa, *Inorg. Chem.*, **9**, 1476 (1970).

7) J. B. Goddard and F. Basolo, *Inorg. Chem.*, **8**, 2223 (1969).
8) P. Haake and P. C. Turley, *J. Am. Chem. Soc.*, **90**, 2293 (1968).
9) "International Tables for X-Ray Crystallography," Vol. 3 Kynoch Press, Birmingham (1962), pp. 202, 215.
10) W. A. Freeman, *Inorg. Chem.*, **9**, 2235 (1976).
11) M. E. Gress and R. A. Jacobson, *Inorg. Chim. Acta*, **8**, 209 (1974).
12) S. Bagger, *Acta Chem. Scand.*, **A28**, 467 (1974).
13) L. E. Erickson, J. E. Sarneski, and C. N. Reilley, *Inorg. Chem.*, **14**, 3007 (1975).
14) C. J. Hawkins, "Absolute Configuration of Metal Complexes," Wiley-Interscience (1971), Chap. 6.
15) N. Koine, N. Sakota, J. Hidaka, and Y. Shimura, *Chem. Lett.*, **1972**, 543.
16) No differentiation was made here between $\Delta\varepsilon[V_N(R)_{eq}]$ and $\Delta\varepsilon[V_N(R)_{ax}]$, and it was assumed that $\Delta\varepsilon[V_N(R)_{eq}]=\Delta\varepsilon[V_N(R)_{ax}]=\Delta\varepsilon[V_N(R)]$, since the positional change of the N–CH_3 group on the equatorial↔axial interconversion is small compared with the case of the C–CH_3 group.
17) B. Bosnich and J. MacB. Harrowfield, *J. Am. Chem. Soc.*, **94**, 3425 (1972); Ref. 14, p. 202; Ref. 6.
18) The CD data for $[Pt(NH_3)_2(R\text{-pn})]Cl_2$ and $[Pt(NH_3)_2(R,R\text{-chxn})]Cl_2$ are given in Ref. 1. In the text, however, the inverted CD's of these compounds were used as those of the *S*- and *S,S*-analogues.
19) K. Yokoho, K. Matsumoto, S. Ooi, and H. Kuroya, Proceedings of the 25th symposium of coordination chemistry (1975), p. 73.
20) In Ref. 2, it was concluded that the N–CH_3 in *R*-$[Pt(NH_3)_2(Meen)]^{2+}$ is predominantly in the equatorial disposition. However, the fair agreement between the two curves in Fig. 4 suggests that $z\simeq 0.16$ and that the abundance ratio of the equatorial N–CH_3 conformer to the axial conformer is about 58 : 42.

Determination of Rubidium in Biological Materials Using Atomic Absorption Spectroscopy

Gi-ichiro TANAKA, Akeo TOMIKAWA,* and Hisao KAWAMURA

Division of Radioecology, National Institute of Radiological Sciences, Isozaki, Nakaminato 311-12

**Faculty of Agriculture, Tokyo Kyoiku University, Komaba, Meguro-ku, Tokyo 153*

(Received March 14, 1977)

In order to establish a reliable and rapid method for the determination of rubidium in biological materials using atomic absorption spectroscopy, chemical interference as well as ionization interference due to co-existing elements and some organic substances was studied. In the presence of potassium of sufficient concentration, most of the interference was found to be negligible. The temperature of the sample solutions proved to be a possible source of error. The process of sample preparation was examined, including a determination of the loss of rubidium in dry ashing. The accuracy and precision of the method was tested by analyzing NBS SRM 1577 Bovine Liver. The rubidium contents of typical biological materials—foodstuffs, human tissues and urine—were determined by the present method and a possible relationship between the rubidium and potassium concentrations is indicated.

Rubidium is an element the behavior of which in biological systems is similar to that of potassium.[1] However, its data on the transfer of this element from the environment to man and on its distribution in the human body are relatively few.[2,3] Rubidium has a natural radioactive isotope, ^{87}Rb, the half-life of which is 4.8×10^{10} years and the abundance of which is 27.85 %.[4] The radioactivity of ^{87}Rb is calculated to be 52.9 disintegrations per min per milligram of rubidium, which cannot be neglected from the standpoint of radiological health problems. The development of rapid and precise methods for the determination of natural rubidium in biological and environmental materials has recently become urgent.

Rubidium has usually been determined using emission spectrography, X-ray fluorescence analysis, or neutron activation techniques,[5] which require rather complicated equipment and are not considered to be very convenient methods in most laboratories. Flame emission spectrometry, which is claimed to be simple and of satisfactory sensitivity, is subject to unavoidable interference due to the neighboring strong potassium lines even when spectrometers of high spectral resolution are used.[6,7] This problem necessitates wavelength scanning which is time consuming.

Only a few papers have been reported on the determination of rubidium in biological materials by atomic absorption spectroscopy. In this report, in order to establish a rapid method of atomic absorption spectroscopic determination of rubidium, the chemical interference due to the co-existing elements and acids, as well as the ionization interference effect, was studied. It was confirmed that rubidium in typical biological materials can be rapidly determined, free from the effect of interference, using the proposed method, which was proven using a biological standard material.

Experimental

Instrument. Perkin-Elmer Model 303 and 403 atomic absorption spectrophotometers were used with 10-cm slot burner heads for air-acetylene flames. An Osram rubidium discharge lamp covered with filter paper having an 8 mm × 8 mm square aperture was used. Thus, about a two-fold increase in intensity was obtained supposedly due to the integration of the emitted light by reflection. A UV-cut filter (Hoya Glass Works, Tokyo, O-56) was placed just in front of the entrance slit of the Model 303 instrument. A Hitachi 056 strip chart recorder was employed. A Medical Spectrometer (Tokyo Shibaura Electric Co.) with a well-type NaI(Tl) detector was used for gamma scintillation counting.

Reagents. Rubidium chloride and cesium chloride were purchased from E. Merck AG. and used in most of the experiments. A 1000 μg cm^{-3} rubidium stock solution for quantitative determination was prepared by dissolving 1.415 g of Johnson Matthey "Specpure" rubidium chloride in 1000 ml of distilled water. The rubidium-86(tracer with a half-life of 18.66 d, supplied as a chloride, a specific activity of 0.833 mCi/mg-Rb) was obtained from the Radiochemical Centre, U. K., and diluted before use. Most of the other reagents used were of JIS Special Grade or Analytical Grade.

Results and Discussion

Optimum Operating Conditions. Typical operating conditions adopted are summarized in Table 1. The light beam, 2, 6, and 15 mm in height above the burner, approximately sampled the primary, interconal and outer zones, respectively. A comparatively small variation in absorbance was observed over the range of acetylene flow rate examined in the presence of potassium at a height of 7 mm (Fig 1). Some enhancement of the rubidium absorbance was observed when the acetylene cylinder pressure was reduced below 5 kg/cm^2. This effect, which occurred up to 30% of the relative absorbance, was suspected to be due to acetone vapor liber-

TABLE 1. OPERATING CONDITIONS

Wavelength	780.0 nm
Discharge lamp current	350 mA
Slit setting	4 divisions
Spectral band width	1.4 nm
Acetylene flow,	
meter setting	9.0 divisions
flow rate	3.4 dm^3/min
Air flow, meter setting	7.5 divisions
flow rate	17.0 dm^3/min
Beam height above burner (with potassium added)	7 mm

Perkin-Elmer Model 303. Similar conditions were adopted for Model 403.

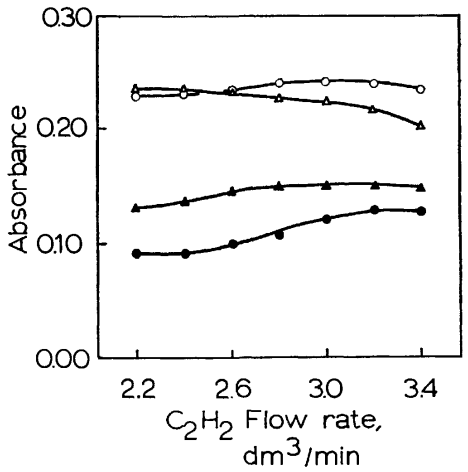

Fig. 1. Effect of acetylene flow rate on rubidium absorbance. Air flow rate: 17.0 dm^3/min (const). 5 μg cm^{-3} Rb, 3 mm (▲) and 7 mm (●) above burner top 5 μg cm^{-3} Rb+1000 μg cm^{-3} K, 3 mm (△) and 7 mm (○) above burner top.

ated from absorbing beds.

Comparison between Atomic Absorption and Emission Spectroscopy. The effect of the spectral band width on the signal-to-noise ratio of the rubidium absorbance signal in the presence of potassium was negligible as expected from theoretical considerations,[8] as is shown in Table 2. The peak-to-background ratio of the emission spectrum seriously deteriorated when wider slit widths were used, revealing the need for time-consuming scanning employing a narrow slit width (Fig. 2). Furthermore, it should be born in mind that many molecular emission bands such as the CrO 777.8- and 781.2-nm bands, the LaO 775.9-nm band, the FeO 777.5-nm band and the VO 785.1-nm band can interfere with the rubidium 780.0-nm line.[8,9]

The Effect of Other Alkali and Alkaline-earth Metals. Lithium, sodium, potassium, and cesium, as chlorides at concentrations greater than 100 μg cm^{-3} caused the rubidium absorbance to increase. In the interconal zone, the enhancement reached saturation at metal concentrations of greater than 1000 μg cm^{-3} while the saturation point shifted to the range from 2500 to 5000 μg cm^{-3} in the outer zone (Fig. 3). In the case of cesium, the rubidium absorbance apparently increases linearly with the concentration of cesium at concentrations greater than 1000 μg cm^{-3}. This was proven to be due to the rubidium impurity in the cesium chloride used (0.40 μg/mg of Cs as determined by atomic absorption) and the absorbance corrected for the reagent blank disclosed saturation at cesium concentrations greater than 500 μg cm^{-3}. The degree of enhancement was compared for these elements on a molar basis. The order was found to be Li<Na<K<Cs, which agrees with the inverse order of their ionization energies: 5.39 eV for Li, 5.14 eV for Na, 4.34 eV for K, and 3.89 eV for Cs.[8] The effect was more marked in the outer zone (Fig. 3). Flame temperatures in the outer zone were found to be higher than in the lower part for an air-acetylene flame closely matched to the flame conditions used here.[10] From these results, it is concluded

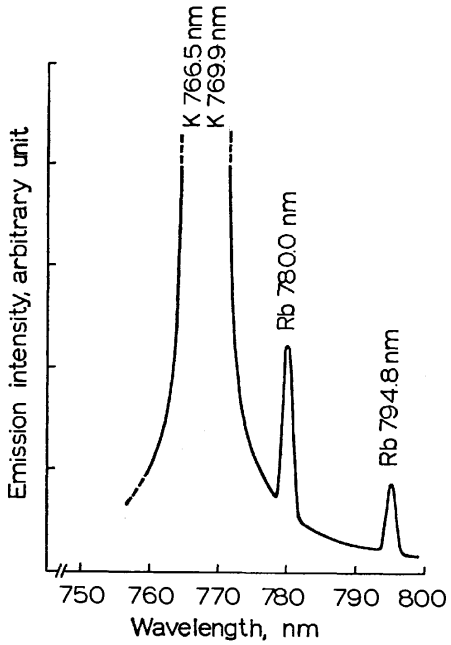

Fig. 2. A typical emission spectra of rubidium in the air-acetylene flame in the presence of potassium obtained by scanning. 2 μg cm^{-3} Rb+2000 μg cm^{-3} K (0.1 mol dm^{-3} HCl). Spectral band width: 1.4 nm; Scanning speed: 10 nm/min.

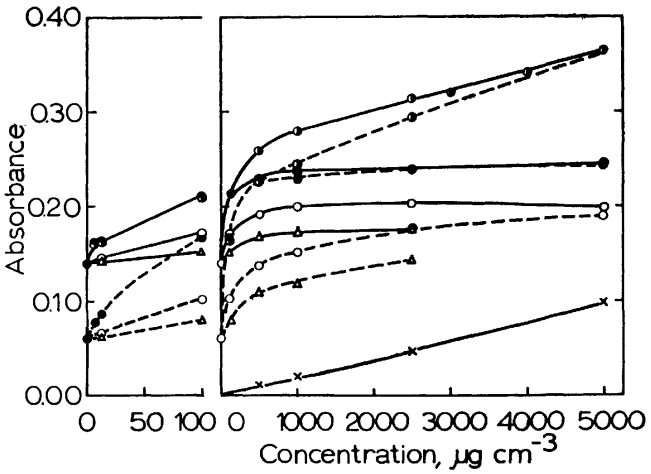

Fig. 3. Effect of other alkali metals. 5 μg cm^{-3} Rb+ Li (△), Na (○), K (●), Cs (◑); Cs only (×). ——: interconal zone; ---: outer zone.

Table 2. The effect of the slit width or spectral band width on rubidium determination by atomic absorption and emission in the presence of potassium

Slit		Spectral band width (nm)	Atomic absorption S/N ratio	Atomic emission Peak/background ratio
Setting (scale)	Width (mm)			
3	0.3	0.4	72	11
4	1	1.4	133	3.2
5	3	4	123	0.9
6	10	14	107	—

2 μg cm^{-3} Rb+2000 μg cm^{-3} K (0.1 mol dm^{-3} HCl).

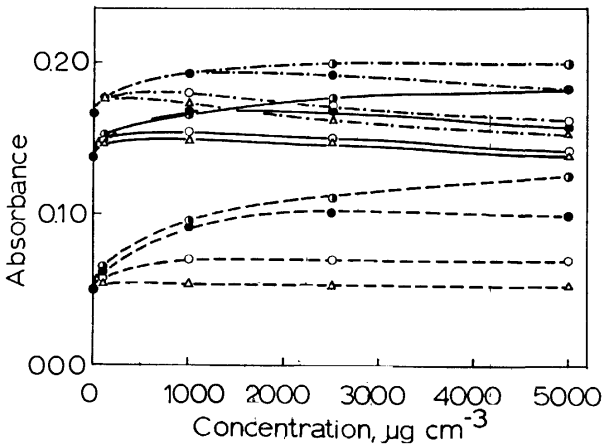

Fig. 4. Effect of alkaline earth metals. 5 μg cm^{-3} Rb+ Mg (△), Ca (○), Sr (●), Ba (◑). —·—·: primary zone; ——: interconal zone; ---: outer zone.

that the suppression of rubidium ionization by other easily ionized alkali metals[11,12] is the essential mechanism of this effect.

Alkaline-earth metals show a less pronounced but similar effect and the enhancement was found to be Mg<Ca<Sr<Ba, which is the inverse of their ionization energies: 7.65 eV for Mg, 6.11 eV for Ca, 5.69 eV for Sr, and 5.21 eV for Ba.[8] Magnesium, calcium, and strontium at greater than 1000 μg cm^{-3}, however, exhibited a slight suppression of the rubidium absorbance which had been enhanced at lower concentration levels. This negative interference was not observed in the outer zone (Fig. 4). It appears that the alkaline-earth metals were ionized to some extent in air-acetylene flames exhibiting ionization interference and that, at higher concentrations (2500 to 5000 μg cm^{-3}), they caused chemical interference by retarding the atomization of rubidium, possibly through occlusion in and/or adsorption to clotlets in the primary and interconal zones.

The enhancements of alkali and alkaline-earth metals at 10—20 mmol dm^{-3} were compared, with the resulting order in the interconal zone: Li, Mg<Ca< Sr<Ba<Na<K<Cs. This is in good agreement with the inverse order of the ionization energies for all these elements except lithium.

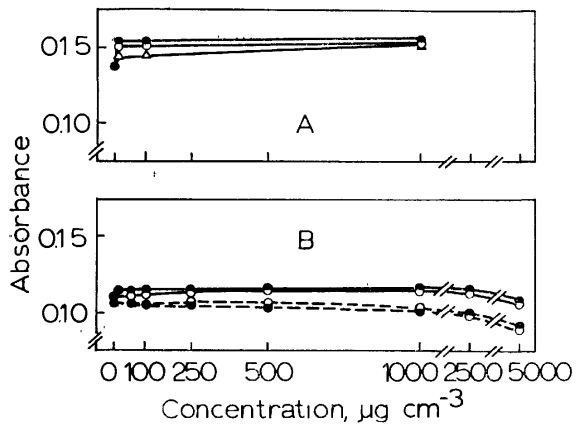

Fig. 5. Effect of transition metals and aluminium.
(A) 5 μg cm^{-3} Rb+Fe, Cr, Zn (●), Cu (○), Mn (△).
(B) 5 μg cm^{-3} Rb+Al as nitrate (●), as chloride (○).
—— interconal zone; ---: primary zone.

The Effect of Several Transition Metals and Aluminium. Iron, chromium, zinc, and copper at concentrations of 10 to 1000 μg cm^{-3} exhibited small positive interference while the effect of manganese was negligible at concentrations below 100 μg cm^{-3} (Fig. 5). Aluminium, as a nitrate at concentrations in the range from 100 to 2500 μg cm^{-3}, exhibited a small enhancement although it noticeably lowered the rubidium absorbance at 5000 μg cm^{-3} as either a nitrate or a chloride. For systems containing 1000 μg cm^{-3} of potassium, sodium showed no influence on the rubidium absorbance up to 1000 μg cm^{-3} and virtually no effect was observed for calcium, iron, copper, zinc, manganese, and aluminium up to 1000 μg cm^{-3} (Fig. 6). A small negative interference due to magnesium was observed in the presence of potassium. The use of nitric acid proved favorable when aluminium is present in sample solutions.

The Effect of Mineral Acids. No appreciable effect due to nitric acid was observed. Hydrochloric and perchloric acid exhibited slight enhancement at 0.1 mol dm^{-3} but a negative interference of about −30% at

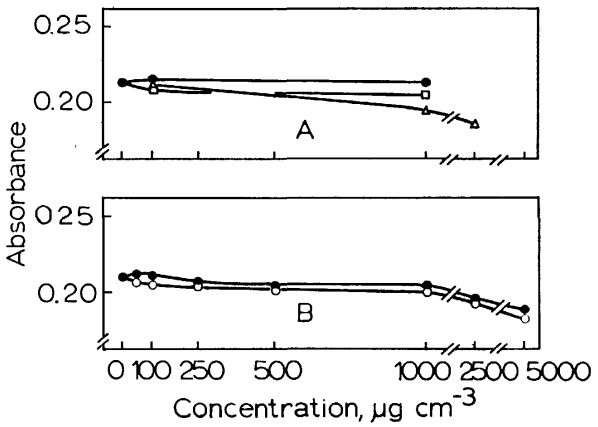

Fig. 6. Effect of transition metals and aluminium in the presence of potassium.
(A) 5 μg cm^{-3} Rb+1000 μg cm^{-3} K. ●: Na, △: Mg, □: Ca, Fe, Cu, Zn, Mn.
(B) 5 μg cm^{-3} Rb+1000 μg cm^{-3} K, Al as nitrate (●) as chloride (○).

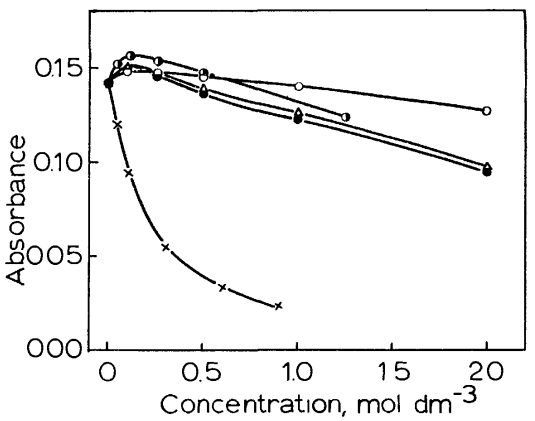

Fig. 7. Effect of mineral acids.
5 μg cm^{-3} Rb. ○: HNO_3, ●: HCl, △: $HClO_4$, ◑: H_2SO_4, ×: H_3PO_4.

2 mol dm^{-3} was observed (Fig. 7). This interference was inferred to be due to the formation of the diatomic molecule, RbCl, in the flame.[13] Phosphoric acid severely interfered causing a −50% decrease in signal even at 0.2 mol dm^{-3}. With sulfuric acid, the absorbance decreased and the aspiration rate of the sample solution was found to be reduced. In the presence of 1000 μg cm^{-3} of potassium, the negative interference for these acids at a concentration of 0.1 mol dm^{-3} was negligible, except for phosphoric acid in which case the interference was reversed to only −22% at 0.2 mol dm^{-3}. Precipitation occurred in solutions containing potassium and of perchloric acid concentrations greater than 0.5 mol dm^{-3}, which perturbed the rubidium absorbance measurements (Fig. 8).

The Effect of Phosphates. Phosphates at concentrations in the form of P below 2500 μg cm^{-3}, including free orthophosphoric acid, exhibited interference, except when the counter cation was potassium (Fig. 9). For an added potassium concentration of 1000 μg cm^{-3}, the interference of phosphoric acid, ammonium phosphate and calcium phosphate was reversed to from −3 to −5% at a P concentration of 1000 μg cm^{-3}. For the purpose of suppressing the phosphate interference, potassium should be added so as to render the K/P ratio greater than two.

The Effect of Silicates. No systematic study on the effect of silicates was carried out but some interference was observed. Since silicates exist in considerable amounts only in plant materials, this interference is expected to be negligible for most biological materials.

The Effect of Organic Acids and Their Ammonium Salts. Several ammonium salts of organic acids are used for separating alkali elements from matrices by ion-exchange column chromatography. In this connection, the effects of formic, acetic, lactic and tartaric acids and their ammonium salts were examined and the results are shown in Fig. 10. Trichloroacetic acid was selected since it is used for precipitating proteins from biological fluids. Acetic acid enhanced the rubidium absorbance while its trichloro derivative caused a severe reduction especially in the presence of 1000-μg cm^{-3} potassium concentrations. The effect of trichloroacetic acid is assumed to be due to liberated chlorine which tends to form RbCl. Ammonium formate, ammonium acetate and ammonium lactate in concentrations up to 0.5 mol dm^{-3} in the presence of 1000 μg cm^{-3} of potassium caused only a negligible effect and these are the most probable cases for practical application. These organic

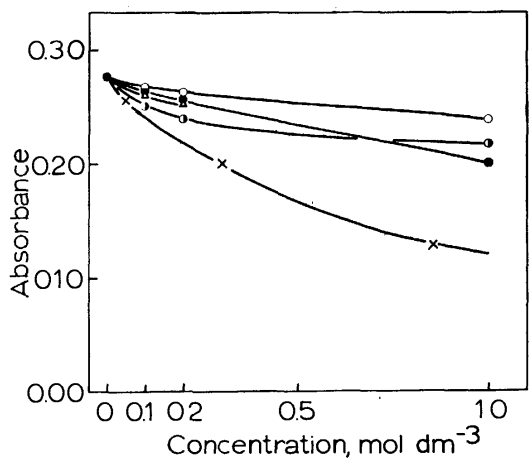

Fig. 8. Effect of mineral acids in the presence of potassium.
5 μg cm^{-3} Rb+1000 μg cm^{-3} K. ○: HNO_3, ●: HCl, △: $HClO_4$, ◑: H_2SO_4, ×: H_3PO_4.

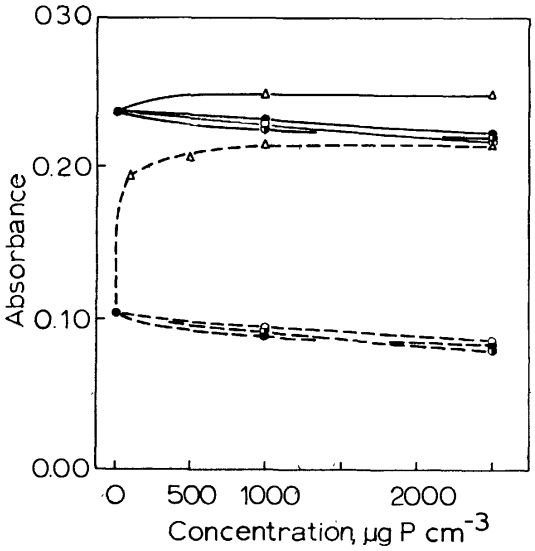

Fig. 9. Effect of phosphates.
---: 5 μg cm^{-3} Rb; ——: 5 μg cm^{-3} Rb+1000 μg cm^{-3} K.
●: H_3PO_4, ○: $(NH_4)_2HPO_4$, ◑: $Ca(H_2PO_4)_2$, △: KH_2PO_4.

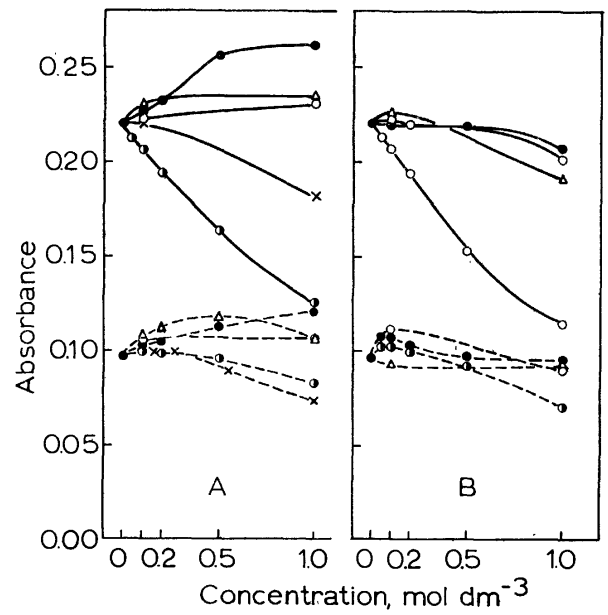

Fig. 10. Effect of organic acids and their ammonium salts.
---: 5 μg cm^{-3} Rb. ——: 5 μg cm^{-3} Rb+1000 μg cm^{-3} K.
(A) ○: HCOOH, ●: CH_3COOH, ◑: CCl_3COOH, △: $CH_3CH(OH)COOH$, ×: $(CH_2(OH)COOH)_2$.
(B) ○: $HCOONH_4$, ●: CH_3COONH_4, ◑: CCl_3COOH/NH_4OH equimolar mixture, △: $CH_3CH(OH)COONH_4$.

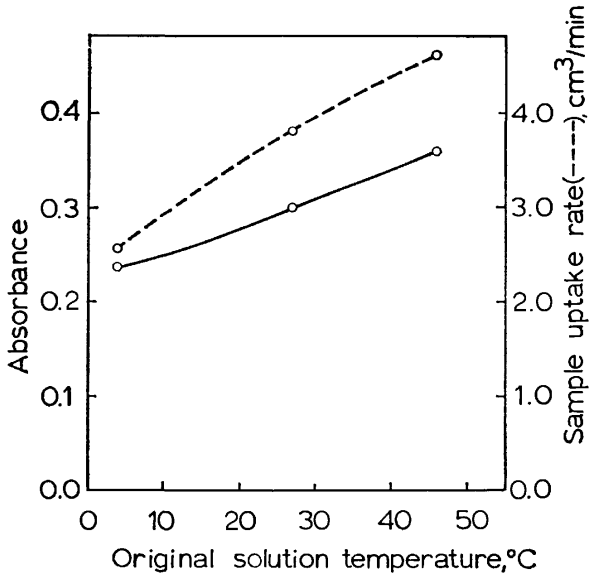

Fig. 11. Effect of sample solution temperature on rubidium absorbance and sample uptake rate.
5 μg cm^{-3} Rb+1000 μg cm^{-3} K.

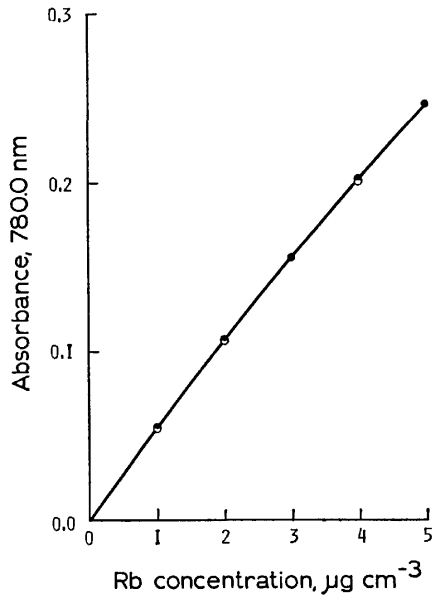

Fig. 12. Working curves for rubidium.
●: 1000 μg cm^{-3} K. ○: 1000 μg cm^{-3} K+500 μg cm^{-3} Na+500 μg cm^{-3} Ca+500 μg cm^{-3} P.

substances, however, should be decomposed prior to nebulization, because they can clog the burner slot.

The Effect of the Solution Temperature. At higher sample solution temperatures, a considerable increase in absorbance was observed (Fig. 11). This phenomenon was accompanied by an increase in the rate of sample aspiration through a capillary. If sample and standard solutions of different temperatures are measured, considerable error will result.

Sensitivity and Detection Limit. Typical analytical curves for rubidium with potassium added are shown in Fig. 12. The slight non-linearity can be attributed to self-absorption in the light source. It is not expected that this can be avoided by replacing the discharge lamp with a hollow cathode, because no essential difference was observed between Na and K analytical curves obtained using metal discharge lamps and those obtained using hollow-cathode lamps. This non-linearity excludes the use of the standard addition method in precision analysis.

Only less than a 1% reduction in sensitivity was observed when further addition of sodium, calcium and phosphorus, each at 500 μg cm^{-3}, were made. The sensitivity for rubidium under these conditions was calculated to be 0.08 μg cm^{-3} for 1% absorption (0.0044 absorbance). The detection limit obtained by digital signal averaging over about 10 s was 6.5 ng cm^{-3}.

TABLE 3. LOSS OF RUBIDIUM DURING DRY ASHING AND PREPARATION OF SILICA-FREE SAMPLE SOLUTIONS DETERMINED BY Rb-86

Material	Wet weight (g)	Ashing temperature (°C)	Ashing time (h)	Recovery (%)
Cabbage	100	450	24	99.6
		550	3	94.5
Beef	100	450	24	99.8
		500	8	97.1

Cabbage was homogenized using a Waring blender, transferred to a porcelain dish, mixed thoroughly with a quantity of Rb-86 tracer and dried at 100 °C prior to ashing in a muffle furnace. Beef was minced, mixed with a quantity of Rb-86 tracer, and treated in a similar manner.

Decomposition of Biological Materials. The loss of rubidium during dry ashing and the conventional procedure for removing silica using concentrated hydrochloric acid (Table 3) was compared with the loss during

TABLE 4. DETERMINATION OF RUBIDIUM IN NBS SRM 1577 BOVINE LIVER

Analysis number	Sample weight[a] (g)	Absorbance[b] (780.0 nm)	Concentration (μg Rb/g)	Content (μg Rb/g)	Certified value (μg Rb/g)
1	0.9221	0.093_8	1.71	18.6	
2	0.9659	0.098_9	1.81	18.7	
3	0.9146	0.092_8	1.69	18.5	18.3±1.0
4	0.9220	0.095_4	1.75	19.0	
5	0.9334	0.094_3	1.72	18.4	
				Mean ± s. d.	
				18.6 ± 0.20	

a) Dried at 90°C for 24 h. The ash was taken up in 10.00 cm^3 of 0.1 mol dm^{-3} HNO_3. b) Mean of five measurements with relative standard deviation of 0.6% for an approximately 10 s digital integration ("100 AVR").

acid digestion (the recovery found, 99.7%). No appreciable rubidium loss was found for dry ashing. When extremely accurate determinations are required, a temperature of 450 °C should be used.

Preparation of Samples. Fifty to two hundred grams of fresh vegetables and cerials were dried at 90 °C for 24 h and ashed. Silica was removed as usual. The edible parts of about 50 g of fresh fish and shellfish were selected and processed as stated above without the removal of silica. About 50 g of meat was processed in the same manner. Two hundred milliliters of milk was evaporated in a porcelain evaporating dish on a water bath and then ashed. Urine sampled for 24 h, about 1.5 dm^3, was digested by repeated treatment with concentrated nitric acid and 30% hydrogen peroxide with heating, then evaporated to dryness and dissolved with distilled water. Regarding human tissue, about 10 g of fresh material was used. Finally, sample solutions were adjusted to 0.1 mol dm^{-3} using nitric or hydrochloric acid and the content of potassium was determined by atomic absorption or by emission in order to confirm that the concentration was in the range of 1000 to 5000 μg cm^{-3}. As necessary, potassium was added to sample solutions.

Accuracy and Precision. A biological reference material, NBS SRM 1577 Bovine Liver, was analyzed and the results are summarized in Table 4. The sample solution contained roughly 1300 μg cm^{-3} of potassium. The analytical results were in good agreement with the certified value.

Rubidium Content of Biological Materials. Some analytical results for typical biological materials made using the present method are listed in Tables 5 and 6. The values of the rubidium content found for these samples were in the range from 0.4 to 7 μg/g fresh weight. Higher figures were found for meat and milk than those for vegetables and fish. This relationship was again found when the results were compared on a potassium weight basis: 2—3 μg-Rb/mg-K for meat and milk as compared to 0.2—0.6 μg-Rb/mg-K for vegetables and fish. Human lung, liver, and spleen were found to contain slightly higher concentrations than the other tissues examined. The Rb/K ratios fall in the range 1.5—3.5 μg-Rb/mg-K for human tissues. From these results it may be inferred that mammals including man concentrate rubidium more than potassium during the incorporation of these alkali metals from precursors.

Table 5. Analytical results for rubidium in food stuffs

Material	Rb concentration		
	mg/g ash	μg/g wet wt	μg/mg-K
Vegetable			
Spinach, leaf	0.187	2.61	0.603
Japanese radish, root	0.149	0.412	0.436
Japanese radish, leaf	0.101	1.65	0.404
Fish			
Carp	0.082	0.747	0.314
Saurel	0.050	0.968	0.280
Mackerel	0.076	0.968	0.263
Bonito	0.083	0.680	0.289
Tuna	0.083	0.643	0.278
Shellfish			
Tapes sp.	0.560		0.196
Pork	0.753	7.11	2.38
Milk, processed	0.555	4.02[a]	2.68

a) Equivalent to 1030 μg-Rb/dm^3 of milk.

The authors are grateful to Professor Y. Ohyagi of Chiba University for valuable discussions.

Table 6. Analytical results for rubidium in human organs and urine

Material	Subject		Rb concentration		
	Age	Sex	mg/g ash	μg/g wet wt	μg/mg-K
Lung	76	Male	0.472	5.05	3.49
Liver	76	Male	0.513	4.36	3.73
	73	Male	0.330	3.44	2.63
	24—81	F, M[a]			1.96±0.75
Kidney	38	Female	0.283		1.87
	79	Male	0.255		1.72
Spleen	38	Female	0.316		1.92
	79	Male	0.217		1.61
Pancreas	60	Male	0.555		3.01
Thyroid	24	Male	0.319		1.91
Diaphragm	55	Female	0.312		1.65
	[b]	Female	0.473		2.14
	24	Male	0.334		1.83
	79	Male	0.196		1.54
Small intestine	73	Male	0.559	1.61	3.38
	24—79	F, M[c]			1.94±0.55
Urine, 24-h	26	Male		1.40	1.80

a) Sample number: 8. b) Age not identified. c) Sample number: 8.

References

1) E. J. Underwood, "Trace Elements in Human and Animal Nutrition," 3rd ed, Academic Press, New York and London (1971), p. 446.
2) N. Yamagata, *J. Radiat. Res.*, **3**, 9 (1962).
3) N. Yamagata, *J. Radiat. Res.*, **3**, 158 (1962).
4) C. M. Lederer, J. M. Hollander, and I. Perlman, "Tables of Isotopes," 6th ed, John Wiley (1967).
5) H. Hamaguchi, "Ultra-trace Analysis 1—Geochemical Materials," Sangyo Tosho Publishing Co., Tokyo (1970), p. 195.
6) T. E. Shellenberger, P. E. Pyke, D. B. Parrish, and W. G. Schrenk, *Anal. Chem.*, **32**, 210 (1960).
7) M. C. Farquhar and J. A. Hill, *Anal. Chem.*, **34**, 222 (1962).
8) R. Mavrodineanu and H. Boiteux, "Flame Spectroscopy," John Wiley, New York (1965).
9) A. M. Ure and R. L. Mitchell, "Flame Emission and Atomic Absorption Spectrometry," Vol. 3, ed by J. A. Dean and T. C. Rains, Marcel Dekker, New York (1975), p. 19.
10) H. Kawamura *et al.*, unpublished data.
11) G. E. Janauer, F. R. Smith, and J. Mangan, *At. Absorption Newslett.*, **4**, 180 (1967).
12) H. Sanui and N. Pace, *Anal. Biochem.*, **24**, 330 (1968).
13) G. Tanaka, A. Tomikawa, H. Kawamura, and Y. Ohyagi, *Nippon Kagaku Kaishi*, **89**, 175 (1968).

A Temperature-Jump Study of the Formation Reactions of Nickel(II)–Pyridine Complexes in Aqueous Solutions

Kiyoshi TAMURA, Shoji HARADA,* and Tatsuya YASUNAGA*

Department of Chemistry, National Defense Academy, Hashirimizu, Yokosuka 239

**Department of Chemistry, Faculty of Science, Hiroshima University, Higashisenda-machi, Hiroshima 730*

(Received March 26, 1977)

A temperature-jump study reveals two relaxation phenomena in aqueous nickel(II)–pyridine solutions. One is observed in a metal-rich and low-concentration system, while the other is found only in a ligand-rich and high-concentration system. The relaxation processes are ascribed to the complex formation reactions:

$$Ni^{2+} + py \underset{k_{-1}}{\overset{k_1}{\rightleftharpoons}} Ni(py)^{2+} \quad \text{and} \quad Ni(py)_2^{2+} + py \underset{k_{-3}}{\overset{k_3}{\rightleftharpoons}} Ni(py)_3^{2+}$$

The rate constants reported are: 3.6×10^3 M^{-1} s^{-1} for k_1 and k_3, 37 s^{-1} for k_{-1}, and 760 s^{-1} for k_{-3}, at 25 °C. The effect of the coordinated pyridine molecules on the reactivity of the metal is discussed.

Considerable information now exists on the kinetics of the complex formation reactions of metal ions with organic and inorganic ligands.[1,2] In particular, much effort has been directed toward characterizing the solvent lifetimes within the inner coordination spheres of the metal ions. However, these studies have been concerned almost entirely with the formation reactions of mono-ligand complexes, and considerably less is known about the kinetics of multi-ligand complexes, in particular, of unidentate ligands. This is because a fundamental difficulty exists in these studies. For obtaining kinetic information on these complexes, experiments have to be made on solutions in a ligand-rich concentration range. However, this condition generally produces many kinds of complexes in solution and introduces a complication in reaction analysis.

In the present study, complex formation reactions in the aqueous nickel(II)–pyridine system were investigated to begin with. Although many studies[1,2] have been made on the kinetics of the reactions of Ni^{2+} with unidentate and multidentate heterocyclic amines, few systematic studies have been made on the nickel(II)–pyridine system, especially from the above point of view. Any information obtained will be helpful in elucidating the detailed reaction mechanism of the formation of multidentate complexes.

Experimental

Pyridine of a reagent grade was dried over KOH and distilled once. The other chemicals used were of a reagent grade and were used without further purification. Distilled water was degassed by boiling it immediately before use. Sample solutions were prepared by mixing appropriate amounts of aqueous stock solutions of $Ni(NO_3)_2$, pyridine and, when necessary, Bromothymol Blue as a colorimetric pH-indicator. The ionic strength, I, was brought to the desired level by the addition of KNO_3. The pH was adjusted by the addition of NaOH and/or HNO_3.

The temperature-jump apparatus used and the experimental procedure have been described elsewhere.[3] The only change in the apparatus was that the cathode follower previously used was replaced by a 1 : 1 probe (Iwatsu 117B2). This improvement has resulted in an increase in the signal-to-noise ratio by a factor of two. The relaxation measurement was carried out at 25±1 °C.

Results

The experimental conditions and the kinetic data obtained are summarized in Table 1. All the solutions studied showed a single relaxation phenomenon. The reciprocal relaxation times, τ_1^{-1} and τ_2^{-1}, quoted in Table 1 represent an average of at least four experiments. The maximum errors are about ±10 and 15%, respectively. As is shown in Table 1, the kinetic studies were carried out for two different concentration ranges.

Table 1. Kinetic data for the nickel–pyridine system at 25 °C[a]

ΣNi (M)	Σpy (M)	pH[b]	τ_1^{-1} (10^2 s^{-1})	τ_2^{-1} (10^2 s^{-1})
		I=0.10[c]		
0.00496	0.00102	7.04	0.573	
0.00496	0.00508	6.78	0.661	
0.00992	0.00254	7.23	0.711	
0.00992	0.0102	6.89	0.837	
0.0101	0.00102	7.13	0.727	
0.0149	0.0102	7.13	0.921	
0.0198	0.00102	7.12	1.11	
0.0198	0.00508	7.29	1.05	
0.0198	0.0203	6.75	1.09	
0.0198	0.0254	7.02	1.15	
0.0236	0.0242	7.16	1.18	
0.0248	0.0101	7.28	1.28	
		I=0.30		
0.100	0.154	6.90		9.0
0.100	0.206	6.87		11.2
0.100	0.257	6.89		13.4
0.100	0.257	6.51		11.7
0.100	0.257	5.96		11.0
0.100	0.309	6.89		14.0
0.100	0.360	6.89		14.7

a) The equilibrium constants used:[5] pK_H=5.44, $\log K_1$ =1.91, $\log K_2$ = 1.28, and $\log K_3$ = 0.52, at 25 °C and I=0.6. b) Converted to $[H^+]$ by the use of γ_H =0.825 and 0.806 at I=0.10 and 0.30, respectively. c) Solutions contain 2×10^{-5} M Bromothymol Blue indicator (pK_{In} = 7.10, I=0.1).[6]

One has relatively low concentrations, mostly in the metal-rich region (I=0.10), and the other, high concentrations in the ligand-rich region (I=0.30).

The low concentration system contained Bromothymol Blue indicator, and the temperature-jump relaxation phenomenon was observed by following the absorbance at the wavelength of 617 nm. A representative relaxation effect is shown in Fig. 1. Blank solutions of the nickel-indicator and pyridine-indicator systems showed no relaxation effect in the same time range.

On the other hand, the indicator method is not effective in the ligand-rich region, because the amplitude of the relaxation signal decreases with an increase in the concentration of pyridine. Therefore, the experiments in this region were carried out at high concentrations and without a pH-indicator. The wavelength of the observation was 605 nm, where the nickel–pyridine solution exhibits an absorbance maximum. Figure 2 shows a representative relaxation effect. A solution containing only 0.1 M $Ni(NO_3)_2$ at pH=6.8 showed no relaxation effect in the same time range.

The above results indicate that the relaxation times in Table 1 are really associated with nickel–pyridine interactions.

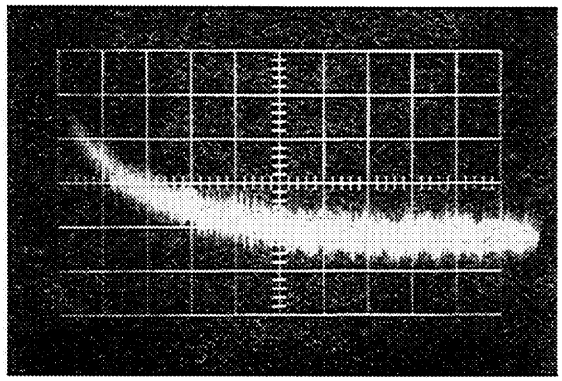

Fig. 1. Relaxation effect in nickel-pyridine system: $\Sigma Ni=9.92\times10^{-3}$ M, Σ py$=2.54\times10^{-3}$ M, pH=7.23, I=0.10 with 2×10^{-5} M Bromothymol Blue as an indicator. The abscissa scale is 10 ms per division, and the vertical scale is in arbitrary unit of absorbency. The relaxation effect corresponds to an increase in absorbance with time.

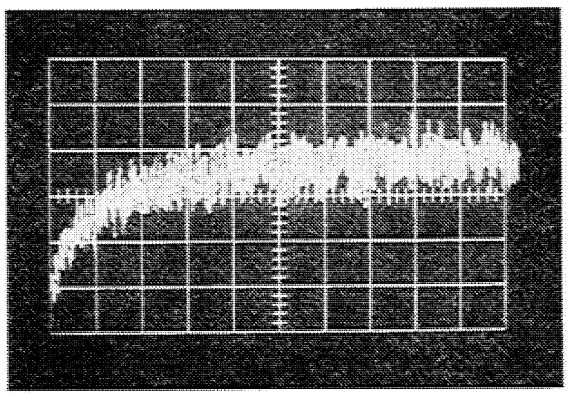

Fig. 2. Relaxation effect in nickel-pyridine system: Σ Ni$=0.100$ M, Σ py$=0.257$ M, pH=6.89, I=0.30. The abscissa scale is 0.5 ms per division, and the vertical scale is in arbitrary unit of absorbency. The relaxation effect corresponds to a decrease in absorbance with time.

Treatment of Data

Under the experimental conditions studied, the formation of nickel(II)–pyridine complexes may proceed most generally by the following reaction mechanism:

$$Hpy^+ \overset{\text{fast}}{\rightleftharpoons} H^+ + py \qquad K_H,$$

$$Ni^{2+} + py \underset{k_{-1}}{\overset{k_1}{\rightleftharpoons}} Ni(py)^{2+} \qquad K_1, \qquad (1)$$

$$Ni(py)^{2+} + py \underset{k_{-2}}{\overset{k_2}{\rightleftharpoons}} Ni(py)_2^{2+} \qquad K_2, \qquad (2)$$

$$Ni(py)_2^{2+} + py \underset{k_{-3}}{\overset{k_3}{\rightleftharpoons}} Ni(py)_3^{2+} \qquad K_3, \qquad (3)$$

where py denotes the pyridine molecule and where K_H, K_1, K_2, and K_3 are the equilibrium constants for the corresponding reactions. If the relaxation process is ascribed to one of the reactions, (1—3), the corresponding relaxation time is given by:

$$\frac{1}{\tau} = k_n\{[Ni(py)_{n-1}^{2+}] + [py]\} + k_{-n}, \quad n=1,\ 2,\ \text{or}\ 3, \qquad (4)$$

where the brackets indicate the molar concentration at equilibrium. The protolytic reactions of pyridine and the pH-indicator (when it is added in solution) reach equilibrium much faster than the metal complex reactions (1—3), and they can be assumed to be in equilibrium at all times. However, the contributions of these equilibria to the relaxation times can be ruled out under the experimental conditions studied,[4] and so this effect has been ignored in Eq. 4.

The equilibrium constants used are listed in the footnote of Table 1. The values of the constants at I=0.6 were used without further corrections to the present systems at I=0.10 and 0.30. This approximation may not cause serious errors in the results because of the charge types of the reactions concerned. The equilibrium concentrations of various species in solution were calculated from the ΣNi, Σpy, and pH values in Table 1 by using these equilibrium constants.

Table 1 shows the two concentration-dependent relaxation times (τ_1 and τ_2), which were observed in very different concentration ranges. Since these relaxation times could be ascribed to different processes, they will be discussed separately.

Low-concentration Time (τ_1). An examination of the equilibrium concentrations shows that the predominant species in the solution are Ni^{2+}, py, and $Ni(py)^{2+}$. Then, the relaxation process can be attributed primarily to the complexation reaction (1). As is shown in Fig. 3, a graph of τ_1^{-1} *vs.* $[Ni^{2+}]+[py]$ plot gives a straight line. The slope and intercept of this line correspond to the rate constants k_1 and k_{-1}, respectively. The ratio of these values, 97±13, conforms with the equilibrium constant for this process. The rate constants obtained are shown in Table 2.

High-concentration Time (τ_2). The relaxation time was observed only in the solutions at high nickel concentrations with a pyridine-rich region. When the concentration of pyridine decreases further than those

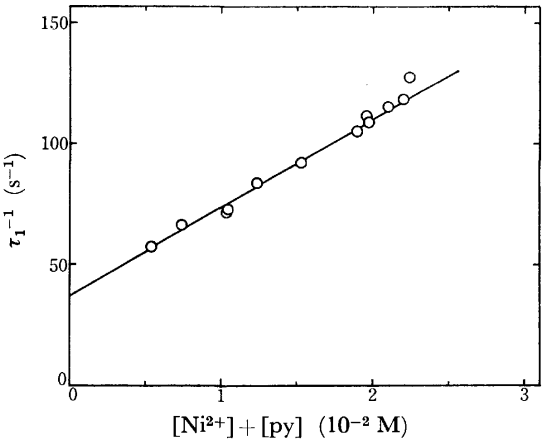

Fig. 3. $1/\tau_1$ *vs.* $[Ni^{2+}]+[py]$ plot of nickel-pyridine system at 25 °C, $I=0.10$.

Table 2. Kinetic results for the formation of nickel-pyridine complexes at 25 °C

n	$k_n(M^{-1}s^{-1})$	$k_{-n}(s^{-1})$
1	$(3.6\pm0.3)\times10^3$	37±4
3	$(3.6\pm1.5)\times10^3$	760±280

studied here, the amplitude of the relaxation effect decreases rapidly. This fact indicates that the relaxation process could not be ascribed to Reaction 1. In fact, the τ_1^{-1} value expected in this concentration range was estimated to be lower by a factor of 0.25—0.41 than the τ_2^{-1} value in Table 1. Therefore, the investigation was carried out by associating the relaxation process with one of the reactions, (2 or 3). By using Eq. 4, it was found that only the case of $n=3$ is consistent with the present data.[7] As is shown in Fig. 4, a graph of τ_2^{-1} *vs.* $[Ni(py)_2^{2+}]+[py]$ plot gives a straight line. From the slope and intercept of this line, the rate constants k_3 and k_{-3} were obtained; they are also shown in Table 2. The ratio of these values gives $K_3=4.7\pm2.7$, which is close to the corresponding value used.

In the system of interest here, an additional complication is introduced by the fact that the contribution of Reaction 2 to the relaxation process must be taken into account. By a relaxation treatment coupling the two reactions, (2 and 3), we obtain:[8]

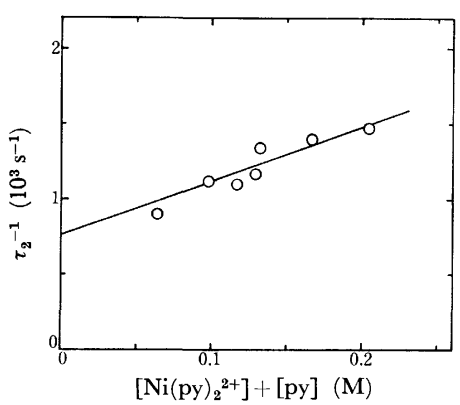

Fig. 4. $1/\tau_2$ *vs.* $[Ni(py)_2^{2+}]+[py]$ plot of nickel-pyridine system at 25 °C, $I=0.30$.

$$\frac{1}{\tau}=\frac{a_{11}+a_{22}}{2}+\left[\left(\frac{a_{11}-a_{22}}{2}\right)^2+a_{12}a_{21}\right]^{1/2}, \quad (5)$$

where $a_{11}=k_2\{[Ni(py)^{2+}]+[py]\}+k_{-2}$, $a_{12}=k_2[Ni(py)^{2+}]-k_{-2}$, $a_{21}=k_3\{[Ni(py)_2^{2+}]-[py]\}$, and $a_{22}=k_3\{[Ni(py)_2^{2+}]+[py]\}+k_{-3}$. The relaxation time was calculated by means of Eq. 5, with the k_3 and k_{-3} values in Table 2, together with appropriately assumed k_2 values and by use of the relation $k_{-2}=k_2/K_2$. Thus, the k_2 value in the range, $(2—5)\times10^3$ M^{-1} s^{-1}, is proven to affect the relaxation time only 8% at most. Therefore, the relaxation process can be ascribed solely to Reaction 3.

Discussion

The k_1 value in Table 2 is close to the corresponding rate constants reported for the reactions of Ni^{2+} with neutral unidentate ligands[1,2] and is also consistent with the first-order rate constant of the water exchange of the nickel ion measured by NMR.[9,10] This result indicates that the formation reaction of $Ni(py)^{2+}$ proceeds *via* the Eigen mechanism,[11] which involves the loss of a water molecule in the rate-determining step. Table 2 shows also that the value of k_3 is the same as that of k_1. This result leads one to conclude that the formation reaction of the $Ni(py)_3^{2+}$ complex proceeds by a mechanism similar to that cited above and that the rate of water release from $Ni(py)_2^{2+}$ is close to that of Ni^{2+}. This conclusion is similar to that already reached by Hammes and Steinfeld[8] for the consecutive formations of nickel(II)–imidazole complexes, although they obtained a slightly decreasing tendency of $k_1>k_2>k_3$.

On the other hand, the dissociation rate constants, k_{-1} and k_{-3}, are very different from each other; these values determine the corresponding stability constants of the complexes. It is interesting to note that the k_{-3} value is much higher than the k_{-1} value, even taking into account the fact that the chance of the liberation of a pyridine molecule from $Ni(py)_3^{2+}$ is three times larger than that from $Ni(py)^{2+}$. The conclusion remark is that the pyridine molecules coordinated to the nickel ion enormously enhance their own lability, but little affect the lability of the coordinated water molecules. This fact suggests that the crowding of the bulky ligand molecules in the inner coordination sphere loosens solely the Ni–N bonds and facilitates their rupture. The dissociation rate constants of the mono-, bis-, and tris-imidazole–nickel(II) complexes[8] and those of the mono- and tris-(2,2′-bipyridine)–nickel(II) complexes[12] also support this idea, although in the latter complexes the absolute values of the rate constants are extremely low as a result of the stabilization effect of chelation.

References

1) M. Eigen and R. G. Wilkins, *Adv. Chem. Ser.*, **49**, 55 (1964).

2) D. J. Hewkin and R. H. Prince, *Coord. Chem. Rev.*, **5**, 45 (1970).

3) K. Tamura, *Bull. Chem. Soc. Jpn.*, **46**, 1581, 3626 (1973).

4) By including the rapid protolytic reactions, the relaxation time is expressed by (Ref. 8): $1/\tau=k_n\{[Ni(py)_{n-1}^{2+}]/(1+\alpha)+[py]\}+k_{-n}$. However, the quantity α is less than 0.01

under the experimental conditions in Table 1 and can be ignored with respect to unity in the above expression.

5) M. S. Sun and D. G. Brewer, *Can. J. Chem.*, **45**, 2729 (1967).

6) I. M. Kolthoff, *J. Phys. Chem.*, **34**, 1466 (1930).

7) From a graph of τ_2^{-1} *vs.* $[Ni(py)^{2+}]+[py]$ plot, the k_2 and k_{-2} values were estimated to be $4.9\times10^3\ M^{-1}\ s^{-1}$ and $670\ s^{-1}$, respectively. However, the ratio of these values, 7.4, is very different from the equilibrium constant for Reaction 2.

8) G. G. Hammes and J. I. Steinfeld, *J. Am. Chem. Soc.*, **84**, 4639 (1962).

9) T. J. Swift and R. E. Connick, *J. Chem. Phys.*, **37**, 307 (1962).

10) R. E. Connick and D. Fiat, *J. Chem. Phys.*, **44**, 4103 (1966); T. J. Swift and G. P. Weinberger, *J. Am. Chem. Soc.*, **90**, 2023 (1968).

11) M. Eigen and L. De Maeyer, "Technique of Organic Chemistry," Vol. VIII, Part II, 2nd ed, ed by S. L. Friess, E. S. Lewis, and A. Weissberger, Interscience Publishers, Div., John Wiley & Sons, New York (1963), p. 1031.

12) R. H. Holyer, C. D. Hubbard, S. F. A. Kettle, and R. G. Wilkins, *Inorg. Chem.*, **4**, 929 (1965).

Transition-metal Complexes of Pyrrole Pigments. XIV.[1] An Electron Spin Resonance Study of Bis(3,3′,5,5′-tetramethyldipyrromethenato)manganese(II)†

Yoshihisa MATSUDA and Yukito MURAKAMI*

Department of Organic Synthesis, Faculty of Engineering, Kyushu University, Hakozaki, Higashi-ku, Fukuoka 812

(Received April 13, 1977)

Bis(3,3′,5,5′-tetramethyldipyrromethenato)manganese(II) in single crystalline and powdered sample states was investigated by means of K-band ESR spectroscopy. The spectral shape for the single crystal depends highly on the angle between the external magnetic field and the crystal axes. Anisotropic parameters D and E evaluated by the simulation method are 0.12 ± 0.01 and 0.032 ± 0.004 cm^{-1}, respectively. These values are considerably larger than those expected for the distorted tetrahedral manganese(II) complexes formed with four equivalent donor atoms. An origin of these large anisotropic parameters has been discussed.

Some bivalent and trivalent manganese complexes of dipyrromethenes were observed previously to show d→d transition bands of unusual high intensity.[2] The high transition probabilities can be attributed to mixing of the excited states of different spin-multiplicity into the ground electronic state through the simple spin-orbit coupling interaction, or else to the strong covalent interaction between manganese and aromatic nitrogen atoms. The ground state of high spin manganese(II) complexes should have d-electrons distributed in a manner of spherical symmetry, *i.e.*, it is in the sextet S-like state. Bis(3,3′,5,5′-tetramethyldipyrromethenato)-manganese(II) (**1**), referred to TMD-Mn(II) hereafter,

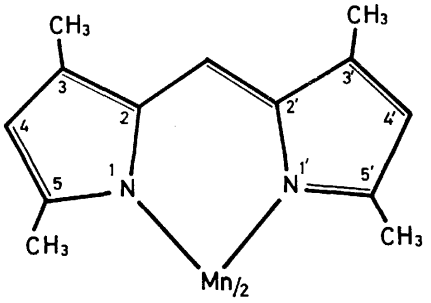

1

shows d→d bands of unusual high intensity ($\varepsilon\simeq160$) with some broadening.[2] This spectral feature indicates that the above mentioned effects are significant for the complex. The purpose of this paper is to discuss the electronic structure of TMD-Mn(II) and to characterize the anisotropic nature of the ground state by means of ESR spectroscopy applied to both single crystalline and powdered samples.

Experimental

The preparative procedure for TMD-Mn(II) has been reported previously.[2] Single crystals were grown by cooling down the saturated hexane solution from refluxing to room temperature.

ESR spectra were recorded on a JEOL JES-3K K-band spectrometer, equipped with a 100-kHz field modulation unit and with a modulation amplitude of 20 G, for both single

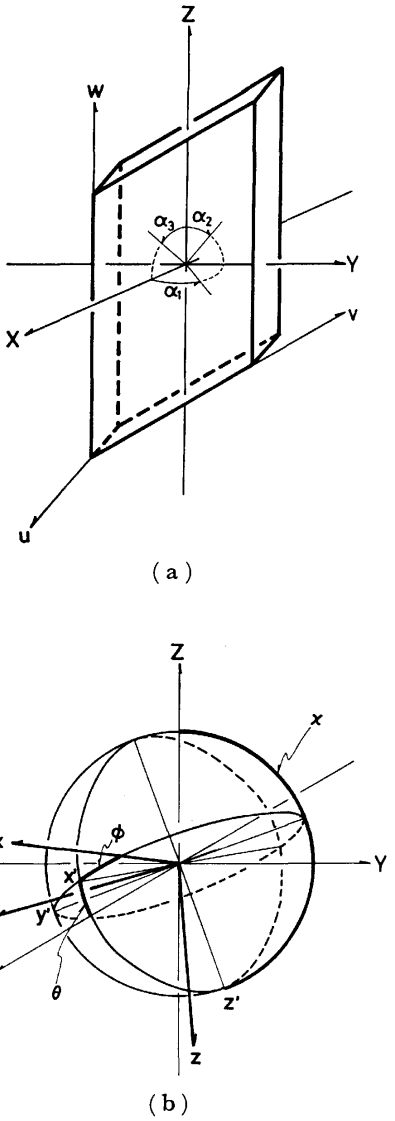

Fig. 1. (a) Correlation between crystal axes (u, v, and w) and experimental axes (X, Y, and Z) about which magnetic field is rotated: Z//w, X⊥vw-plane; α_1,α_2, and α_3 represent rotation angles about Z, X, and Y, respectively. (b) Correlation between molecular axes (x, y, and z) and coventional axes (X, Y, and Z) defined in Fig. 1a: rotations about X-, y′-, and z-axes by χ, θ, and ϕ (Eulerian angles), respectively, in this sequence convert X, Y, and Z coordinates to x, y, and z.

† Contribution No. 400 from this Department.

* To whom correspondence should be addressed.

crystalline and powdered samples. The manganese(II) ion diffused thermally into magnesium oxide was used to provide the reference signals for measurements. The lack of crystallographic data for the single crystal made it difficult to establish *a priori* the relevant axes for ESR measurements in connection with the molecular coordinates. The Cartesian coordinates X, Y, and Z were set up for convenience with respect to the rhombohedral single crystal as shown in Fig. 1a. The crystal axes u, v, and w, defined as shown in Fig. 1a, have no ordinary crystallographic meaning. The Z-axis is parallel to the w-axis, and the X-axis is perpendicular to the vw-plane, while the Y-axis is perpendicular to both X and Z. The single crystal was mounted on a sample holder in a manner that the magnetic field can be applied effectively in a direction perpendicular to one of X, Y, and Z axes, and rotations were performed about these axes for ESR measurements. The rotation angles about these axes (α_1, α_2, and α_3) are defined as shown in Fig. 1a.

Computational Procedures

The ordinary ESR signals for the d^5 system are interpreted by the spin Hamiltonian

$$\mathscr{H} = g\beta H\cdot S + D[S_z^2 - S(S+1)/3] + E[S_x^2 - S_y^2] + AS\cdot I + \text{higher order terms} \quad (1)$$

The contribution of higher order terms is usually very small, in fact confirmed to be so in this work, and can be neglected. In addition, the hyperfine term was neglected due to the absence of such hyperfine ESR structures for the present undiluted chelate system. Then, Eq. 1 is simplified as follows for the six spin states ($m_s = 5/2 \text{——} 5/2$)

$$\mathscr{H} = g\beta H\cdot S + D[S_z^2 - S(S+1)/3] + E[S_x^2 - S_y^2] \quad (2)$$

Computations were performed by substituting sets of D and E values of reasonable magnitude. The level splittings were evaluated by solving the Hamiltonian for every 10° of both Θ and Φ, where Θ and Φ are the polar angles for the direction of magnetic field in the molecular coordinate system (x, y, and z), and the magnetic field intensities at resonance were consequently obtained. The numerical calculations were carried out on a Facom 230-60 computer of the Computer Center of Kyushu University. The anisotropic parameters D and E were obtained roughly from comparison of the ESR spectrum for powdered sample and the calculated resonance positions for the applied magnetic field parallel to the anisotropic axes (molecular axes) as shown in Figs. 3 and 4. The D and E parameters were then reexamined whether or not one set of parameters allows the existence of the corresponding set of reasonable θ, ϕ, and χ values (Fig. 1b), which provide satisfactory elucidation of the ESR spectra for the single crystal.

Results

ESR spectra observed for the single crystal are shown in Fig. 2 for rotation about the Z-axis as an example. The spectra consist of a set of five strong peaks and some weaker ones. Consequently, it is obvious that manganese occupies only a single kind of coordination sites in the unit cell. The spectra depend highly on the rotation angles α_1, α_2, and α_3.

A spectrum for the powdered sample is given in Fig. 3. The spectrum showing a strong peak at $g_{eff} \simeq 2.0$ and weaker one at $g_{eff} \simeq 4.0$ is characteristic of those having anisotropic parameters $D \lesssim h\nu$ and $E \simeq 0.3D$, as clarified by Dowsing and Gibson.[3] The correlation between resonance position and E/D is illustrated in Fig. 4 for the cases that the magnetic field is applied parallel to the x, y, and z axes. Upon comparison of this with Fig. 3, the D and E/D values are estimated as 0.12 cm^{-1} and 0.25, respectively. Resonance positions for magnetic field parallel to the x, y, and z axes are given in Fig. 3 by arrows. The final D and E values evaluated by the computational procedure mentioned in the preceding section are 0.12 ± 0.01 and 0.032 ± 0.004 cm^{-1}, respectively (refer to Figs. 5 and 6).

The computational results due to the manipulation of Eq. 2 are given in Fig. 5 as the correlation between resonance magnetic field and polar coordinates Θ and Φ. The allowed transitions ($\Delta m_s = 1$) are denoted by solid lines, and the forbidden transitions with $\Delta m_s = 2$ and $\Delta m_s > 2$ are represented by broken lines, respectively.

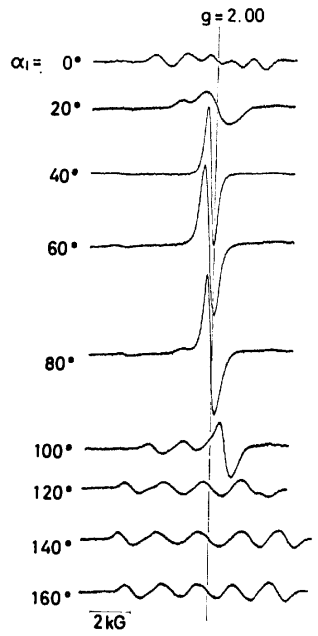

Fig. 2. Single crystal ESR spectra at room temperature (K-band): the magnetic field is rotated about the Z-axis (Fig. 1a) by α_1.

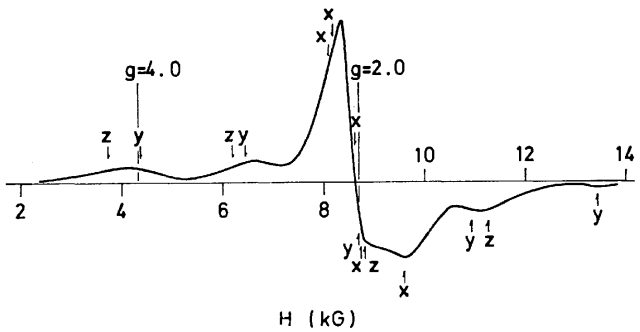

Fig. 3. K-band ESR spectrum of the powdered sample at room temperature. Arrows indicate the predicted resonance positions under the magnetic fields directed along the molecular axes (x, y, and z).

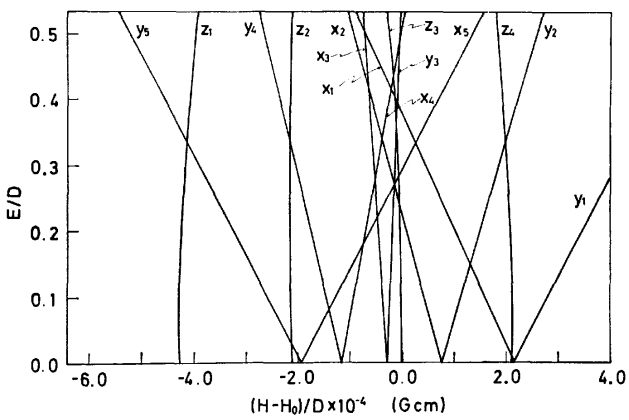

Fig. 4. Correlation between zero-field splitting parameters and resonance positions: $H_0=h\nu/g_0\beta$. Suffixed numbers refer to the transitions: 1, $-5/2\leftrightarrow-3/2$; 2, $-3/2\leftrightarrow-2/1$; 3, $-1/2\leftrightarrow1/2$; 4, $1/2\leftrightarrow3/2$; 5, $3/2\leftrightarrow5/2$.

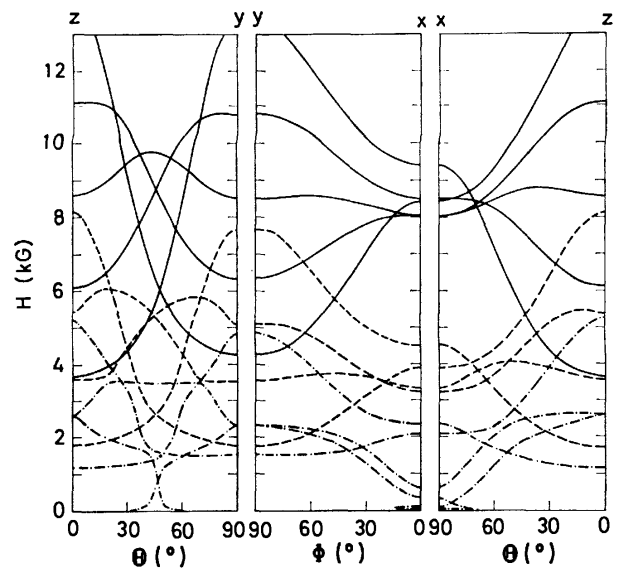

Fig. 5. Predicted ESR transitions for $S=5/2$ with $D=0.12$ cm^{-1}, $E=0.032$ cm^{-1}, and $h\nu=0.81$ cm^{-1}: ——, transitions for $\Delta m_s=1$; ----, transitions for $\Delta m_s=2$; —·—·, transitions for $\Delta m_s>2$.
θ, polar angle between z-axis and magnetic field; Φ, polar angle between x-axis and magnetic field projected on xy-plane.

Subsequently, the Eulerian angles θ, ϕ, and χ were evaluated as 7.7°, 43.3°, and 153.0°, respectively. The calculated correlations between resonance positions and rotation angles (α_1, α_2, and α_3) are illustrated in Fig. 6 along with the experimental results. The agreements between calculated and experimental data are quite satisfactory.

Discussion

Several investigators have reported on the coordination structures of manganese(II) complexes in which the central metal is subject to either regular or distorted tetrahedral ligand field. Since the bivalent manganese is in general favorably placed in the octahedral ligand field, the steric effect may provide primarily a cause for the tetrahedral coordination. Moreover, the distorted tetrahedral coordination is less common for this metal ion. Most of these distortions have been caused by the structural nature of host lattice, which gives a geometrically distorted configuration of four equivalent donor atoms.[4] The rest has been due to the intramolecular repulsive interaction among ligands, where the coordination of electronically different donor atoms takes place. In those cases, the configuration of donor atoms is close to the regular tetrahedron. The anisotropic parameters D and E for manganese(II) placed in those geometrically distorted ligand fields are very close to zero and the corresponding g-value is nearly the free electron value.[4]

On the other hand, the tetrahedral manganese(II) complexes are reported to be subject to the profoundly large anisotropy in a few cases.[5] In those cases, two kinds of electronically different donor atoms are involved for the formation of a complex. Nevertheless, the mechanism responsible for the occurrance of this large anisotropy has not been clearly elucidated. Some iron(III) complexes show anisotropy larger than manganese(II) complexes. Cole and Garrett studied the large anisotropy of the aquapentachloroiron(III) anion, and attributed the origin of the large D value to the tetragonal distortion of coordination geometry.[6]

Judging from the existence of nonzero D and E values, TMD-Mn(II) is obviously in a distorted tetrahedral coordination structure. The electronic property is, however, identical with each other among all the four nitrogen donor atoms due to the resonance interaction within each dipyrromethene molecule. In any case, the bulky methyl groups placed at the 5- and 5′-positions in the present ligand hinder the planar alignment of four nitrogen atoms. Since there is no significant steric reason against attaining the regular tetrahedral geometry, manganese(II) must assume this coordination geometry unless other factors come into play. When the coordinate bonds between manganese(II) and nitrogen atoms attain highly covalent character, the configuration of nitrogen donor atoms can be expected to deviate from the regular tetrahedron toward the planar structure. These effects have been observed for dipyrromethene complexes of transition metals having a partially filled d-shell.[7]

The small D and E values for the geometric distortion can be explained in terms of the splitting of the sextet ground state caused by higher order perturbation due to spin-orbit coupling. On the other hand, TMD-Mn(II) gained the uniquely large D and E values for the complex having four equivalent donor atoms. These large D and E values may be attributed to the strong σ-bonding interaction. The existence of profound σ-bonding between manganese and nitrogen atoms tends to distort the coordination geometry from tetrahedral toward tetragonal, causing the mixing of the excited quartet into the sextet ground state. The π-bonding interaction between the central metal atom and the ligand molecules may be partly responsible for such tetragonal distortion.

In conclusion, the eminent covalent interaction between manganese(II) and donor atoms caused the

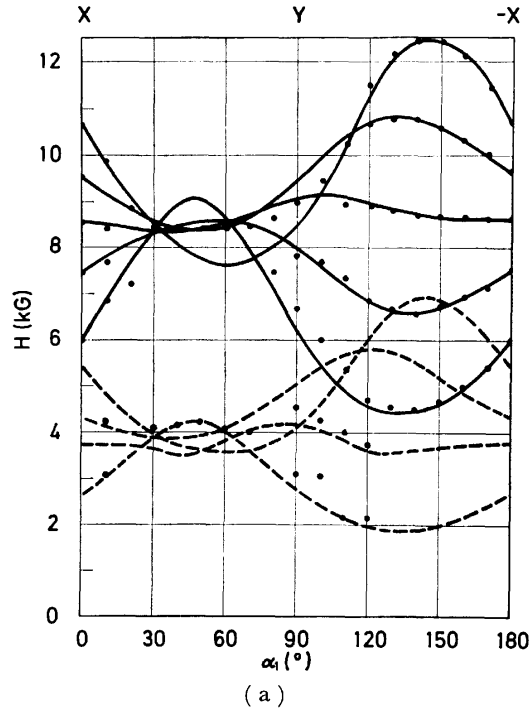

(a)

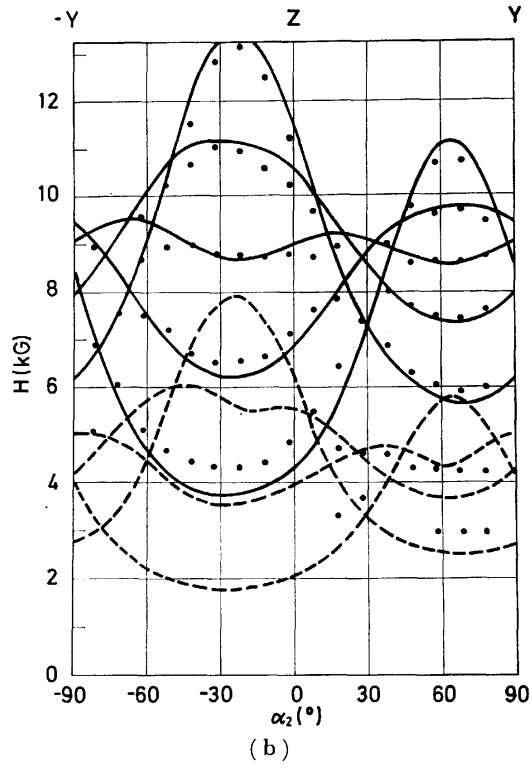

(b)

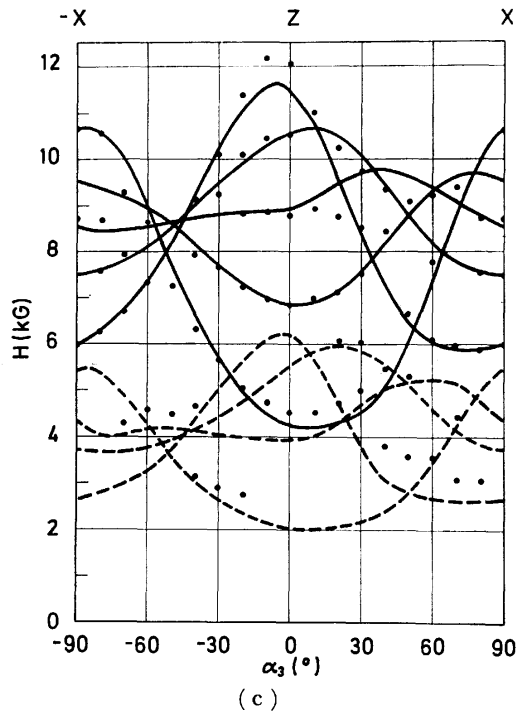

(c)

Fig. 6. Resonance positions for single crystal under the magnetic field rotated by α_1 (a), α_2 (b), and α_3 (c) (refer to Fig. 1a). Solid and broken lines denote the calculated resonance positions ($\Delta m_s = \pm 1$ and ± 2, respectively) for $D = 0.12$ cm^{-1}, $E = 0.032$ cm^{-1}, and $h\nu = 0.81$ cm^{-1}, and solid circles indicate the observed values.

distortion of ligand alignment from the regular tetrahedron, and gives out the nonspherical distribution of d-orbitals. The latter effect is accompanied with spin-orbit interaction with the excited configurations. This mechanism must be responsible for the profound anisotropy existing in the N_4-pseudotetrahedral manganese complex, as well as for the exceedingly high intensity of ligand field bands due to spin forbidden transitions.[2]

References

1) Part XIII: Y. Murakami and Y. Aoyama, *Bull. Chem. Soc. Jpn.*, **49**, 683 (1976).

2) Y. Murakami, K. Sakata, K. Harada, and Y. Matsuda, *Bull. Chem. Soc. Jpn.*, **47**, 3021 (1974).

3) R. D. Dowsing and J. F. Gibson, *J. Chem. Phys.*, **50**, 294 (1969).

4) For example: P. B. Dorain, *Phys. Rev.*, **112**, 1058 (1958).

5) R. D. Dowsing, J. F. Gibson, D. M. L. Goodgame, M. Goodgame, and P. J. Hayward, *J. Chem. Soc., A*, **1969**, 1242.

6) G. M. Cole, Jr. and B. B. Garrett, *Inorg. Chem.*, **13**, 2680 (1974).

7) (a) Y. Murakami, Y. Matsuda, and K. Sakata, *Inorg. Chem.*, **10**, 1728 (1971); (b) Y. Murakami, Y. Matsuda, and K. Sakata, *ibid.*, **10**, 1734 (1971).

Preparation and Resolution of a Complete Series of $[Co(en)_x(tn)_y(tmd)_z]^{3+}$ Complexes

Masaaki KOJIMA, Hiroyuki YAMADA, Hiroshi OGINO,* and Junnosuke FUJITA

Department of Chemistry, Faculty of Science, Nagoya University, Chikusa, Nagoya 464

**Department of Chemistry, Faculty of Science, Tohoku University, Aoba, Aramaki, Sendai 980*

(Received April 19, 1977)

A complete series of ten complexes, $[Co(en)_x(tn)_y(tmd)_z]^{3+}$ (en=ethylenediamine; tn=trimethylenediamine; tmd=tetramethylenediamine) was obtained by preparing four new complexes, $[Co(en)(tmd)_2]^{3+}$, $[Co(tn)_2(tmd)]^{3+}$, $[Co(tn)(tmd)_2]^{3+}$, and $[Co(en)(tn)(tmd)]^{3+}$. The new complexes were resolved into optical isomers by SP-Sephadex column chromatography. The absorption and circular dichroism spectra of all the complexes were recorded and discussed.

Ten complexes are expected for a series of complexes of the type, $[M(AA)_x(BB)_y(CC)_z]^{n+}$ (x, y, z=0, 1, 2, or 3; $x+y+z=3$), where AA, BB, and CC denote different bidentate ligands. However, no example of such a complete series has been reported. In a series of ten complexes, $[Co(en)_x(tn)_y(tmd)_z]^{3+}$ (en=ethylenediamine; tn=trimethylenediamine; tmd=tetramethylenediamine), there remain four unknown complexes, $[Co(en)(tmd)_2]^{3+}$, $[Co(tn)_2(tmd)]^{3+}$, $[Co(tn)(tmd)_2]^{3+}$, and $[Co(en)(tn)(tmd)]^{3+}$, all of which contain a seven membered chelate ring. Recently we prepared two tmd complexes, $[Co(en)_2(tmd)]^{3+}$ [1] and $[Co(tmd)_3]^{3+}$,[2] and resolved them into optical isomers. The en, tn, and tmd ligands are the most representative diamines which form a five-, six-, and seven-membered chelate ring, respectively. The collective data on a complete series of complexes of these diamines will be useful in elucidating such properties as the electronic state and the optical activity of a cobalt(III) complex. This paper is concerned with the preparation and resolution of the four unknown tmd complexes and with the comparison of absorption and circular dichroism spectra of all the complexes of the present series.

Experimental

Ligands. The ligands, en, tn, and tmd were obtained from Wako Pure Chemical Industries Co. and used without further purification.

$[Co(en)(tn)(tmd)]Cl_3\cdot 0.5H_2O$. To a solution of *trans*-$[CoCl_2(en)(tn)]ClO_4$[3] (2.0 g, 5.5 mmol) in *N,N*-dimethylformamide(DMF)(100 cm^3) was added a solution of tmd (0.5 g, 5.5 mmol) in DMF (100 cm^3), and the solution was stirred for 5 h at room temperature. The resultant reddish brown solution was diluted with a 10^{-2} M HCl solution, and passed through an SP-Sephadex column (ϕ 2.7×5 cm). A small portion of the Sephadex charged with the product was poured on the top of an SP-Sephadex column (ϕ 2.7×120 cm), and the adsorbed complexes were eluted with a 0.2 M Na_2SO_4 solution adjusted to pH 2 with HCl. The column showed six bands; pink (very small amount), pink, yellow, orange, violet, and red-violet bands from bottom to top of the column. The effluent of the fourth orange band was diluted with a 10^{-2} M HCl solution and poured again on an SP-Sephadex column (ϕ 1.5×3 cm). The adsorbed complex was eluted with a 1.0 M KBr solution adjusted to pH 2 with HBr, and the effluent was concentrated to dryness in a vacuum desiccator over P_2O_5–NaOH. The residue was extracted with methanol and the extract was mixed with diethyl ether to give an orange precipitate. The precipitate (crude complex bromide) was filtered off and dissolved in a small amount of 10^{-2} M HCl. To this solution was added a solution of $K_3[Co(CN)_6]$ in 10^{-2} M HCl to precipitate hardly soluble hexacyanocobaltate(III) salt of the complex. This salt was filtered off, washed with water, and mixed with the anion exchanger (BIORAD AG 1×8, 200—400 mesh, in the chloride form) in 10^{-2} M HCl. After the mixture had been stirred for several hours, the resin was filtered off, and the filtrate was passed through a column of the anion exchanger of the same type as the above to ensure the conversion into chloride. The effluent was evaporated to dryness under reduced pressure. Recrystallization from 10^{-2} M HCl by the addition of ethanol gave orange crystals. The yield depends on the purity of the starting material, *trans*-$[CoCl_2(en)(tn)]ClO_4$ which is usually contaminated with *trans*-$[CoCl_2(en)_2]ClO_4$ and *trans*-$[CoCl_2(tn)_2]ClO_4$.

Found: C, 27.24; H, 8.02; N, 20.92%. Calcd for $CoC_9H_{31}N_6O_{0.5}Cl_3$=$[Co(en)(tn)(tmd)]Cl_3\cdot 0.5H_2O$: C, 27.25; H, 7.88; N, 21.19%.

Resolution of $[Co(en)(tn)(tmd)]^{3+}$. A solution containing about 120 mg (0.3 mmol) of $[Co(en)(tn)(tmd)]Cl_3\cdot 0.5H_2O$ was poured on an SP-Sephadex column (ϕ 2.7×120 cm) and the adsorbed band was eluted with a 0.18 M sodium $(+)_{589}$-tartratoantimonate(III) solution. Two bands, the $(-)_{589}$- and $(+)_{589}$-isomers, were eluted in this order. Each isomer was isolated as bromide by the same method as that for the racemic complex chloride except that the anion exchanger was used in the bromide form. The complex was recrystallized from 10^{-2} M HBr by the addition of methanol. The complex chloride was hygroscopic. Found: C, 19.68; H, 5.79; N, 15.22%. Calcd for $CoC_9H_{34}N_6O_2Br_3$=$(+)_{589}$-$[Co(en)(tn)(tmd)]Br_3\cdot 2H_2O$: C, 19.41; H, 6.15; N, 15.09%.

$[Co(tn)_2(tmd)]Br_3\cdot 3.5H_2O$. To a solution of *trans*-$[CoCl_2(tn)_2]ClO_4$[4] (4.2 g, 11 mmol) in DMF (300 cm^3) was added a solution of tmd (1 g, 11 mmol) in DMF (200 cm^3) with stirring. The solution was stirred for 1 h at room temperature, and the product was chromatographed by a method similar to that for $[Co(en)(tn)(tmd)]^{3+}$. By developing the adsorbed band with a 0.2 M Na_2SO_4 solution adjusted to pH 2 with HCl, the column gave five bands, blue-violet, violet, reddish orange, violet, and pink in the order of elution. The effluent of the third reddish orange band was reloaded on an SP-Sephadex column (ϕ2.7×5 cm) after dilution with 10^{-2} M HCl. The adsorbed complex was eluted with a 1.0 M KBr solution adjusted to pH 2 with HBr. The eluate was concentrated to a small volume in a rotary evaporator, and the concentrate was kept in a refrigerator to give reddish orange crystals. These were filtered off, and recrystallized from 10^{-2} M HBr. Yield: about 50%. Found: C, 20.02; H, 6.17; N, 14.10%. Calcd for $CoC_{10}H_{39}N_6O_{3.5}Br_3$=$[Co(tn)_2(tmd)]Br_3\cdot 3.5H_2O$: C, 20.08; H, 6.57; N, 14.05%.

Resolution of $[Co(tn)_2(tmd)]^{3+}$. The resolution was

achieved by a method similar to that for $[Co(en)(tn)(tmd)]^{3+}$. The separation of optical isomers was incomplete, but the initial and the final fractions of the eluted complex showed negative and positive CD bands, respectively in the region of the first absorption band. The initial fractions of the effluent were collected, and chromatographed repeatedly until no further increase in dissymmetry factor ($\Delta\varepsilon/\varepsilon$) was observed. The isolation of the optical pure isomer was not attained, because of its small amounts. The quantitative CD curve of the complex was determined with the aid of the ε value of the racemate.

Preparation and Resolution of $[Co(en)(tmd)_2]^{3+}$. A solution of tmd (5.28 g, 60 mmol) and en (1.8 g, 30 mmol) in dimethyl sulfoxide (DMSO) (400 cm³) was added to a solution of $Co(NO_3)_2 \cdot 6H_2O$ (8.8 g, 30 mmol) and tmd·2HBr (3.75 g, 15 mmol) in DMSO (400 cm³) with stirring. The cobalt ions were oxidized by bubbling a stream of air through the solution for 9 h at room temperature. The resultant dark red solution was diluted with 10^{-2} M HCl and poured on SP-Sephadex. The adsorbed complexes were chromatographed by a method similar to that for $[Co(en)(tn)(tmd)]^{3+}$ with a 0.2 M Na_2SO_4 solution adjusted to pH 2 with HCl. The column gave nine bands; blue-violet, red, yellow, orange, pink, orange, pink, orange, and red-violet bands from bottom to top of the column. The effluent of the fourth orange band was a mixture of $[Co(en)(tmd)_2]^{3+}$ and other tris-diamine complexes as described below, and it was used for optical resolution without isolating the complex racemate. The effluent was reloaded on an SP-Sephadex column ($\phi 2.7 \times 120$ cm) after dilution with 10^{-2} M HCl, and the adsorbed band was eluted with a 0.15 M sodium $(+)_{589}$-tartratoantimonate(III) solution. The column gave four pairs of bands (Δ and Λ), yellow ($[Co(en)_3]^{3+}$), yellowish orange ($[Co(en)_2(tmd)]^{3+}$), orange ($[Co(en)(tmd)_2]^{3+}$), and orange (not characterized) bands in the order of elution. Each eluate of the third pair of the orange bands was passed through an SP-Sephadex column ($\phi 1.5 \times 3$ cm) after dilution with 10^{-2} M HCl and the adsorbed complex was eluted with a 1.0 M NaCl solution adjusted to pH 2 with HCl. The isomers were precipitated as hexacyanocobaltate(III) by the addition of $K_3[Co(CN)_6]$ in 10^{-2} M HCl. These salts were converted into chlorides by the use of the anion exchanger as described for $[Co(en)(tn)(tmd)]^{3+}$. Orange crystals were obtained by recrystallizing from 10^{-2} M HCl and methanol. Yield: about 1%. Found: C, 28.62; H, 8.16; N, 19.94%. Calcd for $CoC_{10}H_{34}N_6OCl_3 = (-)_{589}$-$[Co(en)(tmd)_2]Cl_3 \cdot H_2O$: C, 28.61; H, 8.11; N, 20.03%.

$[Co(tn)(tmd)_2]Cl_3$. To a solution of $Co(NO_3)_2 \cdot 6H_2O$ (8.8 g, 30 mmol) and tmd·2HBr (7.6 g, 30 mmol) in DMSO (800 cm³) were added a solution of tmd (6.68 g, 76 mmol) and tn (1.12 g, 15 mmol) in DMSO (1200 cm³) and active charcoal (1 g). The air oxidation of the cobalt ions was carried out for 50 h at room temperature. The reaction mixture was filtered to remove the charcoal. The filtrate was diluted with 10^{-2} M HCl and passed through an SP-Sephadex column ($\phi 7 \times 30$ cm). By developing the adsorbed band with a 0.5 M HCl solution, the column showed seven bands; violet, orange, blue-violet, red, blue-violet, reddish orange, and red-violet in the order of elution. The effluents of the first violet and the second orange bands were collected and reloaded on an SP-Sephadex column ($\phi 5.5 \times 30$ cm) after dilution with 10^{-2} M HCl, and the adsorbed band was eluted with a 0.2 M Na_2SO_4 solution adjusted to pH 2 with HCl. Five bands, violet, violet, orange, brown, and reddish brown were eluted in this order. The effluent of the third band was further loaded on an SP-Sephadex column ($\phi 2.7 \times 120$ cm) after dilution with 10^{-2} M HCl, and the adsorbed complexes were eluted with a 0.15 M sodium $(+)_{589}$-tartratoantimonate(III) solution. The column showed five separate bands; orange ($[Co(tn)_3]^{3+}$), reddish orange ($[Co(tn)_2(tmd)]^{3+}$), red ($[Co(tn)(tmd)_2]^{3+}$), and two purplish red ($(+)_{589}$- and $(-)_{589}$-$[Co(tmd)_3]^{3+}$) bands in the order of elution. The red crystals of $[Co(tn)(tmd)_2]Cl_3$ were obtained from the effluent of the third red band by a method similar to that for $[Co(en)(tn)(tmd)]^{3+}$. Yield: about 0.3%. Found: C, 31.38; H, 8.02; N, 20.22%. Calcd for $CoC_{11}H_{34}N_6Cl_3 = [Co(tn)(tmd)_2]Cl_3$: C, 31.78; H, 8.24; N, 20.22%.

Resolution of $[Co(tn)(tmd)_2]^{3+}$. The resolution was achieved by a method similar to that for $[Co(tn)_2(tmd)]^{3+}$. The bands of enantiomers were separated incompletely, so that the chromatography was repeated until no further increase in dissymmetry factor ($\Delta\varepsilon/\varepsilon$) was observed. No isolation of the isomer was made.

Resolution of $[Co(en)_2(tn)]^{3+}$ *and* $[Co(en)(tn)_2]^{3+}$. The racemic complexes were prepared by the method of Ogino and Fujita[5] and resolved by a method similar to that for $[Co(en)(tn)(tmd)]^{3+}$. The separation of bands of Δ- and Λ-$[Co(en)_2(tn)]^{3+}$ was complete, but that of Δ- and Λ-$[Co(en)(tn)_2]^{3+}$ was not, and the chromatography was repeated to obtain the optically pure isomer. Each isomer adsorbed on SP-Sephadex was eluted with a 1.5 M $NaClO_4$ solution and the effluent was evaporated in a vacuum desiccator over P_2O_5 to give orange crystals. These were recrystallized from a small amount of water by the addition of ethanol. Found: C, 14.32; H, 4.88; N, 14.31%. Calcd for $CoC_7H_{30}N_6O_{14}Cl_3 = (+)_{589}$-$[Co(en)_2(tn)](ClO_4)_3 \cdot 2H_2O$: C, 14.31; H, 5.15; N, 14.30%. Found: C, 17.13; H, 5.06; N, 14.93%. Calcd for $CoC_8H_{28}N_6O_{12}Cl_3 = (+)_{589}$-$[Co(en)(tn)_2](ClO_4)_3$: C, 16.99; H, 4.99; N, 14.86%.

Other complexes, $[Co(en)_3]^{3+}$, $[Co(en)_2(tmd)]^{3+}$, $[Co(tn)_3]^{3+}$, and $[Co(tmd)_3]^{3+}$ were prepared and resolved by the methods given in Table 1.

Measurements. Absorption and circular dichroism spectra were obtained on a Hitachi 323 spectrophotometer and a JASCO J-20 spectropolarimeter, respectively.

Results and Discussion

Preparation and Resolution of the Complexes. All of the new complexes contain the seven-membered chelate ligand. Since such large chelate ligands as tmd tend to coordinate to two metal ions to form polymeric complexes,[5] the reactions were carried out in dilute solutions as described in the Experimental part. Nonaqueous solvents such as DMSO are known to be useful for preparing complexes containing large chelate rings.[5] However, in the reactions of *trans*-$[CoCl_2(en)(tn)]^+$ or of *trans*-$[CoCl_2(tn)_2]^+$ with tmd in DMSO, a partial reduction of Co(III) to Co(II) takes place and disproportionation occurs to yield all possible complexes. Such a reduction may be avoided by use of DMF instead of DMSO, and no disproportionation is observed in the reactions. The perchlorates of the above dichloro complexes as well as the corresponding bis-en complex are fairly soluble in DMF and will be good starting materials for preparing mixed tris-diamine complexes. However, the reactions between *trans*-$[CoCl_2(en)_2]ClO_4$ and tn, and between *trans*-$[CoCl_2(tn)_2]ClO_4$ and en in DMF are accompanied by disproportionation, although no reduction seems to occur. For the preparation of both $[Co(en)(tmd)_2]^{3+}$ and $[Co(tn)(tmd)_2]^{3+}$, *trans*-$[CoCl_2(tmd)_2]^+$ should be useful as a starting material.

TABLE 1. DATA ON OPTICAL RESOLUTION OF $[Co(en)_x(tn)_y(tmd)_z]^{3+}$

Complex	SP-Sephadex column chromatography			Chemical resolution			X-Ray analysis	
	Faster moving isomer	Eluent	Ref.	Less soluble isomer	Resolv. agent	Ref.	Absolute config.	Ref.
$[Co(en)_3]^{3+}$	(+)*(*Λ*)	a	8)	(+)	d	9)	(+)-*Λ*	10)
$[Co(en)_2(tn)]^{3+}$	(+) (*Λ*)	b	This work	(+)	e	11)	(+)-*Λ*	12)
$[Co(en)(tn)_2]^{3+}$	(+) (*Λ*)	b	This work	(+)	e	11)		
$[Co(en)_2(tmd)]^{3+}$	(−) (*Λ*)	b	1)					
$[Co(tn)_3]^{3+}$	(−) (*Λ*)	c	6)	(−) (+)	e f	13) 14)	(−)-*Λ*	15)
$[Co(en)(tn)(tmd)]^{3+}$	(−) (*Λ*)	b	This work				(+)-*Δ*	16)
$[Co(en)(tmd)_2]^{3+}$	(−) (*Λ*)	b	This work					
$[Co(tn)_2(tmd)]^{3+}$	(+) (*Δ*)	b	This work					
$[Co(tn)(tmd)_2]^{3+}$	(+) (*Δ*)	b	This work					
$[Co(tmd)_3]^{3+}$	(+) (*Δ*)	b	2)	(−)	g	2)	(+)-*Δ*	17)

*: (+) or (−) at NaD line (589 nm); a: sodium $(+)_{589}$-tartrate; b: sodium $(+)_{589}$-tartratoantimonate(III); c: see the text; d: barium $(+)_{589}$-tartrate; e: sodium nitro-$(+)_{589}$-camphorate; f: $(-)_{589}$-K[As(cat)$_3$] (cat=catecholate ion=1,2-benzenediolate ion); g: silver $(+)_{589}$-tartratoantimonate(III).

However, this complex may be obtained only a little as a by-product in the preparation of $[Co(tmd)_3]^{3+}$.[2] Attempts to obtain this dichloro complex enough for reactions have all been unsuccessful. Hence, the two bis-tmd complexes of en or tn were prepared by oxidizing mixtures of Co(II) and the corresponding diamines in DMSO and isolated by the aid of SP-Sephadex column chromatography. The yields were extremely low, less than 1%. The same reactions in DMF result in the formation of hardly soluble black precipitates which appear to be a peroxo complex, and the reactions do not proceed further.

The complexes containing the tmd chelate ligand decompose gradually in neutral water, but stable in acidic solutions. The four new tmd complexes behave as monomeric tripositive ions in SP-Sephadex column chromatography; these complexes adsorbed on SP-Sephadex are easily eluted with 0.1—0.2 M Na_2SO_4 solutions.[5]

All the complexes, $[Co(en)_x(tn)_y(tmd)_z]^{3+}$ except $[Co(tn)_3]^{3+}$ can be resolved into their antipodes by SP-Sephadex column chromatography. By elution with sodium $(+)_{589}$-tartratoantimonate(III), the complexes containing the en ligand give *Λ* isomers first, while those of the series, $[Co(tn)_y(tmd)_z]^{3+}$, *Δ* isomers reversely. For $[Co(tn)_2(tmd)]^{3+}$ and $[Co(tn)(tmd)_2]^{3+}$, the separation of enantiomers on a column is insufficient, and repeated chromatography is necessary to obtain optically pure isomers. The $[Co(tn)_3]^{3+}$ complex cannot be resolved by SP-Sephadex column chromatography, but done completely by a modified Sephadex(D-$(-)_{589}$-tartrate form) column chromatography using a sodium L-$(+)_{589}$-tartrate solution as the eluent.[6] The data on optical resolution for all the complexes are given in Table 1.

Absorption and Circular Dichroism Spectra. Figures 1 to 4 show the absorption and circular dichroism spectra of the present series of complexes, $[Co(en)_x(tn)_y(tmd)_z]^{3+}$, and Table 2 lists the numerical data. Both the d-d and the charge-transfer absorption bands shift to longer wavelengths as the number of ring members

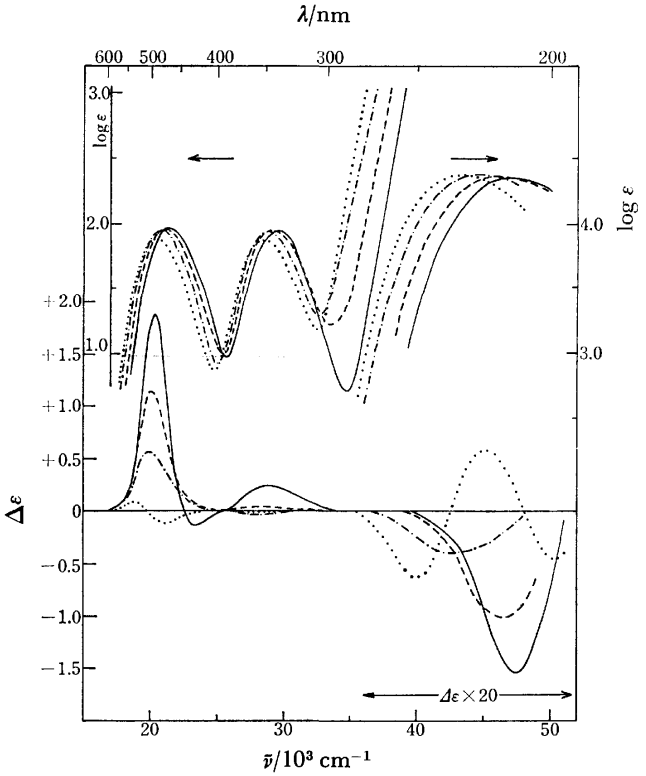

Fig. 1. Absorption and CD spectra of a series of *Λ*-$[Co(en)_x(tn)_y]^{3+}$ complexes; $(+)_{589}$-$[Co(en)_3]^{3+}$ (——), $(+)_{589}$-$[Co(en)_2(tn)]^{3+}$ (----), $(+)_{589}$-$[Co(en)(tn)_2]^{3+}$ (—·—), and $(-)_{589}$-$[Co(tn)_3]^{3+}$ (·····).

of the ligands increases. In Fig. 5 are plotted the maximum positions of these absorption bands against the number of ring members. The magnitude of shifts becomes smaller with increase in the number of ring members. In particular, the charge-transfer band of $[Co(tmd)_3]^{3+}$ shifts very little as compared with that of $[Co(tn)_3]^{3+}$, and those bands in the complexes, $[Co(tn)_y(tmd)_z]^{3+}$, are at nearly the same wavelengths. A similar shift of absorption bands due to the increase

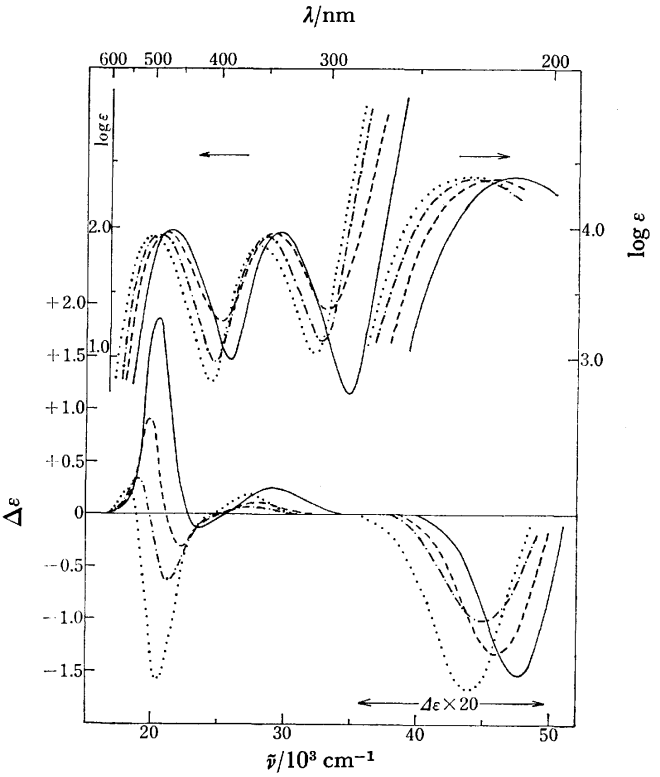

Fig. 2. Absorption and CD spectra of a series of Λ-$[Co(en)_x(tmd)_z]^{3+}$ complexes; $(+)_{589}$-$[Co(en)_3]^{3+}$ (——), $(-)_{589}$-$[Co(en)_2(tmd)]^{3+}$ (----), $(-)_{589}$-$[Co(en)(tmd)_2]^{3+}$ (—·—), and $(-)_{589}$-$[Co(tmd)_3]^{3+}$ (·····).

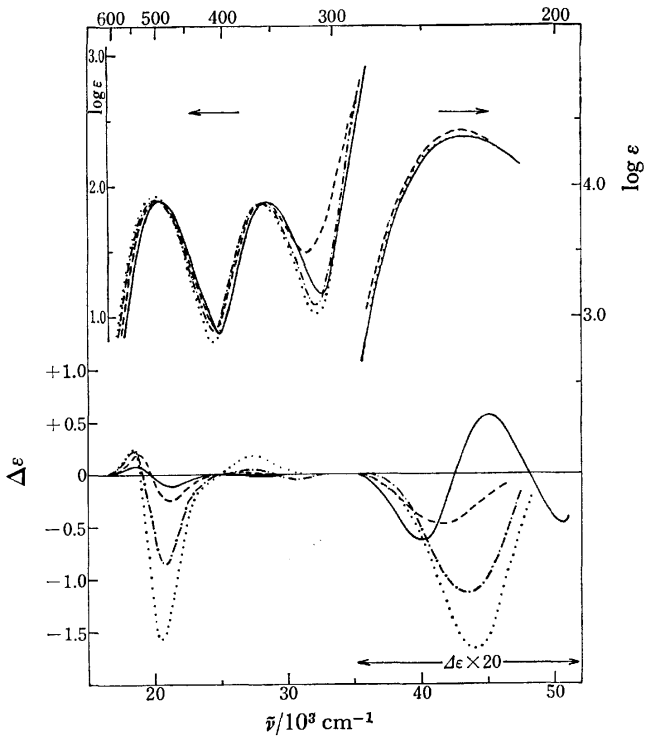

Fig. 3. Absorption and CD spectra of a series of Λ-$[Co(tn)_y(tmd)_z]^{3+}$ complexes; $(-)_{589}$-$[Co(tn)_3]^{3+}$ (——), $(-)_{589}$-$[Co(tn)_2(tmd)]^{3+}$ (----), $(-)_{589}$-$[Co(tn)(tmd)_2]^{3+}$ (—·—), and $(-)_{589}$-$[Co(tmd)_3]^{3+}$ (·····).

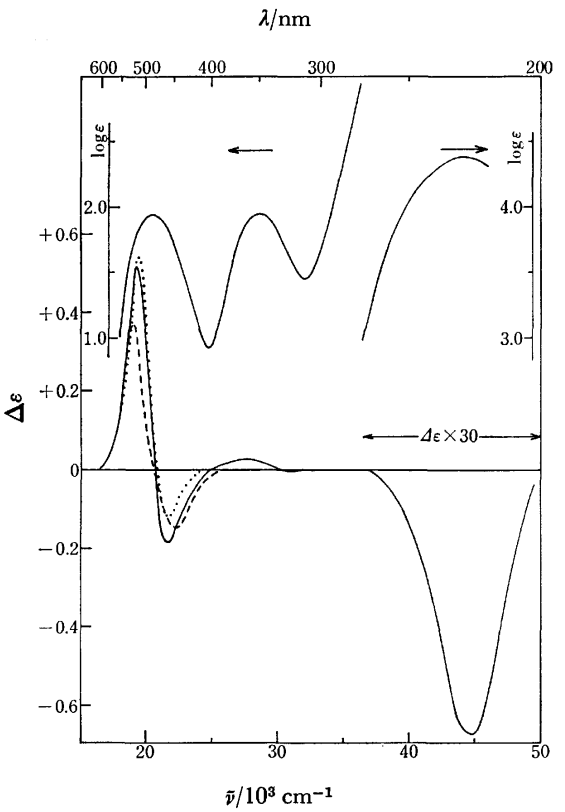

Fig. 4. Absorption and CD spectra of Λ-$(-)_{589}$-$[Co(en)(tn)(tmd)]^{3+}$ (——). Calculated CD curves of Λ-$[Co(en)(tn)(tmd)]^{3+}$ from $1/2\{\Lambda\text{-}[Co(en)_2(tn)]^{3+} + \Lambda\text{-}[Co(tn)_2(tmd)]^{3+} + \Lambda\text{-}[Co(en)(tmd)_2]^{3+}\} - 1/6\{\Lambda\text{-}[Co(en)_3]^{3+} + \Lambda\text{-}[Co(tn)_3]^{3+} + \Lambda\text{-}[Co(tmd)_3]^{3+}\}$ (·····) and $1/3\{\Lambda\text{-}[Co(en)_3]^{3+} + \Lambda\text{-}[Co(tn)_3]^{3+} + \Lambda\text{-}[Co(tmd)_3]^{3+}\}$ (----).

in the ring members was observed for the complexes of the type, $[Co(am)(en)_2]^{2+}$ (am=amino acidate ion); the first absorption bands of $[Co(gly)(en)_2]^{2+}$, $[Co(\beta\text{-ala})(en)_2]^{2+}$, and $[Co(amb)(en)_2]^{2+}$ (amb=4-aminobutanoic acidate ion) are at 20.5, 20.2, and 19.8×10^3 cm^{-1}, respectively.[7]

Although accurate intensity of absorption bands may be determined with difficulty, the apparent intensities (not band area) of the first absorption bands decrease in the order of the complexes of the ligands, en>tmd>tn; the intensities are not proportional to the number of ring members. Such a regular trend is not seen for the second and the charge-transfer absorption bands.

Figures 1—3 show the circular dichroism spectra of three series of complexes, $[Co(en)_x(tn)_y]^{3+}$, $[Co(en)_x(tmd)_z]^{3+}$, and $[Co(tn)_y(tmd)_z]^{3+}$, respectively. Of these complexes, the absolute configurations of $(+)_{589}$-$[Co(en)_3]^{3+}$, $(-)_{589}$-$[Co(tn)_3]^{3+}$, $(+)_{589}$-$[Co(en)_2(tn)]^{3+}$, and $(+)_{589}$-$[Co(tmd)_3]^{3+}$ have been determined by X-ray work to be Λ, Λ, Λ, and Λ, respectively (Table 1). Since the CD spectra of each series show a gradual change in the region of the first absorption band, the configurations of the other complexes shown in Figs. 1—3 can be assigned to Λ. The signs of the main CD bands in this region depend on the number of ring members. However, these nine complexes exhibit all positive CD components at a longer wavelength side

Table 2. Absorption and CD spectral data

Complex	Absorption		CD			
			in water		in 0.2 M Na_2SO_4	
	$\tilde{\nu}/10^3$ cm^{-1}	log ε	$\tilde{\nu}/10^3$ cm^{-1}	$\Delta\varepsilon$	$\tilde{\nu}/10^3$ cm^{-1}	$\Delta\varepsilon$
$(+)_{589}$-$[Co(en)_3]^{3+}$	21.4	1.97	20.4	+1.89	20.3	+1.84
			23.3	−0.12	23.0	−0.36
	29.5	1.93	28.6	+0.25		
	47.1	4.36	47.4	−31		
$(+)_{589}$-$[Co(en)_2(tn)]^{3+}$	21·1	1.96	20.2	+1.14	20.0	+0.98
					22.8	−0.084
	29.2	1.95	27.6	+0.038		
	45.7	4.35	46.5	−20		
$(+)_{589}$-$[Co(en)(tn)_2]^{3+}$	20.7	1.94	19.9	+0.57	19.6	+0.38
					22.9	−0.010
	28.7	1.94	28.2	−0.038		
	44.4	4.37	42.6	−7.9		
$(-)_{589}$-$[Co(en)_2(tmd)]^{3+}$	21.0	1.95	19.7	+0.88	19.6	+0.66
			22.2	−0.33	21.8	−0.65
	29.1	1.94	27.8	+0.11		
	45.5	4.35	46.1	−27		
$(-)_{589}$-$[Co(tn)_3]^{3+}$	20.4	1.88	18.8	+0.083	18.1	+0.023
			21.1	−0.11	20.7	−0.31
	28.5	1.88	28.4	−0.018		
	43.3	4.38	40.0	−13		
			45.3	+12		
			50.5	−9.1		
$(-)_{589}$-$[Co(en)(tn)(tmd)]^{3+}$	20.6	1.95	19.3	+0.51	19.1	+0.35
			21.9	−0.19	21.4	−0.56
	28.6	1.94	27.4	+0.026		
	44.2	4.38	44.8	−20		
$(-)_{589}$-$[Co(en)(tmd)_2]^{3+}$	20.4	1.94	19.0	+0.34	18.7	+0.18
			21.2	−0.64	21.0	−0.94
	28.4	1.91	27.4	+0.061		
	44.1	4.37	45.0	−20		
$(-)_{589}$-$[Co(tn)_2(tmd)]^{3+}$	20.2	1.89	18.8	+0.19	19.5	+0.099
			21.1	−0.24	20.8	−0.44
	28.2	1.87	27.0	+0.01		
			30.3	−0.044		
	43.1	4.41	41.8	−9.4		
$(-)_{589}$-$[Co(tn)(tmd)_2]^{3+}$	20.1	1.90	18.5	+0.22	18.1	+0.050
			20.7	−0.87	20.6	−0.94
	28.2	1.86	27.0	+0.04		
			31.3	−0.04		
	43.1	4.40	43.3	−23		
$(-)_{589}$-$[Co(tmd)_3]^{3+}$	19.9	1.92	18.4	+0.24	17.8	+0.03
			20.5	−1.56	20.3	−2.20
	28.0	1.87	27.4	+0.18		
	43.1	4.38	43.9	−33		

of the first absorption band. The strengths of these components are diminished in the presence of Na_2SO_4, and complementarily the negative CD components are enhanced (Table 2). The signs of the CD bands at the longest wavelengths in the charge-transfer region are all negative. All these observations have been reported for some complexes of the present series (Table 1). The CD spectrum of $(-)_{589}$-$[Co(en)(tn)(tmd)]^{3+}$ shown in Fig. 4 satisfies the above observations, and can be assigned to the same absolute configuration, *A*. The gradual changes of the CD spectra shown in Figs. 1—3 indicate that the CD spectrum of a mixed tris-diamine complex in the region of the first absorption band can be approximated by a sum of the contributions from three pairs of the chelate rings in chiral configuration. For example, the CD curve of [Co(en)(tn)-

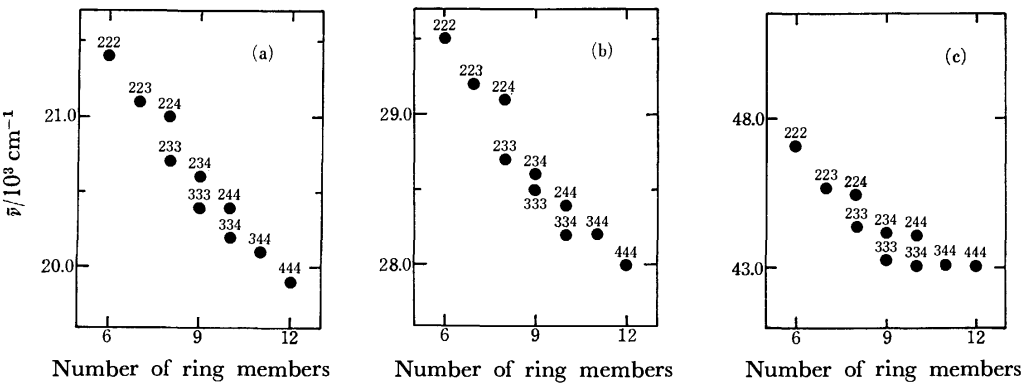

Fig. 5. Positions of (a) the first, (b) the second, and (c) the charge-transfer absorption bands of $[Co(en)_x(tn)_y(tmd)_z]^{3+}$. In the Figs. 2, 3, and 4 indicate en, tn, and tmd in the complex, respectively. For example, 234 denotes $[Co(en)(tn)(tmd)]^{3+}$.

$(tmd)]^{3+}$ which involves three pairs of chiral configurations, en-tn, en-tmd, and tn-tmd may be evaluated from the observed CD spectra of the following six complexes; $[Co(en)(tn)(tmd)]^{3+}=1/2\{[Co(en)_2(tn)]^{3+}+[Co(tn)_2(tmd)]^{3+}+[Co(en)(tmd)_2]^{3+}\}-1/6\{[Co(en)_3]^{3+}+[Co(tn)_3]^{3+}+[Co(tmd)_3]^{3+}\}$. The calculated CD curve of $[Co(en)(tn)(tmd)]^{3+}$ shown in Fig. 4 agrees well with the observed one. If the CD spectrum of a tris-chelate complex can be approximated by a sum of the contributions from each chelate ring, the CD curve of $[Co(en)(tn)(tmd)]^{3+}$ is obtained by the following equation; $[Co(en)(tn)(tmd)]^{3+}=1/3\{[Co(en)_3]^{3+}+[Co(tn)_3]^{3+}+[Co(tmd)_3]^{3+}\}$(or $1/3\{[Co(en)_2(tn)]^{3+}+[Co(tn)_2(tmd)]^{3+}+[Co(en)(tmd)_2]^{3+}\}$). The calculated CD curve is also given in Fig. 4. This curve agrees less satisfactorily with the observed spectrum compared with that approximated by the sum of the contributions of three pairs of the chelate rings.

References

1) H. Ogino and J. Fujita, *Chem. Lett.*, **1973**, 517.
2) J. Fujita and H. Ogino, *Chem. Lett.*, **1974**, 57.
3) M. C. Couldwell, D. A. House, and H. K. J. Powell, *Inorg. Chem.*, **12**, 627 (1973).
4) M. Linhard and G. Stirn, *Z. Anorg. Allg. Chem.*, **268**, 105 (1952).
5) H. Ogino and J. Fujita, *Bull. Chem. Soc. Jpn.*, **48**, 1836 (1975).
6) M. Fujita, Y. Yoshikawa, and H. Yamatera, *J. Chem. Soc., Chem. Commun.*, **1975**, 941.
7) M. Kojima, H. Takayanagi, and J. Fujita, *Bull. Chem. Soc. Jpn.*, **50**, 1891 (1977).
8) Y. Yoshikawa and K. Yamasaki, *Inorg. Nucl. Chem. Lett.*, **6**, 523 (1970).
9) *Inorg. Synth.*, **6**, 183 (1960).
10) Y. Saito, K. Nakatsu, M. Shiro, and H. Kuroya, *Acta Crystallogr.*, **8**, 729 (1955).
11) O. Bang, A. Engberg, K. Rasmussen, and F. Woldbye, *Acta Chem. Scand.*, **A29**, 749 (1975).
12) H. V. F. Schousboe-Jensen, *Acta Chem. Scand.*, **26**, 3413 (1972).
13) F. Woldbye, *Record of Chemical Progress*, **24**, 197 (1963).
14) R. R. Judkins and J. Royer, *Inorg. Chem.*, **13**, 945 (1974).
15) T. Nomura, F. Marumo, and Y. Saito, *Bull. Chem. Soc. Jpn.*, **42**, 1016 (1969).
16) Y. Saito, private communication.
17) S. Sato and Y. Saito, *Acta Crystallogr., Sect. B*, **31**, 1378 (1975).

Circular Dichroism Spectra of Cobalt(III)–Ammine Complexes Containing Optically Active 1,3-Diphenyl-1,3-propanediamine or 1,2-Diphenyl-1,2-ethanediamine*

Sumio Arakawa, Kazuo Kashiwabara,** Junnosuke Fujita,** and Kazuo Saito

Department of Chemistry, Faculty of Science, Tohoku University, Aramaki, Sendai 980

***Department of Chemistry, Faculty of Science, Nagoya University, Nagoya 464*

(Received April 25, 1977)

A series of optically active cobalt(III) ammine complexes containing (*S,S*)-1,3-diphenyl-1,3-propanediamine (dppn) or (*S,S*)-1,2-diphenyl-1,2-ethanediamine (stien) were prepared. The sign of circular dichroism (CD) of $[Co(NH_3)_4(S,S\text{-dppn})]Br_3$ depends on solvents in the first absorption band region. The CD magnitude of *trans*-$[Co(NH_3)_2(S,S\text{-dppn})_2]^{3+}$ varies significantly with solvent variations in the same energy region. The CD curve of the vicinal effect of (*S,S*)-dppn derived from the two diastereomers of *cis*-$[Co(NH_3)_2(S,S\text{-dppn})_2]^{3+}$ is different from the CD spectra of both $[Co(NH_3)_4(S,S\text{-dppn})]^{3+}$ and *trans*-$[Co(NH_3)_2(S,S\text{-dppn})_2]^{3+}$. The CD spectra of the (*S,S*)-stien complexes are insensitive to solvent variations and the vicinal contributions of the (*S,S*)-stien calculated from a variety of the (*S,S*)-stien complexes are similar to one another.

It has been suggested that circular dichroism (CD) of metal complexes are sensitive to environment around a metal ion, *i.e.* conformational change of ligands, the deviation of ligating atoms from the octahedral positions, and interactions between solute and solvent. Recently, cobalt(III) complexes containing six-membered chelate rings have been investigated to show remarkable variations in CD spectra with change in solvent.[1–3] These variations have been primarily ascribed to the flexibility of six-membered chelate rings.

Such a conformational flexibility will differ depending on the kind of substituent on six-membered chelate rings. In a previous paper,[4] we have reported that the CD sign of $[Co(NH_3)_4(S,S\text{-dppn})]Br_3$ in water is opposite to that of $[Co(NH_3)_4(R,R\text{-ptn})](ClO_4)_3$(*R,R*-ptn=(*R,R*)-2,4-pentanediamine) in water in the first absorption band region, although both the diamine ligands are expected to have the same λ-skew conformation. In order to investigate further detailed features of the dppn chelate ligand, we have prepared a series of complexes of the type $[Co(NH_3)_{2n}(S,S\text{-dppn})_{3-n}]^{3+}(n=0, 1, 2)$. This paper will report the preparation and the CD spectra of these complexes together with those of the corresponding (*S,S*)-1,2-diphenyl-1,2-ethanediamine (stien) complexes.

Experimental

Preparation of Ligands. The optically active diamines used were prepared by the methods previously reported; (*S,S*)-dppn[4] and (*S,S*)-stien.[5]

Preparation of the Complexes. *(1)* $[Co(NH_3)_4(S,S\text{-}dppn)]Br_3\cdot H_2O$: Method 1). Sodium hydroxide (2 g) in water (5 cm³) was added dropwise to a suspension of (−)$_D$-dppn-di-*O*-benzoyltartrate (0.6 g) in cold water (5 cm³). The released dppn was extracted with chloroform (20 cm³). After removal of the chloroform under reduced pressure, the oily residue was dissolved in 5 cm³ of dimethyl sulfoxide (DMSO). The solution was mixed with a DMSO solution (10 cm³) of $[Co(NH_3)_5(H_2O)](ClO_4)_3$ (0.46 g) and allowed to stand at room temperature for 10 h with stirring. The resultant solution was passed through a column ($\phi 3\times 20$ cm) of an SP-Sephadex ion exchanger. After washing with water, the adsorbed band was eluted with a 0.5 M aqueous solution of potassium bromide. The first eluted orange yellow band was $[Co(NH_3)_6]^{3+}$. The second orange yellow eluate was concentrated to give orange crystals, which were recrystallized from warm water (50 °C) acidified with a few drops of 60% hydrobromic acid. Yield; 0.1 g. Found: C; 29.67, H; 5.36, N, 13.78%. Calcd for $[Co(NH_3)_4(S,S\text{-dppn})]Br_3\cdot H_2O$ ($C_{15}H_{32}N_6OBr_3Co$): C; 29.48, H; 5.28, N; 13.76%.

Method 2). A DMSO solution (30 cm³) of racemic dppn (1.4 g) was added to a DMSO solution (50 cm³) of $[Co(NH_3)_5(H_2O)](ClO_4)_3$ (2.3 g). The solution was allowed to stand at 50 °C for 4 h with stirring, diluted to 1 dm³ with water and acidified with concd hydrochloric acid. A red precipitate of by-products was filtered off and the orange filtrate was passed through a column ($\phi 5\times 30$ cm) of an SP-Sephadex C-25 ion exchanger. After washing with water, the adsorbed band was eluted with a 0.3 M aqueous solution of potassium bromide. The orange yellow eluate was concentrated to give orange crystals, which were recrystallized from water (25 cm³) by adding ethanol (25 cm³) and by cooling the solution in a refrigerator. Yield: 0.9 g. Found: C; 28.98, H; 5.36, N; 13.63%. Calcd for $[Co(NH_3)_4(dppn)]Br_3\cdot 1.5H_2O$ ($C_{15}H_{33}N_6O_{1.5}Br_3Co$): C; 29.05, H; 5.36, N; 13.55%.

An aqueous solution of the orange yellow crystals was passed through a column ($\phi 4\times 60$ cm) of an SP-Sephadex C-25 ion exchanger. After washing with water, the adsorbed band was eluted with a 0.36 M aqueous solution of sodium (+)$_D$-tartratoantimonate(III). When the adsorbed band was separated into two bands, the eluent was changed to a 0.3 M aqueous solution of potassium bromide. The first eluted orange yellow band was concentrated to give orange crystals, which were the same compound as that prepared by method 1) on the basis of the elemental analysis and the CD spectra. Found: C; 29.24, H; 5.31, N; 13.90%.

The second orange yellow eluate was concentrated to give crystals, the CD spectrum of which is mirror image of that of the first eluted complex. Found: C; 29.47, H; 5.29, N; 14.00%. Calcd for $[Co(NH_3)_4(dppn)]Br_3\cdot H_2O$($C_{15}H_{32}N_6OBr_3Co$): C; 29.48, H; 5.28, N: 13.76%.

(2) $[Co(NH_3)_4(R,S\text{-}dppn)]Br_3$: A DMSO solution (5 cm³) of (*R,S*)-dppn prepared from (*R,S*)-dppn·2HCl (1.6 g) was mixed with a DMSO solution (20 cm³) of $[Co(NH_3)_5(H_2O)](ClO_4)_3$ (2.3 g). The resultant solution was warmed at 70 °C for 10 min with stirring, diluted with water (100 cm³) and acidified with concd hydrochloric acid. A red orange precipitate of by-products was filtered off and the orange filtrate was

* A part of the Ph.D. thesis submitted by S. Arakawa to Tohoku University, 1976.

passed through a column ($\phi 5 \times 30$ cm) of an SP-Sephadex C-25 ion exchanger. After washing with water, the adsorbed band was eluted with a 0.3 M aqueous solution of potassium bromide. The first eluted orange band was $[Co(NH_3)_6]^{3+}$. The second orange eluate was concentrated to give orange crystals, which were recrystallized from hot water (200 cm^3) acidified with a few drops of 47% hydrobromic acid. Yield; 0.7 g. Found: C; 29.98, H; 5.38, N; 13.39%. Calcd for $[Co(NH_3)_4(R,S\text{-dppn})]Br_3 \cdot H_2O$ ($C_{15}H_{32}N_6OBr_3Co$): C; 29.48, H; 5.28, N; 13.76%.

(3) $[Co(NH_3)_4(S,S\text{-}stien)](ClO_4)_3 \cdot 4H_2O$: (*S,S*)-Stien (1.0 g) was added to a DMSO solution (50 cm^3) of $[Co(NH_3)_5(H_2O)](ClO_4)_3$ (2.24 g). The resultant solution was allowed to stand at room temperature for 20 h, and passed through a column ($\phi 5 \times 30$ cm) of an SP-Sephadex C-25 ion exchanger. After washing with water, the adsorbed band was eluted with a 0.5 M aqueous solution of sodium perchlorate. The first eluted red band was $[Co(NH_3)_5(H_2O)]^{3+}$. The second yellow orange eluate was concentrated to give orange crystals, which were recrystallized from ethanol. Yield; 0.4 g. Found: C; 23.99, H; 5.00, N; 11.39%. Calcd for $[Co(NH_3)_4(S,S\text{-stien})](ClO_4)_3 \cdot 4H_2O$ ($C_{14}H_{36}N_6O_{16}Cl_3Co$): C; 23.69, H; 5.11, N; 11.84%.

(4) trans- *and* cis-$[Co(NH_3)_2(S,S\text{-}dppn)_2]^{3+}$: When *trans*-$[CoCl_2(S,S\text{-dppn})_2]Cl \cdot HCl \cdot H_2O$[4] (600 mg) was dissolved in liquid ammonia, the color of solution changed from green to orange instantly. After removal of liquid ammonia at room temperature, the residue was mixed with 2 M hydrochloric acid (10 cm^3) and then dissolved in DMSO. The resultant solution was passed through a column ($\phi 4 \times 45$ cm) of an SP-Sephadex C-25 ion exchanger. After washing with a mixture of water and DMSO (4 : 1), the adsorbed band was eluted with a 0.15 M solution of sodium $(+)_D$-tartratoantimonate(III) in a mixture of DMSO and water (1 : 4). When the adsorbed orange band was separated into two bands (I and II in the order of elution), the eluent was changed to a 0.7 M solution of sodium perchlorate in a mixture of water and methanol (2 : 1). The slowly eluted band, II, was further separated into two bands (IIa and IIb). The eluate of I was concentrated to give crystals, which were recrystallized from a mixture of acetone and ethanol (1 : 5), filtered off, and washed with ethanol and diethyl ether. Yield; 0.2 g. Found: C; 40.33, H; 5.39, N; 9.41%. Calcd for $[Co(NH_3)_2(S,S\text{-dppn})_2](ClO_4)_3 \cdot 3H_2O$ ($C_{30}H_{48}N_6O_{15}Cl_3Co$): C; 40.09, H; 5.39, N; 9.36%. This complex was assigned to the *trans* isomer on the basis of the PMR and CD spectra.

The eluate IIa was diluted about ten times with water and passed through a column ($\phi 2 \times 20$ cm) of an SP-Sephadex C-25 ion exchanger. The adsorbed band was eluted with 1 M hydrochloric acid. Orange crystals (20 mg) were obtained by concentrating the eluate. Found: C; 53.77, H; 6.52, N; 12.47%. Calcd for $[Co(NH_3)_2(S,S\text{-dppn})_2]Cl_3 \cdot H_2O$ ($C_{30}H_{44}N_6OCl_3Co$): C; 53.78, H; 6.62, N; 12.54%. This complex was assigned to the *cis-Λ* isomer on the basis of the CD spectrum.

The precipitate formed by concentrating the eluate IIb was filtered off and dissolved in a mixture of water and methanol (2 : 1). The solution was passed through a column ($\phi 2 \times 20$ cm) of an SP-Sephadex C-25 ion exchanger. The adsorbed band was eluted with 1 M hydrochloric acid. The orange eluate was evaporated to almost dryness and the residue was again dissolved in methanol. The solution was filtered and the filtrate was concentrated to give orange crystals, which were recrystallized from a mixture of methanol and water. Yield; 0.2 g. Found: C; 51.97, H; 6.49, N; 12.26%. Calcd for $[Co(NH_3)_2(S,S\text{-dppn})_2]Cl_3 \cdot 2H_2O$ ($C_{30}H_{46}N_6O_2Cl_3Co$): C; 52.37, H; 6.74, N; 12.21%. This complex was assigned to the *cis-Λ* isomer on the basis of the PMR and CD spectra.

(5) trans- *and* cis-$[Co(NH_3)_2(S,S\text{-}stien)_2]^{3+}$: To liquid ammonia (50 cm^3) was added *trans*-$[CoCl_2(S,S\text{-stien})_2]ClO_4 \cdot H_2O$[1] (0.57 g). The color of the solution changed from green to orange instantly. After removal of liquid ammonia at room temperature, the residue was mixed with 2 M hydrochloric acid (10 cm^3) and then dissolved in DMSO. The resultant solution was passed through a column ($\phi 4 \times 45$ cm) of an SP-Sephadex C-25 ion exchanger. After washing with a mixture of DMSO and water (1 : 4), the adsorbed band was eluted with a 0.15 M solution of sodium $(+)_D$-tartratoantimonate(III) in a mixture of DMSO and water (1 : 4). When the orange band was separated into two bands, the eluent was changed to a 0.7 M solution of sodium perchlorate in a mixture of water and methanol (2 : 1). The first eluted orange band was concentrated to give crystals, which were recrystallized from methanol. Yield; 0.3 g. Found: C; 40.40, H; 5.13, N; 9.82%. Calcd for $[Co(NH_3)_2(S,S\text{-stien})_2](ClO_4)_3(C_{28}H_{38}N_6O_{13}Cl_3Co)$: C; 40.33, H; 4.83, N; 10.08%. This complex was assigned to the *trans* isomer on the basis of the CD spectrum.

The second orange eluate was concentrated to give orange precipitate. The product was dissolved in a mixture of water and DMSO (4 : 1) and rechromatographed with a column ($\phi 4 \times 45$ cm) of an SP-Sephadex C-25 ion exchanger. The adsorbed band was eluted with a 0.15 M solution of sodium $(+)_D$-tartratoantimonate(III) in a mixture of DMSO and water (1 : 4). When the orange band was separated into two bands, the eluent was changed to a 0.5 M aqueous solution of sodium chloride. The first eluted band was concentrated to give orange precipitate. Recrystallization from a mixture of water and methanol (1 : 4) gave orange crystals, which were filtered off and washed with ethanol. Yield; 20 mg. Found: C; 49.42, H; 6.45, N; 12.35%. Calcd for $[Co(NH_3)_2(S,S\text{-stien})_2]Cl_3 \cdot 3H_2O$ ($C_{28}H_{44}N_6O_3Cl_3Co$): C; 49.60, H; 6.54, N; 12.40%. This complex was assigned to the *cis-Λ* isomer on the basis of the CD spectrum.

The second eluted band was concentrated to give orange precipitate, which was recrystallized from water. Yield; 0.1 g. Found: C; 49.74, H; 6.78, N; 12.75%. Calcd for $[Co(NH_3)_2(S,S\text{-stien})_2]Cl_3 \cdot 3H_2O$ ($C_{28}H_{44}N_6O_3Cl_3Co$): C; 49.60, H; 6.54, N; 12.40%. This complex was assigned to the *cis-Λ* isomer on the basis of the CD spectrum.

Measurements. Visible and ultraviolet absorption spectra were recorded on a Hitachi 323 spectrophotometer. CD spectra were obtained with JASCO J-20 and J-40 spectropolarimeters. PMR spectra were recorded on Varian A-60 and HA-100 spectrometers in deuterated solvents using tetramethylsilane (TMS) as the internal standard. All the solvents for optical measurements are of spectroscopic grade and used without further purification.

Results and Discussion

Conformation of the Chelate Rings and Geometrical Isomers of the Complexes. The PMR spectral data for the methylene and methine resonances of the (*R,S*)- and (*S,S*)-dppn complexes are summarized in Table 1 together with those of the (*R,S*)- and (±)-ptn platinum(II) and platinum(IV) complexes. Appleton and Hall[6] suggested that the chair conformation is preferred in the (*R,S*)-ptn platinum complexes and the skew conformation in the (±)-ptn platinum(IV) complex on the basis of the coupling constant $J_{Pt\text{-}N\text{-}C\text{-}H}$. The coupling constants, J_{AX} and J_{AB} of the (*R,S*)-dppn

Table 1. The methylene proton (H_A, H_B) resonances and the coupling constants with the methine proton (H_X) of the dppn and ptn complexes (δ/ppm)

	H_A	H_B	J_{AX}
$[Co(NH_3)_4(R,S\text{-dppn})](ClO_4)_3$	3.01	2.17	11
$[Pt(NH_3)_2(R,S\text{-ptn})]Cl_2$[6]	2.03	3.08	11.0
$[Pt(H_2O)_2(R,S\text{-ptn})_2](ClO_4)_4$[6]	2.68	3.75	11.0
$[Co(NH_3)_4((\pm)\text{-dppn})](ClO_4)_3$	2.62		8
trans-$[Co(NH_3)_2(S,S\text{-dppn})_2](ClO_4)_3$	2.70		8
cis-Λ-$[Co(NH_3)_2(S,S\text{-dppn})_2](ClO_4)_3$	2.53, 2.78		8
$[Pt((\pm)\text{-ptn})(NH_3)_2]Cl_2$[6]	2.87		5.5
$[Pt((\pm)\text{-ptn})(NH_3)_2(H_2O)_2](ClO_4)_4$[6]	3.42		7.5

Solvent: $(CD_3)_2CO$ for dppn complexes and D_2O for ptn complexes. Internal references: TMS for dppn complexes and DSS for ptn complexes.

cobalt(III) complexes are similar to those of the (*R,S*)-ptn platinum complexes. The constants, J_{AX} of the ((±) or *S,S*)-dppn cobalt(III) complexes are also similar to that of $[Pt((\pm)\text{-ptn})(NH_3)_2(H_2O)_2](ClO_4)_4$ as seen in Table 1. It is, therefore, concluded that the (*R,S*)-dppn and the (*R,R* or *S,S*)-dppn chelate rings take chair and skew conformations, respectively. In a previous paper,[4] it was clarified from the CD spectrum of *trans*-$[CoCl_2(S,S\text{-dppn})_2]^+$ that the (*S,S*)-dppn takes a λ-skew conformation upon coordination.

The assignment of the geometrical isomers of $[Co(NH_3)_2(S,S\text{-dppn})_2]^{3+}$ was made on the basis of the PMR spectral patterns (Table 1). This assignment will be supported by the elution order of the isomers of $[Co(NH_3)_2(S,S\text{-dppn})_2]^{3+}$ in SP-Sephadex column chromatography; *trans*>*cis*-Λ>*cis*-Δ. This order is the same as that for the corresponding isomers of the (*R,R*)-ptn complexes.[3]

Circular Dichroism Spectra. The CD data of the (*S,S*)-dppn and (*S,S*)-stien complexes in the first absorption band region are summarized in Table 2 together with the absorption data.

(1) $[Co(NH_3)_4L]^{3+}$(L=(S,S)-dppn and (S,S)-stien): The CD spectra of the complexes, $[Co(NH_3)_4L]^{3+}$ in water are shown in Fig. 1. Both the complexes give only a negative CD band in the first absorption band region. The (*S,S*)-stien is known to take a δ-gauche conformation, the two phenyl groups on the asymmetric carbons adopting equatorial orientation.[7,8] A single negative CD sign of the (*S,S*)-dppn complex predicts that the chelate ring also takes a δ-skew conformation. However, this conformation is unlikely for the (*S,S*)-dppn because the two phenyl groups on the asymmetric carbons become axial orientation. The (*S,S*)-dppn chelate is expected to be stable in the λ-skew conformation with two equatorial phenyl groups. The designation of the absolute configuration for both the diamines is opposite to each other for the same conformation on the basis of the sequence rule.[9] The CD pattern of $[Co(NH_3)_4(S,S\text{-dppn})]^{3+}$ in water is also different from either CD curve of the vicinal contribu-

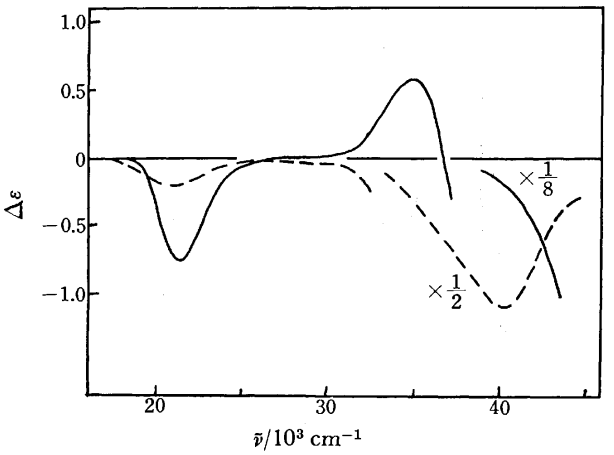

Fig. 1. CD spectra of $[Co(NH_3)_4(S,S\text{-dppn})]Br_3$ (----) and $[Co(NH_3)_4(S,S\text{-stien})](ClO_4)_3$ (——) in water.

Table 2. Absorption (AB) and CD spectral data of the (*S,S*)-dppn and the (*S,S*)-stien complexes in the first absorption band region

	L=(*S,S*)-dppn		L=(*S,S*)-stien	
	AB $\bar{\nu}/10^3$ cm^{-1} (ε)	CD $\bar{\nu}/10^3$ cm^{-1} ($\Delta\varepsilon$)	AB $\bar{\nu}/10^3$ cm^{-1} (ε)	CD $\bar{\nu}/10^3$ cm^{-1} ($\Delta\varepsilon$)
$[Co(NH_3)_4L]^{3+}$	20.88(79.0)*1)	20.83(−0.17)*1)	21.28(83.3)*1)	21.37(−0.75)*1)
	20.83(85.4)*3)	19.34(−0.10)*3)	21.19(91.1)*3)	21.14(−1.49)*3)
		22.94(−0.02)*3)		
		17.24(−0.01)*4)	21.19(91.1)*2)	21.46(−1.02)*2)
		20.62(+0.21)*4)		
		25.32(−0.01)*4)		
$[Co(NH_3)_2L_2]^{3+}$, *cis*-Λ	20.45(106.5)*2)	18.18(−0.03)*2)	21.32(100)*1)	19.49(+0.31)*1)
		20.41(+0.62)*2)		21.88(−0.54)*1)
cis-Δ	20.53(87.7)*2)	19.34(−0.31)*2)	21.32(87)*1)	21.23(−1.69)*1)
trans	20.66(121.9)*2)	19.23(+0.21)*2)	21.46(118)*2)	18.52(+0.04)*2)
		21.83(−0.01)*2)		
	20.75(109.9)*3)	19.57(+0.48)*3)	21.51(119)*3)	19.32(+0.32)*3)
				21.85(−2.03)*3)
		19.76(+0.75)*4)		21.44(−3.17)*4)

* Solvent: 1) water, 2) methanol, 3) DMSO, and 4) KBr matrix.

tion of (*S,S*)-dppn calculated from the two diastereomers, *Δ*- and *Λ*-[Co(*S,S*-dppn)$_3$]$^{3+}$ or from *Δ*- and *Λ*-[Co(en)$_2$(*S,S*-dppn)]$^{3+}$.[4,10] One explanation for the CD spectrum of [Co(NH$_3$)$_4$(*S,S*-dppn)]$^{3+}$ can be based on the flexibility of the (*S,S*)-dppn ligand in connection with the observation that the cobalt(III) complexes containing 2,4-pentanediamine are susceptible to solvent effect.[3]

The solvent effect on the CD spectra of both the (*S,S*)-dppn and the (*S,S*)-stien complexes is shown in Figs. 2 and 3, respectively. The former complex shows a marked solvent effect in the first absorption band region. The CD pattern in KBr matrix resembles that of the vicinal contribution of (*S,S*)-dppn derived from the *Δ*- and *Λ*-[Co(*S,S*-dppn)$_3$]$^{3+}$ complexes in DMSO. On the other hand, [Co(NH$_3$)$_4$(*S,S*-stien)](ClO$_4$)$_3$ shows little variations. The pattern is the same as that of the vicinal contribution of (*S,S*)-stien derived from the two diastereomers of *Δ*- and *Λ*-[Co(*S,S*-stien)$_3$]$^{3+}$.[1] Several explanations have been proposed for the solvent effect; 1) the conformational change of the diamine chelate ring, 2) asymmetric deviation of the coordinated nitrogen atoms from the octahedral positions, 3) asymmetric interaction of the solvent molecule with the solute. These factors are not independent of one another. The fact that the CD spectrum of [Co(NH$_3$)$_4$(*S,S*-dppn)]$^{3+}$ is much more susceptible to solvent ef-

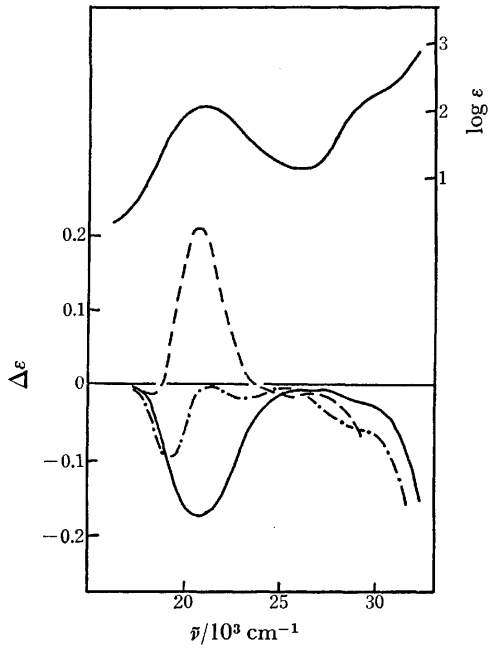

Fig. 2. Absorption and CD spectra of [Co(NH$_3$)$_4$(*S,S*-dppn)]Br$_3$ in water (——), in DMSO (—·—), and KBr matrix (----).

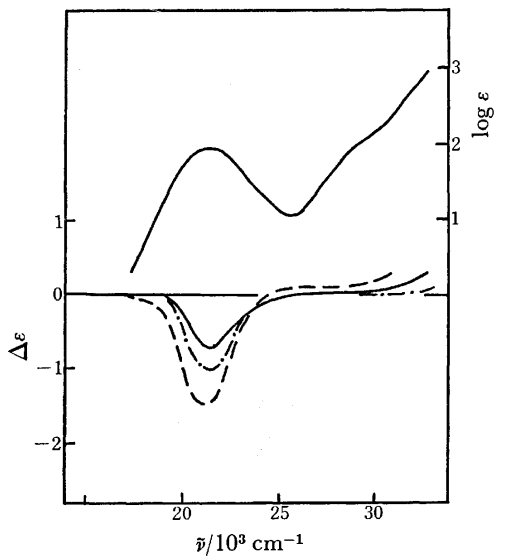

Fig. 3. Absorption and CD spectra of [Co(NH$_3$)$_4$(*S,S*-stien)](ClO$_4$)$_3$ in water (——), in DMSO (—·—), and KBr matrix (----).

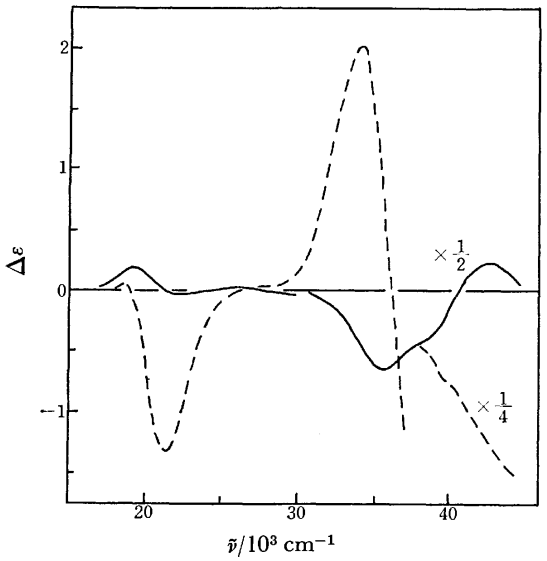

Fig. 4. CD spectra of *trans*-[Co(NH$_3$)$_2$(*S,S*-dppn)$_2$]-(ClO$_4$)$_3$ (——) and *trans*-[Co(NH$_3$)$_2$(*S,S*-stien)$_2$](ClO$_4$)$_3$ (----) in methanol.

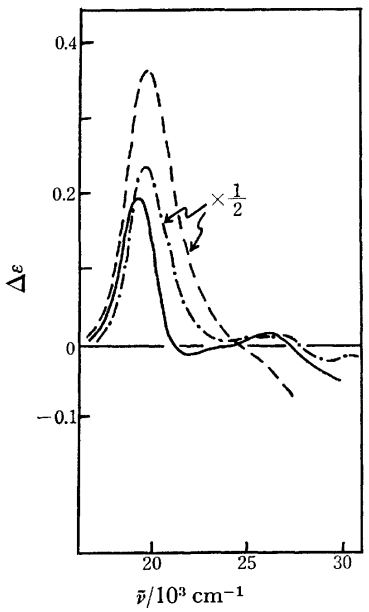

Fig. 5. CD spectra of *trans*-[Co(NH$_3$)$_2$(*S,S*-dppn)$_2$]-(ClO$_4$)$_3$ in methanol (——), in DMSO (—·—), and KBr matirx (----).

fect than that of the corresponding stien complex indicates that the variations may be associated with the flexibility of the six-membered chelate ring. However, the main factor for the solvent variations is not clear at present.

(2) trans-[*Co(NH$_3$)$_2$L$_2$*]$^{3+}$ *(L=(S,S)-dppn and (S,S)-stien)*: The CD spectra of the complexes, *trans*-[Co(NH$_3$)$_2$L$_2$]$^{3+}$ in methanol are shown in Fig. 4. Both the complexes give two CD peaks in the first absorption band region and the sign of the main component is positive for the former and negative for the latter. These patterns coincide with the anticipation that the (*S,S*)-dppn takes a λ-skew conformation and the (*S,S*)-stien a δ-gauche form. The CD strength of the (*S,S*)-dppn complex in the second absorption band region is very weak, in contrast to that of the corresponding (*R,R*)-ptn complex.[11]

The solvent effect on both the (*S,S*)-dppn and the (*S,S*)-stien complexes is shown in Figs. 5 and 6, respectively. The CD strength of the (*S,S*)-dppn complex varies significantly with the solvent variations in the first absorption band region. On the other hand, the CD spectrum of the (*S,S*)-stien complex is rather insensitive to the solvent variations. The CD pattern of *trans*-[Co(NH$_3$)$_2$(*S,S*-dppn)$_2$]$^{3+}$ is entirely different from that of [Co(NH$_3$)$_4$(*S,S*-dppn)]$^{3+}$ in water, while the (*S,S*)-stien complex gives the same pattern as that of [Co(NH$_3$)$_4$(*S,S*-stien)]$^{3+}$. The difference in the CD behavior between the (*S,S*)-dppn and the (*S,S*)-stien complexes may be related with the difference in the conformational behavior of the chelate rings.

(3) cis-[*Co(NH$_3$)$_2$L$_2$*]$^{3+}$*(L=(S,S)-dppn and (S,S)-stien)*: Figures 7—10 show the CD spectra of the isomers of *cis*-[Co(NH$_3$)$_2$L$_2$]$^{3+}$ and the calculated configurational and vicinal (per mole of the ligands) contributions to the CD spectra. The *cis* 1 in Figs. 7 and 9

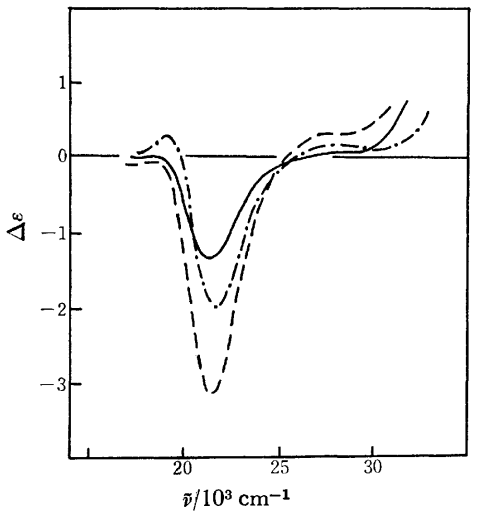

Fig. 6. CD spectra of *trans*-[Co(NH$_3$)$_2$(*S,S*-stien)$_2$]-(ClO$_4$)$_3$ in methanol (——), in DMSO (—·—) and KBr matrix (----).

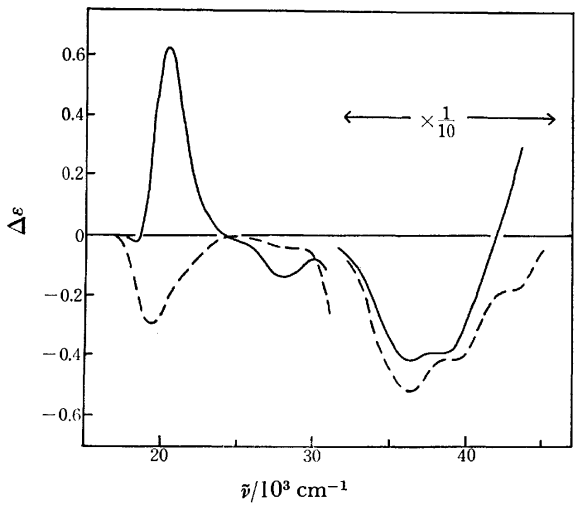

Fig. 7. CD spectra of *cis* 1 (——) and *cis* 2 (----) of [Co(NH$_3$)$_2$(*S,S*-dppn)$_2$]Cl$_3$ in methanol. The solution of *cis* 2 was acidified with hydrochloric acid.

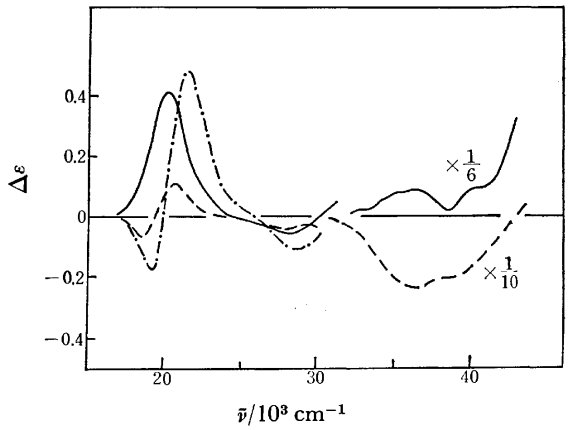

Fig. 8. The configuration (*Λ*) (——) and the vicinal (----) contribution in the CD calculated from the spectra of the two diastereomers of *cis*-[Co(NH$_3$)$_2$(*S,S*-dppn)$_2$]Cl$_3$ in methanol, and the vicinal (—·—) contribution from *Δ*- and *Λ*-[Co(*S,S*-dppn)$_3$]$^{3+}$.

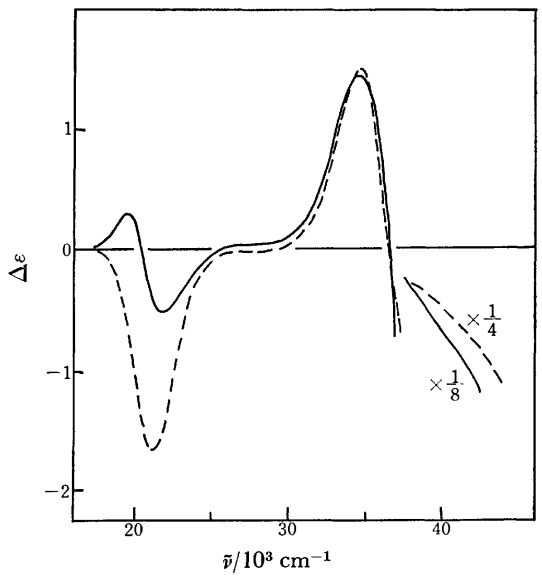

Fig. 9. CD spectra of *cis* 1 (——) and *cis* 2 (----) of [Co(NH$_3$)$_2$(*S,S*-stien)$_2$]Cl$_3$ in 0.02 M aqueous hydrochloric acid.

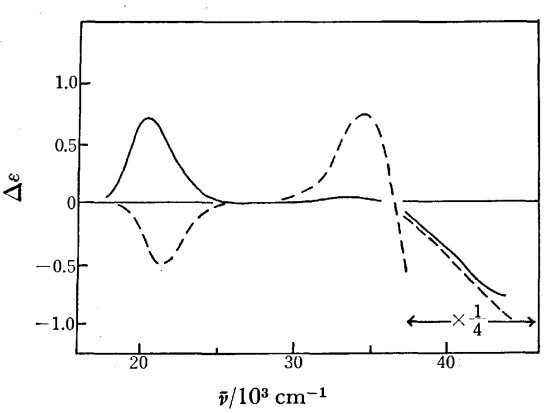

Fig. 10. The configurational (*Λ*) (——) and the vicinal (----) contribution in the CD calculated from the spectra of the two diastereomers of *cis*-$[Co(NH_3)_2(S,S\text{-stien})_2]Cl_3$ in methanol.

were obtained from the first orange eluate and the *cis* 2 from the second orange yellow eluate. The absolute configuration of each isomer can be assigned on the basis of the empirical rule.[12] The calculated configurational contribution of the CD spectra shown in Fig. 8 also supports the assignment: *cis* 1 to *Λ* and *cis* 2 to *Δ*.

Boucher and Bosnich[11] reported that the calculated vicinal contribution of (*R,R*)-ptn derived from the two diastereomers of *cis*-$[Co(NH_3)_2(R,R\text{-ptn})_2]^{3+}$ is entirely different from the CD spectrum of *trans*-$[Co(NH_3)_2(R,R\text{-ptn})_2]^{3+}$. Mizukami *et al.*[13] also claimed that the vicinal contribution of (*R,R*)-ptn derived from $[Co(R,R\text{-ptn})_3]^{3+}$ differs from the CD spectrum of $[Co(NH_3)_4(R,R\text{-ptn})]^{3+}$. The calculated vicinal contribution of (*S,S*)-dppn derived from the two diastereomers of *cis*-$[Co(NH_3)_2(S,S\text{-dppn})_2]^{3+}$ also differs from the CD spectra of both *trans*-$[Co(NH_3)_2(S,S\text{-dppn})_2]^{3+}$ and $[Co(NH_3)_4(S,S\text{-dppn})]^{3+}$. The spectral pattern of the calculated vicinal contribution, however, is similar to that obtained from the CD spectra of *Δ*- and *Λ*-$[Co(S,S\text{-dppn})_3]^{3+}$ in Fig. 8, although the CD strength of the former is weak compared with that of the latter.

The vicinal contribution of the (*S,S*)-stien chelate ring in Fig. 10 is almost the same as the CD spectra of both $[Co(NH_3)_4(S,S\text{-stien})]^{3+}$ and *trans*-$[Co(NH_3)_2(S,S\text{-stien})_2]^{3+}$. This is common to five-membered chelate ring systems such as 1,2-propylenediamine cobalt(III) complexes.[14]

The present work was partially supported by a Grant-in-Aid for Scientific Research from the Ministry of Education.

References

1) B. Bosnich and J. MacB. Harrowfield, *J. Am. Chem. Soc.*, **94**, 3425 (1972); *Inorg. Chem.*, **14**, 828 (1975).
2) P. G. Beddoe, M. J. Harding, S. F. Mason, and B. J. Peart, *Chem. Commun.*, **1971**, 1283.
3) M. Kojima, M. Fujita, and J. Fujita, *Bull. Chem. Soc. Jpn.*, **50**, 898 (1977).
4) S. Arakawa, K. Kashiwabara, J. Fujita, and K. Saito, *Bull. Chem. Soc. Jpn.*, **50**, 2108 (1977).
5) O. F. Williams and J. C. Bailar, Jr., *J. Am. Chem. Soc.*, **81**, 4464 (1959).
6) T. G. Appleton and J. R. Hall, *Inorg. Chem.*, **9**, 1807 (1970); *ibid.*, **10**, 1717 (1971).
7) S. Yano, M. Saburi, S. Yoshikawa, and J. Fujita, *Bull. Chem. Soc. Jpn.*, **49**, 101 (1976).
8) S. F. Mason and R. H. Seal, *J. Chem. Soc., Chem. Commun.*, **1973**, 422.
9) R. S. Cahn, C. K. Ingold, and V. Prelog, *Angew. Chem. Int. Ed. Engl.*, **5**, 385 (1966).
10) S. Arakawa, K. Kashiwabara, J. Fujita, and K. Saito, *Chem. Lett.*, **1976**, 105.
11) H. Boucher and B. Bosnich, *Inorg. Chem.*, **15**, 1471 (1976).
12) C. J. Hawkins, "Absolute Configuration of Metal Complexes," Wiley-Interscience (1971), Chap. 5.
13) F. Mizukami, H. Ito, J. Fujita, and K. Saito, *Bull. Chem. Soc. Jpn.*, **45**, 2129 (1972).
14) B. E. Douglas, *Inorg. Chem.*, **4**, 1813 (1965); A. J. McCaffery, S. F. Mason, B. J. Norman, and A. M. Sargeson, *J. Chem. Soc., A*, **1968**, 1304; K. Ogino, K. Murano, and J. Fujita, *Inorg. Nucl. Chem. Lett.*, **4**, 351 (1968).

The Effect of a Solvent on the Carbonylation of Methanol Catalyzed by Rhodium Complexes in the Presence of Methyl Iodide

Toshio MATSUMOTO, Kunio MORI, Tsutomu MIZOROKI, and Atsumu OZAKI

Research Laboratory of Resources Utilization, Tokyo Institute of Technology, Ohokayama, Meguro-ku, Tokyo 152

(Received March 13, 1976)

In the synthesis of acetic acid by the carbonylation of methanol catalyzed by $RhCl_3 \cdot 3H_2O$ or $Rh_2Cl_2(CO)_4$ in the presence of methyl iodide, it was found that ketone solvents, such as acetophenone and benzophenone, keep both the catalytic activity and selectivity high, even at an elevated temperature. The kinetic results in acetophenone are in agreement with the mechanism proposed by Paulik and Roth.[11] The effect of the ketone solvent was discussed by taking account of the competitive oxidative addition of hydrogen iodide with methyl iodide.

The oxidative addition of aryl iodide to nickel(0),[1,2] palladium(0),[3-8] and rhodium(I)[9,10] has been shown to play an important role in the catalytic carbonylation and arylation of olefin. It has been reported that, in the carbonylation of iodobenzene catalyzed by palladium-black in a basic medium to give methyl benzoate, the oxidative addition of iodobenzene to a palladium(0) complex is the rate-determining step, a step which is considerably influenced by ligands weakly bonded to the palladium complex.[4] Recently the oxidative addition of methyl iodide was demonstrated to be the rate determining step in the carbonylation of methanol catalyzed by rhodium compounds in liquid[11,12,16] and gas-phase reactions.[13-15] In this methanol carbonylation, the effect of ligands (including solvents) should also be reflected in its rate, as may be seen in the palladium-catalyzed carbonylation of iodobenzene. It was observed, however, that, when methanol was used as the solvent, the selectivity was very low (<20%) because of the formation of dimethyl ether in considerable amounts. The formation of dimethyl ether made it very difficult to elucidate the kinetic results. Thus, we examined the effects of the solvents in increasing the selectivity, and found that both the rate and the selectivity are highest in a ketone solvent, such as acetophenone or benzophenone.

During the preparation of this paper, a kinetic study of the carbonylation of methanol in an acetic acid solvent was reported,[16] and it was also noticed that much dimethyl ether was formed on initiating the carbonylation in a pure methanol solvent. The effect of solvents, however, was not described.

The purpose of this work is to investigate the effect of the solvent on the rate and selectivity of the rhodium complex-catalyzed carbonylation of methanol in the presence of methyl iodide and to discuss the role of solvents.

Experimental

Materials. Dichlorotetracarbonyldirhodium(I), $Rh_2Cl_2(CO)_4$, was prepared from $RhCl_3 \cdot 3H_2O$ and carbon monoxide according to the literature[17] (Found: C, 11.2; Cl, 18.8 %. Calcd: C, 12.4; Cl, 18.2%.). $RhCl_3 \cdot 3H_2O$ (Koso Chemical Co., Ltd,), carbon monoxide (>98%), methanol (>99%), methyl iodide (Tokyo Kasei's extra pure grade), and all the solvents used in this work were obtained from commercial sources. The solvents listed in Table 1 were checked by gas chromatography before use, and were used without purification.

Procedure. All the carbonylations were carried out using a Ti–Mn alloy autoclave (100 ml) equipped with a magnetic stirrer. A given amount of $RhCl_3 \cdot 3H_2O$ or $Rh_2Cl_2(CO)_4$ (0.125—1.00 mmol) and a mixture of methyl iodide (5—20 mmol), methanol (50—250 mmol) and a solvent (20 ml) were placed in the autoclave. Carbon monoxide was then introduced up to the desired pressure (7—90 kg/cm^2). Subsequently the autoclave was heated up to a reaction temperature within 15—20 min, the temperature and the pressure being kept constant for 1—4 h. The autoclave was then cooled rapidly to room temperature with water, and the carbon monoxide was purged out. The product solution was analyzed by gas chromatography. The reaction rate was measured as follows. A rhodium catalyst and a solution were placed in the autoclave, and it was heated up to a reaction temperature before introducing carbon monoxide. The carbonylation was initiated by introducing carbon monoxide. The pressure was kept constant during the reaction by supplying carbon monoxide from a high-pressure gas reservoir (100 ml). The amount of carbon monoxide consumed was measured by means of the pressure decrease in the gas reservoir.

Analysis. The product solutions were quantitatively analyzed by means of gas chromatography. A glass column (3 mmϕ, 3 m, carrier gas of H_2) of diethylene glycol succinate polyester on Celite was used at 100—200 °C for carboxylic acids with an internal standard substance (C_6H_5Br or 1-$C_{10}H_7Br$). For the determination of the methyl acetate, methanol, and methyl iodide, a copper column (3 mmϕ, 3 m, carrier gas of H_2) of 3,3′-oxy-dipropionitrile on an insulating brick was used at 70 °C with dibutyl ether as the internal standard substance.

Results and Discussion

Effect of Solvents. The carbonylation of methanol catalyzed by $RhCl_3 \cdot 3H_2O$ and methyl iodide was examined in various solvents under the same reaction conditions. The results are summarized in Table 1. The use of the solvents with a carbonyl group improved the yield and selectivity of the carbonylation of methanol. The yield and selectivity of more than 100% in the methyl benzoate solvent seemed to be caused by the hydrolysis of methyl benzoate or by its ester exchange with acetic acid. This idea was supported by the detection of benzoic acid in the reaction product.[25] The methyl iodide was restored almost completely after the carbonylation except in the case of the *N,N*-dimethylacetamide solvent. Acetophenone was employed to show the effectiveness of the ketone solvents in Table 2. The addition of acetophenone significantly increases

Table 1. Effect of solvent

CH_3OH 50 mmol, CH_3I 20 mmol, Solvent 20 ml, $RhCl_3 \cdot 3H_2O$ 0.5 mmol, P_{CO} 20 kg/cm² (at room temp), temp 140 °C, and time 90 min.

Solvent	Yield[a] (%)	Select.[b] (%)	Resid. CH_3I (mmol)
$C_6H_5COOCH_3$	109	177	19
	82	90	19
$CH_3COC_2H_5$	81	94	17
$C_6H_5COCH_3$	80	96	19
$C_2H_5COC_2H_5$	71	93	16
$C_6H_5OCH_3$	58	98	18
C_6H_5CN	50	99	18
C_6H_5Cl	49	99	19
DMA	32	51	8.9
$C_6H_5CH_3$	31	81	20
n-C_6H_{14}	16	26	16
$C_6H_5NO_2$	2.0	9.5	17

a) $\text{Yield}(\%) = \dfrac{[\text{AcOH}]+[\text{AcOCH}_3]}{[\text{CH}_3\text{OH}]_{\text{init.}}} \times 100$,

b) $\text{Selet.}(\%) = \dfrac{([\text{AcOH}]+[\text{AcOCH}_3]) \times 100}{[\text{CH}_3\text{OH}]_{\text{init.}} - [\text{CH}_3\text{OH}]_{\text{resid.}} - [\text{AcOCH}_3]}$

(AcO = CH_3COO, DMA = N,N-dimethylacetamide).

Table 2. Effects of acetophenone

CH_3I 10 mmol, $RhCl_3 \cdot 3H_2O$ 0.25 mmol, P_{CO} 30 kg/cm² (at room temp), temp 173 °C, and time 60 min.

CH_3OH (ml)	$C_6H_5COCH_3$ (ml)	Total AcOH[a] (mmol)	Select.[b] (%)	$(CH_3)_2O$[c] (mmol)
25	0	42	13	140
20	5	68	37	60
15	10	69	43	48
10	15	76	65	23
5	20	71	83	6.6

a) Total AcOH = AcOH + $AcOCH_3$. b) Defined in Table 1. c) The amount of $(CH_3)_2O$ formed was calculated as follow: $(CH_3)_2O = 1/2 \times ([CH_3OH]_{\text{init.}} - [\text{AcOH}] - 2[AcOCH_3] - [CH_3OH]_{\text{resid.}})$.

the amount of total acetic acid, retarding the formation of dimethyl ether, at a smaller volume ratio of methanol to acetophenone. The effect of acetophenone on the rate of carbonylation at 156 °C is shown in Fig. 1; anisole or toluene was added to keep the concentrations of the methyl iodide, the rhodium catalyst, and the methanol constant. In both cases, the rates effectively increase with an increase in the volume ratio of acetophenone added and reach a constant rate (138 mmol/h) above the ratio of 1. In no runs was any metallic substance detected in the product solutions.

A kinetic study of the carbonylation was undertaken in the acetophenone solvent. The amounts of carbon monoxide absorbed during the reaction are plotted against the time at various amounts of the rhodium catalyst and methyl iodide under 30 kg/cm² of carbon monoxide at 112 °C in Figs. 2 and 3. The total consumption of carbon monoxide almost corresponded to

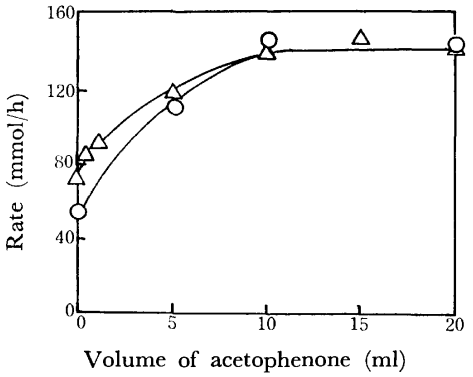

Fig. 1. Effect of acetophenone.
CH_3OH 125 mmol, CH_3I 20 mmol, $RhCl_3 \cdot 3H_2O$ 0.5 mmol, Total volume of solvent 20 ml, P_{CO} 30 kg/cm² (at 156 °C), and temp 156 °C.
△ In anisole-acetophenone and ○ in toluene-acetophenone.

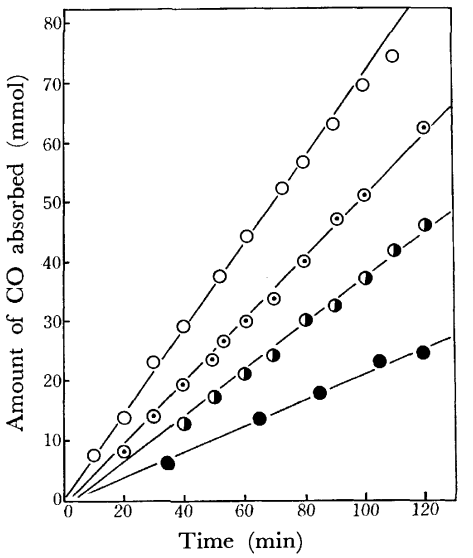

Fig. 2. Effect of the amount of $RhCl_3 \cdot 3H_2O$ on the rate.
CH_3OH 125 mmol, CH_3I 40 mmol, acetophenone 20 ml, P_{CO} 30 kg/cm² (at 112 °C), and temp 112 °C. $RhCl_3 \cdot 3H_2O$: ● 0.25 mmol, ◑ 0.50 mmol, ⊙ 0.75 mmol, and ○ 1.00 mmol.

the amount of total acetic acid produced in each run. Accordingly, the rates of carbonylation are independent of the feed of methanol. The rate is first order with respect to the amount of methyl iodide, and also with respect to that of the rhodium catalyst. The rate was also independent of the pressure of carbon monoxide (10—90 kg/cm²). These kinetic relations were independently confirmed in the higher-temperature range.

Effect of Temperature. The effect of the temperature was examined in stable solvents, such as acetophenone, benzophenone, anisole, and toluene (Figs. 4 and 5). Benzonitrile and chlorobenzene, which gave a high selectivity at 140 °C, as is shown in Table 1, were not investigated in detail, since the hydrogenolysis of benzonitrile and the oxidative addition of chlorobenzene seemed to interfere with the carbonylation of methanol at higher temperatures. In the toluene sol-

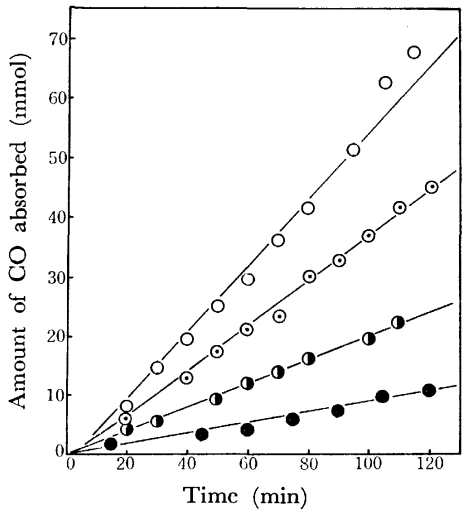

Fig. 3. Effect of the amount of CH_3I on the rate.
CH_3OH 125 mmol, $RhCl_3 \cdot 3H_2O$ 0.5 mmol, acetophenone 20 ml, P_{CO} 30 kg/cm² (at 112 °C), and temp 112 °C. CH_3I: ● 10 mmol, ◑ 20 mmol, ⊙ 40 mmol, and ○ 60 mmol.

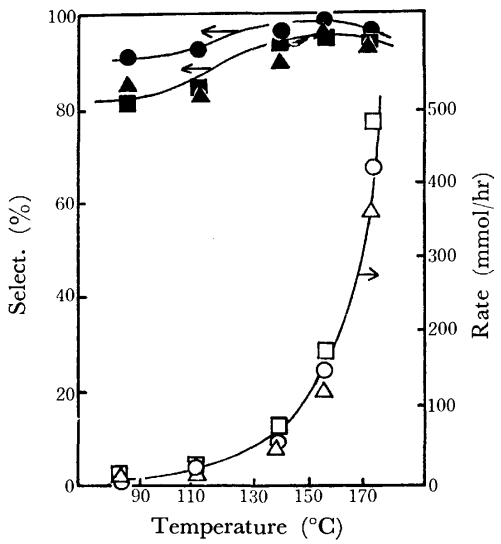

Fig. 4. Effect of temperature in acetophenone or benzophenone.
CH_3OH 125 mmol, CH_3I 20 mmol, $RhCl_3 \cdot 3H_2O$ 0.5 mmol or $Rh_2Cl_2(CO)_4$ 0.25 mmol, solvent 20 ml, P_{CO} 30 kg/cm² (at react temp), and time 120 min.
□ and ■: in benzophenone with $RhCl_3 \cdot 3H_2O$,
○ and ●: in acetophenone with $RhCl_3 \cdot 3H_2O$,
△ and ▲: In acetophenone with $Rh_2Cl_2(CO)_4$.

vent, the selectivity is very low because of the formation of dimethyl ether in considerable amounts. At 173 °C, the rates in the ketone solvents were 6 to 8 times larger than in anisole and 13 to 18 times larger than in toluene. There was no essential difference between $RhCl_3 \cdot 3H_2O$ and $Rh_2Cl_2(CO)_4$ with respect to the rate and selectivity of carbonylation, as is shown in Fig. 4. Arrhenius plots of the rates in ketone solvents gave good linearities, from which the apparent activation energy was estimated to be 19 kcal/mol (Fig. 6).

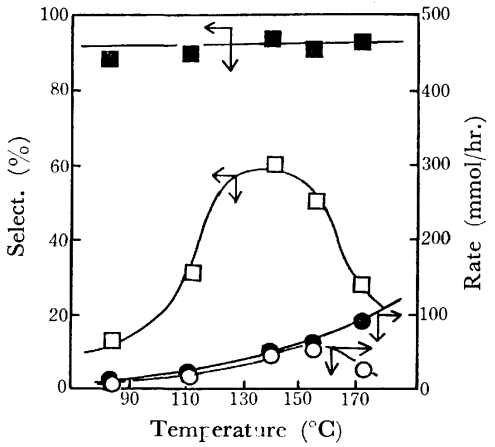

Fig. 5. Effect of temperature in toluene or anisole.
CH_3OH 125 mmol, CH_3I 20 mmol, $RhCl_3 \cdot 3H_2O$ 0.5 mmol, solvent 20 ml, P_{CO} 30 kg/cm² (at react temp), and time 120 min.
○ and □: in toluene, ● and ■: in anisole.

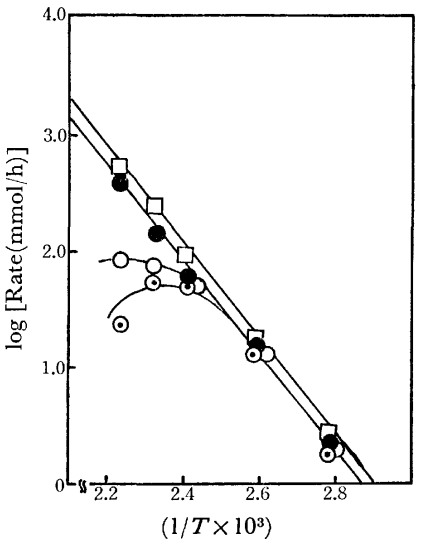

Fig. 6. Arrhenius plot of the rates with $RhCl_3 \cdot 3H_2O$.
□ In benzophenone, ● in acetophenone, ○ in anisole, and ⊙ in toluene.

To examine whether or not low rates in anisole or toluene at elevated temperatures were caused by an irreversible deactivation of the catalyst, the dependence of the rates on temperature was reinvestigated. The rate in anisole initially measured at 173 °C for 30 min under the conditions specified in Fig. 5 was 75±10 mmol /h. After the temperature had been lowered to 156 °C within 5 min, the rate was measured again for 45 min to give the value of 65±5 mmol/h. The temperature was, then, further lowered to 140 °C within 5 min; the rate measured for 40 min was 32±5 mmol/h. These rates were almost entirely consistent with those obtained by the separate experimental runs shown in Fig. 6, namely, 80, 67, and 40 mmol/h at 173, 156, and 140 °C respectively. The rates obtained in toluene by the same manner were 52(50), 40(38), and 15(16) mmol/h at 156, 140, and 112 °C respectively; the rates given in Fig. 6 are shown in parentheses. These results indicate that the catalytic activity is reproducible with

respect to the reaction temperature. It seems most likely that there is no essential change in the mechanism, since the kinetic behavior in anisole or toluene is almost the same as in acetophenone, even at higher temperatures.

The effect of hydrogen on the methanol carbonylation was examined in the acetophenone solvent using $RhCl_3 \cdot 3H_2O$. Under a lower pressure of carbon monoxide (P_{H_2} 40 kg/cm^2, P_{CO} 10 kg/cm^2, 140 °C), acetophenone was hydrogenated to give ethylbenzene and a trace amount of styrene, while practically no hydrogenation of acetophenone was observed under a higher pressure of carbon monoxide (P_{CO}>20 kg/cm^2). Neither acetaldehyde nor ethanol was detected in the product solutions in any case. The treatment of methyl iodide without methanol under 60 kg/cm^2 of a H_2–CO (H_2/CO=1) mixture gave only a trace amount of acetic acid, but no acetaldehyde, and more than 80% of the methyl iodide was recovered in the product solution.

Role of the Solvent. The kinetic results suggest that the carbonylation of methanol in ketone solvents proceeds *via* a scheme similar to that proposed by Roth *et al.*[12] Recently a more elaborate scheme has been reported by Forster.[18] The most reasonable rate-determining step is the oxidative addition of methyl iodide to the rhodium(I) complex, assuming that the equilibrium between methyl iodide and hydrogen iodide ($CH_3OH + HI \rightarrow CH_3I + H_2O$) is much shifted to the formation of methyl iodide during the carbonylation. Figure 6 shows that the rates at lower temperatures (<140 °C) are almost the same in any solvent examined, indicating no essential role of solvent molecules as ligands.[19] Accordingly, the active species in ketone solvents is probably the same as that observed by Forster during a catalytic carbonylation of methanol in a heptanoic acid solvent, using $RhCl_3 \cdot 3H_2O$ as the catalyst precursor.[18] The reaction scheme with this species is illustrated.[20] It was reported that the oxidative addition of alkyl halide to a rhodium(I) complex such

$$[Rh(CO)_2I_2]^- \xrightarrow{CH_3I} [CH_3Rh(CO)_2I_3]^- \xrightarrow{CO}$$

$$[CH_3CORh(CO)_2I_3]^-\ ^{21)} \xrightarrow[-AcOCH_3 \text{ or } AcOH]{+CH_3OH \text{ or } H_2O}$$

$$[HRh(CO)_2I_3]^- \xrightarrow[+Solvent\text{-}HI]{+Solvent} [Rh(CO)_2I_2]^-$$

$$Solvent\text{-}HI + CH_3OH \rightleftharpoons CH_3I + Solvent + H_2O$$

as $RhCl(CO)(PPh_3)_2$ and $RhCl(CO)_2(PPh_3)$ proceeds *via* electrophilic attack of alkyl halide.[22–24] Since hydrogen iodide is less crowded and more electrophilic, a small amount of hydrogen iodide in the solution should be competitive with the methyl iodide for the oxidative addition. The equilibrium concentration of hydrogen iodide should increase with elevating the temperature, because the formation of methyl iodide is exothermic. In ketone solvents, hydrogen iodide may be effectively solvated so as to prevent its oxidative addition to the rhodium(I) complex.

References

1) M. Nakayama and T. Mizoroki, *Bull. Chem. Soc. Jpn.*, **42**, 1124 (1969).
2) L. Casser and M. Foa, *J. Organomet. Chem.*, **51**, 381 (1973).
3) K. Mori, T. Mizoroki, and A. Ozaki, *Bull. Chem. Soc. Jpn.*, **46**, 1505 (1973).
4) T. Ito, K. Mori, T. Mizoroki, and A. Ozaki, *Bull. Chem. Soc. Jpn.*, **48**, 2091 (1975).
5) R. F. Heck and J. P. Nolley, Jr., *J. Org. Chem.*, **37**, 2320 (1972).
6) A. Schoenberg, I. Bartoletti, and R. F. Heck, *J. Org. Chem.*, **39**, 3318 (1974).
7) A. Schoenberg, and R F. Heck, *J. Org. Chem.*, **39**, 3327 (1974).
8) H. A. Dieck and R. F. Heck, *J. Am. Chem. Soc.*, **96**, 1133 (1974).
9) J. Tsuji and K. Ono, *J. Am. Chem. Soc.*, **90**, 99 (1968); *Tetrahedron Lett.*, **1966**, 4713.
10) K. Mori, T. Mizoroki, and A. Ozaki, *Bull. Chem. Soc. Jpn.*, **49**, 758 (1976).
11) F. E. Paulik and J. F. Roth, *Chem. Commun.*, **1968**, 1578.
12) J. F. Roth, J. H. Craddock, A. Hershman, and F. E. Paulik, *Chemtech*, **1971**, 600.
13) K. K. Robinson, A. Hershman, J. H. Craddock, and J. F. Roth, *J. Catal.*, **27**, 389 (1972).
14) R. G. Schultz and P. D. Montgomery, *J. Catal.*, **13**, 105 (1969).
15) A. Krzywicki and G. Pannetier, *Bull. Soc. Chem. Fr.* **1975**, 1093.
16) J. Hjortkjaer and V. W. Jensen, *Ind. Eng. Chem., Prod. Res. Dev.*, **15**, 46 (1976).
17) *Inorg. Synth.*, Vol. 8, McGraw-Hill (1966), p. 211.
18) D. Forster, *J. Am. Chem. Soc.*, **98**, 846 (1976).
19) The activation energy in acetic acid has been reported to be 14.7 kcal/mol,[16] suggesting that an activated complex is in a highly polar state.
20) The counter cation may be a solvated proton.
21) Forster *et al.* prepared a dimeric anion of the rhodium acetyl complex $[CH_3CORh(CO)I_3]_2^{2-}$, which is held together by Rh–I–Rh bridges.[18]
22) I. C. Douck and G. Wilkinson, *J. Chem. Soc., A*, **1969**, 2604.
23) P. Uguagliati, A. Palazzi, G. Deganello, and U. Belluco, *Inorg. Chem.*, **9**, 724 (1970).
24) A. J. Hart-Davis and W. A. G. Graham, *Inorg. Chem.*, **9**, 2685 (1970); **10**, 1653 (1970).
25) The product solution contained AcOH (35.5 mmol), $AcOCH_3$ (19.2 mmol), C_6H_5COOH (19.5 mmol), and no methanol, indicating that 20—24 mmol of methyl benzoate were consumed during the carbonylation to give benzoic acid.

Studies of Peptide Antibiotics. XXXVI.[1] Synthesis and Biological Activity of [5,5′-Leucine]-gramicidin S[2]

Okitoshi ABE, Yoko UTSUMI, and Nobuo IZUMIYA*

Laboratory of Chemistry, Fukuoka Dental College, Nishi-ku, Fukuoka 814

**Laboratory of Biochemistry, Fuculty of Science, Kyushu University 33, Hakozaki, Higashi-ku, Fukuoka 812*

(Received April 25, 1977)

An analog of gramicidin S, in which 5,5′-proline residues were replaced by leucine, was prepared in order to investigate the effect of the introduction of hydrophobic side groups on the antibacterial activity and on the conformation. Also the solubility problems encountered during the synthesis of this analog are described. No significant effect was observed on the cyclization reaction by the replacement of 5,5′-proline to leucine residues. This analog exhibited comparable biological activity and the similar conformation to the natural gramicidin S. These studies suggested that the imino groups of 5,5′-proline residues have no significant roles on both antibacterial activity and conformation of this antibiotic.

Synthetic analogs of gramicidin S (GS, Fig. 1) in which 5,5′-Pro residues are replaced by Gly,[3] Sar,[4] β-Ala,[5] α-aminoisobutyric acid (Aib),[6] or Phe[7] have been reported by Izumiya and his collaborators. Some of them, such as [5,5′-Gly]-,[3] [5,5′-Sar]-,[4] and [5,5′-Phe]-GS,[7] exhibited substantial biological activities. On the other hand, very weak or no antibacterial activity was observed on the other two analogs, *i.e.* [5,5′-β-Ala]-[5] and [5,5′-Aib]-GS.[6]

In this study was synthesized an analog in which 5,5′-Pro residues of the natural GS were replaced by Leu residues, namely [5,5′-Leu]-GS. Leucine residue possesses bulky hydrophobic side chain and its effect on the antibacterial activity has also been studied. In addition, as a strategy of the synthesis of this analog, the sequence of the linear intermediate was selected such a way that the 3- or 3′-Leu located to the carboxyl terminus in consideration of its similarity to the biosynthetic intermediate of GS.[8] The problems caused by this sequence are also discussed. Possibility of racemization during the cyclization reaction was overcome by the employment of the azide procedure.[9,10]

The intermediate peptides were protected on the α amino terminus by the *t*-butoxycarbonyl group (Boc–), on the δ amine of ornithines by the benzyloxycarbonyl group (Z–), and on α carboxyl groups by the ethyl ester (–OEt). Selective deprotection of Boc-group was

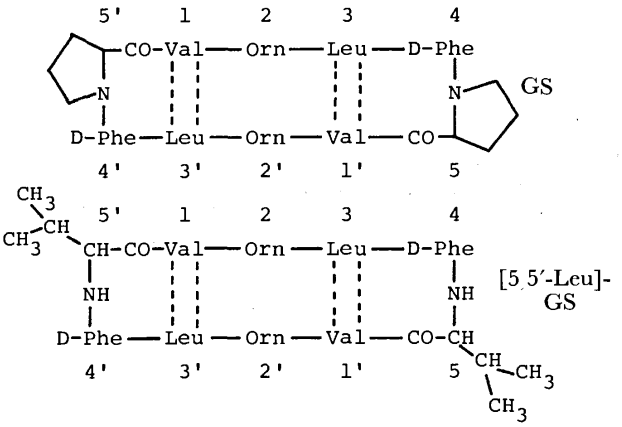

Fig. 1. Structure of GS (upper) and [5,5′-Leu]-GS (bottom).

carried out with hydrogen chloride in formic acid and of Z-group by hydrogenolysis in the presence of palladium black. As for the coupling reaction, the azide procedure of Curtius[9] and of Honzl and Rudinger[10] were mainly employed.

Scheme 1 indicates a route for the synthesis of the protected decapeptide (**6**) with 3-Leu as the carboxyl terminus. This route was designed to imply the similarity of the amino acid sequence to that of the bio-

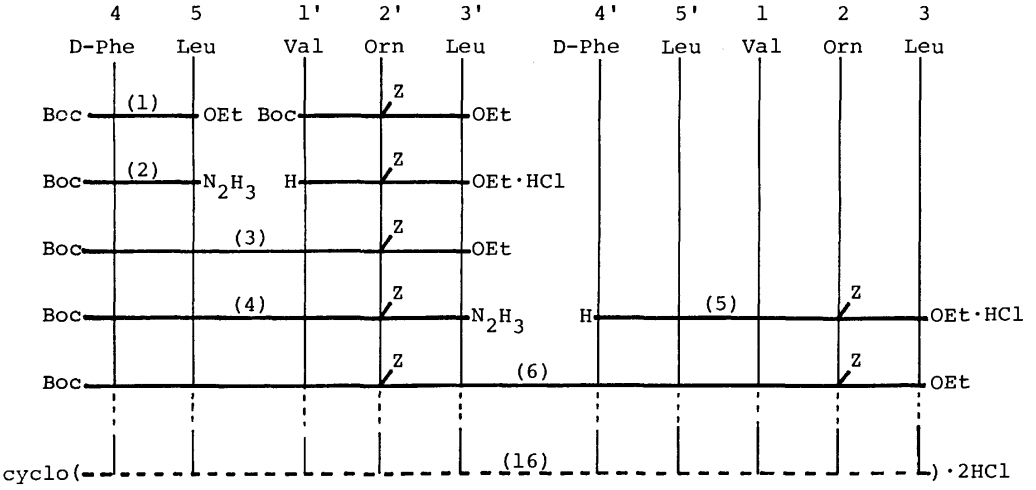

Scheme 1. Synthesis of [5,5′-Leu]-GS with 3-Leu as carboxyl terminus.

synthetic intermediate of GS.[8]

The first dipeptide derivative (**1**) was obtained by the mixed anhydride method with isobutyl chloroformate as the coupling reagent. Product **1** was obtained in 65% yield and then converted without difficulty to its hydrazide (**2**) by the addition of 20 molar excess of hydrazine hydrate. Boc-pentapeptide ester (**3**) was obtained by the coupling of the product **2** with H–Val–Orn(Z)–Leu–OEt[11] using azide procedure[9] in 80% yield. First problem was encountered in the following step, conversion of the ester (**3**) to the hydrazide (**4**). At first the same condition as described for the preparation of **2** was employed, however, the reaction was incomplete. Therefore, the amount of hydrazine was increased to 40 molar excess and also the reaction time prolonged. On standing for eight days, precipitates were formed and the reaction mixture was revealed to contain almost no ester on a thin-layer plate, yielding 82% of the product **4**. Deblocking of Boc-group from **3** yielded the product **5** in 96%.

The second problem was in the coupling of the product **4** with **5**. Compound **4**, sparingly soluble in common organic solvents, was dissolved on two hours of stirring in the mixed solvent DMF–DMSO (1 : 1, v/v) and the coupling was carried out using the azide procedure of Honzl and Rudinger.[10] The product was revealed to be a mixture of several components and all the efforts for their separation and purification resulted in vain, mainly because of their insolubility. No better result was obtained when the coupling reaction was repeated several times. These facts forced to change the strategy of the synthetic route.

In the alteration of the synthetic route, first to be considered was the use of the intermediate peptide derivatives synthesized in Scheme 1. As shown in Scheme 2, two peptide derivatives, Boc–Val–Orn(Z)–Leu–OEt and the dipeptide derivative (**1**), could be successfully used. Conversion of the Boc-tripeptide ester to its hydrazide (**7**) with 20 molar excess of hydrazine hydrate and deblocking of the Boc-group of the compound **1** were performed without trouble. Subsequent coupling of **7** with **8** was carried out by means of the azide procedure to produce Boc-pentapeptide ester (**9**) in the yield of 54%. The next step, conversion of ester (**9**) to its hydrazide (**10**), was much easier than the corresponding step (**3** to **4**) in Scheme 1. It took two days to complete the reaction with 40 molar excess of hydrazine hydrate. Decapeptide derivative (**12**) was also obtained without difficulty in pure form by the azide method and the yield was fairly good (88%).

In the synthetic route of Scheme 2, the most troublesome step was the conversion of **12** to the hydrazide (**13**). The amount of hydrazine was increased from 40 to 80 and finally to 200 molar equivalents. Under the final condition, the product **13** was obtained in good yield (96%).

After removal of Boc-group from **13**, the product **14** was cyclized by the azide procedure as described in Experimental part. Crude cyclic peptide thus obtained was dissolved in aqueous methanol and passed through a column of Dowex 50X8. Recrystallization from methanol–water gave the pure Z-protected cyclic petide (**15**) in the yield of 58%. Hydrogenolysis of **15** produced the final product, [5,5′-Leu]-GS (**16**), in the yield of 67%. Homogeneity of **16** was ascertained by paper and thin-layer chromatographies with various solvent systems, paper electrophoresis, elemental analysis and by amino acid analysis. Also the final product was subjected to antibacterial test and ORD measurements.

In general, from the standpoint of synthesis, deblocking of Boc-groups with hydrogen chloride in formic acid was performed without any trouble. On the contrary,

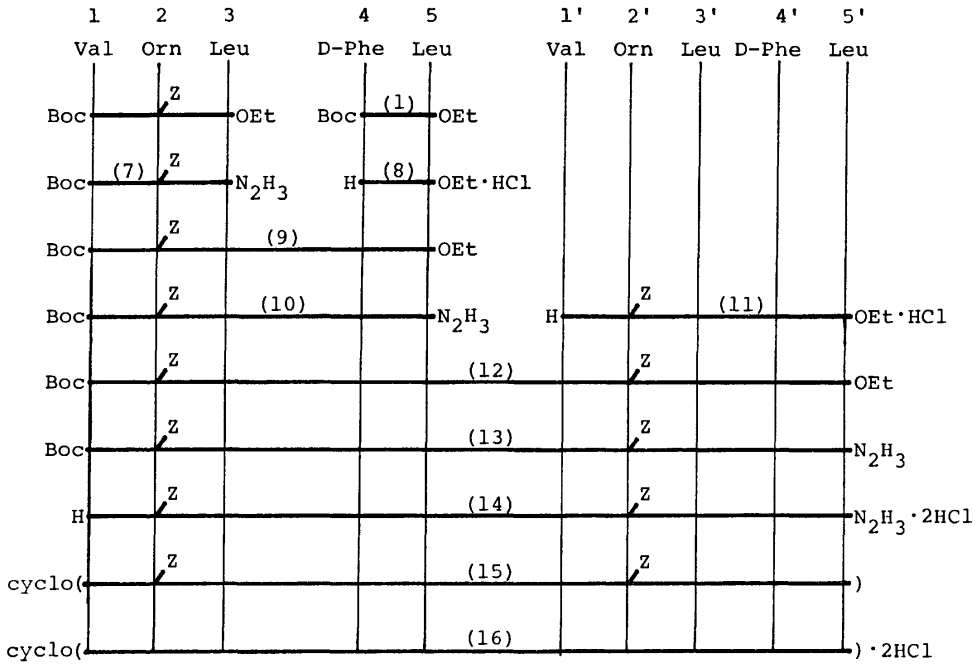

Scheme 2. Synthesis of [5,5′-Leu]-GS with 5′-Leu as carboxyl terminus.

Table 1. Antibacterial activity of the synthetic GS analog, [5,5′-Leu]-GS (**16**)
(Minimum inhibitory concentration, μg/ml)

Strain	[5,5′-Leu]-GS (**16**)		GS	
	A[a]	B[b]	A[a]	B[b]
Escherichia coli	>50	>50	>50	>50
Proteus vulgaris	>50	>50	>50	>50
Staphylococcus aureus	10	10	2	5
Bacillus subtilis	5	5	2	5
Mycobacterium 607	>50	>50	>50	>50
Mycobacterium avium	>50	>50	>50	>50

a) Nutrient agar medium, pH 7. b) Synthetic medium.

Table 2. Antibacterial activities of the 5,5′-position substituted GS analogs[a]

5,5′-Residues	*S. aureus*		*B. subtilis*		Reference No.
	A[b]	B[c]	A[b]	B[c]	
Gly	5 (2)	5 (5)	5 (2)	2—5 (5)	12)
Sar	10 (5)	10 (5)	5 (5)	5 (5)	4)
β-Ala[d]	100 (6)		100 (3)		5)
Aib[e]	>100 (3)		>100 (3)		6)
Phe	10 (5)	20 (5)	10 (2)	10 (5)	7)
Leu	10 (2)	10 (5)	5 (2)	5 (5)	This work

a) ( ): Activity of the natural GS used as the control. b) Bouillon agar medium. c) Synthetic agar medium. d) Assay conditions not clearly shown. e) Assayed by paper disk method.

the conversion of the esters to their hydrazides produced several difficulties in some cases. And the insolubility of some hydrazides made the subsequent reaction difficult. Although the imino acid proline was replaced by the amino acid leucine, the cyclization step by the azide method was carried out without trouble and resulted in good yield.

Antibacterial activities of [5,5′-Leu]-GS measured in both nutrient agar and synthetic medium are listed in Table 1. Compared to natural GS, the synthetic analog exhibited considerable inhibitory activities against some organisms tested. From these data, the 5,5′-Pro residues of the natural GS seem to be exchangeable to bulky hydrophobic amino acid residues such as Leu without any significant effect on the antibacterial activity. In Table 2 are listed antibacterial activities of the 5,5′-position substituted GS analogs reported thus far. These data also indicate the insignificance of 5,5′-Pro residues of GS on its antibacterial activity.

The ORD curves of [5,5′-Leu]-GS measured in both ethanol and 8 M urea were presented in Fig. 2. In both media the synthetic analog exhibited similar curves as those of the natural GS with a negative trough at 234—235 nm. The fact that no shift of the trough had been observed even in the strong denaturing reagent such as 8 M urea suggested the rigid and stable conformation of the synthetic analog as well as the natural GS molecule, which has the intramolecular antiparallel β-form with four hydrogen bondings between the valyl and the leucyl residues.[13] Correlation between the rigid structure and the antibacterial activity is also suggested.

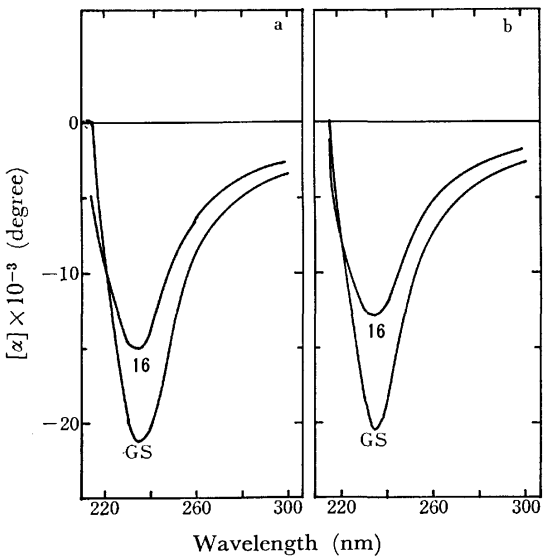

Fig. 2. ORD curves of [5,5′-Leu]-GS (**16**) and natural GS.
Solvent: a, EtOH; b, 8 M urea.

Experimental

All melting points are uncorrected. Prior to elemental analysis, all the compounds were dried over P_2O_5 to a constant weight at 80 °C and 2 Torr. TLC was carried out on silica gel G (Merck) with the following solvent systems: R_f^1, chloroform–MeOH (5 : 1, v/v), R_f^2, chloroform–MeOH–AcOH (95 : 5 : 1, v/v), R_f^3, chloroform–MeOH (9 : 1, v/v), R_f^4, 1-butanol (BuOH)–AcOH–pyridine–H_2O (4 : 1 : 1 : 2, v/v), R_f^5, BuOH–AcOH–pyridine–H_2O (15 : 3 : 10 : 12, v/v). Paper chromatography (PPC) was performed on Toyo Roshi No. 52 paper with the solvent system, either R_f^4 or R_f^5. The optical rotations were determined with a polarimeter at the 589 sodium line. Amino acid analysis was carried out on the sample which had been hydrolyzed for 24 h in a evacuated sealed tube at 110 °C.

*Boc-D-Phe-Leu-OEt (**1**).* To a solution of Boc-D-Phe-OH (2.65 g, 10 mmol) in THF (20 ml), were added triethylamine (TEA, 1.40 ml) and isobutyl chloroformate (1.31 ml, 10 mmol) at 0—4 °C. The mixture was stirred for 10 min at 0—4 °C and to this was added a solution of H-Leu-OEt·*p*TsOH[14] (3.31 g, 10 mmol) and TEA (1.4 ml) in chloroform (20 ml). After the mixture was stirred overnight at a room temp, the solvent was evaporated *in vacuo* and the residue was taken up in AcOEt. The AcOEt solution was then washed successively with 0.5 M citric acid, 4% sodium hydrogen carbonate and water, and then dried (Na_2SO_4). The solvent was evaporated *in vacuo* and the product was precipitated by the addition of ether and petroleum ether. Recrystallization was carried out from ether–petroleum ether; yield, 2.64 g (65%); mp 111—112 °C; $[\alpha]_D^{25}$ −4.6° (*c* 1, DMF); R_f^1 0.96.
Found: C, 64.96; H, 8.44; N, 7.04%. Calcd for $C_{22}H_{34}N_2O_5$: C, 65.00; H, 8.43; N, 6.89%.

*Boc-D-Phe-Leu-N_2H_3 (**2**).* Hydrazine hydrate (2.91 ml, 60 mmol) was added with stirring to the solution of **1** (1.22 g, 3 mmol) in DMF (6 ml) and the mixture was left to stand at a room temp. After stirring for 48 h, the reaction mixture showed a single spot, which was distinguished from that of **1**, on a TLC plate. Excess hydrazine was evaporated

in vacuo, and then the product was precipitated with water (200 ml). The precipitates were washed with water and desiccated overnight (P_2O_5); yield, 1.03 g (87%); mp 163—164 °C; $[\alpha]_D^{25}$ −12.0° (*c* 1, DMF); R_f^1 0.77.

Found: C, 61.13; H, 8.30; N, 14.28%. Calcd for $C_{20}H_{32}N_4O_4$: C, 61.20; H, 8.22; N, 14.28%.

Boc-D-Phe-Leu-Val-Orn(Z)-Leu-OEt (**3**). In a mixture of glacial AcOH (40 ml) and 1 M HCl (3 ml) was dissolved **2** (0.59 g, 1.5 mmol) and the solution was cooled to −5 °C. To the solution was added, with stirring, a cold concentrated aq solution of sodium nitrite (0.103 g, 1.5 mmol). After 10 min, the azide was precipitated by the addition of cold water (200 ml) and the precipitates were filtered, washed successively with ice-cold water, 5% sodium hydrogen carbonate, and again with water. After brief drying (P_2O_5), the azide was added to the solution of H-Val-Orn(Z)-Leu-OEt·HCl[11] (0.815 g, 1.5 mmol) and TEA (0.21 ml, 1.5 mmol) dissolved in DMF (10 ml). After standing overnight at 0 °C and then for 2 days at a room temp, the reaction mixture was concentrated *in vacuo* and the product was precipitated on adding water. The crude product was recrystallized with EtOH–ether; yield, 1.04 g (80%); mp 237—238 °C (dec); $[\alpha]_D^{20}$ −14.0° (*c* 1, DMF); R_f^1 0.98, R_f^2 0.98.

Found: C, 63.45; H, 8.19; N, 9.71%. Calcd for $C_{46}H_{70}N_6O_{10}$: C, 63.72; H, 8.14; N, 9.69%.

Boc-D-Phe-Leu-Val-Orn(Z)-Leu-N$_2$H$_3$ (**4**). A solution of **3** (0.867 g, 1 mmol) and hydrazine hydrate (1.94 ml, 40 mmol) in DMF (20 ml) was left to stand for 8 days at a room temp and hydrazide precipitated in the reaction mixture was filtered, washed with water and with a small amount of EtOH, and then dried (P_2O_5); yield ,0.72 g (82%); mp 237—238 °C (dec); $[\alpha]_D^{20}$ −11.8° (*c* 1, DMF); R_f^1 0.98, R_f^2 0.94, R_f^5 0.98.

Found: C, 60.55; H, 9.86; N, 12.50%. Calcd for $C_{44}H_{68}N_8O_9$: C, 60.52; H, 10.16; N, 12.83%.

H-D-Phe-Leu-Val-Orn(Z)-Leu-OEt·HCl (**5**). Compound **4** (434 mg, 0.5 mmol) was dissolved in 0.075 M HCl in formic acid (8.0 ml) and allowed to stand for 2 h at a room temp. After the reaction mixture was evaporated to dryness *in vacuo*, the product was solidified by the addition of ether; yield, 387 mg (96%); mp 231 °C (dec); $[\alpha]_D^{20}$ +4.0° (*c* 1, DMF); R_f^1 0.66, R_f^2 0.10, R_f^5 (PPC) 0.95.

Found: C, 60.48; H, 7.95; N, 10.23%. Calcd for $C_{41}H_{63}N_6O_8Cl\cdot 1/2H_2O$: C, 60.61; H, 7.94; N, 10.34%.

Boc-(D-Phe-Leu-Val-Orn(Z)-Leu)$_2$-OEt (**6**). To a solution of **4** (175 mg, 0.2 mmol) in a mixed solvent of DMF (25 ml) and DMSO (25 ml) were added 3.97 M HCl in dioxane and then isoamyl nitrite (0.031 ml, 0.22 mmol) at −30 °C. After 30 min of stirring at −10 °C, hydrazide test[15] of the reaction mixture turned negative. And the mixture was neutralized by the addition of TEA (0.084 ml, 0.6 mmol). After 5 min at 0 °C, a solution of **5** (176 mg, 0.22 mmol) was added to the mixture. After stirring for 3 days at 4 °C, 0.5 M citric acid (100 ml) was added to the reaction mixture concentrated *in vacuo* to *ca.* 30 ml, and the mixture was kept at 4 °C for 3 h. The colloidal product, which was hard to filter, was collected by centrifugation at 4000×*g* for 10 min and washed with water several times. The resulting residue was dried over P_2O_5.

Boc-Val-Orn(Z)-Leu-N$_2$H$_3$ (**7**). To a solution of Boc-Val-Orn(Z)-Leu-OEt[11] (1.03 g, 1.7 mmol) in DMF (3 ml), hydrazine hydrate (1.65 ml, 34 mmol) was added and allowed to stand overnight at a room temp. After the excess hydrazine had been evaporated *in vacuo*, water (50 ml) was added to the mixture.Precipitates formed were filtered, washed with water, and dried (P_2O_5); yield ,988 mg (98%); mp 209—210 °C; $[\alpha]_D^{20}$ −19.2° (*c* 0.5, AcOH); R_f^1 0.70, R_f^5 0.95.

Found: C, 59.05; H, 8.22; N, 14.21%. Calcd for $C_{29}H_{48}O_7N_6$: C, 58.76; H, 8.16; N, 14.18%.

H-D-Phe-Leu-OEt·HCl (**8**). The compound **1** (813 mg, 2 mmol) was dissolved in 0.113 M HCl in formic acid (21.2 ml) and allowed to stand at a room temp. After 30 min, the solution was evaporated *in vacuo*. The addition of ether and subsequent evaporation were repeated several times and the oily product was obtained; yield of the oil, 686 mg (100%); R_f^1 0.73.

Boc-Val-Orn(Z)-Leu-D-Phe-Leu-OEt (**9**). The compound was obtained from **7** (890 mg, 1.5 mmol) and **8** (686 mg, 2 mmol) by the azide procedure[10] as described for the preparation of **6**. The product was crystallized twice from AcOEt–ether–petroleum ether; yield, 701 mg (54%); mp 211—213 °C; $[\alpha]_D^{20}$ −12.9° (*c* 1, DMF); R_f^3 0.73.

Found: C, 63.47; H, 8.10; N, 9.63%. Calcd for $C_{46}H_{70}O_{10}N_6$: C, 63.72; H, 8.14; N, 9.69%.

Boc-Val-Orn(Z)-Leu-D-Phe-Leu-N$_2$H$_3$ (**10**). The compound **9** (607 mg, 0.7 mmol) was dissolved in DMF (10 ml) and hydrazine hydrate (1.36 ml, 28 mmol) was added. After standing for two days at a room temp, the solvent was evaporated *in vacuo* to a small volume and water was added to the residue. After brief standing at 4 °C, the precipitates were filtered and dried over P_2O_5; yield, 622 mg (96%); mp 207—209 °C; $[\alpha]_D^{20}$ −11.3° (*c* 0.5, DMF); R_f^1 0.67.

Found: C, 61.61; H, 8.21; N, 13.00%. Calcd for $C_{44}H_{68}O_9N_8$: C, 61.95; H, 8.04; N, 13.14%.

H-Val-Orn(Z)-Leu-D-Phe-Leu-OEt·HCl (**11**). Deblocking of Boc-group from **9** (780 mg, 0.9 mmol) was performed by the similar method described in the preparation of **5** by the action of 0.13 M HCl in formic acid (7.6 ml); yield, 694 mg (96%); mp 211—213 °C; $[\alpha]_D^{20}$ +3.8° (*c* 1, DMF) R_f^3 0.17.

Found: C, 61.17; H, 7.92; N, 10.36%. Calcd for $C_{41}H_{63}O_8N_6Cl$: C, 61.29; H, 7.90; N, 10.46%.

Boc-(Val-Orn(Z)-Leu-D-Phe-Leu)$_2$-OEt (**12**). This compound was prepared from **10** (512 mg, 0.6 mmol) and **11** (627 mg, 0.78 mmol) by the similar method described for the preparation of **3**, except that a mixed solvent, DMF–DMSO (5 : 1, v/v), was used in this case. Crude product was recrystallized from MeOH; yield, 839 mg (88%); mp 239—241 °C; $[\alpha]_D^{20}$ −13.4° (*c* 0.5, DMF); R_f^1 0.93.

Found: C, 63.57; H, 7.97; N, 10.58%. Calcd for $C_{85}H_{126}O_{17}N_{12}\cdot H_2O$: C, 63.57; H, 8.08; N, 10.53%.

Boc-(Val-Orn(Z)-Leu-D-Phe-Leu)$_2$-N$_2$H$_3$ (**13**). To the compound **12** (250 mg, 0.157 mmol) dissolved in DMF (10 ml), was added 200 molar equivalents of hydrazine hydrate (1.52 ml, 31.4 mmol) and allowed to stand at a room temp for 2 days and treated as described for the preparation of **2**; yield, 226 mg (96%); mp >250 °C; $[\alpha]_D^{20}$ −14.6° (*c* 0.5, DMF–DMSO (2 : 1, v/v)); R_f^2 0.01, R_f^3 0.41.

Found: C, 63.20; H, 8.01; N, 12.20%. Calcd for $C_{83}H_{124}O_{16}N_{14}$: C, 63.33; H, 7.94; N, 12.46%.

H-(Val-Orn(Z)-Leu-D-Phe-Leu)$_2$-N$_2$H$_3$·2HCl (**14**). The compound **13** (200 mg, 0.127 mmol) was treated with 0.12 M HCl in formic acid (2.5 ml) at a room temp. After an hour, the reaction mixture was evaporated *in vacuo*, AcOEt added to the residue and evaporation repeated. To the residue was added ether and the mixture was kept at 4 °C; yield, 199 mg (100%); mp >250 °C; $[\alpha]_D^{20}$ −32.2° (*c* 0.2, DMF–DMSO (2 : 1, v/v)); R_f^1 0.41.

Found: C, 60.11; H, 7.74; N, 12.53%. Calcd for $C_{78}H_{116}O_{14}N_{14}\cdot 2HCl\cdot H_2O$: C, 59.86; H, 7.73; N, 12.53%.

cyclo(*-(Val-Orn(Z)-Leu-D-Phe-Leu)$_2$-*) (**15**). To the solution of **14** (193 mg, 0.13 mmol) in DMF–DMSO (2 : 1, v/v, 6 ml) was added at −30 °C, 2.7 M HCl in AcOEt (0.096 ml) and then 10% isoamyl nitrite in DMF (0.182 ml,

0.13 mmol). The reaction mixture was stirred at −20 °C until hydrazide test[15] became negative. After 15 min of stirring, the resulting pale yellow solution was added at 0 °C to pyridine (65 ml) and the mixture was kept stirring at 0 °C. After 3 days, pyridine and DMF were evaporated *in vacuo* from the mixture and 5 M citric acid (80 ml) was added. White precipitates formed were filtered, washed with water and dried (P_2O_5). The crude product (199 mg) was dissolved in a mixture of MeOH (100 ml) and H_2O (10 ml), and passed through a column (1.5×7.0 cm) of Dowex 50x8 and the elution was performed with the same solvent. The combined eluates were evaporated *in vacuo*. The white residue was filtered with the aid of small amount of water and dried over P_2O_5. The product (125 mg) was recrystallized from MeOH–H_2O; yield, 109 mg (58%); mp >250 °C; $[\alpha]_D^{20}$ −122° (*c* 0.2, DMF); R_f^3 0.53.

Found: C, 64.01; H, 7.82; N, 11.17%; mol wt,[16] 1441. Calcd for $C_{78}H_{112}O_{14}N_{12}\cdot H_2O$: C, 64.17; H, 7.87; N, 11.51 %; mol wt, 1460.

cyclo*(−(Val–Orn–Leu–*D*-Phe–Leu)$_2$−)·2HCl* (**16**).

The compound **15** was dissolved in 0.07 M HCl in EtOH (1.2 ml) and hydrogenolysis was performed in the presence of palladium black. After 2 h, additional 0.07 M HCl was added to the reaction mixture and the hydrogenolysis was continued overnight at 4 °C. After the catalyst had been filtered and washed several times with EtOH, the filtrate was evaporated to dryness and the residual solid was collected with the aid of ether. The crude product was recrystallized from EtOH–ether; yield, 29 mg (67%); mp 251—255 °C; $[\alpha]_D^{20}$ −156° (*c* 0.2, DMF); R_f^3 0.01, R_f^4 0.91, R_f^4 (PPC) 0.92. Amino acid ratios in acid hydrolyzate; Val 2.16, Orn 2.00, Leu 4.00, Phe 2.30.

Found: C, 56.52; H, 8.24; N, 12.33%. Calcd for $C_{62}H_{100}O_{10}N_{12}\cdot 2HCl\cdot 4H_2O$: C, 56.47; H, 8.40; N, 12.75%.

Electrophoresis Electrophoresis on Toyo Roshi No. 52 paper was carried out with a solvent system, formic acid–AcOH–MeOH–H_2O (1 : 3 : 6 : 10, v/v, pH 1.8) at 500 V/30 cm for 3 h. As shown in Fig. 3, [5,5′-Leu]-GS migrated more slowly toward cathode than the control GS, *i.e.* the former migrated 7.4 cm and the latter 8 cm by length.

ORD Measurements These were performed with a JASCO spectropolarimeter Model ORD/UV-5 over a range 215—300 nm. A cell of the path length 0.1 cm was used and the runs were at ambient temperature. Patterns in EtOH and 8 M urea are shown in Fig. 2.

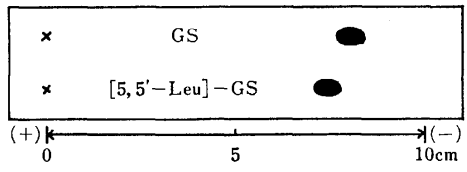

Fig. 3. Paper electrophoresis of [5,5′-Leu]-GS (**16**) and natural GS.

Microbiological Assays. The results of the assay and the microorganisms employed are listed in Table 1. The minimum amount of the compound necessary for the complete inhibition of growth was determined by a dilution method using a bouillon agar medium and a synthetic medium. As shown in Tables 1 and 2, [5,5′-Leu]-GS (**16**) was found to exhibit a considerable antibacterial activity against *Bacillus subtilis* and *Staphylococcus aureus*.

The authors are indebted to Dr. K. Kuromizu for his useful suggestions and discussions, Mr. Y. Shimohigashi for ORD measurements ,and the staffs of Takeda Chemical Industries, Ltd., for the biological assays.

References

1) Part XXXV of this series: K. Sato, H. Abe, T. Kato, and N. Izumiya, *Bull. Chem. Soc. Jpn.*, **50**, 1999 (1977).
2) All optically active amino acids, except D-Phe, are of the L configuration.
3) H. Aoyagi, T. Kato, M. Ohno, M. Kondo, M. Waki, S. Makisumi, and N. Izumiya, *Bull. Chem. Soc. Jpn.*, **38**, 2139 (1965).
4) H. Aoyagi and N. Izumiya, *Bull. Chem. Soc. Jpn.*, **39**, 1747 (1966).
5) S. Matsuura, M. Waki, S. Makisumi, and N. Izumiya, *Bull. Chem. Soc. Jpn.*, **43**, 1197 (1970).
6) H. Takiguchi, H. Nishikawa, K. Matsudai, and N. Izumiya, *Fukuoka Univ. Sci. Reports*, **3**, 31 (1974).
7) H. Takiguchi, H. Nishikawa, and N. Izumiya, *Fukuoka Univ. Sci. Reports*, **5**, 139 (1975).
8) I. W. Pollard, N. V. Bhagavan, and J. B. Hall, *Biochemistry*, **7**, 1153 (1968).
9) T. Curtius, *Ber.*, **35**, 3226 (1902).
10) J. Honzl and J. Rudinger, *Collect. Czech. Chem. Commun.*, **26**, 2333 (1961).
11) H. Abe, K. Sato, T. Kato, and N. Izumiya, *Bull. Chem. Soc. Jpn.*, **49**, 3113 (1976).
12) S. Matsuura, M. Waki, and N. Izumiya, *Bull. Chem. Soc. Jpn.*, **45**, 863 (1972).
13) D. C. Hodgkin and B. M. Oughton, *Biochem. J.*, **65**, 752 (1957).
14) T. Kato, S. Makisumi, M. Ohno, and N. Izumiya, *Nippon Kagaku Zasshi*, **83**, 1151 (1962).
15) H. Ertel and L. Horner, *J. Chromatogr.*, **7**, 268 (1962).
16) Molecular weight was determined on a Hitachi Osmometer, type 115, with methanol as a solvent.

The Photobromination of β-Styrenesulfonamides and Syntheses of 2-Arylacetylene-1-sulfonamides

Kiyoshi HASEGAWA, Syuzi HIROOKA, Hiroshi KAWAHARA, Atsushi TANAKA, Masahiro NOMURA, and Yutaka HORI

Department of Industrial Chemistry, Faculty of Engineering, Toyama University, Takaoka 933

(Received November 4, 1976)

The photobromination of *trans*-β-styrenesulfonamides in acetic acid at 16—18 °C gave about 75 : 25 mixtures of *threo* (*cis* adducts)- and *erythro*-1,2-dibromo-2-arylethane-1-sulfonamides (*trans* adducts). A similar photobromination of *cis*-β-styrenesulfonamide afforded a 33 : 67 mixture of the *threo* (*trans* adduct)- and the *erythro*-dibromides (*cis* adduct). The diastereomers could be separated by fractional recrystallization. The *cis* adducts were shown to be formed neither by secondary isomerization nor by (presumably) ionic addition. The *trans* dehydrobromination of the *threo*- and the *erythro*-dibromides with Et_3N gave (*Z*)- and (*E*)-β-bromo-β-styrenesulfonamides respectively, which underwent further facile dehydrobromination with aqueous 1 M NaOH at 45—50 °C to afford 2-arylacetylene-1-sulfonamides. They were also prepared from (*Z*)-α-chloro-β-styrenesulfonamide by an analogous procedure.

Triple bonds are more subject to nucleophilic attack than are double bonds.[1] It was, therefore, of interest to synthesize new 2-arylacetylene-1-sulfonic acids and -sulfonyl chlorides and to investigate their reactions with nucleophiles.

Rondestvedt, Jr. previously reported that the sulfonation of phenylacetylene or its acetylide was unsuccessful and the dehydrobromination of β-bromo-β-styrenesulfonic acid and -sulfonyl chloride gave only decomposed products involving no sulfonyl group.[2] He assumed that the *cis* configuration with respect to H and Br atoms makes the dehydrobromination difficult. Since then, acetylenesulfonic acid derivatives have not been studied.

Since an alkali-soluble sulfonamide group would promote dehydrobromination by alkali, we attempted to synthesize 2-arylacetylene-1-sulfonamides (**5**) from β-bromo- (**3**) and α-chloro-β-styrenesulfonamides (**4**). This paper will describe the stereochmistry of 1,2-dibromo-2-arylethane-1-sulfonamides (**2**), **3**, and **4**, and the synthesis of **5** from them.

Results and Discussion

Photobromination of trans- *and* cis-*β-Styrenesulfonamides.* It is known that bromine adds to *trans*-β-styrenesulfonyl chloride in CCl_4[2-4] or to *trans*-β-styrenesulfonamide (*trans*-**1a**, R=H) in acetic acid[2,3] by (presumably) a free-radical mechanism which is catalyzed by light and inhibited by oxygen. However, the stereochemistry of these adducts has not been estabilshed.

According to the procedure of Bordwell *et al.*,[3] *trans*-**1** was photobrominated by sunlight irradiation at 16—18 °C for 30 min. All of the crude products was shown by NMR spectroscopic and high-speed liquid chromatographic analyses to be mixtures of the *threo*- and *erythro*-**2**, predominantly the *threo*. On the contrary, *cis*-β-styrenesulfonamide (*cis*-**1a**) gave a mixture of the diastereomers in which the *erythro* predominated. Table 1 shows the distribution of the diastereomers and their NMR spectroscopic data. The stereochemical relationships are presented in Scheme 1. As the *erythro*-dibromides (R= H, CH_3, and NO_2) are more soluble in benzene than the *threo*, the two isomers could be separated by fractional recrystallization (Table 2). However, the *p*-halogeno-substituted dibromides could not be separated into their diastereomers. The *threo* and *erythro* configurations were assigned to **2** on the basis of the coupling constants (J_{AB}) and the configuration of **3** produced from **2** by *trans* elimination. It is known that the magnitude of the vicinal coupling constant (J_{AB}) depends upon the dihedral angle involved.[5] The diastereomers which have the larger coupling constants were assigned to the *erythro*-**2**, since it seems evident, from a consideration of the steric repulsion by large bromine atoms, that the

Table 1. Addition products of an equimolar amount of bromine to *trans*-**1** and *cis*-**1a** (0.0010 mol) in acetic acid (15 ml) at 16—18 °C for 30 min

R	Yield %	Ratio(%)[a] *threo*	NMR data[b] *threo* H_A	*threo* H_B	*threo* J_{AB}	*erythro* H_A	*erythro* H_B	*erythro* J_{AB}
H[c]	85	74	5.54	5.89	4.0	5.73	5.88	6.5
H[d]	84	33						
CH_3[c]	85	81	5.55	5.88	5.0	5.74	5.86	6.5
Cl[c]	89	76	5.65	5.85	5.0	5.80	5.87	6.5
Br[c]	86	74	5.66	5.84	5.0	5.79	5.88	6.5
NO_2[c]	79	77	5.88	6.01	5.5		e)	

a) Determined by the NMR analysis of the crude products. b) Measured in DMSO-d_6, with TMS as the internal standard; chemical shifts reported in δ(ppm) and coupling constants(J_{AB}) in Hz units. c) *trans*-**1**. d) *cis*-**1a**. e) The chemical shifts are ambiguous.

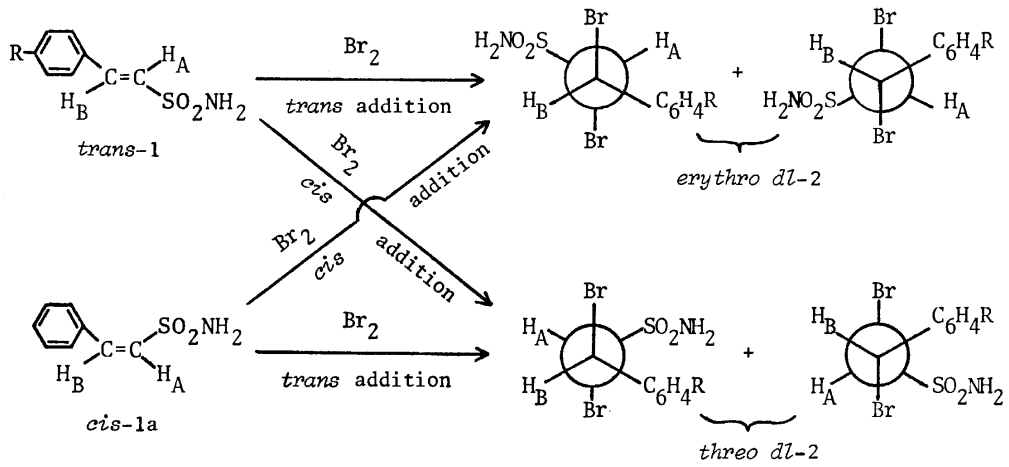

Scheme 1.

TABLE 2. *threo-* AND *erythro*-DIBROMIDES **2**

Compd	R	Mp(°C)	Found(%)				Calcd(%)				IR(KBr)
			C	H	N	S	C	H	N	S	$NH_2(cm^{-1})$
threo-**2a**	H	158—160[a]	28.01	2.80	4.31		28.01	2.64	4.08	9.35	3300, 3400
erythro-**2a**	H	122—123	28.25	2.65	4.02	9.52					3300, 3400
threo-**2b**	CH_3	123—124	30.02	3.12	3.92	8.72	30.27	3.11	3.99	8.97	3260, 3350
erythro-**2b**	CH_3	147—148	30.12	2.91	3.87	8.74					3280, 3390
2c[b]	Cl	142—145	25.71	2.38	3.68	8.60	25.45	2.14	3.71	8.49	3240, 3340 3280, 3400
2d[b]	Br	157—160	22.92	1.96	3.05	7.66	22.77	1.91	3.32	7.60	3240, 3340 3280, 3400
threo-**2e**	NO_2	173—176	24.69	2.07	7.14	8.42	24.76	2.08	7.22	8.26	3240, 3350

a) Lit,[3] mp 161—162 °C. b) They are mixtures of *threo-* and *erythro*-**2**. *threo*(%) : *erythro*(%); (**2c**) = 75 : 25 and (**2d**) = 73 : 27.

conformers shown in Scheme 1 will contribute more heavily to the rotational isomers of the *erythro-* and *threo*-**2**. Figure 1 shows the NMR spectra of *threo-* and *erythro*-**2a** in their methine-field regions. As the AB patterns of both diastereomers could be clearly distinguished, the evaluation of the signal intensities gave an

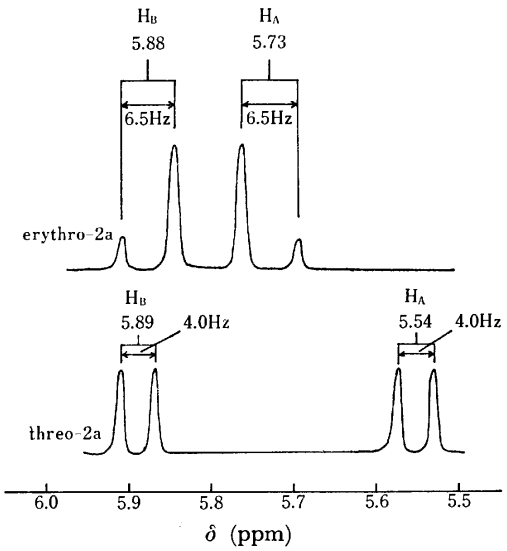

Fig. 1. NMR spectra of *threo-* and *erythro*-**2a** in methine region (DMSO-d_6).

estimate of the amounts of each isomer present. Our conclusion, to be drawn from the subsequent discussion of the configuration of **3**, also supports the stereochemical assignment based upon the coupling constants. The IR spectra of *threo*-**2b**—**e** showed a pair of NH_2 bands at a lower frequency region than the NH_2 bands of the *erythro* isomers.

As Bordwell and Rondestvedt, Jr., reported previously,[3] the addition was accelerated by light irradiation. Upon sunlight irradiation at 16—18 °C, the addition was completed within 5 min, but in the dark **2** was prepared in yields of less than 8%. The influence of the reaction time and the temperature on the stereochemistry of the addition was studied in order to find out whether the *cis* adducts were formed in the addition step or whether they arose from the subsequent isomerization of the initially formed *trans* adducts. Under the conditions used, the absence of isomerization between *trans-* and *cis*-**1** prior to the addition was proved by a blank test. The results summarized in Table 3 show that the isomerization of the products is negligible even at high temperatures and that the addition becomes non-stereospecific as the temperature increases. The *cis* addition under sunlight irradiation is a striking feature; however, its explanation must await the results of mechanical studies.

Syntheses of **5** *by Dehydrobromination.* The stereospecific *trans* dehydrobromination of *threo-* and *erythro*-**2**

Table 3. Influence of reaction time and temperature on the distribution of **2**[a]

R	Time (min)	Temp (°C)	Ratio(%) *threo*
H[b]	5	16—18	75
	30	16—18	74
	60	16—18	75
	5	48—50	63
	30	48—50	64
	5	68—70	58
	30	68—70	57
H[c]	5	16—18	33
	30	16—18	33
	5	48—50	49
	5	68—70	54

a) The experiments were carried out under the conditions described in Table 1. b) *trans*-**1a**. c) *cis*-**1a**.

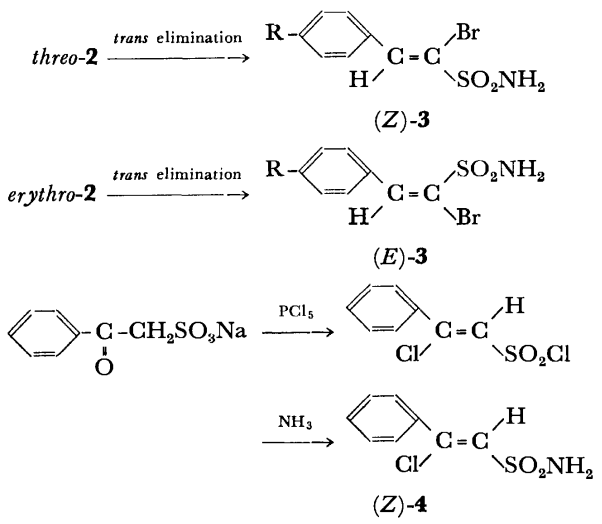

with Et_3N gave *Z* and *E* isomers of **3** respectively. On the other hand, the *Z* isomer of **4** was prepared by the route described below. The results are summarized in Table 4. The *Z* and *E* configurations were assigned to **3** and **4** on the basis of the NMR data and the relative rate measurement of the dehydrobromination from them. The vinyl protons of **3** and **4** resonate about 0.30 ppm upfield from the chemical shifts calculated by the application of the NMR rules[6] of additivity. Since no substituent shielding constants for the SO_2NH_2 group have been reported, the value for the SO_2R group was used. The error must be caused by the shield effect of the NH_2 group. The dehydrobromination experiments of both isomers of **3** in five equiv of aqueous 1 M NaOH at 40 °C for 30 min revealed that not only (*Z*)-**3** is capable of undergoing a facile *β-trans* elimination to

(*Z*)-**3** : δ_{CH}(ppm)=5.25+1.38+1.16+0.55=8.34

(*E*)-**3** : δ_{CH}(ppm)=5.25+1.38+0.45+0.93=8.01

(*Z*)-**4** : δ_{CH}(ppm)=5.25+1.55+0.36+0.13=7.29

give **5**, but, surprisingly, (*E*)-**3** also. The only difference is that the *cis* elimination is slower than the *trans* process. The **5a** sulfonamide was also prepared by the dehydrochlorination of (*Z*)-**4** under the same conditions as held with **3**. The extent of the elimination was measured by the increase in **5** at the expense of **3** and **4** in high-speed liquid chromatography. The configuration and *p*-substituent effects on the elimination are as follows: (*Z*)-**3**; R(reaction %)=NO_2(100) > Cl(23) > Br(22) > H(16) > CH_3(5), (*E*)-**3a**; H(8), and (*Z*)-**4**; H(14). This order is in accord with the idea that electron-attracting groups facilitate elimination reactions.[7] The reason for the greater ease of

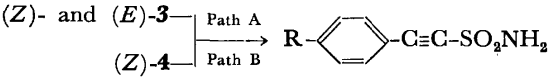

5

Table 4. (*Z*)- and (*E*)-monobromides **3** and (*Z*)-monochloride **4**

Compd	R	Mp(°C)	Crystals[a]	NMR in DMSO-d_6 CH(δ)	Found(Calcd), % C	H	N	S	UV $\lambda_{max}^{C_2H_5OH}$ (ε_{max})
(*Z*)-**3a**	H	132—134[b]	needles	8.01	36.38 (36.65)	3.13 (3.08)	5.07 (5.34)	12.26 (12.23)	266 (18500)
(*E*)-**3a**	H	140—142	prisms	7.60	36.50	2.96	5.12	12.32	266 (13400)
(*Z*)-**3b**	CH_3	135—137	plates	8.00	39.23 (39.14)	3.46 (3.65)	4.88 (5.07)	11.93 (11.61)	274 (20600)
(*E*)-**3b**	CH_3	120—122	columns	7.58	38.94	3.49	4.91		276 (14000)
(*Z*)-**3c**[c]	Cl	147—148	plates	8.05	32.69 (32.40)	2.37 (2.38)	4.56 (4.72)	10.91 (10.81)	272 (19500)
(*E*)-**3c**[c]	Cl	133—135	needles	7.60	32.62	2.55	4.62	10.94	272 (14300)
(*Z*)-**3d**[c]	Br	169—171	plates	8.01	28.43 (28.17)	2.16 (2.07)	4.14 (4.11)	9.39 (9.40)	274 (21200)
(*Z*)-**3e**	NO_2	174—176	needles	8.15	31.52 (31.28)	2.28 (2.30)	8.90 (9.12)	10.44 (10.44)	298 (16700)
(*E*)-**3e**	NO_2	159—161	columns	7.58	31.32	2.23	8.88	11.22	294 (14700)
(*Z*)-**4**	H	161—162	needles	7.05	44.36 (44.14)	3.97 (3.70)	6.66 (6.44)	14.64 (14.73)	251 (10300)

a) Recrystallized from benzene. b) Lit,[2] mp 132—133 °C, lit,[3] mp 130—131 °C. c) They were separated by crystal forms.

Table 5. 2-Arylacetylene-1-sulfonamides 5

Compd	R	Yield(%)[a] path A	path B	path C	Mp (°C)	Found(%) C	H	N	S	Calcd(%) C	H	N	S	UV $\lambda_{max}^{C_2H_5OH}$ (ε_{max})
5a	H	72	83	78	136—138	53.16	3.64	7.70	17.47	53.04	3.90	7.73	17.70	248(19800)
5b	CH_3	45		40	149—152	55.16	4.36	7.10		55.37	4.65	7.18		254(21300)
5c	Cl	86		86	162—164	44.37	2.57	6.74	14.90	44.55	2.80	6.50	14.87	256(23500)
5d	Br	84		77	168—169	36.85	2.15	5.13	12.38	36.94	2.33	5.39	12.33	258(26800)
5e	NO_2	76		74	160—161	42.61	2.64	12.44	14.44	42.49	2.67	12.39	14.17	288(17700)

a) Yield after recrystallization from benzene.

the *cis* elimination from (*E*)-**3a** is the previous isomerization to (*Z*)-**3a** and/or the enhanced leaving ability of HBr from such a system when activated by an electron-attracting sulfonyl group.[8] As *cis*-**1a** is known to readily isomerize to *trans*-**1a** upon treatment with aqueous 1 M NaOH,[9] we attempted to detect (*Z*)-**3a** in the reaction mixture of (*E*)-**3a** by high-speed liquid chromatography, but it could not be found. However, this fact does not exclude the idea of the previous isomerization of (*E*)-**3a** if the *trans* elimination proceeds more rapidly than the isomerization.

We concluded that the **3a** sulfonamide (mp 132—133 °C[2] and 130—131 °C[3]), which was previously prepared by the dehydrobromination of the **2a** dibromide (mp 161—162 °C[3]) and by the amidation of β-bromo-β-styrenesulfonyl chloride,[2] has the *Z* configuration, judging from the physical properties and the spectral data.

The **5** sulfonamides were readily synthesized by treating **3** (Path A), (*Z*)-**4** (Path B), or **2** (Path C) with 4—5 equiv of aqueous 1 M NaOH for 5 h at 45—50 °C (Table 5). Both sulfonamides, **2** and **3**, were used without separation into their stereoisomers. The structures of **5** were determined on the basis of the analytical and spectral data. The IR spectrum of **5** displayed a strong absorption band at 2180—2190 cm^{-1} due to the C≡C bond. The **5** sulfonamides are stable enough to be stored for a year.

Experimental

The melting points and the IR, UV, NMR, and mass spectra were measured by the same apparatus as has been reported previously.[9] The high-speed liquid chromatographic analysis was carried out using a JASCO-FLC 150 apparatus on a 0.5 m×2.1 mm column packed with JASCO-DAC SV-O2 (Solvent: methanol (20—40%)-water). The melting points are uncorrected.

cis-*β-Styrenesulfonamide* (cis-*1a*). It was prepared in 100% purity by the method previously described by us.[9] Mp 122—122.5 °C (lit,[10] 96—98 °C).

threo- *and* erythro-*1,2-Dibromo-2-arylethane-1-sulfonamides* (threo *and* erythro-*2*). *General Procedure*: To a solution of *trans*-**1** (0.0010 mol) in purified acetic acid (15 ml) we added an equimolar amount of bromine at 16—18 °C, after which the solution was kept in sunlight at 16—18 °C. Acetic acid in aliquots irradiated for, 5, 30, and 60 min was evaporated *in vacuo* below 30 °C to leave a residue, which was solidified by the addition of ice water. Fractional recrystallization succeeded in separating the *threo* and *erythro* isomers except for the *p*-halogeno-substituted ones. The spectral data for *threo*- and *erythro*-**2a**: *threo*-**2a**: IR(KBr); 3400 and 3300 (NH_2), 1360, 1320, 1160, and 1130 (SO_2), 725 and 700 cm^{-1}. NMR (DMSO-d_6) δ: 5.54 (d, 1, H_A), 5.89 (d, 1, H_B), J_{AB}=4.0 Hz, 7.30—7.50 (m, 5, C_6H_5), and 7.50—7.60 (m, 2, NH_2). MS *m/e*: 343 (M^+). *erythro*-**2a**: IR(KBr); 3400 and 3300 (NH_2), 1350, 1160, and 1145 (SO_2) and 710 cm^{-1}. NMR (DMSO-d_6) δ: 5.73 (d, 1, H_A), 5.88 (d, 1, H_B), J_{AB}=6.5 Hz, 7.30—7.50 (m, 5, C_6H_5), and 7.50—7.60 (m, 2, NH_2). MS *m/e*: 343 (M^+).

(Z,E)-*β-Bromo-β-styrenesulfonamides* ((Z)-*3*, (E)-*3*). *General Procedure*: To a solution of *threo*-**2** (0.00050 mol) in benzene (100 ml) we added Et_3N (0.0020 mol), after which the solution was stirred for 1 h at room temperature. Triethylammonium bromide, which was immediately precipitated, was filtered out, and the filtrate was evaporated to dryness *in vacuo* to leave (*Z*)-**3**. The yields were more than 80%.

Isomers, (*E*)-**3**, were prepared from *erythro*-**2** by using the technique described in the synthesis of (*Z*)-**3**. The spectral data for (*Z*)- and (*E*)-**3a**: (*Z*)-**3a**: IR(KBr); 3350 and 3240 (NH_2), 1330 and 1160 (SO_2) cm^{-1}. NMR(DMSO-d_6) δ; 7.40—7.68 (m, 5, C_6H_5), 7.76—7.86 (m, 2, NH_2), and 8.01 (s, 1, CH). MS *m/e*; 262 (M^+). (*E*)-**3a**: IR(KBr); 3350 and 3240 (NH_2), 1330, 1170, 1160, and 1150 (SO_2) cm^{-1}. NMR(DMSO-d_6) δ; 7.28—7.48 (m, 5, C_6H_5), 7.60 (s, 1, CH), and 7.68 (s, 2, NH_2). MS *m/e*; 262 (M^+).

The dehydrobromination of **2c** (*threo* 75%) and **2d** (*threo* 73%) gave **3c** (*Z* 75%) and **3d** (*Z* 73%) respectively. The (*Z*)- and (*E*)-**3c**, and (*Z*)-**3d** could be separated by crystal forms, but (*E*)-**3d** could not be freed of (*Z*)-**3d**.

(Z)-*α-Chloro-β-styrenesulfonamide* ((Z)-*4*). Sodium benzoylmethanesulfonate (5.0 g, 0.023 mol) was refluxed with PCl_5 (18.7 g, 0.090 mol) for 10 h. The product was worked up in a way analogous to that reported in the synthesis of β-styrenesulfonyl chloride[11] and distilled under reduced pressure to give α-chloro-β-styrenesulfonyl chloride; bp 60—110 °C/3 mmHg (58% yield). Without further purification, it was converted to (*Z*)-**4** by treatment with a 28% ammonia solution. The *E* isomer could not be detected.

2-Arylacetylene-1-sulfonamides (*5*). *Paths A and C*: *General Procedure*: A solution of **3** (Path A) or **2** (Path C) in aqueous 1 M NaOH (50 ml, 0.050 mol) was stirred for 5 h at 45—50 °C and then acidified with concd HCl under cooling to give **5**. Recrystallization from benzene afforded thin plates.

Path B: Sulfonamide **5a** was prepared from (*Z*)-**4** and 1 M NaOH by using the procedure described for Paths A and C.

The spectral data for **5a**: IR(KBr); 3320 and 3210 (NH_2), 2180 (C≡C), 1330, 1180, and 1150 (SO_2) cm^{-1}. NMR (DMSO-d_6) δ; 7.55—7.60 (m, 5, C_6H_5) and 8.24 (s, 2, NH_2). MS *m/e*; 181 (M^+).

References

1) J. March, "Advanced Organic Chemistry, Reactions, Mechanism, and Structure," McGraw-Hill, International Student Ed., Tokyo (1968), p. 575 and cited references.

2) C. S. Rondestvedt, Jr., *J. Am. Chem. Soc.*, **76**, 1926 (1954).

3) F. G. Bordwell and C. S. Rondestvedt, Jr., *J. Am. Chem. Soc.*, **70**, 2429 (1948).

4) C. S. Rondestvedt Jr., R. L. Grimsley, and C. D. Ver Nooy, *J. Org. Chem.*, **21**, 206 (1956).

5) L. M. Jackman and S. Sternhell, "Applications of Nuclear Magnetic Resonance Spectroscopy in Organic Chemistry," 2nd ed, Pergamon Press, Germany (1969), p. 291.

6) a) C. Pascual, J. Meier, and W. Simon, *Helv. Chim. Acta*, **49**, 164 (1966); b) S. W. Tobey, *J. Org. Chem.*, **34**, 1281 (1969).

7) Abdel-Hamid A. Youssef and Hamdy M. Abdel-Maksoud, *J. Org. Chem.*, **40**, 3227 (1975).

8) a) Y. Amiel, *J. Org. Chem.*, **39**, 3867 (1974); b) F. G. Bordwell, J. Weinstock, and T. F. Sullivan, *J. Am. Chem. Soc.*, **93**, 4728 (1971).

9) K. Hasegawa, S. Hirooka, T. Sasaki, S. Ikeda, and K. Hashimoto, *Nippon Kagaku Kaishi*, **1975**, 1028.

10) A. P. Terentév, R. A. Gracheva, and Z. F. Shcherbatova, *Chem. Abstr.*, **47**, 3262e (1953).

11) C. S. Rondestvedt, Jr., and F. G. Bordwell, *Org. Synth.*, Coll. Vol. IV, 846 (1963).

Diphosphine–Rhodium Complex-Catalyzed Hydroformylation of α,β-Unsaturated Esters

Masato TANAKA, Teruyuki HAYASHI, and Ikuei OGATA

National Chemical Laboratory for Industry, Honmachi, Shibuya-ku, Tokyo 151

(Received December 14, 1976)

The product distribution in the hydroformylation of α,β-unsaturated esters (ethyl acrylate, methyl methacrylate, methyl crotonate, and methyl tiglate) catalyzed by $Rh_2Cl_2(CO)_4$ was studied at 150 °C under 100 atm of synthesis gas ($CO/H_2=1/1$) in the absence or presence of various additional phosphorus ligands. In order to attain a high selectivity of α-formylation (>80%), the addition of shorter methylene-chained diphosphines ($R_2P(CH_2)_nPR_2$, R=phenyl or cyclohexyl, $n=2$—4) to the reaction system was essential, while the use of $Rh_2Cl_2(CO)_4$ alone or in combination with triphenylphosphine or a longer diphosphine, $Ph_2P(CH_2)_5PPh_2$, resulted in a very low α-selectivity. The effects of the reaction variables on the product distribution were also examined for acrylate and methacrylate using $Ph_2P(CH_2)_4PPh_2$ and $Ph_2P(CH_2)_2PPh_2$, respectively, as additional ligands.

Among many types of polar olefins, α,β-unsaturated esters have received much attention as substrates for hydroformylation. The selective β-formylation of the ethylenic linkage of acrylates, followed by cyclization to afford γ-butyrolactone, has been accomplished by the use of a cobalt carbonyl catalyst.[1] On the other hand, it has been noted in a patent claim that a rhodium catalyst favors α-formylation, though the selectivity attained is not very high.[2] The composition of the products from ethyl acrylate under a wide range of the reaction conditions has also been examined in detail by the use of cobalt[3] as well as rhodium catalyst.[4] In the hydroformylation of methyl methacrylate by a rhodium catalyst, the addition of a large amount of a phosphorus ligand to the reaction system or a much elevated pressure of synthesis gas as high as 1000 atm is required for selective α-formylation.[5,6] Methyl crotonate undergoes formylation mainly on the β-carbon, and a relatively large amount of the hydrogenation by-product is also formed.[5]

In this report, the authors will describe the hydroformylation of various α,β-unsaturated esters by the use of the diphosphine–rhodium catalyst system, and it will be shown that this catalyst system is extremely efficient for selective α-formylation.

Experimental

Materials. Benzene and ethylbenzene were distilled under nitrogen. All of the substrates were commercial products, and were freshly distilled under nitrogen of a reduced pressure before use. Triphenylphosphine and 1,2-bis(diphenylphosphino)ethane were used as purchased. Tetracarbonyldi-μ-chlorodirhodium,[7] 1,3-bis(diphenylphosphino)propane,[8] 1,4-bis(diphenylphosphino)butane,[9] 1,5-bis(diphenylphosphino)pentane,[9] 1,2-bis(dicyclohexylphosphino)ethane,[10] 1,4-bis(dicyclohexylphosphino)butane,[11] and 1,2-bis(5*H*-dibenzophospholyl)ethane[12] were prepared by the previously reported methods.

Reaction Procedure. A 37-ml Schlenk-tube-type high-pressure reaction vessel, made of stainless steel (SUS 316), was charged under a nitrogen atmosphere with 3 ml of a solvent (ethylbenzene for ethyl acrylate and benzene for the other substrates), 1.3 mg of tetracarbonyldi-μ-chlorodirhodium (6.7×10^{-6} mol with respect to the rhodium atom), a desired amount of a phosphine, and 1.5 ml of a substrate. The reaction vessel was then sealed and flushed with carbon monoxide. Then, carbon monoxide and hydrogen were introduced up to their given partial pressures. The temperature was elevated in an oil bath. The reaction solution was then agitated magnetically.

Analysis of the Products. An aliquot of the reaction mixture was analyzed by gas chromatography. A Shimadzu model GC-3B gas chromatograph, equipped with a stainless steel column packed with diethylene glycol succinate polyester on Neopak AS (3 mm i.d.×2.5 m) was used at an oven temperature of 120 °C for most cases. The remainder of the reaction mixture was submitted to distillation, and the products were identified spectroscopically. The IR and NMR spectra were recorded on a Shimadzu IR 27G apparatus, and a JEOL C-60HL apparatus, respectively.

Results

The reaction was carried out at 150 °C under 100 atm of synthesis gas ($CO/H_2=1/1$), with $Rh_2Cl_2(CO)_4$ as a catalyst precursor, in the absence or presence of a variety of phosphines. The phosphorus-to-rhodium ratio of 4 : 1 was used in every case. The boiling points and spectral data of the products are summarized in Table 1. The NMR spectra of some α-formylated isomers show that these isomers are present in equilibrium with the corresponding enol forms. The approximate ratio of enol to aldehyde under the conditions of the NMR measurement (carbon tetrachloride solution, 31.5 °C) is also shown in the table.

Hydroformylation of Ethyl Acrylate. The results are summarized in Table 2. The catalytic activity of the rhodium complex was, in the absence of a phosphine, very low, and ethyl β-formylpropionate was mainly formed. The addition of triphenylphosphine to the reaction system much improved the α-selectivity, though the reaction was still sluggish. In contrast, when carried out in the presence of α,ω-bis(diphenylphosphino)-alkanes, $Ph_2P(CH_2)_nPPh_2$ ($n=2$—4), the reaction proceeded extremely fast, and the α-carbon was formylated almost exclusively. It was also found that the extent of the competitive hydrogenation was enhanced by the use of these diphosphines. As the carbon chain between the two phosphorus atoms of the diphosphine got longer from C_2 to C_4, the amount of the hydrogenation by-product much decreased and the α-selectivity became slightly higher. However, when the still longer diphosphine, $Ph_2P(CH_2)_5PPh_2$, was used, a very low α-selectivity was caused, and the competitive hydrogenation intensively occurred again. In addition, a much

TABLE 1. BOILING POINTS AND SPECTRAL DATA OF THE REACTION PRODUCTS

Structure	Bp (°C/Torr)	IR[a] (cm^{-1})	^{1}H-NMR[b] (τ ppm)	Enol/Aldehyde
$CH_3CH(CHO)COOCH_2CH_3$			0.36 (1H, d, J=1.4 Hz, CHO), 5.83 (2H, q, CH_2), 6.72 (1H, dq, CH), 8.75 (3H, d, J=7.2 Hz, CH_3CH), 8.75 (3H, t, J=6.9 Hz, CH_3CH_2)	
CH_3-C(=CH-OH)-$COOCH_2CH_3$	47.0—49.5/10	2730 ($\nu_{C(=O)H}$), 1745, 1720, 1668 (ν_{CO}), 1616 ($\nu_{C=C}$)	−1.21 (1H, d, OH), 3.09 (1H, d, J=12.6 Hz, CH), 5.81 (2H, q, CH_2), 8.35 (3H, s, CH_3C=), 8.73 (3H, t, J=6.7 Hz, CH_2CH_3) 0.35 (1H, s, CHO), 5.87 (2H, q, CH_2CH_3)	1.7/1.0
$OHC-CH_2CH_2COOCH_2CH_3$	56.5—57.3/3	2820, 2715 ($\nu_{C(=O)H}$), 1730 (ν_{CO})	7.15—7.55 (4H, m, $2CH_2$), 8.75 (3H, t, J=7.0 Hz, CH_3)	
$(CH_3)_2C(CHO)COOCH_3$	41.0—42.5/12	2820, 2710 ($\nu_{C(=O)H}$), 1730 (ν_{CO})	0.48 (1H, s, CHO), 6.28 (3H, s, OCH_3), 8.71 (6H, s, $2CH_3$)	
$OHC-CH_2CH(CH_3)COOCH_3$	49.0—49.3/3	2825, 2720 ($\nu_{C(=O)H}$), 1730 (ν_{CO})	0.36 (1H, s, CHO), 6.38 (3H, s, OCH_3), 7.0—7.6 (3H, m, $CHCH_2$), 8.82 (3H, d, J=7.0 Hz, $CHCH_3$)	
$CH_3CH_2CH(CHO)COOCH_3$			0.36 (1H, d, J=2.1 Hz, CHO), 6.25 (3H, s, OCH_3), 6.83 (1H, dt, CH), 8.10 (2H, m, CH_2), 9.06 (3H, t, J=7.5 Hz, CH_3CH_2)	1/1
CH_3CH_2-C(=CH-OH)-$COOCH_3$	43.0—46.0/10	2710 ($\nu_{C(=O)H}$), 1730, 1666 (ν_{CO}), 1605 ($\nu_{C=C}$)	−1.22 (1H, d, OH), 3.01 (1H, d, J=12.5 Hz, CH), 6.22 (3H, s, OCH_3), 8.04 (2H, q, CH_2CH_3), 9.00 (3H, t, J=7.5 Hz, CH_3CH_2)	
$CH_3CH(CHO)CH_2COOCH_3$	49.0—51.0/3	2800, 2700 ($\nu_{C(=O)H}$), 1730 (ν_{CO})	0.41 (1H, s, CHO), 6.35 (3H, s, OCH_3), 8.1—8.8 (3H, m, $CHCH_2$), 8.85 (3H, d, J=7.4 Hz, CH_3CH)	
$OHC-(CH_2)_3COOCH_3$	—	2810, 2700 ($\nu_{C(=O)H}$), 1730 (ν_{CO})	0.35 (1H, t, J=1.5 Hz, CHO), 6.38 (3H, s, OCH_3), 7.3—8.3 (6H, m, $3CH_2$)	
$CH_3CH_2C(CH_3)(CHO)COOCH_3$	33.0—36.0/3	2815, 2715 ($\nu_{C(=O)H}$), 1720 (ν_{CO})	0.42 (1H, s, CHO), 6.31 (3H, s, OCH_3), 8.19 (2H, m, CH_2), 8.77 (3H, s, CCH_3), 9.14 (3H, t, J=7.5 Hz, CH_3CH_2)	

a) Neat. b) In a carbon tetrachloride solution (10—20% solution); internal standard: TMS.

TABLE 2. HYDROFORMYLATION OF ETHYL ACRYLATE[a]

Phosphine	Reaction time (min)	Conversion (%)	Product distribution (%)[b]			α-Selectivity (%)[c]
			α	β	Dihydro	
—	36	6	28.6	66.7	4.8	22.9
PPh_3	180	27	71.5	27.0	1.5	72.5
$Ph_2P(CH_2)_2PPh_2$	42	100	64.2	2.6	32.0	96.1
$Ph_2P(CH_2)_3PPh_2$	22	≈100	72.3	2.9	24.8	96.1
$Ph_2P(CH_2)_4PPh_2$	5	≈100	85.4	2.3	12.3	97.4
$Ph_2P(CH_2)_5PPh_2$	550	≈100	49.9	17.0	33.1	74.6
$Cy_2P(CH_2)_2PCy_2$	7	100	79.9	3.8	16.3	95.5
$Cy_2P(CH_2)_4PCy_2$	12	≈100	67.2	1.1	31.7	98.4
DBP-$(CH_2)_2$-DBP[d]	76	100	32.1	17.3	50.5	65.0

a) Reaction conditions: 150 °C, 100 atm (CO/H_2=1/1), phosphorus/rhodium=4/1. b) α, β and dihydro stand for ethyl α-formylpropionate, ethyl β-formylpropionate, and ethyl propionate, respectively. c) α-Selectivity denotes $100\times\alpha/(\alpha+\beta)$. d) DBP stands for the 5*H*-dibenzophospholyl group.

longer reaction time was required for complete conversion in the case of this diphosphine.

The electronic effects on the product distribution were examined by the use of dicyclohexylphosphino analogues of 1,2-bis(diphenylphosphino)ethane and 1,4-bis(diphenylphosphino)butane. These effects are apparently not separable from steric effects, and no clear trends in either the reaction rate or the extent of the competitive hydrogenation could be found. The α-selectivity remained practically unchanged upon the exchange of the phenyl groups for the cyclohexyl ones.

The effect of the structure of the diphosphine was further studied using 1,2-bis(5H-dibenzophospholyl)-ethane, some rhodium complexes of which efficiently catalyzed the hydroformylation of olefinic hydrocarbons.[13] However, for ethyl acrylate, this diphosphine was much inferior in its catalytic activity as well as in its α-selectivity to 1,2-bis(diphenylphosphino)ethane.

Hydroformylation of Methyl Methacrylate. The results of the hydroformylation of methyl methacrylate are collected in Table 3. Unlike ethyl acrylate, methyl methacrylate was rapidly hydroformylated in the absence of phosphines. The β-isomer was mainly formed, accompanied by a considerable amount of the hydrogenation by-product. The addition of tertiary phosphines to the reaction system much retarded the reaction and increased the content of the α-isomer. In addition, it suppressed the competitive hydrogenation except the reaction with 1,3-bis(diphenylphosphino)-propane. The highest α-selectivity accomplished by the use of 1,2-bis(diphenylphosphino)ethane, 81.4%, was lower than that observed in the reaction of ethyl acrylate, probably because of the steric hindrance of the α-methyl substituent. 1,2-Bis(dicyclohexylphosphino)ethane and 1,4-bis(dicyclohexylphosphino)butane, which caused high α-selectivities similar to the diphenylphosphino counterpart in the reaction of ethyl acrylate, gave inferior results for methyl methacrylate. Probably, this is also attributable to the steric hindrance due to the presence of the α-methyl substituent on the double bond as well as to the large ligand cone angle[14] of the bis(dicyclohexylphosphino)alkanes.

Hydroformylation of Methyl Crotonate. The results are shown in Table 4. In comparison with the reactions of ethyl acrylate and methyl methacrylate, the hydroformylation of methyl crotonate gave very diverse results for the product distribution depending on the nature of the added ligands. Competitive hydrogenation was often the main reaction. Nevertheless, some of the diphosphines, such as $Ph_2P(CH_2)_{2(or\ 4)}PPh_2$ and $Cy_2P(CH_2)_2PCy_2$, showed high α-selectivities, suppressing the formation of the β- and γ-isomers which were the main products when the reaction was carried out either in the absence of any additional ligands or in the presence of triphenylphosphine.

Hydroformylation of Methyl Tiglate. The results

Table 3. Hydroformylation of methyl methacrylate[a]

Phosphine	Reaction time (min)	Conversion (%)	Product distribution (%)[b]			α-Selectivity (%)[c]
			α	β	Dihydro	
—	16	100	7.2	73.4	19.6	8.7
PPh_3	200	100	38.5	56.1	5.4	40.8
$Ph_2P(CH_2)_2PPh_2$	105	100	79.5	17.6	2.9	81.8
$Ph_2P(CH_2)_3PPh_2$	250	51	45.9	17.5	36.6	72.4
$Ph_2P(CH_2)_4PPh_2$	360	92	75.5	19.2	5.3	79.8
$Ph_2P(CH_2)_5PPh_2$	420	98	14.7	74.3	11.0	16.5
$Cy_2P(CH_2)_2PCy_2$	450	98	50.2	44.7	5.1	52.9
$Cy_2P(CH_2)_4PCy_2$	280	98	54.9	40.5	4.7	57.6

a) Reaction conditions: 150 °C, 100 atm ($CO/H_2=1/1$), phosphorus/rhodium=4/1. b) α, β and dihydro stand for methyl α-formylisobutyrate, methyl β-formylisobutyrate, and methyl isobutyrate, respectively. c) α-Selectivity denotes $100\times\alpha/(\alpha+\beta)$.

Table 4. Hydroformylation of methyl crotonate[a]

Phosphine	Reaction time (min)	Conversion (%)	Product distribution (%)[b]				α-Selectivity (%)
			α	β	γ	Dihydro	
—	160	100	0.0	51.7	30.0	18.0	0.0
PPh_3	210	100	17.2	52.6	12.6	17.6	20.9
$Ph_2P(CH_2)_2PPh_2$	150	100	22.9	2.0	0.0	75.1	91.8
$Ph_2P(CH_2)_3PPh_2$	210	93	8.8	4.6	0.0	86.6	65.5
$Ph_2P(CH_2)_4PPh_2$	240	92	80.1	5.2	0.0	14.7	93.9
$Ph_2P(CH_2)_5PPh_2$	360	94	3.6	40.6	27.9	28.0	5.0
$Cy_2P(CH_2)_2PCy_2$	360	71	43.5	2.6	0.1	53.8	94.2
$Cy_2P(CH_2)_4PCy_2$	210	40	41.4	28.2	4.7	25.7	55.7

a) Reaction conditions: 150 °C, 100 atom ($CO/H_2=1/1$), phosphorus/rhodium=4/1. b) α, β, γ, and dihydro stand for methyl α-formylbutyrate, methyl β-formylbutyrate, methyl γ-formylbutyrate, and methyl butyrate, respectively. c) α-Selectivity denotes $100\times\alpha/(\alpha+\beta+\gamma)$.

TABLE 5. HYDROFORMYLATION OF METHYL TIGLATE[a)]

Phosphine	Reaction time (h)	Conversion (%)	Yield[b)] (%)	α-Selectivity (%)[c)]
—	5	≈100	44	1.8
$Ph_2P(CH_2)_2PPh_2$	24	24	19	74.9
$Ph_2P(CH_2)_4PPh_2$	24	16	12	73.4

a) Reaction conditions: 150 °C, 100 atm ($CO/H_2=1/1$), phosphorus/rhodium=4/1. b) Total yield of the four aldehydes based on the amount of methyl tiglate charged (see the text). c) α-Selectivity denotes the percentage of methyl α-formyl-α-methylbutyrate in the total amount of the four aldehydes formed.

are shown in Table 5. Unlike the other substrates examined, a significant amount of unidentified high boiling by-product(s) was formed, especially in the absence of phosphine. As concerns the aldehyde formation, after comparing the gas chromatogram of the reaction mixture with that of methyl crotonate, the authors presume that all of the possible four isomeric aldehydes were produced. However, only the α-isomer could be isolated and identified. The other isomers could not be separated in a pure state because of the similarity of their boiling points. The α-selectivity, which was very low without added phosphines, was markedly enhanced by the use of the diphosphines.

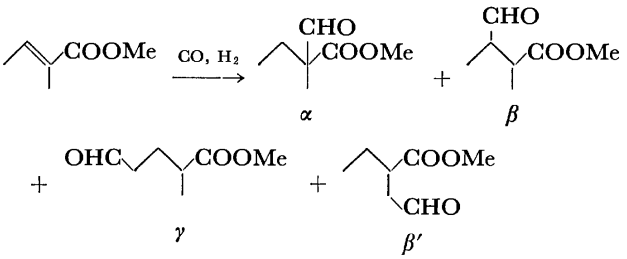

Effects of the Reaction Variables. Tables 2 and 3 show that 1,4-bis(diphenylphosphino)butane and 1,2-bis(diphenylphosphino)ethane are the most beneficial α-formylating ligands for ethyl acrylate and methyl methacrylate respectively. Therefore, using those most beneficial combinations of the ligand and the substrate, the effects of the reaction variables, such as the phosphorus-to-rhodium ratio, the reaction temperature, and the partial pressures of carbon monoxide and hydrogen, on the product distribution were briefly examined in order to search for the optimum conditions for selective α-formylation and to shed more light on the role of the diphosphines during the course of the reaction. The results are illustrated in Figs. 1—5.

Figure 1 shows that, in the reaction of ethyl acrylate, the decrease in the amount of the diphosphine slightly lowered the α-selectivity. Competitive hydrogenation was almost completely inhibited at phosphorus-to-rhodium ratios smaller than 2. A similar but more profound influence on the α-selectivity was also observed for methyl methacrylate (Fig. 2), while the effect on the hydrogenation by-product formation was just the reverse of that with ethyl acrylate, and, at the ratio of 2, the extent of hydrogenation was markedly intensive.

Lowering the reaction temperature increased the α-

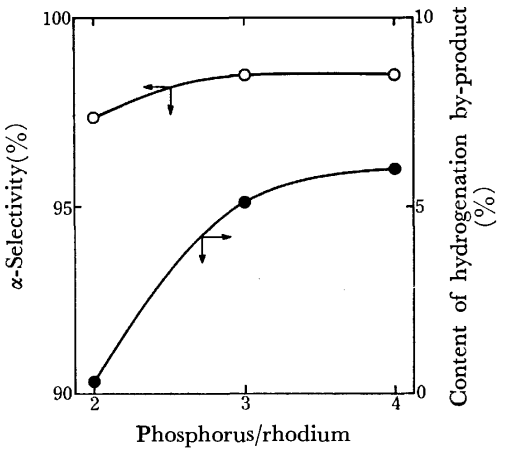

Fig. 1. Effects of the ratio of phosphorus/rhodium in hydroformylation of ethyl acrylate.
100 °C, 100 atm ($CO/H_2=1/1$), phosphine; $Ph_2P(CH_2)_4PPh_2$.

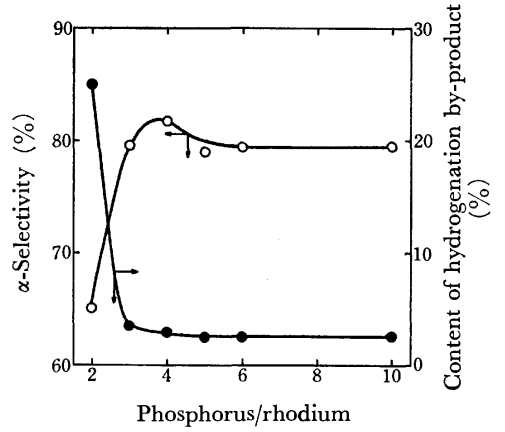

Fig. 2. Effects of the ratio of phosphorus/rhodium in hydroformylation of methyl methacrylate.
150 °C, 100 atm ($CO/H_2=1/1$), phosphine; $Ph_2P(CH_2)_2PPh_2$.

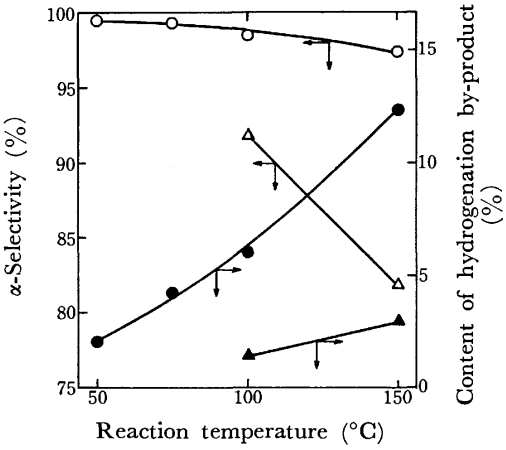

Fig. 3. Effects of the reaction temperature.
○,●: Ethyl acrylate: 100 atm ($CO/H_2=1/1$), phosphine; $Ph_2P(CH_2)_4PPh_2$, phosphorus/rhodium=4/1.
△,▲: Methyl methacrylate: 100 atm ($CO/H_2=1/1$), phosphine; $Ph_2P(CH_2)_2PPh_2$, phosphorus/rhodium=4/1.

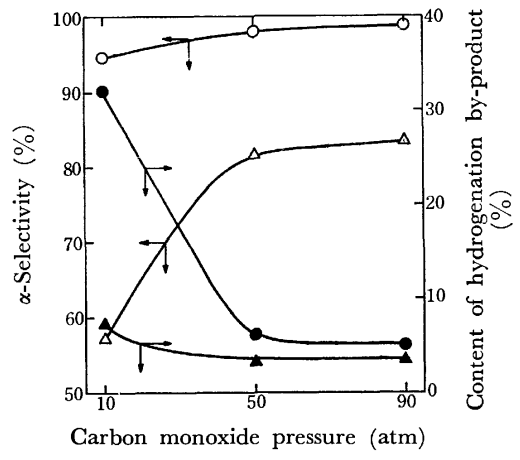

Fig. 4. Effects of the carbon monoxide pressure.
○,●: Ethyl acrylate: $p(H_2)=50$ atm, 100 °C, phosphine; $Ph_2P(CH_2)_4PPh_2$, phosphorus/rhodium=4/1.
△,▲: Methyl methacrylate: $p(H_2)=50$ atm, 150 °C, phosphine; $Ph_2P(CH_2)_2PPh_2$, phosphorus/rhodium=4/1.

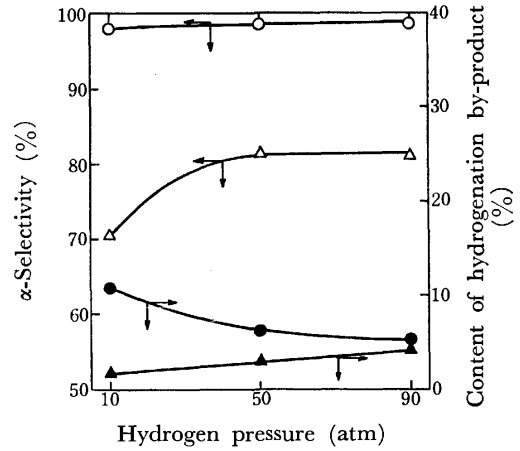

Fig. 5. Effects of the hydrogen pressure.
○,●: Ethyl acrylate: $p(CO)=50$ atm, 100 °C, phosphine; $Ph_2P(CH_2)_4PPh_2$, phosphorus/rhodium=4/1.
△,▲: Methyl methacrylate: $p(CO)=50$ atm, 150 °C, phosphine; $Ph_2P(CH_2)_2PPh_2$, phosphorus/rhodium=4/1.

selectivity and decreased the extent of hydrogenation for ethyl acrylate as well as methyl methacrylate (Fig. 3); therefore, it provides a very favorable condition for selective α-formylation. For example, when ethyl acrylate was allowed to react with synthesis gas (100 atm, $CO/H_2=1/1$) at 100 or 75 °C by the use of 1,4-bis(diphenylphosphino)butane (phosphorus/rhodium=4/1), the reaction was completed within 12 or 65 min respectively, and ethyl α-formylpropionate was obtained in a 92.6 or 95.1% yield (98.5 or 99.3% α-selectivity) respectively.

For both the substrates, the α-selectivity and the amount of hydrogenation by-product increased and decreased respectively with an increase in the carbon monoxide pressure up to *ca.* 50 atm; thereafter it remained practically unchanged (Fig. 4).

As Fig. 5 shows, the effect of the hydrogen pressure on the α-selectivity was smaller than, but similar to, that of the carbon monoxide pressure for both ethyl acrylate and methyl methacrylate. On the other hand, concerning the hydrogenation by-product formation, acrylate and methacrylate behaved differently from each other on a variation in the hydrogen pressure. Thus, for acrylate, a higher pressure suppressed the competitive hydrogenation. The influence of the hydrogen pressure on methacrylate was the reverse.

Discussion

As has been described above, the rhodium–diphosphine system is a very beneficial catalyst for the selective α-formylation of α,β-unsaturated esters. As concerns the isomer distribution, Takegami and his co-workers[4] have examined the hydroformylation of ethyl acrylate catalyzed by rhodium carbonyl under various reaction conditions. On the basis of the results, they have suggested that the extent of the skeletal isomerization of the α-metalated intermediate, which is preferably formed initially, is an important factor in deciding the product distribution. With the present catalyst system, the effects of the reaction variables on the α-selectivity in the reaction of ethyl acrylate were qualitatively the same as the above authors had observed. In addition, γ- and/or β′-isomers were also produced in the reaction of crotonate and tiglate. These results seem to indicate that such an isomerization occurs also with the diphosphine–rhodium catalysts (Scheme 1). The α-selectivity for methyl methacrylate was more sensitive to the reaction conditions than for ethyl acrylate. This can also be reasonably explained from the point of view of the skeletal isomerization; *i.e.*, the possibility of the skeletal isomerization of the α-metalated intermediate from methacrylate is greater than that from acrylate, because the former has two carbons onto which the rhodium can migrate through isomerization, while the latter has only one such carbon. However, judging from the extremely high α-selectivity and its low sensitivity to the reaction conditions compared with those reported by Takegami *et al.*, it might be better to consider that the extent of the skeletal isomerization is not so great with the present catalyst system. The shorter carbon-chained (C_2–C_4) diphosphines may coordinate tightly to rhodium because of their chelating power, and may thus stabilize the α-metalated intermediate predominantly formed initially, retarding the possible skeletal isomerization prior to the CO insertion. This may be at least one of the reasons why the high α-selectivity is realized by the use of these shorter-chained diphosphines as additional ligands, though the possibility that the chelation of the diphosphines facilitates the CO insertion itself, considering the unexpected acceleration of the reaction of ethyl acrylate by the shorter-chained diphosphines, can not be ruled out. Such a retardation of skeletal isomerization due to the stabilization of the reaction intermediates caused by the addition of a phosphine to the reaction system is also observed in the palladium-catalyzed isomerization of straight-chained acyl halides to the corresponding branched-chained ones.[15]

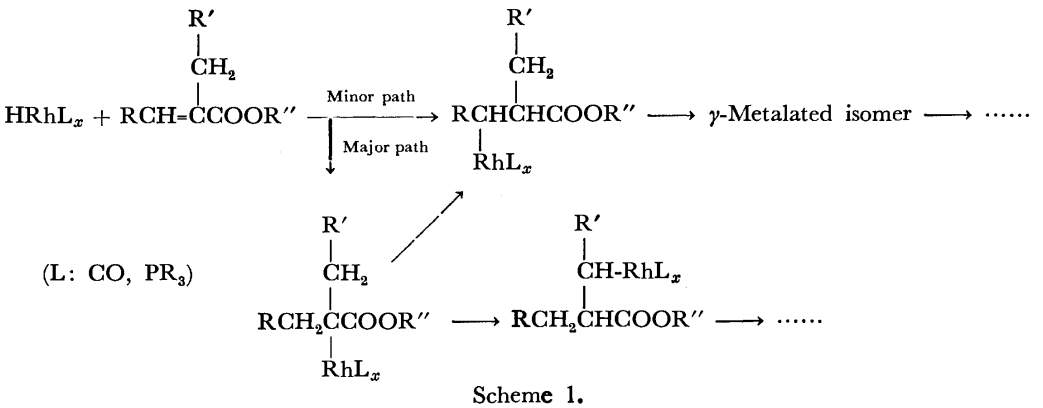

Scheme 1.

On the other hand, the α-selectivity varied sensitively depending on the chain length of the diphosphine. Moreover, the effect of the chain length on the α-selectivity appeared in a different manner from substrate to substrate. These results indicate that the size and the conformation of the chelate ring have much to do with the α-selectivity and the reaction rate. Concerning the hydrogenation of olefinic compounds, Kagan and his co-workers[16] have reported that the catalytic activity of some diphosphine–rhodium complexes heavily depends on the combination of the diphosphine and the substrate.

In consideration of the effect of the size and the conformation of the chelate ring formed by α,ω-bis(diphenylphosphino)alkanes in the present reaction system, it may be reasonable to assume that any factors weakening the coordination of a diphosphine as a bidentate ligand are harmful to a high α-selectivity, because the addition of a diphosphine is essential for selective α-formylation. The chelate ring formed by the coordination of a diphosphine with a longer methylene chain linking the two diphenylphosphino groups should become progressively less stable as the rings become larger. Moreover, the so-called medium rings, such as the eight-membered ring formed by 1,5-bis(diphenylphosphino)pentane, suffer a further destabilization due to the transannular steric repulsion. Therefore, it is likely that the longer-chained diphosphine functions as a monodentate ligand with a free phosphorus end. The low α-selectivity observed with 1,5-bis(diphenylphosphino)pentane, which lies on a level with that with $Rh_2Cl_2(CO)_4$ alone or in the presence of triphenylphosphine, may be because of the above reasons.

The reaction with 1,3-bis(diphenylphosphino)propane also caused a relatively low α-selectivity, with the exception of the case of ethyl acrylate. This may be explained as follows: 1,3-bis(diphenylphosphino)propane forms a six-membered ring on chelating coordination, the ring being preferably of a chair form. As is well known in the cyclohexane chemistry, there arises a serious steric repulsion between 1,3-diaxial substituents of chair-formed cyclohexanes. Regarding the present six-membered ring containing a rhodium and two phosphorus atoms, a pair of phenyl groups bonded to the separate phosphorus atoms cannot help occupying the 1,3-diaxial position. This may weaken the coordination of the diphosphine and bring about the formation of some non-α-selective catalytic species in which the diphosphine does not effectively chelate the rhodium. The relatively lower α-selectivity for methyl methacrylate as well as for methyl crotonate with 1,3-bis(diphenylphosphino)propane than that with 1,2-bis(diphenylphosphino)ethane or 1,4-bis(diphenylphosphino)butane may be ascribable to the partial participation of these non-α-selective species. However, the above-mentioned tendency for this diphosphine to cause a lower α-selectivity did not appear explicitly in the case of ethyl acrylate. In consideration of this point, careful attention should be paid to the reaction rate: the reaction without any additional ligand or in the presence of triphenylphosphine proceeded very sluggishly. On the other hand, the reaction with the shorter diphosphines was extremely fast. Judging from this great difference in the reaction rate between these two cases, it may be reasonable to consider that the species in which 1,3-bis(diphenylphosphino)propane does not effectively chelate the rhodium can scarcely participate in the reaction to such a great extent as to influence the results, while the species with the chelating diphosphine effects a rapid and highly α-selective formylation. This may be the reason why a high α-selectivity was attained for ethyl acrylate even by the use of 1,3-bis(diphenylphosphino) propane.

As another factor playing an important role during the reaction, a steric interaction of the substrate with the catalyst should be taken into account. The introduction of a methyl group into the α-position of acrylate (methyl methacrylate) lowered the α-selectivity, probably because of the increased steric repulsion around the α-carbon to be preferentially metalated. However, unexpectedly, the introduction of a methyl group into the β-carbon (methyl crotonate) also lowered the α-selectivity. Moreover, 1,2-bis(5*H*-dibenzophospholyl)-ethane, in which the rotation of the phenyl groups around the phenyl-to-phosphorus-bond axis is inhibited by the connection of the two phenyl groups on each phosphorus atom to each other at the ortho position, caused a much poorer activity and a far lower α-selectivity in the hydroformylation of ethyl acrylate than the more flexible 1,2-bis(diphenylphosphino)ethane. These results suggest that a delicate steric interaction between the substituents of the catalyst ligands and those of the substrates should be taken into consideration. The steric requirement for the coordination of a substrate should be more severe as the steric bulk of both the substrate and the other ligands increases. This is

supported by the fact that the α-selectivity for methyl methacrylate and crotonate varied more sensitively with the structure of the catalyst than that for ethyl acrylate. However, the mode and the extent of this kind of steric interaction must be very dependent on the conformation of the ligand, and more precise knowledges about the real structure of the catalyst under the reaction conditions will be necessary in order to develop a more subtle argument.

Finally, concerning the electronic aspects, the authors did not find any direct and distinct evidence that the variation in the α-selectivity as well as in the reaction rate observed with various diphosphines, including such powerful electron donors as α,ω-bis(dicyclohexylphosphino)alkanes, was dependent on the electronic factor of the diphosphines. Probably, this is because the steric factors much more seriously affect the results.

The authors wish to thank Mr. Tohru Arakawa and Mr. Hirokatsu Takyu for their experimental assistance.

References

1) J. Falbe, N. Huppes, and F. Korte, *Chem. Ber.*, **97**, 863 (1964).
2) M. Takesada, H. Wakamatsu, Y. Iwanaga, and J. Kato, Japanese Patent 3020 (1964); *Chem. Abstr.*, **60**, 15741e (1964).
3) Y. Takegami, C. Yokokawa, and Y. Watanabe, *Bull. Chem. Soc. Jpn.*, **39**, 2430 (1966).
4) Y. Takegami, Y. Watanabe, and H. Masada, *Bull. Chem. Soc. Jpn.*, **40**, 1459 (1967).
5) J. Falbe and N. Huppes, *Brennstoff-Chem.*, **48**, 46 (1967).
6) R. L. Pruett and J. A. Smith, *J. Org. Chem.*, **34**, 327 (1969).
7) "Inorganic Syntheses," ed by H. F. Holtzclaw, Vol. 8, McGraw-Hill, New York (1966), p. 211.
8) T. Yoshida, M. Iwamoto, and S. Yuguchi, Japanese Patent 11934 (1967); *Chem. Abstr.*, **68**, 105358e (1968).
9) L. Sacconi and J. Gelsomini, *Inorg. Chem.*, **7**, 291 (1968).
10) K. Issleib and G. Döll, *Chem. Ber.*, **96**, 1544 (1963).
11) K. Issleib and D. -W. Müller, *Chem. Ber.*, **92**, 3175 (1959).
12) E. H. Braye, I. Caplier, and R. Saussez, *Tetrahedron*, **27**, 5523 (1971).
13) M. Tanaka, T. Hayashi, and I. Ogata, manuscript in preparation.
14) C. A. Tolman, *J. Am. Chem. Soc.*, **92**, 2956 (1970).
15) T. A. Foglia, P. A. Barr, and M. J. Idacavage, *J. Org. Chem.*, **41**, 3452 (1976).
16) J. -C. Poulin, T. -P. Dang, and H. B. Kagan, *J. Organomet. Chem.*, **84**, 87 (1975).

Catalysis and Mechanism of the Isomerization of a Δ^5-3-Keto Steroid

Tadashi OKUYAMA, Akira KITADA, and Takayuki FUENO

Department of Chemistry, Faculty of Engineering Science, Osaka University, Toyonaka, Osaka 560

(Received February 25, 1977)

The acid- and base-catalyzed isomerizations of Δ^5- to Δ^4-testosterone have been kinetically studied in aqueous solution. Solvent isotope effects of $k_{H_3O^+}/k_{D_3O^+}=0.69$ and $k_{OH^-}/k_{OD^-}=3.1$ were obtained. It was thus concluded that the acid-catalyzed isomerization proceeds through rate-determining enolization but the base-catalyzed reaction through rate-determining protonation of an enolate ion. It was found that primary amines efficiently catalyze the isomerization *via* an iminium ion intermediate. Possible bifunctional catalysis was suggested for the high catalytic activity of polyfunctional primary amines.

The isomerization of β,γ-unsaturated ketones to their conjugated isomers has been shown to be catalyzed by both acids[1–6] and bases.[4,6] The acid-catalyzed isomerization involves the formation of a dienol intermediate followed by protonation at the γ carbon to give an α,β isomer.[3,5] A similar pathway through a dienolate anion intermediate has been presented for the base-catalyzed reaction.[4,6] The rate-determining step of these reactions seems to depend on the ketone structure.[5,6] Recently, a primary amine has been found to efficiently catalyze the isomerization through a dienamine intermediate.[7,8] Closely related enzymatic reactions have received considerable attention.[9,10] The Δ^5-3-keto steroid isomerase from *P. testosteroni* has most extensively been studied, although the mechanism for this reaction has yet to be fully elucidated.[9]

In this paper, acid- and general base-catalyzed isomerization of Δ^5-(**1**) to Δ^4-testosterone (**2**) has been investigated to determine the rate-determining step.

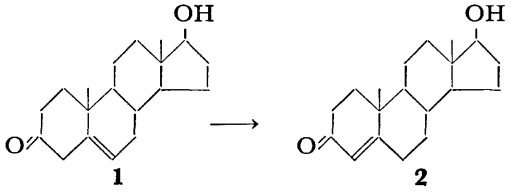

1 **2** (1)

Various primary amines, including polyfunctional amines, have been examined for their catalytic activities.

Experimental

Materials. Δ^5-Testosterone (**1**) was prepared by the isomerization of testosterone (**2**) catalyzed by potassium *t*-butoxide in *t*-butyl alcohol.[11] Crude products were recrystallized from acetone to give white plates melting at 160 °C. Calcd for $C_{19}H_{28}O_2$: C, 79.17; H, 9.72%. Found: C, 79.40; H, 9.72%.

Inorganic salts of reagent grade were used without further purification. Organic buffers were distilled or recrystallized before use. Freshly boiled, glass distilled water was used for all the rate determinations.

Kinetics. Rates were measured at 30±0.1 °C in aqueous buffer solutions containing 1% methanol, ionic strength being maintained at 0.50 with the addition of KCl. Three ml of buffer solution was equilibrated at 30 °C in a stoppered quartz cuvette inserted in a water-jacketted cell holder. Into the buffer solution was injected 30 μl of stock solution of **1** in methanol (4×10^{-3} M) with use of a microsyringe. After thorough mixing, the reaction was monitored spectrophotometrically using a Shimadzu spectrophotometer UV-200. First-order plots were linear over 90% conversion as monitored at 245 nm (λ_{max} of **2**) in the absence of primary amines.

Values of pH of buffer solutions and reaction mixtures were determined with a Hitachi-Horiba pH meter CTE F-5 calibrated in +0.01 pH unit.

To determine solvent isotope effects, D_2O and DCl and NaOD solutions supplied by E. Merck (isotopic purity >99.5 %) were used. Protic methanol was used for the preparation of the stock solution of **1**. Thus, deuterium purity of the reaction mixture was >98%.

Results and Discussion

Acid-catalyzed Isomerization. The rates of isomerization of **1** were measured in HCl (H_2O) and DCl (D_2O) solutions. An inverse isotope effect of $k_{H_3O^+}/k_{D_3O^+}=0.69\pm0.02$ was observed (Table 1). The result is consistent with the rate-determining enolization and in agreement with that observed for androst-5-ene-3,17-dione.[3]

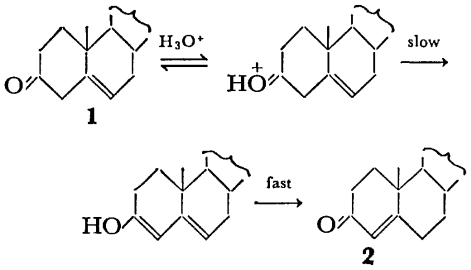

1 **2** (2)

With 3-cyclohexen-1-one a normal isotope effect was found, indicating the rate-determining protonation of

Table 1. Acid-catalyzed isomerization of **1**

Acid	Acid concn, M	$10^3\ k_{obsd}$, s^{-1}	$10^2\ k_2$, $M^{-1}\,s^{-1}$
HCl	0.099	1.12	1.13
		1.07	1.08
		1.14	1.15
	0.0495	0.553	1.12
		0.532	1.07
		0.556	1.12
		Av	1.11±0.013
DCl	0.104	1.71	1.63
		1.64	1.58
	0.052	0.837	1.61
		0.802	1.54
		Av	1.60±0.024

Table 2. Base-catalyzed isomerization of **1**

Base	Base concn, M	$10^3\ k_{obsd}$, s^{-1}	k_2, $M^{-1}\,s^{-1}$
NaOH	0.00495	5.37	1.08
		5.77	1.17
		5.70	1.15
	0.0099	10.5	1.06
		11.7	1.19
		11.6	1.17
	0.0198	21.5	1.09
		20.7	1.05
		23.6	1.19
		Av	1.13±0.02
NaOD	0.00496	1.61	0.325
		1.65	0.332
	0.00993	3.59	0.363
	0.00960	3.69	0.384
		3.65	0.380
	0.0199	7.29	0.366
		7.53	0.378
		Av	0.361±0.009

a dienol intermediate.[5a] The reason for the mechanistic difference of the latter reaction was nicely interpreted by the conformational aspects.[6]

Base-catalyzed Isomerization. The rate of the isomerization of **1** were compared in NaOH (H_2O) and NaOD (D_2O) solutions (Table 2). The isotope effect is normal $k_{OH^-}/k_{OD^-}=3.13\pm0.14$, indicating an equilibrium formation of a dienolate ion intermediate, followed by the rate-determining protonation of the intermediate by water.

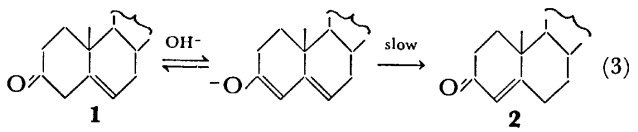

This observation is consistent with the preferential α-protonation (deconjugation) of a dienolate anion in *t*-butyl alcohol.[11,12] That is, even in aqueous solution the base-catalyzed isomerization proceeds by the rate-determining protonation or the dienolate anion undergoes the preferential α-C protonation. A similar observation has recently been made with 3-cyclohexen-1-one.[6]

General Base Catalysis. The isomerization was also carried out in various buffer solutions. The observed rates were strongly dependent on buffer concentrations. Buffer-dependent rate constants were partitioned into the acid- and base-catalytic constants in a usual way as seen in Fig. 1. The acid-catalytic term was negligible at pH>7 except for primary amine buffers. The general base catalytic constants obtained are given in Table 3 and the Brønsted plots are shown in Fig. 2 ($\beta=0.48$). The apparent general base catalysis observed here must be a consequence of combined specific hydroxide and general acid catalyses since the rate-determining step is protonation (Eq. 3). In the same way, the apparent general acid catalysis

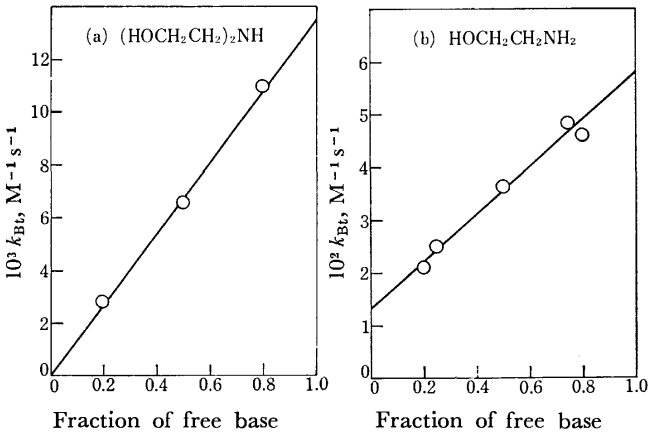

Fig. 1. Buffer-dependent rate constants, k_{Bt}, for the isomerization of **1** in (a) 2,2′-iminodiethanol and (b) 2-aminoethanol buffer solutions.

Table 3. General base catalysis in the isomerization of **1**

No.	Base	pK_a[a]	$10^2\ k_B$, $M^{-1}\,s^{-1}$
1	$(C_2H_5)_2NH$	11.1	19.7
2	$(C_2H_5)_3N$	10.9	7.8
3	Caps[b]	10.4	5.3
4	CO_3^{2-}	9.8	7.0
5	$HOCH_2CH_2NH_2$	9.6	5.8
6	$(HOCH_2CH_2)_2NH$	9.1	1.34
7	Morpholine	8.7	5.0
8	$(HOCH_2CH_2)_3N$	7.9	0.328
9	Imidazole	7.0	0.155

a) pH of a buffer solution of [acid]/[base]=1. b) Cyclohexylaminopropanesulfonate.

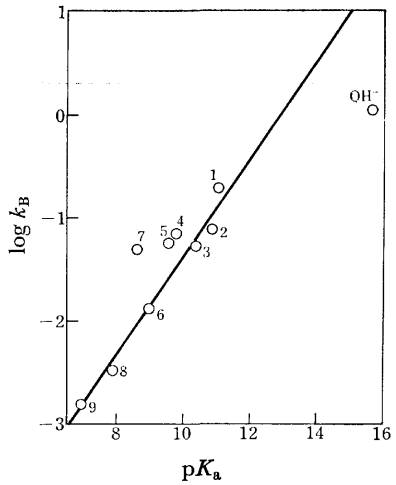

Fig. 2. Brønsted plot for general base catalysis of the isomerization of **1**. For numbering see Table 3.

is actually specific oxonium-general base catalysis. Thus, the reasoning previously made by Jones and Wigfield[4] that the phenolic group of the enzyme acts as a general acid because of insufficient base catalytic activity of phenolate anion is weak.

Primary Amine Catalysis. The reactions in primary amine buffers showed some induction period with higher concentrations, and rates showed non-linear buffer de-

pendence. With 2-aminoethanol as a buffer, the rate constants obtained with low buffer concentrations (< 0.06 M) showed an acid-catalytic term as is seen in Fig. 1(b). With primary amine buffers of lower pK_a, the anomalous behavior was more apparent and the transient intermediate formation was observed by the scannings of UV spectra of the reaction mixture. An intermediate having the absorption maximum at ≈280 nm appeared rapidly, followed by slower decay for all the primary amines of $pK_a<9$ studied here. Similar observations were noted previously with trifluoethylamine[7] and glycylglycine[8] and the intermediate of λ_{max} ≈280 nm was identified as an α,β-unsaturated iminium ion of type **5**.

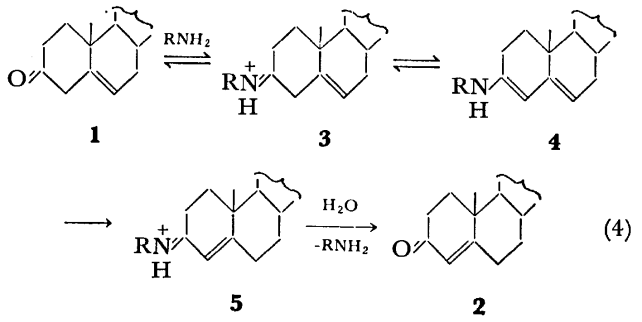

(4)

Kinetics of the primary amine-catalyzed isomerization of 3-methyl-3-cyclohexen-1-one has recently been investigated with trifluoroethylamine as a buffer, and a mechanism similar to Eq. 4 has been presented by Pollack and Kayser.[7] Some kinetic results preliminarily obtained with our system are consistent with the mechanism 4.[13] Because of the kinetic complexity and the publication of Pollack's data, thorough kinetic investigation of the present system was abandoned.

We compared relative catalytic effects of various primary amines. For the sake of kinetic simplicity,

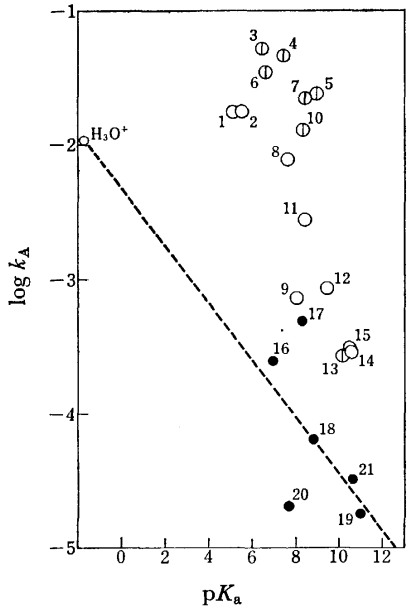

Fig. 3. Amine catalysis of the isomerization of **1**. For numbering see Table 4. ○, Primary amines. ⓓ, Polyfunctional primary amines. ●, Sceondary and tertiary amines.

Table 4. Amine catalysis in the isomerization of **1** in phosphate buffer[a]

No.	Amine	pK_a[b]	$10^4\ k_A$, $M^{-1}\ s^{-1}$
1	$NCCH_2NH_2$	5.3	176
2	$CF_3CH_2NH_2$	5.6	174
3	$(CH_3)_2\overset{+}{N}HCH_2CH_2NH_2$	6.7	520
4	$H_3\overset{+}{N}CH_2CH_2NH_2$	7.5	450
5	$[H(NHCH_2CH_2)_2NH_2]H^+$	9.0[c]	240
6	$[H(NHCH_2CH_2)_3NH_2]H_2^{2+}$	6.8[d]	334
7	$[H(NHCH_2CH_2)_4NH_2]H_2^{2+}$	8.5[e]	225
8	$NCCH_2CH_2NH_2$	7.7	78.9
9	$(HOCH_2)_3CNH_2$	8.1	7.4
10	$^-OCOCH_2NHCOCH_2NH_2$	8.4	130
11	$ClCH_2CH_2NH_2$	8.5	28
12	$HOCH_2CH_2NH_2$	9.5	8.6
13	$^-OCOCH_2CH_2NH_2$	10.2	2.7
14	$CH_3CH_2NH_2$	10.6	2.9
15	CH_3NH_2	10.6	3.1
16	Imidazole	7.1	2.5
17	Morpholine	8.4	5.0
18	$(HOCH_2CH_2)_2NH$	8.9	0.64
19	$(CH_3CH_2)_2NH$	11.0	0.18
20	$(HOCH_2CH_2)_3N$	7.8	0.21
21	$(CH_3CH_2)_3N$	10.7	0.33

a) [Phosphate]=0.1 M, pH=6.6±0.1. Without added amines, $k_{obsd}=2.04\times10^{-5}\ s^{-1}$. b) Values taken from "CRC Handbook of Biochemistry," H. A. Sober, Ed, Chem. Rubber Co., Cleveland (1968), unless otherwise noted. c) R. L. Pecsok, R. A. Garber, and L. D. Shields (*Inorg. Chem.*, **4**, 447 (1965)) report pK_a=4.22, 8.95, 9.79 at 26 °C. d) D. B. Rorabacher, W. J. MacKeller, F. R. Shu, and S. M. Bonavita (*Anal. Chem.*, **43**, 561 (1971)) report pK_a=3.39, 6.75, 9.31, 10.09 at 25 °C. e) D. B. Rorabacher, W. J. MacKeller, F. R. Shu, and S. M. Bonavita (*Anal. Chem.*, **43**, 561 (1971)) report pK_a=2.40, 4.70, 8.50, 9.65, 10.36 at 25 °C.

very low concentrations of amines (≦0.02 M) were employed to determine the catalytic constants at pH near neutrality. To maintain pH constant (pH=6.6± 0.1), phosphate buffer of 0.1 M was used. Under these conditions, the formation of **2** (245 nm) was of the first-order in rate. From the rate increase by the addition of an amine, the apparent catalytic constant k_A was calculated and given in Table 4.

Logarithms of k_A are plotted against pK_a of the conjugate acid in Fig. 3. A reference line was drawn through the points for usual general acids because the acidic term of primary amine catalysis is important in mechanism 4.[7,13] Points for primary amines show large upward deviations from the reference line by the magnitude of *ca.* 2 in the log unit. The reaction in a 1-M buffer of *N,N*-dimethylethylenediamine of neutral pH would be more than 10^5 times as rapid as the uncatalyzed reaction at the same pH. A primary amine effectively attacks the β,γ-unsaturated ketone as a nucleophile to give an iminium ion followed by rapid isomerization to the α,β-unsaturated iminium ion, which is finally hydrolyzed to give the α,β-unsaturated ketone

(Eq. 4). During the conversion of the iminium intermediate, a second molecule of an amine or an external buffer acts as a general base or acid.

When a bifunctional primary amine having a second base group is used as a catalyst, intramolecular base (acid) catalysis may operate in manners like **6**—**8** in each step of Eq. 4.

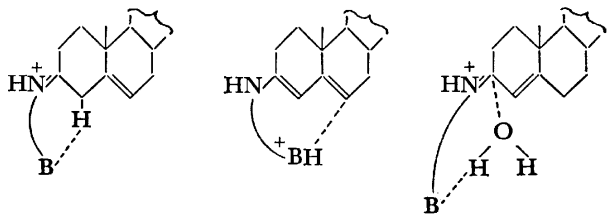

6 **7** **8**

Some polyfunctional primary amines were examined and are included in the plots of Fig. 3. Small such effects seem to be actually operative, though not definite. Intramolecular catalysis similar to **8** was previously found in the dehydration of a carbinolamine (the reverse of the present reaction).[14] Although the catalysis like **6** may also be possible, the step that follows (γ protonation) would hardly be catalyzed intramolecularly because of the remoteness of an acid group (**7**). Thus, whether or not the bimolecular catalysis by primary amines is actually effective depends on the rate-determining step of the overall reaction. Further details on this problem is now under investigation.

References

1) F. S. Kawahara, S. -F. Wang, and P. Talalay, *J. Biol. Chem.*, **237**, 1500 (1962).
2) W. R. Nes, E. Loesser, R. Kirdant, and J. Marsh, *Tetrahedron Lett.*, **1963**, 299.
3) S. K. Malhotra and H. J. Ringold, *J. Am. Chem. Soc.*, **87**, 3228 (1965).
4) J. B. Jones and D. C. Wigfield, *Can. J. Chem.*, **47**, 4459 (1969).
5) a) D. S. Noyce and M. Evett, *J. Org. Chem.*, **37**, 394 (1972); b) *ibid.*, **37**, 397 (1972).
6) D. L. Whalen, J. F. Weimaster, A. M. Ross, and R. Radhe, *J. Am. Chem. Soc.*, **98**, 7319 (1976).
7) a) R. H. Kayser and R. M. Pollack, *J. Am. Chem. Soc.*, **97**, 952 (1975); b) R. M. Pollack and R. H. Kayser, *ibid.*, **98**, 4174 (1976).
8) W. F. Benisek and A. Jacobson, *Bioorg. Chem.*, **4**, 41 (1975).
9) P. Talalay and A. M. Benson, *Enzymes, 3rd ed*, **6**, 591 (1972).
10) R. L. Jones, *Biochem. J.*, **139**, 381 (1974).
11) H. J. Ringold and S. K. Malhotra, *Tetrahedron Lett.*, **1962**, 669
12) S. K. Malhotra and H. J. Ringold, *J. Am. Chem. Soc.*, **85**, 1538 (1963).
13) Presented in part at the Third IUPAC Conference on Physical Organic Chemistry, La Grande-Motte, France, September, 1976.
14) J. Hine, M. S. Cholod, and W. K. Chess, Jr., *J. Am. Chem. Soc.*, **95**, 4270 (1973).

Syntheses of 4′-Deoxykanamycin[1] and 4′-Deoxykanamycin B

Toshiaki MIYAKE, Tsutomu TSUCHIYA, Sumio UMEZAWA, and Hamao UMEZAWA*

Institute of Bioorganic Chemistry, 1614 Ida, Nakahara-ku, Kawasaki 211

**Institute of Microbial Chemistry, Kamiosaki, Shinagawa-ku, Tokyo 141*

(Received March 1, 1977)

4′-Deoxykanamycin (**9**) was prepared from kanamycin *via* *N*-benzyloxycarbonylation, 4″,6″-*O*-cyclohexylidenation, selective benzoylation at 2′,3′, and 2″-hydroxyl groups, 4′-*O*-mesylation, 4′-iodination, 4′-hydrogenation, and removal of the protective groups. 4′-Deoxykanamycin B (**19**) was analogously prepared from kanamycin B. 4′-*O*-Tosyl derivative of kanamycin B was also led to **19**. Selective formylation of the 3′-hydroxyl group of a protected kanamycin B derivative with *N*,*N*-dimethylformamide-tosyl chloride followed by mesylation of the unstable 3′-*O*-formyl derivative also led to 4′-deoxykanamycin B. Throughout the syntheses, the 4′-hydroxyl group of the protected kanamycins was found to be least reactive for benzoylation among the 2′,3′,4′, and 2″-hydroxyl groups. The ^{13}C NMR spectrum of **9** was also measured. It was concluded that 4′-deoxygenation of antibiotics structurally related to kanamycin caused the resonances of ^{13}C-6′ downfield shift.

As reported[2] previously, 4′-deoxykanamycin (**9**) synthesized by a condensation method has been found to have antibacterial activity in the similar strength as that of parent antibiotic, kanamycin and moreover to have activity against some strains of *Pseudomonas aeruginosa*. Naito *et al.*[3] have also prepared **9** starting from kanamycin *via* the 4′,6′-carbamate formation[4] followed by selective liberation of the 4′-hydroxyl group or *via* the 4′-*O*-acetyl migration to the 6′-amino group. This paper describes another synthesis of 4′-deoxykanamycin (**9**) starting from kanamycin and three processes for the synthesis of 4′-deoxykanamycin B (**19**) strating from kanamycin B.

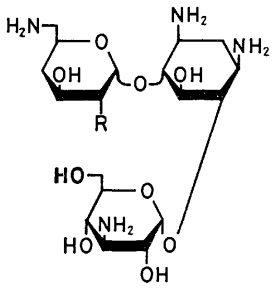

9 R=OH
19 R=NH_2

In preliminary experiments we have found that the 4′-hydroxyl groups of kanamycin, kanamycin B and their derivatives were least reactive for benzoylation among the 2′,3′,4′, and 2″-hydroxyl groups. We, therefore, utilized this finding for the syntheses of **9** and **19**.

Synthesis of 4′-Deoxykanamycin (9). Tetrakis(*N*-benzyloxycarbonyl)kanamycin (**1**) was treated with 1,1-dimethoxycyclohexane in *N*,*N*-dimethylformamide (DMF) in the presence of *p*-toluenesulfonic acid. The 4″,6″-*O*-cyclohexylidenation was achieved almost quantitatively without formation of other mono-*O*-cyclohexylidene or di-*O*-cyclohexylidene derivatives. This exclusive 4″,6″-*O*-cyclohexylidenation was rather unexpected, because in a similar treatment of a *N*-protected kanamycin B derivative, the 3′,4′-*O*-cyclohexylidenation occurred[5] more or less in addition to the 4″,6″-*O*-cyclohexylidenation.

Treatment of the 4″,6″-*O*-cyclohexylidene derivative (**2**) with 6 mol equivalents of benzoyl chloride in pyridine gave a mixture of tri- and tetra-*O*-benzoyl (**4**) derivatives. If the amount of benzoyl chloride used

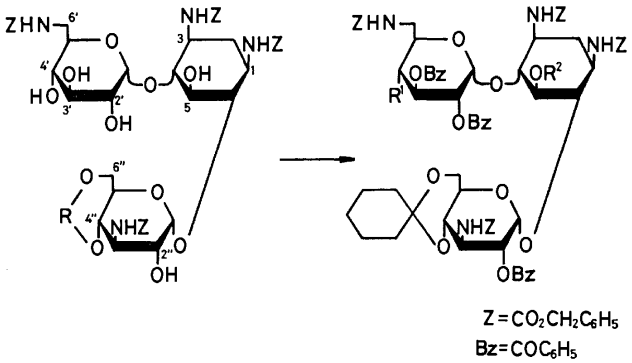

Z=$CO_2CH_2C_6H_5$
Bz=COC_6H_5

		R¹	R²
1	R=H, H		
2	R=$C(CH_2)_5$		
		3 OH	H
		4 $OCOC_6H_5$	H
		5 OSO_2CH_3	H
		6 OSO_2CH_3	SO_2CH_3
		7 I*	H
		8 H	H

* A mixture of epimers

was reduced, the production of tri-*O*-benzoyl derivatives was increased with the decrease of **4**. However, the apparent increase of tri-*O*-benzoyl derivatives did not necessarily mean the yield increase of the desired 2′,3′,2″-tri-*O*-benzoyl derivative (**3**), since **3** was found to be contaminated with other minor tri-*O*-benzoyl isomer(s) and this made the purification of **3** difficult even by column chromatography (**3** and the isomer(s) had the same mobility). The contamination was shown by the PMR spectrum of the mesylated mixture of the tri-*O*-benzoylated products; that is, in the spectrum, at least two peaks assignable to the methyl protons of mesyls were observed, indicating that the tri-*O*-benzoyl products were a mixture of the position isomers. By increasing the amount of benzoyl chloride up to 6 mol equivalents for **2**, a mixture of **3** and **4** was formed exclusively. The tetra-*O*-benzoyl isomer (**4**), which was formed concomitantly in high proportion, could be converted again to **2** in 90% yield by treatment with sodium methoxide. The doubtless structure of **3** was deduced from the fact that **3** was led to 4′-deoxykanamycin after a sequence of reactions described below.

Mesylation of **3** gave 4′-*O*-mesyl (**5**, 65%) and 5,4′-di-*O*-mesyl (**6**, 9.5%) derivatives. It should be noted that mesylation of an *N*-ethoxycarbonyl-kanamycin B

derivative[6] (compound **5** in that literature) gave 3′,4′-di-*O*-mesyl derivative in 96% yield without formation of the 5-*O*-mesyl derivative. This means that 4′-*O*-mesylation of **3** is somewhat hindered by the neighboring groups (possibly by 3′-*O*-benzoyl and 6′-*N*-benzyloxycarbonyl groups) and consequently the mesylation can occur at the 4′- and 5-hydroxyl groups in a similar level. Tosylation of **3**, in contrast to mesylation, occurred scarcely. Treatment of **5** with 50% (w/v) sodium iodide in DMF at 100 °C gave an epimeric mixture of 4′-iodo derivatives (**7**). This displacement reaction required 40 h heating. Since the similar iodination of **22** and **26** described later required a shorter reaction period for completion, the displacement reaction of **5** was considered to be somewhat hindered by the groups in the vicinity of the 4′-mesyloxy group. Hydrogenolysis of **7** with Raney nickel gave the 4′-deoxy derivative (**8**), which, after deblocking, gave 4′-deoxykanamycin (**9**).

The structure of **9** was confirmed by acidic solvolysis of the tetrakis(*N*-benzyloxycarbonyl) derivative of **9**. One of the alcoholyzed products which showed the same mobility was identified to the anomeric mixture of benzyl 6-benzyloxycarbonylamino-4,6-dideoxy-D-*xylo*-hexopyranosides (**10**) which consumed periodate, indicating that **10** has a pair of vicinal diols. Acidic hydrolysis of **9** followed by paper chromatography also supported the conclusion (Chart 1).

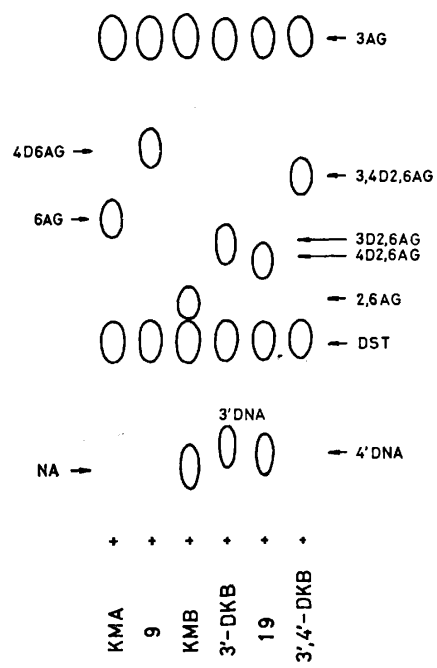

Chart 1. The paper chromatogram of acidic hydrolyzates (6M HCl 100 °C 0.5 h for KMA and **9**, and 6.5 h for other compounds) of kanamycin (KMA), 4′-deoxykanamycin (**9**), kanamycin B (KMB), 3′-deoxykanamycin B (3′-DKB), 4′-deoxykanamycin B (**19**), and 3′,4′-dideoxykanamycin B, descending for 3 days. Abbreviations are: NA (neamine), DST (2-deoxystreptamine), 3AG (3-amino-3-deoxy-D-glucose), 6AG (6-amino-6-deoxy-D-glucose), 2,6AG (2,6-diamino-2,6-dideoxy-D-glucose); the denotions of 3D, 3′D, 4D, 4′D, and 3,4D mean that the numbered positions of the parent compounds (cited after the letter D) are deoxygenated.

Table 1. The ^{13}C chemical shifts[a] of kanamycin (KMA),[b] 4′-deoxykanamycin (**9**), 3′-deoxykanamycin B(3′-DKB),[c] and 3′,4′-dideoxykanamycin B(3′,4′-DKB) (all as free bases)

Carbon	KMA	**9**	3′-DKB	3′,4′-DKB
1′	100.8	101.2	100.8	101.1
2′	72.7	74.5	50.3	50.6
3′	73.7	70.5[d]	35.7	26.2[e]
4′	71.9	36.3	67.1	28.1[e]
5′	73.7	68.0[d]	74.1	70.2
6′	42.4	45.3	42.4	45.4
1	51.2	51.3	51.2	51.1
2	36.3	36.3	36.4	36.3
3	49.8	49.9	50.0	50.3
4	88.2	88.1	87.1	86.9
5	74.9	75.1	75.3	75.4
6	88.7	88.6	89.0	89.0
1″	100.4	100.8	100.3	100.7
2″	72.7	72.6	72.6	72.6
3″	55.1	55.1	55.1	55.1
4″	70.2	70.2	70.2	70.2
5″	73.0	73.0	73.0	73.1
6″	61.2	61.2	61.3	61.3

a) In ppm downfield from TMS calculated as $\delta^{TMS} = \delta^{dioxane} + 67.4$ ppm. b) Shift assignments were based on the shifts of kanamycin (pH 9.6) reported.[8] c) The shifts were substantially the same with those reported by Koch *et al.*[9] d) The values of C-3′ and C-5′ may well be reversed. e) Shift assignments of C-3′ and C-4′ were made based on the corresponding shifts[10] of gentamicin C_{1a} and gentamin C_{1a}.

^{13}C NMR spectral studies were further made. The data of **9**, kanamycin, 3′-deoxykanamycin B (tobramycin), and 3′,4′-dideoxykanamycin B[7] were shown in Table 1. By the spectrum of **9**, the presence of two deoxy groups (δ 36.3 at C-2 and 4′) was clearly shown. Comparison of the C-6′ resonances of kanamycin and 3′-deoxykanamycin B with those of **9** and 3′,4′-dideoxykanamycin B showed downfield shifts $\approx$3 ppm of the latter. By taking the shift difference ($\Delta\delta$) between C-6′ and C-2 of structurally related antibiotics as a measure of downfield shift (the shift of C-2 was selected as a standard because the shift was thought to remain relatively constant throughout kanamycin series), following results were obtained: kanamycin ($\Delta\delta$ 6.1), 3′-deoxykanamycin B (6.0),[9] 3′,4′-dideoxykanamycin B (9.1), gentamicin C_{1a} (9.4),[10] ribostamycin (6.0),[11] 4′-deoxyneamine (9.1),[12] and seldomycin factor 5 (9.2).[13] These results show that the lack of 4′-hydroxyl group causes downfield shift of the resonance of C-6′ by $\approx$3 ppm. This fact is useful to discern the presence of 3′- or 4′-deoxy group. Similar downfield shifts were reported[14] on mannose and galactose, in which the C-4 resonances shifted downfield ($\Delta\delta$ 2.5—5.3) on 6-deoxygenation.

Synthesis of 4′-Deoxykanamycin B. Pentakis(*N*-benzyloxycarbonyl)kanamycin B (**11**), which was prepared from kanamycin B, was treated with 1,1-dimethoxycyclohexane similarly as described for **2** to give the 4″,6″-*O*-cyclohexylidene derivative (**12**).[15] In this reac-

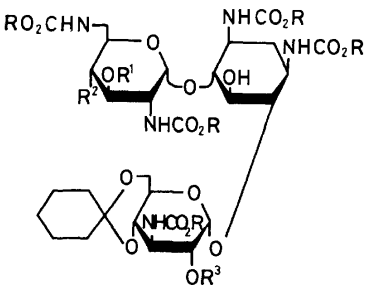

	R	R^1	R^2	R^3
12	$CH_2C_6H_5$	H	OH	H
13	$CH_2C_6H_5$	COC_6H_5	OH	COC_6H_5
14	$CH_2C_6H_5$	COC_6H_5	$OCOC_6H_5$	COC_6H_5
15	$CH_2C_6H_5$	COC_6H_5	OSO_2CH_3	COC_6H_5
17	$CH_2C_6H_5$	COC_6H_5	I*	COC_6H_5
18	$CH_2C_6H_5$	COC_6H_5	H	COC_6H_5
20	C_2H_5	H	OH	COC_6H_5
21	C_2H_5	$SO_2C_6H_4CH_3$-(*p*)	OH	COC_6H_5
22	C_2H_5	H	$SO_2C_6H_4CH_3$-(*p*)	COC_6H_5
24	C_2H_5	CHO	OH	COC_6H_5
25	C_2H_5	CHO	OSO_2CH_3	COC_6H_5
26	C_2H_5	H	OSO_2CH_3	COC_6H_5
27	C_2H_5	H	I*	COC_6H_5
28	C_2H_5	H	H	COC_6H_5

* A mixture of epimers

tion, undesirable 3′,4′-*O*-cyclohexylidenation was inevitable, but this product was mostly hydrolyzed to **12** by addition of water.[5] Benzoylation of **12** with benzoyl chloride gave a mixture of 3′,2″-di-*O*-(**13**) and 3′,4′,2″-tri-*O*-benzoyl (**14**) derivatives, from which **13** was readily separated by chromatography. Mesylation of **13** gave 4′-*O*-mesyl derivative (**15**) and subsequent iodination gave 4′-iodo derivative (**17**). Hydrogenation of **17** with tributyltin hydride[16] or with hydrogen-Raney nickel gave the 4′-deoxy derivative (**18**). Finally, removal of the protecting groups gave 4′-deoxykanamycin B (**19**).

The structure of **19** was confirmed by another synthesis, that is, the 4′-*O*-tosyl derivative[17] (**22**) of 2″-*O*-benzoyl-4″,6″-*O*-cyclohexylidene-pentakis(*N*-ethoxycarbonyl)kanamycin B (**20**), was led to **19**. Iodination of **22** gave the 4′-iodo derivative (**27**) and it was hydrogenated with Raney nickel to give the 4′-deoxy derivative (**28**), which after deblocking gave 4′-deoxykanamycin B (**19**) identical with that obtained by the first synthesis. Paper chromatogram of the acidic hydrolyzates of **19** was shown in Chart 1.

To further improve the synthesis of **19**, we tried to protect the 3′-hydroxyl group of **20** by formylation with *N*,*N*-dimethylformamide in the presence[18] of tosyl chloride. Treatment of **20** in DMF with tosyl chloride in the presence of pyridine gave a product (**24**) which was considered to be a mono-*O*-formyl compound. Since the compound could not be purified by column chromatography owing to its instability, **24** was mesylated without purification and the mesyl derivative (**25**) was treated with aqueous ammonia to remove the formyl group. The 4′-*O*-mesyl derivative (**26**) was thus obtained in a yield of 62% from **20**. This formylation reaction did not proceed smoothly, if pyridine was omitted, and higher temperature and longer reaction period were required for completion of the reaction and the yield of **26** was much lower. The structure of **26** was confirmed by leading it to **27** by treatment with sodium iodide. Above results indicate that the formylation occured at 3′-hydroxyl group fairly selectively, although the mode of acylation was different from that of benzoylation for the preparation of **13**. In the above 4′-*O*-sulfonylation step, if tosyl chloride was used instead of mesyl chloride, the 4′-*O*-tosylation hardly occurred. This suggests that the 3′-*O*-formyl group of **24** fairly prevents the 4′-*O*-tosylation as in the case of 3′-*O*-benzoyl group in **3** described before.

The structure of **19** was further confirmed by determination of $\Delta[M]_{TACu}$[19] values (Table 2). TACu can form complex only with a pair of vicinal amino and hydroxyl groups having relative spacial orientations of $\approx 60°$ dihedral angle and the $\Delta[M]_{TACu}$ shows a value

Table 2. The $\Delta[M]_{TACu}$[19] values measured at 20 °C

Kanamycin	+870°
4′-Deoxykanamycin (**9**)	+890°
Kanamycin B	−500°
3′-Deoxykanamycin B	+780°
4′-Deoxykanamycin B (**19**)	−570°
3′,4′-Dideoxykanamycin B	+820°

Table 3. Antibacterial spectra of **9**, **19**, kanamycin (KMA), and kanamycin B (KMB)

Test organisms[a]	Minimal inhibitory concentration (mcg/ml)			
	9	KMA	**19**	KMB
Staphylococcus aureus 209P	0.78	0.78	0.39	0.39
Sarcina lutea PCI 1001	12.5	12.5	1.56	12.5
Klebsiella pneumoniae PCI 602	1.56	0.78	0.39	0.39
Escherichia coli K-12	3.12	1.56	0.78	0.78
Escherichia coli K-12 ML 1629[b]	>100	>100	>100	>100
Pseudomonas aeruginosa A3	1.56	50	6.25	25
Pseudomonas aernginosa A3 No. 12	6.25	12.5	12.5	12.5
Pseudomonas aeruginosa TI-13	6.25	>100	50	100
Mycobacterium smegmatis ATCC 607[c]	0.78	0.78	0.78	0.78

a) Agar dilution streak method (nutrient agar, 37 °C, 18 h). b) A strain of clinical origin having the ability of phosphorylating the 3′-hydroxyl groups of kanamycins. c) 48 h.

of $\approx\pm900°$. The accordance of the difference of the $\Delta[M]_{TACu}$ values between kanamycin and kanamycin B with that between 3′-deoxy- and 4′-deoxykanamycin B (**19**) shows that a copper complex was formed between 2′-amino and 3′-hydroxyl groups in **19**.

Antibacterial activities of 4′-deoxykanamycin[2] (**9**) and 4′-deoxykanamycin B (**19**) are shown in Table 3.

Experimental

PMR spectra were recorded at 60, 90, and 100 MHz with Hitachi R-24A, Varian EM-390, and Varian XL-100 spectrometers, respectively. ^{13}C NMR spectra were recorded on a Varian XL-100 spectrometer with Varian 620-L data processing system (25.2 MHz) in $\approx$0.5 M deuterium oxide solution containing dioxane as internal reference. Thin-layer chromatography (TLC) was performed on Wakogel B-5 unless otherwise stated or on E. Merck silica gel 60 F_{254}. Paper chromatography (PPC) was carried out on Toyo-Roshi paper No. 50 with 1-butanol–pyridine–water–acetic acid=6 : 4 : 3 : 1, descending for 7—8 days unless otherwise stated and spots were visualized by 0.5% ninhydrin in pyridine. For column chromatography, silica gel (Wakogel C-200) was used. For experiments at lower than 0 °C, cooling assembly of Haake constant circulator KS60W was used. Reprecipitation was carried out by adding the last-cited solvent to a solution of the first-cited solvent (or the mixture of the first and the second-cited solvents).

*Tetrakis(*N*-benzyloxycarbonyl)kanamycin (**1**).* To an ice-cold suspension of kanamycin sulfate (54.2 g as kanamycin·H_2SO_4·H_2O) and anhydrous sodium carbonate (52 g) in aqueous acetone (1 : 1, 1 l), benzyl chloroformate (50 ml) was gradually added under vigorous stirring and the mixture was stirred for 1.5 h in the cold. Precipitates occurred were filtered, washed with water and then with ether to give a solid of **1**, 78.0 g (90%), $[\alpha]_D^{25}$ +68° (*c* 2, DMF); IR (KBr): 1690, 1530 cm^{-1}; PMR (DMSO-d_6) δ: 5.05 (8H s, C_6H_5-CH_2).

Found: C, 58.89; H, 6.18; N, 5.41%. Calcd for $C_{50}H_{60}N_4O_{19}$: C, 58.81; H, 5.92; N, 5.49%.

*Tetrakis(*N*-benzyloxycarbonyl)-4″,6″-*O*-cyclohexylidenekanamycin (**2**).* To a solution of **1** (297 mg) in dry DMF (3 ml), anhydrous *p*-toluenesulfonic acid (11 mg) and 1,1-dimethoxycyclohexane (0.07 ml, $\approx$1.5 mol equivalents for **1**) were added and the solution was heated at 50 °C under reduced pressure (25—30 Torr) for 1 h. The resulting solution showed, on TLC with $CHCl_3$–EtOH (6 : 1), a single spot at R_f 0.5 (*cf.* **1**, R_f 0.12). The solution was poured into aqueous sodium hydrogencarbonate solution with stirring and the precipitates occurred were filtered, washed with water, and dried. The solid was reprecipitated from dioxane–water, 314 mg (98%), $[\alpha]_D^{20}$ +60° (*c* 1, DMF).

Found: C, 60.78; H, 6.14; N, 4.82%. Calcd for $C_{56}H_{68}N_4O_{19}$: C, 61.08; H, 6.22; N, 5.09%.

*2′,3′,2″-Tri-*O*-(**3**) and 2′,3′,4′,2″-Tetra-*O*-benzoyl-tetrakis(*N*-benzyloxycarbonyl)-4″,6″-*O*-cyclohexylidenekanamycin (**4**).* To an ice-cold solution of **2** (39.4 g) in dry pyridine (800 ml), benzoyl chloride (8.35 ml, 2 mol equivalents for **2**) was added and the solution was kept in the cold for 1 h. Another benzoyl chloride (8.35 ml) was added and the solution was kept in the cold for further 1 h. Benzoyl chloride (8.35 ml) was again added and the solution was kept at room temperature overnight. The resulting solution showed, on TLC with $CHCl_3$–2-propanol (IPA) (40 : 1), spots of **3** (R_f=0.15) and **4** (R_f=0.2) in almost equal color strength. After addition of water (20 ml) followed by heating at 40 °C for a while, the solution was concentrated. The chloroform solution (1.2 l) of the residual syrup was washed with 5% aqueous potassium hydrogensulfate, 2% aqueous sodium hydrogencarbonate, and water, dried ($MgSO_4$), and concentrated. The pale-brown solid was chromatographed over silica gel with the same solvent system to give a colorless solid of **3**, 24.3 g (48%) and **4**. Since **4** thus obtained was contaminated with color impurities, it was purified by column chromatography again as described above and the pale-yellow solid obtained was reprecipitated from $CHCl_3$–ether–hexane to give a colorless solid of **4**, 341 mg (50%).

3: $[\alpha]_D^{25}$ +106° (*c* 1, $CHCl_3$).

Found: C, 65.61; H, 5.79; N, 3.77%. Calcd for $C_{77}H_{80}N_4O_{22}$: C, 65.43; H, 5.70; N, 3.96%.

4: $[\alpha]_D^{25}$ +109° (*c* 1, $CHCl_3$); PMR ($CDCl_3$): the areal ratio of the signals at δ 6.8—7.7 ($CH_2C_6\underline{H}_5$ and *m* and *p* of COC_6H_5) and those at δ 7.7—8.2 (*o* of COC_6H_5) were $\approx$4 : 1.

Found: C, 66.16; H, 5.69; N, 3.74%. Calcd for $C_{84}H_{84}N_4O_{23}$: C, 66.48; H, 5.58; N, 3.69%.

*Conversion of **4** to **2**.* To a solution of **4** (68.5 mg) in dioxane (1.4 ml), 1 M sodium methoxide in methanol (0.14 ml) was added and the solution was kept at room temperature for 1.5 h. After addition of Dowex 50Wx8 (H form, pretreated with methanol) the mixture was filtered and the filtrate was concentrated to give a syrup. Washing the syrup thoroughly with water gave a solid (45.0 mg, 90%) identical with **2**.

*2′,3′,2″-Tri-*O*-benzoyl-tetrakis(*N*-benzyloxycarbonyl)-4″,6″-*O*-cyclohexylidene-4′-*O*-mesylkanamycin (**5**).* To a solution of **3** (20.0 g) in dry pyridine (300 ml), mesyl chloride (3.32 ml, $\approx$3 mol equivalents for **3**) were added and the solution was kept at 50 °C overnight. The solution showed, on TLC with $CHCl_3$–IPA (25 : 1), three spots of R_f 0.22 (**3**), 0.3 (major, **5**) and 0.45 (**6**). After addition of water (3.8 ml), the solution was concentrated *in vacuo* and the chloroform solution (600 ml) of the residual syrup was washed with 5% aqueous potassium hydrogensulfate, 2% aqueous sodium hydrogencarbonate, and water, dried ($MgSO_4$), and concentrated. The brown solid (21.3 g) was vigorously stirred with benzene (100 ml) and the mixture was centrifuged. The solid was treated likewise twice more to give a colorless solid of **5**, 13.8 g (65%). The benzene-soluble part (6.4 g), which was a mixture of **3**, **5**, and **6**, was repeatedly chromatographed over silica gel with $CHCl_3$–IPA to give a colorless solid of **6**, 2.1 g (9.5%).

5: $[\alpha]_D^{22}$ +120° (*c* 1, $CHCl_3$); PMR ($CDCl_3$): δ 2.85 (3H s, SO_2CH_3).

Found: C, 62.81; H, 5.62; N, 3.52; S, 2.07%. Calcd for $C_{78}H_{82}N_4O_{24}S$: C, 62.81; H, 5.54; N, 3.75; S, 2.15%.

6: $[\alpha]_D^{25}$ +82° (*c* 1, $CHCl_3$); PMR ($CDCl_3$): δ 2.87 and 2.96 (each 3H s, SO_2CH_3).

Found: C, 60.26; H, 5.26; N, 3.37; S, 3.83%. Calcd for $C_{79}H_{84}N_4O_{26}S_2$: C, 60.45; H, 5.39; N, 3.57; S, 4.08%.

*2′,3′,2″-Tri-*O*-benzoyl-tetrakis(*N*-benzyloxycarbonyl)-4″,6″-*O*-cyclohexylidene-4′-deoxy-4′-iodokanamycin (**7**).* A mixture of **5** (5.00 g) and sodium iodide (50 g) in DMF (100 ml) was heated at 100 °C for 40 h in an atmosphere of nitrogen. The solution, which solidified on cooling, was shaken with chloroform and the organic layer was concentrated *in vacuo* with several additions of toluene (to remove DMF) to give a residue. The solution of the residue in chloroform was washed with aqueous sodium thiosulfate and water, dried ($MgSO_4$), and concentrated. The brown solid was chromatographed over silica gel with $CHCl_3$–IPA (45 : 1) to give a pale-yellow solid, 3.34 g (65%). The solid contained two components, on checked by TLC, of R_f 0.3 (major) and 0.4 (the 3′-epimer); $[\alpha]_D^{23}$ +102° (*c* 1, $CHCl_3$).

Found: C, 60.70; H, 5.41; N, 3.69; I, 8.17%. Calcd for $C_{77}H_{79}N_4O_{21}I$: C, 60.71; H, 5.23; N, 3.68; I, 8.33%.

2',3',2''-Tri-O-benzoyl-tetrakis(N-benzyloxycarbonyl)-4'',6''-O-cyclohexylidene-4'-deoxykanamycin (8). A solution of **7** (2.38 g) in dioxane–methanol (1 : 1, 14 ml) containing a few drops of triethylamine was hydrogenated with hydrogen under pressure (50 lb/in^2) with Raney nickel at room temperature. After 1 h, the catalyst was replaced with fresh one and the mixture was treated likewise for further 1 h, then the procedure was repeated again. Filtration followed by evaporation gave a solid, which was chromatographed over silica gel with $CHCl_3$–IPA (45 : 1) to give a solid of **8**, 1.93 g (89%). The solid was reprecipitated from dioxane–water, $[\alpha]_D^{20}$ +160° (*c* 0.5, $CHCl_3$).

Found: C, 66.33; H, 5.87; N, 3.85%. Calcd for $C_{77}H_{80}N_4O_{21}$: C, 66.18; H, 5.77; N, 4.01%.

4'-Deoxykanamycin (9). To a solution of **8** (502 mg) in dry dioxane–methanol (1 : 1, 10 ml), 1 M sodium methylate in methanol (0.5 ml) was added and the solution was kept at room temperature for 4.5 h. Dowex 50Wx8 (H form) resin pretreated with methanol was added and the neutral solution was filtered and the filtrate was concentrated. The solid was washed with vigorous stirring with ether and then with hot acetone to give a solid, 304 mg (78% as debenzoyl product). A suspension of the solid in 80% aqueous acetic acid (11 ml) was heated at 80 °C for 1 h. The resulting clear solution was concentrated *in vacuo* to give a solid (295 mg). The decyclohexylidenated product was suspended in a mixture of dioxane–acetic acid–water (2 : 2 : 1, 20 ml) and the mixture was hydrogenated with atmospheric hydrogen in the presence of palladium black at room temperature for 20 min. Filtration followed by evaporation *in vacuo* gave a pale-brown syrup, which was chromatographed over CM-Sephadex C-25 (NH_4 form) with aqueous ammonia (0.02→0.15 M, gradually increased). The ninhydrin-positive fractions were concentrated to give a solid, 121 mg (62% as monocarbonate hemihydrate), $[\alpha]_D^{20}$ +137° (*c* 1, H_2O) (lit[2] +129° as 2/3 hydrate; +134°[3] as free base); PPC: $R_{f\ kanamycin}$ 1.2, TLC: $R_{f\ kanamycin}$ 1.7 (Avicel (microcrystalline cellulose powder, Funakoshi Co.), BuOH–EtOH–$CHCl_3$–17% NH_3=4 : 4 : 2 : 3, doubly developed).

Found: C, 42.45; H, 7.30; N, 10.08%. Calcd for $C_{18}H_{36}N_4O_{10}\cdot H_2CO_3\cdot 1/2H_2O$: C, 42.29; H, 7.29; N, 10.38%.

Benzyl 6-Benzyloxycarbonylamino-4,6-dideoxy-α- and β-D-xylo-hexopyranosides (10). A suspension of **9** (51.1 mg as $H_2CO_3\cdot 1/2H_2O$ salt) and anhydrous sodium carbonate (57 mg) in aqueous methanol (1 : 1, 1 ml) was treated with benzyl chloroformate (0.07 ml) in a similar manner as described to give tetrakis-(*N*-benzyloxycarbonyl)-4'-deoxykanamycin (85 mg, 89%). This was suspended in 2 M hydrogen chloride in benzyl alcohol (1.5 ml) and the mixture was heated at 100 °C for 15 min. The resulting clear solution showed, on TLC with $CHCl_3$–EtOH (10 : 1), three spots of R_f 0.05 (2-deoxystreptamine), 0.30 (3-amino-3-deoxy-D-glucose), and 0.38 (**10**). Basic lead carbonate (0.8 g) was added and the mixture was vigorously stirred for hours. Centrifugation followed by concentration of the upper layer gave a syrup, which was chromatographed over silica gel with $CHCl_3$–EtOH (40 : 1) to give a colorless solid of **10**, 32 mg (98%). PMR ($CDCl_3$–D_2O): δ 1.36 (≈0.7H q, J≈12 Hz, H-4_{ax} (α-anomer)), 1.39 (≈0.3H q, H-4_{ax} (β-anomer)), 1.75—2.05 (1H, m H-4_{eq}), 4.24 (≈0.3H d, J=7.5 Hz, H-1 (β)), 4.53 (≈1.4H AB q, J_{AB}=11.5 Hz, $C_6H_5C\underline{H}_2OC(1)(\alpha)$), 4.69 (≈0.6H AB q, J_{AB}=11.5 Hz, $C_6H_5C\underline{H}_2OC(1)(\beta)$), 4.93 (≈0.7H d, J=4.0 Hz, H-1(α)), 5.85 (2H s, $C_6H_5C\underline{H}_2OCO$).

Periodate Oxidation of 10. A sample of **10** (≈1 mg) was dissolved in a drop of dioxane and a drop of 0.01 M aqueous metaperiodate solution was added. The solution was checked by TLC with $CHCl_3$–EtOH (10 : 1). After keeping at room temperature for 10 min, the solution showed a spot of R_f 0.33 (**10**) and that of 0.43 in almost equal color strength, and after 1 h, the former spot disappeared. The latter spot was active for triphenyltetrazolium chloride, a reagent for reducing substances.

Pentakis(N-benzyloxycarbonyl)kanamycin B (11). Kanamycin B sulfate was treated similarly as described for **1** to give **11** in a yield of 85%, $[\alpha]_D^{25}$ +72° (*c* 1, DMF).

Found: C, 60.13; H, 5.81; N, 6.05%. Calcd for $C_{58}H_{67}N_5O_{20}$: C, 60.36; H, 5.85; N, 6.07%.

Pentakis(N-benzyloxycarbonyl)-4'',6''-O-cyclohexylidenekanamycin B (12). A mixture of **11** (6.65 g), 1,1-dimethoxycyclohexane (1.7 ml, 2 mol equivalents for **11**), and anhydrous *p*-toluenesulfonic acid (220 mg) was treated in a similar manner as described for **2**. The resulting sloution showed, on TLC with $CHCl_3$–EtOH (10 : 1), two spots of R_f 0.3 (**12**) and 0.7 (dicyclohexylidene isomer, major) (*cf.* **11**, R_f 0.12). After addition of water (0.05 ml, 0.5 mol equivalent for **11**), the solution was kept at room temperature overnight. The formation of **12** became major. Aqueous sodium hydrogencarbonate (480 mg) was added with vigorous stirring and the mixture was concentrated *in vacuo* with several additions of toluene. The residual colorless solid (5.9 g) was stirred with hot benzene (30 ml×3), centrifuged, and dried to give pure **12**, 5.67 g (80%). The benzene-soluble portion (217 mg) contained the dicyclohexylidene derivative as a major component.

12: $[\alpha]_D^{25}$ +62° (*c* 1, DMF) (lit,[15] +47° in pyridine).

Found: C, 62.43; H, 6.18; N. 5.68%. Calcd for $C_{64}H_{75}N_5O_{20}$: C, 62.28; H, 6.12; N, 5.67%.

3',2''-Di-O- (13) and 3',4',2''-Tri-O-benzoyl-tetrakis(N-benzyloxycarbonyl)-4'',6''-O-cyclohexylidenekanamycin B (14). To a solution of **12** (495 mg) in dry pyridine (10 ml), benzoyl chloride (0.12 ml, 2.5 mol equivalents for **12**) was added and the solution was kept at room temperature overnight. This reaction conditions were established by mesylating the product followed by examining its PMR spectrum several times, as in the preparation of **3**. The solution showed, on TLC (E. Merck) with $CHCl_3$–methyl ethyl ketone (MEK) (3 : 1), two spots of R_f 0.15 (**13**) and 0.22 (**14**) in almost equal strength. Work up as described for **3** gave a mixture of **13** and **14** (611 mg). The solid (195 mg) was chromatographed over silica gel (E. Merck silica gel 60, prepacked column 2.5×25 cm) with $CHCl_3$–MEK (3 : 1) to give **13** (81.6 mg, 44%), **14** (56.9 mg, 29%) and a mixture of **13** and **14** (25.7 mg).

13: mp 237—238 °C, $[\alpha]_D^{25}$ +112° (*c* 0.8, $CHCl_3$).

Found: C, 64.70; H, 5.75; N, 4.82%. Calcd for $C_{78}H_{83}N_5O_{22}$: C, 64.94; H, 5.80; N, 4.86%.

14: mp 139—140 °C, $[\alpha]_D^{25}$ +96° (*c* 1, $CHCl_3$).

Found: C, 65.74; H, 5.74; N, 4.45%. Calcd for $C_{85}H_{87}N_5O_{23}$: C, 66.01; H, 5.67; N, 4.53%.

3',2''-Di-O-benzoyl-pentakis(N-benzyloxycarbonyl)-4'',6''-O-cyclohexylidene-4'-O-mesylkanamycin B (15). A solution of **13** (197 mg) and mesyl chloride (0.05 ml, 5 mol equivalents for **13**) in dry pyridine (4 ml) was kept at room temperature for 2 h. The solution showed, on TLC (E. Merck) with $CHCl_3$–MEK (3 : 1), two spots of R_f 0.23 (**15**) and 0.44 (minor, di-*O*-mesyl derivative). Work up as described for **5** gave a solid (195 mg), which was chromatographed over silica gel with $CHCl_3$–MEK (3 : 1) to give a solid of **15**, 155 mg (75%) and a solid of 5,4'-di-*O*-mesyl derivative (**16**), 18 mg (8.3%).

15: mp 211—212 °C, $[\alpha]_D^{25}$ +97° (*c* 1, $CHCl_3$); PMR ($CDCl_3$): δ 2.78 (3H s, CH_3SO_2).

Found: C, 62.66; H, 5.73; N, 4.58; S, 1.88%. Calcd for $C_{79}H_{85}N_5O_{24}S$: C, 62.40; H, 5.63; N, 4.61; S, 2.11%.

16: mp 162—163 °C, $[\alpha]_D^{25}$ +70° (*c* 0.5, $CHCl_3$); PMR ($CDCl_3$): δ 2.78 and 3.07 (each 3H s, CH_3SO_2).

Found: C, 59.86; H, 5.43; N, 4.46; S, 4.01%. Calcd for $C_{80}H_{87}N_5O_{26}S_2$: C, 60.10; H, 5.49; N, 4.38; S, 4.01%.

*3′,2″-Di-O-benzoyl-pentakis(N-benzyloxycarbonyl)-4″,6″-O-cyclohexylidene-4′-deoxy-4′-iodokanamycin B (**17**).* Compound **15** (147 mg) was treated with sodium iodide (1.5 g) in DMF (3 ml) at 100 °C for 40 h. Work up as described for **7** gave a mixture of 4′-iodo epimers (R_f 0.2 and 0.38 (minor) with $CHCl_3$–MEK=3 : 1), 68 mg (45%).

*3′,2″-Di-O-benzoyl-pentakis(N-benzyloxycarbonyl)-4″,6″-O-cyclohexylidene-4′-deoxykanamycin B (**18**).* To a solution of **17** (35.6 mg) in dry dioxane (0.7 ml), tributyltin hydride (0.07 ml) and α,α′-azobisisobutyronitrile (≈3 mg) were added and the solution was heated at 80 °C for 2 h under the atmosphere of nitrogen. The solution showed, on TLC with $CHCl_3$–MEK (3 : 1), a single spot at R_f 0.2. Concentration gave a residue, which was chromatographed over silica gel with $CHCl_3$–MEK (3 : 1) to give a solid, which was reprecipitated from chloroform–ether, 26.5 mg (81%), mp 247—248 °C, $[\alpha]_D^{25}$ +120° (*c* 0.8, $CHCl_3$).

Found: C, 65.62; H, 5.84; N, 4.85%. Calcd for $C_{78}H_{83}N_5O_{21}$: C, 65.67; H, 5.86; N, 4.91%.

*4′-Deoxykanamycin B (**19**).* *A. From **18***: Compound **18** (26.5 mg) was treated likewise as described in the preparation of 4′-deoxykanamycin (**9**) to yield **19**, 7.0 mg (64% as dicarbonate), $[\alpha]_D^{20}$ +117° (*c* 0.5, H_2O); PPC: $R_{f\ \text{kanamycin B}}$ 1.2 (*cf.* tobramycin, 1.3); PMR (D_2O): δ 1.0—1.5 (2H two overlapped q, $J\approx12$ Hz, H-2_{ax}, H-$4'_{ax}$), 1.75—2.1 (2H m, H-2_{eq}, H-$4'_{eq}$), 4.99 (1H d, J=3.5 Hz, H-1′ or 1″), 5.35 (1H d, J=3.5 Hz, H-1′ or 1″).

Found: C, 40.75; H, 6.96; N, 11.90%. Calcd for $C_{18}H_{37}N_5O_9\cdot2H_2CO_3$: C, 40.61; H, 6.99; N, 11.84%.

*B. From **28***: Compound **28** (97.4 mg) was treated similarly as described[17] (preparation of **10** from **7** in that litrature) to give **19**, 20.0 mg (35% as dicarbonate) and a ureylene derivative,[20] 15.6 mg.

*2″-O-Benzoyl-4″,6″-O-cyclohexylidene-pentakis(N-ethoxycarbonyl)-3′-O-(**21**), 4′-O- (**22**), and di-O-tosylkanamycin B (**23**).* A solution of **20**[17] (4.17 g) and *p*-toluenesulfonyl chloride (3.90 g, 5 mol equivalents for **20**) in dry pyridine (50 ml) was kept at room temperature overnight. The solution showed, on TLC with $CHCl_3$–IPA (15 : 1), three spots of R_f 0.30 (**21**, major), 0.36 (**22**), and 0.38 (**23**). After addition of water, the reaction mixture was treated likewise as descibed[17] (preparation of **5** in that literature) to give **21** (2.76 g, 58%; mp 149—150 °C (lit, [17]149—150 °C), $[\alpha]_D^{20}$ +88° (*c* 1, MeOH) (lit,[17] +88°)), **22** (0.60 g, 12.5%), and **23** (0.36 g, 6%).

22: mp 152—153 °C (dec), $[\alpha]_D^{20}$ +118° (*c* 1, DMF); PMR ($(CD_3)_2SO$): δ 2.42 (3H s, CH_3(Ts)).

Found: C, 53.78; H, 6.15; N, 5.88; S, 2.85%. Calcd for $C_{53}H_{75}N_5O_{23}S$: C, 53.84; H, 6.40; N, 5.93; S, 2.71%.

23: $[\alpha]_D^{25}$ +79° (*c* 1, MeOH); PMR ($CDCl_3$): δ 2.47 (6H s, CH_3(Ts)).

Found: C, 54.08; H, 6.12; N, 5.36; S, 4.71%. Calcd for $C_{60}H_{81}N_5O_{25}S_2$: C, 53.92; H, 6.11; N, 5.24; S, 4.80%.

*2″-O-Benzoyl-4″,6″-O-cyclohexylidene-pentakis(N-ethoxycarbonyl)-4′-O-mesylkanamycin B (**26**).* To a cold (−20 °C) solution of **20** (101 mg) in dry DMF (1 ml) containing dry pyridine (0.048 ml, 6 mol equivalents for **20**), tosyl chloride (38.2 mg) was added and the solution was kept for 2 h in the cold. The solution showed, on TLC with $CHCl_3$–IPA (10 : 1), a single spot at R_f 0.2 (mainly **24**) (*cf.* **19**, R_f 0.1). Concentration of the solution below 30 °C gave a syrup, which was dissolved in chloroform. The solution was washed with 5% aqueous sodium hydrogencarbonate and water, dried ($MgSO_4$), and concentrated *in vacuo* with several additions of toluene to give a colorless solid (114 mg). The solid was vigorously stirred with ether and filtered. The solid (108 mg) contained a trace amount of di-*O*-formyl(?) product (R_f 0.21). To a solution of the solid in pyridine (2 ml), mesyl chloride (0.024 ml, 3 mol equivalents for **20**) was added and the solution was kept at room temperature for 4 h. The solution showed, on TLC (E. Merck), a single spot at R_f 0.49 (mainly **25**) *cf.* mono-*O*-formyl product, R_f 0.42). Work up as described for **5** gave a solid (112 mg). A solution of the solid in dioxane (1 ml) and 28% aqueous ammonia (0.1 ml) was kept at room temperature for 15 min. The solution showed, on TLC, a single spot at R_f 0.40. Concentration followed by washing of the residue with water gave a solid (100 mg). The solid was washed with ethyl acetate (1 ml×2) with vigorous stirring to give a colorless solid of **26**, 68 mg (62% based on **20**). The ethyl acetate-soluble part (30 mg) is mainly composed of **20**. Compound **26** has fairly low solubility in usual organic solvents.

26: $[\alpha]_D^{25}$+105° (*c* 1, DMF); PMR (Py-d_5): δ 3.43 (3H s, CH_3SO_2).

Found: C, 51.14; H, 6.44; N, 6.16; S, 2.88%. Calcd for $C_{47}H_{71}N_5O_{23}S$: C, 51.03; H, 6.47; N, 6.33; S, 2.90%.

*2″-O-Benzoyl-4″,6″-O-cyclohexylidene-4′-deoxy-pentakis(N-ethoxycarbonyl)-4′-iodokanamycin B (**27**).* *A. From **22***: A mixture of **22** (517 mg) and sodium iodide (5.0 g) in DMF (10 ml) was heated at 100 °C for 3 h. Work up as described for **7** gave a solid of **27**, 359 mg (72%), $[\alpha]_D^{20}$ +78° (*c* 1, MeOH).

Found: C, 48.69; H, 5.91; N, 6.01; I, 10.80%. Calcd for $C_{46}H_{68}N_5O_{20}I$: C, 48.55; H, 6.02; N, 6.15; I, 11.15%.

*B. From **26***: A mixture of **26** (49.3 mg) and sodium iodide (500 mg) in DMF (1 ml) was heated at 100 °C for 10 h. Work up as described in A gave **27**, 46.8 mg (92%). Compounds **27** obtained by A and B were identical in every respect.

*2″-O-Benzoyl-4″,6″-O-cyclohexylidene-4′-deoxy-pentakis(N-ethoxycarbonyl)kanamycin B (**28**).* Compound **27** (49.6 mg) was treated as described for **8** to give a solid of **28**, 37.3 mg (85%), mp 256—257 °C, $[\alpha]_D^{20}$ +93° (*c* 1, MeOH),

Found: C, 54.47; H, 6.73; N, 6.65%. Calcd for $C_{46}H_{69}N_5O_{20}$: C, 54.59; H, 6.87; N, 6.92%.

The authors are grateful to Dr. Hiroshi Naganawa of Institute of Microbial Chemistry for collaboration on ^{13}C NMR spectral studies.

References

1) A part of this paper was briefly presented at the 192nd Meeting of Japan Antibiotics Research Association, March 22, 1974.

2) S. Umezawa, Y. Nishimura, Y. Hata, T. Tsuchiya, M. Yagisawa, and H. Umezawa, *J. Antibiot.*, **27**, 722 (1974).

3) T. Naito, S. Nakagawa, Y. Abe, K. Fujisawa, and H. Kawaguchi, *J. Antibiot.*, **27**, 838 (1974).

4) D. Ikeda, T. Tsuchiya, S. Umezawa, and H. Umezawa, *Bull. Chem. Soc. Jpn.*, **47**, 3136 (1974).

5) T. Miyake, T. Tsuchiya, S. Umezawa, and H. Umezawa, *Carbohydr. Res.*, **49**, 141 (1976).

6) S. Umezawa, H. Umezawa, Y. Okazaki, and T. Tsuchiya, *Bull. Chem. Soc. Jpn.*, **45**, 3624 (1972).

7) H. Umezawa, S. Umezawa, T. Tsuchiya, and Y. Okazaki, *J. Antibiot.*, **24**, 485 (1971); S. Umezawa, H. Umezawa, Y. Okazaki, and T. Tsuchiya, *Bull. Chem. Soc. Jpn.*, **45**, 3624 (1972).

8) G. Kotowycz and R. U. Lemieux, *Chem. Rev.*, **73**, 669 (1973).

9) K. F. Koch, J. A. Rhoades, E. W. Hagaman, and E. Wenkert, *J. Am. Chem. Soc.*, **96**, 3300 (1974).

10) J. B. Morton, R. C. Long, P. J. L. Daniels, R. W. Tkach, and J. H. Goldstein, *J. Am. Chem. Soc.*, **95**, 7464 (1973).
11) S. Omoto, S. Inouye, M. Kojima, and T. Niida, *J. Antibiot.*, **26**, 717 (1973).
12) R. S. Egan, A. C. Sinclair, R. L. Vault, J. B. McAlpine, S. L. Mueller, P. C. Goodley, R. S. Stanaszek, M. Cirovic, R. J. Mauritz, L. A. Mitscher, K. Shirahata, S. Sato, and T. Iida, *J. Antibiot.*, **30**, 31 (1977).
13) J. B. McAlpine, A. C. Sinclair, R. S. Egan, R. L. Vault, R. S. Stanaszek, M. Cirovic, S. L. Mueller, P. C. Goodley, R. J. Mauritz, N. E. Wideburg, L. A. Mitscher, K. Shirahata, H. Matsushima, S. Sato, and T. Iida, *J. Antibiot.*, **30**, 39 (1977).
14) D. E. Dorman and J. D. Roberts, *J. Am. Chem. Soc.*, **92**, 1355 (1970).
15) T. Nishimura, T. Tsuchiya, S. Umezawa, and H. Umezawa, *Bull. Chem. Soc. Jpn.*, **50**, 1580 (1977).
16) G. J. M. Van Der Kerk, J. G. Noltes, and J. G. A. Luijten, *J. Appl. Chem.*, **7**, 366 (1957); H. Arita and Y. Matsushima, *J. Biochem.*, **70**, 795 (1971); H. Arita, N. Ueda, K. Fukukawa, and Y. Matsushima, *Bull. Chem. Soc. Jpn.*, **45**, 567, 3614 (1972).
17) Y. Takagi, T. Miyake, T. Tsuchiya, S. Umezawa, and H. Umezawa, *Bull. Chem. Soc. Jpn.*, **49**, 3649 (1976).
18) J. D. Albright, E. Benz, A. E. Lanzilotti, and L. Goldman, *Chem. Commun.*, **1965**, 413; An example of *O*-formylation by DMF–mesyl chloride was reported by M. E. Evans, L. Long, Jr., and F. W. Parrish, *J. Org. Chem.*, **33**, 1074 (1968).
19) S. Umezawa, T. Tsuchiya, and K. Tatsuta, *Bull. Chem. Soc. Jpn.*, **39**, 1235 (1966).
20) T. Yamaguchi, T. Tsuchiya, and S. Umezawa, *J. Antibiot.*, **30**, 71 (1977).

Synthesis of a Lividomycin B Analogue, 5-*O*-[3-*O*-(2-Amino-2-deoxy-α-D-glucopyranosyl)-β-D-ribofuranosyl]-3′-deoxyparomamine

Isamu WATANABE, Tsutomu TSUCHIYA, Tsuneyuki TAKASE,* Sumio UMEZAWA, and Hamao UMEZAWA**

Institute of Bioorganic Chemistry, 1614 Ida, Nakahara-ku, Kawasaki 211

**Department of Applied Chemistry, Faculty of Engineering, Keio University, Hiyoshi, Kohoku-ku, Yokohama 223*

***Institute of Microbial Chemistry, Kamiosaki, Shinagawa-ku, Tokyo 141*

(Received March 1, 1977)

5-*O*-[3-*O*-(2-Amino-2-deoxy-α-D-glucopyranosyl)-β-D-ribofuranosyl]-3′-deoxyparomamine was prepared by two different routes. The first route involves glycosylation of a protected 1-*N* : 6-*O*-carbonyl-3′-deoxyparomamine with a protected 3-*O*-(2-amino-2-deoxy-α-D-glucopyranosyl)ribofuranosyl bromide and subsequent removal of the protecting groups. In the second route, 1-*N* : 6-*O*-carbnyl-3′-deoxyparomamine was glycosylated with a protected ribosyl bromide having 3-*O*-benzylthiocarbonyl group to give a pseudotrisaccharide and, after de-3-*O*-benzylthiocarbonylation, the product was further condensed with a protected 1-bromide of 2-amino-2-deoxy-D-glucose. This synthesized lividomycin B analogue showed only very weak antibacterial activity and the role of the 6″-amino group of lividomycin in the action was suggested.

Lividomycin B[1] is an aminoglycoside antibiotic which belongs to a pseudotetrasaccharide. Since its pseudotrisaccharide[2] portion which lacks the 2,6-diamino-2,6-dideoxy-L-idopyranose moiety has only very weak antibacterial activity, this diaminohexose moiety has been suggested to enhance the antibacterial activity in a great extent. However, it has not yet been certain, which amino group in this diaminohexose moiety has the predominant role to increase the activity. Therefore, we attempted to replace this diaminohexose moiety of lividomycin B with 2-amino-2-deoxy-D-glucose.

Among two synthetic routes considered, we at first prepared this lividomycin B analogue by condensation of a disaccharide with a pseudodisaccharide. The disaccharide was prepared by condensation of 3,4,6-tri-*O*-acetyl-2-deoxy-2-(*p*-methoxybenzylidene)amino-α-D-glucopyranosyl bromide[3] (**1**) with 5-*O*-benzoyl-1,2-*O*-isopropylidene-α-D-ribofuranose[4] (**2**) in benzene in the presence of mercury(II) cyanide as catalyst. Acid hydrolysis of the *N*-(*p*-methoxybenzylidene) group of the condensation product followed by *N*-benzyloxycarbonylation gave the protected disaccharide (**3**) in 54% yield (based on **2**). The high yield formation of the α-D-glucoside may be ascribed in part to the presence of the 2-*N*-(*p*-methoxybenzylidene) group.[5] To confirm the α-D-glucoside linkage of **3**, the *O*-acyl and *N*-benzyloxycarbonyl groups of **3** were removed. The PMR spectrum and the optical rotation of the deacylated product (**4**) substantiated the α-D-glucoside linkage. Then, the isopropylidene group of **3** was removed by 95% formic acid treatment without affecting the glucosyl bond and the *O*-acyl groups, and the resulting free hydroxyl groups at C-1 and 2 were *p*-nitrobenzoylated to give **5**. The presence of the 2-*O*-(*p*-nitrobenzoyl) group prevents undesirable orthoester[6] formation in the subsequent glycosylation. Treatment of **5** with hydrogen bromide in dichloromethane gave the corresponding 1-bromide.

The protected pseudodisaccharide, namely 3,2′-bis(*N*-benzyloxycarbonyl)-1-*N* : 6-*O*-carbonyl-3′-deoxy-4′,6′-di-*O*-(α-naphthoyl)paromamine (**6**), which is moderately soluble in organic solvents, was prepared by treatment of tris(*N*-benzyloxycarbonyl)-3′-deoxyparomamine[7] with sodium hydride in *N*,*N*-dimethylformamide (DMF)[8] followed by regioselective acylation with α-naphthoyl chloride. The positions of the α-naphthoyl groups in **6** were confirmed by the hydrolysis of mono-*O*-mesyl derivative (**7**) of **6**. Paper chromatography of the acidic hydrolyzate of **7** gave no detectable 2-deoxystreptamine, whereas the same treatment of **6** gave 2-deoxystreptamine, indicating that the 5-hydroxyl group of **6** was mesylated. Condensation of **6** with the abovementioned 1-bromide of **5** was carried out in dichloromethane in the presence of mercury(II) cyanide, and, the condensation products having β-D (**8**) and α-D (**8′**) glycoside linkages were separated by silica gel chromatography in yields of 33 and 47%, respectively. Treatment of **8** and **8′** with sodium benzylate in benzyl alcohol removed all the *O*-acyl groups and, simultaneously cleaved the 1,6-carbamate into 1-benzyloxycarbonylamino and 6-hydroxyl groups to give **9** and **9′**, respectively. Hydrogenolysis of **9** and **9′** with palladium black removed the benzyloxycarbonyl groups and gave the desired pseudotetrasaccharide (**10**) and its α-D-anomer (**10′**), respectively.

The anomeric configurations of **10** and **10′** were identified by their PMR spectra, and their pseudotetrasaccharide structures were supported by paper chromatography of their methanolyzates.

In another route, the pseudodisaccharide derivative (**6**) was successively glycosylated with a protected ribofuranosyl bromide and then with the glucosamine derivative (**1**). The aforementioned protected ribose **2** was led to 3-*O*-benzylthiocarbonyl derivative (**11**) by treatment with benzylthiocarbonyl chloride in pyridine. This protecting group[9] was chosen because of its easy elimination by oxidation with hydrogen peroxide to liberate the free hydroxyl group at C-3 of the ribose moiety. Acidic solvolysis of **11** to remove the isopropylidene group followed by *p*-nitrobenzoylation gave methyl 3-*O*-benzylthiocarbonyl-2-*O*-(*p*-nitrobenzoyl)-β-D- and α-D-riboside (**12** and **12′**). The structures of **12** and **12′** were confirmed by their PMR spectra as well as by those of the debenzylthiocarbonylated product (**13** and **13′**) of **12** and **12′**. In the spectrum of **12′** a virtual coupling[10] between H-1 and 3 was observed and it was further observed that 2-*O*→3-*O*-(*p*-nitrobenzoyl) migration gradually occurred when the solu-

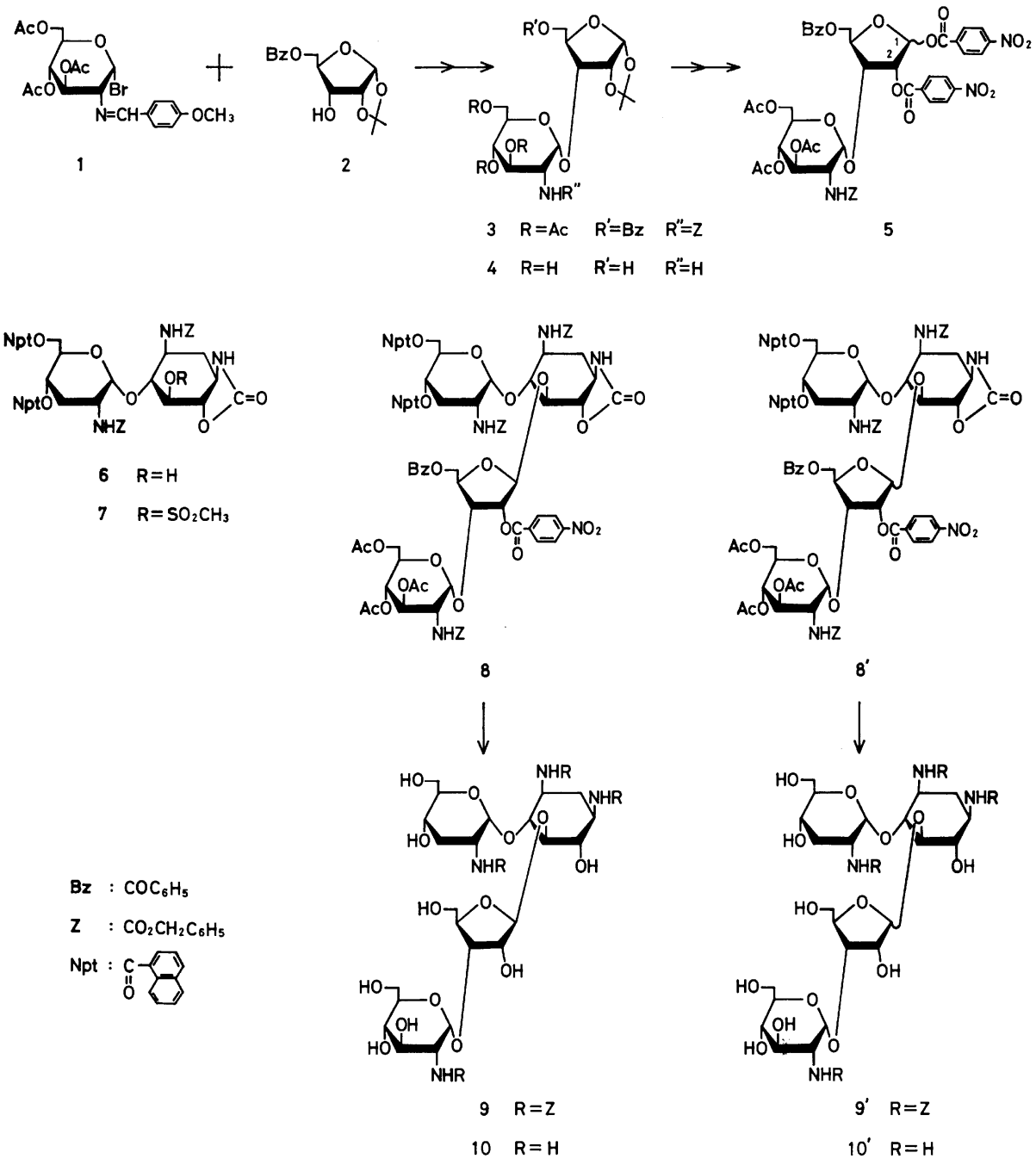

tion (in pyridine-d_5 containing deuterium oxide) of **13** and **13'** were allowed to stand (see Experimental).

Treatment of **12** with hydrogen bromide in acetic acid gave the 1-bromide, which was used without purification, for coupling with **6** in a manner described above to give the condensation product (**14**) in 66% yield. The β-anomeric configuration (at C-1") of **14** could not be determined at this stage, but was made clear at the last step which gave **10** identical with that prepared by the alternative route aforementioned. Removal of the benzylthiocarbonyl group with hydrogen peroxide in acetic acid gave the product (**15**) having a free hydroxyl group at C-3". In this reaction, a slight amount of 3"-*O*-(*p*-nitrobenzoyl) derivative was formed by migration. The structure of **15** was confirmed by recovery of **14** from **15** with the benzylthiocarbonyl chloride treatment. The condensation of **15** with **1** was achieved in benzene in the presence of silver reagents to give **8**, in 30% yield, which was led to the desired product (**10**).

The overall yield of **10** by the second route was lower than that by the first route. However, it should be noted that the first route gave a larger amount of the α-riboside (**8'**) than the desired β-riboside (**8**). In the second route no α-riboside was obtained.

The synthesized pseudotetrasaccharide (**10**) showed much weaker antibacterial activities than lividomycin B and this result suggested that the 6"'-amino group

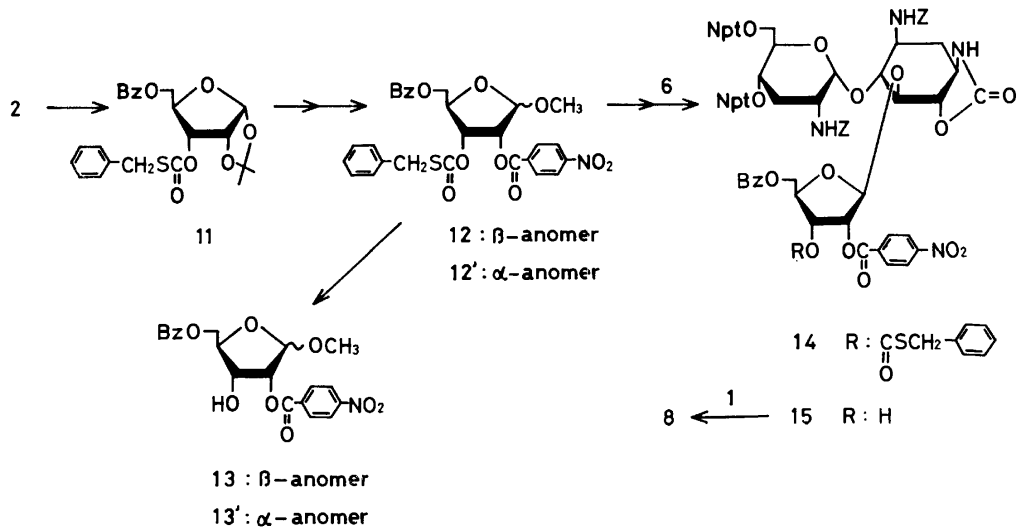

of lividomycin B has a predominant role in increasing the antibacterial activity. The corresponding α-anomer (**10′**) showed no antibacterial activity.

Experimental

Thin-layer chromatography (TLC) was carried out on Wakogel B-5 with sulfuric acid spray for detection unless otherwise stated. For column-chromatography, silica gel (Wakogel C-200) was used. Descending paper chromatography was performed on Toyo-Roshi Paper No. 50 with 1-butanol–pyridine–water–acetic acid (6 : 4 : 3 : 1), and spots were visualized by spraying 0.5% ninhydrin in pyridine. PMR spectra were recorded at 60 and 90 MHz with Hitachi R-24A and Varian EM-390 spectrometers, respectively.

*5-O-Benzoyl-1,2-O-isopropylidene-α-D-ribofuranose (**2**).* The compound was prepared in a different way from the reported one.[4] 5-*O*-Benzoyl-1,2-*O*-isopropylidene-D-*erythro*-pentofuranos-3-urose[11] (2 g) dissolved in methanol was treated with sodium borohydride in a usual manner to give **2** as needles (from ethyl acetate–diisopropyl ether, 1.7 g, 86%), mp 81—82 °C (lit,[4] 78—79 °C), $[\alpha]_D^{26}$ +32° (*c* 1, $CHCl_3$) (lit,[4] +20.05° in $CHCl_3$).

*3-O-(3,4,6-Tri-O-acetyl-2-benzyloxycarbonylamino-2-deoxy-α-D-glucopyranosyl)-5-O-benzoyl-1,2-O-isopropylidene-α-D-ribofuranose (**3**).* To a solution of 3,4,6-tri-*O*-acetyl-2-deoxy-2-(*p*-methoxybenzylidene)amino-α-D-glucopyranosyl bromide[3] (**1**, 1.34 g) in dry benzene (18 ml), 5-*O*-benzoyl-1,2-*O*-isopropylideneribofuranose[2] (**2**, 0.58 g,) mercury(II) cyanide (1.3 g), and calcium sulfate (Drierite 2.7 g) were added and the mixture was stirred at room temperature overnight. After addition of chloroform (100 ml), the mixture was centrifuged. The organic layer separated was washed with aqueous sodium hydrogencarbonate and water, dried (Na_2SO_4), and concentrated. The resulting syrup was dissolved in a mixture of methanol (36 ml) and 50% aqueous acetic acid (16 ml) and the solution was kept at room temperature for 4 h. After addition of powdered sodium carbonate (7.1 g), the solution was concentrated. The residue was extracted with acetone and the extract was concentrated to dryness. To an ice cold solution of the residue in aqueous acetone (3 : 10, 50 ml), sodium carbonate (900 mg) and benzyl chloroformate (1.8 g) were added and the mixture was stirred for 1 h in the cold. Evaporation followed by extraction with chloroform and evaporation of the solvent gave a syrup. Since **2** which remained unreacted had the same mobility with that of **3** on column chromatography, **3** was separated after acetylation of the remaining **2**. A mixture of the syrup and acetic anhydride (2 ml) in pyridine (40 ml) was allowed to stand at 37 °C overnight. Evaporation, extraction of the residue with chloroform, washing of the solution (aqueous potassium hydrogensulfate, aqueous sodium hydrogencarbonate, and water), drying (Na_2SO_4), and evaporation of the solvent gave a syrup. The syrup was chromatographed over silica gel with benzene–ethyl acetate (8 : 1) to give **3** (syrup), 748 mg (54%), $[\alpha]_D^{20}$ +102° (*c* 1, $CHCl_3$); IR (KBr): 1740, 1720 cm^{-1}; PMR ($CDCl_3$) δ: 1.22 and 1.53 (each 3H s, $C(CH_3)_2$), 1.94, 2.00, and 2.02 (each 3H s, Ac), 5.07 (1H d, J=3.5 Hz, H-1′), 5.91 (1H d, J=3.5 Hz, H-1).

Found: C, 58.67; H, 5.78; N, 1.78%. Calcd for $C_{35}H_{41}NO_{15}$: C, 58.74; H, 5.77; N, 1.96%.

*3-O-(2-Amino-2-deoxy-α-D-glucopyranosyl)-1,2-O-isopropylidene-α-D-ribofuranose (**4**).* A solution of **3** (100 mg) in methanol containing 5% ammonia (5 ml) was kept at room temperature overnight and the solution was concentrated. To a solution of the residue in dioxane (2 ml), water (1 ml) and two drops of acetic acid were added and the mixture was hydrogenated with palladium black in an atmospheric pressure of hydrogen. After filtration, the filtrate was concentrated to give a syrup, which was chromatographed over CM-Sephadex C-25 (NH_4 form) with 0.05 M aqueous ammonia to give a ninhydrin-positive solid of **4** as hemihydrate, 20 mg (40%), $[\alpha]_D^{18}$ +165° (*c* 0.5, H_2O); PMR (D_2O) δ: 1.43 and 1.61 (each 3H s, $C(CH_3)_2$), 2.78 (1H q, $J_{1',2'}$=3.7 Hz, $J_{2',3'}$=9.5 Hz, H-2′), 4.95 (1H m, H-2), 5.12 (1H d, J=3.7 Hz, H-1′), 5.96 (1H d, J=3.8 Hz, H-1).

Irradiation of H-2′ collapsed the doublet of H-1′ to a singlet and irradiation of H-1′ collapsed the quartet of H-2′ to a doublet (J=9.5 Hz). Irradiation of H-1 (δ 5.96) collapsed the multiplet of H-2 to an incomplete triplet ($J \approx 1.9$ Hz).

Found: C, 46.75; H, 6.96; N, 3.70%. Calcd for $C_{14}H_{25}NO_{19} \cdot 1/2H_2O$: C, 46.66; H, 7.27; N, 3.89%.

*3-O-(3,4,6-Tri-O-acetyl-2-benzyloxycarbonylamino-2-deoxy-α-D-glucopyranosyl)-5-O-benzoyl-1,2-bis-O-(p-nitrobenzoyl)-D-ribofuranose (**5**).* A solution of **3** (621 mg) in 95% aqueous formic acid (30 ml) was kept at room temperature for 3.5 h. Concentration *in vacuo* at room temperature gave a syrup. The chloroform solution of the syrup was washed with aqueous sodium hydrogencarbonate and water, dried (Na_2SO_4), and concentrated. To a solution of the resulting syrup in dry pyridine (8 ml), *p*-nitrobenzoyl chloride (626 mg) was added and the solution was kept at room temperature overnight.

After addition of water (0.1 ml), the solution was concentrated. The chloroform solution (50 ml) of the residue was washed with aqueous potassium hydrogensulfate, aqueous sodium hydrogencarbonate, and water, dried (Na_2SO_4), and concentrated. The resulting syrup was chromatographed over silica gel with benzene–ethyl acetate (10 : 1) to give a syrup of **5**, 572 mg (68%), $[\alpha]_D^{23}$ +72° (*c* 1, $CHCl_3$); IR (KBr): 1725, 1520 cm^{-1}.

Found: C, 56.82; H, 4.65; N, 4.02%. Calcd for $C_{46}H_{43}N_3O_{21}$: C, 56.73; H, 4.45; N, 4.31%.

*3,2′-Bis(*N*-benzyloxycarbonyl)-1-*N*:6-O-carbonyl-3′-deoxy-4′,6′-di-O-(α-naphthoyl)paromamine (6).* To an ice-cold solution of 1,3,2′-tris(*N*-benzyloxycarbonyl)-3′-deoxyparomamine[7] (3.0 g) in DMF (60 ml), 50% oily suspension (600 mg) of sodium hydride was added under nitrogen atmosphere and the mixture was stirred vigorously for 2.5 h. After addition of acetic acid (0.8 ml), the mixture was poured into ice-water. The precipitates of 1,6-carbamate were filtered and dried (2.35 g). To a cold (−20 °C) solution of the solid in pyridine (45 ml), α-naphthoyl chloride (610 mg×3) was added and the solution was kept at −10 °C for 9 h (3 h×3). After concentration, the residue was dissolved in chloroform. The solution was washed (with aq $KHSO_4$, aq $NaHCO_3$, and H_2O) as described for **3** to give a solid, which was chromatographed over silica gel with chloroform–ethanol (50 : 1) to give a solid of **6**, 2.78 g (76%), $[\alpha]_D^{22}$ +69° (*c* 1, $CHCl_3$); IR (KBr): 1775 cm^{-1} (shoulder, cyclic carbamate).

Found: C, 67.31; H, 5.26; N, 4.64%. Calcd for $C_{51}H_{47}N_3O_{13}$: C, 67.32; H, 5.21; N, 4.62%.

*3,2′-Bis(*N*-benzyloxycarbonyl)-1-*N*:6-O-carbonyl-3′-deoxy-5-O-mesyl-4′,6′-di-O-(α-naphthoyl)paromamine (7).* To a solution of **6** (180 mg) in dry pyridine (4 ml), methanesulfonyl chloride (200 mg) was added and the solution was kept at room temperature overnight. The solution showed, on TLC with chloroform–methanol (30 : 1), a single spot at R_f 0.33. Work up in a usual manner gave a solid of **7**, 172 mg (88%), $[\alpha]_D^{24}$ +49° (*c* 1, $CHCl_3$); IR (KBr): 1180, 1350 (Ms) cm^{-1}; PMR: δ of SO_2CH_3: 3.07 (in $CDCl_3$), 3.18 (in $CDCl_3$–CD_3OD=1 : 1), 3.43 (in C_5D_5N).

Found: C, 63.00; H, 5.16; N, 4.16; S, 3.47%. Calcd for $C_{52}H_{49}N_3O_{15}S$: C, 63.21; H, 5.00; N, 4.25; S, 3.25%.

Acidic Methanolysis of 7. A solution of **7** in 2 M methanolic hydrogen chloride was heated at 80 °C for 40 h. As a control experiment, **6** was similarly treated. Paper chromatography of the methanolyzate of **7** gave no 2-deoxystreptamine, whereas that of **6** did.

*5-O-[3-O-(3,4,6-Tri-O-acetyl-2-benzyloxycarbonylamino-2-deoxy-α-D-glucopyranosyl)-5-O-benzoyl-2-O-(*p*-nitrobenzoyl)-β-* and *α-D-ribofuranosyl]-3,2′-bis(*N*-benzyloxycarbonyl)-1-*N*:6-O-carbonyl-3′-deoxy-4′,6′-di-O-(α-naphthoyl)paromamine (8 and 8′).* *A. From 5 and 6*: To a cold (−10 °C) solution of **5** (1.75 g) in dry dichloromethane (50 ml), hydrogen bromide was introduced until saturation and the solution was kept at −10 °C for 30 min. Colorless needles of *p*-nitrobenzoic acid was deposited. Filtration followed by concentration of the filtrate at room temperature gave a syrup, which was dissolved in dichloromethane (11 ml). To the solution, **6** (516 mg), mercury(II) cyanide (1.85 g), and calcium sulfate (Drierite 3.75 g) were added and the mixture was vigorously stirred at room temperature overnight. On TLC with chloroform–ethanol (30 : 1), the reaction mixture showed two marked spots at R_f 0.37 (**8**), 0.29 (**8′**). The mixture was filtered with aid of chloroform. The filtrate was concentrated to give a syrup, which was chromatographed over silica gel with chloroform–ethanol (100 : 1) to give a solid of **8**, 316 mg (33% from **6**) and a solid of **8′**, 456 mg (47% from **6**).

Compound **8**: $[\alpha]_D^{20}$ +51° (*c* 1, $CHCl_3$): IR(KBr): 1780 (s), 1725, 1530 cm^{-1}.

Found: C, 62.59; H, 5.05; N, 4.05%. Calcd for $C_{90}H_{85}N_5O_{30}$: C, 62.97; H, 4.99; N, 4.08%.

Compound **8′**: $[\alpha]_D^{20}$+69° (*c* 0.5, $CHCl_3$): IR(KBr): 1780 (s), 1725, 1530 cm^{-1}.

Found: C, 63.04; H, 5.05; N, 4.04%.

B. From 1 and 15: To a solution of **1** (222 mg) in dry benzene (4 ml), **15** (194 mg), freshly prepared silver carbonate (230 mg), silver perchlorate (23 mg), and calcium sulfate (Drierite 550 mg) were added and the mixture was stirred at room temperature overnight in a dark place. The reaction mixture was filtered with aid of chloroform (20 ml) and the filtrate was concentrated. The residue was dissolved in a mixture of chloroform (2 ml), methanol (4 ml), acetic acid (1 ml) and water (1 ml), and the solution was kept at room temperature overnight. After addition of powdered sodium carbonate (930 mg), the mixture was concentrated *in vacuo*. The residue was extracted with chloroform and the extract was washed with water, dried (Na_2SO_4), and concentrated to give a solid. To a cold (0 °C) solution of the solid in aqueous acetone (1 : 2, 6 ml), benzyl chloroformate (150 mg) and sodium carbonate (600 mg) were added and the mixture was stirred at 0 °C for 1.5 h. After evaporation of the mixture was extracted with chloroform. The solution was washed with water, dried (Na_2SO_4), and evaporated to give a solid, which was chromatographed over silica gel with chloroform–ethanol (60 : 1) to give a solid of **8**, 77 mg (30% based on **14**), $[\alpha]_D^{23}$ +52° (*c* 1, $CHCl_3$). Recovered **15** by the chromatography was 80 mg (41%).

Found: C, 62.61; H, 5.11; N, 3.87%. Calcd for $C_{90}H_{85}N_5O_{30}$: C, 62.97; H, 4.99; N, 4.08%.

*1,3,2′-Tris(*N*-benzyloxycarbonyl)-5-O-[3-O-(2-benzyloxycarbonylamino-2-deoxy-α-D-glucopyranosyl)-β-* and *α-D-ribofuranosyl]-3′-deoxyparomamines (9 and 9′).* To a solution of **8** (42 mg) in dry dioxane (0.17 ml), 0.27 M sodium benzylate in benzyl alcohol (0.63 ml, benzyl alcohol was dried over molecular sieves 4A) were added and the solution was kept at 37 °C for 2 h. After addition of chloroform (27 ml), the organic solution was washed thoroughly with water, dried (Na_2SO_4), and concentrated to give a syrup. The syrup was chromatographed over silica gel with chloroform (to elute the alcohol remained) and then with chloroform–ethanol (4 : 1) to give **9**, 23 mg of solid (83%), $[\alpha]_D^{19}$ +58° (*c* 0.4, MeOH).

Found: C, 56.65; H, 5.89; N, 4.94%. Calcd for $C_{55}H_{68}N_4O_{22}\cdot H_2O$: C, 57.19; H, 6.11; N, 4.85%.

Compound **9′** was obtained from **8′** in a similar manner as described above in a yield of 83%; $[\alpha]_D^{19}$ +113° (*c* 0.5, MeOH).

Found: C, 56.90; H, 5.98; N, 4.88%.

5-O-[3-O-(2-Amino-2-deoxy-α-D-glucopyranosyl)-β- and *α-D-ribofuranosyl]-3′-deoxyparomamines (10 and 10′).* A mixture of **9** (80 mg) in aqueous dioxane (1 : 3, 4 ml) containing two drops of acetic acid was hydrogenated with palladium black in an atmospheric pressure of hydrogen. On TLC (E. Merck, silica gel 60 F_{254}) with chloroform–methanol–17% aqueous ammonia (1 : 4 : 3), the solution showed a major spot at R_f 0.51 (in the case of **10′**, R_f 0.59). Concentration of the solution gave a solid, which was chromatographed over CM-Sephadex C-25 (NH_4 form) with 0.05 M aqueous ammonia to give **10** as a solid of monocarbonate, 34 mg (73%); PPC, $R_{f\ \text{Hydromycin B}}$ 1.49, $[\alpha]_D^{23}$ +77° (*c* 0.7, H_2O); PMR (D_2O+DCl, pH ≈3) δ: 5.34 (1H d, J≈4 Hz, H-1′ or 1‴), 5.36 (1H s, H-1″), 5.53 (1H d, J=3.0 Hz, H-1′ or 1‴).

Found: C, 43.27; H, 7.28; N, 8.26%. Calcd for $C_{23}H_{44}N_4O_{14}\cdot H_2CO_3$: C, 43.50; H, 6.99; N, 8.45%.

Compound **10′** was obtained from **9′** in a similar manner

as described above in a yield of 77.5% as monocarbonate; PPC, R_f lividomycin B 1.63, $[\alpha]_D^{23}$ +119° (*c* 0.7, H_2O); PMR (D_2O)δ: 4.95 (1H d, $J\approx4$ Hz), 5.13 (1H d, $J\approx2.7$ Hz), 5.23 (1H d, $J\approx3$ Hz) (each anomeric proton); in D_2O+DCl (pH≈3): δ: 5.34 (1H d, $J\approx3$ Hz), 5.35 (1H d, $J\approx4$ Hz), and 5.48 (1H d, $J\approx2.5$ Hz) (each anomeric proton).

Found: C, 43.63; H, 7.22; N, 8.29%.

Acidic Methanolysis of ***10*** *and* ***10′***. A solution of **10**, **10′**, or lividomycin B in 0.4 M methanolic hydrogen chloride was heated at 65 °C for 25 h, and the solution was examined by TLC (E. Merck, silica gel 60 F_{254}) with chloroform–methanol–17% aqueous ammonia (2 : 2 : 1). The methanolyzates of **10** and **10′** gave the same TLC pattern. From the comparison of the R_f values of the spots on the chromatograms with those of the hydrolyzate of lividomycin B and other reference substances, assignments of the spots were made: R_f 0.12 (2-deoxystreptamine), 0.25 (3′-deoxyparomamine), 0.52 [methyl 3-O-(2-amino-2-deoxy-α-D-glucopyranosyl)riboside], 0.58 (methyl 2-amino-2-deoxy-D-glucoside), 0.62 (methyl 2-amino-2,3-dideoxy-D-glucoside).

*5-O-Benzoyl-3-O-benzylthiocarbonyl-1,2-O-isopropylidene-α-D-ribofuranose (****11****).* To a solution of **2** (3.0 g) in pyridine (50 ml), benzylthiocarbonyl chloride (3 ml) was added and the solution was kept at room temperature overnight. After addition of water (0.5 ml), the solution was concentrated and the chloroform solution of the residue was washed (with aq $KHSO_4$, aq $NaHCO_3$, and H_2O), dried (Na_2SO_4), and concentrated. The residue was recrystallized from methanol to give colorless needles, 4.2 g (93%), mp 68—69 °C, $[\alpha]_D^{23}$ +141° (*c* 1, $CHCl_3$); PMR ($CDCl_3$) δ: 1.38 and 1.60 (each 3H s, $C(CH_3)_2$), 4.17 (2H s, CH_2S), 5.94 (1H m, J=5 Hz, H-1).

Found: C, 62.27; H, 5.47; S, 7.12%. Calcd for $C_{23}H_{24}O_7S$: C, 62.15; H, 5.44; S, 7.12%.

*Methyl 5-O-Benzoyl-3-O-benzylthiocarbonyl-2-O-(p-nitrobenzoyl)-β- and α-ribofuranosides (****12*** *and* ***12′****).* To a solution of **11** (3.5 g) in dry dichloromethane (21 ml), 0.4 M methanolic hydrogen chloride (50 ml) was added and the solution was kept at room temperature for 40 h. Pyridine (3 ml) was added and the solution was concentrated with intermittent additions of pyridine to give a syrup. To a solution of the syrup in pyridine (30 ml), a solution of *p*-nitrobenzoyl chloride (3.3 g) in dichloromethane (8 ml) was added and the solution was kept at room temperature for 3 h. On TLC with benzene–ethyl acetate (30 : 1), the solution showed two spots at R_f 0.54 (major **12**) and 0.50 (minor, **12′**). Work up as described for **11** gave a syrup, which was chromatographed over silica gel with benzene–ethyl acetate (100 : 1) to give a pale-yellow syrup of **12**, 2.96 g (66%), and pale-yellow needles (recrystallized from methanol) of **12′**, 1.05 g (24%).

Compound **12**: $[\alpha]_D^{24}$ +90° (*c* 1, $CHCl_3$).

Found: C, 59.52; H, 4.50; N, 2.41; S, 5.41%. Calcd for $C_{28}H_{25}NO_{10}S$: C, 59.25; H, 4.44; N, 2.47; S, 5.65%.

PMR ($CDCl_3$) δ: 3.43 (3H s, OCH_3), 4.07 (2H s, CH_2S), 5.15 (1H s, H-1), 5.6—5.85 (2H m, H-2,3). In pyridine-d_5: δ 5.38 (1H s, which sharpend on irradiation at δ 6.0, H-1), 6.0 [1H d, $J_{2,3}$=5 Hz, with small splittings ($J_{1,2}\approx1$ Hz), which disappeared, on irradiation at δ 5.38, to give a sharp d, H-2], 6.08 (1H t, $J_{2,3}=J_{3,4}$=5 Hz, H-3). On irradiation at δ 4.8, the triplet of H-3 collapsed to a doublet.

Compound **12′**: mp 110—110.5 °C, $[\alpha]_D^{20}$ +147° (*c* 1, $CHCl_3$).

Found: C, 58.95; H, 4.46; N, 2.39; S, 5.45%. Calcd for $C_{28}H_{25}NO_{10}S$: C, 59.25; H, 4.44; N, 2.47; S, 5.65%.

PMR (in $CDCl_3$ at 90 MHz) δ: 3.49 (3H s, OCH_3), 4.13 (2H AB q, J_{gem}=13 Hz, CH_2S), 5.2—5.45 (2H m, H-1,2), 5.55—5.75 (1H m, H-3). Since any signal distance of H-1,2 multiplet and that of H-3 multiplet did not accord each other, the occurrence of virtual coupling[10] between H-1 and H-3 was suggested. To clarify this, the solvent was changed: among the solvents tested, pyridine-d_5 was found most suitable and the signals of **12′** assignable to H-1,2, and 3 were separated each other without virtual coupling as follows: δ (at 90 MHz) 3.46 (3H s), 4.27 (2H s, CH_2S), 4.7—5.0 (3H, H-4,5,5′), 5.60 (1H d, $J_{1,2}$=4.7 Hz, H-1), 5.78 (1H q, J=4.7 and 7.2 Hz (=$J_{2,3}$), H-2), 6.12 (1H double q, J=7, ≈2, and ≈1 Hz, H-3). Irradiation at δ 4.8, the multiplet of H-3 collapsed to a doublet (J=7 Hz).

*Methyl 5-O-Benzoyl-2-O-(p-nitrobenzoyl)-β- and α-D-ribofuranosides (****13*** *and* ***13′****).* To a solution of **12** (or **12′**) (100 mg) in chloroform (1 ml), acetic acid (3 ml) and 30% aqueous hydrogen peroxide (1 ml) was added and the solution was kept at room temperature overnight. The solution was pound, with stirring, into an ice–water (150 ml) containing sodium hydrogencarbonate (4.5 g). The mixture was extracted with chloroform and the solution was washed with water, dried (Na_2SO_4), and concentrated to give a solid of **13** (or **13′**).

Compound **13**: Yield 67 mg (91%), colorless needles (from benzene–hexane), mp 134—135 °C, $[\alpha]_D^{23}$ +6° (*c* 1, $CHCl_3$).

Found: C, 57.46; H, 4.63; N, 3.23%. Calcd for $C_{20}H_{19}NO_9$: C, 57.55; H, 4.59; N, 3.36%.

PMR (pyridine-d_5) δ: 3.45 (3H s, OCH_3), 5.34 (1H s, H-1), 5.80 (1H d, J=4.4 Hz, H-2). On addition of D_2O followed by keeping the solution at room temperature for 1 h, the doublet of H-2 (δ 5.79) was gradually weakened with concomitant increase in intensity of a quartet at 5.91 (J=4.0 and 7.0 Hz, H-3 of **13m**) although the singlet of H-1 (δ 5.40) remained unchanged. This shows that an acyl migration occurred as shown below.

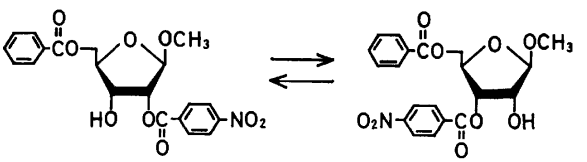

13 **13m**

Compound **13′**: Yield 58 mg (79%), pale-yellow needles (from benzene–hexane); mp 73.5—74.5 °C, $[\alpha]_D^{23}$ +80° (*c* 0.8, $CHCl_3$).

Found: C, 57.73; H, 4.63; N, 3.38%. Calcd for $C_{20}H_{19}NO_9$: C, 57.55; H, 4.59; N, 3.36%.

PMR (pyridine-d_5) δ: 3.55 (3H s, OCH_3), 5.53 (1H d, $J_{1,2}$=4.5 Hz, H-1), 5.70 (1H q, J=4.5 and 5.9 Hz(=$J_{2,3}$), H-2). On addition of water, the signal pattern was gradually changed possibly by the similar migration described above, but the migration was much slower than that for **13**.

*5-O-[5-O-Benzoyl-3-O-(benzylthiocarbonyl)-2-O-(p-nitrobenzoyl)-β-D-ribofuranosyl]-3,2′-bis(N-benzyloxycarbonyl)-1-N : 6-O-carbonyl-3′-deoxy-4′,6′-di-O-(α-naphthoyl)paromamine (****14****).*
To a solution of **12** (1.9 g) in dry dichloromethane (5 ml), hydrogen bromide saturated in acetic acid (6 ml) was added and the solution was kept at room temperature for 1 h. The solution was concentrated *in vacuo* and the resulting syrup was dissolved in dichloromethane (40 ml). The solution was washed as fast as possible with aqueous sodium hydrogencarbonate and water, dried (Na_2SO_4), and concentrated to give a syrup. Immediately, to a solution of the syrup in dichloromethane (9 ml), **6** (1.0 g), mercury (II) cyanide (1.9 g) and calcium sulfate (Drierite, 3.8 g), were added and the mixture was vigorously stirred at room temperature overnight. The reaction mixture was filtered with aid of chloroform and the filtrate was concentrated. The resulting syrup was chromato-

graphed over silica gel with chloroform–ethyl acetate (5 : 1) to give a solid of **14**, 1.05 g (66% based on **6**), $[\alpha]_D^{23}$ +33° (*c* 0.5, $CHCl_3$); IR (KBr): 1780, 1725, 1530 cm^{-1}.

Found: C, 64.50; H, 4.89; N, 3.79; S, 2.38%. Calcd for $C_{78}H_{68}N_4O_{22}S$: C, 64.81; H, 4.74; N, 3.88; S, 2.22%.

5-O-[*5*-O-*Benzoyl-2*-O-(p-*nitrobenzoyl*)-β-D-*ribofuranosyl*]-*3,2'*-*bis*(N-*benzyloxycarbonyl*)-*1*-N : *6*-O-*carbonyl-3'-deoxy-4',6'-di*-O-(α-*naphthoyl*)*paromamine* (**15**). To a solution of **14** (600 mg) in acetic acid (18 ml), 30% aqueous hydrogen peroxide (2.1 ml) was added and the solution was kept at room temperature overnight. On TLC with chloroform–ethanol–acetic acid (150 : 5 : 1), the solution showed two spots at R_f 0.49 (major, **15**) and 0.41 (trace, 3″-*p*-nitrobenzoate isomer?). The solution was concentrated at room temperature and the residue was dissolved in chloroform. The solution was washed with water, dried (Na_2SO_4), and concentrated. The resulting solid was chromatographed over silica gel with chloroform–ethanol–acetic acid (500 : 10 : 1) to give a solid of **15**, 424 mg (79%), $[\alpha]_D^{23}$ +18° (*c* 0.5, $CHCl_3$).

Found: C, 65.03; H, 4.96; N, 4.17%. Calcd for $C_{70}H_{62}N_4O_{21}$: C, 64.91; H, 4.82; N, 4.33%.

References

1) T. Mori, Y. Kyotani, I. Watanabe, and T. Oda, *J. Antibiot.*, **25**, 149 (1972).
2) T. Yamaguchi, K. Kamiya, T. Mori, and T. Oda, *J. Antibiot.*, **30**, 332 (1977).
3) L. Zervas and S. Konstas, *Chem. Ber.*, **93**, 435 (1960).
4) K. Oka and H. Wada, *Yakugaku Zasshi*, **83**, 890 (1963).
5) S. Umezawa, T. Miyazawa, and T. Tsuchiya, *J. Antibiot.*, **25**, 530 (1972).
6) P. A. J. Gorin, *Can. J. Chem.*, **40**, 275 (1962).
7) I. Watanabe, A. Ejima, T. Tsuchiya, D. Ikeda, and S. Umezawa, *Bull. Chem. Soc. Jpn.*, **50**, 487 (1977).
8) D. Ikeda, T. Tsuchiya, S. Umezawa, and H. Umezawa, *Bull. Chem. Soc. Jpn.*, **47**, 3136 (1974).
9) J. J. Willard and E. Pacsu, *J. Am. Chem. Soc.*, **82**, 4347 (1960).
10) L. M. Jackman and S. Sternhell, "Applications of Nuclear Magnetic Resonance Spectroscopy in Organic Chemistry," 2nd ed, Pergamon Press (1969), p. 133.
11) H. Yanagisawa, M. Kinoshita, S. Nakada, and S. Umezawa, *Bull. Chem. Soc. Jpn.*, **43**, 246 (1970).

Synthesis of Streptolidine Lactam, a Guanidine-containing Amino-acid Lactam Moiety of Streptothricin Antibiotic Group

Mitsuhiro KINOSHITA and Yoshiharu SUZUKI

Department of Applied Chemistry, Faculty of Engineering, Keio University, Hiyoshi, Kohoku-ku, Yokohama 223

(Received March 5, 1977)

Streptolidine lactam (**3**) present in streptothricin antibiotics was stereospecifically synthesized. 3,4-Anhydro-1,2 : 5,6-di-*O*-isopropylidene-D-iditol (**4**) was converted into the 3,4-bis(benzyloxycarbonylamino)-3,4-dideoxy-D-mannitol derivative **7** *via* the 3,4-diazido-3,4-dideoxy-D-mannitol derivative **6**. De-*O*-protection of **7** followed by two-stage oxidation with periodate–bromine afforded 2,3-bis(benzyloxycarbonylamino)-2,3-dideoxy-D-*arabono*-1,4-lactone (**8**), which was transformed into the azide lactone **9**. Selective hydrogenolysis of **9** with Raney Ni gave the *N*-protected amino sugar lactam **10**. *O*-Tetrahydropyranylation of **10** followed by hydrogenolysis afforded the *O*-protected amino sugar lactam **12**. Treatment of **12** with cyanogen bromide in water gave the *O*-tetrahydropyranylated streptolidine lactam **13**, which on mild acid hydrolysis afforded **3** (hydrochloride). The amino sugar lactam **14** obtained by hydrogenolysis of **9** with palladium black was also treated with cyanogen bromide to yield **3** (hydrobromide). Acid hydrolysis of **3** gave streptolidine (**2**)(dihydrochloride) identical with that derived from the antibiotics.

The ingenious studies on construction of the streptolin-streptothricin group of *streptomyces* antibiotics by Van Tamelen *et al.*[1] revealed the presence of a lactam ring in the streptolidine unit **A** of the intact antibiotic **1**.[2] Borders *et al.*[3] verified the lactam structure by comparison of the PMR spectra of antibiotic LL-AC-541 belonging to the streptothricin family and of streptolidine(**2**), a common degradation product of various streptothricin type antibiotics.

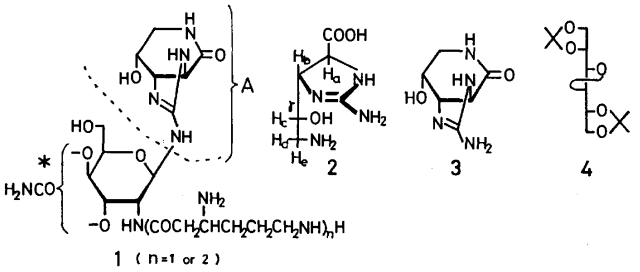

Chart 1.

During the course of synthetic studies on streptothricin antibiotics, we found it necessary to synthesize the streptolidine lactam **3** which corresponds to the cyclic guanidine-containing lactam moiety **A**, for use in a streptothricin antibiotic synthesis and for a biological test in connection with the role of **A** in the biological activity of the antibiotics.[1,5] This paper presents the first synthesis of **3** and its *O*-protected derivative **13**. Streptolidine(**2**) has been synthesized independently by Kusumoto *et al.*,[6] and Goto and Ohgi[7] *via* the amino sugar lactam **14** from D-ribose and D-xylose.[8] In the synthesis of streptolidine lactams, we also adopted the condensation reaction of amino sugar lactam with cyanogen bromide[6,7] for the cyclic guanidine ring formation. Consideration was given to the following points: (i) protection of the free hydroxyl group of the amino sugar lactam **14** stabilizes the lactam ring during the condensation reaction and (ii) the use of equivalent amounts of the pure amino sugar lactam and cyanogen bromide for the reaction minimizes any side reactions which might be caused by excess cyanogen bromide. The *O*-protected amino sugar lactam **12** and free lactam **14** were synthesized in moderate overall yields through the new stereospecific route from the 3,4-anhydro-D-iditol derivative **4** prepared from D-mannitol.[9,10]

* The indicated pattern for the carbamate group substitution has been shown to be most likely vaild for streptolin-streptothricin group (**1**) by Borders *et al.*[4]

Results and Discussion

Starting material, 3,4-anhydro-1,2 : 5,6-di-*O*-isopropylidene-D-iditol(**4**),[9] prepared *via* *trans*-3,4-didehydro-3,4-dideoxy-1,2 : 5,6-di-*O*-isopropylidene-D-*threo*-hexitol[10] from D-mannitol, was subjected to azidolysis with sodium azide in the presence of ammonium chloride in aqueous methyl cellosolve and the resulting azido hydroxy compound, without purification, was *O*-mesylated in the usual way, affording 3-azido-3-deoxy-1,2:5,6-di-*O*-isopropylidene-4-*O*-mesyl-D-talitol(**5**) in 61% overall yield from **4**. The mesylate **5** was allowed to react with sodium azide in DMSO to give 3,4-diazido-3,4-dideoxy-1,2 : 5,6-di-*O*-isopropylidene-D-mannitol (**6**) in 47% yield. Hydrogenolysis of **6** over palladium black in methanol followed by *N*-benzyloxycarbonylation with benzyl chloroformate in pyridine at −20 °C afforded 3,4-bis(benzyloxycarbonylamino)-3,4-dideoxy-1,2 : 5,6-di-*O*-isopropylidene-D-mannitol (**7**) in 77% yield. De-*O*-isopropylidenation of **7** with warm aqueous acetic acid followed by periodate oxidation with 1.2 equivalent of sodium periodate in aqueous acetone and subsequent oxidation with bromine in aqueous dioxane at room temperature gave 2,3-bis(benzyloxycarbonyl-

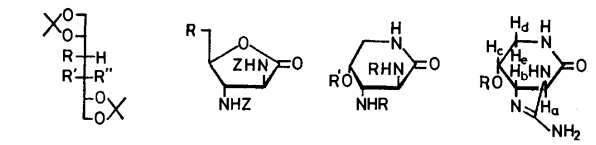

5 R=N_3, R'=MsO, R''=H
6 R=R''=N_3, R'=H
7 R=R''=ZHN, R'=H
8 R=HO
9 R=N_3
10 R=Z, R'=H
11 R=Z, R'=THP
12 R=H, R'=THP
14 R=R'=H
13 R=THP
3 R=H

Z=$PhCH_2OCO$ THP=

Chart 2.

amino)-2,3-dideoxy-D-*arabono*-1,4-lactone (**8**) in 59% yield. *O*-Mesylation of **8** in the usual way followed by treatment with sodium azide in DMSO at 100 °C afforded 5-azido-2,3-bis(benzyloxycarbonylamino)-2,3,5-trideoxy-D-*arabono*-1,4-lactone (**9**) in 61% yield.

Selective hydrogenolysis of the azido group in **9** over Raney Ni in methanol led directly[11] to 5-amino-2,3-bis-(benzyloxycarbonylamino)-2,3,5-trideoxy-D-*arabono*- 1,5-lactam (**10**) in 63% yield after recrystallization. The 4-*O*-(tetrahydro-2-pyranyl) derivative **11** (an epimeric mixture about the 2-position of the pyran) was obtained by treatment of **10** with dihydropyran and a catalytic amount of *p*-toluenesulfonic acid in DMF at 37—40 °C in 80% yield after recrystallization. Hydrogenolysis of **11** over 10% palladium on charcoal in methanol at 50 psi affroded, after silica gel column chromatography, an almost pure sample of the *O*-protected sugar lactam **12**, whose IR spectrum($CHCl_3$) showed a δ-lactam band at 1660 cm^{-1}, in 77% yield. Treatment of **12** in water with 0.95 equivalent of cyanogen bromide gave the *O*-protected cyclic guanidine lactam **13** as a crystalline hydrobromide in 51% yield after recrystallization. The ring proton coupling constants in the PMR spectrum of the hydrobromide of **13** were very similar to those of the spectral data[3] reported for the lactam structure of the streptolidine moiety in antibiotic LL-AC541 (Table). Treatment of the hydrobromide with silver carbonate followed by mild hydrolysis with 0.5 M hydrochloric acid afforded the hydrochloride of streptolidine lactam(**3**) as needles in 87% yield after recrystallization. The PMR spectrum of **3** also shows peaks consistent with the lactam structure.

On the other hand, hydrogenolysis of **9** over palladium black in methanol gave, after silica gel column chromatography, an almost pure sample of 2,3,5-triamino-2,3,5-trideoxy-D-*arabono*-1,5-lactam(**14**)[6,7] in 71 % yield. *N*-benzyloxycarbonylation of **14** with *N*-(benzyloxycarbonyloxy)succinimide[14] in aqueous DMF yielded **10** in 90% yield. Treatment of **14** in water with one equivalent of cyanogen bromide for 2 h at room temperature afforded the crystalline hydrobromide of **3** in 62% yield after recrystallization. The CD curve of **3** shows the positive Cotton effect at 220 nm. In the plain negative ORD curve of **3**, however, no first positive extremum expected for the positive Cotton effect in the CD spectrum is observed. The ORD curves of streptothricin and its family show a first extremum at 227 nm in positive field through negative field.[12] This indicates that the ORD curve of **3** is more strongly affected by back ground rotation[13] than those of the antibiotics.

Hydrolysis of **3** with 3 M hydrochloric acid overnight at room temperature gave the crystalline dihydrochloride of **2** (85% yield) identical in IR, PMR (Table), and optical rotation with those derived from streptothricin antibiotics. The stereochemistry of synthetic **3** was thus completely confirmed.

In preliminary microbial tests, the synthetic streptolidine lactams **13** and **3** showed no inhibition against test microorganisms sensitive to the streptothricin antibiotic group at the concentration of 100 μg/ml.

TABLE. COMPARISON OF 90 MHz PMR DATA (D_2O)[a] OF SYNTHETIC STREPTOLIDINE LACTAM (**13** and **3**) AND STREPTOLIDINE (**2**) WITH THE REPORTED PMR DATA (100 MHz, D_2O)[a,b] OF ANTIBIOTIC LL-AC541 AND NATURAL STREPTOLIDINE

(δ, Hz)	**13**	**3**	LL-AC541	**2**	
				Synthetic	Natural
H_a	5.15	5.03	5.16	5.06	5.07
H_b	4.55	4.47	4.59	4.73	4.74
H_c	≈5.20	5.14	≈5.20	4.57	4.59
H_d	4.22	4.28	4.32	3.77	3.76
H_e	3.99	3.85	3.89	3.53	3.54
J_{ab}	14.2	14.0	14.8	4.7	4.7
J_{bc}	2.5	2.8	2.7	3.6	3.6
J_{cd}	4.5	5.5	5.5	3.4	3.4
J_{ce}	1.8	1.5	1.2	9.8	9.8
J_{de}	15.0	14.8	15.0	13.2	13.2

a) All chemical shifts are based on external reference of TMS. b) See Ref. 3.

Experimental

Melting points were detemined on a micro hot-stage and are uncorrected. IR spectra were taken on a Hitachi 225 spectrophotometer, PMR spectra on Varian A-60D and EM-390 spectrometers using TMS as internal and external standard. Specific rotations were determined with a Zeiss Photoelectric Polarimeter. CD and ORD spectra were taken on a JASCO J-20 spectropolarimeter. TLC was performed on Wakogel B-5 and colum chromatography on Wakogel C-200. Paper chromatography was conducted on Toyoroshi No. 525 with 1-butanol–acetic acid–water (3 : 1 : 1). Paper electrophoresis was carried out with a Savant IV-5000A in formic acid–acetic acid–water (1 : 3 : 36). Unless otherwise stated, hydrogenolysis was conducted at room temperature over catalyst under bubbling with hydrogen. In general, concentration was carried out under reduced pressure below 40 °C.

1) 3-Azido-3-deoxy-1,2 : 5,6-di-O-isopropylidene-4-O-mesyl-D-talitol (5). A solution of 3,4-anhydro-1,2 : 5,6-di-*O*-isopropylidene-D-iditol (**4**)[9] (36.0 mg) in 80% aqueous methyl cellosolve (1 ml) was heated with sodium azide (78.8 mg) and ammonium chloride (32.6 mg) at 120 °C for 7 h. The reaction mixture was evaporated after filtration and the residue was extracted with ethyl acetate. The dried extract was evaporated to afford a pale brown syrup. The syrup (40 mg) was mesylated with mesyl chloride (0.012 ml) in dry pyridine (0.8 ml) at room temperature for 1 h. Work-up in the usual way gave a brown syrup, which was chromatographed on silica gel with benzene–acetone (20 : 1) to afford **5** (32.6 mg, 60%) as a colorless syrup: $[\alpha]_D^{17}$ −26° (*c* 0.78, $CHCl_3$); $\nu_{max}^{CCl_4}$ 2105 (N_3), 1370 and 1180 cm^{-1} (sulfonate).

Found: C, 42.94; H, 6.25; N, 11.22; S, 8.53%. Calcd for $C_{13}H_{23}N_3O_7S$: C, 42.73; H, 6.34; N, 11.50; S, 8.78%.

2) 3,4-Diazido-3,4-dideoxy-1,2 : 5,6-di-O-isopropylidene-D-mannitol (6). Sodium azide (365 mg) was added to a solution of **5** (379.4 mg) in dry DMSO (7.6 ml) and the mixture was heated at 120 °C for 3.5 h. The reaction mixture was poured into cold water and extracted with chloroform. The extracts were washed with saturated NaCl solution, dried, and evaporated. The residual brown syrup was chromatographed on silica gel with benzene–acetone (40 : 1) to afford **6** (153.3 mg, 47%) as a colorless syrup: $[\alpha]_D^{28}$ +15° (*c* 0.67, $CHCl_3$), $\nu_{max}^{CCl_4}$ 2100 cm^{-1} (N_3); δ ($CDCl_3$), 1.40 and

1.46 [each s, 6H, $(CH_3)_2C$], and 3.60—4.39 (m, 8H).

Found: C, 46.49; H, 6.55; N, 26.54%. Calcd for $C_{12}H_{20}N_6O_4$: C, 46.14; H, 6.45; N, 26.91%.

*3) 3,4-Bis(benzyloxycarbonylamino)-3,4-dideoxy-1,2 : 5,6-di-O-isopropylidene-*D*-mannitol (7).* A sample of **6** (220 mg) was hydrogenolysis in methanol (6 ml) for 3 h over palladium black. The resulting colorless syrup (200 mg) was dissolved in dry pyridine (4 ml) and cooled to −20 °C, and benzyl chloroformate (0.375 ml) was added to this solution under stirring. After being stirred at −20 °C for 1.5 h, the reaction mixture was diluted with water and extracted with chloroform. The extracts were washed with saturated NaCl solution, dried and evaporated. The residue was subjected to silica gel column chromatography with benzene–acetone (20 : 1) to give **7** (288.6 mg, 77%) as a colorless syrup: $[\alpha]_D^{28}$ +13° (*c* 3.74, $CHCl_3$); δ ($CDCl_3$), 1.32 and 1.42 [each s, 6H, $(CH_3)_2C$], 3.75—4.45 (m, 8H), 5.12 (s, 4H, $PhCH_2$), 5.59—5.86 (br, 2H, NH), and 7.34 (s, 10H, Ph).

Found: C, 63.46; H, 6.88; N, 5.19%. Calcd for $C_{28}H_{36}N_2O_8$: C, 63.62; H, 6.87; N, 5.30%.

*4) 2,3-Bis(benzyloxycarbonylamino)-2,3-dideoxy-*D*-arabono-1,4-lactone (8).* A solution of **7** (82.0 mg) in acetic acid (1.6 ml) was diluted with water (0.8 ml) and warmed at 60 °C for 1 h. The solution was evaporated and the residue was co-evaporated with ether in order to remove acetic acid. The residual solid (70 mg) was dissolved in a mixture of acetone (2.1 ml) and water (0.28 ml), and solid sodium metaperiodate (39.9 mg) was added to the solution in small portions with stirring under ice-cooling. After 1 h, acetone (2 ml) was added to the mixture. The precipitate was filtered off and evaporated to give a colorless solid. Bromine (0.032 ml) was added dropwise to the ice-cooled solution of the solid in dioxane (2.5 ml) and water (0.77 ml), and the mixture was stirred for 1 h. After being kept at room temperature for 3 h, a saturated $Na_2S_2O_3$ solution (4.5 ml) was added to the reaction mixture under ice-cooling. The resulting mixture was extracted with ethyl acetate and extracts were washed with saturated NaCl solution and saturated $NaHCO_3$ solution, dried, and evaporated. The residual solid was dissolved in a small amount of ethyl acetate and filtered in order to remove sulfur. Evaporation of the filtrate afforded a pale yellow solid, which was chromatographed on silica gel with chloroform–methanol (10 : 1) to give a colorless solid. Recrystallization from ethyl acetate and petroleum ether (bp 30—60 °C) afforded needles of **8** (38.6 mg, 59%): mp 149.0—150.5 °C (dried for 24 h at 60 °C in 1 Torr over CaH_2); $[\alpha]_D^{26}$ −51° (*c* 0.89, CH_3OH): ν_{max}^{KBr} 1800 (γ-lactone), 1680 (amide I), and 1530 cm^{-1} (amide II).

Found: C, 59.82; H, 5.44; N, 6.70%. Calcd for $C_{21}H_{22}N_2O_7 \cdot 1/2H_2O$: C, 59.570 H, 5.48; N, 6.62%.

*5) 5-Azido-2,3-bis(benzyloxycarbonylamino)-2,3,5-trideoxy-*D*-arabono-1,4-lactone (9).* A sample of **8** (34.0 mg) was mesylated with mesyl chloride (0.0254 ml) in pyridine (1 ml) at room temperature for 1 h. Work-up in the usual way followed by silica gel column chromatography with benzene–acetone (6 : 1) afforded an almost pure sample of the mesylate (36.1 mg, 89%); δ ($CDCl_3$), 3.85 (s, 3H, CH_3SO_3), 4.02—4.62 (5H, H-2,3,4,5-CH_2), 4.91 (s, 4H, $PhCH_2$), 5.31—5.90 (br, 2H, NH), and 7.15 (s, 10H, Ph). The mesylate (11.5 mg) was treated with sodium azide (6.1 mg) in dry DMSO (0.3 ml) at 100 °C for 0.5 h. Work-up in the suual way followed by silica gel column chromatography with benzene–acetone (10 : 1) gave colorless crystals of **9** (6.8 mg, 68%): mp 84.0—85.0 °C (dried for 24 h at 60 °C in 1 Torr over CaH_2); $[\alpha]_D^{26}$ +20° (*c* 1.72, CH_3OH), $\nu_{max}^{CHCl_3}$ 2100(N_3), 1790(γ-lactone), 1710 (amide I), and 1500 cm^{-1} (amide II).

Found: C, 56.36; H, 4.84; N, 15.63%. Calcd for $C_{21}H_{21}N_5O_6 \cdot 1/2\ H_2O$: C, 56.24; H, 4.95; N, 15.62%.

*6) 5-Amino-2,3-bis(benzyloxycarbonylamino)-2,3,5-trideoxy-*D*-arabono-1,5-lactam (10).* (a) A sample of **9** (37.5 mg) was hydrogenolyzed in methanol with Raney Ni R-100 (Nikko Scientific and Chemical Industries Ltd.) for 4 h. Recrystallization of the crystalline product from methanol gave **10** (22.0 mg, 63%) as fine needles: mp 208—209 °C $[\alpha]_D^{25}$ −122° (*c* 0.84, DMF); ν_{max}^{KBr} 3370 (OH), 3310 (NH), 1680 (amide I), 1650 (δ-lactam), and 1530 cm^{-1} (amide II).

Found: C, 60.74; H, 5.56; N, 10.34%. Calcd for $C_{21}H_{23}N_3O_6$: C, 61.01; H, 5.61; N, 10.16%.

(b) A sample of **9** (231.5 mg) was hydrogenolyzed in methanol (8.5 ml) over palladium black for 5 h. During this period a fresh catalyst was added every hour. Evaporation of the filtered solution afforded the crude triamino sugar lactam **14** as a pale yellow syrup. A solution of *N*-(benzyloxycarbonyloxy)succinimide (283 mg) in DMF (1 ml) was added to a solution of the syrup in DMF (3 ml) and water (0.5 ml). After being kept at room temperature for 1 h, the reaction mixture was neutralized with triethylamine and evaporated. The residue (pale brown semisolid) was chromatographed on silica gel with chloroform–methanol (10 : 1) to give **10** (127.3 mg, 60% overall yield from **9**): mp 203—207 °C; $[\alpha]_D^{20}$ −127° (*c* 0.79, DMF). This sample was identical with that obtained in (a) on mixture melting point.

*7) 5-Amino-2,3-bis(benzyloxycarbonylamino)-2,3,5-trideoxy-4-O-(tetrahydro-2-pyranyl)-*D*-arabono-1,5-lactam (11).* A mixture of **10** (107.2 mg), dihydropyran (0.54 ml), *p*-toluenesulfonic acid (4.8 mg), and dry DMF (1.75 ml) was warmed at 37—40 °C for 2 h. The reaction mixture was neutralized with triethylamine and evaporated. The residual pale brown syrup was chromatographed on silica gel with chloroform–methanol (25 : 1) to afford **11** (124.6 mg, 97%) as a colorless solid. Crystallization took place on slow evaporation of the methanol solution, giving colorless needles of **11** (80% overall yield): mp 163—166 °C; $[\alpha]_D^{20}$ −59° (*c* 1.28, $CHCl_3$); δ ($CDCl_3$), 1.12—1.90 (m, 6H, 3′,4′,5′-CH_2), 3.10—4.76 (m, 8H, 5,6′-CH_2, H-2′, 2, 3, 4), 5.05 (s, 4H, $PhCH_2$), 5.50—6.33 (br, 3H, NH), and 7.30 (s, 10H, Ph).

Found: C, 62.65; H, 6.26; N, 8.53%. Calcd for $C_{26}H_{31}N_3O_7$: C, 62.76; H, 6.28; N, 8.45%.

*8) 2,3,5-Triamino-4-O-(tetrahydro-2-pyranol)-2,3,5-trideoxy-*D*-arabono-1,5-lactam (12).* A sample of **11** (150.8 mg) was hydrogenolyzed in methanol (3 ml) at 50 psi for 4 h using 10% Pd/C catalyst (total 180 mg). The catalyst was divided into four 45 mg-portions, one portion being added every hour during the reaction period. Filtration followed by removal of solvent afforded a pale yellow-green syrup. Chromatography over silica gel (0.7 g) with chloroform–methanol–17% aqueous ammonia (20 : 20 : 1) gave almost pure **12** (53.2 mg, 77%) as a colorless syrup: $\nu_{max}^{CHCl_3}$ 3580—3140 (NH_2), 3400 (NH), and 1660 cm^{-1} (δ-lactam).

9) O-(Tetrahydro-2-pyranyl)streptolidine Lactam (13) Hydrobromide. Cyanogen bromide (23.5 mg, 0.95 equiv) was added to a solution of **12** (53.2 mg) in water (0.5 ml) and the mixture was allowed to stand at room temperature for 5 h. Evaporation of the reaction mixture afforded a pale yellow solid, which was crystallized on slow evaporation of the methanol solution to give colorless needles of the hydrobromide of **13** (40.1 mg, 51%): mp 295 °C (dec); $[\alpha]_D^{20}$ −128° (*c* 0.975, H_2O); ν_{max}^{KBr} 3100 (NH), 1670 (lactam and guanidium I), and 1590 cm^{-1} (vw, guanidium II).

Found: C, 39.44; H, 5.76; N, 16.60%. Calcd for $C_{11}H_{18}N_4O_3 \cdot HBr$: C, 39.41; H, 5.71; N, 16.72%.

10) Streptolidine Lactam (3) Hydrochloride. A solution of **13** hydrobromide (37.5 mg) in water (0.9 ml) was treated with Ag_2CO_3 (15.4 mg, 0.5 equiv) for 10 min. Additional

Ag_2CO_3 (7 mg) was added to the mixture and the precipitates were filtered and washed with water (1 ml). The combined filtrates (1.9 ml) were acidified with 2M HCl (0.6 ml), and kept at room temperature for 0.5 h. The reaction mixture was neutralized (pH 7) with Amberlite CG-4B and evaporated after filtration to afford colorless crystals. Recrystallization from methanol–acetone (1 : 1) gave a pure sample of the hydrochloride of **3** (20.0 mg, 87%) as needles: mp 146—147.5 °C; $[\alpha]_D$ −124°, $[\alpha]_{436}$ −250°, and $[\alpha]_{365}$ −386° (*c* 0.99, H_2O at 16 °C); $[\theta]_{220}$ +3794 (*c* 0.11, H_2O at 18 °C); ν_{max}^{KBr} 1680 (lactam and guanidium I), and 1600 cm^{-1} (sh, guanidium II).

Found: C, 34.72; H, 5.58; N, 26.76%. Calcd for $C_6H_{10}N_4O_2 \cdot HCl$: C, 34.78; H, 5.37; N, 27.12%.

11) Preparation of Streptolidine Lactam (3) Hydrobromide from Triamino Sugar Lactam (14). A crude sample of **14** (Exp. 6b) was chromatographed through a short column of silica gel with chloroform–methanol–17% aqueous ammonia (6 : 6 : 1) to afford a practically pure sample of **14** in 72% yield. Cyanogen bromide (30.0 mg, 1 equiv) was added to a solution of the sample (39.7 mg) of **14** in water (0.4 ml), and the mixture was kept at room temperature for 2 h and then neutralized (pH 7) with Amberlite CG-4B, and evaporated. The pale yellow crystalline residue (70 mg) was recrystallized twice from methanol–acetone to give **3** hydrobromide (42 mg, 60%): mp 147—148 °C; $[\alpha]_D$ −102°, $[\alpha]_{436}$ −210°, and $[\alpha]_{365}$ −329° (*c* 0.638, H_2O at 19 °C); ν_{max}^{KBr} 1680 (lactam and guanidium I) and 1600 cm^{-1} (guanidium II). The PMR spectrum (D_2O) of the sample was identical with that of **3** hydrochloride.

Found: C, 29.02; H, 4.66; N, 22.00%. Calcd for $C_6H_{10}N_4O_2 \cdot HBr$: C, 28.70; H, 4.42; N, 22.31%.

12) Streptolidine (2) Dihydrochloride. A solution of **3** hydrochloride (10.5 mg) in 3 M HCl (0.2 ml) was allowed to stand at room temperature for 22 h. The solution was evaporated and the crystalline residue was washed with a mixture of methanol–acetone (2 : 1) to afford **2** dihydrochloride (11.0 mg, 83%). Recrystallization from water–ethanol gave an analytical sample: mp 175—180 °C (dec) [lit,[15] mp 173—190 °C (dec)]; $[\alpha]_D$ +52°, $[\alpha]_{436}$ +126°, $[\alpha]_{365}$ +195° (*c* 0.988, H_2O at 16 °C) [lit,[15] $[\alpha]_D^{22}$ +56.8° (*c* 2.35, H_2O)]; ν_{max}^{KBr} 1725 (COOH), 1680 (guanidium I), 1580 cm^{-1} (guanidium II). R_f-values on paper chromatopraghy and mobility of paper electrophresis of the synthetic product and the natural one were identical.

Found: C, 27.70; H, 5.21; N, 21.41%. Calcd for $C_6H_{12}N_4O_3 \cdot 2HCl$: C, 27.60; H, 5.41; N, 21.46%.

The authors wish to thank Dr. Shinpei Aburaki for the measurements of PMR, CD, and ORD spectra, Mr. Nakada for the microanalyses, and Mr. Yoichi Niimura for his technical assistance. We are also indebted to Dr. Masa Hamada, Institute of Microbial Chemistry, for the microbiological test.

References

1) E. E. Van Tamelen, J. Dyer, H. A. Whaley, H. E. Carter, and G. B. Whitfield, Jr., *J. Am. Chem. Soc.*, **83** 4295 (1961).
2) H. E. Carter, D. K. Clark, Jr., J. W. Rothrock, W. R. Taylor, C. A. West, G. B. Whitfield, and W. G. Jackson, *J. Am. Chem. Soc.*, **76**, 566 (1954).
3) D. B. Borders, K. J. Sax, J. E. Lancaster, W. K. Hausmann, L. A. Mitcher, E. R. Wetzel, and E. L. Patterson, *Tetrahedron*, **26**, 3123 (1970).
4) D. B. Borders, J. P. Kirby, E. R. Wetzel, M. C. Davis, and W. K. Hausmann, *Antimicrob. Agents Chemother.*, **1**, 403 (1972).
5) H. Taniyama, Y. Sawada, and T. Kitagawa, *J. Antibiot.*, **24**, 662 (1971).
6) S. Kusumoto, S. Tsuji, and T. Shiba, *Tetrahedron Lett.*, **1974**, 1417; S. Kusumoto, S. Tsuji, and T. Shiba, *Bull. Chem. Soc. Jpn.*, **47**, 2690 (1974).
7) T. Goto and T. Ohgi, *Tetrahedron Lett.*, **1974**, 1413.
8) S. Kusumoto, S. Tsuji, K. Shima, and T. Shiba, *Bull. Chem. Soc. Jpn.*, **49**, 3611 (1976).
9) G. O. Aspinall, N. W. H. Cheetham, J. Frdova, and S. C. Tam, *Carbohydr. Res.*, **36**, 257 (1974).
10) R. S. Tipson and A. Cohen, *Carbohydr. Res.*, **1**, 338 (1965).
11) S. Hanessian and T. H. Haskell, *J. Heterocyclic Chem.*, **1**, 55 (1964).
12) H. Taniyama and Y. Sawada, *Chem. Pharm. Bull.*, **20** 596 (1972); Our unpubliched data.
13) P. Crabbe, "ORD and CD in Chemistry and Biochemistry," Academic Press, New York (1972), p. 8.
14) H. Kawaguchi, T. Naito, S. Nakagawa, and K. Fujisawa, *J. Antibiot.*, **25**, 695 (1972).
15) H. E. Carter, C. C. Sweeley, E. E. Daniels, J. E. Mcnary, C. P. Schaffner, C. A. West, E. E. Van Tamelen, J. R. Dyer, and H. A. Whaley, *J. Am. Chem. Soc.*, **83**, 4296 (1961).

Ketyl Radicals Formed in Grignard Reaction. IV.[1] Sterically Hindered Ketyl Radicals in Nuclear Replacement and Conjugate Addition

Masao Ōkubo

Department of Chemistry, Faculty of Science and Engineering, Saga University, Honjō-machi, Saga 840

(Received March 9, 1977)

The reaction in which 4′-methoxy and 4′-cyano substituents on 2,3,5,6-tetramethylbenzophenone are effectively replaced by benzyl- and *t*-butylmagnesium chloride was examined by means of ESR measurements. Both the original and the "replaced" ketyl radicals were identified, and an electron-transfer mechanism similar to that of S_{RN}-type reactions was proposed. Some sterically hindered $\alpha\beta$-enones were also found to form detectable amounts of ketyl radicals. The factors governing the production ratio of the normal and the conjugate adduct were discussed.

Several reports have been given on evidence for the electron-transfer(ET) mechanism of Grignard reaction.[2,3] The course of the reaction of PhMgBr with benzophenone is affected greatly by the steric hindrance of *ortho*-methyl groups; the group on the former reagent tends to form benzopinacol whereas the same group on the latter to form the nuclear phenylated product.[1] The formation of these "abnormal" products can be explained by the ET-mechanism *via* ketyl radicals. Not only the mode of appearance but also the spin-distribution on the radicals have turned out to be dependent upon the magnitude of the steric effect. Thus, similar steric effects are expected to be operative in the Grignard reactions of the several different types of ketones. This paper gives the results of the ESR studies on the two "abnormal" Grignard reactions: 1) the nuclear replacement of anionoid substituents on hindered benzophenones, and 2) the conjugate addition to the *ortho*-methyl derivatives of chalcone, 2-benzoylbenzofuran, and 3-benzylidenecamphor.

Results and Discussion

Nuclear Replacement of Hindered Benzophenones. Recently the ET-mechanism for the nuclear *ortho*-phenylation of benzoylmesitylene in the reaction with PhMgBr was proposed.[4] Benzophenone itself undergoes unclear *t*-butylation, which has been explained also by the ET-mechanism.[5] Fuson and his co-workers pointed out that some anionoid substituents (methoxyl, cyano, and acetoxyl) were effectively available for the analogous nuclear alkylation or arylation.[6] As the first step in the present work, the "replacement" reaction of the 4′-MeO and 4′-CN substituents of 2,3,5,6-tetramethylbenzophenone (benzoyldurene) with $PhCH_2MgCl$ (Scheme 1) was examined by ESR technique.

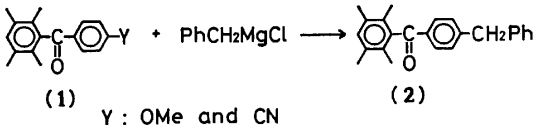

Scheme 1.

For the sake of simple analysis of ESR spectra, the 2,3,5,6-tetramethylphenyl(duryl) group is advantageous since it gives no resolvable splitting[7] as a result of the inhibition of spin-delocalization due to the twisting of the group out of the plane of the carbonyl group.[8] Though all the spectra were not fully-resolved, they can be analyzed by considering only the hydrogen atoms of the unhindered aryl groups. The structure and the coupling constants of the radicals identified are summarized in Table 1.

When the two 4′-substituted benzoyldurenes(**1**) were treated with five equivalents of $PhCH_2MgCl$ in tetrahydrofuran(THF) in a vacuum and at room temperature, the colorless (Y=OMe) or pale yellow (Y=CN) solution turned first pink and then reddish brown rapidly. Replacement product(**2**) was obtained after 1 h in a good yield. The highest radical concentrations, observed after 30 min after mixing, were estimated to be *ca.* 6 mol% based on the concentration of the original ketones. The ESR spectrum (Fig. 1a) obtained after the reaction solution had turned reddish brown, was independent of the 4′-substituents. When $PhCD_2MgCl$ is used, the spectrum changes to the one which has weak narrow quintets (Fig. 1b). The spectrum is thus ascribed to a ketyl radical (Rp)· which has been "replaced" by the benzyl group. The large coupling constant of the benzylic hydrogen, a_{α}^{H} (Table 1), seems to reflect the fact that the $Q_{C-CH_2}^{H}$ value (27.2) is larger than the Q_{C-H}^{H} value (23.7).[9]

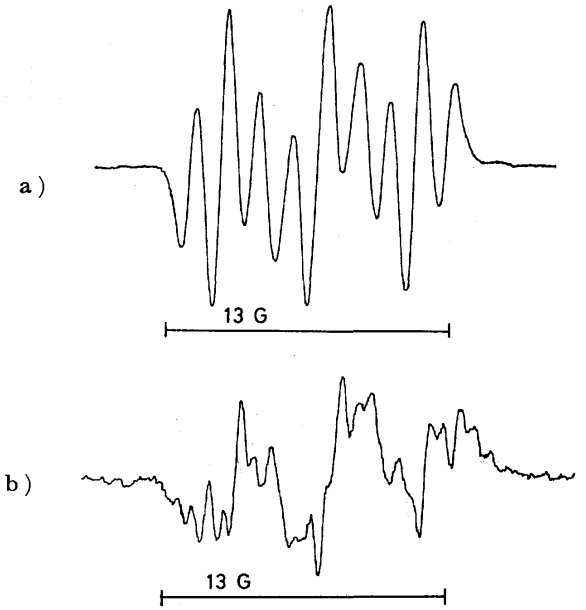

Fig. 1. ESR Spectra obtained in the benzyl-MgCl reaction of 4′-MeO- and 4′-CN-benzoyldurene: (a) usual benzyl-MgCl was used, (b) benzyl-α-d_2-MgCl was used.

Table 1. Coupling constants of Grignard ketyls of some benzoyldurenes

No.	Structure of ketyls	Coupling constants (G) a_p^H	a_o^H	a_m^H	a_α^H	Spectrum corresponding to Fig.
1	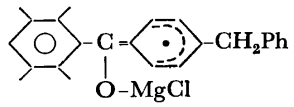	—	4.44	1.39	4.0	Fig. 1a
2	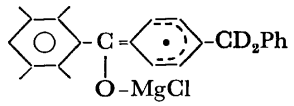	—	4.44	1.39	$a_\alpha^D=0.62$	Fig. 1b
3	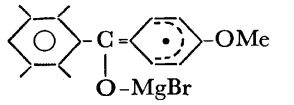	—	4.44	1.52	—	Fig. 2
4	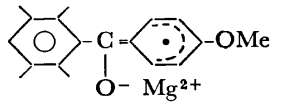	—	4.44	1.52	—	(Fig. 2)
5	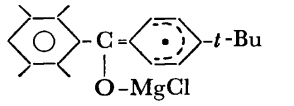	—	4.44	1.46	—	Fig. 3
6	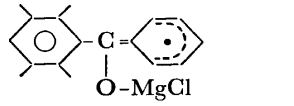	5.69	4.38	1.32	—	Fig. 4
7	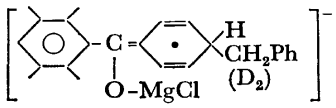	2.91	5.83	1.39	—	Fig. 4

When PhMgBr was used instead of $PhCH_2MgCl$, the solution turned pink, the coloration becoming deep purple. The radical concentration increased gradually and reached *ca.* 30 mol% of the original ketone after 5 h. A partially resolved spectrum (Fig. 2) was obtained. It was identical with that of the Mg-ketyl prepared by use of Mg-amalgam. However, only the original ketone was recovered when the deeply colored solution was hydrolyzed after 1 h. Thus, the pink coloration observed transiently in the initial stage of the $PhCH_2MgCl$ reaction can be ascribed to the ketyl radical of **1**.

t-Butylmagnesium chloride reacts similarly with **1** (Y=OMe) giving *para*-*t*-butylated ketone in a high yield.[10] A color change similar to that of $PhCH_2MgCl$ reaction was observed though the radical concentration was low (*ca.* 2 mol%). This low radical concentration is recognizable as a result of the higher reactivity

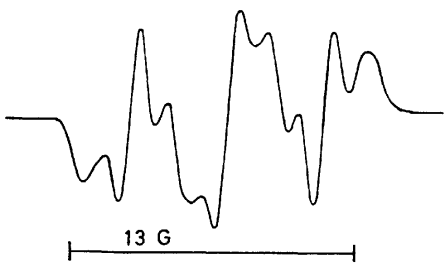

Fig. 2. ESR Spectrum obtained in the phenyl-MgBr and/or Mg-amalgam treatment of 4′-MeO-benzoyldurene.

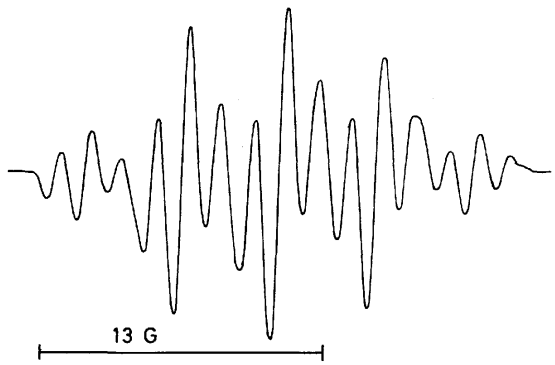

Fig. 3. ESR Spectrum obtained in the *t*-butyl-MgCl reaction of 4′-MeO-benzoyldurene.

of *t*-butyl reagent than that of benzyl reagent.[2] The obtained ESR spectrum is shown in Fig. 3. Since the spectrum differs from that of the original ketyl of **1**, it can be ascribed to that of the "replaced" ketyl radical (Table 1). The difference between the values of a_m^H of No. 1, 3, and 5 is understood as that between the magnitudes of electron-repelling ability of the respective substituents.

Since both the original and the "replaced" ketyl radicals were identified and the low radical concentration in the $PhCH_2MgCl$ and/or *t*-BuMgCl reaction is attributable to the high reactivity of these reagents, the replacement reaction can be explained by the ET-mechanism shown in Scheme 2.

The benzyl radical produced in step i) is in the coordi-

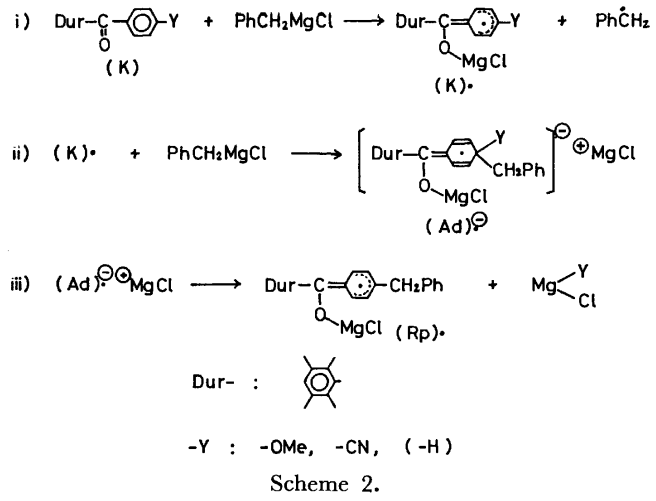

Scheme 2.

nating state to the Mg atom, and would be less reactive than the ordinarily generated "free" radicals; the radical does not necessarily react with the ketyl radical (K)· in the recombination manner. In fact, most part of the benzyl radical escapes out of the solvent cage and abstracts hydrogen from the THF molecule.[11] Since neither benzyl methyl ether nor benzyl cyanide was detected, the substituent Y would be eliminated as anoin Y^- and the process can be formulated by the sequence of steps ii) and iii). The formation of the adduct radical anion species $(Ad)^{\cdot-}$ ^+MgCl is possible since the O–Mg linkage in (K)· is covalent due to the largest electronegativity of Mg among the alkali and alkaline-earth elements; (K)· should thus be neutral. The formation of such an aggregated state[4] is compatible with the observation of the highly aggregated Grignard species in the presence of oxygen-containing compounds.[12]

The postulate on the formation of $(Ad)^{\cdot-}$ ^+MgCl is rationalized by the following study on the nuclear substitution reaction of benzoyldurene itself (**3**) with $PhCH_2MgCl$ (Scheme 3).[13] The *para*-benzylated product (**2**) was isolated (yield 23%) after the reaction solution had been left to stand at room temperature for 4 h. The ESR spectrum consists of thirteen lines (Fig. 4) and is not influenced by the use of $PhCD_2MgCl$, in contrast with the case of **1**. The original ketyl of **3** has thirteen lines with the relative strength of 1 : 2 : 1 : 2 : 5 : 4 : 2 : 4 : 5 : 2 : 1 : 2 : 1, whereas the adduct radical anion (Scheme 2; $(Ad)^{\cdot-}$, Y=H) shows also thirteen lines but with different relative strength of 1 : 2 : 2 : 2 : 3 : 4 : 4 : 4 : 3 : 2 : 2 : 2 : 1 (*cf.* Table 1, No. 6 and 7). The spectrun (Fig. 4) with the apparent relative strength of 1 : 1.9 : 1.2 : 1.0 : 2.4 : 2.6 : 1.6 : 2.6 : 2.4 : 1.0 : 1.2 : 1.9 : 1 was reconstructed by superposing the stronger signals of the original ketyl (No. 6) on the weaker ones of the adduct radical anion (No. 7). The $(AdH)^{\cdot-}$ species does not undergo the hydrogen-transfer (Scheme 4a)[4] as easily as the $(Ad)^{\cdot-}$ species undergoes the Y^--transfer. Thus, the $(AdH)^{\cdot-}$ becomes detectable, but not the "replaced" radical (Rp)·. The formation of **2** would be caused by the air-oxidation of AdH during the course of isolation (Scheme 4b).[5]

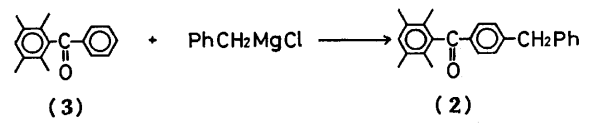

Scheme 3.

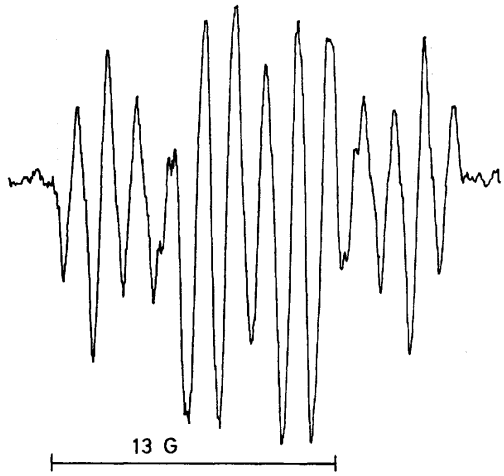

Fig. 4. ESR Spectrum obtained in the benzyl-MgCl and/or benzyl-α-d_2-MgCl reaction of benzoyldurene.

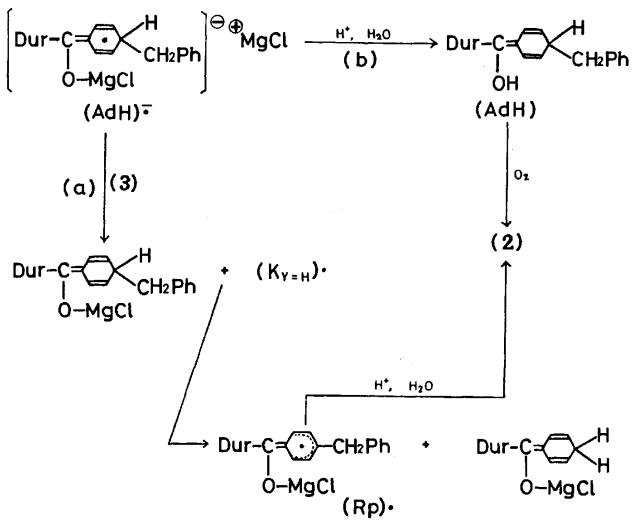

Scheme 4.

If we compare the reaction profiles of **1** with those of **3**, the former reaction is characterized in terms of "replacement", the latter in terms of "addition." The definitive ease of the former reaction is consistent not only with the high spin-density on the unhindered aryl groups,[8] but also with the formation of $(Ad)^{\cdot-}$ favoring the elimination of Y^-. Such an intermediacy of the radical anion species resembles what was postulated in a number of S_{RN}-type reactions.[14] The electrolytically reductive elimination,[15,16] as well as the Grignard replacement,[17] of the anionoid substituents from benzonitrile derivatives have also been reported.

In order to estimate the effect of 4′-anionoid substituents on the ET-process, the initial concentrations of ketyl radicals produced on the PhMgBr treatment of 4′-F-, 4′-Cl- and 4′-MeO-benzoylmesitylenes were

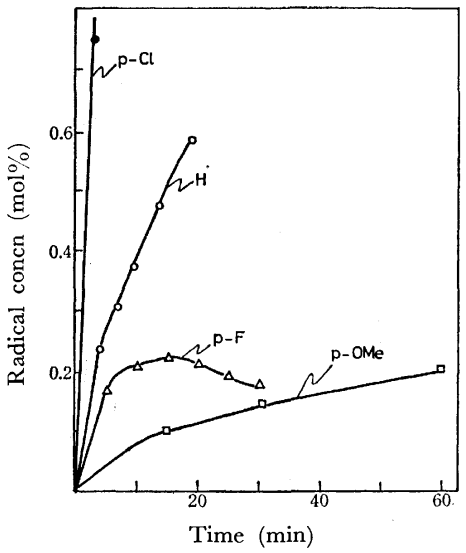

Fig. 5. Radical concentrations at the initial stage of the phenyl-MgBr treatment of benzoylmesitylenes.

compared. Despite the high radical concentrations, no replacement product was obtained after this treatment for 1 h. The radical concentrations, measured by the over-modulation technique, were tentatively corrected on the basis of the relative total width of the well-resolved spectra, respectively (see Experimental). As shown in Fig. 5, the chloro derivative accelerates and the methoxy derivative retards the ET-velocity, whereas the fluoro derivative greatly reduces the radical concentration. However, the estimation by means of visible spectral absorbance verified the high ET-velocity of the fluoro derivative comparable to that of the chloro derivative. The seemingly low radical concentration, as well as the noticeably reduced fluidity of the deeply colored solution, suggests the presence of aggregated diamagnetic dimers which might be formed by the coordination of unhindered fluorine atoms to Mg atom. Probably such an additional coordination through the lone-pair electrons of substituents, when it is located on a position appropriate for the reactivity of the Grignard reagent used, favors the replacement reaction. In fact, the introduction of anionoid substituents such as methoxyl group[18] or bromine atom[19] on the *ortho*-position of benzophenones is effective for the nuclear *ortho*-phenylation in the "replacement" manner.

Considering the difference between the markedly slow *ortho*-phenylation of benzoylmesitylene[4] and the rather rapid *para*-benzylation of benzoyldurene,[13] the C_{phenyl}–Mg linkage is stronger than the C_{benzyl}–Mg linkage.

Conjugate Addition to αβ-Enones. The earliest systematic work by Kohler[20] on the mode of the Grignard addition to open-chain αβ-enones (Scheme 5) reveals the steric effect of R_1, R_2, and R. If R_2 is H(aldehydes), only the normal 1,2-addition takes place. As R_2 becomes bulkier, the conjugate 1,4-addition becomes predominant. This is understandable since the bulky R_2 favors the *s-cis* conformation which is appropriate for the six-membered cyclic structure of transition state. When R_1 is phenyl and R_2 is ethyl, some alkylmagnesium bromides and benzylmagnesium chloride gave 68—70% yields of the conjugate adducts whereas phenylmagnesium bromide gave only the 40% yield.[20] This reveals the strength of C_{phenyl}–Mg linkage, which may be loosened only slightly in the transition state, making it suitable for normal addition.

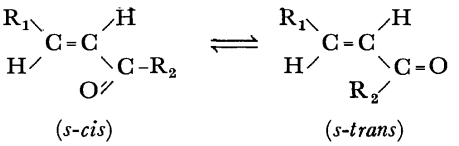

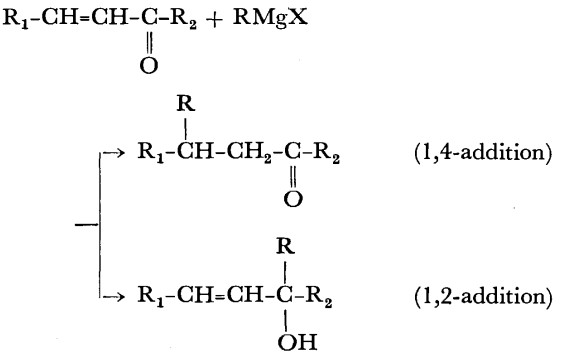

Scheme 5.

Even in the PhMgBr reaction, chalcone(**4**) has been reported to give the conjugate adduct almost exclusively.[20] Though the product resulting from the radical dimerization at the β-carbon has been reported,[21] detection of the Grignard ketyl of **4** could not be made because it should react more rapidly than benzophenone[1] owing to its less-crowded molecular structure resulting from the interposition of the –CH=CH– group. Thus, the present author used the sterically hindered chalcones (Table 2) which have one or two mesityl groups instead of the phenyl groups. Attempts to detect ketyl radicals at room temperature in the PhMgBr reaction were unsuccessful even with the use of these chalcones. The electrolytic reduction method was applied. Though all the radical anions of **5**, **6**, and **7** were short lived and the ESR spectra obtained

Table 2. Beta-hydrogen coupling constants and apparent life-times of chalcones

	Chalcones	a^H_β	Order[a] of life-time
(**4**)	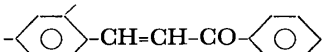	11.3—12.2	3
(**5**)		13.3—13.9	2
(**6**)	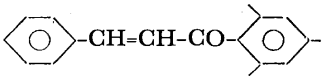	—[b]	(4)
(**7**)		14.1—15.2	1

a) The radical anion which has the apparently longest life-time is indicated by 1. b) The radical anion is very short-lived and a^H_β could not be determined.

were poorly resolved, they consisted of the widely separated two equivalent parts due to the large β-H coupling constants.[22,24] The observed a_β^H values accompanied by the order of the apparent life-times are summarized in Table 2.

The a_β^H values of **5** and **7** larger than the value of **4** indicate that the spin-delocalization is suppressed by the mesityl substitution. The life-times in cases of **5** and **7** longer than those of **4** and **6** can be explained by the steric hindrance due to the β-mesityl group against the dimerization at the β-carbon.[22] However, all the chalcones **4**—**7** gave the conjugate adducts in the PhMgBr reaction.

In the o-MeC_6H_4MgBr treatment, **5** solely produced the short-lived Grignard ketyl detectable at room temperature; a_β^H=17.7—18.9 G.[25] This is attributable to the following: 1) slower addition process of the o-tolyl reagent than that of the phenyl reagent,[1] 2) lower spin-density on the β-carbon than that of **7**, and 3) the steric hindrance due to the β-mesityl group against addition. The explanation suggests the existence of a correlation between the mode of addition and the spin-distribution. This is supported by the HMO-calculation which shows the high spin-density on the β-carbon comparable to that on the carbonyl-carbon.[24] This is exemplified also by the following examples.

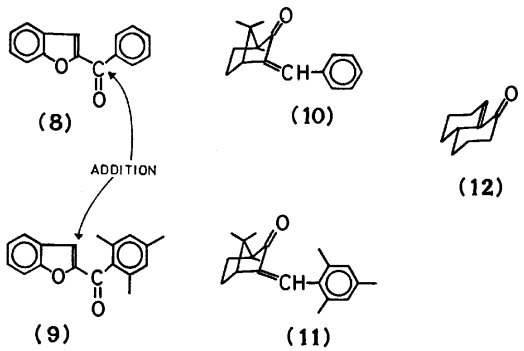

2-Benzoylbenzofuran(**8**) reacts in the normal mode, and its trimethyl derivative(**9**) in the conjugate mode.[26] The latter displays a pink color of the Grignard ketyl for *ca.* 1 h in the o-MeC_6H_4MgBr treatment at room temperature; a_β^H=7.8 G. The fair stability as well as the large a_β^H is explained in terms of the nuclear phenylation of benzoylmesitylene.[4]

The bridged cyclic enones, 3-benzylidenecamphor(**10**) and its trimethyl derivative(**11**), gave the conjugate adducts exclusively.[27] On the treatment of **10** and **11** with o-MeC_6H_4MgBr, the fairly long-lived ketyl radical of the latter camphor was detected at room temperature; a_β^H=4.3 G. The small coupling constant is explicable by the incomplete co-planarity of the grouping O=C–C=CH–; the mode of addition in this case is governed solely by the rigid *s-cis* conformation.

It can be suggested that 1) the spin-distribution in the ketyl radical, 2) the conformation of $\alpha\beta$-enones, and 3) the strength of C–Mg linkage are the three main factors governing the mode of the Grignard addition to $\alpha\beta$-enones. The result showing that $\Delta^{8,8a}$-1-octalone (**12**) gave only the 43% yield of the conjugate adduct in the PhMgBr reaction[28] is partly attributable to the strong C_{phenyl}–Mg linkage which favors the normal 1,2-addition.

General Discussion. Holm[2] studied the behavior of some alkyl Grignard reagents in the electrolytic oxidation and their thermographically-measured kinetic behavior in the reaction with benzophenone, and discussed the correlation between the two kinds of behavior on the basis of the ET-mechanism. House and Weeks[29] utilized the *cis-trans* isomerization of enone-radical anion, as well as the skeletal rearrangement of radical anion, as means to distinguish the ET-mechanism from the direct nucleophilic attack mechanism in the reaction with methyl-carbanionic reagents. The effect of the strength of C–Mg linkage has not been taken into account. The steric effect would be an additional factor affecting the boundary between the two mechanisms. However, the fact that the steric hindrance of both ketones and Grignard reagents makes it possible to detect the intermediate ketyl radicals by the ordinary ESR technique suggests the possibility of the ET-mechanism of Grignard reaction.

Experimental

Materials. All the benzoyldurenes and benzoylmesitylenes were prepared from durene and mesitylene respectiveley by the Friedel-Crafts reaction with the corresponding benzoyl chlorides.[4,6] Chalcones **4**—**7** were prepared by the aldol condensation of the corresponding benzaldehydes and acetophenones.[20] 2-Benzoylbenzofurans **8** and **9**[26] and 3-benzylidenecamphors **10** and **11**[27] were prepared according to the reported methods. Commercial halogen compounds, including benzyl-α-d_2 chloride, were used for the preparation of Grignard reagents.

Procedures. Grignard reagents in THF were prepared as usual, and stored in sealed bottles under N_2 atmosphere. The preparation of samples for ESR measurements were similar to those described previously;[1,8] the molar concentrations of ketones and Grignard reagents were 1.4×10^{-4} and 7.0×10^{-4}, respectively.

Radical concentrations were determined by the over-modulation technique using a reference solution of galvinoxyl in THF.[1] The values obtained by the PhMgBr treatment of benzoylmesitylenes (Fig. 5) were corrected on the basis of the total widths of the resolved spectra: benzoylmesitylene 20.9 G, chloro derivative 16.3 G, fluoro derivative 29.6 G, and methoxy derivative 16.8 G. In order to obtain a well-resolved spectrum, a small portion of the reaction mixture in the measurement cell was diluted by the vaucum distillation of THF from the reaction vessel; the spectra (Figs. 1—4) were not resolvable any further. The visible absorption measurement was also carried out.[1]

For the electrolytic reduction of chalcones **4**—**7**, a similarly shaped simple glass apparatus equipped with two platinum-wire electrodes(the one on the top, anode, and the other at the bottom, cathode, of the cell) was used. Tetrabutylammonium perchlorate(1.0 M) and one of the chalcones (0.2 M) were dissolved in acetonitrile and the apparatus was degassed and sealed off. Since all the radical anions of **4**—**7** were short-lived, the cathode-part of the cell was placed at the center of the ESR cavity. When direct current (0.2 V) was supplied, the green or blue color of radical anions appeared. The apparent life-times(Table 2) were compared based ron the relative time in which the radical anion had been

detected by ESR after the direct current was cut off.

Reaction products were separated by means of TLC and/or column chromatography, and identified by their mp and NMR spectra.

Financial support by the Scientific Research Fund of the Japanese Ministery of Education is gratefully acknowledged.

References

1) Part III; M, Ōkubo, *Bull. Chem. Soc. Jpn.*, **48**, 2057 (1975).
2) T. Holm, *Acta Chem. Scand., B*, **28**, 809 (1974).
3) C. Blomberg, H. H. Grootveld, T. H. Gerner, and F. Bickelhaupt, *J. Organomet. Chem.*, **24**, 549 (1970); H. W. H. J. Bodewitz, C. Blomberg, and F. Bickehaupt, *Tetrahedron*, **29**, 719 (1972); F. Bickelhaupt, *Angew. Chem. Int. Ed. Engl.*, **13**, 419 (1974).
4) M. Ōkubo, *Bull. Chem. Soc. Jpn.*, **48**, 1327 (1975).
5) T. Holm and I. Crossland, *Acta Chem. Scand.*, **25**, 59, 1158 (1971).
6) R. C. Fuson and R. Gaertner, *J. Org. Chem.*, **13**, 496 (1948); R. C. Fuson, W. P. Emmons, and R. Tull, *ibid.*, **16**, 648 (1951); R. C. Fuson and W. P. Emmons, *J. Am. Chem. Soc.*, **73**, 5175 (1951).
7) S. Terabe, K. Kuruma, and R. Konaka, *J. Chem. Soc., Perkin Trans. 2*, **1973**, 1253.
8) M. Ōkubo, *Bull. Chem. Soc. Jpn.*, **48**, 1057 (1975).
9) P. H. Rieger and G. K. Fraenkel, *J. Chem. Phys.*, **37**, 2795 (1962).
10) R. C. Fuson and W. Friedlander, *J. Am. Chem. Soc.*, **75**, 5410 (1953).
11) The NMR analysis of the toluene recovered after the hydrolysis of the reaction mixture with D_2SO_4–D_2O shows that *ca.* 18% of $PhCH_3$ is present in $PhCH_2D$. A small amount of dibenzyl was also detected.
12) H. O. House, R. A. Latham, and G. M. Whitesides, *J. Org. Chem.*, **32**, 2481 (1967); A. D. Vreugdenhill and C. Blomberg, *Recl. Trav. Chim. Pays-Bas*, **84**, 39 (1965).
13) R. C. Fuson and B. C. McKusick, *J. Am. Chem. Soc.*, **65**, 60 (1943).
14) R. A. Rossi and J. F. Bunnett, *J. Am. Chem. Soc.*, **94**, 683 (1972); *ibid.*, **96**, 112 (1974); N. Kornblum, *Angew. Chem. Int. Ed. Engl.*, **14**, 734 (1975).
15) P. H. Rieger, J. Bernal, W. H. Reinmuth, and G. K. Fraenkel, *J. Am. Chem. Soc.*, **85**, 683 (1963).
16) D. E. Bartak, K. J. Houser, B. C. Rudy, and M. D. Hawley, *J. Am. Chem. Soc.*, **94**, 7526 (1972).
17) H. Richtzenhain and P. Nippus, *Ber.*, **77**, 1, 566 (1944).
18) R. C. Fuson and S. B. Speck, *J. Am. Chem. Soc.*, **64**, 2446 (1942).
19) C. Jongsma and F. Bickelhaupt, *Recl. Trav. Chim. Pays-Bas*, **92**, 1143 (1973).
20) E. P. Kohler, *Am. Chem. J.*, **38**, 511 (1907); E. P. Kohler and W. D. Peterson, *J. Am. Chem. Soc.*, **55**, 1073 (1933).
21) R. A. Kretchmer, *J. Org. Chem.*, **37**, 2747 (1972).
22) K. W. Bowers, R. W. Griese, T. Grinshaw, H. O. House, N. Koladny, K. Kronberger, and D. K. Roe, *J. Am. Chem. Soc.*, **92**, 2783 (1970).
23) G. A. Russell and G. R. Stevenson, *J. Am. Chem. Soc.*, **93**, 2432 (1971).
24) J. Harbour and A. V. Guzzo, *Mol. Phys.*, **20**, 565 (1971); *ibid.*, **23**, 151 (1973).
25) The reason for this larger a_β^H value than that of the electrolytically generated radical anion is not obvious, but the coordination to the Grignard species would modify the conformation of the enone and then change the spin-distribution.
26) R. C. Fuson, E. W. Kaiser, and S. B. Speck, *J. Org. Chem.*, **6**, 845 (1941).
27) A. Haller and E. Bauer, *C. R. Acad. Sci.*, **142**, 971 (1906); N. Wolf, *Ann. Chim. (Paris)*, **20**[9], 82 (1923).
28) H. O. House and H. W. Thompson, *J. Org. Chem.*, **28**, 360 (1963).
29) H. O. House and P. D. Weeks, *J. Am. Chem. Soc.*, **97**, 2770, 2778 (1975).

Reduction by a Model of NAD(P)H. XV. Kinetics for the Reduction of Methyl Benzoylformate

Atsuyosi OHNO, Hiroyuki YAMAMOTO, Tadashi OKAMOTO, Shinzaburo OKA, and Yutaka OHNISHI*

Institute for Chemical Research, Kyoto University, Uji, Kyoto 611

**Sagami Chemical Research Center, Nishiohnuma, Sagamihara, Kanagawa 228*

(Received April 16, 1977)

Kinetics for the reduction of methyl benzoylformate (**1**) with *N*-α-methylbenzyl-1-propyl-1,4-dihydronicotinamide (**2**) in the presence of magnesium perchlorate in acetonitrile at 25 °C has been studied. The reaction follows first-order in **1**, first-order in **2**, and zero-order in magnesium ion when [**2**] ≪ [**1**], [$Mg(ClO_4)_2$]. When [**2**] = [$Mg(ClO_4)_2$] ≪ [**1**], the kinetics is best explained by Eqs. 6 and 7. The results indicate that **2** and magnesium ion form a complex, which reacts with **1** at the rate-determining step. It is concluded that magnesium ion activates **2** to promote the release of an electron.

It has been reported that biomimetic reduction of α-keto esters by a model of NAD(P)H takes place in acetonitrile in the presence of magnesium or zinc perchlorate.[1] In addition to the promotion of the reduction, these metal salts also catalyze the asymmetric induction with a chiral model of NAD(P)H.[1] Lithium perchlorate is effective, although the efficiency is much less than that of magnesium or zinc perchlorate, to promote the reduction, but the stereospecificity is absolutely absent with this lithium salt.[2]

In a preceeding paper of this series,[2] we proposed a mechanism of stereospecific magnesium ion-catalyzed reduction of methyl benzoylformate (**1**) with *N*-α-methylbenzyl-1-propyl-1,4-dihydronicotinamide (**2**), where the importance of the initial formation of a complex between **2** and magnesium ion was suggested.

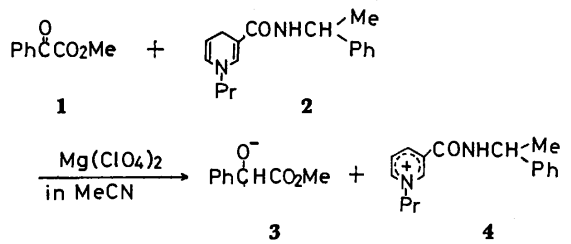

However, the existence of the complex prior to the reduction of **1** remained equivocal, and in order to confirm the previously proposed mechanism we studied the kinetics of the reduction.

Results and Discussion

Kinetics was followed at 25 °C by observing the decrease in the intensity of absorption at 354 nm. The absorption is characteristic of **2**. Pseudo-first-order rate constants, k_{obsd}, under various concentrations of **1** and of magnesium perchlorate are listed in Tables 1 and 2. In Tables 1 and 2 are also listed second-order rate constants, k_{calcd}, calculated by dividing k_{obsd} by the concentration of **1**. The result clearly indicates that the reaction kinetics is first-order in **1**, first-order in **2**, and zero-order in magnesium perchlorate under the conditions employed. The independency of the reaction rate from the concentration of magnesium perchlorate rules out the possibilities of initial formation of a complex between **1** and magnesium ion and of termolecular reaction with free reagents.

Table 1. Dependence of the rate on the concentration of methyl benzoylformate

[**2**] × 10^4, M	[$Mg(ClO_4)_2$] × 10^3, M	[**1**] × 10^3, M	k_{obsd} × 10^2, min^{-1}	k_{calcd}, $M^{-1}\,min^{-1}$
2.00	5.89	5.90	3.84±0.15	6.51×0.30
1.99	12.05	6.11	4.79±0.18	6.75±0.30
2.00	5.96	7.41	5.14±0.20	6.94±0.31
1.99	6.03	12.21	8.26±0.31	6.76±0.30
2.00	5.99	13.61	9.62±0.37	7.06±0.31
2.00	5.99	15.03	10.82±0.40	7.20±0.33
2.00	6.01	16.52	11.82±0.45	7.15±0.31

Table 2. Dependence of the rate on the concentration of magnesium perchlorate

[**2**] × 10^4, M	[$Mg(ClO_4)_2$] × 10^3, M	[**1**] × 10^3, M	k_{obsd} × 10^2, min^{-1}	k_{calcd}, $M^{-1}\,min^{-1}$
2.00	3.91	11.92	8.16±0.30	6.84±0.31
2.00	6.06	11.74	7.86±0.30	6.70±0.30
1.99	6.03	12.21	8.26±0.31	6.76±0.30
2.00	11.91	11.92	8.53±0.31	7.15±0.31
2.00	23.81	12.34	8.36±0.31	6.77±0.30
2.00	35.70	12.40	8.00±0.30	6.45±0.30

It may be safely assumed that the first dissociation of magnesium perchlorate is practically complete in acetonitrile under the conditions where the concentrations of the salt are 10^{-2}—10^{-3} M.[3,4] Thus, the present result is best interpreted, in agreement with the previously suggested mechanism, with the following reaction scheme:

$$Mg(ClO_4)_2 \overset{K_1}{\rightleftharpoons} Mg(ClO_4)^+ + ClO_4^-$$

$$Mg(ClO_4)^+ + \mathbf{2} \overset{K_2}{\rightleftharpoons} \mathbf{2}\cdot Mg(ClO_4)^+$$

$$\mathbf{2}\cdot Mg(ClO_4)^+ + \mathbf{1} \xrightarrow{k_3} \mathbf{3}\cdot Mg^+ + \mathbf{4}\cdot ClO_4^-$$

It should be noted that the absorption at about 354 nm is not affected appreciably by the presence of magnesium perchlorate.[2] That is, what we can observe by measuring the intensity of this absorption is the sum of concentrations of free and complexed **2**. This is an important point, because otherwise the observed kinetics does not predict the above scheme.

The validity of the proposed scheme can be tested

in another way: when initial concentrations of **2** and magnesium perchlorate are set to be equal, Eq. 1 holds because the equilibrium constant K_1 has been assumed to be very large:

$$[\mathbf{2}]_T = [Mg(ClO_4)^+]_T, \quad (1)$$

where the subscript T denotes the sum of concentrations of free and complexed species.
Since

$$K_2 = [\mathbf{2}\cdot Mg(ClO_4)^+]/[Mg(ClO_4)^+][\mathbf{2}]$$
$$= [\mathbf{2}\cdot Mg(ClO_4)^+]/[\mathbf{2}]^2, \quad (2)$$

therefore

$$[\mathbf{2}]_T = [\mathbf{2}] + K_2[\mathbf{2}]^2. \quad (3)$$

When Y is defined by Eq. 4

$$Y = (1 + 4K_2[\mathbf{2}]_T)^{1/2} \quad (4)$$

the kinetic expression according to the proposed reaction scheme can be written as in Eq. 5,

$$-d[\mathbf{2}]_T/dt = k_3[\mathbf{2}\cdot Mg(ClO_4)^+][\mathbf{1}]$$
$$= K_2k_3[\mathbf{2}]^2[\mathbf{1}]$$
$$= k_3[\mathbf{1}](Y-1)^2/4K_2. \quad (5)$$

Finally, we obtain Eqs. 6 and 7 under the conditions of $[\mathbf{2}]=[Mg(ClO_4)_2]\ll[\mathbf{1}]$

$$(Y-1)^{-1} - \ln(Y-1) = k_3[\mathbf{1}]t/2 + C, \quad (6)$$

$$C = (Y_0-1)^{-1} - \ln(Y_0-1), \quad (7)$$

where Y_0 is the value of Y at $t=0$.

The values for K_2 and k_3 were obtained by computer-assisted iteration with the Newton's method[5] and the result is summarized in Table 3. The excellent agreement between the values for k_3 and k_{calcd} proves the validity of the proposed reaction scheme. The value for K_2 also agrees with the idea that practically all molecules of **2** in the reaction system are complexed by magnesium ion under the conditions with which the pseudo-first-order kinetics was studied.

Hughes and Prince reported that the rate of reduction of 2-pyridinecarbaldehyde exibits a half-order dependence on total metal salt concentration.[6] Indeed, our kinetic result obtained under the conditions of $[\mathbf{2}]=[Mg(ClO_4)_2]\ll[\mathbf{1}]$ is very well processed by a two-third order dependence on total concentration of **2**. Therefore, it may provide another possibility that the rate depends on the first-order in **2** and a half-order in magnesium perchlorate. However, such a kinetics comes out only when the dissociation constant of magnesium perchlorate in acetonitrile is very small. If this were the case, the kinetics under the conditions of $[\mathbf{2}]<[Mg(ClO_4)_2]\ll[\mathbf{1}]$ should deviate from the first-order in **2** in contrast to the observed result. Thus, the assumption that K_1 has a large value has been proved to be valid.

Table 3. Computed values for rate and equilibrium constants

$[\mathbf{2}]\times10^4$, M	$[Mg(ClO_4)_2]\times10^4$, M	$[\mathbf{1}]\times10^3$, M	k_3, $M^{-1}\,min^{-1}$	$K_2\times10^{-3}$, M^{-1}
1.99	1.99	24.00	6.91	1.98
1.99	1.99	24.15	6.86	1.82
1.99	2.00	23.82	6.99	1.65
1.99	1.99	12.08	6.96	2.03

The kinetics has revealed that the complex, $\mathbf{2}\cdot Mg(ClO_4)^+$, is the reacting species and the role of magnesium ion is not only to activate the substrate but also to activate the model compound.[7] In this way, **2** releases an electron, a proton, and an electron, successively. This conclusion is different from that proposed by Gase and his coworkers, who assigned free **2** as a reacting species.[8]

Lithium perchlorate gave a quite complex kinetics which could not be interpreted. The reaction rate depended on the concentration of lithium ion even in the region of 15×10^{-3} M against 2×10^{-4} molar concentration of **2**. The result may probably due to the formation of various types of aggregates in concordance with the idea previously proposed in a simplified form.[2]

Partial support in the form of a Scientific Resarch Grant from the Ministry of Education, Japan, is acknowledged.

Experimental

Materials. Acetonitrile was distilled once on phosphorus pentaoxide and kept over molecular sieves 4A. Magnesium and lithium perchlorates were dried at 120 °C *in vacuo* for 5 h and used immediately. Preparations of methyl benzoylformate and *N*-α-methylbenzyl-1-propyl-1,4-dihydronicotinamide were described previously.[9]

Procedure. Acetonitrile was flushed with dry argon prior to the use. In a glove-box filled with dry argon, solutions for kinetic studies were prepared and placed in a UV-cell (1 cm) equipped with a silicone-rubber stopper. Kinetics was followed spectrophotometrically with a Union Giken SM-401 spectrophotometer, the cell-compartment of which was filled with dry argon and kept at 25.0+0.1 °C. The order of incubation of reagents did not affect the kinetics.

Kinetics. In the presence of a large excess of magnesium perchlorate, the reactions gave good first-order plots over three half-lives ($r>0.9997$). In the presence of a small amount of magnesium perchlorate, the kinetics over 75% conversion of the reaction was processed well with Eqs. 6 and 7. Iterations of K_2 and k_3 by a FACOM 230 OS2/VS with a FORTRAN IV program gave constants which reproduced experimentally obtained plots exactly.

References

1) Y. Ohnishi, M. Kagami, and A. Ohno, *J. Am. Chem. Soc.*, **97**, 4766 (1975).
2) A. Ohno, T. Kimura, H. Yamamoto, S. G. Kim, S. Oka, and Y. Ohnishi, *Bull. Chem. Soc., Jpn.*, **50**, 1535 (1977).
3) It is highly unprobable to expect that the second dissociation of magnesium perchlorate is complete.
4) *Cf.* a) R. L. Kay, J. B. Hales, and G. P. Cunningham, *J. Phys. Chem.*, **71**, 3925 (1967); b) D. J. Creighton, J. Hajdu, and D. S. Sigman, *J. Am. Chem. Soc.*, **98**, 4619 (1976).
5) G. J. Kynch, "Mathematics for the Chemist," Butterworths Scientific Publ., London (1955), p. 19.
6) M. Hughes and R. H. Prince, *Chem. Ind. (London)*, **1975**, 648.
7) The donisities, DN, of tertiary amines are much larger than those of carbonyl compounds. See V. Gutman, *Coordin. Chem. Rev.*, **18**, 225 (1976).
8) R. A. Gase, G. Boxhoorn, and U. K. Pandit, *Tetrahedron Lett.*, **1976**, 2899.
9) A. Ohno, T. Kimura, S. G. Kim, H. Yamamoto, S. Oka, and Y. Ohnishi, *Bioorg. Chem.*, **6**, 21 (1977).

Synthesis of α Substance-I_B in *Saccharomyces cerevisiae*[1,2]

Haruhiko Aoyagi and Nobuo Izumiya

Laboratory of Biochemistry, Faculty of Science 33, Kyushu University, Higashi-ku, Fukuoka 812

(Received April 18, 1977)

Two hexapeptides, H–Arg–Gly–Pro–Phe–Pro–Ile–OH (**1a**) and H–Arg–Pro–Gly–Phe–Pro–Ile–OH (**1b**), have been proposed for a factor inducing sexual agglutination in the yeast and were synthesized by a conventional method. Compound **1a** was completely identical with the natural peptide in thin-layer chromatography, mass spectrometric measurements, and biological assay on agglutination. Compound **1b** showed the same biological activity as **1a** though distinct differences in the chemical data were observed. Strong bitterness of the **1a** and **1b** was discovered.

Sakurai *et al.*[3] reported the isolation of a peptidyl factor named α substance-I from α type cells (H15 strain) of heterothallic yeast *Saccharomyces cerevisiae*. The active principle induces sexual agglutinability in opposite a (ei) type cells (H22 strain) prior to the mating reaction. It was later found that the factor could be separated into two components by further purification and one of them was designated as α substance-I_B (abbreviated as I_B).[4] Sakurai *et al.* intended to determine the amino acid sequence of I_B by means of mass spectrometry and postulated a tentative structure as H–Arg–Gly–Pro–Phe–Pro–Ile–OH (**1a**). In the beginning, however, an alternate structure of H–Arg–Pro–Gly–Phe–Pro–Ile–OH (**1b**) for I_B could not be excuded because of presence of the unexpected fragment ions. We intended to ascertain the correct structure of the I_B by the syntheses of the supposed hexapeptides, **1a** and **1b**.

The present paper deals with the syntheses of **1a**·2AcOH and **1b**·2AcOH by a conventional method and the comparison of the synthetic peptides with the natural I_B by thin-layer chromatography, mass spectrometry and biological assays.

The syntheses of **1a**·2AcOH and **1b**·2AcOH are outlined in Figs. 1 and 2. The mixed anhydride method[5] was employed through all coupling reactions and the removal of Boc groups of the intermediates was performed by the action of hydrogen chloride in ethyl acetate. The protected hexapeptide **8a** prepared from Z–Arg(NO_2)–OH and **7a**·HCl was hydrogenated in the presence of palladium black, and the desired product (**1a**) was obtained as diacetate by lyophilization. The similar procedure was employed for the preparation of **1b**. The intermediate **8b** contained minor by-products and was purified by silica gel column chromatography, and the desired product (**1b**) was obtained as diacetate. The homogeneity of **1a**·2AcOH and **1b**·2AcOH was confirmed by paper and thin-layer chromatography, paper electrophoresis and elemental analysis.

For the comparison of the synthetic peptides with natural I_B, thin-layer chromatography was performed at first using four different systems, the result being given in Table 1. In all cases, the **1a**·2AcOH revealed com-

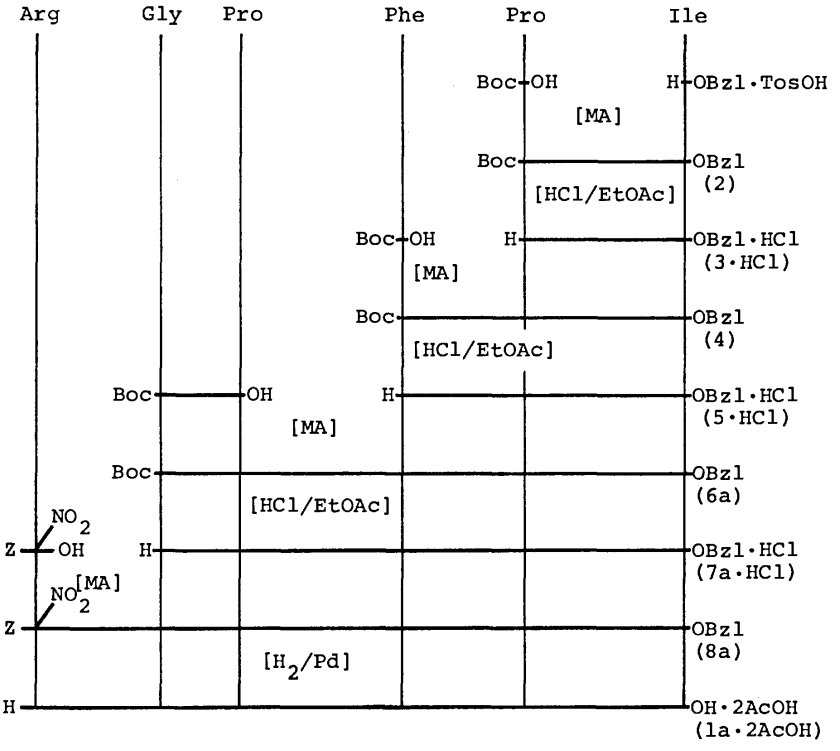

Fig. 1. Synthesis of the hexapeptide, **1a**.

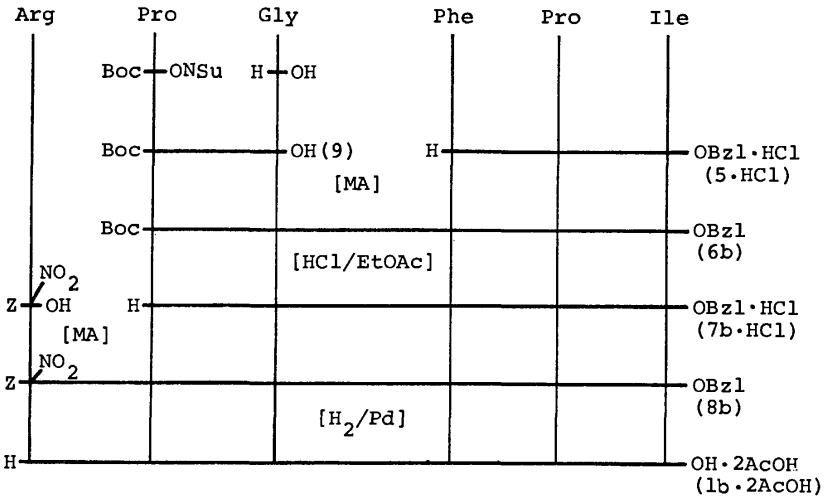

Fig. 2. Synthesis of the hexapeptide, **1b**.

Table 1. Thin-layer chromatography of natural and synthetic peptides

Solvent	Carrier	R_f[a]		
		I_B	**1a**·2AcOH	**1b**·2AcOH
1-BuOH–AcOH–H_2O (4 : 1 : 5, upper phase)	Silica gel[b]	0.18	0.18	0.17
1-BuOH–AcOH–pyridine–H_2O (15 : 3 : 10 : 12)	Silica gel[b]	0.59	0.59	0.57
1-BuOH–1-PrOH–0.2 M AcOH (2 : 1 : 3, upper phase)	Silica gel[b]	0.11	0.11	0.09
1-BuOH–1-PrOH–0.2 M AcOH (2 : 1 : 3, upper phase)	Cellulose[c]	0.58	0.58	0.63

a) The chromatograms were stained with ninhydrin followed by chlorine–toluidine. b) The plates coated with siligel gel GF_{254} (Merck) in 0.25-mm thickness were used. c) The plates coated with cellulose (Merck) in 0.1-mm thickness were used.

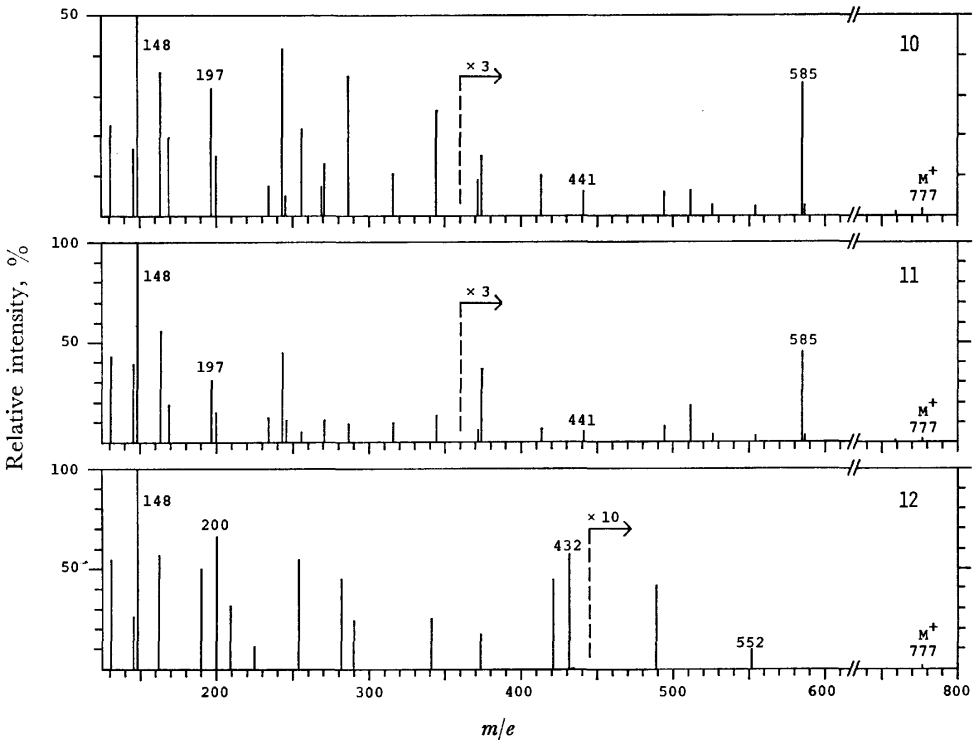

Fig. 3. Mass spectra of the derivative (**10**) of I_B and the derivatives (**11** and **12**) of the hexapeptides (**1a** and **1b**).

plete identity with I_B. The difference between R_f's of **1b**·2AcOH and I_B obvious.

Prior to comparison of mass spectra, the N-terminal arginine residues in I_B, **1a**·2AcOH, and **1b**·2AcOH were converted to α-*N*-acetyl-δ-*N*-pyrimidyl-ornithines and the C-terminus to methyl esters according to the literature.[6] The spectra of the derivatives, which named [Ac–Orn(Pyr)[1]]–I_B–OMe (**10**), [Ac–Orn(Pyr)[1]]–**1a**–OMe (**11**) and [Ac–Orn(Pyr)[1]]–**1b**–OMe (**12**), respectively, from I_B, **1a**, and **1b** are shown in Fig. 3. Compound **11** showed ion peaks at *m/e* 777 (M^+), 585, 441, 197, and 148, which were exactly the same as those observed for the corresponding **10** from I_B. On the contrary, the spectra of **12** were quite different in fragmentation pattern from those of **10** and **11**. From these results, the identity of **1a** with I_B was verified unambiguously.

The biological activities of the natural and synthetic peptides to induce agglutinability in a (ei) type cells were examined, and the I_B and **1a**·2AcOH showed the activity in the same degree at dosages at 2—20 ng/ml. Contrary to our expectation, the **1b**·2AcOH also showed almost the same activity as I_B, the finding suggesting that a strict structure is not always required for activity. This phenomenon is interesting because the replacement of amino acid residue by another in a biologically active peptide gives generally an influence for activity of the peptide.

Recently, Ribadeau Dumas *et al.* elucidated the whole primary structure of bovine β-casein,[7] which contained the partial sequence of –Arg[202]–Gly–Pro–Phe–Pro–Ile[207]–Ile–Val–OH[209] in the C-terminal portion. It is noteworthy that the part of –Arg[202]–Gly–Pro–Phe–Pro–Ile[207]– is identical with the I_B, On the other hand, two Japanese groups isolated the peptides having the structures of H–Arg–Gly–Pro–Pro–Phe–Ile–Val–OH (**13**)[8] and H–Gly–Pro–Phe–Pro–Val–Ile–OH (**14**)[9] from the enzymatic hydrolyzate of casein as bitter principles. Neither amino acid sequence of **13** nor that of **14** can be found in any part of the primary structure of casein, but both peptides are very similar to C-terminal portion of casein and I_B. We observed that the synthetic **1a**·2AcOH and **1b**·2AcOH showed strong bitter taste in almost the same threshold value. From these results, we assume that the partial structure of a substance corresponding to **13** will be H–Arg–Gly–Pro–Phe–Pro–Ile–, and that of **14** will be H–Gly–Pro–Phe–Pro–Ile–.

Experimental

Melting points are uncorrected. The ratio in parentheses after a solvent system was indicated by vol. TLC was carried out on silica gel G (Merck) with the solvent systems: R_f^1, $CHCl_3$–MeOH (5 : 1); R_f^2, 1-BuOH–AcOH–pyridine–H_2O (15 : 3 : 10 : 12). Paper chromatography was carried out on Toyo Roshi No. 52 paper with the solvent system: R_f^3, 1-BuOH–AcOH–pyridine–H_2O (4 : 1 : 1 : 2). Optical rotations were measured on a Union high sensitivity polarimeter PM-71. Amino acid analyses were performed with a Hitachi amino acid analyzer, KLA-5.

*Boc–Pro–Ile–OBzl (**2**).* To a chilled solution of Boc–Pro–OH (3.23 g, 15 mmol) and TEA (2.10 ml, 15 mmol) in THF (30 ml) was added isobutyl chloroformate (1.97 ml, 15 mmol) at −5 °C. After 15 min, a chilled solution of H–Ile–OBzl·TosOH (5.90 g, 15 mmol) and TEA (15 mmol) in $CHCl_3$ (30 ml) was added. The mixture was left to stand overnight at room temperature, evaporated *in vacuo*, and the oily residue was dissolved in EtOAc. The solution was washed successively with 4% $NaHCO_3$, 10% citric acid and water, and then dried (Na_2SO_4). The solvent was evaporated *in vacuo*; yield of an oil, 6.06 g (96%); R_f^1 0.91.

*Boc–Phe–Pro–Ile–OBzl (**4**).* Compound **2** (5.86 g, 14 mmol) was dissolved in 3.0 M hydrogen chloride in EtOAc (50 ml). The solution was allowed to stand for 40 min at room temperature and then evaporated; yield of oily H–Pro–Ile–OBzl·HCl (**3**·HCl), 4.87 g (98%). Then, **4** was prepared from Boc–Phe–OH (3.58 g, 13.5 mmol) and **3**·HCl (4.79 g, 13.5 mmol) as described for **2**; the yield of oily **4**; 7.20 g (94%); R_f^1 0.90.

*Boc–Gly–Pro–Phe–Pro–Ile–OBzl (**6a**).* Compound **4** (5.66 g, 10 mmol) was treated with 3.0 M hydrogen chloride in EtOAc (35 ml) as described for **3**·HCl; yield of oily H–Phe–Pro–Ile–OBzl·HCl (**5**·HCl), 4.75 g (95%). Then, **6a** was prepared from Boc–Gly–Pro·OH[10] (1.22 g, 4.5 mmol) and **5**·HCl (2.26 g, 4.5 mmol) as described for **2**; yield of oily **6a**, 3.00 g (93%); R_f^1 0.69.

*H–Gly–Pro–Phe–Pro–Ile–OBzl·HCl (**7a**·HCl).* Compound **6a** (2.88 g, 4 mmol) was treated as described for **3**·HCl. The oily product was solidified by the addition of ether; yield, 2.13 g (80%); mp 145—148 °C; $[\alpha]_D^{20}$ −69.8° (*c* 1, DMF); R_f^1 0.35, R_f^2 0.85.

Found: C, 61.28; H, 6.94; N, 10.48%. Calcd for $C_{34}H_{46}O_6N_5Cl\cdot 1/2H_2O$: C, 61.38; H, 7.12; N, 10.53%.

*Z–Arg(NO_2)–Gly–Pro–Phe–Pro–Ile–OBzl (**8a**).* This compound was prepared from Z–Arg(NO_2)–OH (1.06 g, 3 mmol) and **7a**·HCl (1.99 g, 3 mmol) as described for **2**. The product was recrystallized from EtOAc–ether; yield, 2.09 g (72%); mp 99—103 °C; $[\alpha]_D^{20}$ −58.0° (*c* 1, DMF); R_f^1 0.71, R_f^2 0.92.

Found: C, 59.31; H, 6.44; N, 14.41%. Calcd for $C_{48}H_{62}O_{11}N_{10}\cdot H_2O$: C, 59.24; H, 6.63; N, 14.40%.

*H–Arg–Gly–Pro–Phe–Pro–Ile–OH·2AcOH (**1a**·2AcOH).* Compound **8a** (389 mg, 0.4 mmol) was dissolved in a mixture of MeOH (5 ml), AcOH (2 ml) and water (3 ml), and treated with hydrogen in the presence of Pd black overnight. The filtrate of the reaction mixture was evaporated and the evaporation was repeated several times on the addition of water. The residue was dissolved in water and lyophilized to leave a solid; yield, 312 mg (95%); mp 102—108 °C; $[\alpha]_D^{21}$ −87.6° (*c* 1, H_2O). The homogeneity of **1a** was confirmed by ninhydrin and Sakaguchi reagent on paper electrophoresis and paper chromatography; R_f^3 0.88. Amino acid ratios in an acid hydrolyzate; Pro 2.12, Gly 1.00, Ile 0.98, Phe 0.96, Arg 0.97.

Found: C, 54.18; H, 7.53; N, 15.55%. Calcd for $C_{33}H_{51}O_7N_9\cdot 2CH_3COOH\cdot H_2O$: C, 53.93; H, 7.46; N, 15.30%.

*Boc–Pro–Gly–OH (**9**).* To a solution of glycine (1.13 g, 15 mmol) and TEA (15 mmol) in water (70 ml) at 5 °C was added Boc–Pro–ONSu[11] (3.89 g, 12.5 mmol) in dioxane (50 ml). The mixture was stirred for 30 min at 5 °C and overnight at room temperature. After the dioxane was evaporated, the aqueous solution was acidified with 10% citric acid and extracted with EtOAc. The organic layer was washed with water, dried and evaporated to leave a solid. The product was recrystallized from EtOAc–ether; yield, 2.37 g (70%); mp 159—160 °C; $[\alpha]_D^{20}$ −60.8° (*c* 1, DMF); R_f^1 0.22.

Found: C, 52.78; H, 7.40; N, 10.14%. Calcd for $C_{12}H_{20}O_5N_2$: C, 52.93; H, 7.40; N, 10.29%.

*Boc–Pro–Gly–Phe–Pro–Ile–OBzl (**6b**).* This compound was prepared from **9** (0.95 g, 3.5 mmol) and **5**·HCl (1.76 g,

3.5 mmol) as described for **2**; yield of an oil, 2.47 g (98%); R_f^1 0.72.

*H-Pro-Gly-Phe-Pro-Ile-OBzl·HCl (**7b**·HCl).* Compound **6b** (2.16 g, 3 mmol) was treated as described for **3**·HCl. The oily product was solidified by the addition of ether; yield, 1.70 g (84%); mp 91—94 °C; $[\alpha]_D^{20}$ −39.6° (*c* 1, DMF); R_f^1 0.34, R^2 0.82.

Found: C, 60.38; H, 7.07; N, 10.34%. Calcd for $C_{34}H_{46}O_6N_5Cl\cdot H_2O$: C, 60.56; H, 7.18; N, 10.39%.

*Z-Arg(NO$_2$)-Pro-Gly-Phe-Pro-Ile-OBzl (**8b**).* This compound was prepared from Z-Arg(NO$_2$)-OH (0.88 g, 2.5 mmol) and **7b**·HCl (1.68 g, 2.5 mmol) as described for **2**. The oily product was obtained in 2.30 g. For purification, a half (1.15 g) of the product was dissolved in a solvent of $CHCl_3$–MeOH–AcOH (95 : 5 : 1), applied on a column (2.4 × 84 cm) with silica gel, and eluted with the same solvent. The fractions with the desired product were evaporated to leave an oil which was solidified by the addition of ether, the remainder (1.15 g of the product) being purified by the same procedure. Recrystallization from EtOAc–ether gave 0.92 g (38%) of pure **8b**; mp 98—105 °C; $[\alpha]_D^{20}$ −33.8° (*c* 1, DMF); R_f^1 0.68; R_f^2 0.91.

Found: C, 59.79; H, 6.59; N, 14.40%. Calcd for $C_{48}H_{62}O_{11}N_{10}\cdot 1/2H_2O$: C, 59.80; H, 6.59; N, 14.53%.

*H-Arg-Pro-Gly-Phe-Pro-Ile-OH·2AcOH (**1b**·2AcOH).* Compound **8b** (386 mg, 0.4 mmol) was treated as described for **1a**·2AcOH; yield of a solid, 314 mg (95%); mp 107—112 °C; $[\alpha]_D^{21}$ −56.2° (*c* 1, H_2O); R_f^3 0.89. Amino acid ratios in an acid hydrozate: Pro 2.11, Gly 1.00, Ile 0.97, Phe 0.96, Arg 0.95.

Found: C, 53.67; H, 7.45; N, 15.52%. Calcd for $C_{33}H_{51}O_7N_9\cdot 2CH_3COOH\cdot H_2O$: C, 53.93; H, 7.46; N, 15.30%.

*Comparison of the Natural Peptide (I_B) and Synthetic Peptides (**1a** and **1b**).* *TLC*: TLC was carried out using four different systems, the results being shown in Table 1.

Mass Spectrometric Measurements: The I_B, **1a**·2AcOH, and **1b**·2AcOH were modified according to the literature,[6] and the measurements were performed on a Hirachi RMU-6L at 70 eV. The results are shown in Fig. 3.

Agglutinability Assays: The activities of I_B, **1a**·2AcOH, and **1b**·2AcOH to induce agglutinability in a (ei) type cells (H 22 strain) were assayed according to the literature.[3] The I_B and **1a**·2AcOH showed the activity in the same degree at 2—20 ng/ml. Compound **1b**·2AcOH also showed the same activity.

Bitterness Evaluation. Each synthetic peptide (**1a**·2AcOH or **1b**·2AcOH) was dissolved in water and a series of solution of decreasing concentration were prepared. The degree of bitterness was organoleptically determined by a panel of five men in our laboratory according to the literature.[12] Compounds **1a**·2AcOH and **1b**·2AcOH showed the bitter taste in the same degree at 0.13—0.25 mM (0.1—0.2 mg/ml).

We wish to express our thanks to Professor S. Tamura, University of Tokyo, for his helpful discussion, and to Dr. A. Sakurai, Institute of Physical and Chemical Research, Saitama, for TLC and agglutinability assays for the comparision of the synthetic peptides with I_B. We also thank to Drs. A. Isogai and K. Aizawa, University of Tokyo, for the measurements of mass spectra.

References

1) Part of this work has been briefly communicated: H. Aoyagi, N. Izumiya, A. Sakurai, K. Sakata, and S. Tamura, *Experientia*, in press.

2) The abbreviations recommended by the IUPAC-IUB Commission of Biochemical Nomenclature (*J. Biol. Chem.*, **247,** 977 (1972)) have been used throughout. Additional abbreviations: AcOH, acetic acid; 1-BuOH, 1-butanol; DMF, *N,N*-dimethylformamide; MA, mixed anhydride method; 1-PrOH, 1-propanol; Pyr, pyrimidyl; TEA, triethylamine; THF, tetrahydrolyfuran; TosOH, *p*-toluenesulfonic acid. Amino acid symbols except Gly denote the L-configuration.

3) A. Sakurai, S. Tamura, N. Yanagishima, and C. Shimoda, *Proc. Jpn. Acad.*, **51**, 291 (1975).

4) A. Sakurai, K. Sakata, S. Tamura, K. Aizawa, N. Yanagishima, and C. Shimoda, *Agric. Biol. Chem.*, **40**, 1451 (1976).

5) T. R. Vaughan, Jr. and R. L. Osato, *J. Am. Chem. Soc.*, **74**, 676 (1952).

6) M. M. Shemyakin, E. I. Vinogradova, Yu. A. Ovchinnikov, A. A. Kiryushkin, M. Yu. Feigina, N. A. Aldanova, Yu. B. Alakhov, V. M. Lipkin, B. V. Rosinov, and L. A. Fonina, *Tetrahedron*, **25**, 5785 (1969).

7) B. Ribadeau Dumas, G. Bringnon, F. Grosclaude, and J. C. Mercier, *Eur. J. Biochem.*, **25**, 505 (1972).

8) N. Minamiura, Y. Matsuura, F. Fukumoto, and T. Yamamoto, *Agric. Biol. Chem.*, **36**, 588 (1972).

9) T. Matoba, R. Hayashi, and T. Hata, *Agric. Biol. Chem.*, **34**, 1235 (1970).

10) J. C. Anderson, M. A. Barton, P. M. Hardy, G. W. Kenner, and R. C. Sheppard, *J. Chem. Soc.*, **1967**, 108.

11) G. W. Anderson, J. E. Zimmerman, and F. M. Callahan, *J. Am. Chem. Soc.*, **86**, 1839 (1964).

12) T. Matoba and T. Hata, *Agric. Biol. Chem.*, **36**, 1423 (1972).

^{13}C-NMR-Spektren von thermischen Oligomeren des Cyclopentadiens

Kiyoshi NAKAGAWA, Shoji IWASE, Yasutaka ISHII,
Sawako HAMANAKA, und Masaya OGAWA
Abteilung für Angewandte Chemie, Technische Fakultät der Universität Kansai, Senriyama, Suita, Osaka 564

(Received April 11, 1977)

Die zwei Isomere des Dicyclopentadiens und vier Isomere des Tricyclopentadiens werden isoliert und ihre ^{13}C-NMR-Spektren werden vorgelegt, wobei die Trimerisationsstufe des Cyclopentadiens systematisch in allen Einzelheiten behandelt wird. Die ^{13}C-NMR-Spektren von Oligomeren des Cyclopentadiens werden durch Vergleich mit Spektren von Vergleichssubstanzen zugeordnet. Es ist beachtenswert, dass zwei neue Stereoisomere des Tricyclopentadiens isoliert und nachgewiesen werden.

Die Oligomere des Cyclopentadiens erregen von früher her die Aufmerksamkeit.[1] Die Entstehung des Tricyclopentadiens spielt eine bedeutende Rolle für alle folgenden Oligomerisationsprozesse. Die Addition des dritten Cyclopentadiens an den Cyclopentenring des *endo-* oder *exo*-Dicyclopentadiens wurde bisher noch nicht systematisch untersucht. Die ^{13}C-NMR-Spektroskopie hat sich in den letzten Jahren zu einem leistungsfähigen Hilfsmittel des organischen Chemikers entwickelt. In der vorliegenden Arbeit werden die ^{13}C-MNR-spektroskopischen Daten einer oligomeren Reihe von Cyclopentadien interpretiert, wobei die Trimerisationsstufe des Cyclopentadiens ausführlich diskutiert wird.

Ergebnisse und Diskussion

*^{13}C-NMR-Spectren von Dicyclopentadienen **1** und **2**.*

Das ^{13}C-NMR-Spektrum von **1**, das schon von Johnson und Jankowski berichtet wurde[2], konnte nicht vollständig zugeordnet werden. Die in der Tabelle 1 angegebenen Zuordnungen der ^{13}C-Signale von **1** und **2** ergeben sich aus folgenden Gesichtspunkten. Bei Verbindung **7** liegen drei ^{13}C-Signale um 5 bis 43.7 ppm bei tieferem Feld als bei **1**. Der Substituenteneinfluss der Hydroxylgruppe auf die chemische Verschiebung des C-1-Signals ist α-Effekt von $\Delta\delta_\alpha=43.7$ ppm (vgl. ^{13}C-NMR-Spektren von Cyclopentanol[3] und 2-Hydroxynorbornan[4]). Daher entspricht dem C-1-Atom das Signal bei $\delta=34.7$ ppm. Der Einfluss der Hydroxygruppe auf das C-2- oder C-7a-Signal ist β-Effekt von $\Delta\delta_\beta=5$ oder 11.7 ppm. Charakteristisch getrennt von dem C-7a-Signal (sp^3-Kohlenstoff) erscheint das C-2-Signal (sp^2-Kohlenstoff). Somit entspricht dem C-2-Atom das Signal bei $\delta=132.1$ ppm, so dass das Signal bei $\delta=41.3$ ppm dem C-7a-Atom entspricht. Bei Verbindung **8** liegen zwei sp^3-Kohlenstoff-Signale *ca.* 5 ppm bei höherem Feld als bei **1**. Da diese Hochfeldverschiebungen aufgrund der Hydrierung von Norbornendoppelbindung sind, entsprechen den C-4- und C-7-Atomen diese zwei sp^3-Kohlenstoff-Signale bei $\delta=$ 45.3 und 46.3 ppm in **1**, wobei die Verschiebungsdifferenz zwischen C-4 und C-7 nicht zu unterscheiden ist. Bei Verbindung **9** wird das Signal des C-4-Atoms (γ-ständiges Kohlenstoffatom zu Cyclopentendoppelbindung in **8**) mit 1.7 ppm nach tieferem Feld im Vergleich zu **8** verschoben, während das δ-ständige C-7-Atom durch Hydrierung der Cyclopentendoppelbindung nahezu unbeeinflusst bleibt. Das Signal bei $\delta=45.3$ ppm muss also C-4 zugeordnet werden und das

TABELLE 1. ^{13}C-CHEMISCHE VERSCHIEBUNGEN (δ IN ppm, $\delta_{TMS}=0$) UND MULTIPLIZITÄTEN VON DICYCLOPENTADIENEN UND IHREN DERIVATEN

		C-1	C-2	C-3	C-3a	C-4	C-5	C-6	C-7	C-7a	C-8
1	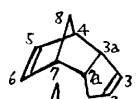	34.7 (t)	132.1 (d)	135.6 (d)	54.8 (d)	45.3 (d)	131.9[a] (d)	132.2[a] (d)	46.3 (d)	41.3 (d)	50.3 (t)
7	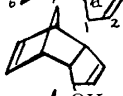	78.4 (d)	137.1 (d)	135.2 (d)	54.5 (d)	44.5 (d)	132.2 (d)	134.6 (d)	44.5 (d)	53.0 (d)	51.1 (t)
8	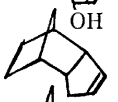	32.3 (t)	130.2 (d)	132.8 (d)	53.1 (d)	39.8 (d)	25.4 (t)	22.1 (t)	41.4 (d)	42.7 (d)	41.4 (t)
9	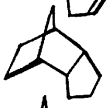	27.0 (t)	28.7 (t)	27.0 (t)	45.5 (d)	41.5 (d)	23.1 (t)	23.1 (t)	41.5 (d)	45.5 (d)	43.3 (t)
2	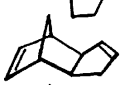	36.5 (t)	132.9 (d)	132.0 (d)	51.4 (d)	45.5 (d)	137.2[a] (d)	137.0[a] (d)	48.0 (d)	41.8 (d)	41.3 (t)
10	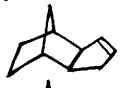	40.0 (t)	132.5[a] (d)	131.6[a] (d)	56.0 (d)	40.6 (d)	29.3[b] (t)	29.0[b] (t)	43.3 (d)	44.1 (d)	31.8 (t)
11	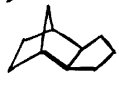	32.6 (t)	27.4 (t)	32.6 (t)	48.4 (d)	40.8 (d)	28.9 (t)	28.9 (t)	40.8 (d)	48.4 (d)	32.2 (t)

a), b) Tauschbare Zuordnungen.

Signal bei $\delta=46.3$ ppm entspricht C-7 in **1**. Somit können die Verschiebungen bei 135.6 und 54.8 ppm C-3 und C-3a in **1** zugeordnet werden.

Die Zuordnung der Signale von C-5, C-6, und C-8 in Verbindung **2** ergibt sich, wenn man berücksichtigt, dass C-5 und C-6 durch sterischen Kompressionseffekt des Cyclopentenringes nicht beeinflusst werden, während C-8 durch diesen Effekt nach höherem Feld verschoben wird. Für C-5 und C-6 in **2** beobachtet man die Tieffeldverschiebungen im Vergleich zu **1**.

Wie bei **1** können die Signale von anderen Kohlenstoffatomen in **2** durch Vergleich mit Spektren von Vergleichssubstanzen **10** und **11** zugeordnet werden. Die Ergebnisse sind in Tabelle 1 zusammengefasst.

Longitudinale Relaxationszeiten T_1 von Dicyclopentadienen. Wenn Relaxationsvorgänge durch intramolekulare C-H-Dipol-Dipol-Wechselwirkungen beherrscht werden, sollte die longitudinale Relaxationszeit T_1 von ^{13}C charakterisch von der Anzahl direkt an Kohlenstoff gebundener Wasserstoffatome abhängen.[5] T_1 von Dicyclopentadienen sind in Schema 1 zusammengefasst. Diese Ergebnisse unterstützen die oben erwähnten Zuordnungen der ^{13}C-chemischen Verschiebungen von Dimeren des Cyclopentadiens.

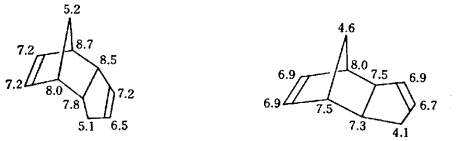

Schema 1. T_1 von Dimeren des Cyclopentadiens (in Sek).

*^{13}C-NMR-Spektren von Tricyclopentadienen **3** und **4**.*

Lässt man frisch destilliertes Cyclopentadien bei normaler Temperatur stehen, so erstarrt es zum *endo*-Dicyclopentadien, aber das *exo*-Dicyclopentadien tritt bei höherer Temperatur in Erscheinung.[1d] Die Angliederung des dritten Cyclopentadiens ist eine 1,4-Addition von Monomeren an die Norbornendoppelbindung oder Cyclopentendoppelbindung des *endo*- oder *exo*-Dicyclopentadiens (s. Tabelle 2). Unter den denkbaren 14 Isomeren sind 4 Isomere molekülmässig unwahrscheinlich.

Was die Norbornendoppelbindung betrifft, kommt man zu dem Schluss, dass Cyclopentadien in *exo*-Stellung addiert wird.[1d] Innerhalb der *exo*-Stellung bleibt noch die Entscheidung für die gegenseitige Lage der Brücken zu treffen. Diese Alternative zwischen *exo-endo*- und *exo-exo*-Addition von Cyclopentadien an die Norbornendoppelbindung wurde von Soloway,[6] Stille und Frey[7] und de Vries und Winstein[8] entschieden. Daher kann man sagen, dass *exo-endo*-Addukte **3** und **4** bevorzugt gebildet werden.[1f,1g]

Somit können die ^{13}C-Signale von Norbornanringen (C-3a, C-4, C-4a, C-8a, C-9, C-9a, und C-10) in **3** und **4** mit Hilfe von Schema 2 zugeordnet werden, wobei man Norbornenring als symmetrischen Substituenten betrachten kann und daher die ^{13}C-chemischen Verschiebungen des Norbornanringes in **3** oder **4** durch Norbornenring symmetrisch beeinflusst werden.

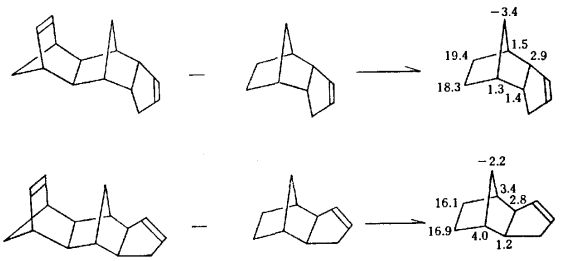

Schema 2. Einfluss von Norbornenring auf die ^{13}C-chemischen Verschiebungen Norbornanring in **3** order **4**.

TABELLE 2. DENKBARE TRICYCLOPENTADIENE

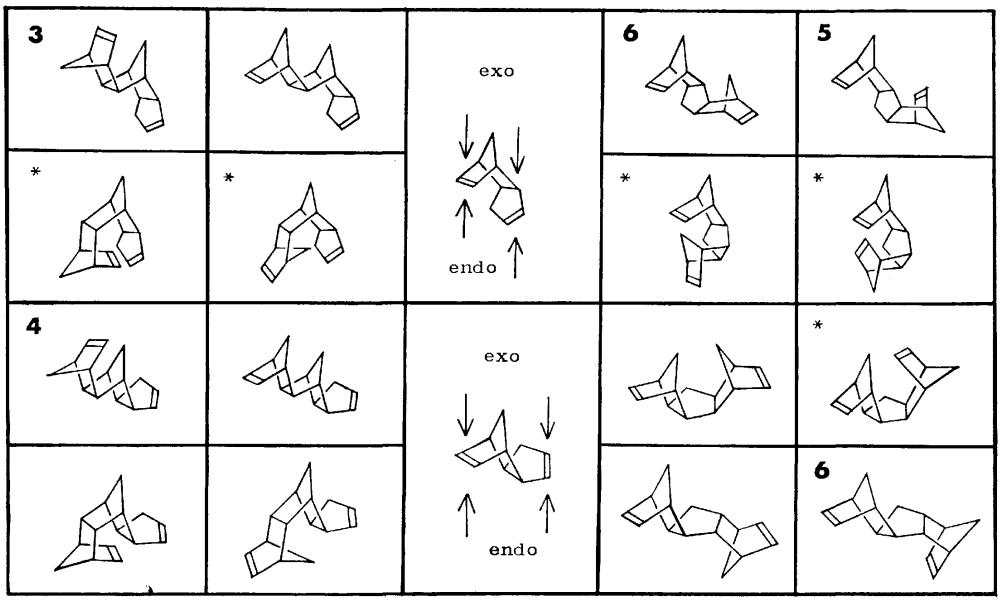

* Stereochemisch unmögliche Verbindungen.

Tabelle 3. ^{13}C-Chemische Verschiebungen (δ in ppm, $\delta_{TMS}=0$) und Multiplizitäten der tricyclopentadiene **3** und **4**

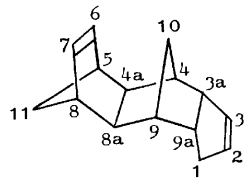

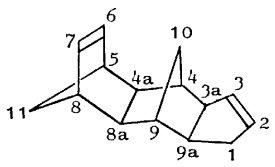

	3	**4**
C-1	31.3(t)	38.9(t)
C-2	132.0(d)	132.4(d)
C-3	131.2(d)	131.5(d)
C-3a	56.0(d)	58.8(d)
C-4	41.3(d)	42.4(d)
C-4a	44.8(d)	48.6(d)
C-5 oder C-8	46.9(d), 47.2(d)	46.6(d)
C-6 oder C-7	135.7(d), 136.3(d)	135.2(d), 135.4(d)
C-8a	40.4(d)	49.6(d)
C-9	42.7(d)	44.8(d)
C-9a	44.4(d)	46.6(d)
C-10	38.9(t)	26.8(t)
C-11	53.3(t)	53.2(t)

Andererseits können die ^{13}C-Signale von Norbornenringen (C-5, C-6, C-7, C-8, und C-11) durch Vergleich der ^{13}C-chemischen Verschiebungen von **1** und **2** zugeordnet werden. Die ^{13}C-Signale von Cyclopentenringen (C-1, C-2, und C-3) können durch Vergleich der Verbindungen **8** und **10** zugeordnet werden. Die Ergebnisse sind in Tabelle 3 zusammengefasst.

*^{1}H- und ^{13}C-NMR-Spektren von Tricyclopentadienen **5** und **6**.* Was die Addition des dritten Cyclopentadiens an die Cyclopentendoppelbindungen der Dimere betrifft, ist es bisher noch nicht möglich, zwischen der *endo-* und *exo-* Stellung zu entscheiden. Die Isolierung einheitlicher Isomere des Cyclopentadiens ist zwar mit Schwierigkeiten verbunden, aber doch ist es uns gelungen, zwei neue Isomere, **5** und **6**, neben **3** und **4** durch geeignete Variation der Versuchsbedingungen zu isolieren (s. exp. Teil).

Die Elementaranalysen und das in den Massenspektren von **5** und **6** beobachtete Auftreten eines Molekul-Ions bei $m/e=198$ weisen beide Verbindungen als Trimere des Cyclopentadiens aus. In den IR-Spektren von **5** und **6** treten C=C-Valenzschwingungen des Norbornenringes auf, aber keine C=C-Valenzschwingungen des Cyclopentenringes (s. Tabelle 4), was die folgende Tatsache zeigt, dass **5** und **6** zueinander Stereoisomere sind, die durch Addition von Cyclopentadien an Cyclopentendoppelbindungen der Dimere gebildet werden.

Dem Nachweis, dass die neuen Trimere im Verhältnis der Stereoisomere zueinander stehen, schliesst sich eine weitgehende Klärung der konfigurativen Verhältnisse an. Tabelle 5 bietet Daten für Zusammensetzung der Tricyclopentadiene bei der Reaktion von Cyclopentadien an *endo-* oder *exo*-Dicyclopentadien(s. exp. Teil). Da die Norbornendoppelbindung bei weitem reaktiver als die Cyclopentendoppelbindung ist, tritt Trimer **4** auf als Nebenprodukt bei der ersten Reaktion durch *exo-endo*-Addition von Cyclopentadien an Norbornendoppelbindung des *exo*-Dicyclopentadiens, das infolge der Isomerisierung des *endo*-Dicyclopentadiens entsteht, und tritt Trimer **3** auf als Nebenprodukt bei der zweiten Reaktion durch *exo-endo*-Addition von Cyclopentadien an Norbornendoppelbindung des *endo*-Dicyclopentadiens, das infolge der leichten Dimerisierung des Cyclopentadiens entsteht. Es ist bemerkenswert, dass kein Trimer **6** bei der ersten Reaktion nachgewiesen wird und dass kein Trimer **5** bei der zweiten Reaktion gefunden wird. Dieses Resultat führt zwangsläufig zu der Folgerung, dass Trimer **5** durch Addition von Cyclopentadien an Cyclopentendoppelbindung des *endo*-Dicyclopentadiens gebildet wird und dass Trimer **6** durch Addition von Cyclopentadien an Cyclopentendoppelbindung des *exo*-Dicyclopentadiens gebildet wird. Eine Fülle zusätzlicher Informationen steuern die NMR-Messungen bei.

Tabelle 4. Die charakteristischen Absorptionsbanden der IR-spektren von Tricyclopentadienen

Tricyclopentadiene	C=C (cm^{-1})	
	Norbornenring	Cyclopentenring
3	1570	1620
4	1570	1617
5	1568	—
6	1570	—

Tabelle 5. Die Zusammensetzung der Trimere bei der Reaktion von Cyclopentadien und *endo-* oder *exo*-Dicyclopentadien in Benzol (180 °C 1 Stde.)

Reaktionen	Zusammensetzung der Trimere (%)			
	3	**4**	**5**	**6**
Cyclopentadien + *endo*-Dicyclopentadien	66.8	16.0	17.2	0.0
Cyclopentadien + *exo*-Dicyclopentadien	14.6	74.5	0.0	10.9

Das ^{1}H-NMR-Spektrum von Tricyclopentadien **5** (s. Abb. 1) oder **6** (s. Abb. 2) weist ein oder zwei Multipletts für olefinische Protonen des Norbornenringes ($\delta=$ 5.65—6.10) und kein Multiplett für olefinische Protonen des Cyclopentenringes($\delta=5.20$—5.60) auf, was mit dem Ergebn s der Tabelle 4 übereinstimmt. Die olefinischen Protonen des Norbornenringes von **5** sind äquivalent und die von **6** sind nicht äquivalent. Somit kann man sagen, dass Trimer **5** die symmetrische Verbindung ist und dass Trimer **6** die asymmetrische Verbindung ist. Aus alledem ergibt sich, dass das symmetrische Trimer **5** durch *exo-endo*-Addition von Cyclopentadien an Cyclopentendoppelbindung des *endo*-Dicyclopentadiens gebildet wird und dass das asymmetrische Trimer **6** nicht durch *exo-endo*-Addition von Cyclopentadien an Cyclopentendoppelbindung des *endo*-Dicyclopentadiens ge-

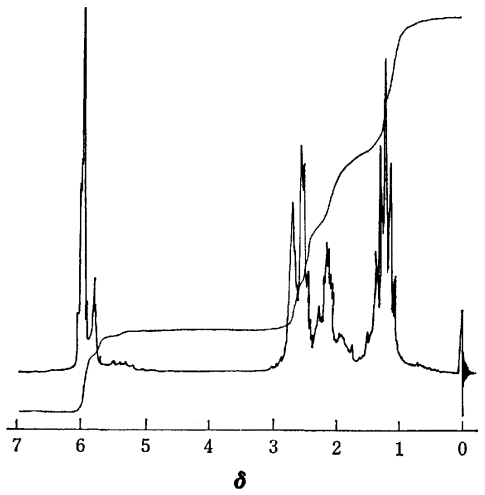

Abb. 1. 100 MHz ^{1}H-NMR-Spektrum von Tricyclopentadien **5** in CCl_4(Reinbeit; 80%).

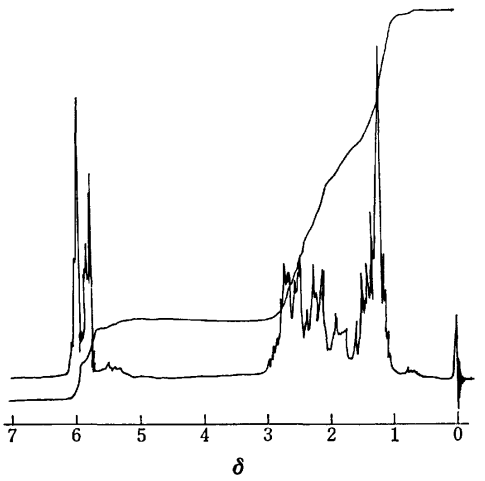

Abb. 2. 100 MHz ^{1}H-NMR-Spektrum von Tricyclopentadien **6** in CCl_4(Reinbeit; 71%).

bildet wird, sondern durch *endo-endo*-Addition von Cyclopentadien an Cyclopentendoppelbindung des *exo*-Dicyclopentadiens. Es ist schwer, die anderen Wasserstoffe, mit Ausnahme der Brücken-Methylene ($\delta = 1.05$—1.50), vollständig zuzuordnen, da die Signalgruppen überlappen.

Daher kann man nur sieben ^{13}C-Signale für die symmetrische Verbindung **5** erwarten. In der Tat beobachtet man sieben Signale im ^{13}C-NMR-Spektrum von **5**. Die Zuordnung der Signale von **5** ergibt sich, wenn man die Ergebnisse der Tabelle 1 und die Off-Resonance-Technik benutzt(s. Tabelle 6). Das ^{13}C-NMR-Spektrum der asymmetrischen Verbindung **6** weist die Existenzen von sp^2-Kohlenstoffatomen der *exo*- und *endo*-Norbornentypen und Brücken-Kohlenstoffatome der *exo*- und *endo*-Norbornentypen auf(s. Tabelle 6), was mit der Struktur **6** in Tabelle 2 übereinstimmt. In diesem Fall sind die unsicheren Zuordnungen von C-1, C-4, C-4a usw. kein grosses Problem. Die in dieser Arbeit angegebenen Zuordnungen der ^{13}C-NMR-Spektren von thermischen Oligomeren des Cyclopentadiens werden nach Einführungen von Deuterium und anderen Substituenten festgestellt werden.

TABELLE 6. ^{13}C-CHEMISCHE VERSCHIEBUNGEN (δ IN ppm, $\delta_{TMS} = 0$) UND MULTIPLIZITÄTEN DER TRICYCLOPENTADIENE **5** UND **6**

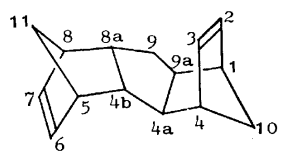

5

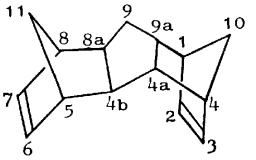

6

C-1, C-4	47.6(d)	C-2 oder C-3	135.6(d) oder 136.3(d)
C-5, C-8			
C-2, C-7	136.5(d) oder 136.8(d)	C-6 oder C-7	137.0(d) oder 137.2(d)
C-3, C-6			
C-4a, C-4b	52.9(d) oder 53.1(d)	C-9	34.2(t)
C-8a, C-9a		C-10	50.9(t)
C-9	32.9(t)	C-11	43.4(t)
C-10, C-11	51.9(t)	C-1, C-4, C-4a, C-4b, C-5, C-8, C-8a, C-9a	47.8, 48.6, 48.7, 49.3, 50.5, 51.0, 51.5, 52.1

Angesichts der vielen theoretischen Möglichkeiten der Tricyclopentadiene ist es besonders auffällig, dass nur vier Vertreter bekannt sind. Offenbar findet bei der Bildung der Tricyclopentadiene eine weitgehende Stereoauslese statt. Da sich in ähnlicher Weise Argumente für die Konstitution der höheren Oligomere des Cyclopentadiens beibringen lassen, bilden dieso Ergebnisse den Schlüssel für das Verständnis des Aufbaues der ganzen oligomeren Reihe.

Experimenteller Teil

Die Aufnahme der ^{1}H-NMR-Spektren erfolgte mit einem JEOL-Gerät PS-100 in CCl_4(TMS als innerer Standard), während die Massenspektren mit LEOL-Gerät JMS-OlSG aufgenommen wurden(75 eV). Die IR-Spektren wurden mit einem Shimadzu-Gerät IR-27G aufgenommen. Zur Aufnahme der Puls-Fourier-Transform-^{13}C-NMR-Spektren diente ein JPS-EC-100 von JEOL-Gerät mit einer Messfrequenz von 25.15 MHz, wobei die Reproduzierbarkeit der ^{13}C-chemischen Verschiebungen ± 0.05 ppm beträgt. Alle Substanzen wurden als 50%-ige Lösungen in $CDCl_3$ gemessen(TMS als innerer Standard). Das Deuteriumsignal des Lösungsmittels diente als Lock(Lockfrequenz 15.36 MHz). Die FT-^{13}C-NMR-Spektren wurden unter Akkumulation von 200 Pulsinterferogrammen bei einer Pulsbreite von 12.5 μsek(Pulswinkel 45°) und einem Pulsintervall von 6 sek durch Fourier-Transformation des akkumulierten Interferogramms mit einem JEC-6-Rechner erhalten(Spektrumbreite 5 kHz; Datenpunkte 16382). Die in den Tabellen 1, 3, und 6 angegebenen Multiplizitäten berhen auf Off-Resonance-Technik. Die Messung von T_1 beruhte auf Inversion-Wiederherstellung-^{13}C-Experimenten (180°-t-90°), wobei ein JEOL-Auto-T_1-Programm verwendet wurde. Die Genauigkeit von T_1 beträgt ± 0.7 sek.

Darstellung und Isolierung der Verbindungen 1—6. Dimer **1** wurde durch Dimerisierung des Cyclopentadiens, das durch thermische Zersetzung des verkäuflichen *endo*-Dicyclopentadiens gewonnen wurde[9], bei Zimmertemperatur gewon-

nen, während Dimer **2** nach der Methode von Bartlett und Goldstein gewonnen wurde.[10] Trimere **3**—**6** wurden auf folgende Weise gewonnen. Frisch destilliertes Cyclopentadien wurde unter N_2 im Autoklaven 5 Stdn. auf 150 °C erhitzt. Nach der Entfernung des Dicyclopentadiens wurde das Produktgemisch durch Behandeln mit siedendem Methylalkohol, in dem Tetracyclopentadien und die höheren Oligomere unlöslich sind, von dem Tricyclopentadien völlig befreit.[1b] Nach dem Umkristallisieren aus Methylalkohol erhielt man Trimer **3** (*m/e* 198, 132, 66). Durch Rektifikation der Mutterlauge erhielt man Trimer **5** ($C_{15}H_{18}$, Ber. C, 91.0; H, 9.0%. Gef. C, 90.9; H, 9.1%. *m/e* 198, 132, 66). Äquimolare Mengen frisch destillierten Cyclopentadiens und Dimer **2** wurden unter N_2 im Autoklaven 2 Stdn. auf 250 °C erhitzt. Durch Umkristallisieren aus Methylalkohol und Rektifikation der Mutterlauge erhielt man Trimere **4** und **6** (Gef. C, 91.1; H, 8.9%. *m/e* 198, 132, 66).

Darstellung der Verbindungen ***7***—***11***. α-1-Hydroxy-dicyclopentadien **7** wurde nach der Methode von Rosenblum gewonnen.[11] 5,6-Dihydro-dicyclopentadien **8** oder **10** wurde durch Hydrierung der Norbornendoppelbindung von **1** oder **2** mittels Raney-Nickel-Katalysators bei Zimmertemperatur unter Wasserstoffdruck von 140 kg/cm² gewonnen. 2,3,5,6-Tetrahydro-dicyclopentadien **9** oder **11** wurde durch Hydrierung der Cyclopentendoppelbindung von **8** oder **10** mittels Raney-Nickel-Katalysators bei 150 °C unter Wasserstoffdruck von 140 kg/cm² gewonnen. Alle diese Verbindungen wurden mit Hilfe von ^{1}H-NMR-Spektren bestätigt.

Reaktion von Cyclopentadien und endo- *oder exo-Dicyclopentadien.* Äquimolare Mengen(5×10^{-2} Mol) frisch destillierten Cyclopentadiens und *endo*- oder *exo*-Dicyclopentadien wurden in 160 ml Benzol unter N_2 im 300 ml Autoklaven 1 Std. auf 180 °C erhitzt. In dieser Reaktionsbedingung waren Ausbeuten von Trimeren 2—3% und wurden keine weiteren Oligomere des Cyclopentadiens nachgewiesen. Gaschromatographische Bestimmung des Mengenverhältnisses der Isomere des Tricyclopentadiens erfolgte mit einem Shimazu-Gerät GC-3AF mit Flammenionisationsdetektor; Säulenfüllung: PEG 6000 10 wt%; Säulendimension: 3 mm$\phi \times$ 3 m; Trägergas: N_2.

Literatur

1) z.B. a) H. Staudinger und A. Rheiner, *Helv. Chim. Acta*, **7**, 23 (1924); b) H. Staudinger und H. A. Bruson, *Liebigs Ann. Chem.*, **447**, 97 (1926); c) K. Alder und G. Stein, *ibid.*, **485**, 211, 228 (1931); d) *idem.*, *Angew. Chem.*, **52**, 837 (1934); e) B. Raistrick, R. H. Sapiro und D. M. Newitt, *J. Chem. Soc.*, **1939**, 1761; f) R. G. Foster und M. C. Mclvor, *J. Chem. Soc., B*, 188 (1969); g) S. Tsuchida, S. Hamanaka, und M. Ogawa, *J. Japan Petrol. Inst.*, **15**, 159 (1972).

2) L. F. Johnson und W. C. Jankowski, Carbon-13 NMR Spectra, Wiley, New York (1967), S. 372.

3) J. D. Roberts, F. J. Weigert, J. I. Kroschwitz und H. J. Reich, *J. Am. Chem., Soc.* **92**, 1338 (1970).

4) J. B. Grutzner, M. Jautelat, J. B. Dence, R. A. Smith, J. D. Roberts, *J. Am. Chem. Soc.*, **92**, 7107 (1970).

5) K. F. Kuhlmann, D. M. Grant und P. K. Harris, *J. Chem. Phys.*, **52**, 3439 (1970).

6) S. B. Soloway, *J. Am. Chem. Soc.*, **74**, 1027 (1952).

7) J. K. Stille und D. A. Frey, *J. Am. Chem. Soc.*, **81**, 4273 (1959).

8) L. de Vries und S. Winstein, *J. Am. Chem. Soc.* **82**, 5363 (1960).

9) *Org. Synth.*, **32**, 41 (1952).

10) P. D. Bartlett und S. Goldstein, *J. Am. Chem. Soc.*, **69**, 2553 (1947).

11) M. Rosenblum, *J. Am. Chem. Soc.*, **79**, 3179 (1957).

Photolytic Oxidation of Alkylbenzenesulfonic Acids by Aqueous Sodium Hypochlorite[1]

Masao NAKAMURA and Yoshiro OGATA*

Department of Applied Chemistry, Faculty of Engineering, Nagoya University, Chikusa-ku, Nagoya 464

(Received December 4, 1976)

Photolyses of alkylbenzenesulfonic acids, such as benzene-, *p*-toluene-, and *p*-ethylbenzenesulfonic acids, in aqueous solution by sodium hypochlorite have been studied. In the presence of a large excess of hypochlorite, benzenesulfonic acid is completely photolyzed to give carbon dioxide and sulfuric acid. Irradiation of an equimolar mixture of substrate and hypochlorite in an aqueous solution yields the corresponding alkylbenzene, alkylphenol, arylalkyl alcohol and arylalkylaldehyde, some of which may be produced by an attack of the oxidant on alkyl chain. In some cases, small amounts of diaryl sulfones and chlorinated compounds are also detected.

Interest has recently centered on the decontamination of surfactants, sodium alkylbenzenesulfonate in particular, from waste water. Practically, the removal of surfactants has been done by biochemical or physical (*e.g.* adsorption) methods and sometimes by irradiation of sunlight or ultraviolet light in the presence of oxygen or appropriate oxidizing agents such as alkali hypochlorite and hydrogen peroxide. However, these methods are often insufficient for certain surfactants.

Matsuura and Smith[2,3] reported from kinetic and product analysis (GLC) studies that the photochemical autoxidation of aqueous alkali dodecylbenzenesulfonate (DBS) gives products containing formaldehyde, formic acid and acetaldehyde, which are finally oxidized to CO_2. On the other hand, a loss of surface activity of some surfactants by hypohalite on UV irradiation was observed.[4]

Recently, an effective industrial process[5] was developed for the photo-oxidative removal of several organic contaminants in waste water by aqueous alkali hypochlorite in excess, by which most organic materials are completely decomposed into CO_2, HCl and H_2O. Decontamination of organic compounds in waste water was accomplished by the combined use of irradiation with UV light in the presence of Cl gas or hypochlorite and activated sludge treatment.[6]

However, there is no detailed information on the intermediary products and reaction mechanism for the hypohalite oxidation. Some products might cause secondary pollution. We have examined the intermediary products and mechanism for the UV photolyses of anionic surfactants by aqueous sodium hypochlorite. As model compounds of alkylbenzenesulfonate type surfactants, simple sulfonates such as benzene-, *p*-toluene-, and *p*-ethylbenzenesulfonic acids were chosen. They were photolyzed under conditions of short irradiation time and a nearly equivalent amount of sodium hypochlorite. Analyses were carried out by means of GLC-mass spectra along with a comparison of the retention times of products with those of authentic samples by GLC.

Experimental

Gas chromatograms were recorded with a Yanagimoto Model GCG550 chromatograph employing a flame ionization detector and a 1.5 m × 3 mm copper column packed with Silicone OV17 5% on Celite. The mass spectra were measured with a Shimadzu Model GCMS-7000 mass spectrometer.

Materials. *Sodium Hypochlorite*: The aqueous solution of sodium hypochlorite was prepared as follows. Gaseous chlorine was bubbled into an aqueous 1 M-NaOH with ice-cooling, and the sodium chloride precipitated was filtered off. The solution can be stored for severl days in a refrigerator. The concentration was determined by iodometry before use.

Alkylbenzenesulfonic Acids: All the alkylbenzenesulfonic acids were commercial products of the best grade.

Irradiation of Benzenesulfomic Acid. A mixture of benzenesulfonic acid (0.099 M), aqueous sodium hypochlorite (0.103 M), and 1 M-NaOH solution (100 ml) were diluted with distilled water until the total volume became 400 ml. The solution was degassed with nitrogen and irradiated by quartz-filtered UV light employing a 300 W high pressure mercury lamp, nitrogen being bubbled at room temperature. Irradiation was stopped before complete disappearance of sodium hypochlorite. After irradiation, the excess sodium hypochlorite was removed with sodium sulfite, the aqueous solution being extracted with 100 ml ether. The aqueous layer was acidified to pH 2—3 with HCl and again extracted with 100 ml ether. The combined extracts, after being dried over anhydrous sodium sulfate, were concentrated, and then analyzed by means of GLC and GLC-mass spectrometry. The work-up for other alkylbenzenesulfonic acids is similar to that mentioned above.

Estimation of Evolved Carbon Dioxide. Carbon dioxide produced by photolysis was kept absorbed in the aqueous alkaline solution. The solution was acidified with sulfuric acid, carbon dioxide being expelled by N_2 stream from the reaction mixture. The CO_2 evolved was absorbed by aqueous 0.05 M-$Ba(OH)_2$ and determined by titration with 0.1 M-HCl.

Estimation of Sulfate Ion. Analysis of sulfate ion in the products was achieved gravimetrically by adding excess aqueous barium chloride to the acidified reaction mixture, barium sulfate precipitated being weighed.

Results and Discussion

Irradiation of an aqueous solution of benzenesulfonic acid in the presence of a 20-fold equivalent of sodium hypochlorite gives, after complete disappearance of hypochlorite, carbon dioxide and sulfate, their yields by photolysis being 95.7 and 83.5%, respectively. Benzenesulfonic acid is decomposed almost completely to give CO_2 and inorganic materials.

In the photolysis of an equimolar mixture of benzene-

* To whom all correspondence should be addressed.

sulfonate and hypochlorite by means of quartz-filtered UV light (>180 nm) for a short time, the yield of CO_2 was only *ca.* 3%. The organic products extracted with ether are given in Table 1. The products were identified by direct comparison of the GLC peaks with those of the authentic samples and also the parent ion peak and its pattern of fragmentation in mass spectra. Crystals of mp 128.5—129° C (lit, mp 128—129 °C) were isolated by condensation of the ether extract, and identified by GLC using three different columns (Silicone OV17 5% on Celite, Apiezon grease L 3% on Celite and PEG 20M 10% on Chromosorb) as diphenyl sulfone.

Table 1. Partial mass spectra of photo-oxidation products of benzensulfonic acid[a)]

Parent ion peak *m/e*	Fragment ion peak	Compound	Relative mole ratio
94	66 65 55 39	Phenol	1
154	153 152 115 77 76 64 51	Biphenyl	0.01
218	152 125 97 77 51	Diphenyl sulfone	0.06

a) Initial concentration: $PhSO_3H$ 247.5 mM, NaOCl 257.5 mM; pH≈11; room temperature. Conversion of $PhSO_3H$ into products was *ca.* 8%.

Table 2. Partial mass spectra of photo-oxidation products of *p*-toluenesulfonic acid[a)]

Parent ion peak *m/e*	Fragment ion peak	Compound	Relative mole ratio
92	91 65 63 51 50 39	Toluene	1
106	105 78 77 51	Benzaldehyde	0.16
108	107 91 79 77	Benzyl alcohol	2.18
108	107 91 90 79 77 53 51	*p*-Cresol	0.42

a) Initial concentration: *p*-toluenesulfonic acid 25.0 mM, NaOCl 31.2 mM; pH≈11; room temperature. Conversion of toluenesulfonic acid into products was *ca.* 10%.

Table 3. Partial mass spectra of photo-oxidation products of *p*-ethylbenesulfonic acid[a)]

Parent ion peak *m/e*	Fragment ion peak	Compound	Relative mole ratio
106	91 79 78 77 65 51	Ethyl-bennzene	1
94	66 65 55 39	Phenol	0.18
122	107 91 79 77 51 43	1-Phenyl-ethanol	0.41
120	105 91 77 51 43	Acetophenone	3.26
122	107 91 79 77 51 39	2-Phenyl-ethanol	5.97
122	107 94 91 77 39	*p*-Ethylphenol	2.15

a) Initial concentration: *p*-ethylbenzenesulfonic acid 23.0 mM, NaOCl 22.5 mM; pH≈11; room temperature. Conversion of ethylbenzenesulfonic acid into products was *ca.* 7%.

The results of photolysis of *p*-toluene- and *p*-ethylbenzenesulfonate, with equimolar hypochlorite by quartz-filtered light, are given in Tables 2 and 3, respectively. Reports[7)] on mass spectrometry are cited for identification of the products.

The photolytic oxidation of alkylbenzenesulfonic acid with hypochlorite gives rise mainly to alkylbenzene, alkylphenol, arylakyl alcohol, and arylalkyl aldehyde. Small amounts of chlorinated compounds such as monochlorophenols were also detected.

Typical conversion curves for the photodecomposition of aqueous sodium hypochlorite in the presence and absence of benzenesulfonic acid are shown in Fig. 1. Decomposition is rather fast with light of over 180 nm, and is accelerated by the addition of benzenesulfonic acid which probably acts as a sensitizer.

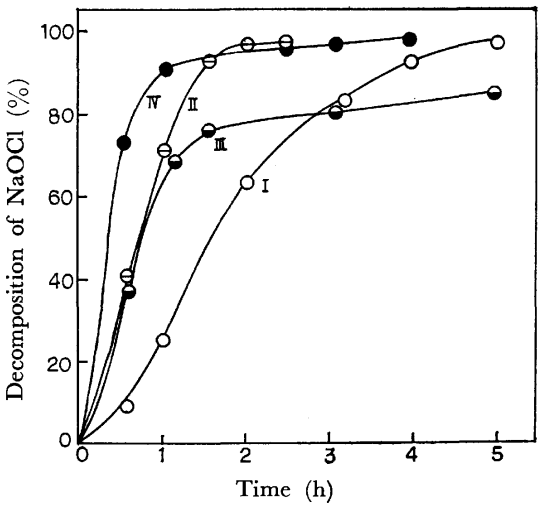

Fig. 1. Photodecomposition of aqueous sodium hypochlorite at room temperature and pH≈11 in the presence and absence of $PhSO_3H$.

Curve	Initial concentration (mM) NaOCl	Initial concentration (mM) $C_6H_5SO_3H$	Light
I	89.5	0	>300 nm
II	89.5	0	>180 nm
III	83.4	84.2	>300 nm
IV	102.7	98.8	>180 nm

The photodecomposition of aqueous hypochlorite has been studied, but the overall mechanism of photochemical decomposition does not seem to have been clarified. Earlier workers[8)] showed that the products of the photolysis of aqueous hypochlorite are oxygen, chloride and chlorate ions and that the amount of decomposed hypohalite is proportional to the light energy absorbed. Recently, Buxton and Subhani[9)] demonstrated with flash photolysis technique that the primary products of the photolysis of hypochlorite ion at 365 nm are O (triplet oxygen atom), O^-, Cl, and Cl^- and that, at 313 and 253.7 nm, O (singlet oxygen atom) and Cl^- are also produced. The stoichiometry is expressed as follows.

$$ClO^- \xrightarrow{h\nu} Cl^- + O\ (^3P) \quad (1a)$$
$$ClO^- \xrightarrow{h\nu} Cl + O^- \quad (1b)$$
$$ClO^- \xrightarrow{h\nu} Cl^- + O\ (^1D). \quad (1c)$$

We employed quartz-filtered light (>180 nm) for *p*-ethylbenzenesulfonic acid in which non-selective oxidation on α- and β-carbon atoms of alkyl chain with little chlorination was observed (Table 3). Thus, the photo-oxidation should proceed mostly by an attack of oxygen atom produced from hypochlorite by the above mechanism (1a and 1c) to give the observed products.

A probable mechanism for an initial stage in the photolysis is as follows (R: H, *p*-Me, *p*-Et).

$$RC_6H_4SO_3H \xrightarrow{h\nu} RC_6H_4\cdot + \cdot SO_3H, \quad (1)$$
$$\cdot SO_3H \xrightarrow{h\nu} SO_2 + \cdot OH, \quad (2)$$
$$SO_2 + O + H_2O \xrightarrow{h\nu} H_2SO_4. \quad (3)$$

Formation of sulfur dioxide from benzenesulfonic acid (Eqs. 1 and 2) was confirmed by the Fuchsine test for the photolysis of aqueous benzenesulfonic acid alone. As regards Eq. 3, we have reported on the photo-oxidation of aqueous sulfur dioxide to sulfuric acid with H_2O_2 and O_2.[10] There are other reports[11] which support this kind of photo-oxidation.

The aryl and hydroxyl radicals produced might undergo reactions as follows in view of the observed products.

1) Phenyl radical:

$$Ph\cdot + \cdot OH \longrightarrow PhOH, \quad (4)$$
$$2Ph\cdot \longrightarrow Ph\text{-}Ph. \quad (5)$$

2) *p*-Tolyl radical:

$$\cdot C_6H_4CH_3 \longrightarrow C_6H_5CH_2\cdot, \quad (6)$$
$$C_6H_5CH_2\cdot + \cdot OH \longrightarrow C_6H_5CH_2OH, \quad (7)$$
$$\cdot C_6H_4CH_3 \text{ (or } C_6H_5CH_2\cdot \text{ or another radical)} + C_6H_5CH_2OH \longrightarrow C_6H_5CH_3 \text{ (etc.)} + C_6H_6\dot{C}HOH, \quad (8)$$
$$C_6H_5\dot{C}HOH + O \longrightarrow C_6H_5CHO + \cdot OH, \quad (9)$$
$$\cdot C_6H_4CH_3 + \cdot OH \longrightarrow HOC_6H_4CH_3. \quad (10)$$

3) *p*-Ethylphenyl radical:

$$\cdot C_6H_4CH_2CH_3 \longrightarrow C_6H_5\dot{C}HCH_3, \quad (11)$$
$$\cdot C_6H_4CH_2CH_3 \longrightarrow C_6H_5CH_2CH_2\cdot, \quad (12)$$
$$C_6H_5\dot{C}HCH_3 + \cdot OH \longrightarrow C_6H_5CH(OH)CH_3, \quad (13)$$
$$C_6H_5CH_2CH_2\cdot + \cdot OH \longrightarrow C_6H_5CH_2CH_2OH, \quad (14)$$
$$\cdot C_6H_4CH_2CH_3 + SH \longrightarrow C_6H_5CH_2CH_3 + S\cdot, \quad (15)$$
$$C_6H_5\dot{C}HCH_3 + SH \longrightarrow C_6H_5CH_2CH_3 + S\cdot, \quad (16)$$
$$C_6H_5CH_2CH_2\cdot + SH \longrightarrow C_6H_5CH_2CH_3 + S\cdot, \quad (17)$$
(SH: $C_6H_5CH(OH)CH_3$, $C_6H_5CH_2CH_2OH$)
$$S\cdot + O \longrightarrow C_6H_5COCH_3 \text{ or } C_6H_5CH_2CHO, \quad (18)$$
$$\cdot C_6H_4CH_2CH_3 + \cdot OH \longrightarrow HOC_6H_4CH_2CH_3. \quad (19)$$

The aryl radical, $RC_6H_4\cdot$, produced might abstract a hydrogen atom from its own alkyl chain to give aryl-alkyl radical *via* successive internal *o*- and *m*-H atom shifts (Eqs. 6, 11, and 12), giving alcohols and carbonyl compounds. Aryl radical can also abstract a hydrogen atom from another molecule to give alkylbenzene (Eqs. 8 and 15), but the yield is very low and the contribution of intermolecular H-atom abstraction seems to be small. Polymerization of aryl radical might be impossible in consideration of the absence of $(-C_6H_4-R)_2$ except biphenyl. The product distribution shows that the H-abstraction is preferable to coupling of $RC_6H_4\cdot$ with hydroxyl radical to form alkylphenol. The absence of products formed by chlorine addition to radicals or by chlorination of the side chain suggests that the hydrogen abstraction by Cl· is unimportant. Higher yields of *p*-alkylphenol than *o*- and *m*-substituted phenols may be due to the greater resonance stability of *p*-$RC_6H_4\cdot$ radical. The higher yield of $PhCH_2CH_2OH$ than $PhCH(OH)CH_3$ is of interest, since the radical stability in the latter is greater. This suggests that the attack of ·OH on these arylalkyl radicals is very fast, giving a statistical distribution of the OH position of alcohols. The unsubstituted phenol formation, though small, from ethylbenzenesulfonate but not from toluenesulfonate implies easier elimination of the larger alkyl chain to give the phenyl radical.

There are reports stating that (i) benzyl phenyl sulfone can be formed by coupling of benzyl and phenylsulfonyl radicals produced from phenyl radical and SO_2[12] and (ii) the ESR evidence of methylsulfonyl radical photochemically formed from methyl radical and SO_2.[13] The results suggest the following mechanism for this diaryl sulfone formation.

$$Ph\cdot + SO_2 \xrightarrow{h\nu} PhSO_2\cdot, \quad (20)^{14}$$
$$\text{(or } PhSO_3H \xrightarrow{h\nu} \cdot PhSO_2\cdot + \cdot OH), \quad (21)$$
$$PhSO_2\cdot + \cdot Ph \longrightarrow PhSO_2Ph, \quad (22)$$
$$Ph\cdot + PhSO_3H \longrightarrow PhSO_2Ph + \cdot OH, \quad (23)$$
$$PhSO_2\cdot + PhSO_3H \longrightarrow PhSO_2Ph + \cdot SO_3H. \quad (24)$$

The phenol produced might subsequently be chlorinated to give mono- and di-chlorinated phenols. In fact, mono- and di-chlorophenols were formed on irradiation of a mixture of phenol and aqueous sodium hypochlorite (Table 4). However, the poor yield of chlorinated phenol in the photo-oxidation of alkylbenzenesulfonate shows that an attack of Cl species is not important.

We found that the photo-oxidation by aqueous hypochlorite proceeds even by Pyrex-filtered light (>300

Table 4. Partial mass spectra of photo-oxidation products of phenol[a]

Parent ion peak *m/e*	Fragment ion peak	Compound	Relative mole ratio
128	130 95 94 66 65 55 39	Monochloro-phenols	1
162	166 164 94 66 65	Dichloro-phenols	0.08

a) Initial concentration: phenol 49.6 mM, NaOCl 46.0 mM; pH≈11; room temperature.

nm), where a grater variety of products were observed, since the substrate cannot be excited and thus only a random attack of oxygen atom predominates. In photo-oxidation employing a Pyrex filter, slightly larger amounts of various chlorinated compounds were also detected. An attack of Cl· on the unexcited substrate might become significant in this case.

This work was supported by a Grant-in-Aid for Science Research from the Ministry of Education (No. 147078).

References

1) Contribution No. 228.

2) T. Matsuura and J. M. Smith, *Ind. Eng. Chem., Fundam.*, **9**, 252 (1960).

3) T. Matsuura and J. M. Smith, *Ind. Eng. Chem., Fundam.*, **10**, 316 (1971).

4) K. E. Conroe, I. Kaplan, J. S. Roscoe, and S. I. Trotz, Water & Sewage Works, **113**, 237 (1966).

5) Y. Kojima, *PPM*, 42 (1973).

6) S. Arai, K. Taguchi, and M. Fukuhira, Japan Open Patent 7444553; *Chem. Abstr.*, **81**, 96142u (1974).

7) a) J. H. Beynon, G. R. Lester, and A. E. Williams, *J. Phys. Chem.*, **63**, 1861 (1959); b) T. Aczel and H. E. Lumpkin, *Anal. Chem.*, **32**, 1819 (1960); c) S. Meyerson and P. N. Rylander, *J. Am. Chem. Soc.*, **79**, 1058 (1957); d) S. Meyerson, P. N. Rylander, E. L. Eliel, and J. D. McCollum, *ibid.*, **81**, 2606 (1959); e) E. L. Eliel, J. D. McCollum, S. Meyerson, and P. N. Rylander, *ibid.*, **83**, 2481 (1961); f) J. D. McCollum and S. Meyerson, *ibid.*, **85**, 1739 (1963); g) S. Meyerson, H. Drews, and E. K. Fields, *Anal. Chem.*, **36**, 1294 (1964).

8) a) W. C. Lewis, *J. Chem. Soc.*, **1912**, 2371; b) L. Spencer, *ibid.*, **1914**, 2565; c) A. J. Allmand, P. W. Cunliffe, and R. E. Maddison, *ibid.*, **1928**, 655; d) K. W. Young and A. J. Allmand, *Can. J. Res.*, **27B**, 318 (1949).

9) a) G. V. Buxton and M. S. Subhani, *J. Chem. Soc., Faraday Trans. 1*, **68**, 947 (1972); b) G. V. Buxton and M. S. Subhani, *ibid.*, **68**, 958 (1972).

10) Y. Ogata, K. Takagi, and S. Yamada, *Bull. Chem. Soc. Jpn.*, **50**, 2183 (1977).

11) a) R. A. Cox and S. A. Peukett, *Amtos. Environ.*, **4**, 425 (1970); *Chem. Abstr.*, **74**, 6224a (1971); b) R. A. Cox, *J. Aerosol Sci.*, **4**, 473 (1973); *Chem. Abstr.*, **80**, 87052s (1974); c) J. P. Friend, R. Leifer, and M. Trichon, *J. Atmos. Sci.*, **30**, 465 (1973); *Chem. Abstr.*, **78**, 149878k (1973).

12) J. M. Squire and W. A. Waters, *J. Chem. Soc.*, **1962**, 2068.

13) T. Kawamura, P. J. Krusic, and J. K. Kochi, *Tetrahedron Lett.*, **1972**, 4075.

14) Equation 20 is supported by several authors in the sulfoxidation of saturated carbons, *e.g.*, L. Orthner, *Angew. Chem.*, **62**, 302 (1950); R. Graf, *Ann. Chem.*, **578**, 50 (1952); Y. Ogata *et al.*, *Tetrahedron*, **21**, 1349 (1965).

Coenzyme Models. IX. Micellar Catalysis of Isoalloxazine (Flavin) Oxidation of Dithiol*

Seiji SHINKAI and Toyoki KUNITAKE

Department of Organic Synthesis, Faculty of Engineering, Kyushu University, Fukuoka 812

(Received January 31, 1977)

The influence of micelles on the reaction of isoalloxazines and 1,4-butanedithiol(BDT) was studied. The pK_a of BDT was lowered by 0.3 pK unit in the presence of the hexadecyltrimethylammonium bromide(CTAB) micelle, indicating the formation of "hydrophobic ion pairs." The apparent second-order rate constant for the reaction of 3-methyl-10-ethylisoalloxazine and BDT increased by 18-fold on addition of CTAB(3 mM). The UV-visible spectrum of 3-hexadecyl-10-butylisoalloxazine in the presence of the CTAB micelle was similar to that in organic solvents, the rate being enhanced by more than 400-fold as compared with that in a nonmicellar system. Anionic(SDS) and nonionic(Brij-35) micelles suppressed the reaction. The results show that the flavin oxidation of dithiol is facilitated by the environments of the CTAB micelle.

Reduction of flavins by dihydrolipoic acid is one of the interesting oxidation-reduction reactions catalyzed by flavoenzymes(*e.g.*, lipoamide dehydrogenase). Gascoigne and Radda[1] found that dihydrolipoic acid reacts with flavins in the absence of enzyme to produce lipoic acid and reduced flavins(Eq. 1). The subsequent examination established the fact that flavin oxidation of dithiol is of first-order in dithiol concentration and buffer-catalyzed, while that of monothiol is of second-order in monothiol concentration, not being subjected to buffer-catalysis.[2-4]

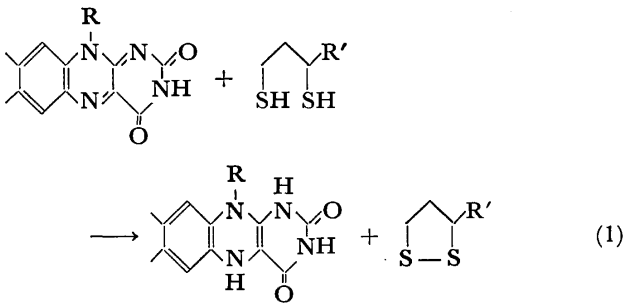

(1)

We have found that the reactivity of some coenzymes and their model compounds are markedly affected by the microenvironments of micelles and polysoaps.[5-7] This is of interest from the viewpoint that the reactivity of coenzymes must a priori be very susceptible to the microenvironments of apoenzymes. In particular, the nucleophilic reactivity of some anions (including thiolate anions such as glutathione and coenzyme A) is drastically enhanced in the presence of the cationic hydrophobic aggregates.[7,8] This unusual activation of anions is conceivably derived from the formation of a "hydrophobic ion pair" between the surfactant cation and the anionic nucleophile.[9,10] Since flavins are reduced by dissociated species of dithiol,[1-3] it occurred to us that the efficiency of this biologically important reaction would be markedly affected by the hydrophobic environment.

In this paper, we wish to report on the micellar effect on the reaction of isoalloxazines and 1,4-butanedithiol(BDT: an analogue of dihydrolipoic acid). Isoalloxazines chosen are 3-methyl-10-ethylisoalloxazine(**1**) and 3-hexadecyl-10-butylisoalloxazine(**2**).

* Contribution No. 418 from this department.

Isoalloxazine:

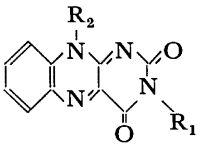

(**1**) $R_1=CH_3-$, $R_2=CH_3CH_2-$

(**2**) $R_1=CH_3(CH_2)_{15}-$, $R_2=CH_3(CH_2)_3-$

Surfactant:

CTAB, $CH_3(CH_2)_{15}N^+(CH_3)_3Br^-$

SDS, $CH_3(CH_2)_{11}OSO_3Na$

Brij-35, $CH_3(CH_2)_{11}(CH_2CH_2O)_{23}OH$

Experimental

Materials. 3-Methyl-10-ethylisoalloxazine(**1**) and 10-butylisoalloxazine were supplied by Professor F. Yoneda(for preparation, *cf.* Ref. 11). 3-Hexadecyl-10-butylisoalloxazine was obtained by treating 10-butylisoalloxazine(130 mg: 0.5 mmol) with hexadecyl iodide(176 mg: 0.5 mmol) at room temperature in *N,N*-dimethylformamide containing excess powdered K_2CO_3(500 mg). The progress of the reaction was monitored by the TLC method (silica gel–ethyl acetate). The insoluble parts were filtered off after two days, and the solvent was evaporated *in vacuo*. The residual brown oil was extracted with carbon tetrachloride, the extract being washed with an aqueous solution of 0.1 M NaOH and water, dried over anhydrous K_2SO_4. The reaction mixture was concentrated to dryness, and the yellow residue was recrystallized from ethanol–acetonitrile; mp 77—80 °C. Found: C, 72.15; H, 9.44; N, 10.98%. Calcd for $C_{30}H_{46}N_4O_2$: C, 72.83; H, 9.37; N, 11.33%.

1,4-Butanedithiol was distilled under N_2 stream before use: bp 98—102 °C/17 mmHg (lit,[12] bp 74.5 °C/10 mmHg). Hexadecyltrimethylammonium bromide was recrystallized from ethanol before use, and other surfactants(sodium dodecylsulfate, Brij-35) were used without further purification.

Titration of 1,4-Butanedithiol. The spectrophotometric titration was carried out under anaerobic conditions with a Thunberg cuvette. Absorbance at 240 nm(thiolate anion) was chosen. The detailed procedure has been described.[7,13]

Kinetics. All the kinetic measurements were carried out anaerobically at 30±0.1 °C at a calculated ionic strength (μ=0.06 with KCl) unless otherwise stated. The reactions were followed spectrophotometrically by monitoring the reduction of isoalloxazine (λ_{max}, 433 nm for **1** and 440 nm for **2**). The stock solution of BDT was prepared in ethanol just before the experiment. Since excess BDT was present in all the cases, the pseudo first-order behavior was observed. The pH of the reaction mixture was confirmed

not to vary from pH measurements (TOA Digital pH Meter, Model HM-15A) before and after the reaction.

Results

Spectrophotometric Titration of 1,4-Butaneditiol(BDT). Prior to the kinetic measurements, the equilibrium constants for the –SH ionization(K_a) were estimated in the absence and presence of the CTAB micelle. Since the critical micelle concentration (CMC) for CTAB is estimated to be about 8×10^{-4} M under the present conditions,[14] the titration for the latter system was conducted in the presence of 3 mM CTAB. The results are shown in Fig. 1.

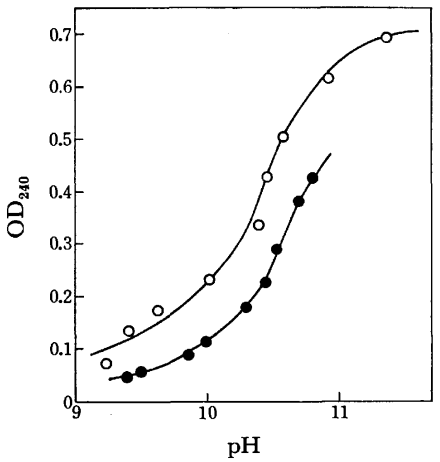

Fig. 1. Spectrophotometric titration of 1,4-butanedithiol. [1,4-Butanedithiol]$=2.20\times10^{-4}$ M, $\mu=0.06$ with KCl.
(○), [CTAB]$=3.0\times10^{-3}$ M; (●), CTAB was not added.

Under the anaerobic conditions at pH 9.2—11.4, only one inflection point was observed. The titration curve monitored by the absorbance(OD) at 240 nm(thiolate anion) is expressed by Eq. 2, where ε is the molar absorption coefficient of thiolate anion. The linear correlation between a_H and $1/OD_{240}$ is indicated by Eq. 3.

$$OD_{240} = \varepsilon[BDT]\left(\frac{K_a}{K_a+a_H}\right) \quad (2)$$

$$\frac{1}{OD_{240}} = \frac{1}{\varepsilon[BDT]} + \frac{a_H}{\varepsilon[BDT]K_a} \quad (3)$$

Good linear relationships($r>0.99$) were observed for the treatment of the experimental data by Eq. 3. From the slope and the intercept, K_a and ε were determined: in the presence of CTAB (3 mM), $pK_a=10.4$, $\varepsilon=3.41\times10^3$ $M^{-1}cm^{-1}$; in the absence of CTAB, $pK_a=10.7$, $\varepsilon=3.30\times10^3$ $M^{-1}cm^{-1}$. According to Benesch and Benesch,[15a] the molar absorption coefficients for aliphatic thiolate anions are $(4—6)\times10^3$ $M^{-1}cm^{-1}$. The observed inflections may correspond to the first dissociation(K_{a1}) of two SH groups.[15b] The pK_{a1} value was lowered in the presence of the CTAB micelle by *ca.* 0.3 pK unit.

Absorption Spectra of Isoalloxazines. Figure 2 shows absorption spectra of oxidized and reduced forms of isoalloxazines. The isoalloxazine **1** shows an absorption maximum at 433 nm($\varepsilon=14200$ $M^{-1}cm^{-1}$). the reduction by BDT giving a tight isosbestic point at 323 nm. The spectra were hardly affected by addition of CTAB above CMC. At the completion of the reaction, admittance of O_2 regenerated **1** quantitatively. In the presence of the CTAB micelle(λ_{max} 440 nm, $\varepsilon=11500$ $M^{-1}cm^{-1}$), the spectrum of **2** shows distinct shoulders at 420 nm and 460—470 nm(Fig. 2), isosbestic points for the reduction by BDT appearing at 278, 324, 367, and 385 nm. Since similar shoulders are observable in organic solvents(acetonitrile, dioxane), the isoalloxazine ring of **2** should be present in the hydrophobic region of the micelle.

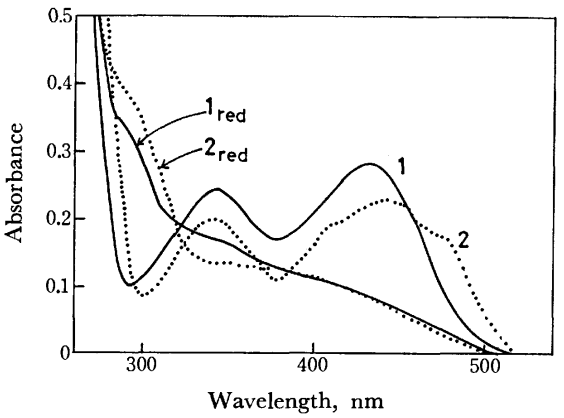

Fig. 2. Spectra of oxidized and reduced forms of isoalloxaznes. [isoalloxazine]$=2.0\times10^{-5}$ M, [CTAB]$=3.0\times10^{-3}$ M, pH 10.05.
——, **1** and reduced **1** ($\mathbf{1}_{red}$); ----, **2** and reduced **2** ($\mathbf{2}_{red}$). Reduction was performed with 1.04×10^{-3} M 1,4-butanedithiol.

Rate Measurements. With excess BDT, isoalloxazine concentration as a function of time gave good pseudo

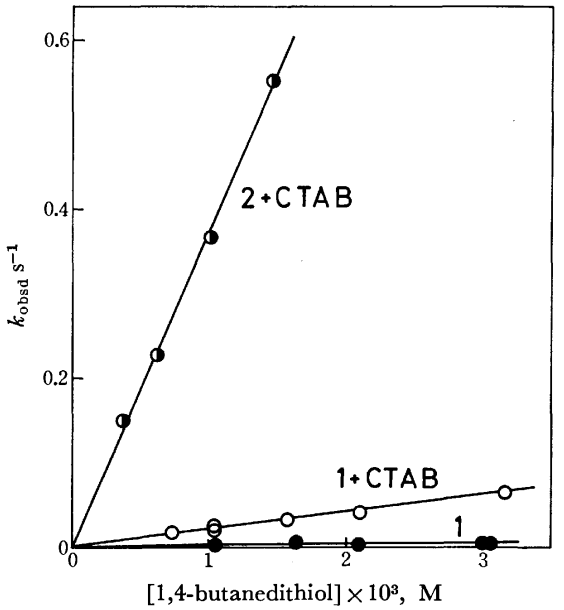

Fig. 3. Pseudo-first order rate constant (k_{obsd}) *vs.* [1,4-butanedithiol].
[Isoalloxazine]$=(1—3)\times10^{-5}$ M, [CTAB]$=3.0\times10^{-3}$ M, pH 10.05+0.02.

first-order plots up to 3 half-lives under all reaction conditions in the present work. When the concentration of BDT was varied, plots of pseudo first-order rate constants(k_{obsd}) against the BDT concentration showed linearity(Fig. 3), indicating that the reaction is of first-order with respect to the concentrations of isoalloxazine and BDT. The apparent second-order rate constants(k_2') can be obtained by dividing k_{obsd} by the total concentration of BDT.

The apparent second-order rate constants at pH 10.05+0.02 are given in Table 1. At this pH, the rate constant for the reaction of **1** and BDT was accelerated by a factor of 23 by the CTAB micelle. The rate for the reaction of **2** and BDT is further accelerated, being more than 400 times greater than that of **1** and BDT in a nonmicellar system. The results suggest that the cationic environments remarkably improve the electrophilicity of isoalloxazine ring and/or the reductive activity of the thiolate anion.

The apparent second-order rate constants for the reaction of **1** and BDT are plotted against the concentration of CTAB in Fig. 4. The plots give a sigmoidal curve: around the CMC, the rate constants rose rapidly with increasing the CTAB concentration. At optimal CTAB concentration(*ca.* 5 mM), 35 times rate augmentation was observed. In contrast, addition of anionic (SDS) and nonionic(Brij-35) surfactants suppressed the reaction above their CMC (Fig. 5). Thus,

TABLE 1. APPARENT SECOND-ORDER RATE CONSTANTS AND pH_{max}

Isoalloxazine	CTAB mM	k_2' at pH 10.05 $M^{-1}s^{-1}$	$k_{2'max}$ $M^{-1}s^{-1}$	pH_{max}
1	0	0.904	1.78	10.9
1	3.0	21.0	32.0	10.4
2	3.0	375	447	10.3

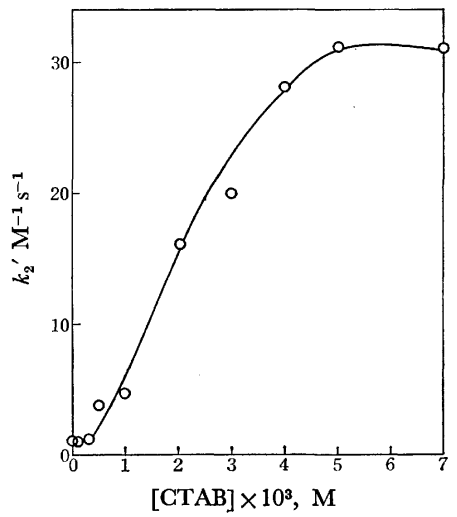

Fig. 4. Apparent second-order rate constants for the reaction of **1** and 1,4-butanedithiol plotted as a function of CTAB.
[**1**]=3.01×10⁻⁵ M, [1,4-butanedithiol]=1.05×10⁻³ M, pH 10.05±0.02, μ=0.06 with KCl.

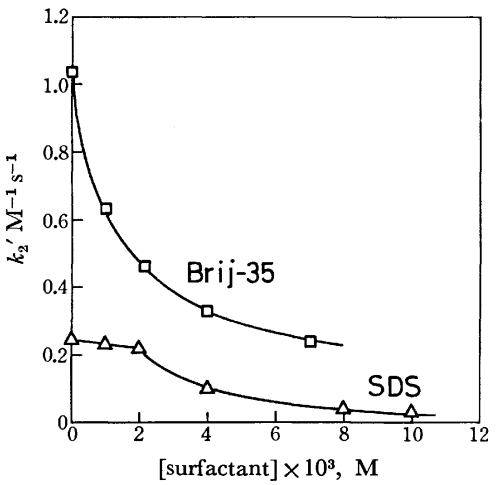

Fig. 5. Apparent second-order rate constants for the reaction of **1** and 1,4-butanedithiol plotted as a function of anionic (SDS) and nonionic (Brij-35) surfactants. (△), SDS, pH 9,10±0.03; (□), Brji-35, pH 10.05± 0.02. Other reaction conditions are recorded under Fig. 4.

only the cationic micelle acts as a catalyst for the reaction of **1** and BDT.

Effects of pH, Salt Concentration, and Buffer Concentration. The logarithm of the apparent second-order rate constant is plotted as a function of pH in Fig. 6. Plots of log k_2' *vs.* pH give bell-shaped curves.[3,4] The pH values(pH_{max}) and the rate constants($K_{2'max}$) at the rate maxima are summarized in Table 1. We see that the pH_{max} values are lowered by 0.5—0.6 pK unit on addition of CTAB(3 mM). The maximal rate constant for the reaction of **1** and BDT is enhanced 18 times in the presence of the CTAB micelle and that of **2** 250 times, as compared with that for **1** and BDT in a nonmicellar system.

The rate of micelle-catalyzed system is influenced by

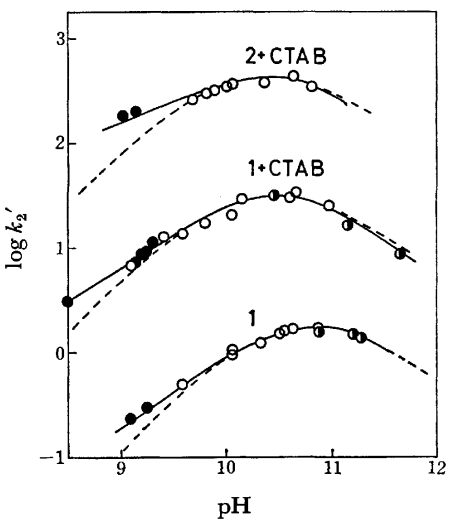

Fig. 6. pH Dependence.
[CTAB]=3.0×10⁻³ M. pH was adjusted with KOH (◑), carbonate (○), and borate (●). Ionic strength was maintained at 0.06 with KCl. Dotted curves (theoretical pH-rate profiles) are obtained from Eq. 6.

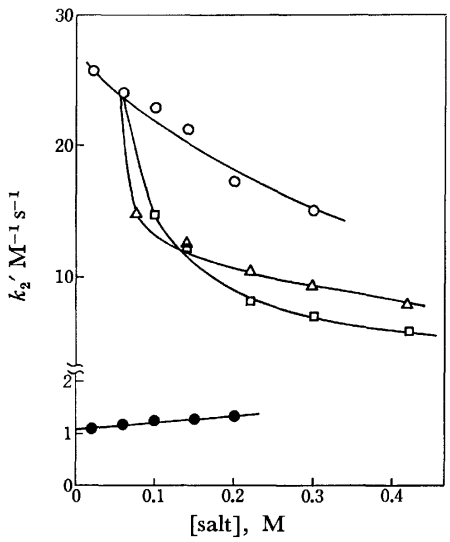

Fig. 7. Effect of ionic strength and buffer concentration on the reaction of **1** and 1,4-butanedithiol.
pH 10.05±0.03, [CTAB]=3.0×10^{-3} M. (○), Carbonate; (●), carbonate without CTAB; (□), KCl; (△), K_2SO_4. pH of the latter two systems was maintained with 0.06 M carbonate.

the salt concentration of the reaction medium. The second-order rate constants for the reaction of **1** and BDT in the presence of the CTAB micelle are suppressed by increase in salt concentration (KCl, K_2SO_4; Fig. 7). Increase in the carbonate buffer($KHCO_3$–K_2CO_3) concentration does not retard the reaction as conspicuously as KCl and K_2SO_4. As shown by Gascoigne and Radda[1] and Loechler and Hollocher,[3] the flavin oxidation of dithiol is subjected to general catalysis. In the present system, the reaction of **1** and BDT in a nonmicellar system was slightly accelerated with increasing carbonate buffer concentration(black circles in Fig. 7); third-order rate constant for general catalysis(*i.e.*, slope for the plots of black circles), 1.3 $M^{-2}s^{-1}$. Supposedly, the micelle-catalyzed reaction is also subjected to general catalysis. The increase in carbonate buffer concentration would provide two opposing effects: the rate deceleration due to the increased ionic strength and the rate acceleration due to the increased local concentration of bicarbonate ion as an acid around the micelle surface. As a result, the rates would become less susceptible to the change in buffer concentration.

Discussion

Micellar catalysis provides suitable model systems of the enzymatic catalysis.[16,17] Micelles can influence rates and equilibria of biologically important reactions. The micellar environment evaluated with the fluorescent emission is akin to that of the active site of enzymes.[17,18] Thus, it seems significant to assess the influence of the micellar enviroments on the enzyme-like reactions, especially on the coenzyme-dependent reactions.

One of the most significant findings on the micellar catalysis would be the unusual enhancement of nucleophilicity of a variety of anionic species when they are bound to the cationic micellar and polymer micellar phase.[8,10] In studies on nucleophilic reactions of thiolate anions, we found that the thiolate anion bound to the cationic micellar phase is very susceptible to air oxidation.[7,13] This suggests that the formation of the hydrophobic ion pair would enhance not only the nucleophilicity but the reactivity as a reducing agent. This led us to investigate the effect of micellar environments on the oxidation-reduction reactions containing thiol groups.

The most plausible mechanism for the reaction of flavins and dithiols is the formation of adduct followed by the nucleophilic attack of intramolecular thiolate anion. The free radical mechanism can be disregarded on the basis of kinetic evidence.[3,4] Two kinetically equivalent mechanisms were suggested: (i) nucleophilic attack by thiolate anion on C(4a), aided by a general acid catalysis at N(5)(k_{4a} process in Eq. 4), and (ii) nucleophilic attack on N(5)(k_5 process) followed by 5→4a migration of RS^+(k_M process).**

According to Loechler and Hollocher,[3] buffer catalysis is observed only when the 4a-addition(*i.e.*, k_{4a} process) is involved in the rate-limiting step. This is based on the fact that the negative charge on N(5) developed by 4a-addition is energetically unfavorable ($pK_a\approx24$), unless the adduct formation is aided by acid catalysis. The present system is buffer-catalyzed in the absence and probably in the presence of the CTAB micelle(Fig. 7). Therefore, mechanism (i) is not incompatible with the present kinetic situation. 5-Addition(*i.e.*, mechanism (ii)) is presumed not to be buffer-

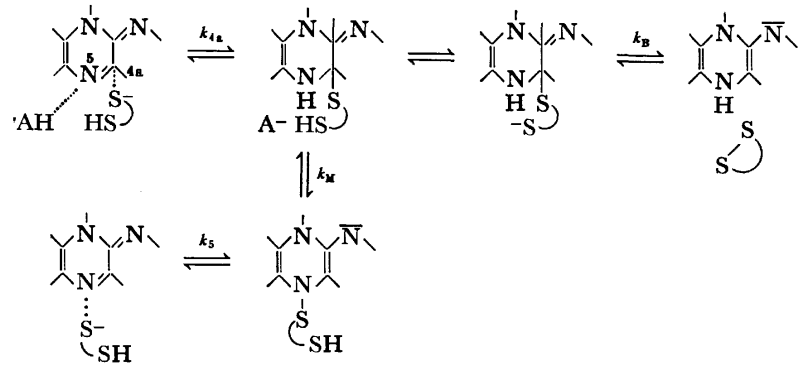

(4)

** This mechanism was proposed for the reaction of flavins and monothiols.[4]

catalyzed, since the anionic charge is developed on N(1), the pK_a of which is much lower ($\approx$6.6).[19] If 5-adduct is formed, 5→4a migration of RS^+ becomes obligatory prior to breakdown(k_B process). Since the reaction which yields the cationic charge in the transition state is extremely suppressed by the cationic micelle,[5,6] the migration should be significantly inhibited by the CTAB micelle. However, the CTAB micelle acts as catalyst for the isoalloxazine oxidation of BDT. Thus, mechanism (ii) is unlikely in the present system.

Similar reaction orders and pH-rate profiles observed for the micellar and nonmicellar systems indicate that the reaction mechanism is not essentially changed by the micelle. The result of spectrophotometric titration of BDT shows that the pK_{a1} is lowered by 0.3 pK unit in the presence of the CTAB micelle. pH_{max} values (Table 1) are lowered by 0.5—0.6 pK unit. The lowering of pK_a is generally observed for anionic species bound to the cationic micelle,[9,13,20] and such anions are greatly activated with no apparent exceptions. For example, the nucleophilic reaction of coenzyme A and *p*-nitrophenyl acetate is accelerated by a factor of 290 in the presence of the CTAB micelle, the pK_a being lowered by 0.5 pK unit as compared with the corresponding value in a nonmicellar system.[7] On the other hand, spectral data(Fig. 2) indicate that **1** is not much concentrated in the micellar phase. Thus, the rate increase for the reaction of **1** and BDT would be attributed to the concentration of BDT in the micellar phase and to the enhanced nucleophilicity of BDT anion therein.

The 18—23 fold rate augmentation in **1** oxidation of BDT seems rather small. It has been shown that **1** oxidation of monothiols shows a remarkable rate enhancement by a factor of 10^2—10^5 times.[21] Some mechanistic difference between monothiol and dithiol may cause the different susceptibility to the micellar catalysis. Possible interpretation might be as follows. (i) The k_B process is presumed to be rate-limiting for flavin oxidation of monothiol.[3,4] Since the k_B process is a simple nucleophilic attack on flavin–S– by RS^-, the rate would directly reflect the enhanced nucleophilicity of RS^-. On the other hand, the k_{4a} process, a rate-limiting step for dithiol,[3] is a nucleophilic attack concerted with acid catalysis. In most cases, the cationic micelle retards acid catalyzed reactions.[5,6,22,23] Therefore the total reaction rate would not be greatly enhanced despite the favorable influence on the nucleophilicity. (ii) The monoanion of BDT is subjected to micellar activation to a smaller extent due to the intramolecular hydrogen bond with the undissociated SH group. There is a precedent that reactivity of naked anion in aprotic environment is efficiently quenched by a single intramolecular hydrogen bonding.[24] Micellar desolvation of anion stabilized by intramolecular hydrogen bonding might be considerably difficult.

Isoalloxazine **2** is scarcely soluble in an aqueous solution. The isoalloxazine ring of **2** resides in relatively hydrophobic region of the micelle(Fig. 2). Both **1**+CTAB and **2**+CTAB systems employ similar pH_{max} (10.4 and 10.3, respectively), indicating that both systems oxidize similar species of BDT. Thus, a mechanistic change in the **2**+CTAB system is hardly expected. The rate increase in this system could be derived from the concentration effect of **2** in the micellar phase and the facilitation of flavin oxidation due to the change in the oxidation potential of **2**. The latter conjecture is supported by the fact that flavin oxidation is more facile in dipolar aprotic solvents[25] to which the cationic micellar environment is said to be akin.[17]

The requirement of a general acid catalysis for 4a-addition is discussed by Bruice *et al.*[4,26,27] in detail on the basis of the libido rule of Jencks.[28] Since H_3O^+ catalysis is *completely* inhibited by the cationic micelle when the substrate is buried in the micellar phase,[6] H_3O^+ dependent processes (k_3 and k_6 in Loechler and Hollocher's scheme) should be disregarded in the cationic micellar system. Thus, acid species present in the cationic micellar solution are H_2O, buffer acid, and intramolecular SH group. When the reaction system is buffered by H_2O–OH^-, intramolecular SH group would play the role of a general acid(Eq. 5).

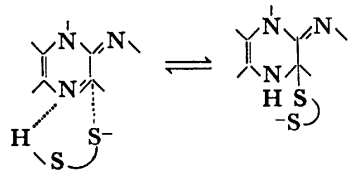

(5)

If the reaction is of first-order in BDT monoanion as expressed by $v_{obsd}=k_2[HS(CH_2)_4S^-][isoallozaxine]$, the corresponding pH-rate profile is given by

$$k_2' = k_2 a_H K_{a1}/(a_H^2 + a_H K_{a1} + K_{a1}K_{a2}) \quad (6)$$

where k_2 denotes a true second-order rate constant. Theoretical curves(Fig. 6, dotted line) derived from Eq. 6*** show that the experimental data satisfy Eq. 6 at $pH > pH_{max}$, while the observed rate is greater at $pH < pH_{max}$. In the latter pH region, buffer acid would significantly contribute to the observed rate.

In conclusion, the reactivity of BDT as a reducing agent is remarkably enhanced in the presence of the cationic micelle, and the electrophilicity of isoalloxazines can be affected by the micellar environements.

The authors express their thanks to Professor F. Yoneda for his valuable discussion. They also express their appreciation to Miss R. Ando for technical assistance.

References

1) I. M. Gascoigne and G. K. Radda, *Biochim. Biophys. Acta*, **131**, 498 (1967).
2) M. J. Gibian and D. V. Winkelman, *Tetrahedron Lett.*, **1969**, 3901.
3) E. L. Loechler and T. C. Hollocher, *J. Am. Chem. Soc.*, **97**, 3236 (1975).
4) I. Yokoe and T. C. Bruice, *J. Am. Chem., Soc.* **97**, 450 (1975).

*** Based on the relationships, $pK_{a2} \approx pK_{a1} + 1.0$[3] and $pH_{max} = 0.5(pK_{a1} + pK_{a2})$, appropriate k_2, K_{a1}, and K_{a2} were chosen by the trial-and-error method. Best fit values are: for **1**, $k_2 = 2.9\ M^{-1}\ s^{-1}$, $pK_{a1} = 10.4$, $pK_{a2} = 11.4$; for **1**+CTAB, $k_2 = 52.2\ M^{-1}\ s^{-1}$, $pK_{a1} = 9.9$, $pK_{a2} = 10.9$; for **2**+CTAB, $k_2 = 730\ M^{-1}\ s^{-1}$, $pK_{a1} = 9.8$, $pK_{a2} = 10.8$.

5) S. Shinkai, R. Ando, and T. Kunitake, *Bull. Chem. Soc. Jpn.*, **48**, 1914 (1975).
6) S. Shinkai, R. Ando, and T. Kunitake, *Bull. Chem. Soc., Jpn.*, **49**, 3652 (1976).
7) S. Shinkai and T. Kunitake, *Bull. Chem. Soc. Jpn.*, **49**, 3219 (1976).
8) P. Heitmann, *Eur. J. Biochem.*, **5**, 305 (1968); W. Tagaki, T. Amada, Y. Yamashita, and Y. Yano, *J. Chem. Soc., Chem. Commun.*, **1972**, 1131.
9) T. Kunitake, S. Shinkai, and Y. Okahata, *Bull. Chem. Soc. Jpn.*, **49**, 450 (1976); S. Shinkai and T. Kunitake, *Chem. Lett.*, **1976**, 109.
10) S. Shinkai and T. Kunitake, *J. Chem. Soc., Perkin Trans. 2*, **1976**, 980.
11) F. Yoneda, Y. Sakuma, M. Ichiba, and K. Shinomura, *J. Am. Chem. Soc.*, **98**, 830 (1976).
12) W. P. Hall and E. E. Reid, *J. Am. Chem. Soc.*, **65**, 1466 (1943).
13) S. Shinkai and T. Kunitake, *Makromol. Chem.*, **178**, 1613 (1977).
14) Y. Okahata, R. Ando, and T. Kunitake, *Polym. Prepr. Jpn.*, **25**, 54 (1976).
15) a) R. E. Benesch and R. Benesch, *J. Am. Chem. Soc.*, **77**, 5877 (1955); b) However, *cf.* Ref. 1 and G. M. Whitesides, J. E. Lilburn, and R. P. Szajewski, *J. Org. Chem.*, **42**, 332 (1977).
16) J. H. Fendler and E. J. Fendler, "Catalysis in Micellar and Macromolecular Systems," Academic Press, New York, N. Y. (1975).
17) E. H. Cordes and C. Gitler, *Progr. Bioorg. Chem.*, **2**, 1 (1973).
18) D. C. Turner and L. Brand, *Biochemistry*, **7**, 3381 (1968).
19) R. F. Williams, S. Shinkai, and T. C. Bruice, *J. Am. Chem., Soc.*, **99**, 921 (1977).
20) T. Kunitake, Y. Okahata, and T. Sakamoto, *J. Am. Chem. Soc.*, **98**, 7799 (1976).
21) S. Shinkai, R. Ando, and F. Yoneda, *Chem. Lett.*, **1977**, 147.
22) R. B. Dunlop, G. A. Ghanim, and E. H. Cordes, *J. Phys. Chem.*, **73**, 1898 (1969).
23) B. M. Dunn and T. C. Briuce, *J. Am. Chem. Soc.*, **92**, 6589 (1970).
24) D. S. Kemp, D. O. Cox, and K. G. Paul, *J. Am. Chem. Soc.*, **97**, 7312 (1975).
25) J. A. Rynd and M. J. Gibian, *Biochem. Biophys. Res. Commun.*, **41**, 1097 (1070).
26) T. C. Bruice, L. Hevesi, and S. Shinkai, *Biochemistry*, **12**, 2083 (1973).
27) T. C. Bruice and J. P. Taulane, *J. Am. Chem. Soc.*, **98**, 7769 (1976).
28) W. P. Jencks, *Chem. Rev.*, **72**, 705 (1972).

5-Fluorouracil Derivatives. I. The Synthesis of 1-Carbamoyl-5-fluorouracils

Shoichiro OZAKI,* Yoshimasa IKE, Haruo MIZUNO, Katsutoshi ISHIKAWA, and Haruki MORI

Research Center, Mitsui Toatsu Chemicals, Inc. Kasama-cho, Totsuka-ku, Yokohama 247

(Received February 21, 1977)

The toxicity and tumor affinity of 5-fluorouracil (**1**) have been modified by the introduction of a carbamoyl group. Carbamoylation by three general methods were studied extensively: (i) The reaction of **1** with isocyanate, (ii) the reaction of 1-chloroformyl-5-fluorouracil with amine, and (iii) the reaction of **1** with carbamoyl chloride. These three methods usually give 1-carbamoyl-5-fluorouracils (**2**). 3-Carbamoyl-5-fluorouracils were not obtained by any method. The **2** substances take a hydrogen-bonded structure in chloroform, a non hydrogen-bonded structure in DMSO at 80 °C, and mixed structures in DMSO at 25 °C. Thirty-six homologues shown by **2** were prepared all of these compounds showed antitumor activity. Of them, 1-hexylcarbamoyl-5-fluorouracil (HCFU) appeared to be the most promising antitumor agent when administered orally in that HCFU retains well balanced lipo- and hydro-philicity, is stable in acid in the stomach, and moreover, decomposed moderately in a tumor. Isocyanate was obtained from the reaction of amine with trichloromethyl chloroformate (TCF) by simply heating these two reagents in toluene; this offers a convenient new method for synthesizing isocyanate from amine. Several new isocyanate were obtained from amino acids.

As the combination of long-standing research on isocyanate chemistry[1] and the synthetic work on 5-fluorouracil derivatives, searching for useful products, the reaction of isocyanate with 5-fluorouracil (**1**) has been studied in detail; it has led to the discovery of the powerful antitumor agents.[2]

1, though an effective antitumor agent,[3] has a strong toxicity and poor tumor affinity. Chemical modifications of **1** by introducing β-cyanoethyl,[4] 2-tetrahydrofuryl,[5] 2-oxo-3-tetrahydrofuryl,[6] β-amino-β-carboxyethyl,[7] methyl,[8] hydroxy,[9] benzyloxy,[9] 2,3-dihydroxypropyl,[10] acyl,[11] alkyl- and aryl- sulfonyl,[11] and alkoxycarbonylmethyl[12] groups have been reported. However many of these masked compounds have no or only weak activities toward tumors, because the chemical bonds between **1** and the substituents are too strong to undergo biodegradation. Some of the 5-fluorouracil derivatives retaining weakly bonded substituents, though, show no difference in action toward tumors when compared with **1** itself.

In order to adapt the biological activities of **1** for practical purposes, especially for oral administration, hundreds of new structual analogs have been synthesized. The antitumor activities of these compounds were examined at the Pharmacology Division, National Cancer Center Research Institute, Tokyo. Some of the screening results for biological activity have been published.[13,14] In the present paper we wish to report the synthesis of 1-carbamoyl-5-fluorouracils (**2**) in detail.

Although the reaction of uracil and isocyanate has been reported to be sluggish,[15] the treatment of uracil with methyl isocyanate in a dimethyl sulfoxide solution gave 1-methylcarbamoyluracil.[16] We have extensively explored the reactions of **1** with isocyanate, with phosgene and amine, and with carbamoyl chlorides, and have obtained a number of **2** substances by three general synthetic methods.

Results and Discussion

Method 1. The reaction of **1** with isocyanates affords **2**.

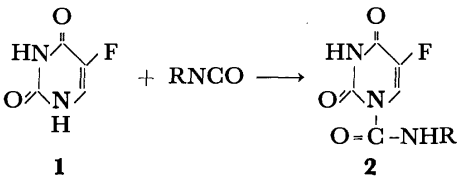

1 **2**

Scheme 1.

This reaction was originally carried out in *N,N*-dimethylformamide. However, our thorough study of the solvent effect revealed that pyridine (Method 1-A) was the best solvent and that the reaction proceeded almost quantitatively. In other solvents, such as *N,N*-dimethylacetamide (Method 1-B) and dimethyl sulfoxide (Method 1-C), however, the yield does not exceed 70% as is shown in Table 1. The best reaction temperature is 90—100 °C. The best molar ratio of isocyanate/**1** is 1.5. The reaction is catalyzed by organic bases, such as triethylamine, triethylenediamine, and DBU (1,8-diazabicyclo[5.4.0]undecene-7).

This method gives products of the best quality and in good yields as well. 1-Arylcarbamoyl-5-fluorouracil is obtained only by this method. It is known[11] that

Table 1. Solvent effects on the conversion of 5-fluorouracil to 1-hexylcarbamoyl-5-fluorouracil[a]

Solvent	Conversion[b] (%)
Pyridine	99
N,N-Dimethylformamide	70
N,N-Dimethylacetamide	70
Dimethyl sulfoxide	40
Hexamethylphosphoric triamide	60
o-Dichlorobenzene	40
Triethylamine	trace
N,N-Dimethylaniline	60
Quinoline	60
Acetonitrile	70
Nitromethane	70

a) The n-$C_6H_{13}NCO$-to-5-fluorouracil molar ratio was 1.5. The reaction was carried out at 90 °C for 2 h. b) The conversion was measured by comparing the TLC spots of premixed 5-fluorouracil and **22**.

* To whom correspondence should be addressed.

the reaction of **1** with an electrophile like alkyl chloride introduces substituents at the 3- and 1-positions of **1**. However, 3-carbamoyl-substituted 5-fluorouracils (**3** and **4**) were not obtained by the treatment of 5-fluorouracils with isocyanate, even when a higher temperature, a large excess of isocyanate, or a catalyst such as triethylamine was employed. This may result from the acidic character of the proton on the nitrogen at the 3-positions of **1** and **2**, or from the easy dissociation of once-formed carbamoyl groups at the 3-positions of **3** and **4**.

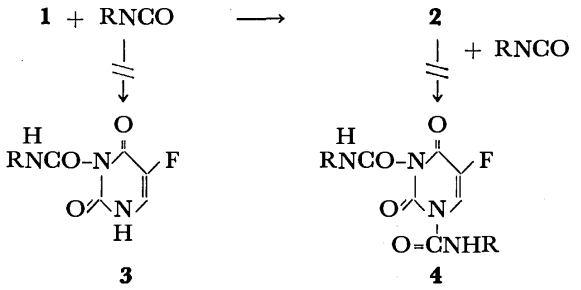

Scheme 2.

Method 2. Phosgene can be condensed with **1**, but the resulting 1-chloroformyl-5-fluorouracil (**5**) is too unstable to be isolated; nevertheless, it is stable enough in a basic solvent such as pyridine at low temperatures. Accordingly, **5** treated with aliphatic amines *in situ* afforded **2**.

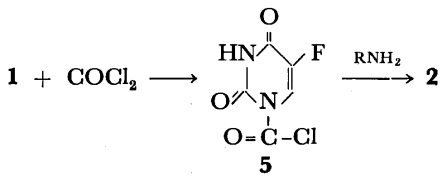

Scheme 3.

On the contrary, aromatic amine does not react with **5**, indicating that a strong basicity is necessary for the amine to react with **5**.

In this reaction, a small amount of triethylamine increases the yield, while excess amines lower the yield, because of the following further reaction:

$$2 + RNH_2 \longrightarrow 1 + RNHCONHR$$

Method 2, shown in Scheme 3, is a convenient method to prepare **2**, as amine is more easily available than isocyanate. One more practical advantage is that amines retaining a hydroxy moiety, like thyrosine, **6**, can condense with **5**.

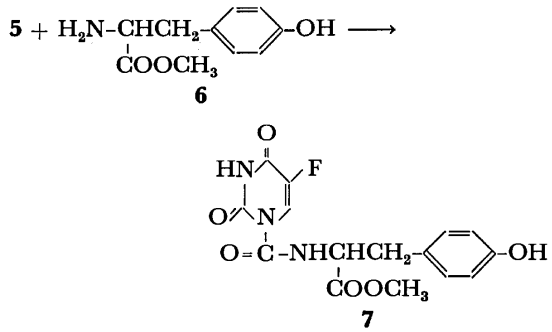

Scheme 4.

The carbamoyl uracil (**7**) can not be obtained by Method 1, because hydroxy isocyanate can not be prepared.

Method 3. Amine and phosgene condense to give carbamoyl chloride. The carbamoyl chloride of secondary amine (**8**) reacted with **1** to give 1-(*N*,*N*-disubstituted carbamoyl)-5-fluorouracil (**9**).

When an excess of carbamoyl chloride (**8**) was employed, 1,3-dicarbamoyl-5-fluorouracil (**10**) was also produced, along with 1-carbamoyl-5-fluorouracil (**9**).

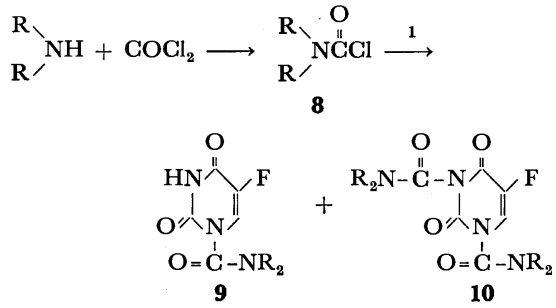

Scheme 5.

The carbamoyl chloride of primary amine (**11**) and **1** do not give **2**, even in the presence of triethylamine at low temperatures, but they do give **2** in low yields at a high temperature (80 °C).

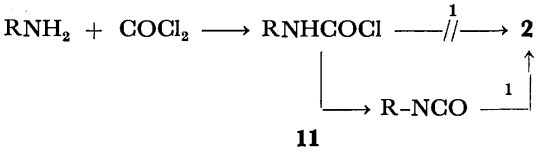

Scheme 6.

The nucleophilicity of **1** is too weak to attack the carbonyl of **11** at low temperatures. At a high temperature (80 °C), **11** decomposes to isocyanate, and eventually the isocyanate reacts with **1** to give **2**.

The structure of **2** was confirmed by elemental analysis and by its infrared and NMR spectra.**

In a polar solvent like dimethyl sulfoxide, the **2** substances take two mixed structures at room temperature, as is shown in Fig. 1 and Table 3. These two structures are presumed to be a hydrogen-bonded[16] **12** and a non hydrogen-bonded structure, **13**.

With an increase in the temperature, **13** predominates over **12**, as polar dimethyl sulfoxide affects the hydrogen bond unfavorably. At 80 °C, for example, 1-hexylcarbamoyl-5-fluorouracil (**22**) mostly exists in the form of

** The position of substituents was clearly distinguished on the basis of UV at varying pH and NMR spectra of 1-alkoxymethyl-, 3-alkoxymethyl-, and 1,3-bis(alkoxymethyl)-5-fluorouracils. The NMR spectra of 1-substituted uracils showed a sharp doublet at around 7.5 ppm due to C_6–H (coupling with F), while non-substituted and 3-monosubstituted uracils gave the corresponding triplets (coupling with F and N_1–H) at around 8 ppm. A fuller account will be given in detail in the third article of this series. The NMR spectrum of **2** showed a doublet due to C_6–H, indicating the 1-carbamoyl structure.

Table 2. 1-Carbamoyl-5-fluorouracils 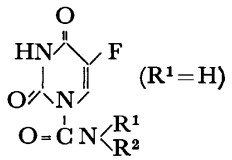 ($R^1=H$)

Compd	R_2	Synthetic method	Yield %	Mp °C	Molecular formula	Found (Calcd) % C	H	F	N
15	CH_3	1-C	86.1	170	$C_6H_6FN_3O_3$	38.23 (38.51)	3.22 (3.23)	10.10 (10.15)	22.31 (22.46)
16	C_2H_5	1-B	65.1	165	$C_7H_8FN_3O_3$	41.41 (41.80)	4.12 (4.01)	9.46 (9.44)	20.72 (20.89)
17	C_3H_7	1-B	80.1	145	$C_8H_{10}FN_3O_3$	44.61 (44.65)	4.76 (4.65)	8.67 (8.84)	19.81 (19.53)
18	i-C_3H_7	1-B	61.5	145	$C_8H_{10}FN_3O_3$	44.29 (44.65)	4.60 (4.65)	8.98 (8.84)	19.26 (19.53)
19	n-C_4H_9	1-B	72.3	137	$C_9H_{12}FN_3O_3$	47.29 (47.16)	5.32 (5.28)	8.18 (8.29)	18.80 (18.33)
20	t-C_4H_9	1-B	50.2	108	$C_9H_{12}FN_3O_3$	46.99 (47.16)	5.76 (5.28)	8.41 (8.29)	18.78 (18.33)
21	n-C_5H_{11}	1-B	40.2	117	$C_{10}H_{14}FN_3O_3$	49.56 (49.38)	5.81 (5.80)	7.57 (7.81)	17.02 (17.28)
22	n-C_6H_{13}	1-A	95.0	110—111	$C_{11}H_{16}FN_3O_3$	51.19 (51.36)	6.37 (6.23)	7.27 (7.39)	16.60 (16.34)
23	n-C_7H_{15}	1-B	58.4	103	$C_{12}H_{18}FN_3O_3$	53.37 (53.13)	7.02 (6.69)	7.02 (7.00)	15.36 (15.49)
24	n-C_8H_{17}	1-B	53.2	98—100	$C_{13}H_{20}FN_3O_3$	55.12 (54.72)	7.42 (7.07)	6.33 (6.65)	14.34 (14.73)
25	n-$C_{12}H_{25}$	2	60.1	107—108	$C_{17}H_{28}FN_3O_3$	59.20 (59.80)	8.35 (8.27)	5.52 (5.56)	11.92 (12.31)
26	n-$C_{18}H_{37}$	1-B	62.1	107—108	$C_{23}H_{40}FN_3O_3$	65.25 (64.91)	9.81 (9.41)	4.06 (4.46)	9.72 (9.87)
27	cyclo-C_6H_{11}	1-B	55.2	156—157	$C_{11}H_{14}FN_3O_3$	52.14 (51.76)	5.72 (5.49)	7.02 (7.45)	16.17 (16.47)
28	$CH_2C_6H_5$	1-A	91.8	177—178	$C_{12}H_{10}FN_3O_3$	55.45 (55.75)	4.10 (3.83)	7.05 (7.21)	16.30 (15.96)
29	$CH_2CH_2C_6H_5$	1-A	58.9	161	$C_{13}H_{12}FN_3O_3$	56.73 (56.32)	4.48 (4.36)	6.86 (6.85)	15.66 (15.16)
30	CH_2-CH=CH_2	2	31.8	130—131	$C_8H_8FN_3O_3$	44.76 (45.08)	3.57 (3.78)	8.51 (8.91)	19.27 (19.71)
31	CH=CH_2	1-A	70.3	150—160	$C_7H_6FN_3O_3$	41.95 (42.22)	3.03 (3.04)	9.25 (9.54)	20.90 (21.09)
32	COC_6H_5	1-A	28.1	168	$C_{12}H_8FN_3O_4$	52.21 (51.99)	3.21 (2.91)	7.22 (6.85)	14.79 (15.16)
33	C_6H_5	1-C	81.4	280	$C_{11}H_8FN_3O_3$	52.83 (53.02)	3.19 (3.24)	7.64 (7.63)	16.43 (16.86)
34	o-CH_3-C_6H_4	1-C	73.4	280—283	$C_{12}H_{10}FN_3O_3$	55.15 (54.75)	3.97 (3.85)	7.02 (7.22)	15.67 (15.96)
35	o-NO_2-C_6H_4	1-C	46.0	216—242	$C_{11}H_7FN_4O_5$	45.32 (44.91)	2.87 (2.40)	6.03 (5.46)	18.62 (19.04)
36	$(CH_2)_6$[a]	1-A	89.0	172—173	$C_{16}H_{18}F_2N_6O_6$	44.90 (44.87)	4.38 (4.24)	8.39 (8.87)	20.00 (19.61)
37	m-$CH_2C_6H_4CH_2$[b]	1-A	50.2	178—180	$C_{18}H_{14}F_2N_6O_6$	48.22 (47.70)	3.15 (3.40)	8.46 (8.05)	18.51 (18.05)
38	CH_2COOCH_3	1-A	70.5	149—150	$C_8H_8FN_3O_5$	39.19 (39.12)	3.29 (3.27)	7.75 (7.50)	17.14 (16.90)
39	$CH_2CH_2COOC_2H_5$	1-A	86.5	151—153	$C_{10}H_{12}FN_3O_5$	43.96 (44.12)	4.43 (4.38)	6.95 (7.03)	15.38 (15.42)
40	$CHCH_2C_6H_5$ $COOCH_3$	1-A	92.1	64— 65	$C_{15}H_{14}FN_3O_5$	53.73 (54.13)	4.21 (4.34)	5.67 (5.61)	12.33 (11.94)
41	$CHCH_2C_6H_5$ $COOC_2H_5$	1-A	92.1	55— 56	$C_{16}H_{16}FN_3O_5$	55.01 (55.41)	4.62 (4.92)	5.44 (5.18)	12.03 (12.48)
42	$CHCH_2C_6H_5OH(p)$ $COOC_2H_5$	2	25.8	76— 78	$C_{16}H_{16}FN_3O_6$	52.60 (52.90)	4.41 (4.59)	5.00 (4.57)	10.82 (10.50)

TABLE 2. (Continued)

Compd	R^2	Synthetic method	Yield %	Mp °C	Molecular formula	Found (Calcd) % C	H	F	N
43	$CHCH_2CH_2SCH_3$ $COOC_2H_5$	1-A	73.2	104—105	$C_{12}H_{16}FN_3O_5S$	43.24 (43.27)	4.84 (4.99)	5.70 (5.69)	12.61 (12.31)
44	$CHCH_2CH(CH_3)_2$ $COOCH_3$	1-A	87.6	95— 96	$C_{12}H_{16}FN_3O_5$	47.84 (47.92)	5.35 (5.44)	6.31 (5.91)	13.95 (13.94)
45	$CHCH_2CH_2COOCH_3$ $COOCH_3$	2	78.5	59	$C_{12}H_{14}FN_3O_7$	43.51 (43.51)	4.26 (4.27)	5.73 (5.46)	12.69 (12.52)
46	$R_1=R_2=CH_3$	3	71.1	194—196	$C_7H_8FN_3O_3$	41.80 (41.71)	4.01 (4.13)	9.44 (9.24)	20.89 (20.93)
47	$R_1=R_2=C_2H_5$	3	75.5	157—160	$C_9H_{12}FN_3O_3$	47.16 (47.23)	5.28 (5.27)	8.29 (8.11)	18.33 (18.09)
48	$R_1=R_2=C_6H_5$	3	70.8	256—258	$C_{17}H_{12}FN_3O_3$	62.77 (63.05)	3.72 (3.80)	5.84 (5.96)	12.92 (12.69)
49	$R_1=R_2=CH_2CH_2Cl$	3	43.7	176—177	$C_9H_{10}Cl_2FN_3O_3$	36.26 (36.06)	3.38 (3.36)	6.37 (6.14)	14.09 (13.95)
50	$R_1=R_2=C_6H_{13}$	3	52.8	88	$C_{17}H_{28}FN_3O_3$	59.81 (60.03)	8.27 (7.82)	5.57 (5.30)	12.30 (11.98)
51	1,3-Bis$(C_2H_5)_2$[c]	3	31.0	147—148	$C_{14}H_{21}FN_4O_4$	51.21 (51.11)	6.45 (6.44)	5.80 (5.75)	17.06 (16.87)

a) Prepared from hexamethylene diisocyanate. b) Prepared from *m*-xylene-α,α'-diyl diisocyanate. c) 1,3-Bis-(diethylcarbamoyl)-5-fluorouracil.

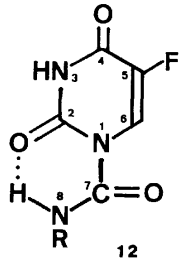

12

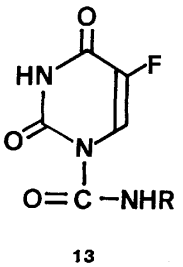

13

13. In a poorly solvating chloroform, only the **12** structure is observed at 25 and 60 °C. The ratio of **12** to **13** can be calculated based on the peak-intensity ratio of two doublets at 8.38 ppm (J=8 Hz, C_6–H of **12**) and at 7.70 ppm (J=6 Hz, C_6–H of **13**), or the ratio of two broad triplets at 9.11 ppm (J=6 Hz, N_8–H of **12**) and 5.68 ppm (J=6 Hz, N_8–H of **13**).

In contrast to the fact that the **2** substances decompose gradually in neutral water, they are generally resistant to acid hydrolysis because of their hydrogen bonding. Especially alkylcarbamoyl compounds like **22** are strongly resistant to acid hydrolysis. Indeed, their dormant nature in acid conditions suggests a possible application as oral administrative drugs which can survive acid in the stomach.

1-Alkylcarbamoyl-5-fluorouracil (**2**) can be absorbed into the blood. The lipophilic alkyl group of **2** helps it reach tissues or a tumor, and it moderately decomposes into **1** or other metabolites in tumor cells where the pH is nearly neutral.

The antitumor activities of **2** were evaluated by Hoshi *et al.*[13,14] by oral administration along with two reference compounds, **1** and 1-(2-tetrahydrofuryl)-5-fluorouracil (FT-207). The compounds tested in the L-1210 system were methyl-, ethyl-, isopropyl-, phenyl-, hexyl- and cyclohexyl-carbamoyl-5-fluorouracil; the therapeutic ratios ($ILSmax/ILS_{30}$) of these compounds were 1.9, 2.2, 2.3, 1.0, 4.5, and 3.3 respectively, while

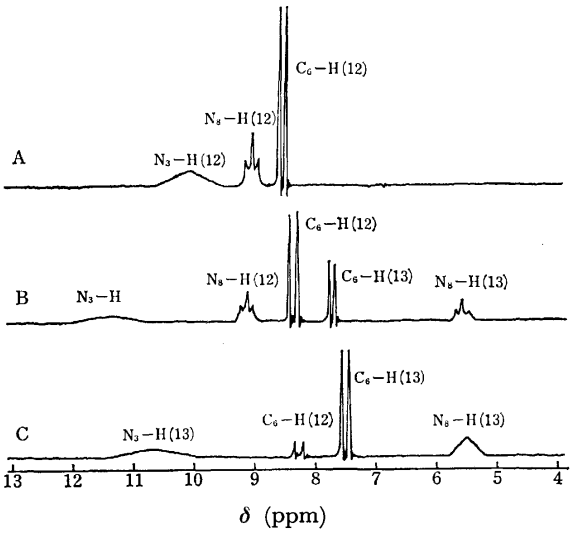

Fig. 1. Partial ^1H NMR spectra of 1-hexylcarbamoyl-5-fluorouracil.
A: In $CDCl_3$ solvent at 25 °C (hydrogen-bonded structure 12),
B: in DMSO-d_6 solvent at 25 °C (60% 12 and 40% 13),
C: in DMSO-d_6 solvent at 80 °C (non hydrogen-bonded structure 13).

those of the two reference compounds were 1.7 and 1.0. Among these compounds **22** showed the most effective results. The therapeutic ratio in the C-1498 system of **22** was 11, while those of **1** and FT-207 were 3.3 and 2.5 respectively. **22** was also showed activities toward solid tumors like Nakahara Fukuoka sarcoma and adenocarcinoma-755, and ascites tumors like sarcoma-180A, and was moderately active against Ehrlich ascites carcinoma. This compound had a wider tumor spectrum than **1** and FT-207 upon oral administration.

Table 3. ^{1}H NMR spectral data of 1-carbamoyl-5-fluorouracils

Compd	Carbamoyl groups						Uracil rings				Temp, °C	Solvent
	CH_3	CH_2	CH_nNH	h,[a] $NHC{=}O$	nh,[b] $NHC{=}O$	h[c]	N_3-H	h, C_6-H	nh,C_6-H	h(%)		
15			2.52 nh 2.83 h	9.01	5.68	38	11.23	8.37	7.71	41	25	D[e]
15			2.55	—[d]	5.49	0	—	—	7.58	0	80	D
16	1.12		3.30	9.10	5.65	64	11.32	8.37	7.72	67	25	D
17	0.88	1.48	3.14	9.32	5.80	51	11.56	8.50	7.82	44	25	D
17	0.95	1.68	3.38	9.09	—	100	—	8.58	—	100	25	C[f]
18	1.10		3.75	9.02	5.45	41	—	8.38	7.73	43	25	D
19	0.96	1.56	3.45	9.19	—	100	—	8.62	—	100	25	C
20	1.37			9.33	—	100	—	8.48	—	100	25	C
21	0.91	1.47	3.42	9.11	—	100	—	8.63	—	100	25	C
22	0.93	1.47	3.44	9.15	—	100	—	8.62	—	100	25	C
22	0.87	1.28	3.17	9.11	5.68	66	11.20	8.38	7.70	59	25	D
22	0.87	1.28	3.10	—	5.47	0	10.70	8.28	7.50	8	80	D
23	0.89	1.45	3.42	9.15	—	100	—	8.60	—	100	25	C
23	0.88	1.31	3.23	9.21	5.73	73	—	8.47	7.78	67	25	D
24	0.90	1.37	3.34	9.26	—	100	12.44	8.47	—	100	25	C
25	0.90	1.28	3.43	9.12	—	100	—	8.60	—	100	25	C
26	0.88	1.27	3.40	9.00	—	100	—	8.59	—	100	25	C
28			4.55	9.67	—	100	—	8.46	7.75	95	25	D
29		2.70	3.27	—	5.97	0	—	—	7.76	0	25	D+H_2O
30		5.3	4.20	9.72	—	100	—	8.75	—	100	25	P[g]
32				4.33	—	100	12.02	8.31	—	100	25	D
36		1.32	3.30	—	—		—	—	7.78	0	25	D+H_2O
37			4.52	9.65	—	100	12.38	8.47	—	100	25	D
38	3.72, 3.67		4.71, 3.85	9.98	6.60	50	12.00	8.49	7.81	54	25	D
39	1.21	2.56, 4.1	4.2	9.42	6.06	65	11.60	8.46	7.78	72	25	D
40	3.76	3.18	4.85	9.65	—	100	10.14	8.43	—	100	25	C
41	1.41	3.15, 4.15	4.23	9.65	—	100	—	8.43	6.55	95	25	D
42	1.29	3.07, 4.29	4.73	9.45	—	100	—	8.33	—	100	25	C
43	1.33, 2.13	2.4, 4.3	4.75	9.65	—	100	—	8.54	—	100	25	C
44	1.0, 3.82	1.78	4.65	9.75	—	100	11.90	8.50	—	100	25	C
45	2.30	3.76	4.55	9.57	—	100	—	8.50	—	100	25	C
46	2.90, 2.96						—	—	7.96	0	25	C
47	1.18		3.27				—	—	8.15	0	25	C
48							11.85	—	8.45	0	25	D
49		3.80					12.20	—	8.18	0	25	D
50	0.90	1.30	3.30				9.50	—	7.48	0	25	C

a) Hydrogen-bonded. b) Non-hydrogen-bonded. c) (h/h+nh)×100. d) Not detected. e) DMSO-d_6. f) $CDCl_3$. g) Pyridine-d_5.

In one continuing research on antitumor drugs a convenient new method of preparing isocyanate was also found. Isocyanates are obtained by the treatment of amines with trichloromethyl chloroformate (TCF)[17] in toluene at 100—110 °C, followed by distillation. In this reaction, the use of amine hydrochloride is preferable to avoid the formation of 1,3-disubstituted urea. When free amine is used, amine and TFC must be added to the solution so that the TCF is in excess in solution. Otherwise, heating at a high temperature for a long time is necessary for disubstituted ureas to react with TCF. By this method, several new isocyanates, **52**—**55**, were prepared.[18]

Experimental

The melting points were recorded on a Büchi melting-point aparatus and are uncorrected. Most 1-alkylcarbamoyl-5-fluorouracils (**2**) melt instantaneously at 95—170 °C and solidify. This melting point is likely to be overlooked, how-

ever. Nevertheless, differential thermal and gravimetric analysis revealed that **2** dissociated to **1** and isocyanates in this melting region, and a loss in weight of the isocyanates was observed. **1** decomposes at 280—283 °C. Therefore, in patents[2] in 1975, we mistakenly observed some decomposition temperatures of **2** to be 280—283 °C. The ^{1}H NMR spectra were recorded on a JEOL-60HL apparatus and the ^{13}C NMR spectra at 15 MHz on a JEOL-FX-60 apparatus. The IR spectra were obtained on a JASCO IR-A-1 apparatus. The mass spectrum was recorded on a Varian CH 7 apparatus. Microanalysis was done by the staff of the Analytical Laboratories of the Mitsui Toatsu Research Center.

*1-Hexylcarbomoyl-5-fluorouracil (**22**) (HCFU). Method 1-A. Reaction in a Pyridine Solution*: Hexyl isocyanate (19.08 g, 0.15 mol) and **1** (13.0 g, 0.1 mol) were heated in 40 ml of pyridine at 90 °C for an hour. The reaction mixture was then cooled to room temperature. About 30 ml of the pyridine were evaporated at 50 °C under reduced pressure. To the resulting residue, 50 ml of ethanol were added at 55 °C. Then the solution was kept at 0—5 °C overnight. Cyrstalline **22** (22.5 g, 87.4%) was thus obtained. As a second crop 2.90 g of product was obtained: mp 110—111 °C.

^{13}C NMR 157.27 (d, $J_{C_4-F}=1.87$ Hz, C-4), 150.35 (s, C-2), 149.31 (s, C-7), 140.90 (d, $J_{C_5-F}=16.05$, C-5), 123.43 (d, $J_{C_6-F}=2.47$ Hz, C-6), 41.52 (s, C-9), 31.38 (s, C-10), 29.11 (s, C-11), 26.51 (s, C-12), 22.55 (s, C-13), 13.97 (s, C-14).

MS *m/e* (rel. intensity) 257 (0.49) (M^+), 131 (7.9), 130 (88.4), 128 (1.3), 126 (1.7), 114 (2.0), 113 (1.3), 112 (14.5), 100 (4.9), 99 (70.7), 88 (5.6), 87 (37.4), 86 (2.2), 85 (27.0), 84 (19.8), 83 (1.9), 82 (6.0), 74 (1.3), 71 (3.4), 70 (7.5), 69 (8.6), 68 (1.7), 67 (4.2), 60 (27.0), 59 (8.5), 58 (16.6), 56 (56.2), 55 (49.9), 54 (4.6), 53 (8.0), 51 (2.0), 46 (1.9), 44 (9.5), 43 (35.4), 42 (35.4), 41 (87.4), 40 (7.8), 39 (8.3), 38 (27.0), 37 (2.6), 32 (4.6), 31 (11.4), 30 (11.4), 29 (49.9), 28 (73.8), 27 (43.7), 26 (4.2). IR (KBr) 3320, 3230, 3080, 2920, 1720—1740 (s), 1680, 1660, 1510, 1445, 1340, 1272, 1200, 1090, 1042, 802, 770, 750 cm^{-1}. UV ($CHCl_3$), λ_{max} 258, E 451, $\varepsilon=1.16\times10^4$.

Method 1-B. Reaction in a Dimethylacetamide Solution: Hexyl isocyanate (19.1 g, 0.15 mol), **1** (13.0 g, 0.1 mol) and triethylamine (1.0 g) in 52 ml of *N,N*-dimethylacetamide were heated at 90 °C for 3 h. The reaction mixture was then cooled and stirred into dilute aqueous hydrochloric acid (pH 1; 100 ml). The resulting precipitate was filtered, washed with water, and dried *in vacuo* to yield 21.4 g (83.1%) of crude **22,** which was then recrystallized from ethanol as white crystals.

Method 2. Into a cold (5 °C) solution containing **1** (1.30 g, 0.01 mol) in 40 ml of pyridine, phosgene (2.97 g, 0.03 mol) was bubbled over a 1 h period at 10 °C. Nitrogen gas was passed through to expel the excess phosgene. Hexylamine (1.01 g, 0.01 mol) was then added, and the mixture was stirred 1 h. The resulting pyridine hydrochloride was filtered off, and the reaction mixture was evaporated to dryness. The residue, taken up in 50 ml of chloroform, was washed twice with 30 ml of a dilute hydrochloric acid solution. The chloroform sloution was then dried (Na_2SO_4) and evaporated to afford **22** (2.05 g, 80.0%).

*1-Phenylcarbamoyl-5-fluorouracil (**33**). Method 1-C. In a Dimethyl Sulfoxide Solution*: To a solution containing **1** (10.4 g, 0.08 mol) in 100 ml of dimethyl sulfoxide, phenyl isocyanate (14.3 g, 0.12 mol) was added, and the mixture was stirred at room temperature for 1 h. When the milky reaction mixture was then filtered, fine precipitates were obtained. The precipitates were suspended in hot ethanol and filtered again to afford **33** (16.2 g, 81.4%); mp 280 °C.

*1-[α-Ethoxycarbonyl-β-(p-hydroxyphenyl) ethylcarbamoyl]-5-fluorouracil (**42**). Method 3.* To a cold pyridine solution containing a 0.04 molar amount of 1-chloroformyl-5-fluorouracil (**5**), a solution of L-thyrosine ethyl ester hydrochloride (9.80 g, 0.04 mol) in triethylamine (12.14 g) was added at 0 °C over a period of 2 h. The pyridine hydrochloride thus formed was filtered off. The filtrate was evaporated to dryness, and the residue, dissolved in 200 ml of chloroform, was washed twice with 200 ml of dilute hydrochloric acid. The chloroform layer was evaporated and column chromatographed on silica gel C-200. Elution with benzene–ethyl acatate (10 : 1) gave 5.10 g (25.8%) of **42**; mp 76.5—78 °C.

*1-Diethylcarbamoyl-5-fluorouracil (**47**). Method 3.* To 1.3 g (0.01 mol) of **1** dissolved in 20 ml of *N,N*-dimethylacetamide was added 0.48 g (0.01 mol) of 50% sodium hydride in mineral oil. Subsequently, diethylcarbamoyl chloride (1.36 g, 0.01 mol) in 5 ml of *N,N*-diethylacetamide was added, drop by drop, at 30 °C. After stirring at 30 °C for 5 h, the reaction mixture was left to stand overnight at room temperature and then filtered; the filtrate was subsequently evaporated *in vacuo*. The chloroform extract of the residue yielded 2.14 g of a crude product which was washed with diethyl ether to afford pure **47** (1.73 g, 75.5%); mp 157—160 °C.

*1,3-Bis(diethylcarbamoyl)-5-fluorouracil (**51**). Method 3.* To **1** (2.6 g, 0.02 mol) in 30 ml of *N,N*-dimethylformamide was added powdered potassium carbonate (3.32 g, 0.024 mol), and then a mixture of diethylcarbamoyl chloride (7.06 g, 0.052 mol) and 20 ml of *N,N*-dimethylformamide. The reaction mixture was heated at 80 °C for 2 h. The product was extracted into chloroform after the removal of the solvent *in vacuo*. The extract was washed with water, dried (Na_2SO_4), and evaporated to give a viscous oil. The oil was triturated with 5 ml of ethanol, and ether was added to complete the crystallization. The crystal was washed with ether to afford **51** (1.18 g, 31.0%); mp 147—148 °C.

*L-α-Ethoxycarbonyl-β-phenylethyl Isocyanate (**52**).* TCF (16.0 g, 0.07 mol) is added, drop by drop, to a mixture of L-phenylalanine ethyl ester hydrochloride (16.0 g, 0.07 mol) and active carbon (0.1 g) in 200 ml of toluene. The reaction mixture was gradually being heated to 80 °C over a 1 h period, the addition of the TCF being adjusted so as to finish at the time when the temperature reached 80 °C. The reaction was continued for an additional 2 h at 100—110 °C. The subsequent removal of the toluene and distillation of the reaction mixture gave **52** (13.75 g, 89.6%); bp 141—142 °C (5 mm); IR (neat), 2980, 2250(vs), 1735(s), 1208(s), 1197, 1025, 700 cm^{-1}; NMR (neat), 1.12 (3H, t, $J=8$ Hz), 2.95 (2H, d, $J=6$ Hz), 4.09 (2H, q, $J=8$ Hz), 4.0—4.2 (1H, m,) 7.21 (5H, s). Found: C, 65.54; H, 5.91; N, 6.14%. Calcd for $C_{12}H_{13}NO_3$: C, 65.74; H, 5.98; N, 6.39%.

*L-α-Ethoxycarbonyl-β-(methylthio)propyl Isocyanate (**53**).* Into a mixture of methionine ethyl ester hydrochloride (14.96 g, 0.07 mol), active carbon (0.01 g), and 200 ml of toluene, TCF (10.4 g, 0.0525 mol) was added dropwise with stirring. Then the reaction mixture was gradually heated up to reflux, and the reflux was continued for 2 h. The subsequent distillation of the reaction mixture gave 7.37 g (51.8%) of **53** as a colorless liquid: bp 133 °C (7 mm); IR (neat), 2995, 2950, 2270(s), 1752(s), 1450, 1225(s), 1040 cm^{-1}; NMR (neat), 1.32(3H, t, $J=8$ Hz), 2—2.2(2H, m), 2.1(3H, s), 2.67(2H, t, $J=7$ Hz), 4.3(2H, q, $J=8$ Hz), 4.2—4.4(1H, m). Found: C, 46.89; H, 6.52; N, 6.66; S, 15.46%. Calcd for $C_8H_{13}NO_3S$: C, 47.27; H, 6.45; N, 6.89; S, 15.74%.

*α-Methoxycarbonyl-β-methylbutyl Isocyanate (**54**).* TCF (19.8 g, 0.1 mol) was added, drop by drop, to a mixture of L-leucine methyl ester hydrochloride (26.62 g, 0.13 mol), active carbon (0.2 g), and toluene (200 ml). The mixture was

gradually heated to reflux, and heating at reflux was continued for 2 h. The subsequent distillation of the reaction mixture afforded 15.51 g (69.7%) of **54** as a colorless liquid; bp 74 °C (5 mm); n_D^{25} 1.4322; IR (neat), 3420, 2960, 2270(s), 1755, 1445, 1280, 1220 cm^{-1}; NMR (neat) 0.93(6H, d, J= 6 Hz), 1.67 (3H, m), 3.78 (3H, s), 4.05 (1H, t, J=8 Hz). Found: C, 56.61; H, 7.65; N, 7.43%. Calcd for $C_8H_{13}NO_3$: C, 56.31; H, 7.65; N, 8.18%.

*β-(Ethoxycarbonyl)ethyl Isocyanate (**55**).* The treatment of β-alanine ethyl ester hydrochloride (15.3 g, 0.1 mol) with TCF (19.8 g, 0.1 mol) in the usual way in **52** afforded 10.2 g (71.2%) of **53** as a colorless liquid; bp 69 °C (8 mm); IR (neat) 3000, 2280, 1750, 1390, 1200 cm^{-1}.

*Phenethyl Isocyanate (**56**).* Into a solution of TCF (19.8 g, 0.1 mol) in 200 ml of toluene, phenethylamine (24.15 g, 0.2 mol) and active carbon (0.1 g) were added, drop by drop, with strring. Then the reaction mixture was gradually heated to 50 °C and TCF (9.9 g, 0.05 mol) was added, drop by drop. The reaction was subsequently continued for 2 h at 100—110 °C. The removal of the solvent and distillation of the residue afforded 25.0 g (85.3%) of **56**: bp 124—126 °C (33 mm).

*Benzyl Isocyanate (**57**).* The treatment of benzylamine (21.4 g, 0.2 mol) with TCF (30.0 g, 0.15 mol) in the same way in was used for **56** afforded 23.0 g (86.4%) of **57**; bp 95 °C (19 mm).

The authors wish to thank Drs. K. Kuretani and A. Hoshi, National Cancer Center Research Institute in Tokyo, for the evaluation of the antitumor activity, and also Mitsui Toatsu Chemicals, Inc., and Mitsui Pharmaceuticals, Inc. (The Pharmaceutical Division of Mitsui Toatsu Chemicals, Inc.) for permission to publish this paper.

References

1) S. Ozaki, *Chem. Rev.*, **72**, 457 (1972).
2) Mitsui Pharmaceutical, Inc, and Mitsui Toatsu Chemicales, Inc., Japan Patent Open, 50—148365 (1975); German Patent Open, 2455423 (1975), 2639135 (1977); Belg. Patent 846956 (1977).
3) C. Heidelberger, N. K. Chauduri, P. Danneberg, M. Mooren, L. Griesbach, R. Duschinsky, R. J. Schnitzer, E. Pleven, and L. Scheneider, *Nature*, **179**, 663 (1957).
4) R. Paegle, M. Lidaks, and Yu. P. Shvachkin, *Khim. Geterotsikl. Soedin., Aka. Nauk Latv. SSR* (2) 316 (1966).
5) S. A. Hiller, R. A. Zhnk, and M. Lidak. *Dokl. Akad. Nauk SSSR*, **176**, 332 (1967).
6) S. A. Hiller, R. A. Zhuk, and G. Ya. Nashatyr, *Khim. Geterotsikl. Soedin.*, (3) 557 (1968); *Chem. Abstr.*, **69**, 96641h (1968).
7) M. Lidaks, R. Paegle, M. Plata, K. Ya. Pets, and Yu. P. Shvachkin, *Khim. Geterotsikl. Soedin.*, (2) 379 (1968); *Chem. Abstr.*, **69**, 96640g (1968).
8) T. T. Sakai, A. L. Pogolotti, and D. V. Santi, J. *Heterocycl. Chem.*, **5**, 849 (1968).
9) W. Klotzer and M. Herberz, *Monatsh. Chem.*, **99**, 847 (1968).
10) T. Seita, M. Kinoshita, and M. Imoto, *Bull. Chem. Soc. Jpn.*, **46**, 1572 (1973).
11) M. Tada, *Chem. Lett.*, **1975**, 129.
12) M. Tada, *Bull. Chem. Soc. Jpn.*, **48**, 3427 (1975).
13) A. Hoshi, M. Iigo, M. Yoshida, and K. Kuretani, *Gann*, **66**, 673 (1975).
14) A. Hoshi, M. Iigo, A. Nakamura, M. Yoshida, and K. Kuretani, *Gann*, **67**, 725 (1976).
15) A. S. Jones and J. H. Warren, *Tetrahedron*, **26**, 791 (1970).
16) R. Parthathy, J. Ohrt, S. P. Dutta, and G. B. Chheda, *J. Am. Chem. Soc.*, **95**, 8141 (1973).
17) O. Masuyama, *J. Synth. Org. Chem. Jpn.*, **34**, 431 (1976).
18) Mitsui Toatsu Chemicals, Inc., Japan Patent applied for.

Studies on Separation of Amino Acids and Related Compounds. VIII.[1] Preparative Separation of Isomeric L-Aspartyl-L-phenylalanine Methyl Esters and Related Dipeptide Esters by Ion-Exchange Chromatography

Akira YASUTAKE, Haruhiko AOYAGI, and Nobuo IZUMIYA

Laboratory of Biochemistry, Faculty of Science, 33 Kyushu University, Higashi-ku, Fukuoka 812

(Received February 21, 1977)

Authentic peptides, α- and ω-isomers of L-aspartyl (or L-glutamyl)-L-phenylalanine (or L-tyrosine) methyl ester, were synthesized by conventional methods. Among these eight peptides, α-L-glutamyl-L-phenylalanine methyl ester showed the tendency to convert to the corresponding dipeptide anhydride even under mild conditions. The experiments on a small column of Dowex 50 cation exchange resin were carried out with a model mixture composed of the α- and ω-isomers, and the optimum conditions for the complete separation of both isomers were determined. A synthetic mixture composed of the α- and ω-isomers was prepared readily through the coupling of benzyloxycarbonyl-L-aspartic acid (or glutamic acid) anhydride with L-phenylalanine (or L-tyrosine) methyl ester and subsequent hydrogenation. The synthetic mixture was separated by the use of a large ion exchange column and each isomer was obtained in a good yield.

In 1969, Mazur *et al.* discovered that α-APM[2] was 100—200 times sweeter than sucrose.[3] Although Davey *et al.* synthesized α-APM in 1966 by the hydrogenation of Z–Asp(OBzl)–Phe–OMe,[4] the large-scale preparation of α-APM by a simpler method has been desired. As described in a previous paper,[1] we have developed a convenient procedure for the separation of the α- and β-isomers of H–Asp–His–OH by column chromatography with Dowex 50.

In the present study, we attempted to separate in quantity α- and β-APM from a synthetic mixture by similar chromatographic methods. The synthetic mixture was prepared easily as shown in Fig. 1 by coupl ing and subsequent hydrogenation of the resulting mixture containing Z–Asp(OH)–Phe–OMe and Z–Asp(Phe–OMe)–OH. Additionally, we intended to separate α- and β-ATM, α- and γ-GPM, and α- and γ-GTM, from corresponding synthetic mixtures

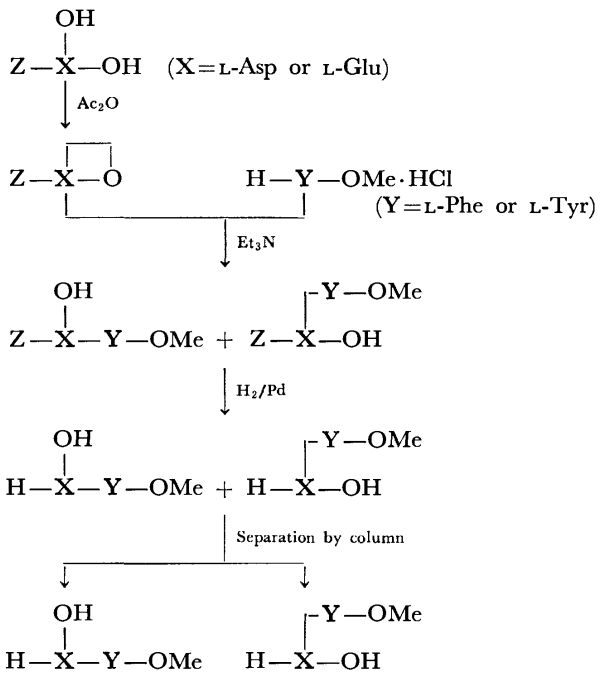

Fig. 1. Preparation of a synthetic mixture composed of α- and ω-dipeptide ester and subsequent saparation of the mixture.

which were also prepared by the coupling and hydrogenation procedure outlined in Fig. 1. These dipeptide esters are considered as interesting compounds from the standpoint of possible structure-taste relationships related to α-APM.

Experimental

TLC was carried out on Merck silica gel G, and PPC on Toyo Roshi No. 52 paper. R_f (TLC) and R_f (PPC) values are reported for the following solvent system: 1-butanol–acetic acid–pyridine–water (15 : 3 : 10 : 12, v/v). Material possessing a free terminal amino group (*e.g.*, α-APM) was detected by spraying with 0.2% ninhydrin solution in 80% ethanol, followed by heating at 100 °C. Material having blocked amino groups (*e.g.*, dipeptide anhydride) was detected by spraying with 10% H_2SO_4, followed by heating on a hot plate. $[\alpha]_D$ was measured with a Union high sensitivity polarimeter PM-71 (Kyoto).

*Authentic Peptides. Z-Asp(OBzl)-Phe-OMe (**1**), Z-Asp(OBzl)-Tyr-OMe (**3**), Z-Glu(OBzl)-Phe-OMe (**5**), Z-Glu(Phe-OMe)-OBzl (**6**), Z-Glu(OBzl)-Tyr-OMe (**7**)*: Mazur *et al.* prepared these compounds by the coupling of the Z-amino acid *p*-nitrophenyl ester, *e.g.*, Z–Asp(OBzl)–ONp, and H–Phe(or Tyr)–OMe in yields of 57—97%.[3] We prepared these compounds by the coupling of a mixed anhydride[5] of the Z-amino acid with H–Phe(or Tyr)–OMe in yields of about 70% as described for the preparation of **2**. Melting points and specific rotations of the products agreed with literature values[3] with the exceptions of mp 99—100 °C for **5** (lit, 78—80 °C), $[\alpha]_D^{20}$ −6.4° for **7** (*c* 2, MeOH) (lit, −44°). We observed that the synthesis of Z–Asp(OH)–OBzlNO_2[6] was easier than that of Z–Asp(OH)–OBzl;[7] therefore, the intermediate compounds (**2** and **4**) were prepared as follows.

*Z-Asp(Phe-OMe)-OBzlNO_2 (**2**)*: To a chilled solution of Z–Asp(OH)–OBzlNO_2 (4.02 g, 10 mmol) and triethylamine (1.4 ml, 10 mmol) in tetrahydrofuran (25 ml) was added isobutyl chloroformate (1.31 ml, 10 mmol) at −10 °C. After 15 min, a chilled solution of H–Phe–OMe·HCl (2.16 g, 10 mmol) and triethylamine (1.4 ml, 10 mmol) in chloroform (20 ml) was added. The reaction mixture was left to stand at room temperature overnight, evaporated *in vacuo*, and the oily residue was dissolved in ethyl acetate (300 ml). The solution was washed successively with 4% $NaHCO_3$, 2% HCl and water, dried (Na_2SO_4), and evaporated. The crystals were collected with the aid of ether; yield, 3.84 g (68%); mp 162—164 °C; $[\alpha]_D^{20}$ −40.9° (*c* 1, MeOH).

Found: C, 61.73; H, 5.16; N, 7.28%. Calcd for $C_{29}H_{29}O_9N_3$: C, 61.80; H, 5.19; N, 7.46%.

Z-Asp(Tyr-OMe)-OBzlNO$_2$ (4): This compound was prepared from Z-Asp(OH)-OBzlNO$_2$ (10 mmol) and H-Tyr-OMe·HCl (10 mmol), as described for the preparation of **2**; yield, 4.18 g (72%); mp 163—164 °C; $[\alpha]_D^{20}$ −40.4° (*c* 1, MeOH).

Found: C, 60.04; H, 5.06; N, 7.19%. Calcd for $C_{29}H_{29}O_{10}N_3$: C, 60.10; H, 5.04; N, 7.25%.

Z-Glu(Tyr-OMe)-OBzl (8): This compound was prepared from Z-Glu(OH)-OBzl[8] (10 mmol) and H-Tyr-OMe·HCl (10 mmol), as described above; yield, 3.50 g (64%); mp 149 °C; $[\alpha]_D^{20}$ −9.2° (*c* 1, MeOH).

Found: C, 65.54; H, 6.05; N, 5.07%. Calcd for $C_{30}H_{32}O_8N_2$: C, 65.68; H, 5.88; N, 5.11%.

α-APM, β-APM, α-ATM, β-ATM, α-GPM, γ-GPM, α-GTM: These compounds were prepared by the hydrogenation of **1**—**7**, as described for the preparation of γ-GTM. Their specific rotations agreed with literature values[3] with the exceptions of $[\alpha]_D^{20}$ +6.1° (*c* 2, H_2O) for β-APM (lit, +4°)[3] and $[\alpha]_D^{20}$ +15.8° for γ-GPM (*c* 2, H_2O) (lit, +21°).[3]

γ-GTM: A solution of **8** (0.55 g, 1 mmol) in a mixture of methanol (12 ml) and acetic acid (3 ml) was treated with hydrogen in the presence of palladium black, and the filtrate was evaporated *in vacuo*. The resulting solid was recrystallized from hot water; yield, 0.30 g (93%); mp 197—199 °C; $[\alpha]_D^{20}$ +6.9° (*c* 2, H_2O), $[\alpha]_D^{20}$ +39.2° (*c* 2, AcOH); R_f (TLC) 0.68, R_f (PPC) 0.54.

Found: C, 55.40; H, 6.23; N, 8.51%. Calcd for $C_{15}H_{20}O_6N_2$: C, 55.55; H, 6.22; N, 8.64%.

H-α-Glu-Phe-OH Anhydride (9): α-GPM (62 mg, 0.2 mmol) was dissolved in methanol (10 ml) previously saturated with ammonia, and the solution was allowed to stand at room temperature for 2 days. The solvent was removed by evaporation, the residue was dissolved in water (10 ml), and the solution was acidified with 1 M HCl (0.2 ml). After the solution was evaporated to dryness, the resulting crystals were collected by the filtration with the aid of cold water; yield, 42 mg (71%); mp 235—236 °C (dec); $[\alpha]_D^{20}$ +28.8° (*c* 1, AcOH); R_f (TLC) 0.75.

Found: C, 60.54; H, 5.93; N, 10.18%. Calcd for $C_{14}H_{16}O_4N_2$: C, 60.56; H, 5.84; N, 10.14%.

Column Chromatography. A column was packed with Dowex 50X8 (200—400 mesh) equilibrated with a specified eluting solvent. The eluting solvents used were aqueous pyridinium acetate at different concentrations and pHs as follows; S_1=0.1 M at pH 4, S_2=0.2 M at pH 4, S_3=0.2 M at pH 5, S_4=1 M at pH 5. A mixture of dipeptide esters was applied to a column and eluted with one of these eluting solvents at room temperature. An aliquot (0.5 ml) of each fraction was subjected to a test to determine the amount of ninhydrin-positive material present using the Yemm and Cocking method.[9]

Results and Discussion

Column Chromatography of a Model Mixture Containing Isomeric Dipeptide Esters. Preliminary experiments on a model mixture were performed as follows with a small column in order to find the optimum conditions for the separation. A model mixture was prepared by dissolving 0.01 mmol each of α- and β-APM in water (0.5 ml). Other model mixtures (α- and β-ATM, α- and γ-GPM, and α- and γ-GTM) were prepared similarly. The model mixture was applied to a column (0.9×20 cm) and eluted with a specified eluting solvent,

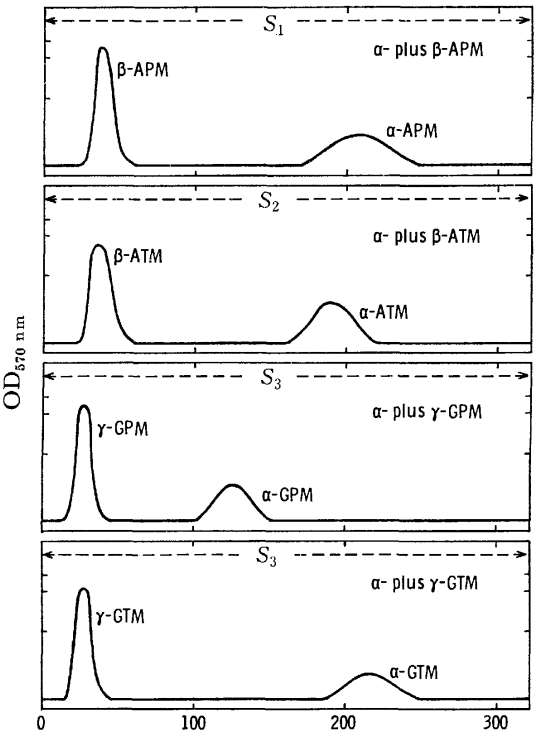

Fig. 2. Chromatography on a 0.9×20 cm column of Dowex 50 of model mixtures. For example, α- plus β-APM represents a model mixture composed of α-APM and β-APM (total, 0.02 mmol).

2-ml fractions being collected at a flow rate of 20 ml/h. The peptide in each fraction was identified by means of TLC or PPC after concentration of the corresponding fraction by evaporation.

We applied pyridinium acetate in various concentrations and pHs to determine necessary separation conditions of the α- and ω-isomers in a model mixture. An example with satisfactory results is shown in Fig. 2. When higher concentrations of pyridinium acetate and more alkaline pHs were used, the distance of separation between the α- and ω-isomers was diminished.

As seen in Fig. 2, the α-isomer was eluted more slowly than the corresponding ω-isomer in every case. We can give no definite explanation for this phenomenon, but we can point out that the same phenomenon was observed in the previous study in which H-β-Asp-His-OH or H-γ-Glu-His-OH was eluted faster than the corresponding α-dipeptide.[1]

Preparative Separation of α-APM and β-APM from a Synthetic Mixture. A synthetic mixture was prepared according to Fig. 1 and each isomer was separated with a large column. To a solution of Z-Asp-OH anhydride[10] (2.49 g, 10 mmol) in tetrahydrofuran (10 ml) was added a solution of H-Phe-OMe·HCl (2.38 g, 11 mmol) and triethylamine (1.54 ml, 11 mmol) in chloroform (20 ml) while stirring at room temperature. After stirring overnight, the reaction mixture was evaporated to dryness and the residue was dissolved in a mixture of methanol (40 ml) and acetic acid (10 ml). The solution was treated with hydrogen in the presence of palladium black. The filtrate was evaporated to dry-

Table 1. Elution data for preparative separation of synthetic mixture

Material	Elution solvent	Eluate volume (ml)	Portion for evaporation (ml)	Peptide present
Mixture of				
α- and β-APM	S_1	0—1000	580—980	β-APM
	S_3	1000—2000	1340—1760	α-APM
α- and β-ATM	S_2	0—1000	660—900	β-ATM
	S_3	1000—2000	1620—1900	α-ATM
α- and γ-GTM	S_3	0—1000	300—520	γ-GTM
	S_4	1000—1600	1400—1700	α-GTM
α- and γ-GPM	S_3	0—500	300—420	γ-GPM
	S_4	500—1200	900—1100	α-GPM[a]

a) α-GPM was converted into H-Glu-Phe-OH anhydride mostly after evaporation of the portion (900—1100 ml).

Table 2. Yields and physical constants of peptides

Peptide	Yield (%)	Melting point (°C dec)	$[\alpha]_D^{20}$ (c 1)		R_f	
			H_2O	AcOH	TLC	PPC
β-APM	32	181—182	+6.2°	+40.4°	0.69	0.67
α-APM	37	239—242	+0.2°	+33.0°	0.74	0.72
β-ATM	31	200—202	+14.8°	+38.4°	0.65	0.55
α-ATM	34	266—268	+5.2°	+36.2°	0.69	0.61
γ-GTM	27	201—202	+7.0°	+39.0°	0.69	0.55
α-GTM	34	215—217	+15.6°	+46.0°	0.72	0.76
γ-GPM	27	160—162	+1.2°	+38.4°	0.69	0.71
H-α-Glu-Phe-OH anhydride	31	234—236	—[a]	+28.6°	0.76[b]	
Authentic α-GPM[c]		105—109	+1.2°	+45.2°	0.74[b]	0.80

a) H-α-Glu-Phe-OH anhydride was slightly soluble in water, hence an accurate determination of $[\alpha]_D$ in water was difficult. b) When chloroform-methanol-acetic acid (25 : 5 : 1, v/v) was used as a solvent on TLC, R_f values were 0.54 for H-α-Glu-Phe-OH anhydride and 0.14 for authentic α-GPM. c) Data of this peptide synthesized by the conventional method are given as reference values.

ness, and the resulting powder (a synthetic mixture) was used in the next step.

The powder was dissolved in S_1 (20 ml) and put on a column (2.7×50 cm) of Dowex 50. The sample was eluted with 1000 ml of eluant S_1 at a flow rate of 40 ml/h, and 20-ml fractions were collected. Then, the eluant was changed to S_3 in order to shorten elution time, and 1000 ml of S_3 was eluted. The eluting solvents used in this study are summarized in Table 1. The elution pattern is shown in Fig. 3 as a representative example among similar experiments. A portion of 580—980 ml was evaporated in a bath at about 50 °C *in vacuo*, the evaporations being repeated several times by the additions of water.

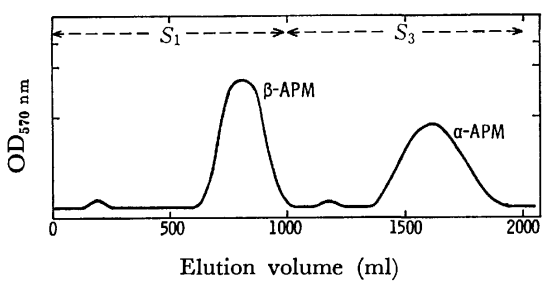

Fig. 3. Chromatography on a 2.7×50 cm column of Dowex 50 of a synthetic mixture (10 mmol) composed of α-and β-APM.

The residual product was recrystallized from hot water; yield of β-APM, 0.95 g (32% from Z-Asp-OH anhydride), the data being shown in Table 2. A portion of 1340—1760 ml was treated similarly; yield of α-APM, 1.09 g (37% from Z-Asp-OH anhydride).

As mentioned above, we could isolate pure α- and β-APM in good yields from a synthetic mixture by the use of a column with ion-exchange resin. Ariyoshi *et al.* prepared a similar synthetic mixture by the coupling of L-aspartic acid anhydride (1 equivalent) and H-Phe-OMe (4 equivalents); this procedure is advantageous because it avoids the hydrogenation step as seen in Fig. 1, but suffers from the contamination of the product with excess H-Phe-OMe and polymers that are produced by over reaction of L-aspartic acid anhydride.[11] The same investigators reported the isolation of α-APM hydrochloride, which was less soluble than β-APM hydrochloride, by means of fractional crystallization from their synthetic mixture.[11]

Preparative Separations of α-ATM and β-ATM, and α-GTM and γ-GTM, from Each Synthetic Mixture. Each synthetic mixture was prepared from Z-Asp-OH anhydride (10 mmol) and H-Tyr-OMe·HCl (11 mmol), and from Z-Glu-OH anhydride[12] (10 mmol) and H-Tyr-OMe·HCl (11 mmol), respectively, as described for the preparation of the synthetic mixture containing α- and β-APM. Subsequently, each mixture was subjected to column chromatography as described for the

isolation of α- and β-APM, the data of eluting solvents being summarized in Table 1. Each isomer was obtained in yields of 0.97 g (31%) for β-ATM, 1.06 g (34%) for α-ATM, 0.87 g (27%) for γ-GTM and 1.09 g (34%) for α-GTM. The physical constants are summarized in Table 2.

Preparative Separation of H–α-Glu–Phe–OH Anhydride and γ-GPM from a Synthetic Mixture. The synthetic mixture prepared from Z–Glu–OH anhydride (10 mmol) and H–Phe–OMe·HCl (11 mmol) was treated on a column as described above. A portion of the eluate (300—420 ml) yielded 0.84 g (27%) of pure γ-GPM (see Tables 1 and 2). It was observed that a portion of the 900—1100 ml fraction contained α-GPM; however, the residual powder obtained after evaporation of this fraction was a mixture of H–α-Glu–Phe–OH anhydride as a major product and α-GPM as a minor product. The residual powder was collected by filtration with the aid of cold 0.1 M HCl to remove α-GPM, and subsequently washed with cold water; yield of H–α-Glu–Phe–OH anhydride, 0.91 g (31%); mp 234—236 °C (dec) (see Table 2).

At the beginning stages of this experiment, we had assumed that the product with mp 234—236 °C was either Pyroglu–Phe–OMe or H–α-Glu–Phe–OH anhydride. Since the results of IR and NMR of the product indicated no presence of methyl ester group, we compared the product with authentic H–α-Glu–Phe–OH anhydride(**9**), and were able to identify the product as the anhydride. We discovered that the H–α-Glu–Phe–OH anhydride was produced during evaporation of the eluate and the amount produced was dependent upon the temperature of the bath and the extent of reduced pressure during the evaporation. For example, the residual powder after evaporation at 30 °C with a good aspirator at 15—20 mmHg was a 3 : 7 mixture of the anhydride to α-GPM. Since these results suggested the lability of α-GPM compared with other dipeptide esters, we carried out the following experiments.

Stability of Dipeptide Esters. Authentic dipeptide methyl esters (eight kinds) were stored in bottles at room temperature for about 4 months, and each was examined by TLC and PPC. The results indicated that α-GPM was converted mostly into H–α-Glu–Phe–OH anhydride and only a small amount of the original peptide ester remained. On the contrary, the seven other peptide esters remained unchanged after 4 months.

The experiment was also carried out in solution. 25 μmol of each of the pure authentic dipeptide esters (eight kinds) was dissolved in S_4 (1 ml), and the solution was allowed to stand at 25 °C. Aliquots withdrawn at selected intervals up to 6 days were subjected to TLC, and examined for the appearance of new peptides. After 6 days, an incubation solution of α-GPM contained an appreciable amount (about 20%) of H–α-Glu–Phe–OH anhydride, and each solution of α-APM, α-ATM, and α-GTM also contained some amounts (5—10%) of new products which are presumably the corresponding dipeptide anhydrides. On the contrary, each solution of ω-dipeptide esters was stable producing no new product.

No definite explanation for the marked tendency of α-GPM to convert to the corresponding anhydride can be given at present. Recently, Furda *et al.* examined the relative stabilities of α-APM and its hydrochloride in aqueous solution, and detected the presence of H–α-Asp–Phe–OH anhydride as a major product.[13]

Sweetness Evaluation. The sweetness of these compounds was organoleptically determined by panel evaluation in our laboratory according to the literature.[14] α-APM and α-ATM, isolated from the synthetic mixture, had intense sweet tastes similar to the corresponding authentic samples. Other β-aspartylpeptide esters and all glutamylpeptide esters, including γ-GTM which was prepared newly in this study, showed weak bitter tastes. Mazur *et al.* reported the intense sweet tastes of α-APM and α-ATM, and the bitter tastes of many β-aspartyl and glutamylpeptide esters.[3]

References

1) M. Hirata, K. Noda, and N. Izumiya, *Bull. Chem. Soc. Jpn.*, **45**, 1290 (1972).
2) Standard amino acid symbols denote the L-configuration. One letter abbreviations used are: A, Asp; G, Glu; P, Phe; T, Tyr; M, methyl ester. Thus, *e.g.* α-APM represents α-L-aspartyl-L-phenylalanine methyl ester, γ-GTM γ-L-glutamyl-L-tyrosine methyl ester. Other abbreviations used are: Z, benzyloxycarbonyl; OBzl, benzyl ester; OBzl-NO_2, *p*-nitrobenzyl ester; TLC, thin-layer chromatography; PPC, paper chromatography.
3) R. H. Mazur, J. M. Schlatter, and A. H. Goldkamp, *J. Am. Chem. Soc.*, **91**, 2684 (1969).
4) J. M. Davey, A. H. Laird, and J. S. Morley, *J. Chem. Soc., C*, **1966**, 555.
5) J. R. Vaughan, Jr. and R. L. Osato, *J. Am. Chem. Soc.*, **74**, 676 (1952).
6) E. Schröder and E. Klieger, *Justus Liebigs Ann. Chem.*, **673**, 208 (1964).
7) T. Hayakawa, Y. Fujiwara, and J. Noguchi, *Bull. Chem. Soc. Jpn.*, **40**, 1205 (1967).
8) E. Klieger and H. Gibian, *Justus Liebigs Ann. Chem.*, **655**, 195 (1962).
9) E. W. Yemm and E. C. Cocking, *Analyst*, **80**, 209 (1955).
10) W. D. John and G. T. Young, *J. Chem. Soc.*, **1954**, 2870.
11) Y. Ariyoshi, T. Yamatani, N, Uchiyama, Y. Aoki, and N. Sato, *Bull. Chem. Soc. Jpn.*, **46**, 1893 (1973).
12) W. J. LeQuesne and G. T. Young, *J. Chem. Soc.*, **1950**, 1954.
13) I. Furda, P. D. Malizia, M. G. Kolor, and P. J. Vernieri *J. Agric. Food Chem.*, **23**, 340 (1975).
14) Y. Ariyoshi, N. Yasuda, and T. Yamatani, *Bull. Chem. Soc. Jpn.*, **47**, 326 (1974).

Effects of Metal Ions on Reactivity Patterns in the Reactions of 1-Methoxycarbonyl-2-imidazolidinone and Its Derivatives with Butylamine

Noboru MATSUMURA, Hiroshi KAWAI, Yoshio OTSUJI, and Eiji IMOTO

Department of Applied Chemistry, College of Engineering, University of Osaka Prefecture, Sakai, Osaka 591

(Received Feberuary 28, 1977)

The reactions of 1-methoxycarbonyl-2-imidazolidinone, 3-acetyl-1-methoxycarbonyl-2-imidazolidinone and 1-methoxycarbonyl-*cis*-perhydrocyclopenta[*d*]imidazol-2-one with butylamine were studied in the absence and presence of various metal ions. Certain bivalent ions such as Mg^{2+}, Ca^{2+}, and Mn^{2+} enhanced an electrophilic reactivity of the methoxycarbonyl group and facilitated the transfer reaction of this group to butylamine, especially when the imidazolidinone moiety of substrates bears the methoxycarbonyl group at one N-position and a hydrogen atom at the other N-position. Whereas monovalent ions such as Na^+ and Ag^+, and bivalent ions such as Zn^{2+} and Cu^{2+}, had no appreciable effect on the reactivity, and exhibited almost the same reactivity patterns as those observed in the reactions in the absence of metal ions. A possible explanation is given in terms of the stability of coordination complexes which are formed by the interaction between the imidazolidinone moiety of substrates and added ions.

It has been postulated that a carboxylated biotin-enzyme, most probably carboxylated at the 1-N position of the biotin moiety of the enzyme, is a key intermediate in the biotin-enzyme-promoted carboxylations, and that the carbonyl group is transferred from this intermediate to a nucleophilic carbon of acyl-CoA or α-keto acids.[1,2] In order to elucidate the chemical mechanism of these enzymatic carboxylations, many model studies have been carried out by use of compounds related to biotin.[3] However, no definitive information has yet been obtained. We have recently investigated the chemistry of 1-methoxycarbonyl-2-imidazolidinone and its derivatives in a hope to gain a more insight into the chamical functions of biotin in the enzymatic carboxylations.[4]

Upon treatment with an amine, 1-methoxycarbonyl-2-imidazolidinone (**1**) is preferentially converted into 1-alkylcarbamoyl-4-methoxycarbonylethylenediamine (**2**), and the transfer of the methoxycarbonyl group to the amine is not observed.[4] Consequently, this experiment does not become in any sense a model reaction for the enzymatic carboxylations. On the other hand, it has been found that certain metal ions such as Mg^{2+} and Mn^{2+} are required for the enzymatic carbonylations.[5] These metal ions also depress the decarboxylation of 1-carboxy-2-imidazolidinone.[6] On the bases of these findings, we studied the effects of several metal ions on the reactivities of **1** and its derivatives in their reactions with butylamine. The addition of some ions including Mg^{2+} and Mn^{2+} to the reaction system exerted a dramatic change in the reactivity patterns and promoted the transfer of the methoxycarbonyl group from **1** and its derivatives to butylamine. The results are summarized in this paper.

Results and Discussion

*Reaction of **1** with Butylamine.* Treatment of **1** with butylamine in the absence and presence of various metal ions gave the products listed in Table 1. The results of Table 1 demonstrate that the reaction takes place through two different paths, depending on the constituents of the reaction system (Scheme 1). In the absence of metal ions, 1-butylcarbamoyl-4-methoxycarbonylethylenediamine (**2a**) was obtained as a sole product (path A). The addition of monovalent ions such as Na^+ and Ag^+ and some bivalent ions such as Zn^{2+} and Cu^{2+} to the reaction system did not alter the above reactivity pattern. However, the addition of Mg^{2+}, Ca^{2+}, and Mn^{2+} brought about a dramatic change in the reactivity pattern and resulted in the formation of methyl butylcarbamate (**3**) and 2-imidazolidinone (**4**) (path B).

TABLE 1. REACTION OF **1** WITH BUTYLAMINE IN THE PRESENCE OF METAL IONS[a]

Added salt	Reaction path	Products, %		
		2	**3**	**4**
None	A	95	—[b]	—
AgCl	A	96	—	—
NaCl	A	94	—	—
$CuCl_2$	A	88	—	—
$ZnCl_2$	A	86	—	—
$MgCl_2$	B	—	74	67
$MnCl_2$	B	—	63	40
$CaCl_2$	B	—	62	56

a) The reaction was carried out by refluxing an equimolar mixture of **1** and a metal chloride in butylamine for 17 h. b) The dash(—) signifies that the product was unable to be isolated.

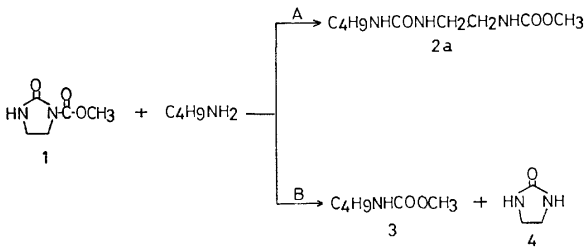

Scheme 1.

The methoxycarbonyl transfer reaction of path B occurs by an attack of butylamine on the carbonyl carbon of the methoxycarbonyl group of **1**. An analogous transfer reaction did not take place upon treatment of **2a** with butylamine in the presence of Mg^{2+} under the similar conditions.

Table 2. Reaction of **5** with butylamine in the presence of magnesium chloride[a)]

Added salt	Products, %				
	2	**3**	**4**	**6**	**7**
None	17	66	42	55	24
$MgCl_2$	—[b)]	71	67	85	—

a) The reaction was carried out by refluxing an equimolar mixture of **5** and magnesium chloride in butylamine for 17 h. b) The dash(—) signifies that the product was unable to be isolated.

Reaction of 3-Acetyl-1-methoxycarbonyl-2-imidazolidinone (5) with Butylamine. The reaction of **5** with butylamine was carried out in the absence and presence of Mg^{2+}. The products isolated are listed in Table 2. In the absence of metal ion, the reaction yielded **2a**, **3**, **4**, *N*-acetylbutylamine (**6**), and 1-acetyl-4-(butylcarbamoyl)ethylenediamine (**7**). In contrast, the reaction in the presence of Mg^{2+} afforded **3**, **4**, and **6**. These results show that the reactivity pattern is also altered by the addition of Mg^{2+}; *i.e.*, the production of ring-opening compounds, **2a**, and **7**, is completely depressed by the addition of Mg^{2+}.

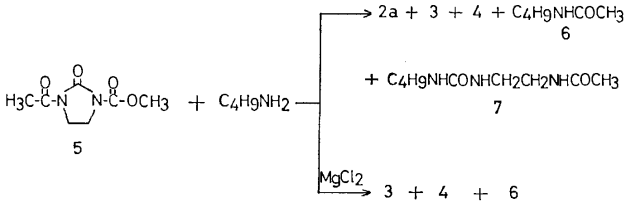

Scheme 2.

*Reaction of 1-Methoxycarbonyl-*cis*-perhydrocyclopenta*[d]*imidazol-2-one (8) with Butylamine.* The reaction of **8** with butylamine was studied somewhat in detail. The results are summarized in Table 3 and Scheme 3. In the absence of metal ions, **3**, 1-butylcarbamoyl-*cis*-perhydrocyclopenta[*d*]imidazol-2-one (**9**), *N*,*N*′-disubstituted *cis*-1,2-diaminocyclopentane (**10**), and *cis*-perhydrocyclopenta[*d*]imidazol-2-one (**11**) were obtained. For this reaction, a main reaction was an attack of butylamine on the 1-methoxycarbonyl carbon to produce **9**. Whereas the methoxycarbonyl transfer to produce **3** and **11** *via* the same mode of attack became a side-reaction. This observation implies that a leaving ability of the *cis*-perhydrocyclopenta[*d*]imidazol-2-one anion is lower than that of methoxide anion.

Table 3. The reaction of **8** with butylamine in the presence of various metal ions[a)]

Added salt	Products, %			
	3	**9**	**10**	**11**
None	7	55	15	13
AgCl	8	51	20	7
$CuCl_2$	10	52	17	15
$MgCl_2$	66	28	—[b)]	38
$MnCl_2$	68	22	—	44

a) The reaction was carried out by refluxing an equimolar mixture of **8** and a metal chloride in butylamine for 17 h. b) The dash(—) signifies that the product was unable to be isolated.

No essential change in the reactivity pattern was observed by the addition of Ag^{+} and Cu^{2+}. However, the addition of Mg^{2+} again brought about a considerable change in the reactivity pattern. The formation of **10** was completely depressed, and the methoxycarbonyl transfer leading to **3** was highly facilitated.

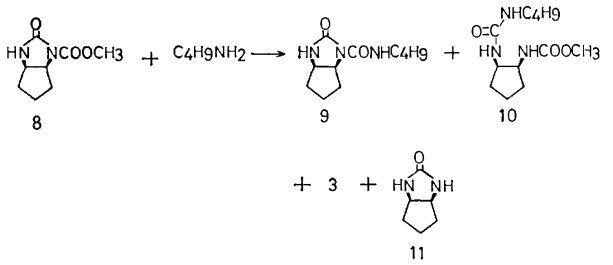

Scheme 3.

Discussion. In a previous paper,[4)] we have studied the reactions of **1**, **5**, and **8** with nucleophilic reagents in the absence of metal ions, and proposed probable pathways for these reactions. The reaction of **1** with an amine proceeds by way of the isocyanate intermediate (**12**) which has been produced by the removal of an acidic NH proton on the imidazolidinone ring of **1** by amine.

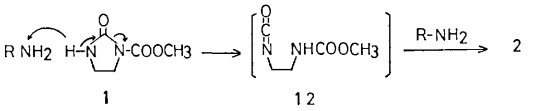

Compound **5** bears no acidic proton on the ring. For this compound, the methoxycarbonyl or acetyl group is removed at the first step by the nucleophilic attack of an amine on their carbonyl carbons. 1-Acetyl-2-imidazolidinone and **1** thus produced are converted into **7** and **2** *via* the corresponding isocyanate intermediates, **13** and **12**. These pathways explain the formation of all the products isolated. Finally, **8** is of special interest from the viewpoint that it has a more close structural resemblance to biotin than do **1** and **5**. Although **8** bears an acidic NH proton on the imidazolidinone ring, its 1-methoxycarbonyl group is attacked to produce **3**, **9**, and **11** in moderate yields. Obviously, **10** is produced *via* the isocyanate intermediate **14**.

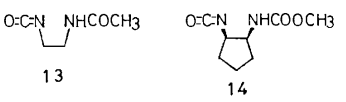

The above reactivity patterns observed in the absence of metal ions change upon the addition of certain bivalent ions such as Mg^{2+}, Ca^{2+}, and Mn^{2+} to the reaction mixtures. These ions enhance an electrophilic reactivity of the methoxycarbonyl group and facilitate breaking of the N–$COOCH_3$ bond, especially when the imidazolidinone moiety of substrates bears the methoxycarbonyl group at one N-position and a hydrogen atom at the other N-position. In the case of **5** which bears

no hydrogen on the nitrogen atoms of the imidazolidinone moiety, the compound is, as pointed out above, at first transformed into **1** and 1-acetyl-2-imidazolidinone regardless the addition of metal ions. Since both of the products have a hydrogen on the N-position of the imidazolidinone moiety, **1** is preferentially converted into **3** and **4**, and 1-acetyl-2-imidazolidinone into **4** and **6** upon the addition of Mg^{2+}.

There is little doubt that the formation of coordination complexes as represented in formula 15 by chelating interaction between metal ions and imidazolidinone moiety is responsible for these changes. The formation of stabilized chelate ring depresses the conversion of the imidazolidinone derivatives, **1**, **5**, and **8** into the corresponding isocyanate intermediates, **12**, **13**, and **14**. It also enhances an electrophilic reactivity of the methoxycarbonyl group by its increased polarization.

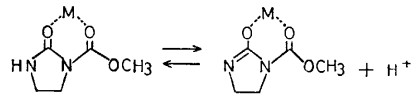

$M = Mg^{2+}, Ca^{2+}, Mn^{2+}$

15

The experimental results suggest that the formation of stabilized chelate rings is favored by an association of the imidazolidinato ligand with bivalent ions, Mg^{2+}, Ca^{2+}, and Mn^{2+}, that belong to the hard metal ions in Pearson's classification.[7]

Bivalent ions, Zn^{2+} and Cu^{2+}, that belong to the borderline class in his classification and all monovalent ions do not give stabilized chelate rings.

Experimental

Materials. 1-Methoxycarbonyl-2-imidazolidinone (**1**), mp 178—179 °C, 3-acetyl-1-methoxycarbonyl-2-imidazolidinone (**5**), mp 143—144.5 °C, and 1-methoxycarbonyl-*cis*-perhydrocyclopenta[*d*]imidazol-2-one (**8**), mp 153.5—154.5 °C, were prepared by the methods described previously.[4]

*Reaction of **1**, **5**, and **8** with Butylamine.* The reaction of an imidazolidinone, **1**, **5**, or **8**, with butylamine in the absence of metal ion were conducted by refluxing a solution of 2 mmol of the respective imidazolidinone in 10 ml of butylamine for 17 h, and the products were isolated and identified by the procedures described previously.[4]

The reactions in the presence of metal ions were carried out as follows: A mixture of 2.08 mmol of an imidazolidinone, **1**, **5**, or **8**, and 2.08 mmol of a metal ion (as chloride) in 10 ml of butylamine was refluxed for 17 h. An excess of butylamine was removed by distillation, and the residue was subjected to a chlomatographic separation on silica gel column: chromatographic separations were successfully accomplished by use of the solvent systems[4] employed for the reactions in the absence of metal ions.

The products were identified by the comparisons of melting points and spectral properties such as IR, NMR, and mass spectra with those of the respective authentic specimens.

References

1) J. Moss and M. D. Lane, *Adv. Enzymol.*, **35**, 321 (1971).
2) M. C. Scrutton and M. R. Young, "The Enzymes," Vol. 6, ed by P. D. Boyer, Academic Press, New York (1972), pp. 1—35.
3) a) H. J. Schaeffer and P. S. Bhargava, *Biochem. Biophys. Res. Commun.*, **14**, 468 (1964); b) A. F. Hegarty and T. C. Bruice, *J. Am. Chem. Soc.*, **92**, 6568 (1970); c) M. Caplow, *J. Am. Chem. Soc.*, **87**, 5774 (1965); d) R. F. Pratt and T. C. Bruice, *Biochemistry*, **10**, 3178 (1971); e) Y. Akasaka and A. Ohno, *J. Am. Chem. Soc.*, **96**, 1957 (1974); f) M. G. Ahmed and R. W. Alder, *Chem. Commun.*, **1969**, 1389; g) M. Caplow, *J. Am. Chem. Soc.*, **90**, 6795 (1968); h) S. L. Johnson and D. L. Morrison, *J. Am. Chem. Soc.*, **94**, 1323 (1972).
4) N. Matsumura, Y. Yagyu, H. Kawai, Y. Otsuji, and E. Imoto, *Nippon Kagaku Kaishi*, **1977**, 362.
5) J. Moss and M. D. Lane, *Adv. Enzymol.*, **35**, 386 (1971).
6) M. Caplow, *J. Am. Chem. Soc.*, **90**, 6795 (1968).
7) P. G. Pearson, *J. Chem. Educ.*, **45**, 581, 643 (1968).

A Macrocyclic Enzyme Model System. Catalytic Properties of 10-Amino-[20]paracyclophane in the Deacylation of *p*-Nitrophenyl Carboxylates

Yukito MURAKAMI,* Junzo SUNAMOTO, Hiroki KONDO, and Hiroshi OKAMOTO

**Department of Organic Synthesis, Faculty of Engineering, Kyushu University, Hakozaki, Higashi-ku, Fukuoka 812*

Department of Industrial Chemistry, Faculty of Engineering, Nagasaki University, Nagasaki 852

(Received April 21, 1977)

The catalytic efficiency of 10-amino[20]paracyclophane in the deacylation of *p*-nitrophenyl carboxylates was investigated in 10.9 or 20.8% (v/v) aqueous ethanol at $\mu=0.10$ (KCl). The present catalyst exhibited marked catalytic effects not only in the free amine but in the ammonium form. The observed saturation-type kinetics is consistent with a reaction mechanism which involves pre-equilibrium complexation between the aminoparacyclophane and the substrate at a 1 : 1 molar ratio, followed by pseudo-intramolecular catalysis effected by the amino group of the macrocycle. Studies on the inhibition effect by 1-dodecanol and the modification of the catalyst by 2,4-dinitrofluorobenzene confirmed the effective binding ability of the present paracyclophane toward hydrophobic substrates. The free amine form of the catalyst acted as an effective nucleophile to give the acylated aminoparacyclophane as confirmed by the product analysis. On the other hand, the protonated amine form also enhanced the ester degradation, retaining a turnover behavior. On the basis of the kinetic solvent isotope effect and the exceedingly minor kinetic effect of [10-oxo[20]paracyclophan-22(23)-ylmethyl]trimethylammonium chloride in the ester degradation in the neutral pH region, a plausible reaction mechanism has been discussed.

[20]Paracyclophanes are synthetic macrocycles designed to have a hydrophobic cavity of sizable diameter into which an appropriate hydrophobic substrate can be incorporated. Upon formation of the inclusion complex, the cleavage of an ester bond of the incorporated substrate is subjected to the catalysis by a functional group or groups placed on the edge of a macrocyclic skeleton. The previously developed catalysts in this series, *i.e.*, 10-hydroxy-11-hydroxyimino[20]paracyclophane (**1**)[1,2] and substituted 10-hydroxyimino[20]paracyclophanes,[3] have shown characteristic enzyme-like behavior in the deacylation of *p*-nitrophenyl carboxylates bearing a long aklyl chain. In those systems, the reaction had to be carried out at relatively high pH's to observe moderate catalysis because of relatively high pK_a values of the hydroxyimino group. Another macrocycle, 10-amino[20]paracyclophane (**2**), was prepared previously by Murakami *et al.*[4] and investigated as for its catalytic efficiency in this work. Since a free amino group is expected to act as either a nucleophile or a general base and a protonated amino group as either a general acid or an electrostatic catalyst in a moderate pH region, some novel catalysis different from those demonstrated by the hydroxyimino group would be expected in this study.

Amino acid residues as components constituting many enzymes often bear primary amine substituents. These amino groups play indispensable roles in the enzymatic reactions in one way or another. While the aminolysis of carboxylic esters is one of the most thoroughly investigated reactions,[5] the catalytic roles of amino groups seem less understood in the enzymatic reactions in spite of their importance. In the present investigation, the catalytic functions of an amino group placed in the hydrophobic field are to be clarified to obtain a clue to development of more elaborated enzyme model systems.

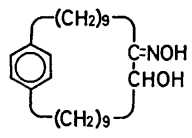

1

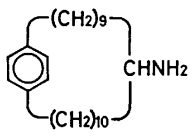

2

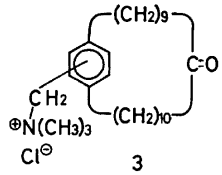

3

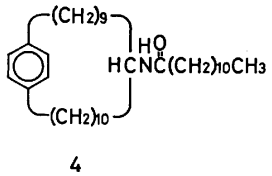

4

Experimental

Materials. 10-Amino[20]paracyclophane (**2**) was prepared by a three-step procedure from 11-hydroxy[20]paracyclophan-10-one and isolated as the hydrochloride form.[4] Preparation of [10-oxo[20]paracyclophan-22(23)-ylmethyl]-trimethylammonium chloride (**3**) was described previously.[3] *p*-Nitrophenyl dodecanoate (PNPL) and hexadecanoate (PNPP) were the same as those described previously.[1,2] 2,4-Dinitrofluorobenzene was obtained as a guaranteed reagent from Nakarai Chemicals, Ltd. 1-Dodecanol was also obtained as a guaranteed grade from Nakarai Chemicals, Ltd. and distilled *in vacuo* before use. Deuterium oxide (99.75%) and ethanol-d_1 (99%) were the products of E. Merck AG and Commissariat al' Energie Atomique de France, respectively, and used without further purification.

Kinetic Measurements.[6] The deacylation rates of *p*-nitrophenyl carboxylates were determined by measuring the absorption at 400 nm either on a Hitachi 124 recording spectrophotometer or on a Shimadzu-Bausch & Lomb Spectronic 88 equipped with a Riken Denshi SP-G3 recorder. The procedure for the kinetic measurements was essentially the same as those described previously.[1,2] Each run was initiated by adding an appropriate amount of a substrate dissolved in ethanol to a reaction medium which was pre-equilibrated at an appropriate temperature in a thermostatted cell set in the spectrometer. The reaction medium was prepared by mixing appropriate amounts of 10-amino[20]paracyclophane, ethanol, potassium chloride, and buffer salts. The initial substrate concentration was always maintained at 1.00×10^{-5} M in order to make critical comparisons of kinetic data possible, since the hydrolytic rates of *p*-nitrophenyl carboxylates bearing a long alkyl chain

were reported to vary by the change in their initial concentrations.[7,8]

pH Measurements. The pH and pD values of reaction mixtures were measured with a TOA HM-5A pH meter equipped with a TOA GS-135C combined electrode. The pH meter was calibrated by using a combination of appropriate aqueous buffer solutions. The pH values thus determined were converted into stoichiometric hydrogen ion concentrations (−log[H+]) by titrating perchloric acid with standard sodium hydroxide in the same solvent as used for the kinetic runs (10.9 or 20.8% (v/v) aqueous ethanol). The difference between pH in 20.8% (v/v) aqueous ethanol and pD in 20.8% (v/v) ethanol-d_1–79.2% (v/v) deuterium oxide was directly estimated from the pH-meter readings measured in phosphate buffer for both solvent systems.

Product Analysis.[9] A solution of **2** (14 mg) and PNPL (50 mg) dissolved in a mixture of aqueous borate-carbonate buffer (pH 9.4, μ=0.1 with KCl, 800 ml) and ethanol (200 ml) was stirred at 40 °C for 58 h, and the mixture was extracted with ether (150 ml×6). The ether extracts were washed with water (200 ml×2), dried over sodium sulfate, and evaporated to give an oil. The oily material was chromatographed on a column (2.4×15 cm) of silica gel (Wakogel C-100) with dichloromethane–benzene (1 : 1) as an eluant to afford *ca.* 4 mg of the acylated amine (**4**). The authentic sample was prepared independently as follows for the identification of the product. A solution of **2** (20 mg) and dodecanoyl chloride (100 mg) in dry ether (25 ml) was stirred under reflux for 8 h. The cooled solution was washed with 5% aqueous sodium carbonate (20 ml×3), 5% aqueous sodium hydroxide (20 ml×5), and then water (30 ml×2) in this sequence. The usual work-up gave an oily material (*ca.* 40 mg) which was applied on a chromatographic column in a manner as described above. The amide fraction eluted with dichloromethane–benzene (1 : 1) was further purified by a Hitachi 635 liquid chromatograph equipped with a column of Hitachi gel 3019. Methanol was used as eluant and components eluted were detected by UV absorption at 254 nm. Spectral data identified the acylated amine (**4**) with the isolated authentic sample (*ca.* 5 mg). IR (neat): 3280 (NH str.), 1635 (amide C=O str.), and 1552 cm^{-1} (amide NH bend. and CN str.). NMR ($CDCl_3$, TMS): δ 7.11 (s, aromatic), 5.13 (broad d, NH), 3.51 (m, *H*CNHCO), 2.64 (t, benzyl methylene), 2.16 (t, CH_2CO), and 1.9—0.8 (m, methylene).

Results

The deacylation reaction of *p*-nitrophenyl carboxylates was investigated in aqueous ethanol both in the absence and in the presence of **2** as listed in Table 1. The initial concentration of a substrate was adjusted at 1.00×10^{-5} M and total amount of **2** was in the same concentration range. The pseudo-first-order rate constants were obtained from the early stage, since good first-order correlations were observed for that range under the present conditions. While **2** showed little catalytic effect in the degradation of substrates bearing a comparatively short alkyl chain in a manner as observed with **1**,[1,2] it showed marked rate acceleration in the reaction of carboxylic esters bearing a longer alkyl chain, such as PNPL and PNPP. The extents of rate acceleration in the ester decomposition are 1380- and 4750-fold for PNPL and PNPP, respectively, relative to their spontaneous hydrolyses as shown in Table 2.

pH-Rate profiles for the reaction between **2** and PNPL in 20.8% (v/v) aqueous ethanol and in 20.8% (v/v) ethanol-d_1–79.2% (v/v) deuterium oxide are a characteristic sigmoid type for which the acid dissociation process is responsible (Fig. 1). This feature is consistent with the presence of two forms for the present catalyst, *i.e.*, protonated (**2a**) and free amine species (**2b**), the latter being far more effective (Eq. 1). Figure 2 shows the solvent isotope effect on the specific base catalyzed hydrolysis of PNPL, plotted as log k_{hyd} *vs.* −log [H+] or −log [D+].

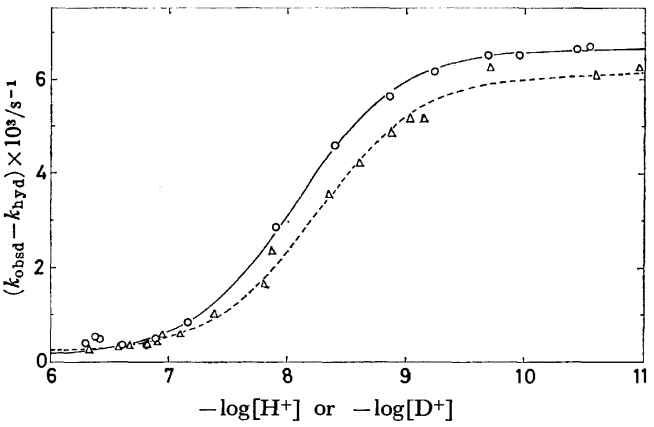

Fig. 1. pH-Rate profiles for the deacylation of PNPL as catalyzed by **2** in 20.8%(v/v) aqueous ethanol (○) and in 20.8%(v/v) ethanol-d_1–79.2%(v/v) deuterium oxide (△) at 40.0±0.1 °C and μ=0.10 (KCl) with the initial concentrations: PNPL, 1.00×10^{-5} M; **2**, 0.998×10^{-5} M. Solid lines are theoretical curves calculated by using parameters given in Table 3.

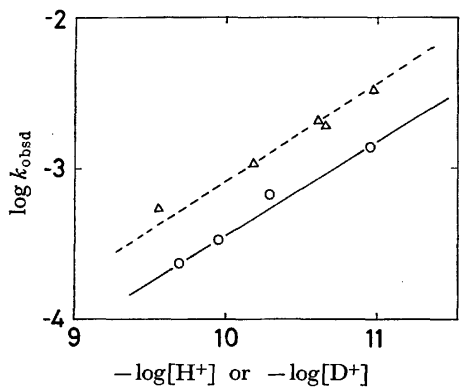

Fig. 2. pH-Rate profiles for the hydrolysis of PNPL as catalyzed by the specific base (hydroxide ion) in 20.8 %(v/v) aqueous ethanol (○) and in 20.8%(v/v) ethanol-d_1–79.2%(v/v) deuterium oxide (△) at 40.0± 0.1 °C and μ=0.10 (KCl) with the initial PNPL concentration of 1.00×10^{-5} M. The kinetic solvent isotope effect ($k^{(H)}/k^{(D)}$) is 0.47.

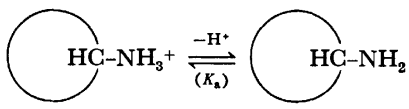

(1)

The kinetic pK_a values for the aminoparacyclophane in the presence of PNPL and PNPP are listed in Table 3 along with their deacylation rates as catalyzed by the two functional species, **2a** and **2b**. It must be noted

Table 1. Apparent first-order rate constants for the *p*-nitrophenol release from *p*-nitrophenyl carboxylates in the presence of **2** in aqueous ethanol at 40.0±0.1 °C and μ=0.10 (KCl)

$-\log[H^+]$	$[\mathbf{2}]\times10^5$/M	$[S]^{a)}\times10^5$/M	$k_{obsd}\times10^3/s^{-1}$	$-\log[H^+]$	$[\mathbf{2}]\times10^5$/M	$[S]^{a)}\times10^5$/M	$k_{obsd}\times10^3/s^{-1}$
Substrate:	PNPL[b]			6.83[d]	0.998	1.00	0.363
6.30	0.998	1.00	0.387, 0.403	6.90[d]	0.998	1.00	0.423
6.39	0.998	1.00	0.403	6.95[d]	0.998	1.00	0.583
6.42	0.998	1.00	0.300	7.10[d]	0.998	1.00	0.587, 0.590
6.61	0.998	1.00	0.290, 0.333	7.38[d]	0.998	1.00	1.01
6.82	0.998	1.00	0.370, 0.330	7.81[d]	0.998	1.00	1.65
6.89	0.998	1.00	0.473	7.87[d]	0.998	1.00	2.35
7.00	0.300	1.00	0.148	8.35[d]	0.998	1.00	3.54
7.00	0.400	1.00	0.190	8.61[d]	0.998	1.00	4.21
7.00	0.500	1.00	0.271	8.87[d]	0.998	1.00	4.83
7.00	0.700	1.00	0.348	9.03[d]	0.998	1.00	5.13
7.00	0.800	1.00	0.398	9.15[d]	0.998	1.00	5.15
7.00	0.900	1.00	0.490	9.55[d]	0	1.00	0.555
7.00	0.998	1.00	0.571	9.71[d]	0.998	1.00	6.25
7.00	1.00	1.00	0.571	10.18[d]	0	1.00	1.08, 1.07
7.00	1.10	1.00	0.692	10.61[d]	0.998	1.00	8.17
7.00	1.20	1.00	0.833	10.65[d]	0	1.00	2.10
7.00	1.40	1.00	1.07	10.66[d]	0	1.00	1.95
7.00	1.50	1.00	1.05	10.97[d]	0	1.00	3.38
7.00	1.60	1.00	1.20	10.97[d]	0.998	1.00	9.62
7.00	2.00	1.00	1.41	Substrate:	PNPP[e]		
7.16	0.998	1.00	0.825	6.43	0.995	1.00	0.625
7.90	0.998	1.00	2.89	6.97	0.301	0.996	0.072
8.40	0.998	1.00	4.66	6.97	0.502	0.996	0.162
8.40	0	1.00	0.023	6.97	0.703	0.996	0.213
8.86	0.998	1.00	5.79	6.97	0.904	0.996	0.353
8.86	0	1.00	0.059	6.97	1.00	0.996	0.410
9.24	0.998	1.00	6.29	6.97	1.21	0.996	0.532
9.24	0	1.00	0.073	6.97	1.41	0.996	0.517
9.69	0.998	1.00	6.77	6.97	1.51	0.996	0.748
9.69	0	1.00	0.233	6.97	1.61	0.996	0.895
9.95	0	1.00	0.328	6.97	1.71	0.996	0.998
9.95	0.300	1.00	1.90	6.97	1.81	0.996	1.15
9.95	0.400	1.00	2.77	6.97	1.91	0.996	1.23
9.95	0.500	1.00	3.46	6.97	2.01	0.996	1.23
9.95	0.700	1.00	5.15	7.44	0.955	1.00	0.583
9.95	0.800	1.00	5.85	7.74	0.955	1.00	1.67
9.95	0.900	1.00	6.54	8.24	0.955	1.00	3.02
9.95	0.998	1.00	6.84	8.61	0.955	1.00	4.53
9.95	1.00	1.00	7.29	8.99	0.955	1.00	5.41
9.95	1.10	1.00	8.25	9.61	0.955	1.00	5.53
9.95	1.20	1.00	8.80	9.94	0.955	1.00	5.90
9.95	1.30	1.00	9.00	10.27	0.955	1.00	6.20
9.95	1.40	1.00	9.75	10.29	0	0.996	0.067
9.95	2.00	1.00	10.8	10.29	0.301	0.996	1.14
10.29	0	1.00	0.658	10.29	0.401	0.996	1.68
10.44	0.998	1.00	7.33	10.29	0.502	0.996	2.35
10.54	0.998	1.00	7.50	10.29	0.703	0.996	3.50
10.77	0	1.00	0.962	10.29	0.803	0.996	4.19
10.96	0	1.00	1.39	10.29	0.904	0.996	4.89
Substrate:	PNPL[c]			10.29	1.00	0.996	5.77
6.33[d]	0.998	1.00	0.250	10.29	1.11	0.996	5.54
6.58[d]	0.998	1.00	0.303	10.29	1.21	0.996	6.38
6.67[d]	0.998	1.00	0.326	10.29	1.31	0.996	6.64
6.82[d]	0.998	1.00	0.347	10.29	1.41	0.996	6.92

Table 1. continued

$-\log[H^+]$	$[2]\times10^5$/M	$[S]^{a)}\times10^5$/M	$k_{obsd}\times10^3/s^{-1}$	$-\log[H^+]$	$[2]\times10^5$/M	$[S]^{a)}\times10^5$/M	$k_{obsd}\times10^3/s^{-1}$
10.29	1.51	0.996	7.00	Substrate:	PNPP[f]		
10.29	2.01	0.996	7.72	6.38	0.955	1.00	1.66
10.67	0.955	1.00	6.23	6.81	0.955	1.00	2.20
10.79	0.955	1.00	6.16	7.38	0.955	1.00	3.59
				7.86	0.955	1.00	4.16

a) Initial concentration of a *p*-nitrophenyl carboxylate. b) Buffer systems: KH_2PO_4-$Na_2B_4O_7$ for $-\log[H^+]$ values of 6.0—9.0; Na_2CO_3-$Na_2B_4O_7$ for $-\log[H^+]>9.0$. Solvent: 20.8%(v/v) aqueous ethanol. c) Buffer systems: KH_2PO_4-Na_2HPO_4 for $-\log[D^+]$ values of 6.33—7.87; KH_2PO_4-$Na_2B_4O_7$ for $-\log[D^+]$ values of 8.35—9.15; Na_2CO_3 for $-\log[D^+]>9.55$. Solvent: 20.8%(v/v) ethanol-d_1-79.2%(v/v) deuterium oxide. d) $-\log[D^+]$. e) Buffer systems: KH_2PO_4-$Na_2B_4O_7$ for $-\log[H^+]$ values of 6.0—9.0; Na_2CO_3-$Na_2B_4O_7$ for $-\log[H^+]>9.0$ but Na_2CO_3 for $-\log[H^+]=10.29$. Solvent: 20.8%(v/v) aqueous ethanol. f) Buffer system: KH_2PO_4-$Na_2B_4O_7$. Solvent: 10.9%(v/v) aqueous ethanol.

Table 2. Rate enhancement effected by 10-amino-[20]paracyclophane (**2**) in the deacylation of PNPL and PNPP[a)]

Substrate	$[2]\times10^5$/M	k_{OH}[b)] $M^{-1}s^{-1}$	k_c[c)] $M^{-1}s^{-1}$	k_c/k_{OH}
PNPL	None	0.49±0.00[d)]		1380
	0.998		683[e)]	
PNPP[f)]	None	0.12		4750
	1.00		570	

a) Solvent, 20.8%(v/v) aqueous ethanol; $\mu=0.10$(KCl); 40.0±0.10 °C. b) $k_{OH}=k_{hyd}/[OH^-]$. c) $k_c=(k_{obsd}-k_{hyd})/[2]$. d) $[PNPL]_0=1.00\times10^{-5}$ M; $-\log[H^+]=$ 9.95—10.97 e) $[PNPL]_0=1.00\times10^{-5}$ M; $-\log[H^+]=$ 9.95. f) $[PNPP]_0=0.996\times10^{-5}$ M; $-\log[H^+]=10.29$.

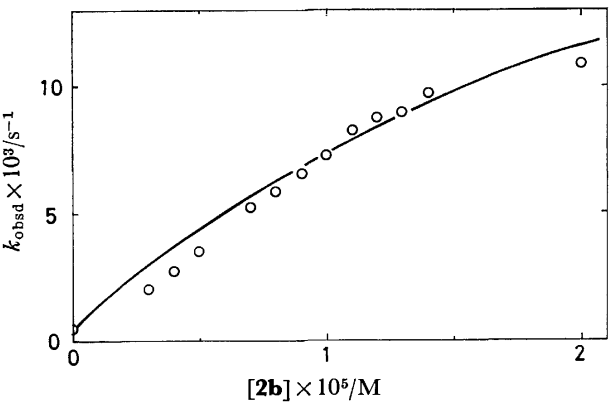

Fig. 3. Saturation-type kinetics for the reaction of PNPL with **2b** in 20.8% (v/v) aqueous ethanol at 40.0±0.1 °C, $\mu=0.10$ (KCl), and $-\log[H^+]=9.95$ with the initial substrate concentration of 1.00×10^{-5} M. Solid line is the theoretical curve calculated by using parameters listed in Table 5.

that the kinetic pK_a value decreases with the decrease in an ethanol content, even though it is little effected by a small change in the alkyl-chain length of the substrates. The equilibrium solvent isotope effect ($pK_a^{(D)}-pK_a^{(H)}$) is 0.20. The kinetic solvent isotope effects for reactions of PNPL with **2a** and **2b**, $k^{(H)}/k^{(D)}$, are 0.67 and 1.09, respectively.

The saturation-type kinetics was observed as exemplified by the correlation between concentration of aminocyclophane **2b** and rate constant for the deacylation of PNPL (Fig. 3). These results are consistent with a reaction mechanism which involves pre-equilibrium complexation of the aminoparacyclophane and the substrate at a 1 : 1 molar ratio, followed by the pseudo-intramolecular catalysis effected by the amino group of the paracyclophane.

The addition of 1-dodecanol resulted in the depression of the catalytic efficiency of **2** in the degradation of PNPL and PNPP, while the alcohol alone (10^{-4} M, 10-fold amount of the substrates) did not show any effect on the hydrolysis of both substrates.

The extent of inhibition by 1-dodecanol increased with the increase in its concentration, and both PNPL- and PNPP-systems show a similar behavior (Fig. 4). On the other hand, 2,4-dinitrofluorobenzene (DNFB) in-

Table 3. Acid dissociation constants of the protonated amino group of **2** and rate constants for the degradation of PNPL and PNPP as catalyzed by conjugated functional species **2a** and **2b**[a)]

Substrate	$[2]\times10^5$/M	Ethanol content %(v/v)	k_{OH}[b)]/$M^{-1}s^{-1}$	$k_{(2a)}\times10^4/s^{-1}$	$k_{(2b)}\times10^3/s^{-1}$	pK_a
PNPL	0.998	20.8	0.49±0.00	1.4±0.5	6.65±0.10	8.07
PNPL[c)]	0.998	20.8	1.06±0.00	2.1±0.3	6.11±0.31	8.25
PNPP	0.995	20.8	0.12	2.4±0.2	6.14±0.43	8.26
PNPP	0.995	10.9	—	1.0±0.1	4.74±0.14	7.08

a) $[Substrate]_0=1.00\times10^{-5}$ M; 40.0±0.1 °C; $\mu=0.10$ (KCl). pK_a-Values were evaluated graphically for the first approximation from the corresponding pH-rate profiles (see Fig. 1), and $k_{(2a)}$ and $k_{(2b)}$ values as well as pK_a were determined from computations which provide best fits to the corresponding kinetic (pH-rate) data. b) The second-order rate constant for the specific base catalyzed hydrolysis in the absence of **2**; $k_{OH}=k_{hyd}/[OH^-]$ or $k_{hyd}/[OD^-]$. c) In 20.8% (v/v) ethanol-d_1-79.2% (v/v) deuteruim oxide.

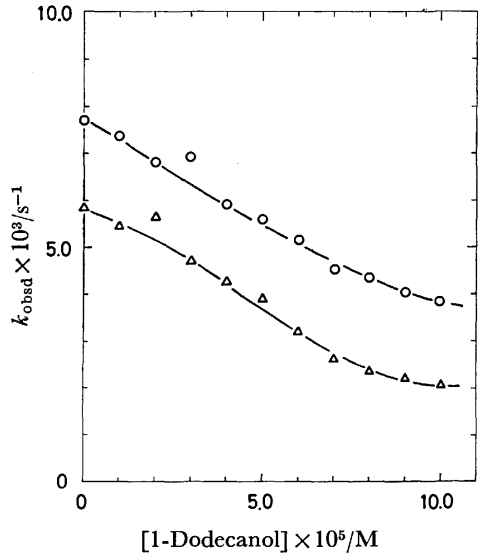

Fig. 4. Inhibition of the **2**-catalyzed degradation of PNPL (○) or PNPP (△) by 1-dodecanol in 20.8% (v/v) aqueous ethanol at 40.0±0.1 °C, μ=0.10 (KCl), and $-\log[H^+]=10.29$ with the initial concentrations: PNPL, 0.997×10^{-5} M; PNPP, 0.996×10^{-5} M; **2**, 1.00×10^{-5} M.

Table 4. The effect of chemical modification of **2** with 2,4-dinitrofluorobenzene in the catalytic degradation of PNPL[a)]

$[2]\times10^5$ M	$[DNFB]\times10^5$ M	Incubation time h	$k_{obsd}\times10^4$ s^{-1}
None	None	—	1.53
1.00	None	—	62.7
1.00	0.515	24	16.7
1.00	0.515	60	16.3
1.00	1.03	24	1.03
1.00	1.03	60	1.11
1.00	5.15	24	1.13
1.00	5.15	60	0.92

a) $[PNPL]_0=1.00\times10^{-5}$ M; solvent, 20.8%(v/v) aqueous ethanol; μ=0.10(KCl); $-\log[H^+]=9.26$; 40.0±0.1 °C.

hibited the aminoparacyclophane-catalyzed reaction in a manner different from 1-dodecanol. The pre-incubation of **2** with DNFB resulted in an appreciable reduction of the catalytic efficiency as listed in Table 4. Examination of the effects of incubation time and DNFB concentration on the reaction rate confirms that the amino group of **2** reacted quantitatively with DNFB at a 1 : 1 molar ratio in 24 h. It must be noted that the dinitrophenylated aminoparacyclophane reduced the rate of PNPL decomposition even below the catalyst absence level.

Discussion

10-Amino[20]paracyclophane is characterized by two functions: a hydrophobic binding site formed by polymethylene chains and a benzene ring, and a catalytic center provided by an amino group. In fact, dinitrophenylation of **2** with DNFB, which is the potent re-

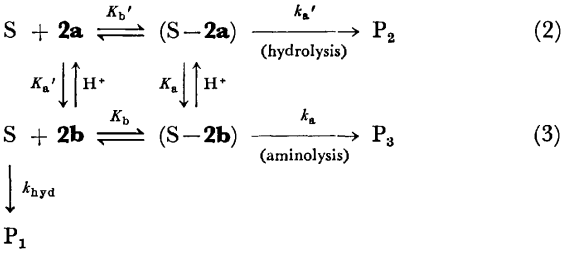

P_1: Carboxylate and *p*-nitrophenolate ions,
P_2: carboxylate, *p*-nitrophenolate, and regenerated **2a**,
P_3: *p*-nitrophenolate ion and acylated **2**.

Scheme 1.

agent to modify an essential amino group of enzymes,[10] resulted in the complete disappearance of catalytic effect. Accordingly, it is evident that the amino group placed on the paracyclophane skeleton plays an indispensable role in the catalytic degradation of the carboxylic esters. Formation of an inclusion complex between **2** and the substrate was confirmed by the inhibition experiment with 1-dodecanol. The catalytic efficiency exhibited by **2** gradually decreases with the increase in inhibitor concentration as shown in Fig. 4. Since the inhibitor and the substrate (PNPL or PNPP) bear a hydrophobic alkyl chain of similar length, they can compete with each other in occupying the hydrophobic cavity of the catalyst.

In consistent with the pH-rate correlation (Fig. 1) and the saturation-type kinetics (Fig. 3), the reaction scheme is given by Scheme 1 in a manner similar to those applied to the hydroxyiminoparacyclophane catalysis described previously.[2] This reaction scheme means that the pre-equilibrium complexation of the aminoparacyclophane with the substrate at a 1 : 1 molar ratio is followed by the pseudo-intramolecular catalysis to decompose the substrate. Reactions 2 and 3 in Scheme 1 can be treated separately by analyzing the kinetic data obtained in sufficiently lower and higher pH regions, respectively, relative to the pK_a value of the catalyst. The binding constant K_b and the rate constant for substrate decomposition k_a were computed by the nonlinear least-squares method to obtain best fit to the kinetic data (see Appendix). The rate constants of simple hydroxide-catalyzed hydrolysis (k_{hyd}) were obtained independently from kinetic runs in the absence of the catalyst (Table 5).

Nucleophilic Catalysis in the Higher pH Region.[11] In general, the free amine takes part in the decomposition of carboxylic esters in two different ways;[5] the general base catalysis to give the same product as observed in the corresponding spontaneous hydrolysis, and the direct nucleophilic attack of the amino group on the ester carbonyl to give the acylated amine. When both substrate and amine bear long hydrocarbon chains, the overall rate of ester degradation was accelerated drastically due to the mutual hydrophobic interaction which facilitate to place the amino group in a close vicinity of the ester carbonyl.[7,12] At the same time, the aminolysis becomes the major reaction among competing ones. Similar proximity effect is expected for the present paracyclophane system and the amino group attacks on the ester carbonyl as confirmed by the prod-

Table 5. Kinetic parameters for the deacylation reactions of PNPL and PNPP as catalyzed by **2b**[a]

Substrate	$-\log[H^+]$	$k_{hyd}\times10^4/s^{-1}$	$k_a\times10^2/s^{-1}$	$K_b\times10^{-3}/M^{-1}$	U[b]
PNPL	9.95	3.28	2.40	59	4.32×10^{-6}
PNPP	10.29	*ca.* 0.1—0.5	1.38	100	2.76×10^{-6}

a) $[PNPL]_0=1.00\times10^{-5}$ M and $[PNPP]_0=0.996\times10^{-5}$ M; solvent, 20.8% (v/v) aqueous ethanol; 40.0±0.1 °C; μ=0.10 (KCl). b) A residual sum of squares for the computational procedure, see Appendix.

uct analysis. The observed small isotope effect on the specific rate constant, $k_{(2b)}^{(H)}/k_{(2b)}^{(D)}=1.09$ for PNPL as shown in Table 3, is consistent with the direct nucleophilic attack by the amino group. For the nucleophilic displacement, the kinetic solvent isotope effect is usually very close to unity: phenyl acetate with imidazole, 1.07;[13] *p*-nitrophenyl acetate with imidazole, 1.0;[13] and *p*-nitrophenyl acetate with trimethylamine, 0.9.[14]

The ester degradation was even slower than the corresponding spontaneous hydrolysis in the presence of the dinitrophenylated aminoparacyclophane. This means that the modified paracyclophane can still incorporate the substrate and the incorporated substrate is less susceptible to the nucleophilic attack by hydroxide ion due to the steric hindrance effect exerted by the bulkyl substituent. A similar state of affairs has been noted by Bender *et al.* for the reaction between phenyl acetates and dodecamethylcyclohexaamylose.[15] Since the present and related paracyclophanes may be regarded to exist largely in a monomeric form under the kinetic conditions,[3] the inclusion complex is most plausibly formed at a 1 : 1 molar ratio as shown in Scheme 1. The cyclic skeleton of **2b** shows a profound tendency to bind the substrates in a manner similar to those observed for other [20]paracyclophanes.[1-3] Thus, there is no doubt that [20]paracyclophane skeleton provides an effective hydrophobic binding site for carboxylic esters bearing a long alkyl chain.

Another prominent feature found in the present study is that the acyl transfer rates as catalyzed by the amino group (**2b**) are comparable to those by the hydroxyimino group (**1**); $k_a=1.82\times10^{-2}$ s^{-1} at 43.1 °C and pH 10.3 for PNPL, and 4.45×10^{-2} s^{-1} at 39.9 °C and pH 10.7 for PNPP with the hydroxyimino group in 10.9% (v/v) aqueous acetone.[1] This result seems to be rather surprising since the basicity of the hydroxyimino group of **1** is greater than that of the amino group of **2b** by an order of approximately 10^4. The large basicity as well as the additional α-effect should in general enhance the nucleophilic reactivity of the hydroxyimino group relative to the amine. The complexation of **2b** with the substrate bearing a long alkyl chain may provide a profound hydrophobic reaction field for the amino group of **2b**. This field effect (microsolvent effect) as well as the proximity effect seems to enhance the nucleophilicity of the amino group in the present system.

Rate Acceleration in the Neutral pH Region. The present paracyclophane gave out an appreciable catalysis in the degradation of PNPL and PNPP in a pH region where the amino group is protonated predominantly and the spontaneous hydrolysis of the substrate esters proceeds to a negligible extent. In an alkaline region where **2b** is the dominant species, the rate plots always deviated downwards, relative to the linear first-order correlation line, because the catalytic amino group was consumed along with the progress of reaction. On the other hand, the rate plots deviated upwards in the neutral pH region in a manner as observed in the spontaneous hydrolysis of PNPP over the whole pH range. In the cases of the hydrophobic substrates, such as PNPL or PNPP, the substrate becomes progressively free from the intermolecular aggregation along with the progress of reaction because of the decrease of substrate concentration.[8] The kinetic behavior mentioned above suggests that the deaggregated substrate is more favorably incorporated into the paracyclophane. In the neutral pH region, in addition, it is clear that the catalytic group is not consumed during the course of reaction. The protonated amino group most plausibly plays a catalytic function by either of the following two mechanisms in the hydrolysis of carboxylic esters. The first one is the electrostatic catalysis effected by the positively charged ammonium group which stabilizes the anionic tetrahedral intermediate. The alkaline hydrolysis of acetylcholine proceeds 32 times as fast as that of 2-(dimethylamino)ethyl acetate.[16] This acceleration effect was attributed to the electrostatic stabilization of the anionic tetrahedral intermediate by the positively charged ammonium group of the former species. An appropriate spatial orientation of an ammonium group relative to an ester carbonyl was suggested to be responsible for the development of such electrostatic catalysis.[17] In a previous work,[3] [10-hydroxyimino[20]paracyclophan-22(23)-ylmethyl]trimethylammonium chloride was found to enhance the deacylation of PNPL and PNPP in an alkaline solution due to an electrostatic effect provided by the positively charged ammonium group. In order to examine the possibility of electrostatic catalysis by the protonated amino group of **2a**, the kinetic effect of [10-oxo[20]paracyclophan-22(23)-ylmethyl]trimethylammonium chloride (**3**) in the degradation of PNPL was investigated under the following conditions: pH 7.28; solvent, 20.8% (v/v) aqueous ethanol; temp, 40.0 °C; ionic strength, 0.10 with KCl; initial concentration of PNPL, 1.00×10^{-5} M.[9] The observed first-order rate constants (2.33×10^{-5} s^{-1} with 0.88×10^{-5} M of **3**, and 2.92×10^{-5} s^{-1} with 1.53×10^{-5} M of **3**) are much smaller than those observed in the presence of **2a**, even though they are larger than that of the spontaneous hydrolysis (*ca.* 1.3×10^{-5} s^{-1}) under the same conditions. Thus, it is concluded that contribution of electrostatic effect may be ruled out under the present experimental conditions, even if the structural difference between **2a** and **3** needs to be taken into consideration. In addition, the observed solvent isotope effect (0.67) seems

to support this view, since no isotope effect would be expected for the electrostatic catalysis which involves no proton transfer process. An alternative mechanism is the general acid catalysis[18] in which the ammonium group of **2a** attacks on the ester carbonyl as a general acid and the nucleophilic attack of a water molecule is facilitated accordingly. Even though the solvent deuterium isotope effect is usually greater than unity for this mechanism, there are other examples in which the isotope effect is smaller than unity: the dehydration step of oxime formation, 0.30;[19] the acid-catalyzed addition of thiol to aldehyde, 0.59.[20] Thus, the protonated amino group most plausibly attacks on the ester carbonyl as a general acid catalyst. This work presents undoubtedly a novel type of catalysis in any sense played by the protonated amino group placed on the hydrophobic cyclic skeleton in the hydrolysis of carboxylic esters.

In brief summary, the present aminoparacyclophane demonstrated marked catalytic effects on the deacylation of *p*-nitrophenyl carboxylates bearing a long alkyl chain not only in the free base but also in the protonated form. The nucleophilic attack of the free amino group of **2** on the ester carbonyl takes place pseudo-intramolecularly upon complexation with the substrate, which afforded the acylated aminocyclophane. On the other hand, the general acid catalysis is exercised by the protonated amino group of **2** in the deacylation of the same substrates. Even though its absolute catalytic efficiency is not so large as that of the free base group, a characteristic turnover behavior was observed.

Appendix

Determination of Kinetic Parameters for Saturation-type Kinetics. When the reaction is carried out in a sufficiently high pH region relative to the pK_a value of the catalyst, the predominant catalyst species is **2b** and Scheme 1 can be simplified to Scheme 2.

$$\mathrm{S} + \mathrm{C} \overset{K_b}{\rightleftharpoons} (\mathrm{S-C}) \overset{k_a}{\rightleftharpoons} \mathrm{P}$$
$$\Big\downarrow k_{hyd}$$
$$\mathrm{P'}$$

Scheme 2.

The kinetic parameters given in Scheme 2 are evaluated by the following computations. Abbreviations are made here for convenience.

S: a substrate species
C: a catalyst species (**2b**)
S–C: a substrate-catalyst inclusion complex
P and P′: products
K_b: a binding constant
k_a: a catalytic rate constant for the aminolysis step
k_{hyd}: a rate constant for spontaneous or simple alkaline hydrolysis
k_ϕ: an overall rate constant

Mass balances in consistent with Scheme 2 are established as follows.

$$[\mathrm{S}]_T = [\mathrm{S}] + [\mathrm{S-C}] \tag{4}$$

$$[\mathrm{C}]_T = [\mathrm{C}] + [\mathrm{S-C}] \tag{5}$$

The binding constant is given by

$$K_b = \frac{[\mathrm{S-C}]}{[\mathrm{S}][\mathrm{C}]} \tag{6}$$

Combination of Eqs. 4, 5, and 6 gives

$$[\mathrm{S-C}] = \frac{1}{2}\left[[\mathrm{S}]_T + [\mathrm{C}]_T + \frac{1}{K_b} - \left\{\left([\mathrm{S}]_T + [\mathrm{C}]_T + \frac{1}{K_b}\right)^2 - 4[\mathrm{S}]_T[\mathrm{C}]_T\right\}^{1/2}\right] \tag{7}$$

The overall rate can be expressed as follows:

$$k_\phi[\mathrm{S}]_T = k_{hyd}[\mathrm{S}] + k_a[\mathrm{S-C}] \tag{8}$$

$$k_\phi = \left(1 - \frac{[\mathrm{S-C}]}{[\mathrm{S}]_T}\right)k_{hyd} + \frac{[\mathrm{S-C}]}{[\mathrm{S}]_T}k_a \tag{9}$$

The equation derived by combination of Eqs. 7 and 9 is nonlinear with respect to parameters K_b and k_a. An iterative calculation was performed to minimize the residual sum of squares (U):

$$U = \sum_{i=1}^{n}\{k_\phi(\mathrm{obsd})_i - k_\phi(\mathrm{calcd})_i\}^2,$$

where n is the number of observations at different concentrations of the catalyst and i is the observation-number index.

All calculation processes were programmed by means of the Fortran language for use with a FACOM 270-20/30 electronic computer of the Computation Center of Nagasaki University.

References

1) Y. Murakami, J. Sunamoto, and K. Kano, *Bull. Chem. Soc. Jpn.*, **47**, 1238 (1974).
2) Y. Murakami, J. Sunamoto, H. Okamoto, and K. Kawanami, *Bull. Chem. Soc. Jpn.*, **48**, 1537 (1975).
3) Y. Murakami, Y. Aoyama, and K. Dobashi, *J. Chem. Soc., Perkin Trans. 2*, **1977**, 24 and 32.
4) Y. Murakami, Y. Aoyama, K. Ohno, K. Dobashi, T. Nakagawa, and J. Sunamoto, *J. Chem. Soc., Perkin Trans. 1*, **1976**, 1320.
5) T. C. Bruice and S. J. Benkovic, "Bioorganic Mechanisms," Vol. 1, W. A. Benjamin, Inc., New York (1966).
6) The kinetic experiments were aided in part by Miss Tomiko Hamada of Nagasaki University.
7) D. Oakenful, *J. Chem. Soc., Perkin Trans. 2*, **1973**, 1006.
8) J. P. Guthrie, *Can. J. Chem.*, **51**, 3494 (1973).
9) This experiment was performed by Dr. Yasuhiro Aoyama of Kyushu University.
10) C. H. W. Hirs, M. Halmann, and J. H. Kycia, *Arch. Biochem. Biophys.*, **111**, 209 (1965).
11) Nucleophilic catalysis is referred practically to the aminolysis of *p*-nitrophenyl carboxylates by aminoparacyclophane (**2**). Such aminolysis reactions are considered to be quite important processes and the corresponding nucleophiles are often called nucleophilic catalysts in enzymatic reactions (Ref. W. P. Jencks, "Catalysis in Chemistry and Enzymology," McGraw-Hill Book Co., New York (1969), Chap. 2). We prefer to use such classification here.
12) C. A. Blyth and J. R. Knowles, *J. Am. Chem. Soc.*, **93**, 3017 (1971).
13) B. M. Anderson, E. H. Cordes, and W. P. Jencks, *J. Biol. Chem.*, **236**, 455 (1961).
14) M. L. Bender, E. J. Pollock, and M. C. Neven, *J. Am. Chem. Soc.*, **84**, 595 (1962).

15) R. L. Van Etten, G. A. Clowes, J. F. Sebastian, and M. L. Bender, *J. Am. Chem. Soc.*, **89**, 3253 (1967).
16) W. Davis and W. C. J. Ross, *J. Chem. Soc.*, **1950**, 3056.
17) G. F. Holland, R. C. Durant, S. L. Friess, and B. Witkop, *J. Am. Chem. Soc.*, **80**, 6031 (1958).
18) An intramolecular general acid catalysis was observed in the aminolysis reaction of 4-[2-(acetylthio)ethyl]morpholine hydrochloride with methoxyamine: P. E. Anderson, G. M. Blackburn, and S. Murphy, *J. Chem. Soc., Chem. Commun.*, **1972**, 171.
19) A. Williams and M. L. Bender, *J. Am. Chem. Soc.*, **88**, 2508 (1966).
20) G. E. Lienhard and W. P. Jencks, *J. Am. Chem. Soc.*, **88**, 3982 (1966).

A New Method for Measuring Surface Acidity. The Titration of Silica–Alumina with the Indicator Itself[1]

Jun-ichiro TAKE, Haruyuki KAWAI,[2] and Yukio YONEDA

Department of Synthetic Chemistry, Faculty of Engineering, The University of Tokyo, Hongo, Bunkyo-ku, Tokyo 113

(Received July 23, 1976)

A new method has been proposed for measuring the surface acidity of solid acids. The method involves the titration of a solid acid with the indicator itself in a nonpolar solvent; it determines the number of acid sites from the amount of the indicator chemisorbed at saturation. The titration of silica-aluminas with 4-anilinoazobenzene ($pK_a=1.5$) itself yielded an acid content smaller than the butylamine titration method with the same indicator. This difference in acid content was ascribed to the difference in the base strength of the titrants. Similarly, titration with *trans*-azobenzene ($pK_a=-2.9$)itself produced an acid content smaller than that with 4-anilinoazobenzene itself.

Walling's[3] and the butylamine titration (or Benesi's)[4] methods have been employed for measuring the acidic properties of solid acid surfaces in nonpolar solvents. The former is for measuring the acid strength from the color change in indicators adsorbed on surfaces. The latter method, for measuring the acid-strength distributions, can be interpreted in the following way: it is primarily designed to determine the number of acid sites capable of chemisorbing each H_0 indicator on the basis of the amount of butylamine which must be added until the chemisorbed indicator changes in color. In our recent studies[5–7] it was pointed out that the assumption underlying the latter method is not valid from a practical point of view. This argument is based on the fact that neither the amine nor the any indicator reaches an adsorption equilibrium with the acid sites under the conventional conditions of operation.

Since butylamine is much more basic than the usual indicators, it may reasonably be inferred that the acid sites capable of chemisorbing the amine are not all capable of chemisorbing indicators, and also that the amine chemisorbed is less mobile than the chemisorbed indicators. The former inference is equivalent in essence to the generalized one that acid sites on a solid acid vary in number depending on the base strength of the base used. When no asdorption equilibrium is attained, a substantial part of the amine added may be chemisorbed on acid sites incapable of chemisorbing an indicator, and thus wasted. Consequently, the butylamine titration method may overestimate the number of acid sites.

Therefore, if solid acid surfaces are titrated with indicators themselves different in base stregth, accurate information may be obtained on acid-strength distributions from both the amount chemisorbed at saturation and the base strength of each indicator. The amount of a chemisorbed indicator at saturation will correspond to the number of acid sites capable of chemisorbing the indicator. The base strength of the indicator (*e.g.*, its pK_a value) will determine an arbitrary scale of the acid strength of the acid sites. Also this method will not require, in principle, that the adsorption be at equilibrium, if only the amount of a chemisorbed indicator itself is measurable even in the presence of the physically adsorbed indicator.

The present study was undertaken in order to see whether or not the titration of solid acid surfaces worked out in practice with an indicator itself, and also to examine whether or not the above inference was valid. This attempt was carried out with silica–alumina catalysts as solid acids, silica gel as an inert diluent of the catalysts, and 4-anilinoazobenzene or *trans*-azobenzene as an indicator.

Experimental

Materials. The original and Na-poisoned silica-alumina catalysts (SA-1, SA-1-Na-2 and -3) were described elsewhere.[8] The additional catalyst (SA-1-Na-4) was prepared by the impregnation of SA-1 with an aqueous solution of sodium hydroxide. Its surface area and Na^+- content were 452 m^2/g and 0.807 mg-ion/g respectively. The silica gel (S-3) was taken from the same batch as was used earlier.[6] The 4-anilinoazobenzene (BADA, $pK_a=1.5$) and *trans*-azobenzene (TAB, $pK_a=-2.9$) were of a GR and an EP grade respectively, and both were purified by recrystalization from ethanol. Their solutions in cyclohexane were prepared in the way described previously.[6] Thoroughly purified cyclohexane was sealed in a small Y-shaped glass ampoule under a vacuum;[6] its volume (around 3 ml) was determined from the difference in the weight of the ampoule before and after sealing. Gaseous nitrogen from a cylinder was also purified.[6]

Apparatus. The specially designed UV-cell, which provides two light-paths rectangular to each other, was shown in a previous paper.[6] A single wafer was used in each of the present runs, so that concurrent spectral measurements were possible of both the wafer and the liquid phase. The spectra were recorded on a Shimadzu multipurpose recording spectrophotometer, Model MSP-50L, at room temperature. The control was atmospheric air.

Procedures. Most of the procedures have been described in detail earlier.[6] In most experiments, the powdered catalysts were diluted with inert S-3 powder (for a reason to be stated later) by mixing them well for 2—5 min in a mixing grinder; they were then pressed into self-supporting wafers.

A wafer was activated in the cell at 450 °C and at pressures of 10^{-4} to 10^{-5} mmHg for 2 h after pretreatment in air at 550 °C for 5 h. After the introduction of the sealed cyclohexane, the background spectra were recorded of both the liquid phase and the wafer, plus the liquid phase. The background spectra of the wafer itself were obtained as a difference between the two spectra. A known, small amount of each indicator solution (around 0.3 or 0.5 ml) was added to the cell, and then the cell was allowed to stand at 60 °C for at least 4 days before spectral measurements. This addition was repeated until the amount of a chemisorbed indicator became virtually constant. A previous study[6] showed that the BADA adsorbed on non-acidic sites transmigrated

effectively onto acid sites when it was allowed to stand as above. In the present titration, therefore, the added indicator can be regarded as being approximately in an adsorption equilibrium.

Results

Spectra of BADA and Molar Absorption Coefficients. BADA shows a band at 386 nm in cyclohexane, at 440 nm on S-3, and at 545 nm on SA-1. The bands at 440 and 545 nm are ascribable to species hydrogen-bonded to non-acidic sites and chemisorbed on acid sites respectively.[6] The molar absorption coefficients were determined for each species from the Beer plots. They are listed in Table 1. The values for adsorbed species were obtained with undiluted wafers (*ca.* 25 mg). For each species, an excellent linearity was confirmed up to an absorbance of at least 2 at an absorption maximum. This critical absorbance corresponded to surface concentrations of around 3.5×10^{-3} and of around 7×10^{-3} mmol/g for chemisorbed and hydrogen-bonded BADA respectively.

Table 1. Molar absorption coefficients of BADA

System	Molar absorption coefficient	
	Symbol	$\varepsilon\times10^{-4}$
In cyclohexane	$\varepsilon_{l,386}$	2.78
On S-3	$\varepsilon_{p,440}$	2.00
	$\varepsilon_{p,545}$	0.07
On SA-1 or	$\varepsilon_{c,545}$	3.72
SA-1-Na-4	$\varepsilon_{c,440}$	0.29

With S-3 wafers, the BADA remained in part unadsorbed in the liquid phase, even on the first addition (about 3×10^{-5} mmol). Also, no spectral evidence was found to indicate the presence of chemisorbed BADA, not even at the above critical surface concentration. The adsorption isotherm of hydrogen-bonded BADA followed the Freundlich equation well. With undiluted SA-1 wafers, the spectra showed not only the presence of chemisorbed BADA alone on the surface, but the absence of BADA in the liquid phase, even at a surface concentration of about 8×10^{-3} mmol/g, indicating that the chemisorption was far from saturation even at this surface concentration. The same things were noted with undiluted SA-1-Na-4 wafers. Therefore, it was necessary for the titration of the catalysts with BADA itself to reduce greatly the amount of acid sites in a wafer. For this purpose, it seemed advisable to dilute the catalysts with inert S-3. This is the reason for the use of a diluted wafer.

Evaluation of the Amount of Chemisorbed BADA. The spectra of diluted wafers showed the coexistence of both chemisorbed and hydrogen-bonded BADA, even on the first addition of $3—5\times10^{-5}$ mmol. When the addition was repeated, the BADA increased gradually in both the liquid-phase and surface concentrations. Hence, the material balance is given by the following equations:

$$m_0 = m_a + m_l, \tag{1}$$

$$m_a = m_p + m_c, \tag{2}$$

where m is the amount of BADA; the 0, a, l, p, and c subscripts denote the BADA added, adsorbed, remaining in the liquid phase, hydrogen-bonded, and chemisorbed respectively. The m_l quantity is readily determinable from the data on both the liquid-phase concentration of BADA and the cumulative volume of cyclohexane added; hence, the m_a can be determined from Eq. 1. The absorbances at the absorption maxima of both adsorbed species (A_{λ_m}) are given by Eqs. 3 and 4:

$$A_{545} = \frac{1}{S}(\varepsilon_{c,545}m_c + \varepsilon_{p,545}m_p), \tag{3}$$

$$A_{440} = \frac{1}{S}(\varepsilon_{c,440}m_c + \varepsilon_{p,440}m_p), \tag{4}$$

where S is the cross section of a wafer; ε, the molar absorption coefficient, and m, in mmol.[6]

It is well known that molar absorption coefficients often vary at high concentrations.[9] When diluted wafers were titrated, the chemisorbed BADA increased in the net surface concentration by a factor of 10 to 50 over the critical concentration below which the Beer law was valid. On the other hand, the concentration of hydrogen-bonded BADA was never beyond the range of the validity of the Beer law. Then, it does not seem to be reasonable to evaluate the amount of chemisorbed BADA directly from Eqs. 3 and 4 with the ε_c and ε_p values given in Table 1. With the assumption that the ratio of $\varepsilon_{c,440}$ to $\varepsilon_{c,545}$ is constant over an extended range of surface concentrations (Eq. 5), Eq. 6 is derived from Eqs. 2, 3, and 4:

$$\frac{\varepsilon_{c,440}}{\varepsilon_{c,545}} = \alpha \text{ (constant value)}, \tag{5}$$

$$m_c = m_a - m_p = m_a - \frac{S(A_{440}-\alpha A_{545})}{\varepsilon_{p,440}-\alpha\varepsilon_{p,545}}. \tag{6}$$

This assumption seems to be reasonable and much more practical than the assumption of the Beer law over an extended range of surface concentrations. For BADA, the value of α was as low as 0.078. Also, the second term ($\alpha\varepsilon_{p,545}$) in the denominator of Eq. 6 was neglected because of its negligibly small value. Thus, the amount of chemisorbed BADA was determined according to Eq. 6.

Adsorption Isotherms of Chemisorbed BADA. The adsorption isotherms were obtained by plotting the amount chemisorbed on a catalyst of a unit weight, M_c (mmol/g), against the liquid-phase concentration, as is exemplified in Fig. 1. Each isotherm conformed well to the Langmuir equation, as is illustrated in Figs. 1 and 2. The solid lines in Fig. 1 denote isotherms derived from the Langmuir equation. Figure 2 shows the Langmuir plots of the isotherm data given in Fig. 1. The isotherm data at zero concentration were excluded from the Langmuir plots because the lower limit for the detectable liquid-phase concentration was about 3×10^{-4} mmol/l. The amount of chemisorbed BADA at saturation (*i.e.*, the number of acid sites capable of chemisorbing BADA) was determined from the Langmuir plots in the usual way. The results are listed in Table 2. Acid contents determined by other methods were also collected in this table for comparison.

Spectra and Adsorption Isotherms of TAB. Titration

TABLE 2. ACID CONTENTS OF SILICA-ALUMINA CATALYSTS

Catalyst	Dilution ratio[b] (Cat : S-3)	Acid contents[a] This work BADA	This work TAB	Amine method with BADA[c]	IR-Py method[d] (L+B)
SA-1	1 : 19.0	0.12_5, 0.07_4	—	0.23	0.09_7
	1 : 6.24	0.06_7	0.01_0		
	1 : 0	—	0.01_1		
SA-1-Na-2	1 : 5.54	0.06_7	—	0.16	0.07_7
SA-1-Na-3	1 : 9.58	0.09_3	—	0.13	0.06_0
SA-1-Na-4	1 : 9.24	0.04_3, 0.05_8	—	—	0.04_6

a) mmol/g. b) Ratio by weight. c) The butylamine titration method, Ref. 8. d) IR spectroscopic method with pyridine (Ref. 10); L+B, Lewis plus Brønsted acid sites; see text. e) Values averaged over the indicated two or three independent titration data.

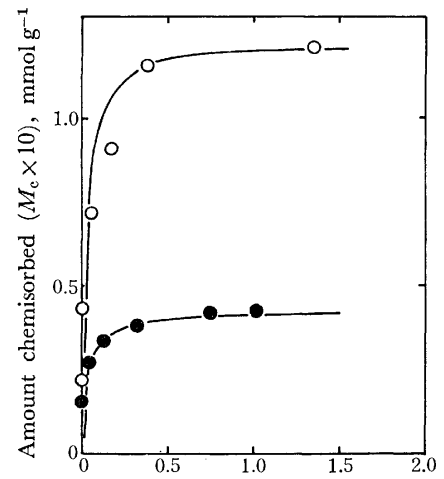

Fig. 1. Adsorption isotherms of chemisorbed BADA.
○: SA-1, ●: SA-1-Na-4.

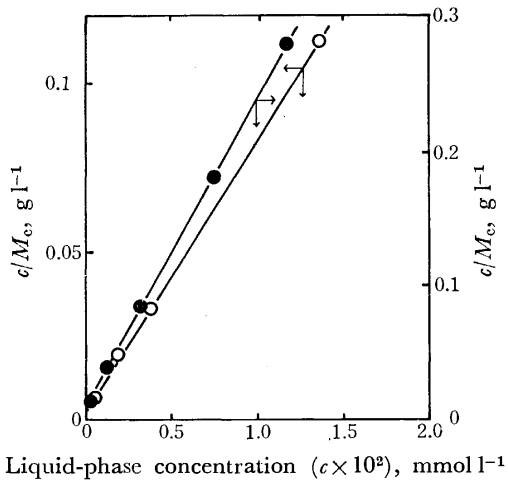

Fig. 2. Langmuir's plots of BADA chemisorption.
○: SA-1, ●: SA-1-Na-4.

with TAB, less basic than BADA, was preliminarily examined. Table 3 summarizes the absorption spectra of TAB, together with the relevant molar absorption coefficients determined from the Beer plots. An inspection of this table leads to the conclusion that the strong bands at 435 nm on SA-1 and at 318 nm on S-3 are due to TAB chemisorbed on acid sites and adsorbed in the neutral (probably, hydrogen-bonded) form on non-acidic sites respectively. The amount of chemisorbed TAB was determined according to the equation corresponding to Eq. 6. For TAB, α was 0.21 and the second term ($\alpha\varepsilon_{p,435}$) in the denominator was again neglected.

TABLE 3. UV SPECTRA OF TAB AND MOLAR ABSORPTION COEFFICIENTS

System	Absorption at[a]			Molar abs. coef. Symbol	$\varepsilon \times 10^{-4}$
In cyclohexan	230(s)	317(vs)	450(vw, b)	$\varepsilon_{1,317}$	2.50
In ethanol	230(s)	318(vs)	420(vw, b)		
On S-3	230(s)	318(vs)	420(vw, b)	$\varepsilon_{p,318}$	1.65
				$\varepsilon_{p,435}$	0.16
In aq H_2SO_4	255(s)	295(vw)	425(vs)		
On SA-1	245(s)	305(vw)	435(vs)	$\varepsilon_{c,435}$	1.57
				$\varepsilon_{c,318}$	0.34

a) nm; (vs), very strong; (s), strong; (vw), very weak; (b), broad.

When a diluted SA-1 wafers was titrated, even the first addition of TAB (about 5 mmol) effected the saturation of the chemisorption, as evidenced by the fact that repeated additions brought about no increase in the amount of chemisorbed TAB. The amount of chemisorbed TAB in each addition was, therefore, taken as the amount of acid sites for TAB. The value listed in Table 2 is the one averaged over four additions.

The adsorption isotherm of chemisorbed TAB was determined with an undiluted SA-1 wafer (Fig. 3). In this titration, TAB was detected in the liquid phase, even at a low surface concentration. In addition, no spectral evidence was observed to show the presence of hydrogen-bonded TAB at any stage of the titration. Figure 3 also shows that the isotherm fits the Langmuir equation. The acid content evaluated from the Langmuir plot is also listed in Table 2.

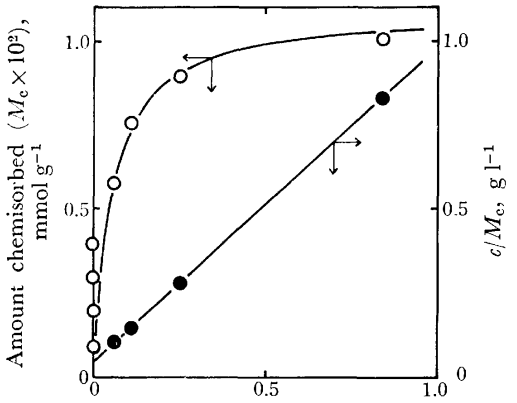

Fig. 3. Adsorption isotherm (○) and Langmuir's plot (●) for TAB chemisorption on SA-1.

Discussion

Table 2 indicates that there are fewer acid sites on SA-1 when TAB is used than when BADA is used, as was expected. This difference can be explained in terms of the difference in the base strength of the two indicators, since TAB is smaller in molecular size than BADA. A similar phenomenon was observed with S-3. Silica gel S-3 behaved as a non-acid to BADA. but as an acid to 4-(1-naphthylamino)azobenzene (pK_a=4.0), which is more basic than BADA. This is also very similar to the well-known fact that even alcohols such as 1-butanol behave as acids toward potasium hydroxide, yielding alkoxide anions. Thus, the present observations substantiate the inference that acid sites on a solid acid vary in number depending on the base strength of the base used.

Also, Table 2 points out that the present titration with BADA itself gives an acid content smaller than the butylamine titration method with BADA for every catalyst used. Two explanations may be offered for this difference. The first is that the observed difference results from the difference in molecular size between BADA and butylamine as titrants. If the acid sites were present mainly in small surface pores which are accessible to butylamine molecules, but inaccessible to BADA molecules larger than the amine, or if such pores were predominant in the surfaces, titration with BADA itself would yield an acid content smaller than the butylamine titration method with BADA. The second is in terms of the difference in the base strengths of the two titrants, as has been described in the Introduction.

The acid-content data shown in the last column of Table 2 give a clue for determining which explanation is valid. These values (for Lewis plus Brønsted acid sites) were determined from the integrated IR absorption intensities for the Lewis-bound pyridine (1455 cm^{-1}) and Brønsted-bound pyridine (1540 cm^{-1}) bands,[10] using the apparent integrated molar absorption coefficients reported by Hughes and White.[11] The IR spectra were recorded after a catalyst wafer had been exposed to pyridine vapor and then evacuated at 150 °C for 1 h.[10] When an undiluted SA-1 wafer was pretreated with pyridine in the same way as above, its UV spectra revealed that such a wafer was capable of chemisorbing only a small amount of BADA. This fact implies that the prechemisorbed pyridine has occupied almost all the acid sites capable of chemisorbing BADA. It should be noted here that pyridine is substantially the same in molecular size as butylamine. According to the first explanation, therefore, the IR-pyridine method would produce an acid content larger than the present titration method. On the other hand, according to the second explanation, almost the same acid contents will be obtained by both methods. Table 2 shows clearly that the two methods yielded almost the same acid content for each catalyst except for SA-1-Na-3. This fact proves the second explanation and, hence, our inference to be valid, although the cause of the exceptional value for SA-1-Na-3 is not clear at present.

Tiration with TAB produced the same acid content for both diluted and undiluted SA-1 wafers, as is shown in Table 2. In the case of the former wafer, its acid content was obtained without the determination of the adsorption isotherms, as has been described above. These facts imply that the present titration method does not necessarily require the time-consuming determination of adsorption isotherms.

The authors are grateful to Mr. Akira Watanabe for his help in part of the measurements, and to Dr. Yasukazu Saito for his valuable discussion.

References

1) Presented partly at the 25th Symposium on Catalysis of the Catalysis Society of Japan, Fukuoka, October 1969.
2) Present address: Chidori Plant, Showa Denko K.K., 4 Chidori-cho, Kawasaki-ku, Kawasaki-shi, Kanagawa, Japan.
3) C. Walling, *J. Am. Chem. Soc.*, **72**, 1164 (1950).
4) H. A. Benesi, *J. Phys. Chem.*, **61**, 970 (1957); O. Johnson, *J. Phys. Chem.*, **59**, 827 (1955).
5) J. Take, Y. Nomizo, and Y. Yoneda, *Bull. Chem. Soc. Jpn.*, **46**, 3568 (1973).
6) J. Take, H. Kawai, and Y. Yoneda, *J. Catal.*, **36**, 356 (1975).
7) J. Take, K. Mizuno, and Y. Yoneda, *J. Catal.*, **42**, 471 (1976).
8) J. Take, T. Tsuruya, T. Sato, and Y. Yoneda, *Bull. Chem. Soc. Jpn.*, **45**, 3409 (1972).
9) C. N. R. Rao, "Ultra-Violet and Visible Spectroscopy; Chemical Applications," Butterworths, London (1961), p. 3.
10) J. Take, T. Ueda, and Y. Yoneda, presented at the 28 th National Meeting of the Chemical Society of Japan, Tokyo, April 1973.
11) T. R. Hughes and H. M. White, *J. Phys. Chem.*, **71**, 2192 (1967).

Emission Spectra of Phenol, Anisole, and Phenetole by Controlled Electron Impact

Masaharu Tsuji,* Teiichiro Ogawa, Yukio Nishimura,* and Nobuhiko Ishibashi

Faculty of Engineering, Kyushu University, Hakozaki, Fukuoka 812

(Received November 2, 1976)

Upon the impact of an electron beam (100—450 eV) on PhOH, $PhOCH_3$, $PhOC_2H_5$, $PhCOCH_3$, and $(Ph)_2CO$ at low pressures, the S_1 emission of the parent molecule (not from $PhCOCH_3$ and $(Ph)_2CO$) and the photoemissions from such fragments as H, CH, CO, CO^+, and OH were observed in the 200—520 nm region. It was concluded that the S_1 emission of the parent molecule originates through both the $S_0 \rightarrow S_1$ and $S_0 \rightarrow S_2$ (cascade) $\rightarrow S_1$ excitation processes and that the direct excitation into the lower vibronic levels of S_1 is responsible for the appearance of the vibrational structures. Most excited species including $CO^+(A)$ from PhOH were confirmed to be primarily produced; however, $CO^+(A)$ from $PhOCH_3$, $PhOC_2H_5$, and $PhCOCH_3$, and CO(b) from $PhCOCH_3$ were found to be produced competitively through one-electron and two-electron excitation processes in relation to the intensity measurements. The relative contribution of the two-electron excitation process in producing $CO^+(A)$ increased with a larger substituent, and it was larger than that for CO(b) in $PhCOCH_3$.

The spectroscopic analysis of the optical emission resulting from the collision of an electron with molecules at a low pressure provides direct information about the energy states not only of ionic products, which have been well investigated by mass spectrometry, but also of radical and neutral ones. In the previous papers,[1-7] we have reported the emission spectra of various aromatic molecules in the ultraviolet and visible regions as studied by means of the crossed electron-beam and molecular-jet method. Many aromatic molecules showed the characteristic S_1 emission of the parent molecule, and in the case of naphthalene[5] the cascading processes from S_2 and S_3 to S_1 were concluded to be mainly responsible for the S_1 emission. Photoemissions from several excited fragments were also observed; most of them were confirmed to be primarily produced in relation to their intensity measurements. The formation of $CO^+(A)$ from three isomers of dimethoxybenzenes[6] was an exceptional case, which involves a secondary reaction, and the results were interpreted in terms of the competition between the one-electron and the two-electron excitation processes. However, no studies have been carried out on the emission spectra and the mechanism of the dissociative excitation of monosubstituted benzene with an oxygen atom, except for our previous communications on anisole[1] and nitrobenzene.[4] In this paper, we will describe the emission spectra of phenol, anisole, phenetole, acetophenone, and benzophenone under a controlled electron-impact excitation (100—450 eV) and will discuss the mechanism of the S_1 emission of the parent molecule and that of the formation of the excited species.

Experimental

The apparatus and the experimental conditions were essentially identical with those described previously.[3] The electron-beam current in the collision chamber ranged between 10 and 3000 μA for electron energies from 100 to 450 eV. The pressure of the sample gases in the collision chamber, which was proportional to that in the gas reservoir, was estimated to be of the order of 10^{-3} Torr.

The photoemission in the 200—520 nm region was detected by the use of a JASCO CT-50 scanning spectrometer in the first order of a 1200 grooves/mm grating blazed at 300 nm. The spectra were recorded at a resolution of about 4 Å (FWHM). An EMI 9558QB photomultiplier and a Burr-Brown 3421K OP amplifier were used for recording the spectra. The current and pressure dependences of the emission intensities were measured with the aid of a HTV R585 photomultiplier, and the output pulses from the photomultiplier were amplified and counted by means of an NF-PC 545A photon counter. The absence of changes in the observed spectra when a suppressor electrode was put just above the electron target or when an aluminum target was replaced by a golden one reinforced the conclusion that the excitation by secondary electrons ejected from the target was negligible.

The reagents were obtained either from the Wako Pure Chemical Co. or from Kishida Chemical Ind. They were subjected to several freeze-pump-thaw cycles to remove dissolved atmospheric gases.

Results

A typical emission spectrum of phenol excited by an electron beam of 300 eV at 2 mA is shown in Fig. 1. The continuous features with discrete structures in the 275—340 nm region were assigned to the $S_1(^1B_1) \rightarrow S_0$ $(^1A_1)$ transition of the parent molecule. No appreciable alteration in the shape or position of the S_1 emission was found by changing the excitation energies between 100 and 450 eV. Prakash[8] measured photographically the fluorescence spectrum of phenol at the vapor phase excited by the radiation from a condensed iron spark and analyzed the observed S_1 emission in the 275—303 nm region. He found the 0-0 band at 2751 Å; this band was very weak because of the self-absorption by the unexcited molecules. In the present spectrum, taken under a very low pressure, where such a self-absorption effect and collisional deactivation within the lifetime of the excited species are expected to be negligible, the 0-0 band appears intensively at the shortest wavelength. Although our spectrum is less resolved, several features at the shorter wavelengths can be interpreted as an overlapping of some fluorescence bands given by Prakash.

Since energetic electrons bring about not only the excitation but also the dissociation of target molecules, photoemissions from the excited fragments can be ob-

* Research Institute of Industrial Science, Kyushu University, Hakozaki, Fukuoka 812,

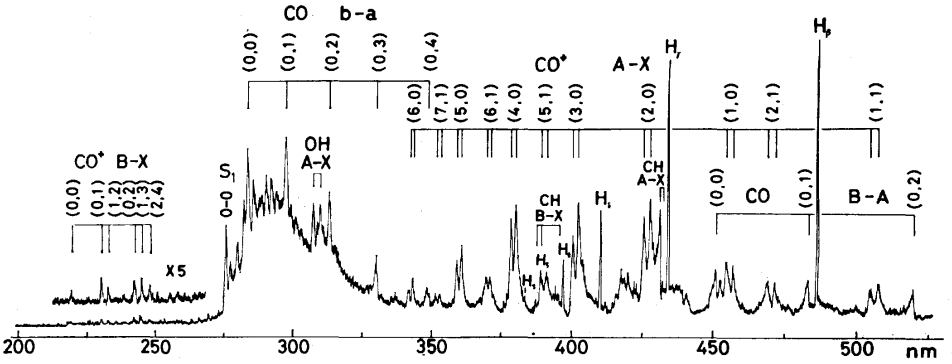

Fig. 1. Emission spectrum of phenol by controlled electron impact. Electron energy 300 eV, electron-beam current 2 mA.

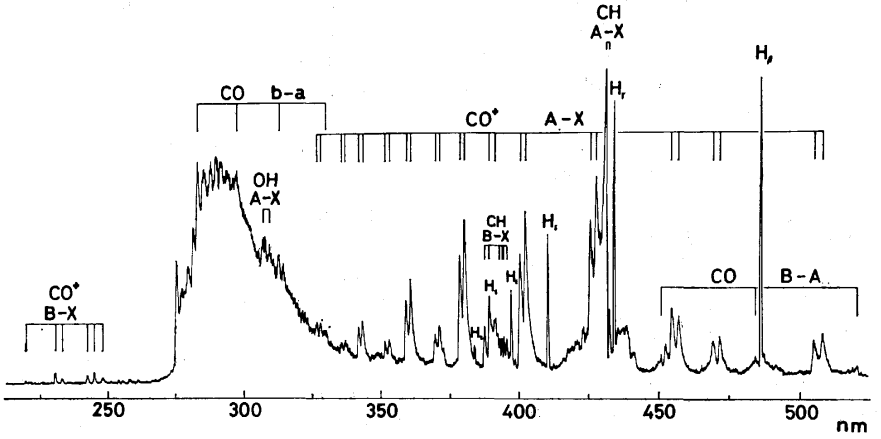

Fig. 2. Emission spectrum of anisole by controlled electron impact. Electron energy 300 eV, electron-beam current 1 mA.

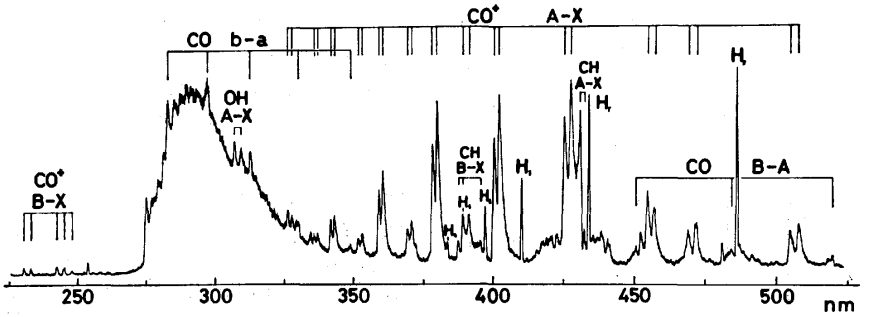

Fig. 3. Emission spectrum of phenetole by controlled electron impact. Electron energy 300 eV, electron-beam current 1 mA.

served. The Balmer series of the hydrogen atom ($H_{\beta-\eta}$) and the two systems of CH, the 4300 Å system ($A^2\Delta$-$X^2\Pi$) and the 3900 Å system ($B^2\Sigma^-$-$X^2\Pi$), were identified in the 384—486 nm region. The features around 306 nm and the bands at 283, 298, 313, and 331 nm, superimposed upon the intense S_1 emission of the parent molecule, were assigned to the 3064 Å system of OH ($A^2\Sigma^+$-$X^2\Pi$) and the third positive system of CO ($b^3\Sigma^+$-$a^3\Pi$). The bands at 451, 484, and 520 nm were assigned to the Ångström system of CO ($B^1\Sigma^+$-$A^1\Pi$). The numerous other bands were ascribed to the comet tail system ($A^2\Pi$-$X^2\Sigma^+$) and the first negative system ($B^2\Sigma^+$-$X^2\Sigma^+$) of CO^+.

Figures 2 and 3 show the emission spectra of anisole and phenetole excited by an electron beam of 300 eV at 1 mA. The S_1 emission of the parent molecule, the shape and position of which were independent of the excitation energy (100—450 eV), can be observed at the identical wavelength region in the case of phenol, and the 0-0 band is found at 275 nm in both spectra. Their vibrational structures are very similar to those of phenol, although the fraction of the unresolved continuum becomes larger with an enlargement of the substituent. Several features of anisole at the shorter wavelengths can be interpreted as an overlapping of some fluorescence bands measured and assigned by Prakash and Singh in the vapor phase.[9] The S_1 emission of phenol, anisole, and phenetole are more diffuse than the spectrum of benzene,[3] while they are sharper than the spectrum of naphthalene.[5] Photoemissions from

the same atomic and diatomic fragments can be identified in both spectra.

The striking optical features of benzene monoderivatives with a carbonyl group are the appearance of strong phosphorescence instead of fluorescence in the solution and in the low-temperature matrix.[10] In the electron-impact excitation of acetophenone and benzophenone at low pressures, no photoemission from the excited parent molecule could be observed, just as in the case of the optical excitation; all the observed bands were attributed to the photoemissions from the excited fragment species: H, CH, CO, and CO^+. Both spectra were similar to the emission spectrum of nitrobenzene,[4] except for the absence of the band systems of NO and CN.

The current and pressure dependences of the photoemission intensities of the parent molecule and the fragment species were measured in order to elucidate the reaction mechanism. Figure 4 shows such intensity measurements on anisole. The band intensities of the parent molecule, H, and CH are proportional both to the electron-beam current and to the gas pressure, just as in the cases of other aromatic molecules.[2-7] However, the band intensity of CO^+(A) varies non-linearly with the electron-beam current, although it is proportional to the gas pressure. The pressure dependence of the intensity of CO^+(A) from CO[11] and CH_3OH[7] has been found to be linear at a low pressure, and a similar linear relationship has been presumed on $PhNO_2$[4] and $Ph(OCH_3)_2$.[6] The present observation of the linearity in anisole indicates the validity of the previous assumption.

The photoemission intensities of the parent molecule, H, and CH produced from phenol, phenetole, and acetophenone, and that of OH from phenol were also proportional to the electron-beam current. However, their pressure dependence could not be measured in the present study because of the low vapor pressures of these compounds. Figure 5 shows the dependence

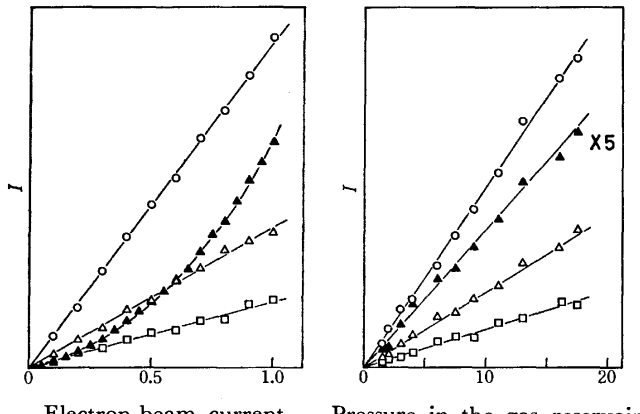

Fig. 4. Dependence of band intensities (I, arbitrary units) from anisole on the electron-beam current (mA) and on the pressure in the gas reservoir (mmHg). Electron energy 300 eV, electron-beam current in the measurement of the pressure dependence 50 μA.
○: $PhOCH_3$(285 nm), △: CH(431 nm), □: H_δ, ▲: CO^+(402 nm).

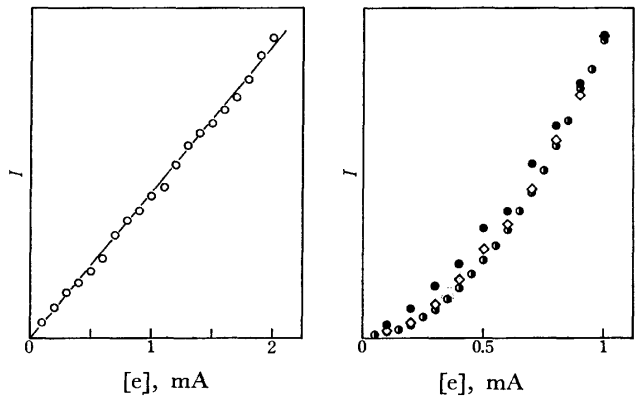

Fig. 5. Dependence of photoemission intensities (I, arbitrary unit) on the electron-beam current [e]. Electron energy 300 eV.
Left; ○: CO^+(A) from phenol (402 nm).
Right; ●: CO(b) from acetophenone (298 nm), ◇: CO^+(A) from acetophenone (402 nm), ◑: CO^+(A) from phenetole (380 nm).

of the photoemission intensity of CO^+(A) from phenol and phenetole, and that of CO(b) and CO^+(A) from acetophenone, where the intensities in the right figure are normalized at the value of 1 mA. A significant deviation from the linearity is observed in the intensity of CO^+(A) from phenetole, and that of CO(b) and CO^+(A) from acetophenone, while a linear relationship is established in the intensity of CO^+(A) from phenol.

The non-linearity of the photoemission intensity (I) may be interpreted by considering the quadratic term with respect to the electron-beam current [e]:

$$I = K_1[e] + K_2[e]^2, \quad (1)$$

where K_1 and K_2 are constant. It is convenient to divide this equation by the electron-beam current and to plot $I/[e]$ as a function of [e]:

$$I/[e] = K_1 + K_2[e]. \quad (2)$$

The current dependence of the emission intensities of CO^+(A) and CO(b) described in this form is given in Figs. 6 and 7. The reasonable fit to a straight line in all cases indicates the validity of this equation. The measurement of the intensity of CO(b) from the other

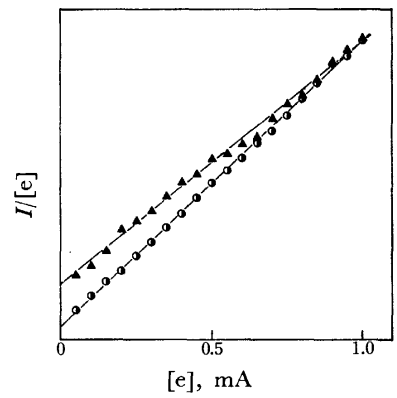

Fig. 6. Dependence of $I/[e]$ (arbitrary unit) on [e].
▲: CO^+(A) from anisole, ◑: CO^+(A) from phenetole.

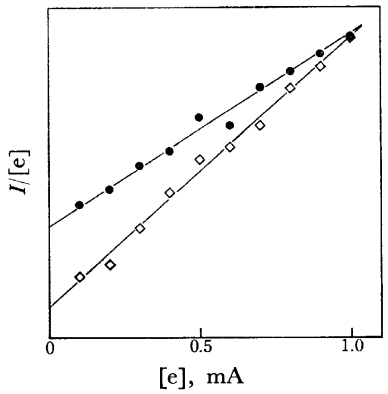

Fig. 7. Dependence of $I/[e]$ (arbitrary unit) on [e]. ●: CO(b) from acetophenone, ◇: CO^+(A) from acetophenone.

compounds was difficult because of the weak intensity and the band overlapping with the intense S_1 emission of the parent molecule.

Discussion

The Emission of the Parent Molecule. There is a significant difference in the excitation into the neutral states between the photon and the electron. The former pumps molecules resonantly into one or a few specific vibronic levels; on the other hand, the latter excites them simultaneously into all the vibronic levels below the electron energy. Therefore, phenol, anisole, and phenetole are expected to be primarily excited into any of the S_1, S_2, and higher singlet states under the impact of fast electrons. However, photoemission can be observed almost exclusively from the S_1 state; this indicates that the radiationless transition occurs with a high efficiency at higher excited singlet states under a very low pressure.

The probability of excitation by fast electrons into an upper state, s, with an energy, E_s, is known to be proportional to $M_s^2=f_sR/E_s$ in the case of an optically allowed transition according to the Bethe theory,[12-14] where f stands for the optical oscillator strength, which can be obtained from the energy-loss (absorption) spectrum, and where R is the Rydberg constant. The efficiency of the radiative transition from an excited state is given by the fluorescence quantum yield Φ, which can be measured in an optical excitation. Hence, the relative contribution of the S_1 emission from the various primary excitation processes can be estimated by the product, $\Phi_s(S_1)M_s^2$. Although the energy-loss spectra of phenol, anisole, and phenetole have not been reported, it is justifiable to use the oscillator strengths obtained by the ultraviolet absorption spectra, because the oscillator strengths obtained through the two methods agreed well with each other.[15] Kimura and Nagakura[16] measured the f values of these molecules in the vapor phase and found them to be 0.020—0.028 for $S_0\rightarrow S_1$ (E_1=4.59 eV), 0.132—0.188 for $S_0\rightarrow S_2$ (E_2=5.75—5.82 eV), and 0.529—0.636 for $S_0\rightarrow S_3$ (E_3=6.60—6.70 eV). These values show that the $S_0\rightarrow S_2$ and $S_0\rightarrow S_3$ excitation is 5—6 and 13—22 times stronger than the $S_0\rightarrow S_1$ excitation. The quantum yield of the S_1 emission as a function of the excitation energy has, to our knowledge, been measured only on phenol in dilute solutions in the 280—200 nm region;[17] the quantum yield in a nonpolar solvent is almost constant within the first absorption band ($\Phi_1(S_1)=7.5\times10^{-2}$) and within the second one ($\Phi_2(S_1)=3.0\times10^{-2}$). The non-zero value of the quantum yield in the S_2 region shows the existence of some contribution of the S_1 emission, followed by a fast internal conversion from S_2 to S_1. Assuming that the value of the quantum yield in a dilute solution can be carried over to that in the low-pressure vapor, the relative contribution of the S_1 emission from the two excited states is obtained as follows: $\Phi_1(S_1)M_1^2$: $\Phi_2(S_1)M_2^2$ $=1.0:2.1$. This result indicates that the contribution of the S_1 emission through the $S_0\rightarrow S_2$ excitation, followed by the fast internal conversion from S_2 to S_1, is larger than that through the direct $S_0\rightarrow S_1$ excitation. The routes of the S_1 emission of anisole and phenetole are probably similar to that of phenol.

From the investigations of the resonance fluorescence of aromatic molecules, the S_1 emission has been established to become increasingly diffuse as the molecules are excited into the higher vibronic levels.[18] For instance, no vibrational fine structure could be observed when toluene was excited into the higher vibronic levels at 1189 cm^{-1} above the 0-0 level of the $S_0\rightarrow S_1$ transition.[19] The present S_1 emissions of phenol, anisole, and phenetole exhibit some vibrational structures on a broad continuum, and it is reasonable to consider that the vibrational structure and the continuum come from different origins; the direct excitation into the lower vibrational levels of the S_1 state is responsible for the vibrational structure and the excitation into the higher levels for the continuum photoemission. The density of the vibrational levels increases with a larger substituent; therefore, the fraction of the broad continuum increases in the order of phenol, anisole, and phenetole.

It has been found that the predominant process of the S_1 emission of benzene[20-22] contrasts with that of naphthalene.[5,23] The former emission exhibits a sharp vibrational structure[3] and arises mostly from the lower vibrational levels of the S_1 state. The latter emission is very broad, shifts to the red in comparison with the resonance fluorescence obtained at low excitation energies, and occurs mostly from the highly excited vibrational levels of the S_1 state populated through rapid internal conversion from the primarily excited S_2 and S_3 states. In the present study, it was concluded that the S_1 emission of phenol originates through both the $S_0\rightarrow S_1$ and $S_0\rightarrow S_2$ (cascade)$\rightarrow S_1$ excitation processes; probably this is the case for anisole and phenetole also.

The S_1 emission could not be observed from acetophenone and benzophenone. In these carbonyl compounds, the lowest excited singlet state is of the n,π^* type, and a rapid intersystem crossing to the triplet state occurs. The quantum yields of the intersystem crossing in these molecules have been reported to be unity in benzene at room temperature.[24]

The Kinetic Study of the Reaction. In the crossed electron-beam and molecular-jet method, most emitting excited species produced from aromatic molecules have been confirmed to be primary products in terms of the

current and pressure dependences of the emission intensity.[2-7] In the present study, the intensities of the parent molecule, H, and CH from phenol, anisole, phenetole, and acetophenone have been found to be proportional to the electron-beam current. Their intensities from anisole were also found to be proportional to the gas pressure, and similar linear relationships can be expected to hold for the other molecules, because their pressures in the reaction chamber were still lower than that in the case of anisole. Therefore, it can be concluded that the formation of excited parent molecule, H, and CH from such compounds proceeds through a primary collision of an electron with a molecule.

It has been found that the current dependence of the band intensity of $CO^+(A)$ from small molecules, such as CO[6] and CH_3OH,[7] differs from that from larger aromatic molecules, such as $PhNO_2$[4] and $Ph(OCH_3)_2$;[6] the former was linearly proportional, while the latter was non-linear. The linear relationship of the band intensities of $CO^+(A)$ and OH from phenol shows that these fragments are also primary products. However, since the intensities of $CO^+(A)$ from anisole, phenetole, and acetophenone, and CO(b) from acetophenone are represented by Eq. 1, a secondary collision with another electron participates in the formation of such excited fragments.

Several similar relationships have been pointed out, and the excited species which show non-linear relationships have been classified in the following two groups:[6] (a) fragments which are produced through the scission of two skeletal bonds—*e.g.*, CN(anilines[4]) and CO^+ (dimethoxybenzenes[6]) and (b) a new chemical bond is created on its formation—*e.g.*, HCl^+(chlorobenzene[7]) and HBr^+(bromobenzene[7]). The formation of CO^+ (A) from anisole and phenetole can be classified in Group (a). It should be noticed that aromatic molecules with a large substituent containing an oxygen atom give fragments abundantly produced in the non-linear process.

For the interpretation of the empirical Eq. 1, the following reaction scheme is assumed:

$$\mathrm{M} + \mathrm{e} \xrightarrow{k_1} \mathrm{CO}^{+}{}^{*}, \quad \mathrm{M} + \mathrm{e} \xrightarrow{k_2} \mathrm{X}$$

$$\mathrm{X} + \mathrm{e} \xrightarrow{k_3} \mathrm{CO}^{+}{}^{*}, \quad \mathrm{X} + \mathrm{e} \xrightarrow{k_4} \mathrm{Y}$$

$$\mathrm{X} \xrightarrow{k_5} \mathrm{Z}$$

$$\mathrm{CO}^{+}{}^{*} \xrightarrow{k_6} \mathrm{CO}^{+}(\mathrm{X}) + h\nu,$$

where M and CO^+* denote a target molecule and the $A^2\Pi$ state of CO^+. X, which stands for some unidentified neutral or ionic intermediates, disappears upon another collision with an electron, producing CO^+* or other products (Y). It is also removed from the reaction zone mainly by the evacuation process, where the removed species are represented as Z.[25] The radiative lifetime of CO^+*, reported as 2.1—3.8 μs,[26] is short enough to emit radiation within the observation region. A similar reaction scheme is applicable to the formation of CO(b) from acetophenone. The observed emission intensity is proportional to $k_6[CO^+*]$:

$$I = ak_6[CO^+*], \tag{3}$$

where a is a proportionality constant. The rates of the formation of CO^+* and X are represented as follows:

$$d[CO^+*]/dt = k_1[M][e] + k_3[X][e] - k_6[CO^+*], \tag{4}$$

$$d[X]/dt = k_2[M][e] - k_3[X][e] - k_4[X][e] - k_5[X]. \tag{5}$$

Since the photoemission was observed in a flowing system at the stationary state, the steady-state conditions hold; therefore, the following equations can be derived:

$$[X] = k_2[M][e]/\{(k_3+k_4)[e]+k_5\}, \tag{6}$$

$$I = ak_1[M][e] + ak_2k_3[M][e]^2/\{(k_3+k_4)[e]+k_5\}. \tag{7}$$

If $(k_3+k_4)[e] \ll k_5$, an equation identical with the one obtained empirically, Eq. 1, is derived by substituting $ak_1[M]/k_5=K_1$ and $ak_2k_3[M]/k_5=K_2$. Therefore, we can conclude that $CO^+(A)$ and CO(b) are produced competitively through one-electron and two-electron excitation processes where most of the X is removed by the evacuation process. The relative contribution of the two-electron excitation process to the one-electron excitation process, K_2/K_1, was evaluated, by means of the slope and the intercept of the straight line, as 1.0: 2.0 : 5.2 : 0.39 for $CO^+(A)$ from anisole, acetophenone, and phenetole, and for CO(b) from acetophenone, respectively. The relative contribution of the two-electron excitation process in the formation of $CO^+(A)$ from dimethoxybenzenes has been attributed to the difference in the intra-molecular interaction of two adjacent groups.[6] In the present study, an increase in the mass of the substituent, taking phenol as a limiting case, enhances the relative rate (K_2/K_1) of the two-electron excitation process. In the competitive formation of $CO^+(A)$ and CO(b) from acetophenone, the relative rate of the two-electron excitation process for producing $CO^+(A)$ is about 5 times faster than that for producing CO(b).

The authors wish to thank Professor Fumiyuki Nakashio and Dr. Minoru Toyoda for their discussions. They are also indebed to Professor Tomoo Oyama for the use of his CT-50 monochromator.

References

1) T. Ogawa, M. Tsuji, M. Toyoda, and N. Ishibashi, *Chem. Lett.*, **1972**, 233.
2) T. Ogawa, M. Tsuji, M. Toyoda, and N. Ishibashi, *Bull. Chem. Soc. Jpn.*, **46**, 1063 (1973).
3) T. Ogawa, M. Tsuji, M. Toyoda, and N. Ishibashi, *Bull. Chem. Soc. Jpn.*, **46**, 2637 (1973).
4) M. Tsuji, T. Ogawa, and N. Ishibashi, *Bull. Chem. Soc. Jpn.*, **46**, 3380 (1973).
5) M. Tsuji, T. Ogawa, and N. Ishibashi, *Chem. Phys. Lett.*, **26**, 586 (1974).
6) T. Ogawa, T. Imasaka, M. Toyoda, M. Tsuji, and N. Ishibashi, *Bull. Chem. Soc. Jpn.*, **48**, 645 (1975).
7) K. Hirota, M. Hatada, and T. Ogawa, *Int. J. Radiat. Phys. Chem.*, **8**, 205 (1976).
8) S. Prakash, *Nature*, **210**, 521 (1966).
9) S. Prakash and N. L. Singh, *Indian J. Phys.*, **37**, 59 (1963).

10) R. S. Becker, "Theory and Interpretation of Fluorescence and Phosphorescence," John Wiley & Sons (1969).
11) J. F. M. Aarts and F. J. de Heer, *Physica (Utrecht)*, **49**, 425 (1970).
12) H. A. Bethe, *Ann. Phys. (Leipzig)*, **5**, 325 (1930).
13) R. L. Platzman, *Radiat. Res.*, **17**, 419 (1962).
14) M. Inokuti, *Rev. Mod. Phys.*, **43**, 297 (1971).
15) For example R., H. Huebner, S. R. Mielczarek, and C. E. Kuyatt, *Chem. Phys. Lett.*, **16**, 464 (1972).
16) K. Kimura and S. Nagakura, *Mol. Phys.*, **9**, 117 (1965).
17) G. Köhler and N. Getoff, *Chem. Phys. Lett.*, **26**, 525 (1974).
18) C. S. Parmenter, "Spectroscopy," ed by D. A. Ramsay, Butterworth, London (1972), p. 297.
19) J. M. Blondeau and M. Stockburger, *Ber. Bunsenges. Phys. Chem.*, **75**, 450 (1971).
20) K. C. Smyth, J. A. Schiavone, and R. S. Freund, *J. Chem. Phys.*, **61**, 1782 (1974).
21) C. I. M. Beenakker, F. J. de Heer, and L. J. Oosterhoff, *Chem. Phys. Lett.*, **28**, 320 (1974).
22) T. Ogawa, Abstr. Invited Paper 3Q1, 32th National Meeting of the Chemical Society of Japan, Tokyo, April 1975.
23) K. C. Smyth, J. A. Schiavone, and R. S. Freund, *J. Chem. Phys.*, **62**, 136 (1975).
24) A. Lamola and G. Hammond, *J. Chem. Phys.*, **43**, 2129 (1965).
25) The CO^{+*} formation from dimethoxybenzenes in Ref. 6 was analyzed in the identical formulation; however, k_5 does not appear explicitly, and this has induced some confusion.
26) G. R. Möhlmann and F. J. de Heer, *Chem. Phys. Lett.*, **43**, 170 (1976).

The Formation of $VOSO_4$ on the Surface of V_2O_5 in the Oxidation of SO_2 as Studied by ESR

Yoshiya KERA and Keiji KUWATA

Department of Chemistry, Faculty of Science, Osaka University, Toyonaka, Osaka 560

(Received December 27, 1976)

To obtain information on the arrangements of the $VOSO_4$ phase in the surface layer of the V_2O_5 single crystal, the angular dependencies of an asymmetric ESR spectrum which has been found in the crystal under the conditions of SO_2 oxidation and assigned to the $VOSO_4$ phase were examined in detail. Two types of the angular dependency of the spectrum on the static magnetic field were clearly differentiated from each other. In the main spectrum, the direction of $g_{//}$ was completely consistent with the b-axis of the V_2O_5 crystal, while, on the other hand, in the minor spectrum, it took rather random orientations. From comparisons of the crystal structures between V_2O_5 and $VOSO_4$, it was deduced, preliminarily, that the α-$VOSO_4$ phase with a layer structure, was regularly aligned along the layer of the V_2O_5 lattice and that the β-$VOSO_4$ phase without a layer structure took a relatively random orientation to the lattice.

Vanadium oxides, which were promoted with alkali metals and/or supported on silica and alumina gels, have been used as catalysts in the production of sulfuric acid and organic acids. Numerous investigators have attempted to make clear their catalytic properties and reaction mechanisms, especially in SO_2 oxidation.[1] Their results, however, seem to conflict with each other. This is because of some changes in the surface states to which catalysts are subjected in preparation[2] and working.[3] On the other hand, a simple and reversible change in the ESR spectrum was found in the highly purified V_2O_5 single crystal under the conditions of SO_2 oxidation. It was previously reported that, at lower temperatures, the $VOSO_4$ phase existed stably, while at higher temperatures oxygen vacancies remained in the surface layer under the conditions of SO_2 oxidation.[4]

In the present study, in order to obtain information on the structure of the $VOSO_4$ formed in the surface layer of the V_2O_5 crystalline lattice, the angular dependencies of the asymmetric ESR spectrum on the static magnetic field were examined in detail. The growth of $VOSO_4$ in the surface layer of V_2O_5 crystal will be preliminarily discussed.

Experimental

Preparation and Treatment of V_2O_5 Single Crystal. The V_2O_5 powder which was used as the starting material was obtained by the thermal decomposition of NH_4VO_3 (special grade, Wako Pure Chem. Co.) at 600 °C for 3 h in an air stream. The purification of the V_2O_5 powder was carried out chemically according to the procedures reported by McCarley *et al.*[5] The V_2O_5 single crystal was prepared by a zone-melting method in a Pt boat. The crystal was cut out in a size (mm^3) of about $1.4\times0.5\times9$ (wt 0.021 g) and was placed in a quartz tube (4 mm in outer diameter) for the reaction and for ESR measurement. The sample was preliminarily heated at about 500 °C for 1 h under evacuation. After the sample had then cooled to room temperature, a gaseous mixture (SO_2 : air = 37 : 20) of 500 mmHg* was introduced and the tube was sealed. The inner volume of the sealed tube was 6 cm^3. The reaction temperature was kept at 617 °C (±1 °C). At time, the reaction tube was taken out from the furnace, and the intensities and line shapes of the ESR spectrum were checked.

* 1 mmHg = 1.333×10^2 Pa.

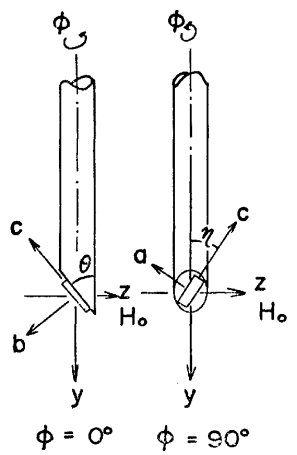

Fig. 1. Rotating operations and relations among crystal axes, experimental coordinates and H_0.

After treatment for 312 h, the crystal was taken out from the reaction tube and was cut out again in a size (mm^3) of about $1.4\times0.3\times4$, in order to measure the angular dependencies of the ESR spectrum.

Rotation Apparatus and Crystal Settings. A quartz rod, the end of which was cut out at a given angle (the angle is denoted as θ) to the rod axis, was mounted on a rotating divice around the vertical axis (the angle of the rotation is denoted as ϕ). In this experiment, six quartz rods, the θ values of which equal 0, 30, 45, 60, and 90° respectively, were used. The accuracy in θ was about 1°. The crystal was placed on the cut plane of the rod at a given angle between the long axis of the elliptical-cut plane of the rod and the c-axis of the crystal (the angle is denoted in η). The relations among the crystal axes and the laboratory coordinates are illustrated in Fig. 1. The three ways of rotation were chosen as follows:

θ: rotation angle around the x-axis (experimental coord.) at $\phi=0°$

ϕ: rotation angle around the y-axis (experimental coord.)

η: rotation angle around the b-axis (crystal axis).

η was determined by use of a micrometerscope (10X) with a graduator; the accuracy was about 1°. ϕ was changed from 0 to 180° at 5° intervals, and accuracy in ϕ was about 0.5°.

ESR Measurements. The ESR measurements were carried out at 77 K by means of a home made X-band spectrometer. The modulation frequency was 455 kHz. The microwave frequency was determined by means of a wave meter,

and the calibration of the magnetic field was done by the use of DPPH and Mn(II) ions doped in MgO. The determination of the concentration of the unpaired electron was done by comparing the integrated intensities with those of a known amount of the $CuSO_4 \cdot 5H_2O$ single crystal. The growth of the spectrum was estimated by comparing the intensities with the DPPH. For the check of the line shape, the spectrum was observed in several different directions of the magnetic field in each measurement.

Results

V_2O_5 Single Crystals Heated in SO_2+Air. No ESR signal was found initially in the V_2O_5 crystal, which was prepared from cautiously purified V_2O_5 powder. The crystal exposed to a gaseous mixture of SO_2 and air at 617 °C for 32 h, however, showed an asymmetric ESR signal. The intensity increased with the time up to about 180 h. The growth of the spectrum with the time is illustrated in Fig. 2. Finally, the spin concentration increased up to about 2×10^{17}. The line shape did not change with the time.

Angular Dependencies of ESR Spectrum. Sharp Signal: When both θ and η are fixed at zero, the change in the spectrum with ϕ is demonstrated in Fig. 3. The figure shows clearly that a strong sharp signal is gradually moving toward a low field as the direction of the magnetic field changes from H_0//b to H_0//a in the ba-plane of the crystal. Besides this, a minor signal, which seems to consist of more than one component, was seen, but the angular behavior is not clear. The sharp signal also behaved similarly when θ was fixed at 0 and at a η of any value from 0 to 90°. When η was fixed at 0° and the θ was of any value between 0 and 90°, the moving range of the sharp component with ϕ was not constant; the larger θ was, the narrower the moving range became. In the limiting case of $\eta=0°$ and a θ value close to 0°, the sharp signal seems always to be at the lowest magnetic field during the change in ϕ, as is demonstrated in Fig. 4. These results for the sharp signal clearly indicate that the ***g***-tensor has approximately an axial symmetry, that the direction of $g_{//}$ coincides with the b-axis of the crystal, and that $g_\perp$ is in the ac-plane.

The g-values of the sharp signal at each θ are plotted against ϕ in Fig. 5. The full lines are the theoretical one, calculated using the values of $g_{//}=1.924$ and $g_\perp=1.970$ obtained by the least-square treatment of the data by the use of the familiar equation, $g^2=g_{//}^2\cos^2\delta+g_{//}^2\sin^2\delta$, where δ denotes the angle between $g_{//}$ and H_0.

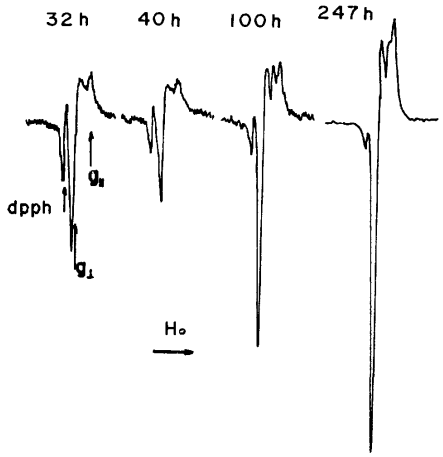

Fig. 2. Change in the intensity of ESR spectrum in V_2O_5 single crystal during SO_2 oxidation reaction.

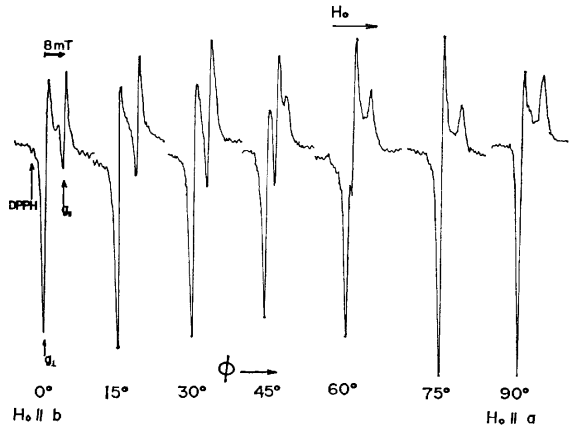

Fig. 3. Change in ESR spectrum with change in the direction of H_0 in the crystal ab-plane from H_0//b to H_0//a.

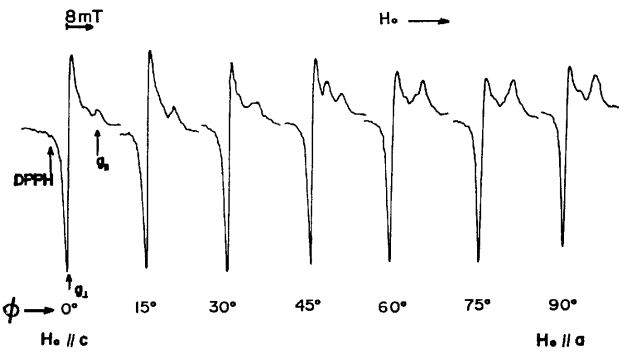

Fig. 4. Change in ESR spectrum with the change in the direction of H_0 in the crystal ac-plane from H_0//c to H_0//a.

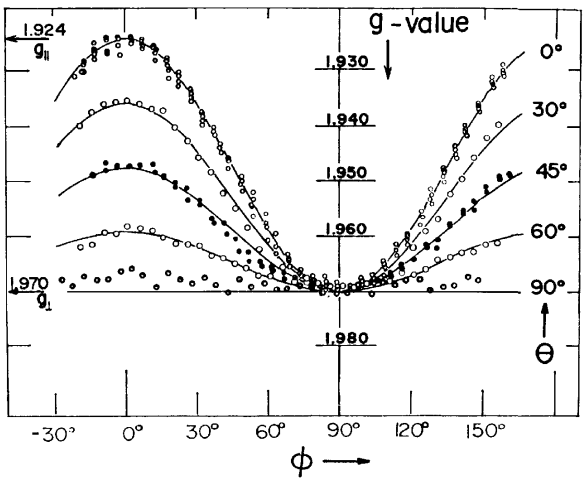

Fig. 5. Angular dependency of the sharp signal on θ. Figure shows following cases: at $\theta=0°$ with $\eta=0$, 30, 45, 60, and 90°; at $\theta=45°$ with at $\eta=0$ and 45°; and with $\theta=30$, 60, and 90° only at $\eta=0°$.

In the case of $\theta=0°$, at η values of 0, 30, 45, 60, and 90°, and in the case of $\theta=45°$, at η values of 0° and 45°, the results are given together. In the other cases, only results at $\eta=0°$ are given. Except in the case of $\theta=90°$, the g-values concentrate close to the theoretical curves. The fluctuations of the g-values in the case of $\theta=90°$ seem to due to the overlap of some minor components, as will be discussed below.

Other Minor Signals: It may be seen in Fig. 4 that the other minor signals in the spectrum move from a low to a high field with the change in the direction of the H_0 in the ac-plane from $H_0//c$ to $H_0//a$. As several components overlap complicatedly and seem to move independently of each other, the centers of the groups of these signals can not be preciesly determined. In the case of $\theta=90°$ and $\phi=0°$, however, the g-values estimated from the distances between the center of the group and that of DPPH can be plotted against ϕ, as is shown in Fig. 6. A periodical change is seen, especially near the maximum point in the figure. The dotted

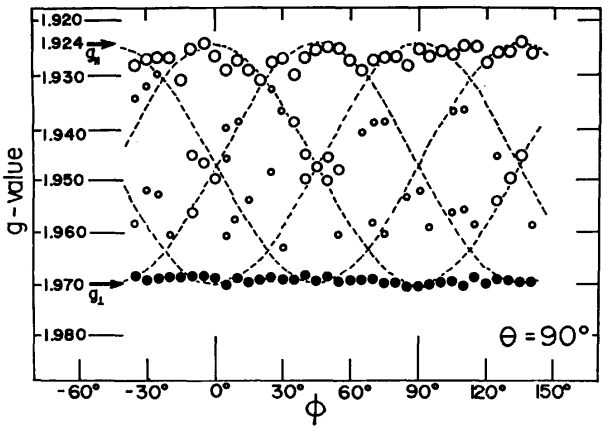

Fig. 6. Angular variations of the minor signal with the change in H_0 in the ac-plane. Dotted lines denote the theoretical calculations under the assumptions that $g_{//}$ is in the ac-plane and is parallel to a-, c-axis and the axes deviated by ±45° from a- or c-axis. Closed circles denote the values of the sharp signal. Large open circles denote the values of relatively clear signal and the small circles that of not so clear signal.

lines are the theoretical ones, calculated by the use of the same equation and parameters as those used in the case of the sharp signal. To obtain a good fit, several directions of g were tried parallel to the a- and c- axes and deviating by ±45° from the axes in the ac-plane; the best fit was thus obtained. It may be seen in the figure that there are also other groups of points which are not distributed on any of the dotted lines. This may indicate that there are other components which have $g_{//}$ components out of the ac-plane. Nearly the same periodicities as in the case of the H_0 change in the ac-plane (*cf.* Fig. 6) were also seen near the c- and a-axes in the case of the H_0 variations in the ab- and bc-planes of the V_2O_5 crystal. However, the minor signals can not be determined practically because they are extensively disturbed by the sharp signal.

Discussion

Possible Structures of the $VOSO_4$ Formed in the V_2O_5 Crystal in the Oxidation of SO_2 with Air. Many investigators have found several types of ESR spectra in the V_2O_5 crystal, in some cases by the addition of metal impurities.[6-10] The results have always indicated that the direction of $g_{//}$ coincides with the b-axis, and the spectra show hfs due to V (IV) ions which are diluted inside the V_2O_5 lattice and are sufficiently isolated from each other. Therefore, the sharp and asymmetric spectrum in the present study can not be ascribed to these species. On the other hand, the possibilities of ascribing this ESR spectrum to some lower vanadium oxide compounds (*e.g.*, V_3O_7, V_6O_{13}, and VO_2) can also be excluded. On the contrary, existence of the $VOSO_4$ phase has been strongly supported by previous study.[4]

Two types of crystal structures have been reported in $VOSO_4$:[11] the α-form (tetragonal) and the β-form (orthorhombic). The α-form has the layer structure shown in Fig. 7,[12] and the vanadium-oxygen bond (V=O) takes only one direction, which coincides with the c-axis in the crystal. In the β-form, the layer structure is completely destroyed, as is shown schematically in Fig. 8.[13] The vanadium-oxygen bond (V=O) takes two directions deviating by about ±22° from the a-

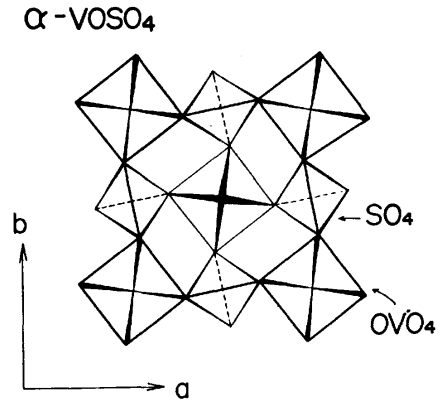

Fig. 7. A schematic representation of α-$VOSO_4$ crystal structure by Ladwig.[12] A layer structure is kept, although crystal coordinate differ from that in V_2O_5.

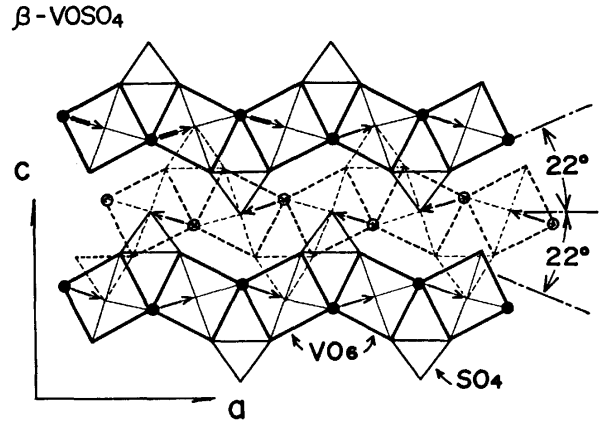

Fig. 8. A schematic representation of the crystal structure of β-$VOSO_4$ by Kierkegaard *et al.*[13]

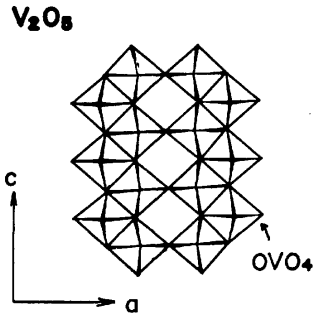

Fig. 9. A schematic representation of V_2O_5 crystal structure by Byström *et al.*[14] and Bachmann *et al.*[15] Construction of a sheet from zig-zag double chains.

axis on the ac-plane of the crystal. On the other hand, V_2O_5 is orthorhombic (Pnmn) and has a layer structure, as is shown in Fig. 9.[14,15] All the V=O bonds are alined on a straight line, which is parallel to the b-axis.

α-$VOSO_4$ in the crystalline state could be realized from the V_2O_5 crystal, keeping the layer structure in such a manner that the oxygen ions in the four corners of the VO_5 square-pyramid unit of V_2O_5 are simply replaced by the oxygen atoms of the four SO_4^{2-} tetrahedrons. On the other hand, in the β-$VOSO_4$ the same replacement of the oxygen of the VO_5 unit by the oxygen of SO_4^{2-} could occur only after the destruction of the layer structure. Therefore, we can expect that the growth of the α-phase in the V_2O_5 crystal occurs more easily than that of the β-phase.

Arrangement of the $VOSO_4$ Phases in the V_2O_5 Lattice under the SO_2 Oxidation. The directions of the V=O bond, which are coincident with the $g_{//}$ of the $\boldsymbol{g}$-tensor in these crystals, may be clearly summarized as follows: in V_2O_5 and α-$VOSO_4$, it takes only one direction, parallel to the b-axis, but in β-$VOSO_4$, a pair of directions, deviating from the a-axis by about $\pm 22^\circ$ on the ac-plane. The $\boldsymbol{g}$-tensor should have the same value in both α- and β-$VOSO_4$ because they have the same local field around the vanadyl ion.

The alignments of the V=O bond and principal axes of the $\boldsymbol{g}$-tensor in the $VOSO_4$ crystal can be primarily known from the crystal structure. By connecting the crystal structures with the results of the $\boldsymbol{g}$-tensor analysis, therefore, the possible arrangements of $VOSO_4$ phase in the V_2O_5 lattice can be discussed.

The finding that the axis for the $g_{//}$ of the sharp signal in the spectrum was completely coincident with the b-axis of the V_2O_5 crystal strongly suggests that the $VOSO_4$ formed in the V_2O_5 lattice is the α-form. Both α-$VOSO_4$ and V_2O_5 have the same layer structure, except only for such differences that the oxygen atoms in the four corners of the VO_5 square-pyramid in V_2O_5 are replaced by the oxygen atoms of the SO_4^{2-} tetrahedron in α-$VOSO_4$. The change from V_2O_5 to α-$VOSO_4$ seems to be possible in the crystalline states in such a manner that the oxygen atoms in the four corners of the VO_5 square-pyramidal unit in V_2O_5 are simply replaced by the oxygen atoms of the four SO_4^{2-} tetrahedrons; then the layer structure and the direction of V=O bonds are kept unchanged in the α-$VOSO_4$ lattice.

In the case of the minor components of the spectrum, as has been preliminarily described above, the axis for $g_{//}$ exists on the ac-plane and on the other planes as a pair of $\boldsymbol{g}$-tensors, which take an angle of about 45° toward each other. From the correspondence of the directions of the $\boldsymbol{g}$-tensor with that of the V=O bond in β-$VOSO_4$, the minor components can possibly be ascribed to β-$VOSO_4$. Besides, the possibility of the growth of α-$VOSO_4$ on dislocation or some other imperfection of the crystal can not, of cause, be ruled out.

It can reasonably be expected that a clear-cut and reversible transformation between the formation and decomposition of the $VOSO_4$ phase in the V_2O_5 crystalline lattice occurs more favorably in the case of the α-$VOSO_4$ than the β-$VOSO_4$ phase. The fact that a surface brilliance always remained after repetitions of the formation and the decomposition of the $VOSO_4$ phase in the V_2O_5 lattice[4] also suggests strongly that, in the cleaven plane (the ac-plane) of the V_2O_5, α-$VOSO_4$ phase easily grows with a topochemical relation. From this suggestion, the important role of the ac-plane in catalysis can be understood in the case of SO_2 oxidation as well as in the case of CO oxidation.[16]

References

1) For instance (a) P. Mars and J. G. H. Maessen, *Proc. Int. Congr. Catal. 3rd, Amsterdom*, **1**, 266 (1964); *J. Catal.*, **10**, 1 (1968); (b) G. K. Boreskov, R. A. Buyanov, and A. A. Ivanov. *Kinet. Katal.*, **8**, 153 (1967); G. K. Boreskova, L. P. Davydova, V. M. Mastikhin, and G. M. Polyakova, *Dokl. Akad. Nauk. SSSR*, **210**, 626 (1973); (c) A. R. Glueck and C. N. Kenney, *Chem. Eng. Sci.*, **23**, 1257 (1968).

2) H. Tanaka and A. Matsumoto, *Bull. Chem. Soc. Jpn.*, **39**, 874 (1966).

3) G. K. Boreskov, L. P. Davydova, V. M. Mastikhin, and G. M. Polyakova, *Dokl. Akad. Nauk. SSSR*, **171**, 648 (1966); V. M. Mastikhin, G. M. Polyakova, Ya. Zyulkovskii, and G. K. Boreskov, *Kinet. Katal.*, **11**, 1463 (1970).

4) Y. Kera and K. Kuwata, *Bull. Chem. Soc. Jpn.*, to be submitted.

5) R. E. McCarley and J. W. Roddy, *J. Less-Common Met.* **2**, 29 (1960); J. Haemers, *Bull. Soc. Chim. Belg.* **79**, 473 (1970).

6) J. L. Ragle, *J. Chem. Phys.* **38**, 2020 (1963).

7) V. A. Ioffe and I. B. Patrina, *Soviet Phys. -Solid State*, **6**, 2425 (1964); *ibid.*, **10**, 639 (1968).

8) E. Gilis and E. Boesman, *Phys. Status Solidi*, **14**, 337, 349 (1966).

9) K. Hirota, K. Kuwata, and Y. Kera, *Bull. Chem. Soc. Jpn.*, **43**, 3017 (1970).

10) G. Sperlich, *Z. Phys.*, **250**, 335 (1972).

11) J. Selbin, *Chem. Rev.*, **65**, 153 (1965).

12) V. G. Ladwig, *Z. Anorg. Allg. Chem.*, **364**, 225 (1969).

13) P. Kierkegaard and J. M. Longo, *Acta Chem. Scand.*, **19**, 1906 (1965).

14) A. Byström, K. A. Wilhelmi, and O. Brotzen, *Acta Chem. Scand.*, **4**, 1119 (1950).

15) H. G. Bachmann, F. R. Ahmed, and W. H. Barnes, *Z. Kristallogr.*, **115**, 110 (1961).

16) K. Hirota, Y. Kera, and S. Teratani, *J. Phys. Chem.*, **72**, 3133 (1968); Y. Kera, K. Hirota, *ibid.*, **73**, 3973 (1969).

Indirect Chemiluminescence from the Air Oxidation of Ketones and Carboxylic Acids in Alkaline Aprotic Solvents Containing 9,10-Diphenylanthracene and 9,10-Dibromoanthracene

Isao KAMIYA and Takashi SUGIMOTO

Department of Chemistry, College of General Education, Nagoya University, Chikusa-ku, Nagoya 464

(Received March 15, 1977)

A number of ketones and carboxylic acids have been examined for direct and indirect chemiluminescence with 9,10-diphenylanthracene and 9,10-dibromoanthracene by air oxidation. From the finding that the efficiency of the chemiluminescence was dramatically influenced by the class of the C–H bond adjacent to the carbonyl group, it was concluded that the molecules with a –COCH– group surely give an excited product during air oxidation in alkaline aprotic solvents. The reaction scheme was consistent with the evidence that most simple carboxylic acids exhibited no chemiluminescence, probably because the C–H bond adjacent to the carboxyl group is no more acidic, but keto acids exhibited emission. In several compounds, however, the chemiluminescent reaction was retarded by other functional groups.

In the previous studies of the chemiluminescence from the air oxidation of 3,5-dihalogeno-4-hydroxyphenylpyruvic acid[1] and succinylfluorescein[2] in alkaline aprotic solvents, a mechanism involving dioxetane intermediate was proposed for the luminescent reactions, and the reaction pathway leading to the dioxetanes which will be formed by the oxygenation of the anion of these compounds, formed by the loss of a proton from the carbon adjacent to the carbonyl or 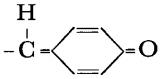 group, was discussed as a possible mechanism for the generation of the excited products.

These results suggest that other simple molecules with a –COCH– group should also follow the same reaction pathways, involving a dioxetane, to yield a product in an excited state. In order to test this hypothesis, we carried out a preliminary study to investigate the chemiluminescent reaction of several carbonyl compounds by means of the indirect chemiluminescence technique with 9,10-diphenylanthracene(DPA) and 9,10-dibromoanthracene(DBA); we found that excited acetone and benzoic acid, mainly in the triplet state, were generated by air oxidation of 3-methyl-2-butanone and benzoin respectively in dimethyl sulfoxide(DMSO) or *N*,*N*-dimethylformamide(DMF) containing potassium *t*-butoxide (*t*-BuOK) as the base.[3]

In the present study, we have examined a number of simple ketones and carboxylic acids for the chemiluminescence from the air oxidation under the same experimental condition in order to test the validity of, and to broaden the scope of this interesting reaction mechanism.

Results and Discussion

The indirect chemiluminescence was observed upon adding a *t*-BuOK solution in *t*-BuOH to an aerated solution of ketones in DMSO or DMF containing DPA or DBA. However, no direct chemiluminescence could be detected on an appreciable scale except with some aromatic ketones (see below). The intensity of the indirect chemiluminescence with DBA was markedly higher than with DPA, in spite of the much higher fluorescence efficiency of the latter. From these findings, we concluded that the excited species, predominantly in the triplet rather than the singlet state, were produced during the air oxidation of the ketones, because DBA is more capable of converting the energy of excited triplet species into singlet energy than is DPA because of the increased spin-orbit coupling and mixing of singlet and triplet states by the heavy-atom effect.[4]

The features of the chemiluminescent reaction were affected by the experimental conditions— *i.e.* the temperature, solvents, and the concentrations of the ketones,

Table 1. Relative intensities (i_M) and 1/4-lifetimes ($t_{1/4}$) of the indirect chemiluminescence of aliphatic ketones with DBA in a DMSO-*t*-BuOK system at 313 K, and the colors of the spent reaction solutions[a]

Compound		i_M[b]	$t_{1/4}$(s)	Colors of spent reaction solns
$CH_3COCH(CH_3)_2$	(**1**)[c]	1.0	40	colorless
$CH_3COCH(CH_3)CH_2CH_3$	(**2**)	1.2	40	colorless
$CH_3COCH_2CH(CH_3)_2$	(**6**)	0.3	20	reddish brown
$CH_3COCH_2CH_2CH(CH_3)_2$	(**7**)	0.2	15	reddish brown
$CH_3COCH_2CH_3$	(**8**)	0.5	10	dark red
$CH_3COC(CH_3)_3$	(**12**)	0.0	—	light brown
$CH_3COCH(OH)CH_3$	(**5**)	0.0	—	yellowish brown
$(CH_3)_2CHCOCH(CH_3)_2$		0.2	20	colorless
$CH_3CH_2CH_2COCH_2CH_2CH_3$		0.1	15	brown
$CH_3CH_2CH_2COCH(CH_3)_2$		0.0	—	colorless
$CH_3CH_2COCH_2CH_3$		0.1	15	light reddish brown
$CH_3(CH_2)_{20}CO(CH_2)_{20}CH_3$		0.0	—	colorless
CH_3COCH_3		0.0	—	dark orange

a) The intensity of the emission peak from **1** was defined as 1.0. b) The ratios of the (total) light emission were given approximately by $i_M \cdot t_{1/4}$. c) The quantum yield for the indirect chemiluminescence of **1** at an infinite concentration of DBA was estimated to be 2.1×10^{-7} einstein mol^{-1} (the details of the measurement will be reported in the next paper).

Table 2. The values of i_M and $t_{1/4}$ of the indirect chemiluminescence of aromatic ketones with DBA in a DMSO-*t*-BuOK system at 313 K, and the colors of the spent reaction solutions

Compound		i_M[a]	$t_{1/4}$(s)	Colors of spent reaction solns
$C_6H_5COCH(CH_3)_2$	(**3**)[b]	200	20	colorless
$C_6H_5COCH(OH)$-C_6H_5	(**4**)	25	5	colorless
$C_6H_5CO(CH_2)_2CH_3$	(**10**)	15	12	brown
$C_6H_5CO(CH_2)_4CH_3$	(**11**)	15	12	orange
$C_6H_5COCH_2CH_3$	(**9**)	7	10	dark orange
$C_6H_5COCH_3$		1.0	10	brown
$C_6H_5CH_2COCH_2C_6H_5$		0.5	10	brown
$C_6H_5COCH_2C_6H_5$		0.0	—	yellow
$C_6H_5COCH_2COC_6H_5$		0.0	—	colorless
$(C_6H_5)_2CHCOCH_3$		0.0	—	colorless

a) The values of i_M were also estimated by comparison with the i_M value from **1**, which was defined as 1.0. b) The quantum yield for the indirect chemiluminescence of **3** at an infinite concentration of DBA was estimated to be 2.6×10^{-5} einstein mol^{-1}.

t-BuOK, and the fluorescers, and also, more essentially, by the chemical structure of the ketones. In general, the intensity was much higher with aromatic ketones than with aliphatic ketones. The relative intensities of the emission peaks (i_M) and the times for the decay of intensities to one fourth of the maxima ($t_{1/4}$), as measured in a DMSO solution with equal concentrations of ketones, *t*-BuOK, and DBA at 313 K, are listed in Tables 1 and 2 for aliphatic and aromatic ketones respectively, together with the colors of the spent reaction solutions. The results in the tables clearly show that the efficiency of the emission is dramatically influenced by the class of the C–H bond adjacent to the carbonyl group, as was expected.

3-Methyl-2-butanone(**1**) and 3-methyl-2-pentanone (**2**), which possess a tertiary C–H bond, exhibited the most intensive chemiluminescence among all the aliphatic ketones examined. Among the aromatic ketones, isopropyl phenyl ketone(**3**) exhibited the most intensive emission; it could be easily observed even by the naked eye in a dark place. These ketones, **1**, **2**, and **3**, absorbed equimolar amounts of oxygen and yielded acetone, 2-butanone, and both acetone and benzoic acid respectively, as the main products. Thus, the chemiluminescent reaction of these ketones can be explained reasonably by the following mechanism:

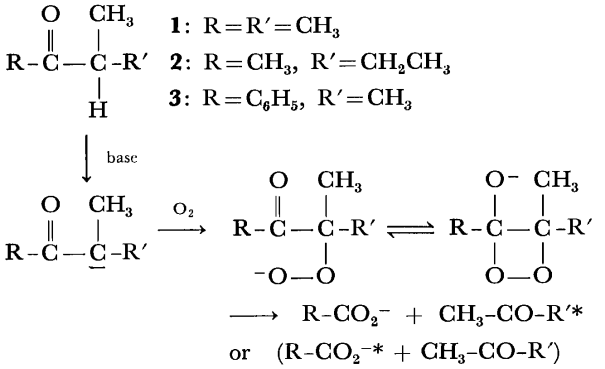

A similar reaction mechanism has been proposed for the decomposition of α-hydroperoxy ketones, which are known to be intermediates in the autoxidation of the parent ketones.[5]

Benzoin(**4**), whose emission was fairly intensive but rapidly decayed, yielded benzoic acid as the main product in a 59% yield (based on the two moles of the acid). This result implies that excited triplet benzoic acid is generated by the oxidation of benzoin, presumably *via* a dioxetane intermediate:

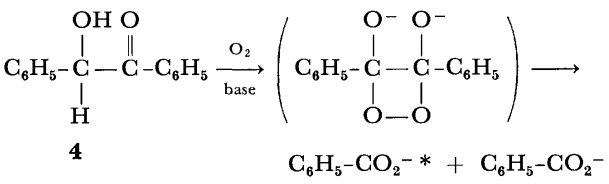

Acetoin(**5**), though it absorbed equimolar oxygen upon oxidation, showed no appreciable indirect chemiluminescence with DBA or DPA. This is probably because a large amount of energy, greater than the sum of the reaction enthalpy and activation energy, would be required to excite the acetic acid produced. Therefore, it is more reasonable to assert that excited triplet acetone and 2-butanone, rather than excited triplet acetic acid, are generated in the air oxidation of **1** and **2** respectively. However, it is difficult to decide which, acetone or benzoic acid, is the excited species in the case of **3**.

4-Methyl-2-pentanone(**6**), 5-methyl-2-hexanone(**7**), and 2-butanone(**8**), whose C–H bond adjacent to the carbonyl group is not tertiary but secondary, showed a much weaker emission than **1** and **2**. Similarly, ethyl phenyl ketone(**9**), phenyl propyl ketone(**10**), and pentyl phenyl ketone(**11**) exhibited a medium indirect chemiluminescence emission. In the system of **6** and **7**, where the molar ratios of absorbed oxygen to the ketones were about 2 : 1 and 3 : 1 respectively, acetone was formed, though in low yields. The difference in the amounts of absorbed oxygen and the formation of acetone can be best explained by the following consecutive reaction mechanism, in which the aldehydes formed by the initial oxidation undergo a sequential oxidation reaction to give acetone:

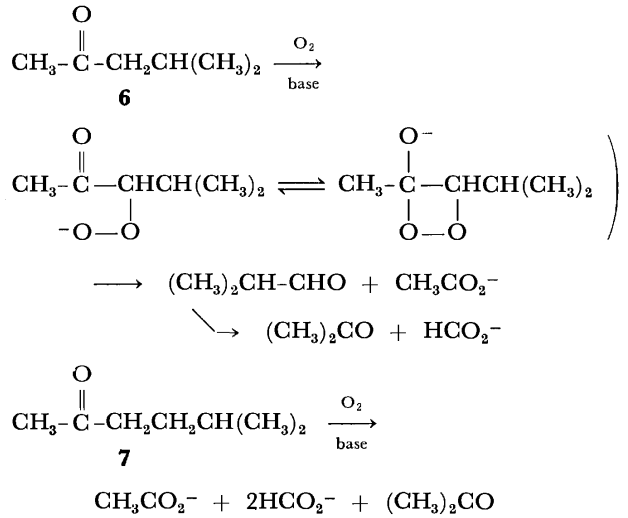

However, no aldehydes could be detected in the spent reaction solutions of these ketones, probably because they were quickly consumed by sequential oxidation or by other concurrently proceeding reactions, such as addition and polymerization. In fact, the spent reaction solutions were colored probably because of the concurrent reactions (see Tables 1 and 2). The aromatic ketones, **9**, **10**, and **11**, reacted similarly and gave benzoic acid in yields of 38, 57, and 23% respectively. Thus it may be reasonable to decide that excited triplet benzoic acid is generated from **9**, **10**, and **11** in the same way as it is from benzoin. However, we cannot exclude the possibility that aldehydes in the excited state are generated from **8**.[b]

Such ketones as 3,3-dimethyl-2-butanone(**12**), acetone, and acetophenone, whose C–H bond adjacent to the carbonyl group is primary, exhibited little or very feeble emission.

We also examined the chemiluminescent reaction of carboxylic acids. With simple carboxylic acids, such as acetic acid, propionic acid, isobutyric acid, phenyl acetic acid, diphenylacetic acid, and α(and β)-naphthylacetic acids, neither direct nor indirect chemiluminescence could be detected. However, β-benzoylpropionic acid(**13**) and β-phenylpyruvic acid(**14**), which possess a carbonyl group in addition to a carboxyl group, exhibited indirect chemiluminescence with the emission characteristics shown in Table 3. The results obtained from these keto acids also support our reaction scheme for the luminescent reaction shown above.

TABLE 3. THE VALUES OF i_M AND $t_{1/4}$ OF THE INDIRECT CHEMILUMINESCENCE OF CARBOXYLIC ACIDS WITH DBA IN A DMSO-*t*-BuOK SYSTEM AT 313 K, AND THE COLORS OF THE SPENT REACTION SOLUTIONS

Compound		i_M[a]	$t_{1/4}$(s)	Colors of spent reaction solns
$C_6H_5COCH_2CH_2$-COOH	(**13**)	1.0	40	dark orange
$C_6H_5CH_2COCOOH$	(**14**)	2.5	60	dark brown

a) The values were estimated by comparison with the i_M value from **1**, which was defined as 1.0.

β-Phenylpyruvic acid(**14**) exhibited a direct chemiluminescence whose spectral distribution was similar to that of the fluorescence spectrum of benzaldehyde. This implies that both excited singlet and triplet benzaldehydes are produced, presumably *via* a dioxetane intermediate:

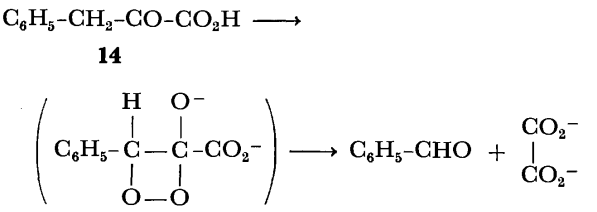

Cilento *et al.* have proposed the same reaction mechanism for the oxidation of the phenylthio ester of 3-indoleacetic acid.[7] β-(*p*-Hydroxyphenyl)pyruvic acid (**15**) also exhibited both direct and indirect chemiluminescence. It should be noted here that the intensity of the indirect chemiluminescence of **15** with DPA was higher than that with DBA, while the total intensity of the emissions was lower compared to the case of **14**. Ethyl *p*-hydroxyphenyl ketone(**16**) also exhibited both direct and indirect chemiluminescence with emission features similar to those from **15**. The relative intensities of the direct and the indirect chemiluminescence with DPA and DBA are listed in Table 4. These results indicate that the substitution of a hydroxyl group at the 4 position of the benzene ring in aromatic ketones increases the yield of the excited singlet product, but causes a reduction in the total yield of excited products. An analogous substitution effect was observed in the cleavege of dioxetanes. Turro and coworkers reported that tetramethyl-1,2-dioxetane(**17**) gave excited triplet acetone in high yields and a little amount of excited singlet acetone.[8] On the other hand, it has been shown that relatively low and nearly equal yields of excited singlet and triplet 2-hexanone were formed upon the cleavage of 3,4-dibutyl-3,4-dimethyl-1,2-dioxetane(**18**).[18]

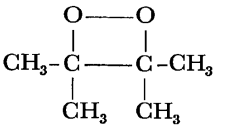

17

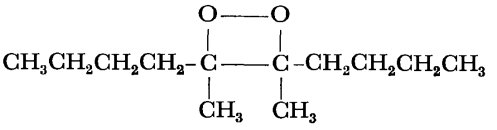

18

Ethyl *o*-hydroxyphenyl ketone(**19**) exhibited neither direct nor indirect chemiluminescence, probably because the reaction route is entirely altered by the substituent.

TABLE 4. RELATIVE INTENSITIES[a] OF THE DIRECT AND INDIRECT CHEMILUMINESCENCE IN THE SYSTEMS OF **14**, **15**, AND **16**

Compound		Direct CL	Indirect CL		Colors of spent reaction solns
			DPA	DBA	
$C_6H_5CH_2COCOOH$	(**14**)	1.0	1.2	2.5	dark brown
p-$HOC_6H_4CH_2COCOOH$	(**15**)	0.3	0.6	0.3	light yellow
$C_6H_5COCH_2CH_3$	(**9**)	0.0	0.5	7	dark orange
p-$HOC_6H_4COCH_2CH_3$	(**16**)	0.4	0.6	0.4	colorless
o-$HOC_6H_4COCH_2CH_3$	(**19**)	0.0	0.0	0.0	bright yellow

a) These values were also estimated by comparison with the i_M value from **1**, which was defined as 1.0.

Table 5. The emission features (i_M and $t_{1/4}$) of the indirect chemiluminescence with DBA of the *p*-substituted isopropyl phenyl ketones, and the colors of the spent reaction solutions

Substituent (and compound)		i_M[a)]	$t_{1/4}$(s)	Colors of spent reaction solns
p-CH_3	(**20**)	180	20	colorless
p-OCH_3	(**21**)	50	20	colorless
p-Cl	(**22**)	50	15	light yellow
p-Br	(**23**)	20	18	yellowish brown
p-F	(**24**)	0	—	colorless
p-SCH_3	(**25**)	0	—	colorless

a) The values were also estimated by comparison with the i_M value from **1**, defined as 1.0.

In Table 5, the relative intensities of the indirect chemiluminescence of several substituted isopropyl phenyl ketones with DBA are listed. We can find that the emission efficiencies of the *p*-methyl(**20**), *p*-methoxy (**21**), *p*-chloro(**22**), and *p*-bromo derivatives(**23**) decrease in this order. The *p*-fluoro(**24**) and *p*-methylthio derivatives(**25**) exhibited little emission.

Summarizing the results of the present study, we conclude that excited products are surely generated *via* dioxetane intermediates in the air oxidation of those molecules with a –COCH– group in alkaline aprotic solvents and that the dioxetanes are formed by the oxygenation of the anion formed by the loss of the proton from the carbon atom adjacent to the carbonyl group. However, it should be kept in mind that the luminescent reaction is debased by the competitive and sequential processes brought about by other functional groups.

Recently, we have found that several aldehydes with a –CHCHO group exhibited similar indirect chemiluminescence with DPA and DBA under comparable experimental conditions.[10)]

Experimental

The commercially available ketones (except the substituted isopropyl phenyl ketones), carboxylic acids, and fluorescers, DPA and DBA (Nihon Kasei, extra pure grade) were used without further purification. The substituted isopropyl phenyl ketones(**21**, **22**, **23**, **24**, and **25**) were synthesized by Friedel-Crafts condensation of the appropriately substituted benzene with isobutyric anhydride in carbon disulphide under reflux, using aluminum chloride as the catalyst. The products were purified by fractional distillation under reduced pressure (except for **25**, which was purified by recrystallization from hexane and melted at 42—43 °C): **20**, bp 132.5—133.5 °C/27 mmHg; **21**, bp 116—117 °C/2 mmHg; **22**, bp 89—92 °C/3 mmHg; **23**, bp 85—87 °C/3 mmHg; **24**, bp 49.5—50 °C/3 mmHg. The structures of these compounds were confirmed by means of their ^1H NMR spectra.

The concentrations of the solution of the ketones or carboxylic acids in DMSO (*A*), the solution of *t*-BuOK in *t*-BuOH (*B*), and the solution of DPA or DBA in DMSO (*C*) were usually 3.0×10^{-4}, 3.3×10^{-2}, and 1.0×10^{-3} mol l^{-1} respectively.

A mixed solution composed of 1 ml of *A* and 1 ml of *C* was placed in a quartz cell, which was kept at 313 K by means of a thermostatically controlled cell holder. The intensity of the indirect chemiluminescence at 430 nm (the peak of the spectral distribution) was measured immediately after adding 0.2 ml of *B* into the mixed solution on a Hitachi MPF-2A type fluorescence spectrophotometer, with the exciting source off.

The reaction products, acetone, 2-butanone, benzoic acid, and the *p*-substituted benzoic acids, were detected as follows:

General Procedures for the Isolation of Benzoic Acid and Its p-Substituted Derivatives. A solution of *t*-BuOK (2.3 g) in DMF (70 ml) was saturated with oxygen by stirring vigorously under the gas. A solution of isopropyl phenyl ketone (1.50 g) in DMF (30 ml) was then added to the solution through a dropping funnel, and the mixture was stirred under oxygen at 17—18 °C for 15 min, during which period 280 ml of oxygen was absorbed. After being diluted with water (100 ml), the solution was evaporated to dryness under reduced pressure. The residue, dissolved in water (20 ml) and acidified with hydrochloric acid, gave benzoic acid (1.13 g, 92%); mp 122—123 °C (recrystallized from water).

In a similar way, benzoic acid was isolated from the oxidation solution of the following compounds (the yield of the acid is shown in parentheses); benzoin (59%); phenyl propyl ketone (38%); pentyl phenyl ketone (57%); ethyl phenyl ketone (23%); β-benzoylpropionic acid (50%).

The substituted isopropyl phenyl ketones (**20**, **21**, **22**, **23**, **24**, and **25**) were similarly oxidized and gave, respectively, the following *p*-substituted benzoic acids, which were all recrystallized from water and identified by means of their melting points: *p*-methylbenzoic acid (80%, mp 182—183 °C), *p*-methoxybenzoic acid (68%, mp 183.5—185 °C), *p*-chlorobenzoic acid (90%, mp 241—242 °C), *p*-bromobenzoic acid (40%, mp 255—256 °C), *p*-fluorobenzoic acid (50%, mp 184.5—186 °C), and *p*-(methylthio)benzoic acid (90%, mp 193.5—194 °C).

General Procedures for the Detection of Acetone and Other Ketones. A solution of *t*-BuOK (2.5 g) in DMF (100 ml) was saturated with oxygen as above. After adding 3-methyl-2-butanone (0.74 g), the solution was stirred under oxygen at 23 °C for 30 min, during which period 220 ml of oxygen was absorbed. To the solution, 1 M HCl (20 ml) and then 2,4-dinitrophenylhydrazine (1.0 g) in methanol (300 ml) were added. The solution was stirred at 25 °C for 30 min and then under reflux for 20 min. Evaporation to dryness under reduced pressure and trituration with water (30 ml) gave a yellow solid. The crystallization of the solid from methanol gave yellow needles (1.15 g) of acetone 2,4-dinitrophenylhydrazone, identified with an authentic sample by a mixed mp (125—126 °C) and by TLC developed by a mixture of benzene (15 v/v) and ethyl acetate (5 v/v) on a Merck pre-coated silica gel 60 F_{254} plate.

In a similar way, we detected acetone from an oxidation solution of **3**, **6**, and **7** and 2-butanone from **2**, both as the 2,4-dinitrophenylhydrazones; they were identified by means of TLC as above.

References

1) G. Cilento, M. Nakano, H. Fukuyama, K. Suwa, and I. Kamiya, *Biochem. Biophys. Res. Commun.*, **58**, 296 (1974).
2) I. Kamiya and K. Aoki, *Bull. Chem. Soc. Jpn.*, **47**, 1744 (1974).
3) I. Kamiya and T. Sugimoto, *Chem. Lett.*, **1976**, 33.
4) V. A. Belyakov and R. F. Vassilév, *Photochem. Photobiol.*, **11**, 179 (1970); T. Wilson and A. P. Schaap, *J. Am. Chem. Soc.*, **93**, 4126 (1971); N. J. Turro, P. Lechtken, G. Schuster, J. Orell, H. -C. Steinmetzer, and W. Adam, *ibid.*, **96**, 1627 (1974); M. J. S. Dewar and S. Kirschner, *ibid.*, **96**,

7578 (1974); W. Adam, G. A. Simpson, and F. Yany, *J. Phys. Chem.*, **78**, 2559 (1974); I. Simo and J. Stauff, *Chem. Phys. Lett.*, **34**, 326 (1975); G. B. Schuster, N. J. Turro, H. -C. Steinmetzer, A. P. Schaap, G. Faler, W. Adam, and J. C. Liu, *J. Am. Chem. Soc.*, **97**, 7110 (1975); W. Adam, N. Duran, and G. A. Simpson, *ibid.*, **97**, 5464 (1975); M. A. Umbreit and E. H. White, *J. Org. Chem.*, **41**, 479 (1976); T. Wilson, D. E. Golan, M. S. Harris, and A. L. Baumstark, *J. Am. Chem. Soc.*, **98**, 1086 (1976).

5) W. H. Richardson, V. H. Hodge, D. L. Stiggall, M. B. Yelvington, and F. C. Montgomery, *J. Am. Chem. Soc.*, **96**, 6652 (1974).

6) The 2-butanone produced in the **2** system was not further oxidized under the experimental conditions employed, and the spent reaction solution of **2** was almost colorless.

7) N. Durán, K. Zinner, R. C. DE Baptisa, C. C. C. Vidigal, and G. Cilento, *Photochem. Photobiol.*, **24**, 383 (1976).

8) N. J. Turro and P. Lechtken, *J. Am. Chem. Soc.*, **94**, 2886, (1972).

9) T. R. Darling and C. S. Foote, *J. Am. Chem. Soc.*, **96**, 1625, (1974).

10) K. Aoki and I. Kamiya, unpublished results.

Yields of Excited Triplet Products Generated from the Air Oxidation of 3-Methyl-2-butanone and Isopropyl Phenyl Ketone in a Dimethyl Sulfoxide Solution Containing Potassium *t*-Butoxide

Isao KAMIYA

Department of Chemistry, College of General Education, Nagoya University, Chikusa-ku, Nagoya 464

(Received April 12, 1977)

An attempt has been made to evolve the kinetic scheme in order to evaluate the yields (ϕ^*_{react}) of excited triplet products generated from the air oxidation of 3-methyl-2-butanone (**1**) and isopropyl phenyl ketone (**2**). Expressions for the total light emission and quantum yield of the indirect chemiluminescence (CL) can be derived, from which the rates of energy transfer from excited triplet products to singlet 9,10-dibromoanthracene (DBA), k_{TS}, and ϕ^*_{react} were determined on the basis of the CL intensity measured for various DBA concentrations. The values of k_{TS} from **1** and **2** (4×10^8 and 1×10^9 l mol^{-1} s^{-1}) are in fair agreement with the values proposed by several investigators who measured the indirect CL from the thermal cleavage of 1,2-dioxetanes. The markedly small ϕ^*_{react} values (1×10^{-5} and 1×10^{-3}) result from the fact that the CL arises from a minor reaction.

In previous studies,[1] Kamiya and Sugimoto have found that many simple ketones exhibit indirect chemiluminescence (CL) by air oxidation in alkaline aprotic solvents containing 9,10-diphenylanthracene (DPA) or 9,10-dibromoanthracene (DBA), and that the intensity for solvents containing DBA was markedly higher than for those containing DPA, in spite of the much higher fluorescence efficiency of DPA. The results indicate that excited species, mainly in the triplet state, are produced during the oxidation of the ketones, since DBA is more efficient at converting the energy of the excited triplet species into singlet energy than is DPA due to the heavy-atom effect.[2] Further, they observed that the CL intensity was dramatically affected by the class of C–H bonds adjacent to the carbonyl group; generally, the intensity increased in the order, primary <secondary<tertiary. The results suggest that the CL efficiency depends upon the tendency to loose a proton from the C–H bond. This argument was supported by evidence that the ordinary carboxylic acids, having a C–H bond adjacent to the carboxyl group, are very weakly acidic and exhibit neither direct nor indirect CL. However, such keto acids as β-benzoylpropionic and β-phenylpyruvic acids exhibit emission.

Summarizing their results, they concluded that excited products, predominantly in the triplet rather than in the singlet state, were surely generated during air oxidation of those compounds having a –CO–CH– group *via* dioxetane intermediates. These intermediates were generated by oxygenation of the anion of the compounds formed *via* the loss of a proton from the α-carbon atom.

The overall reaction in systems of several ketones is very complicated, since the molar ratios of the absorbed oxygen to the reactants were found to be greater than 2 and the spent reaction solutions were dark orange or red owing to other competitive and/or sequential reactions. However, two ketones, 3-methyl-2-butanone (**1**) and isopropyl phenyl ketone (**2**), which possess a tertiary C–H bond adjacent to the carbonyl group and exhibited relatively intense emission, showed rather simple reaction characteristics: an equimolar amount of oxygen was absorbed, and acetone and acetic acid, and acetone and benzoic acid were produced as main products from **1** and **2**, respectively. No color change was observed in the spent reaction solutions under the experimental conditions employed in this study. (See experimental section.)

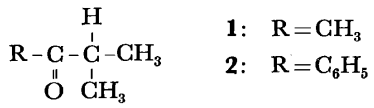

In the present study, an attempt has been made to evolve the kinetic scheme for indirect CL with DBA in order to evaluate the yields of the excited triplet products generated from **1** and **2**.

Results and Discussion

From the results described above, the following kinetic scheme appears plausible for indirect CL.

The ketones (AH) transfer their proton to the *t*-butoxide ion (*t*-BuO$^-$) when a potassium *t*-butoxide (*t*-BuOK) solution in *t*-butyl alcohol (*t*-BuOH) is added to solutions of **1** and **2**:

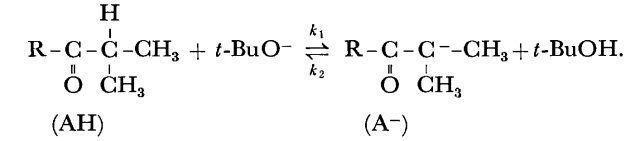

A possible mechanism for the reaction of A$^-$ with oxygen would be oxygenation *via* a *radical pair*:[3]

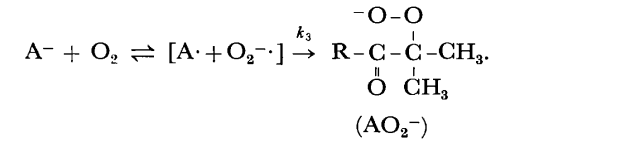

Of the decomposition processes of the hydroperoxy ketone anion (AO_2^-), one is cleavage *via* a dioxetane intermediate (**3**) generating two products, one in the excited state (mainly in the triplet state, P*(T)) and the other in the ground state;[4]

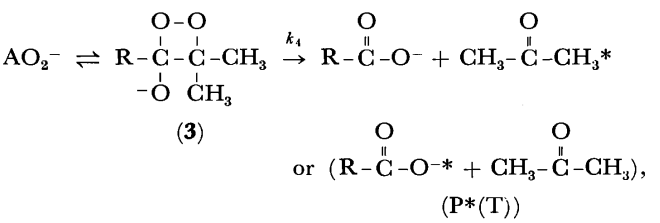

or, both in the ground state,

$$AO_2^- \rightleftharpoons \mathbf{3} \xrightarrow{k_5} R\text{-}\overset{O}{\overset{\|}{C}}\text{-}O^- + CH_3\text{-}\overset{O}{\overset{\|}{C}}\text{-}CH_3.$$

Other AO_2^- cleavage processes *via* acyclic intermediates[5] will compete with cleavage *via* the dioxetane intermediate. Let us write all the reactions together in the following scheme:

$$AO_2^- \rightleftharpoons AO_2H \rightarrow \text{(acyclic intermediate)} \xrightarrow{k_6} \text{products.}$$

In the presence of DBA, the following steps will occur:
triplet-singlet energy transfer from P*(T) to DBA,

$$P^*(T) + DBA \xrightarrow{k_{TS}} P + DBA^*(S),$$

triplet-triplet energy transfer form P*(T) to DBA,

$$P^*(T) + DBA \xrightarrow{k_{TT}} P + DBA^*(T)$$

(where DBA*(S) and DBA*(T) are the excited singlet and triplet states of DBA, respectively),
radiationless deactivation of P*(T),

$$P^*(T) \xrightarrow{k_7} P,$$

quenching of P*(T) by oxygen,

$$P^*(T) + O_2 \xrightarrow{k_8} P + O_2^*(\Delta),$$

fluorescence emission from DBA*(S),

$$DBA^*(S) \xrightarrow{k_f} DBA + h\nu,$$

radiationless deactivation of DBA*(S),

$$DBA^*(S) \xrightarrow{k_9} DBA,$$

and intersystem crossing from DBA*(S) to DBA*(T),

$$DBA^*(S) \xrightarrow{k_{10}} DBA^*(T).$$

Since the emission intensity with DPA was much lower than that with DBA (DPA and DBA are often used as monitors for excited singlet and triplet products, respectively[6]), the step for generating excited singlet products is ignored. Moreover, triplet-triplet annihilation of DBA*(T), DBA*(T)+DBA*(T)→DBA*(S)+DBA, is not taken into account, because the process has been reported to occur with low probability.[7]

According to the above scheme, the intensity of the indirect CL emission (I_{CL}) is given by:

$$I_{CL} = k_f[DBA^*(S)].$$

Using the steady-state approximation for which $d[P^*(T)]/dt=0$ and $d[DBA^*(S)]/dt=0$, I_{CL} can be written as

$$I_{CL} = \frac{k_4 k_{TS} \phi_f [DBA][AO_2^-]}{\{(k_{TS}+k_{TT})[DBA]+k_7+k_8[O_2]\}}, \quad (1)$$

where ϕ_f is the fluorescenec efficiency of DBA and is given by

$$\phi_f = k_f/(k_f+k_9+k_{10}).$$

If $[O_2]$ and [DBA] are maintained constant during the air oxidation, the total light emission is given by:

$$\int I_{CL}dt = \frac{k_4 k_{TS} \phi_f [DBA]}{\{(k_{TS}+k_{TT})[DBA]+k_7+k_8[O_2]\}} \times \int [AO_2^-]dt. \quad (2)$$

Furthermore, from the scheme we can write

$$-d[AH]/dt = k_1[AH][t\text{-}BuO^-] - k_2[A^-][t\text{-}BuOH], \quad (3)$$

$$d[A^-]/dt = k_1[AH][t\text{-}BuO^-] - k_2[A^-][t\text{-}BuOH] - k_3[A^-][O_2], \quad (4)$$

and

$$d[AO_2^-]/dt = k_3[A^-][O_2] - (k_4+k_5+k_6)[AO_2^-], \quad (5)$$

thence,

$$-\int d[AH] - \int d[A^-] - \int d[AO_2^-] = (k_4+k_5+k_6)\times \int [AO_2^-]dt = [AH]_0, \quad (6)$$

since

$$\int d[A^-] = \int d[AO_2^-] = 0$$

and

$$-\int d[AH] = [AH]_0,$$ where $[AH]_0$ is the initial ketone concentration.

Upon substituting Eq. 6 for Eq. 2, the total light emission is found to be:

$$\int I_{CL}dt = \frac{k_4 k_{TS}[DBA]\phi_f[AH]_0}{(k_4+k_5+k_6)\{(k_{TS}+k_{TT})[DBA]+k_7+k_8[O_2]\}}, \quad (7)$$

The curves of the emission intensity *versus* time (*I-t* curves) for the indirect CL upon adding a solution of *t*-BuOK in *t*-BuOH to solutions of **1** and **2** of various concentrations in dimethyl sulfoxide (DMSO) containing DBA, are illustrated in Figs. 1 and 2, respectively. The results indicate that both the intensity and total light emission are proportional to the initial concentration of the ketone ($[AH]_0$) when $[AH]_0$ is comparably low.[8] The *I-t* curves obtained by adding *t*-BuOK solutions of different concentrations to solutions of **1** and **2** are illustrated in Figs. 3 and 4, respectively. The results indicate that the peak of the emission increases and that duration of the emission decreases with increasing *t*-BuOK concentration, while the total light emission remains almost constant provided that $[AH]_0$ is kept constant. Thus, it may be concluded that the

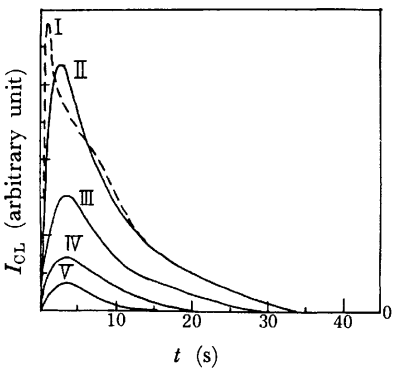

Fig. 1. Effect of the concentration of 3-methyl-2-butanone (**1**) on *I-t* curve of the indirect CL from **1** in a DMSO-*t*-BuOK/*t*-BuOH system containing DBA at 313 K. The initial concentration of **1** in 10^{-3} mol l^{-1}: I, 2.4; II, 1.2; III, 0.60; IV, 0.30; V, 0.15. The initial concentrations of *t*-BuOK and DBA are 3.0×10^{-3} and 5×10^{-4} mol l^{-1}, respectively.

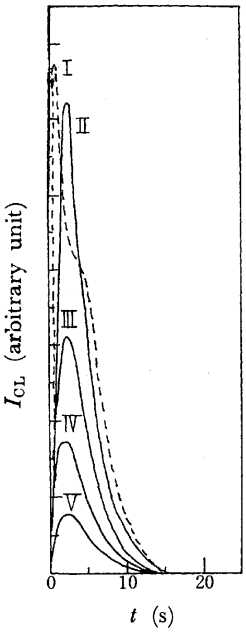

Fig. 2. Effect of the concentration of isopropyl phenyl ketone (**2**) on *I-t* curve of the indirect CL from **2** in a DMSO-*t*-BuOK/*t*-BuOH system containing DBA at 313 K. The initial concentration of **2** in 10^{-4} mol l^{-1}: I, 14; II, 7.0; III, 3.5; IV, 1.8; V, 0.9. The initial concentrations of *t*-BuOK and DBA are 3.0×10^{-3} and 5×10^{-4} mol l^{-1}, respectively.

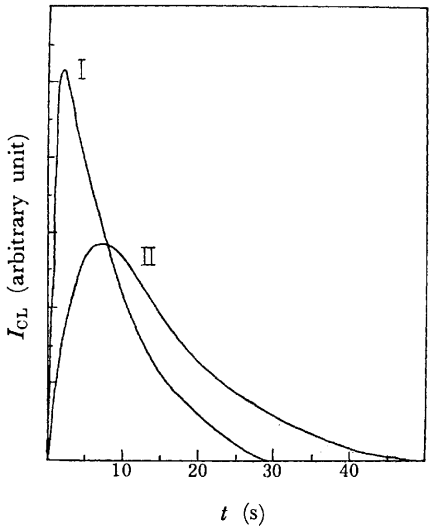

Fig. 3. Effect of the concentration of *t*-BuOK on *I-t* curve of the indirect CL from 3-methyl-2-butanone (**1**) in a DMSO-*t*-BuOK/*t*-BuOH system containing DBA at 313 K. The initial concentration of *t*-BuOK in 10^{-3} mol l^{-1}: I, 3.0; II, 0.75. The initial concentrations of **1** and DBA are 3.0×10^{-4} and 5×10^{-4} mol l^{-1}, respectively.

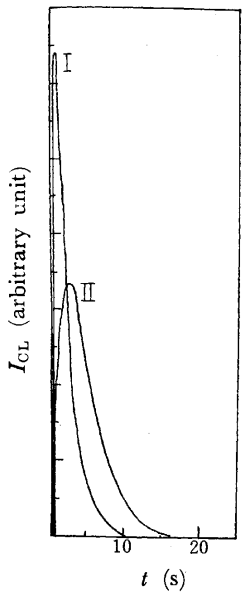

Fig. 4. Effect of the concentration of *t*-BuOK on *I-t* curve of the indirect CL from isopropyl phenyl ketone (**2**) in a DMSO-*t*-BuOK/*t*-BuOH system containing DBA at 313 K. The initial concentration of *t*-BuOK in 10^{-3} mol l^{-1}: I, 3.0; II, 0.75. The initial concentrations of **2** and DBA are 1.8×10^{-4} and 5×10^{-4} mol l^{-1}, respectively.

experimental results support the validity of Eq. 7.

From Eq. 7, the indirect CL quantum yield can be written as

$$\phi_{CL}=\frac{\int I_{CL}dt}{[AH]_0}=\frac{k_4k_{TS}[DBA]\phi_f}{(k_4+k_5+k_6)\{(k_{TS}+k_{TT})[DBA]+k_7+k_8[O_2]\}},$$

or

$$\frac{1}{\phi_{CL}}=\frac{1}{\phi^*_{react}\phi_{ET}\phi_f}\left(1+\frac{k_7+k_8[O_2]}{(k_{TS}+k_{TT})[DBA]}\right), \quad (8)$$

where

$\phi^*_{react}=k_4/(k_4+k_5+k_6)$ and $\phi_{ET}=k_{TS}/(k_{TS}+k_{TT})$.

The quantum yields for the indirect CL of **1** and **2** were determined from the *I-t* curves measured by varying the DBA concentration. (See experimental section.) Plots of $1/\phi_{CL}$ *versus* 1/[DBA] are shown in Figs. 5 and 6 for **1** and **2**, respectively. These linear plots indicate that Eq. 8 is plausible.

The values of the *abscissa intercept* ($1/\phi_{CL}$ at infinite DBA concentration, $1/\phi^\infty_{CL}$) were found from the figures to be 5.0×10^6 and 3.8×10^4 mol einstein^{-1} for **1** and **2**, respectively. Thus, the values of ϕ^∞_{CL} for **1** and **2** were calculated to be 2.0×10^{-7} and 2.6×10^{-5} eins mol^{-1}, respectively.

From Eq. 8, the value of $(k_7+k_8[O_2])/(k_{TS}+k_{TT})$ is given by the *line slope/intercept*, which is found from Figs. 5 and 6 to be $2.5\times10^3/5.0\times10^6=5.0\times10^{-4}$ and $7.5/3.8\times10^4=2.0\times10^{-4}$ mol l^{-1} for **1** and **2**, respectively. Considering that the stationary concentration of dissolved oxygen is lower than the initial concentration due to consumption during oxygenation, the decay rate of P*(T), $k_7+k_8[O_2]$, is assumed to be $\approx10^6$ s^{-1}, although

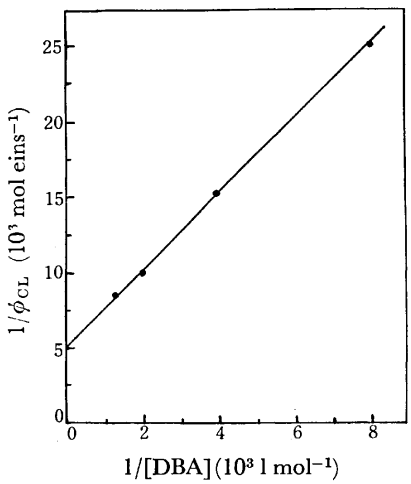

Fig. 5. Effect of the concentration of [DBA] on the quantum yield of the indirect CL from 3-methyl-2-butanone (**1**) in a DMSO-*t*-BuOK/*t*-BuOH system at 313 K. The initial concentrations of **1** and *t*-BuOK are 1.2×10^{-3} and 3.0×10^{-3} mol l^{-1}, respectively.

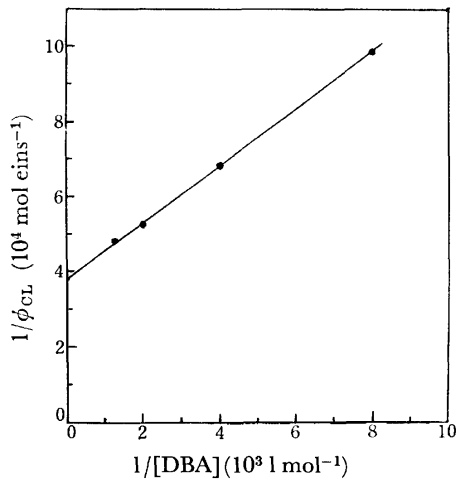

Fig. 6. Effect of the concentration of DBA on the quantum yield of the indirect CL from isopropyl phenyl ketone (**2**) in a DMSO-*t*-BuOK/*t*-BuOH system at 313 K. The initial concentrations of **2** and *t*-BuOK are 7.0×10^{-4} and 3.0×10^{-3} mol l^{-1}, respectively.

this value is an order of magnitude smaller than that proposed by Turro *et al.*[9] Then, using the value $\phi_{ET}=k_{TS}/(k_{TS}+k_{TT})=0.2$ reported by Wilson *et al.*,[6] the k_{TS} values for **1** and **2** were calculated to be 4×10^8 and 1×10^9 l mol^{-1} s^{-1}, respectively. These values are in fairly good agreement with the values reported by Belyakov and Vassilév,[10] Turro *et al.*[9] and Wilson *et al.*[6] for the rate of energy transfer from triplet carbonyl compounds to singlet DBA.

The yield of the excited triplet product (ϕ^*_{react}) can be written as:

$$\phi^*_{react} = \phi^{\infty}_{CL}/\phi_{ET}\phi_f.$$

Since $\phi^{\infty}_{CL}=2.0\times10^{-7}$ and 2.6×10^{-5} eins mol^{-1} (for **1** and **2**, respectively), $\phi_{ET}=0.2$, and $\phi_f=0.1$,[9] the values of ϕ^*_{react} for **1** and **2** were calculated to be 1×10^{-5} and 1×10^{-3}, respectively. These values are markedly lower than the yields of excited triplet products generated in the thermal cleavage of various 1,2-dioxetanes (0.5—0.02[11]). These very small values are presumably due to the fact that CL *via* a dioxetane intermediate arises from a minor reaction.[12]

Experimental

Commercially available 3-methyl-2-butanone, isopropyl phenyl ketone, DBA (all from Tokyo Kasei and of guaranteed reagent grade), and *t*-BuOK (from Merck, for synthesis) were used without further purification. Luminol (from Nakarai Kagaku) was recrystallized from dilute hydrochloric acid prior to use. All solvents, DMSO (from Merck, for spectroscopy) and *t*-BuOH (from Tokyo Kasei, extra pure grade), were used without further purification.

The luminescent reaction was initiated by adding 0.2 ml of a *t*-BuOK solution (in *t*-BuOH) to 2 ml of an aerated solution of **1** or **2** with stirring in a quartz cell ($10\times10\times45$ mm) which was situated in a thermostatically-controlled cell holder.

The CL intensity at 430 nm (the peak of the DBA fluorescence) *versus* time was measured on a Hitachi MPF-2A fluorescence spectrophotometer with no exciting source. The total light emission was determined graphically from the *I-t* curves.

A standard solution of luminol in anhydrous DMSO having an optical density at 359.5 nm (the absorption peak) of 0.010 (1.26×10^{-6} mol l^{-1}) was prepared, and the *I-t* curve of the CL initiated by adding 0.2 ml of a *t*-BuOK solution to 2 ml of the standard solution was measured on the same apparatus at 313 K.

Using the value of 1.28×10^{-2} eins mol^{-1} proposed by Lee *et al.* for the CL exhibited from the luminol solution,[13] the quantum yields for indirect CL from **1** and **2** were determined from the ratios of the total light emitted from the luminol solution to the total measured light emission from the ketone solutions.

Support for this research from a Scientific Research Grant from the Ministry of Education is gratefully acknowledged.

References

1) I. Kamiya and T. Sugimoto, *Chem. Lett.*, **1976**, 33; *Bull. Chem. Soc. Jpn.*, **50**, 2442 (1977).

2) (a) V. A. Belyakov and R. F. Vassilév, *Photochem. Photobiol.*, **11**, 179 (1970); (b) T. Wilson and A. P. Schaap, *J. Am. Chem. Soc.*, **93**, 4126 (1971).

3) J. W. Haap, E. G. Janzen, and B. C. Rudy, *J. Org. Chem.*, **35**, 3382 (1970).

4) For example, N. J. Turro, P. Lechtken, N. E. Schore, G. Schuster, H.-C. Steinmetzer, and A. Yekta, *Acc. Chem. Res.*, **7**, 97 (1974).

5) Y. Sawaki and Y. Ogata, *J. Am. Chem. Soc.*, **97**, 6983 (1975).

6) T. Wilson, D. E. Golan, M. S. Harris, and A. L. Baumstark, *J. Am. Chem. Soc.*, **98**, 1086 (1976).

7) J. W. Hastings and T. Wilson, *Photochem. Photobiol.*, **23**, 461 (1976).

8) The *I-t* curves indicate that the luminescent reaction arises from consecutive reactions. An expression for I_{CL} can be derived from Eqs. 1, 3, 4, and 5 by assuming that $d[A^-]/dt=0$, $k_2[A^-][t\text{-BuOH}]\gg k_3[A^-][O_2]$, and that $k_1[t\text{-BuO}^-]/k_2[t\text{-BuOH}]$ remains constant during the luminescent reaction, thus

$$I_{CL} = \frac{k[AH]_0k_4k_{TS}\phi_f[DBA]}{(k-\sum k_i)\{(k_{TS}+k_{TT})[DBA]+k_7+k_8[O_2]\}}\times \{\exp(-\sum k_i t) - \exp(-kt)\},$$

where $k = k_1[t\text{-BuO}^-]/k_2[t\text{-BuOH}]$

and $\sum k_i = k_4+k_5+k_6$.

9) k_T(decay rate of P*(T)) 10^7 s^{-1}: N. J. Turro, P. Lechtken, G. Schuster, J. Orell, H.-C. Steinmetzer, and W. Adam, *J. Am. Chem. Soc.*, **96**, 1627 (1974).

10) $k_{TS}=3\times10^8$ l mol^{-1} s^{-1} (Ref. 2 (a)); 1×10^9 l mol^{-1} s^{-1} (Ref. 9).

11) For example, M. A. Umbreit and E. H. White, *J. Org. Chem.*, **41**, 479 (1976). See also Ref. 7.

12) Y. Sawaki and Y. Ogata, *J. Org. Chem.*, **42**, 40 (1977).

13) L. Lee, A. S. Wesley, J. F. Ferguson, III, and H. H. Seliger in "Bioluminescence in Progress," ed by F. H. Johnson and Y. Haneda, Princeton Univ. Press (1966), p. 35.

Stereochemistry of Cobalt(III) Complexes with Thioethers. III.[1] Vicinal Circular Dichroism due to the Chiral Sulfur Donor Atom

Kazuaki YAMANARI, Jinsai HIDAKA,* and Yoichi SHIMURA

Department of Chemistry, Faculty of Science, Osaka University, Toyonaka, Osaka 560

(Received February 21, 1977)

Two kinds of mixed type cobalt(III) complexes, [(2-aminoethylthio)acetato](L-methioninato)cobalt(III) chloride and [3-(2-aminoethylthio)propionato](L-methioninato)cobalt(III) chloride, have been prepared and chromatographically separated into seven and eight isomers, respectively. The characterization of isomers based on their electronic absorption and ^{1}H NMR spectra leads to the conclusion that there have been obtained four pairs of diastereomers due to the sulfur chirality of the coordinated L-methioninate. The circular dichroism spectra of isomers have been measured and discussed in relation to the absolute configurations. The vicinal CD contribution due to the chiral sulfur atom of L-methioninate has been estimated by applying an additivity rule for the three diastereomeric pairs.

A large number of investigations for the vicinal circular dichroism (CD) of asymmetric carbon[2] and nitrogen[3] atoms have been undertaken and the results have indicated that the vicinal chirality makes a relatively smaller CD contribution than the configurational one. The sulfur atom of a thioether ligand also becomes chiral by coordination to a metal ion,[4-8] leaving on itself a single lone-pair which can give a fixed configuration for the donor center at ordinary temperature. However, no optical resolution has been reported for the coordinated sulfur atom of cobalt(III) complexes with thioethers, though some examples were known for the complexes of other metals such as $[Pt^{IV}Cl_4(NH_2CH_2CH_2SCH_2CH_2NH_3)]Cl$.[9]

The present paper is concerned with the isolation of diastereomers arising from the chiral sulfur donor atom and the estimation of vicinal CD contribution due to the sulfur donor in two mixed-complex systems, [Co(terdentate-*N,S,O*)(L-met)]$^+$ [L-Hmet=L-methionine; terdentate-*N,S,O*=(2-aminoethylthio)acetic acid (Haeta), and 3-(2-aminoethylthio)propionic acid (Haetp)]. For the mixed complex six geometrical isomers, *tr.tr.tr.*, *trans(S)*, *trans(O)*, *trans(N)*, *cisciscis-I*, and *cisciscis-II*, are possible as seen in Fig. 1. As compared with [Co(terdentate-*N,S,O*)$_2$]$^+$ complexes,[1] isomer distribution is altered; *meridional* isomer becomes impossible and two *cisciscis* isomers, *cisciscis-I* and *-II*, appear in the present mixed type complexes. In addition, a pair of another type isomers are formally expected for each of the six geometrical isomers, arising from the absolute configuration (*R*) or (*S*) of the sulfur donor atom of coordinated L-methioninate ligand.

Experimental

Preparation and Separation of Isomers. [(2-Aminoethylthio)acetato](L-methioninato)cobalt(III) Chloride, [Co(aeta)(L-met)]Cl: To a hot solution (*ca.* 75 °C) of 9.0 g of cobalt(II) chloride hexahydrate in 60 cm^3 of water was added a mixed solution of 5.95 g of (2-aminoethylthio)acetic acid hemihydrochloride,[10] 5.65 g of L-methionine, and 0.75 g of sodium hydroxide dissolved in 80 cm^3 of water. Nine grams of lead dioxide was gradually added to the solution, and this was stirred at 70—75 °C for 40 min, whereupon the color of the solution became violet. The mixture was filtered to remove an excess of the lead dioxide after cooling to room temperature.

The filtrate was poured into a cation-exchange column of Dowex 50Wx8 (Na^+ form, 200—400 mesh, 4.5×40 cm). After the column had been swept with water, the adsorbed band was eluted with 0.15 M aqueous solution of sodium chloride at the rate of 1 cm^3 per min. Seven colored bands were eluted. It was confirmed from the measurements of the CD and electronic absorption spectra of these eluates, that the second eluate (brownish violet) was *tr.tr.tr.*-[Co(aeta)$_2$]$^+$, the third one (purple) *trans(S)*-[Co(L-met)$_2$]$^+$,[8] the fourth one (purple) *trans(O)*-[Co(aeta)$_2$]$^+$, and the seventh one (red) *trans(N)*-[Co(aeta)$_2$]$^+$,[1] and that the isomers of the desired complex, therefore, exist in the remaining three eluates, first, fifth, and sixth ones. It was also found that the first dark violet eluate is a single band (C-1), but the fifth and sixth reddish purple ones consist of bands more than two. The three eluates were concentrated separately in a vacuum evaporator, and then the deposit, NaCl, was filtered off. The complex in C-1 eluate was obtained by adding a large amount of ethanol to the concentrated solution and recrystallized from a small amount of water.

Each concentrated solution of the fifth and sixth eluates was again poured into a column of SP-Sephadex C-25 (K^+ form, 4.5×120 cm). The adsorbed band was eluted with 0.05 M aqueous solution of $K_2[Sb_2(d\text{-tart})_2]\cdot 3H_2O$ (*d*-H_4tart $=C_4O_6H_6$) at the rate of 0.5 cm^3/min. For the column of the fifth eluate, five colored bands, a brownish red one (C-2), a violet one which was *trans(O)*-[Co(L-met)$_2$]$^+$,[8] a reddish

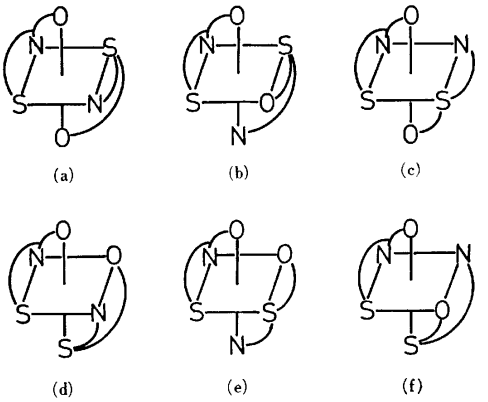

Fig. 1. Six possible geometrical isomers for the [Co(terdentate-*N,S,O*)(L-met)]$^+$ type complex: (a) *tr.tr.tr* (b) *trans(S)*, (c) *trans(O)*, (d) *trans(N)*, (e) *cisciscis-I*, and (f) *cisciscis-II*; methyl group in L-methioninate is omitted.

* Present address: Department of Chemistry, The University of Tsukuba, Ibaraki, 300-31.

purple one (C-3), a brownish red one (C-4), and another brownish red one which was *trans(N)*-[Co(L-met)$_2$]$^+$,[8] were eluted in this order. On the other hand, for the column of the sixth eluate four colored bands, a brownish red one (C-2), a red one (C-5), another red one (C-6), and a violet one (C-7), were eluted in this order. CD measurements showed that each band consists of a single species. The desired eluates, C-2 to C-7, were concentrated separately in a vacuum evaporator, and the deposit, $K_2[Sb_2(d\text{-tart})_2]\cdot 3H_2O$, was filtered off. The concentrated eluate was poured into an anion exchange column of Dowex 1x8 (Cl^- form) and converted into the chloride salt. The desired complex was obtained by adding a large amount of ethanol to the eluate. The product was recrystallized from a minimum quantity of water by adding a small amount of ethanol and washed with ethanol and then acetone, and dried in a vacuum desiccator over $CaCl_2$. Found for C-1: C, 28.09; H, 4.79; N, 7.34%. Calcd for [Co(aeta)(L-met)]Cl=$C_9H_{18}N_2S_2O_4ClCo$: C, 28.69; H, 4.82; N, 7.44%. Found for C-2: C, 27.69; H, 4.76; N, 7.09%. Calcd for [Co(aeta)(L-met)]Cl·0.5H_2O·1/10 KCl=$C_9H_{19}N_2S_2O_{4.5}ClCo$·1/10 KCl: C, 27.49; H, 4.87; N, 7.12%. Found for C-3: C, 25.79; H, 5.30; N, 6.54%. Calcd for [Co(aeta)(L-met)]Cl·2H_2O·1/10 KCl=$C_9H_{22}N_2S_2O_6ClCo$·1/10 KCl: C, 25.72; H, 5.28; N, 6.67%. Found for C-4: C, 26.42; H, 5.35; N, 6.60%. Calcd for [Co(aeta)(L-met)]Cl·2H_2O=$C_9H_{22}N_2S_2O_6ClCo$: C, 26.17; H, 5.37; N, 6.79%. Found for C-5: C, 25.33; H, 4.89; N, 6.75%. Calcd for [Co(aeta)(L-met)]Cl·1.5H_2O·3/10 KCl=$C_9H_{21}N_2S_2O_{5.5}ClCo$·3/10 KCl: C, 25.37; H, 4.97; N, 6.57%. Found for C-6: C, 24.99; H, 4.94; N, 6.86%. Calcd for [Co(aeta)(L-met)]Cl·1.5H_2O·3/10 KCl=$C_9H_{21}N_2S_2O_{5.5}ClCo$·3/10 KCl: C, 25.37; H, 4.97; N, 6.57%. Found for C-7: C, 26.15; H, 5.36; N, 6.93%. Calcd for [Co(aeta)(L-met)]Cl·2H_2O=$C_9H_{22}N_2S_2O_6ClCo$: C, 26.19; H, 5.37; N, 6.79%.

[3-(2-Aminoethylthio)propionato](L-methioninato)cobalt(III) Chloride, [Co(aetp)(L-met)]Cl: The preparation and separation of isomers were carried out according to the method similar to that for the corresponding [Co(aeta)(L-met)]Cl complex, by use of Haetp·HBr·0.5H_2O[10] instead of Haeta·0.5HCl.

Nine colored bands were eluted. From the measurements of the electronic absorption and CD spectra, it was confirmed that the first eluate (brownish violet) is *tr.tr.*-[Co(aetp)$_2$]$^+$, the third one (purple) *trans(S)*-[Co(L-met)$_2$]$^+$,[8] the fourth one (purple) *trans(O)*-[Co(aetp)$_2$]$^+$, and the sixth one (brownish red) *trans(N)*-[Co(aetp)$_2$]$^+$.[1] Thus, the second eluate (dark violet, D-1), the fifth one (purple, D-2), the seventh one (reddish purple, D-3+D-4), the eighth one (purple, D-5), and the ninth one (red, D-6) were the desired isomers. These eluates were concentrated separately in a vacuum evaporator, and then the deposit, NaCl, was filtered off.

Each concentrated filtrate was again poured into a column containing SP-Sephadex C-25 (K^+ form, 4.5×120 cm). The adsorbed band was eluted with 0.05 M aqueous solution of $K_2[Sb_2(d\text{-tart})_2]\cdot 3H_2O$ at the rate of about 0.5 cm^3/min. For the column of the seventh eluate, three bands, a brownish red one (D-3), a purple one which was *trans(O)*-[Co(L-met)$_2$]$^+$,[8] and a red one (D-4), were eluted in this order. For the other columns there was apparently a single band. However, careful CD measurements showed that D-4 and D-6 bands consist of two bands, which were designated as D-4a and D-4b for D-4 eluate, and D-6a and D-6b for D-6 one according to the elution order though the separation of the latter two isomers was insufficient. The desired eluate was concentrated in a vacuum evaporator and the deposit, $K_2[Sb_2(d\text{-tart})_2]\cdot 3H_2O$, was filtered off, and then converted into the chloride salt by using an anion exchange resin (Dowex 1x8, Cl^- form). To the eluate a large amount of ethanol and acetone was added. The product was recrystallized from a minimum quantity of water by adding ethanol and acetone, and washed with acetone and then diethyl ether, and dried in a vacuum desiccator over $CaCl_2$. The isomers obtained were contaminated with a small amount of potassium chloride or sodium chloride, because of the relatively lower yields of isomers as compared with those of [Co(L-met)$_2$]$^+$ and [Co(aetp)$_2$]$^+$ complexes. The CD spectra of D-4a, D-4b, D-6a, and D-6b isomers were measured with the eluates, and their concentrations were calculated from the optical densities referring to that of the mixture, D-4 or D-6. Found for D-1: C, 23.88; H, 4.72; N, 5.49%. Calcd for [Co(aetp)(L-met)]Cl·2H_2O·1.4NaCl=$C_{10}H_{24}N_2S_2O_6ClCo$·1.4NaCl: C, 23.61; H, 4.76; N, 5.51%. Found for D-2: C, 27.76; H, 5.36; N, 6.47%. Calcd for [Co(aetp)(L-met)]Cl·2H_2O·1/5KCl=$C_{10}H_{24}N_2S_2O_6ClCo$·1/5KCl: C, 27.19; H, 5.48; N, 6.34%. Found for D-3: C, 29.38; H, 5.12; N, 6.84%. Calcd for [Co(aetp)(L-met)]Cl·0.5H_2O·0.13KCl=$C_{10}H_{21}N_2S_2O_{4.5}ClCo$·0.13KCl: C, 29.33; H, 5.17; N, 6.84%. Found for D-4 (=mixture of D-4a and D-4b): C, 27.68; H, 5.61; N, 5.89%. Calcd for [Co(aetp)(L-met)]Cl·1.5H_2O·CH_3OH·2/5KCl=$C_{10}H_{23}N_2S_2O_{5.5}ClCo$·$CH_3OH$·2/5KCl: C, 27.54; H, 5.67; N, 5.84%. Found for D-5: C, 28.01; H, 5.08; N, 6.56%. Calcd for [Co(aetp)(L-met)]Cl·H_2O·3/10NaCl=$C_{10}H_{22}N_2S_2O_5ClCo$·3/10NaCl: C, 28.17; H, 5.20; N, 6.57%. Found for D-6 (=mixture of D-6a and D-6b): C, 26.17; H, 5.23; N, 6.13%. Calcd for [Co(aetp)(L-met)]Cl·2H_2O·2/5KCl=$C_{10}H_{24}N_2S_2O_6ClCo$·2/5KCl: C, 26.30; H, 5.30; N, 6.13%.

Measurements. The electronic absorption spectra were measured on a Shimadzu UV-200 spectrophotometer in aqueous solution. The CD spectra were recorded with a JASCO MOE-1 spectropolarimeter. The ^1H NMR spectra were measured in deuterium oxide on a Varian XL-100-15 spectrometer with DSS as the internal reference. All measurements were made at room temperature.

Results and Discussion

Absorption Spectra and Structural Assignments. In the [Co(aeta)(L-met)]$^+$ complex, seven isomers were obtained. Their absorption spectra, are shown in Fig. 2

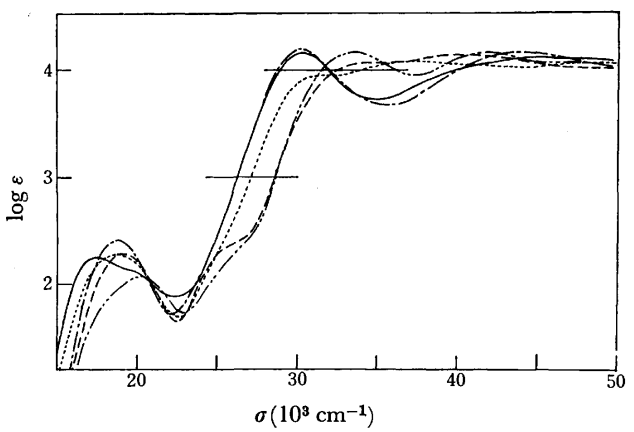

Fig. 2. Absorption spectra of the isomers of [Co(aeta)(L-met)]Cl: C-1 (——), C-2 (– – – –), C-3 (— — —), C-6 (——), and C-7 (- - - -); the spectra of C-4 and C-5 isomers are similar to those of C-2 and C-6 ones, respectively.

Table 1. Absorption data of isomers of [Co(aeta)(L-met)]Cl and [Co(aetp)(L-met)]Cl

Isomer	Assignment	σ_{max}[a] (log ε) First d-d band	Second d-d band	Charge transfer band region
[Co(aeta)(L-met)]Cl				
C-1	*tr. tr. tr.*	17.5(2.25)		30.3(4.16)
		20.0(2.10)[b]		44.9(4.11)
C-2	*trans(N)*	sh[c]	25.5(2.10)[b]	33.5(4.16)
		20.2(2.07)		41.9(4.16)
				47.7(4.07)
C-3	*trans(S)*	18.8(2.41)		30.3(4.18)
				44.1(4.16)
C-4	*trans(N)*	sh[c]	25.5(2.20)[b]	33.0(4.08)
		19.9(2.07)		42.2(4.12)
C-5	*cisciscis-I*	19.1(2.28)	25.5(2.30)[b]	34.0(4.10)
				42.8(4.10)
C-6	*cisciscis-I*	19.2(2.29)	25.5(2.30)[b]	34.2(4.06)
				40.3(4.14)
C-7	*trans(O)*	18.8(2.28)		31.3(3.95)[b]
		sh[c]		37.5(4.08)
				41.7(4.05)[b]
				48.8(4.07)
[Co(aetp)(L-met)]Cl				
D-1	*tr. tr. tr.*	19.2(2.26)		29.0(4.20)
				46.7(4.16)
D-2	*trans(S)*	18.6(2.24)		29.2(4.02)
				44.3(4.00)
D-3	*trans(N)*	18.4(1.99)[b]	25.5(2.30)[b]	33.4(4.20)
		20.4(2.11)		47.5(4.08)
D-4	*cisciscis-I*	19.0(2.39)	25.5(2.40)[b]	33.0(4.13)
				42.4(4.07)
D-5	*trans(O)*	17.9(2.37)	sh[c]	31.9(4.04)
		sh[c]		34.5(4.02)[b]
				42.4(4.01)
D-6	*cisciscis-II*	18.8(2.39)	sh[c]	33.3(4.11)
				46.3(4.05)

a) The wave numbers are given in 10^3 cm^{-1} unit. b) A shoulder. c) The wave number cannot be determined.

and Table 1. The spectral behavior of the present isomers is very similar to that of $[Co(aeta)_2]^+$, and this is due to the fact that both complexes have the same chromophore $[Co(N)_2(O)_2(S)_2]$. Furthermore both complexes have the geometrical isomers of the same types. Therefore, the interpretation of the electronic absorption spectra described in the previous paper[1] could be applied for the present isomers in the same manner.

Of seven isomers, the long wavelength thioether charge transfer bands for C-1 (30300 cm^{-1}, log ε=4.16) and C-3 (30300 cm^{-1}, log ε=4.18) locate at lower energy side than those for the other five isomers. This indicates that the former two isomers have two ligating sulfur atoms in *trans* positions and the latter five in *cis* positions. The isomers C-1 shows a broad first absorption band with a shoulder at high energy side, while C-3 shows a sharp peak. Therefore, C-1 and C-3 can be assigned to *tr.tr.tr.* and *trans(S)* structures, respectively.

On the other hand, of the latter five isomers, C-2 and C-4 show a shoulder at low energy side of the major peak at 20200 and 19900 cm^{-1}, respectively, and C-7 shows a band at 18800 cm^{-1} with a vague shoulder at high energy side, while C-5 and C-6 apparently a sharp peak at 19100 and 19200 cm^{-1}, respectively. From these absorption patterns it was affirmed that C-2 and C-4 isomers are *trans(N)*, C-5 and C-6 *cisciscis*, and C-7 *trans(O)*. As shown in Fig. 1, there exists the only one geometrical isomer for the *trans(N)* geometry. Accordingly, C-2 and C-4 isomers with *trans(N)* structure should be diastereomers due to the sulfur atom chirality (*R*) or (*S*) of the coordinated L-methioninate. For the *cisciscis* form, two geometrical isomers, *cisciscis-I* and *cisciscis-II*, are expected, but it is impossible to decide the configuration of C-5 and C-6 isomers from their electronic absorption spectra. In order to achieve the assignments, NMR spectra of C-5 and C-6 isomers were measured in D_2O by adding a small amount of DCl; the spectra are entirely similar to each other all over the measured region. Furthermore, in the region of amine protons, there are four peaks at 6.35, 5.85, 5.18, and 4.48 ppm from DSS for both isomers. These results indicate that both isomers have either *cisciscis-I* or *cisciscis-II* structure. The C-5 and C-6 isomers, therefore, are diastereomers due to the sulfur atom chirality (*R*) or (*S*) of the coordinated L-methioninate. Referring to the characterization of *cisciscis-I* and *cisciscis-II* isomers for the $[Co(aetp)(L\text{-met})]^+$ complex, which will be described below, the C-5 and C-6 isomers are assigned finally to have the *cisciscis-I* structure (see Figs. 1 (e) and (f)).

In the $[Co(aetp)(L\text{-met})]^+$ complex, eight isomers were obtained chromatographically and their absorption spectra are shown in Fig. 3 and Table 1. These isomers can be assigned in the same manner described above; D-1 is *tr.tr.tr.*, D-2 *trans(S)*, D-3 *trans(N)*, D-4a and D-4b *cisciscis*, D-5 *trans(O)*, and D-6a and D-6b *cisciscis*. It is reasonable from their chromatographic behavior to consider that D-4a and D-4b (or D-6a and D-6b) have the same geometrical structure.

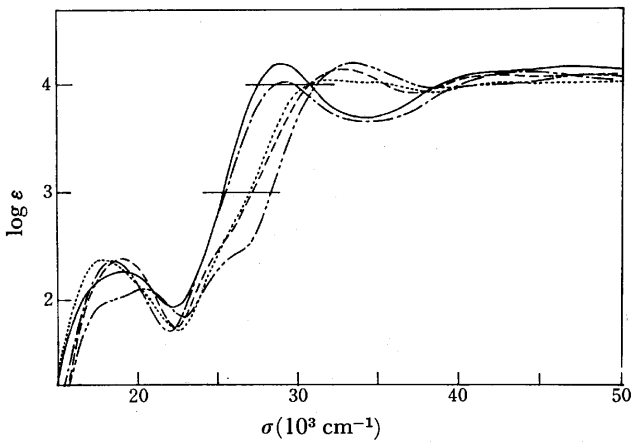

Fig. 3. Absorption spectra of the isomers of [Co(aetp)-(L-met)]Cl: D-1 (——), D-2 (– – –), D-3 (— — —), D-4a (——), and D-5 (----); the spectra of D-4b, D-6a, and D-6b isomers are similar to that of D-4a one.

The assignment of *cisciscis-I* and *cisciscis-II* was made on the basis of ^{1}H NMR spectra. D-4 complex which is a mixture of D-4a and D-4b isomers, showed a methine signal at 3.91 ppm from DSS, and D-6 one which is a mixture of D-6a and D-6b, showed at 3.45 ppm. This very large difference of the chemical shift between D-4 and D-6 isomers is explained on the basis of C–O deshielding effect[11] as follows; in the *cisciscis-I* structure, the methine proton is located just above a line drawn down the C–O bond of the other ligand and will be deshielded by the anisotropy associated with the C–O bond, while in the *cisciscis-II* form, this effect does not occur. From these reasons, D-4 and D-6 isomers can be assigned to the *cisciscis-I* and *cisciscis-II* structures, respectively. In addition, in the region of the amine protons, D-4 isomer showed three peaks at 4.31, 5.03, and 6.19 ppm, whereas D-6 isomer one peak at 5.97 ppm from DSS. Since the *cisciscis-I* structure has each of two amine groups in the deshielded and shielded positions and the *cisciscis-II* one has two amine groups in the shielded positions, it is also expected that D-4 isomer is *cisciscis-I* and D-6 one *cisciscis-II*. The similar consideration was applied for the assignment of *cisciscis-I* structure of the C-5 and C-6 isomers of [Co(aeta)(L-met)]$^+$. Thus, four diastereomeric pairs, C-2 and C-4, C-5 and C-6, D-4a and D-4b, and D-6a and D-6b, are discovered, which are arising from the chiral sulfur donor atom of the coordinated L-methioninate.

The structural assignments described above were able to be made mainly on the basis of electronic absorption spectra. This indicates that the absorption spectral behavior in the mixed type complexes is similar on the whole to that of the bis(terdentate-*N,S,O*) type complexes. However, there appear some interesting differences in details. Firstly, two *trans(N)* isomers of $[Co(aeta)_2]^+$ and $[Co(aetp)_2]^+$ show no splitting in the first absorption band region, but four *trans(N)* isomers of the present mixed type complexes and of the $[Co(L\text{-met})_2]^+$ complex exhibit an explicit shoulder at low energy side of the major peak. Two bis(terdentate) type *trans(O)* isomers show more explicit shoulder at high energy side of the major peak than the *trans(O)* isomers of the mixed type and $[Co(L\text{-met})_2]^+$ complex. These differences indicate that the sulfur atom in the linear terdentate-*N,S,O* ligands has a strong ligand field strength than that in L-methioninate. Secondly, the thioether charge transfer band positions of the mixed type *trans(O)* isomers apparently differ from those of the bis type *trans(O)* isomers: 31300 cm^{-1} for [Co(aeta)(L-met)]$^+$ (C-7); 31900 cm^{-1} for [Co(aetp)(L-met)]$^+$ (D-5); 35100 cm^{-1} for $[Co(aeta)_2]^+$; 34200 cm^{-1} for $[Co(aetp)_2]^+$. The present mixed complexes have two kinds of sulfur atoms, one in the ligand aeta$^-$ or aetp$^-$ and the other in L-met$^-$. The *trans(O)* isomer of $[Co(L\text{-met})_2]^+$ shows the thioether charge transfer band at 32700 cm^{-1}, a considerably lower energy position than that of $[Co(aeta)_2]^+$ or $[Co(aetp)_2]^+$. Therefore, the thioether charge transfer bands due to two kinds of sulfur atoms appear separately in this case. In fact, C-7 isomer shows another intense band at 37500 cm^{-1} and D-5 one at 34500 cm^{-1} (sh), which correspond roughly to the positions of the bis type complexes.

CD Spectra. CD spectra of fifteen mixed type complexes are shown in Figs. 4—9 and Table 2. The CD patterns hardly change with the substitution of the aetp ligand for the aeta one, especially in the first absorption band region. This suggests that the difference in size of the *S*-carboxylate chelate ring has not large effect on the CD spectra as in the case of the bis(terdentate-*N,S,O*) type complexes.[1] In contrast to this, drastic changes were reported for the cobalt(III) complexes of bis(terdentate-*O,N,O*) type.[12]

The *tr.tr.tr.* isomers show two CD bands in the first absorption band region; the low energy band has a positive sign and the high energy negative (Fig. 4). This is good agreement with the fact that both isomers have *Λ* configurations[13] according to the ring pairing method.[14]

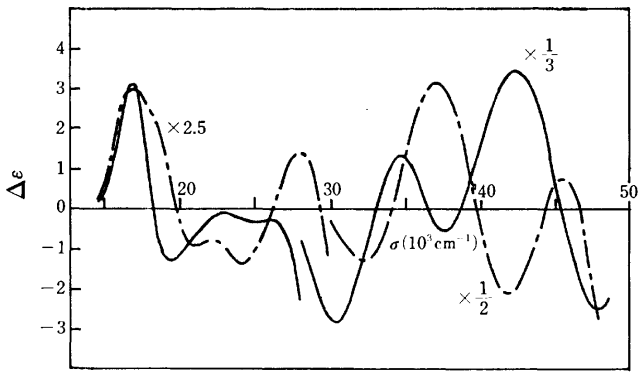

Fig. 4. CD spectra of *tr.tr.tr.* complexes: [Co(aeta)(L-met)]Cl (——) and [Co(aetp)(L-met)]Cl (———).

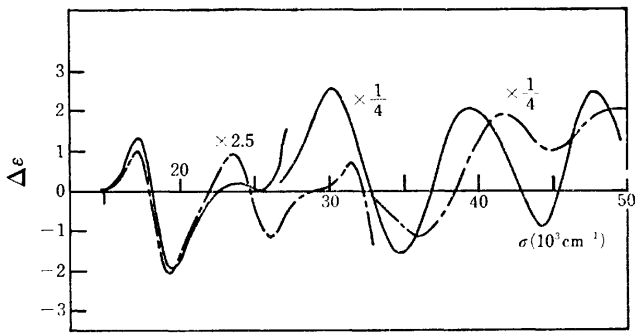

Fig. 5. CD spectra of *trans(S)* complexes: [Co(aeta)(L-met)]Cl (——) and [Co(aetp)(L-met)]Cl (———).

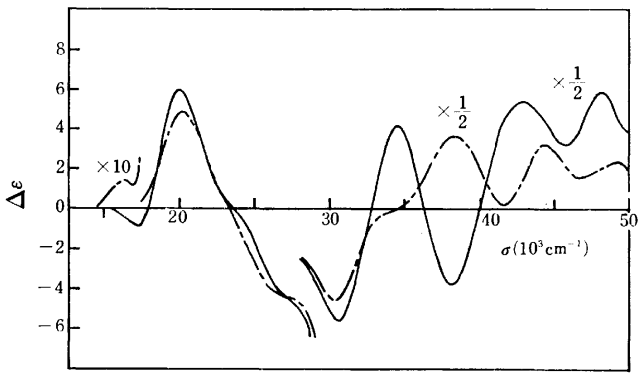

Fig. 6. CD spectra of *trans(O)* complexes: [Co(aeta)(L-met)]Cl (——) and [Co(aetp)(L-met)]Cl (———).

TABLE 2. CD DATA OF ISOMERS OF [Co(aeta)(L-met)]Cl AND [Co(aetp)(L-met)]Cl

Isomer	σ_{ext}[a] ($\Delta\varepsilon$) First d-d band region	Second d-d band region	Charge transfer band region
[Co(aeta)(L-met)]Cl			
tr. tr. tr. (C-1)	16.9(+3.16)	24.9(−0.33)	30.5(−8.48)
	19.5(−1.28)		34.8(+3.98)
			37.6(−1.51)
			42.4(+10.5)
			48.0(−7.55)
trans(N) (C-2)	18.0(−1.19)	25.6(+0.96)	30.4(+0.36)
	20.7(+2.14)		35.3(−9.99)
			42.1(−11.8)
			47.6(+19.1)
trans(S) (C-3)	17.2(+1.31)	23.7(+0.20)	30.1(+10.2)
	19.5(−1.96)		34.8(−6.42)
			39.5(+8.23)
			44.3(−3.73)
			47.8(+9.99)
trans(N) (C-4)	17.9(+1.31)	27.4(+2.54)	31.6(+6.74)
	20.7(−3.29)		35.3(−4.09)
			44.3(+3.20)
cisciscis-I (C-5)	18.5(+0.53)	26.4(−0.69)	29.9(+0.22)
	23.6(+0.17)		32.4(−0.70)
			34.4(+0.11)
			37.7(−2.64)
			42.1(+9.11)
			46.4(−3.38)
cisciscis-I (C-6)	17.8(−0.84)	26.0(−0.45)	33.3(+2.04)
	20.1(+0.69)		39.5(+5.36)
			44.5(−3.65)
trans(O) (C-7)	17.2(−0.89)	27.0(−4.30)[b]	30.6(−11.2)
	20.0(+6.01)		34.5(+8.33)
			38.1(−7.59)
			42.8(+10.8)
			48.3(+11.8)
[Co(aetp)(L-met)]Cl			
tr. tr. tr. (D-1)	16.8(+1.22)	24.2(−0.55)	28.2(+0.58)
	17.3(+0.97)[b]		32.3(−2.56)
	21.1(−0.35)		37.1(+6.40)
			41.9(−4.29)
			45.3(+1.54)
trans(S) (D-2)	17.2(+0.39)	23.5(+0.38)	31.5(+0.27)
	19.2(−0.83)	26.1(−0.49)	36.0(−4.56)
			41.7(+7.68)
			49.1(+8.39)
trans(N) (D-3)	16.5(+0.03)	25.8(+0.87)	30.8(+3.61)
	17.7(−0.05)		35.9(−18.9)
	20.6(+2.06)		46.3(+15.3)
cisciscis-I (D-4)	17.0(+0.08)		31.5(+2.30)
	18.3(+0.12)		35.9(−0.90)
	20.6(−0.44)		40.3(−0.42)
			44.8(+0.32)
cisciscis-I[c] (D-4a)	17.8(+1·30)	26.9(+0.59)	32.5(−7.11)
	20.7(−0.88)		37.7(+2.05)
			40.8(−0.24)
			43.6(+1.94)
			47.7(−3.99)
cisciscis-I[c] (D-4b)	17.7(−1.13)	24.3(−0.17)	31.9(+11.9)
	20.5(+0.11)		36.8(−3.65)
			43.5(−1.26)
			46.7(+3.28)
trans(O) (D-5)	16.1(+0.14)	27.0(−4.40)[b]	30.4(−9.17)
	20.2(+4.89)		38.3(+7.37)
			44.4(+6.60)
			49.3(+4.86)
cisciscis-II (D-6)	17.2(−0.17)	25.7(−0.48)	37.0(+7.04)
	19.3(+0.14)		45.0(−4.73)
cisciscis-II[c] (D-6a)	15.6(+0.04)	25.5(−0.29)	36.8(+7.47)
	17.3(−0.07)		44.4(−5.63)
	20.5(−0.21)		
cisciscis-II[c] (D-6b)	16.0(+0.05)[b]	26.2(−0.28)	37.9(+5.31)
	19.5(+0.64)		45.5(−2.09)

a) The wave numbers are given in $10^3\,cm^{-1}$ unit. b) A shoulder. c) CD spectra were measured for the eluates.

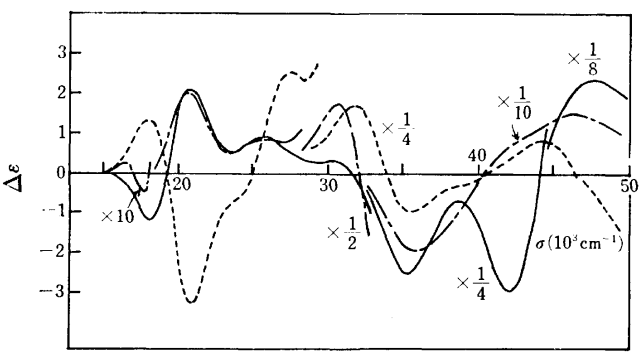

Fig. 7. CD spectra of *trans(N)* complexes: [Co(aeta)-(L-met)]Cl, C-2 (——) and C-4 (----); [Co(aetp)-(L-met)]Cl (——).

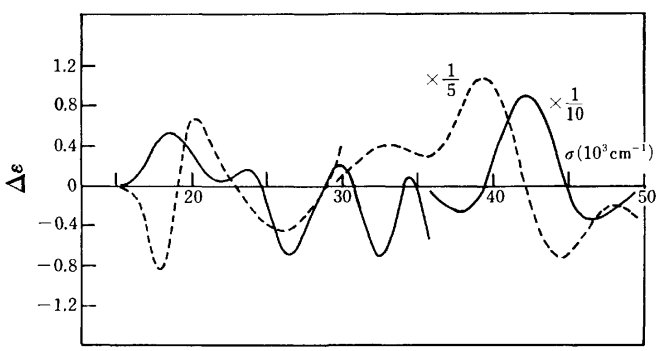

Fig. 8. CD spectra of *cisciscis-I*-[Co(aeta)(L-met)]Cl, C-5 (——) and C-6 (----).

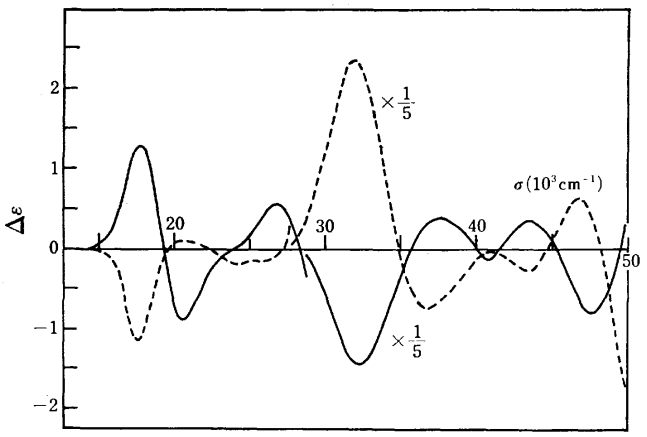

Fig. 9. CD spectra of *cisciscis-I*-[Co(aetp)(L-met)]$^+$, D-4a (——) and D-4b (----).

The two *trans(S)* isomers (Fig. 5) exhibit the same pattern as that of the *tr.tr.tr.* isomers in the first absorption band region. Since both *trans(S)* isomers also have *A* absolute configuration but the $^1A \rightarrow {}^1A + {}^1B_b(C_2)$ transition should be in higher energy for this geometry, this result indicates that CD spectral pattern cannot be always related to the ring pairing method for the complexes containing L-methioninate. A similar case has been reported for another system.[15]

Both *trans(O)* isomers exhibit a major positive CD band at high energy side, though a weak positive or negative band occurs in low energy (Fig. 6). This may suggest that the high energy positive band represents a composite transition $^1A \rightarrow {}^1B_a + {}^1B_b(C_2)$. However, these mixed *trans(O)* isomers have formally no configurational chirality according to the ring pairing method. Thus it may be more reasonable to consider that the CD contributions due to the chiral sulfur donor atoms become dominant.

For the *trans(N)* isomers, this viewpoint becomes more important; two *trans(N)* isomers of the aeta complex, C-2 and C-4, exhibit completely enantiomeric CD patterns in the first absorption band region (Fig. 7), which can be attributed mainly to the enantiomeric configurations of chiral sulfur atom of the coordinated L-methioninate. In the case of the aetp complex, the only one *trans(N)* isomer was obtained. Its CD spectral pattern is similar to that of C-2 isomer and its structure is considered to be same as that of C-2. The D-4a *cisciscis-I* isomer shows the CD spectrum almost enantiomeric to the D-4b *cisciscis-I* isomer (Fig. 9).

Of the fifteen mixed type complexes, eight ones which are classified into diastereomeric pairs, C-2 and C-4, C-5 and C-6, D-4a and D-4b, and D-6a and D-6b, have of course a definite configuration, (*R*) or (*S*), with respect to the chiral sulfur donor atom of L-methioninate. Furthermore, the remaining five isomers except two *tr.tr.tr.* ones take also a definite configuration of the chiral sulfur atom of L-methioninate on the basis of the following reasons; firstly, all fractions of each isomer on the chromatographic separation shows the same CD spectra. Secondly, ^1H NMR spectra of these isomers showed a single peak in the *S*-methyl proton region (Fig. 10). Thirdly, corresponding geometrical isomers of the mixed aeta and aetp complexes show very similar CD spectra, and stereomodel examination reveals that the isomers except *tr.tr.tr.* one prefer (*S*) configuration, since the S-CH_3 group in (*R*) configuration interacts with the chelate ring of the other ligand.

For the present mixed type complexes, there are two kinds of chiral sulfur atoms, one in the ligand aeta$^-$ or aetp$^-$, and the other in L-met$^-$. Therefore, the CD signs in the thioether charge transfer band region cannot

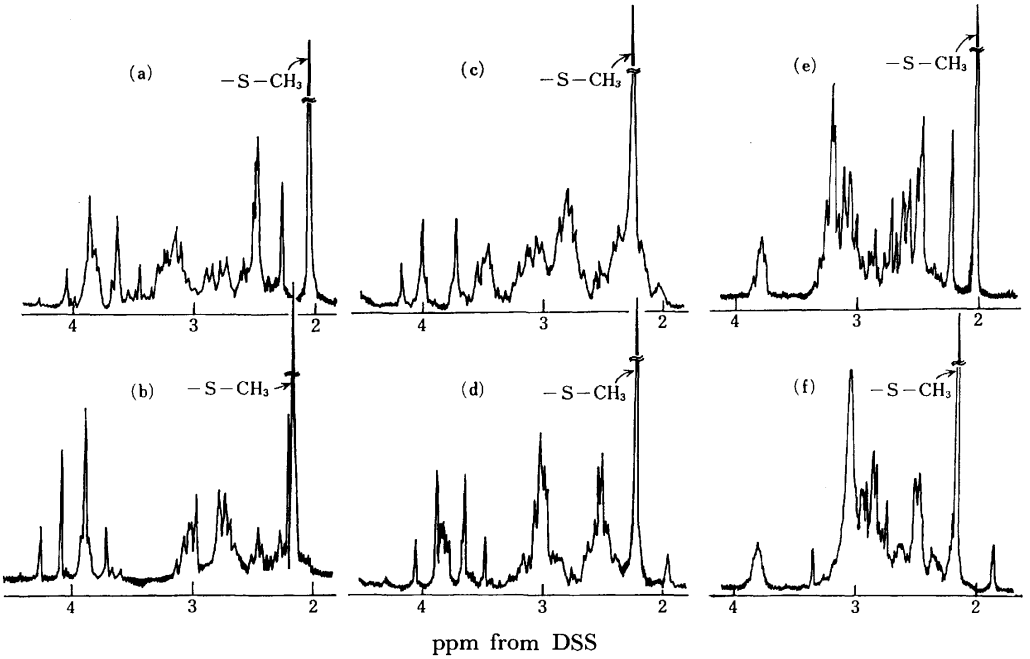

Fig. 10. The ^1H NMR spectra of the isomers of [Co(aeta)(L-met)]Cl, [(a) *trans(N)*=C-2, (b) *trans(N)*=C-4, (c) *trans(S)*, and (d) *trans(O)*] and [Co(aetp)(L-met)]Cl [(e) *trans(N)* and (f) *trans(O)*].

be simply related to the absolute configurations. However, some correlations are found for the *trans*(*S*) and *trans*(*N*) isomers. Namely, both *trans*(*S*) isomers show two CD bands, (+) and (−) from low energy side, and both *trans*(*N*) isomers (C-2 and D-3) also two CD bands of opposite signs (Table 2).

CD Contribution due to the Chiral Sulfur Donor Atom. In order to estimate the vicinal CD contribution of the chiral sulfur donor atom of L-methioninate, an additivity rule was applied to the CD spectra of the diastereomeric pairs C-2 and C-4, C-5 and C-6, and D-4a and D-4b isomers; the chiral sulfur contribution can be obtained by subtracting the observed CD of one isomer from that of the counterpart, while the overall CD contribution due to the remaining factors such as the chiral carbon atom of L-methininate and the chiral sulfur atom of the terdentate-*N,S,O* ligand and/or the configurational chirality due to the skew pair of chelate rings can be obtained by summing up the two observed CD curves. The calculated CD curves are shown in Figs. 11—13.

In the case of *trans*(*N*)-[Co(aeta)(L-met)]$^+$ (Fig. 11), the CD contribution of the chiral sulfur donor atom of L-methioninate is very large in the first absorption band region ($\Delta\varepsilon=-1.24$ at 18000 cm^{-1} and $\Delta\varepsilon=+2.72$ at 20700 cm^{-1}). Similarly, for the *cisciscis-I*-[Co(aeta)-(L-met)]$^+$ and -[Co(aetp)(L-met)]$^+$ complexes (Figs. 12 and 13), their L-methioninate sulfur vicinal CD are

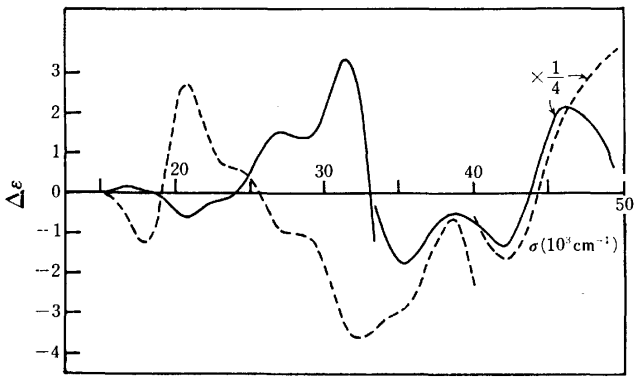

Fig. 11. Curve analysis of *trans(N)*-[Co(aeta)(L-met)]Cl complexes: $1/2\times\{\Delta\varepsilon(\text{C-2})+\Delta\varepsilon(\text{C-4})\}$ (——) and $1/2\times\{\Delta\varepsilon(\text{C-2})-\Delta\varepsilon(\text{C-4})\}$ (----).

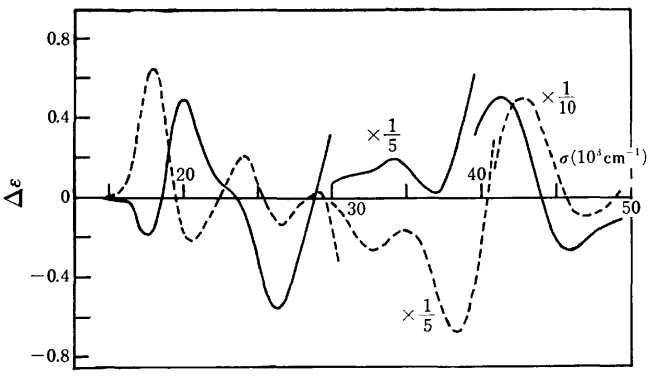

Fig. 12. Curve analysis of *cisciscis-I*-[Co(aeta)(L-met)]Cl complexes: $1/2\times\{\Delta\varepsilon(\text{C-5})+\Delta\varepsilon(\text{C-6})\}$ (——) and $1/2\times\{\Delta\varepsilon(\text{C-5})-\Delta\varepsilon(\text{C-6})\}$ (----).

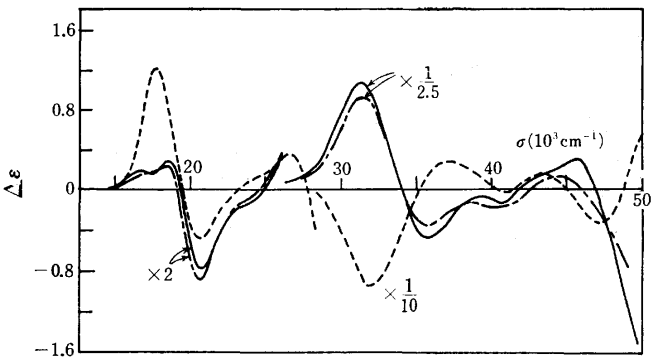

Fig. 13. Curve analysis of *cisciscis-I*-[Co(aetp)(L-met)]$^+$ complexes: $1/2\times\{\Delta\varepsilon(\text{D-4a})+\Delta\varepsilon(\text{D-4b})\}$ (——), $1/2\times\{\Delta\varepsilon(\text{D-4a})-\Delta\varepsilon(\text{D-4b})\}$ (----), and D-4 mixture of diastereomers (———).

dominant in the first absorption band region. It is interesting to note that the observed CD curve of the D-4 mixture is very similar to the calculated contribution of chiralities other than the sulfur atom chirality of L-methioninate. This indicates that the D-4 complex is composed of equal amounts of D-4a and D-4b isomers.

In conclusion, the sulfur chirality of the coordinated L-methioninate has large vicinal CD contribution even in the first absorption band region. In this respect, there are some differences between the chiral sulfur and nitrogen[3] donor atoms. Therefore, care must be taken in relating the CD spectra to the absolute configurations of the complexes containing L-methioninate ligand.

References

1) Part II of this series: K. Yamanari, J. Hidaka, and Y. Shimura, *Bull. Chem. Soc. Jpn.*, in contribution.

2) C. T. Liu and B. E. Douglas, *Inorg. Chem.*, **3**, 1356 (1964); B. E. Douglas and S. Yamada, *ibid.*, **4**, 1562 (1965); T. Yasui, J. Hidaka, and Y. Shimura, *Bull. Chem. Soc. Jpn.*, **39**, 2417 (1966); C. J. Hawkins and P. J. Lawson, *Inorg. Chem.*, **9**, 6 (1970); N. Matsuoka, J. Hidaka, and Y. Shimura, *ibid.*, **9**, 719 (1970); C. J. Hawkins and P. J. Lawson, *Aust. J. Chem.*, **23**, 1735 (1970); N. Matsuoka, J. Hidaka, and Y. Shimura, *Bull. Chem. Soc. Jpn.*, **45**, 2491 (1972). *ibid.*, **48**, 458 (1975); K. Yamanari, J. Hidaka, and Y. Shimura, *ibid.*, **48**, 1653 (1975).

3) D. A. Buckingham, S. F. Mason, A. M. Sargeson, and K. R. Turnbull, *Inorg. Chem.*, **5**, 1649 (1966); B. Halpern, A. M. Sargeson, and K. R. Turnbull, *J. Am. Chem. Soc.*, **88**, 4630 (1966); M. Saburi and S. Yoshikawa, *Inorg. Chem.*, **7**, 1890 (1968); M. Saburi, H. Homma, and S. Yoshikawa, *ibid.*, **8**, 367 (1969); K. Okamoto, J. Hidaka, and Y. Shimura, *Bull. Chem. Soc. Jpn.*, **44**, 1601 (1971); *ibid.*, **46**, 3134 (1973); M. Fujita, Y. Yoshikawa, and H. Yamatera, *Chem. Lett.*, **1976**, 959.

4) F. P. Dwyer and F. Lions, *J. Am. Chem. Soc.*, **72**, 1545 (1950); F. P. Dwyer, N. S. Gill, E. C. Gyarfas, and F. Lions, *ibid.*, **74**, 4188 (1952); *ibid.*, **75**, 2443 (1953).

5) J. H. Worrell and D. H. Busch, *Inorg. Chem.*, **8**, 1563 (1969); *ibid.*, **8**, 1572 (1969).

6) B. Bosnich, W. R. Kneen, and A. T. Phillip, *Inorg. Chem.*, **8**, 2567 (1969); B. Bosnich and A. T. Phillip, *J. Chem. Soc., A*, **1970**, 264.

7) R. J. Magee, W. Mazurek, M. J. O'Connor, and A. T. Phillip, *Aust. J. Chem.*, **27**, 1629 (1974).

8) J. Hidaka, S. Yamada, and Y. Shimura, *Chem. Lett.*, **1974**, 1487.
9) F. G. Mann, *J. Chem. Soc.*, **1930**, 1745.
10) K. Yamanari, J. Hidaka, and Y. Shimura, *Bull. Chem. Soc. Jpn.*, **50**, 2299 (1977).
11) E. A. Brends and J. G. Brushmiller, *Inorg. Nucl. Chem. Lett.*, **6**, 531 (1970); *ibid.*, **6**, 847 (1970); L. G. Stadtherr and J. G. Brushmiller, *ibid.*, **6**, 907 (1970).
12) K. Okamoto, J. Hidaka, and Y. Shimura, *Bull. Chem. Soc. Jpn.*, **46**, 475 (1973).
13) Absolute configurations are designated by the IUPAC rule: *Inorg. Chem.*, **9**, 1 (1970).
14) J. I. Legg and B. E. Douglas, *J. Am. Chem. Soc.*, **88**, 2697 (1966).
15) J. Hidaka, S. Yamada, and B. E. Douglas, *J. Coord. Chem.*, **2**, 123 (1972); J. I. Legg and J. A. Neal, *Inorg. Chem.*, **12**, 1805 (1973).

Cobalt(III) Complexes Containing Large Chelate Rings. II.[1] Syntheses and Properties of Cobalt(III)–Ammine Complexes Containing α,ω-Alkanediamines

Hiroshi OGINO

Departemnt of Chemistry, Faculty of Science, Tohoku University, Aoba, Aramaki, Sendai 980

(Received March 17, 1977)

Reactions of $[Co(H_2O)(NH_3)_5](ClO_4)_3$ with $H_2N(CH_2)_nNH_2$ (N–N) in dimethyl sulfoxide were examined by changing the number of methylene groups in N–N (n=2—5, 7, 8, 10, 12, and 14). Complexes of the $Co(NH_3)_4$-(N–N)$^{3+}$ type were found to be formed for n=2—4, 12, and 14, but, not for n=5, 7, 8, and 10. In addition to these products, a number of new cobalt(III) complexes were isolated.

In the previous paper, a number of new cobalt(III) complexes were isolated as products of the reactions of $[CoCl_2(en)_2]Cl$ with α,ω-alkanediamines $H_2N(CH_2)_n$-NH_2 (N–N) in dimethyl sulfoxide (DMSO), where en denotes 1,2-ethanediamine.[1] Among them, complexes of the $[Co(en)_2(N–N)]X_3$ and $[Co_2(en)_4(N–N)_2]$-X_6 types which contain large chelate rings were found.

Recently, $[Co(NH_3)_{6-2p}(en)_p]X_3$ (p=0, 1, 2, and 3) and $[Co(NH_3)_5(enH)]X_4$ were isolated as products of the reaction of $[Co(H_2O)(NH_3)_5](ClO_4)_3$ with en in DMSO.[2] It seemed that it would be interesting and worthwhile to know, when this reaction is applied to various diamines, what kinds of products are formed. If a diamine with a long methylenic chan is used, the formation of the complexes containing large chelate rings might be expected. In this paper, the products of the reactions of $[Co(H_2O)(NH_3)_5](ClO_4)_3$ with α,ω-alkanediamines (N–N) in DMSO are examined. The diamines, $H_2N(CH_2)_nNH_2$, used in this work are n= 2 (en), 3 (tn), 4 (tmd), 5 (pmd), 7 (hepn), 8 (ocn), 10 (den), 12 (don), and 14 (tden).

Several attempts have been made to prepare cobalt(III) complexes in non-aqueous solvents.[3] The results indicate that the non-aqueous solvents are useful for obtaining novel cobalt(III) complexes. The present study will also help to understand the features of the reactions of cobalt(III) complexes in such a solvent.

Experimental

Preparation of Cobalt(III) Complexes. All the cobalt(III) complexes were obtained from the products of the reactions of $[Co(H_2O)(NH_3)_5](ClO_4)_3$ with N–N in DMSO. The species formed in the reactions were separated by the use of an SP-Sephadex C-25 column (ϕ5×40 cm). Usually, KBr solutions were used as the eluents. In order to isolate the products, each eluate was concentrated to a small volume by means of a rotary evaporator.

When it was difficult to obtain bromide salt because of its high solubility, the eluate was diluted with water and then poured into another SP-Sephadex column. The adsorbed species was then eluted with an appropriate eluent, *e.g.*, a HCl, $LiClO_4$, or NaI solution. When a $LiClO_4$ solution was used as the eluent, the column was washed first with a dilute HCl solution to remove potassium ions; otherwise, the deposition of insoluble $KClO_4$ crystals in the column was unavoidable. The eluate was then concentrated again. The addition of ethanol or ethanol–ether to the resulting solution was often necessary to ensure crystallization.

The elution of highly charged species with KBr solutions sometimes caused a crystallization of the bromide salt in the column. In such a case, the eluent was changed to a sodium acetate–acetic acid solution and the eluate was concentrated. Then, the bromide salt was obtained by the addition of an HBr solution to the concentrated eluate.

The analytical data for the complexes prepared in this work are summarized in Table 1.

1) Products of the Reaction of $[Co(H_2O)(NH_3)_5](ClO_4)_3$ with en. To 100 ml of a DMSO solution containing 9.2 g of $[Co(H_2O)(NH_3)_5](ClO_4)_3$ (0.02 mol) were added 1.2 g of en (0.02 mol). The solution was kept at 85 °C for 20 min. The resulting deep yellowish orange solution was neutralized with concd HCl and diluted to 1.5 l with water. This was poured into a Sephadex column, and then the column was washed with water. When the adsorbed bands were developed with NaBr solutions, the column showed three bands; reddish orange (a trace amount), yellow, and yellowish orange, in the order of elution. The first and second species were eluted with a 0.25 M NaBr solution. The first reddish orange species was found to be $Co(H_2O)(NH_3)_5^{3+}$. When the second yellow eluate was concentrated, crystals of $[Co(NH_3)_6]Br_3$ appeared; they were filtered off, and the filtrate was diluted with water and then poured into a Sephadex column. The adsorbed species were eluted with a 0.08 M Na_3PO_4 solution. The single band was progressively separated into three bands. The eluates were labeled F1, F2, and F3, in the order of elution. Each eluate was neutralized with a HCl solution and poured into a Sephadex column. The F1 species was eluted with a 0.3 M HCl solution. The concentration of the eluate gave yellow crystals, which were characterized as $[Co(en)_3]Cl_3 \cdot 3H_2O$ by the measurements of the infrared, electronic, and PMR spectra. The F2 and F3 species were eluted out with 0.5 M KI solutions. The concentration of these eluates gave *cis*-$[Co(NH_3)_2(en)_2]I_3$ and $[Co(NH_3)_4(en)]I_3$ respectively. The *cis* configuration of $[Co(NH_3)_2(en)_2]I_3$ was confirmed by the measurement of the PMR spectrum.

The last yellowish orange species was eluted with a 0.7 M NaBr solution. When the eluate was concentrated with a rotary evaporator, yellowish orange crystals of $[Co(NH_3)_5$-$(enH)]Br_4$ were obtained. Yield: 0.6 g.

The yield of the products was found to be in the order: $Co(NH_3)_6^{3+} > Co(NH_3)_4(en)^{3+} > Co(NH_3)_2(en)_2^{3+} > Co$-$(NH_3)_5(enH)^{4+} > Co(en)_3^{3+}$

When a mixture of 0.6 g of en (0.01 mol) and 2.6 g of $en \cdot 2HClO_4$ (0.01 mol) was used in place of 1.2 g of en, 0.8 g of $[Co(NH_3)_5(enH)]Br_4$ was obtained. The other products were found to be $[Co(NH_3)_{6-2p}(en)_p]Br_3$ (p=0—3).

When 100 ml of a DMSO solution containing 6.8 g of $[Co$-$(NH_3)_6](ClO_4)_3$ and 0.9 g of en was kept at 90 °C for 10 min, 30 mg of $[Co(NH_3)_5(enH)]Br_4$ was obtained from the reaction products.

2) $[Co(NH_3)_5(en)]Br_3$. Crystals of $[Co(NH_3)_5(enH)]$-Br_4 (0.2 g) were dissolved into 4 ml of 1.5 M aqueous ammonia. Solid NaBr was added to the solution until a small amount

Table 1. Summary of analytical data for the complexes prepared in this work

Complex	C, %		H, %		N, %	
	Calcd	Found	Calcd	Found	Calcd	Found
$[Co(NH_3)_6]Br_3$[a]	0	—	4.53	4.54	20.97	21.19
$[Co(NH_3)_4(en)]I_3$	4.23	4.12	3.55	3.64	14.80	14.60
$[Co(NH_3)_2(en)_2]I_3$	8.09	7.84	3.73	4.00	14.15	14.04
$[Co(NH_3)_5(enH)]Br_4$	4.58	4.37	4.61	4.53	18.68	18.78
$[Co(NH_3)_5(enH)](ClO_4)_4$	3.98	4.27	4.01	4.09	16.26	16.02
$[Co(NH_3)_5(en)]Br_3$	5.41	5.68	5.22	5.34	22.09	21.82
$[Co(NH_3)_4(tn)](ClO_4)_3$	7.21	7.16	4.44	4.68	16.82	16.64
$[Co(NH_3)_2(tn)_2](ClO_4)_3$	13.36	13.08	4.86	5.12	15.57	15.74
$[Co(tn)_3](ClO_4)_3 \cdot H_2O$	18.08	17.90	5.39	5.67	14.06	14.25
$[Co(NH_3)_5(tnH)]Br_4$	6.69	6.98	4.86	5.15	18.20	18.10
$[(NH_3)_5Co(tn)Co(NH_3)_5]Br_6$[b]	4.21	4.68	4.79	5.28	19.97	19.66
$[Co(NH_3)_4(tmd)](ClO_4)_3$	9.36	9.60	4.71	4.90	16.36	16.43
$[Co(NH_3)_5(tmdH)]Br_4$	8.69	8.82	5.10	5.24	17.73	17.73
$[Co(NH_3)_4(tmdH)_2](ClO_4)_5$	11.97	12.14	4.77	5.00	13.96	13.77
$[Co(NH_3)_4(tmdH)_2]I_5$	10.22	10.01	4.07	4.07	11.92	11.97
$[(NH_3)_5Co(tmd)Co(NH_3)_5]Br_6$[b]	5.61	5.87	4.95	5.80	19.63	18.16
$[Co(NH_3)_5(pmdH)]Br_4$	10.59	10.63	5.33	5.48	17.30	17.62
$[Co(NH_3)_5(pmdH)](ClO_4)_4$	9.31	9.41	4.69	4.75	15.20	14.95
$[Co(NH_3)_4(pmdH)_2](ClO_4)_5$	14.46	14.08	5.10	5.12	13.49	13.28
$[(NH_3)_5Co(pmd)Co(NH_3)_5]Br_6 \cdot 3H_2O$	6.50	6.59	5.46	5.36	18.19	18.25
$[Co(NH_3)_5(hepnH)]Br_4$	14.13	14.14	5.76	5.86	16.49	16.80
$[Co(NH_3)_5(hepnH)](ClO_4)_4$	12.49	12.62	5.09	5.20	14.57	14.38
$[Co(NH_3)_4(hepnH)_2]Cl_5 \cdot 2H_2O$	27.89	27.90	9.03	9.12	18.59	18.58
$[Co(NH_3)_5(ocnH)]Br_4$	15.78	16.10	5.96	6.23	16.10	16.28
$[Co(NH_3)_4(ocnH)_2]Cl_5 \cdot 3H_2O$	29.62	29.32	9.32	8.95	17.27	17.49
$[Co(NH_3)_4(ocnH)_2]I_5 \cdot 2H_2O$	17.66	17.37	5.37	5.02	10.30	10.57
$[Co(NH_3)_5(denH)]Br_4$	18.85	19.14	6.33	6.55	15.39	15.48
$[Co(NH_3)_4(denH)_2]Br_5$	27.51	27.40	7.16	7.20	12.83	12.72
$[Co(NH_3)_3(denH)_3]Cl_6 \cdot 2H_2O$	41.00	40.98	10.09	10.01	14.35	14.18
$[(NH_3)_5Co(den)Co(NH_3)_5]Br_6 \cdot 2H_2O$	12.31	12.36	5.99	5.91	17.22	17.00
$[(NH_3)_4Co(den)_2Co(NH_3)_4]Br_6 \cdot 3H_2O$	21.22	21.45	6.94	7.03	14.85	14.76
$[Co_2(NH_3)_8(den)(denH)_2]Br_8 \cdot 2H_2O$	24.88	24.72	7.10	6.99	13.54	13.31
$[Co(NH_3)_4(don)]Br_3$	25.41	25.45	7.11	7.33	14.82	14.84
$[Co(NH_3)_5(donH)]Br_4$	21.67	21.73	6.67	6.71	14.74	15.02
$[Co(NH_3)_5(donH)](ClO_4)_4$	19.39	19.47	5.97	6.04	13.19	12.91
$[Co(NH_3)_4(donH)_2](ClO_4)_5$	28.07	28.26	6.87	6.69	10.91	10.45
$[(NH_3)_5Co(don)Co(NH_3)_5]Br_6$	14.89	15.06	6.04	6.30	17.36	17.31
$[Co(NH_3)_4(tden)]Br_3 \cdot 1.5H_2O$	27.07	27.11	7.63	7.58	13.53	13.64
$[Co(NH_3)_5(tdenH)]Br_4$	24.26	24.35	6.98	7.29	14.15	14.20

a) This sample was isolated from the products of the reaction of $[Co(H_2O)(NH_3)_5](ClO_4)_3$ with en in DMSO.
b) The analytical results were not improved by repeated crystallizations. The salt might contain a small amount of $[(NH_3)_4Co(N\text{-}N)_2Co(NH_3)_4]Br_6$.

of crystals of $[Co(NH_3)_5(en)]Br_3$ appeared. Ethanol and then ether were added to insure the crystallization.

3) Products of the Reaction of $[Co(H_2O)(NH_3)_5](ClO_4)_3$ with tn, tmd, pmd, hepn, ocn, den, don, or tden. To a DMSO solution containing $[Co(H_2O)(NH_3)_5](ClO_4)_3$ were added the title N–N. The solution was then treated with the way described in 1). The species adsorbed on a Sephadex column were eluted with KBr solutions.

a) Products of the Reaction with tn: To 100 ml of a DMSO solution containing 9.2 g of $[Co(H_2O)(NH_3)_5](ClO_4)_3$ (0.02 mol) were added 1.5 g of tn (0.02 mol). Four bands were observed on a Sephadex column. The lowest reddish orange species was found to be a small amount of $Co(H_2O)(NH_3)_5^{3+}$. The upper three bands were of yellowish orange colors. The eluates were labeled F1, F2, and F3 in the order of elution. F1 was found to contain a mixture of $Co(NH_3)_{6-2p}(tn)_p^{3+}$ (p=0, 1, 2, and 3). The concentration of the eluate yielded crystals of $[Co(NH_3)_6]Br_3$. The filtrate was diluted, and then the solution was poured into a Sephadex column. After the column had been washed with dil HCl, the adsorbed species were eluted out with a 0.5 M $LiClO_4$ solution. The concentration of the solution gave crystals of $[Co(NH_3)_{6-2p}(tn)_p](ClO_4)_3$ (p=1, 2, and 3). The separation of $[Co(NH_3)_4(tn)](ClO_4)_3$, $[Co(NH_3)_2(tn)_2](ClO_4)_3$, and $[Co(tn)_3](ClO_4)_3 \cdot H_2O$ was achieved by fractional crystallization. From F2, crystals of $[Co(NH_3)_5(tnH)]Br_4$ were obtained. The concentration of F3 gave orange crystals which were considered to contain $[(NH_3)_5Co(tn)Co(NH_3)_5]Br_6$ as the main component

(see Table 1).

b) Products of the Reaction with tmd: To 100 ml of a DMSO solution containing 9.2 g of $[Co(H_2O)(NH_3)_5](ClO_4)_3$ (0.02 mol) were added 1.8 g of tmd (0.02 mol). The Sephadex column showed six bands. The lowest species was found to be a small amount of Co^{2+}. Then, the band of a small amount of $Co(H_2O)(NH_3)_5^{3+}$ followed. The eluates of the other four bands were labeled F1, F2, F3, and F4 in the oder of elution. The concentration of F1 gave $[Co(NH_3)_6]Br_3$. The filtrate contained $Co(NH_3)_4(tmd)^{3+}$, which could be crystallized as the perchlorate salt. When F2 was concentrated, crystals of $[Co(NH_3)_5(tmdH)]Br_4$ were obtained. The KBr medium in F3 was replaced by $LiClO_4$ with the aid of a Sephadex column. Upon the evaporation of the solution, crystals of $[Co(NH_3)_4(tmdH)_2](ClO_4)_5$ were precipitated. The concentration of F4 gave yellowish orange crystals, which were considered to consist of $[(NH_3)_5Co(tmd)Co(NH_3)_5]Br_6$ and a small amount of $[(NH_3)_4Co(tmd)_2Co(NH_3)_4]Br_6$ (see Table 1).

c) Products of the Reaction with den: To 750 ml of a DMSO solution containing 9.2 g of $[Co(H_2O)(NH_3)_5](ClO_4)_3$ (0.02 mol) were added 3.4 g of den (0.02 mol). The Sephadex column showed the presence of a small amount of Co^{2+}, $Co(H_2O)(NH_3)_5^{3+}$, and many yellow-to-orange species. From the fractions with yellow to orange colors, the following salts were obtained, in the order of elution (the yield (%), based on $[Co(H_2O)(NH_3)_5](ClO_4)_3$, is given in parentheses): $[Co(NH_3)_6]Br_3$ (25), $[Co(NH_3)_5(denH)]Br_4$ (26), $[Co(NH_3)_4(denH)_2]Br_5$ (9), $[Co(NH_3)_3(denH)_3]Cl_6\cdot 2H_2O$ (0.3),[4] $[(NH_3)_5Co(den)Co(NH_3)_5]Br_6\cdot 2H_2O$ (7),[5] and $[(NH_3)_4Co(den)_2Co(NH_3)_4]Br_6\cdot 3H_2O$ (9).[5]

Even after these species had been eluted out, several species remained in the column. These species could be crystallized as bromides. One of the species was found to be $[Co_2(NH_3)_8(den)(denH)_2]Br_8\cdot 2H_2O$. Yield: 3%.[5]

d) Products of the Reaction with don: To 700 ml of a DMSO solution containing 6.9 g of $[Co(H_2O)(NH_3)_5](ClO_4)_3$ (0.015 mol) were added 3.0 g of don (0.015 mol). The Sephadex column showed many bands. Crystals of $[Co(NH_3)_6]Br_3$, $[Co(NH_3)_4(don)]Br_3$, $[Co(NH_3)_5(donH)]Br_4$, $[Co(NH_3)_4(donH)_2](ClO_4)_5$,[4] and $[(NH_3)_5Co(don)Co(NH_3)_5]Br_6$ were obtained, in that order of elution. Even after these species had been eluted out, several species remained in the column.

e) Products of the Reaction with pmd, hepn, ocn, or tden: To 1000 ml of a DMSO solution containing 4.6 g of $[Co(H_2O)(NH_3)_5](ClO_4)_3$ (0.01 mol) were added 0.01 mol of N–N (1.0 g for pmd, 1.3 g for hepn, 1.4 g for ocn, and 2.3 g for tden). From the eluates, various complexes containing pmd, hepn, ocn, or tden, which are shown in Table 1, were isolated as crystals. $[Co(NH_3)_6]Br_3$ was also obtained, regardless of the kind of N–N used. No formation of $Co(NH_3)_4(N–N)^{3+}$ was observed for any of the diamines except the tden. The $[Co(NH_3)_4(tden)]^{3+}$ ions moved faster than $Co(NH_3)_5(tdenH)^{4+}$, but slower than $Co(NH_3)_6^{3+}$. The formation of more positively charged species than six was not observed in any of the diamines under the conditions employed.

Apparatus. The electronic spectra were recorded with a Union Giken SM-401 or a Hitachi EPS-3 recording spectrophotometer. The PMR spectra were recorded with a Varian A-60 spectrometer.

Results and Discussion

Product Distribution. The analytical results given in Table 1 are in good agreement with the formulas assigned to the products isolated in this work. All these products are yellow to yellowish orange in color; hence, they must be of the CoN_6 type (*vide infra*). This is also consistent with the assigned formulas. Furthermore, these complex ions show reasonable flow rates on Sephadex columns.[1]

A semi-quantitative determination of the product distribution of the reactions in question was also carried out; the results are shown in Table 2. Complex ions, $Co(NH_3)_6^{3+}$ and $Co(NH_3)_5(\underline{N}–NH)^{4+}$,[6] were always formed as the products, regardless of the kind of N–N. The pH titration of the solutions containing $Co(NH_3)_5(\underline{N}–NH)^{4+}$ with standard NaOH solutions reveals that the complex ions are mono-basic acid. The value of pK increases with the increase in the number of methylene groups in the N–N.[7]

Table 2 shows that the change in the concentration of the reactants affects the product distribution considerably. The formation of highly charged species becomes significant with the increase in the concentration of the reactants. This is a trend similar to that found in the reactions of $[CoCl_2(en)_2]Cl$ with N–N in DMSO.[1]

Table 2. Product distribution of the reactions of $[Co(H_2O)(NH_3)_5](ClO_4)_3$ with N–N in DMSO[a]

	N–N used	en	tn[b,c]	tn	tmd[b,d]	tmd	pmd	hepn	ocn	den[e]	don[e]	tden
	Concentration of reactants/M ($[Co(H_2O)(NH_3)_5^{3+}]=[N–N]$)	0.20	0.010	0.20	0.010	0.20	0.010	0.010	0.010	0.027	0.021	0.010
Products	Co^{2+}	0	0	0	25	f	f	f	f	f	f	f
	$Co(NH_3)_6^{3+}$	f	42	f	26	18	18	26	23	25	27	29
	$Co(NH_3)_4(N–N)^{3+}$	f	f	f	22	21	0	0	0	0	5	6
	$Co(NH_3)_2(N–N)_2^{3+}$	f	f	f	0	0	0	0	0	0	0	0
	$Co(N–N)_3^{3+}$	f	f	f	0	0	0	0	0	0	0	0
	$Co(NH_3)_5(\underline{N}–NH)^{4+}$	6	6	16	8	29	36	33	26	26	30	48
	$Co(NH_3)_4(\underline{N}–NH)_2^{5+}$	0	0	0	1	6	1	3	5	9	7	—[g]
	$(NH_3)_5Co(N–N)Co(NH_3)_5^{6+}$ [h]	0	0	1[f]	0	6[f]	0.8	—[g]	—[g]	7	17	—[g]

a) The reactants were allowed to react at 85 °C for 20 min, unless otherwise stated. The numerical values given in this table denote the yield (%) based on $[Co(H_2O)(NH_3)_5](ClO_4)_3$. The f symbol denotes that the product indicated is formed. b) The reactants were allowed to react at 92 °C for 20 min. c) The recovered $Co(H_2O)(NH_3)_5^{3+}$ amounted to 8% of the initial $Co(H_2O)(NH_3)_5^{3+}$. d) The recovered $Co(H_2O)(NH_3)_5^{3+}$ amounted to 14% of the initial $Co(H_2O)(NH_3)_5^{3+}$. e) The species with charges higher than 6+ were formed in considerable amounts. f) The product is not sufficiently pure (see Table 1). g) The product indicated is considered to be formed, but no pure sample has been isolated. h) The yield was calculated by means of the following relation: Yield = 2 × (mol of the indicated product) × 100/(mol of $[Co(H_2O)(NH_3)_5](ClO_4)_3$ used as the starting material).

The formation of $Co(NH_3)_4(N-N)^{3+}$, which contains an N–N chelate ring, is observed for en, tn, tmd, don, or tden, but not for pmd, hepn, ocn, or den. These facts support the previous conclusion in which the medium-size chelate ring is unstable.[1)]

In the en and tn systems, $Co(NH_3)_2(N-N)_2^{3+}$ and $Co(N-N)_3^{3+}$ were formed, and the formation of complexes more positively charged than four was not significant. The yield of $Co(NH_3)_5(\underline{N}-NH)^{4+}$ was also low. However, when the diamines with more methylene groups than tn were used, the formation of appreciable amounts of $Co(NH_3)_5(\underline{N}-NH)^{4+}$ was observed. Furthermore, the formations of $Co(NH_3)_4(\underline{N}-NH)_2^{5+}$ and $(NH_3)_5Co(N-N)Co(NH_3)_5^{6+}$ were also significant. These tendencies become notable with the increase in the number of methylene groups, as is shown in Table 2. These facts indicate that, when the methylenic chain of N–N is long, the N–N tends to coordinate to a cobalt(III) ion as a unidentate ligand, or to two cobalt(III) ions as a bridging ligand, rather than as a chelate ligand. In the systems of the diamines higher than tn, Co^{2+} ions were always formed during the reactions in DMSO. Their amounts increased with the increase in the reaction time and with the elevation of the reaction temperature. In the en and tn systems, the formation of Co^{2+} ions was found to be negligible.

Mechanism of the Reaction of $[Co(H_2O)(NH_3)_5](ClO_4)_3$ with N–N in DMSO. When a DMSO solution containing $[Co(H_2O)(NH_3)_5](ClO_4)_3$ is heated, the aqua ligand in $Co(H_2O)(NH_3)_5^{3+}$ is known to be replaced by DMSO.[3g)] Here, it is assumed tentatively that the formation of $Co(DMSO)(NH_3)_5^{3+}$ occurs prior to the attack of $Co(H_2O)(NH_3)_5^{3+}$ by N–N; that is, the reaction occurs in the following sequence:

$$Co(H_2O)(NH_3)_5^{3+} + DMSO \longrightarrow Co(DMSO)(NH_3)_5^{3+} + H_2O, \quad (1)$$

$$Co(DMSO)(NH_3)_5^{3+} + N\text{–}N \longrightarrow Co(NH_3)_5(\underline{N}-N)^{3+} + DMSO. \quad (2)$$

Upon the acidification of the solution, the $Co(NH_3)_5(\underline{N}-N)^{3+}$ complex should be converted into $Co(NH_3)_5(\underline{N}-NH)^{4+}$. This explains the formation of $[Co(NH_3)_5(\underline{N}-NH)]X_4$.

As has been mentioned above, the product distributions of the en and tn systems are quite different from those for the higher N–N systems. The products indicate that the predominant reactions in the systems of en and tn can be expressed as follows:

$$Co(NH_3)_5(\underline{N}-N)^{3+} \rightarrow Co(NH_3)_4(N-N)^{3+} + NH_3, \quad (3)$$

$$Co(DMSO)(NH_3)_5^{3+} + NH_3 \rightarrow Co(NH_3)_6^{3+} + DMSO, \quad (4)$$

$$Co(NH_3)_4(N-N)^{3+} + N\text{–}N \rightarrow Co(NH_3)_2(N-N)_2^{3+} + 2NH_3, \quad (5)$$

$$Co(NH_3)_2(N-N)_2^{3+} + N\text{–}N \rightarrow Co(N-N)_3^{3+} + 2NH_3, \quad (6)$$

$$Co(NH_3)_6^{3+} + N\text{–}N \rightarrow Co(NH_3)_5(\underline{N}-N)^{3+} + NH_3. \quad (7)$$

Reaction 7 was comfirmed by the product survey of the direct reaction of $Co(NH_3)_6^{3+}$ with en in DMSO (see Experimental section). The occurrence of Reactions 3, 5, and 6 reveals that the successive substitution of the ammonia molecules from $Co(NH_3)_5(\underline{N}-N)^{3+}$ with en or tn molecules leads to the formation of $Co(NH_3)_{6-2p}(N-N)_p^{3+}$ containing the diamine chelate(s), where $1 \leq p \leq 3$. In the systems of the higher N–N's, however, Reactions 5 and 6 are absent. The successive substitution of ammonia molecules from $Co(NH_3)_5(\underline{N}-N)^{3+}$ with these N–N molecules leads to the formation of

Table 3. Electronic spectral data for the complexes prepared in this work

Wave numbers are in $10^3\ cm^{-1}$, while the intensities are given by $\log \varepsilon$ in parentheses.

Complex	I band	II band
$[Co(NH_3)_6](ClO_4)_3$[a)]	21.0(1.76)	29.5(1.67)
$[Co(NH_3)_4(en)]I_3$	21.2(1.87)	—
$[Co(NH_3)_4(en)](SO_4)_{1.5}\cdot 2H_2O$[a)]	21.2(1.83)	29.5(1.76)
cis-$[Co(NH_3)_2(en)_2]I_3$	21.4(1.89)	—
cis-$[Co(NH_3)_2(en)_2](ClO_4)_3\cdot H_2O$[a)]	21.5(1.79)	29.8(1.74)
trans-$[Co(NH_3)_2(en)_2](ClO_4)_3\cdot H_2O$[a)]	21.4(1.77)	29.7(1.73)
$[Co(en)_3](ClO_4)_3$[b)]	21.3(1.94)	29.6(1.89)
$[Co(NH_3)_4(tn)](ClO_4)_3$	20.9(1.82)	29.1(1.76)
$[Co(NH_3)_4(tn)]Br_3\cdot H_2O$[c)]	20.9(1.79)	29.2(1.78)
$[Co(NH_3)_2(tn)_2](ClO_4)_3$	20.7(1.86)	28.9(1.83)
$[Co(tn)_3](ClO_4)_3$[b)]	20.3(1.88)	28.5(1.87)
$[Co(NH_3)_4(tmd)](ClO_4)_3$	20.7(1.84)	29.0(1.77)
$[Co(tmd)_3]Br_3$[d)]	19.9(1.89)	27.9(1.85)
$[Co(NH_3)_4(don)]Br_3$	20.6(1.86)	29.0(1.81)
$[Co(NH_3)_4(tden)]Br_3\cdot 1.5H_2O$	20.7(1.88)	29.0(1.83)
$[Co(NH_3)_5(enH)](ClO_4)_4$	20.8(1.80)	29.2(1.71)
$[Co(NH_3)_5(tnH)](ClO_4)_4$	20.8(1.83)	29.2(1.75)
$[Co(NH_3)_5(tmdH)](ClO_4)_4$	20.8(1.82)	29.2(1.74)
$[Co(NH_3)_5(pmdH)](ClO_4)_4$	20.8(1.82)	29.2(1.74)
$[Co(NH_3)_5(hepnH)](ClO_4)_4$	20.8(1.86)	29.2(1.80)
$[Co(NH_3)_5(ocnH)](ClO_4)_4$	20.8(1.85)	29.2(1.81)
$[Co(NH_3)_5(denH)]Br_4$	20.8(1.83)	29.2(1.77)
$[Co(NH_3)_5(donH)](ClO_4)_4$	20.8(1.87)	29.2(1.81)
$[Co(NH_3)_5(tdenH)]Br_4$	20.8(1.87)	29.2(1.83)
$[Co(NH_3)_4(tmdH)_2](ClO_4)_5$	20.6(1.88)	29.0(1.83)
$[Co(NH_3)_4(pmdH)_2](ClO_4)_5$	20.7(1.88)	29.0(1.82)
$[Co(NH_3)_4(hepnH)_2]Cl_5\cdot 2H_2O$	20.7(1.91)	29.0(1.85)
$[Co(NH_3)_4(ocnH)_2]Cl_5\cdot 3H_2O$	20.7(1.90)	29.0(1.84)
$[Co(NH_3)_4(denH)_2]Br_5$	20.7(1.89)	29.0(1.84)
$[Co(NH_3)_4(donH)_2](ClO_4)_5$	20.7(1.91)	29.2(1.99)
$[Co(NH_3)_3(denH)_3]Cl_6\cdot 2H_2O$	20.4	28.6
$[(NH_3)_5Co(tn)Co(NH_3)_5]Br_6$[e)]	20.8	29.2
$[(NH_3)_5Co(tmd)Co(NH_3)_5]Br_6$[e)]	20.8	29.2
$[(NH_3)_5Co(pmd)Co(NH_3)_5]Br_6\cdot 3H_2O$[f)]	20.9(2.13)	29.3(2.06)
$[(NH_3)_5Co(den)Co(NH_3)_5]Br_6\cdot 2H_2O$[f)]	20.8(2.11)	29.4(2.07)
$[(NH_3)_5Co(don)Co(NH_3)_5]Br_6$[f)]	20.8(2.11)	29.2(2.07)
$[(NH_3)_4Co(den)_2Co(NH_3)_4]Br_6\cdot 3H_2O$[f)]	20.6(2.20)	29.1(2.15)
$[Co_2(NH_3)_8(den)(denH)_2]Br_8\cdot 2H_2O$[f)]	20.7(2.18)	29.1(2.15)

a) From Ref. 8. b) From Ref. 1. c) From Ref. 10. d) From Ref. 3i. e) The sample is not pure (see Table 1). f) The intensities are given per complex ion, *i.e.*, per two cobalt(III) ions.

$Co(NH_3)_{6-p}(\underline{N}\text{–}N)_p^{3+}$:

$$Co(NH_3)_5(\underline{N}\text{–}N)^{3+} + (p-1)N\text{–}N \longrightarrow Co(NH_3)_{6-p}(\underline{N}\text{–}N)_p^{3+} + (p-1)NH_3, \quad (8)$$

where $p>1$. Upon the acidification of the solution, the $Co(NH_3)_{6-p}(\underline{N}\text{–}N)_p^{3+}$ complex should be converted into the highly charged $Co(NH_3)_{6-p}(\underline{N}\text{–}NH)_p^{(3+p)+}$ complex. This would explain the formation of $Co(NH_3)_4(\underline{N}\text{–}NH)_2^{5+}$ and $Co(NH_3)_3(denH)_3^{6+}$. Reaction 8 is absent in the systems of en and tn, This result and the occurrence of Reactions 3, 5, and 6 show the remarkable tendency for the en or tn to take the chelate form.

The formation of the dimeric complex can be expressed as:

$$Co(DMSO)(NH_3)_5^{3+} + Co(NH_3)_5(\underline{N}\text{–}N)^{3+} \longrightarrow (NH_3)_5Co(N\text{–}N)Co(NH_3)_5^{6+} + DMSO. \quad (9)$$

The amount of the dimer becomes appreciable with the increase in the number of methylene groups in the N–N. In the N–N with a long methylenic chain, a close approach between two positively charged cobalt(III) ions is not necessary. This would favor the formation of the dimer.

Spectral Properties of the Complexes. The numerical data for electronic absorption spectra of the complexes are summarized in Table 3. The positions of the first absorption bands of all the complexes prepared in this work are located around 21000 cm^{-1}. Therefore, it can be concluded that all the complexes have CoN_6 moieties. The increase in the number of en chelate(s) in $Co(NH_3)_{6-2p}(en)_p^{3+}$ causes shifts in the absorption maxima to shorter wavelengths,[9] while those of the other N–N chelate(s) shift to longer wavelengths. The absorption bands of $Co(NH_3)_4(N\text{–}N)^{3+}$ shift to longer wavelengths as the methylenic chain of the N–N becomes longer; hence, the ligand-field strength for N–N chelates is in this order: en>$(NH_3)_2$>tn>tmd≃don≃tden. The successive substitution of ammonia molecules in $Co(NH_3)_6^{3+}$ with monoprotonated diamines causes shifts in the absorption maxima to longer wavelengths. However, the absorption positions for $Co(NH_3)_5(\underline{N}\text{–}NH)^{4+}$ and $Co(NH_3)_4(\underline{N}\text{–}NH)_2^{5+}$ are almost independent of the kind of diamine. The absorption positions of the dimeric complexes are also insensitive to the kind of diamine.

The author wishes to thank Professor Nobuyuki Tanaka, Tohoku University, and Professor Junnosuke Fujita, Nagoya University, for their encouragement and support.

References

1) Part I of this series: H. Ogino and J. Fujita, *Bull. Chem. Soc. Jpn.*, **48**, 1836 (1975).

2) H. Ogino and N. Tanaka, *Chem. Lett.*, **1975**, 687.

3) For instance; a) F. P. Dwyer and A. M. Sargeson, *J. Am. Chem. Soc.*, **81**, 5269 (1959); b) E. S. Gould, *J. Am. Chem. Soc.*, **87**, 4730 (1965); c) R. B. Jordan, A. M. Sargeson, and H. Taube, *Inorg. Chem.*, **5**, 1091 (1966); d) M. Muto, T. Baba, and H. Yoneda, *Bull. Chem. Soc. Jpn.*, **41**, 2918 (1968); e) R. J. Balahura and R. B. Jordan, *J. Am. Chem. Soc.*, **92**, 1533 (1970); f) H. Yoneda, M. Muto, and K. Tamaki, *Bull. Chem. Soc. Jpn.*, **44**, 2863 (1971); g) C. R. P. Mac-Coll and L. Beyer, *Inorg. Chem.*, **12**, 7 (1973); h) H. Ogino and J. Fujita, *Chem. Lett.*, **1973**, 517; i) J. Fujita and H. Ogino, *Chem. Lett.*, **1974**, 57.

4) As it was difficult to separate the bromide complex from KBr, the complex was converted to the chloride or perchlorate with the aid of a Sephadex column.

5) The yield in % was calculated by means of the following equation:

Yield = 2× (mol of the indicated product) × 100/(mol of $[Co(H_2O)(NH_3)_5](ClO_4)_3$ used as the starting material)

6) Co(N–NH) denotes that the ω-aminoalkylammonium ion N–NH^+ is coordinated to the cobalt moiety through the ω-amino group. Similarly, Co(N–N) denotes that the N–N acts as the monodentate ligand.

7) H. Ogino, to be published.

8) Y. Shimura, *Bull. Chem. Soc. Jpn.*, **31**, 311 (1958).

9) Shimura pointed out that the successive substitution of ammonia molecules by en causes somewhat irregular shifts of the band maxima.[8]

10) F. Mizukami, H. Ito, J. Fujita, and K. Saito, *Bull. Chem. Soc. Jpn.*, **45**, 2129 (1972).

The Crystal Structure and Magnetic Property of Di-μ-propionato-*O,O'*-bis[*N*-*p*-tolylsalicylideneaminatocopper(II)]

Masahiro MIKURIYA, Sigeo KIDA, Ikuhiko UEDA,* Tadashi TOKII,** and Yoneichiro MUTO**

Department of Chemistry, Faculty of Science, Kyushu University 33, Hakozaki, Higashi-ku, Fukuoka 812

**College of General Education, Kyushu University 01, Ropponmatsu, Fukuoka 810*

***Department of Chemistry, Faculty of Science and Engineering, Saga University, Saga 840*

(Received May 23, 1977)

The crystal structure of di-μ-propionato-*O,O'*-bis[*N*-*p*-tolylsalicylideneaminatocopper(II)] was determined by X-ray diffraction method using the data collected by counter diffractometer techniques. The space group is $P\bar{1}$ and the cell constants are $a=12.565(2)$, $b=13.040(2)$, $c=12.230(2)$ Å, $\alpha=107.73(1)$, $\beta=115.72(1)$, $\gamma=100.18(1)°$, and $Z=2$. The structure was solved by the heavy atom method and refined by the block-diagonal least-squares method to an R factor of 0.029. The crystal is composed of one-dimensional chains extended along the c axis, where the two copper atoms coordinated by the Schiff bases are bridged by two propionate groups. The magnetic property was discussed on the basis of the crystal structure.

Recently, Tokii *et al.*[1] found that bis(*N*-R-salicylideneaminato)copper(II), Cu(Sal·*N*-R)$_2$ reacts with copper(II) carboxylates, Cu(R'COO)$_2$, to form a series of the complexes with the formula, [Cu(Sal·*N*-R)R'-COO], where R=phenyl and *p*-tolyl and R'=ethyl. These complexes show antiferromagnetic behavior and the temperature dependence of the magnetic susceptibility (80—300 K) is well expressed by the Bleaney-Bowers equation 1[2]

$$\chi_A = \frac{Ng^2\beta^2}{3kT}\left[1 + \frac{1}{3}\exp\left(\frac{-2J}{kT}\right)\right]^{-1} + N\alpha, \qquad (1)$$

where $-2J$ is equal to the energy separation between the lowest singlet and triplet levels, which gives the degree of the magnetic interaction. By the best fit of the observed cryomagnetic data to Eq. 1, assuming $N\alpha=60\times10^{-6}$ emu/mol, they evaluated the values of $-2J=101$ cm^{-1} and $g=2.14$ for [Cu(Sal·*N*-*p*-tolyl)C$_2$H$_5$-COO]. On the basis of the magnetic properties and the IR spectral data, they concluded that the complexes possess the binuclear structure shown in **1**.[3]

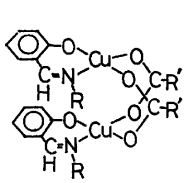

1

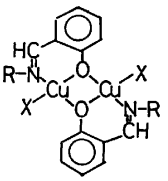

2

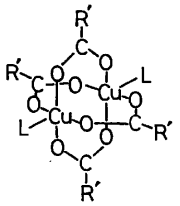

3

Binuclear copper(II) complexes with monatomic bridges and with triatomic bridges as shown in **2** and **3** have been studied extensively. However, the binuclear structure consisting of only two triatomic bridges as shown in **1** is rare so far. Only one example of the copper complex of this structure has been reported.[4] Hence, in this study, the crystal structure of [Cu(Sal·*N*-*p*-tolyl)C$_2$H$_5$COO], was determined by the single-crystal X-ray diffraction method, in order to clarify the structure and to discuss the magnetic property in more detail in relation to the structure.

Experimental

Dark green crystals of the title complex were prepared according to Ref. 1. Most of the crystals were twins, and accordingly a crystal which had been confirmed to be a single-crystal by the Weissenberg photographs was used for the measurement of the cell parameters and intensities. Preliminary Weissenberg photographs revealed no systematic absences and showed the triclinic symmetry. The cell parameters and intensities were measured on a Syntex $P\bar{1}$ automated diffractometer with monochromated Mo $K\alpha$ radiation ($\lambda=0.71073$ Å). The crystal used was ground to a sphere of radius 0.225 mm. The cell parameters were determined by the least-squares refinement from 15 reflections within a range of $24<2\theta<35°$. The values are $a=12.565(2)$, $b=13.040(2)$, $c=12.230(2)$ Å, $\alpha=107.73(1)$, $\beta=115.72(1)$, $\gamma=100.18(1)°$, and $V=1604.3(4)$ Å^3. The density $D_m=1.43(1)$ g/cm^3 obtained by floatation in hexane-carbon tetrachloride solutions agrees well with the density $D_c=1.435$ g/cm^3 calculated for two dimer units per cell. Of the two possible triclinic space groups, the centrosymmetric space group $P\bar{1}$ was assumed on the basis of its more frequent occurrence. Successful solution and refinement in this space group support this choice.

Intensity data were collected by the θ-2θ scan technique with a variable scan rate of 4.0 to 24.0 °/min. Three standard reflections were monitored every 50 reflections, and their intensities showed a good stability. A total of 4154 independent reflections with $2\theta<45°$ were collected. 3421 reflections with I greater than $3\sigma(I)$ were considered as "observed" and were used for the structure analysis, where $\sigma(I)$ was calculated for each reflection on the basis of counting statistics. The Lorentz and polarization corrections were applied, but no absorption correction was made on account of $\mu r=0.33$.

Solution and Refinement of the Structure

The structure was solved by the heavy atom method. The positions of the copper atoms were obtained from a three-dimensional Patterson synthesis. Successive Fourier syntheses and difference Fourier syntheses revealed all the nonhydrogen atoms. Refinement was carried out by the block-diagonal least-squares method. In the course of refinement, it became apparent that the carbon atom C(6) of the ethyl group was subjected to disorder. A difference Fourier map revealed two largest chemically reasonable peaks in the vicinity of C(6). Thus, in further refiements two partial atoms, C(6A) and C(6B), were used. The occupancy factors, 0.4 and 0.6 for C(6A) and C(6B) respectively, were based on the peak heights. The bolckdiagonal least-squares refinement introducing anisotropic thermal pa-

TABLE 1. FRACTIONAL POSITIONAL PARAMETERS AND ANISOTROPIC TEMPERATURE FACTORS ($\times 10^5$) OF NON-HYDROGEN ATOMS WITH THEIR ESTIMATED STANDARD DEVIATIONS IN PARENTHESES

Temperature factors are of the from: $\exp[-(h^2B_{11}+k^2B_{22}+l^2B_{33}+2hkB_{12}+2hkB_{12}+2hlB_{13}+2klB_{23})]$.

Atom	x	y	z	B_{11}	B_{22}	B_{33}	B_{12}	B_{13}	B_{23}
Cu(1)	−2205(3)	−3830(3)	10253(4)	566(4)	604(3)	784(5)	181(3)	375(4)	303(3)
Cu(2)	3755(4)	1228(3)	39354(4)	712(4)	592(3)	842(5)	162(3)	483(4)	244(3)
O(1)	15664(21)	−2176(22)	19502(25)	612(22)	1058(25)	1090(30)	328(19)	457(22)	592(23)
O(2)	17973(22)	−1832(23)	38653(25)	818(25)	1053(25)	1035(30)	388(21)	550(24)	413(23)
O(3)	−6813(22)	−19116(19)	9595(23)	937(25)	584(19)	941(27)	232(18)	508(23)	287(19)
O(4)	−6477(23)	−15168(19)	28806(24)	1106(28)	589(20)	1081(31)	166(19)	710(26)	258(20)
O(5)	3318(20)	11031(18)	10656(23)	700(22)	582(19)	1012(28)	200(16)	514(21)	284(19)
O(6)	−10535(21)	2992(19)	40361(24)	758(23)	613(19)	1214(32)	229(17)	609(23)	297(20)
N(1)	−19399(24)	−3518(23)	4914(27)	598(26)	689(24)	839(32)	156(20)	385(25)	309(23)
N(2)	12871(27)	18010(24)	48051(28)	855(30)	657(24)	836(33)	118(22)	483(27)	264(23)
C(1)	21566(31)	−2432(30)	30510(35)	707(34)	825(32)	967(41)	310(27)	489(32)	394(30)
C(2)	34374(40)	−3255(48)	34817(46)	959(44)	1985(64)	1314(56)	808(44)	625(43)	930(50)
C(3)	38428(51)	−4961(66)	25085(66)	1303(59)	2948(97)	2448(95)	1383(65)	1256(65)	1627(83)
C(4)	−8377(33)	−21887(29)	17949(36)	864(36)	592(28)	1032(43)	211(26)	503(34)	316(29)
C(5)	−12797(55)	−34516(35)	14585(55)	2330(81)	534(33)	1923(73)	271(41)	1200(66)	386(41)
C(6A)	−7845(200)	−40896(104)	6862(180)	4650(391)	713(104)	3286(306)	1300(170)	2974(313)	1087(153)
C(6B)	−18559(114)	−43248(75)	1472(97)	3101(188)	912(78)	1620(126)	46(95)	1153(130)	357(81)
C(7)	−1091(32)	19306(28)	13495(32)	841(34)	599(27)	694(36)	217(25)	389(30)	230(26)
C(8)	6231(36)	30694(31)	17601(40)	944(39)	700(31)	1329(50)	211(28)	710(38)	335(33)
C(9)	2100(41)	39605(32)	20949(46)	1259(47)	622(31)	1621(59)	246(31)	863(45)	368(35)
C(10)	−9379(43)	37636(34)	20159(48)	1471(52)	756(34)	1815(64)	575(35)	1104(51)	547(39)
C(11)	−16837(37)	26646(34)	15827(42)	1000(41)	891(35)	1391(52)	425(31)	774(40)	503(35)
C(12)	−12930(30)	17250(28)	12589(33)	737(33)	698(29)	887(39)	291(26)	495(31)	370(28)
C(13)	−21587(31)	5961(30)	7549(34)	659(32)	782(30)	913(40)	275(26)	460(31)	369(29)
C(14)	−30045(29)	−14068(28)	−1106(34)	579(30)	654(28)	916(39)	155(24)	379(30)	306(28)
C(15)	−36143(40)	−15884(36)	5412(42)	1137(46)	957(39)	1166(50)	−49(34)	720(41)	155(35)
C(16)	−46277(43)	−25934(39)	−583(49)	1228(51)	1092(44)	1679(65)	−71(37)	977(51)	403(43)
C(17)	−50253(36)	−34376(34)	−12942(44)	776(38)	798(35)	1491(57)	87(29)	455(39)	319(37)
C(18)	−43928(38)	−32357(34)	−19150(42)	997(43)	800(35)	1153(50)	137(31)	448(39)	86(34)
C(19)	−33862(34)	−22318(33)	−13428(38)	817(37)	866(34)	1066(45)	164(29)	563(35)	300(32)
C(20)	−61146(47)	−45585(41)	−19236(60)	1230(55)	902(43)	2394(89)	−186(39)	876(59)	269(50)
C(21)	−13764(34)	12144(31)	41647(34)	935(37)	809(31)	815(39)	346(28)	521(33)	337(29)
C(22)	−26165(39)	11051(37)	38452(45)	1043(44)	1083(41)	1487(58)	485(35)	749(43)	501(40)
C(23)	−29955(46)	20375(47)	39691(54)	1356(55)	1624(58)	1875(73)	966(48)	966(55)	805(54)
C(24)	−21634(54)	31160(44)	44336(55)	2191(77)	1331(52)	1987(76)	1189(54)	1385(67)	904(53)
C(25)	−9644(48)	32598(37)	47445(49)	1756(61)	880(38)	1631(62)	601(40)	1038(53)	611(40)
C(26)	−5368(37)	23150(31)	46042(37)	1184(43)	687(30)	965(43)	376(29)	637(36)	366(30)
C(27)	7540(38)	25482(30)	49502(36)	1231(44)	574(29)	893(42)	112(28)	561(36)	230(29)
C(28)	26216(35)	22848(31)	52944(36)	904(38)	723(32)	882(41)	−6(27)	481(34)	153(29)
C(29)	34752(41)	22697(41)	64320(47)	1071(47)	1208(45)	1449(60)	224(37)	644(45)	575(43)
C(30)	47732(41)	27712(46)	69325(51)	888(45)	1507(55)	1571(65)	173(39)	530(46)	504(48)
C(31)	51929(42)	32385(45)	62850(50)	926(46)	1447(55)	1466(63)	−155(39)	666(46)	−85(46)
C(32)	43280(52)	32327(59)	51574(57)	1463(65)	2262(81)	1683(75)	−310(57)	948(60)	701(63)
C(33)	30250(46)	27432(52)	46217(49)	1197(53)	2053(71)	1223(58)	−199(49)	528(47)	774(53)
C(34)	66016(53)	37655(65)	68357(71)	1122(62)	2438(94)	2502(107)	−173(59)	1088(71)	172(79)

rameters yielded discrepancy factors $R_1=\Sigma||F_o|-|F_c||/\Sigma|F_o|=0.045$ and $R_2=[\Sigma w(|F_o|-|F_c|)^2/\Sigma w|F_o|^2]^{1/2}=0.067$. At this stage, a difference Fourier map revealed all the hydrogen atoms except for those bound to the disordered carbon atom C(6). Further refinement including the hydrogen atoms yielded final values of 0.029 and 0.042 for R_1, and R_2, respectively. The final shift in the atomic parameters of the nonhydrogen atoms averaged 0.05σ with a maximum of 0.42σ, with the exception of several parameters of the disordered carbon atom C(6) which were undergoing poorly damped oscillations of 0.05—2.15σ. A final difference Fourier map showed no important features, the highest peak being 0.25 e/Å^3 except for some peaks of 0.26—0.29 e/Å^3 corresponding to the hydrogen atoms bound to C(6).

In the least-squares refinement the function minimized was $\Sigma w(|F_o|-k|F_c|)^2$, and the weighting scheme was

Table 2. Fractional positional parameters ($\times 10^4$) and isotropic temperature factors of hydrogen atoms

The average of estimated standard deviations of the isotropic temperature factors is 1.2 Å.

Atom	x	y	z	B Å^2
H(C2)	3477(49)	−856(44)	3849(55)	9.6
H(C2)'	4092(50)	247(47)	4387(59)	10.6
H(C3)	4736(53)	−493(49)	2903(61)	11.0
H(C3)'	3885(61)	141(53)	2284(69)	13.4
H(C3)''	3191(71)	−1240(63)	1719(82)	17.0
H(C5)	−1881(48)	−3666(43)	1678(54)	9.3
H(C5)'	−346(57)	−3595(52)	1950(64)	12.0
H(C8)	1436(33)	3210(31)	1720(37)	5.0
H(C9)	746(32)	4769(29)	2369(35)	4.5
H(C10)	−1164(36)	4426(33)	2263(41)	5.7
H(C11)	−2504(34)	2489(31)	1510(38)	5.2
H(C13)	−3009(31)	552(28)	642(33)	3.9
H(C15)	−3411(36)	−998(33)	1351(41)	5.9
H(C16)	−5016(54)	−2774(49)	414(62)	11.2
H(C18)	−4573(41)	−3800(38)	−2707(46)	7.4
H(C19)	−2935(28)	−2115(25)	−1683(30)	3.0
H(C20)	−6738(55)	−4683(48)	−2712(62)	11.5
H(C20)'	−6372(51)	−4597(47)	−1420(59)	11.0
H(C20)''	−5886(50)	−5204(45)	−2009(54)	9.8
H(C22)	−3114(38)	378(34)	3601(41)	6.1
H(C23)	−3877(37)	1869(33)	3699(40)	5.8
H(C24)	−2446(45)	3759(41)	4540(50)	8.6
H(C25)	−298(37)	4011(34)	5126(42)	6.3
H(C27)	1280(35)	3416(32)	5412(39)	5.5
H(C29)	3183(40)	1854(36)	6833(45)	7.0
H(C30)	5304(54)	2686(50)	7743(62)	11.5
H(C32)	4544(71)	3642(67)	4753(84)	17.5
H(C33)	2362(51)	2749(46)	3799(58)	10.1
H(C34)	6463(55)	4188(50)	6448(63)	12.4
H(C34)'	7016(72)	3370(65)	6942(82)	16.9
H(C34)''	6956(61)	4192(55)	7808(69)	13.5

$w=(6.0+|F_o|+0.01|F_o|^2)^{-1}$.[5] Atomic scattering factors for Cu, O, N, C_{val}, and H, and the anomalous dispersion corrections, $\Delta f'$ and $\Delta f''$ for Cu, were taken from International Tables for X-ray Crystallography.[6]

The final positional and thermal parameters with their estimated standard deviations are given in Tables 1 and 2.***

The calculations were carried out at the Computer Center of Kyushu University, with the UNICS-II program system.

Description of the Structure and Discussion

The molecular structure obtained is shown in Fig. 1. The bond distances and angles with their estimated standard deviations are listed in Tables 3 and 4, respectively. Some least-squares planes with the deviations of atoms from the planes are given in Table 5.

The asymmetric unit contains two crystallographi-

*** A list of structure factors has been deposited with the Chemical Society of Japan as a Document No. 7716.

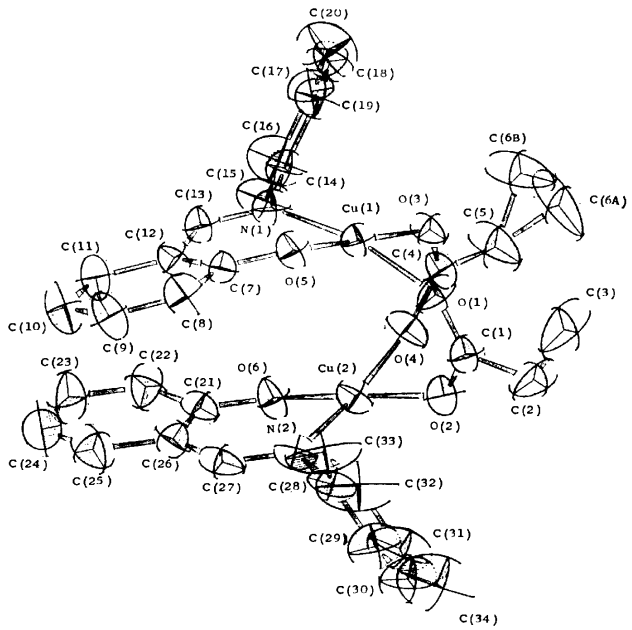

Fig. 1. A perspective view of the molecule.

Table 3. Interatomic distances (l/Å) with their estimated standard deviations in parentheses

Copper coordination spheres			
Cu(1)-O(1)	1.960(2)	Cu(2)-O(2)	1.929(3)
Cu(1)-O(3)	1.941(3)	Cu(2)-O(4)	1.949(2)
Cu(1)-O(5)	1.917(3)	Cu(2)-O(6)	1.901(3)
Cu(1)-N(1)	1.979(3)	Cu(2)-N(2)	1.968(3)
Cu(1)-O(5)^{II}	2.371(3)	Cu(2)-O(6)^{II}	2.519(3)
Propionate groups			
O(1)-C(1)	1.238(5)	O(3)-C(4)	1.260(6)
O(2)-C(1)	1.248(6)	O(4)-C(4)	1.237(5)
C(1)-C(2)	1.496(7)	C(4)-C(5)	1.502(6)
C(2)-C(3)	1.460(11)	C(5)-C(6A)	1.478(26)
		C(5)-C(6B)	1.408(10)
N-p-tolylsalicylideneamine moieties			
O(5)-C(7)	1.320(5)	O(6)-C(21)	1.314(5)
C(7)-C(8)	1.402(5)	C(21)-C(22)	1.400(7)
C(8)-C(9)	1.377(7)	C(22)-C(23)	1.372(8)
C(9)-C(10)	1.374(8)	C(23)-C(24)	1.368(8)
C(10)-C(11)	1.358(6)	C(24)-C(25)	1.345(9)
C(11)-C(12)	1.409(6)	C(25)-C(26)	1.422(7)
C(12)-C(7)	1.412(6)	C(21)-C(26)	1.402(5)
C(12)-C(13)	1.425(5)	C(26)-C(27)	1.433(7)
C(13)-N(1)	1.289(5)	C(27)-N(2)	1.288(6)
N(1)-C(14)	1.450(4)	N(2)-C(28)	1.447(5)
C(14)-C(15)	1.364(8)	C(28)-C(29)	1.347(6)
C(15)-C(16)	1.375(6)	C(29)-C(30)	1.405(7)
C(16)-C(17)	1.372(7)	C(30)-C(31)	1.349(10)
C(17)-C(18)	1.360(8)	C(31)-C(32)	1.331(8)
C(18)-C(19)	1.375(5)	C(32)-C(33)	1.401(8)
C(19)-C(14)	1.364(5)	C(33)-C(28)	1.358(9)
C(17)-C(20)	1.515(6)	C(31)-C(34)	1.521(8)
Nonbonded contacts			
Cu(1)-Cu(1)^{I}	3.1828(12)	O(5)-O(5)^{I}	2.9093(44)
Cu(2)-Cu(2)^{II}	3.2106(13)	O(6)-O(6)^{II}	3.1000(52)
Cu(1)-Cu(2)	3.1217(9)		

I) $-x, -y, -z$. II) $-x, -y, 1-z$.

TABLE 4. BOND ANGLES (φ/°) WITH THEIR ESTIMATED STANDARD DEVIATIONS IN PARENTHESES

Copper coordination spheres			
O(1)-Cu(1)-O(3)	89.3(1)	O(2)-Cu(2)-O(4)	90.1(1)
O(1)-Cu(1)-O(5)	87.3(1)	O(2)-Cu(2)-O(6)	174.6(1)
O(1)-Cu(1)-N(1)	167.5(1)	O(2)-Cu(2)-N(2)	91.9(1)
O(3)-Cu(1)-O(5)	175.7(1)	O(4)-Cu(2)-O(6)	85.9(1)
O(3)-Cu(1)-N(1)	92.5(1)	O(4)-Cu(2)-N(2)	173.1(1)
O(5)-Cu(1)-N(1)	91.4(1)	O(6)-Cu(2)-N(2)	92.5(1)
O(1)-Cu(1)-O(5)$^{I)}$	89.7(1)	O(2)-Cu(2)-O(6)$^{II)}$	88.1(1)
O(3)-Cu(1)-O(5)$^{I)}$	92.6(1)	O(4)-Cu(2)-O(6)$^{II)}$	86.1(1)
O(5)-Cu(1)-O(5)$^{I)}$	84.7(1)	O(6)-Cu(2)-O(6)$^{II)}$	87.9(1)
N(1)-Cu(1)-O(5)$^{I)}$	102.5(1)	N(2)-Cu(2)-O(6)$^{II)}$	100.6(1)
Propionate groups			
Cu(1)-O(1)-C(1)	125.6(3)	Cu(2)-O(2)-C(1)	133.1(3)
Cu(1)-O(3)-C(4)	128.0(2)	Cu(2)-O(4)-C(4)	129.1(3)
O(1)-C(1)-O(2)	126.2(4)	O(3)-C(4)-O(4)	126.2(3)
O(1)-C(1)-C(2)	118.0(5)	O(3)-C(4)-C(5)	117.4(4)
O(2)-C(1)-C(2)	115.8(4)	O(4)-C(4)-C(5)	116.5(5)
C(1)-C(2)-C(3)	117.3(5)	C(4)-C(5)-C(6A)	111.6(9)
		C(4)-C(5)-C(6B)	123.0(7)
N-*p*-tolylsalicylideneamine moieties			
Cu(1)-O(5)-C(7)	125.4(3)	Cu(2)-O(6)-C(21)	127.1(3)
Cu(1)-O(5)-Cu(1)$^{I)}$	95.3(1)	Cu(2)-O(6)-Cu(2)$^{II)}$	92.1(1)
C(7)-O(5)-Cu(1)$^{I)}$	119.5(2)	C(21)-O(6)-Cu(2)$^{II)}$	113.7(3)
Cu(1)-N(1)-C(13)	122.6(2)	Cu(2)-N(2)-C(27)	123.6(3)
Cu(1)-N(1)-C(14)	120.7(2)	Cu(2)-N(2)-C(28)	121.5(3)
C(13)-N(1)-C(14)	116.5(3)	C(27)-N(2)-C(28)	114.9(3)
O(5)-C(7)-C(8)	119.0(4)	O(6)-C(21)-C(22)	119.5(4)
O(5)-C(7)-C(12)	123.0(3)	O(6)-C(21)-C(26)	123.2(4)
C(8)-C(7)-C(12)	118.0(4)	C(22)-C(21)-C(26)	117.3(4)
C(7)-C(8)-C(9)	120.8(5)	C(21)-C(22)-C(23)	121.6(4)
C(8)-C(9)-C(10)	121.3(4)	C(22)-C(23)-C(24)	120.9(6)
C(9)-C(10)-C(11)	119.1(5)	C(23)-C(24)-C(25)	119.5(6)
C(10)-C(11)-C(12)	121.8(5)	C(24)-C(25)-C(26)	121.5(4)
C(7)-C(12)-C(11)	118.9(3)	C(21)-C(26)-C(25)	119.1(4)
C(7)-C(12)-C(13)	122.9(4)	C(21)-C(26)-C(27)	123.2(4)
C(11)-C(12)-C(13)	118.0(4)	C(25)-C(26)-C(27)	117.6(4)
N(1)-C(13)-C(12)	126.7(4)	N(2)-C(27)-C(26)	126.7(3)
N(1)-C(14)-C(15)	121.1(3)	N(2)-C(28)-C(29)	119.2(5)
N(1)-C(14)-C(19)	119.0(4)	N(2)-C(28)-C(33)	121.2(4)
C(15)-C(14)-C(19)	119.9(3)	C(29)-C(28)-C(33)	119.7(4)
C(14)-C(15)-C(16)	119.8(4)	C(28)-C(29)-C(30)	119.3(6)
C(15)-C(16)-C(17)	121.3(6)	C(29)-C(30)-C(31)	121.9(5)
C(16)-C(17)-C(18)	117.5(4)	C(30)-C(31)-C(32)	117.5(5)
C(16)-C(17)-C(20)	120.8(6)	C(30)-C(31)-C(34)	121.1(5)
C(18)-C(17)-C(20)	121.6(4)	C(32)-C(31)-C(34)	121.4(7)
C(17)-C(18)-C(19)	122.2(4)	C(31)-C(32)-C(33)	122.6(7)
C(14)-C(19)-C(18)	119.2(5)	C(28)-C(33)-C(32)	119.0(5)

I) $-x, -y, -z$. II) $-x, -y, 1-z$.

cally independent copper(II) atoms, two *N*-*p*-tolylsalicylideneamine ligands, and two propionate groups. The structure essentially agrees with that proposed by Tokii *et al.* The copper atoms Cu(1) and Cu(2) are bridged by two propionate groups in a "*syn-syn*" configuration, and each copper atom is coordinated by the amino nitrogen and the phenolic oxygen atoms of *N*-*p*-tolylsalicylideneamine and by the two oxygen atoms of propionate groups with the distances of the normal Cu–O and Cu–N in-plane coordination. These four coordinating atoms slightly deviate from the least-squares plane (plane A and A′ in Table 5). Such a slight distortion from a plane toward the tetrahedron has been reported for a number of copper complexes. In addition to these coordinations, the phenolic oxygen atoms coordinate to neighbouring copper atoms from the apical direction with the bond distances of 2.371(3) and 2.519(3) Å, respectively.

Table 5. Deviations of the atoms from least-squares (l/Å) and dihedral angles between them (φ/°)

(A)	Plane through O(1), O(3), O(5), and N(1) (plane A)										
	O(1)	0.130	O(3)	−0.123	O(5)	−0.128	N(1)	0.120	Cu(1)	−0.087	
(A′)	Plane through O(2), O(4), O(6), and N(2) (plane A′)										
	O(2)	0.083	O(4)	−0.089	O(6)	0.087	N(2)	−0.082	Cu(2)	0.028	
(B)	Plane through C(7), C(8), C(9), C(10), C(11), and C(12) (plane B)										
	C(7)	0.007	C(8)	−0.011	C(9)	0.003	C(10)	0.010	C(11)	−0.013	C(12) 0.005
(B′)	Plane through C(21), C(22), C(23), C(24), C(25), and C(26) (plane B′)										
	C(21)	0.009	C(22)	0.002	C(23)	−0.010	C(24)	0.007	C(25)	0.005	C(26) −0.012
(C)	Plane through C(14), C(15), C(16), C(17), C(18), C(19), and C(20) (plane C)										
	C(14)	0.004	C(15)	0.009	C(16)	−0.013	C(17)	−0.010	C(18)	−0.005	
	C(19)	0.002	C(20)	0.013	N(1)	0.016					
(C′)	Plane through C(28), C(29), C(30), C(31), C(32), C(33), and C(34) (plane C′)										
	C(28)	0.010	C(29)	−0.009	C(30)	0.006	C(31)	−0.002	C(32)	0.005	
	C(33)	−0.009	C(34)	−0.001	N(2)	0.038					
(D)	Plane through O(5), N(1), C(7), C(8), C(9), C(10), C(11), C(12), and C(13) (plane D)										
	O(5)	0.012	N(1)	0.029	C(7)	0.002	C(8)	−0.025	C(9)	−0.005	
	C(10)	0.020	C(11)	0.007	C(12)	0.018	C(13)	−0.058	Cu(1)	0.584	
(D′)	Plane through O(6), N(2), C(21), C(22), C(23), C(24), C(25), C(26), and C(27) (plane D′)										
	O(6)	0.037	N(2)	−0.066	C(21)	0.015	C(22)	−0.017	C(23)	−0.036	
	C(24)	−0.000	C(25)	0.023	C(26)	0.014	C(27)	0.030	Cu(2)	−0.389	
(E)	Plane through O(5), N(1), C(7), C(12), and C(13) (plane E)										
	O(5)	−0.010	N(1)	0.027	C(7)	−0.002	C(12)	0.031	C(13)	−0.045	Cu(1) 0.557
	C(8)	−0.029	C(9)	0.010	C(10)	0.051	C(11)	0.037	C(14)	−0.178	
(E′)	Plane through O(6), N(2), C(21), C(26), and C(27) (plane E′)										
	O(6)	0.023	N(2)	−0.030	C(21)	−0.021	C(26)	−0.012	C(27)	0.039	Cu(2) −0.356
	C(22)	−0.088	C(23)	−0.130	C(24)	−0.084	C(25)	−0.028	C(28)	0.106	
(F)	Plane through O(1), O(2), C(1), and C(2) (plane F)										
	O(1)	0.003	O(2)	0.003	C(1)	−0.007	C(2)	0.002	Cu(1)	−0.318	
	Cu(2)	0.219	C(3)	−0.124							
(F′)	Plane through O(3), O(4), C(4), and C(5) (plane F′)										
	O(3)	0.002	O(4)	0.002	C(4)	−0.004	C(5)	0.001	Cu(1)	−0.109	
	Cu(2)	0.529	C(6A)	0.756	C(6B)	−0.362					
(G)	Plane through Cu(1), Cu(1)[I], O(5), and O(5)[I] (plane G)										
	Cu(1)	0.000	O(5)	0.000	Cu(1)[I]	0.000	O(5)[I]	0.000			
(G′)	Plane through Cu(2), Cu(2)[II], O(6), and O(6)[II] (plane G′)										
	Cu(2)	0.000	O(6)	0.000	Cu(2)[II]	0.000	O(6)[II]	0.000			

Dihedral angles between the planes

A and A′	35.9	A and D	28.2	A′ and D′	17.3	B and C	51.5
B and D	0.7	B and E	1.4	B′ and C′	66.3	B′ and D′	1.1
B′ and E′	2.5	C and D	51.9	D and D′	10.9	D and E	0.8
C′ and D′	66.4	D′ and E′	1.4	A and G	83.6	A′ and G′	82.6

Equations of planes[a)]

(A)	$-0.3587X+0.0881Y+0.9293Z=1.2826$	(E)	$-0.0903X-0.3031Y+0.9487Z=0.7441$
(A′)	$-0.1178X-0.4768Y+0.8711Z=4.2711$	(E′)	$-0.2168X-0.2209Y+0.9509Z=4.8016$
(B)	$-0.0657X-0.3095Y+0.9486Z=0.6983$	(F)	$0.2298X+0.8709Y+0.4345Z=-0.1688$
(B′)	$-0.2588X-0.2146Y+0.9418Z=4.9144$	(F′)	$0.8337X-0.3117Y+0.4559Z=0.0875$
(C)	$0.4717X-0.7646Y+0.4393Z=-0.9120$	(G)	$0.8260X-0.3126Y+0.4690Z=0.0000$
(C′)	$-0.2993X+0.7965Y+0.5254Z=3.0862$	(G′)	$0.2455X+0.7629Y+0.5981Z=0.8104$
(D)	$-0.0781X-0.3106Y+0.9473Z=0.7105$		
(D′)	$-0.2402X-0.2121Y+0.9473Z=4.8531$		

I) $-x$, $-y$, $-z$. II) $-x$, $-y$, $1-z$. a) Equations have the from $AX+BY+CZ=D$ where X, Y, and Z are Cartesian axes lying along a×c*, b, and c*, respectively.

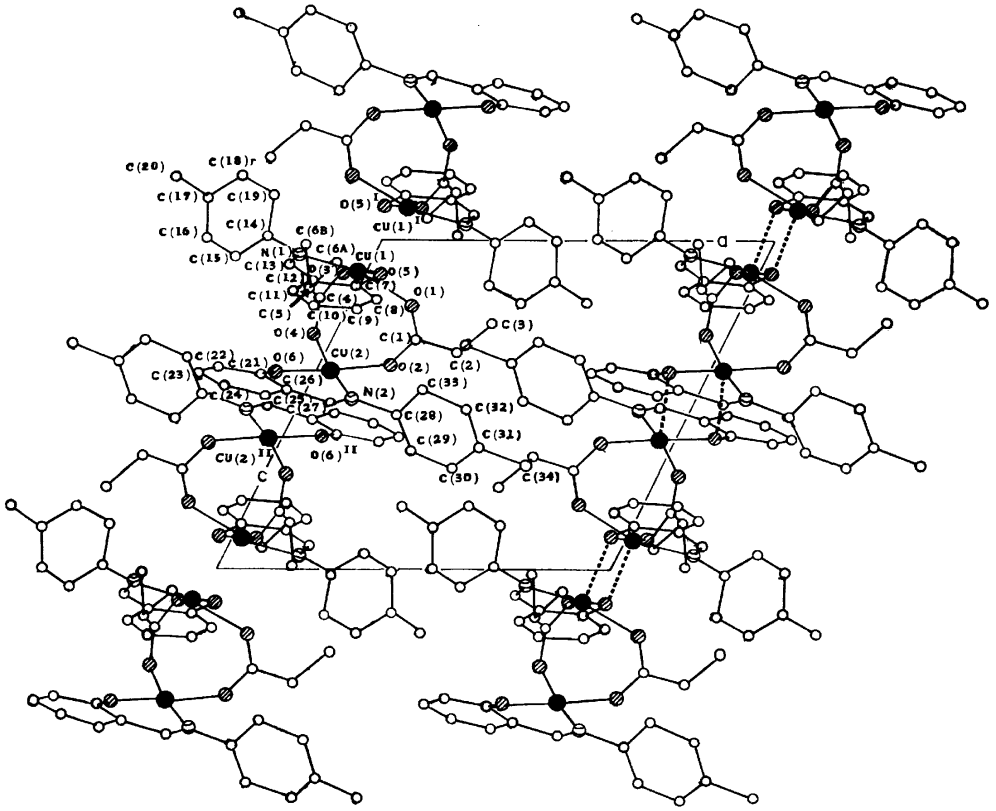

Fig. 2. A view of the packing along the b axis.

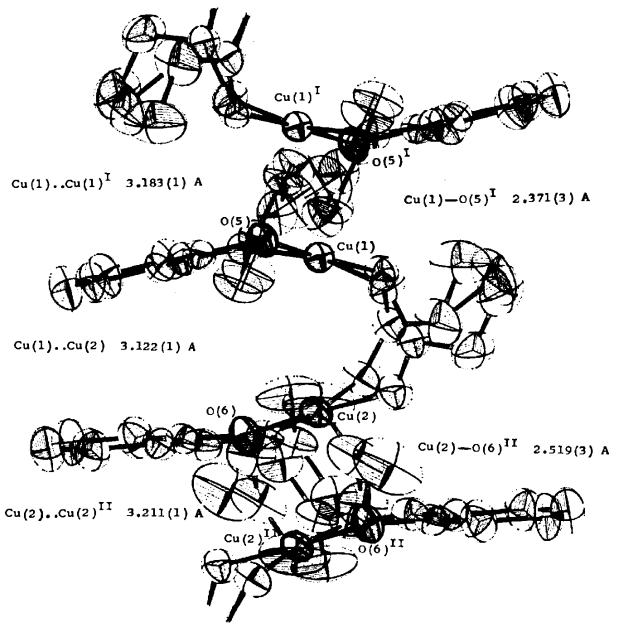

Fig. 3. A portion of the chain structure.

(A view of the packing along the b axis is shown in Fig. 2.) The apical O–Cu–basal atom angles for Cu(1) vary from 84.7(1) to 102.5(1)° and those for Cu(2) vary from 86.1(1) to 100.6(1)°, implying that the coordination sphere about each copper atom is a distorted square pyramid. The C–O distances O–C–O and O–C–C angles of the propionate groups are normal,[7–11] with average values of 1.246 Å, 126.2 and 116.9°, respectively. The $\begin{matrix}O\\O\end{matrix}\!\!>$C–C planes retain their planarity (Table 5). Such planarity was also observed for dimeric copper(II) carboxylates.[12–16] The Cu(1)–Cu(2) distance is 3.122(1) A, being longer than the Cu–Cu distances of dimeric copper(II) carboxylates (*ca.* 2.5—2.8 Å). When the number of bridging carboxylate groups is reduced from 4 to 2, the metal-metal distance becomes longer. Such a tendency was also found in the rhodium(II)[17] and molybdenum(II)[18] complexes with structures similar to the present one. The two basal planes of the distorted square pyramids around copper atoms incline toward each other making a dihedral angle of 35.9°, whereas those of copper(II) carboxylates are parallel. The Cu–O–C angles of the carboxylate groups have a mean value of 129.0°, larger than the angles observed in copper(II) acetate (a mean value of 123.1°). The above facts imply that a reduction of the number of bridging carboxylate groups weakens the binding force between the two copper atoms and opens the carboxylate group bridges.

The binuclear units are linked in a mode of out-of-plane coordination by the phenolic oxygens of upper and lower binuclear units, forming a one-dimensional polymeric chain along the c axis. The chains are separated from each other with the shortest interchain contact (excluding hydrogen atoms) of 3.594(19) Å. Consequently, any interchain magnetic interactions should be very small. There are two types of magnetic interaction between copper ions in the one-dimensional chain (Fig. 3). One is the magnetic interaction *via* two triatomic bridges of the propionate groups (Cu(1)–

Cu(2) 3.122(1) Å), and the other is the interaction *via* monatomic out-of-plane bridges of the phenolic oxygen atoms (Cu(1)–Cu(1)^{I} 3.183(1) Å, Cu(2)–Cu(2)^{II} 3.211(1) Å). Because the Cu–Cu separations of both types are longer than 3 Å, a direct interaction can not be maintained. Therefore, a "superexchange" mechanism should be operative in this system. Considered from the fact that the magnetic behavior of the present complex can be explained by a binuclear model, it is reasonable that the observed magnetic interactions are within each binuclear unit and inter-dimer interactions are negligible. It has been known that the out-of-plane interaction in copper(II) complexes is very weak compared to the interaction *via* triatomic carboxylate bridges.[19,20] Accordingly, it is natural that the antiferromagnetic behavior of the present complex can be explained mainly by a pairwise interaction between Cu(1) and Cu(2) *via* two triatomic carboxylate bridges. This view seems to be compatible with the fact that the $2J$ value of the present complex is about one third of that of copper(II) carboxylate (for example, $2J=-284$ cm^{-1} for copper(II) acetate monohydrate,[21] $2J=-300$ cm^{-1} for anhydrous copper(II) propionate[22]).

The authors are grateful to Dr. Yuzo Nishida of Kyushu University for his kind advice and help in the operation of the Syntex P$\bar{1}$ diffractometer. Thanks are also due to Professor Tetsuya Komori of Kyushu University for allowing us to use the diffractometer.

References

1) T. Tokii, S. Emori, and Y. Muto, *Bull. Chem. Soc. Jpn.*, **47**, 2887 (1974).
2) B. Bleaney and K. D. Bowers, *Proc. R. Soc. London, Ser. A*, **214**, 451 (1952).
3) T. Tokii and Y. Muto, *Bull. Chem. Soc. Jpn.*, **49**, 1849 (1976).
4) D. B. W. Yawney, J. A. Moreland, and R. J. Doedens, *J. Am. Chem. Soc.*, **95**, 1164 (1973).
5) J. S. Rollett, Ed., "Computing Methods in Crystallography," Pergamon Press, Oxford (1965), p. 114.
6) "International Tables for X-Ray Crystallography," Vol. IV, Kynoch Press, Birmingham (1974).
7) M. M. Borel, A. Busnot, and A. Leclaire, *J. Inorg. Nucl. Chem.*, **38**, 235 (1976).
8) M. M. Borel, and A. Leclaire, *Acta Crystallogr., Sect. B*, **32**, 1273 (1976).
9) M. M. Borel and A. Leclaire, *Acta Crystallogr., Sect. B*, **32**, 1275 (1976).
10) M. M. Borel and A. Leclaire, *Acta Crystallogr., Sect. B*, **32**, 3333 (1976).
11) M. M. Borel, A. Busnot, and A. Leclaire, *J. Inorg. Nucl. Chem.*, **38**, 1557 (1976).
12) D. B. W. Yawney and R. J. Doedens, *Inorg. Chem.*, **9**, 1626 (1970).
13) G. M. Brown and R. Chidambaram, *Acta Crystallogr., Sect. B*, **29**, 2393 (1973).
14) P. de Meester, S. R. Fletcher, and A. C. Skapski, *J. Chem. Soc., Dalton*, **1973**, 2575.
15) F. Hanic, D. Stempelova, and K. Hanicova, *Acta Crystallogr.*, **17**, 633 (1964).
16) G. Davey and F. S. Stephens, *J. Chem. Soc., A*, **1970**, 2803.
17) J. Halpern, E. Kimura, J. Molin-Case, and C. S. Wong, *Chem. Comm.*, **1971**, 1207.
18) D. M. Collins, F. A. Cotton, and C. A. Murillo, *Inorg. Chem.*, **15**, 1861 (1976).
19) E. Sinn, *Inorg. Chem.*, **9**, 2376 (1970).
20) W. E. Hatfieled, *Inorg. Chem.* **11**, 216 (1972).
21) B. N. Figgis and R. L. Martin, *J. Chem. Soc.*, **1956**, 3837.
22) R. L. Martin and H. Waterman, *J. Chem. Soc.*, **1957**, 2545.

NOTES

BULLETIN OF THE CHEMICAL SOCIETY OF JAPAN, VOL. 50 (9), 2471—2472 (1977)

ESR Study of the *t*-Pentyl Derivative of Yang's Biradical

Kazuo MUKAI, Koichi YORIMITSU, and Tadashi MISHINA

Department of Chemistry, Faculty of Science, Ehime University, Matsuyama 790

(Received January 17, 1977)

Synopsis. An asymmetrical *t*-pentyl derivative of Yang's biradical was prepared, and the ***g***- and ***D***-tensor values of the biradical were determined from an analysis of an asymmetric ESR spectrum of a frozen solution containing the biradical. The result may be understood by assuming that the benzene ring onto which two pentyl groups are substituted is twisted more than the other two benzene rings. On the other hand, the fluid solution ESR spectrum shows seven hyperfine splittings due to six equivalent meta ring protons in the three benzene rings of the pentyl derivative.

Yang's biradical (I) is a ground-state triplet molecule which has structural three-fold symmetry and degenerate partially-filled levels.[1,2] The evidence for the triplet state (S=1) has been demonstrated by the ESR observation of zero-field splitting in rigid media.[3,4] The triplet ground state has actually been confirmed by susceptibility measurements,[5] that is, the susceptibility of powder samples of Yang's biradical follows the Curie-Weiss law with a paramagnetic Curie constant of 1.0 K·emu/mol and a Weiss constant of −4 K in the temperature region between 4.2 and 300 K. In a previous paper, Mukai *et al.* analyzed the toluene rigid-matrix ESR spectrum of Yang's biradical, obtained with $D=34.1$ G and $E=2.3$ G,[6] as the characteristic spectrum of a non-axially symmetrical triplet. This result was explained by assuming that at least one of the twist angles of the three benzene rings is different from the other two rings in the low-temperature rigid matrix. It was suggested that both Jahn-Teller distortion and the asymmetric environment due to frozen solvent molecules may contribute to such a molecular distortion in Yang's biradical. In that publication, the effect of asymmetric deuterium substitution on molecular distortion in Yang's biradical was also reported, indicating that the effect is negligible.

In work reported here, for the purpose of obtaining further information about the molecular distortion, a less symmetrical di-*t*-pentyl derivative (see Fig. 1(a)) of Yang's biradical was synthesized, and the effect of the pentyl substitution on the unpaired spin distribution and symmetry of Yang's biradical was studied.

Experimental

2,6-Di-*t*-butylphenol is commercially available. 2,6-Di-*t*-pentylphenol (bp 100—110 °C/2 mmHg) was synthesized by the reaction of phenol with 2-methyl-2-butene in the presence of aluminium phenoxide as a catalyst in an autoclave according to the method of Kolka *et al.*[7] The bisphenol precursor of the di-*t*-pentyl derivative (see Fig. 1(a)) of Yang's biradical was synthesized from 2,6-di-*t*-butylphenol and 2,6-di-*t*-pentylphenol, following a method similar to that used with the bisphenol precursor of Yang's biradical.[1] Mp 245—247 °C. Found: C, 82.55; H, 10.15%. Calcd for $C_{45}H_{66}O_3$: C, 82.53; H, 10.16%. UV spectrum ($\lambda_{max}=266$ nm, $\log\varepsilon=4.24$; 412 nm, $\log\varepsilon=4.57$ in cyclohexane).

ESR spectra were obtained in the X band using a JES-ME-3X spectrometer equipped with a Takeda-Riken microwave frequency counter, which was used to measure the klystron frequency. The ESR splittings were determined using $(KSO_3)_2NO$ ($a^N=13.05\pm0.03$ G) as a standard. The *g*-values were measured relative to the value of Li-TCNQ powder, calibrated with $(KSO_3)_2NO$ ($g=2.0054$).[8]

Results and Discussion

The initial slight oxidation of the bisphenol precursor of the di-*t*-pentyl derivative of Yang's biradical in toluene gives a five line hyperfine pattern ($a_m^H=1.30\pm0.04$ G and $g_{iso}=2.00442\pm0.00003$) due to the equivalent four meta ring protons of the monoradical precursor. As the oxidation process proceeds further, the spectrum of the monoradical is altered to a seven-line spectrum with an equivalent splitting constant of $a=0.86\pm0.04$ G and with $g_{iso}=2.00447\pm0.00003$, as shown in Fig. 1(b). This spectrum is believed to be due to the magnetically equivalent six meta ring protons of the di-*t*-pentyl derivative of Yang's biradical. The g_{iso}-value for the pentyl derivative is in good agreement with that ($g_{iso}=2.00451\pm0.00003$) for Yang's biradical.[6] The hyperfine splitting constant (a_m^H) due to the meta ring hydrogen atoms of the pentyl derivative is also the same as that ($a_m^H=0.91\pm0.04$) for Yang's biradical, to within experimental error.

When a solution containing the biradical is frozen into rigid glass at 77 K, one can observe dipolar splittings, as is shown in Fig. 2. Assuming non-axial symmetry, the zero-field splitting parameters *D* and *E* and the ***g***-tensor values were tentatively estimated from the

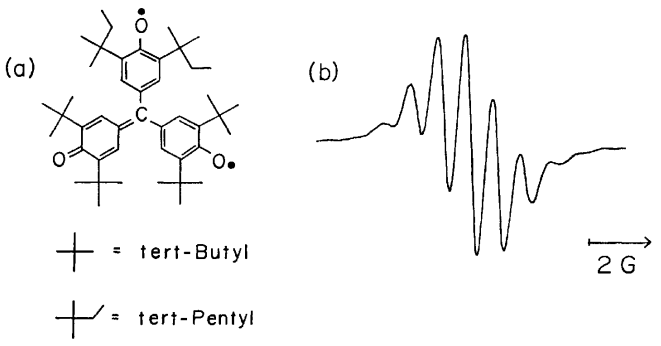

Fig. 1. (a) Molecular structure of the di-*t*-pentyl derivative of Yang's biradical, and (b) ESR spectrum of the biradical in toluene at 20 °C.

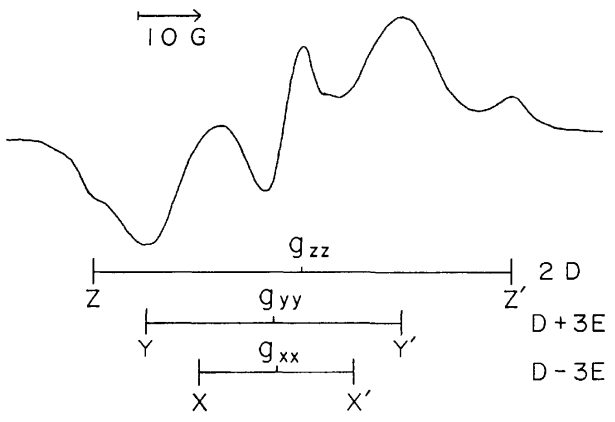

Fig. 2. ESR spectrum of the di-*t*-pentyl derivative of Yang's biradical in toluene at 77 K.

positions of the three pairs of turning points ZZ', YY', and XX' in Fig. 2, as performed for Yang's biradical in Ref. 6. The separation of the two outermost lines (ZZ') is $2D=66.6\pm0.4$ G. Due to the delocalization of each unpaired electron, the principal Z-axis of the D-tensor, corresponding to a maximum separation $2D$, is probably parallel to the $2p_z$ orbital of the center triphenylmethyl carbon atom. The remaining pairs, YY' and XX' ,are separated by $(D+3E)=40.6\pm1.2$ G, and $(D-3E)=24.5\pm1.2$ G, respectively. The E values calculated from the separations ,YY' and XX', assuming $D=33.3$ G, are 2.4 and 2.9 G, respectively. These values will give lower and higher limits of the E value, considering the overlapping of the two inner pairs of lines. The average value is $E=2.7\pm0.4$ G. Corresponding separations for Yang's biradical are $ZZ'=68.3\pm0.4$ G, $YY'=40.0\pm1.2$ G, and $XX'=26.0\pm1.2$ G, respectively.[6] The experimental errors in the absolute values of these separations were estimated by considering the overlapping of the lines. On the other hand, comparing the rigid-matrix ESR spectra of Yang's biradical and its pentyl derivative, the relative decrease in the $ZZ'=2D$ separation and the relatively small increase in the $YY'=D+3E$ separation in the pentyl derivative compared to those of Yang's biradical are obvious. Therefore, it appears reliable that the values, $D=33.3$ G and $E=2.7$ G, show a relatively small decrease and increase, respectively, compared with the values ($D=34.1$ G and $E=2.3$ G) for Yang's biradical reported previously. The frequency centers of these three pairs of absorption lines, ZZ', YY', and XX', give $g_{zz}=2.0025\pm0.0002$, $g_{yy}=2.0053\pm0.0002$, and $g_{xx}=2.0050\pm0.0002$, respectively. The average $g_{av}=1/3(g_{xx}+g_{yy}+g_{zz})=2.0043\pm0.0002$ is in agreement with the isotropic $g_{iso}=2.00447\pm0.00003$ value measured at room temperature, indicating that the g-tensor values obtained by the above analysis are consistent.

Yang's biradical may be considered to be triphenylmethyl derivatives. A molecular model indicates that the main steric interaction in Yang's biradical operates between the ring protons, although weak interactions can be seen between the substituted tertiary butyl groups. Thus, the radical most probably adopts a propeller configuration, with a twist angle of about 30°.[2] By substituting a tertiary pentyl group for the tertiary butyl group, the steric interaction between the substituted groups increases to some extent. Consequently, the benzene ring onto which the pentyl groups are substituted will be twisted more than the other two benzene rings. This results in a decrease in the D-parameter and an increase in the E-parameter in the pentyl derivative in comparison to those for Yang's biradical. Therefore, in addition to both Jahn-Teller distortion and the asymmetric environment due to the frozen solvent molecules, as is observed for Yang's biradical, the asymmetric pentyl substitution may also contribute to the molecular distortion found for the pentyl derivative of Yang's biradical in the low-temperature rigid matrix.

On the other hand, the fluid-solution ESR spectrum of Yang's biradical exhibits seven equally-spaced lines due to the six equivalent protons in the biradical.[3,6] The results of NMR and ENDOR studies[4,9] in solution also indicate that the six ring protons are magnetically equivalent, resulting in a hyperfine splitting for the six meta ring protons. The ESR spectrum of the pentyl derivative at 20 °C also appears to correspond to the hyperfine interaction with six equivalent meta ring protons. The difference in the proton splittings for the pentyl derivative is expected to be less than the line widths.

We are very grateful to Prof. Kazuhiko Ishizu for his encouragement.

References

1) N. C. Yang and A. J. Castro, *J. Am. Chem. Soc.*, **82**, 6208 (1960).
2) D. Kearns and S. Ehrenson, *J. Am. Chem. Soc.*, **84**, 739 (1962).
3) R. Kreilick, *J. Chem. Phys.*, **43**, 308 (1965).
4) H. V. Willigen, M. Plato, K. Möbius, K. P. Dinse, H. Kurreck, and J. Reusch, *Mol. Phys.*, **30**, 1359 (1975).
5) K. Mukai, K. Ishizu, and Y. Deguchi, *J. Phys. Soc. Jpn.*, **27**, 783 (1969).
6) K. Mukai, T. Mishina, and K. Ishizu, *J. Chem. Phys.*, **66**, 1680 (1977).
7) A. J. Kolka, J. P. Napolitano, A. H. Filbey, and G. G. Ecke, *J. Org. Chem.*, **22**, 642 (1957).
8) J. J. Windle and A. K. Wiersma, *J. Chem. Phys.*, **39**, 1139 (1963).
9) P. W. Kopf and R. W. Kreilick, *J. Am. Chem. Soc.*, **91**, 6569 (1969).

BULLETIN OF THE CHEMICAL SOCIETY OF JAPAN, VOL. 50 (9), 2473—2474 (1977)

Variations in the Vibrational Structures of Fluorescence Spectra of Naphthalene and Pyrene in Water and in Aqueous Surfactant Solutions

Akira NAKAJIMA

Department of Electronic Engineering, Saitama Institute of Technology, Fusaiji, Okabemachi, Ohsatogun, Saitama 369-02

(Received December 27, 1976)

Synopsis. Variations in the vibrational structures of the fluorescence spectra of naphthalene and pyrene in water and in aqueous solutions of sodium dodecyl sulfate (SDS) have been studied by comparison with those in various organic solvents. The results were applied to the determination of the critical micelle concentration of SDS.

In studies on the effect of solvent polarity on vibrational structures in the absorption and fluorescence spectra of condensed aromatic hydrocarbons,[1-5] remarkable intensity enhancement of the forbidden vibronic bands in various organic polar solvents was observed for some aromatic hydrocarbons.

The electronic spectra of condensed aromatic hydrocarbons in aqueous solutions might be important in view of solvent effects.[6,7] However, they have not been studied much. It is of interest to examine whether a similar band enhancement is observed in water, a highly polar solvent.

On the other hand, in view of recent interest in the spectroscopic studies in micellar systems,[8-10] the effects can be applied to micellar solutions to provide useful information on the micellar interior and permit determination of the critical micelle concentration (CMC).

In this work, the fluorescence spectra of naphthalene and pyrene have been investigated in water and in aqueous solutions of sodium dodecyl sulfate (SDS), a typical anionic surfactant.

Experimental

Naphthalene and pyrene were purified by recrystallization, sublimation, and zone-refining. SDS was repeatedly recrystallized from methanol. Water was distilled three times. All the organic solvents were of spectroscopic grade. The aqueous solutions of the aromatic hydrocarbons were prepared in the following way. Small amounts of the hydrocarbons were immersed in given quantities of water and the mixtures were treated with an ultrasonic cleaner to accelerate dissolution. In order to eliminate the undissolved microcrystals, the saturated solutions were carefully filtered with finest Whatman glass fiber papers, diluted with water, treated with an ultrasonic apparatus, and allowed to stand for a day before spectroscopic measurements. The solutions contained various amounts of SDS, the concentrations of hydrocarbons being constant. This was confirmed by measuring the absorbances at strong UV bands which were found to be *ca.* 2×10^{-5} and 3×10^{-7} M for naphthalene and pyrene, respectively. The fluorescence spectra were recorded on a Hitachi MPF-2A spectrofluorometer and the absorption spectra on a Hitachi EPS-3 spectrophotometer.

Results and Discussion

The fluorescence spectra of naphthalene and pyrene have been observed in organic solvents of varying polarities (Figs. 1 and 2). In the vibrational structures of these spectra, the intensities of the forbidden vibronic bands A, B, and C increase remarkably with the solvent polarity relative to the intensity of the allowed vibronic

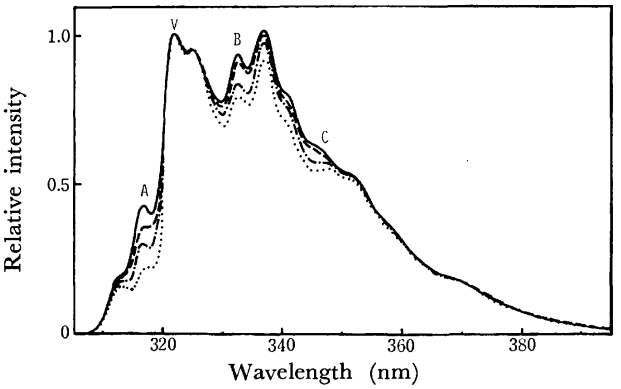

Fig. 1. Fluorescence spectra of naphthalene in several organic solvents. Solvent: cyclohexane (·····), diethyl ether (·-·-·), 1,2-dichloroethane (----), and acetonitrile (——).

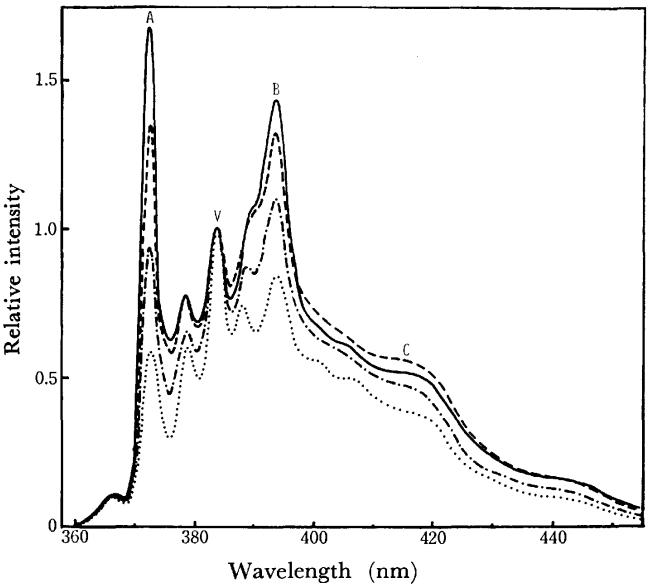

Fig. 2. Fluorescence spectra of pyrene in several organic solvents. Solvent: cyclohexane (·····), diethyl ether (·-·-·), 1,2-dichloroethane (----), and acetonitrile (——).

band V, which is almost insensitive to the solvents.[1,2,4] Thus, these aromatic hydrocarbons can be employed as fluorescent probes for the characterization of their environments.

The fluorescence spectra of naphthalene (Fig. 3) and pyrene (Fig. 4) have been studied in aqueous solutions of various concentrations. The vibronic bands are considerably broadened in water as compared with those in organic solvents, the red shifts being small. Relatively large broadenings indicate the specific solvent effects of water. The relative intensities of bands A, B, and C are markedly enhanced in water, which is reasonable considering its high polarity. In aqueous surfactant solutions, the spectra at lower SDS concentrations are practically the same as those in pure water, whereas at higher SDS concentrations the band intensities are reduced to those as observed in a much less polar solvent. The CMC can thus be determined by means of the present medium effects.

The intensity enhancement can be expressed in terms of the intensity ratio of band A to band V, I_A/I_V. In

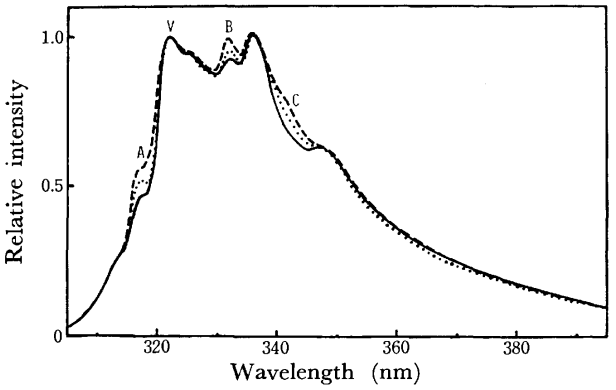

Fig. 3. Fluorescence spectra of naphthalene in water and in aqueous SDS solutions. SDS concentration: 0 and 5.22×10^{-3} M (----), 1.22×10^{-2} M (·····), and 1.86×10^{-2} M (——).

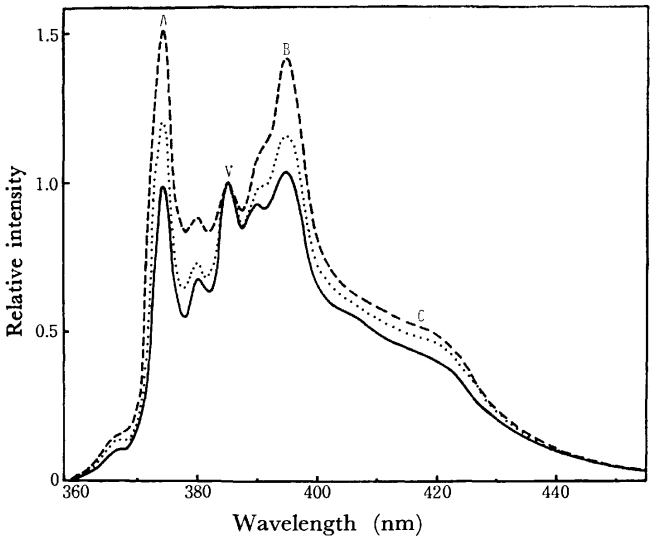

Fig. 4. Fluorescence spectra of pyrene in water and in aqueous SDS solutions. SDS concentration: 0 and 1.30×10^{-3} M (----), 8.16×10^{-3} M (·····), and 4.99×10^{-2} M (——).

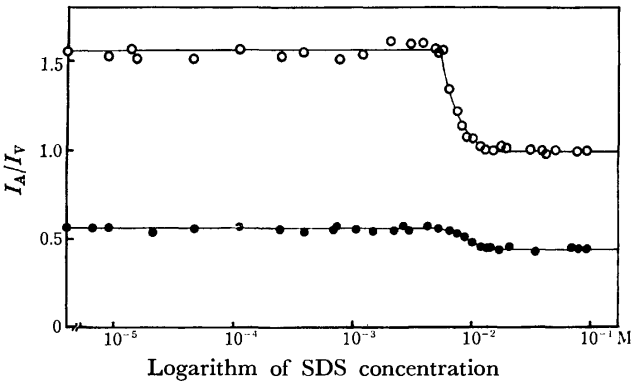

Fig. 5. Plots of relative intensities, I_A/I_V, *vs.* SDS concentration for naphthalene (●) and pyrene (○) probes.

Fig. 5, the ratios are plotted against the concentration of SDS. Changes in ratio occur in the relatively narrow concentration range, on either side of which the ratios remain constant. The concentration at which the breaks are observed may be taken as the CMC of SDS. Its values are estimated as 0.0065 and 0.007 M for naphthalene and pyrene, respectively (Fig. 5). These values are in rough agreement with those reported,[11,12] being slightly smaller. In the presence of aromatic hydrocarbons, the micellar formation may be more or less influenced; thus, the CMC values are somewhat reduced by the induction effects of probes.

In view of the band intensities in pyrene, the environment in the interior of micelle is considerably less polar than in ethanol but a little more polar than in diethyl ether. Such a weak polar environment might be caused by the influence of the ionic atmosphere around the micelles as well as the polarization of the surrounding water. In the case of naphthalene, however, a comparison of spectra indicates that the environment in micellar solution is much more polar than in organic polar solvents, implying that the probe molecules are preferably located near the micellar surface.[13]

References

1) A. Nakajima, *Bull. Chem. Soc. Jpn.*, **44**, 3272 (1971).
2) A. Nakajima, *Bull. Chem. Soc. Jpn.*, **46**, 2602 (1973).
3) A. Nakajima, *J. Luminescence*, **8**, 266 (1974).
4) A. Nakajima, *Spectrochim. Acta*, **30A**, 860 (1974).
5) A. Nakajima, *J. Mol. Spectrosc.*, **61**, 467 (1976).
6) N. S. Bayliss and L. Hulme, *Australian J. Chem.*, **6**, 257 (1953).
7) E. H. Kosower, "An Introduction to Physical Organic Chemistry," Wiley, New York (1968), p. 259.
8) E. J. Fendler and J. H. Fendler, *Adv. Phys. Org. Chem.*, **8**, 271 (1970).
9) R. R. Hautala and N. J. Turro, *Mol. Photochem.*, **4**, 545 (1972).
10) S. C. Wallace and J. K. Thomas, *Radiat. Res.*, **54**, 49 (1973).
11) T. Tachibana, ed, "Jikken Kagaku Koza (A Course in Experimental Chemistry)," Vol. 7, Kaimenkagaku (Surface Chemistry), Maruzen, Tokyo (1956).
12) The Chemical Society of Japan, ed, "Kagaku Binran (Handbook of Chemistry)," Kisohen (Fundamentals) II, Maruzen, Tokyo (1975), p. 644.
13) S. Riegelman, N. A. Allawala, M. K. Hrenoff, and L. A. Strait, *J. Colloid Sci.*, **13**, 208 (1958).

BULLETIN OF THE CHEMICAL SOCIETY OF JAPAN, VOL. 50 (9), 2475—2476 (1977)

ESR and ENDOR Study of the Carbonization of Rubrene

Yoshio YAMADA and Yuzo SANADA*

National Research Institute for Pollution and Resources, Kawaguchi, Saitama 332

(Received January 18, 1977)

Synopsis. An ESR spectrum of the radical produced during the carbonization of rubrene was measured and analyzed from an ENDOR spectrum and using computer simulations.

It is well-known that the initial thermal reactions of organic materials are of particular importance in determining the course of the subsequent carbonization and graphitization processes.[1-3] The reaction mechanism and the precursor of the carbon produced have been investigated by X-ray diffraction,[1] mass spectrometry,[3] chromatography,[4] *etc.* Singer and Lewis[5] have pointed out that the electron spin resonance (ESR) spectrometer is a powerful tool for obtaining information about the individual steps of the carbonization process when pyrolysis is carried out in an inert solvent such as *m*-quinquephenyl. In many cases, however, it appears rather difficult to analyze the many ESR spectral lines due to radicals of large molecular size.[6]

The purpose of the present study is to identify the radicals produced during initial carbonization by combining the ESR technique with electron nuclear double resonance (ENDOR) and to clarify the reaction process involving the mechanism of radical formation. This paper is concerned with the structure of the radical formed by the pyrolysis of rubrene, *i.e.*, 5,6,11,12-tetraphenylnaphthacene ($C_{42}H_{28}$), and with the associated reaction mechanism. The reason why rubrene was selected as the starting material is that the carbonization reaction rate is moderate compared with that of naphthacene.

Experimental

Rubrene and *m*-quinquephenyl were purchased from the Aldrich Chem. Co., Inc., and the K & K Laboratories, Inc., respectively. The preparation of the sample and the procedure for ESR measurement are described elsewhere.[6] The ENDOR spectra were obtained using a Japan Electron Optics Laboratory ES-EDX1 ENDOR spectrometer.

Results and Discussion

Rubrene dissolved in *m*-quinquephenyl in a weight ratio of 1 : 10 began to exhibit a large number of ESR spectral lines for pyrolysis at 450 to 470 °C. Figure 1(a) shows the spectrum observed at 150 °C for the heat treatment of rubrene at 500 °C for 5 min. This spectrum consists of about 57 lines with the same interval of 0.44 G, which are overlapped by a broad line. The spectrum illustrated in Fig. 1(a) is spread over about 25 G. The spin concentration is of the order of about 1.2 species per 1000 molecules of rubrene heat-treated at 450 °C. A similar spectrum was observed also when only rubrene was pyrolyzed at 425 °C for 1 h or at 450 °C for 10 min and then dissolved in *m*-quinquephenyl. Accordingly, it appears reasonable that the *m*-quinquephenyl used in this experiment does not participate in the rubrene carbonization.

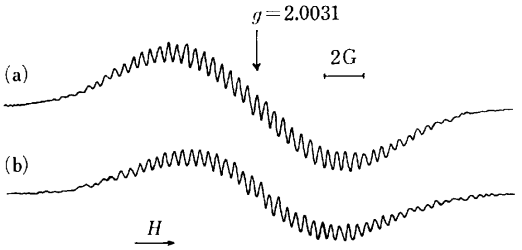

Fig. 1. (a) Experimental ESR spectrum of the radical produced when rubrene was heat-treated in *m*-quinquephenyl at 500 °C for 5 min. The spectrum was measured at 150 °C. (b) The calculated spectrum. Line spape is Gaussian, with a peak to peak linewidth of 0.35 G. The spectrum consists of 8 equivalent protons with a^H=0.884 G, 6 protons with 1.230, 4 protons with 1.724, 2 protons with 1.964, and 2 protons with 2.412.

When the rubrene was treated in *m*-quinquephenyl at 500 °C for a period longer than 5 min, the intensity of the broad line gradually increased but the relative intensity of the hyperfine spectral lines scarcely changed. Also, when the spectra were measured at various temperatures between 130 and 190 °C, the line widths became sharper with increasing temperature, whereas no significant variation of the intensity ratio was observed in this temperature range. Assuming a single radical on the basis of these observations, one can explain the odd lines of the hyperfine structure in terms of the interaction with even hydrogen nuclei.

An ENDOR spectrum was recorded at 150 °C for the sample heat-treated in *m*-quinquephenyl at 500 °C for 5 min (Fig. 2). Five pairs of lines which were reduced to hyperfine splitting constants of 0.884, 1.230, 1.724, 1.964, and 2.412 G, were observed above and below the free-proton frequency.

On the basis of the values of the splitting constants determined from the ENDOR signal, the ESR spectrum was simulated using the SESRS computer program of Stone and Maki.[8] As a result, two calculated spectra were found to fit the observed spectrum best by trial and error. One consists of 8 equivalent protons at a^H= 0.884 G, 6 protons at 1.230, 4 protons at 1.724, 2 protons at 1.964, and 2 protons at 2.412. The other is composed of 8 protons at 0.884 G, 6 protons at 1.230, 4 protons at 1.724, 4 protons at 1.964, and 2 protons at 2.412. The former spectrum is represented in Fig. 1(b).

* Present address: Faculty of Engineering, Hokkaido University, Sapporo 060.

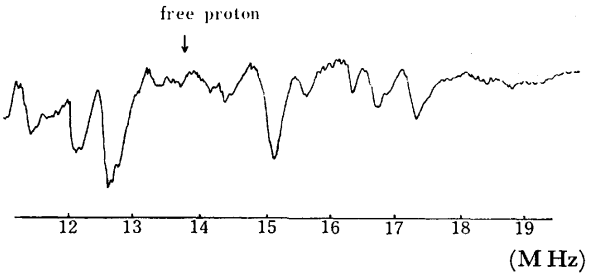

Fig. 2. ENDOR spectrum of the radical produced when rubrene was heat-treated in *m*-quinquephenyl at 500 °C for 5 min. The spectrum was measured at 150 °C.

π-Radicals, such as perinaphthenyl, are generally known to be stable at the intermediate stage of early carbonization.[7] These radicals always contain an odd number of carbon atoms. In this case, since carbon-carbon bond cleavage within the benzene and/or naphthacene ring in the rubrene is impossible at as low a temperature as 500 °C, the radical produced from the rubrene is considered to be located in the carbon-frame composed of 11 rings, such as bi-naphthacene.

In order to confirm the existence of a biradical, on the other hand, the lines due to the $\Delta M_s = \pm 2$ transition were examined and temperature variations of the spectrum were measured over the range 123—373 K, for which a single line was observed. No line corresponding to this transition was found at low field, but the absorption intensity significantly decreased with decreasing temperature. This result may suggest the existence of a biradical. Also, it can be considered that dimerization of the radical causes a reduction in the signal intensity.[10] But the large molecular size of the radical formed in the carbonization of rubrene may make dimerization difficult in the solid phase at the low temperature tested. Accordingly, identification of the radicals is expected after further experimentation.

As an approach to estimating the molecular weight of the reaction product, the mass spectrum of the sample carbonized at 450 °C with no solvent was observed. New intense peaks appeared in the range 608—684, in addition to a group of peaks at $m/e=532$, which were assigned to the unreacted parent molecular ion.[9] The thermal reaction of rubrene involves the elimination of substituted phenyl groups, subsequent polymerization and aromatization to a condensed aromatic layer. The development of such a plane as the precursor of carbon is thought to result in a well-ordered graphite product, the *c*-spacing of which is 3.356 Å.[11]

References

1) W. Ruland, *Carbon*, **2**, 365 (1965).
2) I. C. Lewis and L. S. Singer, *Am. Chem. Soc., Div. Fuel. Chem.*, **13**, 86 (1969).
3) S. Evans and H. Marsh, *Carbon*, **9**, 733 (1971).
4) J. Janak, *J. Gas Chromatogr.*, **10**, 20 (1963).
5) L. S. Singer and I. C. Lewis, *Carbon*, **2**, 115 (1964).
6) Y. Yamada and S. Toyoda, *Bull. Chem. Soc. Jpn.*, **46**, 3571 (1973).
7) I. C. Lewis and L. S. Singer, *Carbon.* **7**, 93 (1969).
8) E. W. Stone and A. H. Maki, *J. Chem Phys.*, **38**, 1999 (1963).
9) Y. Yamada and Y. Sanada, Abstracts of the 13 th ESR Symposium, Nagoya, p. 30 (1974).
10) F. Gerson, *Helv. Chim. Acta*, **49**, 1463 (1966).
11) T. Edstrom and I. C. Lewis, *Carbon*, **7**, 85 (1969).

BULLETIN OF THE CHEMICAL SOCIETY OF JAPAN, VOL. 50 (9), 2477—2478 (1977)

Preparation of Vitamin E Using Cation Exchange Resin Complexes of Metal Ions

Yoji TACHIBANA

Ueda Factory, Nisshin Chemical Co., Ltd., Kamishiojiri, Ueda, Nagano 386

(Received February 17, 1977)

Synopsis. A series of cation exchange resin complexes of metal ions were prepared. These resins are effective catalysts for the preparation of vitamin E and were recycled for use several times with little activity loss. The effect of solvents and metal ions on the reaction is discussed.

Incresed attention has recently been paid to anchoring homogeneous transition metal catalysts to polymers. Heterogenized catalysts have some advantages over their homogeneous counterparts such as (1) the ease in separation from the product,[1-5] (2) enhanced size and positional selectivity,[6] and (3) the ability to carry out sequential catalytic reactions.[7] In this respect, insoluble polymers also have been used widely in organic synthesis,[8] for example, as protecting groups[9-11] or in esterification.[12-13]

The cation exchange resins were employed for the preparation of vitamin E, but their catalytic activity was very low. The present paper describes the preparation of cation exchange resin complexes of metal ions and the use of these materials as catalyst for the preparation of vitamin E.

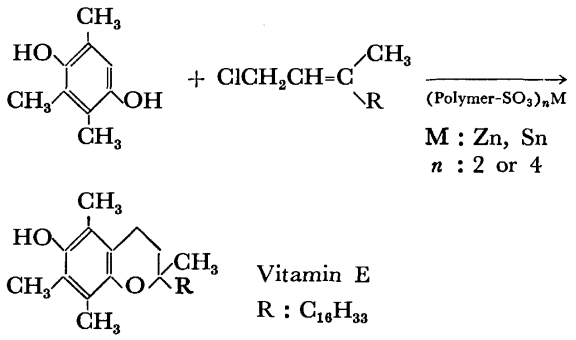

It was shown that the catalysts can be used as heterogenous catalysts. Furthermore, the investigation of the preparation of vitamin E using the resin complexes as catalysts was prompted by the following advantages offered by resins: the ability to remove the catalyst from the reaction product by simple filtration, thus avoiding contamination of the latter and generating economic savings effected by repeated use of the resin, which exhibits good stability of activity. The stabilities of the catalysts decrease in the order $Sn^{4+}>Sn^{2+}>Zn^{2+}$. This agrees well with the stability order for chelate rings. In benzene, the catalysts were recycled several times with little loss in activity. However, in highly polar solvents such as acetonitrile, repeated use of the catalysts was not possible. This may be due to the elimination of metal ions from the resin by strong solvation. With recycling of the catalyst, a decrease in activity was observed. This is ascribed to the elimination of metal ions through reactions. The catalysts can be regenerated to their initial activity by the addition of the amount of metal ions equal to that lost in the reactions. The results are summarized in Table 1 and Fig. .

TABLE 1. EFFECT OF RECYCLING CATALYSTS
Trimethylhydroquinone: 50 mmol, phytyl chloride: 50 mmol, catalyst: 20 mmol (as metal ion), benzene: 50 ml and time: 3.0 h.

Metal ion	Run	Yield (%)	Purity (%)
Sn^{4+}	1	86.7	96.4
	2	86.0	94.1
	3	85.6	90.8
	4	82.5	89.5
	5	80.2	85.4
Sn^{2+}	1	87.4	94.9
	2	85.7	90.0
	3	84.7	88.5
	4	81.2	83.6
	5	75.4	80.1
Zn^{2+}	1	85.0	92.4
	2	83.5	90.6
	3	81.3	86.4
	4	75.6	80.4
	5	70.1	76.9

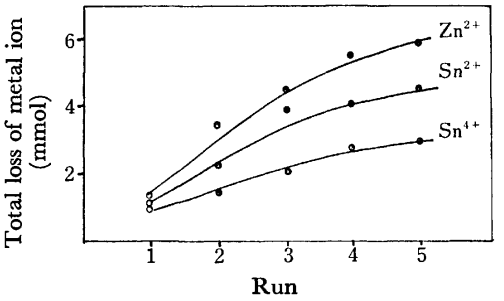

Fig. 1. Loss of metal ions.
Trimethylhydroquinone 50 mmol, phytyl chloride 50 mmol, catalyst 20 mmol (as metal ion), benzene 50 ml and time 3 h.

One practical limitation of this method is the very low catalytic activity and the inability to employ recycling when phytol or isophytol is used. In the course of the reaction, about 70% of the metal ions in the resin catalyst were detected. This strongly indicates that the catalytic species is a metal halide. These reactions were effectively assisted by the addition of a trace amount of a protonic acid, such as *p*-toluenesulfonic or methanesulfonic acid. This may be due to the promotion of cyclization in the reaction.[14] From the results, a plausible mechanism for this catalytic

system is shown below. The detailed nature of the catalytic process reported here requires further clarification and work in progress is aimed at exploring the synthetic utility of this technique.

$$2\,\text{Polymer-SO}_3\text{H} + \text{ZnCl}_2 \longrightarrow (\text{Polymer-SO}_3)_2\text{Zn} + 2\text{HCl}$$

2 trimethylhydroquinone + 2 phytyl chloride

$$\xrightarrow[(\text{Polymer-SO}_3)_2\text{Zn}]{} 2\ \text{Vitamin E} + \underline{\text{ZnCl}_2 + 2\ \text{Polymer-SO}_3\text{H}}$$

$$\Downarrow$$

$$\underline{(\text{Polymer-SO}_3)_2\text{Zn} + 2\ \text{HCl}}$$

or,

trimethylhydroquinone + phytyl chloride + ZnCl_2

$$\xrightarrow[\text{H}^+(\text{HCl or Polymer-SO}_3\text{H})]{} \text{Vitamin E} + \text{ZnCl}_2 + \text{HCl}$$

Experimental

GLC and atomic absorption spectra were recorded on a Hitachi 023 gas chromatograph equipped with a flame ionizer detector and a Hitachi 208 atomic absorption spectrometer, respectively.

General Procedure. Zinc chloride (12.3 g, 0.09 M) was dissolved in 100 ml of ethyl acetate. Amberlyst 15 in hydrogen ion form (30 g, 4.8 meq/g dry resin) was added to the solution and the mixture was maintained at 40 °C for 2 h and allowed to stand overnight at room temperature. The resin complex was filtered and washed well with acetone to remove hydrogen chloride and unbounded zinc chloride. A theoretical amount of zinc ions were shown to be bounded to the resin (analyzed by atomic absorption spectroscopy). A benzene solution (100 ml) containing 30 g of trimethylhydroquinone, 65 g of phytyl chloride and 30 g of the catalyst was allowed to reflux for 3 h. After standing overnight, the catalyst was filtered off and washed with acetone. The filtrate was concentrated under reduced pressure and the residue was subsequently distilled. The product thus obtained was analyzed by GLC. The catalyst could be recycled for use in the next reaction.

The author wishes to thank the Nisshin Chemical Co., Ltd., for permission to publish this report. The author is also grateful to Drs. K. Nakagawa and H. Fukawa of the Central Research Laboratory, Nisshin Flour Milling Co., Ltd., for their interest throughout this work.

References

1) C. P. Tsonis and M. F. Farona, *J. Organomet. Chem.*, **114**, 293 (1976).
2) K. G. Allum, R. D. Hancock, I. V. Howell, S. McKenzie, R. C. Pitkethly, and R. J. Robinson, *J. Organomet. Chem.*, **87**, 203 (1975).
3) K. G. Allum, R. D. Hancock, I. V. Howell, T. E. Lester, S. Mckenzie, R. C. Pitkethly, and P. J. Robinson, *J. Organomet. Chem.*, **107**, 393 (1976).
4) C. U. Pittman, Jr., L. R. Smith, and R. M. Hanes, *J. Am. Chem. Soc.*, **97**, 1742 (1975).
5) J. Basset, R. Mutin, G. Descotes, and D. Sinou, *C. R. Acad. Sci. Paris*, **280**, 1181 (1975).
6) C. U. Pittman, Jr., S. E. Jacobson, and H. Hiramoto, *J. Am. Chem. Soc.*, **97**, 4774 (1975).
7) C. U. Pittman, Jr., and L. R. Smith, *J. Am. Chem. Soc.*, **97**, 1749 (1975).
8) P. Hodge and G. Richardson, *J. Chem. Soc., Chem. Commun.*, **1975**, 622.
9) E. C. Blossey, L. M. Turner, and D. C. Neckers, *J. Org. Chem.*, **40**, 959 (1975).
10) J. M. J. Frechet and K. E. Haque, *Tetrahedron Lett.*, **35**, 3055 (1975).
11) J. M. J. Frechet and G. Pelle, *J. Chem. Soc., Chem. Commun.*, **1975**, 225.
12) G. D. Nageshwar, D. M. Pandharpurker, and P. S. Mene, *Chem. Age. India*, **26**, 365 (1975).
13) J. Yamanis and M. Adelman, *Can. J. Chem. Eng.*, **53**, 536 (1975).
14) P. A. Wehrli, R. I. Fryer, and W. Metlesics, *J. Org. Chem.*, **36**, 2910 (1971).

BULLETIN OF THE CHEMICAL SOCIETY OF JAPAN, VOL. 50 (9), 2479—2480 (1977)

Adsorption of Phosphate on Synthetic Silica–Alumina Possessing Lewis-acid Sites

Kazuto TAKIMOTO, Akira FUJITA, and Satoru TSUDA
Department of Chemistry, Faculty of Engineering, Hiroshima University, Senda-machi, Hiroshima 730

(Received February 24, 1977)

Synopsis. It was confirmed from measurements of the adsorption isotherms of phosphates in aqueous solutions that there were adsorption sites with very high reactivity on the surface of silica–alumina. The concentration of adsorption sites which is estimated from the adsorption amount extrapolated to zero equilibrium concentration is nearly twice the concentration of Lewis-acid sites for silica–alumina of higher alumina content. Furthermore, the concentration of phosphate adsorbed on the surface of various silica–alumina is relatively well correlated with the concentration of Lewis-acid sites.

It is well known that inorganic phosphates play an important role in the abnormal growth of phytoplankton in an area of the sea or a lake, which is called red tide. Nishimura[1] has reported that the average concentration is 0.015 ppm for P and 0.14 ppm for N in a given sea area. The pollution source of the phosphates is mainly domestic sewage. Even in the effluent of so-called secondary sewage treatment, phosphate in concentrations of 3 to 5 ppm as P is usually detected.[2] Complete phosphate removal, which is relatively easy and economical compared with that of nitrogen, may offer the best solution for returning aquatic environments to their pristine state.[3] Although many workers have widely studied phosphate removal,[4–6] some clay minerals containing aluminium atoms are reported to be effective for the removal of phosphate at the very low concentrations described above. The aluminium atoms responsible for the phosphate removal are not the internal atoms of the adsorbent but the surface atoms. Therefore, it is expected that the concentration of Lewis-acid sites associated with surface aluminium atoms correlates with that of the phosphate adsorbed. To the authors' knowledge, no work has been done from such a viewpoint.

In the study reported here, synthetic silica–alumina samples having strong Lewis-acid sites, which also react with electron-donating polyaromatic hydrocarbons[7] were used as adsorbents. The object of the present paper is to clarify the correlation between the concentration adsorbed of Lewis-acid sites, the concentration of phosphate and the alumina content of the silica–alumina samples.

Experimental

Aluminium isopropoxide and tetraethyl orthosilicate purified under reduced pressure were mixed in various proportions and were hydrolyzed for 12 h. The gels thus obtained were treated at 600 °C for 8 h. The particles which passed through 100 mesh sieve were used as adsorbents. Each silica–alumina sample is represented as % silica–alumina which indicates the alumina content in wt%. The surface area of these silica–alumina samples were measured by means of the BET method. The concentration of Lewis-acid sites on the surface of the silica–alumina samples was measured by the Leftin method,[8] after heating *in vacuo* at 400 °C for 2 h.

The phosphate was adsorbed onto various silica–alumina samples at 20 °C. The adsorbents were suspended in aqueous KH_2PO_4 solutions having concentrations in the range from 1 to 10 mmol/l and the mixture were stirred for 48 h. It was confirmed that the adsorption equilibrium was reached within 48 h. After centrifugation, the phosphate concentration in the supernatant solutions was determined by the molybdenum blue method.[9]

Results and Discussion

The isotherms for the adsorption of phosphate onto the silica–alumina samples are shown in Fig. 1. The phosphate is only slightly adsorbed on samples ranging from pure silica gel to 25% silica–alumina, whereas adsorption clearly occurs on samples ranging from 40% silica–alumina to pure alumina. Thus, adsorption is enhanced with increasing alumina content. For pure alumina, however, the adsorption concentration, is slightly lower than that for 90% silica–alumina.

The phosphate adsorption concentration is fairly large even near zero equilibrium concentration in the cases from 50% silica–alumina to pure alumina. This result suggests that highly reactive sites responsible for the adsorption exist on the surface.

In order to confirm this, the Muljadi adsorption isotherm[10] and the Langmuir isotherm for alumina are shown in Fig. 2. The Langmuir theory assumes that all the adsorption sites are equivalent. This theory is

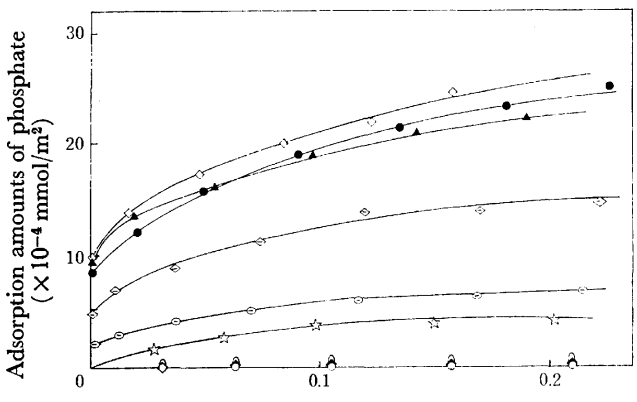

Fig. 1. Adsorption isotherms of phosphate on the surface of silica–alumina (S.A).
▲: Alumina, ◇: 90% S.A, ●: 75% S.A, ◁: 60% S.A, ⊖: 50% S.A, ☆: 40% S.A, ▯: 25% S.A, ◆: 10% S.A, ○: silica gel.

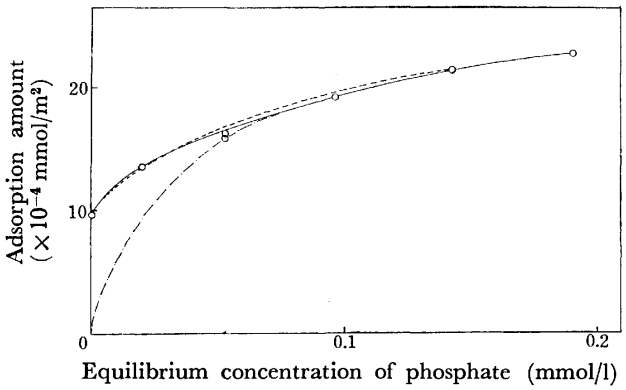

Fig. 2. Adsorption isotherms of phosphate on the surface of alumina.
—○—: Observed adsorption isotherm, —·—·: Langmuir adsorption isotherm, ----: Muljadi adsorption isotherm.

not applicable to the present results obtained at low phosphate concentrations. On the contrary, the adsorption isotherm obtained is in rather good accord with the Muljadi isotherm. Muljadi and his co-workers[10] have revealed that there are two types of adsorption sites on the surface of kaolinite, gibbsite and pseudo-boehmite.

The concentration of highly-reactive sites estimated from the phosphate adsorption concentration extrapolated to zero equilibrium concentration is shown in Table 1. Since the reactive sites responsible for the adsorption are essentially surface aluminium atoms, it can be expected that the concentration of Lewis-acid sites is a good parameter for estimating the phosphate adsorption. The Lewis-acid sites associate with bare aluminium atoms due to the removal of water which is produced by a reaction between adjacent hydroxyl groups on the surface. The concentration of highly-reactive sites is nearly twice that of Lewis-acid sites for silica–aluminas of higher alumina content. This difference may be due to the following reason: there are weakly and strongly-bonded hydroxyl groups on the surface of silica–alumina, corresponding to strong and weak basic sites, respectively.[11] The phosphate can easily exchange with weakly-bonded hydroxyl groups in the aqueous solution, forming a surface complex with aluminium atoms. In the case of the strongly bonded groups, the ability of the phosphate to exchange with the hydroxyl groups may be less.

On the other hand, the weakly-bonded hydroxyl groups may be preferentially eliminated by heat treatment at 400 °C for 2 h *in vacuo*, forming weak Lewis-acid sites. All hydroxyl groups on the surface are not eliminated by the heat treatment.[12] Therefore, it is believed

Table 1. The relation between the concentration of phosphate adsorbed and the concentration of Lewis-acid sites

Silica–alumina	Specific surface area (m^2/g)	Concentration of phosphate adsorbed ($\times 10^{-4}$ mmol/m^2)	Concentration of Lewis-acid sites ($\times 10^{-4}$ mmol/m^2)
Alumina	164.3	8.95	4.72
90% S.A	323.6	9.47	4.02
75% S.A	178.4	8.42	3.41
60% S.A	142.7	4.21	1.99
50% S.A	343.7	1.89	1.89
40% S.A	97.4	0.42	1.80
25% S.A	118.5	0	0.88
10% S.A	309.1	0	0.34
Silica gel	378.9	0	0.13

that strongly-bonded hydroxyl groups which form Lewis-acid sites with difficulty, have possibly an exchange ability in the aqueous solution, although this ability is weak. Another reason may be the positively-charged spots proposed by Cloos *et al.*[13]

Table 1 indicates that the concentration of Lewis-acid site increases with the alumina content in silica–alumina. However, the adsorption concentration is zero up to 25% silica–alumina and, thereafter, it increases with the alumina content. This should be due to the negatively-charged surface caused by the isomorphous replacement of four-fold coordinating aluminium atoms into the tetrahedral silica framework. As the alumina content in silica–alumina is increased, the surface negativity decreases due to the increase in Al–OH cations with alumina content.[13]

Reference

1) H. Nishimura, *Kagaku*, **45**, 49 (1973).
2) F. Mukai, Japan Patent, Kokai 74-81290 (1975); *Chem. Abstr.*, **82**, 64087J (1975).
3) J. C. Goldman, *Water Res.*, **10**, 97 (1973).
4) R. Coleman, *Soil Sci. Soc. Am., Proc.*, **7**, 134 (1943).
5) K. R. Kar, *J. Sci. Ind. Res. (India)*, **17B**, 175 (1958).
6) Y. Ouikura, *Kyushu Nogyo Shikensho Iho.*, **9**, 51 (1963).
7) K. Takimoto and M. Miura, *Bull. Chem. Soc. Jpn.*, **44**, 1534 (1971); *ibid.*, **45**, 2231 (1972).
8) H. P. Leftin and E. K. Hall, *Actes Deuxième Congr. Int. Catal. Paris.*, Vol. I (a) p. 1353, (b) p. 1307.
9) Japanese Industrial Standards, K0102-1971.
10) D. Muljadi, A. M. Posner, and J. P. Quirk, *J. Soil Sci.*, **117**, 212 (1966).
11) K. Takimoto, *Bull. Chem. Soc. Jpn.*, **45**, 2391 (1972).
12) T. Morimoto, M. Nagao, and J. Imai, *Bull. Chem. Soc. Jpn.*, **44**, 1282 (1971).
13) P. Cools, A. Herbillon, and J. Echeverria, *Trans., Int. Congr. Soil Sci., 9th*, **2**, 733 (1968).

BULLETIN OF THE CHEMICAL SOCIETY OF JAPAN, VOL. 50 (9), 2481—2482 (1977)

Asymmetric Shape of Charge-transfer Absorption in Crystalline Ion Radical Salts

Yôichi IIDA

Department of Chemistry, Faculty of Science, Hokkaido University, Sapporo 060

(Received Aplil 6, 1977)

Synopsis. Using the one-dimensional Hubbard model, we proposed an asymmetric band shape for the charge-transfer transition between ion radicals in crystalline ion radical salts. The charge-transfer band of the anion radical salts derived from 2,3-dicyano-*p*-benzoquinone was explained in terms of such a model.

In a number of solid ion radical salts, the planar ion radical molecules are known to form, in themselves, a face-to-face stacking into infinite one-dimensional columns so as to make a large overlap between their half-filled molecular orbitals.[1-3] In this case, since any individual radical molecule interacts through charge-transfer most strongly with two other neighboring radicals, the electronic spectrum of the solid salt differs distinctly from the monomer spectrum of the radical ion in solution but shows a charge-transfer transition between ion radicals in the low-energy region.[1-3]

The 2,3-dicyano-*p*-benzoquinone (*p*-H_2QCy_2) and 2,3-dichloro-5,6-dicyano-*p*-benzoquinone (*p*-Cl_2QCy_2) molecules are known to be strong electron acceptors and to form stable anion radical salts with some diamagnetic alkali metal cations. Several years ago,[2] we measured the diffuse reflection spectra of the solid anion radical salts of Na^+ *p*-$H_2QCy_2^{\cdot-}$, K^+ *p*-$H_2QCy_2^{\cdot-}$, Na^+ *p*-$Cl_2QCy_2^{\cdot-}$ and K^+ *p*-$Cl_2QCy_2^{\cdot-}$, and found strong absorptions due to the charge-transfer transition between anion radicals in the low-energy region. The observed spectra of the charge-transfer absorptions are reproduced in Fig. 1, where the Kubelka-Munk function, $f(R)=(1-R)^2/2R$, was plotted against wave number. In the case of the Na^+ *p*-$Cl_2QCy_2^{\cdot-}$ salt (see (a) or Fig. 1), the peak position of the charge-transfer band is around 12600 cm^{-1} and its band shape is found to be almost symmetrical with respect to the axis of peak energy. On the other hand, the solid-state spectrum of the Na^+ *p*-$H_2QCy_2^{\cdot-}$ salt (see (c) of Fig. 1) shows the charge-transfer band with the peak position around 10700 cm^{-1}. However, its band shape is not symmetrical with respect to the axis of peak energy, but has a shoulder in the higher-energy region. Regardless of the species of the counter cations, these distinct differences are also observed for the K^+ *p*-$Cl_2QCy_2^{\cdot-}$ and K^+ *p*-$H_2QCy_2^{\cdot-}$ salts as are shown in (b) and (d) of Fig. 1. When we first reported those solid-state spectra,[2] we could not fully explain why the anion radical salts derived from *p*-H_2QCy_2 have asymmetric charge-transfer band with a shoulder in the higher-energy region.

In order to understand the character of this charge-transfer absorption in more detail, we studied in a previous paper the transition energy and the theoretical line shape of such absorption by the use of one-dimensional Hubbard model and the Green's function method.[3] For half-filled band system of simple ion

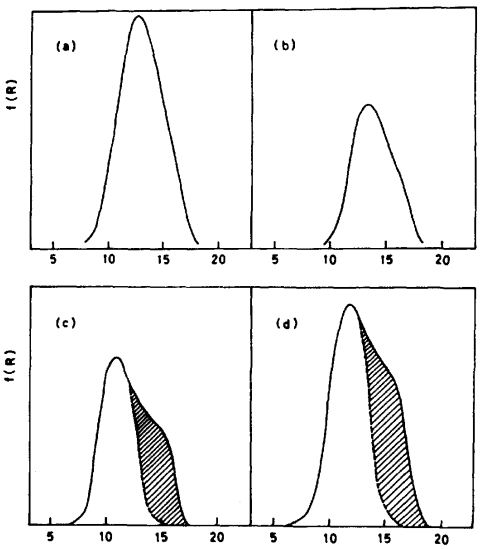

Fig. 1. The observed charge-transfer absorptions of solid anion radical salts as studied by diffuse reflection method (see Ref. 2); (a) Na^+ *p*-$Cl_2QCy_2^{\cdot-}$, (b) K^+ *p*-$Cl_2QCy_2^{\cdot-}$, (c) Na^+ *p*-$H_2QCy_2^{\cdot-}$ and (d) K^+ *p*-$H_2QCy_2^{\cdot-}$. The Kubelka-Munk function, $f(R)=(1-R)^2/2R$, was plotted *versus* wave number. For shaded and unshaded parts, see text.

radical salt, we consider non-alternant one-dimensional stack of ion radical molecules with paramagnetic state. We assumed a δ-function for each elementary transition in which the spin and the wave vector of an electron are conserved. The intermolecular charge-transfer absorption, $\sigma(\omega)$, at very low temperature is given by

$$\sigma(\omega) \propto \frac{e^2}{4}\frac{I^2}{\omega^2\sqrt{\omega^2-I^2}}\sqrt{4T^2-\omega^2+I^2}, \qquad (1)$$

where I is the intra-site Coulomb repulsion energy, and $T(<0)$ is the transfer matrix element between nearest neighbor sites in such one-dimensional column.

The theoretical charge-transfer absorption has a sharp divergent peak at the energy $\omega=I$, where the spectrum has a van Hove singularity in the lower energy side. The spectrum has no absorption in the energy region $\omega<I$, but has an absorption intensity in the region $\omega>I$. The intensity is the greatest at $\omega=I$, and decreases progressively with the increase of ω. The highest energy of the absorption takes place at $\omega=\sqrt{I^2+4T^2}$, where the intensity falls down to zero. The spectrum has a shoulder in the region $I<\omega<\sqrt{I^2+4T^2}$. These spectroscopic features are illustrated in Fig. 2.

In this model, the line width, $\sqrt{I^2+4T^2}-I$, of the charge-transfer absorption is solely caused by the ex-

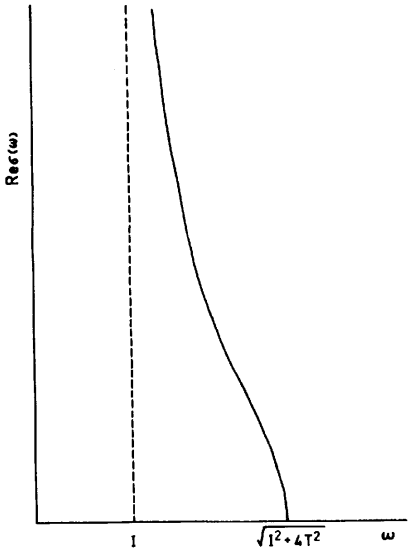

Fig. 2. The theoretical absorption line shape of Eq. 1 due to the charge-transfer transition between ion radical molecules in one-dimensional Hubbard model. See text and Ref. 3.

istence of non-zero transfer matrix element, T. However, as has been mentioned in the previous paper,[3] the actual elementary absorption is not a simple δ-function but involves finite width. Therefore, the actual charge-transfer absorption will have extra width and become more smoothed. If the band width due to the transfer matrix element is much smaller than that of the elementary absorption, the charge-transfer absorption will be governed predominantly by the band shape of the elementary absorption, so that we can well expect almost symmetrical line shape of the charge-transfer absorption with the peak position at $\omega=I$. The charge-transfer absorption of the Na^+ p-$Cl_2QCy_2^-$ and K^+ p-$Cl_2QCy_2^-$ salts should correspond to this case. In the case of the Na^+ p-$Cl_2QCy_2^-$ salt (see (a) of Fig. 1), the observed absorption peak value, 12600 cm^{-1}, corresponds to $I=12600$ cm^{-1}. The band width due to the transfer matrix element, $\sqrt{I^2+4T^2}-I$, will be very small compared to that of the elementary absorption, 4000 cm^{-1}, and the $|T|$ value appears less than 1000 cm^{-1}. In a similar way, $I=13300$ cm^{-1} is estimated for the K^+ p-$Cl_2QCy_2^-$ salt, and the $|T|$ value of this salt will again be less than 1000 cm^{-1}. In both of these salts, we can well see that a narrow band system with strong electron correlation (*i.e.*, $|T|\ll I$) takes place in one-dimensional column of the p-$Cl_2QCy_2^-$ anion radicals.

On the other hand, we consider the case when the band width due to transfer matrix element is comparable to or larger than that of the elementary absorption. In this case, the peak position of the charge-transfer absorption is still at $\omega=I$, but the line shape is no longer symmetrical with respect to $\omega=I$. Because of asymmetric component of Fig. 2, the charge-transfer absorption will have a distinct shoulder in the energy region $\omega>I$, and the total band width will arise partly from the width due to the elementary absorption but partly from the width due to the non-zero transfer matrix element. As are shown in (c) and (d) of Fig. 1, the charge-transfer absorption of the Na^+ p-$H_2QCy_2^-$ and K^+ p-$H_2QCy_2^-$ salts should correspond to this case. In the case of the Na^+ p-$H_2QCy_2^-$ salt, the observed absorption peak value, 10700 cm^{-1}, thus corresponds to $I=10700$ cm^{-1}. As for the band shape, note that the effect of transfer matrix element gives no contribution to the absorption intensity in the region $\omega<I$. Therefore, we divide, for the sake of simplicity, the observed charge-transfer absorption into symmetrical and asymmetrical parts by subtracting, with respect to $\omega=I$, the lower-energy side from the higher-energy side. This is shown in (c) of Fig. 1, where the unshaded and shaded parts are the symmetrical and asymmetrical ones, respectively. Then, the band width of the shaded part will come mostly from the width due to the non-zero transfer matrix element, $\sqrt{I^2+4T^2}-I$, and this width is found to be of the order of 3000 cm^{-1} or less. By putting $I=10700$ cm^{-1} into this relation, the magnitude of the transfer matrix element is estimated to be $|T|\lesssim 4300$ cm^{-1}. Similarly, in the case of the K^+ p-$H_2QCy_2^-$ salt, it is found that $I=11700$ cm^{-1} and $\sqrt{I^2+4T^2}-I\lesssim 3000$ cm^{-1}, so that the magnitude of the transfer matrix element is estimated to be $|T|\lesssim 4500$ cm^{-1}.

On the basis of these considerations, we can well understand the spectroscopic features of the charge-transfer absorptions characteristic of the Na^+ p-$H_2QCy_2^-$ and K^+ p-$H_2QCy_2^-$ salts as well as of the Na^+ p-$Cl_2QCy_2^-$ and K^+ p-$Cl_2QCy_2^-$ salts. The magnitude of $|T|$ of the p-H_2QCy_2 anion radical salts appears to be considerably larger than that of the p-Cl_2QCy_2 anion radical salts. This result is also strongly supported by the following reason. The p-Cl_2QCy_2 anion radical molecule includes bulky chlorine substituents, while the p-H_2QCy_2 anion radical molecule does not. Therefore, in one-dimensional stacking of anion radicals, the p-H_2QCy_2 anion radicals will stack, in themselves, more closely than do the p-Cl_2QCy_2 anion radicals, so that the magnitude of $|T|$ of the p-H_2QCy_2 anion radical salts will be definitely larger than that of the p-Cl_2QCy_2 anion radical salts.

At the present time, it is desirable to make sure of the magnitudes of $|T|$ of those anion radical salts by another approach. For this purpose, it will be quite useful to measure the exchange interaction parameters in their magnetic properties and the energy gaps in their semiconductivities. However, more useful approach is to measure absolute intensity of the charge-transfer absorption, because the total intensity will be roughly proportional to $|T|^2$. In this respect, the intensites of the charge-transfer absorptions of the p-H_2QCy_2 anion radical salts may be much stronger than those of the p-Cl_2QCy_2 anion radical salts.

References

1) Y. Iida, *Bull. Chem. Soc. Jpn.*, **42**, 71, 637 (1969).
2) Y. Iida, *Bull. Chem. Soc. Jpn.*, **44**, 1777 (1971), and the references cited therein.
3) Y. Iida, *Bull. Chem. Soc. Jpn.*, **50**, 1445 (1977).

BULLETIN OF THE CHEMICAL SOCIETY OF JAPAN, VOL. 50 (9), 2483—2484 (1977)

A Modified Method of Discrete Fourier Transform Application to Electron Spin Resonance Spectral Data

Toshio NISHIKAWA and Kazuo SOMENO

National Chemical Laboratory for Industry, Honmachi, Shibuya-ku, Tokyo 151

(Received February 18, 1977)

Synopsis. With the development of signal processing techniques, the spectral data obtained from analytical instruments have been collected and searched with the aid of a digital computer. Recognition of the spectrum as a wave pattern is adequate in such situations. The previous study[1] demonstrated signal processing based on this idea, involving the discrete Fourier transform (DFT) applied to ESR spectral data, and the advantages of this method with respect to memory capacity and searching speed. In that study, however, the spectral data were limited to symmetrical traces from organic free radicals in solution, in which case the ESR spectra exhibit isotropic hyperfine structure. This paper describes some modifications of the method rendering it applicable to asymmetrical traces, thus, for general use.

Modification of the Procedure

For the ESR spectral data, which are considered as a time series, values of $f(nT)$ $(0 \leq n \leq N-1)$ consisting of N samples, the discrete Fourier transform (DFT), $F(k\Omega)$ $(0 \leq k \leq N-1)$, may be calculated using the Fourier processing algorithm. The notation and details of formulation are the same as in a previous paper.[1]

Mathematically, $f(nT)$ and $F(k\Omega)$ are complex numbers, but for an actual DFT sequence, the real part of $F(k\Omega)$ is even and the imaginary part is odd due to the nature of the DFT,[2] since the values of $f(nT)$ are real numbers as obtained from experiment. In a method presented previously,[1] only the imaginary parts of $F(k\Omega)$ appear due to the nature of the symmetrical ESR pattern, and these are stored in the file. The present method, which is intended for application to asymmetrical patterns, however, requires both the real and imaginary parts of the DFT terms in addition to the k-values. This requires 50% more storage than the previous method.

For the file search, the known DFT, $P(k\Omega)$, and the unknown DFT, $Q(k\Omega)$, are treated in an expression for the absolute value and the argument,

$$\left.\begin{array}{ll} \text{known:} & P(k\Omega) = |P_k| \exp(ip_k) \\ \text{unknown:} & Q(k\Omega) = |Q_k| \exp(iq_k) \end{array}\right\}, \quad (1)$$

although the comparison procedure should be modified.

For the shift between the known and unknown traces, the absolute values, $|P_k|$ and $|Q_k|$, may be directly compared, since the absolute values of the DFT are invariant for the shifted traces.

On the other hand, the argument cannot be compared as it is. The comparison procedure is modified by utilizing the relationship that the shift in the time domain results in rotation of the argument in the frequency domain. In other words, the difference in argument angles due to the shift is linearly related to the difference in the magnetic fields to the order k, if the microwave frequency is assumed to remain unchanged. The arguments for unknown data are modified in the following manner:

$$\left.\begin{array}{l} q'_k = q_k - (k/k_{max})(q_{k_{max}} - p_{k_{max}}),\ k_{max} \neq 0 \\ q'_{k_{max}} = p_{k_{max}} \end{array}\right\}. \quad (2)$$

These equations indicate that the DFT arguments are rotated proportionally to the k/k_{max} ratio, so that the argument for an unknown k_{max} th DFT becomes equal to that for the known. Then, the modified argument q'_k can be compared with the standard argument p_k.

Results and Discussion

The applicability of the modified method was tested on asymmetrical ESR spectra. The hyperfine structure of the dialkyldithiocarbamate complex in solution is asymmetrical, because the line widths are dependent on the magnetic quantum number, m_I, of the central metal nucleus due to insufficient averaging for the anisotropy.[3,4]

The examples of ESR spectra were measured on diethyldithiocarbamate of Cu(II) in toluene under different conditions, such as for different signal heights, shifts, and signal-to-noise ratios. Traces 1a and 2a in Fig. 1 are taken as examples of known and unknown spectra, respectively.

The number of sampling points, N, is 512, since N should be a power of 2 for fast Fourier transform computation.[2] The DFT waveforms obtained are shown

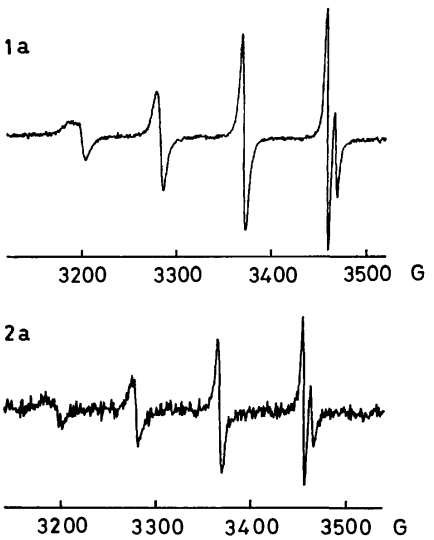

Fig. 1. Original spectral traces of Cu(II) diethyldithiocarbamate. 1a and 2a, assumed as known and unknown, are contrasted in respect of signal height, shift, and S/N ratio.

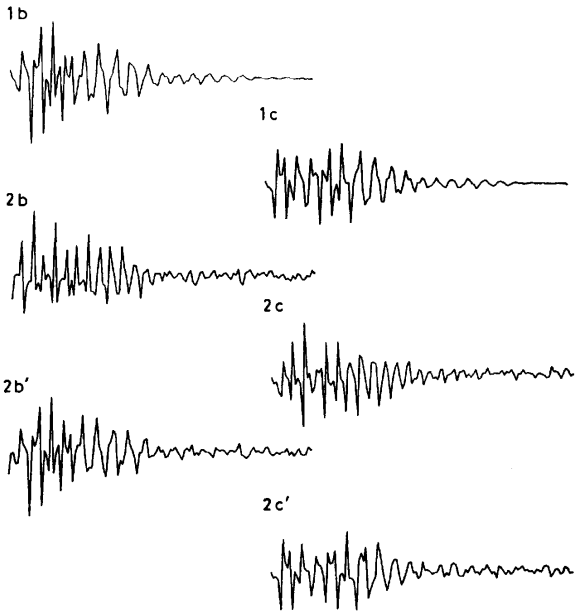

Fig. 2. DFT plots corresponding to 1a and 2a. 1b, 2b, and 2b′ are real-part plots and 1c, 2c, and 2c′ are imaginary-part plots. 2b′ and 2c′ are modified DFT plots.

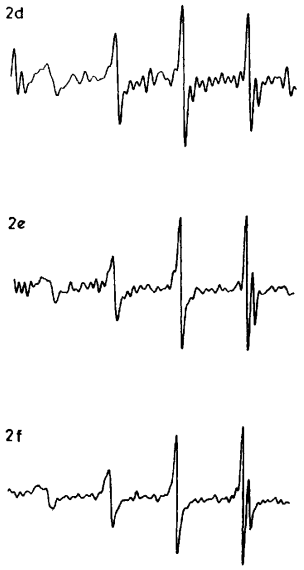

Fig. 3. The reproduced traces by inverse Fourier transform on modified DFT's 2b′ and 2c′. 2d, 2e, and 2f are transformed from 20, 40, and 60 DFT terms in the largest order, respectively.

in Fig. 2. Plots 1b and 1c are the real and imaginary parts, respectively, corresponding to 1a, and plots 2b and 2c the real and imaginary parts, respectively, corresponding to 2a. As comparisons between 1b and 2b, and between 1c and 2c indicate, these are completely different.

To obtain the unknown argument, q'_k, in Eq. 2, a problem arises from multi-valued arctangent function. Although the argument should change linearly with the magnetic field, the actual angle may differ by 2π radians.

Moreover, since the argument, p_k, is computed using the FORTRAN statement, "ATAN2(AIMAG(P(K)), REAL(P(K)))", p_k will fall within the range $-\pi$ to π. Such angles were corrected using the fact that the advanced trace shift corresponding to greater magnetic field results in a gain of the argument, as was discussed previously.[1)]

In comparing known and unknown data for search, another problem occurs: when angle p_k is near π or $-\pi$ radians, the comparison may be unsuccessfull because of deviation errors and the discontinuity of the arctangent function in these regions. For this reason, the DFT are returned as real and imaginary numbers. Therefore, the parameters obtained for the unknown data can be compared with those for the standard data.

Modified DFT plots for the unknown trace, 2a, are shown as 2b′ and 2c′ in Fig. 2. It is seen that 2b′ is almost identical with 1b, and, similarly, 2c′ with 1c, although small differences are present.

The inverse Fourier transform using some of the largest terms may reproduce the original pattern as described previously.[1)] This is demonstrated for the largest twenty, forty, and sixty DFT terms in Fig. 3. Fairly good reproduction is realized for sixty terms, but the number of terms required for an asymmetrical trace is greater than that for a symmetrical trace. The symmetrical wave pattern would be more sinusoidal, requiring fewer DFT terms. On the other hand, an asymmetrical wave pattern, being composed of higher DFT terms, might be less favorable to Fourier processing. Fourier processing, however, might still be effective with respect to data normalization for search and with a reduction of computer memory compared with the storage of original spectral values. It is believed that the present method may be applicable, in general, to analytical spectral data, as well as ESR data.

References

1) T. Nishikawa and K. Someno, *Anal. Chem.*, **47**, 1290 (1975).
2) B. Gold and C. M. Radar, "Digital Processing of Signals," McGraw-Hill, New York, N. Y. (1969).
3) T. Vänngård and S. Åkerström, *Nature*, **184**, 183 (1959).
4) R. Pettersson and T. Vänngård, *Arkiv Kemi*, **17**, 249 (1960).

BULLETIN OF THE CHEMICAL SOCIETY OF JAPAN, VOL. 50 (9), 2485—2486 (1977)

Low-spin Cobalt(II) Complexes with 6,13-Diaryl-1,8-dihydrodibenzo[*b,i*][1,4,8,11]tetraazacyclotetradecene[1)]

Yuzo NISHIDA, Akira SUMITA, and Sigeo KIDA
Department of Chemistry, Faculty of Science, Kyushu University 33, Fukuoka 812

(Received April 4, 1977)

Synopsis. The ESR spectra of the title compounds were measured at 77 K. From the results, it was concluded that an unpaired electron is localized in the d_{yz} orbital of the cobalt atom of the complexes.

In the last several years we have investigated the electronic structures of low-spin square planar cobalt(II) complexes in terms of their ESR spectra. Very recently we found that 6,13-diaryl-1,8-dihydrodibenzo[*b,i*][1,4,8,11]tetraazacyclotetradecene, **1**(a) and **1**(b), shown in Fig. 1, can be readily obtained from the reaction mixture of 4-aryl-1,2-dithiolium salt and *o*-phenylenediamine.[2)] In this study we have synthesized the cobalt(II) complexes with **1**(a) and **1**(b) and measured their ESR spectra. This is the first report on the ESR spectra of low-spin square planar cobalt(II) complexes with a 14-membered tetraazacyclotetradecene.

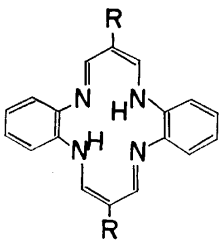

Fig. 1. Tetraaza-macrocyclic ligands. **1**(a): R=phenyl
1(b): R=*p*-tolyl

Experimental

Preparation of the Ligands. The ligand, **1**(a)(or **1**(b)), was obtained from the reaction mixture of 4-phenyl(or 4-*p*-tolyl)-1,2-dithiolium hydrogensulfate and *o*-phenylenediamine.[2)]

Preparation of the Cobalt(II) Complexes. A DMF solution(15 ml) containing cobalt(II) acetate tetrahydrate (0.001 mol) and the ligand(0.001 mol) was refluxed at 150 °C for 3 h. On cooling the solution, the complex was separated as dark violet needles.

Measurements. ESR spectra were obtained with a JEOL ESR spectrometer model JES-ME-3X at 77 K. For the ESR measurements, cobalt(II) complexes were diluted in the corresponding nickel(II) complexes. DPPH was employed as a standard marker. Magnetic susceptibilities were measured at room temperature by the Faraday method, Pascal's constants being used for diamagnetic correction.

Results and Discussion

The magnetic moments of the cobalt(II) complexes with **1**(a) and **1**(b) were 2.28 BM and 2.30 BM at room temperature, respectively, indicating that these complexes are of low-spin type. These cobalt(II) complexes are stable against air in the solid state.

The ligands, **1**(a) and **1**(b), are 14-membered tetraazamacrocyclic ligands with 16 π-electrons, while porphyrins are 16-membered tetraaza-macrocyclic ligands with 18 π-electrons. Therefore it is interesting to compare the electronic states of the complexes of **1**(a) and **1**(b) with those of cobalt(II) porphyrins.

In Fig. 2, the ESR spectrum of cobalt(II) complex with **1**(a) is shown, which is very similar to that of **1**(b). One absorption (g_1=4.256) with eight hyperfine structures due to ^{57}Co was observed in the range 1000—2200 G(G=10^{-4} T). In the range of 3700—4500 G, two absorptions(g_2=1.71, g_3=1.53) were observed, their

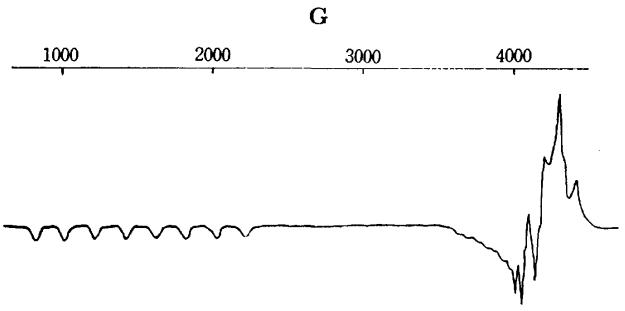

Fig. 2. ESR spectrum of cobalt(II) with **1**(a).

Table 1. ESR parameters of cobalts(II) complexes

Type	Complexes	g_x	g_z	g_y	$\lvert A_x\rvert$	$\lvert A_z\rvert$ (10^{-4} cm^{-1})	$\lvert A_y\rvert$	Ref.
I	[Co(tpp))]	3.322	1.798	3.322	315	197	315	3
	[Co(pc)]	2.92	1.91	2.89	270	160	260	5
II	[Co(acen)]	3.26	2.00	1.88	116	34	38	6
	[Co(sacsac)$_2$]	3.280	1.899	1.904	105	35	35	7
	Co-**1**(a)	4.256	(1.71, 1.53)[a)]		397	(30, 55)[b)]		
	Co-**1**(b)	4.057	(1.70, 1.55)[a)]		352	(——)[c)]		

a) The definite assignment of the experimental values to g_z and g_y is difficult. b) Roughly estimated.
c) Unresolved.

hyperfine splittings being smaller than that observed for g_1. It should be noted that this ESR pattern is quite different from that of Co-tpp,[3] where H_2tpp represents $\alpha,\beta,\gamma,\delta$-tetraphenylporphyrin. The latter complex shows an axial pattern with $g_{//}=1.798$ and $g_{\perp}=3.322$, and the hyperfine splitting observed for $g_{//}$ is very large. (*cf.* Table 1).

Recently we have investigated the ESR spectra of low-spin cobalt(II) complexes in detail[4] and found that square planar cobalt(II) complexes can be classified into two types, Type-I and Type-II, in terms of their ESR parameters, as shown in Table I. These two types are different from each other in two points, (1) the anisotropy of $\boldsymbol{g}$-tensors and (2) the value of $|A_z|$. The origin of such differences was attributed to the different ground state configurations, $(d_{x^2-y^2})^2(d_{xz})^2(d_{yz})^2(d_{z^2})^1$ for Type-I and $(d_{x^2-y^2})^2(d_{z^2})^2(d_{xz})^2(d_{yz})^1$ for Type-II.[4,*)]

As clearly seen in Table I, the cobalt(II) complexes with **1**(a) and **1**(b) belong to Type-II, and their ESR parameters can be elucidated in terms of our calculated results[4] based on the $(d_{x^2-y^2})^2(d_{z^2})^2(d_{xz})^2(d_{yz})^1$ ground state configuration.

References

1) Part VIII of the series, "Investigation on Low-spin Cobalt(II) Complexes."
2) Y. Nishida, A. Sumita, and S. Kida, to be published.
3) J. M. Assour, *J. Chem. Phys.*, **43**, 2477 (1965).
4) Y. Nishida and S. Kida, submitted to *Inorg. Chem.*
5) J. M. Assour and W. K. Kohn, *J. Am. Chem. Soc.*, **87**, 207 (1965).
6) F. Cariati, F. Marazzoni, C. Busetto, E. D. Piero, and A. Zaaetta, *J. Chem. Soc., Dalton Trans.*, **1976**, 342.
7) A. K. Gregason, R. L. Martin, and S. Mitra, *Chem. Phys. Lett.*, **5**, 310 (1970).

*) In this paper, x and y axes were adopted to be in the molecular plane and to bisect the nitrogen-cobalt bond angles, z axis being perpendicular to the plane.

BULLETIN OF THE CHEMICAL SOCIETY OF JAPAN, VOL. 50 (9), 2487—2488 (1977)

^{13}C-NMR-Spektren von mono- und disubstituierten Cyclohexenen

Kiyoshi NAKAGAWA, Michimasa SAWAI, Yasutaka ISHII, und Masaya OGAWA

Abteilung für Angewandte Chemie, Technische Fakultät der Universität Kansai, Senriyama, Suita-shi, Osaka 564

(Received December 17, 1976)

Synopsis. ^{13}C-NMR-Spektren von mono- und disubstituierten Cyclohexenen werden vorgelegt. Für die ^{13}C-chemischen Verschiebungen von disubstituierten Cyclohexenen gelten gute Additivitäten, sofern nicht sterische Wechselwirkungen auftreten und daraus einige Gesetzmässigkeiten abgeleitet werden können, die in der Konfigurations- und Konformationsanalyse von Bedeutung sind.

Was die ^{13}C-NMR-Spektren von Cyclohexenderivaten betrifft, werden nur die Monoalkylcyclohexene vorgelegt.[1] In der vorliegenden Arbeit werden ^{13}C-NMR-spektroskopische Daten einer Reihe mono- und disubstituierter Cyclohexenderivate interpretiert.

Resultat und Diskussion

4-Substituierte Cyclohexene werden durch Diels-Alder-Reaktionen von Butadien mit monosubstituierten Äthylenen gewonnen.[2] Die Zuordnung der ^{13}C-Signale von 4-substituierten Cyclohexenen beruhen auf ^{1}H-Off-Resonance-Entkopplung und Substituenteneinfluss auf den Cyclohexenring. Die ^{13}C-chemischen Verschiebungen von 4-substituierten Cyclohexenen sind in Tabelle 1 zusammengefasst. Trägt man α-Effekte von 4-substituierten Cyclohexenen gegen die von CH_3X auf, so stellt man eine lineare Korrelation fest. Da viele α-Effekte von CH_3X bekannt sind[3], kann man α-Effekte von unbekannten 4-substituierten Cyclohexenen schätzen.

TABELLE 1. ^{13}C-CHEMISCHE VERSCHIEBUNGEN (δ in ppm, $\delta_{TMS}=0$) VON 4-SUBSTITUIERTEN CYCLOHEXENEN

R	C-1	C-2	C-3	C-4	C-5	C-6	R
H	127.2	127.2	25.5	23.1	23.1	25.5	
CN	127.2	123.9	28.6	24.8	25.7	23.2	122.5
COOH	126.7	125.1	27.3	39.3	24.9	24.5	182.7
$COOCH_3$	126.7	125.4	27.8	39.4	25.4	24.8	175.7; 51.4
CHO	127.1	124.9	24.4	46.0	22.1	23.8	203.7
C_6H_5	126.8	128.3	33.6	40.3	29.9	26.0	a)

a) C_α: 147.1, C_o: 126.8, C_m: 128.3, C_p: 125.9.

Bei der Diels-Alder-Reaktionen von Isopren mit monosubstituierten Äthylenen können zwei Regioisomeren entstehen.[2] Diese Regioisomeren werden nicht durch gebräuchliche Methoden getrennt. Aber die Zuordnung der ^{13}C-Signale von den Regiosiomeren wird im Gemisch erreicht, da die ^{13}C-NMR-Spektren die chemischen Verschiebungen der C-Atome nicht nur direkter, sondern auch deutlicher anzeigen als ^{1}H-NMR-Spektren. In Tabelle 2 und 3 sind die berechneten und beobachteten ^{13}C-chemischen Verschiebungen von 4- und 5-substituierten 1-Methylcyclohexenen zusammengestellt.

Tabelle 2 und 3 zeigen die guten Additivitäten. Man erhält die linearen Korrelationen zwischen den α-Effekten von CH_3X und denen von 4- und 5-substituierten 1-Methycyclohexenen.

Bei der Diels-Alder-Reaktionen von *trans*-1,3-Pentadien mit monosubstituierten Äthylenen können Stereo- und Regioisomeren entstehen.[2] Da die *meta*-Isomeren nur in geringem Anteil entstehen, sind die Isolierung dieser Isomeren schwer. Demnach behandeln wir die *ortho*-Isomeren. Jedes *ortho*-Isomer kann als Gleichgewicht zweier Konformeren auftreten. In der Regel ist das diaxiale Konformer thermolabiler als das diäquatoriale Konformer, was dafür spricht, dass das diäquatoriale Konformer gegenüber dem diaxialen Konformer bevorzugt ist. Für *ortho-cis*-Isomere erwartet man das zeitmittlere Spektrum. Im Vergleich zum *ortho-trans*-Isomer erlei den die Signale von C-3, -4, -5, -6, Methylkohlenstoff und Substituentskohlenstoff in ortho-cis-Isomeren die erwarteten Hochfeldverschiebungen infolge des sterischen Kompressionseffektes. In Tabelle 4 sind die berechneten und beobachteten ^{13}C-chemischen Verschiebungen von 4-substituierten 3-Methyl-cyclohexenen zusammengestellt. Wegen der

TABELLE 2. BERECHNETE UND BEOBACHTETE ^{13}C-CHEMISCHE VERSCHIEBUNGEN (δ in ppm, $\delta_{TMS}=0$) VON 4-SUBSTITUIERTEN 1-METHYLCYCLOHEXENEN

R	C-1	C-2	C-3	C-4	C-5	C-6	CH_3	R
H	134.2	122.3	26.7	24.4	24.4	31.5	23.8	
CN	134.2 (134.2)	117.8 (119.0)	28.6 (27.8)	25.9 (26.1)	27.8 (27.0)	27.8 (29.2) a)	23.4	122.5
COOH	133.7 (133.7)	119.2 (120.2)	27.5 (28.5)	39.2 (40.6)	25.3 (26.2)	29.2 (30.5)	23.4	182.8
$COOCH_3$	133.6 (133.7)	119.5 (120.5)	28.0 (29.0)	39.3 (40.7)	25.7 (26.7)	29.5 (30.8)	23.5	175.8; 51.4
CHO	134.2 (134.1)	118.9 (120.0)	24.6 (25.6)	45.9 (47.3)	22.6 (23.4)	28.6 (29.8)	23.5	204.0
C_6H_5	133.5 (134.7)	120.9 (121.0)	33.7 (34.6)	40.7 (41.5)	30.8 (32.1)	30.2 (31.9)	23.5	b)

a) Die Werte in Klammern bedeuten die berechneten ^{13}C-chemischen Verschiebungen. b) C_α: 147.1, C_o: 126.8, C_m: 128.3, C_p: 125.9

Tabelle 3. Berechnete und beobachtete ^{13}C-chemische Verschiebungen (δ in ppm, $\delta_{TMS}=0$) von 5-substituierten 1-Methylcyclohexenen

R	C-1	C-2	C-3	C-4	C-5	C-6	CH_3	R
H	134.2	122.3	26.7	24.4	24.4	31.5	23.8	
CN	130.7	121.0	23.4	25.3	25.1	32.9	23.6	122.5
	(130.9)	(122.3)	(24.3)	(27.0)	(26.1)	(34.6)[a]		
COOH	132.1	120.7	24.8	24.8	39.9	32.0	23.4	182.8
	(132.1)	(121.8)	(25.7)	(26.2)	(40.6)	(33.3)		
$COOCH_3$	132.3	120.8	24.8	25.1	39.9	32.4	23.5	175.8; 51.4
	(132.4)	(121.8)	(26.0)	(26.7)	(40.7)	(33.8)		
CHO	131.8	121.2	24.0	22.0	46.7	29.1	23.5	203.8
	(131.9)	(122.2)	(25.0)	(23.4)	(47.3)	(30.4)		
C_6H_5	133.5	120.9	25.9	30.2	40.2	38.5	23.5	b)
	(133.0)	(122.7)	(27.1)	(32.1)	(41.5)	(39.4)		

a) Die Werte in Klammern bedeuten die berechneten ^{13}C-chenmischen Verschiebungen. b) C_α: 147.1, C_o: 126.8, C_m: 128.3, C_p: 125.9

Tabelle 4. Berechnete und beobachtete ^{13}C-chemische Verschiebungen (δ in ppm, $\delta_{TMS}=0$) vom 4-substituierten 3-Methylcyclohexenen

R	C-1	C-2	C-3	C-4	C-5	C-6	CH_3	R
H	126.6	134.0	32.6	30.9	22.4	26.1	22.4	
CN	(126.6)	(130.7)	(35.7)	(32.6)	(25.0)	(23.8)[a]		
cis	126.2	129.9	31.4	31.1	24.1	22.4	18.5	120.4
trans	126.0	130.1	33.8	32.9	25.1	23.5	20.2	122.0
COOH	(126.1)	(131.9)	(34.4)	(48.0)	(24.2)	(25.1)		
cis	125.8	131.7	30.9	43.6	19.1	24.9	16.4	181.7
trans	125.5	131.7	32.4	47.7	24.5	25.7	20.4	182.9
$COOCH_3$	(127.1)	(131.9)	(34.4)	(48.0)	(24.2)	(25.1)		
cis	125.8	131.7	31.1	43.5	19.4	24.9	16.5	175.0; 51.1
trans	125.5	132.0	32.6	47.7	24.6	25.8	20.3	176.3; 51.4
CHO	(126.5)	(131.7)	(31.5)	(53.8)	(21.3)	(24.4)		
cis	126.5	131.8	29.7	50.5	18.5	24.3	16.9	204.0
trans	125.8	131.5	29.6	53.6	21.5	23.7	20.3	204.7
C_6H_5	(127.0)	(135.1)	(40.7)	(48.1)	(29.2)	(26.6)		
cis	125.7	133.5	35.2	43.2	22.1	26.2	15.7	b)
trans	126.0	133.4	37.0	48.9	30.9	26.0	20.0	c)

a) Die Werte in Klammern bedeuten die berechneten ^{13}C-chemischen Verschiebungen. b) C_α: 145.0, C_o: 128.0, C_m: 128.2, C_p: 125.7. c) C_α: 146.4, C_o: 127.4, C_m: 128.2, C_p: 126.0.

Tabelle 5. Diels-Alder-Reaktionen von acyclischen Dienen mit monosubstituierten Äthylenen

Dien	Dienophil(CH_2CHX) X=	Literatur
	CN	4)
	COOH	5)
	$COOCH_3$	6)
	CHO	7)
	C_6H_5	8)
	CN	9)
	COOH	10)
	$COOCH_3$	11)
	CHO	12)
	C_6H_5	10)
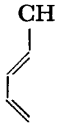	CN	10)
	COOH	13)
	$COOCH_3$	14)
	CHO	12)
	C_6H_5	10)

sterischen Faktoren erhalt man die linearen Korrelationen zwischen den α-Effekten von CH_3X und denen von *cis*- und *trans*-4-substituierten 3-Methylcyclohexenen im einzelnen.

Experimenteller Teil

Zur Aufnahme der PFT-^{13}C-NMR-Spektren diente ein PS-100 von JEOL-Gerät mit einer Messfrequenz von 25.15 MHz. Alle Substanzen wurden als 50%-ige Lösung in $CDCl_3$ gemessen(TMS als innerer Standard). ^{1}H-Rauschentkopplung-PFT-^{13}C-NMR-Spektren wurden unter Akkumulation von 200 Pulsinterferogrammen bei einer Pulsbreite von 12.5 µsek (Pulswinkel 45°) und einem Pulsintervall von 6 sek durch Fourier-Transformation des akkumulierten Interferogramms mit einem JEC-6-Rechner erhalten(Spektrumbreite 5 kHz; Datenpunkte 8191). Die mono- und disubstituierten Cyclohexene wurden durch bekannte Diels-Alder-Reaktionen von acyclischen Dienen mit monosubstituierten Äthylenen gewonnen(150°—200 °C; 2—7 Stdn.). Vgl. Tabelle 5.

Literatur

1) T. Pehk, S. Rang, O. Eisen, und E. Lippmaa, *Eesti NSV Tead. Akad. Toim. Keem. Geol.*, **17**, 296 (1968).

2) z. B., A. S. Onishenko, Diene Synthesis, Oldbourne Press, London (1964); H. Wollweber, Diels-Alder-Reaktion, Georg Thime Verlag, Stuttgart (1972).

3) G. Miyajima und K. Nishimoto, *Org. Magn. Reson.*, **6**, 313 (1974), und vgl. die angeführten Literaturen dort.

4) z. B., S. Murahashi, B. Ryutani, und Y. Shuto, *Nippon Kagaku Zasshi*, **78**, 324 (1957).

5) z. B., F. X. Werber, J. E. Jansen, und T. L. Gresham, *J. Am. Chem. Soc.*, **74**, 532 (1952).

6) z. B., N. P. Sopov, *Zh. Obsch. Chim.*, **25**, 2082 (1955).

7) z. B., R. W. Schortridge, R. A. Craig, K. W. Greenlee, J. M. Derfer, und C. E. Boord, *J. Am. Chem. Soc.*, **70**, 946 (1948).

8) z. B., C. Konigsberger und G. Salomon, *J. Polym. Sci.*, **1**, 353 (1946).

9) z. B., J. C. Soula, D. Lumbroso, M. Hellin, und F. Coussemant, *Bull. Soc. Chim. Fr.*, **1966**, 2059.

10) I. N. Nazarov, A. I. Kuznetsova, und N. V. Kuznetsov, *Zh. Obsch. Chim.*, **25**, 88 (1955).

11) z. B., H. E. Hennis, *J. Org. Chem.*, **28**, 2570 (1963).

12) A. A. Petrov und N. P. Sopov, *Zh. Obsch. Chim.*, **27**, 1795 (1957).

13) z. B., K. Alder und W. Vogt, *Justus Liebigs Ann. Chem.*, **564**, 120 (1949).

14) z. B., B. S. Eljanov, S. K. Sachova, S. V. Vitt, und M. G. Gonikberg, *Izv. Akad. Nauk SSSR, Ser. Khim.*, **1969**, 565.

BULLETIN OF THE CHEMICAL SOCIETY OF JAPAN, VOL. 50 (9), 2489—2490 (1977)

Photochromism of 2,2,4,6-Tetraphenyl-1,2-dihydro-1,3,5-triazine

Taro HAYASHI

Institute of Physical and Chemical Research, Wako, Saitama 351

(Received September 17, 1976)

Synopsis. 2,2,4,6-Tetraphenyl-1,2-dihydro-1,3,5-triazine shows temperature dependent photochromism only in a solid state at temperatures above *ca.* −70 °C under UV(320—380 nm) irradiation, giving several absorption maxima in the visible region, but no change in the IR spectrum. *N*-Substituted derivatives show no photochromism.

It was briefly reported by Lottermoser[1] that 2,2,4,6-tetraphenyl-1,2-dihydro-1,3,5-triazine (TPDT) exhibits photochromism in a solid state. No investigation has been made since the phenomenon was confirmed by von Walthers.[2] In this note the specificity of the photochromism of TPDT is reported.

TPDT turned brownish pink on irradiation in a solid state with the light 320—380 nm of sunlight or a Xenon lamp, the coloration reaching a limit with continual irradiation. TPDT which showed λ_{max} 257 and 325 nm (broad; assigned to an n,π^*-transition[3]) in a solid state before irradiation showed λ_{max} 430, 447, 487, 502, 533, 565, and 584 nm in a solid state after irradiation (Fig. 1).

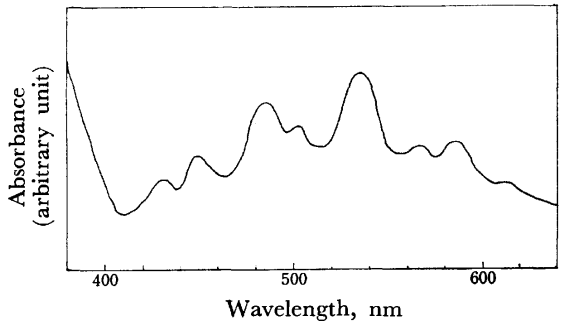

Fig. 1. The electronic absorption spectrum of TPDT measured in a solid state after irradiation at room temperature (the paraffin paper method).

It seems that the absorption at 325 nm indicates the start of photochromism. The color hardly faded at all at room temperature in the dark and also under irradiation with visible light, but it reverted thermally to the original colorless state in the dark slowly at temperatures above room temperature, somewhat rapidly with a rise in temperature. TPDT showed no change in the IR spectrum in the range 650—4000 cm^{-1} on irradiation in solid state, showing no ESR signal in both solid state not irradiated and solid state irradiated. The photochromic characteristic was lost by repetition of photochromic treatment.

It was found that TPDT exhibits photochromism only in solid state, since TPDT exhibits photochromism neither in solutions at various temperatures nor in rigid glasses in mixed solvents such as isopentane–methylcyclohexane(1 : 1) at *ca.* −196 °C. In addition, no absorption of the light in the visible region was recorded at room temperature on high density excitation by the 337 nm light of a nitrogen laser pulse with a nanosecond time-resolved spectrosco pytechnique.[4] The result indicates that TPDT does not yield even a transient colored species with a short lifetime on irradiation in solution. Very few compounds have been reported[5,6] which exhibit photochromism only in a solid state.

The photochromism of TPDT is temperature dependent. It was not observed at low temperatures below *ca.* −70 °C down to *ca.* −196 °C. A weak photochromic coloration was first observed at *ca.* −70 °C, deepening with a rise in temperature to about room temperature. No such temperature dependence seems to have been reported.[6]

TPDT containing a solvent of crystallization, such as acetone, benzene and chloroform, exhibited photochromism accompanied by the absorption of light in visible region, similar to that of TPDT free from a solvent of crystallization. TPDT containing methanol or ethanol as a solvent of crystallization, in which formation of a hydrogen bond between the alcohol and NH of TPDT was confirmed by IR analysis, exhibited no photochromism. Salts of TPDT, such as hydrochloride, and *N*-substituted TPDT, such as *N*-methyl-, *N*-ethyl-, and *N*-nitroso-TPDT, exhibited no photochromism. This shows that the photochromism of TPDT requires the presence of free H in NH.

The results suggest that the mechanism of the photochromism of TPDT is of a new type[6] attributed to an intermolecular interaction in a crystalline structure, presumably an interaction between free H in NH and excited C=N, rather than an intramolecular change of the molecular structure.

Experimental

The crystals of 2,2,4,6-tetraphenyl-1,2-dihydro-1,3,5-triazine(TPDT), $C_{27}H_{21}N_3$, were prepared according to the method of von Walthers;[2] colorless fine crystalline powder, mp 197—198 °C; $\lambda_{max}^{C_2H_5OH}$ 242($\varepsilon=3.62\times10^4$), 307($\varepsilon=1710$), 330 nm ($\varepsilon=1100$), $\lambda_{max}^{C_6H_6}$ 274($\varepsilon=6.84\times10^4$), 310(sh)($\varepsilon=1170$), 333 nm ($\varepsilon=884$); IR(KBr) 3405(m, ν_{NH}), 1685(w), 1612 cm^{-1}(m, ν_{CN}); NMR(δ ppm) 6.12 (1H, NH; missing on treatment with D_2O), 7.20—8.60 (aromatic protons). TPDT exhibits no thermochromism both in solid state and in solution. TPDT containing methanol, ethanol, benzene, acetone, or chloroform as solvent of crystallization was obtained as colorless fine crystals by recrystallization of TPDT from the solvents respectively; $C_{27}H_{21}N_3\cdot CH_3OH$(IR 3190 cm^{-1}, m, ν_{NH} (hydrogen-bonded)), $C_{27}H_{21}N_3\cdot C_2H_5OH$ (IR 3155 cm^{-1}, m,) $C_{27}H_{21}N_3\cdot CH_3COCH_3$(IR 3420 cm^{-1}, m, ν_{NH}), $C_{27}H_{21}N_3\cdot 1/3\ C_6H_6$ (IR 3415 cm^{-1}, m), $C_{27}H_{21}N_3\cdot 1/5\ CHCl_3$ (IR 3415 cm^{-1}, m). *N*-Methyl-TPDT, mp 198—200 °C, and *N*-ethyl-TPDT, mp 218—219 °C, were prepared[7] from alkyl iodide and TPDT-potassium which was obtained by heating TPDT with metallic potassium in dioxane. *N*-Nitroso-TPDT, $C_{27}H_{20}ON_4\cdot 2H_2O$, mp 171—173 °C, was prepared by a reaction of an aqueous

solution of sodium nitrite with TPDT-hydrochloride, $C_{27}H_{21}N_3 \cdot HCl$, obtained from TPDT and 2M HCl.

The electronic absorption spectra were measured with a Cary 14 spectrophotometer. The spectrum in a solid state was recorded with a thin layer of the specimen on paraffin paper obtained by rubbing crystals of the specimen on paraffin paper with an agate pestle and also with KBr disk. The infrared spectra were recorded with a Hitachi 215 grating spectrophotometer. The nuclear magnetic resonance spectrum was recorded with a Varian HA 100D spectrometer. The electron spin resonance was recorded with a JES 3B electron spin resonance spectrometer of Japan Electron Optics Laboratory.

The author wishes to express his gratitude to Dr. H. Midorikawa, Dr. K. Yamamoto, Dr. T. Kobayashi, and Dr. R. Nakagaki, Institute of Physical and Chemical Research, and Dr. K. Maeda, Ochanomizu University, for their kind help throughout this work.

References

1) A. Lottermoser, *J. Prakt. Chem.*, [2], **54**, 113 (1896).
2) R. von Walthers, *J. Prakt. Chem.*, [2], **67**, 446 (1905).
3) The absorption λ_{max} 325 nm is reasonably assigned to an n,π^*-transition in C=N, since $\lambda_{max}^{C_2H_5OH}$ 307, 330 nm and $\lambda_{max}^{C_6H_6}$ 310, 333 nm measured in the solutions are assigned to an n,π^*-transition in C=N.
4) The nanosecond time-resolved spectroscopic measurement was carried out by Drs. K. Kobayashi and R. Nakagaki, Institute of Physical and Chemical Research.
5) J. M. Tien and I. M. Hunsberger, *J. Am. Chem. Soc.*, **79**, 6604 (1955).
6) "Photochromism," ed by G. H. Brown, Wiley-Interscience, New York (1971) and literatures subsequently published.
7) *N*-Methyl- and *N*-ethyl-TPDT were supplied by Dr. K. Maeda, Ochanomizu University.

BULLETIN OF THE CHEMICAL SOCIETY OF JAPAN, VOL. 50 (9), 2491—2492 (1977)

Para Tolylation of Pyridine by Photolysis of Di-*p*-Tolyl Sulfone and Related Compounds

Takeshige NAKABAYASHI, Toyokazu HORII, Shunichi KAWAMURA, and Masayuki HAMADA

Radiation Center of Osaka Prefecture, Shinke-cho, Sakai, Osaka 593

(Received February 16, 1977)

Synopsis. Di-*p*-tolyl sulfone, sulfoxide and sulfide, *p*-toluoyl peroxide, and *p*-iodotoluene were respectively photolyzed in pyridine with a mercury arc lamp. It was found that all the compounds decompose photochemically to yield the isomeric *p*-tolylpyridines (α, β, and γ). The isomer distribution ratios ($\beta > \alpha > \gamma$) obtained with the sulfone differ from those ($\alpha > \beta > \gamma$) with the other compounds. The presence of acetone in the reaction system remarkably promoted the photochemical conversion of both the sulfone and sulfoxide.

Kharasch and Khodair[1] first reported that the photolysis of diaryl sulfone, sulfoxide, and sulfide in benzene produces aryl radicals which afford the corresponding biphenyl derivatives in good yields. They proposed the following intermolecular mechanism: the photolytic cleavage of the C–S bond of the sulfone, sulfoxide, or sulfide gives the aryl radical which, in turn, reacts with benzene to form the intermediate arylcyclohexadienyl radical, and finally the corresponding biphenyls are produced by the hydrogen atom abstraction from the intermediate. The mechanism was confirmed by Nakai *et al.*[2] in the photolysis of a benzene solution of diphenyl-1,1′-$^{14}C_2$ sulfone. Khodair *et al.*[3] reported that the photolysis of a series of symmetrical and unsymmetrical aromatic sulfones in benzene solutions gives rise to only the corresponding monosubstituted biphenyls but no disubstituted biphenyls. Diphenyl sulfone in selected aromatic solvents undergoes photolysis to afford the corresponding isomeric biphenyl derivatives (*o*-, *p*-, and *m*-).[4] This also supports the above mechanism involving the attack of aryl radical on aromatics used as the solvent. In the course of studies on the photolysis of aromatic sulfones, it was found[5] that the photolysis of diphenyl sulfone in a pyridine solution gives rise to three isomeric phenylpyridines whose isomer distribution ratios ($\beta > \alpha > \gamma$) differ from those ($\alpha > \beta > \gamma$) for a free-radical phenylation of pyridine. The purpose of the present work is to examine whether or not the order of the isomer distribution ratios of *p*-tolylpyridines produced by the photolysis of di-*p*-tolyl sulfone in pyridine coincides with that obtained with the diphenyl sulfone.

Di-*p*-tolyl sulfone (1.5 mmol, 369.5 mg) in 100 ml of pyridine or pyridine–acetone (1 : 1 in volume) was irradiated for 20 h or 50 h at room temperature, with a 400-W medium pressure mercury arc lamp. After irradiation, the unchanged sulfone and isomeric *p*-tolylpyridines produced in the reaction mixture were identified and estimated by gas chromatography. For the sake of comparison, di-*p*-tolyl sulfoxide and sulfide, *p*-toluoyl peroxide, and *p*-iodotoluene were photolyzed in the same way as for the sulfone. The results are summarized in Table 1. We see that acetone photosensitized the degradation of both sulfone and sulfoxide in pyridine solutions, but decreased markedly the yield of the isomeric *p*-tolylpyridines with sulfoxide. The isomer distribution ratios of the *p*-tolylpyridines were hardly or not at all affected by the acetone present in the reaction mixture. Either di-*p*-tolyl sulfoxide or sulfide was photolyzed in acetone to give *p*-tolyl radical which abstracts a hydrogen atom from acetone affording toluene in a good yield. Accordingly, the low yields of the *p*-tolylpyridines both with the sulfoxide and sulfide in the presence of acetone seem to be ascribed to the competitive formation of toluene with the *p*-tolylpyridines. The isomer distribution ratios ($\beta > \alpha > \gamma$) with the sulfone differ from those ($\alpha > \beta > \gamma$) obtained with the other compounds (Table 1), being comparable to those with diphenyl sulfone.[5] The gross isomer distribution ratios

TABLE 1. PARA TOLYLATION OF PYRIDINE BY PHOTOLYSES OF DI-*p*-TOLYL SULFONE AND RELATED COMPOUNDS

Compound	Irrad. time (h)	Pyridine (ml)	Acetone (ml)	Photolysis[a] (%)	Yield[b] of *p*-tolylpyridines (%)	Isomer ratios[c] of *p*-tolylpyridines (%)		
						α	β	γ
$(p\text{-}CH_3C_6H_4\text{-})_2SO_2$	50	100	0	15.6	104.0	21.7	66.4	11.9
$(p\text{-}CH_3C_6H_4\text{-})_2SO_2$	20	50	50	50.8	92.4	26.3	64.9	8.8
$(p\text{-}CH_3C_6H_4\text{-})_2SO$	20	100	0	19.6	99.1	47.2	35.4	17.4
$(p\text{-}CH_3C_6H_4\text{-})_2SO$	20	50	50	100.0	51.2	51.9	29.9	18.2
$(p\text{-}CH_3C_6H_4\text{-})_2S$	20	100	0	65.5	58.2	50.3	31.7	18.0
$(p\text{-}CH_3C_6H_4\text{-})_2S$	20	50	50	54.0	35.2	50.7	27.5	21.7
$(p\text{-}CH_3C_6H_4COO\text{-})_2$	20	100	0	d)	d)	46.8	32.0	21.2
$p\text{-}IC_6H_4CH_3$	20	100	0	d)	d)	44.2	38.4	17.5

a) Determined by estimation of the unchanged starting compounds. b) Based on the amount which actually underwent photolysis and on the assumption that 1 mole of the starting compound gives 1 mole of *p*-tolylpyridines. c) Preliminary work indicated that authentic *p*-tolylpyridines do not isomerize mutually under our reaction conditions. d) Not determined.

in a free-radical phenylation of pyridine are essentially independent of the source of phenyl radicals.[6,7] Abramovitch and Saha[8] reported that in the reaction with *p*-tolyl radical generated by the Gomberg-Hey reaction, the isomer distribution ratios of *p*-tolylpyridines are $\alpha=58.0\%$, $\beta=26.2\%$, and $\gamma=15.7\%$. This suggests that the *p*-tolylation of pyridine with compounds other than the sulfone proceeds *via* simple *p*-tolyl radical generated from the radical sources themselves under UV irradiation. Although the reason for the characteristic result obtained with the sulfone is ambiguous, we propose the following mechanism based on the fact that the yield of the *p*-tolylpyridines with the sulfone does not decrease substantially even in the presence of acetone : the sulfone in pyridine interacts on UV irradiation with pyridine to form a sulfone-pyridine complex[9] which decomposes exclusively into the *p*-tolylpyridines giving the isomer distribution ratios of $\beta>\alpha>\gamma$.

Experimental

Materials. Commercial di-*p*-tolyl sulfone (mp 160 °C), di-*p*-tolyl sulfoxide (mp 96—97 °C), and *p*-iodotoluene were purified by recrystallization or preparative gas chromatography. *p*-Toluoyl peroxide (mp 134—135 °C, dec : lit[10] 136—137 °C, dec) was prepared by the method given in literature from the reaction of *p*-toluoyl chloride with sodium peroxide and purified by recrystallization from ethanol. Di-*p*-tolyl sulfide (mp 56—57.5 °C) was supplied by Dr. S. Tamagaki, Osaka City University. Pyridine and acetone were of spectroscopic grade and used without further purification. Authentic α-*p*-tolylpyridine was prepared from the corresponding bromopyridine according to the procedure of Abramovitch and Saha.[11] Authentic β-*p*-tolylpyridine was prepared by a slight modification of the procedure since it was found that a mixture of β-*p*-tolylpyridine and 4-methyl-1-(3-pyridyl)-1-cyclohexene was produced by the procedure; additional dehydrogenation of the above mixture was carried out with elemental sulfur at 200 °C. The two *p*-tolylpyridines thus obtained were purified by preparative gas chromatography on a 5 m×3 mm column packed with 20% OV-210 on Shimalite W (210 D), using a JEOL Chromatograph, JGC-650. Authentic γ-*p*-tolylpyridine was prepared by the dehydrogenation of γ-*p*-tolyl-1,2,3,6-tetrahydropyridine obtained from *p*-α-dimethylstyrene, ammonium chloride, and formaldehyde.[12] The compound was purified by recrystallization twice from hexane (mp 90—91 °C, lit,[12] 90—91 °C).

General Procedure for the Photolysis of Di-p-Tolyl Sulfone and Related Compounds. The procedure for the sulfone is described here as a typical run. A 0.015 M-solution of di-*p*-tolyl sulfone in 100 ml of pyridine or pyridine–acetone (1 : 1 in volume) was placed in a quartz cylinder. The solution was irradiated for 50 h or 20 h at room temperature, with a 400 W-medium pressure mercury arc lamp. After the irradiation, the photolysate was transferred to a round-bottomed flask, acetone or pyridine being removed by means of a rotary evaporator. The residue was treated with benzene in order to remove benzene-insoluble materials. The benzene solution was washed with water and dried over anhydrous sodium sulfate. After most of the solvent had been evaporated, the oily residue was placed in a volumetric flask, adjusted to an appropriate volume with acetone, and subjected to GLC analysis to determine the unchanged sulfone and isomeric *p*-tolylpyridines produced in the reaction. All the GLC analyses were carried out with use of a Shimadzu Gas Chromatograph GC-3AF equipped with a flame ionization detector. The unchanged sulfone and isomeric *p*-tolylpyridines obtained were identified by comparison of their retention times with those of authentic specimens, their amounts being estimated by use of calibration curves for the authentic compounds. A 3 m× 3 mm column packed with 5% OV-210 on Shimalite W (210 D) was employed in the GLC analyses.

References

1) N. Kharasch and A. I. Khodair, *Chem. Commun.*, **1967**, 98

2) M. Nakai, N. Furukawa, S. Oae, and T. Nakabayashi, *Bull. Chem. Soc. Jpn.*, **45**, 1117 (1972).

3) A. I. Khodair, T. Nakabayashi, and N. Kharasch, *Int. J. Sulfur Chem.*, **8**, 37 (1973).

4) T. Nakabayashi, Y. Nagata, and J. Tsurugi, *Int. J. Sulfur Chem.*, **A**, **1**, 54 (1971).

5) T. Nakabayashi, Y. Abe, and T. Horii, *Phosphorus and Sulfur, and Related Elements*, **1**, 285 (1976).

6) R. A. Abramovitch and J. C. Saha, "Advances in Heterocyclic Chemistry," ed by A. R. Katritzky and A. J. Boulton, Academic Press, Vol. 6, New York and London (1966), p. 322.

7) R. M. Elofson, F. F. Gadallah, and K. F. Schuly, *J. Org. Chem.*, **36**, 1526 (1971).

8) R. A. Abramovitch and J. G. Saha, *J. Chem. Soc.*, **1964**, 2181.

9) Preliminary UV spectral work showed no indication of the formation of the complex at least in the ground state.

10) C. G. Swain, W. H. Stockmayer, and J. T. Clarke, *J. Am. Chem. Soc.*, **72**, 5432 (1950).

11) See Ref. 8, p. 2175.

12) C. J. Schmidle, J. E. Locke, and R. C. Mansfield, *J. Org. Chem.*, **21**, 1194 (1956).

BULLETIN OF THE CHEMICAL SOCIETY OF JAPAN, VOL. 50 (9), 2493—2494 (1977)

Reaction of Dioxygen Complexes with Catechols

Shigeaki MUTO, Kazuaki TASAKA, and Yoshio KAMIYA

Department of Reaction Chemistry, Faculty of Engineering, The University of Tokyo, Hongo, Bunkyo-ku, Tokyo 113

(Received February 22, 1977)

Synopsis. The square planar dioxygen complexes $MO_2(PPh_3)_2$(M=Pt, Pd) reacted with catechols at low temperature to give H_2O_2 and the corresponding catecholato complexes, characterized by their physical properties, in high yields. A similar treatment of $PtO_2(PPh_3)_2$ with *o*-substituted anilines afforded the corresponding adducts and H_2O_2 in moderate yields.

A number of reports have appeared on the formation of catecholato complexes by oxidative addition of *o*-quinones to metal complexes having mainly d^6, d^8, and d^{10} electron configurations.[1-7] We have found that these complexes can also be obtained in high yields by an other route. In this paper we deal with the reaction of dioxygen complexes with catechols which results in the selective formation of catecholato complexes and H_2O_2. The reactivity of dioxygen complexes toward *o*-substituted anilines was also studied, the reactions of square planar dioxygen complexes $MO_2(PPh_3)_2$-(M=Pt, Pd)[8-10] with catechlos being carried out in CH_2Cl_2 or CH_2Cl_2–EtOH(1 : 1 by volume) solvent at low temperature. Hydrogen peroxide formed during the course of reaction was transferred under vacuum (*ca.* 10^{-2} Torr) and then titrated by the conventional iodometric method. The transfer efficiency for H_2O_2 was about 98 percent.

Table 1. Yield of H_2O_2 and catecholato complexes in the reaction of dioxygen complexes with phenols or aromatic diamines at 2 °C[a]

Dioxygen complex (1.97×10^{-2} M)	Phenol or diamine (8.25×10^{-2} M)	Yield (%) H_2O_2	Yield (%) Catecholato complex
$PtO_2(PPh_3)_2$	**1a**[b]	85.1	87.8
	1a[b]	1.22[c]	87.8
	1b	68.3	77.6
	1c	66.5	75.7
	o-Aminophenol	83.2	64.0
	o-Phenylenediamine	57.6	51.5
	Hydroquinone	5.34	
	p-Aminophenol	7.40	
	p-Phenylenediamine	—[d]	
$PdO_2(PPh_3)_2$[e]	**1a**	72.1	68.9
	1b	65.7	63.7
	1c	59.1	65.7
	o-Aminophenol	36.5	
	o-Phenylenediamine	3.58	
	p-Aminophenol	4.44	
	p-Phenylenediamine	—[d]	

a) All the reactions were carried out in 4 ml of CH_2Cl_2-EtOH(1 : 1 by volume) under N_2 for 1 h. b) Reacted in 4 ml of CH_2Cl_2. c) Treated with catalase prior to titration. d) No peroxide was detected by iodometry. e) $[PdO_2(PPh_3)_2]$ was 1.68×10^{-2} M.

$PtO_2(PPh_3)_2$ reacted with catechol(**1a**), 4-*t*-butylcatechol(**1b**), and 3,5-di-*t*-butylcatechol(**1c**) under nitrogen atmosphere to give peroxide in 66—85% yields based on the dioxygen complexes (Table 1). The fact that the amount of peroxide formed considerably decreases by treatment with catalase prior to titration indicates that the peroxide transferred is principally H_2O_2. H_2O_2 was also obtained in moderate yields in the reaction of $PtO_2(PPh_3)_2$ with *o*-aminophenol and *o*-phenylenediamine. Similarly reaction of $PdO_2(PPh_3)_2$ with **1a**, **1b**, and **1c** gave H_2O_2 in 59—72% yields. No H_2O_2 is formed under N_2 in the absence of $MO_2(PPh_3)_2$. This suggests that the peroxide titrated was driven from the coordinated molecular oxygen of $MO_2(PPh_3)_2$. The yields of H_2O_2 obtained in the reactions of the dioxygen complexes with *p*-substituted phenols were much less than those obtained by use of the corresponding *o*-isomers. A possible explanation may beth at catechol dianions are suitable ligands for the formation of these complexes.

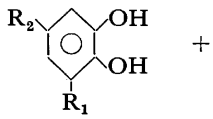

+ $MO_2(PPh_3)_2$ ⟶

1a; $R_1=R_2=H$ M=Pt, Pd
1b; $R_1=H$, $R_2=t$-Bu
1c; $R_1=R_2=t$-Bu

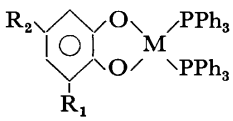

+ H_2O_2

2a; M=Pt, $R_1=R_2=H$
2b; M=Pt, $R_1=H$, $R_2=t$-Bu
2c; M=Pt, $R_1=R_2=t$-Bu
2d; M=Pd, $R_1=R_2=H$
2e; M=Pd, $R_1=R_2=t$-Bu

1a reacted with $MO_2(PPh_3)_2$ to yield, along with H_2O_2, new four-coordinate complexes, **2a** and **2d**, as yellow and blue crystals, respectively. Similarly **1b** and **1c** reacted with $PtO_2(PPh_3)_2$ to yield orange complexes, **2b** and **2c**, respectively. The results of elemental analyses are in line with the proposed structures(**2a** Found: C, 60.03; H, 4.01; P, 6.99%. Calcd for $C_{42}H_{34}O_2P_2Pt$: C, 60.94; H, 4.15; P, 7.48%. **2b** Found: C, 62.35; H, 4.62; P, 6.98%. Calcd for $C_{46}H_{42}O_2P_2Pt$: C, 62.50; H, 4.82; P, 7.01%. **2c** Found: C, 63.98; H, 5.35; P. 6.69%. Calcd for $C_{50}H_{50}O_2P_2Pt$: C, 63.88; H, 5.37; P, 6.59%. **2d** Found: C, 68.81; H, 4.60; P, 8.36%. Calcd for $C_{42}H_{34}O_2P_2Pd$: C, 68.25; H, 4.65; P, 8.38%. NMR($CDCl_3$)[11] **2a**: δ 7.21(m, 30H, PPh_3) *ca.* δ 6.42(m, 4H, C_6H_4). **2b**: δ 7.23(m, 30H, PPh_3), δ 6.50—6.41(m, 3H, C_6H_3), δ 1.23(s, 9H, Bu^t). **2c**:

Table 2. IR data (cm^{-1}) of the complexes in Nujol[a)]

Complex	Bands characteristic of the *o*-diolato ligands						$\nu(PPh_3)$	$\nu(O\text{-}O)$
2a	1570 w		1267 s	1256 s	1093 sh	998 w	1098 s	
2b	1564 w	1282 m		1259 s	1096 sh	998 w	1098 s	
2c	1557 m	1290 s		1244 s	*ca.* 1097[b)]	996 w	1099 s	
2d	1565 w		1264 s	1253 s	1094 sh	998 w	1098 s	
2e	1551 m	1283 s		1244 s	*ca.* 1097[b)]	996 w	1098 s	
$PtO_2(PPh_3)_2$[c)]							1098 s	821 s
$PdO_2(PPh_3)$[c)]							1098 s	869 s

a) The IR spectra were calibrated with polystyrene film. w weak, m medium, s strong, sh shoulder.
b) Overlapping with the strong PPh_3 band. c) In CH_2Cl_2 solution.

δ 7.26(m, 30H, PPh_3), δ 6.43(br d, 2H, C_6H_2), δ 1.23 (s, 9H, 5-Bu^t), δ 0.99(s, 9H, 3-Bu^t). **2e**: δ 7.24(m, 30H, PPh_3), δ 6.33(br s, 2H, C_6H_2), δ 1.23(s, 9H, 5-Bu^t), δ 0.92(s, 9H, 3-Bu^t).). The infrared spectra (Table 2) of the complexes are similar to each other. The parent catechols show intense hydroxyl absorption at *ca.* 3500 cm^{-1}, but none in the 4000—3100 cm^{-1} region. In the 1800—1500 cm^{-1} region no bands were observed except for a weak band at 1570—1551 cm^{-1} which seems to be the characteristic of the reduced form of the ligand as reported for $Pt(C_6Cl_4O_2)(PPh_3)_2$.[5] All the complexes exhibited intense IR absorption at 1098 cm^{-1} characteristic of the coordinated PPh_3. Other new bands in the complexes were observed at *ca.* 1260, 1093, and 998 cm^{-1} where the parent catechols show no characteristic absorption. The results support the structures illustrated above.

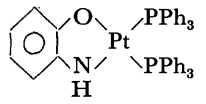

3

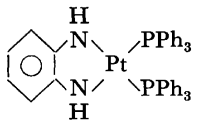

4

3 and **4** were obtained in moderate yields as brown and reddish brown crystals, respectively, by similar reactions of $PtO_2(PPh_3)_2$ with *o*-aminophenol and *o*-phenylenediamine. Analytical data of complexes **3** and **4** are as follows: **3** Found: C, 61.47; H, 4.48; N, 1.44%. Calcd for $C_{42}H_{35}ONP_2Pt$: C, 61.01; H, 4.28; N, 1.66%. **4** Found: C, 60.51; H, 4.54; N, 3.17%. Calcd for $C_{42}H_{36}N_2P_2Pt$: C, 61.08; H, 4.40; N, 3.39%. IR(Nujol) **3**: 3410, 1572, 1291, 1270, 1098, and 997 cm^{-1}, **4**: 3400, 1567, 1298, 1098, and 997 cm^{-1}. Complex **4** is unstable in solution at ambient temperature, decomposing in a few hours to give black precipitates. However, the NMR spectrum of **4** in $CDCl_3$ solution exhibits a singlet absorption at 5.25 and a multiplet at 7.21 ppm. This also indicates the formula $Pt(C_6H_4NHO)(PPh_3)_2$ and $Pt(C_6H_4N_2H_2)(PPh_3)_2$ for **3** and **4**, respectively.

Experimental

Melting points were determined on a Yazawa hot-stage apparatus and are uncorrected. IR spectra were recorded as Nujol mulls on a Nippon Bunko IR-G spectrophotometer (4000—400 cm^{-1}), calibrated with polystyrene film. ^1H NMR spectra were measured in $CDCl_3$ solution on a JEOL JMN PMX 60 spectrometer.

Preparation of Catecholato Complexes. The general procedure for the preparation of catecholato complexes is as follows. Excess catechol(0.22 g, 2.0 mmol) dissolved in EtOH (10 ml) was added dropwise to a stirred solution of $PtO_2(PPh_3)_2 \cdot 1.5C_6H_6$(0.44 g, 0.5 mmol) in CH_2Cl_2(2 ml) at 0 °C. The solution was then stirred for 1 h at 0 °C. At the end of the reaction, the mixture containing an appreciable amount of precipitates was filtered and washed twice with EtOH. Recrystallization from $CHCl_3$ gave yellow crystals in 88% yield. A similar procedure for the preparation of other complexes was employed(yields were 50—80%). Infrared data for individual complexes are given in Table 2.

The authors wish to thank Dr. E. Niki, the University of Tokyo, for his valuable discussions.

References

1) J. S. Valentine and D. Valentine, Jr., *J. Am. Chem. Soc.*, **92**, 5795 (1970).
2) Y. S. Sohn and A. L. Balch, *J. Am. Chem. Soc.*, **93**, 1290 (1971).
3) G. LaMonica, G. Navazio, P. Sandrini, and S. Cenini, *J. Organomet. Chem.*, **31**, 89 (1971).
4) D. M. Barlex, R. D. W. Kemmitt, and G. W. Littlecott, *J. Organomet. Chem.*, **34**, 225 (1972).
5) Y. S. Sohn and A. L. Balch, *J. Am. Chem. Soc.*, **94**, 1144 (1972).
6) A. L. Balch and Y. S. Sohn, *J. Organomet. Chem.*, **30**, C 31 (1971).
7) S. Cenini, R. Ugo, and G. LaMonica, *J. Chem. Soc., A*, **1971**, 416.
8) L. Malatesta and M. Angoletta, *J. Chem. Soc.*, **1957**, 1186.
9) L. Malatesta and C. Cariello, *J. Chem. Soc.*, **1958**, 2323.
10) S. Takahashi, K. Sonogashira, and N. Hagihara, *Nippon Kagaku Zasshi*, **87**, 610 (1966).
11) No NMR spectrum of **2d** was available owing to its low solubility in usual solvents.

BULLETIN OF THE CHEMICAL SOCIETY OF JAPAN, VOL. 50 (9), 2495—2496 (1977)

Friedel-Crafts Reaction of Benzene with 2-Phenylbutanedioic Anhydride

Iwao HASHIMOTO and Ryozo TAKATSUKA

Department of Industrial Chemistry, Wakayama Technical College, Noshima, Nada-cho, Gobo 649-15

(Received March 1, 1977)

Synopsis. The $AlCl_3$-catalyzed acylation of benzene with 2-phenylbutanedioic anhydride was found to give a mixture of 3-benzoyl-2-phenylpropanoic acid, isomeric 3-benzoyl-3-pehnylpropanoic acid, and 3-oxoindan-1-carboxylic acid. The distribution of the products was affected markedly by the amount of $AlCl_3$ or solvents used.

It has been reported in earlier publications[1-5] that the acylation of benzene with 2-phenylbutanedioic anhydride (**1**) gave only the intermolecular acylation products, 3-benzoyl-2-phenylpropanoic acid (**2**) and 3-benzoyl-3-phenylpropanoic acid (**3**), in low yields (6.9 and 7.5%, respectively). However, the reaction mechanism discussed on the basis of such low yields does not appear to afford a rational mechanism, and furthermore, there is the possibility of intramolecular acylation of **1** itself. In the present work, the acylation of benzene with **1** was studied in more detail and the solvent effect was examined.

Results and Discussion

Ten mmol of **1** reacted almost quantitatively with 20 mmol of $AlCl_3$ in a large excess of benzene (550 mmol) to give a mixture of **2** and **3**, in which the yield of **3** was about twice as much as that of **2**.

When acylation using a lesser amount of benzene (10 mmol) was carried out in the presence of 20 mmol of $AlCl_3$ in 1,2-dichloroethane, a considerable amount of **4**, an intramolecular acylation product, was formed along with **2** and **3**. A high yield (93%) of **4** was also obtained in the absence of benzene using 1,2-dichloroethane as a solvent. These facts indicate that both inter- and intramolecular acylations occur competitively in the reaction system. A decrease in the amount of $AlCl_3$ in 1,2-dichloroethane resulted in a greater decrease in the yield of **3** than those of **2** and **4**, or higher (**2**+**4**)/(**3**) ratio.

Acylation in nitrobenzene gave the same products, accompanied by a small amount of 2,4-diphenyl-3-buten-4-olide (**5**). However, the yield of **3** was low even with a greater amount (30 mmol) of $AlCl_3$ and it was always less than that of **2**.

These results suggest the following reaction paths: In the presence of a sufficient amount (20 mmol) of $AlCl_3$, the acylating agent should be the acyl halide complexes (**2b** and **3b**), because one molecule of dibasic acid anhydride requires two molecules of $AlCl_3$ to form an acyl halide complex.[6] The electrophilic reactivity of **3b** having an electron-attracting phenyl group closer to the acylium cation may be greater than that of **2b**, hence, **3** is formed preferentially, even though the concentration of **3b** is lower than that of species **2b** (or **2a**).

However, for an insufficient amount of $AlCl_3$ (10 mmol), complexes of the entire anhydride molecule

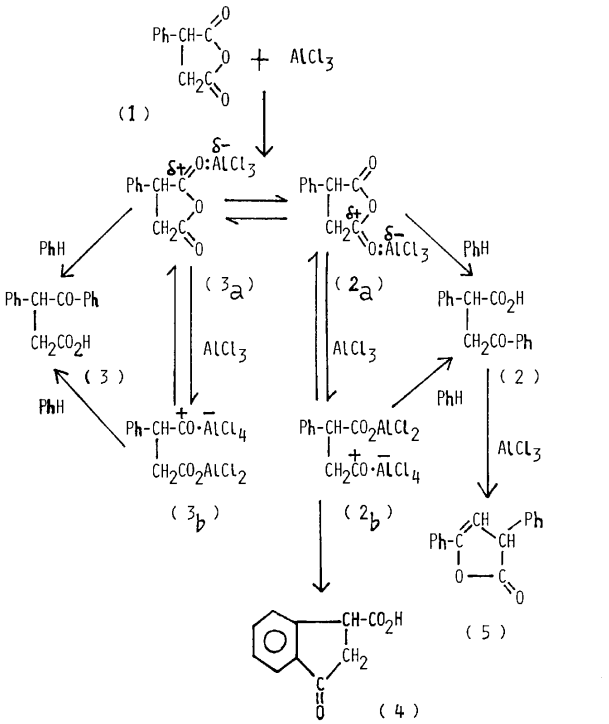

Scheme 1.

coordinated with one molecule of $AlCl_3$ (**2a** and **3a**) should appear as the actual acylating agents.[7] The concentration of the complex, **2a**, in which $AlCl_3$ is added to the oxygen atom separated from the phenyl group, should be higher than that of **3a** (or **3b**). Complex **2a** should afford **2** and **4** upon acylation, although **4** may be formed preferentially *via* **2b**. Therefore, a decrease in the amount of $AlCl_3$ leads to an increase in the ratio (**2**+**4**)/(**3**).

Since nitrobenzene is a polar solvent, the polarized complexes (**2b** and **3b**) should be strongly solvated by nitrobenzene to form bulky acylating species. Such bulky acylating species may be unfavorable for the electrophilic attack on the benzene molecule, hence, the yields of **2** and **3** become low. Furthermore, the complex formation between nitrobenzene and $AlCl_3$ may decrease the effective amount of $AlCl_3$ and thus unfavorably affect the formation of **3a** (or **3b**) with the result that the yield of **3** is low.

The reaction of isolated **2** with $AlCl_3$ in nitrobenzene gave **5** *via* the enolization of **2**.

Experimental

General Procedure for the Acylation of Benzene with 2-Phenylbutanedioic Anhydride (1). To a solution of benzene and $AlCl_3$ in $ClCH_2CH_2Cl$ was gradually added a solution of **1** in $ClCH_2CH_2Cl$. The reaction mixture was stirred at 25 °C for 5 h, poured onto crushed ice containing 6 ml of concd

Table 1. $AlCl_3$-catalyzed acylation of benzene with 2-phenylbutanedioic anhydride (10 mmol) at 25 °C for 5 h

Solvent	$AlCl_3$ (mmol)	C_6H_6 (mmol)	Product yields[a] (%)			(2+4)/(3)
			2	3	4	
None	10	550	19	29	trace	0.7
	20	550	29	69	trace	0.4
	30	550	30	69	trace	0.4
$(ClCH_2)_2$	20	0	—	—	93	
10 ml	30	0	—	—	93	
	5	10	3	7	6	1.3
	10	10	7	18	12	1.1
	20	10	21	59	19	0.7
	10	20	11	28	9	0.7
	20	20	24	66	9	0.5
$C_6H_5NO_2$[b]	30	0	—	—	39	
10 ml	20	10	10	5	16	5.2
	30	10	14	10	23	3.7[c]
	30	20	25	15	23	3.3[c]

a) Calculated on the basis of the amount of 2-phenylbutanedioic anhydride used. b) The reaction time was one day. c) **5** was obtained in a yield of less than 1%.

HCl, and then extracted with ether. After removal of the solvent, the crude keto carboxylic acids were methylated with an ethereal solution of diazomethane. The resulting esters were analyzed by means of GLPC employing a Yanagimoto G 800 T Model chromatograph on a 1.5 m×3 mm column packed with Apiezon Grease M (5 wt%) with a He flow of 40 ml/min at 205 °C. Benzyl benzoate was used as an internal standard.

The authors are very grateful to Professor Yoshiro Ogata of Nagoya University for valuable discussions concerning this work.

References

1) A. Ali, R. D. Desai, R. F. Hunter, and S. M. M. Muhammad, *J. Chem. Soc.*, **1937**, 1013.
2) M. A. Saboor, *J. Chem. Soc.*, **1945**, 922.
3) F. G. Badder, H. A. Fahim, and A. M. Fleifel, *J. Chem. Soc.*, **1955**, 2199.
4) M. A. Wali, A. K. Khalli, R. L. Bhatia, and S. S. Ahamad, *Proc. Indian Acad. Sci.*, **14 A**, 139 (1941).
5) D. P. N. Satchell, *J. Chem. Soc.*, **1961**, 3822.
6) A. G. Peto, "Acylation with Di- and Polycarboxylic Acid Derivatives in Friedel-Crafts and Related Reactions," Vol. 3, Part 1, ed by G. A. Olah, Interscience Publishers, New York (1964), p. 536.
7) W. R. Edwards, Jr., and R. J. Eckert, Jr., *J. Org. Chem.*, **28**, 674 (1963).

BULLETIN OF THE CHEMICAL SOCIETY OF JAPAN, VOL. 50 (9), 2497—2498 (1977)

An Efficient Synthesis of Bicyclo[3.1.0]hex-3-en-2-one

Masaji ODA,* Yoshinori KANAO, Masaji KASAI, and (the late) Yoshio KITAHARA

Department of Chemistry, Faculty of Science, Tohoku University, Sendai 980

(Received March 19, 1977)

Synopsis. Bicyclo[3.1.0]hex-3-en-2-one is synthesized in fair yield in five steps from 4-cyclopentene-1,3-dione-furan Diels-Alder adduct.

Although a good number of derivatives of bicyclo-[3.1.0]-hex-3-en-2-one (**1**) have been described, there is only one paper dealing with the synthesis of the parent componnd.[1] The preparation starts from 2-cyclopentenone and the total yield is poor. We have recently reported the preparation of 4-cyclopentene-1,3-dione-furan Diels-Alder adduct (*exo*-10-oxatricyclo[5.2.1.$0^{2,6}$]-dec-8-en-3,5-dione) (**2**).[2] In view of ready thermal cycloreversion of furan–Diels-Alder adducts[3] and of high reactivities of 1,3-diones, the adduct (**2**) could be a versatile synthetic intermediate for cyclopentenoids. We here describe an efficient synthesis of the parent compound (**1**) from **2**.

Treatment of **2** with a slight excess of triethyloxonium tetrafluoroborate[4] in the presence of triethylamine in methylene chloride afforded the enol ether (**3**) in quantitative yield. The enol ether (**3**) was then converted into the cyclopentenone derivative (**4**) by reduction with lithium aluminum hydride and following acid hydrolysis of the resulting hydroxy enol ether with aqueous acetic acid in 54% overall yield.

Cyclopropanation of **4** using dimethylsulfoxonium methylide[5] in dimethyl sulfoxide gave the cyclopropyl ketone (**5**) in 84% yield. The configuration of the cyclopropane ring is tentatively assigned to be *anti* to the 2,5-dihydrofuran moiety on the basis of steric hindrance.

As expected, the thermal cycloreversion of **5** to **1** was fairly easy: on heating in a short-path distillating apparatus[6] at 120—140 °C at the pressure of 200 mmHg, **5** gave almost pure material of **1** in 76% yield.

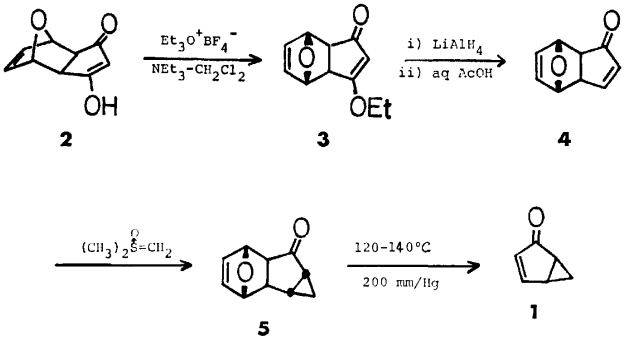

Chart.

Experimental

Melting points were uncorrected. IR spectra were recorded with a Hitachi 215 grating spectrometer and PMR with a Varian A-60A and a JEOL PMX-60 spectrometers. Microanalyses were performed at the Microanalytical Laboratory in this department.

*5-Ethoxy-10-oxatricyclo[5.2.1.$0^{2,6}$]deca-4,8-dien-3-one (**3**).* To a solution of 10-oxatricyclo[5.2.1.$0^{2,6}$]deca-8-en-3,5-dione (**2**)[2] (10.0 g, 61 mmol) and triethylamine (7.88 g, 78 mmol) in methylene chloride (100 ml) was added rapidly triethyloxonium tetrafluoroborate (14.0 g, 74 mmol) at room temperature. After stirring for one hour, the reaction mixture was washed with water (30 ml×5), dried over $MgSO_4$, and the solvent evaporated off under reduced pressure to give 11.7 g (100%) of **3** as solids. Recrystallization from benzene gave pure materials, mp 137—138 °C. IR (KBr) 1674, 1582 cm^{-1}; PMR ($CDCl_3$) δ 6.53 (2H, s), 5.37 (1H, s), 5.12 (1H, br. s), 5.04 (1H, br. s), 4.14 (2H, q, J 7.0 Hz), 2.88 (1H, d, 5.6), 2.57 (1H, d, 5.6), 1.44 (3H, t, 7.0). Found: C, 68.66; H, 6.54%. Calcd for $C_{11}H_{12}O_3$: C, 68.73; H, 6.29%.

*9-Oxatricyclo[5.2.1.$0^{2,6}$]deca-4,8-dien-3-one (**4**).* To a suspension of lithium aluminum hydride (1.14 g, 30 mmol) in ether (150 ml) was added dropwise a solution of the crude **3** (11.7 g, 61 mol) in tetrahydrofuran (150 ml) under stirring in an ice-bath. The mixture was then stirred at room temperature for two hours. Water (10 ml) was cautiously added to the reaction mixture under ice-cooling and then 20 g of $MgSO_4$. The solids were filtered with suction and washed with tetrahydrofuran (50 ml×3), and the filtrate concentrated to leave 11.2 g of oil which on standing mostly crystallized. The crude product was then dissolved in 60% aqueous acetic acid (50 ml) and the solution was allowed to stand at room temperature for two days. The mixture was added with methylene chloride (250 ml), and the organic layer was washed with water (50 ml×3), saturated aqueous sodium carbonate until no more carbon dioxide evolved, and finally with brine, and the organic layer dried. Removal of the solvent left 8.6 g of pale yellow oil. Chromatography on silica gel (100 g) using benzene–ethyl acetate as eluent afforded 4.9 g (54%) of **4**, mp 69—70 °C. IR (KBr) 1692, 1584 cm^{-1}; PMR ($CDCl_3$) δ 7.65 (1H, ddd, J 5.6, 2.5, 0.5 Hz), 6.5 (2H, m), 6.24 (1H, dd, 5.6, 1.3), 4.99 (1H, m), 4.78 (1H, m), 3.01 (1H, ddd, 5.0, 2.5, 1.3), 2.39 (1H, d, 5.0). Found: C, 72.99; H, 5.44%. Calcd for $C_9H_8O_2$: C, 72.96; H, 5.44%.

*11-Oxatetracyclo[6.2.1.$0^{2,7}$.$0^{4,6}$]undec-9-en-3-one (**5**).* To a solution of dimethylsulfoxonium methylide prepared *in situ* from trimethylsulfoxonium iodide (4.0 g, 18 mmol) and sodium hydride (450 mg, 18.8 mmol) in dimethyl sulfoxide (25 ml) was added **4** (2.40 g, 16 mmol) under nitrogen atmosphere at room temperature. After one hour, ice-water (150 ml) was added and the mixture extracted with methylene chloride (50 ml×3), and the organic layer was washed with water (25 ml×2), and dried. After removal of the solvent, the residue was passed through a short silica gel column (30 g) to afford 2.20 g (84%) of **5**, mp 46—48 °C. IR (KBr) 1712 cm^{-1}; PMR (CCl_4) δ 6.4 (2H, m), 4.9 (2H, m), 2.28 (1H, d, J 6.0 Hz), 2.1—1.8 (3H, m), 1.15 (1H, dddd, 8.5, 7.5, 4.5, 1.3), 0.61 (1H, dt, 4.5, 4.0). Found: C, 74.10; H, 6.33%. Calcd for $C_{10}H_{10}O_2$: C, 74.05; H, 6.22%.

*Bicyclo[3.1.0]hex-3-en-2-one (**1**).* The cyclopropyl ketone (**5**) (207 mg) was heated in a short-path distillating apparatus[6] at 120—140 °C under the reduced pressure of

200 mmHg. After about 20 min, 91 mg (76%) of almost pure **1** was distilled. IR (liquid film) 1712, 1692, 1568 cm^{-1}; UV (MeOH) λ 210 (sh, ε 4940), 251 (2060), 325 nm (90). PMR data were identical with the reported ones.[1)]

References

1) G. A. Russel and G. R. Stevenson, *J. Am. Chem. Soc.*, **93**, 2432 (1971).
2) M. Oda, M. Kasai, and Y. Kitahara, *Chem. Lett.*, **1977**, 307.
3) For a recent application of ready cycloreversion of a furan Diels-Alder adduct, see S. Takano and K. Ogasawara, *Synthesis*, **1974**, 42.
4) H. Meerwein, *Org. Synth.*, **46**, 113 (1966).
5) E. J. Corey and M. Chaykovsky, *J. Am. Chem. Soc.*, **84**, 867 (1962); **87**, 1353 (1965).
6) The apparatus used here for short-path distillation is a sublimator attached with a small dish at the bottom of the cold finger.

BULLETIN OF THE CHEMICAL SOCIETY OF JAPAN, VOL. 50 (9), 2499—2500 (1977)

The Structure of Sendanolactone, a New Triterpenoid from *Melia azedarach* L. *var. japonica* Makino

Masamitsu Ochi, Hiyoshizo Kotsuki, Takashi Tokoroyama,* and Takashi Kubota**

Faculty of Science, Kochi University, Asakura, Kochi 780

**Faculty of Science, Osaka City University, Sugimoto-cho, Sumiyoshi-ku, Osaka 558*

***School of Medicine, Kinki University, Sayama-cho, Osaka 589*

(Received March 24, 1977)

Synopsis. Sendanolactone, a new tetracyclic triterpenoid from the bark of *M. azedarach* L. *var. japonica* Makino, was determined as 3,6-dioxo-13α,14β,17α-lanosta-7,24-dien-21,16β-olide on the basis of chemical and spectroscopic evidence.

In the course of an investigation of limonoids of *M. azedarach* L. *var. japonica* Makino,[1] a new tetracyclic triterpenoid was obtained. In this paper, the isolation and structural elucidation of this compound designated as sendanolactone is treated.

Sendanolactone (I), $C_{30}H_{42}O_4$, mp 208.5—209 °C, $[\alpha]_D^{14.5}$ −30° (*c* 0.1, EtOH), was isolated in a 0.008% yield from an methanol extract of the bark of *M. azedarach* L. *var. japonica* Makino by partitioning and careful silica gel column chromatography. The IR, UV, and NMR spectra of I indicate the presence of the following groups: one γ-lactone (1780 cm^{-1}), one six-membered ring ketone (1715 cm^{-1}), one α,β-unsaturated ketone [1655 and 1625 cm^{-1}; 246 nm (ε 16400)], five tertiary methyls [δ 1.00, 1.13, 1.34 (3H each, s), and 1.38 (6H, s)], two vinylic methyls [δ 1.64 and 1.72 (3H each, br s)], and one trisubstituted double bond [δ 5.11 (1H, m)]. The reduction of I with sodium borohydride in methanol, followed by acetylation, gave II, $C_{35}H_{52}O_7$, mp 204.5—205 °C, and III, $C_{36}H_{54}O_7$, mp 154.5—155 °C. The UV spectra of both products still showed the presence of the conjugated enones. The NMR spectrum of II indicates signals due to two acetate groups [δ 2.00 and 2.07 (3H each, s)] and a methyl ester [δ 3.62 (3H, s)], whereas that of III shows the presence of three acetate groups [δ 1.99, 2.04, and 2.07 (3H each, s)] and an acetylated hydroxymethyl [δ 4.03 (2H, d, J=4 Hz)], instead of the methyl ester. The formation of these products is explained as follows. The opening of the γ-lactone ring due to transesterification occurs concurrently with the reduction of the saturated ketone both in II and III during the sodium borohydride treatment, and further reduction of the resultant methoxycarbonyl group ensued in the latter.

These facts and the analogy with the structures of the triterpenes isolated from the *Melia* species[2] suggest a euphane or tirucallane skeleton for I, the side chain of which contains a double bond between C_{24} and C_{25}.

The location of the conjugated enones was proven by the following data. The NMDR experiments of I show the presence of a $-CO-CH_A=\overset{|}{C}-\overset{|}{C}H_B-$ grouping [δ_A 5.78 (1H, d, J=3 Hz) and δ_B 2.96 (1H, m)], in which the dihedral angle between H_A and H_B is roughly 90°. In the NMR spectrum of I, the signal due to the methine proton adjacent to the carbonyl appears as a sharp singlet (δ 2.46). Consequently, the conjugated enone

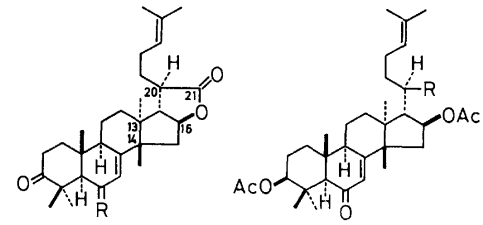

I R = O II R = CO_2Me

IV R = H,H III R = CH_2OAc

must be located on the B-ring (7-en-6-one). Possible locations of γ-lactone are C_{21}–C_{23} and C_{21}–C_{16}. The NMR spectrum of I contains a signal due to the methine proton on an oxygenated carbon as a doublet of paired doublets (J=10, 10, and 8 Hz) at δ 4.18. This observation indicates that the oxy linkage of the lactone is at C_{16} and is β-oriented. From biogenetic considerations, it would be most reasonable to place the remaining carbonyl in I at C_3. This was verified by the following evidence. The NMR spectrum of I includes signals due to the methyls at C_4 and C_{10} at a rather low field [δ 1.38 (6H) and 1.33 (3H)], while those of II and III exhibit the corresponding signals at a somewhat higher field [II: δ 1.21 (6H) and 1.23 (3H); III: δ 1.19 (6H) and 1.21 (3H)]. Moreover, the solvent shifts ($\Delta=\delta^{CDCl_3}-\delta^{C_6D_6}$) of these signals in I, given in Table 1, are consistent with the case of 3,6-dione.[3]

Table 1. Solvent shifts ($\Delta=\delta^{CDCl_3}-\delta^{C_6D_6}$) of C_4 and C_{10}-methyls in I

	δ^{CDCl_3}	$\delta^{C_6D_6}$	Δ
C_4-α-Me	1.38	1.64	−0.26
C_4-β-Me	1.38	1.42	−0.04
C_{10}-Me	1.33	0.82	+0.51

Therefore, sendanolactone must be represented by structure I.[4] The proposed structure is quite analogous to that of kulactone (IV)[2e] isolated from *M. azedarach* L., the typical variety, except for the presence of the ketonic group at C_6, and the spectral data of I are in good agreement with those of IV, except for the environment of the conjugated enone.

The structure of sendanolactone was eventually established from an X-ray analysis as 3,6-dioxo-13α,14β,17α-lanosta-7,24-dien-21,16β-olide (I),[5] which is in full agreement with the structure derived from the chemical and spectral data mentioned above.

Sendanolactone is the first compound of the euphane

series which has an oxygen substituent at C_6.

Experimental

All mps are uncorrected. The IR and UV spectra were recorded on a JASCO model IR-S and a Hitachi EPS-3T spectrophotometer, respectively. The NMR spectra were determined, using a JEOL PS-100 spectrometer, in $CDCl_3$ solutions with TMS as an internal standard unless otherwise stated. A Rex Optical Works model NEP-2 apparatus was used for the rotation measurement.

Isolation. Air-dried bark of *M. azedarach* L. *var. japonica* Makino (6 kg), collected in Kochi, in July 1974, was cut into small pieces and extracted with methanol (50 l) for one month. The methanol extract was concentrated up to about 5 l and washed with petroleum ether. The methanol layer was again concentrated up to 1 l, diluted with water (2 l), and extracted with ether. The ether layer was dried over Na_2SO_4 and evaporated to dryness. The residue (32 g) was repeatedly subjected to chromatography over silicic acid. Elution with $CHCl_3$–MeOH (49 : 1) gave sendanolactone (I) (470 mg): needles from methanol; mp 208.5—209 °C, $[\alpha]_D^{14.5}$ −30° (*c* 0.1, EtOH); MS *m/e* 466 (M^+). Found: C, 76.89; H, 9.12%. Calcd for $C_{30}H_{42}O_4$: C, 77.21; H, 9.07%.

Reduction of I With $NaBH_4$. To a solution of I (200 mg) in methanol (50 ml) were added excess amounts of $NaBH_4$ (200 mg). The mixture was stirred for 30 min at 0 °C. The solution was then concentrated, diluted with water (100 ml), and extracted with ether. The ether layer was washed with water, dried over Na_2SO_4, and evaporated to dryness. The residue was subjected to chromatography over silicic acid; subsequent elution with $CHCl_3$–MeOH (99 : 1) gave a diol and a triol.

The diol (84 mg) was acetylated with acetic anhydride (2 ml) and pyridine (2 ml) and then worked up in the usual manner to afford II (65 mg): needles from methanol, mp 204.5—205 °C; IR (Nujol) 1735 and 1660 cm^{-1}; UV (EtOH) 244 nm (ε 16700). Found: C, 71.93; H, 9.06%. Calcd for $C_{35}H_{52}O_7$: C, 71.88; H, 8.96%.

The triol (40 mg) was acetylated in the same manner as described above to give III (21 mg): needles from aqueous ethanol, mp 154.5—155 °C; IR (Nujol) 1740 and 1670 cm^{-1}; UV (EtOH) 245 nm (ε 12700). Found: C, 72.16; H, 9.06%. Calcd for $C_{36}H_{54}O_7$: C, 72.21; H, 9.09%.

We are grateful to Drs. M. Shiro and H. Nakai of Shionogi Research Laboratory for carring out the X-ray analysis and to Dr. Y. Hirose and Mr. H. Naoki of the Institute of Food Chemistry for recording the mass spectrum.

References

1) M. Ochi, H. Kotsuki, K. Hirotsu, and T. Tokoroyama, *Tetrahedron Lett.*, **1976**, 2877.

2) (a) D. Lavie, M. K. Jain, and I. Kirson, *Tetrahedron Lett.*, **1966**, 2049; (b) D. Lavie, M. K. Jain, and I. Kirson, *J. Chem. Soc., C*, **1967**, 1347; (c) D. Lavie, M. K. Jain, and S. R. Shpan-Gabrielith, *Chem. Commun.*, **1967**, 910; (d) F. C. Chang and C. Chiang, *ibid.*, **1968**, 1156; (e) F. C. Chang and C. Chiang, *Tetrahedron Lett.*, **1969**, 891; (f) Y. Inubushi and T. Hibino, *Yakugaku Zasshi*, **90**, 99 (1970).

3) (a) N. S. Bhacca and D. H. Williams, *Tetrahedron Lett.*, **1964**, 3127; (b) D. H. Williams and N. S. Bhacca, *Tetrahedron*, **21**, 2021 (1965).

4) The configuration at C_{20} is based on X-ray analysis. See also Ref. 5.

5) Private communication. M. Shiro and H. Nakai, *Acta Crystallogr.*, to be published.

BULLETIN OF THE CHEMICAL SOCIETY OF JAPAN, VOL. 50 (9), 2501—2502 (1977)

A Convenient and General Preparation of Diphenyl Tellurium Dicarboxylates

Seizo TAMAGAKI, Isao HATANAKA, and Seizi KOZUKA

Department of Applied Chemistry, Faculty of Engineering, Osaka City University, Sugimoto-cho, Sumiyoshi-ku, Osaka 558

(Received March 24, 1977)

Synopsis. A number of diphenyl tellurium dicarboxylates were readily prepared from diphenyl telluroxide and carboxylic acids or anhydrides. Some of them were also derived through the carboxylate exchange from readily available tellurium carboxylates.

While several diaryl tellurium dicarboxylates have been prepared either by the reaction between the corresponding tellurium dichlorides and metal carboxylates[1] or *via* the lead tetraacetate oxidation of tellurides,[2] little attention has been paid to the preparation in which telluroxides serve as starting materials.

$$Ar_2TeCl_2 + 2AgOCOR \longrightarrow Ar_2Te(OCOR)_2 + 2\,AgCl$$

$$Ar_2Te + Pb(OAc)_4 \longrightarrow Ar_2Te(OAc)_2 + Pb(OAc)_2$$

Herein we wish to present facile methods for the preparation of a number of tellurium dicarboxylates from diphenyl telluroxide.

Results and Discussion

Diphenyl telluroxide, easily prepared from diphenyl tellurium dichloride by aqueous sodium hydroxide hydrolysis,[3] was allowed to react with an equiv of acetic anhydride in chloroform for 30 min at room temperature and evaporation of the solvent and recrystallization of the resulting residue from chloroform–hexane gave a crystalline product (I) almost quantitatively.

$$\text{a)}\ Ph_2Te{=}O + Ac_2O \xrightarrow[30\,min]{r.t.,} Ph_2Te(OAc)_2 \qquad (I)$$

TABLE 1. PRODUCT YIELDS AND PHYSICAL PROPERTIES OF TELLURIUM DICARBOXYLATES

Dicarboxylate	Method	Yield, %	Mp, °C	IR[d]	NMR[e]	Elemental anal. Found	Calcd
$Ph_2Te(OCOH)_2$	b	95	122—124	1637	8.22(s) 7.25—8.06(m)	C, 45.31 H, 2.99	45.22 3.25
	c	79					
$Ph_2Te(OCOCH_3)_2$	a	89	143—145	1645	7.30—7.95(m) 1.95(s)	lit, mp 138—141 °C[1]	
	b	97					
$Ph_2(OCOPr^i)_2$	a	93	108—109	1637	7.27—7.94(m) 2.20—2.70(m) 1.00(s) 1.12(s)	C, 51.97 H, 5.09	52.68 5.30
	b	91					
	c	68					
$Ph_2Te(OCOBu^t)_2$	b	87	137—140	1642	7.25—7.97(m) 1.08(s)	C, 54.46 H, 5.79	54.59 5.83
	c	56					
$Ph_2Te(OCOPh)_2$	a	88	161—163	1650	8.01—7.30(m)	lit, mp 159—161 °C	
	b	77					
	c	77					
$Ph_2Te(OCOCH_2Ph)_2$	b	92	99—100	1644	7.09—7.79(m) 7.79(m) 7.17(s) 3.49(s)	C, 60.63 H, 4.29	60.91 4.38
	c	79					
$Ph_2Te(OSO_2Tol)_2$	a	79	282—285	1218 1195 1180	7.10—7.95(m) 2.26(s)	C, 48.83 H, 3.80	50.03 3.88
	b	71					
	c	74					
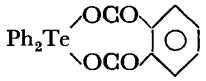	a	93	181—185	1643	7.20—8.12(m)	C, 54.42 H, 3.25	53.87 3.16
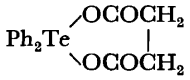	a	99	115—119	1645	7.25—8.04(m) 2.43(s)	C, 48.36 H, 3.74	48.30 3.55

a) From carboxylic anhydrides. b) From carboxylic acids. c) By carboxylate exchange reaction. The values indicated are unreacted amounts of the starting diacetate, which were determined by NMR measurements 5 minutes after diphenyl tellurium diacetate was mixed with two moles of acids. d) $\nu_{C=O}$ (KBr) cm^{-1}. e) Spectra were measured in $CDCl_3$. Line positions are reported in δ (ppm).

Likewise, other commercially available acid anhydrides could be employed for the synthetic purposes and the treatment of diphenyl telluroxide with sulfonic anhydride such as *p*-toluenesulfonic anhydride afforded diphenyl tellurium bistoluenesulfonate (II) in good yield.

$$Ph_2Te{=}O + (TolSO_2)_2O \longrightarrow Ph_2Te(OSO_2Tol)_2 \qquad (II)$$

Various dicarboxylates thus obtained were satisfactorily characterized by elemental analyses, and IR and NMR spectra. The data are summarized in Table 1.

When desired carboxylic anhydrides are not available on hand, instead the corresponding carboxylic acids may be used as well. Thus, treatment of the telluroxide with 2 equiv of acetic acid in chloroform at room temperature resulted in the formation of the tellurium diacetate (I) quantitatively.

$$\text{b)}\ Ph_2Te{=}O + 2AcOH \xrightarrow{\text{r.t., 30 min}} I + H_2O$$

Quite recently McWhinnie *et al.*[4] have reported that sodium salt of ortho-phthalic acid reacts with diaryl tellurium dichlorides to give dimeric tellurium phthalates. It is of particular interest, however, that the methods described here are applicable to dicarboxylic anhydrides and acids such as phthalic, maleic, malonic, and succinic acids giving quantitative yields of monomeric or oligomeric esters. Especially, the melting point of monomeric compound III (mp: 181—185 °C) is markedly different from that of the dimeric ester (mp: 108—110 °C) provided by McWhinnie *et al.*

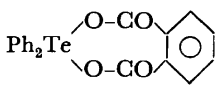

(III)

MW(obsd): 438

The application of this method to propiolactones failed to give discrete monomeric compounds, but led to the formation of oligomeric compounds with molecular weight larger than 1000.

$$Ph_2Te{=}O + O{=}C(CH_2)O \longrightarrow -(Ph_2Te{-}OCOCH_2CR_2O)-_{n=3-4}$$

(R = H, Ph)

Meanwhile, although McWhinnie's attempt to obtain a pure product from formic acid was unsuccessful, the preparation of diphenyl tellurium diformate was attained in a nearly quantitative yield by the reaction of the telluroxide with a slight excess of formic acid. Alternatively, the same formate ester could be given by the ligand exchange reaction of the corresponding diacetate with a large excess of formic acid. In general, less acidic carboxylic acids tend to be more readily expelled from the tellurium center than more acidic ones do.

$$\text{c)}\ Ph_2Te(OAc)_2 + 2HCOOH \xrightarrow{\text{r.t., 10 min}} Ph_2Te(OCOH)_2$$

The methods described are quite simple and hence convenient because a variety of carboxylic acids and anhydrides is commercially available and can be directly used without conversion into their sodium or silver salts.

Experimental

A typical procedure was as follows: diphenyl telluroxide and an equimolar amount of carboxylic anhydrides or acids were dissolved in dry chloroform. The reaction mixture was allowed to react at room temperature for 30 min. After evaporation of the solvent, the residue was recrystallized from chloroform–hexane. A similar procedure was also employed for carboxylate exchange reactions by using excess of desired carboxylic acids. Yields and physical properties of products are listed in Table 1.

References

1) B. C. Pant, *J. Organomet. Chem.*, **65**, 51 (1974).
2) B. C. Pant, *Tetrahedron Lett.*, **1972**, 4779.
3) F. Kraft and R. E. Lyons, *Ber.*, **27**, 1768 (1894).
4) N. Dance and W. R. McWhinnie, *J. Orgamomet. Chem.*, **104**, 317 (1976).

BULLETIN OF THE CHEMICAL SOCIETY OF JAPAN, VOL. 50 (9), 2503—2504 (1977)

Alicyclic Terpenoids from Cyclocitryl Phenyl Sulfides. V. A Synthesis of Ferruginol

Sigeru TORII,* Kenji UNEYAMA, and Kazuhide HAMADA

Department of Industrial Chemistry, School of Engineering, Okayama University, Okayama 700

(Received April 30, 1977)

Synopsis. Ferruginol a precursor for taxodione synthesis, was prepared by the coupling of C(10) units between 2-(phenylsulfonylmethyl)-1,3,3-trimethylcyclohexane and 3-isopropyl-4-methoxybenzyl bromide followed by desulfonation and acid-catalyzed cyclization.

Taxodione (**1**), a tumor-inhibitory diterpene, has been isolated from *Taxodium distichum* Rich (Taxodiaceae) by Kupchan *et al.*[2] Because of its significant tumor-inhibitory activity, its synthesis attracted our attention. Mori *et al.* succeeded the transformation of podocarpic acid into **1** *via* ferruginol (**2**) by several modifications on B and C rings.[3] Matsumoto *et al.* prepared **1** starting from 2,3-dimethoxyisopropylbenzene by C→B →A ring construction[4a] and also from abieta-8,11,13-trienoate (**3**).[4b] Recently, the same authors reported a new route to **1** from methyl ether of **2**.[5]

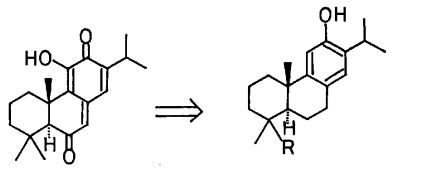

1 2 R=Me ; 3 R=CO_2H

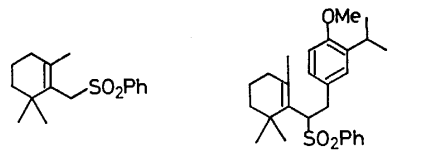

4 5

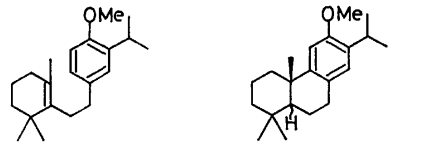

6 7a cis ; 7b trans

Considering the synthetic design of **1**, ferruginol (**2**) must be one of the desirable precursors of **1** and therefore should be prepared by a simple and practical method, since the reported syntheses involved many steps and unsatisfactory yields.[6] Here, we describe an efficient synthesis of **2** by the coupling of C(10) units between 2-(phenylsulfonylmethyl)-1,3,3-trimethylcyclohexene (**4**) and 3-isopropyl-4-methoxybenzyl bromide followed by desulfonation and acid-catalyzed cyclization.

The sulfone, **4**, is a synthon of cyclocitral and can react effectively with carbonyls, halides, and epoxides[7] as a nucleophile. Thus, the reaction of **4** with 3-isopropyl-4-methoxybenzyl bromide afforded **5** in 92% yield on treatment with butyllithium in THF at −70 C°. Desulfonation of **5** was accomplished selectively in 80% yield, without reducing the anisole ring, by the action of potassium in liquid ammonia at −65 °C. Cyclization of **6** thus obtained was performed quantitatively by stirring in AcOH–H_2SO_4 (9 : 1) to afford **7** as a mixture (6 : 4) of *cis*-**7a** and *trans*-**7b**. The isomers were separated by VPC and identified spectroscopically with those reported.[8] Demethylation of *trans*-**7b** with boron tribromide in dichloromethane gave **2** as a sole product. The spectral data of **2** was consistent with those reported.[3,6g]

Experimental

Melting point is uncorrected. IR spectra were determined with a JASCO IRA-1 infrared spectrophotometer. NMR spectra were obtained at 100 MHz with a JEOL FX-100 spectrometer and the chemical shift values are expressed in δ value (ppm) relative to Me_4Si in $CDCl_3$. The mass spectra were determined at 70 eV with a Finnigan 3300F.

*2-[1-Phenylsulfonyl-2-(3-isopropyl-4-methoxyphenyl)ethyl]-1,3,3-trimethylcyclohexane (**5**).* To a solution of 181 mg (0.65 mmol) of **4** in 2 ml of dry THF was added 0.63 ml (0.98 mmol) of BuLi–ether at −70 °C under N_2. After 5 min tsirring, the reaction mixture was treated with 3-isopropyl-4-methoxybenzyl bromide (221 mg, 0.91 mmol) dissolved in 2 ml of dry THF and stirred at −70 °C for 2 h. After adding 2 ml of saturated NH_4Cl, the organic substances were extracted three times with ethyl acetate. The combined extracts were washed with saturated NaCl, dried (Na_2SO_4), and concentrated *in vacuo*. The residue was chromatographed (SiO_2, benzene–AcOEt/10 : 1) to afford **5** (359 mg, 92%) as colorless crystals: mp 116—117 °C; IR (Nujol) 1506 (Ar), 1306, 1156 (SO_2) cm^{-1}; NMR ($CDCl_3$) δ 7.82—7.30 (5H, m, $ArSO_2$), 6.80—6.52 (3H, m, Ar), 3.98 (1H, dd, J=6 and 8 Hz, $CHSO_2$), 3.75 (3H, s, CH_3O), 3.55—3.00 (3H, m, CH_2Ar, CH), 2.30—1.92 (2H, m, CH_2C=), 2.14 (3H, s, CH_3), 1.70—1.18 (4H, m, CH_2), 1.11 (3H, d, J=7 Hz, CH_3), 1.08 (3H, d, J=7 Hz, CH_3), 0.99 (3H, s, CH_3), 0.36 (3H, s, CH_3); MS *m/e* (rel. intensity) 440 (m^+, 1), 299 (M^+-SO_2Ph, 69), 163 (81), 137 (71), 123 (100). Found: C, 73.66; H, 8.08%. Calcd for $C_{27}H_{36}O_3S$: C, 73.60; H, 8.24%.

*2-[2-(3-Isopropyl-4-methoxyphenyl)ethyl]-1,3,3-trimethylcyclohexene (**6**).* To a solution of 132 mg of **5** in 2 ml of dry THF and 20 ml of liq. NH_3 was added 100 mg of potassium at −70 °C and the mixture was vigorously stirred at −70—−65 °C for 2 h. After quenching with 1 ml of EtOH and evaporating the solvent under reduced pressure, 2 ml of saturated NH_4Cl was added to the residue and the organic substance was extracted with ether. The combined ether extracts were washed with saturated NaCl, dried (Na_2SO_4), and concentrated *in vacuo*. The residue was chromatographed (SiO_2, hexane–benzene/10 : 1), affording **6** (72 mg, 80%). Subsequent elution with hexane–AcOEt (10 : 1) provided **5** (10 mg, 8%): IR (neat) 2840 (MeO), 1610 (Ar), 1500,

1460, 1240 cm^{-1}; NMR ($CDCl_3$) δ 7.02 (1H, d, J=2 Hz, ArH), 7.00 (1H, dd, J=9 and 2 Hz, ArH), 6.75 (1H, d, J=9 Hz, ArH), 3.80 (3H, s, CH_3O), 3.28 (1H, sept, J=7 Hz, CH), 2.44—2.70 (2H, m, CH_2Ar), 2.10—2.37 (2H, m, CH_2), 1.82—2.02 (2H, m, CH_2), 1.67 (3H, s, CH_3C=), 1.30—1.72 (4H, m, CH_2), 1.22 (6H, d, J=7 Hz, CH_3), 1.05 (6H, s, CH_3); MS *m/e* 300 (M^+, 8), 163 (100). Found: C, 84.04; H, 10.76%. Calcd for $C_{21}H_{32}O$: C, 83.94: H, 10.73%.

12-Methoxyabieta-8,11,13-triene (7). Into 46 mg of **6** was added a mixture of AcOH (1.8 ml) and concd H_2SO_4 (0.2 ml) under ice cooling. The reaction mixture was stirred vigorously at 5 °C for 5 min and at 15—18 °C for 20 h. After adding 5 ml of ice water, the organic substance was extracted with hexane–ether (1 : 5). The combined extracts were washed with saturated $NaHCO_3$ and saturated NaCl, dried (Na_2SO_4), and concentrated *in vacuo*. The residue was chromatographed (SiO_2, hexane–benzene 10 : 1), affording **7** (45 mg, 99%) as a mixture (6 : 4) of *cis*-**7a** and *trans*-**7b**. Both isomers were separated by VPC (SE-30, 3 m, 4ϕ, 210 °C) and identified in comparison with the reported spectral data.

Ferruginol (2). To a solution of 1.4 mg of **7b** in 1.5 ml of dry CH_2Cl_2 was added 10 mg of BBr_3 at −70 °C under stirring. The mixture was stirred for 1 h while the reaction temperature was allowed to rise to −30 °C and then at 15—18 °C for additional 1 h. After adding 0.02 ml of saturated $NaHCO_3$, the mixture was dried (Na_2SO_4) and concentrated under reduced pressure. The residue was chromatographed (SiO_2, benzene), affording **2** (1.1 mg, 84%) as a sole product. The NMR and IR spectra were consistent with those reported.

The authors are grateful to Messrs M. Oka and K. Nara, Kuraray Co., Ltd. for mass spectral analysis.

References

1) Part IV. K. Uneyama and S. Torii, *Chem. Lett.*, **1977**, 39.

2) S. M. Kupchan, A. Karim, and C. Marcks, *J. Am. Chem. Soc.*, **90**, 5923 (1968); S. M. Kupchan, A. Karim, and C. Marcks, *J. Org. Chem.*, **34**, 3912 (1969).

3) K. Mori and M. Matsui, *Tetrahedron*, **26**, 3467 (1970).

4) (a) T. Matsumoto, Y. Tachibana, J. Uchida, and K. Fukui, *Bull. Chem. Soc. Jpn.*, **44**, 2766 (1971); (b) T. Matsumoto Y. Ohsuga, and K. Fukui, *Chem. Lett.*, **1974**, 297.

5) T. Matsumoto and S. Usui, Preprint on the 36 th National Meeting of the Chemical Society of Japan, Osaka, April (1977).

6) (a) C. W. Brandt and L. G. Neubauer, *J. Chem. Soc.*, **1939**, 1031; (b) W. P. Campbell and D. Todd, *J. Am. Chem. Soc.*, **64**, 928 (1942); (c) F. E. King, T. J. King, and J. G. Topliss, *J. Chem. Soc.*, **1957**, 573; (d) P. N. Rao and K. Raman, *Tetrahedron*, **4**, 294 (1958); (e) W. L. Meyer, G. B. Clemans, and R. W. Hufman, *Tetrahedron Lett.*, **1966**, 4255; (f) J. Wolinsky, R. Lau, J. J. Hamsher, and C. M. Cimarusti, *Synth. Commun.*, **2**, 327 (1972); (g) W. L. Meyer, G. B. Clemans, and R. A. Manning, *J. Org. Chem.*, **40**, 3686 (1975).

7) S. Torii, K. Uneyama, and M. Ishihara, *Chem. Lett.*, **1975**, 479; S. Torii, K. Unayama, and M. Kuyama, *Tetrahedron Lett.*, **1976**, 1513; K. Uneyama and S. Torii, *Tetrahedron Lett.*, **1976**, 443.

8) M. Fetizon and G. Moreau, *Bull. Soc. Chim. Fr.*, **1965**, 3479.

BULLETIN OF THE CHEMICAL SOCIETY OF JAPAN, VOL. 50 (9), 2505—2506 (1977)

Photochemical Dimroth Rearrangement of 1,4-Diphenyl-5-amino- and 4-Phenyl-5-anilino-1,2,3-triazoles[1]

Yoshiro OGATA, Katsuhiko TAKAGI, and Eiji HAYASHI

Department of Applied Chemistry, Faculty of Engineering, Nagoya University, Chikusa-ku, Nagoya 464

(Received May 14, 1977)

Synopsis. Irradiation of 1,4-diphenyl-5-amino-1,2,3-triazole (**1a**) gives 4-phenyl-5-anilino-1,2,3-triazole (**2a**) and the reverse photochemical reaction is possible. Hence, the reaction is reversible, the ratio of **1a** : **2a** in equibrium being 1.2—1.7, which is different from the ratio 0.33 in the thermal reaction (Dimroth rearrangement). The mechanism is discussed on the basis of spectral data and analogous reactions.

Dimroth discovered a rearrangement of 1-aryl-5-amino-1,2,3-triazoles(**1**) to 5-anilino-1,2,3-triazoles(**2**) in boiling pyridine or in boiling ethanolic sodium ethoxide.[2] The rearrangement is essentially complete in the above solvent,[3] but in some other solvents or in melts, **1** gives an equilibrium mixture of **1** and **2** in which the acidic isomer(**2**) usually predominates.[4,5] The reverse thermal reaction of **2** to **1** (retro-Dimroth rearrangement) leading to the equilibrium state was also reported.[6]

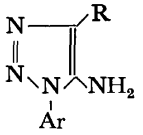

(**1**)

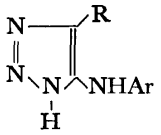

(**2**)

We wish to report here a photo-equilibrium between the amino(basic) isomer(**1**) and the anilino (acidic) isomer(**2**).

Results and Discussion

1,4-Diphenyl-5-amino-1,2,3-triazole(**1a**)[7] (2.0 g) in absolute ethanol(250 ml) was irradiated with a 100-W high-pressure mercury lamp for 40 h under N_2. The irradiated products were separated by TLC, and the rearrangement product(**2a**) (34.9%), unreacted **1a** (53.5%) and unidentified products(12.1 wt%) were obtained.

On the other hand, the irradiation of **2a** (1.9 g) under N_2 in absolute ethanol (200 ml) for 40 h gave a mixture of **1a** (36.6%), unreacted **2a** (30.7%) and unidentified products (32.7 wt%). The longer irradiation, which is sufficient for establishment of the equilibrium, afforded an equilibrium mixture containing **1a** and **2a** in a mole ratio of 1.53 by means of preparative TLC. Whereas, the irradiation of **2a** gave an equilibrium mixture of isolated **1a** and **2a** in the ratio of 1.20. The slight difference in the ratio may be due to the difference of extent of side reactions from **1a** and **2a**.

The amount of acidic isomer(**2a**) was determined by acidimetry with aq KOH at appropriate time intervals. As a result, the ratio of **1a** : **2a** became constant approaching to 1.70. This ratio is close to that obtained above by TLC analysis.

Generally, **1a** is favored in the photo-equilibrium of **1a** : **2a**. It is in contrast to the thermal reaction in which the equilibrium mixture consists of a larger amount of **2** than that of **1**, *i.e.*, the reported equilibrium ratio of 0.33 in melts,[6] while the ratio for photolysis in ethanol is 1.2—1.7, and suggests the difference in mechanism between thermal and photochemical reactions.

The thermal Dimroth rearrangement was postulated to involve a diazonium intermediates(**3** or **4**).[5] In the case of photolysis, this mechanism is not suitable, because the diazonium intermediate(**3** or **4**) is expected to react

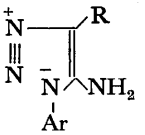

(**3**)

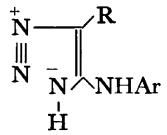

(**4**)

with the solvent.[8] In our attempt for spectral detection of the intermediates (**3** and **4**), the UV peak around 400 nm[9] and IR absorption in a range of 2150—2170 cm^{-1},[9] which are characteristic to diazonium group (C–N_2^+; *e.g.*, a diazonium ketone has UV peaks at 410 and 417 nm[10] and IR peak at 2137 cm^{-1} [10]), could not be detected at room temperature. These facts also disfavor the intermediacy of **3** and **4** possessing a diazonium group. But the possibility cannot completely be precluded at present, since the diazonium intermediate should be diluted and short-lived.

It is likely that this photo-rearrangement of **1** to **2** involves a valence isomerization which is characteristic to the photolysis of aromatic compound;[11] *i.e.*, the photolysis may proceed *via* diarines (**5** and **6**), and may

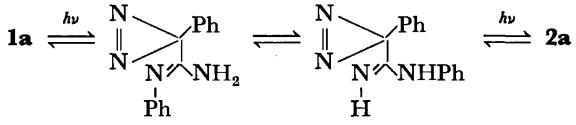

(**5**) (**6**)

involve a process of ring contraction and expansion together with a proton shift of **5** to **6**. A similar mechanism was suggested for five-membered hetero aromatics such as the photo-rearrangement of 3,5-diphenylisoxazole to 2,5-diphenyloxazole *via* a three-membered azirine which was detected spectroscopically.[12]

Experimental

Materials. 1,4-Diphenyl-5-amino-1,2,3-triazole(**1a**) and 4-phenyl-5-anilino-1,2,3-triazole(**2a**) were prepared by the method of Libers;[7] **1a**, mp 171—172 °C (lit,[7] 169—171 °C), λ_{max}(EtOH) 268 nm (log ε 4.18), IR (KBr)(cm^{-1}) 1620(s), 1265(s); NMR (DMSO-d_6, internal TMS) δ 7.95

(m, 3H), 7.72(s, 5H), 7.32(m, 2H), 6.82(s, 2H). **2a**, mp 167—168 °C (lit,[7] 167—169 °C); λ_{max}(EtOH) 238 nm(log ε 4.24), 360 nm(sh); IR(KBr)(cm^{-1}) 1580(s); NMR (DMSO-d_6, internal TMS) δ 8.14(s, 1H), 7.94(m, 2H), 7.50(m, 4H), 7.38(s, 1H), 7.20(d, 3H), 6.90(t, 1H).

*Photolysis of 1,4-Diphenyl-5-amino-1,2,3-triazole(**1a**).* **1a**(2.0 g) in absolute ethanol(250 ml) was irradiated with a 100-W high-pressure mercury lamp for 40 h, and the reaction mixture was evaporated to yield a brown crystalline solid which was separated and analyzed by TLC.

*Photolysis of 4-Phenyl-5-anilino-1,2,3-triazole(**2a**).* **2a** (1.9 g) in absolute ethanol(200 ml) was irradiated similarly, and condensed *in vacuo* to yield brown tarry material which was analyzed by TLC.

TLC Analysis. TLC was carried out on a plate (200×200 mm) uniformly coated with Kieselgel 60PF$_{254}$ (1 mm thickness) by using a mixture of benzene–ethyl acetate (3 : 1) as an eluant. The TLC analysis afforded three substances from the reaction mixture of **1a**(200 mg). The first (R_f=0.52) was unreacted **1a**(107 mg), the second (R_f=0.65) was **2a**(69.8 mg), and the rest (R_f=0.75) was unidentified(20.4 mg). Four substances were obtained from the reaction mixture of **2a**(200 mg). The first (R_f=0.52) and **1a**(73.2 mg), the second (R_f=0.85) (30.0 mg) was unidentified. Identification of the isolated products was done by means of comparison of UV, IR, and NMR spectra with those of authentic specimen.

Actinometry. An ethanol solution (200 ml) of **1a** (503 mg) was irradiated with a 300-W high-pressure mercury lamp, and aliquots (10 ml) were pipetted out at 2 h intervals and titrated by 0.0146 M KOH using phenolphthalein as an indicator. The final aliquot was that of 40 h irradiation.

References

1) Contribution No. 230.
2) O. Dimroth, *Ann.*, **364**, 185 (1904).
3) E. Lieber and T. S. Chao, *J. Org. Chem.*, **22**, 654 (1957).
4) E. Lieber, C. N. R. Rao, and T. S. Chao, *J. Am. Chem. Soc.*, **79**, 5962 (1957).
5) D. R. Sutherland and G. Tennant, *J. Chem. Soc., C*, **1971**, 706.
6) E. R. Brown and D. L. Hammick, *J. Chem. Soc.*, **1953**, 3280.
7) E. Lieber, T. S. Chao, and C. N. Rao, *Org. Synth.*, Coll. Vol. IV, 380 (1963).
8) R. E. Hoover and A. R. Day, *J. Am. Chem. Soc.*, **78**, 5352 (1956).
9) J. F. Ogilive, *J. Mol. Struct.*, **3**, 513 (1969).
10) E. Fahr and L. Neuman, *Ann.*, **715**, 15 (1968).
11) N. J. Turro, "Molecular Photochemistry," W. A. Benjamin Inc., New York (1965), p. 175.
12) E. F. Ullman and S. Singh, *J. Am. Chem. Soc.*, **89**, 6911 (1967).

BULLETIN OF THE CHEMICAL SOCIETY OF JAPAN, VOL. 50 (9), 2507—2508 (1977)

Synthesis of 10-Hydroxy-2-decenoic Acid (Royal Jelly Acid) from the Butadiene Telomer

Jiro TSUJI, Kazutaka MASAOKA, Takashi TAKAHASHI, Akira SUZUKI,* and Norio MIYAURA*

Faculty of Engineering, Tokyo Institute of Technology, Meguro, Tokyo 152

**Faculty of Engineering, Hokkaido University, Sapporo, Hokkaido 060*

(Received May 18, 1977)

Synopsis. Ethyl 2-acetyl-4,9-decadienoate obtained by palladium catalyzed reaction of butadiene and ethyl acetoacetate was converted to 4,9-decadienoate. Hydroboration of the terminal olefin gave 10-hydroxy-4-decenoate. After hydrogenation and protection of the hydroxyl group, the double bond was created at the conjugated position by introduction of phenylseleno group and subsequent oxidative removal to give 10-hydroxyl-2-decenoic acid.

Royal jelly is a nutrient of queen bee *lavae*. Investigation of the lipids of royal jelly has revealed that their free acid fraction contained a complex mixture of C_{10} acids which are called royal jelly acids. The structure of the main component of the royal jelly acids was determined by Butenandt and Rembold as 10-hydroxy-2-decenoic acid.[1] Several synthetic methods for this physiologically interesting acid have been reported.[2] These syntheses are based on chain elongation of the shorter compounds *via* somewhat lengthy steps. We now wish to report a simple synthetic method for this acid starting from an easily available butadiene telomer which has the right carbon numbers and suitable functional groups for the synthesis of the acid.

Butadiene and ethyl acetoacetate react to give 2-acetyl-4,9-decadienoate (**1**)[3] in 80% yield (bp 91—93 °C/2 Torr) using palladium acetate and triphenylphosphine as a catalyst. It is apparent that this easily prepared compound has an ideal structure for the construction of the royal jelly acid, which was synthesized by the following sequences.

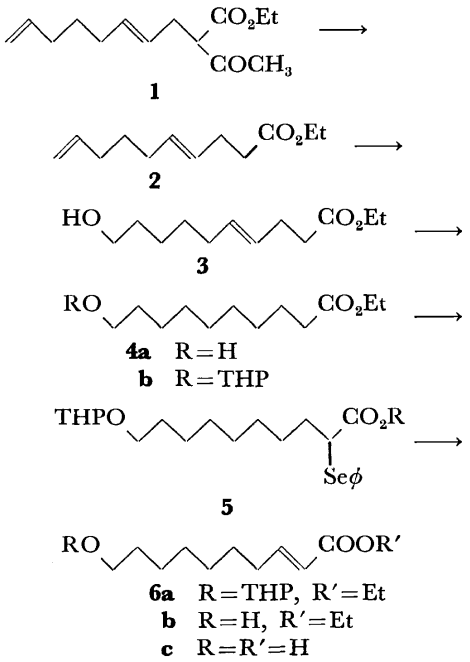

The acetyl group was removed by treatment of the ester **1** (63.5 g, 267 mmol) with sodium ethoxide in absolute ethanol (5.3 g, 78 mmol, 241 ml) to give, in 86% yield, ethyl 4,9-decadienoate **2**: bp 83 °C/1 Torr; NMR (CCl_4) δ 4.7—6.15 (m, 5H, olefin), 4.05 (q, J=7.0 Hz, 2H), 1.75—2.45 (m, 6H), 1.45—1.75 (m, 2H), 1.2 (t, J=7.0 Hz, 3H); IR (neat) 1735, 970, 910 cm^{-1}. Then the terminal double bond was converted to alcohol by hydroboration[4] using 1.1 equivalent of bis(1,2-dimethylpropyl)borane in dry THF and subsequent oxidation with 30% hydrogen peroxide in 3M sodium hydroxide solution to give, in 82% yield, 10-hydroxy-4-decenoate **3**: bp 118 °C/1 Torr; NMR (CCl_4) δ 5.3—5.6 (bt, 2H, olefin), 4.1 (q, J=7.0 Hz, 2H), 3.55 (bt, J=6.0 Hz, 2H), 3.2 (br, 1H, -OH), 2.3 (bs, 4H), 1.85—2.2 (br, 2H), 1.25 (t, J=7.0 Hz, 3H); IR (neat) 3600—3200, 1735, 975 cm^{-1}. The isomerization of the double bond at the position 4 of the ester **3** to the conjugated position would complete the synthesis. However, the attempted isomerization with various catalysts such as strong base, $RhCl(PPh_3)_3$, platinic acid, gave no clear result. Thus the double bond was hydrogenated by using palladium on carbon to give the saturated ester **4a** in 90% yield. The hydroxyl group was protected by converting to tetrahydropyranyl ether **4b** in 77% yield: NMR (CCl_4) δ 4.55 (br, 1H), 4.1 (q, J=7.0 Hz, 2H), 3.15—3.80 (m, 4H), 2.0—2.4 (m, 2H), 1.24 (t, J=7.0 Hz, 3H); IR (neat) 1738, 1040 cm^{-1}. Generation of the anion of saturated ester **4b** (900 mg, 3 mmol) with lithium isopropylcyclohexylamide (3.6 mmol) in dry THF at −78 °C was followed by the reaction of phenylselenenyl bromide[5] (991 mg, 4.2 mmol) to give, in 47% yield after column chromatography, the selenide **5**: NMR (CCl_4) δ 7.0—7.6 (m, 5H, phenyl), 4.4 (br, 1H), 3.95 (q, J=7.0 Hz, 2H), 3.2—3.7 (m, 5H), 1.12 (t, J=7.0 Hz, 3H). The purified selenide **5** (636 mg, 1.4 mmol) was oxidized with sodium periodate[5] (899 mg, 4.2 mmol) in aqueous methanol to give, in 81% yield after column chromatography, the desired unsaturated ester **6a**: NMR (CCl_4) δ 6.83 (dt, J=15.6 and 6.0 Hz, 1H, olefin), 5.67 (d, J=15.6, 1H, olefin), 4.4 (br, 1H), 4.10 (q, J=7.0 Hz, 2H), 3.2—3.7 (m, 4H), 1.8—2.4 (br, 2H), 1.25 (t, J=7.0 Hz, 3H). The removal of tetrahydropyranyl ether from ester **6a** (337 mg, 1.1 mmol) with copper sulfate (400 mg) in a mixture of methanol (8 ml) and water (2 ml) under reflux gave quantitatively the ethyl ester of royal jelly acid **6b**: NMR (CCl_4) δ 6.83 (dt, J=15.8 and 6.0 Hz, 1H, olefin), 5.67 (d, J=15.6, 1H, olefin), 4.10 (q, J=7.0 Hz, 2H), 3.50 (dt, 2H), 1.8—2.4 (br, 3H), 1.25 (t, J=7.0 Hz, 3H); IR (neat) 3100—3600, 1720, 1650, 980 cm^{-1}. The coupling constants of 15.6 and 15.8 for the olefinic protons of **6a** and **6b**

support the trans configuration of the olefins. Hydrolysis of the ester with 10% potassium hydroxide in aqueous methanol produced the royal jelly acid **6c** which was identified by its melting point, 63—64 °C (reported 64—65 °C).[2a]

References

1) A. Butenandt and H. Rembold, *Z. Phys. Chem.*, **308**, 284 (1957).

2) a) O. P. Vig, A. K. Vig, J. S. Man, and K. C. Gupta, *J. Indian Chem. Soc.*, **52**, 538 (1975); b) E. E. Smissman, J. F. Muren, and N. A. Dahle, *J. Org. Chem.*, **29**, 3517 (1964); and references cited therein.

3) G. Hata, K. Takahashi, and A. Miyake, *J. Org. Chem.*, **36**, 2116 (1971).

4) H. C. Brown and G. Zweifel, *J. Am. Chem. Soc.*, **83**, 1241 (1961).

5) K. B. Sharpless, R. F. Lauer, and A. Y. Teranishi, *J. Am. Chem. Soc.*, **95**, 6137 (1973); R. J. Reich, I. L. Reich, and J. M. Renga, *J. Am. Chem. Soc.*, **95**, 5813 (1973).

Exciplex and EDA Complex Fluorescence in 1,4-Dicyanonaphthalene with Alkylbenzenes and Alkylnaphthalenes

Michiya Itoh,*[1] Shu-ichi Furuya, and Toshihiko Okamoto

*Faculty of Pharmaceutical Sciences, Kanazawa University, Takara-machi, Kanazawa 920
Faculty of Pharmaceutical Sciences, The University of Tokyo, Bunkyo-ku, Tokyo 113

(Received January 17, 1977)

The exciplex (at room temperature) and EDA complex (at low temperature) fluorescence was observed in 3-methylpentane solution of 1,4-dicyanonaphthalene with several alkylbenzenes and alkylnaphthalenes. The fluorescence behavior provides evidence for an identical fluorescent state of the exciplex and EDA complex.

Intermolecular electron donor-acceptor (EDA) interaction leads to the formation of molecular complexes stable in the ground state and also the exciplexes stable only in the excited state. Formation of an exciplex can be observed in the fluorescence quenching of the component molecule and/or in the appearance of a new red-shifted fluorescence band. By transient absorption spectroscopy both the singlet excited states of the EDA complex and the exciplex are seen to show absorption bands of cation and anion radicals of the electron donor and acceptor, which indicates their strong charge transfer (CT) character in the excited state.[2]

Itoh and Mimura[3] and others[4,5] reported on the exciplex and EDA complex formation in the nonpolar solution of 9,10-dicyanoanthracene (DCA) and several naphthalene and benzene derivatives, demonstrating an experimental evidence for an identical fluorescent state of the exciplex and EDA complex. Similar evidence was reported for the identical fluorescent state in the tetracyanobenzene and *p*-xylene system by Gaweda and Prochorow.[6] This paper describes further examples of evidence for their identical fluorescent state in the simple EDA system of 1,4-dicyanonaphthalene (DCN) and alkylbenzenes (alkylnaphthalenes).

Experimental

1,4-Dicyanonaphthalene was prepared from naphthalene by bromination and cyanogenation, and purified several times by silica gel chromatography (solvent; benzene–hexane) and recrystallization. The sample has no fluorescent impurity in solution as verified by thinlayer chromatography. Purification of alkylbenzenes, alkylnaphthalenes, and solvents was carried out as reported.[4,5]

Measurement of fluorescence spectra was carried out with Hitachi MPF-2A and MPF-4 spectrophotometers, and that of absorption spectra with Cary 11 and Hitachi 323 spectrophotometers. Determination of fluorescence polarization was described previously.[4] The fluorescence lifetimes and time-resolved fluorescence spectra were determined by analyzing exponential decay curves measured with an oscilloscope and a coaxial N_2 gas laser.

Results and Discussion

The exciplex fluorescence in the 3-methylpentane (MP) solution of 1,4-dicyanonaphthalene (DCN) and alkylbenzenes was observed at room temperature. Figure 1 shows the fluorescence and fluorescence excitation spectra of MP solution of DCN and pentamethylbenzene (PMB) at room temperature. The fluorescence maxima and lifetimes of the exciplexes in

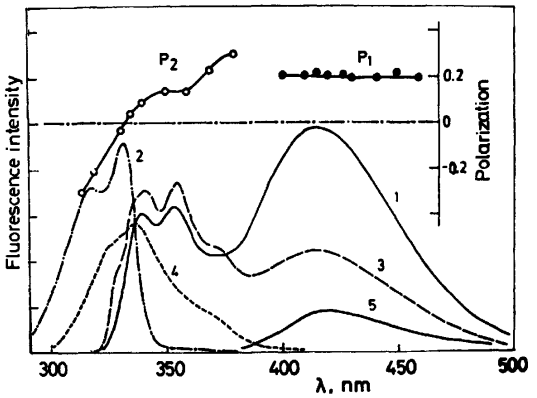

Fig. 1. Fluorescence and fluorescence excitation spectra, and their polarizations of MP solutions of DCN and PMB. *Spectra* 1 (excited at 310 nm) and 2 (monitored at 450 nm) are fluorescence and excitation spectra at room temperature, respectively (Concentration: DCN, 3×10^{-6} M: PMB, 1.5×10^{-2} M). *Spectra* 3 (excited at 310 nm) and 5 (excited at 370 nm) are fluorescence spectra at 77 K, and 4 (monitored at 450 nm) is a fluorescence excitation spectrum. P_1 (excited at 370 nm) and P_2 (monitored at 420 nm) are fluorescence and excitation polarizations at 77 K, respectively (Concentration: DCN, 9×10^{-7} M; PMB, 1×10^{-3} M).

Table 1. Fluorescence maxima and lifetimes of the exciplex (at room temperature) and the EDA complex (at 77 K) in MP solution of DCN and alkylbenzenes and alkylnaphthalenes

Donor	Exciplex		EDA complex	
	λ, nm	τ, ns[a]	λ, nm	τ, ns[a]
Hexamethylbenzene	430	86	430	71
Pentamethylbenzene	416	69	415	66
Durene	413	69	405[b]	50
Mesitylene	390	43	400[b]	40
p-Xylene	390	38	400[b]	37
Toluene	376[c]	15[c]	—	—
1,5-Dimethylnaphthalene	440	59	434	58
2-Methylnaphthalene	436	52	430	50
Naphthalene	430	51	427	48

a) Errors are approximately ± 1 ns. b) Determined by time-resolved fluorescence spectra. c) Determined in the concentrations of DCN = 6×10^{-6} M and toluene = 1.1 M.

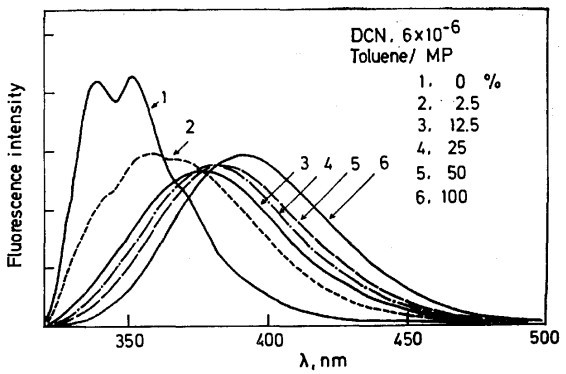

Fig. 2. Fluorescence spectra of MP solutions of DCN and toluene at room temperature.

MP, summarized in Table 1, show a slight concentration dependence of the electron donor. In the DCN and toluene system, however, the fluorescence maxima and lifetimes show remarkable concentration dependence (Fig. 2). Data of these exciplexes determined in almost the same concentrations of electron donor ($\approx 10^{-1}$ M) and acceptor ($\approx 10^{-6}$ M) are given in Table 1. The concentration dependence is due to the increasing solvent polarity with donor concentration.[7]

The exciplex fluorescence was gradually quenched with decrease in temperature. Almost the same fluorescence band as that of exciplex increases in intensity with further decrease in temperature. The temperature region of the decrease and increase of the long wavelength fluorescence is dependent on the concentrations of donor and acceptor. The fluorescence spectra of the MP solution of DCN with low concentration of alkylbenzene show no exciplex fluorescence band at room temperature but a similar fluorescence to that of the exciplex at low temperature. The fluorescence and excitation spectra of MP solution of DCN and PMB at 77 K are also shown in Fig. 1. The absorption spectra of the MP solution of DCN–alkylbenzene system at room temperature are completely superimposed by those of the component molecules, while the spectra show the EDA complex formation at low temperature as shown in Fig. 3 (DCN–PMB). The electronic absorption spectra at 77 K are similar to the corresponding excitation spectra monitored at long wavelength fluorescence

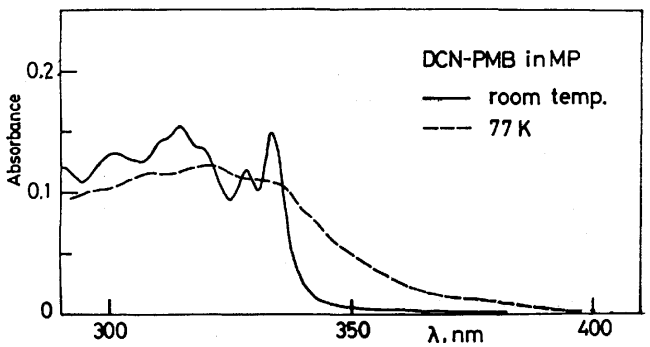

Fig. 3. Electronic absorption spectra of an MP solution of DCN and PMB at room temperature and 77 K (Concentration: DCN, 1.6×10^{-5} M; PMB, 7.5×10^{-3} M). Volume change at 77 K was corrected.

(Fig. 1). From the absorption and fluorescence excitation spectra in the MP solutions of DCN–alkylbenzenes, the long wavelength fluorescences at room temperature and at low temperature are ascribed to the exciplex and to the EDA complex, respectively. The absorption and excitation spectra indicate a small absorption band in the EDA complex at 350—400 nm as will be mentioned later. The fluorescence maxima and fluorescence lifetimes of the EDA complex in the MP solution at 77 K are summarized in Table 1. In the EDA complexes of DCN with durene, mesitylene and *p*-xylene, fluorescence maxima were determined with time-resolved fluorescence spectra because of their low solubility in MP at 77 K. The DCN–toluene system shows no detectable EDA complex formation.

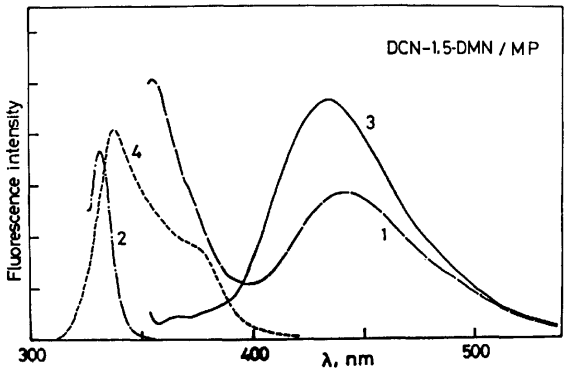

Fig. 4. Fluorescence and excitation spectra of MP solutions of DCN and 1,5-dimethylnaphthalnene. *Spectra* 1 (excited at 335 nm) and 2 (monitored at 450 nm) are fluorescence and excitation spectra at room temperature, respectively (Concentration: DCN, 2×10^{-6} M; 1,5-DMN, 2.2×10^{-2} M). *Spectra* 3 (excited at 340 nm) and 4 (monitored at 450 nm) are fluorescence and excitation spectra at 77 K, respectively (Concentration: DCN, 2×10^{-6} M; 1,5-DMN, 3.4×10^{-3} M).

The DCN and methylnaphthalene system shows exciplex formation at room temperature with the excitation of DCN and the EDA complex formation at low temperature, spectra of which are shown in Fig. 4 (DCN–1,5-dimethylnaphthalene). With the excitation of electron donor, however, no exciplex fluorescence but only alkylnaphthalene fluorescence was observed. The excitation spectra monitored at long wavelength fluorescence of the EDA complex of DCN–DMN (Fig. 4) give a similar absorption band at 350—400 nm to that in DCN–PMB.

The fluorescence maxima and lifetimes of both exciplex and EDA complex increase with decreasing ionization potential of alkylbenzene (alkylnaphthalene), indicating an increase of CT character of their fluorescent state with decreasing ionization potential of the electron donor. The fluorescent behavior in DCN–alkylbenzene (alkylnaphthalene) is similar to that in the DCA–alkylbenzene (alkylnaphthalene).[4,5] The fluorescence of the EDA complex in the DCN–alkylbenzene system at 77 K shows positive polarization with excitation at 370 nm, and negative with excitation at 320 nm. On the other hand, the electronic absorption spectra

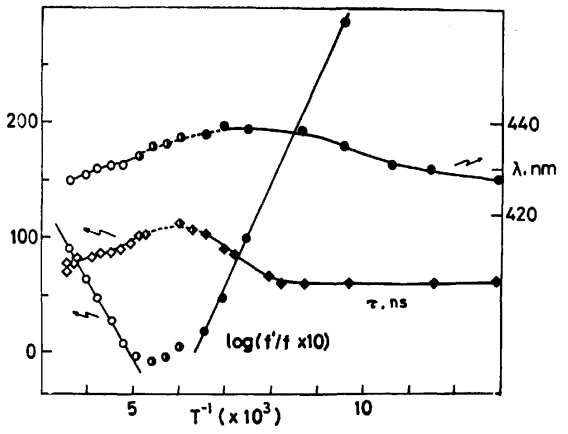

Fig. 5. Temperature dependence of fluorescence maxima (—○— exciplex and —●— EDA complex) and lifetimes (—◇— exciplex and —◆— EDA complex) in MP solutions of DCN and PMB, and of intensity ratio of the long wavelength fluorescence (f′ at λ_{max} 415 nm) and DCN fluorescence (f at λ_{max} 355 nm); —◑—, —◈— and —◑— are fluorescence indistinguishable from each other between exciplex and EDA complex.

and the excitation spectra of the EDA complex give a small absorption band at 350—400 nm. The results indicate that the absorption is a CT band between DCN and the electron donor. In the DCA–alkylbenzene system reported previously, small positive polarization with the local excitation of DCA and rather small fluorescence lifetimes of the EDA complex as well as the exciplex suggest that the fluorescent states mostly consist of the locally excited state of DCA.[5] The results of the EDA complex and the exciplex in DCN–alkylbenzene (alkylnaphthalene) show marked CT character in their fluorescent states.

The fluorescence maxima and lifetimes of the long wavelength fluorescence of MP solution of DCN–PMB at serveral temperatures, plotted in Fig. 5, both show continuous variation from room temperature to 77 K. On the other hand, the temperature dependence of intensity ratio of the long wavelength fluorescence to the DCN fluorescence completely differ between exciplex

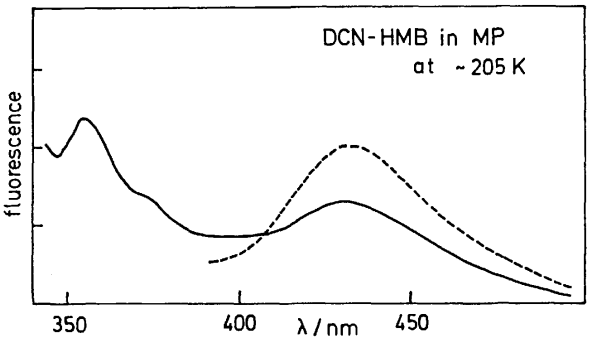

Fig. 6. Fluorescence spectra of an MP solution of DCN and HMB at 205 K in the excitations at 320 nm (——) and at 380 nm (------), (concentration; DCN, 3×10^{-6} M and HMB, 6×10^{-3} M).

and EDA complex.[4] If the exciplex and EDA complex have different fluorescence behavior, different fluorescence should be observed in the intermediate temperature (200—140 K). However, no distinguishable fluorescence is observed between exciplex and EDA complex in DCN–HMB system at ≈205 K, the fluorescence being observed in the excitation of DCN absorption band and CT band of the complex (Fig. 6). Appearance of one fluorescence species in this temperature region and the continuous change in fluorescence maxima and lifetime indicate an identical fluorescent state of the exciplex and EDA complex.[3]

References

1) To whom correspondence should be addressed at Kanazawa University.
2) M. Ottolenghi, *Acc. Chem. Res.*, **6**, 153 (1973).
3) M. Itoh and T. Mimura, *Chem. Phys. Lett.*, **24**, 551 (1974).
4) M. Itoh, *J. Am. Chem. Soc.*, **96**, 7390 (1974).
5) M. Itoh, Y. Kumano, and T. Okamoto, *Bull. Chem. Soc. Jpn.*, **49**, 42 (1976).
6) E. Gaweda and J. Prochorow, *Chem. Phys. Lett.*, **30**, 155 (1975).
7) N. Mataga, T. Okada, and N. Yamamoto, *Chem. Phys. Lett.*, **1**, 119 (1967).

NMR Studies of Picolyl-type Carbanions. IV.[1] Anions Produced by Reactions of 2-Substituted Pyridines with Butyllithium

Kazuyori KONISHI and Kensuke TAKAHASHI*

The Industrial Technology Center of Mie Prefecture, Takajaya-komori-cho, Tsu 514

**Department of Industrial Chemistry, Nagoya Institute of Technology, Gokiso-cho, Showa-ku, Nagoya 466*

(Received January 26, 1977)

The ^{13}C and ^{1}H NMR spectra of 2-pyridylmethyl (α-picolyl), 2-pyridylamino, 2-pyridyloxy, and 2-pyridylthio anions were observed in polar solvents with lithium as a counter ion. The chemical shifts are compared with the electron densities calculated using the PPP and CNDO/2 MO methods. A linear relationship was obtained between the ^{13}C chemical shifts and π-electron densities. The charge distributions on the anions are discussed, and it is found that the 2-pyridylamino anion and its methyl derivatives can be regarded as delocalized anions with the same significance as a series of picolyl anions.

In the benzyl carbanion, a simple Hückel MO theory predicts that the excess charges are distributed at the α-, *o*-, and *p*-positions, respectively.[2] Therefore, it is reasonable to consider that carbanions which have more electronegative atoms at the *o*- or *p*-positions are more stable than the benzyl carbanion. Picolyl-type carbanions have been studied as models of these carbanions.[1,3,4] This study was extended to anions having α-atoms of nitrogen, oxygen, and sulfur. The anions prepared are numbered from II to IX as follows: (I, which was reported previously,[3,4] is presented for comparison.)

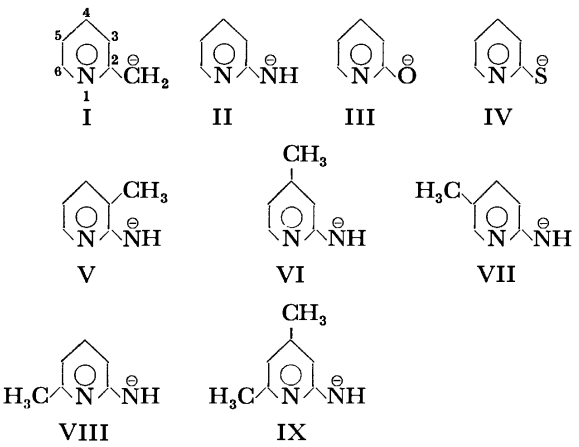

Experimental

The procedures used in this study are similar to those described in previous reports.[3,4] All the starting materials are commercially available. These materials were used after vacuum sublimation.

The ^{13}C NMR spectra were measured using a Hitachi R-20B spectrometer operating in the CW mode at 15.085 MHz. Sample concentrations were about 1.0 mol/l or more. Chemical shifts were evaluated with solvent peaks used as an internal reference. These peaks were taken to be 26.4 ppm for tetrahydrofuran (THF) and 37.0 ppm for hexamethylphosphoramide (HMPA) with respect to TMS. In the ^{1}H NMR spectra, the solvent peaks used as an internal reference were taken to be 1.79, 2.15, 2.58, and 3.28 ppm from TMS for THF, TMEDA (*N,N,N',N'*-tetramethylethylenediamine), HMPA, and DME (1,2-dimethoxyethane), respectively.

The PPP and CNDO/2 MO calculations were carried out using the Okitac-4300C and Hitachi-8450 computer systems installed at The Industrial Technology Center of Mie Prefecture and at Nagoya Institute of Technology, respectively, using modified versions of programs taken from the book of Kikuchi.[5] All the parameters used in the calculation were taken from this book and other references.[6,7] The skeletal coordinates of the anions were taken to be the same as those of pyridine.[8] The bond lengths between the 2-carbon and the α-atom used in the calculation are 1.39, 1.36, 1.31, and 1.75 Å for I, II, III, and IV, respectively.

Results and Discussion

Typical spectra of the anions are shown in Figs. 1 and 2. The ^{1}H and ^{13}C chemical shifts of both the anions and the starting materials are given in Tables 1 and 2. The results are of first order analysis.

NMR Spectra of the Anions. Typical PMR (^{1}H NMR) spectra of the anions are shown in Fig. 1. The well-separated signals permitted easy assignment. For example, the spectrum of the aromatic proton region of II, shown in Fig. 1(a), consists of four parts. The peaks appear as a doublet, a triplet, a doublet, and a triplet in passing from lower to higher field, with an integrated ratio of 1 : 1 : 1 : 1. They can, therefore, be identified as signals due to the 6-, 4-, 3-, and 5-protons. Typical CMR (^{13}C NMR) spectra are shown in Fig. 2. The signals were assigned in several ways, such as by comparison with the PMR spectra and by substitution of a methyl group for a hydrogen atom in the pyridyl ring.

From an inspection of the PMR spectra of VI, VIII, and IX shown in Fig. 1(b)—(d), the reaction sites of the starting materials having a 2-amino and 4- or 6-methyl groups with butyllithium were confirmed using chemical-shift considerations. The metal-proton exchange reaction occurred at the 2-amino group, indicating that the 2-amino group is more reactive than the 6-methyl group. The methyl protons in these anions show upfield shifts similar to the ring protons, but the shifts are about 0.1 ppm and are smaller than about 0.6 ppm in α-picolyl anions.[4] In the PMR spectra of II, V, and VII in HMPA shown in Fig. 1(a), (e)—(f), one relatively broad signal is observed in the range of 3.4—3.7 ppm. This signal may be attributed to the 2-NH.

Chemical Shift and Charge Density. In the CMR spectra of I—IV, the 5-carbon of each anion is the most shielded of the ring carbons, *i.e.*, its signal appears at a

Table 1. The proton chemical shifts of the anions and the starting materials, at 60 MHz and 31.5 °C in ppm[a]

Compound	Solvent	Assignment				
		3-H	4-H	5-H	6-H	CH_2, CH_3
I	THF[b]	5.64_5	6.06	4.84	6.90	$2.54(CH_2)$
	DME[b]	5.58	6.01	4.77	6.82	$2.52(CH_2)$
	HMPA	5.16	5.68	4.33	6.81	c) (CH_2)
II	TMEDA	5.96	6.84	5.79	7.47	
	THF	5.96	6.84	5.77	7.50	
	HMPA	5.75	6.58	5.42	7.44	
III	THF[d]	6.27	7.14	6.19	7.73	
	HMPA	6.24	7.01	5.98	7.75	
IV	HMPA	7.03	6.81	6.24	7.66	
V	HMPA		6.66	5.55	7.49	$1.89(CH_3)$
VI	DME	5.83		5.70_5	7.43_5	$1.99(CH_3)$
VII	HMPA	5.71	6.50		7.34	$1.90(CH_3)$
VIII	DME	5.89	6.84	5.77		$2.18(CH_3)$
IX	DME	5.71		5.65		1.98, $2.14(CH_3)$
2-Methylpyridine	THF[b]	7.16	7.57	7.07	8.46	$2.48_5(CH_3)$
	DME[b]	7.13	7.54	7.05	8.42_5	$2.48(CH_3)$
	HMPA	7.30	7.74	7.21	8.42	c) (CH_3)
2-Aminopyridine	TMEDA	6.32	7.20	6.38	7.90_5	
	THF	6.41	7.30	6.48	7.95	
	HMPA	6.60	7.29	6.38	7.86	
2-Hydroxypyridine	THF	6.46	7.43[e]	6.19	7.43[e]	
	HMPA	6.27	7.44[e]	6.15	7.44[e]	
2-Mercaptopyridine	HMPA	7.21	7.44	6.75	7.61	
2-Amino-3-methylpyridine	HMPA		7.18	6.37	7.76	$2.16(CH_3)$
2-Amino-4-methylpyridine	DME	6.26		6.31	7.79	$2.16(CH_3)$
2-Amino-5-methylpyridine	HMPA	6.51	7.12		7.69	$2.09(CH_3)$
2-Amino-6-methylpyridine	DME	6.23	7.19	6.31		$2.29(CH_3)$
2-Amino-4,6-dimethylpyridine	DME	6.06		6.17		2.10, $2.22(CH_3)$

a) Errors are estimated to be within ± 0.03 ppm. b) From Table 1 of Ref. 4, in which the measuring temperature should be 31.5 °C. c) Chemical shifts are not available because of overlapping of the large solvent peak. d) Measured at 50 °C. e) Center peak of complex multiplet.

Table 2. The carbon chemical shifts of the anions and the starting materials, in ppm[a]

Compound	Solvent	Assignment					
		2-C	3-C	4-C	5-C	6-C	CH_2,CH_3
I	THF	164.0	115.8	131.3	97.9	148.5	$56.1(CH_2)$
	HMPA	161.5	113.7	129.9	92.5	149.2	$58.8(CH_2)$
II	THF	173.7	113.0	135.9	104.4	147.8	
	HMPA	173.0	111.7	134.0	101.3	148.2	
III	HMPA	173.3	114.0	135.8	106.3	146.6	
IV	HMPA	183.5	128.6[b]	132.2[b]	110.9	146.1	
V	HMPA	172.2	115.6	133.4	101.7	146.1	$18.9(CH_3)$
VII	HMPA	171.6	111.4	135.6	107.9	147.2	$17.3(CH_3)$
2-Methylpyridine	THF	159.0	123.2	136.2	120.8	149.8	$24.4(CH_3)$
	HMPA	157.9	122.9	136.0	120.5	149.0	$24.1(CH_3)$
2-Aminopyridine	THF	160.9	108.9	137.9	113.2	148.7	
	HMPA	160.5	108.5	136.8	111.7	147.8	
2-Hydroxypyridine	HMPA	162.7	120.3	136.1	104.6	140.3	
2-Mercaptopyridine	HMPA	179.9	133.6[b]	135.8[b]	111.3	137.3	
2-Amino-3-methylpyridine	HMPA	158.6	116.4	137.1	113.2	145.4	$16.9(CH_3)$
2-Amino-5-methylpyridine	HMPA	158.3	108.4	138.0	121.0	147.4	$17.1(CH_3)$

a) Errors are estimated to be within ± 0.3 ppm. b) Assignment uncertain.

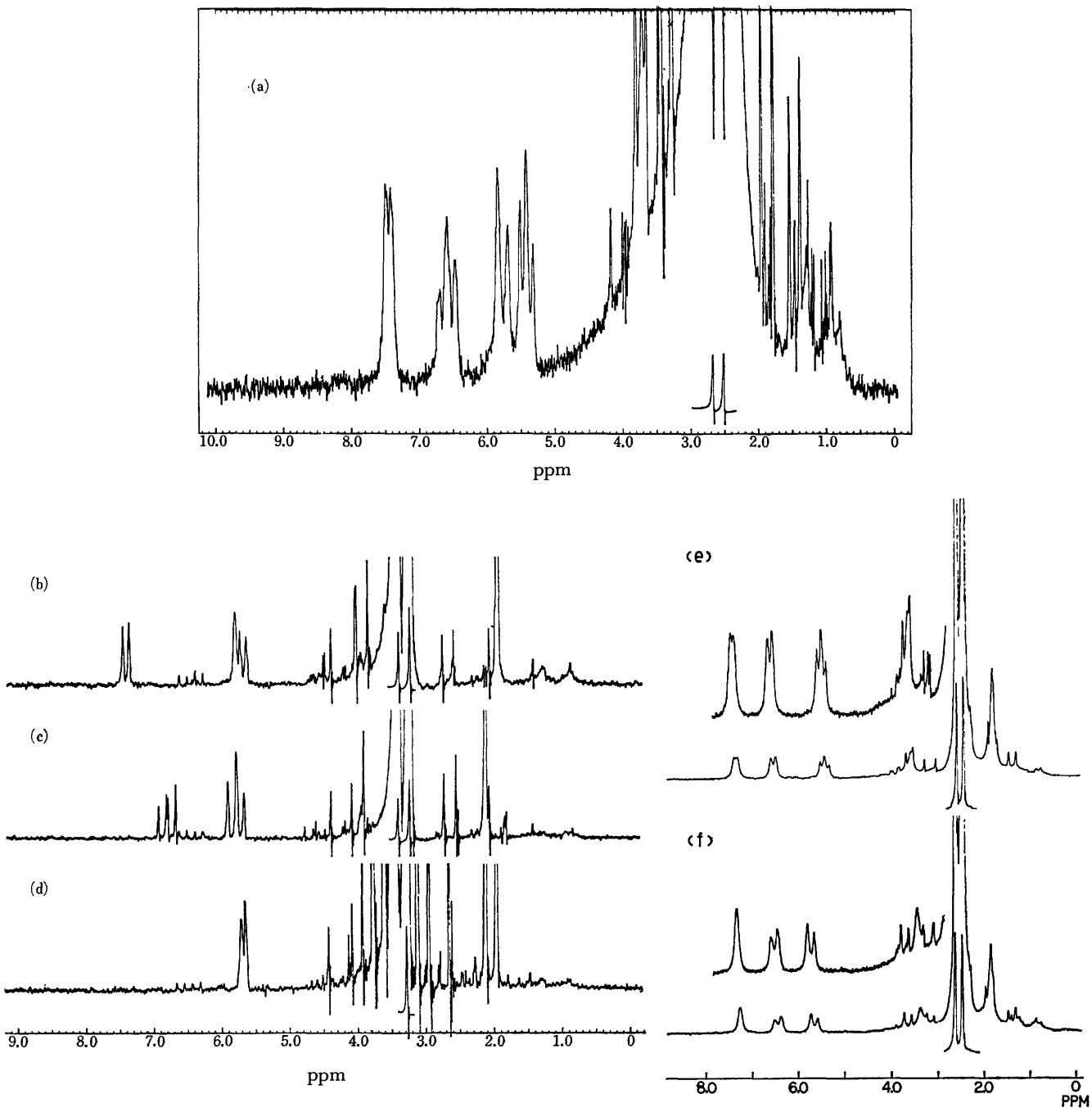

Fig. 1. PMR spectra of pyridylamino anions; (a) II in HMPA, (b) VI, (c) VIII, (d) IX in DME, and (e) V, (f) VII in HMPA.

higher field. In addition, the 5-carbon signals of I and II are shifted appreciably in the upfield direction relative to those of the starting materials. In the PMR spectra, the same tendency is observed for the 5-protons. It is apparent that the excess charges transferred from the α-atom to the pyridyl ring in I and II have the strongest influence at the 5-position, *i.e.*, the 5-carbon and proton chemical shifts are most affected by the charges. The 5-carbon and proton signals appear at higher field in the increasing order, IV, III, II, and I. Thus, it may be possible to consider that the excess charges transferred onto the ring increase in the same order.

In order to clarify the relationship between the carbon or proton chemical shifts and the π-electron densities, these densities were calculated using the PPP and CNDO/2 MO methods for I—IV and I—III, respectively. The π-electron densities calculated using the PPP method are plotted against the carbon chemical shifts in Fig. 3. The plot is linear although the 2-carbons and the methylene carbon of I deviate from linearity. One cause of this deviation may be the hybridization change in the α-atoms. On the other hand, in Fig. 4 are plotted the π-electron densities

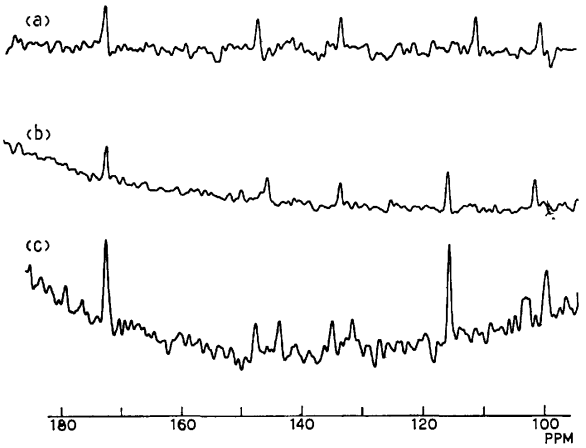

Fig. 2. CMR Spectra of the aromatic carbon region of pyridylamino anions; (a) II, (b) V in HMPA (proton noise decoupling), and (c) V in HMPA (off resonance decoupling).

calculated using the CNDO/2 method. The plot of the 4-carbons deviates considerably from linearity, as compared with the plot of the others, that is, the densities are underestimated. The cause of this is unclear at present. Next, the relation between the ring-proton chemical shifts for each anion in I—III and the π-electron densities of the adjacent carbons calculated using the PPP method is linear, and the plot of I is most distinctly linear.

The charge distributions on I—IV are discussed on the basis of the relationship shown in Fig. 3. This relationship implies that, in spite of changes in the α-atoms, the π-electron densities of the ring carbons in these anions can be evaluated from the carbon chemical shifts using an identical scale. The δ-values of the ring-carbon chemical shifts of each anion increase in the order 5-, 3-, 4-, 6-, and 2-carbons, indicating that the π-electron densities decrease in the same order. Of these anions, the 6-carbon chemical shifts are almost the same, the shift range is about 3 ppm, and, of course, is smaller than about 18 ppm for the 5-carbons. This may be due to the strong induction effect caused by the neighboring nitrogen atom. Here, from an assignment of both the 3- and 4-carbon signals of IV, the calculated charge densities distinguish the 3- from the 4-carbon. In this sense, this assignment may be uncertain. Therefore, at least in I—III, the π-electron distribution patterns are clearly analogous, *i.e.*, I—III are anions of the same type. The ring nitrogens in I—III are expected to follow the same tendency as the 5-carbons, over which the charges transferred from the α-atoms are largely distributed and the π-electron densities increase in the order III, II, and I. The π-electron densities of the ring nitrogen calculated using both the PPP and CNDO/2 methods also increase in the order III, II, and I.

The PMR spectra of I in THF were temperature dependent; chemical shifts of the ring protons at −25 °C were 0.10—0.15 ppm upfield from the 31.5 °C values. This variation is larger than those for benzyllithium and 1- and 2-naphthylmethyllithium.[9] This relatively large temperature dependence shows that solvent separation in I occurs to an appreciable extent. In addition to this fact, the ring proton and carbon signals in HMPA move to higher field in comparison with those in THF, *i.e.*, the excess charges on the α-atom are transferred more into the ring for HMPA than for

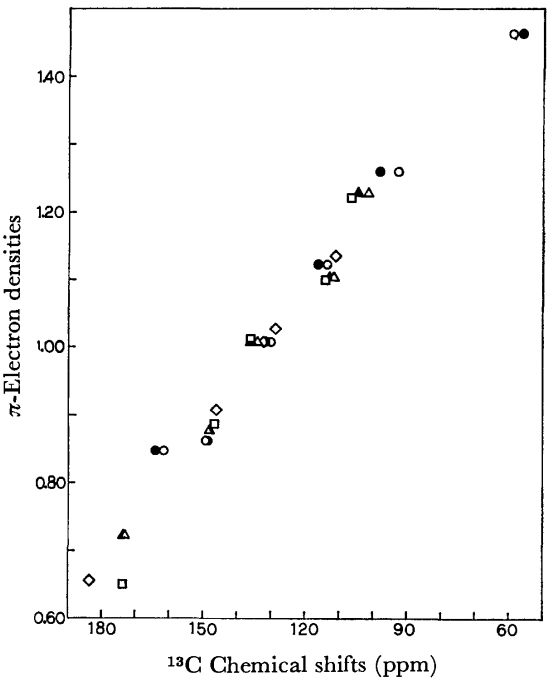

Fig. 3. π-Electron densities (PPP method) *vs.* ^{13}C chemical shifts.
○ I in HMPA, ● I in THF, △ II in HMPA, ▲ II in THF, □ III in HMPA, ◇ IV in HMPA.

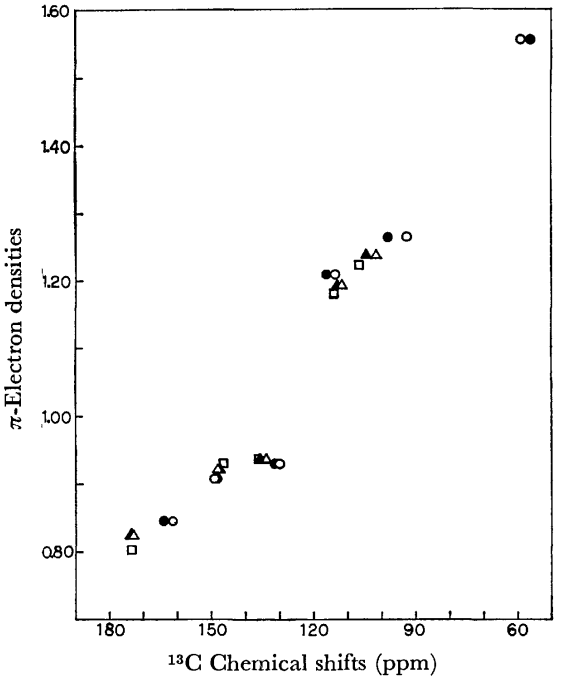

Fig. 4. π-Electron densities (CNDO/2 method) *vs.* ^{13}C chemical shifts.
○ I in HMPA, ● I in THF, △ II in HMPA, ▲ II in THF, □ III in HMPA.

Table 3. Comparison of charge densities calculated using the PPP and CNDO/2 MO methods for the 2-pyridylmethyl, -amino, -oxy, and -thio anions

Compd	I			II			III			IV
Atom	PPP	CNDO/2		PPP	CNDO/2		PPP	CNDO/2		PPP
		$\pi(P_z)$	Total		$\pi(P_z)$	Total		$\pi(P_z)$	Total	
1-N	1.437	1.292	5.305	1.391	1.247	5.296	1.380	1.229	5.300	1.269
2-C	0.847	0.846	3.802	0.722	0.822	3.753	0.650	0.802	3.712	0.655
3-C	1.122	1.209	4.153	1.103	1.193	4.157	1.099	1.180	4.166	1.027
4-C	1.008	0.928	3.941	1.008	0.934	3.944	1.012	0.936	3.946	1.008
5-C	1.260	1.265	4.171	1.227	1.237	4.156	1.221	1.222	4.149	1.135
6-C	0.863	0.907	3.871	0.878	0.920	3.880	0.887	0.928	3.882	0.907
α-X	1.462	1.554	4.366	1.672	1.647	5.520	1.751	1.702	6.592	2.000
3-H			1.046			1.042			1.039	
4-H			1.070			1.069			1.070	
5-H			1.060			1.058			1.057	
6-H			1.090			1.090			1.089	
α-H			1.064 1.061			1.035				

THF. In this sense, I is more stable in HMPA than in THF. Consequently, I exists as either solvent separated ion pairs or free ions in HMPA. The ring protons of II—III and the ring carbons of II in HMPA are also more shielded than those in THF. The 5-proton chemical shift of each anion in I—III shows the largest variation with a change in solvents from THF to HMPA, and the magnitudes are 0.21, 0.35, and 0.51 ppm for III, II, and I, respectively. For the 5-carbon chemical shifts of both I and II, the same tendency is observed, and the magnitudes are 5.4 and 3.1 ppm. With a change in solvents, the densities at the 5-position vary greatly. In HMPA, the PMR spectral patterns of II and III are similar to that of I. From these results for II and III in polar solvents and the relationship among I—III as shown in Fig. 3, it is possible to consider that II and III also exist as analogous ions in HMPA, as does I, and, furthermore, so may IV.

The 5-carbons in V and VII show upfield shifts of about 10 ppm similar to that in II. This magnitude is smaller than about 25 ppm in I, but much larger than about 0 ppm in III and IV. This suggests that the excess charges on the α-nitrogen atoms are appreciably transferred onto the pyridyl rings with a change in starting materials to lithium salts in polar solvents. Therefore, anions II and V—IX, whose α-atoms are nitrogens, can be regarded as delocalized anions with the same significance as a series of picolyl anions.

References

1) Part III in this series: K. Konishi, Y. Onari, S. Goto, and K. Takahashi, *Chem. Lett.*, **1975**, 717.
2) A. Streitwieser, Jr., *J. Am. Chem. Soc.*, **74**, 5290 (1952).
3) K. Konishi, K. Takahashi, and R. Asami, *Bull. Chem. Soc. Jpn.*, **44**, 2281 (1971).
4) K. Takahashi, K. Konishi, M. Ushio, M. Takaki, and R. Asami, *J. Organomet. Chem.*, **50**, 1 (1973).
5) Osamu Kikuchi, "Bunshi Kidoho," Kodansha, Tokyo (1971).
6) J. Hinze and H. H. Jaffé, *J. Am. Chem. Soc.*, **84**, 540 (1962).
7) J. A. Pople and D. L. Beveridge, "Approximate Molecular Orbital Theory," McGraw-Hill Book Company, New York (1970).
8) B. Bak, L. Hansen-Nygaard, and J. Rastrup-Andersen, *J. Mol. Spectrosc.*, **2**, 361 (1958).
9) F. J. Kronzer and V. R. Sandel, *J. Am. Chem. Soc.*, **94**, 5750 (1972).

Synthetic Zeolites as Catalysts for the Ring Conversion of γ-Butyrolactone into 1-Substituted 2-Pyrrolidinones

Kou HATADA* and Yoshio ONO

Department of Chemical Engineering, Tokyo Institute of Technology, Ookayama, Meguro-ku, Tokyo 152

(Received January 31, 1977)

Synthetic zeolites were found to be effective catalysts for the synthesis of 1-substituted 2-pyrrolidinone by the reaction of γ-butyrolactone with amines. 1-Propyl-2-pyrrolidinone was obtained in the equilibrium yield with practically 100% selectivity over copper exchanged Y-zeolite at 280 °C. The effects of reaction temperature, contact time and partial pressures of the reactants were examined. A reaction mechanism is proposed for the ring transformation based on the kinetic studies of the reaction of γ-butyrolactone with propylamine.

Transformation of heterocycles into compounds containing a ring system differing from that of starting substance provides a convenient method for the synthesis of some heterocycles. As an example, 2-pyrrolidinone can be obtained by the reaction of γ-butyrolactone and ammonia.[1] Usually, the reaction is carried out in a liquid phase under pressure. The ring transformations of cyclic ethers or lactones into the corresponding cyclic imines or lactams can be effectively carried out in a vapor phase by using synthetic zeolites as catalysts.[2-7] Over copper-exchanged Y zeolites, 2-pyrrolidinone was obtained from γ-butyrolactone in 80—90% yield.[4] We have carried out the synthesis of 1-substituted 2-pyrrolidinones from γ-butyrolactone in a vapor phase with use of zeolites as catalysts. A detailed study has been carried out on the kinetics of the reaction and a reaction mechanism is proposed in the case of the reaction of γ-butyrolactone with propylamine to form 1-propyl-2-pyrrolidinone.

Experimental

Measurements. All the boiling points are uncorrected. The determination of infrared spectra was made on a Shimadzu IR-6 spectrophotometer. The NMR spectra were recorded in tetrachlorometane solution with a spectrometer using tetramethylsilane as an internal reference. Gas chromatograms were obtained using a 2 m column packed with a 10% PEG-6000 on Shimalite-F operating at 200 °C.

Materials. γ-Butyrolactone (Tokyo Chemical Industry) was distilled just before each reaction. Amines (Wako Pure Chemical Industry) were used without purification.

Catalyst. NaY-zeolite (Linde SK-40) was used as the starting material for all the catalysts. Various cation forms of zeolites were prepared by the conventional cation exchange procedure using salt solutions. The cation exchanged zeolites were pelleted without a binder and crushed and sized into 9—16 mesh.

Apparatus and Procedure. A continuous flow reactor was used under atomspheric pressure. The reactor is a silica tubing (13 mm i.d.) placed in a vertical furnace. Prior to the reaction, the catalyst in the reactor was heated in an air stream at 500 °C (or 450 °C for HY) for 60 min. The liquid reactants were pumped with microfeeders into the preheating zone of the reactor containing 10 ml quartz or α-alumina (about 24 mesh). The gaseous materials were fed through flowmeters. Nitrogen was used as a diluent for regulating the initial pressure of reactants. Reaction products collected in the receiver maintained at 0 °C was withdrawn at certain intervals during the run and were analyzed by gas chromatography. 2-Pyrrolidinone, 1-methyl-2-pyrrolidinone and 1-ethyl-2-pyrrolidinone were identified by comparison of their infrared spectra with that of authentic samples. Other products were assignd by IR, NMR, and the elemental analysis methods.

1-Propyl-2-pyrrolidinone. Bp 94—96 °C, 9 mmHg. C=O band 1693 cm^{-1}. NMR (CCl_4, δ) 0.80—1.00 (t, 3H), 1.24—1.80 (m, 2H), 1.90—2.40 (m, 4H), 3.06—3.47 (m, 4H). Found: C, 66.33; H, 10.46; N, 11.27%. Calcd for $C_7H_{13}NO$: C, 66.10; H, 10.30; N, 11.01%.

1-Butyl-2-pyrrolidinone. Bp 116—118 °C, 10 mmHg. C=O band 1686 cm^{-1}. NMR (CCl_4, δ) 0.80—1.85 (t, 3H), 1.16—1.61 (m, 4H), 1.86—2.41 (m, 4H), 3.09—3.46 (m, 4H). Found: C, 67.83; H, 10.79; N, 10.30%. Calcd for $C_8H_{15}NO$: C, 68.04; H, 10.71; N, 9.92%.

1-Isobutyl-2-pyrrolidinone. Bp 96—98 °C, 10 mmHg. C=O band 1676 cm^{-1}. NMR (CCl_4, δ) 0.80—0.91 (d, 6H), 1.64—2.40 (m, 5H), 2.92—3.02 (d, 2H), 3.20—3.40 (t, 2H). Found: C, 67.82; H, 10.69; N, 9.77%. Calcd for $C_8H_{15}NO$: C, 68.04; H, 10.71; N, 9.92%.

1-s-Butyl-2-pyrrolidinone. Bp 102—103 °C, 10 mmHg. C=O band 1677 cm^{-1}. NMR (CCl_4, δ) 0.75—0.96 (t, 3H), 1.04—1.16 (d, 3H), 1.25—1.70 (m, 2H), 1.86—2.37 (m, 4H), 3.12—3.33 (t, 2H), 3.70—4.21 (m, H). Found: C 68.31; H, 10.89; N, 10.20%. Calcd for $C_8H_{15}NO$: C, 68.04; H, 10.71; N, 9.92%.

1-t-Butyl-2-pyrrolidinone. C=O band 1672 cm^{-1}.

1-Pentyl-2-pyrrolidinone. Bp 124—126 °C, 14 mmHg. C=O band 1676 cm^{-1}. NMR (CCl_4, δ) 0.80—0.99 (t, 3H), 1.15—1.59 (m, 6H), 1.86—2.34 (m, 4H), 3.09—3.44 (m, 4H). Found: C, 69.60; H, 11.14; N, 8.99%. Calcd for $C_9H_{17}NO$: C, 69.63; H, 11.04; N, 9.02%.

1-Hexyl-2-pyrrolidinone. 133—134 °C, 10 mmHg. C=O band 1681 cm^{-1}. NMR (CCl_4, δ) 0.80—0.99 (t, 3H), 1.15—1.60 (m, 8H), 1.80—2.35 (m, 4H), 3.07—3.45 (m, 4H). Found: C, 71.55; H, 11.46; N, 8.45%. Calcd for $C_{10}H_{19}NO$: C, 70.96; H, 11.23; N, 8.28%.

1-Phenyl-2-pyrrolidinone. Mp 67—68 °C. C=O band 1676 cm^{-1}. NMR (CCl_4, δ) 1.86—2.64 (m, 4H), 3.68—3.91 (t, 2H), 7.03—7.70 (m, 5H). Found: C, 74.60; H, 6.83; N, 8.79%. Calcd for $C_{10}H_{11}NO$: C, 74.51; H, 6.88; N, 8.69%.

Results and Discussion

Catalytic Activity of Various Cation Forms of Zeolite. The catalytic activities of various cation forms of Y-zeolite for the reaction of γ-butyrolactone and propylamine were compared under the following conditions:

* Present address: Faculty of Education, Saitama University, Urawa, Saitama 338.

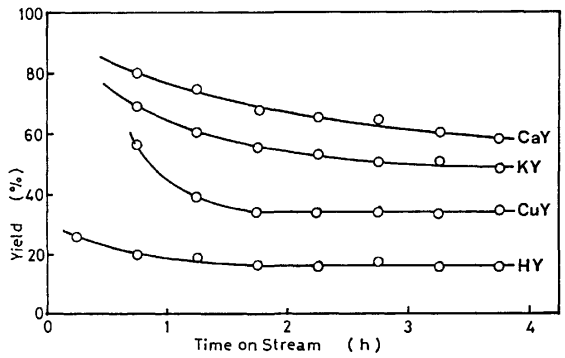

Fig. 1. Change in the yield of 1-propyl-2-pyrrolidinone over various zeolites at 280 °C.

reaction temperature 280 °C, catalyst weight 1 g, flow rate of reactants; γ-butyrolactone 24×10^{-3} mol/h, propylamine 122×10^{-3} mol/h, flow rate of nitrogen 99×10^{-3} mol/h. The catalytic activities decreased with time (Fig. 1). The activity and selectivity for the production of 1-propyl-2-pyrrolidinone on various cation forms of zeolites are given in Table 1. The values refer to the data obtained after the reaction had proceeded for 3 h. Besides 1-propyl-2-pyrrolidinone, a small amount of *N*-propyl-4-hydroxybutyramide was produced. Selectivity is defined as follows.

$$\text{Selectivity (\%)} = \frac{\text{mol of pyrrolidinone produced}}{\text{mol of } \gamma\text{-butyrolactone reacted}} \times 100.$$

The highest yield of the pyrrolidinone was obtained over CaY (calcium exchanged Y zeolite), followed by alkaline cation forms (Table 1). The best selectivity for the pyrrolidinone was observed for CuY, the most stable catalyst for the reaction (Fig. 1). Thus, CuY was used exclusively for further investigations. Though the activity decreased gradually with stream hours, it is completely recovered by calcining the used catalyst under air stream at 500 °C.

Reaction of γ-Butyrolactone with Various Amines. The reactions of γ-butyrolactone (I) with various primary amines were carried out with CuY as a catalyst

Table 1. Activity and selectivity for the reaction of γ-butyrolactone over various Y-zeolites

Cation	Conversion of I %	Yield of III %	Selectivity for III %
H	23	15	65
Li	47	36	77
Na	38	30	80
K	58	50	86
Rb	54	46	85
Cs	54	44	81
Mg	24	15	63
Ca	73	62	85
Sr	20	10	50
Ba	16	6	38
Cu	37	34	92
Ni	35	27	77
Co	23	16	70
Zn	16	6	38

Catalyst 1 g. Reaction temperature 260 °C. Feeding rate of I 24.0×10^{-3} mol/h. Reactant ratio II/I=5.08. Total feed (I+II+N_2) 225×10^{-3} mol/h.

at 280 °C. The results are summarized in Table 2. The yield of 2-pyrrolidinones depends on the nature of the amines, but the selectivity of the reaction is quite high. In addition to neat amines, the amine in aqueous solution can be used for the synthesis.

The yield of 2-pyrrolidinone in the reaction of I with ammonia was lower than that with primary amines. This may be caused by the difference in the basicity of ammonia and primary amines. The steric effect also seems to be important for the reactions; the yield of 2-pyrrolidinones depends on the starting amine in the following order.

$$CH_3NH_2 \approx C_3H_7NH_2 > C_4H_9NH_2 > C_5H_{11}NH_2 > C_6H_{13}NH_2 > PhNH_2$$

$$C_4H_9NH_2 > \text{Iso-}C_4H_9NH_2 > s\text{-}C_4H_9NH_2 > t\text{-}C_4H_9NH_2$$

Since the basicity of alkylamines hardly depends at

Table 2. Activity and selectivity for the reaction of γ-butyrolactone with various amines over Cu–Y

Amine	P_I (atm)	R_I ($\times10^{-3}$ mol/h)	P_{amine} (atm)	R_{amine} ($\times10^{-3}$ mol/h)	Yield of pyrrolidinone (%)	Selectivity (%)
Ammonia	0.098	24	0.497	122	12	68
Methylamine	0.098	24	0.497	122	98	98
Methylamine[a)]	0.052	20	0.192	73	56	—
Ethylamine[b)]	0.075	20	0.258	67	80	—
Propylamine	0.098	24	0.497	122	96	98
Butylamine	0.098	24	0.409	101	86	94
Isobutylamine	0.098	24	0.508	124	85	96
s-Butylamine	0.098	24	0.404	99	64	92
t-Butylamine	0.098	24	0.571	140	4	88
Pentylamine	0.098	24	0.522	128	60	92
Hexylamine	0.098	24	0.440	108	49	95
Aniline	0.098	24	0.446	109	8	—

Catalyst Cu–Y 3 g. Reaction temperature 280°C. Total feed(I+amine+N_2): 245×10^{-3} mol/h. *P*: partial pressure. *R*: feeding rate. a) 40% aqueous solution. b) 70% aqueous solution.

all on the kind of alkyl group, the difference in the yield of 2-pyrrolidinone seems mainly to be caused by the steric effect. The bulkier the alkyl group, the less the reactivity of amine toward I. Since propylamine (II) has a high reactivity toward I with high selectivity, the various parameters determining the yield of 1-propyl-2-pyrrolidinone (III) were examined by using propylamine as a strating amine.

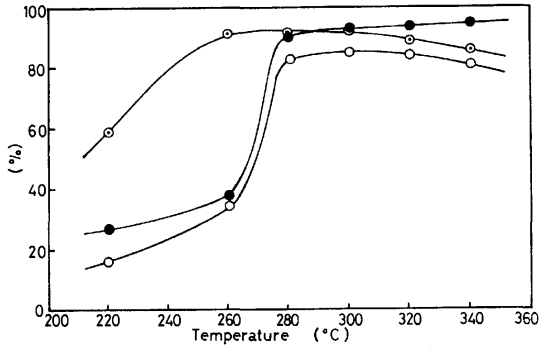

Fig. 2. Effect of reaction temperature on the catalytic behavior of CuY in the reaction of γ-butyrolactone with propylamine.
●: Conversion of γ-butyrolactone, ○: yield for 1-propyl-2-pyrrolidinone, ⊙: selectivity for 1-propyl-2-pyrrolidinone.

Influence of the Reaction Temperature. Figure 2 shows the temperature dependence of the yield of III by the reaction of I with II. The yield of III increases with temperature up to 320 °C, decreasing slightly above 320 °C. Thus, the optimum temperature seems to lie around 300 °C.

Effect of Contact Time. Effect of the contact time (W/F) on the yield of III from I and II over CaY and CuY was examined. W/F is defined as follows.

$$W/F = \frac{\text{Weight of catalyst (g)}}{\text{Total feed (I+II+N}_2\text{) (mol/h)}}$$

The results are illustrated in Fig. 3. The partial pressure of I was kept constant at 0.098 atm and that of II was varied in the range 0.088—0.497 atm. The yield of III increased with contact time, reaching a constant value which does not depend on the nature of the catalyst. Thus, the reaction seems to proceed until equilibrium is reached. The apparent equilibrium constant (K_P)

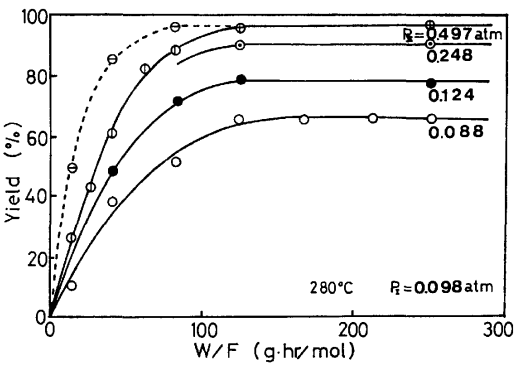

Fig. 3. Effect of contact time (W/F) on the yield of 1-propyl-2-pyrrolidinone over CuY (——) and CaY (------).

values estimated from the data in Fig. 3 are given in Table 3. The K_P value does not depend on the initial reaction conditions, suggesting that the reaction proceeds nearly to equilibrium.

Reaction Kinetics. The kinetics of the reaction of I and II was studied with CuY as a catalyst. Reaction kinetics was examined in the temperature range 240—280 °C under small contact time conditions for the reaction of I and II. The effect of the partial pressure of I (P_I) on the reaction rate was examined by keeping the partial pressure of II (P_{II}) at 0.348 atm. The partial pressure of nitrogen was adjusted to keep the contact time constant. The result is given in Fig. 4.

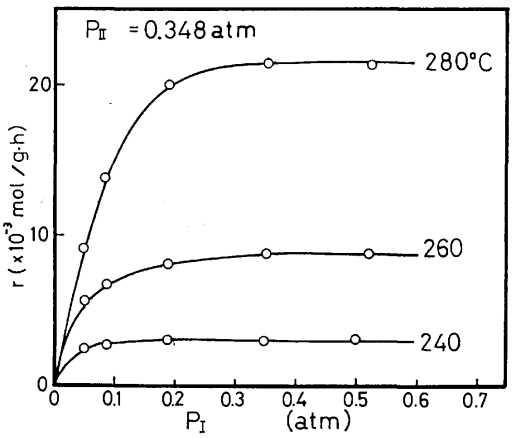

Fig. 4. Dependence of the reaction rate on the partial pressure of γ-butyrolactone.

Table 3. Apparent equilibrium constant of the reaction of γ-butyrolactone with propylamine

Catalyst	Feeding rate of reactant I ×10⁻³ mol/h	Feeding rate of reactant II ×10⁻³ mol/h	Formation rate of III ×10⁻³ mol/h	Yield of III %	Apparent equilibrium constant K_p
CuY, CaY	24.0	121.6	23.0	95.8	5.4
CuY	24.0	60.8	21.6	90.0	5.0
CuY	24.0	30.4	18.5	77.1	5.6
CuY	24.0	21.5	15.8	65.8	5.3

Catalyst 3 g. Reaction temperature 280 °C. Total feed (I+II+N_2) 245×10⁻³ mol/h.

$$K_p = \frac{P^*_{III} \cdot P^*_{H_2O}}{P^*_I \cdot P^*_{II}} = \frac{P^{*2}_{III}}{P^*_I \cdot P^*_{II}}$$

P^*: partial pressure at the reactor exit.

The dependence of the rate (r) on the partial pressure of I can be expressed by

$$r = k_I \cdot \frac{K_I P_I}{1+K_I P_I}, \quad (1)$$

were k_I and K_I are constants. By rearrangement, we have

$$\frac{P_I}{r} = \frac{1}{k_I K_I} + \frac{P_I}{k_I}, \quad (2)$$

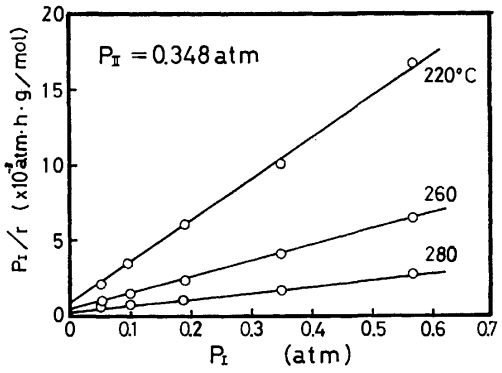

Fig. 5. P_I/r *vs.* P_I plot.

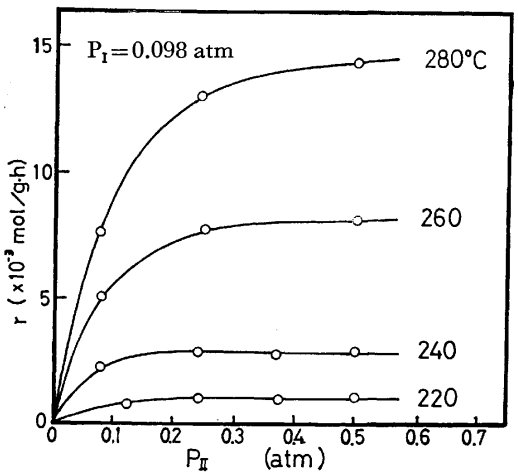

Fig. 6. Dependence of the reaction rate on the partial pressure of propylamine.

Straight lines are obtained by plotting P_I/r against P_I (Fig. 5). The slope and the intercept give the values of $1/k_I$ and $1/k_I K_I$, respectively.

The dependence of the reaction rate on the partial pressure of II was examined by keeping P_I at 0.098 atm (Fig. 6). It was found to be represented also by

$$r = k_{II} \cdot \frac{K_{II} P_{II}}{1+K_{II} P_{II}}, \quad (3)$$

which, on rearrangement, gives

$$\frac{P_{II}}{r} = \frac{1}{k_{II} K_{II}} + \frac{P_{II}}{k_{II}}. \quad (4)$$

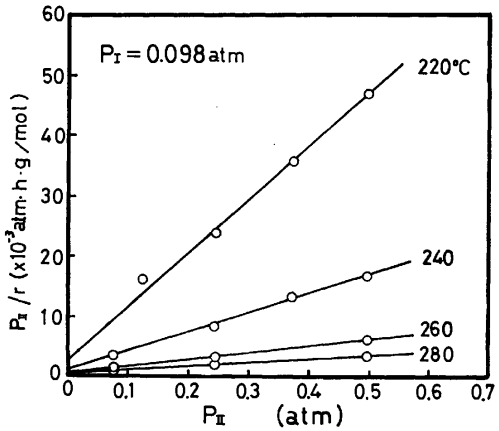

Fig. 7. P_{II}/r *vs.* P_{II} plot.

The relation was checked (Fig. 7) and the values of k_{II} and K_{II} were obtained.

Thus, the following kinetic expression is obtained from Eqs. 1 and 3:

$$r = k \cdot \frac{K_I P_I}{1+K_I P_I} \cdot \frac{K_{II} P_{II}}{1+K_{II} P_{II}}, \quad (5)$$

where

$$k_I = k \cdot \frac{K_{II} P_{II}}{1+K_{II} P_{II}} \quad \text{and} \quad k_{II} = k \cdot \frac{K_I P_I}{1+K_I P_I}.$$

From the values of k_I, k_{II}, K_I, and K_{II}, obtained experimentally, the value of k was determined uniquely. The values of K_I, K_{II} are given in Table 4.

Equation 5 indicates that there are independent adsorption sites for I and amine and that the reaction of the adsorbed I and adsorbed amine is rate determining. The activation energy of the reaction, the heats of adsorption of I and II were determined to be 23 kcal/mol, 9.0 kcal/mol, and 9.9 kcal/mol, respectively.

It was also confirmed that rate does not depend on the partial pressure of water or III, by addition of water or III to the feeding reactant.

Reaction Mechanism. The reaction kinetics represented by Eq. 5 suggests that there is an independent adsorption site for each reactant. In a previous work on the reaction of I and ammonia, it was postulated that polarization of the carbonyl group of I to the strong electrostatic field in the neighborhood of the metal cation is essential. The same should hold for the reaction with primary amines. The adsorption sites for I are probably metal cations.

The adsorption site for primary amines might be the oxygen ions next to aluminum cations in the zeolitic framework. Dissociative adsorption of ammonia has been observed on the oxide ions of alumina surface.[8]

TABLE 4. KINETIC PARAMETERS FOR THE REACTION OF γ-BUTYROLACTONE AND PROPYLAMINE OVER CuY

Temperature (°C)	k_I (×10^{-3} mol/g·h)	K_I (atm^{-1})	k_{II} (×10^{-3} mol/g·h)	K_{II} (atm^{-1})	k (×10^{-3} mol/g·h)
220	—	—	1.11	45.2	—
240	3.66	32.1	3.15	24.9	4.1
260	9.28	26.3	9.62	20.8	12.1
280	23.25	21.5	16.39	15.3	20.9

Thus, we proposed the following reaction mechanism.

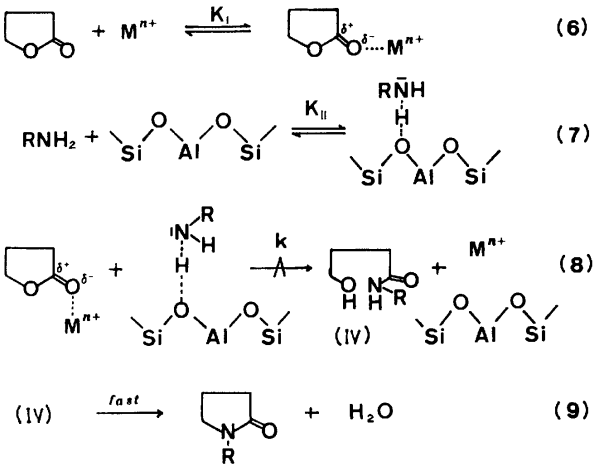

Equations 6 and 7 represent the adsorption of I and primary amine on metal cation and oxygen anion in the zeolite framework, respectively. The activated reactants react with each other to form an acid amide like intermediate IV (Eq. 8), the step being rate determining. The dehydration of the intermediate to the lactam is fast. This mechanism is in line with Eq. 5, if we put the adsorption equilibrium constant of I and primary amine, K_I and K_A and the rate constant of the elementary reaction (Eq. 8), k. This mechanism also expresses the effect of the kind of amines on their reactivity toward I. The elementary reaction (Eq. 8) should be faster, if the basicity of the amine increases; primary normal alkylamines react more readily with I than ammonia. The large steric effect is expected since the reaction occurs on the surface of zeolite. The interaction between the carbonyl group of I and the lone pair of the amine may need very specific special arrangement.

Low activity of hydrogen form of the zeolite (HY) should be noted since the origin of catalytic activity of the zeolite is very often ascribed to the protonic acidity of the zeolite. In the case of the reaction studied, protonic acid probably reacts with amines to form ammonium ions.

$$NH_2R + H^+ \rightleftharpoons NH_3R^+.$$

This explains the low activity of HY.

The authors acknowledge the helpful discussion of Professor Tominaga Keii. One of us (Y. O.) wishes to thank the Kurata Foundation for financial assistance.

References

1) E. Späth and J. Lintner, *Chem. Ber.*, **69**, 2727 (1936).
2) K. Hatada, M. Shimada, K. Fujita, Y. Ono, and T. Keii, *Chem. Lett.*, **1974**, 439.
3) K. Fujita, K. Hatada, Y. Ono, and T. Keii, *J. Catal.*, **35**, 325 (1974).
4) K. Hatada, M. Shimada, Y. Ono, and T. Keii, *J. Catal.*, **37**, 166 (1975).
5) Y. Ono, K. Hatada, K. Fujita, A. Halgeri, and T. Keii, *J, Catal.*, **41**, 322 (1976).
6) Y. Ono, Y. Takeyama, K. Hatada, and T. Keii, *Ind. Eng. Chem., Prod. Res. Dev.*, **15**, 180 (1976).
7) Y. Ono, M. Kaneko, A. Halgeri, and K. Hatada, "Molecular Sieves-II," ACS Symposium Series, No. 40, ed by J. R. Katzer, American Chemical Society, Washington (1977), p. 596.
8) J. B. Peri, *J. Phys. Chem.*, **69**, 231 (1969).

Application of Infrared ATR Spectroscopy to Liquid Crystals. I. Surface-Induced Orientation in Thin Films of Nematic MBBA[1]

Aritada HATTA

Laboratory of Interface Science of Metals, Faculty of Engineering, Tohoku University, Aramaki Aoba, Sendai 980

(Received February 8, 1977)

Infrared dichroism of nematic liquid *N*-(*p*-methoxybenzylidene)-*p*-butylaniline (MBBA) was measured using a conventional transmission method and an ATR method. In the former, KBr windows were used as substrates. The degree of orientation order of the homogeneous structure, which was achieved by a rubbing procedure, was obtained to be $S=0.40$. Using the measured dichroic ratios, the angles between the transition moments and the long axis of the molecule were calculated. The calculated values are in satisfactory agreement with the molecular conformation already suggested. In the ATR method, In_2O_3-coated glass plates were used as substrates. Rubbing of the In_2O_3 surface gave a uniform homogeneous orientation with an S value of 0.57. An In_2O_3 surface treated with dimethyldichlorosilane gave a homeotropic texture with an S value of 0.53. The directions of the transition moments relative to the long axis of the molecule closely agreed with those obtained from transmission spectra.

The orientation of the thin liquid-crystal film in contact with the solid surface is very often determined by the orientation of the liquid-crystal molecules interacting with the solid surface. Therefore, if the interaction between the molecules and the solid surface is very strong, the surface orientation can greatly contribute to the long-range ordering of the liquid crystal. Such an orientation behavior is not only a phenomenon of fundamental interest, but is also a practical problem for application to display elements.[2] In this connection, it is interesting to observe the infrared dichroism arising from molecular orientation in thin films of the liquid crystals in contact with various substrate surfaces.

The effects of temperature[3] and electric field[4] on molecular orientation have been investigated by the infrared dichroism method. All of these studies, however, have resorted to the use of the transmission method. Absorption measurements on liquid crystals using transmission techniques are often difficult because of the strong absorption and, therefore, extremely thin films are required. This difficulty does not arise when the ATR method[5] is used, because the observed intensities are determined by an electric-field penetration into the sample of a few microns and are independent of the sample thickness.

The most significant advantage of using the ATR method is that the electric fields exist in all spatial directions at the reflecting interface. Therefore, the ATR technique is capable of giving information about any orientational state of the liquid crystal.

Vergoten and Fleury[6] have recently reported infrared and Raman spectra of *N*-(*p*-methoxybenzylidene)-*p*-butylaniline (MBBA) in the solid state and in nematic and isotropic liquids. However, no infrared dichroism measurements have yet been reported.

The objective of this report is to show the versatility of the infrared ATR method in studying the structure of oriented liquid films of MBBA induced by the surface effect of the substrate.

Experimental

ATR spectra were recorded using a JASCO model IR-G grating spectrophotometer equipped with a double-beam ATR attachment and a conventional AgCl polarizer. Two trapezoidal prisms made from high-purity monocrystalline silicon were used as internal reflection elements in an optically-balanced double-beam system; one prism was put in the sample beam and the other in the reference beam.

The prisms were cut and polished so as to provide an internal reflection angle of incidence of 40° and give one reflection. The Si prism used has a constant transmittance (55%) from 2.5 to 6.6 μ. Beyond 6.6 μ, however, the transmittance of silicon falls off due to impurities and lattice bands, for example, three weak bands appear between 6.6 and 8 μ and a strong band appears at 9 μ. Careful balancing of the sample and reference beams provided a flat background level over the 2.5—10 μ wavelength range with sufficient sensitivity. In the present study, mainly the 6—10 μ range was investigated.

The sandwich cell shown in Fig. 1 was used for the ATR measurements. The sample of the liquid crystal is sandwiched between the Si prism and a substrate plate which is separated from the prism by a polyester spacer. The substrate chosen for the present study was an In_2O_3-coated conducting glass plate. The substrate was in contact with the wall of a brass box containing a nichrome wire heater. The tempera-

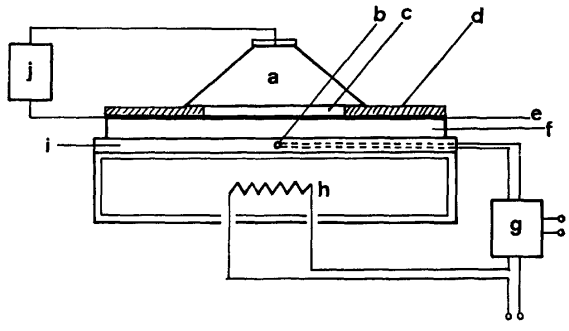

Fig. 1. Liquid crystal cell for ATR measurements. a: Si prism, b: thermocouple, c: liquid crystal, d: spacer, e: In_2O_3 electrode, f: glass plate, g: temperature regulator, h: heater, i: single-bored glass plate, j: voltage generator.

ture of the liquid crystal was controlled by a conventional on-off power supply. The accuracy of the temperature was ±2 °C. Guaranteed-grade MBBA reagent was obtained from Tokyo Chemical Industry Co. and was used without further purification.

To obtain homeotropic alignment, the substrate of the In_2O_3-coated glass plate was immersed in a 5% toluene solution of $(CH_3)_2SiCl_2$, following the experimental procedure given by Uchida *et al.*[14] After standing for 30 min at room temperature, the substrate was taken out of the solution and then rinsed with toluene to remove the remaining $(CH_3)_2SiCl_2$. The substrate thus treated was dried at 100°C for 1 h.

Results and Discussion

First, the transmission spectra of oriented MBBA at 30 °C will be discussed. The MBBA sample was held between two KBr windows whose surfaces were rubbed in one direction with a buff.

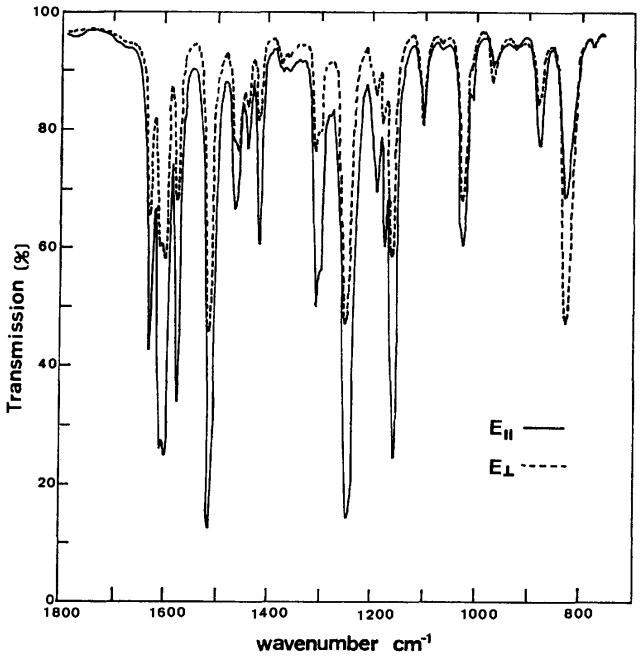

Fig. 2. The polarized transmission spectra of oriented thin MBBA film at 30 °C. $E_{//}$ and $E_{\perp}$ refer to the electric vector of radiation polarized parallel and perpendicular to the optic axis (rubbing direction), respectively.

Spectra were taken for radiation with the electric vector polarized parallel and perpendicular to the rubbing direction. Because of the high degree of absorption, no spacer was used between the windows. The polarized transmission spectra for MBBA are shown in Fig. 2. The observed dichroic ratios and vibrational assignments for several important bands are given in Table 1.

The degree of orientational order in liquid crystals is generally defined by the degree of order, S[7]

$$S = \frac{1}{2}(3\cos^2\alpha - 1), \tag{1}$$

where α is the angle between the long axis of the molecule and the optical axis of the uniformly oriented liquid crystal.

Table 1. Observed frequencies, vibrational assignments, and dichroic ratios for homogeneously-oriented MBBA (S=0.40; α=39.2°)

Observed (cm^{-1})	Assignment	R	β[a]
1630	C=N stretching	2.03	29.4°
1600	phenyl ring stretching	2.51	19.3°
1578	phenyl ring stertching	2.85	10.2°
1520	phenyl ring stretching	2.52	19.0°
1250	C–O–C asym. stretching	2.51	19.2°
1160	phenyl C–H in-plane deformation	2.63	16.4°
1030	CH_3–O stretching (C–O–C sym. str.)	1.34	44.8°
830	phenyl C–H out-of-plane deformation	0.50	90.0°[b]

a) The angle between the direction of the transition moment and the long axis of the molecule. b) Assumed.

On the other hand, the dichroic ratio is given by[8]

$$R = \frac{k_{//}}{k_{\perp}} = \frac{4\cos^2\beta\cos^2\alpha + 2\sin^2\beta\sin^2\alpha}{2\cos^2\beta\sin^2\alpha + \sin^2\beta(1+\cos^2\alpha)}. \tag{2}$$

In Eq. 2, $k_{//}$ and $k_{\perp}$ are the absorption coefficients measured with the infrared radiation polarized parallel and perpendicular to the optical axis, respectively. The angle β designates the angle between the long axis and the vibrational transition moment of the molecule. The coordinate system defined above is shown in Fig. 3. In this figure, all the long axes of the molecules are assumed to be inclined at a common angle α with respect to the optical axis. Furthermore, the molecules are assumed to rotate freely about their own long axes.

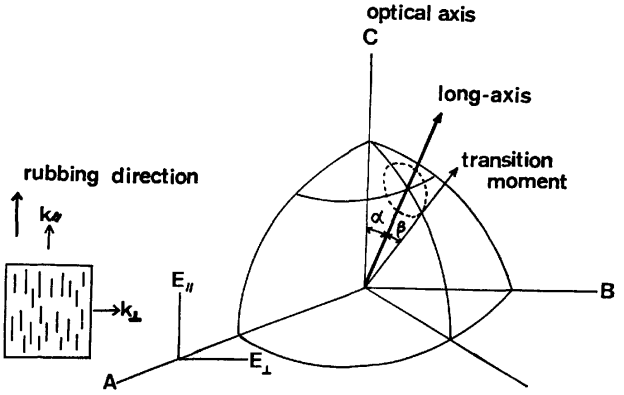

Fig. 3. Uniaxial orientation of the long-axis of the molecule around the optical axis and of the transition moment around the long-axis of the molecule.

From Eqs. 1 and 2, the degree of order is expressed in the simple form,

$$S = \frac{R-1}{S_\beta(R+2)}, \tag{3}$$

where

$$S_\beta = \frac{1}{2}(3\cos^2\beta - 1).$$

Thus, the degree of order is expressed in terms of R and

S_β. Accordingly, if the angle β is known for a given vibrational band, the value of S can be obtained from its R value. Furthermore, by using the S value obtained above, the β value can be calculated for any other vibrational band.

According to Eq. 1, the S value in Eq. 3 should vary from -0.5 to 1, the former corresponding to liquids oriented with the long axes of molecules perpendicular to the rubbing direction and the latter to liquids oriented with the long axes parallel to that direction. If the liquid crystal is isotropic, that is $R=1$, the S value becomes zero.

On the other hand, there is a high tendency for nematic molecules to line up with their long axes parallel to the direction of rubbing[3,9] and, therefore, the optical axis of the uniaxial liquid crystal can be assumed to coincide with the rubbing direction, as shown in Fig. 3. Accordingly, we may consider only the case in which the long axis of the molecule is oriented preferably parallel to the optical axis of the liquid so that the long axis has a positive S value. If the vibrational transition moment is oriented along the long axis of the molecule, Eq. 3 reduces to $S=(R-1)/(R+2)$. Because R varies between 1 and infinity in this case, the degree of order varies from 0 and 1, the former corresponding to an isotropic liquid and the latter to a liquid oriented parallel to the optical axis. On the other hand, when the transition moment is directed perpendicular to the long axis, the degree of order is given by $S=2(1-R)/(R+2)$. In this case, R would vary from 0 and 1, and then S is positive with a maximum value of 1 which also corresponds to a completely parallel liquid. Consequently, the degree of order S varies from 0 and 1 provided the $k_{//}$ component of the absorption coefficients is taken to be parallel to the optical axis of MBBA molecule.

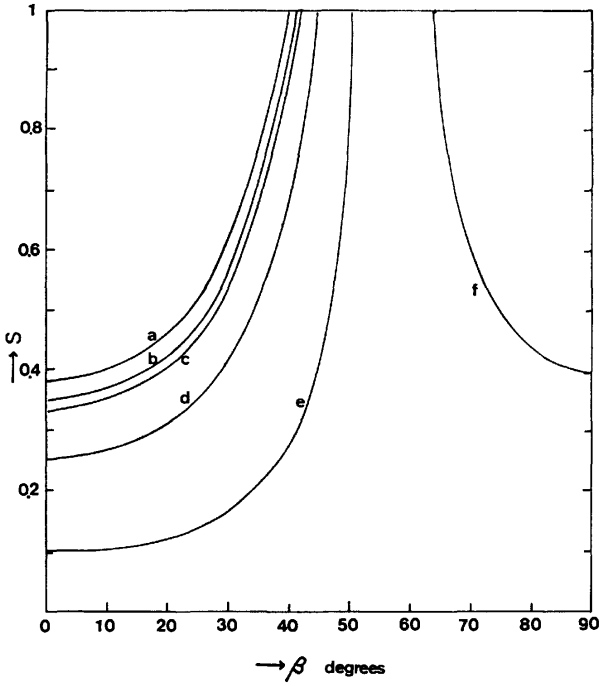

Fig. 4. The degree of orientation order S as a function of angle calculated from experimental dichroic ratio. a: 1578 cm^{-1}, b: 1160 cm^{-1}, c: 1600 cm^{-1}, d: 1630 cm^{-1}, e: 1030 cm^{-1}, f: 830 cm^{-1}.

The S values estimated from Eq. 3 are plotted against β in Fig. 4, using the R values listed in Table 1. The plots vary in a characteristic way and provide useful information about molecular structure: they afford the relative direction of the transition moment of the molecule and can, therefore, give confirmation of assignments already given. It is evident from Fig. 4 that the angle for the 1578 cm^{-1} band must have the lowest value; its transition moment is oriented nearly parallel to the direction of the long axis of the molecule. In contrast to this band, the 830 cm^{-1} band very probably has a much different direction of transition moment from that of the above band.

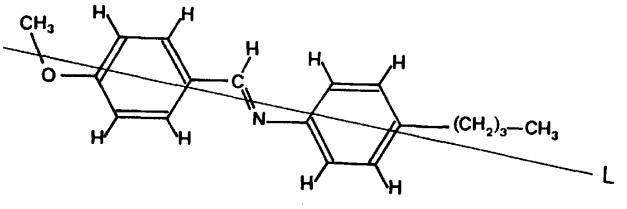

Fig. 5. Structural model for MBBA. L is the approximate direction of the long-axis of the molecule (from Ref. 10).

Based on the NMR study, Pines and Chang[10] suggested the structure of the MBBA molecule as shown in Fig. 5, where the long axis **L** is shown as the line passing through the centers of the co-planar benzene rings. If the transition moment of the 830 cm^{-1} band is assumed to be perpendicular to the long axis, *i.e.*, $\beta=\pi/2$, the S value is found, from Fig. 4, to be 0.40. From Eq. 1, the value of α is calculated to be 39.2°. If an S value of 0.40 is used, one can estimate β values for the remainder of the vibrational bands. The results are presented in Table 1.

The angle β between the transition moment of the phenyl ring stretching mode at 1578 cm^{-1} and the long axis of the molecule is calculated to be 10.2°, which is in excellent agreement with the experimental value of 9° given by Pines and Chang.[10] The above-mentioned value $S=0.40$ is rather low compared with the 0.62 value obtained from optical anisotropy measurements.[11] Nevertheless, in view of the fact that a sample in the form of very thin film was used, the uniformity of orientation may be affected by the container surfaces.

Saupe and Maier[7] have pointed out that the observed dichroic ratios contain a contribution from the anisotropy in the refractive indices, *viz.*, birefringence, $\Delta n=n_e-n_o$, where the extraordinary index n_e and ordinary index n_o correspond to the directions parallel and perpendicular to the optical axis of the medium, respectively: the correction factor to the dichroic ratio should increase with increasing S. If we conveniently assume that the birefringence of MBBA[12] obtained at 6328 Å is applicable to the present case, the corrected S value is found to be 0.44. In this case, however, the resulting β value for the 1578 cm^{-1} band is as large as 22°, which cannot be considered reasonable in view of the structural model mentioned above. Therefore,

the birefringence in the infrared region is probably small compared with that in the visible region. Support for this deduction is given by the ATR measurements of highly-oriented MBBA.

In the ATR method,[13] electromagnetic fields interacting with the absorbing medium are present in three directions at the reflecting interface and then the measurement of the reflectivity losses provides information about the anisotropy of the medium. In this respect, the ATR method is valuable for all types of oriented liquid crystals. However, no ATR spectra of liquid crystals have yet been reported. Brief mention is made of a procedure for the determination of the orientation of MBBA induced by substrate surfaces.

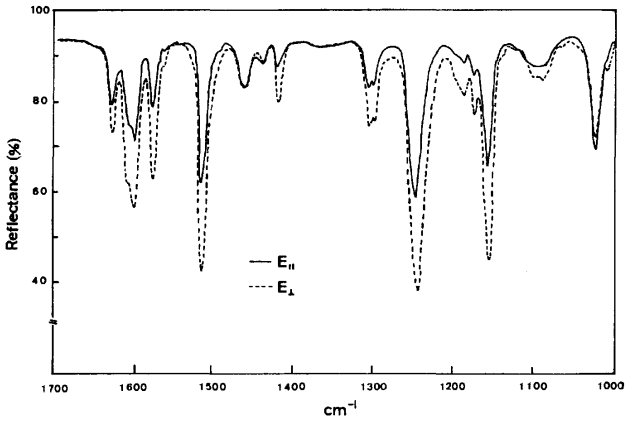

Fig. 6. The ATR spectra of uniformly homogeneous MBBA kept at 25 °C, measured with the electric vector of the radiation polarized parallel (solid line) and perpendicular (broken line) to the plane of incidence.

Figure 6 shows the polarized ATR spectra of a 25-μ sandwich of nematic MBBA between indium-oxide coated glass and a single reflection silicon prism. The temperature of the liquid cell was maintained at 25 °C and the incident angle was 40°. In order to obtain homogeneous orientation, the In_2O_3 surface was rubbed with alumina in one direction. The rubbed substrate was positioned to form the liquid cell so that the direction of rubbing coincided with the x-axis of the prism (see Fig. 8).

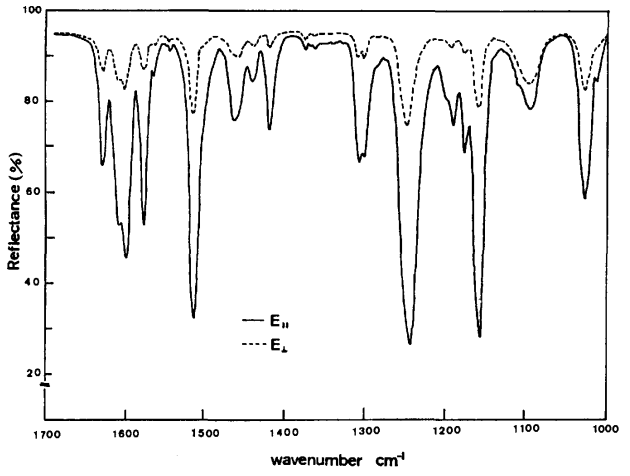

Fig. 7. The ATR spectra of homeotropic MBBA kept at 25 °C, measured with the electric vector of the radiation polarized parallel (solid line) and perpendicular (broken line) to the plane of incidence.

Figure 7 shows the polarized ATR spectra of homeotropically-oriented MBBA film at a constant temperature of 25 °C with the long axis of the molecule perpendicular to the substrate. This homeotropic structure was attained when the surface of the In_2O_3 coated glass was treated with dimethyldichlorosilane[14] or lecithin. The dichroic behavior exhibited in Fig. 7 shows clearly that the sample is quite well oriented, in agreement with the literature.[14] The observed dichroic ratios, D, taken from Figs. 6 and 7 are listed in Table 2.

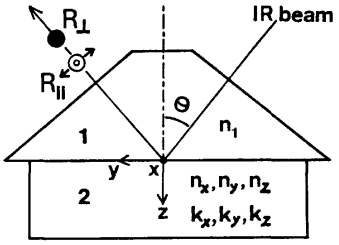

Fig. 8. Coordinate system for the attenuated total reflection from anisotropic absorbing medium. 1: Silicon prism, 2: anisotropic liquid crystal.

Table 2. Observed dichroic ratios, calculated β values, and S values for homogeneous and homeotropic liquids of MBBA

Wavenumber (cm^{-1})	Homogeneous			Homeotropic		
	D_{obsd}	k_x/k_z	β	D_{obsd}	k_z/k_x	β
1630	0.74	2.556	31.6°	4.35	2.277	32.6°
1600	0.53	3.568	20.9°	5.72	3.144	22.1°
1578	0.42	4.502	11.0°	7.18	4.068	10.0°
1520	0.51	3.708	19.6°	5.90	3.258	20.9°
1250	0.51	3.708	19.6°	5.74	3.156	22.0°
1160	0.46	4.110	15.5°	6.48	3.625	16.3°
1030	1.19	1.589	43.6°	3.29	1.606	42.4°
	$S=0.57$; $\alpha=32.4°$			$S=0.53$; $\alpha=34.0°$		

We now consider the two-phase system having a flat boundary shown in Fig. 8. In the figure, medium **1** is the Si ATR prism (refractive index of 3.42)[15] from which the infrared radiation is incident on medium **2**, which is a semi-infinite absorbing liquid crystal. The plane of incidence is the yz plane, the x-axis being perpendicular to this plane.

When total reflection occurs, the electromagnetic wave penetrates into medium **2** beyond the reflecting interface. For bulk material in which the thickness is much greater than the penetration depth of the evanescent wave, the change in reflection absorbance is respectively expressed for radiation polarized perpendicular and parallel with respect to the plane of incidence,[16] as

$$\ln\left(\frac{R_0}{R_\perp}\right) = pk_x$$

and

$$\ln\left(\frac{R_0}{R_{//}}\right) = qk_y + rk_z, \tag{4}$$

with

$$p = \frac{4n_{x1}^2}{\tan\theta(1-n_{x1}^2/\sin^2\theta)^{1/2}(1-n_{x1}^2)},$$

$$q = r(1-n_{z1}^2/\sin^2\theta), \tag{5}$$

and

$$r = \frac{4n_{y1}n_{z1}}{\tan\theta(1-n_{z1}^2/\sin^2\theta)^{1/2}(1-n_{z1}^2/\sin^2\theta+n_{y1}^2n_{z1}^2\cot^2\theta)}.$$

In Eq. 4, R_0 is the reflectivity when the absorption of medium **2** is zero and k_x, k_y, and k_z are the components of the absorption coefficient along the x, y, and z axes, respectively. In Eq. 5, θ is the incident angle and n_{x1}, n_{y1}, and n_{z1} are the components of the ratio of the refractive index of medium **2** to that of medium **1**.

From Eq. 4, the experimental dichroic ratio D, obtained from ATR spectra can be written as

$$D = \frac{q}{p}\left(\frac{k_y}{k_x}\right) + \frac{r}{p}\left(\frac{k_z}{k_x}\right). \tag{6}$$

In a particular case where the liquid is isotropic, *i.e.*, where $k_x=k_y=k_z$, D becomes $(q+r)/p$. Since the nematic liquid crystal has a uniaxial symmetry about the optical axis, the Eq. 6 can be reduced to a simpler expression.

If the molecules are oriented normal to the Si prism surface (homeotropic orientation), one finds $k_x=k_y$ from Fig. 8, and Eq. 6 reduces to

$$D = \frac{q}{p} + \frac{r}{p}\left(\frac{k_z}{k_x}\right). \tag{7}$$

If the molecules are oriented parallel to the x axis (homogeneous orientation), one has $k_y=k_z$ and then obtains

$$D = \frac{q+r}{p}\left(\frac{k_z}{k_x}\right). \tag{8}$$

Thus, if the values of p, q, and r can be calculated from Eq. 5, the value of the degree of order, S, can be obtained as a function of β in the manner described above for the case of transmission spectra. One should note that the k_z/k_x in Eq. 7 corresponds to the R in Eq. 3 in the case of homeotropic orientation, while in the case of homogeneous orientation the k_x/k_z in Eq. 8 corresponds to the R in Eq. 3. In order to calculate coefficients p, q, and r, however, it is necessary to know the anisotropic refractive indices in the infrared region for truly-oriented MBBA, however, no data are available at present.

On the other hand, in the visible region, detailed determinations of the birefringence and indices of refraction of MBBA at two wavelengths have been made by Haller, Huggins, and Freiser.[12] Their results are $n_o=1.54$ and $\Delta n=0.22$ at 6328 Å. These values are in good agreement with those obtained by Labrunie and Valette[17] at the same wavelength. Therefore, the values of p, q, and r were calculated assuming the above values.

Using an appropriate β value and the D value observed for any one vibration band, we can determine the degree of order S by the combined use of Eq. 3 and Eq. 7 or 8 corresponding to the case of homeotropic or homogeneous orientation. The β values for any other vibration can be derived using the S value thus determined. In the present study, the S value was changed independently for the homeotropic and the homogeneous cases so as to obtain agreement of the resulting β values for all vibration bands listed in Table 2 for both cases, because the β values cannot be altered by changes of orientation and the degree of orientation order. However, no set of reasonable S values could be obtained that fit the corresponding β values for both cases. Therefore, the most reasonable set of β values was obtained by changing only Δn, because the contribution of Δn to the calculated β and S values is much more sensitive than that of n_o. For these calculations, a least-squares refinement gave S values of 0.57 for the uniform homogeneous orientation and 0.53 for the homeotropic orientation. In these cases, the values of α are calculated to be 32.4 and 34.0° for the homogeneous and homeotropic cases, respectively. As a result of the above calculations, the most probable birefringence was obtained to be 0.05. In view of the experimental accuracy, however, a birefringence of 0.10 should also be considered to give good fit to the observations. The values of β obtained for the two liquid crystals are presented in Table 2, together with the values of k_z/k_x and k_x/k_z. The values of the degree of order S thus derived are compatible with the value of 0.62 for MBBA given by Chang.[11] In addition, values of β for the vibrational bands investigated here are in satisfactory agreement with those obtained by the transmission method mentioned previously.

It should be noted that the dichroisms observed for the two types of oriented film both arise from orientations of the liquid crystal very near the Si surface. In spite of this fact, dichroic analysis revealed a high degree of orientation, as mentioned above, which strongly suggests that the influence of the silicon surface on the orientational structure is much weaker than the aligning forces of the wall of the substrate side.

For practical reasons, several techniques for obtaining uniform orientation of liquid crystals have been investigated.[18] In order to understand the alignment mechanism, it is important to elucidate the structure of the liquid crystal as well as the surface structure of the substrate.[14,19] The infrared ATR technique permits experiments directed towards these problems.

Another important objective of the present ATR study on liquid crystals was to observe the molecular orientation under electric fields. This has been partly completed and the results of the experiment will be reported in the near future.

The author wishes to thank the Ōsaka Titanium Co., Ltd., for providing a high-purity single crystal of Si. The author also wishes to thank Professor W. Suĕtaka of Tohoku University, for help in the preparation of the manuscript.

References

1) A preliminary report of this work was presented in part at the 2nd Symposium on Liquid Crystals, August, 1976, Sapporo, Abstract, p. 34.

2) G. W. Gray and P. A. Winsor, "Liquid Crystals and Plastic Crystals," Vols. I and II, John Wiley & Sons, New

York (1974).
3) W. Maier and G. Englert, *Elektrochem.*, **64**, 689 (1960); W. Maier and K. Markau, *Z. Phys. Chem., N.F.*, **28**, 190 (1961); V. L. Khodzhaeva, M. V. Shishkina, and I. I. Konstantinov, *Mol. Cryst. Liq. Cryst.*, **31**, 21 (1975); J. R. Fernandes and S. Venugopalan, *ibid.*, **35**, 113 (1976).
4) V. D. Neff, L. W. Gulrich, and G. H. Brown, *Mol. Cryst.*, **1**, 225 (1966).
5) N. J. Harrick, *J. Phys. Chem.*, **64**, 1110 (1960); J. Fahrenfort, *Spectrochim. Acta*, **17**, 698 (1961).
6) G. Vergoten and G. Fleury, *Mol. Cryst. Liq. Cryst.*, **30**, 213 (1975).
7) A. Saupe and W. Maier, *Z. Naturforsch., Teil A*, **16**, 816 (1961); A. Saupe, *ibid.*, **19**, 161 (1964).
8) R. D. B. Fraser, *J. Chem. Phys.*, **21**, 1511 (1953).
9) P. Chatelain, *C. R. Acad. Sci., Paris*, **213**, 875 (1941).
10) A. Pines and J. J. Chang, *Phys. Rev., A*, **10**, 946 (1974).
11) R. Chang, *Mol. Cryst. Liq. Cryst.*, **30**, 155 (1975).
12) I. Haller, H. A. Huggins, and M. J. Freiser, *Mol. Cryst. Liq. Cryst.*, **16**, 53 (1972).
13) N. J. Harrick, "Internal Reflection Spectroscopy," Interscience, New York (1967).
14) T. Uchida, C. Shishido, and M. Wada, *Denki Tsushin Gakkaishi*, **58C**, 224 (1975).
15) M. Herzberger and C. D. Salzberg, *J. Opt. Soc. Am.*, **52**, 420 (1962).
16) P. A. Flournoy and W. J. Schaffers, *Spectrochim. Acta*, **22**, 5 (1966).
17) G. Labrunie and S. Valette, *Appl. Opt.*, **13**, 1802 (1974).
18) F. J. Kahn, G. N. Taylor, and H. Schonhorn, *Proc. IEEE.*, **61**, 823 (1973); W. Urbach, M. Boix, and E. Guyon, *Appl. Phys. Lett.*, **25**, 479 (1974); S. Matsumoto, M. Kawamoto, and N. Kaneko, *ibid.*, **27**, 268 (1975); J. C. Dubois, M.Gazard, and A. Zann, *J. Appl. Phys.*, **47**, 1270 (1976).
19) T. Uchida, H. Watanabe, and M. Wada, *Jpn. J. Appl. Phys.*, **11**, 1559 (1972).

The Heat of Solution of Poly(oxyethylene) Dodecyl Ethers in Dodecane

Takayasu MIURA* and Masao NAKAMURA

Department of Chemistry, Faculty of Science, Tokai University, Kitakaname, Hiratsuka 259-12

(Received February 9, 1977)

The heats of mixing of nonionic surfactants, poly(oxyethylene) dodecyl ethers $C_{12}H_{25}(OC_2H_4)_nOH$ (n=0—5) with a nonpolar liquid, dodecane were measured directly with a twin conduction microcalorimeter. A discontinuity appears on the heat of mixing *vs.* concentration curve except for n=0, the concentration of which decreases exponentially with n. This was regarded as the critical micelle concentration. It was deduced from the heat of solution at infinite dilution, $\Delta_s h_2^{\ominus}$, that the poly(oxyethylene) chain is in a cyclic state in dodecane due to intramolecular hydrogen bonding of the terminal OH group with an oxygen atom in the chain. In addition, the energy of the solute-solvent interaction, $\Delta_t u_2^{\ominus}$, was estimated from $\Delta_s h_2^{\ominus}$ and the heat of evaporation of the solute, $\Delta_e h^0$. As a consequence, the interaction energies of the OH group with nonpolar hydrocarbon are similar, regardless of whether or not the OH group is intramolecularly hydrogen bonded.

The use of nonionic surfactants in nonaqueous solutions has been developed,[1] but the dissolved states are not well understood.[2] In a previous paper,[3] the molecular state of poly(oxyethylene) dodecyl ethers, a typical series of nonionic surfactants were deduced, in the vapor phase, in which the poly(oxyethylene) chains are not extended but in cyclic states due to the intramolecular hydrogen bonding of the terminal OH group with an oxygen atom in the chain. Poly(oxyethylene) chains are also expected to be in cyclic states in a nonpolar liquid, because the vapor phase may be regarded as the most nonpolar medium. Dodecane may be the most desirable solvent in nonpolar liquids for poly(oxyethylene) dodecyl ethers, because the hydrophobic dodecyl group cannot be discerned from the solvent dodecane. In the present paper, the dissolved states of nonionic surfactant molecules in nonpolar liquids are elucidated by calorimetrically determining the heats of mixing of poly(oxyethylene) dodecyl ethers with dodecane.

Experimental

Poly(oxyethylene) dodecyl ethers, $C_{12}H_{25}(OC_2H_4)_nOH$ (n= 1, 2, 3, 4, and 5), and 1-dodecanol (corresponding to n=0) were kindly provided by Nihon Surfactant Kogyo K. K., which have the same order of purity as those used in a previous paper.[3] The solvent was prepared by distilling G. R. grade dodecane (Wako Junyaku Co.) after drying over a sodium wire for one week.

The heats of mixing were measured with a twin conduction microcalorimeter using a mixing device for ampoules (Oyodenki Kenkyujo Co., CM-502).[4] The temperature of the cells was maintained at 29.00±0.05 °C by circulating thermostatically-controlled water around the apparatus installed in an air thermostat. A small glass ampoule containing a weighed amount of solute was immersed in 25 cm³ of dodecane in the cell. After the establishment of thermal equilibrium, the ampoule was crushed and the liquid was stirred for 1 min. The difference in temperature between the two cells, one ampoule in either cell being empty, was recorded. This difference is due to the liberation or absorption of heat which accompanies the mixing of the solute and dodecane. The heat was estimated similarly using the method described by Murakami and Fujishiro.[5]

* Present address: Nihon Surfactant Kogyo K. K., 3-24-3, Itabashi, Tokyo 174.

Results and Discussion

Critical Micelle Concentration. When n_1 mol of solvent and n_2 mol of solute are mixed, the heat of mixing, ΔH, is given by

$$\Delta H = n_1 \Delta h_1 + n_2 \Delta h_2, \quad (1)$$

where $\Delta h_i = h_i^0 - h_i$ and h_i and h_i^0 are the partial molar enthalpy in the solution and the molar enthalpy in the pure state, respectively, of component i. Then,

$$\Delta h_2 = \left(\frac{\partial \Delta H}{\partial n_2}\right)_{T,p,n_1}, \quad (2)$$

where T is the absolute temperature and p the pressure. The relations between ΔH and n_2 measured for poly(oxyethylene) dodecyl ethers with dodecane are shown in Figs. 1—6, when the amount of solvent dodecane is 25 cm³. Since T, p, and n_1 are maintained constant under the present experimental conditions, the tangent at any point on the curves in Figs. 1—6 is equal to Δh_2 at that concentration.

For 1-dodecanol (n=0), ΔH is proportional to n_2 and, therefore, Δh_2 is constant over the measurement range, as shown in Fig. 1. This means that such concentrations

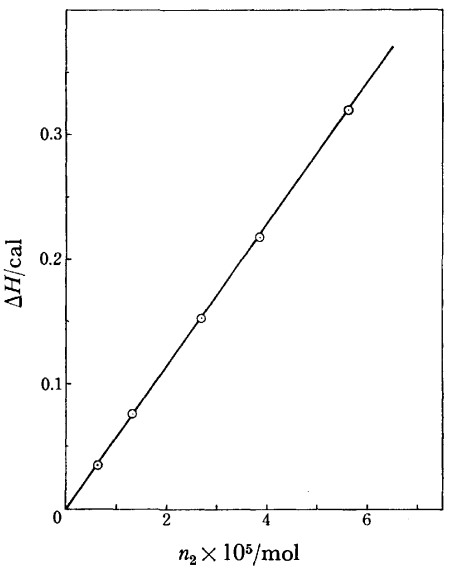

Fig. 1. Heat of mixing ΔH of n_2 mol of 1-dodecanol with 25 cm³ of dodecane at 29 °C.

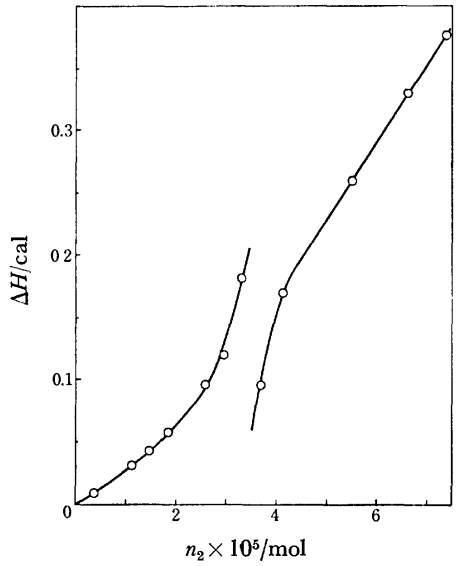

Fig. 2. Heat of mixing ΔH of n_2 mol of $C_{12}H_{25}OC_2H_4OH$ with 25 cm³ of dodecane at 29 °C.

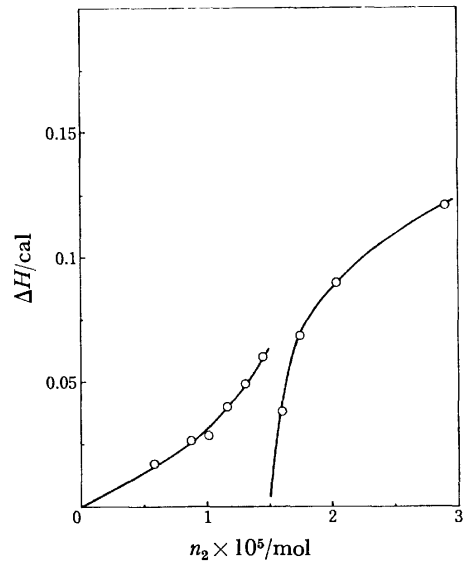

Fig. 4. Heat of mixing ΔH of n_2 mol of $C_{12}H_{25}(OC_2H_4)_3$-OH with 25 cm³ of dodecane at 29 °C.

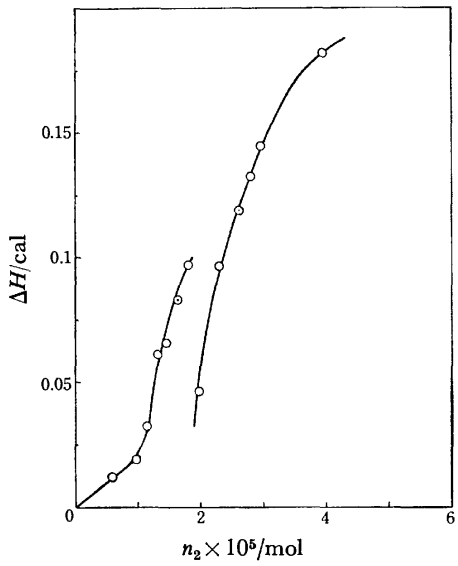

Fig. 3. Heat of mixing ΔH of n_2 mol of $C_{12}H_{25}(OC_2H_4)_2$-OH with 25 cm³ of dodecane at 29 °C.

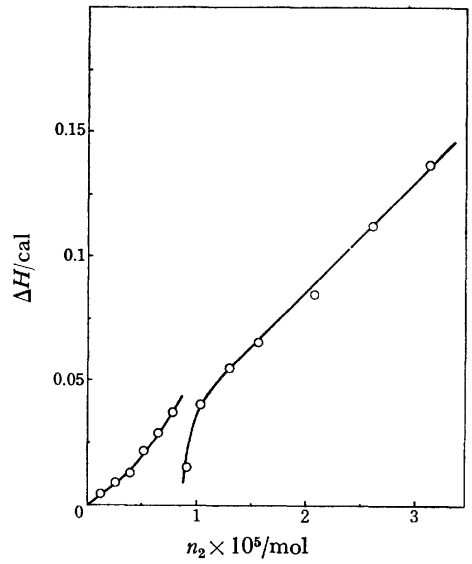

Fig. 5. Heat of mixing ΔH of n_2 mol of $C_{12}H_{25}(OC_2H_4)_4$-OH with 25 cm³ of dodecane at 29 °C.

are dilute enough so that the solutions can be regarded as ideal dilute solutions. Thus, the value of Δh_2 estimated from the inclination is equal to the heat of solution at infinite dilution, $\Delta_s h_2^{\ominus}$.

For $n=1$—5, ΔH is not proportional to n_2 and Δh_2 is not constant even in the same concentration region where the solution of 1-dodecanol is ideally dilute, as shown in Figs. 2—6. In such a concentration region, the solution not only deviates from the condition of an ideal dilute solution, but also there appears a discontinuous point on the curve of ΔH *vs.* n_2, where ΔH decreases abruptly with increasing concentration, regardless of n. Such discontinuous phenomena have been found by Hutchinson *et al.*[6] for aqueous sodium alkyl sulfates solutions. They have shown that the discontinuity concentration, DC, is in good agreement with the critical micelle concentration, CMC. Then, the observed DC is also assumed to correspond to the CMC of poly(oxyethylene) dodecyl ethers in dodecane, the values of which are listed in Table 1.

The plot of log DC was found to decrease linearly with n, the number of oxyethylene units in a poly(oxyethylene) chain, as shown in Fig. 7. Such a relationship resembles those between CMC for aqueous solutions and the number of methylene groups in a hydrophobic alkyl chain of a homologous series of surfactants.[7] According to the theory of micellization,[8] the linear relation means that each methylene group of the homologs makes an equal energy contribution, when an alkyl group is transferred from the aqueous solution into a micelle. The linear relation between log DC and n, therefore, confirms the assumption that the DC corre-

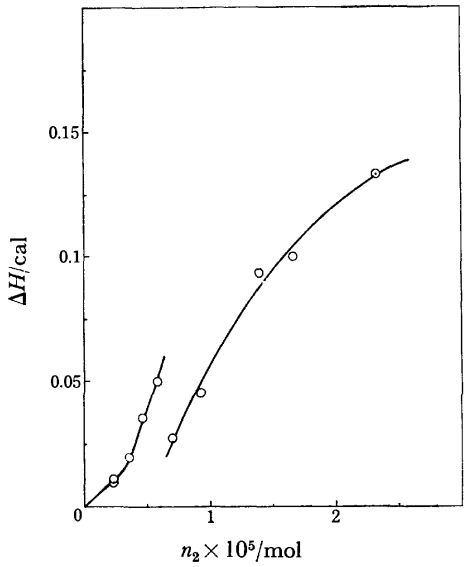

Fig. 6. Heat of mixing ΔH of n_2 mol of $C_{12}H_{25}(OC_2H_4)_5$-OH with 25 cm³ of dodecane at 29 °C.

TABLE 1. CRITICAL MICELLE CONCENTRATIONS CMC, HEATS OF MICELLIZATION $\Delta_m h_2$, HEATS OF SOLUTION AT INFINITE DILUTION $\Delta_s h_2^\ominus$, AND INTERACTION ENERGIES WITH SOLVENT $\Delta_i u_2^\ominus$ OF $C_{12}H_{25}(OC_2H_4)_nOH$ IN DODECANE AT 29 °C

n	CMC / mol m^{-3}	$\Delta_m h_2$ / kcal mol^{-1}	$\Delta_s h_2^\ominus$ / kcal mol^{-1}	$\Delta_i u_2^\ominus$ / kcal mol^{-1}
0			5.6	−8.9
1	1.40	5.0	2.3	−14.8
2	0.75	4.0	1.5	−17.6
3	0.60	3.2	2.6	−22.2
4	0.35	4.0	3.2	−27.2
5	0.26	6.0	4.1	−31.9

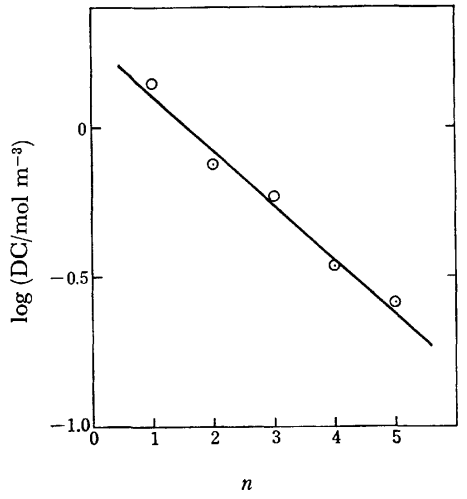

Fig. 7. The relationship between discontinuity concentration DC and degree of polymerization n of $C_{12}H_{25}$-$(OC_2H_4)_nOH$ in dodecane at 29 °C.

sponds to the CMC. In addition, the state of an oxyethylene unit in the lipophobic chain would not be different depending whether it exists in micelle or in dodecane.

Hutchinson *et al.* have also shown that the discontinuous change in the heat of mixing per mol of solute at the CMC corresponds to the heat of micellization.[6] The values of the heat of micellization, which are listed in Table 1, were estimated by dividing the abrupt changes in ΔH at the DC by n_2. They exhibit no tendency to increase linearly with n, which is expected from the linear relation between log CMC and n. These may not always reflect equilibrium properties, because of the complexity of the dissolving process of the surfactant, especially around the CMC, involving the alternate formation and destruction of micelles. Actually, both endothermic and exothermic parts were often found in a chart at such concentrations. Even if the heat of micellization cannot always be obtained correctly, the measurement of the heat of mixting is recommended as the preferred method for determining the CMC, especially for organic solutions.

Heat of Solution at Infinite Dilution. From Eq. 2, the heat of solution at infinite dilution, $\Delta_s h_2^\ominus$, is expressed by

$$\Delta_s h_2^\ominus = \lim_{n_1 \to 0} \Delta h_2 = \lim_{n_1 \to 0} \left(\frac{\partial \Delta H}{\partial n_2} \right)_{T,p,n_1} . \quad (3)$$

Then, $\Delta_s h_2^\ominus$ can be obtained from the initial slope of the straight lines passing through the origin in Figs. 1—6. The values thus estimated are listed in Table 1. It was found that $\Delta_s h_2^\ominus$ increases linearly with n in the range 2—5, as shown in Fig. 8. This means that all oxyethylene units in a poly(oxyethylene) chain of n= 2—5 are in equal states in dodecane, as has been described previously for the heats of evaporation of these compounds.[3] From the slope of the line, it requires *ca.* 0.8 kcal mol^{-1} for the oxyethylene unit to transfer a poly(oxyethylene) dodecyl ether from the pure liquid state to the dodecane solution for n=2—5.

The straight line in Fig. 8 passes through the origin, which is *ca.* 5.6 kcal mol^{-1} less than the value for 1-dodecanol (n=0). These phenomena suggest that the terminal OH group of the poly(oxyethylene) chain is

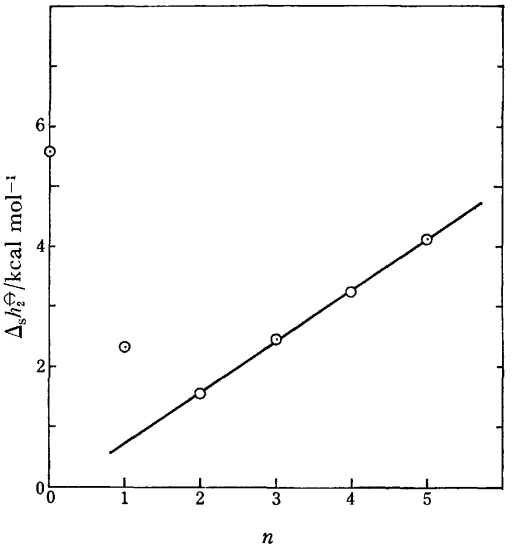

Fig. 8. Heat of solution at infinite dilution $\Delta_s h_2^\ominus$ *vs.* n plot for $C_{12}H_{25}(OC_2H_4)_nOH$ in dodecane at 29 °C.

not in the same state as the alcoholic OH group dissolved in dodecane, because both the alcoholic and terminal OH groups in their pure states are considered not to be so different energetically but to interact with one of the neighboring molecules due to intermolecular hydrogen bonding. As already deduced for the vapor phase,[3] for the nonpolar dodecane solution the terminal OH group of the poly(oxyethylene) chain is believed to interact with an oxygen atom in the chain and thus the chain is in a cyclic state due to intramolecular hydrogen bonding. A signal due to intramolecular hydrogen bonding has been observed by means of infrared spectroscopy for similar substances, the monomer and dimer of ethylene glycol and their monomethyl ethers, in nonpolar carbon tetrachloride.[9,10] Because an energy of 5.6 kcal mol^{-1}, the difference between $\Delta_s h_2^{\ominus}$ for 1-dodecanol and the straight line for $n=2$—5, corresponds exactly to that of 1 mol of a hydrogen bond[11] (although this is slightly less than the corresponding value for evaporation, 6.2 kcal mol^{-1}), almost all the molecules would be in cyclic states due to intramolecular hydrogen bonding.

The value of $\Delta_s h_2^{\ominus}$ for $n=1$ is *ca.* 1.5 kcal mol^{-1} higher than that expected from the linear relation for $n=2$—5. This increase in energy can be interpreted from the fact that the molecule of $n=1$ can only form a 5-membered ring, for intramolecular hydrogen bonding. The 5-membered ring is expected to have a higher energy for hydrogen bonding than 8-membered or larger rings,[12] because it has been found that the infrared absorption-band shift of the OH group due to the 8-membered ring is appreciably larger than that due to the 5-membered ring.[10]

Solute-solvent Interaction. The heat of condensation of 1 mol of solute from the vapor phase to solution at infinite dilution, $\Delta_i h_2^{\ominus}$, may be expressed in terms of the heat of evapration, $\Delta_e h_2^0$, and the heat of solution at infinite dilution, $\Delta_s h_2^{\ominus}$, as

$$\Delta_i h_2^{\ominus} = \Delta_s h_2^{\ominus} - \Delta_e h_2^0, \tag{4}$$

according to the Born-Harber cycle:

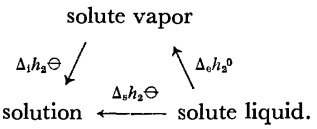

When the interaction between solute molecules is neglected in the vapor phase, the interaction energy of the solute with the surrounding solvent molecules in the solution, $\Delta_i u_2^{\ominus}$, can be expressed as

$$\Delta_i u_2^{\ominus} = \Delta_i h_2^{\ominus} + RT, \tag{5}$$

where R is the gas constant. $\Delta_i u_2^{\ominus}$ is considered to be the most suitable measure of the affinity for a given solute and solvent combination. The values of $\Delta_i u_2^{\ominus}$ for poly(oxyethylene) dodecyl ethers in dodecane listed in Table 1 were calculated from the data for $\Delta_s h_2^{\ominus}$ in the present paper and those for $\Delta_e h_2^0$ from a previous paper.[3] The relationship between $\Delta_i u_2^{\ominus}$ and n is shown in Fig. 9. A linear relation holds not only for $n=2$—5, as in Fig. 8, but also for $n=0$ for which the value of $\Delta_i u_2^{\ominus}$ falls near the straight line. This reveals that the

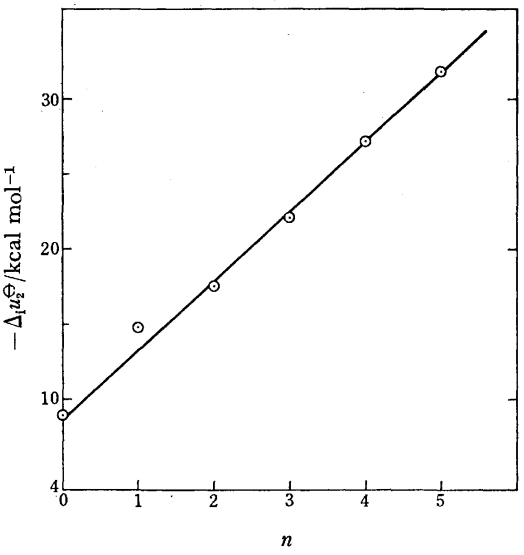

Fig. 9. Intraction energy with dodecane $\Delta_i u_2^{\ominus}$ *vs.* n plot for $C_{12}H_{25}(OC_2H_4)_nOH$ at 29 °C.

interaction of an alcoholic OH group with dodecane is indistinguishable from that of the terminal OH group of the poly(oxyethylene) chain for $n=2$—5. Thus, it is concluded that the energy of interaction of the OH group with dodecane does not depend on whether it is free or intramolecularly bonded to an ether oxygen atom. If this is true, the upward deviation of $n=1$ from the straight line can be ascribed to changes in the energy of the intramolecular hydrogen bond in the 5-membered ring and/or in the rate for the 5-membered ring to free an OH group, when the molecules are transferred from the vapor phase to the dodecane solution. The slope of the straight line gives an energy of *ca.* −4.7 kcal mol^{-1}, which is the interaction energy of an oxyethylene unit with dodecane. Since the cohesive energy of a hydrocarbon is estimated to be *ca.* −0.8 kcal mol^{-1} of the methylene group,[13] the interaction energy of an ether oxygen atom with dodecane results in an energy of *ca.* −3.1 kcal mol^{-1}, provided that the additivity holds for the interaction energy in oxyethylene unit.

The authors wish to express their thanks to Professor Kiiti Kosiyama for his encouragement throughout this work.

References

1) N. Schonfelt, "Surface Active Ethylene Oxide Adducts," Pergamon Press, Oxford (1969), p. 368.
2) F. M. Forkes, "Solvent Properties of Surfactant Solutions," ed by K. Shinoda, Marcel Dekker, New York (1967), p. 65.
3) M. Nakamura, K. Eda, and K. Kosiyama, *Bull. Chem. Soc. Jpn.*, **47**, 2877 (1974).
4) M. Koishi, *Bull. Chem. Soc. Jpn.*, **39**, 2406 (1966).
5) S. Murakami and R. Fujishiro, *Bull. Chem. Soc. Jpn.*, **40**, 1784 (1967).
6) E. Hutchinson, K. E. Manchester, and L. Winslow, *J. Phys. Chem.*, **58**, 1124 (1954).

7) K. Shinoda, T. Yamaguchi, and R. Hori, *Bull. Chem. Soc. Jpn.*, **34**, 237 (1961); H. B. Klevens, *J. Am. Oil Chem. Soc.*, **30**, 74 (1953).
8) K. Shinoda, T. Nakagawa, B. Tamamushi, and T. Isemura, "Colloidal Surfactants," Academic Press, New York (1963), p. 1.
9) L. S. Probhumirashi and C. I. Jose, *J. Chem. Soc., Faraday Trans. 2*, **71**, 1545 (1975).
10) C. Quivoron and J. Néel, *J. Chim. Phys.*, **63**, 1210 (1966).
11) G. C. Pimentel and A. L. McClellan, "The Hydrogen Bond," Freeman, San Francisco (1960).
12) S. N. Vinogradov and R. H. Linnell, "Hydrogen Bonding," Van Nostrand Reinhold, New York (1971), p. 138.
13) Nipponkagakukai, "Kagakubenran (Kisohen I)," Maruzen, Tokyo (1975), p. 916.

Dye-sensitization on the Photocurrent at Zinc Oxide Electrode in Aqueous Electrolyte Solution

Michio MATSUMURA, Yoichi NOMURA, and Hiroshi TSUBOMURA

Department of Chemistry, Faculty of Engineering Science, Osaka University, Toyonaka, Osaka 560

(Received February 10, 1977)

The dye-sensitized photocurrents generated from the electrochemical systems <zinc oxide|aq solution|platinum> have been studied. The action spectra for the photocurrent, its dependence on the concentration of the dye solution and other experimental results have revealed that the photocurrent is caused by the dye adsorbed on the electrode, not from that dissolved in the liquid phase. From the analysis of the decay of the photocurrent with the time of illumination, the quantum yield for the electron injection from the excited dye has been determined. Rose Bengal showed the quantum yield of 22%. The influence of halide ions on the photocurrent has also been studied.

"Wet-type" photocells, consisting of a semiconductor electrode, an aqueous solution, and a metal counter electrode, are attracting growing attention as a device to convert light energy into electrical or chemical energy.[1-4] The photovoltaic effect in such cells arises essentially from generation of electrons and holes in the illuminated semiconductor electrode and their efficient separation by the built-in electric field inside the space charge layer of the semiconductor. One of the characteristics of the "wet" cells is that the photocurrent is accompanied by redox reactions of the solute or the solvent in the electrolyte solution.

When the electrolyte solution contains a dye, a photocurrent often flows by the excitation of the dye with photon energy less than the band gap of the semiconductor. In this case, the current is called the dye-sensitized photocurrent, on which many reports have been made.[5-9]

We have succeeded in constructing a dye-sensitized semiconductor photo-cell having an energy conversion efficiency of 1.5% under monochromatic illumination.[10] In order to increase the energy conversion efficiency further, it will be necessary to increase both the quantity of light absorbed by the dye and the quantum yield of electron injection from the excited dye. For this purpose, it is essential to deepen our understanding on the mechanism of electron transfer in such systems. In this paper, we describe some of our results on such problems.

Experimental

Zinc oxide sinter disks were used as the electrodes. They were prepared by moulding zinc oxide powder by compression and heating at 1300 °C in the air for 1 h. It was found that the adsorptive activity of the zinc oxide sinter for the dye depends on the source of the zinc oxide powder. In the following experiments, we made the sinter out of zinc oxide powder obtained from Kanto Chemical Co. without any purification or pre-treatment. The sinter had low adsorptive activity but gave a reproducible photocurrent. One of the surfaces of the zinc oxide disk was coated with indium by employing the evaporation method so as to make an ohmic contact, and a copper wire was attached with silver paste. The structure of the electrode was mostly the same as that described previously.[9,10] Before each measurement, the electrode was polished with silicon carbide abrasive, etched with hydrochloric acid or nitric acid, washed with water, and dried.

The potential of the semiconductor electrode *versus* the reference electrode (SCE) was controlled by use of a Hokutodenko HA-101 potentiostat and the current was measured with a Yokogawa-Hewlett-Packard 4304B electrometer. A 500 W xenon lamp of Ushio Electric Inc. was used as the light source. The light was monochromatized by use of a Japan Jarrel-Ash, 0.25 m Ebert type monochromator. The light intensity was measured with an Eppley, bismuth-silver type thermopile. A Shimadzu MPS-50L Spectrometer was used for the measurements of absorption spectra.

All the solutions used contained 0.2 M (mol·dm^{-3}) Na_2SO_4 or KNO_3 as the supporting electrolyte. Oxygen was removed by bubbling high purity nitrogen gas through the solutions before measurement. All chemicals were of reagent grade and used without further purification. The structual formulas of the dyes used are given below:

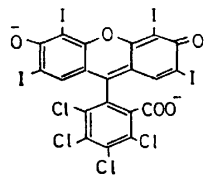

Rose Bengal.

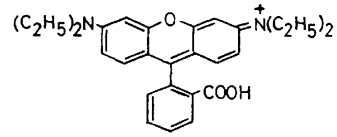

Rhodamine B.

Results

Figure 1 shows the dye-sensitized photocurrent-potential curves for the case of Rose Bengal. The anodic current was negligible in the dark, while it rose up under illumination in the wavelength range of the absorption band of Rose Bengal. When the solution contained no dye, the photocurrent was less than 0.03

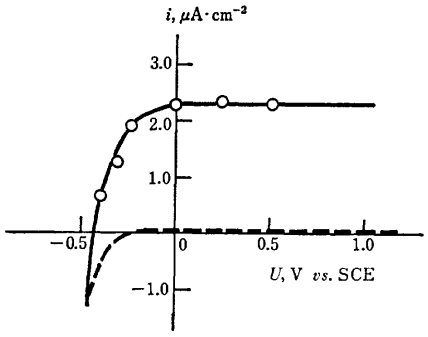

Fig. 1. Current-potential curves in the presence of 6.5×10^{-7} M Rose Bengal and 0.2 M Na_2SO_4, ——dark current, ——under illumination (λ 562 nm).

$\mu A \cdot cm^{-2}$ under illumination at the same wavelength and at the electrode potential of 0.35 V. Since the photocurrent decayed during the course of illumination, the photocurrent curve was plotted by using the value obtained immediately after the light had been turned on. The photocurrent appeared at the electrode potential more positive than −0.5 V *vs.* SCE, which nearly agreed with the flat band potential of the zinc oxide electrode reported by Lohmann,[11] and became constant at the potential more positive than 0.0 V. Therefore, most of the experiments were made at 0.35 V.

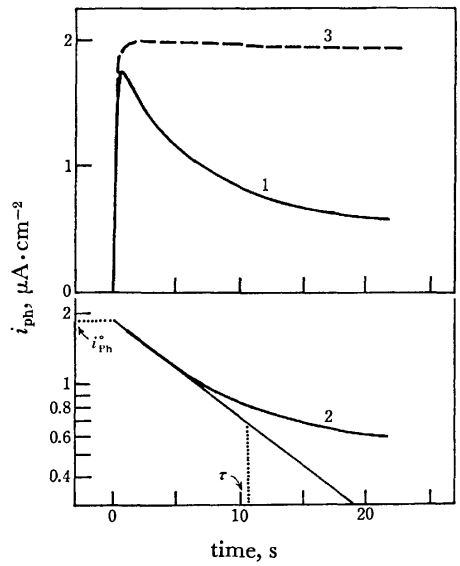

Fig. 2. The change of the photocurrent *vs.* time. Curve 1, for the solution of 6.7×10^{-7} M Rose Bengal and 0.2 M KNO_3. Curve 2, the logarithmic plot of the same result. Curve 3, for the case where 0.1 M KI is added.

The photocurrent decayed rather quickly with time as shown in Fig. 2. The photocurrent was not restored to the initial value, if the electrode was kept in the dye solution for a few minutes. The photocurrent fell down to zero when the light was turned off, and no overshoot to the cathodic side was observed. The decay of the photocurrent was suppressed or stopped by adding a reducing agent, *e.g.*, potassium iodide, as shown by curve 3. The logarithm of the photocurrent gave a straight line for the first several seconds as shown by curve 2, from which we can obtain the initial value of the photocurrent, i^0_{ph}, and the decay time constant, τ, namely the period of illumination for which the current decays to 1/e.

The surface of the zinc oxide electrode faintly colored pink, if it was dipped into the Rose Bengal solution. After prolonged illumination in the same solution at closed circuit, the color changed to brown-red. The color was not removed by washing with water. On the other hand, no color change occurred when the elctrode was illuminated at open circuit or at closed circuit in the presence of a reducing agent.

Figure 3 shows the photocurrent action spectrum obtained for a solution containing a sufficient amount of potassium iodide. Almost the same action spectrum was obtained for a solution without any reducing agent

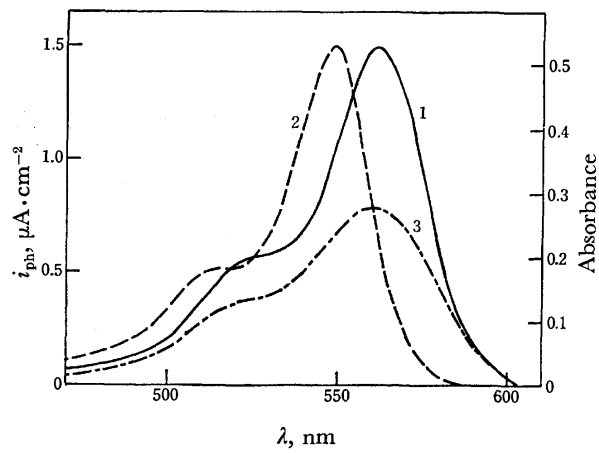

Fig. 3. (1) The action spectrum for the photocurrent for the solution of 5.3×10^{-7} M Rose Bengal and 0.1 M KI at the electrode potential: 0.35 V *vs.* SCE. (2) Absorption spectrum of the same solution, measured with a 10 cm cell. (3) Diffuse reflectance spectrum of the dye adsorbed on zinc oxide powder. The dye was adsorbed in the aqueous solution of 1.4×10^{-5} M Rose Bengal.

by scanning rapidly under weak illumination. The peak of the action spectrum for the photocurrent shifted by 13 nm toward the longer wavelength from that of the absorption spectrum of the dye solution, and nearly coincided with that of the reflection spectrum of the dye adsorbed on zinc oxide powder.

The initial value of the photocurrent increased proportionally with the illumination intensity, while the decay time constant was inversely proportional to it (Fig. 4). The value of i^0_{ph} and τ scarcely changed over the electrode potential range 0.0—1.0 V. Figure 5 shows the change of i^0_{ph} and that of τ with the concentration of Rose Bengal in the solution. The i^0_{ph} value increased with the concentration of the dye and ap-

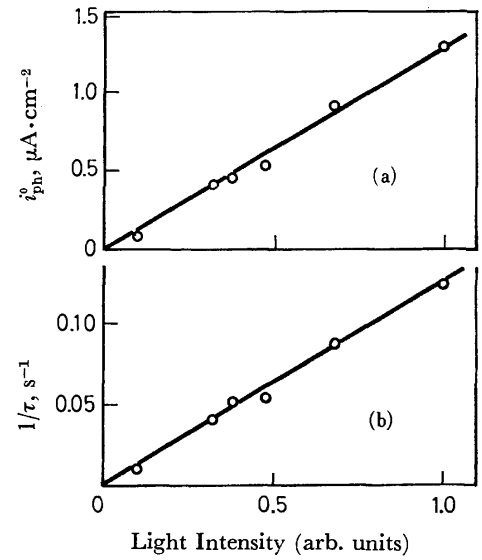

Fig. 4. The change of the initial value of the photocurrent (a), and the decay time constant of the photocurrent (b) with the light intensity: Rose Bengal, 6.5×10^{-7} M; Na_2SO_4, 0.2 M; electrode potential, 0.2 V *vs.* SCE.

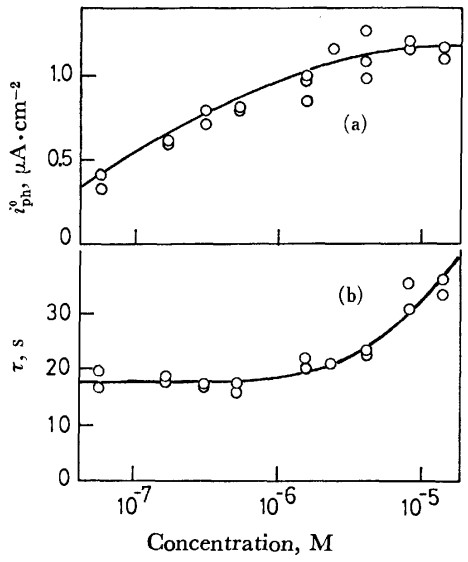

Fig. 5. The initial value of the photocurrent (a) and the decay time constant of the photocurrent (b) *versus* the concentration of Rose Bengal: Na_2SO_4, 0.2 M; electrode potential, 0.35 V *vs.* SCE.

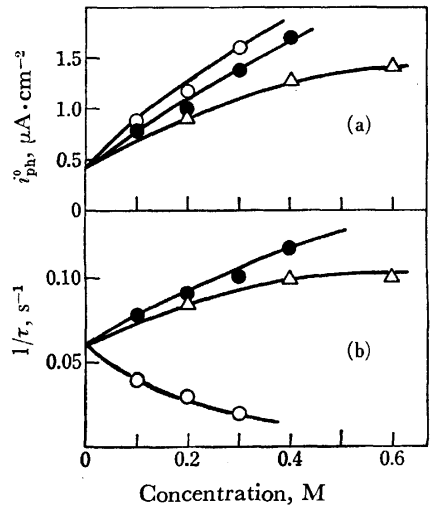

Fig. 6. The initial value of the photocurrent (a) and the decay time constant of the photocurrent (b) *versus* the concentration of the halide ions, Rhodamine B: 1.0×10^{-6} M, Na_2SO_4: 0.2 M, electrode potential: 0.2 V *vs.* SCE; △, chloride ion; ●, bromide ion; ○, iodide ion.

proached a constant. The τ was constant for the concentration of Rose Bengal up to 10^{-6} M, and increased by the concentration above 10^{-6} M.

The photocurrent for Rhodamine B increased by addition of halide ions to the dye solution, while the dependence of the decay time constant of the photocurrent on the concentration of the halide ions was more complicated (Fig. 6a and b).

Discussion

The mechanism of the dye-sensitized photocurrent can be explained by the energy diagram such as shown in Fig. 7, for the case of an n-type semiconductor. The

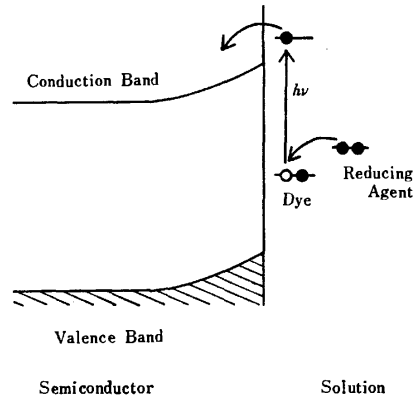

Fig. 7. A model for the electron injection.

electron injection from an excited dye (D*) into a conduction band is suggested by the fact that only those dyes whose excited energy levels are considerably higher than the conduction band of the semiconductor at the interface can act as effective sensitizers.[12] The electron deficient dye (D^+) may undergo irreversible reaction, causing the color change of the electrode. The total reaction scheme can be represented as follows:

$$D + h\nu \longrightarrow D^*, \quad (1)$$

$$D^* \longrightarrow D^+ + e(\text{electrode}), \quad (2)$$

$$D^+ \longrightarrow \text{reaction product}. \quad (3)$$

It has been tacitly assumed by many authors so far that the dye-sensitized photocurrent is caused by the dye adsorbed on the electrode and not by that dissolved in solution. However, there has been no strong evidence for this. Now, we can pick up the following three facts as such evidence from our experimental results.

1. The shift of the action spectrum for the photocurrent from the absorption spectrum of the solution, as shown in Fig. 3, indicates that the photocurrent is caused mainly by the dye adsorbed on the electrode.

2. From the initial value of the photocurrent shown in Fig. 2, the apparent quantum yield of the photocurrent (η), defined as the number of electrons transferred divided by the number of incident photons, can be calculated to be 1.8%, which means that at least 1.8% of the photons are absorbed by the dye. If the photocurrent is assumed to be caused only by the dye in the bulk of the solution, 3 mm of the light path length in the solution is required to make the absorption factor of the light 1.8% at λ=562 nm. However, the same photocurrent was observed with a light path length of 0.2 mm or shorter. This result indecates that the contribution of the dye in the solution is small or negligible.

3. As shown in Fig. 5, the photocurrent indicates the tendency of saturation at a relatively low concentration of the dye, *i.e.*, 5×10^{-6} M. It would be difficult to explain this by attributing the photocurrent to the dissolved dye. From our preliminary experiments, the adsorption isotherm of the dye adsorbed on the electrode surface has been found to be saturated at about the same low dye concentration as above.

The Decay Curve of the Photocurrent and the Quantum Yield of Electron Injection from the Excited Dye. The photocurrent of some semiconductor-aqueous solution

photocell decays with time owing to the deposition of opaque substance on the surface of the electrode, produced by the reaction with the holes generated. The photocurrent in the case of zinc oxide electrode does not decay, because in this case the products, zinc ion and oxygen, do not accumulate on the surface.[13]

In the case of the dye-sensitized photocurrent for zinc oxide, the photon energy is less than the band gap, and so it is clear that the decay is not caused by the reaction of the electrode itself, since no free hole exists in the electrode. The decay of the photocurrent should then be attributable either to the decrease of the number of the unoxidized dye molecules (or ions) adsorbed on the electrode or to an accumulation of the deteriorated dye (Reactions 1—3).

The influence of the dye (D_{soln}) or the reducing agent (R_{soln}) in solution on the decay of the photocurrent, as shown in Figs. 2 and 5, is explained by the following dye regeneration processes:

$$D^+ + D_{soln} \longrightarrow D + D^+_{soln}, \quad (4)$$

$$D^+ + R_{soln} \longrightarrow D + R^+_{soln}. \quad (5)$$

Process 4 can be achieved either by the electron transfer or by the exchange of D^+ and D_{soln}. The decay of the photocurrent is suppressed if the reaction velocities for processes 4 and 5 are greater than those for processes 2 and 3.

When the solution contains no reducing agent, the number of dye molecules (or ions), N, per unit area of the electrode surface will change according to

$$dN/dt = -\eta_0 SN + kC(N_0 - N), \quad (6)$$

where η_0 is the quantum yield of the electron injection from the excited dye, S the frequency of excitation of a dye molecule (or ion), N_0 the number of the dye molecules (or ions) per unit area of the electrode before illumination, C [M] the concentration of the dye in the solution, and k the rate constant. The second term of the right hand side of Eq. 6 corresponds to the restoring rate of the oxidized dye on the electrode surface by Reaction 4.

When the concentration of the dye in the solution is very low, the second term of Eq. 6 can be neglected, and N can be written as

$$N = N_0 \exp(-\eta_0 St). \quad (7)$$

The photocurrent, assumed to be proportional to N, can be written as

$$i_{ph} = i^0_{ph} \exp(-\eta_0 St), \quad (8)$$

and, hence

$$\eta_0 = 1/\tau S. \quad (9)$$

The exponential decay of the photocurrent, as observed experimentally at the initial stage, coincides with Eq. 8.

The dependence of τ on the concentration of the dye shown in Fig. 5b can be explained as follows. When the concentration of the dye is high, the second term of Eq. 6 cannot be neglected. Therefore, Eqs. 7—9 are valid only in the range of the concentration where τ does not depend on C. Figure 5 shows that such a condition is satisfied when C is lower than 10^{-6} M.

The absorbance of the dye on the electrode can be written as

$$\log I_0/I = 1000\varepsilon N/N_A, \quad (10)$$

where ε [M^{-1} cm^{-1}] is the molar extinction coefficient of the dye, N_A the Avogadro constant, I_0 the number of the photons incident on a unit area of the dye layer on the electrode per second, and I the number of the photons transmitted through the same layer. Since the absorption of light by the dye layer is small, the equation can be approximated as

$$(I_0 - I)/I_0 = 1000(\ln 10)\varepsilon N/N_A, \quad (11)$$

and

$$I_0 - I = SN. \quad (12)$$

From these equations, S can be written as

$$S = 1000(\ln 10)\varepsilon I_0/N_A. \quad (13)$$

The relation that τ is inversely proportional to I_0, as shown in Fig. 4b, can be derived from Eqs. 9 and 13.

The quantum yield η_0 for Rose Bengal was determined to be 22% by applying Eqs. 9 and 13 to the experimentally obtained photocurrent decay curves. The quantum yield was obtained for the illumination at the peak wavelength, and the molar extinction coefficient was assumed to be the same as that at the peak of the absorption spectrum of the solution. The reflection factor of light at the surface of the electrode was estimated to be 0.7 from the comparison of the reflected light intensity with that from magnesium oxide powder. This means that seven tenths of the incident light, which passes through the dye layer toward the inside of zinc oxide sinter, is reflected and passes again through the dye layer on the surface of the electrode. Therefore, we employed the value of measured number of photons incident upon the sample multiplied by 1.7 for I_0 in Eqs. 10—13.

Effect of Halide Ions on the Dye-sensitized Photocurrent. Hauffe *et al.*[14] found that the dye-sensitized photocurrent at a zinc oxide electrode was increased by addition of halide ions to the dye solution. The results shown in Fig. 6a indicate similar effects of the halide ions on the photocurrent. The increase in the photocurrent becomes greater in the sequence $Cl^- < Br^- < I^-$. This order is the same as that of the electron donating ability of the ions, *i.e.*, the oxidation potential increases in the reverse order.

Essentially, the visible spectra of the dye solution were not changed by addition of halide ions. Therefore, the effect of halide ions can be explained by assuming the formation of the exciplex between the excited dye and halide ions, the exciplex injecting an electron into the electrode efficiently. It is expected that the $1/\tau$ increases with the quantum yield of electron injection (Eq. 9). The result for chloride and bromide ions (Fig. 6b) is consistent with the expectation and supports the mechanism mentioned above. By addition of ioide ion, τ as well as i^0_{ph} increased. Iodide ion suppresses the deterioration of the dye by supplying an electron to the oxidized dye as described earlier. Therefore, in this case, the decrease of $1/\tau$ is attributable to the restoration of the oxidized dye by iodide ion, but not to the decrease of the quantum yield of electron injection.

Hauffe *et al.* proposed the reduced dye formation by the electron transfer from halide ions to the excited

dye, the reduced dye injecting an electron into the electrode. According to their mechanism, the dye should not deteriorate, in contradiction with the experimental results that the decay is faster in the presence of chloride and bromide ions.

The authors wish to express their gratitude to Wireless Research Laboratory, Matsushita Electric Industrial Co., Ltd. for the supply of zinc oxide sinter disks at the early state of this work. The present work was partially supported by a Grant-in-Aid for Scientific Research from the Ministry of Education (No. 911504).

References

1) A. Fujishima and K. Honda, *Nature*, **238**, 37 (1972).
2) H. Gerischer and J. Gobrecht, *Ber. Bunsenges. Phys. Chem.*, **80**, 327 (1976).
3) M. S. Wrighton, D. L. Morse, A. B. Ellis, D. S. Ginley, and H. B. Abrahamson, *J. Am. Chem. Soc.*, **98**, 44 (1976).
4) G. Hodes, J. Manassen, and D. Cahen, *Nature*, **261**, 403 (1976).
5) H. Tributsch and H. Gerischer, *Ber. Bunsenges. Phys. Chem.*, **73**, 251 (1969); H. Tributsch, *ibid*, **73**, 582 (1969).
6) K. Hauffe, H. Danzmann, H. Pusch, J. Range, and H. Voltz, *J. Electrochem. Soc.*, **117**, 993 (1970); K. Hauffe and U. Bode, *Faraday Discuss. Chem. Soc.*, **58**, 281 (1974).
7) R. Memming and H. Tributsch, *J. Phys. Chem.*, **75**, 562 (1971). R. Memming, *Photochem. Photobiol.*, **16**, 325 (1972).
8) A. Fujishima, T. Iwase, T. Watanabe, and K. Honda, *J. Am. Chem. Soc.*, **97**, 4134 (1975); T. Watanebe, A. Fujishima, O. Tatuoki, and K. Honda, *Bull. Chem. Soc. Jpn.*, **49**, 8 (1976).
9) M. Matsumura, K. Yamamoto, and H. Tsubomura, *Nippon Kagaku Kaishi*, **1976**, 399; M. Matsumura, Y. Nomura, and H. Tsubomura, *Bull. Chem. Soc. Jpn.*, **49**, 1409 (1976).
10) H. Tsubomura, M. Matsumura, Y. Nomura, and T. Amamiya, *Nature*, **261**, 402 (1976).
11) F. Lohmann, *Ber. Bunsenges. Phys. Chem.*, **70**, 428 (1966).
12) H. Tsubomura, M. Matsumura, K. Nakatani, K. Yamamoto, and K. Maeda, *Solar Energy*, to be published.
13) H. Gerischer, *J. Electrochem. Soc.*, **113**, 1174 (1966).
14) U. Bode, K. Hauffe, Y. Ishikawa, and H. Pusch, *Z. Phys. Chem. (N. F.)*, **85**, 144 (1973).

Studies of the Measurement of the Intermicellar Concentration of Surfactants by Gel Filtration

Tsunetaka SASAKI,* Misako YASUOKA,** and Hitoshi SUZUKI***

Department of Chemistry, Faculty of Science, Tokyo Metropolitan University, Setagaya, Tokyo 158

(Received February 21, 1977)

Equations are derived which are used to calculate the intermicellar concentration (C_s) of a surfactant from measurements of the elution volumes of micelles, the elution front and the intermicellar monodisperse molecules or ions. These quantities are obtained by the gel filtration of a surfactant charged in band form through a gel column previously filled with the same surfactant at a lower concentration. The C_s values found are not constant, but increase and the increase becomes less pronounced with the concentration (C) of the surfactant, both for sodium dodecyl sulfate and α-dodecyl-ω-hydroxyhexa(oxyethylene). This confirms that the concentration $C-C_s$ of the micelles which move during the gel filtration is smaller than the usually-employed concentration $C-C_m$ of micelles in a stationary state, where C_m denotes the critical micelle concentration.

Many problems remain unsolved regarding the properties of aqueous surfactant solutions, especially the dissolution state of the surfactants.[1] The intermicellar concentration of the aqueous surfactant, for instance, is usually believed to be constant for a solution of concentration C above the critical micelle concentration (CMC), C_m, and the micellar concentration is equated with $C-C_m$.[2,3] Here, constancy of the intermicellar solution is assumed from the constancy of the surface tension of the aqueous surfactant solution above the CMC[4] or from the result of equilibrium dialysis.[5] However, the surface tension of, for instance, a sodium dodecyl sulfate (SDS) solution shows a gradual decrease with increasing concentration of the SDS above the CMC.[1,6] Also, equilibrium dialysis cannot be applied to such a system, consisting of single ions and micelles with rapid equilibrium established between them, since the micelles eventually pass through a semipermeable membrane, if the intermicellar concentration or the activity increases above the CMC.[7]

T. Sasaki *et al.* have studied the dissolution state of aqueous surfactant solutions by gel filtration[8] and have found the method to be suitable also for the study of intermicellar concentrations. The present paper describes studies of the measurements of intermicellar concentrations of the aqueous solutions of SDS and α-dodecyl-ω-hydroxyhexa(oxyethylene) ($D(EO)_6$).

Experimental

Materials. SDS was prepared from 1-dodecanol and chlorosulfuric acid according to the Dreger method[9] and was purified by extraction with diethyl ether and recrystallization from ethanol. $D(EO)_6$ of more than 99% purity, as measured by gas chromatography, was obtained from the Nikko Chemical Company. Both SDS and $D(EO)_6$ were confirmed to be free from surface-active impurities by the absence of a minimum in the surface tension *vs.* concentration curve. Distilled water was used after degassing by boiling.

Apparatus. The gel filtration apparatus is shown in Fig. 1. In this figure, Sephadex G-50 fine gel from Pharmacia

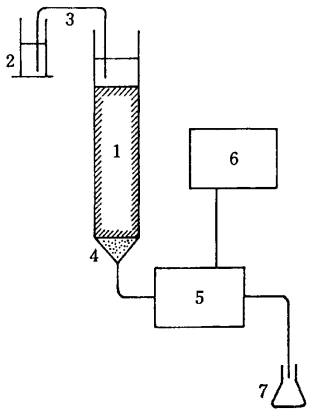

Fig. 1. Gel filtration apparatus.
(1) Gel column, (2) reservoir vessel, (3) siphon, (4) glass wool, (5) differential refractometry monitor, (6) recorder, (7) weighing vessel.

Products was packed in gel column 1 after sufficient swelling in water. The gel beds used were of 1.18 cm inner diameter and 24 and 30 cm in length. For the measurements, a given amount (8 to 30 cm^3) of sample solutions of varying concentrations was placed in vessel 2, from which the solution was introduced through a siphon onto the gel column that had previously been filled with the same solution at a different concentration which is hereafter abbreviated to a preset solution. The sample solution was then eluted by similarly introducing water from vessel 2 through the siphon onto the gel column. This ensures elution under a constant hydrostatic pressure. The rate of liquid flow was 30 and 24 cm^3/h in the cases of SDS and $D(EO)_6$, respectively. The monitor used for the sample flow was a flow-type differential refractometer (LDC-Mitsumi Model 1103 refractomonitor) which detects and records the change of the refractive index at the outlet of the gel column due to the concentration change. The whole apparatus, with the exception of the recorder, was maintained in an air thermostat at 30 ± 1 °C for SDS and 25 ± 1 °C for $D(EO)_6$.

Principle of the Intermicellar Concentration Measurements. Figure 2 shows the elution profile of a surfactant solution of concentration C, which is larger than C_m, charged in band form and eluted with water through a gel column previously swollen with water. As is seen, the tail part of the elution curve forms two steps, corresponding to the fast- and slow-flowing tails of the micelles and the intermicellar single molecules or ions, respectively.

At the elution front, fast-flowing micelles precede the inter-

* Present address: Department of Chemistry, Faculty of Science, Tokai University, Kitakaname, Hiratsuka 259-12.

** Present address: c/o Hosoyama, 1-632 Marukodōri, Nakahara, Kawasaki 211.

*** Present address: 3-2-10 Honchō, Koganei 184.

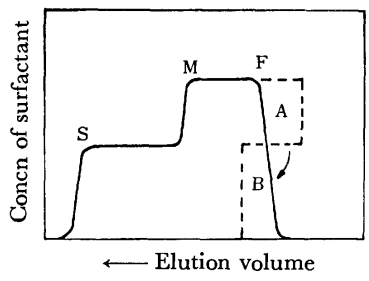

Fig. 2. Elution profile of a surfactant solution.

micellar solution. However, since micelles without the intermicellar solution containing single molecules or ions are unstable, A in Fig. 2 decomposes to form intermicellar molecules or ions, B, with which the rest of the micelles are brought into equilibrium, as is shown in Fig. 2. Because of such a docomposition, the micellar front moves slower than the micelles eluting without decomposition or than the tail of the micelles. Now, if the gel column is previously filled with a preset solution of the same surfactant at concentration C', which is lower than C_m, decomposition of the sample solution at the elution front decreases and the difference in elution rate between the micellar front and tail may become smaller. Then the preset concentration which makes this difference zero is considered to be the intermicellar concentration.

Actually, the concentration of such a preset solution,which contains only single molecules or ions, is not available when the intermicellar concentration C_s is larger than C_m. Therefore, in the present experiment, the concentration of the preset solution, C', was first made slightly lower than C_m. This also avoids the change in structure of the gel due to the change in the solution concentration as elution proceeds. Figure 3 shows the principle of the calculation of C_s. Figure 3(a) shows the state of the preset solution and the sample solution before elution and Fig. 3(b) represents the behavior of the solution during elution. In this figure, R_f, R_m, and R_s denote the elution rates of the solution front, of the tails of micelles, and of the intermicellar molecules or ions, respectively, C is the total concentration of the surfactant, and A_t and A_0 are the cross-sectional area of the gel column through which the

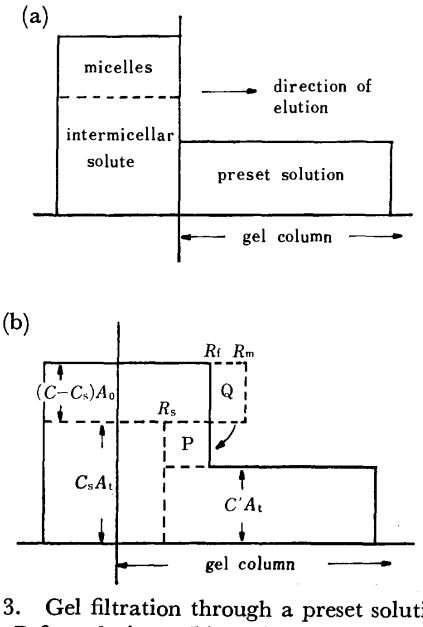

Fig. 3. Gel filtration through a preset solution.
(a) Before elution, (b) during elution.

intermicellar solute and micelles flow, respectively.

In Fig. 3(b), the broken lines indicate the elution profile of each component of solutions of concentrations C and C', the former being assumed to flow without micelle decomposition. Actually, however, as shown by the arrow, part Q of the micellar front of the solution of concentration C decomposes and fills up the solute gap, P. Thus, the entier elution profile assumes the form represented by the solid lines. From this consideration, we obtain

$$(R_m-R_f)(C-C_s)A_0 = (R_f-R_s)(C_s-C')A_t. \quad (1)$$

Taking into account that

elution rate $R \propto$ elution volume V^{-1}

and that

cross sectional area $A \propto$ elution volume V, } (2)

Eq. 1 can be rewritten as

$$C_s = \frac{(V_f-V_m)(C-C')}{V_s-V_m} + C', \quad (3)$$

where V_m, V_f, and V_s represent the elution volumes of the micelles, the solution front and the intermicellar single molecules or ions, respectively. Equation 3 enables us to calculate C_s from measurements of V_m, V_f, and V_s for a solution of concentration C eluted through the gel column filled with a preset solution of concentration C'. Here, V_m and V_s can be measured from the elution tail of the corresponding constituent.

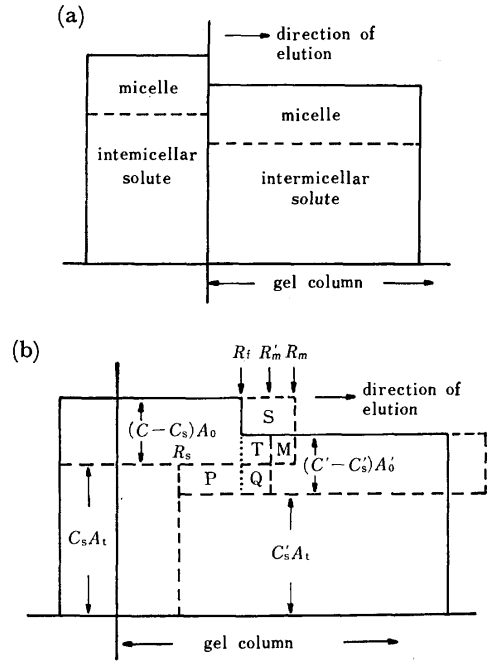

Fig. 4. Gel filtration through a preset solution.
(a) Before elution, (b) during elution.

Furthermore, in case the concentration C' of the preset solution is larger than C_m, so that $C_m<C'<C$, the elution diagram becomes somewhat more complicated, as is shown in Fig. 4. Here, R_m' and C_s' represent the elution rates of the micelles and the intermicellar concentration of the preset solution, respectively, and A_0' denotes the cross-sectional area of the gel column available for micellar flow of the preset solution. The broken lines indicate both the elution tail of the preset solution when eluted alone and the elution front of the solution

of concentration C, assumig that the micelles do not decompose. The solid lines indicate the actual elution front.

From this diagram, it is confirmed that the frontal part of the micelles S+(overlapped)M decomposes to fill up the solute gaps, P and Q, or that the S+M+T part fills up parts P and Q+T. Thus, we obtain

$$(R_m-R_f)(C-C_s)A_o = (R_f-R_s)(C_s-C_s')A_t + (R_m'-R_f)(C'-C_s')A_o'. \quad (4)$$

Again, applying Eq. 2, Eq. 4 can be rewritten as

$$C_s = \frac{C(V_f-V_m)-C'(V_f-V_m')+C_s'(V_s-V_m')}{V_s-V_m}, \quad (5)$$

where the primes indicate preset solution quantities. Equation 5 enables us to calculate the intermicellar concentration, C_s, of the sample solution from measurements of V_f, V_m, and V_s for a solution of concentration C passing through the gel filled with a preset solution of concentration C', intermicellar concentration C_s' and elution volume V_m'. Thus, we can obtain the intermicellar concentration of a surfantant of successively higher concentrations, C.

Results and Discussion

Intermicellar concentration obtained, C_S, is plotted against the total concentration for the aqueous SDS and $D(EO)_6$ solutions in Figs. 5 and 6, respectively. It is seen that C_s increases with increasing concentration of the surfactants both for SDS and $D(EO)_6$, but the increase becomes less marked with the concentration. It is worthwhile to refer to the fact that, according to

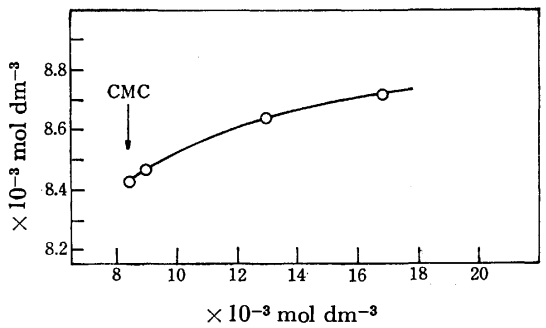

Fig. 5. Intermicellar concentration of SDS.
Abscissa; Concentration of SDS,
ordinate; intermicellar concn of SDS.

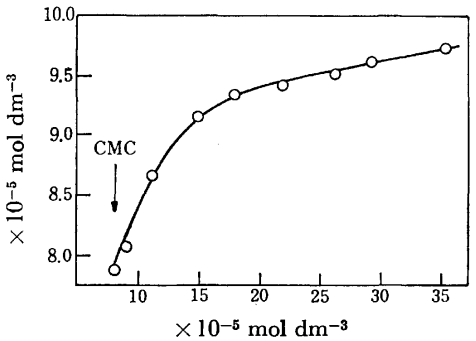

Fig. 6. Intermicellar concentration of $D(EO)_6$.
Abscissa; Concentration of $D(EO)_6$,
ordinate; intermicellar concn of $D(EO)_6$.

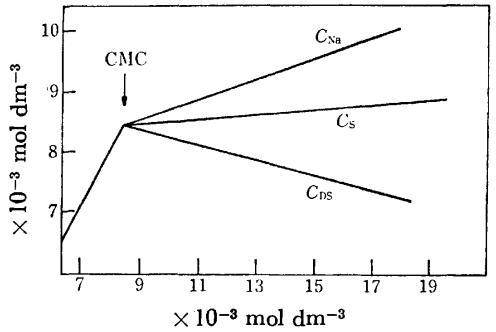

Fig. 7. Intermicellar concentration of SDS at stationary and elution states.
Abscissa; Concentration of SDS,
ordinate; concns of C_{Na}, C_{DS}, and C_s.

the results of EMF measurements,[1] the intermicellar concentration of Na^+ ions increases while that of dodecyl sulfate ions, DS^-, decreases with the total concentration above the CMC as shown in Fig. 7, where the curve for C_S is also depicted. As is seen, the C_S curve is situated between the Na^+ and DS^- curves. This means that the micelles in the stationary state have a net negative charge, but when the micelles precede the intermicellar Na^+ and DS^- ions during elution, they are constrained to move as electrically-neutral units. This requirement is satisfied by the dissociation and the detachment of a part of the excess negative DS^- ions of the micelles and at the same time by the attachment of Na^+ ions to the micelles from the intermicellar solution, thus leaving the solution also electrically neutral.

Actually, Fig. 7 indicates that the amounts of DS^- ion detachment and Na^+ ion attachment are roughly equal and the following relation results,

$$C_{Na} - X = C_{DS} + X = \frac{C_{Na}+C_{DS}}{2} = C_s, \quad (6)$$

where C_{NS} and C_{DS} express the intermicellar concentration of Na^+ and DS^- ions, respectively, and X is the amount of DS^- ions detached from and Na^+ ions attached to micelles. Equation 6 may be the physical meaning of the intermicellar concentration C_S, although the actual intermicellar concentrations in the stationary state are C_{Na} and C_{DS} for Na^+ and DS^- ions, respectively, both of which are different from C_s. Furthermore, the micellar concentration of SDS in the stationary state, or more strictly, the concentration of DS^- ions in the form of micelles is expressed by $C-C_{DS}$, which is larger than the usually-employed value of $C-C_m$,[3] while the concentration of micelles which move during the gel filtration is $C-C_s$ which is considerably smaller than $C-C_{DS}$ and is slightly smaller than $C-C_m$, as is seen from Fig. 7. The difference in concentration of the micelles in the stationary and in the gel filtration states results from the requirement that the micelles be negatively charged in the former case and electrically neutral in the latter case.

The situation may be far simpler in the case of $D(EO)_6$, since it produces no ions. Here also, the micellar concentration is $C-C_s$, and not $C-C_m$. As is seen in Fig. 6, the former is smaller than the latter. It may

also be mentioned that, strictly speaking, $C-C_s$ is the concentration of those micelles which move during gel filtration, while the micellar concentration in the stationary state may differ from $C-C_s$, as in the case of SDS. Although this concentration has not yet been determined experimentally, the value may prove to be close to $C-C_s$, because of the nonionic nature of $D(EO)_6$.

References

1) T. Sasaki, M. Hattori, J. Sasaki, and K. Nukina, *Bull. Chem. Soc. Jpn.*, **48**, 1397 (1975).
2) K. J. Mysels, *J. Colloid Sci.*, **10**, 507 (1955).
3) C. Botré, V. L. Crescenzi, and A. Mele, *J. Phys. Chem.*, **63**, 650 (1959).
4) K. Shinoda and E. Hutchinson, *J. Phys. Chem.*, **66**, 577 (1962).
5) J. T. Yang and J. F. Foster, *J. Phys. Chem.*, **57**, 628 (1953).
6) H. Elworthy and K. J. Mysels, *J. Colloid Interfac. Sci.*, **21**, 331 (1966).
7) M. Abu-Hamdiyyah and K. J. Mysels, *J. Phys. Chem.*, **71**, 418 (1967).
8) T. Sasaki and Y. Ogihara, "Proc. 5th International Congress on Surface Activity," Barcelona, 915 (1968); H. Suzuki and T. Sasaki, *Bull. Chem. Soc. Jpn.*, **44**, 2630 (1971); T. Sasaki, K. Tanaka, and H. Suzuki, "Proc. 6th International Congress on Surface Activity," Zürich, 849 (1972); M. Kodama and T. Sasaki, *Bull. Chem. Soc. Jpn.*, **47**, 1368 (1974).
9) E. E. Dreger, *Ind. Eng. Chem.*, **36**, 610 (1944).

The Behavior of Aqueous Solution of Sodium Deoxycholate in Capillary Flow

Gohsuke SUGIHARA, Mitsuru TANAKA, and Ryohei MATUURA*

Department of Chemistry, Faculty of Science, Fukuoka University, Nishi-ku, Fukuoka 814
**Department of Chemistry, Faculty of Science, Kyushu University, Higashi-ku, Fukuoka 812*

(Received March 9, 1977)

Primary micelles form secondary, polymer-like aggregates in a capillary flow of aqueous solution of sodium deoxycholate (SDC). The formation of the polymer-like aggregate is promoted by mechanical action, degradation being simultaneously caused by shearing stress. The viscosity of the SDC solution in the capillary flow attains equilibrium value between polymerization and degradation. The viscosity changes a great deal with the time of observation and pH. Under given conditions the SDC solution behaves as a non-Newtonian fluid obeying a power-law.

The flow of colloid-dispersed systems is of practical and theoretical interest as regards transportation through pipe and humors in a capillary *in vivo*. The motion of material *in vivo* can be classified into two types, permeation through an interface (membrane) and the flow in a capillary. Flow systems accompanied by reactions are of special interest. Attention has been paid to the variation in particle size or particle structure during the course of flow which considerably affects the flowing characteristics.

Sodium deoxycholate (SDC), a bile salt which is a surfactant *in vivo*, was chosen. Vochten and Joos[1] studied the viscosity of SDC solutions with an Ubbelohde type viscometer. They measured the viscosity at pH=7 for SDC of constant concentration containing NaCl in different concentrations, and found that the viscosity varies with time. Fontell performed viscosity measurement of aqueous solutions of various bile salts and pointed out that micelles at higher concentrations are voluminous and anisometric, indicating the formation of a secondary structure by the interlinking of primary micelles.[2] However, Fontell ignored the time dependency in the viscosity of the aqueous solution of SDC. We have regarded the viscous behavior in the capillary flow as a process of polymer-like aggregation of primary micelles. The aggregation is accelerated by mechanical action, degradation being caused by shearing stress simultaneously. Blow and Rich[3] observed this phenomenon for the first time by viscosity measurement with an Ostwald-type viscometer. However, they did not carry out analysis.

We have investigated aqueous solutions of SDC in detail, and found that the solution has a rheologically complex character, which might be clarified by means of an improved method of viscosity measurement on non-Newtonian flow.

The present study was carried out with the use of horizontal viscometers in order to clarify the effect of shearing stress on the flow and to correlate the result with SDC concentration, pH, and temperature.

Experimental

Horizontal viscometers were so constructed as to enable us to observe flow volume and flow time of the solution by connecting a 2 cm^3 mess-pipet to the capillary. Two viscometers were used: (a) capillary length 10 cm, and inner diam. 1.64×10^{-2} cm and (b) capillary length 10 cm, inner diam. 1.66×10^{-2} cm. The Reynold number was less than 60 under hydraulic pressure of 100 cm. The viscosity measurement was carried out by immersing the viscometer in a thermostated water bath, putting the SDC solution in the viscometer and giving an arbitrary shearing stress. The temperature was kept constant within ±0.01 °C.

A pressure-generator was set up by combination of two water-tanks (20 dm^3), U-tube for manometer (180 cm in height) and cocks. This makes it possible to give an arbitrary difference of pressure and observe both forward and backward processes by use of T-cocks. For the simultaneous measurement of viscosity and pH, the horizontal viscometer was fitted with a combination-type electrode (Hitachi-Horiba 6028-10T for test tube) near the exit of capillary (Fig. 1). The variation of pH with time was measured with a Hitachi-Horiba pH meter, model F-5 and recorded automatically with a recorder (QPD-54, Hitachi).

The solutions were prepared as follows. Aqueous SDC and inorganic salt solutions (buffer) were prepared separately with concentration twice higher than necessary for the experiments. Both solutions were kept at a constant temperature. The

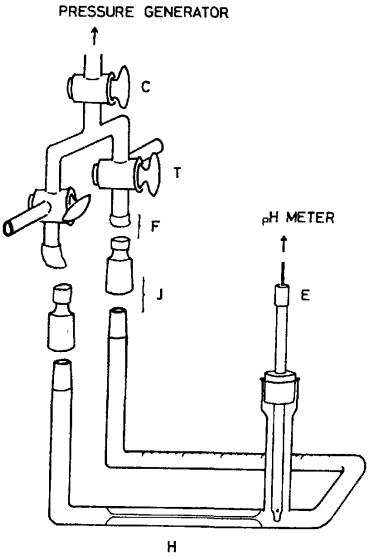

Fig. 1. Horizontal viscometer for the simultaneous measurement of pH and viscosity.
Key C: cock, T: T-cock, F: flexible pipe ,J: glass joint, H: horizontal viscometer, E: combination-type electrode (for test-tube use).

same amount of each was mixed in a vessel, and the mixture was freed from dust by a Millipore 47 mm membrane filter. 5 cm^3 of filtered solution was immediately put into the viscometer immersed in thermostated bath, and then subjected to incessant flow. The pH of the solutions was adjusted to 6.8, 7.0, or 7.2 by the Sørensen buffer solution.

SDC (E. Merck Co.) was thrice crystallized from ethanol and dried at 110 °C *in vacuo* for a day. Twice distilled water was used. Other chemicals were of guaranteed reagent-grade.

Results and Discussion

Correlation of Viscosity with Flow Time. After the initial Newtonian flow the viscosity rises abruptly, showing a characteristic peak and stationary value (Fig. 2). The viscosity is expressed in time (s) required

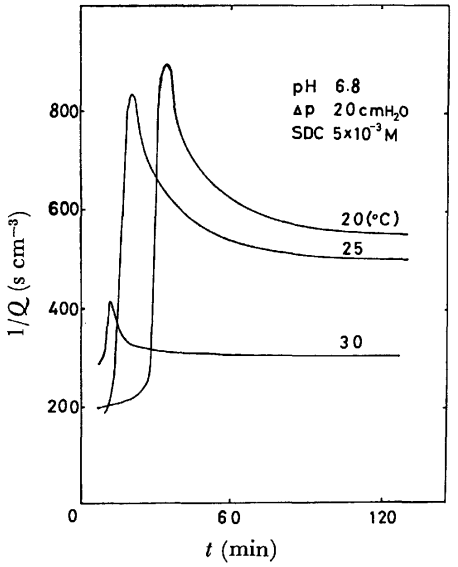

Fig. 2. An example of viscosity change with time in the capillary flow.

for the flow of the unit volume of liquid. The abrupt rise in viscosity with time seems to be correlated with various factors. The reproducibility is not always good because of sensitivity to the delicate difference of running or existence of impurity. We might interpret the initial part of the curve as follows. It is assumed that the polymer-like aggregation of SDC takes place by crystallization or phase transition. The growth of crystalline nuclei may be hindered by thermal and mechanical motions. The temperature of the whole system is kept constant during the observation, but minute, local variation is unavoidable. The rate of producing nuclei depends largely on the temperature nearer to that of phase transition, increasing rapidly with a lowering temperature. Thus, there is a possibility for effective nuclei to exist whose rate of production and growth exceed that of collapse during the minute, local variation of temperature. Once the effective nuclei are produced, polymer-like aggregation is accelerated in the field of flow. On the other hand, the degradation of the aggregates proceeds in the flow. The curves in Fig. 2 can be regarded as the result of polymerization and degradation.

The time-dependent equation of the number-average degree of polymerization $P_{(t)}$ at time t is[5]

$$P_{(t)} = \frac{qe^{qkt}}{e^{qkt}-1+qT/(t+T)}, \quad (1)$$

where T denotes the half-life of particle (monomer) number, k the rate constant of degradation of polymer-like aggregates, and $q=2g-1$, g being the limiting degree of polymerization. If we denote the mass of primary particle (monomer) by m and the Avogadro number by N, the time-dependent weight average molecular weight $[M]_{w,t}$ is given by[5]

$$[M]_{w,t} = \frac{2mNqe^{qkt}}{e^{qkt}-1+qT/(t+T)}, \quad (2)$$

where parameters T, q, and k have the same meaning as in Eq. 1. These parameters and m should be determined by separate experiments. No complete analysis can be carried out from only the curves shown in Fig. 2. We see from Eqs. 1 and 2 that $P_{(t)}$ and $[M]_{w,t}$ attain the values q and $2mNq$, respectively, after a sufficiently long time. These two values correspond to the dynamic equilibrium after the peak in Fig. 2.

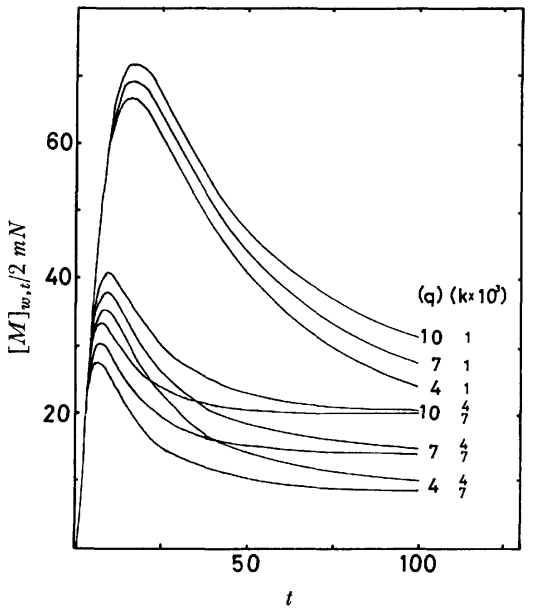

Fig. 3. Simulation curves for the relation between the weight-average degree of polymerization, computed with various values of each parameter and time t.

Figure 3 shows simulation curves computed by substituting appropriate values for the parameter in Eq. 2. The equilibrium value varies with concentration of SDC, temperature and pH. This is of dynamic equilibrium related directly to shearing stress or shear rate. The value of dynamic equilibrium does not depend on the history (the half-life T and the rate constant of degradation k) but on only the limiting degree of polymerization g determined by given conditions. Thus only the treatment of dynamic equilibrium is required for the analysis of the characteristics of the

flow system.

Apparent and Real Viscosity in Dynamic Equilibrium. The behavior of capillary flow of aqueous SDC solution was investigated by examining the relation between the value of dynamic equilibrium and various conditions. All systems in Fig. 2 behave as non-Newtonian flow.

In the case of non-Newtonian flow the coefficient of viscosity η is a function of shearing stress p_t or shear rate $\dot{e}_t$:

$$\eta = \frac{p_t}{\dot{e}_t} = \frac{g(\dot{e}_t)}{\dot{e}_t} = \frac{p_t}{f(p_t)}. \quad (3)$$

The shearing stress P and shear rate V on the wall-surface of capillary are

$$P = \frac{R\Delta p}{2l}, \quad (4)$$

$$V = \frac{4Q}{\pi R^3}, \quad (5)$$

where R is the radius of capillary, l the length, Δp the pressure difference on the unit area of cross-section of liquid cylinder in the capillary, and Q the amount of flowing liquid per unit time. Q is expressed as a function of P (or Δp) as follows.[6]

$$Q = (2l/\Delta p)^3 \int_0^P p_t^2 f(p_t) dp_t = (\pi R^3/P^3) \int_0^P p_t^2 f(p_t) dp_t. \quad (6)$$

It is desirable to find the relation between the measured Q and Δp, but the type of function $f(p_t)$ is unknown. The function can be obtained, if we use the following equation.[6-9]

$$f(P) = V(3/4 + (1/4)\, d \log Q/d \log P). \quad (7)$$

If we determine the slope of the curve $\log P$-$\log Q$, we obtain the second term in parenthesis. Since P is proportional to Δp, we can use $\log \Delta p$ instead of $\log P$.

In the Newtonian flow $d \log Q/d \log P$ is equal to unity and we have $f(P) = V$. While V in Newtonian flow gives a real shear-rate on the capillary-wall, V in non-Newtonian flow gives only an apparent one. Thus, P/V gives the apparent viscosity η_a. The real coefficient of viscosity η is given by $P/f(P)$.

When the non-Newtonian flow is of a power function type, $f = kp_t^n$, we obtain the following equation from Eqs. 6 and 4.

$$Q = \frac{\pi R^3 k}{n+3} P^n = \frac{\pi k R^{n+3}}{(n+3)(2l)^n} (\Delta p)^n. \quad (8)$$

Thus we have $d \log Q/d \log P = n$. Hence Eq. 7 gives the relation $f(P) = (3+n)V/4$. The value of real viscosity η is given by

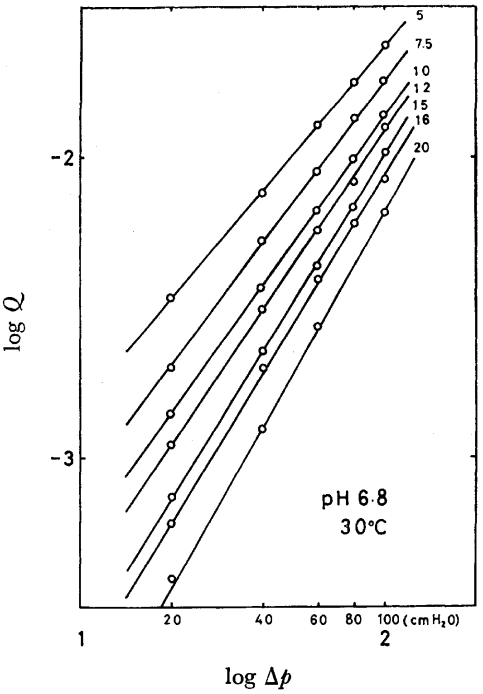

Fig. 4. The plot of $\log \Delta p$ *vs.* $\log Q$ at pH 6.8 and 30 °C. The figures at the right hand of curves indicate the concentration of SDC in mM. The slope of the straight line gives the power n in Eq. 8.

$$\eta = \frac{4}{n+3} \eta_a. \quad (9)$$

Straight lines are obtained by plotting $\log Q$ against $\log \Delta p$ in dynamic equilibrium (Fig. 4). This indicates that the flow of the SDC solution is non-Newtonian and of the power function type. The values n obtained from the slopes of $\log \Delta p$-$\log Q$ curves are given in Table 1. The value of n may give a criterion of the deviation from Newtonian type, or a degree of non-Newtonian. Although the real physical meaning of n is not known, it seems to correspond to the degree of interaction among aggregated particles. We see from Table 1 that the value of n is larger in higher concentration range for any temperature and pH.

Relation between Real Viscosity, Concentration of SDC, and Shearing Stress at Various Temperatures and pH. The dynamic equilibrium value of real viscosity η at pH 7.0 and 25 °C is shown in Fig. 5, in which (a) is the plot of η *vs.* concentration of SDC and (b) the plot of η *vs.* shearing stress, where the pressure difference Δp (cm

Table 1. The power value n of SDC solution

		20 °C			25 °C			30 °C	32.5 °C	35 °C
	pH	6.8	7.0	7.2	6.8	7.0	7.2	6.8	6.8	6.8
SDC concn (mM)	5	1.25	1.23	1.26	1.20	1.22	1.10	1.20	1.08	—
	7.5	1.37	1.32	1.39	1.32	1.35	1.24	1.35	1.31	1.21
	10	1.49	1.35	1.45	1.42	1.47	1.41	1.41	1.40	1.35
	12	1.58	1.42	1.49	1.50	1.51	1.50	1.49	1.46	1.45
	15	1.75	1.46	1.60	1.57	1.56	1.59	1.63	1.57	1.58
	16	1.77	1.50	1.61	1.59	1.60	1.59	1.70	1.59	1.60
	20	1.88	1.64	—	1.73	1.68	—	1.81	1.80	1.77

TABLE 2. THE REAL VISCOSITY η (C.P.) OF SDC SOLUTION AT DYNAMIC EQUILIBRIUM

SDC concn	Temperature (°C)	pH	Pressure difference between both ends of the capillary Δp in cm H_2O				
			20	40	60	80	100
1.00×10^{-2} M	20	6.8	6.61	4.61	3.63	3.20	2.82
		7.0	5.30	4.15	3.51	3.15	2.77
		7.2	5.11	3.82	3.13	2.76	2.50
	25	6.8	4.58	3.67	2.97	2.76	2.48
		7.0	4.74	3.43	2.82	2.51	2.19
		7.2	3.56	2.73	2.26	2.04	1.87
	30	6.8	3.60	2.76	2.29	2.09	1.80
	32.5	6.8	3.11	2.38	2.00	1.86	1.69
	35	6.8	2.33	1.86	1.54	1.44	1.27
1.60×10^{-2} M	20	6.8	15.56	9.33	6.51	5.33	4.60
		7.0	9.90	7.23	5.87	4.98	4.45
	25	6.8	9.15	6.55	5.31	4.55	4.10
		7.0	9.65	6.37	4.93	4.21	3.75
	30	6.8	7.50	5.02	3.75	3.18	2.80
	35	6.8	5.38	3.23	2.51	2.15	1.84

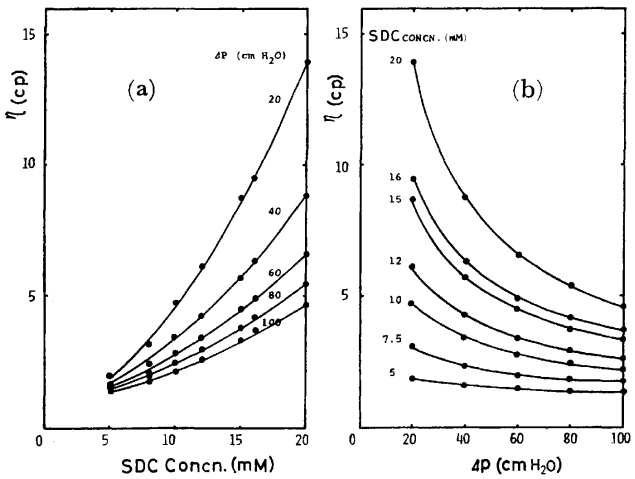

Fig. 5. The correlation of the real viscosity (cp) with SDC concentration (mM) and pressure difference Δp (cm H_2O) at pH 7.0 and 25 °C. (a) The plot of SDC concentration *vs.* η, where numerical values indicate the pressure difference Δp in cm H_2O. (b): The plot of Δp *vs.* η, where numerical values indicate the SDC concentration in mM.

H_2O) is used instead of the real shearing stress. Numericals at the end of respective curves refer to the pressure difference (in cm H_2O) in (a) and to the concentration (in mM** (mol m^{-3})) of SDC in (b). Though the value of η varies with pH and temperature, all the results are similar. Decrease in shearing stress tends to increase the viscosity, and the higher the concentration of SDC, the greater the dependence of real viscosity on shearing stress. The values of η of the 1.00×10^{-2} M** solution and 1.60×10^{-2} M solution in the dynamic equilibrium under various conditions are given in Table 2.

Effect of Shearing Stress on the Molecular Weight of Polymer-like Aggregate. As shown in Fig. 5, the shearing stress (Δp) considerably affects viscosity and the molecular weight of the polymer-like aggregate in dynamic equilibrium.

The dimension of polymer-like aggregate can be estimated from the molecular weight determined by viscometry. If the reduced values η_{sp}/c and $\ln \eta_r/c$ are plotted against c (in grams of SDC per 100 cm^3) and extrapolated to $c=0$, both curves intersect at the same point of ordinate (Fig. 6). The coincidence of intercept of the two curves affords a reasonable value as the limiting viscosity number $[\eta]$.

The correlation of $[\eta]$ with Δp illustrates the fact that decrease in shearing stress tends to increase considerably $[\eta]$ or the dimension of polymer-like aggregate. The plot of log Δp *vs.* $[\eta]$ gives straight lines (Fig. 7). We see that the product $[\eta]\,\Delta p^{\beta}$ is constant, where β is a

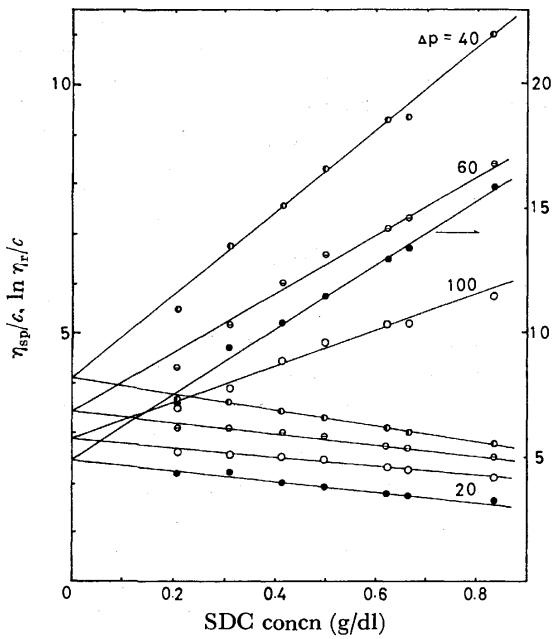

Fig. 6. The plot of $\ln \eta_r/c$ and η_{sp}/c *vs.* the SDC concentration c(g/dl). The reading value extrapolated to the zero concentration affords an apparent intrinsic viscosity $[\eta]$.

** Throughout this paper 1M=1 mol dm^{-3} and 1 mM=1 mol m^{-3}.

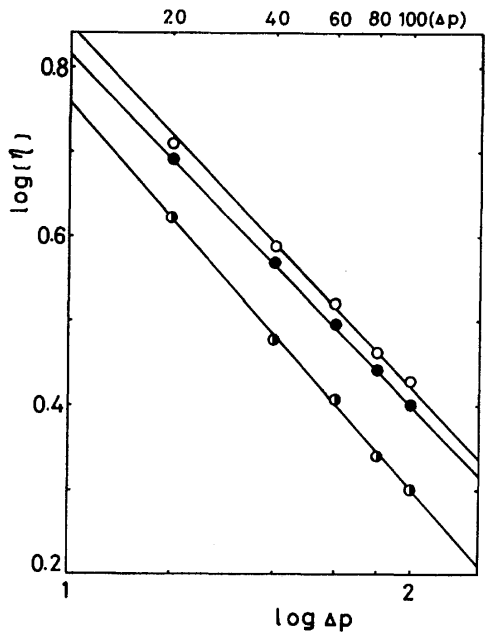

Fig. 7. The relation between log Δp and log $[\eta]$.
Key ○ pH 6.8, 25 °C, ● pH 7.2, 20 °C, ◑ pH 6.8, 30 °C. Empirical formula is expressed as follows.
at pH 6.8, 20 °C $\log[\eta]=-0.46\log(\Delta p)+1.33$
at pH 6.8, 25 °C $\log[\eta]=-0.46\log(\Delta p)+1.31$
at pH 6.8, 30 °C $\log[\eta]=-0.46\log(\Delta p)+1.22$
at pH 7.0, 20 °C $\log[\eta]=-0.37\log(\Delta p)+1.20$
at pH 7.2, 20 °C $\log[\eta]=-0.42\log(\Delta p)+1.24$

constant.

The intercept of the log (Δp) *vs.* log $[\eta]$ curve might be utilized as an index of limiting dimension of the aggregate at the pressure difference $\Delta p=1$ cm H_2O. Though the physical meaning of the slope or the power of pressure difference cannot be grasped, the value seems to correspond to pH. Temperature seems to have no effect on the slope. When pH is constant, curves at various temperatures have the same slope.

In the case of linear polymer the molecular weight is estimated by the relation $[\eta]=KM^{\alpha}$. However, this relation is not applicable to the SDC system, since the parameters K and α are unknown. The molecular weight of SDC aggregates can be estimated roughly by use of the computed data for q-value and the data for m obtained by means of light scattering. We assume that q is 5—10 (Fig. 3) and mN or the micellar weight of primary micelle is 2.6×10^4 at 36.5 °C. Thus from Eq. 2, the value of $[M]_{w,t}$ in dynamic equilibrium is estimated to be 2.6×10^5 to 5.2×10^5. The micellar weight of the polymer-like aggregate is calculated to be several millions at 10 °C.[10]

pH Change with Flow. The SDC solution undergoes specific hydrolysis when it forms a gel.[4,11] This can be explained by a kinetic consideration that the abrupt rise of pH is due to the hydrolysis of SDC. When gel formation takes place, the pH rise is linear against logarithm of the reaction time t in the early stage with the same slope of unity. If we denote the initial concentration of the reactant deoxycholate ion by C, the concentration of the product by x, the rate constant by k, and the ionic product of water by K_w, we obtain the relation

$$pH = \log t + \log(kC/K_w), \qquad (10)$$

where it is assumed that $x \ll C$ in the initial stage of reaction and therefore only the first term of the expansion of $\ln[C/(C-x)]$ is taken. Equation 10 gives the relation $\mathrm{d\,pH/d\log}\,t=1$. It was found that the rate constant varies from 1.6×10^{-7} to 20×10^{-7} ($\mathrm{min^{-1}}$) at temperatures 5—35 °C, the activation energy of hydrolysis being calculated to be 14 kcal. We studied the behavior of the counter ions Na^+ and H^+ through the measurement of their activity change with concentration. We have concluded that the adsorption of proton on the micelle surface (or hydrolysis) is necessary for the structure-making of micelle or gel, and that the counter ion Na^+ undergoes exchange with a proton on micelle (gel) formation, and the proton exchanged contributes to the formation of hydrogen bond between deoxycholate molecules.[11]

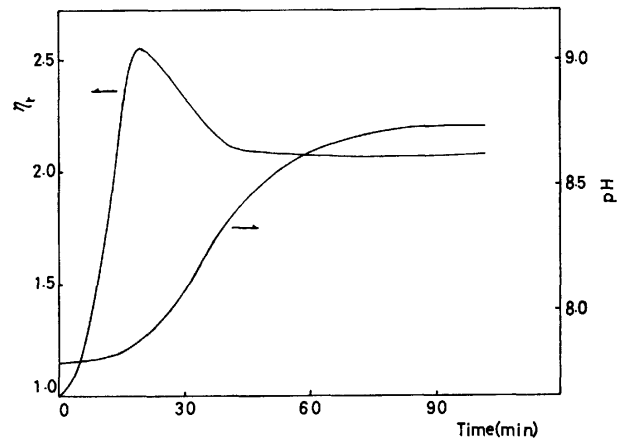

Fig. 8. The time-dependent changes of viscosity and pH which were caused simultaneously in the capillary flow. 1.6×10^{-2} M solution of SDC with addition of 0.5 M NaCl at 15 °C under $\Delta p=80$ cm H_2O.

A special viscometer (Fig. 1) was used in order to determine the pH change accompanied by the change in viscosity. The solution containing SDC of given concentration and 0.5 M NaCl showed a specific rise in pH when viscosity began to rise. However, the rise in pH was gradual, no peak being observed as in viscosity. The dynamic equilibrium in viscosity and pH was reached at the same time. Figure 8 shows an example of both changes in pH and viscosity with time. The measurement of pH shifts was carried out for different concentrations of SDC, shear-rates and temperatures. The results show that the pH shift is independent of concentration and shear-rate, but depends on temperature. On the other hand, viscosity is affected distinctly by shear-rate, concentration and temperature. The characteristic pH behavior indicates that the secondary aggregation or polymerization is not parallel to hydrolysis. The value of pH in equilibrium corresponds to that of the system (Fig. 2, the preceding paper[11]) and the range of pH shifts corresponds to the deviation from the straight line with slope 1/2 extrapolated from the singly dispersed region. The mixing of two solutions (SDC and NaCl) indicates that the SDC

solution is diluted with NaCl solution, the micelles being broken abruptly due to the shift of equilibrium. After micelles are broken by dilution, new micelles are formed again. In this state the environment of new micelles and singly dispersed species are now rich in sodium ions, almost all the counterions being sodium ions. Micelles of a more stable structure are then formed gradually, the counterions of Na^+ being replaced by protons. This can be considered a relaxation phenomena. Though the exchange reaction is slow, it can be accelerated by mixing or by being carried out in a field of flow. Alternatively, in the early stage of the capillary flow when no rise of viscosity appears, the exchange reaction takes place and stable primary micelles are formed by hydrogen bonding. As soon as sufficient protons are adsorbed on deoxycholate ions in the micelle, the primary micelles begin to associate secondarily forming polymer-like aggregates.

The indispensable role of hydrogen bond in the formation of SDC aggregate was revealed by other studies on pH and pNa behavior of aqueous solution of SDC[11] and the sol-gel transition under high pressure.[12]

We would like to acknowledge the valuable suggestions given by Prof. Dr. Kinsi Motomura, Kyushu University. We are indebted to Mr. Yoshio Aogame, Miss Machiko Hiraishi, Mr. Kiyofumi Hiramatsu, and Mrs. Makiko Taka, Fukuoka University, for their technical assistance.

References

1) R. Vochten and P. Joos, *J. Chim. Phys. Phys.-Chim. Biol.*, **67**, 1373 (1970).
2) K. Fontell, *Kolloid Z. Z. Polym.*, **246**, 614 (1971).
3) D. M. Blow and A. Rich, *J. Am. Chem. Soc.*, **82**, 3566 (1960).
4) G. Sugihara, K. Motomura, and R. Matuura, *Mem. of Fac. of Sci., Kyushu Univ., Ser. C.*, **7**, 103 (1970).
5) G. Sugihara, *Fukuoka Univ. Sci. Reports*, **3**, 37 (1974).
6) T. Nakagawa and H. Kambe, "Rheology," Misuzu Shobo, Tokyo (1959), p. 330.
7) B. Rabinowitch, *Z. Phys. Chem.*, **A 145**, 1 (1929).
8) O. H. Clark and M. L. Deutch, *J. Appl. Phys.*, **21**, 713, 1195 (1950).
9) A. B. Bestul and H. V. Belcher, *J. Colloid Sci.*, **5**, 303 (1950).
10) T. Furusawa, *Fukuoka Acta Medica*, **53**, 124 (1962).
11) G. Sugihara and M. Tanaka, *Bull. Chem. Soc. Jpn.*, **49**, 3457 (1976).
12) G. Sugihara, S. Kaneshina, T. Ueda, and M. Tanaka, *Bull. Chem. Soc. Jpn.*, **50**, 604 (1977).

Comparison of Experimental and Calculated Oscillator Strengths for Condensed Ring Compounds

Tetsutaro YOSHINAGA, Hiroshi HIRATSUKA, and Yoshie TANIZAKI
Department of Chemistry, Tokyo Institute of Technology, Meguro-ku, Tokyo 152
(Received March 18, 1977)

The electronic absorption spectra of eighteen aromatic condensed ring compounds (C_{2v} or D_{2h}) were studied by means of comparison between the calculated and experimental results in terms of three fundamental factors: the electronic transition energy, the direction of the electronic transition moment, and the oscillator strength. The three experimental factors were obtained from the component spectra polarized to the long and short axes of the molecule, which were determined by means of the dichroism analysis technique. The calculated oscillator strengths were obtained by the dipole-length, dipole-velocity, and mixed-dipole methods. From the comparison between experimental and calculated results, it was found that the mixed-dipole method gives the best fit of the values to the experimental ones.

As is well known, the electronic absorption spectrum is assigned on the basis of comparison between calculated and experimental results for three fundamental factors: the electronic transition energy, the direction of the electronic transition moment, and the oscillator strength. In most cases, however, the experimental results to be compared with the theory are not always valid for these items, since the results are obtained through band spectra in which most bands are composed of two or more overlapping transition bands. In order to make more precise assignments, therefore, it is necessary to separate the overlapping bands. One of the most useful methods for separating such bands for some symmetrical molecules is dichroism analysis using a stretched PVA [poly(vinyl alcohol)] film.

For a planar molecule of C_{2v} symmetry, for instance, the polarization direction of the π-π^* electronic transitions are restricted to directions parallel or perpendicular to the C_2 axis in the molecular plane. In such cases, the directions of polarization can easily be distinguished from one another by the use of the dichroism analysis. By means of this method, an absorption spectrum observed in non-stretched PVA film can be divided into two kinds of spectra in which the polarization directions are orthogonal to each other. When the divided spectra thus obtained are employed as experimental data, the comparison with the calculated results will become more precise in terms of the three factors mentioned above.

As for the theoretical calculation of the oscillator strength, the dipole-length method[1] has been extensively used. In recent years, however, the mixed-dipole method[2] and the dipole-velocity method[3-5] have also been employed, and comparisons of calculated with experimental values have been reported.

The first purpose in the present study is to determine the oscillator strength experimentally using the component spectra for many symmetrical molecules, such as condensed-ring compounds. The second purpose is to compare the oscillator strengths obtained by the dipole-length, mixed-dipole, and dipole-velocity methods with the experimental values.

Experimental

Materials. The chemical structures and the names of the compounds used are shown in Fig. 1, along with the sample number to be referred to throughout this work.

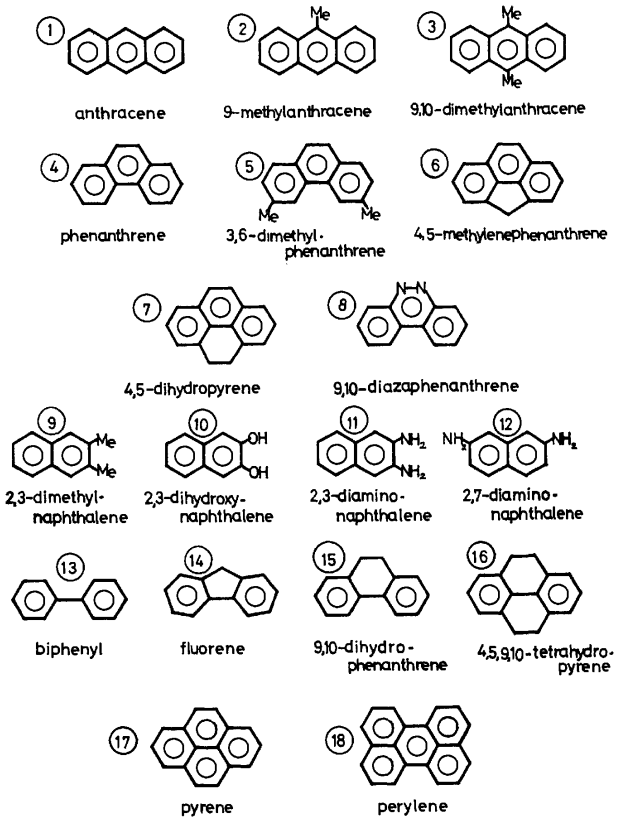

Fig. 1. Name, structures, and numbers for the compounds. (In Table 1, these numbers are employed instead of respective name of compound.)

The anthracene (U.P.; ultra-pure reagent), 9-methylanthracene (G.R.; guaranteed reagent), 9,10-dimethylanthracene (G.R.), 3,6-dimethylphenanthrene (G.R.), 4,5-methanophenanthrene (G.R.), 2,3-dimethylnaphthalene (G.R.), 2,3-naphthalenediol (G.R.), 2,3-naphthalenediamine (E.P.; extra pure reagent), 2,7-naphthalenediamine (E.P.), pyrene (U.P.), biphenyl (E.P.: >99%, G.C.), fluorene (U.P.), 9,10-dihydrophenanthrene (G.R.), and 4,5,9,10-tetrahydropyrene (G.R.) were commercially obtained from the Tokyo Kasei Kogyo Co., Ltd. The phenanthrene(fluorescence grade) and 5,6-phenanthroline were obtained from the Aldrich Chemical Company. Highly purified perylene was kindly offered by the Inokuchi Laboratory at the Institute for Solid State Physics, the University of Tokyo. The biphenyl, 2,3-dimethyl-

naphthalene, and other naphthalene derivatives were repeatedly recrystallized from the respective appropriate solvents. For 9,10-dihydrophenanthrene and 4,5,9,10-tetrahydropyrene, further purification was made by the Tokyo Kasei Kogyo Co., Ltd., at our request. For other compounds, no purification was made.

Measurement. The measurement of the polarized absorption spectra and the determination of the component spectra were carried out using the methods previously reported.[6]

After the assignment of the electronic transition bands for the component spectra had been established, the experimental oscillator strength (f^{exp}) for the respective bands were determined by means of the well-known formula:*

$$f^{exp} = 4.32 \times 10^{-9} \int \varepsilon_\sigma d\sigma$$

where σ is the wave number in cm^{-1} and where ε_σ is the molar extinction coefficient in the PVA substrate. In the present work, however, we used ε_σ in ethanol instead of that in PVA, since the absorption curves in the PVA film generally resemble those in ethanol. In fact, for some compounds, such as anthracene, and phenanthrene, it was found that the ε_σ values in PVA were nearly equal to those in ethanol.

Calculation

The MO calculations were carried out using the Pariser-Parr-Pople SCF CI method.[7,8] The one- and two-center electron repulsion integrals were evaluated by the Pariser-Parr equation[7] and the Nishimoto-Mataga equation[9] respectively. The valence-state ionization potentials (I_p(r)) and the electron affinities (E_a(r)) were as follows: I_p(C)=11.16 eV, E_a(C)=0.03 eV, I_p(–N=)=14.12 eV, E_a(–N=)=1.78 eV, I_p(–NH_2)=24.80 eV, E_a(–NH_2)=8.04 eV, I_p(–OH)=33.00 eV, and E_a(–OH)=11.47 eV.

For the "methyl" group, the hyperconjugation effect was taken into account after Morita,[10] and the following values were used: $I_p(H_3)$=10.08 eV and $E_a(H_3)$=0.19 eV, the resonance integrals were β(C–C')=–2.24 eV and β(C'–H_3)=–5.27 eV where the primed carbon is for methyl carbon. For the methylene group, the same parameters were used as for the methyl group. All the molecules, including biphenyl, were regarded as planar. The geometrical structure of fluorene was determined by reference to the crystal structure.[11]

The theoretical oscillator strengths, f^{cal}, were calculated by means of the following equations:[2,3]

$$f_l = 1.085 \times 10^{11}\, \sigma M_l^2 \quad (1)$$

$$f_v = 1.463 \times 10^{5}\, D_v^2/\sigma, \quad (2)$$

$$f_m = (f_l \cdot f_v)^{1/2}, \quad (3)$$

$$M_l = \langle \Psi_p | \sum_i r_i | \Psi_q \rangle,$$

$$D_v = \langle \Psi_p | \sum_i \mathrm{grad}\, i | \Psi_q \rangle,$$

where σ is the transition energy in cm^{-1}, for which the calculated values were used. The calculation methods using Eqs. 1, 2, and 3 are referred to as the dipole-length, dipole-velocity, and mixed-dipole methods respectively. In these calculations, Slater's atomic orbitals were employed, and the overlap integrals were not neglected. Moreover, all the elements of the transition density matrix were included.

* In general, f^{exp} is little affected by the medium. However, we neglected this correction in the present work, since there is some disagreement about this matter. See also Ref. 5 and especially the Ref. 17 in the Ref. 5.

Results

Table 1 shows the experimental and calculated results for the allowed transitions of eighteen compounds. Roman numerals represent the calculated transition numbers. For example, in the case of anthracene (Sample Number 1), the I st, II nd, and VI th transitions are allowed, while the others are forbidden, in the region above 200 nm. Even if a transition is allowed, when the corresponding absorption is too low to be determined, the relevant columns for the experimental transition energy and also the oscillator strength (f^{exp}) are left blank, as may be seen for the 1st transition of Sample No. 5, for example. Moreover, even if a transition energy is determined, when not all of the band is observed, f^{exp} can not be determined and the relevant column is blank (see the Xth transition of Sample No. 5).

In Table 1, the transition directions are designated by x and y for the long and short axes of the molecule respectively, and Platt's notations are shown in parentheses. The oscillator strengths calculated by the dipole-length, dipole-velocity, and mixed-dipole methods are denoted by f_l, f_v, and f_m respectively.

According to Table 1, the calculated transition energies as well as the transition directions agree very well with the experimental values. As for the oscillator strength, however, the calculated values are considerably different from the experimental ones in some cases. Moreover, some considerable differences between f_l and f_v are observed.

Figure 2 shows the distributions of the experimental (f^{exp}) and calculated (f^{cal}) oscillator strengths for the about seventy transitions listed in Table 1. In the figure, the abscissa is divided into sections at 0.1 intervals: for example, the f^{exp} value, 1.54, of the VI th transition of Sample No. 1 is placed in the column between 1.5 and 1.6. Thus, the distributions for f^{exp}, f_l, f_v, and f_m are obtained as shown in Figs. 2(a), (b), (c), and (d) respectively. The f^{exp} and f^{cal} values did not exceed 1.6 and 2.6 respectively. Nearly 90% of all the f values fall in the range of $0<f<1$. The frequencies within $0<f<0.1$ are 30—40% and are the greatest in all classes.

Now, let us investigate the relation between the f^{exp} and f^{cal} values. First, let us select sample molecules in Table 1 for which the π-electron approximation will be completely valid in the present calculation; that is, the five molecules of Samples No. 1, 4, 8, 17, and 18 have a planar structure and no substituent groups. The ratios of the oscillator strength, $R(=f^{cal}/f^{exp})$, for the corresponding transitions are plotted in Fig. 3, in which the abscissa is the same as in Fig. 2 and in which the ordinate represents the frequency of R values. In Fig. 3, the R values for $f^{exp}<0.1$ are marked by oblique lines to distinguish them from the others.

According to Fig. 3(c) all the values of $R_v(=f_v/f^{exp})$

TABLE 1. COMPARISON OF EXPERIMENTAL AND CALCULATED OSCILLATOR STRENGTHS

Sample No.[c]	Transition No.	Transition energy		Oscillator strength				Polarization[b]	
				Calcd[a]			Exptl		
		Calcd kcm^{-1}	Exptl kcm^{-1}	f_l	f_v	f_m	f^{exp}		
①	I	26.91	26.2	0.2437	0.0152	0.0609	0.0763	y	(L_a)
	II	28.10	27.6	0.0120	0.0063	0.0087	0.0194	x	(L_b)
	VI	39.17	38.9	2.4135	1.2801	1.7577	1.545	x	(B_b)
2	I	26.11	25.5	0.2614	0.0169	0.0664	0.0867	y	(L_a)
	II	27.82	27.0	0.0202	0.0063	0.0113	0.0201	x	(L_b)
	VI	38.83	38.4	2.4780	1.2159	1.7358	1.455	x	(B_b)
3	I	25.62	24.9	0.2775	0.0255	0.0841	0.127	y	(L_a)
	II	27.70	24.9	0.0188	0.0052	0.0099	0.0232	x	(L_b)
	VI	38.63	37.9	2.4427	1.1884	1.7038	1.080	x	(B_b)
④	I	29.00	28.9	5.9×10^{-4}	4.6×10^{-4}	5.2×10^{-4}	0.0027	y	(L_b)
	II	32.96	33.7	0.3298	0.1225	0.2010	0.171	x	(L_a)
	IV	39.85	(39)	0.4563	0.1213	0.2353	0.272	y	(B_b)
	V	39.87	39.2	1.3009	0.6735	0.8762	0.737	x	(B_a)
	VII	45.25	45.0	0.3078	0.1429	0.2097	0.101	y	
	X	48.85	(46)	0.0790	0.0263	0.0456		(x)	
5	I	28.67		7.3×10^{-4}	4.2×10^{-4}	5.5×10^{-4}		(y)	(L_b)
	II	32.15	33.1	0.4255	0.1847	0.2803	0.198	x	(L_a)
	IV	39.60	(38)	0.4591	0.1227	0.2373	0.352	y	(B_b)
	V	39.64	38.8	1.2838	0.7003	0.9482	0.613	x	(B_a)
	VII	43.79	43.9	0.4943	0.2475	0.3498	0.247	y	
	X	48.46	(46)	0.3208	0.1854	0.2439		(x)	
6	I	28.54		2.5×10^{-5}	1.0×10^{-5}	1.6×10^{-5}		y	(L_b)
	II	32.52	32.9	0.3107	0.1103	0.1851	0.187	x	(L_a)
	IV	38.28	39.1	0.7817	0.4645	0.6026	0.665	x	(B_a)
	V	38.67	37.6	0.4378	0.1192	0.2284	0.317	y	(B_b)
	VII	44.74	44.6	0.2920	0.1205	0.1876	0.223	y	
	X	47.39	43.9	0.4402	0.1885	0.2881	0.217	x	
7	I	28.63		0.0011	4.9×10^{-4}	7.3×10^{-4}		y	(L_b)
	II	32.69	33.1	0.3023	0.0959	0.1702	0.149	x	(L_a)
	IV	38.51	38.2	1.0222	0.5483	0.7486	0.396	x	(B_a)
	V	38.83	37.4	0.4475	0.1424	0.2524	0.279	y	(B_b)
	VII	44.82	43.9	0.3150	0.1232	0.1970	0.169	y	
	X	47.54	45.7	0.5597	0.2505	0.3391	0.317	x	
⑧	I	27.02	27.7	0.0457	0.0062	0.0168	0.0249	y	(L_b)
	II	29.36	31.8	0.5021	0.1364	0.2617	0.154	x	(L_a)
	V	40.11	39.2	1.0652	0.5262	0.7487	0.734	x	(B_a)
	VI	40.57	39.8	0.4609	0.1328	0.2474	0.191	y	(B_b)
	VIII	46.37	45.6	0.0704	0.0268	0.0434	0.071	y	
	IX	48.88	>46.5	0.2405	0.1102	0.1628		x	
9	I	30.66	31.3	0.0046	0.0022	0.0032	0.0011	x	(L_b)
	II	34.02	34.3	0.1596	0.0254	0.0637	0.0879	y	(L_a)
	III	42.90	43.5	1.9731	1.0321	1.4270	1.040	x	(B_b)
	IV	43.57		0.0036	0.0018	0.0026			
10	I	29.72	30.5	0.0439	0.0192	0.0290	0.0267	x	(L_b)
	II	33.41	33.9	0.1324	0.0189	0.0500	0.0581	y	(L_a)
	III	41.55	42.5	0.8730	0.4517	0.6280	0.836	x	(B_b)
	IV	43.04		0.6136	0.3260	0.4473		x	
	VI	44.61	44.1	0.3027	0.1237	0.1935	0.258	y	
11	I	26.55	28.9	0.1206	0.0474	0.0756	0.0572	x	(L_b)
	II	31.13	32.6	0.0382	0.0004	0.0039	0.0346	y	(L_a)
	IV	37.18	39.6	0.7162	0.3668	0.5125	0.642	x	(B_b)
	V	39.88		0.2168	0.1216	0.1624			
	VI	42.72	40.6	0.1215	0.0584	0.0842	0.274	y	
	VIII	45.37	46.0	0.5515	0.2917	0.4011		x	
12	I	26.88	29.4	0.0855	0.0334	0.0534	0.0409	x	(L_b)
	II	30.02	32.1	0.0658	0.0037	0.0156	0.0168	y	(L_a)
	III	36.09	39.6	1.0014	0.5530	0.7442	1.033	x	(B_b)
	V	41.97	45.8	0.3496	0.1490	0.2282	0.147	y	
	IX	48.05	48.0	0.3319	0.1438	0.2185		x	
13	I	34.63	34.5	6.0×10^{-4}	1.5×10^{-4}	3.0×10^{-4}	0.6×10^{-4}	y	
	III	36.40	39.0	0.7684	0.4420	0.5828	0.293	x	
	VI	48.85		0.8038	0.2970	0.4886		y	
14	I	33.95	32.6	0.0008	0.0026	0.0015	1.0×10^{-4}	y	
	II	34.62	33.1	0.0558	0.0230	0.0358	0.0623	x	
	III	35.76	37.6	0.4751	0.2811	0.3654	0.404	x	
	IV	45.09	44.9	0.2724	0.0986	0.1638		x	

TABLE 1. (continued)

Sample No.[c]	Transition No.	Transition Energy Calcd kcm^{-1}	Transition Energy Exptl kcm^{-1}	Oscillator strength Calcd[a] f_l	Calcd[a] f_v	Calcd[a] f_m	Exptl f^{exp}	Polarization[b]	
15	I	34.15	31.7	8.2×10^{-5}	2.7×10^{-5}	4.7×10^{-5}	2.0×10^{-4}	y	
	II	34.59	33.2	0.0020	0.0029	0.0024	0.0369	x	
	III	35.86	37.3	0.6394	0.3472	0.4712	0.296	x	
	IV	45.33	45.3	0.1438	0.0444	0.0789	0.103	x	
	V	46.54	46	0.1709	0.0988	0.1299		y	
16	I	33.56	32.6	7.0×10^{-6}	1.1×10^{-5}	8.8×10^{-6}	4.4×10^{-4}	y	
	III	35.03	33.9	0.5460	0.3130	0.4143	0.298	x	
	VI	46.71	45.3	0.8172	0.4047	0.5751	0.578	y	
	VII	47.28	(46)	1.2852	0.4185	0.7334		x	
⑰	I	27.05	26.8	0.0034	0.0014	0.0022	0.0014	y	(L_b)
	II	28.00	29.4	0.6723	0.1841	0.3518	0.326	x	(L_a)
	V	38.17	36.4	0.8322	0.2401	0.4470	0.418	y	(B_b)
	IX	43.57	41.2	1.3143	0.6054	0.8920	0.750	x	(B_a)
⑱	I	23.40	22.6	0.8037	0.2126	0.4611	0.332	x	
	II	28.60	(27.3)	0.0121	0.0046	0.0074	(0.019)	y	
	IX	40.04	37.8	1.4677	0.5515	0.8025	0.592	y	

a) The calculated oscillator strengths, f_l, f_v, and f_m, represent the values from the dipole-length method, the dipole-velocity method, and the mixed-dipole method respectively. b) Where x and y show the polarization directions paralle to and perpendicular to the molecular long axis respectively; the signs in parentheses are Platt's notations. c) Circles indicated in the first column show the selected samples.

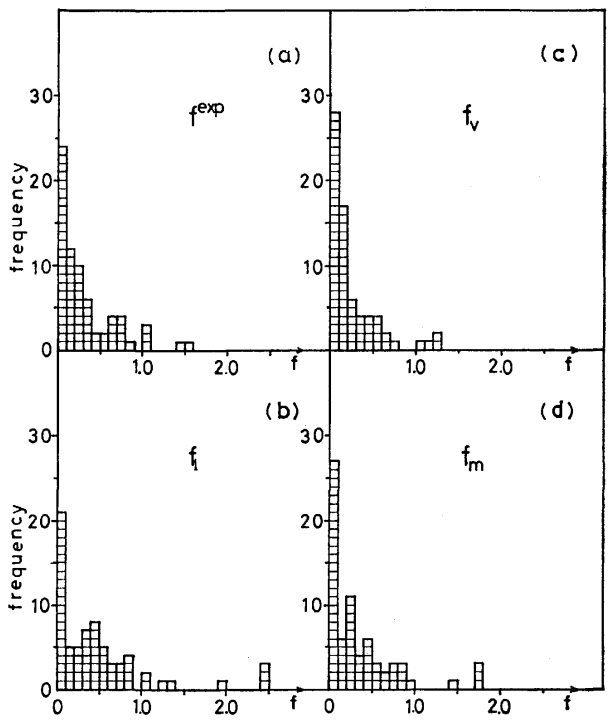

Fig. 2. Distributions of absolute oscillator strength for f^{exp} (a), f_l (b), f_v (c), and f_m (d); The ordinate, the number of frequencies and the abscissa, the absolute oscillator strength classed at 0.1 intervals.

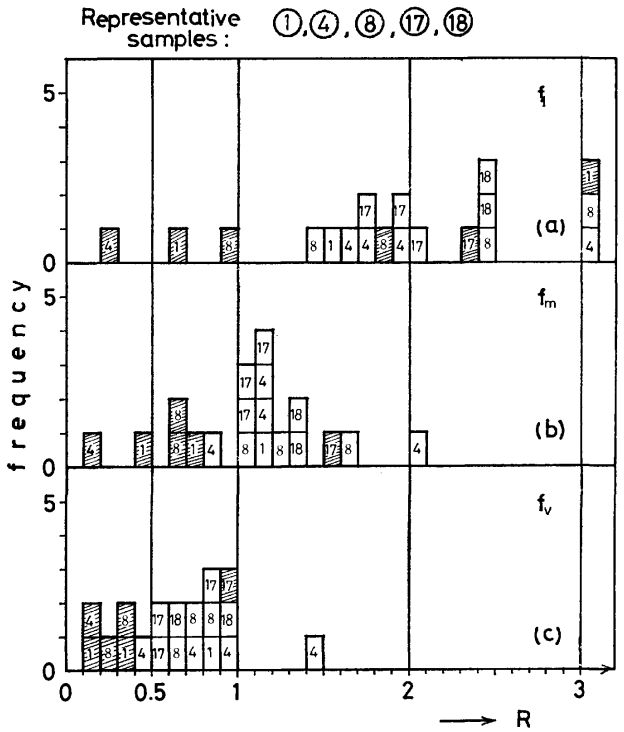

Fig. 3. Distributions of relative oscillator strength; (f_l/f^{exp}) (a), (f_m/f^{exp}) (b), and (f_v/f^{exp}) (c) for the representative compounds. The ordinate, the frequencies and the abscissa, the relative values, $R=(f^{cal}/f^{exp})$ at 0.1 intervals. The shaded parts represent the R values for $f^{exp}<0.1$.

except one ($R_v=1.5$, the VIth transition of Sample No. 2) are less than unity, and most of those for $f^{exp}<0.1$ are less than those for $0.1<f^{exp}$. On the other hand, Fig. 3(a) shows that the values of $R_l(=f_l/f^{exp})$ are scattered widely around 3. The values of $R_m(=f_m/f^{exp})$ shown in Fig. 3(b) fall between the former two values, and it is noticed that the values for $0.1<f^{exp}$ are concentrated in the range of 1.0—1.5.

Figure 4 shows the distributions of the R values for all the transitions in Table 1. The interrelation among R_v, R_m, and R_l is similar to that for the selected samples in Fig. 3.

From these results, the following relations are generally obtained:

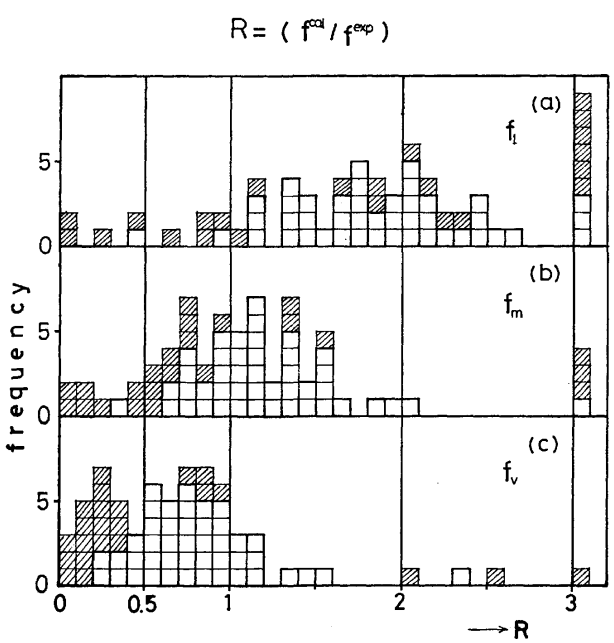

Fig. 4. Distributions of relative oscillator strength, $R=f^{cal}/f^{exp}$, for all compounds used in the present work. The shaded parts represent the R values for $f^{exp}<0.1$.

$$f_v \lesssim f^{exp} \lesssim f_l, \text{ and } f_v \lesssim f_m \lesssim f_l.$$

Moreover, in the comparison of the experimental and calculated values, since, in practical absorption spectra, intensity-borrowing phenomena usually occur, even if the calculated values are exact ones, for weak intensity bands the $f^{cal}<f^{exp}$ relation is to be expected. In fact, in the figures of distributions of the R values for f_m and f_v, the shaded parts ($f^{exp}<0.1$) mainly lie in the classes with relatively low values.

Discussion

In the present investigation, we determined the experimental oscillator strength (f^{exp}) from the component spectra obtained by the application of the dichroism analysis, thinking that the f^{exp} value to be compared with the calculated value should be determined for the corresponding single electronic band. That the f^{exp} values thus obtained are quite reasonable can be shown by the following example. For the first band of anthracene, the experimental oscillator strength has been given as 0.10—0.11.[13-15] It is well known that this band is composed of ^1L_a and ^1L_b bands. According to Table 1 (Sample No. 1), they are $f^{exp}(L_a)=0.0763$ and $f^{exp}(L_b)=0.0194$, the sum of these values gives 0.096, which is very close to the above conventional value. For the strong second band (^1B_b) of anthracene, the conventional values reported are 1.4—2.8;[13,15,16] among them, the value of $f=1.56$ is considered as the best one.[5] Table 1 shows that $f^{exp}(^1B_b)=1.545$. Since it is known that this band is a little overlapped, the value of $f=1.56$ may be regarded as reasonable.

In view of the above, the f^{exp} values which used to be compared with f^{cal} in the studies of the oscillator strength were not always reliable. However, if the band in question is not overlapped, such as the first band of linear polyenes, its f^{exp} value is reliable.

From the study of the oscillator strength for the linear polyenes, biphenyl linear polyenes, *etc.*, Chong *et al.*[3,4] found that the f_l/f^{exp} ratio ranges from 2 to 5, whereas f_v/f^{exp} varies from 1 to 0.5; they concluded that f_v is much better than f_l. The same conclusion was derived from the study of naphthalene, anthracene, *etc.* by McHugh and Gouterman.[5] They obtained a quantity relatively independent of the overlapped bands and intensity borrowing by integration over the complete experimental absorption curve. Using these quantities, they compared M_l and D_v (see Eqs. 1—3) and found that D_v is superior to M_l and that consequently, f_v is superior to f_l, in comparison with the experimental (f^{exp}) value. Furthermore, they concluded that f_v is superior to the f_m employed by Hansen.[2]

On the other hand, as is shown in our results, both f_v and f_m are much better than f_l in comparison with the experimental (f^{exp}) values; moreover, f_m is superior to f_v, as is shown in Figs. 3 and 4. It is natural from the forms of Eqs. 1—3 that f_m falls between f_l and f_v. According to Hansen,[2] when the doubly excited configuration is taken into account, f_l and f_v are considerably changed, while f_m shows less sensitivity. This means that even if the electron correlation is taken into account, f_m is still superior to f_l and f_v.

Incidentally, one advantage of employing f_m is that the transition energy is unnecessary in the calculation. Therefore, in contrast to f_l and f_v, one can avoid the problem of whether to use the experimental or theoretical transition energy in the calculation of the oscillator strength. (In this connection, Chong *et al.* used the experimental values.)

De Bruijn[17] calculated f_l and f_v by considering the overlap integral and CI for alternant hydrocarbons. He concluded that a complete CI does not give much improvement in f^{cal} and that the failure in f^{cal} is partly attributable to the deficiency of the simpler MO-levels and partly to the neglect of the polarization of the σ-electrons. He pointed out that the overlap integral is effective in the f_v calculation. Especially, from a comparison of f_l and f_v for the S_j-S_o transitions of naphthalene and anthracene, he concluded that the inference of Chong *et al.* is not generally valid. However, as has been already pointed out, these considerations do not seem appropriate, since the f^{exp} values employed in his study have some problems.

Finally, it should be emphasized here that the inclusion of the off-diagonal terms of the transition density matrix in the calculation of the oscillator strength, especially by the dipole-length method, sometimes becomes very important, though the off-diagonal elements have been disregarded in almost all cases.[18,19] An example is indicated for the very weak transitions on the longest-wavelength sides of the first bands for pyrene, phenanthrene, biphenyl, *etc.*, which are well known to be ^1L_b bands. (Ex.: for pyrene, $f^{exp}=1.4\times10^{-3}$). For these transitions, the conventional calculated values are always zero; *i.e.*, f_l(diagonal)=0.000. On the other hand, relatively good values for the corresponding f^{exp} values are obtained by the inclusion of off-diagonal terms. (Ex.: for pyrene,

f_l(diag.+off-diag.)$=3.4\times10^{-3}$.) (See Table 1.) The same relation holds for naphthalene, which was not taken up in the present study. This may also be extended to a general case; that is, the inclusion of the off-diagonal terms gives a non-zero finite value for a transition which is group-theoretically allowed, but f_l(diagonal) is zero.

References

1) R. S. Mulliken, *J. Chem. Phys.*, **51**, 137 (1939).
2) A. E. Hansen, *Mol. Phys.*, **13**, 425 (1967).
3) D. P. Chong, *Mol. Phys.*, **14**, 275 (1968).
4) C. P. Yue and D. P. Chong, *Mol. Phys.*, **14**, 487 (1968).
5) A. J. McHugh and M. Gouterman, *Theor. Chim. Acta*, **13**, 249 (1969).
6) Y. Tanizaki and S. Kubodera, *J. Mol. Spectrosc.*, **24**, 1 (1967).
7) R. Pariser and R. G. Parr, *J. Chem. Phys.*, **21**, 466 767 (1953).
8) J. A. Pople, *Proc. Phys. Soc.*, **A68**, 81 (1955).
9) N. Mataga and K. Nishimoto, *Z. Physik. Chem. N.F.*, **13**, 13 (1957).
10) T. Morita, *J. Chem. Phys.*, **25**, 1290 (1956); *Bull. Chem. Soc. Jpn.*, **31**, 322 (1958); *ibid.*, **33**, 1486 (1960).
11) D. M. Burns and J. Iball, *Proc. R. Soc. London, Ser. A*, **227**, 200 (1955).
12) K. Inuzuka and R. S. Becker, *Bull. Chem. Soc. Jpn.*, **47**, 88 (1974).
13) J. R. Platt, H. B. Klevens, and W. C. Price, *J. Chem. Phys.*, **17**, 466 (1949); H. B. Klevens and J. R. Platt, *J. Chem. Phys.*, **17**, 470 (1949).
14) A. Matsui and Y. Ishii, *J. Phys. Soc. Jpn.*, **23**, 581 (1967).
15) M. Tanaka and J. Tanaka, *Theor. Chim. Acta*, **30**, 81 (1973).
16) T. Kitagawa, *J. Mol. Spectrosc.*, **26**, 1 (1968).
17) S. de Bruijn, *Chem. Phys. Lett.*, **5**, 428 (1970).
18) F. Momicchioli and A. Rastelli, *J. Chem. Soc., B*, **1970**, 1353.
19) C. C. Bott and T. Kurucsev, *J. Chem. Soc., Faraday Trans. 2*, **71**, 749 (1975).

ESR Studies of the Photoreduction of Quinones. II. The Reinterpretation of Semiquinone Intermediates from Halogenated *p*-Benzoquinones in Ethanol

Yoshihiko KAMBARA, Hiroshi YOSHIDA, and Bengt RÅNBY*

Faculty of Engineering, Hokkaido University, Kita-ku, Sapporo 060
**Institute of Polymer Technology, Royal Institute of Technology, Stockholm 70, Sweden*

(Received March 22, 1977)

A reinterpretation was made of the electron spin resonance spectrum of semiquinone intermediates during the photolysis of a flowing solution of tetrachloro-*p*-benzoquinone (chloranil) in ethanol. The photoinduced spectrum with a width of 0.06 mT with an unresolved hyperfine structure was found to be identical with the spectrum of the semiquinone anion generated by reducing chloranil in an alkaline ethanol solution. This and other observations indicated that the photoinduced spectrum was due to the chloranil semiquinone anion formed primarily by the one-electron transfer to chloranil from the solvent ethanol, rather than to the semiquinone radical. The photoinduced one-electron transfer reaction was found, though qualitatively, to proceed more efficiently for chloranil and fluoranil, with a larger electron affinity, than for *p*-benzoquinone and dichloro-*p*-benzoquinones.

Because of the interesting nature of semiquinone intermediates and their important role in biological systems, the photochemistry of quinones has attracted much attention.[1] One of the quinones, tetrachloro-*p*-benzoquinone (chloranil), had thus far been studied by means of the flash-photolysis and the electron spin resonance methods.[2-6] However, controversy still remains as to the identification of semiquinone intermediates upon photolyzing chloranil in alcoholic solutions. Kemp and Porter observed an optical absorption at 420 nm in their laser-flash-photolysis study of the ethanol solution and attributed it to the semiquinone radical resulted from the hydrogen abstraction of the triplet excited chloranil from the solvent.[2] Wong *et al.* observed an ESR spectrum with an unresolved hyperfine structure by flash-photolyzing chloranil in 2-propanol and attributed it also to the semiquinone radical,[4] mainly by the analogy to other simple quinones, such as *p*-benzoquinone and duroquinone, from which semiquinone radicals has been inferred to be the photoinduced intermediates in alcoholic solutions.[7-9] On the contrary, Hales and Bolton assigned a similar ESR spectrum recorded from the solution in ethanol or methanol to the chloranil semiquinone anion on the basis of the measured *g*-values.[3] In the flash-photolysis study, Kawai *et al.* reported the formation of both the semiquinone anion and the radical from chloranil in ethanol.[5]

We also found the generation of the ESR spectra of both the anion and the radical recorded during the continuous photolysis of *p*-benzoquinone and its methyl-substituted derivatives in methanol and ethanol,[10-11] and have recently revealed that the *p*-benzosemiquinone anion is generated by a photoinduced one-electron transfer from the solvent to the quinone and that the *p*-benzosemiquinone radical results from a subsidiary reaction between the quinone and hydroquinone.[12] These results raised a question as to our previous interpretation of an ESR spectrum observed during the photolysis of chloranil in alcoholic solutions[6]—that the transient intermediate involved was the semiquinone radical.

Our primary concern in the present investigation is the reinterpretation of the ESR spectra of chloranil semiquinone intermediates. Experimental evidence will be given that the photoinduced one-electron transfer takes place for chloranil and other halogenated *p*-benzoquinones in ethanol, just as for *p*-benzoquinone.[12]

Experimental

Chloranil, fluoranil (tetrafluoro-*p*-benzoquinone), 2,5-, and 2,6-dichloro-*p*-benzoquinones of an analytical grade were purified by sublimation several times, and their purity was checked from their melting point. Ethanol of a specrtoscopic grade was usually used as received, without further purification. Occasionally ethanol was purified as has been described before,[12] but the purification of the solvent caused no change in the results. Sodium ethoxide of an analytical grade was used as received.

The photogenerated semiquinone intermediates were studied by observing their ESR spectrum during the continuous photolysis of a solution of the quinones (usually 1×10^{-3} mol dm^{-3}) flowing through a flat quartz cell in the ESR resonant cavity after being purged with helium gas for at least half an hour to remove any dissolved oxygen. The photolysis was carried out with unfiltered light from a super-high pressure mercury arc (Philips, SP-500), except when otherwise mentioned. The effective volume of the cell was 0.045 cm^3, which results in the total photolysis time of 30 ms when the solution flows, for example, at the rate of 1.5 cm^3 s^{-1}. A more detailed description of the experimental apparatus has been given in our previous papers.[12,13] The solution sealed in a quartz sample tube was studied under photolyzing light, but no good ESR signal could be recorded because of the rapid depletion of the quinones.

Results and Discussion

Photolysis of Chloranil. Figure 1A shows a typical ESR spectrum recorded during the photolysis of chloranil in neutral ethanol. It indicates no resolved hyperfine structure with a spectral width (peak-to-peak in the derivative spectral curve, ΔH_{msl}) of 0.06 mT, and agrees with the spectra in our previous investigation, where the widths were precisely determined to be 0.055, 0.062, and 0.063 mT in 2-propanol, ethanol, and methanol respectively.[6] It is essentially the same as

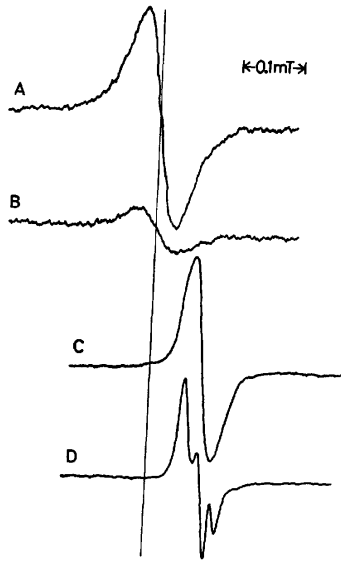

Fig. 1. ESR spectra of semiquinone intermediates generated from chloranil (1×10^{-3} mol dm^{-3}) in ethanol at room temperature (A) during photolysis, or by the addition of (B) 1×10^{-3}, (C) 3×10^{-3}, or (D) 1×10^{-2} mol dm^{-3} of sodium ethoxide. Solutions are flowing at the rate of 0.15 cm^3 s^{-1} for (A) and (B), and are sealed in sample tubes for (C) and (D).

the spectrum reported by Wong *et al.* (0.058 mT in 2-propanol)[4] and that reported by Hales and Bolton (0.08 mT in ethanol and methanol).[3]

When the solution was made alkaline with a small amount of sodium ethoxide, it gave an ESR spectrum without photolyzing light, as is shown in Fig. 1B. This "dark spectrum" showed a *g*-value and width exactly identical with those of the photospectrum in the neutral solution. Successive ESR recording under the photolyzing light, the other conditions being the same, gave a much more intense spectrum without any change in the *g*-value and the width, and confirmed the identity of the dark spectrum with the photospectrum. Thus, the photospectrum is attributable to the chloranil semiquinone anion, the same entity as that in alkaline ethanol,[3,14] resulting from photoinduced one-electron transfer from the solvent ethanol to chloranil. Previously we assigned the photospectrum to the semiquinone radical resulting from the hydrogen abstraction of excited chloranil from the solvent, on the basis of the observed difference in *g*-value between the photospectrum and the dark spectrum.[6] However, such an assignment has been found to be incorrect, as will be described below.

When the solution was made acidic with acetic acid, the photospectrum did not change in shape, but only decreased in intensity. Dissolved oxygen also reduced the intensity. By analogy with the semiquinone anion formation from *p*-benzoquinone previously studied,[12] these observations may be interpreted in terms of the inhibiting effect of oxygen and acid on the photoinduced one-electron transfer to chloranil, and in terms of the protonation of the semiquinone anion being too slow to compete with its decay reaction. When the flow rate was changed from 2 to 0.15 cm^3 s^{-1}, the intensity decreased monotonically. This result indicates a lifetime of the semiquinone anion equal to, or less than, some tens miliseconds under the present conditions. Otherwise, the intensity should have increased as a result of the accumulation of the generated semiquinone anion during the longer photolysis time. The observed decrease in the intensity may be attributed to the depletion of chloranil. Some stable photoproduct seems to have been deposited on the cell surface and to have screened the solution from the photolyzing light at low flow rates, so that no quantitative measurement could be made of the effect of the flow rate.

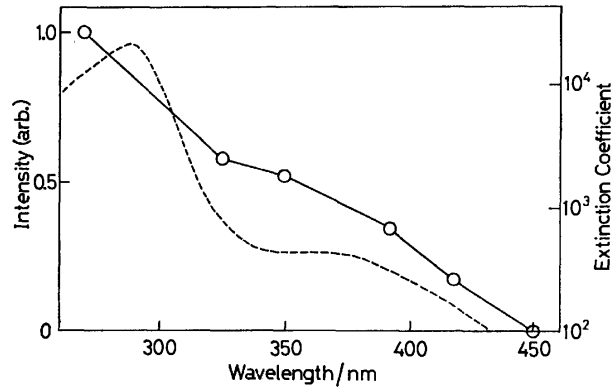

Fig. 2. Dependence of the intensity of ESR spectrum observed during the photolysis of flowing (0.15 cm^3 s^{-1}) solution of 1×10^{-3} mol dm^{-3} chloranil in ethanol on the wavelength of photolyzing light examined by discriminating the light with long-pass filters. Optical absorption spectrum of chloranil in ethanol reported in Ref. 15 is shown by dashed line for comparison.

When the shorter wavelength region of the light was successively descriminated by long-pass filters, the intensity of the spectrum decreased as is shown in Fig. 2. The intensity observed without a filter was plotted at 270 nm, which was effectively the shortest wavelength of the light source used. The plot at 325 nm shows the intensity observed with a filter of a 50% transmission at this wavelength, and so forth. The light of wavelengths longer than 450 nm is found to be ineffective to generate the photospectrum. The optical absorption spectrum of chloranil in ethanol was studied with a conventional recording spectrophotometer, and was found to agree with that reported by Shcheglova *et al.*,[15] though it gradually changed even in the absence of light under oxygen-free conditions. Taking into account this optical absorption spectrum and the spectral distribution of the light sourse supplied by the manufacturer, the relative quantum efficiency of the semiquinone anion formation can be calculated from the data in Fig. 2:

Wavelength (nm)	Efficiency
295—330	0.1
330—370	0.02
370—405	1.0
405—450	0.8

Admitting the uncertainty in the above values mainly caused by the tailing of the filters (though this uncertainty was taken into account in calculating the efficien-

cy), one can notice that the longer-wavelength region of the absorption spectrum is effective for the semiquinone anion formation. This observation is consistent with the previous result that the *p*-benzosemiquinone anion was the most efficiently generated by the light of wavelengths at the $n\pi^*$ band of *p*-benzoquinone.[12]

Chloranil in Alkaline Ethanol. The dark formation of the chloranil semiquinone anion by adding sodium ethoxide was studied in more detail for a fixed concentration of chloranil, 1×10^{-3} mol dm^{-3}, sealed in sample tubes under a vacuum. For concentrations of sodium ethoxide lower than 2×10^{-3} mol dm^{-3}, the ESR spectrum was the one due to the semiquinone anion. However, the spectrum changed, as is shown in Fig. 1C, when the ethoxide concentration was raised to 3×10^{-3} mol dm^{-3}. It narrowed to the width of 0.04 mT and was shifted to a resonant field higher by 0.09 mT (the *g*-value was smaller by 0.0006). We had assigned this shifted spectrum incorrectly to the chloranil semiquinone anion.[6] The increase in ethoxide concentration caused a further change in the spectral shape, it becoming complex, as is shown in Fig. 1D.

Sasaki *et al.* studied the reduction of chloro-*p*-benzoquinone by ethoxide and found that the semiquinone anion primarily formed was further transformed into the diethoxy-*p*-benzosemiquinone anion.[16] The present spectral change in the reduction of chloranil may be interpreted analogously: the substitution of one of the chlorine atoms in the chloranil semiquinone anion with an ethoxyl group may have caused the narrowing and shift of the spectrum. Further substitution resulted in the complex and resolved hyperfine structure shown in Fig. 1D, though no exact interpretation has been made. Because chlorine isotopes make the hyperfine structure complicated and unresolved, the decrease in the number of chlorine nuclei involved should resolve the hyperfine structure. Because of the large spin-orbit coupling of the chlorine atom, it is also conceivable that the loss of the chlorine nucleus caused the change in the *g*-value and, therefore, the shift in the resonant magnetic field.

Assignment of Semiquinone Intermediates. Hales and Bolton compared spectral parameters between the photoinduced ESR spectrum in neutral alcohols and that of the semiquinone anion generated from chloranil in alkaline alcohols in the dark, and concluded that the photoinduced spectrum was also due to the semiquinone anion.[3] Later Wong *et al.* argued that the difference in the *g*-value between the semiquinone anion and the semiquinone radical might be too small to give an unequivocal identification of semiquinone intermediates.[4] In the present investigation, however, the identity of the photospectrum with that of the authentically generated semiquinone anion was proven almost unequivocally, especially by the photolysis of the alkaline solution, where the semiquinone anion was present even in the dark. In addition, it was strongly suggested that the photoinduced one-electron transfer took place between an ethoxide ion and chloranil.

Wong *et al.* assigned the photospectrum to the chloranil semiquinone radical by analogy with other simple quinones, such as *p*-benzoquinone and duroquinone.[4] Since Porter's pioneering work by the flash photolysis-optical absorption method,[7] the photochemical generation of semiquinone radicals from these quinones in alcohols has been widely accepted. ESR studies seem to have supported such a view by detecting photospectra unquestionably attributable to the corresponding semiquinone radicals from their resolved hyperfine structure.[8,9] Recently, however, we reported ESR evidence that the semiquinone anion is a unique intermediate generated by photolyzing the fresh solution of the simple non-halogenated quinones in alcohols, and that the ESR spectra of the semiquinone radicals may, when observed, have resulted from a subsidiary reaction between the quinones and the corresponding hydroquinones.[10,12] Therefore, we believe that the photochemical analogy mentioned above is no longer pertinent.

Naturally it is a difficult task to identify an ESR spectrum without a resolved hyperfine structure, such as shown in Fig. 1A. Perhaps the ENDOR study will give a firm answer to the question of whether the photoinduced semiquinone intermediate is an anion or a radical, when the measurements are carried out during the photolysis, by proving the absence (or the presence) of a proton hyperfine splitting. In such a study, attention should be paid to eliminate the perplexing effect of the corresponding hydroquinone in the chloranil solution.

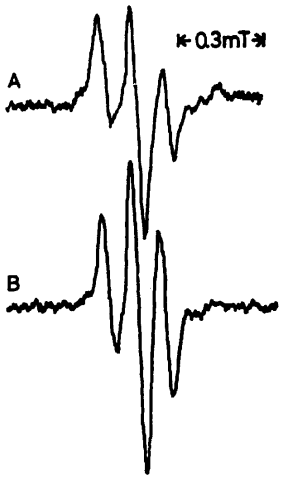

Fig. 3. ESR spectra of semiquinone intermediates observed during the photolysis of the solution, flowing at a rate of 1.5 cm^3 s^{-1}, of 1×10^{-3} mol dm^{-3} (A) 2,5-dichloro-*p*-benzoquinone or (B) 2,6-dichloro-*p*-benzoquinone in ethanol at room temperature.

Photolysis of Other Halogenated p-*Quinones.* When 2,5- and 2,6-dichloro-*p*-benzoquinones were photolyzed in ethanol at a comparatively high flow rate of the solution, the spectra with three hyperfine lines shown in Fig. 3 were recorded. The observed hyperfine splittings were 0.23 and 0.20 mT, essentially the same as those determined for the 2,5- and 2,6-dichloro-*p*-benzosemiquinone anions generated by the air oxidation of the corresponding hydroquinones.[17] Therefore, the semiquinone anions are believed to form from these dichloro-*p*-benzoquinones, as from chloranil, by photoinduced

one-electron transfer reactions. With a decrease in the flow rate, the spectra decreased in their intensity and were distorted simply because of an overlapping of the broad spectrum without a resolved hyperfine structure. The latter spectrum is thought to be due to the semiquinone radicals, which are generated preferentially at a low flow rate through the photoreaction between dichloro-*p*-benzoquinones and their corresponding hydroquinones, because of the depletion of the quinone concentration and the increase in the concentration of the product hydroquinones. Such a dependence on the flow rate is just the same as that reported previously for *p*-benzoquinone.[12]

The *g*-values for the authentically generated semiquinone aions of chloranil, 2,5-, and 2,6-dichloro-*p*-benzoquinones and *p*-benzoquinone have been reported to be 2.00568, 2.00516, 2.00503, and 2.00468 respectively.[18] The spectra assigned to these semiquinone anions in this and previous[12] investigations were all consistent with the reported *g*-values. Evidently the increasing number of chlorine atoms in the semiquinone anions results in an increase in the *g*-value because of the large spin-orbit coupling in the chlorine atom. Keeping in mind the negligible difference in the *g*-value between the *p*-benzosemiquinone anion and the *p*-benzosemiquinone radical, one might be convinced that the shift of the spectra to the higher field (*i.e.*, to the smaller *g*-value) in the solution of chloranil in the highly alkaline ethanol is attributable to the elimination of some of the chlorine atoms by ethoxy-substitution.

Fluoranil in ethanol gave, under the photoillumination, a spectrum with five hyperfine lines of the binomial intensity ratio, just as has been reported previously by Hudson and Lewis.[19] They interpreted this spectrum as being due to a rapid proton transfer between the two oxygen atoms of the semiquinone radical, which was presumed to be the primary intermediate in the photoreduction of fluoranil in ethanol. However, the spectrum was found to decrease in its intensity without changing its shape if the solution was made highly acidic by adding water and sulfuric acid. The interconversion between the semiquinone anion and the radical, which was a part of proposed rapid proton transfer, is believed to be slow for fluoranil, as for *p*-benzoquinone.[12] There is no reason why the observed five-line spectrum cannot be attributed to the fluoranil semiquinone anion generated primarily by the photoinduced one-electron transfer.

No spectrum attributable to the semiquinone radical was observed from either fluoranil or chloranil, even by decreasing the flow rate of solution. In contrast, the superposition of the spectrum of the semiquinone radical on that of the semiquinone anion was observed at a low flow rate for *p*-benzoquinone[12] and dichloro-*p*-benzoquinones. The generation of the *p*-benzosemiquinone radical was found previously to be the result of the hydrogen abstraction of the quinone from hydroquinone, the concentration of which became high enough because of the long photolysis time. The electron affinity increases in the order of *p*-benzoquinone, dichloro-*p*-benzoquinones, fluoranil and chloranil.[20] The photoinduced one-electron transfer is slow for quinones of a low electron affinity, so that the hydrogen abstraction reaction competes. The one-electron transfer for quinones of a high electron affinity, such as fluoranil and chloranil, proceeds so rapidly that their semiquinone anions are exclusively observed by ESR during the photolysis.

References

1) See for example, J. M. Bruce, "The Chemistry of Quinonoid Compounds, Part 1," ed by S. Patai, John Wiley and Sons, London (1974), p. 465.
2) D. R. Kemp and G. Porter, *J. Chem. Soc., Chem. Commun.*, **1969**, 1029.
3) B. J. Hales and J. R. Bolton, *Photochem. Photobiol.*, **12**, 239 (1970).
4) S. K. Wong, L. Fabes, W. J. Green, and J. K. S. Wan, *J. Chem. Soc., Faraday Trans. 1.*, **68**, 2211 (1972).
5) K. Kawai, Y. Shirota, H. Tsubomura, and H. Mikawa, *Bull. Chem. Soc. Jpn.*, **45**, 77 (1972).
6) H. Yoshida, Y. Kambara, and B. Rånby, *Bull. Chem. Soc. Jpn.*, **47**, 2599 (1974).
7) D. R. Kemp and G. Porter, *Proc. R. Soc. London, Ser. A*, **326**, 131 (1972).
8) T. A. Claxton, T. E. Gough, and M. C. R. Symons, *Trans. Faraday Soc.*, **62**, 279 (1966).
9) S. K. Wong, W. Sytnyk, and J. K. Wan, *Can. J. Chem.*, **50**, 3052 (1972).
10) H. Yoshida, K. Hayashi, and T. Warashina, *Bull. Chem. Soc. Jpn.*, **45**, 3515 (1972).
11) T. Warashina, O. Edlund, and H. Yoshida, *Bull. Chem. Soc. Jpn.*, **48**, 636 (1975).
12) Y. Kambara and H. Yoshida, *Bull. Chem. Soc. Jpn.*, **50**, 1367 (1977). Part I of the present series of studies.
13) H. Yoshida and T. Warashina, *Bull. Chem. Soc. Jpn.*, **44**, 2950 (1971).
14) B. G. Segal, M. Kaplan, and G. K. Fraenkel, *J. Chem. Phys.*, **43**, 4191 (1965).
15) N. A. Shcheglova, D. N. Shigorin, G. G. Yakobson, and L. Sh. Tushishvili, *Zh. Fiz. Khim.*, **43**, 1984 (1969).
16) M. Sasaki and J. Osugi, *Nippon Kagaku Zasshi*, **90**, 1231 (1969).
17) B. Venkataraman, B. G. Segal, and G. Fraenkel, *J. Chem. Phys.*, **30**, 1006 (1959).
18) B. G. Segal, M. Kaplan, and G. K. Fraenkel, *J. Chem. Phys.*, **43**, 4191 (1965).
19) A. Hudson and J. W. Lewis, *J. Chem. Soc., B*, **1969**, 531.
20) E. C. M. Chen and W. E. Wentworth, *J. Chem. Phys.*, **63**, 3183 (1975).

Light Scattering by Oligostyrene Solutions

Toshio KAMATA, Hisae NAKAHARA, and Shigeru HATTORI

National Chemical Laboratory for Industry, Honmachi, Shibuya-ku, Tokyo 151

(Received March 23, 1977)

Light-scattering photometers were partially modified in order to measure light scattering by low molecular-weight molecules. Corrections to the molecular weights were then theoretically estimated, when the light scattering due to fluid density fluctuations were approximated by that due to the density fluctuations of a pure solvent. The molecular weight of benzene was determined, in an ethyl methyl ketone solvent, using the light-scattering method prior to the determination of the molecular weights of oligostyrene molecules. Measurements of light scattering by oligostyrene molecules with molecular weights from 600 to 20000 were then carried out. The weight-average molecular weight observed by the light-scattering method was compared with the number-average molecular weights which were determined by the vapor-phase osmometric and NMR methods. The molecular-weight heterogeneity of the specimen is discussed. The second virial coefficient, in the ethyl methyl ketone solvent system, was found to change from negative to positive with increasing molecular weight. It is also shown that the molecular optical anisotropy changes markedly in the range of molecular weights between 2000 and 3000, the change being considered to reflect the conformational changes of oligostyrene molecules.

Oligomers are not only useful for practical uses but are also attracting considerable interest in the study of solution properties. It is especially interesting to determine the range of molecular weights in which the recent theory of solutions for high molecular-weight polymers can be applied. For this purpose it is desirable to measure molecular weights in the range from oligomers to high molecular-weight compounds using the same technique, because mean values should be compared on the same basis. The light-scattering method is most suitable for the measurement of molecular weights over such a wide range. There are several technical problems in the measurement of low molecular weights as noted below:

(1) Minute amounts of scattered light must be accurately measured, because the scattering intensity may be very weak.

(2) Scattering due to a fluctuation in the fluid density cannot be approximated by that due to the fluctuation of the solvent density.

(3) The correction to the degree of depolarization of the scattered light due to a fluctuation in the orientation of anisotropic molecules should be made accurately when unpolarized light is used as the incident light.

The method for measuring molecular weights utilizing minute amounts of scattered light has already been reported by Kamata and Nakahara.[1] In the present paper, a method for correcting the observed molecular weights, as the result of density fluctuations and methods for correcting the depolarization are reported. In addition, the characteristic behavior of oligomer molecules in solution are discussed based on the results of light-scattering measurements of oligostyrene.

Experimental

Materials. Polystyrenes, batch 16a, 15a, 12b, 11b, 8b, and 2b, obtained from the Pressure Chemical Co., were used. Dibenzyl of G.R. grade, used as the substance corresponding to the dimer for the measurement of the specific refractive index increment, was obtained from the Tokyo Kasei Kogyo Co. The solvent, ethyl methyl ketone (special grade), was purchased from the Kanto Chemical Co. and used after distillation. The benzene (DOTITE Primazol) used, after distillation, for the calibration of the light-scattering photometers was purchased from the Dojin Chemical Co.

Light-Scattering Measurements. It is difficult to accurately measure the depolarization and the scattered light produced by a solution containing a low molecular-weight substance using a single light-scattering photometer. Thus, the Rayleigh factor and the depolarization were separately measured using two photometers. A light-scattering photometer, Shimadzu Model PG-21, was used for measuring the Rayleigh factor, and a high-gain photomultiplier, Hamamatsu TV. Co. Model R-105 UH, having an anode sensitivity= 1530 μA/μlm, was used for accurately measuring weakly scattered light. A Shimadzu Model DL-10A light scattering photometer was used with some modifications for the depolarization measurements. It is necessary that the zero point be easy to monitor during the experiments and the observed values be stable in order to accurately determine the depolarization of the weakly scattered light. For this purpose, a solenoid shutter was placed in front of the photomultiplier. This shutter can be opened and closed by means of an external switch. The zero point was very easily checked using this shutter, which also rendered the observed values very stable, since there was no need to shut off the power supply for the photomultiplier during the course of the experiments. A Glan-Thompson prism was also used as a polarizer and an analyzer.

The solvents and solutions used were all centrifuged for 1 h at about 60000 g using a Beckman (Spinco) Model L_4 preparative ultracentrifuge, and then directly filtered into the light-scattering cell through a Corning ultrafine glass filter.

The light scattering was measured using mercury radiation at a wavelength of 436 nm in vacuo at room temperature. Calibration of the light-scattering photometer was carried out using the Rayleigh ratio, $R_{90}=45.88\times10^{-6}$ cm^{-1}(20.0 °C), for benzene. Depolarization was measured using the Shimadzu Model DL-10A light-scattering photometer with the cell containing the specimen the same as that used for the Rayleigh factor measurements. The isotropic part was calculated from the Cabannes factor.[2]

The determination of the specific refractive index increment was carried out at room temperature using a Shimadzu differential refractometer.

Measurement of the Number Average Molecular Weight. The number average molecular weight was determined from values of the vapor pressure which was obtained using a

Hitachi-Perkin Elmer Model 115 vapor pressure osmometer and from the NMR spectra obtained in a CCl_4 solvent system using a JEOL Model HL-60 NMR spectrometer.

Gel Permeation Chromatography. Gel permeation chromatography was carried out at 35 °C using a Waters Ana-Prep GPC with four columns (4 feet long with pore sizes of 3×10^5, 10^4, 10^3, and 10^2 nm) connected in series, tetrahydrofuran being used as the solvent.

Results and Discussion

Light Scattering Due to Fluctuations in the Fluid Density and Its Influence on Molecular Weight Determination. The total isotropic light scattering of the binary solution is expressed by

$$R_{is} = R_c + R_d + R^*, \quad (1)$$

where R_c and R_d indicate the scattering intensity due to fluctuations in the densities of solute concentrations and those of the densities of the pure solvent, respectively. R^* is the cross term. The scattering due to fluctuations in the solute concentrations, which is necessary for determining the molecular weight using the light-scattering method, is usually obtained by subtracting the scattering by a pure solvent from that by the solution. As indicated by Eq. 1, the scattering due to fluctuations in the binary solution density is not equal to that due to fluctuations in the pure solvent density. The influence of this difference causes no problem for determining molecular weights larger than 10^4. The determination of low molecular weights, such as those in the range between several tens and several hundreds, however, is considerably affected by this difference.

According to Bullough,[3] when the scattering due to fluctuations in the solution density is approximated by the scattering due to fluctuations in the density of the pure solvent, a correction of the molecular weight obtained by the light-scattering method is given approximately by

$$\Delta M \approx N_A\lambda_0^2(\tau_0\kappa_0kT/8\pi^3)^{1/2}/n_0(dn/dc), \quad (2)$$

where N_A is Avogadro's constant, λ_0 the wavelength of the incident light in vacuo, τ_0 the turbidity, κ_0 the isothermal comressibility, k Boltzmann's constant, T the absolute temperature, n_0 the refractive index of the solvent, and dn/dc the specific refractive index increment. For isotropic molecules, $\tau_0=(16/3)\pi R_{90}$. Therefore, Eq. 2 becomes

$$\Delta M \approx \{(N_A\lambda_0^2/n_0(dn/dc)\}(2R_{90}\kappa_0kT/3\pi^2)^{1/2}. \quad (3)$$

The values of ΔM obtained from measurements at $\lambda_0=436$ nm in several solvents are given in Table 1.

The contribution to the light scattering due to the density fluctuation was found to be rather large when a determination of the molecular weight of benzene was attempted in an ethyl methyl ketone (EMK) solvent using the light-scattering method. The displacement of the estimated molecular weight was up to 13% and was not negligible when the scattering due to fluctuations in the solution density was approximated by that due to fluctuations in the pure solvent density. The influence of such as approximation on estimations of the molecular weights of oligostyrenes, which are larger than 1000, in an EMK solvent using the light-scattering technique, however, was found to be negligible when compared with the experimental errors in the light-scattering measurement.

Measurement of Light Scattering of Benzene in an EMK Solvent. Since styrene polymers contain phenyl groups which are strongly optically anisotropic, it is believed that oligomers may strongly be affected by the phenyl groups and exhibit strong optical anisotropy. It is, therefore, important to correct for the degree of depolarization in the light-scattering measurements of anisotropic molecules using unpolarized incident light. In the present study, as mentioned above, two photometers were used for measurements of the light-scattering intensity and the degree of depolarization. In order to verify the method adopted in this study, a measurement of the molecular weight of benzene dissolved in an EMK solvent was carried out prior to measurements on oligostyrenes.

The equation which is well known for the calculation of molecular weights,

$$Kc/R_\theta = 1/(M_wP(\theta)) + 2A_2c + \cdots, \quad (4)$$

was used. When unpolarized incident light is used, K and $P(\theta)$ are given respectively by

$$K = 2\pi^2n_0^2(dn/dc)^2/(N_A\lambda_0^4) \quad (5)$$

and

$$P(\theta) = 1-(1/3)(4\pi/\lambda)^2R_G^2\sin^2(\theta/2) + \cdots, \quad (6)$$

where R_θ is the isotropic excess light scattering, c the solution concentration (g/cm³), M_w the weight average molecular weight of the solute, A_2 the second virial coefficient and R_G the radius of gyration. R_θ in Eq. 4

Table 1. Molecular weight corrections calculated for various solutions of low molecular-weight substances

Substance	Solvent	n_0[a]	dn/dc[a] (cm³/g)	$R_{90}\times10^6$[a] cm⁻¹	$\kappa_0\times10^{12}$ (cm²/dyne)	ΔM	M[b]	δ[c] (%)
Benzene	EMK[d]	1.388	0.154	12.0	108[e]	10.1	78.1	13
Benzene	Cyclohexane	1.436	0.100	12.5	112[g]	15.6	78.1	20
Toluene	EMK	1.388	0.150	12.0	108[e]	10.3	92.1	11
Carbon tetrachloride	EMK	1.388	0.055	12.0	108[e]	28.2	153.8	18
Oligostyrene (16a)	EMK	1.388	0.222	12.0	108[e]	7.0	600[f]	1
Oligostyrene (16a)	Benzene	1.523	0.082	45.9	95[g]	31.6	600[f]	5
Sucrose	Water	1.340	0.149	2.84	45.7[h]	3.4	342.3	1

a) Experimental conditions: 20 °C, $\lambda_0=436$ nm. b) Calculated from molecular formula. c) $\delta=(\Delta M/M)\times100$.
d) Ethyl methyl ketone. e) Ref. 8. f) Nominal molecular weight. g) Ref. 9. h) Ref. 10.

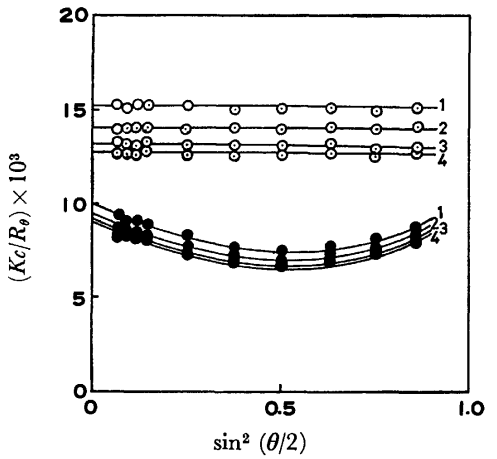

Fig. 1. Light Scattering diagram for benzene in ethyl methyl ketone.
●: Uncorrected, ○: corrected for optical anisotropy. Concentration of benzene: (1) 0.293, (2) 0.219, (3) 0.146, (4) 0.0974 (g/cm³).

was calculated, using the King equation (Eq. 8),[4] from the Rayleigh factor $(R_\theta)_u$, which was measured with unpolarized light,

$$R_\theta = (R_\theta)_u/f_u(\theta) \quad (7)$$

with

$$f_u(\theta) = [6+6\rho_u\{(1-\cos^2\theta)/(1+\cos^2\theta)\}]/(6-7\rho_u), \quad (8)$$

where ρ_u is the degree of depolarization. The scattering diagram for benzene in an EMK solvent is shown in Fig. 1. Since the benzene molecule is optically anisotropic, the curves in Fig. 1 curve downward sharply. A straight line was obtained after correction for depolarization, indicating a proper correction for depolarization. In addition to this, the value of Kc/R_θ in Eq. 4 exhibited no angle dependency and the value of $P(\theta)$ is approximately equal to 1, since the benzene molecule is considerably smaller than the wavelength of the incident light. Thus, the molecular weight of benzene can be calculated from only the 90° scattering.

TABLE 2. MOLECULAR WEIGHT OF BENZENE ESTIMATED FROM LIGHT-SCATTERING MEASUREMENTS

M_{app}	ΔM	M(expt)[a]	M(formula)[b]
88.5	10.1	78.4	78.1

a) $M(\text{expt})=M_{app}-\Delta M$. b) Calculated from molecular formula of benzene.

Since the contribution from the cross term, in Eq. 1, is rather large for the benzene molecule, the molecular weight estimated using the conventional double extrapolation method (Zimm plot) resulted in a considerable deviation from the true value. The measured values of the molecular weight of benzene are shown in Table 2. M_{app} indicates the apparent molecular weights evaluated by the conventional extrapolation method. ΔM gives the correction to the molecular weights, calculated using Eq. 3 and neglecting the cross term in Eq. 1. M is the molecular weight compensated for by the cross term. M(formula) is the molecular weight calculated from the molecular formula of benzene. The corrected molecular weights of benzene agree well with the formula weight of this compound, although Eq. 3 can only give a rough correction. The results given in Table 2, therefore, suggest that molecular weights of low molecular-weight substances may be determined with sufficient accuracy by means of the light-scattering method, if the solvent system is so chosen as to make the molecular weight correction due to the cross term as small as possible.

Light-Scattering Measurements of Oligostyrenes in an EMK Solvent. The scattering diagram of polystyrene (16a) is given in Fig. 2, showing a rather intense optical anisotropy.

The results of measurements on oligostyrene are

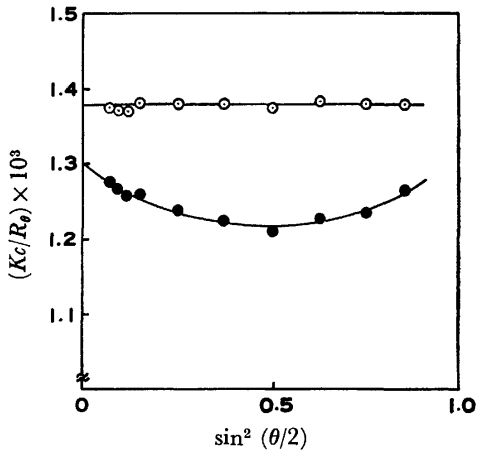

Fig. 2. Light scattering diagram for oligostyrene(16a) in ethyl methyl ketone.
●: Uncorrected, ○: corrected for optical anisotropy. Concentration of oligostyrene: 2.05×10^{-2} (g/cm³).

TABLE 3. EXPERIMENTAL RESULTS FOR OLIGOSTYRENES IN AN ETHYL METHYL KETONE SOLVENT

Oligostyrene sample[a]	dn/dc[b] (cm³/g)	ΔM	$(M_w)_{app}$	M_w	M_n	$A_2\times10^4$ (mol cm³/g²)	$f_u(90°)$	M_w/M_n Exptl	Calcd[c]	Ref[d]
16a	0.2221	7.0	702	695	580	−11	1.115	1.20	1.18	<1.10
15a	0.2257	6.9	1780	1770	1230	3.8	1.156	1.14	1.09	<1.10
12b	0.2297	6.7	2250	2240	2100	−3.3	1.178	1.07	1.05	<1.10
11b	0.2297	6.7	3790	3780	3100[d]	0.12	1.038	1.22[e]	1.03	<1.10
8b	0.2309	6.7	11000	11000	9800[d]	1.0	1.019	1.12[e]	1.01	<1.10
2b	0.2309	6.7	20800	20800	20200[d]	2.0	1.019	1.03[e]	1.005	<1.06

a) Commercial samples obtained from the Pressure Chemical Co. were used. b) Experimental conditions: 20 °C, λ_0=436 nm. c) Calculated from Eq. 10 on the assumption that living polymerization proceeded under ideal conditions. d) Pressure Chemical Co. data sheet. e) The values of M_n given on the Pressure Chemical Co. data sheet were used for the calculation of M_w/M_n.

summarized in Table 3. The factor indicating the optical anisotropy, $f_u(90°)$, was calculated with

$$f_u(90°) = [(Kc/R_{90})_u]_{c\to 0}/(Kc/R_{90})_{c\to 0} = [(R_{90})_u/R_{90}]_{c\to 0}, \quad (9)$$

where $(R_{90})_u$ is the excess light scattering observed at an angle of 90°, without correction for depolarization, and R_{90} is the isotropic excess light scattering calculated from the King equation. Values in the "exptl" column for M_w/M_n were calculated from the values obtained using the light-scattering and vapor-pressure measurements. The values under "calcd" in the table indicate the heterogeneity of the molecular weights of polymers calculated, for conditions under which living polymerization would ideally be performed, using

$$M_w/M_n = 1 + 1/P_n, \quad (10)$$

where P_n is the number average polymerization degree. When the observed, reference, and calculated values were compared with each other, the reference value for specimen 16a turned out to be markedly smaller than the calculated value. Since the calculated values were estimated assuming ideal polymerization, the heterogeneity of the molecular weights of real specimens should not be lower than this calculated value. The observed value for specimen 16a, on the other hand, was not in disagreement with the calculated value.

In addition to specimen 16a, there exist considerable discrepancies between the observed values and the reference values for specimens 15a and 11b, the discrepancy being marked for 15a. The heterogeneity of the molecular weights of this specimen is extremely high when compared with other specimens. This appears to be due to incomplete living polymerization. Since the calculated value of the heterogeneity of molecular weights is dependent upon the number average polymerization degree, it is important to accurately measure the number average molecular weight. The number average molecular weight of specimen 16a was estimated from the NMR spectrum of this compound, which is given in Fig. 3. The chemical structure of this substance was thought to contain a terminal butyl group based on its polymerization mechanism. Thus, the degree of polymerization may be estimated by taking the ratio of the H_ϕ contributed by protons in the phenyl group

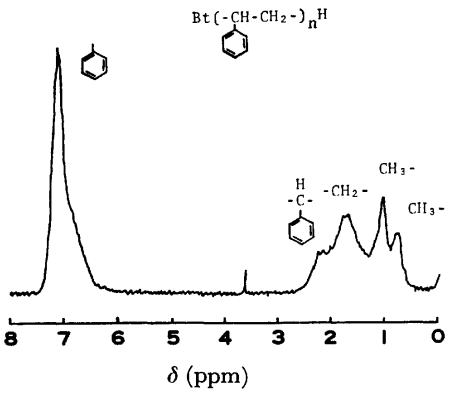

Fig. 3. NMR spectrum of oligostyrene(16a) in carbon tetrachloride.

to that, the H_b, from protons in other groups in the expression

$$H_\phi/H_b = 5P_n/(10+3P_n). \quad (11)$$

The value of H_ϕ/H_b was estimated from the areas occupied by each spectrum and then the value of P_n for oligostyrene was calculated. The P_n value was calculated to be 4.64, and the number average molecular weight estimated from the P_n was found to be 541.

The results obtained for specimen 16a are summarized in Table 4. The values of M_w/M_n were calculated using the number average polymerization degrees obtained from the number average molecular weights observed using various methods and from Eq. 10 on the assumption that living polymerization proceeded under ideal conditions. The values of M_w/M_n are in the range between 1.18 and 1.20. Therefore, the true M_w/M_n value of specimen is thought to be greater than 1.18 and is unlikely to be smaller than 1.10. Although the value of M_w/M_n obtained using the GPC method was slightly higher than those obtained from the light-scattering and VPO methods, it appears to be reasonable judging from the calculated value.

Molecular Optical Anisotropy of Oligostyrene. It is interesting to study the dependency of the molecular optical anisotropy of styrene polymers on their molecular weights because this involves a phenyl group which exhibits strong optical anisotropy. The relation between the molecular optical anisotropies, $f_u(90°)$, and the

Table 4. Molecular weights and molecular weight heterogeneities of oligostyrene (16a)

Method		M_w	M_n	M_w/M_n Exptl	M_w/M_n Calcd[a)]
LS[b)]	Present work	695	—	1.20	—
VPO[c)]		—	580	—	1.18
NMR		—	541	—	1.19
GPC		684	544	1.26	—
VPO(A)[d)]	Pressure Chemical Co. data sheet	—	524±7%	—	1.20
VPO(B)[e)]		—	585±7%	—	1.18
Rast[f)]		—	581±5%	—	1.18
Kinetic		—	550±10%	—	1.19

a) Calculated from Eq. 10 on the assumption that living polymerization proceeded under ideal conditions. b) Light scattering. c) Vapor pressure osmometry. d) Analysis performed at the Mellon Institute. Experimental conditions: benzene solvent, duplicate determinations. e) Crobaugh Laboratories, chloroform solvent, duplicate determinations. f) Camphor solvent, duplicate determinations.

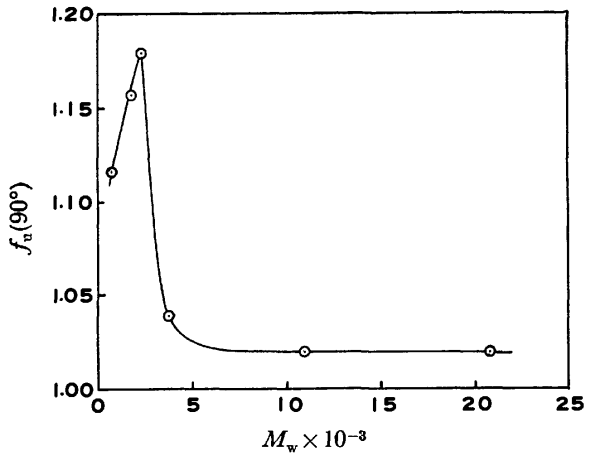

Fig. 4. Molecular weight dependence of the molecular optical anisotropy for oligostyrene in ethyl methyl ketone.

molecular weights of oligostyrenes is shown in Fig. 4. Values of $f_u(90°)$ most fluctuated in the range between molecular weights of 2000 and 3000 and became almost constant at about 10000. This tendency has been observed by Nomura and Miyahara[5] who reported the dependency of the partial specific compressibility on the molecular weight. This phenomenon has been considered to reflect the transition process of conformation of the polystyrene molecule from a rod-like rigid form to a random coil caused by internal rotation of the molecular chain.

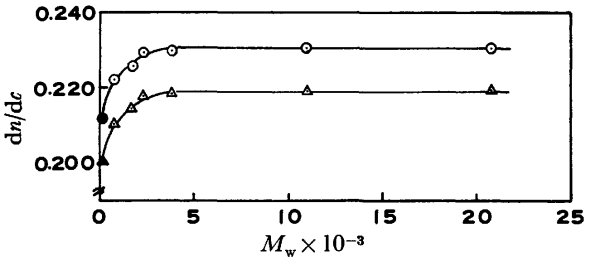

Fig. 5. Molecular weight dependence of the specific refractive index increment for oligostyrene in ethyl methyl ketone.
○: λ_0=436 nm, △: λ_0=546 nm, ●▲: data for dibenzyl.

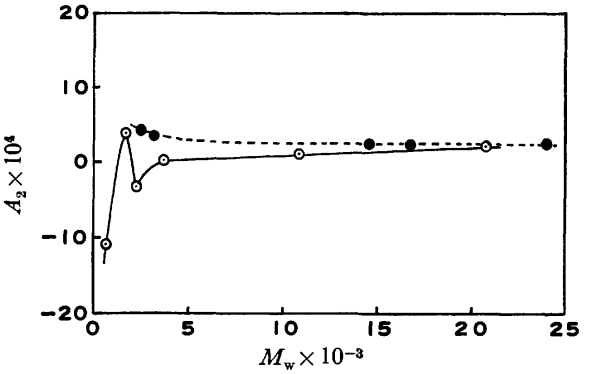

Fig. 6. Molecular weight dependence of the second virial coefficient for oligostyrene.
○: Present work, ●: Outer *et al.*[6]

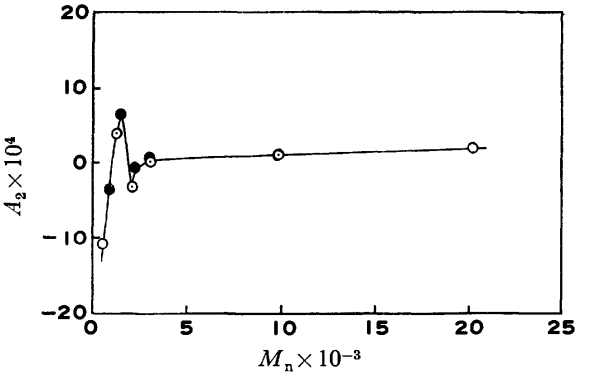

Fig. 7. Molecular weight dependence of the second virial coefficient for oligostyrene.
○: Present work, ●: Nomura and Miyahara.[5]

Dependency of the Specific Refractive Index Increment and the Second Virial Coefficient on Molecular Weight. The data given in Table 3 are plotted in Figs. 5 and 6. The values of dn/dc show considerable fluctuations for molecular weights smaller than 20000. The second virial coefficient of the oligostyrene–EMK solution changed from negative to positive and exhibited a maximum with increasing molecular weight. It has been reported by Outer *et al.*[6] that the second virial coefficient monotonically decreases with increasing molecular weight when light scattering by polystyrenes of molecular weights from 2460 to 1770000 were measured in an EMK solvent. The results obtained in the low molecular-weight range, in the present study, are thus different from their results. Sotobayashi and Ueberreiter[7] have measured the second virial coefficient by means of a cryoscopic method. Nomura and Miyahara[5] have also measured this using vapor-pressure osmometry. They obtained results similar to those reported here. Figure 7 shows the plots of the second virial coefficients against the number average molecular weights, M_n, and also compares the results obtained in the present study with those of Nomura and Miyahara.[5] Since, in the present study, the second virial coefficients were obtained from light-scattering measurements, they could not be compared with those of Nomura and Miyahara[5] because of the influence of the molecular-weight distribution. The overall tendency, however, showing a conversion from negative to positive of the value of A_2 with the molecular weight and the appearance of a maximum, agree well with their results. It has been suggested by Sotobayashi and Ueberreiter,[7] as mentioned above, that this may be due to the transition of the molecular conformation of styrene polymers from rod-like rigid molecules to random coil structures. It appears improper to discuss the nature of this phenomenon in further details, because there is no evidence to prove the homogeneity of the chemical structure of terminal groups and because the heterogeneity of the molecular weights of oligostyrenes are slightly different for each of the specimens used in the present study.

Since the properties of oligomers in solution are greatly influenced by the chemical structure of the terminal groups of the oligomer molecules, it may be necessary, first of all, to prepare specimens with

homogeneous molecular weights and with identical terminal groups in the molecules and then to measure these properties, in order to discuss them in detail over the oligomer molecular-weight range.

The authors wish to express their thanks to Dr. Sueo Nishi for his kind permission to use the vapor pressure osmometer and his helpful advice regarding its operation.

References

1) T. Kamata and H. Nakahara, *J. Colloid Interface Sci.*, **43**, 89 (1973).
2) J. Cabannes, "La Diffusion Moléculaire de la Lumière," Les Presses Universitaires de France, Paris (1929), Chap. 10.
3) R. K. Bullough, *Proc. R. Soc. London, Ser. A*, **275**, 271 (1963).
4) L. V. King, *Proc. R. Soc. London, Ser. A*, **104**, 333 (1923).
5) H. Nomura and Y. Miyahara, *Nippon Kagaku Kaishi*, **89**, 142 (1968).
6) P. Outer, C. I. Carr, and B. H. Zimm, *J. Chem. Phys.*, **18**, 830 (1950).
7) H. Sotobayashi and K. Ueberreiter, *J. Polym. Sci.*, **A 2**, 1257 (1964).
8) S. H. Maron and R. L. Lou, *J. Polym. Sci.*, **14**, 273 (1954).
9) G. A. Holder and E. Whalley, *Trans. Faraday Soc.*, **58**, 2095 (1962).
10) I. L. Fabelinskii, "Molecular Scattering of Light," Plenum Press, New York (1968), p. 563.

The Molecular Structure of Dimethyl Sulfide*

Takao IIJIMA, Shuzo TSUCHIYA, and Masao KIMURA
Department of Chemistry, Faculty of Science, Hokkaido University, Sapporo 060
(Received March 25, 1977)

The gas-phase molecular structure of dimethyl sulfide, $(CH_3)_2S$, has been investigated by means of electron diffraction. By a joint analysis of the diffraction results and the spectroscopic moments of inertia by Pierce and Hayashi, the structure parameters, the distances in r_g and the angles in φ_{a_v}, were determined (with parenthesized limits of error) to be as follows: S–C=1.807(2) Å, C–H=1.116(3) Å, ∠CSC=99.05(4)°, and ∠HCH=109.3(5)°. A tilt of 2.35° and the local C_{3v} symmetry of the methyl groups were assumed. The isotope effects of deuterium substitution were examined, and the DCD angle was found to be larger than HCH in the zero-point average structure.

The present authors have, for some time, been investigating the structures of molecules which contain one or two methyl groups. The combined use of diffraction and spectroscopic data has been successful in obtaining more accurate values of the structure parameters. By this technique, the uncertainties of the hydrogen parameters were especially reduced to ±0.003—6 Å for C–H distances and ±0.5—1.0° for the HCH angles.[1] Furthermore, it was possible in some favourable cases to obtain information on the isotope effects in structure parameters for the deuterium substitution.[2] In the present study, the structure of dimethyl sulfide was determined by applying the technique of the joint analysis.

The microwave spectra of this molecule were extensively studied by Pierce and Hayashi.[3] They measured and analyzed the spectra of several isotopic species as well as the parent species. The spectrum of the parent species was measured also by Rudolph, Dreizler, and Maier.[4] As for the diffraction study, there were the visual works by Brockway and Jenkins[5] and by Schomaker,[6] but no high-precision data have been available.[7] Therefore, the electron-diffraction data were newly obtained in the present study by the sector-microphotometer method. The moments of inertia reported by Pierce and Hayashi were used in the joint analysis.

Experimental

A sample of grade G. R. purchased from Nakarai Chemicals, Ltd., was used without further purification. The diffraction experiments were made by means of the Hokkaido University apparatus[8] at room temperature, using an r^3-sector and two nozzle-to-plate distances, 244.3 and 109.3 mm. The other experimental conditions are as follows: accelerating voltage, 42 kV; beam current, 0.1 μA; exposure times, 100—180 s; and sample pressure, 60—70 Torr (1 Torr=133.322 Pa). The scale factor for $L\lambda$ was calibrated using the diffraction patterns of CS_2 taken in the same sequence of exposures. Data obtained from three selected plates for the long and short camera distances covered the approximate s ranges of 3—17, and 7—40 $Å^{-1}$ respectively.[9]

The theoretical molecular intensities from the best-fit model and the differences (experimental minus theoretical) are shown in Fig. 1.[10] The vertical scale of the difference is four times as large as that of the molecular intensity. The narrower shaded boundaries in the difference correspond to ±2 in the last digit of the digital voltmeter used in photometry, that is the, limit of the detectable changes in the intensity. The outer boundaries, drawn in broken lines, indicate the normally expected range of the random scattering of differences. Some points are outside this boundary for accidental reasons. A least-squares refinement with zero-weights for these points showed that the effects of these extraordinary data on the final parameter-values were negligibly small.

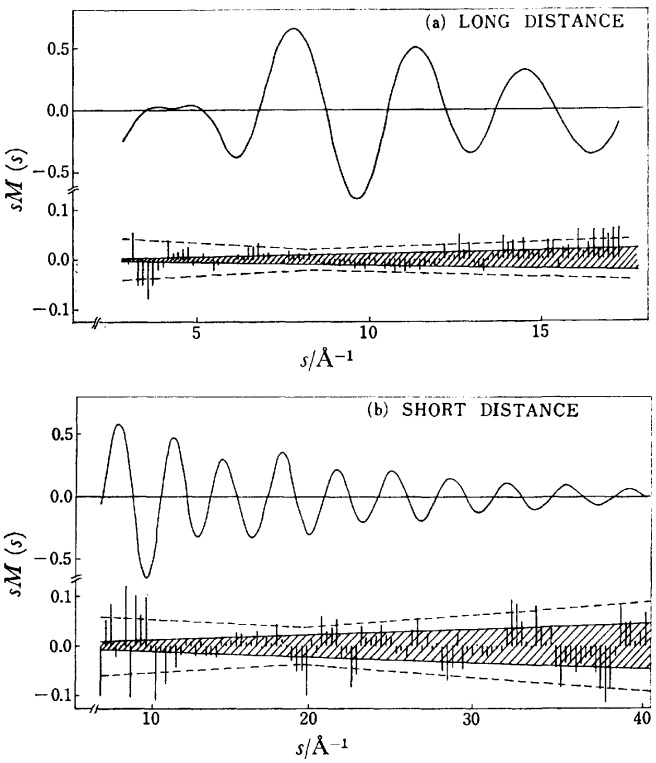

Fig. 1. Theoretical $sM(s)$ from the best-fit model and the differences (experimental minus theoretical) for the long (a) and short (b) camera distances. The vertical scale of the difference is four times as large as that of the $sM(s)$. See text.

Analysis of the Diffraction Data

The skeletal parameters, S–C, S···H, and C···C distances, were determined by the least-squares method.[9] The C–H and H···H r_a distances of the methyl group were fixed at 1.107, and 1.783 Å respectively. The local C_{3v} symmetry of the methyl

* 1 Å=100 pm is used throughout this paper.

group was assumed. The other non-bonded distances were fixed at the values calculated from the reported r_s-structure.[3] The rms amplitudes of vibration were fixed at the values calculated by Gebhardt and Cyvin.[11] The Hartree-Fock elastic scattering factors were generated by a computer program for the partial-waves method.[12] The inelastic scattering factors were taken from the literature.[13] The results of the least-squares procedure are summarized in Table 1.

Table 1. Results of the least-squares analysis of the diffraction data for dimethyl sulfide (in Å units)[a]

	S–C	S···H	C···C
Long camera distance			
r_a	1.8056	2.4098	2.7616
σ_1[b]	8	37	91
σ_2	3	37	64
ε[c]	31	101	243
Short camera distance			
r_a	1.8055	2.3943	2.7567
σ_1	10	91	201
σ_2	3	22	60
ε	33	239	524
Weighted averages			
r_a	1.805_6[d]	2.408_1	2.76_1
ε	2_2	9_3	2_2

a) Index of resolution; 0.82—0.94. b) For the definitions of σ_1 and σ_2, see Ref. 14. c) The limit of error, ε, was estimated from $2.6\sigma_1$ and the systematic error of the scale factor, 0.13% for the long, and 0.11% for the short, camera distance. d) r_g(S–C); 1.806_9 Å.

The r_a values from the data of the long and short camera distances are in good agreement with each other for all three distances. The weighted averages of them give the most probable values of the bond distances as obtained by the diffraction method. For the S–C distance, the long- and short-distance data make nearly equal contributions, while for the S···H and C···C distances, the weights of the long-distance data are much larger than those of the short-distance data.

It is noted that the S–C distance might be affected by the assumed value of the intra-methyl H···H distance, because they are very close to each other. Thus, in the final refinement the value of the H···H was changed to 1.804 Å, a value which was given from the results of the joint analysis, and the least-squares procedure was carried out again. The values of the parameters shifted within only 10% of the standard deviations.

Joint Analysis of the Diffraction Results and the Spectroscopic Moments of Inertia

More detailed structure information was obtained by a joint analysis of the diffraction data and the spectroscopic data on the moments of inertia. Since the data from both methods were combined on the r_z-basis (the zero-point average structure),[15] the vibrational effects of the moments of inertia or the vibrational corrections were calculated by using the force field reported by Gebhardt and Cyvin.[11] The barrier to the internal rotation of the methyl top of this molecule is reported to be about 2.1 kcal/mol.[3] The method of calculating the vibrational corrections for molecules with large-amplitude internal motion was applied.[16,17] The moments of inertia and the vibrational corrections are shown in Table 2.

Table 2. Moments of inertia of dimethyl sulfide (in amu Å^2 units)[a]

	$I^{(0)}$	ΔI	$I^{(z)}$
$(CH_3)_2S$			
a	28.376	0.143(0.143)	28.519
b	66.314	0.209(0.210)	66.522
c	88.387	0.101(0.101)	88.488
γ[b]	(3.262)	0.015(−0.004)	3.277
$(CD_3)SCH_3$			
a	32.646	0.151	32.797
b	76.619	0.227	76.846
c	99.731	0.112	99.843

a) $I^{(0)}$: observed effective values for the ground vibrational state, taken from Ref. 3. The numerical values are, however, slightly different from Ref. 3 because of the use of the conversion factor of 505376 Mc amu Å^2 in this work. ΔI; calculated vibrational corrections. The values in parentheses were obtained by an approximate method. See text. $I^{(z)}$: moments of inertia for the zero-point average structure. b) γ indicates the torsional coordinate of the methyl tops.

For the vibrational correction in the case of a large-amplitude torsional motion, it is necessary to calculate the n_{is} matrix as well as the l_{is} matrix.[16] The n_{is} is the derivative of the l_{is} viewed on the top-fixed axis with respect to the torsional coordinate. The requirement of calculating the n_{is} matrix makes the whole procedure tedious and complicated. If the n_{is} matrix can be neglected, though, the l_{is} matrix may easily be obtained by ordinary normal-cordinate calculations. The vibrational corrections for the parent species calculated by neglecting the n_{is} matrix were found to be good approximations for ΔI except for ΔI_γ, as is shown in the parentheses in Table 2. A similar comparison was made for propane and 2-fluoropropane. The maximum deviation of the approximate value was found to be 0.006 amu Å^2. The vibrational corrections for the CD_3SCH_3 species in Table 2 were calculated by this approximated method.

The r_g(C–S) distance by diffraction, 1.806_9 Å, was converted into r_α^0 ($\approx r_z$), $1.804_8 \pm 0.002$ Å, by the use of anharmonic stretching, 0.0003 Å, the correction for the perpendicular motion, 0.0009 Å, and centrifugal stretching, 0.0009 Å. All these corrections were calculated by the use of the force field by Gebhardt and Cyvin.[11]

As was the case in our previous papers,[1,2] the structure of the molecule including the isotope effects for the deuterium substitution was determined by using the $I^{(z)}$ values of $(CH_3)_2S$ and CD_3SCH_3 species and r_α^0(S–C) from diffraction. The value of r_α^0(S–C) and its limit of error determine the allowable region of the S–C distance. For each S–C value within this region, three

structure parameters, C–H ∠HCH, and ∠CSC, were determined from the three moments of inertia of the parent species, by assuming a local C_{3v} symmetry of the methyl top and a tilt of 2.35°.[18] The equilibrium conformation of the methyl group was determined by the microwave study[3] to be such that one of the C–H bonds lies on the CSC plane in the position trans to the S–C bond.

By using the structure parameters of the parent species, the deuterium-isotope effects were determined from the $I^{(z)}$ values of the d_3-species. The isotope effects in C–D, ∠DCD, and ∠CSC were also taken into consideration. Among them the isotope effect in C–D was estimated by assuming a Morse-type potential and using a diatomic approximation.[19] The values of ∠DCD and ∠CSC were adjusted to give a good fit for the three $I^{(z)}$ values of the d_3-species. It was found that there was no satisfactory solution for them in the r(S–C)<1.803 Å region, just outside the region allowed by the diffraction results. The moments of inertia of the ^{13}C and ^{34}S species were found to be consistent with the parameters of the parent species, in and around the region of the S–C distance examined by the present analysis. The variations of the parameters with the change in the S–C distance are shown in Fig. 2.

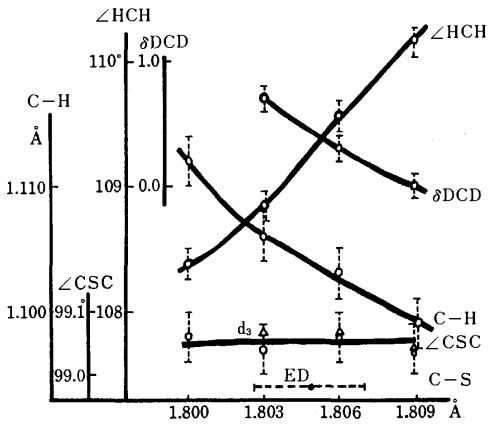

Fig. 2. Variations of structure parameters determined by moments of inertia along the change of the S–C distance. Vertical broken lines show the uncertainties due to ±0.01 amu Å² of $I^{(z)}$. Δ show the CSC angle of d_3-species. The range of S–C allowed by the diffraction result is indicated as ED. No solution was found for ∠DCDh and ∠CSC (d_3) in the region of S–C<1.803.

Table 3. Zero-point average structure of dimethyl sulfide[a]

	r_{av}, ϕ_{av}	ε_1	ε_2	ε_3	ε_4	ε_0
S–C	1.805	0.002	—	—	—	0.002
C–H	1.104	0.002	0.002	—	—	0.003
∠CSC	99.05	0.01	0.04	—	—	0.04
∠HCH	109.30	0.48	0.12	—	0.03	0.50
δ(CSC)[b]	0.01	0.02	0.03	0.01	—	0.04
δ(DCD)[b]	0.40	0.20	0.10	0.08	—	0.25

r_g; S–C 1.807, C–H 1.116

a) The distances are in Å, and the angles, in degree units. ε_1 through ε_4 are uncertainties from various origins, and ε_0 is the estimate of the total uncertainty. See text. b) δ(CSC)=∠CSC(in d_3)−∠CSC(h_6); δ(DCD)=∠DCD−∠HCH.

The structure parameters obtained by the analysis are summarized in Table 3. Uncertainties from various origins were estimated and are also listed in the table. They are: ε_1, from the half-width of the variation of the parameter values in the allowed region; ε_2, from the uncertainties of $I^{(z)}$, assumed to be ±0.01 amu Å²; ε_3, from the uncertainty of the estimated isotope effect in C–D ±0.0015 Å, and ε_4, from the uncertainty in the tilt, ±0.37°.[20] The total estimates of the uncertainty are shown as ε_0, obtained by means of the square-root of the sum of the squares of ε_1 through ε_4.

Discussion

The bond-angles in the zero-point average structure shown in Table 3 are close to the values of the r_s-structure reported by Pierce and Hayashi, while the r_z distances are longer than r_s.[21] The final structure in Table 3 leads to the r_a values of 2.418, 2.748, and 1.804 Å for S···H, C···C, and H···H respectively, neglecting the anharmonicity in bond-angles. The S···H and C···C distances are judged to be consistent with the diffraction results in Table 1. The HCH angle, 109.3(5)°, of this molecule is in the range, 107.9—110.8°, of the HCH angles of acetyl halides,[1] acetone,[2] acetaldehyde,[16] propane,[22] and 2-chloropropane,[23] which were determined by the technique of joint analysis. The C–H distance, 1.116 Å, in r_g is, however, longer than the C–H distances of these molecules, 1.101—1.109 Å. This may be an effect of the neighbouring hetero-atom sulfur, used in place of carbon, on the structure of the methyl group.

A positive isotope effect in the DCD angle (the effect giving a ∠DCD larger than ∠HCH) is similar to that found in acetone and several other molecules. As was discussed in a previous paper on acetone,[2] it may be attributed to the repulsive interaction between the two methyl tops. It is interesting to note that the nearest H···H distance between the two tops is 2.82 Å in acetone and 2.76 Å in dimethyl sulfide. The skeletal bond-distances are very different in the two molecules, but the smaller CSC angle of dimethyl sulfide compensates for the longer S–C distance, and the H···H distance becomes almost the same. Therefore, the effect of the H···H interaction, if any, may be expected to exist to a similar extent.

In the case of acetone, the isotope effect in the CCC angle was found to be 17′(2); that is, the angle for the d_6-species is less than that for the h_6-species. For dimethyl sulfide, however, the isotope effect in the CSC angle of the d_3-species is essentially zero. According to the idea that the isotope effect in the CSC angle is due to the anharmonicity of the symmetric rocking mode of the two methyl groups,[2] the effect in the d_3-species may be roughly estimated to be about one third of what would be observed for the d_6-species. The present result for the d_3-species does not necessarily exclude the possibility of the existence of the isotope effect in the d_6-species of an amount similar to that of acetone. Unfortunately, the spectroscopic data of the d_6-species

are not available.

The authors wish to thank Miss Kumiko Ohtaki for her help in an early stage of this work. The numerical computation was performed on a FACOM 230-75 of the Hokkaido University Computing Center, and also on a FACOM 270-20 in the laboratory of Professor Kimio Ohno, to whom the authors' thanks are due.

References

1) *E.g.*, S. Tsuchiya, *J. Mol. Struct.*, **22**, 77 (1974).
2) T. Iijima, *Bull. Chem. Soc. Jpn.*, **45**, 3526 (1972).
3) L. Pierce and M. Hayashi, *J. Chem. Phys.*, **35**, 479 (1961).
4) H. D. Rudolph, H. Dreizler, and W. Maier, *Z. Naturforsch.*, **15a**, 742 (1960).
5) L. O. Brockway and H. O. Jenkins, *J. Am. Chem. Soc.*, **58**, 2036 (1936).
6) V. Schomaker, quoted in P. W. Allen and L. E. Sutton, *Acta Crystallogr.*, **3**, 46 (1950).
7) Professor I. Hargittai has recently investigated this molecule by means of gas electron-diffraction. (private communication).
8) Y. Murata, K. Kuchitsu, and M. Kimura, *Jpn. J. Appl. Phys.*, **9**, 591 (1970).
9) S. Konaka and M. Kimura, *Bull. Chem. Soc. Jpn.*, **43**, 1693 (1970).
10) The numerical experimental data on the leveled total intensity, the background, and the correlation matrix have been deposited with the Chemical Society of Japan (Document No. 7717).
11) O. Gebhardt and S. J. Cyvin, *J. Mol. Struct.*, **12**, 205 (1972).
12) M. Kimura, S. Konaka, and M. Ogasawara, *J. Chem. Phys.*, **46**, 2599 (1967).
13) C. Tavard ,D. Nicolas, and M. Rouault, *J. Chim. Phys.*, **64**, 540 (1967).
14) Y. Morino, K. Kuchitsu, and Y. Murata, *Acta Crystallogr.*, **18**, 549 (1965).
15) For the definitions of the various representations of structure parameters, see, *e.g.*, K. Kuchitsu and S. J. Cyvin, "Molecular Structures and Vibrations," ed by S. J. Cyvin, Elsevier, Amsterdam (1972), Chap. 12.
16) T. Iijima and S. Tsuchiya, *J. Mol. Spectrosc.*, **44**, 88 (1972).
17) Equation 33 of Ref. 16 contains an error. It should read

$$I_{\alpha T} = \Sigma_i m_i\{\lambda_\alpha \boldsymbol{\sigma}_i^2 - (\boldsymbol{\sigma}_i)_\alpha(\lambda\cdot\boldsymbol{\sigma}_i)\} + \Sigma_i(l_{is}\times n_{is})_\alpha Q_s^2 - (\lambda\times L_{R's})_\alpha Q_s.$$

The same applies to Eq. 8 of Ref. 2.
18) The tilt angle is determined from ∠CSC and the angle between the two top-axes, 2θ. The value of 2θ was determined to be 103.77 ° by the analysis of the torsional splittings.[3] In the present analysis, the variation in the ∠CSC within the allowed region was so small that the tilt was fixed at 2.35°.
19) K. Kuchitsu, *J. Chem. Phys.*, **49**, 4456 (1968).
20) One and a half of the reported uncertainty in 2θ in Ref. 3, namely, three times as much as that of the tilt. Note that the uncertainty in ∠CSC is much smaller.
21) r_s-structure: S–C 1.802(2) Å, C–H 1.091(5) Å, ∠CSC 98.9(2)°, and ∠HCH 109.6(3)°. Ref. 3.
22) T. Iijima, *Bull. Chem. Soc. Jpn.*, **45**, 1291 (1972).
23) T. Iijima, S. Seki, and M. Kimura, *Bull. Chem. Soc. Jpn.*, **50**, 2568 (1977).

Molecular Structure of 2-Chloropropane, as Determined by a Combined Use of the Electron Diffraction Data and the Spectroscopic Moments of Inertia*

Takao IIJIMA, Schigenori SEKI, and Masao KIMURA**

Department of Chemistry, Faculty of Science, Hokkaido University, Sapporo 060

(Received March 25, 1977)

The gas-phase molecular structure of 2-chloropropane, $(CH_3)_2CHCl$, has been investigated by means of electron diffraction and by a joint analysis of the diffraction results and the spectroscopic moments of inertia. The structure parameters, distances in r_g and angles in φ_{av}, were determined (with parenthesized limits of error) to be as follows; C–Cl 1.812(1) Å, C–C 1.527(1) Å, C···Cl 2.720(2) Å, C–H 1.104(4) Å, ∠CCC 112.7(4)° and ∠HCH 108.5(8)°. The CCH_{sec} angle was assumed to be 109.8(20)°. The present results, together with the data for other molecules, confirmed a systematic elongation of the C–Cl r_g-distance in the series of methyl, ethyl, isopropyl, and *t*-butyl chlorides.

The systematic elongation of the C–Cl distances in the series of chloroalkanes (*viz.*, methyl, ethyl, isopropyl, and *t*-butyl chlorides) was first pointed out by Lide and Jen.[1] In the corresponding series of fluorides, a similar trend has also been observed.[2,3] These notable appearances of the environment effect on structure parameters are worth careful investigation, perhaps next after the environment effect on carbon-carbon bonds.[4]

For the series of chlorides mentioned above, the r_s-structures were determined by means of microwave spectroscopy. For *t*-butyl chloride, Hilderbrandt and Wieser obtained the r_z- and r_g-structure by an electron-diffraction investigation and a joint analysis of both the diffraction data and the spectroscopic moments of inertia.[5,6] For the other three molecules of the series, there has so far been no high-precision study by gas-electron diffraction. The present paper will report the structure determination of isopropyl chloride, or 2-chloropropane, by means of a joint analysis of the diffraction data and the spectroscopic moments of inertia. A similar study for the structures of ethyl chloride and methyl chloride will be reported in succeeding papers.[7,8]

A brief comment must be added to clarify why we are not content with the r_s-structures which are already available. The r_s-structure is the only existing structural information which can be obtained by making the optimal use of the experimental values of the ground-state rotational constants, without any knowledge of the molecular force field. It is widely accepted that the r_s-structure is useful, not only qualitatively, but, to a considerable extent, quantitatively as well.

In some favorable cases, the r_s-structure can be a good estimate of the r_e-structure. Watson[10] showed that the $I_s=(1/2)(I_e+I_0)$ relation holds for linear, planar, and symmetric top molecules. It is, then, possible to derive the r_e-structure from the r_s-structure and the observed ground-state rotational constants. The relation is theoretically approximate, but it is sufficiently good for molecules which do not contain light atoms, *e.g.*, hydrogen. For the molecules which contain hydrogen atoms, it seems that much is still left to be investigated about the physical nature of the r_s-structure.

In several recent determinations of accurate r_g-distances which were obtained by the combined use of spectroscopic and diffraction information, it was found, contrary to one's expectation, that the differences between r_g and r_s are not necessarily the same for similar bonded distances in different molecules.[11] The C–C distance of *t*-butyl chloride is one such case, the r_g-value being smaller than the r_s-value. This suggests that the r_s-structure (r_0-structure, too) may not be suitable for critical comparison and quantitative discussion of structural parameters.

Table 1. The r_s- and r_g-distances of C–Cl and C–C bonds in the series of chlorides (in Å units)[a]

		C–Cl	C–C	Reference
CH_3Cl	r_s	1.781(1)	—	12
	r_g	1.783(2)	—	8
CH_3CH_2Cl	r_s	1.788(2)	1.520(3)	13
	r_g	1.797(3)	1.526(4)	7
$(CH_3)_2CHCl$	r_s	1.798 (+8, −4)	1.520 (+4, −6)	14, 15
	r_g	1.812(1)	1.527(1)	b)
$(CH_3)_3CCl$	r_s	1.803(2)	1.530(2)	1
	r_g	1.830(5)	1.528(3)	5

a) The uncertainties to be attached to the last significant digit are shown in the parentheses. b) This work.

In the series of chlorides shown in Table 1, the documented r_s-values of C–Cl distances can not clearly establish the longer C–Cl of *t*-butyl chloride as compared with that of isopropyl chloride, if the quoted uncertainties are taken into consideration. In the present study, the uncertainties have been reduced by the use of joint analysis, and the difference in C–Cl distances has been clarified in terms of the r_g-structure, as is summarized in Table 1. The C–C r_g distances are nearly constant in this series of molecules, contrary to the difference observed in the r_s-structure.

Experimental

A guaranteed reagent of the Tokyo Kasei Co., Ltd., was used without further purification. The diffraction photographs were taken at room temperature on a unit with an

* 1Å=100 pm is used throughout this paper.

** To whom correspondence should be addressed.

r^3-sector,[16] under the following conditions: camera length, 109.3 mm; accelerating voltage, 40 kV; beam current, 0.2 μA; exposure time, 1 min; and sample pressure, 60 Torr (1 Torr= 133.322 Pa). The total range of s covered was from 7 to 38 Å^{-1}.

Five sets of plates were taken during a week, each set containing six plates obtained in a sequence of exposures. The first set, like the last, was of the diffraction patterns of carbon disulfide, by which the scale factor was calibrated. The scale factors yielded by the two sets of carbon disulfide patterns agreed with each other within 0.1%. The relative stability of the accelerating voltage was monitored by a digital voltmeter and found to be within 0.05% during the term of a week. The nozzle setting was kept untouched so that the camera length was kept constant. Six plates of 2-chloropropane were selected from eighteen plates and analyzed by the least-squares method.

Analysis of the Diffraction Data

The procedure used to analyze the diffraction data of this molecule was much like that for 2-fluoropropane previously reported.[3] Four distances, C–C, C–Cl, C–H, and C···Cl, were adjusted by the least-squares method for molecular intensity. The remaining eighteen distances were fixed initially at the r_s-values by Tobiason and Schwendeman[14] and finally at values consistent with the converged values of the four adjusted distances, the r_s-values being still used for the parameters which could not be deduced from the four converged values. All the mean amplitudes were fixed at the values calculated by Cyvin and Cyvin.[17] The other details followed the routine procedure described in Ref. 18. The results of the least-squares adjustment are listed in Table 2.

Table 2. Results of the least-squares analysis of the diffraction data for 2-chloropropane[a]
(in Å units)

	C–C	C–Cl	C–H	C···Cl
r_a	1.523_1	1.807_6	1.098_5	2.715_2
σ_1[b]	0.001_6	0.001_6	0.002_9	0.001_9
σ_2	0.001_3	0.000_7	0.001_6	0.000_8
ε[c]	0.004_3	0.004_4	0.007_3	0.005_4
r_g	1.525	1.809	1.104	2.717

a) Index of resolution: 0.95—1.00 b) For the definitions of σ_1 and σ_2, see Ref. 19. c) Limits of error estimated from $2.5\sigma_1$ and the systematic error originating in the uncertainty of the scale factor.

The best-fit calculated molecular intensity and the residuals of the observed are shown in Fig. 1.[20] The residuals are shown in an enlarged scale, four times as great as that of $sM(s)$ curve. The narrower boundaries with shading correspond to ±2 of the last digit of the digital voltmeter, that is, the limits of detection in the photometry. The outer boundaries (shown by the broken lines) are the estimated limits of error in the intensity measurement; they indicate the normally expected range of scattering in the intensity data. Some of the points exceeded the boundary, more or less for accidental reasons. These points were zero-weighted in the final refinement and are shown by vertical broken lines in Fig. 1. The shifts of the converged values of the parameters caused by the use of the modified weight were within the standard deviations, which were reduced to about two thirds of the standard deviations in the unmodified case.

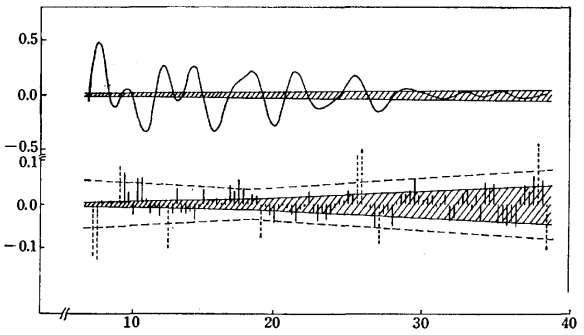

Fig. 1. The best-fit theoretical molecular intensity and the residuals of 2-chloropropane. See text.

Joint Analysis

The effective moments of inertia, as determined by Tobiason and Schwendeman,[14] were corrected for the vibrational effect and converted into $I^{(z)}$, the moments of inertia for the zero-point average structure.[4] The corrections were calculated by the use of the force constants obtained by Cyvin and Cyvin.[17] Since the barrier to the methyl torsion has been reported to be greater than 3.45 kcal/mol,[14] the torsional motions were treated as small amplitude vibrations. The r_g distances of the C–C, C–Cl, and C···Cl atom-pairs determined by electron diffraction were converted into r_α^0 distances[21] by correcting for the anharmonic term, the centrifugal stretching, and the perpendicular vibration. The Morse parameter, a_3, was assumed to be 2.0 Å^{-1} for C–C and C–Cl distances and zero for the non-bonded C···Cl distance. The numerical values of these vibrational corrections are summarized in Table 3.

Table 3. Moments of inertia, vibrational correction, and r_α^0-distances of 2-chloropropane[a]

	$I^{(eff)}$ [b]	ΔI[c]	$I^{(z)}$ (in amu Å^2)
a	62.639	0.073	62.712
b	110.566	0.084	110.650
c	157.557	0.063	157.620
	$r_g-r_\alpha^0$		r_α^0 [d] (in Å)
C–C	0.0030		1.522_1
C–Cl	0.0034		1.805_8
C···Cl	0.0021		2.715_1

a) Similar tables for isotopic species are omitted. b) Calculated from the rotational constants[14] by means of the conversion factor of 505376 Mc amu Å^2. c) Vibrational correction for $I^{(eff)}$. $I^{(z)}=I^{(eff)}+\Delta I$. d) See Ref. 6 for the definition.

The uncertainty of $I^{(z)}$ was assumed to be 0.01 amu Å^2, while that of r_α^0 was taken to be equivalent to the limits of error of the r_a values. The zero-point average

structure (r_{av}-structure)[21] was determined by a joint analysis of the r_α^0 by diffraction and of $I^{(z)}$ by spectroscopy. $(CH_3)_2CH^{35}Cl$, -^{37}Cl, -$D^{35}Cl$, and $(CH_3)(CD_3)$-$CD^{35}Cl$ (the C's are all ^{12}C) were selected for the structure analysis in the present work.

It has been our experience that the moments of inertia of the isotopic species of such heavy atoms as ^{13}C and ^{37}Cl can not give additional information independent of that of the parent species. This comes about for two reasons. First, the range of parameters which can account for the $I^{(z)}$ of both the parent species and the isotopic species is usually rather wide. Thus, the use of $I^{(z)}$ for the isotopic species is of no help in reducing the range of parameters already limited by the results of electron diffraction, if the uncertainties of $I^{(z)}$, which are of the order of 0.01 amu Å^2, are taken into consideration. Secondly, the border between the acceptable region and the unacceptable region of the parameters is very vulnerable to the estimated isotope effects in structure parameters and to the amount of the uncertainty of $I^{(z)}$, for which no quantitative method of estimation has been established.[22]

The deuterated species, on the other hand, can provide independent information. In this case, however, the isotope effect on the structure parameters becomes important. For the bonded distances, the isotope effect may be estimated fairly well by assuming a Morse-type anharmonic potential and using a diatomic approximation.[23] For the bond angles, usually almost nothing is known about the anharmonicity.

It seems to be a sound approach to the problem to let the isotope effects in the bond angles be adjustable and to determine the values from the $I^{(z)}$ of the deuterated species, as has already been attempted in some of the previous studies.[24–26] Fortunately, the deuterated species are very effective in reducing the allowed range of parameters, even if additional freedom is introduced by adjustable isotope effects. Moreover, the discrepancy between the calculated and observed values of $I^{(z)}$ develops markedly with small changes in the parameters, so that the final conclusion for the structure is not sensitive to the estimated amount of the uncertainty in $I^{(z)}$.

Therefore, in the present study, the structure parameters were first determined chiefly by the use of the $I^{(z)}$ of the parent species. The $I^{(z)}$ of the ^{37}Cl species were calculated by the same parameter values only in order to confirm that they were consistent with the observed values. The allowable ranges of the parameters are naturally very wide at this stage, covering an area bounded only by the limits of error in the results of electron diffraction. They were then reduced by the use of the deuterated species. The isotope effects in $\angle ClCD_s$, $\angle DCD$ in the methyl tops and $\angle CCC$ in the D-4 species were adjusted, while the isotope effect in the C–H bond was assumed to be the value calculated by the diatomic approximation, with an estimated uncertainty of ± 0.0015 Å.[27]

The local C_{3v} symmetry was assumed for the methyl tops. The tilting angle was assumed to be zero. The methyl C–H distance and the secondary C–H distance were assumed to be equivalent in their r_g values. Therefore, their difference in r_{av}-structure was fixed at the calculated value, 0.007_5 Å. A pertinent piece of information from the microwave study is that one of the methyl C–H bonds lies on the CCC plane in the trans position to the C–C bond.[14] There are still seven independent structure parameters left, —— C–C, C–Cl, C···Cl, $\angle CCC$, C–H, and $\angle HCH$ in the methyl top and $\angle CCH_s$. For the C–C, C–Cl, and C···Cl distances, the most probable values and the uncertainties by which the parameters may vary have been determined by electron diffraction. Therefore, three more parameters can be determined by the three moments of inertia of the parent species. By considering that the $I^{(z)}$ values are least sensitive to a change in $\angle CCH_s$, it was assumed at the value in the r_s-structure, 109.8°, with an estimated uncertainty of $\pm 2°$.

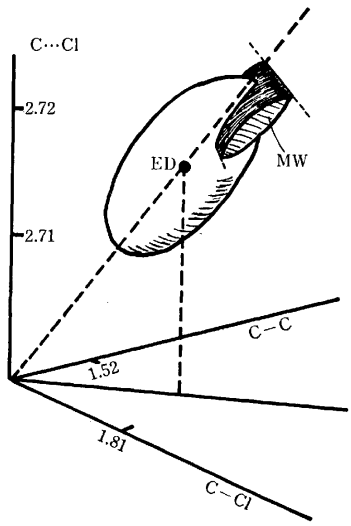

Fig. 2. The allowable range of structure parameters shown in the three-dimensional parameter space. The limits of error of electron diffraction is shown by a boundary like a rugby ball. The region compatible with spectroscopic moments of inertia is shown by the shaded portion of the space, which extends to both sides more than depicted.

The range of parameters compatible with the $I^{(z)}$ of the deuterated species as well as the parent species is shown schematically in Fig. 2; it is denoted as MW, with shading. The most probable values can be determined by the portion of the MW region which is inside the error boundary of electron diffraction. Figure 3 shows the section of Fig. 2 by means of a plane defined by the C···Cl axis and a straight line connecting the origin and the ED point. In the sections parallel to that shown in Fig. 3, the situation is more or less similar.

The results obtained are summarized in Table 4. Uncertainties originating from the several different factors are also shown: ε_1, the half-width of the variation in the parameter value corresponding to the allowed region; ε_2, the uncertainty originating in the uncertainty of $I^{(z)}$, ± 0.01 amu Å^2, although the correlations among the parameters are not shown; ε_3, the uncertainty due to the assumed $\angle CCH_s$, $\pm 2°$; and ε_4, that due to the

TABLE 4. ZERO-POINT AVERAGE STRUCTURE OF 2-CHLOROPROPANE[a]
(in Å and degrees units)

	r_{av}, ϕ_{av}	ε_1	ε_2	ε_3	ε_4	ε_0
C–Cl	1.808_4	0.001	—	—	—	0.001
C–C	1.524_2	0.001	—	—	—	0.001
C···Cl	2.718_2	0.002	—	—	—	0.002
(∠CCCl	109.00)					
∠CCC	112.7_1	0.20	0.09	0.27	—	0.4
$C–H_{Me}$	1.093[b]	0.002	0.001	0.003	—	0.004
∠HCH	108.4_7[b]	0.55	0.12	0.57	—	0.8
$\delta(CCD_{sec})$[c]	0.24[d]	0.03	0.1	—	—	0.1
δ(DCD)	0.26	0.17	0.1	—	0.07	0.2
δ(CCC)	0.0	0.0	0.03	—	0.01	0.03

r_g: C–Cl 1.812, C–C 1.527, C···Cl 2.720, C–H 1.104 Å.

a) ε_1 through ε_4 are uncertainties from various sources. ε_0 is the total estimate of uncertainty. See text.
b) The effect of methyl torsion is eliminated by adding 0.010 Å to C–H and 0.17° to ∠HCH. See text.
c) $\delta(CCD_{sec})$, $\angle CCD_{sec}-\angle CCH_{sec}$; δ(DCD), ∠DCD−∠HCH; δ(CCC), $\angle CCC(D_1)-\angle CCC(H)$.
d) This amount is equivalent to −0.5° in $\delta(ClCD_{sec})$.

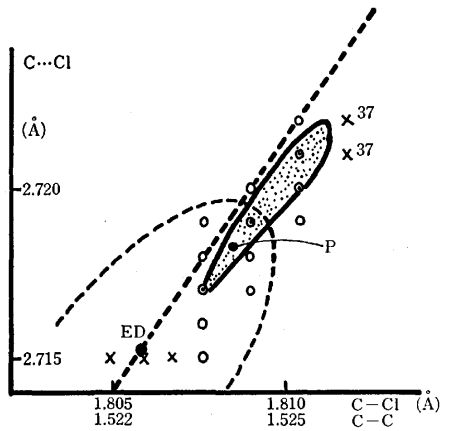

Fig. 3. A section of Fig. 2. See text.
× ; Points not compatible with $I^{(z)}$ of the D_s-species.
$\times^{37}$; Points not compatible with $I^{(z)}$ of ^{37}Cl species.
○ ; Points compatible with $I^{(z)}$ of D_s-species, but not with those of D-4 species.
⊙ and the area shown with dots; Points compatible with $I^{(z)}$ of D_s and D-4 species as well as those of the parent species.

uncertainty of the assumed isotope effect in the C–H(D) distance, ±0.0015 Å. The total estimates of uncertainty are then shown in the last column as ε_0.

The parameters of the structure of methyl tops, C–H and HCH, apparently decrease upon averaging over the torsional motion. For comparative purposes, however, it is desirable to get structure parameters which correspond to that of the large-amplitude treatment,[24] or a structure in which the average over the torsional motion is excluded. In the values listed in Table 4, the averaging effect of the torsional motion is eliminated by adding 0.010 Å to the determined C–H distance and 0.17° to the HCH angle. Thes corrections were evaluated from the differences between the present results and those of the large-amplitude treatment.[28] They were also in good agreement with the estimates by a simple model-calculation that the apparent shrinking of the C–H distance is due only to the perpendicular amplitude of the torsional mode and that the decrease in the HCH angle is caused by a slight bending of the shrunken C–H bonds, so that all the hydrogen atoms may lie on the same plane as that in the torsional-equilibrium configuration.

Discussion

The skeletal structure has already been discussed in the introductory part, where it was compared with the structures of other normal alkyl chlorides. The structure of the methyl top of this molecule is much like that of acetone, including a positive isotope effect in the DCD angle, which was interpreted as being due to the repulsive interaction between two methyl tops.[29] The isotope effect in the CCC angle was −0.3° in D-6 acetone, while it is zero in the present case. This is not in perfect conformity with the picture of the repulsive interaction, although the amount of δ(CCC) is expected to be smaller in the present species, for which only one of the two methyl tops is deuterated.

The positive isotope effect in $\angle CCD_s$, obtained as 0.24°, corresponds to a negative one in the $ClCD_s$ angle, −0.5°. This may be manifestation of the anharmonicity due to a repulsive interaction between the chlorine and the secondary hydrogen.

In the present study, the anharmonicity in non-bonded C···Cl was neglected in obtaining r_a^o from r_g. If the Morse-type parameter, a_3, had a non-zero value, the ellipse shown in Fig. 3 by the broken curve would be shifted parallel to the C···Cl axis downwards or upwards, according to whether it has a positive value or a negative one. The overlapping area and, therefore, the structure parameters would be almost the same for a negative value within 0—2 $Å^{-1}$. However, for a positive a_3, the overlapping area would decrease rapidly, and the consistency between the diffraction results and the spectroscopic moments of inertia would diminish. A possibility of a non-bonded anharmonicity which could be expressed by a Morse-type potential with a negative a_3 value has also been found in recent studies of $CHCl_3$[30] and $CHBr_3$[31] molecules.

Table 5. Comparison between r_s and r_{av} structure of 2-chloropropane[a] (in Å and degrees units)

	I	II	III
C–Cl	1.797	1.797—1.807	1.808
C–C	1.520	1.505—1.523	1.524
$C–H_{Me}$	1.092 1.099[b]	1.091—1.099	1.093
$C–H_s$	1.091	1.091—1.117	1.093
CCCl	109.5		109.0
CCC	112.8	112.5—114.6	112.7
$HCH(\alpha\beta,\beta\gamma)$	109.1	108.9—109.2	108.5
$HCH(\alpha,\gamma)$	108.3		108.5
CCH_β	110.0	110.0—111.9	110.4
H_sCCl	105.2	103.5—105.4	106.1
CCH_s	109.8		(109.8)[c]

a) I: the complete r_s-structure; Ref. 14. II: the range of variation in the r_s-structure; Ref. 15. III: the r_{av}-structure of the present study. b) According to Ref. 15. c) Assumed.

Tobiason and Schwendeman determined the complete r_s-structure for this molecule by the use of the species isotopically substituted for all non-equivalent atoms.[14] It is compared in Table 5 with the r_{av}-structure determined in the present study. There also are shown the ranges in the variation of the r_s-values reported by Schwendeman.[15] These variations are what would be caused by different analytical methods as well as by an insufficient number of isotopic species. It may be noted that the complete r_s-structure is in fair agreement with the r_{av}-structure except for the C–Cl distance, and that the maximum deviation of an incomplete r_s-value from the r_{av}-value may be about 2° in bond-angles. It seems, then, appropriate to assume an uncertainty of $\pm 2°$ when some bond angle in the r_s-structure are used as complementary information in determining the r_{av}-structure.

The numerical computations were performed on a FACOM 230-75 of the Hokkaido University Computing Center and on a FACOM 270-20 in the laboratory of Prefessor Kimio Ohno, to whom the authors' thanks are due.

References

1) D. R. Lide, Jr. and M. Jen, *J. Chem. Phys.*, **38**, 1504 (1963).
2) L. Nygaard, *Spectrochim. Acta*, **22**, 1261 (1966).
3) H. Kakubari, T. Iijima, and M. Kimura, *Bull. Chem. Soc. Jpn.*, **48**, 1984 (1975).
4) K. Kuchitsu, "MTP International Review of Science, Physical Chemistry Series One," Vol. 2, ed by G. Allen, Medical and Technical Publishing Co., Ltd., Oxford (1972), Chap. 6.
5) R. L. Hilderbrandt and J. D. Wieser, *J. Chem. Phys.*, **55**, 4648 (1971); *ibid.*, **56**, 1143(1972).
6) For the definitions of r_s, r_g, r_α, r_z, r_{av}, see K. Kuchitsu and S. J. Cyvin, "Molecular Structures and Vibrations," ed by S. J. Cyvin, Elsevier, Amsterdam (1972), Chap. 12.
7) M. Hirota and M. Kimura, to be published.
8) H. Kunimi and M. Kimura, to be published.
9) C. C. Costain, *J. Chem. Phys.*, **29**, 864 (1058).
10) J. K. G. Watson, *J. Mol. Spectrosc.*, **48**, 479 (1973).
11) K. Kuchitsu, "Critical Evaluation of Chemical and Physical Structure Information," ed by D. R. Lide, Jr., and M. A. Paul, National Academy of Sciences (1974), p. 135.
12) R. H. Schwendeman and J. D. Kelly, *J. Chem. Phys.*, **42**, 1132 (1965).
13) R. H. Schwendeman and G. D. Jacobs, *J. Chem. Phys.*, **36**, 1245 (1962).
14) F. L. Tobiason and R. H. Schwendeman, *J. Chem. Phys.*, **40**, 1014 (1964).
15) R. H. Schwendeman, Ref. 11, p. 94.
16) Y. Murata, K. Kuchitsu, and M. Kimura, *Jpn. J. Appl. Phys.*, **9**, 591 (1970).
17) B. N. Cyvin and S. J. Cyvin, *Acta Chem. Scand.*, **36**, 3943 (1972).
18) S. Konaka and M. Kimura, *Bull. Chem. Soc. Jpn.*, **43**, 1693 (1970).
19) Y. Morino, K. Kuchitsu, and Y. Murata, *Acta Crystallogr.*, **18**, 549 (1965).
20) The numerical data of the total intensity and the background, together with the elements of the correlation matrix, are deposited with the Chemical Society of Japan (Document No. 7718).
21) For the definitions of r_α^0 and r_{av}, see Ref. 6.
22) The major terms of the vibrational correction to the rotational constants are of the $1/\omega$ type, where ω is the frequency of normal vibrations.[24] The discrepancy between the true ω and the value calculated by the use of an available set of force constants may be estimated to be less than 10% of ω. In the present study, the uncertainty of the correction was, then, estimated to be about 10% of the amount of the correction itself, rounded out to the order of 0.01 amu Å^2.
23) K. Kuchitsu, *J. Chem. Phys.*, **49**, 4456 (1968).
24) T. Iijima and S. Tsuchiya, *J. Mol. Spectrosc.*, **44**, 88 (1972).
25) T. Iijima, *Bull. Chem. Soc. Jpn.*, **45**, 3526 (1972).
26) S. Tsuchiya, *J. Mol. Struct.*, **22**, 77 (1974).
27) Estimated from an uncertainty of ± 0.5 Å^{-1} in a_3.
28) In the present study, the vibrational correction was also calculated by the large-amplitude treatment. Then the process of eliminating the effect of the torsional motion might seem to be meaningless. However, it is intended that the step discussed here shall be applied to other molecules for which the torsional barrier is high, and the analysis may be performed solely by the small-amplitude treatment. The values of the vibrational correction for the parent species in the large-amplitude treatment are: ΔI_a 0.161, ΔI_b 0.213, and ΔI_c 0.149 amu Å^2.
29) The methyl structure of acetone: r_{av}(C–H) 1.091(3) Å, ϕ_{av}(HCH) 108.5(5)°, and δ(DCD) 0.17(20)°. See Ref. 25.
30) H. Kunimi and M. Kimura, to be published.
31) K. Tamagawa and M. Kimura, to be published.

Crystal and Molecular Structure of 3-(Adenin-9-yl)propiontryptamide

Minoru OHKI, Akio TAKENAKA, Hirotaka SHIMANOUCHI, and Yoshio SASADA

Laboratory of Chemistry for Natural Products, Tokyo Institute of Technology, Ookayama, Meguro-ku, Tokyo 152

(Received March 31, 1977)

The crystal structure of 3-(adenin-9-yl)propiontryptamide (3-(adenin-9-yl)-*N*-[2-(3-indolyl)ethyl]propionamide) has been investigated as a model for adenine-tryptophan interaction. The space group of the crystal is $P2_1/c$, with dimensions $a=8.512(2)$, $b=16.884(3)$, $c=12.405(3)$ Å, $\beta=105.54(2)°$, and $Z=4$. The structure was solved by the direct method and refined by a block-diagonal least-squares method. A slight overlapping between adenine and indole moieties is found, but it may not be sufficient to produce a strong π-π interaction. The adenine base is paired with that related by the centre of symmetry through two N(6)H···N(1) hydrogen bonds, and also with the other centrosymmetrically related adenine base through two N(6)H···N(7) hydrogen bonds. Adenine and indole are bound through a hydrogen bond between N(7) of adenine and imino nitrogen of indole.

Interaction between nucleic acid and protein plays an important role in several biological processes, though the precise molecular mechanism is still unknown. Some elementary binding patterns between amino acid and purine-pyrimidine base, if any, would provide a stereochemical basis for the mechanism of mutual recognition between nucleic acid and protein.

We have reported some common hydrogen bond schemes between cytosine and acidic amino acid through X-ray crystallographic studies of complexes between nucleotide bases and amino acid derivatives.[1-3] The preparation of complex crystals is very difficult owing to the physico-chemical properties of the compounds; only a few complex crystals of restricted combination of components have been obtained. We have tried to use other type of model compounds containing a nucleotide base and a side group of amino acid in a molecule. They might provide interaction modes for any combinations between nucleotide bases and amino acids.

Intermolecular stacking interaction between adenine and tryptophan was suggested from spectroscopic studies.[4-7] On the other hand, in the crystal of 9-ethyladenine–indole complex[8] there is no stacking interaction between the two components. They are bound through a hydrogen bond between N(3) of adenine and imino nitrogen of indole. We have found the same hydrogen bond in the monohydrate crystal[9] of the title compound. In the present paper, we report another mode of hydrogen bond between adenine and indole moieties.

Experimental

3-(Adenin-9-yl)propiontryptamide (3-(adenin-9-yl)-*N*-[2-(3-indolyl)ethyl]propionamide) was synthesized from 9-(β-carboxyethyl)adenine[10] and tryptamine by the dicyclohexylcarbodiimide method. Plate crystals were obtained by evaporating a solution of benzene and methanol (10: 1) at room temperature. Oscillation and Weissenberg photographs showed the space group to be $P2_1/c$ from the systematic absence of reflexions. The density was determined by flotation in a mixture of cyclohexane and carbon tetrachloride. A crystal, $0.2\times0.3\times0.4$ mm, was mounted on a Rigaku four-circle automated diffractometer. Unit-cell parameters were calculated by least-squares refinement of 2θ values for 22 high-angle reflexions (Mo$K\alpha$; $\lambda=0.71069$ Å). Crystallographic data are summarized in Table 1.

Table 1. Crystal data

3-(Adenin-9-yl)propiontryptamide	
$C_{18}H_{19}N_7O$	$F.W.=349.40$
Crystal system: monoclinic	
Systematic absences: $h0l$, $l=2n+1$; $0k0$, $k=2n+1$	
Space group: $P2_1/c$	$Z=4$
$a=8.512(2)$ Å	$D_x=1.350$ g cm^{-3}
$b=16.884(3)$	$D_m=1.34_7$ g cm^{-3}
$c=12.405(3)$	μ(Mo$K\alpha$)
$\beta=105.54(2)°$	$=0.98$ cm^{-1}
$U=1719.6(6)$ Å^3	

Intensity data were collected on the diffractometer by use of graphite-monochromated Mo$K\alpha$ radiation, with a $\omega/2\theta$ scanning technique ($2\theta\leq50°$). Five reference reflexions monitored periodically showed no significant intensity fluctuations during the course of data collection. Corrections were made for the Lorentz and polarization factors, but not for absorption. A total of 3030 independent reflexions were obtained, zero-reflexions ($I\leq\sigma(I)$) numbering 810.

Structure Determination and Refinement

The structure was solved by the symbolic addition procedure.[11] The atomic parameters were refined by the block-diagonal least-squares method; the quantity minimized was $\Sigma\omega(|F_o|-|F_c|)^2$, with $\omega=1/(\sigma^2_p+qF_o^2)$ where σ_p is due to counting statistics and q is 1.25×10^{-5} derived from the intensity variance of the monitored reflexions. In the refinement, the zero-reflexions were included by assuming $|F_o|=F_{lim}$ and $\omega=\omega(F_{lim})$ where F_{lim} is 2.43, an observational threshold value. However, zero-reflexions for which $|F_c|<F_{lim}$ were omitted. When the R value reached 0.11, a difference synthesis revealed all the hydrogen atoms. The refinement was terminated when the maximum shift of parameters for hydrogen was less than 0.49σ. The final R value was 0.088 for 2504 reflexions ($R=0.073$ for $F_o\geq3/\sqrt{\omega}$). Atomic scattering factors were taken from "International Tables for X-Ray Crystallography."[12] A comparison between observed and calculated structure factors is given in Table 2.[13] The final positional and thermal parameters are listed in Table 3.

Table 3. Final positional and thermal parameters

Standard deviations are given in parentheses. The anisotropic temperature factor has the form $\exp[-(B_{11}h^2+B_{22}k^2+B_{33}l^2+B_{12}hk+B_{13}hl+B_{23}kl)]$.

Atom	x*	y*	z*	B_{11}*	B_{22}*	B_{33}*	B_{12}*	B_{13}*	B_{23}*
N(1)	−3764(3)	−491(2)	1369(2)	83(4)	46(1)	42(2)	3(4)	29(5)	6(3)
C(2)	−3318(4)	−679(2)	2460(3)	109(6)	48(2)	53(3)	−1(6)	76(7)	2(4)
N(3)	−1841(3)	−879(2)	3110(2)	101(5)	41(1)	38(2)	11(4)	44(5)	2(3)
C(4)	−720(3)	−858(2)	2521(2)	86(5)	25(1)	38(2)	4(5)	16(6)	0(3)
C(5)	−1005(3)	−656(2)	1411(2)	70(5)	27(1)	43(2)	4(4)	27(6)	2(3)
C(6)	−2593(4)	−470(2)	816(2)	101(6)	30(1)	42(3)	−10(5)	25(6)	−4(3)
N(6)	−3003(3)	−280(2)	−273(2)	89(5)	54(2)	38(2)	8(4)	12(5)	26(3)
N(7)	438(3)	−698(2)	1079(2)	96(5)	35(1)	42(2)	13(4)	37(5)	4(3)
C(8)	1527(4)	−912(2)	2001(3)	89(5)	33(2)	51(3)	13(5)	45(6)	−2(3)
N(9)	911(3)	−1020(1)	2897(2)	88(4)	27(1)	36(2)	12(4)	15(5)	3(3)
C(9)	1851(4)	−1259(2)	4024(3)	116(6)	31(2)	43(3)	27(5)	21(6)	11(3)
C(10)	2230(4)	−555(2)	4823(2)	114(6)	29(1)	47(3)	17(5)	30(6)	0(3)
C(11)	2989(4)	126(2)	4344(2)	96(6)	35(2)	39(3)	0(5)	−2(6)	−5(3)
O(1)	3832(3)	13(1)	3692(2)	133(4)	50(1)	63(2)	−19(4)	90(5)	−34(3)
N(10)	2671(3)	841(2)	4699(2)	135(5)	33(1)	43(2)	9(4)	53(5)	1(3)
C(12)	3311(4)	1568(2)	4363(3)	156(7)	34(2)	64(3)	−30(6)	16(8)	−1(4)
C(13)	1953(5)	2167(2)	3923(3)	219(8)	32(2)	64(3)	11(6)	1(8)	−16(4)
C(14)	705(4)	1895(2)	2889(3)	191(8)	26(2)	46(3)	17(6)	26(7)	2(3)
C(15)	988(4)	1544(2)	1969(3)	161(7)	45(2)	71(3)	21(6)	28(8)	−11(4)
N(11)	−459(3)	1401(2)	1180(2)	185(6)	44(2)	54(3)	3(5)	36(6)	−16(3)
C(16)	−1726(4)	1650(2)	1582(3)	169(7)	29(2)	62(3)	0(6)	43(8)	12(4)
C(17)	−1019(4)	1969(2)	2667(3)	180(7)	24(1)	59(3)	5(5)	58(8)	19(4)
C(18)	−2064(5)	2273(2)	3262(3)	249(9)	31(2)	81(4)	3(7)	148(9)	25(4)
C(19)	−3718(5)	2258(2)	2781(4)	240(9)	38(2)	154(5)	−8(7)	233(12)	15(5)
C(20)	−4375(5)	1944(2)	1708(4)	181(9)	40(2)	175(6)	−36(7)	126(11)	20(6)
C(21)	−3410(4)	1628(2)	1096(3)	177(8)	37(2)	98(4)	−29(7)	15(9)	12(5)

*$\times 10^4$

Atom	x**	y**	z**	B/Å^2	Atom	x**	y**	z**	B/Å^2
H(2)	−422(3)	−66(2)	286(2)	1.3(0.7)	H(122)	419(3)	182(2)	504(2)	2.7(0.8)
H(61)	−412(3)	−8(2)	−67(2)	2.2(0.8)	H(131)	251(3)	268(2)	377(2)	1.5(0.7)
H(62)	−223(3)	−14(2)	−53(2)	2.1(0.8)	H(132)	132(3)	232(2)	449(2)	2.2(0.8)
H(8)	268(3)	−99(1)	203(2)	0.9(0.7)	H(15)	205(4)	143(2)	185(2)	3.4(0.9)
H(91)	288(3)	−151(2)	393(2)	1.7(0.7)	H(11)	−52(4)	114(2)	53(2)	3.6(0.9)
H(92)	115(3)	−167(2)	428(2)	1.4(0.7)	H(18)	−161(3)	248(2)	403(2)	2.1(0.8)
H(101)	310(3)	−77(2)	555(2)	2.6(0.8)	H(19)	−446(4)	248(2)	311(3)	5.6(1.1)
H(102)	120(3)	−38(1)	500(2)	1.1(0.7)	H(20)	−560(4)	194(2)	134(3)	4.4(1.0)
H(10)	219(3)	88(2)	528(2)	3.1(0.8)	H(21)	−383(4)	140(2)	30(3)	3.9(0.9)
H(121)	393(3)	146(2)	379(2)	2.2(0.8)					

**$\times 10^3$

Results and Discussion

Molecular Structure. Bond lengths and angles are given in Table 4 and those involving non-hydrogen atoms in Fig. 1. The least-squares planes of adenine, indole and amide moieties are given in Table 5, together with the displacements of atoms from the planes. The molecular structure is shown in Fig. 2, torsion angles being given in Table 6.

The bond lengths and angles of the adenine ring are in good agreement with those found in related compounds.[14] The purine base is highly planar with a maximum shift of 0.011 Å for N(1) from the least-squares plane.

In the six-membered ring of indole, the bond lengths of C(18)–C(19) and C(20)–C(21) are shorter than the others, the bond angle of C(16)–C(21)–C(20) being the smallest. This is a common feature in the related compounds.[15,16] The indole ring is highly planar with a maximum displacement of 0.010 Å for C(20) from the least-squares plane. The exocyclic atom of C(13) significantly deviates from the plane.

As shown in Fig. 2, the molecule is folded as torsions around C(9)–C(10) and C(12)–C(13) are in skew arrangement (Table 6), in contrast to the extended form in its monohydrate crystal.[9] The dihedral angle between the adenine and indole rings in the molecule is 38.3°. The shortest intramolecular contact between the adenine and indole rings is 3.612 Å for C(6)···N(11).

Crystal Structure. The crystal structure viewed along the a axis is shown in Fig. 3, and that along the

Table 4. Bond lengths and angles

Length (l/Å)					
N(1)–C(2)	1.343(4)	C(2)–N(3)	1.343(4)	N(3)–C(4)	1.350(4)
C(4)–C(5)	1.374(4)	C(5)–C(6)	1.393(4)	C(6)–N(1)	1.354(4)
C(6)–N(6)	1.340(4)	C(5)–N(7)	1.399(4)	N(7)–C(8)	1.316(4)
C(8)–N(9)	1.363(4)	N(9)–C(4)	1.370(4)	N(9)–C(9)	1.469(4)
C(9)–C(10)	1.525(4)	C(10)–C(11)	1.517(4)	C(11)–O(1)	1.232(4)
C(11)–N(10)	1.337(4)	N(10)–C(12)	1.450(4)	C(12)–C(13)	1.524(5)
C(13)–C(14)	1.501(5)	C(14)–C(15)	1.364(5)	C(15)–N(11)	1.374(5)
N(11)–C(16)	1.371(4)	C(16)–C(17)	1.424(5)	C(17)–C(14)	1.425(5)
C(17)–C(18)	1.398(5)	C(18)–C(19)	1.376(6)	C(19)–C(20)	1.401(6)
C(20)–C(21)	1.369(6)	C(21)–C(16)	1.400(5)		
C(2)–H(2)	1.02(3)	N(6)–H(61)	1.00(3)	N(6)–H(62)	0.84(3)
C(8)–H(8)	0.99(3)	C(9)–H(91)	1.01(3)	C(9)–H(92)	1.03(3)
C(10)–H(101)	1.07(3)	C(10)–H(102)	1.00(3)	N(10)–H(10)	0.93(3)
C(12)–H(121)	1.01(3)	C(12)–H(122)	1.05(3)	C(13)–H(131)	1.03(3)
C(13)–H(132)	1.03(3)	C(15)–H(15)	0.98(3)	N(11)–H(11)	0.90(3)
C(18)–H(18)	0.99(3)	C(19)–H(19)	0.93(4)	C(20)–H(20)	1.02(3)
C(21)–H(21)	1.03(3)				

Angle (ϕ/°)			
C(2)–N(1)–C(6)	118.0(3)	N(1)–C(2)–N(3)	129.1(3)
C(2)–N(3)–C(4)	110.8(3)	N(3)–C(4)–C(5)	126.0(3)
N(3)–C(4)–N(9)	127.6(3)	C(5)–C(4)–N(9)	106.4(3)
C(4)–C(5)–C(6)	118.2(3)	C(4)–C(5)–N(7)	110.5(3)
C(6)–C(5)–N(7)	131.3(3)	N(1)–C(6)–C(5)	118.0(3)
N(1)–C(6)–N(6)	119.2(3)	C(5)–C(6)–N(6)	122.8(3)
C(5)–N(7)–C(8)	103.2(2)	N(7)–C(8)–N(9)	114.2(3)
C(4)–N(9)–C(8)	105.8(2)	C(4)–N(9)–C(9)	128.6(3)
C(8)–N(9)–C(9)	125.6(3)	N(9)–C(9)–C(10)	111.8(3)
C(9)–C(10)–C(11)	112.0(3)	C(10)–C(11)–O(1)	121.6(3)
C(10)–C(11)–N(10)	114.2(3)	O(1)–C(11)–N(10)	124.2(3)
C(11)–N(10)–C(12)	123.0(3)	N(10)–C(12)–C(13)	111.0(3)
C(12)–C(13)–C(14)	113.5(3)	C(13)–C(14)–C(15)	127.2(3)
C(13)–C(14)–C(17)	126.6(3)	C(15)–C(14)–C(17)	106.2(3)
C(14)–C(15)–N(11)	110.3(3)	C(15)–N(11)–C(16)	109.3(3)
N(11)–C(16)–C(17)	106.5(3)	N(11)–C(16)–C(21)	130.6(3)
C(17)–C(16)–C(21)	122.9(3)	C(14)–C(17)–C(16)	107.7(3)
C(14)–C(17)–C(18)	134.3(3)	C(16)–C(17)–C(18)	118.0(3)
C(17)–C(18)–C(19)	119.2(3)	C(18)–C(19)–C(20)	121.4(4)
C(19)–C(20)–C(21)	121.9(4)	C(16)–C(21)–C(20)	116.7(4)
N(1)–C(2)–H(2)	116(1)	N(3)–C(2)–H(2)	115(1)
C(6)–N(6)–H(61)	122(2)	C(6)–N(6)–H(62)	116(2)
H(61)–N(6)–H(62)	117(3)	N(7)–C(8)–H(8)	122(2)
N(9)–C(8)–H(8)	124(2)	N(9)–C(9)–H(91)	106(2)
N(9)–C(9)–H(92)	106(2)	H(91)–C(9)–H(92)	110(2)
C(10)–C(9)–H(91)	111(2)	C(10)–C(9)–H(92)	112(2)
C(9)–C(10)–H(101)	105(2)	C(9)–C(10)–H(102)	109(1)
H(101)–C(10)–H(102)	111(2)	C(11)–C(10)–H(101)	109(2)
C(11)–C(10)–H(102)	111(1)	C(11)–N(10)–H(10)	120(2)
C(12)–N(10)–H(10)	116(2)	N(10)–C(12)–H(121)	111(2)
N(10)–C(12)–H(122)	111(2)	H(121)–C(12)–H(122)	104(2)
C(13)–C(12)–H(121)	111(2)	C(13)–C(12)–H(122)	109(2)
C(12)–C(13)–H(131)	106(2)	C(12)–C(13)–H(132)	115(2)
H(131)–C(13)–H(132)	105(2)	C(14)–C(13)–H(131)	111(2)
C(14)–C(13)–H(132)	106(2)	C(14)–C(15)–H(15)	127(2)
N(11)–C(15)–H(15)	123(2)	C(15)–N(11)–H(11)	123(2)
C(16)–N(11)–H(11)	127(2)	C(17)–C(18)–H(18)	120(2)
C(19)–C(18)–H(18)	121(2)	C(18)–C(19)–H(19)	123(2)
C(20)–C(19)–H(19)	115(2)	C(19)–C(20)–H(20)	122(2)
C(21)–C(20)–H(20)	117(2)	C(20)–C(21)–H(21)	125(2)
C(16)–C(21)–H(21)	118(2)		

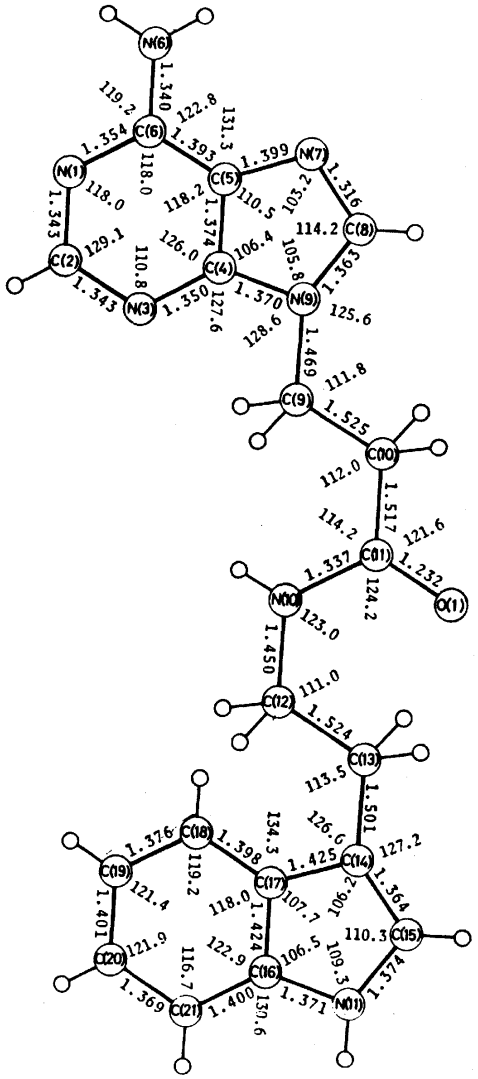

Fig. 1. Bond lenghts (l/Å) and angles (ϕ/°).

b axis in Fig. 4. As seen from Fig. 4, the folded molecules come together around the 2_1 axes, and stack along them. Short intermolecular contacts are 3.474 for N(9)···C(17), 3.479 for N(9)···C(18), and 3.129 Å for C(8)···C(18), the last one being fairly shorter than the normal van der Waals separation.[17] Figure 5 shows the stacking geometry of the adenine and indole rings, (a) being a

Table 5. Least-squares planes

X, Y, and Z are in Å along the directions **a***, **c**×**a***, and **c**, respectively.

Plane 1 (adenine ring)

$0.1902X-0.9615Y+0.2074Z+6.018=0$

Plane 2 (indole ring)

$-0.0479X-0.9007Y+0.4318Z+1.429=0$

Plane 3 (amide group)

$0.8171X-0.0635Y+0.5730Z-4.691=0$

	Deviation (l/Å)				
	Plane 1		Plane 2		Plane 3	
N(1)*	−0.011	C(14)*	−0.003	C(10)*	0.001
C(2)*	0.009	C(15)*	−0.001	C(11)*	−0.003
N(3)*	0.001	N(11)*	−0.006	O(1)*	0.001
C(4)*	−0.004	C(16)*	0.006	N(10)*	0.001
C(5)*	0.009	C(17)*	0.004	C(9)	−0.696
C(6)*	−0.001	C(18)*	0.004	C(12)	0.029
N(7)*	0.001	C(19)*	−0.003	H(10)	0.152
C(8)*	0.001	C(20)*	−0.010		
N(9)*	−0.006	C(21)*	0.009		
N(6)	−0.014	C(13)	−0.036		
C(9)	−0.010	H(15)	−0.036		
H(2)	0.050	H(11)	0.054		
H(8)	−0.008	H(18)	0.037		
H(61)	0.095	H(19)	−0.063		
H(62)	0.220	H(20)	−0.030		
		H(21)	−0.020		

* Atoms included in the calculation of the least-squares plane.

Dihedral angles between the planes (ϕ/°)

No.	2	3
1	141.7	78.2
2		74.6

Table 6. Selected torsion angles of the molecule

C(4)–N(9)–C(9)–C(10)	−78.4°
C(8)–N(9)–C(9)–C(10)	101.4
N(9)–C(9)–C(10)–C(11)	−51.3
C(9)–C(10)–C(11)–O(1)	−29.9
C(9)–C(10)–C(11)–N(10)	150.6
O(1)–C(11)–N(10)–C(12)	−0.9
C(10)–C(11)–N(10)–C(12)	178.5
C(11)–N(10)–C(12)–C(13)	128.6
N(10)–C(12)–C(13)–C(14)	−62.9
C(12)–C(13)–C(14)–C(15)	−44.9
C(12)–C(13)–C(14)–C(17)	136.4

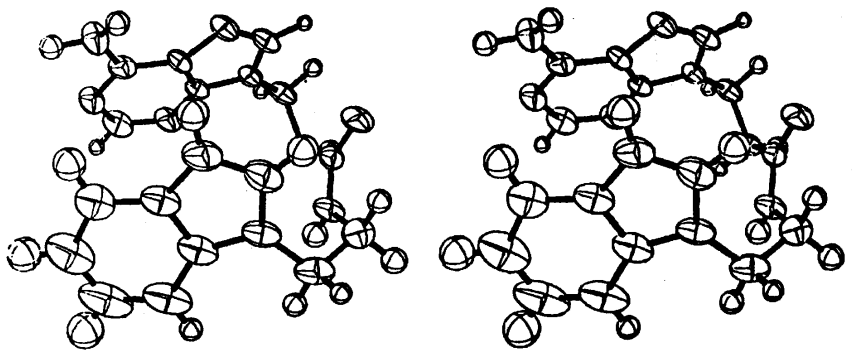

Fig. 2. A stereoscopic view of 3-(adenine-9-yl)propiontryptamide. Thermal ellipsoids are drawn at the 50% probability level.

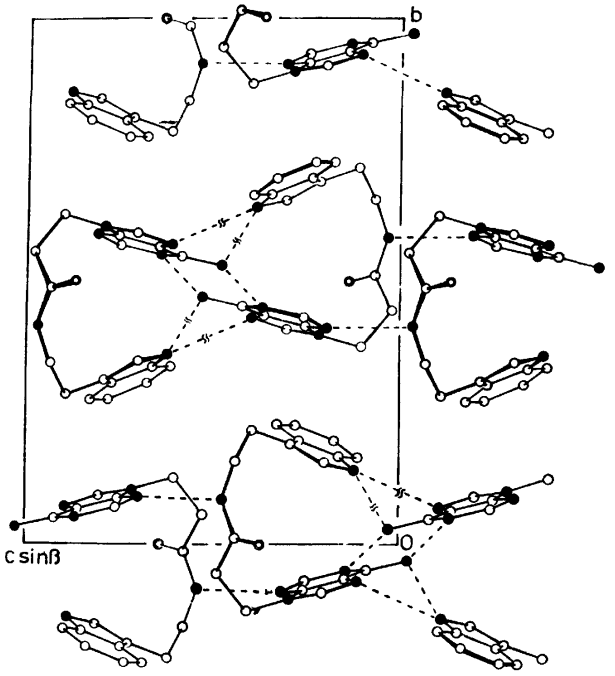

Fig. 3. The crystal structure viewed along the a axis.

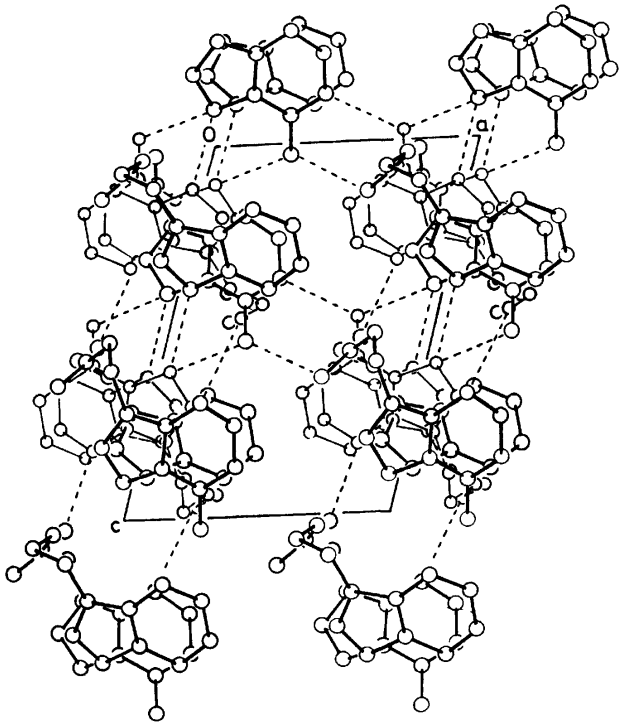

Fig. 4. The crystal structure viewed along the b axis.

projection onto the adenine plane and (b) that onto the indole. These planes make an angle of 18.7°, and the overlapping area is very small, so that there is no strong π-π interaction between them.

The hydrogen bond arrangement is shown in Fig. 6, relevant distances and angles being given in Table 7. The adenine base is paired with that related by the centre of symmetry through two N(6)H···N(1) hydrogen bonds and also with the other centrosymmetrically

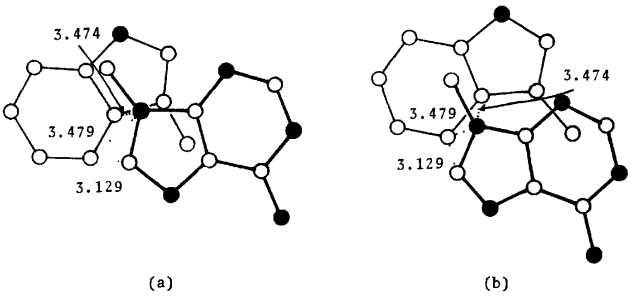

Fig. 5. The stacking geometry of adenine and indole rings. (a) is a projection onto the adenine plane and (b) is that onto the indole.

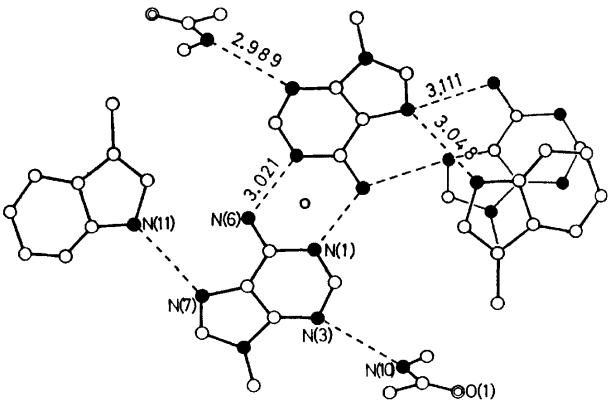

Fig. 6. Hydrogen bond arrangement in the crystal.

Table 7. Distances and angles of the hydrogen bonds (X–H···Y)

				Distance (l/Å)	Distance (l/Å)	Angle (ϕ/°)
X	H	Y		X···Y	H···Y	X–H···Y
N(6)	H(61)	N(1)	(a)	3.021	2.03	171
N(10)	H(10)	N(3)	(b)	2.987	2.09	162
N(11)	H(11)	N(7)	(c)	3.048	2.16	170
N(6)	H(62)	N(7)	(c)	3.111	2.32	158
			(a)	at $-1-x$,	$-y$,	$-z$
			(b)	at $-x$,	$-y$,	$1-z$
			(c)	at $-x$,	$-y$,	$-z$

related adenine bases through two N(6)H···N(7) hydrogen bonds. From a comparison of the hydrogen bond lengths and angles between these two pairing modes (Table 7), it is suggested that the mode by two N(6)H···N(1) hydrogen bonds is more stable than that by two N(6)H···N(7) bonds. This is consistent with the relative stability of these modes calculated by Pullman *et al.*[18] using molecular orbital methods.

N(3) of the adenine ring is hydrogen bonded with N(10) of the amide group in the molecule related by the centre of symmetry. The same kind of hydrogen bonding between nucleotide bases and amide groups is proposed by Gurskii *et al.*[19] as a model of interaction of nucleic acid with regulatory proteins. Furthermore, it is found that N(7) of the adenine ring is hydrogen bonded with N(11) of the indole. Thus N(7) acts as an acceptor

for two hydrogen bonds from N(11) of indole and N(6) of adenine. A similar situation was found for N(1) of adenine in the crystal of *N*-[3(adenin-9-yl)propyl]-3-carbamoylpyridinium bromide.[20] This would be attributable to the large basicity of the nitrogen atoms.[21] Judging from the lengths and angles (Table 7), the N(11)H···N(7) hydrogen bond should be stronger than N(6)H···N(7). The hydrogen bonded adenine and indole rings make an angle of 18.7°.

Interaction Mode between Adenine and Aromatic Moiety of Amino Acid. Crystals of 3-(adenin-9-yl)propiontyramide dihydrate,[22] 3-(adenin-9-yl)propiontryptamide (the present molecule), its monohydrate,[9] and 9-ethyladenine–indole complex[8] are systems in which adenine and aromatic moieties co-exist. Although a π-π interaction between adenine bases in nucleic acid and aromatic side groups in protein is suggested by spectroscopic studies,[4-7] these crystal structures show that there is no stacking between the two components except for the present crystal. Even in the overlapping between adenine and indole rings found in the present crystal (Fig. 5), the relative arrangement may not be sufficient to produce a strong π-π interaction. This is consistent with the calculations of Pullman and Pullman,[23] which indicate both adenine and indole to be π-electron donating. Thus, we consider that hydrogen bonding is more important than the stacking in the system of adenine and the aromatic amino acids.

Two interaction modes between adenine and indole have been found. One is the hydrogen bonding between N(3) of the former and N(11) of the latter found in the crystals of 9-ethyladenine–indole complex[8] and 3-(adenin-9-yl)propiontryptamide monohydrate.[9] The other is the hydrogen bonding between N(7) of the former and N(11) of the latter found in the present crystal. All the adenine bases interacting with indole are paired with other symmetry-related adenines in the crystals. Thus, the hydrogen bonds between adenine and indole provide models of interaction between paired adenine and the side group of tryptophan. We have tried to fit the interaction geometries found in our studies into a double helical nucleic acid (conformation B), atomic coordinates of which are taken from the work of Arnott and Hukins.[24] The indole ring bound to N(7) can be situated in the major groove of DNA without any stereochemical difficulties (Fig. 7); the shortest intermolecular contact is 4.67 Å. On the other hand, the indole ring bound to N(3) in the minor groove gives very short approach to the ribose part, so that some modification of the DNA structure might be required.

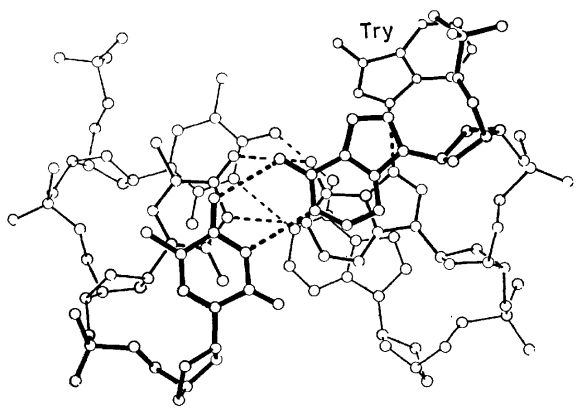

Fig. 7. Indole fitted into a double helical nucleic acid which is constituted with three adenine: thymine base pairs in the B conformation.

Part of the expenses connected with this research was defrayed by grants from the Ministry of Education and from the Kawakami Foundation, to which the authors' thanks are due.

References

1) M. Ohki, A. Takenaka, H. Shimanouchi, and Y. Sasada, *Bull. Chem. Soc. Jpn.*, **48**, 848 (1975).
2) M. Ohki, A. Takenaka, H. Shimanouchi, and Y. Sasada, *Bull. Chem. Soc. Jpn.*, **49**, 3493 (1976).
3) M. Ohki, A. Takenaka, H. Shimanouchi, and Y. Sasada, *Bull. Chem. Soc. Jpn.*, **50**, 90 (1977).
4) T. Monteray-Garestier and C. Hélène, *Biochemistry*, **10**, 300 (1971).
5) F. Brun, J. J. Toulmé, and C. Hélène, *Biochemistry*, **14**, 558 (1975).
6) F. Morita, *J. Biol. Chem.*, **242**, 4501 (1967).
7) F. Morita, *Biochim. Biophys. Acta*, **343**, 674 (1974).
8) T. Kaneda and J. Tanaka, *Bull. Chem. Soc. Jpn.*, **49**, 1799 (1976).
9) M. Ohki, A. Takenaka, H. Shimanouchi, and Y. Sasada, *Acta Crystallogr., Sect. B*, in press (1977).
10) K. Kondo, M. Miyata, and K. Takemoto, *Bull. Chem. Soc. Jpn.*, **44**, 2554 (1971).
11) J. Karle and I. L. Karle, *Acta Crystallogr.*, **21**, 849 (1966).
12) "International Tables for X-Ray Crystallography," Vol. III, Kynoch Press, Birmingham (1962), p. 201.
13) Table 2 has been deposited at the Chemical Society of Japan (Document No. 7715).
14) S. T. Rao and M. Sundaralingam, "Synthetic Procedures in Nucleic Acid Chemistry," Vol. II, ed by W. W. Zorbach and R. S. Tipson, John Wiley & Sons, New York (1973), p. 399.
15) M. Cotrait and Y. Barrans, *Acta Crytallogr., Sect. B*, **30**, 510 (1974).
16) G. L. Gartland, G. R. Freeman, and C. E. Bugg, *Acta Crystallogr., Sect. B*, **30**, 1841 (1974).
17) L. Pauling, "The Nature of the Chemical Bond," Cornell University Press, Ithaca (1960), p. 260.
18) B. Pullman, P. Claverie, and J. Caillet, *Proc. Natl. Acad. Sci. U. S. A.*, **55**, 904 (1966).
19) G. V. Gurskii, V. G. Tumanyan, A. S. Zasedatelev, A. L. Zhuze, S. L. Grokhovskii, and B. P. Gottikh, *Molekularnaya Biobgiya*, **9**, 635 (1975).
20) P. L. Johnson, C. A. Maier, and I. C. Paul, *J. Am. Chem. Soc.*, **95**, 5370 (1973).
21) R. E. Marsh, "Structural Chemistry and Molecular Biology," ed by A. Rich and N. Davidson, Freeman, San Francisco (1968), p. 484.
22) M. Ohki, A. Takenaka, H. Shimanouchi, and Y. Sasada, *Acta Crystallogr., Sect. B*, in press (1977).
23) B. Pullman and A. Pullman, *Proc. Natl. Acad. Sci. U. S. A.*, **44**, 1197 (1958).
24) S. Arnott and D. W. L. Hukins, *Biochem. Biophys. Res. Commun.*, **47**, 1504 (1972).

The Oxidation Activity and Acid-base Properties of V_2O_5-based Binary Catalysts

Mamoru Ai

Research Laboratory of Resources Utilization, Tokyo Institute of Technology, Ookayama, Meguro-ku, Tokyo 152

(Received April 9, 1977)

The oxidation of *cis*-2-butene, butadiene, and acetic acid was carried out by using a series of V_2O_5–X_nO_m (atomic ratio=9: 1) catalysts with more than twenty metal oxides (X_nO_m). The results were compared with the dehydration activity for isopropyl alcohol (IPA), as a measure of acidity, and with the ratio, dehydrogenation activity for IPA/dehydration activity for IPA, used as a measure of the basicity of catalyst. The activity for the oxidation of butadiene and that for the isomerization of butene are correlated with the acidity, and the activity for the oxidation of acetic acid with the basicity of the catalyst. The selectivity to maleic anhydride from butene and butadiene is scarcely influenced by the introduction of metal oxides. Butene is mainly oxidized to acetic acid as a result of C–C fission. The selectivity to acetic acid is enhanced when the catalyst is highly acidic, decreasing with increase in basicity. It is concluded that the introduction of metal oxides into V_2O_5 modifies the acid-base properties of the catalyst, inducing a change in oxidation activity and selectivity.

Catalysts based on V_2O_5 have been used for a long time in the synthesis of sulfuric acid from sulfur dioxide and of carboxylic acids from aromatic hydrocarbons; they play an important part in the partial oxidation of organic substances. The characteristic feature of these catalysts is their effective specificity in "acid formation."

As a practical catalyst, pure V_2O_5 is rarely used. In most cases V_2O_5 is modified by combining it with oxides of other metals in order to enhance the catalytic action. Attempts have been made to determine the role of the additives as regards the structural,[1–6] electronic,[7–12] and other physico-chemical properties of the catalyst system.[4,13–16] It should be noted that the selectivity of acrolein to acrylic acid is connected with the electronegativity of the metal oxides used as second components added to V_2O_5 catalysts.[17]

The acid-base properties and their correlation with the oxidation activity and selectivity were studied in the case of many MoO_3 and V_2O_5-based binary catalysts, such as MoO_3–P_2O_5,[18] MoO_3–Bi_2O_3–P_2O_5,[19,20] MoO_3–V_2O_5,[21] MoO_3–TiO_2,[22] MoO_3–SnO_2,[23] MoO_3–Fe_2O_3,[24] V_2O_5–P_2O_5,[25] V_2O_5–TiO_2,[22] V_2O_5–SnO_2,[26] and V_2O_5–Fe_2O_3.[24] The catalytic activity for the oxidation of electron-donating (basic) reactants such as olefinic and aromatic hydrocarbons is correlated with the acidic nature of the catalyst surface, and that of acidic reactants such as carboxylic acids with the basic nature of the catalyst. The activity and selectivity in mild oxidations are governed by the acid-base properties of the catalyst and the reactant.[18–26]

The following two functions are required for a catalyst to be active in an oxidation reaction;

(1) activation of oxygen,

(2) activation of reactant molecules.

When a catalyst is potent in the activation of oxygen, *i.e.*, when it has high oxidizing power, the reaction takes place without requiring any activation of the reactant: it proceeds non-selectively toward CO_2 and H_2O. This is the case of deep oxidation.[27] On the other hand, when the oxidizing power of a catalyst is not very high, the reaction requires the activation of the reactant molecule as well as of oxygen. Thus the difference in the mode or degree of this reactant-activation brings about the selectivity of the catalyst.

The acidic sites, probably consisting of metal ions with a particularly high electron affinity, play a role in the electron transfer from reactant to the sites, resulting in the formation of a cationic intermediate and a reduced metal ion;[28–30] the acidic sites contribute to the activation of the elctron-donating (basic) reactants, such as olefins. On the other hand, the basic sites, because of their electron-donating ability, serve to adsorb and activate the acidic reactants such as carboxylic acids.

The fact that V_2O_5 is a typical acidic oxide leads us to the prediction that the addition of metal oxide to V_2O_5 modifies the acid-base properties of the catalyst system, and that this modification, in turn, induces a change in the catalytic behavior.

In the present work, we have attempted to confirm how the addition of a small amount of metal oxide to V_2O_5 modifies the acid-base properties as well as the oxidation activity and selectivity and to find the correlation between the acid-base properties and catalytic behavior.

Experimental

Catalysts. The catalysts used in this study were a series of V_2O_5-based binary oxides, V_2O_5–X_nO_m. As the second component, X_nO_m, more than twenty metal oxides, including almost all those used in practice, were tested. As starting materials, we used nitrates for Al, Sb, Bi, Te, Fe, Ni, Cr, Co, and Zn, ammonium salts of oxo-acid for V, Mo, and W, chlorides (converted into hydroxides with dilute ammonia) for Sn and Ti, hydrates for Ca, Mg, and K, acetate for U, H_2SO_4 for S, and H_3PO_4 for P. The surface area of these catalysts were determined by the BET method, using nitrogen at −196 °C.

Determination of Acidic and Basic Properties. Since the V_2O_5-based mixed oxides are colored and small in surface area, it is not easy to determine their acidity and basicity by the ordinary titration method[31,32] or by studying the adsorption of a basic or acidic molecule in the gas phase. However, from a comparison of the catalytic activities for isopropyl alcohol (IPA) with the acidity-basicity data directly measured on many kinds of mixed catalysts, such as MoO_3–Bi_2O_3–P_2O_5,[20] MoO_3–TiO_2,[22] MoO_3–SnO_2,[23] MoO_3–Fe_2O_3,[24] V_2O_5–TiO_2,[22] V_2O_5–SnO_2,[26] V_2O_5–Fe_2O_3,[24] and TiO_2–

X_nO_m (X_nO_m=various kinds of metal oxides),[33] it has been found that the activity for the dehydration of IPA to propylene (r_p) represents the acidity of the catalyst and that the value of the r_a/r_p ratio, where r_a is the activity for the dehydrogenation of IPA to acetone, is also valid as an index of basicity;

$$\text{acidity} \propto \text{dehydration rate} \quad (1)$$

$$\text{basicity} \propto \frac{\text{dehydrogenation rate}}{\text{dehydration rate}}. \quad (2)$$

The results indicate that acidic and basic sites take part almost equally in the dehydrogenation of IPA;

$$\text{dehydrogenation rate} \propto (\text{acidity})(\text{basicity}). \quad (3)$$

This reaction may proceed by means of a concerted mechanism, *e.g.*,[34]

$$\geq C\text{-}H^{\ominus} \rightarrow \text{acidic site}$$
$$O\text{-}H^{\oplus} \rightarrow \text{basic site}$$

Thus we used the values of r_p and r_a/r_p as measures of the acidity and basicity, respectively, of the catalysts.

Catalytic Activity Measurements. The vapor-phase oxidation of *cis*-2-butene, 1,3-butadiene, and acetic acid, and the dehydration and dehydrogenation of isopropyl alcohol (IPA) were carried out in an ordinary continuous-flow-type reaction system. The concentrations of butene, butadiene, acetic acid, and IPA were 0.67, 0.67, 1.5, and 1.65 mol%, in the air; the total flow rate (at 25 °C) was kept constant at 1.5 l/min, the amout of catalyst used being 2—30 g. The reactor and experimental procedures were the same as those employed in previous works.[18-26]

Results and Discussion

Acidic and Basic Properties. A gaseous mixture of IPA with air was passed through a bed of the catalyst (2—6 g) held at 175 °C. The rates of dehydration (r_p) and dehydrogenation (r_a) [mol/h g-cat], which are known to be almost of zero-order with respect to the IPA concentration,[18-26] were obtained for each catalyst.

The values of r_p together with the surface areas, S (m^2/g) are given in Fig. 1. Introduction of the additives (X_nO_m) causes a remarkable change both in the surface area and the specific acidity (r_p/S) of the catalyst. It should be noted that introduction of TeO_2, K_2SnO_3, and K_2SO_4 into V_2O_5 decreases the acidic property significantly.

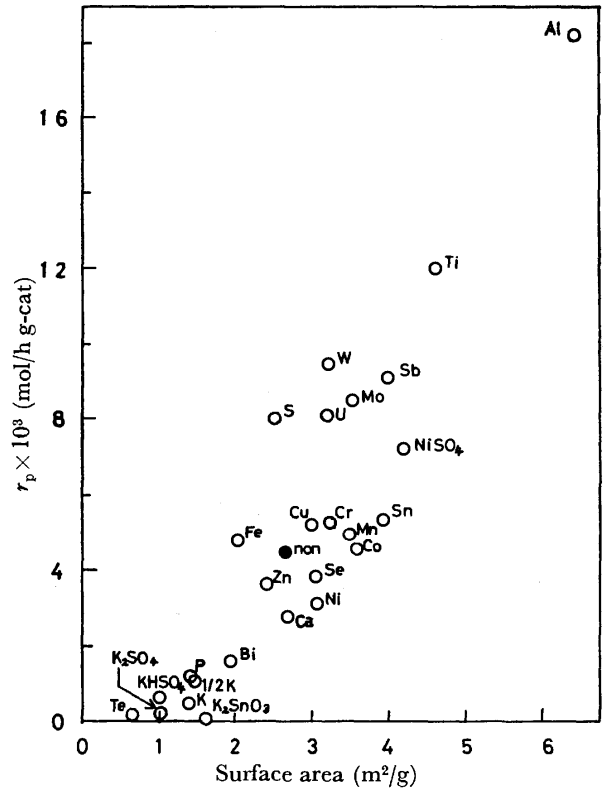

Fig. 1. Influence of the second components (X_nO_m) on the acidity (r_p) and the surface area.

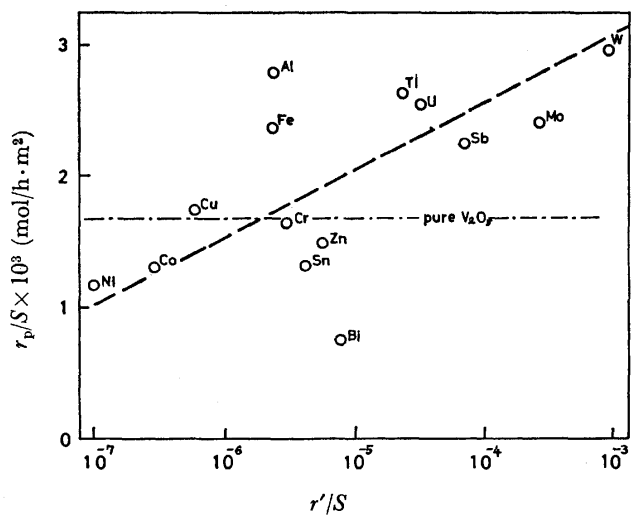

Fig. 2. The specific acidity of the binary system (V_2O_5–X_nO_m), r_p/S, as a function of that of the second component (X_nO_m) alone, r'_p/S.
r_p: The dehydration rate at 175 °C,
r'_p: the dehydration rate at 190 °C.

In Fig. 2 the specific acidity of the binary system, r_p/S, is plotted as a function of that of the second component (X_nO_m) alone, r'_p/S, obtained previously.[35] A rough correlation holds between r_p/S and r'_p/S, though a disparity and some exceptions are found. Addition of such acidic elements as P_2O_5 and TeO_2 decreases the acidity.

Figure 3 shows the relationship between the specific acidity, r_p/S, and the basicity, r_a/r_p. The basicity decreases a great deal with an increase in acidity, as might be expected in the case of a liquid acid-base, except for the cases of P_2O_5 and TeO_2. Introduction of P_2O_5 decreases both the acidity and the basicity.

Isomerization Activity for Butene. The oxidation of butene over a V_2O_5-based catalyst is always accompanied by its isomerization. The influence of the additives on the activity for the isomerization of butene was studied. The experiments were carried out at the *cis*-2-butene concentration of 0.67 mol % in the air, at a total flow rate of 1.5 l/min, and at 220 °C, the catalyst amount being varied in the 2.5—30 g range. The ratio of (*trans*-2-butene + 1-butene)/(*cis*-2-butene + *trans*-2-butene + 1-butene) corresponding to the surface area of 5 m^2, I, which is far from the thermodynamic equilibrium (I_e) of *ca.* 0.65, was adopted as a measure of the specific activity for isomerization. The data are plotted against the value of r_p/S in Fig. 4.

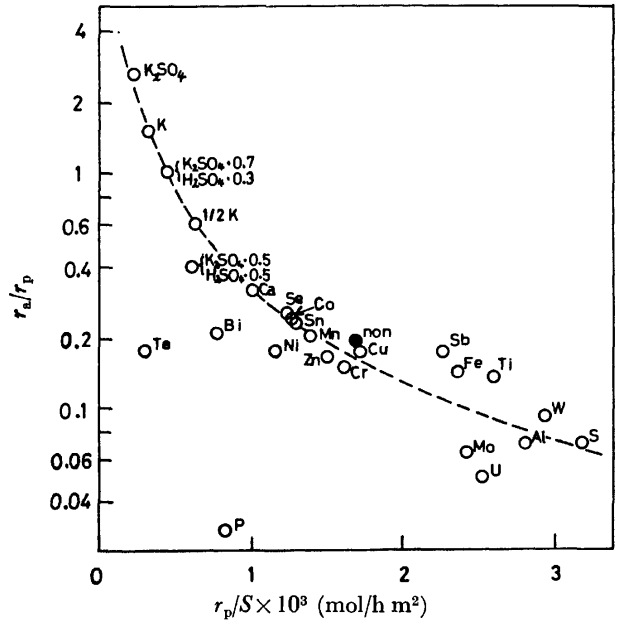

Fig. 3. Relation between the acidity (r_p/S) and the basicity (r_a/r_p).

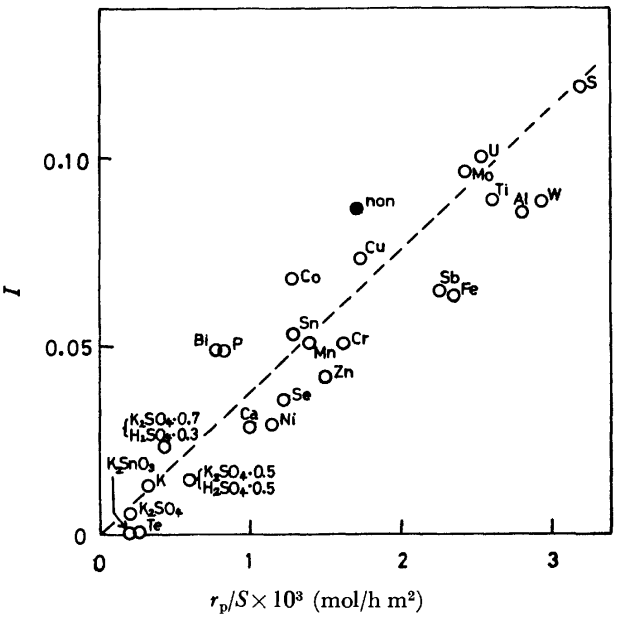

Fig. 4. The isomerization activity (I) against the acidity (r_p/S.)

A linear relationship is obtained between isomerization activity and acidity of the catalyst. This indicates[22,23,26] that, under the circumstances of the oxidation reaction in a flow system, the isomerization is catalyzed only by the acidic sites, and that the basic sites which can also catalyze the isomerization in the absence of oxygen in a closed[36] or pulse-reaction system[37] are poisoned by CO_2 or other acidic products.

Oxidation Activity for Olefin. The promotive effect of the additives on the oxidation activity for such basic reactants as olefins was also examined. The oxidation of 1,3-butadiene was chosen as a model reaction for convenience of experimental procedure. It was carried out over a seires of V_2O_5–X_nO_m catalysts at 285 °C, the amount of the catalyst being varied from 2.5 to 25 g. The initial rate of butadiene disappearance, r_B (mol/h g-cat), was adopted as a measure of activity. The specific activity, r_B/S, is plotted as a function of the specific acidity, r_p/S, in Fig. 5.

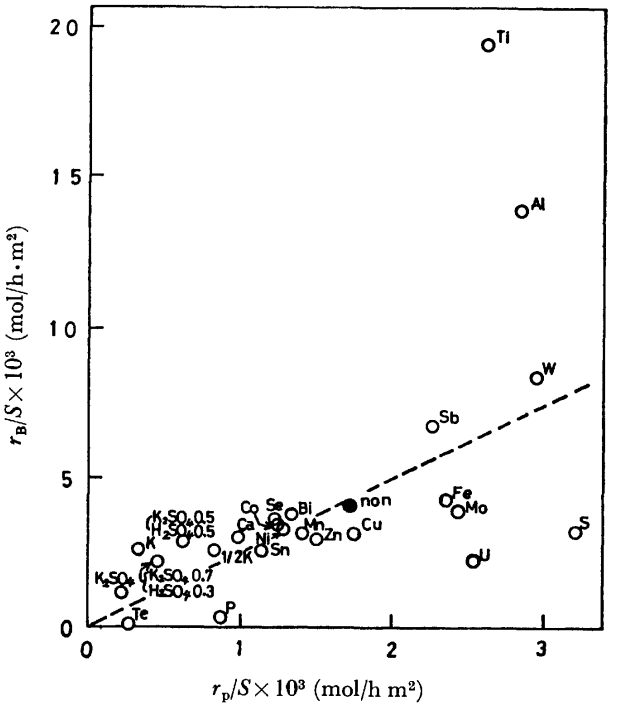

Fig. 5. The oxidation activity for butadiene (r_B/S) as a function of the acidity (r_p/S).

A moderately good correlation is obtained between oxidation activity and acidity, except for several oxides such as TiO_2, Al_2O_3, P_2O_5, SO_3, and U_3O_8. The data are in line with the results obtained previously,[18–26] indicating that the acidic sites play an important role in catalyzing the oxidation of olefin. It seems that the large deviation of V_2O_5–TiO_2 and V_2O_5–Al_2O_3 is connected to their large surface area. When the oxidation activity per unit volume of catalyst is very high, the evolution of heat per unit volume of catalyst becomes great and, the real temperature of the catalyst surface becomes much higher than the measured temperature, which gives rise to a large increase in apparent activity. The disparity of these results may arise in part from the participation of another factor in the catalysis; *e.g.*, the activation of oxygen which seems to be associated with (1) the strength of metal-oxygen bonding and (2) the possibility of incorporation of gaseous oxygen into the crystal lattice oxygen by electron donation from the catalyst.

Oxidation Activity for Acid. The influence of the additives on the oxidation activity for acidic compounds was also examined. Acetic acid was chosen as the reactant. The initial rate of oxidation to CO_2 at 325 °C, r_A (mol/h g-cat), was adopted as a measure of activity.

The specific activity, r_A/S, is plotted as a function of the basicity, r_a/r_p, in Fig. 6. The basic sites of the catalyst are considered to contribute to the activation of acidic compounds.[19–22,24]

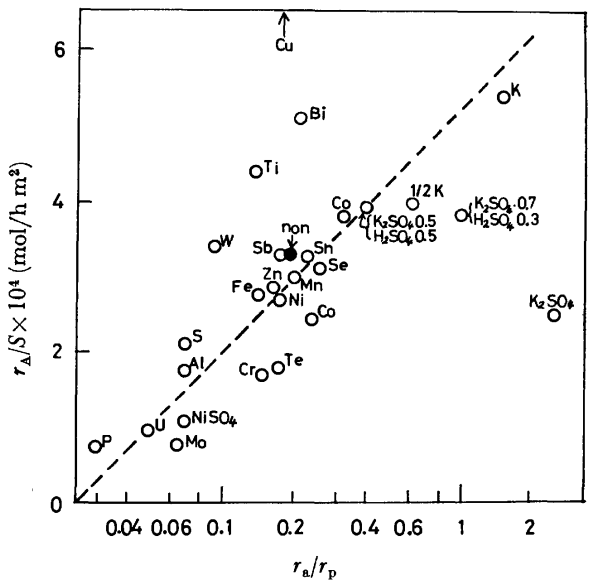

Fig. 6. The oxidation activity for acetic acid (r_A/S) as a function of the basicity (r_a/r_p).

A relatively good correlation is found between r_A/S and r_a/r_p. This supports the validity of the above conception that the basic sites of catalysts contribute to the activation of an acidic compound and oxygen (electron-accepting compound). The large deviation of CuO and K_2SO_4 is supposed to be caused by the strength of metal-oxygen bonding.

Selectivity in Oxidation. The effect of additives on selectivity in the oxidation of olefins was examined. Butadiene was oxidized in the presence of excess air (butadiene=0.67 mol %) over the series of V_2O_5–X_nO_m catalysts with a variety of second components, X_nO_m. At a high conversion of *ca.* 80—95%, the main product, besides CO_2 and CO, was maleic anhydride as in earlier results. The amount of acetic acid was fairly small.

The selectivity of butadiene to maleic anhydride at a conversion of 80—90% is plotted as a function of the basicity of the catalyst, r_a/r_p, in Fig. 7. The selectivity is *ca.* 50 mol % and nearly independent of the additives, except in the cases of K_2SO_4 and K_2SnO_3 where the oxidation activity is extremely low. Since V_2O_5-based catalysts are acidic enough, *viz.*, they are inactive for acidic compounds, the selectivity is not limited by the consecutive decomposition of the maleic anhydride produced, but by the selectivity in the steps from butadiene to maleic anhydride.

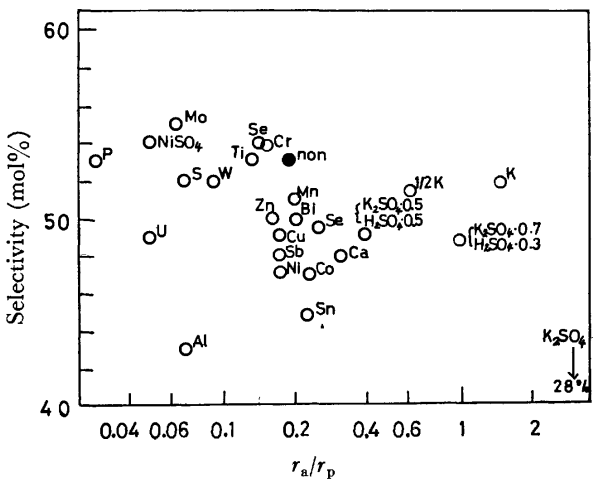

Fig. 7. The selectivity from butadiene to maleic anhydride at a conversion of 80—95% as a function of the basicity of the catalyst (r_a/r_p).

Concerning maleic anhydride formation, the selectivity from butene is fairly small as compared with that from butadiene. A significant amount of acetic acid is formed at the expense of maleic anhydride as has been reported by Brockhaus.[38] The selectivities to maleic anhydride and acetic acid at a 80—95% conversion are plotted as a function of the basicity of the catalyst, r_a/r_p, in Fig. 8.

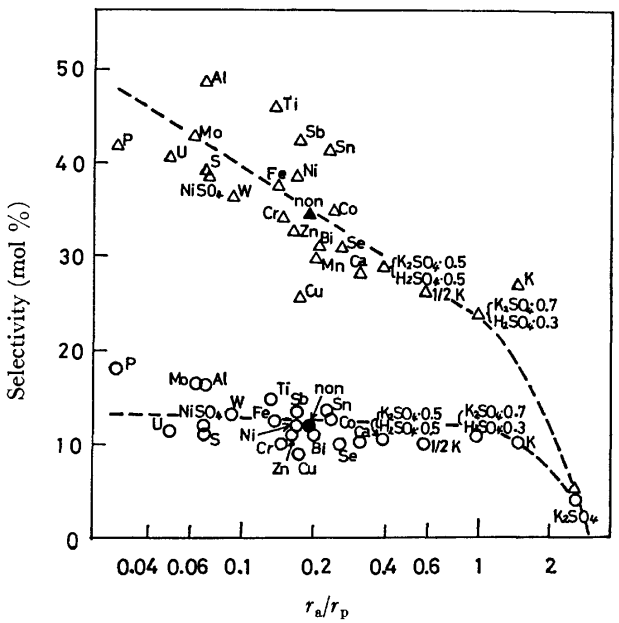

Fig. 8. The selectivity from *cis*-2-butene to maleic anhydride and acetic acid at a conversion of 80—95% as a function of the basicity (r_a/r_p).
○ =Maleic anhydride, △ =acetic acid + maleic anhydride.

The selectivity to maleic anhydride is *ca.* 12 mol % for each catalyst, while selectivity to acetic acid decreases with an increase in the basicity, r_a/r_p. The results in Fig. 8, which coincide with the data of the oxidation activity for acetic acid (Fig. 6), reveal that acetic acid is decomposed more easily than maleic anhydride by means of the basic sites of the catalyst. It is of interest that, in contrast to butadiene, butene is mainly oxidized to acetic acid.

The selectivity to maleic anhydride over V_2O_5-based catalysts not containing a large amount of P_2O_5 is mainly

limilted by the selectivity at the step of allylic oxidation, butene→butadiene.[39] This is because butene is more susceptible to the C–C fission than to the allylic C–H fission.

Thus it can be said that the V_2O_5-based catalysts, if they are highly acidic and moderately basic, are effective for the oxidation of butene to acetic acid.

Conclusion

The introduction of a small amount (10 atom %) of metal oxides into a V_2O_5 catalyst causes a remarkable change in the surface area and the acid-base properties.

The acidity of the binary system, V_2O_5–X_nO_m (9: 1), is roughly correlated to that of the second component, X_nO_m, itself, though there are many exceptions. In general the basicity decreases markedly with acidity.

The activity for the isomerization of 1-butene is proportional to the acidity of catalyst. The oxidation activity for olefin is roughly correlated with the acidity and that for acid is correlated with the basicity of the catalyst.

Since the V_2O_5–X_nO_m (9: 1) catalysts are rather acidic, the selectivity of butadiene to maleic anhydride, which is relatively stable, is *ca.* 50 mol % and is scarcely influenced by the introduction of any metal oxides except for X_nO_m=K_2SO_4 and K_2SnO_3. Over these V_2O_5–X_nO_m catalysts, butene is mainly oxidized to acetic acid as a result of the C–C fission which takes place in preference to the allylic C–H fission, little butadiene being formed from butene. The selectivity to acetic acid decreases with an increase in the basicity of the catalyst, since acetic acid is decomposed easily with the basic sites.

This agrees with the results of our earlier works and leads us to conclude that the introduction of metal oxides into V_2O_5 modifies the acid-base properties of the catalysts, and that this modification induces the main change in oxidation activity and selectivity.

References

1) J. K. Dixon and J. E. Longfield, "Catalysis," Vol. 7, ed by P. H. Emmett, Reinhold, New York (1960), p. 281.
2) I. I. Ioffe, Z. I. Ezhkova, and A. G. Lyubarskii, *Kinet. Katal.*, **3**, 194 (1962).
3) R. H. Munch and E. D. Pierron, *J. Catal.*, **3**, 406 (1964).
4) K. Tarama, S. Teranishi, S. Yoshida, and N. Tamura, Proc. Intern. Congr. Catal., 3 rd, (Amsterdam, 1964), **1**, 282 (1965).
5) G. A. Kursheva, O. Ya. Polotnyuk, L. I. Konsheva, Z. I. Ezhkova, and B. E. Zaitsev, *Kinet. katal.*, **13**, 459 (1972).
6) M. Nakamura, K. Kawai, and Y. Fujiwara, *J. Catal.*, **34**, 345 (1974).
7) G. K. Boreskov, L. A. Kasatkina, V. V. Popovskii, and Yu. A. Balovnev, *Kinet. Katal.*, **1**, 229 (1960).
8) J. D. Butler and B. G. Weston, *J. Catal.*, **2**, 8 (1963).
9) Z. I. Ezhkova, I. I. Ioffe, V. B. Kazanskii, A. V. Krylova, A. G. Lyubarskii, and L. Ya. Margolis, *Kinet. Katal.*, **5**, 861 (1964).
10) V. Ya. Volifson and L. N. Gunuk, *Kinet. Katal.*, **6**, 306 (1965).
11) A. V. Krylova, L. Ya. Margolis, and E. S. Aleksandrova, *Kinet. Katal.*, **7**, 69 (1966).
12) Ya. A. Gavar, M. V. Shimanskaya, and L. Ya. Margolis, *Kinet. Katal.*, **14**, 1274 (1973).
13) A. P. Dzisyak, G. K. Boreskov, L. A. Kasatkina, and V. E. Kochurkhin, *Kinet. Katal.*, **2**, 727 (1961).
14) V. B. Kazanskii, Z. I. Ezhkova, A. G. Lyubarskii, V. V. Voevodskii, and I. I. Ioffe, *Kinet. Katal.*, **2**, 862 (1961).
15) B. E. Zaitsev, Z. I. Ezhkova, and I. I. Ioffe, *Kinet. Katal.*, **7**, 755 (1965).
16) V. A. Shvet and V. B. Kazanskii, *J. Catal.*, **25**, 123 (1972).
17) N. Kominami and H. Nakajima, *Kogyo Kagaku Zasshi*, **69**, 237 (1966).
18) M. Ai and S. Suzuki, *J. Catal.*, **30**, 362 (1973).
19) M. Ai and S. Suzuki, *Bull. Chem. Soc. Jpn.*, **46**, 1208 (1973).
20) M. Ai and T. Ikawa, *J. Catal.*, **40**, 203 (1975).
21) M. Ai and S. Suzuki, *Nippon Kagaku Kaishi*, **1973**, 260.
22) M. Ai, *Bull. Chem. Soc. Jpn.*, **49**, 1328 (1976).
23) M. Ai, *J. Catal.*, **40**, 327 (1975).
24) M. Ai and T. Ikawa, *Shokubai*, **17**, 10p (1975).
25) M. Ai and S. Suzuki, *Bull .Chem. Soc. Jpn.*, **47**, 3074 (1974).
26) M. Ai, *J. Catal.*, **40**, 318 (1975).
27) W. M. H. Sachtler and N. H. De Boer, Proc. Intern. Congr. Catal., 3 rd (Amsterdam, 1964), **1**. 252 (1965).
28) J. J. Rooney and G. Webb, *J. Catal.*, **3**, 488 (1964).
29) N. S. Butt and A. Fish, *J. Catal.*, **5**, 205 (1966).
30) J. M. Peacock, M. J. Sharp, A. J. Parker, P. G. Ashmore, and J. A. Hockey, *J. Catal.*, **15**, 379 (1969).
31) H. A. Benesi, *J. Am. Chem. Soc.*, **78**, 5490 (1956).
32) K. Tanabe, "Solid Acids and Bases," Kodansha, Tokyo, Academic Press, New York/London (1970).
33) M. Ai, Preprint of 37 th Shokubai (Catalyst) Meeting (Fukuoka), p. 58 (1975).
34) P. Mars, "The Mechanism of Heterogeneous Catalysis," ed by J. H. De Boer, Elsevier, Amsterdam (1959), p. 49.
35) M. Ai and S. Suzuki. *Shokubai*, **15**, 159p (1973).
36) M. Itoh, H. Hattori, and K. Tanabe, *J. Catal.*, **43**, 192 (1976).
37) H. Hattori and A. Satoh, *J. Catal.*, **45**, 32 (1976).
38) R. Brockhaus, *Chem. Ing. Tech.*, **36**, 1039 (1966).
39) M. Ai, *Bull. Chem. Soc. Jpn.*, **43**, 3590 (1970); **44**, 761 (1971).

A Study of the Transport of Tetraalkylammonium Ions through Ion-exchange Membranes

Kiyotoshi INENAGA, Akira YAMAUCHI, and Hideo KIMIZUKA
Department of Chemistry, Faculty of Science, Kyushu University, Fukuoka 812
(Received May 6, 1977)

The membrane potential and conductance of the cation-exchange membrane–aqueous quaternary tetraalkylammonium chloride systems have been measured by using NH_4^+, tetramethyl-(Me_4N^+), tetraethyl-(Et_4N^+), tetrapropyl-(Pr_4N^+), and tetrabutylammonium ions (Bu_4N^+). The potential change in the concentration cell with these salts was about 58 mV for a tenfold change of concentration. The membrane conductance in the concentration cell increased with the concentration. The membrane permeability, as estimated from the potential and conductance data, was in the order of $NH_4^+ > Me_4N^+ > Et_4N^+ > Pr_4N^+ > Bu_4N^+$; it is proportional to the geometric mean of the activities of exterior solutions. The effective pore size of the membrane was deduced from the conductance data and found to be *ca.* 10 Å. The selective permeation coefficient has been determined from the potential data of the two- and multi-ionic systems. The selectivity data obtained with the two-ionic system were in agreement with those obtained with the multi-ionic system. The selectivity increased with the chain length of the cation, in contrast to the reversed order of the membrane permeability in the concentration cell. This was attributed to the decreasing mobility with the increasing chain length.

So far, only a few studies of the transport phenomena of organic ions have been reported[1–10] in spite of their importance from the industrial and biological points of view. It is well known that quaternary tetraalkylammonium ions, such as tetramethyl-(Me_4N^+), tetraethyl-(Et_4N^+), tetrapropyl-(Pr_4N^+), and tetrabutylammonium ions (Bu_4N^+), are spherical and that the conductances of these ions in aqueous solutions are generally smaller than those of simple inorganic ions.[12] However, as to the transport of these ions through ion-exchange membranes, it has rarely been reported.[5]

The purpose of this study is to estimate the membrane permeability, the mobility, the selectivity coefficient, and the pore size of the membrane on the basis of measurements of the membrane potential and the membrane conductance of the ion-exchange membrane–organic ion system by using various quaternary ammonium ions and to discuss these physical properties.

Experimental

Materials. The membrane used in this study was a CL-2.5T cation-exchange membrane kindly supplied by the Tokuyama Soda Industry Co., Ltd.; after conditioning it was prepared by immersing the sodium-form membrane in 0.1 M tetraalkylammonium chloride for over a week. The water contents in the membranes of the ammonium and sodium forms were determined from the difference between the weights of the wet and dried membranes. The dried membrane was prepared by heating the wet membrane for a few days at 110 °C until the weight of the membrane attained a constant value. The ion-exchange capacity was measured by means of the back titration of alkali after treating the membrane of the hydrogen form with an excess of a 0.5 M sodium hydroxide solution. The exchange capacity was calculated with respect to the dry weight in the sodium form. The membrane of each form was washed thoroughly with redistilled water and blotted quickly with the filter paper to remove the adhered liquid; its thickness was then measured with the micrometer. The concentration of each counter ion in the wet membrane was calculated on the basis of the exchange capacity and the wet volume of the membrane in the sodium form. The ion-exchange capacity, the water content, and the thickness of the cation-exchange membrane in various forms are summarized in Table 1. The concentrations of the tetraalkylammonium chlorides were determined by the method of Fajans, in which Tween 80 (a nonionic surfactant) was used to decide the end point readily.

TABLE 1. SPECIFIC PROPERTIES OF MEMBRANE[a]

Substance	Thickness × 10^4 / cm	$\bar{C}$[b] / eq/l	Water content / wt %
Na^+	1.56	1.6	27
NH_4^+	1.57	1.6	27
Me_4N^+	1.61	1.6	—
Et_4N^+	1.66	1.5	—
Pr_4N^+	1.72	1.5	—
Bu_4N^+	1.77	1.4	—

a) Exchange capacity of membrane: 1.70 meq/g.
b) Molarity in membrane.

Membrane Potential and Conductance. The membrane potential and the conductance were measured by the method described in previous papers.[13,14] There are several methods for conductance measurement.[15–17] Lakshminarayanaiah *et al.*[14] have reported that the mercury method yields a steady value of membrane conductance for the range of the frequencies of the applied electric field of 1000—10000 Hz. Thus, this method was employed for the conductance measurement, and values measured with 1000 Hz were taken throughout this study. The area of the membrane for the measurement was 0.785 cm^2. The experiments were carried out at room temperature, 20±0.5 °C.

Mean Activity Coefficient. In order to analyze the experimental results, the mean activity coefficient should be known. Since the mean activity coefficients of tetraalkylammonium ions in concentrations bellow 10^{-1} M have never been reported, they were calculated from the data of the freezing point depression.[18] For concentrations above 10^{-1} M, the values obtained by the gravimetric isopiestic vapor pressure technique[19] were used.

Results and Discussion

Consider the system in which two aqueous phases, I and II, contain electrolytes, M^+X^- and N^+X^-, and in which the aqueous phases are separated by an ion-

exchange membrane. According to earlier papers,[13,14,20] the equations for the membrane potential, V_o, and the membrane conductance, G_m, are expressed by:

$$V_o = \frac{RT}{F} \ln \frac{P_M a_M^I + P_N a_N^I + P_X a_X^{II}}{P_M a_M^{II} + P_N a_N^{II} + P_X a_X^I}, \quad (1)$$

and:

$$G_m = \frac{F^2}{RT}(P_M a_M^{II} + P_N a_N^{II} + P_X a_X^I) \exp\left(\frac{FV_o}{2RT}\right) = \frac{F^2}{RT}(P_M a_M^I + P_N a_N^I + P_X a_X^{II}) \exp\left(-\frac{FV_o}{2RT}\right), \quad (2)$$

respectively. In Eqs. 1 and 2, the superscripts, I and II, refer to the aqueous phases, I and II, respectively, and the subscripts, M, N, and X, the ion M, N, and X, respectively; R denotes the gas constant; T, the absolute temperature; F, the Faraday constant; P_α, the membrane permeability to the ion, α, and a_α, the activity of the ion, α.

When the two phases contain a single electrolyte, M^+X^-, Eqs. 1 and 2 reduce to:

$$V_o = \frac{RT}{F} \ln \frac{P_M a_M^I + P_X a_X^{II}}{P_M a_M^{II} + P_X a_X^I}, \quad (3)$$

and:

$$G_m = \frac{F^2}{RT}(P_M a_M^{II} + P_X a_X^I) \exp\left(\frac{FV_o}{2RT}\right) = \frac{F^2}{RT}(P_M a_M^I + P_X a_X^{II}) \exp\left(-\frac{FV_o}{2RT}\right), \quad (4)$$

respectively.

For the cation-exchange membrane, which is highly permselective to cations, P_X is very small as compared to P_M and P_N. In this case, Eqs. 1—4 can be reduced to:

$$V_o = \frac{RT}{F} \ln \frac{P_M a_M^I + P_N a_N^I}{P_M a_M^{II} + P_N a_N^{II}}, \quad (5)$$

$$G_m = \frac{F^2}{RT}(P_M a_M^I + P_N a_N^I) \exp\left(-\frac{FV_o}{2RT}\right) = \frac{F^2}{RT}(P_M a_M^{II} + P_N a_N^{II}) \exp\left(\frac{FV_o}{2RT}\right), \quad (6)$$

$$V_o = \frac{RT}{F} \ln \frac{a_M^I}{a_M^{II}}, \quad (7)$$

and:

$$G_m = \frac{F^2}{RT} P_M a_M^I \exp\left(-\frac{FV_o}{2RT}\right) = \frac{F^2}{RT} P_M a_M^{II} \exp\left(\frac{FV_o}{2RT}\right), \quad (8)$$

respectively.

When Phase I contains M^+X^- and Phase II, N^+X^-, *i.e.*, when the system is two-ionic, Eqs. 5 and 6 are reduced to:

$$V_o = \frac{RT}{F} \ln \frac{P_M a_M^I}{P_N a_N^{II}}, \quad (9)$$

and:

$$G_m = \frac{F^2}{RT} P_M a_M^I \exp\left(-\frac{FV_o}{2RT}\right) = \frac{F^2}{RT} P_N a_N^{II} \exp\left(\frac{FV_o}{2RT}\right), \quad (10)$$

respectively.

Thus, the membrane permeability can be estimated providing that the potential, the conductance, and the activity data are known.

Concentration Cells. In Fig. 1, the membrane potentials are shown for the concentration cells of Pr_4N^+ and Bu_4N^+ chloride as typical examples. The concentration of the salt in Phase II was kept at 10^{-2} M while that in Phase I was altered. The potential change was about 58 mV for a tenfold change in the concentrations from 10^{-3} to 10^{-1} M and the apparent transference numbers of Pr_4N^+ and Bu_4N^+ were 0.97 or 0.98

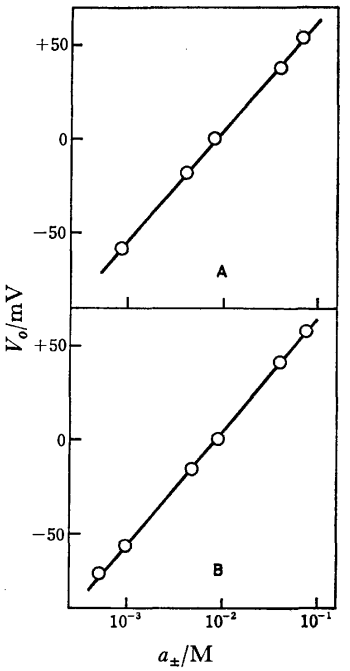

Fig. 1. Membrane potentials as functions of the mean activity of Phase I for the concentration cells.
A: Pr_4N^+, B: Bu_4N^+.

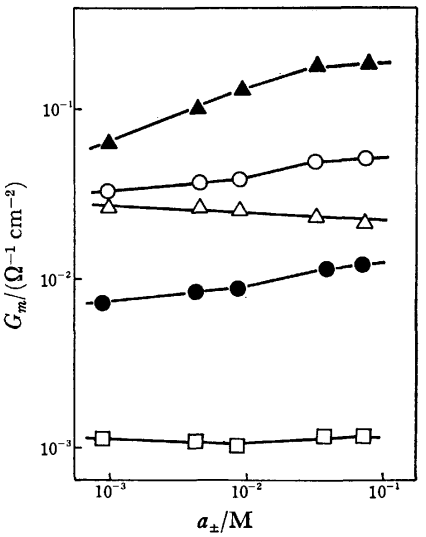

Fig. 2. Membrane conductances as functions of the mean activity of Phase I for various concentration cells. Concentration of Phase II was kept at 10^{-2}M.
▲: NH_4^+, ○: Me_4N^+, △: Et_4N^+, ●: Pr_4N^+, □: Bu_4N^+.

respectively. The same results were also obtained with NH_4^+, Me_4N^+, and Et_4N^+. All the data of membrane conductance are shown in Fig. 2. It has been shown that the membrane conductance becomes larger[16,17,21] as the concentration of the external solution increases except for the case of Et_4NCl. In the case of Et_4NCl, a small decrease in the conductance was observed at higher concentrations. The reason for this decrease is not still clear at present. The order of magnitude of the membrane conductance was $NH_4^+ > Me_4N^+ > Et_4N^+ > Pr_4N^+ > Bu_4N^+$. As has been mentioned previously,[13] the membrane permeability, P_α, was estimated according to Eqs. 7 and 8 by using the experimental results of the membrane potentials and conductances. The membrane permeabilities are plotted against the mean activities in Fig. 3. The results indicate that the membrane permeability decreases with an increase in the concentration and decreases in the order: $NH_4^+ > Me_4N^+ > Et_4N^+ > Pr_4N^+ > Bu_4N^+$.

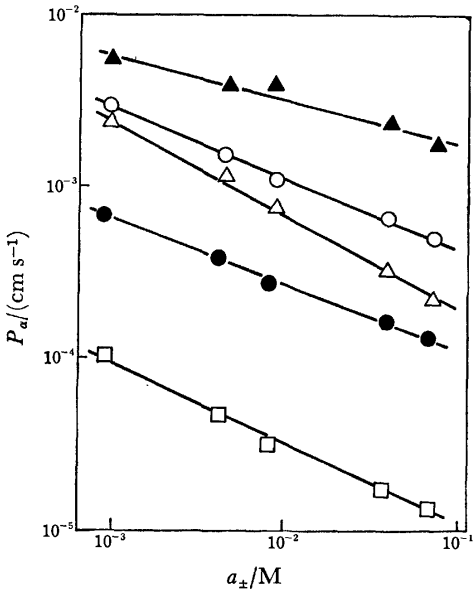

Fig. 3. Permeability *vs.* mean activity diagram for various concentration cells.
▲: NH_4^+, ○: Me_4N^+, △: Et_4N^+, ●: Pr_4N^+, □: Bu_4N^+.

The values of P_{Cl} were found to be very small as compared with those of cations; *i.e.*, P_{Cl}/P_{NH_4} and P_{Cl}/P_{R_4N} were less than 1/100, where R_4N denotes the tetraalkylammonium ion.

According to a previous paper,[20] the membrane permeability is expressed by:

$$P_\alpha = \frac{RT}{|Z_\alpha|F} \frac{\bar{U}_\alpha \bar{C}_\alpha}{\delta (a_\alpha^{\mathrm{I}} \cdot a_\alpha^{\mathrm{II}})^{1/2}}, \qquad (11)$$

provided the membrane is permselective to the ion, α, and the process is membrane-controlling, where Z_α denotes the ionic charge; $\bar{U}_\alpha$, the mobility; $\bar{C}_\alpha$, the concentration of the ion, α, within membranes; δ, the membrane thickness and a_α^{I} and a_α^{II}, the activities of the ion, α, in Phases I and II respectively.

Thus, the permeabilities are plotted against $(a_\alpha^{\mathrm{I}} \cdot a_\alpha^{\mathrm{II}})^{-1/2}$ in Fig. 4. Figure 4 indicates that P_α is

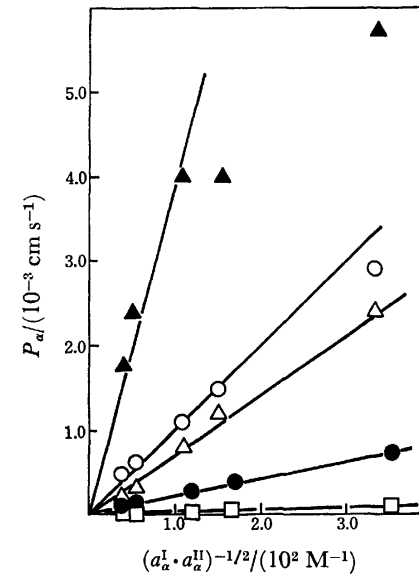

Fig. 4. Permeabilities as functions of the reciprocal of geometric means of the activities of Phase I and Phase II.
▲: NH_4^+, ○: Me_4N^+, △: Et_4N^+, ●: Pr_4N^+, □: Bu_4N^+.

approximately proportional to $(a_\alpha^{\mathrm{I}} \cdot a_\alpha^{\mathrm{II}})^{-1/2}$ for all the systems studied. According to Eq. 11, this implies that $\bar{U}_\alpha \bar{C}_\alpha$ is almost constant. Since the concentration of the cation in the membrane may be regarded as constant within the range of concentrations studied,[22] this means that the mobilities are constant. The mobilities were then evaluated according to Eq. 11; they are summarized, together with the limiting equivalent conductance[11] and ionic radii,[12] in Table 2. The mobility in the membrane in Table 2 are plotted against the limiting equivalent conductance of each ion, λ_α, in Fig. 5.

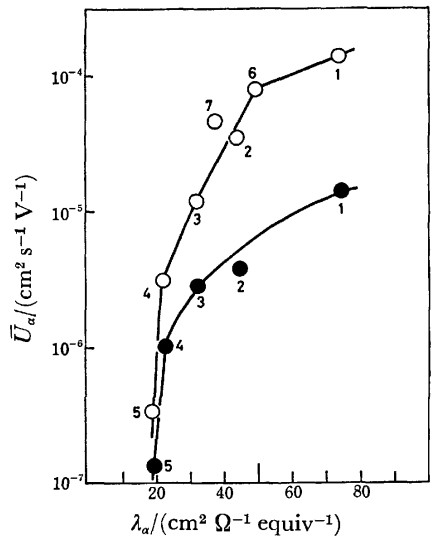

Fig. 5. Mobility in the membrane as a function of the limiting equivalent conductance in aqueous solution.
1: NH_4^+, 2: Me_4N^+, 3: Et_4N^+, 4: Pr_4N^+, 5: Bu_4N^+, 6: Na^+, 7: Li^+.
●: The data obtained in this study with Cl-2.5T.
○: The data obtained by Kawabe *et al.*[5] with AC-1 (Asahi Chem.) at 10^{-1} M.

Table 2. Mobility in the membrane and limiting equivalent conductances in aqueous solution and ionic radii

Substance	$\bar{U}_\alpha$ / $cm^2\ s^{-1}\ V^{-1}$	λ_α / $cm^{-2}\ \Omega^{-1}\ equiv^{-1}$	r_α / Å
NH_4^+	1.4×10^{-5}	73.50	3.31
Me_4N^+	4.2×10^{-6}	44.92	3.67
Et_4N^+	3.0×10^{-6}	32.66	4.00
Pr_4N^+	1.0×10^{-6}	23.42	4.52
Bu_4N^+	1.3×10^{-7}	19.47	4.94

Kawabe *et al.*[5] measured the membrane conductances with the alkali metal cation and tetraalkylammonium ions in order to estimate the effective pore size of the ion-exchange membranes. According to their method, the mean pore size of a membrane was estimated from our experimental results of Et_4N^+, Pr_4N^+, and Bu_4N^+. These quaternary ions may be regarded as indicating that they are not hydrated.[12] By comparing the results of Et_4N^+–Pr_4N^+ and Pr_4N^+–Bu_4N^+, the pore radii of the membrane in this study were found to be 5.4 Å and 5.2 Å respectively. Thus, it can be suggested that the mean effective pore size of the membrane is approximately 10 Å, since the ionic radius of Bu_4N^+ is 4.94 Å and the mobilities of Pr_4N^+ and Bu_4N^+ decrease steeply, as is shown in Fig. 5.

Two-ionic System. The two-ionic membrane potentials for the system expressed by the following scheme were studied.

(II)		(I)
NH_4Cl	Membrane	Tetraalkylammonium chloride
10^{-2} M		10^{-3} M to 10^{-1} M

The concentration of the salt in Phase II was kept at 10^{-2} M NH_4Cl, while that in Phase I was altered from 10^{-3} M to 10^{-1} M. The results are shown in Fig. 6.

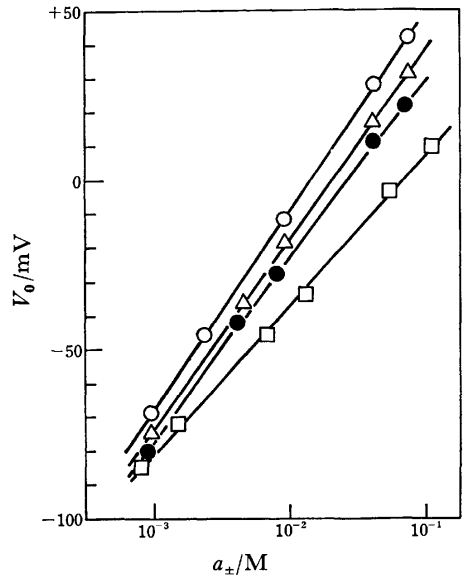

Fig. 6. Membrane potentials as functions of the mean activity of Phase I for two-ionic systems.
○: Me_4N^+, △: Et_4N^+, ●: Pr_4N^+, □: Bu_4N^+.

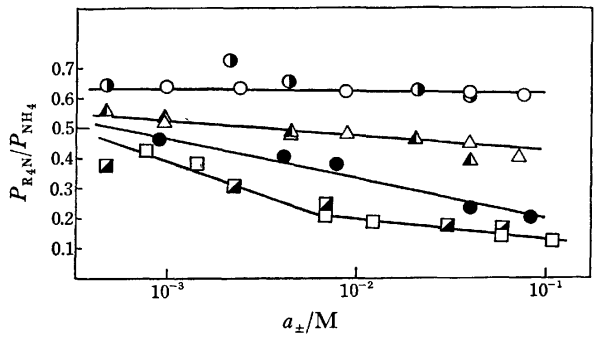

Fig. 7. Permeability ratios as functions of the mean activity of Phase I for two-ionic and multi-ionic systems.
Two-ionic system;
○: Me_4N^+, △: Et_4N^+, ●: Pr_4N^+, □: Bu_4N^+.
Multi-ionic system;
◑: Me_4N^+, ◭: Et_4N^+, ◪: Bu_4N^+.

For the NH_4^+–Me_4N^+ and NH_4^+–Et_4N^+ systems, the plots of the potentials *vs.* the logarithmic activities were found to be linear, with the slope of 58 mV. The results are in agreement with that expected from Eq. 9 provided the membrane permeability ratios are constant. Small deviations from the slope of 58 mV, however, were observed with the NH_4^+–Pr_4N^+ and –Bu_4N^+ systems. The membrane permeability ratios, P_{R_4N}/P_{NH_4}, calculated according to Eq. 9 are shown in Fig. 7. It may be seen in this figure that the longer the chain, the smaller the values of P_{R_4N}/P_{NH_4}, and that the tendency to decrease with the concentration becomes greater as the ionic radius increases. A more detailed study will be required to elucidate the concentration dependence of the permeability ratio.

Multi-ionic System. The multi-ionic potentials of the following system were examined:

(II)		(I)
NH_4Cl	Membrane	$R_4NCl:NH_4Cl=1:1$
10^{-2} M		5×10^{-4} M to 5×10^{-2} M

The concentration of the salt in Phase I, where the concentration ratio of R_4N^+ to NH_4^+ was kept at 1:1, was altered from 5×10^{-4} M to 5×10^{-2} M. Here, the activity coefficient was used without further correction for the mixed electrolyte solutions. The permeability ratio was calculated according to Eq. 5 and shown in Fig. 7. As shown in this figure, P_{R_4N}/P_{NH_4} in the two-ionic system was agreed with that in the multi-ionic system.

According to Eq. 11, $P_\alpha/\bar{U}_\alpha$ may give the measure of the partition of the ion, α, in the membrane; hence:

$$K_{NH_4}^{R_4N} = \frac{P_{R_4N}\bar{U}_{NH_4}}{\bar{U}_{R_4N}P_{NH_4}} \qquad (12)$$

corresponds to the ion-exchange selectivity coefficient. The values of $K_{NH_4}^{R_4N}$ calculated according to Eq. 12 are shown in Table 3. $K_{NH_4}^{R_4N}$ shows an increase with an increase in the alkyl chain length which agrees with the result reported by Kressman and Kitchener.[23,24] At this stage, it is interesting to compare the relative permeabilities, P_{R_4N}/P_{NH_4}, in the two- and multi-ionic systems with those calculated from the permeabilities

TABLE 3. SELECTIVITY COEFFICIENT[a)]

Substance	$K^{R_4N}_{NH_4}$
Me_4N^+	2.2
Et_4N^+	2.2
Pr_4N^+	5.3
Bu_4N^+	19

a) The data were calculated at 10^{-1} M.

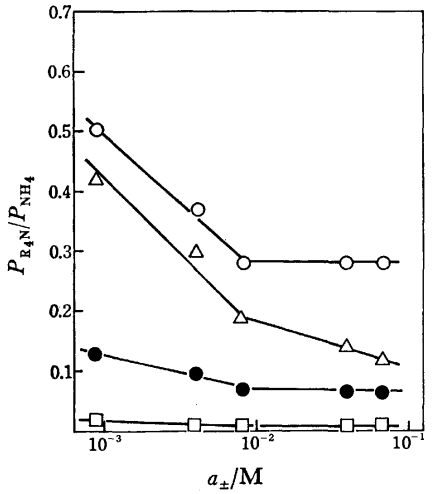

Fig. 8. Permeability ratio, P_{R_4N}/P_{NH_4}, *vs.* mean activity diagram for concentration cells.
○: Me_4N^+, △: Et_4N^+, ●: Pr_4N^+, □: Bu_4N^+.

in the concentration cell given in Fig. 8. Those permeability ratios showed a tendency to decrease against the increase in the concentration of the external solution, *i.e.*, Phase I. However, the values in the concentration cell were found to be much smaller than those in the two- and multi-ionic systems. It is noted that the longer the chain of the organic ion, the smaller the value of P_{R_4N}/P_{NH_4}. This behavior is more or less different from the earlier results in the case of simple inorganic ions.[13,14] These facts imply that the transport phenomena of the organic ions are strongly dependent on the compositions of the ionic species present in the membrane. That is, when only a single species of an ion is present in the membrane, the permeability to the quaternary tetraalkylammonium ion decreases remarkably as their ionic radii increase, as may be seen in Fig. 3. On the other hand, when two species of ions are present together in the membrane, it may be presumed that the relative permeability is governed by the interdiffusion in the membrane and that, therefore, the permeabilities of coexisting ions become closer. However, a more detailed study of the permeability in the two- and multi-ionic systems will be required to confirm the deduction described here.

References

1) R. H. Henderson, *J. Phys. Chem.*, **70**, 2694 (1966).
2) M. A. Peterson and H. G. Gregor, *J. Electrochem. Soc.*, **106**, 1051 (1959).
3) D. Hutchings and R. J. P. Williams, *Discuss. Faraday Soc.*, **21**, 192 (1956).
4) K. Sollner, S. Dray, E. Grim, and R. Neihof, "Ion Transport across Membranes," Academic Press, New York (1954), p. 144.
5) H. Kawabe, H. Jacobson, I. Miller, and H. P. Gregor, *J. Colloid Interface Sci.*, **21**, 79 (1966).
6) A. S. Tombalakian, M. Worsley, and W. F. Graydon, *J. Am. Chem. Soc.*, **88**, 661 (1966).
7) J. H. B. George, R. A. Horne, and C. R. Schlaikjer, *J. Electrochem. Soc.*, **117**, 892 (1970).
8) K. Kaibara, T. Nakahara, I. Satake, and R. Matuura, *Mem. Fac. Sci. Kyushu Univ. Ser. C*, **7**, 1 (1970).
9) B. J. Birch and D. E. Clarke, *Anal. Chim. Acta*, **61**, 159 (1972).
10) K. Shirahama, *Kolloid Z. Z. Polym.*, **250**, 620 (1972).
11) R. A. Robinson and R. H. Stokes, "Electrolyte Solutions," Butterworths, London (1959), p. 463.
12) E. R. Nightingale, Jr., *J. Phys. Chem.*, **63**, 1381 (1959).
13) A. Yamauchi and H. Kimizuka, *J. Theor. Biol.*, **30**, 285 (1971).
14) K. Kaibara, A. Yamauchi, and H. Kimizuka, *Mem. Fac. Sci. Kyushu Univ. Ser. C*, **8**, 247 (1973).
15) V. Subrahmanyan and N. Lakshminarayanaiah, *J. Phys. Chem.*, **72**, 4314 (1968).
16) W. J. McHardy, P. Meares, A. H. Sutton, and J. F. Thain, *J. Colloid Interface Sci.*, **29**, 116 (1968).
17) Y. Matsuda and T. Ishino, *Denki Kagaku*, **30**, 778 (1962).
18) J. Lange, *Z. Phys. Chem. (Leipzig)*, **168A**, 147 (1934).
19) S. Lindenbaum and G. E. Boyd, *J. Phys. Chem.*, **68**, 911 (1964).
20) H. Kimizuka and K. Kaibara, *J. Colloid Interface Sci.*, **52**, 516 (1975).
21) F. Hellferich, "Ion Exchange," McGraw Hill, N. Y. (1962), Chap. 8.
22) K. Kaibara, K. Saito, and H. Kimizuka, *Bull. Chem. Soc. Jpn.*, **46**, 3712 (1973).
23) T. R. E. Kressman and J. A. Kitchener, *J. Chem. Soc.*, **1949**, 1208.
24) J. I. Bregman, *Ann. N. Y. Acad. Sci.*, **75**, 125 (1953).

Structure of Aqueous Isomeric Butyl Alcohols—Sound Velocity Studies

N. Manohara MURTHY and S. V. SUBRAHMANYAM
Department of Physics, Post-Graduate Centre, Anantapur 515003, India

(Received November 1, 1976)

The effect of isomeric butyl alcohols on the temperature of sound velocity maximum in water (TSVM) was studied using a variable path interferometer working at 3 MHz. The structural contribution to the shift in TSVM, $[\Delta T_{str}]_{exp}$, was evaluated for the butyl alcohols and the results are compared with those obtained from studies on the effect of these solutes on the temperature of adiabatic compressibility minimum and density maximum of water. The results indicate that the butyl alcohols enhance the hydrogen-bonded structure of water at low concentrations and at any given concentration, the order of increasing structural contribution to the shift in TSVM being *t*-butyl >*s*-butyl>isobutyl>butyl alcohols. The structural propensities of the butyl alcohols as revealed by TSVM studies are in line with the information obtained from the temperature of adiabatic compressibility minimum and density maximum studies. The results of the present study indicate that TSVM studies are useful in understanding the solution structure in aqueous mixtures.

Many studies have been reported on the solution structure of aqueous alcohols. They mainly deal with the observation of non-ideal thermodynamic behaviour of aqueous mixtures such as viscosity composition,[1] ultrasonic velocity,[2,3] and absorption[4,5] maxima as a function of concentration and negative partial molal volumes.[6,7] At any given temperature water can be considered to consist of essentially two species, one hydrogen bonded and the other non-hydrogen bonded, this being the most common of the many theories.[8] Water exhibits a density maximum at 3.98 °C, adiabatic compressibility minimum at 64 °C and sound velocity maximum at 74 °C. Any parameter which can affect the structural equilibrium of water will also influence the temperature at which the extrema are observed. Hence a study of the effect of non-electrolytes on these physical properties of water helps one to understand the structural propensities of these solutes in water. Wada and Umeda[9] studied the effect of isomeric butyl alcohols on the temperature of density maximum of water. In an earlier communication[10] we reported the effect of these solutes on the temperature corresponding to the adiabatic compressibility minimum of water. Both studies indicate that isomeric butyl alcohols hehave as structure promoters when added in small amounts to water.

According to Eyring and Kincaid[11] a sound wave in a liquid is supposed to travel with infinite velocity within a molecule and with gas kinetic velocity in the intermolecular space. On this assumption, the conversion of hydrogen-bonded into close-packed ones (due to rise in temperature) results in a positive temperature coefficient of sound velocity and the simultaneous volume expansion of both species gives rise to a negative temperature coefficient of velocity. The competition between these two opposing tendencies leads to the sound velocity maximum observed at 74 °C, where thermal expansion balances the effect due to the equilibrium shift. Above 74 °C the structural expansion plays a dominant role and the velocity decreases with increasing temperature.

Any parameter which can affect the structural equilibrium in water would also influence the temperature of sound velocity maximum (TSVM). Hence ultrasonic velocity measurements in aqueous solutions in the vicinity of TSVM are likely to throw some light on the structural effects of different molecules. However, ultrasonic velocity is not generally considered to be a primary thermodynamic quantity. It can be considered to be dependent on density and adiabatic compressibility. Density and adiabatic compressibility of aqueous solutions show a complex temperature dependence, each becoming maxima and minima, respectively, at certain temperatures which are not the same. Under these conditions, we are not certain whether the condition $(du/dt)_{t=TSVM}=0$ can be considered to be a criterion for structure breaking or structure promotion where u denotes ultrasonic velocity and t temperature. The present paper deals with the studies on the effect of isomeric butyl alcohols on the TSVM of water with a view to comparing the results with those obtained from density maximum[9] and adiabatic compressibility minimum[10] studies and thereby evaluate the usefulness of velocity measurements.

Experimental

A. R grade isomeric butyl alcohols were used after purification. Ultrasonic velocity in the pure components and aqueous mixtures was determined using a single crystal variable path interferometer working at 3 MHz with an accuracy of ± 0.003 percent. The details of the experimental technique and the method of measurement of velocity and temperature of liquid were reported.[10]

Solutions of desired concentration were prepared by weighing the samples using triple distilled, degassed water. Ultrasonic velocity in the solutions were determined at $\simeq 2$ °C intervals over a range of 5 °C on either side of TSVM. The velocities were corrected for diffraction effects, following the procedure developed by Subrahmanyam *et al.*[12] At low concentrations of the organic solute, the temperature dependence of sound velocity in the aqueous solutions is parabolic and resembles that of pure water. Hence a transparent template of the curve for pure water was employed to fix TSVM. The accuracy in fixing TSVM is $\pm$ 0.2 °C.

Results

Diffraction corrected ultrasonic velocities in dilute aqueous solutions of isomeric butyl alcohols as a function of temperature at different concentrations are given in Table 1. Some typical results are shown in Fig. 1.

Table 1. Ultrasonic velocity in aqueous solutions of isomeric butyl alcohols at different temperatures

Water + *t*-butyl alcohol

Temperature t(°C)	Velocity u(m/s)	Temperature t(°C)	Velocity u(m/s)
$X_2=0$		$X_2=0.0013$	
	1550+		1550+
68.05	4.60	68.50	6.37
69.60	4.84	69.20	6.52
71.10	5.06	70.20	6.80
72.20	5.19	71.95	7.03
73.55	5.27	72.65	6.95
75.05	5.26	74.60	6.92
76.15	5.21	76.35	6.79
77.55	5.10	78.35	6.56
78.60	4.86		
79.95	4.60		
$X_2=0.0025$		$X_2=0.0037$	
	1550+		1550+
68.50	7.90	68.25	9.27
70.55	8.19	69.55	9.49
72.75	8.43	71.35	9.69
75.30	8.34	73.15	9.67
77.15	8.23	74.85	9.58
79.40	7.67	77.50	9.33
$X_2=0.0046$		$X_2=0.0062$	
	1550+		1550+
68.25	10.62	64.60	12.90
70.15	10.82	66.70	13.15
72.00	11.02	68.55	13.40
72.90	11.03	70.00	13.41
74.10	10.94	72.05	13.23
76.05	10.87	74.20	12.97
78.50	10.50	76.65	12.19
$X_2=0.0075$			
	1550+		
62.20	15.17		
64.00	15.45		
65.80	15.51		
67.30	15.39		
69.25	15.29		
71.35	14.96		

Water + *s*-butyl alcohol

Temperature t(°C)	Velocity u(m/s)	Temperature t(°C)	Velocity u(m/s)
$X_2=0.0014$		$X_2=0.0024$	
	1550+		1550+
68.10	5.64	66.60	7.01
70.30	6.00	68.80	7.44
72.65	6.05	70.95	7.49
74.60	5.89	73.35	7.44
75.95	5.71	76.10	7.12
78.30	5.30	78.10	6.71
$X_2=0.0048$		$X_2=0.0077$	
	1550+		1550+
61.30	9.02	59.20	12.90
63.60	9.53	61.45	13.32
66.55	9.89	64.00	13.38
68.75	9.96	66.40	13.41
71.30	9.72	68.60	13.06
73.40	9.37	70.00	12.86
$X_2=0.0107$			
	1550+		
55.10	16.13		
55.80	16.25		
57.05	16.46		
59.50	16.82		
61.75	16.78		
64.20	16.60		
66.00	16.24		

Water + isobutyl alcohol

Temperature t(°C)	Velocity u(m/s)	Temperature t(°C)	Velocity u(m/s)
$X_2=0.0017$		$X_2=0.0037$	
	1550+		1550+
68.05	5.72	65.95	7.14
70.60	5.98	68.30	7.53
72.85	6.03	70.35	7.49
75.15	5.86	72.00	7.49
77.20	5.50	74.50	7.14
79.10	5.02	76.00	6.84
$X_2=0.0056$		$X_2=0.0082$	
	1550+		1550+
62.60	9.28	57.30	11.16
64.55	9.64	59.85	11.50
67.15	9.65	62.35	11.73
69.35	9.58	65.20	11.61
71.35	9.30	61.75	11.24
74.00	8.80	69.65	10.94

Water + butyl alcohol

Temperature t(°C)	Velocity u(m/s)	Temperature t(°C)	Velocity u(m/s)
$X_2=0.0014$		$X_2=0.0028$	
	1550+		1550+
68.35	3.87	64.50	4.45
70.15	4.12	66.40	4.65
72.50	4.20	68.55	4.87
74.35	4.27	70.40	5.02
75.85	4.02	72.15	4.96
77.70	3.72	74.15	4.72
		75.95	4.36
$X_2=0.0038$		$X_2=0.0064$	
	1550+		1550+
63.15	5.75	59.05	7.75
65.00	6.10	61.55	8.26
67.25	6.35	63.70	8.47
69.20	6.38	65.75	8.51
71.05	6.27	67.90	8.41
73.15	6.00	70.55	8.00
$X_2=0.0080$		$X_2=0.0098$	
	1550+		1550+
56.45	9.80	54.60	11.63
58.10	10.10	57.20	11.90
60.25	10.28	59.55	11.95
62.65	10.19	61.55	11.80
64.92	9.94	63.55	11.44
67.35	9.58	65.10	11.20

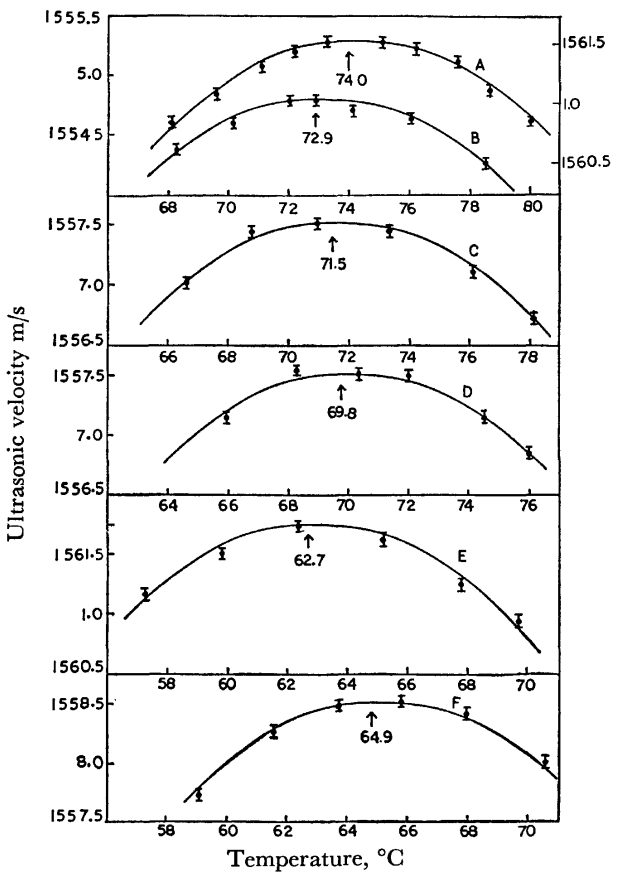

Fig. 1. Ultrasonic velocity in dilute aqueous solutions of isomeric butyl alcohols at different temperatures. A: Pure water. B: water+*t*-butyl alcohol, X_2=0.0046, C: water+*s*-butyl alcohol, X_2=0.0024, D, E: water+isobutyl alcohol, X_2=0.0037, 0.0082, F: water+butyl alcohol, X_2=0.0064.

Discussion

In order to understand the structural propensities of solutes in aqueous mixtures from TSVM studies, it is necessary to obtain an expression for the TSVM of the solution in terms of known quantities. For this purpose it is neccessary to express the sound velocity in the mixture in terms of the velocities in the pure components. Since there is no agreed view regarding the method of evaluation of sound velocity in an ideal mixture, we have taken up the additivity of adiabatic compressibility on volume fractions. The adiabatic compressibility of an aqueous solution can be represented by

$$\beta = \phi_1\beta_1 + \phi_2\beta_2 + \beta^E, \quad (1)$$

where β_1, β_2, and ϕ_1, ϕ_2 refer to the adiabatic compressibilities and volume fractions of water and the organic solute, respectively, and β^E represents the excess adiabatic compressibility. Since

$$\beta = \frac{1}{u^2\rho}, \quad (2)$$

where u is the ultrasonic velocity and ρ density, we can rewrite Eq. 1 as

$$\frac{1}{u^2\rho} = \frac{\phi_1}{u_1^2\rho_1} + \frac{\phi_2}{u_2^2\rho_2} + \beta^E. \quad (3)$$

It is not necessary to use $\rho=\phi_1\rho_1+\phi_2\rho_2+\rho^E$ in the above equation since the effect of ρ^E, the excess density, on the velocity of the solution is negligibly small. Hence we can rewrite Eq. 3 as

$$\frac{1}{u^2} = \frac{\phi_1^2}{w_1u_1^2} + \frac{\phi_2^2}{w_2u_2^2} + \rho\beta^E, \quad (4)$$

where w_1 and w_2 refer to the weight fractions of water and the organic solute, respectively, in the solution.

According to Willard[13] the velocity in pure water conforms to the relation

$$u_1 = 1557 - 0.0245(74-t)^2, \quad (5)$$

where t is the temperature in °C. Over a small range of temperature the sound velocity in the organic solute is given by

$$u_2 = u_2^\circ - \alpha_u t, \quad (6)$$

where α_u is the temperature coefficient of sound velocity in the solute and u_2° is the velocity at 0 °C.

By substitution of Eqs. 5 and 6 in Eq. 4, differentiation with respect to temperature, and use of the conditions $(du/dt)_{t=TSVM}=0$, we obtain the following expression for TSVM in the solution:

$$T = 74 - \left(\frac{\phi_2}{\phi_1}\right)^2\left(\frac{w_1}{w_2}\right)\left(\frac{\alpha_u}{0.049}\right)\left(\frac{u_1^3}{u_2^3}\right) - \left(\frac{w_1}{\phi_1^2}\right)\left(\frac{u_1^3}{0.098}\right)\left[\rho\frac{d\beta^E}{dt}+\beta^E\frac{d\rho}{dt}\right]. \quad (7)$$

The shift produced in the TSVM of water due to the presence of the organic solute, ΔT_{obsd}, is given by

$$\Delta T_{obsd} = -\left(\frac{\phi_2}{\phi_1}\right)^2\left(\frac{w_1}{w_2}\right)\left(\frac{\alpha_u}{0.049}\right)\left(\frac{u_1}{u_2}\right)^3 - \left(\frac{w_1}{\phi_1^2}\right)\left(\frac{u_1^3}{0.098}\right)\left[\rho\frac{d\beta^E}{dt}+\beta^E\frac{d\rho}{dt}\right]. \quad (8)$$

ΔT_{obsd} can be thought of as being due to two effects; structural effects caused by interaction of the two molecules and dilution. The effect of dilution is always to lower the TSVM. The first term on the right hand side of Eq. 8 represents the shift which can be called the ideal shift ΔT_{id}. If there is no interaction between the two types of molecules, we have $\Delta T_{obsd}=\Delta T_{id}$. The second term refers to the structural contribution to the shift in TSVM, ΔT_{str}, which can be evaluated either from the values of $d\beta^E/dt$ and $d\rho/dt$ of the solution or by means of the relation

$$[\Delta T_{str}]_{exp} = T_{exp} - T_{id}, \quad (9)$$

where

$$T_{id} = 74 - \left(\frac{\phi_2}{\phi_1}\right)^2\left(\frac{w_1}{w_2}\right)\left(\frac{\alpha_u}{0.049}\right)\left(\frac{u_1}{u_2}\right)^3. \quad (10)$$

T_{id} can be evaluated using α_u, u_1, and u_2 and following the method of successive approximations. The values of u_2° and α_u for the isomeric butyl alcohols evaluated from a study of temperature dependence of ultrasonic velocity are given in Table 2. Since the temperature dependence of ϕ_1 and ϕ_2 is very small, ϕ_1 and ϕ_2 used for determining T_{id} were evaluated at the TSVM of the solution found experimentally.

The values of T_{exp}, T_{id}, and $[\Delta T_{str}]_{exp}$ at different concentrations for the isomeric butyl alcohols are given in Table 3. The variation of T_{exp} with mole fraction

Table 2. Ultrasonic velocity at 0 °C, $u_2°$, and temperature coefficient of sound velocity, α_u, for isomeric butyl alcohols

Solute	$u_2°$(m/s)	α(m/s °C)
t-Butyl alcohol	1227.20	−4.21
s-Butyl alcohol	1306.45	−3.75
Isobutyl alcohol	1271.95	−3.35
Butyl alcohol	1323.58	−3.36

Table 3. T_{exp}, T_{id}, and $[\Delta T_{str}]_{exp}$ at different mole fractions X_2 for isomeric butyl alcohols

Mole fraction X_2	T_{exp} (°C)	T_{id} (°C)	$[\Delta T_{str}]_{exp}$ (°C)
	t-Butyl alcohol		
0.0013	73.6	70.2	+3.4±0.2
0.0025	73.4	67.0	+6.4±0.2
0.0037	73.0	64.1	+8.9±0.2
0.0046	72.9	61.9	+11.0±0.2
0.0062	69.0	58.5	+10.5±0.2
0.0075	66.0	56.2	+9.8±0.2
	s-Butyl alcohol		
0.0014	72.3	71.6	+0.7±0.2
0.0024	71.5	69.8	+1.7±0.2
0.0048	68.0	66.1	+1.9±0.2
0.0077	64.2	62.0	+2.2±0.2
0.0107	60.5	58.5	+2.0±0.2
	isobutyl alcohol		
0.0017	71.9	71.2	+0.7±0.2
0.0037	69.8	68.2	+1.6±0.2
0.0056	67.1	65.6	+1.5±0.2
0.0082	62.7	62.2	+0.5±0.2
	Butyl alcohol		
0.0014	72.4	72.1	+0.3±0.2
0.0028	70.2	70.3	+0.1±0.2
0.0038	68.5	69.1	−0.6±0.2
0.0064	64.9	65.9	−1.0±0.2
0.0080	61.0	64.0	−3.0±0.2
0.0098	58.5	62.1	−3.6±0.2

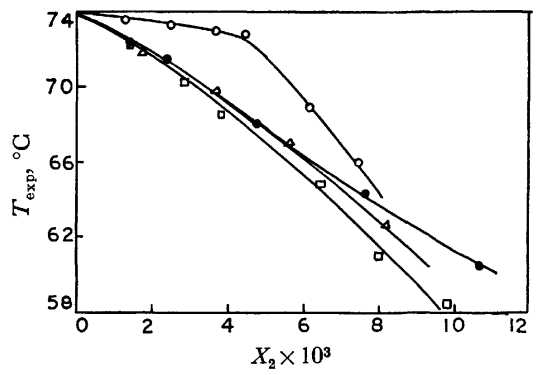

Fig. 2. Variation of T_{exp} with mole fraction X_2 of isomeric butyl alcohols.
○: *t*-Butyl alcohol, △: isobutyl alcohol, ●: *s*-butyl-alcohol, □: butyl alcohols.

X_2 for the butyl alcohols is shown graphically in Fig. 2.

Plots of $[\Delta T_{str}]_{exp}$ *versus* X_2 for the butyl alcohols are shown in Figs. 3A—3D. Also included in these

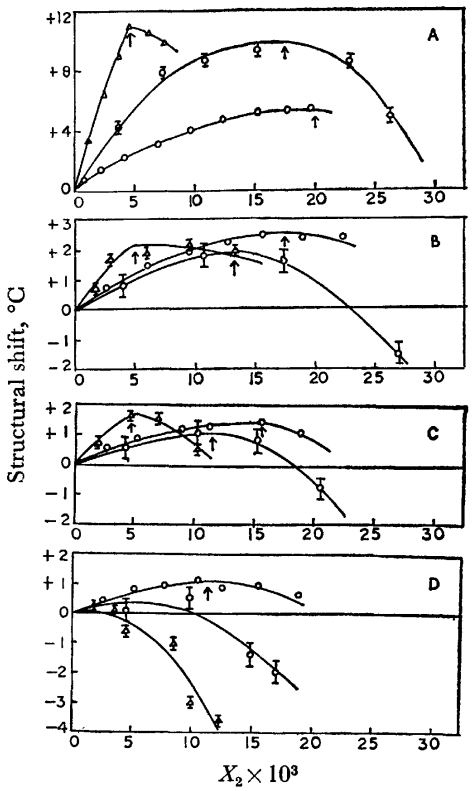

Fig. 3. Structural shifts versus molefraction X_2 of isomeric butanols.
$\bar{\Upsilon}$: $[\Delta T_{str}]_{exp}$, $\bar{\Phi}$: $[\Delta T_{\beta str}]_{exp}$, ○: $[\Delta T'_{str}]_{exp}$.
A: Water+*t*-butyl alcohol, B: water+*s*-butyl alcohol, C: water+isobutyl alcohol, D: water+butyl alcohol.

figures are the variation of $[\Delta T'_{str}]_{exp}$ (structural contribution to the shift in the temperature of maximum density of water) and $[\Delta T_{\beta\ str}]_{exp}$ (structural contribution to the shift in the temperature of adiabatic compressibility minimum of water) taken from literature[9,10] to facilitate a comparison of the different studies.

$[\Delta T_{str}]_{exp}$ is positive at low concentrations for *t*-butyl, *s*-butyl, and isobutyl alcohols indicating stabilization of the hydrogen-bonded structure of water. $[\Delta T_{\beta\ str}]_{exp}$ and $[\Delta T'_{str}]_{exp}$ are also positive for these solutes. $[\Delta T_{str}]_{exp}$ and $[\Delta T_{\beta\ str}]_{exp}$ are positive for butyl alcohol though small in magnitude, in the very low concentration range, becoming negative at high concentrations. It is quite possible that the structure stabilizing propensity of this molecule becomes weak at high temperatures. At any given concentration, the structure enhancing efficiency of the butyl alcohols found from TSVM studies is in the order, *t*-butyl>*s*-butyl>isobutyl>butyl alcohol. The same order is found in studies on the effect of these butyl alcohols on the temperature density maximum[9] and adiabatic compressibility minimum[10] of water.

For the butyl alcohols, the optimum concentration at which the quantities $[\Delta T_{str}]_{exp}$, $[\Delta T_{\beta\ str}]_{exp}$, and $[\Delta T'_{str}]_{exp}$ become maxima are not the same (Figs. 3A—3D and Table 4). T_{exp}, $T_{\beta\ exp}$, and T'_{exp} (temperature of maximum density of the solution) for the aqueous isometric butyl alcohols at the optimum concentrations evaluated from the graphs (Fig. 2 and

TABLE 4 $(X_2)_{opt}$ FOR DIFFERENT SOLUTES

Solute	$[\Delta T_{str}]_{exp}$		$[\Delta T_{\beta\ str}]_{exp}$		$[\Delta T_{str}]_{exp}$	
	$(X_2)_{opt}$	T_{exp} (°C)	$(X_2)_{opt}$	$T_{\beta\ exp}$ (°C)	$(X_2)_{opt}$	T' (°C)
t-Butyl alcohol	0.0047	72.4	0.0175	43.5	0.0200	0.87
s-Butyl alcohol	0.0040	69.0	0.0106	52.0	0.0140	2.36
Isobutyl alcohol	0.0038	69.8	0.0092	53.2	0.0124	1.65
Butyl alcohol	0.0027	71.2	0.0090	50.6	0.0090	2.48

literature[9,10]) are also given in Table 4.

The results indicate that the structural effects as revealed from density and adiabatic compressibility measurements have similar concentration dependence. In all cases $[\Delta T_{str}]_{exp}$ becomes maximum at much lower X_2 than either that of $[\Delta T_{\beta\ str}]_{exp}$ or $[\Delta T_{str}]_{exp}$. Even though the concentration at which $[\Delta T_{\beta\ str}]_{exp}$ becomes maximum is less than that at which $[\Delta T_{str}]_{exp}$ becomes maximum, for a given solute, they are close to each other. This indicates that there is a close similarity between the temperature of density maximum and adiabatic compressibility minimum in revealing the structural propensities of solutes in water. However, there is a large difference with respect to the concentration dependence of structural effects as revealed from TSVM studies. This is because $[\Delta T_{str}]_{exp}$ becomes maximum at a lower X_2 as compared to $[\Delta T_{\beta\ str}]_{exp}$ or $[\Delta T'_{str}]_{exp}$ for a given solute. It is difficult to interpret this behaviour from the fact that each study was confined to different temperature (TSVM studies around 74 °C, adiabatic compressibility minimum studies around 64 °C, and density maximum studies around 4 °C). The $(X_2)_{opt}$ of each study is not commensurate to the temperature differences as is clear from Table 4. The occurrance of the maximum in $[\Delta T_{str}]_{exp}$ *versus* X_2 at very low X_2 values as compared to the other two studies may very likely be due to the dependent nature of ultrasonic velocity on density and adiabatic compressibility. However, the TSVM studies, in general, indicate correctly whether a solute behaves as a structure promoter or disrupter.

It is clear that even though ultrasonic velocity is not a primary thermodynamic quantity, TSVM studies could be used to classify the solutes as structure makers or breakers.

References

1) W. Herz and E. Lorentz, *Z. Phys. Chem.*, **A140**, 406 (1929).
2) Ch. Burton, *J. Acoust. Soc. Am.*, **20**, 186 (1948).
3) E. K. Baumgartner and G. Atkinson, *J. Phys. Chem.*, **75**, 2337 (1971).
4) H. Endo and O. Nomoto, *Bull. Chem. Soc. Jpn.*, **46**, 3004 (1973).
5) M. J. Blandamer, D. E. Carke, N. J. Hidden, and M. C. R. Symons, *Chem. Commun*, **1968**, 342.
6) V. S. Griffiths, *J. Chem. Soc.*, **1952**, 860.
7) G. N. Malcolm and J. S. Rowlinson, *Trans. Faraday Soc.*, **53**, 921 (1957).
8) F. Franks and D. J. G. Ives, *Quart. Rev.*, **20**, 1 (1966).
9) G. Wada and S. Umeda, *Bull. Chem. Soc. Jpn.*, **35**, 1797 (1962).
10) S. V. Subrahmanyam and N. Manohara Murthy, *J. Sol. Chem.*, **4**, 347 (1975).
11) H. Eyring and J. F. Kincaid, *J. Chem. Phys.*, **5**, 587 (1937).
12) S. V. Subrahmanyam, V. Hyder Khan, and C. V. Raghavan, *J. Acoust. Soc. Am.*, **46**, 272 (1969).
13) G. Willard, *J. Acoust. Soc. Am.*, **19**, 236 (1947).

Ultraviolet Spectral Study of *o*- and *p*-(Halomercurio)phenols

P. L. YADAV,* N. K. JHA, and V. RAMAKRISHNA**
Department of Chemistry, I. I. T., New Delhi, India
(Received December 13, 1976)

The ultraviolet spectra of *o*- and *p*-(halomercurio)phenols, *o*- and *p*-OHC_6H_4HgX(X=F, Cl, Br, or I) have been recorded in ethanolic solution and λ_{max} and log ε_{max} have been recorded. The spectra of these compounds have been interpreted in terms of the correlation with the spectra of benzene. HgX group is shown to be having electron-withdrawing effect on the benzene ring. Variation in the values of λ_{max} and log ε_{max} on changing from *o*- to *p*-derivative for a particular (halomercurio)phenol and on changing the halogen attached to mercury has been explained.

A very large number of organomercury compounds are known but only a few of them have been subjected to UV spectral study; such a study is specially limited when one considers aromatic organomercurials. Leandri and Tundo[1] have reported and interpreted the UV spectral data (220 to 350 nm) of *p*-XC_6H_4HgCl and $XC_6H_4HgC_6H_4X$ where X=OH, CH_3, Cl, NO_2, and NH_2. Gowenlock and Trotman[2] restudied the *p*-XC_6H_4HgCl compounds in a wider range (200 to 350 nm) and also included compounds where $X=O^-$ or NH_3^+. In addition, they have reported the spectra of some ortho derivatives ($X=O^-$ or OH). Baliah and Subharayan[3] have reported the spectral study of some of the *o*- and *p*- compounds reported earlier and they have enlarged their list to include compounds where $X=(CH_3)_2N$, $(C_2H_5)_2N$, and CH_3O; however, their data were collected upto 220 nm and they have referrred to the work of Leandri and Tundo only but not that of Gowenlock and Trotman.

The spectral study of *o*- and *p*-(halomercurio)phenols reported so far have been confined to the chloromercurio derivatives only. Gowenlock and Trotman[2] predicted from their spectral analysis of *o*- and *p*-chloromercurio derivatives that the spectra of bromo- and iodomercurio derivatives would be more complicated because of the interference from HgBr and HgI groups as observed in the case of HgCl group. In the present work the spectra of *o*- and *p*-OHC_6H_4HgX where X=F, Cl, Br, or I are reported and interpreted.

Experimental

o- and *p*-(Halomercurio)phenols were prepared according to a method reported earlier.[4] The spectral data were recorded using ethanolic solutions of these compounds (ethanol was purified by treating with clean and dry magnesium turnings and a little iodine and refluxing for half an hour; the fraction distilling at 78.3 °C was collected). Solutions of concentration varying from 1×10^{-4} to 7×10^{-5} M were employed. The spectra were recorded on Unicam SP 700 UV and visible spectrophotometer. The spectra are shown in Figs. 1 and 2.

All the eight compounds studied showed three bands in the UV region. λ_{max} was recorded for each band and the corresponding value of log ε_{max} was also calculated. These

Table 1. UV Spectral data of *o*- and *p*-(haromercurio)phenols

Compound	λ_{max} (nm)	log ε	λ_{max} (nm)	log ε	λ_{max} (nm)	log ε
o-OHC_6H_4HgF	210	3.86	225	3.49	284	3.25
p-OHC_6H_4HgF	207	4.05	232	3.51	282	3.23
o-OHC_6H_4HgCl	212	4.13	225	3.80	282	3.51
p-OHC_6H_4HgCl	207	4.14	234	4.05	275	3.30
o-OHC_6H_4HgBr	210	4.16	225	3.82	284	3.52
p-OHC_6H_4HgBr	208	4.17	234	4.07	282	3.39
o-OHC_6H_4HgI	209	4.38	232	4.05	284	3.60
p-OHC_6H_4HgI	208	4.39	237	4.27	282	3.54

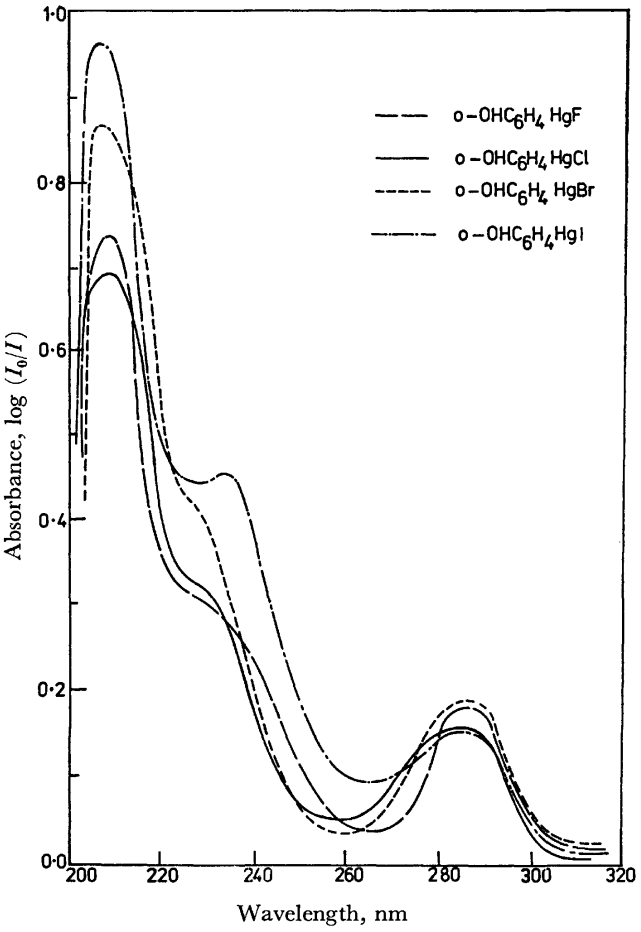

Fig. 1. UV spectra of *o*-(halomercurio)phenols.

* Present address: Department of Chemistry, Engineering College, Bhagalpur, Bihar, India.

** Present address: Ministry of Defence, South Block, New Delhi, India.

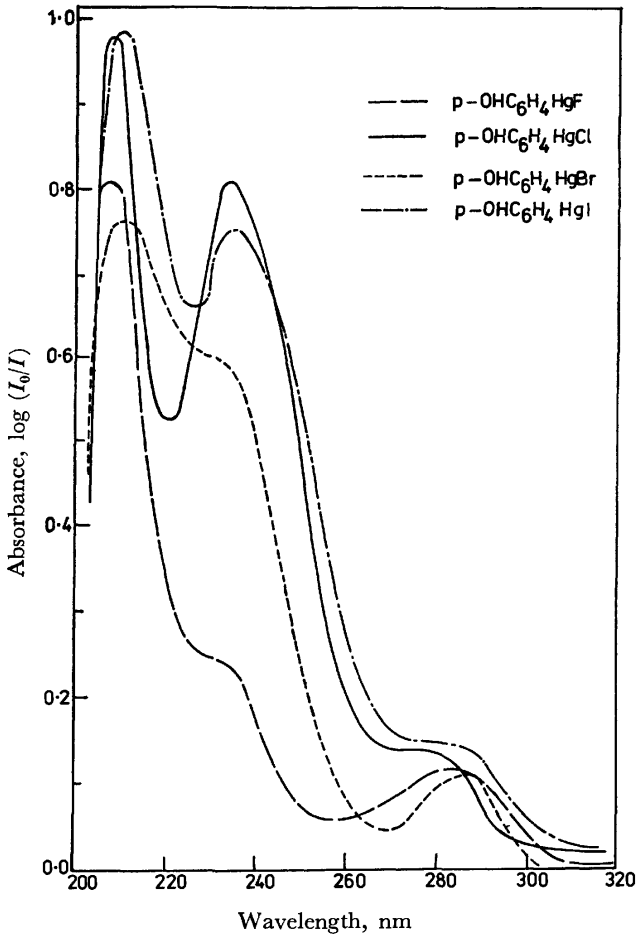

Fig. 2. UV spectra of *p*-(halomercurio)phenols.

values are shown in Table 1. In certain cases, *viz.* *o*-derivatives the band at 225 nm was not distinct, rather observed as an inflection point (Fig. 1).

Discussion

As *o*- and *p*-(halomercurio)phenols are disubstituted benzene derivatives, their spectral data may be correlated with those of benzene. Benzene shows three absorption bands at 256, 203, and 180 nm attributed to $^1B_{2u}\leftarrow{}^1A_{1g}$ $^1B_{1u}\leftarrow{}^1A_{1g}$, and $^1E_{1u}\leftarrow{}^1A_{1g}$ transitions respectively.[5] The 256 and 203 nm bands usually called secondary and primary bands respectively have been studied extensively in benzene derivatives. These bands are usually present in the spectra of substituted benzenes, though shifted due to substitution.[6]

Effect of HgCl Group on the Spectra of Benzene. The two bands of phenylmercury(II) chloride at 210 and 258 nm may be considered as bathochromically shifted primary and secondary bands of benzene.[1-3] It is difficult to assess the amount of shift in the primary band because HgCl group itself absorbs in this region. In fact most of the mercury compounds (though not derivatives of benzene) have absorption bands in this region, *e.g.* $HgCl_2$ 211 nm, $HgBr_2$ 206 and 234 nm, HgI_2 215 and 273 nm,[2] and CH_3HgCl 206 nm.[7] Thus, the bands in the first column of Table 1 may be ascribed to HgX groups and the bands in the second and third columns may be treated as the shifted primary and secondary bands of benzene respectively.

In spite of the overlap of the primary band of C_6H_5-HgCl by that of HgCl group, it is possible to estimate a value of λ_{max} for the former using the observation by Doub and Vandenbelt[6a] that the ratio of λ_{max} (secondary) to λ_{max} (primary) in monosubstituted benzenes is nearly constant, *viz.* 1.19 to 1.28. Taking an average value of 1.23 for this ratio and the known value of λ_{max} (secondary) for C_6H_5HgCl, 258 nm, the value of λ_{max} (primary) for C_6H_5HgCl comes out to be 258/1.23= 210 nm.

Electronic Effect of HgCl Group. It is not possible to conclude from the shifts alone in phenylmercury(II) chloride (203→210 nm, 256→258 nm) whether HgCl group is acting like electron acceptor or electron donor since both electron acceptor and electron donor groups are known to cause shift (bathochromic and hyperchromic) in the primary and secondary bands of benzene.[6,8,9] Gowenlock and Trotman[2] have concluded by comparing the effect of ionization OH→O^- on the secondary band for both *o*- and *p*-substituted phenols that HgCl group is *o*-, *p*-directing. However, their conclusion is not very convincing; for example, for the *p*-substituents SMe, Cl, HgCl, CHO, COMe, and NO_2 the ionization leads to a displacement of λ_{max} to a longer wavelength by 7, 19, 30, 46.5, 49, and 85 nm respectively and from this observation they conclude that HgCl group is similar to Cl group and is *o*-, *p*-directing. However, the value of the shift for HgCl, 30 nm, happens to be between the value for an *o*-, *p*-directing group (Cl, 19 nm) and that for a *m*-directing group (CHO, 46.5 nm) and thus it is not possible to say definitely whether HgCl group is *o*-, *p*-directing or *m*-directing. Unfortunately there is no direct experimental evidence of the *o*-, *p*-directing or *m*-directing nature of HgCl group in literature since most reagents used in substitution in the benzene ring remove the HgCl group from the ring.

Some idea about the electron withdrawing or electron releasing nature of HgCl group may be obtained by using the observation of Doub and Vandenbelt[6] that in a *p*-disubstituted benzene, the shift in the primary band is not much different from the sum of the shifts by

Table 2. Effect of para disubstitution A-C_6H_4-B on the primary band of benzene

A	Shift (nm)[a] for A	B	Shift (nm) for B	Ref.	Shift for *p*-A-C_6H_4-B		
					Calcd Sum A+B	Obsd	Ref.
HgCl	7.0	NO_2	57.0	1	64.0	66.0	1
HgCl	7.0	CH_3	3.5	1	10.5	21.5	1
HgCl	7.0	Cl	6.5	1	13.5	23.0	1
HgCl	7.0	NH_2	31.0	1	38.0	50.0	1
HgCl	7.0	OH	7.0	1	14.0	31.0	Table 1
HgCl	7.0	OCH_3	13.5	10	20.5	30.0	3
HgCl	7.0	$N(CH_3)_2$	47.5	10	54.5	76.0	3
HgCl	7.0	O^-	31.5	10	38.5	43.0	2

a) Calculated from the present work.

the individual substituents (as observed in corresponding monosubstituted derivatives) if the substituents are of the same character (*i.e.* both electron withdrawing or both electron releasing) but the shift is larger than the sum of the two shifts if the substituents are of opposite character. Table 2 shows that when HgCl group is in *p*-position to *o*-, *p*-directing groups (OH, NH_2 *etc.*) the shift is much larger than the sum of the shifts due to two substituents individually. Further when HgCl group is in *p*-position to an electron withdrawing group, namely NO_2, the shift is nearly the same as the sum of the shifts due to NO_2 and HgCl groups individually. These two observations clearly indicate that HgCl group acts like an electron withdrawing group.

The electron withdrawing capacity of Hg group can be ascribed to the fact that mercury has two vacant p orbitals in its valence shell which can accommodate the withdrawn electrons. These must be a conjugative interaction of HgCl group with the electron-releasing group, for example, the following structure would make an important contribution to the excited state of *p*-(halomercurio)phenol:

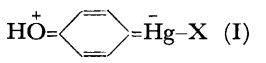

(I)

which causes a considerable bathochromic shift in the primary band of benzene.

Comparison of the Spectra of o- *and* p-*(Halomercurio)-phenols.* It is observed in Table 1 that the shift in primary band is greater in *p*-compounds than in *o*-compounds and also that the intensities of these bands are greater for *p*-compounds than for *o*-compounds. In fact, for *o*-compounds usually inflection points are observed rather than peaks which are distinct for the *p*-compounds (Figs. 1 and 2). The decrease in the shift and intensity of the primary band in *o*-compounds can be ascribed to the steric interference with coplanarity. The steric overlap between the *o*-substituents sets up appreciable interference which prevents the attainment of uniplanar configuration by the benzene derivatives. Steric inhibition of electronic interaction thus raises the energy level of the ground state but since the phenyl-oxygen and phenyl-mercury links postulated in the excited state contain a larger amount of double bond character and since the interplanar angle cannot from theoretical consideration (Franck-Condon principle) change during transition, the energy level of the excited state will be raised even more than that of the ground state. Thus the transition energy is increased in *o*-compound as compared to *p*-compound resulting in a smaller bathochromic shift and also a reduced transition probability, resulting in a loss of absorption intensity.

In case of secondary bonds *p*-compounds show lesser bathochromic and hyperchromic shifts as compared to *o*-compounds. A reason for such a behaviour is not apparent since one might expect that the secondary bands would be effected in a similar way as the primary bands in changing from a *p*-isomer to *o*-isomer.

Effect of Change in Halogen Atom on the Spectra of o- *and* p-*(Halomercurio)phenols.* It may be noted that the prediction by Gowenlock and Trotman[2] regarding the complex nature of the spectra of bromo and iodo derivatives compared to that of chloro derivatives does not appear to be correct. Table 1 shows that the spectra of all the halo derivatives are similar and there are only three bands in each case.

It is seen in Table 1 that for the *o*-derivatives the intensity of the primary band increases in the order F<Cl<Br<I. The secondary bands behave in a similar way. However, the λ_{max} values for the secondary bands remain nearly constant (282—284 nm) and λ_{max} values for primary bands are also constant except for *o*-iodo derivative which has a longer λ_{max} value than other *o*-halo derivatives. For *p*-derivatives the situation is similar.

The excited state of *p*-(halomercurio)phenol may be represented by the structure I mentioned earlier where HgX group is acting like an electron acceptor. Since the iodo derivative shows the maximum intensity of the primary band, the excited state must be stabilized most in its case and stability of the excited state should decrease in the order I>Br>Cl>F. On the basis of inductive effect of halogen atoms it would appear that the excited state should be most stable in the case of fluoro derivatives (fluorine being the most electronegative amongst the halogens) and the order should be F>Cl>Br>I. Thus, the inductive effect cannot be used to explain the observed order. No other explanation is apparent for the observed order.

References

1) G. L. Leandri and A. Tundo, *J. Chem. Soc.*, **1954**, 3377.
2) B. G. Gowenlock and J. Trotman, *J. Chem. Soc.*, **1955**, 1554.
3) V. Baliah and P. Subharayan, *J. Ind. Chem. Soc.*, **40**, 638 (1963).
4) P. L. Yadav, N. K. Jha, and V. Ramakrishna, *Ind.J. Chem.*, **13**, 1095 (1975).
5) H. H. Jaffe and M. Orchin, "Theory and Application of Ultraviolet Spectroscopy," 4th ed, John Wiley & Sons, Inc., London (1966), p. 244.
6) L. Doub and J. M. Vandenbelt, a) *J. Am. Chem. Soc.*, **69**, 2714 (1974); b) *ibid.*, **71**, 2414 (1949).
7) K. Hartley, H. O. Pritchard, and A. A. Skinner, *Trans. Faraday Soc.*, **46**, 1019 (1905).
8) W. F. Hammer and F. A. Matsen, *J. Am. Chem. Soc.*, **70**, 2842 (1948).
9) F. A. Matsen, *J. Am. Chem. Soc.*, **72**, 5243 (1950).
10) A. E. Gilman and E. S. Stern, "An Introduction to Electronic Absorption Spectroscopy," 2nd ed, Edward Arnold Publishers, London (1957), p. 140.

Studies on the Mechanism and Kinetics of Propylene Oligomerization and Hydrooligomerization on Zeolites

Shawky M. HASSAN, G. M. PANCHENKOV,* and O. I. KUZNETSOV*

Department of Chemistry, Faculty of Science, The University of Almansoura, Almansoura, Egypt
**Department of Physical and Colloid Chemistry, Institute of Petrochemicals and Gas Industry, Moscow U.S.S.R.*

(Received May 12, 1975)

The propylene conversion process has been studied in the presence of synthetic zeolites of different types and metal ions. The NiX zeolite is selective for the oligomerization of propylene. On the zeolites of different other metal ions, the hydro-oligomerization process took place. It has been found that the obtained 3-methylpentenes are primary products of the propylene oligomerization. A scheme mechanism has been proposed assuming an intermediate of a cyclobutane derivative. The mechanism explains the formation of all the obtained products of propylene conversion on the synthetic zeolites.

Oligomerization of olefins is one of the most complicated reactions owing to its high exothermic effect. The heat liberated during the reaction accelerates different undesirable side reactions such as cracking, hydrogen transfer, double bond migration, and coke formation.[1-5] It is, therefore, difficult to study either the mechanism or the kinetics of this reaction, especially, on a solid catalyst.

To facilitate this study, two problems had to be solved. The first is the unstability of the temperature during the reaction, and the second is the competition of the side reactions, *i.e.* the selectivity of the used catalyst.

The first problem is solved[6] by making a reactor with a special construction which allows to withdraw the released heat out of the reaction zone and maintains the reaction proceed at constant temperature.

It is of interest to study the propylene oligomerization in the presence of synthetic faujasites of various metal ions for the purpose to obtain a selective catalyst. For this purpose the cations such as cobalt, nickel, manganese, and magnesium were used, the oxides of which possess a high selectivity in the propylene oligomerization.[7-10] Other cations were used for comparison.

Experimental

The various di- and trivalent cationic X and Y zeolites were prepared by exchanging the russian synthetic NaX ($Na_2O \cdot Al_2O_3 \cdot 2.4SiO_2 \cdot nH_2O$) and NaY ($Na_2O \cdot Al_2O_3 \cdot 48SiO_2 \cdot nH_2O$ zeolites).[3] The degree of exchange was maintained at ≈65% for the X Zeolites and ≈85% for the Y Zeolites. A catalyst with 80% of nickel-exchange was also prepared from the NaX zeolite. The ion-exchanged powders were compressed without binders into tablets, 4 mm in diameter and 5—6 mm in thickness.

Propylene conversion activity was measured under atmospheric pressure with 40 ml of catalyst in a fixed bed reactor of conventional design. The catalyst was calcined at 550 °C in a flow of dry air for 4 h and then in a flow of nitrogen for 1 h. After calcination the temperature was adjusted to the desired value. The feed in each run was 4 liters of 100% propylene.

Both gaseous and liquid products were collected separately. Each was analyzed by the gas and liquid chromatography. Liquid products were also analyzed by the infrared spectroscopy. The olefin products were determined quantitatively and separated by the thin layer chromatography using a fluorescene indicator[11]. The total catalytic activity of the catalyst was calculated by the percentage of converted propylene.

The initial temperature was 190 °C, but due to the exothermic behaviour of the studied reaction, it quickly increased by about 20—25 °C depending on the treated zeolite catalyst. For kinetic experiments a reactor of special design[6] was used which allowed to maintain the temperature constant.

The part of liquid products which cannot be obtained by suction after the run, was cracked by raising the temperature slowly to 550 °C. Gases and liquids of C_1—C_8 paraffins were formed and the colour of the catalyst became dark due to the formation of coke. The amount of the latter was determined.

Results and Discussion

Catalytic Activity of Zeolites. The catalytic activity of various ion-exchanged zeolites was tested at an initial temperature of 190 °C and space velocity of propylene 40 ml (ml catalyst)$^{-1}$ h^{-1} (Table 1). The overall order of activity is LaY≃LaX≃CeX≃MgY>NiY>CoY>AlY>MgX>MnY>NiX>CoX>CaX.

When cations are of the same group in the periodic table a certain relation may be obtained.[12] Attempts have failed to correlate the obtained catalytic activities with the ionic radii or ionization potential of the exchanged metal cations of different groups of the periodic table. Thus, each metal ion has its own ability to perform a certain change in the zeolite lattice depending on its own electronic configuration.

Selectivity of Zeolites. Depending on the zeolite form it is possible to obtain liquid products which contain only olefins, paraffins or mixtures of both. In the presence of all the tested zeolites no aromatics are detected by the infrared spectral analysis.

In the cases of CoX, MnX, and MgX, 18.9, 10.1, and 20.2% olefins are, respectively, separated from the liquid products by the thin layer column chromatography. The other products are C_4—C_9 paraffins. The IR spectra of the separated olefins indicate the presence of two bands at 910 and 965 cm^{-1} characteristic for double bonds of the vinyl and transvinyl types.[13] The 890 cm^{-1} band characteristic for the double bond of vinylidene type is absent.

In the presence of all tested zeolites except NiX only paraffinic hydrocarbons are formed, as indicated by both chromatographic and infrared spectral analyses. The composition of these paraffins are presented in

Table 1. Propylene conversion on various zeolite catalysts at 190 °C and 0.025 h

Catalyst	MgY	NiY	CoY	CaY	AlY	LaY	CaY	CeX	LaX
Propylene conversion, wt %	98.7	92.0	90.7	62.4	88.1	98.4	32.6	98.8	98.3
Liquid products, wt %	18.7	32.4	31.0	32.0	22.4	7.8	28.4	2.0	5.24
Propane, wt %	3.9	8.8	5.7	6.3	1.6	15.1	3.0	12.2	14.3
C_2, C_4, and C_5 paraffins, wt %	10.8	3.6	5.0	14.5	6.1	25.9	10.2	13.2	27.0
Unrecovered liquid converted into gas and liquid by heating,[a] wt %.	54.6	26.2	30.3	23.9	58.6	38.0	35.0	57.1	35.6
Unrecovered liquid converted into coke,[a] wt %.	9.8	28.9	27.6	21.7	10.9	13.2	22.5	15.1	17.8

a) These products were obtained by raising the temperature of the catalyst to 550 °C after the run.

Table 2. Products of propylene conversion on zeolites at 190 °C and 0.025 h

Product	MgY	NiY	CoY	CaY	AlY	LaX	CaX	CeX	LaX
Isobutane	7.68	3.86	2.51	3.72	0.28	0.10	0.00	0.83	5.34
Butane	0.89	0.24	0.03	4.52	0.00	0.00	0.00	2.54	0.48
2-Methylbutane	28.05	21.40	17.83	11.22	8.59	5.02	2.77	18.11	23.11
Pentane	0.89	0.56	0.13	0.00	0.83	0.29	0.00	0.98	0.98
2,3-Dimethylbutane +2-Methylpentane	27.63	32.47	32.47	28.15	22.18	29.25	11.29	24.62	31.92
3-Methylpentane	9.90	18.43	11.65	8.74	7.70	12.92	4.62	13.11	14.81
Hexane	0.89	3.37	0.33	0.00	0.62	0.97	0.74	1.39	1.18
2,4-Dimethylpentane	4.43	3.21	6.17	8.00	6.47	4.47	5.74	3.61	3.50
2-Methylhexane	5.02	4.92	5.77	6.32	5.39	9.91	9.44	7.62	5.44
2,3-Dimethylpentane	6.21	3.47	8.56	10.40	8.68	6.21	13.14	4.92	3.05
3-Methylhexane	4.88	4.15	7.77	6.88	6.32	11.66	8.51	8.19	6.48
3-Ethylpentane	0.00	0.14	0.24	0.00	0.18	0.49	1.11	0.39	0.20
Heptane	0.00	0.17	0.30	0.00	0.28	0.47	0.00	0.08	0.00
2,2-Dimethylhexane	0.34	0.84	0.17	1.00	2.59	1.63	0.00	1.18	0.28
2,4- + 2,5-Dimethylhexane	2.17	1.39	0.41	4.28	5.54	3.47	12.76	2.52	0.38
2,3,4-Trimethylpentane	0.59	0.04	0.02	0.33	0.09	0.00	0.02	0.03	0.71
2,3,3-Trimethylpentane +2-Methylheptane	0.93	0.82	0.64	3.72	2.95	2.38	9.07	1.71	0.56
2,3-Methylethylpentane	1.25	0.64	0.30	0.40	1.80	1.28	0.00	0.10	0.02
2,3-Dimethylhexane	0.00	0.00	0.00	0.00	2.22	0.48	0.00	0.28	0.01
4-Methylheptane	0.35	0.29	0.21	0.46	0.92	1.04	2.04	0.72	0.02
3-Methylheptane + 3,4-Dimethylhexane	1.14	0.97	0.45	1.55	0.24	3.15	4.81	2.52	0.66
3-Ethylhexane	0.22	0.18	0.16	0.31	0.10	0.28	1.32	0.24	0.00
Total C_9	1.04	2.97	4.15	0.00	16.13	3.58	12.62	4.26	0.92
Calculated octane number	83.1	80	85	78	—	—	—	—	82

Table 2. Presence of hexane, methylpentanes, and dimethylbutane gives evidence that a hydrodimerization reaction takes place on these zeolites. The C_9 paraffins are formed by hydrotrimerization of propylene. In addition to that, C_2, C_4, C_5, C_7, and C_8 paraffins are formed. This suggests that hydrodimerization of propylene into trimers and tetramers is accompanied by a cracking and then by subsequent hydrogen transfer to the cracking products. The distribution of C_4—C_9 paraffins in the liquid products seems to depend on the exchanged cations (Table 2). The zeolites NiY and LaX give more dimers (47.9, 49.7%), while AlY and CaX give more trimers (16.1; 12.6%). Also the quantity of propylene converted into propane, and the part of the liquid which remained on the zeolite (Table 1) depend on the nature of the exchanged cation and the SiO_2: Al_2O_3 ratio.

The products which remain on the zeolites are probably propylene high oligomers, formed and captured within the pores of zeolites, which on heating crack into C_1—C_8 molecules and pass through the windows of the zeolite pores.

The most interesting zeolite catalyst is the NiX. The reaction products of this catalyst are pure oligomers and 95.49% of which are dimers (Table 3). The calculated octane number of these products is about 94. They contain more than 34% of hexenes which usually[14] do not exceed 10% if an acid catalyst is used. Within the other dimers 3-methylpentenes are present. The presence of these dimers were previously[15] attributed to secondary rearrangement.

In the presence of NiX with a higher degree of nickel ions (80%), C_5, C_7, and C_8 olefins are formed. Thus replacement of the more difficultly exchangeable sodium ions by nickel, enhances the cracking of the formed propylene oligimers.

TABLE. 3. COMPOSITION OF PROPYLENE OLIGOMERS OBTAINED ON NiX AT 190 °C AND 0.025 h

Propylene oligomer	wt %
2-Methyl-2-pentene	27.40
trans-2-Hexene	23.50
trans-3-Methyl-2-pentene + *cis*-2-hexene	11.50
trans- and *cis*-3-hexene	10.24
cis-4-Methyl-2-pentene	1.57
trans-4-Methyl-2-pentene	8.35
2-Methyl-1-pentene + 1-hexene	8.53
cis-4-Meth-l-1-pentene	0.79
cis-3-Methyl-2-pentene	1.26
2,3-Dimethyl-2-butene	1.09
2,3-Dimethyl-1-butene	1.26
Trimers	4.51
Octone number	94

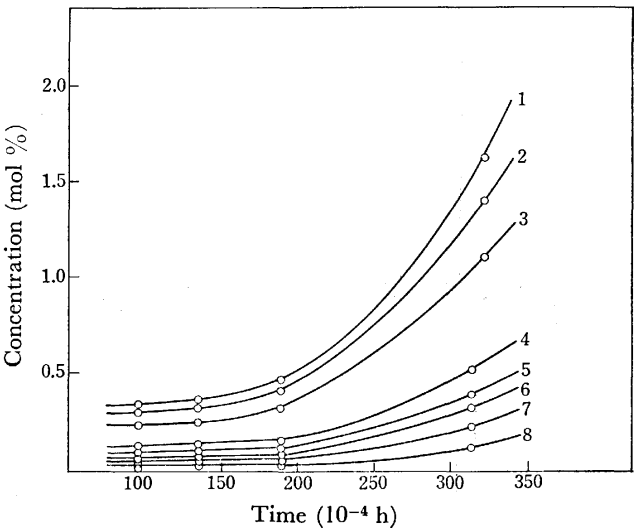

Fig. 1. Distribution of propylene dimers against contact time at a reaction temperature of 225 °C.
1: 2-Methyl-2-pentene, 2: *trans*-2-hexene, 3: *trans*-3-methyl-2-pentene+*cis*-2-hexene, 4: *trans*- and *cis*-3-hexene, 5: 2-methyl-1-pentene, 6: *trans*-4-methyl-2-pentene+1-hexene, 7: *cis*-3-methyl-2-pentene, 8: 2,3-dimethyl-2-butene.

Kinetics of Oligomerization. It is of interest to determine the kinetic curves of the oligomerization to obtain information on the 3-methylpentenes, *i.e.* whether they are secondary products or not. Thus the oligomerization was carried out on the NiX zeolite at different temperatures (190, 205, 217, and 225 °C) and contact times (0.01—0.037 h). Figure 1 reveals a similar character of the decrease of the different dimer contents, as well as that of the 3-methylpentenes with the decrease of the contact time. The same results were obtained at the temperatures of 190, 205, and 217 °C. If 3-methylpentenes are secondary products, then their contents should decrease with a higher degree than the other dimers. With respect to the 3-methylpentane the same results were obtained[16] over the HNaY zeolite as an example of the zeolites over which hydrooligomerization takes place. These experimental facts indicate that the 3-methylpentenes and the 3-methylpentane are primary products of propylene dimerization and hydrodimerization, respectively. They cannot be produced under the used experimental conditions by secondary skeletal isomerization of either hexenes or 2-methylpentenes.

Reaction Mechanism. The 3-methylpentenes cannot be explained as the primary products of propylene dimerization neither by a carbonium-ion mechanism nor by any other mechanism which assumes an open-chain hydrocarbon as the activated intermediate. A mechanism of dimerization has been proposed,[8] over the nickel oxide on silica-alumina catalyst, which

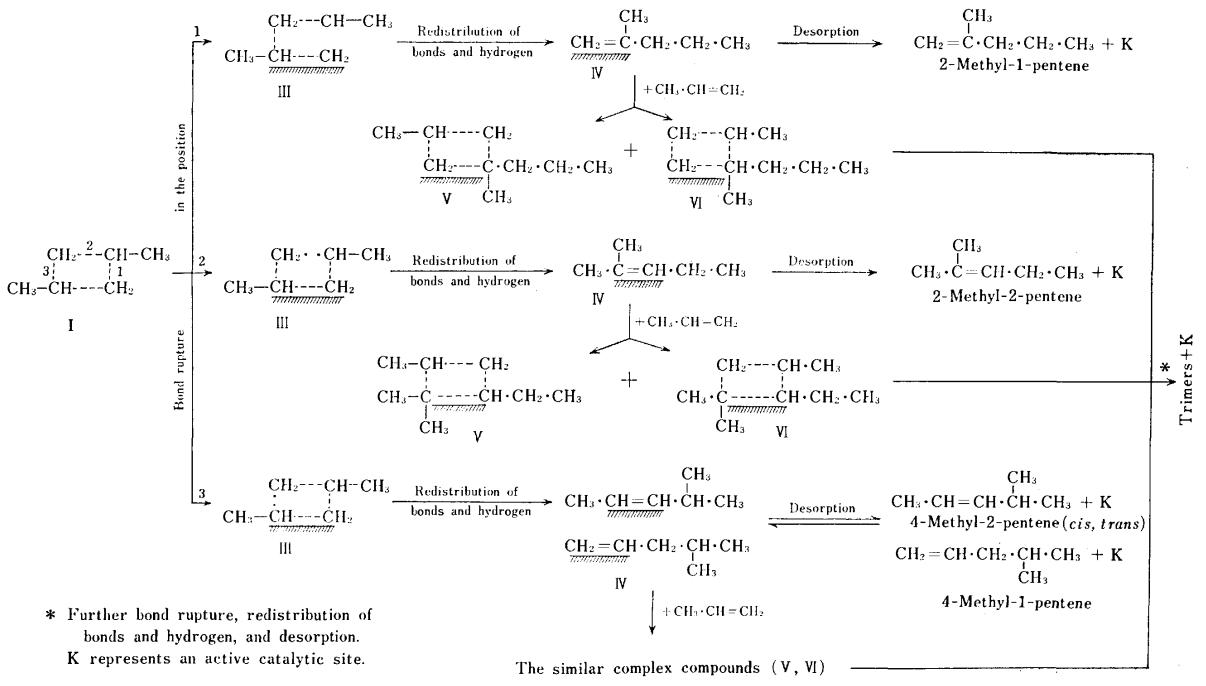

* Further bond rupture, redistribution of bonds and hydrogen, and desorption.
K represents an active catalytic site.

Scheme 1.

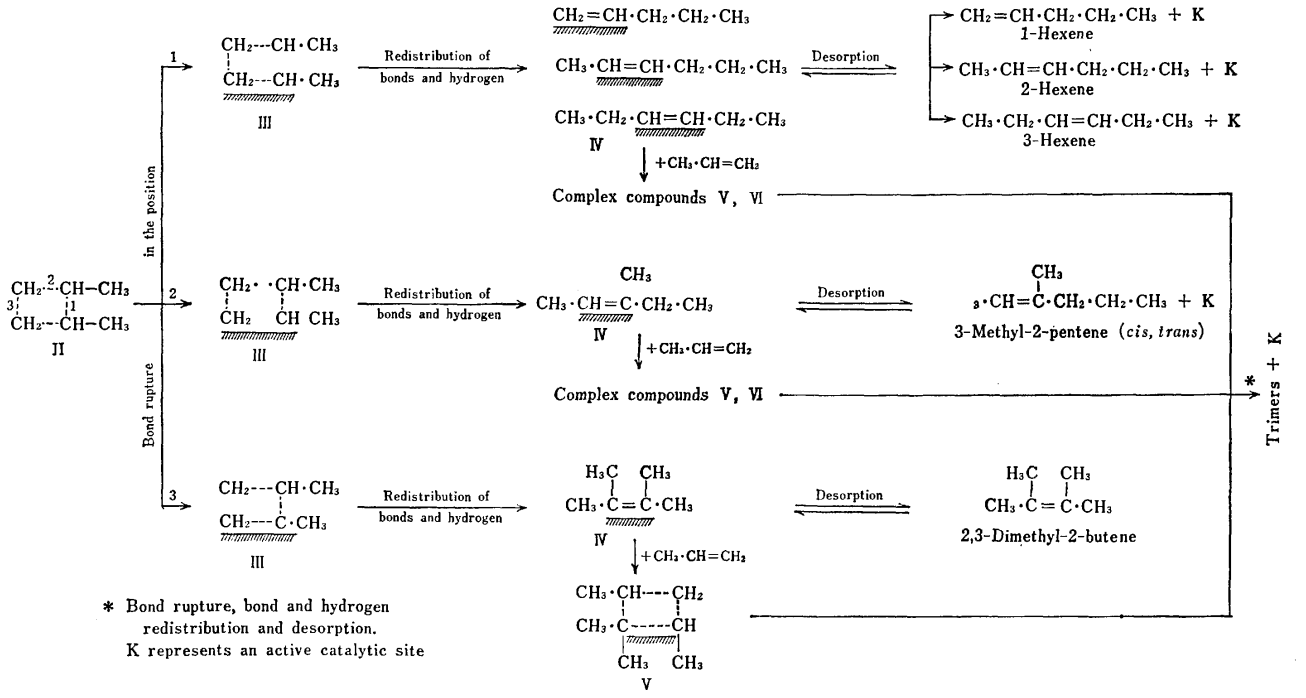

Scheme 2.

assumes an intermediate of a cyclobutane derivative. Examination of the present results has shown that the same mechanism may hold for the conversion of propylene on the investigated zeolites.

It is possible that these intermediate compounds can be formed when a propylene molecule reacts with an adsorbed one on the zeolite surface as follows:

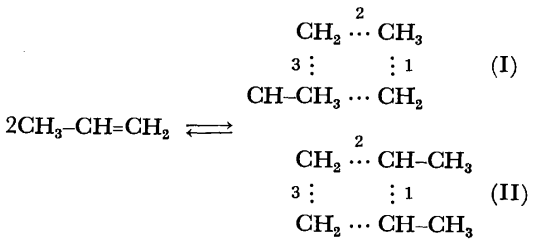

The formed dimethylcyclobutanes, I and II, are unstable complexes, and therefore they either converted to the initial molecules or undergo a bond rupture. The latter may take place in the bond 1, 2, or 3. The bond rupture of complex I (Scheme 1) or complex II (Scheme 2) leads to the formation of extremely unstable complexes III, which undergo rearrangement and hydrogen redistribution. As a result, the propylene dimers, II, are formed on the zeolite surface.

Depending on the catalyst selectivity and the experimental conditions the redistribution of hydrogen can lead to the formation of propylene dimers as in the case of NiX zeolite (Table 3) and hydrodimers (paraffins) as in the case of other zeolites (Table 2).

The hydrodimerization leads to the formation of hydrodimers and compounds of poor hydrogen content. Dimers (Table 3) and hydrodimers (Table 2) of different structures are formed due to the rupture of different bonds of I and II. Thus if the rupture occurs at positions 1, 2, or 3, then 4- or 2-methylpentenes are formed in the case of complex I (Scheme 1), and hexenes, 3-methylpentenes or 2,3-dimethylbutenes in the case of complex II (Scheme 2). The formation of 2-methyl-2-pentene and *trans*-2-hexene in large quantities (Table 3, Fig. 1) indicates that the rupture at position 2 (complex I) and position 1 (complex II) occurs much easier than at other positions.

If the rate of desorption is relatively slow, the formed dimers, IV, on the zeolite surface can adsorb another propylene molecule forming the complex V or VI which are unstable as well as complexes I and II. They are converted either to the initial state or undergo bond rupture, bond and hydrogen redistribution and desorption to give propylene trimers or hydrotrimers.

The presence of C_2, C_4, C_5, C_7, and C_8 paraffinic hydrocarbons (Table 2) indicates that bond ruptures may take place for two bonds of complexes V and VI.

Similarly if trimers are not relatively rapidly desorbed they can adsorb another propylene molecules forming, in the same manner, tetramers and so on.

The above mechanism explains the formation of obtained products during the propylene conversion over the zeolites studied. However, the difference in the selectivity of the various cation-exchanged zeolites is not clear. This difference can be explained in view of some recent works[17-20] which reported the existence of two types of active sites with different acidic strengths on faujasite. Barthomeuf and Beaumont[21] reported that weak active sites are related to the cationic sites which are easily exchangeable. Thus, it can be concluded that hydrooligomerization and the accompanied cracking reaction require the stronger active sites compared to the oligomerization. This conclusion is supported by the fact that exchange of the more difficult-

ly exchangable sodium ions by nickel cations, leads to cracking of some of the formed propylene oligomers. On the other hand, it is evident[17,22] that the ratio of strong acidic sites to all the sites on faujasite increases with the increase of the SiO_2: Al_2O_3 ratio. This may explain the reason why the hydrooligomerization takes place on NiY (SiO_2: Al_2O_3=4.8) and oligomerization takes place on NiX (SiO_2: Al_2O_3=2.4). As the conclusion, the difference in selectivity of the various cation-exchanged zeolites in propylene conversion, probably, relates to the change in the acidic strength distribution of the active sites on the zeolite surface, which is due to the SiO_2: Al_2O_3 ratio and the different effect of each cation. However, this conclusion requires further studies on the quantitative basis.

References

1) T. J. Weeks, Jr., C. L. Angell, I. R. Ladd, and A. P. Bolton, *J. Catal.*, **33**, 256 (1974).

2) Ya. T. Eidus, A. L. Lanidus, L. N. Rudakova, Ya. I. Isakov, and Kh. M. Minachev, *Izv. AN USSR, Ser. Khim.*, **1974**, 129.

3) G. M. Panchenkov, O. I. Kuznetsov, and M. H. Shawky, *Neftekhimiya*, **9**, 63 (1969).

4) M. Repas, *Chem. Tech. (Berlin)*, **1965**, 222; **1971**, 278.

5) G. A., Oblad Mills and H. Heinemenn, "Catalysis," Vol. 6, ed by Paul H. Emmett (1958), p. 353.

6) O. I. Kuznetsov, G. M. Panchenkov, M. H. Shawky, *NTS. Ser. Neftepererabotka, Neftekhimiya, Slantsepererabotha*, No. 7 (1971).

7) G. R. Schultz, J. M. Schvek, and R. C. Wildi, *J. Catal.*, **6**, 385 (1966).

8) H. Imai, T. Hasegawa, and H. Uchida, *Bull. Chem. Soc. Jpn.*, **41**, 45 (1968).

9) E. L. Pollitzer, E. E. Meisinger, U. S. Patent 3148157 (1967).

10) M. L. Becher and K. L. Fresh, Belg. Patent 632055 (1963).

11) G. M. Panchenkov, M. Zhorov, K. A. Venkachalam, and I. P. Gurevich, *Neftekhimiya*, **4**, 128 (1964).

12) P. B. Venuto and P. S. Landis, *Adv. Catal.*, **18**, 260 (1963).

13) N. Sheppard, D. M. Simpson, *Quart. Rev. London Chem. Soc.*, **6**, 1 (1962).

14) M. Repas, M. Marko, and F. Gregor, *Chem. Prum.*, **18**, 34 (1968).

15) A. Wachter, *Ind. Eng. Chem.*, **30**, 822 (1938).

16) G. M. Panchenkov, O. I. Kuznetsov, and M. H. Shawky, *Neftekhimya*, **10**, 45 (1970).

17) K. Tsutsumi, H. Kajiwara, and H. Takahashi, *Bull. Chem. Soc. Jpn.*, **47**, 801 (1974).

18) P. A. Jacobs, H. E. Leeman, and J. B. Uytterhoeven, *J. Catal.*, **33**, 31 (1974).

19) Ho Shi Thoang, K. V. Topchieva, and B. V. Ramonovskii, *Kinet. Katal.*, **15**, 1053 (1974).

20) R. Beaumont and D. Barthomeuf, *J. Catal.*, **27**, 45 (1972).

21) D. Barthomeuf and R. Beaumont, *J. Catal.*, **30**, 288 (1973).

22) K. V. Topchieva and Ho Shi Thoang, *Dokl. AN USSR*, **205**, 642 (1972).

Hydrogen Bonding between Phenols and Nitriles

Inam JAWED*

Institute of Physical Chemistry, Peshawar University, Peshawar, Pakistan

(Received May 16, 1975; in revised form, February 28, 1977)

Hydrogen bonding between a number of para-substituted phenols and nitriles was studied by means of infrared spectroscopy using a longer cell. Thermodynamic quantities were determined and found to be the functions of the electronegativity and inductive effect of the phenol and nitrile substituents respectively except for the complexes of *t*-butyl cyanide for which the $-\Delta H$ values were lower than expected. Some correlations among thermodynamic quantities were also established. Both the sample and the reference cells were heated simultaneously by means of a special heating arrangement which minimized the base line errors and made the intensity measurements more accurate.

Phenol has been one of the most extensively used proton donor molecules in hydrogen bond studies. Systematic data, however, for phenol–nitrile systems are relatively scarce and there are only a few reports available in literature.[1,2] Data on substituted phenols is even more scarce. It was, therefore, considered worthwhile to make a detailed and systematic study of the thermodynamic properties of hydrogen bonds between a number of substituted phenols and nitriles using improved techniques and under more desirable experimental conditions. This study was carried out by means of infrared spectroscopy. The phenols and nitriles were chosen so as to give a rather wide range of acidity and basicity values respectively. Para-substituted phenols were preferred to avoid complications arising from intramolecular associations and steric effects.

Experimental

The infrared spectroscopic measurements were made on a Perkin-Elmer model 125 infrared grating spectrophotometer using an expanded scale (1 cm=5 wave numbers). Quartz cells, 20 mm long, were used. As shown by Russell and Thompson,[3] the slit width should be at least one-fifth of the half width of the absorption band in order to obtain true band intensities. Hence, a slit program was chosen which gave a spectral slit width of about one-seventh of the half width of the hydroxyl stretching vibrational band of phenols, ν_{OH}. Tetrachloroethylene was chosen as the solvent because of its high boiling point (121 °C) to make measurements within a wide range of temperatures, 20 to 65 °C.

A special heating jacket was designed because of the rather large size of the cells. It consisted of two solid brass pieces carefully cut from inside so that when the two pieces were brought together by means of a screw, they formed a round hole in the center of which the cell fitted almost exactly. The brass pieces were fitted through an asbestos insulator onto a brass backing plate. Copper tubes were soldered round the brass pieces through which water could be circulated from a thermostat. By means of this arrangement, it was possible to control the temperature of the cell within ± 1 °C of the desired values for any length of time. Measurements were made at 20, 30, 39.5, 50, and 60 or 61.5 °C. The temperature of the solutions in the cell was measured by means of an iron-constantan thermocouple.

For each phenol, a preliminary investigation was first carried out to determine approximately the maximum concentration at which self-association disappears. Concentrations much lower than this were used keeping the absorption of the bands within 25—60 percent for accurate measurements of the intensities. The following concentrations were used for actual measurements of the thermodynamic parameters:

p-Methoxyphenol and phenol	7.0×10^{-4} M	Cl_3CCN	1.20 M
		C_6H_5CN	0.20 M
		CH_3CN	0.16 M
		$(CH_3)_3CCN$	0.12 M
p-Chlorophenol	7.0×10^{-4} M	Cl_3CCN	0.80 M
		C_6H_5CN	0.12 M
		CH_3CN	0.12 M
		$(CH_3)_3CCN$	0.08 M
p-Cyanophenol and *p*-nitrophenol	4.0×10^{-4} M	Cl_3CCN	1.00 M
		C_6H_5CN	0.06 M
		CH_3CN	0.06 M
		$(CH_3)_3CCN$	0.04 M

The concentrations of the proton donors and acceptors are expected to change as a result of change in solution density with increase in temperature. The correction in the concentration for density changes was made as suggested by Powell and West.[4] Since the densities of the solutions which had quite low concentrations of the proton donors and accep-

TABLE 1. ASSOCIATION CONSTANTS FOR HYDROGEN BONDS BETWEEN *p*-METHOXYPHENOL AND TRICHLOROACETONITRILE

Temperature (°C)	Association constants		
	K	*K*	*K*
21.0	0.51	0.53	0.52
30.0	0.46	0.48	0.45
39.5	0.38	0.39	0.38
50.5	0.32	0.33	0.31
60.0	0.30	0.27	0.29
K(25 °C)	0.48	0.49	0.48 (l/mol)
$-\Delta G$	−0.44	−0.43	−0.43 (kcal/mol)
$-\Delta H$	2.97	2.91	3.00 (kcal/mol)
$-\Delta S$	11.4	11.2	11.5 (cal/mol/deg)

* Present address: Martin Marietta Laboratories, 1450 South Rolling Road, Baltimore, Maryland 21227, U.S.A.

Table 2. Association constants for hydrogen bonds between *p*-chlorophenol and acetonitrile

Temperature (°C)	Association constants		
	K	*K*	*K*
20.0	10.0	11.2	10.5
30.0	6.90	7.0	7.10
39.5	4.67	4.84	4.79
50.5	3.60	3.54	3.80
61.5	2.69	2.80	2.75
K(25 °C)	8.22	8.37	8.32 (l/mol)
$-\Delta G$	1.25	1.26	1.25 (kcal/mol)
$-\Delta H$	6.06	6.16	5.99 (kcal/mol)
$-\Delta S$	16.1	16.4	15.9 (cal/mol/deg)

tors were found to be very similar to that of the solvent. corrections were made using the density of the solvent only.

The phenols and nitriles were purified by the usual methods of drying, recrystallization or fractional distillation. The solvent, tetrachloroethylene, was also dried carefully and fractionally distilled. After purification they were stored in vacuum dessicators or over nitrogen atmosphere in a dry box.

The association constants were calculated using the method described by Lopes and Thompson.[2] Tables 1 and 2 give the typical examples of the measurements of the association constants at different temperatures together with the values of $-\Delta G$, $-\Delta H$, and $-\Delta S$. Three measurements were made for each system at almost the same concentrations of the phenols and nitriles. The thermodynamic quantities were calculated separately and then averaged. Figures 1 and 2 give examples of plot of log *K* *vs.* $1/T$.

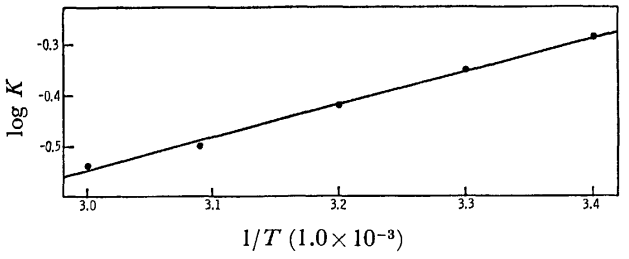

Fig. 1. Plot of log *K* against $1/T$ for *p*-methoxyphenol–Cl_3CCN complex.

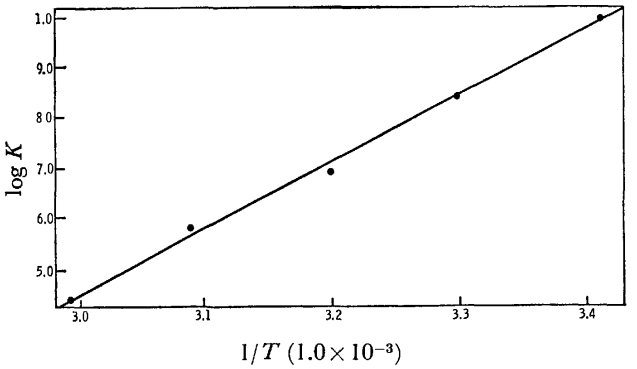

Fig. 2. Plot of log *K* against $1/T$ for *p*-chlorophenol–CH_3CN complex.

Results and Discussion

The values of the thermodynamic quantities of the various systems studied are given in Table 3. As can be seen, for the complexing of any particular nitrile with different phenols, the association constant, and the enthalpy and entropy changes generally follow the same order as the electronegativity of the para-substituents in phenols. For any particular phenol complexing with different nitriles, the association constant follows the same order as the inductive effect of the nitrile substituents. The enthalpy and entropy changes, however, increase from Cl_3CCN to CH_3CN, but, are lower for $(CH_3)_3CCN$ complexes than for CH_3CN complexes although the values of association constants are higher for the complexes of the former. This result was observed for the complexes of $(CH_3)_3CCN$ with every phenols studied, and although the difference is within the error of measurements, repeated measurements confirmed the observed pattern. It seems unlikely that steric hindrance of the bulkier *t*-butyl group plays a significant part here because of the higher values of the association constants and some spectral characteristics like infrared frequency shifts for $(CH_3)_3CCN$ complexes relative to CH_3CN complexes. Solvent effects as suggested by Pullin and co-workers[5] also cannot account for this change as the effect persists even in the gas phase as shown by Thomas[6] in his thermodynamic studies of the hydrogen fluoride–ether complexes in the gas phase. He explains this discrepancy in terms of the heat of conformational rearrangement of the ether molecule on hydrogen bond formation. In

Table 3. Thermodynamic quantities (Solvent: Tetrachloroethylene)

Proton donor	Proton acceptor	*K* (25 °C) l/mol	$-\Delta G$ kcal/mol	$-\Delta H$ kcal/mol	$-\Delta S$ cal/mol/deg
p-Methoxyphenol	Cl_3CCN	0.48	−0.44	2.96	11.4
	C_6H_5CN	3.22	0.69	4.91	14.2
	CH_3CN	3.69	0.77	5.27	15.0
	$(CH_3)_3CCN$	4.73	0.92	4.99	13.7
Phenol	Cl_3CCN	0.67	−0.23	3.03	11.0
	C_6H_5CN	4.46	0.88	4.88	13.4
	CH_3CN	6.75	1.13	5.38	14.3
	$(CH_3)_3CCN$	7.99	1.23	5.11	13.1
p-Chlorophenol	Cl_3CCN	1.18	0.09	3.27	10.6
	C_6H_5CN	7.82	1.22	5.37	13.9
	CH_3CN	8.30	1.25	6.08	16.2
	$(CH_3)_3CCN$	14.6	1.59	5.77	14.1
p-Cyanophenol	Cl_3CCN	1.47	0.23	3.48	10.9
	C_6H_5CN	22.3	1.84	5.66	12.8
	CH_3CN	30.0	2.02	6.07	13.6
	$(CH_3)_3CCN$	39.2	2.18	5.89	12.6
p-Nitrophenol	Cl_3CCN	1.20	0.10	4.35	14.2
	C_6H_5CN	27.4	1.96	6.54	15.4
	CH_3CN	33.5	2.08	6.97	16.4
	$(CH_3)_3CCN$	48.2	2.30	6.73	14.9

$\Delta K = \pm 10\%$ (l/mol), $\Delta(\Delta G) = \pm 0.05$ kcal/mol, $\Delta(\Delta H) = \pm 0.2$ kcal/mol, $\Delta(\Delta S) = \pm 1.0$ cal/mol/deg.

the present case, however, *t*-butyl cyanide is likely to have only one conformation common to the free molecule and the complex. Thus, it is unlikely that an explanation of the reduced $-\Delta H$ along the lines of the hydrogen fluoride–ether complexes is possible unless the bonds throughout the molecule are weakened in such a way that the molecule becomes distorted.

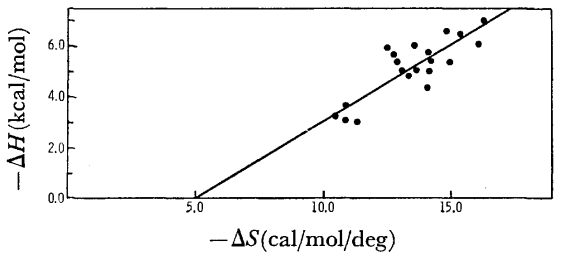

Fig. 3. Plot of $-\Delta H$ against $-\Delta S$ for hydrogen bonds between phenols and nitriles.

The thermodynamic parameters of the hydrogen bonded systems have been reported to show various correlations among themselves. Shepp and Bauer[7] and Person[8] have discussed theoretically the linear relationship between $-\Delta H$ and $-\Delta S$. Several workers have noted this linear relationship.[9–15] The present data for $-\Delta H$ and $-\Delta S$ when subjected to the least squares treatment gave the following equation:

$$-\Delta H\,(\text{kcal/mol}) = -0.60\,\Delta S - 2.97.$$

In view of the considerable scatter (Fig. 3), little meaning can be given to such plots at least for the systems reported here. Person has theoretically predicted a value of 2.0 for the $\Delta H/\Delta S$ slope. The observed value is, however, widely different from this.

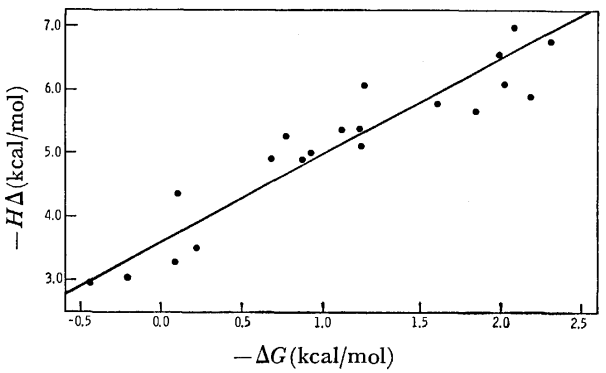

Fig. 4. Plot of $-\Delta H$ against $-\Delta G$ for hydrogen bonds between phenols and nitriles.

All nitriles in the present study show a general increase in $-\Delta H$ with K and hence with $-\Delta G$. The only exception are the complexes of $(CH_3)_3CCN$. These have already been discussed. A least squares treatment of the present data for $-\Delta H$ and $-\Delta G$ gives the following straight line (Fig. 4):

$$-\Delta H\,(\text{kcal/mol}) = -1.38\,\Delta G + 3.6.$$

Several linear correlations have also been reported by other workers.[2,16–18] All these data, however, lead to the conclusion that there is perhaps a more complicated relationship between $-\Delta G$, $-\Delta H$, and $-\Delta S$ than simple equations as shown above and, therefore, not too much weight should be placed on the singificance of these equations.

Before concluding the discussion of the thermodynamic quantities, it is perhaps desirable to make some comments on the difficulties in the interpretation of data from solution phase studies. In fact, no solvent can be regarded as truly inert.[19–21] Jones and Watkinson[22] have shown that there exists an interaction between solvent tetrachloroethylene and phenol molecules. This view seems to be verified from our studies also. Thus, in the course of measurements at various temperatures, we noted that the free or unbonded hydroxyl stretching vibrational frequency shifted to slightly higher values as the temperature raised. The more acidic the phenol, the greater was this shift. This indicates the decrease of a phenol-solvent association by the increase in temperature. Thus the effect of the solvent on the thermodynamic parameters is evident. Moreover, it has been reported that the value of the association constant varies with the concentrations of the proton donor and acceptor molecules.

Figueroa and co-workers,[23] in their studies of association of phenol with sulfoxides, noted that the value of association constant increased with increasing phenol/sulfoxide ratio showing that even in a chosen standard solvent, the concentrations of donor and acceptor molecules may affect the K and $-\Delta H$ values.

Ther are evidences of self-association among nitrile molecules at higher concentrations.[24,25] Such an association would mean that there are less nitrile molecules available to associate with phenol molecules and, consequently, the association constant is lowered. In addition, the heat of formation of hydrogen bond between phenol and nitrile may be partially compensated by the heat of breaking the nitrile-nitrile bond. In the present work, the increased cell thickness enabled us to use very dilute solutions. This, together with the improved heating technique, made the data more reliable.

It is perhaps desirable to include here data on the more accurate values of ν_{OH} obtained by using a longer cell and keeping the temperature more accurate than before. Table 4 gives the values of both the free and bonded ν_{OH} at 20 °C for the phenol–nitrile systems studied.

TABLE 4. FREQUENCIES OF THE FREE AND BONDED ν_{OH} BANDS FOR THE PHENOL–NITRILE SYSTEMS AT 20 °C

Nitrile	ν_{OH} Bonded (cm^{-1})				
	p-Methoxy-phenol	Phenol	*p*-Chloro-phenol	*p*-Cyano-phenol	*p*-Nitro-phenol
Cl_3CCN	3552.5	3544.5	3534.5	3501.5	3494.0
C_6H_5CN	3471.0	3460.0	3442.5	3398.5	3382.5
CH_3CN	3468.0	3456.0	3439.5	3395.0	3380.0
$(CH_3)_3CCN$	3458.0	3445.5	3426.5	3377.0	3363.5
ν_{OH} Free (cm^{-1})	3613.0	3608.0	3605.5	3592.5	3589.5

Accuracy of measurements of the values of $\nu_{OH} = \pm 0.5\ cm^{-1}$. Solvent: tetrachloroethylene. The values of ν_{OH} (bonded) were obtained by extrapolation to infinite dilution of the nitriles.

Table 5. Change in ν_{OH}(Bonded) with concentration of nitriles at 20 °C

Phenol	ν_{OH} Free (cm^{-1})	Nitrile	Nitrile concn mol/l	ν_{OH} Bonded (cm^{-1})
p-Chlorophenol (7.0×10^{-4} M)	3605.5	Cl_3CCN	0.196	3533.5
			1.177	3529.5
		C_6H_5CN	0.041	3441.5
			0.295	3434.0
		CH_3CCN	0.047	3539.0
			0.290	3431.5
		$(CH_3)_3CCN$	0.018	3425.0
			0.126	3420.0
p-Nitrophenol (4.0×10^{-4} M)	3589.5	Cl_3CCN	0.261	3493.0
			1.305	3490.0
		C_6H_5CN	0.028	3381.0
			0.215	3379.0
		CH_3CN	0.032	3381.0
			0.210	3375.5
		$(CH_3)_3CCN$	0.015	3360.0
			0.090	3356.0

Accuracy of measurements of the values of $\nu_{OH}=\pm0.5$ cm^{-1}. Solvent: tetrachloroethylene.

The frequency of the bonded ν_{OH} is also found to depend to some extent on the concentration of the nitrile molecules. Table 5 shows some examples of this concentration dependence. The unbonded or free ν_{OH}, however, remains unchanged.

References

1) S. C. White and H. W. Thompson, *Proc. R. Soc. London, Ser. A*, **291**, 460 (1966).
2) M. S. C. Lopes and H. W. Thompson, *Spectrochim. Acta, Part A*, **24**, 1367 (1968).
3) R. A. Russell and H. W. Thompson, *Spectrochim. Acta, Part A*, **9**, 133 (1955).
4) D. L. Powell and R. West, *Spectrochim, Acta, Part A*, **20**, 989 (1964).
5) T. M. Brakat, M. J. Nelson, S. M. Nelson, and A. D. E. Pullin, *Trans. Faraday, Soc.*, **41**, 65 (1969).
6) R. K. Thomas, *Proc. R. Soc. London, Ser A*, **322**, 137 (1971).
7) A. Shepp and S. H. Bauer, *J. Am. Chem. Soc.*, **76**, 265 (1954).
8) W. B. Person, *J. Am. Chem. Soc.*, **84**, 536 (1962).
9) K. Igarashi, F. Watari, and K. Aida, *Spectrochim. Acta, Part A*, **25**, 1743 (1969).
10) T. M. Brakat, J. Nelson, S. M. Nelson, and A. D. E. Pullin, *Trans. Faraday Soc.*, **41**, 65 (1969).
11) J. Nelson, *Spectrochim. Acta, Part A*, **26**, 109 (1970).
12) Z. Yoshida and N. Ishibe, *Spectrochim. Acta, Part A*, **24**, 893 (1968).
13) T. Gramstad, *Acta Chim. Scand.*, **15**, 1337 (1961).
14) W. B. Person, W. C. Golton, and A. I. Popov, *J. Am. Chem. Soc.*, **85**, 891 (1963).
15) H. Yada, J. Tanaka, and S. Nagakura, *Bull. Chem. Soc. Jpn.*, **33**, 1660 (1960).
16) S. Ghersetti and A. Lusa, *Spectrochim. Acta, Part A*, **21**, 1067 (1965).
17) P. Biscarini, S. Ghersetti, and G. Galloni, *Spectrochim. Acta, Part A*, **20**, 267 (1964).
18) E. M. Arnet *et al.*, *J. Am. Chem. Soc.*, **92**, 2365 (1970).
19) H. E. Hallam, in "Infrared Spectroscopy and Molecular Structure," ed by Mansel Davies, Chap. 12, Elsevier Publishing Co., Amsterdam (1963).
20) A. N. Fletcher, *J. Phys. Chem.*, **74**, 216 (1970).
21) A. N. Fletcher, *J. Phys. Chem.*, **73**, 2217 (1969).
22) D. A. K. Jones and G. J. Watkinson, *J. Chem. Soc.*, **1964**, 2366.
23) R.H. Figueroa, E. Roig, and H.H. Szmant, *Spectrochim. Acta, Part A*, **22**, 1107 (1966).
24) E. L. Zhukova, *Opt. Spektrosk.*, **4**, 750 (1958).
25) R. G. Jones and J. W. Orville-Thomas, *J. Chem. Soc.*, **1965**, 4632.

Multiple Relaxation Processes in Long Chain Molecules at Microwave Frequencies

H. D. PUROHIT and H. S. SHARMA

Microwave Laboratory, Physics Department, University of Jodhpur, Jodhpur, India

(Received January 5, 1977)

The permittivity ε' and dielectric loss ε'' of octanoyl, undecanoyl, and lauroyl chlorides have been measured in benzene for five different concentrations varying from 0.02 to 0.10 wt fraction at three different microwave frequencies, *viz.* 3.31, 9.83, and 26.90 GHz at 35 °C. The static permittivity ε_0 at 100 kHz and the high frequency limiting permittivity ε_∞ have also been measured at the same temperature. The permittivity and dielectric loss at different frequencies have been plotted against concentration and their slopes have been used to draw normalised complex plane plots between $(a'-a_\infty)/(a_0-a_\infty)$ and $a''/(a_0-a_\infty)$ for these compounds. Such plots show a skewed arc dielectric behaviour. The values of distribution parameter β, characteristic relaxation time τ_0, average relaxation time τ_{av}, and dipole moment μ have been reported for the first time. The relaxation mechanism in these three molecules has been explained on the basis of multiple relaxation processes.

Complex plane plots for most of the normal unassociated molecules are semicircular arcs represented by the Debye equation[1] or symmetric Cole-Cole arcs represented by the Cole-Cole equation.[2] However, there are a few exceptions. It has been observed that in case of long chain molecules[3,4] the complex plane plot is a skewed arc and can be represented by the Davidson-Cole equation.[5] Such a behaviour is also exhibited by higher thiols[6] and benzylidyne trifluoride.[7] The present studies have been carried out with three long chain molecules namely octanoyl chloride $CH_3(CH_2)_6COCl$, undecanoyl chloride $CH_3(CH_2)_9COCl$, and lauroyl chloride $CH_3(CH_2)_{10}COCl$ in dilute solutions of benzene.[8] These compounds are highly reactive and when exposed to the atmosphere react with moisture present to form hydrochloric acid. Further in pure liquids the internal field effects[9-11] are pronounced because of large dipolar field. The dielectric behaviour has, therefore, been studied in dilute solutions of benzene so that the solute molecules are in a quasi-isolated state practically unaffected by the dipolar field and solute-solute co-operative phenomenon. These molecules have been chosen because of the likelihood of multiple relaxation mechanism being present in them.

Experimental

Materials. *(a) Solute*: Octanoyl chloride of purum grade (of 98% purity), undecanoyl chloride of purum grade (of 98% purity) and lauroyl chloride of puriss grade (of 99% purity) were obtained from Messrs Fluka, A. G., Switzerland. They were used as such for experimental work.

(b) Solvent: Benzene of A. R. grade was purchased from Messrs British Drug House (India) Ltd. and was dried over sodium and fractionally distilled before use.

Experimental Details. The measurements of permittivity ε' and dielectric loss ε'' for each of the solutes in five dilute solutions of different concentrations (0.02 to 0.10 wt fraction) in benzene were made using the method suggested by Heston *et al.*[12] for low loss liquids and adapted for short circuited termination at three different microwave frequencies *viz.* 3.31, 9.83, and 26.90 GHz. The heterodyne beat method was used for determining the static permittivity ε_0 at 100 kHz. High frequency limiting permittivity ε_∞ was taken as square of the refractive index which was measured by an Abbe's refractometer. All measurements were made at 35 °C and the temperature was maintained within ± 0.5 °C by circulating water from a temperature controlled bath. The values of ε', ε'', ε_0, and ε_∞ thus obtained were plotted against concentration in wt fraction. The slopes a', a'', a_0, and a_∞ are given in Table 1. The accuracy of measurement of a' is ± 1 percent and of a'' is ± 5 percent.

TABLE 1. VALUES OF THE SLOPES OF PLOTS OF ε' AND ε'' *versus* CONCENTRATION

Frequency	a'	a''
(a) Octanoyl chloride		
100 kHz	$a_0=4.58$	—
3.31 GHz	4.00	1.30
9.83 GHz	2.88	2.13
26.90 GHz	0.63	1.19
Optical	$a_\infty=-0.23$	—
(b) Undecanoyl chloride		
100 kHz	$a_0=4.03$	—
3.31 GHz	3.60	1.25
9.83 GHz	2.30	1.81
26.90 GHz	0.65	1.09
Optical	$a_\infty=-0.18$	—
(c) Lauroyl chloride		
100 kHz	$a_0=3.78$	—
3.31 GHz	3.25	1.23
9.83 GHz	2.00	1.70
26.90 GHz	0.40	0.78
Optical	$a_\infty=-0.21$	—

Theory

A system having an asymmetric distribution of relaxation time can be represented by Davidson-Cole type relation.[5] This equation can be modified by substituting a', a'' *etc.* in place of ε', ε'' *etc.* The Davidson-Cole equation can be written for dilute solution as

$$\frac{a^*-a_\infty}{a_0-a_\infty}=\frac{1}{(1+i\omega\tau_0)^\beta}, \qquad (1)$$

where β is a distribution parameter having values between 0 and 1, and τ_0 is the characteristic relaxation time. The average relaxation time τ_{av} is equal to $\beta\tau_0$. Putting the value of $a^*=a'-ia''$ and separating real and imaginary parts, one gets

$$a'-a_\infty = (a_0-a_\infty)(\cos\phi)^\beta \cos\beta\phi, \quad (2)$$

$$a'' = (a_0-a_\infty)(\cos\phi)^\beta \sin\beta\phi, \quad (3)$$

where $\tan\phi = \omega\tau_0$, (4)

hence $$\omega\tau_0 = \tan\left[\frac{1}{\beta}\tan^{-1}\frac{a''}{(a'-a_\infty)}\right]. \quad (5)$$

An approximate value of β can be obtained from the skewed arc in which high frequency side approaches asymptotically a line making an angle $\beta\pi/2$ with real axis of a'. τ_0 can be calculated from Eq. 5 by substituting the measured values of $a''/(a'-a_\infty)$ at a given frequency. The value of β is then adjusted within the experimental range for getting constant value of τ_0 from different frequency data.

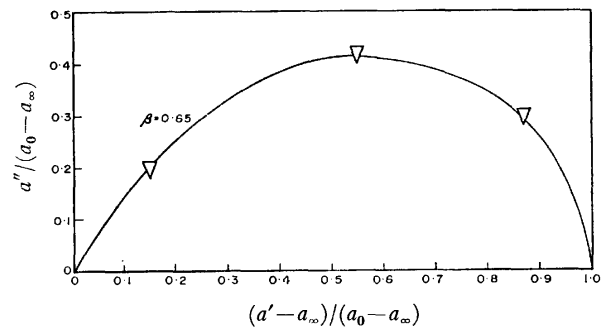

Fig. 1. Normalised plot of $(a'-a_\infty)/(a_0-a_\infty)$ *versus* $a''/(a_0-a_\infty)$ for lauroyl chloride in benzene.

A better method would be to draw curve between $(a'-a_\infty)/(a_0-a_\infty)$ and $a''/(a_0-a_\infty)$ (normalised plots) for different known values of β by varying ϕ by fixed amounts. The values of these quantities obtained experimentally are also plotted on the same graph. The value of β can be found out from the curve which fits the experimental values best. Knowing β, τ_0 can be calculated from Eq. 5 by substituting the measured values of $a''/(a'-a_\infty)$ at a given frequency. A representative normalised plot in case of lauroyl chloride is given in Fig. 1. The normalised maximum loss $a''_m/(a_0-a_\infty)$ which indicates the width of the distribution of relaxation time has also been calculated and reported in Table 2.

Table 2. Values of β, $a''_m/(a_0-a_\infty)$, τ_0, τ_{av}, and μ for octanoyl, undecanoyl and lauroyl chlorides

Compound	β	$a''_m/(a_0-a_\infty)$	τ_0 (ps)	τ_{av} (ps)	μ (D)
Octanoyl chloride	0.75	0.430	18.6	13.6	2.74
Undecanoyl chloride	0.70	0.425	22.3	15.6	2.88
Lauroyl chloride	0.65	0.415	27.3	17.7	2.89

The dipole moments μ of these solute molecules have been calculated by the following equation proposed by Higasi:[13]

$$\mu = A(a_0-a_D)^{1/2} \quad (6)$$

where A is a constant and is given by

$$A = \left[\frac{27kT}{4\pi N}\frac{M_2}{(\varepsilon_1+2)^2 d_1}\right]^{1/2}$$

Here d_1 is the density of the solvent and M_2 is the molecular weight of the solute. The values of μ for all the three solute molecules are reported for the first time and are given in Table 2.

Results and Discussion

The normalised arc plots for all the three solute molecules are skewed arcs which show that there is an asymmetric type of distribution of relaxation time. The value of β increases with the decrease of chain length which means that the distribution of relaxation time decreases with the decrease in chain length. In other words the distribution of relaxation time tends towards a symmetric distribution with decrease in chain length. The width of distribution of relaxation time which is indicated by the normalised maximum loss also increases with the decrease of chain length.

The skewed arc behaviour in liquids has been reported by many workers[14-17] and has been explained in terms of co-operative phenomenon and multiple relaxation processes. In dilute solutions the former possibility is ruled out. The only possible machanism which can explain the asymmetric distribution is due to multiple relaxation processes. This is borne out by the fact that the skewed behaviour increases with the increase in chain length. The molecule becomes less rigid and can relax in more than one way. A particular group or segment of the molecule may rotate, as well as the molecule may rotate as a whole. The former process has a smaller relaxation time as compared to the latter process. These are the limits between which the other relaxation times lie. The orientation of one segment may trigger many other orientations and consequently the rotating group does not relax independently. This intramolecular process has similar effects as intermolecular co-operative phenomenon which has been used to explain the skewed arc behaviour in pure liquids. The decrease in value of β with increase in chain length suggests that the segmental reorientations become increasingly possible with the increase in the number of C–C bonds, whereas with the decrease in chain length or decrease in the number of C–C bonds the segmental reorientation processes are reduced and the distribution becomes symmetric tending towards Cole-Cole behaviour. In the study of such molecules the possibility of solute-solvent interactions can not be ruled out.

The value of dipole moment increases with the increase in chain length. The characteristic relaxation time τ_0 of these compounds in solution increases with the increase in chain length, which is due to the increase in the molecular size. The average relaxation time τ_{av} also increases in the same manner as τ_0.

The authors are indebted to Professor Krishnaji, University of Allahabad, Allahabad for his helpful discussions and for the facilities provided in connection with some measurements. They also wish to thank Prof. A. N. Nigam, Head of Physics Department of this University for providing facilities to continue the present investigations.

References

1) P. Debye, "Polar Molecules," Dover Publication, Inc., New York (1945).
2) R. H. Cole and K. S. Cole, *J. Chem. Phys.*, **9**, 341 (1941).
3) W. E. Vaughan, W. S. Lovell, and C. P. Smyth, *J. Chem. Phys.*, **30**, 753 (1962).
4) F. I. Mopslk and R. H. Cole, *J. Chem. Phys.*, **44**, 1015 (1966).
5) D. Davidson and R. H. Cole, *J. Chem. Phys.*, **19**, 1484 (1951).
6) Krishnaji, V. K. Agarwal, and P. Kumar, *J. Chem. Phys.*, **56**, 5304 (1972).
7) H. S. Sharma, "Dielectric Dispersion and Relaxation Mechanism in Some Trifluoro-compounds," D. Phil. Thesis, Jodhpur University, Jodhpur (1971).
8) H. D. Purohit, "Microwave Absorption and Dielectric Relaxation in Organic Molecules," D. Phil. Thesis, Jodhpur University, Jodhpur (1970).
9) C. P. Smyth, "Dielectric Behaviour and Structure," McGraw Hill Co., New York (1955), Chap. 2.
10) C. J. F. Böttcher, "Theory of Electric Polarization," Elsevier Publishing Co., Amsterdam (1952), Chap. 6.
11) R. H. Cole, *J. Chem. Phys.*, **43**, 637 (1965).
12) W. M. Heston, Jr., A. D. Franklin, E. J. Hennelly, and C. P. Smyth, *J. Am. Chem. Soc.*, **72**, 3443 (1950).
13) K. Higasi, *Bull. Inst. Phys. Chem. Res.*, **22**, 865 (1943).
14) S. W. Tucker and S. Walker, *J. Chem. Phys.*, **45**, 1302 (1966).
15) S. H. Glarum, *J. Chem. Phys.*, **33**, 639 (1960).
16) D. W. Davidson, *Can. J. Chem.*, **39**, 571 (1961).
17) G. E. McDuffie, Jr. and T. A. Litovitz, *J. Chem. Phys.*, **37**, 1699 (1962).

The Stereochemistry and Reactivity of Metal-Schiff Base Complexes. II. High Stereoselectivity in (1*S*,2*S*)-*N*,*N*′-1,2-Cyclohexylenebis(salicylideneaminato)(sal$_2$-(*S*,*S*)-chxn) Cobalt(III) Complexes with Amino Acids and the Optical Resolution of Amino Acids with Cobalt(III)-sal$_2$-(*S*,*S*)-chxn*

Yuki Fujii, Mitsuo Sano, and Yoshiharu Nakano

Department of Chemistry, Faculty of Science, Ibaraki University, Bunkyo-cho, Mito, Ibaraki 310

(Received September 3, 1976)

A series of mixed ligand cobalt(III)–Schiff base complexes with the general formula of [Co(sal$_2$-(*S*,*S*)-chxn)(aa)] (aa=gly$^-$, L- and D-ala$^-$, L- and D-val$^-$, L- and D-leu$^-$, L- and D-thr$^-$, or L- and D-trp$^-$) were newly prepared from [Co(sal$_2$-(*S*,*S*)-chxn)] and amino acids by air oxidation. All the complexes were found to take, stereoselectively, the *Λ-cis-β*$_1$(*fac*)-structure, irrespective of the configuration of the amino acids. On the other hand, the reactions of [Co(sal$_2$-(*S*,*S*)-chxn)] with an excess of DL-amino acids in open air gave [Co(sal$_2$-(*S*,*S*)-chxn) (aa)], in which L-amino acids were selectively coordinated except for proline. These stereospecificities were found from the optical-purity measurement of the unreacted amino acids which had been separated from the reaction solutions by extracting the formed complex with chloroform. The configuration and the optical purities of the unreacted amino acids recovered from 1 : 2 reaction solutions (complex: DL-amino acid) were as follows: ala, (D, 6—10%); leu, (D, 6—8%); met, (D, 6—8%); ser, (D, 10—12%); thr, (D, 27—30%); asp, (D, 16—18%); glu, (D, 6—8%); phe, (D, 29—31%); trp, (D, 41—43%); pro, (L, 48—50%). These stereoselectivities and stereospecificities were explained in terms of the thermodynamic origin and the stereochemical requirement of the complexes.

In recent papers,[1,2] the stereoselectivity in cobalt(III)–Schiff base complexes containing L-amino acids, [Co(sal$_2$en)(L-aa)] and [Co(7,7′-Me-sal$_2$en)(L-aa)], has been reported on. In these complexes, the stereoselectivity was thermodynamic in origin and was well explained in terms of the intramolecular steric repulsion between the alkyl groups of the coordinated amino acids and the H–C=N or CH$_3$–C=N groups of the Schiff base ligands. In this paper, we wish to report on another type of stereoselectivity which comes from a chiral Schiff base ligand in cobalt(III)-sal$_2$-(*S*,*S*)-chxn complexes with amino acids. Also to be reported is a stereospecificity of the cobalt(III)-sal$_2$-(*S*,*S*)-chxn complex to L-amino acids. The study is very interesting because the stereospecificity is thermodynamic in origin and is related to the optical resolution of amino acids with a metal complex[3–13] or to the problem of chiral recognition in metal-coenzyme.[14–19]

Experimental

Preparation of the Complexes. *1)* [*Co(sal$_2$-(S,S)-chxn)*]: This complex was prepared by the method described in Ref. 20 using (1*S*,2*S*)-*N*,*N*′-1,2-cyclohexylenebis(salicylideneamine). The optically active cyclohexanediamine used for the preparation of the optically active Schiff base ligand was resolved by a modification of the literature method.[21] A solution of *d*-tartaric acid (150 g) in 250 ml of water was cooled to about 10 °C. To this solution we then cautiously added 57 g of 1,2-cyclohexanediamine (Tokyo Kasei Co.) in small batches with cooling and stirring, followed by cooling in a refrigerator at about 0 °C for a day. A white powder-like compound was precipitated from the cold solution by scratching the wall of the beaker and subsequently separated by filtration. The white precipitate was the (+)$_D$-component and was recrystallized from a minimum amount of hot water to show a constant optical rotation (5—6 times), $[\alpha]_D$= +27.0°. Yield, 12.5 g. Found: C, 38.68; H, 6.52; N, 6.47%. Calcd for $C_6H_{16}N_2(C_4H_5O_6)_2\cdot H_2O$: C, 38.89; H, 6.53; N, 6.48%. The hydrochloride of the (+)$_D$-component, which was obtained by the usual procedure,[21] showed an $[\alpha]_D$ of +16.0° (lit,[21] +15.8°).

The (−)$_D$-component was obtained as white needles or plates by the slow concentration of the filtrate at room temperature. It was recrystallized from a minimum amount of hot water several times to show a constant optical rotation, $[\alpha]_D$=−12.1° (lit,[22] −12°). Yield, about 7.0 g. Found: C, 44.75; H, 7.65; N, 10.49%. Calcd for $C_6H_{16}N_2(C_4H_4O_6)\cdot 1/4H_2O$: C, 44.69; H, 7.69; N, 10.42%. The hydrochloride showed $[\alpha]_D$ of −16.0°.

The absolute configuration, (1*S*, 2*S*), has been determined for (+)$_D$-chxn by Marumo *et al.* from the X-ray crystal analysis of (−)$_D$-[Co((+)-chxn)$_3$]Cl$_3\cdot$5H$_2$O.[23]

2) [*Co(sal$_2$-(S,S)-chxn)(aa)*]: Since the preparative method is almost the same for all the complexes, only a representative procedure will be described here. The amino acid (1.5×10^{-3} mol) dissolved in 35 ml of water was added to a suspension of [Co(sal$_2$-(*S*,*S*)-chxn)] (0.5 g, 1.3×10^{-3} mol) in 45 ml of methanol. The mixture was stirred vigorously in open air for about 30 min at 60 °C. By this procedure, the complex was dissolved to give green solution. After cooling to room temperature, the solution was concentrated to about 35 ml at room temperature. Chloroform (about 50 ml) was added to extract the formed complex, and the crude product was obtained by evaporating off the chloroform to dryness. It was then recrystallized from methanol (complexes of L-ala, L-thr, D-thr, L-trp, and D-trp) or reprecipitated from chloroform (complexes of gly, D-ala, L-val, D-val, L-leu, and D-leu) by evaporating to dryness. The yields were 80—90%. These complexes can also be prepared from a mixture of a large excess of amino acid (about 1×10^{-2} mol) in 100 ml of water and [Co(sal$_2$-(*S*,*S*)-chxn)(aa)] (1×10^{-3} mol) in 50 ml of methanol, followed by a treatment similar to the method mentioned above. The compounds were identified by their PMR spectra, and their yields were 80—90%. The analytical data are listed in Table 1.

Optical Resolution of Amino Acids. The method for the optical resolution of amino acids is similar for all the amino acids, and so only a representative procedure will be given

* A part of this study was reported in *Chem. Lett.*, **1976**, 745.

Table 1. Elemental analysis data

Complex	C (%) Found(Calcd)	H (%) Found(Calcd)	N (%) Found(Calcd)
$[Co(sal_2\text{-}(S,S)\text{-chxn})(gly)]\cdot H_2O$	56.29(56.06)	5.66(5.56)	8.73(8.91)
$[Co(sal_2\text{-}(S,S)\text{-chxn})(L\text{-ala})]\cdot 4.5H_2O$	50.31(50.37)	6.42(6.43)	7.68(7.66)
$[Co(sal_2\text{-}(S,S)\text{-chxn})(D\text{-ala})]\cdot CHCl_3$	48.65(48.37)	4.48(4.57)	7.11(7.05)
$[Co(sal_2\text{-}(S,S)\text{-chxn})(L\text{-val})]\cdot 0.5CHCl_3\cdot H_2O$	53.39(53.44)	5.67(5.72)	7.23(7.33)
$[Co(sal_2\text{-}(S,S)\text{-chxn})(D\text{-val})]\cdot 0.5CHCl_3\cdot H_2O$	53.68(53.44)	5.64(5.72)	7.22(7.33)
$[Co(sal_2\text{-}(S,S)\text{-chxn})(L\text{-leu})]\cdot 0.5CHCl_3$	55.68(55.92)	5.96(5.76)	7.24(7.33)
$[Co(sal_2\text{-}(S,S)\text{-chxn})(D\text{-leu})]\cdot 0.5CHCl_3$	55.75(55.92)	5.81(5.76)	7.32(7.33)
$[Co(sal_2\text{-}(S,S)\text{-chxn})(L\text{-thr})]\cdot H_2O$	57.61(57.72)	5.52(5.65)	8.30(8.41)
$[Co(sal_2\text{-}(S,S)\text{-chxn})(D\text{-thr})]\cdot H_2O$	57.92(57.72)	5.54(5.65)	8.39(8.41)
$[Co(sal_2\text{-}(S,S)\text{-chxn})(L\text{-trp})]\cdot 3.5H_2O$	57.60(57.67)	5.83(5.93)	8.64(8.68)
$[Co(sal_2\text{-}(S,S)\text{-chxn})(D\text{-trp})]\cdot 4H_2O$	56.92(56.88)	5.92(6.01)	8.66(8.56)

here. The molar ratio of the reactants is 1: 2 (Complex: DL-amino acid). DL-Amino acid (2.6×10^{-3} mol), dissolved in 40 ml of water, was added to a suspension of $[Co(sal_2\text{-}(S,S)\text{-chxn})]$ (0.5 g, 1.3×10^{-3} mol) in 60 ml of methanol. The mixture was then stirred vigorously for 30 min at about 60 °C. After cooling, the green complex was extracted into chloroform (50 ml, twice), and the water layer was concentrated to near dryness. The white precipitate thus obtained was washed with methanol; the yields were 90—100% (a half of the used amino acid corresponds to the yield of 100%). The white precipitate in each case was confirmed to be the corresponding amino acid by a study of its IR spectrum. The opical purity of the recovered amino acids was determined by using the method described in Ref. 24.

Measurements. The IR spectra were recorded as KBr pellets with a Hitachi EPI-S2 spectrophotometer. The electronic Absorption spectra were measured with a Hitachi EPS-3 spectrophotometer at 25 °C. The CD spectra were recorded with a JASCO J-20 Automatic Recording Spectropolarimeter at room temperature. The optical rotation at 435 nm was measured with a JASCO DIP-180 Automatic Polarimeter at 25 °C. The PMR spectra were measured with a Hitachi R-20 spectrometer (60 MHz) at 35 °C in CD_3OD using TMS as the internal reference.

Results and Discussion

Stereoselectivity. The data for the electronic absorption spectra (AB) and the circular dichroism spectra (CD) are summarized in Table 2, while some representative AB and CD spectra are shown in Fig. 1 (and Fig. 1 in *Chem. Lett.*, **1976**, 745). The PMR spectral data are listed in Table 3, while some representative PMR spectra are shown in Fig. 2 (and Fig. 2 in *Chem. Lett.*, **1976**, 745.)

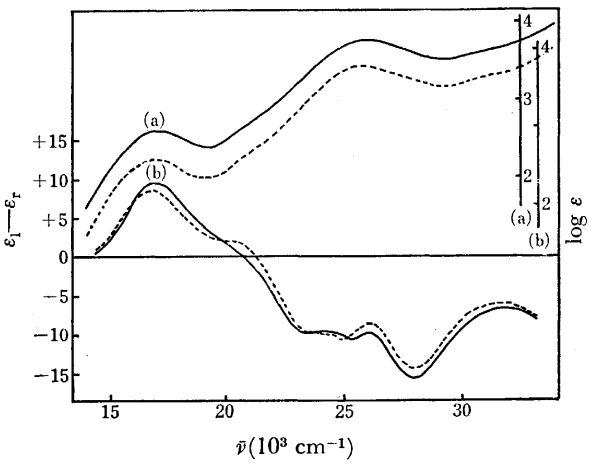

Fig. 1. AB and CD spectra of Λ-$[Co(sal_2\text{-}(S,S)\text{-chxn})(L\text{-val})]$ (——) and Λ-$[Co(sal_2\text{-}(S,S)\text{-chxn})(D\text{-val})]$ (……) in MeOH.

All the complexes exhibit AB and CD spectra which are quite similar to one another. Thus, it is suggested that all the complexes prefer to take the same geometrical structure. All the complexes show CD intensities in the first absorption region (16000—21000 cm^{-1}) as strong as those for optically pure isomers of $[Co(sal_2en)(aa)]$.[2] Thus, it is also suggested that all the complexes prefer to take the same optical form. These speculations are strongly supported by the PMR spectra. All the complexes show almost the same PMR signal for the coordinated $sal_2\text{-}(S,S)$-chxn. Moreover, the PMR signals of the alkyl groups of the coordinated amino acids consist of peaks which correspond to only one isomer. Therefore, it is clear from these data that the

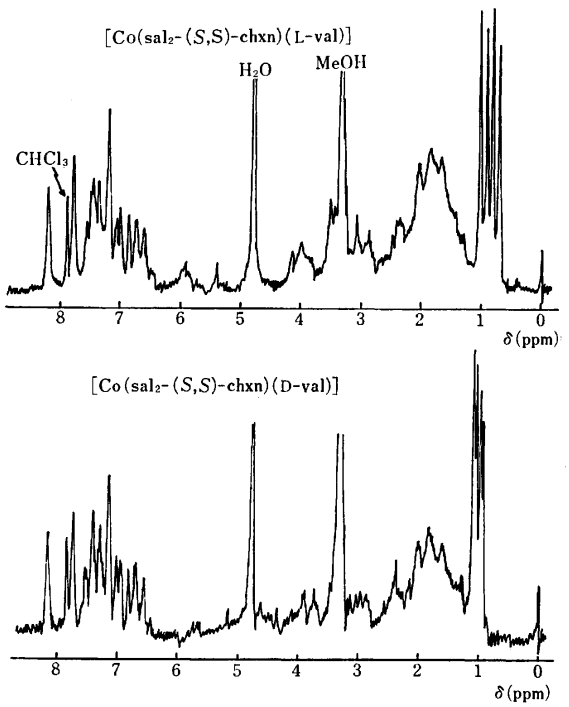

Fig. 2. PMR Spectra of representative complexes in CD_3OD.

TABLE 2. AB AND CD SPECTRAL DATA FOR [Co(sal$_2$-(*S*,*S*)-chxn)(aa)] IN METHANOL
(Wave number are in 10^3 cm^{-1})

Amino acid (aa)	AB (log ε_{max})	CD ($\Delta\varepsilon_{ext}$)	mino acid (aa)	AB (log ε_{max})	CD ($\Delta\varepsilon_{ext}$)
Gly	16.95(2.56)	16.95(+8.35)	D-Leu	16.95(2.59)	16.81(+8.68)
	20.83(2.58)[a]	20.00(+1.01)		21.28(2.74)[a]	20.62(+1.65)
	25.97(3.73)	23.64(−8.33)		25.97(3.88)	23.64(−9.55)
		25.00(−7.81)			25.00(−9.42)
		28.17(−12.94)			28.17(−13.28)
L-Ala	17.09(2.58)	16.95(+10.66)	L-Thr	17.09(2.62)	16.65(+10.82)
	21.28(2.73)[a]	20.00(+1.30)		21.28(2.83)[a]	20.00(+1.87)
	25.97(3.74)	23.64(−10.86)		25.97(3.86)	23.42(−10.95)
		25.00(−10.86)			25.32(−10.93)
		28.17(−15.90)			28.17(−16.50)
D-Ala	17.09(2.64)	16.95(+8.44)	D-Thr	16.95(2.56)	16.81(+9.96)
	21.28(2.72)[a]	20.62(+1.48)		21.28(2.79)[a]	20.62(+2.58)
	25.97(3.81)	23.64(−8.82)		25.97(3.76)	23.64(−10.44)
		25.00(−8.88)			25.32(−9.56)
		28.17(−13.31)			28.17(−15.22)
L-Val	17.09(2.62)	16.95(+9.50)	L-Trp	17.09(2.60)	16.95(+10.62)
	21.28(2.76)[a]	20.00(+2.00)		23.81(3.46)[a]	20.00(+2.31)
	25.97(3.78)	23.26(−9.50)		25.97(3.84)	23.42(−10.00)
		25.32(−10.23)			25.32(−9.28)
		28.17(−15.32)			28.17(−14.20)
D-Val	17.09(2.60)	16.95(+8.53)	D-Trp	16.95(2.56)	16.81(+8.46)
	21.28(2.73)[a]	20.63(+2.10)		22.22(2.98)[a]	20.00(+1.82)
	25.97(3.79)	23.64(−9.33)		25.97(3.87)	23.64(−8.30)
		25.00(−10.37)			25.00(−7.82)
		28.17(−13.98)			28.17(−11.55)
L-Leu	17.09(2.58)	16.95(+8.98)			
	21.28(2.70)[a]	20.00(+1.65)			
	25.97(3.88)	23.64(−9.46)			
		25.00(−9.27)			
		28.17(−13.48)			

a) Shoulder.

complexes exist as only one diastereoisomer in methanol. As will be mentioned later, six diastereomers are possible for each complex: *Λ*- and *Λ-cis-*β_1, *Λ*- and *Λ-cis-*β_2, and *Λ*- and *Λ-cis-*α. However, all the complexes utilize only one diastereoisomer, and their structures are similar to one another whether the coordinated amino acid is L or D. Thus, it may be concluded that 1) the stereoselectivity in the [Co(sal$_2$-(*S*,*S*)-chxn)(aa)] complex is complete, and 2) the stereoselectivity of the coordinated sal$_2$-(*S*,*S*)-chxn is great enough to assume only one optical form.

Although some differences in CD strengths are observed between the complexes with L- and D-amino acids, this is not due to the poor stereoselectivity but to the vicinal effect of the coordinated amino acids. Since the CD strengths in these Schiff base complexes are 2—3 times greater than those in the usual amino acidato cobalt(III) complexes,[25-28] the vicinal effect may also be somewhat stronger in these complexes. Quite a strong vicinal effect has also been observed for [Co(tfac$_2$en)-(L-aa)] (tfac$_2$en=dianion of *N*,*N*′-ethylenebis(trifluoroacetylacetoneamine); the results will be reported elsewhere.

All the complexes show no time-dependence on their CD and PMR spectra in methanol. Thus, the isomerization reaction such as seen in [Co(sal$_2$en)(L-aa)] and [Co(7,7′-Me-sal$_2$en)(L-aa)] may not occur in these sal$_2$-(*S*,*S*)-chxn-complexes.[2] However, these complexes are substitution-labile for the coordinated amino acid. That is, as has been described in the Experimental section, the reaction of these complexes with an excess of another amino acid (aa′H) proceeds comparatively rapidly to give [Co(sal$_2$-(*S*,*S*)-chxn)(aa′)] with a retention of the configuration. These facts mean that the stereoselectivity of sal$_2$-(*S*,*S*)-chxn-complexes is so high that no conversion of the configuration of the coordinated Schiff base ligand is observed. Since the stereoselectivity in substitution-labile complexes can usually be ascribed to thermodynamic origins,[11-13] the stereoselectivity observed here can also be thought to be thermodynamic in origin.

Structure of the Complexes. All the complexes isolated show ν(COO$^-$) at 1625—1630 cm^{-1}, suggesting the coordination of the carboxylate group of the amino acidato ligand to the central cabolt(III) ion.[29] The elemental analysis suggests that all the amino acids act as bidentate ligands. Since the PMR signal of the H–C=N group of the sal$_2$-(*S*,*S*)-chxn ligand is split into

Table 3. PMR Spectral data for [Co(sal$_2$-(*S*,*S*)-chxn)(aa)] in CD_3OD (δ, ppm)

Amino acid (aa)	sal$_2$-(*S*,*S*)-chxn			CH_3 of amino acid[c]
	HC=N[c]	ϕ-protons	chxn[b]	
Gly	8.19(1) 7.72(1)	7.5—6.5 (multiplet)	2.3—1.3 (multiplet)	
L-Ala	8.19(1) 7.70(1)	7.5—6.5 (multiplet)	2.3—1.3 (multiplet)	1.37(1.5) 1.25(1.5) } (doublet)
D-Ala[a]	8.18(1) 7.70(1)	7.5—6.5 (multiplet)	2.3—1.3 (multiplet)	1.56(1.5) 1.44(1.5) } (doublet)
L-Val[a]	8.20(1) 7.77(1)	7.5—6.5 (multiplet)	2.3—1.3 (multiplet)	1.00(1.5) 0.88(1.5) } (doublet)
				0.80(1.5) 0.68(1.5) } (doublet)
D-Val[a]	8.20(1) 7.77(1)	7.5—6.5 (multiplet)	2.3—1.3 (multiplet)	1.09(1.5) 0.97(1.5) } (doublet)
				1.05(1.5) 0.83(1.5) } (doublet)
L-Leu[a]	8.17(1)	7.5—6.5 (multiplet)	2.3—1.3 (multiplet)	0.99(1.5) 0.91(1.5) } (doublet)
				0.96(1.5) 0.88(1.5) } (doublet)
D-Leu[a]	8.17(1) 7.71(1)	7.5—6.5 (multiplet)	2.3—1.3 (multiplet)	1.04(1.5) 0.95(1.5) } (doublet)
				0.97(1.5) 0.88(1.5) } (doublet)
L-Thr	8.23(1) 7.77(1)	7.5—6.5 (multiplet)	2.3—1.3 (multiplet)	1.24(1.5) 1.12(1.5) } (doublet)
D-Thr	8.22(1) 7.77(1)	7.5—6.5 (multiplet)	2.3—1.3 (multiplet)	1.34(1.5) 1.22(1.5) } (doublet)
L-Trp	8.10(1)[d] 7.55(1)[d]	7.5—6.5 (multiplet)	2.0—1.0 (multiplet)	
D-Trp	8.20(1) 7.70(1)	7.5—6.5 (multiplet)	2.0—1.0 (multiplet)	

a) This mcoplex shows a $CHCl_3$ signal at 7.87 ppm. b) Broad multiplet. c) The number of protons is in parentheses. d) The high-field shift of this peak is perhaps due to the anisotropic effect of the phenyl ring.

two peaks of equal intensity, the *cis*-α- and *cis*-β-structures are thought to be possible. However, the *cis*-α-structure is thought to be quite unstable, and such a complex has not yet been reported in cobalt(III)–Schiff base complexes.[30,31] On the other hand, the *cis*-β-structure is well known.[30-34] Since the stereoselectivity in these complexes is thermodymanic in origin, as has been mentioned above, the thermodynamically stable *cis*-β-structure is confidently assigned to the complexes. It is well known that (*S*,*S*)-chxn and its derivatives take the δ-conformation exclusively.[35-37] This is due to the extraordinary stability of the chair form of the cyclohexane ring. Molecular models indicate that the δ-conformation persists in sal$_2$-(*S*,*S*)-chxn and that the Λ-configuration is strain-free in its complex with the *cis*-β form. Therefore, the Λ-configuration is confidently assigned to all the complexes. As will be discussed later, [Co(sal$_2$-(*S*,*S*)-chxn)(L-aa)] is more thermodynamically stable than [Co(sal$_2$-(*S*,*S*)-chxn)-(D-aa)]. This is mainly due to the intramolecular steric repulsion between the alkyl group of the coordinated amino acid and the H–C=N group of the Schiff base ligand. This repulsion is larger in the D-aa-complex than in the L-aa-complex. Molecular models show that the steric repulsion is larger in the Λ_D-*cis*-β_1(*fac*) isomer than in the Λ_L-*cis*-β_1(*fac*) isomer. However, the Λ_L-*cis*-β_2(*mer*) isomer displays somewhat a larger steric repulsion than the Λ_D-*cis*-β_2(*mer*) isomer. Thus, the *cis*-β_1(*fac*)-structure shown in Fig. 3 may be assigned to all the complexes.

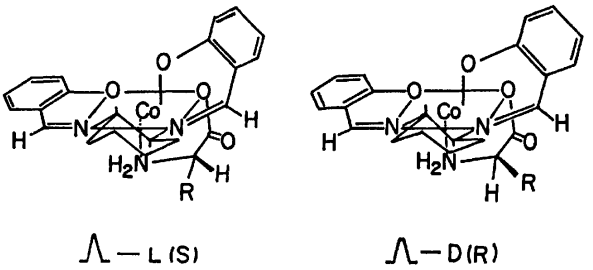

Fig. 3. The proposed structure of [Co(sal$_2$-(*S*,*S*)-chxn)-(aa)].

Stereospecificity. In order to study the stereospecificity of the complexes toward L- or D-amino acids, we examined the reactions of [Co(sal$_2$-(*S*,*S*)-chxn)] with various racemic amino acids in open air. The molar ratio in the reaction was maintained at 1 : 2 (complex: DL-amino acid). The stereospecificity was estimated from the optical purity of the unreacted amino acid which was recovered from the reaction solution by extracting the formed complex with chloroform, followed by the concentration of the amino-acid solution. The optical purities of the unreacted amino acids are sum-

TABLE 4. OPTICAL PURITY OF UNREACTED AMINO ACIDS WHICH WERE RECOVERED FROM THE REACTION SOLUTIONS OF [Co(sal$_2$-(*S*,*S*)-chxn)] AND DL-AMINO ACIDS IN A 1 : 2 MOLAR RATIO

Amino acid	Configuration of unreacted amino acid	Optical purity (%)	Amino acid	Configuration of unreacted amino acid	Optical purity (%)
Ala	D(R)	6—10	Asp	D(R)	16—18
Val	D(R)	6—8	Glu	D(R)	6—8
Leu	D(R)	6—8	Phe	D(R)	29—31
Met	D(R)	6—8	Trp	D(R)	41—43
Ser	D(R)	10—12	Pro	L(S)	48—50
Thr	D(R)	27—30			

marized in Table 4. Since the reaction is stoichiometric, it is written as follows:

$$2[\text{Co(sal}_2\text{-}(S,S)\text{-chxn)}] + 4\text{aaH} + 0.5\text{O}_2 \longrightarrow 2[\text{Co(sal}_2\text{-}(S,S)\text{-chxn)(aa)}] + 2\text{aaH} + \text{H}_2\text{O}. \quad (1)$$

Moreover, since all the complexes are substitution-labile toward the coordinated amino acids, the following equilibrium is also thought to be established in solution:

$$[\text{Co(sal}_2\text{-}(S,S)\text{-chxn)(L-aa)}] + \text{D-aaH} \rightleftarrows [\text{Co(sal}_2\text{-}(S,S)\text{-chxn)(D-aa)}] + \text{L-aaH}. \quad (2)$$

Here, we must consider the possibility of the racemization of amino acids or the assymetric transfer of the coordinated amino acids, but these processes were not observed under our experimental conditions. Therefore, the results in Table 4 indicate that Equilibrium 2 tends to lie toward the left side. Thus, it may be concluded that the cobalt(III)-sal$_2$-(*S*,*S*)-chxn-complex favors L-amino acids more than D-amino acids, with the exception of proline. Since the existence of Equilibrium 2 means that the stereospecificity is thermodynamic in origin, it may be concluded that the L-aa-complex is thermodynamically more stable than the D-aa-complex, again with the exception of proline. In this case, it is known that the stereoselective behavior of proline is markedly different from that of the other amino acids.[1,2]

The stereospecificity increases in the order, ala$\sim$met$\sim$leu$\sim$val$\sim$glu$<$ser$<$asp$<$thr$\lesssim$phe$<$trp$<$pro. This order parallels the increasing order of the stereoselectivity in the [Co(sal$_2$en)(L-aa)] complex and also coincides with the increasing order of the steric crowding of the alkyl group of the amino acid.[2] Therefore, an intramolecular steric repulsion between the alkyl group and the H–C=N group of the Schiff base ligand, such as seen in the [Co(sal$_2$en)(L-aa)] complex,[2] exists in each complex, and it may be larger in the Λ_D-isomer than in the Λ_L-isomer. This is the reason why the L-amino acid is selectively coordinated in the complex. In the case of proline, the molecular model indicates that the steric repulsion is larger in the Λ_L-isomer than in the Λ_D-isomer.

Variation of the Molar Ratio (DL-Amino Acid/Complex) in the Reaction. Figure 4 shows the plots of the optical purity of unreacted amino acid *versus* the molar ratio (m/n) in the reaction of n mol of a complex with $2m$ mol of DL-amino acid. In this figure, the solid lines show the calculated values, and the circles, the observed values. The calculation was carried out by using Eqs. 3 and 4 as derived below. Here, K is the equilibrium constant of Reaction 2 and is equal to

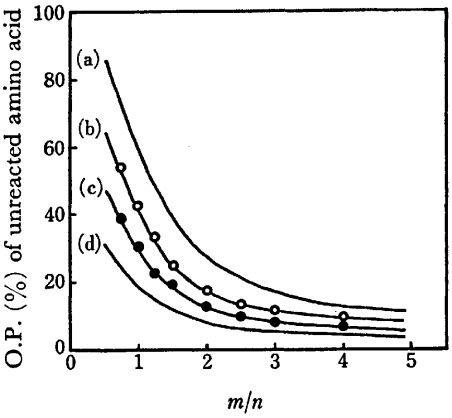

Fig. 4. A plot of optical purity (O.P.) of unreacted amino acid and molar ratio (m/n) in the reaction of n mol of complex with $2m$ mol of DL-amino acid. (a), (b), (c), and (d) are the calculated curve for K=20, K=6.0, K=3.4, and K=2, respectively. ○ and ● are the observed values for tryptophan (○) and phenylalanine (●).

K_L/K_D ($K_L>K_D$ in sal$_2$-(*S*,*S*)-chxn-complex), where K_L and K_D are the stability constants written as follows:

$$K_L = [\text{Co(Y)(L-aa)}]/[\text{Co(Y)}][\text{L-aa}],$$
$$K_D = [\text{Co(Y)(D-aa)}]/[\text{Co(Y)}][\text{D-aa}].$$

Co(Y) indicates the Co(sal$_2$-(*S*,*S*)-chxn)-complex, and the brackets stand for the concentration.

When the reaction of n mol of the complex with $2m$ mol of DL-amino acid ($2m>n$) is considered, the optical purity of the unreacted amino acid is written as follows:

$$\text{O.P. (\%)} = \{[\text{D-aa}]_f - [\text{L-aa}]_f\}/\{[\text{D-aa}]_f + [\text{L-aa}]_f\} \times 100.$$

where $[\text{D-aa}]_f$ and $[\text{L-aa}]_f$ are the concentrations of free D- and L-amino acids respectively. Since the complex formation is quantitative, and if we can neglect the concentration of free complex, [Co(Y)], the O.P.(%) can be written as follows:

$$\text{O.P. (\%)} = \{[\text{D-aa}]_f - (2m-n-[\text{D-aa}]_f)\}/\{[\text{D-aa}]_f + (2m-n-[\text{D-aa}]_f)\} \times 100, \quad (3)$$

where

$$[\text{D-aa}]_f = \{-(3m-n-mK+nK) + [(3m-n-mK+nK)^2 - 4(mn-2m^2)(K-1)]^{1/2}\} \times [2(K-1)]^{-1}. \quad (4)$$

Thus, if K is known, we can estimate the O.P.(%) of the unreacted amino acid by using Eqs. 3 and 4. In Fig. 4, we selected K arbitrarily (K=2 or 20) or as fitted to the

observed values (K=3.4 for phe and K=6.0 for trp).

From these results, it may be seen that the observed values fit the calculated curves quite well at all the reaction molar ratios; the K-values for phe and trp are quite reliable. These K-values are close to the thermodynamic stereoselectivity (Λ_L-*cis*-β_1 isomer/Δ_L-*cis*-β_1 isomer) of the Co(sal$_2$en)-complexes with L-phe and L-trp, respectively (about 4 for phe and 8 for trp).[2] Here, the Λ_L-*cis*-β_1 isomer/Δ_L-*cis*-β_1 isomer ratio is equal to the Λ_L-*cis*-β_1 isomer/Λ_D-*cis*-β_1 isomer ratio; it corresponds to the relative stability constant between the complex with L-aa and that with D-aa. Therefore, these results give strong support for the thermodynamic origin of the stereospecificity.

Finally, it should be pointed out that, although the optical purity at $2m/n$=2 is not very high, it becomes higher as m becomes smaller, and that the use of a chloroform-soluble, non-electrolyte complex is one of the advantages of our method of optical resolution of amino acid, as it provides for the easy separation of the unreacted amino acid and the formed complex by solvent extraction.

The authors wish to express their deep thanks to Professor Y. Yoshino of Tokyo University, and Professor K. Sone and Dr. Y. Fukuda of Ochanomizu University for their kind assistance in the CD spectral measurements. This work was supported in part by a Scientific Research Grant from the Ministry of Education, Japan (No. 154189).

References

1) Y. Fujii, T. Isago, and M. Sano, *Chem. Lett.*, **1975**, 1299.
2) Y. Fujii, T. Isago, M. Sano, N. Yanagibashi, and S. Takahashi, *Bull. Chem. Soc. Jpn.*, **49**, 3509 (1976).
3) A. D. Gott and J. C. Bailar, Jr., *J. Am. Chem. Soc.*, **74**, 4820 (1952).
4) B. D. Sarma and J. C. Bailar, Jr., *J. Am. Chem. Soc.*, **78**, 895 (1956).
5) M. Shibata, Y. Fujita, M. Naito, and K. Hori, *Bull. Chem. Soc. Jpn.*, **36**, 485 (1963).
6) M. Shibata, H. Nishikawa, and K. Hori, *Bull. Chem. Soc. Jpn.*, **41**, 130 (1968).
7) K. Harada, *Nature*, **205**, 590 (1965).
8) M. Shibata, *Kagaku No Ryoiki*, **29**, 334 (1975).
9) V. D. Davankov *et al.*, *J. Chromatogr.*, **60**, 280 (1971); **91**, 174 (1974); and **91**, 439 (1974).
10) V. D. Davankov *et al.*, *J. Inorg. Nucl. Chem.*, **37**, 369 (1975).
11) B. E. Leach and R. J. Angelici, *J. Am. Chem. Soc.*, **91**, 6296 (1969).
12) R. Nakon, R. R. Rechani, and R. J. Angelici, *Inorg. Chem.*, **12**, 2431 (1973).
13) R. V. Snyder, R. J. Angelici, and R. B. Meck, *J. Am. Chem. Soc.*, **94**, 2660 (1972).
14) R. G. Asperger and C. F. Liu, *Inorg. Chem.*, **6**, 796 (1967).
15) R. C. Job and J. C. Bruice, *J. Chem. Soc., Chem. Commun.*, **1973**, 332.
16) J. P. Glusker, H. L. Carrell, R. C. Job, and J. C. Bruice, *J. Am. Chem. Soc.*, **96**, 5741 (1974).
17) R. C. Job and J. C. Bruice, *J. Am. Chem. Soc.*, **96**, 809 (1974).
18) J. E. Hix, Jr. and M. M. Jones, *J. Am. Chem. Soc.*, **90**, 1723 (1968).
19) H. Ogino and K. Ogino, "Coordination Chemistry of Metalloenzymes," Nankodo, Tokyo (1974), p. 194.
20) H. Aoi, M. Ishimori, S. Yoshikawa, and T. Tsuruta, *J. Organomet. Chem.*, **85**, 241 (1975).
21) R. G. Asperger and C. F. Liu, *Inorg. Chem.*, **4**, 1492 (1965).
22) R. S. Treptow, *Inorg. Chem.*, **5**, 1593 (1966).
23) F. Marumo, Y. Utsumi, and Y. Saito, *Acta Crystallogr., Sect. B*, **26**, 1492 (1970).
24) Y. Fujii, S. Hirasawa, and S. Takahashi, *Chem. Lett.*, **1976**, 817.
25) N. Matsuoka, J. Hidaka, and Y. Shimura, *Bull. Chem. Soc. Jpn.*, **48**, 458 (1975).
26) J. Fujita and Y. Shimura, "Spectroscopy and Structure of Metal Chelate Compounds," John Wiley & Sons, New York (1968), p. 197.
27) C. J. Hawkins, "Absolute Configuration of Metal Complexes," John Wiley & Sons, New York (1971), p. 185.
28) Recent papers: a) K. Yamanari, J. Hidaka, and Y. Shimura, *Bull. Chem. Soc. Jpn.*, **48**, 1653 (1975); b) M. Takeuchi and M. Shibata, *ibid.*, **47**, 2797 (1974); c) T. Yasui, *ibid.*, **48**, 454 (1975); d) Y. Kojima and M. Shibata, *Inorg. Chem.*, **12**, 1009 (1973); e) N. Matsuoka, J. Hidaka, and Y. Shimura, *Bull. Chem. Soc. Jpn.*, **45**, 2491 (1972); f) J. P. Glusker, H. L. Carrell, R. C. Job, and C. Bruice, *J. Am. Chem. Soc.*, **96**, 5741 (1974); g) S. Yamada, J. Hidaka, and B. E. Douglas, *Inorg. Chem.*, **10**, 2187 (1971); h) G. R. Brubaker and D. P. Schaefer, *ibid.*, **10**, 2170 (1971); i) J. I. Legg and J. Steele, *ibid.*, **10**, 2177 (1971).
29) K. Ueno and B. Sakaguchi, "Metal Chelate," Nankodo, Vol. II, Tokyo (1963), p. 43.
30) Y. Fujii, A. Osawa, Y. Furukawa, F. Ebina, and S. Takahashi, *Bull. Chem. Soc. Jpn.*, **45**, 2459 (1972).
31) D. Cummins, B. M. Higson, and E. D. McKenzie, *J. Chem. Soc., Dalton Trans.*, **1973**, 1359.
32) M. Caligaris, G. Manzini, G. Nardin, and L. Pandaccio, *J. Chem. Soc., Dalton Trans.*, **1972**, 543.
33) N. A. Bailey, B. M. Higson, and E. D. McKenzie, *J. Chem. Soc., Dalton Trans.*, **1972**, 503.
34) A. Bigotto, G. Costa, G. Mestroni, G. Pellizer, A. Puzeddu, E. Reicenhofer, L. Stefani, and G. Tauzer, *Inorg. Chim. Acta, Rev.*, **4**, 41 (1970).
35) J. B. Hendrickson, D. J. Cram, and C. S. Hammond, "Organic Chemistry," 3rd ed, McGraw-Hill-Kogakusha, Tokyo (1970), p. 190.
36) M. Goto, M. Saburi, and S. Yoshikawa, *Inorg. Chem.*, **8**, 358 (1969).
37) M. Saburi and S. Yoshikawa, *Bull. Chem. Soc. Jpn.*, **47**, 1184 (1974).

The Synthesis of Greigite from a Polysulfide Solution at about 100 °C

Hiroaki WADA

National Institute for Researches in Inorganic Materials, Kurakake, Sakura-Mura, Nihari-Gun, Ibaraki

(Received October 15, 1976)

Favorable synthesis conditions for greigite are examined in $FeSO_4 \cdot (NH_4)_2SO_4$–$Na_2S$–$Na_2S_x$ systems at about 100 °C. It has been found that greigite formation is influenced by the pH adjustment and by the addition of sulfur. When the final pH is about 6.0 and the dissolved iron concentration is in the 10^{-3}—$10^{-1.5}$ M range, greigite is synthesized as a single phase. The unit-cell dimensions of greigite range from 9.840 to 9.877 Å, corresponding to variations in compositions between 45.4 and 42.9 atomic % Fe. The formula of synthetic greigite is represented as $Fe_{3+x}S_4$ (x=0—0.4).

Many reports have been published on the preparation of greigite, Fe_3S_4, in an aqueous solution.[1-3] However, it is not easy to synthesize greigite as a single phase, because greigite formation depends upon many factors, such as the temperature, the pH, the starting source materials, and the redox conditions.[4,5] Recently, Horiuchi *et al.* studied the reaction of tetragonal FeS (mackinawite) with colloidal sulfur and observed the formation of cubic Fe_3S_4 in the semi-dry system by means of electron diffraction.[6] From the results of this work, it was suggested that amorphous sulfur played an important role in Fe_3S_4 formation.

In an aqueous solution, free sulfur is frequently combined with sulfide ions and so changed into the form of polysulfide ions. Paying special attention to sulfur source materials, the present author attemped to prepare greigite from a polysulfide solution.

Experimental

All the chemicals used were of a guaranteed reagent grade. A polysulfide stock solution was prepared by reacting orthorhombic sulfur with a Na_2S solution in a nitrogen gas atmosphere for 2 h at about 100 °C. After the residual solid sulfur had been taken away by filtration, the polysulfide solution was kept in polyethylene bottles in a cold and dark place. Prior to the experiments, the concentrations of sodium and sulfur were determined by the methods of flame-photometry and conventional gravimetry respectively. 0.20 M $Na_2S_{3.89}$ solution was used in the synthesis of greigite.

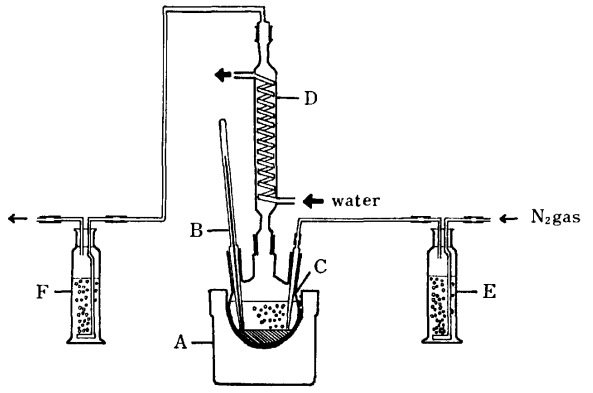

Fig. 1. Schematic diagram of the reaction vessel for synthesis of iron sulfides. A: Heating mantles. B: Mercury thermometer. C: 500 ml of round bottom flask with four necks. D: Dimroth condenser. E and F: Washing gas bottles. E is filled with 40 per cent pyrogallol–NaOH solution to remove oxygen in nitrogen gas. H_2S gas which is expelled from the vessel is absorbed in F, filled with 10 per cent NaOH solution.

$FeSO_4 \cdot (NH_4)_2SO_4$ and Na_2S were dissolved in a proper volume of distilled water in every other experiment. Less than 10 ml of a $Na_2S_{3.89}$ solution was added into large amounts of the Na_2S solution as a part of the sulfur source. Two hundred ml of a 0.0834 ± 0.0006 M $FeSO_4 \cdot (NH_4)_2SO_4$ solution were mixed with 200 ml of a 0.1468 ± 0.0006 M Na_2S solution containing polysufide ions, as is shown in Fig. 1. Purified nitrogen gas was flowed through the solution at the rate of about 170 ml/min in order to avoid the contamination of products by air oxidation. A colloidal suspension of iron sulfides precipitated was heated at the boiling temperature (103 °C) for 15—20 h.

At the termination of each experiment, the final pH of solution was measured by means of a pH meter (TOA Electronics Ltd., HM-7A type). The concentration of ferrous ions in the clear supernatant solution was determined by the titration method using 1.67×10^{-2} M $K_2Cr_2O_7$ or a colorimetric method using 1,10-phenanthroline. The iron sulfide product was separated from the solution by a centrifuge, washed by water, aqueous ammonia, and acetone, dried in a vacuum, and identified by means of X-ray and electron diffraction. An X-ray diffractometer (Shimadzu VDR-11) and an electron microscope (100 kV: Hitachi 11 D) were employed to identify the specimens.

The compositions of the iron sulfide products were determined by the analytical method of Kolthoff and Sandell.[7] About 200-mg portions of the specimens were decomposed into an ionic state on the basis of oxidation in the wet way using bromine with nitric acid. The sulfur was determined gravimetrically as $BaSO_4$. After the dissolved iron had been reduced to Fe^{2+} ions with $NH_2OH \cdot HCl$, the iron content was determined by the spectrophotometric method,[8] using 1,10-phenanthroline.

Results and Discussion

Greigite was obtained under the preferred synthesis conditions, listed in Table 1. Meanwhile, phase transformations were observed in the order of mackinawite, greigite, and pyrite (cubic FeS_2) with an increase in the amounts of the $Na_2S_{3.89}$ solution added. When the $Na_2S_{3.89}$ solution was not added, only mackinawite was formed. Greigite was produced as a single phase by the addition of 3—6 ml of the $Na_2S_{3.89}$ solution. Pyrite was formed together with greigite by the addition of 7—10 ml of the $Na_2S_{3.89}$ solution.

The analytical results of the products showed that the S/Fe atomic ratio of iron sulfides increased linearly with an increase in the amount of polysulfide solution

TABLE 1. EFFECT OF SULFUR FROM A 0.20 M $Na_2S_{3.89}$ SOLUTION UPON PRODUCTS, ON HEATING FOR 15—20 h AT ABOUT 100 °C

Source materials			Final pH	Product
$FeSO_4 \cdot (NH_4)_2SO_4 \cdot 6H_2O$ in g	$Na_2S \cdot 9H_2O$ in g	$Na_2S_{3.89}$ in ml		
6.5401	7.0269	—	6.38	mackinawite
6.4972	7.0227	3	6.00	greigite
6.5807	7.0733	5	6.10	greigite
6.5988	7.0158	5.5	6.01	greigite
6.6023	7.0279	6	6.03	greigite
6.5211	7.0322	10	6.00	greigite +pyrite

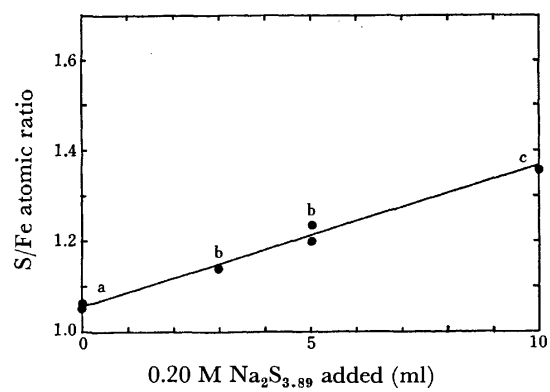

Fig. 2. Relation of S/Fe atomic ratio of products with 0.20 M $Na_2S_{3.89}$ solution added. Products: a=mackinawite, b=greigite, c=greigite+pyrite.

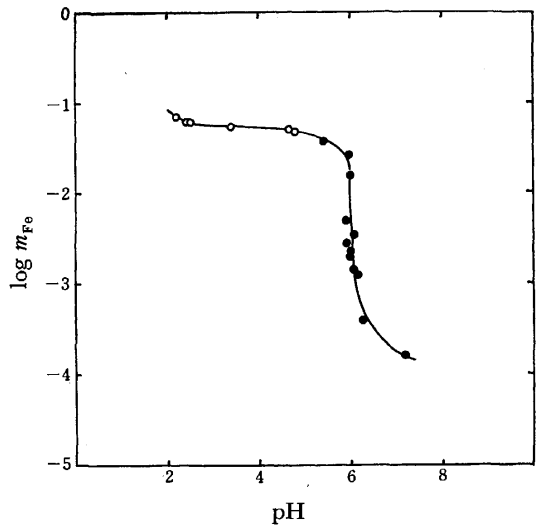

Fig. 3. Relations of the final pH with iron concentration in solutions. The pH is adjusted with variation of mixing ratio of $FeSO_4 \cdot (NH_4)_2SO_4$ and Na_2S (●), and addition of 1.13 M H_2SO_4 (○).

added (Fig. 2). The dissolved iron content in the clear supernatant solution increased by the order of 2.5, from 10^{-4} to $10^{-1.5}$ M/l, corresponding to the pH change from 7 to 5.8 (Fig. 3). The final pH values of the solutions associated with greigite ranged from 5.8 to 6.1. The region of greigite formation was consistent with the conspicuous increase in the solubility of mackinawite. These results indicate that (1) forms of the resulting iron sulfide are controlled systematically by the amounts of sulfur added and by the pH of the solution and (2) the region of greigite formation as a single phase in solutions is restricted to the extremely narrow pH range between 5.8 and 6.1.

It was found that the correct pH adjustment of the solution was important in preparing greigite as a single phase. However, the rapid pH change upon the addition of mineral acids was not suitable for its synthesis. In order to acidify solutions mildly and gradually from the alkaline side in the heating process, proper mixing ratios of $FeSO_4 \cdot (NH_4)_2SO_4$ and Na_2S solutions, described above, were selected. Pure greigite was formed when (1) 2 $m_{SO_4^{2-}} > m_{Na^+}$ and (2) $m_{S^{2-}} + m_{HS^-} > m_{Fe^{2+}}$ (all the iron was transformed initially into the form of precipitated FeS).

After the solution had been dried in a vacuum, synthetic greigite was obtained as a fine sooty black powder with strong magnetic properties. The grain size of greigite was calculated to be 200—300 Å on the basis of the measurement of the half-width of the diffraction peak. Fresh greigite synthesized in acidic solution sometimes showed a pyrophoric property. When exposed to the atmosphere, it was burned with fumes of S_2 and SO_2, being thus completely altered to a mixture of magnetite (Fe_3O_4) and hematite (Fe_2O_3).

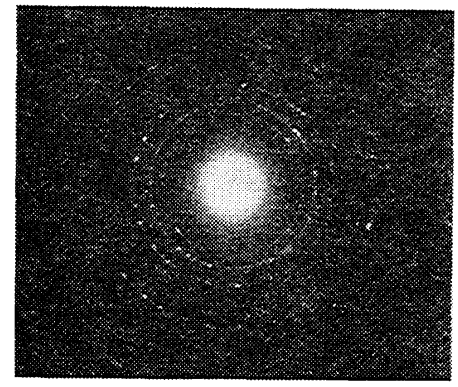

Fig. 4. Electron diffraction pattern of synthetic greigite.

Figure 4 shows a typical electron-diffraction pattern from a synthetic greigite. This pattern contains only the reflections allowed for the spinel structure, with the space group Fd3m. Both the d-spacings and the relative intensities observed are listed in Table 2 in comparison with the X-ray data of natural greigite. There is a close correspondence of d-spacings and intensities between synthetic greigite and the natural mineral.[9]

The product, stable in air was examined by the X-ray powder diffraction method, and its composition was determined by chemical analysis. The compositions of synthetic greigite ranged from 45.4 to 42.9 atomic per cent of iron and explicitly showed a deviation from stoichiometric Fe_3S_4. The chemical formula of synthetic greigite was given by $Fe_{3+x}S_4$ (x=0—0.4). With respect to the compositions, this iron-rich greigite ($Fe_{3+x}S_4$) was analogous to natural iron-rich smythite ($Fe_{3+x}S_4$), which

Table 2. Electron-diffraction data for synthetic greigite in comparison with X-ray diffraction data for mineral greigite (Skinner, Erd, and Grimaldi (1964))

hkl	Synthetic greigite		Natural greigite	
	d_{obsd}	I[a)]	d_{obsd}	I
111	5.68	w	5.720	8
220	3.51	s	3.500	30
311	3.00	vs	2.980	100
222	2.88	w	2.855	4
400	2.49	vs	2.470	55
331	2.29	w	2.260	2
422	2.03	w	2.017	10
333, 511	1.91	vs	1.901	30
440	1.75	vs	1.746	75
531			1.671	1
620	1.57	vw	1.563	4
533	1.50	w	1.506	10
622			1.488	2
444	1.43	w	1.425	8
711, 551	1.39	vw	1.383	1
642	1.32	vw	1.320	4
731, 553	1.29	vw	1.286	12
800	1.23	vw	1.235	10
733			1.210	1
644			1.198	1
822, 660			1.164	1
751, 555	1.14	vw	1.140	2
840	1.10	w	1.105	16
753, 911			1.084	1
664			1.054	2
931	1.03	vw	1.035	8
844	1.01	w	1.001	30

a) Intensities were estimated visually. vs=very strong, s=strong, w=weak, vw=very weak.

was found at Silverfields Mine, Cobalt, Ontario.[10)]

The cell edges of synthetic greigite ranged from 9.840 Å to 9.877 Å with corresponding variations in the compositions. They increased with a decrease in the iron content in the compositional range between 45.4 and 42.9 atomic % Fe.

The density determination with a pycnometer was made at 25 °C on synthetic greigite. The specific gravities of $Fe_{3.33}S_4$ and Fe_3S_4 were 4.60 and 4.02 respectively.

The results presented above may be indicative of the possibility that excess iron occupies an interstitial site in the spinel structure. Further detailed researches on the crystal structure are, however, necessary for a better understanding of the nonstoichiometry of greigite.

The author wishes to express his thanks to Dr. Shigeto Yamaguchi for his encouragement and guidance throughout this work and to Dr. Shigeo Horiuchi for his valuable discussions. Thanks are also due to Mr. Kousuke Sakaguchi for his operation of the electron microscope.

References

1) S. Yamaguchi and T. Katsurai, *Kolloid Zeit.*, **170**, 147 (1960).
2) S. Yamaguchi and H. Wada, *Naturwissenschaften*, **54**, 515 (1967).
3) M. Uda, *Am. Mineral.*, **50**, 1487 (1965).
4) R. A. Berner, *J. Geol.*, **72**, 293 (1964).
5) D. T. Rickard, *Stockholm Contr. Geology*, **20**, 67 (1969).
6) S. Horiuchi, H. Wada, and T. Noguchi, *Naturwissenschaften*, **57**, 670, (1970).
7) I. M. Kolthoff and E. B. Sandell, "Textbook of Quantitative Inorganic Analysis," 3 rd ed, Macmillan, New York (1952), p. 333.
8) E. B. Sandell,"Colorimetric Determination of Traces of Metals," Intersci. Publishers (1959), p. 1032.
9) B. J. Skinner, R. C. Erd, and E. S. Grimaldi, *Am. Mineral.*, **49**, 543 (1964).
10) L. A. Taylor, *Carnegie Inst. Wash. Year Book*, **68**, 259 (1970).

Preparation and Properties of the Uni- and Binuclear [Co(III)N_2O_4] Type Complexes Containing (*S*)-2-Amino-1-propanol

Toshikazu NISHIDE and Kazuo SAITO

Chemistry Department, Faculty of Science, Tohoku University, Aramaki, Sendai, 980

(Received November 9, 1977)

Reactions of (*S*)-2-amino-1-propanol (*S*-praH) with the tricarbonatocobaltate(III) solution gave binuclear complexes bridged by carbonates, or carbonate and hydroxide. The carbonate was replaced by oxalate (ox^{2-}) to give binuclear complexes $[(S\text{-praH})_2Co(ox)_2Co(S\text{-praH})_2]^{2+}$ and uninuclear *trans*(*N*)*cis*(*O*)-[Co(ox)(*S*-pra)-(*S*-praH)]. Another uninuclear complex $[Co(ox)(S\text{-praH})_2]^+$ was obtained by direct synthesis from *S*-praH and cobalt(II) acetate by oxidation with lead dioxide. Column chromatography with SP-Sephadex C-25 was useful for separating the geometrical isomers, which were identified by PMR, IR, visible, and UV absorption spectra. Their circular dichroism (CD) spectra changed depending on pH of the aqueous solution. All the *S*-pra$^-$ chelates have δ-conformation, which is characterized by an intensive plus CD component in the 25000 cm^{-1} region, regardless of the skeletal structure of the complexes.

In the previous papers[1,2] we reported the preparation of mixed ligand complexes of the type $[Co^{III}N_5O]$ containing various amino alcohols (amOH), and ammines or diamines. The alcohol protons of coordinated aminoalkanols in complexes of the type $[Co^{III}(amOH)(L)]X_3$ (amOH=2-aminoethanol [etaH], (*S*)-2-amino-1-propanol [*S*-praH] *etc.*; L=$(NH_3)_4$, $(en)_2$, and ((*R*,*R*)-1,2-diaminocyclohexane)$_2$; X=chloride, bromide and perchlorate) were deprotonated easily (p*K* 3 to 3.5 at 25 °C and ionic strength 0.05), and the aminoalkanolato complexes exhibited larger CD components than the protonated did in the first and second absorption band regions. Especially $[Co(S\text{-amO})(L)]^{2+}$ gave characteristic large plus vicinal CD components at *ca.* 25000 cm^{-1} (second band region), which were due to the δ-conformation of the *S*-amO$^-$ chelate.

The study has been extended to related complexes containing two moles of aminoalkanol ligands per cobalt(III), and this paper deals with the preparation of complexes of $[CoN_2O_4]$ type, *i.e.* the uninuclear complexes $[Co(ox)(S\text{-praH})_2]ClO_4$ and *trans*(*N*)*cis*(*O*)-[Co(ox)(*S*-pra)(*S*-praH)], and the binuclear complexes $[(S\text{-pra})_2Co(CO_3,OH)Co(S\text{-pra})(S\text{-praH})]$, $[(S\text{-pra})(S\text{-praH})Co(CO_3)_2Co(S\text{-pra})(S\text{-praH})]$, and $[(S\text{-praH})_2Co(ox)_2Co(S\text{-praH})_2](ClO_4)_2$. Their structure and CD pattern have been discussed with reference to the characteristic nature of the coordinated aminoalkanolato ligand.

Experimental

Material. The *S*-praH ligand was synthesized by Vogl and Pöln's method.[3] The outline of the syntheses is shown in Fig. 1.

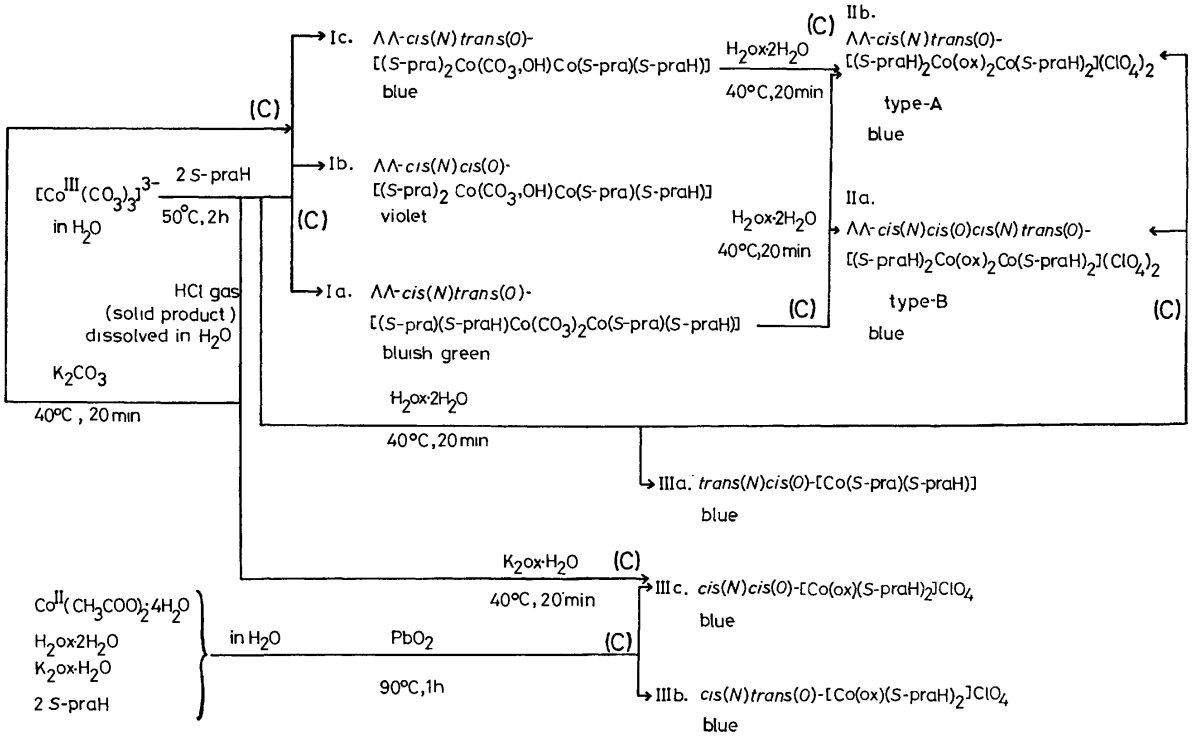

Fig. 1. Outline of the preparation. (C); Column chromatography (see the text).

Syntheses and Separation of μ-Carbonato Complexes: The tricarbonato $[Co(CO_3)_3]^{3-}$ solution (0.042 mol, 50 cm^3)[4] was heated with *S*-praH (0.1 mol) at 60 °C for 2 h and evaporated to dryness under a reduced pressure. The complexes were extracted with ethanol (300 cm^3), the solution was evaporated to dryness and the residue was extracted with a small amount of water. The aqueous solution was poured onto a column (3.5×60 cm) of Dowex 50W-X8 (Na form, 100—200 mesh). The adsorbed band was eluted with water to give three bands. The eluates were collected individually and each was evaporated to dryness under a reduced pressure at 40 °C to give higroscopic powder. The complexes were recrystallized from ethanol and found to have the following formulae. They were named Ia, Ib, and Ic in the order of elution.

Ia: $[(S\text{-pra})(S\text{-praH})Co(CO_3)_2Co(S\text{-pra})(S\text{-praH})]\cdot 2NaHCO_3\cdot 2H_2O$. Found: C, 26.16; H, 5.54; N, 7.06%. Calcd for $Co_2C_{14}H_{34}N_4O_{10}\cdot 2NaHCO_3\cdot 2H_2O$: C, 25.95; H, 5.45; N, 7.57%.

Ib: $[(S\text{-pra})_2Co(CO_3,OH)Co(S\text{-pra})(S\text{-praH})]$. Found: C, 32.18; H, 7.13; N, 11.20%. Calcd for $Co_2C_{13}H_{33}N_4O_8$: C, 31.78; H, 6.77; N, 11.41%.

Ic: $[(S\text{-pra})_2Co(CO_3,OH)Co(S\text{-pra})(S\text{-praH})]\cdot 2H_2O$. Found: C, 29.75; H, 7.36; N, 10.67%. Calcd for $Co_2C_{13}H_{33}N_4O_8\cdot 2H_2O$; C, 29.61: H, 7.07; N, 10.63%.

These complexes were also prepared by the following method. When the residue on the extraction of the initial reaction products with ethanol was treated with hydrogen chloride gas, blue violet hygroscopic powder was obtained with the composition $[CoCl_2(S\text{-praH})_2]Cl$. Reaction of its aqueous solution with potassium carbonate gave a blue solution, which was treated with a similar ion exchange column to that mentioned above for separating Ia, Ib, and Ic from one another.

Syntheses and Separation of μ-Oxalato Complexes: The initial reaction mixture containing the μ-carbonato complexes (0.042 mol) was heated with oxalic acid (6.35 g, 0.05 mol) at 40 °C for 20 min. Blue prisms were filtered off and identified as the uninuclear complex *trans(N)cis(O)*-$[Co(ox)(S\text{-pra})(S\text{-praH})]\cdot 0.5\,H_2O$. (IIIa, *vide infra*) The filtrate was submitted to column (4.5×82 cm) chromatography with SP-Sephadex C-25 and eluted with sodium perchlorate solution (0.2 mol·dm^{-3}). Three bands were observed, of which the first band was too small to be collected. Eluates from the remaining two bands were individually made acid to pH 1 with perchloric acid, and evaporated under a reduced pressure at 40 °C to decrease the volumes to *ca.* 20 cm^3. Both solutions were filtered, made pH 3 with sodium hydroxide solution (1 mol·dm^{-3}) and kept overnight in a refrigerator to give blue crystals. They were filtered off, washed with ethanol, and recrystallized from water, and named IIa and IIb in the order of elution.

IIa: $[(S\text{-praH})_2Co(ox)_2Co(S\text{-praH})_2](ClO_4)_2\cdot 6H_2O$. Found: C, 21.03; H, 5.00; N, 6.05%. Calcd for $Co_2C_{16}H_{36}N_4O_{10}Cl_2\cdot 6H_2O$: C, 21.32; H, 5.37; N, 6.22%.

IIb: $[(S\text{-praH})_2Co(ox)_2Co(S\text{-praH})_2](ClO_4)_2\cdot 2.5H_2O$. Found: C, 23.24; H, 5.38; N, 6.31%. Calcd for $Co_2C_{16}H_{36}N_4O_{10}Cl_2\cdot 2.5H_2O$: C, 22.92; H, 4.93; N, 6.69%.

Reaction of a concentrated aqueous solution of Ia with an equivalent amount of oxalic acid at 40 °C for 20 min gave a blue solution, which was treated with a similar column to that mentioned above to give two bands consisting of IIa and IIb respectively. On the other hand, when a concentrated solution of Ic was caused to react with an equivalent amount of oxalic acid at 40 °C for 20 min, a blue solution was obtained, which gave only one band consisting of IIb on a similar column chromatography.

Preparation of Uninuclear Complexes Containing Oxalate: Among the three geometrical isomers the *trans(N)cis(O)* isomer (IIIa) was obtained as shown before. The other two isomers were synthesized directly as in the following. An aqueous solution of cobalt(II) acetate (0.02 mol) was mixed with oxalic acid (0.024 mol), potassium oxalate (0.016 mol) and *S*-praH (0.048 mol) in water (total 140 cm^3). The solution was oxidized with lead dioxide (5 g) at 80—90 °C for 1 h. The product was filtered and the filtrate was poured into a column (4.5×45 cm) of SP-Sephadex C-25. The adsorbed band was eluted with sodium perchlorate solution (0.2 mol·dm^{-3}). A blue and a violet band were observed in the order of elution. Blue (IIIb) and violet (IIIc) crystals were obtained by treating the respective eluates similarly to those of the μ-oxalato complexes. They were assigned as follows.

IIIa: *trans(N)cis(O)*-$[Co(ox)(S\text{-pra})(S\text{-praH})]\cdot 0.5H_2O$. Found: C, 31.18; H, 6.36; N, 9.22%. Calcd for $CoC_8H_{17}N_2O_6\cdot 0.5H_2O$: C, 31.48; H, 5.95; N, 9.18%.

IIIb: *cis(N)trans(O)*-$[Co(ox)(S\text{-praH})_2]ClO_4\cdot 2.5H_2O$. Found: C, 21.89; H, 5.01; N, 6.53%. Calcd for $CoC_8H_{18}N_2O_{10}Cl\cdot 2.5H_2O$: C, 21.75; H, 5.24; N, 6.34%.

IIIc: *cis(N)cis(O)*-$[Co(ox)(S\text{-praH})_2]ClO_4\cdot H_2O$. Found: C, 23.31; H, 5.13; N, 6.62%. Calcd for $CoC_8H_{18}N_2O_{10}Cl\cdot H_2O$: C, 23.17; H, 4.86; N, 6.76%.

An aqueous solution of the hygroscopic blue violet powder ($[CoCl_2(S\text{-praH})_2]Cl$) was treated with an equivalent amount of potassium oxalate at 40 °C for 20 min to give a blue solution, which was similarly treated with a column containing SP-Sephadex C-25 to give only IIIc isomer.

Measurements. Visible and ultraviolet absorption spectra were recorded with a Hitachi 323 Recording Spectrophotometer. Circular dichroism (CD) spectra were recorded with a JASCO Model ORD/UV-5 Spectrometer with CD attachment. Proton NMR spectra were recorded with Varian T-60 and A-60 Spectrometers. A JASCO IR-A-2S Spectrophotometer was used for the measurement of infrared spectra in KBr disks. The acid dissociation constants of the complexes were determined by the titration with sodium hydroxide solution (0.1 mol·dm^{-3}) with a Metrohm Combi Titrator 3D at 25 °C and ionic strength 0.1. The pH of complex solutions for spectroscopic measurement was adjusted with perchloric acid (0.1 mol·dm^{-3}), sodium hydroxide (0.025 mol·dm^{-3}), or potassium carbonate solution (*ca.* 10^{-2} mol·dm^{-3}).

Results and Discussion

Determination of the Skeletal Structure. The skeletal structure has been identified on the basis of elemental analysis, column chromatography, and infrared (IR) spectroscopy.

Binuclear Complexes with Carbonate Bridges: Each of the complexes Ia, Ib, and Ic in aqueous solution gave an absorption peak in the region from 30000 to 31000 cm^{-1}. Hence they must have bi- or multinuclear structures. They gave antisymmetric stretching absorption of the carbonate ions in the region from 1500 to 1520 cm^{-1} in KBr disks (Fig. 2). Gatehause *et al.*[5] found that the antisymmetric CO stretching absorptions of bi- and unidentate carbonato ligands appeared in higher energy regions than 1520 cm^{-1} and 1493 cm^{-1}, respectively. The uninuclear complex *cisβ*-$[Co(CO_3)(N,N'\text{-}Me_2\text{-}(S,S)\text{-mhydaH})]$ gives the $\bar{\nu}_{as}(CO)$ value 1600 cm^{-1}.[6] The μ-carbonato complex $[(NH_3)_5Co(CO_3)Co(NH_3)_5](SO_4)_2\cdot 4H_2O$ gives the $\bar{\nu}_{as}(CO)$ value 1480 cm^{-1}.[7] Wieghardt prepared various binuclear complexes of the type $[(NH_3)_3Co(OH,OH,RCO_2)Co(NH_3)_3]^{3+}$, and found a linear relationship between the

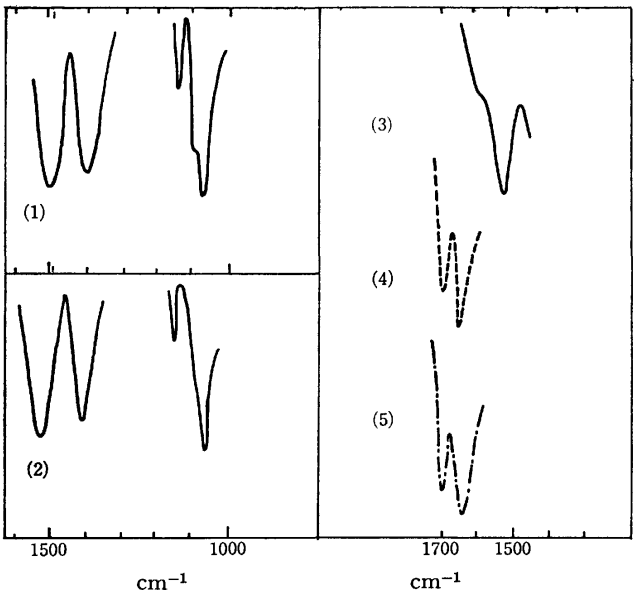

Fig. 2. IR Spectra of the binuclear complexes.
(1) $[(S\text{-pra})_2Co(CO_3,OH)Co(S\text{-pra})(S\text{-praH})]\cdot 2H_2O$ (Ic).
(2) $[(S\text{-pra})(S\text{-praH})Co(CO_3)_2Co(S\text{-pra})(S\text{-praH})]\cdot 2NaHCO_3\cdot 2H_2O$ (Ia).
(3) $[(S\text{-praH})_2Co(ox)_2Co(S\text{-praH})_2](ClO_4)_2\cdot 2.5H_2O$ (——) (IIb).
(4) $[(S\text{-praH})_2Co(ox)_2Co(S\text{-praH})_2](ClO_4)_2\cdot 6H_2O$(----) (IIa).
(5) *trans(N)cis(O)*-$[Co(ox)(S\text{-pra})(S\text{-praH})]\cdot 0.5H_2O$ (—·—) (IIIa).

$\bar{\nu}_{as}(CO)$ in cm^{-1} and the pK_a value of the carboxylic acid.[8] The $\bar{\nu}_{as}(CO)$'s observed for the present binuclear complexes fall on the same line. On the basis of these facts the carbonate ligands in our complexes can be reckoned to bridge two cobalt(III) ions. Reactions with oxalic acid converted all the μ-carbonato complexes into μ-oxalato complexes (Fig. 1). This fact also supports binuclear structure of the carbonato complexes.

Nakamoto *et al.* measured the IR spectrum of the binuclear complex $K_4[(ox)_2Co(OH)_2Co(ox)_2]$, and assigned the band near 1100 cm^{-1} to the Co–O–H bending.[9] Both the complexes Ib and Ic give the same absorption bands. Thus hydroxide ions must bridge two cobalt(III) ions in these complexes. The complex Ia gives no such IR absorption band. On the basis of these data we give the formulae to Ia, Ib, and Ic as mentioned before.

Binuclear Complexes Bridged by Oxalate: Chromatographic behavior of IIa and IIb and the presence of UV absorption bands in 30000—31000 cm^{-1} suggest that they have binuclear structure. The pH titration and IR spectra indicate the absence of unidentate ligands.

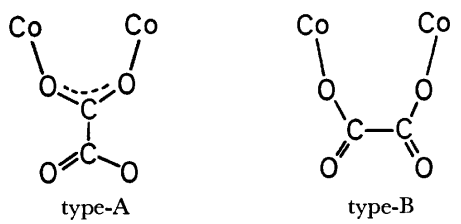

Fig. 3. Types of the bridging oxalate.

Hence these complexes should be doubly bridged.

The oxalate can bridge cobalt(III) in two ways as shown in Fig. 3; *i.e.* by coordinating to two cobalt(III) through two oxygen atoms on one carbon atom (Type-A), or through two oxygens on different carbon atoms (Type-B). IR Spectroscopy was useful for distinguishing these bridges. Scott *et al.* found the $\bar{\nu}(CO)$ of oxalate in the Type-A bridging binuclear complex $[(NH_3)_4Co(NH_2,ox)Co(NH_3)_4]^{3+}$ at 1640 and 1616 cm^{-1} and in $[(NH_3)_3Co(OH,OH,ox)Co(NH_3)_3]^{2+}$ at 1634 and 1600 cm^{-1}.[10] The complex IIb gave $\bar{\nu}(CO)$'s 1620 and 1570 cm^{-1} (Fig. 2). These are slightly lower in wave number than those of Scott *et al*'s complexes. However, such a shift can be caused by the difference in other bridging ligands between ours and theirs. So we conclude that IIb has two bridging oxalates of Type-A.

The complex IIa gave $\bar{\nu}(CO)$ 1700 and 1675 cm^{-1} (Fig. 2). These wave numbers are similar to those of the five-membered oxalate chelate. However, we tend to consider that the oxalates in this complex bridge two cobalt(III) through Type-B by the following reasons. First, the Type-B bridge will have a similar electronic state to chelating oxalate, so that the $\bar{\nu}(CO)$ can be similar to that of chelating oxalate. Scott *et al.* observed four $\bar{\nu}(CO)$'s, 1721, 1701, 1629, and 1670 cm^{-1} for the Type-B binuclear complex $[(NH_3)_5Co(ox)Co(H_2O)(NH_3)_4]^{4+}$.[10] They considered these bands to be the split peaks of the two bands of chelated oxalate at 1696 and 1667 cm^{-1} in $[Co(ox)(NH_3)_4]^+$. IR peaks of our complex fail to show such a splitting, presumably because of the increase in symmetry around the bridging moiety. Second, an alcohol is a weaker ligand than amines and carboxylates toward cobalt(III). If amino alcohols doubly bridged two cobalt(III), the Co–O bonds would be compared to those between Co(III) and (*O*-coordinated) unidentate amino alcohol. Further, each cobalt(III) in such a complex is considered to be chelated by a large chelate ring consisting of two amino alcohols and one cobalt(III). Such a ring may not be stable enough to give a crystalline product. Thus we conclude the structure of IIa and IIb as shown before.

Uninuclear Complexes Containing Oxalates: The complexes IIIa, IIIb, and IIIc gave $\bar{\nu}(CO)$ values of oxalate ligands *ca.* 1700 and 1667 cm^{-1} (Fig. 3). Absence of UV peaks in the 30000 cm^{-1} region, as well as their chromatographic behavior, indicates that these complexes are uninuclear.

Synthetic Method. The tricarbonato method has been recognized as a very useful tool for preparing a variety of uninuclear cobalt(III) complexes containing bidentate carbonate. These products are also useful intermediates for synthesizing further varieties of uninuclear complexes containing other ligands.[4] However, no binuclear complexes have ever been known among the products. We have succeeded in preparing a few binuclear species with carbonate bridges and thus extended the usefulness of this method to the preparation of binuclear complexes.

Reactions of oxalic acid with such binuclear complexes under a mild condition gave binuclear species bridged by oxalate. These reactions appear to involve local substitution of the bridging part.

TABLE. NUMERICAL DATA OF ABSORPTION (AB) AND CD SPECTRA UNINUCLEAR OXALATO COMPLEXES

	Geometrical isomerism		I band		II band	
			AB $\bar{\nu}/10^3$ cm^{-1} (log ε)	CD $\bar{\nu}/10^3$ cm^{-1} ($\Delta\varepsilon$)	AB $\bar{\nu}/10^3$ cm^{-1} (log ε)	CD $\bar{\nu}/10^3$ cm^{-1} ($\Delta\varepsilon$)
IIIa	*trans*(*N*) *cis*(*O*)	a	17.61 (1.81)	16.05 (+1.12)	25.13 (2.12)	27.47 (+0.4)
			19.88 (1.83)	18.69 (−1.25)		
		b	17.57 (2.14)	16.13 (+0.64)	23.06 (2.07)	23.70 (+1.74)
				18.12 (−2.05)	sh. 28.17 (2.10)	
IIIb	*cis*(*N*) *trans*(*O*)	a	17.92 (2.03)	18.02 (−0.51)	24.81 (2.21)	25.32 (+0.11)
		b	18.12 (2.17)	17.86 (−1.18)	sh. 23.60 (2.26)	22.94 (+1.17)
					sh. 25.20 (2.29)	
IIIc	*cis*(*N*) *cis*(*O*)	a	18.38 (1.99)	16.67 (+0.52)	26.11 (2.18)	25.77 (+0.22)
				19.23 (−0.62)		
		b	18.08 (2.11)	15.92 (+0.84)	25.13 (2.30)	23.47 (+1.50)
				18.45 (−1.69)		

a: Protonated form $[Co(ox)(S\text{-praH})_2]^+$. b: Deprotonated form $[Co(ox)(S\text{-pra})_2]^-$.

Acid-base Equilibria. The uninuclear complexes IIIb and IIIc were titrated with sodium hydroxide, and their pK_1 and pK_2 values were determined to be *ca.* 3.2 and *ca.* 6, respectively, at 25 °C and ionic strength 0.1. The pK_1 values are similar to the pK_a values of uninuclear complexes containing one amino alcohol.[1,2] The pK_2 values are similar to the pK_a values of aqua ligands in various cobalt(III) complexes. The pK_a values of other complexes were not determined by technical reasons. These data, as well as the pH dependence of the absorption and CD spectra, and the chromatographic behavior, indicate that all the complexes containing oxalate have *S*-praH ligands in protonated form in an aqueous solution of pH≤1, and in completely deprotonated form at pH≥9. μ-Carbonato complexes are only stable in aqueous solutions of pH≥7, so that the amino alcohol logands are in deprotonated forms.

Geometrical Isomerism and Absorption Spectra of the Uninuclear Complexes. Octahedral cobalt(III) complexes containing two *S*-praH and one oxalate exist in three geometrical isomers, *trans*(*N*)*cis*(*O*), *cis*(*N*)*trans*(*O*), and *cis*(*N*)*cis*(*O*), which have C_2, C_2, and C_1 symmetry, respectively. The absorption spectra of protonated and deprotonated forms of IIIa, IIIb, and IIIc are shown in Fig. 4. Change in pH always brings about reversible change of the absorption spectra between the protonated and the deprotonated form. IIIa in the protonated form gives split bands in the first band region and is assigned to *trans*(*N*)*cis*(*O*) isomer. IIIb and IIIc give similar absorption patterns to each other. The IIIc isomer gives more complicated methyl signals in the pmr spectra than the IIIb isomer does, so that they are assinged to *cis*(*N*)*cis*(*O*) and *cis*(*N*)*trans*(*O*) isomer, respectively.

Data of the absorption and CD spectra in the d-d transition region are shown in the Table for both the protonated and the deprotonated form of the complexes. The locations of absorption peaks of the protonated forms are almost equal to those of the corresponding isomers of $[Co(ox)(gly)_2]^-$ (gly=glycinate ion).[11] Hence the alcoholic hydroxyl group has the same position in the spectrochemical series with carboxylates.

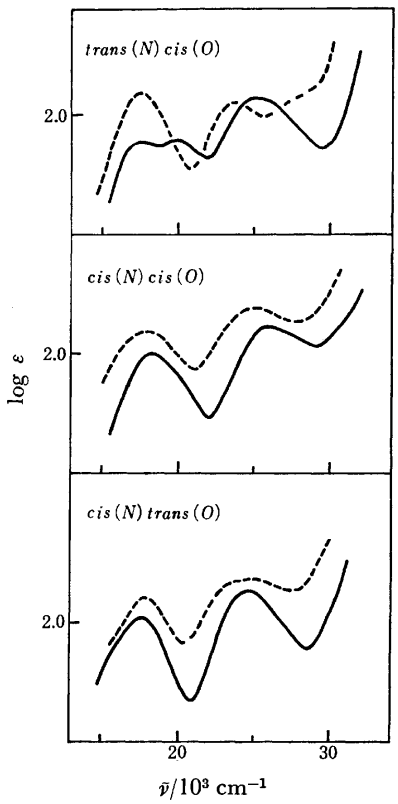

Fig. 4. Absorption spectra of geometrical isomers of $[Co(ox)(S\text{-praH})_2]^+$ (protonated form) (——) and $[Co(ox)(S\text{-pra})_2]^-$ (deprotonated form) (----).

On deprotonation of the hydroxyl groups, peaks in the first band region change in quite characteristic ways depending on the geometrical isomerism. Split peaks of the *trans*(*N*)*cis*(*O*) isomer unite apparently into one peak. The *cis*(*N*)*trans*(*O*) isomer gives blue shift, whereas the *cis*(*N*)*cis*(*O*) isomer red shift. (In the $[CoN_5O]$ type complex containing one (*S*)-2-amino-1-propanol, the peak in the first band region gives blue shift in a basic solution[2]). In the second band region, the peaks of *trans*(*N*)*cis*(*O*) and *cis*(*N*)*trans*(*O*) isomers split on deprotonation. The *cis*(*N*)*cis*(*O*) isomer gives apparently only a broad band. Since all these absorption

bands consist of more than one component, the deprotonation brings about not only splitting but also shift and intensity change of the component peaks. It also causes increase in number of lone pair electrons on coordinating oxygen atoms. These factors give influence in a complicated manner, to result in very diverse change in the absorption pattern.

CD Spectra of the Uninuclear Complexes. Attempts to resolve the isomers were unsuccessful. Intensity of the PMR methyl signals of IIIb and IIIc suggests that these complexes consist of almost equal amounts of *Λ*- and *Δ*-isomers. Hence their CD patterns should reflect the vicinal contribution of *S*-praH and *S*-pra$^-$.

In the first band region, large minus components are commonly seen for both protonated and deprotonated forms of all the geometrical isomers. Such minus components reflect *δ*-conformation of the *S*-praH or *S*-pra$^-$ chelate.[1,2] The $\Delta\varepsilon$ values are large for the deprotonated than for protonated forms. These facts were also seen in $[CoN_5O]$ type complexes with one optically active amino alcohol.[2] The spectral patterns are, however, different among the geometrical isomers. They should be dependent on the symmetry, and related to the change in absorption patterns.

In the second band region, the change of CD pattern with pH is more marked than in the first band region. All the three isomers in the deprotonated form give characteristic large plus components at 23000 to 24000 cm^{-1}. Such a marked plus CD was also observed in the deptonated forms of $[CoN_5O]$ type complexes. We considered that it reflected *δ*-conformation of *S*-pra$^-$ and the unusually large $\Delta\varepsilon$ values in this region were related to the presence of three lone pairs in alcoholate $-O^-$ moiety.[2] The same consideration is

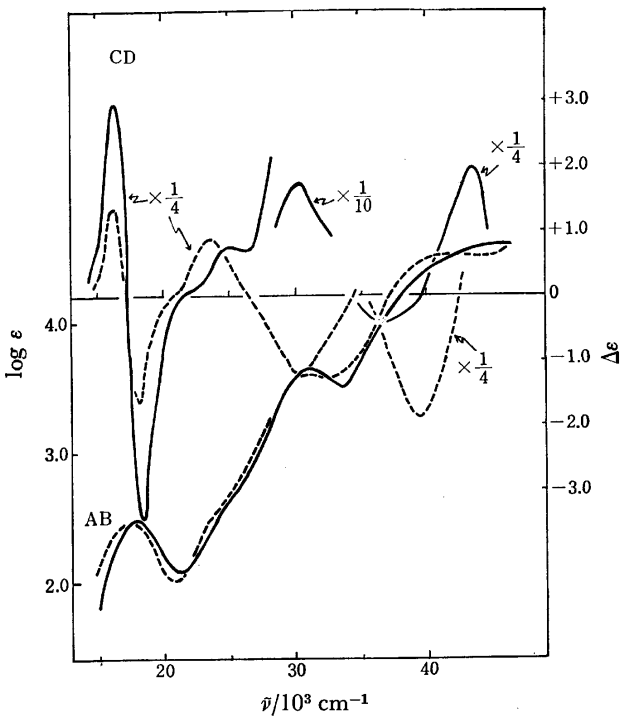

Fig. 5. Absorption and CD spectra of $[(S\text{-praH})_2Co(ox)_2Co(S\text{-praH})_2]^{2+}$ (——) and $[(S\text{-pra})_2Co(ox)_2Co(S\text{-pra})_2]^{2-}$ (------) (IIb).

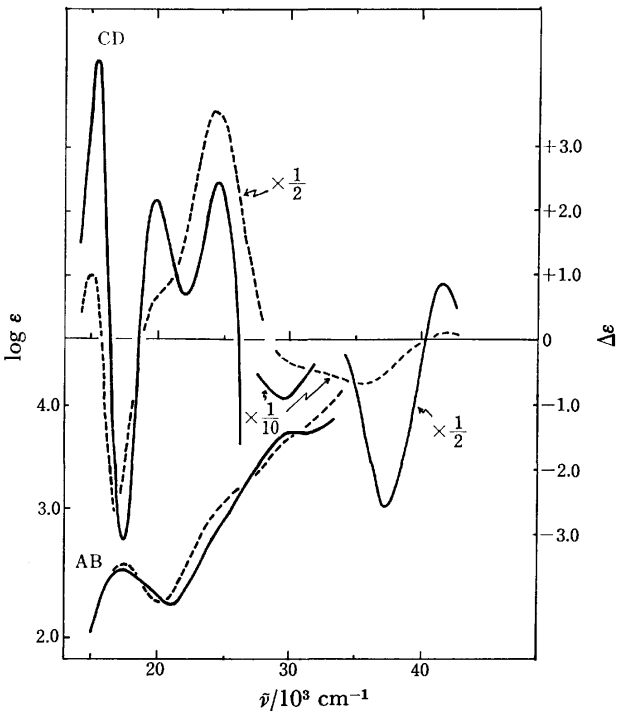

Fig. 6. Absorption and CD spectra of $[(S\text{-praH})_2Co(ox)_2Co(S\text{-praH})_2]^{2+}$ (——) and $[(S\text{-pra})_2Co(ox)_2Co(S\text{-pra})_2]^{2-}$ (------) (IIa).

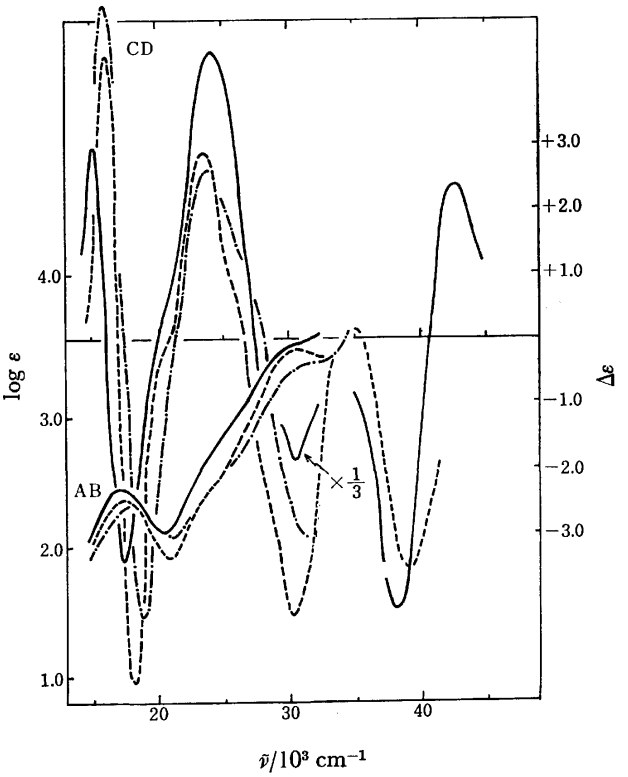

Fig. 7. Absorption and CD spectra of *μ*-carbonato complexes.
$[(S\text{-pra})_2Co(CO_3)_2Co(S\text{-pra})_2]^{2-}$ (——) (Ia),
$[(S\text{-pra})_2Co(CO_3,OH)Co(S\text{-pra})_2]^{-}$ (—·—) (Ib), and
$[(S\text{-pra})_2Co(CO_3,OH)Co(S\text{-pra})_2]^{-}$ (------) (Ic).

applicable to the present complexes containing two *S*-pra$^-$ ligands.

Geometrical Isomerism and CD Spectra of the Binuclear Complexes. A large number of geometrical isomers can exist for such types of binuclear complexes. Only two μ-oxalato complexes and three μ-carbonato complexes have been obtained. Attempts to assign the crystalline products to individual isomers have turned out unsuccessful, because of too complicated absorption and CD patterns.

The CD spectra of μ-oxalato complexes are shown in Figs. 5 and 6, and those of μ-carbonato complexes in Fig. 7. Each of these complexes gives a large plus component in the first band region. It must be due to the $\Lambda\Lambda$-configurational effect around cobalt(III). It appears as if the $\Lambda\Lambda$-isomers were preferentially formed. The reason may be related to the larger stability of lel- than ob-structure, because the chelated *S*-praH ligands give δ-conformation exclusively.

There is one common characteristic pattern in the second band region; *i.e.* the deprotonated forms give remarkable plus CD components. The $\Delta\varepsilon$ values are nearly equal to four times of that of $[Co(S\text{-pra})(NH_3)_4]^{2+}$ ($\Delta\varepsilon=0.85$). The vicinal effect of *S*-pra$^-$ ligand in the second band region does not appear to be much affected by the skeletal structure throughout all the cobalt(III) complexes.

The authors thank the Ministry of Education for financial support.

References

1) K. Ogino, T. Uchida, T. Nishide, J. Fujita, and K. Saito, *Chem. Lett.*, **1973**, 679.
2) T. Nishide, K. Ogino, J. Fujita, and K. Saito, *Bull. Chem. Soc. Jpn.*, **47**, 3057 (1974).
3) O. Vogl and M. Pöln, *Monatsh.*, **83**, 541 (1952).
4) M. Shibata, *Proc. Jpn. Acad.*, **50**, 779 (1974).
5) a) B. M. Gatehause, S. E. Livingstone, and R. S. Nyholm, *J. Chem. Soc.*, **1958**, 3137; b) E. Kyuno, *Nippon Kagaku Zasshi*, **80**, 849 (1959).
6) Unpublished data. *N,N'*-Me_2-(*S,S*)-mhydaH_2=(2*S*,7*S*)-2,3,6,7-tetramethyl-1,8-dihydroxy-3,6-diazaoctane.
7) E. Kramer and C. R. P. Mac-Coll, *Inorg. Chem.*, **10**, 2182 (1971).
8) K. Wieghardt, *J. Chem. Soc., Dalton Trans.*, **1973**, 2548.
9) K. Nakamoto, "Infrared Spectra of Inorganic and Coordination Compounds," Willey (1970), p. 171.
10) K. L. Scott, K. Wieghardt, and A. G. Sykes, *Inorg. Chem.*, **12**, 655 (1973).
11) N. Matsuoka, J. Hidaka, and Y. Shimura, *Bull. Chem. Soc. Jpn.*, **40**, 1868 (1967).

Circular Dichroism Spectra of Cobalt(III) Complexes Containing One or Two Azido, Isothiocyanato, and Nitro Ligands. II.[1] *trans*-Type Bis[(1*R*,2*R*)-1,2-cyclohexanediamine] Complexes

Kiyoshi YAMASAKI,* Jinsai HIDAKA,** and Yoichi SHIMURA

Department of Chemistry, Faculty of Science, Osaka University, Toyonaka, Osaka 560

(Received February 7, 1977)

The *trans* dianiono type complexes of cobalt(III) containing (1*R*,2*R*)-1,2-cyclohexanediamine, *trans*-$[Co(X)_2(R,R\text{-chxn})_2]^+$, and -$[Co(X)(X')(R,R\text{-chxn})_2]^+$ (X and X′=N_3^-, NCS^-, or NO_2^-) were prepared and their circular dichroism (CD) spectra measured in the visible and ultraviolet regions. The CD and absorption behaviors in the so-called specific absorption band region are compared with those of *cis*-type bis(ethylenediamine) complexes and discussed in relation to the origin of the specific band. In addition, three isomers of the $[Co(NCS)(NH_3)(R,R\text{-chxn})_2]^{2+}$ complex are assigned on the basis of their CD spectra.

In a previous paper,[1] circular dichroism (CD) spectra of bis(ethylenediamine) complexes of cobalt(III) with a *cis* configuration were discussed, especially with emphasis on the so-called specific absorption band in the near ultraviolet region. The specific absorption band is moderately intense, and specific for certain aniono ligands, such as azido, isothiocyanato, nitro, and sulfito ligands. The origin of these bands has been attributed to charge-transfer transitions between the aniono ligand and the central metal, or to intraligand transitions. A previous study[1] suggests an interaction between two aniono ligands in the *cis* positions through the central cobalt(III) ion. This kind of electronic interaction between two NCS^-, NO_2^-, or Cl^- ligands have frequently been proposed for complexes which have two aniono ligands in the *trans* positions.[2-6] Thus, the specific band of a *trans* dianiono complex is more bathochromic than that of the corresponding *cis* isomer,[4,5] with some exceptions.[6]

The present paper deals with *trans* dianiono type complexes, including mixed complexes, of cobalt(III) containing (1*R*,2*R*)-1,2-cyclohexanediamine (abbreviated as *R,R*-chxn) for the purpose of studying their CD spectra in the region of the specific absorption bands of azido, isothiocyanato, and nitro ligands.

Experimental

Preparation and Optical Resolution. (1) (1R,2R)-1,2-Cyclohexanediamine: The ligand was optically resolved by the method of Asperger and Liu.[7] The less soluble diastereomer, (*R,R*-chxnH_2) (*d*-tart), showed a constant optical rotation $[\alpha]_{589}=+12.1°$ (*d*-tart denotes the $(+)_{589}$-tartrate(2−) ion). Found: C, 45.18; H, 7.60; N, 10.55%. Calcd for $C_{10}H_{20}N_2O_6$: C, 45.45; H, 7.63; N, 10.60%. For preparative purposes, a stock solution of *R,R*-chxn was conveniently prepared by the addition of a calculated amount of $Ba(OH)_2\cdot 8H_2O$ to a hot suspension of the less soluble diatereomer. After cooling overnight in a refrigerator, the precipitated $BaSO_4$ was removed.

(2) trans-$[CoCl_2(R,R\text{-chxn})_2]Cl\cdot H_2O$: This complex was prepared following exactly the method of Treptow.[8] Found: C, 35.79; H, 7.41; N, 13.60%. Calcd for $[CoCl_2(C_6H_{11}N_2)_2]Cl\cdot H_2O$: C, 35.01; H, 7.35; N, 13.61%.

(3) trans-$[Co(N_3)_2(R,R\text{-chxn})_2]Cl\cdot 0.5H_2O$: The dichloro complex, *trans*-$[CoCl_2(R,R\text{-chxn})_2]Cl\cdot H_2O$ (0.4 g), was dissolved in 20 cm^3 of methanol at 30 °C, and 25 mg of LiN_3 was added with stirring. The azide of the dichloro complex, *trans*-$[CoCl_2(R,R\text{-chxn})_2]N_3\cdot nH_2O$, quickly separated out. The suspension in methanol was vigorously stirred at 30 °C until the azide salt dissolved (about 5 min). Then another 25 mg of LiN_3 was added to the solution and the resulting suspension was further stirred for 15 min. To the resulting blue-violet solution of the azidochloro complex was added 50 mg of LiN_3, and the mixture was heated to 50 °C and stirred for 40 min. This was then cooled in ice to stop the reaction, and concentrated to about 10 cm^3 with a vacuum evaporator. After cooling in a refrigerator overnight, the dark blue-violet crystals that separated out were filtered, washed with ether and air-dried. 110 mg. Recrystallization was performed from methanol by the addition of ether. Found: C, 34.86; H, 6.93; N, 32.78%. Calcd for $[Co(N_3)_2(C_6H_{14}N_2)_2]Cl\cdot 0.5H_2O$: C, 34.66; H, 7.03; N, 33.33%.

(4) trans-$[Co(NCS)_2(R,R\text{-chxn})_2]Cl\cdot H_2O$: To a solution of 0.4 g of the dichloro complex in 20 cm^3 of methanol was added 340 mg of $LiSCN\cdot H_2O$, and the mixture was stirred for 30 min at 65 °C. Then, crystals began to separate out. After further stirring for 15 min, the mixture was ice-cooled for half an hour. The resulting reddish-orange crystals were filtered, washed with ice-cold methanol and ether, and air-dried. 180 mg. Recrystallization was carried out from hot methanol (60 °C, 8 cm^3). Found: C, 36.64; H, 6.66; N, 18.72%. Calcd for $[Co(NCS)_2(C_6H_{14}N_2)_2]Cl\cdot H_2O$: C, 36.80; H, 6.62; N, 18.39%.

(5) trans-$[Co(NO_2)_2(R,R\text{-chxn})_2]Cl\cdot 2.5H_2O$: To a solution of the dichloro complex (0.4 g) in 20 cm^3 of methanol was added 140 mg of $LiNO_2\cdot H_2O$. The mixed solution was stirred at 60 °C for 2 h, and the separated crystals were filtered off. The filtrate was evaporated to 7 cm^3 and stored in a refrigerator overnight. The resulting crystals were filtered off. The yellow-orange lustrous crystals obtained (both the first and second crops) were the *cis*-isomer. The filtrate was evaporated to dryness. The residual solid was suspended in 4 cm^3 of ethanol and filtered. 99 mg. The product was recrystallized from ethanol by the addition of ether, and the resulting fine yellow-orange crystals were filtered, washed with ether, and air-dried. Found: C, 31.75; H, 7.32; N, 18.35%. Calcd for $[Co(NO_2)_2(C_6H_{14}N_2)_2]Cl\cdot 2.5H_2O$: C, 31.35; H, 7.23; N, 18.28%.

(6) trans-$[CoCl(NCS)(R,R\text{-chxn})_2]Cl\cdot 3H_2O$: To a solution of the dichloro complex (0.4 g) in 20 cm^3 of methanol at 30 °C was added 85 mg of $LiSCN\cdot H_2O$. When the mixed solution was stirred for 10 min, the color of the solution changed from green to dark violet. The solution was evaporated to 5 cm^3

* Present address: Osaka Prefectural Industrial Research Institute, Enokojima, Nishi-ku, Osaka 550.

** Present address: Institute of Chemistry, The University of Tsukuba, Ibaraki 300-31.

and stored in a refrigerator overnight. After the removal of the reddish-violet precipitate of the *cis*-chloroisothiocyanato complex, the filtrate was again stored overnight in a refrigerator. The resulting blue-violet precipitate of the desired complex was filtered with suction and washed with ether. 35 mg. The second crop of the blue-violet precipitate was obtained when the filtrate was stored in a refrigerator for further 3 days. 32 mg. The two crops of the crude *trans* complex were combined and reprecipitated from methanol (2 cm^3) by adding ether (8 cm^3). The reprecipitated product was filtered and washed with ether and air-dried. Found: C, 34.51; H, 7.29; N, 14.87%. Calcd for $[CoCl(NCS)(C_6H_{14}N_2)_2]Cl\cdot 3H_2O$: C, 33.19; H, 7.29; N, 14.89%.

(7) trans-$[CoCl(NO_2)(R,R\text{-}chxn)_2]Cl\cdot 1.5H_2O$: The reaction was carried out at 30 °C by adding 70 mg of $LiNO_2\cdot H_2O$ to a solution containing 0.4 g of the dichloro complex in 20 cm^3 of methanol. After stirring for 10 min, the reacted solution of dark orange color was cooled in ice for 2 h. The resulting crystals (the *cis*-chloronitro complex) were removed by filtration, 10 cm^3 of ether was added to the filtrate, and then the mixture was stored in a refrigerator overnight. The second crop of *cis* complex crystals separated out was filtered off, and the filtrate was further cooled for 3 days in a refrigerator. The third crop of crystals yielded in a small quantity, and this was filtered off. The fourth crop, which was obtained upon evaporating the filtrate to about 4 cm^3, was a mixture of *cis* and *trans* complexes. To the filtrate from the fourth crop was added 2 cm^3 of ether, and after a period the *trans* complex separated out. After storage in a refrigerator for 2 h, the crystals were filtered, washed with a little cold methanol and ether, and air-dried. 75 mg. Reddish-orange fine crystals were obtained by recrystallization from methanol (3 cm^3) upon the addition of ether (4 cm^3). Found: C, 33.87; H, 7.31; N, 15.97%. Calcd for $[CoCl(NO_2)(C_6H_{14}N_2)_2]Cl\cdot 1.5H_2O$: C, 33.42; H, 7.25; N, 16.24%.

(8) trans-$[Co(NCS)(NO_2)(R,R\text{-}chxn)_2]Cl\cdot 1.5H_2O$: To a solution of 0.4 g of the dichloro complex in 20 cm^3 of methanol was added 70 mg of $LiNO_2\cdot H_2O$. After the mixture had been stirred for 10 min at 30 °C, 80 mg of $LiSCN\cdot H_2O$ was added to it and the reaction temperature was raised to 60 °C. After stirring for 70 min, the reacted solution was evaporated to dryness. The resulting solid was dissolved in water and the solution was adsorbed on a column (20×220 mm) containing a cation-exchange resin (Dowex 50W×8, K^+ form). The eluting agent, a 0.1 M KCl solution, was made to flow at a rate of 2 cm^3/min. While 6.8—11.5 dm^3 of the eluting agent flowing, the yellow-to-orange colored eluate (4.7 dm^3) was collected in 20-cm^3 portions in a fraction collector. The middle (56—180 th) fractions were confirmed to contain the desired *trans*-isothiocyanatonitro complex by checking the absorption spectra. These were combined and evaporated at 30 °C. After the separated KCl crystals had been removed by filtration several times, the eluate was evaporated to dryness. The complex was extracted from the residual solid using 20 cm^3 of methanol, and the undissolved KCl crystals were filtered off. In order to remove the remaining KCl, careful fractional precipitation was carried out by the addition of ether to the methanol extract. The desired complex obtained as a later fraction was filtered, washed with ether, and air-dried. Found: C, 34.45; H, 6.84; N, 18.66%. Calcd for $[Co(NCS)(NO_2)(C_6H_{14}N_2)_2]Cl\cdot 1.5H_2O$: C, 34.40; H, 6.88; N, 18.52%.

(9) trans-$[Co(N_3)(NCS)(R,R\text{-}chxn)_2]^+$: As in the course of preparing the diazido complex (3), four 25-mg portions of LiN_3 were added over a 30-min period to a stirred solution containing 0.8 g of the dichloro complex in 40 cm^3 of methanol at 30 °C. To the blue-violet reaction mixture (the *cis*- and *trans*-azidochloro complexes) was added 165 mg of $LiSCN\cdot H_2O$, and the solution was heated to 60 °C and stirred for 15 min. The color of the solution turned to red-violet. After the reaction had been stopped by ice-cooling, an equal volume of ether was added to the solution and the resulting mixture was evaporated to dryness with a vacuum evaporator. The solid was dissolved in water and subjected to chromatography on a column containing a cation-exchanger CM-Sephadex C-25 using a 0.1 M NaCl solution as the eluting agent. The earlier eluate contained the desired *trans*-azidoisothiocyanato complex. The isomerization to *cis* occurred even at 25 °C and the *trans* complex could not be isolated in crystal.

(10) trans-$[Co(N_3)(NO_2)(R,R\text{-}chxn)_2]^+$: To a solution of 0.8 g of the dichloro complex in 40 cm^3 of methanol at 30°C was added 140 mg of $LiNO_2\cdot H_2O$ with stirring. This stirring was continued for 10 min. Upon the addition of 100 mg of LiN_3, the azide salt of the dichloro complex separated out. The suspension was heated to 60 °C and stirred for 20 min. The resulting solution was evaporated to dryness, and the solid obtained was dissolved in water and subjected to chromatography on a column (27×980 mm) containing CM-Sephadex C-25 with a 0.1 M NaCl solution at a rate of 0.23 cm^3/min. When 1.5 dm^3 of the eluting agent was passed over the column, the *trans* species reached the bottom of the column. At this time, the eluate began to be collected in 10-cm^3 portions and the 28—38 th fractions were confirmed to contain the desired *trans*-azidonitro complex (the *trans*-dinitro and -diazido complexes were contained in the 1—15 th and 44—50 th fractions, respectively). The isomerization to *cis* occurred rapidly, and isolation of the complex was unsuccessful.

(11) Three Isomers of the $[Co(NCS)(NH_3)(R,R\text{-}chxn)_2]^{2+}$ *Complex*: To a solution containing 0.8 g of the dichloro complex in 40 cm^3 of methanol at 30 °C was added 170 mg of $LiSCN\cdot H_2O$, and the mixed solution was stirred for 10 min. After adding an equal volume of ether, the reaction mixture was evaporated to dryness with a vacuum evaporator. The resulting violet solid was placed in a 250-cm^3 pressure cylinder, which was placed in a dry ice-methanol bath, and ammonia was condensed over the solid. After about 15 cm^3 of ammonia had been condensed, the container was tightly capped and allowed to stand at room temperature (21°C) for about 15 min. The color of the ammonia solution changed to reddish-orange. Then, the cap was removed and the ammonia was evaporated. After the resulting orange product had been dried over P_2O_5 *in vacuo*, it was dissolved in an appropriate amount of water and subjected to chromatography on a cation-exchanger column (CM-Sephadex C-25, 25×850 mm) with a 0.15 M NaCl solution. While 12.4—19.6 dm^3 of the eluting agent was made to flow through the column in one month, the three desired isomers were eluted out in well separated bands. Each of the three eluates was evaporated to dryness on a vacuum evaporator at 30 °C, and the resulting solid was extracted with a minimum amount of methanol and undissolved NaCl was removed by filtration. After evaporating each of the methanol solutions to dryness at 10 °C, the resulting solid (contaminated with a small amount of NaCl) was dissolved in 3 to 4 cm^3 of water.

1) To the aqueous solution obtained from the first eluted band (Fl) was added 0.3 g of NaI with stirring The iodide salt precipitated was filtered, washed with a small amount of ethanol and ether, and air-dried. 100 mg. The iodide dissolved in 15 cm^3 of water, and changed to a chloride solution by employing a cation-exchange resin (Cl^- form). The chloride solution was evaporated to dryness by the freeze-drying method, and the resulting chloride salt was dissolved in 2 cm^3 of water and the solution was evaporated gently to dryness in a vacuum desiccator over P_2O_5. Reddish-orange crystals. 55

mg (Fl). Found: C, 32.39; H, 7.62; N, 17.36%. Calcd for $[Co(NCS)(NH_3)(C_6H_{14}N_2)_2]Cl\cdot 2.5H_2O$: C, 32.34; H, 7.52; N, 17.40%.

2) To the aqueous solutions obtained from the second and third eluted bands (F2 and F3) were added 0.5 and 1.5 g of $LiClO_4\cdot 3H_2O$ with stirring, respectively. The perchlorate salts precipitated were filtered, washed with an ethanol–ether mixture and then ether, and air-dried. 144 mg (F2) and 200 mg (F3). The perchlorate salts were dissolved in an appropriate amount of water, and the solutions were changed to chloride solutions using an ion-exchange method. The chloride solutions were evaporated to dryness by freeze-drying, the resulting powders were dissolved in 3 and 4 cm^3 of water, respectively, and then to the solutions were added 1.0 and 0.75 g of $LiClO_4\cdot 3H_2O$ with stirring. After storage in a refrigerator for 2 days, the perchlorate salts were filtered, washed sufficiently with an ethanol–ether mixture to eliminate the contaminant $LiClO_4\cdot 3H_2O$, then with ether, and air-dried. Reddish-orange crystals. 50 mg (F2) and 73 mg (F3). Found for F2: C, 29.51; H, 5.70; N, 15.70%. Found for F3: C, 29.62; H, 5.89; N, 15.74%. Calcd for $[Co(NCS)(NH_3)(C_6H_{14}N_2)_2](ClO_4)_2$: C, 29.46; H, 5.89; N, 15.85%.

(12) Bis(ethylenediamine) Complexes: The *trans* complexes were prepared according to methods described in the literature, except for the two new complexes, for which the methods will be described below. *Cis* and *trans* isomers of chloronitrobis(ethylenediamine)cobalt(III) chloride were prepared by the method of Werner.[9,10]

trans-$[Co(N_3)(NCS)(en)_2]ClO_4$: To a solution of 12.0 g of *cis*-$[CoCl(NCS)(en)_2]ClO_4$[10] in 75 cm^3 of water (60 °C) was added 2.5 g of NaN_3. The resulting solution was stirred at 60 °C for about 2 h. After diluting with an appropriate amount of water, the solution was subjected to chromatography on a column (26×800 mm, Dowex 50W×8, H^+ form) using a 0.2 M $LiClO_4$ solution as the eluting agent. The elution was continued at a rate of 1.5—2.0 cm^3/min until the first series of bands (containing *trans* complexes) were eluted out. The eluates were fractionated and the intermediate fractions, with the first d-d absorption band at about 528 nm, were combined and evaporated to dryness on a vacuum evaporator below 35 °C. In order to remove the eluting agent, $LiClO_4\cdot 3H_2O$, the solid obtained was suspended in ethanol, filtered, washed sufficiently with ethanol. This was recrystallized from water (55 °C), filtered, washed with water, ethanol, and then ether, and air-dried. Found: C, 15.46; H, 4.21; N, 29.63%. Calcd for $[Co(N_3)(NCS)(C_2H_8N_2)_2]ClO_4$: C, 15.86; H, 4.26; N, 29.59%.

trans-$[Co(N_3)(NO_2)(en)_2]ClO_4$: To a solution containing 4.0 g of *trans*-$[CoCl(NO_2)(en)_2]Cl\cdot H_2O$[9] in 40 cm^3 of water (60 °C) was added 1.0 g of NaN_3. Then the azide salt of chloronitro complex precipitated out. The resulting suspension was stirred at 60 °C for 90 min. After diluting with water, the solution was subjected to chromatography on a column (Dowex 50 W×8, H^+ form) with a 0.1 M LiCl solution. When the elution was continued for 8 days using a 0.1 M LiCl solution of about 25 dm^3, the first series of bands containing *trans* complexes were eluted out. The earlier fractions, which showed the first d-d absorption band at about 481 nm, were combined and evaporated to 20 cm^3 below 35 °C. To the concentrated eluate was added a solution of 2.0 g of $LiClO_4\cdot 3H_2O$ in 4 cm^3 of water. After a period, the perchlorate salt of the desired complex crystallized out. After standing for 1 h, the crystals were filtered (0.8 g), recrystallized from warm water (55 °C), filtered, washed with water, ethanol, and then ether, and air-dried. Lustrous red-orange flakes. 0.5 g. Found: C, 12.92; H, 4.42; N, 30.27%. Calcd for $[Co(N_3)(NO_2)(C_2H_8N_2)_2]ClO_4$: C, 13.11; H, 4.40; N, 30.57%.

Measurements. The absorption spectra were measured using Shimadzu UV-200 and Beckman DU spectrophotometers. The CD spectra were recorded with Jasco ORD/UV-5, J-10, and J-20 spectropolarimeters. The optical rotation was checked using Yanagimoto Model 185 and Jasco ORD/UV-5 spectropolarimeters. The measurements were made at room temperature in aqueous or methanol solutions ranging in concentration from 0.005 to 0.0001 M. The cell lengths were 1, 0.2, and 0.1 cm.

Results and Discussion

Characterization of trans *Dianiono Complexes.* Eight cobalt(III) complexes of *trans*-dianionobis[(1*R*,2*R*)-1,2-cyclohexanediamine] type were derived from *trans*-$[CoCl_2(R,R\text{-chxn})_2]Cl\cdot H_2O$ upon treatment with LiN_3, LiSCN, or $LiNO_2$ in methanol. Only one of these, the *trans*-dinitro complex, is a known complex, which was recently prepared by Brennan and Douglas for the first time.[11] *trans*-to-*cis* isomerization was observed in the isolation procedure of some *trans* complexes containing azido ligand from the eluates, and the azidoisothiocyanato and azidonitro complexes could not be isolated as crystals. The *trans* structures of all the complexes were determined by comparing the visible and ultraviolet absorption bands with those of *cis* and *trans* isomers of the corresponding ethylenediamine complex (Table 1).

Configuration of Three Isomers of the Ammineisothiocyanato Complex. Three isomers are possible for the $[Co(NCS)(NH_3)(R,R\text{-chxn})_2]^{2+}$ ion: one is the *trans* isomer and the other two are the diastereomeric *cis* isomers. All the isomers of the $[Co(NCS)(N)_5]$ type show very similar absorption spectra, and they are indistinguishable on the basis of their absorption spectra. The configurations of the three isomers are assigned, therefore, on the basis of their CD spectra. The *cis* isomers have two kinds of chiralities: one is the "configurational" chirality (Δ or Λ) due to the two chxn chelate rings and the other the "vicinal" chirality due to the asymmetric carbon atom of the *R,R*-diamine (including "conformational" chirality). It has been established that the CD contributions of the two kinds of chiralities are separable and additive in several cobalt(III) complexes containing five-membered chelate rings.[12–15] Thus, for the CD of the diastereomeric *cis* ammineisothiocyanato isomers, ΔRR and ΛRR, the following equations can be written, where *R* represents the *R,R*-chxn ligand,

$$\Delta\varepsilon(\Lambda RR) = \Delta\varepsilon(\Lambda) + 2\Delta\varepsilon(R) \quad (1)$$

and

$$\Delta\varepsilon(\Delta RR) = \Delta\varepsilon(\Delta) + 2\Delta\varepsilon(R). \quad (2)$$

Because $\Delta\varepsilon(\Lambda)$ should be equal to $-\Delta\varepsilon(\Delta)$, one obtains

$$\Delta\varepsilon(\Lambda) = \frac{1}{2}[\Delta\varepsilon(\Lambda RR) - \Delta\varepsilon(\Delta RR)] \quad (3)$$

and

$$\Delta\varepsilon(R) = \frac{1}{4}[\Delta\varepsilon(\Lambda RR) + \Delta\varepsilon(\Delta RR)]. \quad (4)$$

Therefore, if a pair of *cis* isomers can be selected from the three isomers, the configurational CD contribu-

Table 1. Absorption peak positions (in 10^3 cm^{-1}) and intensities (log ε in parenthesis) of the $[Co(X)(X')(diamine)_2]^+$ complexes

(X)(X')	Diamine	Config.	First d-d band	"Specific" or charge transfer bands	
$(N_3)_2$	*R,R*-chxn	*trans*	17.7 (2.52)	29.8 (4.08)	46.5 (4.38)
	en	*trans*	17.8 (25.4)	30.0 (4.13)	46.0 (4.28)
	en	*cis*[1]	19.3 (2.52)	33.1 (4.06)	46.5 (4.30)
$(NCS)_2$	*R,R*-chxn	*trans*	19.6 (2.43)	32.5 (3.54)	47 (4.4)
	en	*trans*	19.7 (2.44)	31.6 (3.49)	
	en	*cis*[1]	20.4 (2.54)	32.5 (3.46)	
$(NO_2)_2$	*R,R*-chxn	*trans*	23.1 (2.28)	29.3 (3.53)	40.2 (4.38)
	en	*trans*	23.4 (2.28)	29.5 (3.56)	40.3 (4.31)
	en	*cis*[1]	22.8 (2.23)	31.1 (3.56)	41.7 (4.32)
$(N_3)(NCS)$	*R,R*-chxn	*trans*	18.9	32.6	46.6
	en	*trans*	18.9 (2.49)	32.3 (3.94)	47 (4.4)
	en	*cis*[1]	19.6 (2.51)	32.4 (3.91)	47 (4.3)
$(N_3)(NO_2)$	*R,R*-chxn	*trans*	20.7	29	33.4
	en	*trans*	20.8 (2.60)	29 (3.7)	33.8 (4.00)
	en	*cis*[1]	20.4 (2.65)	33.1 (3.92)	
$(NCS)(NO_2)$	*R,R*-chxn	*trans*	21.6 (2.38)	32 (3.3)	41 (4.3)
	en	*trans*	21.8 (2.38)	34 (3.4)	42 (4.2)
	en	*cis*[1]	21.2 (2.48)	31.0 (3.52)	41 (4.1)
Cl(NCS)	*R,R*-chxn	*trans*	18.1 (2.12)	31 (3.3)	37 (3.6)
	en	*trans*	17.9 (2.16)	30.9 (3.30)	37 (3.4)
	en	*cis*[1]	19.9 (2.24)	32 (3.2)	
$Cl(NO_2)$	*R,R*-chxn	*trans*	21.5 (1.98)	29.9 (3.03)	42 (4.3)
	en	*trans*	21.6 (1.98)	29.4 (3.21)	40.1 (4.26)
	en	*cis*	20.1 (1.94)	29.9 (3.20)	41.6 (4.21)

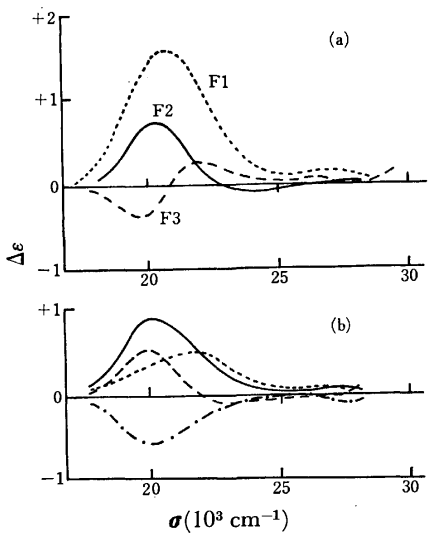

Fig. 1. CD spectra of three isomers of $[Co(NCS)(NH_3)(R,R\text{-chxn})_2]^{2+}$ (a), and calculated curves of (1/2)[Δε(F1) − Δε(F3)] (——), (1/2)[Δε(F2) − Δε(F3)] (------), and (1/2)[Δε(F1) − Δε(F2)] (·····) (b). The CD curve (Δε×2) of $\Delta(-)_{589}$-$[Co(NCS)(NH_3)(en)_2]^{2+}$ is also shown in (b) (-·-·-).

tion can be calculated from their observed CD spectra. The configurational CD curve thus calculated is considered to be similar in shape to the observed CD curve of the corresponding en complex. Fig. 1(a) shows the CD curves in the d-d absorption band region for the three isomers which are designated as F1, F2, and F3 in the order of elution, and Fig. 1(b) shows the calculated curves for (1/2)[Δε(F1) − Δε(F3)], (1/2)[Δε(F2) − Δε(F3)], and (1/2)[Δε(F1) − Δε(F2)] together with the observed CD curve of $\Delta(-)_{589}$-$[Co(NCS)(NH_3)(en)_2]^{2+}$. The calculated (1/2)[Δε(F1) − Δε(F3)] curve is similar in shape to (but reverse in sign to and about twice as intense as) the observed curve of Δ-$[Co(NCS)(NH_3)(en)_2]^{2+}$. It is therefore concluded that F1 and F3 form the *cis* pair and F2 is the *trans* isomer and that F1 is the $\Delta(ob)$ isomer and F3 the $\Delta(lel)$ isomer (this is consistent with the fact that the formation ratio of F1 to F3 is 1: 1.19). Furthermore, if the configurational contribution of the chxn complex is of the same magnitude as that of the en complex, it can be deduced that the optical purity of the $(-)_{589}$-$[Co(NCS)(NH_3)(en)_2]^{2+}$ complex derived from the resolved $[CoCl(NCS)(en)_2]^+$ complex was a little lower than 50% and that its true CD intensity may be about twice the reported value.[1]

CD and Absorption Spectra. It is acceptable, from the first d-d absorption band positions, that the ligand strength of chxn is almost the same as that of en. Two or three CD bands are observed in the first d-d absorption band region (Table 2). Although the *trans*-$[Co(X)_2(R,R\text{-chxn})_2]^+$ complexes are of D_2 symmetry, if they are considered to be of the *trans*-$[Co(X)_2(N)_4]^+$ type, they are approximately of D_{4h} symmetry. Accordingly, the first spin-allowed d-d transition, $^1A_{1g} \rightarrow {}^1T_{1g}$, in O_h is split into the $^1A_{1g} \rightarrow {}^1E_g$ and $^1A_{1g} \rightarrow {}^1A_{2g}$ transitions. Then, the CD bands observed at about 21000 cm^{-1} are considered to correspond to the nondegenerate com-

TABLE 2. CD DATA OF THE *trans*-[Co(X)(Y)-(*R*,*R*-chxn)$_2$]$^{n+}$ COMPLEXES IN THE FIRST d-d BAND REGION

(Wave numbers are given in 10^3 cm^{-1})

(X)(Y)	$\sigma_{ext}(\Delta\varepsilon)$ in H_2O	$\sigma_{ext}(\Delta\varepsilon)$ in CH_3OH	Fig. No.
$(N_3)_2$	17 (+0.19)	16.1(+0.56)	Fig. 2
	18 (+0.18)	18 (+0.20)	
	21.3(−0.24)	21.2(−0.12)	
$(NCS)_2$	19.7(+0.76)	19.2(+0.76)	Fig. 3
	22.9(−0.28)	22.8(−0.20)	
$(N_3)(NCS)$	19.1(+0.40)[a]		Fig. 6
	22.0(−0.21)[a]		
Cl(NCS)		17.5(+0.75)	
		21.3(−0.14)	
$(NCS)(NH_3)$	20.3(+0.75)		Fig. 5
	23.7(−0.06)		
$(NO_2)_2$	21.8(−1.01)	21.9(−1.04)	Fig. 4
	24.6(+0.52)	24.9(+0.24)	
$(N_3)(NO_2)$	18.4(−0.28)[a]		Fig. 7
	20.9(+0.25)[a]		
	23.3(−0.02)[a]		
$(NCS)(NO_2)$	19.8(−0.17)	19.8(−0.12)	Fig. 8
	22.4(+0.37)	22.2(+0.31)	
$Cl(NO_2)$		18.7(−0.06)	
		20.8(+0.23)	

a) These $\Delta\varepsilon$ values are estimated by assuming that the molar extinction coefficients of the first d-d absorption band are the same as those of the corresponding en complexes.

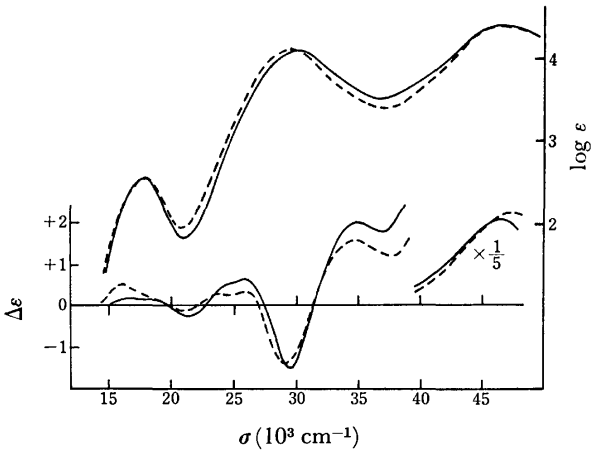

Fig. 2. Absorption and CD spectra of *trans*-[Co(N$_3$)$_2$-(*R*,*R*-chxn)$_2$]Cl·0.5H$_2$O in water (——) and in methanol (------).

ponent, $^1A_{1g}\rightarrow{}^1A_{2g}$, and those observed at the lower (X=N_3^- and NCS^-) or higher (X=NO_2^-) energy positions to the degenerate component, $^1A_{1g}\rightarrow{}^1E_g$. In the diazido complex, however, two CD bands corresponding to the $^1A_{1g}\rightarrow{}^1E_g$ component are observed at about 16000 and 18000 cm^{-1} (Fig. 2). This band splitting can be reasonably interpreted by symmetry lowering to D_2. It is remarkable that the CD band assigned to the $^1A_{1g}\rightarrow{}^1A_{2g}$ transition in the diazido complex, which is observed at 21300 cm^{-1} in an aqueous solution, is located just in the trough of the absorption curve. This appears to suggest that, in this complex, the absorption band intensity of this nondegenerate component is very weak and the observed absorption peak corresponds to the degenerate component.

In the diazido complex, two strong CD bands of opposite signs are observed in the specific band region, exactly corresponding to the main absorption peak and the shoulder on its higher energy side (Fig. 2 and Table 3). The two positive CD bands at 24000—26000 cm^{-1} are then thought to belong to the second d-d band which is completely hidden. Also in the diisothiocyanato complex, two CD bands of opposite signs are observed in the specific band region (Fig. 3 and Table 3). In this case, the lower energy band of negative sign is much weaker than the higher energy one of positive sign. The negative band is considered to be partly

TABLE 3. CD DATA OF THE *trans*-[Co(X)(Y)(*R*,*R*-chxn)$_2$]$^{n+}$ COMPLEXES IN THE ULTRAVIOLET REGION (wave numbers are given in 10^3 cm^{-1})

(X)(Y)	Solvent	$\sigma_{ext}(\Delta\varepsilon)$ Second d-d band region		$\sigma_{ext}(\Delta\varepsilon)$ "Specific" band region		$\sigma_{ext}(\Delta\varepsilon)$ Intense band region	
$(N_3)_2$	H_2O	25 (+0.5)	25.9(+0.63)	29.7(−1.5)	35.0(+2.0)	46.7(+10.6)	
	CH_3OH	24.0(+0.3)	26.1(+0.36)	29.3(−1.45)	35.0(+1.6)	47.3(+11.6)	
$(NCS)_2$	H_2O			28 (−0.1)	34 (+1.2)	44.0(+11.0)	
	CH_3OH			27 (−0.1)	34 (+1.0)	45.0(+11.6)	
$(N_3)(NCS)$[a]	H_2O	25 (+0.2)	28 (+0.2)	30.8(−0.2)	35 (+1.3)	45 (+11.4)	
Cl(NCS)	CH_3OH	26.0(+0.1)		31.0(+0.43)	34.8(−0.8)	40.7(+10.2)	
$(NCS)(NH_3)$	H_2O	29.0(+0.05)		31.0(−0.04)	36 (+1)	44.7(+12.5)	
$(NO_2)_2$	H_2O	29.3(+0.12)		32 (−0.7)	34.3(−1.1)	41.3(+8.0)	
	CH_3OH			31.8(−0.6)	37 (+1.7)	41.3(+6.2)	45.7(−2.4)
$(N_3)(NO_2)$[a]	H_2O	26.4(+0.2)		30.3(+0.1)	33.1(−0.5)	43.3(+9.3)	
$(NCS)(NO_2)$	H_2O	28.1(+0.18)		33.2(−0.6)		42.5(+10.3)	
	CH_3OH	28.0(+0.05)		30.3(−0.2)	32.8(−0.3)	43.0(+8.9)	
$Cl(NO_2)$	CH_3OH	27.2(+0.28)		34.1(−1.5)		41.0(+8.0)	

a) The $\Delta\varepsilon$ values are estimated by assuming that the molar extinction coefficients of the fisrt d-d absorption band are the same as those of the corresponding en complexes.

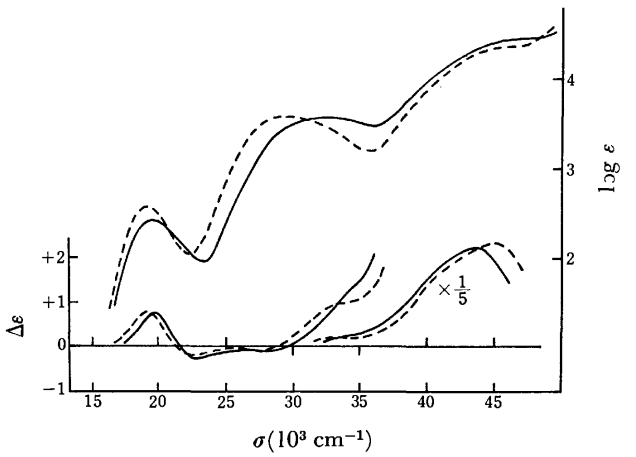

Fig. 3. Absorption and CD spectra of *trans*-$[Co(NCS)_2(R,R\text{-chxn})_2]Cl\cdot H_2O$ in water (——) and in methanol (------).

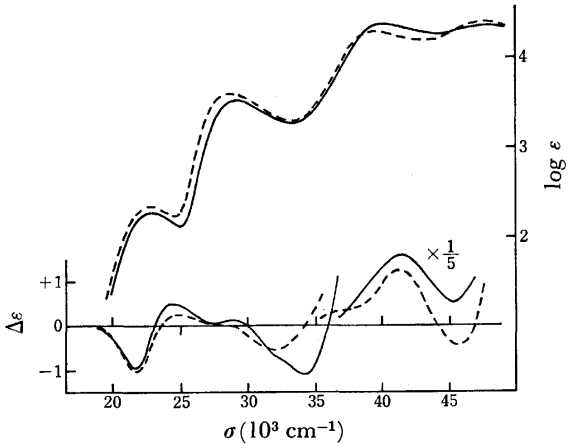

Fig. 4. Absorption and CD spectra of *trans*-$[Co(NO_2)_2(R,R\text{-chxn})_2]Cl\cdot 2.5H_2O$ in water (——) and in methanol (------).

cancelled by the CD bands for the second d-d transition, which probably have a positive net sign like the analogous *trans*-$[Co(X)_2(R,R\text{-chxn})_2]^+$ complexes ($X=F^-$, Cl^-, Br^-,[8] and N_3^-).

In the two pseudohalogeno complexes, a positive CD band is observed in an energy region higher than the specific absorption band.

If the specific absorption bands of the present pseudohalogeno complexes are assigned to the p_π(ligand)→d_{z^2} charge-transfer transitions, the relatively weaker absorption intensity of the higher energy component can be explained by the electric-dipole forbidden character of the p_{π_g}(ligand)→d_{z^2}(e_g→a_{1g} in D_{4h}) transition and the relatively stronger CD intensity of the component can be interpreted by its magnetic-dipole allowed character. Furthermore, the red shift of the specific absorption band of the *trans*-dianiono type complexes (in comparison with the *cis*-dianiono complexes) can be attributed to the relatively stronger absorption intensity of the lower energy electric-dipole allowed component, the p_{π_u}→d_{z^2}(e_u→a_{1g} in D_{4h}) transition. A similar interpretation has been made for the CD spectra of the charge-transfer band region of the halogeno complexes, *trans*-$[Co(X)_2(R,R\text{-chxn})_2]^+$ ($X=Cl^-$ and Br^-), although the signs of these two CD bands are the reverse of the present complexes.[8]

The assignment of the specific bands of the present pseudohalogeno complexes to the p_π→d_{z^2} charge-transfer transitions is consistent with the previous CD study of the *cis*-type bis(ethylenediamine) complexes. The same assignment has also been made in absorption spectral studies of $[Co(X)(NH_3)_5]$ and $[Co(X)(CN)_5]$ complexes[16,17] and a redox study of $[Co(NCS)(NH_3)_5]^{3+}$.[18]

For the corresponding nitro complex (Fig. 4 and Table 2) in aqueous solution, two CD bands of opposite signs are observed under the "nitro-specific band" and the lower energy positive band is weaker than the higher energy negative band. However, the signs of these are reverse to the pseudohalogeno complexes. On the other hand, it has been reported that the analogous $(-)_{589}$-*trans,trans*-$[Co(NO_2)_2(N\text{-Me-en})_2]^+$ complex shows the same CD pattern in this region as that of the present pseudohalogeno complexes.[19]

Concerning the solvent effect on the absorption and CD spectra of the three dianiono complexes, it was found that the specific absorption bands apper at higher energies in water than in methanol; the shift is very wide especially for the isothiocyanato complex (2600 cm^{-1} interval). The shift is in the same direction as that reported for the charge-transfer band in some halogeno complexes.[20]

In a previous paper[1] on the *cis*-type bis(ethylenediamine) complexes, it was found that the dipseudohalogeno complexes show two CD bands in the specific band region, while the amminepseudohalogeno complexes show a single CD band. In Fig. 5, the calculated CD curve of the configurational effect for the *cis*-$[Co(NCS)(NH_3)(R,R\text{-chxn})_2]^{2+}$ complexes and the observed CD curve for the *trans* complex are shown together with their absorption spectra. The configurational CD

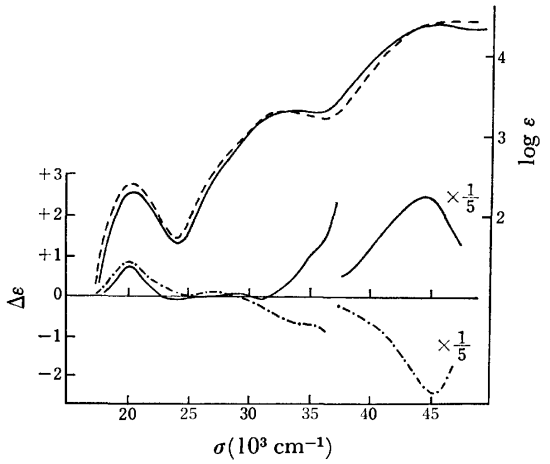

Fig. 5. Absorption and CD spectra of *trans*-$[Co(NCS)(NH_3)(R,R\text{-chxn})_2](ClO_4)_2$ (——) and calculated *Λ* configurational curve of *cis*-$[Co(NCS)(NH_3)(R,R\text{-chxn})_2]^{2+}$ (-·-·-). Absorption spectrum of *Λ*-$[Co(NCS)(NH_3)(R,R\text{-chxn})_2](ClO_4)_2$ is shown in broken line.

curve has the same pattern as the observed CD curve[1] of Δ-$[Co(NCS)(NH_3)(en)_2]^{2+}$ over all the regions, and has a single CD band corresponding to the absorption peak of the specific band. The CD band can be assigned to the degenerate charge-transfer transition, p_π(ligand) $\rightarrow d_{z^2}$($e \rightarrow a_1$ in C_{4v}). However, in the case of the *trans*-$[Co(NCS)(NH_3)(R,R\text{-chxn})_2]^{2+}$ complex which has the same approximate symmetry, C_{4v}, as the *cis* complex, the positive CD band in shoulder and another very weak negative CD band on the lower energy side appear to correspond to the specific absorption band, because the positive shoulder is located rather far from the absorption peak.

The absorption curves in the specific band region of the *trans* mixed complexes $[Co(X)(X')(diamine)_2]^+$ (X and X'=N_3^-, NCS^-, and NO_2^-) are very different

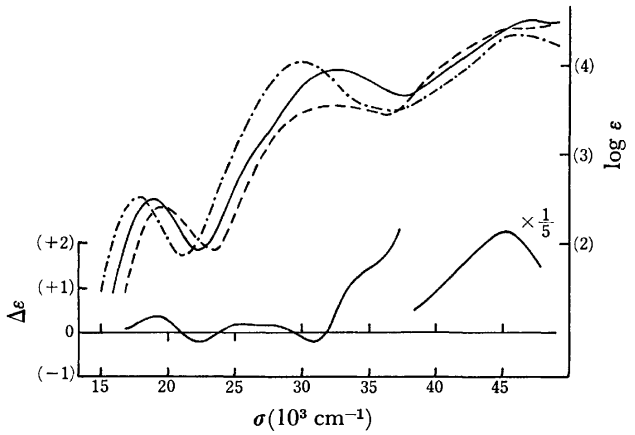

Fig. 6. Absorption and CD spectra of *trans*-$[Co(N_3)(NCS)(R,R\text{-chxn})_2]^+$ eluate (——). (The intensities are estimated by assuming that the molar extinction coefficient of the first d-d band is the same as the corresponding en complex.) Absorption spectra of *trans*-$[Co(N_3)_2(R,R\text{-chxn})_2]Cl \cdot 0.5H_2O$ (-·-·-) and -$[Co(NCS)_2(R,R\text{-chxn})_2]Cl \cdot H_2O$ (------) are shown for comparison.

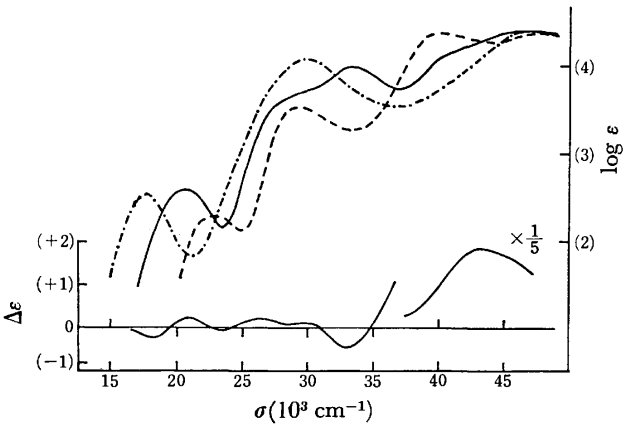

Fig. 7. Absorption and CD spectra of *trans*-$[Co(N_3)(NO_2)(R,R\text{-chxn})_2]^+$ eluate (——). (The intensities are estimated by assuming that the molar extinction coefficient of the first d-d band is the same as the corresponding en complex.) Absorption spectra of *trans*-$[Co(N_3)_2(R,R\text{-chxn})_2]Cl \cdot 0.5H_2O$ (-·-·-) and -$[Co(NO_2)_2(R,R\text{-chxn})_2]Cl \cdot 2.5H_2O$ (------) are shown for comparison.

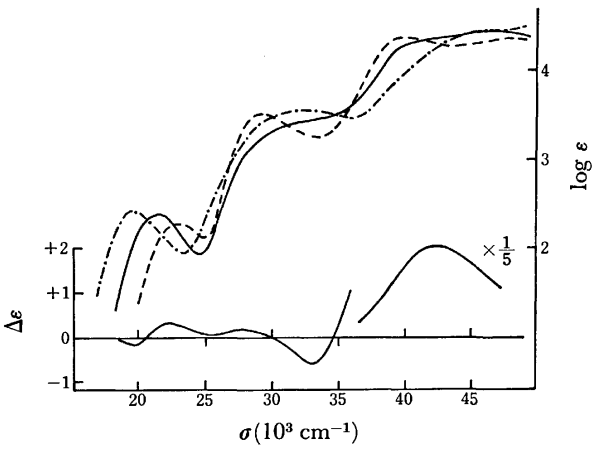

Fig. 8. Absorption and CD spectra of *trans*-$[Co(NCS)(NO_2)(R,R\text{-chxn})_2]Cl \cdot 1.5H_2O$ (——). Absorption spectra of *trans*-$[Co(NCS)_2(R,R\text{-chxn})_2]Cl \cdot H_2O$ (-·-·-) and -$[Co(NO_2)_2(R,R\text{-chxn})_2]Cl \cdot 2.5H_2O$ (------) are shown for comparison.

from the intermediate of the "parent" complexes $[Co(X)_2(diamine)_2]^+$ and $[Co(X')_2(diamine)_2]^+$ (see Figs. 6—8). This absorption behavior suggests that the specific bands are not due to the intraligand transitions and that there is some strong interaction, for example, a p_π-d_π interaction, between the ligands in the *trans* positions through the central cobalt(III) ion. The CD data of the *trans*-$[Co(X)(X')(R,R\text{-chxn})_2]^+$ (X, X'= N_3^-, NCS^-, NO_2^-, and Cl^-) complexes are presented in Tables 2 and 3 and Figs. 6—8. The azidoisothiocyanato complex shows two CD bands under the specific absorption band (Fig. 6): one is the weaker negative CD band of lower energy and the other the stronger positive one of higher energy. The CD behavior is the same as that of the "parent" complexes, *trans*-$[Co(N_3)_2(R,R\text{-chxn})_2]^+$ and -$[Co(NCS)_2(R,R\text{-chxn})_2]^+$. Accordingly, the two CD bands at about 25000 and 28000 cm^{-1} are considered to belong to the second d-d band. The azidonitro complex (Fig. 7) exhibits a very strange absorption spectrum which is remarkably different from the intermediate of the "parent" complexes, and a negative CD band is located under the intense absorption band at 33400 cm^{-1} and two positive CD bands are observed under the shoulder at about 29000 cm^{-1}. It is more probable to consider that the lowest energy CD band corresponds to the second d-d absorption band, which is hidden. Then, the weak positive and strong negative CD bands at 30300 and 33100 cm^{-1} are assigned to the specific absorption band. A single strong positive CD band is observed under another intense absorption band in the higher energy region. In summary, the CD behavior of the mixed complexes in the specific absorption band region is complicated as in the case of the *cis*-type bis(ethylenediamine) complexes, but it seems a common behavior that two CD bands are observed under the specific band, and the higher energy one of which is the stronger.

Finally, the four complexes containing only N_3^- or NCS^-, that is, $(N_3)(N_3)$, $(NCS)(NCS)$, $(N_3)(NCS)$, and $(NCS)(NH_3)$ complexes, exhibit the (—, +) CD pattern under the specific absorption band. The five

complexes containing Cl^- or NO_2^-, namely, $(NO_2)(NO_2)$, $(NCS)(NO_2)$, $(N_3)(NO_2)$, $Cl(NCS)$, and $Cl(NO_2)$ complexes, appear to exhibit the reverse CD pattern, (+, −), under the specific band. Furthermore, the higher energy CD component of the specific band is stronger than the lower energy CD component for all nine complexes. Lastly, it was observed that all the complexes exhibit one strong CD band in the region of 41000—48000 cm^{-1} and that the sign is always positive (Table 3).

The authors are grateful to Dr. Wasuke Mori of Osaka University, and to Dr. Keiji Matsumoto of Osaka City University for their help in the measurements of the CD spectra.

References

1) Part I of this series: K. Yamasaki, J. Hidaka, and Y. Shimura, *Bull. Chem. Soc. Jpn.*, **49**, 3060 (1976).
2) Y. Shibata, *Tokyo Kagaku Kaishi*, **36**, 1243 (1915).
3) R. Tsuchida, *Bull. Chem. Soc. Jpn.*, **13**, 388, 436 (1938).
4) F. Basolo, *J. Am. Chem. Soc.*, **72**, 4393 (1950).
5) Y. Shimura, *J. Am. Chem. Soc.*, **73**, 5079 (1951).
6) K. Ohkawa, J. Hidaka, and Y. Shimura, *Bull. Chem. Soc. Jpn.*, **40**, 2830 (1967).
7) R. G. Asperger and C. F. Liu, *Inorg. Chem.*, **4**, 1492 (1965).
8) R. S. Treptow, *Inorg. Chem.*, **5**, 1593 (1966).
9) A. Werner and L. Gerb, *Chem. Ber.*, **34**, 1734 (1901).
10) A. Werner, *Justus Liebigs Ann. Chem.*, **386**, 1-272 (1912).
11) B. J. Brennan and B. E. Douglas, *J. Coord. Chem.*, **1**, 297 (1971).
12) C. T. Liu and B. E. Douglas, *Inorg. Chem.*, **3**, 1356 (1964); B. E. Douglas, *ibid.*, **4**, 351 (1968).
13) K. Ogino, K. Murano, and J. Fujita, *Inorg. Nucl. Chem. Lett.*, **4**, 351 (1968).
14) K. Yamasaki, J. Hidaka, and Y. Shimura, *Bull. Chem. Soc. Jpn.*, **42**, 119 (1969).
15) N. Matsuoka, J. Hidaka, and Y. Shimura, *Inorg. Chem.*, **9**, 719 (1970); *Bull. Chem. Soc. Jpn.*. **45**, 2491 (1972); *ibid.*, **48**, 458 (1975).
16) J. Fujita, Ph. D. Thesis, Osaka University, Osaka, Japan, 1958.
17) V. M. Miskowski and H. B. Gray, *Inorg. Chem.*, **14**, 401 (1975).
18) K. Schug, M. D. Gilmore, and L. A. Olson, *Inorg. Chem.*, **6**, 2180 (1967).
19) D. A. Buckingham, L. G. Marzilli, and A. M. Sargeson, *Inorg. Chem.*, **7**, 915 (1968).
20) J. C. Barnes and P. Day, *J. Chem. Soc.*, **1964**, 3886.

Metal Complexes of Amino Acids. X.[1] The Preparation and Characterization of Cobalt(III) Complexes of the Type $[Co(N)_2(O)_4]$ Containing β-Alanine

Tomoharu AMA, Matsutake HIGA,* Norio KOINE,* and Takaji YASUI

Department of Chemistry, Faculty of Sciences, Kochi University, Asakura, Kochi 780

**Department of Industrial Chemistry, Faculty of Engineering, Ehime University, Bunkyo-cho, Matsuyama 790*

(Received February 7, 1977)

Three geometrical isomers of the bis(β-alaninato)(oxalato)cobaltate(III) and of the (β-alaninato)(glycinato)-(oxalato)cobaltate(III) complexes have been prepared and resolved into their optical isomers. Their structures were assigned on the basis of the electronic absorption, ^1H NMR and ^{13}C NMR spectra. The circular dichroism spectra of these complexes have been measured and compared with those of the bis(glycinato)(oxalato)cobaltate(III) complexes.

Optically active cobalt(III) complexes containing amino acids are important for clarifying the relationships between their electronic absorption and circular dichroism (CD) spectra and the structures of the complexes. A number of investigators have studied α-amino acid–cobalt(III) complexes.[1-8] However, only a few cobalt(III) complexes containing β-alanine have been reported and further investigation is necessary.

β-Alanine can coordinate to a cobalt(III) ion with both carboxyl and amino groups as in the case of α-amino acids. Consequently, in complexes of the type bis(amino acidato)(oxalato)cobaltate(III) anion, β-alanine complexes provide the same geometrical isomers as α-amino acid complexes. However, β-alanine forms a six-membered chelate ring, unlike α-amino acids. It has been pointed out that the difference in size of chelate rings affects the CD spectra.[9,10] Thus, it would be interesting to compare the CD spectra of the complexes which contain β-alanine with those of the complexes containing α-amino acids.

The present paper deals with the separation and optical resolution of the isomers of bis(β-alaninato)-(oxalato)cobaltate(III) and (β-alaninato)(glycinato)-(oxalato)cobaltate(III) complexes and with their electronic absorption and CD spectra. Their spectra are compared with those of optically active bis(glycinato)-(oxalato)cobaltate(III) complexes.

Experimental

Preparation of Complexes. Isomers of Potassium Bis(β-alaninato)-(oxalato)cobaltate(III): A solution of 20 g of cobalt(II) chloride hexahydrate in 20 ml of hot water was added to a solution containing 18.5 g of potassium oxalate monohydrate and 15 g of β-alanine in 80 ml of water. The resulting dark red solution was oxidized with 20 g of lead dioxide at 60 °C for about 22 h. After the mixture had been cooled to room temperature, a large amount of insoluble material was removed by filtration. The filtrate was poured into a column (30 mm × 600 mm) containing an anion exchange resin (Dowex 1×8, 200—400 mesh, acetate form). A small quantity of non-electrolyte complexes was eluted when the column was flushed with water. The adsorbed band was eluted with a 0.05 M aqueous solution of potassium acetate, giving three colored bands. The bands, in the order of elution, were blue-violet, purple and blue. Another blue band remained at the top of the column. The second and third eluted bands were determined from their electronic absorption spectra and column chromatographic behavior to be C_1-*cis*(N)- and C_2-*cis*(N)-$[Co(\beta\text{-ala})_2(ox)]^-$ ions, respectively. The first eluted band was confirmed to be *trans*(N)-$[Co(\beta\text{-ala})_2(ox)]^-$ ion from its absorption spectrum. Each eluted solution was evaporated to a few milliliters in a vacuum evaporator. To each concentrated solution was added a large amount of ethanol. The complex precipitated was washed with methanol. Each complex was recrystallized from hot water by addition of methanol. The yields were 5.0 g for the C_1-*cis*(N) isomer and 1.5 g for the C_2-*cis*(N) isomer. Found: C, 22.77; H, 4.48; N, 6.55%. Calcd for C_1-*cis*(N)-$K[Co(\beta\text{-ala})_2(ox)]\cdot 3.5H_2O$: C, 22.59; H, 4.50; N, 6.59%. Found: C, 23.18; H, 4.22; N, 6.67%. Calcd for C_2-*cis*(N)-$K[Co(\beta\text{-ala})_2(ox)]\cdot 3H_2O$: C, 23.08; H, 4.35; N, 6.73%.

Isomers of Potassium (β-Alaninato)(glycinato)(oxalato)cobaltate-(III): A solution containing 4.5 g of potassium oxalate monohydrate, 1.6 g of glycine and 3.5 g of β-alanine in 20 ml of water (50 °C) was added to a solution containing 4.5 g of cobalt(II) sulfate heptahydrate in 10 ml of water (50 °C). The solution was oxidized with 3 g of lead dioxide. The resulting mixture was stirred at 50 °C for about 30 min. After the mixture had been cooled in an ice bath for about 3 h, a large amount of insoluble material was removed by filtration. The filtrate was poured into a column (35 mm × 900 mm) containing an anion exchange resin (Dowex 1×8, 200—400 mesh, acetate form). After the column had been swept with four liters of water, the adsorbed band was eluted with a 0.04 M aqueous solution of potassium acetate. Ten colored bands were separated: (i) blue-violet, (ii) blue-violet, (iii) violet, (iv) purple, (v) blue, (vi) violet-red, (vii) red-violet, (viii) pale violet, (ix) red-violet and (x) pale blue-violet. The symbols (i)—(x) represent the fractions eluted from each band. The complex/or isomer obtained from each fraction is abbreviated as **1**—**10**. Thus, (i) represents the fraction from the first band and **1** denotes the complex/or isomer from fraction (i), and so on. Each fraction was concentrated in a vacuum evaporator at 35—40 °C. A mixture of a small amount of methanol and a large amount of acetone was added to each concentrated solution to give two liquid layers, a cloudy colorless layer and a clear colored layer. After the cloudy layer was removed by decantation, a mixture of a small amount of methanol and a large amount of acetone was added to the clear layer, and the resulting new cloudy layer was discarded. This procedure was repeated several times, and finally a large amount of ethanol was added to the residual solution. The crude product deposited was filtered and washed with ethanol. Purification of the complex was carried out by addition of ethanol to a concentrated aqueous solution.

The visible absorption and NMR spectra of the isolated complexes indicate that the complexes **1**, **4**, and **5** are three

geometrical isomers of $[Co(\beta\text{-ala})_2(ox)]^-$ and the complexes **3**, **9**, and **10** are those of $[Co(gly)_2(ox)]^-$. The complexes obtained from the (ii), (vi), (vii), and (viii) fractions are the isomers of $[Co(\beta\text{-ala})(gly)(ox)]^-$. The yield of the complex from the band (viii) was so small that we could not isolate complex **8** in pure form. The yields of **2**, **6**, and **7** were 0.15, 0.2, and 0.1 g, respectively. Found for complex **2**: C, 23.31; H, 3.04; N, 7.86%. Calcd for $K[Co(\beta\text{-ala})(gly)(ox)]\cdot 0.5H_2O$: C, 23.54; H,3.10; N, 7.80%. Found for complex **6**: C, 21.85; H, 3.65; N, 7.22%. Calcd for $K[Co(\beta\text{-ala})(gly)(ox)]\cdot 2H_2O$: C, 21.88; H, 3.67; N, 7.29%. Found for complex **7**: C, 22.34; H, 3.50; N, 7.32%. Calcd for $K[Co(\beta\text{-ala})(gly)(ox)]\cdot 1.5H_2O$: C, 22.41; H, 3.49; N, 7.47%.

Optical Resolution of the Complexes. The Second Eluted Isomer of Potassium Bis(β-alaninato)(oxalato)cobaltate(III): A suspension of 2 g of $(+)_{546}$-$[Co(en)_2(ox)]I$ in 14 ml of water was stirred with 0.9 g of silver acetate at 50 °C for about 10 min. The silver iodide precipitated was filtered and washed with a small amount of ice water. To the combined filtrate and washings was added 2 g of C_1-*cis*(N)-$K[Co(\beta\text{-ala})_2(ox)]\cdot 3.5H_2O$ (the second eluted isomer), and the solution was chilled in an ice bath for about 4 h. The red-brown diastereomer which deposited, $(+)_{546}$-$[Co(en)_2(ox)](+)_{546}$-$[Co(\beta\text{-ala})_2(ox)]\cdot 7H_2O$, was filtered, washed with a small amount of ice water, methanol and then ether, and dried in the air. The diastereomer was recrystallized repeatedly from hot water by addition of methanol until no further increase in optical rotation was observed. $[\alpha]_{546}+1490°$. Found: C, 23.38; H, 6.07; N, 11.57%. Calcd for $(+)_{546}$-$[Co(en)_2(ox)](+)_{546}$-$[Co(\beta\text{-ala})_2(ox)]\cdot 7H_2O$: C, 23.47; H, 5.92; N, 11.73%.

A solution containing 0.7 g of the $(+)_{546}$ diastereomer in a small amount of water was passed through a column (20 mm ×200 mm) containing a cation exchange resin (Dowex 50W ×8, 200—400 mesh, potassium form). The complex anion, $(+)_{546}$-$[Co(\beta\text{-ala})_2(ox)]^-$, was eluted when the column was flushed with water, while the resolving agent, $(+)_{546}$-$[Co(en)_2(ox)]^+$, was adsorbed on the top of the column. The eluate (solution) was evaporated to a few milliliters in a vacuum evaporator, methanol being added to the residue. The complex which precipitated was filtered, washed with a water–methanol mixture and then methanol, and dried in the air. The complex was recrystallized from hot water by addition of methanol. $[\alpha]_{546}+1710°$. Found: C, 23.62; H, 4.34; N, 6.80%. Calcd for $(+)_{546}$-$K[Co(\beta\text{-ala})_2(ox)]\cdot 2.5H_2O$: C, 23.59; H, 4.21; N, 6.88%.

The Third Eluted Isomers of Potassium Bis(β-alaninato)(oxalato)cobaltate(III): A suspension containing 1.1 g of $(+)_{546}$-$[Co(en)_2(ox)]I$ in 10 ml of water was stirred with 0.5 g of silver acetate at 50 °C for about 10 min. The silver iodide which precipitated was filtered and washed with a small amount of water. To the combined filtrate and washings was added 1.1 g of C_2-*cis*(N)-$K[Co(\beta\text{-ala})_2(ox)]\cdot 3H_2O$ (the third eluted isomer). A red-brown diastereomer which deposited immediately, $(+)_{546}$-$[Co(en)_2(ox)](+)_{546}$-$[Co(\beta\text{-ala})_2(ox)]\cdot 4H_2O$, was filtered, washed with a small amount of ice water, methanol and then ether, and dried in the air. The diastereomer was recrystallzed repeatedly from hot water by addition of methanol until no further increase in optical rotation was observed. $[\alpha]_{546}+840°$. Found: C, 25.39; H, 5.57; N, 12.61%. Calcd for $(+)_{546}$-$[Co(en)_2(ox)](+)_{546}$-$[Co(\beta\text{-ala})_2(ox)]\cdot 4H_2O$: C, 25.38; H, 5.49; N, 12.69%.

Separation of $(+)_{546}$-$K[Co(\beta\text{-ala})_2(ox)]$ from the diastereomer was carried out by the same method as described for the separation of $(+)_{546}$ isomer from the second eluted band. The complex obtained was recrystallized from hot water by addition of methanol. $[\alpha]_{546}+590°$. Found: C, 24.87; H, 4.16; N, 6.93%. Calcd for $(+)_{546}$-$K[Co(\beta\text{-ala})_2(ox)]\cdot 1.5H_2O$: C, 24.69; H, 3.88; N, 7.19%.

The Potassium Salt of Complex 3: The recemate, (±)-*trans*-(N)-$K[Co(\beta\text{-ala})(gly)(ox)]\cdot 0.5H_2O$ (0.51 g), was dissolved in 70 ml of water, and the solution was treated with a cation exchange resin (Dowex 50W×8, 200—400 mesh, lithium form). The resolving agent, $(+)_{546}$-$[Co(en)_2(ox)]Br\cdot H_2O$ (0.25 g) was dissolved in 200 ml of water, and the solution was treated with an anion exchange resin (Dowex 1×8, 200—400 mesh, acetate form). The two solutions were mixed, the mixture was evaporated to 50 ml, and then 15 ml of ethanol was added to the concentrated solution. The less soluble diastereomer deposited was filtered and washed with warm water. It is sparingly soluble in water. $[\alpha]_{546}+940°$. Found: C, 25.90; H, 4.72; N, 13.94%. Calcd for $(+)_{546}$-$[Co(en)_2(ox)](+)_{546}$-$[Co(\beta\text{-ala})(gly)(ox)]\cdot 1.5H_2O$: C, 25.88; H, 4.85; N, 13.93%.

The cation exchange resin (Dowex 50W×8, 200—400mesh, potassium form) was added to a suspension of the $(+)_{546}$ diastereomer in water. The mixture was stirred for about 1 h and the resin was removed by filtration. The filtrate containing $(+)_{546}$-$K[Co(\beta\text{-ala})(gly)(ox)]$ was concentrated in a vacuum evaporator, ethanol being added to the concentrated solution. The $(+)_{546}$ isomer obtained was reprecipitated repeadedly from aqueous solution by addition of ethanol until optical rotation attained a constant value. The isomer was gelatinous. $[M]_{546}+2040°$ (concentration of the solution was determined from its absorption spectrum).

The Potassium Salt of Complex 6: A 50 ml of aqueous solution of $K[Co(\beta\text{-ala})(gly)(ox)]\cdot 2H_2O$ (obtained from the eluted band (vi), 0.8 g) was treated with a cation exhange resin (lithium form). An aqueous solution of $(+)_{546}$-$[Co(en)_2(ox)]Br\cdot H_2O$ (0.5 g) was passed through an anion exchange resin (acetate form). These two solutions were mixed, the mixture was evaporated to 50 ml in a vacuum evaporator, and then 50 ml of ethanol was added to the concentrated solution. On cooling the solution in an ice bath for 2 h, the less soluble diastereomer precipitated as a red-violet powder. The precipitate was filtered and washed with ethanol. The diastereomer was recrystallized repeatedly from hot water by addition of ethanol until no further increase in optical rotation was observed. $[\alpha]_{546}$ −940°. Found: C, 25.36; H, 4.99; N, 13.57%. Calcd for $(+)_{546}$-$[Co(en)_2(ox)](-)_{546}$-$[Co(\beta\text{-ala})(gly)(ox)]\cdot 2H_2O$: C, 25.50; H, 4.94; N, 13.73%.

The $(-)_{546}$ diastereomer, $(+)_{546}$-$[Co(en)_2(ox)](-)_{546}$-$[Co(\beta\text{-ala})(gly)(ox)]\cdot 2H_2O$, was dissolved in water and the solution was passed through a small column of cation exchange resin (Dowex 50W×8, 200—400 mesh, potassium form). The solution was evaporated to a few milliliters. Violet-red flakes were deposited by adding ethanol to the concentrated solution. The complex was recrystallized from water by addition of ethanol. $[\alpha]_{546}-1830°$. Found: C, 22.25; H, 3.70; N, 7.25%. Calcd for $(-)_{546}$-$K[Co(\beta\text{-ala})(gly)(ox)]\cdot 2H_2O$: C, 21.88; H, 3.67; N, 7.29%.

The Potassium Salt of Complex 7. The complex was resolved in the same way as described for complex **6**. The racemate, $(\pm)$-$K[Co(\beta\text{-ala})(gly)(ox)]\cdot 1.5H_2O$ (obtained from the eluted band (vii), 1.10 g), was dissolved in 50 ml of water, and the solution was treated with a cation exchange resin (Dowex 50W×8, 200—400 mesh, lithium form). The resolving agent, $(+)_{546}$-$[Co(en)_2(ox)]Br\cdot H_2O$ (0.69 g), was dissolved in 60 ml of water at 60 °C, and the solution was treated with an anion exchange resin (Dowex 1×8, 200—400 mesh, acetate form). The two solutions were mixed. The mixture was evaporated to 75 ml in a vacuum evaporator, and then 25 ml of ethanol was added to the concentrated solution. After 1 h, red-violet crystals deposited were filtered and washed with water–ethanol mixture. They were recrystallized from water by addition of

ethanol. $[\alpha]_{546}+980°$. Found: C, 24.48; H, 5.07; N, 13.55%. Calcd for $(+)_{546}$-$[Co(en)_2(ox)](+)_{546}$-$[Co(\beta\text{-ala})(gly)(ox)]\cdot 3H_2O$: C, 24.77; H, 5.11; N, 13.33%.

The $(+)_{546}$ diastereomer was dissolved in water, and the solution was passed through a column of a cation exchange resin (Dowex 50W×8, 200—400 mesh, potassium form) in order to remove the resolving agent. The resulting solution was evaporated to a few milliliters, and then ethanol was added to the concentrated solution. After the solution had been allowed to stand for about 30 min at room temperature, crystalline powder deposited was filtered. It was recrystallized from a mixture of water and ethanol. $[\alpha]_{546}+1210°$. Found: C, 22.81; H, 3.30; N, 7.58%. Calcd for $(+)_{546}$-K-$[Co(\beta\text{-ala})(gly)(ox)]\cdot H_2O$: C, 22.96; H, 3.30; N, 7.65%.

Measurements. The electronic absorption spectra of the complexes were measured with a Hitachi Model EPS-3T spectrophotometer in aqueous solution. The CD spectra were recorded on a JASCO Model MOE-1 spectropolarimeter, the ^1H NMR spectra on a JEOL Model MH-100 spectrometer with DSS as an internal standard, and the ^{13}C NMR spectra on a JEOL Model MFT-100 spectrometer in pulse Fourier transform/proton noise decoupling mode at 25.15 MHz. The ^{13}C chemical shifts were measured relative to external benzene and converted into the chemical shifts from TMS using the relation $\delta_{TMS}=\delta_{benzene}-128.5$ ppm.

Results and Discussion

Both $[Co(gly)_2(ox)]^-$ and $[Co(\beta\text{-ala})_2(ox)]^-$ ions provide three geometrical isomers, *trans*(N), C_1-*cis*(N) and C_2-*cis*(N). On the other hand, the mixed complex ion, $[Co(\beta\text{-ala})(gly)(ox)]^-$, exists in four geometrical isomers of *trans*(N), *cis*(N)*trans*(O_β,N) (O_β represents the coordinating oxygen atom in β-alanine), *cis*(N)*trans*-(O_g,N) (O_g represents the coordinating oxygen atom in glycine) and *cis*(N)*trans*(O_β,O_g) (this isomer has a pseudo C_2 axis, the glycine being regarded as β-alanine; it is therefore referred to as C_2-*cis*(N) in this paper) (Fig. 1).

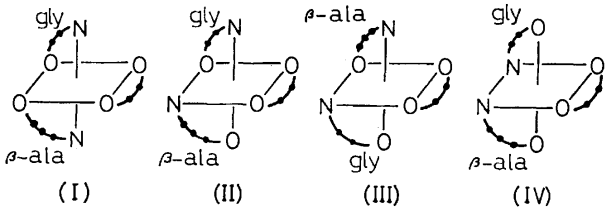

Fig. 1. The geometrical structures of four isomers in the mixed complex ion, $[Co(\beta\text{-ala})(gly)(ox)]^-$.
(I), *trans*(N); (II), *cis*(N)*trans*(O_β,N); (III), *cis*(N)*trans*-(O_g,N); (IV), *cis*(N)*trans*(O_β,O_g) (pseudo C_2 symmetry).

Structural Assignments of the Isomer $[Co(\beta\text{-ala})_2(ox)]^-$. It is generally recognized that the visible absorption band at lower energy side (the so-called first absorption band) of the *trans*(N) isomer of $[Co(N)_2(O)_4]$ type complex shows a more marked split as compared with that of the corresponding *cis*(N) isomer.[12] The $[Co(\beta\text{-ala})_2(ox)]^-$ complex prepared by Hidaka and Shimura[13] has been assigned to *trans*(N) isomer on the basis of the above. A marked split of the first absorption band was also observed for the complex obtained from the first eluted band in the process of separation of $[Co(\beta\text{-ala})_2(ox)]^-$ ion. Thus we conclude that the isomer obtained from the first eluted band has the *trans*(N) configuration. On the other hand, the other two isomers obtained from the second and third eluted bands showed no such marked split in the first absorption band, so that their configurations can be assigned to *cis*(N).

The assignments of the C_1- and C_2-*cis*(N) isomers can be verified by their ^{13}C NMR spectra. Since the chemical environments of the ethylene-carbons of the two β-alanine ligands are equivalent in the C_2-*cis*(N) isomer but not in the C_1-*cis*(N) isomer, two and four resonance lines resulting from ethylene-carbons are expected for the former and the latter, respectively. In addition, one resonance line due to the carboxyl-carbons in the coordinated β-alanines is expected for the C_2-*cis*(N) isomer, and two lines for the C_1-*cis*(N) isomer. The second eluted isomer showed four resonance lines resulting from ethylene-carbons and two resonance lines from carboxyl-carbons (Table 1). On the other hand, the third eluted isomer showed only two resonance lines and one for these carbons. Thus the structures of the second and third eluted isomers can be assigned to C_1-*cis*(N) and C_2-*cis*(N), respectively.

Table 1. ^{13}C CHEMICAL SHIFTS OF THE COORDINATED β-ALANINE

Complex ion	Ethylene-carbons		Carboxyl-carbon
trans(N)-$[Co(\beta\text{-ala})_2(ox)]^-$	33.9 ppm	38.6 ppm	184.4 ppm
C_1-*cis*(N)-$[Co(\beta\text{-ala})_2(ox)]^-$	33.7 (slightly split)	38.0	183.1
		38.6	184.2
C_2-*cis*(N)-$[Co(\beta\text{-ala})_2(ox)]^-$	33.6	38.0	183.3

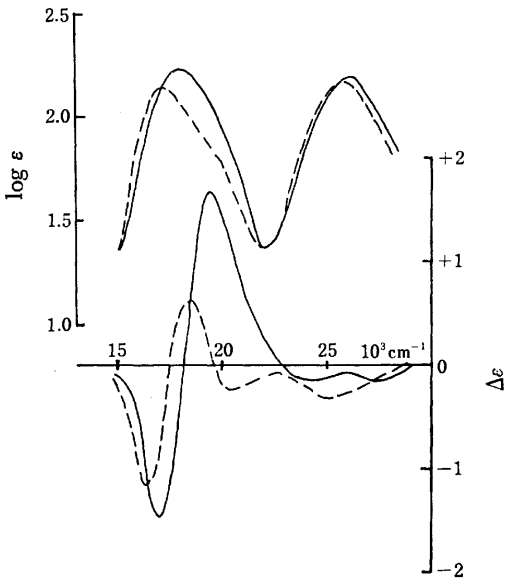

Fig. 2. The absorption and CD spectra of C_1- and C_2-*cis*(N) isomers of $[Co(\beta\text{-ala})_2(ox)]^-$ ion.
—— $(+)_{546}$-C_1-*cis*(N)-$[Co(\beta\text{-ala})_2(ox)]^-$, and
------ $(+)_{546}$-C_2-*cis*(N)-$[Co(\beta\text{-ala})_2(ox)]^-$.

The assignments of the C_1-*cis*(N) and C_2-*cis*(N) isomers can be made also on the basis of the energy difference in the first absorption bands. Matsuoka *et al.*[12] reported three geometrical isomers of a bis(amino acidato)-(oxalato)cobaltate(III) complex, and pointed out that the first absorption maxima of the C_2-*cis*(N) isomers are located in a lower energy region than those of the C_1-*cis*(N) isomers. As shown in Fig. 2, the first absorption maximum (18070 cm^{-1}) of the second eluted isomer was observed in a higher energy region as compared with that (17300 cm^{-1}) of the third eluted isomer. It can be concluded that the second and third eluted isomers take C_1-*cis*(N) and C_2-*cis*(N) structures, respectively. These assignments are in line with those from the ^{13}C NMR data.

Structural Assignments of Four Isomers in [Co(β-ala)(gly)-(ox)]⁻ Ion. Ten chromatographic bands ((i)—(x)) appeared on separation of [Co(β-ala)(gly)(ox)]⁻ (see Experimental). For complexes **3**, **9**, and **10**, the ^1H NMR resonance lines due to only the methylene-protons of the coordinated glycine were observed in the region 3.37—3.67 ppm. On the other hand, for complexes **1**, **4**, and **5**, the resonance lines due to only the ethylene-protons of the coordinated β-alanine were observed in the region 2—3 ppm. However, for complexes **2**, **6**, **7**, and **8**, both signals of the coordinated glycine and β-alanine were observed. The absorption spectra of complexes **1**, **3**, **4**, **5**, **9**, and **10** agree well with those of *trans*(N)-[Co(β-ala)$_2$(ox)]⁻, *trans*(N)-[Co(gly)$_2$(ox)]⁻, C_1-*cis*(N)-[Co(β-ala)$_2$(ox)]⁻, C_2-*cis*(N)-[Co(β-ala)$_2$(ox)]⁻, C_1-*cis*(N)-[Co(gly)$_2$(ox)]⁻, and C_2-*cis*(N)-[Co(gly)$_2$-(ox)]⁻, respectively. It is therefore expected that the remaining complexes, **2**, **6**, **7**, and **8**, are four isomers of the [Co(β-ala)(gly)(ox)]⁻ ion.

Of four isomers of the (β-alaninato)(glycinato)-(oxalato)cobaltate(III) complex, the structure of isomer **2** can be assigned to *trans*(N) since a marked split was observed in the first absorption band, which is characteristic of the complexes of *trans*(N)-[Co(N)$_2$(O)$_4$] type. The other three isomers, **6**, **7**, and **8**, exhibited no such marked split in the first absorption band, and thus would have the *cis*(N) configuration. Of these three *cis*(N) isomers, isomer **8** showed the first absorption band maximum (17670 cm^{-1}) in the lowest energy region (Table 2 and Fig. 3). The absorption maximum of C_2-*cis*(N) isomer was observed in a lower energy region than for the C_1-*cis*(N) isomer in bis(amino acidato)-(oxalato)cobaltate(III) complexes. Isomer **8** is thus expected to take C_2-*cis*(N) structure, as shown in Fig. 1 (IV). The structures of the remaining two isomers **6** and **7** can be assigned to either *cis*(N)*trans*(O_β,N) (Fig. 1 (II)) or *cis*(N)*trans*(O_g,N) (Fig. 1 (III)).

^1H NMR Spectra. The ^1H NMR spectra of the complexes are shown in Fig. 4. The methylene-proton

Table 2. Absorption and CD data of bis(amino acidato)cobaltate(III) complexes

Elution order		Complex ion	Band I		Band II	
			AB_{max} 10^3 cm^{-1} (log ε)	CD_{ext} 10^3 cm^{-1} (Δε)	AB_{max} 10^3 cm^{-1} (log ε)	CD_{ext} 10^3 cm^{-1} (Δε)
(iii)	**3**	(+)$_{546}$-*trans*(N)-[Co(gly)$_2$(ox)]⁻ [a]	*ca.* 16.7 (1.7) 18.87 (2.00)	*ca.* 16.7 (−1.4) 18.88 (−2.07)	25.83 (2.23)	26.17 (+0.69)
(ii)	**2**	(+)$_{546}$-*trans*(N)-[Co(β-ala)(gly)(ox)]⁻	16.30 (1.75) 18.81 (2.01)	*ca.* 16.3 (−1.1) 18.55 (−1.46)	25.97 (2.19)	23.70 (−0.13) 26.11 (+0.54)
(i)	**1**	(+)$_{546}$-*trans*(N)-[Co(β-ala)$_2$(ox)]⁻ [a]	16.00 (1.76) 18.83 (2.00)	15.70 (−0.43) *ca.* 16.7 (−0.3) 19.53 (−0.57)	26.30 (2.12)	23.80 (−0.13) 26.53 (+0.71)
(ix)	**9**	(−)$_{546}$-C_1-*cis*(N)-[Co(gly)$_2$(ox)]⁻ [a]	18.33 (2.15)	17.70 (+2.48) *ca.* 22.3 (+0.04)	25.77 (2.24)	23.93 (+0.09) 26.30 (−0.32) 29.00 (+0.10)
(vi)	**6**	(−)$_{546}$-*cis*(N)*trans*(O_β,N)-[Co(β-ala)(gly)(ox)]⁻	18.52 (2.19)	17.09 (+3.81) 19.49 (−1.88)	25.84 (2.24)	24.27 (+0.49) 26.11 (−0.09) 28.17 (+0.17)
(vii)	**7**	(+)$_{546}$-*cis*(N)*trans*(O_g,N)-[Co(β-ala)(gly)(ox)]⁻	18.02 (2.20)	17.15 (−1.50) 19.80 (+0.24)	26.04 (2.24)	23.98 (−0.10) 26.11 (+0.20) 28.74 (−0.04)
(iv)	**4**	(+)$_{546}$-C_1-*cis*(N)-[Co(β-ala)$_2$(ox)]⁻	18.07 (2.24)	17.00 (−1.45) 19.43 (+1.71)	25.90 (2.18)	24.57 (−0.13) 27.23 (−0.12)
(x)	**10**	(+)$_{546}$-C_2-*cis*(N)-[Co(gly)$_2$(ox)]⁻ [a]	17.83 (2.08)	18.03 (−3.39) *ca.* 22.5 (+0.04)	25.90 (2.20)	25.97 (+0.52)
(viii)	**8**	*cis*(N)*trans*(O_β,O_g)-[Co(β-ala)(gly)(ox)]⁻ (pseudo C_2 symmetry)	17.67 (qualitative)		26.14 (qualitative)	
(v)	**5**	(+)$_{546}$-C_2-*cis*(N)-[Co(β-ala)$_2$(ox)]⁻	17.30 (2.12)	16.47 (−1.19) 18.47 (+0.62) 20.83 (−0.24)	25.77 (2.17)	25.30 (−0.29)

a) Refs. 11 and 13.

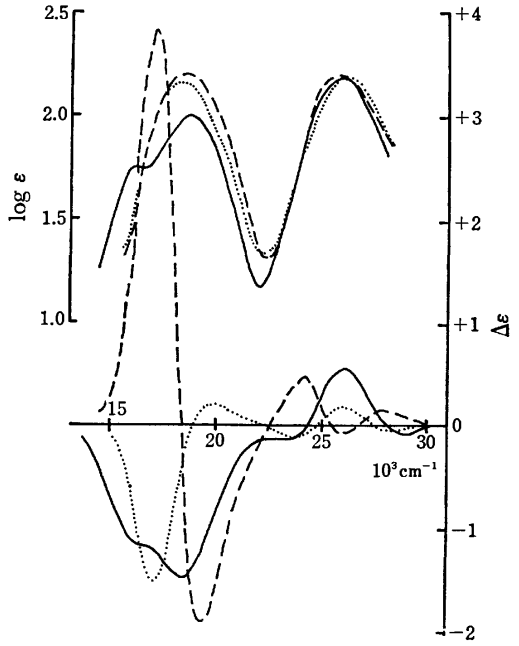

Fig. 3. The absorption and CD spectra of the isomers in $[Co(\beta\text{-ala})(gly)(ox)]^-$ complex ion.
—— $(+)_{546}$-*trans*(N)-$[Co(\beta\text{-ala})(gly)(ox)]^-$,
------ $(-)_{546}$-*cis*(N)*trans*(O_β,N)-$[Co(\beta\text{-ala})(gly)(ox)]^-$,
····· $(+)_{546}$-*cis*(N)*trans*(O_g,N)-$[Co(\beta\text{-ala})(gly)(ox)]^-$.

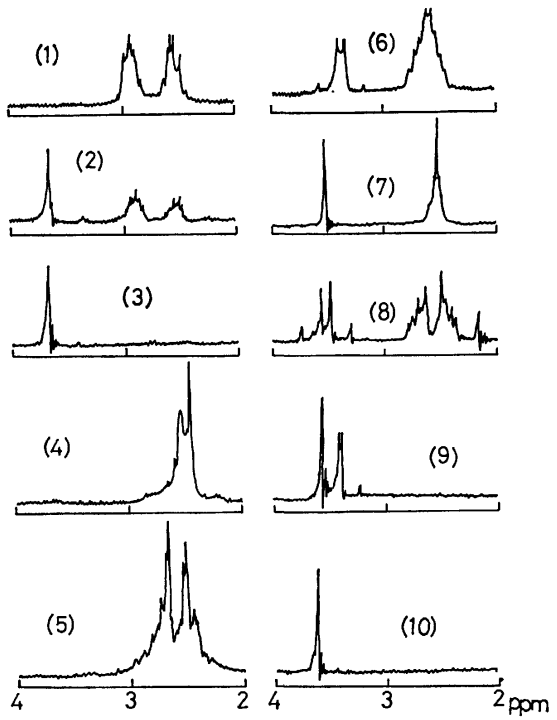

Fig. 4. The ^1H NMR spectra of $[Co(\beta\text{-ala})_{2-x}(gly)_x(ox)]^-$ (x=0—2) ions.
(1), *trans*(N)-$[Co(\beta\text{-ala})_2(ox)]^-$; (2), *trans*(N)-$[Co(\beta\text{-ala})(gly)(ox)]^-$; (3), *trans*(N)-$[Co(gly)_2(ox)]^-$; (4), C_1-*cis*(N)-$[Co(\beta\text{-ala})_2(ox)]^-$; (5), C_2-*cis*(N)-$[Co(\beta\text{-ala})_2(ox)]^-$; (6), *cis*(N)*trans*($O_\beta$,N)-$[Co(\beta\text{-ala})(gly)(ox)]^-$; (7), *cis*(N)-*trans*($O_g$,N)-$[Co(\beta\text{-ala})(gly)(ox)]^-$; (8), *cis*(N)*trans*($O_\beta$, O_g)-$[Co(\beta\text{-ala})(gly)(ox)]^-$ (pseudo C_2 symmetry, containing some contamination); (9), C_1-*cis*(N)-$[Co(gly)_2(ox)]^-$; and (10) C_2-*cis*(N)-$[Co(gly_2(ox)]^-$.

signals of the chelated glycine appear in the region 3.3—3.7 ppm. The *trans*(N) isomer **3** of the bis(glycinato)(oxalato)cobaltate(III) complex showed a single resonance at 3.67 ppm, and the C_2-*cis*(N) isomer **10** one at 3.52 ppm. However, two different resonance signals (a singlet at 3.52 ppm and a quartet at 3.37 ppm) were observed in the C_1-*cis*(N) isomer **9**. This suggests that the methylene-protons of the two glycines in isomer **9** are present in different chemical environments. Sakaguchi *et al.* pointed out the importance of the effect of magnetic anisotropy which is induced on the central Co(III) chromophore. They applied the anisotropy to the assignments of protons in ethylenediamine-Co(III) complexes[14] and amino acidato-Co(III) complexes.[15] They suggested that, in C_1-*cis*(N)-$[Co(gly)_2(ox)]^-$, the methylene-protons of the chelated glycine located in the plane including N-Co(III)-N would be observed in a lower field than the other methylene-protons of the chelated glycine which is not located in the plane. Thus the singlet at 3.52 ppm can be assigned to H_b and H_b', and the quartet at 3.37 ppm to H_a and H_a' (Fig. 5 (I)).

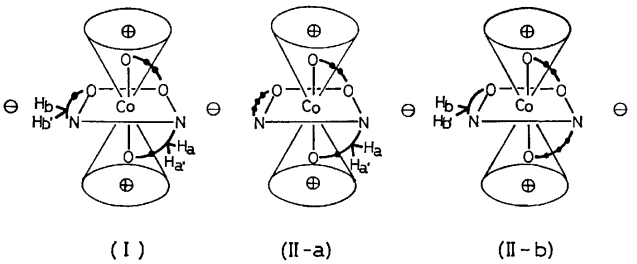

Fig. 5. The magnetic anisotropy induced on cobalt(III) chromophore.
(I); C_1-*cis*(N)-$[Co(gly)_2(ox)]^-$, (II-a); *cis*(N)*trans*(O_β, N)-$[Co(\beta\text{-ala})(gly)(ox)]^-$, and (II-b); *cis*(N)*trans*(O_g,N)-$[Co(\beta\text{-ala})(gly)(ox)]^-$.
+: Shift to up field, —: shift to down field.

The ^1H NMR data of isomer **6** gave a quartet signal due to the methylene-protons of glycine, at 3.38 ppm (Fig. 4). From the chemical shift and splitting pattern, it seems that these methylene-protons are in similar chemical environments to the higher field methylene-protons (H_a and H_a') of the C_1-*cis*(N) isomer of bis(glycinato)(oxalato)cobaltate(III) complex. The resonance line due to the methylene-protons of the glycinato chelate in isomer **7** (a singlet at 3.54 ppm) corresponds to that of the lower field methylene-protons (H_b and H_b') of C_1-*cis*(N)-$[Co(gly)_2(ox)]^-$. The correspondence leads to the conclusion that the structure of isomer **6** is *cis*(N)*trans*(O_β,N) and that of isomer **7** is *cis*(N)*trans*-(O_g,N) (Fig. 5, (II-a) and (II-b)).

The signals in the region 2—3 ppm should be assigned to the ethylene-protons of the β-alaninato chelate.

Electronic Absorption and CD Spectra. Electronic absorption and CD data of *trans*(N) complexes are given in Table 2. The absorption spectra of these complexes are very similar to each other. The intensity ratio of sub- and major-band of the first absorption band, (ε_{max}(sub)/ε_{max} (major)), for the *trans*(N)-$[Co(\beta\text{-ala})_2(ox)]^-$ is 0.58 and that for the *trans*(N)-$[Co(gly)_2(ox)]^-$ is

0.50. The ratio of the *trans*(N)-[Co(β-ala)(gly)(ox)]$^-$ is 0.55, greater than that of *trans*(N) bis(glycinato) and smaller than that of the *trans*(N) bis(β-alaninato) complex. The maximum of the second absorption band of the *trans*(N) (β-alaninato)(glycinato) complex was observed in a higher energy region than that of the bis(glycinato) complex, but in a lower energy region than that of the bis(β-alaninato) complex. For the second absorption bands of these three *trans*(N) complexes, the bis(β-alaninato) complex shows the lowest intensity (log ε_{max}) and the bis(glycinato) complex the highest intensity.

The CD curve of the $(+)_{546}$-*trans*(N) bis(glycinato) complex shows two negative bands in the first absorption band region and a positive band in the second absorption band region (Table 2). The CD curve of the $(+)_{546}$-*trans*(N) bis(β-alaninato) complex shows three negative bands in the first absorption band region, their intensities being significantly smaller compared with those of the bis(glycinato) complex.[13] However, the positive CD band of the bis(β-alaninato) complex observed in the second absorption band region is nearly equal to that of the bis(glycinato) complex. The CD curve of the $(+)_{546}$-*trans*(N)-[Co(β-ala)(gly)(ox)]$^-$ in the first absorption band region shows two negative bands which have somewhat smaller intensities than those of the $(+)_{546}$-*trans*(N) bis(glycinato) complex. The positive CD band of the mixed *trans*(N) complex in the second absorption band region is nearly equal in intensity to those of the other two *trans*(N) complexes. From the CD spectrum of the $(+)_{546}$-*trans*(N)-[Co(β-ala)$_2$(ox)]$^-$ in the first absorption band region, it is possible to assign its absolute configuration to Δ, as in the case of the $(+)_{546}$-*trans*(N) bis(glycinato) complex.[11]

For the four C_1-*cis*(N) complexes (**9**, **6**, **7**, and **4**) in Table 2, the first absorption maximum of the *cis*(N)*trans*-(O_β,N) (β-alaninato)(glycinato) complex **6** was observed in the highest energy region and that of the *cis*(N)*trans*-(O_g,N) (β-alaninato)(glycinato) complex **7** in the lowest energy region. However, the first absorption maximum of the *cis*(N)*trans*(O_β,O_g) (β-alaninato)(glycinato) complex **8** (pseudo C_2 symmetry) is located in a lower energy region than that of the C_2-*cis*(N) bis(glycinato) complex **10**, but in a higher energy region than that of the C_2-*cis*(N) bis(β-alaninato) complex **5**. The maxima of the first absorption band of the C_2-*cis*(N) complexes were observed in a lower energy region than those of the C_1-*cis*(N) complexes.

The *cis*(N)-[Co(α-am)$_2$(ox)]$^-$ type complexes containing glycine or L-serine show only one CD band in the first absorption band region. On the other hand, *cis*(N)-[Co(ida)$_2$]$^-$,[16] [Co(edta)]$^-$ [16,17] and *cis*(N)-[Co(L-alama)$_2$]$^-$ (L-alama: L-alanine-monoacetic acid)[18] have two CD bands of the opposite signs with comparable intensities. The *cis*(N)*trans*(O_β,N) (β-alaninato)(glycinato) complex **6** and the C_1-*cis*(N) bis(β-alaninato) complex **4** belong to the latter group, revealing two CD bands of the opposite signs and of nearly comparable intensities. The CD curves of the *cis*(N)*trans*(O_g,N) (β-alaninato)(glycinato) complex **7** and C_2-*cis*(N) bis(β-alaninato) complex **5** show different patterns from those of C_1-*cis*(N) bis(β-alaninato) and *cis*(N)*trans*(O_β,N) (β-alaninato)(glycinato) complexes in the first absorption band region. Namely, complex **5** shows three CD bands in the first absorption band region, while complex **7** shows two CD bands of opposite signs in the first absorption band region, but the CD intensity at 19800 cm^{-1} is significantly smaller than that of the opposite sign at 17150 cm^{-1}. The differences in the CD spectra would be caused by the difference in ligand field strength between O_g and O_β, and the difference in size of the chelate ring between the glycinato and β-alaninato chelates. However, the dominant factor is unknown.

The absolute configuration of the *cis*(N)-[Co(ida)$_2$]$^-$ isomer for which the CD bands in the first absorption band region show positive and negative signs listing from the lower energy side, was assigned to Λ by Van Saun and Douglas.[16] The Λ $(-)_{546}$-isomer of [Co(edta)]$^-$ shows a similar CD pattern in this region. From a comparison of CD patterns, it is concluded that the $(+)_{546}$-C_1- and $(+)_{546}$-C_2-*cis*(N) isomers of the bis(β-alaninato) complex and $(+)_{546}$-*cis*(N)*trans*(O_g,N) isomer of the (β-alaninato)(glycinato) complex take Δ configuration and the $(-)_{546}$-*cis*(N)*trans*(O_β,N) isomer of the (β-alaninato)(glycinato) complex takes Λ configuration.

References

1) Part IX of this series: T. Ama and T. Yasui, *Bull. Chem. Soc. Jpn.*, **49**, 472 (1976).
2) T. Yasui, J. Hidaka, and Y. Shimura, *Bull. Chem. Soc.* Jpn., **39**, 2417 (1966).
3) M. B. Ćelap, S. R. Niketic, and T. J. Janic, *Inorg. Chem.*, **6**, 2063 (1967).
4) T. Yasui and B. E. Douglas, *Inorg. Chem.*, **10**, 97 (1971).
5) N. Koine, N. Sakota, J. Hidaka, and Y. Shimura, *Inorg. Chem.*, **12**, 859 (1973).
6) R. D. Gillard, S. H. Laurier, D. C. Price, D. A. Phipps, and C. F. Weick, *J. Chem. Soc., Dalton Trans.*, **1974**, 1385.
7) N. Matsuoka, J. Hidaka, and Y. Shimura, *Bull. Chem. Soc. Jpn.*, **48**, 458 (1975).
8) T. Yasui, *Bull. Chem. Soc. Jpn.*, **48**, 454 (1975).
9) J. Fujita and H. Ogino, *Chem. Lett.*, **1974**, 57 (1974).
10) K. Yamasaki, J. Hidaka, and Y. Shimura, *Bull. Chem. Soc. Jpn.*, **42**, 119 (1969).
11) N. Matsuoka, J. Hidaka, and Y. Shimura, *Inorg. Chem.*, **9**, 719 (1970).
12) N. Matsuoka, J. Hidaka, and Y. Shimura, *Bull. Chem. Soc. Jpn.*, **40**, 1868 (1967).
13) J. Hidaka and Y. Shimura, *Bull. Chem. Soc. Jpn.*, **40**, 2312 (1967).
14) U. Sakaguchi, S. Yamazaki, and H. Yoneda, *Bull. Chem. Soc. Jpn.*, **49**, 402 (1976).
15) H. Yoneda, U. Sakaguchi, anb Y. Nakashima, *Bull. Chem. Soc. Jpn.*, **48**, 209 (1975).
16) C. W. Van Saun and B. E. Douglas, *Inorg. Chem.*, **8**, 1145 (1969).
17) B. E. Douglas, R. A. Haines, and J. G. Brushmiller, *Inorg. Chem.*, **2**, 1194 (1963).
18) K. Okamoto, J. Hidaka, and Y. Shimura, *Bull. Chem. Soc. Jpn.*, **44**, 1601 (1971).

The Formation and Structure of $Bi_{1.34}CrNbO_6$

Yasuyoshi Torii and Kanemitsu Hasegawa

Government Industrial Research Institute, Nagoya, Hirate-machi, Kita-ku, Nagoya 462

(Received February 18, 1977)

A new ternary oxide $Bi_{1.34}CrNbO_6$ was prepared and characterized. The unit cell is face-centered cubic with $a=10.455$ Å. The structure is assumed to be of the pyrochlore type based on the space group Fd3m and was refined by trial and error to a reliability factor R of 0.0564. This pyrochlore phase was confirmed to have vacancies at the A sites and also at the special oxygen sites, and may be considered to be a rare case in this respect. The Cr^{3+} and Nb_5^+ ions are bonded octahedrally to six oxygen atoms at 2.03 Å, while the Bi^{3+} ions are bonded to six oxygen atoms at 2.56 Å. The structure consists of bismuth tetrahedra, the centers of which are vacant. The highly polarizable Bi^{3+} ion plays an important role in the formation of the defect pyrochlore structure. Related pyrochlores were also prepared.

A number of mixed oxides with pyrochlore structure are known by the formula $A_2B_2O_7$,[1] and have provided a rich source of new materials exhibiting ferroelectricity[2] and promising electrooptic effects.[3] In recent years, many defect pyrochlores have been prepared based on the correlation between the perovskite and pyrochlore phases, and their structures and electrical properties have been investigated.[4-7] Most are oxygen deficient pyrochlores having the formula $A_2B_2O_{7-x}$ ($0<x\leqq 1$). Like $Pb_{1.5}Nb_2O_{6.5}$[2] and $TlSbWO_6$,[8] there are few pyrochlores which have vacancies at the A sites. During a study on the synthesis of Bi-containing mixed oxides, a new phase, $Bi_{1.34}CrNbO_6$, was found which exhibits an X-ray pattern of pyrochlore structure. As can be estimated from the chemical formula, this phase may be regarded as a rare defect pyrochlore which has vacancies at the A sites. In $TlSbWO_6$[8] and $Tl_{1-\alpha}(Ta_{1+\alpha}W_{1-\alpha})O_6$,[9] however, the A ions occupy special sites and, therefore, the latter is a nonstoichiometric pyrochlore. It is of interest to know how the structure of the defect pyrochlores can tolerate a balanced deficiency of both bismuth and oxygen ions. A suggestion can be given on the basis of systematic synthesis of defect pyrochlores. In the present study, the defect pyrochlore, $Bi_{1.34}CrNbO_6$, was prepared and are characterized. The position of the Bi^{3+} ions in the cubic unit cell was determined and is discussed, and the formula of this compound is established. Also, related pyrochlores, $Bi_{1.34}B'B''O_6$, where B′=Cr and Fe and B″=Nb, Ta, and Sb were prepared and their dielectric properties were measured.

Experimental

For sample preparations, starting materials were employed in the form of metal oxides. The reactants were all of reagent or better grade. Appropriate mixtures of metal oxides were fired at 950 °C for 2 h, ground and refined at 1050 °C for 3 h in air. An examination of the samples was carried out using the powder diffraction method employing a Philips diffractometer with Cu$K\alpha$ and occasionally Fe$K\alpha$ radiation. The lattice constants were determined from the reflection lines of (662) and (840). The X-ray intensity data were measured integrally for each peak. The theoretical intensity of a group of equivalent reflection lines was taken to be $I=KM(\mathrm{Lp})F^2$, where K is the scale factor, M the multiplicity, Lp the Lorentz-polarization factor, and F the structure factor.[10] For structural refinement, the observed intensity was compared with the sum of the calculated intensities which appeared at the same value of 2θ. The scattering factors for Bi^{3+}, Cr^{3+}, Nb^{5+}, and O^{2-} ions were taken from Moore.[11] The calculated structure factors were also corrected for anomalous dispersion using values given by Cromer.[12] The intensity computations were performed using a FACOM 270-30 computer with a Fortran program developed by this laboratory for the minimization of the reliability factor $R=\Sigma|I_{\mathrm{obsd}}-I_{\mathrm{calcd}}|/\Sigma I_{\mathrm{obsd}}$. Stereographic pictures of the pyrochlore structure were drawn using a computer program.[13] The dielectric constants were measured on a YHP universal bridge at 1 kHz. For the measurements, disks about 1 cm in diameter and 0.15 cm thick were coated with silver paint.

Results

Formation of $Bi_{1.34}CrNbO_6$ and Related Pyrochlores. The new phase was prepared by firing a powdered mixture of Bi_2O_3, Cr_2O_3, and Nb_2O_5 having a molar ratio of 4: 3: 3. The X-ray diffraction powder pattern was completely indexed on the basis of a face-centered cubic unit cell with the dimension $a=10.455$ Å, as shown in Table 1. This pattern exhibits the reflection lines characteristic of pyrochlore structure. The chemical formula of the new phase $Bi_{1.34}CrNbO_6$, however, does not differ from that of normal or oxygen deficient pyrochlore. When mixtures of metal oxides corresponding to the formulae Bi_2CrNbO_7 and $Bi_{1.5}CrNbO_{6.25}$ were fired separately, the formation of phases other than the cubic pyrochlore phase was observed. In the case of Bi-rich components, the reacted products were partly melted even when fired at 900 °C. In all cases, there was almost not change in the relative intensity ratio and in the positions of the reflection lines observed in the powder patterns. The best preparation of this new pyrochlore phase resulted from the mixture with a molar ratio of 4: 3: 3, and it was found that no nonstoichiometric pyrochlore phase appears to exist.

Thermal analysis was carried out in order to determine whether oxidation or reduction occurs in the sample during the formation process. In the TG and DTA curves, an increase in weight began at *ca.* 520 °C and then the broad peak of the exothermic reaction was observed at 700 °C at a heating rate of 10 °C/min. An X-ray diffraction analysis of the intermediate stage showed the formation of $(BiO)_2CrO_4$ and supported the hypothesis that the oxidation of Cr ion in the sample took place during the heating run in air. Upon heating above

Table 1. X-Ray powder diffraction data for $Bi_{1.34}CrNbO_6$

$h\ k\ l$	d_{obsd}	I_{obsd}	I_{calcd}
1 1 1	6.03	10.0	10.8
3 1 1	3.15	9.4	9.6
2 2 2	3.02	100.0	100.0
3 3 1	2.40	28.2	29.8
5 1 1 3 3 3	2.01	2.4	1.8
4 4 0	1.848	30.1	31.7
5 3 1	1.766	1.7	0.5
6 2 0	1.652	0.9	0.1
5 3 3	1.594	0.2	0.1
6 2 2	1.575	23.3	23.3
4 4 4	1.513	6.0	5.2
7 1 1 5 5 1	1.463	0.9	0.6
8 0 0	1.307	2.4	2.5
7 5 1 5 5 5	1.207	0.9	0.5
6 6 2	1.199	6.2	5.2
8 4 0	1.169	5.8	4.1
9 1 1 7 5 3	1.147	0.4	0.5
9 3 1	1.096	0.2	0.2
8 4 4	1.067	3.0	2.7
9 5 1 7 7 3	1.011	0.4	0.1
6 6 6 10 2 2	1.006	3.0	2.5
8 8 0	0.924	0.6	0.6

760 °C, however, loss of oxygen occurred and the TG curve returned to its original level at *ca.* 950 °C. This level remained unchanged up to 1050 °C. After heating at this temperature for 2 h and then cooling, only formation of the new pyrochlore phase was found in the product. During a reheating run, the product showed no change in thermal analysis. Consequently, the Cr ions in this compound were assumed to be trivalent.

Table 2. Lattice and dielectric constants for some $Bi_{1.34}B'B''O_6$ pyrochlores

Compound	a (Å)	ε
$Bi_{1.34}CrNbO_6$	10.455	72
$Bi_{1.34}CrTaO_6$	10.449	35
$Bi_{1.34}CrSbO_6$	10.374	56
$Bi_{1.34}FeNbO_6$	10.506	116
$Bi_{1.34}FeTaO_6$	10.501	43
$Bi_{1.34}FeSbO_6$	10.421	39

The preparation of related compounds, all of which were of the pyrochlore type, was attempted. These lattice constants are shown in Table 2. The Cr^{3+}-containing pyrochlores are olive green in color, while the Fe^{3+}-containing compounds are dark organge, with a slight difference in hue. Attempts to prepare the V^{5+}-containing pyrochlores were unsuccessful even at high pressure (900 °C, 60 kb, 45 min). The lattice constant of $Bi_{1.34}CrNbO_6$ was slightly larger than that of $Bi_{1.34}CrTaO_6$, although both Nb^{5+} and Ta^{5+} ions are of the same size (0.64 Å) according to Shannon and Prewitt.[14] In this respect the Fe^{3+}-containing defect pyrochlores gave the same result as in the Cr^{3+}-containing ones. This is valid evidence for the existence of a defect pyrochlore type, since six pyrochlores could be prepared with starting compositions of $Bi_{1.34}B'B''O_6$.

Refinement of $Bi_{1.34}CrNbO_6$. The cell dimension and qualitative intensities of $Bi_{1.34}CrNbO_6$ strongly suggest that this compound has the pyrochlore structure belonging to the space group Fd3m.[15] Assuming $Bi_{1.34}CrNbO_6$ is of the pyrochlore type, one-third of the Bi^{3+} ions and one-seventh of the oxygen ions are missing in comparison with normal pyrochlore. Such a defect pyrochlore is rare. In $Pb_{1.5}Nb_2O_{6.5}$, the Pb^{2+} ions have been assumed to occupy the 16(d) sites.[2] In $TlSbWO_6$, the Tl^{1+} ions have been reported to occupy the 32(e) sites between the 8(b) and 16(d) sites.[8] Although the pyrochlore structure itself has been studied extensively, it is important in the establishment of the defect pyrochlore structure to determine the arrangement of atoms in the new phase, $Bi_{1.34}CrNbO_6$. Since there are only one or two positional parameters for the pyrochlore structure, the 23 reflection lines observed in the powder pattern are considered to be sufficient for structural analysis. Their intensities were calculated using the positions listed in Table 3. The site with $\bar{3}$m symmetry

Table 3. Atomic positions for $Bi_{1.34}CrNbO_6$

		Space group: Fd3m (No. 227)
		Lattice constant: 10.455 Å
		Cell content: $8Bi_{1.34}CrNbO_6$
	(0,0,0; 0,1/2,1/2; 1/2,0,1/2; 1/2,1/2,0)+	
Bi	16(d)	1/2,1/2,1/2; 1/2,1/4,1/4; 1/4,1/2,1/4; 1/4,1/4,1/2 occupancy probability: 67%
Cr(Nb)	16(c)	0,0,0; 0,1/4,1/4; 1/4,0,1/4; 1/4,1/4,0
O	48(f)	u,1/8,1/8; $\bar{u}$,7/8,7/8; 1/4−u,1/8,1/8; 3/4+u,7/8,7/8; 1/8,u,1/8; 7/8,$\bar{u}$,7/8; 1/8,1/4−u,1/8; 7/8,3/4+u,7/8; 1/8,1/8,u; 7/8,7/8,$\bar{u}$; 1/8,1/8,1/4−u; 7/8,7/8,3/4+u u=0.330
O	8(b)	3/8,3/8,3/8; 5/8,5/8,5/8 occupancy probability: 0%

was chosen as the origin. Firstly, the bismuth and oxygen vacancies were assumed to lie on one-third of the 16(d) sites and on the 8(b) sites, respectively, as shown in Fig. 1. Then, minimization of the reliability factor R to the final value of 0.0564 yielded the following results, u=0.330 and B=4.18 Å^2. The observed and calculated intensities for these parameters are listed on the right side of Table 1, and good agreement between both intensities is obtained. The density of the sample measured with a pycnometer was 6.01 g/cm^3, which corresponds to 8 formula weights of $Bi_{1.34}CrNbO_6$ per unit cell (theoretical density, 6.04 g/cm^3). When the random distribution of Bi^{3+} ions in the 16(d) and 8(b) sites or of oxygen ions in the 48(f) and 8(b) sites was assumed, the minimum values of R became considerably larger. This fact indicates erroneous assumptions. Next, when the Bi^{3+} ions were assumed to lie only on the

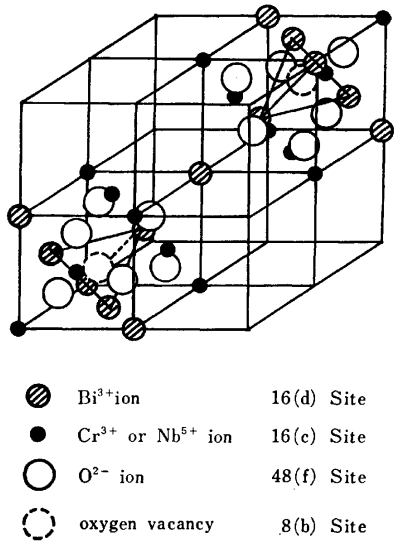

Fig. 1. Crystal structure of defect pyrochlore $Bi_{1.34}CrNbO_6$.

32(e) sites, instead of the 16(d) sites, the final R value was refined to be 0.0562 with $u_a=0.495$ (32(e) positional parameter) and $B=4.04$ Å^2. The slight decrease in the R value might be related with experimental errors in the intensity measurement. The u_a value obtained is close to 0.500, a value indicating the 16(d)-site occupancy of Bi^{3+} ions, differing from that ($u_a=0.403$) in $TlSbWO_6$.[8] From these results, it is not necessary to conclude that the Bi^{3+} ions lie on the 32(e) sites and that they deviate slightly from the 16(d) sites. The selected interatomic distances and angles in $Bi_{1.34}CrNbO_6$ were calculated on the first assumption, and are shown in Table 4. These values are in reasonable accord with the ionic sizes of Shannon and Prewitt.[14] The O–Cr(Nb)–O angles are a measure of the distortion of the oxygen octahedra, since all of these angles are 90° in the case of a regular octahedron.

Table 4. Selected interatomic distances and angles for $Bi_{1.34}CrNbO_6$

Distance	Å	Angle	Deg.
Bi–O	2.56	O–Bi–O	63.5
Cr(Nb)–O	2.03	O–Bi–O	116.5
O–O	2.70	O–Bi–O	180.0
O–O	3.03	O–Cr(Nb)–O	83.3
Bi–Bi	3.70	O–Cr(Nb)–O	96.7

In order to further examine this defect pyrochlore phase, the values of the reliability factor R for two series of proposed formulae, $Bi_{2-x}CrNbO_{7-3x/2}$ and $Bi_{2-x}Cr_{2-3x/2}Nb_{3x/2}O_6$, were calculated using the two parameters ($u=0.330$ and $B=4.18$ Å^2) determined previously. Figure 2 shows the relationship between R and x. In both curves, the R values are minima respectively when $x=2/3$, the x value of which corresponds to the chemical formula of $Bi_{1.34}CrNbO_6$. The R values rapidly increase with any deviation from this x value. This result provides conclusive proof that the defect pyrochlore phase has the true composition, $Bi_{1.34}CrNbO_6$.

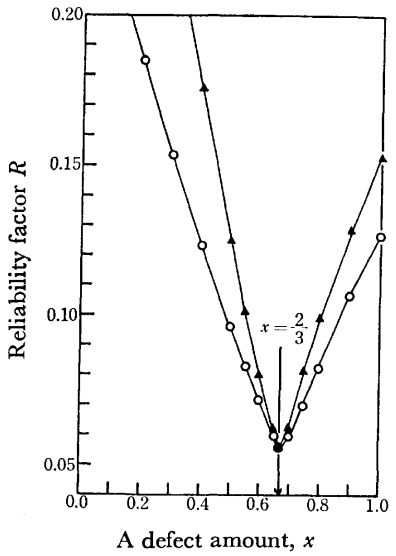

Fig. 2. Relation between R and x for two series of proposed formula.
○: $Bi_{2-x}CrNbO_{7-3x/2}$.
▲: $Bi_{2-x}Cr_{2-3x/2}Nb_{3x/2}O_6$.

Dielectric Properties. The six defect pyrochlores prepared had dielectric constants of *ca.* 30—110 at room temperature, as shown in Table 1, although no correction was made in regard to sample porosity. These values are relatively high in general, which fact renders them worth examining. The dielectric constants of Nb^{5+}-containing pyrochlores are considerably higher than those of Ta^{5+}- and Sb^{5+}-containing pyrochlores. Since these defect pyrochlores are of the cubic and centrosymmetric space group, the dielectric measurements were carried out in the temperature range from −150 to 20 °C. Figure 3 shows the temperature dependence of ε and tan δ for $Bi_{1.34}CrNbO_6$ and $Bi_{1.34}FeNbO_6$. No dielectric anomaly was observed, and ε and tan δ increased monotonically with increasing temperature. These defect pyrochlores are considered to be paraelectric in this temperature range. They have high electric resistivities which, although not

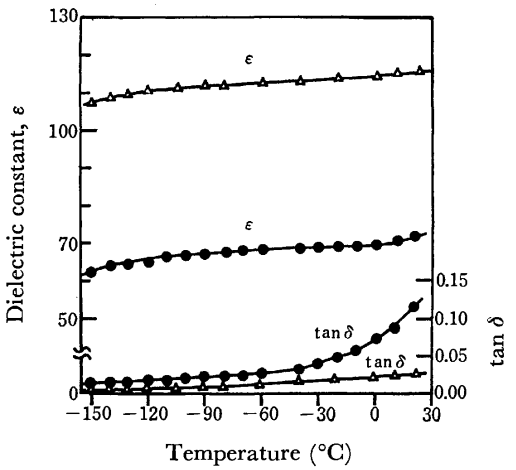

Fig. 3. Temperature dependence of ε and tan δ for two defect pyrochlores.
●: $Bi_{1.34}CrNbO_6$. △: $Bi_{1.34}FeNbO_6$.

measured directly, were high enough to balance a capacitance bridge. There should be a little change even when transition metal ions are present in the ambivalent oxidation state, since the electrical resistivity is expected to be sensitive to the state.

Discussion

The A cations in the pyrochlore structure are usually in eightfold coordination. In the case of $Bi_{1.34}CrNbO_6$, however, the Bi^{3+} ions have a sixfold coordination with an equivalent distance of 2.56 Å, since the 8(b) sites are not occupied by oxygen ions. The Cr^{3+} and Nb^{5+} ions are bonded octahedrally to six oxygen ions at a distance of 2.03 Å. The positional u parameter of 0.330 is within the range of 0.305 to 0.355 reported by Sleight[16] for twelve pyrochlores and is close to the values for rare-earth pyrochlores. The oxygen octahedra are slightly distorted because of the deviation from the 0.3125 value for a regular octahedron. The oxygen-oxygen distances in the octahedra are 2.70 and 3.03 Å. The octahedra form corners with other octahedra to form a three-dimensional framework, as shown in Fig. 4. The 8(b)-site vacancies are located at the

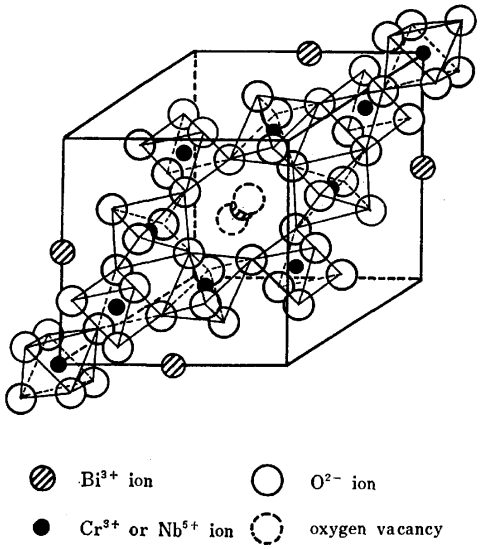

Fig. 4. Framework structure of defect pyrochlore $Bi_{1.34}CrNbO_6$.

centers of bismuth tetrahedra and the occupancy probability of Bi^{3+} ions is 67% at the tetrahedral corners. The Bi-Bi distance was 3.70 Å and the bismuth ions are in close proximity to each other, being unscreened. In normal pyrochlores, the 8(b) sites are filled by oxygen ions and, therefore, the defect pyrochlore structure should be unstable because of the repulsion between the Bi^{3+} ions, judging only from electrostatic considerations. No pyrochlore phases, however, were formed when the Bi^{3+} ion was replaced by a La^{3+} or Y^{3+} ion as the A-site ion in the $A_{1.34}CrNbO_6$ and A_2CrNbO_7 forms. Occupancy by a La^{3+} or Y^{3+} ion appears to be unfavorable for the formation of such a defect pyrochlore structure, while occupancy by a Bi^{3+} ion appears favorable. The ionic sizes of La^{3+}, Y^{3+}, and Bi^{3+} ions are 1.18, 1.015, and 1.11 Å respectively,[14] and these ions are of suitable size for the A-site ion in the pyrochlore structure. Consequently, the essential nature of A-site ions must be considered in the formation of defect pyrochlores. That is to say, the La^{3+} and Y^{3+} ions are of ionic character and the Bi^{3+} has a significant contribution of covalent character. Even though the Bi atom is completely ionized to the valence state of +3, the Bi^{3+} ion has outer $6s^2$ core electrons which easily polarize the neighiboring oxygen ions and exhibit directional bonding. The remarkable arrangement of unscreened Bi^{3+} ions in $Bi_{1.34}CrNbO_6$ has often been found for oxides containing an inert-pair ion, as in PbO, Bi_2O_3, and SnO.[17] The abnormal stereochemistry of these compounds is due to s-p hybridization. The trap-mediated metal-metal bond pointed out by Goodenough *et al.*[4] may also be responsible for the defect pyrochlore formation of $Bi_{1.34}CrNbO_6$. The 8(b)-vacancy sites act as traps for the outermost electrons of the Bi^{3+} ions, and the 6s and 6p orbitals spread out into the vacancy sites, where considerable electron density is concentrated. The electrostatic repulsion between the Bi^{3+} ions may be counteracted by the transfer of the outermost electrons to the vacancy sites, and the defect pyrochlore structure of $Bi_{1.34}CrNbO_6$ is stabilized by this Bi-Bi bonding. A 67% occupancy of Bi^{3+} ions at the 16(d) sites is naturally determined from the electroneutrality condition, considering that the Cr^{3+} and Nb^{5+} ions contribute to the framework of the defect pyrochlore structure. The value itself exhibits no significant meaning in this case. However, the case appears to be different for $TlSbWO_6$ where the occupancy probability of Tl^{1+} ions is only 50%. In the case of $TlSbWO_6$, the 32(e) positional parameter for the Tl^{1+} ion has been determined to be $u_a=0.403$.[8] The 32(e) site lies on a straight line between the 16(d) and 8(b) sites. As shown in Fig. 1, the 16(d) and 8(b) sites are the corners and center of the cationic tetrahedron, respectively. The 32(e) site corresponds to the 16(d) site at $u_a=0.500$, and to the 8(b) site at $u_a=0.375$. Consequently, the Tl-Tl distance becomes smaller with decreasing u_a. In $TlSbWO_6$, the 32(e)-site occupancy of Tl^{1+} ions, which deviates considerably from the 16(d) site, would enable the outermost electrons to overlap sufficiently at the vacancy sites despite the low occupancy probability. The circumstances under which the trap-mediated bond is formed may be severe because of the rather large Tl-Tl distance under the condition that the Tl^{1+} ions occupy half of the 16(d) sites. For that reason, the assumption that the Bi^{3+} ions occupy the 32(e) site with $u_a=0.495$ in $Bi_{1.34}CrNbO_6$ might be correct, although deviation from the 16(d) sites is slight. This slight deviation is probably due to the fact that the occupancy probability of A-site ions is higher in $Bi_{1.34}CrNbO_6$ than in $TlSbWO_6$. Thus, the Bi^{3+} ions not only occupy open spaces in the framework, but also play an important role in the formation of defect pyrochlore structures. $Bi_{1.34}CrNbO_6$ and related compounds are rare examples of a defect pyrochlore type which has vacancies at the A sites and also at special oxygen sites.

References

1) E. Aleshin and R. Roy, *J. Am. Ceram. Soc.*, **45**, 18 (1962).
2) F. Jona, G. Shirane, and R. Pepinsky, *Phys. Rev.*, **98**, 903 (1955).
3) C. H. Hokmes, E. G. Spencer, A. A. Ballman, and P. V. Lenzo, *Appl. Opt.*, **4**, 551 (1965).
4) J. M. Longo, P. M. Raccah, and J. B. Goodenough, *Mater. Res. Bull.*, **4**, 191 (1969).
5) J. M. Longo, P. M. Raccah, J. A. Kafalas, and J. W. Pierce, *Mater. Res. Bull.*, **7**, 137 (1972).
6) N. Ramadass, T. Palanisamy, J. Gopalakrishnan, G. Aravamudan, and M. V. C. Sastri, *Solid State Commun.*, **17**, 545 (1975).
7) Y. Torii and H. Matsumoto, *Bull. Chem. Soc. Jpn.*, **49**, 671 (1976).
8) C. Michel, D. Grout, and B. Raveau, *Mater. Res. Bull.*, **8**, 201 (1973).
9) C. Michel and B. Raveau, *Mater. Res. Bull.*, **8**, 451 (1973).
10) L. E. Alexander and H. P. Klug,"X-Ray Diffraction Procedures," John Wiley & Sons, New York (1959), pp. 147, 157.
11) F. H. Moore, *Acta Crystallogr.*, **16**, 1169 (1963).
12) D. T. Cromer, *Acta Crystallogr.*, **18**, 17 (1965).
13) Y. Torii, Y. Hori, and Y. Yamada, The Fall Meeting of the Ceramic Society of Japan, Nov. 1976, Nagoya, p. 28.
14) R. D. Shannon and C. T. Prewitt, *Acta Crystallogr., Sect. B*, **25**, 925 (1969).
15) "International Tables for X-Ray Crystallography," Vol. 1, Kynoch Press, Birmingham (1965), p. 341.
16) A. W. Sleight, *Inorg. Chem.*, **7**, 1704 (1968).
17) A. F. Wells, "Structural Inorganic Chemistry," 3 rd ed, Oxford University Press, London (1962), p. 887.

Stereochemistry of Cobalt(III) Complexes with Thioethers. II.[1] Geometrical Isomers, Absorption, and Circular Dichroism Spectra of Bis(terdentate-*N,S,O*) Complexes

Kazuaki YAMANARI, Jinsai HIDAKA,* and Yoichi SHIMURA

Department of Chemistry, Faculty of Science, Osaka University, Toyonaka, Osaka 560

(Received February 21, 1977)

Two cobalt(III) complexes containing terdentate thioethers, bis[(2-aminoethylthio)acetato]cobalt(III)(1+), and bis[3-(2-aminoethylthio)propionato]cobalt(III)(1+) were prepared and separated into five and six geometrical isomers, respectively, by ion-exchange column chromatography. The isomers were identified on the basis of their electronic absorption and NMR spectra. The circular dichroism spectra of optically resolved isomers were measured and discussed in relation to the absolute configurations.

Some cobalt(III) complexes with multidentate thioether ligands have so far been reported.[2-15] It appears that the presence of thioether donor atoms induces an extreme specificity concerning the formation of geometrical isomers.[6-9] As an example, of the bis(terdentate) type cobalt(III) complexes with linear terdentate ligands having the donor atom sequence N–S–N[11,14] or O–S–O,[15] only one or two geometrical isomers of three possible ones have been isolated. Recently, a bis(L-methioninato)cobalt(III) complex[11] of the $[Co(N)_2(O)_2(S)_2]$ type has been prepared and its three geometrical isomers obtained. The complex is the first example for the isolation of all the possible isomers of a complex with multidentate thioethers.

In the present work, two linear terdentate ligands having the donor atom sequence N–S–O, (2-aminoethylthio)acetic acid (Haeta=$NH_2CH_2CH_2SCH_2CO_2H$) and 3-(2-aminoethylthio)propionic acid (Haetp=$NH_2CH_2CH_2SCH_2CH_2CO_2H$), were used, and the absorption and circular dichroism (CD) spectra of their cobalt(III) complexes studied. For the bis(terdentate-*N,S,O*) type cobalt(III) complexes, six geometrical isomers are possible. So far no report seems to have appeared with respect to the isolation of six geometrical isomers of such $[Co(A–B–C)_2]$ type complex, though two isomers of $[Co(aeta)_2]^+$ have recently been reported.[16]

Experimental

Preparation, Separation, and Optical Resolution of the Complexes. (1) Bis[(2-aminoethylthio)acetato]cobalt(III) Chloride, [Co(aeta)$_2$]Cl: To a hot solution (*ca.* 70 °C) of 9 g cobalt(II) chloride hexahydrate in 80 cm^3 of water was added a solution of 9.35 g of (2-aminoethylthio)acetic acid hemihydrochloride[1] and 1.51 g of sodium hydroxide dissolved in 80 cm^3 of water. Fifteen grams of PbO_2 was gradually added to the mixed solution on a water bath, whereupon the solution turned violet. The mixture was stirred at 70 °C for *ca.* 40 min. The reaction mixture was filtered in order to remove excess lead dioxide after being cooled to room temperature. A considerable amount of brownish violet precipitate appeared which was filtered off.

The filtrate was poured into an ion exchange column containing Dowex 50 W×8 resin (200—400 mesh, Na^+ form, 4.5×40 cm). After the column had been swept with water, the adsorbed band was eluted with a 0.15 M aqueous solution of NaCl at the rate of 1 cm^3 per min. Five colored bands, brownish violet (A-1), purple (A-2), red (A-3), another red (A-4), and reddish purple (A-5), were eluted in this order. The eluates of these bands were separately concentrated in a vacuum evaporator and then the deposit, NaCl, was filtered off. To each of the filtrates was added a large amount of ethanol. The complexes thus obtained were crystallized from a minimum quantity of water by adding ethanol and then acetone, and dried in a vacuum desiccator over $CaCl_2$. The isomers were obtained in comparable yields, except for A-2 which showed a somewhat higher yield. Found for A-1: C, 25.76; H, 4.44; N, 7.71%. Calcd for $[Co(aeta)_2]Cl=C_8H_{16}N_2S_2O_4ClCo$: C, 26.49; H, 4.45; N, 7.72%. Found for A-2: C, 26.28; H, 4.62; N, 7.82%. Calcd for $[Co(aeta)_2]Cl=C_8H_{16}N_2S_2O_4ClCo$: C, 26.49; H, 4.45; N, 7.72%. Found for A-3: C, 25.04; H, 4.83; N, 7.81%. Calcd for $[Co(aeta)_2]Cl\cdot H_2O=C_8H_{18}N_2S_2O_5ClCo$: C, 25.24; H, 4.77; N, 7.36%. Found for A-4: C, 24.46; H, 5.10; N, 7.56%. Calcd for $[Co(aeta)_2]Cl\cdot 1.5H_2O=C_8H_{19}N_2S_2O_{5.5}ClCo$: C, 24.65; H, 4.91; N, 7.15%. Found for A-5: C, 24.80; H, 4.85; N, 7.75%. Calcd for $[Co(aeta)_2]Cl\cdot H_2O=C_8H_{18}N_2S_2O_5ClCo$: C, 25.24; H, 4.77; N, 7.36%.

Of the five isomers, four except A-1 were optically resolved.

A-2, $(-)_{589}$-[Co(aeta)$_2$]Cl, (trans(O)): This isomer was resolved by using $(-)_{589}$-K[Co(edta)]·2H_2O as a resolving agent. The racemic chloride (0.36 g) and the resolving agent (0.21 g) were dissolved in 2 cm^3 of water at 40 °C. After being cooled to room temperature, the mixed solution was allowed to stand overnight in a refrigerator. A small amount of less soluble diastereomer was deposited as violet needles and recrystallized from a minimum quantity of water. The yield was 0.25 grams. Found: C, 27.91; H, 4.87; N, 7.33%. Calcd for $(-)_{589}$-$[Co(aeta)_2][Co(edta)]\cdot 5H_2O=C_{18}H_{38}N_4S_2O_{17}Co_2$: C, 28.28; H, 5.01; N, 7.33%.

Optically active chloride was obtained from the diastereomer by using an anion exchange resin (Dowex 1×8, Cl^- form). Found: C, 26.23; H, 4.49; N, 7.71%. Calcd for $(-)_{589}$-$[Co(aeta)_2]Cl=C_8H_{16}N_2S_2O_4ClCo$: C, 26.49; H, 4.45; N, 7.72%.

A-3, $(-)_{589}$-[Co(aeta)$_2$]Cl·H$_2$O, (trans(S)): Attempts to resolve this isomer by means of the resolving agents $(-)_{589}$-K[Co(edta)]·2H_2O, $(+)_{589}$-Na[Co(ox)$_2$(en)]·H_2O, $Na_2[Sb_2(d\text{-tart})_2]\cdot 2H_2O$, and $Ag_2(d\text{-}H_2tart)$; (d-$H_4tart=C_4O_6H_6$), were unsuccessful. However, spontaneous resolution[17] was observed for the crystals prepared as follows: 0.5 g of the racemic chloride monohydrate was dissolved in 5 cm^3 of water at 40 °C and the solution was kept standing in a refrigerator for several days for crystallization. Crystals arbitrarily chosen then showed optical activity. No hemihedral facets, however, were found for the crystals. Found: C, 24.93; H, 4.83; N, 7.45%. Calcd for $(-)_{589}$-[Co(aeta)$_2$]-

* Present address: Department of Chemistry, The University of Tsukuba, Ibaraki, 300-31.

$Cl \cdot H_2O = C_8H_{18}N_2S_2O_5ClCo$: C, 25.24; H, 4.77; N, 7.36%.

A-4, $(+)_{589}$-[Co(aeta)$_2$]$^+$, (cisciscis): The racemic chloride (0.39 g), dibenzoyl-*d*-tartaric acid (*d*-H_2tart-bz_2) (0.38 g), and sodium hydroxide (0.08 g) were dissolved in 10 cm^3 of water at 40 °C. The mixed solution was then evaporated to 2 cm^3 and cooled in a refrigerator overnight. The red diastereomer deposited was recrystallized from 2 cm^3 of hot water by adding acetone. Found: C, 36.47; H, 4.75; N, 4.92%. Calcd for $(+)_{589}$-[Co(aeta)$_2$]$_2$(*d*-tart-bz_2)$\cdot 5.5H_2O$ = $C_{34}H_{55}N_4S_4O_{21.5}Co_2$: C, 36.79; H, 4.99; N, 5.05%.

Optically active chloride was obtained from the diastereomer by using an anion exchange resin (Dowex 1×8, Cl^- form). The CD spectrum of this complex was measured with the eluate, and the concentration was calculated from the CD intensity referring to that of the diastereomer.

A-5, $(-)_{589}$-[Co(aeta)$_2$]Cl$\cdot 2.25H_2O$, (trans(N)): The racemic chloride (0.39 g) and the resolving agent $Na_2[Sb_2$(*d*-tart$)_2]\cdot 2H_2O$ (0.16 g) were dissolved in 3 cm^3 of water at 40 °C. The mixed solution was allowed to stand for a few days in a refrigerator to crystallize. The less soluble diastereomer (reddish purple) precipitated was filtered off and recrystallized from 2 cm^3 of hot water by adding ethanol. This was converted into the optically active chloride by using an anion exchange resin (Dowex 1×8, Cl^- form). Found: C, 23.46; H, 4.94; N, 6.90%. Calcd for $(-)_{589}$-[Co(aeta)$_2$]-$Cl \cdot 2.25H_2O = C_8H_{20.5}N_2S_2O_{6.25}ClCo$: C, 23.83; H, 5.12; N, 6.95%.

(2) Bis[3-(2-aminoethylthio)propionato]cobalt(III) Chloride, [Co(aetp)$_2$]Cl: This complex was prepared and separated according to the same method as that for [Co(aeta)$_2$]Cl with use of 3-(2-aminoethylthio)propionic acid[1] instead of (2-aminoethylthio)acetic acid.

Five colored bands, brownish violet (B-1), purple (B-2), another purple (B-3+B-4), reddish purple (B-5), and violet (B-6), were eluted in this order. The yields for B-1 and B-2 isomers were very low. It was confirmed by the absorption spectral behavior in the thioether charge transfer band region that the third eluate consists of two isomers B-3 and B-4, and that the B-1, B-2, and B-4 have a configuration in which the two sulfur atoms occupy *trans* positions. The eluates were separately concentrated in a vacuum evaporator and the deposit, NaCl, was filtered off. To each of the concentrated solution was added a large amount of ethanol. The desired complex was collected by filtration and recrystallized from a small amount of water by adding ethanol and acetone, and then dried in a vacuum desiccator over $CaCl_2$. However, complete separation of B-3 and B-4 isomers by means of an ion exchange resin (Dowex 50 W×8 or SP-Sephadex C-25) was unsuccessful. The pure products of these two isomers were obtained as follows. After removal of excess laed dioxide, the reaction mixture was evaporated to 50 cm^3 and cooled in an ice bath, and B-3 isomer was then crystallized as the bromide salt. On the other hand, the pure product of B-4 isomer could be fractionally crystallized from the mixed eluate of B-3 and B-4 isomers because of its low solubility. Found for B-1: C, 27.52; H, 5.70; N, 6.44%. Calcd for [Co(aetp)$_2$]$Cl \cdot 2.5H_2O = C_{10}H_{25}N_2S_2O_{6.5}ClCo$: C, 27.56; H, 5.78; N, 6.43%. Found for B-2: C, 26.76; H, 6.14; N, 5.90%. Calcd for [Co(aetp)$_2$]$Cl \cdot 4H_2O = C_{10}H_{28}N_2S_2O_8ClCo$: C, 25.95; H, 6.10; N, 6.05%. Found for B-3: C, 21.74; H, 5.06; N, 5.23%. Calcd for [Co(aetp)$_2$]$Br \cdot 3.5H_2O \cdot 1/2NaBr = C_{10}H_{27}N_2S_2O_{7.5}BrCo \cdot 1/2$-NaBr: C, 21.85; H, 4.95; N, 5.10%. Found for B-4: C, 27.96; H, 5.43; N, 6.58%. Calcd for [Co(aetp)$_2$]$Cl \cdot 2H_2O = C_{10}H_{21}N_2S_2O_6ClCo$: C, 28.14; H, 5.67; N, 6.56%. Found for B-5: C, 29.18; H, 5.50; N, 6.90%. Calcd for [Co(aetp)$_2$]-$Cl \cdot H_2O = C_{10}H_{22}N_2S_2O_5ClCo$: C, 29.38; H, 5.42; N, 6.85%. Found for B-6: C, 27.60; H, 5.73; N, 6.47%. Calcd for [Co(aetp)$_2$]$Cl \cdot 2.5H_2O = C_{10}H_{25}N_2S_2O_{6.5}ClCo$: C, 27.56; H, 5.78; N, 6.43%.

B-3, $(-)_{589}$-[Co(aetp)$_2$]Cl$\cdot 2H_2O$, (trans(O)): The racemic bromide (0.55 g) and the resolving agent $K_2[Sb_2$(*d*-tart$)_2]\cdot 3H_2O$ (0.32 g) were dissolved in 5 cm^3 of water at 50 °C. After cooling to room temperature, the mixed solution was allowed to stand for a week in a refrigerator. The less soluble diastereomer deposited was recrystallized from a small amount of water, and converted into the chloride salt by using an anion exchange resin (Dowex 1×8, Cl^- form). Found: C,23.47; H,4.68; N,5.40%. Calcd for $(-)_{589}$-[Co(aetp)$_2$]$Cl \cdot 2H_2O \cdot 1.2KCl = C_{10}H_{24}N_2S_2O_6ClCo \cdot 1.2KCl$: C,23.26; H,4.69; N,5.43%.

B-2, $(+)_{589}$-[Co(aetp)$_2$]$^+$, (mer-trans(S)); *B-4, $(+)_{589}$-[Co(aetp)$_2$]$^+$*, (trans(S)); *B-5, $(+)_{589}$-[Co(aetp)$_2$]$^+$*, (cisciscis); *and B-6, $(+)_{589}$-[Co(aetp)$_2$]$^+$*, (trans(N)): These four isomers were partially or completely resolved into their optical antipodes by chromatographic technique.

An aqueous solution containing 0.1 g of the complex was poured into a column of SP-Sephadex C-25 (Na^+ form, 3×120 cm). The adsorbed band was eluted with a 0.1 M aqueous solution of $K_2[Sb_2$(*d*-tart$)_2]\cdot 3H_2O$ at the rate of 0.3 cm^3/min. Under these conditions, 7—10 days were necessary for the complete elution of the complex, which produced a broad band. The eluate was separated into fractions of 5 cm^3 each. A few fractions eluted first, which showed CD spectra completely enantiomeric to those of the last fractions, were collected and after removal of the excess elution agents converted into the chloride salt by using an anion exchange resin (Dowex 1×8, Cl^- form). This eluate of the chloride salt was used to measure the CD spectrum, and its concentration was calculated from the optical density referring to that of the racemate.

In all of the four isomers, the first eluates showed positive optical rotations for the Na-D line. A complete band separation into the antipodes was only observed for B-4 isomer.

Measurements. The electronic absorption spectra were measured on a Shimadzu UV-200 spectrophotometer in aqueous solutions. The CD spectra were obtained with a Jasco MOE-1 spectropolarimeter, by use of a cell with 1 cm pathlength. A Jasco DIP-4 digital polarimeter was used to check the optical rotations. The ^1H NMR spectra were recorded in deuterium oxide on a Varian XL-100-15 spectrometer with DSS as the internal reference. All the measurements were carried out at room temperature.

Results and Discussion

Separation of Isomers. For the present [Co(terdentate-*N,S,O*)$_2$]$^+$ type complexes, six geometrical isomers are possible. They are denoted by *tr.tr.tr.*, *trans(S)*, *trans(O)*, *trans(N)*, *cisciscis*, and *mer-trans(S)*, respectively, as shown in Fig. 1.

In the [Co(aeta)$_2$]$^+$ complex, five geometrical isomers were obtained. A-1 and A-2 seem to correspond to the two isomers reported by Hori[16] from a comparison of absorption spectra. For the [Co(aetp)$_2$]$^+$ complex, six geometrical isomers were separated chromatographically, which is the first example for the isolation of all the possible isomers of the [Co(A–B–C)$_2$] type complex. A molecular model examination reveals that the aeta ligand, which forms two five-membered chelate rings by coordination, strongly prefers the facial coordina-

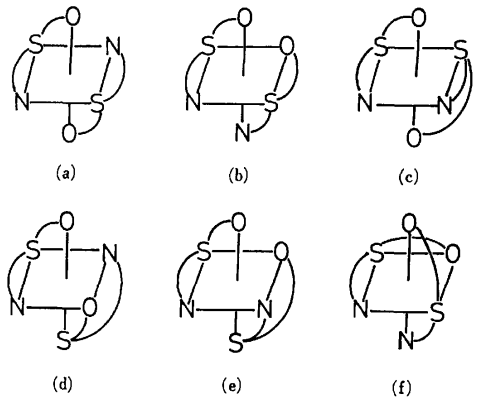

Fig. 1. Six possible geometrical isomers for the [Co(terdentate-*N,S,O*)$_2$]$^+$ type complex: (a) *tr.tr.tr.*, (b) *trans(S)*, (c) *trans(O)*, (d) *trans(N)*, (e) *cisciscis*, and (f) *mer-trans(S)*.

tion, whereas the aetp ligand which forms a five- and a six-membered chelate ring will take the meridionally coordinated form readily. It is therefore reasonable to expect that the *mer-trans(S)* isomer does not exist in the aeta complex. These circumstances seem to be common with the bis(terdentate) type cobalt(III) complexes containing linear *O,S,O*-[15] or *O,N,O*-terdentate[18-21] ligands.

An optical antipode exists for each five isomers of the six geometrical ones, except for *tr.tr.tr.* which has an inversion center. Accordingly, A-1 and B-1 isomers which could not be optically resolved are expected to have the *tr.tr.tr.* geometry.

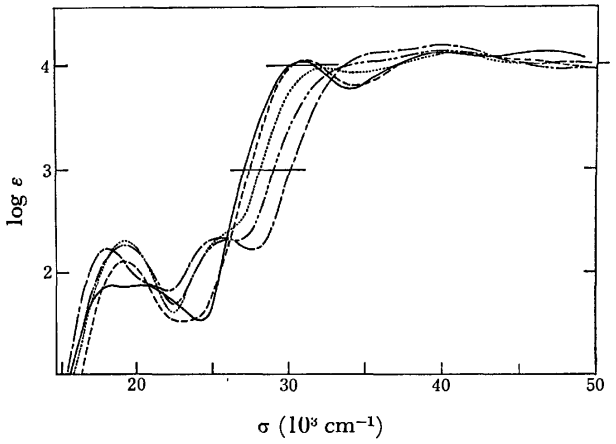

Fig. 2. Absorption spectra of the isomers of [Co(aeta)$_2$]-Cl: A-1 *tr.tr.tr.* (——), A-2 *trans(O)* (·—·—·), A-3 *trans(S)* (-----), A-4 *cisciscis* (—··—··—), and A-5 *trans(N)* (·····).

Absorption Spectra and Configuration Assignments. The absorption spectra of [Co(aeta)$_2$]$^+$ are shown in Fig. 2 and summarized in Table 1. In the near-ultraviolet region, the complexes show intense sulfur-to-metal charge transfer bands. The bands for A-1 and A-3 are located at lower energy side than those for the other three isomers. The charge transfer band of this type has been recognized to occur at a lower energy side for the cobalt(III) complexes with two ligating S atoms

Table 1. Absorption data of isomers of [Co(aeta)$_2$]Cl and [Co(aetp)$_2$]Cl

[Co(aeta)$_2$]Cl[a] Isomer	Configuration	σ_{max}[b] (log ε) First d-d band	Second d-d band	Charge transfer band region
A-1	*tr.tr.tr.*	18.4(1.87)		30.9(4.04)
		20.4(1.87)		40.1(4.11)
				46.3(4.11)
A-2	*trans(O)*	18.1(2.24)	25.3(2.34)	35.1(4.09)[c]
		20.8(1.88)[c]		40.0(4.17)
				48.3(4.04)
A-3	*trans(S)*	19.2(2.10)		31.2(4.04)
				40.2(4.12)
A-4	*cisciscis*	19.2(2.27)	26.1(2.32)	33.7(3.98)[e]
				40.0(4.12)
A-5	*trans(N)*	19.2(2.31)	25.5(2.36)[c]	32.4(3.97)
				40.7(4.11)
				47.8(4.01)
[Co(aetp)$_2$]Cl[a]				
B-1	*tr.tr.tr.*	17.5(1.92)		29.2(4.13)
		20.7(2.02)		39.1(4.02)
				47.2(4.13)
B-2	*mer-trans(S)*	18.9(2.59)	25.3(2.55)[c]	31.2(4.26)
				39.7(4.04)
B-3[d]	*trans(O)*	17.8(2.32)	26.4(2.40)[c]	34.2(4.19)
		21.1(2.05)		40.5(4.00)
B-4	*trans(S)*	18.8(2.60)		29.7(4.15)
				39.3(4.03)
				47.4(4.08)
B-5	*cisciscis*	19.0(2.42)	25.6(2.46)[c]	33.0(4.15)
				42.1(4.06)
B-6	*trans(N)*	sh[e]	25.3(2.62)[c]	31.8(4.10)
		18.8(2.60)		40.9(4.08)

a) The racemates. b) Wave numbers are given in 10^3 cm^{-1} unit. c) A shoulder. d) Bromide salt. e) The wave number could not be determined.

in *trans* positions than for the corresponding *cis* complexes.[12,13,15] Additional support was recently given to this absorption spectral criterion by the X-ray crystal structure analysis of *trans(S)*-[Co(*S*-methyl-L-cysteinato)$_2$]ClO$_4$·H$_2$O.[22] Thus, A-1 and A-3 isomers can be assigned to the *trans(S)* or *tr.tr.tr.* configuration and others to the *trans(O)*, *trans(N)*, or *cisciscis* one.

In the first d-d absorption band region, the expected splittings can be calculated semiempirically;[23] the *tr.tr.tr.* and *trans(N)* isomers should have the component of lowest energy, since the sulfur atom in the present terdentate ligands is between the oxygen of the carboxyl group and the nitrogen of the amino group in the spectrochemical series.[1] The *tr.tr.tr.* and *trans(O)* isomers should have one component in close proximity to the transition of [Co(N)$_6$], and the splitting for *tr.tr.tr.* isomer should be greater than those for *trans(N)* and *trans(O)* forms. The *trans(S)* and *cisciscis* isomers should have two and three components, respectively, in about the same region.

Of the two isomers assigned to the *trans(S)* or *tr.tr.tr*, A-1 exhibits two splitting components with the same molar extinction coefficients in the first absorption band

region, while A-3 shows apparently a sharp band. This indicates that A-1 is *tr.tr.tr.* and A-3 *trans(S)*.

On the other hand, of the three isomers assigned to the *trans(O)*, *trans(N)*, or *cisciscis*, A-2 exhibits an explicit shoulder at the high energy side of the major peak in the first absorption band region, while both A-4 and A-5 show a sharp peak. In the [Co(L-methioninato)$_2$]-Br[12] complex, both *trans(N)* and *trans(O)* isomers showed a marked splitting in the first absorption band region, their splitting patterns differing from each other; the *trans(O)* isomer showed a broad band with a shoulder at high energy side of the major peak, the *trans(N)* one at low energy side. This confirms that A-2 isomer is *trans(O)*.

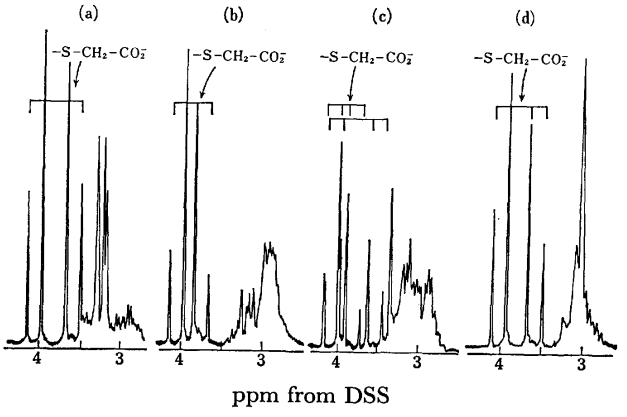

Fig. 3. The NMR spectra of the isomers of [Co(aeta)$_2$]-Cl in D_2O: (a) A-2 *trans(O)*, (b) A-3 *trans(S)*, (c) A-4 *cisciscis*, and (d) A-5 *trans(N)*.

The absorption spectra of A-4 and A-5 isomers are similar to each other, though there is a difference with respect to the position of thioether charge transfer band. ^{1}H NMR spectra of these isomers are shown in Fig. 3. A-2, A-3, and A-5 isomers exhibit a quartet due to methylene protons between carboxyl group and sulfur atom,[15] whereas A-4 shows two sets of quartet. The *trans(S)*, *trans(O)*, and *trans(N)* structures have C_2 symmetry, the *cisciscis* structure C_1. The latter isomer should show the most complicated pattern. Accordingly, A-4 can be assigned to *cisciscis*, and A-5 to *trans(N)*. Further support is given by the signals in the region of amine protons. The amine signals appear at 6.17 and 6.58 ppm from DSS for A-2, at 4.62 and 4.98 ppm for A-3, at 4.49, 4.90, and 6.36 ppm for A-4, and at 5.26 and 6.67 ppm for A-5. This is explained qualitatively in terms of the magnetic anisotropy associated with the C–O single bond.[24-27] In each of the present isomers there are two amine groups; two groups of *trans(S)* and *trans(N)* isomers and one group of *cisciscis* isomer are in the shield position from the C–O bond of the other ligand, whereas one group of *cisciscis* isomer and two groups of *trans(O)* isomer are deshielded by the C–O bond of the other ligand. It is possible to expect that *cisciscis* isomer with C_1 symmetry shows the most complicated signals over the wider region than the other three isomers with C_2 symmetry.

The absorption spectra of six isomers of [Co(aetp)$_2$]$^+$ are shown in Fig. 4 and summarized in Table 1. According to the same discussion as described above, B-1

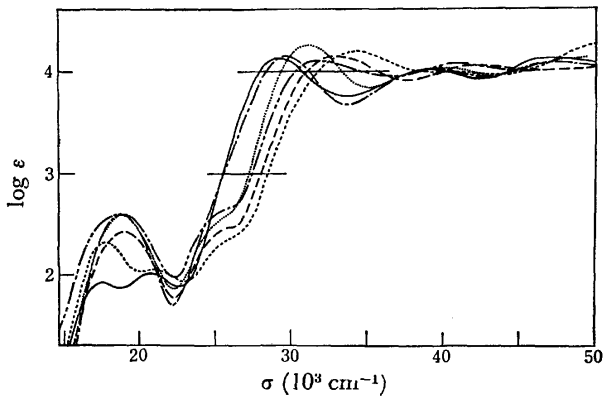

Fig. 4. Absorption spectra of the isomers of [Co(aetp)$_2$]-Cl: B-1 *tr.tr.tr.* (——), B-2 *mer-trans(S)* (·····), B-3 *trans(O)* (------), B-4 *trans(S)* (·-·-·), B-5 *cisciscis* (—·—·), and B-6 *trans(N)* (—···—); B-3 isomer is a bromide salt.

isomer can be assigned to *tr.tr.tr.* and B-3 to *trans(O)*. Of the remaining four isomers, B-5 and B-6 have the thioether charge transfer bands at the higher energy side than B-2 and B-4. Therefore, the former two and the latter two isomers can be assigned to the configurations with two ligating S atoms in *cis* and *trans* positions, respectively. In the first absorption band region, B-5 shows a sharp band, while B-6 exhibits a vague shoulder at the low energy side of the major peak. The spectral behavior corresponds to the expectation from semiempirical theory, and B-5 can be assigned to *cisciscis* and B-6 to *trans(N)*. The B-2 and B-4 isomers were assigned to *mer-trans(S)* and *fac-trans(S)* configurations, respectively, on the basis of the low yield of B-2 (see Experimental), and of absorption spectral behavior in which the low energy thioether charge transfer band of B-2 occurs at an exceptional position. These assignments have good correlation with the column chromatographic behavior. Namely, the complexes [Co(aeta)$_2$]$^+$ and [Co(aetp)$_2$]$^+$ have the same elution order of isomers except for B-2-*mer-trans(S)* isomer; the order is *tr.tr.tr.*, *trans(O)*, *trans(S)*, *cisciscis*, and *trans(N)* for both series.

Thus, the electronic absorption spectra of the corresponding isomers between [Co(aeta)$_2$]$^+$ and [Co(aetp)$_2$]$^+$ complexes are similar to each other but differ in detail. Firstly, the first d-d band intensities of the isomers of [Co(aetp)$_2$]$^+$ are two or three times larger than those of the corresponding isomers of [Co(aeta)$_2$]$^+$. Such kind of intensity difference has been observed between *trans(N)-RR*-[Co(L-promp)$_2$]$^-$ and *trans(N)-RR*-[Co(L-proma)$_2$]$^-$ complexes,[28] where L-promp and L-proma are L-prolinate-*N*-monopropionate and L-prolinate-*N*-monoacetate, respectively. Secondly, in the aetp complexes, the thioether charge transfer band is shifted to a lower energy side than that of the corresponding aeta isomer, and the shift direction is the same as that of the first d-d absorption band.

CD Spectra. The CD spectra are shown in Figs. 5—8 and Table 2. The complexes have two CD contributions, one from the configurational chirality due to the skew pair of chelate rings and the other from the chirality due to the sulfur donor atoms, though both contributions can not be separated. The observed CD

TABLE 2. CD DATA OF ISOMERS OF $[Co(aeta)_2]Cl$ AND $[Co(aetp)_2]Cl$

$[Co(aeta)_2]Cl$ Isomer	Rotation for Na-D line	σ_{ext}[a] ($\Delta\varepsilon$) First d-d band region	Second d-d band region	Charge transfer band region
trans(O)	(−)	17.8 (−4.04)	25.4 (−1.23)	36.4 (+10.7)
		21.5 (+2.64)		42.1 (−17.2)
				47.6 (+22.2)
trans(S)	(−)	17.9 (−0.52)	23.7 (−0.15)	30.9 (+23.5)
		20.3 (−0.13)		35.7 (−10.4)
				39.6 (−14.9)
				44.9 (+23.3)
cisciscis	(+)	18.0 (+2.51)	24.6 (+0.82)	32.5 (−5.72)
		20.4 (−1.19)		38.7 (−15.5)
				43.2 (+14.5)
trans(N)[b]	(−)	18.7 (−1.63)	26.0 (+2.24)	31.7 (+13.6)
		20.0 (−1.48)[c]		35.5 (−2.09)
				40.3 (+16.5)
				44.8 (−19.5)
$[Co(aept)_2]Cl$				
mer-trans(S)[b]	(+)	17.3 (+0.37)	25.1 (+0.21)	31.5 (−3.88)
		19.6 (−0.44)		36.1 (+1.17)
				38.6 (−0.43)
				44.4 (+4.22)
trans(O)	(−)	18.0 (−4.51)	25.8 (−1.25)	31.7 (−8.09)
		21.1 (+4.56)		34.8 (+4.22)
				37.7 (−6.59)
				44.2 (+14.0)[c]
				48.3 (+21.6)
trans(S)[b]	(+)	17.2 (−1.59)	26.2 (−2.47)	30.1 (−4.36)
		19.6 (+5.87)		36.6 (−13.6)
				43.5 (+8.12)
cisciscis[b]	(+)	17.7 (+1.52)	24.2 (+0.19)	31.9 (−14.7)
		20.7 (−0.17)	26.5 (+0.25)	37.2 (+3.97)
				43.3 (+2.59)
				46.8 (−3.16)
trans(N)[b]	(+)	17.2 (−0.27)	25.6 (−0.75)	31.1 (−6.85)
		19.8 (+1.25)		36.1 (−4.28)
				42.9 (+10.6)

a) Wave numbers are given in 10^3 cm^{-1} unit. b) CD spectra were measured with eluates. c) A shoulder.

spectra differ significantly among the different geometrical isomers, but resemble the corresponding geometrical isomers of $[Co(aeta)_2]^+$ and $[Co(aetp)_2]^+$. Accordingly, it is convenient to discuss each pair of geometrical isomers individually.

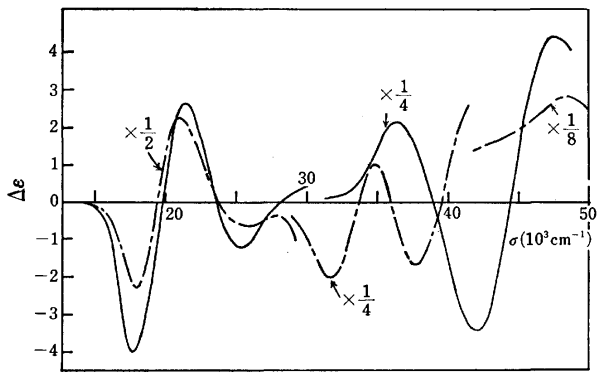

Fig. 5. CD spectra of *trans(O)* complexes: $(-)_{589}$-$[Co(aeta)_2]^+$ (——) and $(-)_{589}$-$[Co(aetp)_2]^+$ (·–·–·).

In the first absorption band region, both $(-)_{589}$-*trans(O)* aeta and $(-)_{589}$-*trans(O)* aetp complexes have two CD components, (−) and (+) from low energy side (Fig. 5), though three bands, (+), (−), and (+), have been observed for *trans(O)*-$[Co(L\text{-methioninato})_2]^+$ [12] and *trans(O)*-$[Co(S\text{-methyl-L-cysteinato})_2]^+$ [13] in the corresponding region. In the present *trans(O)* isomers with C_2 symmetry, there is a weaker field along the unique axis (O–Co–O) than along the other axes perpendicular to it. Thus it is predicted that the $^1A+{}^1B_b(C_2)$ level would be lower in energy than the $^1B_a(C_2)$ level. Consequently, the negative CD components at low energy are assigned to be $^1A+{}^1B_b(C_2)$, and the positive CD components at high energy $^1B_a(C_2)$. The absolute configurations of $(-)_{589}$-*trans(O)*-$[Co(aeta)_2]^+$ and $(-)_{589}$-*trans(O)*-$[Co(aetp)_2]^+$ are assigned to *ΔΔΛ*-(*RR*) and *ΔΔΛ*-(*SS*),[29] respectively, according to the CD sign of the $^1A+{}^1B_b(C_2)$ transition, where (*RR*) and (*SS*) represent the chiralities of the chiral sulfur atoms. The absolute configuration of $(-)_{589}$-*trans(O)*-$[Co(NH_2CH_2CH_2NHCH_2CO_2)_2]^+$,[30] which exhibits two CD

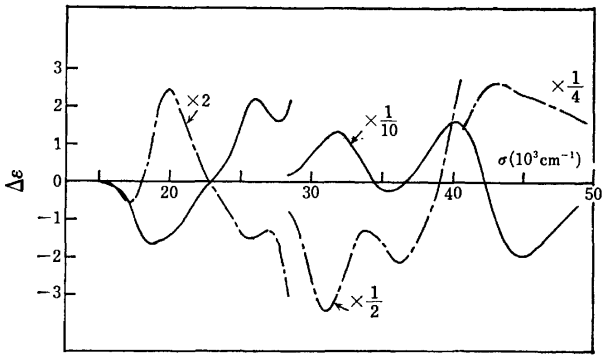

Fig. 6. CD spectra of *trans(N)* complexes: $(-)_{589}$-[Co(aeta)$_2$]$^+$ (——) and $(+)_{589}$-[Co(aetp)$_2$]$^+$ (·—·—·).

peaks of opposite sign, (−) and (+) from low energy side, in the first absorption band region, has been assigned to *ΔΔΛ*.

For the *trans(N)* isomers (Fig. 6), the aeta $(-)_{589}$-complex exhibits two negative CD bands at 18700 cm^{-1} ($\Delta\varepsilon=-1.63$) and *ca.* 20000 cm^{-1} ($\Delta\varepsilon=-1.48$), but the aetp $(+)_{589}$-complex shows two bands of opposite sign at 17200 cm^{-1} ($\Delta\varepsilon=-0.27$) and 19800 cm^{-1} ($\Delta\varepsilon=+1.25$). On the basis of a consideration similar to that mentioned above, the low energy band is assigned in each case to the $^1A\rightarrow{}^1B_a(C_2)$ transition and the high energy component to $^1A\rightarrow{}^1A+{}^1B_b(C_2)$. Worrell and Busch[7] studied some complexes containing a flexible quadridentate ligand, 1,8-diamino-3,6-dithiaoctane (dadt). Of these complexes, $(+)_{546}$-*sym-cis*-[Co(dadt)Cl$_2$]$^+$, $(+)_{546}$-*sym-cis*-[Co(dadt)ClH$_2$O]$^{2+}$ and $(+)_{546}$-*sym-cis*-[Co(dadt)(H$_2$O)$_2$]$^{3+}$, which have the two ligating NH_2 groups in *trans* positions and show a negative and a positive CD component from low energy side of the first absorption band region, were assigned to *Λ* absolute configurations, because in all three cases, the sign pattern is in agreement with that exhibited by the corresponding ethylenediamine and triethylenediamine complexes of *Λ* absolute configuration. The same argument is applied to the present system. The absolute configurations of $(-)_{589}$-*trans(N)*-[Co(aeta)$_2$]$^+$ and $(+)_{589}$-*trans(N)*-[Co(aetp)$_2$]$^+$ are assigned to *ΔΔΛ*-(*SS*) and *ΔΔΛ*-(*SS*) configurations, respectively, according to the sign of the $^1A+{}^1B_b(C_2)$ transition.

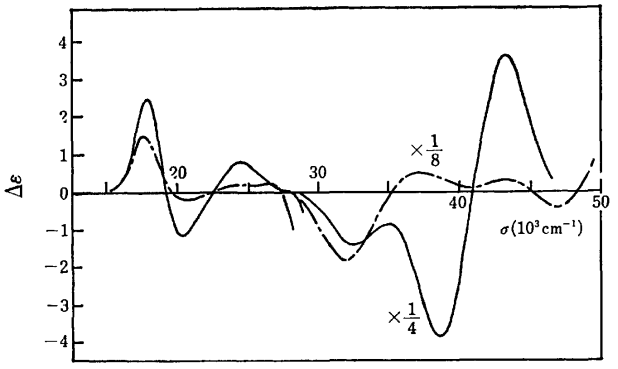

Fig. 7. CD spectra of *cisciscis* complexes: $(+)_{589}$-[Co(aeta)$_2$]$^+$ (——) and $(+)_{589}$-[Co(aetp)$_2$]$^+$ (·—·—·).

In the *cisciscis* isomers (Fig. 7), the parential arguments as above seem to have limited applicability because of the lowering of symmetry and the difficulty in the assignment of three components. However, the CD contribution of this geometrical isomer is mainly due to the configurational chirality, since the two chiral sulfur atoms form a meso combination ((*R*) and (*S*)). Therefore, the major CD component in the first absorption band region is related to the molecular framework; *cisciscis* isomers of both aeta and aetp $(+)_{589}$-complexes exhibit a strong positive and a negative band and can be assigned to *ΔΔΔ* configuration.

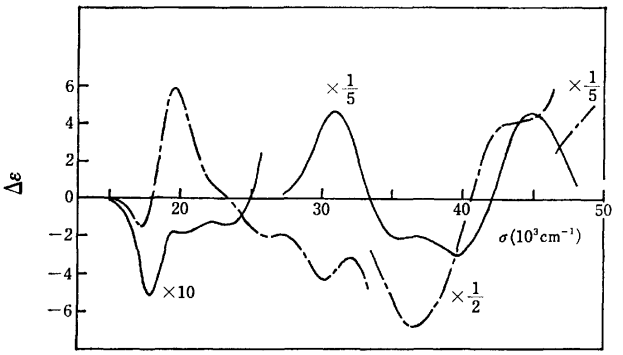

Fig. 8. CD spectra of *trans(S)* complexes: $(-)_{589}$-[Co(aeta)$_2$]$^+$ (——) and $(+)_{589}$-[Co(aetp)$_2$]$^+$ (·—·—·).

For the *trans(S)* isomers (Fig. 8), the aeta $(-)_{589}$-complex exhibits two weak CD components in the first absorption band region and a strong CD band in the thioether charge transfer band region, whereas the aetp $(+)_{589}$-complex shows a strong major CD band in the first absorption band region and a relatively weak band in the thioether charge transfer band region. These CD patterns cannot be related directly to their absolute configurations, because the *trans(S)* forms do not have CD contribution due to the skew pair of chelate rings according to the ring pairing method[31] but only the contribution due to the two chiral sulfur donor atoms.

In the low energy thioether charge transfer band region, medium or strong CD bands are generally observed for all isomers. The correlation of the charge transfer CD spectra of the *trans(N)* isomers between the aeta and aetp complexes is good as regards position and sign; the aeta *ΔΔΛ*-(*SS*)-complex has a (+) band, the aetp *ΔΔΛ*-(*SS*)-complex a (−) band.

References

1) Part I of this series: K. Yamanari, J. Hidaka, and Y. Shimura, *Bull. Chem. Soc. Jpn.*, **50**, 2299 (1977).
2) F. P. Dwyer and F. Lions, *J. Am. Chem. Soc.*, **72**, 1545 (1950).
3) F. P. Dwyer, F. Lions, and D. P. Mellor, *J. Am. Chem. Soc.*, **72**, 5037 (1950).
4) F. P. Dwyer, N. S. Gill, E. C. Gyarfas, and F. Lions, *J. Am. Chem. Soc.*, **74**, 4188 (1952).
5) F. P. Dwyer, N. S. Gill, E. C. Gyarfas, and F. Lions, *J. Am. Chem. Soc.*, **75**, 2443 (1953).
6) J. H. Worrell and D. H. Busch, *Inorg. Chem.*, **8**, 1563 (1969).

7) J. H. Worrell and D. H. Busch, *Inorg. Chem.*, **8**, 1572 (1969).
8) B. Bosnich, W. R. Kneen, and A. T. Phillip, *Inorg. Chem.*, **8**, 2567 (1969).
9) B. Bosnich and A. T. Phillip, *J. Chem. Soc., A*, **1970**, 264; R. J. Magee, W. Mazurek, M. J. O'Connor, and A.T. Phillip, *Aust. J. Chem.*, **27**, 1629 (1974).
10) K. Travis and D. H. Busch, *Inorg. Chem.*, **13**, 2591 (1974).
11) K. Hori, *Nippon Kagaku Zasshi*, **11**, 62 (1970).
12) J. Hidaka, S. Yamada, and Y. Shimura, *Chem. Lett.*, **1974**, 1487 .
13) J. Hidaka, S. Yamada, and Y. Shimura, Presented at the 23 th Symposium on Coordination Chemistry of Japan, Fukuoka, October, 1973; Abstract 2B14, p. 163.
14) G. H. Searle and E. Larsen, *Acta Chem. Scand.*, **A30**, 143 (1976).
15) H. Kanamori, T. Sudani, and K. Kawai, *Bull. Chem. Soc. Jpn.*, **49**, 2739 (1976).
16) K. Hori, *Bull. Chem. Soc. Jpn.*, **49**, 569 (1977).
17) K. Yamanari, J. Hidaka, and Y. Shimura, *Bull. Chem. Soc. Jpn.*, **46**, 3724 (1973).
18) M. Mori, M. Shibata, E. Kyuno, and F. Murayama, *Bull. Chem. Soc. Jpn.*, **35**, 75 (1962).
19) J. Hidaka, Y. Shimura, and R. Tsuchida, *Bull. Chem. Soc. Jpn.*, **35**, 567 (1962).
20) D. W. Cooke, *Inorg. Chem.*, **5**, 1141 (1966).
21) K. Okamoto, J. Hidaka, and Y. Shimura, *Bull. Chem. Soc. Jpn.*, **44**, 1601 (1971).
22) P. D. Meester and D. J. Hodgson, *J. Chem. Soc., Dalton Trans.*, **1976**, 618.
23) H. Yamatera, *Bull. Chem. Soc. Jpn.*, **31**, 95 (1958).
24) A. A. Bothner-By and C. Naar-Colin, *J. Am. Chem. Soc.*, **80**, 1728 (1958).
25) E. A. Berends and J. G. Brushmiller, *Inorg. Nucl. Chem. Lett.*, **6**, 531 (1970).
26) E. A. Berends and J. G. Brushmiller, *Inorg. Nucl. Chem. Lett.*, **6**, 847 (1970).
27) L. G. Stadtherr and J. G. Brushmiller, *Inorg. Nucl. Chem. Lett.*, **6**, 907 (1970).
28) K. Okamoto, J. Hidaka, and Y. Shimura, *Bull. Chem. Soc. Jpn.*, **46**, 475 (1973).
29) Absolute configurations of the complexes are as designated by the IUPAC rule: *Inorg. Chem.*, **9**, 1 (1970).
30) K. Igi and B. E. Douglas, *Inorg. Nucl. Chem. Lett.*, **10**, 587 (1974).
31) J. I. Legg and B. E. Douglas, *J. Am. Chem. Soc.*, **88**, 2697 (1966).

One-dimensional System of Square-planar Bis(1,2-dicyanovinylene-1,2-dithiolato)metal Complexes. I. The Crystal Structure of $[(C_4H_9)_4N]_2[Ni(mnt)_2]$ and $[(C_2H_5)_4N][Ni(mnt)_2]$

Akiko KOBAYASHI and Yukiyoshi SASAKI

Department of Chemistry, Faculty of Science, The University of Tokyo, The Research Centre for Spectrochemistry, Hongo, Tokyo 113

(Received March 19, 1977)

X-Ray crystal structure analyses of $[(C_4H_9)_4N]_2[Ni(mnt)_2]$ (I) and $[(C_2H_5)_4N][Ni(mnt)_2]$ (II) {mnt: 1,2-dicyanovinylene-1,2-dithiolato $C_4N_2S_2^{2-}$} have been carried out from the viewpoint of one-dimensional system. Crystals of (I) belong to triclinic system: $a=12.360(6)$, $b=11.138(12)$, $c=9.833(9)$ Å, $\alpha=118.43(9)$, $\beta=92.05(6)$, $\gamma=91.91(6)°$, space group $P\bar{1}$ with $Z=1$. The compound (II) forms monoclinic crystals, $P2_1/a$: $a=20.018(18)$, $b=16.079(9)$, $c=7.118(6)$ Å, $\beta=110.43(6)°$, $Z=4$. Both structures, solved by the heavy-atom method, have been refined anisotropically by least-squares procedure to $R=0.049$ and 0.050 for (I) and (II), respectively. The bond distances of diamagnetic $Ni(mnt)_2^{2-}$ anion and paramagnetic $Ni(mnt)_2^{1-}$ anion are compared. A columnar structure was found in the structure of (II). The $Ni(mnt)_2^{1-}$ ions form a diadic unit, that is a repeating unit of two anions, within the columns. The electrical conductivity data are measured along the direction parallel to the $Ni(mnt)_2^{1-}$ stacks in the temperature range from room temperature to 373 K. This compound behaves as a semiconductor in this temperature range.

Recent studies of high conductive platinum complex of $K_2Pt(CN)_4Br_{0.3}\cdot xH_2O$ and TCNQ salts[1] have revealed their metallic behavior. Their magnetic, electrical and optical properties are also originated from one-dimensional interactions associated with a columnar crystallographic structure.[1] Like TCNQ, bis(1,2-dicyanovinylene-1,2-dithiolato)metal complexes are known in some cases to form compounds with high electrical conductivities.[2,3] Furthermore these dithiolene complexes form a series of stable compounds with the same central metal ion in different oxidation states *e.g.*, in the Ni, Pd, Pt, the 0, −1, −2 charged complexes are well known.[4]

We report here X-ray diffraction studies on single crystals of tetrabutylammonium salt of diamagnetic $Ni(mnt)_2^{2-}$ and tetraethylammonium salt of paramagnetic $Ni(mnt)_2^{1-}$. Electrical conductivity measurements were also performed on single crystals of $[(Et)_4N][Ni(mnt)_2]$ by the use of the four-probe methods. We are interested in the relationship between the crystal structures and electrical properties of one-dimensional system.

Experimental

Data Collections and Structure Analyses. The compounds $[(n\text{-}Bu)_4N]_2[Ni(mnt)_2]$ (I) and $[(Et)_4N][Ni(mnt)_2]$ (II) were prepared by the published method.[4] The tetrabutylammonium salt and tetraethylammonium salt were chosen because we could obtain suitable single crystals for experiments. The red crystals of (I) and black crystals of (II) were obtained from the original product through recrystallization by slow evaporation from acetone solution. For the purpose of the X-ray diffraction work, a specimen $0.25\times0.20\times0.37$ mm was used for (I) and $0.075\times0.125\times0.38$ mm for (II). The intensity data set were collected with monochromatized Mo$K\alpha$ radiation by the ω-2θ scan technique out to $2\theta=60°$. Reflections were scanned at a rate of 2 ° minute in 2θ. Background counts of 10 s were taken at each end of the scan range. Independent 3559 significant reflections for which $|F|\geqq3\sigma(F)$ were obtained for (I) and 2635 for (II), respectively. The data were corrected for Lorentz and polarization effects. No corrections were made for absorption.

The crystal data are as follows:

$[(n\text{-}Bu)_4N]_2[Ni(mnt)_2]$ (I)	$[(Et)_4N][Ni(mnt)_2]$ (II)
triclinic $P\bar{1}$	monoclinic $P2_1/a$
$a=12.360(6)$ Å	$a=20.018(18)$ Å
$b=11.138(12)$	$b=16.079(9)$
$c=9.833(9)$	$c=7.118(6)$
$\alpha=118.43(9)°$	$\beta=110.43(6)°$
$\beta=92.05(6)$	$V=2147.0$ Å^3
$\gamma=91.91(6)$	$Z=4$
$V=1187.7$ Å^3	$d_m=1.24$ g/cm^3
$Z=1$	$d_c=1.235$ g/cm^3
$d_m=1.07$ g/cm^3	$\mu=13.23$ cm^{-1}
$d_c=1.074$ g/cm^3	
$\mu=6.29$ cm^{-1}	

Since Wilson's statistics indicated the presence of a center of symmetry, the space group $P\bar{1}$ was assumed for (I). For solution and refinement of the structure usual heavy-atom methods were employed. The atomic parameters were refined by the block-diagonal least-squares method, using anisotropic temperature factors for all the nonhydrogen atoms and isotropic ones for hydrogen atoms. The effects of the anomalous dispersion of Ni and S atoms were included in the calculation. Final reliability factors are: (I), $R=0.049$, (II), $R=0.050$. The positional and thermal parameters of all atoms are presented in Tables 1 and 2.

The calculations were performed on a HITAC 8700/8800 computer at the Computer Center of the University of Tokyo using a local version of UNICS.[5] The atomic scattering factors and the values of $\Delta f'$ and $\Delta f''$ were taken from the International Tables for X-Ray Crystallography.[6] The weighting scheme used were: (I), $w=1$ for $|F_o|\geqq4.25$ (F_o: absolute scale), $w=0.0$ otherwise; (II), $w=1$ for $|F_o|\geqq15.15$, $w=0.2$ otherwise. The F_o-F_c tables are kept at the office of this Bulletin as Document No. 7726 and 7727.

Conductivity Measurements. $[(Et)_4N][Ni(mnt)_2]$ single crystals are black needles with long axis parallel to the crystallographic c axis, giving good optical reflections. Comparatively high electrical conductivity is expected for $[(Et)_4N][Ni(mnt)_2]$ single crystals because of its columnar structure:

TABLE 1. FRACTIONAL COORDINATES AND THERMAL PARAMETERS ($\times 10^4$) FOR $[(C_4H_9)_4N]_2[Ni(mnt)_2]$

Thermal parameters are for the expression $\exp\{-(h^2B_{11}+k^2B_{22}+l^2B_{33}+2hkB_{12}+2hlB_{13}+2klB_{23})\}$.

a) Nonhydrogen atoms.

Atom	X	Y	Z	B_{11}	B_{22}	B_{33}	B_{12}	B_{13}	B_{23}
Ni	0	0	0	76(1)	95(1)	127(1)	−1(1)	−5(1)	55(1)
S(1)	−1370(1)	−417(1)	1073(1)	93(1)	108(1)	186(2)	0(1)	11(1)	75(1)
S(2)	−283(1)	2168(1)	1079(2)	114(1)	102(1)	200(2)	4(1)	37(1)	69(1)
N(1)	−3662(3)	1270(5)	3458(5)	91(4)	204(7)	270(9)	4(1)	16(5)	123(7)
N(2)	−2241(5)	4628(5)	3532(7)	253(8)	172(7)	377(13)	95(6)	162(8)	149(8)
N(3)	2787(3)	855(3)	3761(4)	66(3)	117(4)	141(5)	0(3)	−10(3)	69(4)
C(1)	−1914(3)	1166(4)	2066(5)	78(3)	113(5)	137(6)	3(3)	−2(4)	69(5)
C(2)	−1434(4)	2284(4)	2068(5)	101(4)	111(5)	138(7)	12(4)	12(4)	63(5)
C(3)	−2884(4)	1241(4)	2844(5)	83(4)	133(6)	179(8)	3(4)	−11(4)	81(5)
C(4)	−1881(5)	3597(5)	2896(6)	137(5)	146(6)	230(10)	30(5)	59(6)	111(7)
C(5)	2576(3)	1931(4)	3246(5)	79(3)	126(5)	143(6)	15(3)	−2(4)	79(5)
C(6)	3521(4)	2946(4)	3544(5)	95(4)	121(5)	164(7)	5(4)	8(4)	78(5)
C(7)	3232(5)	3817(5)	2781(6)	149(6)	169(7)	200(9)	−14(5)	−13(6)	117(7)
C(8)	4044(6)	5018(6)	3232(8)	180(7)	168(8)	334(14)	−34(6)	−8(8)	157(9)
C(9)	3720(3)	−10(4)	2918(5)	70(3)	126(5)	177(7)	20(3)	7(4)	75(5)
C(10)	3594(4)	−679(5)	1149(5)	112(5)	167(7)	170(8)	42(5)	27(5)	67(6)
C(11)	4468(4)	−1722(5)	417(6)	109(5)	168(7)	238(10)	21(5)	31(6)	70(7)
C(12)	4275(6)	−2992(6)	547(8)	164(7)	165(8)	394(17)	34(6)	46(9)	112(10)
C(13)	1726(3)	−23(4)	3375(5)	65(3)	137(5)	158(7)	−11(3)	−12(4)	74(5)
C(14)	1764(4)	−1196(5)	3745(7)	97(5)	190(8)	324(12)	−38(5)	−56(6)	173(8)
C(15)	765(4)	−2074(6)	3240(7)	104(5)	205(9)	350(14)	−38(5)	−30(7)	168(9)
C(16)	739(5)	−3261(6)	3580(7)	123(6)	186(8)	330(13)	−33(5)	−13(7)	144(9)
C(17)	3121(3)	1534(4)	5492(5)	81(3)	132(5)	130(6)	−8(3)	−19(4)	70(5)
C(18)	2271(4)	2358(4)	6556(5)	92(4)	138(6)	139(7)	−6(4)	−11(4)	66(5)
C(19)	2780(4)	3227(5)	8204(5)	124(5)	152(6)	148(7)	−23(4)	−17(5)	64(6)
C(20)	1953(5)	4082(5)	9315(6)	161(6)	175(8)	161(8)	−11(6)	−5(6)	68(7)

b) Hydrogen atoms.

Fractional coordinates $\times 10^3$; Isotropic thermal parameters $\times 10$.

Atom	X	Y	Z	B	Atom	X	Y	Z	B
H(1)	198(4)	241(5)	380(5)	53(12)	H(19)	380(4)	219(4)	561(5)	47(12)
H(2)	237(4)	145(4)	214(5)	48(12)	H(20)	335(4)	79(5)	575(5)	49(12)
H(3)	422(4)	244(5)	332(5)	55(13)	H(21)	178(4)	179(5)	662(5)	53(12)
H(4)	360(4)	359(5)	462(5)	50(12)	H(22)	200(4)	301(5)	624(5)	54(12)
H(5)	252(4)	405(5)	301(6)	65(14)	H(23)	339(4)	380(5)	818(5)	53(12)
H(6)	319(4)	330(5)	173(6)	66(14)	H(24)	302(4)	262(5)	864(6)	64(14)
H(7)	378(4)	−64(4)	337(5)	45(11)	H(25)	473(4)	476(5)	321(5)	59(13)
H(8)	441(4)	75(5)	338(5)	50(12)	H(26)	405(4)	573(5)	443(6)	68(14)
H(9)	362(4)	16(5)	93(6)	60(13)	H(27)	417(4)	540(5)	246(6)	67(14)
H(10)	281(4)	−108(5)	92(6)	59(13)	H(28)	43(4)	−262(5)	459(6)	69(14)
H(11)	527(4)	−125(5)	80(6)	61(13)	H(29)	141(4)	−360(5)	342(6)	68(14)
H(12)	441(4)	−214(5)	−84(6)	66(14)	H(30)	2(4)	−400(5)	283(6)	67(14)
H(13)	158(4)	−40(4)	222(5)	45(11)	H(31)	138(4)	359(5)	941(5)	58(13)
H(14)	120(4)	58(5)	411(5)	50(12)	H(32)	161(4)	464(5)	907(5)	58(13)
H(15)	176(4)	−63(5)	499(6)	70(15)	H(33)	239(4)	463(5)	1023(6)	62(13)
H(16)	240(4)	−161(5)	374(6)	68(14)	H(34)	481(4)	−361(5)	−19(6)	67(14)
H(17)	59(4)	−245(5)	206(6)	68(14)	H(35)	340(4)	−340(5)	19(6)	68(14)
H(18)	11(4)	−147(5)	376(6)	67(14)	H(36)	440(4)	−279(5)	161(6)	69(14)

the details of the crystal structure will be mentioned later. Four-probe resistance measurements were made on single crystals (3—6 mm long and 0.45—0.5 mm in diameter) along the needle axis paralled to the $Ni(mnt)_2^{1-}$ stacks. The crystals were attached by four 0.025 mm gold wires on a Teflon sample holder. Electrical contact was made by wetting the gold wires with silver-paste paint. The resistivity data ($R=\sigma^{-1}$) are presented in Fig. 1a, where $\ln R/R_0$ is plotted as a function of T^{-1} in the limited range from room temperature to 373 K which shows straight-line behavior. Thus this compound is semiconductive. From this slope, one obtains the value of 0.35 eV for the activation energy. The room temperature resistivity parallel to $Ni(mnt)_2^{1-}$ stacks is $(3.5\pm1.2)\times10^5\ \Omega$ cm. Another type of $[(Et)_4N][Ni(mnt)_2]$ crystals (parallolepiped pillar) show different kinds of resistivity behavior in the temperature

TABLE 2. FRACTIONAL COORDINATES AND THERMAL PARAMETERS ($\times 10^4$) FOR $[(C_2H_5)_4N][Ni(mnt)_2]$

Thermal parameters are for the expression $\exp\{-(h^2B_{11}+k^2B_{22}+l^2B_{33}+2hkB_{12}+2hlB_{13}+2klB_{23})\}$.

a) Nonhydrogen atoms.

Atom	X	Y	Z	B_{11}	B_{22}	B_{33}	B_{12}	B_{13}	B_{23}
Ni	432(1)	496(1)	2852(2)	22(0)	32(0)	165(2)	2(0)	25(1)	3(1)
S(1)	1427(1)	1157(2)	3814(4)	22(1)	37(1)	271(7)	2(1)	23(2)	8(2)
S(2)	−174(1)	1619(2)	1871(4)	22(1)	35(1)	232(6)	2(1)	27(2)	5(2)
S(3)	1053(1)	−607(2)	3938(4)	25(1)	39(1)	276(7)	4(1)	21(2)	12(3)
S(4)	−553(1)	−186(2)	1908(4)	23(1)	35(1)	216(6)	1(1)	22(2)	6(2)
N(1)	2155(5)	3282(6)	4025(17)	36(4)	55(5)	562(43)	−12(4)	33(10)	5(12)
N(2)	86(5)	3887(6)	1355(15)	34(3)	42(4)	495(36)	5(3)	54(9)	24(11)
N(3)	831(6)	−2895(6)	4348(16)	60(5)	41(5)	440(36)	17(4)	53(11)	20(11)
N(4)	−1235(5)	−2348(6)	1693(16)	41(4)	38(4)	474(37)	−9(3)	32(9)	−1(11)
N(5)	1866(4)	5083(5)	9373(11)	20(2)	33(3)	221(20)	−3(2)	24(6)	7(7)
C(1)	1177(5)	2179(6)	3225(14)	24(3)	33(4)	226(26)	−1(3)	21(7)	9(9)
C(2)	471(5)	2378(6)	2373(14)	24(3)	30(4)	234(27)	0(3)	37(7)	10(8)
C(3)	1721(5)	2792(7)	3677(17)	29(3)	39(5)	339(34)	4(3)	34(9)	21(11)
C(4)	253(5)	3220(7)	1801(16)	24(3)	45(5)	293(31)	−3(3)	36(8)	2(10)
C(5)	427(5)	−1375(6)	3448(14)	33(3)	32(4)	231(28)	4(3)	34(8)	−2(8)
C(6)	−283(5)	−1199(6)	2534(13)	29(3)	30(4)	160(23)	2(3)	23(7)	1(8)
C(7)	667(5)	−2231(7)	3957(16)	34(4)	44(5)	281(31)	5(4)	34(9)	11(10)
C(8)	−818(5)	−1840(6)	2064(15)	33(4)	36(5)	226(27)	5(3)	20(8)	10(9)
C(9)	1621(5)	5910(6)	8242(16)	31(4)	33(5)	308(32)	0(3)	31(9)	15(10)
C(10)	2167(7)	6610(7)	8844(22)	46(5)	32(5)	602(55)	−13(4)	46(3)	9(14)
C(11)	1224(5)	4515(6)	8874(16)	24(3)	38(4)	342(32)	−7(3)	30(8)	22(11)
C(12)	866(6)	4312(8)	6597(17)	37(4)	55(6)	298(34)	−8(4)	3(9)	−12(12)
C(13)	2434(5)	4716(7)	8579(16)	26(3)	47(6)	297(30)	1(3)	43(8)	3(10)
C(14)	2712(6)	3869(7)	9399(20)	30(4)	43(5)	502(46)	7(4)	48(11)	4(13)
C(15)	2184(5)	5191(7)	11619(14)	31(3)	60(6)	161(24)	−1(4)	20(7)	2(10)
C(16)	1696(7)	5622(10)	12463(18)	50(5)	107(10)	270(34)	1(6)	62(11)	−32(16)

b) Hydrogen atoms.

Fractional coordinates $\times 10^3$; isotropic thermal parameters $\times 10$.

Atom	X	Y	Z	B	Atom	X	Y	Z	B
H(1)	124(6)	603(7)	866(16)	49(29)	H(11)	220(6)	670(8)	1037(18)	68(35)
H(2)	145(5)	576(6)	655(15)	38(26)	H(12)	43(5)	402(7)	610(15)	45(28)
H(3)	85(5)	479(7)	942(15)	43(27)	H(13)	74(5)	482(6)	572(14)	37(26)
H(4)	137(5)	405(7)	996(15)	44(28)	H(14)	116(5)	392(7)	617(16)	45(28)
H(5)	282(5)	509(7)	878(15)	42(27)	H(15)	284(6)	387(8)	1093(17)	60(32)
H(6)	221(5)	470(6)	698(14)	29(23)	H(16)	309(5)	368(7)	861(16)	45(28)
H(7)	262(5)	560(6)	1189(13)	25(22)	H(17)	232(6)	340(7)	875(17)	57(31)
H(8)	233(5)	460(6)	1208(13)	28(23)	H(18)	133(6)	535(8)	1253(18)	63(34)
H(9)	201(6)	706(7)	778(16)	51(30)	H(19)	151(6)	619(7)	1167(16)	49(29)
H(10)	260(6)	641(8)	887(18)	66(34)	H(20)	197(7)	581(8)	1377(19)	80(39)

range of 323—363 K (Fig. 1b) and the resistivity of the room temperature is $R=(4.9\pm1.5)\times10^7\ \Omega$ cm. From the X-ray check both crystals are crystallographically identical but the latter data shows that the crystallization is bad. The accuracy of the absolute value of the conductivity is evidently limited by the crystalline imperfection.[7] It seems likely that the imperfections involved are microcracks or other large scale defects which limit the effective cross-sectional area of the samples.

Description of the Structure and Discussion

[(n-Bu)$_4$N]$_2$[Ni(mnt)$_2$]. Molecular geometry of the $Ni(mnt)_2^{2-}$ anion is shown in Fig. 2a. A projection of the structure as viewed along the c axis are presented in Fig. 3. This Ni^{2+} complex is isomorphous with Co^{2+} [8] and Cu^{2+} [9] complexes. The planar diamagnetic $Ni(mnt)_2^{2-}$ ion has a center of symmetry at the nickel atom and the two tetra-*n*-butylammonium ions are related to each other by a center of symmetry. The bond lengths and angles of the anion are listed in Table 3a. The nickel atoms are very well separated with the closest distance of approach in the shortest axial length of 9.84 Å. The anion is closely planar with the sulfur atoms in a square arrangement around the nickel atom and Ni, S(1), S(2), C(1), and C(2) make the five-membered ring. The distance of the various atoms from the least-squares plane are listed in Table 4a. The average Ni–S bond length is 2.175(1) Å, S–C 1.730(5), and C–C 1.410(7), respectively. The bond distance of

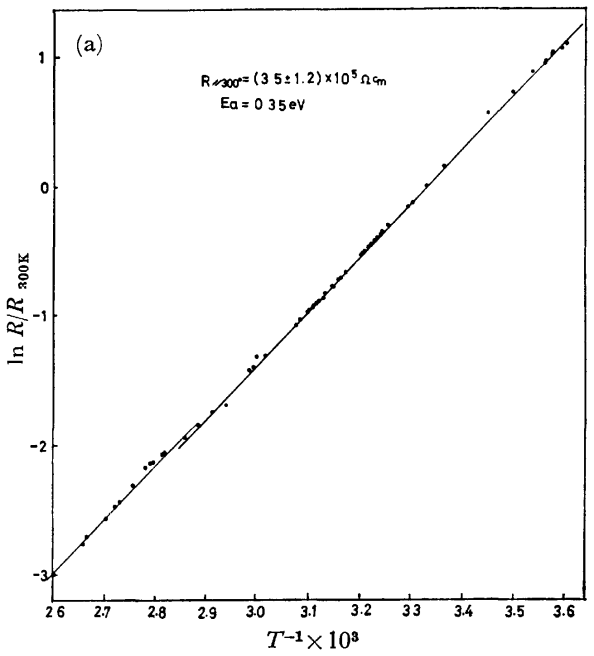

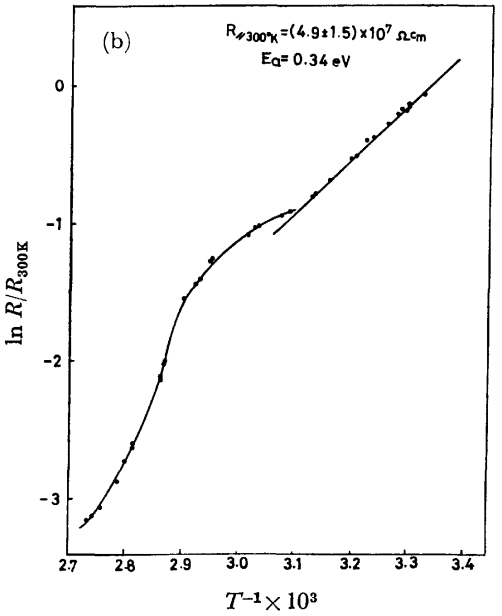

Fig. 1. Temperature dependence of electrical resistivity of $[(Et)_4N][Ni(mnt)_2]$, showing resistivity parallel to the anion stacks (crystallographic c axis).

C–C agrees well with those found in the conjugated C–C system like the benzene molecule. The S–Ni–S bond angle within the five-membered ring is found to be 92°. The bond lengths and angles of the cation is listed in Table 5a. Three of the butyl chains adopt the *trans* conformation, but one (C(9)—C(12)) adopts a *gauche* conformation. The dihedral angles for all the chains are listed in Table 6. The dihedral angle for the *gauche* chain is 72.4°.

$[(Et)_4N][Ni(mnt)_2]$. Molecular geometry of the anion is shown in Fig. 2b. A projection of the structure along the c axis is shown in Fig. 4. The anions are stacked in columns whose axes are parallel to c and

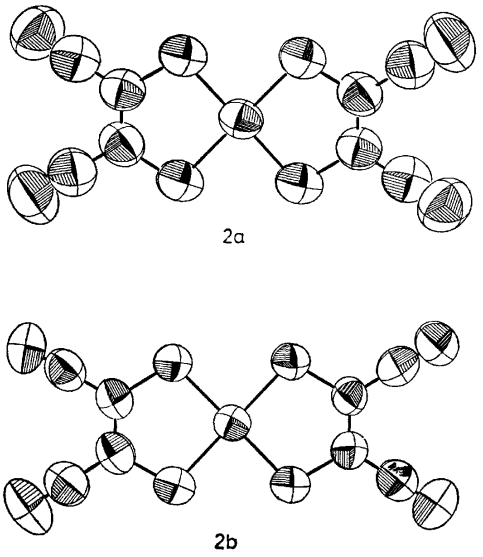

Fig. 2. Molecular geometry of the $Ni(mnt)_2^{2-}$ (2a) and $Ni(mnt)_2^{-1}$ (2b) anions. The 50% probability ellipsoids are shown.

Table 3. Bond lengths and angles of the anions

a) $Ni(mnt)_2^{2-}$			
Ni–S(1)	2.176(1)Å	C(1)–C(3)	1.428(6)Å
Ni–S(2)	2.173(1)	C(2)–C(4)	1.435(6)
S(1)–C(1)	1.732(4)	C(3)–N(1)	1.147(7)
S(2)–C(2)	1.725(5)	C(4)–N(2)	1.130(7)
C(1)–C(2)	1.360(7)		
S(1)–Ni–S(2)	92.2(1)°	C(2)–C(1)–C(3)	121.9(4)°
Ni–S(1)–C(1)	103.1(1)	C(1)–C(2)–C(4)	120.4(4)
Ni–S(2)–C(2)	103.0(2)	C(1)–C(3)–N(1)	178.4(5)
S(1)–C(1)–C(2)	120.3(3)	C(2)–C(4)–N(2)	179.2(5)
S(2)–C(2)–C(1)	121.4(3)		
b) $Ni(mnt)_2^{1-}$			
Ni–S(1)	2.147(3)Å	C(5)–C(6)	1.370(12)Å
Ni–S(2)	2.151(3)	C(1)–C(3)	1.420(14)
Ni–S(3)	2.148(3)	C(2)–C(4)	1.437(14)
Ni–S(4)	2.149(3)	C(5)–C(7)	1.462(14)
S(1)–C(1)	1.727(10)	C(6)–C(8)	1.439(13)
S(2)–C(2)	1.722(9)	C(3)–N(1)	1.133(14)
S(3)–C(5)	1.705(10)	C(4)–N(2)	1.135(14)
S(4)–C(6)	1.724(9)	C(7)–N(3)	1.124(14)
C(1)–C(2)	1.367(12)	C(8)–N(4)	1.131(14)
S(1)–Ni–S(2)	92.5(1)°	S(4)–C(6)–C(5)	119.9(7)°
S(3)–Ni–S(4)	92.5(1)	C(3)–C(1)–C(2)	122.1(9)
Ni–S(1)–C(1)	103.6(3)	C(1)–C(2)–C(4)	120.7(8)
Ni–S(2)–C(2)	103.3(3)	C(6)–C(5)–C(7)	120.6(9)
Ni–S(3)–C(5)	103.5(3)	C(5)–C(6)–C(8)	121.8(8)
Ni–S(4)–C(6)	103.3(3)	C(1)–C(3)–N(1)	179.5(11)
S(1)–C(1)–C(2)	119.8(7)	C(2)–C(4)–N(2)	179.5(11)
S(2)–C(2)–C(1)	120.7(7)	C(5)–C(7)–N(3)	177.9(11)
S(3)–C(5)–C(6)	120.9(7)	C(6)–C(8)–N(4)	179.5(11)

those columns are surrounded by cations. This arrangement is very different from that found in $[R_4N]_2[M(mnt)_2]$, where the metal atoms are separated by about 10 Å. The dimensions of the anion are listed in

TABLE 4. LEAST-SQUARES PLANE FOR $Ni(mnt)_2^{n-}$ ANIONS AND DEVIATIONS FROM THE PLANES

a) $Ni(mnt)_2^{2-}$

Plane equation:

$0.56445X+(-0.24625)Y+(0.78788)Z=0$

Atom	Deviation (Å)	Atom	Deviation (Å)
Ni	0.0	C(3)	−0.0882
S(1)	0.0306	C(4)	−0.0456
S(2)	0.0284	N(1)	−0.1431
C(1)	−0.0172	N(2)	−0.0882
C(2)	−0.0121		

b) $Ni(mnt)_2^{1-}$

Plane equation:

$0.41049X+(-0.13374)Y+(-0.90201)Z+1.76906=0$

Atom	Deviation (Å)	Atom	Deviation (Å)
Ni	0.0107	N(1)	0.0020
S(1)	0.0093	N(2)	0.0506
S(2)	−0.0387	C(7)	0.0124
S(3)	−0.0067	C(8)	0.0403
S(4)	0.0122	N(3)	0.0147
C(3)	−0.0044	N(4)	0.0678
C(4)	0.0176	C(1)	−0.0014
C(5)	−0.0102	C(2)	−0.0244
C(6)	0.0115		

TABLE 6. DIHEDRAL ANGLES FOR THE FOUR BUTYL CHAINS IN $(C_4H_9)_4N^+$ CATION

Plane (1)	Plane (2)	Dihedral angles
C(5)–C(6)–C(7)	C(6)–C(7)–C(8)	9.45°
C(9)–C(10)–C(11)	C(10)–C(11)–C(12)	72.41
C(13)–C(14)–C(15)	C(14)–C(15)–C(16)	0.41
C(17)–C(18)–C(19)	C(18)–C(19)–C(20)	0.38

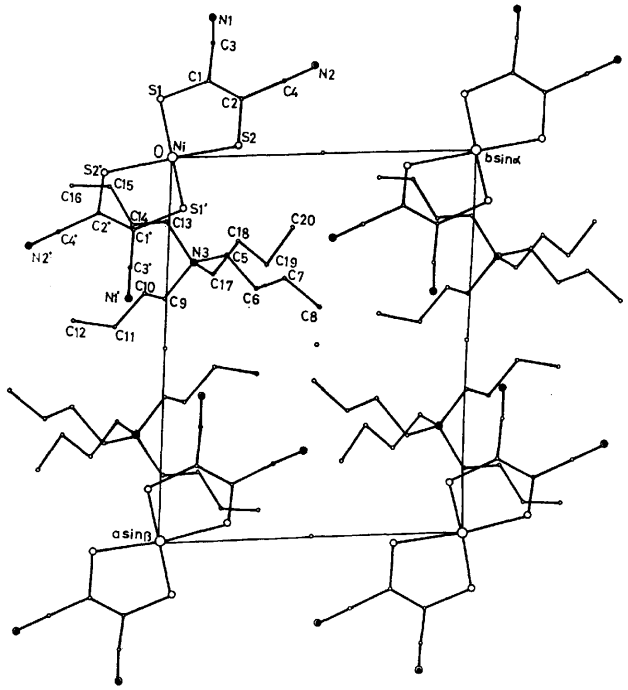

Fig. 3. A projection of the structure of $[(n\text{-}Bu)_4N]_2[Ni(mnt)_2]$ as viewed along the c axis.

Table 3b, and compared with those found for the $Ni(mnt)_2^{2-}$ anion in the $[(n\text{-}Bu)_4N]_2[Ni(mnt)_2]$. The paramagnetic anion is approximately planar, but deviations from planarity are considerably smaller than those in the $Ni(mnt)_2^{2-}$ ion. One of the cyanide group is bent a little out of the plane. The deviations of the atoms from the least-squares plane are listed in Table 4b. The average Ni–S bond length is 2.149 Å, S–C 1.725 Å, and C–C (in the five-membered ring) 1.369 Å. The S–Ni–S bond angle is 92.5°. Table 7 shows comparison of the bond lengths of $Ni(mnt)_2^{n-}$ ($n=1$, 2) in our structure analyses and those found in other $M(mnt)_2^{n-}$ structures. In $[(Et)_4N][Ni(mnt)_2]$ bond distances of the ligand agree well with our result of $[(n\text{-}Bu)_4N]_2[Ni(mnt)_2]$ and $[TMPD]_2[Ni(mnt)_2]$[11] by less than two standard deviations except Ni–S. Namely, Ni–S in (I)

TABLE 5. BOND LENGTHS AND ANGLES OF THE CATIONS

a) $(C_4H_9)_4N^+$

N(3)–C(5)	1.533(7)Å	N(3)–C(9)	1.525(5)Å	N(3)–C(5)–C(6)	115.4(4)°	C(5)–C(6)–C(7)	108.7(4)°
C(5)–C(6)	1.516(6)	C(9)–C(10)	1.531(6)	N(3)–C(9)–C(10)	114.8(4)	C(6)–C(7)–C(8)	112.7(5)
C(6)–C(7)	1.526(9)	C(10)–C(11)	1.542(7)	N(3)–C(13)–C(14)	114.8(4)	C(9)–C(10)–C(11)	110.2(4)
C(7)–C(8)	1.519(8)	C(11)–C(12)	1.491(10)	N(3)–C(17)–C(18)	115.3(4)	C(10)–C(11)–C(12)	113.3(5)
N(3)–C(13)	1.532(5)	N(3)–C(17)	1.530(5)	C(5)–N(3)–C(9)	111.0(4)	C(13)–C(14)–C(15)	112.9(5)
C(13)–C(14)	1.515(9)	C(17)–C(18)	1.506(6)	C(9)–N(3)–C(13)	111.2(3)	C(14)–C(15)–C(16)	116.0(6)
C(14)–C(15)	1.464(7)	C(18)–C(19)	1.533(6)	C(13)–N(3)–C(17)	111.7(3)	C(17)–C(18)–C(19)	109.9(4)
C(15)–C(16)	1.509(11)	C(19)–C(20)	1.516(7)	C(17)–N(3)–C(5)	110.9(3)	C(18)–C(19)–C(20)	111.7(4)
				C(5)–N(3)–C(13)	105.8(3)		
				C(9)–N(3)–C(17)	106.4(3)		

b) $(C_2H_5)_4N^+$

N(5)–C(9)	1.543(12)Å	C(9)–C(10)	1.522(15)Å	N(5)–C(9)–C(10)	115.1(8)°	C(9)–N(5)–C(11)	108.0(6)°
N(5)–C(11)	1.514(12)	C(11)–C(12)	1.561(15)	N(5)–C(11)–C(12)	114.5(9)	C(9)–N(5)–C(13)	106.1(8)
N(5)–C(13)	1.553(14)	C(13)–C(14)	1.510(15)	N(5)–C(13)–C(14)	114.9(9)	C(9)–N(5)–C(15)	113.2(7)
N(5)–C(15)	1.510(11)	C(15)–C(16)	1.485(19)	N(5)–C(15)–C(16)	112.8(9)	C(11)–N(5)–C(13)	110.7(7)
						C(11)–N(5)–C(15)	109.1(7)
						C(13)–N(5)–C(15)	109.7(7)

TABLE 7. COMPARISON OF BOND DISTANCES FOUND FOR $M(mnt)_2^{n-}$ ANIONS

Bond	$[(n\text{-}Bu)_4N]_2[Ni(mnt)_2]$	$[(Et)_4N]^{*g)}[Ni(mnt)_2]$	$[TMPD]_2[Ni(mnt)_2]^{a)}$	$[(Me)_4N]_2[Ni(mnt)_2]^{b)}$	$[(n\text{-}Bu)_4N]_2[Cu(mnt)_2]^{c)}$	$[(Et)_4N]_2[Cu(mnt)_2]^{d)}$	$[(n\text{-}Bu)_4N]^*[Cu(mnt)_2]^{e)}$	$[(n\text{-}Bu)_4N]_2[Co(mnt)_2]^{f)}$
M–S(1)	2.176(1) Å	2.148(2)	2.173(2)	2.16(1)	2.286(1)	2.264(1)	2.174(4)	2.163(3)
M–S(2)	2.173(1)	2.150(2)	2.179(2)	2.16(1)	2.265(1)	2.271(1)	2.158(5)	2.159(3)
S(1)–C(1)	1.732(4)	1.716(7)	1.731(5)	1.75(1)	1.727(3)	1.725(2)	1.73(1)	1.731(7)
S(2)–C(2)	1.725(5)	1.723(6)	1.727(5)	1.75(1)	1.729(3)	1.729(2)	1.70(1)	1.715(7)
C(1)–C(2)	1.360(7)	1.369(9)	1.378(6)	1.30(2)	1.359(4)	1.365(3)	1.32(2)	1.34(1)
C(1)–C(3)	1.428(6)	1.441(10)	1.413(7)	1.44(1)	1.434(4)	1.432(3)	1.42(2)	1.40(1)
C(2)–C(4)	1.435(6)	1.438(10)	1.427(6)	1.42(1)	1.430(4)	1.433(3)	1.43(2)	1.40(1)
C(3)–N(1)	1.147(7)	1.129(10)	1.148(6)	1.13(2)	1.143(4)	1.140(3)	1.17(2)	1.15(1)
C(4)–N(2)	1.130(7)	1.133(10)	1.137(6)	1.13(2)	1.147(4)	1.146(3)	1.12(2)	1.16(1)

a) Reference 11. b) Reference 10. c) Reference 9b. d) Reference 12. e) Reference 8. f) Reference 9a.
g) The asterisk indicates the existence of the columnar structure of $M(mnt)_2^{n-}$ anions.

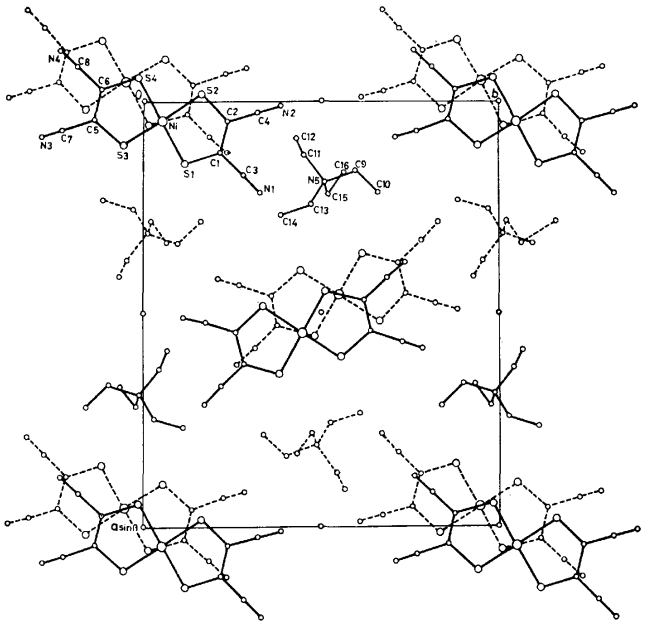

Fig. 4. A projection of the structure of $[(Et)_4N][Ni(mnt)_2]$ as viewed along the c axis.

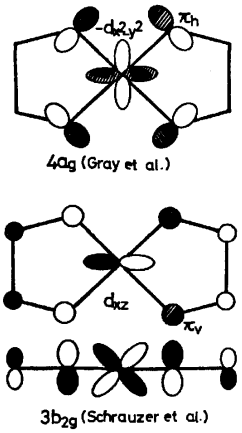

Fig. 5. Schematic drawing of highest occupied orbitals of $Ni(mnt)_2^{n-}$ ($n=1, 2$). The π_v is the ligand π-MO vertical to the plane of the molecule and π_h is in the plane of the molecule.

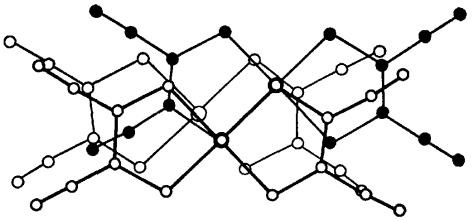

Fig. 6. Nearest neighbor overlapping within a $Ni(mnt)_2^{1-}$ column in $[(Et)_4N][Ni(mnt)_2]$.

is 2.175(1) Å and 2.149(2) Å in (II).

It is well known in organic compounds that bond lengths of molecules become longer or shorter in accordance with the change of the bond order or electronic state of molecules. When a molecular orbital which has the same sign on the neighboring two atoms is occupied with electrons, the bonding is strengthend and the bond length becomes shorter. If the sign is the reverse, the bonding is weakened. Similarly this discussion can be applied to complexes such as $Ni(mnt)_2^{n-}$ whose oxidation state could change with the molecular structure almost remaining unchanged.

The paramagnetic $Ni(mnt)_2^{1-}$ anion is thought to have the same electronic structure as that of the $Ni(mnt)_2^{2-}$ whose one electron is removed from the highest occupied level. The electronic structures of $Ni(mnt)_2^{n-}$ were studied by Gray and Schrauzer *et al.*[13,14] Gray's highest occupied orbital is $4a_g$ and Schrauzer's is $3b_{2g}$ (Fig. 5). These wave functions have the reverse sign on the Ni and S atoms, and the Ni–S bond length will be longer according to changing from $Ni(mnt)_2^{2-}$ to $Ni(mnt)_2^{1-}$. This agrees with the result of our crystal structure analyses. Similar relationship will be hold between $[(n\text{-}Bu)_4N]_2[Cu(mnt)_2]$ and $[(n\text{-}Bu)_4][Cu(mnt)_2]$ as to Cu–S bond distances (Table 7).

A characteristic feature of the crystal structure of $Ni(mnt)_2^{1-}$ complexes is the presence of columns of the $Ni(mnt)_2^{1-}$ anions weakly connected with each other. The mode of nearest neighbor overlapping within a $Ni(mnt)_2^{1-}$ column is shown in Fig. 6. The $Ni(mnt)_2^{1-}$ ions form a diadic unit within the columns. Similar columnar structure has been found in $[(n\text{-}Bu)_4N][Cu(mnt)_2]$, where columns are composed with tetradic units of $Cu(mnt)_2^{1-}$. The average interplanar

spacing of $Ni(mnt)_2^{1-}$ anion pairs in Fig. 6 is 3.5 Å and that of $Cu(mnt)_2^{1-}$ is 3.6 Å. In $Ni(mnt)_2^{1-}$ anion columns, overlapping of the Ni and S atoms is especially large, a similar columnar structure is also found in $[(n\text{-}Bu)_4N][Cu(mnt)_2]$.

References

1) A. J. Heeger and A. F. Garito,"Low Dimensional Cooperative Phenomena," ed by H. J. Keller, Plenum Press, New York (1975).

2) L. Alcacerand and A. H. Maki, *J. Phys. Chem.*, **78**, 215 (1974).

3) R. C. Wheland and J. L. Gillson, *J. Am. Chem. Soc.*, **98**, 3916 (1976).

4) E. Billig, R. Williams, I. Bernal, J. H. Waters, and H. B. Gray, *Inorg. Chem.*, **3**, 663 (1964); A. Davison, N. Edelstein, R. H. Holm, and A. H. Maki, *ibid.*, **2**, 1227 (1963).

5) The Universal Crystallographic Computation Program System, Crystallographic Society of Japan (1967).

6) "International Tables for X-Ray Crystallography," Kynoch Press, Birmingham (1962), Vol. III.

7) L. B. Coleman, J. A. Cohen, A. F. Garito, and A. J. Heeger, *Phys. Rev. B*, **7**, 2122 (1973).

8) J. D. Forrester, A. Zalkin, and D. H. Templeton, *Inorg. Chem.*, **3**, 1500 (1964).

9) a) J. D. Forrester, A. Zalkin, and D. H. Templeton, *Inorg. Chem.*, **3**, 1507 (1964); b) K. W. Plumlee, B. M. Hoffman, J. A. Ibers, and Z. G. Soos, *J. Chem. Phys.*, **63**, 1926 (1975).

10) R. Eisenberg, J. A. Ibers, R. J. Clark, and H. B. Gray, *J. Am. Chem. Soc.*, **86**, 113 (1964).

11) M. T. Hove, B. M. Hoffman, and J. A. Ibers, *J. Chem. Phys.*, **56**, 3490 (1972).

12) a) K. W. Plumlee, B. M. Hoffman, M. T. Ratjack, and C. R. Kannewurf, *Solid State Commun.*, **15**, 1651 (1974). b) K. W. Plumlee, B. M. Hoffman, and J. A. Ibers, (to be published).

13) S. I. Shupack, E. Billig, R. J. H. Clark, R. Williams, and H. B. Gray, *J. Am. Chem. Soc.*, **86**, 4594 (1964).

14) G. N. Schrauzer and V. P. Mayweg, *J. Am. Chem. Soc.*, **87**, 3585 (1965).

The Study of Thermochemical Hydrogen Preparation. III.[1] An Oxygen-evolving Step through the Thermal Splitting of Sulfuric Acid

Masayuki DOKIYA, Tetsuya KAMEYAMA, Kenzo FUKUDA, and Yoshihide KOTERA*

National Chemical Laboratory for Industry, 2-19-19 Mita, Meguro-ku, Tokyo 153

(Received March 31, 1977)

The thermal decomposition of sulfuric acid is used as a step in the oxygen evolution in some thermochemical water-splitting cycles. The catalytic activity of metal oxides was studied in an attempt to find some suitable catalysts for sulfuric acid decomposition. The catalytic activity of SiO_2, Al_2O_3, ZnO, CuO, NiO, CoO, Fe_2O_3, MnO, Cr_2O_3, V_2O_5, TiO_2 was measured at high temperatures (800—870 °C) and at atmospheric pressure. Iron(III) oxide was found to have the highest activity as a catalyst. Low catalytic activity was observed for the oxides (Al_2O_3, ZnO, NiO, CoO, MnO) which change to their sulfates under the present reaction conditions. Since the reaction conditions were very severe (more than 800 °C and in the presence of steam), a rapid decrease in both the specific surface area and the catalytic activity was observed. In order to avoid these disadvantages and in order to prepare practically useful catalysts, iron(III) oxide was pelletized and sintered (1000 °C, 6 h). Upon this procedure, this catalyst showed an almost constant activity for 120 hours' reaction.

Among the many thermochemical water-splitting cycles[2-5] proposed thus far, the following cycle is thought to be one of the most promising ones. The most difficult problem of this cycle is, though, how to separate the hydroiodic acid from the sulfuric acid in Reaction 1:

$$I_2 + 2H_2O + SO_2 \longrightarrow H_2SO_4 + 2HI, \quad (1)$$

$$H_2SO_4 \longrightarrow H_2O + SO_2 + 1/2O_2, \quad (2)$$

$$2HI \longrightarrow H_2 + I_2. \quad (3)$$

Three solutions have been proposed for this problem by the present authors[1] and by others.[6-10]

The most simple solution is to omit Reaction 3 and to replace Reaction 1 by a Reaction 4 evolving hydrogen by electrolysis.[1,6-8,10] In this case, the electric power will be reduced to one-third of that needed in the electrolysis of water:

$$2H_2O + SO_2 \xrightarrow{\text{electrolysis}} H_2SO_4 + H_2. \quad (4)$$

Another solution was proposed by Russel *et al.*[9] They tried to separate hydroiodic acid from sulfuric acid by adding a large amount of iodine to the reaction mixture of Reaction 1, and then to separate it into two liquid phases.

The present authors showed the possibility of performing Reaction 1 as a cell reaction using a cation-exchange membrane, which serves as a diaphragm and a separator of hydroiodic acid and sulfuric acid at the same time.[1]

In every case, Reaction 2 serves as an oxygen-evolving reaction. The decomposition of sulfur trioxide seemed feasible when studied by Spewock *et al.*;[8] however, the composition of the catalyst has not been reported:

$$SO_3 \longrightarrow SO_2 + 1/2O_2. \quad (5)$$

Moreover, there exists a difference between Reactions 2 and 5; that is, steam is also present in Reaction 2 and not in Reaction 5. Thus, in the latter case, one more process step will be needed before Reaction 5 — the dehydration of sulfuric acid.

In this paper, the catalytic activities of various metal oxides have been studied for Reaction 2.

* Present address: Central Research Center, Showadenko Co., Ltd., 2-24-60 Tamagawa, Ohta-ku, Tokyo 146.

Experimental

The experimental system is shown in Fig. 1. To find out the most suitable chemical species for use as the catalyst for Reaction 2, the reaction vessel, C, was used. The same volume (2.8 cmϕ × 0.4 cm = 2.5 ml) of powder oxides of Si, Al, Zn, Cu, Ni, Co, Fe, Mn, Cr, V, and Ti were put in the reaction vessel, C. These oxides were all guaranteed reagents and were commercially available. The 60 wt% sulfuric acid was used as a reactant, as the concentration of sulfuric acid yielded in Reaction 1 could be expected to be 60 wt% on the basis of another experiment.[1] The sulfuric acid was introduced into the reaction vessel, C, which was kept at 820 ± 10 °C or 860 ± 10 °C, by the use of a microfeeder at the rate of 0.85 ± 0.04 ml/min. The reaction mixture, consisting of unreacted gaseous sulfuric acid, sulfur dioxide, and oxygen, was then cooled to room temperature at the cold trap, and the unreacted sulfuric acid was condensed out. The sulfur dioxide and oxygen gas mixture was washed with a sodium hydroxide solution, in which the sulfur dioxide was absorbed almost completely (less than 0.1 %); the amount of oxygen evolved per unit of time was measured by means of a conventional gas meter.

The decomposition of sulfuric acid with the sintered iron-(III) oxide catalyst was carried out by the use of the same

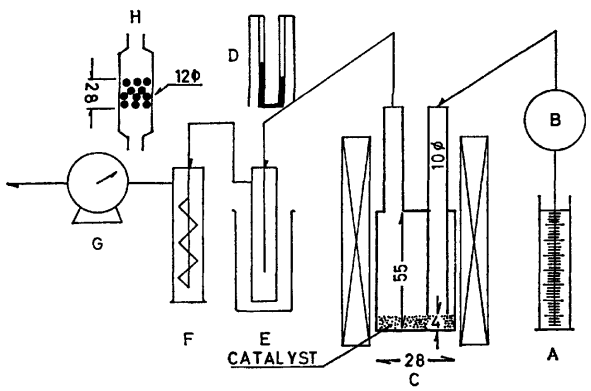

Fig. 1. Apparatus.
A: 60 wt%H_2SO_4, B: microfeeder, C: reaction vessel, D: manometer, E: cold trap, F: NaOH solution, G: gas meter, H: reaction vessel.

apparatus as in Fig. 1, except that the reaction vessel, C, was replaced by the vessel, H, as may be seen in the figure. The volume of the catalyst bed was 1.2 cmϕ×2.8 cm=3.2 ml. The iron(III) oxide catalyst was prepared as follows: iron(III) oxide powder was pressed at 5 tons/cm^2 into cylindrical pellets 4 cm in diameter and 1 cm in height. These pellets were sintered at 1000 °C for 6 h, and then crushed. Particles of 2—4 mm were used as the catalysts. The other procedure was almost the same as has been described above, except for the feeding rate of sulfuric acid.

Results and Discussion

Some typical results on the iron(III) oxide powder catalyst are shown in Fig. 2, where the amount of oxygen evolved per unit of time is plotted against the time. The rapid increase and decrease in the reaction rate observed at the initial stage at 820 °C was due to the time lag, during which the evolved sulfur dioxide and oxygen replaced the air in the experimental system. As may be seen in Fig. 2, the amount of oxygen evolved per unit of time gradually decreased with the reaction time at 860 °C. Such a tendency was observed with almost all kinds of chemical species the catalytic activity of which was examined.

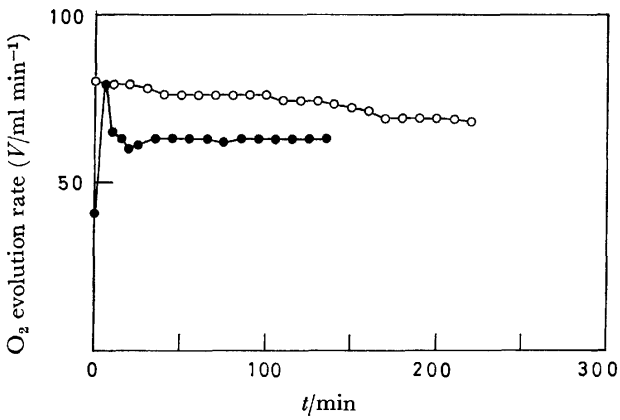

Fig. 2. The change of catalytic activity of Fe_2O_3 with time.
● 820 °C, ○ 865 °C.

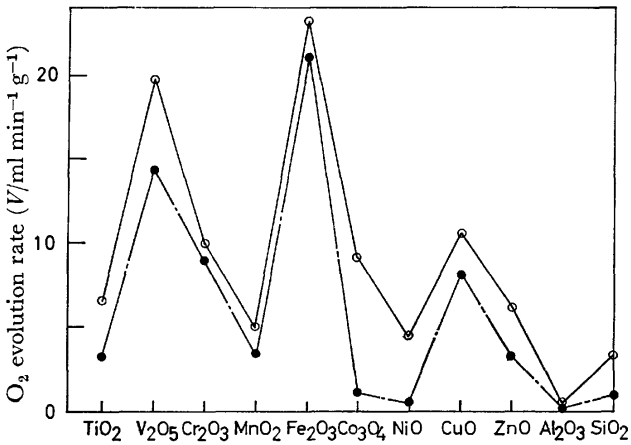

Fig. 3. The comparison of activity per unit weight of various oxides.
● 820±10 °C, ○ 860±10 °C.

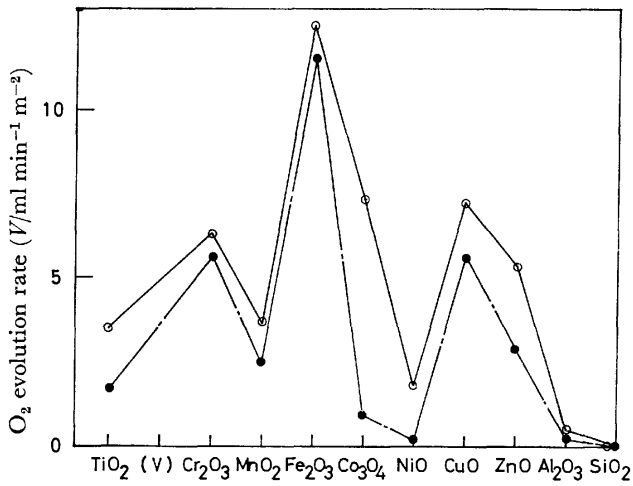

Fig. 4. The comparison of activity per specific surface area of various oxides.
● 820±10 °C, ○ 860±10 °C.

In Figs. 3 and 4, the amount of oxygen evolved per unit of time is plotted against the metal oxides used as catalysts. The ordinates of Figs. 3 and 4 are the amount of oxygen evolved per unit of time per unit of weight of the catalyst and the amount of oxygen evolved per unit of time per unit of the specific surface area, respectively. In Fig. 4, the value for vanadium(V) oxide is omitted because vanadium(V) oxide is a liquid at these reaction temperatures. Here, the amount of oxygen evolved per unit of time 4—5 h after the initiation of the reaction was chosen as the representative value of the amount of oxygen evolved per unit of time for each oxide. As may be seen from these results, iron(III) oxide has the highest activity among the oxides used.

Table 1. The crystal structure and specific surface area of catalysts

Catalyst		Surface area S/m^2 g^{-1}	
Original	Used	Original	Used
TiO_2	rutile≫ anatase	2.50	1.86
V_2O_5	V_2O_5	—	fused
Cr_2O_3	eskolaite	3.10	1.58
MnO_2	$MnSO_4$	31.8	1.43
Fe_2O_3	Fe_2O_3	9.21	1.85
Fe_3O_4	Fe_2O_3	—	—
SiO_2(am)	SiO_2(am)	655.0	95.5
Co_3O_4	Co_3O_4, CoO α-$CoSO_4$	0.88	1.24
CoO	Co_3O_4, CoO α-$CoSO_4$	—	—
NiO	NiO $NiSO_4$	0.42	2.48
CuO	CuO≫ $CuO(SO_4)$	1.84	1.48
ZnO	$ZnSO_4$ $Zn_5O_2(SO_4)_3$ $Zn_3O_2(SO_4)_2$	5.26	1.15
α-Al_2O_3	α-Al_2O_3 $Al_2(SO_4)_3$	6.20	1.41

As may be seen in Table 1, the speicfic surface area and the crystal structure of the catalysts used changed during the reaction. The specific surface area decreased except in the cases of cobalt(II) oxide and nickel(II) oxide. This fact and the gradual decrease in the amount of oxygen evolved per unit of time are noteworthy for the practical preparation of catalysts.

The oxides of Al, Zn, Ni, Co, and Mn, which were found as sulfates after the reaction (Table 1), showed low catalytic activity, as can be seen in Figs. 3 and 4. Among the active oxides (V, Cr, Cu, and Fe), iron(III) oxide was chosen as a candidate for catalyst for practical use, considering the cost of the catalyst and the environmental safety.

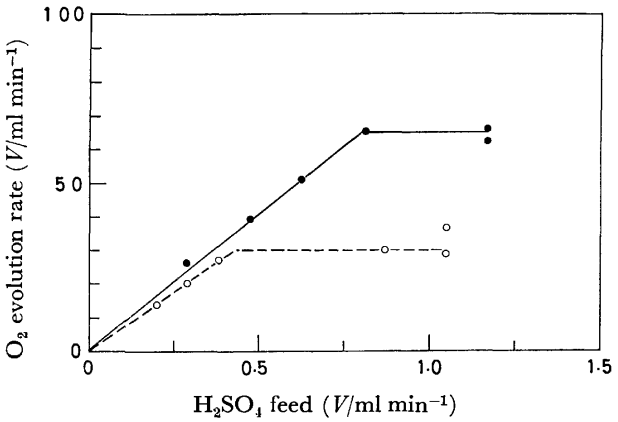

Fig. 5. The dependence of oxygen evolution rate upon the feeding rate of H_2SO_4.
○ 800 °C, ● 850 °C.

Five g of well-sintered particles of iron(III) oxide were used for each reaction, having been placed in the reaction vessel, H, shown in Fig. 1. In Fig. 5, the amount of oxygen evolved per unit of time *vs.* the feeding rate of the sulfuric acid is plotted. A linear dependence of the amount of oxygen evolved per unit of time on the feeding rate below 0.5 or 0.8 ml/min at 800 °C or 850 °C was observed. These results indicate that the space velocities based on the sulfur dioxide and oxygen gas produced are 560 ml/ml-catalyst-h (800 °C) and 1200 ml/ml-catalyst-h (850 °C). Their conversion were 69 and 79% respectively. On the basis of these results, the feeding rates of sulfuric acid at 1.1 ml/min (800 °C) and 1.3 ml/min (850 °C) were chosen as the feeding rates for the following experiments.

In Fig. 6, the results of the long-time examination of the stability of catalyst at 800 °C and 850 °C are shown. In each case, an increase of activity was observed around 25 hours' reaction. After that increase, the iron(III) oxide catalyst showed a constant activity up to 120 h. The specific surface area of the catalysts used were compared with those of the original ones; the results are summarized in Table 2. At 800 °C, an increase in the specific surface area was observed with the catalyst which was used for 28 hours' reaction (open square in Fig. 6); then the specific surface area of the catalyst remained substantially constant up to 120 h (solid square in Fig. 6). At 850 °C, the specific surface area still increased from 28 hours' reaction up to 120 h.

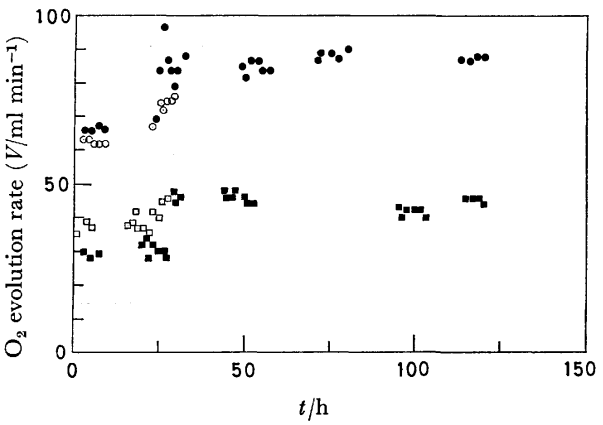

Fig. 6. The change of catalytic activity of sintered Fe_2O_3 with time.
□,■ 800 °C, ○,● 850 °C.

Table 2. The specific surface area of ferric oxide catalysts

	Surface area S/m^2 (5 g)$^{-1}$		
	Original	Used 28 h	Used 120 h
850 °C	2.20	3.09	6.41
800 °C	2.20	2.80	2.74

No sulfate species were observed by means of X-ray diffractometry. However, it was observed that a few particles changed color from violet to red and that the crushing strength of the pellets was lowered in spite of the fact that their shape did not change at all.

From these results, the authors concluded that, from a practical stand point, the well-sintered iron(III) oxide catalyst has a high possibility of being utilized in the sulfuric acid thermal splitting reaction. The next problem may be whether this catalyst can be applied for a long term or not (for example, one year's operation), because of the necessary reaction conditions of a high temperature and the presence of steam. Silica or alumina would not be proper for a catalyst support, as they are not stable enough under the reaction conditions described above, as is shown in Table 1.

This work was done as part of the Sunshine Project of the Ministry of International Trade and Industry of Japan.

References

1) Part II: M. Dokiya, T. Kameyama, K. Fukuda, Y. Kotera, and S. Asakura, *Denki Kagaku*, **45**, 139 (1977).
2) R. E. Chao, *Ind. Eng. Chem., Process Des. Dev.*, **14**, 94 (1974).
3) E. D. Glandt and S. L. Myers, *Ind. Eng. Chem., Process Des. Dev.*, **15**, 100 (1976).
4) "Round Table on Direct Production of Hydrogen with Nuclear Heat," EUR/ClS/1062/1/69e, C.C.R. Euratom, Ispra, Italy (1969).
5) H. Tagawa,"Thermodynamic Considering on the Constitution of Multi-thermochemical Water Splitting Process," JAERI-M6421, Japan Atomic Energy Research Institute (1976).

6) M. G. Bowman and E. I. Onstott, Abstract No. 232, Extended Abstracts, Fall Meeting, The Electrochemical Soc. (1974), pp. 574—575.

7) L. E. Brecher, S. Spewock, and C. J. Warde, "Conference Proceedings of Ist World Hydrogen Energy Conference," Vol. 1. 9A-1, The Univ. of Miami, Coral Gables, Florida (1976).

8) S. Spewock, L. E. Brecher, and F. Talko,"Conference Proceedings of Ist World Hydrogen Energy Conference," Vol. 1. 9A-53 (1976).

9) J. L. Russel, Jr., K. H. McCorkle, J. H. Norman, J. T. Porter II, T. S. Roemer, J. R. Schuster, and R. S. Sharp, "Conference Proceedings of Ist World Hydrogen Energy Conference," Vol. 1. 1A-105 (1976).

10) Westinghouse Electric Corp. Astronuclear Laboratory, "The Conceptual Design of Integrated Nuclear-Hydrogen Production Plant Using the Sulfur Cycle Water Decomposition System," NASA CR-134976 (1976).

Conversion of Cobalt(II) and Nickel(II) Fixed on the Ion Exchange Resin into Their Trifluoroacetylacetonates and Gas Chromatography of the Chelates

Tooru TAMURA, Kunio OHZEKI, and Tomihito KAMBARA

Department of Chemistry, Faculty of Science, Hokkaido University, Sapporo 060

(Received April 18, 1977)

The conversion of cobalt(II) and nickel(II) ions collected on the ion exchange resin into the chelate compounds with trifluoroacetylacetone (Htfa) has been studied in various solvents. In the presence of pyridine, cobalt and nickel ions were quantitatively extracted from the resin into organic phase in the form of the base adducts $[Co(tfa)_2(py)_2]$ and $[Ni(tfa)_2(py)_2]$, respectively. The thermogravimetric and gas chromatographic behaviors of these compounds have been investigated. A gas chromatographic separation of $[Ni(tfa)_2]$ from $[Co(tfa)_2]$ was successfully performed.

The gas chromatography of metal chelates, particularly those with ligands of the β-diketone type, has been noted and reviewed.[1,2] The application of the gas chromatography to inorganic analysis has been limited by the problems involved in the quantitative conversion of metal ions in aqueous solution into the suitable metal chelates with adequate volatility and thermal stability for elution from gas chromatographic column.[3] The application of gas chromatography to divalent transition metal ions in the form of β-diketonates has proved particularly difficult, since the dihydrates of the bis chelates are hardly volatile.[4] Attempts have been made to separate cobalt(II) and nickel(II) ions as their 2-thenoyltrifluoroacetonates by gas chromatography,[5,6] and it was reported that the peak shapes of the chelates could be improved when the chelates were injected as the corresponding adducts with diethylamine.[6]

We have reported that iron(III),[7] copper(II),[8] nickel(II),[9] and cobalt(II)[10] ions fixed on the ion exchange resins were quantitatively extracted with acetylacetone or 2-thenoyltrifluoroacetone into organic medium by the aid of a small amount of pyridine or pyridine-water mixture.

It is worthwhile to examine the utility of the synergistic extraction of metal ions previously fixed on the ion exchange resin in the preparation of the chelate compounds suitable for gas chromatography. In this work, the synergistic extraction of cobalt(II) and nickel(II) with trifluoroacetylacetone in the presence of pyridine is studied and the gas chromatographic behavior of the resulting chelates is discussed.

Experimental

Apparatus. A Hitachi 508 atomic absorption spectrometer was used for the cobalt and nickel absorption measurements at 240.7 and 231.4 nm, respectively, in air-acetylene flame. The thermogravimetric data were obtained using a Shimadzu TG-20 thermogravimetric analyzer with *ca.* 5 mg of sample. The heating rate was programmed at 5 °C min^{-1} and helium was passed through the sample chamber at a flow rate of 30 cm^3 min^{-1}. A Hitachi 063 gas chromatograph equipped with a thermal conductivity detector was used.

Reagents. Trifluoroacetylacetone (1,1,1-trifluoropentane-2,4-dione, Wako Pure Chemicals Co.) was distilled and used. Pyridine and all other reagents used were of the guaranteed reagent grade.

Extraction of Metal Ions from the Resin with Htfa. The resin used was a sulfonate cation exchanger, Amberlyst 15, with a macroreticular structure. The Co(II)- and Ni(II)-form resins were prepared according to the method reported previously.[9,10] It was found that 3.43 meq of cobalt and 3.31 meq of nickel ions were adsorbed on 1.00 g of the airdried Co(II)- and Ni(II)-form resins, respectively. A 5-cm^3 portion of 0.1 mol l^{-1} Htfa in organic medium was poured onto the 25 mg of airdried Co(II)- or Ni(II)-form resin in an eggplant type flask and a small amount of pyridine was added. The mixture was shaken at a room temperature for 20 min for cobalt and 10 min for nickel. The resin was separated by filtration and washed with ethanol and then water. The cobalt or nickel ion remaining on the resin was eluted by 2 mol l^{-1} hydrochloric acid and determined by atomic absorption spectrometry.

Preparation of Chelates. A 100-cm^3 portion of 0.5 mol-l^{-1} Htfa in benzene was poured onto 4 g of the air-dried Co(II)- or Ni(II)-form resin in an eggplant type flask and 8 cm^3 of pyridine was added. The mixture was shaken for 1 h at a room temperature. After filtration, the filtrate was gently warmed and the solvent was removed with a stream of nitrogen gas. The residue was dissolved in benzene or ethanol and the adduct $[Co(tfa)_2(py)_2]$ or $[Ni(tfa)_2(py)_2]$ was recrystallized from the solution. The results of elemental analysis were: Found: C, 45.50; H, 3.86; N, 5.21; Co, 11.23%. Calcd for $[Co(tfa)_2(py)_2]$: C, 45.91; H, 3.47; N, 5.35; Co, 11.26%. Found: C, 45.62; H, 3.58; N, 5.58; Ni, 11.15%. Calcd for $[Ni(tfa)_2(py)_2]$: C, 45.92; H, 3.47; N, 5.36; Ni, 11.22%.

Results and Discussion

Extraction of Nickel(II) and Cobalt(II) from the Resin with Htfa. The removal of nickel and cobalt ions from the resin with Htfa into the organic solvent was successfully carried out in the presence of a small amount of pyridine, as shown in Figs. 1 and 2. Upon the addition of pyridine blue or dark orange color was immediately developed in the organic phase, indicating the formation of the base adduct, $[Ni(tfa)_2(py)_2]$ or $[Co(tfa)_2(py)_2]$. Nickel(II) ions on the resin were quantitatively extracted into Htfa-carbon tetrachloride and Htfa-benzene solution in the presence of pyridine in 1—6 and 1—4% (v/v), respectively. Cobalt(II) ions were also quantitatively extracted into Htfa-carbon tetrachloride, Htfa-benzene, and Htfa-cyclohexane solu-

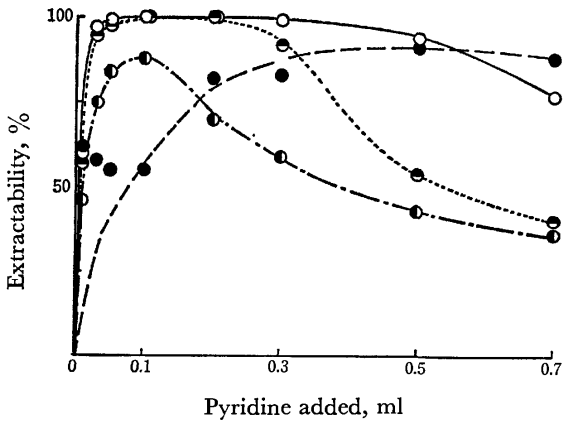

Fig. 1. Effect of pyridine on the extractability of Ni(II) ions from the resin with 0.1 mol l^{-1} Htfa in various solvents.
○: Carbon tetrachloride, ◓: benzene, ◐: chloroform, ●: cyclohexane.

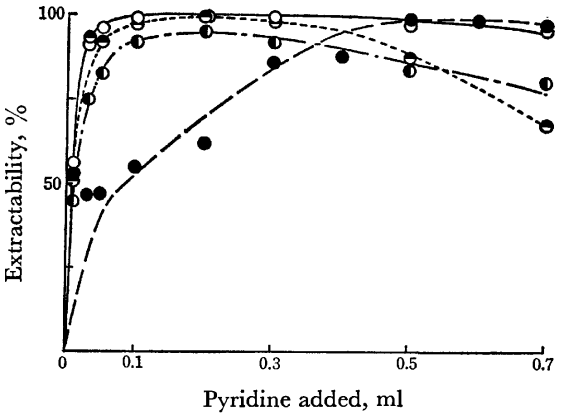

Fig. 2. Effect of pyridine on the extractability of Co(II) ions from the resin with 0.1 mol l^{-1} Htfa in various solvents. Keys to the symbols are similar to those in Fig. 1.

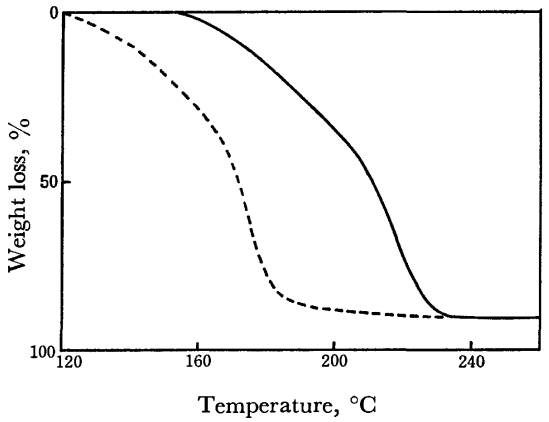

Fig. 3. Thermogravimetric analysis of $[Co(tfa)_2(py)_2]$ (----) and $[Ni(tfa)_2(py)_2]$ (——).

tion in the presence of pyridine in 2—6, 2—4 and 10—14% (v/v), respectively.

Thermogravimetric Analysis. Thermogravimetric behavior of the chelates is shown in Fig. 3. A considerable volatility difference between the chelates was observed, while both chelates were not completely volatile. Some black residue was left in the sample pan after each run. The loose weight loss observed at the beginning of thermograms is attributed to the thermal dissociation of pyridine from the adduct. For comparison with the gas chromatographic behavior, the thermograms were obtained under the conditions in which the chelates were sublimated through a small amount of the column packing, *i.e.* 10% SE-30 or 5% Apiezon L on Chromosorb WAW was placed on the chelate in the sample pan. No remarkable differences were found with and without the column packing.

Thermal Dissociation of Pyridine from the Adducts. The thermal dissociation of pyridine from the adducts was investigated by gas chromatography as follows. A 25-cm glass column packed with 30% PEG 4000 on Celite 545 was used. The column temperature was held at 75 °C and injection port temperature was varied from 100 to 300 °C. An appropriate dead space was placed between the packing and injection port to avoid the thermal decomposition of the packing. The sample solution containing 33.8 mg of $[Co(tfa)_2(py)_2]$ or 42.1 mg of $[Ni(tfa)_2(py)_2]$ in 1.5 cm^3 of benzene was prepared and a 10-μl portion of ethylbenzene was added. Sample size injected was 2 μl for cobalt and 4 μl for nickel, respectively. The relationship between the injection port temperature and the amount of dissociated pyridine was examined with ethylbenzene as the internal standard. As shown in Fig. 4, the peak height ratio of

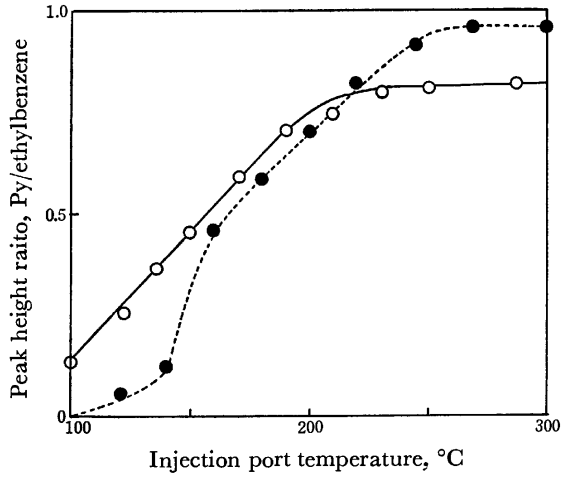

Fig. 4. Thermal dissociation of pyridine from the adduct.
○: $[Co(tfa)_2(py)_2]$, ●: $[Ni(tfa)_2(py)_2]$.

pyridine to ethylbenzene became constant above the injection port temperature around 230 and 270 °C for cobalt and nickel chelates, respectively. It is safely assumed that under the appropriate gas chromatographic conditions the liberation of pyridine takes place immediately after the sample injection, and hence, cobalt and nickel are eluted from the column in the form of $[Co(tfa)_2]$ and $[Ni(tfa)_2]$, respectively.

Choice of Column Packing. The following experiment was carried out to select the column packing suitable to elute the chelates. A J-shaped glass tube, the round part of which was packed with column packing, was affixed to injection port in the column oven.

The linear part of the tube stuck through a hole out of the wall of the oven, so that it was cooled to a room temperature resulting in the deposition of the metal complex at the inner wall of glass tube. The injection port temperature and column temperature were held at 210 and 230 °C, respectively. A benzene solution containing a known amount of the chelate was injected successively. Then the chelate condensed at the inner wall of the protruding section of tube was washed with methyl isobutyl ketone into a volumetric flask and the metal ion content was determined by atomic absorption spectrometry and compared with the injected amount. Among the several stationary liquids examined, the best result was obtained with silicone SE-30. With the use of 5% SE-30 on silanised Chromosorb W (80—100 mesh), 80, 84, and 86% of the injected amount of the cobalt chelate were found to be eluted from the glass tube, the packed length of which was 26, 10.5, and 4.5 cm, respectively. For nickel chelate 77% of the injected amount were found to be in the effluent from a 28 cm packed tube. On the other hand, no detectable amount of the chelate was found in the effluent from the tube packed with Apiezon L. This fact clearly indicates that the recovery does not depend on the packing length, but seriously depends on the packing material. No evidence of the thermal decomposition of the chelate at the injection port was found. It is supposed that the loss of the chelate is mainly due to the adsorption of chelate on the column packing adjacent to the injection port.[11]

Gas Chromatography. A glass column (25 cm long and 4 mm i.d.) packed with 10% SE-30 on Chromosorb WAW (60—80 mesh) was used. Gas chromatographic conditions were as follows. For $[Co(tfa)_2(py)_2]$, column temperature, 170 °C; injection port temperature, 210 °C; detector temperature, 200 °C. For $[Ni(tfa)_2(py)_2]$, column temperature, 230 °C; injection port temperature 260 °C; detector temperature, 240 °C. Detector current, 115 mA; helium flow rate, 25 cm^3 min^{-1}. The typical chromatograms are shown in Fig. 5. Sample quantities are 32 μg $[Co(tfa)_2(py)_2]$ and 113.4 μg $[Ni(tfa)_2(py)_2]$ in benzene. In the case of cobalt, a good separation of

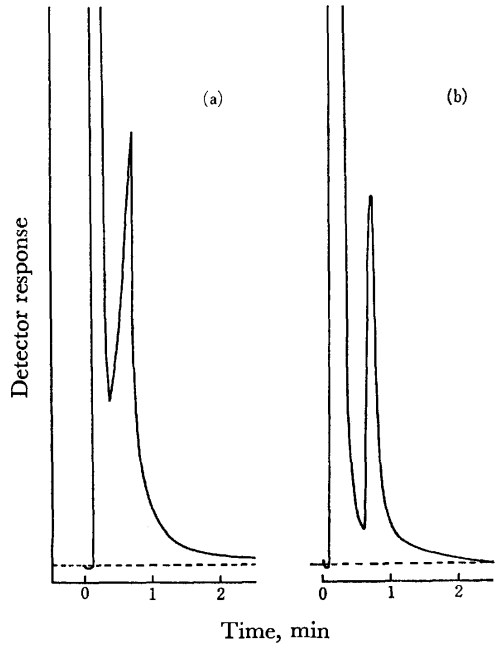

Fig. 5. Chromatograms of (a) $[Ni(tfa)_2]$ and (b) $[Co(tfa)_2]$. Column: 25 cm long × 4 mm i.d., borosilicate glass, filled with 10% SE-30 on 60—80 mesh Chromosorb WAW.

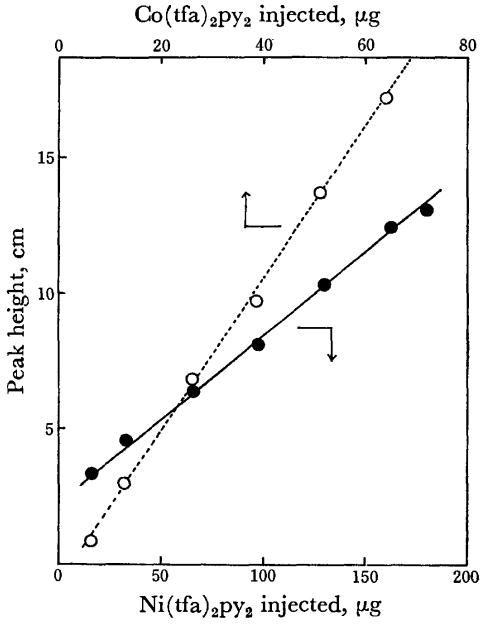

Fig. 6. Plot of the chelate peak height against the sample amount injected. ○: $[Co(tfa)_2(py)_2]$, ●: $[Ni(tfa)_2(py)_2]$.

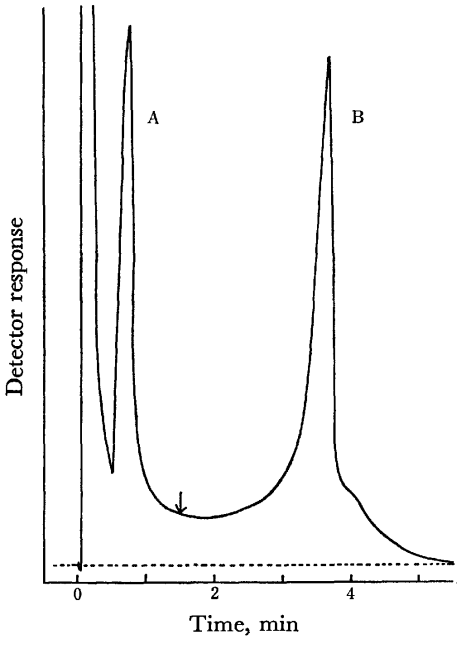

Fig. 7. Separation of Co(II) and Ni(II) trifluoroacetylacetonates by the programmed temperature method. Column: 25 cm long × 4 mm i.d., borosilicate glass, filled with 2% SE-30 on 80—100 mesh Chromosorb WHP. Temperature was programmed at the point indicated by an arrow from 165 to 230 °C at 20 °C min^{-1}. (A) $[Co(tfa)_2]$, (B) $[Ni(tfa)_2]$.

the chelate from the solvent was obtained. On the other hand, an isothermal separation of nickel chelate from the solvent was unsuccessful under the condition employed. The column temperature was too low for the chelate and too high for the solvent to give symmetrical peak shapes. The increase in the peak height with sample size was found to be linear as shown in Fig. 6.

Separation of Nickel(II) and Cobalt(II) Trifluoroacetylacetonates. The programmed temperature method was examined to separate these compounds. A 25-cm glass column packed with 2% SE-30 on Chromosorb WHP (80—100 mesh) was used. The temperatures of injection port and detector were held at 250 °C and 210 °C, respectively. The detector current was 125 mA and helium flow rate was 45 $cm^3\ min^{-1}$ at 165 °C. A mixture of 98.4 μg of $[Co(tfa)_2(py)_2]$ and 205.0 μg of $[Ni(tfa)_2(py)_2]$ in benzene was injected. The column temperature was held at 165 °C until the cobalt chelate was eluted, then programmed to 230 °C at 20 °C min^{-1}. A fair separation of cobalt and nickel trifluoroacetylacetonates was observed as shown in Fig. 7. A small shoulder was found for nickel chelate. An attempt was also made to separate these compounds in the extract from the resin. The column temperature was held at 110 °C until the solvent and the excess reagents were eluted, then programmed to 230 °C at 10 °C min^{-1}. A fairly good separation was attained, which indicates that the synergistic extraction of nickel(II) and cobalt(II) ions from the ion exchange resin onto which the metal ions are previously collected from the aqueous solution is effective in the preparation of metal chelates to be separated by gas chromatography.

References

1) R. W. Moshier and R. E. Sievers, "Gas Chromatography of Metal Chelates," Pergamon Press, Oxford (1965).
2) V. A. Komarov, *Zh. Anal. Khim.*, **31**, 366 (1976).
3) R. S. Barratt, R. Belcher, W. I. Stephen, and P. C. Uden, *Anal. Chim. Acta*, **59**, 59 (1972).
4) R. Belcher, R. J. Martin, W. I. Stephen, D. E. Henderson, K. Kamalized, and P. C. Uden, *Anal. Chem.*, **45**, 1197 (1973).
5) P. Jacoquelot, J. P. Weille, and G. Thomas, *Anal. Chim. Acta*, **60**, 335 (1972).
6) P. Jacoquelot and G. Thomas, *J. Chromatogr.*, **66**, 121 (1972).
7) K. Ohzeki, M. Ikeuchi, and T. Kambara, *Bull. Chem. Soc. Jpn.*, **48**, 67 (1975).
8) T. Okamura, K. Ohzeki, and T. Kambara, *Bull. Chem. Soc. Jpn.*, **48**, 469 (1975).
9) K. Ohzeki, T. Tamura, and T. Kambara, *Bull. Chem. Soc. Jpn.*, **48**, 2829 (1975).
10) T. Tamura, K. Ohzeki, and T. Kambara, *Bull. Chem. Sco. Jpn.*, **49**, 2108 (1976).
11) P. C. Uden and C. R. Jenkins, *Talanta*, **18**, 429 (1971).

Synthesis and Absorption Spectra of the $[Co(O-O)_2(py)_2]^-$-type Complexes

Yayoi IDA, Shuhei FUJINAMI, and Muraji SHIBATA

Department of Chemistry, Faculty of Science, Kanazawa University, Kanazawa 920

(Received April 22, 1977)

Five bis(dicarboxylato)bis(pyridine)-type complexes, *trans*-$[CoCO_3ox(py)_2]^-$, *trans*- and *cis*-$[Co(ox)_2(py)_2]^-$, and *trans*- and *cis*-$[Co(mal)_2(py)_2]^-$, have been isolated as crystals and characterized on the basis of the absorption spectra, the PMR spectra, *etc.* The *trans* isomers of the carbonatooxalato and bis(oxalato) complexes reveal spectra similar to that of the *trans*-$[Co(CO_3)_2(py)_2]^-$ complex synthesized previously; the splittings of the absorption bands are not observed in the I bands, but are observed in the II bands. On the other hand, the *trans* isomer of the bis(malonato) complex reveals no splittings in either the I band or the II band. The assignment of these absorption bands has been made from considerations based on the Angular Overlap Model.

In the studies previously carried out in our laboratory,[1-3] some dicarbonato complexes of the $[Co(CO_3)_2(a)_2]^{n-}$ type, where a represents unidentate ligands such as NH_3, NO_2^-, and CN^-, were synthesized by a method called the "tricarbonato method."[4] However, every complex isolated was of *cis* isomer. Under the circumstances, efforts were continued to find a *trans* isomer of this type of complex, and we finally succeeded in obtaining the isomer; the action of pyridine on an aqueous potassium bicarbonate solution of tricarbonatocobaltate(III) yielded not only the *cis* isomer, but also the *trans* one of the $[Co(CO_3)_2(py)_2]^-$ complex.[5] In addition to this success, it was found that the *trans* isomer revealed an unusual absorption spectrum; it showed a single maximum in the first absorption-band region (I band) and two maxima in the second absorption-band region (IIa and IIb bands).

Then, studies of the synthesis of the $[Co(O-O)_2(py)_2]^-$-type complexes were undertaken by using CO_3^{2-}, $C_2O_4^{2-}$, and $C_3H_2O_4^{2-}$ (malonate) ions as the bidentate O–O donor ligands. This paper will deal with the results of the studies; the synthesis gave a pair of *cis* and *trans* isomers for the $[CoCO_3ox(py)_2]^-$, $[Co(ox)_2(py)_2]^-$, and $[Co(mal)_2(py)_2]^-$ complexes. The *trans* isomers of the former two complexes revealed spectra similar to that of the *trans*-$[Co(CO_3)_2(py)_2]^-$ complex, while the *trans* isomer of the latter complex exhibited no splittings in either the first or the second absorption band.

Experimental

Synthesis. *1) Carbonatooxalatobis(pyridine)cobaltate(III).* *a) Potassium Salt of the* trans *Isomer,* trans-*K*$[CoCO_3ox(py)_2]\cdot 2.5H_2O$: To a green solution containing mainly the $[Co(CO_3)_2(ox)]^{3-}$ species, which had been prepared by the literature method[2] ($Co(NO_3)_2\cdot 6H_2O$, 15 g scale, 0.05 mol), we added pyridine (8 ml, 0.1 mol); the mixture was then stirred at 50 °C for 1.5 h. The resulting violet solution was kept in a refrigerator until red-violet crystals were deposited. The crystals were filtered and recrystallized from warm water (*ca.* 50 °C). The filtrate was preserved for the synthesis of the subsequent *cis* isomer. The yield was about 2.5 g. Found: C, 34.71; H, 3.66; N, 6.58%. Calcd for $K[CoCO_3(C_2O_4)(C_5H_5N)_2]\cdot 2.5H_2O$: C, 34.70; H, 3.36; N, 6.23%.

b) cis *Isomer,* cis-$[CoCO_3ox(py)_2]^-$: A portion of the filtrate (*ca.* 1/5 volume) was charged on a column of Dowex 1-X8 resin (100—200 mesh) in the Cl-form (4.0×25.0 cm). After washing with water, the column was treated with a 0.1 M NaCl aqueous solution; three bands were thus separated. The first-descending band was of *cis*-$[Co(CO_3)_2(py)_2]^-$, and the last band, *cis*-$[Co(ox)_2(py)_2]^-$, while the middle band was the desired one. This was collected in a fraction and concentrated to a small volume, but no crystals were obtained because of its great solubility.

2) Bis(oxalato)bis(pyridine)cobaltate(III). *a) Potassium Salt of the* trans *Isomer,* trans-*K*$[Co(ox)_2(py)_2]\cdot 3H_2O$: To an aqueous solution of $K_3[Co(ox)_3]\cdot 3H_2O$[6] (25 g, 0.05 mol in 60 ml H_2O), we added pyridine (8 ml, 0.1 mol) and activated charcoal (1 g); the mixture was then stirred at 60 °C for 2 h. The resulting solution was filtered once to remove the charcoal and any precipitated material, and then concentrated until pink crystals began to be deposited. After the whole had been cooled for a while, the crystals were collected by filtration and recrystallized from warm water (*ca.* 50 °C). The filtrate was preserved for the subsequent *cis* isomer. The yield was *ca.* 2 g. Found: C, 34.86; H, 3.55; N, 6.00%. Calcd for $K[Co(C_2O_4)_2(C_5H_5N)_2]\cdot 3H_2O$: C, 34.51; H, 3.31; N, 5.75%.

b) Lithium Salt of the cis *Isomer,* cis-*Li*$[Co(ox)_2(py)_2]\cdot H_2O$: The filtrate in *a*) was poured into a column of Dowex 50W-X8 resin (100—200 mesh) in the Li-form (5.0×10.0 cm) in order to obtain the lithium salt of the desired isomer. The effluent was collected and evaporated almost to dryness. The residue was then extracted with warm ethanol (*ca.* 50 °C), and the solution was kept in a refrigerator until violet crystals were deposited. The yield was about 1.5 g. Found: C, 40.23; H, 3.21; N, 6.75%. Calcd for $Li[Co(C_2O_4)_2(C_5H_5N)_2]\cdot H_2O$: C, 40.12; H, 2.89; N, 6.68%.

3) Bis(malonato)bis(pyridine)cobaltate(III). *a) Potassium Salt of the* trans *Isomer,* trans-*K*$[Co(mal)_2(py)_2]\cdot 2H_2O$: To a solution of potassium tris(malonato)cobaltate(III), which had been prepared by the literature method[7] ($Co(NO_3)_2\cdot 6H_2O$, 30 g scale, 0.1 mol), we added pyridine (16 ml, 0.2 mol); the mixture was then stirred at 50 °C for 40 min. After the insoluble material had been removed by filtration, the filtrate was concentrated to a small volume and then kept in a refrigerator until purple crystals separated out. The crystals were collected by filtration and recrystallized from warm water (*ca.* 50 °C). The filtrate was preserved for the subsequent *cis* isomer. The yield was about 2 g. Found: C, 38.73; H, 3.55; N, 5.68%. Calcd for $K[Co(C_3H_2O_4)_2(C_5H_5N)_2]\cdot 2H_2O$: C, 38.72; H, 3.66; N, 5.64%.

b) Bis(ethylenediamine)oxalatocobalt(III) Salt of the cis *Isomer,* $[Co(ox)(en)_2]\cdot$cis-$[Co(mal)_2(py)_2]\cdot 3H_2O$: The filtrate in *a*) was evaporated almost to dryness, after which the residue was extracted with methanol. The methanol solution was then dried, and the residue was again dissolved with a minimum amount of water. To this solution, we added an aqueous solution of bis(ethylenediamine)oxalato-

cobalt(III) acetate[8] (in excess). The whole was kept in a refrigerator until red-brown crystals were deposited. Recrystallization was performed from warm water (*ca.* 50 °C). The yield was about 3.5 g. Found: C, 35.73; H, 4.84; N, 11.03%. Calcd for $[Co(C_2O_4)(C_2H_5N_2)_2]\cdot[Co(C_3H_2O_4)_2(C_5H_5N)_2]\cdot 3H_2O$: C, 35.59; H, 4.88; N, 11.32%.

An attempt to resolve this complex was successful; the racemate (3.5 g, 0.005 mol) was ground in a mortar with water (5 ml), and then NaI (0.83 g, 0.005 mol) was added. The mixture was filtered to remove precipitates of $[Coox(en)_2]I$. To an aqueous solution of $(-)_{589}[Coox(en)_2]^+$ (0.003 mol in 7 ml H_2O), which had been prepared in the acetate form according to the literature method,[8] we added the above filtrate; the mixture was then cooled in an ice bath, and a small amount of ethanol was added. After the sides of the vessel had been scratched with a glass rod for some time, the whole was kept for an hour in an ice bath. The crystals thus deposited were recrystallized several times from water (*ca.* 40 °C). The less soluble diastereoisomer was found to be $(-)_{589}[Coox(en)_2]\cdot(+)_{589}[Co(mal)_2(py)_2]\cdot 3H_2O$.

4) Dicarbonatobis(pyridine)cobaltate(III), trans- *and* cis-*$K[Co(CO_3)_2(py)_2]\cdot 3H_2O$*: The syntheses of these isomers have been described in a previous paper.[5]

The synthesis was attempted using 3- or 4-methylpyridine in place of pyridine; the *trans* isomers could be isolated, but no *cis* isomers were isolated because of their great solubility in ethanol. In the case of 2-methylpyridine, no substitution reaction proceeded.

Measurements. For the measurement of the absorption spectra in solution, a Hitachi 323 recording spectrophotometer was used. The spectra of the *trans*- and *cis*-$[Co(CO_3)_2(py)_2]^-$ complexes were measured with aqueous solutions containing a small amount of $KHCO_3$ in order to prevent the decomposition of the complex species. For the $[Coox(en)_2]\cdot$*cis*-$[Co(mal)_2(py)_2]$ complex, the spectrum was measured with the effluent obtained by passing its aqueous solution through a column of Dowex 50W-X8 resin in the Na-form. The absorption spectrum of the *trans*-$[Coox(H_2O)_2(py)_2]^+$ species was measured with an acidified solution of the *trans*-$[CoCO_3ox(py)_2]^-$ complex with 10% $HClO_4$; the acid-hydrolyzed species was chromatographically pure, and its absorption spectrum was reformed into the original spectrum of the parent carbonato complex when $KHCO_3$ was added to the acidified solution. This fact was evidence for the complete retention of the configuration during the acid-hydrolysis. The crystal absorption spectra were measured with a microspectrophotometer constructed in our laboratory.[9]

The proton magnetic resonance (PMR) spectra were recorded on a JEOL JNM PS-100 NMR spectrometer at 25 °C, using TMSP as the internal reference. The infrared absorption (IR) spectra in the 700—4000 cm^{-1} region were measured by means of a KBr disc method using a JASCO IRA-2 grating infrared spectrophotometer. The far-infrared spectra were taken by the Nujol method using a JASCO IR-F far-infrared spectrophotometer.

The isomerization of the *trans*-$[Co(CO_3)_2(py)_2]^-$ species was monitored spectrophotometrically at 400 and 560 nm at 25 °C under the following conditions: $[Co^{III}\ complex]=(4.30-4.72)\times10^{-3}$ M, $[HCO_3^-]=0.25$ M, $[H^+]=3.98\times10^{-9}$ M and $[py]=6.18\times10^{-6}$ M. The ionic strength was made up to 1.0 M with KCl. The pH measurement was carried out with a Hitachi-Horiba M-7E pH-meter.

The calculations for curve analysis were carried out at Data Processing Center, Kanazawa University.

Results and Discussion

Characterization. In a previous work,[5] we characterized two isomers of the $[Co(CO_3)_2(py)_2]^-$ complex on the basis of the electronic absorption and the far-infrared spectra; the isomer which exhibits a distinct splitting in the second absorption band and a very simple pattern of the far-infrared spectrum was determined to be the *trans* isomer. Figure 1 shows the solution spectra for the isomers obtained at the earlier stage in each synthesis of the $[CoCO_3ox(py)_2]^-$ and $[Co(ox)_2(py)_2]^-$ complexes, the spectrum of the *trans*-$[Co(CO_3)_2(py)_2]^-$ being included for comparison. Both the isomers exhibit splittings of the second absorption bands (IIa and IIb), although the extents of the splittings are considerably reduced compared with that for *trans*-$[Co(CO_3)_2(py)_2]^-$. The absorption spectrum of the isomer obtained at the later stage in the synthesis of the $[Co(ox)_2(py)_2]^-$ complex and the spectrum of the *cis*-$[Co(CO_3)_2(py)_2]^-$ complex are compared in Fig. 2.

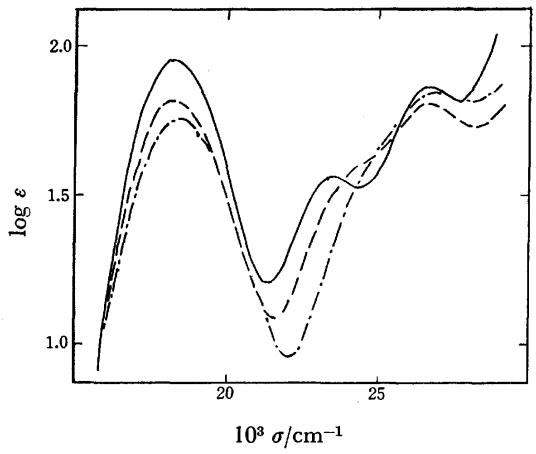

Fig. 1. Absorption spectra of *trans* isomers of; - - - $[CoCO_3ox(py)_2]^-$, —·—$[Co(ox)_2(py)_2]^-$, and —— $[Co(CO_3)_2(py)_2]^-$.

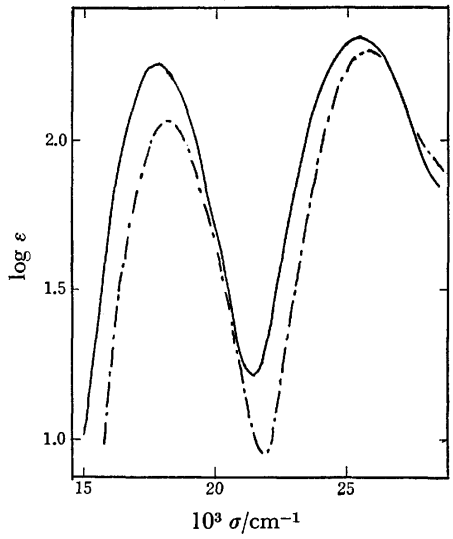

Fig. 2. Absorption spectra of *cis* isomers of; —·— $[Co(ox)_2(py)_2]^-$ and —— $[Co(CO_3)_2(py)_2]^-$.

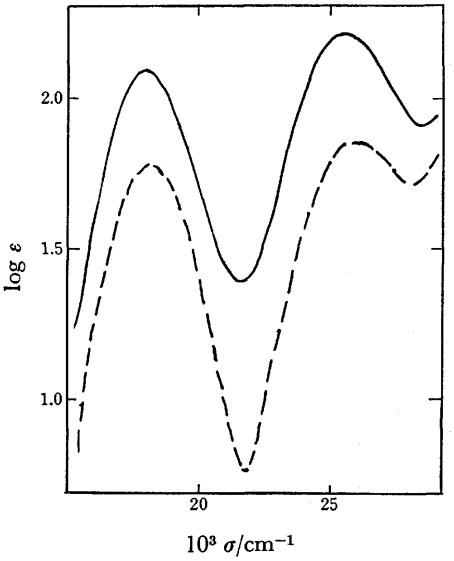

Fig. 3. Absorption spectra of;
---- *trans*-$[Co(mal)_2(py)_2]^-$ and
—— *cis*-$[Co(mal)_2(py)_2]^-$.

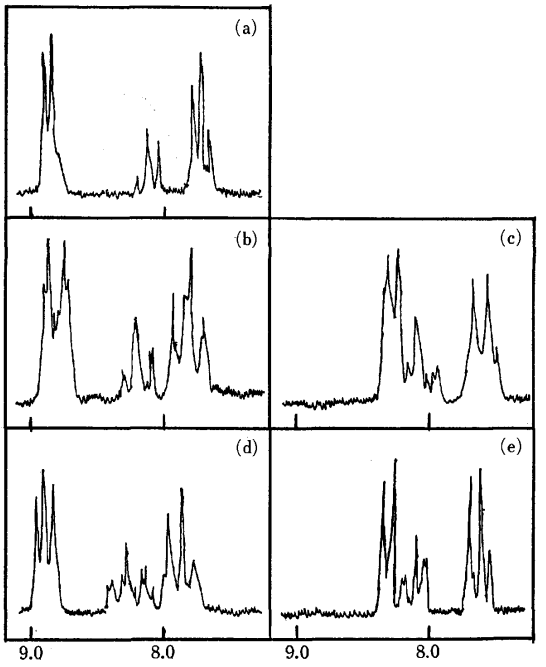

Fig. 4. PMR spectra of;
a) *trans*-$[CoCO_3ox(py_2)]^-$, b) *trans*-$[Co(ox)_2(py)_2]^-$, c) *cis*-$[Co(ox)_2(py)_2]^-$, d) *trans*-$[Co(mal)_2(py)_2]^-$ and e) *cis*-$[Co(mal)_2(py)_2]^-$.

The spectra in the two figures are quite similar to each other. From a comparison of the spectra, the present isomers can be characterized.

The absorption spectra of the two isomers of the $[Co(mal)_2(py)_2]^-$ complex are shown in Fig. 3. The spectra are similar to each other except that there is a considerable difference in ε value between the isomers. However, as a successful resolution was effected with the isomer obtained at a later stage in the synthesis, the *cis* configuration is assigned to that isomer. Consequently, the remainder is regarded as the *trans* isomer. In this connection, the optical resolution was performed with one isomer of the $[Co(CO_3)_2(py)_2]^-$ complex and one of the $[Co(ox)_2(py)_2]^-$ complex. Our CD spectral studies of these *cis*-$[Co(O-O)_2(N)_2]^-$-type complexes[10] will be reported in a subsequent paper.

The PMR spectra of the present bis(pyridine) complexes are shown in Fig. 4. It is well known that, in free pyridine, the α-, γ-, and β-protons resonate at 8.50, 7.36, and 6.98 ppm (*vs.* TMSP) respectively. In the present complexes, these protons resonate at lower fields; for the *trans* isomers, at 8.9—8.7 ppm (α), 8.2—8.0 ppm (γ), and 8.0—7.6 ppm (β), while for the *cis* isomers, at 8.4—8.2 (α), 8.2—7.9 (γ), and 7.7—7.4 (β). A marked difference in chemical shift is observed between the α-protons of a *trans* isomer and those of the corresponding *cis* isomer. This phenomenon can be understood by the empirical rule of Watabe *et al.*[11] found from the studies of α-amino carboxylato complexes of cobalt(III): "The methine proton adjacent to the coordinated N atom resonates at a higher magnetic field when the O atom occupies the site *trans* to the N atom than when the N atom occupies the same site." The former case applies to the present *cis* isomer, which exhibits the resonance due to the α-protons at a higher magnetic field, the latter case, to the *trans* isomer.

Properties. The present compounds are all soluble in water, methanol, and ethanol. No *cis* isomer could be isolated as potassium or sodium salt because of their great solubilities in either an aqueous or an alcoholic medium. The use of the $[Coox(en)_2]^+$ ion as a counter ion was effective for the isolation of the *cis*-$[Co(mal)_2(py)_2]^-$ complex. The *cis*-$[Co(ox)_2(py)_2]^-$ complex was isolated as the lithium salt. The isolation of the *cis*-$[CoCO_3ox(py)_2]^-$ complex was unsuccessful in spite of various attempts. With respect to the corresponding *trans* isomers, all of the complexes were isolated as potassium salts.

Davies and Hung[12] investigated the kinetics of the reaction between the $[Co(CO_3)_3]^{3-}$ species and excess pyridine in an aqueous sodium hydrogencarbonate medium and reported that the reaction produced only the *cis*-$[Co(CO_3)_2(py)_2]^-$ species. Contrary to their statement, we found an isomerization of the *trans*-$[Co(CO_3)_2(py)_2]^-$ species; under the conditions mentioned in Experimental, *ca.* 40% of the initial amount of the *trans* species isomerized to the *cis* species after 12 h, and *ca.* 70% after 22 h, while the reaction was completed after 3 days.

The *trans*-$[CoCO_3ox(py)_2]^-$ species was acid-hydrolyzed in aqueous perchloric acid to give the *trans*-$[Coox(H_2O)_2(py)_2]^+$ species; the hydrolysis proceeded slowly. In a 10% perchloric acid medium, it took about an hour to complete the reaction. The absorption spectrum of the diaqua complex species thus produced is shown in Fig. 5.

The *trans*- and *cis*-$[Co(CO_3)_2(py)_2]^-$ species are also hydrolyzed in the same acid medium to give diaquacarbonato species. However, the species produced are not pure chromatographically because of the rather unstable nature of the parent dicarbonato species in an aqueous medium.

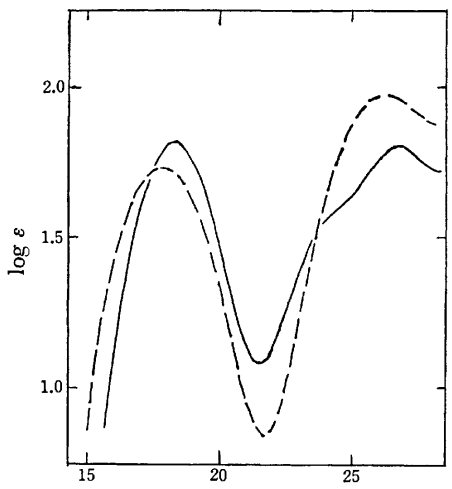

Fig. 5. Absorption spectra of;
—— *trans*-[Coox$(H_2O)_2(py)_2]^+$ and —— *trans*-[$CoCO_3$-ox$(py)_2]^-$.

When excess ammonia reacts on the $[Co(CO_3)_3]^{3-}$ complex, the reaction proceeds successively, yielding *cis*-$[Co(CO_3)_2(NH_3)_2]^-$ and then $[CoCO_3(NH_3)_4]^+$.[1] In contrast, the action of excess pyridine on the $[Co(CO_3)_3]^{3-}$ complex gives only the *trans*- and *cis*-$[Co(CO_3)_2(py)_2]^-$ complexes, no further reaction to give the tetrakis(pyridine) complex occurring. Springborg and Schäffer[13] reported that the action of excess pyridine on an aqueous potaasium bicarbonate solution of the $[Co(CO_3)_3]^{3-}$ complex, which had been prepared using $CoCl_2 \cdot 6H_2O$, at room temperature, yielded the $[CoClCO_3(py)_3]$ complex after 2—3 days. Further, the action of pyridine on this tris(pyridine) complex in the presence of bis(pyridine)mercury(II) perchlorate gave the tetrakis(pyridine) complex $[CoCO_3(py)_4]^+$. The acid decomposition of this carbonato complex to give carbon dioxide is unusually slow and results in the formation of the *trans*-$[Co(H_2O)_2(py)_4]^{3+}$ species.[13]

The coordination of the O–O donor ligands was ascertained from the IR spectral data according to the literature.[14,15] As to the IR spectra of pyridine complexes, Gill *et al.*[16] pointed out that coordinated pyridine is usually distinguished from the free base by the presence of a weak band between 1235 and 1250 cm^{-1}, by a shift of the strong 1578 cm^{-1} band to 1600 cm^{-1}, and by shifts of the 601 and 403 cm^{-1} bands to 625 and

Table 1. Absorption spectral data of *trans*(*N*) complexes ($\tilde{\nu}$ in 10^3 cm^{-1})

Complex		I		IIa		IIb	
		$\tilde{\nu}_{max}$ (log ε)	Half-width	$\tilde{\nu}_{max}$ (log ε)	Half-width	$\tilde{\nu}_{max}$ (log ε)	Half-width
trans-$[Co(CO_3)_2(py)_2]^-$	obsd	18.2 (1.95)	3.00	23.5 (1.56)		26.7 (1.86)	
	calcd[a]	18.2 (1.95)	2.93	23.3 (1.55)	3.42	26.5 (1.76)	2.48
trans-$[CoCO_3ox(py)_2]^-$	obsd	18.2 (1.82)	3.12	*ca.* 23.8		26.7 (1.80)	
	calcd[a]	18.2 (1.82)	3.06	23.8 (1.47)	2.92	26.6 (1.75)	3.02
trans-$[Co(ox)_2(py)_2]^-$	obsd	18.4 (1.76)	3.25	*ca.* 24.2		26.7 (1.84)	
	calcd[a]	18.4 (1.76)	3.12	24.0 (1.25)	2.57	26.7 (1.79)	3.53

Complex	I		II	
	$\tilde{\nu}_{max}$ (log ε)	Half-width	$\tilde{\nu}_{max}$ (log ε)	Half-width
trans-$[Co(mal)_2(py)_2]^-$	18.1 (1.78)	3.31	26.0 (1.85)	4.05
trans-$[Co\ ox(H_2O)_2(py)_2]^+$	17.9 (1.73)	3.70	26.5 (1.95)	4.12

Complex	Ia	Ib	II
trans(*N*)-$[Co\ ox(gly)_2]^-$ [b]	16.7 (1.70)	18.9 (2.00)	25.8 (2.23)
trans(*N*)-$[Co(ida)_2]^-$ [b]	16.7 (1.05)	20.4 (1.72)	27.8 (1.75)
trans(*N*)-$[Co(L\text{-}asp)_2]^-$ [b]	15.9 (1.16)	19.5 (1.90)	26.5 (1.90)

a) Results from Gaussian Analysis. b) Ref. 17.

Table 2. Absorption spectral data of the *cis* complexes ($\tilde{\nu}$ in 10^3 cm^{-1})

Complex	I		II	
	$\tilde{\nu}_{max}$ (log ε)	Half-width	$\tilde{\nu}_{max}$ (log ε)	Half-width
cis-$[Co(CO_3)_2(py)_2]^-$	17.7 (2.24)	2.94	25.5 (2.34)	3.77
cis-$[Co(Cx)_2(py)_2]^-$	18.2 (2.06)	2.89	25.8 (2.29)	3.58
cis-$[Co(mal)_2(py)_2]^-$	18.0 (2.07)	3.23	25.4 (2.20)	3.72
C_2-*cis*(*N*)-$[Coox(gly)_2]^-$ [a]	17.8 (2.08)	—	25.9 (2.20)	—
C_1-*cis*(*N*)-$[Coox(gly)_2]^-$ [a]	18.3 (2.15)	—	25.8 (2.24)	—
cis(*N*)-$[Co(ida)_2]^-$ [a]	17.8 (2.18)	—	26.3 (2.13)	—
cis(*N*)*trans*(O_6)-$[Co(L\text{-}asp)_2]^-$ [a]	*ca.* 16.7 (1.90) 19.2 (2.25)	—	26.2 (1.87)	—
cis(*N*)*trans*(O_5)-$[Co(L\text{-}asp)_2]^-$ [a]	17.2 (2.09) *ca.* 20.0 (1.88)	—	26.5 (1.80)	—

a) Ref. 17.

420 cm^{-1} respectively. In our spectra, a similar trend was observed; a weak 1250 cm^{-1} band was observed in the spectrum of each of the dicarbonato and carbonato-oxalato complexes (in the spectra of the other complexes, this absorption region was hidden by other bands). The strong band at *ca.* 1580 cm^{-1} in the free base shifted to 1600—1610 cm^{-1}. The shifts in the *ca.* 600 and 400 cm^{-1} bands could not be identified, because other bands due to the coordinated O-O ligands occurred. There was little difference in the spectrum of the 700—4000 cm^{-1} region between any isomeric pair of the complexes. In the far-infrared region, however, a marked difference was observed between the *trans* and *cis* isomers of the $[Co(CO_3)_2(py)_2]^-$ complex,[5] while the spectra of the other isomeric complexes were weak and broad.

Absorption Spectra. In order to discuss this subject in some detail, we summarize the numerical data on the absorption spectra in Tables 1 and 2, also including the spectral data[17] on some related complexes. As to all the *trans* isomers except for the *trans*-bis(malonato) complex, the observed spectra were divided into three Gaussians (I, IIa, and IIb);[18] the calculations were repeated until the corrections became sufficiently small. The calculated data are included in Table 1 and are illustrated in Fig. 6.

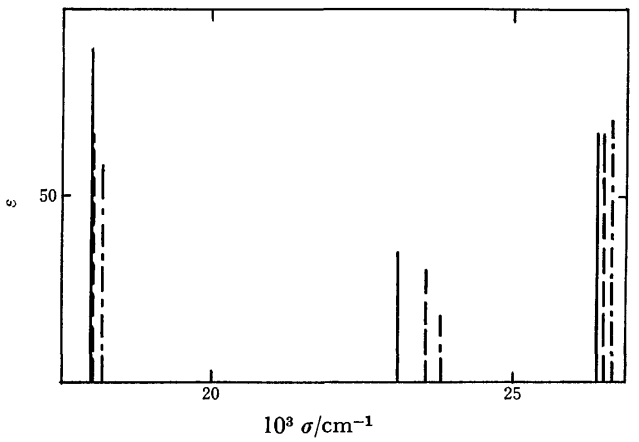

Fig. 6. Calculated positions and intensities for absorption maxima;
----- $[CoCO_3ox(py)_2]^-$, —·— $[Co(ox)_2(py)_2]^-$ and
—— $[Co(CO_3)_2(py)_2]^-$.

Most of the $[CoN_2O_4]^-$-type complexes thus far prepared contain the N-donor in the form of an amino acidate, iminodiacetate, or nitrilotriacetate ion, and their *trans*(*N*) isomers exhibit explicit splittings of their first absorption bands (Table 1).[17,19-21] The situation differs in the present complexes, which contain unidentate pyridine molecules; the *trans*-$[Co(CO_3)_2(py)_2]^-$, *trans*-$[CoCO_3ox(py)_2]^-$ and *trans*-$[Co(ox)_2(py)_2]^-$ complexes exhibit the first bands which can be expressed by only one Gaussian and the second bands which can be divided into two Gaussians, while the *trans*-$[Co(mal)_2(py)_2]^-$ complex shows no splittings in either the first or the second absorption band. As far as the *cis* isomers are concerned, their spectra are typical of the *cis*-$[CoN_2O_4]^-$-type (Table 2).

When the spectral data of the above-mentioned three *trans* isomers are compared with each other, the following tendencies can be found:

1) The maximum positions of the I bands are similar to each other. This was a rather unexpected fact in view of the ligand-field-strengths of the two ligands (the Δ values for octahedral $[Co(O-O)_3]^{3-}$ complexes are 17300 cm^{-1} (CO_3^{2-}) and 18000 cm^{-1} ($C_2O_4^{2-}$)).[22] The ε_{max} values decrease in the order of the dicarbonato, carbonatooxalato, and bis(oxalato) isomers.

2) The half-widths of the I bands are all narrow, but they tend to broaden progressively from the dicarbonato to the bis(oxalato) isomer.

3) The maximum positions of the IIa bands shift to shorter wavelengths in the order of the dicarbonato, carbonatooxalato, and bis(oxalato) isomers, and the ε_{max} values decrease in the same order. The half-widths also decrease in this order.

4) The IIb maxima are located at almost the same positions, and the ε_{max} values are nearly identical. The half-widths increase from the dicarbonato to the bis(oxalato) isomer.

Let us first discuss the assignment of the absorption bands for the three *trans* isomers besides the bis(malonato) isomer. It is well known that, under the D_{4h} symmetry, the $^1T_{1g}$ component in the O_h parentage splits into the $^1E_g{}^a$ and $^1A_{2g}$ components and the $^1T_{2g}$ into the $^1E_g{}^b$ and $^1B_{2g}$. From a comparison of our spectral data on the $^1T_{1g}$ region with those of the related *trans*(*N*)-$[CoN_2O_4]^-$-type complexes, it can be said that the observed I bands (18200—18400 cm^{-1}) are mainly due to the $^1A_{1g}\rightarrow{}^1E_g{}^a$ transition; the transitions to the $^1A_{2g}$ component are perhaps hidden by the feet of the I bands.

For the assignment of the IIa and IIb bands, the π contributions from the N and O donors must be considered. Schäffer *et al.*[23] have recently reported π-back bonding due to the N ligators with respect to the *trans*-$[Cr(py)_4AB]^{n+}$-type complexes. On the other hand, we previously reported that the positions of the IIa and IIb bands for the *trans*-$[Co(CO_3)_2(py)_2]^-$ complex calculated by means of Yamatera's prediction[24] roughly agreeded with the observed positions, although any π contribution was ignored in the calculation. We shall discuss this subject in more detail below.

According to the Angular Overlap Model,[25] the energies of the $(t_{2g})^6\rightarrow(t_{2g})^5(e_g)$ transition in a complex whose holohedrized symmetry is D_{4h} are expressed as follows:

$$\mathbf{E}(A_{2g}) = \langle x^2-y^2|\mathbf{A}|x^2-y^2\rangle - \langle xy|\mathbf{A}|xy\rangle - C \quad (1)$$

$$\mathbf{E}(B_{2g}) = \langle z^2|\mathbf{A}|z^2\rangle - \langle xy|\mathbf{A}|xy\rangle + 16B - C \quad (2)$$

$$\begin{vmatrix} E_g{}^a & \begin{matrix}3/4\langle z^2|\mathbf{A}|z^2\rangle \\ +1/4\langle x^2-y^2|\mathbf{A}|x^2-y^2\rangle \\ -\langle yz|\mathbf{A}|yz\rangle - C - \mathbf{E}\end{matrix} & \begin{matrix}\sqrt{3}/4\{\langle z^2|\mathbf{A}|z^2\rangle \\ -\langle x^2-y^2|\mathbf{A}|x^2-y^2\rangle\}\end{matrix} \\ E_g{}^b & \begin{matrix}\sqrt{3}/4\{\langle z^2|\mathbf{A}|z^2\rangle \\ -\langle x^2-y^2|\mathbf{A}|x^2-y^2\rangle\}\end{matrix} & \begin{matrix}1/4\langle z^2|\mathbf{A}|z^2\rangle \\ +3/4\langle x^2-y^2|\mathbf{A}|x^2-y^2\rangle \\ -\langle yz|\mathbf{A}|yz\rangle + 16B \\ -C-\mathbf{E}\end{matrix} \end{vmatrix} = 0 \quad (3)$$

where **A** represents a one-electron potential operator, and

where B and C denote Racah parameters. From these relations, the energies of the degenerate E_g states can be expressed by the parameters B and C, and the energies $\mathbf{E}(A_{2g})$ and $\mathbf{E}(B_{2g})$ and the energy difference between d_{yz} antibonding energy and d_{xy} antibonding energy, $\langle yz|\mathbf{A}|yz\rangle - \langle xy|\mathbf{A}|xy\rangle$ ($\equiv\Delta\mathbf{E}(\pi)$). Actually the $\mathbf{E}(B_{2g})$ value as well as the $\mathbf{E}(E_g{}^b)$ value can be estimated from the observed IIa maximum and the IIb maximum, and the $\mathbf{E}(A_{2g})$ value from the related complexes which exhibit remarkable splittings in their I band region. Thus, assuming C=4B,[26] the variation in the $\mathbf{E}(E_g{}^a)$ or the $\Delta\mathbf{E}(\pi)$ with varying B values is found.

Let us take the *trans*-$[Co(ox)_2(py)_2]^-$ complex as a representative example; we assume two cases, one of which is that the IIb band is assumed to be the $^1A_{1g}\rightarrow{}^1B_{2g}$ transition (Case a), and the other is that the IIb band is assumed to be the $^1A_{1g}\rightarrow{}^1E_g{}^b$ transition (Case b). For the $\mathbf{E}(A_{2g})$ value, various values are adopted in the 16000—17000 cm^{-1} region. The B parameter varies in the 400—520 cm^{-1} range. The results are illustrated in Figs. 7 and 8.

In Case a, the calculated $\mathbf{E}(E_g{}^a)$ values are almost independent of the varying $\mathbf{E}(A_{2g})$ values, and the estimated $\Delta\mathbf{E}(\pi)$ has positive values. On the other hand, in Case b the $\mathbf{E}(E_g{}^a)$ values are sensitive to the variation in the $\mathbf{E}(A_{2g})$, and the $\Delta\mathbf{E}(\pi)$ has negative values, which are evidence for a net π back-bonding from metal(III) to ligand. In this connection, for the other *trans* bis(pyridine) complexes similar situations were obtained.

The most suitable B value can be evaluated by fitting a calculated $\mathbf{E}(E_g{}^a)$ value to the observed I maximum; the value is estimated to be less than 400 cm^{-1} in Case a, while in Case b it is *ca.* 480 cm^{-1}. In view of the separation between the I maximum and the II maximum for the *cis*-$[Co(ox)_2(py)_2]^-$ complex, the value in Case a

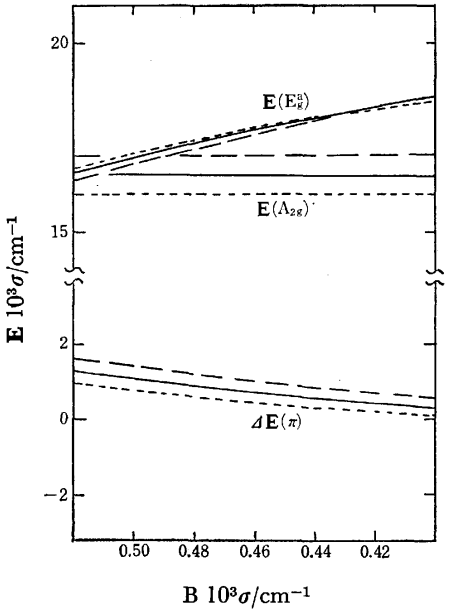

Fig. 7. The variation of $\mathbf{E}(E_g{}^a)$ or $\Delta\mathbf{E}(\pi)$ with B (Case a);
----$\mathbf{E}(A_{2g})=17000$, ——$\mathbf{E}(A_{2g})=16500$ and ·····$\mathbf{E}(A_{2g})=16000$ cm^{-1}.

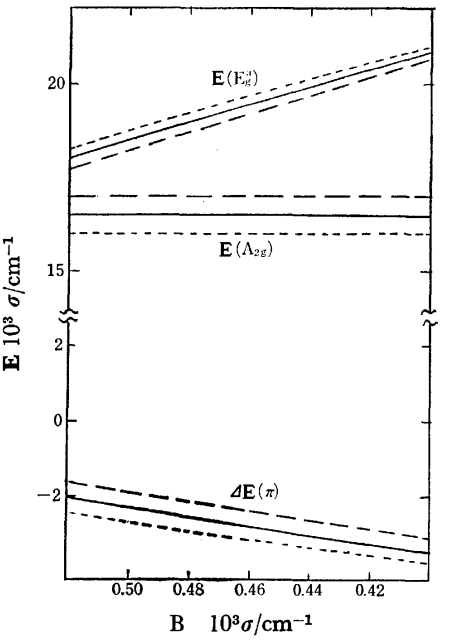

Fig. 8. The variation of $\mathbf{E}(E_g{}^a)$ or $\Delta\mathbf{E}(\pi)$ with B (Case b);
----$\mathbf{E}(A_{2g})=17000$, ——$\mathbf{E}(A_{2g})=16500$ and ·····$\mathbf{E}(A_{2g})=16000$ cm^{-1}.

($\approx$400 cm^{-1}) seems to lose its physical meaning.

Since the $^1A_{1g}\rightarrow{}^1A_{2g}$ and the $^1A_{1g}\rightarrow{}^1B_{2g}$ transitions correspond to the $xy\rightarrow x^2-y^2$ and the $xy\rightarrow z^2$ transitions respectively, the ratio of the transition oscillator strengths can be derived in a way similar to that used for the O_h transitions:[27]

$$\frac{f_{A_2}}{f_{B_2}}=\frac{3\times\mathbf{E}(A_2)}{\mathbf{E}(B_2)}\times\left(\frac{\mathbf{E}(B_2)-\mathbf{E}(CT)}{\mathbf{E}(A_2)-\mathbf{E}(CT)}\right)^2. \qquad (4)$$

Using this equation, the intensity of the $^1A_{1g}\rightarrow{}^1A_{2g}$ transition can be evaluated for the *trans*-$[Co(ox)_2(py)_2]^-$ complex; the $\mathbf{E}(A_{2g})$ value is estimated to be *ca.* 17000 cm^{-1} in view of the Ia maxima of the *trans*(*N*)-$[Co(ida)_2]^-$ and *trans*(*N*)-$[Coox(gly)_2]^-$ complexes (Table 1). The $\mathbf{E}(CT)$ value is assumed to be 41000 cm^{-1}, which corresponds to the CT maximum for the $[Co(ox)_3]^{3-}$ complex. Thus, the ε_{max} value due to the $^1A_{1g}\rightarrow{}^1A_{2g}$ transition is calculated to be *ca.* 42 in Case a and *ca.* 19 in Case b. If the fact that the observed I maximum has $\varepsilon_{max}=57.5$ is taken into consideration, then the ε_{max} in Case a seems to be too large. As to the *trans*-$[Co(CO_3)_2(py)_2]^-$ complex, it is difficult to adopt the same discussion about the intensity because the symmetry of this complex is actually lower than D_{4h}; in addition, the $\mathbf{E}(A_{2g})$ value is hard to estimate. On the basis of these considerations, we now assign the IIa band to the $^1A_{1g}\rightarrow{}^1B_{2g}$ transition and the IIb band to the $^1A_{1g}\rightarrow{}^1E_g{}^b$ transition.

In this connection, the same procedure was applied to the spectral data for the *trans*(*N*)-$[CoCO_3(mda)(NH_3)]^-$ (mda=*N*-methyliminodiacetate ion) complex[28] in order to find the variation in $\mathbf{E}(E_g{}^a)$ or $\Delta\mathbf{E}(\pi)$ with B. The results were quite similar; this fact suggests the minor contribution of the π bonding character due

to coordinated py molecules in the present bis(pyridine) complexes.

We adopt the more reasonable B value, 480 cm^{-1}. The $\langle xy|\mathbf{A}|xy\rangle$ value is assumed to be zero, because two p orbitals of any O donor in xy molecular plane are already used for σ hybridizations and so cannot be of any use in the π bondings. Using such a value, the π antibonding energy in the yz plane is evaluated to be:

$$\langle yz|\mathbf{A}|yz\rangle = -2200\,cm^{-1}. \quad (5)$$

This is expressed alternatively in terms of ligand-field parameters;

$$\Delta(O) + \Delta(N) = -4400\,cm^{-1}. \quad (6)$$

This value is more negative than the $\Delta(N)$ value (-3400——2000 cm^{-1}) for the *trans*-$[Cr(py)_4AB]^{n+}$-type complexes.[23] When the energies from the ligand to metal-charge-transfer transitions are compared between the $[Co(acac)_3]$ and $[Cr(acac)_3]$ complexes,[29] it is found that the metal orbitals in the cobalt(III) complex lie at rather lower levels than those in the chromium(III) complex, suggesting the existence of π-bonding contributions due to O-O donors in the present cobalt(III) complexes.

Let us next consider the spectrum of the *trans*-$[Co(mal)_2(py)_2]^-$ complex. No shoulder is observed in the I band, but the maximum shifts to a longer wavelength compared with those for the other *trans* isomers, and the half-width is enhanced. These facts suggest that the absorption due to the $^1A_{1g}\rightarrow{}^1A_{2g}$ transition gains a certain amount of intensity. The II band maximum also shifts to a considerably longer wavelength compared with the maxima of the IIb bands for the other isomers, and the half-width is also enhanced. These facts suggest that the absorptions due to the $^1A_{1g}\rightarrow{}^1B_{2g}$ and $^1A_{1g}\rightarrow{}^1E_g{}^b$ transitions occur in a closely-neighboring region with the comparable intensities. The same facts can be found more clearly in the spectrum of the *trans*-$[Coox(H_2O)_2(py)_2]^+$ complex (Fig. 5 and Table 1).

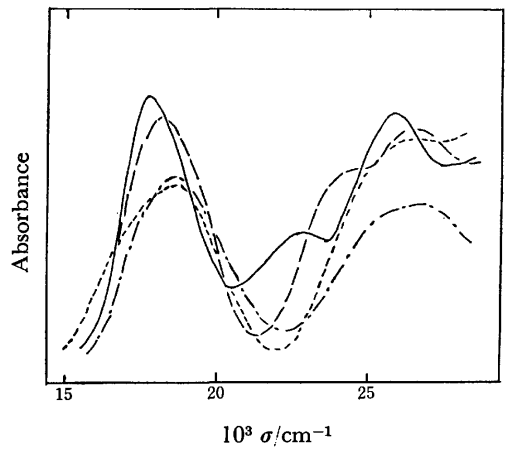

Fig. 9. Crystal spectra of *trans* isomers of;
—— $K[Co(CO_3)_2(py)_2]\cdot 3H_2O$,
---- $K[CoCO_3ox(py)_2]\cdot 2.5H_2O$,
-·-·- $K[Co(ox)_2(py)_2]\cdot 3H_2O$,
····· $K[Co(mal)_2(py)_2]\cdot 2H_2O$.

Figure 9 shows the nonpolarized crystal spectra of the *trans*-isomers; every spectrum resembles the corresponding solution spectrum in shape, but it is noteworthy that the spectrum of the *trans*-$[Co(mal)_2(py)_2]\cdot 2H_2O$ shows a shoulder on the longer-wavelength side (*ca.* 16400 cm^{-1}) of the main I band (18600 cm^{-1}). This may be due to the $^1A_{1g}\rightarrow{}^1A_{2g}$ transition, which disappears in the solution spectrum.

References

1) M. Shibata, *Nippon Kagaku Zasshi*, **87**, 771 (1966).
2) H. Ichikawa and M. Shibata, *Bull. Chem. Soc. Jpn.*, **42**, 2873 (1969).
3) S. Fujinami and M. Shibata, *Bull. Chem. Soc. Jpn.*, **46**, 3443 (1973).
4) M. Shibata, *Proc. Jpn. Acad.*, **50**, 779 (1974).
5) Y. Ida, K. Kobayashi, and M. Shibata, *Chem. Lett.*, **1974**, 1299.
6) *Inorg. Synth.*, Vol. 1, 37 (1939).
7) N. C. Kneten and S. T. Spees, *J. Inorg. Nucl. Chem.*, **33**, 2437 (1971).
8) F. P. Dwyer, I. K. Reid, and F. L. Garvan, *J. Am. Chem. Soc.*, **83**, 1285 (1961).
9) S. Nagasaki and M. Shibata, *Bull. Chem. Soc. Jpn.*, **49**, 2329 (1976).
10) S. Muramoto and M. Shibata, Presented in part at the 26 th Symposium of Coordination Chemistry, Sapporo, August, 1976.
11) M. Watabe, K. Onuki, and S. Yoshikawa, *Bull. Chem. Soc. Jpn.*, **48**, 687 (1975).
12) G. Davies and Y. Hung, *Inorg. Chem.*, **15**, 704 (1976).
13) J. Springborg and C. E. Schäffer, *Acta Chem. Scand.*, **27**, 3312 (1973).
14) K. Nakamoto, J. Fujita, S. Tanaka, and M. Kobayashi, *J. Am. Chem. Soc.*, **79**, 4904 (1957).
15) J. Fujita, K. Nakamoto, and M. Kobayashi, *J. Phys. Chem.*, **61**, 1014 (1957).
16) N. S. Gill, R. H. Nuttall, D. E. Scaife, and D. W. A. Sharp, *J. Inorg. Nucl. Chem.*, **18**, 79 (1961).
17) S. Yamada, J. Hidaka, and B. E. Douglas, *Inorg. Chem.*, **10**, 2187 (1971).
18) L. M. Schwarz, *Anal. Chem.*, **43**, 1336 (1971).
19) N. Matsuoka, J. Hidaka, and Y. Shimura, *Bull. Chem. Soc. Jpn.*, **40**, 1868 (1967).
20) N. Koine, N. Sakota, J. Hidaka, and Y. Shimura, *Bull. Chem. Soc. Jpn.*, **42**, 1583 (1969).
21) N. Matsuoka, J. Hidaka, and Y. Shimura, *Inorg. Chem.*, **9**, 719 (1970).
22) C. K. Jørgensen,"Absorption Spectra and Chemical Bonding in Complexes," Pergamon Press (1962), p. 110.
23) J. Glerup, O. Monsted, and C. E. Schäffer, *Inorg. Chem.*, **15**, 1399 (1976).
24) H. Yamatera, *Bull. Chem. Soc. Jpn.*, **31**, 95 (1958).
25) C. E. Schäffer, *Structure and Bonding*, **5**, 68 (1968); C. E. Schäffer, *Pure Appl. Chem.*, **24**, 361 (1970).
26) Since the parameter C is involved in each transition energy to the same extent, the relation between B and C has no influence upon the results of the calculating process.
27) R. F. Fenske, *J. Am. Chem. Soc.*, **89**, 252 (1967).
28) S. Nakashima and M. Shibata, *Bull. Chem. Soc. Jpn.*, **48**, 3128 (1975).
29) Y. Murakami and K. Nakamura, *Bull. Chem. Soc. Jpn.*, **39**, 901 (1966).

Association Constants of Optically Active $[Co(en)_3]^{3+}$ with (+)-Tartrate and Fumarate Ions Determined from the Kinetic Data of Hydrogen-Deuterium Exchange

Miho FUJITA* and Hideo YAMATERA

Department of Chemistry, Faculty of Science, Nagoya University, Chikusa, Nagoya 464

(Received April 25, 1977)

The hydrogen-deuterium exchange rates of *Λ*- and *Δ*-$[Co(en)_3]^{3+}$ were measured in D_2O solutions containing (+)-tartrate ions. From the kinetic data, the ion-association constants of the *Λ*- and *Δ*-isomers with (+)-tartrate ions were determined to be 40 and 32 (I=0.1) respectively. Similar measurements with fumarate resulted in the association constant of 16 (I=0.1).

In a previous paper,[1] we preliminarily reported the stereoselective hydrogen-deuterium exchange reaction of *Λ*- and *Δ*-$[Co(en)_3]^{3+}$ in D_2O solutions in the presence of (+)-tartrate ions.

The present paper will give a further analysis of the experimental results on the exchange reaction rates, from which the association constants of *Λ*- and *Δ*-$[Co(en)_3]^{3+}$ with the (+)-tartrate ion and with the fumarate ion will be derived.

Experimental

$[Co(en)_3]Br_3 \cdot H_2O$ was prepared by the usual method and resolved into the optical isomers by using silver (+)- and (−)-tartrate. The *Λ*- and *Δ*-$[Co(en)_3]Br_3 \cdot H_2O$ obtained showed $[\alpha]_D$ values of +125 ° and −124 ° respectively. (+)-Tartrate buffer solutions of a constant pH value (pH=5.00±0.03)** were prepared by dissolving the acid and its sodium salt at a given ratio in a E. Merck D_2O with an isotopic purity of 99.75%; the concentrations of sodium (+)-tartrate in these buffer solutions ranged from 0.006 to 0.15 M (=mol dm^{-3}). The fumarate buffer solutions (pH=5.33±0.03, 0.025—0.12 M) were similarly prepared.

After the complex had been dissolved in the buffer solutions at a constant concentration (0.03 M), the hydrogen-deuterium exchange rates were measured at 25.0 °C. The first-order rate constants were determined in the way described in a previous paper.[1]

Results and Discussion

Table 1 shows the first-order rate constants, k, of hydrogen-deuterium exchange reactions of *Λ*- and *Δ*-$[Co(en)_3]^{3+}$ in the presence of (+)-tartrate and of fumarate. The rate constants decreased with the increase in the (+)-tartrate concentration; the change in the rate constant was greater for *Λ*-$[Co(en)_3]^{3+}$ than for the *Δ*-isomer, showing a stereoselectivity between *Λ*- and *Δ*-$[Co(en)_3]^{3+}$ in the interaction with (+)-tartrate ions. Fumarate ions had a smaller effect without stereoselectivity. These data were analyzed in order to determine the association constants of *Λ*- and *Δ*-$[Co(en)_3]^{3+}$ with (+)-tartrate ions and with fumarate ions on the following assumptions:

Table 1. First-order rate costants of hydrogen-deuterium exchange reactions of *Λ*- and *Δ*-$[Co(en)_3]^{3+}$ in D_2O[a]

[(+)-tartrate]/M[b]	$10^4 k/s^{-1}$ *Λ*	$10^4 k/s^{-1}$ *Δ*	[fumarate]/M[c]	$10^3 k/s^{-1}$ *Λ*, *Δ*
0.00614	13.7	13.9	0.0240	3.05
0.0191	11.3	11.9	0.0248	3.00
0.0254	10.5	10.6	0.0359	2.53
0.0487	7.63	8.23	0.0467	2.38
0.0664	6.02	6.70	0.0700	2.02
0.0988	4.97	5.28	0.1079	1.73
0.1035	4.77	5.17	0.1228	1.51
0.1225	3.93	4.42		
0.1485	2.72	3.28		
0.2045	2.55	3.05		

a) The $[Co(en)_3]^{3+}$ concentration was 0.03 M in all cases. b) pH 5.00±0.03. c) pH 5.33±0.03.

i) There is the ion-association equilibrium:

$$RH^{3+} + B^{2-} \rightleftharpoons RHB^{+}$$

where RH^{3+} and B^{2-} represent the complex cation and the buffer anion respectively. The association constant, K, is given by:

$$K = \frac{[RHB^+]}{[RH^{3+}][B^{2-}]} \frac{f_1}{f_3 f_2} = \frac{x}{(c_A - x)(c_B - x)} \frac{f_1}{f_3 f_2}, \quad (1)$$

where c_A and c_B are the total concentrations of RH^{3+} and B^{2-} respectively, and x the concentration of the ion-pair, RHB^+, at equilibrium. The f_z (z=1, 2, and 3) notation represents the activity coefficient of the ions with the charge of z or $-z$.

ii) The hydrogen-deuterium exchange proceeds in the following steps:

$$RH^{3+} + OD^- \overset{K_{OD}}{\rightleftharpoons} RHOD^{2+}$$

$$K_{OD} = \frac{[RHOD^{2+}]}{[RH^{3+}][OD^-]} \frac{f_2}{f_3 f_1}, \quad (2)$$

$$RHOD^{2+} \overset{k'}{\longrightarrow} R^{2+} + HOD, \quad (3)$$

$$R^{2+} + D_2O \longrightarrow RD^{3+} + OD^-. \quad (4)$$

Step 3 with the rate constant, k', is rate-determining, and Step 4 is very fast. The activity coefficients were assumed to be identical for ions of the same $|z|$ value.

iii) The rate of the hydrogen-deuterium exchange of RHB^+ is very slow compared with that of RH^{3+}.

* Present address: Department of Chemistry, Nagoya City University, Mizuho, Nagoya 467.

** The pH values in this paper are the apparent ones of D_2O solutions measured with an ordinary pH meter. Two relations, pD=pH(apparent)+0.40[2] and $K_{W(D_2O)}=0.160\times K_{W(H_2O)}$,[3] were used for the determination of $[OD^-]f_{OD^-}$.

On these assumptions, the observed exchange rate, first-order in the concentration of the complex, c_A, is related to the rate of Step 3:

$$kc_A = k'[\mathrm{RHOD}^{2+}]. \quad (5)$$

Equations 2 and 5 give:

$$kc_A = k'K_{OD}[\mathrm{RH}^{3+}]\frac{f_3}{f_2}[\mathrm{OD}^-]f_1. \quad (6)$$

On the other hand, Eq. 1 is transformed to:

$$[\mathrm{RH}^{3+}] = c_A\{1+(c_B-x)\frac{f_3f_2}{f_1}K\}^{-1}. \quad (7)$$

Substituting Eq. 7 into Eq. 6, one obtains:

$$k(f_2/f_3) = k'K_{OD}[\mathrm{OD}^-]f_1\{1+(c_B-x)\frac{f_3f_2}{f_1}K\}^{-1}, \quad (8)$$

or

$$\log k(f_2/f_3) = \log k_{OD} + \log([\mathrm{OD}^-]f_1) - \log\{1+(c_B-x)\frac{f_3f_2}{f_1}K\}, \quad (9)$$

where k_{OD} is substituted for $k'K_{OD}$. Since the values of k_{OD} and $[\mathrm{OD}^-]f_1$ (activity of OD^- ions) are constant in the present experiments, a $-\log(1+X)$ *vs.* $\log X$ curve will fit the $\log k(f_2/f_3)$ *vs.* $\log\{(c_B-x)(f_3f_2/f_1)\}$ plots of the experimental results. The association constant and the k_{OD} value can be determined from the asymptotes of the curve.

The activity coefficient, f_z, was calculated by using the extended Debye-Hückel equation:

$$\log f_z = -\frac{Az^2\sqrt{I}}{1+Ba\sqrt{I}} + bI, \quad (10)$$

with the values of $a=6$ Å and $b=0.1$ z^2. The ionic strength (I) ranged from 0.18 to 0.64 for the sample solutions containing (+)-tartrate and from 0.12 to 0.43 for the fumarate solutions. All the kinetic data were corrected to $I=0.1$ by means of Eq. 10.

An approximate K value was obtained from the curve-fitting with the first approximation of $(c_B-x)(f_3f_2/f_1)=c_B(f_3f_2/f_1)$ and $I=6c_A+3c_B$, and was then used to calculate the value of x with Eq. 1. Then, f_1, f_2, and f_3 were recalculated with $I=6c_A+3c_B-6x$. The second curve-fitting for the $\log k(f_2/f_3)$ *vs.* $\log\{(c_B-x)(f_3f_2/f_1)\}$ plots gave a better K value. Further repetition of the procedure reproduced the K value within the limits of experimental error.

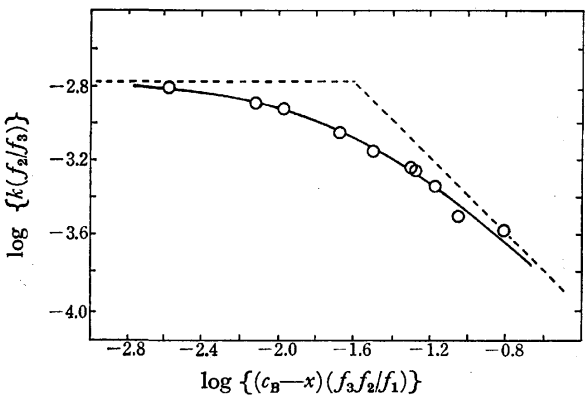

Fig. 1. The curve-fitting for the results on the Λ-[Co(en)$_3$]$^{3+}$-(+)-tartrate(2−) system. ○: Experimental values, ——: the normalized curve, ----: asymptotes for the curve.

Table 2. Values of the association constant, K, and of the rate constant, k_{OD}, at 25 °C

Ion-pair	K This work	K Ref. 4[a]	K Ref. 5[b]	$10^{-6}k_{OD}$/M^{-1} s^{-1} This work
Λ + (+)-tart(2−)	40	26±2	55.8±1.4	4.2
Δ + (+)-tart(2−)	32	21±2	50.4±1.8	4.1
Λ(Δ) + fumarate(2−)	16			4.5

a) Measured at $I=0.1$ (adjusted with $NaClO_4$). b) Corrected to $I=0.1$ using the equation: $\log f_z = -Az^2\sqrt{I}/(1+Ba\sqrt{I})$, with the value of $a=6$Å.

Figure 1 shows a typical example of the curve-fitting for Λ-[Co(en)$_3$]$^{3+}$ after repeated successive approximations as has been described above, while Table 2 summarizes the resulting K and k_{OD} values, together with the literature values. Our K values for the Λ- and Δ-[Co(en)$_3$]$^{3+}$-(+)-tartrate ion-pairs are intermediate between the two sets of literature values[4,5] obtained from spectrophotometric measurements. Yoneda *et al.*[5] have claimed that the smaller K values obtained by Ogino and Saito[4] may be ascribed to the neglect of the association of [Co(en)$_3$]$^{3+}$ with ClO_4^-; the latter authors added $NaClO_4$ to the sample solutions to adjust the ionic strength. In the present experiments, the sample solutions contained a constant amount of bromide ions derived from [Co(en)$_3$]$Br_3\cdot H_2O$. Therefore, our K values may be slightly too small because of the neglect of the association of [Co(en)$_3$]$^{3+}$ with Br^-.

The k_{OD} values given in Table 2 can be compared with the value of 2.4×10^6 M^{-1} s^{-1} obtained by Palmer and Basolo[6] in an acetate buffer solution, considering that different methods were used for the estimation of the OD^- concentrations. As is shown in Table 2, the K values are about twice as large for (+)-tartrate ions as for fumarate ions. This is consistent with the conclusion from our previous circular-dichroism studies that the (+)-tartrate ion would be favored in the formation of hydrogen bonds through N–H hydrogens of the complex ion.[7]

References

1) H. Yamatera and M. Fujita, *Bull. Chem. Soc. Jpn.*, **42**, 3043 (1969).
2) P. K. Glasoe and F. A. Long, *J. Phys. Chem.*, **64**, 188 (1960).
3) V. K. LaMer, *Chem. Rev.*, **19**, 363 (1936).
4) K. Ogino and U. Saito, *Bull. Chem. Soc. Jpn.*, **40**, 826 (1967).
5) H. Yoneda, K. Miyoshi, S. Suzuki, and T. Taura, *Bull. Chem. Soc. Jpn.*, **47**, 1661 (1974).
6) J. W. Palmer and F. Basolo, *J. Inorg. Nucl. Chem.*, **15**, 279 (1960).
7) M. Fujita and H. Yamatera, *Bull. Chem. Soc. Jpn.*, **49**, 1301 (1976).

Complex Formation of Silver(I) Ion with Some Aliphatic Diamines

Hitoshi OHTAKI and Kenji CHO

Department of Electronic Chemistry, Tokyo Institute of Technology at Nagatsuta, Nagatsuta-cho, Midori-ku, Yokohama 227

(Received June 7, 1977)

Complex formation of silver(I) ion with 1,3-propanediamine and 1,4-butanediamine has been studied potentiometrically at 25 °C in 3 mol dm^{-3} $LiClO_4$ aqueous solution. Some additional experiments have been carried out in the system of silver–1,2-ethanediamine of large diamine/Ag ratios, the system having been examined in a previous work at small diamine/Ag ratios. Over the pH range of 6—10.4, the emf data obtained in the silver–diamine solutions could be explained in terms of the formation of the following complexes (L denotes the free diamine molecule): In a solution of low pH (pH=6—8), the $AgHL^{2+}$ and $AgH_2L_2^{3+}$ complexes are formed. In an alkaline solution, the AgL^+, $Ag_2L_2^{2+}$, and AgL_2^+ complexes are formed, and the relative amounts of the complexes depend on the concentrations of the metal and ligand (L) and also the ratio of these concentrations. The Ag(OH)L complex becomes a main species at the highest pH examined. In some cases the formation of the $AgHL_2^{2+}$, $Ag_2HL_2^{3+}$, and Ag_2L^{2+} complexes is suggested from the graphical or computer analysis of the data, but the formation constants of the complexes are rather uncertain. Over the whole pH range examined, the $AgHL^{2+}$, $AgH_2L_2^{3+}$, AgL^+, and $Ag_2L_2^{2+}$ complexes are predominant in all the systems.

In a previous work we studied the complex formation of silver(I) ion with 1,2-ethanediamine and 1,2-propanediamine, and found various protonated and polynuclear complexes.[1] The equilibria between silver(I) and the diamines were more complicated than those described in the preceding papers.[2,3] In addition to the study on the effect of the methyl group attached to the methylene chain previously examined,[1] the effect of the length of the methylene chain on the reaction between silver(I) and diamines was explored in the present work.

Experimental

Reagents. 1,3-Propanediammonium perchlorate and 1,4-butanediammonium perchlorate were prepared from the corresponding diamines and perchloric acid. 1,3-Propanediamine and 1,4-butanediamine were purchased from Wako Pure Chemicals Co., Osaka and Aldrich Chemical Co., Inc., Milwaukee, USA, respectively. The method of preparation of the reagents was described in the previous paper.[1] Other chemicals were the same as those used previously.[1]

Apparatus. Beckman (Nos. 40495 and 40498) glass electrodes were used in combination with the Kawai-type of the half cell[4] for emf measurements. An Orion Digital pH Meter Model 801 was used.

Method of Measurements. During the potentiometic titrations the total concentration of perchlorate ions was kept constant at 3 M (M=mol dm^{-3}) by using lithium perchlorate. The concentrations of silver and diamines were changed over the range of 2—40 mM and 5—160 mM, respectively. The ratio of the concentration of the diamines to that of silver ion (C_L/C_{Ag}) was changed from 0.5—40.

Twelve titrations for silver–1,3-propanediamine and fifteen titrations for silver–1,4-butanediamine solutions were performed at 25.00±0.01 °C in a paraffin oil thermostat, which was placed in a room thermostated at 25±1 °C. Some additional titrations were carried out for silver–1,2-ethanediamine solutions under the same experimental conditions. The C_L/C_{Ag} ratio was 5 and 10 in this work, whereas the ratio had been 2—4 in the previous work.[1]

Details of the method of measurements were described elsewhere.[1]

Results

Titration curves of silver–1,3-propanediamine and –1,4-butanediamine solutions are shown in Figs. 1 and

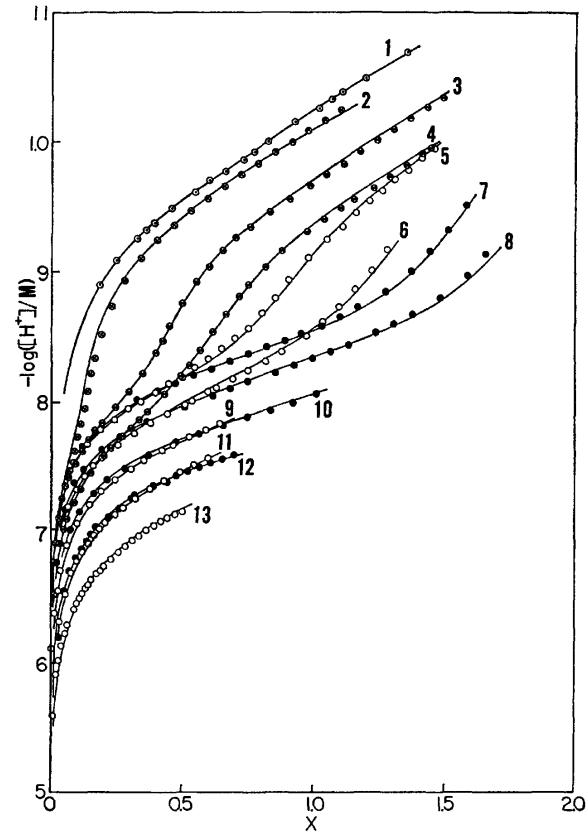

Fig. 1. Titration curves of 1,3-propanediamine and silver–1,3-propanediamine solutions. Curve 1: C_{Ag} (mM)=0.0, C_L (mM)=20.00; 2: 2.488, 39.99*; 3: 2.488, 20.02; 4: 5.169, 39.99; 5: 2.494, 10.01; 6: 5.170, 20.42; 7: 2.518, 5.035; 8: 5.017, 10.02; 9: 10.09, 39.99; 10: 9.993, 20.01; 11: 20.37, 80.08; 12: 20.10, 39.80; 13: 40.37, 160.1.

* The concentration of the ligand was changed by dilution during the titration. Curves are calculated ones by using constants in Table 2.

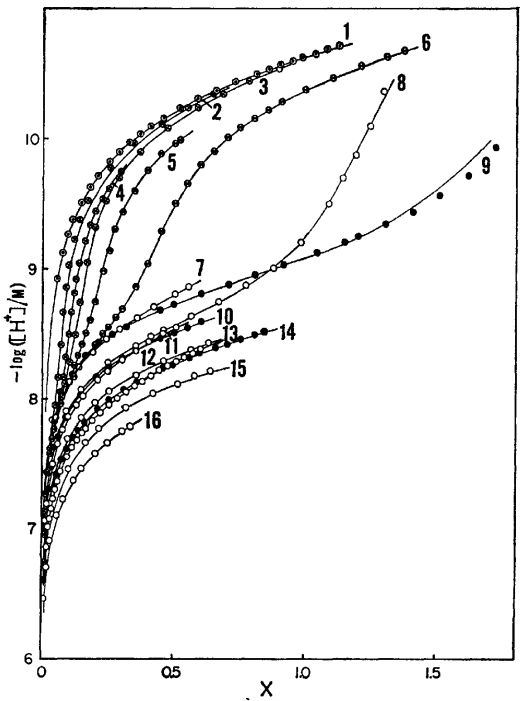

Fig. 2. Titration curves of 1,4-butanediamine and silver–1,4-butanediamine solutions. Curve 1: C_{Ag} (mM)= 0.0, C_L (mM) =5.004; 2: 2.516, 80.06*; 3: 2.516, 39.97*; 4: 2.526, 80.03; 5: 2.519, 40.01; 6: 2.524, 20.00; 7: 2.513, 9.990; 8: 5.044, 9.973*; 9: 2.540, 5.012; 10: 5.012, 9.990; 11: 5.008, 20.01; 12: 10.06, 9.973*; 13: 9.993, 40.62; 14: 10.01, 20.32; 15: 19.86, 10.03*; 16: 20.01, 80.03.
* The concentration of the ligand was changed by dilution during the titration. Curves are calculated ones by using constants in Table 2.

2, respectively.

The pK Values of the Diammonium Perchlorates were obtained from the titration curves of the solutions without silver ion (curve 1 in Figs. 1 and 2). The pK values are tabulated in Table 1, together with the pK

Table 1. Acid dissociation constants of 1,2-ethanediamine, 1,3-propanediamine and 1,4-butanediamine (25 °C, 3 M $LiClO_4$).

	en	pn	bn
pK_1	7.93	9.71	10.39
pK_2	10.74	10.93	11.05
$\Delta pK=pK_2-pK_1$	2.81	1.22	0.66

values of 1,2-ethanediammonium perchlorate which were recalculated in the present work. Compared with the values reported by Ohtaki and Tanaka in a 0.1 M NaCl medium,[5] the pK values found in the 3 M $LiClO_4$ medium were larger, but $\Delta pK=pK_2-pK_1$ more rapidly converged to the statistical value of 0.6.

Estimation of the Composition and Formation Constants of Silver–Diamine Complexes. Along the line described in the previous paper,[1] we estimated the composition and the formation constants of the silver–diamine complexes first with the graphical method and then the mathematical treatment by using a high speed electronic computer in order to refine the constants. In the course of the computer calculations, some complexes were assumed in addition to the complexes graphically estimated in order to obtain a better fit of calculated titration curves with experimental ones.

At lower pH where most diamine molecules are present as H_2L^{2+} (L denotes the free base of diamine), the equilibrium between silver ion and a diamine may be written by Eq. 1.

$$pAg^+ + rH_2L^{2+} = Ag_pH_qL_r^{(p+q)+} + (2r-q)H^+. \quad (1)$$

The equilibrium constant is defined as follows:

$$\kappa_{pqr} = \frac{[Ag_pH_qL_r^{(p+q)+}][H^+]^{(2r-q)}}{[Ag^+]^p[H_2L^{2+}]^r} = \beta_{pqr}K_1^rK_2^r, \quad (2)$$

where β_{pqr} is the overall formation constant of the complex $Ag_pH_qL_r^{(p+q)+}$;

$$\beta_{pqr} = \frac{[Ag_pH_qL_r^{(p+q)+}]}{[Ag^+]^p[H^+]^q[L]^r}. \quad (3)$$

Here [ ] represents the concentration (M=mol dm^{-3}) of the species. From the material balance of the metal ion, Eq. 4 can be readily derived.

$$\frac{C_M-[Ag^+]}{[Ag^+]} = \phi - 1 = \sum_p\sum_q\sum_r p\kappa_{pqr}[Ag^+]^{p-1}[H^+]^{-(2r-q)}[H_2L^{2+}]^r. \quad (4)$$

If we assume as a first approximation that only one complex is formed in this pH range, the summations in Eq. 4 are dropped. If the assumption is acceptable, the plot of log $(\phi-1)$ against $-\log [H^+]$ should give straight lines with a slope of $(2r-q)$, the lines depending on the concentrations of the silver ion and diamine. However, the plots were independent of the concentration of the silver ion as is seen in Fig. 3. Therefore, it is obvious that the main species formed in the pH range shown in Fig. 3 is mononuclear with respect to silver. Since the slope of the line was approximately unity, $(2r-q)$ should be unity. Since it is readily found that the family of the straight lines is a function of log C_L (C_L is approximately equal to $[H_2L^{2+}]$ under the

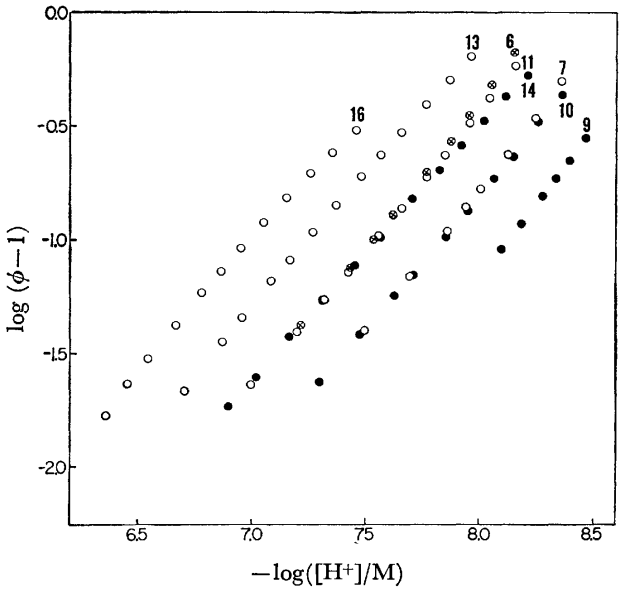

Fig. 3. Relationships between log $(\phi-1)$ and $-\log [H^+]$. Numbers in the figures correspond to those of Fig. 2.

present conditions), r should be unity, and thus $q=1$. Thus the composition of the species was determined to be $AgHL^{2+}$. Another species was found from the analysis of the second approximation of Eq. 4 by assuming two complexes, $AgHL^{2+}$ and $Ag_{p'}H_{q'}L_{r'}^{(p'+q')+}$, because the slope of the lines in Fig. 3 was slightly larger than unity. In order to avoid duplication of description, the treatment of the data is not described here and should be referred to the previous paper, Eqs. 14—17 of Ref. 1.[6] The second species $Ag_{p'}H_{q'}L_{r'}$ was $AgH_2L_2^{3+}$.

At higher pH the AgL^+ complex was found. In solution containing a large excess of a diamine compared with the silver ion, the $Ag_2L_2^{2+}$ and AgL_2^+ complexes were found in the same pH range.[7]

At the highest pH a hydrolyzed species Ag(OH)L formed.

The formation constants of the complexes, together with some other complexes which were not detected by the graphical treatment, were refined by the least squares method in which the error square sum $U=\sum(X-X_{calcd})^2$ was minimized by searching the best values of β_{pqr} for a set of the complexes $Ag_pH_qL_r^{(p+q)+}$. Here X denotes the ratio of the concentration of hydroxide ions added to the total concentration of a diamine in the solution, and X_{calcd} represents the calculated value of X and is given by Eq. 5.

$$X_{calcd}=\frac{2C_L+K_w/[H^+]-[H^+]-\sum_p\sum_q\sum_r q\beta_{pqr}[Ag^+]^p[H^+]^q[L]^r}{C_L}, \quad (5)$$

where K_w denotes the autoprotolysis constant of water in the 3 M $LiClO_4$ and is $10^{-13.867\pm0.009}$ M^2.[8]

The results are summarized in Table 2 in terms of $\log\beta_{pqr}$. For the silver–1,2-ethanediamine complexes, the formation constants of the complexes reported in the previous paper were recalculated by using all the data given in Ref. 1 and obtained in the present work. Some other complexes such as $AgHL_2^{2+}$, $Ag_2HL_2^{3+}$, and AgL_2^+ were found in the present calculation; these complexes have not been obtained in solutions of relatively small C_L/C_{Ag} ratios in the previous work.[1] On the other hand, the formation constant of the Ag_2L^{2+} complex was not detected with reasonable accuracy in the present calculation.

The $Ag_2HL_2^{3+}$ complex was not detected with reasonable certainty in both the systems of silver–1,3-propanediamine and –1,4-butanediamine. The formation constant of the AgL_2^+ complex was also not obtained in the former system by the least squares calculations. The value estimated by the graphical method is given in parentheses as reference in Table 2. For the silver–1,4-butanediamine solutions, the formation constant of the AgL^+ complex was uncertain as is shown in parentheses in Table 2. Some minor complexes added in the least squares caculation may sometimes refine the results, but the existence of the complexes is less certain and the formation constants obtained are rather unreliable. The $Ag_2HL_2^{3+}$ complex detected as a minor species in the present calculation is uncertain with this reason.

Table 2. Formation constants of the $Ag_pH_qL_r^{(p+q)+}$ complexes, $\log\beta_{pqr}$, in 3 M $LiClO_4$ at 25°C
$\beta_{pqr}=[Ag_pH_qL_r^{(p+q)+}]/[Ag^+]^p[H^+]^q[L]^r$ $M^{-(p+q+r-1)}$.

Complex	en	pn	bn	en[2]	pn[3]	bn[3]
HL	10.74	10.96	11.05	10.03	10.64	10.82
H_2L	18.67	20.65	21.44	17.25	19.52	20.42
AgHL	13.53	14.32	14.68	12.38	13.2	13.9
AgH_2L_2	27.48	28.90	29.83	—	—	—
$AgHL_2$	18.8_6	19.2_5	19.1_5	—	—	—
Ag_2HL_2	21.9_2	—	—	—	—	—
Ag(OH)L	-4.8_1	-3.5_7	-4.4_0	—	—	—
AgL	5.2_6	6.59	(6.4)[a]	4.7	5.8	5.9
Ag_2L_2	14.90	15.90	15.27	13.2	—	—
AgL_2	9.45	(9.8)[a]	8.6_2	7.7	—	—
Ag_2L	—	—	7.2_3	6.5	6.4	—

a) Values in parentheses are those estimated by curve-fitting in the concentration ranges where appreciable amounts of the relevant complexes are expected to be present, but these constants are not refined by the least-squares calculations with reasonable certainty.

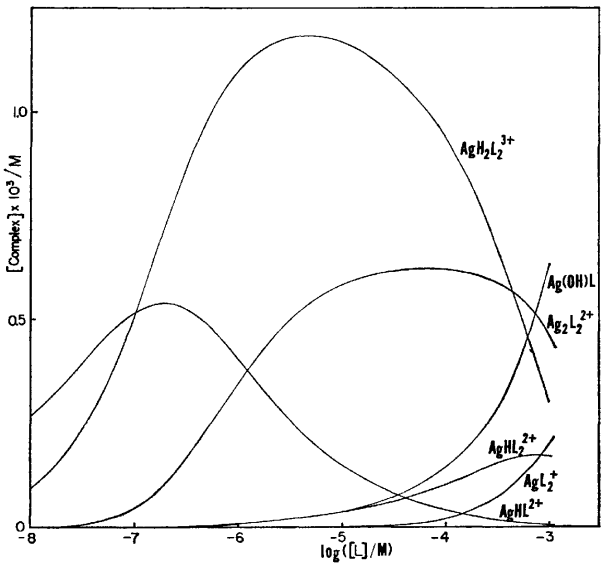

Fig. 4. Distribution of silver–1,4-butanediamine complexes.
$C_{Ag}=2.542$ mM, $C_L=20.00$ mM.

A typical set of the distribution curves of the complexes listed in Table 2 is shown for the 1,4-butanediamine system in Fig. 4. Similar sets of the distribution curves of the complexes were obtained for the 1,2-ethanediamine and 1,3-propanediamine systems. As is seen from the figure, $AgHL^{2+}$ is a major component of the complexes at the lowest pH's (pH=6—7). The $AgH_2L_2^{3+}$ complex is a main species over a wide range of pH examined. The $Ag_2L_2^{2+}$ complex and sometimes the AgL^+ complex become the main species. In the highest pH range the Ag(OH)L complex becomes one of the most important species in the solution.

Discussion

Stepwise formation constants of the $AgHL^{2+}$ and $AgH_2L_2^{3+}$ complexes are readily calculated from the values in Tables 1 and 2.

$$Ag^+ + HL^+ = AgHL^{2+}, \quad (6)$$

$$\log K(AgHL/HL) = 2.79(L=en),\ 3.39(pn),\ 3.63(bn),$$

and

$$AgHL^{2+} + HL^+ = AgH_2L_2^{3+}, \quad (7)$$

$$\log K(AqH_2L_2/HL) = 3.16(L=en),\ 3.65(pn),\ 4.10(bn),$$

where the constants $K(AgHL/HL)$ and $K(AgH_2L_2/HL)$ are defined as follows:

$$K(AgHL/HL) = \frac{[AgHL^{2+}]}{[Ag^+][HL^+]},$$

$$\text{and}\quad K(AgH_2L_2/HL) = \frac{[AgH_2L_2^{3+}]}{[AgHL^{2+}][HL^+]}, \quad (8)$$

and en, pn, and bn denote 1,2-ethanediamine, 1,3-propanediamine and 1,4-butanediamine, respectively.

The second formation constant $K(AgH_2L_2/HL)$ is larger than the first one $K(AgHL/HL)$ in all the cases, as has been pointed out in the previous paper.[1] The values of log $K(AgHL/HL)$ and log $K(AgH_2L_2/HL)$ approach the corresponding stepwise formation constants of the silver–ammine complexes, log $K_1=3.58$ and log $K_2=4.19$[9] with the length of the methylene chain. The values of the stepwise formation constants of the silver–1,4-butanediamine complexes are very close to those of the silver–ammine complexes. This fact suggests that the electrostatic repulsion between protons on the diamine molecules and the silver ion becomes negligible when they are separated by four methylene groups. The result that ΔpK of 1,4-butanediamine was close to the statistical value (0.6, see Table 1) supports this consideration. That the first stepwise formation constant is smaller than the second one is a known fact for a complex having a linear structure.

The stepwise formation constants of the AgL_n complex are given as follows:

$$Ag^+ + L = AgL^+, \quad (9)$$

$$\log K(AgL/L) = 5.2_6(L=en),\ 6.59(pn),\ (6.4)(bn),$$

and

$$AgL^+ + L = AgL_2^+, \quad (10)$$

$$\log K(AgL_2/L) = 4.1_9(L=en),\ (3.2)(pn),\ (2.2)(bn).$$

The values in parentheses are uncertain because the overall formation constants of these complexes were not determined with reasonable accuracy. However, we may still say that $K(AgL/L)$ is larger than $K(AgL_2/L)$, and the values of $K(AgL/L)$ for all the diamine complexes are smaller than β_2 of the diammine silver(I) complex. It is seen that $K(AgL/L)$ is much larger than K_1 of the monoammine silver complex and $K(AgHL/HL)$ of the $AgHL^{2+}$ complex. Therefore, we concluded that the diamine molecule combines with the silver ion as a bidentate ligand. The AgL_2^+ complex may have a tetrahedral configuration. The AgL^+ complex would have either a bent linear or a distorted tetrahedral structure with additional two water molecules attached to the vacant sites of the tetrahedron. As we will discuss later for the formation constant of the Ag(OH)L complex, the latter structure seems to be more possible than the former.

A large dimerization constant of the AgL^+ complex suggests a ring structure of the $Ag_2L_2^{2+}$ complex, as has been described by Schwarzenbach, *et al.*[2]

The formation constant of the $AgHL_2^{2+}$ complex from the AgL^+ and HL^+ complexes is given as follows:

$$AgL^+ + HL^+ = AgHL_2^{2+};$$

$$K(AgHL_2/HL) = \frac{[AgHL_2^{2+}]}{[AgL^+][HL^+]}, \quad (11)$$

$$\log K(AgHL_2/HL) = 2.8_6(L=en),\ 1.7_0(pn),\ (1.7)(bn).$$

Stabilization of the $AgHL_2^{2+}$ complex by combination of AgL^+ with HL^+ suggests that the $AgHL_2^{2+}$ complex has also a ring structure. The formation constant $K(AgHL_2/HL)$ smaller than $K(Ag_2L_2/AgL)$ may be attributed to the weaker H_2N–H^+–NH_2 bond than the H_2N–Ag^+–NH_2 bond in the ring structures.

The hydrolysis constant of the AgL^+ complex is given by Eq. 12.

$$AgL^+ + H_2O = Ag(OH)L + H^+;$$

$$K(Ag(OH)L/H_2O) = \frac{[Ag(OH)L][H^+]}{[AgL^+]}, \quad (12)$$

$$\log K(Ag(OH)L/H_2O) = -10.0_8(L=en),\ -10.1_6(pn),\ (-10.8)(bn).$$

These values are almost the same as the hydrolysis constant of the aqua silver(I) ion:

$$Ag^+ + H_2O = AgOH + H^+;$$

$$\log K(AgOH/H_2O) = -11.1\ (1\ M\ AgNO_3[10]). \quad (13)$$

The fact may show that no H_2N–Ag bond cleavage occurs by the hydrolysis of the AgL^+ complex. Therefore, the silver ion within the Ag(OH)L complex might be combined with at least three ligand atoms (two N and one O), and more probably the metal ion would be coordinated with two amino groups, one hydroxide ion and one water molecule.

The authors thank Dr. Takayoshi Kawai for his kind assistance.

References

1) H. Ohtaki and Y. Ito, *J. Coord. Chem.*, **3**, 131 (1973).
2) G. Schwarzenbach, B. Maissen, and H. Ackermann, *Helv. Chim. Acta*, **35**, 2333 (1952).
3) G. Schwarzenbach, H. Ackermann, B. Maissen, and G. Anderegg, *Helv. Chim. Acta*, **35**, 2337 (1952).
4) H. Tsukuda, T. Kawai, M. Maeda, and H. Ohtaki, *Bull. Chem. Soc. Jpn.*, **48**, 691 (1975).
5) H. Ohtaki and N. Tanaka, *J. Phys. Chem.*, **75**, 90 (1971).
6) Equation 16 of Ref. 1 should read $[HL^+]=[\{(1+K_1^{-1}[H^+]+\beta_{111}K_2[Ag^+])^2+8\beta_{122}K_2^2[Ag^+]C_L\}^{1/2}-(1+K_1^{-1}[H^+]+\beta_{111}K_2[Ag^+])]/4\beta_{122}K_2^2[Ag^+]$.
7) The third term of the right hand side of Eq. 19 of Ref. 1 should read $K_1^{-1}K_2^{-1}[H^+]^2[L]$. Equation 22 should read $[L]=\{(B^2+8AC)^{1/2}-B\}/4A$.
8) T. Kawai, Doctor Thesis, Tokyo Institute of Technology, 1975.
9) R. Arnek, G. Biedermann, and M. Maeda, unpublished results.
10) G. Biedermann and S. Hietanen, *Acta Chem. Scand.*, **14**, 711 (1960).

Phthalimides. I. Base-catalyzed Lossen Rearrangement and Acid-catalyzed Beckmann Rearrangement with *N*-(Arylsulfonyloxy)phthalimides

A. F. M. Fahmy, N. F. Aly, A. Nada, and N. Y. Aly
Faculty of Science, Ain Shams University, Abbassia, Cairo, A.R.E.

(Received August 2, 1976)

N-(Arylsulfonyloxy)phthalimides undergo base-catalyzed Lossen rearrangement with amines, and amino acids to give *N,N'*-diaryl ureas and amine salts. They behave similarly with phenylhydrazine in alcohol to give a mixture of *N*-hydroxyphthalimide and phenylhydrazine salts. However, *N*-(arylsulfonyloxy)phthalimides undergo isomerization followed by Beckmann rearrangement to give a mixture of 4-aryl-1*H*-2,3-benzoxazin-1-ones and diarylsulfones.

N-(Hydroxy)phthalimides undergo Beckmann rearrangement but fail to undergo Lossen reangement.[1] We have reinvestigated the imide rearrangement starting with *N*-(arylsulfonyloxy)phthalimides (I) in order to see the effect of the introduction of *N*-arylsulfonyl group on the mode of rearrangement. It was found that Ia and b undergo base-catalyzed Lossen rearrangement and acid-catalyzed isomerization followed by Beckmann rearrangement.

Lossen Rearrangement of N-*(Arylsulfonyloxy)phthalimides. (A) Rearrangement in the Presence of Amines*: When *N*-(arylsulfonyloxy)phthalimides (Ia and b) are allowed to react with aromatic amines in refluxing benzene, they undergo aminolysis followed by base-catalyzed Lossen rearrangement to give the corresponding mixtures of *N*-[2-(arylcarbamoyl)phenyl]-*N'*-arylureas (IIa—d), and aromatic amine salts of aryl sulfonic acids (IIIa—h).

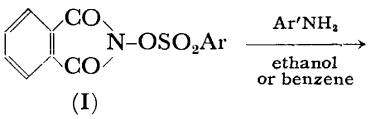

(I)

Ar'
a; C_6H_5
b; $C_6H_4CH_3(p)$
c; $C_6H_4OCH_3(p)$
d; $C_6H_4Cl(p)$

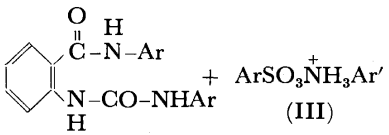

(II) (III)

	Ar	Ar'
a;	C_6H_5	C_6H_5
b;	C_6H_5	$C_6H_4CH_3(p)$
c;	C_6H_5	$C_6H_4OCH_3(p)$
d;	C_6H_5	$C_6H_4Cl(p)$
e;	$C_6H_4CH_3(p)$	C_6H_5
f;	$C_6H_4CH_3(p)$	$C_6H_4CH_3(p)$
g;	$C_6H_4CH_3(p)$	$C_6H_4OCH_3(p)$
h;	$C_6H_4CH_3(p)$	$C_6H_4Cl(p)$

Structure (II) was confirmed by the following:

IR spectra: $\nu_{C=O}$ (anilide, 1710—1700 cm^{-1}), $\nu_{C=O}$[2] (*N,N'*-diarylureas, 1660—1640 cm^{-1}), and $\nu_{NH's}$ (3300—3200 and 3120—3100 cm^{-1}).

MS of IId: (molecular ion, m/e=399).

Pyrolysis of IIa—d to give the corresponding 3-aryl-1,2,3,4-tetrahydroquinazoline-2,4-diones (IVa—d).

Structure (IIIa—h) was confirmed by the following:

(i) IR spectra: $\nu^{+}_{NH_3}$ (3020—3000 cm^{-1}), $\overset{+}{N}H_3$ asymm. bending (1600—1575 cm^{-1}), $\overset{+}{N}H_3$[3] symm. bending (1500 cm^{-1}).

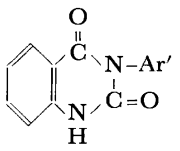

(IV)

a; Ar'=C_6H_5, b; Ar'=$C_6H_4CH_3(p)$,
c; Ar'=$C_6H_4OCH_3(p)$, d; Ar'=$C_6H_4Cl(p)$

(ii) Identity with authentic products.[4] The above reactions are summarized in the following scheme (Scheme 1).

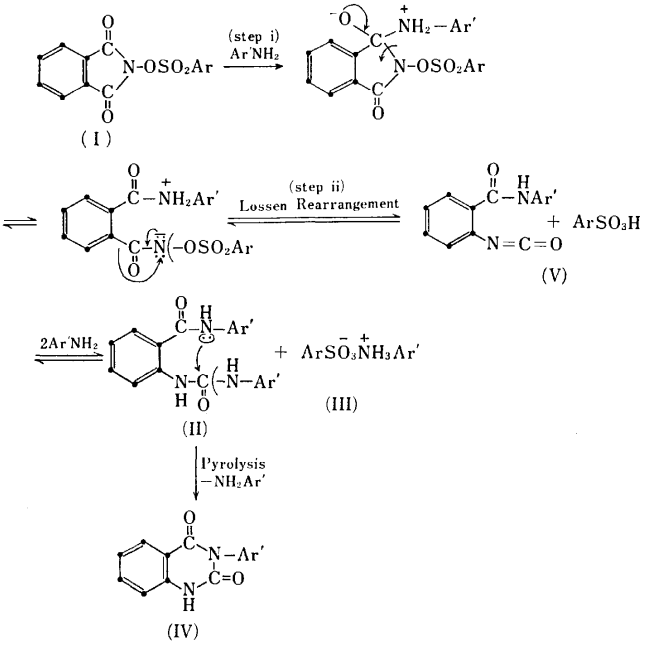

Scheme 1.

(B) Rearrangement in the Presence of Aminobenzoic Acids: *N*-(Arylsulfonyloxy)phthalimides (Ia and b) undergo base-catalyzed Lossen rearrangement with (*p*- and *m*-) aminobenzoic acids to give the corresponding mixtures of *N,N'*-diarylureas (VIa and b) and amino acid salts with sulfonic acids (VIIa—d).

Structure (VI) was confirmed by the following:

IR spectra: ν_{NH} (3320—3300 cm^{-1}), and $\nu_{C=O}$ (acid, 1720—1700 cm^{-1}).

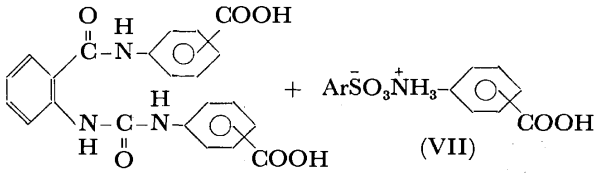

(VI)
a; COOH(*p*-)
b; COOH(*m*-)

(VII)
a; Ar=C_6H_5, COOH(*p*-)
b; Ar=$C_6H_4CH_3$(*p*-), COOH(*p*-)
c; Ar=C_6H_5, COOH(*m*-)
d; Ar=$C_6H_4CH_3$(*p*-), COOH(*m*-)

Structure (VII) was confirmed by the following:

(i) IR spectra: $\nu^{+}_{NH_3}$ [3] (3000 cm^{-1}), and $\nu_{C=O}$ (acid, 1700—1680 cm^{-1}).[5]

(ii) Identity with products obtained by the reaction of arylsulfonic acids (V) with the corresponding amino acids.

(C) Rearrangement in the Presence of Phenylhydrazine: *N*-(Arylsulfonyloxy)phthalimides (Ia and b) undergo base-catalyzed Lossen rearrangement with phenylhydrazine in refluxing ethanol to give mixtures of VIII, and phenylhydrazine salts of sulfonic acids (IX).

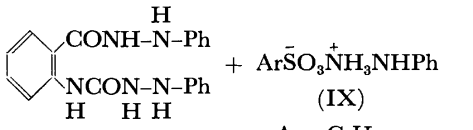

(VIII)

(IX)
a; Ar=C_6H_5
b; Ar=$C_6H_4CH_3$(*p*-)

Structure (VIII) was confirmed by the following:

IR spectra: $\nu_{NH's}$ at (3320—3280 cm^{-1}) and $\nu_{C=O's}$ at (1680—1660 cm^{-1}); pyrolysis to give 3-anilino-1,2,3,4-tetrahydroquinazoline-2,4-diones (X).

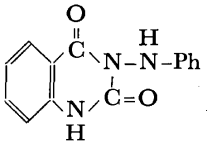

(X)

(II) Beckmann Rearrangement of N-(Arylsulfonyloxy)-phthalimides. *N*-(Arylsulfonyloxy)phthalimides undergo isomerization to 3-(arylsulfonyloxyimino)-phthalide followed by Beckmann rearrangement with anhydrous aluminium chloride as a Lewis acid.

N-(Arylsulfonyloxy)phthalimides (Ia and b) react with anhydrous aluminium chloride in 1,1,2,2-tetrachloroethane to give a mixture of phthalic acid and arylsulfonic acid (V).

It was also found that *N*-(arylsulfonyloxy)phthalimides (Ia and Ib) react with reactive aromatic substrates (benzene, toluene, anisole, and chlorobenzene) in the presence of anhydrous $AlCl_3$ to give the corresponding mixtures of 4-aryl-1*H*-2,3-benzoxazin-1-ones (XIa—d), and diarylsulfones (XIIa—g).

Structure (XI) was confiermd by the following:

(i) IR spectra: $\nu_{C=O}$ in six membered heterocyclic compounds, 1750—1740 cm^{-1}.

(ii) Identity with authentic products.[6-9]

Structure (XII) was confirmed by the following:

(i) IR spectra: ν_{SO_2} asymm. st. 1320—1310 cm^{-1}.

(ii) Identity with authentic products.[10-12]

The reaction is assumed to take place according to Scheme 2.

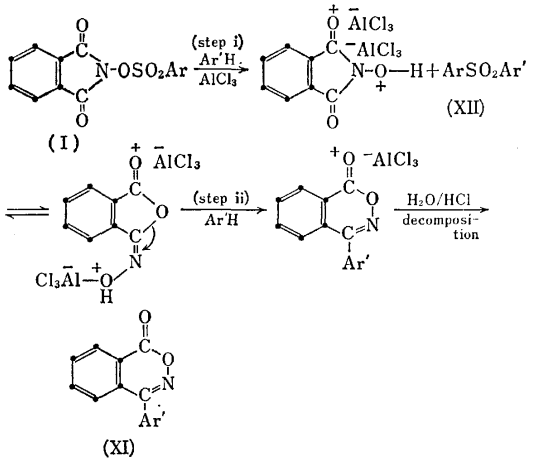

Scheme 2.

The above scheme was confirmed by the fact that *N*-hydroxyphthalimide (XIII) reacts with aromatic substrates in the presence of anhydrous $AlCl_3$ to give 4-aryl-1*H*-2,3-benzoxazin-1-ones.[1]

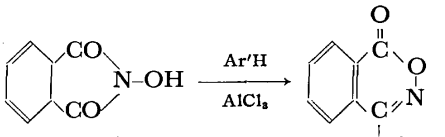

(XIII) (XI)

The results show that *N*-(arylsulfonyloxy)phthalimides undergo two types of molecular rearrangement. Lossen rearrangement occurs with amines, amino acids, and hydrazines; isomerization followed by Beckmann rearrangement occurs with Lewis acids such as anhydrous $AlCl_3$.

Experimental

Melting points were not corrected. IR spectra were carried out on an Unicam SP 1200 spectrophotometer by means of KBr Wafer technique.

Reaction of N-(Arylsulfonyloxy)phathalimides with Aromatic Amines in Ethanol. A mixture of *N*-(arylsulfonyloxy)-phthalimides (I) (0.1 mol) and primary aromatic amines

Table 1. Action of aromatic amines on *N*-(arylsulfonyloxy)phthalimides (Ia and b)

Reactants start amine		Products: *N*-2-(Arylcarbamoyl)-*N'*-arylureas (II) No.	Mp, °C	Yield %	M.F.	Analysis Req.	Found	Amine salts of aryl sulfonic acid (II) No.	Mp, °C	Mmp, °C	Yield
Ia	Aniline	IIa	218—220	58	$C_{20}H_{17}N_3O_2$	C 72.50 H 5.13	72.3 5.4	IIIa	222	222	60
	p-Toluidine	IIb	204—205	54	$C_{22}H_{21}N_3O_2$	C 73.5 H 5.8	74.0 5.0	IIIb	194—196	195	61
	p-Anisidine	IIc	208	60	$O_{22}H_{21}N_3O_4$	C 67.53 H 5.37	67.00 5.17	IIIc	168—170	169	64
	p-Chloro-aniline	IId	225—226	40	$C_{20}H_{15}N_3O_2Cl$	C 60.0 H 3.75	60.5 3.4	IIId	213—215	214—215	68
Ib	Aniline	IIa	218—220	60				IIIe	224—225	223	60
	p-Toluidine	IIb	204—205	58				IIIf	184—185	184	48
	p-Anisidine	IIc	208	62				IIIg	180	180	61
	p-Chloro-aniline	IId	225—226	49				IIIh	230	230	58

(0.4 mol) in ethanol or benzene (20 ml) were heated under reflux for (6 h) and then cooled. The solid product was treated with ethanol and filtered off.

The residual solid was recrystallized from ethanol to give *N*-[2-(arylcarbamoyl)phenyl]-*N'*-arylureas (II) as white crystals. The mother liquor was concentrated by evaporation and trated with a few drops of benzene to give III as a solid product (Table 1).

It was proved to be an amine salt of arylsulfonic acids by mp and mixed mps with authentic samples prepared from the reaction of arylsulfonic acids (Va and b) with the corresponding amines.[3]

Pyrolysis of N-[*2-(Arylcarbamoyl)phenyl*]-N'-*arylureas*: *N*-[2-(Arylcarbamoyl)phenyl]-*N'*-arylureas (IIa—d) were heated above their mps on a sand bath for 2 h. The solid product was obtained in sublimed needles and collected in an air condenser. The product was proved to be 3-aryl-1,2,3,4-tetrahydroquinazoline-2,4-diones (IVa—d) by mp and mixture mp and IR spectra.[4]

I-B) Reaction of N-*(Arylsulfonyloxy)phthalimides with Aminobenzoic Acids.* A mixture of *N*-(arylsulfonyloxy)-phthalimide (I) (0.1 mol), aminobenzoic acid (0.3 mol) and a few drops of pyridine in benzene (10 ml) was heated under reflux for 4 h, then cooled. The solid product was treated with ethanol and filtered off. The residual solid was recrystallized from acetic acid to give *N,N'*-diarylureas (VIa and b) as white crystals (Table 2). The mother liquor was concentrated, and treated with a few drops of benzene to give-VII as a product (Table 2).

It was proved to be arylsulfonic acid salts of aminobenzoic acid by mp and mixture mp.

Reaction of Arylsulfonic Acids (V) with Aminobenzoic Acids: A mixture of arylsulfonic acids (V) (0.1 mol) and aminobenzoic acids (0.3 mol) and a few drops of pyridine in benzene was heated under reflux for 2 h, then cooled. The solid product obtained was filtered off, recrystallized from benzene and a few drops of ethanol were added to give white crystals. It was proved to be arylsulfonic acid salts of aminobenzoic acids by mp and mixture mp.

Reaction of N-*(Arylsulfonyloxy)phthalimides with Phenylhydrazine in Ethanol*: A mixture of *N*-(arylsulfonyloxy)phthalimides (I) (0.1 mol) and phenylhydrazine (0.3 mol) in ethanol was heated under reflux for (3 h), then cooled. The solid product was obtained, filtered off, recrystallized from ethanol to give VIII as white crystals, mp 193 °C. Found: C, 66.6; H, 5.0%. Calcd for $C_{20}H_{19}H_5O_2$: C, 66.48; H, 4.9%.

The mother liquor was concentrated by evaporation. A solid product was obtained. It was proved to be phenyl-

Table 2. Action of aminobenzoic acids on *N*-[arylsulfonyloxy]phthalimides

Reactants start amino acids		Products: *N,N'*-Diarylureas (VI) No.	Mp °C	Yield %	M.F.	Analysis % Calcd (Found) C	H	Aminobenzoic acid salts (VII) No.	Mp °C	Yield %	M.F.	Analysis, % Calcd (Found) C	H
Ia	*p*-Amino-benzoic acid	VIa	over 360	75	$C_{22}H_{17}N_3O_6$	63.0 (63.34)	4.06 (3.69)	VIIa	173—175	40	$C_{13}H_{13}NO_5S$	52.42 (53.3)	4.4 (4.6)
Ib	*p*-Amino-benzoic acid	VIa	over 360	75				VIIb	295—297	38	$C_{14}H_{15}NO_5S$	54.37 (54.5)	4.85 (4.6)
Ia	*m*-Amino-benzoic acid	VIb	over 360	78	$C_{22}H_{17}N_3O_6$	63.0 (63.7)	4.06 (4.2)	VIIc	238—240	43	$C_{13}H_{13}NO_5S$	52.45 (53.3)	4.40 (4.6)
Ib	*m*-Amino-benzoic acid	VIb	over 360	78				VIId	253—255	41	$C_{14}H_{15}NO_5S$	54.37 (54.4)	4.85 (4.6)

Table 3. Reaction of anhydrous aluminium chloride in aromatic solvents with *N*-[arylsulfonyloxy]phthalimides

Reactants aromatic solvents	Products: 4-Aryl-1*H*-2,3-benzoxazin-1-ones (XI) No.	Mp °C	Mixed mp °C	Yield %	Ref.	Diarylsulfones (XII) No.	Mp °C	Mixed mp °C	Yield %	Ref.	M.F.	Analysis % Calcd (Found) C	H
Ia Benzene	XIa	160	160	35	5	XIIa	128	127	85	9	—	—	—
Toluene	XIb	158	158	33	6	XIIb	124	123	83	—	$C_{13}H_{12}O_2S$	58.7 (58.3)	4.6 (4.3)
Anisole	XIc	141	140	30	7	XIIc	72	72	84	—	$C_{13}H_{12}O_3S$	62.9 (62.65)	4.84 (4.9)
p-Chlorobenzene	XId	187	186	28	8	XIId	93	93	80	10	—	—	—
Ib Benzene	XIa	160	—	—	—	XIIb	124	—	86	—	—	—	—
Toluene	XIb	158	—	—	—	XIIe	158	157	84	11	—	—	—
Anisole	XIc	141	—	—	—	XIIf	100	98	86	—	$C_{14}H_{14}O_3S$	64.12 (63.72)	5.33 (5.61)
p-Chlorobenzene	XId	186	—	—	—	XIIg	128	127	81	—	$C_{13}H_{11}O_2SCl$	54.6 (54.2)	4.5 (5.0)

hydrazine salt of arylsulfonic acids (IX) by mp and mixed mps.[3]

Pyrolysis of VIII: VIII was heated above its mp on a sand bath for one hour, then cooled. A solid product obtained was filtered off, and recrystallized from ethanol to give a solid product. It was proved to be Xa—d by mp and mixed mp, and IR spectra. The mother liquor was concentrated by evaporation to give an oil.

It was proved to be phenylhydrazine by condensation with benzophenone to give benzophenone hydrazone.

IIA. Action of Anhydrous Aluminium Chloride in Dry 1,1,2,2-Tetrachloroethane on N-(Arylsulfonyloxy)pathalimides (I). Anhydrous aluminium chloride was added while stirring to a solution of *N*-(arylsulfonyloxy)phthalimides (I) in dry 1,1,2,2-tetrachloroethane. The reaction mixture was heated under reflux for 1/2 h, and the complex formed was decomposed with ice-cold dilute hydrochloric acid. The solvent was steam distilled. The solution was extracted with ether. The ethereal layer was separated, dried over anhydrous sodium sulfate, and the solvent was concentrated by evaporation.

The solid product obtained was filtered off, recrystallized from ethanol to give white crystals, mp 206 °C. It was proved to be phthalic acid by mp and mixed mp. The mother liquor was concentrated to dryness to give arylsulfonic acids.

IIB. Action of Anhydrous Aluminium Chloride in Aromatic Solvents on N-(Arylsulfonyloxy)phthalimides. Anhydrous aluminium chloride (0.6 mol) was added under stirring to a solution of *N*-(arylsulfonyloxy)phthalimide (I) (0.1 mol) in dry aromatic solvents. The reaction mixture was heated under reflux for 1 h, and the complex formed was decomposed with ice-cold dilute hydrochloric acid. The solvent was steam distilled. The residual solid was filtered off.

The crude product was dissolved in ethanol, concentrated, then cooled, and the solid obtained was filtered off and recrystallized from ethanol to give diarylsulfone (XII) as white crystals (*cf.* Table 3).

The mother liquor was concentrated then cooled to give solid product. It was proved to be 4-aryl-1*H*-2,3-benzoxazin-1-ones (XI), (*cf.* Table 3).

References

1) A. F. M. Fahmy, N. F. Aly, M. Oraby, *J. Chem. A. R. E.*, **19** (2) (1976).
2) F. Scheinmann, "An Introduction to Sepctroscopic Methods for Identification of Organic Compounds," Vol. 7, Pergamon Press, New York (1970), p. 182.
3) Ref. 2, p. 185.
4) A. F. M. Fahmy, N. F. Aly, A. Nada, and N. Y. Aly, *J. Chem. A.R.E.* (received for publication).
5) Ref. 2, p. 179.
6) R. E. Rose, *J. Am. Chem. Soc.*, **33**, 392 (1911).
7) F. G. Baddar, A. F. M. Fahmy, and Nawal F. Aly, *J. Chem. Soc., Perkin Trans. 1*, **1973**, 2448.
8) G. Runti and S. Galimberti, *Ann. Chim.*, **47**, 250 (1957).
9) J. M. Sprague, F. C. Novello, and A. A. Deana, U.S. Patent 3322631 (CL. 167—168), May 30, 1967.
10) Ed. Bourgeois, *Ber.*, **28**, 2323 (1895).
11) H. Meyer, *Ann.*, **433**, 337 (1923).
12) H. Meyer, *Ann.*, **433**, 349 (1923).

Thermally Dissociative Degradation of Polymers Containing Dicyclopentadiene Ring in Main Chains

Masatoshi MIURA, Fumihiko AKUTSU, Shigeo HIROSE, Yoshiyuki IKENO, and Kuniharu NAGAKUBO

Department of Synthetic Chemistry, Faculty of Engineering, Chiba University, Yayoi-cho, Chiba 280

(Received December 13, 1976)

Polymers containing dicyclopentadiene units in their main chain were prepared by the polycondensation of dicyclopentadienedicarbonyl dichloride with bis(*p*-hydroxyphenyl) ether or 2,2-bis(*p*-hydroxyphenyl)propane. Thermal analysis showed that the dicyclopentadiene units dissociate reversibly. The results of thermal degradation in a nitrobenzene solution indicate that a reversible degradation occurs at 10% concentration of the polymer, and an irreversible one at concentration below 1%. The activation energy of the dissociation of dicyclopentadiene units in the main chain of the polymer was estimated to be 30 kcal/mol.

It is well-known that a molecule of dicyclopentadiene reversibly dissociates into two molecules of cyclopentadiene on heating. Thus, a polymer containing dicyclopentadiene ring in the main chain is expected to dissociate reversibly into polymers of lower molecular weight. Stille and Plummer attempted to synthesize polymer having such a structure by the Diels-Alder type polyaddition of bis(cyclopentadienyl)alkanes,[1] but obtained only polymers of low molecular weight. Thus the behavior of the thermally dissociative degradation of these polymers has not been clarified.

We obtained polymers of high molecular weight containing the dicyclopentadiene ring in the main chain by the polycondensation of dicyclopentadienedicarbonyl dichloride (DCPC) with bis(*p*-hydroxyphenyl) ether (HPE) or 2,2-bis(*p*-hydroxyphenyl)propane (HPP), and investigated their thermal behavior. This paper deals with thermally dissociative degradation of these polymers in solid state and in a nitrobenzene solution.

Experimental

Materials. HPP was recrystallized from toluene just before use, mp 160—161 °C. HPE was prepared[2] from bis(*p*-aminophenyl) ether as a starting material *via* the diazonium salt and then acetate; it was recrystallized from water, mp 167—168 °C; 15% yield (based on the starting material). DCPC was obtained by the chlorination of dicyclopectadienedicarboxylic acid with thionyl chloride,[3] and recrystallized from petroleum ether, mp 61.5—62.5 °C (lit, 62 °C[3]).

Model compound (diphenyl dicyclopentadienedicarboxylate). A solution of 2.21 g (8.9 mmol) DCPC in 10 ml dichloromethane was added to a mixture of 9.19 g (23.2 mmol) phenol, 3.23 ml (27.1 mmol) pyridine and 20 ml dichloromethane at 19—23 °C, followed by stirring at the same temperature. The reaction mixture was washed with a dilute aqueous solution of sodium carbonate and then with water. The oily layer was separated and dried with anhydrous calcium chloride, the solvent being removed. The viscous liquid so obtained was dissolved in methanol, poured into water to give a solid product, which was recrystallized from heptane to yield colorless crystals, mp 90.5—91.5 °C (lit, 92—94 °C[4]); 57.4% yield. Found: C, 77.38%; H, 5.32%. Calcd for $C_{24}H_{20}O_4$: C, 77.42%; H, 5.41%. The IR spectra showed absorptions for ester group at 1200 and 1735 cm^{-1} and for double bonds of dicyclopentadiene ring at 1600 and 1635 cm^{-1}.

Polycondensation. A typical procedure is as follows. A solution of 0.643 g (2.5 mmol) DCPC in 3.8 ml dichloromethane was added dropwise to a solution of 0.505 g(2.5 mmol) HPE and 0.8 ml (5.5 mmol) triethylamine in 7.5 ml dichloromethane under stirring at −3 °C. Stirring was continued for 45 min at −3——2 °C. The reaction mixture was poured into acetone containing 20% water to precipitate polymer. The polymer obtained was reprecipitated in benzene–methanol system and dried *in vacuo* to yield 80.8% of a white powdery polymer. The inherent viscosity(0.5% concn, *m*-cresol, 30 °C) was 0.67 dl/g. Found: C, 74.30%; H, 4.77%. Calcd for $C_{24}H_{18}O_5$: C, 74.60%; H, 4.70%. The IR spectra showed absorptions for the ester group at 1190 and 1700 cm^{-1} and for double bonds of the dicyclopentadiene ring at 1600 and 1630 cm^{-1}.

The polycondensation of DCPC with HPP gave high molecular weight polymers under the same reaction conditions as those described above except that reaction time was 10 minutes. The inherent viscosity (0.5% concn, *m*-cresol, 30 °C) was 0.84 dl/g. Found: C, 77.71%; H, 6.23%. Calcd for $C_{27}H_{24}O_4$: C, 78.62%; H, 5.86%. IR spectra showed not only the IR absorptions decribed for the polymer of DCPC with HPE, but also absorption for methyl group at 2960 and 1375 cm^{-1}.

Degradation and Measurement. DTA and TGA were carried out on a Rigaku Denki thermal analyzer (Cat. No 8085Dl) at a heating rate of 20 °C/min under a nitrogen stream.

Thermal degradation of a polymer solution was carried out in a sealed viscometer[5] for a dilute solution containing less than 1% of the polymer. A nitrobenzene solution of the polymer was added to the viscometer, degassed by a freeze-thaw procedure and sealed. The viscometer was heated at a specified temperature for a certain time, then rapidly cooled, viscosity being measured at 30 °C.

In the case of a solution of 10% concentration, a degassed polymer solution in a sealed glass tube was heated at a specified temperature for the desired time, and then diluted with nitrobenzene to 0.5%. The viscosity of the solution so obtained was measured at 30 °C with an Ubbelohde viscometer.

Results and Discussion

Preparation of Polymer. The polycondensation of DCPC with bisphenol was carried out in dichloromethane by low temperature solution polycondensation. The results are given in Table 1. The high molecular weight polymer of DCPC with HPE could be obtained at the reaction conditions of No. 5 in Table 1. With

Table 1. Low temperature solution polycondensation of DCPC with bisphenol

No.	Bispheonl	Concn of acid chloride[a] mol l^{-1}	Ratio of triethylamine to acid chloride mol mol^{-1}	Temp °C	Reaction time[b] h	Conversion %	η_{inh}[c] dl g^{-1}
1	HPE	0.167	2	2—3	1	76.4	0.12
2	HPE	0.187	2	1.5—3	6	60.1	0.11
3	HPE	0.220	2	2—3	1	78.1	0.40
4	HPE	0.220	2.2	−3—−2	0.75	80.8	0.67
5	HPE	0.220	2.2	−3—−2	2	—	—[d]
6	HPE	0.333	2	2—3	2	—	—[d]
7	HPP	0.220	2.2	−2—−1	2	71.2	0.29
8	HPP	0.267	2.2	−3—−1	0.16	61.1	0.84
9	HPP	0.267	2.2	−3—−2	2	—	—[d]

a) Concn of acid chloride in reaction mixture. b) Reaction time after addition of acid chloride soln. c) 0.5% *m*-cresol soln at 30 °C. d) Insoluble in *m*-cresol.

decrease in the concentrations of reactants, molecular weight of polymer decreased (Nos. 1 and 2). When the concentration of reactants was increased, a polymer insoluble in *m*-cresol was formed; it may be crosslinked (No. 6). An unnecessarily long reaction time also resulted in the formation of insoluble polymers. The polycondensation of DCPC with HPP proceeded in a similar way to that of DCPC with HPE with respect to the concentrations of reactants and the reaction time.

The resulting polymers were identified by elemental analysis and IR spectroscopy. Since the structure of DCPC was assigned by Peters[3,6] as endo-4,9-bis-(chloroformyl)tricyclo[5.2.1.$0^{2,6}$]deca-3,8-diene, the structures of the polymers obtained in this investigation are as follows.

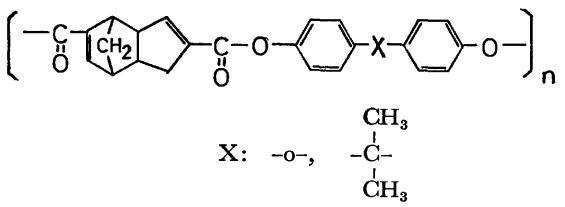

Degradation in Solid State. TGA and DTA curves of the model compound show two endothermic peaks at 92 and 190—305 °C respectively (Fig. 1, Curve A). The one at lower temperature corresponds to the melting point of the model compound. The other accompanied by 93% weight loss is due to the dissociation of the model compound and the volatilization of dissociated compounds. TGA and DTA of the polymer of DCPC with HPE show two endothermic peaks at 190—250 and 300—420 °C (Curve B). The first peak of curve B seems to be caused by the dissociation of polymer chains, since the thermal dissociation of the model compound starts at almost the same temperature. This was confirmed by the following experiment. Thus the polymer heated to 237 °C (at this temperature, the first endothermic peak can be observed, but not the second one) was allowed to cool down to room temperature; on reheating of this polymer, an endothermic peak appeared at 223—260 °C. The endothermic peak on reheating may be responsible for some chemical change of polymer by heating. The second peak at 300—420 °C accompanied by *ca.* 70% weight loss is due to further degradation and volatilization of dissociated and degradated fragments. TGA and DTA of the polymers of DCPC with HPP gave endothermic peaks at 190—250 and 250—400 °C accompanied by *ca.* 75% weight loss. The temperature at which the dissociation of polymer chains begins was similar to that for the polymers of DCPC with HPE, but endothermic peaks were observed at slightly higher temperature (Fig. 1).

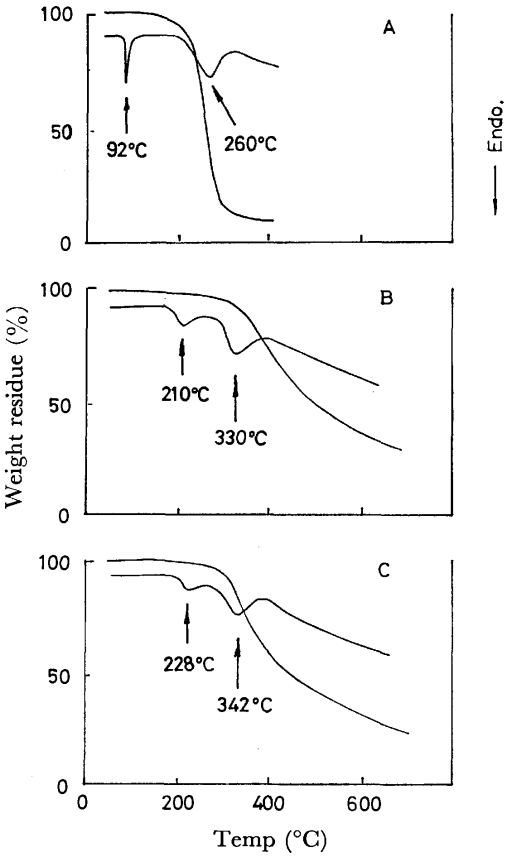

Fig. 1. TGA and DTA of model compound and polymers:
A, model compound; B, polymer of DCPC with HPE
C, polymer of DCPC with HPP; N_2 flow, 100 ml/min; rate of temperature increase, 20 °C/min.

Degradation in a Solution. Thermal degradation

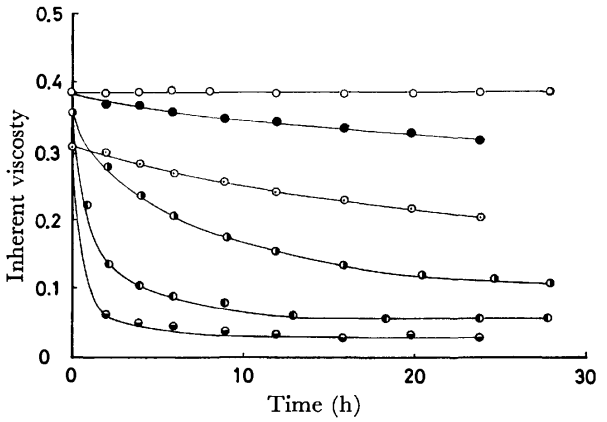

Fig. 2. Effect of temperature on viscosity decrease of polymer: temperature; ○, 30 °C; ●, 40 °C; ⊙, 50 °C; ◑, 60 °C; ◐, 80 °C; ◒, 100 °C; polymer concentration, 0.5%; samples of different molecular weight were used for the measurements at 50 and 60 °C.

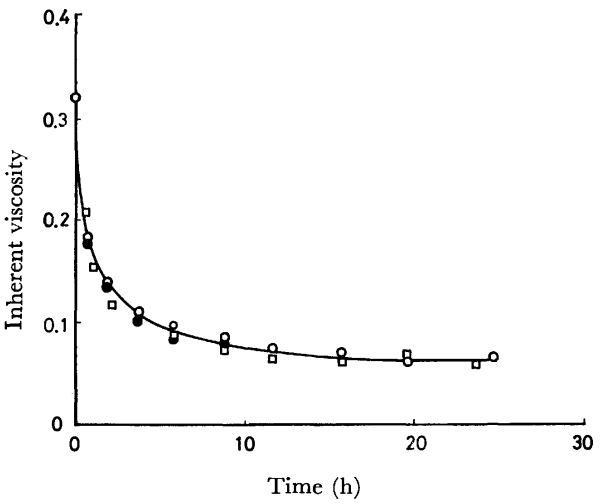

Fig. 3. Effect of polymer concentration on viscosity decrease of polymer at 80 °C: polymer concentration; ○, 1.0%; ●, 0.5%; □, 0.1%.

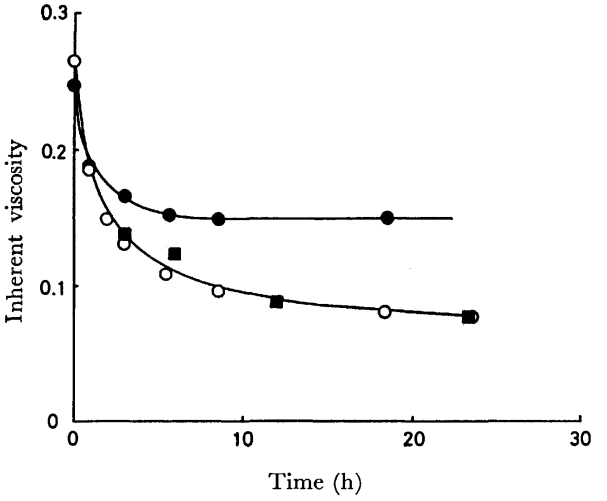

Fig. 4. Effects of polymer concentration and maleimide addition on viscosity decrease of polymer at 80 °C: ●, 10% polymer solution; ○, 1% polymer solution; ■, five times as much the molar quantity of *N*-phenylmaleimide as the dicyclophntadiene unit of the polymer was added to the 10% polymer solution. In the case of 10% polymer solutions viscosities were measured in 0.5%, and in the case of 1% no dilution was done.

processes of the polymers in a nitrobenzene solution were followed by viscometry. Figure 2 shows the viscosity change of a solution of the polymer of DCPC with HPE at a concentration of 0.5% at various temperatures. At 30 °C, no change in viscosity of the solution was observed for 30 h. This indicates that hardly any of the dicyclopentadiene ring in the main chains of the polymers dissociate at this temperature. With increasing temperature the viscosity decreased rapidly. At temperature higher than 80 °C, viscosity decreased a great deal at the initial stage of heating. When the polymers of DCPC with HPP were used, almost the same curves showing viscosity decrease as above were observed at 30 and 80 °C. Thus, further experiments were carried out on the polymers of DCPC with HPE only. For the polymer concentration from 0.1 to 1.0%, decrease in viscosity is not influenced by polymer concentration, (Fig. 3). This indicates that the polymer degrades irreversibly in a solution of concentration less than 1%. If the degradation of the polymer proceeds reversibly, the decay curve of the viscosity should be affected by the concentration of the polymer, since the forward reaction is of first-order with respect to the concentration of dicyclopentadiene unit and the reverse reaction is of second-order with respect to the concentration of cyclopentadienyl groups produced. Thermal degradation of the polymer in a solution of 10% concentration is shown in Fig. 4 together with that of the 1% polymer solution. In the case of the 10% polymer solution, the viscosity was measured for 0.5% polymer solution obtained by diluting the heat-treated 10% polymer solution with nitrobenzene. At 10% polymer concentration, viscosity fell to a constant value in a relatively short time, the value being higher than that of the 1% polymer solution. The 10% polymer solution heated for 18.5 h at 80 °C was allowed to stand for 48 h at room temperature, but no increase in viscosity of the polymer from the equilibrium value could be observed.

If the polymer is degraded in the presence of excess dienophile such as *N*-phenylmaleimide, cyclopentadienyl groups produced by the dissociation of dicyclopentadiene units in the polymers react exclusively with *N*-phenylmaleimide; thus a recombination reaction of two cyclopentadienyl groups present as end groups of the degraded polymers would be disturbed. As shown in Fig. 4, addition of the maleimide to the 10% polymer solution has predominant effect of the decrease of molecular weight of the polymers. The decay curve of the viscosity in the presence of the maleimide was similar to that observed for the 1% polymer solution in which irreversibly dissociative degradation took place. The addition of maleimide to the 1% polymer solution had no effect on the relationship between the viscosity of the polymers and heating time.

From the effect of polymer concentration and that of maleimide addition on viscosity decrease, it is concluded that in the 10% polymer solution the degradation of the polymers proceeds by a reversible process, the molecular weight of the polymer reaching an equilibrium value. In this case, however, no viscosity recovery could be observed by letting the solution to stand for 48 h at room temperature. This might be responsible for the very slow rate of the recombination reaction because of the low reaction temperature. In a dilute solution below 1%, recombination of cyclopentadienyl groups is disturded by dilution; consequently irreversible degradation was observed.

If the polymers degrade irreversibly under random scission of the main chain, a linear relationship can be expected to exist between the reciprocal of the degree of polymerization and heating time. The plots of $(1/[\eta])^{1/\alpha}$ against heating time should be linear, where α donates the exponential term of the Mark-Houwink equation and $[\eta]$ intrinsic viscosity. However, α has not yet been estimated for this polymer solution. By assuming that α equals 1/2, plots of $(1/\eta_{inh})^2$ against heating time were found to be linear at temperatures lower than 60 °C, using the data in Fig. 2, (Fig. 5). The Arrhenius plot of the slope of lines gave satisfactory linear relationship. The activation energy for the degradation of the polymer was calculated to be 30 kcal/mol. The activation energy corresponds to that for the dissociation of dicyclopentadiene units in the main chain of the polymer into cyclopentadienyl group, since the scission of the main chain seems to occur exclusively at the dicyclopentadiene units at a temperatures below 60 °C. The activation energy for the dissociation of dimethyl dicyclopentadienedicarboxylate was reported to be 30 kcal/mol in a tetraglyme solution.[7] It is interesting to note that the activation energy of the dissociation of dicyclopentadiene units in a polymer main chains agreed with that for a low molecular weight compound.

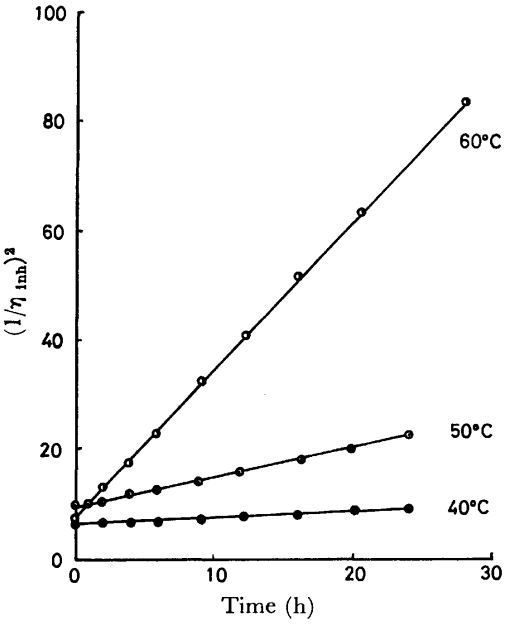

Fig. 5. Plots of $(1/\eta_{inh})^2$ against time.

References

1) J. K. Stille, and L. Plummer, *J. Org. Chem.*, **26**, 4026 (1961).
2) G. Koga, M. Yasaka, and Y. Nakayama, *Org. prep. Proced.*, **1**, 205 (1969).
3) D. Peters, *J. Chem. Soc.*, **1960**, 1832.
4) W. E. Franklin, C. H. Mack, and S. P. Rowland, *J. Org. Chem.*, **33**, 626 (1968).
5) R. B. Mesrobian, and A. S. Tobolsky, *J. Polym. Sci.*, **2**, 463 (1947).
6) D. Peters, *J. Chem. Soc.*, **1960**, 1761.
7) W. E. Franklin and C. H. Mack, *Anal. Calorimetry Proc. Am. Chem. Soc. Symp.*, 155 th (1968) 181.

Kinetic Study of the Reactions of Phenacyl Benzoates with Trialkyl Phosphites

Shizunobu HASHIMOTO, Isao FURUKAWA, and Takao TATSUMI

Department of Applied Chemistry, Faculty of Engineering, Doshisha University, Karasuma-imadegawa, Kamigyo-ku, Kyoto 602

(Received December 16, 1976)

The reactions of phenacyl benzoates, X-$C_6H_4COCH_2OCOC_6H_4$-Y (**1a—i**), with trialkyl phosphites (**2a—c**) giving dialkyl 1-arylvinyl phosphates (**3a—d**) in high yields were studied kinetically using the GLC technique. The overall reactions are second order, and exhibit a moderate solvent effect and catalysis upon the addition of certain organic acids. The activation energy, E_a=16.5 kcal/mol, and entropy, $\Delta S^{\neq}$=−38.5 e.u., were obtained from the reaction of **1a** with **2b**, and the ρ value obtained using σ for reactions of the two series of **1a** with **2b** was ρ_X=3.4 and ρ_Y=1.0, respectively. The reactivity of **2** in this reaction is markedly increased in the order, Me<Et<*i*-Pr. These and other data accumulated support a mechanism for this reaction involving a rate-determining addition of phosphorus atoms in **2** to the carbonyl carbon of the phenacyl group followed by rearrangement of the phosphorus moiety to the carbonyl oxygen of the phenacyl group.

Various studies have been published on the scope and mechanism of the Perkow reaction with α-halo ketones.[1-8] It is well known that the reactions of these ketones with trialkyl phosphites (**2**) lead to ketophosphonates (the Arbuzov reaction) and/or enol phosphates (**3**) (the Perkow reaction) (Scheme 1), and that the nature of the halogen atom in the α-halo ketones and the reaction temperature have a substantial effect on the course of the reaction.

It has been found that the reactions of phenacyl benzoates (**1**) with **2** form only **3** in high yields.[9] In this paper, kinetic studies on the reactions of two series of **1** with **2**, and to discuss the mechanism of the reactions.

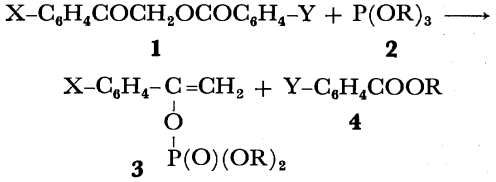

1a: X=H, Y=H
1b: X=H, Y=*p*-CH_3
1c: X=H, Y=*p*-CH_3O
1d: X=H, Y=*m*-CH_3
1e: X=H, Y=*p*-Cl
1f: X=H, Y=*m*-Cl
1g: X=*p*-CH_3, Y=H
1h: X=*p*-CH_3O, Y=H
1i: X=*p*-Cl, Y=H
1j: X=2,4,6-$(CH_3)_3$, Y=H

2a: R=CH_3
2b: R=C_2H_5
2c: R=$(CH_3)_2CH$

3a: X=H, R=C_2H_5
3b: X=*p*-CH_3, R=C_2H_5
3c: X=*p*-CH_3O, R=C_2H_5
3d: X=*p*-Cl, R=C_2H_5

Scheme 1.

Results

The reaction of **1** with **2**, which quantitatively yields enol phosphates (**3**), was studied kinetically in solution using the GLC technique (see Experimental). The reactions obey good second-order kinetics, and are first order with respect to both **1** and **2**, as shown by linear plots of log $(a-x)/(b-x)$ *vs.* time. The relative constancy of k_2 for the reaction of **1a** with **2b** for differing ratios of reactants is shown in Table 1. The rate law is expressed as

$$v = k_2[\text{triethyl phosphite}][\text{phenacyl benzoate}]. \quad (1)$$

Table 1. Reaction of **1a** with **2b** at 140 °C in tetralin

[**1a**], M	[**2b**], M	[**2b**]/[**1a**]	$10^4 k_2$, $M^{-1} s^{-1}$
0.40	0.40	1.0	1.13
0.20	0.80	4.0	1.16
0.50	0.30	0.6	1.19

Table 2. Reaction of phenacyl benzoates (**1a—i**) with **2b** at 140 °C in tetralin[a]

Compound	$10^4 k_2$, $M^{-1} s^{-1}$
1a	1.16
1b	0.77
1c	0.72
1d	1.23
1e	2.22
1f	3.40
1g	0.28
1h	0.11
1i	5.14

a) 0.2 M/l of **1**, 0.8 M/l of **2b**.

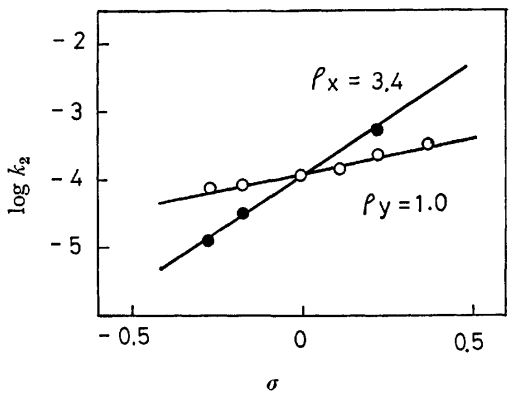

Fig. 1. Hammett plots of rates on the reaction of phenacyl benzoates (X-$C_6H_4COCH_2OCOC_6H_4$-Y) with triethyl phosphite in tetralin at 140 °C.

The rates of the reactions of phenacyl benzoates (**1a—i**) with **2b** at 140 °C are give in Table 2. The kinetic data gave a straight lines for Hammett plots with ρ_X=+3.4 and ρ_Y=+1.0 using the σ values shown in Fig. 1.

The rate constants ($M^{-1}\,s^{-1}$) of the reaction of **1a** with **2b** in tetralin at various temperatures were 3.10×10^{-5} at 110 °C, 4.64×10^{-5} at 120 °C, 1.16×10^{-4} at 140 °C, and 1.90×10^{-4} at 150 °C. The plots of log k_2 *vs.* $1/T$ produced a straight line, from which the energy, 16.5 kcal/mol, and the entropy of activation, −38.5 e.u., were obtained.

Table 3. Solvent effect on the rate of the reaction of **1a** with **2b** at 140° C[a)]

Solvent	Dielectric constant, ε	$10^4\,k_2$, $M^{-1}\,s^{-1}$
Tetralin	2.77	1.16
Phenetole	4.22	1.85
Acetophenone	17.39	3.13

a) 0.2 M/l of **1a**, 0.8 M/l of **2b**.

Table 4. Effect of propionic acid and *m*-chlorobenzoic acid on the reaction of **1a** with **2b**[a)]

Added acid	Concn, M/l	$10^4\,k_2$, $M^{-1}\,s^{-1}$
None	—	1.13
C_2H_5COOH	0.014	1.35
C_2H_5COOH	0.020	1.41
C_2H_5COOH	0.030	1.55
m-ClC_6H_4COOH	0.014	1.44

a) 0.4 M/l of **1a**, 0.4 M/l of **2b** in tetralin at 140 °C.

The solvent effect on the reaction of **1a** with **2b** at 140 °C is shown in Table 3. The rate constants increase with increasing solvent dielectric constant. When organic acids are added to the reaction mixture, the rate constants at 140 °C increase for the incipient step of the reaction (up to a conversion of about 30%) as shown in Table 4. The plots of k_2 *vs.* [propionic acid] show a straight line with a slope of $+1.40\times10^{-3}$ as expressed by

$$k_2 = 1.13\times10^{-4} + 1.40\times10^{-3}\,[\text{propionic acid}]. \quad (2)$$

The effect of the alkyl groups of **2** in the reactions with **1a** in tetralin was also studied, and the results are shown in Table 5. The reaction rates decrease in the order, *i*-Pr>Et>Me, corresponding to the nucleophilicity order of the phosphites.

Table 5. Effect of alkyl groups on the reaction of **2a**—**c** with **1a**[a)]

Compound	σ^*	$10^4\,k_2$, $M^{-1}\,s^{-1}$
2a	0	0.10 (110 °C)
2b	−0.10	0.26 (110 °C)
2b	−0.10	1.16 (140 °C)
2c	−0.19	3.34 (140 °C)

a) 0.2 M/l of **1**, 0.8 M/l of **2** in tetralin.

Discussion

Although various mechanisms have been proposed for the Perkow reaction, the most likely for the reaction of **1** with **2** include pathway A: the addition of **2** to the carbonyl oxygen of the phenacyl group gives directly an enol phosphonium salt (**5**), and pathway B: the addition of phosphite to the carbonyl carbon of the phenacyl groups followed by rearrangement of the phosphorus moiety to oxygen giving **5** (Scheme 2).

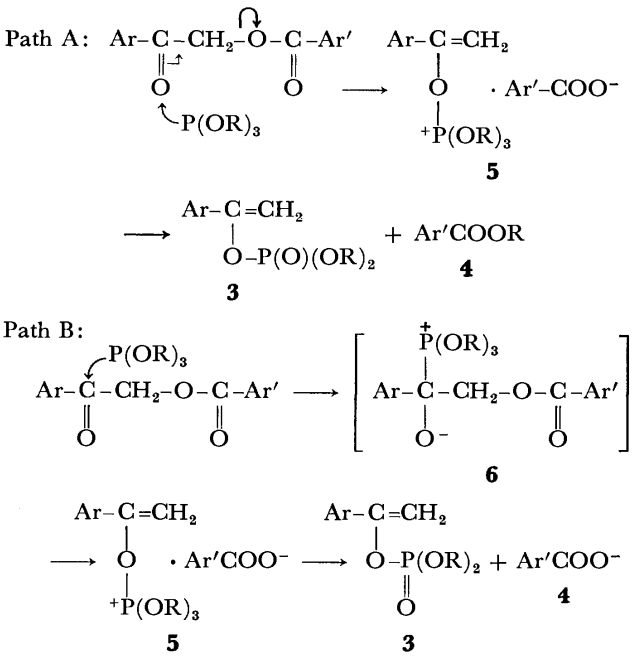

Scheme 2.

Pathway A, formally an S_N2' type reaction, involves the loss of a benzoate anion in the rate-determining step. From the ρ value obtained and the solvent effect, the rate along this pathway, which was proposed by Miller,[10] Trippett,[11] and Ramirez *et al.*[12] may be considerable. However, this pathway appears to be unacceptable in our experiments from a consideration of the role of the acid catalysis. Therefore, pathway A is excluded.

On the other hand, pathway B, involving a rate-determining addition of phosphite to the carbonyl carbon of the phenacyl group followed by fast rearrangement and Arbuzov cleavage, is supported by the following facts.

A) The ρ values, $\rho_X=+3.4$ and $\rho_Y=1.0$, obtained from the reaction with X-$C_6H_4COCH_2OCOC_6H_4$-Y show that the reaction rate is determined by the nucleophilic addition of phosphite to the carbonyl carbon of the phenacyl group. The reaction of 2,4,6-trimethylphenacyl benzoate (**1j**) with **2b** with no solvent did not occur at 140 °C for 10 h because of steric hindrance due to the mesityl group.

B) When the solvent is changed from tetralin ($\varepsilon=2.77$) to acetophenone ($\varepsilon=17.39$), the rate increases by a factor of 2.7 (Table 3). The reaction *via* a charge-separated complex (**6**) should be facilitated by an increase in the polarity of the solvent.[13]

C) When organic acids are added to the mixture of **1a** and **2b**, the rate constant increases in the incipient step of the reaction as shown in Table 4. As the reaction proceeds, however, the accelerating effect gradually decreases. This phenomenon is due to the fact that a reaction of **2** with an acid occurs. In the presence of the acid, **1** may form weak hydrogen bonds

$$>C{=}O + HA \rightleftarrows >\overset{\delta+}{C}{=}O\cdots H\cdots\overset{\delta-}{A}$$

$$(RO)_3P + >\overset{\delta+}{C}{=}O\cdots H\cdots\overset{\delta-}{A} \rightleftarrows (RO)_3\overset{+}{P}-\underset{|}{C}-\overset{-}{O} + H{-}A$$

Scheme 3.

between the phenacyl group and the acid added, and the resulting bonds activate the carbonyl group for the nucleophilic attack by **2**. The reaction is believed to progress as shown in Scheme 3.

m-Chlorobenzoic acid is a more effective catalyst in this reaction (Table 4), because it is more acidic and, thus, more effective in forming a hydrogen bond with the carbonyl group. The acid catalysis and solvent effect, which have been observed for the reaction of α-halo ketones[4,5,8,13,14] and benzil[15] with trivalent phosphorus compounds, are similar to those obtained in this work. According to this mechanism, the second step, a rearrangement of the phosphorus moiety to oxygen, is not rate-determining in terms of the acid effect. The last step, Arbuzov cleavage of the alkyl group by the benzoate anion, which has been shown to be rapid and not rate-determining in the reaction of phosphite with ethyl iodide,[16] should not be accelerated in a polar solvent.

D) In view of the σ^* of Taft,[17] the nucleophilicity of the phosphites is considered to be in the order $(MeO)_3P<(EtO)_3P<(i\text{-}PrO)_3P$. The observed reactivity for the reaction of **1** with **2** is in agreement with the nucleophilicity of trialkyl phosphite.

E) For the reaction of aryl-substituted α-haloisobutyrophenones with **2b**, in which the rate-determining step is carbonyl addition, $E_a = 12.8$—13.3 kcal/mol and $\Delta S^{\neq} = -41$—-42 e.u.[4] These data are quite similar to those presented here. Also, the reaction of benzil with **2** has been postulated to proceed *via* a similar mechanism.[15] The large negative entropy of activation obtained should be consistent with a dipolar transition state **6**.[18,19]

F) This reaction leads exclusively to enol phosphate in very high yields.[9] Since the facility of the elimination of a leaving group in an S_N2 reaction is generally in the order $I>Br>Cl>OCOCH_3$,[20] the elimination of a benzoate anion should be more difficult than that of a halide anion. Consequently, it is believed that this reaction proceeds along pathway B shown in Scheme 2.

Experimental

Materials. Phenacyl benzoates (**1a**—**i**) were prepared from corresponding phenacyl bromides and sodium benzoates.[9] **1j** was prepared by the method described above. Mp 87.5—88.3 °C. NMR (CD_3Cl): δ 2.20 (s, 9H, $(CH_3)_3$), 5.02 (s, 2H, CH_2), 6.60—8.10 (m, 7H, aromatic-H). MS: *m/e* 283 (M^+). Trialkyl phosphites (**2a**—**c**) were prepared from a reaction of phosphorus trichloride with alcohols in the presence of a base and were distilled from metallic sodium.[21] All of the solvents used were purified by the usual method.[22]

Instruments. NMR spectra were recorded on a Hitachi Model R-24 (60 Mc) spectrometer using TMS as an internal standard. Mass spectra were recorded on a Hitachi Model RM-50GC gas chromatograph-mass spectrometer. GLC measurements were carried out on a Shimadzu Model GC-4BPT instrument equipped with a 0.5×2 m silicone SE-30 (5 wt%) on Chromosorb G (60—80 mesh) column at 200 °C, using H_2 as the carrier gas (90 ml/min). Melting points were determining on a Yanaco MP apparatus and uncorrected.

Kinetic Measurements. The reactions were carried out in a rubber-stoppered glass tube maintained at a given temperature using a stirred thermostatically-controlled bath. The reaction rates were estimated from the relative peak areas (corrected), which were determined by means of the internal standard method using the GLC technique. Pyrene was used as the internal standard. In a typical reaction, 2 mmol of **1**, 8 mmol of **2** and 0.3 g of pyrene were placed in a 10-ml volumetric flask. Then this solution was quickly increased to 10 ml with the addition of tetralin. This solution was transferred into a tube displaced with nitrogen, and was allowed to react at 140 °C. Aliquots were taken out by syringe at appropriate time intervals and their compositions were determined immediately by the GLC technique. No reaction of **1j** with **2b** occurred for 10 h at 140 °C, and both **1j** and **2b** were recovered.

The authors are indebted to Mr. S. Isogai for carrying out some of the kinetic determinations.

References

1) F. W. Lichtenthaler, *Chem. Rev.*, **61**, 607 (1961).
2) R. F. Hudson, "Structure and Mechanism in Organophosphorus Chemistry," Academic Press, New York (1965), p. 153.
3) A. Arcoria and S. Fisichella, *Tetrahedron Lett.*, **1971**, 3347.
4) I. J. Borowitz, S. Firstenberg, G. B. Borowitz, and D. Schuessler, *J. Am. Chem. Soc.*, **94**, 1623 (1972).
5) P. A. Chopard, V. M. Clark, R. F. Hudson, and A. J. Kirby, *Tetrahedron*, **21**, 1961 (1965).
6) E. M. Gaydon, G. Buono, and R. Freze, *Bull. Soc. Chim. Fr.*, **1973**, 2284.
7) J. Konecny, R. Dousse, and J. Rosales, *Helv. Chim. Acta*, **55**, 3048 (1972).
8) I. J. Borowitz, M. Anschel, and S. Firstenberg, *J. Org. Chem.*, **32**, 1723 (1967).
9) S. Hashimito and I. Furukawa, *Sulfur and Phosphorus*, in press.
10) B. Miller, *J. Am. Chem. Soc.*, **88**, 1841 (1966).
11) S. Trippett, *J. Chem. Soc.*, **1962**, 2337.
12) F. Ramirez, N. Ramanathan, and N. B. Desai, *J. Am. Chem. Soc.*, **85**, 3465 (1963).
13) R. Huisgen and P. Otto, *J. Am. Chem. Soc.*, **90**, 5342 (1970).
14) I. J. Borowitz and L. J. Grossman, *Tetrahedron Lett.*, **1962**, 471.
15) Y. Ogata and M. Yamashita, *J. Am. Chem. Soc.*, **92**, 4670 (1970).
16) G. Aksnes and D. Aksnes, *Acta Chem. Scand.*, **18**, 38 (1964).
17) R. W. Taft, Jr., *J. Am. Chem. Soc.*, **75**, 4231 (1953).
18) A. J. Speziale and D. E. Bissing, *J. Am. Chem. Soc.*, **85**, 3878 (1963).
19) E. S. Gould, "Mechanism and Structure in Organic Chemistry," Henry Holt and Co., New York (1960), p. 182.
20) E. R. Thornton, "Solvolysis Mechanism," Ronald Press Co., New York (1964), p. 165.
21) A. H. Ford-Moore and B. J. Perry, *Org. Synth.*, Vol. 31, 111 (1951).
22) J. A. Riddick and W. B. Bunger, "Organic Solvent," 3rd ed, John Wiley & Sons, Inc., New York (1970).

Syntheses of D-Arabinofuranosyl and 2'-Deoxy-D-ribofuranosyl 1,2,3-Triazolecarboxamides

Osamu MAKABE,* Hiroshi SUZUKI, and Sumio UMEZAWA**

Department of Applied Chemistry, Faculty of Engineering, Keio University, Hiyoshi, Kohoku-ku, Yokohama, Kanagawa 223

(Received February 14, 1977)

Several D-arabino- and 2'-deoxy-D-ribonucleosides of 1,2,3-triazolecarboxamides were synthesized by two methods, one involving acid-catalyzed fusion reactions of 1-*O*-acetyl derivatives (**3**, **5**) of the corresponding sugars and 1,2,3-triazole-4-carboxylate (**1**), and the other by glycosylation of the trimethylsilyl derivative (**2**) of **1** with glycosyl halides (**4**, **6**). Evidence for the *N*-glycosylation sites and anomeric configurations of the resulting nucleosides is presented.

Because of antiviral activity, some azole-carboxamides such as pyrazomycin[1,2] and virazole[3] have attracted attention. The synthesis of 1-(β-D-ribofuranosyl)-1,2,3-triazole-4-carboxamide, which is active *in vitro* against vaccinia viruses, has been reported.[4,5] Modifications of the glycosyl moiety of these nucleosides were of interest for the determination of structure-activity relationships. A report was given on the syntheses of D-arabinofuranosyl and 2'-deoxy-D-ribofuranosyl pyrazolecarboxamides.[6] The present paper deals with an extention of the work;[4] *i.e.* the synthesis of some 1,2,3-triazole nucleosides with modifications of the glycosyl moiety, including the arabinofuranosyl and 2-deoxyribofuranosyl derivatives of 1,2,3-triazole-4-carboxamide. Two methods have been employed to prepare these *N*-glycosyl-1,2,3-triazoles. One method (method A) is the acid-catalyzed fusion reaction of 1-*O*-acetyl derivatives of *O*-blocked sugars and ethyl 1,2,3-triazole-4-carboxylate (**1**), and the other (method B) is the glycosylation of the trimethylsilyl derivative (**2**) of ethyl 1,2,3-triazole-4-carboxylate with *O*-blocked glycosyl halides.

Results and Discussion

Since D-arabinosylation of purine and pyrimidine bases has often been successful in yielding antiviral and cytotoxic activities as exemplified[7] by 9-(β-D-arabinofuranosyl)adenine and 1-(β-D-arabinofuranosyl)cytosine, we performed the synthesis of 1-*N*-(β-D-arabinofuranosyl)-1,2,3-triazole-4-carboxamide (**13β**). Synthesis of the 1',2'-*cis* nucleoside was first performed by use of 1-*O*-acetyl-2,3,5-tri-*O*-benzyl-D-arabinofuranose[4] (**3**) in which the hydroxyl group at C-2 is blocked with benzyl group (a nonparticipating group). However, fusion of **3** with ethyl 1,2,3-triazole-4-carboxylate[8] in the presence of bis(*p*-nitrophenyl) hydrogenphosphate[9] gave a mixture of isomeric products (total yield 95.8%), *viz.*, ethyl 1-*N*-(2,3,5-tri-*O*-benzyl-β-D-arabinofuranosyl)-1,2,3-triazole-4-carboxylate (**7β**), its α-anomer (**7α**), ethyl 2-*N*-(2,3,5-tri-*O*-benzyl-β-D-arabinofuranosyl)-1,2,3-triazole-4-carboxylate (**8β**) and its α-anomer (**8α**) in a ratio of 1: 5: 7: 13.5, which were separated by chromatography. An improved yield of **7β** (16.7%) was obtained by application of the Lewis acid-catalyzed silyl Hilbert-Johonson reaction.[10] The trimethylsilyl derivative (**2**) of ethyl 1,2,3-triazole-4-carboxylate was treated with 2,3,5-tri-*O*-benzyl-D-arabinofuranosyl chloride[11] (**4**) in the presence of stannic chloride in 1,2-dichloroethane to give a mixture of **7β**, **7α**, **8β**, **8α**, and ethyl 1-*N*-(2,3,5-tri-*O*-benzyl-α-D-arabinofuranosyl)-1,2,3-triazole-5-carboxylate (**9α**) (total yield 83%) in a ratio of 1: 1.5: 1: 1.5: 1.2, which were readily separated by chromatography. The products (**7β**, **7α**, **8β**, **8α**, and **9α**) were converted into the corresponding carboxamides (**10β**, **10α**, **11β**, **11α**, and **12α**) by treatment with methanolic ammonia. The benzyl groups were readily removed by catalytic hydrogenolysis on palladium black to give 1-*N*-(β-D-arabinofuranosyl)-1,2,3-triazole-4-carboxamide (**13β**), its α-anomer (**13α**), 2-*N*-(β-D-arabinofuranosyl)-1,2,3-triazole-4-carboxamide (**14β**), its α-anomer (**14α**), and 1-*N*-(α-D-arabinofuranosyl)-1,2,3-triazole-5-carboxamide (**15α**), respectively.

The structures of these arabinonucleosides were assigned on the basis of their PMR (Table 1) and UV spectra (Table 2). The anomeric proton of **15α** (δ 6.81) appears at lower field than those of **13α** and **13β** (δ 6.16 and 6.40, respectively) and **14α** and **14β** (δ 6.00 and 6.29, respectively). The downfield shift of H-1' of nucleosides having a carbamoyl group adjacent to the site of glycosylation has been attributed to the anisotropic effect of the carbonyl group.[12,13] The signals for the H-5 of **13α** and **13β** (δ 8.86 and 8.70, respectively) appear at lower field than those of the isomeric **14α** and **14β** (δ 8.39 and 8.31, respectively), indicating[6,14] that **13α** and **13β** are 1-*N*-glycosides and **14α** and **14β** are

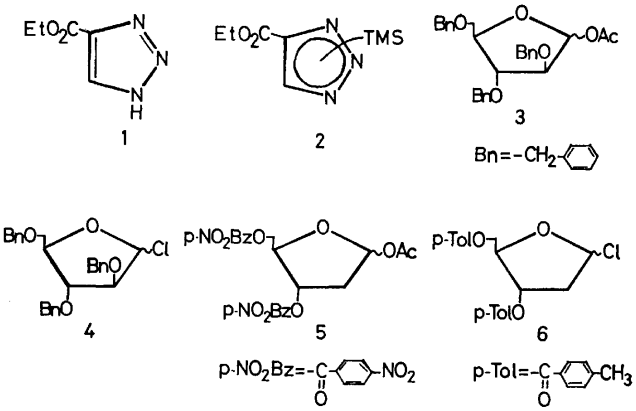

Chart 1.

* Present address: Research Laboratories, Meiji Seika Kaisha, Morooka-cho, Kohoku-ku, Yokohama, Kanagawa 222.

** Present address: Institute of Bio-organic Chemistry, Nakahara, Kawasaki, Kanagawa 211.

TABLE 1. PMR SPECTRAL DATA IN DMSO-d_6

Arabino-nucleosides	Anomeric proton	$J_{1',2'}$	H-5	2'-Deoxyribo-nucleosides	Anomeric proton	$J_{1',2'}$ $J_{1',2''}$	H-5
13α	δ 6.16	3.8 Hz	δ 8.86	**20α**	δ 6.43	2.5, 7.0 Hz	δ 8.72
13β	6.40	5.2	8.70	**20β**	6.40	6.0, 6.0	8.78
14α	6.00	5.3	8.39	**21α**	6.30	5.5, 6.5	8.20
14β	6.29	6.4	8.31	**21β**	6.31	5.0, 6.0	8.13
15α	6.81	4.6	8.35(H-4)				

2-*N*-glycosides. Comparison of **13β** and **14β** with their α-anomers (**13α** and **14α**, respectively) shows downfield shifts for the anomeric protons of the β-anomers as expected for 1',2'-*cis* nucleosides.[15] The coupling constants for the anomeric protons of **13α**, **13β**, **14α**, and **14β** also support their α- and β-configurations. The anomeric configuration of **15α** was deduced by its specific rotation.

TABLE 2. ULTRAVIOLET ABSORPTION DATA

Compound No.	Solvents λ_{max} nm and ε: pH 7 (H_2O) λ_{max}	ε	pH 1 (HCl) λ_{max}	ε	pH 13 (NaOH) λ_{max}	ε
13α	212	11200	211	10800	224	8600
13β	211	12000	211	12200	223	9800
14α	229	11900	230	12000	230	10500
14β	229	11600	229	12700	230	11500
15α	218	9700	217	10200	225	6150
20α	213	11100	212	11800	225	8000
20β	213	11900	213	12200	224	11000
21α	228	11400	227	10900	228	11500
21β	228	11600	228	12000	230	11300

The synthesis of 2'-deoxyribofuranosyl nucleosides was also performed by the two methods. The fusion reaction of 1-*O*-acetyl-2-deoxy-3,5-di-*O*-(*p*-nitrobenzoyl)-D-*erythro*-pentofuranose[6] (**5**) and **1** gave ethyl 1-*N*-[2-deoxy-3,5-di-*O*-(*p*-nitrobenzoyl)-β-D-*erythro*-pentofuranosyl]-1,2,3-triazole-4-carboxylate (**18β**), its α-anomer (**18α**), ethyl 2-*N*-[2-deoxy-3,5-di-*O*-(*p*-nitrobenzoyl)-β-D-*erythro*-pentofuranosyl]-1,2,3-triazole-4-carboxylate (**19β**) and its α-anomer (**19α**) in a ratio of 1.25: 1: 2.5: 1.75 (total yield 78.9%). Protection of hydroxy-groups with substituted benzoyl groups facilitates separation of the anomers usually formed in the synthesis of 2'-deoxyribonucleosides.[6,16] Glycosylation of the trimethylsilyl derivative (**2**) with 2-deoxy-3,5-di-*O*-(*p*-toluoyl)-D-*erythro*-pentofuranosyl chloride[17] in the presence of stannic chloride in 1,2-dichloroethane gave ethyl 1-*N*-[2-deoxy-3,5-di-*O*-(*p*-toluoyl)-β-D-*erythro*-pentofuranosyl]-1,2,3-triazole-4-carboxylate (**16β**), its α-anomer (**16α**), ethyl 2-*N*-[2-deoxy-3,5-di-*O*-(*p*-toluoyl)-β-D-*erythro*-pentofuranosyl]-1,2,3-triazole-4-carboxylate (**17β**), and its α-anomer (**17α**) in a ratio of 1.77: 2.4: 1: 1.1 (total yield 90.5%). Their treatment with methanolic ammonia afforded the corresponding carboxamides, **20β**, **20α**, **21β**, and **21α**, respectively. It should be noted that in the synthesis of the 2'-deoxyribonucleosides by method B, no formation of isomeric 5-carboxylate was detected as compared with a 14.7% yield of **9α** in the synthesis of arabinonucleosides. The H-5 protons of **20α** and **20β** appear at significantly lower field than those of **21α** and **21β**, indicating that the former are 1-*N*-glycosyl derivatives and the latter 2-*N*-glycosyl derivatives. Their UV spectra also show a characteristic difference[4] (Table 2). The anomeric proton of **20β** appears as a pseudotriplet with a peak width of 12 Hz which is in line with the β-configuration.[18,19] The anomeric proton of **20α** appears as a quartet whose *J*-values indicate the α-configuration. The anomeric configuration of **21α** and **21β** was deduced by their specific rotation, though their PMR spectra provided no definite assignments.

Of the nucleosides prepared, 1-*N*-(β-D-arabinofuranosyl)-1,2,3-triazole-4-carboxamide (**13β**) and 1-*N*-(2-deoxy-β-D-*erythro*-pentofuranosyl)-1,2,3-triazole-4-carboxamide (**20β**) were found to have antiviral and cytotoxic activities.[5]

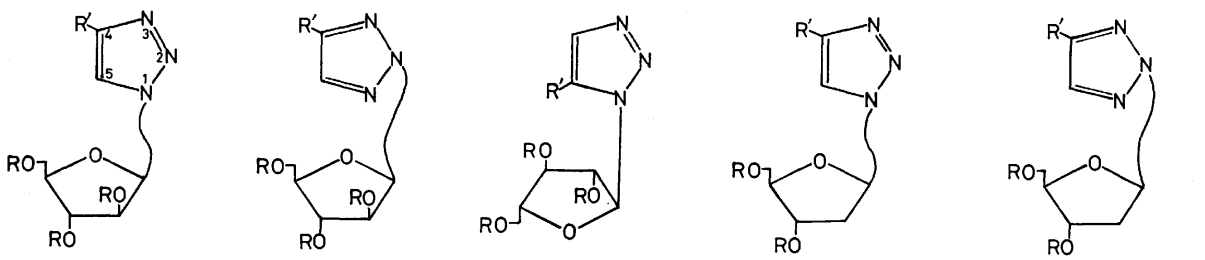

7α, R'= CO_2Et, R= Bn
7β, R'=CO_2Et, R= Bn
10α, R'=$CONH_2$, R=Bn
10β, R'=$CONH_2$, R=Bn
13α, R'=$CONH_2$, R=H
13β, R'=$CONH_2$, R=H

8α, R'=CO_2Et, R=Bn
8β, R'=CO_2Et, R=Bn
11α, R'=$CONH_2$, R=Bn
11β, R'=$CONH_2$, R=Bn
14α, R'=$CONH_2$, R=H
14β, R'=$CONH_2$, R=H

9α, R'=CO_2Et, R=Bn

12α, R'=$CONH_2$, R=Bn

15α, R'=$CONH_2$, R=H

16α, R'=CO_2Et, R=p-NO_2Bz
16β, R'=CO_2Et, R=p-NO_2Bz
18α, R'=CO_2Et, R=p-Tol
18β, R'=CO_2Et, R=p-Tol
20α, R'=$CONH_2$, R=H
20β, R'=$CONH_2$, R=H

17α, R'=CO_2Et, R=p-NO_2Bz
17β, R'=CO_2Et, R=p-NO_2Bz
19α, R'=CO_2Et, R=p-Tol
19β, R'=CO_2Et, R=p-Tol
21α, R'=$CONH_2$, R=H
21β, R'=$CONH_2$, R=H

Chart 2.

Experimental

Melting points were determined on a micro hot stage and are uncorrected. Thin layer chromatography (TLC) was carried out with Wakogel B-5, silica gel column chromatography with Wakogel C-200. UV spectra were taken with a Hitachi Perkin-Elmer UV-VIS spectrometer 139 and PMR spectra with a Varian A-60D spectrometer with TMS as an internal standard.

Silylation of Ethyl 1,2,3-Triazole-4-carboxylate. To a solution of ethyl 1,2,3-triazole-4-carboxylate[8] (**1**, 5.0 g, 35.5 mmol) and chlorotrimethylsilane (7.45 g, 67.5 mmol) in dried 1,4-dioxane (48 ml) was added dropwise, with stirring, a solution of triethylamine (6.9 g) in dried 1,4-dioxane (3 ml). The reaction mixture was stirred for 12 h at room temperature. The precipitated triethylamine hydrochloride was filtered off and washed with two 5 ml portions of dried 1,4-dioxane. The filtrate and washings were combined and evaporated under reduced pressure. The resulting oil was distilled at 114 °C/1 mmHg, to give 6.86 g (91%) of a colorless oil (**2**).

Ethyl 1-N-(2,3,5-Tri-O-benzyl-β-D-arabinofuranosyl)-1,2,3-triazole-4-carboxylate (7β), Its α-Anomer (7α) and Ethyl 2-N-(2,3,5-Tri-O-benzyl-β-D-arabinofuranosyl)-1,2,3-triazole-4-carboxylate (8β), Its α-Anomer (8α) and Ethyl 1-N-(2,3,5-Tri-O-benzyl-α-D-arabinofuranosyl)-1,2,3-triazole-5-carboxylate (9α). *Method A*: A mixture of ethyl 1,2,3-triazole-4-carboxylate (**1**, 890 mg, 6.30 mmol) and 1-*O*-acetyl-2,3,5-tri-*O*-benzyl-D-arabinofuranose[4] (**3**, 2.19 g, 6.30 mmol) was heated at 143°C. To the melt was added bis(*p*-nitrophenyl) hydrogenphosphate (4 mg), and the mixture was heated at 143°C under reduced pressure for *ca.* 20 min until the evolution of acetic acid ceased. The resulting mixture was dissolved in a minimum amount of ethyl acetate and was placed on a column of silica gel (180 g, 2.8×70 cm, packed with 2:1 hexane–diisopropyl ether) and successively eluted with 2:1- (120 ml) and 1:1 hexane–diisopropyl ether. The effluent was fractionated into 12 ml-fractions.

Fractions 37—53 gave **8α**, colorless syrup, 1.38 g (40.2%). Fractions 54—63 gave a mixture of **8α** and **8β**, 820 mg (23.9 %), α:β=2:3 (from PMR). Fractions 64—69 gave **8β**, colorless syrup, 390 mg (11.4%). Fractions 81—91 gave **7α**, colorless syrup, 530 mg (15.4%). Fractions 92—98 gave a mixture of **7α** and **7β**, 90 mg (2.6%), α:β=1:1 (from PMR). Fractions 99—105 gave **7β**, colorless syrup, 80 mg (2.3%).

Method B: To a solution of 2,3,5-tri-*O*-benzyl-D-arabinofuranosyl chloride[11] (**4**, 2.00 g, 4.6 mmol) and silylated ethy-1,2,3-triazole-4-carboxylate (**2**, 1.00 g, 4.8 mmol) in 1,2-dichloroethane (50 ml) was added a solution of redistilled $SnCl_4$ (1.2 ml, 2.0 mmol) in 1,2-dichloroethane (3 ml) at 0 °C under stirring. The reaction mixture was stirred at room temperature for 12 h. After dilution with 1,2-dichloroethane (20 ml), the reaction mixture was washed with saturated aqueous $NaHCO_3$ solution. The organic layer separated by centrifugation was dried (Na_2SO_4), and evaporated under reduced pressure. The resulting mixture was dissolved in a minimum amount of ethyl acetate and chromatographed on a column of silica gel (140 g, 2.8×60 cm, packed with 1:1 hexane–diisopropyl ether) and eluted with the same solvent system. The effluent was fractionated into 11 ml-fractions.

Fractions 40—44 gave **8α**, colorless syrup, 396 mg (17.3%); $[\alpha]_D^{20}$ +58.4° (*c* 1.0, $CHCl_3$). PMR ($CDCl_3$): δ 8.25 (s, 1H, H-5), 7.40 (d, 15H, Ar), 6.39 (d, 1H, $J_{1',2'}$=3.7 Hz, H-1'), 5.05 (dq, 1H, H-2'), 4.70—4.30 (m, 10H, CH_2-ester, CH_2-Ar, H-3', H-4'), 3.75 (d, 2H, H-5',5''), 1.45 (t, 3H, CH_3-ester). Found: C, 68.14; H, 6.16; N, 7.53%. Calcd for $C_{31}H_{33}O_6N_3$: C, 68.49; H, 6.12; N, 7.73%.

Fractions 45—48 gave a mixture of **8α** and **8β**, 85 mg (3.7 %), α:β=1:1 (from PMR).

Fractions 49—52 gave **8β**, colorless crystal, 236 mg (10.3%); mp 101—102 °C. $[\alpha]_D^{20}$ −54.5° (*c* 1.0, $CHCl_3$). PMR ($CDCl_3$): δ 8.35 (s, 1H, H-5), 7.45 (d, 15H, Ar), 6.67 (d, 1H, $J_{1',2'}$= 4.8 Hz, H-1'), 4.50 (m, 11H, H-2', CH_2-Ar, CH_2-ester, H-3', H-4'), 3.75 (d, 2H, H-5',5''), 1.41 (t, 3H, CH_3-ester). Found: C, 68.63; H, 6.11; N, 7.86%. Calcd for $C_{31}H_{33}O_6N_3$: C, 68.49; H, 6.12; N, 7.73%.

Fractions 63—66 gave **9α**, colorless syrup, 358 mg (14.7%); $[\alpha]_D^{20}$ +55.0° (*c* 1.0, $CHCl_3$). PMR ($CDCl_3$): δ 8.12 (s, 1H, H-4), 7.30 (d, 15H, Ar), 6.85 (d, 1H, $J_{1',2'}$=3.3 Hz, H-1'), 5.20 (dq, 1H, H-2'), 4.70—4.20 (m, 10H, CH_2-Ar, CH_2-ester, H-3', H-4'), 3.69 (d, 2H, H-5',5''), 1.39 (t, 3H, CH_3-ester). Found: C, 68.58; H, 6.18; N, 7.51%. Calcd for $C_{31}H_{33}O_6N_3$: C, 68.49; H, 6.12; N, 7.73%.

Fractions 75—83 gave **7α**, colorless syrup, 465 mg (20.3%); $[\alpha]_D^{20}$ +61.0° (*c* 1.0, $CHCl_3$). PMR ($CDCl_3$): δ 8.44 (s, 1H, H-5), 7.45 (d, 15H, Ar), 6.42 (d, 1H, $J_{1',2'}$=1.5 Hz, H-1'), 4.75—4.20 (m, 11H, CH_2-Ar, CH_2-ester, H-2', H-3', H-4'), 3.73 (d, 2H, H-5',5''), 1.40 (t, 3H, CH_3-ester). Found: C, 68.26; H, 6.12; N, 7.55%. Calcd for $C_{31}H_{33}O_6N_3$: C, 68.49; H, 6.12; N, 7.73%.

Fractions 85—91 gave **7β**, colorless syrup, 380 mg (16.7%); $[\alpha]_D^{20}$ −30.2° (*c* 1.0, $CHCl_3$). PMR ($CDCl_3$): δ 8.65 (s, 1H, H-5), 7.45 (d, 15H, Ar), 6.65 (d, 1H, $J_{1',2'}$=4.0 Hz, H-1'), 4.70—4.10 (m, 11H, CH_2-Ar, CH_2-ester, H-2', H-3', H-4'), 3.75 (d, 2H, H-5',5''), 1.40 (t, 3H, CH_3-ester). Found: C, 68.69; H, 6.25; N, 7.63%. Calcd for $C_{31}H_{33}O_6N_3$: C, 68.49; H, 6.12; N, 7.73%.

1-N-(2,3,5-Tri-O-benzyl-α-D-arabinofuranosyl)-1,2,3-triazole-4-carboxamide (10α). A sample of **7α** (400 mg, 0.74 mmol) in absolute methanol (40 ml) saturated with ammonia at 0 °C was kept at room temperature for 12 h and evaporated under reduced pressure at 40 °C. The residual syrup was washed with hexane and the resulting gum was crystallized from ethyl acetate and diisopropyl ether to give **10α**, 315 mg (85%); mp 135—136 °C. $[\alpha]_D^{20}$ +67.2° (*c* 1.0, $CHCl_3$). PMR ($CDCl_3$): δ 8.48 (s, 1H, H-5), 7.40 (m, 15H, Ar), 6.40 (d, 1H, $J_{1',2'}$= 1.9 Hz, H-1'), 6.30 (br d, 2H, $CONH_2$), 4.65 (m, 8H, CH_2-Ar, H-2', H-3'), 4.30 (m, 1H, H-4'), 3.73 (d, 2H, H-5',5''). Found: C, 67.54; H, 5.81; N, 10.70%. Calcd for $C_{29}H_{30}O_5N_4$: C, 67.69; H, 5.88; N, 10.89%.

1-N-(2,3,5-Tri-O-benzyl-β-D-arabinofuranosyl)-1,2,3-triazole-4-carboxamide (10β). By a procedure similar to that for **10α**, **7β** (153 mg, 0.28 mmol) gave **10β**. Recrystallization from benzene–diisopropyl ether gave a pure sample, 110 mg (76%); mp 122—123 °C. $[\alpha]_D^{20}$ −47.5° (*c* 0.61, $CHCl_3$). PMR($CDCl_3$): δ 8.62 (s, 1H, H-5), 7.40 (m, 15H, Ar), 6.60 (d, 1H, $J_{1',2'}$= 4.3 Hz, H-1'), 5.85 (br d, 2H, $CONH_2$), 4.85—4.20 (m, 9H, CH_2-Ar, H-2', H-3', H-4'), 3.75 (d, 2H, H-5',5''). Found: C, 67.69; H, 5.97; N, 10.70%. Calcd for $C_{29}H_{30}O_5N_4$: C, 67.69; H, 5.88; N, 10.89%.

2-N-(2,3,5-Tri-O-benzyl-α-D-arabinofuranosyl)-1,2,3-triazole-4-carboxamide (11α). By a procedure similar to that for **10α**, **8α** (883 mg, 1.62 mmol) gave **11α**. Recrystallization from ethyl acetate and diisopropyl ether gave 701 mg (84%); mp 89.5°C. $[\alpha]_D^{20}$ +67.6° (*c* 1.4, $CHCl_3$). PMR ($CDCl_3$): δ 8.30 (s, 1H, H-5), 7.40 (m, 15H, Ar), 6.50 (br d, 2H, $CONH_2$), 6.30 (d, 1H, $J_{1',2'}$=3.5 Hz, H-1'), 5.00 (t, 1H, H-2'), 4.75—4.25 (m, 8H, CH_2-Ar, H-3', H-4'), 3.72 (d, 2H, H-5',5''). Found: C, 67.64; H, 6.05; N, 10.66%. Calcd for $C_{29}H_{30}O_5N_4$: C, 67.69; H, 5.88; N, 10.89%.

2-N-(2,3,5-Tri-O-benzyl-β-D-arabinofuranosyl)-1,2,3-triazole-4-carboxamide (11β). By a procedure similar to that for **10α**, **8β** (706 mg, 1.3 mmol) gave **11β**. Recrystallization from benzene–diisopropyl ether gave 535 mg (80%). mp 131—132 °C.

$[\alpha]_D^{20}$ −57.5° (*c* 1.2, $CHCl_3$). PMR ($CDCl_3$): δ 8.31 (s, 1H, H-5), 7.40 (m, 15H, Ar), 6.48 (d, 1H, $J_{1',2'}$=5.5 Hz, H-1'), 6.30 (br d, 2H, $CONH_2$), 4.80—4.20 (m, 9H, CH_2–Ar, H-2', H-3', H-4'), 3.90 (d, 2H, H-5',5''). Found: C, 67.82; H, 5.91; N, 10.82%. Calcd for $C_{29}H_{30}O_5N_4$: C, 67.69; H, 5.88; N, 10.89%.

1-N-(2,3,5-Tri-O-benzyl-α-D-arabinofuranosyl)-1,2,3-triazole-5-carboxamide (12α). By a procedure similar to that **10α**, **9α** (200 mg, 0.37 mmol) gave **12α**. Recrystallization from benzene-diisopropyl ether gave 153 mg (81%); mp 122—123 °C. $[\alpha]_D^{20}$ +65.5° (*c* 1.0, $CHCl_3$). PMR ($CDCl_3$): δ 8.00 (s, 1H, H-4), 7.30 (d, 15H, Ar), 6.92 (d, 1H, $J_{1',2'}$=3.1 Hz, H-1'), 6.60 (br s, 2H, $CONH_2$), 5.20 (dq, 1H, H-2'), 4.70—4.20 (m, 8H, CH_2–Ar, H-3', H-4'), 3.73 (d, 2H, H-5',5''). Found: C, 68.00; H, 6.10; N, 11.07%. Calcd for $C_{29}H_{30}O_5N_4$: C, 67.69; H, 5.88; N, 10.89%.

1-N-(α-D-Arabinofuranosyl)-1,2,3-triazole-4-carboxamide (13α). A sample of **10α** (300 mg, 0.583 mmol) in 6 ml methanol was hydrogenated over palladium black catalyst at 3.5 atm for 24h. After removal of the catalyst, the methanol layer was evaporated and the residue was crystalilzed from methanol and benzene to give **13α**, 101 mg (78%); mp 185—185.5 °C. $[\alpha]_D^{20}$ +89.1° (*c* 0.73, H_2O). PMR (DMSO-d_6): δ 8.86 (s, 1H, H-5), 7.80 (br d, 2H, $CONH_2$), 6.16 (d, 1H, $J_{1',2'}$=3.8 Hz, H-1'), 6.06 (d, 1H, OH), 5.67 (d, 1H, OH), 5.00 (t, 1H, OH), 4.60 (t, 1H, H-2'), 4.20 (m, 2H, H-3', H-4'), 3.69 (m, 2H, H-5,5''). Found: C, 39.37; H, 5.03; N, 23.22%. Calcd for $C_8H_{12}O_5N_4$: C, 39.34; H, 4.95; N, 22.94%.

1-N-(β-D-Arabinofuranosyl)-1,2,3-triazole-4-carboxamide (13β). A sample of **10β** (100 mg, 0.19 mmol) was hydrogenated and worked up in a similar manner to that described above. Recrystallization from methanol gave **13β**, 42 mg (84%); mp 163—164 °C. $[\alpha]_D^{20}$ −31.0° (*c* 1.0, H_2O). PMR (DMSO-d_6): δ 8.70 (s, 1H, H-5), 7.75 (br d, 2H, $CONH_2$), 6.40 (d, 1H, $J_{1',2'}$=5.2 Hz, H-1'), 5.70 (m, 2H, OH), 5.18 (d, 1H, OH), 4.40—3.90 (m, 3H, H-2', H-3', H-4'), 3.75 (m, 2H, H-5',5''). Found: C, 39.00; H, 4.88; N, 22.65%. Calcd for $C_8H_{12}O_5N_4$: C, 39.34; H, 4.95; N, 22.94%.

2-N-(α-D-Arabinofuranosyl)-1,2,3-triazole-4-carboxamide (14α). Similar hydrogenation of **11α** (515 mg, 1.0 mmol) followed by recrystallization from methanol gave **14α**, 181 mg (74%); mp 188—189 °C. $[\alpha]_D^{20}$ +89.0° (*c* 0.87, H_2O). PMR (DMSO-d_6): δ 8.39 (s, 1H, H-5), 7.89 (br d, 2H, $CONH_2$), 6.00 (d, 1H, $J_{1',2'}$=5.3 Hz, H-1'), 5.95 (d, 1H, OH), 5.61(d, 1H, OH), 4.90 (m, 2H, OH, H-2'), 4.15 (m, 2H, H-3', H-4'), 3.68 (m, 2H, H-5',5''). Found: C, 39.10; H, 4.94; N, 23.19%. Calcd for $C_8H_{12}O_5N_4$: C, 39.34; H, 4.95; N, 22.94%.

2-N-(β-D-Arabinofuranosyl)-1,2,3-triazole-4-carboxamide (14β). Similar hydrogenation of **11β** (118 mg, 0.23 mmol), followed by recrystallization from isopropyl alcohol, gave amorphos **14β**, 35.4 mg (63%); $[\alpha]_D^{20}$ −44.6° (*c* 0.42, H_2O). PMR (DMSO-d_6): δ 8.31 (s, 1H, H-5), 7.80 (br d, 2H, $CONH_2$), 6.29 (d, 1H, $J_{1',2'}$=6.4 Hz, H-1'), 5.60 (d, 1H, OH), 5.47 (d, 1H, OH), 4.78 (t, 1H, OH), 4.45 (m, 2H, H-2', H-3'), 3.80 (m, 3H, H-4', H-5',5''). Found: C, 39.35; H, 5.15; N, 22.65%. Calcd for $C_8H_{12}O_5N_4$: C, 39.34; H,4.95; N, 22.94%.

1-N-(α-D-Arabinofuranosyl)-1,2,3-triazole-5-carboxamide (15α). A sample of **12α** (80 mg, 0.16 mmol) in 5 ml methanol was hydrogenated over palladium black catalyst at 3.5 atm for 72 h. After removal of the catalyst, the methanol layer was evaporated and the residue was crystallized from methanol to give **15α**, 12 mg (31.6%); mp 189—190 °C. $[\alpha]_D^{20}$ +85.5° (*c* 0.5, H_2O). PMR (DMSO-d_6): δ 8.35 (s, 1H, H-4), 7.80 (br d, 2H, $CONH_2$), 6.81 (d, 1H, $J_{1',2'}$=4.6 Hz, H-1'), 6.00 (d, 1H, OH), 5.65 (d, 1H, OH), 4.80 (m, 2H, OH, H-2'), 4.18 (m, 2H, H-3', H-4'), 3.68 (d, 2H, H-5',5''). Found: C, 39.08; H, 4.97; N, 22.69%. Calcd for $C_8H_{12}O_5N_4$: C, 39.34; H, 4.95; N, 22.94%.

Ethyl 1-N-[2-Deoxy-3,5-di-O-(p-nitrobenzoyl)-β-D-erythro-pentofuranosyl]-1,2,3-triazole-4-carboxylate (16β), Its α-Anomer (16α) and Ethyl 2-N-[2-Deoxy-3,5-di-O-(p-nitrobenzoyl)-β-D-erythro-pentofuranosyl]-1,2,3-triazole-4-carboxylate (17β), Its α-Anomer (17α). Ethyl 1,2,3-triazole-4-carboxylate (**1**, 560 mg, 3.59 mmol) and 1-*O*-acetyl-3,5-di-*O*-(*p*-nitrobenzoyl)-D-2-deoxyribofuranose (**2**, 1.70 g, 3.59 mmol) were heated at 143 °C. To the melt was added bis(*p*-nitrophenyl) hydrogenphosphate (4 mg) and the mixture was heated at 143 °C under reduced pressure for *ca.* 20 min until the evolution of acetic acid cessed. The resulting gum was dissolved in ethyl acetate (5 ml). Silica gel (2.5 g) was added and the suspension was evaporated to dryness. The residue was placed on a column of silica gel (170 g, 3.2×70 cm, packed with benzene) and eluted with 10: 1 benzene–ethyl acetate. The effluent was fractionated into 9.2 ml-fractions.

Fractions 47—53 gave colorless crystals. Recrystallization from benzene gave **17β**, 430 mg (21.6%); mp 178.5—179 °C. $[\alpha]_D^{20}$ −37.5° (*c* 1.0, $CHCl_3$). PMR ($CDCl_3$): δ 8.43 (s, 8H, Ar), 8.25 (s, 1H, H-5), 6.79 (t, 1H, H-1'), 6.10 (m, 1H, H-3'), 4.75 (br s, 3H, H-4', H-5',5''), 4.53 (q, 2H, CH_2-ester), 3.60—2.75 (m, 2H, H-2',2''), 1.41 (t, 3H, CH_3-ester). Found: C, 51.89; H, 3.88; N, 12.82%. Calcd for $C_{24}H_{21}O_{11}N_5$: C, 51.90; H, 3.81; N, 12.82%.

Fractions 54—60 gave a mixture of **17β** and **17α**, 388 mg (19.6%).

Fractions 61—68 gave colorless crystals. Recrystallization from acetone gave **17α**, 212 mg (10.7%); mp 128—129°C. $[\alpha]_D^{20}$ +33.5° (*c* 1.0, $CHCl_3$). PMR ($CDCl_3$): δ 8.45 (d, 8H, Ar), 8.26 (s, 1H, H-5), 6.85 (t, 1H, H-1'), 5.90 (m, 1H, H-3'), 5.10 (m, 1H, H-4'), 4.83 (d, 2H, H-5',5''), 4.58 (q, 2H, CH_2-ester), 3.28 (t, 2H, H-2',2''), 1.47 (t, 3H, CH_3-ester). Found: C, 51.93; H, 3.90; N, 12.58%. Calcd for $C_{24}H_{21}O_{11}N_5$: C, 51.90; H, 3.81; N, 12.61%.

Fractions 76—96 gave a mixture of **16α** and **16β**, 566 mg. The crude gum of the mixture was crystallized from ethyl acetate giving **16β**, 256 mg (12%); mp 204.5—205.0 °C. $[\alpha]_D^{20}$ −33.0° (*c* 1.0, DMSO). PMR (DMSO-d_6): δ 9.18 (s, 1H, H-5), 8.50 (m, 8H, Ar), 6.87 (t, 1H, H-1'), 6.08 (m, 1H, H-3'), 4.80 (m, 3H, H-4', H-5',5''), 4.45 (q, 2H, CH_2-ester), 3.10 (m, 2H, H-2',2''), 1.35 (t, 3H, CH_3-ester). Found: C, 51.80; H, 3.97; N, 12.52%. Calcd for $C_{24}H_{21}O_{11}N_5$: C, 51.90; H, 3.81; N, 12.61%.

The mother liquor contains **16β** and **16α** (about 1: 4 from PMR). **16α** could not be isolated by recrystallization or chromatography with silica gel.

Ethyl 1-N-[2-Deoxy-3,5-di-O-(p-toluoyl)-β-D-erythro-pentofuranosyl]-1,2,3-triazole-4-carboxylate (18β), Its α-Anomer (18α) and Ethyl 2-N-[2-Deoxy-3,5-di-O-(p-toluoyl)-β-D-erythro-pentofuranosyl]-1,2,3-triazole-4-carboxylate (19β), Its α-Anomer (19α).
To a solution of 3,5-di-*O*-(*p*-toluoyl)-D-2-deoxyribofuranosyl chloride[17] (**6**, 3.99 g, 10.3 mmol) and silylated ethyl 1,2,3-triazole-4-carboxylate (**2**, 2.72 g, 12.7 mmol) in 1,2-dichloroethane (70 ml) was added a solution of redistilled $SnCl_4$ (1.73 ml, 14.1 mmol) in 1,2-dichloroethane (40 ml) at 0 °C under stirring. The reaction mixture was stirred at room temperature for 12 h. After dilution with 1,2-dichloroethane (60 ml), the reaction mixture was washed with saturated $NaHCO_3$ solution and the resulting emulsion was separated by centrifugation. The organic layer was dried (Na_2SO_4) and evaporated under reduced pressure. The resulting syrup was triturated with benzene and the insoluble product obtained by filtration was recrystallized from benzene to give **18β**, 1.13 g (22.3%); mp 157—158°C. $[\alpha]_D^{20}$ −64.5° (*c* 1.0, $CHCl_3$). PMR ($CDCl_3$): δ 8.32 (s, 1H, H-5), 7.90 (m, 4H, Ar), 7.30 (m, 4H, Ar), 6.58 (t, 1H, H-1'), 5.80 (m, 1H, H-3'), 4.70

(m, 3H, H-4′, H-5′,5″), 4.40 (q, 2H, CH_2-ester), 3.10 (m 2H, H-2′,2″), 2.40 (d, 6H, CH_3-Ar), 1.40 (t, 3H, CH_3-ester). Found: C, 63.03; H, 5.42; N, 8.70%. Calcd for $C_{26}H_{27}O_7N_3$: C, 63.27; H, 5.51; N, 8.52%. The filtrates were combined and evaporated. The resulting syrup was dissolved in ethyl acetate and was placed on a column of silica gel (150 g, 3.2 ×60 cm, packed with benzene) and eluted with 10: 1 benzene–ethyl acetate. The effluent was fractionated into 10 ml-fractions.

Fractions 52—57 gave colorless crystals. Recrystallization from ethanol gave **19β**, 761 mg (15.0%); mp 121—122 °C, $[\alpha]_D^{20}$ −33.0° (*c* 1.0, $CHCl_3$). PMR ($CDCl_3$): δ 8.15 (s, 1H, H-5), 8.00 (m, 4H, Ar), 7.28 (m, 4H, Ar), 6.65 (dt, 1H, H-1′), 5.98 (m, 1H, H-3′), 4.68 (m, 3H, H-4′, H-5′,5″), 4.37 (q, 2H. CH_2-ester), 3.6—2.4 (m, 2H, H-2′,2″), 2.43 (d, 6H, CH_3-Ar), 1.40 (t, 3H, CH_3-ester). Found: C, 63.40; H, 5.64; N, 8.51%. Calcd for $C_{26}H_{27}O_7N_3$: C, 63.27; H, 5.51; N, 8.52%.

Fractions 59—64 gave **19α**, colorless syrup, 780 mg (15.4%); $[\alpha]_D^{20}$ +35.0° (*c* 1.0, $CHCl_3$). PMR ($CDCl_3$): δ 8.12 (s, 1H, H-5), 7.90 (m, 4H, Ar), 7.25 (m, 4H, Ar), 6.58 (t, 1H, H-1′), 5.63 (m, 1H, H-3′), 4.94 (m, 1H, H-4′), 4.60 (d, 2H, H-5′,5″), 4.40 (q, 2H, CH_2-ester), 3.10 (m, 2H, H-2′,2″), 2.40 (d, 6H, CH_3-Ar), 1.37 (t, 3H, CH_3-ester). Found: C, 63.14; H, 5.59; N, 8.50%. Calcd for $C_{26}H_{27}O_7N_3$: C, 63.27; H, 5.51; N, 8.52%.

Fractions 77—88 gave **18α**, colorless syrup, 1.70 g (33.5%); $[\alpha]_D^{20}$ +72.0° (*c* 1.0, $CHCl_3$). PMR ($CDCl_3$): δ 8.35 (s, 1H, H-5), 7.80 (m, 4H, Ar), 7.20 (m, 4H, Ar), 6.55 (q, 1H, H-1′), 5.65 (m, 1H, H-3′), 4.80 (m, 1H, H-4′), 4.62 (d, 2H, H-5′5″), 4.40 (q, 2H, CH_2-ester), 3.08 (m, 2H, H-2′,2″), 2.38 (d, 6H, CH_3-Ar), 1.37 (t, 3H, CH_3-ester). Found: C, 63.00; H, 5.58; N, 8.61%. Calcd for $C_{26}H_{27}O_7N_3$: C, 63.27; H, 5.51; N, 8.52%.

Fractions 90—96 gave **18β**, colorless crystal, 218 mg (4.3%).

*1-N-(2-Deoxy-β-*D*-*erythro*-pentofuranosyl)-1,2,3-triazole-4-carboxamide (20β).* A sample of **18β** (600 mg, 1.45 mmol) in absolute methanol (60 ml) saturated with ammonia at 0 °C was kept at room temperature for 2 days and evaporated under reduced pressure below 40 °C. The residual syrup was dissolved in water (30 ml) and washed with ethyl acetate (10 ml ×3). The aqueous layer was evaporated to dryness. The crude syrup was crystallized from methanol and benzene to give **20β**, 264 mg (80%); 156—157 °C. $[\alpha]_D^{20}$ −32.2° (*c* 1.0, CH_3OH). PMR (DMSO-d_6): δ 8.78 (s, 1H, H-5), 7.60 (br d, 2H, $CONH_2$), 6.40 (t, 1H, H-1′), 5.30 (d, 1H, OH), 4.88 (t, 1H, OH), 4.45 (m, 1H, H-3′), 3.95 (m, 1H, H-4′), 3.55 (m, 2H, H-5′,5″), 2.90—1.90 (m, 2H, H-2′,2″). Found: C, 41.89; H, 5.16; N, 24.61%. Calcd for $C_8H_{12}O_4N_4$: C, 42.11; H, 5.30; N, 24.55%.

*1-N-(2-Deoxy-α-*D*-erythro-pentofuranosyl)-1,2,3-triazole-4-carboxamide (20α).* A sample of **18α** (1.00 g, 2.03 mmol) was subjected to ammonolysis and worked up in a similar manner to that described for **20β**. The crude syrup was crystallized from ethanol and benzene to give **20α**, 364 mg (78.5%); mp 161—162 °C. $[\alpha]_D^{20}$ +85.0° (*c* 1.0, CH_3OH). PMR (DMSO-d_6): δ 8.72 (s, 1H, H-5), 7.60 (br d, 2H, $CONH_2$), 6.43 (q, 1H, H-1′), 5.42 (d, 1H, OH), 4.80 (t, 1H, OH), 4.28 (m, 2H, H-3′, H-4′), 3.50 (m, 2H, H-5′,5″), 3.01—2.11 (m, 2H, H-2′, 2″). Found: C, 41.79; H, 5.22; N, 24.52%. Calcd for $C_8H_{12}O_4N_4$: C, 42.11; H, 5.30; N, 24.55%.

*2-N-(2-Deoxy-β-*D*-*eyythro*-pentofuranosyl)-1,2,3-triazole-4-carboxamide (21β).* Ammonolysis of **19β** (600 mg, 1.22 mmol) in a similar manner to that described above gave crude syrup which was crystallized from methanol and benzene to give **21β**, 233 mg, (84%); mp 139 °C. $[\alpha]_D^{20}$ −45.5° (*c* 1.0. CH_3OH). PMR (DMSO-d_6): δ 8.13 (s, 1H, H-5), 7.67 (br d, 2H, $CONH_2$), 6.31 (dt, 1H, H-1′), 5.30 (d, 1H, OH), 4.60 (m, 2H, OH, H-3′), 3.90 (m, 1H, H-4′), 3.40 (m, 2H, H-5′,5″), 3.05—2.10 (m, 2H, H-2′,2″). Found: C, 41.88; H, 5.20; H, 24.10%. Calcd for $C_8H_{12}O_4N_4$: C, 42.11; H, 5.30; N, 24.55 %.

*2-N-(2-Deoxy-α-*D*-erythro-pentofuranosyl)-1,2,3-triazole-4-carboxamide (21α).* Ammonolysis of **19α** (600 mg, 1.22 mmol) was subjected to and worked up in a similar manner to that described for the preparation of **20β**. The residual syrup was crystallized from ethanol and benzene to give **21α**, 210 mg (76 %); mp 125—126 °C. $[\alpha]_D^{20}$ +74.5° (*c* 1.0, CH_3OH). PMR (DMSO-d_6): δ 8.20 (s, 1H, H-5), 7.70 (br d, 2H, $CONH_2$), 6.30 (q, 1H, H-1′), 5.22 (d, 1H, OH), 4.75 (t, 1H, OH), 4.20 (m, 2H, H-3′ H-4′), 3.55 (m, 2H, H-5′, 5″), 2.90—2.20 (m, 2H, H-2′, 2″). Found; C, 41.88; H, 5.20; N, 24.80%. Calcd for $C_8H_{12}O_4N_4$: C, 42.11; H, 5.30; N, 24.55%.

The authors wish to thank Mr. Saburo Nakada, Department of Chemistry, Keio University, for the microanalysis. The research was supported in part by a grant for cancer research, Ministry of Education, Science and Culture.

References

1) K. Gerzon, R. H. Williams, M. Hoehn, M. Gorman, and D. C. DeLong, 2nd Intern. Cong. Heterocyclic Chemistry, Montpellier, France, July 10, 1969, Abstr. C-30.

2) J. Farkas, Z. Flegelova, and F. Sorm, *Tetrahedron Lett.*, **1972**, 2279.

3) J. T. Witkowski, R. K. Robins, R. W. Sidwell, and L. N. Simon, *J. Med. Chem.*, **15**, 1150 (1972).

4) O. Makabe, S. Fukatsu, and S. Umezawa, *Bull. Chem. Soc. Jpn.*, **45**, 2577 (1972).

5) O. Makabe, S. Umezawa, and T. Aota, *Saishin Igaku*, **30**, 1056 (1975).

6) O. Makabe, J. Yajima, and S. Umezawa, *Bull. Chem. Soc. Jpn.*, **49**, 3552 (1976).

7) L. T. Chien, F. M. Schabel Jr., and C. A. Alford Jr., "Arabinosyl Nucleosides and Nucleotides," in "Selective Inhibitors of Viral Functions," ed by W. A. Carter, CRC Press, Cleaveland, Ohio (1973), p 213.

8) S. Yamada, T. Mizoguchi, and A. Ayata, *Yakugaku Zasshi*, **77**, 452 (1957).

9) T. Hashizume and H. Iwamura, *Tetrahedron Lett.*, **1965**, 3095; *J. Org. Chem.*, **33**, 1796 (1968).

10) U. Niedballa and H. Vorbrüggen, *Angew. Chem.*, **82**, 449 (1970); *J. Org. Chem.*, **39**, 3654 (1974).

11) C. P. J. Glaudemans and H. G. Fletcher, Jr., in "Synthetic Procedures in Nucleic Acid Chemistry," ed by W. W. Zorbach and R. S. Tipson, Vol. 1, Wiley-Interscience, New York, N. Y. (1968), p. 126.

12) T. C. Thurber, R. J. Pugmire, and L. B. Townsend, *J. Heterocycl. Chem.*, **11**, 645 (1974).

13) S. R. Naik, J. T. Witkowski, and R. K. Robins, *J. Heterocycl. Chem.*, **11**, 57 (1974).

14) F. A. Lehmkuhl, J. T. Witkowski, and R. K. Robins, *J. Heterocycl. Chem.*, **9**, 1195 (1972).

15) L. B. Townsend, "Synthetic Procedures in Nucleic Acid Chemistry," ed by W. W. Zorbach and R. S. Tipson, Vol. 2, Wiley-Interscience, New York, N. Y. (1973), p. 331.

16) L. F. Christensen, A. D. Broom, M. J. Robins, and A. Block, *J. Med. Chem.*, **15**, 735 (1972).

17) M. Hoffer, *Chem. Ber.*, **93**, 2777 (1960).

18) M. J. Robins and R. K. Robins, *J. Am. Chem. Soc.*, **87**, 4934 (1965).

19) M. J. Robins, T. A. Khwaja, and R. K. Robins, *J. Org. Chem.*, **35**, 636 (1970).

1,3-Dipolar Cycloadditions to Bicyclic Olefins. I. 1,3-Dipolar Cycloadditions to Norbornadienes[1]

Hisaji TANIGUCHI, Toshikazu IKEDA, Yoshihiro YOSHIDA, and Eiji IMOTO

Department of Applied Chemistry, College of Engineering, University of Osaka Prefecture, Mozu-Umemachi, Sakai, Osaka 591

(Received February 16, 1977)

The 1,3-dipolar cycloadditions of phenylglyoxylonitrile oxide, benzonitrile-*N*-phenylimine, or *N*-phenyl-*C*-*p*-nitrophenylnitrone to norbornadiene, 2,3-dicyanonorbornadiene, and 2,3-bis(methoxycarbonyl)norbornadiene give the *endo*-adducts, together with the *exo*-adducts. These findings show that the 1,3-dipolar cycloadditions to norbornadienes do not follow the "*exo* rule." It is suggested that the present 1,3-dipolar cycloadditions are kinetically controlled reactions. The *endo*-side of norbornadienes is found to be homoconjugated by their NMR spectra. The homoconjugation must be responsible for the observed phenomenon.

The "*exo* rule" has been deduced by Alder and Stein on the basis of the facts that phenyl azide (**7**) undergoes 1,3-dipolar cycloadditions to various bicyclic olefins with a moiety of a bicyclo[2.2.1]heptane skeleton to afford *only exo*-adducts.[2] In fact, the 1,3-dipolar cycloadditions to norbornenes which have thus far been examined follow the "*exo* rule" without exception.[3] Most norbornadienes also undergo cycloadditions by the "*exo* rule."[4] However, in the cycloadditions of **7** to norbornadiene (**1**) and of benzonitrile oxide to **1**, small amounts of the *endo*-adducts were found to be formed in addition to large amounts of the *exo*-adducts.[5,6] This fact stimulated us to elucidate whether or not the "*exo* rule" is applicable to 1,3-dipolar cycloadditions to norbornadienes; the formation of the *endo*-adduct is general. We carried out the 1,3-dipolar cycloadditions of phenylglyoxylonitrile oxide (**4**), benzonitrile-*N*-phenylimine (**5**), *C*,*N*-diphenylnitrone (**6a**), or *N*-phenyl-*C*-*p*-nitrophenylnitrone (**6b**) to **1**, 2,3-dicyanonorbornadiene (**2**), and 2,3-bis(methoxycarbonyl)norbornadiene (**3**). In these reactions, we found that the *endo*-adducts are formed in addition to the *exo*-adducts. On the basis of these results, we will discuss here the reason for the formation of the *endo*-adducts.

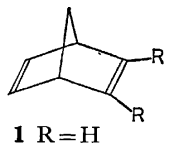

1 R=H
2 R=CN
3 R=CO_2CH_3

C_6H_5–CO–$\overset{+}{C}$=N–$\bar{O}$ **4**

C_6H_5–$\overset{+}{C}$=N–$\bar{N}$–C_6H_5 **5**

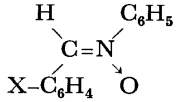

6a X=H
b X=*p*-NO_2

C_6H_5–$\bar{N}$=N–$\overset{+}{N}$ **7**

Results and Discussion

1,3-*Dipolar Cycloadditions.* The 1,3-dipolar cycloaddition of **4** to **1** was carried out as follows. To a stirred solution of α-chloro-α-hydroxyiminoacetophenone (**8**) with an excess of **1** in THF cooled in an ice bath, a solution of triethylamine in THF was added, drop by drop, over a period of one hour. The subsequent work-up of the reaction mixture gave a mixture of 5-benzoyl-3-oxa-4-azatricyclo[5.2.1.$0^{2,6exo}$]deca-4,8-diene (**9a**), 5-benzoyl-3-oxa-4-azatricyclo[5.2.1.$0^{2,6endo}$]deca-4,8-diene (**10a**), and bisadducts. Judging from the TLC, the bisadducts were composed of at least three isomers. Among the isomers, only 5,11-dibenzoyl-3,9-dioxa-4,10-diazatetracyclo[5.5.1.$0^{2,6exo}$0.^{8,12exo}]trideca-4,10-diene (**11**) has been isolated and characterized.

The cycloadditions of **4** to **2** and **4** to **3** were carried out by a method like that described above. In these reactions, the reagent, **4**, attacked the more electron-rich unsubstituted double bond of **2** and **3** to give 5-benzoyl-8,9-dicyano-3-oxa-4-azatricyclo[5.2.1.$0^{2,6exo}$]-deca-4,8-diene (**9b**) and 5-benzoyl-8,9-bis(methoxycarbonyl)-3-oxa-4-azatricyclo[5.2.1.$0^{2,6exo}$]deca-4,8-diene (**9c**) as the *exo*-adducts and 5-benzoyl-8,9-dicyano-3-oxa-4-azatricyclo[5.2.1.$0^{2,6endo}$]deca-4,8-diene (**10b**) and 5-benzoyl-8,9-bis(methoxycarbonyl)-3-oxa-4-azatricyclo[5.2.1.$0^{2,6endo}$]deca-4,8-diene (**10c**) as the *endo*-adducts. The bisadducts and the monoadducts produced by the attack of **4** on the more electron-poor double bond were not detected at all. These findings show that **4** acts as an electron-accepting 1,3-dipole toward **2** and **3**.

The nitrilimine, **5**, which was prepared from *N*-phenylbenzenecarbohydrazonoyl chloride (**12**) and triethylamine in benzene, reacted with an excess of **1** in benzene to afford a mixture of 3,5-diphenyl-3,4-diazatricyclo[5.2.1.$0^{2,6exo}$]deca-4,8-diene (**13**), 3,5-diphenyl-3,4-diazatricyclo[5.2.1.$0^{2,6endo}$]deca-4,8-diene (**14**),[7] and bisadducts.

The reaction of the nitrone **6a** with an excess of **1** in toluene gave two *exo*-monoadducts(4,5^{endo}-diphenyl-3-oxa-4-azatricyclo[5.2.1.$0^{2,6exo}$]dec-8-ene (**15a**) and 4,5^{exo}-diphenyl-3-oxa-4-azatricyclo[5.2.1.$0^{2,6exo}$]dec-8-ene (**16a**)[8]) and bisadducts. When a solution of the nitrone **6b** in benzene containing an excess of **1** was refluxed, however, an *endo*-adduct (4-phenyl-5^{exo}-*p*-nitrophenyl-3-oxa-4-azatricyclo[5.2.1.$0^{2,6endo}$]dec-8-ene (**17b**)) was obtained, together with two *exo*-monoadducts (4-phenyl-5^{endo}-*p*-nitrophenyl-3-oxa-4-azatricyclo[5.2.1.$0^{2,6exo}$]dec-8-ene (**15b**) and 4-phenyl-5^{exo}-

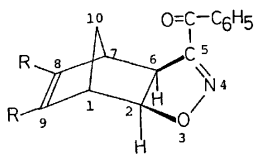

9a R=H
b R=CN
c R=CO_2CH_3

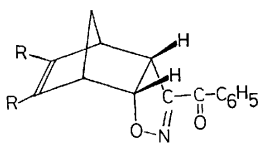

10a R=H
b R=CN
c R=CO_2CH_3

Table 1. Yield and product composition

Olefin	1,3-Dipole	Product: Monoadduct Yield[a] (%)	Composition (%) exo	Composition (%) endo	exo/endo	Bisadduct Yield[a] (%)
1	**4**	76	**9a** (81)	**10a** (19)	4.3[b]	17
2	**4**	90	**9b** (68)	**10b** (32)	2.1	0
3	**4**	95	**9c** (75)	**10c** (25)	3.0[b]	0
1	**5**	95	**13** (87)	**14** (13)	6.7	4
1	**5**	79[c]	**13**[c]	—c)		6
1	**6a**	73	**15a** (56) and **16a** (44)	**17a** (0)		7
1	**6a**	54[d]	**15a**[d]	—d)		2.8
1	**6b**	76	**15b** (67) and **16b** (29)	**17b** (4)	24	7
1	**7**	67[e]	**18**[e] (92)	**19**[e] (8)	11[e]	f)

a) The yields are based on the starting 1,3-dipoles. b) The ratio is different from that shown in a previous communication.[g] c) Ref. 4d. d) Ref. 4c. e) Ref. 5. f) A small amount of bisadducts was obtained in the reaction reported in Ref. 5. g) Ref. 1.

p-nitrophenyl-3-oxa-4-azatricyclo[5.2.1.$0^{2,6exo}$]dec-8-ene (**16b**)) and bisadducts.

The yields of the adducts and the product compositions are summarized in Table 1, together with the data of Findlay *et al.*[5] and Huisgen *et al.*[4c,d] As has been described above, the formation of the *endo*-adducts was observed in all reactions except for that of **6a** with **1**. This fact led us to conclude that the "*exo* rule" is not applicable to 1,3-dipolar cycloadditions to norbornadienes.

Analyses of NMR Spectra of Adducts. The *exo*- and *endo* assignments of each mono-adduct were based on the NMR data (Tables 2 and 3). The coupling contant between the bridgehead proton and the adjacent *endo*-proton of an *exo*-isomer was in the range from 0 to 1 Hz, while the coupling constant between the bridgehead proton and the adjacent *exo*-proton of an *endo*-isomer was in the range from 4 to 5 Hz. These coupling constants were consistent with the values cited in the literature.[9]

Table 3. Coupling constants in adducts[a,b]

Adducts	*exo* or *endo*	Coupling constants $J_{1,2}$	$J_{2,6}$	$J_{5,6}$	$J_{6,7}$
9a	*exo*	~0	9.0	—	~0
9b	*exo*	0—1	9.5	—	0—1
9c	*exo*	0—1	8.5	—	0—1
10a	*endo*	4.0	9.5	—	4.0
10b	*endo*	4.0	10.0	—	4.0
10c	*endo*	4.0	10.0	—	4.0
13	*exo*	~0	9.0	—	~0
14	*endo*	4.0	11.0	—	4.0
15a	*exo*	~1	7.0	9.0	~1
15b	*exo*	~1	7.0	9.5	~1
16a	*exo*	~1	7.0	7.0	~1
16b	*exo*	~1	7.0	7.0	~1
17b	*endo*	4.5	8.0	6.5	4.5

a) The spectra were recorded at 60 MHz. b) J values in Hz.

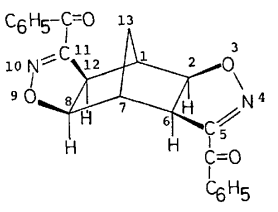

11

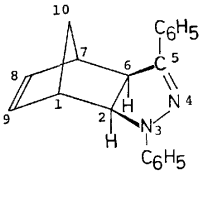

13

The *exo*-adduct **9c** exhibited the chemical shifts of methyl groups of two methoxycarbonyl groups at δ 3.78 and 3.81 ppm, while the *endo*-adduct **10c** at δ 3.33 and 3.78 ppm. The value of δ 3.33 ppm was assinged as being due to the methoxycarbonyl group attached to the C_8 position of **10c**. The molecular model of **10c**

Table 2. Chemical shifts of adducts[a,b]

Adducts	Protons H_1 and H_7	H_2	H_5	H_6	H_8 and H_9
9a	3.31	4.99	—	3.78	6.07 and 6.35
9b	3.78 and 3.92	5.20	—	4.06	—
9c	3.73	5.19	—	4.05	—
10a	3.40	5.37	—	4.09	6.05
10b	3.96	5.77	—	4.55	—
10c	3.71 and 3.82	5.57	—	4.40	—
13	3.25 and 3.46	4.39	—	3.77	6.15 and 6.34
14	3.46 and 3.60	4.79	—	4.12	5.89
15a	2.26 and 3.06	4.57	4.67	2.90	6.05 and 6.14
15b	2.20 and *ca.* 3	4.66	4.83	3.04	6.07 and 6.17
16a	2.85 and 3.00	4.52	3.80	2.63	6.03 and 6.19
16b	2.89 and 3.00	4.53	3.95	2.58	6.06 and 6.22
17b	2.8—3.3	5.12	3.88	3.16	6.23 and 6.33

a) The spectra were recorded at 60 MHz. b) Expressed in δ ppm units, with TMS as the internal standard, in $CDCl_3$ solution.

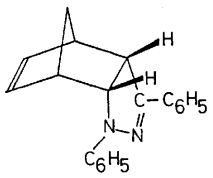

14

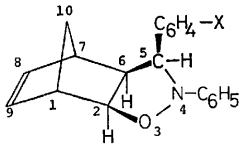

15a X=H
b X=*p*-NO_2

reveals that one of the two methoxycarbonyl groups lies in the shielding cone of the benzene ring of the benzoyl group attached on the C_5 position. The vinyl protons of **14** which are placed above the carbon-nitrogen double bond appeared in a field higher by 0.26—0.45 ppm than that of the corresponding vinyl protons of **13**. This upfield shift is probably due to the diamagnetic anisotoropy effect of the carbon-nitrogen double bond.[10] The chemical shifts of H_2 and H_5 of the *exo*-adduct **15a** were determined by means of the following observation. The former proton appeared as a doublet of triplets with a small coupling constant (J=*ca.* 1 Hz), while the latter proton appeared as a simple doublet. The small coupling was attributed to a "W-letter" coupling between $H_{10\text{-}anti}$ and $H_{2\text{-}endo}$ and to the coupling between H_1 and $H_{2\text{-}endo}$. The chemical shifts of H_2 and H_5 of the adducts **15b**, **16a**, and **16b** were also determined in the same way. The configurations of each isoxazoline moiety of **15a** and **16a**, both of which were *exo*-adducts, as shown in Table 3, were determined on the basis of the magnitude of the coupling constant between H_5 and H_6: the larger value (J=9.0 Hz) was assigned to the *cis*-coupling constant between H_5 and H_6 of **15a**, and the smaller value (J=7.0 Hz) to the *trans*-coupling constant between H_5 and H_6 of **16a**. Such an assignment has also been carried out for the two *exo*-adducts formed by the cycloaddition of the nitrone **6a** to norbornene.[4c] In the Δ^2-isoxazoline system, J_{cis} has been observed to be always larger than J_{trans}.[11] The assignments of the configurations of **15b** and **16b** were carried out in the same manner. The value (J= 6.5 Hz) of the coupling constant between H_5 and H_6 of the endo-adduct **17b** corresponds reasonably to the *trans*-coupling constant.

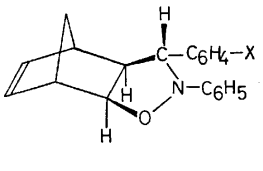

16a X=H
b X=*p*-NO_2

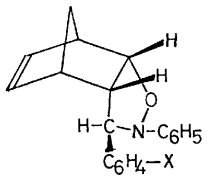

17a X=H
b X=*p*-NO_2

The presence of the symmetry along a C_2 axis of the bisadduct **11** was confirmed by a double-resonance technique: when the bridging methylene protons were irradiated with an additional radio frequency at their resonance position, the broad singlet was sharpened, but not divided into two singlets.

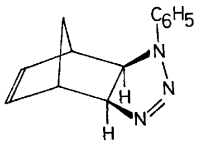

18

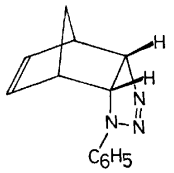

19

Thermal Stability of the exo-*Adducts (**9b** and **9c**) and the* endo-*Adducts (**10b** and **10c**).* When the *exo*-adduct, **9c**, and the *endo*-adducts, **10b** and **10c**, were each heated under reflux in THF for 2 h, they were recovered unchanged. The *exo*-adduct **9b**, when heated under the same conditions, gave a dirty mixture including **9b**, but not **10b**. The mass spectra of **9b** and **10b** showed the same fragmentation pattern (*m/e* 173, *m/e* 116, and no molecular ion peak; sample injection at 200 °C). This finding implies that the adducts **9b** and **10b** are liable to undergo the retro-Diels-Alder reaction by thermal decomposition to 2,3-dicyanocyclopentadiene and 3-benzoylisoxazole, rather than to the starting moieties, **2** and **4**. In addition, isoxazoles can not act as dipolarophiles.[3i]

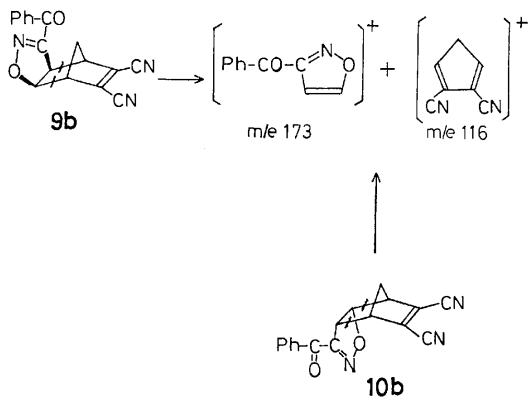

Scheme 1.

From above findings, we suggest that the present 1,3-dipolar cycloadditions are kinetically controlled reactions.

An Explanation for the Formation of the endo-*Adducts.* 1,3-Dipoles cannot undergo cycloadditions from the *endo*-side of norbornene. This is probably because of the steric hindrance of the *endo*-5,6-hydrogens. On the other hand, in the case of norbornadiene, it is possible that, 1,3-dipoles attack the carbon-carbon double bond from the *endo*-side because of the absence of such steric hindrance. This is insufficient, however, to explain the formation of the *endo*-adducts. If the *endo*-side of norbornadiene suffers from no steric hindrance, the *endo*-adduct should be produced in a higher yield than the *exo*-adduct, or at least in an amount equal to that of the *exo*-adduct. As the results shown in Table 1 do not accord with this prediction, an alternative factor must be responsible for the observed phenomena.

We show in Fig. 1 that there is a good linear relationship between the δ values of the vinyl protons of five norbornadienes (**1**, **2**, **3**, **20**, and **21**) and the values of

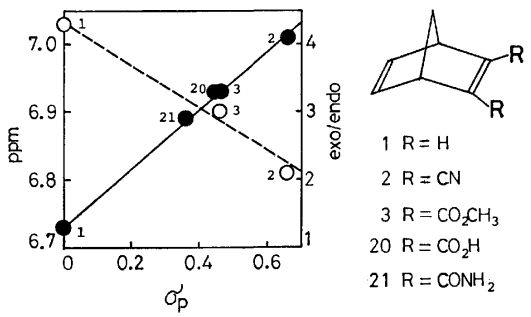

Fig. 1. Chemical shifts (TMS as an internal standard, in DMSO-d_6 solutions) of vinyl protons of 2,3-disubstituted norbornadienes *vs.* Hammett's σ_ps (—●—), and the exo/endo product ratios *vs.* Hammett's σ_ps (---○---)

Hammett's δ_ps[12] of the substituents. The phenomenon that the δ values of the vinyl protons are shifted to lower fields by the electron-withdrawing groups is likely to be attributable to homoconjugation on the *endo*-side of norbornadienes. The presence of homoconjugation between the two non-neighbouring carbon-carbon double bonds has also been found by investigating the photoelectron spectroscopy of norbornadiene.[13]

Inagaki *et al.* have proposed that the π-electron distribution of norbornene extends to the *exo*-side more than to the *endo*-side because of the interaction between the π-orbital and the methano-bridge orbital or the back-side of the anti C–H bond orbital at the C_7 position.[14] Such an interaction may also be present in norbornadiene. On the *endo*-side of norbornadiene, however, homoconjugation is present, as has been described above. This homoconjugation may result in extending the π-electron distribution toward the *endo*-side. Consequently, the difference in the π-electron distribution between the *exo*- and *endo*-sides of norbornadiene may be smaller than that of norbornene.

Thus, we may assume that the homocinjugation on the *endo*-side of norbornadiene brings about the formation of the *endo*-adducts in the cycloadditions of the electron-accepting 1,3-dipoles to norbornadienes.

Experimental

Materials. The precursors of 1,3-dipoles(**8**[15] and **12**[4d]), 1,3-dipoles(**6a**[16] and **6b**[16]), a norbornadiene **3**,[17] and norbornadiene-2,3-dicarboxylic acid(**20**)[17] were prepared by the method described in the literature. The **1** was purchased and distilled before use.

Preparation of **2**. Into a solution of ammonium chloride (24 g) in aq ammonia (240 cm³), **3** (47 g, 0.226 mol) was added, after which the mixture was stirred vigorously for 5 h at room temperature. The resulting white solid was separated by filtration, washed with ether, dried, and recrystallized from MeOH–EtOH to yield norbornadiene-2,3-dicarboxamide(**21**) mp 209—211 °C (dec) (lit,[18] 211—212 °C) in a quantitative yield. To a stirred suspension of **21**(5.0 g, 2.8 mmol) in DMF (28 g), cooled in an ice bath, a solution of thionyl chloride (10.0 g, 84 mmol) in DMF (10 g) was added, drop by drop, over a 30-min period. When the addition of the thionyl chloride solution was complete, the reaction mixture became a clear yellowish liquid. Then, the ice bath was removed and the solution was stirred for 2 days at room temperature. The resulting brown solution was poured into 150 g of ice–water, neutralized (aq Na_2CO_3), and extracted (ether 100 cm³ × 3). The resulting solution was dried($MgSO_4$) and evaporated to dryness to give a yellowish solid (3.77 g). It was chromatographed on alumina. Elution with benzene afforded colorless pure **2** (3.38 g, 85%): mp 44—46 °C (lit,[18] 44—45 °C).

Reaction of **4** *with* **1**. Into a stirred solution of **1** (2.00 g, 21.7 mmol) and **8** (1.84 g, 10.0 mmol) in dry THF (30 cm³) cooled in an ice bath, a solution of triethylamine (TEA)(1.30 g, 13 mmol) in dry THF (20 cm³) was added, drop by drop, over a 1-h period. After an additional 1 h of stirring at the same temperature, the resulting triethylammonium chloride was removed by filtration. It was chlomatographed on silica gel (200—300 mesh). Elution with benzene gave 1.81 g (76%) of a mixture of **9a** and **10a**. The NMR spectrum of the mixture showed that the exo/endo ratio was 81/19. Further elution with benzene afforded 0.316 g (17%) of a mixture of bisadducts ($C_{23}H_{18}O_4N_2$ by elemental analysis). The TLC of the mixture showed three spots (elution with benzene–ether (9:2)). It was recrystallized from EtOH–benzene to give 0.18 g of **11**: mp 181—182 °C; IR(KBr) 1650 (C=O) and 1565 cm^{-1}; NMR ($CDCl_3$) δ=1.55 (s, 2, CH_2), 3.15 (s, 2, H_1 and H_7), 3.83 (d, 2, J=8 Hz, H_6 and H_{12}), 4.76 (d, 2, J=8 Hz, H_2 and H_8), and 7.3—8.3 ppm (m, 10).

Found: C, 71.63; H, 4.82; N, 6.99%. Calcd for $C_{23}H_{18}O_4N_2$: C, 71.49; H, 4.70; N, 7.25%.

A mixture of **9a** and **10a** was column chromatographed on silica gel once again. Elution with benzene–hexane (6:1) gave **9a**. It was recrystallized from EtOH to afford colorless needles: mp 65—66 °C; IR(KBr) 1640 (C=O) and 1557 cm^{-1}.

Found: C, 75.20; H, 5.35; N, 5.77%. Calcd for $C_{15}H_{13}O_2N_1$: C, 75.30; H, 5.48; N, 5.85%.

Further elution with the same solvent gave **10a**. It was recrystallized from EtOH–H_2O to yield colorless needles: mp 53—54 °C; IR(KBr) 1655 (C=O) and 1560 cm^{-1}.

Found: C, 75.28; H, 5.35; N, 5.55%. Calcd for $C_{15}H_{13}O_2N_1$: C, 75.30; H, 5.48; N, 5.85%.

Reaction of **4** *with* **2**. Into a stirred solution of **2** (710 mg, 5.00 mmol) and **8** (460 mg, 2.50 mmol) in dry THF (40 cm³), cooled in an ice bath, a solution of TEA (330 mg, 3.26 mmol) in dry THF (10 cm³) was added, drop by drop, over a 1-h period. After an additional 1 h's stirring, the resulting triethylammonium chloride was removed by filtration. After the removal of the solvent, the residue was chromatographed on silica gel. Elution with benzene gave 351 mg of **2**. Further elution with benzene afforded **9b** (440 mg, 61%), which was subsequently recrystallized from EtOH to give colorless prisms: mp 140—141 °C; IR(KBr) 2220(C≡N), 1640(C=O), and 1570 cm^{-1}.

Found: C, 70.73; H, 3.67; N, 14.56%. Calcd for $C_{17}H_{11}O_2N_3$: C, 70.58; H, 3.83; N, 14.53%.

Elution with benzene–ethyl acetate (1:1) gave **10b** (208 mg, 29%). It was recrystallized from MeOH to afford colorless sticks: mp 127—127.5 °C; IR(KBr) 2225(C≡N) and 1660 cm^{-1} (C=O).

Found: C, 70.73; H, 3.64; N, 14.81%. Calcd for $C_{17}H_{11}O_2N_3$: C, 70.58; H, 3.83; N, 14.53%.

Reaction of **4** *with* **3**. To a stirred solution of **3** (1.04 g, 5.00 mmol) and **8** (0.92 g, 5.00 mmol) in dry THF (15 cm³), cooled in an ice bath, a solution of TEA (0.65 g, 6.50 mmol) in dry THF (10 cm³) was added, drop by drop, over a 1-h period. After an additional 1 h's stirring at the same temperature, the resulting ammonium chloride was removed by filtration. After the evaporation of the solvent, a yellowish oily residue was solidified by the addition of a few drops of

95% EtOH. The solid was separated by filtration and dried under a vacuum to give 1.69 g (95%) of a mixture of **9c** and **10c**. The NMR spectrum of the mixture showed that the exo/endo ratio was 75/25. The mixture was chromatographed on sillica gel. Elution with benzene–ether (20: 1) gave **9c**. It was recrystallized from 95% EtOH to give colorless sticks: mp 113—114 °C; IR(KBr) 1740 (ester C=O), 1715 (ester C=O), 1657 (C=O), 1635, and 1573 cm^{-1}.

Found: C, 64.14; H, 4.61; N, 3.76%. Calcd for $C_{19}H_{17}O_6N_1$: C, 64.22; H, 4.82; N, 3.94%.

Further elution with the same solvent afforded **10c**. It was recrystallized from 95% EtOH to give colorless sticks: mp 151—153 °C; IR(KBr) 1740(ester C=O), 1650(C=O), and 1620 cm^{-1}.

Found: C, 64.07; H, 4.65; N, 3.94%. Calcd for $C_{19}H_{17}O_6N_1$: C, 64.22; H, 4.82; N, 3.94%.

*Reaction of **5** with **1**.* A mixture of **1** (3.00 g, 32.6 mmol) and **12** (576 mg, 2.50 mmol) was dissolved in dry benzene 10 cm^3). Into the solution, TEA (1.3 cm^3) was added all at once, after which the solution was stirred for 24 h at room temperature. The resulting ammonium chloride was removed by filtration. The evaporation of the solvent left a yellow residue. It was chromatographed on alumina. Elution with benzene gave 680 mg (95%) of a mixture of **13** and **14**. The *exo/endo* ratio was 87/13 (from NMR). The developing solvent was changed to ethyl acetate to give 55 mg (4%) of a mixture of bisadduts (mp 281—305 °C (dec); $C_{33}H_{28}N_4$). A mixture of the monoadducts was chromatographed on alumina once again. Elution with hexane–benzene (3: 7) gave **13**. It was recrystallized from EtOH to give pale yellow needles: mp 134—135 °C (lit,[4d] 133—135 °C). Further elution with the same solvent afforded **14**. It was recrystallized from EtOH to give pale yellow needles: mp 110—111 °C; IR(KBr) 1595, 1550, and 1500 cm^{-1}.

Found: C, 83.65; H, 6.39; N, 9.86%. Calcd for $C_{20}H_{18}N_2$: C, 83.88; H, 6.34; N, 9.78%.

*Reaction of **6a** with **1**.* A mixture of **1** (1.84 g, 20.0 mmol) and **6a** (978 mg, 5.00 mmol) was dissolved in dry toluene (5 cm^3) and heated under reflux for 4 h. A large amount of the solvent was removed *in vacuo*. Then, the concnetrated solution was chromatographed on silica gel. Elution with toluene gave **15a** (595 mg, 41%). It was recrystallized from MeOH to afford colorless needles: mp 110—111 °C (lit,[4c] 111° C). Further elution with toluene afforded **16a** (467 mg, 32%). It was recrystallized from MeOH to give colorless needles: mp 76—77 °C; IR(KBr) 1595, 1490, and 1450 cm^{-1}.

Found: C, 83.26; H, 6.56; N, 4.71%. Calcd for $C_{20}H_{19}O_1N_1$: C, 83.01; H, 6.62; N, 4.84%.

The final elution with toluene gave a mixture of bisadducts in a 7% yield (88 mg): mp 218—233 °C (dec)(elemental analysis; $C_{33}H_{30}O_2N_2$).

*Reaction of **6b** with **1**.* A solution of **1** (1.84 g, 20.0 mmol) and **6b** (1.21 g, 5.00 mmol) in dry benzene (20 cm^3) was heated under reflux for 18 h. The solution was concentrated and chromatographed on silica gel. Elution with benzene gave the following products: **15b** (859 mg, 51%): mp 121—122 °C (pale yellow sticks from MeOH); IR(KBr) 1600, 1520 (NO_2), 1495, and 1350 cm^{-1} (NO_2).

Found: C, 72.06; H, 5.47; N, 8.31%. Calcd for $C_{20}H_{18}O_3N_2$: C, 71.84; H, 5.43; N, 8.38%. **16b** (353 mg, 22%): mp 153—154 °C (pale yellow sticks from MeOH); IR(KBr) 1595, 1510 (NO_2), 1490, and 1350 cm^{-1} (NO_2).

Found: C, 71.86; H, 5.44; N, 8.63%. Calcd for $C_{20}H_{18}O_3N_2$: C, 71.84; H, 5.43; N, 8.38%. **17b** (43 mg, 3%): mp 138—140 °C (pale yellow needles from MeOH); IR(KBr) 1595, 1510(NO_2), 1490, and 1355 cm^{-1} (NO_2).

Found: C, 71.81; H, 5.49; N, 8.15%. Calcd for $C_{20}H_{18}O_3N_2$: C, 71.84; H, 5.43; N, 8.38%. A mixture of bisadducts (83 mg; 7%): mp 231—246 °C (dec)($C_{33}H_{28}O_6N_4$).

*Examination of the Thermal Stability of **9b**, **9c**, **10b**, and **10c**.* A solution of **10b** (53 mg) in THF (3 cm^3) was heated under reflux for 2 h. The solvent was then evaporated to give a white solid composed of only one component (TLC). The NMR spectrum of the solid was identical with that of **10b**. **9c** and **10c** were treated in the same way. They were also recovered unchanged. When a solution of **9b** (53 mg) in THF (3 cm^3) was heated under the same conditions, a dirty mixture was obtained. It contained **9b**, but not **10b** (TLC, NMR).

The mass spectra of **9b** and **10b** showed the same pattern. MS (80 eV) *m/e* 173, 116, 105, 89, 77, 51, and 28.

*NMR Measurements of Norbornadienes (**1**, **2**, **3**, **20**, and **21**).* The NMR spectra of norbornadienes (**1**, **2**, **3**, **20**, and **21**) were recorded at 60 MHz, using TMS as the internal standard, in DMSO-d_6 solutions (10% solutions); δ values of vinyl protons: 6.73 (**1**), 7.01 (**2**), 6.93 (**3**), 6.93 (**20**), and 6.89 ppm (**21**).

References

1) The present paper is concerned with only 1,3-dipolar cycloadditions to 7-unsubstituted norbornadienes. A preliminary communication on this subject has been made: H. Taniguchi, T. Ikeda, Y. Yoshida, and E. Imoto, *Chem. Lett.*, **1976**, 1139.

2) a) K. Alder and G. Stein, *Ann. Chem.*, **485**, 211, 223 (1931); b) K. Alder and G. Stein, *ibid.*, **501**, 1 (1933); c) K. Alder and G. Stein, *ibid.*, **515**, 165, 185 (1935); d) K. Alder, H-J. Ache, and F. H. Flock, *Chem. Ber.*, **93**, 1888 (1960).

3) a) R. Huisgen, R. Grashey, and J. Sauer, in S. Patai, "The Chemistry of Alkenes," Interscience, New York (1964), p. 739, and the references cited therein; b) R. Huisgen, *Angew. Chem. Int. Ed. Engl.*, **2**, 565, 633 (1963); c) R. Huisgen, L. Möbius, G. Muller, H. Stangle, G. Szeimies, and J. M. Vernon, *Chem. Ber.*, **98**, 3992 (1965); d) D. Barraclough, J. S. Oakland, and F. Scheinmann, *J. Chem. Soc., Perkin Trans. 1*, **1972**, 1500; e) J. S. Oakland and F. Scheinmann, *ibid.*, **1973**, 800; f) A. C. Oehlschlarger, P. Tillmann, and L. H. Zalkow, *Chem. Commun.*, **1965**, 596; g) L. H. Zalkow and C. D. Kennedy, *J. Org. Chem.*, **28**, 3309 (1963); h) A. C. Oehlschlager and L. H. Zalkow, *Can. J. Chem.*, **47**, 461 (1969); i) R. Huisgen and M. Christl, *Angew. Chem. Int. Ed. Engl.*, **6**, 456 (1967); *Chem. Ber.*, **106**, 3291 (1973); j) R. Huisgen, H. Stangl, H. J. Sturm, R. Raab, and K. Bunge, *Chem. Ber.*, **105**, 1258 (1972).

4) a) J. W. Wilt and T. P. Malloy, *J. Org. Chem.*, **38**, 277 (1973); b) H. Cohen and C. Benezra, *Can. J. Chem.*, **54**, 44 (1976); c) R. Huisgen, R. Grashey, H. Hauck, and H. Seidl, *Chem. Ber.*, **101**, 2043 (1968). d) R. Huisgen, M. Seidel, G. Wallbillich, and H. Knupfer, *Tetrahedron*, **17**, 3 (1962).

5) a) S. McLean and D. M. Findlay, *Tetrahedron Lett.*, **1969**, 2219; b) D. M. Findlay, M. L. Roy, and S. McLean, *Can. J. Chem.*, **50**, 3186 (1972).

6) R. Lazar, F. G. Cocu, and N. Barbulescu, *Rev. Chim. (Bucharest)*, **20**, 3 (1969); *Chem. Abstr.*, **70**, 114341n (1969).

7) The *endo*-isomer was not isolated in the reaction reported in Ref. 4d.

8) The isomer **16a** was not isolated in the reaction reported in Ref. 4c.

9) a) P. Laszlo and P. von R. Schleyer, *J. Am. Chem. Soc.*, **86**, 1171 (1964); b) *Cf.* J. L. Marshall and S. R. Walter, *ibid.*, **96**, 6358 (1974).

10) L. M. Jackman and S. Sternhell, "Application of Nuclear Magnetic Resonance Spectroscopy in Organic Chem-

istry," 2nd ed, Pergamon Press, London (1969), Chap. 2-2.
11) R. Sustmann, R. Huisgen, and H. Huber, *Chem. Ber.*, **100**, 1802, (1967).
12) a) D. H. McDaniel and H. C. Brown, *J. Org. Chem.*, **23**, 420 (1958); b) M. Charton, *ibid.*, **28**, 3121 (1963).
13) a) H. Bock and B. G. Ramsey, *Angew. Chem. Int. Ed. Engl.*, **12**, 734 (1973); b) P. Bishof, J. H. Hashmall, E. Heilbronner, and V. Hornung, *Helv. Chim. Acta*, **52**, 1745 (1969).
14) S. Inagaki, H. Fujimoto, and K. Fukui, *J. Am. Chem. Soc.*, **98**, 4054 (1976).
15) Y. Otsuji, Y. Tsujii, A. Yoshida, and E. Imoto, *Bull. Chem. Soc. Jpn.*, **44**, 223 (1971).
16) S. R. Sandler and W. Karo, "Organic Functional Group Preparations III," Academic Press, New York (1972), p. 307.
17) O. Diels and K. Alder, *Ann. Chem.*, **490**, 236 (1931).
18) A. T. Blomquist and E. C. Winslow, *J. Org. Chem.*, **10**, 1490 (1945).

The Glow-discharge Reactions of Pyrrole, Pyrrolidine, and Butylamine*

Shōichi KIKKAWA, Masakatsu NOMURA, and Noritaka HOSOKAWA

Department of Applied Chemistry, Faculty of Engineering, Osaka University, Suita, Osaka 565

(Received February 25, 1977)

The glow-discharge reactions of pyrrole, pyrrolidine, and butylamine were carried out. Pyrrolidine produces a complex mixture of products, the most prevalent of which is 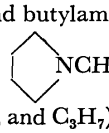 NCH(R)CN (R: H, CH_3, and C_2H_5), and butylamine yielded primarily $CH_3(CH_2)_3N{=}CHR$ (R: CH_3, C_2H_5, and C_3H_7) along with $CH_3(CH_2)_3NHCH_2CN$, whereas pyrrole afforded a mixture of acrylonitrile, crotononitrile, benzene, α-methylpyrrole and β-methylpyrrole, together with large amounts of HCN. The formation of characteristic products, α-(1-pyrrolidinyl) nitrile derivatives with pyrrolidine, and the yield of butylaminoacetonitrile with butylamine can be explained by considering the formation of a resonance-stabilized α-cyanoalkyl radical as the most probable intermediate which attacks a nitrogen atom of pyrrolidine and that of butylamine or which recombines with pyrrolidine-*N*-radical and butylamine-*N*-radical.

Extensive studies of the reaction of organic compounds in a radiofrequency discharge have been carried out.[1-3] There has, however, been little or no attempt to study the discharge reaction of a series of simple amine derivatives. In this paper, the individual reactions of pyrrole, pyrrolidine, and butylamine (three different types of C_4 amine) in a radiofrequency discharge will be reported. These compounds were chosen in an attempt to ascertain the behavior of these three amines under the influence of radiofrequency discharge and to observe the formation of the various products resulting therefrom.

Experimental

The radiofrequency generator was operated at a fixed frequency of 28 MHz, with an output of up to 150 W. The operating pressure in the system was 2.0 Torr through all the runs. The products were collected in a liquid nitrogen trap (−196 °C), as has previously been described.[4]

Analysis. Gas chromatography was employed for quantitative analysis. A Shimadzu GC-4BPTF instrument was used with the following columns: 4.5 m, Silicon SE-30 for the analysis of liquid products (oven temp: 30—270 °C, program rate: 10 °C/min), with H_2 as the carrier gas. The gaseous products were analyzed on a 3-m column packed with silica gel at 150 °C, using N_2 as the carrier gas.

Radiofrequency Decomposition of Pyrrole. Pyrrole vapor was passed through the glow discharge (see Table 1). The major portion of the gas fraction collected in the liquid nitrogen traps was a mixture of ethylene (44.1%), acetylene (31.2%), ethane (20.0%), propylene (0.8%), and propane (0.9%) (Table 1, Run No. 2). Noncondensable products were obtained from the exhaust gas of the vacuum pump connected to the nitrogen traps. Upon gas-chromatographic analysis, they were found to contain only hydrogen and methane (0.21 g; CH_4 22%, H_2 78% in Run No. 2). The fractional distillation of the liquid products collected from several runs and NMR measurements of the resulting fractions showed the presence of hydrogen cyanide (bp 28—29 °C), acetonitrile, propionitrile, acrylonitrile, crotononitrile,[3] benzene, α-methylpyrrole, and β-methylpyrrole. Their mass spectra also confirmed these assignments. The NMR data of these compounds are shown below. Acrylonitrile: NMR (δ ppm in CCl_4): 5.60 (1H, m, C<u>H</u>$_3$CN), 5.92 (1H, m, *trans* β-H), 6.10 (1H, m, *cis* β-H). Crotononitrile: NMR (δ ppm in CCl_4): 1.98 (3H, d.d, C<u>H</u>$_3$CH), 5.24 (1H, d.q, C<u>H</u>CN), 6.46 (1H, d.q, CH$_3$C<u>H</u>). Benzene: NMR (δ ppm in CCl_4): 7.24 (s, aromatic H). α-Methylpyrrole: NMR (δ ppm in CCl_4): 2.12 (3H, s, CH_3), 5.72 (1H, m, C_3–H), 5.94 (1H, m, C_4–H), 6.34 (1H, m, C_5–<u>H</u>). β-Methylpyrrole: NMR (δ ppm in CCl_4): 2.07 (3H, s, C<u>H</u>$_3$), 5.88 (1H, m, C_4–H), 6.28 (1H, m, C_2–H), 6.40 (1H, m, C_5–H).

Radiofrequency Decomposition of Pyrrolidine. For 20 min, a 7.7-g portion of pyrrolidine was passed through a radiofrequency glow discharge (Table 2, Run No. 5). The condensable gaseous products consisted of ethylene (62.4%), acetylene (18.9%), propylene (9.6%), ethane (7.6%), and propane (1.5 %), while the noncondensable products were hydrogen and methane. Gas-chromatographic analysis indicated the presence of twelve constituents in the liquid products. A fractional distillation of the reaction mixture isolated acetonitrile, propionitrile, and butyronitrile. Three major unknown compounds were separated by preparative gas chromatography (Shimadzu GC-2C, Silicon DC 550, 4.5 m, H_2). By referring to their NMR spectra, these three compounds were identified 1-pyrrolidinylacetonitrile, 2-(1-pyrrolidinyl)propionitrile, and 2-(1-pyrrolidinyl)butyronitrile respectively.

The analytical data of the identified products were as follows. Acetonitrile: NMR (δ ppm in CCl_4): 1.94 (s, C<u>H</u>$_3$-CN). IR: complete superimposable spectrum with an authentic sample. Propionitrile: NMR (δ ppm in CCl_4): 1.26 (3H, t, C<u>H</u>$_3$CH$_2$), 2.32 (2H, q, C<u>H</u>$_2$CN). Butyronitrile: NMR[δ ppm in $(CD_3)_2CO$]: 1.00 (3H, t, C<u>H</u>$_3$CH$_2$), 1.62 (2H, m, CH$_3$C<u>H</u>$_2$CH$_2$), 2.38 (2H, t, C<u>H</u>$_2$CN). Pyrrole: NMR (δ ppm in CCl_4): 6.02 (2H, m, β-H), 6.52 (2H, m, α-H). 1-Pyrrolidinylacetonitrile: NMR (δ ppm in $CDCl_3$): 1.86 (4H, m, C<u>H</u>$_2$C<u>H</u>$_2$), 2.68 (4H, m, C<u>H</u>$_2$NC<u>H</u>$_2$), 3.68 (2H, s, C<u>H</u>$_2$CN). IR (cm^{-1}): 2800 (=N–), 2230 (C≡N). MS (*m/e*): 110 (M^+). Found: C, 65.32; H, 9.00; N, 25.15%. Calcd for $C_6H_{10}N_2$: C, 65.42; H, 9.15; N, 25.43%. 2-(1-Pyrrolidinyl)propionitrile: NMR (δ ppm in $CDCl_3$): 1.48 (3H, d, C<u>H</u>$_3$CH), 1.83 (4H, m, C<u>H</u>$_2$C<u>H</u>$_2$), 2.65 (4H, m, C<u>H</u>$_2$NC<u>H</u>$_2$), 3.88 (1H, q, CH$_3$C<u>H</u>), IR (cm^{-1}): 2800 (=N–), 2220 (C≡N). MS(*m/e*): 124 (M^+). Found: C, 67.43; H, 9.80; N, 22.60%. Calcd for $C_7H_{12}N_2$: C, 67.70; H, 9.74; N, 22.56%. 2-(1-Pyrrolidinyl)-butyronitrile: NMR (δ ppm in $CDCl_3$): 1.08 (3H, t, C<u>H</u>$_3$CH$_2$), 1.84 (6H, m, CH$_3$C<u>H</u>$_2$CH,C<u>H</u>$_2$C<u>H</u>$_2$), 2.68 (4H, m, C<u>H</u>$_2$NC<u>H</u>$_2$), 3.67 (1H, t, CH$_2$C<u>H</u>CN). IR (cm^{-1}): 2810 (=N–), 2240 (C≡N). MS (*m/e*) :138 (M^+).

Radiofrequency Decomposition of Butyronitrile. The glow-discharge reaction was carried out by means of a procedure similar to that described above. The condensable gaseous products in Run No. 9 were ethylene (44.2%), acetylene

* Organic Reaction Employing the Glow Discharge. VII. Part VI: S. Kikkawa, M. Nomura, and Y. Morita, *J. Syn. Org. Chem. Jpn.*, **34**, 36 (1976).

(7.2%), propylene (15.3%), butene (2.0%), ethane (18.6%), and propane (12.7%).

The compounds with the same retention times as acetonitrile were separated from the reaction mixtures and were identified as such. Butylaminoacetonitrile was separated by preparative gas chromatography and identified on the basis of its NMR spectrum. Two other major components were identified as *N*-ethylidenebutylamine and *N*-butylidenebutylamine[5] by comparing the retention times with authentic samples, and the mass spectra of the individual fraction (obtained by the use of Hitachi RMU-6MG type GC-MS), with authentic sample. Acetonitrile: NMR (δ ppm in $CDCl_3$) 2.01 (s, $C\underline{H}_3CN$). IR: complete superimposable spectrum with an authentic sample. Butylaminoacetonitrile: NMR (δ ppm in $CDCl_3$): 0.93 (3H, t, $C\underline{H}_3CH_2$), 1,30 (1H, s, $N\underline{H}$), 1.42 (4H, m, $CH_3C\underline{H}_2C\underline{H}_2CH_2$), 2.65 (2H, t, $C\underline{H}_2NH$), 3.48 (2H, s, $NHC\underline{H}_2CN$). IR (cm^{-1}): 3320 (–N–), 2240 (C≡N). MS (*m/e*): 112 (M^+). Found: C, 63.65; H, 11.01; N, 24.97%. Calcd for $C_6H_{12}N_2$: C, 64.24; H, 10.78; N, 24.98%. *N*-ethylidenebutylamine: MS (*m/e*): 99 (M^+), 84 $CH_3CH_2CH_2CH_2\overset{+}{N}{\equiv}CH$ (67.6), 57 $CH_3CH_2\overset{+}{N}{=}CH_2$ (54.0), 56 $CH_3CH{=}\overset{+}{N}{=}CH_2$ (100). *N*-Butylidenebutylamine: MS (*m/e*)[6]: 127 (M^+), 112 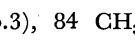 (12.5), 99 (15.3), 84 $CH_3CH_2CH_2CH{=}\overset{+}{N}{=}CH_2$ (100), 70 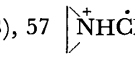 (27.8), 57 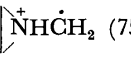 (75.0), 56 $CH_2{=}\overset{+}{N}HCH{=}CH_2$ (75.0). *N*-Propylidenebutylamine: MS (*m/e*): 113 (M^+), 98 (7.4), 84 $CH_3CH_2CH_2CH_2\overset{+}{N}{\equiv}CH$ (100), 71 (38.9), 70 (70.4), 57 (50.0), 56 (92.6).

Results and Discussion

The product distributions with the discharge reactions of pyrrole and pyrrolidine are shown in Tables 1 and 2 respectively, along with the reaction conditions. Under the influence of radiofrequency discharge, pyrrole produced HCN, CH_3CN, C_2H_5CN, $CH_2{=}CHCN$, *trans*-$CH_3CH{=}CHCN$, C_6H_6, α-$CH_3C_4H_4N$, and β-$CH_3C_4H_4N$ as the primary products, whereas pyrrolidine yielded the characteristic products of α-(1-pyrrolidinyl) nitrile, 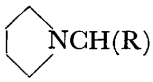 NCH(R)CN (R=H, CH_3, and C_2H_5), in addition to other nitrile derivatives.

Table 1. Experimental conditions and yields of the liquid products for the glow discharge reaction of pyrrole[a)]

Reaction conditions	Run No. 1	2	3
Applied voltage (kV)	1.23	1.50	1.63
Anodic current of discharge (mA)	70	80	90
Reactant fed in (g)	4.6	4.8	4.4
Liquid products (g)	4.1	4.2	3.5
Polymeric materials (g)	0.35	0.42	0.44
Condensable gaseous products (g)	0.11	0.22	0.30
Liquid products (%)			
HCN	5.0	12.5	16.3
CH_3CN	0.7	1.4	2.4
$CH_2{=}CHCN$	1.3	5.2	6.3
CH_3CH_2CN	0.4	1.1	2.0
trans-$CH_3CH{=}CHCN$	3.7	3.2	3.4
C_6H_6	0.2	0.7	1.3
α-$CH_3C_4H_4N$	2.0	2.9	3.3
β-$CH_3C_4H_4N$	1.3	2.1	2.4
Otheres	2.1	4.4	7.8
C_4H_5N	83.3	66.5	54.8
% Conversion	16.7	33.5	45.2

a) Duration of reaction: 20 min.

Table 2. Experimental conditions and yields of the liquid products for the glow discharge reaction of pyrrolidine[a)]

Reaction conditions	Run No. 4	5	6	7
Applied voltage (kV)	1.33	1.50	1.70	1.95
Anodic current of discharge (mA)	70	80	90	100
Reactant fed in (g)	7.5	7.7	7.7	7.3
Liquid products (g)	6.8	6.5	5.5	4.1
Polymeric materials (g)	0	0	0.01	0.03
Condensable gaseous products (g)	0.4	0.6	1.5	2.3
Liquid products (%)				
HCN	t	t	5.6	32.9
CH_3CN	t	t	3.0	5.9
CH_3CH_2CN	t	t	0.4	2.2
$CH_3CH_2CH_2CN$	1.6	4.3	8.9	9.6
C_4H_5N	0.3	1.0	2.9	5.4
 NCH$_2$CN	1.9	7.4	20.4	7.0
 NCH(CH$_3$)CN	3.2	8.6	16.0	9.6
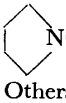 NCH(C$_2$H$_5$)CN	1.4	4.5	11.0	9.9
Others (20 peaks)	2.9	6.2	11.4	17.6
C_4H_9N	88.6	67.9	19.9	0
% Conversion	11.4	32.1	80.1	100

a) Duration of reaction: 20 min.

First, we will discuss the discharge reaction of pyrrole. In the experiment with a discharge current of 70 mA at 1.23 kV (Run No. 1), the primary products were HCN and crotononitrile. If this discharge reaction is assumed to proceed *via* the radical mechanism suggested in a previous paper,[7] the formation of crotononitrile may be explained by the following scheme, where the initial homolytic fission of C–N bond is accompanied by both the subsequent rotation of the C–C bond and the double-bond shift, leading to crotononitrile.

When the discharge current was changed from 70 to 90 mA, the crotononitrile yield decreased among the products while, the yields of HCN and acrylonitrile

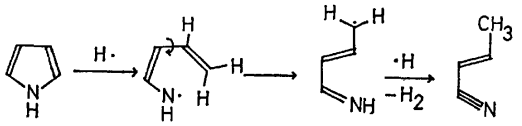

Scheme 1.

increased. In view of these findings and its chemical structure, the formation of acrylonitrile is considered to proceed by means of the generation of crotononitrile. The fact that no detectable amounts of butyronitrile were found in the reaction mixture suggests that propionitrile was formed not by the hydrogenation of acrylonitrile, but by the recombination of $\cdot CH_2CN$ with the methyl radical. By analogy with the reactions of the atomic hydrogen produced by electric discharge with CH_3CN,[8] it seems likely that hydrogen atoms first attack one of the primary products, crotononitrile, to abstract the CN radical or methyl radical to produce HCN, CH≡CH, and the methyl radical, or CH_4, CH≡CH, and the CN radical, respectively. The formation of CH≡CH may partly compensate for the energy needed for the above bond cleavage. Accordingly, these cyano and methyl radicals which stem from crotononitrile produce C_2H_6 and CH_3CN *via* recombination. It is evident that the methyl radical formed in the discharge zone also attacks pyrrole to generate α- and β-methylpyrrole.

With the reaction of pyrrolidine, the radiofrequency discharge initiates a homolytic fission of the C–N bond, which is surely the weakest bond[9] in this molecule, accompanied by a subsequent dehydrogenation similar to that described above to deliver various saturated aliphatic nitriles, such as acetonitrile, propionitrile and butyronitrile, that is outlined in the following scheme.

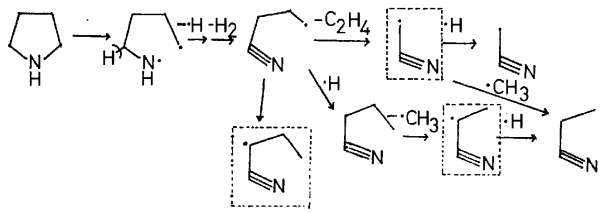

Scheme 2.

Pyrrolidine produces, unlike pyrrole, the characteristic products of α-(1-pyrrolidinyl)nitrile derivatives, whose yields amount to 47.8%, on the basis of the converted pyrrolidine (Run No. 6). The product distribution indicates that, with anodic currents of 70, 80, and 90 mA (Run No. 4, 5, and 6), α-(1-pyrrolidinyl) nitriles are the main products, while small amounts of acetonitrile, propionitrile and butyronitrile are detected which are the alternative constituents of the α-(1-pyrrolidinyl) nitrile derivatives. These findings strongly suggest that pyrrolidine reacts with the resonance-stabilized α-cyanoalkyl radicals[10] to produce α-(1-pyrrolidinyl) nitrile. In this case it appears that α-cyanoalkyl radicals such as $\cdot CH_2CN$, $CH_3\dot{C}HCN$, and $CH_3CH_2\dot{C}HCN$ are not re-formed from the corresponding nitriles by the abstraction of a hydrogen atom, but are generated by the initial radical fission of the C–N bond of pyrrolidine, followed by dehydrogenation subsequent migration to a more stable radical, and the elimination of ethylene, ultimately forming an acetonitrile radical. Scheme 2 shows this, together with the production of saturated nitriles. In Scheme 2, the first-stage intermediate, $\cdot CH_2CH_2CH_2CN$, may rapidly abstract a hydrogen atom to yield butyronitrile, because it is an unstable primary radical. This route competes with another rearrangement leading to a more stable α-radical. Such an idea is supported by the fact that the amounts of butyronitrile were appreciable relative to the trace amounts of acetonitrile and propionitrile produced under rather mild conditions (Run No. 4 and Run No. 5).

Concerning the formation of α-(1-pyrrolidinyl) nitrile derivatives, two possible mechanisms may be considered; one is the recombination of the α-cyanoalkyl radical with the pyrrolidine-*N*-radical, and the other is the electrophilic attack of the α-cyanoalkyl radical towards the basic nitrogen atom of pyrrolidine, accompanied by the subsequent release of the H atom.

TABLE 3. EXPERIMENTAL CONDITIONS AND YIELDS OF THE LIQUID PRODUCTS FOR THE GLOW DISCHARGE REACTION OF BUTYLAMINE[a]

Reaction conditions	Run No 8	9	10
Applied voltage (kV)	1.60	1.95	2.25
Anodic currrent of discharge (mA)	70	85	100
Reactant fed in (g)	4.2	4.8	3.7
Liquid products (g)	3.7	4.2	2.3
Polymeric materials (g)	0.04	0.05	0.07
Condensable gaseous products (g)	0.3	0.4	0.9
Liquid products (%)			
CH_3CN	0.6	0.4	2.8
$CH_3CH_2CH_2CH_2N{=}CHCH_3$	9.4	15.4	21.0
$CH_3CH_2CH_2CH_2N{=}CHCH_2CH_2CH_3$	3.8	2.8	1.3
$CH_3CH_2CH_2CH_2NHCH_2CN$	0.6	2.5	27.7
Others (13 peaks)	2.5	3.3	8.4
$CH_3CH_2CH_2CH_2NH_2$	83.0	75.6	38.8
% Conversion	17.0	24.4	61.2

a) Duration of reaction: 10 min.

The product distribution and the reaction conditions with butylamine are shown in Table 3. The reaction mixture was found to contain acetonitrile, *N*-butylidenebutylamine, *N*-ethylidenebutylamine, and butylaminoacetonitrile, together with other unidentified products. In this case, the probable mechanism of butylaminoacetonitrile formation is considered to be the same as that for the formation of α-(1-pyrrolidinyl) nitrile derivatives in the discharge reaction of pyrrolidine; *e.g.*, α-acetonitrile radical resulting from ethylene-elimination and the dehydrogenation of butylamine either attacks a nitrogen atom of butylamine or combines with the butylamine-*N*-radical, forming butylaminoacetonitrile. *N*-Butylidenebutylamine is assumed to be formed by the recombination of intermediate radicals, $CH_3CH_2CH_2\dot{C}HNH_2$ and $CH_3CH_2CH_2CH_2\dot{N}H$, followed by the elimination of ammonia whose formation was confirmed in this experiment.

An inspection of Table 3 shows that the combined yield of $CH_3CH_2CH_2CH_2N{=}CHCH_3$ and $CH_3CH_2CH_2CH_2N{=}CHCH_2CH_2CH_3$ increases almost linearly with the anodic currents of discharge (70, 85, and 100 mA). As the release of the ethyl radical from the latter to

yield $CH_3CH_2CH_2CH_2N{=}CHCH_2\cdot$ seems to be an energetically preferred process, so the latter produced may be easily converted to $CH_3CH_2CH_2CH_2N{=}CHCH_3$ under these discharge conditions. Therefore, the formation of $CH_3CH_2CH_2CH_2N{=}CHCH_3$ may be supposed to be contingent upon the prior generation of CH_3CH_2-$CH_2CH_2N{=}CHCH_2CH_2CH_3$.

References

1) B. D. Blaustein, "Chemical Reactions in Electrical Discharges," American Chemical Society, Washington, D. C. (1969), p. 289.

2) J. R. Hollahan and A. T. Bell, "Techniques and Applications of Plasma Chemistry," John Wiley & Sons (1974), p. 57.

3) H. Suhr, *Angew. Chem., Int. Ed. Engl.*, **11**, 781 (1972).

4) S. Kikkawa, M. Nomura, and Y. Morita, *J. Synth. Org. Chem. Jpn.*, **34**, 36 (1976).

5) Zakhdrov Nartsissov, *Tr. Mosk. Khim-Tekhnol. Inst.*, **71**, 191 (1972).

6) M. Fischer and C. Djerassi, *Chem. Ber.*, **99**, 1541 (1966).

7) S. Kikkawa, M. Nomura, Y. Morita, and N. Hosokawa, *Chem. Lett.*, **1974**, 1337.

8) J. W. S. Jamieson, G. R. Brown, and J. S. Tanner, *Can. J. Chem.*, **48**, 3620 (1970).

9) K. W. Egger and A. T. Cocks, *Helv. Chim. Acta*, **56**, 1516 (1973).

10) R. F. Pottie and F. P. Lossing, *J. Am. Chem. Soc.*, **83**, 4737 (1961).

The Oxidative Solvolysis of Durohydroquinone Monobenzoates. A Study of the Mechanism

Makoto TAKAGI, Masato TAZAKI, and Tsutomu MATSUDA

Department of Organic Synthesis, Faculty of Engineering, Kyushu University, Hakozaki, Higashi-ku, Fukuoka 812

(Received February 25, 1977)

Durohydroquinone mono(*p*-substituted benzoate)s (**1a**—**1e**) were oxidized by DDQ in CH_3OH/CH_2Cl_2 at room temperature. The products were duroquinone dimethyl acetal **4** and *p*-substituted benzoic acids (**5a**—**5e**). None of the methyl esters **3** was formed. The details of the mechanism of a series of reactions, which start with the one-electron oxidation of **1**, is elucidated by the isolation and characterization of the intermediates as well as by a kinetic study in an acetonitrile solution. The relation between the mode of oxidation, whether it is a one-electron or two-electron process, and the activation of the acyl group was explicitly discussed in terms of the mechanism. Two-electron oxidation is suggested to offer a better chance for acyl activation. Some generalization of the mechanism is made for other oxidation-induced acyl, phosphoryl and sulfuryl activating systems.

The oxidation of hydroquinone monoesters is of considerable interest as models for biological energy conversion, wherein the free energy associated with redox reaction is conserved in such "energy-rich" bondings as phosphoric or carboxylic anhydrides. Research efforts have especially been focussed on the phosphate esters since some hydroquinone phosphates are believed to be involved in biological phosphorylation.[1-3] The oxidation of hydroquinone phosphates can generate a phosphorylating agent and the reaction mechanism, as well as the synthetic application, has been examined extensively.[4,5] The carboxylates behave similarly, and several implications of the mechanism involved have been made by Wieland and Aquila,[6] Bunton and Hellyer,[7] and Clark *et al.*[8] Thanassi and Cohen[9] have proposed a phosphate-free energy conservation cycle based on the ubihydroquinone monocarboxylate ester in mitochondria.

From the point of view of the mechanism, there have been controversial observations of this oxidation-assisted activation of phosphoryl and acyl groups, since both O–C(aryl) and O–P or O–C(acyl) bond fissions have been observed depending on the oxidation conditions.[4-12] The mode of oxidation, whether it is a one- or two-electron process, and the nature of the specific ionic species involved in the case of phosphate esters should be explicitly formulated in the delineation of the reaction mechanism which links oxidation to the phosphoryl and acyl transfer processes. There has been, however, little work along this line which traces back to the characterization of the reaction intermediates involved and studies the detailed behavior in the isolated state. As a substrate for a study of the mechanism involved the carboxylate has some advantages over the phosphate in that they do not dissociate under ordinary conditions and the physical-organic chemistry of the acyl group in general is much better founded than that of the phosphoryl group. In the present investigation, the mechanism of oxidation of durohydroquinone mono(*p*-substituted benzoate)s (**1**)[13a] by dichlorodicyano-*p*-benzoquinone ((DDQ) was studied by product analysis and by intermediate isolation and characterization, as well as by kinetic measurements. The one-electron oxidation process which does not lead to acyl activation[13b] has been elucidated, and the mechanism has been discussed in comparison with the two-electron oxidation process by bromine or NBS which was found to bring about acyl transfer.

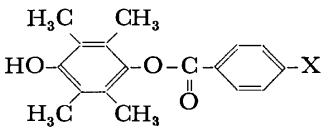

1a: X=H
1b: X=Cl
1c: X=NO_2
1d: X=CH_3
1e: X=OCH_3

Results

Oxidation Products. Substrate **1** reacted with equimolar amounts of DDQ in CH_3OH/CH_2Cl_2 (50/50, v/v) at 30 °C, and the mixture was analyzed directly using GLC for duroquinone (**2**), methyl *p*-X-benzoate (**3**), duroquinone dimethyl acetal (**4**) and *p*-X-benzoic acid (**5**). The results are shown in Table 1. It is obvious that the nature of the products and their yields are the same, irrespective of the *p*-substituent on the benzoyl nucleus. About 90% of the durohydroquinone moiety was recovered as **4**, and 6 to 8%, as **2**. The combined yield accounts for more than 94% of the starting substrate. The benzoyl portions were almost quantitatively converted into the benzoic acids, and methyl benzoates were formed only in trace amounts. After work up, $DDQH_2$ and **5** were isolated in about 90% yield, and the combined yield of isolated **2** and **4** accounted for over 90% of the starting durohydroquinone ester. However, no methyl benzoate **3** was detected. Thus, the reaction can be formulated as

$$\mathbf{1} + DDQ + 2CH_3OH \xrightarrow[1\,h]{r.t.} \mathbf{4} + \mathbf{5} + DDQH_2. \quad (1)$$

Isolation of Reaction Intermediates. Dissolution of DDQ and **1b** in benzene produced a 1:2 (DDQ: **1b**) molecular complex as black-violet crystalline powder, having an IR spectrum very close to the superposition of those of **1b** and DDQ. Since the IR spectrum of the anion radical, $DDQ^{\cdot}$ (potassium salt[14]), was quite different, the structure of this molecular complex appears to involve the usual charge transfer (CT) interaction rather than an ionic or dative one with complete electron transfer. Similar CT complexes were isolated using other nonpolar solvents (1:1 or 1:2 stoichiometry). Recently, McNelis[15] reported a 1:1 CT complex between naphthalenediol monoacetate and DDQ.

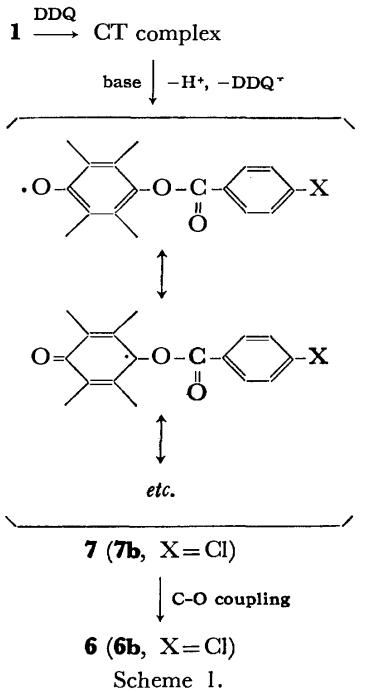

Scheme 1.

When **1b** reacted with DDQ in benzene (CT complex formation) and was then treated with a 2 M NaOH solution, 4-(4-chlorobenzoyloxy)-4-[4-(4-chlorobenzoyloxy)-2,3,5,6-tetramethylphenoxy]-2,3,5,6-tetramethyl-2,5-cyclohexadienone **6b** was produced in a 90% yield as colorless crystals. The ^{1}H NMR spectrum is illustrated in Fig. 1. The assignment is based on a comparison with other structurally-related compounds synthesized in the present study, which are included together in the figure. The formation of **6** from the CT complex upon treatment with a base can be rationalized as follows. The base abstructed the phenolic proton from the CT complex.

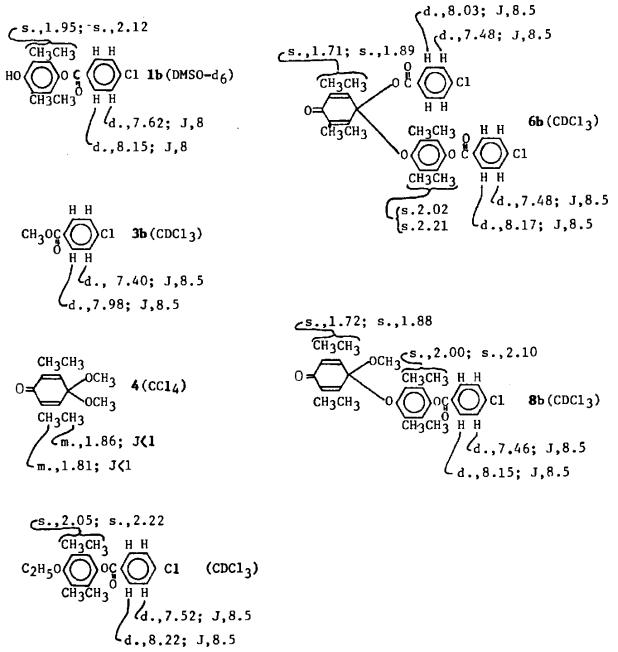

Fig. 1. ^{1}H NMR spectra of the oxidation products and related compounds. Chemical shifts are in ppm from TMS, and coupling constants in Hz.

The CT interaction then proceeded to transfer an electron to form phenoxyl **7**, which in turn coupled bimolecularly at C- and O-terminals giving **6** (Scheme 1).

The reaction of **1** with DDQ in a medium containing alcohols as a major component proceeded rather rapidly (within 1 h) and gave **4**, **5** and $DDQH_2$ as final products (Reaction 1). However, when the reaction was quenched at a very early stage, the products were different. The oxidation of **1b** in $C_2H_5OH/CHCl_3$ (50/50, v/v) according to the similar procedure as described above for the reaction in benzene (1 min of reaction time before treatment with 2 M NaOH) produced **6b** in a 73% yield. In the alcoholic solvent, the CT complex is not a stable entity, but proceeds rapidly to further reactions. It is, therefore, uncertain whether **6b** was formed on contact with the added base (as is the case for the reaction in benzene) or was already being formed in the polar and hydroxylic reaction medium. The reaction mixture was quenched by aqueous ascorbate–sodium hydrogen carbonate. Then, the yield of **6b** was even higher (86%) in $C_2H_5OH/CHCl_3$, while in benzene no **6b** was obtained, and **1b** was recovered quantitatively. This indicates that the ascorbate anion reduced DDQ in the CT complex and completely suppressed the base promoted transformation of the CT complex to *p*-benzoyloxyphenoxyl (**7b**) and DDQ$^{\cdot-}$. These results strongly support the hypothesis that the reactions in Scheme 1 are under way in the initial phase of the reaction in the polar and hydroxylic mediums, such as CH_3OH/CH_2Cl_2 or $C_2H_5OH/CHCl_3$. On the other hand, the reaction does not proceed beyond the CT stage in the benzene solvent.

Scheme 1 describes the one-electron oxidation of **1** by DDQ. The oxidation was carried out with typical one-electron oxidizing agents for comparative purposes. The oxidation of **1b** with potassium hexacyanoferrate(III) in 2 M NaOH produced **6b** in a 70% yield. Oxidation with cerium(IV) ammonium nitrate in methanol turned out to be somewhat different, giving 4-[4-(4-chlorobenzoyloxy)-2,3,5,6-tetramethylphenoxy]-4-methoxy-2,3,5,6-tetramethyl-2,5-cyclohexadienone **8b** (yield 84%). Clark *et al.*[8] conducted a similar cerium(IV) oxidation experiment with **1a** and isolated a yellow solid for which the structure **9a** (X=H) was suggested. The ^{1}H NMR spectra of the preparation reported here (Fig. 1, **8b**) is not in accord with this type of structure. Another structure, **10b**, which is isomeric to **8b**, was excluded on the basis of a detailed comparison of the ^{1}H NMR chemical shifts of the related compounds in

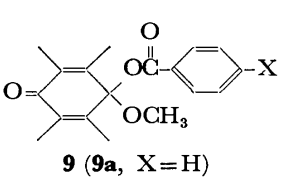

9 (**9a**, X=H)

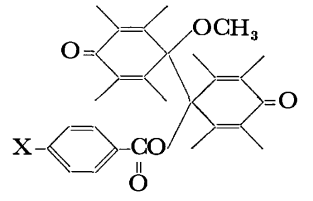

10 (**10b**, X=Cl)

Fig. 1. The product difference between hexacyanoferrate(III) oxidation and cerium(IV) oxidation can be rationalized by the lability of **6b** under acidic conditions.

TABLE 1. DDQ OXIDATION OF **1** IN CH_3OH/CH_2Cl_2[a)]

Substrate	Product, % yield			
	2	**3**	**4**	**5**
1a	6	<1	92	~100
1b	8	<1	92	~100
1c	6	<1	88	b)
1d	—	<1	88	~100
1e	6	<1	88	~100

a) $[\mathbf{1}]_0=[DDQ]_0=0.05$ M, CH_3OH/CH_2Cl_2 (50/50, v/v), 30 °C, 1 h. b) Not determined.

The reaction medium for cerium(IV) oxidation was rather strongly acidic, and it was shown in a control experiment that, under such circumstances, **6b** is readily converted into **8b**.

Chemical Transformations of Reaction Intermediates. The intermediates isolated in the foregoing section were found to be eventually transformed into the final products, **2**, **4**, and **5**, under the reaction conditions described in Table 1. In this context, the behavior of the isolated intermediates was studied with respect to the reactivity of the acetal linkages. Two types of reaction, *i.e.*, heterolytic and homolytic cleavages, were observed.

The acetal **6b** dissolved in $CHCl_3/CH_3OH$ (10/90, v/v) was maintained at 0 °C overnight. Work up of the mixture gave no recoverable **6b** but did give **8b** (in a 83% yield without purification) and *p*-chlorobenzoic acid, **5b**. No evidence was obtained for the formation of **1b**, which should be readily detectable from its characteristic IR absorption (ν_{OH}, 3415 cm^{-1}). This indicates that the acetal linkage C–OCOAr is much more labile than C–OAr′ under neutral to weakly acidic conditions (Reaction 2). Prolonged treatment of **6b** with methanol resulted in a complex mixture containing **2** and **4**, in addition to **5** and **8**. The reaction in ethanol proceeded similarly, but slowly in comparison with that in methanol:

$$\mathbf{6} + CH_3OH \begin{cases} \longrightarrow \mathbf{8} + \mathbf{5} \\ \longrightarrow\!\!\!\!\!\!\times\ \ \mathbf{9} + \mathbf{1} \end{cases} \qquad (2)$$

The time dependence of the ^1H NMR spectrum of a mixture of durohydroquinone monomethyl ether (**11**, 0.10 mmol) and DDQ (0.11 mmol) in $CD_3OD/CDCl_3$ (50/50, v/v, 400 μl) was inspected. The spectra in Fig. 2 indicate that, after 2 h, methyl trideuteriomethyl acetal of duroquinone, **12** (the compound **4** in which one of the CH_3O groups is replaced by CD_3O), was formed quantitatively. After 4 days, the CH_3O group in the acetal **12** was completely exchanged to CD_3O by further reaction with the solvent. A considerable amount of duroquinone was also formed by a reaction with the moisture in the solvent. The first phase of the reaction was very rapid, and the formation of **12** was, in fact, complete within 5 min according to the NMR measurement. The reaction of **11** and DDQ under alkaline conditions gave a quite different product. Thus, the solution of **11** and DDQ in benzene, after treatment with aqueous alkali, afforded 4-methoxy-4-(4-methoxy-2,3,5,6-tetramethylphenoxy)-2,3,5,6-tetramethyl-2,5-

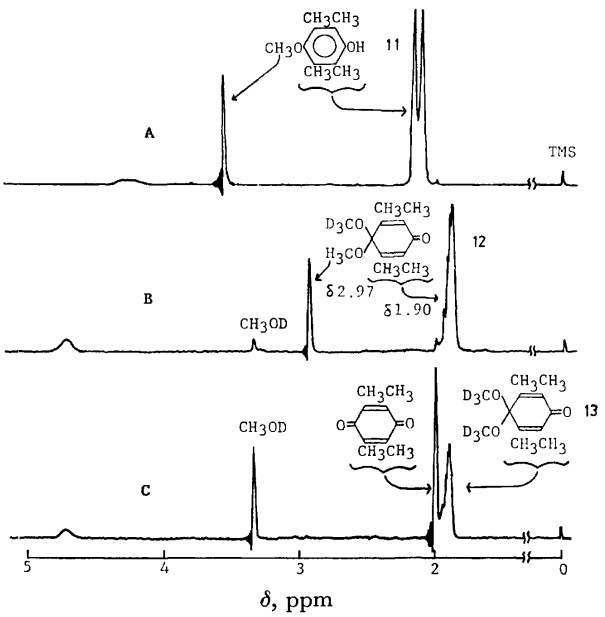

Fig. 2. DDQ oxidation of **11** (0.10 mmol) in $CD_3OD/CDCl_3$ (50/50, v/v, 400 μl) at room temperature. ^1H NMR spectra. A, **11** in $CDCl_3$; B, reaction mixture after 2 h; C, after 4 days.

cyclohexadienone **14** as colorless crystals (yield, 75%). The latter could also be prepared using an alkaline hexacyanoferrate(III) solution as the oxidizing agent.[16] Compound **14** was not only labile to acid forming **4** and **11** in acidified methanol (by the addition of $DDQH_2$) but also readily oxidizable (within 5 min) by DDQ in $CD_3OD/CDCl_3$ to give the acetal **12**. These facts indicate that **14** would be of only transient existence, even if it were formed in the DDQ oxidation of **11** in $CD_3OD/CDCl_3$. The ^1H NMR spectrum of **14** contained unusually broad resonance signals, which were barely assignable to the proposed structure. The ESR measurements made on the solution in benzene/toluene (Fig. 3)

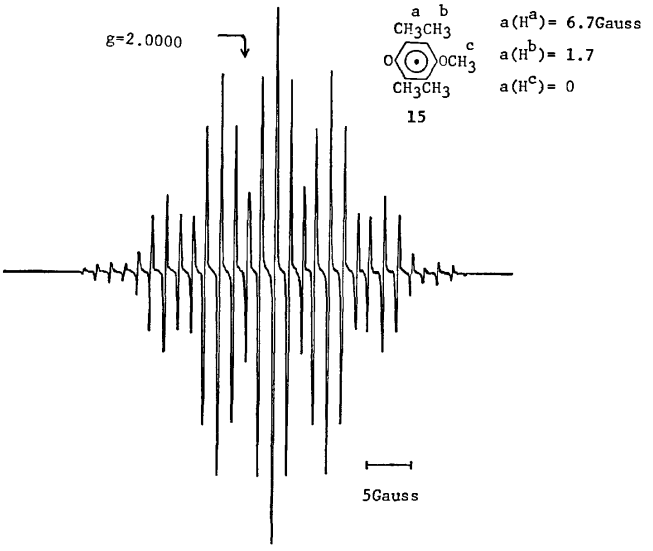

Fig. 3. The ESR spectrum of **14** in $C_6H_6/C_6H_5CH_3$ (40/60, v/v). $[\mathbf{14}]=0.67$M, room temperature. **14** ⇌ **2**·**15**.

clearly indicate the presence of phenoxyl **15** in equilibrium with **14**. Similar behavior has been reported for a related compound.[17]

An equimolar mixture of **6b** and **14** was found to be converted into **8b** simply by dissolving the former in benzene followed by concentration under reduced pressure. This observation indicates that the radical dissociation of **6b** should be considered in addition to that of **14**. The reaction is illustrated in Scheme 2.

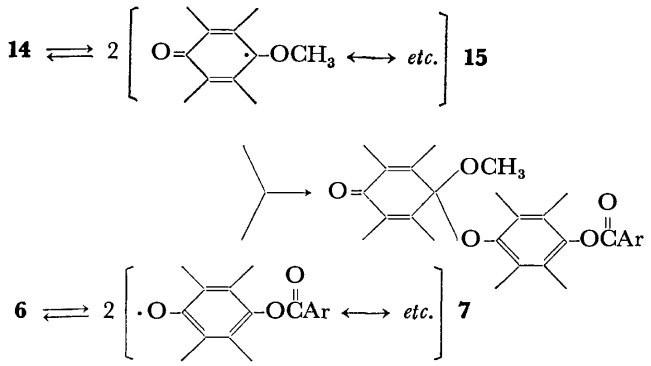

Scheme 2.

The intermediate **8** also appears to undergo facile homolytic cleavage of the acetal linkage, evidence for which has come from the attempted purification of **8b** by column chromatography on silica gel. On elution with benzene/ether, **8b** (1 mmol, contaminated with **5b**) decomposed to **1b** (0.55 mmol), **2** (0.89 mmol), **5b** (0.79 mmol) and **11** (0.26 mmol). Degradation accounts for the difficulty encountered in obtaining **8b**, and, in fact, it was this finding which prompted the examination of the DDQ oxidation of **11**. The reaction can be rationalized by the process illustrated in Scheme 3. A hydrolysis of acetal **8b** to **1b** and **2** should also be considered.

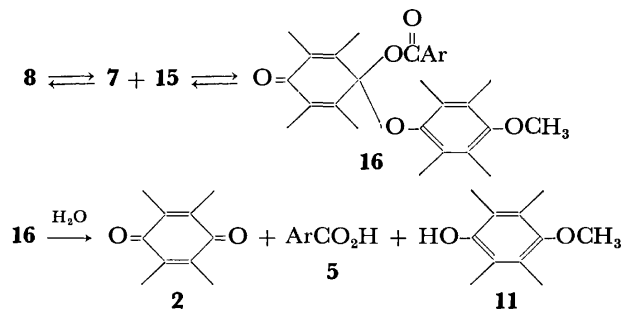

Scheme 3.

Kinetic Study in Dilute Solutions. In the preceeding sections, the chemical events after the completion of one-electron oxidation on the substrate were considered. Now, information is treated regarding the oxidation step using a kinetic method in dilute solutions. The oxidation for the kinetic study was carried out conveniently in CH_3CN or AcOH, and most of the kinetic runs presented herein involve the former as a solvent. When **1a** (0.5 mM) reacted with DDQ (0.5 mM) in dry CH_3CN at room temperature, the electronic spectra indicated the formation of $DDQ^{\cdot}$, in addition to $DDQH_2$ (Fig. 4). In accordance with the acid dissociation and

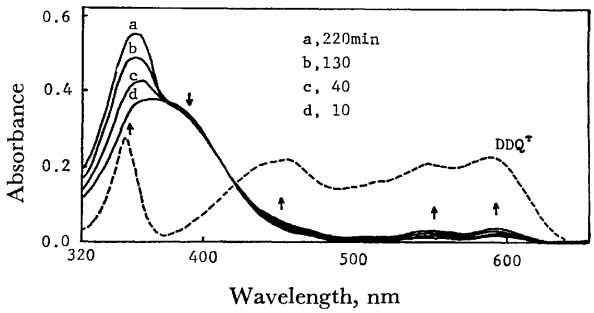

Fig. 4. The variation of electronic spectra accompanying the reaction of DDQ with **1a**. $[DDQ]_0=[\mathbf{1a}]_0=$ 0.5 mM, CH_3CN, 30 °C.

redox equilibrium between DDQ, $DDQH_2$, and $DDQ^{\cdot}$,[18] the relative $DDQ^{\cdot}$ and $DDQH_2$ concentra-

$$2DDQ^{\cdot} + 2H^+ \rightleftharpoons DDQ + DDQH_2, \quad (3)$$

tions formed during the oxidation reactions varied with the acidity of the medium. For example, upon the addition of excess trifluoroacetic acid, no $DDQ^{\cdot}$ was detected, and in the presence of equimolar 2,6-lutidine, $DDQ^{\cdot}$ was the sole product in the oxidation. The presence of basic material (*e.g.*, 2,6-lutidine, pyridine *N*-oxide or lithium acetate) not only affected the nature of the product (*i.e.*, increased the ratio of $DDQ^{\cdot}$/$DDQH_2$) but also drastically accelerated the oxidation rate. For instance, oxidation in the presence of equimolar 2,6-lutidine was instantaneous at room temperature, while the presence of several molar excess amounts of water, methanol, acetic acid or trifluoroacetic acid showed no measurable influence on the rate (*vide infra*). Base-assisted oxidation, which is in accord with Scheme 1, will be more fully treated in a separate communication.

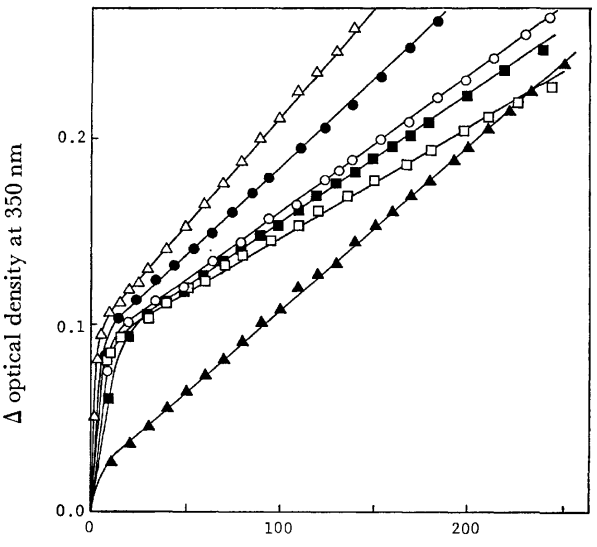

Fig. 5. The time dependence of the increase in absorption at 350 nm in CH_3CN at 30 °C. $[DDQ]_0=[\mathbf{1a}]_0$ =0.5 mM.
—■—, without additive; —○—, 0.06 M CH_3OH; —●—, 0.31 M CH_3OH; —△—, 0.61 M CH_3OH; —□—, 0.22 M AcOH; —▲—, 0.22 M CF_3COOH.

In Fig. 5, the increase in the absorbance at 350 nm, which corresponded to the formation of $DDQH_2$, was plotted against time for the oxidation of **1a** in CH_3CN. A small absorption due to $DDQ^{\cdot}$ was observed under these conditions, except for the case in which trifluoroacetic acid was present as an additive, but this constituted only a trivial correction to the amount of $DDQH_2$ formed on reduction by substrate **1a**. No sign of CT complex formation was observed in the spectra at the low concentration ranges of DDQ and **1a** utilized. Figure 5 exhibits the unusually fast production of $DDQH_2$ at the very early stages of the reaction (<2.5% conversion of DDQ), which was followed by a region (up to ≈8%) with a constant rate (pseudo-zero order kinetics). The first phase of the reaction was probably due to the presence of a small amount of basic impurity in the CH_3CN solvent, although it was carefully purified. The addition of trifluoroacetic acid eliminated most but not all of this irregular region. The relative reaction rates estimated from the slope of the second linear portion of the plots in Fig. 5 are 1.00 (without the additive), 0.83 (AcOH, 0.22 M), 1.23 (CF_3COOH, 0.22 M), 1.06 (CH_3OH, 0.06 M), 1.34 (CH_3OH, 0.31 M), and 1.69 (CH_3OH, 0.61 M). The small effect of the additives on the reaction rate even in the presence of a molar excess of **1a** of 1000 is more likely due to the change in the nature of the medium rather than to the specific effect of the additives. Thus, neither a nucleophilic process nor an acidic catalysis is involved in the rate-determining step of the formation of $DDQH_2$ (or $DDQ^{\cdot}$, refer to Reaction 3). The reaction products from **1** are probably similar to those mentioned in previous sections, but were not identified under the present reaction conditions. Where no nucleophilic additive was intentionally applied, a trace of water in the solvent might have assumed the role of a nucleophile.

Kinetics in acidified CH_3CN (0.16 M CF_3COOH) were studied. The initial concentration of DDQ was maintained constant at 0.5 mM and that of **1a** was varied between 0.25 and 3.99 mM. The pseudo-zero order rates, v_0, for the production of $DDQH_2$ in the early stages of the reaction (<7% conversion of DDQ) were obtained from the slopes of the plots similar to that shown in Fig. 5 and are plotted against the **1a** concentration in Fig. 6. The linear plot with a 1.0 slope indicates the first-order dependence of the rate on [**1a**]. The other series of experiments, in which DDQ (initial concentration, 0.1 mM) reacted with a large excess (4—7 mM) of **1a**, showed that the dependence on DDQ was also of the first order (pseuso-first order production of $DDQH_2$ with up to 90% conversion of DDQ), although the reactions for such low concentrations of DDQ were less reliable in this experiment. Kinetic studies with glacial acetic acid as the solvent also indicated a first-order dependence on both [DDQ] and [**1a**]. The calculated second-order rate constant k (M^{-1} min^{-1}), according to the expression $d[DDQH_2]/dt = k[\mathbf{1a}][DDQ]/2$, was 1.6 in CH_3CN (30 °C) and 2.0 in CH_3COOH (25 °C).

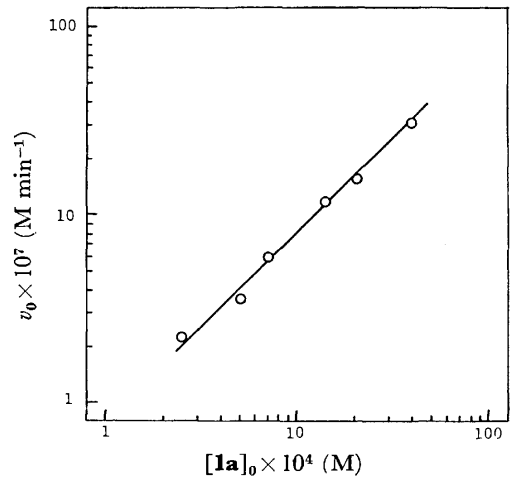

Fig. 6. The dependence of the initial rate of $DDQH_2$ formation on the substrate (**1a**) concentration. $[DDQ]_0$=0.5 mM, $[CF_3COOH]$=0.16 M, CH_3CN, 30 °C.

The effect of a *p*-substituent in the benzoyl group on the rate was investigated. The substrate (**1a**—**1e**, 0.5 mM) was oxidized by DDQ (0.5 mM) at 30 °C in acetonitrile containing 0.16 M trifluoroacetic acid. The previous initial rates were obtained, and the logarithm of the rate ratio was plotted against σ and σ$^+$ (Fig. 7).

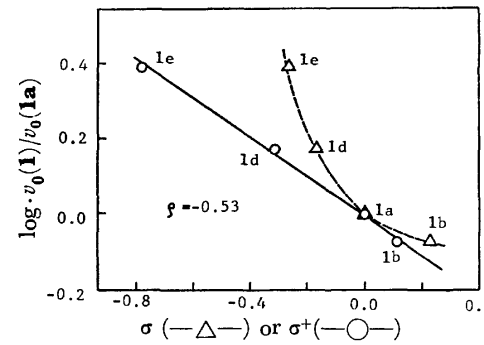

Fig. 7. Hammett's plot of the initial rate for the oxidation of **1a**—**1e** by DDQ. $[DDQ]_0=[\mathbf{1}]_0$=0.5 mM, $[CF_3COOH]$=0.16 M, CH_3CN, 30 °C.

The plot against σ$^+$ gave a straight line with a slope ρ=−0.53. This indicates that a positive charge develops on substrate **1** in the transition state of the rate-limiting step. This is in accord with the expectation that the transition state involves electron transfer or charge separation between **1** and DDQ. The small value of ρ reflects that the substituents are situated rather remote from the durohydroquinone nucleus which suffers oxidation.

Discussion

Reaction Products and Intermediates in DDQ Oxidation. The oxidation products in an alcoholic medium indicated that no activation of an acyl group or acyl transfer occurs (Reaction 1). Even the trace of **3** detected in direct GLC analysis could be an artifact due to the subsequent analytical operation. However, in their extensive study on the oxidation of hydroquinone monocarboxylates, Clark *et al.*[8] reported the activation of an acyl group in a system closely related to that

studied here. In their experiment, **1a**, **1c**, and **1e** reacted separately with DDQ in $C_2H_5OH/CHCl_3$ (50/50, v/v) at room temperature, and the formation of **2** and **3'** (ethyl esters) was observed in yields of 80—95 and 4—33%, respectively, by analyzing the reaction mixture directly using GLC. This reaction was re-examined and their results were reproduced (except for the production of **4**, which they did not mention) but only under subtly specific reaction conditions. Thus, when the GLC analysis was performed immediately after the dissolution of the reactants, the yield of **3'** was much higher than those reported. Analyses at various reaction times indicated a decreasing yield of **3'** with time. Analyses after the conventional work up indicated that no **3'** was formed throughout the reaction. Their results, therfore, do not appear to reflect the real progress of the reaction in the reaction vessel. Quite similar behavior was in fact observed also in the present system (reaction in $CH_3OH/CHCl_3$) and, under suitable conditions, a yield of **3** of more than 60% was realized by direct GLC analysis. These facts obviously indicate that the starting material, or more probably some reaction intermediates therefrom, reacted to give **3** at the high temperature in the injection part of the instrument. The behavior of reaction intermediate **6** was studied in this context. When a solution of **6b** in CH_3OH/CH_2Cl_2 or $C_2H_5OH/CHCl_3$ was injected onto a GLC column, no benzoate, neither **3b** nor **3b'**, was formed. Upon the addition of DDQ to the solution, the formation of 2—4% of the ester was indicated, which could be eliminated by treating the reaction mixture with aqueous sodium ascorbate before injection. Thus, the combination of **6** and DDQ partially simulate the reaction of **1** with DDQ to give benzoates. However, this is obviously not sufficient to explain the origin of the high yield (10—60%) of **3** at the initial stage of the oxidation reaction. It is most likely that the CT complex of **1** and DDQ is responsible for this reactivity:

$$\underset{\text{CT complex}}{\mathbf{1}\cdot DDQ_n} + CH_3OH \xrightarrow{\text{high temp}} \mathbf{2} + \mathbf{3} + DDQH_2 + (n-1)DDQ. \quad (4)$$

The strongly blackish coloration at the onset of the reaction and the isolation of the CT complex support this view.

Hageman *et al.*[15] have studied the oxidation of 2,3-dimethyl-1,4-naphthalenediol monoacetate by manganese dioxide and DDQ to give an oxidatively dimerized product and have suggested that the dimer is formed *via* an *o*-quinone methide intermediate. In the present system, no evidence for the presence of such an intermediate could be obtained, even after all attempts including the possible cyclo-addition of the intermediate with butyl vinyl ether. These same authors[15] have further assumed that the foregoing intermediate was preceeded by still other intermediates, the naphthoxyl and its dimer, which were in equilibrium. This supposition appears to be substantiated by the isolation of **6b** in the present study. Clark *et al.* have mentioned that the oxidation of hydroquinone monobenzoates with cerium(IV) ammonium nitrate produced an oxidatively dimerized compound with concurrent nitration.[8] The structure of this compound was not elucidated, but it could be similar to **6**.

Mechanism of Oxidative Solvolysis. It is reasonable to suppose that ordinary acid catalyzes the acetal exchange process for the degradation of **14** to **4** and **11** in methanol.[16] However, in consideration of the homolytic fission of **14**, it appears also possible to delineate the alternative radical mechanism, in which **15** is first protonated and the subsequent electron transfer results in the net heterolytic cleavage of the acetal bond of **14**:[19]

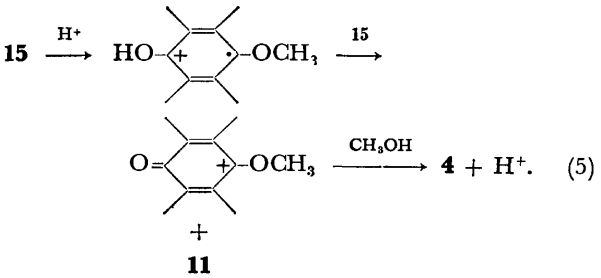

Another possibility would be the disproportionation of **15** involving a quinone methide intermediate.[17] In the presence of DDQ, still another modification can occur due to the Lewis acidity (or CT interaction) of DDQ. The protonated radical in Reaction 5 is then replaced by the CT complex, which subsequently decomposes into DDQ^- and the carbonium ion,[19] thus:

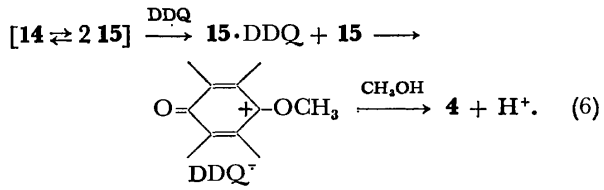

As has been noted, the oxidation of **11** and **14** by DDQ in $CD_3OD/CDCl_3$ is very rapid and is complete within 5 min at room temperature. The acid ($DDQH_2$) catalyzed degradation of **14** into **4** and **11** in the same solvent was also rapid and complete within 5 min under the conditions of the NMR spectral measurements (37 °C). Thus, under the present conditions, it was not possible to assign the major route of degradation of **14** from the alternative oxidation path (giving **4** and **15**, Reaction 6) and acid catalyzed paths (giving **4** and **11**, *e.g.*, *via* Reaction 5).

The homolytic scission of the acetal linkage of **8** poses a question similar to the case of **14** as regards the detailed mechanism of the acid catalyzed solvolytic reaction of **8** in methanol giving the dimethyl acetal **4** and **1** (a reaction similar to Reaction 5). The presence of DDQ here again introduces the possibility of an oxidation route, *i.e.*, the oxidative degradation of **8** to produce **4** and the *p*-aryloxyl radical **7** (which is in equilibrium with **6**) in a manner similar to that in Reaction 6. The data on hand show that both the acid catalyzed path and the oxidation path are again very rapid under the conditions for the NMR spectral measurements (complete within 5 min at 37 °C) and, therefore, it is difficult to determine which path is the major one under the reaction conditions given in Table 1. However, it is interesting to note that **6b** was very

labile to acid, but not to DDQ. An equimolar mixture of DDQ and **6b** in $CD_3OD/CDCl_3$ showed no reaction after 5 min, although after 10 min, the NMR spectra implied the onset of the reaction, which was followed by a great increase in the rate. After 20 min, the reaction was complete and the products were **4** and **5b**. In the presence of $DDQH_2$ (an acid catalyst), **6b** was rapidly converted into **4**, **5b**, and **1b** (within 5 min). The insensitivity of **6b** to DDQ is deemed to reflect the reluctance of **1b** to undergo two-electron oxidation by DDQ.

The chemical events after the formation of **6** (Scheme 1) can now be delineated as in Scheme 4 (in which only the oxidation path is shown for the conversion of **8** into **4** and **7**), thus completing the overall reaction of Reaction 1.

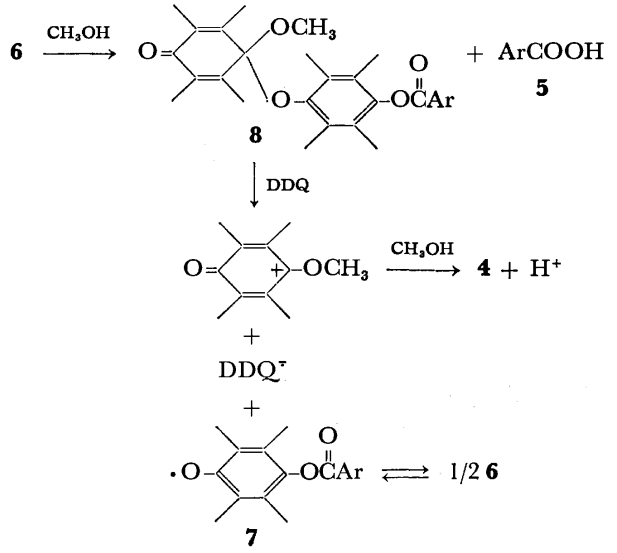

Scheme 4.

One-electron Oxidation of **1** *by DDQ.* The information obtained from this kinetic study can be summarized as follows. Under neutral to acidic conditions, the transition state of the oxidation step (i) contains one molecule each of DDQ and the substrate, (ii) does not involve the direct participation of a nucleophile such as water or methanol, (iii) does not involve acid catalysis, and (iv) carries a cationic character on the substrate. The following mechanism is consistent with these facts:

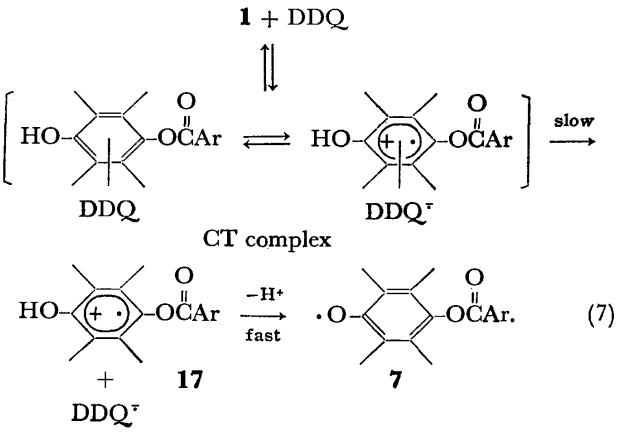

It is assumed that electron transfer within the CT complex is rapid and its dissociation into the solvated radical ion pair is rate determining. The degradation of the CT complex should be strongly facilitated in the presence of a base, since the phenoxyl **7** rather than its conjugate acid **17** can result from the interaction between the base and the CT complex. This view conforms to experimental observation. That the increase in the concentration of methanol in acetonitrile brought about rate enhancement suggests the solvation of the transition state by methanol molecules effectively acting as bases. For the oxidation of phenols by DDQ, both one-electron (as in Scheme 1 and Reaction 7) and two-electron (hydride abstraction mechanism) processes have been proposed,[17,20] and experimental distinction, in many cases, is difficult. The present kinetic evidence itself by no means excludes the alternative hydride abstraction mechanism. The preference for the one-electron oxidation with prior CT complex formation (Reaction 7) is in compliance with the results in the previous sections.

One- and Two-electron Oxidations and the Mechanism of Acyl Activation. Concerning the process of acyl activation *via* oxidation, it would be reasonable to suppose that, as a consequence of oxidation, the hydroquinone moiety of the ester should be converted into a group which exhibits an improved capacity to accommodate the negative charge. For the oxidation of **1** with DDQ, it was shown that **1** is first transformed into the phenoxyl **7** *via* a one electron process. The much stronger acidity of durosemiquinone (pK_a, 4.9—5.9[21]) than that of durohydroquinone (pK_a, 10.5, a guess from Ref. 22) renders the conjugate base of the former much more stable as a product anion. Therefore, from a comparison between the structures of **1** and **7**, we would expect the activated acyl group from **7**, rather than that from **1**. This type of activation should account for somewhat more than the difference in reactivities between phenyl (pK_a (C_6H_5OH) = 10.6) and *p*-nitrophenyl (pK_a (*p*-NO_2-C_6H_4OH) = 7.2) benzoates. The enhanced reactivity of the benzoyl group in **7**, however, could not be observed experimentally because of the involvement of other facile processes, which are initiated by the dimerization of **7** to **6** (Scheme 4). Since the dimerization of radicals is inevitable under ordinary reaction conditions, it is concluded that the acyl activation of hydroquinone monoester cannot generally be expected, when the oxidation is effected by the one-electron process. However, there is a prerequisite for this conclusion in that radical **7** dimerizes to **6** and the latter does not undergo further one-electron oxidation, which would lead in effect to the two-electron oxidation of the substrate, **1**. If the dimerization process is inhibited by certain factors, the expected activation should be observed. The unimolecular conditions (with respect to the substrate) imposed in enzymic reactions or possibly in reaction in a polymer matrix would qualify to be such factors. Concerning two-electron oxidation, there is no evidence up to now that either **6** or **7** is further one-electron oxidized by DDQ. Such a process would produce the very reactive hypothetical cation intermediate:

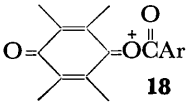

If **18** or a similar species which can conveniently be formulated as **18** on the basis of its reactivity is formed in the reaction mixture, a nucleophilic attack by methanol would be possible at two reactive sites, *i.e.*, at the acyl carbon and the carbonyl carbon of the quinone nucleus. The former gives methyl carboxylate, while the latter would lead eventually to dimethyl acetal (**4**) and carboxylic acid (**5**). Thus, the production of **18** is not necessarily equivalent to experimentally observable acyl activation. The literature indicates that the acyl activation (acyl transfer) has been verified successfully utilizing bromine, NBS, *etc.*, which are apparently two-electron oxidizing agents.[6,8,9] Some of these results were confirmed for the present substrate, **1**. A preliminary study on the mechanism suggests the intervention of **18** or a similar species. Thus, when **1b** reacted with equimolar NBS in benzene at room temperature, *p*-chlorobenzoyl bromide was obtained in a 10% yield, which was identified by IR spectroscopy and its derivation to the anilide. The reaction may be formulated as:

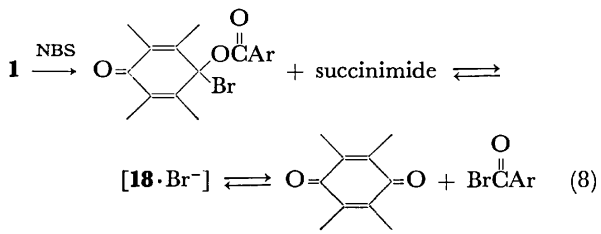

A similar process has been inferred previously.[8,10,23] The reaction with bromine gave similar results, but extensive bromination of the side chain of duroquinone occurred concurrently (acid catalysis by HBr).

It is reasonable to suppose that the actual structure of the intermediate in the two-electron oxidation process can vary according to the nature of the specific oxidizing agent. For NBS, the two electrons are abstracted directly from the hydroquinone nucleus through C–Br bonding (Reaction 8), while the formation of O–I[7,24] and O–Tl[8,25] bonding are assumed for oxidation with periodate and thallic salt, respectively. The efficiency of the nucleophilic attack on the acyl carbon in **18** is also dependent on these variations. A detailed study has yet to be made of this aspect. It is interesting to note in passing that the thermolysis of the CT complexes of **1** and DDQ produced methyl benzoates in a fairly high yield (up to 60%). The mechanism is by no means clear, but it is possible that the thermal decomposition of the CT complex resulted in a net two-electron oxidation and gave an intermediate of type **18**.

Generalization of the Mechanism. As is obvious from the foregoing discussion, two-electron oxidants have a greater probability of activating the acyl group than do one-electron oxidants. This proved also true of the oxidative acyl transfer observed in the reaction of 1,3-dithiol mono carboxylates:[26]

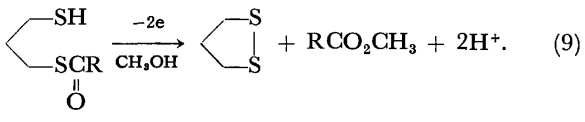

While iodine was the most effective oxidizing agent for the acyl activation, one-electron oxidizing agents lead to the linear disulfide (dimerization of the intermediate thiyl radical) without activating the acyl group. However, if we leave the carboxylate and proceed to the phosphates and sulfates, a different consideration has to be made. The essential difference between the acyl group displacement and that of the phosphoryl and sulfuryl groups resides in the fact that the acylium ion intermediate can never be formed under ordinary conditions, while the corresponding intermediates the metaphosphate anion[5,27] and sulfur trioxide,[28,29] respectively, are of a more realistic entity. There have been reports, although small in number, of one-electron oxidation processes resulting in the observable activation of the phosphoryl group (phosphoryl transfer).[4,11] This means that the radical intermediate corresponding to **7** evolves the metaphosphate anion, the semiquinone anion radical acting as an effective leaving group.[11,12] It is reasonable to assume in these cases that the dimerization of the radical intermediate was inhibited because of the unfavorable charge and steric effects. A similar process may also be possible for the sulfate.[28,30] On the other hand, much of the same above discussion applies to the two-electron oxidation of the phosphates and the sulfates except for allowance for the intervention of metaphosphate and sulfur trioxide intermediates, respectively.

Experimental

General. The melting points were determined on a hot-stage apparatus and are uncorrected. The infrared spectra were recorded in Nujol mulls on a Jasco IR-E instrument unless otherwise noted. The ultraviolet and visible spectra were measured on a Shimazu UV-200 spectrometer, and the NMR spectra were recorded with a Varian A-60 spectrometer for solutions in $CDCl_3$, CCl_4 or deuterated DMSO, using TMS as an internal standard. The ESR spectra were obtained on a Jasco ME-3X X-band spectrometer. The magnetic field was calibrated with Mn^{2+}: MgO. All solvents were purified by standard techniques. The acetonitrile for the kinetic study was retained over 3A Molecular Sieves after a final distillation from K_2CO_3. Kinetic measurements were made in a thermostatically-controlled cell, having an optical path of 10 mm and which was capped with silicone rubber and placed in the spectrometer. The solution was prepared in a nitrogen atmosphere and introduced by means of syringe. The reaction temperature was reproducible to within $\pm$0.2 °C.

Materials. DDQ (reagent grade, purchased from the Tokyo Kasei Kogyo Co.) was repeatedly recrystallized from benzene, and the CT complex therefrom was decomposed under reduced pressure to give pure DDQ. Durohydroquinone was synthesized according to the reported procedure.[31] The durohydroquinone mono *p*-X-benzoates, **1a**, **1c**, and **1e** were prepared according to the literature[8,32] and purified by repeated recrystallization from benzene and then methanol. **1a**: Yield (after purification), 20%; mp 227—228 °C (lit, 221—223°C[32]); IR 3420, 1710, 1292, 1250, and 1097 cm^{-1}; Found: C, 75.65; H, 6.72%. Calcd for $C_{17}H_{18}O_3$: C, 75.53; H, 6.71%. **1c**: Yield, 15%; mp 231.5—233.0 °C (lit, 231 °C[8]); IR 3440, 1720, 1536, 1350, 1290, 1245 and 1093 cm^{-1}; NMR (DMSO-d_6) δ 1.95 (6H, s), 2.15 (6H, s), 8.36 (4H, s); Found: C, 64.65; H, 5.51; N, 4.55%. Calcd for $C_{17}H_{17}NO_5$: C, 64.76; H, 5.43; N, 4.44%. **1e**: Yield, 16%; mp 239—241 °C (lit, 237 °C[8]); IR 3400, 1708, 1290, 1245, and 1100 cm^{-1};

NMR ($CDCl_3$) δ 2.06 (6H, s), 2.15 (6H, s), 3.89 (3H, s), 6.97 (2H, d, J=9 Hz), 8.18 (2H, d, J=9 Hz); Found: C, 71.96; H, 6.71%. Calcd for $C_{18}H_{20}O_4$: C, 71.98; H, 6.71%. The substrates **1b** and **1d** were prepared similarly. **1b**: Yield, 33%; mp 240—241 °C; IR 3415, 1715, 1290, 1245, and 1095 cm^{-1}; NMR, Table 1: Found: C, 67.07; H, 5.71%. Calcd for $C_{17}H_{17}ClO_3$: C, 67.00; H, 5.62%. **1d**: yield, 32%; mp 253.5—255.5 °C; IR 3410, 1712, 1290, 1245 and 1095 cm^{-1}; NMR (DMSO-d_6) δ 1.95 (6H, s), 2.15 (6H, s), 2.41 (3H, s), 7.36 (2H, d, J=8 Hz), 8.03 (2H, d, J=8 Hz); Found: C, 76.06; H, 7.16%. Calcd for $C_{18}H_{20}O_3$: C, 76.03; H, 7.09%. Durohydroquinone monomethyl ether (**11**) was synthesized according to the literature[23] and purified by repeated recrystallization from CCl_4/petroleum ether. Yield, 14%; mp 117—118 °C (lit, 115—116 °C[33]); IR 3330, 1242, 1076, and 1008 cm^{-1}; NMR ($CDCl_3$) δ 2.11 (6H, s), 2.16 (6H, s), 2.59 (3H, s), 4.2—4.5 (1H, broad). Durohydroquinone monoethyl ether was synthesized similarly (mp 122.5—124.5 °C; IR 3370, 1240, 1080, and 1030 cm^{-1}). 4-Ethoxy-2,3,5,6-tetramethylphenyl *p*-chlorobenzoate was prepared in a manner similar to that described for **1** by the reaction of *p*-chlorobenzoyl chloride with durohydroquinone monoethyl ether. Yield, 39%; mp 152—154 °C; IR 1738, 1269, 1235, and 1090 cm^{-1}; NMR, Table 1; Found: C, 68.25; H, 6.35%. Calcd for $C_{19}H_{21}ClO_3$: C, 68.57; H, 6.36%.

The Oxidation of ***1b*** *by DDQ in Methanol.* A mixture of 0.05 mmol of **1** and DDQ in 1 ml of CH_3OH/CH_2Cl_2(50/50, v/v) was stirred at 30°C for 1 h. The initially blackish mixture gradually faded to a brownish and then a reddish-orange color. After 40 min, no further reaction was visually observed, and the reaction mixture was analyzed directly on a GLC column for **2**,**3**,**4**, and **5**. Silicone SE 30 (10% on Celite) was utilized for the former three products (with dinitrodurene as the internal standard), and Polyester FA (10% on Celite) was used for the latter (with dinitrodurene or dimethyl phthalate as the standard). The yield of **2** was dependent on the analytical GLC conditions, and when Polyester FA was utilized, instead of Silicone SE 30, the yield increased to 32—34% at the expense of a decrease in the yield of **4**. This indicates hydrolytic decomposition of **4** during the GLC analysis and, thus, the values for **2** in Table 1 may be considered to be the upper limits of **2** present in the actual reaction mixture. The reddish-orange coloration of the final reaction mixture was caused by the displacement of the chloride atom on DDQ by CH_3OH, although this constituted only a minor side reaction since the reaction was carried out under neutral to acidic conditions.

The reaction was carried out on a preparative scale with 304 mg (1 mmol) of **1b** and 227 mg (1 mmol) of DDQ in 5 ml of CH_3OH at room temperature in a nitrogen atmosphere. After 24 h, the reaction mixture was concentrated under reduced pressure and extracted with 5 ml of CCl_4. The insoluble residue was found to be an approximately equimolar mixture of $DDQH_2$ and **5b** from an inspection of the IR spectrum, which accounted for ≈88% of the DDQ and **1b** utilized. The CCl_4 soluble portion was subjected to chromatography on silica gel to give 39 mg (24%) of **2** and 144 mg (69%) of **4**. The combined yield corresponded to 93% of the starting durohydroquinone ester. No methyl benzoate **3b** was detected. The yields of **2** and **4** were again dependent on the separation conditions, but the combined yield remained constant for duplicate runs. **4**: mp 48—54°C (lit, 56 °C[16]); IR 1678, 1638, 1075, and 1030 cm^{-1}; NMR (CCl_4) δ 1.81 (6H, m, J<1 Hz), 1.86 (6H, m, J<1 Hz), 2.88 (6 H, s). The corresponding diethyl acetal was synthesized according to the known procedure.[16] Mp 88—89.5 °C (lit, 68 °C[16]); IR 1686, 1650 and 1058 cm^{-1} NMR ($CDCl_3$) δ 1.19 (6H, t, J=7.0 Hz), 1.92 (12H, s), 3.05 (4H, q, J=7.0 Hz).

Reaction Intermediates. CT Complex: Upon the addition of DDQ (450 mg, 2 mmol) to a solution of **1b** (304 mg, 1 mmol) in benzene (50 ml), a black-violet crystalline powder (220 mg, dec 107 °C) was immediately separated out. The preparation as obtained gave reasonably good analysis for a 1:2 (DDQ: **1b**) molecular complex. Found: C, 61.35; H, 4.19; N, 3.41%. Calcd for $C_{42}H_{34}N_2Cl_4O_8$: C, 60.30; H, 4.10; N, 3.35%. The complex was unstable in the presence of moisture. **6b**: A mixture of **1b** (102 mg, 0.33 mmol) and DDQ (350 mg, 1.5 mmol) in benzene (20 ml) was stirred for 10 min, and the resultant suspension of the CT complex was treated with a cold 2M NaOH solution. The organic layer which immediately turned colorless was separated from the yellow aqueous solution after further addition of 30 ml of benzene. The organic layer was repeatedly washed with 2M NaOH until the latter became colorless. After the fiinal washing with water, the benzene solution was filtered through dry filter paper and evaporated under reduced pressure. The pale yellowish residue gave **6b** as colorless crystals (92 mg) after purification by reprecipitation from CCl_4/hexane. Yield, 90%; mp 145 °C (dec); UV λ_{max} (CH_3CN) 244 nm (ε 29000); IR (Jasco DS-403G, KBr pellet) 1732, 1720, 1676, 1639, 1594, 1269, 1228, 1088, 1070, 1012, 898, and 759 cm^{-1}; NMR, Table 1; Found: C, 67.32; H, 5.30%. Calcd for $C_{34}H_{32}Cl_2O_6$: C, 67.22; H, 5.31%. **8b**: The compound was isolated according to the procedure outlined in the text. After the addition of $NaHCO_3$, the reactions mixture ($CH_3OH/CHCl_3$) was concentrated under reduced pressure, and the residue was extracted twice with 20 ml of ether. After filtration through fine filter paper, the ether solution was evaporated to dryness, and the residue was purified by reprecipitation from CCl_4/petroleum ether giving colorless crystals of **8b**. Spectral data indicated the presence of *p*-chlorobenzoic acid as a minor contaminant, the complete elimination of which was not successful under the present conditions (also see text). Yield, 84%; mp 131 °C (dec); UV λ_{max} (CH_3CN) 240 nm (ε 36000); IR (Jasco DS-403G, KBr pellet) 1743, 1673, 1636, 1594, 1265, 1229, 1085, 1046, 1010, 948, and 759 cm^{-1}; Found: C, 68.63; H, 6.44%. Calcd for $C_{28}H_{31}ClO_5$: C, 69.63; H, 6.47%. **14**: To a solution of methyl ether **11** (180 mg, 1 mmol) in benzene (20 ml) was added DDQ (650 mg, 2.4 mmol), and the mixture was stirred for 10 min at room temperature. The resultant solution was washed with 2M NaOH until the washing became colorless. Workup of the organic layer in a manner similar to that reported[16] afforded **14** in a 75% yield. White crystals; mp 100—101 °C (lit, 101 °C[16]); IR 1678, 1643, 1247, 1085, 1045, 1010, and 945 cm^{-1}; NMR ($CDCl_3$) δ 1.5—2.3 (24 H, broad), 2.75—3.15 (3H, broad), 3.4—3.8 (3H, broad).

The authors are grateful to Dr. Yoshihisa Matsuda for ESR measurement.

References

1) T. C. Bruice and S. Benkovic, "Bioorganic Mechanisms," Vol. II, ed by W. A. Benjamin, New York (1968), p. 91.

2) C. D. Snyder and H. Rapoport, *J. Am. Chem. Soc.*, **89**, 1269 (1967).

3) P. G. Phillips, B. Revsin, E. G. Drell, and A. F. Brodie, *Arch. Biochem. Biophys.*, **139**, 59 (1970).

4) W. Dürckheimer and L. A. Cohen, *Biochemistry*, **3**, 1948 (1964).

5) R. J. Brooks, C. A. Bunton, and J. M. Hellyer, *J. Org. Chem.*, **38**, 2151 (1973), and references cited therein.

6) Th. Wieland and H. Aquila, *Chem. Ber.*, **102**, 2285 (1969).

7) C. A. Bunton and J. Hellyer, *J. Am. Chem. Soc.*, **89**, 6252 (1967).
8) V. M. Clark, M. R. Eraut, and D. W. Hutchinson, *J. Chem. Soc., C*, **1969**, 79.
9) J. W. Thanassi and L. A. Cohen, *J. Am. Chem. Soc.*, **89**, 5733 (1967); *Biochim. Biophys. Acta*, **172**, 389 (1969).
10) A. Lapidot and D. Samuel, *J. Am. Chem. Soc.*, **86**, 1886 (1964); *Biochim. Biophys. Acta*, **65**, 164 (1962).
11) C. A. Chambers and J. Q. Chambers, *J. Am. Chem. Soc.*, **88**, 2922 (1966).
12) E. P. Meier, J. Q. Chambers, C. A. Chambers, B. R. Eggins, and C.-S. Liao, *J. Electroanal. Chem.*, **33**, 409 (1971).
13) a) Suffixes **a**—**e** are used throughout this paper to denote the *p*-substituent in the benzoyl group. b) "Acyl activation" or similar terminology in this paper refers to the process in which nucleophilic displacement at the acyl carbon is facilitated as a consequence of oxidation . The process in which the O-C (alkyl) bond is cleaved, even though it mey be accelerated, is not apparent.
14) Y. Matsunaga, *J. Chem. Phys.*, **41**, 1609 (1964).
15) L. Hageman and E. McNelis, *J. Org. Chem.*, **40**, 3300 (1975).
16) C. Martius and H. Eilingsfeld, *Justus Liebigs Ann. Chem.*, **607**, 159 (1957).
17) H.-D. Becker, *J. Org. Chem.*, **30**, 982 (1965).
18) J. Q. Chambers, "The Chemistry of the Quinoid Compounds," Part 2, ed by S. Patai, John Wiley & Sons, New York (1974), pp. 737—791.
19) The formation of the carbonium ion in Reaction 5 or 6 should not be conceived literally as it stands therein. For instance, the nucleophilic attack by methanol on the duroquinone nucleus may take place on the CT complex in Reaction 6.
20) P. D. McDonald and G. A. Hamilton, "Oxidation in Organic Chemistry," Part B, ed by W. S. Trahanovsky, Academic Press, New York (1973), p. 97.
21) E. Hayon and M. Simic, *Acc. Chem. Res.*, **7**, 114 (1974).
22) "Constants of Organic Compounds," ed by M. Kotake, Asakura Publishing Co., Tokyo (1963), pp. 644—651.
23) V. M. Clark, D. W. Hutchinson, G. W. Kirby, and A. Todd, *J. Chem. Soc.*, **1961**, 715.
24) E. T. Kaiser and S. W. Weidman, *J. Am. Chem. Soc.*, **86**, 4354 (1964).
25) A. McKillop, B. P. Swann, M. J. Zelesko, and E. C. Taylor, *Angew. Chem.*, **82**, 84 (1970).
26) M. Takagi, S. Goto, R. Ishihara, and T. Matsuda, *J. Chem. Soc., Chem. Commun.*, **1976**, 993.
27) J. Rebek and F. Gavine, *J. Am. Chem. Soc.*, **97**, 3221 (1975).
28) S. W. Weidman, D. F. Mayers, D. R. Zaborsky, and E. T. Kaiser, *J. Am. Chem. Soc.*, **89**, 4555 (1967).
29) S. J. Benkovic and R. C. Hevey, *J. Am. Chem. Soc.*, **92**, 4971 (1970), and references cited therein.
30) Prof. Kaiser, who had studied the oxidation of quinol sulfate,[28] shared this view when he visited this laboratory. We thank him for these discussions.
31) a) L. I. Smith, *Org. Synth.* Coll. Vol. II, 254 (1943). b) T. H. James and A. Weissberger, *J. Am. Chem. Soc.*, **60**, 98 (1938).
32) F. Bergel, A. R. Todd, and T. S. Work, *J. Chem. Soc.*, **1938**, 253.
33) T. H. James, J. M. Snell, and A. Weissberger, *J. Am. Chem. Soc.*, **60**, 2084 (1938).

Metal-catalyzed Organic Photoreactions. Photoreactions of Compounds Containing a Carbon-oxygen or Carbon-nitrogen Multiple Bond with Alcohols in the Presence of Titanium(IV) Chloride or Uranyl Chloride[1]

Tadashi SATO, Shigeo YOSHIIE, Takashi IMAMURA, Kazumi HASEGAWA, Masayuki MIYAHARA, Shigeo YAMAMURA, and Osamu ITO

Department of Applied Chemistry, Waseda University, Nishiookubo 4, Shinjuku-ku, Tokyo 160

(Received February 25, 1977)

α,β-Unsaturated carbonyl compounds and esters, cyclopropyl ketones, β-diketones, Schiff's bases, and nitriles were irradiated in several alcohols in the presence of titanium(IV) chloride or uranyl chloride. In the titanium(IV) chloride-catalyzed reactions, the α-carbon atom of the primary alcohols underwent a bond formation, generally with the C=X (or C≡N) carbon atom of the substrates, while the bond formation occurred on a C=C carbon atom of the substrates in the uranyl chloride-catalyzed reactions. The reactions were examined under several conditions, and a possible scheme for the reactions was suggested.

We previously reported[2] that α,β-unsaturated ketones, when irradiated in alcohols in the presence of titanium(IV) chloride, underwent novel types of reaction with the formation of a C–C bond between the carbonyl carbon atom and the α-carbon atom of the alcohols. Pulegone and dypnone afforded dihydrofurans **2** (Type A), while mesityl oxide and 3-methyl-2-cyclohexenone afforded acetals **3** (Type B); these reactions are shown schematically in Scheme 1.

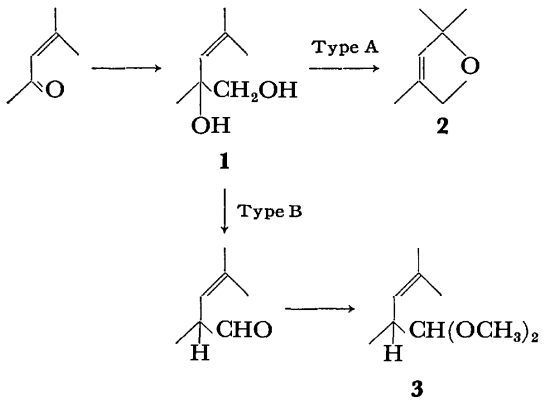

Scheme 1.

In the present study, we found that the reaction is applicable to other types of compounds and that uranyl chloride is also effective as a photocatalyst, but in a different mode from that observed with titanium(IV) chloride.

Results

Photoreactions in Methanol. α,β-Unsaturated carbonyl compounds and esters, cyclopropyl ketones, β-diketones, Schiff's bases, and nitriles were irradiated in methanol in the presence of titanium(IV) chloride or uranyl chloride. Several types of reactions were disclosed; the results are summarized in Tables 1 and 2. Evidently, in view of the observations obtained so far, the compounds containing a newly-formed C–C bond are products formed through the cooperation of light and the catalyst. The details concerning some blank experiments will be described in the Experimental part. The structure determinations of the products were done referring mostly to the spectroscopic data. Further support for the structures was also obtained from the following observations.

Photoreactions in the Presence of Titanium(IV) Chloride. α,β-Unsaturated Ketones: The irradiation of 1-acetylcyclopentene (**4**) gave glycol monomethyl ether **5**, acetal **6**, and methoxy ketone **7** (Run 1). The structure of **5** was supported by oxidizing it to an aldehyde **70**. Compound **5** corresponds to the diol **1**, which had been speculated as an intermediate for the formation of **2** or **3** (Scheme 1). Some reactions which terminated at the diol stage were also discovered in another systems (*vide infra*), and we classify these reactions as Type C. Several efforts to convert **5** into **6** were, however, unsuccessful.

Unlike the case of 3-methyl-2-cyclohexenone, which afforded an acetal *via* a Type B reaction,[2] 2-methyl-2-cyclohexenone (**8**) afforded a product in which two carbon units had been introduced (Run 2). The structure **9** was assigned to the product because it gave *o*-ethyltoluene upon treatment with hydrochloric acid through the elimination of water and methanol and a succeeding proton rearrangement. In order to eliminate the alternative structure **71**, which is also consistent with the observed spectroscopic data, we oxidized **9** with CrO_3–pyridine–HCl. Besides the main product **72** (the structure is not fully conclusive; see Experimental part), a small amount of a methoxy aldehyde **73** was isolated, which definitely supported the structure **9**. Further support for favoring **9** over **71** was obtained because the chemical shift of the *O*-methylene protons in **9** exhibited a greater down-field shift ($\Delta\delta\approx0.6$ ppm) than that of the *O*-methine proton ($\Delta\delta\approx0.1$ ppm) when derived into a phenylurethane derivative.

Reaction **8**→**9** can be shown schematically by the consecutive steps of: (1) the Type B reaction from **8** to form **74**: (2) the isomerization of **74** into an α,β-unsaturated aldehyde **75**, and (3) the Type C reaction from **75** to produce **9**. The photoreactions of α,β-unsaturated aldehydes will be described in the following section.

The absence of a methyl group in the 2-cyclohexenone system induced the reaction to proceed by way of a

TABLE 1. $TiCl_4$-CATALYZED PHOTOREACTIONS

Runs	Starting materials	Products (yields, %)		
1	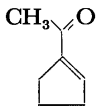 **4**	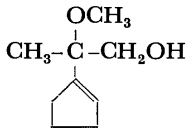 **5** (25)	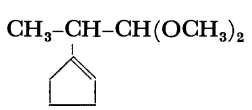 **6** (4)	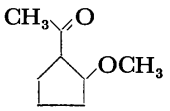 **7** (5)
2	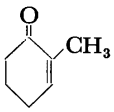 **8**	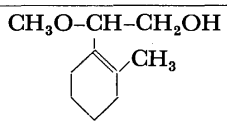 **9** (32)		
3	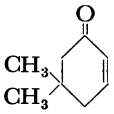 **10**	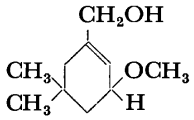 **11** (45)	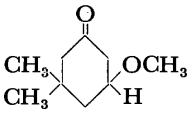 **12** (trace)	
4	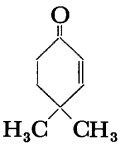 **13**	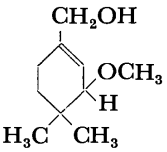 **14** (18)	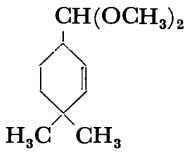 **15** (16)	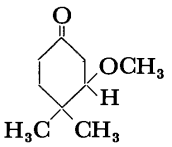 **16** (8)
5	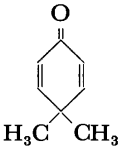 **17**	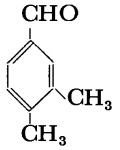 **18** (32)		
6[a)]	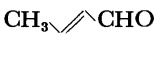 **19**	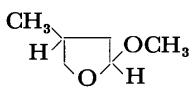 **20** (60)	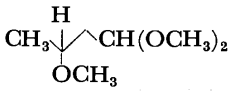 **21** (trace)	
7	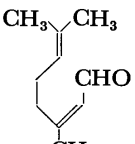 **22**	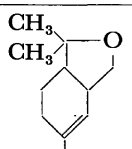 **23** (18)	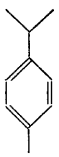 **24** (4)	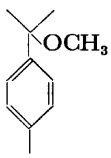 **25** (4)
8	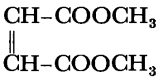 **26**	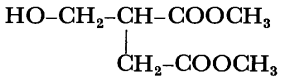 **27** (66:34)	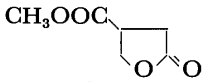 **28**	
9	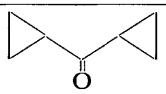 **29**	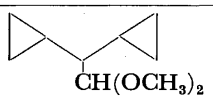 **30** (95)	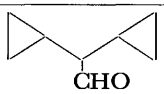 **31** (trace)	
10	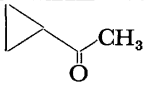 **32**	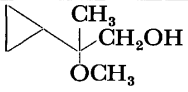 **33** (60)	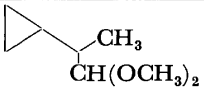 **34** (5)	
11	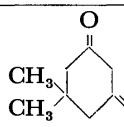 **35**	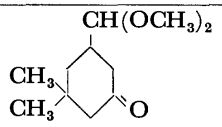 **36** (44—60)	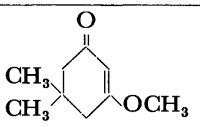 **37** (20—10)	

Table 1. (Continued)

Runs	Starting materials	Products (yields, %)		
12	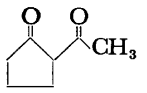	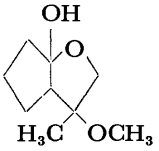		
	38	**39** (60)		
	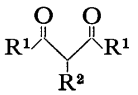	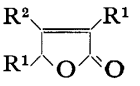	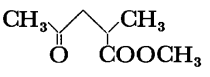	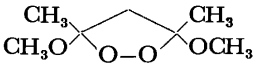
13 ($R^1=CH_3$, $R^2=H$)	**40**	**41** (5)	**42** (18)	**43** (5)
14 ($R^1=$Bu-t, $R^2=H$)	**44**	**45** (65)		
15 $R^1=R^2=CH_3$	**46**	**47** (n.d.)[b]		
	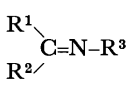	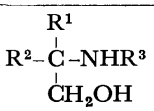	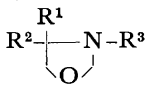	
16 ($R^1=$Ph, $R^2=H$, $R^3=CH_3$)	**48**	**49** (80)	**50** (20)	
17 ($R^1=$Ph, $R^2=H$, $R^3=$ )	**51**	**52** (90)	**53** (trace)	
18 ($R^1=n$-C_5H_{11}, $R^2=H$, $R^3=$ )	**54**	**55** (n.d.)	**56** (n.d.)	
19 ($R^1=$Ph, $R^2=R^3=CH_3$)	**57**	**58** (3:2)	**59**	
20	CH_3CN	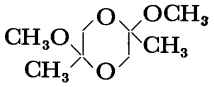		
	60	**61** (8)		
	ArCN	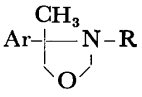	Ar–CH–OH	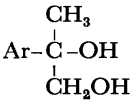
21 Ar=Ph	**62**	R=CH_3 **59** (20)	**63** (trace)	**64** (trace)
22 Ar=p-Tol	**65**	R=H **66** (11)	**67** (trace)	
23 Ar=o-Tol	**68**	R=H **69** (15)		

a) $SnCl_4$-catalyzed reaction. b) Not determined.

Table 2. UO_2Cl_2-catalyzed photoreactions

Runs	Starting materials	Products (yields, %)	
24	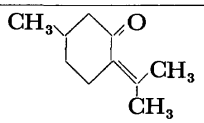	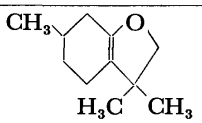	
	91	**92** (71)	
	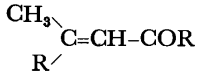	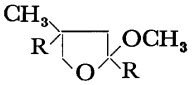	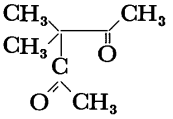
25 R=H	**19**	**20** (19)	
26 R=CH_3	**93**	**94** (45)	**95** (trace)

TABLE 2. (Continued)

Runs	Starting materials	Products (yields, %)		
27	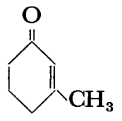 **96**	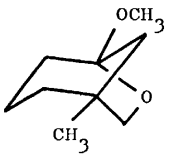 **97** (17)	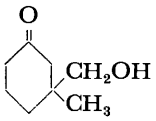 **98** (0—2)	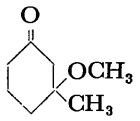 **99** (15)
28	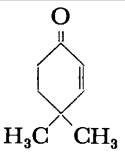 **13**	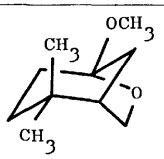 **100** (4)	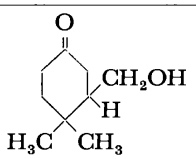 **101** (9)	
	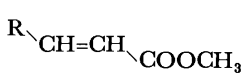	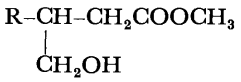	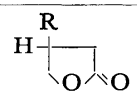	
29	R=$COOCH_3$ **26**		**27** (65)	**28** (6)
30	R=CH_3 **102**		**103** (47)	**104** (11)
31	R=H **105**		**106** (13)	**107** (1)

different course. The irradiation of **10** afforded a methoxy alcohol **11** as a titanium(IV) chloride-catalyzed photoproduct (Run 3). The oxidation of **11** with CrO_3–pyridine–HCl afforded an aldehyde **77**. The formation of **11** can be considered to involve the Type C reaction to produce a diol **76** followed by an S_N' reaction by the methoxyl group.

Since it is widely known that the photoreactions of cyclohexenone and cyclohexadienone systems proceed in a unique way to produce "lumi-products," we carried out the titanium(IV) chloride-catalyzed photoreactions with these substances. The products from **13** were methoxy alcohol **14**, acetal **15**, and a methoxy ketone **16** (Run 4). Evidently **14** and **15** are typical products *via* the titanium(IV) chloride-catalyzed photoreaction, and no products *via* "lumi products" were identified. The structure of **15** was confirmed by hydrolyzing it to an aldehyde **78**, and that of the alcohol **14**, by oxidizing it to an aldehyde **79**. The formation of **14** is another instance of a 2-cyclohexenone system carrying no methyl group.

The irradiation of **17** gave 3,4-dimethylbenzaldehyde (**18**) (Run 5). A possible sequence for the formation of this aromatic aldehyde is an initial hydroxymethylation (Type C), followed by aromatization, with a methyl migration and the succeeding oxidation of the benzyl alcohol to the aldehyde (Scheme 2). However, benzyl alcohol afforded benzyl methyl ether selectively without being oxidized to benzaldehyde under the same reaction conditions.

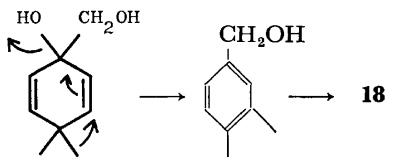

Scheme 2.

α,β-Unsaturated Aldehydes: With a view to comparing the reactivities of ketones and aldehydes, 2-butenal (crotonaldehyde, **19**) and 3,7-dimethyl-2,6-octadienal (citral, **22**) were irradiated under the same conditions. In contrast with the ketone system, **19** afforded a cyclic acetal **20** as the titanium(IV) chloride-catalyzed photoproduct (Run 6). The acetal was isolated as a mixture of *cis*- and *trans*-isomers, which could not be separated by GLC. The NMR spectrum was obtained as a sum of the two spectra, but on adding $Eu(DPM)_3$, each signal separated sufficiently well for the assignment to be made. We assumed that the methyl signal in the *cis*-isomer would exhibit a greater down-field shift when affected by the shift reagent as compared with that in the *trans*-isomer, and estimated the composition of *cis* to *trans* as 42: 58 from the intensities of the methyl signals of the two isomers.

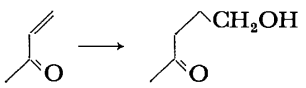

Scheme 3.

It should be noted that the same reaction pattern was observed in the photoreaction under the catalytic action of tin(IV) chloride in place of titanium(IV) chloride. Generally, tin(IV) chloride did not reveal any catalytic activities in reaction to ketones. The formation of a by-product **21** was much less when tin(IV) chloride was used as the catalyst. The present reaction can be schematized as a 1,4-addition, in contrast with the 1,2-additions observed so far (Types A—C), and we would like to classify the reaction as Type D (Scheme 3). It was found that the 1,4-type reaction became the sole reaction pattern, even in a ketone system, when uranyl chloride was used as the catalyst (*vide infra*).

Type D is not necessarily an exclusive reaction type of unsaturated aldehydes. Citral (**22**), when allowed to react under the present reaction conditions, afforded a tetrahydrofuran **23**, along with **24** and **25** resulted from the titanium(IV) chloride-catalyzed dark reaction (Run 7). Evidently the reaction proceeded through the 1,2-type (Type C) to give **80**, followed by a cyclization involving a remote double bond.

α,β-Unsaturated Esters: It was found that the reaction of dimethyl maleate (**26**) was of the 1,4-type and afforded a hydroxymethyl derivative **27** and a lactone **28** (Run 8). Although the sensitized photoadditions of alcohols to α,β-unsaturated esters have been known to produce γ-butyrolactones,[3] the present reaction is considered to proceed through a different mechanism (see Discussion part). The hydroxymethyl derivative cyclized to the corresponding lactone upon heating at 150 °C and it can be assumed to be an intermediate to lactone. The same reaction occurred in the uranyl chloride-catalyzed photoreaction (*vide infra*).

Cyclopropyl Ketones: We observed that saturated alicyclic ketones (cyclohexanone and cycloheptanone) were intact under the present reaction conditions, and we were tempted to see if the cyclopropyl group would activate the carbonyl group to be involved in the present reaction. It was found that the two cyclopropyl ketones **29** and **32** mainly underwent Type B and Type C reactions to produce **30** (Run 9) and **33** (Run 10) respectively. The structure **30** was confirmed by comparing it with the sample prepared from the authentic aldehyde **31**. The structure of **33** was supported because the *O*-methylene protons exhibited an extensive down-field shift ($\Delta\delta\approx 0.6$ ppm) when the alcohol was derived into a phenylurethane derivative (*cf.* Run 2). Upon oxidation with CrO_3–pyridine–HCl, **33** gave an aldehyde **81**. When the work-up was performed after the irradiated solution had been refluxed, the acetal **34** became the sole product. This observation verifies the intermediacy of the diol **1** in the Type B reaction.

β-Diketones: 5,5-Dimethyl-1,3-cyclohexanedione (dimedone, **35**) afforded an acetal **36** and an enol ether **37**, upon the titanium(IV) chloride-catalyzed photoreaction (Run 11). Since the enol ether **37**, which is the exclusive product in the dark reaction of the present system, produced **36** under the same irradiation conditions, the reaction from **35** can be schemed as involving a primary dark step to produce **37**, followed by a Type B reaction to produce **36**. The acetal **36** gave an aldehyde **82** upon hydrolysis with hydrochloric acid.

Although 2-acetylcyclohexanone, under the present reaction conditions, afforded a complicated mixture of products, 2-acetylcyclopentanone (**38**) underwent a clear reaction (Run 12). The extraction of the reaction mixture and the evaporation of the solvent from the extract left an almost pure oil. The structure **39** is tentatively assigned as the product, although we could not eliminate the alternative structures such as **83** and **84**.

Unlike the cases of cyclic β-diketones mentioned above, open-chain β-diketones gave different types of products. Acetylacetone (**40**) afforded butenolide **41**, γ-keto ester **42**, and cyclic peroxide **43** (Run 13). The spectroscopic data of the butenolide **41** coincided with the reported data.[4] The structure of **42** was confirmed by comparing it with the authentic sample prepared from nitroethane and methyl methacrylate.[5] Evidently the oxidation state of the newly-introduced function is higher than those observed so far; we speculate a Cannizzaro-type oxidation of the intermediate aldehyde with the co-operation of the suitably located hydroxyl group and titanium to give the butenolide (*cf.* **86**), which partly undergoes methanolysis to afford a γ-keto ester **42**.

The formation of the cyclic peroxide **43** is without precedent, but it was found that its formation is not characteristic of the titanium(IV) chloride-catalyzed photoreaction. The peroxide was also obtained as the sole product by the hydrochloric acid-catalyzed photoreaction of **40**, although the rate in this case was much slower than the titanium(IV) chloride-catalyzed photoreaction.

The cyclic peroxide **43** was distillable under reduced pressure, but it decomposed cleanly into methyl acetate and methyl propionate at 150 °C (*cf.* **87**). When it was ignited, however, it was detonated violently. Its formation may be shown schematically as a proton-assisted addition of methanol to produce **88**, which was photooxidized to the product, titanium or oxygen in the air presumably serving as the oxidizing agent.

The reaction of 2,2,6,6-tetramethyl-3,5-heptanedione (dipivaloylmethane, **44**) was much more selective: the extraction of the irradiated solution with chloroform and the evaporation of the extract left a butenolide **45** as almost pure crystals in 65% yield (Run 14). The physical data of **45** and those of a reduction product **89** coincided with the reported values.[4]

In the same way, diketone **46** afforded a butenolide **47** under the same conditions (Run 15).

Schiff's Bases: In contrast with the diversity of the photoreactions reported with carbonyl compounds, only a few photoreactions of Schiff's bases have been known. However, it was found in the present study that the reactions of Schiff's bases also proceeded in a reaction pattern similar to that of carbonyl compounds when irradiated in the presence of titanium(IV) chloride.

The photoreaction of **48** afforded an oil which consisted of **49** as the main fraction, contaminated with a minor amount of **50**, as revealed by the NMR analysis (Run 16). No appreciable intensities of signals assignable to the other compounds were observed. Although **49** was stable in the presence of titanium(IV) chloride, it decomposed (probably polymerized) completely after 24 h at room temperature when isolated free from titanium(IV) chloride. From this mixture, a pure sample of **50** was isolated by column chromatography. The structure of **49** was confirmed by deriving it to the bis(*p*-nitrobenzoyl) derivative and the picrate. The formation of **49** is reasonable in view of the Type C reaction observed with carbonyl compounds. The oxazolidine **50** must be a secondary product from **49** and formaldehyde, which had been photolytically produced from methanol and titanium(IV) chloride. Actually, **49** was quantitatively transformed into **50** upon treat-

ment with formalin.

An example of the formation of oxazolidine upon the irradiation of Schiff's base in methanol has been reported by Cerutti and Schmid.[6] In the present case, however, it was confirmed that **49** and **50** were obtained only with the cooperation of light and titanium(IV) chloride. The same authors[7] reported the formation of imidazolidines **90** (*dl* and *meso*) from **48** through photoreductive dimerization, followed by the condensation of formaldehyde. These products were not identified under the present reaction conditions. The formation of the imidazolidines became the main reaction path upon irradiation in the presence of titanium(IV) chloride and sodium methoxide, which will be described in the next section.

A selective photoreaction was also observed in the case of **51** (Run 17). The extraction of the reaction mixture with chloroform and the evaporation of the extract left crystals of **52** in an almost pure state in a high yield. The treatment of **52** with formalin again afforded an oxazolidine **53**. Similarly, **54** afforded **55** and **56** under the same conditions (Run 18).

The photoreaction of ketimine also proceeded in the same way (Run 19). The NMR analysis of the crude reaction mixture from **57** revealed that the products are mainly **58**, accompanied by a small amount of **59**. The treatment of the crude mixture with formalin afforded **59**.

Nitriles: It has been established that the photochemical reaction of aromatic and aliphatic nitriles proceeds mostly on the carbon-carbon double bond (even in an aromatic system), to the exclusion of any products from the reaction at the cyano group. To the best of our knowledge, exceptions have been reported only by Cantrell[8] and recently by Yang,[9] who observed a 2+2 cycloaddition at the nitrile function upon the irradiation of aromatic nitriles with certain electron-rich olefins.

We have now observed that the cyano group was also induced to be involved in the photoreaction in the presence of titanium(IV) chloride. The irradiation of acetonitrile (**60**) gave a mixture of two stereoisomers (3:1) of **61** as the exclusive non-volatile product. Recrystallization furnished the major component as a pure sample which was identical with the crystals separated out from a 50% methanol solution of hydroxyacetone, but the stereochemistry was not elucidated. The reaction can be shown schematically as similar to a Type C reaction, followed by hydrolysis and dimerization (Scheme 4).

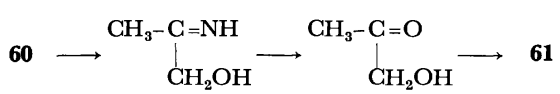

Scheme 4.

In contrast with the simple reaction observed with acetonitrile, the photoreaction of aromatic nitriles gave products exceeding expectations. The major product from benzonitrile (**62**) was a *C*- and *N*-methylated oxazolidine **59** (Run 21), which was identical with the product obtained from *N*-(α-methylbenzylidene)methylamine in Run 19. Similar reactions were observed with *p*- and *o*-tolunitrile, although no *N*-methylation was observed with the tolunitrile system (Runs 22 and 23). The by-product **63** was identified by comparison with an authentic sample. The by-product **64** was identical with the sample obtained in a small amount by the irradiation of acetophenone in methanol in the presence of titanium(IV) chloride.

No reasonable scheme for the *C*- and *N*-methylation can be proposed. For the titanium(IV) chloride-catalyzed photoreactions of ketones, we previously proposed a mechanism involving primary electron transfer from methanol to the carbonyl compound, followed by the proton transfer and cross-coupling of the resulting radicals.[2] In compliance with this scheme, we postulated in our previous communication[1b] a mechanism involving phenylazirine as a possible intermediate for the reaction. The scheme seemed to be attractive, but it has now been found to be unfavorable since phenylazirine did not afford the oxazolidine **59** under the present reaction conditions. Although the structure of the actual product, which was obtained as crystals, has not been determined, the NMR analysis indicated that neither *C*-methylation nor *N*-methylation took place on phenylazirine.

Photoreactions in the Presence of Uranyl Chloride. In contrast with the 1,2-type reactions (Types A—C) observed with most of the α,β-unsaturated carbonyl compounds (except in the cases of Runs 6 and 8), the photoreactions in the presence of uranyl chloride were of the 1,4-type (Type D, Scheme 3). The results are summarized in Table 2.

The primary products from **91** seem to be a mixture of stereoisomers of **108**, as revealed by NMR analysis, but these compounds decomposed cleanly into **92** upon vacuum distillation (Run 24).

The reaction of 2-butenal (**19**) proceeded in the same way (including stereochemistry) as the titanium(IV) chloride- and tin(IV) chloride-catalyzed reactions (Run 25, *cf.* Run 6). Similarly, mesityl oxide (**93**) furnished **94** as the main product, accompanied by a trace amount of **95** (Run 26). Small amount of **95** was also identified in the reactions in other alcohols (ethanol, 1- and 2-propanol, and water–2-methyl-2-propanol (1:1), *vide infra*); it is speculated that this product arose through the addition of the acetyl radical, which had been formed from **93** in a certain stage of the reaction, to another molecule of **93**. The addition of the acetyl radical to **93** to produce **95** has been reported.[10] The hydrolysis of **94** with hydrochloric acid gave a product which could be identified by NMR analysis as a tautomeric mixture of **109a** and **110a** (1:1).[11] The mixture, upon oxidation with CrO_3–pyridine–HCl, afforded a keto aldehyde **111** as the sole product.

The reaction of **96** produced **97** as the main product, accompanied by a small amount of a methanol adduct **99** (Run 27). A vacuum distillation of the mixture induced the elimination of methanol from **99**; the distillate consisted of **97** and the starting ketone **96**. The yields of products in the uranyl chloride-catalyzed reactions are sensitive to the reaction conditions (light intensities, duration of irradiation, quality of the catalyst, and pH of the solution; *vide infra*), and the

ring-opened product **98** was identified, along with the major product **97**, on some reactions of **96**.

The enone **13** also gave a ring-opened alcohol **101**, as well as a cyclic acetal **100** (Run 28). The reaction path through the "lumi-products" was not observed in the present case either (*cf.* Run 4). The primary alcohols **98** and **101** were oxidized to the aldehydes **112** and **113** respectively.

The same type of reaction as observed with titanium(IV) chloride-catalyzed reaction proceeded with the esters **26**, **102**, and **105** (Runs 29—31). The yields in Run 31 are low because of the extensive polymerization of the starting material. The oxidation of the γ-hydroxy ester **106** with CrO_3–pyridine–HCl gave an aldehydic ester **114**. As has been observed in Run 8, **103** and **106** cyclized to lactones **104** and **107** respectively upon heating. It should be noted that, while shorter-wavelength light (quartz-filtered light) was necessary to induce the reaction in the titanium(IV) chloride-catalyzed reaction, Pyrex-filtered light induced the reaction well with catalytic assistance by uranyl chloride.

Table 3. Concentration effect of $TiCl_4$ upon the product yields in the reaction of **96**

$TiCl_4$ Mol equiv to **96**	**96** (Recovd) (%)	**115** (%)	**116a** (%)	**117a** (%)	**99** (%)
0.1	12	30	trace	trace	25
0.2	29	49	trace	trace	5
0.5	7	65	trace	trace	6
1.0	0	71	5	3	11
2.0	trace	70	5	2	trace
3.0	4	51	6	3	4
4.0	4	46	8	5	4
5.0	2	30	11	5	trace
10	trace	15	17	2	trace

Solutions of **96** (0.1 g, 0.91 mmol) and varying amounts of $TiCl_4$ in methanol (10 ml) were irradiated with Pyrex-filtered light for 7 h. The yields were determined by NMR analysis, using nitrobenzene as the internal reference.

Effects of the Reaction Conditions. Titanium(IV) Chloride-catalyzed Reactions: The effect of the catalyst concentration on the product yields was examined using 3-methyl-2-cyclohexenone (**96**) as the substrate. The yields of the products, as determined by NMR analysis, are summarized in Table 3. Although the maximum yield of the Type B products (**115**, **116a**, and **117a**) was obtained when about an equimolar amount of titanium(IV) chloride was used, it is evident that titanium(IV) chloride functions catalytically rather than stoichiometrically, because the amounts of the products exceed the amount of the catalyst at low concentrations of titanium(IV) chloride. Excess amounts of the catalyst complicated the reaction and afforded large amounts of by-products. At low concentration of titanium(IV) chloride, the polar addition of methanol to give **99** became efficient. Presumably the addition of methanol is catalyzed by the proton formed by the reaction of titanium(IV) chloride with methanol. It was confirmed that the proton-catalyzed photoaddition of methanol to **96** was remarkable at low concentrations of hydrochloric acid. Probably at higher proton concentrations, the thermal reverse reaction (elimination of methanol from **99**) would become efficient.

The reaction medium in the present reaction was acidic as a result of the formation of hydrochloric acid from titanium(IV) chloride and methanol. Since we observed, in our preliminary experiments,[2] that the acidic conditions are necessary to induce the present photoreaction, we carried out the titanium(IV) chloride-catalyzed photoreaction of **96** and **48** while adding varying amounts of sodium methoxide. Evidently the Type B reaction (**96**→**115**+**116a**+**117a**, Table 4) was

Table 4. Concentration effect of $NaOCH_3$ upon the product yields in the reaction of **96**

$NaOCH_3$ Mol equiv to $TiCl_4$	**96** (Recovd) (%)	**115** (%)	**116a** (%)	**117a** (%)	**99** (%)
0.5	trace	72	4	3	0
1.0	trace	63	5	2	0
1.5	0	65	4	2	0
2.0	61	6	trace	0	6
3.0	73	0	0	0	trace
4.0	55	0	0	0	trace

Solutions of **96** (0.1 g, 0.91 mmol), $TiCl_4$ (0.17 g, 0.91 mmol), and varying amounts of $NaOCH_3$ in methanol (10 ml) were irradiated and treated in the way described in the footnote in Table 3.

retarded remarkably when the amount of sodium methoxide exceeded two mole equivalents of that of titanium(IV) chloride. The effect of the sodium methoxide concentration was also observed in the case of the photoreaction **48**→**49**+**50** (Run 16), as is shown in Table 5. Notably, there was a change in the reaction pattern, and imidazolidines **90** (*dl* and *meso*) became the products at higher concentrations of sodium methoxide. Cerutti and Schmid reported the formation of **90** by the irradiation of **48** in methanol with a low-pressure mercury lamp under argon.[7] Although we could not duplicate their results, the spectroscopic data on our

Table 5. Concentration effect of $NaOCH_3$ upon the product yield in the reaction of **48**

$NaOCH_3$ Mol equiv to $TiCl_4$	**50** (%)	*meso*-**90** (%)	*dl*-**90** (%)
0.0	71	0	0
1.0	67	0	0
2.0	66	0	0
3.0	50	0	0
4.0	19	7	6
5.0	5	15	13

Solutions of **48** (0.3 g, 2.5 mmol), $TiCl_4$ (0.17 g, 0.91 mmol), and varying amounts of $NaOCH_3$ in methanol (10 ml) were irradiated with quartz-filtered light for 3 h. An appropriate amount of 37% formalin was then added to the photolysate and the solution was worked-up in the way described in Run 16. The yields were determined by NMR analysis, using 1,1,2,2-tetrachloroethane as internal reference.

imidazolidines coincided with those previously reported.[12] *meso*-Imidazolidine **90** was prepared by the condensation of formaldehyde with an authentic ethylenediamine derivative **118** of mp 137 °C.[13] *dl*-Imidazolidine was also prepared from another isomer of **118**, which remained as an oil after the separation of the crystaline form of **118**.

We found that the imidazolidines were the sole products in the titanocene dichloride-catalyzed photoreaction of **48** in methanol. A decrease in the proton concentration or a change in the nature of the catalyst might be responsible for the effect of sodium methoxide, but no experimental evidence has been obtained.

Uranyl Ion-catalyzed Reactions: The uranyl chloride-catalyzed reaction is very sensitive to the pH of the solution. It was found from the experiment with **96** that the C–C bond-formation reaction proceeded most efficiently at pH 2—3. At pH 7, most of the starting material was recovered, while at pH 1, methanol addition to give **99** became the main reaction pattern.

The effect of the catalyst concentration on the product yields was examined using dimethyl maleate (**26**) as the substrate. In contrast with the case of the titanium(IV) chloride catalyst, the product yield (**27**+**28**) reached its maximum at a catalyst concentration of a one-tenth mole equivalent to that of the substrate, and thereafter held constant with increasing amounts of the catalyst. With increasing amounts of the catalyst, however, the cyclization to lactone (probably through the secondary thermal reaction) became appreciable.

Table 6. Effects of the counter ions in UO_2X_2 upon the product yields in the reaction (**26**→**27**+**28**)

Counter ions (X)	**26** (Recovd) (%)	**27**+**28** (%)
Cl	0	59
NO_3	52	24
OAc	79	8
SO_4	62	6

Solutions of **26** (0.15 g, 1.3 mmol) and uranyl compounds (0.13 mmol) in methanol (12 ml) was irradiated with Pyrex-filtered light for 6 h. The yields were determined by NMR analyses, using benzene as the internal reference. The yields of **28** did not exceed 3% of those of **27**.

It was found that the nature of the counter ions exerts a remarkable influence on the reaction of **26**, as is shown in Table 6. However, the trend should not be considered to be general, because uranyl sulfate was found to be as effective as uranyl chloride in the case of the reaction of mesityl oxide, although the acetate was poor in catalytic activity in both cases.

Reactions in the Other Solvents. Titanium(IV) Chloride-catalyzed Reaction of 3-Methyl-2-cyclohexenone (69): We have previously reported that the reaction of **96** in ethanol proceeded in the same way as in methanol to produce two methyl ketones **116b** (49%) and **117b** (12%).[2] The same type of reaction also occurred in other primary alcohols; the products were **116c** (34%) and **117c** (9%) in 1-propanol; **116d** (30%) and **117d** (8%) in 1-butanol; and **116e** (39%) in 2-methyl-1-propanol. Contrary to the primary alcohols, 2-propanol was found to be unreactive, the major part of the starting material being recovered unreacted, accompanied by a small amount of *m*-cymene (**119**), which is a product of a Type C reaction followed by dehydration and proton rearrangement. The reduced reactivity of 2-propanol was also indicated by the reaction of **96** in a mixed solvent of 2-propanol and methanol (1 : 1 by volume), which afforded a methanol-participated product **115** as the sole product. Most of the starting material was recovered by photoreactions in 2-butanol and 2-methyl-2-propanol.

Uranyl Chloride-catalyzed Reaction of Mesityl Oxide (93): The photoreaction of **93** in ethanol in the presence of uranyl chloride proceeded according to the same pattern as that in methanol and afforded a product which was identified by NMR analysis as a mixture of **109b** and **110b**. The subsequent oxidation of the product mixture by CrO_3–pyridine–HCl afforded **95** as the main product (13% from **93**), along with a small amount of a lactone **120**. The lactone must be a product of the oxidative demethylation from **110b**. In parallel with the observation described above, 2-propanol was also lacking the reactivity, and the products in this solvent were a diketone **95** and a cyclobutanol **121**. The diketone **95** became the major product by Pyrex-filtered light, while the ratio was reversed by quartz-filtered light. Both compounds were also the main products in a hydrochloric acid-catalyzed photoreaction in 2-propanol and in a titanium(IV) chloride-catalyzed photoreaction in water–2-methyl-2-propanol (1 : 1 by volume). The cyclobutanol **121** is known to be a photoproduct from 4-methylpent-4-en-2-one (isomesityl oxide),[14] and it can be presumed that the weak acidic conditions (pH 3) of the present reaction might catalyze the thermal isomerization of **93** into isomesityl oxide, from which the cyclobutanol is derived.

Uranyl Chloride-catalyzed Reactions of α,β-Unsaturated Esters: The reaction of dimethyl maleate (**26**) in ethanol proceeded in the same way as in methanol and furnished a mixture of *threo*-**122a**[15] (23%), *erythro*-**122a** (14%), *cis*-**123a** (13%), and *trans*-**123a** (6%), as revealed by NMR analysis. Heating induced cyclization, and a mixture of *cis*- and *trans*-**123a** was obtained. The assignments of the stereochemistry of the lactones were performed by referring to the reported data.[3b] The stereochemistry of the hydroxy esters **122a** was speculated from the relative amounts prior to and after the thermal cyclization to the lactones (*cf.* Experimental part).

In contrast with the reactions described above, 2-propanol was brought into the reaction with **26** with the catalytic assistance by uranyl chloride; we thus obtained **122b**, which was then further cyclized to a lactone **123b**.

Discussion

All the reactions described thus far can be shown schematically as involving a primary step of the formal addition of the hydroxymethyl radical to C=O, C=N,

and C≡N groups (1,2-type, in the titanium(IV) chloride-catalyzed reactions) or to an unsaturated carbon atom (1,4-type, in the uranyl chloride-catalyzed reactions). The photochemical 1,4-additions of alcohols[16] or ethers[17] to α,β-unsaturated carbonyl compounds by means of aromatic-ketone sensitization have been reported with various systems, and have been shown schematically involving radical species. It seemed conceivable that the present reaction might proceed through a radical initiation, particularly when uranyl chloride was used as the catalyst, since such a catalyst might produce chlorine radicals upon irradiation. This hypothesis was examined and rejected on the basis of the following observations.

No traces of products characteristic of the present metal-catalyzed photoreactions were identified from mesityl oxide upon (1) refluxing in methanol for 50 h while benzoyl peroxide was being added, (2) irradiating in methanol in the presence of benzophenone, or (3) the bubbling of chlorine into the methanol solution under irradiation with a tungsten lamp. The reaction with chlorine gave **124** and one more compound whose structure has not been elucidated. The fact that uranyl sulfate is as effective as uranyl chloride would also eliminate the possible intervention of the chlorine radicals.

Table 7. Solvent effects upon the product yields in the reaction (**125**→**126**+**127**)

Alcohols	UO_2Cl_2-catalyzed 1 h		UO_2Cl_2-catalyzed 6 h		Benzophenone-sensitized 6 h	
	126 (%)	**127** (%)	**126** (%)	**127** (%)	**126** (%)	**127** (%)
Methanol	45	0	65	0	0.6	0
Ethanol	19	0	39	0	0.6	0
2-Propanol	0	7	5	24	1.0	1.3

A solution of **125** (0.15 g, 1.5 mmol) and UO_2Cl_2 (0.044 g, 0.13 mmol) or benzophenone (0.029 g, 0.16 mmol) in alcohol (12 ml) was irradiated with Pyrex-filtered light.

Although the benzophenone-sensitized additions of alcohols to ethyl 2-butenoate (**125**) have been reported to be effected under irradiation for 50—72 h,[3a] no appreciable photoaddition was observed during the present irradiation time (1—6 h, see Table 7). The same authors investigated the photochemical addition of hydroxyalkyl groups to **125** with various alcohol systems, and found that the reactivities increased in the order of: methanol<ethanol<2-propanol, an order which is consistent with the proposed radical-chain mechanism. The same reactions with the catalytic assistance by uranyl chloride were now examined, and it was found that the order of the reactivities of these alcohols is completely reversed (Table 7). The decrease in the reactivities of the secondary alcohols, as observed in the cases described here and in the previous section, could be another evidence against the intervention of the free-radical species.

The uranyl ion-catalyzed photoisomerization of stilbene[18] and the photodimerization of dienone[19] have been reported. Energy transfer and a restricted orientation of dienone by coordination, respectively, have been presented as the mechanisms.

Table 8. Experimental conditions

Runs	Starting materials (g)	$TiCl_4$[a] or UO_2Cl_2 (g)	Methanol (ml)	Tubes[c]	Time (h)
1	**4** (0.3)	0.52	30	P	3
2	**8** (0.45)	0.78	45	P	6
3	**10** (0.10)	0.17	10	Q	5
4	**13** (1.40)	2.42	140	Q	4
5	**17** (0.04)	0.10	10	P	4
6	**19** (0.30)	0.52[d]	36	Q	3
7	**22** (1.40)	2.42	140	Q	3
8	**26** (0.15)	0.26	12	Q	6
9	**29** (0.1)	0.17	13	Q	4
10	**32** (0.1)	0.17	13	Q	4
11	**35** (0.8)	1.4	80	P	5
12	**38** (0.6)	1.04	60	Q	6
13	**40** (1.6)	2.8	80	Q	7
14	**44** (0.4)	0.7	40	P	6
15	**46** (0.1)	0.17	10	Q	6
16	**48** (1.0)	2.1	120	Q	4
17	**51** (0.47)	0.8	56	Q	4
18	**54** (0.5)	1.04	60	Q	4
19	**57** (0.28)	0.7	48	Q	24
20	**60** (1.3)	1.4	80	Q	24
21	**62** (0.38)	0.66	48	Q	24
22	**65** (0.38)	0.66	48	Q	24
23	**68** (0.38)	0.66	48	Q	24
24	**91** (0.6)	0.24	72	P	5
25	**19** (0.8)	0.21	96	P	5
26	**93** (0.8)	0.2	96	P	5
27	**96** (0.8)	0.2	96	P	5
28	**13** (1.0)	0.15	80	P	7
29	**26** (1.0)	0.24	80	P	3
30	**102** (1.5)	0.51	120	P	6
31	**105** (1.5)	0.3	120	P	1

a) Runs 1—23. b) Runs 24—31. c) P: Pyrex, Q: quartz. d) $SnCl_4$.

The photoreaction of mesityl oxide in tetrahydrofuran in the presence of uranyl chloride resulted in the formation of a C–C bond, giving **128** as the main product (17%). The same product was obtained by the benzophenone-sensitized photoreaction, while the direct irradiation (without any additives) under the same conditions resulted in a recovery of the starting material, with a negligible formation of **128**. Evidently uranyl chloride functions as a sensitizer in the reaction in tetrahydrofuran, and the reaction proceeds through an intermediacy of the radical species, in marked contrast with the photoreactions in alcohols.

Some of the titanium(IV) chloride-catalyzed photoreactions were wave-length-dependent. Pyrex-filtered light could not induce the present reaction in the cases of 2-acetylcyclopentanone (**38**), dimethyl maleate (**26**), and acetonitrile (**60**). The acetylcyclopentanone **38** afforded **129**, while **26** and **60** were recovered intact under these conditions.

In considering possible mechanisms for the metal-

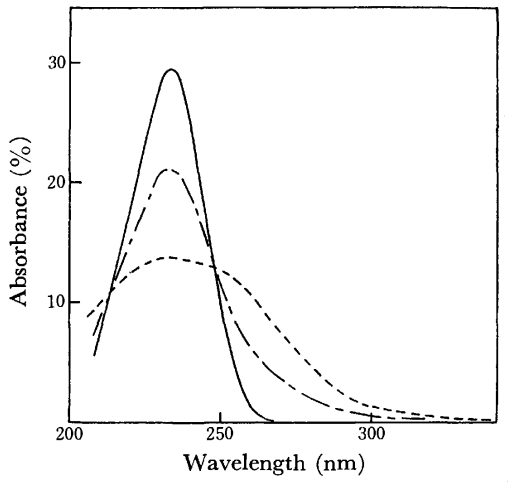

Fig. 1. Absorption spectra of **96** (——, 1.97×10^{-5} M, $\varepsilon=14900$), $TiCl_4$ (– – –, 1.96×10^{-5} M, $\varepsilon=6580$), and a mixture of an equal volume of both solutions (– – – –).

catalyzed photoreactions, it seems important to investigate the absorption characteristics. At low concentrations ($\approx2\times10^{-5}$ M), the mixing of 3-methyl-2-cyclohexenone (**96**) and titanium(IV) chloride did not result in any changes in the absorption curves in the 220—320 nm region; only a sum of the two absorption curves was obtained (Fig. 1). The same phenomena were observed with the uranyl chloride–dimethyl maleate (**26**) and uranyl chloride–mesityl oxide (**93**) systems. It was revealed from the experiments with more concentrated solutions (concentrations corresponding to the actual reactions, 10^{-2}—10^{-1} M), however, that a new absorption band appeared in the 350—480 nm region upon the mixing of the substrate and the metal compound in the **96**–$TiCl_4$, **93**–$TiCl_4$, and **93**–UO_2Cl_2 systems, while no development of the new band was observable in the **26**–UO_2Cl_2, **26**–$TiCl_4$, and **60**–$TiCl_4$ systems. The absorption coefficients (ε) calculated by assuming the formation of a 1 : 1 complex between the substrate and the metal compound were 5—7. We have not identified the character of this new band, and it remains unknown whether or not the light absorption corresponding to this band plays an indispensable role in inducing the present photoreactions. The action spectrum would be informative in this connection, but we have not carried out such an experiment.

The intensity of the new band in the **96**–$TiCl_4$ system increased as a function of the time when kept in the dark. Actually, the color of the solution changed from light yellow (immediately after the mixing) to dark yellow, and became dark green after 24 h when kept in the dark. Despite the remarkable color change though, a work-up resulted in the recovery of only the starting ketone. No such color change in the dark was evident in other systems. Even in cases where no coloration was remarkable upon standing in the dark, most of the reactions are accompanied by a color change to some degree during irradiation. Obviously, it seems difficult to characterize the primary light-absorbing species.

The observations described so far provide convincing evidence that both the substrate and the catalyst are involved in the excited species, although a glance at Fig. 1 might lead one to conclude erroneously that the present photoreaction, particularly with Pyrex-filtered light, is induced by the excitation of the catalyst alone.

All these facts favor our previous proposal of a scheme comprising an initial electron transfer, followed by a proton transfer and succeeding cross coupling.[2] All these processes are considered to proceed consecutively within the coordination sphere of metal compounds, thus providing circumstances favorable for the cross coupling. We have no clear-cut interpretation of the different catalytic behavior between titanium(IV) chloride and uranyl chloride. The different mode of coordination could be responsible, but we have no experimental evidence for this argument at the present stage of our investigation.

Addendum. In their synthetic studies of sesquiterpenes, Isoe and his co-workers recently prepared **131** from **130** by means of the titanium(IV) chloride-catalyzed photoreaction, and established the configuration of the introduced hydroxymethyl group in **131** as exclusively *cis* to the methoxycarbonyl group.[56] Although further work should be done for the full interpretation of the stereoselectivity, an explanation of the selectivity can be obtained in terms of our present proposal that the whole reaction proceeds within the coordination sphere of titanium, which, in this case, might coordinate to oxygen atoms of both the ester and carbonyl groups in **130**.

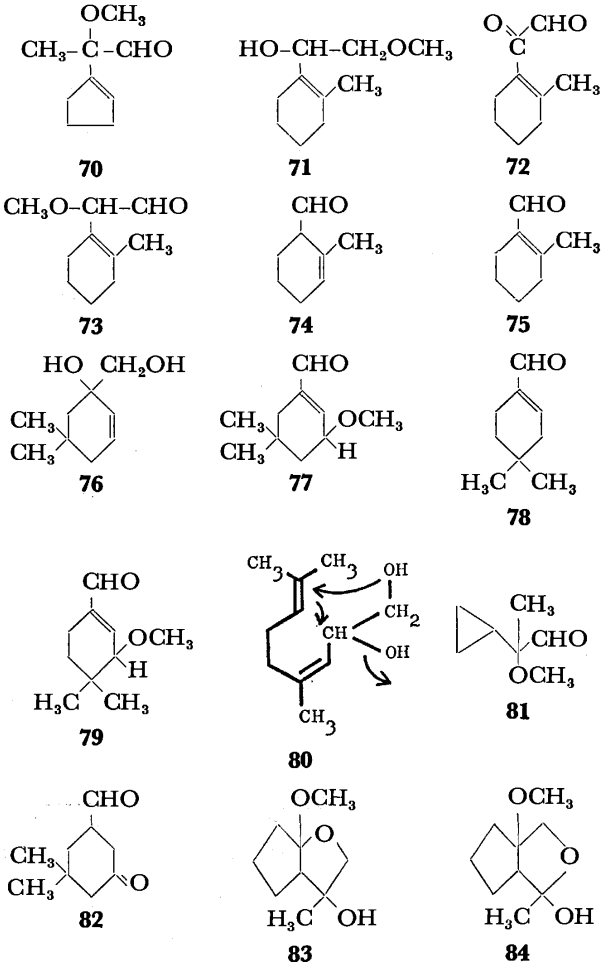

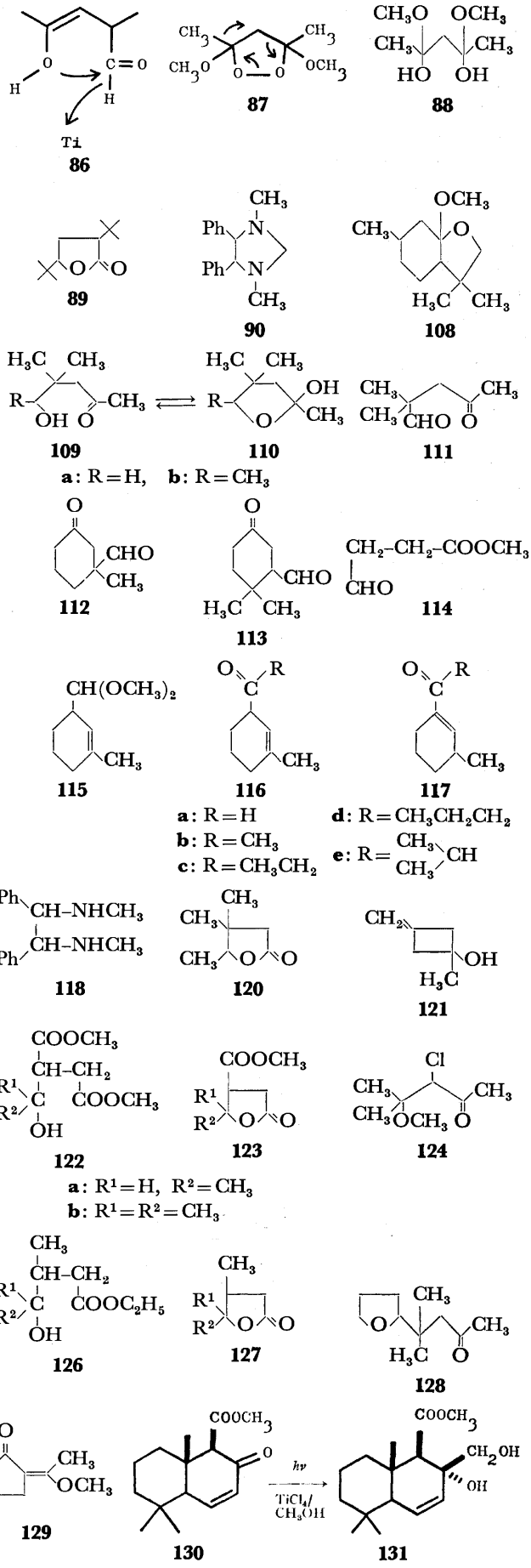

Experimental

General Procedures. The instrumentation was the same as has been described previously.[20] All the irradiations were carried out under the conditions summarized in Table 8, with a high-pressure mercury vapor lamp (Ushio UM 452 (450W)) at the temperature of running water. After the irradiation, the solution was poured into water and shaken with chloroform or dichloromethane. The extract was dried (Na_2SO_4), and the solvent was removed *in vacuo*. The residual substance was treated as indicated in each entry.

Unless otherwise stated, all the spectroscopic data were determined on a sample collected on a preparative GLC, a carbon tetrachloride solution being used for the NMR and IR spectra determinations.

As for the blank experiments in the presence of hydrochloric acid, a solution in methanol and concd hydrochloric acid (10: 1 by volume) was used.

The yields shown in Tables 1 and 2 were determined on a crude reaction mixture by means of NMR and/or GLC analyses, using appropriate internal references. The isolated yields, when determined, are described in each entry.

Materials. *a) Uranyl Chloride*: Prepared (1) according to the previously reported method[21] or (2) by dissolving thoroughly washed $UO_2(OH)_2$, which had been precipitated from $UO_2(NO_3)_2$ by sodium hydroxide, in hydrochloric acid, evaporating the water, and drying the residue on solid sodium hydroxide under reduced pressure. *b)* **4**: Prepared from cyclopentene and acetyl chloride, using tin(IV) chloride as a condensing reagent, according to the reported procedure[22] with the following modifications. Dichloromethane was used as the solvent at the temperature of Dry Ice, and triethylamine in benzene was used in place of *N,N*-dimethylaniline. Bp 67—69 °C (19 mmHg). *c)* **8**: Prepared from 2-methylcyclohexanone according to the reported procedure,[23] using NBS and pyridine as the brominating and dehydrobrominating reagents respectively. Bp 72—73 °C (22 mmHg). *d)* **10**: Prepared from dimedone (**35**) according to the procedure reported for the preparation of cyclohexenone.[24] Bp 76°C (19 mmHg). *e)* **13**: Ref. 25. Bp 34—38°C (3 mmHg). *f)* **17**: Ref. 26. Bp 44 °C (4 mmHg). *g)* **22**: Commercial sample (*cis* 63% and *trans* 35%). *h)* **29**: Ref. 27. Bp 71—75 °C (20—22 mmHg). *i)* **32**: Ref. 28. Bp 106—110 °C. *j)* **38**: Prepared from 4-(1-cyclopentenyl)morpholine and acetic anhydride according to the procedure reported for the preparation of a six-membered ring homologue.[29] Bp 104—106 °C (12 mmHg). *k)* **44**: Ref. 30. Bp 86 °C (22 mmHg). *l)* **46**: Ref. 31. Bp 85—87 °C (45—50 mmHg). *m)* **48**: Ref. 32. Bp 67 °C (15 mmHg). *n)* **51**: Ref. 33. Bp 97—98 °C (3 mmHg). *o)* **54**: Prepared by stirring an aqueous solution (17.5 ml) of hexanal (5 g) and cyclohexylamine (7.5 g) at room temperature for 2 h. Bp 126—142 °C (30 mmHg). (Lit,[34] bp 115 °C (16 mmHg)). IR, 2960, 2925, 2855, 1665, 1550, 1470, 1450, and 1380 cm^{-1}. NMR, δ 0.6—3.1 (m, 22H) and 7.58 (t, J=8 Hz, 1H). *p)* **57**: Prepared according to the previously reported procedure[35] with the following modifications: methylamine (prepared from 30 g of the hydrochloride) was bubbled into a mixture of acetophenone (10 g) and Molecular Sieve 4A (4 g) in methanol (20 ml) at 60—70 °C. The solution was then decanted from the catalyst and fractionated. *q)* **96**: Ref. 36. Bp 65—66 °C (5 mmHg).

The other materials were commercially available and were subjected to the reaction without further purification.

Run 1. The chromatography of the crude oil on a silica gel column and subsequent purification on a preparative GLC afforded **5**, **6**, and **7** as products, although **6** was not

obtained in a highly pure state.

5: MS, *m/e* 125 (M−OMe, base peak), 95, 93, and 67. IR, 3440, 2950, 1370, and 1070 cm^{-1}. NMR, δ 1.30 (s, 3H), 1.6—2.1 (m), 2.1—2.5 (m), 3.10 (s, 3H), 3.28 and 3.52 (ABq, J=10 Hz, 2H), and 5.64 (bs, 1H).

6 (in an impure state): IR, no characteristic bands. NMR, δ 0.95 (d, J=8 Hz, 3H), 1.5—2.5 (m), 3.21 (s, 3H), 3.24 (s, 3H), 4.10 (d, J=8 Hz, 1H), and 5.35 (bs, 1H).

7: (Lit,[37] bp 131—132 °C (140 mmHg)). IR, 2960, 1720, 1360, and 1100 cm^{-1}. NMR, δ 1.4—2.0 (m), 2.15 (s, 3H), 2.83 (bs, 1H), 3.29 (s, 3H), and 3.82 (bs, 1H).

Irradiation in the absence of titanium (IV) chloride afforded a complicated mixture of products irrespective of the presence or absence of hydrochloric acid.

Oxidation of ***5***. A mixture of CrO_3–pyridine–HCl[38] (0.1 g) and **5** (0.066 g), which had been isolated by preparative TLC (silica gel), in dichloromethane (2 ml) was stirred for 1 h at room temperature. The decanted solution was then passed through a short column of Florisil, and the eluant was evaporated. The crude oil was purified by preparative GLC to give a pure sample of an aldehyde **70**. IR, 2960, 1750, and 1120 cm^{-1}. NMR, δ 1.31 (s, 3H), 1.5—2.5 (m), 3.23 (s, 3H), 5.75 (bs, 1H), and 9.38 (s, 1H).

Run 2. A crude oil (0.37 g) was obtained which was chromatographed on an alumina column to give a fraction (0.22 g) of **9**. MS, *m/e* 170 (M), 140, 139 (base peak), 107, 91, and 79. IR, 3420, 2920, and 1100 cm^{-1}. NMR, δ 1.6—2.3 (m), 1.70 (s, 3H), 3.20 (s, 3H), 3.28 (d of d, J=11 and 4 Hz, 1H), 3.49 (d of d, J=11 and 8 Hz, 1H), and 4.10 (d of d, J=8 and 4 Hz, 1H).

Irradiation in either the presence or absence of hydrochloric acid resulted in the recovery of the starting material.

Phenylurethane Derivative of ***9***. A mixture of **9** (0.19 g) and phenyl isocyanate (0.13 g) was heated at 60 °C for 5 min. Chromatography on a silica gel column (benzene–chloroform) gave crystals which were subsequently recrystallized from methanol–water. Mp 85 °C. IR, 2920, 1747, 1601, 1520, 1442, and 1205 cm^{-1}. NMR, δ 1.5—2.0 (m), 1.64 (s, 3H), 3.06 (s, 3H), 3.90 (d, J=8 Hz, 1H), 3.92 (d, J=4 Hz, 1H), and 4.18 (d of d, J=8 and 4 Hz, 1H).

Found: C, 70.53; H, 8.00; N, 4.69%. Calcd for $C_{17}H_{23}NO_3$: C, 70.56; H, 8.01; N, 4.84%.

Treatment of ***9*** *with Hydrochloric Acid.* A mixture of **9** (0.1 g), 3M-hydrochloric acid (15 ml), and ethanol (15 ml) was refluxed for 1.5 h. Subsequent extraction with chloroform gave *o*-ethyltoluene.

Oxidation of ***9***. The oxidation was carried out in the way described above. A small amount of **73** was obtained, along with the main product **72**. The structure of **72** is not conclusive because the fragmentation pattern of the mass spectrum was not consistent with the structure, although the NMR spectrum was satisfactory. The aldehyde **73** could not be completely freed from **72** by preparative GLC, so the spectrum was obtained by subtracting that of **72** from the spectrum of the mixture.

72: NMR, δ 1.5—1.8 (m, 4H), 2.0—2.3 (bs, 7H), and 9.98 (s, 1H).

73: NMR, δ 1.5—1.8 (m), 1.71 (s, 3H), 1.9—2.3 (m), 3.27 (s, 3H), 4.25 (bs, 1H), and 9.63 (bs, 1H).

Run 3. The oil remaining after the work-up was mainly **11**, accompanied by a small amount of **12**.

11: MS, *m/e* 139 (M−OMe, base peak), 107, 93, 91, 79, and 77. IR, 3400, 2950, and 1100 cm^{-1}. NMR, δ 0.90 (s, 3H), 1.02 (s, 3H), 1.5—1.9 (m, 4H), 3.30 (s, 3H), 3.6—3.9 (b, 1H), 3.90 (bs, 2H), and 5.70 (bs, 1H).

12; IR, 2950, 1708, and 1083 cm^{-1}. NMR, δ 0.88 (s, 3H), 1.10 (s, 3H), 1.15—2.3 (m, 6H), 3.30 (s, 3H), and 3.3—3.7 (m, 1H).

Direct irradiation in methanol resulted in the recovery of the starting material. Irradiation in the presence of hydrochloric acid or a dark reaction in the presence of titanium (IV) chloride gave the methanol adduct **12**.

Oxidation of ***11***. An oxidation and work-up in the way described above afforded an aldehyde **77**. MS, *m/e* 168 (M), 139 (base peak), 107, 91, and 79. IR, 2950, 2820, 2700, 1688, 1210, and 1102 cm^{-1}. NMR, δ 0.87 (s, 3H), 1.02 (s, 3H), 1.2—2.3 (m), 3.37 (s, 3H), 3.8—4.1 (b, 1H), and 9.48 (s, 1H).

Run 4. A crude oil was distilled at 4 mmHg into four fractions. Each fraction was found by GLC analyses to contain one or two of the products **14**—**16**. The isolated yields of the products were 12% for **14**, 3% for **15**, and 2% for **16**.

14: MS, *m/e* 170 (M), 139, and 114 (base peak). IR, 3420, 2920, 1209, and 1090 cm^{-1}. NMR, δ 0.85 (s, 3H), 0.95 (s, 3H), 1.0—2.0 (m), 3.22 (bs, 1H), 3.37 (s, 3H), 3.96 (bs, 2H), and 5.67 (bs, 1H).

15: MS, *m/e* 153 (M−OMe), 137, 121, 105, 93, 91, and 75 (base peak). IR, 2950, 1120, and 1055 cm^{-1}. NMR, δ 1.02 (s, 6H), 1.1—2.5 (m), 3.30 (s, 3H), 3.33 (s, 3H), 3.99 (d, J=9 Hz, 1H), and 5.47 (s, 2H).

Found: C, 71.46; H, 10.71%. Calcd for $C_{11}H_{20}O_2$: C, 71.69; H, 10.94%.

16: MS, *m/e* 156 (M), 141, 125, 100, 87, 75, and 70 (base peak). IR, 2920, 1720, and 1100 cm^{-1}. NMR, δ 1.02 (s, 3H), 1.10 (s, 3H), 1.2—1.6 (m, 1H), 1.6—1.9 (m, 1H), 2.1—2.6 (m, 4H), 3.03 (d of d, J=8 and 5 Hz, 1H), and 3.28 (s, 3H).

A dark reaction in the presence of titanium(IV) chloride gave **16** in 63% yield. Irradiation in either the presence or absence of hydrochloric acid gave a complicated mixture of products.

Oxidation of ***14***. The oxidation of **14** in the way described above afforded an aldehyde **79**. MS, *m/e* 168 (M), 112, and 83. IR, 2940, 2820, 2720, 1680, 1640, 1190, and 1095 cm^{-1}. NMR, δ 0.82 (s, 3H), 1.02 (s, 3H), 1.4—1.7 (m, 2H), 2.1—2.3 (m, 2H), 3.50 (s, 4H), 6.67 (bs, 1H), and 9.56 (s, 1H). The signal at δ 3.50 split into a three-proton singlet and a one-proton signal upon the addition of $Eu(FOD)_3$.

Hydrolysis of ***15***. The acetal **15** was treated with 3M-hydrochloric acid in methanol in the way described above to give an aldehyde **78**. MS, *m/e* 138 (M), 123, 109, and 95 (base peak). IR, 2960, 1680, and 1640 cm^{-1}. NMR, δ 1.00 (s, 6H), 1.4—1.6 (m, 2H), 2.0—2.5 (m, 4H), 6.73 (bs, 1H), and 9.57 (s, 1H).

Run 5. The work-up and preparative GLC afforded a pure sample of **18**. MS,[39] *m/e* 134 (M), 133 (base peak), 105, 91, 79, and 77. IR, 2930, 2840, 2720, 1690, 1610, and 1110 cm^{-1}. NMR, δ 2.36 (s, 6H), 7.21 and 7.53 (ABq, J=9 Hz, 2H), 7.57 (s, 1H), and 9.85 (s, 1H). These NMR data are not consistent with those of 2,4-[40] or 2,5-[41] dimethylbenzaldehyde.

No reaction occurred in the dark in the presence of titanium-(IV) chloride. Irradiation in methanol in either the presence or absence of hydrochloric acid gave a complicated mixture of products.

Run 6. The work-up afforded an oil which was an almost pure sample of **20**, accompanied by a small amount of **21**, as revealed by GLC and NMR analyses. The same products were obtained when titanium(IV) chloride was used as the catalyst, but, in this case, the amount of the by-product **21** was much greater.

20: MS, *m/e* 85 (M−OMe, base peak), 71, 56, and 41. IR, 3060, 1450, 1370, 1100, and 1030 cm^{-1}. NMR, [δ 0.98 (d,

J=8 Hz, for *trans*) and 1.02 (d, J=8 Hz, for *cis*)] 3H, 1.3—1.5 (m, 1H), 1.7—2.5 (m, 2H), [3.03 (s, for *trans*) and 3.06 (s, for *cis*)] 3H, 3.15 (t, J=8 Hz, 1H), [3.65 (t, J=8 Hz, for *cis*) and 3.75 (t, J=8 Hz, for *trans*)] 1H, and 4.60 (d, J=5 Hz, 1H). The signal assignments for the *cis*-and *trans*-isomers were performed by adding $Eu(DPM)_3$. From the intensities of the methyl signals, the ratio of the *cis*- to the *trans*-isomer was determined to be 42: 58.

Found: C, 61.59; H, 10.16%. Calcd for $C_6H_{12}O_2$: C, 62.04; H, 10.41%.

21: NMR, δ 1.05 (d, J=6 Hz, 3H), 1.45—1.55 (m, 2H), 3.10 (s, 9H), 3.1—3.2 (m), and 4.26 (d of d, J=4 and 3 Hz, 1H).

The irradiation of **19** in the presence of hydrochloric acid gave **21** as the exclusive product. The direct irradiation gave an oil which is considered from its NMR spectrum to be a mixture of *cis*- and *trans*-**19**, as well as their dimethyl acetals.

Run 7. The oil remaining after the work-up was distilled under reduced pressure to give a mixture of **23**—**25**. Each component was separated by preparative GLC.

23: MS, *m/e* 166 (M), 151, 136, 121, 108, and 93 (base peak). IR, 2950, 1460, 1380, 1170, and 1050 cm^{-1}. NMR, δ 1.0—2.0 (m), 1.14 (s, 6H), 1.68 (s, 3H), 3.33 (d of d, J=9 and 8 Hz, 1H), 3.90 (t, J=8 Hz, 1H), and 5.37 (bs, 1H).

24: The NMR data coincided with the reported data.[42]

25:[43] IR, 2960, 1620, 1360, 1250, 1160, and 1060 cm^{-1}. NMR, δ 1.49 (s, 6H), 2.40 (s, 3H), 3.07 (s, 3H), 7.04 and 7.18 (ABq, J=9 Hz, 4H).

The dark reaction in the presence of titanium(IV) chloride gave **24** and **25** in 31% and 10% yields respectively. Irradiation in either the presence or absence of hydrochloric acid gave a complicated mixture of products.

Run 8. The work-up afforded an oil which was identified by NMR analysis as a mixture of **27** and **28** (66: 34). Details concering the data will be described in Run 29. A dark reaction in the presence of titanium(IV) chloride resulted in the recovery of the starting material.

Run 9. The oil remaining after the work-up was an almost pure sample of **30**, accompanied by a small amount of **31**, as revealed by GLC analysis.

30: IR, 3080, 3000, 2920, 2840, 1470, 1360, and 1080 cm^{-1}. NMR, δ 0.0—0.9 (m, 11H), 3.35 (s, 6H), and 4.15 (d, J=5 Hz, 1H).

Found: C, 69.97; H, 10.32%. Calcd for $C_{10}H_{18}O_2$: C, 70.54; H, 10.66%.

The aldehyde **31** was identical with an authentic sample prepared according to the reported method.[44]

Irradiation in either the presence or absence of hydrochloric acid gave a complicated mixture of products.

Preparation of 30. A mixture of **31** (0.27 g), methyl orthoformate (0.5 g), and ammonium nitrate (0.025 g) in methanol (0.5 ml) was kept at room temperature for 8 h. A saturated solution of sodium carbonate was then added, and the solution was shaken with dichloromethane. The subsequent evaporation of the solvent from the extract left an oil which was identical with **30**.

Run 10. The oil remaining after the work-up was almost pure **33**, accompanied by a small amount of **34**, as revealed by NMR and GLC analyses.

33: MS, *m/e* 99 (M−OMe, base peak), 69, 67, and 41. IR, 3670, 3590, 3070, 1480, 1400, 1080, and 1050 cm^{-1}. NMR, δ 0.0—1.0 (m, 5H), 0.85 (s, 3H), 2.45 (bs, 1H, disappears by D_2O), 3.15 (s, 3H), and 3.20 and 3.30 (ABq, J= 11 Hz, 2H).

Found: C, 64.23: H, 11.33%. Calcd for $C_7H_{14}O_2$: C, 64.58; H, 10.84%.

34: MS, *m/e* 113 (M−OMe), 81, 75 (base peak), and 47 IR, 2960, 2920, 2820, 1450, 1380, and 1070 cm^{-1}. NMR, δ 0.0—0.7 (m, 5H), 0.7—1.1 (m, 4H), 3.12 (s, 6H), and 3.85 (d, J=7 Hz, 1H). The multiplet at δ 0.7—1.1 split into a three-proton doublet (J=8 Hz) and a one-proton distorted sextet (J=7—8 Hz) upon the addition of $Eu(DPM)_3$.

Found: C, 65.75; H, 11.30%. Calcd for $C_8H_{16}O_2$: C, 66.63; H, 11.18%.

When the photolysate was refluxed for 30 min and then worked-up in the same way as above, **34** was obtained as the sole product. The irradiation of **32** in methanol in either presence or absence of hydrochloric acid gave a complicated mixture of products.

Oxidation of 33. The oxidation of **33** in the way described above gave an aldehyde **81**. IR, 3030, 2970, 2830, 1740, and 1090 cm^{-1}. NMR, δ 0.2—1.0 (m, 5H), 1.10 (s, 3H), 3.23 (s, 3H), and 9.45 (s, 1H).

Phenylurethane Derivative of 33. The phenylurethane derivative of **33** was prepared in the way described in Run 2. Although the product seems to be pure, judging from its NMR spectrum, we could not effect the crystallization. NMR (in an impure state), δ 0.05—0.6 (m, 4H), 0.7—1.0 (m, 1H), 0.86 (s, 3H), 3.00 (s, 3H), 3.85 (s, 2H), 6.5—7.1 (m, 5H), and 7.18 (bs, 1H).

Run 11. The oil remaining after the work-up was a mixture of **36** and **37**, judging from the GLC and NMR analyses.

36: MS, *m/e* 169 (M−OMe), 153, 125, 97, and 74 (base peak). IR, 2950, 1700, 1120, and 1050 cm^{-1}. NMR, δ 0.95 (s, 3H), 1.15 (s, 3H), 1.3—2.5 (m, 7H), 3.35 (s, 6H), and 4.10 (d, J=6 Hz, 1H).

The enol ether **37** was identical with a sample prepared according to the reported method.[45]

When **36** was treated with 2,4-dinitrophenylhydrazine, the bis(2,4-dinitrophenylhydrazone) of the keto aldehyde **82** was obtained; it was subsequently recrystallized from dioxane-methanol. Mp 210—212 °C.

Found: C, 48.64; H, 4.13; N, 21.35%. Calcd for $C_{21}H_{22}N_8O_8$: C, 49.03; H, 4.31; N, 21.78%.

Hydrolysis of 36. A crude sample of **36** was refluxed in a mixture of methanol (10 ml) and conc. hydrochloric acid (4 ml) for 4 h. The solution was then diluted with water and extracted with chloroform. The subsequent evaporation of the solvent from the extract left an oil which was purified by preparative GLC to give **82**. MS, *m/e* 139 (M−Me), 126, 83, 69, 57, 55 (base peak), and 41. IR, 2930, 1710, and 1250 cm^{-1}. NMR, δ 0.92 (s, 3H), 1.12 (s, 3H), 1.3—2.8 (m, 7H), and 9.50 (d, J=0.5 Hz, 1H).

Irradiation of **37** *in the Presence of Titanium(IV) Chloride.* Irradiation was carried out under the same conditions as those used with **35**. An acetal **36** was obtained as the sole product.

Run 12. The oil remaining after the work-up was distilled under reduced pressure to give a pure sample of **39**. Bp 58—62 °C (15 mmHg), 0.1 g. MS, *m/e* 172 (M), 157, 155, 143, and 141 (base peak). IR, 3510, 2930, 1770 (weak), 1450, 1400, 1370, 1320, 1200, and 1020 cm^{-1}. NMR, δ 1.15 (s, 3H), 1.1—2.2 (m, 7H), 3.30 (s, 3H), and 3.73 and 3.82 (ABq, J=7 Hz, 2H).

Found: C, 62.67; H, 9.09%. Calcd for $C_9H_{16}O_3$: C, 62.76; H, 9.36%.

When **38** was irradiated in methanol without any additives, or when it was kept in methanol-hydrochloric acid in the dark, it gave an enol ether **129**. IR, 2950, 1740, 1720, 1435, 1360, and 1165 cm^{-1}. NMR, δ 1.45—1.65 (m), 2.05 (s, 3H), 2.1—2.5 (m), and 3.56 (s, 3H).

Run 13. The oil remaining after the work-up was distilled under reduced pressure. An oil, bp 39—45 °C (15

mmHg), was thus obtained which was found by GLC analysis to be a mixture of several compounds; three major fractions (**41**—**43**) were collected in pure states by preparative GLC (temperature, 70 °C).

41: MS, *m/e* 112 (M), 111, 97, and 69 (base peak). The IR and NMR spectra were identical with those previously reported.[4]

42: Identical with the authentic sample prepared according to the reported method.[5]

43: IR, 2940, 1450, 1370, 1320, 1180, and 1050 cm^{-1}. NMR, δ 1.45 (s, 6H), 2.60 (s, 2H), and 3.35 (s, 6H).

Found: C, 52.26; H, 9.00%. Calcd for $C_7H_{14}O_4$: C, 51.84; H, 8.70%.

Irradiation of **40** *in the Presence of Hydrochloric Acid.* A solution of **40** (0.1 g) and concd hydrochloric acid (0.4 ml) in methanol (10 ml) was irradiated in a Pyrex tube for 24 h. The subsequent evaporation of the extract left **43** in an almost pure state (GLC and NMR analyses). The temperature of the GLC should not exceed 70 °C.

Thermolysis of **43**. When a neat sample of **43** was kept at 150 °C for 2 h, an equimolar mixture of methyl acetate and methyl propionate was obtained, as established by GLC and NMR techniques.

Run 14. The crystals obtained after the work-up (0.26 g) were almost pure **45**. Recrystallization from carbon tetrachloride gave white needles; mp 91—92 °C (lit,[4] mp 92—94 °C). The IR and NMR data coincided with the reported values.[4] Hydrogenation over Pd/C gave **89**, which also indicated IR and NMR spectra identical with those previously reported.[4] Mp 73—75 °C (lit, mp 86—88 °C,[4] or 82—83 °C.[46])

Run 15. The oil remaining after the work-up was a mixture of **47** and one more product of an unknown structure. **47**: IR, 2980, 2925, 1760, 1440, 1090, and 1000 cm^{-1}. NMR, δ 1.36 (d, J=7 Hz, 3H), 1.75 (s, 3H), 1.95 (s, 3H), and 4.68 (q, J=7 Hz, 1H).

Run 16. The photolysate was diluted with water and made alkaline with a sodium hydroxide solution. The precipitates of titanium hydroxide were filtered off with the aid of Hyflo Super Cel, and the filtrate was shaken with dichloromethane. The subsequent evaporation of the solvent from the extract left an oil which was found by NMR analysis to be a mixture of **49** and **50** (4: 1). Distillation under reduced pressure gave **49** in an almost pure state. Bp 125—133 °C (6 mmHg), 0.75 g, 59%. (Lit,[47] bp 115—120 °C (4 mmHg)). NMR, δ 2.25 (s, 3H), 3.72 (bs, 2H), 4.72 (bs, 2H), and 7.2—7.7 (m, 5H).

When the crude material of **49** was treated with *p*-nitrobenzoyl chloride in benzene, crystals of bis (*p*-nitrobenzoyl) derivative were obtained. Recrystallization from chloroform-ethanol afforded a pure sample. Mp 167—168 °C.

Found: C, 60.94; H, 4.19; N, 8.99%. Calcd for $C_{23}H_{19}N_3O_7$: C, 61.47; H, 4.26; N, 9.35%.

The picrate of **49** was also obtained. Recrystallization from ethanol afforded a pure sample. Mp 188—191 °C.

Found: C, 46.74; H, 4.04; N, 14.46%. Calcd for $C_{15}H_{16}N_4O_8$: C, 47.37; H, 4.24; N, 14.73%.

Preparation of **50**. An appropriate amount of 37% formalin was added to the photolysate of **48**, and the solution was kept at room temperature for 7 days. The work-up described above afforded an oil which was almost pure **50**. IR, 2880, 2800, 1495, 1455, and 1070 cm^{-1}. NMR, δ 2.30 (s, 3H), 3.53 and 3.67 (d (J=8 Hz) of ABq, J=8 Hz, 2H), 4.08 (d, J=2 Hz, 1H), 4.25 (t, J=8 Hz, 1H), 4.78 (d, J=2 Hz, 1H), and 7.2—7.7 (m, 5H). The signals at δ 3.53 and 3.67 separated into two one-proton triplets (J=8 Hz) upon the addition of $Eu(DPM)_3$.

Run 17. The work-up described in Run 16 afforded crystals of **52**; 0.52 g, mp 87—95 °C. Recrystallization from carbon tetrachloride–hexane afforded a pure sample. Mp 107—109 °C. IR, 3400, 3120, 1445, 1055, and 1030 cm^{-1}. NMR, δ 0.9—1.4 (m, 5H), 1.4—1.8 (m, 4H), 1.8—2.1 (b, 1H), 2.2—2.5 (b, 1H), 2.40 (bs, 2H, disappears by D_2O), 3.48 [d (J=11 Hz) of AB (J=10 Hz), 1H], 3.70 [d (J=4 Hz) of AB (J=10 Hz), 1H], 3.96 (d of d, J=11 and 4 Hz, 1H), and 7.2—7.6 (m, 5H).

Found: C, 75.97; H, 9.57; N, 6.18%. Calcd for $C_{14}H_{21}NO$: C, 76.66; H, 9.65; N, 6.39%.

Preparation of **53**. A mixture of **52** (0.031 g) and 37% formalin (0.018 g) in methanol (0.5 ml) was stirred at 70 °C for 6 h. The work-up afforded a crude sample of **53**. NMR, δ 1.0—2.0 (m, 10H), 2.1—2.7 (bs, 1H), 3.5—3.7 (m, 1H), 4.0—4.3 (m, 2H), 4.5—4.75 (m, 2H), and 7.2—7.6 (m, 5H).

Run 18. The work-up described in Run 16 afforded a crude oil (0.34 g), which partly crystallized upon standing. The crystals were collected and recrystallized from carbon tetrachloride to give white needles of **55**. Mp 71—73 °C. IR (KBr), 3420, 3260, 2960, 2925, 2850, 1450, 1360, 1140, and 1120 cm^{-1}. NMR ($CDCl_3$), δ 0.77—2.1 (m, 2H), 2.07 (bs, 2H, disappears by D_2O), 2.35—2.88 (m, 2H), 3.20 [d (J=7 Hz) of AB (J=11 Hz), 1H], and 3.58 [d (J=4 Hz) of AB (J=11 Hz), 1H].

From the mother liquor separated from the crystals of **55**, a pure sample of **56** was obtained by preparative GLC. MS, *m/e* 225 (M), 194, 182, 154 (base peak), 72, and 55. IR, 2960, 2925, 2855, 1470, 1450, 1375, 1170, and 1028 cm^{-1}. NMR, δ 0.76—2.11 (m, 21H), 2.17—2.57 (m, 1H), 2.89—3.28 (m, 2H), 3.78 (t, J=7 Hz, 1H), and 4.15 and 4.42 (ABq, J=6 Hz, 2H).

Irradiation without any additive or a dark reaction in the presence of titanium(IV) chloride resulted in the recovery of the starting material. Irradiation in the presence of hydrochloric acid afforded a complicated mixture of products.

Run 19. The work-up described in Run 16 afforded a mixture of **58** and **59** (3: 2), as revealed by the NMR spectrum. When the mixture and 37% formalin (0.19 g) in methanol (0.5 ml) were kept at 70 °C for 2 h, and then at room temperature overnight, **59** was obtained; it was identical with the sample obtained in Run 21. The NMR spectrum of **58** was obtained by subtracting that of **59** from the mixture spectrum. δ 1.43 (s, 3H), 2.14 (s, 3H), 3.0—3.6 (b), 3.39 (s), and 7.2—7.6 (m).

Run 20. The work-up afforded white crystals (0.2 g). Recrystallization from methanol afforded white needles of **61**. Mp 122—127 °C. (Lit,[48] mp 125 °C). MS, *m/e* 144 (M—MeOH, base peak), 113, and 73. IR (KBr), 1370, 1285, 1196, 1175, 1065, and 1035 cm^{-1}. NMR, δ 1.15 (s, 6H), 3.20 (s, 6H), and 3.27 and 3.50 (ABq, J=11 Hz, 4H).

Found: C, 55.18; H, 9.59%. Calcd for $C_8H_{16}O_4$: C, 54.53; H, 9.15%.

It was speculated that the crude crystals contain a stereoisomer of **61** (one-third of **61**), since these crystals indicated NMR signals at δ 1.30 (s, 6H), 3.22 (s, 6H), and 3.27 and 3.50 (ABq, J=11 Hz, 4H, overlap with those of **61**), as well as those of **61**.

Compound **61** was identical with the crystals separated out from a 50% methanol solution of hydroxyacetone.

Run 21. The photolysate was made alkaline with a sodium hydroxide solution, and the solid was filtered off (Hyflo Super Cel). The filtrate was made acidic with hydrochloric acid and shaken with chloroform (Extract A). The aqueous solution was made alkaline with sodium hydroxide solution again, and shaken with chloroform (Extract B). Extract A, upon the evaporation of the solvent, gave a trace

amount of an oil from which two products, **63** and **64**, were obtained in pure states by preparative GLC. Compound **63** was identical with the authentic sample. **64**: IR (neat), 3450, 1610, 1505, 1455, 1030, 760, and 695 cm^{-1}. NMR, δ 1.35 (s, 3H), 2.4—2.9 (b, 2H), 3.26 and 3.45 (ABq, J= 11 Hz, 2H), and 6.8—7.1 (m, 5H).

Compound **64** was identical with the sample obtained in a small amount by the irradiation of acetophenone (0.12 ml) in methanol (12 ml) in the presence of titanium(IV) chloride (0.12 ml).

Extract B, upon the evaporation of the solvent, gave an oil which was subsequently distilled under reduced pressure to give 0.13 g of **59**. MS, *m/e* 177 (M), 162 (base peak), 146, 132, and 91. IR (neat), 2980, 2850, 2780, 1440, 1050, 758, and 690 cm^{-1}. NMR δ 1.35 (s, 3H), 2.05 (s, 3H), 3.52 and 3.65 (ABq, J=8 Hz, 2H), 4.07 and 4.27 (dist. ABq, J=2 Hz, 2H), and 6.7—7.2 (m, 5H).

Found: C, 73.82; H, 8.30; N, 7.75%. Calcd for $C_{11}H_{15}NO$: C, 74.54; H, 8.53; N, 7.90%.

Run 22. The photolysate was worked-up in the way described in Run 21. A trace amount of **67** was obtained from the extract from the acidic solution. The amount of the product corresponding to **64** was negligible. **67**: IR (neat), 3320, 2960, 1510, 1440, 1360, 1065, 1005, 890, and 810 cm^{-1}. NMR, δ 1.39 (d, J=7 Hz, 3H), 2.25 (s, 3H), 4.55 (q, J=7 Hz, 1H), and 6.78 and 6.90 (ABq, J=8 Hz, 4H).

The extract from the alkaline solution gave an oil which was subsequently distilled under reduced pressure to give 0.062 g of **66**. IR (neat), 3380, 2950, 2880, 1520, 1460, 1380, 1083, 1018, and 812 cm^{-1}. NMR, δ 1.35 (s, 3H), 2.21 (s, 3H), 3.43 and 3.52 (ABq, J=7 Hz, 2H), 4.03 and 4.23 (ABq, J=6 Hz, 2H), and 6.70 and 6.88 (ABq, J=8 Hz, 4H).

Found: C, 74.54; H, 8.82; N, 7.85%. Calcd for $C_{11}H_{15}NO$: C, 74.54; H, 8.53; N, 7.90%.

Run 23. The work-up was the same as that described in Run 21. The amounts of products corresponding to **63** and **64** were negligible. The extract from the alkaline solution gave an oil which was subsequently distilled under reduced pressure to give 0.088 g of **69**. MS, *m/e* 176 (M−1), 162, 147, 146 (base peak), 133, 132, 105, and 91. IR (neat), 2980, 2890, 1450, 1080, 1015, 900, and 758 cm^{-1}. NMR, δ 1.40 (s, 3H), 2.27 (s, 3H), 3.44 and 3.74 (ABq, J=7 Hz, 2H), 4.06 and 4.30 (ABq, J=6 Hz, 2H), 6.65—6.85 (m, 3H), and 7.17—7.35 (m, 1H).

Found: C, 74.62; H, 8.76; N, 7.71%. Calcd for $C_{11}H_{15}NO$: C, 74.54; H, 8.53; N, 7.90%.

Run 24. The oil remaining after the work-up indicated a complicated NMR spectrum suggestive of the structure **108** of a stereoisomeric mixture. Distillation induced the elimination of methanol from these isomers and gave **92** in an almost pure state; bp 72—78 °C (23 mmHg). IR, 2930, 1710 (weak), 1463, 1172, 1120, and 980 cm^{-1}. NMR, δ 0.97 (d, J=8 Hz, 3H), 1.00 (s, 6H), 1.5—2.1 (m, 7H), and 3.64 (s, 2H).

Found: C, 78.67; H, 11.23%. Calcd for $C_{11}H_{18}O$: C, 79.46; H, 10.92%.

Run 25. The oil remaining after the work-up was distilled to give **20** (bp 56—65 °C (25 mmHg)), which contained a small amount of chloroform. The IR and NMR spectra were identical with those obtained in Run 6.

Run 26. The oil remaining after the work-up was distilled to give **94** (bp 35—56 °C (3 mmHg)), which contained a small amount of chloroform. MS, *m/e* 113 (M−OMe, base peak), 112, and 97. IR, 2965, 2885, 1470, 1378, 1190, 1050, and 1028 cm^{-1}. NMR, δ 1.00 (s, 3H), 1.05 (s, 3H), 1.25 (s, 3H), 1.50 and 1.70 (ABq, J=13 Hz, 2H), 2.96 (s, 3H), and 3.23 and 3.30 (ABq, J=8 Hz, 2H).

From the crude oil prior to the distillation, a small amount of **95**[10] was isolated by preparative GLC. MS, *m/e* 142 (M), 100, 99, 85 (base peak), 82, and 43. IR, 2960, 1715, 1700, 1360, 1170, and 1130 cm^{-1}. NMR, δ 1.15 (s, 6H), 2.00 (s, 3H), 2.10 (s, 3H), and 2.60 (s, 2H).

When **94** was kept in a mixture of tetrahydrofuran–3M-hydrochloric acid (2: 1) at room temperature for 10 min, an oil was obtained which was identified from its NMR spectrum as a mixture of **109a** and **110a**. The oxidation of the oil with CrO_3–pyridine–HCl in the way described above afforded keto aldehyde **111**. MS, *m/e* 100 (M−CO), 85, and 43 (base peak). IR, 2960, 2800, 2650, 1725, and 1370 cm^{-1}. NMR, δ 1.10 (s, 6H), 2.10 (s, 3H), 2.65 (s, 2H), and 9.60 (s, 1H).

Run 27. The oil remaining after the work-up was a mixture of **97** and **99**, as revealed by NMR analysis. Distillation under reduced pressure induced the elimination of methanol from **99** and gave a mixture of the starting material and **97** (bp 68—94 °C (18 mmHg), 0.66 g). On some occasions, the product contained **98** (0—10% of **97**).

97: MS, *m/e* 156 (M), 141, 125, 113 (base peak), and 111. IR, 2990, 2900, 1457, 1195, 1105, 1030, and 1012 cm^{-1}. NMR δ 0.98 (s, 3H), 1.05—2.25 (m, 8H), 3.05 (s, 3H), and 3.30 and 3.40 (ABq, J=6 Hz, 2H).

98: MS, *m/e* 142 (M), 125, 112, 111 (base peak), and 99. IR, 3400, 1710, 1230, and 1050 cm^{-1}. NMR, δ 0.90 (s, 3H), 1.7—2.4 (m, 8H), and 3.25 (s, 2H).

99: IR, 2960, 2870, 1715, 1213, 1112, and 1065 cm^{-1}. NMR, δ 1.15 (s, 3H), 1.5—2.5 (m, 8H), and 3.00 (s, 3H).

Found: C, 66.79; H, 9.95%. Calcd for $C_8H_{14}O_2$: C, 67.57; H, 9.93%.

No reaction occurred in the dark in the presence of uranyl chloride. Irradiation in methanol in the presence of an ordinary amount of hydrochloric acid resulted in the recovery of the starting ketone, while in the presence of a small amount of hydrochloric acid (pH 2—3), a methanol adduct **99** was obtained exclusively.

Oxidation of 98. The oxidation of **98** in the way described above afforded an aldehyde **112**. MS, *m/e* 112 (M−CO), 111, 97, 83, 69, and 55 (base peak). IR, 2960, 2800, 2650, 1720, and 1220 cm^{-1}. NMR, δ 1.11 (s, 3H), 1.2—2.6 (m), and 9.34 (s, 1H).

Run 28. The work-up left an oil which was distilled under reduced pressure to give two fractions: Fraction 1 (bp 36—41 °C (1 mmHg), 0.17 g) contained 32% of **100**, while Fraction 2 (bp 62—68 °C (1 mmHg), 0.22 g) contained 51% of **101**, as revealed by GLC analyses.

100: MS, *m/e* 170 (M), 139, 125, 110, 100, and 99 (base peak). IR, 2960, 1310, 1190, and 1120 cm^{-1}. NMR, δ 0.97 (s, 3H), 1.02 (s, 3H), 1.1—2.0 (m), 3.24 (s, 3H), and 3.89 (m, 2H). The multiplet at δ 3.89 was transformed into a typical ABX type upon the addition of $Eu(DPM)_3$.

Found: C, 70.03; H, 10.50%. Calcd for $C_{10}H_{18}O_2$: C, 70.54; H, 10.66%.

101: MS, *m/e* 156 (M), 126, 125, 85, 83, 69, and 55 (base peak). IR, 3440, 2940, and 1710 cm^{-1}. NMR, δ 1.08 (s, 3H), 1.16 (s, 3H), 0.9—2.6 (m), and 3.3—3.9 (m, 2H).

Oxidation of 101. The oxidation of **101** in the way described above afforded an aldehyde **113**. MS, *m/e* 154 (M), 126, 111, 97, 83, 69, and 55 (base peak). IR, 2960 and 1730 cm^{-1}. NMR, δ 1.14 (s, 3H), 1.31 (s, 3H), 1.6—1.9 (m, 2H), 2.1—2.7 (m, 5H), and 9.98 (s, 1H).

Run 29. An oil (bp 108—110 °C (3.5 mmHg), 0.84 g) was obtained which was found by NMR analysis to be a mixture of **27** and **28** (93: 7). Further purification was not achieved, so the spectroscopic data of **27** were obtained by subtracting those of **28** from the spectra of the mixture. **27**: IR: 3440, 2920, 1740, and 1450 cm^{-1}. NMR, δ 2.57 and

2.64 (d of d, J=7 and 5 Hz, 2H), 2.8—3.0 (m, 1H), 3.30 (bs, 1H), 3.67 (bs, 3H+2H), and 3.70 (s, 3H).

When the mixture was kept at 200 °C for 1 h, **28**[49] was obtained in a 60% yield. Bp 96—97 °C (1.5 mmHg). IR, 1795, 1745, 1450, 1165, and 1015 cm^{-1}. NMR, δ 2.70 (d, J=10 Hz, 1H), 2.71 (d, J=7.5 Hz, 1H), 3.45 (dist. quintet, J=8 Hz, 1H), 3.78 (s, 3H), 4.40[d (J=7 Hz) of AB (J=10 Hz), 1H], and 4.51[d (J=9 Hz) of AB (J=10 Hz), 1H].

Found: C, 49.24; H, 5.63%. Calcd for $C_6H_8O_4$: C, 50.00; H, 5.60%.

Run 30. An oil (bp 63—67 °C (3 mmHg), 1.04 g) was obtained which was found by NMR analysis to be a mixture of **103** and **104** (84:16). Further purification was not achieved, and so the spectroscopic data of **103** were obtained by subtracting those of **104** from the spectra of the mixture. **103**: IR, 3490 and 1740 cm^{-1}. NMR, δ 0.90 (d, J=7 Hz, 3H), 1.85—2.56 (m), 3.35 (bs, 1H, disappears by D_2O), 3.36 (dist. quintet, J=6 Hz, 2H), and 3.57 (s, 3H).

When **103** was kept at 200 °C for 3 h, **104** was obtained. Bp 56—57 °C (3 mmHg) (lit,[50] bp 80—81 °C (10 mmHg)). IR, 2990, 1790, 1165, and 1025 cm^{-1}. NMR, δ 1.11 (d, J=7 Hz, 3H), 1.8—2.2 (m, 1H), 2.4—2.8 (m, 2H), 3.74 (d of d, J=9 and 7 Hz, 1H), and 4.29 (d of d, J=10.5 and 9 Hz, 1H).

Run 31. The oil remaining after the work-up was distilled under reduced pressure. Much of a colorless, viscous material remained undistilled. The distillate (bp 62—65 °C (2 mmHg), 0.28 g) was found by NMR analysis to be a mixture of **106** ans **107** (94:6). Further purification was not achieved, and so the spectroscopic data of **106** were obtained by subtracting those of **107** from the spectra of the mixture. **106** (lit,[51] bp 45—46 °C (0.2 mmHg)): IR, 3420 and 1745 cm^{-1}. NMR, δ 1.80 (quintet, J=7 Hz, 2H), 2.38 (t, J=7 Hz, 2H), 3.23 (bs, 1H), 3.58 (t, J=7 Hz, 2H), and 3.63 (s, 3H).

Found (with a sample of 94% purity): C, 50.69; H, 8.72%. Calcd for $C_5H_{10}O_3$: C, 50.83; H, 8.53%.

When **106** was kept at 200 °C for 3 h, **107** was obtained in a pure state; it was identical with γ-butyrolactone.

Oxidation of ***106***. The oxidation of **106** in the way described above afforded an aldehydic ester **114**. (Lit,[52] bp 79—80 °C (12 mmHg)). MS, m/e 88 (M−CO), 85, 59, and 57. IR, 2960, 2820, 2710, 1740, 1440, and 1175 cm^{-1}. NMR, δ 2.5—2.9 (A_2B_2m, 4H), 3.70 (s, 3H), and 9.95 (s, 1H).

*Irradiation of 3-Methyl-2-cyclohexenone (**96**) in Alcohols in the Presence of Titanium(IV) Chloride.* Solutions of **96** (0.1 g) and titanium(IV) chloride (0.17 g) in the following alcohols (10 ml) were irradiated in Pyrex tubes for 6 h. Subsequent work-ups afforded oils which were analyzed by GLC and NMR to determine the yields.

In 1-Propanol: The product was **116c**. MS, m/e 152 (M), 95 (base peak), 79, 77, and 67. IR, 2900, 1710, 1440, and 1110 cm^{-1}. NMR, δ 1.03 (t, J=8 Hz, 3H), 1.3—2.0 (b, 6H), 1.70 (bs, 3H), 2.41 (q, J=8 Hz, 2H), 2.94 (b, 1H), and 5.47 (bs, 1H).

In 1-Butanol: The products were **116d** and **117d**.

116d: MS, m/e 166 (M), 95 (base peak), 79, 77, 71, and 67. IR, 2920, 1710, and 1130 cm^{-1}. NMR, δ 0.91 (t, J=8 Hz, 3H), 1.0—2.2 (m), 1.68 (bs, 3H), 2.34 (t, J=8 Hz, 2H), 2.92 (b, 1H), and 5.48 (bs, 1H).

117d: IR, 2950, 2930, 1670, and 1200 cm^{-1}. NMR, δ 0.92 (t, J=8 Hz, 3H), 1.13 (d, J=8 Hz, 3H), 1.2—2.0 (m), 2.52 (t, J=8 Hz, 2H), and 6.51 (bs, 1H).

In 2-Methyl-1-propanol: The product was **116e**. MS, m/e 166 (M), 95 (base peak), 79, 77, 71, and 67. IR, 2960, 2930, and 1710 cm^{-1}. NMR, δ 1.06 (d, J=8 Hz, 6H), 1.5—2.0 (m), 1.70 (bs, 3H), 2.72 (heptet, J=8 Hz, 1H), 3.10 (b, 1H), and 5.45 (bs, 1H).

In 2-Propanol: The product was *m*-cymene. IR,[53] 2950, 2910, and 708 cm^{-1}. NMR, δ 1.21 (d, J=7 Hz, 6H), 2.18 (s, 3H), 2.85 (m, J=7 Hz, 1H), and 6.7—7.2 (m, 4H).

*Irradiation of Mesityl Oxide (**93**) in Alcohols in the Presence of Uranyl Chloride.* Solutions of **93** (0.1 g) and uranyl chloride (0.04 g) in the following alcohols (10 ml) were irradiated in Pyrex tubes for 6 h. Subsequent work-ups afforded the following products.

In Ethanol: The irradiation product, which was assumed, on the basis of NMR analysis, to be a mixture of **109b** and **110b** was directly oxidized with CrO_3–pyridine–HCl in the way described above. The products were **95** (13% from **93**) and **120** (trace). The spectroscopic data of **120** were identical with those previously reported.[54]

In 2-Propanol: The products were **95** and **121**. The compound **121** was identical with the one reported previously.[55]

*Irradiation of Dimethyl Maleate (**26**) in Alcohols in the Presence of Uranyl Chloride.* Solutions of **26** (1.0 g) and uranyl chloride (0.24 g) in the following alcohols were irradiated in Pyrex tubes for 1 h, and then treated as follows.

In Ethanol: The oil remaining after the work-up was distilled under reduced pressure to give an oil (bp 106—108 °C (4 mmHg), 0.79 g). Although this oil (Oil A) was assumed to be a mixture of stereoisomeric esters **122a** and lactones **123a** *(vide infra)*, it gave *cis*- and *trans*-lactones **123a** (54:46) (bp 99—102 °C (5 mmHg)) when kept at 200 °C for 2 h. The stereochemistry of the lactones was assigned on the basis of the NMR spectrum by comparing it with those previously reported.[3b] By subtracting the spectra of the lactones from the NMR spectrum of Oil A, we assigned the structure of the γ-hydroxy esters **122a** to the rest of the components. Although the amount of *cis*-lactone exceeds that of the *trans*-isomer in Oil A, amounts became almost equal after the thermal cyclization. We concluded from this result that the major component of the hydroxy esters in Oil A is probably the *threo*-isomer. From the distinctive methyl signals in the NMR spectrum of Oil A, we estimated the yields of the components as follows: *threo*-**122a** (23%), *erythro*-**122a** (14%), *trans*-**123a** (6%), and *cis*-**123a** (13%).

We assigned the NMR signals for **122a** as follows: [δ 1.15 (d, J=7 Hz) for *threo* and 1.18 (d, J=7 Hz) for *erythro*] 3H, 2.6—3.3 (m, 3H), 3.58 (b, 1H, disappears by D_2O), 3.75 (s, 3H), 3.79 (s, 3H), and 4.0—4.3 (m, 1H).

In 2-Propanol: The oil remaining after the work-up was identified by means of NMR analysis as a mixture of **122b**, **123b**, and the starting material (**26**) (76:11:13). Further purification was not achieved, and so the spectroscopic data of **122b** were obtained by subtracting those of **123b** and **26** from the spectra of the mixture. **122b**: IR, 3525, 1740, and 1175 cm^{-1}. NMR, δ 1.16 (s, 3H), 1.20 (s, 3H), 2.6—2.8 (bs, 3H), 3.18 (bs, 1H, disappears by D_2O), 3.63 (s, 3H), and 3.67 (s, 3H).

The distillation under reduced pressure induced the cyclization of **122b** into **123b**; the distillate (bp 108—110 °C (4 mmHg), 0.71 g) was a mixture of **122b**, **123b**, and **26** (9:74:17), as shown by NMR analysis. The spectroscopic data of the purified **123b** were identical with those previously reported.[3b,49]

*Irradiation of Mesityl Oxide (**93**) in Tetrahydrofuran in the Presence of Uranyl Chloride.* A solution of **93** (0.1 g) and uranyl chloride (0.03 g) in tetrahydrofuran (10 ml) was irradiated in a Pyrex tube for 4 h. A subsequent work-up afforded an oil which was almost pure **128**. MS, m/e 113 (M−CH_2COMe), 98, 86, 72 (base peak), and 71. IR (neat), 2950, 2860, 1700, 1355, and 1060 cm^{-1}. NMR, δ 0.89 (s, 3H), 0.98 (s, 3H), 1.4—2.0 (m, 4H), 2.05 (s, 3H), 2.18 and 2.40

(ABq, J=14 Hz, 2H), and 3.4—3.8 (m, 3H).

The authors are grateful to K. Ueda, T. Hamano, H. Kaneko, A. Kohda, K. Nagumo, K. Machida, and M. Morishita, who performed some parts of the experiments.

References

1) Preliminary reports; a) T. Sato, O. Ito, and M. Miyahara, *Chem. Lett.*, **1976**, 295; b) T. Sato and S. Yoshiie, *ibid.*, 415.
2) T. Sato, G. Izumi, and T. Imamura, *J. Chem. Soc., Perkin Trans. 1*, **1976**, 788; *Tetrahedron Lett.*, **1975**, 2191.
3) a) M. Tokuda, Y. Yokoyama, T. Taguchi, A. Suzuki, and M. Itoh, *J. Org. Chem.*, **37**, 1859 (1972); b) S. Mejeti, *J. Org. Chem.*, **37**, 2914 (1972).
4) S. A. M. T. Hussain, W. D. Ollis, C. Smith, and J. F. Stoddart, *J. Chem. Soc., Perkin Trans. 1*, **1975**, 1480.
5) U. S. Patent 3577455; *Chem. Abstr.*, **75**, 197145 (1971).
6) P. Cerutti and H. Schmid, *Helv. Chim. Acta*, **45**, 1992 (1962).
7) P. Cerutti and H. Schmid, *Helv. Chim. Acta*, **47**, 203 (1964).
8) T. S. Cantrell, *J. Am. Chem. Soc.*, **94**, 5929 (1972).
9) N. C. Yang, B. Kim, W. Chiang, and T. Hamada, *J. Chem. Soc., Chem. Commun.*, **1976**, 729.
10) T. M. Patrick, Jr., *J. Org. Chem.*, **17**, 1269 (1952).
11) J. E. Whiting and J. T. Edward, *Can. J. Chem.*, **49**, 3799 (1971).
12) We believe that the chemical shift of the methylene proton in the *meso*-isomer, which has been reported[7] as τ 5.90, should be τ 6.90.
13) G. Balogh and F. C. DeSchryver, *Tetrahedron Lett.*, **1969**, 1371.
14) N. C. Yang and D-M. Thap, *Tetrahedron Lett.*, **1965**, 3671.
15) We designated the isomer leading to the *trans*-lactone as *threo*.
16) B. Fraser-Reid, D. R. Hicks, D. L. Walker, D. E. Iley, M. B. Yunker, S. Y-K. Tam, and R. C. Anderson, *Tetrahedron Lett.*, **1975**, 297; A, Guzmán and J. M. Muchowski, *ibid.*, 2053.
17) Z. Yoshida and M. Kimura, *Tetrahedron*, **31**, 221 (1975).
18) R. Matsushima, T. Kishimoto, and M. Suzuki, *Bull. Chem. Soc. Jpn.* **48**, 3028 (1975).
19) N. W. Alcock, N. Herron, T. J. Kemp, and C. W. Shoppee, *J. Chem. Soc., Chem. Commun.*, **1975**, 785.
20) T. Sato, K. Tamura, K. Maruyama, O. Ogawa, and T. Imamura, *J. Chem. Soc., Perkin Trans. 1*, **1976**, 779.
21) J. D. Hefley, D. M. Mathews, and E. S. Amis, *Inorg. Synth.*, **7**, 146 (1963).
22) W. S. Rapson and R. Robinson, *J. Chem. Soc.*, **1935**, 1285.
23) W. W. Rinne, H. R. Deutsch, M. I. Bowman, and I. B. Joffe, *J. Am. Chem. Soc.*, **72**, 5759 (1950).
24) W. F. Gannon and H. O. House, *Org. Synth.*, Coll. Vol. V, 294 (1973).
25) E. L. Eliel and C. Lukach, *J. Am. Chem. Soc.*, **79**, 5986 (1957).
26) H. E. Zimmerman, P. Klackett, D. F. Juers, J. M. McCall, and B. Schröder, *J. Am. Chem. Soc.*, **93**, 3653 (1971).
27) O. E. Curtis, Jr., J. M. Sandri, R. E. Crocker, and H. Hart, *Org. Synth.*, Coll. Vol. IV, 278 (1963).
28) G. W. Cannon, R. C. Ellis, and J. R. Leal, *Org. Synth.*, Coll. Vol. IV, 597 (1963).
29) G. Stork, A. Brizzolara, H. Landesman, J. Szmuskovicz, and R. Terrell, *J. Am. Chem. Soc.*, **85**, 207 (1963).
30) E. H. Man, F. W. Swamer, and C. R. Hauser, *J. Am. Chem. Soc.*, **73**, 901 (1951).
31) A. W. Johnson, E. Markham, and R. Price, *Org. Synth.*, Coll. Vol. V, 785 (1973).
32) R. B. Moffett, *Org. Synth.*, Coll. Vol. IV, 605 (1963).
33) T. F. West, *J. Soc. Chem. Ind.*, **61**, 158 (1942).
34) T. Cuvigny, H. Normant, and P. Hullot, *Bull. Chim. Soc. Fr.* **1970**, 3876.
35) E. P. Kyba, *Org. Prep. Proced.*, **2**, 149 (1970); *Chem. Abstr.*, **73**, 109422x (1970).
36) S. Natelson and S. P. Gotteried, *J. Am. Chem. Soc.*, **61**, 1001 (1939).
37) *Cf.* I. A. Favorskaya and L. V. Fedorcova, *Zh. Obshch. Khim.*, **23**, 47 (1953); *Chem. Abstr.* **48**, 610i (1954).
38) E. J. Corey and J. W. Suggs, *Tetrahedron Lett.*, **1975**, 2647.
39) *Cf.* H. Schwarz, F. Bohlmann, and W. Volreander, *Org. Mass Spectrum*, **7**, 1005 (1973); *Chem. Abstr.*, **79**, 91180d (1973).
40) "The Aldrich Library of NMR Spectra," Vol. VI, Aldrich Chemical Company, Inc, Milwaukee, Wis. (1974), p. 87D.
41) Ref. 40, p. 88A.
42) Ref. 40, Vol. IV, p. 10D.
43) *Cf.* J. Debrauwere and M. Verzele, *Bull. Soc. Chim. Belg.*, **84**, 167 (1975); *Chem. Abstr.*, **83**, 25073c (1975).
44) S. Tanimoto, A. Kita, M. Okano, and R. Oda, *Yukigosei Kagaku Kyokaishi*, **27**, 444 (1969).
45) D. R. Marshall and T. R. Roberts, *J. Chem. Soc.*, **1971** (B), 797.
46) K. B. Wiberg and T. W. Hutton, *J. Am. Chem. Soc.*, **76**, 5367 (1954).
47) S. M. Davtyan, G. L. Papayan, and S. N. Asratyan, *Arm. Khim. Zh.*, **23**, 251 (1970); *Chem. Abstr.*, **73**, 25030e (1970).
48) G. F. Hennion and W. S. Murray, *J. Am. Chem. Soc.*, **64**, 1220 (1942).
49) K. Fukunichi, Y. Inoue, Y. Kishimoto, and F. Mashio, *J. Org. Chem.*, **40**, 628 (1975).
50) J. Falbe, N. Huppes, and F. Karte, *Chem. Ber.*, **97**, 863 (1964).
51) H. C. Brown and K. A. Keblys, *J. Org. Chem.*, **31**, 485 (1966).
52) P. H. Begemann, V. Lamberti, and W. T. Weller, *Rec. Trav. Chim. Pays-Bas*, **86**, 1335 (1967).
53) F. E. Condon, *J. Am. Chem. Soc.*, **71**, 3544 (1949).
54) D. A. Frost and G. A. Morrison, *J. Chem. Soc. Perkin Trans. 1*, **1973**, 2159.
55) T. Sato, T. Inoue, and K. Yamamoto, *Bull. Chem. Soc. Jpn*, **45**, 1176 (1972).
56) R. Lee, A. Kimura, and S. Isoe, Abstr. No. 1U28, 36th National Meeting of the Chemical Society of Japan, Osaka, April 1977; private communication from Prof. Isoe.

A Wittig-type Reaction of Phosphoranes with Carbon Monoxide Coordinated to Palladium. A Synthetic Route to Isocyanide Palladium Complexes

Jitsuo KIJI,* Akira MATSUMURA, Tomoyuki HAISHI, Satoshi OKAZAKI, and Junji FURUKAWA

Department of Synthetic Chemistry, Faculty of Engineering, Kyoto University, Yoshida, Kyoto 606

(Received March 9, 1977)

The reaction of carbon monoxide with triphenyl(phenylimino)phosphorane proceeded at room temperature in the coordination sphere of palladium to give a mixture of phenyl isocyanide and carbonyl complexes of palladium. Triphenyl(*t*-butylimino)phosphorane gave bis(*t*-butyl isocyanide)palladium chloride in a low yield. Benzophenone triphenylphosphazine and triphenyl(*p*-tolylsulfonylimino)phosphorane failed to react with carbon monoxide.

Although phosphoranes (ylides) and carbon monoxide are versatile reagents in organic synthesis, no reaction between them has been recorded. Coordinated carbon monoxide is susceptible to attack by many nucleophiles. For example, an attack by organolithium leads to the formation of aldehydes[1] or metal–carbene complexes.[2] Ylides possess a nucleophilic character and can be expected to react with coordinated carbon monoxide. In fact, Kaska and his co-workers[3] succeeded in applying the Wittig reaction to transition-metal carbonyl. Iminophosphoranes also react with iron carbonyl to form isocyanide-substituted iron carbonyls *via* a Wittig-type reaction.[4] These reactions seem to provide a method of preparing novel organotransition metal complexes.

While no Pd^{2+}-carbonyl with a definite stoichiometry has been characterized, carbonylation by carbon monoxide is generally accepted to occur in the coordination sphere of the Pd^{2+}-ion.[5] A preliminary work of the present study has been published.[6]

This paper will deal with the Pd^{2+}–assisted Wittig-type reaction of carbon monoxide with iminophosphoranes.

Results and Discussion

Triphenyl(phenylimino)phosphorane (I). Triphenyl(phenylimino)phosphorane (I) reacted with carbon monoxide under an atmospheric pressure in the presence of such palladium chloride complexes (hereafter abbreviated as "$PdCl_2$") as $PdCl_2$(COD) (COD=1,5-cyclooctadiene) or $[PdCl_2(styrene)]_2$. The product was revealed by the IR spectrum to be a mixture of

$$2C_6H_5N{=}P(C_6H_5)_3 + \text{"}PdCl_2\text{"} + CO \longrightarrow$$

I

$$-Pd-\overset{O^-}{\underset{\|}{C}}-\overset{P^+(C_6H_5)_3}{\underset{|}{N}}-C_6H_5 \xrightarrow{-OP(C_6H_5)_3}$$

$$[C_6H_5N{=}P(C_6H_5)_3]PdCl_2(CNC_6H_5) \xrightarrow[-C_6H_5NC]{CO}$$

II

$$[C_6H_5N{=}P(C_6H_5)_3]PdCl_2(CO) \qquad (1)$$

III

Pd²⁺–isocyanide (II) and –carbonyl (III) complexes. The formation of the isocyanide complex indicates an apparent Wittig-type reaction of the ylide (I) with carbon monoxide coordinated to the palladium. Triphenylphosphine oxide, which is the other typical product of the Wittig reaction, was isolated from the solution.

Complex II is soluble in chloroform and slightly soluble in toluene, while complex III is insoluble in common organic solvents. In dimethyl sulfoxide, III decomposed slowly. The separation of II from III could be achieved by extraction with a mixed solvent of toluene and acetone containing a small amount of chloroform. The analytical data of II and III are in accord with the formula of $PdCl_2$(ylide)L (II, L=C_6H_5NC; III, L=CO). The molecular weight (osmometry in $CHCl_3$) indicates that II is monomeric. The infrared and far infrared spectra of II show strong bands at 2200 and 340 cm^{-1} and a medium absorption at 324 cm^{-1}. Complex III has a strong infrared band at 1900 cm^{-1}. In benzene, III reacted slowly with 2 mol of triphenylphosphine, with the evolution of carbon monoxide, to give $PdCl_2[P(C_6H_5)_3]_2$.

It is noteworthy that $PdCl_2$(COD) itself is inactive to carbon monoxide in benzene.[7] All the systems of "$PdCl_2$" and ylide absorbed carbon monoxide slowly.

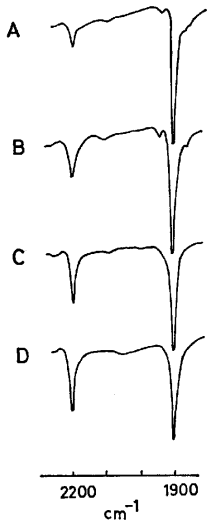

Fig. 1. Typical IR absorptions of ν_{CO} and ν_{CN} of the reaction products obtained from: (A) $PdCl_2$(COD), 27 h; (B) $PdCl_2(C_6H_5CN)_2$, 23 h; (C) $[PdCl_2(styrene)]_2$, 2.5 h. (D) A mixture (1 : 1) of II and III.

* To whom correspondence should be addressed. Present address: Department of Environmental Chemistry and Technology, Faculty of Engineering, Tottori University, Tottori 680.

The absorption continued for 25—30 h. The ratio of II to III depended upon the reaction time. In the early stages of the reaction a considerable amount of II was detected; it was slowly converted into III. Some typical spectra of the reaction products are shown in Fig. 1.

The reaction of II with carbon monoxide is noteworthy. In a toluene solution, II reacted with carbon monoxide to afford III. In the presence of I (I/II$<$1), however, the phenyl isocyanide coordinated to palladium reacted with I under an atmosphere of carbon monoxide to afford diphenylcarbodiimide in a moderate yield.[8] The formation of the carbodiimide was shown by the IR absorptions at 2137 and 2104 (sh) cm^{-1} and by isolating diphenylurea after hydrolyzing it with HCl–AcOH.

Triphenyl(t-butylimino)phosphorane (IV). The IV ylide was allowed to react with carbon monoxide under conditions similar to those described above. The product of the Wittig-type reaction in this case was off-white bis(*t*-butyl isocyanide)palladium chloride (V), which was identified with an authentic sample.[9] The infrared

$$2\,t\text{-}C_4H_9N{=}P(C_6H_5)_3 + 2CO + \text{“}PdCl_2\text{”} \longrightarrow$$
$$\text{IV}$$
$$PdCl_2(CNC_4H_9)_2 + 2OP(C_6H_5)_3 \quad (2)$$
$$\text{V}$$

spectrum coincides completely with that of the authentic sample in the 400—4000 cm^{-1} region. The characteristic bands due to ν_{CN} appear at 2240 and 2260 cm^{-1}. The yield after purification was low, because the separation from triphenylphosphine oxide was difficult (see Experimental). The formation of 2 mol of the isocyanide on palladium shows that basic IV reacts with carbon monoxide more smoothly within the coordination sphere of palladium. In this case, however, the reduction of "$PdCl_2$" with IV occurred competitively and a considerable amount of "$PdCl_2$" was reduced to metal.

Besides V, an insoluble carbonyl complex was also formed. However, it could not identified, because its purification was difficult as a result of poor solubility.

Benzophenone Triphenylphosphazine (VI). In the reaction of VI with carbon monoxide, brown "$PdCl_2$" gradually turned to an insoluble yellow solid. The solid was revealed to be a carbonyl–Pd^{2+} complex (VII).

$$(C_6H_5)_2C{=}N{-}N{=}P(C_6H_5)_3 + \text{“}PdCl_2\text{”} + CO$$
$$\text{IV}$$
$$\longrightarrow [(C_6H_5)_2C{=}N{-}N{=}P(C_6H_5)_3]PdCl_2(CO) \quad (3)$$
$$\text{VII}$$

The analytical data are in accord with VII. The yield was quantitative. The infrared spectrum shows a strong band at 1900 cm^{-1}. Neither isocyanide complex (or Wittig-type product derived from VI) nor triphenylphosphine oxide was detected in the reaction system. From these facts, it is concluded that VI fails to react with carbon monoxide at room temperature. Phosphazine VI, whose negative charge is delocalized, may be represented as follows:[10]

$$R_3P{=}N{-}N{=}C\!\!\prec \longleftrightarrow R_3\overset{+}{P}{-}\overset{-}{N}{-}N{=}C\!\!\prec \longleftrightarrow R_3\overset{+}{P}{-}N{=}N{-}\overset{-}{C}\!\!\prec$$

The lack of reactivity toward the coordinated carbon monoxide may be ascribed to this decreased nucleophilicity.

Other Phosphoranes. No reaction of triphenyl(*p*-tolylsulfonylimino)phosphorane (VIII) with carbon monoxide occurred. The lack of reactivity of VIII may be ascribed to its decreased nucleophilicity, caused by electron-withdrawing sulfonyl group.

$$CH_3\text{–}C_6H_4\text{–}SO_2N{=}P(C_6H_5)_3 \qquad (C_6H_5)_3P{=}C{=}P(C_6H_5)_3$$
$$\text{VIII} \qquad\qquad \text{IX}$$

Hexaphenylcarbodiphosphorane (IX) was allowed to react with carbon monoxide. The brown olefin–palladium complex gradually turned to an insoluble dark green solid which showed infrared bands at 2120 and 1900 cm^{-1}. The former frequency is tentatively assigned to the $\nu_{C\equiv C}$ vibration of $-\overset{|}{\underset{|}{Pd}}-C{\equiv}C-P(C_6H_5)_3$. Triphenylphosphine oxide was isolated from the solution. An analogous reaction has been observed between manganese carbonyl and IX. The absorption band of $Mn(CO)_4Br[C{\equiv}C{-}P(C_6H_5)_3]$ at 2105 cm^{-1} was assigned to the $\nu_{C\equiv C}$ band.[4] The product, which shows the IR band at 2120 cm^{-1}, was relatively stable in the dry state, but exceedingly unstable in solution. All attempts to isolate it in a pure form have been unsuccessful.

Experimental

Materials. The $C_6H_5N{=}P(C_6H_5)_3$[11], $t\text{-}C_4H_9N{=}P(C_6H_5)_3$[12], $(C_6H_5)_2C{=}N{-}N{=}P(C_6H_5)_3$[13], $p\text{-}CH_3C_6H_4SO_2N{=}P(C_6H_5)_3$[14], and $(C_6H_5)_3P{=}C{=}P(C_6H_5)_3$[15] compounds and the palladium complexes were prepared by the known methods. Toluene and benzene were purified by distillation in the presence of benzophenone sodium ketyl and were used under an argon atmosphere. Carbon monoxide (99.5% Matheson Co.) was used without further purification.

General Procedure for the Reactions with Carbon Monoxide. The conventional hydrogenation apparatus under an atmospheric pressure was used. In a round 50-ml flask, ylide, "$PdCl_2$," and toluene (solvent) were placed under an atmosphere of argon. The system was then placed under carbon monoxide by evacuating it by means of an aspirator and by filling it with carbon monoxide several times. Then the flask was shaken under an atmospheric pressure of carbon monoxide at room temperature. After shaking, the resulting solid was filtered off, washed, and dried. Some typical reactions are as follows.

Reaction of I. The ylide (I, 1 mmol) was allowed to react with carbon monoxide in the presence of $[PdCl_2(cyclooctene)]_2$ (0.25 mmol) for 22 h. The solid mass was then extracted with a mixed solvent of toluene, acetone, and chloroform (6:4:1). The subsequent evaporation of the solvent gave II in a 37% yield; mp 99 °C (dec.). Found: C, 58.26; H, 4.27; N, 4.44; P, 4.79%. Calcd for $C_{31}H_{25}N_2PPdCl_2$: C, 58.73; H, 3.95; N, 4.42; P, 4.89%. Complex III (21.6%) remained undissolved; mp 148 °C (dec.). Found: C, 54.20; H, 4.21; N, 2.55; P, 5.30%. Calcd for $C_{25}H_{20}NOPPdCl_2$: C, 53.72; H, 3.58; N, 2.51; P, 5.55%.

Reaction of III with $P(C_6H_5)_3$. III (0.2233 g) was suspended in 2 ml of benzene and was allowed to react with 0.2098 g of $P(C_6H_5)_3$ at a refuxing temperature for 4 h. Filtration gave $PdCl_2[P(C_6H_5)_3]_2$ in a 78% yield (Found: C,

61.65; H, 4.30; P, 8.82%).

Reaction of IV. The reaction of 0.143 g (0.5 mmol) of $PdCl_2(COD)$ with 1 mmol of IV in 10 ml of toluene under carbon monoxide gave gray-green solids after 70 h. After the filtration of the solids, the solution was evaporated to a small volume and ether was added to the concentrated solution. Triphenylphosphine oxide, which was soluble, was removed by this treatment. (In this procedure, a considerable amount of V remained in the solution.) The precipitate, which contained a small amount of the carbonyl compound, was extracted with benzene. The subsequent evaporation of benzene gave pure V; 3 mg (Found: N, 7.23%).

Reaction of VI. The reaction of the VI ylide (1 mmol) with carbon monoxide in the presence of "$PdCl_2$" (1 mmol) for 22 h gave VII in an 80% yield. Found: C, 57.84; H, 3.95; N, 4.46; P, 4.77%. Calcd for $C_{32}H_{25}N_2OPPdCl_2$: C, 58.06; H, 3.78; N, 4.23; P, 4.69.

Reaction of IX. The reaction of ylide IX (1.74 mmol) with "$PdCl_2$" (0.87 mmol) in 10 ml of toluene for 22 h gave 0.436 g of solids, which showed IR absorptions at 2120 and 1900 cm^{-1}.

References

1) M. Ryang, I. Rhee, and S. Tsutsumi, *Bull. Chem. Soc. Jpn.*, **37**, 341 (1964).

2) E. O. Fischer, *Angew. Chem.*, **86**, 651 (1974), and the references cited therein.

3) W. C. Kaska, D. C. Mitchell, R. F. Reichelderfer, and W. D. Korte, *J. Am. Chem. Soc.*, **96**, 2847 (1974).

4) H. Alper and R. A. Partis, *J. Organomet. Chem.*, **35**, 40 (1972).

5) J. Tsuji, M. Morikawa, and J. Kiji, *J. Am. Chem. Soc.*, **86**, 4851 (1964).

6) J. Kiji, A. Matsumura, S. Okazaki, T. Haishi, and J. Furukawa, *J. Chem. Soc., Chem. Commun.*, **1975**, 751.

7) J. Tsuji, S. Hosaka, J. Kiji, and T. Susuki, *Bull. Chem. Soc. Jpn.*, **39**, 141 (1966).

8) The yield could not be determined exactly, because a mixture of II and III was used as the starting material.

9) B. Crociani, T. Boshi, and U. Belluco, *Inorg. Chem.*, **9**, 2021 (1970).

10) A. Maercker, "Organic Reactions," ed by A. C. Cope John Wiley and Sons, New York, Vol. 14 (1965), 270.

11) L. Horner & H. Ödiger, *Justus Liebigs Ann. Chem.*, **627**, 142 (1959).

12) H. Zimmer and G. Singh, *J. Org. Chem.*, **28**, 483 (1963).

13) H. J. Bestmann and H. Fritzche, *Chem. Ber.*, **94**, 2477 (1961).

14) F. Mann and E. J. Chaplin, *J. Chem. Soc.*, **1937**, 527.

15) R. Ramirez, N. B. Desai, B. Hansen, and H. McKelvie, *J. Am. Chem. Soc.*, **83**, 3539 (1961).

Studies of Pyrazines. I. Pyrolyses of Substituted Pyrazines and Their Thermal Stabilities

Takeo KONAKAHARA and Yukio TAKAGI

Department of Applied Chemistry, Science University of Tokyo, Kagurazaka, Shinjuku-ku, Tokyo 162

(Received March 9, 1977)

The pyrolyses and thermal stabilities of 2,5-dialkylpyrazines (**1a—e**), 2,5-diethoxypyrazine (**2**), chloropyrazine (**3**), alkoxypyrazines (**4a—c**), alkylthiopyrazines (**5a, b**), and alkylaminopyrazines (**6a—d**) were studied by means of a mass spectrometer, by which the pyrolysates in the sample reservoir were analyzed. The temperature dependence of the molecular ions and/or fragment ions was also discussed. The thermal dehydrogenation from two α-methine groups makes the **1d** molecule thermally sensitive. The other 2,5-dibutylpyrazines were more stable than it, except for the *t*-butyl derivative, **1e**. Hydroxy- and aminopyrazine, **4a** and **6a**, were very stable. The alkoxypyrazines, **4b** and **4c**, and alkylthiopyrazines, **5**, underwent the thermal elimination of olefine to yield hydroxy- and mercaptopyrazine respectively. The latter disproportionated to form dipyrazinyl sulfide (**11**). At 280 °C, no analogous reactions of alkylaminopyrazines **6b—d** could be observed. The relative thermal stabilities of the compounds were as follows:

2, 4a, 6a, 4b>1c>1e>1b>6c, 5a>3>6b>1d>1a>6d, 5b>4c

The chemistry of pyrazine derivatives has been investigated in various kinds of fields.[1] Recently, several new synthetic methods of the pyrazine ring have been reported. Azirines undergo both acid-catalyzed and photochemical dimerization to give pyrazines.[2,3] Many kinds of pyrazines have been prepared from diaminomaleonitrile and its derivatives.[4,5] Both thermal and photochemical transformations of perfluoroalkyl pyridazines to perfluoroalkylpyrazines have been reported.[6,7] On the other hand, it is well known that the pyrazine ring is isomerized to other diazine rings under both photolytic and pyrolytic conditions.[1] Although many kinds of reactions of substituted pyrazines have been reported, it is difficult to find intramolecular γ-hydrogen abstruction reactions analogous to the Norrish Type II reaction of ketones except for a photoreaction of 2-alkylquinolines.[1,6b,8]

In this paper, we wish to report our findings on the thermal behavior of substituted pyrazines (**1—6**), which can be expected to undergo thermal elimination reactions analogous to those of acetates and of *S*-methyl xantates.[9-11] Indeed, pyrazines (**4c**, **5b**) eliminated propylene at a temperature (250 °C) lower than acetates.[9] Some of the others, (**1b—d**, **4b**, and **5a**), were confirmed to eliminate olefines at higher temperatures. The mercaptopyrazine (**10**) produced by thermal decomposition dispropotionates to give dipyrazinyl sulfide (**11**). The thermal stabilities of these compounds were also discussed.

Results and Discussion

Pyrolysis was carried out in an indirect-inlet system of a mass spectrometer under reduced pressure (see Experimental section). In order to minimize the mass-spectral fragmentations of the thermal decomposition products, the low-energy ionization technique was used. The substituted pyrazines, **1—6**, were heated in the vapor phase at 150—280 °C for a constant period (3—5 min), and then the pyrolysates were transferred into an ionization chamber without fractionation. The total ion current was approximately constant throughout the period. The temperature dependence on the molecular ion abundances (Σ_{26} values) are shown in Figs. 1, 3, 4, and 7, and the relative total ion current $I_r^+(t)$, in Table 1. $I_r^+(t)$ was calculated by means of the following Equation (1):

$$I^+(t) = \sum_{i=26}^{n} I_i^+(t)$$

$$I_r^+(t) = I^+(t)/I^+(150) \qquad (1)$$

where $I_r^+(t)$ is the relative abundance of a "*m/e i*" ion in a 16 eV spectrum at *t* °C and where *n* is the highest mass number in the spectrum. If all of the spectra are obtained under the same operating conditions except for the temperature of the sample reservoir, it is obvious that the changes in the spectra (for example, a change in the ion abundance, and the appearance of a new peak) are attributable to a change in the temperature. The operating conditions are shown in the Experimental section. For that reason, the temperature dependence of the molecular ion intensity and of the relative total ion current $I_r^+(t)$ give us information about the thermal reaction and stability of a compound.

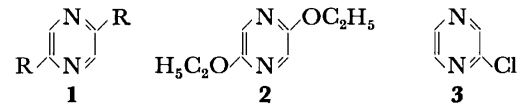

1

a: R=CH_3
b: R=*n*-C_4H_9
c: R=*i*-C_4H_9
d: R=*s*-C_4H_9
e: R=*t*-C_4H_9

2

3

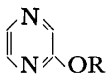

4

a: R=H
b: R=C_2H_5
c: R=*i*-C_3H_7

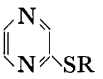

5

a: R=C_2H_5
b: R=*i*-C_3H_7

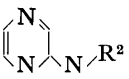

6

a: $R^1=R^2=H$
b: $R^1=C_2H_5$, $R^2=H$
c: $R^1=R^2=C_2H_5$
d: R^1=*i*-C_3H_7, $R^2=H$

Pyrolyses of 2,5-Dialkylpyrazines ***1***. Figure 1 shows the following facts: (i) the molecular ion abundances of the butyl and isobutyl derivatives, **1b** and **1c**,

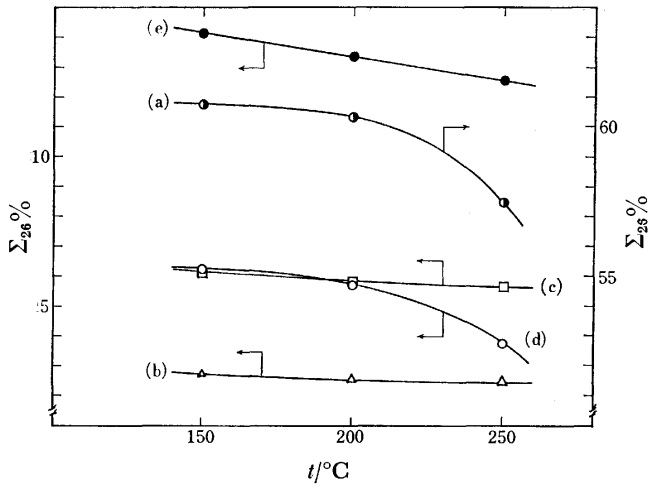

Fig. 1. Temperature dependence of M^+ of 2,5-dialkylpyrazines (**1**) at 16 eV: (a) 2,5-dimethylpyrazine(**1a**), (b) 2,5-dibutylpyrazine (**1b**), (c) 2,5-diisobutylpyrazine (**1c**), (d) 2,5-di-*s*-butylpyrazine (**1d**), (e) 2,5-di-*t*-butylpyrazine (**1e**).

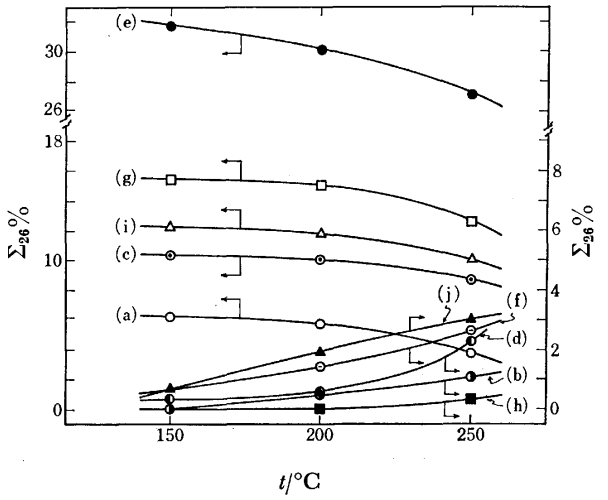

Fig. 2. Temperature dependence of fragment ion abundances of 2,5-di-*s*-butylpyrazine (**1d**): (a) M^+, *m/e* 192.1597 (error −2.8); (b) M−2, 190.1469 (0.0); (c) $M-CH_3$, 177.1391 (0.0); (d) $(M-CH_3)$ −2, 175.1232 (−0.2); (e) $M-C_2H_4$, 164.1306 (−0.6); (f) $(M-C_2H_4)$ −2, 162.1180 (2.4); (g) $(M-C_2H_4)-C_2H_5$, 135.0913 (−0.7); (h) $M-(C_2H_4+C_2H_5)$ −2, 133.0761 (−0.3), (i) $M-C_3H_6$, 150.1142 (−1.3); (j) $(M-C_3H_6)$ −2, 148.0987 mu (−1.2 mmu).

are almost independent of the temperature (150—250 °C), (ii) that of the *t*-butyl derivative (**1e**) decreases slowly with the rise in the temperature, and (iii) those of methyl and *s*-butyl derivatives (**1a**) and **1d**, show a strong temperature dependence at 200—250 °C. These results suggest the thermal unstability of **1a** and **1d**. In order to explain the unstability of **1d**, the temperature dependence of the fragment ions was examined (Fig. 2) and the elemental composition of each ion was determined by means of a high-resolution mass spectrometer. Although the intensity of the molecular ion ($C_{12}H_{20}N_2$, *m/e* 192.1597, error −2.8 mmu) decreases with the rise in the temperature, that of the dehydrogenated ion ($C_{12}H_{18}N_2$, *m/e* 190.1469, error 0.0 mmu) increases. The relative total ion current $I_r^+(t)$ also increases (see Table 1). This suggests that the thermal reaction, Eq. 2, occurs in the sample reservoir before the ionization by electron impact. No thermally induced elimination of ethylene from this compound was

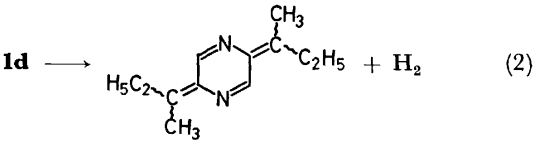

(2)

7

observed at 250 °C (*cf.* Compounds (**4**) and **5**).[13c] In the case of **1a**, however, no increasing ion like (**7**) could be found in spite of the strong temperature dependence of its molecular ion abundance. Therfore, the decrease in the intensity of the molecular ion appears to result from a lack of stabilizing ability of the methyl group.

*Pyrolyses of Chloropyrazine (**3**), Hydroxypyrazine (**4a**), and Aminopyrazine (**6a**).* The temperature dependence of the molecular ions for these compounds is

Table 1. Temperature dependence of the relative total ion current $I_r^+(t)$ and $\Delta I(250)$ at 16 eV

	$I_r^+(t)$				$\Delta I(t)$
t/°C	150	200	250	280	250
1a	1.00	1.01	1.06	—	0.06
1b	1.00	1.00	1.07	—	0.07
1c	1.00	1.03	1.05	—	0.05
1d	1.00	1.05	1.17	—	0.17
1e	1.00	1.03	1.09	—	0.09
2	1.00	0.98	1.02	—	0.02
3	1.00	1.01	1.05	1.07	0.05
4a	—	1.00	0.99	0.98	−0.01
4b	1.00	1.02	1.03	1.08	0.03
4c	1.00	1.15	1.67	1.62	0.67
5a	1.00	1.02	1.08	1.13	0.08
5b	1.00	1.03	1.24	1.36	0.24
6a	1.00	0.99	1.01	0.99	0.01
6b	1.00	1.04	1.13	1.33	0.13
6c	1.00	1.01	1.10	1.17	0.10
6d	1.00	1.05	1.10	1.31	0.10

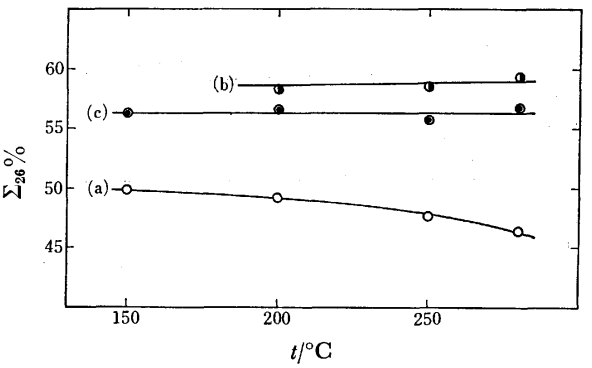

Fig. 3. Temperature dependence of M^+ of (a) chloropyrazine (**3**), (b) hydroxypyrazine (**4a**), and (c) aminopyrazine (**6a**) at 16 eV.

TABLE 2. YIELDS AND PHYSICAL PROPERTIES FOR PYRAZINES (**1**)—(**6**)

Compd No.	Yield (%)	Bp (°C/mmHg)	UV in EtOH λ(nm) (ε)	IR (cm^{-1})	MS m/e	NMR in CCl_4 δ value[o]	Found (Calcd) C%	Found (Calcd) H%
1b	26	95/11.5	274(7100) 279(7200) 312 (840)	3070 1360	192	0.95(t,6H),[a] 1.57(m,8H), 2.74(t,4H),[b]8.20(s,2H)	74.02 $C_{12}H_{20}N_2$ (74.95)	10.41 (10.48)
1c	48	103/13	275(7000) 278(7100) 312(1000)	3075 1365 1155	192	0.93(d,12H),[c] 2.12(m,2H), 2.62(d,4H),[a] 8.26(s,2H)		
1d	45 lit,[m] 60	112/13 lit,[m] 114/13	273(7100) 279(6800) 310(760)	3070 1375 1160	192	0.83(t,6H),[b] 1.28(d,6H),[d] 1.70(q-d,4H),[b,d] 2.78(se,2H),[d] 8.25(s,2H)	192.1597 mu $C_{12}H_{20}N_2$ error −2.8 mmu	
4b	65 lit,[n] 56	58/13 lit,[n] 73/30	211(11200) 279(5500) 295(sh)	3070 1590 1390	124	1.37(t,3H),[b,l] 4.33(q,2H),[b] 8.05(m,2H), 8.18(d,1H)[e]		
4c	51	74.5/22	212(11400) 280(4680) 295(sh)	3050 1585 1170	138	1.33(d,6H),[d,l] 5.28(h,1H),[d] 8.01(d,1H),[f] 8.03(d,1H),[f] 8.13(s, 1H)	60.03 $C_7H_{10}ON_2$ (60.85)	7.19 (7.30)
5a	81	87/10.5	252(9700) 300(sh) 322(4900)	3040 1560	140	1.33(t,3H),[b] 3.12(q,2H),[b] 8.08(d,1H),[q] 8.23(d-d,6H),[g,h] 8.34(d,1H)[h]	51.11 $C_6H_8SN_2$ (51.40)	5.87 (5.75)
5b	59	79/6	253(9910) 300(sh) 322(5030)	3050 1565 1175	154	1.36(d,6H),[a] 3.94(h,1H),[a] 8.08(d,1H),[i] 8.25(d-d,1H),[h,i] 8.32(d,1H),[h]	54.59 $C_7H_{10}SN_2$ (54.51)	6.62 (6.54)
6b	88	90.5/2.5	247(15800) 290(1300) 334(4460)	3270 1600 1530	123	1.19(t,3H),[j] 3.33(q,2H),[j] 5.83(bs,1H), 7.63(d,1H),[i] 7.79(d,1H),[h] 7.87(d-d,1H)[h,i]	57.69 $C_6H_9N_3$ (58.51)	7.50 (7.37)
6c	78	125/26	255(18000) 295(990) 345(4400)	1603	151	1.15(t,6H),[a] 3.45(q,4H),[a] 7.62(m,1H),7.85(m,2H)	63.30 $C_8H_{13}N_3$ (63.54)	8.80 (8.67)
6d	60	82.5/2.0	247(16300) 290(sh) 335(4340)	3270 1600	137	1.18(d,6H),[c] 4.01(h-d,1H)[b,c] 5.64(bd,1H),[b] 7.62(d,1H),[i] 7.77(d,1H),[k] 7.87(d-d,1H)[i,k]	60.81 $C_7H_{11}N_3$ (61.28)	7.82 (8.08)

a) J=7 Hz. b) J=7.5 Hz. c) J=6 Hz. d) 6.5 Hz. e) J=1.35 Hz. f) J=1.9 Hz. g) J=3 Hz. h) J=2 Hz. i) J=2.5 Hz. j) 8 Hz. k) J=1.5 Hz. l) in $CDCl_3$. m) Ref. 22. n) Ref. 25. o) (**1**): at 60 MHz; (**4**)—(**6**): at 100 MHz.

shown in Fig. 3. Hydroxy- and aminopyrazine, **4a** and **6a**, are independent of the temperature. They are stabilized by the electron-donating substituents, while the electron-withdrawing chloro group makes its molecular ion thermally sensitive. This conclusion is also supported by the data in Tables 1 and 3.

*Pyrolyses of Alkoxypyrazines **4b**, **4c** and Alkylthiopyrazines **5a**, **5b**.* Except for **4b**, the pyrazines, **4c**, **5a**, and **5b**, are more thermally sensitive than the others. The molecular ion abundances of both **4c** and **5b** are especially strikingly decreased at 200—250 °C (Fig. 4). The details are shown in Figs. 5 and 6. In Fig. 5, a molecular ion (*m/e* 138) decreases with the rise in the temperature and almost disappears at 280 °C. On the other hand, the *m/e* 96 ion decreases at 150—250 °C and becomes constant at 250—280 °C. The abundance of the *m/e* 42 ion increases with the rise in the temperature and is constricted to a constant value. The behavior

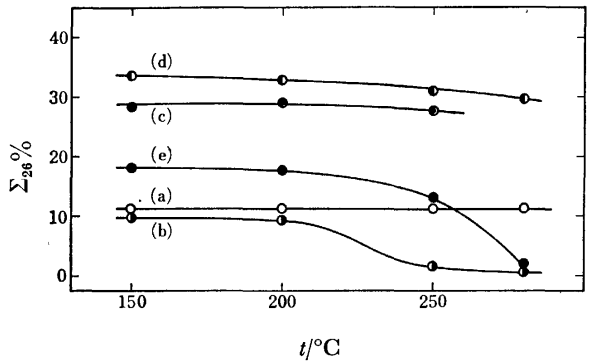

Fig. 4. Temperature dependence of M^+ of (a) ethoxypyrazine (**4b**), (b) isopropoxypyrazine (**4c**), (c) 2,5-diethoxypyrazine (**2**), (d) ethylthiopyrazine (**5a**), and (e) isopropylthiopyrazine (**5b**) at 16 eV.

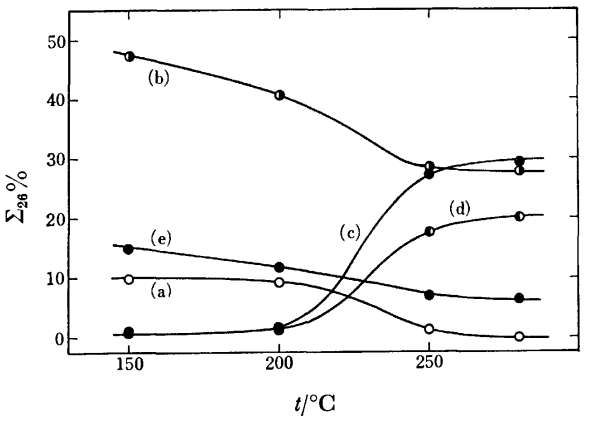

Fig. 5. Temperature dependence of fragment ion abundances of isopropoxypyrazine (**4c**): (a) M^+, *m/e* 138; (b) $M-C_3H_6$, 96; (c) $C_3H_6^+$, 42; (d) $C_3H_5^+$, 41; (e) $M-(C_3H_6+CO)$, 68.

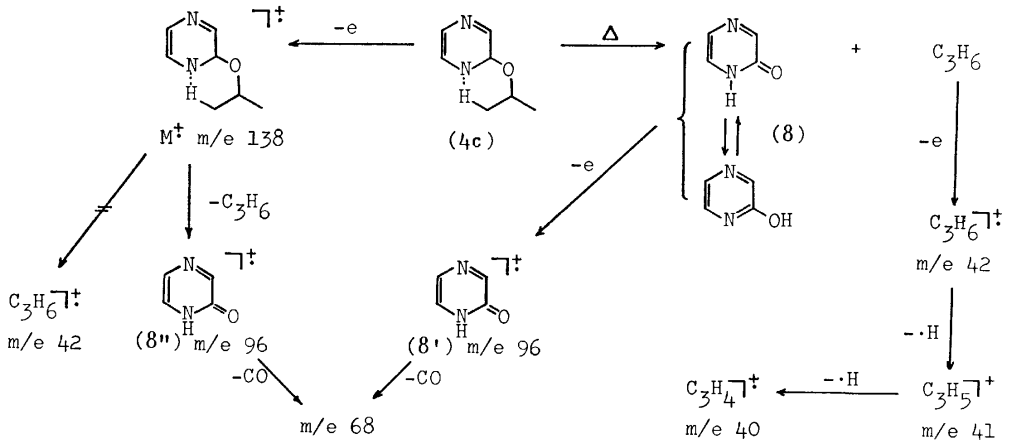

Scheme 1.

of the ions shown in Fig. 5 is explained by means of Scheme 1. In an electron-impact reaction, the abundances of the competing ion products generally reflect their relative ionization potentials (I_p). As the I_p of hydroxypyrazine is smaller than that of propylene, the formation of the ion (**8''**) (charge retention) is more favored than that of propylene ($CH_3CH{=}CH_2^+$/$C_4H_3N_2OH^+$=0.023 at 150 °C).[12] Moreover, hydroxypyrazine is independent of the temperature (Fig. 3). From these facts, it is obvious: (i) that isoproxypyrazine **4c** is thermally decomposed to give hydroxypyrazine **8** and propylene, and (ii) that curve (b) in Fig. 5 is composed of both **8'** and **8''** at 200—250 °C. That is, the low-temperature region is due to **8''** and the high-temperature region, to **8'**. In a kinetic study of the pyrolysis of alkoxypyrazines, it was found that ethoxypyrazine **4b** was decomposed in the same way as **4c**.[13a] Although a similar reaction of 2,5-diethoxypyrazine, **2**, which had two reaction sites, was not observed at these temperatures, it was expected to occur at more elevated temperatures.

A reaction analogous to that of **4c** was also observed in the pyrolysis of isopropylthiopyrazine, **5b**; it is illustrated in Fig. 6 and Scheme 2. Compared with **4c**, this compound showed more drastic changes in the abundances of the ion products, especially in a mass region higher than that of the molecular ion. At 200—250 °C, a new *m/e* 190 peak, the abundance of which was increased by the elevation of the temperature, appeared. It corresponds to the ionized dipyrazinyl sulfide, **11**, produced by the thermal disproportionation reaction of mercaptopyrazine, **10**. This disproportionation reaction was reported by Cheeseman in the pyrolysis of mercaptopyrazine at 220 °C.[14] Curve (b) in Fig. 6 suggests that, in the sample reservoir, most of the molecule of mercaptopyrazine, **10**, is disproportionated so easily that there is no molecule to give the ion radical (**9**) upon electron impact. Ethylthiopyrazine, **5a**, may also be expected to decompose similarly at temperatures higher than 280 °C.

*Pyrolyses of Alkylamino- and Dialkylaminopyrazines (**6b—d**).* As has previously been mentioned, amino-

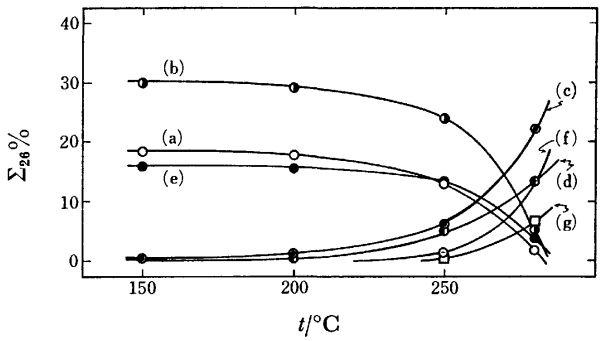

Fig. 6. Temperature dependence of fragment ion abundances of isopropylthiopyrazine (**5b**): (a) M^+, *m/e* 154; (b) $M-C_3H_6$, 112; (c) $C_3H_6^+$, 42; (d) $C_3H_5^+$, 41; (e) $M-(C_3H_6+CO)$, 68; (f) dipyrazinyl sulfide (**11**), 190; (g) (**11**)$-C_3H_4N$, 136.

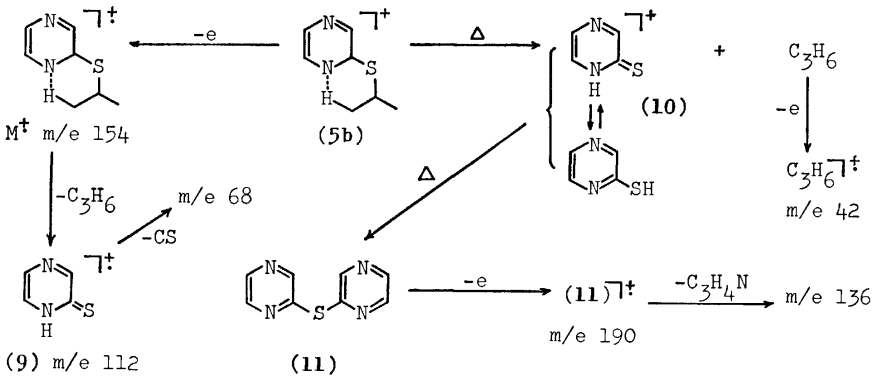

Scheme 2.

pyrazine, **6a**, is thermally stable. Its alkyl derivatives (**6b**—**d**), however, show interesting behavior. Monoalkylation on the amino group destabilizes the molecule more strikingly than dialkylation (see Figs. 3 and 7). This destabilization may be caused by dehydrogenation from the imino and/or alkyl group. The molecular ion abundance of isopropylaminopyrazine (**6d**) is more strongly suppressed at 280 °C than the others. Details of the thermal dehydrogenation from the **6b** and **6d** molecules are shown in Figs. 8 and 9 respectively. The isopropylamino derivative **6d** behaved much like **6b**. Reactions of **6b**, **6c**, and **6d** analogous to that of **4c** were observed at temperatures higher than 280 °C.[13b]

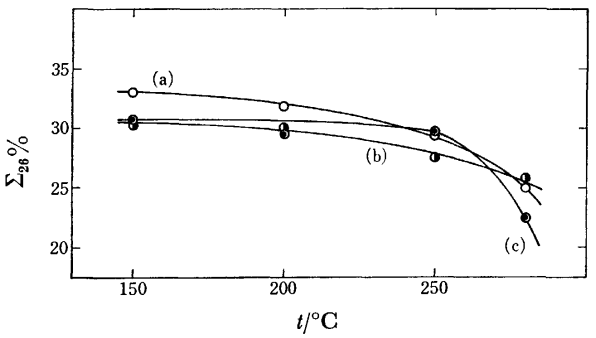

Fig. 7. Temperature dependence of M^+ of (a) ethylaminopyrazine (**6b**), (b) diethylaminopyrazine (**6c**), and (c) isopropylaminopyrazine (**6d**) at 16 eV.

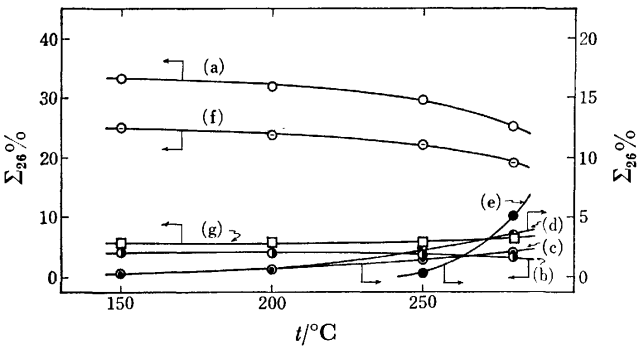

Fig. 8. Temperature dependence of fragment ion abundances of ethylaminopyrazine (**6b**): (a) M^+, *m/e* 123; (b) M−1, 122; (c) M−2, 121; (d) M−3, 120; (e) M−4, 119; (f) M−CH_3, 108; (g) M−C_3H_6, 95.

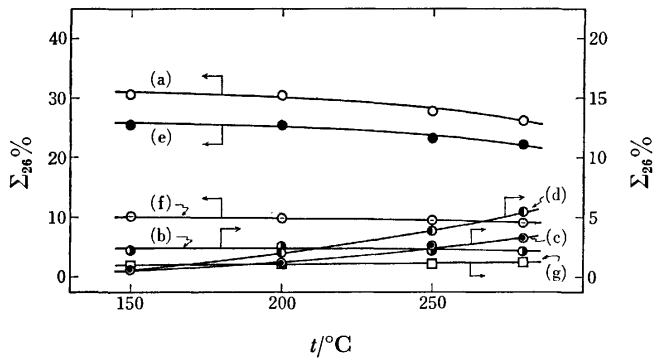

Fig. 9. Temperature dependence of fragment ion abundances of diethylaminopyrazine (**6c**): (a) M^+, *m/e* 151; (b) M−1, 150; (c) M−2, 149; (d) M−3, 148; (e) M−CH_3, 136; (f) M−C_2H_5, 122; (g) M−C_2H_4, 121.

Thermal Stability of Compounds 1—6. Generally, changes in the thermal stability of a series of compounds have been determined by a comparison of half-lives,[15] the amount of evoluted volatile products,[16] the temperatures of the beginning of the evolution of volatile products,[17] and the thermogravimetric curves.[18] From the discussion above, the changes in the ion abundances have proved to be attributable to thermal decomposition reactions. If it is correlated to the reaction temperature, the thermal stability of the compound can be clarified. However, a complete treatment of this subject involves a detailed study of the kinetics of the thermal decomposition reactions, followed by electron-impact reactions, and is very complicated. Therefore, a qualitative treatment was employed in this work. A conversion, α, at a certain temperature is obtained from the following Eq. 3:

$$\alpha = \frac{M(T_0) - M(T)}{M(T_0)} \tag{3}$$

where $M(T)$ is a molecular ion abundance of the pyrazine derivative at T K (see Figs. 1, 3, 4, and 7). When T_0 was 423.15 K, a plot of ln α *vs.* $1/T$ gave a straight line with a negative slope, s. The s values are summarized in Table 3. The most unstable compound, **4c**, showed a small s value (−14.7 kK), and **1c**, more stable than **4c**, a large one (−1.4 kK) (Fig. 10). That is to say, the more unstable a compound is, the smaller the s value is, and *vice versa*. Accordingly, it can be adopted as one of the measures of the thermal stability for the compound. From the data in Table 3, the following order of the thermal stability of the pyrazines **1**—**6** is given:

$$\mathbf{2},\ \mathbf{4a},\ \mathbf{6a},\ \mathbf{4b} > \mathbf{1c} > \mathbf{1e} > \mathbf{1b} > \mathbf{6c},$$
$$\mathbf{5a} > \mathbf{3} > \mathbf{6b} > \mathbf{1d} > \mathbf{1a} > \mathbf{6d},\ \mathbf{5b} > \mathbf{4c} \tag{4}$$

As the molecular ion peaks of **2**, **4a**, **4b**, and **6a** were not affected by the temperature, they were classified into the group of the most stable compound. However,

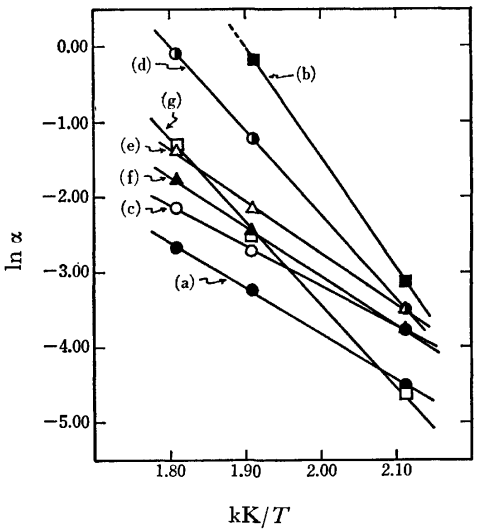

Fig. 10. A plot of ln α *vs.* $1/T$: (a) chloropyrazine (**3**), (b) isopropyrazine (**4c**), (c) ethylthiopyrazine (**5a**), (d) isopropylthiopyrazine (**5b**), (e) ethylaminopyrazine (**6b**), (f) diethylaminopyrazine (**6c**), (g) isopropylaminopyrazine (**6d**). The plot of ln α *vs.* $1/T$ for (**1a**)—(**1e**) was omitted in the Figure.

Table 3. Thermal stability of the pyrazines (1)—(6)

Compds	1a	1b	1c	1d	1e	2	3	4a	4b	4c	5a	5b	6a	6b	6c	6d
s/kK[a)]	−9.8	−3.9	−1.4	−8.0	—	−5.7	—	—	—	−14.7	−5.1	−11.2	—	−6.8	−5.0	−11.0

a) s: the slope obtained from $\ln \alpha$ *vs.* $1/T$.

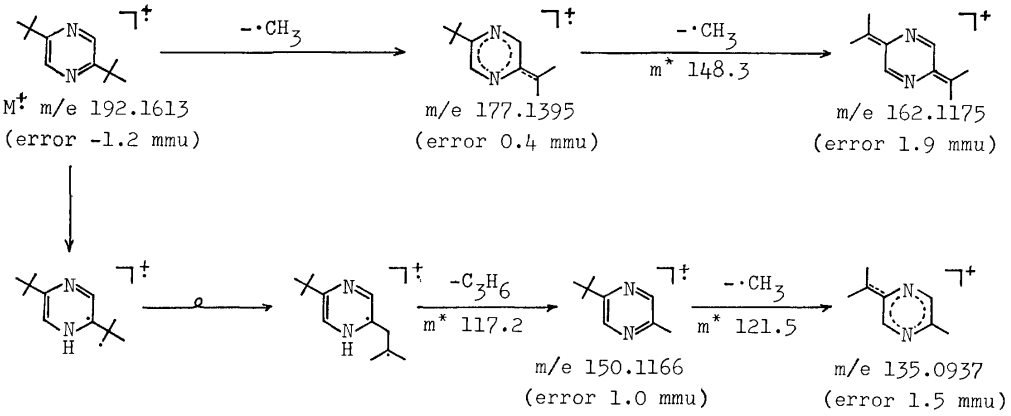

Scheme 3.

4b was decomposed in the same way as **4c**. On the other hand, an attempt to compare the thermal stability of the pyrazines on the basis of the temperature dependence on the $I_r^+(t)$ values in Table 1 was also successful. Although neither $\ln I_r^+(t)$ nor $\ln(I_r^+(t)-1)$ yielded a linear relationship with $1/T$, the order of the thermal stability was obtained by a comparison of $\Delta I(t)$, which was calculated by means of the following Eq. 5.

$$\Delta I(t) = I_r^+(t) - 1 \quad (5)$$

The $\Delta I(250)$ values in Table 1 gave the following order:

$$\mathbf{2, 4a, 6a, 4b} > \mathbf{1c, 3, 1a, 1b, 5a,}$$
$$\mathbf{1e, 6c, 6d} > \mathbf{6b} > \mathbf{1d} > \mathbf{5b} > \mathbf{4c} \quad (6)$$

This is in agreement with the order of (4) except for the cases of **1a** and **6d**. The s value appears to be more suitable for a comparison of the thermal stability of the **1**—**6** pyrazines than $\Delta I(t)$. No theoretical interpretation of the linear relationship between $\ln \alpha$ and $1/T$ can be offered at the present time.

Mass-spectral Reaction. In the mass-spectral fragmentation of **6c**, the McLafferty rearrangement was scarcely observed; this is in contrast with the other cases (except for **1a**, **1e**, **3**, **4a**, and **6a**).[19] This appears to result from a steric effect of the diethylamino group. 2,5-Di-*t*-butylpyrazine, **1e**, produces the rearranged ion ($C_9H_{14}N_2$; *m/e* 150.116; error, 1.0 mmu), which is responsible for the base peak in low-energy spectra at various temperatures. At 70 eV, **1e** loses a methyl radical from one of the *t*-butyl groups to give a base peak.[20] The fragmentation pattern is shown in Scheme 3.

Experimental

All the melting points and boiling points are uncorrected. The melting points were measured with a Meiho micro-melting point apparatus or with a sealed capillary in silicon oil. The ultraviolet spectra were recorded on a Hitachi EPS-3T spectrophotometer. The infrared spectra were recorded on a Hitachi EPI-G2 type spectrometer. The NMR spectra were recorded with either a JNM 4H-100 or a Varian A-60 spectrometer for solutions in deuteriochloroform, carbon tetrachrolide, or deuterium oxide. The chemical shifts are reported in δ(internal tetramethylsilane). The unpublished UV and NMR data are summarized in Table 3. The analitycal GLC determinations were carried out with a Shimadzu GC-4APF apparatus using a 2 m by 4 mm glass column of 10% Silicon GE SE-30 liquid phase on Shimalite W support (60—80 mesh). Elemental analyses were performed at the Institute of Physical and Chemical Research.

Mass Spectra and Pyrolyses of the Compounds. Both normal and high-resolution mass spectra were recorded with a Hitachi RMU-7M double-focusing mass spectrometer at 70 eV. The pyrolyses of the compounds were performed in the indirect inlet system of this instrument. Both a liquid and a solid sample were vaporized at 100 °C under a highly reduced pressure and were transferred into a sample reservior heated previously, in which the gaseous sample was then heated at 150, 200, 250, and 280 °C at 10^{-4}—10^{-5} mmHg for a constant period (3—5 min). An equilibrium mixture of the pyrolysate was introduced into an ionizing chamber through a transfer line heated at the same temperature as the reservior. All of the inlet system was made of Pyrex glass, and a gold orifice (Q_o=0.3 ml/s, molecular leak) was used as the gas leak. The operating conditions in this experiment were fixed as follows: ionizing voltage, 16 eV; chamber temperature, 170 or 200 °C; target current, 10 or 13 μA; total emission current, 10, 12, or 13 μA.

Materials. 2,5-Dimethylpyrazine (**1a**),[21] 2,5-di-*s*-butylpyrazine (**1d**),[22] 2,5-di-*t*-butylpyrazine (**1e**),[20] 2,5-diethoxypyrazine (**2**),[23] and chloropyrazine (**3**)[24] were prepared by known methods.

Hydroxypyrazine (4a): The direct synthetic method devised by Karmas and Spoerri was employed.[24] Both the effect of the reaction temperature and of the addition velocity of alkali on the yield were examined.[25] In consequence, it was found that the following procedure gave the highest yield (the technique was substantially that of Karmas and Spoerri).[24] A solution of glycine amide hydrochloride (22.2 g, 0.2 mol) and water (40 ml) in methanol (400 ml) was stirred at −30——40 °C while a 40% glyoxal solution (34.8 g, 0.24 mol) was added rapidly. The mixture was then cooled at −50——60

°C, and 12.5 M sodium hydroxide (0.50 mol) was added, drop by drop, over a period of 55—60 min. After an additional stirring for 1 h at this temperature, the mixture was stirred at room temperature for 4 h. Then it was treated by the same way as before.[24] The lower the temperature, the higher the yield, unless the reaction mixture was solidified. It was solidified at a temperature lower than −60 °C. On the other hand, the maximum yield was obtained when alkali was added over a period of 55—60 min. Recrystallzation from ethanol using activated carbon was employed instead of purification with silver acetate. The purity of the product, determined by means of its UV spectrum, was 96% (corrected yield, 61%; mp 180 °C; lit,[24] 51%, 188—190 °C). This was used without further purification to prepare chloropyrazine **3**.

*2,5-Dibutylpyrazines (**1b**, **c**)*: The method of Newbold and Spring was applied.[22] The yields and physical properties are shown in Table 2.

*Alkoxypyrazines (**4b**, **c**)*: The following general procedure was used.[26] Chloropyrazine **3** (4 g, 0.035 mol) was added, drop by drop, into a stirred alcoholic solution of sodium alkoxide RONa (R=C_2H_5, *i*-C_3H_7) (from 1.6 g of sodium and 32 ml of the corresponding absolute alcohol), after which the mixture was heated under reflux for 1 h. After cooling, the mixture was poured into a saturated aq sodium chloride solution (200 ml) and then completely extracted with ether. The dried (Na_2SO_4) and evaporated extract was then distilled under reduced pressure (see Table 2).

*Alkylthiopyrazines (**5a**, **b**)*: The following general procedure was used. A solution of 0.045 mol of alkyl thiol RSH (R=C_2H_5, *i*-C_3H_7) and sodium hydroxide (1.9 g, 0.045 mol) in absolute ethanol (20 ml) was heated to boiling and then cooled. Chloropyrazine **3** (5.1 g, 0.045 mol) was subsequently added cautiously with stirring. The mixture was then refluxed for an additional 30 min. After cooling, the mixture was poured into a satulated aq sodium chloride solution (150 ml) and then extracted completely with ether. The dried (Na_2SO_4) and evaporated extract was distilled under reduced pressure (see Table 2).

*Aminopyrazine (**6a**)*: This was prepared by Erickson and Spoerri's method.[26] The crude product was purified by sublimation under reduced pressure (75—80 °C at 1.5 mmHg). Yield, 81%; mp 119 °C (lit,[26] 80%, 118—120 °C).

*Ethylaminopyrazine (**6b**) and Isopropylaminopyrazine (**6d**)*: These substances were prepared by an application of Cheeseman's method.[14] Chloropyrazine **3** (2 g, 0.017 mol), 70% aq ethylamine (or isopropylamine) (0.096 mol), and ethanol (10 ml) were used (see Table 2).

*Diethylaminopyrazine (**6c**)*: Diethylamine (7 g, 0.096 mol) and chloropyrazine **3** (2 g, 0.017 mol) in ethanol (15 ml) were heated in a sealed tube at 150 °C for 7 h. The cooled reaction mixture was then poured into 10 ml of *ca.* 8 M NaOH, extracted with chloroform, and washed with water. The dried (Na_2SO_4) and evaporated extract was then distilled under reduced pressure (see Table 2).

References

1) Recent review: G. W. Cheeseman and E. S. G. Werstiuk, "Advances in Heterocyclic Chemistry," Vol. 14, ed A. R. Katritzky and A. J. Boulton, Academic Press, New York and London (1972), p. 99, and references cited therein.

2) G. Smolinsky, *J. Org. Chem.*, **27**, 3557 (1963).

3) a) A. Hassner and F. W. Fowler, *J. Am. Chem. Soc.*, **90**, 2869 (1968); b) A. Padwa, M. Dharan, J. Smolanoff, and S. I. Wetmore, Jr., *J. Am. Chem. Soc.*, **95**, 1954 (1973).

4) R. W. Begland, D. R. Hartter, D. S. Donald, A. Cairncross, and W. A. Sheppard, *J. Org. Chem.*, **39**, 1235 (1974), and references cited therein.

5) Y. Ohtzuka, *Yuki Gosei Kagaku Kyokai Shi*, **35**, 1 (1977).

6) a) C. G. Allison, R. D. Chambers, Y. A. Cheburkov, J. A. H. MacBride, and W. K. R. Musgrave, *J. Chem Soc. Chem. Commun.*, **1969**, 1200; b) A. L-. Combier, "Photochemistry of Heterocyclic Compound," ed by O. Buchardt, A Wiley-Interscience Publication, John Wiley & Sons, New York (1976), p. 207.

7) R. D. Chambers, M. Clark, J. R. Maslakiewicz, W. K. R. Musgrave, and P. G. Urben, *J. Chem. Soc., Perkin Trans. I*, **1974**, 1513.

8) K. Yamada, K. Katsuura, H. Kashimura, and H. Iida, *Bull. Chem. Soc. Jpn.*, **49**, 1805 (1976).

9) C. H. DePuy and P. W. King, *Chem. Rev.*, **60**, 431 (1960).

10) W. S. Briggs and C. Djerssi, *J. Org. Chem.*, **33**, 1612 (1968).

11) K. Kogami, T. Konakahara, K. Yamada, and J. Kumanotani, *Kogyo Kagaku Zasshi*, **74**, 2304 (1971).

12) F. W. McLafferty, "Interpretation of Mass Spectra," 2nd ed, W. A. Benjamin, London (1973).

13) a) T. Konakahara, T. Kuwana, Y. Takagi, Abstr. No. 3K07, 35th National Meeting of the Chemical Society of Japan, Sapporo, Aug. 1976; b) In the vapor-phase pyrolysis of **6**, it was found that **6d** lost olefine at 550 °C more easily than **6b**, and that **6c** eliminated an appreciable amount of ethylene to give **6b**, which was analyzed by means of GLC. A more detailed investigation is in progress; c) In the vapor-phase pyrolysis at 600 °C, butylpyrazine produced propylene, pyrazine, methylpyrazine, ethylpyrazine, and propylpyrazine; the 2,5-dibuthylpyrazines reacted similarly. A more detailed investigation of this is also in progress.

14) G. W. H. Cheeseman, *J. Chem. Soc.*, **1960**, 242.

15) R. D. Chambers, J. R. Maslakiewicz, and K. C. Srivastava, *J. Chem. Soc., Perkin Trans. I*, **1975**, 1130.

16) T. A. Aganova, F. N. Vishnevskii, G. Ya. Zhigalin, I. I. Skorokhodov, and M. V. Sobolevskii, *Zh. Obshch. Khim.*, **46**, 2034 (1976); *Chem. Abstr.*, **86**, 29238v.

17) T. M. Muinov, *Izv. Akad. Nauk Tadzh. SSR, Otd. Fiz. —Mat. Geol. —Khim. Nauk*, **1976**, 108; *Chem. Abstr.*, **86**, 90676c.

18) S. Dilliand and E. Patsalldes, *Aust. J. Chem.*, **29**, 2369 (1976).

19) At 16 eV, each of the compounds, **1b**—**1d**, **4c**, and **5b**, produced a daughter ion by McLafferty rearrangement as a base peak. The corresponding ion abundances for **6c**, however, was only 1 Σ_{26}%.

20) R. E. Evans and K. N. Mewett, *Aust. J. Chem.*, **25**, 2671 (1972).

21) H. I. X. Mager and W. Berends, *Recl. Trav. Chem. Pays-Bas.*, **77**, 827 (1958).

22) G. T. Newbold and F. F. Spring, *J. Chem. Soc.*, **1947**, 373.

23) K. W. Blake, A. E. A. Porter, and P. G. Sammes, *J. Chem. Soc., Perkin Trans. I*, **1972**, 2494.

24) G. Karmas and P. E. Spoerri, *J. Am. Chem. Soc.*, **74**, 1580 (1952).

25) The details will be reported in the near future.

26) A. E. Erikson and P. E. Spoerri, *J. Am. Chem. Soc.*, **68**, 400 (1946).

$RhCl(PPh_3)_3$-catalyzed Coupling of Diorganomercurials

Kentaro TAKAGI, Naomi HAYAMA, Tadashi OKAMOTO,* Yasumasa SAKAKIBARA,** and Shinzaburo OKA*

College of Liberal Arts and Science, Okayama University, Tsushima, Okayama 700

(Received March 11, 1977)

$RhCl(PPh_3)_3$ has been proved to be an effective catalyst for the reaction of various diorganomercurials to give such coupling products as conjugated diyne, conjugated diene, biaryl, and alkane in good yields under mild conditions. A probable mechanism including the oxidative addition of organomercurials to a rhodium complex and the subsequent reaction of two oxidative-addition adducts to yield the product was presented.

Organomercurials are attractive substrates for organic syntheses,[1] since pure substances, including configurationally pure ones,[2] are easily obtainable. In our previous study of the palladium(0)-catalyzed reaction of organomercurials with acyl halides, the coupling product of organomercurial (R–R) was obtained in a rather large quantity, accompanied by the desired ketone:[3]

$$R_2Hg + R'COBr \xrightarrow{Pd(PPh_3)_4} RCOR' + R\text{–}R \quad \text{(minor product)}$$

As for the decomposition of organomercurials, it is well known that it occurs only at elevated temperatures (generally above 300 °C). In the presence of some transition-metal compounds (Pt, Pd, Ag) the required temperature for the decomposition was lowered, but the conditions were still very drastic.[4] We examined the reaction in detail for the purpose of obtaining the coupling product under mild conditions and found that tris(triphenylphosphine)chlororhodium ($RhCl(PPh_3)_3$) is particularly effective for the reaction. While we have been continuing our study, several papers concerning the palladium-assisted coupling of organomercurials have appeared.[5] Here in this paper we will report the rhodium-catalyzed coupling of organomercurials, which is a more convenient system for the reaction.[6]

Results and Discussion

Reaction Conditions. The decomposition of diphenylmercury was examined with various catalysts and solvents; the results are compared in Table 1. The control experiment showed that a catalyst was essential for the reaction under the conditions examined. The decomposition of $Pd(PPh_3)_4$ occurred, and the reaction was incomplete (Run 1). $RuCl_2(PPh_3)_3$ showed little activity (Run 4). Contrary to palladium or ruthenium complex, $RhCl(PPh_3)_3$ was very effective as a catalyst and biphenyl was obtained quantitatively (Run 5 and Table 2). This implies that two phenyls in diphenylmercury are available for the reaction. Mercury metal was also separated quantitatively. Thus, the stoichiometry of rhodium-catalyzed coupling can be represented by the following equation:

$$(C_6H_5)_2Hg \xrightarrow{RhCl(PPh_3)_3} (C_6H_5)_2 + Hg$$

Table 1. Catalytic coupling of Ph_2Hg[a]

Run	Catalyst	Solvent	Time h	Biphenyl[b] %
1	$Pd(PPh_3)_4$	HMPA	4	13
2	$Pd(PPh_3)_4$	CH_3CN	8	31
3	$Pd(PPh_3)_4$	THF	8	16
4	$RuCl_2(PPh_3)_4$	HMPA	4	1
5	$RhCl(PPh_3)_3$	HMPA	4	100
6	$RhCl(PPh_3)_3$	CH_3CN	4	96
7	$RhCl(PPh_3)_3$	DMF	15	36
8	$RhCl(PPh_3)_3$	DMSO	4	20
9	$RhCl(PPh_3)_3$	toluene	4	13
10	$RhCl(PPh_3)_3$	THF	4	4
11[c]	$RhCl(PPh_3)_3$	HMPA	4	49
12[d]	$RhCl(PPh_3)_3$	HMPA	4	10
13[e]	$RhCl(PPh_3)_3$	HMPA	1	8

a) Catalyst; 0.0065 mmol, Ph_2Hg; 0.25 mmol, solvent; 2 ml, temp.; 80 °C, under N_2. b) GLC analysis using an internal standard. c) PPh_3; 0.065 mmol. d) Under air. e) Galvinoxyl; 0.04 mmol.

Amoung the solvents examined, HMPA and acetonitrile gave better results. The reaction was pronouncedly retarded with galvinoxyl or oxygen. Inhibition by excess triphenylphosphine was also observed.

Syntheses of Conjugated Diynes, Conjugated Dienes, Biaryls, and Alkanes. Rhodium-catalyzed coupling was applied to the syntheses of various hydrocarbons. The results are listed in Table 2. In all cases, pure products were isolated with simple treatments. Thus, this catalytic reaction may be valuable for the syntheses of symmetrical conjugated diyne, symmetrical conjugated diene, and biaryl. The case of dibutylmercury was exceptional; the coupling product, octane, was never detected, as is shown in Run 25, although dibutylmercury undoubtedly reacted with the rhodium catalyst, even at room temperature. The red color of the catalyst

Table 2. $RhCl(PPh_3)_3$-catalyzed synthesis of diyne, diene, biaryl, and alkane

Run	R_2Hg R	Temp °C	Time h	R_2Hg/Rh mol ratio	R–R %
21	PhC≡C	50	1	200	95
22	(*E*)-PhCH≡CH	70	1	50	99[a]
23	*p*-CH_3–C_6H_4	80	4	30	86
24	*p*-Cl–C_6H_4	80	4	30	91
25	Bu	130	4	30	0[b]
26	$PhCH_2$	130	8	30	44[b]

a) (*E*,*E*). b) GLC analysis using an internal standard.

* Institute for Chemical Research, Kyoto University, Uji, Kyoto 611.

** Chemical Laboratory of Textile Fibers, Kyoto University of Industrial Arts and Textile Fibers, Kyoto 606.

immediately changed into black when dibutylmercury was added. Presumably some side reaction, *e.g.* β-elimination of hydrorhodium in the organorhodium intermediate, would occur preferentially. Dibenzylmercury afforded 1,2-diphenylethane only on being heated to an elevated temperature.

Reaction Mechanism. The initial stage of the reaction is probably an oxidative addition of organomercurials to the rhodium catalyst:

$$R_2Hg + RhCl(PPh_3)_2 \longrightarrow \underset{\mathbf{1}}{(R)(RHg)RhCl(PPh_3)_2} \quad (1)$$

There are examples of the oxidative addition of organomercurials to such transition-metal complexes as Pd, Rh, Ir, and Pt.[7] The present result of the supression of the catalytic reaction by the addition of triphenylphosphine supports the idea.[8]

The coupling products are expected to be produced by the reaction of the oxidative-addition adduct(s). There is evidence that the reaction is not such a simple unimolecular demercuration as is shown in Eq. 2, which was suggested by Birch *et al.* for the reaction of Ref. 5a:[9]

$$R_2Hg + Rh \longrightarrow \underset{\mathbf{1}}{R\text{-}Rh\text{-}HgR} \xrightarrow{-Hg} R\text{-}Rh\text{-}R \longrightarrow R\text{-}R + Rh \quad (2)$$

A competitive reaction of an equimolar mixture of diphenylmercury and bis(*p*-tolyl)mercury afforded biphenyl, 4-methylbiphenyl, and 4,4′-dimethylbiphenyl (Table 3). The statistical ratio in diaryls indicates that the catalytic reaction does not follow Eq. 2; if it did, the molar ratio of Ph–Ph: Ph–Tol: Tol–Tol should be 1: 0: 1. Here, it should be noticed that the redistribution between diphenylmercury and bis(*p*-tolyl)mercury does not take place rapidly.[10]

Table 3. Competitive reaction of Ph_2Hg and $(p\text{-Tol})_2Hg$[a]

$$Ph_2Hg + (p\text{-Tol})_2Hg \xrightarrow{Rh} Ph\text{-}Ph + Ph\text{-}Tol\text{-}p + p\text{-}Tol\text{-}Tol\text{-}p$$

Conversion[b] %	Relative mol ratio		
	Ph–Ph	Ph–Tol-*p*	*p*-Tol–Tol-*p*
8	1.3	2.0	0.9
30	1.3	2.0	0.8
90	1.1	2.0	1.0

a) Ph_2Hg; 0.1 mmol, $(p\text{-Tol})_2Hg$: 0.1 mmol, $RhCl(PPh_3)_3$; 0.0065 mmol, HMPA; 2 ml, 80 °C, under N_2. b) Converison based on Ph_2Hg consumed.

At the present time, we propose the next reaction as the most plausible mechanism for the reductive elimination; in this reaction two molecules of **1** yield a coupling product:

$$2\underset{\mathbf{1}}{(R)(RHg)RhCl(PPh_3)_2} \longrightarrow R\text{-}R + 2RhCl(PPh_3)_2 + R_2Hg + Hg \quad (3)$$

Similar "complex" bimolecular reactions yielding organic coupling products are frequently found in organo-transition metal chemistry.[12]

Experimental

Materials. Commercial diphenylmercury and galvinoxyl were used without further purification. The $RhCl(PPh_3)_3$,[13] $RuCl_2(PPh_3)_3$,[14] $Pd(PPh_3)_4$,[15] and bis(2-phenylethynyl)mercury[16] were prepared by previously reported methods. The other organomercurial was prepared from a Grignard reagent and $HgCl_2$ according to a procedure in the literature[17] and was distilled or recrystallized from ethanol or benzene. The solvents were dried over a molecular sieve (3A).

Procedure. Preparation of Biphenyl: In a typical run (Run 5), a solution of diphenylmercury (89 mg, 0.25 mmol), $RhCl(PPh_3)_3$ (6 mg, 0.0065 mmol), and HMPA (2 ml) was stirred at 80 °C for 4 h under nitrogen. After the mercury metal had then been separated by decantation, aqueous sodium chloride (5 ml, 12.5%) was added to the resulting solution, and the organic materials, extracted with 4 ml of ether, were washed with 5 ml of 12.5% aqueous sodium chloride. Then the ether layer was treated with an ether solution of iodine to decompose the unreacted diphenylmercury. Subsequent analysis by GLC (Hitachi Perkin-Elmer F6D, 35% silicon DC 200 on Celite 545, 1 m, 170 °C, 0.5 kg cm^{-2} of N_2) revealed 38.6 mg (0.25 mmol) of biphenyl and a trace amount of iodobenzene. The separated mercury metal, after it had been washed several times with acetone and air-dried, weighed 48.2 mg (0.24 mmol).

Preparation of 1,4-Diphenyl-1,3-butadiyne: A mixture of bis(2-phenylethynyl)mercury (503.5 mg, 1.25 mmol), $RhCl(PPh_3)_3$ (6 mg, 0.0065 mmol), and HMPA (3 ml) was stirred at 50 °C for 1 h under nitrogen. Aqueous sodium chloride (10 ml, 12.5%) was then added to the mixture, and the organic materials were extracted with 10 ml of ether. The aqueous layer was extracted two times with 5-ml portions of ether. After the ether extract had been washed with two 5-ml portions of 12.5% aqueous sodium chloride, the ether was removed under reduced pressure. The purification of the residual solid by column chromatography on silica gel (2 g), using hexane as the eluant, gave 239 mg of 1,4-diphenyl-1,3-butadiyne (94.5%). Mp 86—86.5 °C (lit,[18] 87—88 °C) Found: C 95.13; H, 4.90%. Calcd for $C_{16}H_{10}$: C, 95.01; H, 4.99%.

Preparation of (E,E)-1,4-Diphenyl-1,3-butadiene: A mixture of bis((*E*)-2-phenylethenyl)mercury (101.7 mg, 0.25 mmol), $RhCl(PPh_3)_3$ (4.6 mg, 0.005 mmol), and HMPA (1 ml) was stirred at 70 °C for 1 h under nitrogen. Treatment similar to that described above gave 50.4 mg of (*E,E*)-1,4-diphenylbutadiene (99%). Mp 153.5—154 °C (lit,[19] 153—153.5 °C) Found: C, 93.16; H, 6.86%. Calcd for $C_{16}H_{14}$: C, 93.15; H, 6.85%.

Preparation of 4,4′-Dimethylbiphenyl: A mixture of bis(*p*-tolyl)mercury (574.8 mg, 1.50 mmol), $RhCl(PPh_3)_3$ (46.3 mg, 0.050 mmol), and HMPA (5 ml) was stirred at 80 °C for 4 h under nitrogen. Treatment similar to that above gave 234 mg of 4,4′-dimethylbiphenyl (86%). Mp 121.5 °C (lit,[20] 122 °C). Found: C, 91.97; H 7.86%. Calcd for $C_{14}H_{14}$: C, 92.24; H, 7.76%.

Preparation of 4,4′-Dichlorobiphenyl: A mixture of bis(*p*-chlorophenyl)mercury (635.4 mg, 1.50 mmol), $RhCl(PPh_3)_3$ (46.0 mg, 0.050 mmol), and HMPA (5 ml) was stirred at 80 °C for 5 h under nitrogen. Treatment similar to that above gave 304 mg of 4,4′-dichlorobiphenyl (91%). Mp 147—147.5 °C (lit,[21] 147—148 °C). Found: C, 64.55; H, 3.63%. Calcd for $C_{12}H_8Cl_2$: C, 64.60; H, 3.62%.

References

1) For example, D. E. Bergstrom and J. L. Ruth, *J. Am. Chem. Soc.*, **98**, 1587 (1976); A. J. Bloodworth and M. E. Loveitt, *J. Chem. Soc., Chem. Commun.*, **1976**, 94; H. Horino and N. Inoue, *ibid.*, **1976**, 500; R. C. Larock and J. C. Bernhardt, *Tetrahedron Lett.*, **1976**, 3097.

2) R. C. Larock and H. C. Brown, *J. Organomet. Chem.*, **36**, 1 (1972); R. C. Larock, S. K. Gupta, and H. C. Brown, *J. Am. Chem. Soc.*, **94**, 4371 (1972).

3) K. Takagi, T. Okamoto, Y. Sakakibara, A. Ohno, S. Oka, and N. Hayama, *Chem. Lett.*, **1975**, 951.

4) L. G. Makarova and A. N. Nesmeyanov,"The Organic Compounds of Mercury," (English translation), North Holland Publishing Co., Amsterdam (1967), p. 409.

5) a) $Pd(PPh_3)_4$-catalyzed reaction of divinylmercury: E. Vedejs and P. D. Weeks, *Tetrahedron Lett.*, **1974**, 3207; b) Pd(II)-assisted stoichiometric reaction of vinylmercury: R. C. Larock, *J. Org. Chem.*, **41**, 2241 (1976); c) Pd(II)-assisted stoichiometric reaction of arylmercury: R. A. Kretchmer and R. Glowinski, *ibid.*,**41**, 2661 (1976); see also M. O. Unger and R. A. Fouty, *ibid.*, **34**, 18 (1969).

6) More recently, a review article has appeared describing the effectiveness of the rhodium complex for a similar coupling reaction: R. C. Larock,"New Applications of Organometallic Reagents in Organic Synthesis," ed by D. Seyferth, Elsevier, Amsterdam (1976), p. 271.

7) Ir, Rh: G. M. Intille and M. J. Braithwaite, *J. Chem. Soc., Dalton Trans.*, **1972**, 645; Pt, Pd: V. I. Sokolov, V. V. Bashilov, L. M. Anishchenko, and O. A. Reutov, *J. Organomet. Chem.*, **71**, C41 (1974); Rh: W. C. Baird, Jr., and J. H. Surridge, *J. Org. Chem.*, **40**, 1364 (1975).

8) For example, J. Halpern and C. S. Wong, *J. Chem. Soc., Chem. Commun.*, **1973**, 629; J. Halpern, T. Okamoto, and A. Zakhariev, *J. Mol. Catal.*, **1** (1976).

9) A. J. Birch and I. D. Jenkins,"Transition Metal Organometallics in Organic Synthesis," Vol. 1, ed by H. Alper, Academic Press, New York (1976), p. 11.

10) The GLC analysis of the reaction solution at an 8% conversion (Table 3) revealed *ca.* 0.002 mmol of (Ph)(*p*-Tol)Hg. Thus, the coupling was accompanied by a slow catalytic redistribution[11] (see Eq. 3). The analysis (Hitachi 163, 2% silicon OV-17 on Chromosorb W, 1 m, 200 °C, 15 ml min^{-1} of N_2), however, is not very accurate because some redistribution occurs in the GLC column.

11) The non-catalytic redistribution between diorganomercurials fails when the organo groups are similar in size and nature. Subsequently, diphenylmercury and bis(tolyl)-mercury never form phenyltolylmercury: J. C. Lockhart, *Chem. Rev.*, **65**, 131 (1965); B. J. Aylett, "Comprehensive Inorganic Chemistry," Vol. 3, ed by J. C. Bailar, Jr., H. J. Emeleus, R. Nyholm, and A. F. Trontman-Dickenson, Pergamon Press, Oxford (1973), p. 321.

12) For example, P. M. Maitlis,"The Organic Chemistry of Palladium," Vol. 2, Academic Press, New York (1971), p. 64; F. R. S. Clark, R. O. C. Norman, and C. B. Thomas, *J. Chem. Soc., Perkin Trans. I*, **1975**, 121.

13) J. A. Osborn and G. Wilkinson, *Inorg. Synth.*, **10**, 67 (1967).

14) P. S. Hallman, T. A. Stephenson, and G. Wilkinson, *Inorg. Synth.*, **12**, 238 (1970).

15) D. R. Coulson, *Inorg. Synth.*, **13**, 121 (1972).

16) J. R. Johnson and W. L. McEwen, *J. Am. Chem. Soc.*, **48**, 471 (1926).

17) P. Borgstrom and M. M. Dewar, *J. Am. Chem. Soc.*, **51**, 3387 (1929).

18) I. D. Cambell and G. Eglinton, *Org. Synth.*, Coll. Voll., **5**, 518 (1973).

19) F. B. Kipping and J. J. Wren, *J. Chem. Soc.*, **1959**, 2465.

20) F. Kögl and G. C. van Wessem, *Recl. Trav. Chim. Pays-Bas*, **63**, 5 (1944).

21) T. Migita, N. Morikawa, and A. Simamura, *Bull. Chem. Soc. Jpn.*, **36**, 980 (1963).

Imidazopteridines. I. Synthesis of Imidazo[1,2-*c*]pteridine and Its Alkyl Derivatives

Takashi SUGIMOTO, Keiko SHIBATA, and Sadao MATSUURA

Department of Chemistry, College of General Education, Nagoya University, Chikusa-ku, Nagoya 464

(Received March 25, 1977)

The synthesis of imidazo[1,2-*c*]pteridine and its alkyl derivatives is described. The reaction of 4-aminopteridine with chloroacetaldehyde gave the ring-opened 2-formamido-3-(2-imidazolyl)pyrazine and the isomeric 2-amino-3-(1-formyl-2-imidazolyl)pyrazine but no imidazopteridine. 4-Amino-2-methylpteridine and chloroacetaldehyde similarly gave 2-acetamino-3-(2-imidazolyl)pyrazine in high yield. Hydrolysis of these compounds gave 2-amino-3-(2-imidazolyl)pyrazine, which was used as the key intermediate for the synthesis of the title compounds. Thus it reacted with triethyl orthoformate and homologues to give respectively the parent imidazo-[1,2-*c*]pteridine and its 6-methyl and 6-ethyl homologues. Their 2,3-dimethyl derivatives were prepared likewise from 2-amino-3-(2-imidazolyl)-5,6-dimethylpyrazine, which in turn was prepared from 4-amino-6,7-dimethyl- or 4-amino-2,6,7-trimethylpteridine.

Interest in tricyclic imidazoazines with a bridgehead nitrogen atom has been enhanced by the isolation and structural elucidation of the fluorescent imidazo[1,2-*a*]-purines from baker's yeast ^{Phe}t-RNA[1] and *T. utilis* ^{Phe}t-RNA.[2] Also, imidazo[2,1-*i*]purines[3–8] and analogous systems[9,10] have been studied extensively; several phosphate derivatives of ribofuranosyl imidazo[2,1-*i*]-purine have been found to be active in several enzymatic systems.[4,5]

In continuing our research programs on tricyclic imidazoazines,[2,10,11] we became interested in the chemistry and possible biological activities of hitherto unknown imidazopteridines, since several hydrogenated derivatives of imidazo[1,2-*c*]quinazoline, the 1,4-deaza analogues of imidazo[1,2-*c*]pteridine, have interesting pharmacological activities on the central nervous system.[12,13] In this paper we describe the synthesis of the parent imidazo[1,2-*c*]pteridine (**6a**) and some of its alkyl derivatives (**6b**—**f**).

We first attempted to prepare the unsubstituted imidazo[1,2-*c*]pteridine (**6a**) by condensation of 4-aminopteridine (**1a**) with chloroacetaldehyde. The condensation in water gave several fluorescent compounds, but not the desired imidazopteridine (**6a**). From the mixture, three compounds (**A**, **B**, and **C**) were isolated; the remaining were too little to be isolated Compound **A** with the molecular formula $C_8H_7N_5O$ exhibited weak sky blue fluorescence. Acid hydrolysis of **A** in hot dilute hydrochloric acid afforded the intensely blue fluorescent 2-amino-3-(2-imidazolyl)pyrazine (**5a**). The ^{1}H NMR spectrum of **5a** in trifluoroacetic acid showed a singlet at δ 7.41 for both protons of the imidazole ring and a pair of doublets at δ 7.87 and 8.12 (J=3 Hz) for the protons of the pyrazine ring. The results suggest that compound **A** is a formyl derivative of **5a**, either 2-formamido-3-(2-imidazolyl)pyrazine (**2a**) or 2-amino-3-(1-formyl-2-imidazolyl)pyrazine (**3**). We assigned the structure **2a** to this compound, since its ^{1}HNMR spectrum showed a sharp singlet at δ 7.70 for the imidazole ring protons indicating that the two protons are chemically equivalent, a pair of doublets at δ 8.77 and 8.84 (J=3 Hz) for the pyrazine ring protons, and a singlet at δ 9.12 for the formyl group. The second product (**B**) was found to be the isomer of **A** from elemental analysis and gave **5a** on hydrolysis in dilute hydrochloric acid. The ^{1}H NMR spectrum of **B** showed two pairs of AB doublets at δ 7.27 and 7.42 (J=2 Hz) representing the imidazole ring protons and at δ 8.22 and 8.33 (J=3 Hz) representing the pyrazine ring protons, and a singlet at δ 9.54 for the formyl group. This indicates that the protons of the imidazole ring are no longer equivalent, and hence, compound **B** was assigned as 2-amino-3-(1-formyl-2-imidazolyl)pyrazine (**3**).

The third compound (**C**) was yellow, showing λ_{max} at a wavelength longer than **2a**: the neutral molecule absorbed at 371 nm and the cation at 380 nm (see Table 1). The mass spectrum of **C** exhibited the molecular ion(M) peak at *m/e* 221 and M+2 peak with an intensity about one third of the M peak, suggesting that **C** contains a chlorine atom. From these data and the fact that **C** yielded **5a** on heating in 1 M sodium hydroxide at 70 °C, we determined the compound **C** to be 2-(2-chloroethylideneamino)-3-(2-imidazolyl)pyrazine (**4**), a Schiff base formed by the condensation of **5a** with chloroacetaldehyde. This conclusion was supported by the ^{1}H NMR spectrum, in which the 2-chloroethylidene group appears as a set of a doublet at δ 4.00 (J=2 Hz) and a triplet at δ 6.70 (J=2 Hz), the imidazole ring protons as a sharp singlet at δ 7.55, and the pyrazine ring protons as a pair of doublets at δ 7.91 and 8.03 (J=3 Hz).

The relative yield of the three compounds depends a great deal on the acidity of the reaction solution. In general, when the reaction was carried out in a neutral solution at pH 6—7, **2a** was formed as the main product; in contrast, **4** became predominant in an acidic solution at pH 3—4. In either case, **3** was formed only in a small amount.

4-Amino-6,7-dimethylpteridine (**1c**) reacted similarly with chloroacetaldehyde, yielding 2-formamido-3-(2-imidazolyl)-5,6-dimethylpyrazine (**2c**) in a low yield.

It is obvious that these imidazolylpyrazines (**2a**, **3**, and **2c**) were produced by a ring-opening reaction of the initially formed **6a** or **6d** from 4-aminopteridine (**1a**) or the 6,7-dimethyl homologue (**1c**) with chloroacetaldehyde, respectively. This reaction took place most probably *via* a nucleophilic addition of water to the 6,5-double bond of **6a** or **6d**. We therefore expected that introduction of a blocking methyl group[14] at the

site of the nucleophilic addition would impede ring-opening, and accordingly investigated the reaction of of 4-amino-2-methylpteridine (**1b**) with chloroacetaldehyde in order to obtain 6-methylimidazo[1,2-*c*]-pteridine (**6b**). However, although the reaction was carried out under various conditions, no imidazopter-

Table 1. The pK_a values and UV spectra of 2-amino-3-(2-imidazolyl)pyrazines and imidazo[1,2-*c*]pteridines

Compound	pK_a	pH and ionic species[a]	λ_{max} (log ε)[b]
2a	3.13±0.01	1.0 (+)	264(4.04), 311(3.94)
		5.5 (0)	226(4.04), 283(4.10), 339(4.05)
2b	3.84±0.02	1.5 (+)	215(3.79), 265(3.80), 303(4.14)
		6.0 (0)	225(3.85), 283(3.97), 335(3.90)
2c	3.94±0.01	2.0 (+)	266(4.06), 315(4.02)
		6.0 (0)	225(4.03), 284(4.16), 341(4.12)
2d	4.57±0.01	2.0 (+)	214(4.04) ,268(4.01), 311(4.06)
		7.5 (0)	223(4.01), 283(4.16), 333(4.10)
3	3.10±0.01	1.0 (+)	265(4.03), 312(3.92)
		5.5 (0)	226(4.05), 283(4.11), 338(4.06)
4	4.06±0.02	2.0 (+)	256(3.93), 270(3.84), 380(4.03)
		6.0 (0)	216(4.17), 268(3.74), 371(4.12)
5a	0.10±0.05	−2.5 (++)	212(4.00), 254(3.88), 361(4.03)
	3.82±0.02	2.0 (+)	213(3.91), 259(3.95), 353(3.99)
		6.0 (0)	212(3.92), *254(3.91)*, 270(3.90), 359(4.11)
5b	0.53±0.03	−2.5 (++)	213(4.03), 269(4.03), 377(4.16)
	4.33±0.02	2.5 (+)	215(4.01), 264(3.99), 356(4.06)
		6.5 (0)	213(4.01), 270(4.02), 363(4.16)
6a[c]		MeOH	218(4.25), 261(3.96), 304(3.66), 345(3.90)
6b	2.21±0.01	0.0 (+)	215(4.27), 266(3.65), 318(3.96)
		4.5 (0)	220(4.31), 262(3.92), *304(3.58)*, 343(3.94)
6c	2.49±0.01	0.5 (+)	214(4.32), *265(3.71)*, 321(4.00)
		4.5 (0)	219(4.32), 262(3.93), *303(3.61)*, 344(3.94)
6d	2.98±0.04	0.5 (+)	214(4.20), 277(3.88), 317(4.00)
		5.0 (0)	225(4.37), 264(3.88), 304(3.72), 343(3.96)
6e	2.84±0.01	0.5 (+)	220(4.48), 272(3.72), *281(3.70)*, 326(4.11), *341(4.09)*
		5.0 (0)	225(4.43), 262(3.86), *301(3.69)*, 344(4.05)
6f	3.02±0.01	1.0 (+)	220(4.45), 271(3.71), *280(3.70)*, 326(4.10), *340(4.00)*
		5.0 (0)	224(4.42), 261(3.85), *300(3.68)*, 344(4.04)

a) Negative figures are H_0 values; ionic species are shown by 0 (neutral molecule), + (monocation), and ++ (dication). b) Wavelength in nm and inflexions or shoulders in italics. c) Accurate pK_a value could not be obtained. The observed pK_a value was 2.65±0.13 and the UV spectra at pH 1.0 (+) : 220(4.48), 272 (3.72), *281(3.70)*, 317(4.00); at pH 5.0 (0) : 225(4.43), 262(3.86), *301(3.69)*, 344(4.05) were recorded.

Table 2. The ^{1}H NMR spectra of 2-amino-3-(2-imidazolyl)pyrazines and imidazo[1,2-*c*]pteridines

Compound	Solvent	δ[a]
2a	TFA-*d*	7.70(s, 2), 8.77(d, J=3, 1), 8.84(d, J=3, 1), 9.12(s, 1)
2b	TFA-*d*	2.39(s, 3), 7.50(s, 2), 8.62(d, J=3, 1), 8.76(d, J=3, 1)
2c	TFA-*d*	2.74(s, 3), 2.96(s, 3), 7.53(s, 2) 8.07(d, J=3, 1), 8.37(d, J=3, 1), 9.58(s, 1)
2d	TFA-*d*	2.39(s, 3), 2.72(s, 3), 2.77(s, 3), 7.51(s, 2)
3[b]	Acetone-d_6	7.27(d, J=2, 1), 7.42(d, J=2, 1), 8.22(d, J=3, 1), 8.33(d, J=3, 1), 9.54(s, 1)
4	TFA-*d*	4.00(d, J=2, 2), 6.70(t, J=2, 1), 7.55(s, 2), 7.91(d, J=3, 1), 8.03(d, J=3, 1)
5a	TFA-*d*	7.41(s, 2), 7.87(d, J=3, 1), 8.12(d, J=3, 1)
5b	TFA-*d*	2.53(s, 3), 2.64(s, 3), 7.44(s, 2)
6a[b]	DMSO-d_6	7.79(d, J=2, 1), 8.24(d, J=2, 1), 8.97(s, 2), 9.54(s, 1)
6b[b]	DMSO-d_6	2.95(s, 3), 7.81(d, J=2, 1), 8.25(d,J=2, 1), 8.94(s, 2)
6c[b]	DMSO-d_6	1.46(t, J=7, 3), 3.30(q, J=7, 2), 7.82(d, J=2, 1), 8.31(d, J=2, 1), 8.94(s, 2)
6d[b]	DMSO-d_6	2.69(s, 3), 2.72(s, 3), 7.71(d, J=2, 1), 8.17(d, J=2, 1), 9.45(s, 1)
6e[b]	DMSO-d_6	2.68(s, 3), 2.52(s, 3), 2.91 (s, 3), 7.75(d, J=2, 1), 8.17(d, J=2, 1)
6f[b]	DMSO-d_6	1.43(t, J=7, 3), 3.25(q, J=7, 2), 2.68(s, 3), 2.72(s, 3), 7.74(d, J=2, 1), 8.21 (d, J=2, 1)

a) Relative to TMS; coupling constants(J) in Hz. Suffixes: s, singlet; d, doublet; t, triplet; q, quartet.
b) Measured on a Varian HA-100 NMR spectrometer.

idine was obtained. Instead, only the ring-opened 2-acetamido-3-(2-imidazolyl)pyrazine (**2b**) was obtained in a high yield from **1b** and chloroacetaldehyde. The location of the acetyl group on the amino group, as in **2a**, was confirmed by the ^{1}H NMR spectrum which exhibits a sharp singlet at δ 7.50 for both protons of the imidazole ring (see Table 2).

4-Amino-2,6,7-trimethylpteridine (**1d**) and chloroacetaldehyde similarly gave 2-acetamido-3-(2-imidazolyl)-5,6-dimethylpyrazine (**2d**). Both **2b** and **2d** were converted in high yield into their 2-amino analogues (**5a** and **5b**), respectively, by boiling in dilute hydrochloric acid.

We then used the aminoimidazolylpyrazines (**5a** and **5b**) for the synthesis of imidazo[1,2-*c*]pteridine (**6a**) and its alkyl homologues and found that they are excellent precursors. Heating **5a** in a mixture of triethyl orthoformate and toluene under reflux gave the parent compound (**6a**) in a high yield. The compound was unstable in an aqueous solution, undergoing the ring-opening reaction. The change could be easily monitored by TLC on a Merck silica gel G plate developed by ethyl acetate.

Synthesis of 6-methylimidazo[1,2-*c*]pteridine (**6b**) from **5a** and triethyl orthoacetate required more severe conditions: **5a** was boiled in the ortho ester in the presence of trifluoroacetic acid as a catalyst. In the absence of the catalyst, **5a** was converted only to a small extent into **6b** after prolonged refluxing. Triethyl orthopropionate and **5a** similarly gave 6-ethylimidazo-[1,2-*c*]pteridine (**6c**). Likewise, their 2,3-dimethyl derivatives (**6d**, **6e**, and **6f**) were synthesized by the reaction of **5b** with an appropriate ortho ester. The structures of these imidazo[1,2-*c*]pteridines (**6a**—**f**) were confirmed by elemental analyses, pK_a values (Table 1), UV spectra (Table 1), and ^{1}HNMR spectra (Table 2).

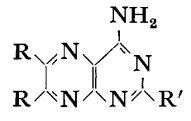

1

	R	R′
a:	H	H
b:	H	CH_3
c:	CH_3	H
d:	CH_3	CH_3

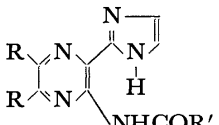

2

	R	R′
a:	H	H
b:	H	CH_3
c:	CH_3	H
d:	CH_3	CH_3

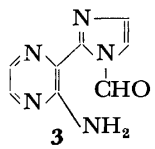

3

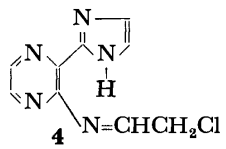

4

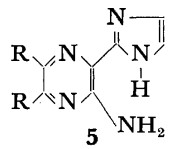

5

a: R=H
b: R=CH_3

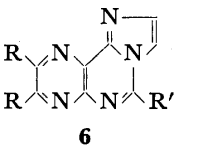

6

	R	R′
a:	H	H
b:	H	CH_3
c:	H	CH_2CH_3
d:	CH_3	H
e:	CH_3	CH_3
f:	CH_3	CH_2CH_3

Experimental

The elemental analyses were carried out at the Analytical Section, Faculty of Agriculture, Nagoya University, and at the Analytical Section, Meijo University, Nagoya. The pK_a values were determined by a spectroscopic method and the UV spectra on a JASCO UVIDEC-1 spectrophotometer. The ^{1}H NMR spectra were determined on a JEOL JNM-MH-60 or Varian HA-100 NMR spectrometer with TMS as an internal standard.

*2-Formamido-3-(2-imidazolyl)pyrazine (**2a**) and 2-Amino-3-(1-formyl-2-imidazolyl)pyrazine(**3**).* A solution of 4-aminopteridine[15] (0.50 g) and chloroacetaldehyde (50% aqueous solution, 5 g) in water (150 ml) was kept at 60 °C for 5 h; during this time the solution was maintained at pH 6—7 with sodium acetate. After being chilled in a refrigerator overnight, the solid (0.25 g) was collected by filtration. The solid was extracted with hot ethyl acetate to remove a little insoluble material and then chromatographed on five Merck silica gel 60 PLC plates (20×20 cm) using ethyl acetate as a solvent to give **2a** (150 mg) and **3** (15 mg). The main product (**2a**) melted at 214—215 °C (from ethyl acetate) (Found: C, 50.95; H, 3.57; N, 37.03%. Calcd for $C_8H_7N_5O$: C, 50.77; H, 3.74; N, 37.03%). The isomer (**3**) melted at 228—228.5 °C (from ethyl acetate) (Found: C, 50.62; H, 3.56; N, 36.99%).

*2-(2-Chloroethylideneamino)-3-(2-imidazolyl)pyrazine (**4**).* A solution of 4-aminopteridine (0.50 g) and chloroacetaldehyde (50%, 2 g) in water (150 ml) was kept at 60 °C for 24 h without the addition of alkali for neutralization; the pH of the solution reached *ca.* 3 at the end of the reaction. After neutralization with sodium acetate, the solution was concentrated to *ca.* 30 ml under reduced pressure and chilled to give a solid. Crystallization of the solid from methanol (about 50 ml) gave crude **2a**. The mother liquor was concentrated to *ca.* 10 ml and chilled to give yellow needles (0.18 g) of **4**, mp 173—173.5 °C (from ethyl acetate) (Found: C, 48.78; H, 3.71; N, 31.48%. Calcd for $C_9H_8ClN_5$: C, 48.76; H, 3.64; N, 31.61%).

*2-Formamido-3-(2-imidazolyl)-5,6-dimethylpyrazine (**2c**).* A solution 4-amino-6,7-dimethylpteridine[16] (0.40 g) and chloroacetaldehyde (50%, 20 g) in water (300 ml) was maintained at 60 °C for 10 h. The pH of the solution was adjusted at 6—7 with sodium acetate and then the solution was concentrated to *ca.* 50 ml under reduced pressure. A small amount of solid was removed by filtration and the filtrate was chilled in a refrigerator overnight to give a solid. The solid was purified by preparative layer chromatography (PLC) as above to give almost colorless needles (80 mg) of **2c**, mp 218.5—220 °C (from ethyl acetate) (Found: C, 55.29; H, 4.98; N, 32.22%. Calcd for $C_{10}H_{11}N_5O$: C, 55.29; H, 5.10; N, 32.24%).

*2-Acetamido-3-(2-imidazolyl)pyrazine (**2b**).* A solution of 4-amino-2-methylpteridine[17] (1.0 g) and chloroacetaldehyde (50%, 10 g) in water (200 ml) was heated at 60 °C for 5 h. The solution was neutralized with sodium acetate, concentrated to *ca.* 60 ml under reduced pressure, and chilled to give colorless needles (0.75 g) of **2b**, mp 227—228 °C (from methanol) (Found: C, 53.57; H, 4.48; N, 34.39%. Calcd for $C_9H_9N_5O$: C, 53.19; H, 4.47; N, 34.47%).

*2-Acetamido-3-(2-imidazolyl)-5,6-dimethylpyrazine (**2d**).* Replacement of 4-amino-2-methylpteridine by 4-amino-2,6,7-trimethylpteridine[18] (1.0 g) in the foregoing reaction gave colorless needles (0.76 g) of **2d**, mp 218—219 °C (from methanol) (Found: C, 57.33; H, 5.64; N, 30.08%. Calcd for $C_{11}H_{13}N_5O$: C, 57.12; H, 5.68; N, 30.29%).

2-Amino-3-(2-imidazolyl)pyrazine (5a). A solution of **2b** (200 mg) in 0.1 M hydrochloric acid (20 ml) was heated under reflux for 4 h. The solution was made alkaline with ammonia and chilled to give slightly yellow leaflets (160 mg) of **5a**. The analytical sample was prepared by sublimation at 140 °C/2 mmHg, mp 203—203.5 °C(Found: C, 52.25; H, 4.41; N, 43.64%. Calcd for $C_7H_7N_5$: C, 52.16; H, 4.39; N, 43.46%).

The same compound was obtained in a similar way from **2a** in 92% yield and from **3**. Heating of **4** in 1 M sodium hydroxide at 70 °C for 20 h and subsequent extraction with ether afforded **5a** in 80% yield.

2-Amino-3-(2-imidazolyl)-5,6-dimethylpyrazine (5b). A solution of **2d** (200 mg) in 1 M hydrochloric acid (40 ml) was heated at 80 °C for 4 h. The solution was evaporated to dryness under reduced pressure at *ca.* 40 °C. The residue, dissolved in water (10 ml) and made alkaline with ammonia, gave slightly yellow leaflets (130 mg) of **5b**, mp 226—226.5 °C (sublimed at 140 °C/2 mmHg)(Found: C, 57.23; H, 6.01; N, 37.04%. Calcd for $C_9H_{11}N_5$: C, 57.11; H, 5.87; N, 37.01%).

The same compound was obtained in 93% yield by boiling **2C** (90 mg) in 0.1 M hydrochloric acid (5 ml) under reflux for 4 h, followed by neutralization with ammonia and chilling in a refrigerator.

Imidazo[1,2-c]pteridine (6a). 2-Amino-3-(2-imidazolyl)-pyrazine (80 mg) was dissolved in triethyl orthoformate (60 ml) by gentle heating. After addition of toluene (30 ml), the solution was heated under reflux for 24 h. The solution was evaporated to dryness under reduced pressure and the residue triturated with a small amount of ethyl acetate and filtered. Sublimation of the solid at 180 °C/2 mmHg gave a colorless solid (60 mg), analytically pure **6a**, mp 303—304 °C (dec) (Found: C, 56.25; H, 2.90; N, 40.93%. Calcd for $C_8H_5N_5$: C, 56.13; H. 2.95; N, 40.92%).

6-Methylimidazo[1,2-c]pteridine (6b). To a solution of **5a** (65 mg) in triethyl orthoacetate (20 ml) was added trifluoroacetic acid (30 μl). The solution was heated under reflux for 2.5 h. After cooling, the solution was diluted with acetone (60 ml), treated with Dowex 1X2 anion exchange resin(OH form) for neutralization, and then evaporated to dryness under reduced pressure. The residue was triturated with cold ethanol (2 ml) and filtered to give colorless needles (45 mg) of **6b**, mp 278—279 °C (dec)(sublimed at 180 °C/2 mmHg)(Found: C, 58.42; H, 3.87; N, 37.72%. Calcd for $C_9H_7N_5$: C, 58.36; H, 3.82; N, 37.82%).

6-Ethylimidazo[1,2-c]pteridine (6c). Aminoimidazolyl-pyrazine(**5a**)(160 mg), trifluoroacetic acid (160 μl), and triethyl orthopropionate (30 ml) were heated under reflux for 7 h. After dilution with acetone (100 ml) and neutralization with Dowex 1X2 resin as above, the solution was evaporated to dryness under reduced pressure. The residue was crystallized from ethyl acetate to give colorless prisms (155 mg) of **6c**, mp 184—184.5 °C (sublimed at 155 °C/2 mmHg)(Found: C, 60.58; H, 4.52; N, 35.16%. Calcd for $C_{10}H_9N_5$: C, 60.28; H, 4.52; N, 35.16%).

2,3-Dimethylimidazo[1,2-c]pteridine (6d). A solution of **5b** (100 mg) in triethyl orthoformate (10 ml) and toluene (30 ml) was heated under reflux for 9 h. Evaporation to dryness under reduced pressure and subsequent crystallization from toluene gave colorless needles (99 mg) of **6d**, mp 304—305 °C (dec)(sublimed at 200 °C/2 mmHg)(Found: C, 59.90; H, 4.56; N, 35.38%. Calcd for $C_{10}H_9N_5$: C, 60.28; H, 4.52; N, 35.16%).

2,3,6-Trimethylimidazo[1,2-c]pteridine (6e). A solution of **5b** (65 mg) in a mixture of triethyl orthoacetate (30 ml) and trifluoroacetic acid (50 μl) was heated under reflux for 6 h. Dilution with acetone (50 ml), neutralization with Dowex 1X2 resin, and evaporation to dryness under reduced pressure gave a solid. The solid was crystallized from ethanol to give colorless needles (47 mg) of **6e**, mp 308—309 °C (dec)(sublimed at 195 °C/2 mmHg)(Found: C, 62.01; H, 5.28; N, 32.61%. Calcd for $C_{11}H_{11}N_5$: C, 61.94; H, 5.21; N, 32.84%).

6-Ethyl-2,3-dimethylimidazo[1,2-c]pteridine (6f). A solution of **5b** (320 mg) and trifluoroacetic acid (300 μl) in triethyl orthopropionate (30 ml) was heated under reflux for 5 h. The solution was chilled to give slightly brown prisms (280 mg) which were collected by filtration and washed with ether. The prisms were then dissolved in cold ethanol and treated with Dowex 1X2 anion exchange resin (OH form) till the solution became neutral. After removal of the resin by filtration, the filtrate was evaporated to dryness under reduced pressure and the residue was triturated with a little ether. The solid was collected by filtration and sublimed at 160 °C/2 mmHg to give colorless needles (250 mg) of **6f**, mp 235—235.5 °C(Found: C, 63.50; H, 5.84; N, 30.96%. Calcd for $C_{12}H_{13}N_5$: C, 63.41; H, 5.78; N, 30.82%).

We thank Miss N. Itoh for measuring the pK_a values and UV spectra, Dr. D. Uemura for measuring the 100 MHz ^{1}HNMR spectra, and Prof. T. Sakaki for his interest in this work. We are also grateful to Dr. D. J. Brown, Australian National University, for his disucssion.

References

1) K. Nakanishi, N. Furutachi, M. Funamizu, D. Grundeger, and I. B. Weinstein, *J. Am. Chem. Soc.*, **92**, 7617 (1970).
2) H. Kasai, M. Goto, S. Takemura, T. Goto, and S. Matsuura, *Tetrahedron Lett.*, **1971**, 2725.
3) N. K. Kochetkov, V. N. Shibaev, and A. A. Kost, *Tetrahedron Lett.*, **1971**, 1993.
4) J. A. Secrist III, J. R. Barrio, N. J. Leonard, and G. Weber, *Biochemistry*, **11**, 3499 (1972).
5) J. A. Secrist III, J. R. Barrio, and N. J. Leonard, *Science*, **175**, 646 (1972).
6) K. -F. Yip and K. -C. Tsou, *J. Org. Chem.*, **40**, 1066 (1975).
7) R. B. Meyer, Jr., D. A. Shuman, R. K. Robins, J. P. Miller, and L. N. Simon, *J. Medicinal Chem.*, **16**, 1319 (1973).
8) G. B. Chheda, S. P. Dutta, A. Metteleman, and L. Baczynsyj, *Tetrahedron Lett.*, **1974**, 433.
9) K. Senga, R. K. Robins, and D. E. O'Brien, *J. Heterocyclic Chem.*, **12**, 1043 (1975).
10) T. Sugimoto and S. Matsuura, *Bull. Chem. Soc. Jpn.*, **50**, 1359 (1977).
11) H. Kasai. M. Goto, K. Ikeda, M. Zama, Y. Mizuno, S. Takemura, S. Matsuura, T. Sugimoto, and T. Goto, *Biochemistry*, **15**, 898 (1976).
12) O. Schindler, U. S. Patent, 3309369; *Chem. Abstr.*, **67**, 73617 (1967).
13) T. S. Sulkowski and S. J. Childress, U. S. Patent, 3329679; *Chem. Abstr.*, **68**, 49646 (1968).
14) A. Albert and W. L. F. Armarego, *Adv. Heterocyclic Chem.*, **4**, 1 (1965).
15) A. Albert, D. J. Brown, and G. Cheeseman, *J. Chem. Soc.*, 474 (1951).
16) J. W. Daly and B. E. Christensen, *J. Am. Chem. Soc.*, **78**, 225 (1956).
17) R. M. Evans, P. G. Jones, P. J. Palmer, and F. F. Stephens, *J. Chem. Soc.*, **1956**, 4106.
18) J. Weinstock, R. Y. Dunoff, J. E. Carevic, J. G. Williams, and A. J. Villani, *J. Medicinal Chem.*, **11**, 618 (1968).

Preparation and the Properties of π-Allylic Palladium(II) Complexes of Amino Acid

Yoshihiro NAKAGAWARA, Kiyoshi KIKUKAWA, Makoto TAKAGI, and Tsutomu MATSUDA

Department of Organic Synthesis, Faculty of Engineering, Kyushu University, Hakozaki, Higashi-ku, Fukuoka 812

(Received March 29, 1977)

The preparation of π-allylic and related organopalladium(II) complexes with amino acid anions as bidentate ligands is described. The complexes were characterized by means of ^{1}H NMR.

In a previous communication[1] we reported a variable-temperature ^{1}H NMR spectral survey of π-allylic palladium complexes of α-amino acid without giving details of the preparation of the complexes. Some complexes were later found to show an interesting catalytic activity in oligomerizing butadiene preferentially to tetramers.[2] We report herewith on the preparation and characterization of the metal complexes concerned.

Results and Discussion

The principle in preparing the complexes was to displace the di-μ-chloro bridge of dimeric organopalladium complexes by bidentate and chelating amino acid anions. The latter was used as silver salts. After publication of our communication, Benedetti *et al.*[3] reported the preparation of similar amino acid complexes, in which potassium salts of amino acids were utilized. The alkali metal salts can not always be prepared. However, the corresponding silver salts are readily available. Thus the use of the latter salts is preferable for the present study. The π-allylic palladium complexes prepared are given in Table 1 along with the ^{1}H NMR chemical shifts of allylic protons. The aryl- or alkylpalladium(II) amino acid complexes of similar type could also be

TABLE 1. π-ALLYLIC PROTON CHEMICAL SHIFTS OF PALLADIUM COMPLEXES
(δ, ppm from TMS, 60 MHz, 35 °C)[a]

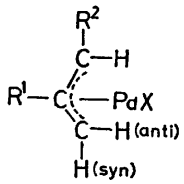

Complex	R^1	R^2	X[b]	Solvent[c]	*syn*-H	*anti*-H	R^1(H,CH_3)
1	H	H	Gly	D_2O	4.10	3.02	5.43
2	H	H	Ala	M	3.93	2.86	5.46
				D_2O	3.70	2.99	5.41
3	H	H	Val	M	3.93	2.84	5.44
4	H	H	Phe	D_2O	3.95	2.73	5.48
5	H	H	Pro	M	3.92	2.96, 2.82	5.52
				C	3.91	2.89, 2.67	5.40
				D_2O	4.05	3.05, 2.95	5.61
6	H	H	Bz-Ala	C	3.90	2.86	5.30
7	H	H	Cbz-Gly	C	3.8—4.0	2.85	5.40
8	CH_3	H	Gly	M	3.70	2.71	2.10
9	CH_3	H	Ala	M	3.70	2.70	2.10
10	CH_3	H	Phe	M	3.56	2.41	1.99
11	CH_3	H	Pro	M	3.65	2.77, 2.63	2.12
12	CH_3	H	His	M	3.6—3.9	2.7—3.1	2.12
13	CH_3	H	Bzl-Ala	M	3.95, 3.82	2.56, 2.1—2.3	1.85
14	CH_3	H	6-MP	M	4.15	3.17	2.20
15	CH_3	H	BTA	M	3.90	2.95	2.04
16	H	CH_3[d]	Ala	M	3.5—4.1	2.62	5.31
17	H	C_6H_5	Ala	M	3.92	4.56, 2.97	5.94
18	H	$CO_2C_2H_5$	Ala	C	4.0—4.3	3.21, 3.53	6.05

a) When signals were broad or no definite assignment could be made, the region where the signals appeared is indicated. Coupling constants between the central and terminal protons were 6.5—7.5 Hz and 11—12.5 Hz for *syn* and *anti* positions, respectively. Geminal couplings of the terminal protons were $\lesssim$1 Hz. b) Amino acids are of natural (L-) configuration. Bz-Ala, *N*-benzoylalaninate; Cbz-Gly, *N*-benzyloxycarbonylglycinate; Bzl-Ala, *N*-benzylalaninate; 6-MP, 6-methylpicolinate; BTA, (benzylthio)acetate. c) M, CD_3OD; C, $CDCl_3$. d) The methyl group is in *anti* position.

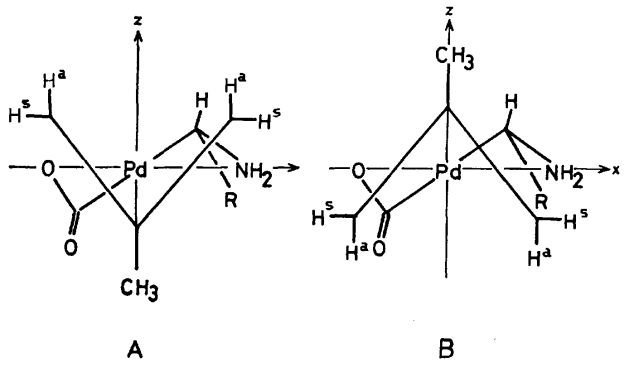

Fig. 1. Schematic view of [π-(2-methylallyl)]Pd(II) complex of α-amino acid.

prepared, including those derived from *N,N*-dimethylbenzylamine-,[4] *N*-benzylideneaniline-[5] or methoxydicyclopentadiene[6]-palladium(II) chloride (see Experimental).

Figure 1 shows a schematic picture of π-(2-methylallyl)palladium complex of amino acid as viewed down Cartesian y axis. Because of the "ligand atom effect" and "chirality effect,"[1] the four front octants in which allylic protons H^s and H^a are placed should differ from each other in their magnetic environment. If the relative configuration of the allylic ligand and the amino acid ligand is fixed as in pictures A and B, then four *anti* proton signals as well as the same number of *syn* proton signals should be observed. The low temperature ^1H NMR at 90 MHz was studied for π-(2-methylallyl)-palladium glycinate (**8**), alaninate (**9**) and prolinate (**11**) complexes at temperatures between 0 and −90 °C. No further change in spectral pattern was observed by lowering the temperature below −40 °C in line with the previous study at 60 MHz. However, the signals were sharpened, and additional small splittings (1—3 Hz) were disclosed. A schematic representation of the experimentally observed spectra is given in Fig. 2 for selected signals. Splittings of *syn* or *anti* proton signal(s) into four signals or less for **9** and **11** are in line with the expectation that the relative configuration of the two ligands on the metal is fixed at low temperature, and all or at least three out of the four front octants differ from each other in their magnetic environment. Examination of intensities of the signals reveals that the relative population of configuration A and B are equal. This is reasonable since no direct steric or dipolar interaction can be expected between the coordinated allylic ligand and the amino acid ligand. Glycinate complex **8** gave the splitting of *syn* and *anti* proton signals (which are singlets at room temperature) into doublets, but the absence of chirality in the glycine molecule allowed no further splitting. The freezing of the chelate ring conformation of the glycine ligand might have occurred at low temperature (−90 °C), but the effect was not sufficient to bring about measurable splittings of the signals.

The dynamic process as revealed by the temperature-dependent ^1H NMR signals was most satisfactorily rationalized either by π-allyl rotation[1] or base assisted N,O-ligand atom exchange of amino acid ligand.[1,7] No

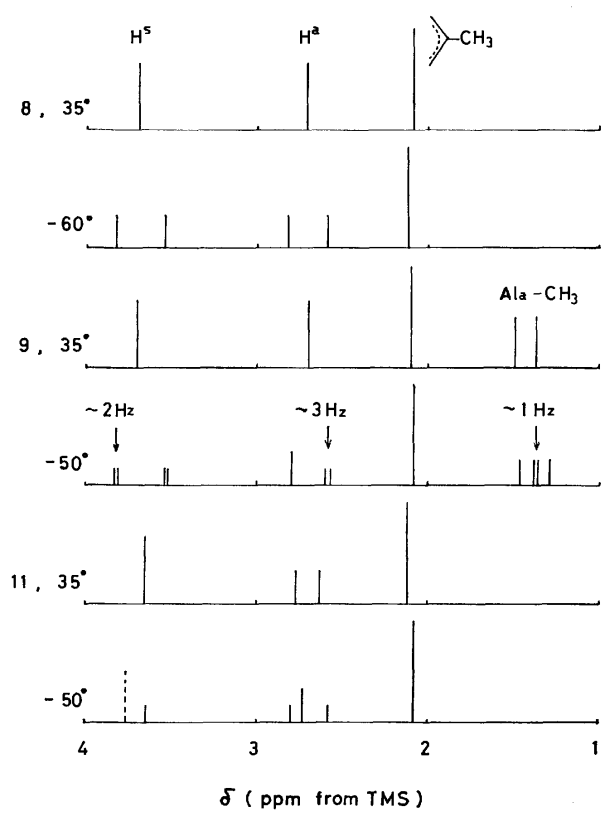

Fig. 2. A schematic representation of selected proton signals observed for π-allylic complexes. Low temperature spectra (−50, −60 °C) were obtained at 90 MHz, and those at 35 °C were at 60 MHz.

effect of the complex concentration[7] on the spectral shape was observed, indicating that the process is unimolecular with respect to the complex. Preference of the π-allyl rotation as a plausible mechanism is suggested. However, the possibility that the solvent molecule (methanol-d_4) acts effectively as base and that the process is the N,O-ligand atom exchange can not be excluded. As to the ^1H NMR behavior of other π-allyl- or π-(2-methylallyl)palladium complexes (Table 1), most of them seem to be grouped into one of the three typical types (Fig. 2). Complex **13** shows a complicated temperature-dependent behavior, rejecting simplified spectral interpretation.

Experimental

General. The ^1H NMR spectra were obtained with a Varian A-60 spectrometer at 60 MHz and a Hitachi R-22 spectrometer at 90 MHz. Natural (L-) amino acids and their derivatives were used. π-Allylic palladium(II) chloride complexes were prepared according to the reported procedures[8] and used as obtained or after purification by column chromatography.

Silver Salts of Amino Acid. The general procedure for the preparation of the salts is as follows. Silver nitrate (1 mmol) dissolved in water or aqueous methanol was added under stirring to an equimolar mixture (1 mmol each) of lithium hydroxide monohydrate and an amino acid in a similar solvent. Silver salt precipitated as withe powder. The solvent was chosen considering the solubility of the starting material and the product. For silver salt easily

hydrolyzable in water (typically, those of proline, *N*-phenylglycine and tryptophan), 80—90% methanol was used. For the stable salts (*e.g.*, those of glycine and β-phenylalanine), water was used. In each case the use of minimum amount of the solvent was preferred. Yields were 60% to quantitative.

π-Allylic Palladium(II) Complexes of Amino Acid. The complexes were prepared according to the following general procedure. π-Allylic palladium(II) chloride (1 mmol) was stirred with the suspension of excess silver salt of amino acid (3 mmol) in methanol or chloroform (20—40 ml) in the dark until the yellow coloration due to the starting complex disappeared (5—20 min). Filtration and concentration of the reaction mixture followed by gradual addition of ether produced the amino acid complex as pale yellowish crystalline powder. Yields were 60% to quantitative. The product was in most cases analytically pure, but in some cases reprecipitation was needed for further purification after treatment with decolorizing charcoal. The stable complexes could be purified by recrystallization. Numerous complexes other than those given in Table 1 were also prepared according to the procedure outlined above. The complexes of Phe were the most stable, while those containing Pro were air-sensitive, the manipulation of the solution being preferably carried out under dry nitrogen. The proline complexes could not be stored more than a week. The elemental analyses of the complexes were statisfactory except for a few cases. No analyses were made for **12** and **17**. The IR and NMR spectra are in line with the composition and structure of the complexes. Details for the selected complexes are given in the following. **4.** π-Allylpalladium(II) chloride[8] was reacted with silver salt of Phe in methanol. The complex was recrystallized from water or water containing a small amount of ethanol, yield 73—95%, dec 160—175 °C, $\nu_{C=O}$ 1600 cm^{-1}. NMR for Phe (δ, ppm from TMS; D_2O): 2.2—2.6 (t, J=5.0 Hz, >CH–), 3.31 (d, J=5.0 Hz, –CH_2–), 7.75 (s, –C_6H_5). Found: C, 46.24; H, 4.76; N, 4.52%. Calcd for $C_{12}H_{15}NO_2Pd$: C, 46.25; H, 4.85; N, 4.49%. **9.** π-(2-Methylallyl)palladium(II chloride[8] was reacted with silver alaninate in chloroform, yield 80—87%, dec 138—150 °C, MW (vapour pressure osmometer) 236 (Calcd: 249.6), $\nu_{C=O}$ 1603 cm^{-1}. NMR for Ala (CD_3OD): 3.54 (q, J=7.0 Hz, >CH–), 1.41 (d, J=7.0 Hz, –CH_3). Found: C, 33.04; H, 5.21; N, 5.54%. Calcd for $C_7H_{13}NO_2Pd$: C, 33.69; H, 5.25; N, 5.61%. **11.** π-(2-Methylallyl)palladium(II) chloride[8] was reacted with silver prolinate in chloroform, yield 60—90%, dec 110—138 °C, MW 294 (Calcd: 275.6), $\nu_{C=O}$ 1608 cm^{-1}. NMR for Pro (CD_3OD): 1.7—2.2(m, C–CH_2CH_2–C), 3.1—3.4 (m, N–CH_2–C), 3.7—3.9 (m, >CH–). Found: C, 39.00; H, 5.41; N, 5.01%. Calcd for $C_9H_{15}NO_2$-Pd: C, 39.22; H, 5.49; N, 5.08%. **15.** The silver salt of BTA was obtained as white precipitate from aqueous reaction mixture. The reaction with π-(2-methylallyl)palladium(II) chloride[8] was carried out in chloroform, yield 76%, dec 110—125 °C, $\nu_{C=O}$ 1634 cm^{-1}. NMR for BTA ($CDCl_3$): 3.47 (s, benzyl-CH_2–), 4.08 (s, –$COCH_2S$–), 7.38 (s, –C_6H_5). Found: C, 45.69; H, 4.70%. Calcd for $C_{13}H_{16}O_2PdS$: C, 45.56; H, 4.71%. π-(1-Ethoxycarbonylallyl)palladium(II) glycinate. π-(1-Ethoxycarbonylallyl)palladium(II) chloride[8] was reacted with silver glycinate in methanol, yield 80—97%, dec 150—160 °C, $\nu_{C=O}$ 1600, 1620 cm^{-1}. Found: C, 32.73; H, 4.33; N, 4.95%. Calcd for $C_8H_{13}NO_2Pd$: C, 32.73; H, 4.33; N, 4.77%. The complex is stable at room temperature. Other complexes. *o*-(Dimethylaminomethyl)-phenylpalladium(II) alaninate. The organopalladium chloride[4] was reacted with silver alaninate in chloroform in the usual way, white crystalline powder, yield 97%, $\nu_{C=O}$ 1625 cm^{-1}. NMR (CD_3OD): 6.8—7.0 (m, Ar–H), 3.88 (s, benzyl CH_2), 3.57 (q, J=7.0 Hz, –CH–), 2.79 (s, N–CH_3), 1.49 (d, J=7.0 Hz, C–CH_3). Found: C, 42.82; H, 5.58; N, 8.47%. Calcd for $C_{12}H_{18}N_2O_2Pd$: C, 42.85; H, 5.52; N, 8.52%. 3a,4,7,7a-Tetrahydro-*exo*-6-methoxy-*endo*-4,7-methanoindene-*endo*-5σ,2π-palladium(II) alaninate. The organopalladium(II) chloride[6] was reacted with silver alaninate in methanol. Manipulation under nitrogen produced white powder, yield 88%, $\nu_{C=O}$ 1632, ν_{C-O} 1090 cm^{-1}. NMR for Ala (CD_3OD): 3.3—3.6 (q, >CH–), 1.58 (d, J=7.5 Hz, –CH_3). The signals for the π-enyl moiety were similar to those of the chloride complex.[6]

The authors' acknowledgements are due to Prof. Y. Tsuno and Dr. M. Mishima, Faculty of Science, Kyushu University, for the measurement of low temperature ^{1}H NMR spectra.

References

1) Y. Nakagawara, K. Kikukawa, M. Takagi, and T. Matsuda, *Chem. Lett.*, **1972**, 611.

2) Presented at the 30 th annual meeting of the Chemical Society of Japan, Higashi-Osaka, April, 1974.

3) E. Benedetti, G. Maglio, R. Palumbo, and C. Pedone, *J. Organomet. Chem.*, **60**, 189 (1973).

4) A. C. Cope and E. C. Friedlich, *J. Am. Chem. Soc.*, **90**, 909 (1968).

5) S. P. Molnar and M. Orchin, *J. Organomet. Chem.*, **16**, 196 (1969).

6) J. K. Stille and R. A. Morgan, *J. Am. Chem. Soc.*, **88**, 5135 (1966).

7) E. Ban, A. Chan, and J. Powell, *J. Organomet. Chem.*, **34**, 405 (1972).

8) a) W. T. Dent, R. Long, and A. J. Wilkinson, *J. Chem. Soc.*, **1964**, 1585; b) R. Hüttel, H. Dietl, and H. Christ, *Chem. Ber.*, **97**, 2037 (1964); c) E. O. Fischer and H. Werner, *ibid.*, **95**, 695 (1962); d) J. Tsuji and S. Imamura, *Bull. Chem. Soc. Jpn.*, **40**, 197 (1967).

Reactions of Thiocarboxylic Acids with Oximes and Nitrones. A New Synthesis of Thiones

Kazuhiko KIMURA, Hiroaki NIWA, and Shinichi MOTOKI

Department of Chemistry, Faculty of Science, Science University of Tokyo, Kagurazaka, Shinjuku-ku, Tokyo 162

(Received March 29, 1977)

The reactions of ketone derivatives containing carbon-nitrogen double bond such as oximes (**3**), *N*-alkyloximes (nitrones, **11**), oxime *O*-alkyl ethers, phenylhydrazones and semicarbazones with thiocarboxylic acids were studied for the purpose of preparing thioketones. Both **3** and **11** reacted with thiocarboxylic acids to give thioketones in good yields. The reaction did not proceed in the cases of other ketone derivatives, the starting materials being recovered. The reaction of benzophenone oxime with thiobenzoic acid gave thiobenzophenone, dibenzoyl disulfide and ammonium benzoate, while that of benzophenone-*N*-methylnitrone with thioacetic acid gave thiobenzophenone and *N*-acetyl-*N*-methylhydroxylamine. The mechanisms of these reactions are presented.

Various procedures for the preparation of thiones including the thionation of ketones by hydrogen sulfide or phosphorus pentasulfide have been worked out.[1,2] Conversion of ketodichlorides[3] or ketimines[4] (Scheme 1) into thiones by the action of thiocarboxylic acids have been used for preparing diaryl or heterocyclic thiones. We were interested in these simple synthetic methods using thiocarboxylic acids and have examined the reaction of more readily available derivatives of ketones such as oximes, nitrones, hydrazones, and semicarbazones with thiobenzoic (**1**) or thioacetic acid (**2**).

$$Ph_2C{=}NPh + RCOSH \longrightarrow$$

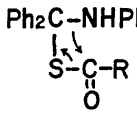

$$\longrightarrow Ph_2C{=}S + RCONHPh \quad (1)$$

Results and Discussion

When benzophenone oxime (**3a**) was mixed with an equimolar amount of **1** in benzene at room temperature, thiobenzophenone (**4a**) was obtained in low yield after being left to stand for 3 days. However, ammonium benzoate (**5**) and dibenzoyl disulfide (**6**) were formed as by-products instead of benzohydroxamic acid (**7**) which was expected to be formed according to the following scheme. Since **7** does not react with **1**, **3a**

$$Ph_2C{=}NOH + PhCOSH \longrightarrow$$

3a **1**

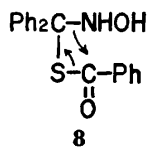

$$\longrightarrow Ph_2C{=}S + PhCONHOH \quad (2)$$

4a **7**

8

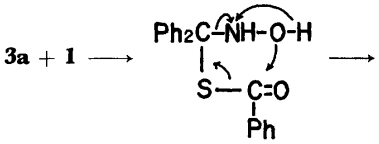

$$Ph_2C{=}S + H_2NOCPh \quad (3)$$

4a **9**

or **4a** to form **5** or **6** under the same reaction conditions, another pathway involving intramolecular nucleophilic attack of oxygen to carbonyl carbon followed by proton transfer in the intermediate (**8**) to form **4a** and *O*-benzoylhydroxylamine (**9**) has been considered. *O*-Acylhydroxylamines react readily with various nucleophiles at nitrogen atom to form carboxylate ion.[5,6]

$$RCO_2NH_2 + :Nu \longrightarrow RCO_2^- + NH_2Nu \quad (4)$$

It seems probable that a portion of **1** in the reaction mixture would react as nucleophile with **9** to afford **5** and **6** as follows. If these steps take part in the reaction

$$\mathbf{9} + \mathbf{1} \longrightarrow PhCO_2H + (PhCOSNH_2)$$
$$(PhCOSNH_2) + \mathbf{1} \longrightarrow \mathbf{6} + NH_3$$
$$PhCO_2H + NH_3 \longrightarrow \underset{\mathbf{5}}{PhCO_2NH_4} \quad (5)$$

and proceed relatively rapid, overall reaction would be as follows. Support for this proposal is supplied by the

$$Ph_2C{=}NOH + 3PhCOSH \longrightarrow$$

3a **1**

$$Ph_2C{=}S + PhCO_2NH_4 + PhCOSSCOPh \quad (6)$$

4a **5** **6**

fact that **9** prepared from *p*-nitrophenyl benzoate and hydroxylamine reacts with 2 mol of **1** at room temperature to give **5** and **6** and that the yield of **4a** increases to *ca.* 80% by using over 3 mol of **1** (Table 1). The other ketoximes reacted similarly to give the corresponding thiones in relatively good yields. The results are given in Table 2.

Table 1. Relation of molar ratio (thiobenzoic acid (**1**)/oximes) and yield of thiobenzopehnone (**4a**)

Molar ratio	1	2	3
Yield of **4a** (%)	30	50	78

The reactions of ketoximes with thioacetic acid (**2**) proceeded rapidly to give thioketones and acetamide along with a small amount of diacetyl disulfide. No ammonium acetate was obtained.

No reaction took place with **1** and benzophenone oxime *O*-methyl ether (**10**), which structurally cannot cause proton transfer in the intermediate.

Nitrones were found to react with thiocarboxylic acids much more readily than oximes. When benzo-

TABLE 2. PREPARATION OF THIONES BY THE REACTION OF OXIMES WITH THIOBENZOIC ACID AND THIOACETIC ACID

$R_1-\underset{\underset{S}{\|}}{C}-R_2$

	R_1	R_2	Molar ratio (RCOSH/oxime)	Condition: Solvent	Condition: Time (day)	R (in RCOSH): Ph Yield (%)	R (in RCOSH): CH_3 Yield (%)
4a	C_6H_5	C_6H_5	1	B	4	30	40
			3			78	80
4b	CH_3	C_6H_5	1	B	3		
			3			trace	trace
4c	*p*-$CH_3OC_6H_4$	*p*-$CH_3OC_6H_4$	1	B	4	30	36
			3			60	65
4d	*p*-$CH_3OC_6H_4$	C_6H_5	1	B	3	30	30
			3			60	70
4e	*p*-$CH_3C_6H_4$	C_6H_5	1	B–E	3	25	35
			3			60	70
4f	2-Thienyl	*p*-ClC_6H_4	1	B	7	26	30
			3			60	78
4g	*p*-ClC_6H_4	*p*-ClC_6H_4	1	B	4	20	35
			3			50	67
4h	*p*-ClC_6H_4	C_6H_5	1	B–E	3	20	40
			3			70	75

Solvent. B: benzene, B–E: benzene–ether (4: 1)

TABLE 3. PREPARATION OF THIONES BY THE REACTION OF N-METHYLNITRONES WITH THIOACETIC ACID

$R_1-\underset{\underset{S}{\|}}{C}-R_2$

	R_1	R_2	Reaction time (day)	Yield (%)
4a	C_6H_5	C_6H_5	2	76
4b	CH_3	C_6H_5[21]	1	44
4c	*p*-$CH_3OC_6H_4$	*p*-$CH_3OC_6H_4$	2	70
4e	*p*-$CH_3C_6H_4$	C_6H_5	2	81
4g	*p*-ClC_6H_4	*p*-ClC_6H_4	2	75

phenone-*N*-methylnitrone (**11a**) was allowed to react with **2**, **4a** and *N*-acetyl-*N*-methylhydroxylamine (**12**) were obtained.* The latter was identified by elementary analyses and comparison of its IR spectra with those of an authentic sample. Thus, the reaction is considered to proceed by intramolecular nucleophilic attack of nitrogen on carbonyl carbon in the intermediate (**13**)

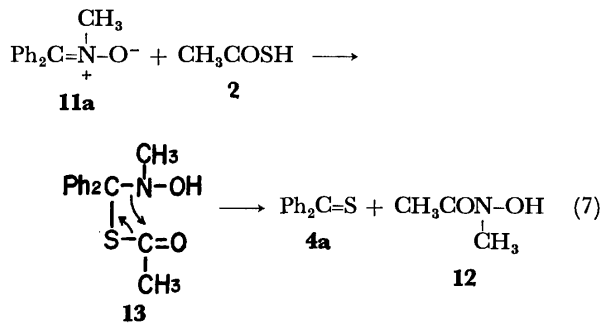

* The reactions of **11** with **1** proceeded similarly, but gave unsatisfactory results in the yield and purity of **4**.

as in the case of Scheme 1. The other thiones were obtained similarly (Table 3).

The cause of such differences in the mechanisms of the reaction of oximes and nitrones has not been clarified.

Phenylhydrazones and semicarbazones did not react with thiocarboxylic acids even in refluxing benzene, the starting materials being recovered. In these compounds, the following resonance effects may markedly lower the reactivity of imino carbon toward uncleophilic addition of thiocarboxylic acids, retarding the reaction.

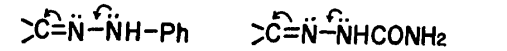

Experimental

All melting and boiling points were uncorrected. The IR spectra were measured on a Hitachi EPI-21G spectrometer. The mass spectra were obtained on a Hitachi RMU-7M mass spectrometer operating at an ionization energy of 70 eV. Silica gel column chromatography was performed with Wakogel C-200 (Wako Pure Chem.).

Materials. Commercial benzophenone and acetophenone were used without further purification. The other ketones were prepared by the Friedel-Crafts reaction of the corresponding acid chlorides. Oximes were prepared by the usual methods. **3f** was prepared from the corresponding ketone and hydroxylamine hydrochloride in pyridine.[7] *N*-Methylnitrones were prepared by the reaction of the corresponding oximes with dimethyl sulfate[8] or methyl iodide.[9] Acetophenone-*N*-methylnitrone was prepared from acetophenone diethyl acetal and *N*-methylhydroxylamine hydrochloride.[10] *O*-Benzoylhydroxylamine was synthesized from *p*-nitrophenyl benzoate and hydroxylamine hydrochloride in the presences of sodium hydroxide.[11] *N*-Acetyl-*N*-methylhydroxylamine was prepared according to the method given by Exner.[10] Thioacetic and thiobenzoic acid were

prepared according to general methods.[12,13]

Preparation of Thiobenzophenone (4a). Reaction of Benzophenone Oxime (3a) With Thiobenzoic Acid (1): A solution of **1** (12.4 g, 0.09 mol) in bry benzene (30 ml) was added to a solution of **3a** (6 g, 0.03 mol) in dry benzene (140 ml) at room temperature under nitrogen atmosphere. The solution gradually turned blue, white precipitates separating. The reaction mixture was allowed to stand in the dark for 4 days. Filtration of the precipitate gave ammonium benzoate (2.7 g, mp 189—191 °C (from EtOH), lit, mp 190 °C). The blue filtrate was evaporated under reduced pressure. The residue was chromatographed on a silica gel column (80 g) by elution with petroleum ether to afford **4a** (4.7 g, 78%, bp 120—125 °C/1 mmHg, mp 47—50 °C (from petroleum ether (bp 60—80 °C); lit,[14] mp 53—54 °C). Further elution with benzene gave dibenzoyl disulfide (3 g, mp 128 °C (from EtOH); lit,[15] mp 130 °C).

Reaction of 3a with Thioacetic Acid (2): A solution of **2** (6.8 g, 0.09 mol) in dry benzene (15 ml) was added to a solution of **3a** (6 g, 0.03 mol) in dry benzene (140 ml) at room temperature under nitrogen atmosphere and the mixture was allowed to stand in the dark for 4 days. The blue solution obtained was evaporated under reduced pressure. The residue was chromatographed on a silica gel column (80 g) by elution with petroleum ether to afford **4a** (4.8 g, 80%). Further elution with benzene–ethanol (1: 1) gave acetamide (1 g, mp 80—81 °C; lit, mp 81—82 °C) and diacetyl disulfide (0.2 g, bp 72—74 °C/2 mmHg, lit[16] bp 60—61 °C/1 mmHg). Acetamide was identified by its IR spectra and by admixture with an authentic sample. **4b—h** were obtained by a similar procedure. The thiones obtained were identified by their physical constants (**4c**,[3] **4d**,[17] **4e**,[18] **4f**,[19] **4g**,[20] **4h**[18]) and conversion into 2,4-dinitrophenylhydrazone.

Reaction of O-Benzoylhydroxylamine (9) with Thiobenzoic Acid (1). A solution of **9** (2.2 g, 0.016 mol) in dry benzene (15 ml) was added to a solution of **1** (4.4 g, 0.032 mol) in dry benzene (50 ml) with stirring at room temperature under nitrogen atmosphere and allowed to stand for 3 days. The white precipitate separated was removed by filtration to give ammonium benzoate (1.4 g, mp 190—193 °C). The filtrate was evaporated under reduced pressure and the residue was recrystallized from ethanol to give dibenzoly disulfide (2.6 g, mp 127—128 °C).

Reaction of Benzophenone-N-methylnitrone (11a) with Thioacetic Acid (2). A solution of **2** (7.1 g, 0.092 mol) in dry benzene (15 ml) was added to a solution of **11a** (19.5 g, 0.092 mol) in dry benzene (100 ml) at room temperature under nitrogen atmosphere. The reaction mixture which rapidly turned blue was allowed to stand in the dark for 2 days. After removal of the solvent, fractional distillation under reduced pressure gave **4a** (15 g, 76%, bp 120—125 °C/1 mmHg, mp 48—50 °C) and *N*-acetyl-*N*-methylhydroxylamine (5 g, bp 93—95 °C/3 mmHg; lit,[10] bp 80 °C/2 mmHg); IR(liquid): 3150, 2850, and 1630 cm^{-1}; MS *m/e* 73 (M^+—O), 58, and 43. **4b**, **4c**, **4e**, and **4g** were obtained by a similar procedure.

References

1) E. Campaigne, "The Chemistry of the Carbonyl Group," Interscience Publishers, New York (1966) Chap. 17, pp. 917—956.

2) D. Paquer, *Int. J. Sulfur Chem.*, **7**, 269 (1972); *ibid.*, **8**, 173 (1973).

3) A. Schönberg, O. Schütz, and S. Nickel, *Chem. Ber.*, **61**, 1375 (1928).

4) B. M. Mikhaĭlov and I. S. Saveléva, *Bulletin of the Academy of Science of the U.S.S.R. Division of Chemical Sciences* No. **7**, 1255 (1959).

5) P. A. S. Smith, H. R. Alul, and R. L. Baumgarten, *J. Am. Chem. Soc.*, **86**, 1139 (1964).

6) L. A. Carpino, *J. Am. Chem. Soc.*, **82**, 3133 (1960).

7) C. Tsuchiya, *Nippon Kagaku Zasshi*, **82**, 1395 (1961).

8) L. Semper and L. Lichtenstadt, *Chem. Ber.*, **51**, 936 (1918).

9) P. A. S. Smith and J. E. Robertson, *J. Am. Chem. Soc.*, **84**, 1197 (1962).

10) O. Exner, *Collect. Czech. Chem. Commun.*, **16**, 258 (1951).

11) W. P. Jencks, *J. Am. Chem. Soc.*, **80**, 4581 (1958).

12) P. Nobel, Jr., and D. S. Tarbell, *Org. Synth.*, Coll. Vol. IV, 924 (1963).

13) E. K. Ellingboe, *Org. Synth.*, Coll. Vol. IV, 928 (1963).

14) B. F. Gofton and E. A. Braude, *Org. Synth.*, Coll. Vol. IV, 927 (1963).

15) R. L. Frank and J. Blegen, *Org. Synth.*, Coll. Vol. III, 116 (1955).

16) L. Field and J. Lawson, *J. Am. Chem. Soc.*, **80**, 838 (1958).

17) N. Lozach and G. Guillouze, *Bull. Soc. Chim. Fr.*, **1957**, 1221.

18) H. Tokunaga, K. Akiba and N. Inamoto, *Bull. Chem. Soc. Jpn.*, **45**, 506 (1972).

19) C. Andrieu, *Bull. Soc. Chim. Fr.*, **1965**, 2457.

20) A. Luttringhaus and J. Grohmann, *Z. Naturforsh.*, **10b**, 365 (1955).

21) R. Mayer and H. Berthold, *Chem. Ber.*, **96**, 3098 (1963).

Synthesis of Tetrahydrospectinomycin

Tetsuo SUAMI,* Shigeru NISHIYAMA, Hikaru ISHIKAWA,
Hiroshi OKADA, and Takeshi KINOSHITA
Department of Applied Chemistry, Faculty of Engineering, Keio University, Hiyoshi, Yokohama 223
(Received April 5, 1977)

Condensation of 1,3-bis-*N*-(benzyloxycarbonyl)actinamine (**2**) with 2-*O*-chloroacetyl-4,6-dideoxy-3-*O*-*p*-nitrobenzoyl-α-D-xylohexopyranosyl chloride (**8**), followed by deacylation and catalytic hydrogenation afforded 5-*O*-(4,6-dideoxy-β-D-xylohexopyranosyl)actinamine (**11**). Compound **11** was found to be identical with one of the four tetrahydrospectinomycins. ^{1}H and ^{13}C NMR spectra were determined and analyzed.

Spectinomycin is an unique aminocyclitol antibiotic produced by the fermentation of *Streptomyces spectabilis*,[1,2] and is widely used in clinical treatment. Its structure was established by Wiley *et al.*,[3] the configuration being assigned by X-ray diffraction study,[4] as shown in Scheme 1.

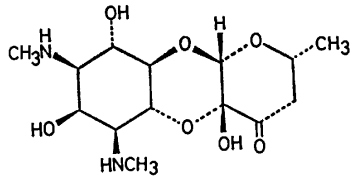

Spectinomycin

Scheme 1.

Reduction of spectinomycin with sodium borohydride or hydrogen in the presence of a catalyst gave two epimeric dihydrospectinomycins,[3] further reduction of the dihydrospectinomycins yielding four tetrahydrospectinomycins.[5]

We have directed our studies toward a total synthesis of spectinomycin, and wish to report the synthesis of tetrahydrospectinomycin by the following reaction route (Schemes 2 and 3).

Actinamine dihydrochloride (**1**) was prepared by the hydrolysis of hexa-*N*,*O*-acetylactinamine[6] in 6 M hydrochloric acid. Treatment of **1** with benzyl chloroformate gave 1,3-bis-*N*-(benzyloxycarbonyl)actinamine (**2**).

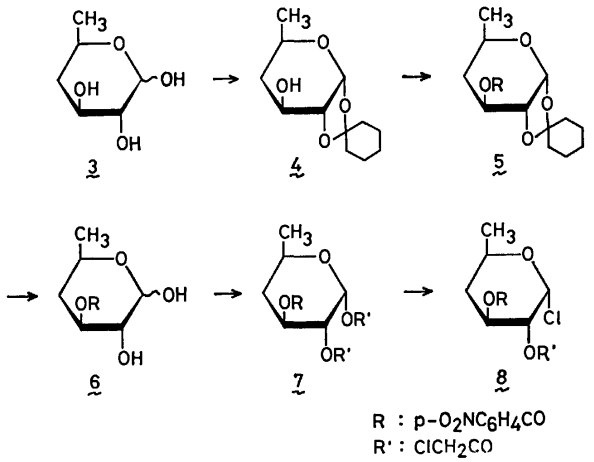

Scheme 2.

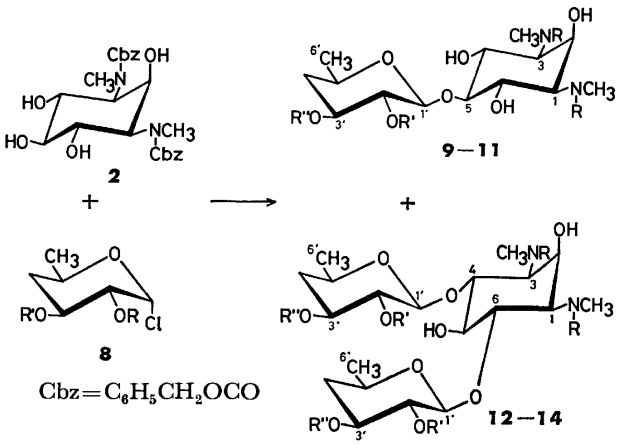

8 R=$ClCH_2CO$, R′=*p*-$O_2NC_6H_4CO$
9 R=Cbz, R′=$ClCH_2CO$, R″=*p*-$O_2NC_6H_4CO$
10 R=Cbz, R′=R″=H
11 R=R′=R″=H
12 R=Cbz, R′=$ClCH_2CO$, R″=*p*-$O_2NC_6H_4CO$
13 R=Cbz, R′=R″=H
14 R=R′=R″=H

Scheme 3.

2-*O*-Chloroacetyl-4,6-dideoxy-3-*O*-*p*-nitrobenzoyl-α-D-xylohexopyranosyl chloride (**8**) was prepared from 4,6-dideoxy-D-xylohexopyranose[7] (**3**) in five steps. A chloroacetyl group was used as protecting group on the hydroxyl group of C-2 because of relative ease of removal under milder conditions as compared with the *p*-nitrobenzoyl group.[8] This was demonstrated by the preparation of methyl 4,6-dideoxy-3-*O*-*p*-nitrobenzoyl-β-D-xylohexopyranoside (**17**) from methyl 2-*O*-chloroacetyl-4,6-dideoxy-3-*O*-*p*-nitrobenzoyl-β-D-xylohexopyranoside (**16**) in an aqueous pyridine solution.

Condensation of **2** with **8** in dry benzene in the presence of mercury(II) cyanide and "Drierite" gave a mixture of three products (R_f 0.28, 0.34, and 0.38) which were detectable on TLC. The mixture was fractionated on a silica gel column with benzene–ethanol as an eluant. Fractions showing a single spot at R_f 0.28 on TLC were combined and evaporated to give the desired compound: 1,3-bis-*N*-(benzyloxycarbonyl)-5-*O*-(2-*O*-chloroacetyl-4,6-dideoxy-3-*O*-*p*-nitrobenzoyl-β-D-xylohexopyranosyl)actinamine (**9**) as crystals in 7.8% yield.

Besides compound **9**, 1,3-bis-*N*-(benzyloxycarbonyl)-4,6-bis-*O*-(2-*O*-chloroacetyl-4,6-dideoxy-3-*O*-*p*-nitrobenzoyl-β-D-xylohexopyranosyl)actinamine (**12**) was obtain-

* To whom correspondence should be addressed.

ed from the fractions (R_f 0.38) in 13% yield. From the fractions (R_f 0.34), an isomer of **9** (**15**) was obtained in 1.7% yield, the structure of which has not been clarified.

By removing the protecting group, **9** gave 5-*O*-(4,6-dideoxy-β-D-xylohexopyranosyl)actinamine (**11**) which was found to be identical with one of the four tetrahydrospectinomycins described by Knight and Hoeksema.[5]

By removing the protecting group, **12** gave 4,6-bis-*O*-(4,6-dideoxy-β-D-xylohexopyranosyl)actinamine (**14**). The β-anomeric configuration of the two glycosidic linkages in **14** were established by ^{1}H NMR spectroscopic study, and their positions attached to the actinamine were confirmed by carbon-13 NMR spectrum in connection with that of **11**.

The normal proton-decoupled natural-abundance carbon-13 Fourier transform spectra of **11** and **14** were determined. The resonances were separated into those originating from an actinamine moiety and those from 4,6-dideoxy-β-D-xylohexopyranosyl group.

When the spectra were determined at pD<1, the resonances arising from the actinamine moiety shifted more or less from those determined in a free base by the effect of protonation on an amino group.[9]

The spectrum of **11** revealed the presence of 14 carbon atoms. The resonance at 33.3 ppm (2 carbons) was attributed to the two *N*-methyl carbons shifted to 31.6 ppm at pD<1, the resonance at 62.9 ppm (2 carbons) being ascribed to C-1 and C-3 which shifted to 62.0 and 61.7 ppm respectively, at pD<1. The resonance at 63.7 ppm is due to C-2, since a large upfield shift (3.6 ppm) was observed at pD<1. These assignments were established in connection with those of spectinomycin.[10] The resonance at 88.0 ppm was assigned to C-5, since methylation of a hydroxyl group causes a large downfield shift of the carbon bearing this hydroxyl group,[11] the result being extended to the glycosidation of a hydroxyl group.[12] C-5 of hyosamine in hygromycin B_2 revealed its resonance at 86.4 ppm[13] and that of 2-deoxystreptamine in ribostamycin at 85.0 ppm.[14] The two resonances at 71.3 and 72.0 ppm were ascribed to the remaining C-4 and C-6, respectively, owing to a large upfield shift at pD<1.

The other 6 resonances were attributed to 6 carbon atoms of the 4,6-dideoxy-β-D-xylohexopyranosyl group. The resonances at 20.6 and 40.6 ppm were clearly due to C-6′ and C-4′, respectively. The resonances at 104.5 and 76.2 ppm were ascribed to C-1′ and C-2′, respectively, since those of methyl β-D-glucopyranoside resonate at 104.2 and 74.1 ppm.[15] The resonance at 69.7 ppm was ascribed to C-5′, since the corresponding carbon atom of spectinomycin revealed its resonance at 69.2 ppm.[10] Thus, the remaining resonance at 71.1 ppm is attributable to C-3′. The assignment was rationalized by the fact that C-4′ of nebramine shows its resonance with a large upfield shift (5.2 ppm) as compared to C-4′ of neamine.[16]

The assignments of the resonances are given in Table 1.

The resonances of the spectrum of **14** were assigned in connection with those of **11**. In the spectrum of **14**, resonances originating from 4,6-dideoxy-β-D-xylohexopyranosyl groups were readily recognized by the formation of pairs of signals at the same position observed in the spectrum of **11**. The two glycosyloxy groups were linked to C-4 and C-6 of the actinamine, since two resonances at 82.7 and 84.8 ppm were ascribed to the carbon atoms where the glycosyloxy groups attached[12] and the resonances of C-4 and C-6 (71.3 and 72.0 ppm) in the spectrum of **11** were not observed in the spectrum of **14**, C-5 showing its resonance at 75.5 ppm instead.

Table 1. ^{13}C NMR chemical shifts[a] of **11**, **14**, and spectinomycin hydrate

	11		**14**		Spectinomycin hydrate[10]
	base	pD<1	base	pD<1	pD 4.6
C-1	62.9	62.0	62.7[c]	61.5	62.5
C-2	63.7	60.1	62.9[c]	59.8	60.7
C-3	62.9	61.7	61.9	60.8	59.5
C-4	71.3[b]	68.2	82.7[d]	77.1	66.5
C-5	88.0	84.2	75.5	73.4	70.7
C-6	72.0[b]	69.0	84.8[d]	79.3	66.9
1-NCH_3	33.3	31.6	33.1	32.1	31.8
3-NCH_3	33.3	31.6	32.8	31.7	31.3
C-1′	104.5	104.2	104.5 105.7	103.8 103.8	94.4
C-2′	76.2	76.1	76.2 76.7	75.8 76.0	94.4
C-3′	71.1	71.1	71.3 71.5	71.1 71.1	92.6
C-4′	40.6	40.6	40.5 40.7	40.4 40.6	42.3
C-5′	69.7	69.8	69.7 69.8	69.8 70.2	69.2
C-6′	20.6	20.6	20.7 20.7	20.7 20.7	20.5

a) In parts per million downfield from tetramethylsilane.
b), c), d) The signals may be reversed.

Experimental

General Methods. Melting points were determined in capillary tubes and are uncorrected. Solutions were evaporated under reduced pressure below 40 °C. Opitcal rotations were recorded on a Japan Spectroscopic DIP-SL polarimeter. IR spectra were measured on a Hitachi 225 spectrophotometer in KBr disks. ^{1}H NMR spectra were recorded on a Varian A-60D spectrometer at 60 MHz or a Varian XL-100 spectrometer at 100 MHz in deuteriochloroform or deuterium oxide with tetramethylsilane or sodium 4,4-dimethyl-4-silapentane-1-sulfonate as an internal standard. The peak positions are given in δ-values. ^{13}C NMR spectra were recorded for solutions in deuterium oxide with an internal dioxane reference, the chemical shifts being reported in ppm downfield from tetramethylsilane (δ_C for dioxane= −67.4). The spectra were obtained on a Varian XL-100 transform with Varian VFT-100 computer. TLC was performed on Wakogel B-10 (Wako Pure Chemical Co. Ltd.) plates, silica gel (Wakogel C-300) being employed for column chromatography. Elemental analyses were performed by Mr. Saburo Nakada.

Actinamine Dihydrochloride (1). A 5.63 g portion of hexa-*N*,*O*-acetylactinamine[6] was heated in 6M hydrochloric acid (40 ml) for 6 h under reflux. The solution was evaporated to dryness and the residue was recrystallized from aqueous

acetone giving 3.38 g (99%) of **1**, mp above 250 °C.

Found: C, 34.24; H, 7.08; N, 9.93; Cl, 25.49%. Calcd for $C_8H_{18}N_2O_4 \cdot 2HCl$: C, 34.42; H, 7.22; N, 10.03; Cl, 25.40%.

*1,3-Bis-*N*-(benzyloxycarbonyl)actinamine (2).* A 3.57 g portion of **1** was suspended in 60% aqueous acetone (550 ml) containing sodium carbonate (13.8 g). 30% Benzyl chloroformate in toluene (43.5 g) was added to the suspension under ice cooling with agitation. After being left to stand overnight at room temperature, the reaction mixture was evaporated to dryness and the residue was extracted with warm acetone. The acetone extracts were evaporated and the residue was triturated with ether. The crude product was recrystallized from ethanol–ether to give 5.11 g (84%) of **2**, mp 161—163.5 °C. An analytically pure sample was obtained by further recrystallizartion fom water, mp 164—165 °C.

Found: C, 61.01; H, 6.30; N, 5.98%. Calcd for $C_{24}H_{30}N_2O_8$: C, 60.75; H, 6.37; N, 5.90%.

*4,6-Dideoxy-*D*-xylohexopyranose (3).* The compound was prepared by the method of Jones and his co-workers.[7]

*1,2-*O*-Cyclohexylidene-4,6-dideoxy-α-*D*-xylohexopyranose (4).* Compound **3** (2.10 g) was suspended in cyclohexanone (74 ml) containing *p*-toluenesulfonic acid (60 mg) and "Drierite" (2.0 g). After being stirred overnight at room temperature, the reaction mixture was added with sodium hydrogencarbonate (5.5 g). The mixture was filtered and the filtrate was evaporated. The residue was purified by silica gel column chromatography with 1:3 (v/v) 2-butanone-toluene as an eluant. Fractions showing a single spot at R_f 0.42 on TLC in the same solvent were combined and evaporated to give 2.45 g (76%) of **4** as a syrup, $[\alpha]_D^{22}$ +35.3 ° (*c* 5.8, chloroform). ^{1}H NMR ($CDCl_3$): δ 1.23 (d, 3, J=6.5 Hz, C$\underline{H}_3$), 2.74 (broad s, 1, OH), 5.56 (d, 1, J=4.5 Hz, H-1).

Found: C, 62.84; H, 8.65%. Calcd for $C_{12}H_{20}O_4$: C, 63.13; H, 8.83%.

*1,2-*O*-Cyclohexylidene-4,6-dideoxy-3-*O*-p-nitrobenzoyl-α-*D*-xylohexopyranose (5).* To a suspension of *p*-nitrobenzoyl chloride (4.96 g) in pyridine (90 ml) was added a solution of **4** (2.33 g) in pyridine (5 ml) under ice cooling with agitation. After being stirred overnight at room temperature, the reaction mixture was poured into ice cold water (700 ml) and extracted with chloroform (50 ml×3). The combined chloroform layers were washed with sodium hydrogencarbonate solution and water. After being dried over anhydrous sodium sulfate, the solution was evaporated to give 3.13 g of a syrup. The product was recrystallized twice from ether–pentane to give 2.49 g (65%) of **5**, mp 94—97 °C; $[\alpha]_D^{24}$ +72 ° (c 1.1, chloroform). ^{1}H NMR ($CDCl_3$): δ 1.29 (d, 3, J=6.5 Hz, C$\underline{H}_3$), 5.68 (d, 1, $J_{1,2}$=2.5 Hz, H-1).

Found: C, 60.35; H, 6.06; N, 3.51%. Calcd for $C_{19}H_{23}NO_7$: C, 60.47; H, 6.14; N, 3.71%.

*4,6-Dideoxy-3-*O*-p-nitrobenzoyl-*D*-xylohexopyranose (6).* Compound **5** (1.51 g) was heated in 80% aqueous acetic acid (30 ml) for 1 h under reflux. The solution was evaporated and the residue was dissolved in ethanol. Petroleum ether was added to the ethanolic solution to give 1.01 g (85%) of **6** as amorphous powder, $[\alpha]_D^{22}$ +148.8 °→+142.1 ° (*c* 1.45, pyridine).

Found: C, 52.29; H, 5.27; N, 4.49%. Calcd for $C_{13}H_{15}NO_7$: C, 52.53; H, 5.27; N, 4.71%.

*1,2-Bis-*O*-chloroacetyl-4,6-dideoxy-3-*O*-p-nitrobenzoyl-α-*D*-xylohexopyranose (7).* Compound **6** (456 mg) was dissolved in a mixture of dioxane (5 ml) and pyridine (0.4 ml). To the solution was added chloroacetyl chloride (0.4 ml) under ice cooling with agitation. After 1 h, the reaction mixture was poured into ice cold water (30 ml) and extracted with chloroform (30 ml×3). The combined chloroform layer was washed with sodium hydrogensulfate solution, sodium hydrogencarbonate solution and water. After being dried over anhydrous sodium sulfate, the solution was evaporated to give 778 mg of a crude product. Recrystallization from ethanol gave 382 mg (55%) of **7**, mp 136—138 °C; $[\alpha]_D^{23}$ +128 ° (*c* 0.5, chloroform). ^{1}H NMR ($CDCl_3$): δ 1.14 (d, 3, J=6.0 Hz, C$\underline{H}_3$), 3.95 (s, 2, C$\underline{H}_2$Cl), 4.15 (s, 2, C$\underline{H}_2$Cl), 6.43 (d, 1, $J_{1,2}$=3.0 Hz, H-1).

Found: C, 45.53; H, 3.84; N, 3.06; Cl, 15.44%. Calcd for $C_{17}H_{17}NO_9Cl_2$: C, 45.35; H, 3.81; N, 3.11; Cl, 15.75%.

*2-*O*-Chloroacetyl-4,6-dideoxy-3-*O*-p-nitrobenzoyl-α-*D*-xylohexopyranosyl Chloride (8).* Hydrogen chloride was bubbled into a solution of **7** (610 mg) in dry ether (150 ml) until saturated and the solution was left to settle overnight in a refrigerator. The solution was evaporated and the residue was dissolved in chloroform (30 ml). The chloroform solution was washed with sodium hydrogencarbonate solution and water. After being dried over anhydrous sodium sulfate, the solution was evaporated. The residue was recrystallized from chloroform–ether to give 364 mg (69%) of **8**, mp 147—149 °C; $[\alpha]_D^{15}$ +216 ° (*c* 0.5, chloroform). ^{1}H NMR ($CDCl_3$): δ 1.26 (d, 3, J=6.5 Hz, C$\underline{H}_3$), 3.98 (s, 2, C$\underline{H}_2$Cl), 6.34 (d, 1, $J_{1,2}$=4.0 Hz, H-1).

Found: C, 45.82; H, 3.81; N, 3.46; Cl, 18.11%. Calcd for $C_{15}H_{15}NO_7Cl_2$: C, 45.94; H, 3.86; N, 3.57; Cl, 18.08%.

Condensation of 2 and 8. A mixture of **2** (3.08 g, 6.5 mmol) and **8** (4.82 g, 12.3 mmol) in dry benzene (60 ml) containing mercury(II) cyanide (3.5 g) and "Drierite" (3.1 g) was heated for 41 h under reflux. The mixture was filtered and the filtrate was evaporated. The residue was fractionated on a silica gel column with 20:1 (v/v) benzene–ethanol as an eluant.

Fractions showing a single spot at R_f 0.28 on TLC in the same solvent system were combined and evaporated. The residue was recrystallized from chloroform–ethanol to give 421 mg (7.8%) of 1,3-bis-*N*-(benzyloxycarbonyl)-5-*O*-(2-*O*-chloroacetyl-4,6-dideoxy-3-*O*-*p*-nitrobenzoyl-β-D-xylohexopyranosyl)actinamine (**9**) as crystals, mp 143—144 °C; $[\alpha]_D^{20}$ +45.4 ° (*c* 1.0, chloroform). ^{1}H NMR ($CDCl_3$): δ 1.35 (d, 3, J=6.0 Hz, C$\underline{H}_3$), 3.06 (s, 3, NC$\underline{H}_3$), 3.10 (s, 3, NC$\underline{H}_3$), 4.03 (s, 2, C$\underline{H}_2$Cl).

Found: C, 56.15; H, 5.26; N, 5.05; Cl, 4.39%. Calcd for $C_{39}H_{44}N_3O_{15}Cl$: C, 56.42; H, 5.34; N, 5.06; Cl, 4.27%.

Fractions showing a single spot at R_f 0.34 on TLC were combined and evaporated. The residue was recrystallized from chloroform–ethanol giving 92 mg (1.7%) of 1,3-bis-*N*-(benzyloxycarbonyl)-*O*-(2-*O*-chloroacetyl-4,6-dideoxy-3-*O*-*p*-nitrobenzoyl-D-xylohexopyranosyl)actinamine (**15**), mp 172—173.5 °C; $[\alpha]_D^{22}$ +87.5 ° (*c* 1.0, chloroform). ^{1}H NMR ($CDCl_3$): δ 1.24 (d, 3, J=6.0 Hz, C$\underline{H}_3$), 3.09 (s, 3, NC$\underline{H}_3$), 3.11 (s, 3, NC$\underline{H}_3$), 4.04 (s, 2, C$\underline{H}_2$Cl).

Found: C, 56.37; H, 5.32; N, 5.01; Cl, 4.39%. Calcd for $C_{39}H_{44}N_3O_{15}Cl$: C, 56.42; H, 5.34; N, 5.06; Cl, 4.27%.

Fractions showing a single spot at R_f 0.38 on TLC were combined and evaporated. The residue was recrystallized from chloroform–ether giving 989 mg (13%) of 1,3-bis-*N*-(benzyloxycarbonyl)-4,6-bis-*O*-(2-*O*-chloroacetyl-4,6-dideoxy-3-*O*-*p*-nitrobenzoyl-β-D-xylohexopyranosyl)actinamine (**12**), mp 152—153 °C; $[\alpha]_D^{22}$ +14.0 ° (*c* 1.0, chloroform). ^{1}H NMR ($CDCl_3$): δ 1.21 (d, 3, J=6.5 Hz, C$\underline{H}_3$), 1.40 (d, 3, J=6.5 Hz, C$\underline{H}_3$), 3.05 (s, 6, 2×NC$\underline{H}_3$), 4.02 (s, 4, 2×C$\underline{H}_2$Cl).

Found: C, 54.51; H, 4.93; N, 4.55; Cl, 6.28%. Calcd for $C_{54}H_{58}N_4O_{22}Cl_2$: C, 54.69; H, 4.93; N, 4.72; Cl, 5.98%.

*1,3-Bis-*N*-(benzyloxycarbonyl)-5-*O*-(4,6-dideoxy-β-*D*-xylohexo-*

pyranosyl)actinamine (10). Compound **9** (290 mg) was deacylated in saturated methanolic ammonia (20 ml) overnight at ambient temperature with gentle agitation. The solution was evaporated and the residue was recrystallized from methanol giving 206 mg (98%) of **10**, mp 244—246 °C; $[\alpha]_D^{18}$ −1.1 ° (*c* 1.0, pyridine).

Found: C, 59.37; H, 6.53; N, 4.83%. Calcd for $C_{30}H_{40}N_2O_{11}$: C, 59.59; H, 6.67; N, 4.63%.

5-O-(4,6-Dideoxy-β-D-xylohexopyranosyl)actinamine (11). A solution of **10** (115 mg) in 50% aqueous methanol (20 ml) was hydrogenated in the presence of palladium black (20 mg) overnight in a Parr apparatus in hydrogen atmosphere (3.4 kg/cm²). The filtrate was evaporated after the catalyst had been filtered off. The residue was purified by Amberlite CG-50 (H^+) resin column chromatography with 0.05 M ammonia as an eluant. The product was recrystallized from ethanol to give 59 mg (92%) of **11** as needles, mp 222—225 °C; $[\alpha]_D^{21}$ −21.8 ° (*c* 1.0, water). ^{1}H NMR (D_2O): δ 1.28 (d, 3, *J*=6.5 Hz, $C\underline{H}_3$), 2.41 (s, 6, 2×$NC\underline{H}_3$), 4.58 (d, 1, *J*=7.5 Hz, H-1). IR and ^{1}H NMR spectra of **11** were superimosable on those of an authentic sample of tetrahydrospectinomycin prepared by the method of Knight and Hoeksema.[5] [Lit,[5] mp 227—231 °C; $[\alpha]_D$−22 ° (*c* 1.0, water)].

Found: C, 49.79; H, 8.19; N, 8.35%. Calcd for $C_{14}H_{28}N_2O_7$: C, 49.99; H, 8.39; N, 8.33%.

1,3-Bis-N-(benzyloxucarbonyl)-4,6-bis-O-(4,6-dideoxy-β-D-xylohexopyranosyl)actinamine (13). Compound **12** (0.4 g) was deacylated by a procedure analogous to that described for **10**. The product was purified by column chromatography with 15:1 (v/v) benzene–ethanol. Fractions showing a single spot at R_f 0.58 on TLC in 5:1 (v/v) benzene–ethanol were combined and evaporated. The residue was dissolved in benzene. Hexane was added to the solution giving 190 mg (75%) of **13** as amorphous powder, mp 111—128 °C; $[\alpha]_D^{22}$ −25.0 ° (*c* 1.0, pyridine).

Found: C, 57.52; H, 6.68; N, 3.62%. Calcd for $C_{36}H_{50}N_2O_{14}\cdot H_2O$: C, 57.44; H, 6.96; N, 3.72%.

4,6-Bis-O-(4,6-dideoxy-β-D-xylohexopyranosyl)actinamine (14). Hydrogenolysis of **13** (124 mg) was carried out by a procedure analogous to that described for **11**. The product was recrystallized from ethanol to give 63 mg (82%) of **14**, mp 243—247 °C; $[\alpha]_D^{22}$ −26.0 ° (*c* 1.0, water). ^{1}H NMR (D_2O): δ 1.28 (d, 6, *J*=6.0 Hz, 2×$C\underline{H}_3$), 2.44 (s, 6, 2×$NC\underline{H}_3$), 4.50 (d, 1, *J*=7.5 Hz, anomeric proton), 4.62 (d, 1, *J*=7.5 Hz, anomeric proton).

Found: C, 51.61; H, 8.02; N, 6.01%. Calcd for $C_{20}H_{38}N_2O_{10}$: C, 51.49; H, 8.21; N, 6.00%.

Methyl 2-O-Chloroacetyl-4,6-dideoxy-3-O-p-nitrobenzoyl-β-D-xylohexopyranoside (16). A solution of **8** (340 mg) in dichloromethane (1.5 ml) was added to methanol (5 ml) containing mercury(II) cyanide (340 mg). The mixture was stirred at ambient temperature for 2 h and filtered. The filtrate was evaporated, and the residue was dissolved in chloroform. The chloroform solution was filtered and the filtrate was evaporated. The residue was recrystallized from ethanol to give 238 mg (71%) of **16**, mp 122—123 °C; $[\alpha]_D^{16}$ + 58 ° (*c* 0.5, chloroform). ^{1}H NMR ($CDCl_3$): δ 1.34 (d, 3, *J*=6.0 Hz, $C\underline{H}_3$), 3.50 (s, 3, $OC\underline{H}_3$), 3.98 (s, 2, $C\underline{H}_2Cl$), 4.44 (d, 1, *J*=8.0 Hz, H-1).

Found: C, 49.36; H, 4.70; N, 3.69; Cl, 8.97%. Calcd for $C_{16}H_{18}NO_8Cl$: C, 49.56; H, 4.68; N, 3.61; Cl, 9.14%.

Methyl 4,6-dideoxy-3-O-p-nitrobenzoyl-β-D-xylohexopyranoside (17). Water (4 ml) was added to a solution of **16** (158 mg) in pyridine (7 ml), and the pH of the mixture was adjusted to 7 by addition of 6M hydrochloric acid. The mixture was settled at ambient temperature for 5 h. The mixture was diluted with chloroform, and the solution was washed successively with sodium hydrogensulfate solution, sodium hydrogencarbonate solution and water. After being dried over anhydrous sodium sulfate, the solution was evaporated. The residue was recrystallized from ethanol–petroleum ether to give 103 mg (81%) of **17**, mp 133—134 °C; $[\alpha]_D^{22}$ +30° (*c* 0.5, chloroform). ^{1}H NMR ($CDCl_3$): δ 1.32 (d, 3, *J*=6.0 Hz, $C\underline{H}_3$), 2.66 (broad s, 1, OH), 3.57 (s, 3, $OC\underline{H}_3$), 4.26 (d, 1, *J*=8.0 Hz, H-1).

Found: C, 54.19; H, 5.50; N, 4.56%. Calcd for $C_{14}H_{17}NO_7$: C, 54.02; H, 5.51; N, 4.50%.

This work was supported in part by a grant-in-aid from the Ministry of Education.

References

1) D. J. Mason, A. Dietz, and R. M. Smith, *Antibiot. Chemotherapy*, **11**, 118 (1961).
2) M. E. Bergy, T. E. Eble, and R. R. Herr, *Antibiot. Chemotherapy*, **11**, 661 (1961).
3) P. F. Wiley, A. D. Argoudelis, and H. Hoeksema, *J. Am. Chem. Soc.*, **85**, 2652 (1963).
4) T. C. Cochran, D. J. Abraham, and L. L. Martin, *J. Chem. Soc., Chem. Commun.*, **1972**, 494.
5) J. C. Knight and H. Hoeksema, *J. Antibiot.*, **28**, 136 (1975).
6) T. Suami and H. Sano, *Tetrahedron Lett.*, **1968**, 2655; T. Suami, S. Ogawa, and H. Sano, *Bull. Chem. Soc. Jpn.*, **43**, 1843 (1970).
7) B. T. Lawton, W. A. Szareck, and J. K. N. Jones, *Carbohydr. Res.*, **14**, 255 (1970).
8) A. F. Cook and D. T. Maichuk, *J. Org. Chem.*, **35**, 1940 (1970).
9) G. Kotowycz and R. U. Lemieux, *Chem. Rev.*, **73**, 669 (1973).
10) R. M. Stroshane, M. Taniguchi, K. L. Rinehart, Jr., J. P. Rolls, W. J. Haak, and B. A. Ruff, *J. Am. Chem. Soc.*, **98**, 3025 (1976).
11) D. E. Dorman, S. J. Angyal, and J. D. Roberts, *J. Am. Chem. Soc.*, **92**, 1351 (1970).
12) D. E. Dorman and J. D. Roberts, *J. Am. Chem. Soc.*, **93**, 4463 (1971).
13) N. Neuss, K. F. Koch, B. B. Molloy, W. Day, L. L. Huckstep, D. E. Dorman, and J. D. Roberts, *Helv. Chim. Acta*, **53**, 2314 (1970).
14) S. Omoto, S. Inouye, M. Kojima, and T. Niida, *J. Antibiot.*, **26**, 717 (1973).
15) D. E. Dorman and J. D. Roberts, *J. Am. Chem. Soc.*, **92**, 1335 (1970).
16) K. F. Koch, J. A. Rhoades, E. W. Hagaman, and E. Wenkert, *J. Am. Chem. Soc.*, **96**, 3300 (1974).

Dehydroannulenes. VII. Synthesis of 3,7,10,14-Tetrasubstituted 1,8-Bisdehydro[14]annulenes

Kunisuke FUKUI, Tateo NOMOTO, Shin'ichi NAKATSUJI, Shuzo AKIYAMA, and Masazumi NAKAGAWA*

Department of Chemistry, Faculty of Science, Osaka University Toyonaka, Osaka 560

(Receired April 18, 1977)

It was found that dienyne ketones such as 2,2-dimethyl-7-*t*-butyl-4,6-nonadien-8-yn-3-one, 2,2-dimethyl-7-phenyl-4,6-nonadien-8-yn-3-one and 1,5-diphenyl-2,4-heptadien-6-yn-1-one give the corresponding tetrasubstituted 14-membered cyclic glycols on treatment with a suspension of potassium hydroxide in liquid ammonia. Reactions of the cyclic glycols with tin(II) chloride in organic solvent saturated with hydrogen chloride afforded strongly diatropic tetrasubstituted bisdehydro[14]annulenes.

Oxidative coupling of polyentetrayne glycols (**1** or **2**) with copper(II) acetate in pyridine–methanol–ether in high dilution[1] yielded the corresponding 18-membered (**3**) or 22-membered cyclic glycols (**4**), precursors of tetrakisdehydro[18]-[2] and [22] annulenes,[3] in unexpectedly high yields. This seems to be a reflection of the favorable configuration of the acyclic glycols (**1** and **2**) on intramolecular oxidative coupling, suggesting the possibility of cyclic dimerization of polyenyne ketones (**5**) to give cyclic polyendiyne glycols under suitable conditions. The cyclic glycols may be transformed into bisdehydro[4n+2]annulenes by the reductive dehydroxylation reaction adopted in the conversion of the cyclic tetrayne glycols (**3** and **4**) into tetrakisdehydro[18]- and [22]annulenes.[2,3]

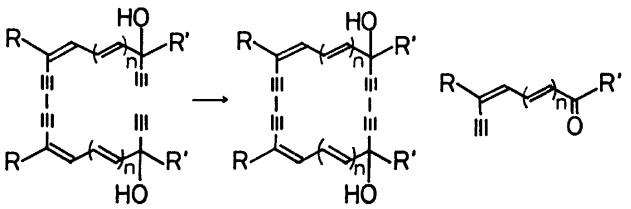

1: n=1 **2**: n=2 **3**: n=1 **4**: n=2 **5**

In this paper we wish to report on the cyclic dimerization of dieyne ketones (**6**) to 14-memberd cyclic glycols (**7**) and their transformation into 3,7,10,14-tetrasubstituted 1,8-bisdehydro[14]annulenes (**8**).[4] The parent compound 1,8-bisdehydro[14]annulene (**8d**) was obtained by Sondheimer and his co-workers by prototropic rearrangement accompanied by an unexpected dehydrogenation by atmospheric oxygen in the course of synthesis of monodehydro[14]annulene.[5] The present studies have opened an efficient route to the synthesis of 1,8-bisdehydro[14]annulenes.

Synthesis. Ethynylation of carbonyl compounds with acetylene or monosubstituted acetylenes in organic solvent in the presence of alkali hydroxide, carbonate or alcoholate is well-known (Favorskii method).[6] Formation of a trace of the cyclic glycol (**7c**) could be recognized on treatment of the diphenyldienyne ketone (**6c**) with potassium hydroxide in tetrahydrofuran or pyridine. No indication of the formation of **7c** could be obtained with alkali amide in liquid ammonia, sodium hydroxide in tetrahydrofuran or pyridine, potassium hydroxide in *N,N*-dimethylformamide or in ether, or sodium hydroxide and calcium carbide in tetrahydrofuran. It was found that slow addition of a solution of **6** in tetrahydrofuran to a stirred suspension of finely powdered potassium hydroxide in liquid ammonia caused the cyclic dimerization of **6** to give a diastereomeric mixture of the desired cyclic glycol (**7**) in a high yield. In the case di-*t*-butyl ethynyl ketone (**6a**), an amorphous solid with an unidentified structure was obtained in addition to the desired cyclic glycol (**7a**).

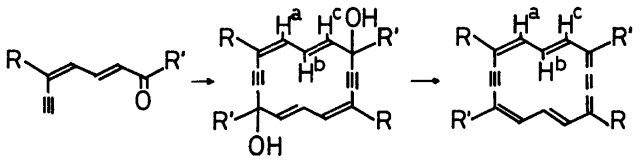

6 **7** **8**

a: R=R′=*t*-Bu; b: R=Ph, R′=*t*-Bu; c: R=R′=Ph ; d: R=R′=H

The cyclic glycols (**7a**—**c**) in an organic solvent were mixed with tin(II) chloride in ether saturated with hydrogen chloride. The resulting deeply colored

TABLE 1. YIELDS AND MELTING POINTS OF **7** AND **8** AND COLOR OF CRYSTALS OF **8**

	Glycol			Annulene		
	Yield (%)	Mp (°C)		Yield (%)	Color	Mp (°C)
7a	19	230.9—232.4 (dec)	**8a**	64	red	298.0—229.0 (dec)
	50	220.0—222.2 (dec)	**8b**	83	brown violet	284.0—284.5 (dec)
7b	96	241.0—243.0 (dec)	**8c**	83	deep violet	>300 (dec)
7c	93	236.0—237.0 (dec)				

* To whom inquiries should be addressed.

TABLE 2. 60 MHz ^{1}H NMR PARAMETERS OF BISDEHYDRO[14]ANNULENES (**8**) (τ-VALUES)

	8a	**8b**	**8c**	**8d**
Outer protons	H^a, H^e 0.58 d J=13.5	H^a 0.12 d J=13.5 H^e 0.47 d J=13.5	H^a, H^e 0.06 d J=13.5	H^a, H^e 0.45 dd J=13.3, 8 R,R′ 1.57 d J=13.3
o-Protons of phenyl		1.2—1.5 m	1.1—1.5 m	
m,p-Protons of phenyl		2.2—2.8 m	2.1—2.6 m	
Protons of *t*-butyl	8.10 s	8.02 s		
Inner protons	14.39 t J=13.5	13.42 t J=13.5	12.56 t J=13.5	15.54 t J=13.3
Solvent	THF-d_8	THF-d_8	THF-d_8	$CDCl_3$

reaction mixtures were worked up in the usual way to give the tetrasubstituted 1,8-bisdehydro[14]annulenes (**8a—c**). The yields and melting points of cyclic glycols (**7a—c**) and annulenes (**8a—c**) together with the color of crystals of the annulenes are given in Table 1.

Properties. The tetrasubstituted 1,8-bisdehydro-[14]annulenes (**8a—c**) were found to be quite stable, no decomposition being observed in the air at room temperature under diffused daylight for a long time. The ^{1}H NMR spectra of **8a—c** indicate that they sustain fairly strong diamagnetic ring current as evidenced by low-field and high-field signals of the outer and inner protons, respectively. The ^{1}H NMR parameters are summarized in Table 2 together with those of the parent compound (**8d**).[5] As a representative example, the ^{1}H spectrum of the tetra-*t*-butyl derivative (**8a**) is shown in Fig. 1. The di-*t*-butyl-diphenyl derivative (**8b**) exhibits two outer proton signals as doublets at τ 0.12 and 0.47. The lower field signal (τ 0.12) could be assigned H^a which undergoes the deshielding effect of the ring current both of the annulene ring and the phenyl groups. The multiplets observed at τ 1.1—1.5 and 2.2—2.8 in the spectra of **8a** and **8c** could be assigned to *o*- and *m,p*-protons of the phenyl groups, since the protons of the phenyl groups are disposed in the deshielding region of diamagnetic ring current of the annulene ring, and lower field shift of the *o*-protons can

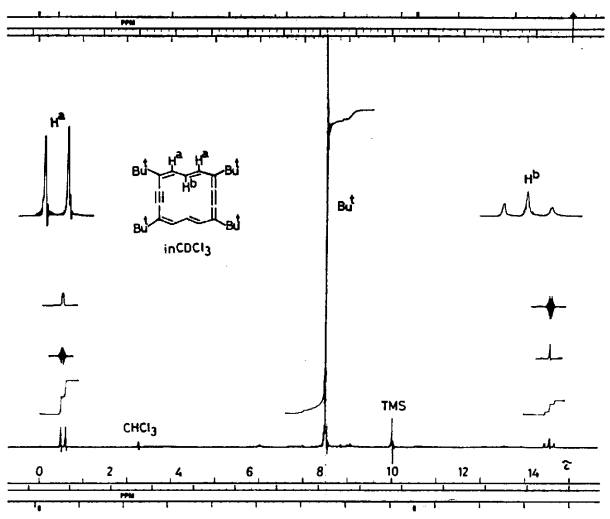

Fig. 1. 100 MHz ^{1}H NMR spectrum of tetra-*t*-butyl-bisdehydro[14]annulene (**8a**) in $CDCl_3$.

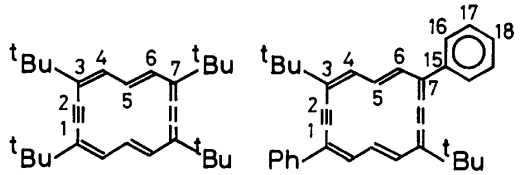

8a **8b**

TABLE 3. ^{13}C NMR PARAMETERS OF **8a** AND **8b** IN $CDCl_3$ (ppm FROM TMS)

8a		**8b**	
t-Bu	32.2(CH_3), 37.8(C)	*t*-Bu	32.3(CH_3), 37.8(C)
C^1,C^2	116.7	C^1,C^2	114.7, 115.7
C^3	131.3	C^3,C^7,C^{15}	119.8, 113.7, 139.9
C^4	130.4	C^4,C^6	130.3, 130.7
C^5	129.0	C^5	132.3
		C^{16},C^{17}	128.0, 128.7
		C^{18}	127.3

be attributed to their proximate position to the 14-membered ring. The most remarkable feature of ^{1}H NMR spectra is the marked low-field shift of signals of inner protons in the tetrasubstituted derivatives (**8a—c**) as compared with that of the parent compound (**8d**). A slight low-field shift of the outer protons of phenyl substituted derivatives (**8b, c**) was also observed.

Carbon-13 NMR spectral parameters of **8a** and **8b** are given in Table 3. The spectrum of **8c** could not be obtained owing to the poor solubility in NMR solvents. Assignment was made on the basis of chemical shift, off resonance technique and the magnitude of NOE. However, the signals of tertiary carbon atoms (C^3, C^7 and C^{15}) and *o,m*-carbons of phenyl groups (C^{16} and C^{17}) could not be discriminated. The sp-hybridized carbon atoms in symmetrical **8a** exhibits only one signal at an intermediate region of acetylene[7,8] and cumulene[8] carbon atoms, suggesting strongly the identity of acetylenic and cumulenic linkages incorporated in aromatic [4*n*+2]π-electron system.[2g,h] On the other hand, two signals were observed in the corresponding region in the spectrum of **8b**. This seems to be ascribable to the difference in electron density between C^1 and C^2 caused by the different inductive effect of *t*-butyl and phenyl groups.

TABLE 4. ELECTRONIC SPECTRA OF **8a—c** IN THF
λ_{max} IN nm (ε)[a)]

8a	228.5(6670), 301 sh(28100), 329(272000), 432 sh (11900), 452(24600) 500 sh(150), 525(100), 548 (210), 567 sh(240), 590(920)
8b	226 sh(12300), 234(14300), 260(13400), 272 sh (10800), 315 sh(27900), 332 sh(41100), 345 sh (76300), 354(195000), 508(50), 571(570), 623(1640)
8c	224 sh(13400), 246(26000), 268(23200), 274.5 (24700), 282.5(24400), 326(18100), 343(30900), 372 sh(68100), 388(289000), 521(26300), 549(53200), 600 sh(830), 658(2520)

a) The absorption curves were given in a preliminary report.[4)]

The electronic spectra of the tetrasubstituted 1,8-bisdehydro[14]annulenes (**8a—c**) consist of three main absorption bands characteristic of aromatic [4*n*+2]-annulenes. The numerical data are given in Table 4.

Increase in the number of phenyl substitution causes a progressive bathochromic shift of the main three absorption bands and appreciable intensification of the medium and the longest wavelength bands indicating electronic perturbation of phenyl groups on the annulene ring. The same trend has been observed in the electronic spectra of tetrakisdehydro[18]-[2e)] and [22]annulenes.[3)]

Tetra-*t*-butyl- (**8a**) and di-*t*-butyl-diphenyl derivatives (**8b**) formed 1:1 CT complexes with 2,4,7-trinitrofluorenone. On the other hand, the tetraphenyl analogue (**8c**) gave CT complex with 2 moles of the nitro compound.

Experimental

All melting points are uncorrected. The IR spectra were measured with a Hitachi EPI-2 or EPI-3G spectrophotometer, the weak, medium and strong absorptions being indicated by w, m and s, respectively. The electronic spectra obtained on a Hitachi EP-3T spectrophotometer were recorded in nm. The ε-values are given in parentheses, the shoulder being denoted by sh. The mass spetra were measured with a Hitachi RM-50 spectrometer (ionization potential 70 eV). The ^{1}H NMR spectra were obtained on a Varian T-60 or a Varian XL-100 spectrometer, and are recorded in τ-values with respect to TMS as an internal standard. The coupling constants (J) are given in Hz. The ^{13}C NMR spectra were measured with an XL-100 spectrometer operated at 25.2 MHz using pulse FT technique with a deuterium internal lock, and given in ppm from TMS as an internal standard. Silica gel (Merck, Kiesel Gel 60) or alumina (Merck, Act. II—III) was used for column chromatography, unless otherwise stated.

1,4,8,11-Tetra-t-butyl-4,6,11,13-cyclotetradecatetraen-2,9-diyn-1,8-diol (7a). A solution of 2,2-dimethyl-7-*t*-butyl-4,6-nonadine-8-yn-3-one (**6a**, 0.21 g, 0.96 mmol)[2d,e)] in THF (50 ml) was added over a period of 8 h to a stirred suspension of finely powdered potassium hydroxide (1.5 g, 27 mmol) in liquid ammonia (200 ml) at −40—−50 °C. After the mixture had been stirred for 5—6 h at −30—−40 °C, powdered ammonium chloride (3.0 g, 56 mmol) was added at −40 °C, and the ammonia was allowed to evaporate. Water was added to the residue and the mixture was extracted with ether. The ethereal solution, after being washed with water and dried (sodium sulfate), was evaporated under reduced pressure. The residue was chromatographed on silica gel (Wako, 15 g). Elution with hexane–benzene gave colorless crystals, mp 202—205 °C (dec), 65 mg, 31%. The IR, NMR and mass spectral data indicate that the colorless srystals are oligomeric, presumably trimeric, cyclic alcohol. However, no further studies on the structure have been performed. Further elution with benzene and benzene–ether (9:1) yielded a diastereomer of **7a**, colorless crystals, mp 230.9—232.4 °C (dec), 39 mg, 19%; Mass (*m/e*) 436 (M^+). Elution with a solvent of increased polarity (benzene–ether) gave another diastereomer of **7c**, colorless crystals, mp 220.0—222.2 °C (dec), 105 mg, 50%; IR(KBr-disk) 3600, 3455 m (OH), 1633 w (C=C), 975 s (*trans* -CH=CH-) cm^{-1}; NMR ($CDCl_3$) 2.34 (dd, 2, J=10.5, 16.0, H^b), 3.67 (d, 2, J=10.5, H^c), 4.06 (d, 2, J=16.0, H^a), 8.45 (s, 2, OH, disappeared on addition of D_2O), 8.85 (s, 18, *t*-butyl adjacent to OH), 8.94 (s, 18, *t*-butyl).

Found: C, 82.75; H, 10.40%; M^+ 436. Calcd for $C_{30}H_{44}O_2$: C, 82.51; H, 10.16%; M 436.

3,7,10,14-Tetra-t-butyl-1,8-bisdehydro[14]annulene (8a). A diastereomeric mixture of **7a** (59 mg, 0.14 mmol) in ether (50 ml) was mixed at −60 °C with the same solvent saturated with hydrogen chloride (10 ml) and finely powdered tin(II) chloride dihydrate (200 mg). After being stirred for 15 min, the resulting deep red solution was worked up in the usual way. Red crystals (57 mg) obtained on evaporating the solvent were dissolved in hexane and chromatographed on alumina (20 g) to give pure **8a**, red crystals, mp 298.0—299.0 °C (dec), 36 mg, 64%; IR(KBr-disk) 963 (*trans* -CH=CH-) 2000 (-C≡C-↔=C=C=) cm^{-1}; NMR($CDCl_3$) 0.65 (d, J=13.5, outer-H), 14.50 (t, J=13.5, inner-H), 8.10 (s, *t*-butyl).

Found: C, 89.49; H, 10.53%; M^+ 402. Calcd for $C_{30}H_{42}$: C, 89.42; H, 10.63%; M 402.

The reaction product obtained on treatment of **6a** with potassium hydroxide in liquid ammonia could be converted without purification under similar reaction conditions into **8a** (67%).

CT Complex of 8a with 2,4,7-Trinitrofluorenone. Brown crystals of CT complex of **8a** with 2,4,7-trinitrofluorenone were obtained on admixing a solution of the nitro compound (9 mg, 0.029 mmol) in ethanol (4 ml) with a hot solution of **8a** (9 mg, 0.022 mmol) in cyclohexane (3 ml).

Found: C, 72.19; H, 6.65; N, 5.91%. Calcd for $C_{30}H_{42}\cdot C_{13}H_5N_3O_5$: C, 71.94; H, 6.60; N, 5.85%.

1,8-Di-t-butyl-4,11-diphenyl-4,6,11,13-cyclotetradecatetraen-2,9-diyn-1,8-diol (7b). 2,2-Dimethyl-7-phenyl-4,6-nonadien-8-yn-3-one (**6b**) was prepared by a slight modification of the reported method[2g,h)] (mp 77.5—76.0 °C, 52% based on 3-phenyl-2-penten-4-ynal). A solution of **6b** (0.500 g, 2.22 mmol) in THF (60 ml) was added over a period of 7 h to a stirred suspension of potassium hydroxide (2.0 g) in liquid ammonia (1000 ml) at the boiling point of the solvent. After the mixture had been stirred overnight at the same temperature, finely powdered ammonium chloride (6 g) was added to the reaction mixture at −65 °C, and then the ammonia was allowed to evaporate. Ethereal extract (500 ml) of the residue was evaporated to yield crystalline material. An examination with TLC indicated predominant formatiom of one of the diastereomers. The material was washed successively with hexane–benzene (9:1) and hexane. Colorless fine crystals (0.480 g, 96%), thus obtained, were recrystallized twice from benzene to give pure **7b**, colorless crystals, mp 241—243 °C (dec); IR(KBr-disk) 970 s (*trans* -CH=CH-), 2220 w (-C≡C-), 3440 w, 3560 m (OH) cm^{-1}; NMR (acetone-d_6) 1.96—2.23 (m, 6, H^b and *o*-H of phenyl), 2.49—2.76 (m, 8, H^a and *m*, *p*-H of phenyl), 3.65 (d, 2, J=15, H^c),

5.23 (s, 2, OH, disapppeared on addition of D_2O), 8.85 (s, 18, *t*-butyl).

Found: C, 85.60; H, 7.58%. Calcd for $C_{34}H_{36}O_2$: C, 85.67; H, 7.61%.

7,14-Di-t-butyl-3,11-diphenyl-1,8-bisdehydro[14]annulene (8b). To a stirred solution of **7b** (0.110 g, 0.23 mmol) in ether (100 ml) kept at −60 °C was added a solution of tin(II) chloride dihydrate (0.40 g) in the same solvent saturated with hydrogen chloride (20 ml). The cooling bath was removed and the reaction mixture was stirred for 20 min. The mixture was worked up in the usual way. Ethereal extract of the product was evaporated under reduced pressure and the crystalline residue was washed thoroughly with hexane to give fairly pure **8b**, reddish brown fine crystals, 85 mg, 83%, which were recrystallized from benzene–ethanol to give an analytical specimen of **8b**, brown violet crystals, mp 284.0—284.5 °C (dec); IR(KBr-disk) 962 (*trans* –CH=CH–), 2020 (–C≡C–↔=C=C=); NMR($CDCl_3$, 60 MHz) 0.12 (d, 2, J=13.5, H^a), 0.53 (d, 2, J=13.5, H^c), 1.2—1.6 (m, 4, *o*-H of phenyl), 2.2—2.7 (m, 6, *m,p*-H of phenyl), 8.07 (s, 18 *t*-butyl), 13.58 (t, 2, J=13.5, H^b); (THF-d_8, 100 MHz) 0.16 (d, 2, J=13, H^a), 0.49 (d, 2, J=13, H^c), 1.39 (m, 4, *o*-H of phenyl), 2.3—2.7 (m, 6, *m,p*-H of phenyl), 8.05 (s, 18, *t*-butyl), 13.45 (*t*, 2, J=13, H^b).

Found: C, 91.96; H, 7.70%. Calcd for $C_{34}H_{34}$: C, 92.26; H, 7.74%.

CT Complex of 8b with 2,4,7-Trinitrofluorenone. A hot solution of 2,4,7-trinitrofluorenone (15.0 mg) in ethanol (6 ml) was mixed with a hot solution of **8b** (15.0 mg) in benzene (2 ml). On cooling the mixture the CT complex was obtained as violet brown crystals.

Found: C, 74.27; H, 5.16; N, 5.57%. Calcd for $C_{34}H_{34}\cdot C_{13}H_5N_3O_7$: C, 74.49; H, 5.19; N,5.54%.

1,8,4,11-Tetraphenyl-4,6,11,13-cyclotetradecatetraen-2,9-diyn-1,8-diol (7c). A solution of 1,5-diphenyl-2,4-heptadien-6-yn-1-one (**6c**, 396 mg, 1.53 mmol)[2c,d,e] in THF (25 ml) was added over a period of 17 h to a suspension of potassium hydroxide (1.6 g, 29 mmol) in liquid ammonia (600 ml) at −55——65 °C. After the mixture had been stirred at −55 °C for 4 h, ammonium chloride (4 g) was added to the reaction mixture, and the ammonia was allowed to evaporate. The residue was digested with ether by decantation. The insoluble material was dissolved in water, and the aqueous solution was extracted with ether. The combined organic layer was worked up in the usual way. Crystalline solid obtained on evaporating the solvent was dissolved in THF and passed through a short column of silica gel (10 g). The filtrate was concentrated under reduced pressure to give pale brown crystals, which were washed with hexane-benzene to give slightly impure **7c** (369 mg, 93%). The material was recrystallized from THF to give colorless crystals, and was found to contain half mole of THF as a solvent of crystallization, mp 236—237 °C (dec); IR(KBr-disk) 974 s (*trans* –CH=CH–), 2210 w (–C≡C–), 3550 w, 3340 broad (OH) cm^{-1}; NMR(THF) 2.23—2.92 (m, 24, H^a, H^b, and phenyl), 3.69 (d, 2, J=15.0, H^c).

Found: C, 85.47; H, 5.72%. Calcd for $C_{38}H_{28}O_2$–1/2 C_4H_8O: C, 85.68; H, 5.75%.

3,7,10,14-Tetraphenyl-1,8-bisdehydro[14]annulene (8c). Finely powdered tin(II) chloride dihydrate (600 mg) was added under nitrogen atmosphere to a solution of **7c** (45.0 mg, 0.087 mmol) in dimethoxyethane (40 ml) at −60 °C. To the stirred mixture was added ether saturated with hydrogen chloride (4 ml) at −50——55 °C. After the mixture had been stirred for 10 min at −55——60°C, the resulting deep purple solution was poured into water and extracted with ethyl acetate. The extract was worked up in the usual way. Deep purple crystals obtained on evaporating the solvent under reduced pressure were washed with hexane–ether (1: 1) to give pure **8c**, deep purple crystals, mp >300 °C (dec.), 35 mg, 83%; IR(KBr-disk) 945 s (*trans* –CH=CH–) cm^{-1}.

Found: C, 94.57; H, 5.43%. Calcd for $C_{38}H_{26}$: C, 94.26; H, 5.45%.

CT Complex of 8c with 2,4,7-Trinitrofluorenone. The bisdehydro[14]annulene (**8c**, 10.0 mg, 0.032 mmol) was dissolved in hot toluene (20 ml), and the solution was mixed with a solution of 2,4,7-trinitrofluorenone (10.0 mg, 0.032 mmol) in ethanol (5 ml) and toluene (5 ml). After addition of ethanol (10 ml), the mixture was kept in a refrigerator to give 1: 2 CT complex as violet crystals.

Found: C, 68.87; H, 3.23; N, 7.59%. Calcd for $C_{38}H_{26}\cdot 2C_{13}H_5N_3O_7$: C, 69.06; H, 3.26; N, 7.55%.

References

1) R. A. Raphael, E. C. Tayler, and H. Wynberg, Ed., "Advances in Organic Chemistry," Vol. 4, Interscience, New York (1963), G. Eglinton and W. McCrae, p. 225.

2) a) J. Ojima, T. Katakami, G. Nakaminami, and M. Nakagawa, *Tetrahedron Lett.*, **1968**, 1115; b) Ojima, T. Katakami, and M. Nakagawa, *Bull. Chem. Soc. Jpn.*, **49**, 292 (1976); c) K. Fukui, T. Okamoto, and M. Nakagawa, *Tetrahedron Lett.*, **1971**, 3121; d) T. Katakami, S. Tomita, K. Fukui, and M. Nakagawa, *Chem. Lett.*, **1972**, 225; e) T. Katakami, K. Fukui, T. Okamoto, and M. Nakagawa, *Bull. Chem. Soc. Jpn.*, **49**, 297 (1976); f) S. Tomita and M. Nakagawa, *Bull. Chem. Soc. Jpn.*, **49**, 302 (1976); g) T. Nomoto, K. Fukui, and M. Nakagawa, *Tetrahedron Lett.*, **1972**, 3253; h) T. Nomoto, K. Fukui, and M. Nakagawa, *Bull. Chem. Soc. Jpn.*, **49**, 305 (1976).

3) a) M. Iyoda, H. Miyazaki, and M. Nakagawa, *J. Chem. Soc., Chem. Commun.*, **1972**, 431; b) M. Iyoda, H, Miyazaki, and M. Nakagawa, *Bull. Chem. Soc. Jpn.*, **49**, 2306 (1967); S. Akiyama, T. Nomoto, M. Iyoda, and M. Nakagawa, *Bull. Chem. Soc. Jpn.*, **49**, 2579 (1976).

4) For a preliminary report, see K. Fukui, T. Nomoto, S. Nakatsuji, and M. Nakagawa, *Tetrahedron Lett.*, **1972**, 3157.

5) F. Sondheimer, Y. Gaoni, *J. Am. Chem. Soc.*, **82**, 5765 (1960); F. Sondheimer, Y. Gaoni, L. M. Jackman, N. A. Bailey, and R. Mason, *ibid.*, **84**, 4595 (1962).

6) *Cf.* W. Ziegenbein, "Athynylierung und Alkinylierung," Verlag Chemie (1963), p. 85.

7) C. Charrier, D. E. Dorman, and J. D. Roberts, *J. Org. Chem.*, **38**, 2644 (1973),.

8) J. P. C. M. van Dongen, M. J. A. de Bie, and R. Steuer, *Tetrahedron Lett.*, **1973**, 1371.

The Synthesis of Peptides by Means of Proteolytic Enzymes

Yoshikazu Isowa, Muneki Ohmori, Tetsuya Ichikawa, Hideaki Kurita, Masanari Sato, and Kaoru Mori

Sagami Chemical Research Center, Nishi-Ohnuma Sagamihara, Kanagawa 229

(Received April 15, 1977)

Nagarse, papain, pepsin and thermolysin were found to catalyze the peptide bond formation between two amino acids or peptides, one protected with a suitable group at the amino group and the other at the carboxyl group. Experiments with various combinations of amino acids and dipeptides show specificity in the catalytic action in varying degree which depending on the nature of the enzyme. Since the condensation takes place efficiently under mild conditions, this method opens up a useful way for the synthesis of peptides.

During the last three decades several important general methods and a large number of coupling reagents for peptide bond formation have been developed.[1] Almost all the coupling methods involve the possibility of side reactions and racemization. Racemization may always be expected to some extent when the carboxyl group of an N-protected amino acid or peptide is activated. Careful control of coupling conditions may be used to minimize or eliminate these side reactions and racemization in chemical synthesis.

On the other hand, proteolytic enzyme is expected to provide a potential method for the peptide synthesis without racemization, if hydrolytic action is supressed.

However, no successful result seems to have been reported except for that of Bergmann and Fraenkel-Conrat which involves the condensation of acylamino acid and amino acid anilide in the presence of papain.[2] Fruton[3] referred to their method as an interesting approach to the synthesis of peptide but one involving difficulties which prevent it from being a general synthetic method.

With the expectation that the above difficulties can be overcome by means of the protecting groups of the substrates, we have examined the possibility of using proteolytic enzymes for practical preparation of peptides since a few years ago. The study has produced a considerable amount of useful findings, and in this paper we give some typical examples from the results obtained so far.

Examination was made of the catalytic action of four representative enzymes[4-7] each from seryl-, thiol-, acid-, and metallo-proteinase groups on the following peptide forming reactions between two amino acids or dipeptides suitably protected at the amino group (carboxyl component) or at the carboxyl group (amine component):

1. Z-X-OH + H-Phe-Val-OBu^t ⟶ Z-X-Phe-Val-OBu^t
2. Z-Phe-X-OH + H-Phe-Val-OBu^t ⟶ Z-Phe-X-Phe-Val-OBu^t
3. Z-X-Y-OH + H-Phe-ODPM ⟶ Z-X-Y-Phe-ODPM
4. Z-X-OH + H-Val-ODPM ⟶ Z-X-Val-ODPM
5. Z-X-OH + H-Phe-Phe-OBu^t ⟶ Z-X-Phe-Phe-OBu^t

In these formulas, X and Y stand for arbitrary amino acid residues with Z, benzyloxycarbonyl; Bu^t, *t*-butyl; and DPM, diphenylmethyl as protecting groups.

Materials and Methods

Enzymes: Papain (2.1×10^2 units/mg, Midori Juji Co.), Nagarse (5×10^2 units/mg, Nagase Co.), Thermolysin (8.08×10^3 units/mg, Daiwa Kasei Co.) and porcine pepsin (1.9×10^3 units/mg, Sigma Chemical Co., U.S.A.) were used without further purification.

Substrates: All the amino acids used had the L-configuration.

Phenylalanine Diphenylmethyl Ester p-*Toluenesulfonate and Valine Diphenylmethyl Ester* p-*Toluenesulfonate*: These were prepared in the same manner as described for the corresponding benzyl ester.[8]

Phenylalanine Diphenylmethyl Ester p-*Toluenesulfonate.* The yield was 83%, mp 217—220 °C (from methanol–ether).

Found: C, 68.88; H, 5.76; N, 2.71%. Calcd for $C_{29}H_{29}NO_5S$: C, 69.16; H, 5.80; N, 2.78%.

Valine Diphenylmethyl Ester p-*Toluenesulfonate.* The yield was 65%, mp 173 °C (from methanol–ether).

Found: C, 65.41; H, 6.51; N, 2.96%. Caldc for $C_{25}H_{29}NO_5S$: C, 65.91; H, 6.42; N, 3.07%.

The following dipeptide derivatives were prepared by the procedure given in literature: H-Phe-Val-OBu^t,[9] H-Phe-Phe-OBu^t,[10] Z-Phe-Gly-OH,[11] Z-Phe-Ser-OH,[12] Z-Phe-Arg-(NO_2)-OH,[13] Z-Leu-Phe-OH,[14] Z-Phe-Tyr-OH.[15]

Z-Phe-Val-OEt. To 48.5 g (0.267 mol) of H-Val-OEt in 180 ml of DMF at −10 °C was added 30 ml (0.270 mol) of *N*-methylmorpholine, 80 g (0.267 mol) of Z-Phe-OH, 36.5 g (0.27 mol) of 1-hydroxy-benztriazole and 56.7 g (0.276 mol) of dicyclohexylcarbodiimide in 180 ml of of DMF. After 20 h, the reaction mixture was worked up by the usual procedure. The product was recrystallized from ethanol–water: yield 107.5 g (94%); mp 103—105 °C; $[\alpha]_D$ −18.4° (*c* 1, ethanol).

Found: C, 67.45; H, 7.09; N, 6.61%. Calcd for $C_{24}H_{30}N_2O_5$: C, 67.58; H, 7.09; N, 6.57%.

Z-Phe-Val-OH. A solution of 60 g (0.141 mol) of Z-Phe-Val-OEt in 350 ml of ethanol was saponified with 180 ml of 1 M aqueous sodium hydroxide for 12 h. The solution was acidified with 2M hydrochloric acid and filtered. The sample was recrystallized from ethanol–water for analysis: yield 52.4 g (93%); $[\alpha]_D$ −7.1° (*c* 1, ethanol).

Found: C, 66.11; H, 6.60; N, 7.05%. Calcd for $C_{22}H_{26}N_2O_5$: C, 66.31; H, 6.58; N, 7.03%.

General procedures of the synthesis with enzymes are as follows.

Peptide Synthesis by Papain: 20 ml of a McIlvaine buffer solution having pH 6.6 was added to 1.0 mmol each of a carboxyl component and an amine component. 150 mg

of papain and 0.1 ml of 2-mercaptoethanol were then added to the mixture. After incubation at 38° for 24 h, the resulting precipitate was filtered off and washed in succession with water, 7% aqueous ammonia, 0.5 M hydrochloric acid and water. The product was dissolved in 50 ml of hot methanol and the solution was treated with active carbon. The solution was concentrated *in vacuo* and the residue was recrystallized from an appropriate solvent to give a pure crystalline product.

Peptide Synthesis by Nagarse: 20 ml of a McIlvaine buffer solution having pH of 7.2 was added to 1.0 mmol each of a carboxyl component and an amine component. 150 mg of nagarse was then added to the mixture. After incubation at 38 °C for 24 h, the product was isolated by the same procedure as described above.

Peptide Synthesis by Pepsin: 20 ml of an acetate buffer solution having pH of 4.5 was added to 1.0 mmol each of a carboxyl component and an amine component. 100 mg of pepsin was then added to the mixture and the mixture incubated at 38 °C for 24 h. The product was isolated by the same procedure as described above.

Peptide Synthesis by Thermolysin: 20 ml of a veronal buffer solution having pH of 7.5 was added to 1.0 mmol each of a carboxyl component and an amine component. 20 mg of thermolysin was then added to the mixture. After incubation at 38 °C for 24 h, the product was isolated by the same procedure as described above.

Results and Discussion

The effect of papain and thermolysin on the reaction of benzyloxycarbonyl amino acids with phenylalanyl-valine *t*-butyl ester is given in Table 1.

Table 1. Effect of enzymes on th ereaction
Z-X-OH+H-Phe-Val-OBu^t→Z-X-Phe-Val-OBu^t

Compound(-X-)	Enzyme Yield (%)	
	Papain	Thermolysin
Gly	43	85
Val	—	47
Tyr	15	63
Ser	31	76
Arg(N_{O_2})	49	58

While papain and thermolysin displayed a similar synthetic activity toward these substrates, nagarse and pepsin were ineffective in reaction 1. Thermolysin appears to be more potent than papain in the tripeptide formation.

The effect of papain, thermolysin and nagarse on the reaction of Z-Phe-X-OH with phenylalanyl-valine *t*-butyl ester is given in Table 2.

Table 2. Effect of enzymes on the reaction
Z-Phe-X-OH^t+H-Phe-Val-OBu^t→Z-Phe-X-Phe-Val-OBu^t

Compound(-X-)	Yield (%)		
	Papain	Thermolysin	Nagarse
Gly	77	79	—
Val	12	50	22
Tyr	—	72	35
Ser	84	65	—
Arg(NO_2)	91	52	21

Papain, thermolysin and nagarse exhibit a synthetic activity, while pepsin was ineffective in these tetrapeptide formations.

A comparison of the results obtained in reactions 1 and 2 shows that acyl dipeptides (Z-Phe-X-OH) are more prone to give condensation products than acyl amino acids (Z-X-OH) as carboxyl component.

The effect of papain and pepsin on the reaction of benzyloxycarbonyl dipeptide acids (Z-X-Y-OH) with phenylalanine diphenylmethyl ester is given in Table 3.

Table 3. Effect of enzymes on the reaction
Z-X-Y-OH+H-Phe-ODPM→Z-X-Y-Phe-ODPM

Compound (-X-Y-)	Yield (%)	
	Papain	Pepsin
Leu-Phe	98	84.7
Phe-Tyr	94	63
Val-Tyr	100	0

Both enzymes show the same synthetic activity in the case of Z-Leu-Phe-OH or Z-Phe-Tyr-OH with phenylalanine diphenylmethyl ester. It is of interest that there is a striking difference between these enzymes in the case of Z-Val-Tyr-OH as carboxyl component. However, nagarse and thermolysin were ineffective in these reactions.

The effect of papain on the reaction of benzyloxycarbonyl amino acids with valine diphenylmethyl ester is given in Table 4.

Table 4. Effect of papain on the reaction
Z-X-OH+H-Val-ODPM→Z-X-Val-ODPM

Compound (X)	Yield (%)	Compound (X)	Yield (%)
Ala	80	Phe	91
Met	81	Glu	61
Thr	66	Asn	25
Gln	69	Arg(NO_2)	83
Lys(z)	70		

Table 5. Effect of papain and thermolysin on the following reaction
Z-X-OH+H-Phe-Phe-OBu^t→Z-X-Phe-Phe-OBu^t

Compound (-X-)	Yield (%)	
	Papain	Thermolysin
Gly	20	68
Ala	80	61
Leu	32	79
Phe	—	28
Tyr	—	50
Ser	8	—
Thr	71	28
Met	95	74
Cys(Bzl)	69	7
Asn	48	89
Glu	52	79
Gln	78	79

Table 6. Physical properties and elemental analysis of the enzymic reaction products

X	Mp(°C)	$[\alpha]_D$	Formula	Calcd (%) (Found) C	H	N	S
1. Z-X-Phe-Val-OBu^t							
Gly	foam	−18.3 (*c* 1, MeOH)	$C_{28}H_{37}N_3O_6$	65.73 (65.75	7.29 7.45	8.21 8.52)	
Val	178	−45.5 (*c* 1, MeOH)	$C_{31}H_{43}N_3O_6$	67.24 (66.98	7.83 7.73	7.59 7.55)	
Tyr	85	−33.4 (*c* 1, MeOH)	$C_{35}H_{43}N_3O_7$	68.05 (67.98	7.02 7.14	6.80 6.91)	
Ser	135	−34.9 (*c* 1, MeOH)	$C_{29}H_{39}N_3O_7$	64.31 (64.00	7.26 7.33	7.76 7.87)	
Arg(NO_2)	125	−24.9 (*c* 1, MeOH)	$C_{32}H_{45}N_7O_8$	58.61 (58.88	6.92 6.98	14.95 14.53)	
2. Z-Phe-X-Phe-Val-OBu^t							
Gly	85—92	−19.9 (*c* 1, MeOH)	$C_{37}H_{46}N_4O_7$	67.46 (67.52	7.04 6.93	8.50 8.58)	
Val	216	−44.8 (*c* 1, MeOH)	$C_{40}H_{52}N_4O_7$	68.55 (68.52	7.48 7.50	7.99 7.97)	
Tyr	110	−40.6 (*c* 1, MeOH)	$C_{44}H_{52}N_4O_8$	69.09 (68.91	6.85 6.89	7.32 7.56)	
Ser	169	−28.3 (*c* 1, MeOH)	$C_{38}H_{48}N_4O_8 \cdot H_2O$	64.57 (64.46	7.13 6.91	7.93 8.01)	
Arg(NO_2)	115	−29.2 (*c* 1, MeOH)	$C_{41}H_{54}N_8O_9$	61.33 (61.79	6.78 6.65	13.96 13.90)	
3. Z-X-Y-Phe-ODPM							
Leu-Phe	172	−24.5 (*c* 1, DMF)	$C_{45}H_{47}N_3O_6$	74.46 (74.62	6.53 6.67	5.79 5.66)	
Phe-Tyr	165	−23.9 (*c* 0.63, DMF)	$C_{48}H_{45}N_3O_7$	74.30 (74.06	5.85 5.84	5.42 5.35)	
Val-Tyr	196	−34.8 (*c* 0.5, DMF)	$C_{44}H_{45}N_3O_7$	72.61 (72.49	6.23 6.22	5.77 5.84)	
4. Z-X-Val-ODPM							
Ala	92—96		$C_{29}H_{32}N_2O_5$	71.29 (71.28	6.60 6.54	5.73 5.82)	
Phe	106		$C_{35}H_{36}N_2O_5 \cdot 2H_2O$	69.98 (70.21	6.71 6.34	4.66 4.80)	
Thr	89—95		$C_{30}H_{34}N_2O_6$	69.48 (69.19	6.61 6.59	5.40 5.26)	
Met	98		$C_{31}H_{36}N_2O_5S$	67.80 (67.83	6.61 6.60	5.12 5.16	5.84 5.79)
Asn	116—125		$C_{30}H_{33}N_3O_6$	67.78 (68.18	6.26 6.27	7.90 7.41)	
Glu	125—131		$C_{31}H_{34}N_2O_7$	68.12 (68.23	6.27 6.31	5.12 4.84)	
Gln	178—183		$C_{31}H_{35}N_3O_6$	68.24 (67.94	6.47 6.39	7.70 7.74)	
Arg(NO_2)	142		$C_{32}H_{38}N_6O_7$	62.12 (62.48	6.19 6.21	13.58 13.40)	
Lys(z)	117		$C_{40}H_{45}N_3O_7$	70.67 (70.28	6.67 6.66	6.18 6.33)	
5. Z-X-Phe-Phe-OBu^t							
Gly	72	−13.6 (*c* 0.5, MeOH)	$C_{32}H_{37}N_3O_6$	68.67 (68.91	6.66 6.76	7.51 7.58)	
Ala	95	−33.5 (*c* 1, MeOH)	$C_{33}H_{39}N_3O_6$	69.09 (68.95	6.85 6.84	7.32 7.21)	
Leu	96	−32.1 (*c* 1, MeOH)	$C_{36}H_{45}N_3O_6$	70.22 (70.38	7.37 7.57	6.82 6.64)	
Phe	104	−29.5 (*c* 1, MeOH)	$C_{39}H_{43}N_3O_6$	72.09 (71.86	6.67 6.66	6.47 6.39)	
Tyr	119	−26.1 (*c* 1, MeOH)	$C_{39}H_{43}N_3O_7$	70.36 (70.37	6.51 6.38	6.31 6.05)	
Ser	103		$C_{33}H_{39}N_3O_7$	67.21 (67.30	6.67 6.91	7.13 6.88)	

Table 5. Continued

X	Mp(°C)	$[\alpha]_D$	Formula	Calcd (%) (Found)			
				C	H	N	S
Thr	94	−24.9 (*c* 1, MeOH)	$C_{34}H_{41}N_3O_7$	67.64 (67.24	6.85 6.70	6.96 6.88)	
Met	106	−31.3 (*c* 1, MeOH)	$C_{35}H_{43}N_3O_6S$	66.32 (66.30	6.84 6.77	6.63 6.53)	
Cys(Bzl)	68	−35.0 (*c* 1, MeOH)	$C_{40}H_{45}N_3O_6S$	69.04 (68.92	6.52 6.48	6.04 6.06)	
Glu	147—152	−17.6 (*c* 1, DMF)	$C_{35}H_{41}N_3O_8$	66.54 (66.54	6.54 6.41	6.65 6.59)	
Asn	185	−29.2 (*c* 1, DMF)	$C_{34}H_{40}N_4O_7$	66.21 (66.22	6.54 6.52	9.09 8.87)	
Gln	188	−18.3 (*c* 1, DMF)	$C_{35}H_{42}N_4O_7$	66.65 (66.51	6.71 6.71	8.88 8.74)	

Papain exhibits wide peptide formation activity for various amino acids as a carboxyl component.

The effects of papain and thermolysin in the reaction of benzyloxycarbonyl amino acids with phenylalanyl-phenylalanine *t*-butyl ester are compared in Table 5.

These two enzymes show similar activities, the specificity as regards the nature of reacting amino acids being low.

It appears that the low specificity in the peptide bond formation is generally associated with the low specificity in the hydrolysis of protein, such as papain[5] and thermolysin.[7]

The results shown that the utilization of proteolytic enzymes as a catalyst in the formation of a peptide linkage is advantageous for practical synthesis of oligopeptides because of ready condensation under mild conditions.

The authors wish to express their deep gratitude to Drs. Y. Morino and O. Shimamura for their constant encouragement throughout the work. Thanks are due to Mrs. K. Kogure for her skilful assistances throughout the experiments.

References

1) (a) E. Schröder and K. Lubke, "The Peptides," Academic Press, New York. Vol. 1 (1965) and Vol. 2 (1966) (b) G. T. Young, Ed., "Amino-acids, Peptides, and Proteins," The Chemical Society, Burlington House, Vols. 1—4, London (1969—1972); R. C. Sheppard, Ed., *ibid*, Vols. 5—7, London (1973—1975); (c) E. Müller, Ed.. "Houben-Weyl: Methoden der Organischen Chemie," Georg Thieme Verlag, Band 15-1 and Band 15-2, Stuttgart (1974); (d) H. Neurath and R. L. Hill, Ed., "The Proteins," 3rd ed, Academic Press, New York (1976), p. 106 257.

2) M. Bergmann and H. Fraenkel-Conrat, *J. Biol. Chem.*, **119**, 707 (1937). O. K. Behrens and M. Bergmann, *ibid.*, 129, 587 (1939).

3) J. S. Fruton, "Advances in Protein Chemistry," Academic Press, Vol. 5, New York (1949), p. 33.

4) F. S. Markland and E. L. Smith, "The Enzyme," ed, P. D. Boyer, Academic Press, Vol. 3, New York and London (1971), p. 561.

5) A. N. Glazer and E. L. Smith, "The Enzyme," ed, P. D. Boyer, Academic Press, Vol. 3, New York and London (1971), p. 502.

6) J. S. Fruton, "The Enzyme," ed, P. D. Boyer, Academic press, Vol. 3, New York and London (1971), p. 120.

7) H. Matsubara and J. Feder, "The Enzyme," ed, P. D. Boyer, Academic Press, Vol. 3, New York and London (1971), p. 765.

8) L. Zervas, M. Winitz, and J. P. Greenstein, *J. Org. Chem.*, **22**, 1515 (1957).

9) E. Wünsch and G. Wendlberger, *Chem. Ber.*, **100**, 160 (1967).

10) K. Inouye, I. M. Voynick, G. R. Delpierre, and J. S. Fruton, *Biochemistry*, **5**, 2473 (1966).

11) E. Scoffone, R. Rocchi, G. Vidali, A. Scatturin, and F. Marchiori, *Gazz. Chim. Ital.*, **94**, 743 (1964).

12) M. Bodansky, J. T. Sheehan, M. A. Ondetti, and S. Lande, *J. Am. Chem. Soc.*, **85**, 991 (1963).

13) M. A. Ondetti, *J. Med. Chem.*, **6**, 10 (1963).

14) F. Weygand, A. Prox, and W. König, *Chem. Ber.*, **99**, 1451 (1966).

15) R. Geiger, G. Jager, A. Valk, and W. Siedel, *Chem. Ber.*, **101**, 2189 (1968).

The Enzymatic Synthesis of Protected Valine-5 Angiotensin II Amide-1

Yoshikazu Isowa, Muneki Ohmori, Masanari Sato, and Kaoru Mori

Sagami Chemical Research Center, Nishi-Ohnuma Sagamihara, Kanagawa 229

(Received April 15, 1977)

An example of the use of proteolytic enzymes to facilitate the peptide synthesis by fragment condensation is provided for the preparation of protected valine-5 angiotensin II amide-1 using *t*-butoxycarbonylpeptides as a carboxyl component and a peptide ethyl ester as an amine component. The proteolytic enzymes used are papain, nagarse (subtilisin BPN') and microbial metalloenzyme isolated from *St. caespitosus*. Papain-catalyzed condensation reaction afforded the corresponding oligopeptide in the ester form, whereas nagarse and microbial metalloenzyme-catalyzed condensation reactions afforded the products in the carboxyl free form. Assignment of the product was made on the basis of a comparison of physical properties with those of the peptide prepared by the solution method.

Previous work in this series has shown that typical proteolytic enzymes, *e.g.*, papain, thermolysin, nagarse (subtilisin BPN') and pepsin, may be capable of catalyzing peptide bond formation between acylamino acids or acyldipeptides and amino acid or dipeptide esters.[1] The first instance of such a reaction was the amide bond formation between an acylamino acid and amino acid anilide in the presence of papain reported by Bergmann and Fraenkel-Conrat,[2] who also examined the effect of the peptide bond formation by chymotrypsin using an amino acid anilide as an amine component.[3,4] These observations indicate that the proteolytic enzymes catalyze the formation of small peptides such as di, tri, and tetrapeptides. However, since the enzymes essentially catalyze the hydrolysis of peptides, it is of interest to examine them with respect to their ability to catalyze the formation of oligopeptides without undesirable reactions.

This investigation was undertaken to provide a fundamental information on the enzymatic synthesis of oligopeptides using papain,[5] nagarse (subtilisin BPN')[6] and microbial metalloenzyme[7] as catalysts. For this purpose, the preparation of protected valine-5 angiotensin II amide-1 *via* the enzymatic fragment condensation was studied. This peptide hormon consists of eight amino acid residues having a L-configuration. Its constructional formula is as follows.

H–Asn^1–Arg^2–Val^3–Tyr^4–Val^5–His^6–Pro^7–Phe^8–OH

The octapeptide was first synthesized by Schwyzer and co-workers.[8] Several angiotensin peptides have since been prepared by means of solution or solid phase method.

It was demonstrated that the angiotensin undergoes cleavage at a tyrosyl residue on the carboxyl side by the action of chymotrypsin or chymotrypsin-like endopeptidases.[9,10] The peptide bond chosen for the fragment condensation was therefore Tyr^4–Val^5 linkage in this synthetic procedure. The scheme for the preparation of N-terminal dipeptide and tetrapeptide used for carboxyl component is given in Fig. 1 and that of C-terminal tetrapeptide for amino component in Fig. 2.

In order to facilitate isolation the side-chain functional groups of Arg, Tyr, and His were protected by nitro or benzyl group.[11] As an amino protecting group for Arg(NO_2), His(BZL), and Pro, 2,4,6-trimethylbenzyloxycarbonyl (TMZ) group, which was readily

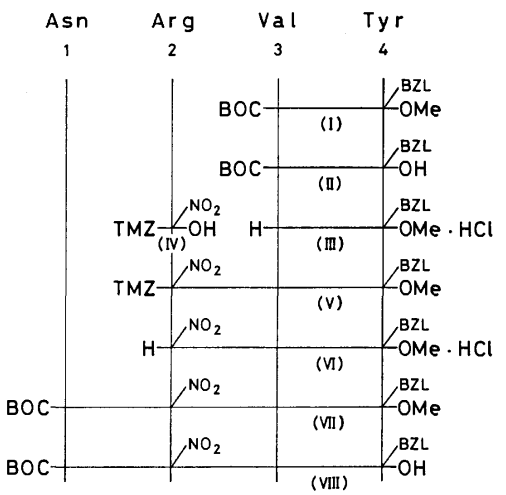

Fig. 1. Preparation of peptide substrates, II and VIII, as carboxyl component; prefix L for amino acids is omitted; BOC, *t*-butoxycarbonyl; TMZ, 2,4,6-trimethylbenzyloxycarbonyl; BZL, benzyl; Me, methyl.

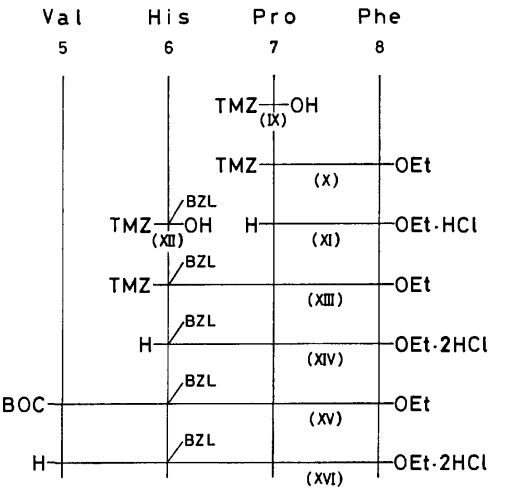

Fig. 2. Preparation of peptide substrate, XVI, as amine component; Et, ethyl.

introduced by the reaction with 2,4,6-trimethylbenzyl 2,4,5-trichlorophenyl carbonate by a modification of the *t*-butoxycarbonylation[12] and smoothly removed by acidolysis, was employed because of the fine crystallization of their peptide derivatives. In a comparison of

VI and XI with samples obtained from the corresponding BOC-derivatives, no detectable amount of optical inpurity was observed.

The reaction sequence for the preparation of the valine-5 angiotensin 3—8 fragment and the protected valine-5 angiotensin II amide-1 as authentic samples is shown in Fig. 3.

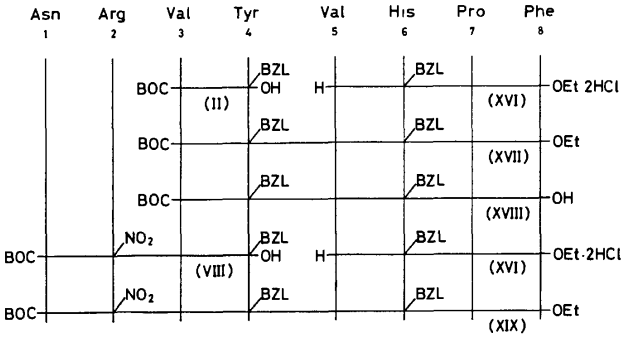

Fig. 3. Preparation of authentic samples, XVII, XVIII, and XIX, by solution method.

In all cases, the coupling reactions were carried out by means of HOBt/DCCI method,[13] the tertiary base being *N*-methylmorpholine, and the solvent *N*,*N*-dimethylformamide. The resulting products were isolated in the usual way. When necessary, the *t*-butoxycarbonyl or 2,4,6-trimethylbenzyloxycarbonyl group was removed by treatment with hydrogen chloride in ethyl acetate. Saponification of the peptide esters was carried out in methanol or *N*,*N*-dimethylformamide solution in the presence of sodium hydroxide at room temperature.

The enzymatic condensation reactions were carried out by incubating the substrates in buffer solutions of the pH comparable to those of the hydrolytic reactions, either in the absence or presence of methanol; the McIlvaine buffer of pH 5.5, 7.5 and Veronal buffer of pH 7.0 were employed for the papain, nagarse and microbial metalloenzyme-catalyzed reactions, respectively. When hydrochloride was used as an amine component, the required quantity of 1 M sodium hydroxide was added. Details of the composition of the reaction mixture and of the reaction conditions are given in Experimental.

All the products obtained in these reactions were identified by direct comparison of their melting point, optical rotation and R_f value of thin layer chromatography with those of samples prepared by the solution method (Fig. 3).

Results and Discussion

1) Syntheses of the Protected Valine-5 Angiotensin II 3-8 Fragment by Papain, Nagarse and Microbial Metalloenzyme-catalyzed Reaction. The possibility of the ploteolytic enzymes to catalyze the formation of oligopeptides was examined in the condensation of BOC–Val–Tyr(BZL)–OH (II) with H–Val–His(BZL)–Pro–Phe–OEt·2HCl (XVI). The results are summarized in Fig. 4.

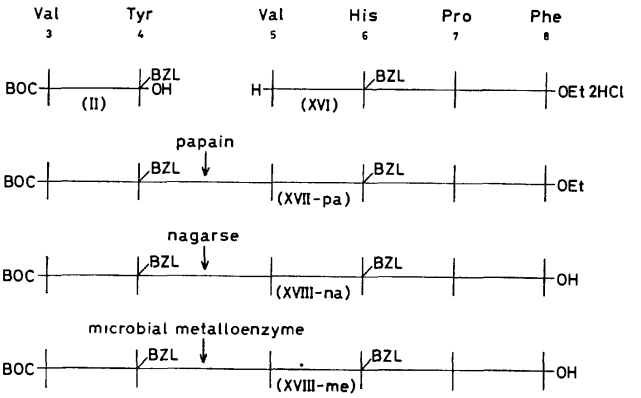

Fig. 4. Enzymatic condensation of BOC–Val–Tyr(BZL)–OH (II) with H–Val–His(BZL)–Pro–Phe–OEt·2HCl (XVI); suffix -pa, -na, and -me indicate the products obtained respectively by papain, nagarse, and microbial metalloenzyme-catalyzed reaction.

The papain-catalyzed reaction in McIlvaine buffer of pH 5.5 containing methanol (1/1, v/v) afforded the corresponding hexapeptide ethyl ester (XVII-pa) as the major product. The presence of all the amino acid residues constituting the hexapeptide and of the ethyl ester were determined by its NMR spectrum (see Experimental). Further structural elucidation was achieved by a comparison of physical properties with those of the peptide ester prepared by the HOBt/DCCI method (Table 1).

Table 1. Comparison of physical properties of XVII-pa with those of XVII prepared by solution method

		Type of condensation	
		Papain-catalyzed condensation (XVII-pa)	HOBt/DCCI (XVII)
Mp(°C)		167—173	164—173
$[\alpha]_D$ (c 1.0)	DMF	−36.0°	−35.3°
	MeOH	−58.5°	−59.2°
R_f (TLC)	system I	0.79	0.79
	system II	0.74	0.75

The observation that the protected hexapeptide ethyl ester (XVII-pa) is mainly obtained by the enzymatic reaction seems to be incompatible with the fact that papain possesses an esterase activity.[5,14] This is of considerable importance from a practical point of view.

The nagarse-catalyzed condensation reaction in McIlvaine buffer of pH 7.5 gave the corresponding hexapeptide in the carboxyl free form (XVIII-na). The melting point, optical rotation and R_f values of thin layer chromatography agree with those of XVIII obtained from the synthetic XVII by saponification (Table 2).

The result is in line with the fact that the serine proteinases catalyze the hydrolysis of ethyl or methyl ester linkage to a great extent.[15,16]

The microbial metalloenzyme-catalyzed reaction in Veronal buffer of pH 7.0 afforded the corresponding

Table 2. Comparison of physical properties of XVIII-na with those of XVIII prepared by saponification of the synthetic XVII

		Type of condensation	
		Nagarse-catalyzed condensation (XVIII-na)	Solution method (XVIII)
MP (°C)[a]		165—169	172—179
$[\alpha]_D$ (c 1.0)	DMF	−27.4°	−28.7°
R_f (TLC)	system I	0.41	0.41
	system II	0.64	0.63

a) Discrepancy in the melting points may be due to the water of crystallization; XVIII-na, $2H_2O$; synthetic XVIII, H_2O.

hexapeptide acid (XVIII-me). In spite of the fact that the microbial metalloenzymes are inactive against the ester substrates,[17,18] no measurable amount of the hexapeptide ester was detected in the condensation product. This might be attributed to an impurity in the microbial metalloenzyme employed.[7]

The investigations into the peptide bond forming ability of the proteolytic enzymes show that the protected hexapeptides can be enzymatically prepared by the fragment condensation of II with XVI without loss of amino acid residues. However, except in the case of the papain-catalyzed reaction, the hexapeptide was obtained in a carboxyl free form even when the condensation reactions were carried out in the presence of methanol.

2) Synthesis of the Protected Valine-5 Angiotensin II Amide-1 by the Papain-catalyzed Reaction. Since the papain-catalyzed reaction afforded the product in the form of the ethyl ester as described in the synthesis of hexapeptide, preparation of the protected valine-5 angiotensin II amide-1 was attempted with use of papain. The product obtained by the papain-catalyzed condensation of fragment 1—4 (VIII) with 5—8 (XVI) in a mixture of McIlvaine buffer of pH 5.5 and methanol (1/1, v/v) was the corresponding octapeptide ester (XIX-pa) containing two of the water of crystallization. Its structure was determined by means of elemental and NMR analysis.

BOC–Asn–Arg(NO_2)–Val–Tyr(BZL)–OH (VIII) + H–Val–His(BZL)–Pro–Phe–OEt (XVI)

↓ papain, in buffer/methanol=1/1 (v/v)

BOC–Asn–Arg(NO_2)–Val–Tyr(BZL)–Val–His(BZL)–Pro–Phe–OEt

Protected valine-5 angiotensin II amide-1 (XIX-pa)

The significant physical properties of XIX-pa were the same as those of XIX prepared by the solution method (Table 3). A small amount of the octapeptide acid was concomitantly obtained when the reaction was carried out in the absence of methanol. It seems to be reasonable to assume that the papain-catalyzed esterolysis is repressed by the addition of methanol to the reaction mixture.

This finding indicates that papain also catalyzes the octapeptide formation *via* fragment condensation without loss of amino acid residues. Furthermore, it is of interest to note that by the addition of methanol to the reaction mixture, the papain-catalyzed reaction affords the product in the form of ethyl ester.

Table 3. Comparison of physical properties of XIX-pa with those of XIX prepared by solution method

		Type of condensation	
		Papain-catalyzed condensation (XIX-pa)	HOBt/DCCI (XIX)
MP (°C)		186—195	189—195
$[\alpha]_D$ (c 1.0)	DMF	−27.3°	−26.5°
	MeOH	−48.3°	−48.4°
R_f (TLC)	system I	0.62	0.63
	system II	0.56	0.55

It is apparent that the proteolytic enzymes, papain, nagarse and microbial metalloenzyme, are capable of synthesizing oligopeptide by fragment condensation. The oligopeptide formation can be attributed to the insolubility of the products, which influences the equilibrium in favor of the peptide bond formation.

In view of the low solubility of the protected oligopeptides, the application of this enzymatic procedure, enzymatic procedure, along with a combination of the solution method, promises a new possibility of facile preparation of the peptide.

Experimental

The melting points were determined on a Yanagimoto micro melting point apparatus and are uncorrected. The optical rotations were measured with a Yanagimoto automatic polarimeter OR-50 type. The NMR spectra were recorded on a Varian HA-100 High Resolution NMR spectrometer, using tetramethylsilane as an internal or external standard. The thin layer chromatography was carried out on precorted plates of silica gel G (E. Merck). The developing solvents commonly used were 2-butanol–3% ammonia water (8: 3, v/v) (system I) and 1-butanol–acetic acid–water (4: 1: 5, v/v) (system II).

Enzymes. All the proteolytic enzymes used in this investigation were commercial preparations; papain (Midori Juji Co., E-2 1200 U/g); nagarse (Nagase Sangyo Co., 50×10^4 PUN/g); microbial metalloenzyme *(St. caespitosus)* (Kyowa Hakko Kogyo Co.). The proteolytic activities of the papain, nagarse and microbial metalloenzyme, assayed by the casein digestion method of Tsuru, Yamamoto, and Fukumoto[19] with the exception that the papain was preincubated with cysteine, were 2.20×10^5, 1.15×10^6 and 2.64×10^5 PU/g, respectively. The microbial metalloenzyme seems to be contaminated with alkaline proteinases, since the proteolytic activity is inhibited by not only EDTA but also diisopropyl fluorophosphate.[7]

BOC–Val–Tyr(BZL)–OMe (I). A mixture of BOC–Val–OH (10.9 g, 50 mmol) and H–Tyr(BZL)–OMe·HCl (16.1 g, 50 mmol) in 120 ml of *N,N*-dimethylformamide was cooled at −5 °C with stirring. To the chilled solution were added *N*-methylmorpholine (5.1 g, 50 mmol) and 1-hydroxybenzotriazole (6.8 g, 50 mmol), followed by a solution of dicyclohexylcarbodiimide (10.7 g, 52 mmol) in 50 ml of *N,N*-dimethylformamide. Stirring was continued at the same temperature

for 1 h and then at room temperature for 8 h. After removal of the urea by filtration the filtrate was evaporated to dryness *in vacuo* and the residue was treated with water. The solid product was collected by filtration and washed with 5% sodium hydrogencarbonate, water, 1 M hydrochloric acid and water. Recrystallization twice from methanol–water yielded 20.3 g (83.7%) of I; mp 114—116 °C; $[\alpha]_D$ −13.0° (*c* 1.0, methanol).

Found: C, 67.17; H, 7.31; N, 5.79%. Calcd for $C_{27}H_{36}N_2O_6$: C, 66.92; H, 7.49; N, 5.78%.

BOC–Val–Tyr(BZL)–OH (II). A solution of I (14.5 g, 30 mmol) in methanol was treated with 1 M sodium hydroxide (33 ml) at room temperature for 2 h. After removal of methanol *in vacuo*, the aqueous solution was acidified with 2 M hydrochloric acid under ice-cooling. The precipitate was collected by filtration and washed with water, and then recrystallized from methanol–water; 11.6 g (82.2%); mp 142—145 °C; $[\alpha]_D$ +0.2° (*c* 1.0, methanol). A sample was further recrystallized from a small volume of methanol for analysis; mp 143—145 °C.

Found: C, 66.51; H, 7.01; N, 6.07%. Calcd for $C_{26}H_{34}N_2O_6$: C, 66.36; H, 7.28 N, 5.95%.

H–Val–Tyr(BZL)–OMe·HCl (III). Eighty milliliter of 5 M hydrogen chloride in ethyl acetate was added to a suspension of I (9.69 g, 20 mmol) in 40 ml of ethyl acetate. The substance dissolved immediately to form a clear solution. After being left to stand for 2 h at room temperature, the solution was evaporated to dryness *in vacuo*. The residue was crystallized by addition of ether; 8.10 g (96.2%); mp 175—179 °C; $[\alpha]_D$ +29.2° (*c* 1.0, methanol).

Found: C, 62.94; H, 6.82; N, 6.45%. Calcd for $C_{22}H_{29}N_2O_4Cl$: C, 62.77; H, 6.94; N, 6.66%.

2,4,6-Trimethylbenzyl 2,4,5-Trichlorophenyl Carbonate. 2,4,6-Trimethylbenzyl alcohol (26.2 g, 174 mmol) was allowed to react with 2,4,5-trichlorophenyl chloroformate (45.2 g, 174 mmol) in 200 ml of dichloromethane in the presence of quinoline (23.2 g, 180 mmol), by the same procedure as that for the preparation of *t*-butyl 2,4,5-trichlorophenyl carbonate.[12] Recrystallization from ligroine yielded colorless needles of the carbonate; 43.0 g (66.1%); mp 113—115 °C.

Found: C, 54.41; H, 4.18; Cl, 28.73%. Calcd for $C_{17}H_{15}O_3Cl_3$: C, 54.64; H, 4.05; Cl, 28.47%.

TMZ–Arg(NO$_2$)–OH (IV). Twenty-eight milliliter of 40% benzyltrimethylammonium hydrxide was added to a suspension of H–Arg(NO$_2$)–OH (10.6 g, 48.5 mmol) in 100 ml of methanol and the resulting mixture was stirred at 55—60 °C until solution was complete (2 h). The solvent was removed *in vacuo* and replaced by a mixture of 200 ml of dioxane and 50 ml of water. To the solution obtained was added 2,4,6-trimethylbenzyl 2,4,5-trichlorophenyl carbonate (18.7 g, 50.0 mmol) and the solution was stirred for 6 h at 55 °C. After removal of the solvent *in vacuo*, the residue was taken up in 250 ml of water and the aqueous solution was washed three times with 100 ml of ether. IV was precipitated by bringing the pH of the solution to 4—5 with citric acid. The crude material was collected, washed with water, and recrystallized from ethanol–ether; 17.2 g (89.7%); mp 176—178 °C; $[\alpha]_D$ +20.7° (*c* 1.0, methanol) and +0.8° (*c* 1.0, tetrahydrofuran).

Found: C, 51.52; H, 6.36; N, 17.48%. Calcd for $C_{17}H_{25}N_5O_6$: C, 51.63; H, 6.37; N, 17.71%.

TMZ–Arg(NO$_2$)–Val–Tyr(BZL)–OMe (V). Condensation of III (4.21 g, 10 mmol) with IV (3.95 g, 10 mmol) was carried out as described for I. Recrystallization of the product twice from methanol–water yielded V as a colorless powder; 5.97 g (78.4%); mp 191—192 °C; $[\alpha]_D$ +3.0° (*c* 1.0, *N,N*-dimethylformamide).

Found: C, 61.33; H, 6.67; N, 12.80%. Calcd for $C_{39}H_{51}N_7O_9$: C, 61.48; H, 6.75; N, 12.87%.

H–Arg(NO$_2$)–Val–Tyr(BZL)·OMe·HCl (VI). Deprotection of V (5.20 g, 6.83 mmol) with 5 M hydrogen chloride in ethyl acetate was carried out in the way as in the preparation of III. The solid product obtained on evaporation was recrystallized from methanol–ether; 4.16 g (98.0%); mp 220—223 °C; $[\alpha]_D$ +25.7° (*c* 1.0, methanol); thin layer chromatography, R_f 0.59 (system I).

Found: C, 53.95; H, 6.43; N, 15.82%. Calcd for $C_{28}H_{40}N_7O_7Cl$: C, 54.05; H, 6.48; N, 15.76%.

This compound was found to be identical with that obtained from the corresponding BOC-derivative (amorphous powder) by comparison of the melting point, optical rotation and R_f value of thin layer chromatography: VI obtained from BOC-derivative; mp 219—223 °C, no depression on admixture with above product; $[\alpha]_D$ +25.4° (*c* 1.0, methanol): thin layer chromatography of a mixed sample, R_f 0.60 (system I).

BOC–Asn–Arg(NO$_2$)–Val–Tyr(BZL)–OMe (VII). To a chilled (−5 °C) solution of BOC–Asn–OH (5.8 g, 25 mmol) and VI (15.6 g, 25 mmol) in 120 ml of *N,N*-dimethylformamide were added *N*-methylmorpholine (2.5 g, 25 mmol) and 1-hydroxybenzotriazole (3.4 g, 25 mmol), followed by dicyclohexylcarbodiimide (5.4 g, 26 mmol) in 20 ml of *N,N*-dimethylformamide. The mixture was stirred at −5 °C for 2 h and then at room temperature for 10 h. The mixture, after removal of urea, was evaporated to dryness *in vacuo* and the residue was treated with 80 ml of water. The resulting solid product was collected by filtration and washed with 5% sodium hydrogencarbonate, water, 1 M hydrochloric acid and water. Recrystallization from *N,N*-dimethylformamide—water gave 16.9 g (85.5%) of VII, mp 198—201 °C. For analysis, a small amount of the product was further recrystallized from *N,N*-dimethylformamide–methanol–water; mp 201—203 °C; $[\alpha]_D$ −5.2° (*c* 1.0, *N,N*-dimethylformamide).

Found: C, 55.80; H, 6.41; N, 15.59%. Calcd for $C_{37}H_{53}N_9O_{11}$: C, 55.56; H, 6.68; N, 15.76%.

BOC–Asn–Arg(NO$_2$)–Val–Tyr(BZL)–OH (VIII). To a stirred solution of VII (1.0 g, 1.25 mmol) in 20 ml of *N,N*-dimethylformamide was added dropwise 0.1 M sodium hydroxide until the pH became 11. The solution was maintained at this pH by gradual addition of sodium hydroxide over a period of 1 h (the total amount of sodium hydroxide required was 30 ml). After stirring for 2 h at room temperature, 4 ml of 1 M hydrochloric acid was added with stirring over 15 min under ice-cooling. The mixture was concentrated *in vacuo* nearly to dryness and the residue was triturated with water. The resulting solid product was collected by filtration, washed thoroughly with water, and recrystallized from ethanol–water; 0.87 g (88.6%); mp 167—170 °C; $[\alpha]_D$ −5.0° (*c* 0.5, methanol); thin layer chromatography, R_f 0.57 (system I) and 0.69 (system II).

Found: C, 54.82; H, 6.49; N, 16.04%. Calcd for $C_{36}H_{51}N_9O_{11}$: C, 55.02; H, 6.54; N, 16.04%.

TMZ–Pro–OH (IX). The 2,4,6-trimethylbenzyloxycarbonylation of H–Pro–OH (11.5 g, 100 mmol) with 2,4,6-trimethylbenzyl 2,4,5-trichlorophenyl carbonate (39.2 g, 105 mmol) was carried out as described for IV. The oily material which separated on acidification of the aqueous solution was extracted with 400 ml of ethyl acetate, the ethyl acetate solution being washed with water and dried over sodium sulfate. Removal of solvent gave 28.6 g (98.2%) of IX as a colorless viscous oil; $[\alpha]_D$ −31.4° (*c* 2.03, methanol). The homogeneity of this product was established by thin layer chromatography, R_f 0.47 (system I) and 0.79 (system II). The oily product was further characterized by the preparation of the corresponding dicyclohexylamine salt; mp 165—168 °C; $[\alpha]_D$ −20.0° (*c* 1.0, methanol).

Found: C, 71.32; H, 9.54; N, 5.82%. Calcd for $C_{25}H_{44}N_2O_4$: C, 71.15; H, 9.38; N, 5.93%.

TMZ-Pro-Phe-OEt (X). Condensation of IX (23.6 g, 81 mmol) with H-Phe-OEt·HCl (18.6 g, 81 mmol) in the presence of *N*-methylmorpholine (8.2 g, 81 mmol), 1-hydroxybenzotriazole (10.9 g, 81 mmol) and dicyclohexylcarbodiimide (17.1 g, 83 mmol) was carred out as described for I. The product was recrystallized twice from ethyl acetate–hexane; 34.5 g (85.9%); mp 97—99 °C; $[\alpha]_D$ −46.0° (*c* 1.0, ethanol).

Found: C, 69.56; H, 7.13; N, 5.95%. Calcd for $C_{27}H_{34}N_2O_5$: C, 69.50; H, 7.35; N, 6.01%.

H-Pro-Phe-OEt·HCl (XI). X (10.0 g, 21 mmol) was treated with 5 M hydrogen chloride in ethyl acetate by the same procedure as for III. The product obtained on evaporation of the reaction mixture was recrystallized from ethanol–ether; 6.51 g (94.9%); mp 151—153 °C; $[\alpha]_D$ −35.0° (*c* 1.0, ethanol).

Found: C, 58.77; H, 7.10; N, 8.62%. Calcd for $C_{16}H_{23}N_2O_3Cl$: C, 58.80; H, 7.09; N, 8.57%.

This compound was found to be identical with that obtained from BOC-Pro-Phe-OEt (oily material) by comparison of melting point, optical rotation and thin layer chromatography: XI obtained from BOC-derivative; mp 151—153 °C, no depression on admixture with a sample prepared above; $[\alpha]_D$ −35.1° (*c* 1.0, ethanol); thin layer chromatography of a mixed sample gave a single spot, R_f 0.68 (system I).

TMZ-His(BZL)-OH (XII). H-His(BZL)-OH (12.3 g, 50 mmol) was allowed to react with 2,4,6-trimethylbenzyl 2,4,5-trichlorophenyl carbonate (19.4 g, 52 mmol) as in the preparation of IV. The product was recrystallized from methanol–water; 17.8 g (84.5%); mp 181—183 °C; $[\alpha]_D$ +34.2° (*c* 1.0, methanol) and +12.0° (*c* 1.0, *N,N*-dimethylformamide).

Found: C, 68.49; H, 6.40; N, 9.98%. Calcd for $C_{24}H_{27}N_3O_4$: C, 68.39; H, 6.46; N, 9.97%.

TMZ-His(BZL)-Pro-Phe-OEt (XIII). A solution of XII (13.1 g, 31.0 mmol) and XI (10.0 g, 30.6 mmol) in 80 ml of *N,N*-dimethylformamide was cooled at −5 °C with stirring. To this solution were added *N*-methylmorpholine (3.10 g, 30.6 mmol) and 1-hydroxybenzotriazole (4.13 g, 30.6 mmol), followed by a solution of dicyclohexylcarbodiimide (6.40 g, 31.0 mmol) in 30 ml of *N,N*-dimethylformamide. Stirring was continued for 2 h at this temperature and 8 h at room temperature. After the urea was filtered off, the filtrate was evaporated *in vacuo* and the residue was taken up in 300 ml of ethyl acetate. The ethyl acetate solution was washed with 7% aqueous ammonia and water, dried over sodium sulfate, and then evaporated to dryness *in vacuo*. The resulting semi-solid product was purified by dissolution in 200 ml of hot ethyl acetate, treated with charcoal, and concentration to a small volume followed by the addition of 100 ml of petroleum ether to yield XIII as an amorphous powder; 20.8 g (97.8%); $[\alpha]_D$ −37.2° (*c* 1.0, methanol). The homogeneity was confirmed by thin layer chromatography; R_f 0.84 (system I) and 0.72 (system II).

Found: C, 68.81; H, 6.68; N, 10.08%. Calcd for $C_{40}H_{47}N_5O_6$: C, 69.24; H, 6.83; N, 10.09%.

All attempts to crystallize the product were unsuccessful. It was thus used for the reaction without further purification.

H-His(BZL)-Pro-Phe-OEt·2HCl (XIV). Fifty milliter of 5 M hydrogen chloride in ethyl acetate was added to a solution of XIII (8.20 g, 11.8 mmol) in 25 ml of ethyl acetate. After being left to stand for 2 h at room temperature, the solution was evaporated *in vacuo* to afford a solid product which was collected by filtration with the aid of ether and washed thoroughly with ether. Recrystallization from ethanol gave colorless needles of XIV; 6.62 g (95.1%); mp 215—218 °C; $[\alpha]_D$ −6.3° (*c* 1.0, methanol).

Found: C, 58.88; H, 6.36; N, 11.89%. Calcd for $C_{29}H_{37}N_5O_4Cl_2$: C, 59.08; H, 6.33; N, 11.88%.

BOC-Val-His(BZL)-Pro-Phe-OEt·2H₂O (XV). BOC-Val-OH (3.74 g, 17.2 mmol) was coupled with XIV (9.98 g, 16.9 mmol) in the presence of *N*-methylmorpholine (3.42 g, 33.8 mmol), 1-hydroxybenzotriazole (2.28 g, 16.9 mmol) and dicyclohexylcarbodiimide (3.51 g, 17.0 mmol) by the same procedure as for XIII. Removal of urea by filtration followed by concentration of the filtrate *in vacuo* gave an oily residue, which was taken up in 200 ml of ethyl acetate. The ethyl acetate solution, after being washed with 7% aqueous ammonia, was dried over sodium sulfate and evaporated to dryness *in vacuo*. Trituration of the residue with a mixture of ether and petroleum ether afforded a solid material. Recrystallization from ethanol–ether gave XV as an amorphous powder with two molecules of the water of crystallization; 11.2 g (88.0%); mp 111—116 °C; $[\alpha]_D$ −36.0° (*c* 1.0, methanol); thin layer chromatography, R_f 0.82 (system I) and 0.70 (system II).

Found: C, 61.97; H, 7.25; N, 11.24%. Calcd for $C_{39}H_{52}N_6O_7\cdot 2H_2O$: C, 62.21; H, 7.49; N, 11.16%.

H-Val-His(BZL)-Pro-Phe-OEt·2HCl (XVI). A suspension of XV (9.03 g, 12.0 mmol) in 40 ml of ethyl acetate was treated with 96 ml of 5 M hydrogen chloride in ethyl acetate. After being left to stand for 2 h at room temperature the solution was evaporated *in vacuo* and the residue was taken up in 150 ml of water. The aqueous layer was washed three times with 50 ml of ethyl acetate, followed by treatment with charcoal. Removal of the solvent by azeotropic distillation *in vacuo* gave an oily material. This was solidified by triturating with ethanol–ether and recrystallized from the same solvent; 7.40 g (89.4%); mp 158—162 °C; $[\alpha]_D$ −15.9° (*c* 1.0, methanol) and −10.4° (*c* 1.0, ethanol).

Found: C, 58.96; H, 6.98; N, 12.33%. Calcd for $C_{34}H_{46}N_6O_5Cl_2$: C, 59.21; H, 6.72; N, 12.19%.

BOC-Val-Tyr(BZL)-Val-His(BZL)-Pro-Phe-OEt·1/2 H₂O (XVII) as an Authentic Sample. To a cooled solution (−5 °C) of II (2.35 g, 5.00 mmol) and XVI (3.45 g, 5.00 mmol) in 50 ml of *N,N*-dimethylformamide were added *N*-methylmorpholine (1.01 g, 10.0 mmol) and 1-hydroxybenzotriazole (0.68 g, 5.00 mmol) with stirring, followed by a solution of dicyclohexylcarbodiimide (1.05 g, 5.10 mmol) in 5 ml of *N,N*-dimethylformamide. The mixture was stirred for 2 h at −5 °C and for 36 h at room temperature. Removal of urea by filtration followed by concentration of the filtrate *in vacuo* gave a solid material, which was collected by suction with water, washed with 7% aqueous ammonia and water, and then dissolved in 20 ml of a mixture of *N,N*-dimethylformamide and water (5: 1, v/v). A small amount of insoluble substance was removed by filtration, the filtrate being passed through a column of Sephadex LH-20. The effluent was evaporated to dryness *in vacuo*, and the product was suspended in water, collected by filtration, and dried. Recrystallization twice from methanol–water gave XVII as a colorless powder; 3.89 g (71.5%); mp 164—173 °C; $[\alpha]_D$ −59.2° (*c* 1.0, methanol) and −35.3° (*c* 1.0, *N,N*-dimethylformamide). The homogeneity of this product was confirmed by thin layer chromatography, R_f 0.79 (system I) and 0.75 (system II). Prior to analysis, the compound was dried over phosphorus pentaoxide at 70 °C and 2 mmHg.

Found: C, 66.77; H, 7.09; N, 10.32%. Calcd for $C_{60}H_{76}N_8O_{10}\cdot 1/2\ H_2O$: C, 66.82; H, 7.19; N, 10.39%.

BOC-Val-Tyr(BZL)-Val-His(BZL)-Pro-Phe-OH·H₂O (XVIII) as an Authentic Sample. To a stirred solution of XVII (2.17 g, 2.0 mmol) in 40 ml of ethanol was added 48 ml of 0.1 M sodium hydroxide dropwise at room temperature

over a period of 1 h. After being stirred for 2 h the reaction mixture was neutralized with Dry Ice according to the method of Schwyzer, *et al.*,[20] and evaporated to a small volume *in vacuo*. The residue obtained was taken up in 40 ml of water and the solution was acidified with citric acid to yield a solid product. Recrystallization from ethanol gave XVIII as colorless needles with one molecule of the water of crystallization; 1.29 g (62.3%); mp 172—179 °C; $[\alpha]_D$ −28.7° (*c* 1.0, *N,N*-dimethylformamide); thin layer chromatography, R_f 0.41 (system I) and 0.63 (system II).

Found: C, 65.86; H, 6.92; N, 10.69%. Calcd for $C_{58}H_{72}N_8O_{10}\cdot H_2O$: C, 65.76; H, 7.04; N, 10.58%.

BOC–Asn–Arg(NO_2)–Val–Tyr(BZL)–Val–His(BZL)–Pro–Phe–OEt·2H_2O(XIX) as an Authentic Sample. *N*-Methylmorpholine (2.02 g, 20 mmol) and 1-hydroxybenzotriazole (1.35 g, 10 mmol) were added with stirring to a cooled (−5 °C) solution of VIII (7.86 g, 10 mmol) and XVI (6.70 g, 10 mmol) in 80 ml of *N,N*-dimethylformamide. To this was added in one portion a solution of dicyclohexylcarbodiimide (2.27 g, 11 mmol) in 10 ml of *N,N*-dimethylformamide. After being stirred for 48 h at room temperature, the reaction mixture was worked up by the same procedure for XVII. Recrystallization from ethanol–water gave XIX as a colorless powder with two molecules of the water of crystallization; 10.6 g (74.3%); mp 189—195 °C; $[\alpha]_D$ −48.4° (*c* 1.0, methanol) and −26.5° (*c* 1.0, *N,N*-dimethylformamide). Only one spot was obtained in thin layer chromatography, R_f 0.63 (system I) and 0.55 (system II).

Found: C, 59.07; H, 6.72; N, 14.75%. Calcd for $C_{70}H_{93}N_{15}O_{15}\cdot 2H_2O$: C, 59.17; H, 6.88; N, 14.79%.

Enzymatic Syntheses of the Protected Valine-5 Angiotensin II 3—8 Fragment. *i) Papain-catalyzed Condensation of II with XVI (XVII-pa)*: Papain (150 mg) and 0.1 ml of 2-mercaptoethanol were added to a solution of II (471 mg, 1.0 mmol) and XVI (690 mg, 1.0 mmol) in a mixture of 15 ml of McIlvaine buffer (pH 5.5) and 15 ml of methanol containing 2 ml of 1 M sodium hydroxide. After being incubated at 38 °C for 2 h, the product precipitated was collected by filtration, washed with 7% aqueous ammonia, 2% citric acid and water, and then dried. Recrystallization from methanol–water gave the hexapeptide ester (XVII-pa) as colorless crystals with a half molecule of the water of crystallization; 615 mg (57.0%); mp 167—173 °C, no depression on admixture with XVII prepared by the solution method; $[\alpha]_D$ −36.0° (*c* 1.0, *N,N*-dimethylformamide) and −58.5° (*c* 1.0, methanol). Only one spot was obtained in thin layer chromatography, R_f 0.79 (system I) and 0.74 (system II).

Found: C, 66.72; H, 7.16; N, 10.55%. Calcd for $C_{60}H_{76}N_8O_{10}\cdot 1/2\ H_2O$: C, 66.82; H, 7.19; N, 10.39%.

The NMR spectrum in DMSO-d_6 showed the following signals in ppm: 0.74 (12H; $-CH_3$ of Val), 1.05 (3H: $-CH_3$ of OEt), 1.36 (9H; $-CH_3$ of BOC), 1.75 (4H; β,γ–CH_2– of Pro), 1.91 (2H; β–CH– of Val), 2.78—3.28 (8H; δ–CH_2– of Pro and β–CH_2– of Phe, His and Tyr), 3.92 (2H; $-CH_2-$ of OEt), 4.98—5.05 (4H; $-CH_2-$ of BZL in His and Tyr), 6.79 and 7.02 (4H; $-C_6H_4-$ of Tyr), and 7.18—7.34 (15H; $-C_6H_5$ of Phe and BZL in His and Tyr).

ii) Nagarse-catalyzed Condensation of II with XVI (XVIII-na): Nagarse (40 mg) was added to a suspension of II (282 mg, 0.60 mmol) and XVI (414 mg, 0.60 mmol) in 8.0 ml of McIlvaine buffer of pH 7.5 containing 1.2 ml of 1 M sodium hydroxide. After being incubated at 38 °C for 6 h, the product precipitated was collected by filtration, washed with 2% citric acid and water, and then dried. The product was purified by solution in 40 ml of hot ethanol, treatment with charcoal, and concentration into a small volume, followed by the addition of ethyl acetate which gave the hexapeptide acid (XVIII-na) as a colorless powder with two molecules of the water of crystallization; 476 mg (73.7%); mp 165—169 °C; $[\alpha]_D$ −27.4° (*c* 1.0, *N,N*-dimethylformamide); thin layer chromatography, R_f 0.41 (system I) and 0.64 (system II).

Found: C, 64.87; H, 6.90; N, 10.52%. Calcd for $C_{58}H_{72}N_8O_{10}\cdot 2H_2O$: C, 64.66; H, 7.11; N, 10.40%.

The NMR spectrum of XVIII-na in DMSO-d_6 showed the following signals in ppm: 0.75 (12H; $-CH_3$ of Val), 1.36 (9H; $-CH_3$ of BOC), 1.69 (4H; β,γ–CH_2– of Pro), 1.92 (2H; β–CH– of Val), 2.80—3.11 (8H; δ–CH_2– of Pro and β–CH_2– of Phe, His and Tyr), 4.97 and 5.07 (4H; $-CH_2-$ of BZL in His and Tyr), 6.79 and 7.01 (4H; $-C_6H_4-$ of Tyr), and 7.18—7.33 (15H; $-C_6H_5$ of Phe and BZL in His and Tyr). No signals of ethyl ester were observed in this spectrum.

iii) Microbial Metalloenzyme-catalyzed Condensation of II with XVI (XVIII-me): Microbial metalloenzyme (50 mg) was added to a suspension of II (235 mg, 0.50 mmol) and XVI (345 mg, 0.50 mmol) in 8.0 ml of Veronal buffer of pH 7.0 containing 1.0 ml of 1 M sodium hydroxide. After being incubated at 38 °C for 6 h, the reaction mixture was worked up in the same way as for XVIII-na. XVIII-me was obtained as a colorless powder with two molecules of the water of crystallization; 222 mg (41.2%); mp 164—169 °C, no depression on admixture with XVIII-na; $[\alpha]_D$ −27.9° (*c* 0.5, *N,N*-dimethylformamide); thin layer chromatography, R_f 0.42 (system I) and 0.65 (system II).

Found: C, 64.89; H, 7.01; N, 10.32%. Calcd for $C_{58}H_{72}N_8O_{10}\cdot 2H_2O$: C, 64.66; H, 7.11; N, 10.40%.

The NMR spectral data of XVIII-me were consistent with those of XVIII-na.

Enzymatic Synthesis of the Protected Valine-5 Angiotensin II Amide-1. Papain-catalyzed Condensation of VIII with XVI (XIX-pa): Papain (100 mg) and 0.07 ml of 2-mercaptoethanol were added to a solution of VIII (472 mg, 0.60 mmol) and XVI (414 mg, 0.60 mmol) in a mixture of 10 ml of McIlvaine buffer (pH 5.5) and 10 ml of methanol containing 1.2 ml of 1 M sodium hydroxide. After being incubated at 38 °C for 2 h, the product precipitated was collected by filtration, washed 7% with aqueous ammonia, 2% citric acid and water. Recrystallization carried out by evaporating an ethanol solution of the product gave a colorless powder of the octapeptide ester (XIX-pa) with two molecules of the water of crystallization; 685 mg (78.1%); mp 186—195 °C, no depression on admixture with XIX prepared by solution method; $[\alpha]_D$ −27.3° (*c* 1.0, *N,N*-dimethylformamide) and −48.3° (*c* 1.0, methanol). Only one spot was obtained in thin layer chromatography, R_f 0.62 (system I) and 0.56 (system II).

Found: C, 59.11; H, 6.62; N. 14.92%. Calcd for $C_{70}H_{93}N_{15}O_{15}\cdot 2H_2O$: C, 59.17; H, 6.88; N, 14.79%.

The NMR spectrum of XIX-pa in DMSO-d_6 showed following signals in ppm: 0.75 (12H; $-CH_3$ of Val), 1.08 (3H; $-CH_3$ of OEt), 1.36 (9H; $-CH_3$ of BOC), 1.50—1.80 (8H; β,γ–CH_2– of Pro and Arg), 3.45 (2H; δ–CH_2– of Arg), 3.92 (2H; $-CH_2-$ of OEt), 4.98—5.21 (4H; $-CH_2-$ of BZL in His and Tyr), 6.80 and 7.12 (4H, $-C_6H_4-$ of Tyr), and 7.20—7.32 (15H; $-C_6H_5$ of Phe, and BZL in His and Tyr).

References

1) Y. Isowa, M. Ohmori, T. Ichikawa, H. Kurita, M. Sato, and K. Mori, "The Synthesis of Peptides by Means of Proteolytic Enzymes," *Bull. Chem. Soc. Jpn*, **50**, 2762 (1977). issue.

2) M. Bergmann and H. Fraenkel-Conrat, *J. Biol. Chem.*, **119**, 707 (1937).

3) M. Bergmann and J. S. Fruton, *J. Biol. Chem.*, **124**, 321 (1938).

4) M. Bergmann and J. S. Fruton, *Ann. N. Y. Acad. Sci.*, **45**, 409 (1944).
5) A. N. Glazer and E. L. Smith, "The Enzymes," 3rd ed, Vol. 3, ed by P. D. Boyer, Academic Press, New York, N. Y. (1971), Chap. 14.
6) M. Ottesen and IB Svendsen, "Method in Enzymology," Vol. 19, ed by G. E. Perlmann and L. Lorand, Academic Press, New York, N. Y. (1970), p. 199.
7) Y. Yokote and Y. Noguchi, *Nippon Nogei Kagaku Kaishi*, **43**, 132 (1969).
8) R. Schwyzer, B. Iseline, H. Kappeler, B. Riniker, W. Ritter, and H. Zuber, *Helv. Chim. Acta*, **41**, 1287 (1958).
9) St. Guttmann, *Helv. Chim. Acta*, **44**, 721 (1961).
10) D. Regoli, B. Rinker, and H. Brunner, *Biochem. Pharmacol.*, **12**, 637 (1963).
11) R. Garner and G. T. Young, *J. Chem. Soc., C*, **1971**, 50.
12) W. Broadbent, J. S. Morley, and B. E. Stone, *J. Chem. Soc., C*, **1967**, 2632.
13) W. König and R. Geiger, *Chem. Ber.*, **103**, 788 (1970).
14) M. L. Bender and L. J. Brubacher, *J. Am. Chem. Soc.*, **88**, 5880 (1966).
15) K. Morihara, T. Oka, and H. Tsuzuki, *Arch. Biochem. Biophys.*, **165**, 72 (1974).
16) S. A. Bizzozero, W. K. Baumann, and H. Dutler, *Eur. J. Biochem.*, **58**, 167 (1975).
17) J. D. McConn, D. Tsuru, and K. T. Yasunobu, *J. Biol. Chem.*, **239**, 3706 (1964).
18) B. Holmquist and B. L. Vallee, *Biochemistry*, **15**, 101 (1976).
19) D. Tsuru, T. Yamamoto, and J. Fukumoto, *Agric. Biol. Chem.*, **30**, 651 (1966).
20) W. Rittel, B. Iselin, H. Kappeler, B. Riniker, and R. Schwyzer, *Helv. Chim. Acta*, **40**, 614 (1957).

Efficient Methods for Oxidation of Alcohols

Koichi NARASAKA, Anri MORIKAWA, Kazuhiko SAIGO,* and Teruaki MUKAIYAMA

Department of Chemistry, Faculty of Science, The University of Tokyo, Hongo, Bunkyo-ku, Tokyo 113

(Received April 18, 1977)

Treatment of alkoxymagnesium bromides, prepared *in situ* from alcohols and Grignard reagent, with *N*-chlorosuccinimide, *m*-chloroperbenzoic acid, or (diacetoxyiodo)benzene in the presence of *t*-butoxymagnesium bromide afforded the corresponding carbonyl compounds in good yields. A wide variety of alcohols, after being converted into their bromomagnesium salts by treatment with propylmagnesium bromide, were also selectively oxidized with 1,1′-(azodicarbonyl)dipiperidine to afford the corresponding ketones or aldehydes in excellent yields.

In the preceding communications, convenient methods were reported for the oxidation of alcohols to the corresponding ketones or aldehydes by the treatment of trialkyltin methoxide[1] or bis(tributyltin) oxide,[2] and by that of alkoxymagnesium bromides with *N*-chlorosuccinimide in the presence of lithium *t*-butoxide.[3]

These reactions were successfully applied to the oxidation of alcohols such as secondary alcohols, allylic alcohols, and benzylic alcohols, but not aliphatic and olefinic primary alcohols. Improvement of the methods was undertaken in order to establish an effective method for the oxidation of a wide variety of alcohols, especially aliphatic and olefinic primary alcohols.

In the previous methods, effective acid captors such as lithium *t*-butoxide, trialkyltin methoxide and bis(tributyltin) oxide were employed in order to scavenge hydrogen halides generated during the course of the reactions. It was found that the yields of the products depend a great deal on the kinds of acid captor. The effects of the other acid captors were reexamined in detail. The yields of the carbonyl compounds increased remarkably when *t*-butoxymagnesium bromide was used as an acid captor instead of lithium *t*-butoxide in the reaction of alkoxymagnesium bromide with *N*-chlorosuccinimide, the carbonyl compounds being obtained in the best yields when the molar ratio of alkoxymagnesium bromide, *t*-butoxymagnesium bromide, and *N*-chlorosuccinimide was 1 : 1.2 : 1.2. When several aliphatic primary alcohols, after being converted into the bromomagnesium salts by propylmagnesium bromide, were treated with a 1.2 molar amount of *N*-chlorosuccinimide in the presence of a 1.2 molar amount of *t*-butoxymagnesium bromide in tetrahydrofuran for 30 min at room temperature, the corresponding aldehyde were produced in good yields (Table 1). In the case of the oxidation of olefinic primary alcohol such as 7-phenyl-4-hepten-1-ol, the desired 7-phenyl-4-heptenal was obtained in low yield (34%), some by-products being produced.

In order to find suitable oxidizing reagents for the oxidation of olefinic primary alcohols, several oxidizing reagents were examined. It was found that when *m*-chloroperbenzoic acid or (diacetoxyiodo)benzene is used for the oxidation of the bromomagnesium salt of 7-phenyl-4-hepten-1-ol in the presence of *t*-butoxymagnesium bromide, 7-phenyl-4-heptenal is obtained in fairly good yields. The bromomagnesium salt of 7-phenyl-4-hepten-1-ol, prepared from the alcohol and propylmagnesium bromide, was treated with a 1.2 molar amount of (diacetoxyiodo)benzene or *m*-chloroperbenzoic acid in the presence of a 1.2 molar amount of *t*-butoxymagnesium bromide in tetrahydrofuran for 30 min at room temperature. The desired 7-phenyl-4-heptenal was isolated in 76 and 74% yields, respectively. In a similar way, several kinds of alcohols such as aliphatic primary alcohol, secondary alcohol, benzylic alcohol, and allylic alcohol were oxidized to the corresponding carbonyl compounds in good yields by use of these reagents (Table 2). The yields of the oxidation

Table 1. Oxidation of alcohols with *N*-chlorosuccinimide

$$R\text{-}CH_2OH \xrightarrow[THF]{n\text{-}PrMgBr} \xrightarrow[THF,\ r.t.,\ 30\ min]{1.2\ t\text{-}BuOMgBr,\ 1.2\ NCS} R\text{-}CHO$$

Alcohol	Yield (%)
1-Octanol	80[a]
1-Heptanol	77[a]
3-Phenyl-1-propanol	81[b]
7-Phenyl-4-hepten-1-ol	34[b]

a) Yield determined by GLC. b) Isolated yield.

Table 2. Oxidation of alcohols with m-chloroperbenzoic acid or (diacetoxyiodo)benzene

$$\begin{matrix} R^1 \\ R^2 \end{matrix}\!\!>\!CHOH \xrightarrow[THF]{n\text{-}PrMgBr} \xrightarrow[THF\ r.t.,\ 30\ min]{1.2\ t\text{-}BuOMgBr,\ m\ oxidant} \begin{matrix} R^1 \\ R^2 \end{matrix}\!\!>\!C{=}O$$

Alcohol	Yield (%),[a] (m)	
	MCPBA	$Ph\text{-}I(OAc)_2$
7-Phenyl-4-hepten-1-ol	74 (1.4)	76 (1.2)
3-Phenyl-1-propanol	79 (1.8)	84 (1.5)
Benzhydrol	82 (1.2)	89 (1.2)
Cinnamyl alcohol	75 (1.2)	—
dl-Menthol	—	90 (1.2)
3β-Cholestanol	—	81 (1.2)

a) Isolated yield.

* Present address: Department of Applied Chemistry, Faculty of Engineering, Saitama Univsersity, Shimo-Okubo 255, Urawa, Saitama 338.

product of the olefinic primary alcohol, 7-phenyl-4-hepten-1-ol, were not so good in comparison with those of the other kinds of alcohols, small amounts of by-products being obtained.

Further examination of suitable oxidizing reagents for the oxidation of olefinic primary alcohol was carried out. Concerning the oxidation of alcohols, an efficient method for ketone synthesis was reported.[4] That is, *s*-alkoxymagnesium bromides were prepared by the reaction of aldehydes with Grignard reagents followed by treatment with diethyl azodicarboxylate or 1,1′-(azodicarbonyl)dipiperidine, resulting in the formation of the corresponding ketones in good yields. Generally these azo compounds are inactive to olefinic linkage, and the use of azo compounds is expected to suppress the side reactions with respect to olefinic linkage of the alcohol. The oxidation of 7-phenyl-4-hepten-1-ol was attempted first by employing diethyl azodicarboxylate as an oxidant. However, the desired oxidation could not be observed and only an ester-exchanging reaction took place to give ethyl 7-phenyl-4-heptenyl azodicarboxylate and bis(7-phenyl-4-heptenyl)azodicarboxylate. To avoid this side reaction, dibenzoyldiimide was used as an oxidizing reagent instead of diethyl azodicarboxylate. The desired 7-phenyl-4-heptenal was obtained in only 20% yield, a by-product, 7-phenyl-4-heptenyl benzoate, being isolated in 38% yield accompanied by the cleavage of carbon-nitrogen bond of dibenzoyldiimide.

On the other hand, when 7-phenyl-4-hepten-1-ol was allowed to react with a 1.2 molar amount of propylmagnesium bromide in tetrahydrofuran and then treated with a 1.2 molar amount of 1,1′-(azodicarbonyl)-dipiperidine at room temperature for 2 h, the desired 7-phenyl-4-heptenal was obtained in 89% yield along with 1,1′-(hydrazodicarbonyl)dipiperidine in 93% yield, 7% of 7-phenyl-4-hepten-1-ol being recovered after the separation by column chromatography (silica gel) (Table 3).

Table 3. Oxidation of 7-phenyl-4-hepten-1-ol with several azo compounds

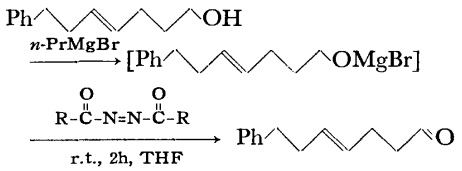

R	Isolated yield (%)
-OEt	0
-OPh	20
-N⟨⟩	89

Similarly, the oxidation of various kinds of alcohols with 1,1′-(azodicarbonyl)dipiperidine afforded the corresponding ketones and aldehydes in excellent yields (89—99%). The results are summarized in Table 4.

An alternative method was adopted for the oxidation of alcohols having the carbonyl group for prevention of the addition reaction of the Grignard reagent to the carbonyl group. When *t*-butoxymagnesium bromide was employed in place of the Grignard reagent for the conversion of testosterone into the bromomagnesium salt, the oxidation of testosterone proceeded successfully, 4-androsten-3,17-dione being obtained in 96% yield (Eq. 1).

Table 4. Oxidation of various alcohols with 1,1′-(azodicarbonyl)dipiperidine

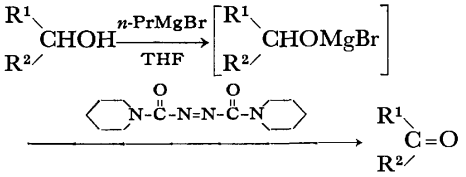

Alcohol	Time	Yield (%)[a]
7-Phenyl-4-hepten-1-ol	2 h	89
Cinnamyl alcohol	2 h	92
Geraniol	2 h	96
Benzhydrol	2 h	99
2-Phenyl-1-butanol	2 h	90
2-Octanol	over night	91[b]
3β-Cholestanol	over night	93
Citronellol	2 h	89

a) Isolated yield. b) Yield determined by GLC.

Similarly, stanolone and 7-phenyl-4-hepten-1-ol were oxidized to give the corresponding carbonyl compounds in excellent yields (Eqs. 2, 3).

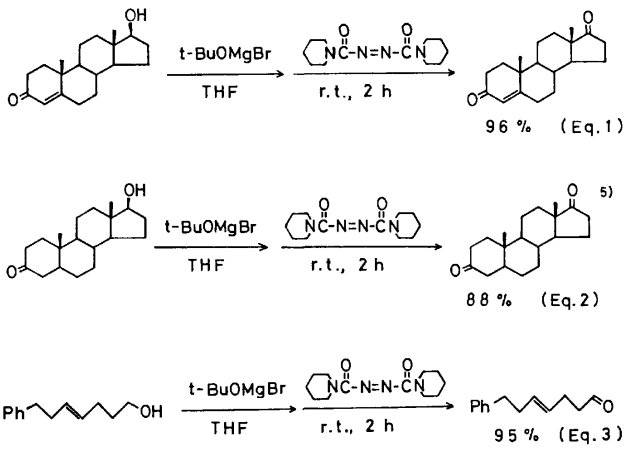

Azo compounds such as diethyl azodicarboxylate[6] and 4-phenyl-1,2,4-triazoline-3,5-dione[7] react with free alcohols to afford the corresponding carbonyl compounds, but the yields are not so good. A long reaction time and elevated temperature are required for the oxidation with diethyl azodicarboxylate. 4-Phenyl-1,2,4-triazoline-3,5-dione is very unstable. Contrary to these results, the oxidation of alcohols proceeded under mild conditions (room temperature) by use of alkoxymagnesium bromide in place of free alcohol, the corresponding carbonyl compounds being obtained in excellent yields. Use of 1,1′-(azodicarbonyl)dipiperidine instead of *N*-chlorosuccinimide, *m*-chloroperbenzoic acid and (diacetoxyiodo)benzene makes it possible to oxidize various kinds of alcohols selectively to the corresponding

carbonyl compounds without addition of acid captors such as lithium *t*-butoxide and *t*-butoxymagnesium bromide.

In general, reagents such as CrO_3–pyridine complex,[8] CrO_3–acetone,[9] dimethyl sulfoxide–dicyclohexylcarbodiimide,[10] dimethyl sulfide–*N*-chlorosuccinimide or chlorine[11] are widely employed for the oxidation of alcohols to the corresponding ketones or aldehydes. However, some of them are very toxic [Cr(VI)], causing side reactions such as further oxidation of produced aldehydes and the formation of alkyl chlorides and sulfides. We have confirmed that a wide variety of alcohols are oxidized selectively to the corresponding ketones or aldehydes in excellent yields by the present procedure utilizing alkoxymagnesium bromides and 1,1′-(azodicarbonyl)dipiperidine.

Experimental

Materials. Commercial *N*-chlorosuccinimide was recrystallized quickly from hot water before use. The purity was determined by iodometry (purity>98%). *m*-Chloroperbenzoic acid was prepared by the reaction of *m*-chlorobenzoyl chloride with aqueous hydrogen peroxide and purified by washing with a phosphate buffer of pH 7.5 according to the procedure given in literature.[12] The purity was determined by iodometry (purity>97.5%). (Diacetoxyiodo)benzene was synthesized by the reaction of iodobenzene with peracetic acid,[13] the purity being determined in a smilar way (purity >97%). 1,1′-(Azodicarbonyl)dipiperidine was prepared by the reaction of diethyl azodicarboxylate with piperidine,[14] and purified by recrystallization from a mixture of benzene and hexane (mp 134—135 °C). 7-Phenyl-4-heptene-1-ol was synthesized from dihydrofuran and 2-phenylethylmagnesium bromide according to the procedure of Brandron *et al.*[15] and purified by distillation (bp 119—120 °C/1.0 mmHg).

General Procedure of Oxidation of Alkoxymagnesium Bromide with N-Chlorosuccinimide. To a solution of propylmagnesium bromide in dry THF (3 ml) prepared from magnesium (58 mg, 2.4 mmol) and propyl bromide (320 mg, 2.6 mmol) was added dropwise a solution of alcohol (1.0 mmol) and *t*-butyl alcohol (89 mg, 1.2 mmol) in THF (4 ml) at room temperature under argon atmosphere. After the reaction mixture had been stirred for 10 min, *N*-chlorosuccinimide (160 mg, 1.2 mmol) was added all at once at room temperature. The reaction mixture was stirred for 30 min, quenched by the addition of brine and solid $Na_2S_2O_3 \cdot 5H_2O$, and extracted with diethyl ether. The ether layer was washed with saturated aqueous $NaHCO_3$ and brine, and dried over anhydrous Na_2SO_4. The yeild of the corresponding aldehyde was determined by vapor phase chromatography or isolation using preparative thin layer chromatography (silica gel).

General Procedure of Oxidation of Alcohols with m-Chloroperbenzoic Acid. A solution of propylmagnesium bromide (1.2 mmol) in THF (3 ml) was prepared in a similar way and treated with a THF (4 ml) solution of an alcohol (1 mmol) and *t*-butyl alcohol (89 mg, 1.2 mmol) at room temperature under argon atmosphere, and stirred for 10–15 min at room temperature. This solution was then treated with crystalline *m*-chlorobenzoic acid (1.2—1.8 mmol) at room temperature, stirred for 30 min at room temperature, and quenched by the addition of brine and solid $Na_2S_2O_3 \cdot 5H_2O$. Benzene was added to the mixture and the resulting precipitate was filtered off. The organic layer was washed with saturated aqueous $NaHCO_3$ and brine, and dried over anhydrous Na_2SO_4. After removal of the solvent, the corresponding carbonyl compound was isolated by preparative thin layer chromatography (silica gel).

General Procedure of Oxidation of Alcohols with (Diacetoxyiodo)-benzene. A solution of alkoxymagnesium bromide (1 mmol) and *t*-butoxymagnesium bromide (1.2 mmol) in THF (7 ml) was prepared in a similar way, treated with crystalline (diacetoxyiodo)benzene (1.2—1.5 mmol) at room temperature. After being stirred for 30 min at room temperature, the mixture was quenched by addition of brine and solid $Na_2S_2O_3 \cdot 5H_2O$, and extracted with ethyl acetate. The organic layer was washed with saturated aqueous $NaHCO_3$ and brine, and dried over anhydrous Na_2SO_4. After removal of the solvent, the yield was determined by isolation using preparative thin layer chromatography (silica gel) or column chromatography (silica gel).

Oxidation of 7-Phenyl-4-hepten-1-ol with (Diacetoxyiodo)benzene. A THF (3 ml) solution of propylmagnesium bromide was prepared from magnesium (58 mg, 2.4 mmol) and propyl bromide (320 mg, 2.6 mmol), then treated with a THF (4 ml) solution of 7-phenyl-4-hepten-1-ol (186 mg, 0.98 mmol) and *t*-butyl alcohol (89 mg, 1.2 mmol) at room temperature under argon atmosphere. The reaction mixture was stirred for 10 min at room temperature, a THF (10 ml) solution of (diacetoxyiodo)benzene (429 mg, 1.33 mmol) being added dropwise within the period of 20 min. The mixture was stirred for additional 30 min. After the usual work-up, 7-phenyl-4-heptenal (140 mg, 76%) was isolated by column chromatography (silica gel).

NMR (CCl_4) δ 2.12—2.80 (m, 8H), 5.32—5.55 (m, 2H), 7.15 (s, 5H), 9.70 (s, 1H); IR 1725 cm^{-1}.

2,4-dinitrophenylhydrazone, mp 96.0—96.2 °C. Found: C, 61.94; H, 5.38; N, 15.02%. Calcd for $C_{19}H_{20}N_4O_4$: C, 61.94; H, 5.47; N, 15.21%.

Oxidation of 7-Phenyl-4-hepten-1-ol with 1,1′-(Azodicarbonyl)-dipiperidine Utilizing Propylmagnesium Bromide. To a THF (3 ml) solution of propylmagnesium bromide (160 mg, 1.3 mmol) was added dropwise a THF (2 ml) solution of 7-phenyl-4-hepten-1-ol (190 mg, 1.0 mmol) at room temperature under argon atmosphere. A THF (4 ml) solution of 1,1′-(azodicarbonyl)dipiperidine (320 mg, 1.2 mmol) was then added dropwise to the mixture. The mixture was stirred for 2 h at room temperature, quenched by addition of brine, and extracted with ethyl acetate. The organic layer was washed with saturated aqueous $NaHCO_3$ and brine, and dried over anhydrous Na_2SO_4. After removal of the solvent, the residue was separated by column chromatography (silica gel). Elution with benzene, methylene chloride, and methanol afforded the desired 7-phenyl-4-heptenal (167 mg, 89%), 7-phenyl-4-hepten-1-ol (13 mg, 7%) and 1,1′-(hydrazodicarbonyl)dipiperidine (234 mg, 92%), respectively.

General Procedure of Oxidation of Alcohols with 1,1′-(Azodicarbonyl)dipiperidine Utilizing Propylmagnesium Bromide. To a solution of propylmagnesium bromide in THF (3 ml) prepared from magnesium (29 mg, 1.2 mmol) and propyl bromide(160 mg, 1.3 mmol) was added dropwise a THF (2 ml) solution of an alcohol (1 mmol) at room temperature under argon atmosphere. A THF (4 ml) solution of 1,1′-(azodicarbonyl)-dipiperidine was then added dropwise at room temperature. The mixture was stirred for 2 h—overnight, quenched by addition of brine, and extracted with ether. After filtration of the precipitate, the organic layer was washed with saturated aqueous $NaHCO_3$ and brine, and dried over anhydrous Na_2SO_4. The yield of the corresponding ketone or aldehyde was determined by isolation using column chromatography (silica gel) or by vapor phase chromatography analysis.

Oxidation of Testosterone with 1,1′-(Azodicarbonyl)dipiperidine

Utilizing t-Butoxymagnesium Bromide. To a THF (3 ml) solution of propylmagnesium bromide prepared from magnesium (29 mg, 1.2 mmol) and propyl bromide (160 mg, 1.3 mmol) was added drowise a THF (2 ml) solution of *t*-butyl alcohol (89 mg, 1.2 mmol). A THF (2 ml) solution of testosterone (388 mg, 1.0 mmol) was then added, and the mixture was treated with a THF (4 ml) solution 1,1'-(azodicarbonyl)-dipiperidine (302 mg, 1.2 mmol). After the usual work-up, the desired 4-androsten-3,17-dione (374 mg, 96%) was isolated by preparative thin layer chromatography (silica gel).

NMR($CDCl_3$) δ 0.93 (s, 3H), 1.23 (s, 3H), 5.72 (s, 1H); IR 1660, 1740 cm^{-1}, mp 170—171 °C (lit, 169—170 °C[10]) Found: C, 79.42; H, 9.30%. Calcd for $C_{19}H_{26}O_2$: C, 79.68; H, 9.15%.

References

1) K. Saigo, A. Morikawa, and T. Mukaiyama, *Chem. Lett.*, **1975**, 145.

2) K. Saigo, A. Morikawa, and T. Mukaiyama, *Bull. Chem. Soc. Jpn.*, **49**, 1656 (1976).

3) T. Mukaiyama, M. Tsunoda, and K. Saigo, *Chem. Lett.*, **1975**, 691.

4) T. Mukaiyama, K. Takahashi, and I. Kuwajima, *Bull. Chem. Soc., Jpn.*, **41**, 1491 (1968).

5) Found: C, 79.36; H, 9.82%. Calcd for $C_{19}H_{28}O_2$: C, 79.12; H, 9.79%. Melting point and NMR spectrum agree with these in literature. *Cf.* J. E. Bridgeman, P. C. Cherry, A. S. Clegg, J. M. Evans, E. R. H. Jones, A. Kasal, V. Kumar, G. D. Meakins, Y. Morisawa, E. E. Richards, and P. D. Woodgate, *J. Chem. Soc., C*, **1970**, 250; H. Nakata, *Tetrahedron*, **19**, 1959 (1963).

6) F. Yoneda, K. Suzuki, and Y. Nitta, *J. Am. Chem. Soc.*, **88**, 2328 (1966).

7) R. C. Cookson, I. D. R. Stevens, and C. T. Watts, *J. Chem. Soc., Chem. Commun.*, **1966**, 744.

8) J. C. Collins, W. W. Hess, and F. J. Frank, *Tetrahedron Lett.*, **1968**, 3363.

9) K. Bowden, I. M. Heilbron, E. R. H. Jones, and B. C. L. Weedon, *J. Chem. Soc.*, **1946**, 39; A. Bowers, J. G. Halsall, E. R. H. Jones, and A. J. Lemin, *ibid.*, **1953**, 2548.

10) K. E. Pfizner and J. G. Moffatt, *J. Am. Chem. Soc.*, **87**, 5661 (1965); A. H. Fenselau and J. G. Moffatt, *ibid.*, **88**, 1762 (1966).

11) E. J. Corey and C. U. Kim, *J. Am. Chem. Soc.*, **94**, 7586 (1972); *Tetrahedron Lett.*, **1973**, 919.

12) R. N. McDonald, R. N. Steppel, and J. E. Dorsey, *Org. Synth.*, **50**, 15 (1970); N. N. Schwartz and J. H. Blumbergs, *J. Org. Chem.*, **29**, 1976 (1964).

13) K. H. Pausacker, *J. Chem. Soc.*, **1953**, 107.

14) E. E. Smissman and A. Makriyannis, *J. Org. Chem.*, **38**, 1652 (1973).

15) R. C. Brandon, J. M. Derfer, and C. D. Boord, *J. Am. Chem. Soc.*, **72**, 2120 (1950).

The Addition Reaction of Acyl Radicals to 9,10-Phenanthrenequinone in the Presence of the Corresponding Aldehydes. A Support for the In-Cage Mechanism of the Photochemical Reaction of 9,10-Phenanthrenequinone with Aldehydes

Kazuhiro MARUYAMA, Hiroshi SAKURAI, and Tetsuo OTSUKI
Department of Chemistry, Faculty of Science, Kyoto University, Kyoto 606
(Received April 18, 1977)

Regarding the photochemical reaction of 9,10-phenanthrenequinone, **1**, with acetaldehyde, **2**, two reaction mechanisms have been proposed: the in-cage mechanism (Eq. 1) and the radical chain mechanism involving an acyl radical as the chain carrier (Eq. 2). For the establishment of the true reaction mechanism, the thermal addition reaction of an acyl radical to 9,10-phenanthrenequinone was investigated. The products in the thermal reaction were the dimeric isomers of the aryloxyl radical, **6**, *i.e.*, **4** and **5**, which were quite different from the product of the photochemical reaction of 9,10-phenanthrenequinone with acetaldehyde, *i.e.*, 9-acetoxy-10-hydroxyphenanthrene, **3**. These results, as well as the estimation of the quantum efficiency for the photochemical reaction, exclude the radical chain mechanism (Eq. 2) and strongly support the in-cage mechanism (Eq. 1) for the photochemical reaction of 9,10-phenanthrenequinone with aldehyde.

The photochemical reactions of quinone have been of great practical significance, providing a method of synthesizing complex organic molecules.[1] The mechanistic elucidation of these reactions are essential to ensure further success in preparative organic photochemistry.

The irradiation of a benzene solution of 9,10-phenanthrenequinone, **1**, and acetaldehyde, **2**, for example, gives 9-acetoxy-10-hydroxyphenanthrene, **3**, in a quantitative yield. The other aldehydes, aliphatic and aromatic, behave similarly to give the corresponding 9-acyloxy-10-hydroxyphenanthrenes in good yields. Recently for the above reaction the present authors proposed the intervening contribution of a radical pair, *i.e.*, the in-cage mechanism, mainly on the basis of an investigation using the ^{1}H-CIDNP technique (Eq. 1).[2] In contrast, Moore and Waters suggested about twenty years ago a radical-chain mechanism involving the acetyl radical as a chain carrier (Eq. 2)[3]

In the present investigation the acetyl radical generated from the hydrogen abstraction of acetaldehyde by the *t*-butoxyl radical was allowed to react with 9,10-phenanthrenequinone, **1**, and the products were compared with those of the photochemical reaction of 9,10-phenanthrenequinone, **1**, with acetaldehyde, **2**.

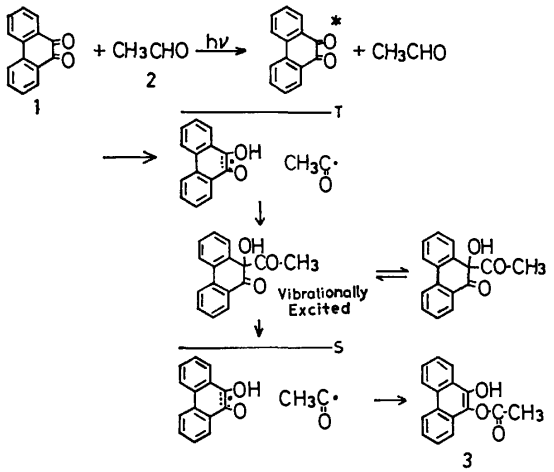

(Eq. 1)

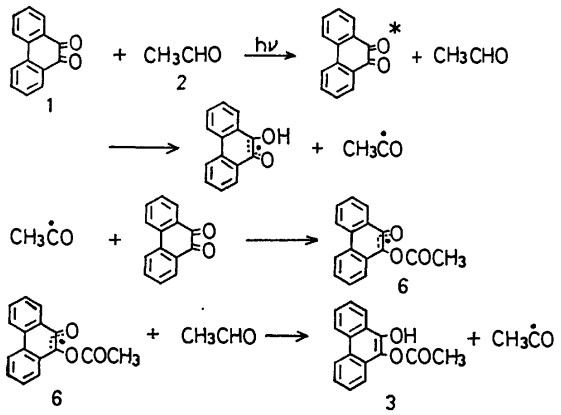

(Eq. 2)

Results and Discussion

Product Analysis. The acetyl radical was generated by the thermal decomposition (70 °C) of di-*t*-butyl diperoxyoxalate[4] dissolved in benzene in the presence of an excess amount of acetaldehyde, **2**. When the acetyl radical was allowed to react with 9,10-phenanthrenequinone, **1**, the yellow color due to **1** disappeared. After the evaporation of the solvent, column chromatography on silica gel gave two white crystals in nearly equal amounts (total yield: 90%). Their molecular weights, as determined by the vapor-pressure method, indicated that both of them are dimers of the aryloxy radical, **6**. The aryloxy radical, **6**, is to be yielded by the addition of an acetyl radical to 9,10-phenan-

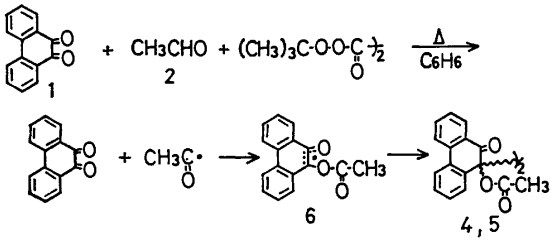

(Eq. 3)

threnequinone. On the basis of their mass analysis and spectral data, the two products were concluded to be configurational isomers with each other and were identified as **4** ("*dl*-form") and **5** ("*meso*-form") respectively[5] (see Eq. 3). The other products were quite small in their amounts, but different from 9-acetoxy-10-hydroxyphenanthrene, **3**, which was the sole product in the photolysis of a solution of **1** and **2**.[2] Further, the possible formation of **4** and **5** *via* **3** was examined by treating **3** with di-*t*-butyl diperoxyoxalate in the presence of acetaldehyde, but no **4** or **5** was found. The exclusive product in this reaction was 9,10-diacetoxyphenanthrene, **7** (Eq. 4). Thus, we can exclude the intermediacy of **3** in the formation of **4** and **5**. As will be described in the following section, the time-dependent parallelism of the amount of **4** relative to **5** also supports

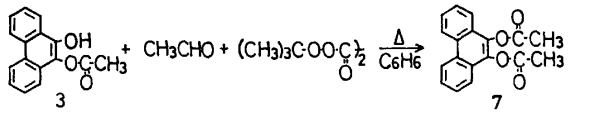

(Eq. 4)

the above consideration. In the reaction with other acyl radicals 9,10-phenanthrenequinone gives dimeric mixtures analogous to that of **4** and **5**. The total yields of the isomeric dimers are summerized in Table 1.

TABLE 1. THE THERMAL REACTION OF 9,10-PHENANTHRENEQUINONE WITH THE ACYL RADICAL

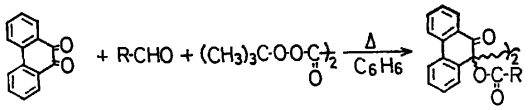

R	Yields of dimers (%)
CH_3–	90
C_3H_7–	83
p-CH_3–C_6H_4–	88
p-CH_3O–C_6H_4–	66

The Yield of **4** *Relative to that of* **5** versus *the Reaction Time.* With the progress of the reaction the amount of **4** relative to **5** was followed; the amounts of **4** and **5** increased monotonously with the time. As was concluded from Fig. 1, the relative yield, **4**/**5**, was invariably constant throughout the reaction. Thus, both **4** and **5** must be primary products in the reaction; hence, **3** cannot be a precursor of **4** and **5**.

Concluding Remarks. Without doubt the acetyl radical adds to 9,10-phenanthrenequinone, **1**, to form the **6** radical in the primary step of the reaction. Subsequently, the **6** radical could undergo dimerization, resulting in the formation of **4** and **5** in nearly comparable amounts. Thus, the *free* acetyl radical adds to **1** even in the presence of a large excess of acetaldehyde, as summarized in Eq. 3.

Contrary to the present reaction, the photochemical reaction of 9,10-phenanthrenequinone, **1**, with acetaldehyde gives **3** in a quantitative yield without **4** or **5**. Therefore, in the photochemical reaction of 9,10-phenanthrenequinone with acetaldehyde the intervention of the *free* acetyl radical, and thus the intermediacy of the aryloxyl radical, **6**, can be excluded completely. That is, the photochemical reaction of 9,10-phenanthrenequinone with acetaldehyde may proceed *via* the in-cage radical pair, *i.e.*, the in-cage mechanism, resulting in the quantitative formation of **3** (Eq. 1). The exclusion of the radical-chain mechanism (Eq. 2) was further supported by the disappearance of 9,10-phenanthrenequinone in the presence of a 10-fold molar quantity of acetaldehyde. Its quantum efficiency was about 0.21.

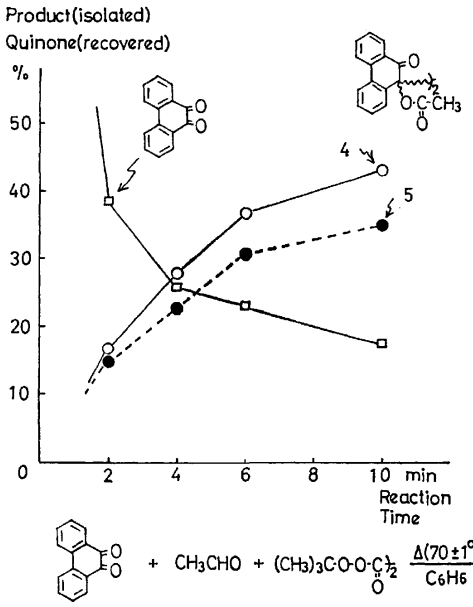

Fig. 1. The effect of the reaction time.

Experimental

Materials. The 9,10-phenanthrenequinone was prepared by the oxidation of phenanthrene with potassium dichromate; mp 202—204 °C. The di-*t*-butyl diperoxyoxalate was prepared according to the method in the literature.[4] All the aldehydes examined here were commercially available and were submitted to the thermal reactions after purification by distillation.

General Procedures. 9,10-Phenanthrenequinone (7.2 mmol) and aldehyde (26.8 mmol) were dissolved in dry benzene (30 ml), while the temperature of the solution was kept at 70 °C. To the solution di-*t*-butyl diperoxyoxalate (10.2 mmol) was added in portions. After an appropriate reaction time, the reaction was quenched by cooling and the reaction mixture was purified by chromatography on silica gel.

Identification of Products. *9,9'-Diacetoxy-9,9',10,10'-tetrahydro[9,9'-biphenanthrene]-10,10'-dione*: yield, 90%. dl-*9,9'-Diacetoxy-9,9',10,10'-tetrahydro[9.9'-biphenanthrene]-10,10'-dione (4)*: white crystals; mp 200.2—201.2 °C. Found; C, 76.76; H, 4.21%. Calcd for $C_{32}H_{22}O_6$; C, 76.48; H, 4.41%. Molecular weight (vapor-pressure method); *m/e*=502 (Calcd for $C_{32}H_{22}O_6$; *m/e*=502). Mass; *m/e*=251 (monomer$^+$), 209, 207, 180, 179. IR (KBr); 1750, 1690 cm^{-1}. ^{1}H-NMR ($CDCl_3$); δ: 1.55 (6H,s), 6.40 (2H,d,J=8Hz), 6.9—8.0 ppm (14H,m). UV max ($CHCl_3$); 339 nm (log ε: 3.68), 252 (4.64), 216 (4.57).

meso-*9,9'-Diacetoxy-9,9',10,10'-tetrahydro[9,9'-biphenanthrene]-10,10'-dione (5)*: white crystals; mp 216—217 °C. Molecu-

lar weight (vapor-pressure method); *m/e*=553 (Calcd for $C_{32}H_{22}O_6$; *m/e*=502), Mass; *m/e*=251 (monomer$^+$), 209, 207, 180, 179. IR (KBr); 1770, 1690 cm^{-1}. ^{1}H-NMR ($CDCl_3$); δ: 2.10 (6H,s), 7.0—7.9 ppm (16H,m). UV max ($CHCl_3$); 339 nm (log ε: 3.56), 227 (4.47), 216 (4.58).

9'9'-Bis(butyryloxy)-9,9',10,10'-tetrahydro[9,9'-biphenanthrene]-10,10'-dione: yield, 83%.

dl-*9,9'-Bis(butyryloxy)-9,9',10,10'-tetrahydro[9,9'-biphenanthrene]-10,10'-dione*: white crystals; mp 190—191 °C. Mass; *m/e*=279 (monomer$^+$). IR (KBr); 1750, 1695 cm^{-1}. ^{1}H-NMR ($CDCl_3$); δ: 0.70 (6H,t,J=6 Hz), 1.32 (4H, sextet, J=6 Hz), 1.84 (4H,t,J=6 Hz), 6.44 (2H,d,J=8 Hz), 7.0—8.1 ppm (14H, m). UV max (CH_2Cl_2); 337, 256, 248 (sh)nm.

meso-*9,9'-Bis(butyryloxy)-9,9',10,10'-tetrahydro[9,9'-biphenanthrene]-10,10'-dione*: white crystals; mp 176—177 °C. Mass; *m/e*=279 (monomer$^+$). IR (KBr); 1750, 1695 cm^{-1}. ^{1}H-NMR ($CDCl_3$); δ: 0.92 (6H,t, J=6 Hz), 1.56 (4H, sextet, J=6 Hz), 2.30 (4H), 2.30 (4H, t, J=6 Hz), 6.8—7.8 ppm (16H,m). UV max (CH_2Cl_2): 337, 255 (sh), 248 nm.

*9,9'-Bis(*p*-toluoyloxy)-9,9',10,10'-tetrahydro[9,9'-biphenanthrene]-10,10'-dione*: yield, 88%; white crystals, mp 195 °C (dec) as a mixture of nearly equal amounts of two isomers. Mass; *m/e*=327 (monomer$^+$). IR (KBr); 1740, 1690 cm^{-1}. ^{1}H-NMR ($CDCl_3$); δ: 2.35 (s,CH_3(*dl*-form)), 2.42 (s, CH_3 (*meso*-form)), 6.42 (d, J=8 Hz, aromatic-H (*dl*-form)), 6.8—8.2 ppm (m). UV max (CH_2Cl_2); 338, 248 nm.

*9,9'-Bis(*p*-arisoyloxy)-9,9',10,10'-tetrahydro[9,9'-biphenanthrene]-10,10'-dione*: yield, 66%; white crystals; mp 151—161 °C as a mixture of nearly equal amounts of isomers. Mass; *m/e*=343 (monomer$^+$). IR (KBr); 1720, 1690 cm^{-1}. ^{1}H-NMR ($CDCl_3$); δ: 2.34 (s, OCH_3(*dl*-form)), 2.40 (s, OCH_3-(*meso*-form)), 6.64 (s, J=8 Hz, aromatic-H(*dl*-form)), 6.8—8.1 (m, aromatic-H(*dl*-form)), 7.0—8.0 ppm (m, aromatic-H (*meso*-form)). UV max (CH_2Cl_2); 337, 255 nm.

9,10-Diacetoxyphenanthrene (**7**): white crystals; mp 196.0—197.5 °C. Mass; *m/e*=294 (M^+). IR (KBr); 1780 cm^{-1}. ^{1}H-NMR($CDCl_3$); δ: 2.52 (6H,s), 7.7—8.0 (6H,m), 8.6—8.8 ppm (2H,m). UV max (CH_2Cl_2); 295, 285, 275, 255, 245 nm. 9,10-Diacetoxyphenanthrene was also yielded by the reductive acetylation (Zn–Acetic anhydride) of 9,10-phenanthrenequinone.

The Estimation of the Quantum Efficiency. The light sourse was a high-pressure Hg arc lamp (300W); by the use of a filter (Toshiba KL-50), the irradiation was carried out by selected light (wavelength: 498±8 nm) at 15.0±0.5 °C. The quanta of light absorbed by the reaction mixture was calibrated using an aqueous solution of potassium tris(oxalo)ferrate(III) as a chemical actinometer.[7] The reaction mixture submitted to the measurement was a benzene solution of 1.92×10^{-3} M of 9,10-phenanthrenequinone and 2.3×10^{-2} M of acetaldehyde. The quantum efficiency, followed by the disappearance of 9,10-phenanthrenequinone, was estimated to be 0.21.

References

1) J. M. Bruce, "The Chemistry of Quinonoid Compounds," ed by S. Patai, John Wiley & Sons, London (1974), p. 465.

2) a) K. Maruyama, A. Takuwa, T. Otsuki, and S. Kako, *Bull. Inst. Chem. Res., Kyoto Univ.*, **50**, 348 (1972; b) K. Maruyama, T. Otsuki, and Y. Naruta, *Bull. Chem. Soc. Jpn.*, **49**, 791 (1976).

3) R. F. Moore and W. A. Water, *J. Chem. Soc.*, **1953**, 238.

4) P. D. Bartlett, E. P. Benzing, and R. E. Pincok, *J. Am. Chem. Soc.*, **82**, 1762 (1960).

5) By inspecting their ^{1}H-NMR spectra and their molecular models, we assigned the stereochemistry of the two isomers to those described in the text on the basis of the fact that the acetyl and the aromatic ring protons in the "*dl*-form," **4**, would be more largely shielded by the anisotropy effect attributable to the carbonyl group and the aromatic rings than those in the "*meso*-form," **5**.

6) The estimated value of the quantum efficiency was far below unity; this suggests that the photolysis did not proceed by the chain mechanism. Moreover, the value is reasonable compared with those observed in the photochemical reaction of quinones with aldehydes. *Cf.* K. Maruyama and Y. Miyagi, *Bull. Chem. Soc. Jpn.*, **47**, 1303 (1974).

7) C. A. Parker, *Proc. R. Soc. London, Ser. A*, **220**, 104 (1952); D. A. Hatchard and C. A. Parker, *Proc. R. Soc. London, Ser. A*, **235**, 518 (1956).

Copper-initiated Decomposition of *N,N*-Dichloromethanesulfonamide

Noboru TORIMOTO, Tadao SHINGAKI,* and Toshikazu NAGAI*

Science Education Institute of Osaka Prefecture, Karita-cho, Sumiyoshi-ku, Osaka 558
**College of General Education, Osaka University, Toyonaka, Osaka 560*

(Received April 25, 1977)

The reactions of *N,N*-dichloromethanesulfonamide (I) with substrates such as hydrocarbons and ethers gave the *N*-substituted methanesulfonamide (II) and methanesulfonamide (III) in the presence of copper. The reaction with 2-methylbutane gave the product only with a tertiary C–H bond, though the singlet nitrene which was generated from methanesulfonyl azide reacted with the primary, secondary, and tertiary C–H bonds in the ratio of 1: 4.2: 9.6. The reactions with the tertiary C–H bonds of *cis*- and *trans*-1,4-dimethylcyclohexanes proceeded non-stereospecifically, in contrast to those of the nitrene with them. The addition of a radical inhibitor, hydroquinone, reduced the yield of II, while it increased the yield of III. The reaction with alcohols led to a quantitative yield of III, accompanied by the corresponding aldehydes. These results suggest that the reaction proceeds not by a nitrene mechanism, but by a metal-radical mechanism.

The existence of a nitrene intermediate has been shown in several reactions which afford the same products or product mixtures *via* two or more independent routes. Phenylnitrene, for example, seems to be the intermediate in the pyrolysis[1] and photolysis[2] of phenyl azide, in the deoxygenation of nitrosobenzene[3] and nitrobenzene,[4] and in the photolyses of oxaziridines,[5] for the intermediate always leads to the same product, 2-dialkylamino-3*H*-azepine, in the presence of a dialkylamine. The species generated by the photolysis[6] and the thermolysis[7] of ethyl azidoformate and by the α-elimination of *N*-(*p*-nitrophenylsulfonyloxy)urethane[8] nearly the same regioselectivities toward the C–H bonds of 2-methylbutane. These demonstrations have been explained by the intervention of ethoxycarbonylnitrene in each instance.

Breslow and Sloan[9] reported that the reaction of dichloramine-T with zinc dust in cyclohexane gave *N*-cyclohexyl-*p*-toluenesulfonamide, and suggested that a free sulfonylnitrene was formed as an intermediate, since the insertion into C–H bonds is a distinctive nitrene reaction:

$$p\text{-}CH_3C_6H_4SO_2NCl_2 + Zn \longrightarrow p\text{-}CH_3C_6H_4SO_2N(Cl)(ZnCl)$$
$$\longrightarrow p\text{-}CH_3C_6H_4SO_2\ddot{N}: + ZnCl_2$$
(sulfonylnitrene)

On the other hand, the thermolysis of *N,N*-dichloromethanesulfonamide in benzene afforded methanesulfonamide in an 82% yield, with gas-chlomatographically detectable biphenyl, but neither *N*-mesylaniline nor azepine derivatives.[10] This finding, by Abramovitch, shows that the formation of nitrene in the reaction might be ruled out. Prior to his paper, we ourselves reported that the reaction of *N,N*-dichloromethanesulfonamide (I) with hydrocarbons and ethers in the presence of copper proceeded by means of a radical mechanism involving no sulfonylnitrene.[11]

We are investigating decomposition mechanisms of chloramide. As a part of this work, the reactions of I with the substrate hydrocarbons, ethers, and alcohols have been studied in further detail. The results will be discussed here in comparizon with those of the direct and the sensitized photolyses of methanesulfonyl azide.

Results and Discussion

Reactions of I in the Presence of Copper. Copper powder was suspended in a substrate (IV), and *N,N*-dichloromethanesulfonylamide (I) was added to the stirred suspension in small portions in a stream of nitrogen. The yields of the products are listed in Table 1.

TABLE 1. REACTION OF I WITH ETHERS AND HYDROCARBONS

	Substrate (IV)		Product (%)[a] II	III
(a)	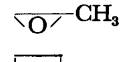	(a)	ND[b]	42
(b)		(b)	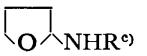 46	46
(c)		(c)	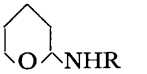 52	41
(d)		(d)	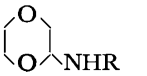 46	48
(e)	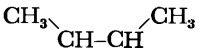	(e)	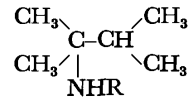 7.0	63
(f)		(f)	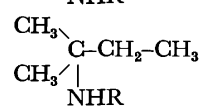 7.0	65
(g)		(g)	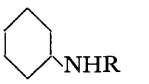 5.4	60
(h)		(h)	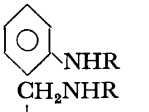 5.6	62
(i)	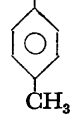	(i)	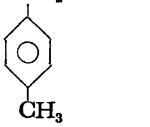 9.1	53

a) Calculated on the basis of the I used. b) ND: not detected. c) R: SO_2CH_3.

Each of the reactions gave the *N*-substituted methanesulfonamide (II) and methanesulfonamide (III).

TABLE 2. REACTION OF I WITH *cis*- AND *trans*-1,4-DIMETHYLCYCLOHEXANES

I or V		IV	Product (%)[a]		
			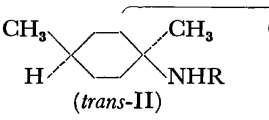 (*trans*-II)	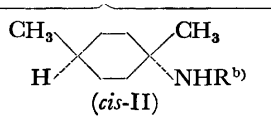 (*cis*-II)	III
$RNCl_2$		*trans*	12.4	11.0	61
		cis	12.1	10.3	60
RN_3	direct	*trans*	3.6	0	35
		cis	0	3.3	49
	sensitized	*trans*	12.9	2.8	22
		cis	13.8	4.3	22

a) Calculated on the basis of the I and V used. b) R: SO_2CH_3.

$$CH_3SO_2NCl_2 + R'\text{-}H \xrightarrow{Cu} CH_3SO_2NHR' + CH_3SO_2NH_2$$
(I) (II) (III)

(R′: hydrocarbon rest or ether rest)

The products, II and III, correspond formally to those from insertion into the C–H bonds, and from the abstraction of the hydrogen atoms, by methylsulfonylnitrene respectively. In the reactions with cyclic ethers, the α-substituted derivatives were isolated in good yields. The preferential formation of the α-substituted derivatives in IVb and IVc parallel those in the direct and sensitized photolyses of ethyl azidoformate in cyclic[13] and acyclic[12] ethers. The reaction of I with propylene oxide gave large quantities of a colorless, viscous substance whose IR spectrum showed a strong O–H stretching absorption. The products with the ring or the methyl C–H bonds were not isolated. The reactions in IVe and IVf gave, besides III, products with only the tertiary C–H bonds. This finding for the reaction with IVf is different from that of the direct photolysis of methanesulfonyl azide (V) in IVf; the singlet sulfonylnitrene generated by the direct photolysis reacted with the primary, secondary, and tertiary C–H bonds of IVf in the ratio of 1: 4.2: 9.6.[14] The difference in the regioselectivities toward the C–H bonds between the present reaction and the photolysis of V means that the singlet sulfonylnitrene is probably not involved in the former.

Attempting the reaction of I with aromatic substrates, the decomposition in *p*-xylene gave the reaction product (IIi) with only the side-chain C–H bond, although the reaction in benzene gave that with the aromatic nucleus, besides III. On the contrary, the thermolysis of V in toluene gave no *N*-benzylmethanesulfonamide corresponding to IIi, but methanesulfonyltoluidide isomers and III in 76.8 and 22.7% yields respectively.[15] Such aromatic nucleus derivatives are formed *via* an aziridine intermediate or a transition state with the sulfonylnitrene.[15,16] The formation of IIi in the present reaction also supports the idea that the reaction proceeds by means of a mechanism involving no singlet nitrene.

Next, the reactions of I were carried out in *cis*- and *trans*-1,4-dimethylcyclohexanes (*cis*-IV and *trans*-IV) in order to obtain information about the stereospecificity. The results are listed in Table 2, where they are compared with those of the direct[11] and the sensitized[17] photolyses of V. The reaction of I with either *cis*-IV or *trans*-IV gave a mixture of *cis*-II and *trans*-II (stereoisomers). On the other hand, in the photolyses of V, only one product isomer (*cis*-II or *trans*-II) was isolated in each reaction; the reaction was virtually completely stereospecific. The insertion of the sulfonylnitrene into the C–H bonds of hydrocarbons is a concerted reaction involving the singlet nitrene. Breslow *et al.* also recently reported that the insertion of methylsulfonylnitrene, generated by the thermolyses of V, into the tertiary C–H bonds of *cis*- and *trans*-1,2-dimethylcyclohexanes proceeded stereospecifically.[18] The stereospecific formation of *cis*-II or *trans*-II shows that the radical, $CH_3SO_2\dot{N}H$, produced by the hydrogen abstraction of the triplet nitrene is not able to recombine with a hydrocarbon radical. Therefore, the non-stereospecific formation of *cis*-II or *trans*-II in the reactions of I means that neither the singlet nor the triplet nitrene takes part in the formation of II. The non-stereospecific formation of *cis*-II or *trans*-II in the sensitized photolyses of V can be explained by the triplet azide mechanism.[17]

The reactions of I with ethyl alcohol and butyl alcohol did not give the product with the O–H bonds, but the hydrogen abstraction product, III, in yields of 97.2 and 97.8% respectively, accompanied by the corresponding aldehydes. The formation of the aldehydes in the alcohols suggests that the reaction of I involves a radical process. Therefore, the reaction of I was repeated in the presence of hydroquinone as a potential inhibitor. When *cis*-IV was employed, the addition of the hydroquinone reduced the yield of the mixture of *cis*-II and *trans*-II from 23% to below 0.3%, while it increased the yield of III from 60 to 77%. When

TABLE 3. REACTION OF I IN THE PRESENCE OF COPPER (I) CHLORIDE

Substrate (IV)	Product (%)[a]				
	II				III
IVb	IIb	57.6			43
trans-IV[b]	*trans*-II	9.7	*cis*-II	7.3	60
cis-IV[b]	*trans*-II	8.6	*cis*-II	6.1	64

a) Calculated on the basis of the I used. b) A mixture of IV and 1,2-dichloroethane in a molar ratio of 0.7: 0.3 was used.

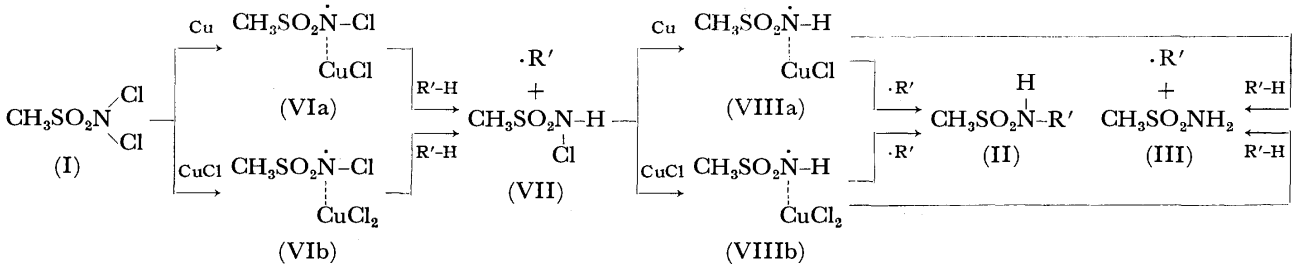

Scheme 1.

IVb was employed, IIb was not detected, while the yield of III increased from 45.6 to 98.4%. These facts show that the reaction of I with the substrates in the presence of copper powder involves a radical mechanism.

Reactions of I in the Presence of Copper(I) Chloride. The reactions of I with the substrates were carried out in the presence of copper(I) chloride instead of copper. The yields of the products are listed in Table 3. The same products as those formed in the presence of copper were obtained. In the reaction with *cis*-IV and *trans*-IV, the products, II, were obtained only when 1,2-dichloroethane was used as a diluent, and the reactions were non-stereospecific.

Reaction Mechanism. A tentative reaction mechanism, which perhaps involves a metal-radical complex, may be outlined as in Scheme 1.

The reactions of I with the substrates do not proceed in the absence of copper or copper(I) chloride under our conditions. The decomposition of I must be initiated by copper or copper(I) chloride. The elimination of one chlorine atom gives a metal-radical complex (VI), followed by the formation of *N*-chloromethanesulfonamide (VII). The sulfonamide radical (VIII) which is formed from VII with copper or copper(I) chloride recombines with the substrate radical (·R'), giving II. On the other hand, VIII abstracts a hydrogen atom from the substrate to give III. It is well known that the metal-radical complex, generated from organic halides and transition metal compounds, behaves somewhat differently from those of radicals generated from such initiators as organic peroxides.[19] As has been mentioned above, the $CH_3SO_2\dot{N}H$ radical generated from V in hydrocarbons, was not able to recombine with a hydrocarbon radical. However, the radical generated by the present reaction would be stabilized by forming the metal-radical complex, as is shown in the Scheme. Consequently, the recombination of the radical with a hydrocarbon radical may be possible.

Photolyses of V in the Presence of Copper(I) Chloride. The presence of a metal compound in the photolysis of V would lead us to expect the recombination of $CH_3SO_2\dot{N}H$ with a hydrocarbon radical. Thus, the direct photolysis of V was carried out in *cis*-IV in the presence of copper(I) chloride. Unexpectedly, the reaction gave only one tertiary isomer, *cis*-II; the reaction was completely stereospecific. The sensitized photolyses of V were carried out in *cis*-IV and *trans*-IV in the presence of copper(I) chloride. As the photolyses proceeded, the solution had a color varying from an initial light yellow to dark green at the end. However, there was no significant difference in the product yields between the absence of copper(I) chloride (shown in Table 2) and its presence (shown in Table 4).

Table 4. Sensitized photolyses of V in the presence of copper(I) chloride

Hydrocarbon (IV)	Product (%)[a]		
	trans-II	*cis*-II	III
trans-IV	5.9	2.4	22
cis-IV	12.7	4.3	27

a) Calculated on the basis of of the I used.

The copper compound did not exhibit any effect on the reaction involving the azide, though it was evident that the copper compound played an important role in the present chloramide system; the absence of copper compound did not result in the formation of the *N*-substituted methanesulfonamide.[10]

Experimental

The IR spectra were recorded on a Hitachi EP-S photometer and a Nippon Bunko (JASCO) Model A-3 photometer, while the NMR spectra were taken on Hitachi R-20 and Hitachi R-24 instruments, using tetramethylsilane as the internal standard. The gas chromatography (VPC) was conducted on Shimadzu GC-2C and Nippon Denshi (JEOL) JGC 20K units by means of the following columns: A, 20% Ucon Oil 5 HB 2000 on Celite (60—80 mesh); B, 10% Polyethylene Glycol Succinate on Neopak 1A (60—80 mesh). The products were separated by VPC, and the structures of the products were determined by means of elemental analyses and by measurements of the IR and NMR spectra. The structures of some of the products were determined by comparing their IR and NMR spectra with those of authentic samples. The quantitative analyses of the products by VPC and testing for the stability of each product during VPC analysis have been described in a previous paper.[20]

Materials. The *N,N*-dichloromethanesulfonamide (I) was prepared by the method of Newcombe.[21] The methanesulfonyl azide (V) was prepared by the method of Reagan and Nickon.[22] The propylene oxide, tetrahydrofuran, tetrahydropyran, 1,4-dioxane, 2,3-dimethylbutane, 2-methylbutane, cyclohexane, benzene, *p*-xylene, ethyl alcohol, butyl alcohol, and 1,2-dichloroethane were used after the commercial reagents had been purified according to the published directions.[23] Analytical-grade reagents of copper(I) chloride, copper, hydroquinone, and acetophenone were used without further purification. The preparation of *cis*- and *trans*-1,4-dimethylcyclohexanes (*cis*-IV and *trans*-IV) has already been described.[17]

Authentic Samples. The preparation of *N*-cyclohexylmethanesulfonamide (IIg), *N*-(*cis*-1,4-dimethylcyclohexyl)methanesulfonamide (*cis*-II), and *N*-(*trans*-1,4-dimethylcyclohexyl)-methanesulfonamide(*trans*-II) has been described previously.[17] *N*-Phenylsulfonamide (IIh) was prepared from aniline and methanesulfonyl chloride in a way similar to that used in the preparation of *N*-cyclohexylurethane;[24] mp 98 °C, IR (Nujol, cm^{-1}): 3270 (NH), 1330, and 1155 (SO_2). NMR ($CDCl_3$, τ): 2.70 (C_6H_5, 5H, s), 2.72 (NH, 1H, bs), and 7.00 (SCH_3, 3H, s).

Reactions of I with Ethers, Hydrocarbons, and Alcohols in the Presence of Copper. Copper powder (4.8 g, 0.075 mol) was suspended in a substrate (0.6 mol of ethers, hydrocarbons, or alcohols), and *N,N*-dichloromethanesulfonamide (I, 4.1 g, 0.025 mol) was added to the stirred suspension in small portions in a stream of nitrogen. The reactions with ethers and alcohols were carried out at 5—7 °C, except for that with dioxane, which was done at 12 °C. After I had been added, the stirring was continued for about another 5 h. Then the suspension was filtered, and the filtrate was concentrated under reduced pressure. In the reactions with hydrocarbons, the residue was analyzed by VPC on Column A and B. On the other hand, the residual material resulted from the filtration of the suspension was extracted with three 50-ml portions of 1M-hydrochloric acid and the hydrochloric acid was evaporated under reduced pressure. The abstraction product (III) contained in the residue was dissolved in ethyl alcohol and analyzed by means of VPC on Column A. In the cases of the ethers and alcohols, the residue was extracted with three 50-ml portions of hot benzene. The colorless crystals (II), obtained by evaporating the benzene, were dried *in vacuo* and weighed. The NMR spectrum of each of the crystals showed it to contain no contaminant. The crystals were then recrystalized from benzene, and the melting points were measured. On the other hand, III was also obtained from the insoluble material in the hot benzene. Methanesulfonamide (III), formed from every experiment, had IR and NMR spectra and a VPC retention time identical with those of the authentic sample.

In Tetrahydrofuran (IVb), Tetrahydropyran (IVc), and 1,4-Dioxane (IVd): *N*-(2-Tetrahydrofuryl)methanesulfonamide (IIb, 1.90 g), *N*-(2-tetrahydropyranyl)methanesulfonamide (IIc, 2.32 g), and *N*-(1,4-dioxan-2-yl)methanesulfonamide (IId, 2.08 g) were isolated respectively. IIb: Mp 75 °C, IR (Nujol, cm^{-1}): 3240 (NH), 1325, and 1170 (SO_2). NMR ($CDCl_3$, τ): 4.44 (NH, 1H, bs), 4.48—4.90 (ring-CH, 1H, m), 5.60—6.34 (ring δ-CH_2, 2H, m), 6.93 (SCH_3, 3H, s), and 7.33—8.52 (ring β- and γ-CH_2, 4H, m). Found: C, 36.10; H, 6.59; N, 8.30%. Calcd for $C_5H_{11}O_3NS$: C, 36.36; H, 6.71; N, 8.48%. IIc: Mp 102 °C, IR (Nujol, cm^{-1}): 3300 (NH), 1330, and 1155 (SO_2). NMR ($CDCl_3$, τ): 3.90 (NH, 1H, bd), 4.82—5.58 (ring-CH, 1H, m), 5.66—6.68 (ring ε-CH_2, 2H, m), 6.85 (SCH_3, 3H, s), and 7.78—8.74 (ring β-, γ- and δ-CH_2, 6H, m). Found: C, 39.81; H, 7.05; N, 7.75%. Calcd for $C_6H_{13}O_3NS$: C, 40.22; H, 7.31; N, 7.82%. IId: Mp 109 °C, IR (nujol, cm^{-1}): 3265 (NH), 1335, and 1155 (SO_2). NMR ($CDCl_3$, τ): 4.05 (NH, 1H, bd), 4.76—5.22 (ring-CH, 1H, m), 5.68—6.78 (ring-CH_2, 6H, m), and 6.90 (SCH_3, 3H, s). Found: C, 32.95; H, 6.01; N, 7.62%. Calcd for $C_5H_{11}O_4NS$: C, 33.14; H, 6.12; N, 7.73%.

In 2,3-Dimethylbutane (IVe), 2-Methylbutane (IVf), and Cyclohexane (IVg): *N*-(1,1,2-Trimethylpropyl)methanesulfonamide (IIe, 0.31 g), *N*-(1,1-dimethylpropyl)methanesulfonamide(IIf, 0.29 g), and *N*-cyclohexylmethanesulfonamide (IIg, 0.24 g) were isolated respectively. The IR and NMR spectra of IIe, IIf, and IIg have been described previously.[17]

In Benzene (IVh) and p-*Xylene (IVi):* *N*-Phenylmethanesulfonamide (IIh, 0.24 g) and *N*-(*p*-tolylmethyl)methanesulfonamide (IIi, 0.45 g) were isolated. The IR and the NMR spectra of IIh were identical with those of the authentic sample. IIi: IR (neat, cm^{-1}): 3260 (NH), 1330, and 1160 (SO_2). NMR ($CDCl_3$, τ): 2.83 (C_6H_4, 4H, s), 5.00 (NH, 1H, bs), 5.75 (CH_2, 2H, d), 7.19 (SCH_3, 3H, s), and 7.66 (CH_3, 3H, s). Found: C, 53.81; H, 6.43; N, 6.92%. Calcd for $C_9H_{13}O_2NS$: C, 54.26; H, 6.58; N, 7.03%.

In trans-*IV*: *N*-(*trans*-1,4-Dimethylcyclohexyl)methanesulfonamide (*trans*-II, 0.63 g) and *N*-(*cis*-1,4-dimethylcyclohexyl)-methanesulfonamide (*cis*-II, 0.56 g) were isolated. The IR and the NMR spectra of *trans*-II and *cis*-II have been described previously.[17]

In cis-*IV*: *trans*-II (0.62 g) and *cis*-II (0.53 g) were isolated.

In Ethyl Alcohol and Butyl Alcohol: For each of the reactions with alcohols, the excess substrate and the volatile product, aldehyde, were trapped in a flask immersed in a dry ice-methanol bath reduced pressure. The trapped solution was added to a 2,4-dinitrophenylhydrazine solution, and the aldehyde was converted to the hydrazone. For ethyl alcohol and butyl alcohol, acetaldehyde and butyraldehyde were isolated as the hydrazones in yields of 2.30 g (41.1%) and 0.42 g (6.7%) respectively.

Reaction of I with IVb and cis-*IV in the Presence of Copper and Hydroquinone.* Hydroquinone (2.8 g, 0.025 mol) was added to the system of I-substrate-copper mentioned above. The reaction with IVb was carried out at 5—7 °C, while that with *cis*-IV was carried out at 70 °C. The reaction mixture was treated with the procedures described for the reaction in the absence of hydroquinone. In the reaction with *cis*-IV, trace amounts (0.01 g) of a mixture of *trans*-II and *cis*-II were isolated. In the reaction with IVb, only the abstraction product (III) was isolated.

Reaction of I with Ether and Hydrocarbons in the Presence of Copper(I) Chloride. Copper(I) chloride (7.1 g, 0.075 mol) was suspended in ether (0.5 mol) or a mixture of hydrocarbon (0.35 mol) and 1,2-dichloroethane (0.15 mol). I (4.1 g, 0.025 mol) in small portions was then added to the stirred suspension in a stream of nitrogen. The reaction with IVb was carried out at 5—7 °C, while those with *trans*-IV and *cis*-IV were carried out at 70 °C. After I had been added, the reaction mixture was treated with the procedures described for the reaction in the presence of copper.

In IVb: IIb (2.37 g) was isolated.

In trans-*IV*: *trans*-II (0.50 g) and *cis*-II (0.37 g) were isolated.

In cis-IV: *trans*-II (0.44 g) and *cis*-II (0.31 g) were isolated.

Sensitized Photolyses of Methanesulfonyl Azide (V) in Hydrocarbons in the Presence of Copper(I) Chloride. A powder of copper (I) chloride (1.9 g, 0.019 mol) was suspended in a mixture of V (1.5 g, 0.0124 mol), hydrocarbon (0.15 mol), 1,2-dichloroethane (0.3 mol), and acetophenone (0.15 mol). The mixture was then irradiated, with stirring at 25 °C, by a high-pressure mercury lamp under an atmosphere of nitrogen. A 1.5M-$CuSO_4$ aqueous solution was circulated as a filter. The filter completely inhibited the direct excitation of V. The irradiation was continued until the evolution of nitrogen was no longer observed. After the copper compound had been filtered out, the excess substrate was removed by distillation at 50—80 °C under 20—30 mmHg. The residue was analyzed by VPC on Columns A and B.

In trans-*IV*: *trans*-II (0.15 g) and *cis*-II (0.06 g) were isolated.

In cis-*IV*: *trans*-II (0.32 g) and *cis*-II (0.11 g) were isolated.

Direct Photolysis of V in cis-*IV in the Presence of Copper(I) Chloride.* A powder of copper(I) chloride (1.9 g, 0.019 mol) was

suspended in a mixture of V (1.5 g, 0.0124 mol), *cis*-IV (0.15 mol), and 1,2-dichloroethane (0.3 mol). The suspension was irradiated, with stirring and cooling at 0 °C, by a low-pressure mercury lamp (mainly 2537 Å) under an atmosphere of nitrogen until the evolution of nitrogen was no longer observed. Then, the reaction mixture was treated with the procedures described for the sensitized photolyses. *cis*-II (0.12 g, 4%) was isolated.

The authors are particulary indebted to Dr. Hisao Arakawa and Dr. Akira Matsumoto of the Science Education Institute of Osaka Prefecture for help in the preparation of this paper and for many useful suggestions.

References

1) R. Huisgen, D. Vossius, and M. Appl, *Chem. Ber.*, **91**, 1, 12 (1958).
2) W. von E. Doering and R. A. Odum, *Tetrahedron*, **22**, 81 (1966).
3) R. A. Odum and M. Brenner, *J. Am. Chem. Soc.*, **88**, 2074 (1966).
4) R. J. Sundberg, W. G. Adams, R. H. Smith, and D. E. Blackburn, *Tetrahedron Lett.*, **1968**, 777.
5) E. Meyer and G. W. Griffin, *Angew. Chem.*, **79**, 648 (1967); J. S. Splitter and M. Calvin, *Tetrahedron Lett.*, **1968**, 1445.
6) W. Lwowski and T. W. Mattingly, Jr., *Tetrahedron Lett.*, **1962**, 277.
7) R. J. Cotter and W. F. Beach, *J. Org. Chem.*, **29**, 751 (1964); M. F. Sloan, T. J. Prosser, N. R. Newburg, and D. S. Breslow, *Tetrahedron Lett.*, **1964**, 2945.
8) W. Lwowski, T. J. Maricich, and T. W. Mattingly, Jr., *J. Am. Chem. Soc.*, **85**, 1200 (1963).
9) D. S. Breslow and M. F. Sloan, *Tetrahedron Lett.*, **1968**, 5349.
10) R. A. Abramovitch, T. D. Bailey, T. Takaya, and V. Uma, *J. Org. Chem.*, **39**, 340 (1974).
11) T. Shingaki, N. Torimoto, M. Inagaki, and T. Nagai, *Chem. Lett.*, **1973**, 1243.
12) N. Torimoto, T. Shingaki, and T. Nagai, *Bull. Chem. Soc. Jpn.*, **50**, 1517 (1977).
13) H. Nozaki, S. Fujita, H. Takaya, and R. Noyori, *Tetrahedron*, **23**, 45 (1967); N. Torimoto, T. Shingaki, and T. Nagai, *Bull. Chem. Soc. Jpn.*, **49**, 2572 (1976).
14) T. Shingaki, M. Inagaki, N. Torimoto, and T. Nagai, *Chem. Lett.*, **1972**, 1181.
15) R. A. Abramovitch, J. Roy, and V. Uma, *Can. J. Chem.*, **43**, 3407 (1965).
16) J. F. Tilney-Bassett, *J. Chem. Soc.*, **1962**, 2517.
17) N. Torimoto, T. Shingaki, and T. Nagai, *J. Org. Chem.*, in press.
18) D. S. Breslow, E. I. Edward, E. C. Linsay, and H. Omura, *J. Am. Chem. Soc.*, **98**, 4268 (1976).
19) Y. Mori and J. Tsuji, *Kagaku No Ryoiki*, **27**, 197 (1973).
20) T. Shingaki, M. Inagaki, M. Takebayashi, and W. Lwowski, *Bull. Chem. Soc. Jpn.*, **45**, 3567 (1967).
21) A. G. Newcombe, *Can. J. Chem.*, **33**, 1250 (1955).
22) M. T. Reagan and A. Nickon, *J. Am. Chem. Soc.*, **90**, 4096 (1968).
23) J. A. Riddic and W. B. Bunger, "Organic Solvents," in "Techniques of Chemistry," Vol. VII, ed by A. Weissberger, Wiley-Interscience, New York, N. Y. (1970).
24) W. Lwowski and T. W. Mattingly, Jr., *J. Am. Chem. Soc.*, **87**, 1947 (1965).

The Thallium(I) Salt-catalyzed Formation of Isothiocyanates from Isocyanides and Disulfides

Sakuya TANAKA, Sakae UEMURA, and Masaya OKANO*
Institute for Chemical Research, Kyoto University, Uji, Kyoto 611
(Received May 11, 1977)

The reactions of various isocyanides with diacyl disulfides or tetraethylthiuram disulfide occur smoothly in the presence of thallium(I) acetate and thiocarboxylates in various organic solvents to give the corresponding isothiocyanates in good yields. Lead(II) acetate has an activity almost identical with that of thallium(I), while cadmium(II) and silver(I) acetates and copper(I) oxide show a slightly lower activity than the above thallium and lead salts. An ionic scheme involving a complex formation between the metal salt and one S atom of the disulfide, followed by a nucleophilic attack of isocyanide on the adjacent S atom, is proposed for this reaction. It is revealed that the reaction of isocyanide with one equivalent of thallium(III) thiobenzoate in refluxing chloroform similarly affords a good yield of the isothiocyanate through the above mechanism after the decomposition of the thallium(III) salt to thallium(I) thiobenzoate and dibenzoyl disulfide, rather than through a pathway involving thiothallation (α-addition).

Several reactions involving the oxymetallation of isocyanides (α-addition) with Hg(II), Tl(III), or Pb(IV) salts have recently been reported.[1] While examining the reaction of isocyanides with similar metal salts containing a S atom, we have found that dibenzoyl disulfide, which can be derived from Tl(III) thiobenzoate, reacts smoothly with isocyanides in the presence of a catalytic amount of Tl(I) salt to afford the corresponding isothiocyanates. We wish now to report the results of the Tl(I)- or some other metal salt-catalyzed formation of isothiocyanates from various disulfides and isocyanides, and to discuss its reaction mechanism. It should be noted here that similar metal salt-promoted reactions of disulfide have been known[2] in the cases of amine and methanesulfinate ion using Ag(I) salt.

Results and Discussion

Reaction of Cyclohexyl Isocyanide (1) with Metal Thiocarboxylates (Table 1). By analogy with the oxidation of isocyanides with Hg(II), Tl(III), or Pb(IV) acetate giving isocyanates,[1c] isothiocyanate formation can be expected to proceed by means of the reaction of isocyanides with these salts of thiocarboxylic acids. When **1** was treated with Tl(III) thiobenzoate in chloroform under reflux, cyclohexyl isothiocyanate (**2**) was obtained in a good yield, whereas none of it was formed by the reaction with Hg(II) thioacetate. If the product is formed through the thiometallation of **1** (Scheme 1), it should also be obtained by the use of Hg(II) thiocarboxylate, since it is generally known that oxymercuration occurs more rapidly than oxythallation.[3]

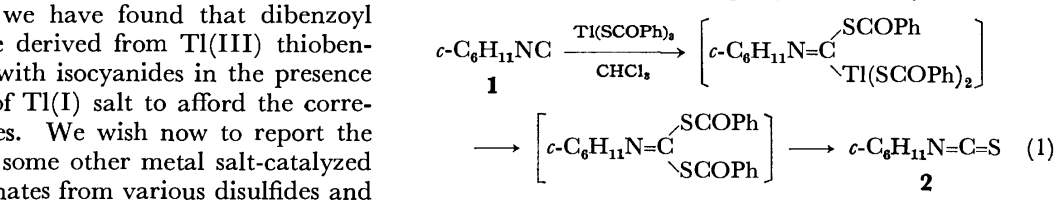

Furthermore, although the reaction with Tl(I) or Pb(II) thiobenzoate did not give **2**, that with Tl(I) thioacetate did afford it.[4] The formation of **2** with the Tl salt of a lower oxidation state can not also be explained by this scheme. Therefore, such a mechanism does not seem to be operative for the isothiocyanate formation. The possibility of the participation of elemental sulfur, which might be formed from the Tl salts in some way or other,[5] can nearly be excluded also, because separate experiments revealed that only a small amount of **2** was formed from **1** and solid sulfur in either the presence or absence of Tl(I) acetate under similar reaction conditions. The most likely route is the nucleophilic attack of **1** upon dibenzoyl or diacetyl disulfide, which can be formed by the thermal decomposition of the corresponding Tl(III)[4a] or Tl(I) thiocarboxylate (Schemes 2 and 3), since similar S–S bond scissions in alkyl, aryl, and acyl disulfides by various O-, S-, N-, P-, As-, and C-nucleophiles have been reported.[2,6,7] In fact, when **1** was treated with dibenzoyl disulfide in the presence of Tl(I) thiobenzoate, **2** was obtained in a good yield. On the other hand, the yield of **2** was quite low without the addition of the Tl(I) salt, suggesting that the electrophilic assistance of Tl(I) salt may be involved, as in the case of other Ag(I)-catalyzed reactions:[2]

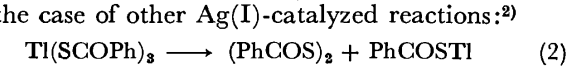

Reaction of Isocyanides with Various Disulfides in the Presence of Tl(I) Salts (Table 2). Since the Tl(I)-assisted interaction between **1** and dibenzoyl disulfide was proved, the scope and limitations of this reaction were examined by using various kinds of disulfides,

TABLE 1. THE REACTION OF **1** WITH METAL THIOCARBOXYLATES IN $CHCl_3$[a]

Metal Salt	**2**(%)[b]	Recovered **1**(%)[b]
$Tl(SCOPh)_3$	66	28
$Hg(SCOMe)_2$	0	86
TlSCOPh	0	100
TlSCOMe	28	63
$Pb(SCOPh)_2$	trace	100
S[c]	3	75
S[c]+TlOAc	8	81

a) **1** (1 mmol), Metal Salt (1 mmol), and $CHCl_3$ (10 ml) were used; at reflux for 3 h. b) By GLC. c) 10 mmol.

* To whom correspondence should be addressed.

Table 2. The reaction of isocyanides with disulfides in the presence of Tl(I) salts

RNC (1 mmol) R	R′SSR′ (1 mmol) R′	Tl(I)Z (1 mmol) Z	Solvent (10 ml)	Temp (°C)	Time (h)	Product (%)[a] RNCS	Product (%)[a] RNC recovered
c-C_6H_{11}	PhCO	—	$CHCl_3$	61	3	9	86
c-C_6H_{11}	PhCO	OCOMe	$CHCl_3$	61	3	96	0
c-C_6H_{11}	PhCO	OCOMe	$CHCl_3$	30	3	44	56
c-C_6H_{11}	PhCO	OCOMe	$CHCl_3$	61	0.5	82	13
c-C_6H_{11}	PhCO	OCOMe	$CHCl_3$[b]	61	0.5	85	trace
c-C_6H_{11}	PhCO	OCOMe	$CHCl_3$[c]	61	0.5	76	15
c-C_6H_{11}	PhCO	OCOMe[d]	$CHCl_3$	61	3	85	14
c-C_6H_{11}	PhCO	OCOMe	Toluene	85	3	94	trace
c-C_6H_{11}	PhCO	OCOMe	C_6H_{10}[e]	83	3	74	0
c-C_6H_{11}	PhCO	OCOMe	EtOH	78	3	83	0
c-C_6H_{11}	PhCO	OCOMe	Dioxane	84	3	81	trace
c-C_6H_{11}	PhCO	SPh	$CHCl_3$	61	3	41	59
c-C_6H_{11}	PhCO	SCOPh	$CHCl_3$	61	3	77	21
Ph	PhCO	OCOMe	$CHCl_3$	61	3	100	0
t-Bu	PhCO	OCOMe	$CHCl_3$	61	3	100	0
n-Bu	PhCO	OCOMe	$CHCl_3$	61	3	100	0
$EtO(CH_2)_4$	PhCO	OCOMe	$CHCl_3$	61	3	100	0
c-C_6H_{11}	Et_2NCS	OCOMe	$CHCl_3$	61	3	66	18
c-C_6H_{11}	MeCO	SCOMe	$CHCl_3$	61	3	48	6
c-C_6H_{11}	$PhCH_2$	OCOMe	$CHCl_3$	61	3	1	82
c-C_6H_{11}	Ph	OCOMe	$CHCl_3$	61	3	2	98
c-C_6H_{11}	*n*-Bu	OCOMe	$CHCl_3$	61	3	0	100

a) By GLC. b) *p*-Benzoquinone (0.5 mmol) was added. c) *t*-Butylcatechol (0.5 mmol) was added. d) TlOAc (0.1 mmol) was used. e) Cyclohexene.

isocyanides, Tl(I) salts, and solvents (Scheme 4). The following points are evident from the table: (i) Dibenzoyl, diacetyl, and tetraethylthiuram disulfides give good yields of isothiocyanates, while dialkyl and diaryl disulfides scarcely react at all. (ii) Tl(I) acetate is the most effective salt among the salts examined, and a catalytic amount of it is enough for the reaction. (iii) The reaction is applicable to both aliphatic and aromatic isocyanides. (iv) The yield of isothiocyanate does not vary significantly when the solvents are changed. (v) The reaction seems to proceed through an ionic pathway, since many radical scavengers exert no effect on the reaction.

$$\text{RNC} + \text{R'SSR'} \xrightarrow[\text{Solvent}]{\text{Tl(I)Z}} \text{RNCS} \qquad (4)$$

R = *c*-C_6H_{11}(**1**), Ph, *n*-Bu, *t*-Bu, $EtO(CH_2)_4$
R′= PhCO, MeCO, Et_2NCS, Ph, $PhCH_2$

Reaction of **1** *with Dibenzoyl Disulfide in the Presence of Various Kinds of Metal Salts (Table 3).* The catalytic effects of several metal salts other than Tl(I) were examined in the reaction of **1** with dibenzoyl disulfide under reflux for 3 h in chloroform. As can be seen from the table, the salts of soft metal ions (soft acid) are generally effective ($Tl^+ \geqslant Pb^{2+} > Cd^{2+} \geqslant Ag^+ \geqslant Cu^+ \geqslant Hg^+$) in the preparation of **2**, while those of hard ones are not at all effective. From the HSAB principle,[8] it can be deduced that the interaction of soft metal ions with either of the two S atoms of the disulfide (soft base) plays an important role in this reaction. Though considerable differences in catalytic activity between two salts of Cu(I) or Fe(II) (depending on the anion component) were observed, it appears to be difficult to offer a reasonable explanation.

Table 3. The reaction of **1** with dibenzoyl disulfide in the presence of various metal salts in $CHCl_3$[a]

Metal Salt	**2** (%)[b]	Recovered **1** (%)[b]
$Pb(OAc)_2 \cdot 3H_2O$	89	11
$Pb(OAc)_2 \cdot 3H_2O$[c]	61	25
$Cd(OAc)_2 \cdot 2H_2O$	75	6
$Cd(OAc)_2 \cdot 2H_2O$[c]	51	46
HgOAc	39	2
AgOAc	65	23
Cu_2O	66	29
CuCl	30	56
$Cu(OAc)_2 \cdot H_2O$	28	72
$Zn(OAc)_2 \cdot 2H_2O$	14	64
$FeSO_4 \cdot 7H_2O$	4	71
$Fe[CH_3CH(OH)CO_2]_2$	26	32
$Co(OAc)_2 \cdot 4H_2O$	30	26[d]
$Ni(OAc)_2 \cdot 4H_2O$	32	16[d]
$Cr(OAc)_3 \cdot H_2O$	2	87
$Mn(OAc)_2 \cdot 4H_2O$	5	59
KSCOMe	3	95

a) **1** (1 mmol), Metal Salt (1 mmol), and $CHCl_3$ (10 ml) were used; at reflux for 3 h. b) By GLC. c) 0.1 mmol. d) In these cases, some polymerized compounds were also formed.

Reaction Scheme. In order to clarify the reaction scheme, the following experiments were carried out in the presence of Tl(I) acetate as a catalyst. First, the

Table 4. The reaction of **1** with *p*-substituted dibenzoyl disulfides in the presence of TlOAc in $CHCl_3$[a]

R'SSR' (1 mmol)	Time (h)	**2** (%)[b]	Recovered **1** (%)[b]
R'=*p*-$NO_2C_6H_4CO$	0.25	87	13
C_6H_5CO	0.25	59	41
p-$MeOC_6H_4CO$	0.25	40	60
R'=*p*-$NO_2C_6H_4CO$	0.5	97	3
C_6H_5CO	0.5	82	13
p-$MeOC_6H_4CO$	0.5	63	37
R'=*p*-$NO_2C_6H_4CO$	3	100	0
C_6H_5CO	3	96	0
p-$MeOC_6H_4CO$	3	100	0

a) **1** (1 mmol), TlOAc (1 mmol), and $CHCl_3$ (10 ml) were used; at reflux. b) By GLC.

competitive reaction between **1** and phenyl isocyanide with dibenzoyl disulfide (1 mmol of each reactant) in chloroform at reflux for 3 h afforded **2** (60%) and phenyl isothiocyanate (40%), the unreacted **1** and phenyl isocyanide amounting to 19% and 38% respectively. Second, the yields of **2** in the reaction of **1** with representative 4,4'-disubstituted dibenzoyl disulfides were compared with that with a non-substituted one (Table 4). As a result, it was revealed that the reaction rate decreases in the following order: *p*-NO_2>H>*p*-MeO. Both results can be explained by assuming that a nucleophilic attack of isocyanide on one S atom of disulfide is an important step in this reaction.

By summarizing all the data described above, we propose Scheme 5 as a reaction scheme. The reaction may involve the initial complex formation between soft metal salt and one S atom of disulfide and the subsequent nucleophilic attack of isocyanide on the adjacent S atom. The latter step would be rate-determining. The removal of the benzoyl cation from the transient imidoyl cation affords isothiocyanate. The last step, namely, the combination of the benzoyl cation with the anion, was explained by the presence of PhCOSPh and PhCOOAc as products of the reactions using TlSPh and TlOAc respectively:

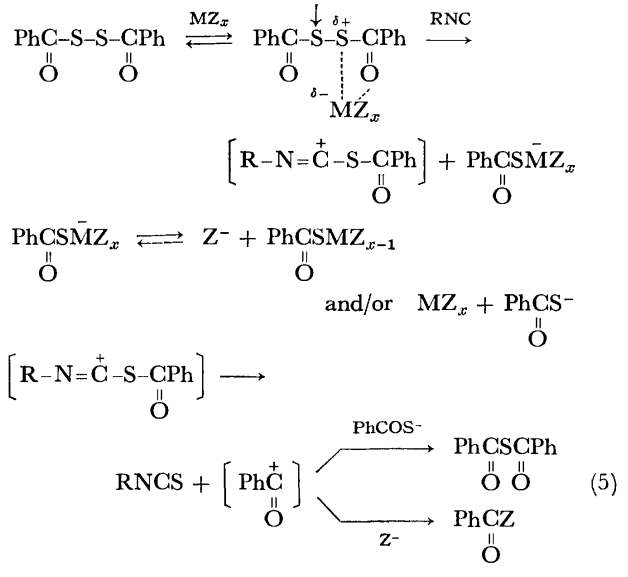

There may be another route involving the attack of the isocyanide-metal salt complex on disulfide, since isocyanides are known to form complexes with various metal salts.[9] It is obvious, however, that the nucleophilic reactivity of isocyanide decreases with complexation,[10] and so such a pathway would be less probable. It was observed in a separate experiment that, when the cyclohexyl isocyanide–CuCl complex prepared separately[9] was treated with dibenzoyl disulfide, **2** (21%) and free **1** (79%) were obtained under reflux for 3 h in chloroform. The result is comparable to that of the reaction catalyzed by CuCl; this suggests that no significant participation of the isocyanide-metal complex is present.

Experimental

The IR and NMR spectra were recorded with a Hitachi EPI-S2 and a Varian EM-360 apparatus respectively. The GLC analyses were carried out on a Shimadzu 4BMPF apparatus, using EGSS-X(30%)-Chromosorb-W(1 m)column (N_2 as the carrier gas).

Materials. Most of the isocyanides (RNC: R=*c*-C_6H_{11}, *n*-Bu, *t*-Bu, Ph) were prepared by the dehydration of *N*-substituted formamides with $POCl_3$,[11] while 4-ethoxybutyl isocyanide[R=$EtO(CH_2)_4$] was prepared by the reaction of the corresponding bromide with AgCN at 75—80 °C for 24 h; bp 89—94 °C/30 mmHg. The cyclohexyl, butyl, *t*-butyl, and 4-ethoxybutyl isothiocyanates (prepared previously in our laboratory[12]) and commercial phenyl isothiocyanate were used as authentic samples for GLC analyses. Some disulfides (R'SSR': R'=MeCO,[4a] PhCO,[4a] Ph,[4a] $PhCH_2$,[4a] *p*-MeO-, and *p*-$NO_2C_6H_4CO$[13]) were prepared by the oxidation of the corresponding thiols or thiocarboxylic acids, while those of R'=*n*-Bu and Et_2NCS were commercial products. Metal salts such as $Tl(SCOPh)_3$,[4a] TlSCOPh,[4a] TlSCOMe,[4a] TlSPh,[4a] and $Pb(SCOPh)_2$[4b] were prepared by the respective reported methods. The $Hg(SCOMe)_2$[mp 140 °C (d)] was prepared by the reaction of yellow HgO with thioacetic acid in chloroform at 5—10 °C for 1 h and then recrystallized from chloroform. The radical scavengers and other metal salts were commercial products and were used without further purification. The organic solvents were purified by distillation before use.

Reaction of 1 with Tl(SCOPh)$_3$. To a stirred suspension of $Tl(SCOPh)_3$(0.62 g, 1 mmol) in chloroform(8 ml) we added **1** (0.11 g, 1 mmol) in chloroform(2 ml) at 55 °C; the resulting mixture was stirred for 3 h under reflux. After being cooled, the solid was filtered off and the filtrate was washed with water, dried over Na_2SO_4, and analyzed by GLC, using iodobenzene as the internal standard. Analysis revealed the presence of 0.66 mmol(66% yield; based on Tl salt) of **2** and 0.28 mmol of unreacted **1**.

From the reaction using **1** (20 mmol), $Tl(SCOPh)_3$ (10 mmol), and chloform(20 ml), **2** was isolated by distillation (1.20 g; bp 72 °C/7 mmHg, $\nu_{N=C=S}$ 2120 cm^{-1}); it was identical with an authentic sample in GLC, NMR, and IR. In addition, 2.4 g of benzoic acid was isolated by the column chromatography of the residue after distillation (Wakogel C-100; diethyl ether as the eluent). No $(PhCO)_2S$ or PhCOSH was obtained by this procedure. These substances may be hydrolyzed to benzoic acid by these treatment.

Reaction of 1 with Dibenzoyl Disulfide in the Presence of TlOAc. To a stirred suspension of TlOAc (0.263 g, 1 mmol) in chloroform (5 ml) we added slowly a mixture of **1** (0.109 g, 1 mmol) and dibenzoyl disulfide (0.274 g, 1 mmol) in chloro-

form (5 ml) at room temperature, after which the resulting mixture was stirred for 3 h under reflux. After being cooled, the solid was filtered off and the filtrate was washed with water and dried over Na_2SO_4. Its GLC analysis reveled the presence of 0.96 mmol (96% yield; based on Tl salt) of **2**. The presence of PhCOOAc was confirmed by the IR of the residue after the evaporation of the solvent from the filtrate.

Competitive Reaction between 1 and Phenyl Isocyanide. A mixture of **1** (0.109 g, 1 mmol), phenyl isocyanide (0.103 g, 1 mmol), and dibenzoyl disulfide (0.274 g, 1 mmol) was stirred for 3 h under reflux in the presence of TlOAc (0.263 g, 1 mmol) in chloroform (10 ml). After treatment as described above, the GLC analysis of the filtrate revealed the presence of 0.60 mmol of **2** (60%), 0.40 mmol of phenyl isothiocyanate (40%), **1** (0.19 mmol, 19%), and phenyl isocyanide (0.38 mmol, 38%).

Reaction of 1 with Dibenzoyl Disulfide in the Presence of TlSPh. A mixture of **1** (1.09 g, 10 mmol), dibenzoyl disulfide (2.74 g, 10 mmol), and TlSPh (3.13 g, 10 mmol) in chloroform (10 ml) was stirred for 3 h under reflux and then treated as above. The GLC analysis of the filtrate revealed the presence of **2** (4.26 mmol, 43%), **1** (5.60 mmol, 56%), diphenyl disulfide (3.84 mmol, 38%), and PhCOSPh (2.37 mmol, 24%). The last two compounds were separated by column chromatography (Wakogel C-100; benzene–ethyl acetate as the eluent), the retention time of GLC, the melting point, and IR spectrum being found identical with those of an authentic sample for each compound.

Reaction of Cyclohexyl Isocyanide-Copper(I) Chloride Complex with Dibenzoyl Disulfide. To a chloroform (10 ml, freed from ethanol) solution of the **1**–CuCl complex[9] (0.208 g, 1 mmol) we added dibenzoyl disulfide (0.274 g, 1 mmol) at room temperature, and the resulting mixture was stirred for 3 h under reflux. After being cooled, the precipitated solid was filtered off. The GLC analysis of the filtrate revealed the presence of 0.21 mmol of **2** (21% yield; based on the complex) and 0.79 mmol of **1** (79%).

References

1) a) F. Kienzle, *Tetrahedron Lett.*, **1972**, 1771; b) H. Sawai and T. Takizawa, *ibid.*, **1972**, 4263; c) S. Tanaka, H. Kido, S. Uemura, and M. Okano, *Bull. Chem. Soc. Jpn.*, **48**, 3415 (1975).

2) a) M. D. Bentley, I. B. Douglass, J. A. Lacadie, D. C. Weaver, F. A. Davis, and S. J. Eitelman, *Chem. Commun.*, **1971**, 1625; b) M. D. Bentley, I. B. Douglass, and J. A. Lacadie, *J. Org. Chem.*, **37**, 333 (1972).

3) See, for example, J. E. Byrd and J. Halpern, *J. Am. Chem. Soc.*, **95**, 2586 (1973).

4) The Tl(III) thioacetate was unstable and rapidly decomposed to the Tl(I) one.[4a] Pb(IV) thiocarboxylates could not be prepared because of their strong oxidizing ability, and so only Pb(II) salts were formed as has previously been reported.[4b] a) S. Uemura, S. Tanaka, and M. Okano, *Bull. Chem. Soc. Jpn.*, **50**, 220 (1977); b) T. Mukaiyama and T. Endo, *Bull. Chem. Soc. Jpn.*, **40**, 2388 (1967).

5) W. Weith, *Ber.*, **6**, 210 (1873).

6) a) A. J. Parker and N. Kharasch, *Chem. Rev.*, **59**, 583 (1959); b) M. Busch and A. Stern, *Ber.*, **29**, 2148 (1896); c) A. Schönberg, *ibid.*, **68**, 163 (1935); d) M. Kodomari, and T. Sodeyama, and K. Itabashi, *Yuki Gosei Kagaku Kyokai Shi*, **31**, 416 (1973).

7) J. L. Kice, *Acc. Chem. Res.*, **1**, 58 (1968).

8) R. G. Pearson, *Chem. Brit.*, **3**, 103 (1967).

9) See, for example, T. Saegusa and Y. Ito, S. Kobayashi, K. Hirota, and H. Yoshioka, *Bull. Chem. Soc. Jpn.*, **42**, 3310 (1969).

10) See, for example, T. Saegusa and Y. Ito, "Isonitrile Chemistry," ed by I. Ugi, Academic Press, New York, N. Y. (1971), p. 223.

11) I. Ugi and R. Meyr, *Chem. Ber.*, **93**, 239 (1960).

12) N. Watanabe, S. Uemura, and M. Okano, *Bull. Chem. Soc. Jpn.*, **48**, 3205 (1975).

13) K. Tsuda and T. Otsu, *Bull. Chem. Soc. Jpn.*, **39**, 2206 (1966).

Carbon-13 NMR Spectra of 4-Chromanone, 4*H*-1-Benzothiopyran-4-one, 4*H*-1-Benzothiopyran-4-one 1,1-Dioxide, and Their Substituted Homologs

Yasuhisa SENDA, Akira KASAHARA,* Taeko IZUMI,* and Toru TAKEDA*

Department of Applied Science, Faculty of Engineering, Tohoku University, Aoba, Sendai 980
**Department of Applied Chemistry, Faculty of Engineering, Yamagata University, Yonezawa 992*

(Received March 25, 1977)

The ^{13}C NMR spectra of 4-chromanone, 4*H*-1-benzothiopyran-4-one, 4*H*-1-benzothiopyran-4-one 1,1-dioxide, and their methyl and phenyl substituted homologs were examined. The salient effect depending on the kinds of the hetero atoms or the group at the 1-position has been observed on the chemical shifts, especially for C-2, C-3, C-8, C-4a, and C-8a.

^{13}C NMR spectroscopy has been used extensively to elucidate the structures of complex molecules. Although ^{13}C NMR studies of several flavones were performed in connection with the structural elucidation of naturally occuring flavonoid compounds,[1] its applications to this field have so far been limited.[2] We wish to report here a study of the ^{13}C NMR spectra of 4-chromanone (**2**), 4*H*-1-benzothiopyran-4-one (**7**), 4*H*-1-benzothiopyran-4-one 1,1-dioxide (**12**), and their methyl and phenyl substituted homologs, undertaken with the object of providing background data for use in future structural studies of the heterocyclic compounds.

Natural-abundance 25.15 MHz ^{13}C FT-NMR spectra in $CDCl_3$ were obtained using the ^1H noise-decoupling technique. The signals were assigned by comparing the signal shifts due to differences in structures between closely related compounds and by the use of the ^1H off-resonance decoupling technique. A shift reagent, $Yb(dpm)_3$ was used to aid the assignments of the resonances to specific carbon atoms.[3] The chemical shifts, δ, thus obtained are listed in Table 1, in which the carbon numbering relates, for purposes of comparison, to the equivalent carbon in the flavanone series (Fig. 1).

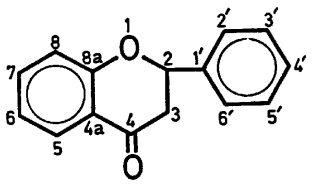

Fig. 1.

Results and Discussion

The resonance of the carbonyl carbon of 1-tetralone (**1**) occurs at δ 197.90. Upon the replacement of the 1-methylene group (the numbering system follows that of **2**) with a hetero atom, the carbonyl carbon signals moved upfield; that of **12** appears at the highest field among the simplest members of each series of compounds, **1**, **2**, **7**, and **12**. Analogous trends were observed in the ^{13}C NMR spectra of cyclohexanone and 1-hetera-4-cyclohexanones.[4] The substituent parameters of a sulfur and an oxygen atom, and a sulfonyl group in simple 1-hetera-4-cyclohexanones are negative (upfield shift) for a γ-carbon. The chemical shifts of C-2 and C-3 of **1**, **2**, **7**, and **12** also exhibited trends similar to those observed in the series of 1-hetera-4-cyclohexanones. The chemical shifts of C-2 are described in the order of the electron-withdrawing abilities of the atoms or the group at the 1-position. The C-3 resonances of **2** and **7** occur at a field lower, while that of **12** appear at one higher than that of **1**. The effect of the sulfonyl group in the C-3 chemical shift indicated a negative value, the reverse of those of the oxygen and the sulfur atom. This may be due to the steric γ-gauche interaction of C-3 with one of the oxygen atoms of the sulfonyl group, which takes an axial-like orientation.[4] The carbonyl chemical shifts of the 2-substituted compounds are similar to those of the corresponding parent compounds. On the other hand, the carbonyl signal of 3-methyl-4-chromanone (**4**) moved downfield by about 3 ppm.

On the addition of $Yb(dpm)_3$ to the solution examined, the carbonyl signal was moved downfield. The magnitude of the lanthanoid-induced shifts (LIS) of **12** and 1-thioflavanone 1,1-dioxide (**15**) were much smaller than those of **2**, flavanone (**5**), **7**, and 1-thioflavanone (**10**). Ytterbium ions may coordinate to the oxygen atoms of the sulfonyl group as well as to the carbonyl oxygen atom.

The signal of the methyl group at the 3-position resonates at an apparently high field (δ 10.55). This indicates that the through-bond interaction of the oxygen atom at the γ-position participates significantly, because the arrangement of the oxygen atom and the methyl carbon is anti-periplanar.[5] However, when a sulfur atom is introduced at the 1-position, the methyl signal appears at δ 13.8; the electronic γ-effect of a sulfur atom, the third-row hetero atom, is negligible.[5] The methyl resonance of 2-methyl-4*H*-1-benzothiopyran-4-one 1,1-dioxide (**13**) occurs at a field slightly higher than that of 2-methyl-4*H*-1-benzothiopyran-4-one (**8**) because of the steric γ-gauche interaction of the oxygen atoms of the sulfonyl group.

The resonances of substituted aromatic carbons are easily distinguished from those of other aromatic carbons by the off-resonance decoupling technique. Since the substituent parameters of the carbonyl group on both α- and β-carbons are positive, the former smaller than the latter, the signals at δ 144.39 and 132.56 of **1** can be ascribed to C-4a and C-8a respectively. The

TABLE 1. CARBON-13 NMR CHEMICAL SHIFTS OF 4-CHROMANONES, 4*H*-1-BENZOTHIOPYRAN-4-ONES AND 4*H*-1-BENZOTHIOPYRAN-4-ONE 1,1-DIOXIDE

No.	Compound	C-1	C-2	C-3	C-4	C-5	C-6	C-7	C-8
1	1-Tetralone	29.60	23.29	39.07	197.90	128.74	126.49	133.29	126.98
2	4-Chromanone Parent		66.92	37.61	191.47	126.96	121.19	135.75	117.76
	ΔYb[a]		2.79	5.83	13.05	4.08	1.79	1.48	1.76
3	2-Methyl-		74.20	44.47	191.96	126.86	121.09	135.78	117.82
4	3-Methyl-		72.25	40.77	194.20	127.32	121.25	135.44	117.70
5	2-Phenyl-(flavanone)		79.47	44.53	191.66	126.93	121.47	136.01	118.00
	ΔYb		2.43	5.52	12.86	3.99	1.75	1.34	1.58
6	3-Phenyl-(isoflavanone)		71.40	52.23	191.90	128.56	121.52	135.93	117.82
7	4*H*-1-Benzothiopyran-4-one Parent		26.45	39.37	193.54	128.98	124.80	133.05	127.40
	ΔYb		2.48	5.52	12.31	4.07	1.69	1.33	1.52
8	2-Methyl-		36.34	47.68	193.78	128.74	124.67	133.11	127.28
9	3-Methyl-		32.94	42.04	196.14	129.35	124.67	132.80	127.16
10	2-Phenyl-(1-thioflavanone)		45.32	46.53	194.02	129.04	125.04	133.47	127.10
	ΔYb		2.30	5.10	11.77	3.82	1.64	1.39	1.40
11	3-Phenyl-(1-thioisoflavanone)		32.51	53.63	193.66	129.59	124.80	132.99	127.22
12	4*H*-1-Benzothiopyran-4-one 1,1-dioxide Parent		49.44	36.82	190.08	128.74	(133.23)[b]	(134.81)	123.64
	ΔYb		1.50	1.83	4.00	1.27	(0.60)	(0.60)	0.73
13	2-Methyl-		54.66	44.28	190.26	128.44	(133.17)	(134.87)	124.19
14	3-Methyl-		55.51	41.37	193.23	128.68	(133.17)	(134.62)	123.34
15	2-Phenyl-(1-thioflavanone 1,1-dioxide)		63.76	42.95	190.81	129.76	(133.19)	(134.90)	124.19
	ΔYb		1.70	2.43	4.85	1.32	(0.66)	(0.54)	0.73
16	3-Phenyl-(1-thioisoflavanone 1,1-dioxide)		55.57	52.90	191.71	129.46	(133.64)	(134.98)	123.76

No.	Compound	C-4a	C-8a	Me	C-1′	C-2′,6′	C-3′,5′	C-4′
1	1-Tetralone	132.56	144.39					
2	4-Chromanone Parent	121.27	161.73					
	ΔYb	5.71	3.11					
3	2-Methyl-	120.79	161.62	20.93				
4	3-Methyl-	120.74	161.81	10.55				
5	2-Phenyl-(flavanone)	120.87	161.43		138.71	126.07	128.71	128.61
	ΔYb	5.62	2.80		1.19	0.61	0.27	0.25
6	3-Phenyl-(isoflavanone)	121.06	161.56		135.07	127.68	128.80	128.56
7	4*H*-1-Benzothiopyran-4-one Parent	130.74	142.03					
	ΔYb	5.34	2.67					
8	2-Methyl-	130.44	141.60	20.32				
9	3-Methyl-	130.38	141.72	14.86				
10	2-Phenyl-(1-thioflavanone)	130.27	141.95		138.27	127.34	128.86	128.31
	ΔYb	5.02	1.33		1.15	0.55	0.24	0.19
11	3-Phenyl-(1-thioisoflavanone)	131.11	141.66		137.96	128.31	128.44	127.22
12	4*H*-1-Benzothiopyran-4-one 1,1-dioxide Parent	130.50	141.72					
	ΔYb	1.75	1.33					
13	2-Methyl-	130.80	141.06	11.70				
14	3-Methyl-	129.89	141.78	16.56				
15	2-Phenyl-(1-thioflavanone 1,1-dioxide)	130.34	141.29		127.95	128.94	129.76	128.51
	ΔYb	2.37	1.70		0.93	0.31	0.12	0.05
16	3-Phenyl-(1-thioisoflavanone 1,1-dioxide)	130.57	142.18		136.06	128.86	129.29	128.51

a) $Yb(dpm)_3$-induced shift (downfield shift), see experimental section. b) The values in parentheses may be interchanged.

magnitude of the LIS values also supports these signal assignments; the LIS value for the C-4a signal is larger than that for C-8a. Taking into account the substituent parameters of a methyl and an acetyl group on a benzene ring, the resonance of C-7, which is placed at the position *para* to the acetyl group, appears at a field lower than that of C-6, which is in the *meta* position in the chromanone system. The chemical shifts of all the aromatic carbons except C-4a and C-8a are supposed to be in the order of: C-7>C-5>C-6>C-8. The resonances of these carbons demonstrate that the more remote from the carbonyl carbon, the smaller were the LIS usually observed in this system.

For **7**, the resonances of C-4a and C-8a were easily distinguished from those of other aromatic carbons as in the case of the chromanone system. The ^{13}C NMR spectrum of thiophenol indicates that the mesomeric effect of the sulfur atom is smaller on the aromatic ring than that of the oxygen atom: substituted-C, δ 130.80; *o*- or *m*-C, δ 129.28 or 128.92; *p*-C, δ 125.40.[6]

Unlike the case of phenol, the resonance of the *para*-related carbon appeared at a field higher than that of the *ortho*-related carbons. The C-4a signal moved downfield by about 10 ppm, and that for C-8a, upfield by about 20 ppm, compared to those of the corresponding carbons of chromanone. This may be a result of the smaller mesomeric effect of the sulfur atom than that of the oxygen atom. Other aromatic carbon signals are tentatively assigned in taking of the effect of the sulfur atom on the aromatic carbons which appeared in the ^{13}C NMR spectrum of thiophenol. These assignments are supported by their LIS values, much as in the case of the chromanone system.

Since the sulfur atom of the sulfonyl group has no lone-pair electrons, and since this group polarizes as $O\diagdown\!\!\!\!\diagup O^-$ (S), this group may act as an electron-attracting group, such as a nitro group. Since the ^{13}C chemical shifts of nitrobenzene are in this order: substituted> *para*->*meta*->*ortho*-related carbons, the resonances at 123—124 and 128—129 are assigned to C-8 and C-5 respectively. The LIS values for these carbons observed in **12** and **15** support these signal assignments. The LIS values suggest that the signals at δ 133.19 and δ 134.90 for **15** correspond to C-6 and C-7 respectively, because carbons which are more remote from the carbonyl group experience smaller shift reagent effects in this system.

Since the resonances of substituted carbons of monoalkylbenzenes are known to occur around δ 140—150, the resonances around δ 140 must correspond to C-1′ in the flavanone system. The resonance of C-1′ of **15** occurs at a field higher than those of other phenyl-substituted compounds. This may be due to the steric γ-gauche interaction with the oxygen atoms of the sulfonyl group, such as the methyl carbon of **13**. When we compare the chemical shifts of alkylbenzenes, the signals of C-2′ and C-6′ or C-3′ and C-5′ may be expected to appear at the same position of the magnetic field, the former carbon atoms appearing at a field slightly higher than those of the latter two.

Experimental

NMR Spectra. The ^{13}C FT-NMR spectra were obtained at 25.15 MHz with a JEOL JNM-MH-100 instrument equipped with a JNM-MFT-100 Fourier transform accessory; the instrument was controlled with a JEC-6 spectrum computer. Samples were observed in 5-mm spinning tubes at 20 $\pm$5% solution in $CDCl_3$ at 28 °C. The solvent provided the internal lock signal. The measurement conditions were as follows: pulse width, 27.5 μs (*ca.* 45°); repetition time, 4 s; spectral width, 6250 Hz; data point, 8192; acquisition time, 0.65 s. All the chemical shifts are expressed in δ (ppm downfield from internal Me_4Si). Each observed chemical shift is estimated to be accurate to δ $\pm$0.06. The LIS values were obtained as follows: each compound (1 mmol) was dissolved in $CDCl_3$ (0.2 ml), and then Yb(dpm)$_3$ (0.15 mmol) was added to the solution, $\Delta Yb = \delta_{Yb} - \delta$.

Materials. The compounds employed in this study have all been previously prepared except **14**: **1**,[7] (bp 82 °C/0.3 mmHg); **2**,[8] (mp 38 °C); **3**,[9] (mp 32 °C); **4**,[10] (bp 125—128 °C/11 mmHg); **5**,[11] (mp 76 °C); **6**,[12] (mp 76—77 °C); **7**,[13] (mp 29—30 °C); **8**,[14] (bp 146—147 °C/9 mmHg); **9**,[14] (bp 188—190 °C/12 mmHg); **10**,[15] (mp 55—56 °C); **11**,[16] (bp 170—176 °C/0.5 mmHg); **12**,[17] (mp 131—132 °C); **13**,[18] (mp 138—139 °C); **15**,[18] (mp 133—134 °C); **16**,[16] (mp 151—152 °C). Compound **14** was prepared as follows: 3-methyl-4*H*-1-benzothiopyran-4-one (1 g) in AcOH (10 ml) was treated with H_2O_2 (30%, 2 ml), and then the solution was allowed to stand for 2 days. The product was precipitated by the addition of water. Crystallization from ethanol afforded **14** as colorless prisms; mp 143—145 °C.

References

1) A. Pelter, R. S. Ward, and T. Ian Gray, *J. Chem. Soc. Perkin Trans. 1*, **1976**, 2475, and the references cited therein.
2) F. W. Wehrli, *J. Chem. Soc., Chem. Commun.*, **1975**, 664; H. Wagner, V. M. Chari, and J. Sonnenbichler, *Tetrahedron Lett.*, **1976**, 1799; K. R. Markham and B. Ternai, *Tetrahedron*, **32**, 2607 (1976).
3) R. E. Sievers, "Nuclear Magnetic Resonance Shift Reagents," Academic Press, New York (1973).
4) J. A. Hirsch and E. Havinga, *J. Org. Chem.*, **41**, 455 (1976).
5) E. L. Eliel, W. F. Bailey, L. D. Kopp, R. L. Willer, D. M. Grant, R. Bertrand, K. A. Christensen, D. K. Dalling, M. W. Duch, E. Wenkert, F. M. Scheli, and D. W. Cookran, *J. Am. Chem. Soc.*, **97**, 322 (1975).
6) L. F. Johnson and W. C. Jankowski, "Carbon-13 NMR Spectra," Wiley-Interscience, New York (1972), p. 164.
7) *Org. Synth.*, **35**, 95 (1955).
8) F. Arndt and G. Kallner, *Ber.*, **57**, 202 (1924).
9) G. W. K. Cavill, F. M. Dean, A. McGookin, B. M. Marshall, and A. Robertson, *J. Chem. Soc.*, **1954**, 4573.
10) J. Colonge and A. Guyot, *Bull. Soc. Chim. Fr.*, **1958**, 325.
11) St. V. Kostaneki and W. Szabranski, *Ber.*, **37**, 2634 (1904).
12) N. Inoue, *Nippon Kagaku Zasshi*, **79**, 112 (1958).
13) F. Krollpfeeffer and H. Scheeltze,*Ber.*, **56**, 1819 (1923).
14) J. C. Petropoulos, M. A. McCall, and D. S. Tarbell, *J. Am. Chem. Soc.*, **75**, 1130 (1953).
15) F. Arndt, *Ber.*, **56**, 1269 (1923)
16) G. F. Katebar and R. M. Thomson, *Aust. J. Chem.*, **25**, 647 (1972).
17) F. Arndt, *Ber.*, **58**, 1612 (1925).
18) T. Nambara, Y. Takemori, and S. Okamoto, *Yakugaku Zasshi*, **81**, 1 (1961).

NOTES

BULLETIN OF THE CHEMICAL SOCIETY OF JAPAN, VOL. 50 (10), 2792 (1977)

The Studies of the Activated Compound. III.[1] A Synthesis of Muscalure: (*Z*)-9-Tricosene

Kyo ABE, Tomio YAMASAKI, Nobuo NAKAMURA, and Takeo SAKAN

Department of Chemistry, Faculty of Science, Osaka City University, Sugimotocho, Sumiyoshi-ku, Osaka 558

(Received May 16, 1977)

Synopsis. A synthesis of muscalure, (*Z*)-9-tricosene, was carried out as an application of metal-induced acylation.

Muscalure, (*Z*)-9-tricosene (**3**), is a sex-attractant pheromone for the female house fly (*Musca domestica L.*). Its synthesis has been accomplished by two groups.[2,3] We ourselves also previously carried out the synthesis of the muscalure as an application of metal-induced acylation.[4,5]

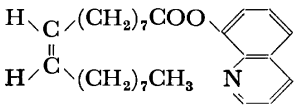

(**1**)

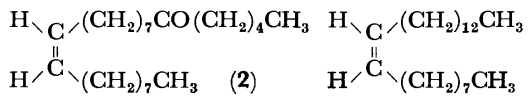

(**2**) (**3**)

The activated starting material, 8-oleoyloxyquinoline (**1**), was prepared from oleoyl chloride and 8-quinolinol in a good yield by the Schotten-Baumann method. A solution of 8-oleoyloxyquinoline (**1**) in dichloromethane was treated with an ethereal solution of pentylmagnesium bromide at −90 °C to give (*Z*)-14-tricosen-6-one (**2**) as the sole product in a 75% yield. The enone (**2**) was reduced by means of Hung-Minlon's procedure to afford muscalure, (*Z*)-9-tricosene (**3**), in an 84% yield. It was found to be identical to an authentic sample by a study of its IR and NMR.[2] An advantage of this route to muscalure (**3**) is in the preparation of the enone (**2**).

Experimental

Synthesis of 8-Oleoyloxyquinoline (1). To a stirred suspension of 8-quinolinol (2.390 g; 0.02 mol) and powdered sodium hydroxide (0.96 g; 0.02 mol) in tetrahydrofuran (20 ml), we added, drop by drop, a solution of oleoyl chloride (6.020 g; 0.02 mol) in tetrahydrofuran (20 ml) at 0 °C over a period of 15 min under an argon atmosphere. The reaction mixture was then kept at 0 °C for 1 h, allowed to stand at room temperature overnight, poured into ice-cooled water, and extracted with ether (30 ml×3). The extracted organic layer was washed with a 1% aqueous solution of sodium hydroxide (20 ml×2) and saturated brine (10 ml), and dried over sodium sulfate. The removal of the solvent from the organic layer gave a crude product (**1**) (7.20 g; 88% yield), which could be used for the next step without any purification. IR (neat): 1770, 1140, 1120 cm^{-1}. NMR (CCl_4): δ 0.83 (3H, t, J=5 Hz), 1.00—1.60 (broad peak centered at 1.26, 22H), 1.60—2.00 (broad peak centered at 1.94, 4H), 2.26 (2H, t, J=7 Hz), 5.18 (2H, m), 7.00—7.60 (4H, m), 7.90 (1H, dd, J=4, 2 Hz).

Synthesis of (Z)-14-Tricosen-6-one (2). An ethereal solution of pentylmagnesium bromide, generated from magnesium turnings (0.178 g; 7.33 mg atom) and pentyl bromide (1.24 g; 7.33 mmol), and a catalytic amount of iodine in dried ether, was added at −90 °C to a solution of 8-oleoyloxyquinoline (**1**) (2.00 g; 4.9 mmol) in dichloromethane (8 ml) under an argon atmosphere. The reaction mixture was then allowed to warm up to room temperature and left to stand overnight. The yellow precipitate in the reaction mixture was then filtered off and the filtrate was washed with a 1 M aqueous hydrochloric acid solution and with saturated brine, and dried over sodium sulfate. By evaporating the solvent, 1.23 g of the residue was obtained. It was purified by preparative TLC (SiO_2, developed with $CHCl_3$) to give the pure enone (**2**). IR (neat): 3015, 2925, 2850, 1715, 1460, 1380, 725 cm^{-1}. NMR (CCl_4): δ 0.88 (6H, t, J=5 Hz), 0.96—1.60 (28H, broad peak), 1.92 (4H, m), 2.23 (4H, t, J=7 Hz), 5.16 (2H, m). Found: C, 81.71; H, 12.83%. Calcd for $C_{23}H_{44}O$: C, 82.07; H, 13.18%. MS *m/e* 336 (M^+).

Synthesis of (Z)-9-Tricosene (3). A mixture of (*Z*)-14-tricosen-6-one (**2**) (127 mg; 1.14 mmol), 80% hydrazine hydrate (71 mg; 1.14 mmol), and potassium hydroxide (76 mg; 1.14 mmol) in 0.8 ml of diethylene glycol was heated at 140 °C for 1.5 h and then at 190 °C for an addition 4 h. After cooling to room temperature, the reaction mixture was diluted with ice water, neutralized with a 6 M hydrochloric acid solution, and then extracted with pentane (10 ml) several times. The extracted organic layer was washed with saturated brine and dried over sodium sulfate. The removal of the solvent from the organic layer gave a crude product. It was purified by means of column chromatography (SiO_2, eluted with hexane) to give (*Z*)-9-tricosene (**3**) (112 mg; 84% yield). Its IR and NMR spectra were both identical with the spectra of an authentic sample. IR (neat): 3015, 2930, 2855, 1460, 725 cm^{-1}. Found: C, 85.60; H, 13.88%. Calcd for $C_{23}H_{46}$: C, 85.63; H, 14.37%. NMR (CCl_4): δ 0.60—1.60 (40H, m), 1.90 (4H, m), 5.16 (2H, t, J=4 Hz). MS *m/e* 322 (M^+).

The authors wish to thank Dr. Gordon W. Gribble and Dr. Robert L. Cargill for sending charts of the IR and NMR spectra of muscalure.

References

1) Part II of this series: K. Abe, T. Sato, N. Nakamura, and T. Sakan, *Chem. Lett.*, **1977**, 817.

2) R. L. Cargill and M. G. Rosenblum, *J. Org. Chem.*, **37**, 3971 (1972).

3) D. A. Carlson, M. S. Mayer, D. L. Silhacek, J. D. James, M. Beroza, and B. A. Bierl, *Science*, **174**, 76 (1971).

4) T. Sakan and Y. Mori, *Chem. Lett.*, **1972**, 793.

5) T. Sakan, Y. Mori, and T. Yamasaki, *Chem. Lett.*, **1973**, 713.

BULLETIN OF THE CHEMICAL SOCIETY OF JAPAN, VOL. 50 (10), 2793—2794 (1977)

Micelle Formation of Purified Dinonylnaphthalenesulfonates in Benzene

Kiyoshi INOUE, Yoshiharu NOSE, and Harumichi WATANABE

Central Technical Research Laboratory, Nippon Oil Co., Ltd., Chidori-cho, Naka-ku, Yokohama 231

(Received January 27, 1977)

Synopsis. The removal of trace amounts of unsulfonated dinonylnaphthalene contained in sulfonates by rubber membrane dialysis in pentane increased the apparent aggregation number of the micelles of dinonylnaphthalenesulfonate measured using vapor-pressure osmometry. The interaction between the cation and sulfonate ion was a factor affecting the aggregation, in addition to the steric factor of the hydrocarbon group and the solute-solvent interaction.

The micelle formation of metal salts of dinonylnaphthalenesulfonic acid (DNNS) in nonpolar solvents has been extensively studied using many methods, such as fluorescence depolarization,[1,2] viscometry,[3] ultracentrifuge separation,[4] and vapor-pressure osmometry.[5] It has been considered that the micelle formation of DNNS in nonpolar solvents is mainly due to the strong interaction between polar groups.[6] Furthermore, considerations of the steric or geometric factor and the solute-solvent interaction are also important. Kaufman and Singleterry[2] have studied the effect of cations on the micelle formation and the apparent molar volume of DNNS anions in benzene. However, the effect of the cation on the aggregation number for DNNS salts, which is a direct measure of the strength of the interaction between polar groups, has not been determined. In the present paper, the effect of the cation on the aggregation number for DNNS salts is reported and the importance of purification of the DNNS salts for vapor-pressure osmometry are also discussed.

Experimental

Alkali and alkaline-earth metal salts of DNNS were synthesized as described previously.[7] Metal salts of DNNS were further purified by rubber-membrane dialysis[8] for 72 h in pentane. This purification period was found to be sufficient to gain the limiting value of the aggregation number. The final product was freed from the solvent by evacuation at 70 °C for 24 h. The benzene used as the solvent for the vapor-pressure osmometric measurements was passed through activated alumina in order to remove water and polar contaminants. The water content in the benzene was determined using the Fischer titration method and was found to be less than 0.01%. The vapor-pressure osmometric measurements were carried out with a Mechrolab Model 301A vapor-pressure osmometer at 38 °C.

Results and Discussion

The relation of the apparent aggregation number for DNNS sodium salt (NaDNNS) and its concentration in benzene are shown in Fig. 1. The apparent aggregation number for NaDNNS was increased by the removal of the trace amount of unsulfonated dinonylnaphthalene contained in the NaDNNS using rubber-membrane dialysis in pentane. Although vapor-pressure osmometry is the most advantageous and accurate technique for investigating the aggregation of a surfactant in a nonpolar and volatile solvent, the result is strongly affected by the presence of trace amounts of low molecular-weight impurities. In addition to the effect mentioned above, the residual impurity in a surfactant which is similar to the surfactant in shape and structure should affect the state of aggregation by solubilization or the formation of co-micelle. To avoid this problem, purification by rubber-membrane dialysis is available for determining the micelle formation of high molecular-weight detergents, such as oil-soluble sulfonates.

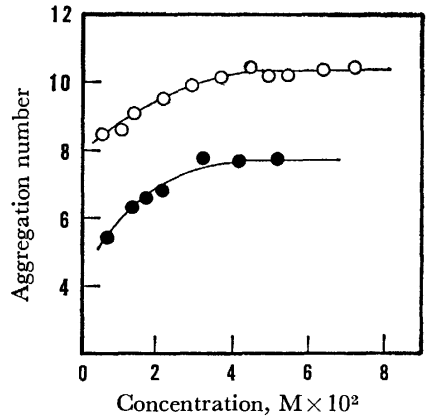

Fig. 1. Effect of purification of sodium dinonylnaphthalenesulfonate by rubber membrane dialysis on the aggregation number in benzene at 38 °C.
(—●— Before dialysis, —○— after dialysis).

Little and Singleterry[5] have studied the micelle formation of DNNS salts in various nonpolar solvents using vapor-pressure osmometry and have reported that the micelle aggregation number in benzene is 7 for Li and Na salts, and 6 for Cs salt. From the consideration that the aggregation of an ionic surfactant in a nonpolar solvent is mainly due to the interaction between the gegenion and the surfactant ion in the micellar cores, it is difficult to understand that the cations have little effect on the micelle aggregation number. Therefore, the present authors reexamined the micelle formation of DNNS salts, which were purified using vapor-pressure osmometry. The effect of the cation radius on the aggregation numbers of metal salts of DNNS in benzene is shown in Fig. 2. The aggregation number plotted in Fig. 2 shows the saturated value in the curve of the concentration-aggregation number as in Fig. 1. A strong correlation is found between the saturated aggregation number and the reciprocal of e^2/r_i for each cation studied, where e and r_i are the charge and radius of the cation, respectively. Kitahara and Kon-no[9] have reported the same effect of halogen ions on the aggregation number of didodecyldimethyl ammonium

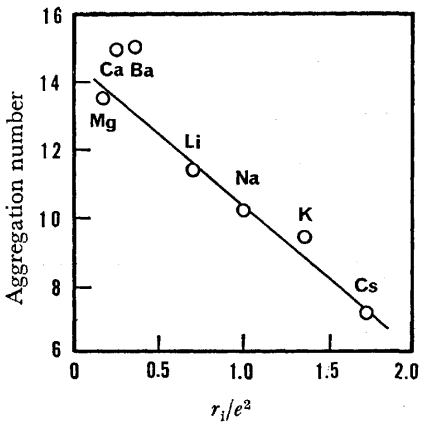

Fig. 2. Effect of cations of dinonylnaphthalenesulfonates on the aggregation number (acid residue/micelle) in benzene at 38 °C.

halides in benzene. Born[10] has suggested that e^2/r_i is proportional to the energy of hydration of gaseous spherical ions and that this value might be considered to be a measure of Lewis acidity. It is clearly seen in Fig. 2 that the driving force for the aggregation of micelles of DNNS salts in nonpolar solvents is the strong acid-base interaction between the polar groups in micellar cores. Kaufman and Singleterry[2] have also reported that such strong acid-base interactions cause a decrease in the apparent molar volume of anions of DNNS salts and an increase in the packing density from solution density measurements. A deviation from the linear relation in Fig. 2 is found in the case of alkaline-earth metal salts of DNNS. The deviation of the bivalent DNNS salts is ascribed to the increased polarity of their ionic head and the different contribution of the hydrocarbon group in the packing of the micelle from that of the monovalent DNNS salts.

Consequently, the micelle formation of DNNS salts in nonpolar solvents is mainly due to the strong interaction between polar groups in micellar cores, in addition to the steric factor and the solute-solvent interaction which have been discussed by Heilweil,[11] and Little and Singleterry,[5] respectively.

References

1) S. Kaufman and C. R. Singleterry, *J. Colloid Sci.*, **10**, 139 (1955).
2) S. Kaufman and C. R. Singleterry, *J. Colloid Sci.*, **12**, 465 (1957).
3) F. M. Fowkes, *J. Phys. Chem.*, **66**, 1843 (1962).
4) T. M. Ford, S. Kaufman, and O. D. Nichols, *J. Phys. Chem.*, **76**, 3726 (1966)
5) R. C. Little and C. R. Singleterry, *J. Phys. Chem.*, **68**, 3453 (1964) and **74**, 1817 (1970).
6) F. M. Fowkes,"Solvent Properties of Surfactant solutions," ed by K. Shinoda, Marcel Dekker (1967), p. 65.
7) K. Inoue, Y. Nose, and H. Watanabe, Proc. 7 th International Conf. Surface Activity, Moscow, 1976, in press.
8) G. I. Jenkins and C. M. Humphreys, *J. Inst. Petrol.*, **51**, 1 (1965).
9) A. Kitahara and K. Kon-no, *J. Colloid Interface Sci.*, **29**, 1 (1969).
10) M. Born, *Z. Physik.*, **1**, 45 (1920).
11) I. J. Heilweil, *J. Colloid Interface Sci.*, **19**, 105 (1964).

BULLETIN OF THE CHEMICAL SOCIETY OF JAPAN, VOL. 50 (10), 2795—2796 (1977)

OH^- as a Possible Cause of the Electron-donor Property of the ZrO_2-TiO_2 System

Kunio ESUMI, Hiroaki SHIMADA, and Kenjiro MEGURO

Department of Chemistry, Science University of Tokyo, Kagurazaka, Shinjuku-ku, Tokyo 162

(Received March 15, 1977)

Synopsis. The electron-donor property of the zirconia-titania system was investigated by means of the adsorption of TCNQ. The TCNQ anion radicals were formed as a result of electron transfer to adsorbed TCNQ from the zirconia-titania surface. The radical concentration on the zirconia-titania system decreased with a increase in the titania content, reached a minimum point at a titania content of 38%, and then increased with the further increase in the titania content. This behavior can explained by the relative amount of OH^- sites, which must be proportional to both, or either one, the relative contents of the pure zirconia phase or the pure titania phase existing on the surface of the zirconia-titania system.

The formation of anion-radical ions on electron-donor sites of some simple metal oxide surfaces has been reported, these electron-donor sites have been also associated with the surface hydroxide ions and the surface oxide ions.[1-5] On the other hand, Flockhart *et al.*[1] studied the electron-donor property of two-component metal oxide systems, they found that silica-aluminas had negligible electron-donating power at low alumina contents, but silica-aluminas of high alumina contents possessed strong electron-donor properties. Hosaka *et al.*[6] studied the electron-donor property of silica-alumina, silica-titania, and alumina-titania systems in the base of the results of the adsorption of 7,7,8,8-tetracyanoquinodimethane (TCNQ), they found that the difference in electron-donor properties among metal oxide systems can be characterized by the change in the concentration of TCNQ anion radicals formed.

These studies are of metal oxides in the Group IV elements. This group, starting with silica, is of interest with respect to changes in size of the metal, coordination, and bonding type. In the present work, the electron-donor property of the zirconia-titania system, estimated by means of the TCNQ adsorption, will be reported.

The preparation of zirconia-titania samples was carried out as follows: Zirconium tetrachloride and titanium one mixtures, in different molar ratios, were dissolved in distilled water, and then, to these solutions, diluted aqueous ammonia was added under vigorous stirring. The precipitates formed were washed with distilled water until free from Cl^- ions. The products were then dried for 48 h at 120 °C. The dried products were calcined in air for 2 h at 500 °C in an electric furnace, followed by cooling *in vacuo*.

The composition of zirconia and titania in each product was determined by means of X-ray fluorometry. The compositions were, respectively, 0, 13, 38, 80, and 100 in the weight-percentage ratio: $TiO_2/(TiO_2+ZrO_2)$. The abbreviations used here are as follows: Z, zirconia; T, titania; Z4T, ZT, and ZT4, zirconia-titania containing 13, 38, and 80% titania.

The surface areas of the zirconia-titania system, as determined by nitrogen adsorption, were as follows: Z, 88; Z4T, 224; ZT, 282; ZT4, 140; T, 69 m^2/g.

The TCNQ was supplied by Dainippon Ink Chemical, Ltd. It was recrystallized from acetonitrile for purification. The acetonitrile used as the solvent was of a reagent grade.

The apparatus and procedure used in this study have been previously described.[7]

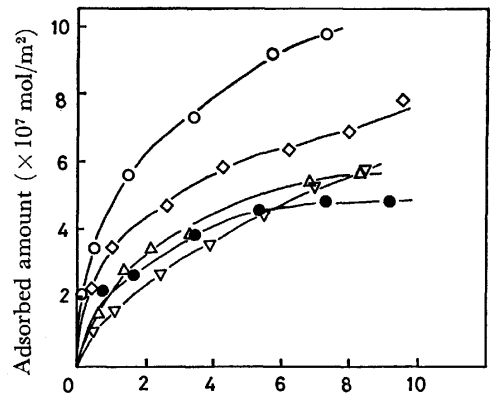

Fig. 1. Adsorption isotherms of TCNQ on zirconia-titania system (at 25 °C): zirconia, △; Z4T, ○; ZT, ▽; ZT4, ◇; titania, ●.

Figure 1 shows the adsorption isotherms of TCNQ from the acetonitrile solution at 25 °C on the zirconia-titania surfaces. All the isotherms follow Langmuir plots.

The radical concentration formed on the surfaces of

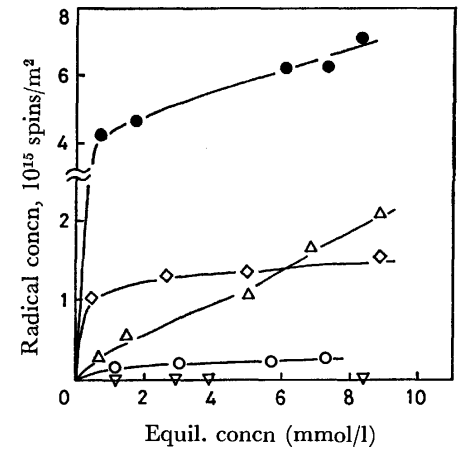

Fig. 2. Radical concentration on zirconia-titania system *vs.* equilibrium concentration of TCNQ: zirconia, △; Z4T, ○; ZT, ▽; ZT4, ◇; titania, ●.

zirconia-titania, plotted against the equilibrium concentration of TCNQ, is shown in Fig. 2.

When TCNQ was adsorbed from a solution in acetonitrile on the surfaces of zirconia-titania, the surfaces of zirconia-titania showed a remarkable coloration, such as violet. The colored samples gave an unresolved ESR spectra with a *g*-value of 2.003, that of TCNQ anion radicals.[6,7] These TCNQ anion radicals were formed as a result of electron transfer from the electron-donor sites of the zirconia-titania surface to adsorbed TCNQ. In the ZT sample, however, the ESR absorption was scarcely observed at all. The unresolved ESR spectra can be explained by the decrease in the freedom of the TCNQ anion radicals adsorbed and by the hyperfine structure becoming obscure of the spectra.

The half-values of the saturated amounts of TCNQ adsorbed, as estimated from the Langmuir plots, are given in the second column of Table I. As can be seen, the half-values are almost the same in all the samples except the Z4T. This indicates that the half-values which consist of neutral TCNQ and TCNQ anion radicals are little affected by the change in the composition of the zirconia-titania system.

For the evaluation of the change in the radical concentration on the surface of zirconia-titania with the composition, the amount of the radical concentration corresponding to the half-values of adsorbed TCNQ in saturation is employed, as is shown in the third column of Table 1. The zirconia-titania (Z4T, ZT, and ZT4) had a much lower radical concentration than titania only. The same tendency has been reported by Hosaka *et al.*[6] in the silica-alumina, silica-titania, and alumina-titania systems. The radical concentration decreased gradually between zirconia and Z4T, but decreased remarkably between Z4T and ZT. On the other hand, in the crystal features of the zirconia-titania system, the pure zirconia phase was present until Z4T, but it became amorphous, as is shown in the fourth column of Table 1. From these results, it may be supposed that the amount of the pure zirconia phase present on the surface of the zirconia-titania system plays an important role in determining the radical concentration. However, the increase in the radical concentration from ZT to ZT4 can be related to the pure titania phase present slightly on the surface of ZT4. It is noteworthy that a weak anatase pattern of ZT4 suggests the presence, in the conglomerate, of a pure titania phase. The steep increase in the radical concentration from ZT4 to the titania corresponds to the increase in the amount of the pure titania phase on the surface.

Table 1. Data of TCNQ adsorption

Sample	Half-values of saturated amounts ($\times 10^7$ mol/m^2)	Radical concn to corresponding half-values of saturated amounts 10^{14} spins/m^2	Phase
Zirconia	3.6	6.8	M*+T(w)
Z4T	5.8	1.7	T(w)
ZT	3.9	negligible	A
ZT4	3.9	11.9	An(w)
Titania	2.8	48.0	An

* M=monoclinic, T=tetragonal, A=amorphous, An=anatase, (w)=weak.

The electron-donor sites of two-component metal oxides are not well known. However, the electron-donor sites of titania, one of the parent oxides in the zirconia-titania system, have been associated with surface hydroxide ions and Ti^{3+} ions.[2,8] Infrared spectroscopy of zirconia has shown that the surface of zirconia contains hydroxide ions.[9] Indeed, Fomin *et al.*[10] have reported that electron transfer from the hydroxide ion can occur in certain solvent systems, provided a suitable acceptor molecule is present. The electron-transfer adsorption of TCNQ on the zirconia-titania system may result from surface hydroxide ions and Ti^{3+} ions. The other product of the electron-transfer adsorption is mainly the OH radical, although only the TCNQ anion radicals are observed in the ESR spectra. The change in the radical concentration of the zirconia-titania system, shown in Table 1, depends on the amount of the pure zirconia phase or the pure titania phase present on the surface of the zirconia-titania system. From the above considerations, it can be expected that the electron-donor sites are surface hydroxide ions(Zr–OH^-) in zirconia-titania of a higher zirconia content, and surface hydroxide ions(Ti–OH^-) and Ti^{3+}ions in the case of zirconia-titania of a higher titania content.

References

1) B. D. Flockhart, I. R. Leith, and R. C. Pink, *Trans. Faraday Soc.*, **65**, 542 (1969).
2) M. Che, C. Naccache, and B. Imelik, *J. Catal.*, **24**, 328 (1972).
3) H. Hosaka, T. Fujiwara, and K. Meguro, *Bull. Chem. Soc. Jpn.*, **44**, 2616 (1971).
4) A. J. Tench and R. L. Nelson, *Trans. Faraday Soc.*, **63**, 2254 (1967).
5) K. Esumi and K. Meguro, *Shikizai Kyokai Shi*, **48**, 535 (1975); **48**, 544 (1975).
6) H. Hosaka, N. Kawashima, and K. Meguro, *Bull. Chem. Soc. Jpn.*, **45**, 3371 (1972).
7) K. Meguro and K. Esumi, *J. Colloid Interface Sci.*, **59**, 93 (1977).
8) K. Esumi and K. Meguro, *Progr. Colloid Polymer Sci.*, in press (1977).
9) P. A. Agron, E. L. Fuller, Jr., and H. F. Holmes, *J. Colloid Interface Sci.*, **52**, 553 (1975).
10) G. V. Fomin, L. A. Blyumenfel'd, and V. I. Sukhorukov, *Proc. Acad. Sci. U.S.S.R.*, **157**, 819 (1964).

BULLETIN OF THE CHEMICAL SOCIETY OF JAPAN, VOL. 50 (10), 2797—2798 (1977)

Measuremets of the Thermal Transpiration Effects of NO at 90 K and of CO, N_2, O_2, CH_4, and He at 77 K

Shozo FURUYAMA

Department of Chemistry, Faculty of Science, Okayama University, Tsushima, Okayama 700

(Received March 18, 1977)

Synopsis. The thermal transpiration effect of the title gases was measured by a relative method by using a diaphragm-type pressure transducer. The data fit the Takaishi-Sensui equation $[P_1/P_2=(AX^2+BX+C\sqrt{X}+\sqrt{T_1/T_2})/AX^2+BX+C\sqrt{X}+1)]$ quite well in the region of X $(=P_2d_2)$ higher than 0.03 mmHg mm. The values for A, B, and C are 25.5, 9.3, and 0.6 for NO at 90 K, 28.5, 10.5, and 0.6 for CO and N_2, 24.0, 9.2, and 0.8 for O_2, 44.0, 11.4, and 1.2 for CH_4, and 2.96, 0.6, and 1.6 for He at 77 k respectively. The values for the temperature-independent constants, A^*, B^*, and C^* deduced from the values for A, B, and C above, were in agreement with the literature values and/or the estimated values.

In studies of the physical adsorption of nitric oxide and carbon monoxide gases,[1] we measured the thermal transpiration effect[2] of NO and CO. Since no data for the thermal transpiration effect of NO and CO are available in the literature, it may be worthwhile to report our data in detail. To check the reliability of our measuring system, other common gases, N_2, O_2, He, and CH_4, were also studied, and the results were compared with existing data.

Experimental

The nominal purities of N_2, He, O_2, CO, NO, and CH_4 were 99.999, 99.99, 99.9, 99.9, 99.9, and 99.9% respectively. NO was further purified by a method described elsewhere.[1]

The thermal transpiration value, P_1/P_2, was obtained as a function of log P_2d_2 by the relative method. The apparatus used is shown schematically in Fig. 1, where the meanings of P_1, P_2, d_2, *etc.* are illustrated. The pressure difference, P_2-P_3, was measured by means of a Datametrics Barocell Pressure sensor-Electronic Manometer. Then, P_3 was determined by evacuating the chamber, B_2, of the pressure sensor to 10^{-5} Torr. P_2 was calculated from the $P_2=P_3+(P_2-P_3)$ relation. Finally, P_1 was determined from P_3 by the usual method.[3,4] The temperature on the lower side was held at 90 K for NO, and at 77 K for the other gases. The temperature on the higher side was always held at 300 ± 1 K. The pressure region extended down to 2×10^{-2} Torr.

The pressure indication of the electronic manometer was calibrated by the gas-expansion method. The accuracy was within 0.2% at pressures above 1 Torr, within 1.2% between 1 and 0.1 Torr, and within 3% between 0.1 and 0.02 Torr.

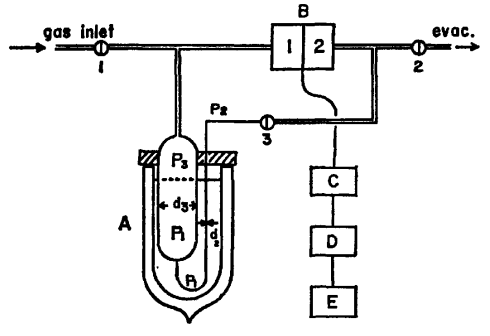

Fig. 1. Schematic representation of the measuring apparatus.
A: Measuring cell, $d_3=46.5$ mm, $d_2=1.45$ mm.
B: Datametrics Barocell Pressure Sensor 570D.
C: Datametrics Barocell Electronic Manometer 1173.
D: Takeda Riken Integrating Digital Voltmeter. TR 66150.
E: Hitachi Recorder 056.

Results and Discussion

The P_1/P_2 and P_3/P_2 values of NO measured at 90.5 K are plotted against log P_2d_2 in Fig. 2. The curves for CO and other gases were obtained at 77.5 K, but are not shown in the present paper.

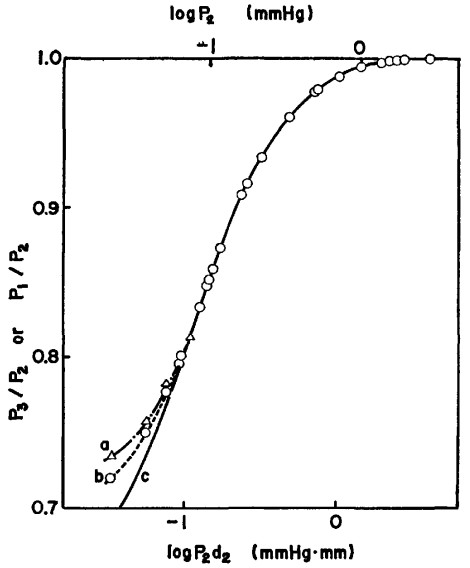

Fig. 2. Plots of thermal transpiration values of NO at 90.5 K.
a: Observed P_3/P_2 *vs.* log P_2d_2,
b: observed P_1/P_2 *vs.* log P_2d_2,
c: calculated P_1/P_2 *vs.* log P_2d_2.

Takaishi and Sensui have proposed the following empirical equation for the thermal transpiration effect:[5]

$$\frac{P_1}{P_2}=\frac{AX^2+BX+C\sqrt{X}+\sqrt{T_1/T_2}}{AX^2+BX+C\sqrt{X}+1} \qquad T_1<T_2, \qquad (1)$$

where A, B, and C are constants and where X is P_2d_2. By substituting the experimental data into the equation, the best-fitting values for A, B, and C have been obtained as summarized in Table 1. The degree of their fitness can be seen from Fig. 2.

Table 1. Values[a] for the constants, A, B, and C, contained in the Takaishi-Sensui equation 1, the viscosity coefficient,[b] and the collision diameter[c]

	A (mmHg mm)$^{-2}$	B (mmHg mm)$^{-1}$	C (mmHg mm)$^{-1/2}$	$10^6\eta$ (poise)	D (Å)
NO	25.5	9.3	0.6	179	3.67
CO	28.5	10.5	0.6	166	3.75
N_2	28.5	10.5	0.6	166	3.75
O_2	24.0	9.2	0.8	192	3.60
CH_4	44.0	11.4	1.2	102	4.26
He	2.96	0.6	1.6	186	2.23

a) Values at 90.5 K for NO and those at 77.5 K for other gases. b) Values at 0 °C. "Kagaku Binran," Chemical Society of Japan, p. 470. c) Values calculated from η (see text).

Takaishi and Sensui have demonstrated that the constants, A, B, and C can be written as:

$$A^* = A \times \bar{T}^2, \quad (2)$$

$$B^* = B \times \bar{T}, \quad (3)$$

$$C^* = C\sqrt{\bar{T}}, \quad (4)$$

where $\bar{T}$ is $(T_1+T_2)/2$ and where A^*, B^*, and C^* are the temperature-independent constants. The determined values for A^*, B^*, and C^* are summarized in Table 2 and compared with the literature values. Since no literature values for NO and CO are available, another way of comparison must be made. The A^*, B^*, and C^* constants of NO and CO are estimated from the following Takaishi-Sensui equations:[5,6]

$$\log A^* = 0.507D + 4.146, \quad (5)$$

$$\log B^* = 0.607D + 0.663, \quad (6)$$

$$C^* = (110/D) - 14. \quad (7)$$

Here, D represents the collision diameter of the gases and is calculated from the viscosity coefficient, η, by the aid of $\eta=5\sqrt{\pi mkT}/16\pi D^2$ relation. By using the values of D summarized in Table 1, the values for A^*, B^*, and C^* are calculated. The results are summarized in Table 2. The agreement between the observed values for the constants and the literature and/or estimated values is reasonably good for all of the gases measured.

Table 2. Constants, A^*, B^*, C^*, contained in Eqs. 2—7

		$10^{-5}A^*$ (deg/mmHg mm)^2	$10^{-2}B^*$ (deg/mmHg mm)	C^* (deg/mmHg mm)$^{1/2}$
NO	obsd	9.7	18	9
	calcd	10	7.8	16
CO	obsd	10	20	8
	calcd	11	8.7	15
N_2	obsd	10	20	8
	lit	12	10	10—18
	calcd	11	8.7	15
O_2	obsd	8.6	17	10
	lit	9—7	16—19	—
	calcd	9.4	7.1	17
CH_4	obsd	16	22	16
	lit	15	15	13
	calcd	20	12	12
He	obsd	1.1	1.1	22
	lit	1.4—1.6	1.2—1.1	18—20
	calcd	1.9	1.0	35

obsd: observed value in the present work. lit.: literature value summarized in Ref. 5. calcd: calculated value in the present work (see text).

This work was supported by a Grant-in-Aid for Research (No. 054182) from the Ministry of Education of the Japanese Government. The author wishes to thank Professor Tetsuo Takaishi (Rikkyo University) for his helpful discussions.

References

1) To be published.
2) M. Knudsen, *Ann. Phys.*, **31**, 210 (1910).
3) S. C. Liang, *J. Appl. Phys.*, **22**, 148 (1951).
4) H. H. Podgurski and F. N. Davis, *J. Phys. Chem.*, **65**, 1343 (1961).
5) T. Takaishi and Y. Sensui, *Trans. Faraday Soc.*, **59**, 2503 (1963).
6) The original equations used to estimate A^* and B^* in Ref. 5 are incorrect. They must be corrected to Eqs. 5 and 6 of the present paper.

BULLETIN OF THE CHEMICAL SOCIETY OF JAPAN, VOL. 50 (10), 2799—2800 (1977)

Relations between the Thermodynamic Properties of Alkali Halides at the Melting Point

Hitoshi KANNO

Department of Chemistry, Meisei University, Hino, Tokyo 191

(Received March 26, 1977)

Synopsis. Two new empirical formulas are presented for alkali halides at the melting point. There is a set of linear relations between the initial slope of melting curve (dT_m/dP) and the solid volume (V_s) for the sequences LiX, NaX, KX, and RbX (X=F, Cl, Br, and I).

Alkali halides are the most typical ionic salt for which theoretical and analytical studies have been made in order to clarify the melting of ionic compounds.[1-3] However, the phenomenon of melting still remains unclarified. It is expected that the relations between various thermodynamic properties associated with fusion might help us understand the mechanism of melting of ionic crystals.

In a previous paper,[4] the following empirical formula was given for the entropy change on fusion (ΔS_m) for the sequences of LiX, NaX, KX, and RbX (X=F, Cl, Br, and I).

$$\Delta S_m = \alpha^{1/3}\left(\frac{A}{r}+B\right) \quad (1)$$

where α and r are the electronic polarizability and interionic distance of the salt, respectively; A and B are constants.

A similar relation holds for the relative volume change on fusion:

$$\frac{\Delta V_m}{V_s} = \alpha^{1/3}\left(\frac{C}{r}+D\right), \quad (2)$$

where ΔV_m and V_s are the volume change on melting and the volume of the solid salt at the melting point, respectively; C and D are constants for the salts with the same cation (LiX, NaX, KX, and RbX, X=halogen ion). Although a small deviation from the straight line is seen for a few salts, good linear correlation for the halides of the same cation (Fig. 1) indicates that electronic polarizability, a measure of the deformation of electron cloud in ion, is a very important factor for characterizing melting of these salts in contrast to the argument of Pauling[5] that apparent irregular variation of thermodynamic properties (melting point, boiling point) of alkali halides is ascribed to the radius-ratio effect. Obviously, regular or irregular variation of a certain property depends on the choice of a set of parameters and coordinates.

Irregular variation of cesium halides (CsCl, CsBr, and CsI) is presumably due to the difference in crystal structure between CsCl (face-centered cubic structure at the melting point) and CsBr and CsI (both simple cubic structure at their melting points). The percentage volume expansion of CsCl on melting (10.0%) is considerably smaller than that of the bromide and iodide (26.8 and 28.5%, respectively).[6,7] However, an extrapolation of the molar volume of the low temperature form of CsCl up to the melting point would give a volume expansion on fusion of 28.3%. Conversely, if the volume expansion (17.6%) associated with the transition in CsCl from simple cubic to face-centered cubic structure is applied to the bromide and iodide, hypothetical cesium bromide and iodide would result in a volume expansion on melting of 9.2 and 10.3%, similar to the value of 10.0% for the chloride. This fact was pointed out by Johnson *et al.*[6] who reasoned that large volume expansion of CsBr and CsI is attributed to the reduction in coordination number from eight to about five on melting, whereas the melting from NaCl structure involves only small change in coordination number (from six to about five). It was proposed and verified by X-ray diffraction study[6,8] that the structure of liquid cesium bromide and iodide is very similar to that of the chloride. It is noteworthy that relations (1) and (2) include lithium halides because it has often been pointed out that lithium salts do not obey the corresponding-state law of other alkali halides.[9,10]

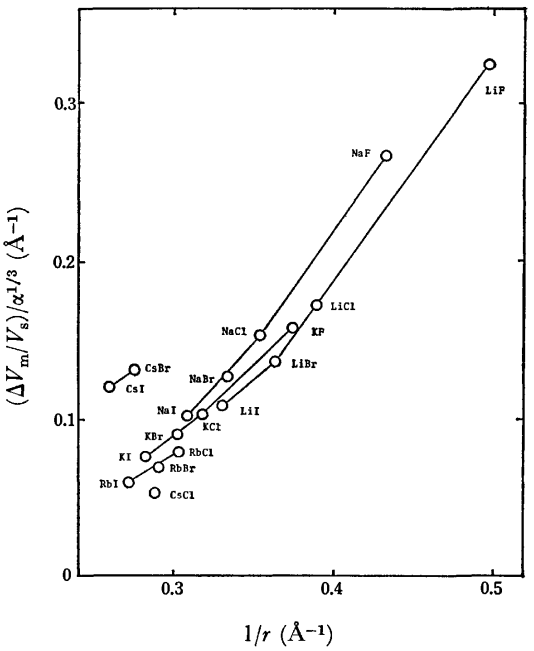

Fig. 1. Relative volume expansion of alkali halide at the melting point. Sources of data: ΔV_m and V_s; H. Spindler and F. Sauerwald, *Z. Anorg. Allg. Chem.*, **335**, 267 (1965), electronic polarizability; J. R. Tessman, A. H. Kahn, and W. Schockley, *Phys. Rev.*, **92**, 890 (1953), Interionic distance; L. Pauling, "The Nature of the Chemical Bond," third ed, Cornell Univ. Press, Ithaca, N. Y. (1960), p. 527.

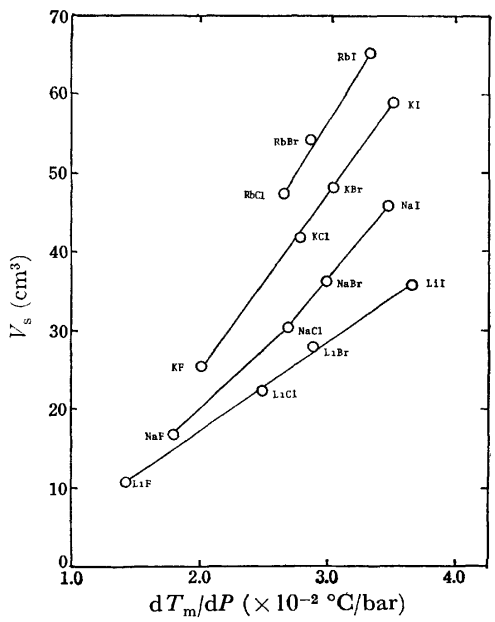

Fig. 2. Linear relation of (d T_m/d P) with solid volume at the melting point ($\bar{V}_s$) for the sequences LiX, NaX, KX, and RbX. Sourece of data: ΔS_m values are calculated from ΔH_m and T_m data compiled by L. Brewer and E. Brackett, *Chem. Rev.*, **61**, 425 (1961).

From relations (1) and (2), we get

$$\left(\frac{dT_m}{dP}\right)_{p=1atm} = \frac{\Delta V_m}{\Delta S_m} = \frac{V_s\left(\frac{C}{r}+D\right)}{\left(\frac{A}{r}+B\right)} = \frac{V_s(C+Dr)}{(A+Br)}$$

$$\simeq EV_s \qquad (3)$$

where E is a constant for the sequence (LiX, NaX, KX, or RbX). Formula (3) suggests that the initial slope of melting curve $(dT_m/dP)_{p=1atm}$ is proportional, as a first approximation, to the volume of the solid salt at the melting point (V_s). As is shown in Fig. 2, there is a good linear relation between the initial slope of the melting curve and the volume of the salt for a sequence of alkali halides of the same cation. It is expected from this relation that at certain high pressures the salt having larger volume should have higher melting point than those of smaller volume if the relation (3) holds up to high pressures. In fact the normal order of melting points of sodium halides is reversed above *ca.* 60 kbars with NaF having the lowest and NaI the highest melting point,[11] and a similar behavior is found for the potassium and rubidium halides at lower pressures.[12,13]

The initial slope of the melting curve $(dT_m/dP)_{p=p_0}$ is expressed as $T_0/a\,c$ by differentiation of the well-known Simon equation, $P-P_0=a\{(T/T_0)^c-1\}$, where T_0 and P_0 are the triple-point temperature and pressure, respectively; a and c are constants. From the corresponding law developed by Reiss *et al.*,[9] the melting point of alkali halide is inversely proportional to ionic distance, *i.e.*, $T_0 \propto 1/r$. Combining this relation and formula (3), we see that $a\,c$ is inversely proportinal to r^4, in accord with the conclusion given by Owens[10] in his analysis of melting curves of alkali halides.

Finally it should be pointed out that the calorimetric heats of fusion of NaI, KI, RbI, and CsI redetermined by Bousquet *et al.*[14] are considerably higher than those of Dworkin and Bredig.[15] However, a comparison of the observed values of the initial slopes of the melting curves of alkali halides[16] with those calculated by means of the Clapeyron-Clausius equation indicates that the data of Dworkin and Bredig are more accurate.

References

1) A. R. Ubbelohde,"Melting and Crystal Structure," Clarendon, Oxford (1965).
2) K. Furukawa, *Discuss. Faraday Soc.*, **32**, 53 (1961).
3) a) C. M. Carlson, H. Eyring, and T. Ree, *Proc. Natl. Acad. Sci. U.S.A.*, **46**, 333 (1960); b) W. L. Lu. T. Ree, V. G. Gerrard, and H. Eyring, *J. Chem. Phys.*, **49**, 797 (1968).
4) H. Kanno, *Bull. Chem. Soc. Jpn.*, **44**, 559 (1971).
5) L. Pauling,"Nature of Chemical Bond," 3 rd ed, Cornell Univ. Press, Ithaca, N.Y. (1960), p. 527.
6) J. W. Johnson, P. A. Agron, and M. A. Bredig, *J. Am. Chem. Soc.*, **77**, 2334 (1955).
7) H. Spindler, *Naturwissenchaften*, **52**, 184 (1965). He reported a little different values of ΔV_m for CsBr (25.9%) and CsI (25.8%) from those of Johnson *et al.* (Ref. 6).
8) H. A. Levy, P, A. Agron, M. A. Bredig, and M. D. Danford, *Ann. N. Y. Acad. Sci.*, **79**, 762 (1960).
9) H. Reiss, S. W. Mayer, and J. L. Katz, *J. Chem. Phys.*, **35**, 820 (1961).
10) B. B. Owens, *J. Chem. Phys.*, **44**, 3144 (1966).
11) C. W. F. T. Pistorius, *J. Chem. Phys.*, **45**, 3513 (1966).
12) C. W. F. T. Pistorius, *J. Phys. Chem. Solids*, **26**, 1543 (1965).
13) C. W. F. T. Pistorius, *J. Chem. Phys.*, **43**, 1557 (1965).
14) J. Bousquet, G. Perachon, and J. C. Remy, *Bull. Soc. Chim. Fr.*, **1967**, 238.
15) A. S. Dworkin and M. A. Bredig, *J. Phys. Chem.*, **64**, 269 (1960).
16) C. W. F. T. Pistorius, *J. Chem. Phys.*, **47**, 4870 (1967).

BULLETIN OF THE CHEMICAL SOCIETY OF JAPAN, VOL. 50 (10), 2801—2802 (1977)

The ESR and ENDOR Spectra of the [2.2](2,7)Pyrenophane Anion Radical

Kazuhiko Ishizu, Yoshinori Sugimoto, Teruo Umemoto,* Yoshiteru Sakata,* and Soichi Misumi*

Department of Chemistry, Faculty of Science, Ehime University, Matsuyama, Ehime 790

**The Institute of Scientific and Industrial Research, Osaka University, Suita, Osaka 565*

(Received April 4, 1977)

Synopsis. The ESR and ENDOR spectra of the [2.2](2,7)-pyrenophane anion, which was prepared by reduction with alkali metal in ethereal solvents, were observed. From a comparison of the spin densities for the anion with those for the pyrene anion, the delocalization of the unpaired electron between the stacked aromatic rings was demonstrated.

Since ESR was successfully used in studies of the intramolecular electron exchange in the [2.2]paracyclophane anion by Weissman,[1] the transannular interaction between the aromatic nuclei has been reported for several cyclophanes, such as [2.2](1,4)naphthalenophane[2] and [2.2](9,10)anthracenophane,[3] where the cyclophane derivative has been regarded as an artificial dimer of the alkyl-substituted aromatics, and the proton hyperfine splitting showed nearly half the value of that for the corresponding monomer anion. In the present note, we wish to report our ESR and ENDOR studies of the [2.2](2,7)pyrenophane anion. Studies of [2.2]-(2,7)pyrenophane have been interesting since, because the pyrenophane MO occupied by the unpaired electron has a node at the bridging positions (2,7) of the pyrene ring, the delocalization of the unpaired electron due to σ-π exchange or the hyperconjugative interaction between the methylene and aromatic groups can be ignored. Therefore, one may expect to elucidate the pure transannular effect on the spin density regardless of either the hyperconjugative or the inductive effect of the bridged ethylene groups in the present case.

Experimental

The synthesis of materials has been described elsewhere.[4] The anion radical was prepared by reduction with sodium in 1,2-dimethoxyethane (DME) and tetrahydrofuran (THF). The ENDOR spectra were recorded with a JEOL-type EX-EDX-1 spectrometer under the operating conditions similar to those described previously.[5]

Results and Discussion

Figure 1 shows the ESR spectrum of the pyrenophane anion, which was prepared by reduction with sodium in DME. The ESR spectrum is composed of 25 hyperfine lines equally spaced, with a line width of 150 mG. The ESR hyperfine structure can be adequately analyzed in terms of the splittings (2.18 G) due to the 8 equivalent protons; the structure is split further into 9 lines attributable to the other equivalent protons with a splitting constant of nearly half. No important changes were detected in the ESR hyperfine structure obtained with THF, and the extra splittings of the alkali metal cation have never been observed anywhere.

The ENDOR spectra of pyrene and pyrenophane anions are shown in Fig. 2. The pyrene anion gives the three ENDOR signals (15.33, 16.88, and 20.71 MHz) above the free proton frequency (13.89 MHz). The splittings were assigned with reference to the previous ESR studies;[6] $a_2^H=a_7^H=1.02$, $a_4^H=a_5^H=a_9^H=a_{10}^H=2.13$, and $a_1^H=a_3^H=a_6^H=a_8^H=4.87$ G. On the other hand, the ENDOR signals of the pyrenophane anion were recorded at 15.40 and 17.05 MHz above the free proton frequency. No ENDOR absorption

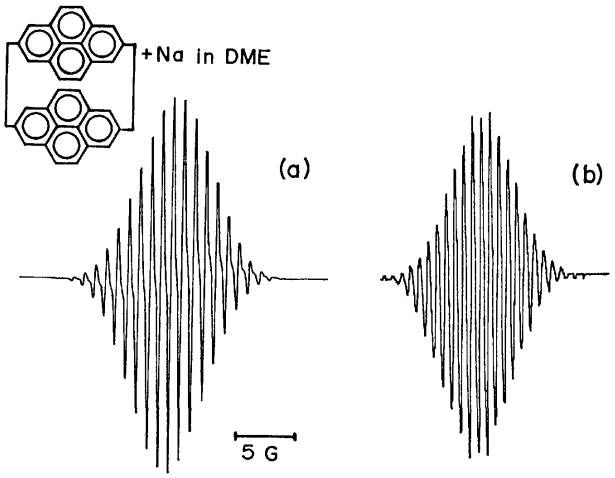

Fig. 1. (a) ESR spectrum of [2.2](2,7)pyrenophane anion recorded at room temperature. (b) A computer simulation of the ESR spectrum.

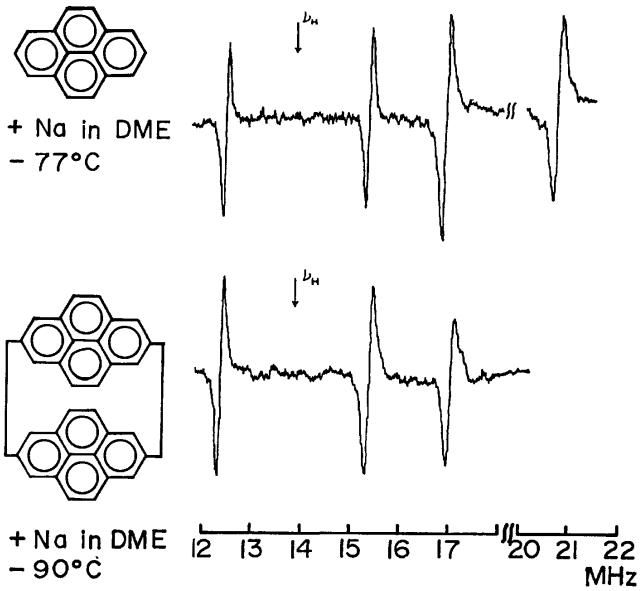

Fig. 2. Higher frequency halves of ENDOR spectra of pyrene and [2.2](2,7)pyrenophane anions. ν_H: free proton frequency.

attributable to the bridging methylene groups can be detected. The splittings of each pyrene group were determined to be 1.08 G for a_4^H, a_5^H, a_9^H, and a_{10}^H and 2.25 G for a_1^H, a_3^H, a_6^H, and a_8^H. Based on the present assumption, computer calculations of the ESR line intensities showed an excellent agreement with the observed spectrum, as is shown in Fig. 1.

The splittings of the pyrene and pyrenophane anions thus determined are summarized in Table 1.

In the previous ESR works on the cyclophane anions, it was pointed out that the spin-density distrubution showed a large dependence on the degree of the transspatial exchange of the unpaired electron in the cyclophane. In [2.2]paracyclophane, however, the doubly degenerated antibonding orbital of the benzene anion causes much difficulty.[7] The importance of the inductive effect of the methylene groups was recently proposed, and the unpaired electron is believed to occupy the orbital which can be expressed by a linear combination of the antisymmetric orbital relative to a plane passing through the two opposite centers and perpendicular to the benzene ring.[8] For [2.2](9,10)anthracenophane, the largest spin densities were assigned to the bridging positions, 9 and 10. Therefore, the possibility of the hyperconjugative interaction of the methylene, which also causes a perturbation on the spin densities, in particular, for the positions with small spin densities, can not safely be ruled out.

Table 1. Proton hyperfine splittings of pyrene and the [2.2](2,7)pyrenophane anion (absolute value in G)

Position	2, 7	4, 5, 9, 10	1, 3, 6, 8
Pyrene	1.02	2.13	4.87
Pyrenophane	$<$150 mG	1.08	2.25

As may be seen in Table 1, the observed ring-proton splittings of the pyrenophane anion are very close to the half-values of those of the pyrene anion radicals, and the methylene proton splitting is very small. This means that the unpaired orbital of the pyrenophane is antisymmetric with respect to the plane passing through the bridging position and perpendicular to the aromatic plane, indicating a negative spin density at the bridging position.

A perturbation of the spin densities due to the hyperconjugative interaction of the methylene group can thus be ignored. A tentative calculation of the methylene proton was performed under the assumptions that the spin densities at the bridging positions, ρ^π, are not affected much by the methylene substitution and that the magnitude of the spin density is reduced to the half-value from that of the pyrene anion.[9] If the methylene protons are tightly fixed in the positions taking the dihedral angle to be $\theta=60°$, the methylene proton splitting can be estimated to be 0.220 G, based on McConnell and Heller's equation, $a^R=B\rho^\pi \cos^2\theta$, $|B|=50$ G.[10] The calculated value is indeed small, and it would be diminished to the order of the ESR linewidth in the real molecule.

References

1) S. I. Weissman, *J. Am. Chem. Soc.*, **80**, 6462 (1958).
2) J. M. Pearson, D. J. Williams, and M. Levy, *J. Am. Chem. Soc.*, **93**, 5478 (1971).
3) T. Hayasi, N. Mataga, Y. Sakata, and S. Misumi, *Bull. Chem. Soc. Jpn.*, **48**, 416 (1975).
4) T. Umemoto, S. Satani, Y. Sakata, and S. Misumi, *Tetrahedron Lett.*, **1975**, 3159.
5) T. Yamamoto, K. Sato, and T. Miyamae, *J. Appl. Phys.*, **11**, 1508 (1971).
6) H. W. Brown and R. C. Jones, *J. Chem. Phys.*, **36** 2809 (1962).
7) A. Ishitani and S. Nagakura, *Mol. Phys.*, **12**, 1 (1967).
8) F. Gerson and W. B. Martin, Jr,. *J. Am. Chem. Soc.*, **91**, 1883 (1969).
9) The spin densities at the 2, 7 positions of the pyrene anion were estimated by taking $|Q^H|=27$ G.
10) C. Heller and H. M. McConnell, *J. Chem. Phys.*, **32**, 1535 (1960).

BULLETIN OF THE CHEMICAL SOCIETY OF JAPAN, VOL. 50 (10), 2803—2804 (1977)

On the Low Dimensionality in Organo-magnetic Material: 9-(α-Fluorenylidene-*p*-chlorobenzyl)-9-fluorenyl

Jun YAMAUCHI and Yasuo DEGUCHI

College of Liberal Arts and Sciences, Kyoto University, Kyoto 606

(Received April 16, 1977)

Synopsis. The low-dimensional character in the organic free radical, *p*-Cl-BDPA, is discussed. The temperature dependence of the *g*-values can provide a method of discrimination between the short- and long-range-ordering effects, and the organic free radical can be regarded as a one-dimensional organo-magnetic material at first approximation, but its interchain interaction is appreciable, amounting to the order of $|J'/J|=0.2$; thus, $|J'|/k=0.88$ K.

Recently the magnetic interactions between unpaired electron spins in crystalline organic free radicals have been of great interest. Especially in the case of neutral organic free radicals, much information has been accumulated so far, and it is generally accepted that there are two regions characteristic of the magnetic interaction between unpaired electron spins in organic free radicals, that is, the short- and long-range-ordered regions.[1] One of the present authors (J.Y.) has discussed in detail the linear antiferromagnetic interaction and the possibility of long-range ordering in organic free radicals.[2] Thus, organic free radicals have been classified as among low-dimensional magnetic materials, that is, low-dimensional organo-magnetic material. An organic free radical, 9-(α-fluorenylidene-*p*-chlorobenzyl)-9-fluorenyl (hereafter abbreviated as *p*-Cl-BDPA),

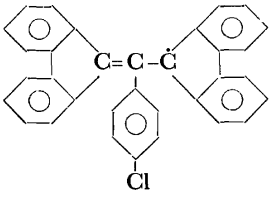

is a typical example, exhibiting magnetic low dimensionality in the short-range-ordered region and experiencing a magnetic phase transition to a long-range-ordered state.[2]

In order to clarify the magnetic interactions in organic free radicals and to obtain more information about low dimensionality and the magnetic structure, various kinds of experiments have been carried out on *p*-Cl-BDPA.[3-8] In the course of these investigations an important question has been arisen— to what extent does the organic free radical, *p*-Cl-BDPA, have a magnetic low dimensional character. This may be one question to which it is not possible to give a definite answer. In this paper, however, attention will be paid mainly to the low dimensionality of the organic free radical, *p*-Cl-BDPA.

It was shown in our previous papers that the low-dimensional character can be found in susceptibility,[2] magnetic heat capacity,[3] ESR linewidth,[2] and NMR intensity[4] as a function of the temperature and that *p*-Cl-BDPA has a nearly one-dimensional magnetic interaction with an exchange interaction parameter of $J/k=-4.4$ K, where k is Boltzmann's constant. In the

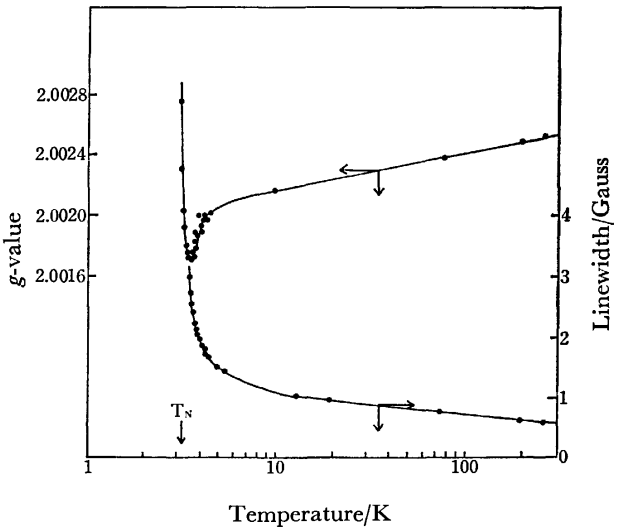

Fig. 1. Temperature dependences of *g*-value and linewidth of *p*-Cl-BDPA. It should be noted that the linewidth is different from that published previously.[2]

microscopic information concerning the ESR linewidth or the NMR intensity, however, the low-dimensional effect could not be discriminated from the long-range-ordering effect.

The experimental results on the ESR *g*-values of polycrystalline *p*-Cl-BDPA as a function of the temperature are shown in Fig. 1, which indicates a *g*-value deviation from a room-temperature *g*-value as the temperature is lowered and its divergence after reaching a minimum at 3.6 K when the temperature approaches the magnetic-phase-transition temperature, 3.25 K. This deviation may be attributed to the magnetic short-range-ordering effect, and the divergence may be due to the magnetic long-range-ordering effect.

Nagata *et al.* classically estimated the simple relations between the anisotropies of the *g*-value and the susceptibility by introducing a small magnetic dipolar interaction and a single ion D-term, both of a uniaxial symmetry referred to the directions of the linear chain interaction.[9] The relationships were as follows:

$$\Delta g_{//}/g = (\chi_{//}-\chi_{\perp})/\chi_{//}, \quad (1)$$

$$\Delta g_{\perp}/g = (\chi_{\perp}-\chi_{//})/2\chi_{\perp}. \quad (2)$$

When we assume the following relation for a powder sample:

$$\Delta g_{iso} = (\Delta g_{//}+2\Delta g_{\perp})/3, \quad (3)$$

equations 1 and 2 give this expression:

$$\Delta g_{iso}/g = -(\chi_{//}-\chi_{\perp})^2/3\chi_{//}\chi_{\perp}. \quad (4)$$

Equation 4 indicates that the *g*-value observed on the powder sample decreases with a decrease in the tem-

perature. The g-value deviation of p-Cl-BDPA is comprehensible from the theory and, therefore, implies a one-dimensional short-range ordering of unpaired electron spins in a linear chain. In the long-range-ordered region, ESR shows an antiferromagnetic resonance pattern, and the resonance shifts to the down-magnetic-field become much larger.[6] This leads to a large g-value anisotropy and to a divergence of the g-value in the short-range-ordered region near the long-range-ordering temperature. This may be the reason why the divergence of g-values can be observed in the case of p-Cl-BDPA.

It is generally accepted that one-dimensional magnetic interactions characterize ESR absorptions at room temperature; that is, the line shape is different from the usual Lorenzian or Gaussian line shapes, and the linewidth angular variation is different from that of the three- or two-dimensional magnetic interaction.[10] These facts are explained at present on the basis of a one-dimensional spin diffusion model. Although the line shape of p-Cl-BDPA was observed, we could not obtain any characteristic behavior such as is mentioned above, but it exhibits a Lorenzian line shape exactly. This fact indicates that p-Cl-BDPA is not a purely one-dimensional magnetic material and implies the presence of fairly large interactions between the magnetic linear chains. As for the angular variations in the linewidth, we can not draw any decisive conclusion because of the lack of the single crystal measurements.

The interchain interaction can not be estimated directly from the experimental results, but the relationship between the intrachain interaction, J, the interchain interaction, J', and the phase transition temperature can be anticipated. Oguchi deduced this relationship in the case of a two-dimensional interchain interaction using the Green function method,[11] which gives the interchain interaction, J', of p-Cl-BDPA. In Table 1 the results obtained are listed, together with those of other organic free radicals for comparison. It can be seen there that $|J'/J|=0.2$ leads to $|J'|/k=0.88$ K and that the interchain interaction is fairly large and not negligible compared with that of the TANOL radical,[12] amounting to the same order of magnitude as in the BDPA-Bz radical.[2,13]

Table 1. Intrachain- and interchain-exchange interaction parameters of several organic free radicals

	J/k	T_N[c]	J/kT_N	$\|J'/J\|$	$\|J'\|/k$
p-Cl-BDPA	−4.4 K	3.25 K	−1.4	0.2	0.88 K
BDPA-Bz[a]	−4.4 K	1.695 K	−2.6	0.04	0.18 K
TANOL[b]	−5.0 K	0.49 K	−10.2	0.004	0.02 K

a) 1,3-Bisdiphenylene-2-phenyl-allyl and benzene complex. b) 2,2,6,6-tetramethyl-4-piperidinol-1-oxyl. c) Antiferromagnetic phase transition temperature.

In conclusion, the temperature dependence of the g-values of the organic free radical, p-Cl-BDPA,can provide a method of discrimination between the short- and long-range-ordering effects, and p-Cl-BDPA can be regarded as a one-dimensional organo-magnetic material at first approximation, but its interchain interaction is appreciable, amounting to the order of $|J'/J|=0.2$; thus, $|J'|/k=0.88$ K.

References

1) L. J. de Jongh and A. R. Miedema, *Adv. Phys.*, **23**, 1 (1974).
2) J. Yamauchi, *Bull. Chem. Soc. Jpn.*, **44**, 2301 (1971).
3) J. Yamauchi, K. Adachi, and Y. Deguchi, *Chem. Lett.*, **1972**, 733; *J. Phys. Soc. Jpn.*, **35**, 443 (1973).
4) K. Uchino, J. Yamauchi, H. O. Nishiguchi, and Y. Deguchi, *Bull. Chem. Soc. Jpn.*, **47**, 285 (1974).
5) K. Watanabe, J. Yamauchi, H. O. Nishiguchi, Y. Deguchi, and K. Ishizu, *Chem. Lett.* **1974**, 489; *Bull. Inst. Chem. Res., Kyoto Univ.*, **53**, 161 (1975).
6) J. Yamauchi, *Chem. Lett.*, **1974**, 1031; *J. Chem. Phys.*, **67**, No. 2, (1977).
7) T. Yoshioka, J. Yamauchi, H. O. Nishiguchi, and Y. Deguchi, *Bull. Chem. Soc. Jpn.*, **48**, 335 (1975).
8) H. Ozaki, H. O. Nishiguchi, and J. Yamauchi, *Phys. Lett.*, **54A**, 227 (1975).
9) K. Nagata and Y. Tazuke, *J. Phys. Soc. Jpn.*, **32**, 337 (1972); K. Nagata, Y. Tazuke, and K. Tsushima, *ibid.*, **32**, 1486 (1972).
10) P. E. Dietz, F. R. Merritt, R. Dingle, D. Hone, B. G. Silbernagel, and P. M. Richards, *Phys. Rev. Lett.*, **26**, 1186 (1971).
11) T. Oguchi, *Phys. Rev.*, **133**, 1098 (1964).
12) J. Yamauchi, T. Fujito, E. Ando, H. Nishiguchi, Y. Deguchi, *J. Phys. Soc., Jpn.* **25**, 1558 (1968); J. P. Boucher, M. Nechtschein, and M. S. Paul, *Phys. Lett.*, **42A**, 397 (1973).
13) W. Duffy, Jr., J. F. Dubach, P. A. Pianetta, J. F. Deck, D. L. Strandburg, and A. R. Miedema, *J. Chem. Phys.*, **56**, 2555 (1972).

BULLETIN OF THE CHEMICAL SOCIETY OF JAPAN, VOL. 50 (10), 2805—2806 (1977)

Formation and Characterization of Lead Monoxide Prepared by the Alkoxy-Method

Osamu YAMAGUCHI, Minoru YAMADERA, and Kiyoshi SHIMIZU

Department of Applied Chemistry, Faculty of Engineering, Doshisha University, Karasuma Imadegawa, Kamigyo-ku, Kyoto 602

(Received March 7, 1977)

Synopsis. Lead alkoxide was hydrolyzed at various temperatures from 28 to 85 °C. The products consisted of only massicot or litharge, or a mixture of the two for modifications of PbO, depending on the reaction temperature and pH of the suspension.

PbO has two polymorphic modifications, litharge (tetragonal) and massicot (orthorhombic). Although litharge transforms into massicot at about 500 °C,[1] the reverse transformation does not occur. On the other hand, massicot transforms readily into litharge by grinding[2-4] or wet ball-milling.[5,6] Commercial PbO, prepared by oxidation of the molten Pb, is usually a mixture of the two modifications.[6] The present paper is concerned with the conditions for the formation of the two modifications and the characterization for the alkoxy-derived PbO.

Experimental

An alcoholic solution containing 6.5 wt% lead alkoxide was prepared by the reaction of anhydrous lead acetate with sodium isopropoxide in the presence of an excess amount of isopropyl alcohol:

$$Na + C_3H_7OH \longrightarrow Na(OC_3H_7) + 1/2H_2, \quad (1)$$

$$Pb(CH_3COO)_2 + 2Na(OC_3H_7) \xrightarrow[C_3H_7OH]{83^\circ C,\ 12\,h} Pb(OC_3H_7)_2 + 2CH_3COONa\downarrow. \quad (2)$$

The purities of anhydrous lead acetate and sodium metal used in the reaction were 99.5 and 99.9%, respectively. Isopropyl alcohol was purified by fractional distillation of the guaranteed reagent. The hydrolysis was carried out as follows. A five-necked flask was equipped with a reflux condenser, a dropping funnel, a stirring rod, a thermometer and a thermo-controller. A definite quantity of water in the range from 100 to 1000 ml was introduced into the flask, and then heated to the desired temperature. A solution of 100 ml of the alkoxide in the dropping funnel was added dropwise to the stirred water in the fiask. After completion of the addition, the suspensions were further stirred for 15 min. The products were separated from the suspensions by filtration, washed repeatedly with water, and dried at 60 °C under reduced pressure. The products were examined by means of X-ray diffraction using Ni filtered Cu$K\alpha$ radiation.

Results and Discussion

All products obtained at various temperatures in 400 ml of water were identified as PbO only as massicot or a mixture of massicot and litharge. The yield was about 67%. Table 1 shows the composition of the two modifications for each PbO powder. The composition was determined by measuring the relative intensities, I_M and I_L, of the strongest peaks in the massicot and litharge spectra. For the alkoxy-derived PbO, as described subsequently, these peaks correspond to $d(002)=2.95$ Å for massicot and $d(002)=2.51$ Å for litharge. The product consisting of only massicot was obtained at 28 °C. A small amount of litharge in addition massicot was formed at 40 °C and the litharge content of the products increased with an increase in temperature up to 85 °C, but no product consisting of only litharge was formed. On the other hand, the products consisted of only litharge when the alkoxide solution was added to water all at once at temperatures ranging from 70 to 85 °C. Judging from the yield described above, it can be assumed that the unreacted sodium alkoxide was involved in the lead alkoxide (see Reaction 2). In view of the fact that sodium alkoxide changes into sodium hydroxide upon hydrolysis, the difference between the results at 70 to 85 °C may be ascribed to a change in

Table 1. Composition of the two modifications for PbO obtained by hydrolyzing lead alkoxide

Run	Temp (°C)	Composition (%)	
		Massicot	Litharge
1	28	100	—
2	40	98.6	1.4
3	50	97.4	2.6
4	60	96.3	3.7
5	70	76.8	23.2
6	85	38.8	61.2
7[a]	70	—	100
8[a]	85	—	100

a) Obtained by rapid hydrolyzation.

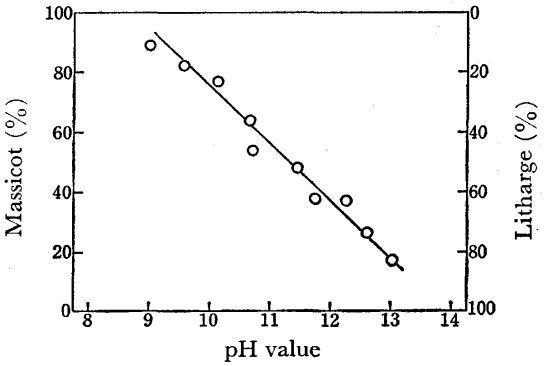

Fig. 1. Relationship between the composition of two modification for PbO and pH of suspensions obtained by hydrolyzing at 85 °C.
The lead alkoxide was in the pH range from 13.6 to 13.8.

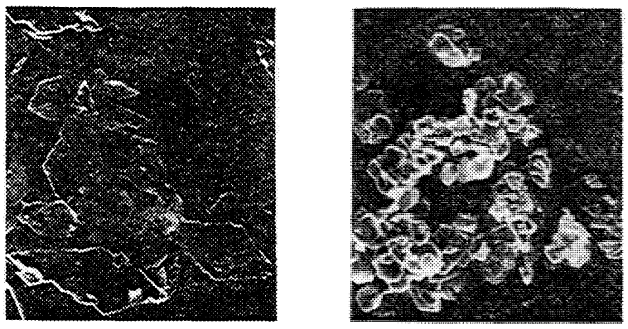

(A) (B) (X800)

Fig. 2. Electron micrographs of the massicot (A) and litharge (B) powders.

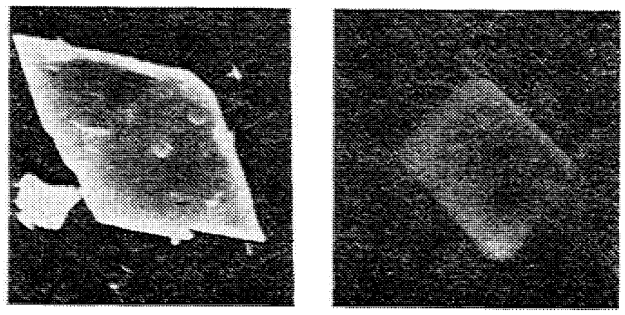

(A) (B) (X1500)

Fig. 3. Electron micrographs of massicot (A) and litharge (B) showing rhombic and tetragonal morphology, respectively.

the pH of the suspensions during the course of hydrolysis. Accordingly, the 100 ml alkoxide solution was added dropwise to various quantities of water at 85 °C. As shown in Fig. 1, an approximately linear relationship exists between the composition of the two modifications in the products and the pH of the suspensions. When the pH value of the suspensions was below about 11.4, the massicot content of the products were greater than the litharge content. A further increase in the pH resulted in the formation of litharge. From the results, it was found that the compositon of the two modifications for PbO prepared by the alkoxy-method is due to the pH of the suspension, as well as the hydrolysis temperature.

Electron micrographs of the PbO powders are shown in Fig. 2. Massicot with an orthorhombic crystal structure consists of rhombic plate-like particles. On the other hand, litharge with a tetragonal crystal structure is composed of tetragonal plate-like particles. The morphology is shown more clearly in Fig. 3, in which well-defined rhombic and tetragonal plates are easily discernible.

X-Ray diffraction patterns of PbO prepared by the

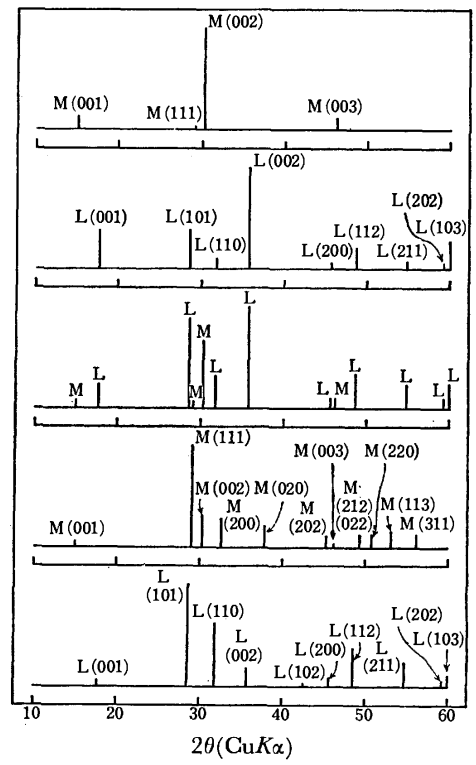

Fig. 4. X-Ray diffraction patterns of PbO prepared by alkoxy-method and described in X-ray powder data file.

M: massicot L: litharge

(A) massicot
(B) litharge } from alkoxide
(C) specimen of run 6 in Table 1

(D) massicot
(E) litharge } from X-ray powder data file

present method showed a preferred orientation in the direction of the c axis in comparison with those of massicot and litharge described in the X-ray powder data file (Fig. 4).[7,8] This phenomenon was observed particularly for massicot.

References

1) For example, R. Soderquist and B. Dickens, *J. Phys. Chem. Solids.*, **28**, 823 (1967).
2) G. L. Clark and R. Rowan, *J. Am. Chem. Soc.*, **63**, 1302 (1941).
3) F. Dachille and R. Roy, *Nature*, **186**, 34, 71 (1960).
4) W. B. White, F. Dachile, and R. Roy, *J. Am. Ceram. Soc.*, **44**, 170 (1961).
5) M. Senna and H. Kuno, *J. Am. Ceram. Soc.*, **54**, 259 (1971).
6) C. A. Sorrel, *J. Am. Ceram. Soc.*, **55**, 47 (1972).
7) X-Ray powder data file (ASTM card 5-0570).
8) X-Ray powder data file (ASTM card 5-0561).

BULLETIN OF THE CHEMICAL SOCIETY OF JAPAN, VOL. 50 (10), 2807—2808 (1977)

The Preparation of Mixed Carbonato Complexes of Cobalt(III) with 2-Pyridinecarboxylic Acid

Yayoi IDA, Masaharu SAKAI, Shigeru SAKAI, and Muraji SHIBATA
Department of Chemistry, Faculty of Science, Kanazawa University, Kanazawa 920
(Received March 25, 1977)

Synopsis. By the successive replacement of CO_3^{2-} ions in the $[Co(CO_3)_3]^{3-}$ complex with 2-pyridinecarboxylic acid (Hpicol), the $[Co(CO_3)_2(picol)]^{2-}$ complex and two geometrical isomers of the $[CoCO_3(picol)_2]^-$ complex have been prepared. By the reaction of the *cis*-$[Co(CO_3)_2(NH_3)_2]^-$ complex and picol, three geometrical isomers of the $[CoCO_3(picol)(NH_3)_2]$ have been prepared.

The most remarkable feature of the preparative method for cobalt(III) complexes starting from a potassium hydrogencarbonate aqueous solution of the tricarbonatocobaltate(III) is the successive replacement of the CO_3^{2-} ions with another ligand, and the first substitution step in the reaction with such a ligand as ammonia, ethylenediamine, pyridine, nitrite ion, or cyanide ion resulted in a dicarbonato complex.[1] However, the action of an α-amino acid (glycine, alanine or valine) on the $[Co(CO_3)_3]^{3-}$ complex resulted not in the dicarbonato complex, but in the carbonatobis (amino acidato) complex.[1] Thus, we adopted 2-pyridinecarboxylic acid (picolinic acid, abbreviated as Hpicol) in order to investigate successive substitution. In addition, the reaction of *cis*-$[Co(CO_3)_2(NH_3)_2]^-$ with 2-pyridinecarboxylic acid to give $[CoCO_3(picol)(NH_3)_2]$ was investigated.

Experimental

2-Pyridinecarboxylic acid was prepared from 2-methylpyridine in the form of hydrochloride by a familiar method.[2]

To a freshly prepared solution of tricarbonatocobaltate(III) ($Co(NO_3)_2 \cdot 6H_2O$, 29.1 g, 0.1 mol), we added a solution of Hpicol (0.1 mol); the mixture was stirred at *ca.* 50 °C for 40 min, whereupon the solution turned blue-green. The resulting solution was allowed to cool in an ice bath. Ethanol was added, to the cold solution for the successive removal of the coexisting salts. Finally, an ethanol–ether (1: 1) mixture was added to the solution, and the whole was kept in a refrigerator until blue-green crystals separated out. Recrystallization was performed by dissolving the crude product in a minimum amount of water, followed by the addition of an ethanol–ether (1: 1) mixture when cold. Yield, *ca.* 15 g. Found: C, 24.77; H, 1.44; N, 3.90%. Calcd for $K_2[Co(CO_3)_2(C_6H_4NO_2)] \cdot 1/2H_2O$: C, 24.75; H, 1.30; N, 3.61%.

A solution of Hpicol (0.05 mol) was added to a freshly prepared solution of $[Co(CO_3)_3]^{3-}$ (0.025 mol); when the mixture was then stirred at 60 °C for 4 h, it turned violet. The resulting solution was concentrated to a small volume with a rotary evaporator at *ca.* 35 °C. To the concentrated solution we added an ethanol–ether mixture (1: 1), and the whole was kept in a refrigerator overnight. The crude product thus obtained was filtered and recrystallized in the way described above. On the other hand, the filtrate was charged on a column containing Dowex 1 X-8 in the Cl-form (9×15 cm). By elution with a 0.3 M KCl aqueous solution, a broad band consisting of univalent anionic species was descended; it was collected in a fraction. This was again chromatographed using a column (5×30 cm) and 0.3 M KCl; three violet bands were then separated. They were collected in fractions labeled A-1—A-3. The absorption spectra of these fractions indicated that the crystals obtained prior to the chromatographic separation were identical with the species in the A-2 fraction. Each fraction was evaporated almost to dryness, the residue being extracted with ethanol. After a small amount of water had been added to the extracted solution, the whole was kept in a refrigerator until crystals separated out. This was successful with the fractions A-2 and A-3, crystallization from the A-1 fraction being unsuccessful because of the poor yield and easy isomerization of the species. Yields, *ca.* 3 g for the A-2 fraction plus the crystallized crop and *ca.* 0.5 g for the A-3 fraction. Found for the A-2 complex: C, 35.82; H, 3.02; N, 6.60%. Calcd for $K[CoCO_3(C_6H_4NO_2)_2] \cdot 2H_2O$: C, 35.62; H, 2.76; N, 6.39%. Found for the A-3 complex: C, 36.44; H, 2.57; N, 6.17%. Calcd for $K[CoCO_3(C_6H_4NO_2)_2] \cdot 3/2H_2O$: C, 36.37; H, 2.58; N, 6.53%.

Three isomers of the diamminecarbonatopicolinatocobalt(III) complex were obtained analogously to those of the $[CoCO_3(gly)(NH_3)_2]$ complex.[3] To a solution of $K[Co(CO_3)_2(NH_3)_2] \cdot H_2O$[1] (10 g, 0.037 mol in *ca.* 20 ml H_2O) we added a solution of the Hpicol ligand (0.05 mol); the mixture was then stirred at room temperature for 3 h. During the reaction, a considerable amount of red-violet crystals separated out as the first crop. The crystals were collected by filtration, and the filtrate was concentrated to a small volume. Ethanol was added to the concentrate, and then the whole was cooled in an ice bath, the second crop of the crystals being thus obtained. The combined first and second crops of crystals were recrystallized from a large quantity of hot water (50 °C).

On the other hand, the filtrate from the second crop of crystals was chromatographed on a column containing 100—200 mesh Dowex 50W-X 8 resin in the Na-form (4.5×25 cm). By washing the column with water, the band of unreacted $[Co(CO_3)_2(NH_3)_2]^-$ was descended first, followed by the three bands of the desired isomers. Since the first-descended band was very poor in yield and was found to be identical with the crystals separated during the reaction, this portion of the eluate was discarded. The second and third bands were collected in fractions. Each fraction was concentrated to a small volume. After the addition of ethanol, the concentrate was kept in a refrigerator overnight. Red needle-like crystals separated out from the fraction of the second band, while pink plates were obtained from the fraction of the third band. Yields, *ca.* 1 g (red-violet crystals), *ca.* 0.5 g (red crystals), and *ca.* 0.5 g (pink crystals). Found for the red-violet crystals: C, 30.53; H, 4.03; N, 14.86%. Calcd for $[CoCO_3(C_6H_4NO_2)(NH_3)_2]$: C, 30.56; H, 3.66 N, 15.07%. Found for the red crystals: C, 27.00; H, 4.87; N, 13.18%. Calcd for $[CoCO_3(C_6H_4NO_2)(NH_3)_2] \cdot 2H_2O$: C, 27.02; H, 4.54; N, 13.51%. Found for the pink crystals: C, 28.79; H, 4.42; N, 14.43%. Calcd for $[CoCO_3(C_6H_4NO_2)(NH_3)_2] \cdot$

H_2O: C, 28.68; H, 4.13; N, 14.34%.

The absorption spectra were measured with a Hitachi Model 323 spectrophotometer. The proton magnetic resonance (PMR) spectra were recorded on a JEOL JNM-PS-100 NMR spectrometer at *ca.* 25 °C, using D_2O as the solvent. The values of the chemical shifts were referred to internal sodium d_4-trimethylsilylpropionate (TMSP).

Results and Discussion

The absorption spectra in solution for the present three kinds of complexes are shown in Figs. 1 and 2. The numerical data are summarized in Table 1, the data[4] on related complexes being included for comparison. When the spectral data of the $[Co(CO_3)_2(picol)]^{2-}$ complex are compared with those of the $[Co(ox)_2(gly)]^{2-}$ complex. a bathochromic shift is observed in the spectrum of the dicarbonato complex. This shift can reasonably be explained by the facts that the CO_3^{2-} is ranked in a position of the spectrochemical series lower than the $C_2O_4^{2-}$ ion, and that the picol lies close to the gly ligand in the series.[5]

The absorption spectra of the two isomers of the $[CoCO_3(picol)_2]^-$ complex are quite similar to each other (Fig. 1); hence, the geometrical configurations have not been determined from the spectral data. Although another isomer had not been isolated as crystals from the eluate, the spectrum of the eluate exhibited the first band at 18200 cm^{-1} which is rather broader than those for the isolated two isomers and the second band at 25200 cm^{-1}. Concerning the $[Coox(gly)_2]^-$ complex, Matsuoka *et al.*[4] reported that one somer, whose structure is determined to be *trans*(*N*)i from the splitting of the first absorption band, corresponds to the first-eluated band in chromatographic separation, and that other two isomers, determined to be C_1-*cis*(*N*) and C_2-*cis*(*N*) on the basis of the PMR spectra, correspond to the second band and the third band respectively. The two isomers isolated in the present work exhibit the proton signals due to the pyridine rings of picol in the region of δ 7.4—9.2 ppm. The patterns were so complicated that the assignments of the peaks have not been performed, but the spectrum of the isomer from the second eluate exhibited a more complex pattern than that from the third eluate. Considering these differences in the absorption spectrum, in the elution order, and in the PMR spectrum, the three isomers are assumed to adopt *trans*(*N*), C_1-*cis*(*N*), and C_2-*cis*(*N*) configurations respectively, according to the order of elution.

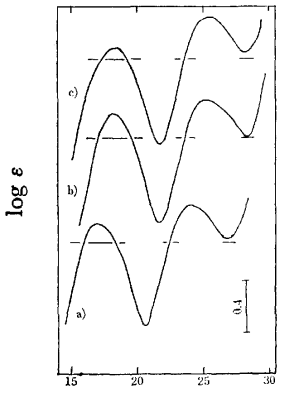

Fig. 1. Absorption spectra of;
a) $[Co(CO_3)_2(picol)]^{2-}$, b) C_1-*cis*(*N*)-$[CoCO_3(picol)_2]^-$ and c) C_2-*cis*(*N*)-$[CoCO_3(picol)_2]^-$.
Short horizontal lines show the levels of log ε=2.00 for each the complexes.

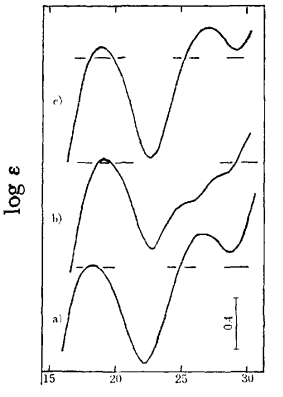

Fig. 2. Absorption spectra of three isomers of $[CoCO_3(picol)(NH_3)_2]$;
a) *mer-cis*(*N*)-isomer, b) *mer-trans*(*N*)-isomer and c) *fac*-isomer.

Table 1. Absorption spectral data ($\bar{\nu}$ in 10^3 cm^{-1})

Complex	I Band		II Band	
	$\bar{\nu}_{max}$	log ε	$\bar{\nu}_{max}$	log ε
$[Co(CO_3)_2(picol)]^{2-}$	17.0	2.16	24.1	2.28
$[Co(ox)_2(gly)]^{2-}$ [4]	17.9	2.20	25.0	2.26
$[CoCO_3(picol)_2]^-$				
trans(*N*) (1)[a]	18.2	—	25.2	—
C_1-*cis*(*N*) (2)	18.2	2.19	25.3	2.27
C_2-*cis*(*N*) (3)	18.4	2.06	25.2	2.30
$[Coox(gly)_2]^-$ [4]				
trans(*N*) (1)	16.7 18.9	1.70 2.00	25.8	2.23
C_1-*cis*(*N*) (2)	18.3	2.15	25.8	2.24
C_2-*cis*(*N*) (3)	17.8	2.08	25.9	2.20
$[CoCO_3(picol)(NH_3)_2]$				
mer-cis(NH_3) (1)	18.3	2.02	26.8	2.26
mer-trans(NH_3) (2)	19.2	2.04	25.0(sh) 28.4(sh)	
fac (3)	18.9	2.07	26.9	2.23
$[CoCO_3(gly)(NH_3)_2]$ [3]				
mer-cis(NH_3) (1)	18.1	2.03	26.5	2.25
mer-trans(NH_3) (2)	18.7	2.07	24.9(sh) 27.3	1.85
fac (3)	18.7	2.02	26.7	2.13

a) Numbers in parentheses indicate the elution order.

The characterization of the three isomers of the $[CoCO_3(picol)(NH_3)_2]$ complex can be made in the same way as that used for the isomers of the $[CoCO_3(gly)(NH_3)_2]$ complex;[3] the isomer, exhibiting splitting of the second absorption band is identified as that of *mer-trans*(NH_3); the isomer exhibiting the first absorption band with the largest half-width, as that of the *mer-cis*-(NH_3) isomer, and the remainder, which was obtained from the last eluate, as the *fac* one.

References

1) M. Shibata, *Proc. Jpn. Acad.*, **50**, 779 (1974), and references therein.
2) "Organic Syntheses," Vol. 20 (1940), p. 79.
3) S. Kanazawa and M. Shibata, *Bull. Chem. Soc. Jpn.*, **44**, 2424 (1971).
4) N. Matsuoka, J. Hidaka, and Y. Shimura, *Bull. Chem. Soc. Jpn.*, **40**, 1868 (1967).
5) N. Matsuoka, Y. Shimura, and R. Tsuchida, *Nippon Kagaku Zasshi*, **82**, 1637 (1961).

BULLETIN OF THE CHEMICAL SOCIETY OF JAPAN, VOL. 50 (10), 2809—2810 (1977)

Electrochemical Fluorination of Ethanethiol

Hajime BABA, Kazuo KODAIRA, Shunji NAGASE, and Takashi ABE

Government Industrial Research Institute, Nagoya, Hirate-machi, Kita-ku, Nagoya 462

(Received May 9, 1977)

Synopsis. The electrochemical fluorination of ethanethiol has been carried out. A number of new fluoroalkyl sulfur compounds have been isolated and characterized.

With bivalent sulfur compounds, the electrochemical fluorination of alkyl sulfides has frequently been carried out,[1] but little work has been reported on the electrochemical fluorination of thiols.[2] The present paper will describe the results of a study of the electrochemical fluorination of ethanethiol, a study initiated in order to examine the possible use of this method for the preparation of partially-fluorinated alkyl sulfur compounds.

The results turned out to be very complex, yielding almost all possibly producible fluoroethyl derivatives of sulfur hexafluoride, most of them new. However, their yields were quite small (<13%). The extensive cleavage of the carbon-sulfur bond of the thiol was observed giving fluorocarbons and sulfur hexafluoride. There were also formed dialkyl sulfur tetrafluoride compounds, that may be yielded as a consequence of the fragmentation of the thiol and the combination of the fragments, showing the complexity of the nature of the electrochemical fluorination of sulfur compounds.[1c,f] The low yields of the fluorinated products may be ascribed partly to the instability of the thiols in hydrogen fluoride[3] and also to the formation of tar-like materials during fluorination.

TABLE 1. FLUOROALKYL SULFUR COMPOUNDS

Compound	Bp[a] (°C)	n_D^{20}	Elemental analysis[b] C (%)	H (%)	F (%)
$CHF_2CF_2SF_5$	31.6	<1.28	10.63 (10.53)	0.70 (0.44)	74.6 (75.0)
$CF_3CH_2SF_5$	39.5	<1.28	11.55 (11.43)	0.95 (0.96)	72.4 (72.4)
CHF_2CHFSF_5	48.0	1.2866	11.57 (11.43)	1.16 (0.96)	72.9 (72.4)
$CHF_2CH_2SF_5$	56.0	1.2967	12.25 (12.50)	1.75 (1.58)	69.0 (69.2)
$C_2H_5SF_5$	59.6	1.3114	15.56 (15.38)	3.67 (3.23)	60.5 (60.9)
$CH_2FCHFSF_5$	62.2	1.3048	12.72 (12.50)	1.77 (1.58)	69.1 (69.2)
cis-$(C_2F_5)_2SF_4$	71.7	1.2832	13.81 (13.88)		76.4 (76.9)
$CF_3CHFSF_4C_2F_5$	81.4	1.2870	14.63 (14.64)	0.50 (0.31)	74.7 (75.3)
$CF_3CH_2SF_4C_2F_5$	88.6	1.2941	15.26 (15.49)	0.85 (0.65)	73.0 (73.5)
$C_2F_5SF_4C_2F_4SF_5$	132.0	1.3057	10.77 (10.58)		75.2 (75.3)

a) Recorded, uncorrected, at atmospheric pressure.
b) The calculated values are given in parentheses.

The physcial constants and elemental analyses of the new sulfur-containing compounds are listed in Table 1. From the kinds of the products, such as $CF_3CH_2SF_5$, $CHF_2CH_2SF_5$, and $C_2H_5SF_5$, it may be said that, during the fluorination, the sulfur atom in the thiols is oxidized to the sexivalent state, mainly in the initial stage of the fluorination, before the fluorination of the alkyl group is complete, as has been shown in the fluorination of alkyl sulfides.[1b,c,f]

The ^{19}F NMR spectroscopy was particularly useful in the structure determination of these kinds of compounds.[4,5] For example, fluoroethylsulfur pentafluorides could be confirmed by indicating the presence of two differently shielded types of fluorine nucleus bonded to the sulfur in the correct intensity ratio of 1:4 in the regions expected. The axial fluorine nuclei are more shielded than the equatorial fluorine nuclei. The ^{19}F and ^1H NMR data are shown in Table 2. Except for the case of bis(pentafluoroethyl)sulfur tetrafluoride, the *trans* configuration of the dialkyl groups of disubstituted derivatives of sulfur hexafluoride was confirmed: all of the $-SF_4-$ fluorine atoms are equivalent, showing a single multiplet expected for only the *trans*-isomer.

The bis(pentafluoroethyl)sulfur tetrafluoride obtained was found to be a mixture of *cis* ($A_2B_2X_4Y_6$ system)- and *trans* ($A_4X_4Y_6$ system)-isomers in an approximate ratio of 1:6, which could be resolved by gas chromatography. For the *trans*-isomer, the $-SF_4-$ signals are a multiplet centered at −26.7 ppm (in CCl_4, with respect to internal CCl_3F). In the case of the *cis*-isomer, in the sulfur-fluorine regions, two triplets of multiplets of an equal intensity, centered at −21.8 and −61.4 ppm, are exhibited. The coupling interaction between SF_{ax} and SF_{eq} is 89.5 Hz. This is the first example of the formation and identification of the *cis*-isomer of bis(perfluoroalkyl)sulfur tetrafluoride in the electrochemical fluorination. Only the *trans*-isomers have been yielded *via* the electrochemical fluorination of the sulfides.[1b-d,4,5]

Experimental

The electrolytic fluorination apparatus and operating procedures were similar to those described previously.[6] The mass spectra were recorded on a Hitachi RMU-7 instrument at 70 eV, the ^{19}F NMR spectra, on a Hitachi R-20B instrument at 56.4 MHz, and the ^1H NMR spectra, on a Hitachi R-22 instrument at 90 MHz.

A representative run and the results obtained will be described below. The sample (25.5 g, 0.410 mol) was dissolved in anhydrous hydrogen fluoride (400 ml) in the cell and fluorinated under the following conditions: sodium fluoride, 20.0 g; anodic current density, 3.5 A/dm^2 (the effective surface areas of the anodes and the cathodes were both 7.7 dm^2); cell voltage, 5.5—6.5 V; cell temperature, 17—18 °C; electricity supplied, 312 A h (690 min); helium, 100 ml/min. (Though this flouorination could be carried out without using a conductivity additive, the use of sodium fluoride increased the yields of partially-fluorinated ethylsulfur pentafluorides). The products (75.5 g) obtained were rectified into four fractions by means of a low-temperature rectification column, and each fraction was then subjected to gas-chromatographic analysis using the following stainless-steel column, 2 m×3 mm, silica gel; 4 m×3 mm, Daifl oil 3 (20%) on Chromosorb P-AW, 4 m×3 mm, Silicone DC QF-1 (15%) on Chromosorb P-AW.

The following compounds were obtained (the compositions were calculated on the basis of the chromatographic peak

Table 2. ^{19}F and ^{1}H NMR spectral data[a,b,c]

Compound	Chemical shifts, ppm	Coupling constants, Hz
$CHF_2{}^aCF_2{}^bSF_5$	F^a 135.1, F^b 101.2, SF_{eq} −41.5, SF_{ax} −64.9	F^a–H 52.2, F^a–F^b 8.1, F^a–SF_{eq} 8.1, F^b–SF_{eq} 13.0, F^b–H 5.2, F^b–SF_{ax} 5.0, SF_{ax}–SF_{eq} 147.2
	H 6.1	H–F^a 52.1, H–F^b 5.2, H–SF_{eq} 0.9
$CF_3{}^aCH_2SF_5$	F^a 65.5, SF_{eq} −70.0, SF_{ax} −76.5	F^a–SF_{eq} 10.5, F^a–H 8.7, SF_{ax}–F^a 2.1, $SF^a{}_x$–SF_{eq} 143.9
	H 4.0	H–F^a 8.9, H–SF_{eq} 7.3
$CH^aF_2{}^aCH^bF^bSF_5$	F^a_A 128.8, F^a_B 132.4, F^b 175.1, SF_{eq} −49.8, SF_{ax} −70.9	F^a_{A-B} 306.3, F^a–H^a 52.2, F^a_A–F^b 12.4, F^a_A–SF_{eq} 9.4, F^a_A–H^b 6.6, F^a_B–F^b 9.4, F^a_B–SF_{eq} 8.1, F^a_B–H^b 8.7, F^b–H^b 44.2, F^b–H^a 6.5, F^b–SF_{eq} 2.3, F^b–SF_{ax} 1.8, SF_{ax}–SF_{eq} 147.5
	H^a 6.0, H^b 5.4	H^a–H^b 3.9, H^b–SF_{eq} 5.2
$CH^aF_2{}^aCH_2{}^bSF_5$	F^a 117.3, SF_{eq} −68.5, SF_{ax} −79.1	F^a–H^a 54.5, F^a–H^b 13.9, F^a–SF_{eq} 9.6, F^a–SF_{ax} 1.5, SF_{ax}–SF_{eq} 146.8
	H^a 6.2, H^b 3.9	H^a–H^b 4.5, H^b–SF_{eq} 8.0
$CH_3{}^aCH_2{}^bSF_5$	SF_{eq} −61.3, SF_{ax} −84.2	SF_{ax}–SF_{eq} 143.9
	H^a 1.5, H^b 3.7	H^a–H^b 7.6, H^a–SF_{eq} 1.5, H^b–SF_{eq} 7.7
$CH_2{}^aF^aCH^bF^bSF_5$	F^a 232.1, F^b 164.0, SF_{eq} −49.1, SF_{ax} −73.6	SF_{ax}–SF_{eq} 145.7, others unresolved
	H^a 4.8, H^b 5.6	H^a–F^a 46, H^b–F^b 46.2, H^b–F^a 25
cis-$(CF_3{}^aCF_2{}^b)_2SF_4$	F^a 81.1, F^b 97.4, SF_{ax} −21.8, SF_{eq} −61.4	F^a–SF_{ax} 8.8, F^a–SF_{eq} 8.6, F^a–F^b 2.2, F^b–SF_{ax} 12.0, F^b–SF_{eq} 9.9, SF_{ax}–SF_{eq} 89.5
$CF_3{}^aCHF^bSF_4CF_2{}^c$-$CF_3{}^d$	F^a 76.1, F^b 170.1, F^c 97.7, F^d 81.2, SF_{eq} −34.7	F^a–SF_{eq} 10.0, F^a–H 5.3, F^b–H 43.3, F^b–F^a 9.3, F^b–SF_{eq} 1.0, F^c–SF_{eq} 15.7, F_d–SF_{eq} 9.0
	H 5.6	H–F^b 43.2, H–F^a 5.2, H–SF_{eq} 5.0
$CF_3{}^aCH_2SF_4CF_2{}^b$-$CF_3{}^c$	F^a 65.1, F^b 97.5, F^c 81.2, SF_{eq} −53.1	F^a–SF_{eq} 10.9, F^a–H 8.6, F^b–SF_{eq} 16.3, F^c–SF_{eq} 9.0
	H 4.1	H–F^a 8.7, H–SF_{eq} 7.7
$CF_3{}^aCF_2{}^bSF_4CF_2{}^c$-$CF_2{}^dS'F_5$	F^a 79.8, F^b 96.6, SF_{eq} −28.5, F^c 91.8, F^d 93.6, $S'F_{eq}$ −44.7, $S'F_{ax}$ −62.4	F^a–SF_{eq} 8.8, F^b–SF_{eq} 15.3, F^c–SF_{eq} 16.1, F^c–$S'F_{eq}$ 13.3, F^d–$S'F_{eq}$ 16.1, F^d–SF_{eq} 13.5, F^d–$S'F_{ax}$ 4.8, F^d–F^c 2.3, $S'F_{ax}$–$S'F_{eq}$ 145.7, $S'F_{ax}$–F^d 4.9, $S'F_{ax}$–F^c 1.4

a) CCl_4 solution. b) The chemical shifts are in δ values with respect to CCl_3F for ^{19}F, and to TMS for ^{1}H as internal references. c) SF_{eq} and SF_{ax} indicate equatorial (basal) and axial (apical) fluorine atoms respectively.

areas): C_1 and C_2 fluorocarbons (29.4 g), SF_6 (12.7 g), *n*-C_4F_{10} (0.2 g), $C_2H_5C_2F_5$ (0.3 g), $C_2F_5SF_5$[1b,c] (12.9 g, 12.8%), *trans*-$(C_2F_5)_2SF_4$[1b] (1.2 g), *cis*-$(C_2F_5)_2SF_4$ (0.2 g), CF_3CHF-SF_5[7] (2.9 g), $CHF_2CF_2SF_5$ (0.5 g), $SF_5C_2F_4SF_5$[2c] (0.4 g), $CF_3CH_2SF_5$ (9.8 g, 11.3%), CHF_2CHFSF_5 (1.1 g), CF_3CHF-$SF_4C_2F_5$ (0.03 g), $CHF_2CH_2SF_5$ (1.5 g), $C_2H_5SF_5$ (0.3 g), $CH_2FCHFSF_5$ (0.1 g), $C_2F_5SF_4C_2F_4SF_5$ (0.04 g), $CF_3CH_2SF_4$-C_2F_5 (0.02 g), others (1.6 g).

trans-$(C_2F_5)_2SF_4$ had bp 70.0 °C (lit,[1b] bp 70.0 °C) and n_D^{20} <1.28. ^{19}F NMR:[4,5] $(CF_3{}^aCF_2{}^b)_2SF_4$; F^a 80.5, F^b 97.7, SF_{eq} −26.7 ppm; F^a–SF_{eq} 8.9. F^b–SF_{eq} 14.9, F^a–F^b 0.6 Hz,

The significant ions from the mass cracking patterns are as follows: *cis*-$(C_2F_5)_2SF_4$; (*m/e*) 189 $[C_2F_5SF_2]$, 119 $[C_2F_5]$, 89 $[SF_3]$, 69 $[CF_3]$. $CHF_2CF_2SF_5$: (*m/e*) 127 $[SF_5]$, 101 $[M-SF_5]$, 89 $[SF_3]$. $CF_3CH_2SF_5$: (*m/e*) 191 $[M-F]$, 127 $[SF_5]$, 89 $[SF_3]$, 83 $[M-SF_5]$, 69 $[CF_3]$. CHF_2CHFSF_5: (*m/e*) 127 $[SF_5]$, 122 $[CH_2SF_4]$, 89 $[SF_3]$, 83 $[M-SF_5]$. CF_3CHFSF_4-C_2F_5: (*m/e*) 119 $[C_2F_5]$, 101 $[C_2HF_4]$, 89 $[SF_3]$, 82 $[C_2HF_3]$, 69 $[CF_3]$. $CHF_2CH_2SF_5$: (*m/e*) 127 $[SF_5]$, 89 $[SF_3]$, 65 $[M-SF_5]$. $C_2H_5SF_5$: (*m/e*) 127 $[SF_5]$, 89 $[SF_3]$, 70 $[SF_2]$. 51 [SF], 29 $[M-SF_5]$, 28 $[C_2H_4]$. $CH_2FCHFSF_5$: (*m/e*) 127 $[SF_5]$, 89 $[SF_3]$, 65 $[M-SF_5]$, 64 $[C_2H_2F_2]$. $C_2F_5SF_4$-$C_2F_5SF_5$: (*m/e*) 189 $[C_2F_5SF_2]$, 119 $[C_2F_5]$, 100 $[C_2F_4]$, 89 $[SF_3]$, 69 $[CF_3]$. $CF_3CH_2SF_4C_2F_5$: (*m/e*) 191 $[C_2H_2F_3SF_4]$, 153 $[C_2H_2F_5S]$, 119 $[C_2F_5]$, 89 $[SF_3]$, 84 $[CH_2F_2S]$, 83 $[C_2H_2$-$F_3]$, 70 $[SF_2]$, 69 $[CF_3]$.

References

1) a) A. E. Clifford, H. K. El-Shamy, H. J. Emeléus, and R. N. Haszeldine, *J. Chem. Soc.*, **1953**, 2372; b) F. W. Hoffmann, T. C. Simmons, R. B. Beck, H. V. Holler, T. Katz, R. J. Koshar, E. R. Larsen, J. E. Mulvaney, F. E. Rogers, B. Singleton, and R. S. Sparks, *J. Am. Chem. Soc.*, **79**, 3424 (1957); c) R. D. Dresdner and J. A. Young, *ibid.*, **81**, 574 (1959); d) J. A. Young and R. D. Dresdner, *J. Org. Chem.*, **24**, 1021 (1959); e) T. Abe, S. Nagase, K. Kodaira, and H. Baba, *Bull. Chem. Soc. Jpn.*, **43**, 1812 (1970); f) S. Nagase, "Fluorine Chemistry Reviews," Vol. 1, ed by P. Tarrant, Marcel Dekker, New York (1967), p. 94.

2) a) R. N. Haszeldine and F. Nyman, *J. Chem. Soc.*, **1956**, 2684; b) Dow Corning Co., Fr. 1512068 (1967); L. A. Lorne, U. S. 3456024 (1969); c) T. Abe, S. Nagase, and H. Baba, *Bull. Chem. Soc. Jpn.*, **46**, 3845 (1973).

3) J. H. Simons, "Fluorine Chemistry," Vol. 1, ed by J. H. Simons, Academic Press, New York (1960), p. 239.

4) N. Muller, R. C. Lauterbur, and G. F. Svatos, *J. Am. Chem. Soc.*, **79**, 1043 (1957).

5) M. T. Rogers and J. D. Graham, *J. Am. Chem. Soc.*, **84**, 3666 (1962).

6) S. Nagase, H. Baba, and T. Abe, *Bull. Chem. Soc. Jpn.*, **40**, 2358 (1967).

7) R. E. Banks, M. G. Barlow, R. N. Haszeldine, and W. D. Morton, *J. Chem. Soc., Perkin Trans. 1*, **1974**, 1266.

BULLETIN OF THE CHEMICAL SOCIETY OF JAPAN, VOL. 50 (10), 2811—2812 (1977)

Synthesis and Properties of 2,8-Dioxabicyclo[3.2.1]octane Derivatives

Hajime IRIKAWA, Tsukasa ISHIKURA, and Yasuaki OKUMURA

Department of Chemistry, Faculty of Science, Shizuoka University, Oya, Shizuoka 422

(Received December 13, 1976)

Synopsis. In order to study the isomerization of daphniphylline into isodaphniphylline, 1,4-dimethyl-2,8-dioxabicyclo[3.2.1]octane-4-carboxylic acid (**3**), a degrada tion product of daphniphylline, was synthesized from the keto diester and transformed into the 3-oxacyclopentanones (**6**, **7**).

A *Daphniphyllum* alkaloid, daphniphylline, undergoes isomerization in hydrochloric acid into isodaphniphylline, by which the 2,8-dioxabicyclo[3.2.1]octane structure is transformed into the 3-oxacyclopentanone skeleton.[1] This paper deals with a model reaction of the isomerization, and the synthesis of 1,4-dimethyl-2,8-dioxabicyclo[3.2.1]octane-4-carboxylic acid (**3**), a degradation product of daphniphylline.

Condensation of diethyl methylmalonate with 4,4-ethylenedioxypentanoyl chloride gave the keto diester (**1**), which afforded acetal alcohol (**2**) on reduction with lithium aluminium hydride followed by treatment with hydrochloric acid. Oxidation of **2** with potassium permanganate gave acetal acid (**3**), whose IR and NMR spectra were identical with those of the authentic sample.[1] Thus, *exo* orientation of the hydroxymethyl group in **2** is clear.

For conversion into the 3-oxacyclopentanone skeleton, the sodium salt of **3** was converted into the diazo ketone (**4**) accompanied by the chloro ketone (**5**) with oxalyl dichloride followed by treatment with diazomethane in ether. Treatment of **4** with methanolic hydrochloric acid gave 3-oxacyclopentanone (**6**), which afforded mesylate (**7**). The IR (3670, 3490, 1762, and 1713 cm^{-1}) and NMR (δ 2.19 ppm, 3H, s) spectra of **6** are in line with the assigned structure. The formation of **6**, which bears the substituents shown in the formula, is explained by a nucleophilic attack on the α-keto methylenediazonium group by the 8-oxygen atom in **4** in close proximity.

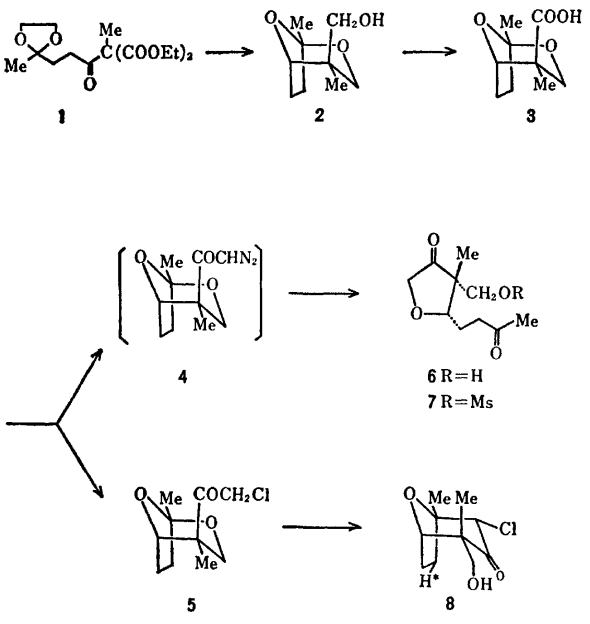

Scheme

An attempt to convert **5** into **6** by treatment with 30% methanolic hydrogen chloride failed, giving isomeric ketone (**8**) instead. The doublet proton signal at 4.55 ppm (–CHCl–) of **8** is due to the long-range coupling with H*, indicating *endo* configuration of the chlorine atom. The isomerization might proceed through an intermediate, which has an enol group bearing the chlorine atom *trans* to the carbon chain.

By analogy with the conversion of **4** into **6**, the isomerization of daphniphylline seems to involve an intramolecular substitution of the protonated acetoxyl group or protonated hydroxyl group (upon hydrolysis) by the bridge-oxygen in close proximity.

Experimental

All melting points and boiling points are uncorrected. The NMR spectra were obtained on a JNM-C-60H in $CDCl_3$ solution, with TMS as an internal standard.

The Keto Diester ***1.*** To a mixture of 17.4 g of diethyl methylmalonate, 4.8 g of 50% NaH and 100 ml of ether was added a solution of 4,4-ethylenedioxypentanoyl chloride in 50 ml of ether, prepared from 18.2 g of sodium 4,4-ethylenedioxypentanoate[2] and 18.5 g of oxalyl dichoride. After being stirred at room temperature for 6 h, the reaction mixture was refluxed for 1 h, and worked up in the usual way to give 16.8 g (53.2% from the sodium salt) of **1** as a colorless oil: bp 148—151 °C/1.2 mmHg; IR(neat) 1755 and 1726 cm^{-1}; NMR δ 1.30 (3H, s), 1.30 (6H, t, J=7 Hz), 1.63 (3H, s), 1.96 (2H, m), 2.74 (2H, m), 3.89 (4H, s) and 4.24 ppm (4H, q, J=7 Hz). Found: C, 57.06; H, 7.74%. Calcd for $C_{15}H_{24}O_7$: C, 56.95; H, 7.65%.

The Acetal Alcohol ***2.*** A mixture of 22.1 g of **1**, 7.6 g of $LiAlH_4$ and 250 ml of ether was refluxed for 6 h, and then treated with 150 ml of 6 M HCl at room temperature overnight. The work-up in the usual way gave 5.1 g (42%) of **2** as a colorless oil: bp 109—110 °C/3.2 mmHg; IR (CCl_4) 3640 and 3480 cm^{-1}; NMR δ 0.74 (3H, s), 1.46 (3H, s), 1.98 (4H, m), 3.22 (1H, s, disappeared on addition of D_2O), 3.40 (1H, d, J=12 Hz), 3.65 (1H, d, J=12 Hz), 3.78 (2H, AB-q, J=11 Hz) and 4.18 ppm (1H, m). Found: C, 63.03; H, 9.43%. Calcd for $C_9H_{16}O_3$: C, 62.76; H, 9.36%.

The Acetal Acid ***3.*** A mixture of 3.1 g of **2**, 0.5 g of NaOH, 6.1 g of $KMnO_4$ and 85 ml of water was stirred at 0 °C for 24 h. Work-up in the usual way gave 1.8 g (55%) of **3** as colorless plates, mp 144—145 °C ($CHCl_3$), whose IR ($CHCl_3$) and NMR spectra were identical with those of the authentic sample. The melting point higher than that of the authentic sample (mp 122—123 °C) indicates that the synthetic **3** is in a form of racemic compound.

Transformation of ***3*** *into Chloro Ketone* ***5*** *and Cyclopentanone* ***6.*** To a mixture of 611 mg of the sodium salt of **3**, 3 drops of

pyridine and 5 ml of benzene was added a solution of 2 ml of oxalyl dichloride in 5 ml of benzene. After being left to stand at room temperature for 3 h, the reaction mixture was concentrated *in vacuo*. Treatment of the residue with ethereal diazomethane (from 5 g of *N*-nitrosomethylurea) at room temperature for 2 days, and then with methanolic hydrochloric acid* (2 ml of 1 M HCl in 3 ml of MeOH) at room temperature for 10 min gave an oily product, which was chromatographed on 5 g of silica gel. Elution with $CHCl_3$ afforded 120 mg (19%) of **5** as colorless needles: mp 76—77 °C (in a sealed tube, diisopropyl ether); IR (Nujol) 1730 cm^{-1}; NMR δ 0.92 (3H, s), 1.47 (3H, s), 2.02 (4H, m), 3.60 (1H, d, J=12 Hz), 4.23 (1H, q, J=12 and 2 Hz), 4.6 (1H, m), and 4.64 ppm (2H, s); MS (70 eV), *m/e*, 218 (M^+), 183 and 141. Found: C, 55.23; H, 7.24%. Calcd for $C_{10}H_{15}O_3Cl$: C, 54.93; H, 6.91%. Elution with 5% MeOH–$CHCl_3$ gave 163 mg (28%) of **6** as a colorless oil; IR ($CHCl_3$) 3670, 3490, 1762, and 1713 cm^{-1}; NMR δ 1.07 (3H, s), 2.00 (2H, m), 2.19 (3H, s), 2.59 (1H, s, disappeared on addition of D_2O), 2.73 (2H, m), 3.69 (2H, s), 3.84 (1H, m), 3.88 (1H, d, J=17 Hz) and 4.12 ppm (1H, d, J=17 Hz); MS (70 eV), *m/e*, 170 (M^+−30), 152, 113, and 112.

The Mesylate 7. Treatment of 127 mg of **6** with 0.3 ml of methanesulfonyl chloride in 1 ml of pyridine at room temperature for 3 h gave 54 mg (31%) of **7** as colorless plates: mp 90—91 °C (EtOH); IR (Nujol) 1759, 1710, 1348, and 1176 cm^{-1}; NMR δ 1.21 (3H, s), 2.01 (2H, m), 2.21 (3H, s), 2.73 (2H, m), 3.03 (3H, s), 3.88 (1H, q, J=9 and 5 Hz), 3.95 (1H, d, J=17 Hz), 4.15 (1H, d, J=17 Hz), and 4.23 ppm (2H, s); MS (70 eV), *m/e*, 278 (M^+), 221 and 191. Found: C, 47.30; H, 6.55%. Calcd for $C_{11}H_{18}O_6S$: C, 47.47; H, 6.52%.

Isomerization of the Chloro Ketone 5. A solution of 51 mg of **5** in 5 ml of 30% methanolic hydrogen chloride was refluxed for 3 h. Evaporation *in vacuo* and subsequent crystallization from benzene–hexane gave 31 mg (61%) of **8** as colorless needles: mp 86—88 °C (in a sealed tube); IR (CCl_4) 3610, 3580 and 1720 cm^{-1}; NMR δ 1.42 (3H, s), 1.60 (3H, s), 1.7—2.2 (5H, m), 3.65 (2H, AB-q, J=12 Hz), 4.20 (1H, q, J=5 and 2 Hz) and 4.55 ppm (1H, d, J=2 Hz); MS (70 eV), *m/e*, 218 (M^+), 183 and 165. Found: C, 54.77; H, 7.01%. Calcd for $C_{10}H_{15}O_3Cl$: C, 54.93; H, 6.91%.

* **5** was also obtained on treatment with AcOH instead of methanolic hydrochloric acid.

References

1) H. Irikawa, N. Sakabe, S. Yamamura and Y. Hirata, *Tetrahedron.*, **24**, 5691 (1968).

2) C. K. Warren and B. C. L. Weedon, *J. Chem. Soc.*, **1958**, 3972.

BULLETIN OF THE CHEMICAL SOCIETY OF JAPAN, VOL. 50 (10), 2813—2814 (1977)

Carbon-13 NMR Spectra of Methyl-1,3-dioxolanes

Yasuhisa SENDA, Jun-ichi ISHIYAMA, and Shin IMAIZUMI

Department of Applied Science, Faculty of Engineering, Tohoku University, Aoba, Sendai 980

(Received February 21, 1977)

Synopsis. The ^{13}C NMR spectra of thirteen methyl substituted 1,3-dioxolanes were measured. The carbon chemical shifts of the methyl groups imply that the 1,3-transannular nonbonded interaction of the methyl groups is negligible, except in the cases of 2,2,4-trimethyl- and 2,2,4,5-tetramethyl-1,3-dioxolanes.

Various attempts have been made to determine the configurations of dimethyl-1,3-dioxolanes by means of the physical constants, such as the boiling point[1] or the reflactive index.[2] Kametani and Sumi have determined the steric configurations of some di- and trimethyl-1,3-dioxolanes by means of the ^1H NMR spectra.[3] In this investigation the ^{13}C NMR spectra of methyl-substituted 1,3-dioxolanes were measured in order to probe the influence of stereochemistry on the carbon chemical shifts of these compounds.

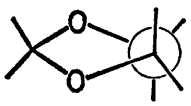

Conformation of 1,3-dioxolane.

The carbon resonance for one of the methyl groups of *cis*-2,4-dimethyl-1,3-dioxolane (*cis*-**5**) that which appeared at δ 20.2 is assigned to the 2-methyl carbon, and at δ 18.9, to the 4-methyl one, on the basis of the chemical shifts of 2-methyl- (**2**) and 4-methyl-1,3-dioxolanes (**3**). The chemical shifts for the methyl groups of *trans*-**5** are similar to those of *cis*-**5**. The 1,3-transannular nonbonded interaction between 2- and 4-methyl groups of *cis*-**5** is practically negligible because of the high flexibility of the five-membered ring system.[4] A similar observation was made in the ^{13}C NMR spectra of stereoisomeric 1,3-dimethylcyclopentanes.[4] The carbon resonances for the methyl groups of *cis*-4,5-dimethyl-1,3-dioxolane (*cis*-**6**) moved upfield by 2.2 ppm compared to that of *trans*-**6**. Such upfield shifts may be due to the dihedral angle of the two vicinal methyl groups of *cis*-**6** being smaller than that of *trans*-**6**.[5] In the case of 2,4,5-trimethyl-1,3-dioxolanes (**7**) the carbon resonances for the methyl groups appeared in two separate regions of the magnetic fields, at δ 20.7—21.3 and 14.3—17.4. Comparing the carbon chemical shifts for the methyl groups of **2**, **5**, and **6**, the signals in the former region are found to be of the 2-methyl, while those in the latter are of the 4- and 5-methyl carbons. Since the carbon chemical shifts for the 2-methyl groups of *trans*-2,2,4,5-tetramethyl-1,3-dioxolane (*trans*-**9**) are δ 27.4, the signal of 2,2,4-trimethyl-1,3-dioxolane (**8**) at δ 27.2 is assigned to the methyl group *cis*, and that at δ 25.9, to the one *trans*, to the 4-methyl group. Much as in the case of **8**, the methyl carbon resonance of the *cis*-**9** at δ 28.7 is ascribed to the one *cis* to the methyl group at the 4- and 5-positions. The chemical shifts for one of the 2-methyl groups of **8** and *cis*-**9** are the same as those for the methyl groups of 2,2-dimethyl-1,3-dioxolane (**4**), while the chemical shifts for the alternative methyl groups *cis* to the 4-methyl one moved downfield by 1.5—3.0 ppm. This indicates the presence of a 1,3-transannular nonbonded interaction between 2-, and 4- and/or 5-methyl groups in the compounds which have two methyl groups at the 2-position. Although the two 2-methyl groups of *trans*-**9** are indistinguishable

TABLE 1. ^{13}C CHEMAICAL SHIFTS OF METHYL-1,3-DIOXOLANES

1,3-Dioxolane	2-Me	4-Me	5-Me	C-2	C-4	C-5
Parent (**1**)				95.1	64.7	64.7
2-Methyl- (**2**)	19.8			101.7	65.0	65.0
4-Methyl- (**3**)		18.1		95.0	72.3	71.0
2,2-Dimethyl- (**4**)	25.7			108.5	64.5	64.5
cis-2,4-Dimethyl- (*cis*-**5**)	20.2	18.9		101.6	73.0	71.0
trans-2,4-Dimethyl- (*trans*-**5**)	20.2	18.5		100.7	71.8	72.0
cis-4,5-Dimethyl- (*cis*-**6**)		14.7	14.7	93.6	74.1	74.1
trans-4,5-Dimethyl- (*trans*-**6**)		16.9	16.9	94.0	78.8	78.8
r-2,*c*-4,*c*-5-Trimethyl- (*r*-2, *c*-4, *c*-5-**7**)	20.9	15.6	15.6	100.3	74.8	74.8
r-2,*c*-4,*t*-5-Trimethyl- (*r*-2, *c*-4, *t*-5-**7**)	20.7	17.4	17.2	100.2	80.0	78.2
r-2,*t*-4,*t*-5-Trimethyl- (*r*-2, *t*-4, *t*-5-**7**)	21.3	14.3	14.3	99.6	74.3	74.3
2,2,4-Trimethyl- (**8**)	27.2(*c*)[a] 25.9(*t*)[b]	18.6		108.7	72.0	70.9
cis-2,2,4,5-Tetramethyl- (*cis*-**9**)	28.7(*c*) 25.8(*t*)	15.6	15.6	107.2	74.0	74.0
trans-2,2,4,5-Tetramethyl- (*trans*-**9**)	27.4	16.9	16.9	107.4	78.3	78.3

a) *cis* to the 4-methyl group. b) *trans* to the 4-methyl group.

in ^{13}C NMR, the carbon resonance at δ 27.4 implies the presence of the 1,3-transannular nonbonded interaction.

Experimental

NMR Spectra. The ^{13}C FT-NMR spectra were obtained at 25.15 MHz with a JEOL JNM-MH-100 instrument equipped with a JNM-MFT-100 Fourier transform accessory. Samples were observed in 5-mm spinning tubes with 25±5% solutions in $CDCl_3$ at 24 °C. All the chemical shifts are expressed in δ (ppm downfield from the internal TMS). Each observed chemical shift is estimated to be accurate to $\delta \pm 0.1$.

1,3-Dioxolanes. The compounds employed in this study were prepared by the methods of Dauben *et al.*[6] and Carmack and Kelley:[7] **1**, bp 74—76 °C; **2**, bp 81—83 °C, **3**, bp 82—85 °C; **4**, bp 92—93 °C; **5**, bp 91 °C, separated by preparative GLC; **6**, bp 74—85 °C, separated by preparative GLC; **7**, bp 80—90 °C, separated by preparative GLC; **8**, bp 95—98 °C; **9**, bp 67—69 °C, separated by preparative GLC. All the compounds were checked by analytical GLC and by means of the IR and ^1H NMR spectra.

References

1) S. A. Baker, E. J. Bourne, R. M. Pinkard, M. Stracy, and D. H. Whiffen, *J. Chem. Soc.*, **1958**, 3232.
2) M. Antheunis and F. Alderweireldt, *Bull. Soc. Chim. Belg.*, **73**, 889 (1964).
3) F. Kametani and Y. Sumi, *Chem. Pharm. Bull.*, **20**, 1479 (1972).
4) M. Christl, H. J. Reich, and J. D. Roberts, *J. Am. Chem. Soc.*, **93**, 3463 (1971).
5) W. E. Willy, G. Binsch, and E. L. Eliel, *J. Am. Chem. Soc.*, **92**, 5394 (1970).
6) H. J. Dauben, Jr., B. Löken, and H. J. Ringold, *J. Am. Chem. Soc.*, **76**, 1359 (1954).
7) M. Carmack and C. J. Kelley, *J. Org. Chem.*, **33**, 2171 (1968).

BULLETIN OF THE CHEMICAL SOCIETY OF JAPAN, VOL. 50 (10), 2815—2816 (1977)

The Radical Addition of Toluene to Fluorocyclobutenes

Hiroshi KIMOTO, Hiroshige MURAMATSU, and Kan INUKAI

Government Industrial Research Institute, Nagoya, Hirate-machi, Kita-ku, Nagoya 462

(Received March 4, 1977)

Synopsis. Fluorine-containing cyclobutane derivatives, 1-benzyl-1,2,2,3,3,4,-hexafluorocyclobutane (**1**) and 1,5,6,6,7,7-hexafluorobenzo[2,3]bicyclo[3.2.0]hept-2-ene (**2**), were synthesized in one step by the radical reaction of toluene and hexafluorocyclobutene. On the other hand, a similar reaction of toluene and 1,2-dichlorotetrafluorocyclobutene gave no adduct, but a substituted product, 1-benzyl-2-chlorotetrafluorocyclobutene (**4**).

In earlier papers, the radical addition reactions of such compounds as alcohols, ethers, and aldehydes to hexafluorocyclobutene (HFCB) and 1,2-dichlorotetrafluorocyclobutene (CFCB) have been reported to give the corresponding 1:1 adducts or their dehydrochlorinated products.[1] However, no investigation is known into the addition of aromatic compounds to these fluorocyclobutenes. In the present work, we carried out a di-*t*-butyl peroxide-induced reaction of toluene to HFCB and CFCB as a part of our synthetic studies of the free-radical addition of aromatic compounds to fluoro olefins.[2,3]

Two different reaction conditions, Methods A and B, were employed. In Method A, excess toluene to fluorocyclic olefins and small amounts of DTBP were used, whereas in Method B, equimolar amounts of toluene and cyclic fluoro olefins were reacted in the presence of large amounts of DTBP in an inert solvent. The conditions employed in Method A had been found suitable for the synthesis of 1:1 adducts, and those in Method B, for the preparation of cycloadducts.[2]

Addition Reaction of Toluene to Hexafluorocyclobutene.

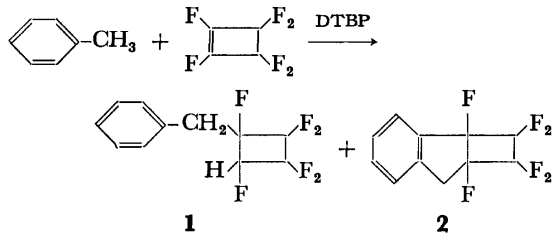

1 **2**

The reaction of toluene and HFCB by Method A afforded 1-benzyl-1,2,2,3,3,4-hexafluorocyclobutane (**1**) as a 1:1 adduct in a 25.6% yield, together with 1,5,6,6,7,7-hexafluorobenzo[2,3]bicyclo[3.2.0]hept-2-ene (**2**) as a cycloadduct in 1.7% yield. The GLC of **1** indicated the presence of two stereoisomers in the ratio of 86:14. The mass and IR spectra of these isomers give an almost identical pattern, and the NMR spectra show complex splitting due to H–F and F–F coupling. The assignment of their configurations is made on the basis of the internal chemical shift values between two non-equivalent fluorine atoms of CF_2 groups. The signals of the fluorine atoms of the CF_2 groups of the predominant isomer appear in the AB quartet (43.1 ppm, 55.3 ppm, $J_{F-F}^{gem}=226$ Hz) and are nearly equivalent as a broad singlet (50.5 ppm). Those of the other isomer appear in two AB quartets (39.4 ppm, 55.6 ppm, $J_{F-F}^{gem}=226$ Hz and 47.4 ppm, 53.4 ppm, $J_{F-F}^{gem}=226$ Hz). The fluorine chemical shifts in the cyclobutane series can be predicted by considering the electric-field effect of the neighboring substituents.[4] Since, in the *cis*-isomer, the electric-field effect of the substituents is additive on the same geminal fluorine nucleus, whereas in the *trans*-isomer this effect is partially compensated for, the *cis*-isomer should show a greater non-equivalence of the fluorine atoms of CF_2 groups than does the *trans*-isomer. Therefore, the predominant isomer is estimated to have the *trans*-configuration, in which a hydrogen and a benzyl group are on opposite sides of the plane of the four-membered ring. As will be mentioned later, the configuration of the *trans*-isomer is supported by the NMR spectrum of its oxidized product.

In order to increase the yield of the cycloadduct (**2**), the reaction was carried out by Method B. However, **2** was obtained in only a 4.9% yield, together with **1** (3.9% yield) and large amounts of a high-boiling residue. As compared with Method A, the yield of **1** in Method B decreased markedly, whereas that of **2** increased, though only slightly. The low yield of **2** may be due to the instability of the strained structure with the fused four-, five-, and six-membered ring.

1-Benzyl-2-methylhexafluorocyclobutane (**3**) was obtained as a by-product in a 2.7% yield. The mechanism for the formation of **3** may be explained in terms of the coupling of the benzyl radical and the 2-methyl-1,2,3,3,4,4-hexafluorocyclobutyl radical generated by the addition of a methyl radical to HFCB.

Although a similar reaction of cumene and HFCB was attempted, most of the HFCB was recovered and neither 1:1 adduct nor cycloadduct was obtained, presumably because of the steric hindrance of methyl groups

Addition Reaction of Toluene to 1,2-Dichlorotetrafluorocyclobutene. The reaction of toluene and CFCB gave benzyl chloride and 1-benzyl-2-chlorotetrafluorocyclobutene (**4**). The corresponding 1:1 adduct was not obtained. In Method A, the conversion of CFCB was low (14.5%) and the yield based on the amounts of CFCB consumed was 48.4%. In Method B, 28.4% of the CFCB was consumed and **4** was obtained in a 12.1% yield.

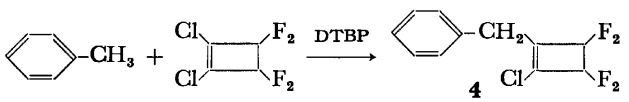

4

Thus, the substitution of a vinylic chlorine by a benzyl group occurred in the reaction of CFCB. The product, **4**, is probably formed by the chlorine elimination from an intermediate radical generated by the addition of a benzyl radical to CFCB. The different behavior between HFCB and CFCB in the radical

reaction with toluene seems to be due mainly to the difference in the carbon-halogen bond dissociation energy. Similar chlorine-substituted products have been reported to be obtained by the radical reaction of alkylbenzenes and chloro olefins.[5]

Oxidation of the Adducts. The methylene groups of **1** and **2** were oxidized to carbonyl groups. The oxidation of **1** by chromium trioxide afforded 1-benzoyl-1,2,2,3,3,4-hexafluorocyclobutane (**5**) in a 72.9% yield. The NMR spectrum of **5** is more simple than that of **1**. The *trans* configuration is also supported by a comparison of the chemical shifts and coupling constants of **5** with those of the 1:1 adduct which was obtained from the photochemical stereospecific *trans*-addition of trichlorosilane and HFCB.[6] A similar oxidation of **2** also gave 1,5,6,6,7,7-hexafluorobenzo[2,3]bicyclo[3.2.0]hept-2-en-4-one (**6**). An attempt to oxidize **4** was unsuccessful and gave only small amounts of benzoic acid. The oxidation of the double bond took place in the case of **4**.

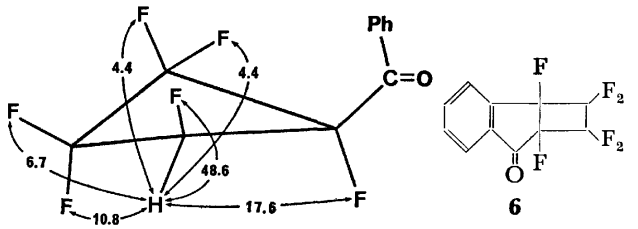

5

6

Experimental

Addition Reaction of Toluene and Hexafluorocyclobutene. *Method A*: A mixture of toluene (115 g, 1.25 mol), HFCB (53 g, 0.327 mol), and DTBP (7.5 g, 0.051 mol) was heated at 130—140 °C for 24 h. After the recovery of unchanged HFCB (11.4 g; conversion, 78.5%), the liquid product was distilled *in vacuo*. A crude 1:1 adduct (16.8 g) and a high-boiling residue (6.2 g) were obtained. Three components, two stereoisomers of the 1:1 adduct and a cycloadduct, were detected by GLC in the ratio of 80.5:13.0:6.5. They were separated by preparative GLC.

Trans-1-Benzyl-1,2,2,3,3,4-hexafluorocyclobutane (13.5 g, 20.6% yield): mp 30.8 °C; bp 188 °C; NMR (50% CCl_4 solution) δ 7.14 (5H, s), 3.13 (2H, d-m, 25.2 Hz), 4.92 (1H, d-m, 48.6 Hz), 92.3 (1F, m), 135.8 (1F, d), 43.1 and 55.3 (2F, AB, 226 Hz), 50.5 (2F, broad s); Found: C, 52.01; H, 3.22%. Calcd for $C_{11}H_8F_6$: C, 51.98; H, 3.17%, *cis*-1-benzyl-1,2,2,3,3,4-hexafluorocyclobutane (2.2 g, 3.3% yield): bp 200 °C; n_D^{20} 1.4363; d_4^{20} 1.385; NMR (20% CCl_4 solution) δ 7.1—7.4 (5H, m), 3.11 (2H, d-m, 25.2 Hz), 4.75 (1H, d-m, 50.8 Hz), 110.0 (1F, t-m), 138.8 (1F, d-m), 39.4 and 55.6 (2F, AB, 226 Hz), 47.4 and 53.4 (2F, AB, 226 Hz); Found: C, 52.08; H, 3.07%. Calcd for $C_{11}H_8F_6$: C, 51.98; H, 3.17% and 1,5,6,6,7,7-hexafluorobenzo[2,3]-bicyclo[3.2.0]hept-2-ene (1.1 g, 1.7% yield): bp 199 °C; n_D^{20} 1.4442; d_4^{20} 1.438; NMR (50% CCl_4 solution) δ 7.1—7.5 (4H, m), 3.2—3.7 (2H, AB), 112.3 (1F, m), 97.0 (1F, m), 47.1 and 53.6 (2F, AB, 218 Hz), 40.6 and 52.1 (2F, AB, 226 Hz); Found: C, 52.39; H, 2.68%. Calcd for $C_{11}H_6F_6$: C, 52.40; H, 2.40%.

Method B: A solution of toluene (46.1 g, 0.500 mol), HFCB (80.0 g, 0.494 mol) and DTBP (75 g, 0.513 mol) in 1,1,2-trichlorotrifluoroethane (187 g, 1.00 mol) was heated at temperatures gradually rising from 130 °C to 160 °C for about 6 h. The product was separated by vacuum distillation and preparative GLC to give **1** (4.9 g, 3.9% yield), **2** (6.1 g, 4.9% yield), and 1-benzyl-2-methylhexafluorocyclobutane[7] (3.6 g, 2.7% yield; bp 198—202 °C; n_D^{20} 1.4325; d_4^{20} 1.322; Found: C, 53.83; H, 3.99%. Calcd for $C_{12}H_{10}F_6$: C, 53.74; H, 3.76%), together with a high-boiling residue (57 g).

Addition Reaction of Toluene and 1,2-Dichlorotetrafluorocyclobutene. *Method A*: By a procedure similar to that described above, the reaction of toluene (115 g, 1.25 mol), CFCB (60.8 g, 0.312 mol), and DTBP (7.5 g, 0.051 mol) gave benzyl chloride (3.6 g), 1-benzyl-2-chlorotetrafluorocyclobutene (5.5 g, 48.4%; bp 209 °C; n_D^{20} 1.4687; d_4^{20} 1.321; IR $\nu_{C=C}$ 1655 cm^{-1}; NMR (50% CCl_4 solution) δ 7.0—7.2 (5H, m), 3.49 (2H, t-m, 2.6 Hz), 36.6 and 37.9 (4F, AA'BB'); Found: C, 52.76; H, 3.25%. Calcd for $C_{11}H_7ClF_4$: C, 52.72; H, 2.82%), and a high-boiling residue (2.3 g).

Method B: By a procedure similar to that described above, the reaction of toluene (46.1 g, 0.500 mol), CFCB (97.5 g, 0.500 mol), and DTBP (75 g, 0.513 mol) in 1,1,2-trichlorotrifluoroethane (187 g, 1.00 mol) gave benzyl chloride (12.7 g), **4** (4.3 g, 12.1% yield), and a high-boiling residue (23.4 g).

Oxidation of the Adducts. 1-Benzoyl-1,2,2,3,3,4-hexafluorocyclobutane (5): To a solution of chromium trioxide (3.0 g, 0.030 mol) in water (5 ml), a solution of **1** (2.6 g, 0.010 mol) in glacial acetic acid (15 ml) was added. The mixture was then refluxed for 16 hr and poured into an ice-cooled aqueous sodium hydrogen sulfite solution. Dichloromethane (100 ml) was then added, and the organic layer separated was washed and dried over magnesium sulfate. The solvent was allowed to evaporate to give an oily residue (2.6 g), which contained **5**, together with small amounts of unchanged **1**. Further purification was done by preparative GLC to give pure **5** (2.0 g, 72.9% yield): bp 215 °C; n_D^{20} 1.4530; d_4^{20} 1.467; IR $\nu_{C=O}$ 1705 cm^{-1}; NMR (50% CCl_4 solution) δ 7.2—7.9 (5H, m), 5.44 (1H, d-m, 48.6 Hz), 85.9 (1F, m), 132.2 (1F, d), 38.1 and 57.5 (2F, AB, 226 Hz), 46.9 (2F, broad s); Found: C, 49.19; H, 2.24%. Calcd for $C_{11}H_6OF_6$: C, 49.27; H, 2.26%.

1,5,6,6,7,7-Hexafluorobenzo[2,3]bicyclo[3.2.0]hept-2-en-4-one (6): By a similar procedure, the oxidation of a mixture (1.3 g) of **1** (40%) and **2** (60%) by chromium trioxide (2.0 g) gave a mixture (1.2 g) of **5** and **6**. They were separated by preparative GLC to give **6**: n_D^{20} 1.4629; IR $\nu_{C=O}$ 1754 cm^{-1}; NMR (5% CCl_4 solution) δ 7.6—8.0 (4H, m), 105.8 (1F, t-d-d), 123.3 (1F, d-d-d-d), 35.5 and 51.3 (2F, AB, 209 Hz), 40.2 and 49.1 (2F, AB, 226 Hz); Found: C, 49.58; H, 1.63%. Calcd for $C_{11}H_4OF_6$: C, 49.64; H, 1.51%.

References

1) H. Muramatsu and K. Inukai, *J. Org. Chem.*, **30**, 544; 2546 (1965); H. Muramatsu, S. Moriguchi, and K. Inukai, *ibid.*, **31**, 1306 (1966).

2) H. Kimoto, H. Muramatsu, and K. Inukai, *Chem. Lett.*, **1974**, 791; *Nippon Kagaku Kaishi*, **1975**, 665.

3) H. Kimoto, H. Muramatsu, and K. Inukai, *Bull. Chem. Soc. Jpn.*, **48**, 1335 (1975); **49**, 1642 (1976).

4) J. Feeney, L. H. Sutcliffe, and S. M. Walker, *Mol. Phys.*, **11**, 117 (1966).

5) L. Schmerling and J. P. West, *J. Am. Chem. Soc.*, **75**, 6216 (1953).

6) C. J. Attridge, M. G. Barlow, W. I. Bevan, D. Cooper, G. W. Cross, R. N. Haszeldine, J. Middleton, M. J. Newlands, and A. E. Tipping, *J. Chem. Soc., Dalton*, **1976**, 694.

7) A mixture of the two stereoisomers in the ratio of 60:40.

BULLETIN OF THE CHEMICAL SOCIETY OF JAPAN, VOL. 50 (10), 2817—2818 (1977)

The Synthesis of 3-Substituted Tropilidenes by the Dehydration of 1-Substituted 2,6-Cycloheptadienols. A New Unambiguous Route

Ken'ichi TAKEUCHI, Takashi MAEDA, and Kunio OKAMOTO

Department of Hydrocarbon Chemistry, Faculty of Engineering, Kyoto University, Sakyo-ku, Kyoto 606

(Received March 8, 1977)

Synopsis. 3-Alkyl-, 3-aryl-, and 3-deuteriotropilidenes are prepared in 21—29% yields by the dehydration of the corresponding 1-substituted 2,6-cycloheptadienols with boric acid. The present method provides an unambiguous route to the title compounds.

Several methods have been proposed for the synthesis of 1-, 2-, or 3-substituted tropilidenes. The relatively simple ones include: (a) the reaction of substituted tropylium ions with metal hydrides,[1] (b) the thermal[2] or photochemical[3] isomerization of 7-substituted tropilidenes, and (c) the ring-expansion of aromatic compounds with carbene.[4] However, such methods generally afford a mixture of isomeric substituted tropilidenes which are separated from each other only with considerable difficulty because of the similarity of the boiling points. Previously we reported an unambiguous route to 3-alkyl-2,4-dimethyltropilidenes which involves the addition of alkyllithiums to 2,7-dimethyl-2,6-cycloheptadienone and the subsequent dehydration of 1-alkyl-2,7-dimethyl-2,6-cycloheptadienols in the presence of boric acid.[5] In the present work the method has been applied to 2,6-cycloheptadienone (I), utilizing lithium aluminum deuteride or various alkyl- and phenyllithiums, in the hope of exploring a selective route to 3-substituted tropilidenes (III) (Eq. 1).

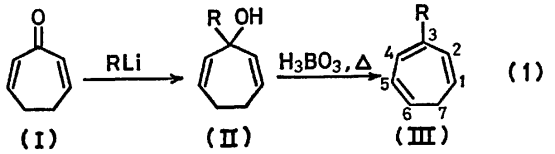

The alcohols (II) were obtained in approximately quantitative yields except for the cases of R=*i*-Pr or *t*-Bu.[6] The dehydration of the crude alcohols with boric acid,[7] followed by a single distillation, afforded 3-substituted tropilidenes (III) in a greater than 96% purity. The results of the synthesis are shown in Table 1. Although the yields of III are generally low (21—29%) because of the formation of polymers during dehydration, the excellent purity of the tropilidenes permits the use of the method applicable to the unambiguous synthesis of III. It should be noted that the present method provides a unique route to highly pure tropilidene-3-*d*, which has never been accessible by any other methods.

For comparison, the dehydration of 1-methyl-2,6-cycloheptadienol with boric anhydride, oxalic acid, or potassium bisulfate was examined. It was found that boric anhydride works much like boric acid, whereas oxalic acid and potassium bisulfate give 3-methyltropilidene in a purity of 89% in each case, the impurities being difficult to separate by repeated distillations.

Table 1. Results of the synthesis of 3-substituted tropilidenes

Lithium compound	3-Substituent	Yield[a] %	Purity %	Boiling point °C (Torr)
$LiAlH_4$	H	24	—	115—116
$LiAlD_4$	D	29	100[b]	115—116
MeLi	Me	25	96[c,d]	45— 48 (21)
i-PrLi	*i*-Pr	21	97[c,d]	99—100 (50)
c-PrLi	*c*-Pr	24	97[c,d]	58— 62 (70)
PhLi	Ph	29	99[c,d]	137—139 (3)

a) Overall isolated yield. b) Determined by NMR. c) Determined by GLC. d) Preparative GLC is required for further purification.

The extension of the present method to the selective synthesis of 1-substituted tropilidenes was attempted starting with 3,5-cycloheptadienone, but such an application was found not to be straightforward, since 3,5-cycloheptadienone, when treated with methyllithium, afforded the corresponding alcohol in a low yield (31%) and the rest of the starting ketone was recovered unchanged. Presumably the enolization of 3,5-cycloheptadienone is preferable to the addition reaction in the presence of methyllithium.

The present method has been successfully applied to the preparation of mixtures of isomeric disubstituted tropilidenes as the precursors of 1,2-disubstituted tropylium ions; the work will be reported elsewhere, together with the results of the one-electron reduction of substituted tropylium ions with chromium (II).[8]

Experimental

Materials. 2,6- and 3,5-Cycloheptadienones were prepared by the procedure of Garbisch.[9]

1-Substituted 2,6-Cycloheptadienols (II). 2,6-Cycloheptadienone was treated with a 30% excess amount of the appropriate lithium compound in anhydrous ether at 0—20 °C, except that the reaction with *t*-butyllithium was conducted at −72 °C. For isopropyllithium, pentane was used in place of ether as the solvent.[10] The NMR spectra of the crude product showed that all the lithium compounds, except for isopropyl- and *t*-butyllithium, gave the expected alcohols (II) in approximately quantitative yields. Isopropyllithium afforded a mixture composed of the expected alcohol and unidentified ketones, which were presumably formed by the 1,4-addition reaction. A detailed characterization of the products has not been carried out. *t*-Butyllithium failed to give 1-*t*-butyl-2,6-cycloheptadienol, as demonstrated by the IR spectrum of the crude product; instead, it afforded a mixture of unidentified ketones and ether-insoluble polymers.

Table 2. NMR spectra of 3-substituted tropilidenes

3-Substituent R	δ, ppm CCl_4, 60 MHz)							Coupling constant, Hz
	H-1	H-2	H-4	H-5	H-6	H-7	R	
D	5.25	6.12	6.48	6.05	5.25	2.20	—	$J_{1,2}=J_{5,6}=9.0$ $J_{1,7}=J_{6,7}=6.4$ $J_{4,5}=3.0$
Me	≈5.20	5.92	6.28	5.97	≈5.20	2.17	2.03 s	$J_{1,2}=J_{5,6}=9.2$ $J_{1,7}=J_{6,7}=6.2$ $J_{4,5}=6.0$
i-Pr	≈5.23	6.02	6.32	6.00	≈5.23	2.15	1.10 d 2.50 m	$J_{1,2}=J_{5,6}=9.2$ $J_{1,7}=J_{6,7}=6.6$ $J_{4,5}=6.0$
c-Pr	≈5.15	5.75	6.21	5.89	≈5.15	2.12	0.63 m 1.57 m	$J_{1,2}=J_{5,6}=9.0$ $J_{1,7}=J_{6,7}=6.0$ $J_{4,5}=6.0$
Ph	≈5.37	6.28	6.80	6.17	≈5.37	2.25	7.25 m	$J_{1,2}=J_{5,6}=8.6$ $J_{1,7}=J_{6,7}=7.0$ $J_{4,5}=6.0$

In each case the crude product was used in the dehydration step without further purification.

Dehydration of 1-Substituted 2,6-Cycloheptadienols. Crude 1-substituted 2,6-cycloheptadienol prepared from 20 mmol of 2,6-cycloheptadienone was mixed with pulverized boric acid (20 mmol) in a short test tube provided with a glass tube connected to a receiver, and the mixture was heated in an oil bath at 150 °C for five min. The pressure of the system was gradually reduced until the products distilled out and thereafter kept constant. The temperature of the oil bath was then gradually raised to 200 °C. The distillate was extracted with ether, dried, and subjected to distillation. The structure of the 3-substituted tropilidenes was determined by means of NMR; the data are shown in Table 2.

References

1) K. Conrow, *J. Am. Chem. Soc.*, **83**, 2343 (1961).
2) A. P. Ter Borg, H. Kloosterziel, and N. Van Meurs, *Rec. Trav. Chim.*, **82**, 717 (1963); A. P. Ter Borg and H. Kloosterziel, *ibid.*, **82**, 741 (1963).
3) A. P. Ter Borg and H. Kloosterziel, *Rec. Trav. Chim.*, **84**, 241 (1965).
4) E. Müller, H. Kessler, H. Fricke, and W. Kiedaisch, *Justus Liebigs Ann. Chem.*, **675**, 63 (1964).
5) K. Takeuchi, K. Yasuda, and K. Okamoto, *Chem. Lett.*, **1976**, 715.
6) See Experimental section.
7) The use of boric acid had been reported in the dehydration of 2,6,6-trimethyl-2,4-cycloheptadienol to 3,7,7-trimethyltropilidene; J. R. B. Campbell, A. M. Islam, and R. A. Raphael, *J. Chem. Soc.*, **1956**, 4096.
8) For the latest publication, see K. Takeuchi, K. Komatsu K. Yasuda, and K. Okamoto, *Tetrahedron Lett.*, **1976**, 3467.
9) E. W. Garbisch, Jr., *J. Org. Chem.*, **30**, 2111 (1965).
10) H. Gilman, F. W. Moore, and O. Baine, *J. Am. Chem. Soc.*, **63**, 2479 (1941).

BULLETIN OF THE CHEMICAL SOCIETY OF JAPAN, VOL. 50 (10), 2819—2820 (1977)

The Effects of Solvents on the Electronic Absorption Spectrum of Sodium 4-Nitrophenoxide in the Presence of 15-Crown-5 Ether

Shinichi UEJI and Masayuki KITADANI

Institute of Chemistry, College of General Education, Kobe University, Tsurukabuto, Nada, Kobe 657

(Received April 14, 1977)

Synopsis. The electronic absorption spectrum of sodium 4-nitrophenoxide was determined in 21 solvents of varying polarities by the aid of the ability of 15-crown-5 ether to solubilize the salt in nonpolar solvents. These spectra showed a marked difference between hydroxylic solvents and nonhydroxylic solvents. A possible interpretation for this difference is presented.

In the course of our study of the relationships between solvent polarity parameters and solvent-induced spectral shifts in spectroscopic investigations, we previously observed interesting solvent effects on the IR frequency shifts[1] and on the NMR chemical shifts.[2] In this report the effects of solvents on the electronic absorption spectrum of sodium 4-nitrophenoxide will be discussed on the basis of the correlation between the solvent shifts and Dimroth's solvent polarity parameter, E_t (hereafter abbreviated as D's E_t), values.[3]

Results and Discussion

The Table summarizes the solvent-induced spectral shifts for sodium 4-nitrophenoxide relative to 4-nitroanisole in a range of solvents. In certain nonpolar solvents, in order to obtain a solubility of the salt sufficient for the measurement of the λ_{max} value, a large excess of the sodium chelatent, 15-crown-5 ether, was used. Since it is desirable that solvent shifts be compared under the same conditions, all the spectra were measured in the presence of a large excess of the crown ether. The crown ether's effects on the spectra are also given in the Table.

It is found that the enhanced red shifts ($-\Delta\nu_{max}$ values in the Table) are correlated well by the D's E_t values (see Figure). As can be seen in the Figure, however, the correlation is separated into two set of straight lines,

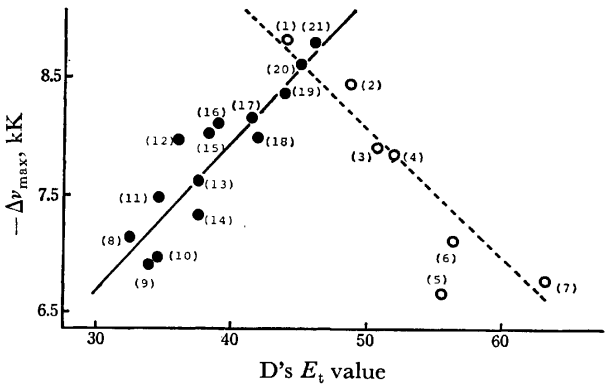

Figure. Correlation between $-\Delta\nu_{max}$ value and D's E_t value.
(○): Hydroxylic solvents, (●): nonhydroxylic solvents.

TABLE ELECTRONIC SPECTRAL SHIFTS FOR SODIUM 4-NITROPHENOXIDE (I) RELATIVE TO 4-NITROANISOLE (II) IN THE PRESENCE OF 15-CROWN-5 ETHER IN A RANGE OF SOLVENTS[a]

Solvents	λ_{max} nm (I)[b]	λ_{max} nm (II)	$-\Delta\nu_{max}$ kK[c]	D's E_t value
(1) *t*-Butyl alcohol	421.0(+1)	307.0	8.82	43.9
(2) Isopropyl alcohol	414.5(0)	307.0	8.44	48.6
(3) *n*-Propyl alcohol	407.0(0)	308.0	7.90	50.7
(4) Ethanol	406.0(0)	308.0	7.84	51.9
(5) Methanol	389.0(0)	309.0	6.65	55.5
(6) Ethylene glycol	407.5(0)	316.0	7.11	56.3
(7) Water	403.5	317.0	6.77	63.1
(8) CCl_4	385.0[d]	302.0	7.14	32.5
(9) Toluene	391.0[d]	308.0	6.89	33.9
(10) Benzene	393.0[d]	308.5	6.96	34.5
(11) Diethyl ether	391.0[d]	302.5	7.48	34.6
(12) Dioxane	407.5(+1)	307.5	7.98	36.0
(13) THF	404.0[d]	309.0	7.61	37.4
(14) Bromobenzene	406.0[d]	313.0	7.32	37.5
(15) 1,2-Dimethoxyethane	410.0(+3)	308.5	8.02	38.2
(16) $CHCl_3$	417.5[d]	312.0	8.10	39.1
(17) Dichloromethane	420.0[d]	313.0	8.14	41.4
(18) Dichloroethane	416.0[d]	312.5	7.98	41.9
(19) DMF	435.5(0)	319.0	8.36	43.8
(20) DMSO	438.0(0)	318.0	8.62	45.0
(21) Acetonitrile	429.0(0)	311.5	8.79	46.0

a) The apporopriate compound (II) was used as a reference standard, because the solvation effects on 4-nitrophenyl portion are assumed to be similar in both compounds; reproducibility <1 nm. b) The λ_{max} value is attributed to a $\pi\rightarrow\pi^*$ transition with the character of an intramolecular charge transfer from the oxygen anion to the hydrocarbon portion. The values in parentheses represent the magnitude of the crown ether effect on the λ_{max} value; positive numbers indicate red shifts. c) Enhanced red shifts for Compound (I) as compared with Compound (II);
$-\Delta\nu_{max}$, kK $= [1/\lambda\,(\mathrm{I}) - 1/\lambda\,(\mathrm{II})] \times 10^4$
d) Not sufficiently soluble in the absence of 15-crown-5 ether.

one for hydroxylic solvents and the other for nonhydroxylic solvents. Furthermore, it should be noted that the slopes of the two straight lines show opposite signs.

In the hydroxylic solvents, the phenoxide anion is presumably present as a cation-free anion rather than as sufficiently tight ion aggregates, because the anion is supposed to be strongly solvated by hydrogen bonding. Indeed, the addition of crown ether produces essentially no effect on the λ_{max} value (see Table). Therefore, it seems reasonable to assume that the hydroxylic solvent-

induced shifts are mainly due to the direct H-bonding solvation of the phenoxide anion. A stronger H-bonding solvation should produce a larger blue shift, because the oxygen of phenoxide is more negative in the ground state than in the excited state. In fact, the decreasing order of the $-\Delta\nu_{max}$ values is consistent with the α-scale of solvent H-bond donor acidities (HBD)[4] reported by Taft and Kamlet, except for the case of methanol. Furthermore, the parallelism between the $-\Delta\nu_{max}$ value and the D's E_t value (see Figure) suggests the operation of similar H-bonding solvation mechanisms, because the D's E_t value is based on the electronic transition of the pyridinium betain with the phenoxide anion site.

On the other hand, the nonhydroxylic solvents are presumed to be poor anion solvators, so that direct solvations of the phenoxide anion can be neglected. The nonhydroxylic solvent shifts can be interpreted by assuming an interaction between the sodium cation bound by the crown ether and the phenoxide anion. It is known[5] that the D's E_t value is correlated with such measures of the ionizing power of solvents as Winstein's Y value[6] and Kosower's Z value.[7] Therefore, the increasing D's E_t value may be expected to cause a larger charge separation between the sodium cation bound by the crown ether and the phenoxide anion, and this charge separation should produce red shifts.[8] Indeed, the observed red shifts are found to be proportional to the D's E_t value (see Figure). Furthermore, the absence of any effect of crown ether in the dipolar aprotic solvents suggests that the salt is a relatively free ion.

Consequently, the $-\Delta\nu_{max}$ value –D's E_t value correlation revealed a difference in the solvation mechanism of sodium 4-nitrophenoxide between the hydroxylic solvents and the nonhydroxylic solvents.[9]

Experimental

The electronic spectra were obtained using a Hitachi 124 automatic recording spectrophotometer. A quartz cell 1.0 cm in length was employed, and the concentration of the sample was of the order of 10^{-4} M.

Sodium 4-nitrophenoxide was prepared by a known method and dried *in vacuo* at 110 °C overnight. The solvents were freshly distilled before use, and the spectro-grade solvents were used without further purification, except for chloroform, which was chromatographed on alumina. The 15-crown-5-ether was a commercial sample (Aldrich Chemical Company, Inc.).

References

1) S. Ueji and T. Kinugasa, *Tetrahedron Lett.*, **1976**, 2037.
2) S. Ueji and M. Nakamura, *Tetrahedron Lett.*, **1976**, 2549.
3) K. Dimroth, C. Reichardt, T. Siepmann, and F. Bohlmann, *Ann.*, **661**, 1 (1963).
4) R. W. Taft and M. J. Kamlet, *J. Am. Chem. Soc.*, **98**, 2886 (1976). The α-scale of HBD increases in the order: [Solvents (1)<(2)<(3)<(4)<(5)<(5)<(6)<(7)].
5) E. M. Kosower,"Physical Organic Chemistry," John-Wiley & Sons, New York (1968), p. 303.
6) E. Grunwald and S. Winstein, *J. Am. Chem. Soc.*, **73**, 2700 (1951).
7) E. M. Kosower, *J. Am. Chem. Soc.*, **80**, 3253, 3261, 3267 (1958).
8) H. E. Haugg and A. D. Schaefer, *J. Am. Chem. Soc.*, **87**, 1587 (1965); J. F. Garst, R. A. Klein, D. Walmsley, and E. R. Zabolotny, *ibid.*, **87**, 4087 (1965); R. C. Kerber, and A. Porter, *ibid.*, **91**, 366 (1969).
9) This result is analogous to the chemical result with regard to the alkylation of phenoxides and naphthoxides [N. Kornblum, P. J. Berrigan, and J. Noble, *J. Am. Chem. Soc.*, **82**, 1257 (1960); **85**, 1141 (1963)].

BULLETIN OF THE CHEMICAL SOCIETY OF JAPAN, VOL. 50 (10), 2821—2822 (1977)

Studies of Lignoids in *Lauraceae*. III.[1] A New Lignan from the Heart Wood of *Cinnamomum Camphora* Sieb.

Daisuke TAKAOKA, Minoru IMOOKA, and Mitsuru HIROI

Department of Chemistry, Faculty of Science, Ehime University, Bunkyo-cho, Matsuyama 790

(Received April 16, 1977)

Synopsis. From the heart wood of *Cinnamomum Camphora* Sieb., a new lignan, (−)-*trans*-2-(3,4-dimethoxybenzyl)-3-(3,4,5-trimethoxybenzyl)butyrolactone [I] and 3-hydroxy-5,7-dimethoxy-3′,4′-methylenedioxyflavan [IV], were isolated, and their structures were determined.

In a previous report,[2] we described the isolation and structural determination of several lignans from the leaves of four kinds of *Cinnamomum Camphora*, the camphor tree.[3] We will report here a new lignan, (−)-*trans*-2-(3,4-dimethoxybenzyl)-3-(3,4,5-trimethoxybenzyl)-butyrolactone [I] and 3-hydroxy-5,7-dimethoxy-3′,4′-methylenedioxyflavan [IV], isolated from the heart wood of the "sesquiterpene tree,"[3] a kind of camphor tree which contains nerolidol as a major component of the leaf oil, along with dimethylmatairesinol [II] and kusunokinin [III].[2]

Results

(−)-trans-*2-(3,4-Dimethoxybenzyl)-3-(3,4,5-trimethoxybenzyl)butyrolactone [I].* This compound is a γ-lactone (ν_{max}^{KBr} 1760 cm^{-1}). The NMR spectrum of aliphatic protons indicates that this compound has a *trans*-substituted γ-lactone ring, as in the case of dimethylmatairesinol;[2] δ (ppm) 2.55 (4H, m), 2.90 (2H, m), and 3.8—4.25 (2H, m). Five methoxyl groups are also detectable.

In the region of aromatic protons, the signal at δ 6.18 ppm (2H, s) indicates two protons of a symmetric trimethoxybenzyl group, *i.e.*, either the 3,4,5-trimethoxybenzyl or the 2,4,6-trimethoxybenzyl group. Of them, the latter can be excluded because the chemical shifts of benzyl C**H**$_2$ are almost identical with those of dimethylmatairesinol; *i.e.*, benzyl CH$_2$ is not flanked by two methoxyl groups.

The signals at δ 6.61 (1H, d, J=8 Hz), 6.68 (1H, br s), and 6.75 ppm (1H, d, J=8 Hz) show three protons of a dimethoxybenzyl group which has two protons located at positions ortho to each other-, *i.e.*, the 3,4-, 2,4- or 2,5-dimethoxybenzyl group. It may be supposed that the 3,4-dimethoxybenzyl group is the most probable from the fact that the signals of the three protons appear in a narrow range and that the two coupled protons are not so equivalent. This supposition is confirmed by the co-occurence of this compound with dimethylmatairesinol [II] and kusunokinin [III].

From these results, this compound is determined to be either *trans*-2-(3,4-dimethoxybenzyl)-3-(3,4,5-trimethoxybenzyl)butyrolactone [I] or *trans*-2-(3,4,5-trimethoxybenzyl)-3-(3,4-dimethoxybenzyl)butyrolactone [Ia].

The MS spectrum shows an ion of *m/e* 208. The fragmentation (Scheme 1) is considered to proceed in the same manner as in the case of kusunokinin,[2] and the formation of this ion can be explained on the basis of [I, but not on that of Ia.]

The CD curve of this compound shows a negative Cotton effect at 235 and 270 nm, as in the case of thujaplicatin methyl ether and related compounds.[4] Therefore, the absolute configuration may be concluded to be 2R, 3R.

(−)-trans-*3-Hydroxy-5,7-dimethoxy-3′,4′-methylenedioxyflavan (IV).* The IR spectrum shows an OH group (3300 cm^{-1}). The NMR spectrum shows a methylenedioxy group, two methoxy groups, and five aromatic protons. The B ring is a 1,3,4-trisubstituted one, because its protons appear as a singlet at δ 7.14 ppm, and there are two doublets (J=8 Hz), at δ 6.91 and 7.06 ppm, all benig finely splitted. The A ring is a 1,2,3,5-tetrasubstituted one, because two protons appear as two doublets (J=3 Hz) at δ 6.19 and 6.27 ppm, as in the case of tetramethylcatechin.[5] H-2 and H-3 are supposed to be located *trans* to each other, because H-2 appears as a doublet (J=2 Hz) at δ 4.99 ppm (equatorial-equatorial coupling). This supposition is confirmed by the very small signal of M$^+$−18 in the

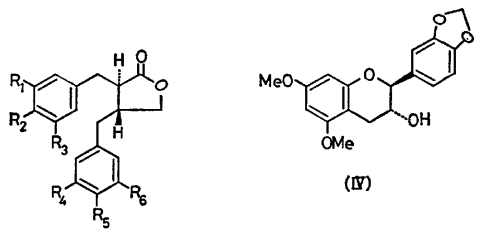

(IV)

(I) R_1, R_2, R_4, R_5, R_6 : OMe , R_3:H

(Ia) R_1, R_2, R_3, R_5, R_6 : OMe , R_4:H

(II) R_1, R_2, R_4, R_5 : OMe , R_3, R_6:H

(III) R_1 R_2 : OCH_2O , R_4, R_5 : OMe , R_3, R_6:H

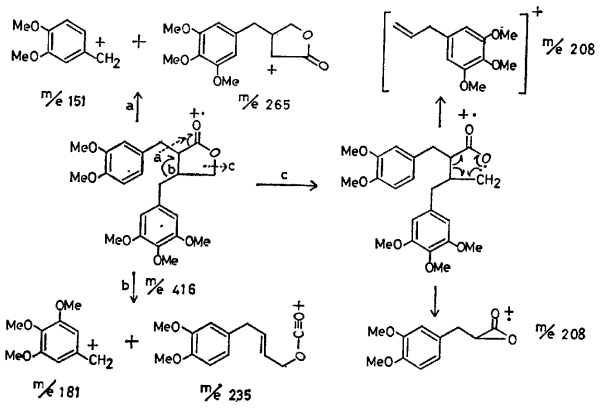

Scheme 1.

MS spectrum (resistant to dehydration[6]). Therefore, this compound is identified as *trans*-3-hydroxy-5,7-dimethoxy-3′,4′-methylenedioxyflavan [IV].

Experimental

Instruments. The CD curve, and the IR, NMR, UV, and MS spectra were obtained by using ORD UV-5 (JASCO), IR-400 (Shimadzu), JNM-4H-100 (JEOL), ESP-3T (Hitachi), and JMS-OlSG-2 (JEOL) apparatuses respectively. $[\alpha]_D$ was measured by the use of a Yanako OR-50 (Yanagimoto) apparatus, and elemental analyses were carried out with a CHN Corder MT-2 (Yanagimoto).

Isolation. Shaves of the heart wood (10 kg) of the tree (10 years old) were extracted with hexane; the hexane solution was then concentrated in *vacuo* and steam-distilled to remove any volatile components. The residue (70 g) was dissolved in hexane and chromatographed on a silica gel column (solvent: hexane: ethyl acetate=100: 0—0: 100) into 22 fractions.

The 19 th fraction (3.7 g) was rechromatographed on a silica gel column (solvent: benzene: ethyl acetate=75: 25) into 18 fractions. From the second fraction, [III] was isolated by TLC.

The 20 th fraction of the first chromatography (4.8 g) was rechromatographed on a silica gel column (solvent: benzene: ethyl acetate=100: 0—0: 100) into 8 fractions. A crystalline material (mp 106—107 °C) was obtained from the second fraction by TLC; this substance shows one spot on TLC with benzene–ethyl acetate (60: 40), but with hexane–chloroform–methanol (6: 3: 1) it shows two spots, which were separated by TLC. The less polar compounds was identified by means of its spectral data as [II].

The more polar compound [I]: a minor component, mp 120—121.5 °C, λ_{max}^{EtOH} 229 nm ($\varepsilon=1.4\times10^4$), 280 nm ($\varepsilon=3.2\times10^3$), $[\alpha]_D$ −17.8° ($c=0.51$ in $CHCl_3$). Found: C, 66.4%; H, 6.2%. Calcd for $C_{23}H_{28}O_7$: C, 66.3%; H, 6.7%. IR cm^{-1} (KBr): 1760, 1590, 1510. NMR (δ ppm in $CDCl_3$): 2.55 (4H, m), 2.90 (2H, m), 3.28 (s), 3.32 (s) (15H), 3.8—4.25 (2H, m), 6.18 (2H, s), 6.61 (1H, d, J=8Hz), 6.68 (1H, br s), 6.75 (1H, d, J=8 Hz). MS: *m/e* 416 (M^+), 386 (M^+-30), 265, 235, 209, 208, 181, 151 (base peak).

The 17 th fraction of the first chromatography (3.0 g) was rechromatographed into 8 fractions in the same manner as in the case of the 19 th fraction. From the 3 rd fraction, a crystalline substance [IV] was isolated by TLC: a minor component, mp 164—165 °C, $[\alpha]_D$ −39.3° ($c=0.84$ in $CHCl_3$), λ_{max}^{EtOH} 286 nm ($\varepsilon=3.4\times10^3$). Found: C, 65.8%; H, 5.2%. Calcd for $C_{18}H_{18}O_6$: C, 65.5%, H, 5.5%. IR cm^{-1} (KBr) 3300, 1610, 1490. NMR (δ in $CDCl_3$): 1.82 (1H, d, J=6 Hz, **OH**), 2.95 (2H, m, H_2-4), 3.83 (6H, s, 2×CH_3O), 4.28 (1H, m, H-3), 4.99 (1H, d, J=2 Hz, H-2), 6.03 (2H, s, OCH_2O), 6.19 (1H, d, J=3 Hz, H-8 or H-6), 6.27 (1H, d, J=3 Hz, H-6 or H-8), 6.91 (1H, d, J=8 Hz, H-5′ or H-6′), 7.05 (1H, d, J=8 Hz, H-6′ or H-5′), and 7.14 ppm (1H, s, H-2′).

References

1) Previous report: D. Takaoka, K. Watanabe, and M Hiroi, *Bull. Chem. Soc. Jpn.*, **49**, 3564 (1976).

2) D. Takaoka, N. Takamatsu, Y. Saeki, K. Kohono, C. Nakaoka, and M. Hiroi, *Nippon Kagaku Kaishi*, **1975**, 2192.

3) N. Hirota, *Mem. Ehime Univ.*, Sect, II, 1, No. 2, 1 (1951).

4) S. Nishibe, S. Hisada, and I. Inagaki, *Yakugaku Zasshi*, **94**, 522 (1974).

5) N. S. Bhacca, D. P. Hollis, L. F. Johnson, and E. A. Pier,"NMR Spectra Catalog," Vol. 2, Varian Associates, Palo Alto, California (1963), Spectr. No. 679.

6) T. Okamoto, T. Murakami, and H. Itokawa,"Tennenbutsu Kagaku," Hirokawa Publishing Co., Tokyo (1963), p. 114.

BULLETIN OF THE CHEMICAL SOCIETY OF JAPAN, VOL. 50 (10), 2823—2824 (1977)

Preparation of Mannich Bases from 6-Methoxy-2*H*-pyran-3(6*H*)-one and Its Epoxide

Sigeru TORII, Hideo TANAKA, and Hisasi TAKAO

Department of Industrial Chemistry, School of Engineering, Okayama University, Okayama 700

(Received March 10, 1977)

Synopsis. 4-Morpholinomethyl-2*H*-pyran-3(6*H*)-ones **3** and **8** were prepared directly from 6-methoxy-2*H*-pyran-3(6*H*)-one (**1**) and its epoxide **4** by treatment with morpholine and aqueous 37% formalin in methanol in 70—88% yield. The mechanisms of the reaction have been discussed on the basis of the intermediates 5,6-dimethoxytetrahydropyran-3-one (**2**), 2,6-dimethoxy-5-hydroxytetrahydropyran-3-one (**5**), 2,6-dimethoxy-2*H*-pyran-3(6*H*)-one (**6**), and 2,5,6-trimethoxytetrahydropyran-3-one (**7**).

Potential biological activities of Mannich bases along with their very reactive properties have aroused great interest.[1] In connection with our interest in the chemistry of 2*H*-pyran-3(6*H*)-ones[2] we report here our studies on 6-methoxy-2*H*-pyran-3(6*H*)-one (**1**) and its epoxide **4**, functionalized with morpholinomethyl group as a Mannich base.

Various studies have been made on Mannich synthesis, but investigations of the reaction at the α position of α,β-unsaturated carbonyl compounds are very limited.[3] No report seems to have appeared on the reaction with α,β-epoxy carbonyl compounds.

The Mannich products **3** and **8** were synthesized directly from the reactive intermediates **1** and **4**.[2] The 4-morpholinomethyl derivatives **3** and **8** could be prepared in several steps *via* 5-methoxytetrahydropyran-3-ones **2** and **7**. The latter case in particular reveals the fact that introduction of methoxyl function as well as the morpholinomethyl group could be achieved at C-2 and C-4 positions of **4**, respectively.

*Conversion of **1** and **2** into **3**.* Stirring **1** in methanol with potassium hydroxide below 5 °C gave **2** in 92% yield.[4] Both **1** and **2** could be converted into the Mannich adduct **3** in 70—84% yields by treatment with morpholine and aqueous formalin in methanol at 45—70 °C for 4—6 h. Under the reaction conditions proton abstraction from C-4 position of **2** followed by nucleophilic attack to formaldehyde would give the Mannich adduct **3**. A possible mechanism for the direct conversion of **1** into **3** can be also rationalized by considering the formation of the intermediate **2**.

*Conversion of **4**, **6**, and **7** into **8**.* Treatment of **4** in methanol with potassium hydroxide at 15—20 °C for 3 h gave **5** in 74% yield together with a small amount of **7**. Addition of the excess base increased the formation of **7**. The treatment of **5** with a mixture of acetic anhydride and pyridine at room temperature for 6 h gave the enone **6**, whereas a similar treatment of **7** afforded the acetate **9** in 97% yield. The transformation of **4**, **6**, and **7** into **8** in 83—88% yields was carried out by heating with morpholine and aqueous 37% formalin in methanol at 40—65 °C for 3—4 h. A plausible mechanism for the formation of the Mannich adduct **8** directly from **4** can be formulated as follows.

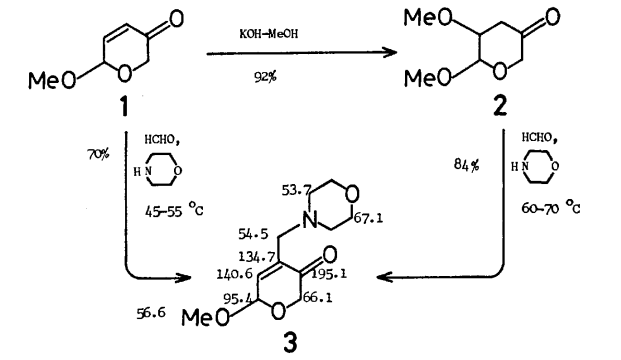

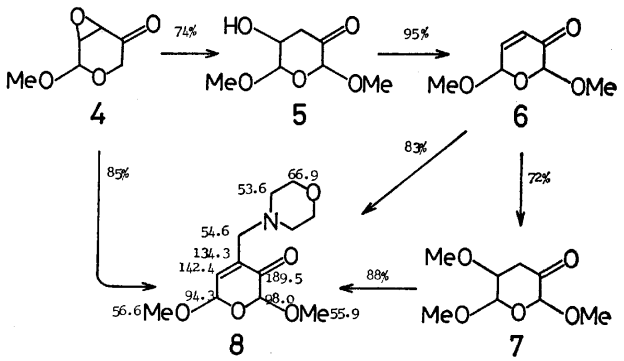

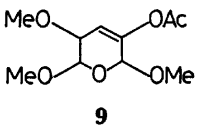

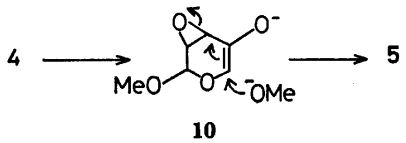

In the presence of morpholine as a base, methoxide ion would be able to react with **10** at C-2 position to give **5**. Subsequent dehydration in the medium would afford **6** smoothly. The assignments of carbon 13 NMR spectra of **3** and **8** are shown on the structural formula.

Experimental

Boiling points are uncorrected. IR spectra were determined with a JASCO IRA-I infrared recording spectrophotometer fitted with a grating. PMR spectra were determined at 60 MHz with a Hitachi R-24 spectrometer. The chemical

shift values are expressed in δ values (ppm) relative to a Me_4Si internal standard. CMR spectra were taken at 25.05 MHz in the Fourier mode with a JEOL FX-100 spectrometer. Samples were dissolved in $CDCl_3$ containing Me_4Si as an internal standard. The mass spectra were obtained with a JEOL Model JMS-OIBM-2, ionizing voltage 75 eV.

5,6-Dimethoxytetrahydropyran-3-one (2). To a mixture of KOH (20 mg) in MeOH (4 ml) was added dropwise a solution of **1**[2] (200 mg, 1.56 mmol) in MeOH (1 ml) at 0—5 °C. The mixture was stirred below 5 °C for 10 min and quenched with 5% aqueous tartaric acid. The mixture was poured into ice water, extracted with AcOEt, washed with brine, and dried ($MgSO_4$). Removal of the solvent gave **2** (239 mg, 92%): bp 61—64 °C/2 Torr; IR (neat) 1732 cm^{-1} (C=O); PMR ($CDCl_3$) δ 2.70 (m, 2, CH_2), 3.39 (s, 3, CH_3O), 3.50 (s, 3, CH_3O), 3.67 (m, 1, CHO), 4.00 (s, 2, CH_2O), 4.77 (d, 1, J=2 Hz, OCHO).

6-Methoxy-4-morpholinomethyl-2H-pyran-3(6H)-one (3). To a solution of **2** (116 mg, 0.72 mmol) and morpholine (73 mg, 0.86 mmol) in MeOH (2 ml) was added dropwise aqueous 37% formalin (67 mg, 0.83 mmol) at room temp. The mixture was stirred at 60—70 °C for 4 h. After removal of the solvent, the residue was chromatographed (SiO_2, benzene–AcOEt/3: 1) to give **3** (137 mg, 84%) as a pale yellow oil: bp 91—96 °C/0.005 Torr; IR (neat) 1688 cm^{-1} (C=O); PMR ($CDCl_3$) δ 2.44 (m, 4, CH_2N), 3.15 (t, 2, J=1 Hz, CH_2N), 3.51 (s, 3, CH_3O), 3.69 (m, 4, CH_2O), 4.10 (d, 1, J=16 Hz, CH_2O), 4.40 (d, 1, J=16 Hz, CH_2O), 5.15 (d, 1, J=4 Hz, CHO), 6.86 (m, 1, HC=C). Found: C, 57.91; H, 7.53%. Calcd for $C_{11}H_{17}NO_4$: C, 58.14; H, 7.54%.

Morpholinomethyl Derivative 3 from 1. To a solution of **1** (136 mg, 1.06 mmol) in MeOH (3 ml) was added dropwise morpholine (130 mg, 1.50 mmol) and aqueous 37% formalin (119 mg, 1.50 mmol). The mixture was stirred at 45—55 °C for 6 h and concentrated. The residue was chromatographed (SiO_2, benzene–AcOEt/3: 1) to give **2** (167 mg, 70%) as a pale yellow viscous oil, whose IR and PMR spectral data were identical with those given above.

2,6-Dimethoxy-5-hydroxytetrahydropyran-3-one (5). To a solution of **4** (287 mg, 1.99 mmol) in MeOH (3 ml) was added dropwise a 0.2 M KOH–MeOH solution (2 ml) at 5—10 °C. The mixture was stirred for 3 h at 15—20 °C and then neutralized with aqueous 5% tartaric acid. After removal of the solvent, the residue was taken up in AcOEt, washed with brine, and dried (Na_2SO_4). Removal of the solvent gave **5** (258 mg, 74%) as a yellow oil, after being chromatographed (SiO_2, benzene–AcOEt/3: 1): IR (neat) 3420 (OH), 1742 cm^{-1} (C=O); PMR ($CDCl_3$) δ 2.73 (d, 1, J=7 Hz, CH_2), 2.75 (d, 1, J=6 Hz, CH_2), 3.14 (broad, 1, OH), 3.53 (s, 3, CH_3O), 3.56 (s, 3, CH_3O), 3.90 (m, 1, CHO), 4.65 (s, 1, CHO), 4.83 (d, 1, J=6 Hz, OCHO). Found: C, 47.73; H, 6.85%. Calcd for $C_7H_{12}O_5$: C, 47.73; H, 6.87%.

2,6-Dimethoxy-2H-pyran-3(6H)-one (6). A mixture of **5**(122 mg, 0.69 mmol), pyridine (0.5 ml) and Ac_2O (0.5 ml) was stirred at room temp for 6 h. The mixture was poured into 2 M HCl. The organic phase was extracted with AcOEt, washed with aqueous $NaHCO_3$, and dried (Na_2SO_4). Removal of the solvent gave **6** (104 mg, 95%) as a pale yellow oil: bp 61—64 °C/1 Torr; IR (neat) 1708 (C=O), 1632 cm^{-1} (C=C); PMR ($CDCl_3$) δ 3.46 (s, 3, CH_3O), 3.52 (s, 3, CH_3O), 4.76 (s, 1, CHO), 5.35 (m, 1, CHO), 6.04 (dd, 1, J=2 Hz, J=11 Hz, HC=C), 6.78 (dd, 1, J=2 Hz, J=11Hz, HC=C); MS *m/e* (rel intensity, %) 158 (M^+, 22), 144 (12), 127 (31), 116 (100), 98 (57), 55 (15), 43 (58). Found: C, 53.31; H, 6.13%. Calcd for $C_7H_{10}O_4$: C, 53.16; H, 6.37%.

2,5,6-Trimethoxytetrahydropyran-3-one (7). To a solution of **6** (218 mg, 1.38 mmol) in MeOH (3 ml) was added dropwise a MeOH–KOH solution (0.2 M, 2 ml) at 0—5 °C. After being stirred at 0—5 °C for 30 min, the mixture was neutralized with aqueous 5% tartaric acid. The mixture was poured into brine and extracted with AcOEt. The extracts were washed with brine, dried (Na_2SO_4), and concentrated, giving **7** (188 mg, 72%) as a pale yellow oil: bp 64—67 °C/1 Torr; IR (neat) 1742 cm^{-1} (C=O); PMR ($CDCl_3$) δ 2.73 (d, 1, J=9 Hz, CH_2), 2.75 (d, 1, J=5 Hz, CH_2), 3.42, 3.53, 3.58 (s, 9, CH_3O), 3.60 (m, 1, CHO), 4.71 (s, 1, CHC=O), 4.88 (d, 1, J=5 Hz, CHO). Found: C, 50.36; H, 7.64%. Calcd for $C_8H_{14}O_5$: C, 50.52; H, 7.42%.

2,6-Dimethoxy-4-morpholinomethyl-2H-pyran-3(6H)-one (8) from 7. A mixture of **7** (116 mg, 0.61 mmol), aqueous 37% formalin (67 mg, 0.82 mmol), and morpholine (75 mg, 0.89 mmol) in MeOH (2 ml) was stirred at 55—65 °C for 4 h. After removal of the solvent, the residue was chromatographed (SiO_2, benzene–AcOEt/3: 1) to give **8** (137 mg, 88%) as a pale yellow oil: bp 81—84 °C/0.04 Torr; IR (neat) 1700 cm^{-1} (C=O); PMR ($CDCl_3$) δ 2.42 (m, 4, CH_2N), 3.14 (t, 2, J=2 Hz, CH_2N), 3.52, 3.54 (s, 6, CH_3O), 3.65 (m, 4, CH_2O), 4.92 (s, 1, CHC=O), 5.47 (m, 1, CHO), 6.84 (m, 1, HC=C); MS *m/e* (rel intensity, %) 257 (M^+, 53), 225 (76), 196 (70), 121 (27), 100 (100), 83 (31), 56 (27), Found: C, 55.99; H, 7.37%. Calcd for $C_{12}H_{19}NO_5$: C, 56.02; H, 7.44%.

Morpholinomethyl Derivative 8 from 6. A mixture of **6** (158 mg, 1.00 mmol), aqueous 37% formalin (97 mg, 1.16 mmol) and morpholine (104 mg, 1.20 mmol), in MeOH (3 ml) was heated for 4 h at 45—55 °C. After work-up in a similar way to that described above, **8** (213 mg, 83%) was obtained.

Morpholinomethyl Derivative 8 from 4. To a solution of **4** (590 mg, 4.09 mmol) and morpholine (460 mg, 5.48 mmol) in MeOH (5 ml) was added dropwise aqueous 37% formalin (443 mg, 5.47 mmol) at room temp and the mixture was heated at 55—65 °C for 4 h. After work-up in a similar way to that above, **8** (892 mg, 85%) was obtained.

3-Acetyl-2,5,6-trimethoxy-5,6-dihydro-2H-pyran (9). A solution of **7** (101 mg, 0.53 mmol) in a mixed solution of pyridine (0.5 ml) and Ac_2O (0.5 ml) was stirred at room temp for 12 h. After work-up in a similar way to that above, **9** (120 mg, 97%) was obtained as a colorless oil: bp 93—97 °C/1 Torr; IR (neat 1764 cm^{-1} (AcO); PMR ($CDCl_3$) δ 2.17 (s, 3, CH_3CO), 3.45, 3.50, 3.57 (s, 9, CH_3O), 3.88 (m, 1, CHO), 4.77 (d, 1, J=6 Hz, HC=C), 5.09 (s, 1, HCC=O), 5.68 (d, 1, J=3 Hz, CHO). Found: C, 51.70; H, 6.86%. Calcd for $C_{10}H_{16}O_6$: C, 51.72; H, 6.94%.

References

1) M. Tramontini, *Synthesis*, **1973**, 703 and references cited therein.

2) S. Torii, H. Tanaka, T. Anoda, and Y. Simizu, *Chem. Lett.*, **1976**, 495.

3) a) K. Bodendorf and P. Kloss, *Justus Liebigs Ann. Chem.*, **677**, 95 (1964); (b) W. J. Serfontein and H. H. E. Schroeder, *J. S. African. Chem. Inst.*, **19**, 38 (1966); *Chem. Abstr.*, **65**, 13700 (1966).

4) O. Achmatowicz, *Rocz. Chem.*, **47**, 99 (1973); *Chem. Abstr.*, **79**, 19026 (1973).

BULLETIN OF THE CHEMICAL SOCIETY OF JAPAN, VOL. 50 (10), 2825—2826 (1977)

Cyclopropanes from Allylic Halides. I. Synthesis of Dimethyl 3-(2-Methyl-1-propenyl)-2,2-dimethylcyclopropane-1,1-dicarboxylate and Pyrocin as Precursors of Chrysanthemic Acid

Sigeru TORII, Hideo TANAKA, and Yosio NAGAI

Department of Industrial Chemistry, School of Engineering, Okayama University, Okayama 700

(Received May 9, 1977)

Synopsis. Dimethyl 3-(2-methyl-1-propenyl)-2,2-dimethyl-cyclopropane-1,1-dicarboxylate and pyrocin as precursors of chrysanthemic acid were synthesized by the reaction of (2-halo-2-methylpropylidene)malonate with 2-methyl-1-propenylmagnesium bromide.

Chrysanthemic acid (**1**), an important moiety of pyrethrins and a naturally occurring pesticide, has been a subject of interest as regards its synthesis.[1] In contrast to the nucleophilic substitution reaction of allylic halides taking place at the α- or γ-position, nucleophilic attack with cyanide at the β-carbon of allylic halides **2**

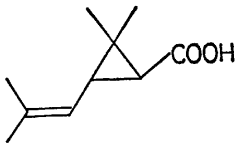

1

bearing alkoxycarbonyl groups in the γ-position followed by cyclization, giving cyclopropanecarboxylates **3**, was observed.[2] The diverse nature of allylic halides prompted us to examine the reaction of dimethyl (2-halo-2-methylpropylidene)malonate (**4**) with various nucleophiles.

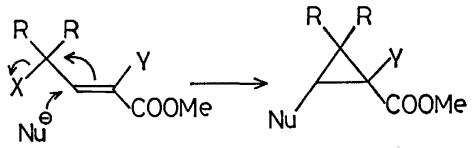

2 **3**

The present paper describes the results obtained in the reaction of **4** with 2-methyl-1-propenylmagnesium bromide[3] as a nucleophile as well as the synthesis of pyrocin (**7b**)[4] using the same starting materials.

(2-Halo-2-methylpropylidene)malonate (**4**) was treated with 2-methyl-1-propenylmagnesium bromide in tetrahydrofuran under the conditions given in Table 1. Chloride **4a** was allowed to react with 2-methyl-1-propenylmagnesium bromide at 24 °C for 45 h to give the desired **5** in 46% yield as well as 11% of **6** and the recovered **4a** (30%) (run 1), whereas the reaction at 45 °C for 18 h resulted in a mixture of 55% of **5**, 19% of **6**, and 14% of **7a** (run 2). When the same reaction was carried out in the presence of catalytic amounts of copper(I) chloride,[5] most of **4a** was consumed within 45 min, giving 51% of **5** and 37% of **6** along with minor product **7a** (4%) (run 3). The presence of a good leaving group in the allylic halide **4** is not sufficient for the reaction, since the same reaction with **4b** (runs 4 and 5) carried out at 24 °C afforded the dehalogenated product **6** principally[6] and **5** showed only 25—32% yields as compared to 46—55% for **5** from **4a**.

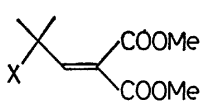

4a, X=Cl
b, X=Br

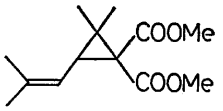

5

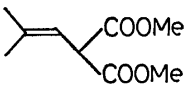

6

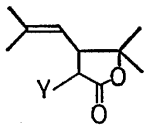

7a, Y=COOMe
b Y=H

The ambident ion **8** is believed to be formed by an unusual nucleophilic reaction of 2-methyl-1-propenide ion on the β-position of **4**. The formation of the cyclopropane ring of **5** can be rationalized by S_N2 type nucleophilic attack of the carbanion of **8** to the γ-position (Path a), while the formation of the parent compound **7a** could be attributed to nucleophilic attack by the enolate ion at the γ-position (Path b).

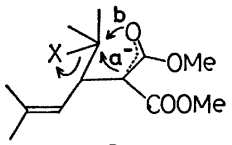

8

When **4b** was heated to 170 °C for 2 h under nitrogen, the 2-butenolide **9** was obtained in 76% yield. Subsequently, Michael addition of **9** with 2-methyl-1-propenylmagnesium bromide gave **7a** in 85% yield.[7] Demeth oxycarbonylation of **7a** in wet dimethyl sulfoxide-sodium chloride at 170 °C afforded pyrocin (**7b**) smoothly.

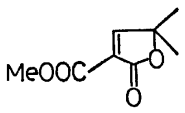

9

Experimental

All boiling points and melting points were uncorrected, the boiling points indicated being air-bath temperatures. Ir spectra were recorded on a Japan Spectroscopic Co., Ltd., IRA-I infrared recording spectrophotometer with a grating.

Table 1. Reaction of **4a** and **4b** with 2-methyl-1-propenylmagnesium bromide

Run	Substrate (mmol)	>=\MgBr mmol	Additive	Temp °C	Time h	Products, %[a]			
						5	**6**	**7a**	**4**
1	**4a** (0.6)	1.4	none	24	45	46	11	—	30
2	**4a** (4.5)	9.0	none	45	18	55	19	14	—
3	**4a** (0.6)	2.0	CuCl[b]	45	0.75	51	37	4	5
4	**4b** (0.7)	0.8	CuCl[b]	24	0.75	25	47	5	7
5	**4b** (0.6)	1.0	none	24	12	32	56	12	—

a) Isolated Yields. b) Copper(I) chloride (10 mg) was added.

NMR spectra were recorded at 60 MHz on a Hitachi R-24 spectrometer with an internal standard of tetramethylsilan. Elemental analyses were carried out in this laboratory.

Dimethyl (2-Chloro-2-methylpropylidene)malonate (4a). A mixture of dimethyl (2-methylpropylidene)malonate[8] (3.0 g, 16.1 mmol), *t*-butyl hypochlorite[9] (2.0 g, 18.4 mmol), and azobisisobutyronitile (AIBN) (30 mg) in CCl_4 (3 ml) was heated under reflux for 2 h. After removal of the volatile substance, CCl_4 (3 ml), *t*-butyl hypochlorite (2.0 g, 18.4 mmol) and AIBN (30 mg) were added to the residue. The resulting mixture was refluxed for 2 h. The operation was repeated 5 times and the resulting **oil** was distilled to give **4a** (1.78 g, 50%): bp 75—77 °C/3 Torr; IR (neat) 1740 (C=O), 1651 cm^{-1}, (C=C); NMR ($CDCl_3$) δ 1.76 (s, 6, CH_3CCl), 3.77 (s, 6 CH_3), 6.93 (s, 1, HC=C). Found: C, 49.17; H, 6.01%. Calcd for $C_9H_{13}O_4$: C, 48.99; H, 5.94%.

Dimethyl (2-Bromo-2-methylpropylidene)malonate (4b). **4b** was prepared by bromination of dimethyl (2-methylpropylidene)malonate with *N*-bromosuccinimide, bp 92—95 °C/18 Torr, according to the reported procedure.[10]

Dimethyl 2,2-Dimethyl-3-(2-methyl-1-propenyl)cyclopropane-1,1-dicarboxylate (5). The reaction conditions and results are given in Table 1. A typical experimental procedure (run 2) is as follows: To aTHF solution (3 ml) of **4a** (1.0 g, 4.5 mmol) was added dropwise a THF solution (7 ml) of 2-methyl-1-propenylmagnesium bromide,[3] prepared from 2-methyl-1-propenyl bromide (1.22 g, 9.0 mmol) and magnesium (0.22 g, 9.0 mmol) at room temperature. After being stirred for 30 min at this temperature and for 18 h at 45 °C, the mixture was quenched with aqueous 10% NH_4Cl, extracted with ether, washed with brine and dried (Na_2SO_4). Removal of the solvent followed by column chromatography (SiO_2, THF–hexane, 1/20) gave **5** (597 mg, 55%), **6** (160 mg, 19%), and **7a** (143 mg, 14%).

Compound 5: Bp 81—84 °C/10 Torr; IR (neat) 1730 cm^{-1} (C=O); NMR ($CDCl_3$) δ 1.23 (s, 3, CH_3), 1.27 (s, 3, CH_3), 1.74 (br s, 6, CH_3C=C), 2.44 (d, 1, J=8 Hz, CH), 3.68 (s, 3, CH_3O), 3.72 (s, 3, CH_3O), 5.02 (diffused d, 1, J=8 Hz, HC=C). Found: C, 64.99; H, 8.59%. Calcd for $C_{13}H_{20}O_4$: C, 64.98; H, 8.39%.

Compound 6: Bp 73—76 °C/8 Torr: IR (neat) 1735 cm^{-1} (C=O); NMR ($CDCl_3$) δ 1.67 (diffused s, 3, CH_3C=C), 1.77 (diffused s, 3, CH_3C=C), 3.71 (s, 6, CH_3O), 4.24 (d, 1, J= 9 Hz, CHCO), 5.43 (diffused d, 1, J=9 Hz, HC=C). Found C, 58.29; H, 7.47%. Calcd for $C_9H_{14}O_4$: C, 58.05; H, 7.58%.

Compound 7a: Mp 81—81.5 °C (hexane–ether, 10/1); IR (Nujol) 1770 (lactone C=O), 1734 (C=O), 1675 cm^{-1} (C=C); NMR ($CDCl_3$) δ 1.27 (s, 3, CH_3), 1.44 (s, 3, CH_3), 1.73 (m, 6, CH_3C=C), 3.48 (d, 1, J=10 Hz, CHC=O), 3.56 (dd, 1, J=5 and 10 Hz, CHC=C), 3.76 (s, 3, CH_3O), 4.98 (diffused d, 1, J=5 Hz, HC=C). Found: C, 63.82; H, 8.05%. Calcd for $C_{12}H_{18}O_4$: C, 63.70; H, 8.02%.

4,4-Dimethyl-2-methoxycarbonyl-2-butenolide (9). The diester **4b** (940 mg, 3.55 mmol) was heated in a Claisen flask to 170 °C for 2 h under N_2 and then distilled to give **9** (456 mg, 76%): bp 90—95 °C/5 Torr; mp 72—73 °C (hexane); IR (Nujol) 1758 (lactone C=O), 1721 (C=O), 1640 cm^{-1} (C=C); NMR ($CDCl_3$) δ 1.54 (s, 6, CH_3), 3.87 (s, 3, CH_3O), 8.08 (s, 1, HC=C). Found: C, 56.43; H, 5.79%. Calcd for $C_8H_{10}O_4$: C, 56,47; H, 5.92%.

4,4-Dimethyl-3-(2-methyl-1-propenyl)-2-(methoxycarbonyl)butanolide (7a). To a THF solution (3 ml) of **9** (100 mg, 0.95 mmol) was added dropwise a THF solution (2 ml) of 2-methyl-1-propenylmagnesium bromide, prepared from 2-methyl-1-propenyl bromide (135 mg, 1.0 mmol) and magnesium (24 mg, 1.0 mmol) at room temperature. After being stirred for 16 h at this temperature, the mixture was quenched with aqueous 10% NH_4Cl, extracted with ether, washed with brine and dried (Na_2SO_4). Removal of the solvents followed by chromatography (SiO_2, hexane–ether, 20/1) gave **7a** (113 mg, 85%): mp 81—81.5 °C (hexane–ether, 10/1). The IR and NMR spectra were identical with those described above.

Pyrocin (7b). A solution of **7a** (40 mg, 0.18 mmol) in DMSO (1.24 ml) containing NaCl (5 mg) and a few drops of water was heated in a sealed tube at 170 °C for 1 h. The mixture was diluted with water and extracted with ether. The extract was washed with brine, dried (Na_2SO_4), and concentrated *in vacuo*. A short-path distillation of the residue gave **7b** (21 mg, 71%): bp 80—85 °C/3 Torr (lit,[4] bp 130—137 °C/17 Torr). The IR and NMR spectra were identical with those reported.[4]

References

1) M. J. Devos, L. Hevesi, P. Bayet, and A. Krief, *Tetrahedron Lett.*, **1976**, 3911 and references cited therein.

2) P. Kolsaker and H. J. Storesund, *J. Chem. Soc., Chem Commun.*, **1972**, 375; similar reactions of **2** (X=Cl, Br; Y= H, Ph; R=Me and/or H) with sodium methoxide and/or phenylmagnesium bromide, giving **3**, have been reported: R. Rambaud, *C. R. Acad. Sci.*, **228**, 1595 (1949); R. S. Ratney and English, Jr., *J. Org. Chem.*, **25**, 2213 (1960).

3) H. Normant,"Advances in Organic Chemistry," Vol II, Intersciences Publishers Inc., New York, N. Y. (1960), p. 1.

4) K. Ueda and M. Mastui, *Agr. Biol. Chem.*, **34**, 1115 (1970) and references cited therein.

5) M. S. Kharash and P. O. Tawney, *J. Am. Chem. Soc.*, **63**, 2308 (1941).

6) H. O. House,"Modern Synthetic Reactions," 2 nd ed, W. A. Benjamin Inc., Menlo Park, Califonia (1972), p. 219.

7) A. Takada, T. Sakai, S. Shinohara, and T. Tsuboi, *Bull. Chem. Soc. Jpn.*, **50**, 1133 (1977).

8) A. C. Cope, C. M. Hofmann, C. Wyckoff, and E. Hardenbergh, *J. Am. Chem. Soc.*, **63**, 3452 (1941).

9) M. J. Mintz and C. Walling, *Org. Synth.*, **49**, 9 (1969).

10) W. Herz, *J. Am. Chem. Soc.*, **78**, 1485 (1956).

BULLETIN OF THE CHEMICAL SOCIETY OF JAPAN, VOL. 50 (10), 2827—2828 (1977)

Aryl Alkanehydrazonates and Their Thio Analogs. Synthesis of Some 2-Alkyl Derivatives of 4*H*-1,3,4-Benzoxadiazines and 4*H*-1,3,4-Benzothiadiazines

Ahmad Sami SHAWALI[1] and Hamdi Mahmoud HASSANEEN*,[2]

Department of Chemistry, Faculty of Science, University of Kuwait, State of Kuwait

**Department of Chemistry, Faculty of Science, University of Cairo, Giza, Egypt*

(Received November 24, 1976)

Synopsis. Synthesis of some *p*-nitrophenyl alkanethiohydrazonates, $RC(SC_6H_4NO_2\text{-}p)=NNHC_6H_3BrNO_2(2,4^-)$, and *p*-nitrophenyl alkanehydrazonates, $RC(OC_6H_4NO_2\text{-}p)=NNHC_6H_3BrNO_2(2,4^-)$ is described. Upon treatment with triethylamine in ethanol at reflux the thiohydrazonates give directly 2-alkyl-4-(*p*-nitrophenyl)-7-nitro-4*H*-1,3,4-benzothiadiazines, whereas the hydrazonates yield the hydrazides, $RCONHN(C_6H_4NO_2\text{-}p)C_6H_3BrNO_2(2,4^-)$. The latter hydrazides can be cyclized, under stronger basic conditions, into 2-alkyl-4-(*p*-nitrophenyl)-7-nitro-4*H*-1,3,4-benzoxadiazines by displacement of the 2-bromine atom.

We have been exploring the synthesis and thermal rearrangement of several hydrazonate esters of type I (Z=aryl, C_2H_5OOC, C_6H_5NHCO, and X=O or S).[3-6] We wish now to describe the synthesis of some alkanethiohydrazonates (II, R=alkyl and X=S) and the use of such esters in the synthesis of 2-alkyl derivatives of 4*H*-1,3,4-benzoxadiazines (III, X=O) and the thiadiazine analogs (III, X=S) respectively.

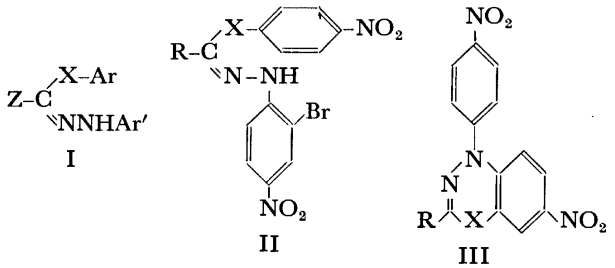

I II III

a, X=S; R=CH_3 d, X=O; R=$(CH_3)_2CH$
b, X=S; R=CH_3CH_2 e, X=O; R=CH_3
c, X=S; R=$(CH_3)_2CH$

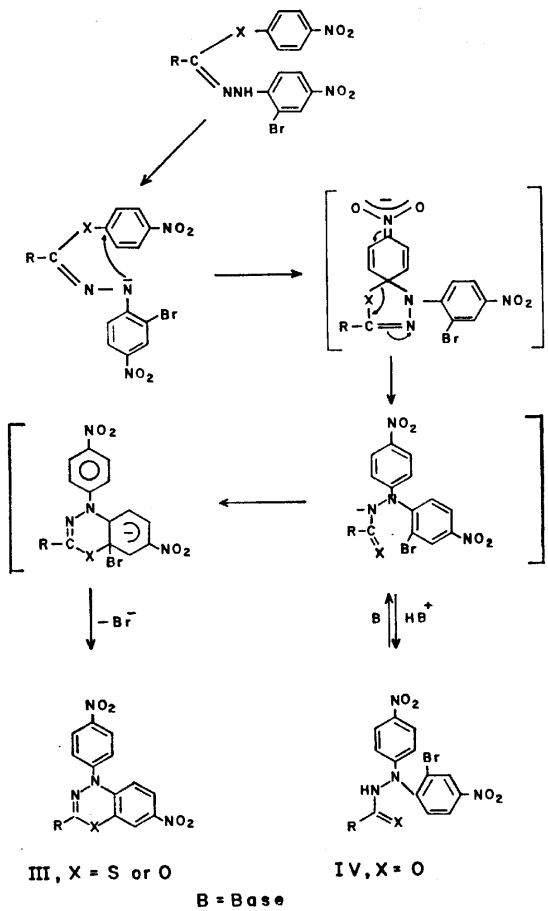

III, X = S or O IV, X = O

B = Base

Scheme 1.

The required *S*-*p*-nitrophenyl alkanethiohydrazonates, IIa to IIc, were obtained by treating the corresponding alkanehydrazonoyl bromides with *p*-nitrobenzenethiol in ethanol in the presence of triethylamine at room temperature. The other alkanehydrazonates, IId and IIe, were similarly prepared using *p*-nitrophenol in place of *p*-nitrobenzenethiol. The structures of these esters were confirmed by their elemental analysis and the spectral data. For example, esters IId and IIe exhibited in infrared spectra bands at 1250 and 1065 cm^{-1} assignable to an aryl ether linkage. Their electronic absorption pattern in ethanol was of typical hydrazones.

Treatment of thiohydrazonate IIa with triethylamine in ethanol at reflux gave the corresponding thiadiazine, IIIa. The other thiohydrazonates, IIb and IIc, similarly gave the thiadiazines, IIIb and IIIc, respectively. The structures of the latter products were evidenced by their elemental analysis and spectra (see Experimental). To account for this, it is assumed that the reaction proceeds through the formation of the anionic species of the rearranged thiohydrazide (IV, X=S), which undergoes cyclization to thiadiazine (III, X=S) as it is formed (Scheme 1). This is analogous to the reaction of arenehydrazonoyl bromides with thioacetate ion[7] and the recently reported rearrangement of aryl thiohydrazonates.[8]

In contrast to thiohydrazonates IIa to IIc, hydrazonates IId and IIe rearranged to the corresponding hydrazides (IV, X=O) in refluxing ethanol-triethylamine generally within 100 min. The structures of the latter hydrazides,

$$R\text{-}CX\text{-}NHN(C_6H_4NO_2\text{-}p)C_6H_3BrNO_2(2,4^-)$$
IV

were evidenced by the appearance of bands at 1680 cm^{-1}

Table 1. *p*-Nitrophenyl alkanehydrazonates and their thio analogs

Compd No.	Mp, °C	Molecular formula	C, % Found	C, % (Calcd)	H, % Found	H, % (Calcd)	N, % Found	N, % (Calcd)
IIa[a]	156	$C_{14}H_{11}N_4O_4BrS$	41.05	(40.88)	2.76	(2.69)	13.60	(13.62)
IIb	132	$C_{15}H_{13}N_4O_4BrS$	42.50	(42.36)	2.87	(3.08)	13.31	(13.17)
IIc	113	$C_{16}H_{15}N_4O_4BrS$	43.74	(43.74)	3.33	(3.44)	12.65	(12.75)
IId[b]	151	$C_{16}H_{15}N_4O_5BrS$	45.44	(45.40)	3.59	(3.57)	13.43	(13.24)
IIe	188	$C_{14}H_{11}N_4O_5Br$	42.39	(42.54)	2.87	(2.80)	14.29	(14.28)

a) λ_{max}^{EtOH} (log ε) 363 (4.383); 320 (4.156) b, nm; $\bar{\nu}$ (KBr) 3297 (NH); 1344 (C–S–C) cm^{-1}; $\delta(CDCl_3)$ 2.14 (s, 3H, CH_3), 7.0—8.40 (m, 8H, ArH and hydrazone NH) ppm. b) λ_{max}^{EtOH} (log ε) 363 (4.321), 325 sh (4.156), 260 sh (4.010) nm; $\bar{\nu}$(KBr) 3375 (NH), 1336, 1038 (aryl ether linkage) cm^{-1}; $\delta(CDCl_3)$ 1.28 (d, 6H, J=7 Hz, $(CH_3)_2CH$), 2.75 (septet, 1H, J=7 Hz, $(CH_3)_2CH$), 7.0—8.6 (m, 8H, ArH and hydrazone NH) ppm.

(CO) and the absence of the Ar–O–C bands in their infrared spectra. This base catalyzed rearrangement of II to IV (X=O) appears to follow nucleophilic substitution mechanism (Scheme 1) rather than the free radical sequence proposed for the thermally induced rearrangement of aryl arenecarbohydrazonates to *N*-aroyl-*N'*,*N'*-diarylhydrazines.[9] The *p*-nitro substituent in the *O*-aryl moiety probably increases the stability of the five-membered cyclic transition state. In this respect the present O→N aryl migration can be seen as a Smiles-type rearrangement;[10] in agreement with the views of Elliott *et al.*[11] who indicated that aryl arenecarbohydrazonates substituted such that the *O*-aryl ring is sufficiently electron deficient, undergo a facile base-catalyzed Smiles rearrangement to give the corresponding hydrazides.

The cyclization of IV (X=O) into III (X=O) was effected only by boiling with an equivalent amount of sodium hydroxide in *N*,*N*-dimethylformamide–triethylamine mixture for 10 h. The structure of the benzoxadiazines prepared followed their elemental analysis and was confirmed by the absence of NH and CO absorption bands in their infrared spectra. The mechanism favoured for this cyclization seems to be analogous to that proposed for the cyclization of IV—III (X=S); *i.e.*, the anionic species derived from the hydrazide is thought to attack the 2-position of the 2-bromo-4-nitrophenyl group to form the heterocyclic ring by nucleophilic displacement of bromine.

Experimental

All melting points are uncorrected. Microanalyses were performed by Alfred Berhardt, Mikroanalytische Laboratorium, West Germany. The IR and UV spectra were recorded with Pye-Unicam SP 1000 and SP 8000 spectrophotometers respectively. PMR spectra were recorded on a Varian T60A spectrometer using tetramethylsilane as an internal reference.

Alkanehydrazonoyl bromides were prepared by literature method;[12] their physical constants (mp.s) corresponded with data reported.[12]

p-Nitrophenyl *N*-(2-bromo-4-nitrophenyl)alkanehydrazonates (IId—e) and their thio analogs (II—ac). General Procedure. A mixture of hydrazonoyl bromide (0.01 mol), *p*-nitrophenol (or *p*-nitrobenzenethiol) (0.01 mol) and triethylamine (0.02 mol) in ethanol (50 ml) was stirred at room temperature for 1 h. The product that precipitated was collected, washed with water and purified by crystallization from ethanol. The results are summarized in Table 1.

N-Isobutyryl-N'-(2-bromo-4-nitrophenyl)-N'-(p-nitrophenyl)-hydrazine (IVd). The hydrazonate IId in 1: 1 (v/v) ethanol–triethylamine mixture was refluxed for 1 h. The reaction mixture was then concentrated, diluted with water and the solid formed was collected. Crystallization from methanol gave the hydrazide IVd, mp 168 °C. Found: C, 45.41; H, 3.50: N, 13.20%. Calcd for $C_{16}H_{15}N_4O_5Br$: C, 45.40; H, 3.57; N, 13.24%. $\bar{\nu}$(KBr) 1680 (CO); 3250 (NH) cm^{-1}; λ_{max}^{EtOH} (log ε) 363 (4.274); 325 (3.997) sh; 260 (3.912) sh; δ ($CDCl_3$) 1.22 (d, 6H, J=7 Hz, $(CH_3)_2CH$) 2.58 (septet, 1H, J=7 Hz, Me_2CH); 7.0—8.6 (m, 8H, ArH and hydrazide NH) ppm.

2-Isopropyl-4-(p-nitrophenyl)-7-nitro-4H-1,3,4-benzoxadiazine, IIId. Equivalent amounts of the hydrazide IVd and sodium hydroxide were dissolved in a mixture of *N*,*N*-dimethylformamide and triethylamine and refluxed for 10 h. The solution was then cooled, poured into excess of 5% acetic acid. The solid that precipitated was collected and washed with water. Crystallization from methanol gave IIId in 50% yield, mp 165 °C. Found: C, 55.98; H, 4.20; N, 16.20%. Calcd for $C_{16}H_{14}N_4O_5$: C, 56.14; H, 4.12; N, 16.36%. $\bar{\nu}$(KBr) 1350, 1040 (cyclic ether).

2-Alkyl-4-(p-nitrophenyl)-7-nitro-4H-1,3,4-benzothiadiazines, IIIa—c. The appropriate thiohydrazonate (0.5 g) was refluxed in a 1: 1 (v/v) mixture of ethanol and triethylamine (40 ml) for 4 h. The solution was then concentrated and the solid that separated on cooling was collected. Crystallization from dioxane gave the following benzothiadiazines.

Compound IIIa, mp 240 °C. Found: C, 50.90; H, 3.13; N, 16.59%. Calcd for $C_{14}H_{10}N_4O_4S$: C, 50.90; H, 3.05; N, 16.96%. λ_{max}^{EtOH} (log ε) 410 (4.163); 295 sh (3.833) nm; $\delta(CDCl_3)$ 2.40 (s, 3H, 2-CH_3); 7.0—8.4 (m, 7H, ArH) ppm.

Compound IIIb, mp 180 °C. Found: C, 51.95; H, 4.10; N, 16.23%. Calcd for $C_{15}H_{12}N_4O_4S$: C, 52.32; H, 3.51; N, 16.27%.

Compound IIIc, mp 160 °C. Found: C, 53.41; H, 3.78; N, 15.41%. Calcd for $C_{16}H_{14}N_4O_4S$: C, 53.62; H, 3.93; N, 15.63%.

References

1) To whom all inquiries should be addressed.
2) Taken in part from the Ph.D. Thesis of H. M. Hassaneen,
3) A. S. Shawali and H. M. Hassaneen, *Tetrahedron Lett.*, **1972**, 1299.
4) A. S. Shawali and H. M. Hassaneen, *Tetrahedron* **28**, 5903 (1972).
5) A. S. Shawali and M. K. Ahmad, *Bull. Chem. Soc. Jpn.*, **46**, 3625 (1973).
6) A. S. Shawali, N. F. Eweiss, H. M. Hassaneen, and M. Sami, *Bull. Chem. Soc. Jpn.*, **48**, 365 (1975).
7) I. I. Barnish, P. D. Callaghan, and M. S. Gibson, *J. Chem. Soc., Perkin Trans. 1*, **1974**, 215.
8) A. J. Elliott, P. D. Callaghan, M. S. Gibson, and S. T. Nameth, *Can. J. Chem.*, **53**, 1484 (1975).
9) A. F. Hegarty, J. A. Kearney, and F. L. Scott, *J. Chem. Soc., Perkin Trans. 2*, **1973**, 1422.
10) J. F. Bunnett and R. E. Zahler, *Chem. Rev.*, **49**, 361 (1951); N. W. Gilman, P. Levitan, and L. H. Sternback, *J. Org. Chem.*, **38**, 373 (1973) and the references cited therein.
11) A. J. Elliott, M. S. Gibson, M. M. Kayser, and G. A. Pawelchak, *Can. J. Chem.*, **51**, 4115 (1973).
12) A. F. Hegarty, M. P. Cashman, and F.L. Scott, *J. Chem. Soc., Parkin Trans 2*, **1972**, 1381.

BULLETIN OF THE CHEMICAL SOCIETY OF JAPAN, VOL. 50 (10), 2829—2830 (1977)

Graft Polymerization on Pulverized Solid Surface. I. Grafting Polystyrene on a Clay Surface Treated with Silane Coupling Agents

Takuo NAKATSUKA, Hitoshi KAWASAKI, and Katsuhiko ITADANI

Industrial Technical Center of Okayama Prefecture, Ifuku-cho, Okayama 700

(Received January 13, 1977)

Synopsis. Styrene was graft-polymerized on kaolin clay treated with silane coupling agents *e.g.* (γ-methacryloyloxypropyl)trimethoxysilane. Although the silane-styrene copolymer was soluble in benzene, the polystyrene-grafted clay swelled in the same medium. A clay-crosslinked, three-dimensional structure is suggested and conditions for gelation are also discussed.

In order to elucidate the interfacial interactions between organic matrices and inorganic fillers in composite materials, studies of the graft polymerization of organic monomers onto inorganic pulverized solid surfaces are of importance.

Many papers appear in the literature dealing with topochemical graft polymerization. But only a single paper has been published on the clay-crosslinked structure of graft polymerization products. Dekking[1] has prepared the adduct of bentonite and 2,2′-azobis-isobutyramidine hydrochloride, which initiated the polymerization of vinyl monomers and gave gel-like compositions.

Although silane coupling agents are often used in many composite materials, neither graft polymerization on kaolin clay treated with silane agents nor the characteristic structure of the products has been reported. In the present paper, the crosslinking role of the clay in the polystyrene-silanized clay composition is described.

Experimental

Materials. X-Ray analysis showed that Kaolinite was the principal mineral in the kaolin clay used. (Found: SiO_2, 44.84; Al_2O_3, 39.59; Fe_2O_3, 0.36; TiO_2, 1.12; CaO, 0.14; MgO, 0.06; Na_2O, 0.07; K_2O, 0.20; Ig. loss, 13.99%. Calcd for kaolin; SiO_2, 46.54; Al_2O_3, 39.49; H_2O, 13.96%). The percentage of water adsorbed on the clay under atmospheric conditions was determined to be 0.56% by the Fischer method and, after the desorption treatment procedure described it was found to be 0.02%. The specific surface area was found to be 6.89 m^2/g by the BET method.

(γ-Methacryloyloxypropyl)trimethoxysilane (**1**) was obtained commercially and used without further purification. Benzene was purified in the usual way and styrene was freshly distilled prior to use. Other organic solvents were of reagent grade. The 2,2′-azobisisobutyronitrile (AIBN) used was also of reagent grade.

Procedure. In a 200-ml two-necked round-bottomed flask equipped with a magnetic stirring bar, a condenser and a three way stopcock was placed 2.0 g of clay. The flask was heated to 70 °C under *ca.* 1 mmHg (1 mmHg≈133 Pa) for 1 h, and then allowed to cool down to room temperature at which time nitrogen was introduced into the vessel. After 5.0 ml of benzene and 0.2 ml of **1** were added to the clay, the mixture was stirred at room temperature for 30 min. Moreover, 5.0 ml of styrene and 40 mg of AIBN were added to the mixture, which was heated at 80 °C with stirring in a nitrogen atmosphere for 2 to 4 h. The reaction mixture was poured into hexane and the precipitate was filtered, dried *in vacuo*, and weighed. Non-graft polymer was extracted from the precipitate with benzene for 12 h. Then, in order to determine the graft polystyrene, the residual solid was submitted to pyrolysis gas chromatography whose decomposing temperature was *ca.* 570 °C.

Results and Discussion

As shown by Solomon and Rosser,[2] and Kawasaki *et al.*,[3] kaolin clay can initiate the polymerization of styrene (conv. 93%) by desorption of water from the clay surface, although no graft polymer is observed on the clay surface. The polymerization is inhibited by the addition of either pyridine or **1**. This is probably due to poisoning of the acidic sites on the clay surface.

Table 1. Styrene graft polymerization on clay

Experiment	I[a]	II	III
Clay (g)	2.0	2.0	2.0
Benzene (ml)	5.0	5.0	5.0
1 (ml)	0.2	0.2	0.2
Styrene (ml)	2.0	2.0	2.0
AIBN (mg)	40	41	40
React. temp (°C)	80	80	80
React. time (h)	2	2	4
St. conv. (%)	35	71	79
Free poly-st/free poly-st and graft poly-st wt ratio	0.85	0.94	0.88
Graft efficiency	0.046	0.041	0.084

a) 0.2 ml of pyridine was added.

The data for styrene graft polymerization are given in Table 1. The graft efficiency is indicated by the weight ratio of the graft polystyrene to the polymer-clay composition. These values varied from 0.041 to 0.084. It is noteworthy that the polystyrene-clay products swelled and formed gels in benzene as do vulcanized rubbers. The conditions for gelation were further explored as explained below.

The amount of **1** adsorbed on the clay was determined. Two kinds of procedures were employed for the treatment of **1** on the clay. (A) One procedure was to add **1** in a solution of methanol–water (9: 1) to the air-dried clay. After evaporation, benzene was added to dissolve the non-adsorbed **1**, which was determined by ir spectroscopy (1716 cm^{-1}; ester band of **1**). The amount of **1** adsorbed was calculated from these data. (B) In the other method, the addition of **1** in a benzene solution

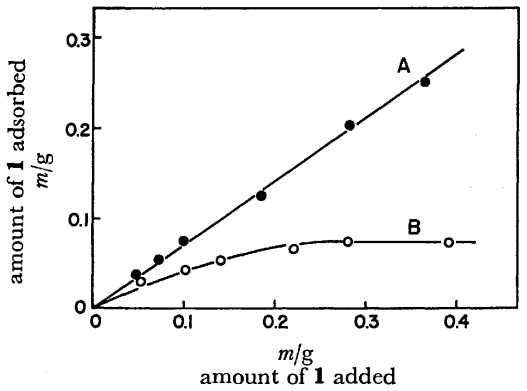

Fig. 1. Amounts of **1** adsorbed on the clay (2.0 g). A) ●: As methanol–water solution (5 ml). B) ○: As benzene solution (5 ml). IR ester band of **1** (1716 cm^{-1}) was used for determination.

was employed. The adsorbed **1** was determined by a similar method. These results are summarized in Fig. 1.

Figure 1 shows that the adsorption of **1** was effective in the presence of enough water to hydrolyze the methoxy moiety of **1** and that the adsorption of **1** increased proportionally to the amount of **1** added in method A. However, in the case of method B, the amount of **1** adsorbed is shown to have a plateau at *ca.* 0.07 g. The specific surface area of the clay is 6.89 m^2/g and the minimum specific surface area of **1** is 314 m^2/g.[4] From these observations, it is considered that **1** forms a multimolecular layer on the clay surface, although it was added as an anhydrous benzene solution.

Subsequently, polymerization was carried out in the presence of the clay which had been treated with various amount of **1** by method A. The results are listed in Table 2. The reproducibility of the graft efficiency and of the amount of *p*-xylene absorbed was rather poor probably due to heterogenity.

As seen in Table 2, when nearly the same amount of **1** was added to the clay, bulk polymerization was found to be preferable to the solution polymerization for the gel compositions. It was also found that gelation of the products brought a considerable increase in the graft efficiency. From the results in Fig. 1, it may be said that the amount of **1** on the clay surface is one of the gelation conditions.

Table 2. Effects of the amount of **1** on the gelation, crosslink density, and graft efficiency of the products

1 (ml)	State of products[a]	Absorbed *p*-xylene[b]	Graft efficiency
0.4	g	0.40	0.247
0.3	g	1.17	0.086
0.2	p	1.10	0.041
0.1	n	—	0.002
0.05	n	—	0.002
0.2[c]	g	0.65	0.250
0.1[c]	g	1.03	0.251
0.05[c]	p	2.98	0.236

a) g: gel, p: partially gel, n: non-gel. b) The amount of *p*-xylene absorbed (g-*p*-xylene/g-composition) was determined by glpc.[5] c) Bulk polymerization was carried out in a manner similar to that for solution one, except for benzene.

The crosslink density of the composition was estimated from the amount of the solvent, such as *p*-xylene, absorbed. Table 2 also shows that the density increases for an increase in the amount of **1** added to the clay.[6]

Then, the polystyrene-clay compositions were compared with the styrene-**1** copolymer (**2**) of the same feed composition. The ir spectra of the two polymers were essentially identical in the 3100—1400 cm^{-1} region. However, the decomposition patterns for differential thermal analysis of the two in air are evidently different (250—450 °C). Therefore, a difference in structure of the organic polymer is suggested. Further work on these results is now in progress.

In contrast to the solubility of copolymer **2** in benzene, the polymer-clay composition swelled by the same solvent. These facts are consistent with the clay-bridged, three-dimensional structure illustrated in Fig. 2.

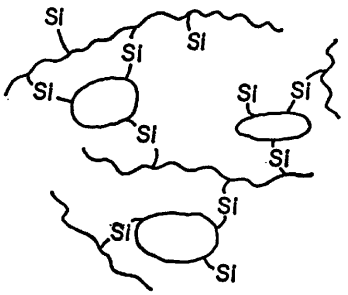

Fig. 2. Model of the polystyrene-clay composition. ⬭: Clay, ～～: styrene-**1** copolymer.

It was hoped to obtain more information about the crosslinking role of the clay. However, attempts to prepare the polymer-clay gel composition by the reaction of copolymer **2** with the clay were not successful. This appears to be due to the decreased accessibility of the silanols or alkoxysilane groups in the copolymer to the clay surface.

References

1) H. G. G. Dekking, *J. Appl. Polym. Sci.*, **11**, 23 (1967).
2) D. H. Solomon and M. J. Rosser, *J. Appl. Polym. Sci.*, **9**, 1261 (1965).
3) H. Kawasaki, K. Itadani, H. Hata, and F. Kusano, *Nippon Gomu Kyokai Shi*, **44**, 59 (1971).
4) I. Murakami, *Nippon Gomu Kyokai Shi.*, **46**, 336 (1973).
5) C. R. Parks and R. J. Brown, *Rubber Chem. Technol.*, **49**, 233 (1976).
6) The increase in crosslink density with **1** in filled rubber has already been examined: M. P. Wagner, *Rubber Chem. Technol.*, **49**, 703 (1976).

On the Behavior of Paramagnetic Species Formed in the Pure V_2O_5 Crystal under SO_2-Oxidation

Yoshiya KERA and Keiji KUWATA

Department of Chemistry, Faculty of Science, Osaka University, Toyonaka, Osaka 560

(Received March 10, 1977)

Two types of ESR spectra were found in the highly purified V_2O_5 crystal under conditions of SO_2 oxidation. The shapes and the intensities of the spectra were investigated in detail in the temperature range from 470 to 656 °C under various mixing ratios of SO_2 to O_2. Below *ca.* 600 °C a sharp and asymmetric spectrum existed stably, while above that temperature it was replaced by a spectrum with an hfs of 29 lines, the intensities of which always were very weak. The low-temperature-type spectrum was reasonably assigned to the $VOSO_4$ phase, and the high-temperature-type, to an oxygen defect surrounded equivalently by four vanadium ions in the V_2O_5 phase. The interchange between the two spectra near 600 °C occurred reversibly and was related favorably to the following process in the surface layer of the V_2O_5 crystal: $2VOSO_4=V_2O_5+SO_3+SO_2$. The change in the working states of a pure V_2O_5 crystal according to the conditions of SO_2 oxidation was discussed.

There have been numerous reports[1–10] on the mechanism of SO_2 oxidation over vanadium oxide catalysts, which are used in the states of a fused mixture of V_2O_5 with alkali sulfates and of a mixture supported on silica and alumina gels. Many authors[5–10] have determined the changes in the mechanisms of SO_2 oxidation over the catalysts at around 450 °C; they have been discussed mainly from the point of view of reaction kinetics. Mastikhin *et al.*[11] have observed the ESR spectra of $V_2O_5 \cdot 3.5\,K_2S_2O_7$ supported on alumina gel during SO_2 oxidation and have suggested that the changes in the kinetics are related to some changes in the working states of the catalyst. However, no full solution to this problem has yet been given for multicomponent catalysts because of the complicated changes in the ESR spectra according to the reaction conditions.

In the highly purified V_2O_5 crystal, however, simple spectra were found under the conditions of SO_2 oxidation. The shapes and the intensities of the spectra showed clear changes depending upon the SO_2/O_2 ratio and the reaction temperature. The purpose of this paper is mainly to give proper assignments to the paramagnetic species and to discuss in detail the behavior of the species on the surface of the pure V_2O_5 crystal depending on the conditions of SO_2 oxidation.

Experimental

Materials. The V_2O_5 powder, which has been obtained by the decomposition of NH_4VO_3 (Special grade, Wako Pure Chem. Ind. Co.) was further chemically purified according to the methods of McCarley *et al.*[12] and Haemers.[13] The V_2O_5 single crystals were prepared by a zone-melting method with a Pt-boat. The crystals were cut into a proper size for contact with the reaction gases and for the ESR measurements. The $VOSO_4 \cdot 3H_2O$ (Special grade, Mitsuwa Chem. Ind. Co.) was used without further purification for the observation of the changes in the ESR spectra by dehydration and sintering.

Procedures. The V_2O_5 single crystal was placed in a quartz tube with an inner diameter of 0.3 cm and a length of 3 cm, which was connected by a gradual joint to a glass tube 0.6 cm in inner diameter. After pretreatment at 500 °C under evacuation for 1 h, it was cooled to room temperature. A given amount of a gaseous mixture of SO_2 and O_2 was introduced into the sample tube, and then the tube was sealed off. The reaction was carried out by heating the sample tube in an electric furnace for a long time. It was quenched by immersing it quickly in cold water before the ESR measurement. The procedure was repeated at various temperatures between 470 and 656 °C, the temperature fluctuation being kept within ±1 °C. The reaction conditions are summarized in Table 1.

TABLE 1. EXPERIMENTAL CONDITIONS OF SO_2 OXIDATION ON V_2O_5 CRYSTAL

Sample	SO_2 Torr[a]	O_2(air) Torr	SO_2/O_2 ratio	V_2O_5 mg	Volume cm^3
S_s-1	370	40(200)	9	29	4
S_s-2	375	34(170)	11	45	25
S_s-3	480	6(31)	80	32	25
S_s-4	556	0	∞	18	5

a) 1 Torr = 1.334×10^2 Pa.

The dehydration of $VOSO_4 \cdot 3H_2O$ and its sintering were done in the same ESR sample tube described above.

ESR Measurements. The ESR spectra were recorded at room temperature and at 77 K with an X-band spectrometer. The modulation frequency of the magnetic field was 455 kHz. The frequency of the microwave was determined to be 9326 MHz by the use of a wave meter. The calibration of the static magnetic field was done with DPPH and the Mn(II) ion doped in MgO as standards.

Determination of Spin Concentration. The spin concentration was determined with a single mode cavity (T_{011}) by the use of $CuSO_4 \cdot 5H_2O$ (single crystal) and DPPH (benzene soln) as the primary and the secondary standards of the spin concentrations respectively. A capillary tube which contained

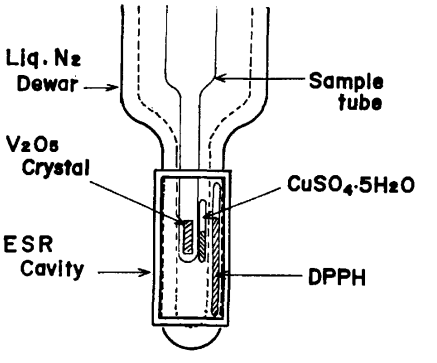

Fig. 1. Arrangement of V_2O_5 crystal and DPPH and $CuSO_4 \cdot 5H_2O$ standards in ESR cavity.

DPPH was always fixed on the outer wall of the quartz Dewar. On the other hand, a capillary tube which contained the $CuSO_4 \cdot 5H_2O$ was placed on the outer wall of the sample tube and was immersed together with it in the Dewar. The arrangement of the sample and the standards in the cavity are shown schematically in Fig. 1. The $CuSO_4 \cdot 5H_2O$ crystal was placed in the capillary tube so as to make the $g_{//}$ and $g_{\perp}$ axes nearly parallel to H_0 during the rotations of the sample tube around the axes. The spin concentrations were mainly obtained by a comparison of the integrated intensities of the standards with those of the samples. In the case of low spin concentrations, the amplitude of the first derivative curve of DPPH was used as a secondary standard.

Results

ESR Spectra in a Single Crystal of Highly Purified V_2O_5 under the Conditions of SO_2 Oxidation. No ESR signal was observed in the single crystal prepared from the cautiously purified V_2O_5 powder in air by the zone-melting method, although the signals ascribed to both vanadium ions (IV) with hfs of 15 lines and to the Fe ion as an impurity were usually found in the spectrum of the unpurified crystal. When the purified V_2O_5 single crystal was placed in contact with a gaseous mixture of SO_2 and O_2, an ESR spectrum with hfs of 15 lines and an hf-splitting constant, $A_{//}$, of 8.8 mT appeared initially. The spectrum is probably the same as has been found in pure and doped V_2O_5 by many authors,[14-16] as has been mentioned below. On prolonged contact the spectrum was replaced by an asymmetric spectrum, and the intensity of new spectrum increased with the time. When the temperatures were raised above *ca.* 600 °C, the asymmetric spectrum abruptly disappeared and a new spectrum with hfs whose splitting constant, $A_{//}$, is about 4.3 mT appeared. The former will hereafter be called the low-temperature-type spectrum, and the latter, the high-temperature-type spectrum.

In Run S_S-4, in which the crystal was treated at 617 °C with SO_2 alone, the spectrum with an hfs of 15 lines appeared initially, but soon disappeared. By this time the brilliance of the surface and the transparency disappeared completely, and the surface was covered with black and velveteen polycrystallines. Except for Run S_S-4, the surface brilliance of the cleaved plane (010) did not vary clearly upon the repetition of the heating and cooling, although the color and the transparency of the crystal did change.

Low-temperature-type Spectrum. The growth of the sharp asymmetric spectrum on Sample S_S-2 during the contacts at 470 °C is illustrated in Fig. 2. The line shapes of the asymmetric spectra at $H_0//b$ and $H_0 \perp b$ in Fig. 2 seem to show a typical randomly oriented paramagnetic species with an axially symmetric g-tensor. In the intermediate direction between $H_0//b$ and $H_0 \perp b$, however, an additional sharp line appeared in the asymmetric spectrum. The sharp line moved from the static magnetic field (position) corresponding to $g_{//}=1.924$ to that corresponding to $g_{\perp}=1.970$, according to the change in the direction of the static magnetic field from $H_0//b$ to $H_0 \perp b$ in the ac-plane. In a previous paper,[17] the angular dependencies of the spectrum

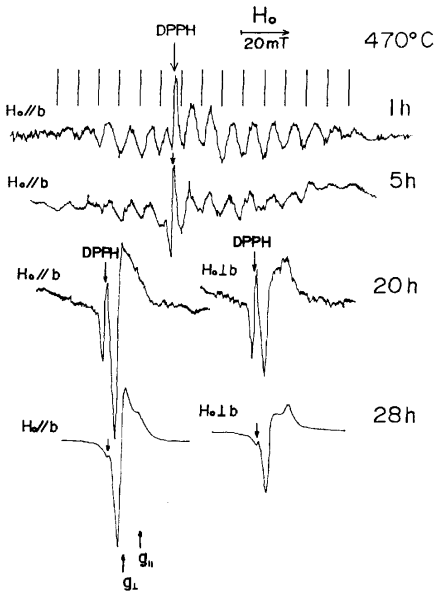

Fig. 2. Changes in ESR spectrum of a highly purified V_2O_5 single crystal during contact with a reaction mixture of SO_2 and O_2 at 470 °C.—Appearance and disappearance of ESR spectrum with hfs of 15-lines and then appearence of a sharp asymmetric spectrum (the so-called low temperature type spectrum).

TABLE 2. CHANGES IN SPECTRUM AND ITS SPIN CONCENTRATION IN SAMPLE S_S-1 WITH THE TEMPERATURE

Temp °C	Time h	Low-temperature type Spin concn $\times 10^{17}$/29 mg	High-temperature type
505	134	8.2	—
639	43	4.7	—
656	17	0.7	hfs 29 lines
656	39	—	hfs 29 lines (4×10^{15})
599	166	3.8	—
549	163	6.8	—
532	70	6.6	—

were examined in detail and it was concluded that the asymmetric sharp spectrum was as a composite: one component was ascribed to the spectrum caused by an axially symmetric g-tensor ($g_{//}=1.924$ and $g_{\perp}=1.970$) taking a relatively random orientation to the crystalline lattice of the V_2O_5 and the other, to that taking a definite orientation, *i.e.*, the $g_{//}$//b-axis of the V_2O_5 crystal.

The changes in the spin concentrations according to the reaction conditions are given for Samples S_S-1, S_S-2, and S_S-3 in Tables 2, 3, and 4 respectively. All the data were also graphically shown together in Fig. 3. In the case of Sample S_S-2, the time responses for the appearance and disappearance of the low-temperature-type spectrum are given in Fig. 4. It may be seen from the figures that the appearance and disappearance occur abruptly within the temperature range between 586 and 595 °C.

High-temperature-type Spectrum. At higher temperatures the low-temperature-type spectrum was re-

Table 3. Changes in spectrum and its spin concentration in sample S_s-2 with temperature

Temp °C	Time h	Low-temperature type Spin concn $\times 10^{17}$/45 mg	High-temperature type
470	229	1.5	—
536	166	4.5	—
595	96	0.1	hfs of 29 lines
640	65	0.08	hfs of 29 lines
586	161	5.2	—
513	180	6.2	—
481	230	8.9	—

Table 4. Changes in spectrum and its spin concentration in sample S_s-3 with temperature

Temp °C	Time h	Low-temperature type Spin concn $\times 10^{17}$/32 mg	High-temperature type
600	45	0.013	—
656	70	0.022	hfs 29 lines
481	167	0.32	—
550	161	0.97	—
572	160	1.1	—
516	180	1.1	—
476	228	4.6	—

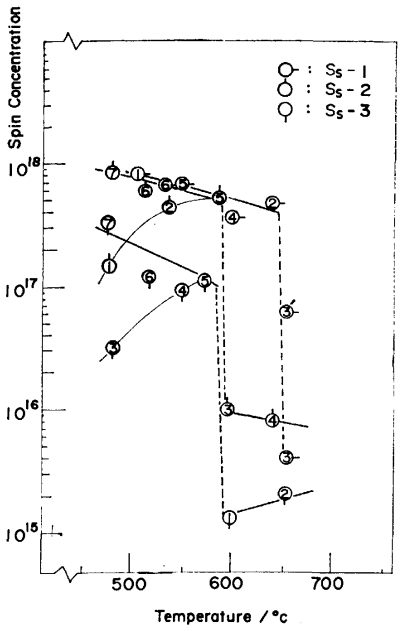

Fig. 3. Temperature dependences of spin concentrations of V_2O_5 single crystals after any periods of the contacts with SO_2+O_2 gases. The concentrations mean the numbers of unpaired electron per weight of used crystal. The figures in the circles indicate sequences of the measurements. Contact conditions are given in Table 1. The spin concentrations, the contact periods and sequences are given in Tables 2, 3, and 4, correspond to S_s-1, S_s-2, and S_s-3, respectively.

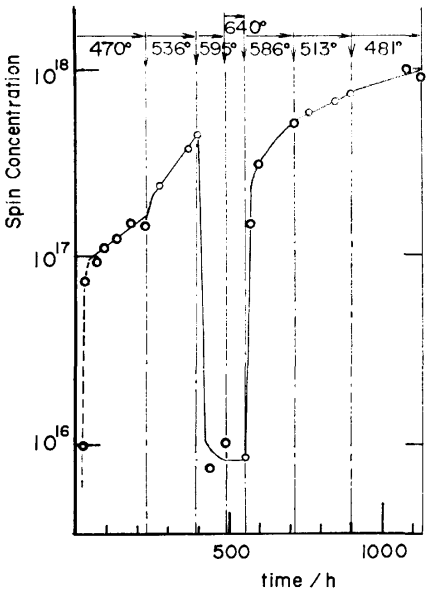

Fig. 4. Changes in the spin concentrations of the crystal, S_s-2 at various temperatures with the contact times.

placed by a new spectrum with hfs of more than twenty lines, whose hf-splitting constant was a half of that of the previous spectrum ($A_{//}$=4.3 mT). Such a change in the spectrum of Sample S_s-1 is illustrated in Fig. 5.

ESR Spectrum of Pure Vanadium Sulfate Powder. In mixtures of V_2O_5 and alkali sulfates under the reaction conditions of SO_2 oxidation, quite similar spectra with low-temperature-type spectra have been reported and ascribed to some states of vanadium sulfates.[11] The ESR spectrum of pure vanadium sulfate was also examined. The ESR spectrum of $VOSO_4 \cdot 3H_2O$ and the spectra obtained after heating $VOSO_4 \cdot 3H_2O$ in air at 490 °C for 24 h and then at 600 °C for 1 h are shown in Fig. 6. The higher the temperature, and the longer the treatment, the sharper and the more asymmetric the line shape. The *g*-values of the spectra are summarized in Table 5. In the limiting case we could obtain the spectrum with a *g*-value similar to that of the low-temperature-type spectrum. Upon heating at 620 °C the sharp asymmetric spectrum disappeared completely.

Discussion

High-temperature-type Spectrum in V_2O_5 Crystal under the Conditions of SO_2 Oxidation. There have been many reports on the ESR spectra of doped and undoped V_2O_5 single crystals. For instance, the spectrum with an hfs of 15 lines was found in Fe-, V-, and Cu-doped crystals,[14,15] and that with an hfs of 29 lines in Li- and Na-doped crystals.[20] In undoped V_2O_5 single crystals, spectra with hfs of 15 and 29 lines[16,18] were also reported; the spectra were ascribed to some kinds of oxygen vacancies in the crystalline lattices. No clear differences in the spectra with an hfs of 15 lines can be found between the doped and undoped crystals so long as only the ESR parameters are compared.

These results indicate that the hf-coupling constants

TABLE 5. COMPARISONS OF ESR PARAMETERS WITH RESPECT TO THE LOW TEMPERATURE TYPE SPECTRUM

Sample	Measurement Temp/K	$g_{//}$	$g_{\perp}$	$\langle g \rangle$	Reference
$V_2O_5 \cdot 3.5K_2S_2O_7$ on α-Al_2O_3 in working states	673	1.920	1.980	1.960	11
$VOSO_4$ on silica gel	300	1.915	1.969	1.951	19
V_2O_5 crystal in the SO_2 oxidation	77	1.924	1.970	1.955	The present work
$VOSO_4 \cdot 3H_2O$ powder	77	—	—	1.980	The present work
$VOSO_4 \cdot 3H_2O$ glyceline soln	77	1.940	1.990	1.973	The present work
$VOSO_4 \cdot 3H_2O$ heated in air at 148 °C for 4 h	77	1.929	1.967	1.954	The present work
$VOSO_4 \cdot 3H_2O$ heated in air at 490 °C for 24 h	77	1.932	1.970	1.957	The present work
$VOSO_4 \cdot 3H_2O$ heated in air at 600 °C for 1 h	77	1.925	1.966	1.952	The present work

TABLE 6. COMPARISONS OF ESR PARAMETERS WITH RESPECT TO THE HIGH-TEMPERATURE-TYPE SPECTRUM (at 77 K)

Sample	No. of hfs -line	$g_{//}$	$g_{\perp}$	$A_{//}$ (mT)	$A_{\perp}$ (mT)	Reference
Doped V_2O_5 crystal (Fe-doped)	15	1.82	1.98	10.5	5.0	14
Doped V_2O_5 crystal (Cu-doped)	15	1.92	1.985	8.6	—	15
Doped V_2O_5 crystal (V-doped)	15	1.92	1.991	9.0	3.7	15
Undoped V_2O_5 crystal	15	1.911	1.983	8.8	3.3	16
	29	1.931	1.982	4.3	—	18
S_s-1 (at 656 °C)	29	1.917		4.3	—	The present work
S_s-2 (at 470 °C, initially)	15	1.924		8.8	3.3	The present work

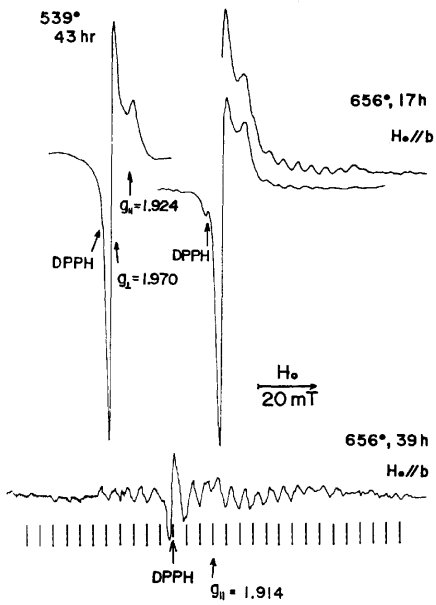

Fig. 5. Low temperature type spectrum at 539 °C, and disappearance of the spectrum and appearance of a new spectrum with hfs of more than 20 lines by the contact at 656 °C (the so-called high temperature type spectrum).

are related inversely to the number of ^{51}V nuclei, interacting equivalently with an unpaired electron, and thus to the number of the hf-lines, as has previously been suggested by Ioffe and Patrina.[14] According to such a rule, the spectrum with an hfs of 15 lines ($A_{//}$= 8.8 mT) in Fig. 2 can be ascribed to an oxygen vacancy of the Gillis type.[16] The high-temperature-type spectrum with the hf-splitting of 4.3 mT at H_0//b in Fig. 5 could also be identified with the spectrum with an hfs of 29 lines,[18] although not all the hf-lines appear and the relative intensities of the hf-lines do not accord with a polynomial distribution. The lack of the full number of hf-lines and the correct intensity distribution might be caused by the relatively low concentration and the small fluctuation in the orientations of the paramagnetic species in the surface layer. Such a low concentration could be understood by thermochemical considerations, as will be mentioned below, and such a fluctuation in the orientations could be expected for the sample quenched from a real working state of SO_2-oxidation.

The positions of the hf-lines, however, were explained well by the following procedure and ESR parameters. Including the magnetic hyperfine interaction to the second order, the resonance field is given approximately by Eq. 1:[21]

$$H(m_I) = H_0 - Km_I/g\beta - (4H_0)^{-1}\cdot(g\beta)^{-2}\cdot A_{\perp}^2\cdot(A_{//}^2+K^2)K^{-2}\cdot \{I(I+1)-m_I^2\} - (2H_0)^{-1}\cdot(g\beta)^{-2}\cdot (A_{//}^2-A_{\perp}^2)K^{-2}\cdot g_{\perp}^2\cdot g_{//}^2\cdot g^{-4}\cdot z^2(1-z^2)m_I^2, \quad (1)$$

where

$$H_0 = h\nu/g\beta,\ g^2 = g_{\perp}^2 + (g_{//}^2-g_{\perp}^2)z^2$$

and

$$K^2g^2 = A_{//}^2g_{//}^2z^2 + A_{\perp}^2g_{\perp}^2(1-z^2).$$

In the limiting case of $z=\cos\delta=1$,

$$H(m_I) = H_{//} - (A_{//}m_I/g_{//}\beta) - (2H_{//})^{-1}\cdot(g_{//}\cdot\beta)^{-2}\cdot A_{\perp}^2\cdot\{I(I+1)-m_I^2\}, \quad (2)$$

can be derived. The positions of the hf-lines (at any m_I, $m=m_{I1}+m_{I2}$ and $m_{I1}+m_{I2}+m_{I3}+m_{I4}$ respectively),

Table 7. Comparisons of spin concentration of the low-temperature-type spectrum with numbers of SO_3 and SO_2 at 580 °C in equilibrium of SO_2 oxidation

Sample	n_{SO_3} SO_3 mols $\times 10^{19}$	n_{SO_2} SO_2 mols $\times 10^{19}$	n_{spin} Spin concn $\times 10^{19}$	$n_{vanad.}$ Vanadium atom $\times 10^{19}$	$n_{spin}/n_{vanad.}$
S_8-1	1.6	6	0.06	20	0.003
S_8-2	5.6	27	0.05	30	0.0017
S_8-3	0.5	41	0.01	21	0.0005

which were calculated by means of Eq. 2 using the parameters of $g_{//}=1.924$; $A_{//}=8.4$, $A_{\perp}=3.3$ mT and $g_{//}=1.917$; $A_{//}=4.3$ mT, are given above and below the spectra in Figs. 2 and 5 respectively. In the latter case the third term of Eq. 2 is neglected. The parameters are listed in Table 6 for the sake of comparison.

From the discussions both the g-values and the hf-coupling constants, it is clear that the ESR spectra, like what those which have previously been observed in doped and undoped V_2O_5 by many authors,[14-18] can also exist in the highly purified V_2O_5 under the conditions of SO_2 oxidation. The spectra with hfs values of 15 lines and more than 20 lines can, then, be conclusively ascribed to the $V^{4+}\cdots V^{5+}$ and $\begin{matrix} V^{4+}\cdots V^{5+} \\ \vdots \quad\quad \vdots \\ V^{5+}\cdots V^{5+} \end{matrix}$ sites, produced by the elimination of lattice oxygens without the interpositions of other metal impurities.

Low-temperature-type Spectrum of the V_2O_5 Crystal under the Conditions of SO_2 Oxidation. The thermal analysis of $V_2O_5\cdot nH_2O$ has been carried out in several atmospheres by many authors.[22-25] From those results, above *ca.* 140 °C $VOSO_4\cdot 3H_2O$ is known to start to change in air to $VOSO_4\cdot H_2O$ and above *ca.* 200 °C to anhydrated $VOSO_4$; this will be followed by further decomposition, $VOSO_4\rightarrow V_2O_5$, on heating above *ca.* 550 °C. On the basis of our present knowledge, the changes in the spectrum from a symmetric and broad type to an asymmetric and sharp one in Fig. 6 seems to correspond to the progress in the dehydration and sintering: $VOSO_4\cdot 3H_2O\rightarrow VOSO_4$. It is known from the suggestion by Ballhausen *et al.*[26] and Ladwig[24] that, in $VOSO_4\cdot 3H_2O$, some of the water molecules remain in the ligand sites and are replaced by SO_4^{2-} ions as the dehydration progresses. Thus, the crystalline-field splittings of the oxovanadium(IV) ion, and thus the g-values, should differ between $VOSO_4\cdot 3H_2O$ and anhydrated $VOSO_4$, as will be discussed below.

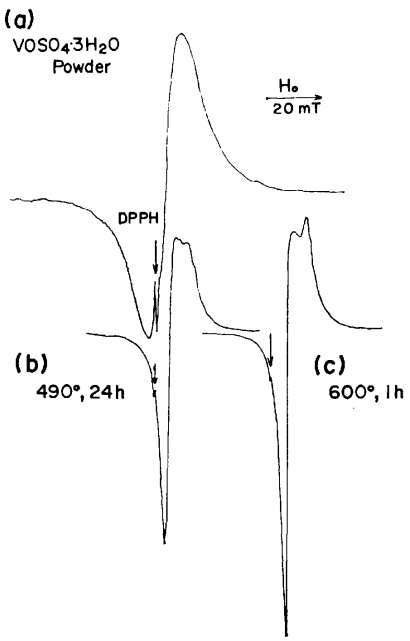

Fig. 6. Changes in ESR spectrum of $VOSO_4\cdot 3H_2O$ powder with heat treatments, see Table 5.

The rather symmetric line shape of the spectrum of $VOSO_4\cdot 3H_2O$ might be caused by a similar extent of increase in the linewidth with the anisotropy of the g-tensor of the spectrum of anhydrated $VOSO_4$ in Fig. 6. Such an increase in the linewidth must be due mainly to some effects of the ligand water on the relaxation time.[27] The reason can not be explained fully now, although the fact that the structure,[24,28] linked tightly by SO_4^{2-} tetrahedrons, is realized by the elimination of the ligand water seems to give a hint.

The g-values of powdered $VOSO_4\cdot 5H_2O$[29] and $VOSO_4\cdot 2H_2O$[30] have been reported to be $\langle g\rangle=1.99$ and 1.96 respectively. The tendency for $\langle g\rangle$ to decrease as the dehydration progresses corresponds closely to the results in Table 5. It is shown in the table, that finally, the g-value became close to the value of the low-temperature-type spectrum. Such a decrease in the g-value could be caused by the increase in the covalency of the vanadyl complex due to the replacement of the water molecules in the ligand sites by the SO_4^{2-} ions.[27] By these comparisons, it seems possible to assign the low-temperature-type spectrum under the conditions of SO_2 oxidation to the $VOSO_4$ phase, formed on the V_2O_5 crystalline lattice.

The amounts of SO_3 formed and SO_2 remaining in the equilibrium at 580 °C were roughly estimated from the initial amounts of SO_2 and O_2 and the equilibrium constant of the reaction, $SO_2+{}^1/_2O_2=SO_3$. The values are given in Table 7, while the total number of vanadium atoms in the V_2O_5 crystal and the spin concentrations for the low-temperature-type spectrum at 580 °C are given in Fig. 3. By comparing the data, especially between Samples S_8-2 and S_8-3, it can be surmised that n_{spin} decreases with a decrease in n_{SO_3} and inversely with an increase in n_{SO_2}. Thus, the spectrum can be ascribed to the $VOSO_4$ phase; in contrast to this, the possibility of a different assignment to some kinds of reduced vanadium oxides can clearly be ruled out.

Formation of the $VOSO_4$ Intermediate and the Reaction Mechanism of SO_2 Oxidation on the V_2O_5 Crystal. It is known that the $(n_{spin}/n_{vanad.})$ ratio is 1/2000—1/330, as is shown in Table 7. This indicates that the

paramagnetic species, ascribed to $VOSO_4$, is formed only in the surface layer of the crystal, even if the reaction is much prolonged. The curves for the increase in intensity of the low-temperature-type spectrum with the time at 470 and 586 °C in Fig. 4 show clearly the existence of a very fast process at the initial stage and a relatively slow process after that. The initial process can be attributed to the growth of the $VOSO_4$ phase on the surface, especially on the (010) plane, and the second process, to the diffusion of the $VOSO_4$ phase into the bulk.

The abrupt increase and decrease in the intensity of the low-temperature-type spectrum near 600 °C seems to occur reversibly in Figs. 3 and 4. The temperature range where the spectrum suddenly disappears may be consistent with the temperature at which the $VOSO_4$ phase in a V_2O_5–SO_2–SO_3–$VOSO_4$ system is decomposed thermally, although the range should change according to the reaction conditions of the SO_2 oxidation on V_2O_5.[31] The disappearance of the spectrum can, therefore, be related to the process of Eq. 3:

$$2VOSO_4 \rightarrow V_2O_5 + SO_3 + SO_2. \quad (3)$$

At low temperatures the SO_2 oxidation reaction on pure V_2O_5 crystal can be expected to proceed through the $VOSO_4$ intermediate as in the following scheme, Eq. 4:

$$2SO_2 + \frac{1}{2}O_2 + V_2O_5 \rightarrow 2VOSO_4 \rightarrow V_2O_5 + SO_3 + SO_2. \quad (4)$$

On the other hand, at high temperatures it would proceed by the participation of the oxygen defect, surrounded equivalently by four vanadium ions on the V_2O_5 surface, as is suggested by the appearance of the spectrum with an hfs of 29 lines.

The findings that the formation and decomposition of the $VOSO_4$ phase in the V_2O_5 crystal occur reversibly and that the surface brilliance of the (010) plane is kept seem to show the possibility of some regular arrangement of the $VOSO_4$ phase on the surface of the V_2O_5 crystal, as was suggested in a previous paper.[17]

References

1) P. Mars and J. G. H. Maessen, *Proc. Int. Congr. Catal., 3rd. Amsterdam*, **1**, 266 (1964); *J. Catal.*, **10**, 1 (1968).
2) G. K. Boreskov, R. A. Buyanov, and A. A. Ivanov, *Kinet. Katal.*, **8**, 153 (1967); G. K. Boreskov, L. P. Davydova, V. M. Mastikhin, and G. M. Polyakov, *Dokl. Akad. Nauk SSSR*, **210**, 626 (1973).
3) A. R. Glueck and C. N. Kenney, *Chem. Eng. Sci.*, **23**, 1257 (1968).
4) H. Livbjerg and J. Villadsen, *Chem. Eng. Sci.*, **27**, 21 (1972).
5) M. Matsui and R. Kiyoura, *Kogyo Kagaku Zasshi*, **40**, 153, 985 (1937).
6) G. K. Boreskov and V. P. Pligunov, *J. Appl. Chem. USSR*, **13**, 653 (1940); *Chem. Abstr.*, **35**, 3396 (1941); E. V. Gerburt-Geibovich and G. K. Boreskov, *Zh. Fiz. Khim.*, **30**, 1801 (1956); *Chem. Abstr.*, **51**, 7818 (1957).
7) H. Kubota, M. Ishizawa, and M. Shindo, *Ryusan*, **12**, 243 (1959).
8) H. Hara, A. Adachi, and N. Kurata, *Kogyo Kagaku Zasshi*, **62**, 669 (1959).
9) P. Jiru, D. Tomkova, V. Jara, and J. Wankova, *Z. Anorg, Allg. Chem.*, **303**, 121 (1960); *Proc. Int. Congr. Catal., 2nd Paris*, **2**, 2113 (1961).
10) G. K. Boreskov, L. P. Davydova, V. M. Mastikhin, and G. M. Polyakova, *Dokl. Akad. Nauk SSSR*, **171**, 648 (1966).
11) V. M. Mastikhin, G. M. Polyakova, Ya. Zyulkovskii, and G. K. Boreskov, *Kinet. Katal.*, **11**, 1463 (1970).
12) R. E. McCarley and J. W. Roddy, *J. Less-Common Met.*, **2**, 29 (1960).
13) J. Haemers, *Bull. Soc. Chim. Belg.*, **79**, 473 (1970).
14) V. A. Ioffe and I. B. Patrina, *Soviet Phys.-Solid State*, **6**, 2425 (1964); *ibid.*, **10**, 639 (1968); L. V. Dmitrieva, V. A. Ioffe, and I. B. Patrina, *ibid.*, **7**, 2228 (1966).
15) J. L. Ragle, *J. Chem. Phys.*, **38**, 2020 (1963).
16) E. Gillis and E. Boesman, *Phys. Status Solidi*, **14**, 337 (1966).
17) Y. Kera and K. Kuwata, *Bull. Chem. Soc. Jpn.*, **50**, 2438 (1977).
18) K. Hirota, K. Kuwata, and Y. Kera, *Bull. Chem. Soc. Jpn.*, **43**, 3017 (1970).
19) H. Tanaka and A. Matsumoto, *Bull. Chem. Soc. Jpn.*, **39**, 874 (1966).
20) G. Sperlich, *Z. Phys.*, **250**, 335 (1972).
21) B. Bleaney, *Philos. Mag.*, **42**, 441 (1951).
22) J. Roch, *C. R. Acad. Sci.*, **249**, 56 (1959).
23) G. Tridot, *Pure Appl. Chem.*, **13**, 543 (1966).
24) G. Ladwing, *Z. Anorg. Allg. Chem.*, **364**, 225 (1969).
25) R. A. Edge, *J. Less-Common Met.*, **18**, 325 (1969).
26) C. J. Ballhausen and H. B. Gray, *Inorg. Chem.*, **1**, 111 (1962); C. J. Ballhausen, B. F. Djurinskij, and K. J. Wastson, *J. Am. Chem. Soc.*, **90**, 3305 (1968).
27) D. Kivelson and R. Neiman, *J. Chem. Phys.*, **35**, 149 (1961).
28) P. Kierkegaard and J. M. Longo, *Acta Chem Scand.*, **19**, 1906 (1965).
29) M. B. Palmer, M. U. Palmer, D. Palumbo, and F. Sgarlata, *Nuovo Cimento*, **3**, 718 (1956).
30) C. A. Hutchison and L. S. Singer, *Phys. Rev.*, **89**, 256 (1953).
31) H. Flood and O. J. Kleppa, *J. Am. Chem. Soc.*, **69**, 998 (1947).

The Adsorption Mechanism of Methanol on Alkali Halides[1)]

Masatoshi CHIKAZAWA and Takafumi KANAZAWA

Department of Industrial Chemistry, Faculty of Technology, Tokyo Metropolitan University, Fukazawa, Setagaya-ku, Tokyo 158

(Received April 14, 1977)

The amounts of methanol adsorbed on (100) planes of the crystals of six alkali halides (LiCl, NaCl, NaBr, KCl, KBr, and KI) and the isosteric heats of their adsorption were measured. For the chloride samples, the order of magnitude of the adsorption heats at a coverage of $\theta=0.5$ was found to be LiCl>NaCl>KCl, while the order for the bromide samples was NaBr>KBr. The monolayer capacities estimated from the adsorption isotherms for KCl and NaBr were in accord with the values calculated by assuming that one methanol molecule is adsorbed on one surface anion of the crystal. In the cases of the NaCl and LiCl salts, whose lattice spacings are smaller than that of NaBr, the methanol molecule was adsorbed on the surface anion with a ratio below 1 : 1. On the other hand, for the KBr and KI samples, whose lattice spacings are larger than that of KCl, alcohol was adsorbed on the surface anion in a ratio above 1 : 1. These phenomena are reasonably interpreted in terms of a relationship between the cross-sectional area of a methanol molecule and the lattice spacing of the salt concerned. An adsorptive mechanism deduced from the isosteric heat curves was compatible with the above explanation.

In the adsorption of polar molecules on the surfaces of alkali halide particles, interaction forces between the surface anions of the salt and the adsorbates will be large. Especially, when the adsorbates form hydrogen bonds with the surface anions, the role of the anions is presumed to be very significant.[2-5)]

A methanol molecule (MeOH) has one OH group expected to form a hydrogen bond with the surface anion. Therefore, in the present paper, MeOH is used as an adsorbate for several alkali halides, and the adsorption characteristics of the samples and the role of the surface anion in MeOH adsorption are discussed.

Experimental

Materials. Samples of five alkali halides (NaCl, NaBr, KCl, KBr, and KI) were purified by two recrystallizations of special-grade reagents using distilled water. A solution of an alkali sample (*ca.* 100 ml, 20—30 wt%) was added to about a five-fold volume of ethanol cooled to −80——90 °C with stirring. The precipitate was filtered, washed four times with absolute ethanol, and then dried under a reduced pressure of 10^{-3} mmHg. Lithium chloride was prepared by the pulverization of a special-grade reagent in a ball-mill for 10 min. The LiCl and NaBr samples, which are able to form the hydrates, were heat-treated at 350 and 450 °C respectively for 2—3 days under a reduced pressure of 10^{-6} mmHg, while the other samples were evacuated with an oil diffusion pump ($<10^{-6}$ mmHg) for 1—2 days at room temperature prior to the adsorption measurements. These samples were found by microscopy to be very small cube crystals (1—8 μm).

The methanol was purified by distillation from a reagent for the UV spectrum measurements, and then used.

Surface Area Measurement. The specific surface areas of the samples were determined by the nitrogen adsorption method at 77 K, assuming the cross-sectional area of a nitrogen molecule to be 16.2 Å^2.

Methanol Adsorption Isotherm. The adsorption isotherms of MeOH on the alkali halides at 10, 20, 30, and 40 °C were determined volumetrically by using the adsorption apparatus reported previously by the present authors.[6)]

Results and Discussion

Adsorption Isotherms. The adsorption isotherms of MeOH on alkali halides are given in Fig. 1. In

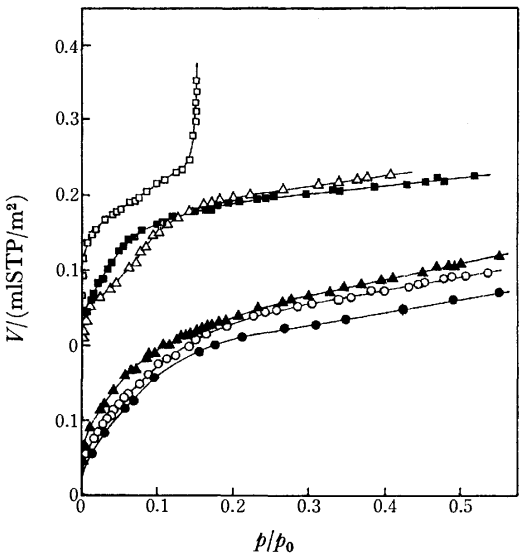

Fig. 1. Adsorption isotherms of MeOH on alkali halides at 20 °C.
—□—: LiCl, —■—: NaCl, —△—: KCl, —▲—: NaBr, —○—: KBr, —●—: KI.

the case of LiCl, it is characteristic that the amount of MeOH adsorbed increased rapidly at pressures above $p/p_0=0.14$ and that, simultaneously, the dissolution of LiCl into the adsorbed MeOH films occurred. The relative vapor pressure of a MeOH solution saturated with LiCl is about $p/p_0=0.15$ at 20 °C. The volume adsorbed at $p/p_0=0.15$ was estimated from the adsorption isotherm to be 0.28 ml STP/m^2. This volume agreed with the amount required to cover the surface of the LiCl particle with a 1.36 molecular layer of MeOH, assuming that the cross-sectional area of a MeOH molecule is 18 Å^2 [7)] (calculated from the density of liquid MeOH at 20 °C). The considerable solubility of LiCl into such a small amount of adsorbed MeOH will be explained on the basis of a strong interaction between the Li ion and the MeOH molecule. This interpretation is supported by the fact that the solubilities[8)] of lithium halides in methanol are higher than those of sodium halides in spite of the considerably larger lattice energies[9)] of the former.

TABLE 1. MONOLAYER CAPACITIES OF MeOH ADSORBED ON ALKALI HALIDES

Sample	V_{BET}(ml STP/m²)	V_B(ml STP/m²)	V_{cal}(ml STP/m²)	V_B/V_{cal}
LiCl	0.23	0.17—0.18	0.282	0.62
NaCl	0.23	0.18—0.19	0.234	0.79
NaBr	0.205	0.24—0.25	0.209	1.17
KCl	0.19	0.18—0.20	0.188	1.01
KBr	0.23	0.24—0.25	0.171	1.40
KI	0.21	0.22—0.23	0.149	1.50

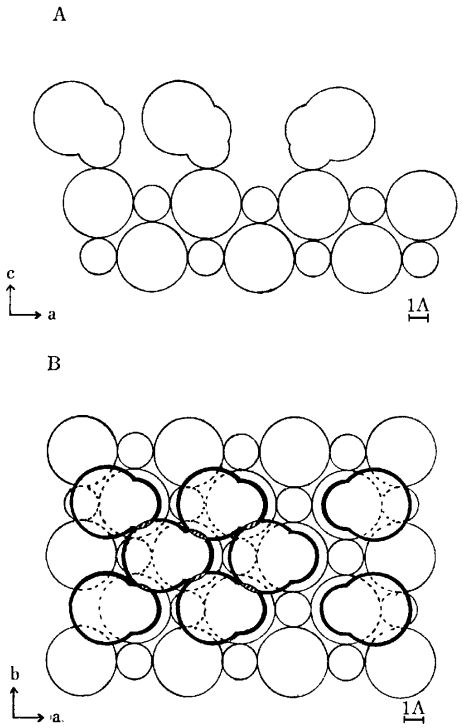

Fig. 2. Schematic diagrams of MeOH adsorption on (100) plane of NaCl.

A: Side view ◯: MeOH, ○: Cl^-, ○: Na^+.

B: Ground plane ◯: MeOH, ○: Cl^-, ○: Na^+.

The monolayer capacities, V_{BET} and V_B, were determined by two methods, the BET and the point B methods respectively. The values thus obtained are summarized in Table 1. As for the salt with a lattice spacing smaller than that of KCl or NaBr, V_B was less than V_{BET}. On the other hand, for the sample whose lattice spacing is larger than that of KCl or NaBr, V_B was greater than V_{BET}. These phenomena may be due to differences in the adsorption mechanisms at a coverage of $\theta=1$. This will also be discussed in the section on the mechanism of adsorption. The disagreement between V_B and V_{BET} values in each sample was within 20%.

Mechanism of Adsorption. The two assumptions introduced here to simplify the mechanism of MeOH adsorption on alkali halides are as follows: (I) all the surfaces of alkali halides particles consist of (100) planes, and (II) one MeOH molecule is adsorbed on one surface anion by an interaction such as a hydrogen bond. The former assumption for the surface structure of the salts will be reasonable in view of two experimental proofs, an electron microscopic observation of alkali halides surfaces made by Yao[2] and the fact found by Young[10] that approximately 80% of the surfaces of pulverized KCl is composed of (100) planes. The amounts of MeOH (V_{cal}) necessary for covering the unit surface area (1 m²) were calculated for all the samples (*cf.*, Table 1). The adsorptive situation of MeOH on the surface, *i.e.*, the (100) plane of NaCl, is illustrated in Fig. 2, in which the OH axis in the molecule is perpendicular to the surface of the crystal. The van der Waals radii of the hydrogen atom, the oxygen atom, and the CH_3 group are assumed to be 1.2, 1.4, and 2.0 Å respectively.[11] In the case of NaCl, some overlaps of neighboring adsorbed MeOH molecules occur, as is shown with the shaded area in Fig. 2-B. Considering this schematic structure of MeOH adsorption, a certain degree of steric hindrance is expected to arise among the adsorbed molecules at the monolayer completion. If an OH axis of MeOH is slightly oblique to the normal surface, such steric hindrance can be avoided in the adsorption. However, since the V_B/V_{cal} value for NaCl was smaller than 1, the steric hindrance is considered to remain to some extent. On the contrary, the V_B/V_{cal} values obtained for KCl and NaBr were approximately equal to 1. Therefore, the lattice spacings of the both salts will be regarded as convenient spacings for MeOH adsorption.

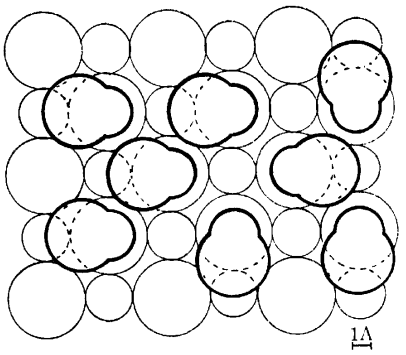

Fig. 3. Schematic diagram of MeOH adsorption on (100) plane of KBr.

○: Br^-, ○: K^+, ◯: MeOH.

In the case of the salt whose lattice spacing is smaller than that of NaCl, the steric hindrance will unavoidably be induced in the adsorbed MeOH, and the number of MeOH molecules adsorbed becomes less than that of anions on the surface. On the other hand, for KBr, whose spacing is larger than that of KCl, MeOH

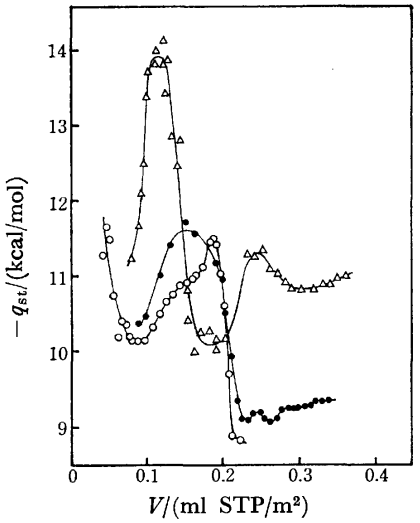

Fig. 4. Isosteric heats of adsorption of MeOH on alkali chlorides.
—△—: LiCl, —●—: NaCl, —○—: KCl.

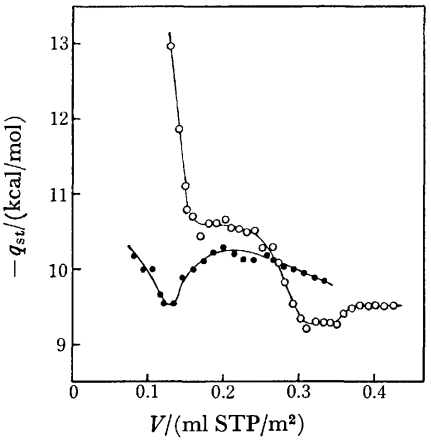

Fig. 5. Isosteric heats of adsorption of MeOH on alkali bromides.
—○—: NaBr, —●—KBr.

is adsorbed first on the surface anion in the ratio of 1 : 1. At this time, however, a vacant space is produced among the adsorbed molecules, as is shown in Fig. 3. In further adsorption, MeOH is packed more closely to diminish the vacant space. Therefore, the monolayer capacity is larger than the value to be expected from the adsorptive structure of one MeOH for one surface anion. When such a vacant space becomes larger, the amount of MeOH necessary for covering the space rises. Hence, the value of V_B/V_{cal} increases with an increase in the lattice spacing of the salt. The change in the V_B/V_{cal} values with the alteration of the samples will be explained in terms of the difference in their lattice spacings. Moreover, this explanation is supported by the discussion in the next section.

Heat of Adsorption. In Figs. 4 and 5, the isosteric heats ($-q_{st}$) of MeOH on the alkali halides are plotted against the amounts adsorbed. In the case of the chloride samples, the order of magnitude of the adsorption heats at $\theta=0.5$ ($V=0.11$ ml STP/m²) was found to be LiCl>NaCl>KCl. For the bromide

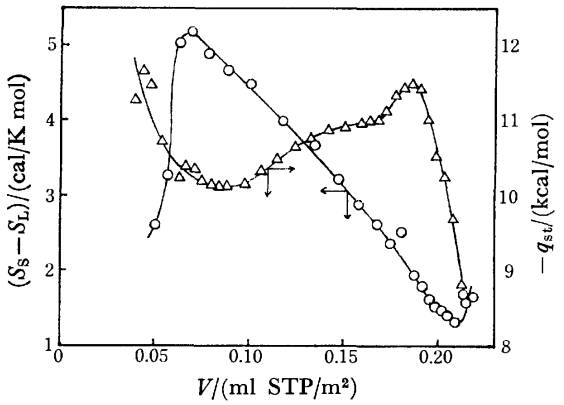

Fig. 6. Molar integral entropy of MeOH adsorbed on KCl.
S_S: Molar integral entropy of adsorbed MeOH.
S_L: Molar integral entropy of liquid MeOH at 20 °C.

samples, the order was NaBr>KBr. The heat of MeOH adsorption rose with an increase in the ionic radius ratio, r_{anion}/r_{cation}, of the crystal. These results are consistent with the adsorptive structure described above that MeOH molecules are adsorbed on the surface anion by the hydrogen bond.

The heats of adsorption for LiCl, NaCl, and KCl were noticed to have maximum values at a coverage below $\theta=1$ (<0.2 ml STP/m²). This phenomenon is considered to be caused by a lateral interaction induced among the adsorbed molecules. The heats of adsorption for NaCl and KCl had smaller values than the liquefaction heat of MeOH at the adsorbed amounts of above $V=0.225$ and 0.21 ml STP/m² respectively. When a MeOH molecule is adsorbed on the surface of the (100) plane, as is shown in Fig. 2, the polar OH group in MeOH is located under the CH_3. Therefore, an interaction between MeOH and the polar groups in the formerly adsorbed molecules is expected to be depressed on the further adsorption of MeOH, *i.e.*, a two-layer adsorption, and the isosteric heat of adsorption will be small at this time. This interpretation is compatible with the molar integral entropy change in MeOH adsorbed on KCl, as is shown in Fig. 6. These entropy values were calculated from adsorption isotherms omitted in this report. At low coverages, $V<0.07$ ml STP/m², the entropy of adsorbed MeOH became small with a decrease in the amounts adsorbed. This entropy change suggests that the MeOH molecule is tightly adsorbed on the surface of KCl in the early stage of the adsorption.

In the case of KBr, MeOH is considered to be adsorbed first on the surface anion, as is illustrated in Fig. 3. The lateral interaction induced among the adsorbed MeOH molecules will be very weak, owing to the long lattice spacing of KBr. It will be stated, in view of such an adsorption mechanism, that the heat of adsorption decreases with the amount adsorbed until the adsorbed molecules come in contact with each other. In the vicinity of the monolayer completion, the adsorbed molecules come in touch with each other, and the lateral interaction increases to cause a peak in the isosteric heat of adsorption at $V=0.21$ ml STP/m². This value is approximately equal to the monolayer

capacity estimated from the cross-sectional area of 18 Å^2 for a MeOH molecule. A peak caused by the lateral interaction was also observed in the curve of the adsorption heat of LiCl in the high-pressure region.

References

1) A part of this paper was presented at the 13th Symposium on Powder Science, Kyoto, November 1975.
2) Y. Y. Yao, *J. Colloid Interface Sci.*, **28**, 376 (1968).
3) P. B. Barraciough and P. G. Hall, *Surf. Sci.*, **46**, 393 (1974).
4) W. C. Price, W. F. Sherman, and G. R. Wilkinson, *Proc. R. Soc. London, Ser. A*, **247**, 467 (1958).
5) R. A. Rad, *Surf. Sci.*, **12**, 37 (1968).
6) M. Chikazawa, F. Yamamoto, E. Saita, M. Kaiho, and T. Kanazawa, *Bull. Chem. Soc. Jpn.*, **50**, 337 (1977).
7) A. L. McClellan and H. F. Harnsberher, *J. Colloid Interface Sci.*, **23**, 577 (1967).
8) A. Seidell and W. F. Linke, "Solubilities of Inorganic and Metal Organic Compounds," 4th ed, American Chemical Society, Washington (1965), p. 402, 1007.
9) K. B. Haevey and G. B. Porter, "Introduction to Physical Inorganic Chemistry," Addison-Wesley Publishing Co. (1963), p. 33.
10) D. M. Young, *Trans. Faraday Soc.*, **50**, 838 (1954).
11) L. Pauling, "The Nature of the Chemical Bond," 2nd ed, Oxford University Press, London (1950), p. 189.

A Study of the Behavior of Surface Oxygen of V_2O_5 Catalysts by the Use of the ^{18}O-Tracer

Yoshiya KERA

Department of Chemistry, Faculty of Science, Osaka University, Toyonaka, Osaka 560

(Received April 15, 1977)

By the use of highly concentrated ^{18}O-carbon dioxide, both the rate of the isotopic exchange of CO_2 and the surface oxygen of a powderd V_2O_5 catalyst and that of the isotopic equilibration of CO_2 on the surface were determined simultaneously in the temperature range from 330 to 450 °C. The rate of the isotopic exchange on the thin-plate crystallines, in which the (010) plane of V_2O_5 crystal was mainly exposed, was also determined. The equilibration rate was 30—40 times faster than the exchange rate. The exchange process on the thin-plate crystallines was found to be extremely rapid, although such a phenomenon has never been found on the powdered catalyst. Based on these results, the relationship of the reaction steps of the isotopic exchange and the isotopic equilibration with those on the triangular scheme of CO-oxidation, previously proposed, was discussed in detail. A small cycle of alternate reduction-oxidation on the top of the surface, especially on the (010) plane, was conclusively confirmed.

The bonding energy of the surface oxygen of metal oxides and its energy distribution have been determined by many authors[1-12] as important parameters for catalytic activities. Information on the dynamical aspects of oxygen species on the surface of metal oxides has also been obtained successfully by the applications of ^{18}O-tracer techniques.[13-16]

In our previous paper[17] the behavior of the surface oxygens of powdered V_2O_5 during the course of CO-oxidation were examined by the use of ^{18}O-tracer techniques, and a mechanism, that is, a "triangular" reaction scheme, was proposed. The very high activity of the surface V=O group, asserted by Tarama *et al.*,[18] was confirmed practically by the simultaneous applications of the IR and ^{18}O-tracer techniques.[19] Evidence of the alternate reduction-oxidation of the oxygen of the V=O group has also been given by the measurements of the reflectance spectra of IR by Fahrenfort *et al.*[20] However, the relationship between the exchangeable oxygen and the most reactive oxygen in CO-oxidation has not been established well enough, as has been pointed out by Sachtler[20] and Emmett.[21]

In this work, first the rates of two processes, the isotopic exchange between CO_2 and the surface oxygen of powdered V_2O_5, Eq. 1, and the isotopic equilibration of oxygen in CO_2 on the surface, Eq. 2, were simultaneously determined and compared with each other:

$$C^{18}O_2 + {}^{16}O(s) = C^{18}O^{16}O + {}^{18}O(s), \quad (1)$$

$$C^{18}O_2 + C^{16}O_2 = 2C^{18}O^{16}O. \quad (2)$$

Secondly, the rate of the exchange process on the powdered V_2O_5 was compared with that on the thin-plate crystallines, in which the (010) plane of V_2O_5 crystal was mainly exposed. On the basis of the results, the relationship of the reaction steps of the isotopic exchange and the isotopic equilibration with those of CO-oxidation was successfully discussed and the triangular scheme, previously proposed, was confirmed further.

Experimental

Materials. A commercial V_2O_5 (special grade, Mitsuwa Chem. Ind. Co.) was used as the powdered catalyst without further treatment. Thin-plate crystallines of V_2O_5, with the (010) plane mainly exposed, were obtained by the pulverization of a single crystal and by sieving with an 80-mesh sieve. Crystal I (smaller size—above 80-mesh) and Crystal II (larger size—below 80-mesh) were used as the catalysts of the thin-plate crystallines. The BET surface area of powdered V_2O_5 and Crystal I were determined to be 2.5 and 0.55 m^2/g respectively.

Gaseous CO_2 containing ^{18}O was prepared by the oxidation of carbon with heavy gaseous oxygen (^{18}O), which had been highly concentrated by the thermal diffusion method.[22] After purification by the usual procedures, no impurities were detected mass-spectrometrically.

Procedure and Experimental Conditions. Reaction systems and procedures similar to those of previous papers[17,19] were adopted. The reaction conditions are summarized in Table 1. The reaction temperatures were controlled within ±1 °C, and the accuracies in the determination of the ^{18}O-concentration were ±0.02—0.05 atom%.

Results

1) Simultaneous Determinations of the Rates of the Isotopic Exchange and the Isotopic Equilibration. Simultaneous determinations of the rates of both the isotopic exchange, Eq. 1, and isotopic equilibration, Eq. 2, over powdered V_2O_5 were attempted. In a preliminary experiment, the determination of the rate of the isotopic equilibration was quite difficult, for the isotopic compositions in carbon dioxide ($C^{16}O_2$, $C^{18}O_2$, and $C^{16}O^{18}O$) were greatly disturbed by the exchange process, which occurred simultaneously. In this experiment, therefore, small amounts of V_2O_5 (0.03 g) were used, and the changes in the isotopic compositions were measured only at the initial stage in order to avoid the trouble as much as possible. The results under the conditions shown in Table 1 are given in Table 2. In the Table, x, γ, and K denote ^{18}O atom% in CO_2, $C^{16}O^{18}O$ molecular percent in CO_2, and the value of $\{C^{16}O^{18}O\}^2/\{C^{16}O_2\}\{C^{18}O_2\}$ at a certain reaction time respectively. The increases in γ and K indicate the progress of the equilibration reaction and the decrease in x the progress in the exchange reaction. When the changes in x become large, the values of γ and K will be affected directly and the rate of the equilibration can not be determined accurately. The changes in x and γ with the time are illustrated again by Fig. 1. It can clearly be seen at 450 °C that γ is practically disturbed by

TABLE 1. REACTION CONDITIONS

Experiment	V_2O_5 Catalyst	Temperature °C	CO_2 Pressure mmHg	Volume cm^3	Catalyst weight g
Exchange and equilibration reactions	Powdered	330—450	12	130	0.03
Exchange reaction	Crystal I (below 80 mesh)	410	23	300	0.3
	Crystal II (above 80 mesh)	410	21	300	0.3
		490	21	300	0.3
	Powdered	410	12	130	0.3

TABLE 2. CHANGES IN THE ISOTOPIC COMPOSITIONS OF CO_2 ON THE POWDERED V_2O_5 AT 450 °C
(x: ^{18}O atomic%, y: $C^{16}O^{18}O$ molecular%, K: $(C^{16}O^{18}O)^2/(C^{16}O)(C^{18}O)$)

		Reaction time/h						
		0	0.25	0.5	1.0	1.5	2.0	3.0
450 °C	x	17.70	17.87	17.37	17.12	16.90	—	—
	y	21.40	24.07	25.34	26.35	27.03	—	—
	K	0.8_8	1.4_3	1.9_4	2.5_3	3.0_3	—	—
410 °C	x	17.57	—	17.45	17.37	17.23	—	—
	y	21.61	—	24.90	26.50	27.34	—	—
	K	0.9_9	—	1.7_5	2.4_8	2.9_2	—	—
370 °C	x	17.66	—	17.60	17.53	17.50	17.44	—
	y	22.16	—	23.75	24.81	25.70	26.37	—
	K	0.9_9	—	1.3_9	1.7_4	2.0_3	2.3_4	—
330 °C	x	17.69	—	17.66	17.66	17.57	17.58	17.50
	y	21.83	—	23.08	24.01	24.68	25.39	26.14
	K	0.9_8	—	1.2_6	1.4_5	1.6_8	1.9_0	2.2_3

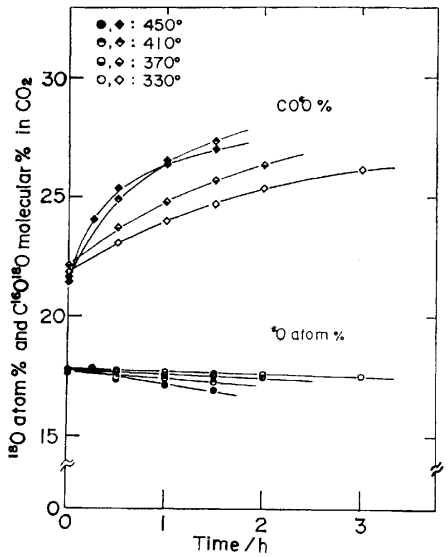

Fig. 1. Changes in ^{18}O atom% and $C^{16}O^{18}O$ molecular % in CO_2 with time over powdered V_2O_5 in the temperature range from 330 to 450 °C.

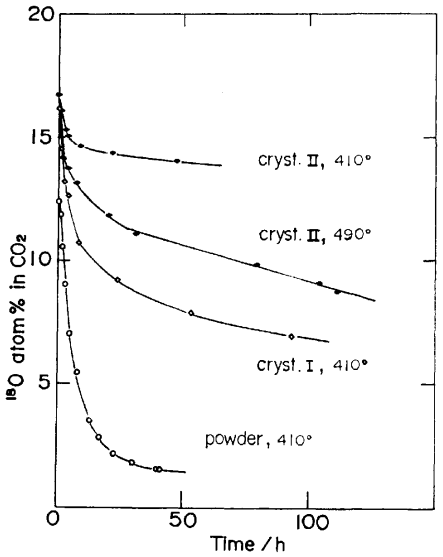

Fig. 2. Changes in ^{18}O atom% in CO_2 with time over powdered V_2O_5 and thin plate crystallines of V_2O_5.

relatively large changes in x.

2) Comparison of the Rates of the Isotopic Exchange on the Powdered V_2O_5 with That on the Thin-plate Crystallines. In order to make clear the effects of the particle size and shapes of V_2O_5 on the catalytic activities and to ascertain the differences in the activities among the crystalline planes, the rate of the isotopic exchange was measured over three types of V_2O_5 samples, shown in Table 1, and compared. The changes in the ^{18}O-concentration-(atom%) in CO_2 with the time are given in Fig. 2. The equilibration reaction took place too fast to determine the rate — the equilibration has already arrived at the first point in the figure. From Fig. 2 it is clear at 410 °C that the rate on the powdered V_2O_5 is faster than that on the Crystal I, while that on the Crystal I faster than that on the Crystal II. These differences must be caused by the differences in the surface areas. In the figure it can also be seen in the initial stage that the rates on the Crystal II are less even at 490 °C

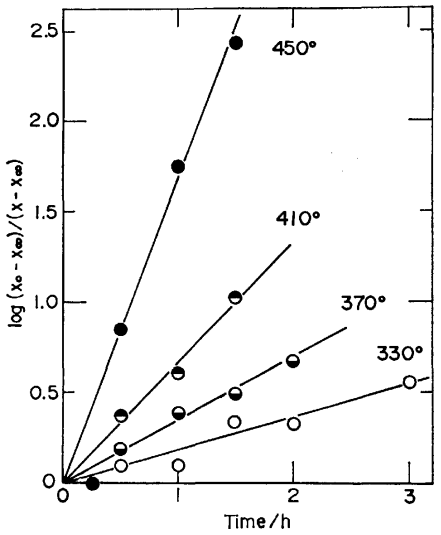

Fig. 3. Kinetical treatment of the data on the isotopic exchange in Table 2 with Eq. 4.

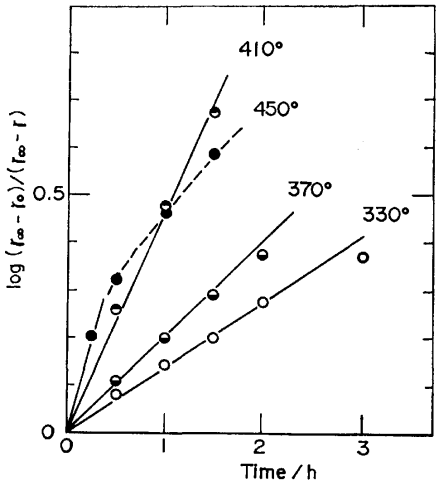

Fig. 4. Kinetical treatment of the data on the isotopic equilibration in Table 2 with Eq. 6.

than those on the Crystal I at 410 °C. The slope of the curve of the ^{18}O-concentration *vs.* the time was kept constant; however, after 30 h on the former sample, it became considerably larger than that on the latter. This feature may correspond to the indication[14,16] that oxygen diffusion in the inner bulk of V_2O_5 crystal is extremely stimulated above 500 °C.

Discussion

Comparison of the Rate of the Isotopic Exchange with That of the Isotopic Equilibration on the Powdered V_2O_5.

The rate of the isotopic exchange can be generally described by Eq. 3 if the oxygen atoms in the oxide (O_1) are alike in exchangeability and if the kinetical isotope effects are neglected:

$$-(dx/dt) = k_{ex}(x-x_\infty). \quad (3)$$

The integrated form is given by Eq. 4:[13-16]

$$\ln\{(x_0-x_\infty)/(x-x_\infty)\} = k_{ex}\cdot t, \quad (4)$$

where x is the ^{18}O-concentration in carbon dioxide at any time, x_0 and x_∞ denote the initial and the final values respectively, and k_{ex} is an apparent rate constant. The total reaction rate, R_{ex}, is obtained by multiplying k_{ex} by the total number of oxygen atoms in carbon dioxide, n_g. x_∞ in Eq. 4 can be estimated using Eq. 5:

$$x_\infty = \{n_g/(n_g+n_{ex})\}x_0. \quad (5)$$

Since the amount of exchangeable oxygen in V_2O_5, n_{ex}, is not known in the present experiment, it is assumed preliminarily that n_{ex} is equal to the total number of oxygen atoms in V_2O_5, n_t. x_∞ was estimated as about 3 atom% by using the values of $n_g=1\times10^{20}$ and $n_t=5\times10^{20}$ atoms. Plots of $\log\{(x_0-x_\infty)/(x-x_\infty)\}$ *vs.* the time are shown in Fig. 3.

The rate of the isotopic equilibration, Eq. 2, can be described by Eq. 6 if there is no disturbance of the isotopic composition in carbon dioxide by the exchange reaction:

$$(d\gamma/dt) = k_{eq}(\gamma_\infty-\gamma). \quad (6)$$

The integrated form is given by Eq. 7:[13-16]

$$\ln\{(\gamma_0-\gamma_\infty)/(\gamma-\gamma_\infty)\}=k_{eq}\cdot t, \quad (7)$$

where γ is the concentration of $C^{16}O^{18}O$ in carbon dioxide, γ_0 and γ_∞ denote the initial and the final values respectively, and k_{eq} is an apparent rate constant. The total reaction rate, R_{eq}, is obtained by multiplying k_{eq} by the total number of CO_2 molecules.

γ_∞ in Eq. 6 can be estimated as follows: when the initial contents of $C^{16}O_2$, $C^{18}O_2$, and $C^{16}O^{18}O$ are denoted by α_0, β_0, and γ_0, the values at equilibrium can be described as (α_0-u), (β_0-u), and (γ_0+2u) respectively, using an unknown value, u. The value of K is approximately equal to 4 in the present temperature range. Therefore, Eq. 8 holds:

$$K = (\gamma_0+2u)^2/(\alpha_0-u)(\beta_0-u) = 4, \quad (8)$$

and thus u can be represented by Eq. 9:

$$u = (4\alpha_0\beta_0-\gamma_0^2)/4. \quad (9)$$

Therefore, γ_∞ is described by Eq. 10:

$$\gamma_\infty = \gamma_0 + 2u = \gamma_0 + (4\alpha_0\beta_0-\gamma_0^2)/2. \quad (10)$$

Plots of $\log\{(\gamma_0-\gamma_\infty)/(\gamma-\gamma_\infty)\}$ *vs.* the time are shown in Fig. 4.

k_{ex} and k_{eq} can be directly estimated from the slopes of the curves in Figs. 3 and 4 respectively, although the errors are rather large. In Fig. 4 the higher the temperature and the longer the reaction time, the larger the deviation from the straight lines. This indicates that the disturbance of the isotopic compositions by the exchange reaction can not be neglected as the temperature increases and as the time becomes longer. At 450 °C especially, disturbance appeared more clearly as time passes; thus, k_{eq} was estimated by considering only the first point in the curve. k_{ex}, k_{eq}, R_{ex}, and R_{eq} are summarized in Table 3. From the comparison of R_{ex} with R_{eq}, the equilibration rate is known to be about 20—40 times faster than the exchange rate. Arrhenius plots of k_{ex} and k_{eq} are given in Fig. 5. The apparent pre-exponential factors and activation energies were evaluated as follows:

$$k_{0,eq} = 1.3\times10^{-2}(cm^{-2}\,s^{-1}), \quad E_{eq} = 14(kcal/mol),$$
$$k_{0,ex} = 5\times10^{-4}(cm^{-2}\,s^{-1}), \quad E_{ex} = 15(kcal/mol),$$

TABLE 3. THE ISOTOPIC EXCHANGE RATE AND THE ISOTOPE EQUILIBRATION RATE

Temperature °C	k_{ex} 10^{-9} cm^{-2} s^{-1}	Exchange rate 10^{11} atoms cm^{-2} s^{-1}	k_{eq} 10^{-7} cm^{-2} s^{-1}	Equilibration rate 10^{13} molecules cm^{-2} s^{-1}
450	14.4	15.8	7.0	3.8
410	5.6	6.1	4.0	2.2
370	3.0	3.3	1.7	0.9
330	1.5	1.6	1.2	0.6

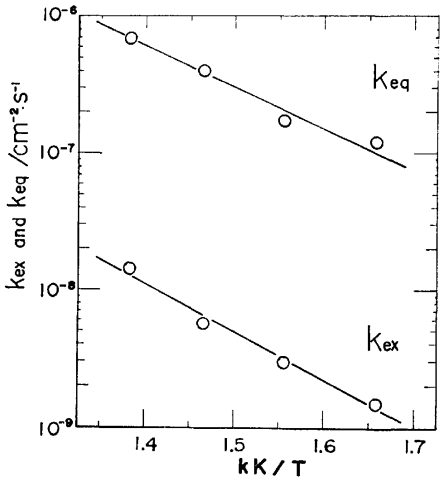

Fig. 5. Arrhenius plots of k_{ex} and k_{eq}.

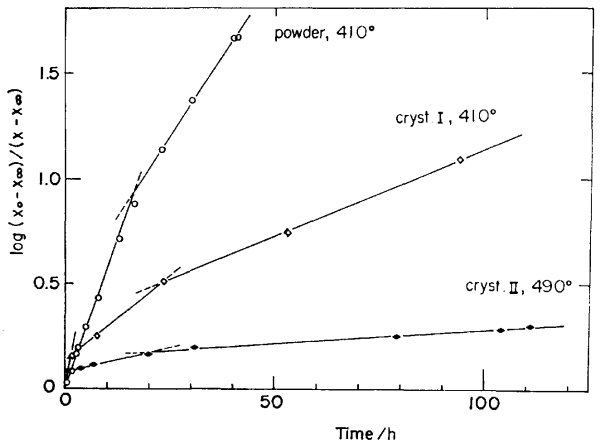

Fig. 6. Comparison of kinetics of the isotopic exchange on the powdered V_2O_5 with that on the thin plate crystallines.

Comparison of the Exchange Rate on the Powdered V_2O_5 with That on the Thin-plate Crystallines. On the application of Eq. 4 to the data of the exchange reaction on the powdered V_2O_5, if an appropriate value is assumed for x_∞, plots of $\log\{(x_0-x_\infty)/(x-x_\infty)\}$ *vs.* the time show two clear straight lines with a break point, as has been mentioned in a previous paper.[17] The appearance of the break suggests that the reactivity or mobility of oxygen in the surface layer of the powdered V_2O_5 can be differentiated from that in the inner bulk during the exchange reaction.

The data on the powdered V_2O_5 (410 °C), the Crystal I (410 °C) and the Crystal II (490 °C), given in Fig. 2, were treated with Eq. 4 assuming appropriate values of x_∞. The results are given in Fig. 6. In the cases of the thin-plate crystallines, an extremely rapid process appeared before the two processes found in the powdered run. The extremely rapid process must have appeared because of relatively high exposure of the (010) plane. This would also give experimental proof that the (010) plane has a considerably higher activity than the other planes. In the case of the powdered V_2O_5, only the process on the (010) plane seems not to be differentiated from that on the other planes; this is because of following reasons: a rapid process would occur not only on the (010) plane, but also on many kinds of surface grain boundaries, and all planes might be exposed with a nearly equal possibility on powdered V_2O_5.

It was found previously by the simultaneous applications of IR and ^{18}O-tracer techniques that the oxygen in the V=O group, projected from the (010) plane, was first exchanged, followed by the oxygen in the V–O–V layer.[19] With reference to these results, of the three straight lines in Fig. 6, the first line corresponds to the exchange of the oxygen in the V=O group, projected perpendicularly to the (010) plane; the second, to that of oxygen in the surface layer (that is, the oxygen near the surface of the other planes or the V–O–V layer), and the third, to the exchange between the surface layer and the inner bulk. Kakioka *et al.*[23] have examined in detail the rate of the isotopic exchange of oxygen in CO_2 with that in powdered V_2O_5 and Mo-doped V_2O_5. They have also demonstrated the existence of two processes — the exchange between the gaseous phase and the surface layer and the diffusion in the inner bulk. The rate and the activation energy of the present second process, R_{ex}, are nearly equal to the rate and the activation energy of the exchange process respectively, as obtained by Kakioka *et al.*

From the intersections of vertical axis with the extrapolated second and third straight lines in Fig. 6, the idealized amounts of exchangeable oxygen atoms corresponding to the top of the surface, n_{S_1}, and the surface layer, n_{S_2}, respectively, could be estimated. Besides, the amounts of the exchangeable oxygen corresponding to the inner bulk, n_b, can be easily estimated as the difference between the total exchangeable oxygen, n_{ex} and $n_{S_1}+n_{S_2}$. The amounts of exchangeable oxygen obtained by those procedures are summarized in Table 4. The overall rates at the initial stage, $R_{0,ex}$, were preliminarily estimated as the decrease in the ^{18}O-concentration for the initial hour. The results are added to Table 4 for the sake of comparison. n_{S_1} is 4—5 times less than n_g in Table 4. The initial rates, $R_{0,ex}$, may not indicate the real values because, in this situation, the exchange between the gaseous phase and the top of the surface possibly arrives at equilibrium within

TABLE 4. AMOUNTS OF EXCHANGEABLE OXYGENS OF V_2O_5 CRYSTAL AND THE INITIAL EXCHANGE RATE

Sample (Temp/°C)	n_g 10^{20} atoms	n_{s_1} 10^{20} atoms	n_{s_2} 10^{20} atoms	n_b 10^{20} atoms	n_t 10^{20} atoms	$R_{0,ex}$ atoms cm^{-2} s^{-1}
Powder (410)	1.03	1.36		7.4	49.4	3.8×10^{11}
Crystal I (410)	1.92	0.37	0.57	2.2	49.4	3.3×10^{12}
Crystal II (490)	1.58	0.30	0.31	35.1	49.4	(1.1×10^{13}) a)

a) The surface area was assumed to be 0.2 m^2/g in this run.

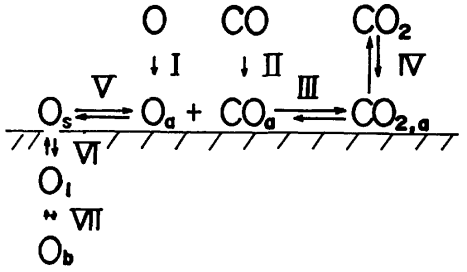

Fig. 7. Relations of reaction paths among the isotopic exchange, the isotopic equilibration, and CO-oxidation. The first, the second, and the third processes of the isotopic exchange are controlled by step V, VI, and VII, respectively and the isotopic equilibration by step V and CO-oxidation by step I and II.
$\{r(+\mathrm{I})=r(+\mathrm{II})=r(+\mathrm{III})-r(-\mathrm{III})$
$=r(+\mathrm{IV})-r(-\mathrm{IV})=r(\pm\mathrm{VI}),\ r(\pm\mathrm{V})\approx30r(\pm\mathrm{VI})\}$

1 h. Practically, larger values could be expected. The exchange rate on the thin-plate crystallines is known, from Table 4, to be more than 10 times faster than that on the powdered V_2O_5. This seems to mean that the exchange rate on the top of the surface of the (010) plane is comparable to the equilibration rate. This could be confirmed, however, only under the experimental condition of $n_g \ll n_{s_1}$.

Relationship of the Reaction Steps on the Isotopic Exchange and the Isotopic Equilibration with Those on the Triangular Scheme of CO-oxidation. The previous reaction scheme[17] of CO-oxidation was further generalized, as is shown in Fig. 7, by adding some steps of oxygen transfer in V_2O_5 crystallines on the basis of the above discussion. In the isotopic exchange on the powdered V_2O_5 Step V could not be observed, only Step VI. In the simultaneous determination of the exchange and the equilibration rates, R_{eq}, which should be related to the rate of Step V, was about 20—40 times faster than R_{ex}, correspondng to the rate of Step VI. On the other hand, on the thin-plate crystallines the rate of Step V was more than 10 times faster than that of Step VI; moreover, R_{ex} on the top of the surface of the (010) plane was suggested to be comparable to the R_{eq}, observed on the powdered V_2O_5. At the steady state of the exchange reaction, therefore, the length of the arrow of Step VI is 20—40 times shorter than the length of the forward and backward arrows in Steps III, IV, and V.

On the powdered V_2O_5, the overall rate of CO-oxidation, R_{oxid}, was nearly equal to R_{ex}, as was shown in a previous paper.[17] It was suggested, furthermore, that the R_{oxid} was controlled by the length of the arrow of Step I or of Step II in Fig. 7. At the steady state the length should be equal to the differences between the forward and backward arrows of Steps III and IV. At the steady state of CO-oxidation, therefore, the length of the arrow of Step VI would be nearly equal to the difference between the forward and the backward arrows in Steps III and IV. With respect to the absolute length of the arrows, Steps III and IV are both also about 20—40 times longer than Step VI. On the basis of the reaction scheme it can easily be understood that the catalytic oxidation proceeds according to a small cycle of alternate reduction-oxidation on the top of the surface, especially on the (010) plane.

In the present experiment the extremely high activity of oxygen on the (010) plane was shown only under the atmosphere of CO_2. The surface composition of vanadium and oxygen seems to be nearly stoichiometric in the working states. An acceleration of the exchange rate has been previously found on the addition of CO.[17] In this case the surface of V_2O_5 is probably kept in reduced states. Therefore, the question of whether or not the small cycle of reduction-oxidation can hold on the strongly reduced surface of V_2O_5 remains for future study.

Recently Boreskov *et al.*[24] and Kazanskii *et al.*[25] examined in detail the reaction of CO-oxidation over vanadium oxide, supported or not supported, and gave valuable suggestions as to the reaction mechanism. However, it is difficult to compare the mechanisms presented by Boreskov, Kazanskii, and the present authors, because the reaction conditions and surface states of the catalysts seem to be very different. In a forthcomming paper the effects on the rate of CO-oxidation will be investigated in detail in connection with the particle sizes and shapes, the degrees of oxidation and reduction of the surface, and the purities of the V_2O_5 catalyst.

References

1) G. K. Boreskov, V. A. Sazonov, and V. V. Popovskii, *Dokl. Akad. Nauk SSSR*, **176**, 1331 (1967); G. K. Boreskov, *Kinet. Katal.*, **8**, 1020 (1967); V. A. Sazonov, V. V. Popovskii, and G. K. Boreskov, *ibid.*, **9**, 307, 312 (1968).
2) T. Uchijima, M. Takahashi, and Y. Yoneda, *Bull. Chem. Soc. Jpn.*, **40**, 2767 (1967); *J. Catal.*, **9**, 403 (1967).
3) K. Klier, *J. Catal.*, **8**, 14 (1967).
4) J. Derén and J. Stoch, *J. Catal.*, **18**, 249 (1967).
5) G. Parravano, *Catal. Rev.*, **4**, 53 (1970).
6) V. I. Marshneva, G. K. Boreskov, and V. D. Sokolovskii, *Kinet. Katal.*, **14**, 210 (1973).
7) A. K. Vijh, *J. Catal.*, **28**, 329 (1973); *ibid.*, **33**, 385 (1974); *ibid.*, **38**, 525 (1975).
8) N. N. Bulgakov, Yu. A. Borisov, and V. V. Popovskii, *Kinet. Katal.*, **15**, 691 (1974).
9) A. Andereev and N. Neshev, *Kinet. Katal.*, **15**, 1237

(1974).
10) B. Halpern and J. E. Germain, *J. Catal.*, **37**, 44 (1975).
11) J. M. Criado, *J. Catal.*, **37**, 563 (1975).
12) N. I. Il'chenko and G. I. Golodets, *J. Catal.*, **39**, 73 (1975).
13) a) J. N. Wilson and R. G. Dickinson, *J. Am. Chem. Soc.*, **59**, 1358 (1937); b) H. A. C. Mckay, *Nature*, **142**, 997 (1938); c) N. Morita, *Bull. Chem. Soc. Jpn.*, **15**, 166 (1940), d) R. B. Duffield and M. Calvin, *J. Am. Chem. Soc.*, **68**, 557 (1946).
14) E. R. S. Winter, *Discuss. Faraday Soc.*, **8**, 231 (1950); *Advan. Catal.*, **10**, 196 (1958); *J. Chem. Soc.*, **1968**, 2889.
15) K. Klier, J. Novakova, and P. Jiru, *J. Catal.*, **2**, 479 (1963); J. Novakova, *Catal. Rev.*, **4**, 77 (1970).
16) G. K. Boreskov, *Adv. Catal.*, **15**, 285 (1964).
17) K. Hirota, Y. Kera, and S. Teratani, *J. Phys. Chem.*, **72**, 3133 (1968).
18) K. Tarama, S. Teranishi, S. Yoshida, and N. Tamura, *Proc. 3rd Int. Congr. Catal., Amsterdam*, **1964**, 262 (1965); K. Tarama, S. Yoshida, S. Ishida, and H. Kakioka, *Bull. Chem. Soc. Jpn.*, **41**, 2840 (1968).
19) Y. Kera and K. Hirota, *J. Phys. Chem.*, **73**, 3973 (1969).
20) a) Y. Fahrenfort and N. C. Rol, unpublished data; *cf. Catal. Rev.*, **4**, 46 (1970); b) W. M. H. Sachtler, *Catal. Rev.*, **4**, 44 (1970).
21) P. H. Emmett, *Catal. Rev.*, **7**, 8 (1973).
22) M. Yamamoto, M. Takahashi, M. Imaoka, T. Hashioka, and K. Hirota, *Nippon Kagaku Zasshi*, **89**, 839 (1968).
23) H. Kakioka, V. Ducarme, and S. J. Teichner, *J. Chim. Phys.*, **68**, 1715, 1722, 1726 (1971).
24) G. K. Boreskov, V. I. Marshneva, and V. D. Solovskii, *Dokl. Akad. Nauk. SSSR*, **199**, 1091 (1971); V. I. Marshneva, G. K. Boreskov, and V. D. Sokolovskii, *Kinet. Katal.*, **13**, 1209 (1972); G. K. Boreskov and V. I. Marshneva, *Dokl. Akad. Nauk SSSR*, **213**, 112 (1973).
25) M. Ya. Kon', V. A. Shets, and V. B. Kazanskii, *Dokl. Akad. Nauk SSSR*, **203**, 624 (1972); *Kinet. Katal.*, **13**, 735 (1972); *ibid.*, **14**, 403 (1973).

Semiconducting Properties of $(Ln_I, Ln_{II})CuO_4$ and of $(Ln, A)_2CuO_4$ (Ln=rare earth, A=alkaline earth)

Tadao KENJO and Seishi YAJIMA

Oarai Branch, Research Institute for Iron, Steel and Other Metals, Tohoku University, Oarai-machi, Ibaraki 311-13

(Received December 13, 1976)

The ternary oxides, $(La,Pr)_2CuO_4$, $(Gd,Tb)_2CuO_4$, $(La,Tb)_2CuO_4$, $(La,Ca)_2CuO_4$ and $(La,Ba)_2CuO_4$, were prepared and their semiconducting properties were investigated. When the mean ionic radius of Ln^{3+} ($\bar{r}$) is increased, the $(La,Pr)_2CuO_4$ compounds transform from semiconductors to metals at a critical $\bar{r}$ value of 1.05 Å. The metal-semiconductor transition which accompanies the shrinkage of the a axis, is explained as being due to the π-bond formation of the Cu–O bond. Compounds in the composition range from $La_{1.3}Tb_{0.7}CuO_4$ to $La_{1.4}Tb_{0.6}CuO_4$ are peculiar to the $(La,Tb)_2CuO_4$ compounds. The crystal structure is the same as that of Ln_2CuO_4, but it is different from Ln_2CuO_4 as regards the c/a ratio and resistivity. The doping of 20 mol% CaO or 10 mol% BaO into La_2CuO_4 lowers the resistivity to tenth of that of La_2CuO_4.

In the CuO-Ln_2O_3 system (Ln=rare earth), there are three different types of compounds, the metallic La_2CuO_4 compound, the semiconductive Ln_2CuO_4 compounds (Ln=Pr—Gd) and the insulating $Ln_2Cu_2O_5$ compounds (Ln=Tb—Lu).[1-3] The resistivities of the Ln_2CuO_4 compounds decrease with increasing ionic radius of the Ln^{3+} ions continuously for Ln=Gd—Pr, but a semiconductor-metal transition takes place between Ln=Pr and La; the La_2CuO_4 compound is metallic.[3] The lattice parameters of these compounds vary with the size of the Ln^{3+} ions in accordance with the electrical behavior. The lattice parameters, both of the *a* and *c* axes, increase with increasing ionic radius of the Ln^{3+} ion continuously for Ln=Gd—Pr, but between Ln=Pr and La they change discontinuously; the *a* parameter for the La_2CuO_4 compound is smaller than that for the Pr_2CuO_4 compound although the La^{3+} ion is larger than the Pr^{3+} ion.[3] The ternary $(La,Pr)_2CuO_4$ compounds are expected to reveal how critically the resistivities and lattice parameters change with variations in the ionic radius between those of the Pr^{3+} and La^{3+} ions, because the ionic radii of the Ln^{3+} ions can be continuously varied by changing the La/Pr ratio.

The ternary $(La,Tb)_2CuO_4$ compounds would continuously cover ionic radii of the Ln^{3+} ion ranging from that of the La^{3+} ion to that of the Tb^{3+} ion, if the La^{3+} ion can freely be replaced by a Tb^{3+} ion. These ternary compounds would reveal how the resistivity and the lattice parameters of Ln_2CuO_4 compounds vary with the $\bar{r}$ value ($\bar{r}$=mean ionic radius of rare earth ions) over the above range and will also reveal whether or not the ternary compounds containig two kinds of rare earth ions, the ionic radii of which are very different from each other, are the same as the binary compounds as regards the variation of structure and resistivity with the $\bar{r}$ value.

The resistivities of the Ln_2CuO_4 compounds decrease with increasing ionic radius of the Ln^{3+} ions.[3] If this trend could be extended to the region of the ionic radius beyond the La^{3+} ion, Ln_2CuO_4 compounds containing larger trivalent ions than La^{3+} ions would show a lower resistivity than that for La_2CuO_4. Such large trivalent ions are very difficult to obtain, but the less electronegative metals, such as alkaline earth metals, can be expected to give the same effect on the resistivity because this trend appears to be related to the electronegativity of atoms in the Ln^{3+} sites. Since the Gd^{3+} ions in the Gd_2CuO_4 compound are partially replaced by alkaline earth ions,[4] the La^{3+} ions in La_2CuO_4 can be expected to be replaced by some alkaline earth ions. CaO and BaO were added to the La_2CuO_4 compound to see if the resistivity decreased.

The composition of the Ln_2O_3–CuO compounds changes discontinuously between Ln=Gd and Tb; Gd_2CuO_4 and $Tb_2Cu_2O_5$ are known,[1,2] but $Gd_2Cu_2O_5$ and Tb_2CuO_4 are unknown. It is of interest to determine whether $Ln_2Cu_2O_5$ and Ln_2CuO_4 compounds coexist in a region of the ionic radius of the Ln^{3+} ion or the Ln_2CuO_4 compound changes into the $Ln_2Cu_2O_5$ compound at a certain critical Gd/Tb atomic ratio. Furthermore, these compounds also have different electrical properties. Gd_2CuO_4 is a semiconductor, while $Tb_2Cu_2O_5$ is an insulator. Since the mean ionic radius of the Ln^{3+} ion can be varied continuously by using ternay $(Gd,Tb)_2CuO_4$ compounds, these discontinuous compositional and electrical changes between Ln=Gd and Tb will be investigated in more detail.

Experimental

Reagents and Materials. Stock solutions of $Ln(NO_3)_3$, $Ba(NO_3)_2$, and $Ca(NO_3)_2$ were obtained by dissolving Ln_2O_3 (Nihon Yttrium Co., 99.9% pure), $BaCO_3$ and $CaCO_3$ (Wako Pure Chemical Co., Ltd., GR grade) into nitric acid (Wako Pure Chemical Co., Ltd., GR grade). A stock solution of $Cu(NO_3)_2$ was obtained by dissolving $Cu(NO_3)_2 \cdot 3H_2O$ (Kanto Chemical Co., GR grade) into distilled water. The solutions were standardized by the EDTA chelatometric titration method.

Procedure. Samples were prepared using the same method as that described in a previous paper.[3] Aliquot portions of the solutions of $Ln(NO_3)_3$, $Cu(NO_3)_2$ (and an alkaline earth nitrate, when necessary) were mixed. A sodium hydroxide solution (1M) (and sodium carbonate solution (1M) for the addition of an alkaline earth nitrate) was added and the mixture was stirred. After the mixture had stood overnight, filtering and washing were repeated until no sodium ions were detected in the filtrate using the flame test. The mixtures of precipitates thus obtained were preheated to 750 °C in air. The dry powder of the oxide mixture thus obtained was milled, pressed into 15 mm diameter pellets and heated to 1000 °C for 15 h in air. The resistivity was measured using the 4-probe method in the same manner as described

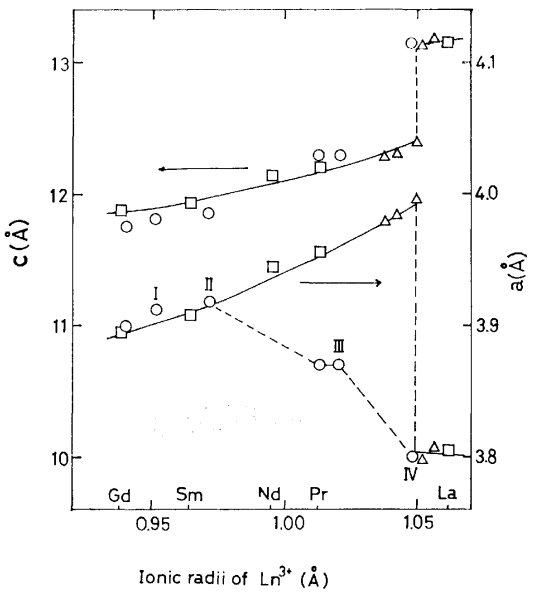

Fig. 1. Variation of lattice parameters of Ln_2CuO_4 with ionic radii or mean ionic radii of rare earth ions. □: Ln_2CuO_4, ○: $(La,Tb)_2CuO_4$, △: $(La,Pr)_2CuO_4$.

in a previous report.[3] An X-ray diffractometer was used for the measurement of lattice parameters and for the solid solubility determination in the ternary system.

Results and Discussion

Figure 1 gives the variation of the lattice parameters of binary Ln_2CuO_4 and ternary $(Ln_I,Ln_{II})_2CuO_4$ compounds with the ionic radius, or the mean ionic radius of the Ln^{3+} ion ($\bar{r}$). Both the a and c axes expand for an increase in the ionic radius of the Ln^{3+} ions for Ln=Gd—Pr. For Ln=La, the c axis expands more than the value estimated by extrapolating the data for Ln=Gd—Pr, and the a axis shortens (□). La_2CuO_4 is electrically metallic, while Pr_2CuO_4 is semiconductive.[3] This marked difference between Ln=La and Pr can be explained as a change in the nature of the Cu–O bond on the a axis ($(Cu–O)_a$) as described below.

The Cu^{2+} ions in the Ln_2CuO_4 lattice are octahedrally surrounded by six O^{2-} ions.[5] According to ligand field theory,[6] in the ground state with the Cu^{2+} ion coordinated octahedrally, the $3d_{z^2}$, $3d_{x^2-y^2}$, 4s and 4p orbitals of the Cu^{2+} ion are used for the σ-bonds. The $3d_{xy}$, $3d_{yz}$, and $3d_{zx}$ orbitals (t_{2g}) can form π-bonds with the coordinating O^{2-} ions, but for Ln=Gd—Pr, they are essentially nonbonding. The upper edge of the valence band originates from the antibonding σ-orbitals (e_g^*). The conduction band is formed of the π-orbitals of higher energy levels, probably the 4d orbitals of the Cu^{2+} ions. For Ln=Gd—Pr the relatively long bond-length of the $(Cu–O)_a$ bond prevents any great overlapping in the π-bond so that the conduction band is located at a higher energy level than the e_g^* orbitals, or the valence band. Therefore, the Ln_2CuO_4 compounds are semiconductive for Ln=Gd—Pr. When the effective change of the O^{2-} ions on the c axis is enhanced, the energy levels of the t_{2g} orbitals are elevated due to the electrostatic repulsive force. Since the less electronegative Ln atom or the atom with the smaller atomic number pushes more electrons toward the O^{2-} ions surrounding the Ln^{3+} ions, the effective charge of the O^{2-} ions increases with decreasing atomic number of the Ln atom so that the energy levels of the t_{2g} orbitals are elevated. For Ln=La, the t_{2g} energy level is maximum so that the La_2CuO_4 lattice becomes unstable. To stabilize it, the $(Cu–O)_c$ bond expands; this weakens the electrostatic repulsive force [$(Cu–O)_c$ is the Cu–O bond on the c axis]. This is the reason why the c axis of La_2CuO_4 expands more than expected from the size of the La^{3+} ion. The lengthening of the $(Cu–O)_c$ bond weakens it, that is, lowers its σ-bond energy but this energy lowering is compensated for by the π-bond formation in the $(Cu–O)_a$ bond composed of the $3d_{xz}$ and $3d_{yz}$ orbitals. This is the reason for the shortening of the a axis in La_2CuO_4. The shortening of the $(Cu–O)_a$ bond also enhances the electron overlap in the conduction band, lowering the energy level of the conduction band to that of the e_g^* band. Thus, the upper edge of the e_g^* band overlaps the lower edge of the conduction band and metallic conduction results. This is the reason why La_2CuO_4 is metallic.

The lattice parameters for the ternary $(La,Tb)_2CuO_4$ compounds are given in Fig. 1 (open circles). In the region of $\bar{r}$ from 0.94 to 0.97 Å, these increase with increasing $\bar{r}$ as do the lattice parameters of binary compounds. This phase is called phase 1. However, when the $\bar{r}$ value increases beyond 0.97 Å, another phase appears as a separated phase and the relative amount of the phase increases with increasing amount of the La^{3+} ions. The X-ray diffraction data reveal that this phase is a single phase in the composition range from $La_{1.3}Tb_{0.7}CuO_4$ to $La_{1.4}Tb_{0.6}CuO_4$ and that the X-ray diffraction patterns can be indexed as Ln_2CuO_4 structures. Since this phase exists as a phase separated from phase 1 and its c/a ratio is different from that of all binary Ln_2CuO_4 compounds, it should be considered to be a new phase which is peculiar to the $(La,Tb)_2CuO_4$ system. This phase is called phase 2.

When the $\bar{r}$ value increases beyond $\bar{r}$=1.015 Å, the La_2CuO_4 phase appears and coexists with phase 2. This fact indicates that phase 2 is different from both phase 1 and the La_2CuO_4 phase. Beyond $\bar{r}$=1.05 Å the La_2CuO_4 phase occurs as a single phase.

The semiconducting properties of this system correspond well to the structural behavior described above. Figure 2 gives the log ρ *vs.* $1000/T$ plots for the $(La,Tb)_2CuO_4$ compounds (ρ=resistivity). The roman numerals refer to the sample numbers given in Fig. 1. The ρ values at a given temperature for phase 1 decrease with increasing $\bar{r}$ value, but with slopes that are essentially the same (I and II). The plots for phase 2 (III) give a less steep slope than those for phase 1, indicating that the activation energy for the phase 2 sample is lower than that of phase 1.

The lowering of the activation energy in phase 2 can be explained as being due to π-bond formation in the $(Cu–O)_a$ bond. As described in the previous sec-

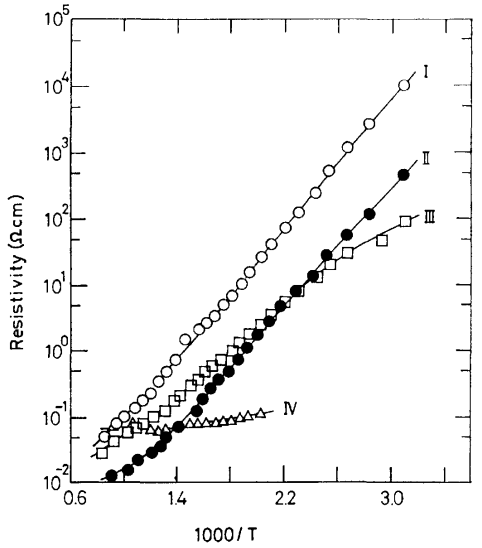

Fig. 2. Temperature dependence of resistivities of (La, Tb)$_2$CuO$_4$ compounds.
○(I): $La_{0.28}Tb_{1.72}CuO_4$, ●(II): $La_{0.6}Tb_{1.4}CuO_4$, □(III): $La_{1.4}Tb_{0.6}CuO_4$, △(IV): $La_{1.8}Tb_{0.2}CuO_4$.

tion, the shortening of the $(Cu–O)_a$ bond can be attributed to the π-bond formation of the t_{2g} orbitals of the Cu^{2+} ions and the degree of π-electron overlap increases with decreasing $(Cu–O)_a$ bond length. The $(Cu–O)_a$ bond length in phase 2 is between that of phase 1 and of La_2CuO_4 so that the $(Cu–O)_a$ bond in phase 2 can be expected to include π-bond characteristic although the electron overlap is not as great as for La_2CuO_4. The π-bond formation lowers the energy of the conduction band, resulting in a lower activation energy.

The fact that the composition range of phase 2 is very narrow and that the La/Tb ratio is two approximately suggests that the phase 2 compound is $La_4Tb_2Cu_3O_{12}$, although no super lattice lines due to ordering of the La^{3+} and Tb^{3+} ions were observed.

The triangles in Fig. 1 show the variation of the lattice parameters for the $(La,Pr)_2CuO_4$ compounds with $\bar{r}$. These lattice parameters change very critically at $\bar{r}=1.05$ Å. No stable specimens of compounds having $\bar{r}\simeq 1.05$ Å could be obtained; the pellets spontaneously reduced to powder when removed from the furnace and cooled to room temperature. Therefore, it was not determined whether or not the critical change in lattice parameters is accompanied by a semiconductor-metal transition, although shortening of the a axis and the very great lengthening of the c axis strongly suggests the same semiconductor-metal transition as that between La_2CuO_4 and Pr_2CuO_4.

As described previously, the La atom, which has the lowest electronegativity of the Ln atoms, causes the π-bond formation of the $(Cu–O)_a$ bond to which the metallic conductivity of La_2CuO_4 is ascribable. One can expect that for metals less electronegative than La, the effective charge of the O^{2-} ions on the c axis are enhanced to a value greater than that for La_2CuO_4 so that the $(Cu–O)_c$ bond is longer and the $(Cu–O)_a$ bond is shorter than in the case of the La atom. Since

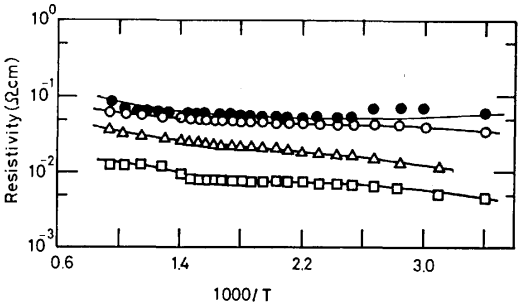

Fig. 3. Temperature dependence of resistivities of CaO-doped La_2CuO_4 compounds.
●: La_2CuO_4, ○: 2.5 mol% CaO-doped, △: 5 mol% CaO-doped, □: 20 mol% CaO-doped.

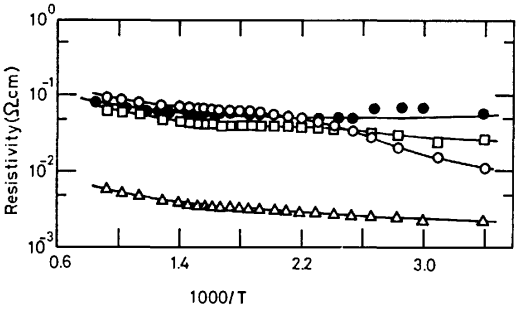

Fig. 4. Temperature dependence of resistivities of BaO-doped La_2CuO_4 compounds.
●: La_2CuO_4, ○: 2.5 mol% BaO-doped, □: 5 mol% BaO-doped, △: 10 mol% BaO-doped.

the shortening of the $(Cu–O)_a$ bond enhances the degree of π-electron overlap and this results in an enhancement of the conducting electron mobility, the replacement of the La^{3+} sites with less electronegative atoms will enhance the conductivity of La_2CuO_4. Calcium and barium are less electronegative than La and it is known that they can replace parts of the Gd^{3+} ions in Gd_2CuO_4.[4] Therefore, Ca^{2+} and Ba^{2+} ions can be expected to replace La^{3+} ions and to enhance the conductivity of La_2CuO_4. Figures 3 and 4 show the log ρ *vs.* $1000/T$ plots for CaO-doped and BaO-doped La_2CuO_4 compounds, respectively. These are seen to be metallic, with the resistivities of the former decreasing with increasing CaO content and, at 20 mol% doping, the ρ value decreases to one-tenth of that of undoped La_2CuO_4. Similarly, the BaO dopant lowers the resistivity; at 10 mol% doping the ρ value becomes one-tenth of that for undoped La_2CuO_4.

Table 1 gives the lattice parameters of undoped and 20 mol% CaO-doped and 10 mol% BaO-doped La_2CuO_4 compounds. Although the Ba^{2+} ion is larger than the La^{3+} ion, the a axis or the $(Cu–O)_a$ bond shortens due to the BaO-doping. This is evidence for

Table 1. Lattice parameters for undoped and CaO- and BaO-doped La_2CuO_4

	a(Å)	c(Å)	c/a
La_2CuO_4	3.808	13.200	3.466
$La_{1.6}Ca_{0.4}CuO_4$	3.790	13.189	3.480
$La_{1.8}Ba_{0.2}CuO_4$	3.796	13.274	3.497

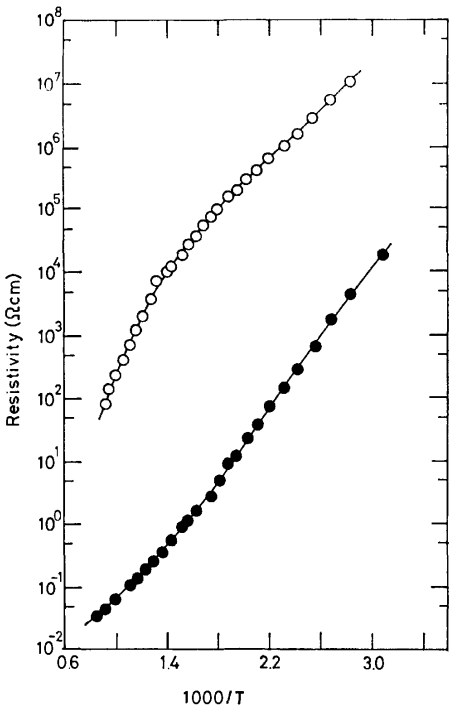

Fig. 5. Temperature dependence of resistivities of $Gd_{0.96}Tb_{1.04}Cu_2O_5$ (○) and $Gd_{0.84}Tb_{1.16}CuO_4$ (●).

an enhancement in the degree of π-electron overlap, which was expected. The CaO dopant shortens the a axis but enhances the c/a ratio. This suggests that the shortening of the a axis due to the CaO dopant is not only due to the smaller size of the Ca^{2+} ion, but is due partly to an enhancement of the π-electron overlap. Thus, the lowering of the resistivity due to doping with alkaline-earth oxides can be attributed to an increase in the degree of π-electron overlap in the conduction band.

The positive-charge deficiency in the La^{3+} site due to doping with divalent alkaline-earth ions may be balanced partly by the oxygen vacancies and partly by the formation of Cu^{3+} ions, as for alkaline-earth doped Gd_2CuO_4. This contributes to a decrease in the number of electron carriers, but the decrease in conductivity due to this effect is negligibly small in comparison with the increase in conductivity due to π-electron overlapping, since La_2CuO_4 is metallic.

The composition of the CuO–Ln_2O_3 system changes discontinuously between Gd and Tb; $CuO/Ln_2O_3=1$ for Ln=La—Gd and $CuO/Ln_2O_3=2$ for Ln=Tb—Lu. Since the $\bar{r}$ value can be varied continuously by varying the Gd/Tb ratio, the ternary system, Gd_2O_3–Tb_2O_3–CuO, will reveal how the CuO/Ln_2O_3 ratio depends upon the $\bar{r}$ value between Gd and Tb. Powder X-ray diffraction data reveal that the limit composition for a compound with $CuO/Ln_2O_3=1$ is $Gd_{0.84}Tb_{1.16}CuO_4$ and that for $CuO/Ln_2O_3=2$ is $Tb_{1.04}Gd_{0.96}Cu_2O_5$. This indicates that overlap occurs in both types of compounds for Gd/Tb ratios ranging from 0.72 to 1.08, that is, there is no critical ionic radius of the Ln^{3+} ions at which the Ln_2CuO_4 type compound transforms into the $Ln_2Cu_2O_5$ type compound.

$Tb_2Cu_2O_5$ is an insulator and Gd_2CuO_4 is a semiconductor.[1,2] It is not known whether this difference in the resistivities is ascribable to the difference in the crystal structures or to the difference in the ionic radii of the Gd^{3+} and Tb^{3+} ions. Figure 5 indicates that the resistivity of the $Tb_{1.04}Gd_{0.96}Cu_2O_5$ compound is still greater than that of the $Gd_{0.84}Tb_{1.16}CuO_4$ compound by three orders of magnitude, although the $\bar{r}$ value of the former is greater than that of the latter. Therefore, the difference in the resistivities of Gd_2CuO_4 and $Tb_2Cu_2O_5$ is not due to the difference in size of the Ln^{3+} ion but due to the difference in the crystal structures.

References

1) R. H. Frushowr and K. S. Vorres, AEC Rept. TID-2207 page E, 1965.
2) O. Schmitz-Dumont and H. Kasper, *Monatsh. Chem.*, **96**, 506 (1965).
3) T. Kenjo and S. Yajima, *Bull. Chem. Soc. Jpn.*, **46**, 1329 (1973).
4) T. Kenjo and S. Yajima, *Bull. Chem. Soc. Jpn.*, **46**, 2619 (1973).
5) R. W. G. Wyckoff, "Crystal Structure," Vol. 3, Interscience Publishers, New York, N. Y. (1965) p. 65.
6) B. N. Figgis, "Introduction to ligand fields," John Wiley & Sons, New York (1966); C. J. Ballhausen, "Introduction to Ligand Field Theory," McGraw-Hill Book Company (1962).

The Determination of the Critical Volume for the Free Motion of Solute Entities in an Aqueous Solution[1)]

Shizuo FUJIWARA, Kozo NAGASHIMA,* Hiroshi MORITA,** and Yasushi KANAOKA
Department of Chemistry, Faculty of Science, The University of Tokyo, Hongo, Tokyo 113
(Received December 27, 1976)

A certain volume of a solution, (20—30 Å)^3 per unit of solute entity, designated the "molecular space," is assigned as the necessary volume for the free motion of the solute. By the use of ESR, the actual size of the molecular space has been determined for the cupric ion and 2,2,5,5-tetramethyl-3-carbamoylpyrollidin-1-oxyl. It is pointed out that the concentrations of the important solutions in nature, such as sea water or human serum, may correspond to the moleuclar space of ions.

Solute entities in solution, such as ions or molecules, undergo diffusional and rotational motions in the solvent media. Those motions depend on the conditions of the solution, such as the concentration, the volume, the temperature, or the chemical propterties of the system, and the behavior of the solutes can be investigated by analogy with gaseous systems, where non-elastic and the elastic collisions characterize ideal and real gases. The free motion of the solute entity colud be defined as the motion in which the solute fulfils any one or a combination of the following conditions; 1) the motion is isotropic, 2) the solute does not exist as an ion-pair, 3) the solute is completely hydrated, or 4) the correlation time τ of the rotational motion obeys Debye's formula, $\tau_c=4\pi\eta a^3/3kT$, where η is the viscosity of the solution; a, the ionic radius; k, the Boltzman constant, and T, the absolute temperature. Whether or not the solute entity is in the state of free motion can be seen by its NMR or ESR spectral features. This paper will report that a certain volume of a solution is required for the maintenance of the free motion of the solute entity. The minimum volume of a solution which allows the solute entity free motion is defined as V_c. The results of the investigation which has been carried out for the measurement of V_c will be presented.

In the investigation, the magnitude of V_c was evaluated first by the examination of the concentration dependence of the linewidths of the ESR spectra of aqueous cupric ions. In this experiment, the conditions of 1, 2, and 3 cited above were taken as measures of the free motion of ions. (Experiment 1).

We planned then to measure V_c more directly by the control of the space of the solution available to the solute entity. Two systems were adopted for this purpose, one silica gel (Experiment 2) and the other, cross-linked poly(vinylalcohol), PVA, gel (Experiment 3). One of the most notable findings of these experiments is that the magnitude of V_c is several times larger than the actual size of the solute entity. The relevance of this finding will be discussed with respect to the recent results of the measurement of the viscosity or the relaxation times of magnetic resonance. The significance of V_c in nature will also be discussed in the text.

* Present address: Tsukuba University, Sakura, Niihari Ibaraki 300-31.

** Present address: Institute for Solid State Physics, Roppongi, Minato-ku Tokyo 160.

Experimental

Experiment 1: Concentration dependence of the ESR linewidth of cupric ions in aqueous solutions. The ESR linewidth of cupric ions in aqueous solutions, ΔH, has been measured as the function of the concentration of ions. As the details of the experimental conditions have already been published elsewhere,[2)] they will not be repeated in this article for except Fig. 1. Figure 1 has been reproduced for convenience, and it has been augmented with some additional data and a recalibration of the scale of the linewidth.

It is evident in Fig. 1 that ΔH is not dependent on the concentration nor on the anion species in the range lower than about 0.1 M. This result has been interpreted in terms of the fact that the cupric ions are wholly hydrated in the concentration range lower than 0.1 M, whereas, in the higher concentration range, ion pairs are formed, resulting in the reduction and the anion dependence of ΔH. Hence, the conditions of the free motion, 1, 2, and 3, which have been raised in the introduction, are fulfilled, and 0.1 M can be taken as the limiting concentration which allows the free motion of ions.

This value of the critical concentration refers to a certain volume of solution (a cube of 20Å) per ion ($=1000\ \text{ml}/2\times 0.1\times 6.02\times 10^{23}$).

Experiment 2: ESR pattern of aqueous solutions of Cu^{2+} adsorbed in silica gel. In order to evaluate V_c more directly, another experiment was undertaken*** with the use of aqueous solutions of cupric sulfate spread over the surface of silica gel.

Two types of experiment were performed: A) with the silica gel dipped in aqueous solutions of different concentra-

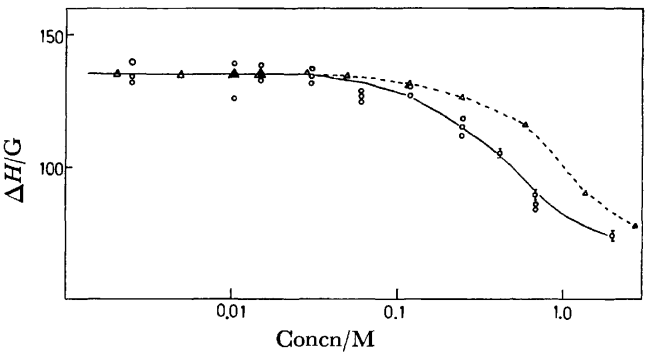

Fig. 1. Concentration dependence of the ESR line widths of aqueous Cu^{2+} ions.
—○— $CuSO_4$ aq. —△— $Cu(NO_3)_2$ aq.

*** This section is a part of the B. Sc. thesis submitted by H. Morita to the University of Tokyo, 1970.

Table 1. Contents of water and cupric sulfate absorbed in silica gel

Sample	Mother solution	H_2O g/g SiO_2	Cu^{2+} mM/g SiO_2
i	0.25 M	1.1	0.26
ii	0.5 M	1.1	0.56
iii	1.0 M	1.1	1.1

The values of water and cupric ions refer to those contained in the silica gel just after it is taken out of the mother solution and after it has been drained.

tions of cupric sulfates, and B) with thin-layered silica gel plates over which the cupric sulfate was developed. In both cases, the ESR of the cupric ions and the contents of ions and water in silica gel were measured.

Conditions of Experiment 2-A:

Silica gel: Wako Gel,

ESR: J 3BS Spectrometer, made by Japan Electron Optics Laboratory Co. X band, 100 kHz modulation.

Procedure. The silica gel was put in equilibrium with three aqueous solutions (i, ii, and iii) with concentrations of 0.25, 0.5, and 1.0 M respectively. No solution with a concentration lower than *ca.* 0.2 M was adopted in the present experiment because of the limitations of the ESR measurements. After filtration, the excess solution was gently removed as drainage. The contents of water and cupric ions in the samples as well as the ESR were measured at the same time at this stage. As a wet sample lowers the Q value of the ESR spectrometer, the sample size must be kept small. This condition brings another difficulty-that the number of cupric ions which are brought into the ESR cavity is reduced. Efforts were made to find out the optimal conditions. Another difficulty lay in the treatment of silica gel. The silica gel which had became wet with the solution showed a tendency to squeeze the solution out of the gel when it was treated for the transference into the capillary sample tube of ESR measurements. Efforts were made to transfer the wet silica gel into the capillary without any distortion. The results of the analysis are shown in Table 1.

Results of 2-A: In Table 1 it may be seen that the water content is the same for all three samples, 1 ml/gSiO_2. This value may be taken as the volume of solution which can "naturally" be held in silica gel. As the results of the analysis of the copper content also show that 1.1 ml of each mother solution is held in the silica gel, *ca.* a 1-ml solution over gSiO_2 would be a good value of water, with reference to the value of V_c. With the values of the surface of the silica gel from 4 to 6, m^2/gSiO_2†, a water layer 20±5 Å thick (=1 ml/4—6 m^2) is taken as the space which allows the solute ions "almost" free motion. The motion in the latter case is called "almost free" because the ions with the concentration of the experiment are assumed to be ion-paired to some extent. There was a slight worry that the samples might hold excess solution as a result of an incomplete removal of the drainage. Accordingly, Experiment 2-B was carried out, where the samples were assumed to be prepared in more homogeneous condition.

Experiment 2-B: Thin-layered silica gel plates were prepared on glass plates according to the usual technique of thin-layer chromatography. The thickness of the silica gel layers was assumed to be a few hundred microns. The silica gel used is the one same used in Experiment 2-A.

Two solutions of cupric sulfate with concentrations of 0.20 and 0.46 M were developed in the layers. After the development, each layer of silica gel was cut into 9 portions, equal in length, from the bottom to the top of the plate. The contents of water, cupric, and sulfate ions were measured as well as the ESR spectra for all samples. Table 2 presents the results of the measurement with respect to the bottom portion of the plates.

† Determined by the nitrogen gas adsorption.

Table 2. Water content in silica gel just after the development of the solution of cupric sulfate

Sample	Mother solution	H_2O Content just after development
iv	0.20 M	1.2 g/g SiO_2
v	0.46 M	1.0 g/g SiO_2

Results of 2-B. In Table 2 it may be seen that the two samples of thin-layered silica gel, iv and v, also hold about 1 ml (actually 1.2 and 1.0 ml) of the solution. Because the patterns of the ESR spectra are of a single line with a fairly good symmetry, it is certain that the cupric ions are in a state of almost "free' motion. Summarizing the results of A and B, the ions in the samples of both cases are in almost "free' motion in the water layer (20±5 Å thick) which is spread over the surface of the silica gel.

Experiment 3††: *Use of the network of γ-irradiated PVA.* For the purpose of the measurement of V_c, the cross-linked network of polyvinyl alcohol, PVA, which was produced by the γ-ray irradiation was utilized. By the γ-ray irradiation of the aqueous solution of PVA, the latter molecules are cross-linked and form a three-dimensional network. The average distance between the end terminals of the PVA molecules, $\langle l \rangle$, can be controlled by the control of the concentration of PVA, C, and the total dose of the γ-rays, R. The value of $\langle l \rangle$ actually refers to the size of the hole in the network which can hold ions in the solution. Thus, the cross-linked PVA gel is used as a convenient medium for the control of the motion of the solutional ions. Some examples of the application have already been reported.[3]

The value of $\langle l \rangle$ may be calculated according to the following equation:[4]

$$\langle l \rangle = 2.5 \times [(5.1 \times 10^8 + 1.37 \times 10^8 C)/R]^{1/2}, \quad (1)$$

where C refers to the value in g PVA per 100 ml of H_2O and R is in rads. In practice, the degree of the polymerization of PVA is about 2000, and C is 5 g PVA/100 g H_2O. The source of the γ rays is the University of Tokyo, the γ-ray source of Co-60 with 3000 Curies, and R is 2×10^6 rads. First in this experiment, a), the symmetry of the ESR spectra was examined by a comparison of the half-maximum linewidths of the two parts of the derivative curve. That is, after recording the derivative of the single line of the ESR absorption spectrum, the half-maximum linewidths, Δh_1 and Δh_2, were measured with respect to both the higher-field and lower-field parts (*cf.* Fig. 2), respectively. It was confirmed that the cupric ions in the gel of $\langle l \rangle$ almost equal to, or smaller than, 25 Å gave Δh_2 values for the lower field side derivative about 5% larger than the Δh_1 values for the higher-field side. However, the ions showed almost symmetric lines in the gel of $\langle l \rangle$ larger than 25 Å. That is, the V_c for Cu^{2+} ions was counted as about 25 Å.

In the b) experiment, the relative heights of the three hyperfine lines of the ESR signal of the radical were compared. The correlation time, τ_c, was then calculated by the use of the observed results and the following equation,[5] where the

†† This section forms a part of the B. Sc. thesis of Yasushi Kanaoka, University of Tokyo, 1975.

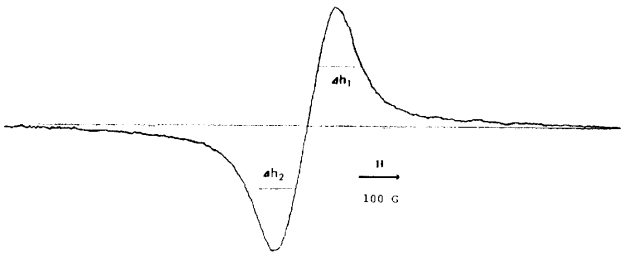

Fig. 2. Derivative of the ESR spectrum of Cu^{2+} 0.01 M solution in PVA gel of $\langle l \rangle = 20$ Å, where $\Delta h_1 > \Delta h_2$ by 5%. When $\langle l \rangle \geqq 25$Å, $\Delta h_1 = \Delta h_2$.

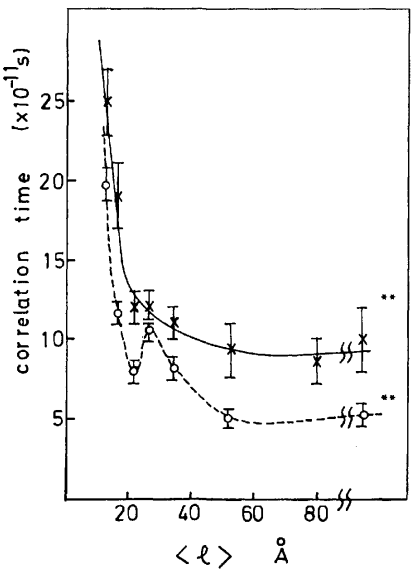

Fig. 3. Correlation time, τ_c, for the motion of 2,2,5,5-tetramethyl-3-carbamoylpyrrolidin-1-oxyl, TMCA, as the function of the molecular space in PVA gel.

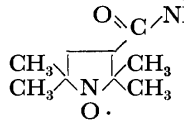

—×—: 0.01 M in PVA gel, —○—: 0.001 M in PVA gel, **: τ_c in bulk solution.

values of the hyperfine constants of A_{xx}, and A_{zz} were obtained from the literature:[6]

$$\tau = \left[\left(\frac{h(0)}{h(1)}\right)^{1/2} + \left(\frac{h(0)}{h(-1)}\right)^{1/2} - 2\right] \times \frac{3\pi\Delta\nu(0)}{2C_2}, \quad (2)$$

where $C_2 = 2\pi/9[A_{zz} - A_{xx}]^2$ and where h refers to the derivative height of each hyperfine line. The results of the measurement are shown in Fig. 3, where a marked increase of τ_c is seen in the gels of $\langle l \rangle$ lower than about 20 Å.

Discussion

According to the results of all the experiments shown above, it is evident that a certain volume of a solution, $(20 \pm 5)^3$ Å per unit solute entity, is required for the free motion of the solute entity of a simple structure, like Cu^{2+} or a low-molecular-weight compound. A problem of current interest is the fact that V_c is several times larger than the real size of the solute entity. This fact may have some connection with the discussion related with the microviscosity, which assumes the presence of a structural sphere surrounding the solute entity.[7] It may also be related to the discussion which has recently been made in the field of magnetic relaxation.[8] It should be stressed that V_c has been measured directly in the present investigation, unlike as in former investigations of microviscosity or magnetic relaxation. Further investigation will be necessary for a real understanding of the structure of V_c. Another point to be noted in this article is the possible significance of V_c in nature. As one considers the situation of the solute entity, where it is held in the concentration range of V_c, the whole system of the solution is assumed to be stabilized by the buffer action of the solute entity. That is, in the solution where the solute entity just holds the space of V_c, each individual solute entity behaves as free from the others and also as free from the external system. Nevertheless, it should easily respond to the action of the external system, for the concentration is not far from the condition which produces the mutual interaction of the solutes or the reaction with the external system. In connection with this statement, reference may be made to the fact that the concentrations of the salt in the important solutions in nature fall in the range of the concentration of V_c. For example, the concentration of the human serum is about 0.1 M, that of the silk worm egg is 0.1 M,[9] and that of the sea water is about 0.5 M. In addition to this, we may refer to the work of Ehrenberg.[10] He assumed the case of an adult human with a body of weight of 70 kg, 50 kg of water and 20 kg other materials, mainly organic. He evaluated the total interface of the macromolecules (and membranes) to be of the order of 10—100 km^2 (10^7—10^8 m^2). If one spreads, according to this formula, the 50 kg of water in an uniform layer over this area, the thickness of the layer becomes 5—50 Å. He assumes that there would be, on the average, less than 20 water molecules between the most distant point in the water and the surface.

Valuable discussions with Professors K. Higasi and A. Ehrenberg are heartily acknowledged.

References

1) Presented at the VIIth International Conference of Magnetic Resonance of Biological Systems, St. Jovite, October, 1976.

2) S. Fujiwara and H. Hayashi, *J. Chem. Phys.*, **43**, 23 (1965).

3) S. Fujiwara, S. Katsumata, and T. Seki, *J. Phys. Chem.*, **71**, 115 (1967).

4) A. Danno, *J. Phys. Soc. Jpn.*, **13**, 722 (1958).

5) R. N. Rogers and G. E. Pake, *J. Chem. Phys.*, **33**, 1107 (1960).

6) O. Griffith, D. Cornell, and H. McConnell, *J. Chem. Phys.*, **43**, 2909 (1965).

7) K. Higasi, *Monogr. Ser., Res. Inst. Appl. Elect., Hokkaido Univ.*, No. 13 (1965), p. 1.

8) See, for example, the references given in p. 29 of "NMR 12, Basic Principles and Progress," by B. Lindman and S. Forsen, Springer-Verlag, Heidelberg (1976).

9) Y. Numata, M. Sc. Thesis, The University of Tokyo, 1976.

10) A. Ehrenberg, Private Communication on his lecture at the Seminar in Skokloster, Sweden, May, 1974. Ref. IVA Meddelande 187, Stockholm 1976.

Studies of the Aqueous Solutions of Guanidinium Salts. VI. Complexes of Guanidinium Halides and Symmetrical Tetraalkylammonium Halides

Koichiro MIYAJIMA, Hiromitsu YOSHIDA, and Masayuki NAKAGAKI

Faculty of Pharmaceutical Sciences, Kyoto University, Yoshidashimoadachi-cho, Sakyo-ku, Kyoto 606

(Received March 22, 1977)

Guanidinium halides (bromide and chloride) form crystalline complexes with symmetrical tetraalkylammonium bromides (tetraethyl-, tetrapropyl-, and tetrabutylammonium bromides and tetrabutylammonium chloride) in aqueous solutions at room temperature. These complexes were analyzed and found to be either binary complexes of two kinds of salts or ternary complexes with water as a third component. Each complex showed complicated peaks in the DSC measurements, which indicated the phase transition in the solid state. The solubility of each salt in ternary systems was measured, and phase diagrams were constructed for some of the ternary systems. A mutual salting- in effect was observed in all the ternary systems, and this effect was discussed in terms of complex formation and the structual change of water.

The guanidinium ion has a strong resemblance to urea in its shape, size, and functional group except for a charge which is distributed around the periphery of the disc-shaped ion. Even in aqueous solutions, the guanidinium ion and urea have a similar effect toward hydrophobic solutes when they are mixed with hydrocarbon gas[1] and symmetrical tetraalkylammonium salts.[2,3] These properties of urea and guanidinium salts are regarded as the main factor in the denaturation of protein in their aqueous solutions.[4] In 1966 Saito *et al.*[5] reported the complex formation of urea with various tetraalkylammonium salts in aqueous solutions. Therefore, it seems worthwhile to investigate the interaction between a hydrophobic solute and a guanidinium salt in an aqueous solution, especially at a high concentration.

From these points of view, we studied the mutual solubility of a guanidinium halide and a symmetrical tetraalkylammonium halide in aqueous solutions and isolated crystalline complexes containing each salt from aqueous ternary solutions. In this paper, we wish to report the preparation and characterization of various crystalline complexes formed by guanidinium halides and tetraalkylammonium halides in aqueous solutions. In addition, the solubilities of these salts were measured in ternary solutions, the total concentrations and the mole ratio being changed. From these data, phase diagrams were constructed for some of the ternary systems.

Experimental

Materials. Symmetrical tetraalkylammonium halides were obtained from the Nakarai Chemical Co., and were purified by recrystalization from appropriate solvents described elsewhere.[6] The guanidinium halides used were the same as those of the previous paper.[7] Reagent-grade urea obtained from Wako Chemical Co., Ltd., was used without further purification after being dried *in vacuo*.

Preperation of Complex. A guanidinium halide and a tetraalkylammonium halide were mixed at an appropriate mole ratio, after which a desired quantity of water was added to dissolve the solid. The solution was then subjected to natural evaporation in an open beaker at room tempetature. The crystals thus formed were collected by filtration, cut to small pieces, and pressed between filter papers to remove the mother liquid. These crystals were powdered and dried for several hours at a relative humidity of 30—50% at room temperature and used for the direct analysis of complexes.

Method of Analysis. For each of the crystalline complexes, wet residues, and saturated solutions, the halide ion was determined by Mohr's method, and the tetraalkylammonium ion, by colorimetry. The latter method is based on the fact that the tetraalkylammonium ion and Metyl Orange form a complex which is slightly soluble in water and soluble in organic solvents, such as chloroform and 1,2-dichloroethane. Therefore, the contents of the tetraalkylammonium ions were determined by measuring the optical densities of extracted solutions of the tetraalkylammonium–Methyl Orange complex at 425 nm. This method was useful in the presence of guanidinium salts. The difference between the contents of the halide and tetraalkylammonium ions correspond to the content of the guanidinium ion. The water content was also deternined from these values and the total weight of the sample.

The phase diagrams were obtained by Schreinmakers' "wet residue" method.[8] In this method, the solid components were dissolved in water at various concentrations, and solutions were agitated in a thermostat until equilibrium was reached. Then the liquid phase and the wet residue were separated, and both were weighed and determined. The compositions obtained by the above procedure are plotted on a triangular diagram in Fig. 1. Let the points a, b, and c represent the compositions of the saturated solutions, and the points a′, b′, and c′, the compositions of the corresponding wet residues. Then, the tie-line a-a′, b-b′, and c-c′, must pass, on the extention past a′, b′, and c′, through the composition of the solid complex P.

Results

Crystalline Complexes and Phase Diagrams. Tetrabutylammonium Bromide [(n-*Bu*)$_4$*NBr*]*–Guanidinium Bromide* [*GuBr*]*–Water.* By applying Scheinmakers' wet residue method, the triangular diagram shown in Fig. 1 was obtained for the (n-Bu)$_4$NBr–GuBr–H_2O system. In this diagram, A and B are the solubilities of (n-Bu)$_4$-NBr and GuBr respectively in water at 25 °C. Curve ACDB shows the compositions of saturated solutions containing both (n-Bu)$_4$NBr and GuBr. As is shown in the plots, Scheinmakers' wet residue method indicated the presence of the P complex, which contains equimolar amounts of (n-Bu)$_4$NBr, GuBr, and H_2O in a crystal. This conclusion was confirmed by the direct analysis of the crystal obtained from mixed solutions containing both salts in different mole ratios. The crystal form

Table 1. Some characteristics of the crystalline complexes formed by guanidinium halides and symmetrical tetraalkylammonium halides

System	Crystal form of complex	Stoichiometric composition in mole ratio	Mp of complex (°C)	Mp of pure R_4NBr (°C)
$(n\text{-Bu})_4NBr\text{-}GuBr\text{-}H_2O$	Prism	1 : 1 : 1	65— 66	119
$(n\text{-Pr})_4NBr\text{-}GuBr\text{-}H_2O$	Plate	2 : 1 : 0	153—155	250
	Flat needle	3 : 5 : 0	108—110	250
$(Et)_4NBr\text{-}GuBr\text{-}H_2O$	Flat needle	1 : 1 : 0	147—149	250
	Needle	1 : 2 : 1	160—161	250
$(n\text{-Bu})_4NBr\text{-}GuBr\text{-}H_2O$	Prism	1 : 1 : 1	60— 63	119
$[(n\text{-Bu})_4NCl\text{-}GuBr\text{-}H_2O]$	Prism	1 : 1 : 1	60— 63	75

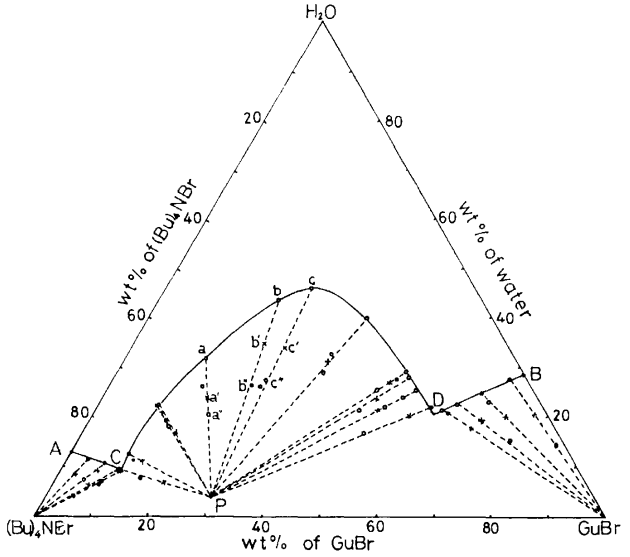

Fig. 1. Triangular diagram for ternary system $(n\text{-Bu})_4NBr\text{-}GuBr\text{-}H_2O$ at 25 °C by Schreinmakers' wet residue method. Complex P $(n\text{-Bu})_4NBr : GuBr : H_2O = 1 : 1 : 1$.

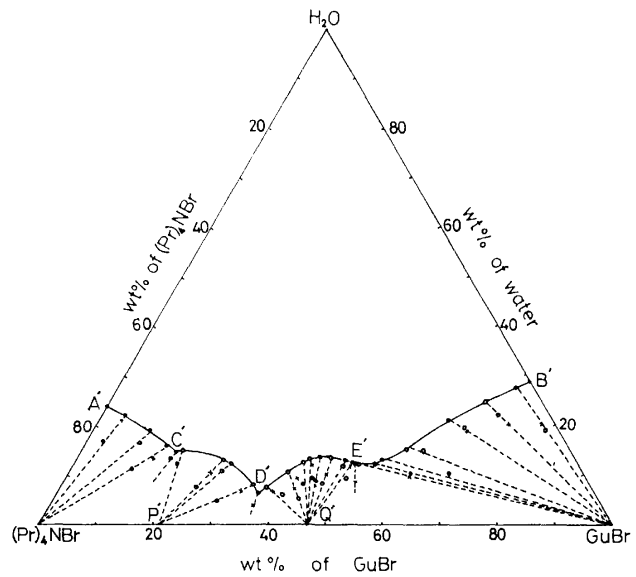

Fig. 2. Triangular diagram for ternary system $(n\text{-Pr})_4NBr\text{-}GuBr\text{-}H_2O$ at 25 °C by Schreinmakers' wet residue method.
Complex P′ $(n\text{-Pr})_4NBr : GuBr = 2 : 1$. Complex Q′ $(n\text{-Pr})_4NBr : GuBr = 3 : 5$.

and the melting point of the complex are shown in Table 1. The crystal of the P complex is stable in an atmosphere at room temperature, but when it was allowed to stand for several hours *in vacuo* at room temperature, it melted by losing water. The amount of water lost corresponded almost exactly to the amount obtained by the direct analysis of the crystal. Tetrabutylammonium bromide forms a clathlate hydrate, $(n\text{-Bu})_4NBr \cdot 32.8H_2O$ at low temperature.[9] Therefore, the same experiment as was done at room temperature was carried out again at 3 °C, no clathlate hydrate was found to form when enough guanidinium bromide was dissolved in the solution. In the $(n\text{-Bu})_4NBr\text{–}GuCl\text{–}H_2O$ or $(n\text{-Bu})_4NCl\text{–}GuBr\text{–}H_2O$ system, a similar crystalline complex was isolated from the mixed solutions, but the half mole of the bromide ion was replaced by the chloride ion in the crystal.

Tetrapropylammonium Bromide $[(n\text{-}Pr)_4NBr]\text{–}GuBr\text{–}H_2O$. As is shown in Fig. 2, the wet residue method indicated the presence of two kinds of complexes, P′ and Q′. These complexes did not contain water, and the mole ratio of $(n\text{-Pr})_4NBr$ and GuBr was 2 to 1 and 3 to 5 for the P′ and Q′ complexes respectively. The crystal forms and melting points are shown in Table 1.

Tetraetylammonium Bromide $[(Et)_4NBr]\text{–}GuBr\text{–}H_2O$. Tetraetylammonium bromide also formed two kinds of complexes with GuBr in aqueous solutions. As is shown in Fig. 3, the P″ complex contained equimolar amounts of the two salts, and no water, while the Q″ complex contained $(Et)_4NBr$, GuBr, and H_2O in the mole ratio of 1 : 2 : 1. The crystal forms and melting points are shown in Table 1.

We did not study ternary systems containing the salts with only a chloride or iodide ion as a common anion, but we may predict with a high possibility of success the formation of crystalline complexes in these systems, judging from the formation of a crystalline complex in the $(n\text{-Bu})_4NBr\text{–}GuCl\text{–}H_2O$ system.

Thermochemical Properties of the Complexes. For the elucidation of the thermochemical properties of these complexes, DSC was employed. Some typical DSC charts and heats of fusion are shown in Fig. 4. and Table 2 respectively. The heats of fusion were determined by comparing the peak area with that of urea. As may be seen in Fig. 4, these DSC charts may be classified into three typical groups. A peak with a shoulder is observed for Type A, a doublet peak for Type C, and two isolated peaks for Type B. No complex shows

Table 2. Some thermochemical properties of the crystalline complexes

Complex	Type of chart	Transition temp by DSC (°C)	Heat of transition (kcal/mol of complex)
$[(n\text{-Bu})_4NBr][GuBr][H_2O]$	A	59.6 (shoulder) 63.7 (peak)	2.68
$[(n\text{-Pr})_4NBr]_2[GuBr]$	B	135.4 (peak) 155.2 (peak)	1.43 1.59
$[(n\text{-Pr})_4NBr]_3[GuBr]_5$	C	103.1 (peak) 106.9 (peak)	2.17
$[(Et)_4NBr][GuBr]$	A	147.2 (shoulder) 149.6 (peak)	0.99
$[(Et)_4NBr][GuBr]_2[H_2O]$	C	154.3 (peak) 159.2 (peak)	2.17
$[(n\text{-Bu})_4NBr][GuCl][H_2O]$	A	58.7 (peak) 61.0 (peak)	2.02

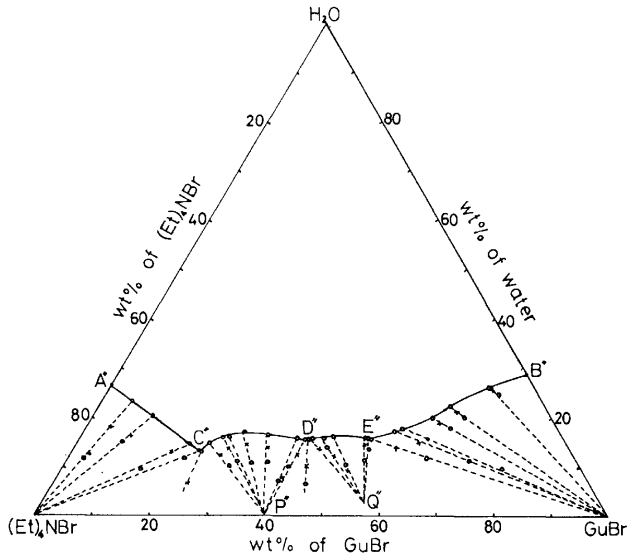

Fig. 3. Triangular diagram for ternary system $(Et)_4NBr$-GuBr-H_2O at 25 °C by Schreinmakers' wet residue method.
Complex P″ $(Et)_4NBr$: GuBr = 1 : 1. Complex Q″ $(Et)_4NBr$: GuBr : H_2O = 1 : 2 : 1.

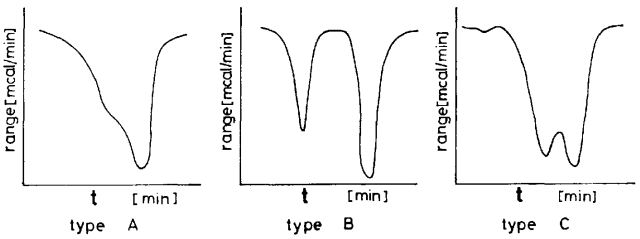

Fig. 4. Typical DSC charts for the crystalline complexes. Range: 8 mcal/min. Temperature-programing rate: 5 °C/min.

a single peak. These phenomena seem to suggest the presence of polymorphism in each complex. As may be seen in Table 2, the melting points, as determined by the usual method, correspond to the temperature of the second peaks in Fig. 4. Therefore, the shoulders of the first peaks in Fig. 4 may arise from the phase change in the solid states. The structure of these complexes are now being studied by means of X-ray diffraction analysis.

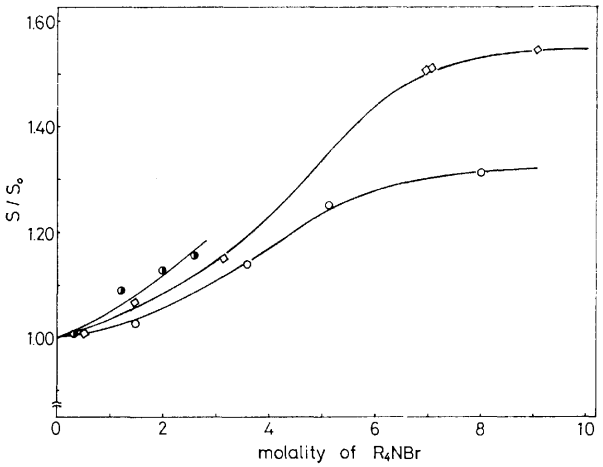

Fig. 5. Solubility ratios (S/S_0) of GuBr *vs.* concentrations of tetraalkylammonium bromides at 25 °C. S: Solubilities of GuBr in aqueous tetraalkylammonium bromides solutions (mol/kg-H_2O). S_0: Solubility of GuBr in water (mol/kg-H_2O). ◑: $(n\text{-Bu})_4NBr$, □: $(n\text{-Pr})_4NBr$, ○: $(Et)_4NBr$.

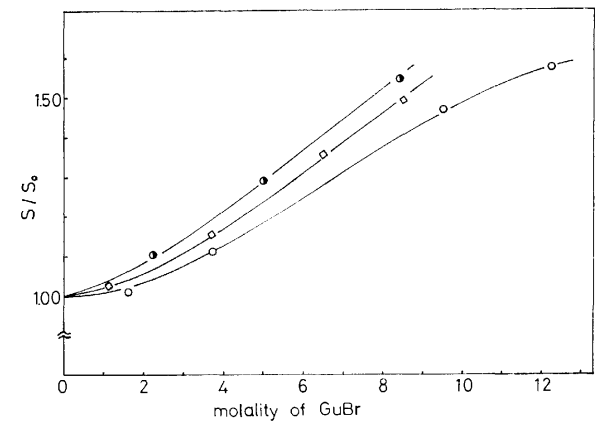

Fig. 6. Solubility ratios (S/S_0) of tetraalkylammonium bromides vs. concentrations of GuBr at 25 °C.
S: Solubilities of tetraalkylammonium bromides in aqueous GuBr solutions. (mol/kg-H_2O). S_0: Solubilities of tetraalkylammonium bromides in water. (mol/kg-H_2O). ◑: $(n\text{-Bu})_4NBr$, □: $(n\text{-Pr})_4NBr$, ○: $(Et)_4NBr$.

Solubility Measurement. As is shown in Fig. 1, 2, and 3, the solubility of each salt in a ternary solution increased as compared with that in pure water. The effect of tetraalkylammonium bromide on the solubility of GuBr is shown in Fig. 5. Each tetraalkylammonium bromide has a salting-in effect toward GuBr in aqueous solutions, $(n\text{-Bu})_4$NBr having the strongest effect among them. As is shown in Fig. 6, GuBr also has a salting-in effect toward tetraalkylammonium bromide and is most effective toward $(n\text{-Bu})_4$NBr. These phenomena constitute the so-called "mutual salting-in" effect. These salting-in effects of GuBr toward tetraalkylammonium bromides are greater than those of urea.[5] This fact is consistent with the effectiveness of GuBr and urea for protein denaturation in aqueous solutions.

Discussion

Guanidinium halides form complexes with symmetrical tetraalkylammonium halides in aqueous solutions just as urea does, though the compositions of complexes are not the same. However, the fact that urea, thiourea,[5] and guanidinium halides form complexes with symmetrical tetraalkylammonium halides suggests that the shape, the size, and the functional group play important roles in the reaction of the complex formation, although there is a quite significant difference (electrolyte and nonelectrolyte) between urea and guanidinium halides.

$(n\text{-Bu})_4$NBr does not form a clathlate hydrate, but does form complexes with guanidinium halides in the presence of enough guanidinium halide, even at low temperatures. This fact indicates the presence of a stronger interaction between guanidinium bromide and $(n\text{-Bu})_4$NBr than between water and $(n\text{-Bu})_4$NBr. As for the structures of crystalline complexes, we must await a detailed X-ray analysis. However, the following things may be deduced. $(n\text{-Bu})_4$NBr forms the clathlate hydrate in which the tetrabutylammonium ion is surrounded by a cage formed by water molecules and bromide ions.[9] In contrast with the clathlate hydrate, the amount of guanidinium bromide and water in the crystalline complex seems to be too small to form a cage. On the other hand, the difference of ionic size between the guanidinium ion and the tetrabutylammonium ion is too much to form a mixed crystal as in the case of alkali halide. Therefore, the crystal structures of these tetraalkylammonium halide-guanidinium halide complexes may be different from those of either a clathlate hydrate or a mixed crystal.

We can postulate two kinds of mechanisms for the mutual salting-in effect in the ternary systems. One is the salting-in due to the formation of a water-soluble complex in the ternary solutions (Mechanism A). If the water-soluble complex is a 1-to-1 complex of GuBr and tetraalkylammonium bromide, and if the specific hydration of the complex is not taken into account, the solubility ratio (S/S_0) must be proportional to the concentration of the solubilizing salt (m) and the slope must correspond to $KS/(1+KS_0)$, where K is the formation constant of the water-soluble complex. As has been stated in the experimental section, tetrabutylammonium bromide and tetraethylammonium bromide form a crystalline complex in which guanidinium bromide and tetraalkylammonium bromide are in a mole ratio of 1-to-1. However, as may be seen in Figs. 5 and 6, a linear relation between (S/S_0) and m was not obtained in either case. This fact suggests that even if the water-soluble complexes were formed in an mixed aqueous solution, the compositions of water-soluble complexes would be different from those of crystalline complexes.

The other mechanism is the salting-in due to the interaction between the guanidinium ion and the tetraalkylammonium ion through the alteration of the water structure (Mechanism B). The guanidinium ion is a structure breaker, while the tetraalkylammonium ions are hydrophobic structure makers. Since an aqueous solutions of tetraalkylammonium bromide is more structured than pure water, the guanidinium ion breaks the water structure in the aqueous solution of tetraalkylammonium bromide more clearly than that in pure water. This effect decreases the activity coefficient of guanidinium bromide. On the other hand, when tetraalkylammonium bromide is added to an aqueous solution of guanidinium bromide, which is less structured than pure water, the ability of the tetraalkylammonium ion to form a water structure will decrease as compared with that in pure water. Thus, the effect of the addition of guanidinium bromide on the structure of water is similar to that of the elevation of the temperature. This effect decreases the activity coefficient of tetraalkylammonium bromide.

We can say that Mechanism A is based on the contribution of the enthalpy change, while Mechanism B is based on that of the entropy change. The thermodynamic way of determining which of these two mechanisms is really working is to measure the free energy and the heat change on mixing these two salts in an aqueous solution. When the free energy change on mixing tetrabutylammonium bromide and guanidinium bromide in an aqueous solution was investigated, large negative free energy changes were obtained.[3] Therefore, a promising avenue to the elucidation of the mutual salting-in effect may be to measure the heat of mixing tetraalkylammonium and guanidinium bromides in aqueous solutions.

References

1) D. B. Wetlaufer, S. K. Malik, L. Stoller, and R. L. Coffine, *J. Am. Chem. Soc.*, **86**, 508 (1966).

2) W-Y. Wen and M. Lee, *J. Phys. Chem.*, **73**, 2895 (1969).

3) K. Miyajima, H. Yoshida, and M. Nakagaki, Abstr. No. 2M 11, 34th National Meeting of the Chemical Society of Japan, Hiratsuka, April 1976.

4) P. H. von Hippel and T. Sheich, "Structure and Stability of Macromolecules," ed by Tismasheff and G. Fasman, Marcel Dekker, Vol. 2, New York (1969), p. 417.

5) S. Saito, M. Lee, and W-Y. Wen, *J. Am. Chem. Soc.* **88**, 5107 (1966).

6) B. E. Conway, R. E. Verrall, and J. E. Desnoyers, *Trans. Faraday Soc.*, **62**, 2738 (1966).

7) K. Miyajima, H. Yoshida, and M. Nakagaki, *Nippon Kagaku Zasshi*, **1976**, 366.

8) S. H. Maron and C. H. Prutton, "Principles of Physical Chemistry," 3rd ed, Macmillan Co., New York (1958), p. 417.

9) W-Y. Wen, "Water and Aqueous Solution," ed by R. A. Horne, Wiley Interscience, New York (1972), p. 614.

^{31}P Magnetic Relaxation in Polynucleotides*

Kazuyuki AKASAKA, Atsuko YAMADA, and Hiroyuki HATANO
Department of Chemistry, Faculty of Science, Kyoto University, Kyoto 606
(Received April 11, 1977)

Phosphorus-31 nuclear spin-lattice relaxation times and nuclear Overhauser enhancement upon nonselective proton saturation were measured on polyriboadenylic acid, polyribocytidylic acid, and polyribouridylic acid. A method is described to separate dipolar contribution from the contribution of chemical shift anisotropy for the phosphorus relaxation by the combined use of T_1 and NOE data. Chemical shift anisotropies ($\delta_{//}-\delta_{\perp}$) of phosphorus in these polynucleotides in solution are estimated to be in the range 120—165 ppm. The molecular motion of the phosphorus moiety becomes faster in the order, poly(A)<poly(C)<poly(U), the thermal activation processes being characterized by single activation energies, *i.e.*, 5.1, 5.3—6.0, and 7.2—8.1 kcal/mol for poly(U), poly(C), and poly(A), respectively.

Phosphorus nucleus plays a key role in the main chain structure of nucleic acids. Its relatively large nuclear moment with its 100% natural abundance makes the ^{31}P nucleus a good sample for nuclear magnetic resonance studies. Numerous reports are available on ^{31}P magnetic resonance of nucleic acid systems, but most of them are based on the analysis of chemical shift[1] and spin-spin coupling constant.[2] Studies of nucleic acids by ^{31}P relaxation measurements have only recently begun, and their relaxation mechanisms and use for the study of nucleic acid structures and dynamics have not been investigated in detail.

Akasaka studied dynamic structure of polyriboadenylic acid using ^{31}P relaxation assuming solely dipolar mechanism for relaxation.[3] Recently Hayashi *et al.* applied ^{31}P relaxation to studies of structures of yeast transfer RNA^{phe} based on more rigorous analysis of ^{31}P relaxation including the contribution from chemical shift anisotropy.[4] In the present paper, a detailed account is given on the method of analysis of ^{31}P relaxation as well as the results of its application to single-stranded polyribonucleotides.

Experimental

Materials. Homopolyribonucleotides (poly(A), poly(C), and poly(U)) (M_r>100,000) from Sigma Chemical Company were used. They were dialyzed extensively in 0.1 M NaCl, mainly to remove paramagnetic metal ions. Samples for ^{31}P NMR measurements were prepared in concentrations of 60—90 mM (in monomer unit) in 99.75% D_2O containing a small amount of EDTA ([EDTA]/[P]=1/20). All the samples were throughly degassed on a vacuum line before NMR measurements.

ApU (from Sigma) was treated with chelex and then prepared for NMR measurements as in the case of polynucleotides.

Methods. Measurements of ^{31}P spin-lattice relaxation times (T_1) were performed on a JEOL PFT-100 Fourier transform NMR spectrometer operating at 40.48 MHz under proton noise irradiation, by utilizing 180°-t-90° (inversion recovery) pulse sequences.

Nuclear Overhauser enhancement of ^{31}P resonance upon proton irradiation was obtained as relative integrated intensity of ^{31}P resonance between conditions with the proton noise-decoupler on and off by using sodium pyrophosphate as an internal standard. The proton decoupling power was kept less than 10 watts to avoid temperature rise in the samples.

* Presented at XVth NMR Symposium of Japan, Tokyo, October 1976.

Analysis of ^{31}P Relaxation

Three major mechanisms are considered to be important in determining ^{31}P longitudinal relaxation in nucleic acids:
(1) dipolar interaction with neighbouring protons, (2) chemical shift anisotropy, and (3) interaction with paramagnetic ions. These interactions are coupled with molecular motions to cause phosphorus relaxation in solution, and must be separated in order to utilize ^{31}P relaxation for a quantitative study of nucleic acid structures and dynamics.

First, the contribution from paramagnetic impurities and dissolved oxygen can be removed almost throughly (see Experimental). The absence of paramagnetic effects can be verified by observation of large nuclear Overhauser enhancements.

Separation of the dipolar contribution from the chemical shift anisotropy contribution is more intricate, requiring inspection into the nature of the relaxation mechanisms. One way frequently used on phospholipid systems[5] is to measure line widths at more than one observing frequency. This is based on the fact that, while the magnitude of the dipolar interaction is independent of the observing frequency ω, that of the chemical shift anisotropy depends on ω^2.[6] However, often in ^{31}P line width, contribution from the component that is linearly dependent ω can not be neglected, leading to errors in the evaluation of chemical shift contribution. Moreover, the availability of ^{31}P NMR spectrometers for a few to several different frequencies can not be usually expected.

In the present work, we have taken an alternative approach for separating two mechanisms, utilizing nuclear Overhauser enhancement of ^{31}P signals upon saturation of proton signals. The utility of the method lies in the fact that the nuclear Overhauser effect occurs only in the case of dipolar relaxation with protons, but not in the case of chemical shift anisotropy relaxation.

Following three basic assumptions are made. (1) The molecular motion of the phosphorus moiety can be approximated as isotropic and is therefore characterized by a single correlation time τ_c. (2) The same correlation time τ_c can be used in common for both the dipolar relaxation and the chemical shift anisotropy relaxation. (3) The geometrical as well as the electronic structure of the phosphorus moiety is invariant in the measured

temperature range so that the distances between the phosphorus atom and the neighbouring protons (*e.g.*, $H_{3'}$, $H_{5'}$, and $H_{5''}$) as well as the anisotropy in the phosphorus chemical shift can be treated as temperature independent quantities.

Assumptions (1) and (2) are expected from simple approaches in NMR theory[6], and can be allowed as a first step. On the other hand, (3) might not be justified easily in a relatively flexible polymer such as a single-stranded polynucleotide. However, as an example, in the case of ApA and UpU phosphorus-proton coupling constants, $^3J_{PH_{5'}}$, $^4J_{PH_{4'}}$, and $^3J_{PH_{3'}}$, show only small variations (less than 10%) in going from 20 °C to 80 °C,[7] indicating relative invariance of rotamer populations about the $C_{3'}$—$O_{3'}$ and $C_{5'}$—$O_{5'}$ bonds with temperature. Unfortunately, no such data are available for polynucleotides, but the variations in rotamer populations might be expected to be even smaller in polynucleotides. In view of this, assumption (3) is considered to be reasonable.

Based on assumptions (1) and (2), the time dependence of the longitudinal magnetization $\langle I_Z\rangle_P$ of phosphorus, in the absence of relaxation contribution from paramagnetic impurities, should obey the equation[8]

$$\frac{d\langle I_Z\rangle_P}{dt}=(\sum_i\rho_{PH_i}+\rho_P)(I_{0P}-\langle I_Z\rangle_P)+\sum_i\sigma_{PH_i}(I_{0H_i}-\langle I_Z\rangle_{H_i}), \tag{1}$$

where I_{0P} and I_{0H_i} denote the magnetization of phosphorus and the i-th proton, respectively, at thermal equilibrium with the lattice, and $\langle I_Z\rangle_P$ and $\langle I_Z\rangle_{H_i}$ the magnetization of phosphorus and i-th proton, respectively, at time t after application of a 180° pulse.

ρ_{PH_i} and σ_{PH_i} are relaxation terms due to dipolar interaction between the phosphorus nucleus and the i-th proton, and expressed by

$$\rho_{PH_i}=\frac{\gamma_P^2\gamma_H^2\hbar^2}{r_i^6}\left\{\frac{1}{10}\frac{1}{1+(\omega_P-\omega_H)^2\tau_c^2}+\frac{6}{10}\frac{1}{1+(\omega_P+\omega_H)^2\tau_c^2}+\frac{3}{10}\frac{1}{1+\omega_P^2\tau_c^2}\right\}\tau_c, \tag{2}$$

$$\sigma_{PH_i}=\frac{\gamma_P^2\gamma_H^2\hbar^2}{r_i^6}\left\{-\frac{1}{10}\frac{1}{1+(\omega_P-\omega_H)^2\tau_c^2}+\frac{6}{10}\frac{1}{1+(\omega_P+\omega_H)^2\tau_c^2}\right\}\tau_c, \tag{3}$$

where r_i represents the distance between the phosphorus atom and the i-th proton, ω_P and ω_H are the Larmor angular frequencies for phosphorus and proton, respectively. ρ_P is the relaxation term due to chemical shift anisotropy and given by[6]

$$\rho_P=\frac{2}{15}(\delta_{//}-\delta_\perp)^2\omega_P^2\frac{\tau_c}{1+\omega_P^2\tau_c^2}, \tag{4}$$

where axial symmetry is assumed for the chemical shift tensor.

Under saturation of all the proton resonances due to proton-noise irradiation, $\langle I_Z\rangle_{H_i}=0$ for all i and Eq. 1 can be solved, giving

$$\langle I_Z\rangle_P=I_{0P}\left(1+\frac{\sum_i\sigma_{PH_i}}{\sum_i\rho_{PH_i}+\rho_P}\cdot\frac{\gamma_H}{\gamma_P}\right)(1-2e^{-t/T_1}), \tag{5}$$

with

$$\frac{1}{T_1}=\left(\frac{1}{T_1}\right)_{dipole}+\left(\frac{1}{T_1}\right)_{c.s.a.}=\sum_i\rho_{PH_i}+\rho_P$$
$$=A\left\{\frac{1}{10}\frac{1}{1+(\omega_P-\omega_H)^2\tau_c^2}+\frac{6}{10}\frac{1}{1+(\omega_P+\omega_H)^2\tau_c^2}+\frac{3}{10}\frac{1}{1+\omega_P^2\tau_c^2}\right\}\tau_c+B\cdot\frac{\tau_c}{1+\omega_P^2\tau_c^2}, \tag{6}$$

where

$$A=\sum_i\frac{\gamma_P^2\gamma_H^2\hbar^2}{r_i^6}, \tag{7}$$

$$B=\frac{2}{15}\omega_P^2(\delta_{//}-\delta_\perp)^2. \tag{8}$$

The fractional increase (η) of phosphorus magnetization upon saturation of proton signals, *i.e.*, the nuclear Overhauser enhancement, is given by

$$\eta=\frac{\sum_i\sigma_{PH_i}}{\sum_i\rho_{PH_i}+\rho_P}\cdot\frac{\gamma_H}{\gamma_P}=\frac{2.47\sum_i\sigma_{PH_i}}{\sum_i\rho_{PH_i}+\rho_P} \tag{9}$$

Under conditions of extreme narrowing ($(\omega_P+\omega_H)^2\tau_c^2\ll1$), Eqs. 6 and 9 become

$$\frac{1}{T_1}=(A+B)\tau_c, \tag{10}$$

$$\eta=1.235\left(\frac{A}{A+B}\right). \tag{11}$$

If we may assume that the average molecular conformation of the ribose-phosphate moiety does not change significantly with temperature (assumption (3)), we may regard A and B as parameters independent of temperature.

$1/T_1$ expressed by Eq. 6 goes through a maximum (or T_1 goes through a minimum) at a certain value of τ_c ($\tau_c\simeq\omega_P^{-1}$), the particular value of which depending on the observing frequency ω_P and the relative values of A and B. On the other hand, the nuclear Overhauser enhancement η, which is nearly zero or very small for $\tau_c>\omega_P^{-1}$ (see Eq. 9), increases monotonically with the decrease of τ_c to a final value given by Eq. 11. Such behavior of T_1 and η is illustrated in Fig. 1, as a function of τ_c for three representative cases, $B=0$, $A/B=1$, and $A=0$.

Information Obtainable from ^{31}P Relaxation and Nuclear Overhauser Enhancement

In practice, if we know the relative values of A and B from measurements obtained under extreme narrowing conditions (Eq. 11), we can determine the τ_c value at the minimum point of T_1 by using Eq. 6. Knowing both the τ_c value and the T_1 value at the minimum point of T_1, we can also determine from Eq. 6 the absolute values of A and B, which in turn, give information as to the effective phosphorus-proton distance, defined by

$$\bar{r}_{P-H}=(\sum_i 1/r_i^6)^{-1/6}, \tag{12}$$

and the magnitude of the effective ^{31}P chemical shift anisotropy ($\delta_{//}-\delta_\perp$) in solution.

Since A and B values are fixed as temperature invariant quantities, the only unknown variable in the right-hand side of Eq. 6 is τ_c. From a measured

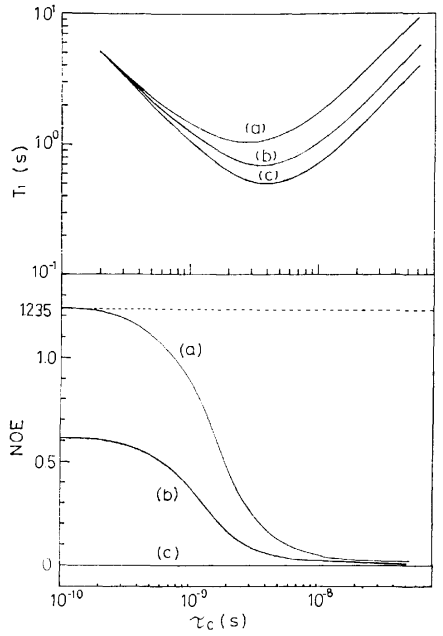

Fig. 1. Theoretical dependence of ^{31}P spin-lattice relaxation time (T_1) and the nuclear Overhauser enhancement (η) upon nonselective proton saturation on the rotational correlation time τ_c for three representative cases of relaxation mechanism:
(a) dipolar 100% ($B=0$ in Eq. 6), (b) dipolar 50%, chemical shift anisotropy 50% ($A/B=1$), (c) chemical shift anisotropy 100% ($A=0$). Isotropic molecular rotation is assumed and the resonance frequency of ^{31}P nucleus at 40.5 MHz is presumed.

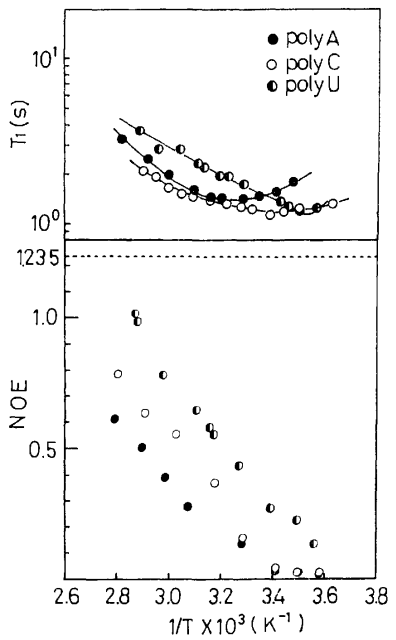

Fig. 2. Temperature dependence of ^{31}P spin-lattice relaxation times and ^{31}P nuclear Overhauser enhancement (η) upon nonselective proton saturation of poly U, poly C, and poly A in neutral D_2O solutions (pH= 6.0+0.1, $[Na^+]=0.1$ M). Concentration of polynucleotides are 92 mM for poly U, 73 mM for poly C, and 60 mM for poly A (monomer unit).

value of T_1 at any desired temperature, we can determine τ_c, a quantity that characterizes the molecular motion around the phosphorus moiety.

Application to Polynucleotides

Figure 2 shows the temperature dependence of spin-lattice relaxation time (T_1) for phosphorus in three polyribonucleotides, poly(U), poly(C), and poly(A), in single-stranded forms in neutral D_2O solutions. Data for poly(A), taken from a previous work[3], are subjected to a more rigorous treatment here. Poly(G) behaves in a distinctly different manner from other polynucleotides, showing neither T_1 minimum nor nuclear Overhauser enhancement ($\omega_p^2\tau_c^2 \gg 1$) because of its unique multi-stranded structure. We notice the following from Fig. 2,
(1) Each polynucleotide shows a minimum value of T_1 in the temperature range of measurement so that the method of analysis described above can be applied.
(2) The temperature at which $T_{1\,\mathrm{min}}$ occurs increases in the order, poly(U)<poly(C)<poly(A), showing that the rate of molecular rotation around the phosphorus atom decreases in this order.

The lower part of Fig. 2 shows the corresponding nuclear Overhauser enhancement (η) for these polynucleotides. We see that:
(3) Nuclear Overhauser enhancement at the highest observed temperature ($\eta=0.6$—1.0) is greater than 50% of that ($\eta=1.235$) expected for the case of 100% dipolar relaxation under extreme narrowing conditions ($B=0$ in Eq. 11), although except for poly(U), the systems may not be under extreme narrowing conditions even at the highest observed temperatures.
(4) At any temperature, the nuclear Overhauser enhancement decreases in the order, poly(U)>poly(C)>poly(A), in line with the rate of molecular motion estimated above from the T_1 data.

Observation (3) shows that $A/(A+B)>0.5$ holds for the three polynucleotides, and the dipolar mechanism is a dominant source of ^{31}P longitudinal relaxation at 40.48 MHz. To ensure measurement of nuclear Overhauser effect under extreme narrowing conditions, a model compound of lower molecular weight ApU was investigated, which indicated $\eta=1.0$.

By using the maximum values of nuclear Overhauser enhancement in the measured temperature range, and the T_1 and τ_c values at $T_{1\,\mathrm{min}}$, the values or the ranges for A and B are determined in each polynucleotide, and the corresponding values or the ranges for $\bar{r}_{P-H}$ and $(\delta_{//}-\delta_{\perp})$ are estimated, according to the method of analysis described. The values are summarized in Table 1. The corresponding quantities for yeast transfer RNA^{Phe}, previously obtained from a similar analysis[4] are given for comparison.

The relatively small variation of $\bar{r}_{P-H}$ values among different polynucleotides seems to indicate that conformational variation is small among the backbone structures of these polynucleotides. The values of chemical shift anisotropy $(\delta_{//}-\delta_{\perp})$ were obtained in the range 120—160 ppm. Differences in $(\delta_{//}-\delta_{\perp})$ values between different polynucleotides can not be discussed in view of the limited accuracy of the present method

TABLE 1. SUMMARY OF ^{31}P RELAXATION DATA AND MOLECULAR PARAMETERS DEDUCED THEREFROM IN HOMOPOLYRIBONUCLEOTIDES AND RELATED SUBSTANCES

Nucleotide	$(T_1)_{min}$ (s)	NOE	Dipolar contribution (%)	$\bar{r}^{a)}_{P-H}$ (Å)	$\delta_{//}-\delta_{\perp}$ (ppm)	E_a (kcal/mol)
poly(U)	1.18	2.0 (72 °C)	$\simeq$ 80	2.33	128	5.1
poly(C)	1.15	1.8 (83 °C)	$>$ 65	2.1—2.4	$<$165	5.3—6.0
poly(A)	1.41	1.6 (83 °C)	$>$ 50	2.2—2.6	$<$158	7.2—8.1
(helix)	1.55			2.49	130	
$tRNA^{phe}_{yeast}$		1.9 (80 °C)	$\simeq$ 73			
(random)	1.80			2.25	120	6.0 (45—80 °C)
ApU[c)]		2.0 (79 °C)	80			

a) Effective P-H distance; $1/\bar{r}^6_{P-H}=\sum_i(1/r_i^6)$. b) Data taken from Ref. 4. c) Measured at 20 mM.

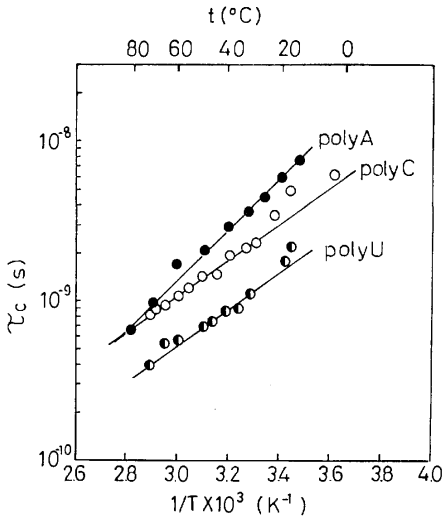

Fig. 3. Temperature dependence of rotational correlation times (τ_c) of poly U, poly C, and poly A as deduced from T_1 and NOE data of Fig. 2.

although the isotropic value of the chemical shift definitely varies.[9] Extreme narrowing conditions are insufficiently fulfilled for poly(A) and poly(C). On the other hand, ApU which is certainly under extreme narrowing conditions in all the temperature ranges measured shows $\eta\simeq 1.0$ or 80% dipolar contribution. By taking account of these facts, we expect that if measurements were done under extreme narrowing conditions for poly(A) and poly(C), the value of η would become as large as that of ApU. Then a probable value of $(\delta_{//}-\delta_{\perp})$ in single stranded polynucleotides in an aqueous solution can be placed in the lower side of the range, *i.e.*, 120—130 ppm.

Furthermore, the τ_c value is obtained as a function of temperature for each polynucleotides (Fig. 3).

It is to be noted that τ_c follows approximately the following equation:

$$\tau_c^{-1}=\tau_0^{-1}\exp(-E_a/RT) \qquad (13)$$

where E_a is the activation energy. The fact that these single-stranded polynucleotides approximately follow a single activation process indicates that their thermal melting is non-cooperative, *i.e.*, the motional activation occurs in a non-cooperative fashion. This makes a sharp contrast with the result for tRNA, which shows a few distinctive steps of activation process.[4]

The τ_c values observed are in the order of 10^{-9} s and can be considered to represent not the whole motion of the molecule ($M_r>100{,}000$) but the local torsional motions around the sugar phosphate backbone. Consequently, the E_a values are considered to represent primarily the torsional barriers around the sugar-phosphate back bone. The observation that the E_a value increases in the order poly(U)$<$poly(C)$<$poly(A) seems to reflect the fact that the incressing tendency of base-stacking gives additional barriers for the molecular motion of the sugar-phosphate moiety.

Conclusion

Important conclusions obtained by inspection of Table 1 and Figs. 2 and 3 may be summarized as follows.

1) The relaxation mechanisms are dipolar dominant (more than 50% in the extreme narrowing region) at this observing frequency (40.48 MHz).

2) Conformations involving the phosphorus atom and the neighbouring protons do not seem to vary significantly between different polynucleotides, as judged from $\bar{r}_{P-H}$ values.

3) Phosphorus chemical shift anisotropy, $(\delta_{//}-\delta_{\perp})$, of single-stranded polynucleotides in solution is in the range 120—165 ppm. It would probably range around 120—130 ppm if measurements could all be made under extreme narrowing conditions.

4) Molecular motions around the phosphate group of single-stranded homopolyribonucleotides become faster in the order, poly(A)$<$poly(C)$<$poly(U). The thermal activation is characterized by single activation energies, 5.1, 5.3—6.0, and 7.2—8.1 kcal/mol for poly(U), poly(C), and poly(A), respectively. These results seem to imply that the base-stacking plays an important role in restricting flexibility of the main chain structure of single-stranded polynucleotides.

We thank Dr. Hayashi for the measurement of the nuclear Overhauser effect in ApU.

References

1) For example, D. G. Gorenstein, and D. Kar, *Biochem. Biophys. Res. Commun.*, **65**, 1073 (1975).

2) For example, M. Tsuboi, S. Takahashi, Y. Kyogoku, H. Hayastu, T. Ukita, and M. Kainosho, *Science*, **166**, 1504

(1969).
3) K. Akasaka, *Biopolymers*, **13**, 2273 (1974).
4) F. Hayashi, K. Akasaka, and H. Hatano, *Biopolymers*, **16**, 655 (1977).
5) For example, J. A. Berden, P. R. Cullis, D. I. Hoult, A. C. Mclaughlin, G. K. Radda, and R. E. Richards, *FEBS Lett.*, **46**, 55 (1974).
6) A. Abragam, "The Principles of Nulcear Magnetism," Oxford University Press (1967), Chap. 8.
7) P. J. Cozzone and O. Jardetzky, *Biochemistry*, **15**, 4860 (1976).
8) J. H. Noggle and R. E. Shirmer, "The Nuclear Overhauser Effect. Chemical Applications," Academic Press, New York & London (1971), p. 45.
9) K. Akasaka, A. Yamada, and H. Hatano, *FEBS Lett.*, **53**, 339 (1975).

Structural Studies of Asymmetric Hydrogenation. III. The Crystal Structure of (*R*)-1-(Methoxycarbonyl)ethyl(*R*)(+)-α-methylbenzylaminebis(dimethylglyoximato)cobalt(III)

Yuji OHASHI and Yoshio SASADA

Laboratory of Chemistry for Natural Products, Tokyo Institute of Technology, O-okayama, Meguro-ku, Tokyo 152

(Received April 12, 1977)

The structure of (*R*)-1-(methoxycarbonyl)ethyl(*R*)(+)-α-methylbenzylaminebis(dimethylglyoximato)cobalt-(III) has been determined by X-ray analysis. The crystal is monoclinic, the space group $P2_1$, $Z=2$ with $a=7.899(5)$, $b=16.397(2)$, $c=9.054(7)$ Å, and $\beta=90.98(7)°$. The structure was deduced by the heavy atom method and refined by the block-diagonal least-squares method to a final R value of 0.048 for 2146 observed reflections. The bis(dimethylglyoximato)cobalt moiety is twisted around its long axis, owing to the steric repulsion from the (*R*)-1-(methoxycarbonyl)ethyl group and the optically active amine. It is proposed that this twist is one of the factors inducing the asymmetry in the hydrogenation catalyzed by the complex of bis(dimethylglyoximato)cobalt and the active amine. At the step of Co–C bond cleavage the reaction proceeds mainly through inversion of the configuration.

The complexes of bis(dimethylglyoximato)cobalt (abbreviated to $Co(dmg)_2$ or cobaloxime) and optically active amine catalyze asymmetric hydrogenation of olefins.[1-6] The hydrogenation proceeds as follows:

$$\begin{array}{l} \qquad\qquad\qquad\quad H_2C{=}CXY \\ \qquad\qquad\qquad\quad \vdots \\ H_2C{=}CXY + \underset{\underset{B^*}{|}}{Co(dmg)_2} \longrightarrow \underset{\underset{B^*}{|}}{Co(dmg)_2} \longrightarrow \quad \tfrac{1}{2}H_2 \\ \\ H_3CC^*XY \\ \quad | \\ \quad \underset{\underset{B^*}{|}}{Co(dmg)_2} \longrightarrow \quad \tfrac{1}{2}H_2 \qquad H_3CC^*HXY + \underset{\underset{B^*}{|}}{Co(dmg)_2}\ , \end{array}$$

where B* is the optically active amine. In order to clarify the mechanism of inducing asymmetry, several crystal structures of related complexes have been determined by X-ray analysis. In Part II of this series on the crystal structure of methyl(*R*)(+)-α-methylbenzylaminebis(dimethylglyoximato)cobalt(III) benzene solvate[7] (abbreviated to methyl complex), it has been shown that the $Co(dmg)_2$ moiety of the catalyzer is deformed by the steric repulsion from the optically active amine coordinated to the cobalt atom so that its symmetry changes from D_{2h} to C_{2h}. We proposed that this deformation is one of the factors inducing asymmetry in the reaction step of π-bond formation. The present study has been undertaken to disclose the mechanism of Co–C(σ) bond formation and its cleavage.

Experimental

Dark red crystals of the title complex were obtained from aqueous methanol solution. The unit cell dimensions were determined from zero layer Weissenberg photographs using Co$K\alpha$ radiation about b and c axes. Spacings of 40 high angle reflections ($\theta \geqq 60°$), calibrated with superposed silicon powder lines, were subjected to the least-squares treatment. The crystal data are summarized in Table 1.

With the use of a crystal of dimensions $0.2\times0.4\times0.3$ mm, the intensities for $3° \leqq 2\theta \leqq 60°$ were collected on a Hilger-Watts linear diffractometer with Mo$K\alpha$ radiation. The balanced Y/Zr filter pair was used. Out of 3055 accessible reflections, 2149 for which $I \geqq 3\sigma(I)$ were regarded as observed. The usual Lorentz and polarization, but no absorption, corrections were made.

TABLE 1. CRYSTAL DATA

Formula	$C_{20}H_{32}N_5O_6Co$
F. W.	497.44
a	7.899(5) Å
b	16.397(2) Å
c	9.054(7) Å
β	90.98(7)°
V	1172(1) Å^3
Systematic absence	$0k0$, k odd
Space group	$P2_1$
Z	2
D_m	1.414 g/cm^3
D_x	1.409 g/cm^3
μ(Mo$K\alpha$)	8.05 cm^{-1}

TABLE 2. PART OF OBSERVED AND CALCULATED INTENSITY RELATIONS BETWEEN hkl AND $h\bar{k}l$

Indices			$\lvert F_c(hkl)\rvert^2$	Observed relations	$\lvert F_c(h\bar{k}l)\rvert^2$
1	1	−3	130	<	595
1	2	1	1183	>	511
1	3	−1	231	>	19
1	5	−1	595	<	1325
1	7	2	493	>	139
2	2	7	520	>	256
2	1	7	353	<	475
2	3	−4	92	<	346
2	4	−3	139	<	424
2	6	1	117	<	475
2	6	3	92	<	493
2	4	7	100	>	13
2	3	7	64	<	262

Structure Determination

The positions of the cobalt and six coordinated atoms were obtained from the three-dimensional Patterson function. The other atoms were revealed on the first

Table 3. Fractional coordinates ($\times 10^4$) and thermal parameters ($\times 10^5$) for the non-hydrogen atoms

The anisotropic thermal parameters are of the form;
$T = \exp(-\beta_{11}h^2-\beta_{22}k^2-\beta_{33}l^2-\beta_{12}hk-\beta_{13}hl-\beta_{23}kl)$.
Estimated standard deviations are in parentheses.

Atom	x	y	z	β_{11}	β_{22}	β_{33}	β_{12}	β_{13}	β_{23}
Co	1135(1)	2500	2740(1)	0852(9)	0143(2)	0529(6)	0126(14)	−0080(11)	0047(12)
N(1)	0514(6)	2298(3)	0752(6)	0803(81)	0244(26)	0731(62)	−0141(59)	0045(114)	−0072(52)
N(2)	2068(7)	1447(3)	2577(6)	1139(100)	0175(21)	0997(74)	0096(72)	0165(136)	0033(63)
N(3)	1869(7)	2748(3)	4675(5)	1184(94)	0292(26)	0546(56)	0196(70)	−0266(115)	0014(54)
N(4)	0253(7)	3559(3)	2892(6)	1073(93)	0155(19)	0750(64)	0214(67)	0017(122)	0107(56)
O(1)	−0328(6)	2843(3)	−0084(5)	1453(95)	0375(23)	0780(57)	0095(73)	−0706(119)	0171(58)
O(2)	2815(8)	1057(3)	3721(6)	2112(118)	0266(22)	1286(80)	0762(82)	−0051(154)	0502(66)
O(3)	2758(7)	2207(3)	5517(5)	1727(105)	0461(28)	0806(63)	0568(82)	−0528(131)	0345(62)
O(4)	−0609(7)	3939(3)	1779(5)	1481(95)	0256(21)	1022(67)	0324(71)	−0336(125)	0252(58)
C(1)	1102(9)	1637(5)	0185(8)	1022(119)	0320(32)	0964(92)	−0291(97)	0459(167)	−0113(84)
C(2)	1987(10)	1109(5)	1265(8)	1282(131)	0274(30)	1114(102)	0095(97)	0283(183)	−0286(86)
C(3)	1563(10)	3462(4)	5160(7)	1601(138)	0242(27)	0606(73)	−0043(95)	−0092(159)	−0166(70)
C(4)	0583(9)	3965(4)	4100(8)	1228(121)	0173(24)	1059(93)	0034(86)	0316(168)	−0146(74)
C(5)	0947(13)	1421(7)	−1443(9)	2355(202)	0558(50)	0903(105)	−0121(160)	0270(231)	−0545(119)
C(6)	2665(15)	0286(6)	0970(13)	3127(259)	0294(39)	2360(197)	0848(159)	1561(363)	−0444(140)
C(7)	2087(15)	3774(7)	6663(10)	3136(246)	0525(49)	0950(109)	0050(172)	−0876(265)	−0701(117)
C(8)	0052(13)	4814(6)	4356(11)	2489(216)	0262(35)	1626(141)	0044(131)	−0045(278)	−0329(110)
N(5)	3427(7)	2917(3)	1974(6)	0848(88)	0202(21)	0900(70)	−0010(68)	−0120(120)	0127(61)
C(9)	3607(9)	3595(4)	0915(7)	1178(115)	0197(24)	0805(79)	−0139(86)	−0101(155)	0122(71)
C(10)	5072(12)	3422(6)	−0090(9)	1993(165)	0349(36)	1155(106)	−0315(124)	1005(212)	−0254(100)
C(11)	3782(8)	4419(4)	1636(8)	0923(108)	0248(28)	1057(90)	−0017(87)	−0175(159)	−0194(81)
C(12)	4785(12)	4539(6)	2875(11)	2023(186)	0409(43)	1714(143)	0172(141)	−2122(271)	−0352(124)
C(13)	4984(15)	5325(6)	3480(13)	2833(247)	0397(46)	2408(193)	0038(166)	−2755(361)	−0707(151)
C(14)	4276(12)	5987(6)	2806(14)	1620(178)	0318(39)	3034(228)	−0005(125)	−0354(308)	−0566(151)
C(15)	3324(12)	5881(6)	1557(12)	1976(185)	0272(37)	2317(180)	0079(130)	−0321(289)	0057(126)
C(16)	3051(10)	5099(5)	0974(9)	1366(141)	0288(32)	1470(121)	−0001(105)	−0133(205)	0301(98)
C(17)	−0972(9)	1930(5)	3586(8)	1202(126)	0268(29)	0921(90)	0061(93)	0325(175)	0051(81)
C(18)	−1983(12)	1422(6)	2510(11)	1651(167)	0422(42)	1704(143)	−0676(137)	0659(249)	−0534(128)
C(19)	−2101(7)	2502(6)	4329(6)	0990(87)	0236(20)	0841(64)	−0225(137)	0039(120)	0183(122)
O(5)	−3325(6)	2827(4)	3772(6)	1116(88)	0500(30)	1471(81)	0494(80)	−0670(137)	0200(77)
O(6)	−1650(6)	2640(4)	5743(5)	1357(79)	0389(32)	0828(52)	0183(81)	0340(102)	−0111(67)
C(20)	−2663(13)	3201(7)	6555(10)	2117(188)	0576(52)	1290(125)	0364(160)	1358(250)	−0457(128)

Fourier map phased with these seven atoms.

The structure was refined by the block-diagonal least-squares method. After several cycles of refinement, the three strongest reflections were excluded because they seemed to be affected by secondary extinction. All the hydrogen atoms were found on the difference map. The final refinement was made including these hydrogen atoms with isotropic temperature factors. The weighting scheme, $w=(34.44/|F_o|)^2$ if $|F_o|>34.44$, $w=1.0$ if $34.44\geqq|F_o|\geqq8.61$, $w=0.3$ if $|F_o|<8.61$, was employed. The final R value became 0.048 for 2146 observed reflections. At the final stage, no peaks higher than 0.30 e Å^{-3}, except for the peaks of 0.45 e Å^{-3} around the cobalt atom, were found on the difference map. Atomic scattering factors were taken from the International Tables for X-Ray Crystallography.[8]

The absolute configuration was determined from Weissenberg photographs using Cu$K\alpha$ radiation. The observed and calculated structure factors of 13 Bijvoet pairs are compared in Table 2.

Final atomic parameters and their standard deviations are given for non-hydrogen atoms and hydrogen atoms in Tables 3 and 4, respectively. A list of the observed and calculated structure factors is kept in the office of the Chemical Society of Japan (Document No. 7719). The computation was done on a HITAC 8800 computer at the University of Tokyo and a HITAC 8700 computer at this Institute.

Description of the Structure

Co(dmg)$_2$ Moiety. The equations of the mean planes of four nitrogen atoms and two dmg's, (I), (II), and (III), are given in Table 5, together with the deviations of atoms from the planes. Figure 1 shows the structure of the complex projected on plane (I) and the short contacts between the non-bonded atoms in the complex. The molecular coordinates, x and y, are taken in plane (I), where x is the projection of the line passing through the mid-points of N(1)···N(2) and N(3)···N(4) on the plane, y being perpendicular to x passing through the cobalt atom. Two arrows indicate

Table 4. Fractional coordinates ($\times 10^3$) and thermal parameters for hydrogen atoms
(Esd's are in parentheses)

Atom	x	y	z	B(Å^2)
H(O1)	−051(11)	346(6)	086(10)	3(2)
H(O2)	278(14)	184(7)	484(12)	4(3)
H(51)	051(13)	093(7)	−170(12)	5(3)
H(52)	137(12)	185(6)	−195(11)	3(2)
H(53)	227(15)	106(8)	−164(14)	6(3)
H(61)	196(15)	−009(7)	033(13)	6(3)
H(62)	358(16)	052(9)	016(15)	9(4)
H(63)	332(14)	−002(7)	140(13)	5(3)
H(71)	123(13)	422(7)	689(13)	5(3)
H(72)	225(14)	337(8)	718(14)	5(3)
H(73)	287(11)	405(6)	674(11)	3(2)
H(81)	−080(12)	497(6)	387(11)	4(2)
H(82)	−037(12)	498(7)	536(12)	4(2)
H(83)	093(13)	518(7)	409(12)	4(3)
H(N51)	414(11)	242(7)	143(9)	4(2)
H(N52)	389(12)	302(6)	273(10)	3(2)
H(9)	261(12)	367(6)	030(11)	3(2)
H(101)	490(12)	378(6)	−084(11)	3(2)
H(102)	520(18)	276(11)	−057(19)	10(5)
H(103)	565(17)	352(9)	063(16)	8(4)
H(12)	535(13)	410(7)	340(13)	5(3)
H(13)	555(16)	532(8)	431(15)	7(4)
H(14)	461(12)	657(6)	339(12)	4(2)
H(15)	261(12)	639(6)	109(11)	3(2)
H(16)	262(15)	508(8)	−001(14)	6(3)
H(17)	−034(12)	166(6)	432(11)	3(2)
H(181)	−260(11)	170(6)	199(10)	3(2)
H(182)	−135(12)	099(6)	206(11)	4(2)
H(183)	−255(16)	087(8)	290(15)	8(4)
H(201)	−346(12)	358(6)	597(10)	3(2)
H(202)	−306(17)	311(9)	726(14)	9(4)
H(203)	−224(15)	352(8)	738(13)	7(3)

the vectors normal to the planes of (II) and (III).

The Co(dmg)$_2$ moiety is significantly bent downward to avoid the short contact with the 1-(methoxycarbonyl)-ethyl group (abbreviated to mce group). The Co(dmg)$_2$ moiety in the methyl complex,[7] which contains the methyl group instead of the mce group and the same amine, is slightly bent in the opposite direction. The cobalt atom in the present complex is significantly displaced upward from the mean plane whereas that in the methyl complex is shifted downward (0.04 Å). Moreover, each dmg is inclined to the y direction. Contacts with the axial ligands, especially between C(18) and N(1) and between H(N51) and N(2), tilt the plane of (II), whereas contacts between C(9), C(11), and N(4), and between N(3), C(3), and O(6) tilt the plane of (III) in the opposite sense. A similar twist of Co(dmg)$_2$ is found in the crystal of 4-pyridyltributylphosphinecobaloxime.[9]

Bond distances and angles are shown in Fig. 2 and Table 6, respectively. In Table 7 the bond lengths in the Co(dmg)$_2$ moiety are compared with those in the methyl complex and the average distances suggested by Bigotto *et al.*[10] In regard to the bond lengths of N–C and C–CH$_3$ and three angles around the endo-cyclic carbon atom, the symmetry of C_{2h} holds good for the present complex.

However, four distances of Co–N are nearly the same and close to the value of Bigotto *et al.*[10] Two bonds of N(3)–O(3) and N(4)–O(4) are longer than N(1)–O(1) and N(2)–O(2). Two hydrogen atoms, H(O1) and H(O2), are bonded to O(4) and O(3), respectively.

Equivalence of four Co–N bonds might be caused

Table 5. Least-squares planes and deviations for equatorial ligands

X, Y, and Z in Å referred to **a**, **b**, and **c*** respectively.

(I) Co(dmg)$_2$ plane:
$-0.8635X-0.3853Y+0.3255Z+1.5507=0.$

(II) dmg plane:
$-0.8595X-0.4588Y+0.2252Z+1.9239=0.$

(III) dmg plane:
$-0.8585X-0.3307Y+0.3919Z+1.0370=0.$

	I	II	III
Co	0.041 (l/Å)	−0.132 (l/Å)	−0.080 (l/Å)
N(1)	−0.020*	0.010*	
N(2)	0.020*	−0.009*	
N(3)	−0.020*		0.001*
N(4)	0.020*		−0.001*
O(1)	−0.047	−0.011	
O(2)	0.109	0.025	
O(3)	−0.025		0.001
O(4)	0.026		−0.031
C(1)	−0.178	−0.016*	
C(2)	−0.115	0.016*	
C(3)	−0.113		−0.001*
C(4)	−0.089		0.001*
C(5)	−0.437	−0.102	
C(6)	−0.149	0.110	
C(7)	−0.205		0.028
C(8)	−0.184		−0.005

* Atoms included in the least-squares calculation.

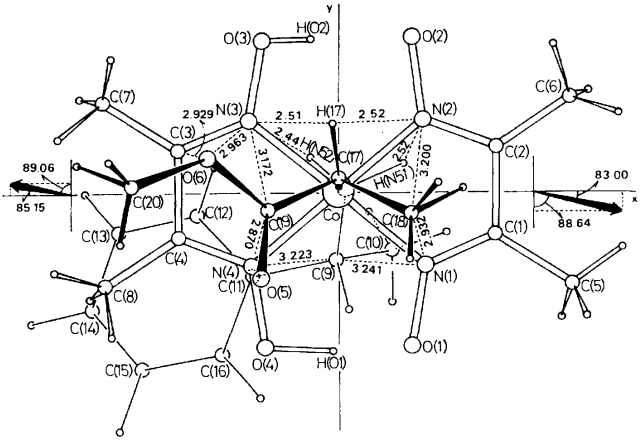

Fig. 1. Projection of the complex to the mean plane of four nitrogen atoms of Co(dmg)$_2$ and the short contacts between non-bonded atoms(l/Å), their threshold values being 3.400 Å for distances between the non-hydrogen atoms and 2.70 Å for those including hydrogen atoms.

Table 6. Bond angles (ϕ/°) (Esd's are in parentheses)
Angles including methyl hydrogens are omitted.

N(1)-Co-N(2)	81.9(2)	N(1)-Co-N(3)	176.1(2)
N(1)-Co-N(4)	98.1(2)	N(1)-Co-N(5)	87.3(2)
N(1)-Co-C(17)	94.4(3)	N(2)-Co-N(3)	99.0(2)
N(2)-Co-N(4)	178.7(2)	N(2)-Co-N(5)	86.0(2)
N(2)-Co-C(17)	86.2(3)	N(3)-Co-N(4)	80.8(2)
N(3)-Co-N(5)	89.1(2)	N(3)-Co-C(17)	89.4(3)
N(4)-Co-N(5)	92.7(2)	N(4)-Co-C(17)	95.1(3)
N(5)-Co-C(17)	171.7(3)	Co-N(1)-O(1)	122.6(4)
Co-N(1)-C(1)	116.0(5)	O(1)-N(1)-C(1)	121.0(6)
Co-N(2)-O(2)	122.8(5)	Co-N(2)-C(2)	116.4(5)
O(2)-N(2)-C(2)	120.7(6)	Co-N(3)-O(3)	121.9(4)
Co-N(3)-C(3)	117.5(5)	O(3)-N(3)-C(3)	120.4(6)
Co-N(4)-O(4)	123.6(4)	Co-N(4)-C(4)	117.7(5)
O(4)-N(4)-C(4)	118.6(6)	N(1)-C(1)-C(2)	113.6(7)
N(1)-C(1)-C(5)	124.0(7)	C(2)-C(1)-C(5)	122.4(7)
N(2)-C(2)-C(1)	111.6(7)	N(2)-C(2)-C(6)	122.5(8)
C(1)-C(2)-C(6)	125.9(8)	N(3)-C(3)-C(4)	113.0(6)
N(3)-C(3)-C(7)	124.9(8)	C(4)-C(3)-C(7)	122.1(7)
N(4)-C(4)-C(3)	110.9(6)	N(4)-C(4)-C(8)	124.1(7)
C(3)-C(4)-C(8)	125.0(7)	Co-N(5)-C(9)	124.2(4)
N(5)-C(9)-C(10)	109.5(6)	N(5)-C(9)-C(11)	113.8(6)
C(9)-C(11)-C(12)	122.0(7)	C(9)-C(11)-C(16)	120.0(7)
C(12)-C(11)-C(16)	117.8(8)	C(11)-C(12)-C(13)	120.5(9)
C(12)-C(13)-C(14)	120.9(11)	C(13)-C(14)-C(15)	119.2(12)
C(14)-C(15)-C(16)	120.7(10)	C(11)-C(16)-C(15)	120.8(8)
Co-C(17)-C(18)	115.7(6)	Co-C(17)-C(19)	112.4(6)
C(18)-C(17)-C(19)	109.4(7)	C(17)-C(19)-O(5)	125.5(9)
C(17)-C(19)-O(6)	113.1(8)	O(5)-C(19)-O(6)	121.5(9)
C(19)-O(6)-C(20)	117.2(8)		
Co-N(5)-H(N51)	111(6)	Co-N(5)-H(N52)	100(7)
C(9)-N(5)-H(N51)	103(6)	C(9)-N(5)-H(N52)	110(7)
H(N51)-N(5)-H(N52)	108(10)	N(1)-O(1)-H(O1)	102(4)
N(2)-O(2)-H(O2)	94(4)	N(3)-O(3)-H(O2)	92(7)
N(4)-O(4)-H(O1)	101(5)	O(1)-H(O1)-O(4)	172(10)
O(2)-H(O2)-O(3)	169(11)	N(5)-C(9)-H(9)	113(6)
C(10)-C(9)-H(9)	108(6)	C(11)-C(9)-H(9)	101(6)
C(11)-C(12)-H(12)	124(7)	C(13)-C(12)-H(12)	116(7)
C(12)-C(13)-H(13)	110(9)	C(14)-C(13)-H(13)	129(9)
C(13)-C(14)-H(14)	113(6)	C(15)-C(14)-H(14)	128(6)
C(14)-C(15)-H(15)	119(5)	C(16)-C(15)-H(15)	120(5)
C(15)-C(16)-H(16)	116(7)	C(11)-C(16)-H(16)	120(7)

Table 7. Bond lengths in $Co(dmg)_2$ (l/Å)

	Methyl complex	Present	Average value of Bigotto *et al.*		Methyl complex	Present	Average value of Bigotto *et al.*
Co-N(1)	1.877	1.888		N(2)-C(2)	1.306	1.312	1.297
Co-N(2)	1.886	1.885	1.879	N(3)-C(3)	1.280	1.275	
Co-N(3)	1.883	1.880		N(4)-C(4)	1.306	1.303	
Co-N(4)	1.906	1.877		C(1)-C(5)	1.514	1.519	
N(1)-O(1)	1.318	1.340		C(2)-C(6)	1.480	1.478	1.500
N(2)-O(2)	1.350	1.344	1.343	C(3)-C(7)	1.484	1.505	
N(3)-O(3)	1.328	1.358		C(4)-C(8)	1.540	1.474	
N(4)-O(4)	1.349	1.358		C(1)-C(2)	1.483	1.474	1.451
N(1)-C(1)	1.257	1.288		C(3)-C(4)	1.447	1.474	

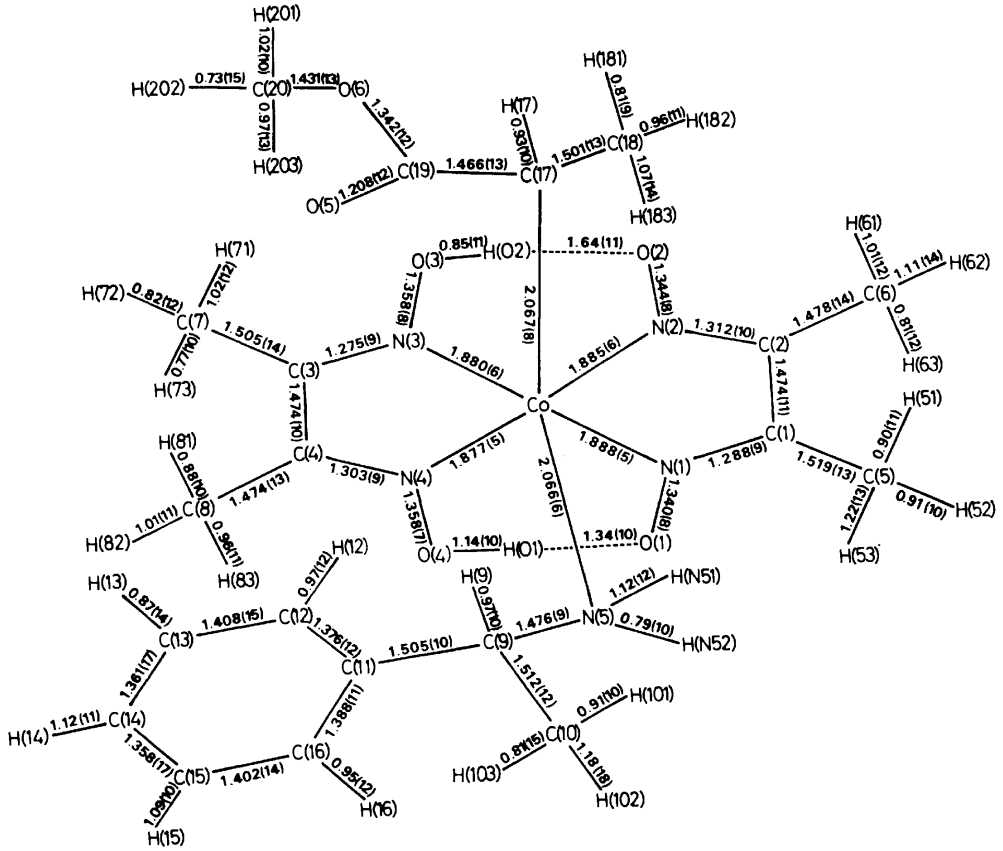

Fig. 2. Bond distances (l/Å). Their standard deviations are in parentheses.

Table 8. Various Co-C(sp^3) distances in cobaloxime complexes

	Co-C distance	Reference
$CH_3Co(dmg)_2(OH_2)$	1.990(5) Å	15
$CH_3Co(dmg)_2(py)$	1.998(5)	10
$CH_3Co(dmg)_2(nmeim)$	2.009(7)	10
$CH_3Co(dmg)_2(mba)$	1.988(19)	7
$(CH_2CO_2CH_3)Co(dmg)_2(py)$	2.04	11
(CH_2CH_2CN)-Co$(dmg)_2$(dphyea)	2.04	16
$(CH(CH_3)CO_2CH_3)$-Co$(dmg)_2$(mba)	2.067(8)	present

py: Pyridine, nmeim: 3-*N*-methylimidazole, dphyea: *erythro*-1,2-diphenyl-2-hydroxyethylamine.

Table 9. Characteristic dimensions of the amine

	Methyl complex	Present
Co-N(5)	2.087(9) Å	2.066(6) Å
N(5)-C(9)	1.463(15) Å	1.476(9) Å
C(9)-C(11)	1.541(16) Å	1.505(10) Å
N(4)-Co-N(5)	96.2(4)°	92.7(2)°
Co-N(5)-C(9)	125.4(7)°	124.2(4)°
Dihedral angle of N(4)-Co-N(5)-C(9)	17.6°	39.7°
Dihedral angle of Co-N(5)-C(9)-C(11)	76.0°	89.9°
Bending of C(9)-C(11) from the phenyl ring	2.2°	4.0°

by the steric repulsions between C(18) and N(1) and between C(19) and N(4). The highly negative O(5) and O(6) atoms would draw the positive H(O1) and H(O2) atoms toward O(4) and O(3), respectively, by electroattractive force. Thus in the step of σ-bond formation, not only the twist of $Co(dmg)_2$ but also slight changes of bond distance occur as a result of electrostatic force and the short contacts between the mce group and $Co(dmg)_2$.

1-(Methoxycarbonyl)ethyl Group. The Co–C(17) distance of 2.067 Å is significantly greater than the usual Co–C(sp^3) length. Various Co–C(sp^3) lengths so far determined in the cobaloxime complexes are summarized in Table 8. As the number of the bulky substituents bonded to the ligating carbon atom increases, the Co–C distance is lengthened. This can be interpreted by the steric repulsion between the substituents and the $Co(dmg)_2$ moiety. The C(17)–C(19) distance of 1.466 Å is significantly smaller than the corresponding one in propionic acid (1.50 Å) and slightly smaller than that in *O*-methyl-(Co–C)carboxymethylpyridinecobaloxime (1.48 Å).[11] Since C(17)–C(18) is shorter than the usual C(sp^3)–C(sp^3) single bond, this suggests that the hybridization of C(17) is modified by coordination. The other distances are in good agreement with the corresponding ones of *O*-methyl-(Co–C)carboxymethylpyridinecobaloxime. The angle of Co–C(17)–C(18), 115.7°, is greater than the tetrahedral angle, probably due to the steric repulsion from $Co(dmg)_2$. Three angles around the C(19) atom, 125.5, 121.5, and 113.1°, are close to those of propionic acid, 125, 122,

and 112°, respectively. Four atoms of C(17), C(19), O(5), and O(6) are coplanar within the limit of 0.001 Å, its plane making an angle of 27.5° with the plane (I) of $Co(dmg)_2$.

α-Methylbenzylamine Ligand. In Table 9, the characteristic dimensions of amine ligand (abbreviated to mba) are compared with those in the methyl complex. The $Co(dmg)_2$ plane is bent toward the amine so that the steric repulsion from the amine should be stronger than that of the methyl complex. To release this, rotation around Co–N(5) and N(5)–C(9) and bending of the phenyl group occur. Co–N(5) rotates from the stable conformation, in which the dihedral angle of N(4)–Co–N(5)–C(9) is 13°.[7] The conformation around N(5)–C(9) is shown in Fig. 3. The N(5)–C(9) bond rotates by about 15° from the conformation of

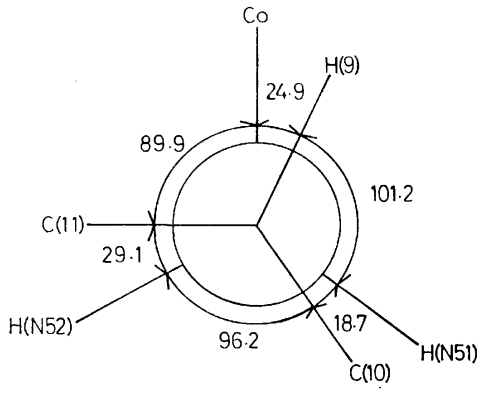

Fig. 3. Newman projection of mba along C(9)–N(5) with the angles (ϕ/°) between the projected bonds.

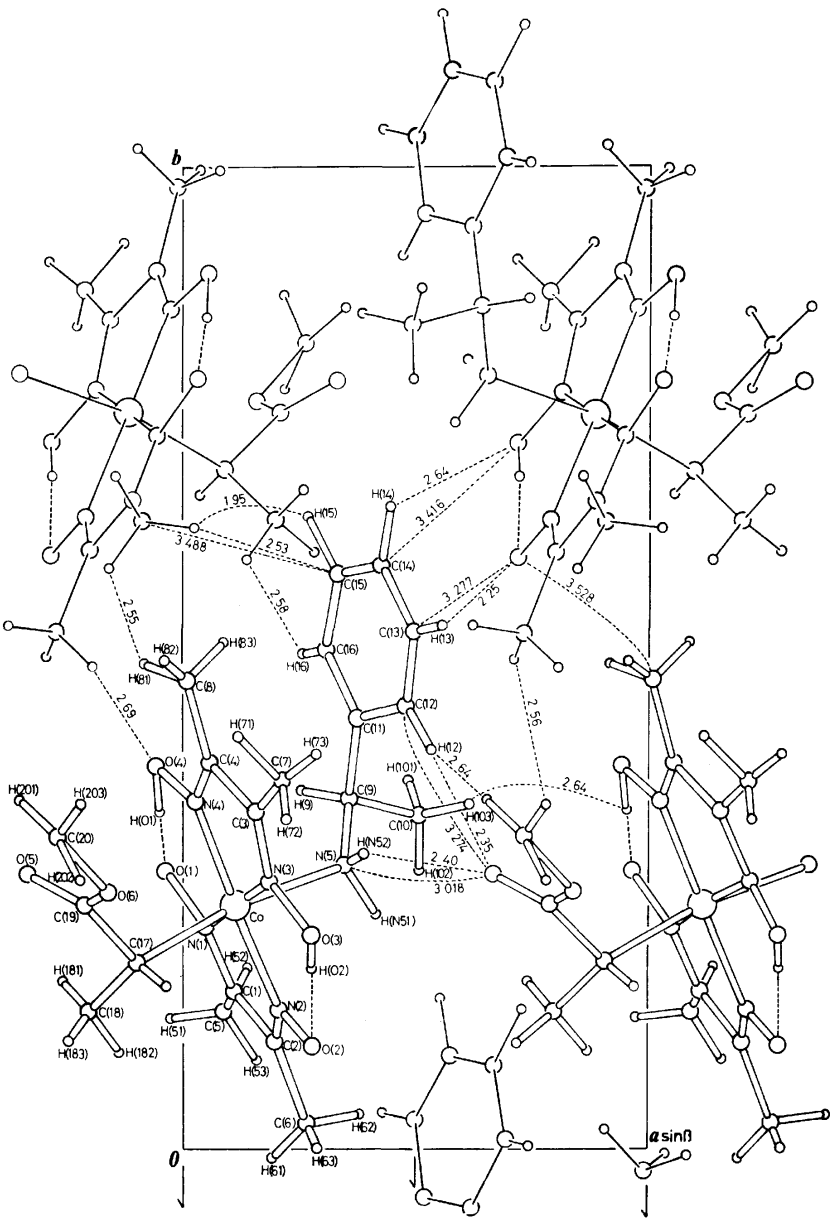

Fig. 4. Projection of the crystal structure along the c axis and short contacts between complexes. Along the c axis the contacts, 3.379 Å for O(3)···C′(5) and 3.580 Å for O(1)···C′(20) are observed.

the methyl complex to the unstable eclipsed form. On the other hand, the Co–N(5) distance is smaller than that in the methyl complex, probably by the effect of the *trans* ligand. The N(5)–C(9) and C(9)–C(11) lengths are in good agreement with the usual distances, 1.472±0.005 and 1.505±0.005 Å, respectively.[12]

Crystal Structure. The crystal structure viewed along the c axis is shown in Fig. 4, the short contacts also being given. There is a fairly short distance, 3.018 Å, between N(5) and O′(5) in the neighbouring complex along the a axis. Although this may be a hydrogen bond of N–H···O in view of N···O distance,[13] O′(5)···H(N52) is not so short and the angle of N(5)–H(N52)···O′(5) is 136°. Therefore, the interaction of N–H···O, if any, should be very weak.[14] Others are normal van der Waals contacts.

Discussion

The $Co(dmg)_2$ moiety is twisted as a 'propeller' by the steric repulsion with the mce group and mba ligand. The N(1) and N(4) atoms are shifted downward and upward, respectively, from the plane, to avoid the short contacts with the methyl of mce group and the asymmetric mba ligand. The carbonyl group with smaller van der Waals radius is located over N(4). If the absolute configuration of the mce group is *S*, as indicated by broken lines in Fig. 5, the methyl of mce group comes close to N(2), which is above the mean plane, giving rise to the strong steric repulsion. It is plausible that the σ-complex containing the *S*-mce group is less stable energetically than that having *R*-mce group, if the asymmetric amine has *R* configuration. We propose that this is one of the factors inducing asymmetry in the step of σ-bond formation of this hydrogenation reaction. This hypothesis, however, is based on the assumption that the *S*-mce group does not change seriously.

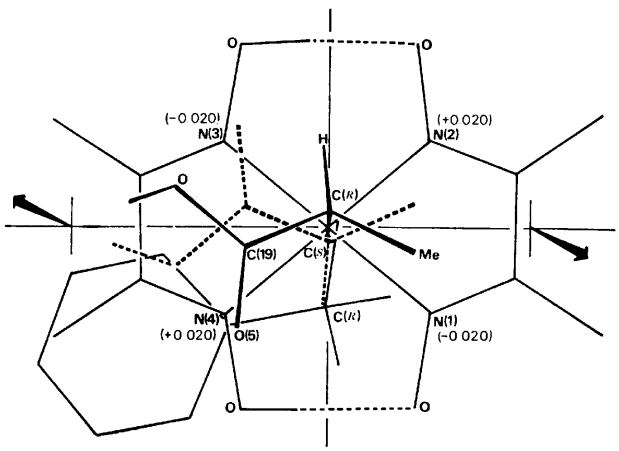

Fig. 5. A presumed conformation of σ-complex containing *S*-mce group (broken lines). The deviations of four nitrogen atoms from the mean plane are in parentheses.

As regards the mechanism of Co–C bond cleavage, the absolute configuration of the mce group was determined to be *R* by an anomalous dispersion method. The reaction product of (+)-methyl propionate-2-*d*, which was obtained by deuterogenation of this complex, was determined to have *S* configuration from the specific rotation.[6] It is, therefore, concluded that the Co–C bond cleavage proceeds mainly through inversion of configuration at the carbon atom.

The authors are grateful to Dr. Yoshiaki Ohgo for supply of the specimens and for valuable discussions.

References

1) Y. Ohgo, S. Takeuchi, and J. Yoshimura, *Bull. Chem. Soc. Jpn.*, **44**, 283 (1971).
2) Y. Ohgo, S. Takeuchi, and J. Yoshimura, *Bull. Chem. Soc. Jpn.*, **44**, 583 (1971).
3) S. Takeuchi, Y. Ohgo, and J. Yoshimura, *Chem. Lett.*, **1973**, 265.
4) Y. Ohgo, S. Takeuchi, Y. Natori, and J. Yoshimura, *Chem. Lett.*, **1974**, 33.
5) Y. Ohgo, Y. Natori, S. Takeuchi, and J. Yoshimura, *Chem. Lett.*, **1974**, 709.
6) Y. Ohgo, Y. Natori, S. Takeuchi, and J. Yoshimura, *Chem. Lett.*, **1974**, 1327.
7) Y. Ohashi and Y. Sasada, *Bull. Chem. Soc. Jpn.*, **50**, 1710 (1977).
8) "International Tables for X-Ray Crystallography," Vol. IV, The Kynoch Press, Birmingham (1974), p. 72.
9) W. W. Adams and P. G. Lenhert, *Acta Crystallogr., Sect. B*, **29**, 2412 (1973).
10) A. Bigotto, E. Zangrando, and L. Randaccio, *J. Chem. Soc., Dalton Trans.*, **1976**, 96.
11) P. G. Lenhert, *Chem. Commun.*, **1967**, 980.
12) L. E. Sutton, "Tables of Interatomic Distances and Configurations in Molecules and Ions. Supplement," Special Publication No. 18, The Chemical Society, London (1965).
13) G. C. Pimentel and A. L. McClellan, "The Hydrogen Bond," W. H. Freeman and Company, San Francisco and London (1960), p. 287.
14) Since estimated standard deviations for the coordinates of H(N52) were large, the geometrical position, H*(N52), was calculated assuming N–H distance to be 1.00 Å. The distance of O′(5)···H*(N52) is 2.22 Å and the angle of N(5)–H*(N52)···O′(5) is 136°.
15) D. L. McFadden and A. T. McPhail, *J. Chem. Soc., Dalton Trans.*, **1974**, 363.
16) Y. Ohashi, Y. Sasada, Y. Tashiro, Y. Ohgo, S. Takeuchi, and J. Yoshimura, *Bull. Chem. Soc. Jpn.*, **46**, 2589 (1973).

The Vibrational Spectra and Rotational Isomerism of Methylvinylsilane and Allylsilane[1)]

Keiichi OHNO, Keijiro TAGA, and Hiromu MURATA

Department of Chemistry, Faculty of Science, Hiroshima University, Higashisenda-machi, Hiroshima 730

(Received April 21, 1977)

The infrared and Raman spectra have been measured for methylvinylsilane, CH_2=$CHSiH_2(-D_2)CH_3$, and allylsilane, CH_2=$CHCH_2SiH_3(-D_3)$. The fundamental vibrations have been assigned, and the normal coordinate treatment for possible molecular forms has been carried out. For methylvinylsilane, the *cis* and *skew* forms coexist in the gaseous and liquid states, while only the former persists in the solid state. In the liquid state the *cis* form is more stable by 0.66±0.05 kcal/mol than the *skew* form. For allylsilane, the form near the *skew* form predominantly exists in the gaseous, liquid, and solid states.

The ultraviolet absorption maximum of allyltrimethylsilane appears at a wavelength longer than that of trimethylvinylsilane.[2)] Previously, the bathochromic effect of the allyl derivative has been commonly cited as evidence of (p-d)π bonding between the double bond and the silicon.[3)] Recently, however, this effect has been interpreted in terms of σ-π hyperconjugation[4,5)] between the double bond and the Si–C σ bond, whose magnitude may vary with the dihedral angle about the axis between the carbon atoms in the α- and β-positions in allylsilane.

In the present paper, we will, therefore, deal with the molecular vibrations of methylvinylsilane and allylsilane in relation to the rotational isomerism in order to obtain information on the stereospecific effect.

Experimental

The samples of methylvinylsilane, CH_2=$CHSiH_2(-D_2)$-CH_3, and allylsilane, CH_2=$CHCH_2SiH_3(-D_3)$, were prepared by the reduction of commercial products of dichloro(methyl)vinylsilane (K & K Co., U.S.A.) and allyltrichlorosilane (Aldrich Chem. Co., U.S.A.) with lithium aluminium hydride or deuteride in dibutyl ether[6)] and were purified by low-temperature bulb-to-bulb distillation in a vacuum. Their purities were checked by means of their nuclear magnetic resonance spectra; CH_2=$CHSiH_2CH_3$ NMR(CCl_4): δ 0.21 (t, 3H, J=4 Hz, Si**C**$\mathbf{H_3}$), 3.94 (dq. 2H, J=1 and 4 Hz, Si**H**$_2$), 5.5—6.5 (m, 3H, **C**$\mathbf{H_2}$=**C**$\mathbf{H}$), CH_2=$CHSiD_2CH_3$ NMR (CCl_4): δ 0.21 (s, 3H, Si**C**$\mathbf{H_3}$), 5.5—6.5 (m, 3H, **C**$\mathbf{H_2}$=**C**$\mathbf{H}$), CH_2=$CHCH_2SiH_3$ NMR(CCl_4): δ 1.69 (sex, 2H, J=4 Hz, **C**$\mathbf{H_2}$Si), 3.53 (t, 3H, J=4 Hz, Si**H**$_3$), 4.8—6.2 (m, 3H, **C**$\mathbf{H_2}$=**C**$\mathbf{H}$), CH_2=$CHCH_2SiD_3$ NMR(CCl_4): δ 1.69 (d, 2H, J=8 Hz, **C**$\mathbf{H_2}$Si), 4.8—6.2 (m, 3H, **C**$\mathbf{H_2}$=**C**$\mathbf{H}$).

The infrared and Raman spectra were recorded on a Perkin-Elmer instrument (Model 621) and a JEOL Raman Spectrometer (Model JRS-400D) with an argon-ion laser respectively. The infrared spectra in the gaseous state were measured using a 10-cm gas cell fitted with CsI windows. The infrared spectra in the liquid state at low temperatures were measured at about 150 K by condensing the gaseous samples on a CsI window cooled with liquid nitrogen. For the Raman spectra in the solid state, the sample in the ampoule was held on a copper block cooled with liquid nitrogen; the solid was obtained by the use of a long period of cooling.

Results

Normal Coordinate Treatment. The normal vibrations were calculated in order to determine the molecular forms and the assignments of the observed spectra to rotational isomers. The valence angles of the CH_2=CH group and the bond lengths used were transferred from those of vinylsilane,[7)] dimethylsilane,[8)] and 1-butene.[9)] The other valence angles were assumed to be tetrahedral, and the dihedral angles were 0° for the *cis* form and 120° for the *skew* form. The modified Urey-Bradley force field was used in the calculation. The force constants of the CH_2=CH group and those of the skeletal torsion were taken so as to predict well the observed frequencies of vinylsilane, CH_2=$CHSiH_3$

TABLE 1. FORCE CONSTANTS FOR METHYLVINYLSILANE AND ALLYLSILANE[a)]

Force const		Force const	
K(C-H), =CH_2	4.651	F(H·C·H), =CH_2	0.0
K(C-H), =CH	4.472	F(C=·C·H)	0.450
K(C-H), CH_3	4.403	F(C·C·H)	0.540
K(C-H), CH_2	4.230	F(Si·C·H)	0.271
K(Si-H), SiH_3	2.578	F(H·Si·H)	0.041
K(Si-H), SiH_2	2.544	F(C·Si·H)	0.149
K(C=C)	7.071	F(C=·C·C)	0.400
K(C-C)	2.800	F(C·C·Si)	0.276
K(C-Si), =C-Si	2.655	F(C·Si·C)	0.040
K(C-Si)	1.991	f(=CH o. p.)	0.252
H(H-C-H), =CH_2	0.360	f(=CH_2 wag.)	0.324
H(H-C-H), CH_3	0.349	Y(C=C)	0.601
H(H-C-H), CH_2	0.331	Y(C-C)	0.088
H(C=C-H)	0.212	Y(C-SiH_3)	0.067
H(C-C-H), =CH	0.123	Y(Si-CH_3)	0.039
H(C-C-H), CH_2	0.278	Y(Si-CH)	0.056
H(Si-C-H), =CH, CH_2	0.123	κ(CH_3)	0.014
H(Si-C-H), CH_3	0.102	κ(CH_2)	−0.040
H(H-Si-H)	0.180	κ(SiH_3)	0.076
H(C-Si-H), =CH	0.123	κ(SiH_2)	0.104
H(C-Si-H), CH_3	0.092	p(C-H), CH_3	−0.084
H(C-Si-H), CH_2	0.094	p(C-H), CH_2	−0.070
H(C=C-C)	0.320	t(C=CH, C=CH)	0.089
H(C=C-Si)	0.090	t(C=CH, C=CY)	0.141
H(C-C-Si)	0.118	t(CSiH_2, $SiCH_3$)	0.057[b)]
H(C-Si-C)	0.133	t(CSiC, $SiCH_3$)	0.030[b)]
F(H·C·H)	0.200	t(CCSi, $CSiH_3$)	0.053[b)]

a) The units of the force constants are mdyn/Å for stretching, K; bending, H; repulsion, F; bond interaction, p; and mdyn Å for out-of-plane bending, f; wagging, f; torsion, Y; intramolecular tension, κ, and *trans* coupling, t. b) The *gauche* coupling constants are assumed to be $g=-0.5\,t$.

TABLE 2. OBSERVED AND CALCULATED FREQUENCIES (cm^{-1}) OF METHYLVINYLSILANE-d_0[a)]

Infrared					Raman[b)]					Calcd		Assignment[c)]
Gas	Int.	Type	Liquid (≈150 K)	Int.	Liquid	Int.	ρ	Solid	Int.	C form	S form	
3064	m	AB(15)	3057	w	3057	vw	dp?	3054	vw	3052 A′	3052	$\nu_a(=CH_2)$
			3013	vvw								1592+1421
2977	m	AB(15)	2972	w	2981	vs	p	2977	vs	2984 A′	2984	$\nu(=CH)$
					2971 sh	vw	p	2974	vs	2964 A″	2964	$\nu_a(CH_3)$
										2964 A′	2964	$\nu_a(CH_3)$
			2951	vw	2953	s	p	2954	vvw	2953 A′	2953	$\nu_s(=CH_2)$
2927	vw							2947	vvw			
2916	vw		2911	vvw	2913	vvw		2907	vw	2900 A′	2900	$\nu_s(CH_3)$
2155	vs				2142	vvs	p	2141		2181 A″	2181	$\nu_a(SiH_2)$
2146	vvs		2138	vs				2133	vvs	2180 A′	2180	$\nu_s(SiH_2)$
								2127				
1920 b	vw		1915	vvw								950×2
1596	vw	AB(15)	1592	vw	1595	vs	p	1595	s	1603 A′	1601	$\nu(C=C)$, $s(=CH_2)$
			1421	vw	1426 sh	vw		1426	vw	1413 A′	1413	$\delta_a(CH_3)$
										1413 A″	1413	$\delta_a(CH_3)$
1408	m	AB(14)	1402	m	1406	m	p	1405	m	1383 A′	1382	$s(=CH_2)$
					1273	s	p	1273	m	1264 A′	1264	$\delta(=CH$ i. p.)
1258	m	AB(14)	1249	m	1255	w	p	1256	vw	1254 A′	1254	$\delta_s(CH_3)$
1012	m	AB(14)	1008	m	1014	vw		1012	vw	1014 A′	1013	$r(=CH_2)$, $\delta(=CH$ i. p.)
								1008	vw	1008 A″	1008	$t(=CH_2)$, $w(=CH_2)$
954	s	AB(20)	950	s	953	w	dp?	955	vs	959 A′	958	$s(SiH_2)$
951	vs		939	s	944 sh	w		942 sh	vw	952 A″	952	$w(=CH_2)$, $t(=CH_2)$
902	vvs	AB(14)	897 sh	vvs	898 b	vw	dp?	893	vw	884 A′	885	$w(SiH_2)$, $r_s(CH_3)$
			886	vvs								
								869 sh	vw			
			864	m	866	vw	dp	865	w	841 A″	840	$r_a(CH_3)$
756	s	AB(14)	751	s	753	w	p	753	m	768 A′	774	$r_s(CH_3)$, $w(SiH_2)$
								731	w			
728	s	C	725	m	726	w	dp?	729	w	721 A′	725	ν(Me-Si), ν(C-Si)
700 sh	w		702	w	700	vs	p	702	vs	704 A″	692	$t(SiH_2)$
629	w	AB(14)	633	w	632	vvs	p	640	vvs	655 A′	662	ν(C-Si), ν(Me-Si)
			527	vw	535 sh	vw		534	w	549 A″		$r(SiH_2)$, $\delta(=CH$ o. p.)
								527	w			
517 b	w		516	vw	522	vw	dp	—			527	$r(SiH_2)$, $\delta(=CH$ o. p.)
477 sh	vw		479	vvw	474	vw		—			499	$\delta(=CH$ o. p.), $r(SiH_2)$
			406	vvw	405	vvw	dp	411	w	462 A″		$\delta(=CH$ o. p.), $r(SiH_2)$
356	vvw	AB(15)	357	vw	357	vw		360	w	330 A′		δ(CCSi), δ(CSiC)
					297	w	p	—			279	δ(CCSi)
					205*	m		—			214	δ(CSiC)
					185	m		176	m	157 A′		δ(CSiC), δ(CCSi)
								145	vw	152 A″	145	τ(Si-Me)
					112*sh	w		118	vs	107 A″	92	τ(C-Si)
								90	m			lattice vibrations
								81	m			
								63	vs			
								57	vs			
								45	vs			
								25	vs			

a) Int.=intensity, s, m, w=strong, medium, weak, v=very, b=broad, sh=shoulder; AB, B, C=*ab*-, *b*-, *c*-type infrared band contours in the asymmetric top case (the values in parentheses indicate the P-R spacing); ρ=polarization, p, dp=polarized, depolarized; C, S=*cis*, *skew*; A′,A″=A′,A″ species of the C_s symmetry. b) Asterisks indicate the Raman lines observed at low temperatures (≈150 K). c) Assignments based on the potential-energy distributions greater than 20% are included; ν, *s*, *w*, *t*, *r*, δ, τ=stretching, scissoring, wagging, twisting, rocking, deformation, torsion, i.p.=in-plane, o.p.=out-of-plane, a, s=asymmetric, symmetric.

Table 3. Observed and calculated frequencies (cm^{-1}) of methylvinylsilane-d_2[a)]

Infrared					Raman[b)]					Calcd		Assignment[c)]
Gas	Int.	Type	Liquid (≈150 K)	Int.	Liquid	Int.	ρ	Solid	Int.	C form	S form	
3065	m	AB(13)	3056	w	3058	vw	dp?	3052	w	3052 A′	3052	$\nu_a(=CH_2)$
			3013	vw								1593+1413
2977	m	AB(13)			2979	m	p	2975	vs	2984 A′	2984	$\nu(=CH)$
			2969	w				2963 sh	m	2964 A″	2964	$\nu_a(CH_3)$
										2964 A′	2964	$\nu_a(CH_3)$
2928	vw		2949	w	2950	vw	p	2945	vw	2953 A′	2954	$\nu_s(=CH_2)$
2918	vw		2908	vw	2911	m	p	2904	s	2900 A′	2900	$\nu_s(CH_3)$
1916 b	vw		1915	vvw								955×2
			1593	w	1594	vs	p	1593	m	1603 A′	1602	$\nu(C=C)$, $s(=CH_2)$
1570	vvs		1562	vvs				1567 sh	s	1576 A″	1576	$\nu_a(SiD_2)$
1560	vvs		1552	vvs	1552	vvs	p	1558	vvs	1559 A′	1559	$\nu_s(SiD_2)$
			1543 sh	vvs	1545 sh	m		1548 sh	s			
1411	m		1413 sh	w	1414 sh	vw		1414 sh	w	1413 A′	1413	$\delta_a(CH_3)$
										1413 A″	1412	$\delta_a(CH_3)$
1404	m		1403	m	1404	w	p	1405	m	1383 A′	1382	$s(=CH_2)$
								1266 sh	w			
1264	m		1264 sh	vvw	1269	m	p	1262	m	1264 A′	1264	$\delta(=CH$ i. p.)
1255	m	AB(12)	1248	m	1253	w	p	1244	vw	1254 A′	1254	$\delta_s(CH_3)$
								1021	vvw	1013 A′	1012	$r(=CH_2)$, $\delta(=CH$ i. p.)
1009	m	C	1005	m	1008	vw	dp?	1008	w	1007 A″	1007	$t(=CH_2)$, $w(=CH_2)$
955	m	C	955	s	960	vvw	dp	961	w	952 A″	952	$w(=CH_2)$, $t(=CH_2)$
812	vvs	AB(12)	805	vvs	814	vvw	p	814	vvw	823 A′	823	$r_s(CH_3)$
										815 A″	815	$r_a(CH_3)$
741	vvs	AB(13)	746	s	745 sh	w		746	m	742 A′		ν(Me-Si), ν(C-Si)
			731	s	732	s	p	—			738	ν(Me-Si)
703 b	vs		689	vs	695	m	p	697	m	706 A′	709	$s(SiD_2)$
688 b	vs							689	m			
			645	w	647	vvs	p	—			648	ν(C-Si), $s(SiD_2)$
			635	vw	637	vs	p	636	vvs	637 A′		ν(C-Si), ν(Me-Si),
618 b	s											$s(SiD_2)$
607 b	s		609	s	617	w	p	610	vw	587 A′	599	$w(SiD_2)$
557 b	m		563	m	569	w		567	m	565 A″		$\delta(=CH$ o. p.), $t(SiD_2)$
			550	m	556	w		—			536	$\delta(=CH$ o. p.), $t(SiD_2)$
			455	vw	455	m	dp	—			482	$t(SiD_2)$, $\delta(=CH$ o. p.)
443 b	w		439	vw	442 sh	w		444	m	473 A″		$t(SiD_2)$, $\delta(=CH$ o. p.)
			413	vw	415*	w		—			412	$r(SiD_2)$
			361	vw				367	vw	386 A″		$r(SiD_2)$
355 b	vvw		347	vw	353	vw		344	m	327 A′		δ(CCSi), δ(CSiC)
					268	m		—			267	δ(CCSi)
					198*	s		—			212	δ(CSiC)
					186	s		189	m	157 A′		δ(CSiC), δ(CCSi)
										150 A″	144	τ(Me-Si)
					103*	w		129	m	104 A″	91	τ(C-Si)
								100	vs			lattice vibrations
								86	s			
								69	s			
								62	s			
								38	m			

a), b), and c): See Footnotes a), b), and c) of Table 2.

($-D_3$),[10] and those of methylvinylsilane and allylsilane respectively. The other force constants were transferred from those of alkylsilanes[11] and olefins.[12] The force constants used are listed in Table 1. The observed and calculated frequencies are summarized in Tables 2—5, together with the assignments based on the predominant potential-energy distributions. As a fair agreement was obtained between the observed and calculated frequencies, further adjustment was not attempted. The vibrational assignments based on the

Table 4. Observed and calculated frequencies (cm^{-1}) of allylsilane-d_0[a)]

Infrared					Raman[b)]					Calcd S form	Assignment[c)]
Gas	Int.	Type	Liquid (≈150 K)	Int.	Liquid	Int.	ρ	Solid	Int.		
3093	vw	AB(14)	3080	vw	3083	vw	dp?	3083	w	3053	$\nu_a(=CH_2)$
			3063	vw							1632+1418
			3036	vvw							1632+1392
3001	vw		2997	vw	3000	m	p	2998	m	3029	$\nu(=CH)$
2987	vw		2975	vw	2977	vw	p	2975	vw	2955	$\nu_s(=CH_2)$
2939	vw		2932	vw	2931	vw		2931	m	2946	$\nu_a(CH_2)$
2915	vw				2912 sh	vw		2907 sh	vw		
2902	vw		2896	vw	2897	m	p	2897	vs	2913	$\nu_s(CH_2)$
					2835	vvw		2839	vvw		1422×2
								2168		2174	$\nu_a(SiH_3)$
2167	vvs	AB(15)	2157	vs	2160	vvs	p	2156	vvs	2174	$\nu_a(SiH_3)$
								2148		2172	$\nu_s(SiH_3)$
1814	vvw	B (14)	1804	vvw							906×2
1636	w	AB(14)	1632	m	1632	vs	p	1631	s	1627	$\nu(C=C)$, $s(=CH_2)$
								1426 sh	vw		
1426	vw	AB(16)	1418	w	1422	w	p	1423	vw	1416	$s(CH_2)$
1397 sh	vw		1394	vw	1400	w	p	1401	w	1404	$s(=CH_2)$
								1301 sh	w		
1300	vvw	AB(16)	1295	vvw	1299	vs	p	1295	m	1303	$\delta(=CH$ i. p.)
1195	vw	AB(15)	1192	vw	1192	w		1196	w	1223	$t(CH_2)$
1163	w	AB(14)	1157	w	1161	vs	p	1159	vs	1175	$w(CH_2)$, $s(CH_2)$
1039	vw	AB(14)	1041	vw	1043	vw		1039	vw	1108	$r(=CH_2)$, $\nu(C-C)$
995 sh	vw		990	w	989 sh	vw	dp?	991	vw	999	$t(=CH_2)$
979 sh	w									968	$w(=CH_2)$
			942 sh	s	941	m	dp?	949	vs	949	$\delta_a(SiH_3)$
931 b	vvs		936 sh	s				935	m	949	$\delta_a(SiH_3)$
923 b	vvs		928	vs				928	m	917	$\delta_s(SiH_3)$
			909	vvs	904	vw	dp?	909	vw	906	$\nu(C-C)$, $r(=CH_2)$
								901	w		
834	m	AB(12)	829	s	829	vvw	dp?	828	vvw	769	$r(CH_2)$, $t(CH_2)$
772	vw							772 sh	vw		
767	vw		764	m	765	s	p	763	m	733	$\nu(C-Si)$
			597 sh	m	599	vs	p	602	vs	589	$r_s(SiH_3)$
589	m	AB(14)	588	s	590 sh	m	p	589	w	582	$r_a(SiH_3)$
527 b	vvw		524	vw	529	vw	dp?	530	w	521	$\delta(=CH$ o. p.)
407	vvw	AB(15)	407	vw	408	s	p	415	m	402	$\delta(CCC)$
					227	vw	dp?	237	vw	239	$\delta(CCSi)$
								228 sh	vvw		
										147	$\tau(C-SiH_3)$
					112*	w		137	m	112	$\tau(C-C)$
								98	s		lattice vibrations
								91	s		
								71	vs		
								58	vs		
								44	vs		
								37	vs		
								31	vs		

a), b), and c): See Footnotes a), b), and c) of Table 2.

relative intensities of the infrared bands and the Raman lines and the comparison with the spectra of analogous molecules[10,11,15)] are consistent with the results of the calculation, except for the assignments of the SiH_2 twisting and Me–Si stretching modes for methylvinylsilane-d_0 and those of the CH_2 wagging and twisting modes for allylsilane-d_0 and -d_3.

Rotational Isomerism. Figures 1 and 2 show the Raman spectra of methylvinylsilane-d_0 and allylsilane-d_0 in the region below 1700 cm^{-1}; the upper and lower spectra are for the liquid state at room temperature and for the solid state at about 100 K respectively. For 1-butene[9)] and methylvinylsilane,[13)] the stable conformations have been confirmed by means of the microwave spectra to be *cis* and *skew* about the C–C or C–Si axes adjacent to the double bond. For methylvinyl-

Table 5. Observed and calculated frequencies (cm^{-1}) of allylsilane-d_3[a)]

Infrared					Raman[b)]					Calcd	Assignment[c)]
Gas	Int.	Type	Liquid (≈150 K)	Int.	Liquid	Int.	ρ	Solid	Int.	S form	
3092	vw	AB(13)	3081	w	3084	vw	dp?	3077	w	3053	$\nu_a(=CH_2)$
			3064	vw							1632+1417
			3033	vvw							1632+1392
3003	vw		3005	vw	3003	m	p	3006	w	3029	$\nu(=CH)$
					2997 sh	w		2993 sh	vw		
2986	vw		2976	w	2978	vw	p	2975	vw	2955	$\nu_s(=CH_2)$
2935	vw		2936	vw	2932	vw	dp	2937	w	2946	$\nu_a(CH_2)$
2913	vw				2911 sh	vw		2910	vw		
2901	vw		2901	vw	2898	m	p	2900	m	2913	$\nu_s(CH_2)$
					2834	vvw		2833	vvw		
1811	vvw	B (13)	1810	vvw							900×2
1636	m	AB(14)	1632	m	1632	vvs	p	1631	vs	1627	$\nu(C=C)$, $s(=CH_2)$
1579	vvs	AB(13)	1574	vs	1574	s	dp?	1579 sh 1573 1568	m vs vs	1572 1572	$\nu_a(SiD_3)$ $\nu_a(SiD_3)$
1558	vvs	AB(14)	1551	vs	1554	vvs	p	1550	vvs	1545	$\nu_s(SiD_3)$
1425	vw	AB(15)	1417	w	1419	w		1422 sh 1417	vvw vw	1416	$s(CH_2)$
1403	vw	AB(12)	1392	w	1397	w		1399 sh 1395	vw w	1404	$s(=CH_2)$
					1310	vvw		1302	vw		
1300	vvw	AB(15)	1293	vvw	1300	vs	p	1298	s	1303	δ(=CH i. p.)
1194	vvw	AB(12)	1190	w	1191	vw	dp?	1196 sh 1191	vw w	1223	$t(CH_2)$
1167	w	AB(14)	1165	w	1167	s	p	1166	w		677+479, 750+404
			1151	w	1155 sh	m	p	1151	vs	1175	$w(CH_2)$, $s(CH_2)$
1036	vw	AB(13)	1037	w	1040	vvw	p	1039	vvw	1107	$r(=CH_2)$, ν(C-C)
990	vw	AB(11)	990	m	990	vw	dp?	994	vw	999	$t(=CH_2)$
930	w	AB(13)	928	w	926	w		929	vw	968	$w(=CH_2)$
906	s	B (10)	900	s	903	w	dp?	908	w	904	ν(C-C), $r(=CH_2)$
786 b	m		792	s	788 sh	vw	dp?	790	vw	764	$r(CH_2)$, $t(CH_2)$
755	m	AB(14)	752	s	750	vs	p	752	vs	744	ν(C-Si), $\delta_s(SiD_3)$
684	vs		677 sh	vs	678	m	dp?	687 680	w w	681	$\delta_a(SiD_3)$
679	vs		669	vvs				674 668	w w	680	$\delta_a(SiD_3)$
580	vvw	AB(12)	579	w	579	vs	p	583	s	657	$\delta_s(SiD_3)$
					493 sh	vw		494	vvw	523	δ(=CH o. p.)
482 b	vvw		479	m	478	vw	dp?	483 479 sh	w w	454	$r_s(SiD_3)$
422	vvw	AB(12)	416	w	416 sh	vw	dp?	422	vw	445	$r_a(SiD_3)$
410	vvw		405 sh	vw	403	s	p	410	s	393	δ(CCC)
					213	vw	dp?	233 225 sh	vvw vw	227	δ(CCSi)
										112	τ(C-SiD_3), τ(C-C)
					100*	w		124	m	108	τ(C-C), τ(C-SiD_3)
								114 sh	w		lattice vibrations
								87	m		
								82 sh	m		
								75 sh	m		
								55	vs		
								40	m		
								30	s		

a), b), and c): See Footnotes a), b), and c) of Table 2.

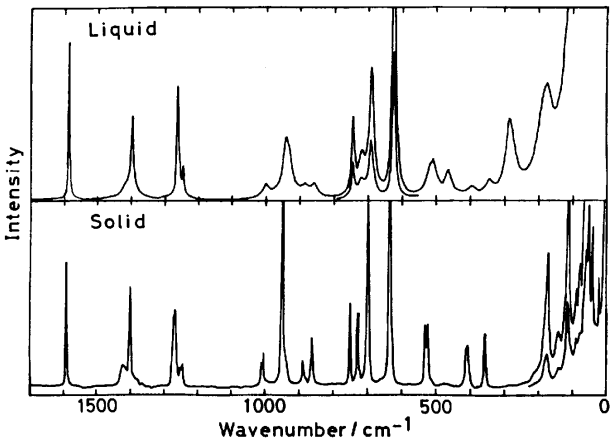

Fig. 1. Raman spectra of methylvinylsilane-d_0.

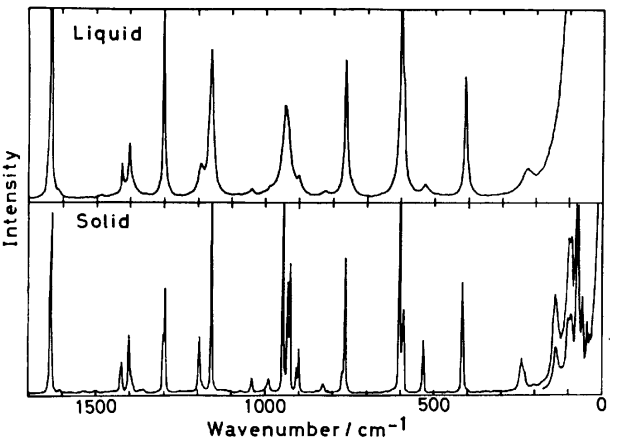

Fig. 2. Raman spectra of allylsilane-d_0.

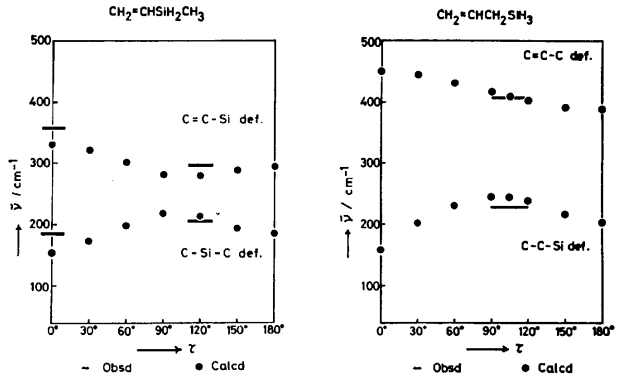

Fig. 3. Dependence of skeletal deformation frequencies on dihedral angle for methylvinylsilane-d_0 and allylsilane-d_0.

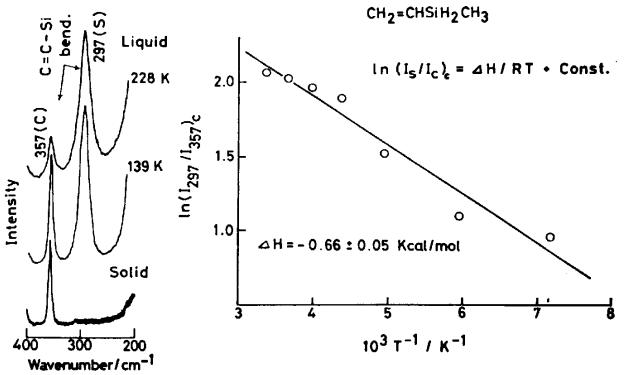

Fig. 4. Raman spectra of methylvinylsilane-d_0 in the 200—400 cm^{-1} region and a plot of $\ln(I_{297}/I_{357})_c$ *vs.* $1/T$.

silane, several Raman lines observed in the liquid state vanish in the solid state, but for allylsilane all the Raman lines observed in the liquid state remain in the solid state. On the other hand, all the vibrational frequencies observed in the solid state for methylvinylsilane and allylsilane are assigned to the fundamental vibrations of one isomer, as Tables 2—5 show. In the 150—450 cm^{-1} region for both the molecules, two skeletal deformation and one torsional vibrations are expected for one isomer; the CH_3 and SiH_3 torsional vibrations may, in general, be very weak in the Raman scattering. For methylvinylsilane-d_0, four Raman lines —at 357, 297, 205, and 185 cm^{-1}—are observed in the liquid state, and two of them remain in the solid state, indicating that two isomers coexist in the liquid state and that one of them persists in the solid state. For allylsilane-d_0, two Raman lines—at 408 and 227 cm^{-1}—are observed in both the liquid and solid states, indicating the existence of only one isomer in both the liquid and solid states. The same results are obtained from methylvinylsilane-d_2 and allylsilane-d_3.

In order to determine the molecular forms, the normal coordinate treatment was carried out for seven possible molecular forms of methylvinylsilane-d_0 and allylsilane-d_0. Figure 3 shows the observed and calculated frequencies of the skeletal deformations. The calculations indicate that, for methylvinylsilane-d_0, *cis* and *skew* forms coexist in the liquid state, while only the *cis* form persists in the solid state, and that for allylsilane-d_0 only the molecular form near the *skew* form exists in both the liquid and solid states.

Enthalpy Difference of the Isomers in Methylvinylsilane. The relative intensities of the Raman lines at 297 and 357 cm^{-1} assigned to the C=C–Si deformation vibrations for the *skew* and *cis* forms of methylvinylsilane-d_0 respectively were measured in the liquid state at temperatures ranging from 297 to 139 K. In the solid state the band at 297 cm^{-1} disappears, but that at 357 cm^{-1} persists. Figure 4 shows some typical examples at 228 and 139 K among seven different temperatures and a plot of $\ln(I_s/I_c)[(1-e^{-h\nu_s/kT})/(1-e^{-h\nu_c/kT})]$ against $1/T$. From the slope of the straight line, the value of the enthalpy difference, $\Delta H(H_{skew}-H_{cis})=0.66\pm0.05$ kcal/mol, is obtained.

Discussion

For allylsilane, the form near the *skew* form is determined on the basis of the normal coordinate treatment to exist predominantly in the liquid and solid states. This result is also supported by the infrared spectra in the gaseous state; no *c*-type bands for the *cis* form were observed, and all the bands were assigned to the fundamental vibrations of only one isomer. On the other hand, for methylvinylsilane, the *cis* and *skew* forms are confirmed to coexist in the gaseous and liquid states; the *cis* form is more stable than the *skew* form by 0.66

±0.05 kcal/mol in the liquid state. For 1-butene, the *skew* form has been reported to be more stable than the *cis* form by only 150±150 cal/mol (from the analysis of microwave spectra[9]) and by −100±50 cal/mol (from the NMR spectra[14]). For allyl halides (X= Cl, Br, I), the *cis* and *skew* forms have been confirmed to coexist in the liquid state, although a larger steric repulsion between the CH_2=CH group and halogen is to be expected.[15]

Recently, Weidner and Schweig have demonstrated, from the photoelectron spectra and CNDO/2 calculations, the importance of σ-π hyperconjugation in trimethylvinylsilane and allyltrimethylsilane.[5] CNDO/2 model calculations have indicated that allyltrimethylsilane has a conformation near the *skew* form as a result of the σ-π hyperconjugation between the Si–C σ bond and the double bond. Thus, the present result on allylsilane is consistent with the conformation of allyltrimethylsilane. Therefore, the form near the *skew* of allylsilane may have a dihedral angle between the 120° of the ordinary *skew* form and the 90° of the maximal σ-π interaction. Actually, Hayashi *et al.* have, from the microwave spectra, reported an estimated dihedral angle of 103°40′ for allylsilane.[16]

The authors wish to express their thanks to Dr. Hiroatsu Matsuura for his valuable discussion.

References

1) Presented in a part at the 34th National Meeting of the Chemical Society of Japan, Tokyo, April 1976.
2) J. Nagy and J. Réffy, *J. Organomet. Chem.*, **22**, 565; *ibid.*, **23**, 79 (1970).
3) For example, E. A. V. Ebsworth, "Organometallic Compounds of the Group IV Elements," ed by A. G. MacDiarmid, Dekker, New York (1968).
4) C. Eaborn, *J. Chem. Soc.*, **1954**, 939; *ibid.*, **1956**, 4858; T. G. Traylor, W. Hanstein, H. J. Berwin, N. A. Clinton, and R. S. Brown, *J. Am. Chem. Soc.*, **93**, 5175 (1971); C. G. Pitt, *J. Organomet. Chem.*, **23**, C35 (1970); M. Kira and H. Sakurai, *Kagaku No Ryoiki*, **29**, 121 (1975).
5) U. Weidner and A. Schweig, *Angew. Chem. Int. Ed. Engl.*, **11**, 146 (1972).
6) M. Kumada, M. Ishikawa, and S. Maeda, *J. Organomet. Chem.*, **2**, 478 (1964).
7) J. M. O'Reilly and L. Pierce, *J. Chem. Phys.*, **34**, 1176 (1961).
8) L. Pierce, *J. Chem. Phys.*, **34**, 498 (1961).
9) S. Kondo, E. Hirota, and Y. Morino, *J. Mol. Spectrosc.*, **28**, 471 (1968).
10) S. G. Frankiss, *Spectrochim. Acta*, **22**, 295 (1966).
11) K. Ohno, M. Hayashi, and H. Murata, *J. Sci. Hiroshima Univ., Ser. A*, **36**, 121 (1972).
12) T. Shimanouchi, Y. Abe, and Y. Alaki, *Polymer J.*, **2**, 199 (1971).
13) M. Hayashi and M. Imachi, *Chem. Lett.*, **1976**, 121.
14) P. B. Woller and E. W. Garrbisch, Jr., *J. Org. Chem.*, **37**, 4281 (1972).
15) R. D. McLachlan and R. A. Nyquist, *Spectrochim. Acta*, **24A**, 103 (1968).
16) M. Hayashi, M. Imachi, and M. Saito, *Chem. Lett.*, **1977**, 221.

The Interaction of Acridine Orange with Poly(*S*-carboxymethyl-L-cysteine)

Toyoko IMAE and Shoichi IKEDA

Department of Chemistry, Faculty of Science, Nagoya University, Chikusa, Nagoya 464

(Received April 25, 1977)

The interaction of Acridine Orange with poly(*S*-carboxymethyl-L-cysteine) has been investigated by observing the solubility behavior, absorption spectra, and circular dichroism of the mixture. When the dye is added to aqueous solution of the polymer, the mixture is homogeneous at higher pH, but precipitation takes place at lower pH; the threshold pH ranges from 3.5 to 6, depending on the mixing ratio. For [P]/[D] 1 or less, the mixture is again homogeneous at very low pH between 4 and 2, when no salt is added. Various type of circular dichroism are induced for the homogeneous solutions, which are characteristic of the bound dye species on the polymer and the structure of dye-polymer complex. The binding of dye with the polymer is mainly caused by electrostatic effect, and the solubility of the mixture is interpreted by considering the ionization of polymer and the binding of dye to the polymer.

The visible absorption spectra of Acridine Orange in water are characterized by two absorption bands at 492 and 470 nm, which are ascribed to the monomer and dimer, respectively, of the dye.[1] The relative abundance of the two forms of the dye depends on its concentration. A structure of antiparallel stacked type has been proposed and accepted[2,3] for the dimeric dye molecule. In highly concentrated dye solutions, higher aggregates of dye are formed, the absorption band shifting down to around 450 nm.

When Acridine Orange is mixed with poly(*S*-carboxymethyl-L-cysteine), its absorption spectra change remarkably from those of free dye in the position and intensity of visible band.[4,5] The peak position indicates the state of aggregation of dye molecules in solution, while the hypochromism suggests the binding of dye to the polymer.

It has also been found that the circular dichroism (CD) is induced on Acridine Orange at its absorption bands in the presence of poly(*S*-carboxymethyl-L-cysteine).[4,5] The induced CD spectra observed at various [P]/[D] (mole of polymer residue/mole of added dye) mixing ratios and pH can be classified into fundamental types or their combinations. The fundamental types are characterized with reference to the bound species of dye molecules on the polymer and the conformation of the polypeptide chain. The latter is deduced from the CD spectra associated with the electronic transitions of peptide groups.

The CD spectrum of Type I was induced on aggregates of dimeric dyes bound to the polymer in the β-conformation.[4,6] Type II CD spectrum was induced on a dissymmetric array of dimeric dyes bound to the randomly coiled polymer at low ionization.[5,7] The CD of Type III was characteristic of low [P]/[D] ratios and was induced on another kind of array of dimeric dyes bound to the randomly coiled polymer at high ionization. Other types of CD, Types II′ and III′, originate from bound monomeric dyes and are considered to be counterparts of Types II and III, respectively.

The experiments so far reported[4,5] were performed on solutions of weakly acidic or higher pH, since the dye–polymer mixture precipitated at lower pH. It was found that the mixture was again homogeneous at very low pH region and for low [P]/[D]. The present work concerns with the interaction of Acridine Orange with poly(*S*-carboxymethyl-L-cysteine), as revealed in the solubility behavior and circular dichroism.

Experimental

Poly(*S*-carboxymethyl-L-cysteine) (code E602) was the same sample as that previously used.[8] Low-molecular-weight poly(*S*-carboxymethyl-L-cysteine) (code E515) was also used for comparison.[8] Acridine Orange was purified from commercial zinc salt and obtained as a hydrochloride salt.[1,4]

The stock solution of dye was added to aqueous solution of polymer. The pH was then adjusted by HCl or NaOH, followed by dilution to the desired dye concentration. For the preparation of solutions at a desired ionic strength, NaCl was added to the stock solution of polymer. The mixed solutions were kept overnight before measurements.

The pH was measured with a Hitachi-Horiba F5-X pH Meter. Absorption spectra were recorded with a 5 mm quartz cell on a Hitachi 323 Recording Spectrophotometer. The CD measurements were performed by using a 10 mm cell on a Jasco J-20 Circular Dichrometer, which was calibrated by use of aqueous solution of *d*-10-camphor sulfonic acid.[9] Measurements were carried out at room temperature.

The molar extinction coefficient, ε_D, and the molar ellipticity, $[\theta_D]$, are expressed on the basis of the total molar concentration of added dye.

Results

Solubility and Phase Separation of Dye–Polymer Mixture. Figure 1 shows the pH region for various [P]/[D] values, indicating where the mixed solution of Acridine Orange and poly(*S*-carboxymethyl-L-cysteine) is homogeneous and where precipitation takes place. A red precipitate is formed when the polymer concentration is high, and a fine gel separates when the polymer concentration is low.

The pH region where the mixture is soluble changes with the [P]/[D] ratio; as [P]/[D] decreases, the pH of phase separation becomes higher. The mixture is soluble above pH 5.8, when [P]/[D] is 0.9. At [P]/[D] lower than 0.9, the pH of phase separation is lowered. When solutions of different concentrations are compared at a given [P]/[D], it is found that the more concentrated mixture precipitates at slightly higher pH.

When [P]/[D] is 1 or less, homogeneous solutions appear at pH between 4 and 2. The upper and lower pH of homogeneous solutions change parallel to the pH

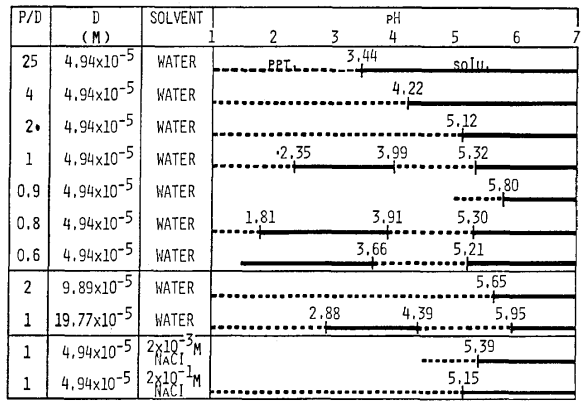

Fig. 1. Solubility of Acridine Orange–poly(*S*-carboxymethyl-L-cysteine) mixture in water and in aqueous NaCl solutions. ——, Solutions; ----, precipitation.

of phase separation around pH 5.5. In the solution of the lowest [P]/[D], 0.6, precipitation does not take place even at pH 1.80. Redissolution occurs for [P]/[D] 1, even when the dye concentration and consequently the polymer concentration are increased by four times. Addition of 0.2 M NaCl prevents the mixture of [P]/[D] 1 from becoming homogeneous in the pH region 4—2, and yields extremely fine gels in this region.

Dye–Polymer Mixture at Higher pH Region. In a higher pH region where no phase separation occurs, the dye molecules on the complex for high [P]/[D] generally form dimers or higher aggregates, while those for low [P]/[D] exist as monomers. The blue shift of the main visible absorption band down to 450 nm occurs for solutions of [P]/[D] higher than 1, suggesting the formation of highly aggregated dye. In the solutions of [P]/[D] 1 and 0.9, the dye molecule is in different states, depending on the pH. For [P]/[D] 0.8 and 0.6, the absorption band of monomeric dye is always dominant. The observed molar extinction coefficient of the main absorption band of dye in the visible region shows hypochromism, which implies extensive binding of dye to the polymer.

The induced CD spectra drastically vary with pH and [P]/[D]. Table 1 gives the wavelength of CD bands belonging to different types of CD. For [P]/[D] higher than 4, the CD of Type I is induced at acidic pH.[4] A strong positive band is located at 466 nm, and a weak negative one at 433 nm. The CD of Type II, which is observed for solutions of [P]/[D] 2 or 1 at pH 6.8 or 5.8, consists of paired bands with a strong negative band at 472 nm and a weak positive band at 415 nm, and of an additional broad positive band around 560 nm. The CD is also induced even at the neutral or alkaline pH when [P]/[D] is lower than 4. It is characterized by three bands, having opposite signs to those of Type II. This type of CD has been called Type III. The other type of CD, Type III′, occurs for solutions of [P]/[D] 0.9—0.6 at acidic pH. A positive band is manifest at 545 nm, and a negative one at 421 nm. Some of the spectral characteristics of the dye–polymer mixtures have already been reported.[5] The pH and [P]/[D] values for the induction of CD of various types are given in Table 2.

Table 1. Wavelength, sign, and magnitude of CD of various types[a]

I	II	III	II′	III′
	560+w	557−w	533−s	545+s
			492−sh	500+sh
466+s	472−s	470+s	465+sh	473−sh
433−m	415+w	422−w	427+m	421−m
	382−w	373+w		
	342+w	343−w	320−m	326+m
	293−sh	294+sh	294+sh	298−sh
269+s	275−s	277+s	273+m	278−m
252−m	251+m	253−m	259+m	250−m
	221+m	222−m	229+m	224−m
			213−m	208+m

a) Wavelength is given in nm. Magnitude is classified into strong (s), medium (m), weak (w), and shoulder (sh).

Dye–Polymer Mixture at Very Low pH Region. The mixtures of [P]/[D] 1 or less are homogeneous at pH 4—2, when no salt is added. However, thier absorption spectra appreciably change from those of the solutions mentioned above. As illustrated in Figs. 2 and 3, the absorption spectra for [P]/[D] 1, 0.8, and 0.6 have two peaks at 492 and 470 nm, and their extinction coefficients differ slightly from those for the free dye at the same concentration.[1,4] This suggests that only a few dye molecules are bound to the polymer.

In this region, the CD behavior is even more complicated. As shown in Fig. 2, the CD for [P]/[D] 1 belongs to Type II at the most acidic pH. Upon raising pH, the three CD bands in the visible region change their signs, while the ultraviolet bands keep them unchanged. However, the solutions of [P]/[D] 0.8 and 0.6 exhibit the CD of Type III′, which has a strong positive band at 541 nm, as seen in Fig. 3. Although the apparent CD is weak in this region, the actual molar ellipticity might be stronger than that shown, if correction is made for the amount of bound dye.

The absorption band of Acridine Orange at 470 nm becomes stronger when the dye concentration increases.[1] Its molar extinction coefficients are slightly influenced by the presence of the polymer for [P]/[D] 1 in very low pH region, which indicates very low binding of dye to the polymer. The CD spectra belong to Type II.

Dye–Low-molecular-weight Polymer Mixture. The low-molecular-weight polymer (E515) has a disordered conformation for all the pH in both absence[8] and presence[5] of Acridine Orange, and it interacts with the dye in a different way from the high-molecular-weight polymer. The induced CD spectra observed in the presence of the dye differ from each other, although the absorption spectra in the visible region are quite similar.

Absorption spectra indicate aggregation of dye in the solution of [P]/[D] 2 and more, as seen in Table 2. In the mixture of [P]/[D] 1, the species of dye changes at both sides of pH 5.4, while for [P]/[D] 0.8 the monomeric dye is dominantly present at all the pH examined. The hypochromism suggests the extensive binding of

Table 2. The pH region for the induction of CD of various types

Polymer code	[P]/[D]	Absorption maximum		Type of CD				
		492 nm	470—450 nm	I	II′	II	III′	III
E602	25		4.0—11	4.0—6.7				
	2		5.8—11			6.8		6.9—10.0
	1	5.5—5.8	5.8—11			5.8		6.1— 9.9
	0.9	5.9—6.4	6.9—11				6.1—6.4	6.9— 9.9
	0.8	5.8—11					5.8—6.6	7.4— 9.9
E515	25		4.0—11			5.6—6.0		
	2		5.1—11			5.1—5.8		
	0.8	4.6—11			4.6—5.2			

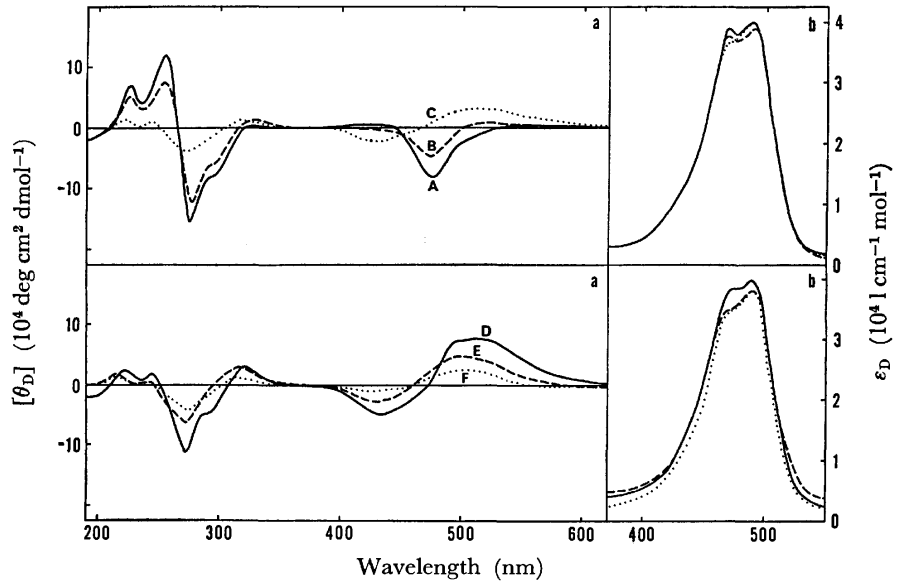

Fig. 2. Circular dichroism (a) and absorption spectra (b) of Acridine Orange-poly(*S*-carboxymethyl-L-cysteine) mixture of [P]/[D] 1 in water at very low pH region. [D]=4.94×10^{-5} M. A, pH 2.57; B, pH 2.68; C, pH 2.75; D, pH 2.91; E, pH 3.39; F, pH 3.81.

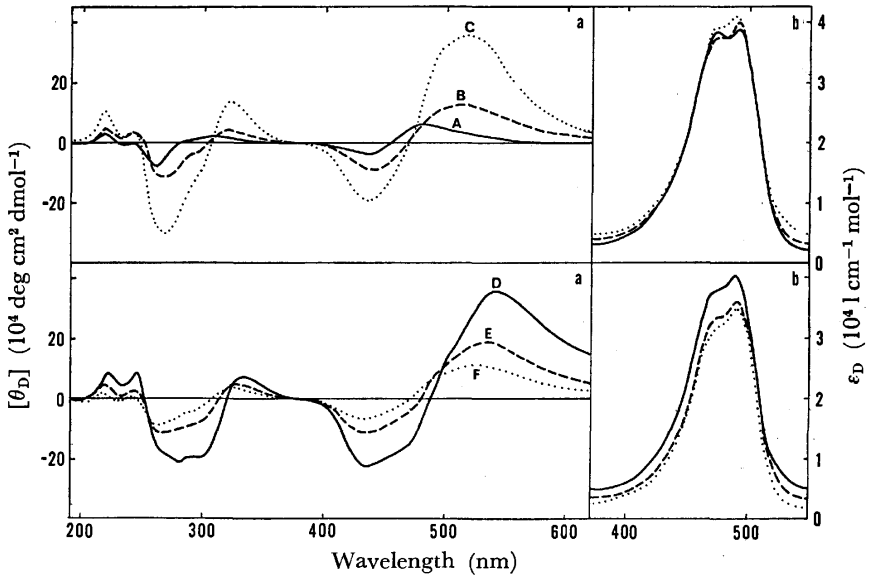

Fig. 3. Circular dichroism (a) and absorption spectra (b) of Acridine Orange-poly(*S*-carboxymethyl-L-cysteine) mixture of [P]/[D] 0.8 in water at very low pH region. [D]=4.94×10^{-5} M. A, pH 2.14; B, pH 2.44; C, pH 3.09; D, pH 3.46; E, pH 3.61; F, pH 3.71.

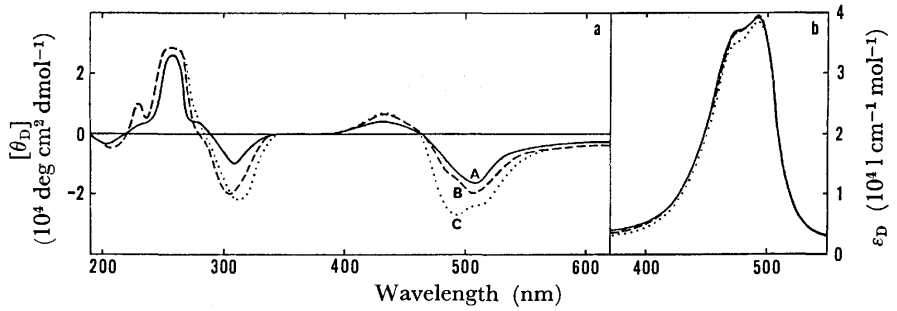

Fig. 4. Circular dichroism (a) and absorption spectra (b) of Acridine Orange-low-molecular-weight poly(*S*-carboxymethyl-L-cysteine) mixture of [P]/[D] 0.8 in water at very low pH region. [D]=4.94×10^{-5} M. A, pH 2.49; B, pH 3.13; C, pH 3.45.

dye to the polymer.

The CD is induced only at pH lower than about 6 for all the [P]/[D] values. The CD of the complexes formed at [P]/[D] higher than 1 belongs to Type II. The observed CD spectrum for [P]/[D] 0.8 consists of a positive band at 427 nm and a negative one at 533 nm, and it has been called Type II′, as shown in Table 1.

The low-molecular-weight polymer (E515) yields precipitates at pH 3.51, 4.98, 4.80, and 4.36 for [P]/[D] 25, 2, 1, and 0.8, respectively. At very low pH, 2.0—3.7, the mixture of [P]/[D] 0.8 is soluble again and exhibits the CD of Type II′ combined with Type II, as shown in Fig. 4. Since the absorption spectra in this region are very similar to those of free dye, indicating very few bound dye on the polymer, the observed CD has to be corrected for the amount of bound dye.

Discussion

Free Acridine Orange in water is dominantly in monomeric form at a concentration of 5×10^{-5} M, while it aggregates at high ionic strengths.[1,4] In the dye–polymer mixtures of low [P]/[D], monomeric form of dye is dominant over all the pH region. On the other hand, for higher [P]/[D], dimeric or higher aggregates of dye are formed on the polymer, since ionized carboxyl groups of the polymer and counter ions behave as the ionic atmosphere surrounding the dye molecules, making the dye molecules stack together.

The binding of dye to the polymer occurs primarily electrostatically, and a nitrogen atom of the cationic dye would be close to an ionized carboxyl group of the polymer, irrespective of whether the dye is monomeric or dimeric. In the absence of dye, the pH for the phase separation of polymer solution is lowered with decrease in concentration. For high [P]/[D], where the binding of dye is relatively low, the solubility of the polymer would not be influenced by such a binding. Thus the complex precipitates at low pH where the polymer is only slightly ionized. However, for [P]/[D] as low as 2, the phase separation occurs at pH as high as 5. When the divalent cationic dimer of Acridine Orange[1,2,10] binds to an ionized carboxyl group of the polymer, the charge on the carboxyl group turns from negative to positive. Thus the phase separation observed around pH 5 can be interpreted as the isoelectric precipitation of ampholytic complex. For [P]/[D] lower than 2, the dye is mainly in monomeric form at low pH. When the monomeric dyes are bound to the polymer, the complex becomes electrically neutral at a certain pH and precipitates.

When greater amounts of cationic dyes are added to the polymer, or when [P]/[D] is lowered further, the pH of phase separation should be higher. However, the pH decreases for [P]/[D] less than 0.9. This could be caused by the decrease in concentration of the polymer. In the same way, more concentrated mixture for [P]/[D] 1 precipitates at slightly higher pH (Fig. 1), reflecting the solubility of the polymer itself.[8]

For the complexes of [P]/[D] 1 or less formed at low pH 4—2, the amount of bound dye is very small, since ionization of carboxyl groups is low and the cationic dye does not bind to uncharged carboxyl groups. However, the net charge of the complex would be positive and the complex becomes soluble. In this complex the polymer chain would be a random coil owing to the electric repulsion between attached positive charges. Thus it is unlikely that the observed CD is of Type I as observed for the β-conformation. The observed CD was either of Type II or Type III′. At very low pH around 2.5, the ionization of the polymer is too low to be soluble in solution.

The same discussion on the solubility behavior of the dye–polymer mixture would apply to that of the dye–low-molecular-weight polymer mixtures, and also to the dye–poly(L-glutamic acid) mixtures.[11]

References

1) V. Zanker, *Z. Phys. Chem.*, **199**, 225 (1952).
2) T. Kurcusev and U. P. Strauss, *J. Am. Chem. Soc.*, **74**, 3081 (1970).
3) R. E. Ballard and C. H. Park, *J. Chem. Soc., A*, **1970**, 1340.
4) S. Ikeda and T. Imae, *Biopolymers*, **10**, 1743 (1971).
5) T. Imae and S. Ikeda, *Biopolymers*, **14**, 1213 (1975).
6) S. Ikeda and T. Imae, *Polymer J.*, **4**, 301 (1973).
7) T. Imae, *Polymer J.*, **9**, No. 6 (1977) in press.
8) S. Ikeda, *Biopolymers*, **5**, 359 (1967).
9) J. Y. Cassim and J. T. Yang, *Biochemistry*, **8**, 1947 (1969).
10) M. E. Lamm and D. M. Neville, *J. Phys. Chem.*, **69**, 3872 (1965).
11) T. Imae and S. Ikeda, *Biopolymers*, **15**, 1655 (1976).

Electronic States of the Crystals of TCNE Complexes with Hexamethylbenzene, Acenaphthene, and Dibenzofuran

Masashi TANAKA

Department of Chemistry, Faculty of Science, Nagoya University, Chikusa, Nagoya 464

(Received May 2, 1977)

The polarized reflection spectra were measured on crystals of tetracyanoethylene and its charge-transfer complexes, and the absolute intensity of the absorption parallel to the crystalline axes has been obtained by the Kramers-Kronig transformation. The charge-transfer degree and the stabilization energy in the ground state were estimated for each complex by analyzing the charge-transfer bands in the crystalline state. In the TCNE–hexamethylbenzene(HMB), acenaphthene, and dibenzofuran complexes, the charge-transfer degrees are 9.05, 12.3, and 4.95% respectively in the ground state.

Tetracyanoethylene, TCNE, is a strong electron acceptor. The formation of charge-transfer complexes with a variety of aromatics in dichloromethane solutions has been studied by Merrifield and Phillips.[1] These complexes are characterized by an intense electronic absorption in the visible or near-ultraviolet region that can be attributed to neither component of the complex alone, but to a new molecular species, the complex itself. Mulliken[2] has developed a theory of the intermolecular charge-transfer (CT) interaction which has been applied successfully to the interpretation of the absorption bands characteristic of molecular complexes. Aihara, Tsuda, and Inokuchi[3] examined the gas-phase spectra of these CT complexes and discussed how an increase in solvent polarity results in a shift of the CT band to a higher-energy region.

The infrared spectra of the complexes showed new bands which appeared on the complex formation,[4,5,16] and the resonance-enhanced Raman band was concluded to be due to the direct participation of the lowest CT state of the complex in the intermediate states of Raman scattering.[6–9]

Some of the molecular complexes of tetracyanoethylene can be obtained as crystalline solids, which often exhibit characteristic absorption bands analogous to the CT bands of the molecular complexes in solution. Kuroda *et al.*[10,11] revealed the presence of marked dichroism in these characteristic bands; the absorption is stronger as the light is polarized parallel to the alternate stack of donor and acceptor molecules, in agreement with the theoretical prediction for a CT transition. Furthermore, the CT interaction between donor and acceptor molecules has been applied to the interpretation of the mechanism of the electrical condition in these crystals of TCNE complexes.[12]

However, no study has been reported hitherto on the correlation of the electronic states of these complexes with the absolute absorption intensity of the CT band. In the present paper, the author shows the crystal absorption spectra obtained by the K-K transformation of the reflection spectra of TCNE complexes with HMB, acenaphthene, and dibenzofuran and gives information about the electronic states of the complexes.

Experimental

The single crystals of TCNE complexes with HMB, acenaphthene, and dibenzofuran were grown by sublimation in bottles. These crystals have the crystal habits shown in

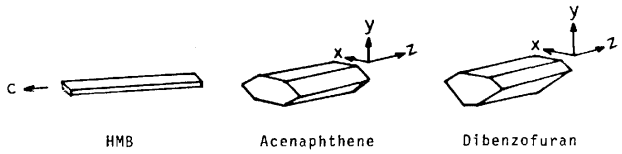

Fig. 1. The crystal habits of TCNE–HMB, acenaphthene, and dibenzofuran.

Fig. 1.

The reflection spectra at the normal incidence have been measured over the range of 10000—40000 cm^{-1} with a reflection spectrophotometer made in our laboratory, while the absorption spectra have been obtained by the Kramers-Kronig transformation. The oscillator strength along the α axis of the crystal may be evaluated by using the following equation:

$$f^{\alpha} = 4.32\times10^{-9}\int n_{\alpha}(\sigma)\varepsilon_{\alpha}(\sigma)\mathrm{d}\sigma,$$

where the integration is calculated over the whole band, σ is the wave number, and n_{α} and ε_{α} are the α components of the refractive index and the molar extinction coefficient. The oscillator strenghts for the three orthogonal axes in the crystal should be compared with that in solution:

$$f^{x} + f^{y} + f^{z} = 3f^{\mathrm{solution}}.$$

Theoretical

The basic theory of the CT complex was given by Mulliken[2]; and the energy diagrams are shown in Fig. 2.

In the AD type, the ground state is partly ionic and

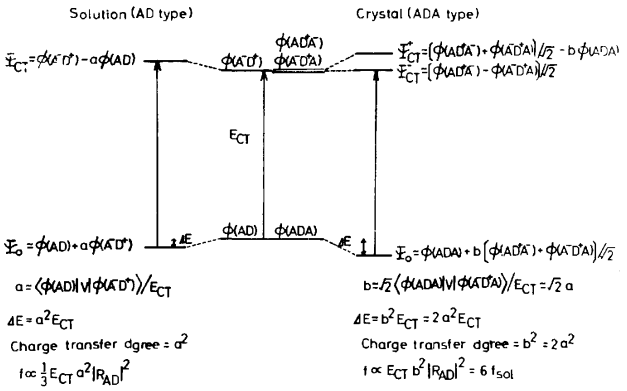

Fig. 2. The energy diagrams of the charge-transfer complexes.

may be described by a wavefunction

$$\Psi_0 \simeq \phi(\mathrm{AD}) + \sum_i a_i\phi_i(\mathrm{A^-D^+}) ,$$

where $\phi(\mathrm{AD})$ represents a non-bonding, and $\phi_i(\mathrm{A^-D^+})$ the i-th CT wavefunction involving the transfer of an electron from D to A. Then, the charge-transfer degree and the stabilization energy are given as $\sum_i a_i^2$ and $\Delta E=\sum_i a_i^2 E_{\mathrm{CT}}{}^i$. For the i-th charge-transfer excited state, we can write the wavefunction, $\Psi_{\mathrm{CT}}{}^i$ given by

$$\Psi_{\mathrm{CT}}{}^i \simeq \phi_i(\mathrm{A^-D^+}) - a_i\phi(\mathrm{AD}).$$

This is responsible for the characteristic color of the complex and the oscillator strengths in the solution and crystal are given as follows:

$$f_i(\mathrm{AD})^{\mathrm{solution}} = 1.085\times10^{11}E_{\mathrm{CT}}{}^i a_i^2|R_{\mathrm{AD}}|^2 ,$$

$$f_i(\mathrm{AD})^{\mathrm{crystal}} = 3f_i(\mathrm{AD})^{\mathrm{solution}} ,$$

where R_{AD} is the vector between the acceptor and donor molecules in the unit of cm and $E_{\mathrm{CT}}{}^i$ the excitation energy in $\mathrm{cm^{-1}}$.

In the ADA type, the ground state can also be described by a wavefunction

$$\Psi_0 \simeq \phi(\mathrm{ADA}) + \sum_i b_i\{\phi_i(\mathrm{AD^+A^-}) + \phi_i(\mathrm{A^-D^+A})\}/\sqrt{2} ,$$

where $\phi(\mathrm{ADA})$ represents a non-bonding, and $\phi_i(\mathrm{AD^+A^-})$ and $\phi_i(\mathrm{A^-D^+A})$ the i-th CT wavefunctions. Then, the charge-transfer degree and the stabilization energy in the ground state are given as $\sum_i b_i^2$ and $\Delta E=\sum_i b_i^2 \cdot E_{\mathrm{CT}}{}^i$. Therefore, it should be noted that they are twice as much as those in the AD type. The wavefunction, $\Psi_{\mathrm{CT}}{}^i(-)$, for the optically allowed i-th excited state is given by

$$\Psi_{\mathrm{CT}}{}^i(-) \simeq \{\phi_i(\mathrm{AD^+A^-}) - \phi_i(\mathrm{A^-D^+A})\}/\sqrt{2} ,$$

and the oscillator strengths in the solution and crystal are as follows:

$$f_i(\mathrm{ADA})^{\mathrm{solution}} = 1.085\times10^{11}E_{\mathrm{CT}}{}^i b_i^2|R_{\mathrm{AD}}|^2,$$

$$f_i(\mathrm{ADA})^{\mathrm{crystal}} = 3f_i(\mathrm{ADA})^{\mathrm{solution}}.$$

Accordingly, by a comparison between the experimental and theoretical oscillator strengths, we can obtain the magnitude values of a_i^2 or b_i^2 and get information about the electronic states of the CT complexes. Furthermore, TCNE complexes form configurations of the AD type in the solution and of the ADA type in the crystal. This means that the oscillator strength in the crystal is six times that in the solution:

$$f_i(\mathrm{ADA})^{\mathrm{crystal}} = 6f_i(\mathrm{AD})^{\mathrm{solution}}.$$

Results

TCNE. TCNE forms monoclinic crystals of the $P2_1/n$ space group, and there are two centrosymmetric molecules in the unit cell. The polarized absorption spectra can be obtained from the reflection spectra, as is shown in Fig. 3. The long-axis transition band of the molecule has a structure; its origin is located at 36300 $\mathrm{cm^{-1}}$, and other vibronic levels appear at 37600, 38800, and 39800 $\mathrm{cm^{-1}}$.

TCNE–HMB Complex. The TCNE–HMB complex forms triclinic crystals,[13] as is shown in Fig. 1. TCNE and HMB molecules are stacked alternately in columns parallel to the c axis. Both molecular planes are perpendicular to the c axis, and the interplanar separation, R_{AD}, is 3.35 Å. The reflection spectra are observed for the polarizations parallel and perpendicular to the c axis, and the absorption spectra are obtained by the K-K transformation of the reflection spectra, as is shown in Fig. 4.

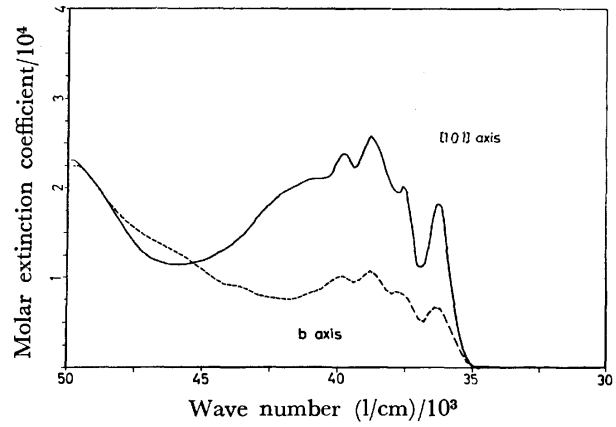

Fig. 3. The absorption spectra of TCNE crystal obtained from the K-K transformation of the reflection spectra.

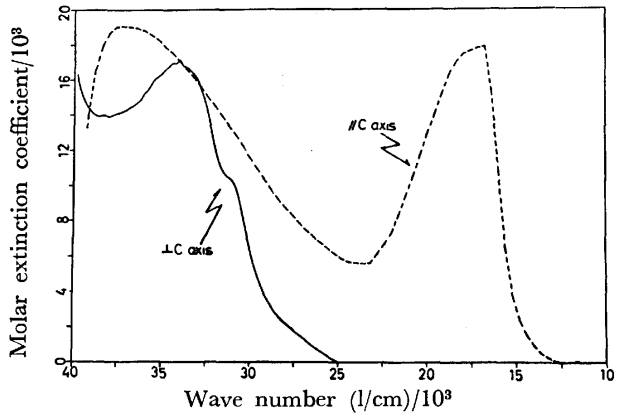

Fig. 4. The absorption spectra of the crystal of TCNE–HMB complex obtained from the K-K transformation of the reflection spectra.

The 17000 $\mathrm{cm^{-1}}$ band is exclusively polarized along the c axis, which can be assigned to a CT band. The oscillator strength of this band is 0.563, and the charge-transfer degree is 9.05%. The stabilization energy in the ground state is given as 4.40 kcal, as is shown in Table 1. The spectrum polarized perpendicular to the c axis consists of the locally excited band of the TCNE molecule, and the broad band in the region of 30000—37000 $\mathrm{cm^{-1}}$ corresponds to the 36000 $\mathrm{cm^{-1}}$ band of the TCNE crystal.

TCNE–Acenaphthene Complex. The crystal of this complex (ρ_{obsd}=*ca.* 1.3 $\mathrm{g/cm^3}$) is a brownish black prism, and its crystal structure is not known. The reflection spectra are observed for the light polarized along the three orthogonal axes (x, y, and z), and the absorption spectra are obtained by the K-K transformation of the reflection spectra, as is shown in Fig. 5.

The z-axis spectrum has three bands— at 14800, 23200, 30000 $\mathrm{cm^{-1}}$— which can be assigned to the CT band. The oscillator strengths of these bands are 0.388,

Table 1. The observed transition energy (E_{CT} in 10^3 cm^{-1}) and oscillator strength (f) and the calculated charge-transfer degree (b^2 in %) and stabilization energy (ΔE in kcal) in the ground state of TCNE complexes

TCNE complex	f	E_{CT}	b^2	ΔE
HMB	0.563	17.0	9.05	4.40
Acenaphthene	0.388	14.8	7.17	3.03
	0.238	23.2	2.80	1.86
	0.250	30.0	2.28	1.96
(Total)			12.3	6.85
Dibenzofuran	0.269	21.4	3.44	2.11
	0.160	29.0	1.51	1.25
(Total)			4.95	3.36

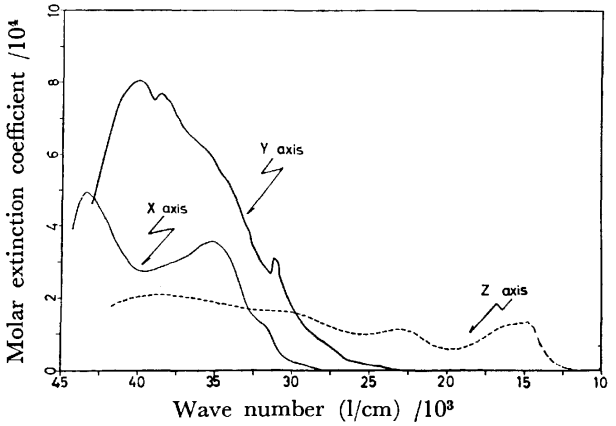

Fig. 5. The absorption spectra of the crystal of TCNE-acenaphthene complex obtained from the K-K transformation of the reflection spectra.

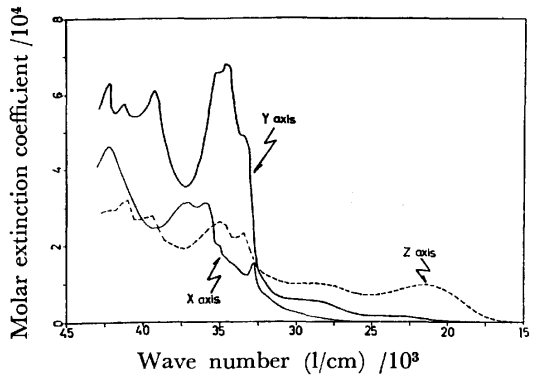

Fig. 6. The absorption spectra of the crystal of TCNE-dibenzofuran complex obtained from the K-K transformation of the reflection spectra.

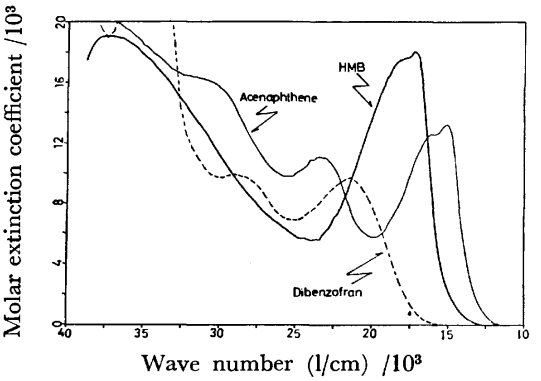

Fig. 7. The absorption spectra characteristic of crystals of TCNE complexes with HMB, acenaphthene, and dibenzofuran.

0.238, and 0.250 respectively. Each band contributes to the charge-transfer degree in the ground state, and the total degree becomes 12.3% by using R_{AD}=3.35 Å, as is shown in Table 1. The stabilization energy is also given as 6.85 kcal. The y-axis spectrum may consist of the α and β bands corresponding to the 30900 and 41800 cm^{-1} bands of the acenaphthene crystal,[14] while the x-axis spectrum consists of the p and β' bands corresponding to two bands at 31400 and 45000 cm^{-1} of the acenaphthene crystal and one band at 36000 cm^{-1} of the TCNE crystal.

TCNE–Dibenzofuran Complex. The crystal of this complex (ρ_{obsd}=*ca.* 1.3 g/cm^3) is a brownish black prism; its crystal structure is not known. The reflection spectra are observed for the light polarized along the three orthogonal axes (x, y, and z), while the absorption spectra are obtained by the K-K transformation of the reflection spectra, as is shown in Fig. 6.

The CT bands located at 21400 and 29000 cm^{-1} are observed in the z and y axes spectra. The total oscillator strengths of these two bands are 0.269 and 0.160, and the total charge-transfer degree in the ground state is estimated to be 4.95% by using R_{AD}=3.35 Å. The stabilization energy is also calculated to be 3.36 kcal, as is shown in Table 1. The y-axis spectrum may consist of the α*, p, and β' bands corresponding to the 33300, 39100, and 46000 cm^{-1} bands of dibenzofuran[15] in addition to two CT bands. The x-axis spectrum may consist of the α and β bands corresponding to two bands at 32600 and 42500 cm^{-1} of the dibenzofuran crystal and one band at 36000 cm^{-1} of the TCNE crystal.

Discussion

The absorption bands characteristic of crystals of TCNE complexes are again depicted in Fig. 7. The first CT band of the TCNE complexes with HMB and acenaphthene splits into doublets, the separation of which are 1500—1200 cm^{-1}. In the crystal of the TCNE–HMB complex,[13] the TCNE residues are disordered in two perpendicular orientations about the normal plane, with relative occupancies of 3 : 1. Therefore, two independent energy bands can be formed in the crystal as a result of the disorder and observed as a doublet.

Another characteristic of the absorption spectra of the TCNE complexes is the appearance of the second and third CT bands. This phenomenon can be observed with complexes of acenaphthene and dibenzofuran. These bands may be assigned to the CT transition from the highest, second highest, and third highest occupied orbitals of the donor to the lowest vacant orbital of TCNE.

The molar extinction coefficient, ε, and the half-

width of the TCNE–HMB complex are 4390[1,9] and 5200[8] cm^{-1} in the CH_2Cl_2 solution, and the oscillator strength is calculated to be $f^{solution}=0.09$; the value of $6f^{solution}=0.54$ is comparable to that of $f^{crystal}=0.563$ which is shown in Table 1.

References

1) R. E. Merrifield and W. D. Phillips, *J. Am. Chem. Soc.*, **80**, 2778 (1958).
2) R. S. Mulliken, *J. Am. Chem. Soc.*, **74**, 811 (1952).
3) J. Aihara, M. Tsuda, and H. Inokuchi, *Bull. Chem. Soc. Jpn.*, **40**, 2460 (1967); **42**, 1824 (1969); **43**, 2439, 3067 (1970).
4) B. Moszynska and A. Tramer, *J. Chem. Phys.*, **46**, 820 (1967).
5) B. Hall and J. P. Devlin, *J. Phys. Chem.*, **71**, 465 (1967).
6) K. Kaya, A. Nakatsuka, N. Kubota, and M. Ito, *J. Raman Spectrosc.*, **1**, 595 (1973).
7) K. H. Michaelian, K. E. Rieckhoff, and E. M. Voigt, *Chem. Phys. Lett.*, **39**, 521 (1976).
8) K. H. Michaelian, K. E. Rieckhoff, and E. M. Voigt, *Proc. Nat. Acad. Sci. USA*, **72**, 4196 (1975).
9) P. W. Jensen, *Chem. Phys. Lett.*, **45**, 415 (1977).
10) H. Kuroda, T. Kunii, S. Hiroma, and H. Akamatu, *J. Mol. Spectrosc.*, **22**, 60 (1967).
11) T. Ohta, H. Kuroda, and T. L. Kunii, *Theoret. Chim. Acta(Berl.)*, **19**, 167 (1970).
12) H. Kuroda, M. Kobayashi, M. Kinoshita, and S. Takemoto, *J. Chem. Phys.*, **36**, 457 (1962).
13) M. Saheki, H. Yamada, H. Yoshioka, and K. Nakatsu, *Acta Crystallogr., Sect. B*, **32**, 662 (1976).
14) M. Tanaka, *Bull. Chem. Soc. Jpn.*, **49**, 2315 (1976).
15) M. Tanaka, *Bull. Chem. Soc. Jpn.*, **49**, 3382 (1976).
16) M. Saheki and H. Yamada, *Spectrochim. Acta, Part A*, **32**, 1425 (1976).

PMR Studies of the Phase Transition in *N,N,N′,N′*-Tetramethyl-*p*-phenylenediamine (Wurster's Blue) Perchlorate

Motomichi INOUE, Hiroyoshi KURAMOTO, and Daiyu NAKAMURA
Department of Chemistry, Nagoya University, Chikusa, Nagoya 464

(Received May 27, 1977)

The powder PMR spectra of $[TMPD]^+(ClO_4)^-$ were recorded in the temperature range 110—300 K. The spectra observed above 140 K consist of two widely separated simple absorption curves of intensity ratio approximately equal to 3 : 1. Spin densities on the carbon and nitrogen atoms of the cation radical were evaluated from the observed field shift ascribable to the Fermi contact interaction. The spin density distribution of the radical ion changes at the transition temperature of 189 K.

The phase transition of *N,N,N′,N′*-tetramethyl-*p*-phenylenediamine (TMPD) perchlorate attracts particular attention, because the crystals display phase transition at *ca.* 189 K accompanied by a novel magnetic behavior.[1,2] X-Ray crystal analysis carried out at 300 and 110 K has revealed that cation radicals, in the high-temperature phase, are stacked equidistantly to form a one-dimensional array, whereas radical ions are dimerized to construct alternating chains in the low-temperature phase.[3] The magnetic interaction between radical ions is closely related to the stacking of cations and also to the distribution of an unpaired electron within radicals.[4,5] The latter can be determined by observing the contact shift of PMR. Kawamori and Suzuki[6] have reported that the PMR absorption curve of TMPD-perchlorate powders consists of two component curves, and that the separation between the centers of the curves varies with temperature in proportion to the magnetic susceptibility of the compound. However, the authors failed to determine the absolute values of the PMR shifts. In the present investigation, we have precisely recorded the PMR spectrum of the radical salt at various temperatures between 110 and 300 K, and have determined the spin density distribution of the TMPD cations in crystals.

Experimental

TMPD perchlorate was prepared by the method of Michaelis and Granick.[7] Crystalline powders obtained were dried *in vacuo* for *ca.* 4 h to eliminate solvent molecules completely.

The PMR spectra were recorded by means of a JEOL JNM-MW-40 NMR spectrometer operating at 40 MHz with a field-modulation amplitude of 0.5 G.* Isohexane (isomeric mixture) was employed as an external standard. The temperature of the specimen was determined with a copper-constantan thermometer inserted directly in the specimen before and after recording each PMR spectrum. The temperature was automatically controlled within ±1° by the following method. Cold vapor evaporated from liquid nitrogen was conducted to the specimen through a transfer tube, in which a heater was mounted. The evaporation of liquid nitrogen was kept at a constant rate, and the temperature of flowing gas was controlled by use of the heater connected to a conventional PID temperature controller. The homogeneity of temperature in the specimen was difficult to keep within ±1°, because of a large volume of the specimen amounting to *ca.* 4 cm^3. The accuracy of the temperature was estimated to be within ±2° over the temperature range investigated.

* The unit corresponds to 10^{-4} T in the SI unit system.

Results

Figure 1 shows some typical derivative curves of PMR absorptions observed at various temperatures. Above *ca.* 140 K, each curve observed can be resolved into two component curves of intensity ratio equal to 3 : 1. The stronger component shifts to a low field, whereas the weaker one does to a high field. From the intensity ratio, the former can be assigned to *N*-methyl protons and the latter to the protons of benzene rings. The amount of the shifts from the external standard is plotted against the temperature for each component as shown in Fig. 2. The temperature dependence of the PMR shifts closely resembles that of the magnetic susceptibility. This is consistent with the results reported by Kawamori and Suzuki.[6]

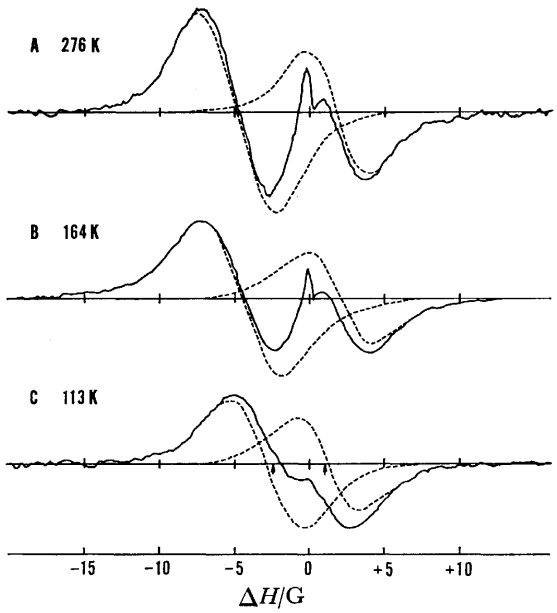

Fig. 1. PMR absorption derivative curves of $[TMPD](ClO_4)$ at various temperatures. Each curve can be resolved into two simple derivative curves (broken curves). Sharp components at $\Delta H=0$ in the spectra A and B are due to isohexane employed as an external standard. The spectrum C dispalys the curve recorded without the external standard to show the inherent curve clearly. The arrows in the spectrum C show the resonance fields estimated by use of the coupling constants of the low-temperature phase.

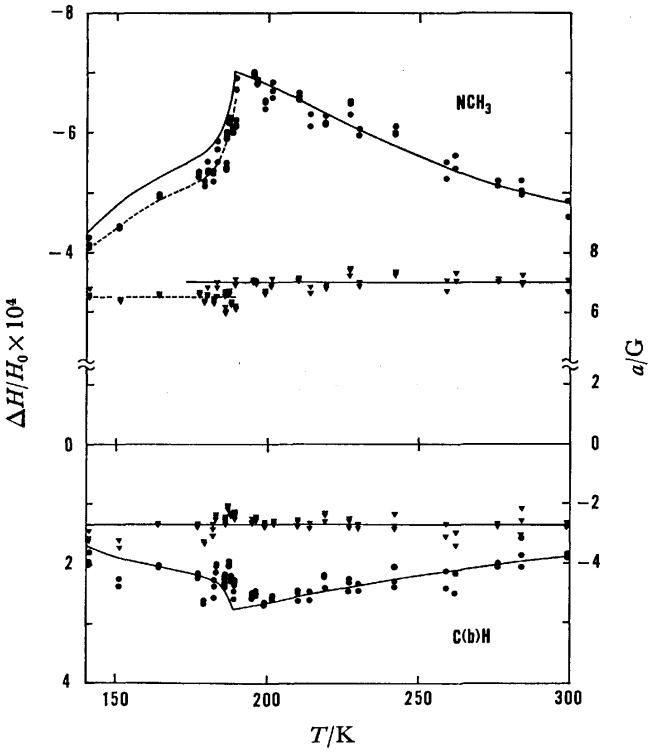

Fig. 2. Observed PMR shifts (●) and the coupling constants (▼) of *N*-methyl protons and ring protons. The straight lines show the respective averaged values of the coupling constants. The solid curves display the shifts evaluated with the coupling constants of the high-temperature phase. The a_{NCH_3} value averaged below T_c gives the broken curve reproducing well the shifts of *N*-methyl protons observed below T_c.

Each curve observed below 140 K can be decomposed into two simple derivative curves, the intensity ratio of which, however, varies with temperature. For example, the spectrum C in Fig. 1 observed at 113 K is made up of two components of intensity ratio nearly equal to 2 : 1. In this paper, the discussion is based solely on the data observed above 140 K.

Discussion

The PMR shift $\Delta H/H$ is attributable to the Fermi contact shift, which is proportional to magnetic susceptibility χ:[8]

$$\frac{\Delta H}{H_0} = -\frac{a_i}{g_N\mu_N}\cdot\frac{\chi}{cN}, \tag{1}$$

where, apart from the usual notations, a_i is the contact coupling constant in Gauss and c is the radical concentration determined from the Curie constant. Thus, the coupling constants, a_{NCH_3} for *N*-methyl protons and $a_{C(6)H}$ for ring protons, can be evaluated from the corresponding PMR shifts and the magnetic susceptibility which has been reported by Duffy, Jr.[1] and Okumura[2] in the temperature range 77—300 K. The temperature, at which the PMR shift shows a sharp decrease, agrees with the transition temperature T_c determined by Okumura rather than by Duffy, Jr. Therefore, the coupling constants were evaluated on the basis of Okumura's data (T_c=189 K and c=0.86$_7$). Each coupling constant is practically constant above T_c as shown in Fig. 2. The averaged values of the constants are listed in Table 1 along with estimated standard deviations. The shifts observed above T_c are well reproduced by the solid curves calculated using Eq. 1.

The coupling constant $a_{C(i)H}$ is proportional to spin density $\rho_{C(i)}$ localized on a carbon atom bonded to the proton:[8]

$$a_{C(i)H} = Q_{CH}\rho_{C(i)}, \tag{2}$$

where Q_{CH} is a proportionality constant. When the rotation of *N*-methyl groups is hindered in >N–CH_3 systems, the contact coupling constant depends on the torsional amplitude ϕ as well as the equilibrium angle θ_j between an N–C–H(j) plane and the axis of the nitrogen p-orbital involving the unpaired electron:[9]

$$a_{NCH_3}(j) = B\langle\cos^2\theta_j\rangle_\phi\rho_N, \tag{3}$$

where j stands for the jth proton of an *N*-methyl group and B is a proportionality constant. For freely rotating methyl groups, all the protons are equivalent so that the coupling constant is simply proportional to the spin density ρ_N of nitrogen:

$$a_{NCH_3} = Q_{NCH_3}\rho_N. \tag{4}$$

The *N*-methyl groups of TMPD cations can be assumed to undergo a free rotation about the threefold axis in the high-temperature phase, because of the following facts: (1) the component curve attributable to *N*-methyl protons has a peak-to-peak width nearly equal to that of the curve due to the ring protons, and shows no appreciable structure, and (2) the absolute values of the coupling constants agree well with the corresponding values determined by an ESR experiment[10] carried out on the radical ions in solution (Table 1), in which *N*-methyl groups perform a free rotation. The proportionality constants have been estimated as Q_{CH}=−28 G and Q_{NCH_3}=25 G.[11] By using these values, the spin density can be evaluated as given in Table 1. All the carbon atoms in the benzene ring carry positive spin densities. The spin density distribution has been calculated on the basis of various MO models.[11,12] The distribution determined by McLachlan[11] yields the best fit to the present result.

Below the transition temperature, the observed shifts of *N*-methyl protons deviate systematically from the solid curve in Fig. 2 calculated with the value of a_{NCH_3} evaluated above T_c, while the broken curve shows the temperature dependence of the shift calculated with a_{NCH_3}=6.52 G, reproducing well the data observed below T_c. The a_{NCH_3} value of the low-temperature phase differs clearly from that of the high-temperature phase. Although the magnetic data reported by Duffy differ slightly from Okumura's data, the coupling constants evaluated on the basis of Duffy's data agree with the corresponding values based on Okumura's data over the whole temperature range except near T_c (180—190 K). Therefore, it can be concluded that the "a_{NCH_3} gap" accompanying the phase transition is inherent in the radical salt. Two interpretations are conceivable for the marked a_{NCH_3} gap: (a) the spin density on nitrogen atoms changes appreciably at the transition

Table 1. Contact coupling constant a_i and spin density ρ_i of a TMPD cation[a)]

	a_{NCH_3}/G	$a_{C(b)H}$/G	ρ_N	$\rho_{C(b)}$	$\rho_{C(a)}$[b)]
$T>189$ K	7.01±0.20	−2.71±0.22	0.28_0	0.09_7	0.02_6
$T<189$ K	6.52±0.21	−2.69±0.35	0.26_1	0.09_6	0.04_7
ESR[c)]	6.76	(−)1.97	0.27_0	0.07_0	0.09_0

a) 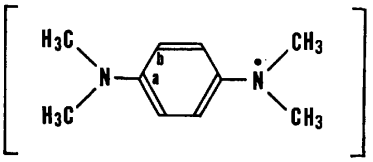 b) $\rho_{C(a)}=\{1-(2\rho_N+4\rho_{C(b)})\}/2$. c) Ref. 10.

temperature, and (b) a hindered rotation of *N*-methyl groups below T_c yields an apparent Q_{NCH_3} value different from that for freely rotating *N*-methyl protons. Equation 3 indicates that, in case (b), three protons within an *N*-methyl group display PMR shifts different from one another, and, hence, the component curve attributable to *N*-methyl protons is expected to display an incipient indication of structure. Contrary to expectation, the component curve obtained below T_c exhibits no appreciable change in shape and line width as compared with that above T_c, suggesting that the *N*-methyl groups practically perform a free rotation even below the temperature. The aforementioned value of Q_{NCH_3} gives a smaller spin density ρ_N in the low-temperature phase than that in the high-temperature phase. This indicates that a fraction of an unpaired electron, in the former phase, is delocalized from nitrogen onto the aromatic ring to a greater extent. X-Ray crystal analysis[3)] has shown that the C–N bond length 1.346 Å at 110 K is evidently shorter than the length of 1.359 Å at 300 K, suggesting a larger double-bond character in the C–N bonds below T_c. This gives support to the present conclusion. The $a_{C(b)H}$ values averaged above and below T_c agree with each other, although the constant is difficult to determine accurately owing to the small absolute value. Hence, it can be presumed that $\rho_{C(b)}$ remains almost unchaged with decreasing temperature through T_c, despite the discernible change of $\rho_{C(a)}$. In fact, X-ray crystal analysis has shown that the C(*a*)–C(*b*) bond distance increases by 0.005 Å at 110 K whereas the C(*b*)–C(*b*) distance remains unchanged, suggesting that there is no significant alteration in the charge distribution on C(*b*) atoms above and below T_c.

The present investigation presents a unique example showing that the phase transition is accompanied by spin-distribution change in a molecule as well as change of molecular arrangement.

This work was partially supported by a Grant-in-Aid for Scientific Research from the Ministry of Education.

References

1) W. Duffy, Jr., *J. Chem. Phys.*, **36**, 490 (1962).
2) K. Okumura, *J. Phys. Soc. Jpn.*, **18**, 69 (1963).
3) J. L. de Boer and A. Vos, *Acta Crystallogr., Sect. B*, **28**, 835, 839 (1972).
4) Z. G. Soos and R. C. Hughes, *J. Chem. Phys.*, **46**, 253 (1967).
5) J. Tanaka, M. Inoue, M. Mizuno, and K. Horai, *Bull. Chem. Soc. Jpn.*, **43**, 1998 (1970).
6) A. Kawamori and K. Suzuki, *Mol. Phys.*, **8**, 95 (1964).
7) L. Michaelis and S. Granick, *J. Am. Chem. Soc.*, **65**, 1747 (1943).
8) H. M. McConnell and C. H. Holm, *J. Chem. Phys.*, **27**, 314 (1957); H. M. McConnell and D. B. Chesnut, *J. Chem. Phys.*, **28**, 107 (1958).
9) E. W. Stone and A. H. Maki, *J. Chem. Phys.*, **37** 1326 (1962).
10) J. R. Bolton, A. Carrington, and J. dos Santos-Veiga, *Mol. Phys.*, **5**, 615 (1962).
11) A. D. McLachlan, *Mol. Phys.*, **1**, 233 (1958).
12) H. J. Monkhorst and J. Kommandeur, *J. Chem. Phys.*, **15**, 391 (1967); R. M. Metzger, *J. Chem. Phys.*, **57**, 1870 (1972); **64**, 2069 (1976), references are cited therein.

The Crystal and Molecular Structures of *trans*-Bis(trimethylphosphine)-[1,2-bis(methoxycarbonyl)vinyl](phenylethynyl)palladium(II)

Takao YASUDA, Yasushi KAI, Noritake YASUOKA, and Nobutami KASAI*

Department of Applied Chemistry, Faculty of Engineering, Osaka University, Yamadakami, Suita, Osaka 565

(Received June 11, 1977)

The X-ray molecular structure of the addition product of *trans*-$HPd(PEt_3)_2(C{\equiv}CPh)$ with dimethyl acetylenedicarboxylate has been determined to be [*trans*-{$(MeO_2C)HC{=}C(CO_2Me)$}$Pd(PEt_3)_2(C{\equiv}CPh)$]. The crystal belongs to the monoclinic system, space group $P2_1/c$, with eight formula units in a cell with dimensions of a= 17.844(3), b=9.476(3), c=36.061(4) Å, β=98.18(1)°. Two independent molecules have similar structures except for the conformation of the phenylethynyl groups and one of the triethylphosphine groups. The 1,2-bis(methoxycarbonyl)vinyl and phenylethynyl groups are σ-bonded to the palladium atom. No significant difference is observed between the Pd-C(sp)[2.04(2) and 2.03(2) Å] and Pd-C(sp^2)[2.05(2) and 2.06(2) Å] bond lengths. The environment of the palladium atom is approximately square-planar: Pd-P=2.321(5), 2.312(5), and 2.305(5), 2.311(5) Å.

It has been reported that a hydridoalkynylmetal complex (I), which is formed by the oxidative addition of a terminal acetylene group to the metal, can be considered to be an intermediate in the oligomerization of terminal acetylenes catalyzed by low-valent transition-metal complexes,[1] and that the hydrido or alkynyl groups of such an intermediate may add to acetylenes to form an alkynylalkenyl (II) or a hydridoalkenyl (III) complex,[2] which can subsequently undergo reductive elimination to the dimer and reform the starting low-valent complex (Scheme).

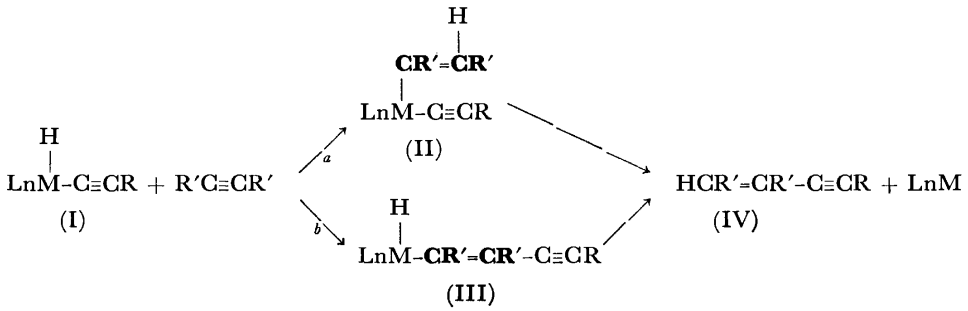

Spectroscopic studies of the reaction products of dimethyl acetylenedicarboxylate with hydridoalkynyl complexes of palladium(II) and platinum(II) suggest that the addition may produce alkenylalkynyl derivatives[3] (Path *a* in the scheme). In order to establish the molecular structure and clarify the reaction mechanism, an X-ray structure analysis of the addition product of *trans*-$HPd(PEt_3)_2(C{\equiv}CPh)$ with dimethyl acetylenedicarboxylate has now been carried out.

Experimental

Yellow needle crystals of the addition product mentioned above were supplied by Professor N. Hagihara and his coworkers. The unit-cell parameters were determined by the least-squares fit, using 35 2θ values of high-angle reflections.

Crystal Data: [*trans*-{$(MeO_2C)HC{=}C(CO_2Me)$}$Pd(PEt_3)_2$-$(C{\equiv}CPh)$], $C_{26}H_{42}O_4P_2Pd$, F. W. 591.0, monoclinic, $P2_1/c$, a=17.844(3), b=9.476(3), c=36.061(4) Å, β=98.18(1)°, U=6036(2) Å^3, λ(Mo$K\alpha$)=0.71069 Å, D_m=1.29 g·cm^{-3}, Z=8, D_c=1.29 g·cm^{-3}, μ(Mo$K\alpha$)=7.59 cm^{-1}.

The intensity data were collected on a Rigaku automated, four-circle diffractometer using the θ-2θ scan technique. The graphite-monochromatized Mo$K\alpha$ radiation was used. The crystal used had dimensions of *ca.* 0.3×0.3×0.2 mm. The integrated intensity was determined by scanning over a peak at a rate of 4° min^{-1} and by subtracting the background obtained by averaging the two values measured for 5 s at both ends of a scan. The scan width in 2θ was $(1.6+0.70\theta_c)°$, where θ_c is the calculated Bragg angle for Mo$K\alpha_1$. A total of 4920 reflections was measured ($\sin\theta/\lambda \leqq 0.46$), of which 954 were less than $\sigma(F)$ and were classed "unobserved". Five standard reflections measured after every 60 reflections showed no significant change in intensity throughout the data collection. The Lorentz and polarization corrections were made in the usual way.

Structure Solution and Refinement

Two independent molecules are contained in an asymmetric unit. The palladium atoms were located from the Patterson map. The non-hydrogen atoms were then located from the subsequent Fourier synthesis. The structure was refined anisotropically by the block-diagonal least-squares procedure, using the HBLS V program.[4] The function minimized was $\Sigma w(\Delta F)^2$, where w was taken as unity. The final refinement reduced the R to 0.075 for 3966 non-zero reflections($\sin\theta/\lambda \leqq 0.46$). Hydrogen atoms were not included in the refinement. The atomic scattering factors were taken from the International Tables for X-Ray Crystallography, Vol. IV.[5] The positional and thermal parameters are given in Table 1.**

* To whom the correspondence should be addressed.

** The table of observed and calculated structure factors is kept as Document No. 7720 at the Chimical Society of Japan.

TABLE 1. ATOMIC PARAMETERS ALONG WITH THEIR ESTIMATED STANDARD DEVIATIONS IN PARENTHESES

Positional parameters in fraction of cell edges and thermal parameters in the form of $\exp[-\{B(11)h^2+B(22)k^2+B(33)l^2+B(12)hk+B(13)hl+B(23)kl\}]$.

ATOM	X	Y	Z	B(11)	B(22)	B(33)	B(12)	B(13)	B(23)
PDA	.19373(7)	.60404(13)	.40338(4)	.00304(5)	.00857(16)	.000850(13)	.00051(4)	.00033(8)	.00049(0)
P(1A)	.16916(26)	.4262 (5)	.35907(14)	.00340(19)	.0104 (6)	.00106 (5)	-.0006 (6)	.00078(15)	-.00101(30)
P(2A)	.20626(26)	.7964 (5)	.44322(13)	.00402(20)	.0084 (6)	.00078 (5)	.0001 (6)	-.00008(15)	.00052(28)
O(1A)	.1550 (7)	.2767 (13)	.45029(34)	.0059 (6)	.0149 (19)	.00114 (14)	-.0060 (18)	.00090(15)	.0003 (8)
O(2A)	.3118 (7)	.2642 (14)	.5000 (4)	.0046 (6)	.0215 (23)	.00133 (15)	.0046 (19)	-.0001 (4)	.0047 (10)
O(3A)	.1674 (7)	.4556 (12)	.40188(32)	.0072 (6)	.0139 (18)	.00090 (13)	-.0001 (18)	.0022 (5)	.0000 (8)
O(4A)	.4733 (7)	.3255 (16)	.4849 (4)	.0043 (6)	.0261 (26)	.00199 (20)	.0038 (20)	.0008 (6)	.0030 (12)
C(1A)	.2435 (9)	.4646 (16)	.4429 (4)	.0036 (7)	.0086 (21)	.00056 (15)	-.0012 (20)	-.0001 (5)	-.0008 (9)
C(2A)	.3187 (9)	.4393 (17)	.4522 (4)	.0033 (7)	.0124 (25)	.00073 (17)	.0013 (21)	-.0008 (5)	.0006 (10)
C(3A)	.1851 (9)	.3841 (17)	.4414 (5)	.0030 (7)	.0101 (24)	.00135 (21)	.0003 (21)	-.0001 (6)	.0018 (12)
C(4A)	.3489 (11)	.3351 (21)	.4806 (6)	.0060 (9)	.0140 (31)	.00148 (26)	.0020 (27)	.0013 (8)	.0009 (15)
C(5A)	.1080 (12)	.3882 (26)	.5103 (6)	.0058 (10)	.029 (4)	.00169 (29)	-.002 (4)	.0033 (9)	.0037 (19)
C(6A)	.4596 (12)	.2234 (27)	.5112 (7)	.0058 (11)	.030 (5)	.00216 (35)	.012 (4)	-.0023 (10)	.0078 (21)
C(7A)	.1437 (9)	.7422 (17)	.3642 (4)	.0037 (7)	.0113 (24)	.00045 (15)	-.0012 (21)	-.0001 (5)	-.0010 (10)
C(8A)	.1124 (8)	.8218 (16)	.3412 (4)	.0027 (6)	.0090 (21)	.00074 (16)	-.0006 (19)	.0007 (5)	.0000 (10)
C(11A)	.0790 (8)	.9181 (16)	.3113 (5)	.0026 (6)	.0070 (21)	.00112 (19)	-.0018 (19)	-.0015 (5)	-.0004 (11)
C(12A)	.0183 (9)	1.0045 (17)	.3192 (5)	.0029 (7)	.0072 (22)	.00170 (24)	-.0019 (21)	-.0012 (6)	-.0018 (12)
C(13A)	-.0147 (9)	1.0944 (19)	.2901 (5)	.0036 (7)	.0134 (26)	.00110 (20)	.0007 (23)	-.0001 (6)	.0009 (12)
C(14A)	.0120 (10)	1.0922 (20)	.2547 (5)	.0049 (8)	.0139 (28)	.00103 (20)	-.0005 (26)	-.0013 (6)	.0004 (13)
C(15A)	.0713 (10)	1.0017 (20)	.2485 (5)	.0048 (8)	.0144 (28)	.00101 (20)	-.0055 (26)	-.0006 (6)	.0002 (13)
C(16A)	.1038 (9)	.9146 (17)	.2769 (4)	.0035 (7)	.0113 (23)	.00061 (16)	.0009 (21)	.0008 (5)	-.0009 (10)
C(21A)	.1792 (12)	.4815 (19)	.3113 (5)	.0094 (12)	.0114 (26)	.00060 (17)	.0060 (30)	.0008 (7)	.0012 (11)
C(22A)	.2269 (15)	.2623 (19)	.3656 (6)	.0113 (15)	.0065 (24)	.00177 (30)	.0061 (31)	.0022 (10)	-.0008 (13)
C(23A)	.0709 (14)	.3579 (33)	.3568 (8)	.0066 (12)	.044 (7)	.0028 (4)	-.021 (5)	.0037 (12)	-.0134 (29)
C(31A)	.1588 (13)	.3653 (24)	.2805 (6)	.0084 (12)	.021 (4)	.00134 (25)	.000 (4)	.002 (9)	-.0045 (16)
C(32A)	.3087 (14)	.2867 (28)	.3591 (7)	.0082 (13)	.029 (5)	.00200 (35)	.016 (4)	.0017 (10)	-.0034 (21)
C(33A)	.0150 (11)	.4276 (33)	.3657 (10)	.0030 (9)	.039 (6)	.0041 (6)	.000 (4)	.0014 (12)	-.0081 (32)
C(41A)	.2511 (11)	.7667 (19)	.4928 (5)	.0066 (10)	.0137 (28)	.00072 (19)	.0013 (27)	-.0007 (7)	-.0011 (12)
C(42A)	.1119 (10)	.8757 (18)	.4474 (5)	.005 (8)	.0116 (26)	.00139 (23)	.0057 (24)	.0022 (7)	-.0001 (13)
C(43A)	.2602 (11)	.9458 (19)	.4251 (6)	.0067 (10)	.0120 (28)	.00157 (27)	-.0076 (27)	.0013 (8)	.0001 (14)
C(51A)	.2547 (13)	.9062 (21)	.5175 (5)	.0102 (13)	.0160 (31)	.00064 (19)	-.0045 (34)	.0000 (8)	.0034 (13)
C(52A)	.0573 (11)	.7675 (23)	.4595 (6)	.0046 (9)	.0193 (35)	.00183 (29)	.0037 (29)	.0014 (8)	.0022 (16)
C(53A)	.3463 (11)	.9110 (27)	.4290 (6)	.0038 (8)	.031 (5)	.0018 (29)	-.0082 (33)	.0018 (8)	-.0019 (19)
PDB	.46689(7)	.49196(14)	.35631(4)	.00322(5)	.00957(17)	.001110(14)	.00050(16)	.00061(4)	.00075(9)
P(1B)	.74866(26)	.6721 (5)	.34650(14)	.00333(19)	.0093 (6)	.00122 (6)	-.0012 (6)	.00032(16)	.00058(31)
P(2B)	.57581(26)	.3308 (5)	.36795(14)	.00321(19)	.0123 (7)	.00113 (6)	-.0013 (6)	.00037(16)	.00142(32)
O(1B)	.8165 (8)	.3458 (13)	.3091 (4)	.0073 (7)	.0123 (18)	.00175 (17)	-.0062 (18)	.0041 (6)	-.0014 (9)
O(2B)	.8713 (7)	.1309 (13)	.3732 (4)	.0052 (6)	.0168 (20)	.00156 (16)	.0079 (18)	.0007 (5)	-.0019 (9)
O(3B)	.7253 (7)	.1885 (12)	.3126 (4)	.0059 (6)	.0101 (17)	.00169 (17)	-.0029 (17)	.0009 (5)	-.0002 (9)
O(4B)	.8971 (7)	.2064 (15)	.4329 (4)	.0045 (5)	.0231 (24)	.00147 (16)	.0059 (19)	-.0003 (5)	.0001 (10)
C(1B)	.7533 (9)	.3461 (16)	.3618 (5)	.0027 (6)	.0084 (23)	.00142 (22)	.0027 (20)	.0016 (6)	.0006 (11)
C(2B)	.7936 (9)	.3110 (18)	.3971 (5)	.0032 (7)	.0105 (24)	.00140 (23)	.0044 (22)	.0005 (6)	.0022 (12)
C(3B)	.7718 (10)	.2933 (16)	.3266 (6)	.0042 (8)	.0060 (21)	.00178 (27)	.0023 (21)	.001 (7)	.0010 (12)
C(4B)	.8557 (9)	.2034 (19)	.3089 (5)	.0025 (7)	.0123 (28)	.00164 (23)	-.0011 (23)	.0010 (6)	.0019 (13)
C(5B)	.7347 (15)	.1465 (29)	.2753 (7)	.0103 (15)	.018 (4)	.00170 (30)	-.005 (4)	.0021 (11)	-.0061 (17)
C(6B)	.9598 (12)	.1064 (25)	.4390 (7)	.0054 (10)	.027 (4)	.00183 (30)	.017 (4)	-.0011 (8)	.0001 (19)
C(7B)	.5784 (10)	.6279 (19)	.3474 (7)	.0032 (7)	.0100 (27)	.00255 (33)	-.0033 (23)	.0009 (8)	.0007 (15)
C(8B)	.5219 (9)	.6977 (18)	.3380 (5)	.0034 (7)	.0099 (24)	.00162 (25)	-.0017 (22)	.0010 (7)	.0001 (13)
C(11B)	.4546 (9)	.7756 (17)	.3285 (5)	.0032 (7)	.0108 (25)	.00115 (21)	.0029 (21)	.0002 (6)	.0001 (12)
C(12B)	.3851 (12)	.7316 (25)	.3406 (7)	.0055 (10)	.023 (4)	.0025 (4)	.0009 (34)	.0032 (10)	-.0037 (20)
C(13B)	.3181 (11)	.8165 (26)	.3278 (7)	.0041 (9)	.023 (4)	.00240 (34)	.0016 (31)	.0013 (9)	-.0048 (20)
C(14B)	.3226 (12)	.9302 (23)	.3067 (7)	.0061 (10)	.019 (4)	.00197 (31)	.0021 (31)	-.0006 (9)	-.0038 (17)
C(15B)	.3885 (13)	.9886 (25)	.2935 (7)	.0069 (12)	.020 (4)	.0023 (4)	.0035 (35)	-.0016 (10)	.0029 (19)
C(16B)	.4556 (11)	.8902 (21)	.3050 (6)	.0052 (9)	.0151 (31)	.00198 (30)	-.0002 (29)	-.0023 (8)	.0026 (16)
C(21B)	.7283 (11)	.8365 (20)	.3681 (6)	.0053 (9)	.0120 (28)	.00185 (28)	.0016 (26)	.0012 (8)	-.0044 (14)
C(22B)	.7454 (14)	.7112 (26)	.2943 (7)	.0078 (12)	.024 (4)	.0022 (4)	-.006 (4)	.0010 (10)	.0071 (21)
C(23B)	.8512 (9)	.6407 (19)	.3615 (7)	.0023 (7)	.0115 (27)	.0027 (4)	-.0003 (22)	.0011 (8)	-.0022 (15)
C(31B)	.7367 (16)	.8211 (27)	.4097 (7)	.0121 (17)	.024 (4)	.00131 (28)	.008 (5)	.0010 (11)	-.0027 (19)
C(32B)	.6743 (14)	.7524 (30)	.2754 (7)	.0084 (14)	.035 (6)	.00152 (30)	-.012 (5)	-.0002 (10)	.0052 (21)
C(33B)	.9037 (11)	.7626 (24)	.3533 (8)	.0039 (9)	.019 (4)	.0030 (4)	-.0050 (29)	.0018 (9)	-.0023 (20)
C(41B)	.4981 (10)	.3109 (22)	.3293 (5)	.0046 (8)	.0200 (34)	.00112 (22)	-.0029 (28)	-.0006 (7)	.0018 (14)
C(42B)	.6063 (10)	.1479 (17)	.3802 (6)	.0047 (8)	.0074 (24)	.00209 (29)	.0004 (23)	.0021 (8)	.0030 (13)
C(43B)	.5256 (10)	.3893 (21)	.4071 (5)	.0042 (8)	.0191 (32)	.00126 (23)	.0010 (27)	.0020 (7)	.0005 (14)
C(51B)	.5286 (14)	.2856 (29)	.2924 (6)	.0090 (14)	.034 (5)	.00110 (25)	-.016 (5)	-.0002 (9)	-.0024 (19)
C(52B)	.5447 (12)	.0559 (20)	.3965 (6)	.0066 (10)	.0141 (31)	.00159 (27)	-.0050 (28)	.0017 (8)	.0048 (15)
C(53B)	.5846 (13)	.4101 (26)	.4430 (6)	.0073 (11)	.029 (4)	.00102 (23)	-.005 (4)	.0016 (8)	-.0037 (17)

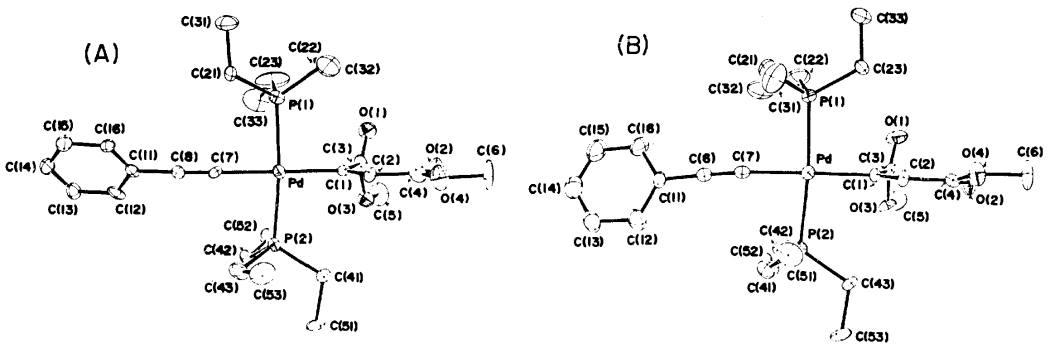

Results and Discussion

Figure 1 shows a stereoscopic view of the two independent molecules in an asymmetric unit. The two molecules (A and B) have similar structures except for the conformation of the phenylethynyl groups and one of the triethylphosphine groups. Selected bond lengths and bond angles are given in Fig. 2.

The main feature of the structure is that the 1,2-bis(methoxycarbonyl)vinyl and phenylethynyl groups are σ-bonded to the palladium atom, and that they are

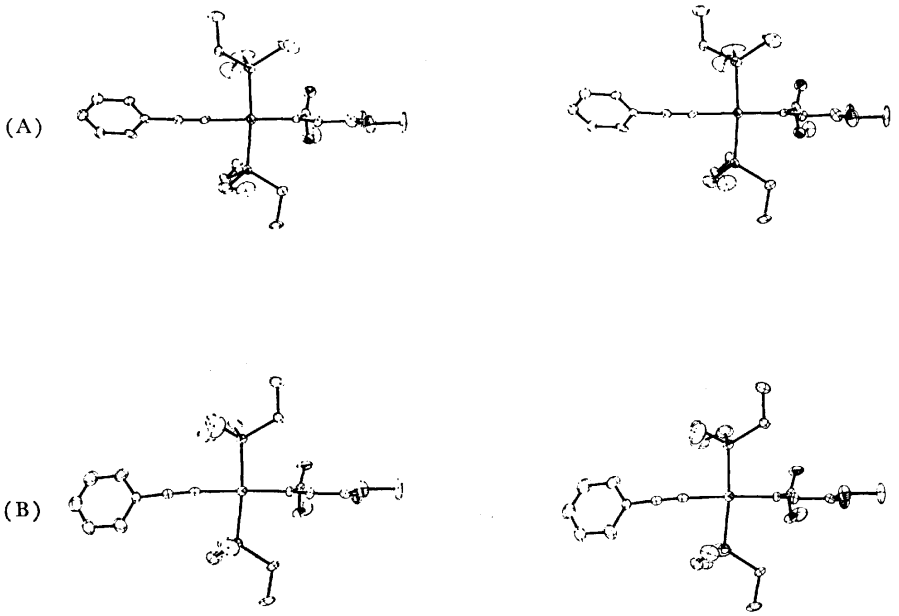

Fig. 1. Stereoscopic drawing of two independent molecules of [*trans*-{$(MeO_2C)HC{=}C(CO_2Me)$}$Pd(PEt_3)_2(C{\equiv}CPh)$].

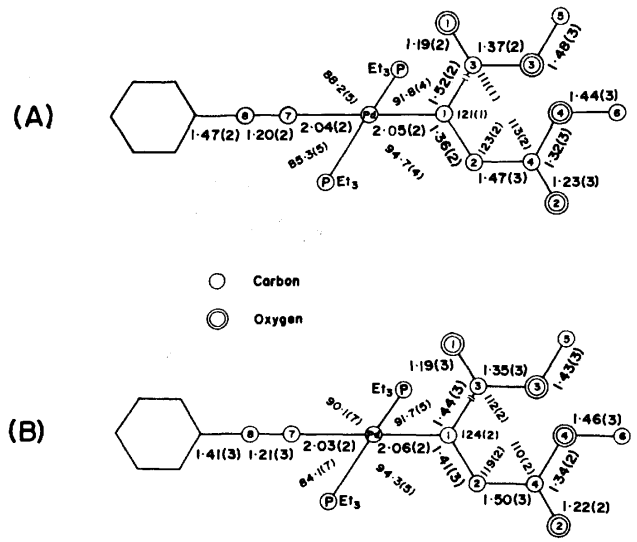

Fig. 2. Selected bond lengths and bond angles. E.s.d.'s in parentheses.

both in the *trans* position. This indicates that, of the two possible reaction paths in the scheme, the terminal acetylene reacted with the hydridoalkynylmetal complex to give the alkenylalkynyl derivative (Path *a* in the scheme). A third feature is that two methoxycarbonyl groups are mutually *cis*, the insertion of dimethyl acetylenedicarboxylate into the palladium atom being found to be a *cis*-insertion. This may be caused by the electronic repulsion between the methoxycarbonyl group and the palladium atom.

The environment of the palladium atom is approximately square-planar: the Pd, P(1), P(2), C(1), and C(7) atoms lie on a plane within 0.13 Å. The two Pd–P lengths are equal [2.321(5), 2.312(5) and 2.305(5), 2.311(5) Å], and no significant difference is found between the Pd–C(sp) [2.04(2) and 2.03(2) Å] and Pd–C(sp^2) lengths [2.05(2) and 2.06(2) Å].

TABLE 2. DIHEDRAL ANGLES

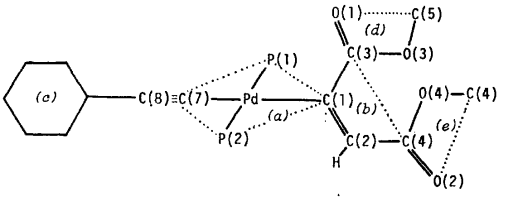

Molecule	Dihedral angles [°] between				
	(*a*) & (*b*)	(*a*) & (*c*)	(*a*) & C(7)≡C(8)	(*b*) & (*d*)	(*b*) & (*e*)
A	82.6	51.2	1.8	89.0	2.7
B	83.2	24.3	9.9	95.5	13.3

The alkenyl group, or, more exactly, the vinyl plane ((*b*) in Table 2), is roughly perpendicular to the co-ordination plane (*a*). The bulkiness of the alkenyl group probably causes the P(1)–Pd–C(1) and P(2)–Pd–C(1) bond angles to be larger than 90°. One of the methoxycarbonyl groups (*d*) is approximately perpendicular to, whereas the other one (*e*) is nearly parallel to, the vinyl plane (*b*). It seems that the C(4)=O(2) double bond lengths [1.23(3) and 1.22(2) Å] are slightly longer than the C(3)=O(1) lengths [1.19(2) and 1.19(3) Å], though this is not really significant; it can be explained by the conjugation of the C(4)=O(2) bond with the vinylic π-system.

The phenylethynyl groups in two molecules have rather different conformations: the C(7)–C(8) bonds make different angles of 1.8 and 9.9° with the co-ordination plane. The dihedral angles between the phenyl ring and the co-ordination plane also have different values [51.2 and 24.3°]. This is probably the result of the difference in the conformations of the triethylphosphine groups (Fig. 1). The bond lengths

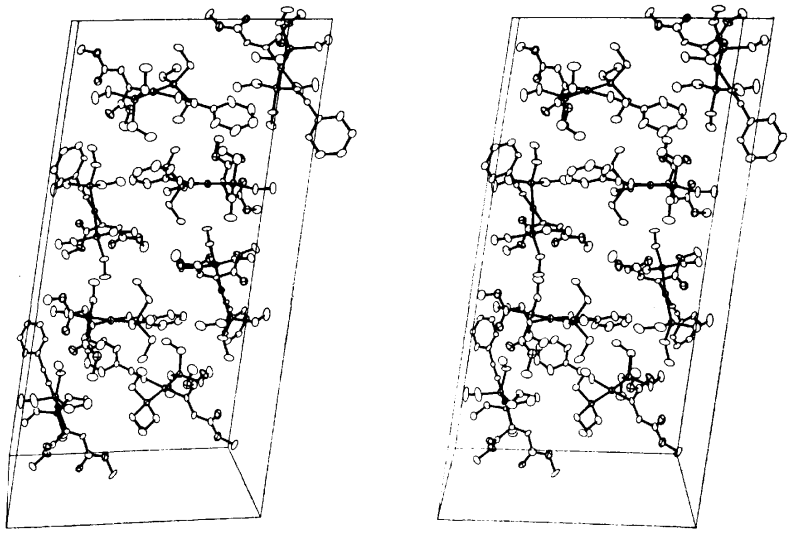

Fig. 3. Stereoscopic view of the crystal structure projected along the b axis. Non-hydrogen atoms are represented by thermal ellipsoid at 50% probability level.

(av. 1.40 and 1.40 Å) and bond angles (av. 120 and 120°) in the phenyl groups are normal.

As has been mentioned before, the triethylphosphine groups, including the P(1) atom have different conformations in two independent molecules: the PEt_3 group in Molecule B is rotated about 120° from that in A (Fig. 1). The exceptionally large thermal parameters of C(23) and C(33) atoms in A and the unusually short C(23A)–C(33A) bond length [1.28(5) Å] suggest disorder in these atoms. The other C–C bond lengths in ethyl groups have normal values (av. 1.55 Å).

The crystal structure is shown in Fig. 3. No close intermolecular atomic contacts less than the usual van der Waals distances can be observed.

All the computations in the present study were carried out on a NEAC 2200-700 computer at Osaka University. Figures 1 and 3 were drawn on a NUMERICON 7000 system at Osaka University, with a local version of ORTEP.[6]

The authors wish to express their deep thanks to Professor Nobue Hagihara, Professor Kenkichi Sonogashira, and their co-workers of Osaka University for their kindness in supplying crystals and for their many helpful discussions.

References

1) E. C. Colthup and L. S. Meriwether, *J. Org. Chem.*, **27**, 3930 (1962); H. Singer and G. Wilkinson, *J. Chem. Soc.*, *A*, **1968**, 190.

2) R. F. Heck, "Organotransition Metal Chemistry," Academic Press, N. Y. (1974), p. 175.

3) Y. Tohda, K. Sonogashira, and N. Hagihara, *J. Organomet. Chem.*, **110**, C53 (1976).

4) T. Ashida, The Universal Crystallographic Computing Program System-Osaka, The Computation Center, Osaka University (1973), p. 55.

5) "International Tables for X-Ray Crystallography," Vol. IV, The Kynoch Press, Birmingham (1974), p. 71.

6) C. K. Johnson, ORTEP, Report ORNL-3794, Oak Ridge National Laboratory, Tennessee, 1965.

Solution Properties of Phycocyanin. IV. Studies of the Self-association Equilibrium of Phycocyanin in a pH 6.8 Solution*

Naomichi Iso, Haruo Mizuno, Takahide Saito, Noriko Nitta, and Katsuaki Yoshizaki**

Department of Food Science and Technology, Tokyo University of Fisheries, Konan, Minato-ku, Tokyo 108

(Received May 7, 1977)

The self-association of phycocyanin in a buffer of pH 6.8 with an ionic strength of 0.1 has been studied by sedimentation equilibrium measurements in the temperature range from 5.2 to 25 °C. The self-association of this system increases with a decrease in the temperature. A quantitative evaluation of the experimental data for this system indicates that the type of the association reaction is not a simple mechanism such as a monomer⇌*n*-mer, but the discrete monomer⇌trimer⇌tetramer mechanism is probable. Several thermodynamic quantities, such as the Gibbs free energy change, $\Delta G°$, the enthalpy change, $\Delta H°$, and the entropy change, $\Delta S°$, accompanying the self-association reaction were computed on the basis of the equilibrium constants. From the results, it is considered that the association process is similar to the ordinary crystallization, and that the formation of a tetramer proceeds at a higher concentration than that in which the trimerization reaction is completed.

Phycocyanin isolated from red or blue-green algae undergoes reversible self-associating reactions according to changes in the environment such as the pH, the ionic strength, the temperature, and the protein concentration of the solution.

In the course of our study of the solution properties of phycocyanin,[1-3] it was supposed, from an analysis of the sedimentation velocity data and of the sedimentation equilibrium data, that the self-association equilibrium was predominantly a monomer⇌hexamer at pH 5.4 and also probably a monomer⇌trimer at pH 6.8, both at the temperature of 25 °C. In the higher-concentration region at pH 6.8, however, the formation of the various aggregates higher than a trimer was probable, judging from the osmotic pressure measurements.

The purpose of the work reported here was to investigate the self-association reacting equilibrium of phycocyanin at pH 6.8 in more detail. That is, the equilibrium constants of the self-association of phycocyanin under various conditions of temperature were determined by sedimentation equilibrium measurements. The characteristic functions, such as the Gibbs free energy change, $\Delta G°$, the enthalpy change, $\Delta H°$, and the entropy change, $\Delta S°$, accompanying the self-association were evaluated on the basis of the equilibrium constants obtained.

Experimental

Materials. The crystalline phycocyanin used in this study was obtained from red alga *Porphyra tenera* by repeated precipitations with ammonium sulfate. The details of the purification of the protein were presented in an earlier paper.[1] The ionic strength was limited to 0.1 in the phosphate buffer in this work.

Sedimentation Equilibruim Measurements. The sedimentation equilibrium measurements were carried out using a magnetically suspended equilibrium-type ultracentrifuge and a Hitachi Model UCA-1 ultracentrifuge, with an interference optical system. All the measurements were made in about a 2-mm liquid column at a given speed for approximately 24 h so as to ensure that an equilibrium was established. The rotor speeds were set at approximately 8000—9000 rpm, and the measurements were done in the temperature range from 5.2 to 25.0 °C.

The apparent weight-average molecular weight at a position, r, in the solution column, $M_w^{app}(r)$, was calculated from the following equation:

$$M_w^{app}(r) = \frac{2RT}{(1-\bar{v}\rho)\omega^2}\frac{\mathrm{d}\ln c}{\mathrm{d}(r^2)}, \quad (1)$$

where $\bar{v}$ is the partial specific volume of the solute; ρ, the density of the solvent; ω, the angular velocity of the rotor; R, the gas constant, and T, the absolute temperature. The concentration, c, was calculated from the concentration difference, Δc, by the use of the formula

$$\Delta c = \Delta N\lambda/(\mathrm{d}n/\mathrm{d}c)L,$$

where ΔN is the number of fringes: λ, the wavelength of light (546 nm); $\mathrm{d}n/\mathrm{d}c$, the refractive-index increment, and L, the thickness of the cell (12 mm).

The Solvent Density and the Partial Specific Volume. The solvent density, ρ, at 16.5—25.0 °C was determined by means of a pycnometer approximately 10 ml in volume. The values of 1.0027 g/ml, 1.0039 g/ml, and 1.0046 g/ml were obtained at 25.0, 20.0, and 16.5 °C respectively. The values of 1.0052 g/ml at 11.5 °C and of 1.0056 g/ml at 5.2 °C were obtained by the linear extrapolation of the values at 16.5—25.0 °C.

Bull and Breese[4] have pointed out that the variation in the partial specific volume of the protein, $\bar{v}$, with the temperature is only *ca.* 0.08% at 5—25 °C. Accordingly, the literature value[5] of 0.744 ml/g was used for the partial specific volume of phycocyanin in all the measurements in this work.

The Refractive-index Increment. The refractive-index increment, $\mathrm{d}n/\mathrm{d}c$, was calculated from the schlieren pattern of a protein solution of a known concentration at 25.0 °C; this pattern has been obtained by using a synthetic-boundary cell. The value of 0.180 ml/g was obtained, and this value was used for the analysis of the experimental data in this work.

Results and Discussion

Figure 1 shows the concentration dependence of the apparent weight-average molecular weight of phycocyanin at pH 6.8, with the open and closed marks being indicative of the experiments performed at 5.2 and 25.0

* Presented at the 25th Annual Meeting of the Society of Polymer Science, Japan, Tokyo, May 30, 1976.

** Department of Chemistry, Tokyo Kyoiku University, Otsuka, Bunkyo-ku, Tokyo 112.

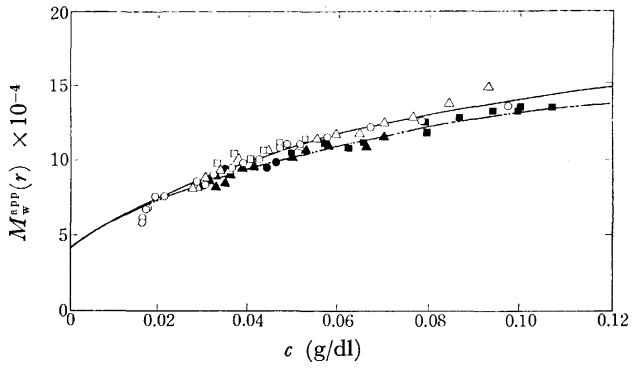

Fig. 1. Plots of $M_w^{app}(r)$ *versus* c for phycocyanin in a buffer of pH 6.8 and ionic strength 0.1 at 5.2 °C (upper curve) and at 25.0 °C (lower curve). The closed mark and the open mark correspond to the values at 25.0 °C and those at 5.2 °C, respectively. The various mark represent the values obtained with solutions of different initial concentration (g/dl): ○, 0.0048; △, 0.0054; □, 0.0031; ●, 0.0053; ▲, 0.0043; ■, 0.0084.

°C respectively. Similar results were obtained from the measurements performed at 20.0, 16.5, and 11.5 °C; these results stood between those at 25.0 °C and those at 5.2 °C in Fig. 1, in the order of the temperature. Consequently, it is clear that the association proceeds with a decrease in the temperature.

In our preceding paper,[3] the molecular weight of the monomer, M_1, of phycocyanin was assumed to be 42000 on the basis of the results of the osmotic pressure measurements. The value of 42000 is, then, used as the molecular weight of the monomer in the following analysis.

Tang and Adams[6] have proposed an analytical method applicable to any monomer⇌n-mer association system; by using it we can determine both the value of n and the equilibrium constant, K_n. According to their theory, the weight fraction of a monomer, f_1, is given as follows:

$$f_1 = \frac{U+2-(2/n)-\{[U+2-(2/n)]^2-8(Un-1)/n\}^{1/2}}{4(n-1)/n}, \tag{2}$$

where

$$U = 2(M_1/M_n^{app}(r)) - (M_1/M_w^{app}(r)) = \frac{2}{c}\int_0^{c_1}\left(\frac{c}{c_1}\right)dc_1 - \left(\frac{c}{c_1}\right)\frac{dc_1}{dc}, \tag{3}$$

$M_n^{app}(r)$ is the apparent number-average molecular weight at a position, r, which can be calculated from the value of $M_w^{app}(r)$ as measured by using the following equation:[7]

$$\frac{M_1}{M_n^{app}(r)} = \frac{1}{c}\int_0^c \frac{M_1}{M_w^{app}(r)}dc, \tag{4}$$

where c indicates the concentrations of all the species and where c_1 is the monomer concentration ($c_1=cf_1$). With the value of f_1, the following equation is derived:

$$(1-f_1)/f_1 = K_n(cf_1)^{n-1}. \tag{5}$$

If the arbitrarily chosen value of n is suitable, a plot of $(1-f_1)$ *versus* $c^{n-1}f_1^n$ will give a straight line which passes through the point of orgin.

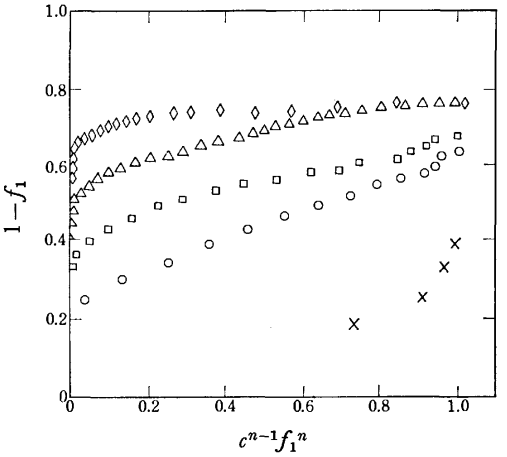

Fig. 2. Plots of $(1-f_1)$ *versus* $c^{n-1}f_1^n$, which are based on Eq. 5, for phycocyanin in a buffer of pH 6.8 and ionic strength 0.1 at 25.0 °C. ×, $n=2$; ○, $n=3$; □, $n=4$; △, $n=6$; ◇, $n=12$.

Their theory was applied to the self-association of phycocyanin in a buffer of pH 6.8 with ionic strength 0.1 at 5.2—25.0 °C. Figure 2 shows the plot of $(1-f_1)$ *versus* $c^{n-1}f_1^n$ at 25.0 °C, in which the n-values are chosen from 2 to 12. As is shown in Fig. 2, the plots were not straight lines passing through the point of origin; similar results were obtained at other temperatures. From these results, it may be concluded that the type of the association of phycocyanin in a buffer of pH 6.8 with an ionic strength 0.1 is not so simple as a monomer⇌n-mer.

In previous works[1,2] it was shown that the type of the association of phycocyanin at pH 6.8 was a monomer ⇌trimer at relatively low concentrations and that various higher aggregates were formed at higher concentrations. Therefore, we assume in this work that the type of the association of phycocyanin at this pH is a monomer⇌trimer⇌tetramer or a monomer⇌trimer⇌hexamer. Adams *et al.*[7,8] have analyzed the multi-component system and have proposed a procedure for evaluating an equilibrium constant for a monomer⇌dimer⇌trimer and a monomer⇌dimer⇌tetramer associations. Extending their treatment to a monomer ⇌trimer⇌tetramer, the following equation may be developed:

$$12M_1/M_w^{app}(r) = 7 + 6f_a e^{-BM_1c} + 6BM_1c - 1/[(M_1/M_w^{app}(r) - BM_1c], \tag{6}$$

where B is the non-ideal parameter. Moreover, the quantity f_a is the apparent weight fraction of the monomer and is obtained from the values of $M_w^{app}(r)$ and c according to the following equation:

$$\ln f_a = \int_0^c \left(\frac{M_1}{M_w^{app}(r)} - 1\right)\frac{dc}{c}. \tag{7}$$

In this work, it is assumed that all of the systems considered here are pseudo-ideal solutions, since the thermodynamic pseudo-ideality of the phycocyanin solution was confirmed by the experimental results from the osmotic pressure measurements.[2]

When the non-ideal parameter, B, is zero, the following equation may be derived for a monomer⇌trimer

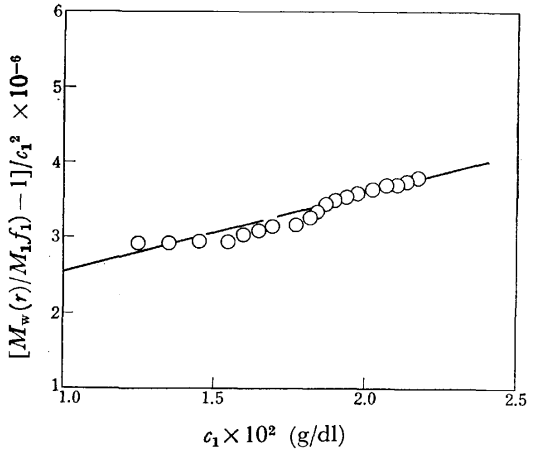

Fig. 3. Plot of $[(M_w(r)/M_1f_1)-1]/c_1^2$ *versus* c_1, which is based on Eq. 8, for phycocyanin in a buffer of pH 6.8 and ionic strength 0.1 at 25.0 °C.

⇌tetramer equilibrium:

$$[(M_w(r)/M_1f_1)-1]/c_1^2 = 3K_3 + 4K_4c_1, \quad (8)$$

where K_3 and K_4, which are calculated on the basis of the weight concentration (g/dl), are the equilibrium constants of a monomer⇌trimer equilibrium and a monomer⇌tetramer equilibrium respectively. According to Eq. 8, the plot of the value of the left-hand side of Eq. 8 *versus* c_1 will be linear. An example of such a plot is shown in Fig. 3, which is obtained from the data of the measurement at 25.0 °C. The plots at all the other temperatures were linear, like that at 25.0 °C, although they were excluded from Fig. 3 for the sake of simplicity. That is, all the plots of $[(M_w(r)/M_1f_1)-1]/c_1^2$ *versus* c_1 were linear. This means that the type of the association of phycocyanin in a buffer of pH 6.8 with an ionic strength 0.1 is probably a monomer⇌trimer⇌tetramer in the temperature range from 5.2 to 25.0 °C.

In the case of a linear plot such as that at 25.0 °C in Fig. 3, the values of K_3 and K_4 may be obtained from the intercept and the slope of the plot respectively. The values thus obtained are summarized in Table 1. These K_3- and K_4- values suggest that the lower aggregate, the trimer, decreases, while the higher aggregate, the tetramer, increases, with a decrease in the temperature. In order to ascertain the obtained values of K_3 and K_4, the values of $M_w(r)$ at some concentrations were calculated by using the K_3- and K_4-values and were compared with the values obtained experimentally. The calculated values were in good agreement with the experimental ones. Table 2 shows an example of the comparison.

A similar analytical procedure was applied to the experimental data assuming a monomer⇌trimer⇌hexamer system. The equilibrium constants of hexamerization, K_6, obtained decreased with a decrease in the temperature. The association proceeds with a decrease in the temperature, as is shown in Fig. 1. On the assumption that the higher aggregate may increase relatively with the process of association, the value of K_6 should increase with a decrease in the temperature. Thus, the associating mechanism of a monomer⇌trimer⇌hexamer system was not considered in this report.

Table 1. The equilibrium constants of the monomer ⇋ trimer and monomer ⇌ tetramer of phycocyanin at pH 6.8 and an ionic strength 0.1

T (°C)	$K_3 \times 10^{-4}$ (dl/g)^2	$K_4 \times 10^{-6}$ (dl/g)^3
5.2	0.36	0.25
11.5	0.34	0.28
16.5	0.45	0.38
20.0	0.75	0.18
25.0	0.68	0.18

Table 2. The comparison of the $M_w(r)$'s obtained at 25.0 °C and calculated by using K_3 and K_4

c (g/dl)	$M_w(r) \times 10^{-4}$	
	Obtained	Calculated
0	4.2_0	4.2_0
0.01	6.0_0	6.8_3
0.02	7.4_0	8.6_9
0.03	8.6_0	9.7_2
0.04	9.6_0	10.4
0.05	10.6	10.9
0.06	11.3	11.2
0.07	12.0	11.5
0.08	12.6	11.7
0.09	12.9	11.9
0.10	13.0	12.1
0.11	13.0	12.2
0.12	13.0	12.4

Figures 4 and 5 show the plots of $\ln k_3$ *versus* $1/T$ and $\ln k_4$ *versus* $1/T$ respectively, where k_3 and k_4 are the molar equilibrium constants. The values of enthalpy change, $\Delta H°$, accompanying the trimerization and the tetramerization were calculated to be 6.4 kcal/mol and −3.8 kcal/mol respectively from the slope in each plot. Table 3 lists the enthaply changes, $\Delta H°$, the Gibbs free energy changes, $\Delta G°$, and the entropy changes, $\Delta S°$, for both reactions.

From the negative value of $\Delta G°$ and the positive value of $\Delta S°$, it is clear that the aggregation process is spontaneous under the experimental conditions in this study. The Gibbs free energy changes in Table 3 correspond to −4——5 kcal/mol per monomer unit. The values are comparable to the values reported for many other proteins.[9] Oosawa and Asakura[10] have suggested that the aggregation process of protein is similar to a crystallization mechanism. Figure 6 shows the relation between the concentration of the aggregate and the total concentration of the solution, which is estimated by using the values of K_3 and K_4 here obtained. The behavior shown in Fig. 6 may be considered to be similar to crystalization. The estimation using the values of K_3 and K_4 shows that the c_4 becomes equal to c_3 when $c=ca.$ 0.78 g/dl. In Fig. 6, the concentration range is limited to that used in the sedimentation equilibrium measurements. After that concentration the tetramer forms quickly.

Table 3. The characteristic thermodynamic functions accompanying the self-association reaction of phycocyanin

The units of ΔH° and ΔG° are (kcal/mol), and that of ΔS°, (cal/mol K)

	k (l/mol)$^{2 \text{ or } 3}$	ΔH°	ΔG°	ΔS°
monomer-trimer	$(2.0—4.0)\times10^{10}$	6.4	−13.1—−14.4	69—70
monomer-tetramer	$(4.5—9.3)\times10^{15}$	−3.8	−20.1—−21.3	59—60

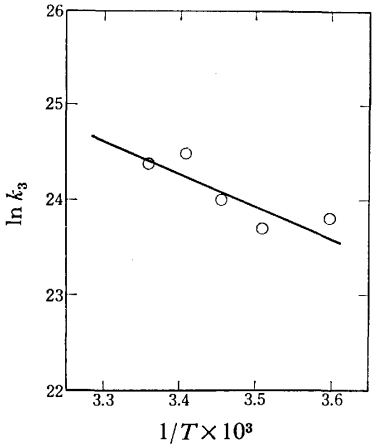

Fig. 4. Plot of $\ln k_3$ *versus* $1/T$.

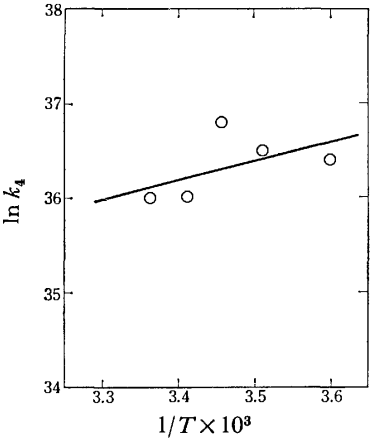

Fig. 5. Polt of $\ln k_4$ *versus* $1/T$.

Although a large part of the aggregate is a trimer in concentrations under 0.1 g/dl at this pH and ionic strength, small amounts of a higher aggregate, which is assigned to a tetramer in this work, also exist in this system. That is the reason why we could not determine the molecular shape of phycocyanin at the pH and ionic strength of a previous work.[2] The number-average molecular weight, M_n of 1.7×10^5 was obtained in the concentration range from 0.5 to 1.5 g/dl from the osmotic pressure measurements.[2] The M_n is calculated to be 1.4×10^5 in the same concentration range by using the values of K_3 and K_4 here obtained. The calculated value of 1.4×10^5 is comparable to the experimental value of 1.7×10^5. Considering the facts

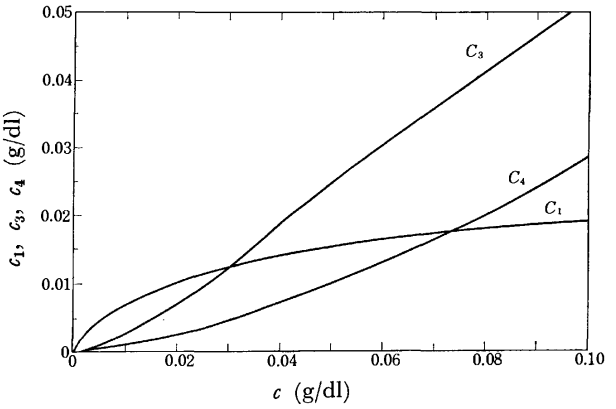

Fig. 6. The relation between the concentration of aggregate (c_3 and c_4) and the concentration of solution, which is estimated by using the values of K_3 and K_4 obtained.

that the phycocyanin molecule is most stable in solution at pH 5.4, and that the predominant species is assumed to be hexamer under this pH condition,[3] the associating system in this work may be intermediate from a monomeric state to a stable polymeric state, the hexamer. This is clear from the thermodynamic analysis of the association reaction of phycocyanin at pH 5.4.

References

1) T. Saito, N. Iso, and H. Mizuno, *Bull. Chem. Soc. Jpn.*, **47**, 1375 (1974).
2) A. Kotera, T. Saito, N. Iso, H. Mizuno, and N. Taki, *Bull. Chem. Soc. Jpn.*, **48**, 1176 (1975).
3) H. Mizuno, T. Saito, and N. Iso, *Bull. Chem. Soc. Jpn.*, **48**, 3496 (1975).
4) H. B. Bull and K. Breese, *J. Phys. Chem.*, **72**, 1817 (1968).
5) A. Hattori, H. C. Crepsi, and J. J. Katz, *Biochemistry*, **4**, 1225 (1965).
6) L.-H. Tang and E. T. Adams, Jr., *Arch. Biochem. Biophys.*, **157**, 520 (1973).
7) E. T. Adams, Jr., and M. S. Lewis, *Biochemistry*, **4**, 1646 (1965).
8) W. E. Ferguson, C. M. Smith, E. T. Adams, Jr., and G. H. Barlow, *Biophys. Chem.*, **1**, 325 (1975).
9) I. M. Klotz, N. R. Langerman, and D. W. Darnall, *Ann. Rev. Biochem.*, **39**, 25 (1970).
10) F. Oosawa and S. Asakura, "Thermodynamics of the Polymerization of Protein," Academic Press, London (1975), p. 25.

Violet Emission Spectra of CN($B^2\Sigma$) Produced in the Photodissociation of HCN and DCN

Setsuko TATEMATSU and Kozo KUCHITSU

Department of Chemistry, Faculty of Science, The University of Tokyo, Hongo, Bunkyo-ku, Tokyo 113

(Received June 17, 1977)

Emission spectra of the CN violet band system ($B^2\Sigma$-$X^2\Sigma$, $\Delta v=0$) produced in the photodissociation of HCN and DCN by Lyman-α radiation (121.6 nm) were observed with resolution of about 0.2 nm and with sample pressures of 0.01—1.5 Torr. The spectral features of the two were similar, but the main peaks ($v'=0$—4) from DCN appeared more sharply than the corresponding peaks from HCN. The relative vibrational populations and the effective rotational temperatures were estimated by a band-envelope analysis. No indication of vibrational population inversion was observed. The CN($B^2\Sigma$) radical produced from DCN is likely to have slightly higher vibrational (0.31 ± 0.08 eV measured from the zero-point energy) and rotational energies (0.15 ± 0.02 eV) than that from HCN (0.23 ± 0.08 and 0.11 ± 0.02 eV, respectively).

There has recently been a spate of theoretical and experimental investigations on the photofragmentation of simple polyatomic molecules. Many of them provide valuable information on the partitioning of internal and kinetic energies of fragments.[1,2] Diatomic radicals produced from linear molecules, particularly the CN($B^2\Sigma$) radicals from various cyanides, have been studied most extensively.[3] For instance, the CN($B^2\Sigma$) radicals from cyanogen halides were analyzed in detail by Mele and Okabe[4] and were recently reinvestigated by Ashfold and Simons[5,6] with much higher resolution.

One of the problems of current interest is the isotope effect on the production of CN($B^2\Sigma$) from HCN/DCN by vacuum ultraviolet radiation. In a number of recent theoretical studies,[7-10] model repulsive potentials for the C–H/C–D bond were estimated by fitting the vibrational distributions of CN($B^2\Sigma$) from HCN observed by Mele and Okabe,[4] and isotope effects on the photofragmentation probability and the vibtational distributions for the krypton and xenon resonance lines were predicted. The predictions made by Band and Freed[7] and by Atabek *et al.*[9,10] differed drastically from each other, but they equally emphasized the importance of an experimental measurement of this isotope effect for the elucidation of the mechanism and dynamics of photodissociation. It should be ideal for this purpose if the CN violet and red emission bands from HCN and DCN by radiations of several different wavelengths were to be measured with high resolution and high accuracy.

The present study is our effort in this direction but only to the limit of our current experimental facilities.[11] Relative vibrational distributions of the CN($B^2\Sigma$) produced from HCN and DCN with various sample pressures by Lyman-α radiation (121.6 nm) have been estimated by analyzing the violet emission spectra measured with medium resolution. The rotational distributions have been estimated by band-envelope simulation.

Experimental

The apparatus and experimental details have been reported previously.[11] The Lyman-α radiation was obtained by 2.45 GHz microwave discharge of a 1 : 3 mixture of hydrogen and helium. Fluorescence in the visible region from the sample cell was detected by a Nikon P-250 grating monochromator (1200 Gr/mm) blazed at 500 nm. The CN violet $\Delta v=0$ bands around 388 nm were observed with slit widths of 40—60 μm. The slit width of 50 μm corresponds to an energy resolution of about 0.2 nm. The signal from a photomultiplier (HTV R585) was measured by a photon counting system.

The sample of HCN was prepared by the reaction[12] of sodium cyanide with sulfuric acid at 60—80 °C. DCN was prepared in a similar way, D_2SO_4 and D_2O being used in place of H_2SO_4 and H_2O. The samples were purified by vacuum distillation. An infrared spectrum of HCN showed no trace of impurity. The isotopic purity of DCN was estimated from the Balmer emission intensities of H and D atoms produced by impact of 200 eV electrons.[13] The upper limit of hydrogen impurity was estimated from the observed intensity ratio to be about 10%.

Analysis

Spectral Features. The $\Delta v=0$ sequences of the CN violet band ($B^2\Sigma$-$X^2\Sigma$) produced from HCN and DCN were observed at pressures ranging from 0.01 to 1.5 Torr. The spectra observed around 388 nm were assigned according to the table prepared by Pearse and Gaydon.[14] The $\Delta v=-1$ sequence was also observed around 420 nm, but it was much weaker than the $\Delta v=$

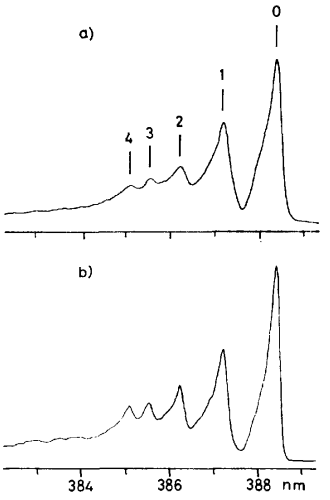

Fig. 1. Emission spectra of the CN violet ($B^2\Sigma$-$X^2\Sigma$) $\Delta v=0$ band from a) HCN, 0.04 Torr and b) DCN, 0.02 Torr with a slit width of 50 μm. The numbers indicate positions of the P-branch heads of the $v'=$ 0—4 bands.

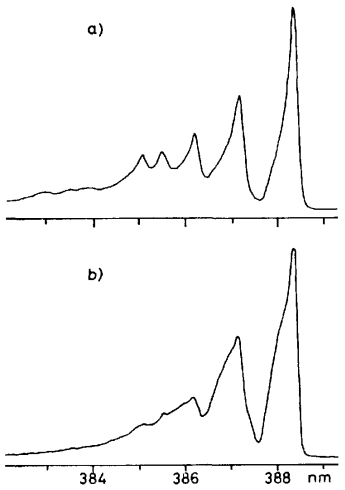

Fig. 2. Typical pressure dependence of the CN($B^2\Sigma$-$X^2\Sigma$) $\Delta v=0$ band from DCN at a) 0.01 Torr and b) 0.62 Torr. The effective rotational temperatures were estimated from best-fit analysis to be a) 1700±200 K and b) 1000±200 K.

0 sequence. Though the isotope effect on the emission yield was not measured quantitatively, there appeared to be no drastic isotope difference at this wavelength. Typical emission spectra measured under similar experimental conditions and at the lowest practicable sample pressures are shown in Fig. 1. The peak intensities of the bands decreased monotonically from $v'=0$ to 4, and no anomalous population distributions were observed. The bands from DCN had sharper peaks than those from HCN. The rotationally perturbed lines[5,6,15] were not observed significantly, but the spectral resolution was insufficient to prove or disprove their presence.

For both species the spectral features were essentially independent of the sample pressure below about 0.4 Torr, but they started to change when the pressure was further increased, as shown in Fig. 2: At a higher pressure the peaks were broadened and those with $v'=2$—4 became obscured. This trend has not been observed clearly for other cyanides studied concurrently[11,16] (BrCN, ICN, and $(CN)_2$).

Band-Envelope Analysis. The vibrational populations, $P_{v'}$, and the effective rotational temperatures, $T_r(v')$, of the CN($B^2\Sigma$) states immediately after production from HCN and DCN, *i.e.*, essentially free from subsequent collisional relaxations, were estimated by a band-envelope analysis.[11,17,19] Since the bands with $v'=5$—10 were buried within those of the lower vibrational levels, only crude estimates of $P_{v'}$ for $v'\geqq 5$ could be obtained. In addition, since the rotational lines were not resolved, the effective rotational temperatures for all the vibrational states were assumed to be equal. The parameters, $P_{v'}$ and T_r, were adjusted by trial and error to obtain the best fit of the calculated band envelope to the observed spectrum. A typical comparison of the observed and calculated band envelopes is shown in Fig. 3. The effective rotational temperatures were thus estimated to be 1300±200 and 1700±200 K for HCN and DCN, respectively. The relative vibrational populations, $P_{v'}/P_0$, in the low-pressure limit are listed in Table 1.

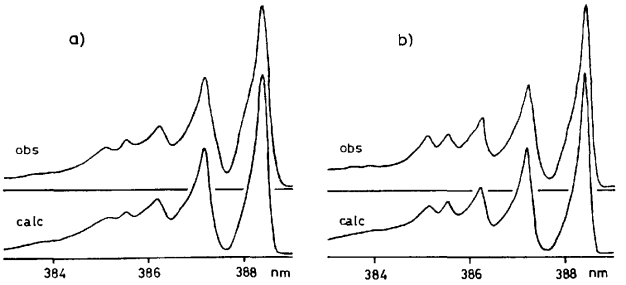

Fig. 3. Comparisons of the observed and best-fit calculated band envelopes of the CN($B^2\Sigma$-$X^2\Sigma$) $\Delta v=0$ from (a) HCN and (b) DCN.

Table 1. Relative vibrational populations ($P_{v'}/P_0$) for CN($B^2\Sigma$) produced in the photodissociation of HCN and DCN

v'	HCN[a]	DCN[a]	HCN[b]
0	1.00	1.00	1.00
1	0.54(5)	0.56(5)	0.40
2	0.20(5)	0.28(5)	0.09
3	0.10(4)	0.17(4)	0.012
4	0.06(3)	0.09(3)	0.006
5	0.04	0.07	—
6	0.02	0.04	—
7	<0.01	0.01	—

a) The present study, by Lyman-α radiation (121.6 nm). Uncertainties represent estimated limits of error in the last significant digits. The relative populations for $v'\geqq 5$ are only crude estimates. b) Crude estimates made by Mele and Okabe (Ref. 4) for the CN($B^2\Sigma$) produced by krypton resonance lines (116.5 and 123.6 nm).

Discussion

Distributions of Internal Energy. By use of the relative populations estimated in Table 1 and the known vibrational energy levels,[20] the average vibrational energies (above the zero-point energy) of the CN($B^2\Sigma$) produced from HCN and DCN are calculated to be 0.23±0.08 and 0.31±0.08 eV, respectively. The average rotational energies, given by kT_r, are estimated to be 0.11±0.02 and 0.15±0.02 eV for HCN and DCN, respectively. The estimated uncertainties include those due to the overlapping of the observable bands, the approximations made in the analysis, and the various sources of experimental error.

The available excess energy in the production of CN($B^2\Sigma$) from HCN corresponds to the difference between the photon energy (10.2 eV) and the sum of the C–H bond dissociation energy (5.2[21] or 5.5[22] eV) and the electronic energy of CN($B^2\Sigma$) from the ground vibrational state of CN($X^2\Sigma$) (3.1 eV).[23] Thus, the fractions of the available energy used for vibrational and rotational excitations are about 15 and 8%, respectively. These estimates agree with those reported by Mele and Okabe[4] for the CN($B^2\Sigma$) produced from HCN by the Kr (and Xe) resonance lines, about 13

and 7%.

Notwithstanding the appreciable uncertainties estimated above, the present study indicates slight isotope effects on the vibrational and rotational excitations of CN($B^2\Sigma$) produced from HCN and DCN.[24] A further more accurate measurement is necessary for a critical comparison of experimental and theoretical distributions of vibrational and rotational energies. In this connection, it is noteworthy that significant isotope effects on the vibrational and rotational distributions of CN($B^2\Sigma$) produced from HCN and DCN have been found in our recent study of electron-impact dissociation (*ca.* 200 eV) with much higher resolution.[25]

Pressure Effect. The observed changes in the spectrum when the sample pressure is higher than 0.4 Torr— the decrease in the peak intensities corresponding to $v'=2$—4 and the apparent decrease in the effective rotational temperatures— may be ascribed to collisional relaxations. If one assumes that the rotational relaxation takes place effectively at about 0.5 Torr, where the mean time between the formation of the CN($B^2\Sigma$) radicals and their collisions with the parent molecules is comparable with their natural radiative lifetime (presumably about 60 ns[26-28]), then it is possible to estimate roughly the effective cross section for the rotational relaxation of CN($B^2\Sigma$). Since the mean velocity of CN($B^2\Sigma$) is estimated to be about 6×10^4 cm/s, the cross section for rotational relaxation is probably of the order of 150 Å^2.

The research has been supported by Science and Technology Grants of Toray Science Foundation.

References

1) S. A. Rice, "Dynamics of Primary Photochemical Processes" in "Excited States," Vol. 2, E. C. Lim, Ed., Academic Press, New York (1975), pp. 111—320.
2) J. P. Simons, "The Dynamics of Photodissociation," Chemical Society Specialist Periodical Reports, Gas Kinetics and Energy Transfer, Vol. 2, London (1977), p. 56.
3) S. Mukamel and J. Jortner, *J. Chem. Phys.*, **65**, 3735 (1976) and the references cited therein.
4) A. Mele and H. Okabe, *J. Chem. Phys.*, **51**, 4798 (1969).
5) M. N. R. Ashfold and J. P. Simons, *Chem. Phys. Lett.*, **47**, 65 (1977).
6) M. N. R. Ashfold and J. P. Simons, *J. Chem. Soc., Faraday Trans. 2*, **73**, 858 (1977).
7) Y. B. Band and K. F. Freed, *Chem. Phys. Lett.*, **28**, 328 (1974).
8) Y. B. Band and K. F. Freed, *J. Chem. Phys.*, **63**, 4479 (1975).
9) O. Atabek, J. A. Beswick, R. Lefebvre, S. Mukamel, and J. Jortner, *J. Chem. Phys.*, **65**, 4035 (1976).
10) O. Atabek, J. A. Beswick, R. Lefebvre, S. Mukamel, and J. Jortner, *Chem. Phys. Lett.*, **45**, 211 (1977).
11) S. Tatematsu, T. Nakagawa, T. Kondow, and K. Kuchitsu, *Bull. Chem. Soc. Jpn.*, **50**, 1056 (1977).
12) G. Bauer, "Handbook of Preparative Inorganic Chemistry," Vol. 1, Academic Press, New York (1963).
13) I. Nishiyama, private communication, 1976.
14) R. W. B. Pearse and A. G. Gaydon, "The Identification of Molecular Spectra," John Wiley & Sons, Inc., New York (1963).
15) H. E. Radford and H. P. Broida, *Phys. Rev.*, **128**, 231 (1962); *J. Chem. Phys.*, **38**, 644 (1963).
16) S. Tatematsu and K. Kuchitsu, unpublished data.
17) T. Urisu and K. Kuchitsu, *Chem. Phys. Lett.*, **18**, 337 (1973).
18) T. Urisu and K. Kuchitsu, *J. Photochem.*, **2**, 409 (1973).
19) I. Tokue, T. Urisu, and K. Kuchitsu, *J. Photochem.*, **3**, 273 (1975).
20) R. J. Fallon, J. T. Vanderslice, and R. D. Cloney, *J. Chem. Phys.*, **37**, 1097 (1962).
21) D. D. Davis and H. Okabe, *J. Chem. Phys.*, **49**, 5526 (1968).
22) B. deB Darwent, "Bond Dissociation Energies in Simple Molecules," NSRDS-NBS 31, U. S. Government Printing Office, Washington, D. C. (1970).
23) W. Jevons, *Proc. R. Soc. London, Ser. A*, **112**, 407 (1926).
24) The difference of 0.07 eV in the available energies, originating from the difference in the zero-point energies of HCN and DCN, is expected to have no appreciable influence on the isotope effect (unless the photon energy is very close to the threshold). This is because only a small fraction of the already small difference in the energies for the isotopic molecules is converted into the internal energy.
25) I. Nishiyama, I. Tokue, and K. Kuchitsu, to be published.
26) H. S. Liszt and J. E. Hesser, *Astrophys. J.*, **159**, 1101 (1970).
27) C. K. Luk and R. Bersohn, *J. Chem. Phys.*, **58**, 2153 (1973).
28) W. M. Jackson, *J. Chem. Phys.*, **61**, 4177 (1974).

The Two-Photon Excitation Spectrum of Phenanthrene Crystal

Hiroshi OTOKOZAWA, Shigehiro INOMATA, Naohiko MIKAMI, and Mitsuo ITO
Department of Chemistry, Faculty of Science, Tohoku University, Aramaki, Aoba, Sendai 980
(Received July 14, 1977)

The two-photon excitation spectrum of phenanthrene crystal was measured and compared with the corresponding usual one-photon absorption spectrum. It was found that the two-photon spectrum consists of a one-photon like system and a system characteristic of a two-photon process. The vibronic couplings in phenanthrene were discussed on the basis of the observed results.

The two photon excitation spectra of benzene and naphthalene have recently been studied by many workers.[1-9] The most characteristic feature of the two-photon absorption of these molecules from the ground state to the lowest excited electronic state $^1B_{2u}(L_b)$ is the appearance of strong vibronic bands involving a b_{2u} vibration whose frequency in the excited state is about 1500 cm^{-1}. This is regarded as evidence of vibronic coupling involving the ground state.[10]

For both phenanthrene and naphthalene, the lowest excited electronic state is ^1L_b. For phenanthrene, it is $^1A_1(L_b)$, for which both one-photon and two-photon transitions from the ground state are allowed under the molecular symmetry C_{2v}. (See Fig. 1.) This is in contrast to naphthalene, where the transition to the $^1B_{2u}(L_b)$ state is one-photon allowed but two-photon forbidden. The purpose of the present work is to see how different the one-photon and two-photon spectra are for phenanthrene, where the electronic transition is simultaneously allowed by both one-photon and two-photon selection rules.

Phenanthrene was purified by zone refining. The single crystal was grown by the Bridgman method, and the ab cleavage plane was normal to incident light. The two-photon excitation spectra were measured at 4.2 K by irradiating with a dye laser over the tunable wavelength region between 580 and 700 nm and detecting the resulting fluorescence. These two-photon energies cover the entire spectral region of the lowest excited electronic state of phenanthrene (300 to 350 nm). The method of the spectral measurements is the same as that reported in our previous paper.[9] The accuracy of the observed frequencies is ±2 cm^{-1} for sharp bands. It was found that a trace of anthracene remaining in the phenanthrene crystal as an imputiry serves as an efficient fluorescence sensitizer. Polarization measurements were attempted. However, no significant difference was found between the main bands of the spectra with light polarized parallel to either the a or the b axis of the crystal. The two-photon excitation spectrum was observed also for the mixed crystal of biphenyl at 4.2 K. It was found that the spectrum of the mixed crystal is essentially the same as that of the pure crystal.

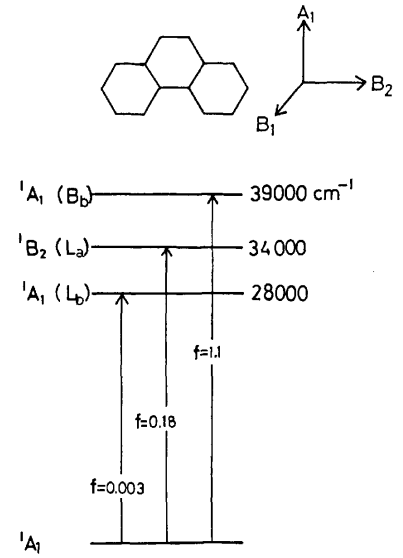

Fig. 1. Low lying electronic states of phenanthrene.

Figure 2 shows the two-photon excitation spectrum of the phenanthrene crystal, together with the corresponding usual absorption spectrum reproduced from a paper by Craig and Gordon.[11] Table 1 lists the observed frequencies of the main bands. It is seen from Fig. 2 that the 0,0 band appears strongly in the two-photon spectrum. This indicates that the electronic transition $^1A_1(L_b)$—$^1A_1$ is two-photon allowed as expected. Details of the Davydov splitting of the 0,0 band are somewhat different for the one-photon and the two-photon cases. In both spectra the lower frequency Davydov component is very sharp and has the same frequency. On the other hand the higher frequency component is very broad in the two-photon spectrum but is sharp in the one-photon spectrum. The maximum of the higher frequency component is

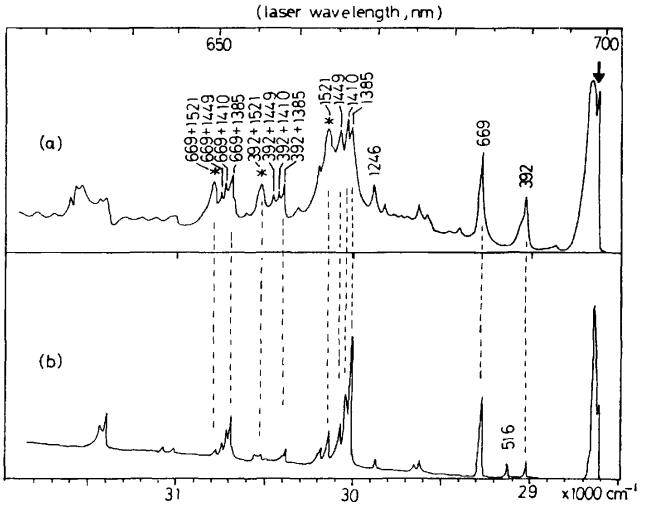

Fig. 2. (a) Two-photon excitation spectrum of phenanthrene crystal at 4.2 K. (b) One-photon absorption spectrum of phenanthrene crystal at 4.2 K taken from Ref. 11. The arrow indicates the position of the average frequency of the Davydov components of the one-photon 0,0 band (28627 cm^{-1}).

Table 1. One-photon and two-photon absorptions of phenanthrene crystal at 4.2 K

One-photon (Craig, Gordon[11])			Two-photon (present work)			Analysis
ν (cm^{-1})	ν (cm^{-1})	Rel. int.	ν (cm^{-1})	ν (cm^{-1})	Rel. int.	
28597 Av. 28656 28627	0	vs vs	28599 (one photon: 28663 28627)	0	vs, sh vs, br	0
29022	395	m	29019	392	m	392 a_1
29143	516	m				516 a_1
29298	671	s	29296	669	s	669 a_1
			29582	955	w	955 a_1
29632	1005	w	29630	1003	w	1003 a_1
29881	1254	w	29873	1246	m	1246 a_1
30003	1376	vs	30012	1385	s	1385 a_1
30034	1407	vs	30037	1410	s	1410 a_1
30073	1446	s	30076	1449	s	1449 a_1
30146	1519	m	30148	1521	s, br	1521 a_1
30215	1588	m	30209	1582	w	1582 a_1
			30313	1686	w	669+1003
30405	1778	w	30405	1778	m	392+1385
			30449	1822	w	392+1410
			30481	1854	w	392+1449
30525	1898	w				516+1385
30555	1928	w	30549	1922	m, br	392+1521
						516+1416
30680	2053	s	30684	2066	m, sh	669+1385
30708	2081	m	30717	2090	m, sh	669+1410
30747	2120	w	30760	2133	w	669+1449
30821	2194	w	30817	2190	m, br	669+1521
31378	2751	s	31392	2765	m, br	2×1385

also shifted by 7 cm^{-1} toward higher frequency from the corresponding one-photon peak. The breadth and frequency shift of the higher frequency band suggest a considerable contribution by a low frequency lattice phonon to the intensity of the 0,0 band of the two-photon spectrum. Coupling with the phonon is also suggested for other broad vibronic bands.

In our vibrational analysis of the two-photon excitation spectrum, the average frequency of the Davydov components of the one-photon 0,0 band (28627 cm^{-1})[11] was taken as the origin from which frequency differences of the main vibronic bands were measured. It is seen from Fig. 2 and Table 1 that the observed frequency differences of the main bands agree very well with those of the one-photon spectrum within experimental error. There is a one-to-one correspondence between the one-photon and two-photon spectra for all the main vibronic bands, showing again the simultaneous one-photon and two-photon allowed transition.* However, the relative intensities of the vibronic bands are somewhat different in the two spectra. The two-photon vibronic bands can be classified into two groups, **A** and **B**, on the basis of their relative intensities in comparison with the intensities of the corresponding one-photon bands. The bands belonging to groups **A** are those for which the intensities relative to that of the 0,0 band are similar to those of the one-photon spectrum. The main bands in this group are 392, 669, 1385, 1410, 1449 cm^{-1} and their combinations. With a few exceptions they are generally very sharp. Group **B** consists of the vibronic bands involving 1521 cm^{-1} shown by asterisk in Fig. 2. These bands are weak in the one-photon spectrum, but fairly strong in the two-photon spectrum. They are also characterized by their broadness.

According to the ordinary absorption studies of the pure and mixed crystals of phenanthrene by Craig and Gordon[11] and by Hochstrasser and Small,[12] all the main bands in the **A** system involve totally symmetric vibrations in the excited state. The most interesting feature of the **A** system is the origin of the 669 cm^{-1} band. Craig and Gordon,[11] Hochstrasser and Small,[12] and Craig and Small[13] concluded that the 669 cm^{-1} band in the one-photon spectrum borrows part of its intensity from higher excited electronic states by vibronic coupling. Since 669 cm^{-1} is a totally symmetric vibration, this is an interesting example of vibronic coupling through a totally symmetric vibration. If this interpretation is correct, we expect some difference in the intensity of the 669 cm^{-1} band relative to that of the 0,0 band between the one-photon and two-photon spectra, because vibronic coupling schemes reflected in the two spectra are generally different. On the other hand, if the 0,1 band is not a vibrationally induced one, the relative intensity should be equal both for the one-photon and the two-photon spectra.

It is difficult to compare quantitatively the intensity

* The one-photon band, 0,0+516 cm^{-1} is missing in the two-photon spectrum. This will be discussed later.

ratio of the 0,0 band and the 0,0+669 cm^{-1} band in the two spectra because of rather large errors in the intensity estimation. However, qualitatively the observed ratios are not greatly different. At least the intensity relation between the 0,0 band and the 0,0+669 cm^{-1} band is similar in the two spectra. The intensity of the 669 cm^{-1} band relative to the 1385 cm^{-1} band, which has a non-vibronic origin according to Craig and Small[13], is also similar. These facts seem to support a non-vibronic origin for the 669 cm^{-1} band, contrary to the conclusion of Craig *et al.* However our qualitative intensity data are not good enough to derive a definite conclusion at the present time. We merely point out here that comparison between the relative intensities of one-photon and two-photon spectra may provide an additional clue for the origin of vibronic bands.

We shall consider next the **B** system, which consists of the vibronic bands involving the totally symmetric excited-state frequency of 1521 cm^{-1}. The **B** system is fairly strong in the two-photon spectrum and weak in the one-photon one. As mentioned before, the strong appearance of vibronic bands whose excited-state frequency is about 1500 cm^{-1} is a common characteristic of the ^1L_b—^1A two-photon absorption spectra of benzene and naphthalene.[1-9] Therefore, the **B** system of phenanthrene may be assumed to arise from the same cause as that of benzene and naphthalene. The effective vibrations of benzene and naphthalene are bond alternating C–C stretching modes. In benzene they are $\nu_{14}(b_{2u})$ (1566 cm^{-1} in the $^1B_{2u}(L_b)$ state and 1309 cm^{-1} in the ground state) and in naphthalene $\nu_{21}(b_{2u})$ (1535 cm^{-1} in $^1B_{2u}(L_b)$ state and 1361 cm^{-1} in the ground state). Mikami and Ito[10] concluded that these vibronic bands are due to vibronic coupling between the ground state and the lowest excited $^1B_{2u}(L_b)$ state through these vibrations. The excited-state vibration at 1521 cm^{-1} of phenanthrene probably corresponds to ν_{14} of benzene and ν_{21} of naphthalene, although it is a totally symmetric vibration in phenanthrene because of reduction of the molecular symmetry. Assuming that the vibronic coupling involving the ground state is similar to the cases of benzene and naphthalene, the corresponding ground state frequency should be smaller than 1521 cm^{-1}. It is expected to be between 1300 and 1400 cm^{-1} by analogy to benzene and naphthalene. There are several totally symmetric vibrations in this frequency region.[14] Unfortunately, it is difficult to pick a specific one because of the lack of knowledge about the detailed vibrational modes.

Finally, it may be worthwhile to mention that the moderately intense one-photon vibronic band 0,0+516 cm^{-1}, reported by Craig and Gordon[11] is entirely missing in our two-photon spectrum (see Fig. 2). In the one-photon spectrum it has about the same intensity as that of the nearby band 0,0+392 cm^{-1}. The latter appears with a considerably intensity in the two-photon spectrum, but the former is absent. This suggests that the 0,0+516 cm^{-1} band has a vibrationally induced origin which occurs selectively in the one-photon spectrum. The excited-state vibration of 516 cm^{-1} was assigned by Craig and Gordon[11] and by Hochstrasser and Small[12] to a totally symmetric vibration. The frequency is close to the excited-state $\nu_6(e_{2g})$ mode of benzene at 520 cm^{-1} [15] (606 cm^{-1} in the ground state) and to the excited-state $\nu_{33}(b_{3g})$ of 438 cm^{-1} of naphthalene[16] (506 cm^{-1} in the ground state). These vibrations are well known to be the most effective perturbing vibrations in mixing the ^1L_b states and ^1B states of benzene and naphthalene. Therefore, it is highly probable that the totally symmetric 516 cm^{-1} vibration of phenanthrene is the perturbing vibration coupling the lowest excited $^1A_1(L_b)$ state and the third lowest $^1A_1(B_b)$ state of this molecule.

We are appreciative to Drs. K. Kaya, Y. Udagawa, and F. A. Miller for the useful comments and discussions.

References

1) R. M. Hochstrasser, J. E. Wessel, and H. N. Sung, *J. Chem. Phys.*, **60**, 317 (1974).
2) L. Wunsch, H. J. Neusser, and E. W. Schlag, *Chem. Phys. Lett.*, **31**, 433 (1975).
3) D. M. Friedrich and W. M. McClain, *Chem. Phys. Lett.*, **32**, 541 (1975).
4) R. G. Bray, R. M. Hochstrasser, and H. N. Sung, *Chem. Phys. Lett.*, **33**, 1 (1975).
5) R. M. Hochstrasser, H. N. Sung, and J. E. Wessel, *J. Chem. Phys.*, **58**, 4694 (1973).
6) R. M. Hochstrasser, H. N. Sung, and J. E. Wessel, *Chem. Phys. Lett.*, **24**, 168 (1974).
7) A. Bergman and J. Jortner, *Chem. Phys. Lett.*, **26**, 323 (1974).
8) R. P. Drucker and W. M. McClain, *Chem. Phys. Lett.*, **28**, 255 (1974).
9) N. Mikami and M. Ito, *Chem. Phys. Lett.*, **31**, 472 (1975).
10) N. Mikami and M. Ito, *J. Chem. Phys.*, **64**, 3077 (1976).
11) D. P. Craig and R. D. Gordon, *Proc. R. Soc. London, Ser. A*, **288**, 69 (1965).
12) R. M. Hochstrasser and G. J. Small, *J. Chem. Phys.*, **45**, 2270 (1966).
13) D. P. Craig and G. J. Small, *J. Chem. Phys.*, **50**, 3827 (1969).
14) V. Schettino, N. Neto, and S. Califano, *J. Chem. Phys.*, **44**, 2724 (1966).
15) H. Sponer, G. Nordheim, A. L. Sklar, and E. Teller, *J. Chem. Phys.*, **7**, 207 (1939).
16) D. P. Craig, J. M. Hollas, M. F. Redies, and S. G. Wait, *Phil. Trans. Faraday Soc.*, **A253**, 543 (1961).

Magnetic Cross-over in Hexa-coordinate Iron(II) Complexes of Several Schiff Bases

Yonezo MAEDA, Shunji SHITE, Yoshimasa TAKASHIMA, and Yuzo NISHIDA

Department of Chemistry, Faculty of Science 33, Kyushu University, Hakozaki, Higashiku, Fukuoka 812

(Received October 26, 1976)

Iron(II) complexes with the Schiff bases of 6-methyl-2-pyridinecarbaldehyde and 2-quinolinecarbaldehyde, and with α,α′-diimine were prepared. The Mössbauer spectra and magnetic susceptibilities of the complexes, $Fe(cbi)_2(NCS)_2\cdot\frac{2}{3}CHCl_3$, $Fe(tbi)_2(NCS)_2\cdot CHCl_3$, $Fe(mpmea)_2(ClO_4)_2$, and $Fe(mepma)_3(ClO_4)_2$, were studied in the range of 80—298 K. It was found that these complexes show a $^5T_2$-$^1A_1$ spin transition in the solid state.

A number of iron(II) complexes have been shown to exhibit a $^5T_2$-$^1A_1$ spin equilibrium.[1-3] In this paper we wish to describe new iron complexes exhibiting such a spin equilibrium. The ligand abbreviations used in this work are as follows.

Abbreviation	*Ligand*
pbi	*N,N′*-diphenyl-2,3-butanediimine
tbi	*N,N′*-di-*p*-tolyl-2,3-butanediimine
cbi	*N,N′*-bis(*p*-chlorophenyl)-2,3-butanediimine
mbi	*N,N′*-bis(*p*-methoxyphenyl)-2,3-butanediimine
mepma	*N*-(6-methyl-2-pyridylmethylene)-methylamine
pmea	*N*-(2-pyridylmethylene)-2-(2-pyridyl)ethylamine
pema	*N*-[1-(2-pyridyl)ethylidene]-(2-pyridyl)methylamine
peea	*N*-[1-(2-pyridyl)ethylidene]-2-(2-pyridyl)ethylamine
mpmma	*N*-(6-methyl-2-pyridylmethylene)-2-pyridylmethylamine
mpmea	*N*-(6-methyl-2-pyridylmethylene)-2-(2-pyridyl)ethylamine
qmma	*N*-(2-quinolylmethylene)-2-pyridylmethylamine
qmea	*N*-(2-quinolylmethylene)-2-(2-pyridyl)ethylamine

Experimental

The preparation of the 2-quinolinecarbaldehyde was accomplished by the reduction of ω,ω-dibromoquinaldine with silver nitrate.[4] 6-methyl-2-pyridinecarbaldehyde, 2-pyridylmethylamine, and 2-(2-pyridyl)ethylamine were purchased from the Aldrich Co., Ltd. The ligands, α,α′-diimines, were isolated before the preparation of the complexes. The other Schiff bases were used without isolating them as solids. The complexes were prepared by mixing iron(II) salts and the Schiff bases in oxygen-free ethanol. The crude products were recrystallized from chloroform or ethanol. All the complexes except $Fe(qmma)_2(ClO_4)_2$ and $Fe(qmea)_2(ClO_4)_2$ were generally stable for oxidation.

The analytical data of the complexes prepared are listed in Table 1. The microanalyses were carried out at the Elemental Analysis Center of Kyushu University. The Mössbauer, electronic reflectance, and infrared spectra, and the conductivities in organic solvents were obtained as has been described elsewhere.[3] The effective magnetic moments, μ_{eff}, were obtained from the $\mu_{eff}=2.83\sqrt{\chi_m^T}$ relation, where χ_m is the molar susceptibility after applying diamagnetic corrections for both the ligands and anions.

Results and Discussion

Characterization of the Samples. The molar conductivities of the complexes listed in Table 2 indicate that the thiocyanates are non-electrolytic in acetone or chloroform, while the perchlorates behave as unibivalent electrolytes. The infrared spectra of the perchlorates show absorptions around 1090 cm^{-1}, which indicate that the perchlorate ion is ionic in these complexes.

Magnetic Susceptibilities. Figure 1 shows the variation in μ_{eff} with the temperature for the complexes which have cross-over points. Although we observed the Mössbauer absorptions of only low-spin states in

Table 1. Analytical data (%)

Complexes	Found				Calcd			
	C	H	N	Fe	C	H	N	Fe
$Fe(pbi)_2(NCS)_2\cdot\frac{1}{2}CHCl_3$	59.27	4.74	12.62	8.05	58.81	4.62	11.93	7.94
$Fe(tbi)_2(NCS)_2\cdot CHCl_3$	56.38	4.97	10.24	6.80	56.97	5.23	10.23	6.81
$Fe(cbi)_2(NCS)_2\cdot\frac{2}{3}CHCl_3$	47.52	3.38	9.62	7.54	48.28	3.33	9.75	7.13
$Fe(mbi)_2(NCS)_2$	58.58	5.27	10.80	7.55	58.64	5.24	10.99	7.31
$Fe(pema)_2(ClO_4)_2$	45.28	3.91	12.07	a)	46.09	3.84	12.41	8.25
$Fe(peea)_2(ClO_4)_2$	47.32	4.71	10.91	a)	47.67	4.26	11.91	7.92
$Fe(pmea)_2(ClO_4)_2$	45.96	3.91	12.25	a)	46.09	3.84	12.41	8.25
$Fe(mpmma)_2(ClO_4)_2\cdot H_2O$	44.29	3.92	11.66	8.46	44.90	4.03	12.09	8.04
$Fe(mpmea)_2(ClO_4)_2$	47.20	4.32	11.58	8.26	47.67	4.26	11.91	7.92
$Fe(qmma)_2(ClO_4)_2$	51.13	3.79	11.29	6.90	51.96	3.92	11.36	7.46
$Fe(qmea)_2(ClO_4)_2$	52.55	3.93	11.72	7.14	53.19	3.91	10.95	7.19
$Fe(mepma)_3(ClO_4)_2$	43.62	4.65	12.64	9.15	43.86	4.57	12.79	8.50

a) Was not analyzed.

TABLE 2. MAGNETIC MOMENTS, MOLAR CONDUCTIVITIES, INFRARED SPECTRA, AND REFLECTANCE SPECTRA OF THE IRON COMPLEXES

Compounds	μ_{eff} (BM) at 295 K	Λ_m[a]	ν_{NCS} (cm^{-1})	Reflectance data (cm^{-1})
$Fe(pbi)_2(NCS)_2 \cdot \frac{1}{2}CHCl_3$	2.87	0(A)	2070, 2080 2120	29000 s, 15700 s, br, 10500 s
$Fe(tbi)_2(NCS)_2 \cdot CHCl_3$	4.26	12.2(A)	2055 2110	29000 s, 16000 s, br, 10300 s
$Fe(cbi)_2(NCS)_2 \cdot \frac{2}{3}CHCl_3$	4.78	0(C)	2049, 2055	29000 s, 15200 s, br, 10000 s
$Fe(mbi)_2(NCS)_2$	3.07	0(C)	2045, 2065 2095, 2110	29000 s, 15700 s, br, 10500
$Fe(pema)_2(ClO_4)_2$	1.09	175.9(A)		24200 s, 20400 sh, 17500 s, br
$Fe(peea)_2(ClO_4)_2$	1.07	187.7(A)		23600, 17100 s, br
$Fe(pmea)_2(ClO_4)_2$	1.22	190.0(A)		25000 s, 19800 sh, 17200 s, br
$Fe(mpmma)_2(ClO_4)_2 \cdot H_2O$	1.86	163.8(A)		24400 s, 20400 sh, 17500 s, br, 16800 s, br
$Fe(mpmea)_2(ClO_4)_2$	4.38	199.9(A)		25000 s, 20200 s, 18000 w, sh, 16700 s, br
$Fe(mepma)_3(ClO_4)_2$	5.58	213.6(A)		18500 s, 9400 sh
$Fe(qmma)_2(ClO_4)_2$	1.60	b)		b)
$Fe(qmea)_2(ClO_4)_2$	5.44	b)		b)

a) cm^{-2} mho mol^{-1} at 25 °C; concn 10^{-3} M in acetone (A) or chloroform (C). b) Was not measured.

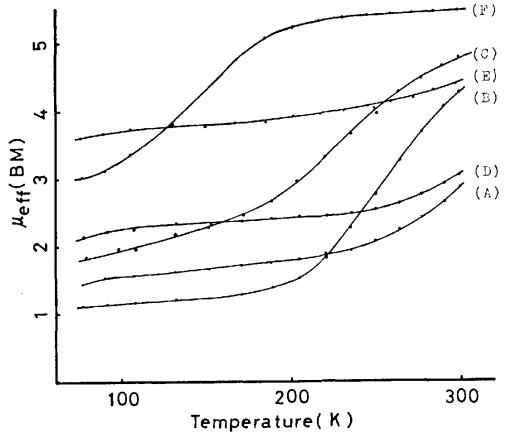

Fig. 1. Variation of the magnetic monemt μ_{eff} with temperature for (A) $Fe(pbi)_2(NCS)_2 \cdot \frac{1}{2}CHCl_3$, (B) $Fe(tbi)_2(NCS)_2 \cdot CHCl_3$, (C) $Fe(cbi)_2(NCS)_2 \cdot \frac{2}{3}CHCl_3$, (D) $Fe(mbi)_2(NCS)_2$, (E) $Fe(mpmea)_2(ClO_4)_2$, and (F) $Fe(mepma)_3(ClO_4)_2$.

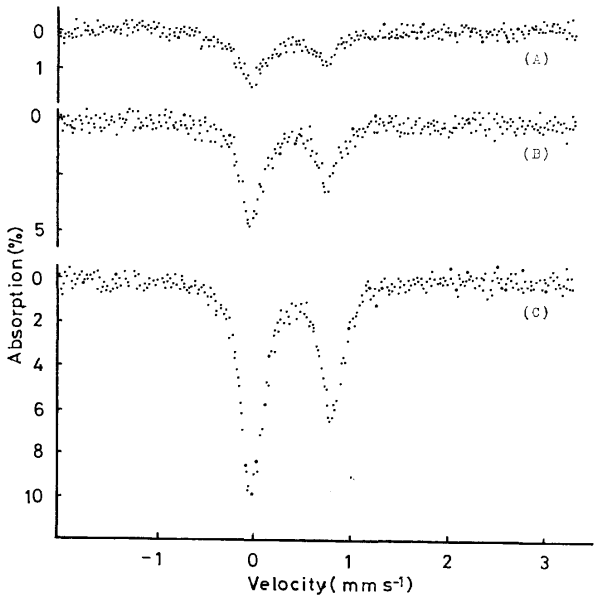

Fig. 2. Mössbauer spectra of $Fe(pbi)_2(NCS)_2 \cdot \frac{1}{2}CHCl_3$ at (A) 296 K, (B) 196 K, and (C) 80 K.

$Fe(pbi)_2(NCS)_2 \cdot \frac{1}{2}CHCl_3$ and $Fe(mbi)_2(NCS)_2$ at 296 K, the magnetic moments of the complexes probably increase at high temperatures, in view of the tendency of the curves. The magnetic data at 295 K show that $Fe(pmea)_2(ClO_4)_2$, $Fe(pema)_2(ClO_4)_2$, $Fe(peea)_2(ClO_4)_2$, $Fe(mpmma)_2(ClO_4)_2 \cdot H_2O$, and $Fe(qmma)_2(ClO_4)_2$ adopt a low-spin configuration (Table 2). A small residual paramagnetism is commonly observed in low-spin iron complexes with imine chelates. A large residual paramagnetism has been observed in the polymorph II of $Fe(phen)_2(NCS)_2$.[5] The origin of the rather high paramagnetism of $Fe(cbi)_2(NCS)_2 \cdot \frac{2}{3}CHCl_3$, $Fe(mbi)_2(NCS)_2$, $Fe(pbi)_2(NCS)_2 \cdot \frac{1}{2}CHCl_3$, and $Fe(mpmma)_2(ClO_4)_2 \cdot H_2O$ at low temperatures is not clear.

$Fe(mpmma)_2(ClO_4)_2 \cdot H_2O$ (five- and five-membered ring) adopts a low-spin configuration, and $Fe(mpmea)_2(ClO_4)_2$ (five- and six-membered ring) is a cross-over complex. $Fe(qmma)_2(ClO_4)_2$ (five- and five-membered ring) and $Fe(qmea)_2(ClO_4)_2$ (five- and six-membered ring) adopt low- and high-spin configurations respectively. These facts show that, in the complexes studied here, the ligands fields of the ligands forming five- and five-membered rings are stronger than those of the ligands forming five- and six-membered rings. The change in the spin multiplicity of iron upon the substitution of the methyl group at the 6-position of the pyridine ring is best attributed to the steric effect of methyl.

Mössbauer Spectra. Table 3 shows the Mössbauer parameters of the complexes. The isomer shifts, δ_{Fe}, were measured relative to the center of the spectrum

TABLE 3. MÖSSBAUER PARAMETERS FOR SEVERAL IRON COMPLEXES (mm/s)

Complexes	At 296 K		At 196 K		At 80 K		Spin state
	δ_{Fe}	ΔE	δ_{Fe}	ΔE	δ_{Fe}	ΔE	
$Fe(pbi)_2(NCS)_2\cdot\frac{1}{2}CHCl_3$		a)				a)	$S=2$
	0.30	0.75			0.38	0.80	$S=0$
$Fe(tbi)_2(NCS)_2\cdot CHCl_3$	0.96	2.91	0.99	3.07		a)	$S=2$
		a)	0.32	0.74	0.37	0.78	$S=0$
$Fe(cbi)_2(NCS)_2\cdot\frac{2}{3}CHCl_3$	0.87	2.74	1.03	2.92		a)	$S=2$
		a)	0.34	0.75	0.37	0.78	$S=0$
$Fe(mbi)_2(NCS)_2$		a)				a)	$S=2$
	0.30	0.74			0.38	0.78	$S=0$
$Fe(pema)_2(ClO_4)_2$	0.21	0.98			0.26	0.99	$S=0$
$Fe(peea)_2(ClO_4)_2$	0.25	0.61			0.39	0.80	$S=0$
$Fe(mpmma)_2(ClO_4)_2\cdot H_2O$	0.27	0.94			0.34	1.15	$S=0$
$Fe(mpmea)_2(ClO_4)_2$	0.94	1.92	0.98	2.14	1.02	2.57	$S=2$
		a)	0.35	0.98	0.35	1.03	$S=0$
$Fe(pmea)_2(ClO_4)_2$	0.32	0.89			0.39	0.89	$S=0$
$Fe(mepma)_3(ClO_4)_2$	1.00	1.06	0.98	1.43	1.09	2.09	$S=2$
		a)	0.46	0.71	0.48	0.73	$S=0$
$Fe(qmma)_2(ClO_4)_2$	0.31	0.60					$S=0$
$Fe(qmea)_2(ClO_4)_2$	0.94	2.59			1.00	2.96	$S=2$

a) Was not observable.

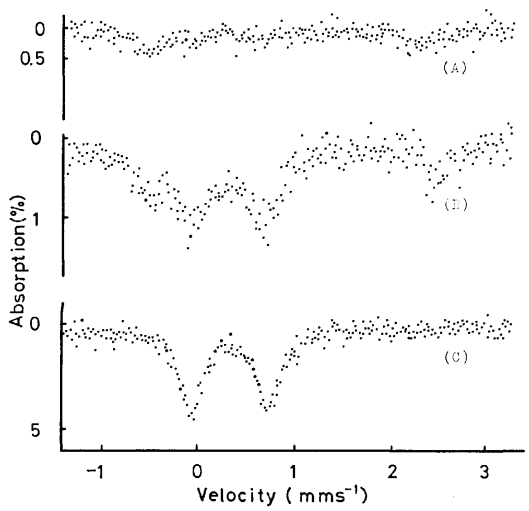

Fig. 3. Mössbauer spectra of $Fe(tbi)_2(NCS)_2\cdot CHCl_3$ at (A) 296 K, (B) 196 K, and (C) 80 K.

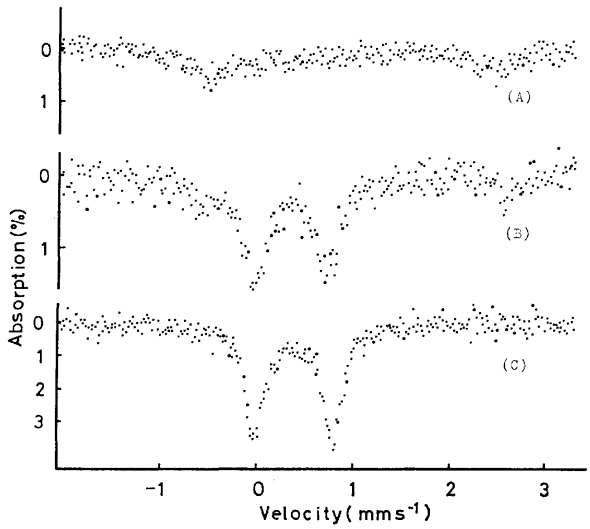

Fig. 4. Mössbauer spectra of $Fe(cbi)_2(NCS)_2\cdot\frac{2}{3}CHCl_3$ at (A) 296 K, (B) 196 K, and (C) 80 K.

of iron foil. The Mössbauer spectrum of $Fe(pbi)_2(NCS)_2\cdot\frac{1}{2}CHCl_3$ shows an asymmetric doublet, the center of which is situated in the range of low-spin iron(II) complexes at 296 and 80 K. The Mössbauer spectrum of $Fe(mbi)_2(NCS)_2$ at 296 K is virtually identical with that of $Fe(pbi)_2(NCS)_2\cdot\frac{1}{2}CHCl_3$, both giving only a low-spin state, though the former spectrum is not shown here. No spectrum of a high-spin state has been observed because of the small recoilless fraction or small populations of the high-spin isomer at 296 K, as can be seen in Fig. 2.

$Fe(tbi)_2(NCS)_2\cdot CHCl_3$ and $Fe(cbi)_2(NCS)_2\cdot\frac{2}{3}CHCl_3$ clearly show the Mössbauer absorptions of the $^1A_1$ and $^5T_2$ states at 196 K, as is shown in Figs. 3 and 4.

The Mössbauer spectra of $Fe(mpmea)_2(ClO_4)_2$ and $Fe(mepma)_3(ClO_4)_2$ in Figs. 5 and 6 show absorptions consisting of two species at 80 K, *i.e.*, high-spin and low-spin states. The component of the low-spin configuration increases as the temperature descends.

Assuming that the Debye-Waller factors, $f(^5T_2)$ and $f(^1A_1)$, are equal, we are able to calculate the proportions of the high-spin isomer, $S(^5T_2)$, from the Mössbauer spectral area and the magnetic data respectively. The magnetic moment values for $S=2$ and $S=0$ states were taken to be 5.30 and 0.80 BM for $Fe(mpmea)_2(ClO_4)_2$, and 5.46 and 0.80 BM for $Fe(mepma)_3(ClO_4)_2$, respectively. The results are shown below:

$Fe(mpmea)_2(ClO_4)_2$;	Temp(K)	196	80	14
(from Mössbauer data)	$S(^5T_2)(\%)$	50	45	50
(from magnetic data)	$S(^5T_2)(\%)$	53	45	—

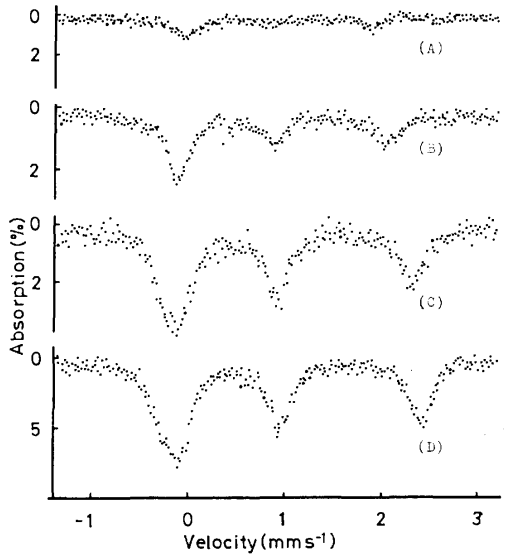

Fig. 5. Mössbauer spectra of $Fe(mpmea)_2(ClO_4)_2$ at (A) 296 K, (B) 196 K, (C) 80 K, and (D) 14 K.

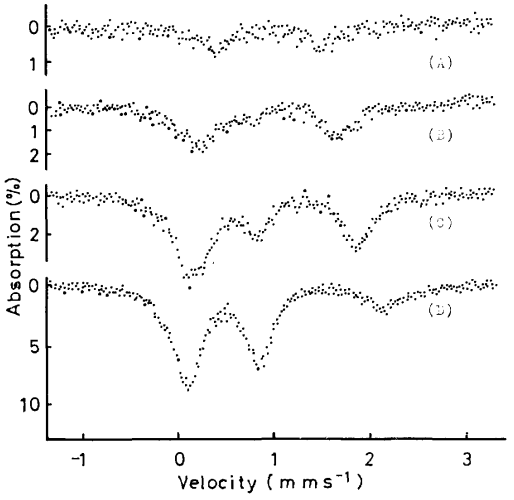

Fig. 6. Mössbauer spectra of $Fe(mepma)_3(ClO_4)_2$ at (A) 296 K, (B) 196 K, (C) 147 K, and (D) 80 K.

$Fe(mepma)_3(ClO_4)_2$;	Temp(K)	196	147	80
(from Mössbauer data)	$S(^5T_2)$(%)	68	63	33
(from magnetic data)	$S(^5T_2)$(%)	91	59	30

The difference between the populations of the high-spin isomer calculated from the Mössbauer spectral area and from the magnetic moment may show that the Debye-Waller factor $f(^5T_2)$ is less than $f(^1A_1)$.

For an axial field resulting from a trigonal ligand symmetry, the quadrupole splitting results primarily from an electron either in $t_{2g}{}^0(d_z{}^2)$ or in $t_{2g}{}^{\pm}$, where the $t_{2g}{}^{\pm}$ are:

$$t_{2g}{}^{+} = \frac{1}{3}(\sqrt{2}\,|d_{x^2-y^2}> - |d_{zx}>),$$

$$t_{2g}{}^{-} = \frac{1}{3}(\sqrt{2}\,|d_{xy}> + |d_{yz}>).$$

For the determination of the orbital ground state it is necessary to know the sign of the electric-field gradient tensor(V_{zz}). In $Fe(mephen)_3(ClO_4)_2$[6] and $Fe(2\text{-Cl-phen})_3(ClO_4)_2$,[7] negative quadrupole splittings have been observed. The lowest orbital of $Fe(mepma)_3(ClO_4)_2$, therefore, may be $d_z{}^2$. In this state, the field splitting of t_{2g} orbitals increases when the temperature is lowered (*i.e.*, from about 165 cm^{-1} at 296 K to 210 cm^{-1} at 80 K) in Ingall's approximation (assuming $\lambda = -80$ cm^{-1}).[8] This result corresponds to an increasing compression of the coordination octahedron over the $^5T_2$-$^1A_1$ transition region as the temperature descends.

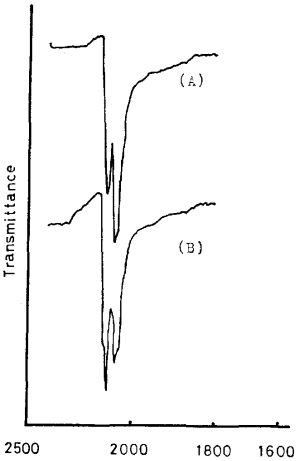

Fig. 7. The C=N stretching vibration region of the infrared spectra of $Fe(pbi)_2(NCS)_2 \cdot \frac{1}{2}CHCl_3$ at (A) 340 K and (B) 298 K.

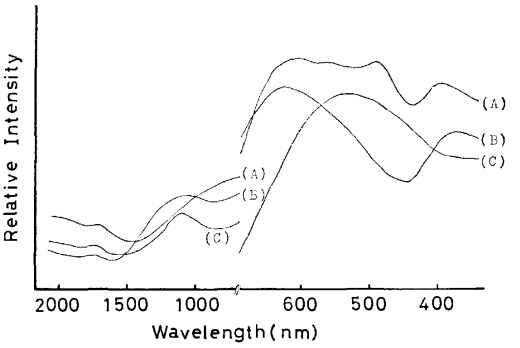

Fig. 8. Electronic reflectance spectra for (A) $Fe(mpmea)_2(ClO_4)_2$, (B) $Fe(cbi)_2(NCS)_2 \cdot \frac{2}{3}CHCl_3$, and (C) $Fe(mepma)_3(ClO_4)_2$.

Infrared Spectra. The data in Table 2 show that, in the $^5T_2$ state, the thiocyanate ion is *N*-bonded.[9] It has been reported that the C–N stretching modes in the $^1A_1$ state are observed in the range of 2100—2128 cm^{-1}.[10] Figure 7 shows the infrared spectra of $Fe(pbi)_2(NCS)_2 \cdot \frac{1}{2}CHCl_3$ in the range of 1800—2400 cm^{-1} at about 298 and 340 K. The spectrum at 340 K may be considered to be predominantly populated in the $^5T_2$ ground state, and the spectrum at 298 K, in the $^1A_1$ ground state.

The splitting of the C–N stretching band has been assigned to a *cis*-configuration of the compound.[10] If $Fe(tbi)_2(NCS)_2 \cdot CHCl_3$ (having an unsplitted C–N stretching band) had a *trans*-configuration, its quadrupole splitting in the low-spin state would be twice as large as that of the other complexes.[11] It seems to be ambiguous, therefore, for the splitting of the ν_{C-N} band

to be used to distinguish between *cis*- and *trans*-configurations.

Electronic Spectra. Figure 8 shows the electronic reflectance spectra of several complexes. The positions of the absorption maxima are listed in Table 2. The d-d spectra for α,α-diimine complexes show a shoulder band at about 10500 cm^{-1}. If we take $\Delta(^5T_2)=10D_q=10500\ cm^{-1}$, $\Delta(^5T_2)$ should be almost equal to the spin-pairing energy $\pi=\frac{5}{2}B+4C=18.5B$ (assuming the usual relation, $C=4B$, between the electron-repulsion parameters). Thus, taking $\Delta(^5T_2)=\pi$, one obtains $B(^5T_2)=568\ cm^{-1}$. Since B is 1058 cm^{-1} for free Fe^{2+}, the nephelauxetic ratio is $\beta=B(\text{complex})/B(\text{free ion})=0.54$. Since the value of D_q for $Fe(H_2O)_6^{2+}$ is estimated to be 1040 cm^{-1},[12] and since the critical D_q has been reported to be in the range of 1160—1340 cm^{-1}, or 1250±80 cm^{-1},[13] the D_q for iron-diimine complexes is considered to be significantly small. There are two plausible reasons for the small D_q of the iron-diimine complexes. First, the peak of 10500 cm^{-1} is one component of the doublet, while the other, on the high-energy side, is masked by the stronger charge-transfer band because site symmetry for the metal is distorted from O_h. Second, the Racah parameters for the free metal ion may be reduced drastically by ligand coordination because of the concomitant reduction of interelectronic repulsions.

References

1) H. A. Goodwin, *Coord. Chem. Rev.*, **18**, 293 (1976).
2) R. L. Martin and A. H. White, *Trans. Met. Chem.*, **4**, 113 (1968).
3) Y. Maeda, Y. Takashima, and Y. Nishida, *Bull. Chem. Soc. Jpn.*, **49**, 2427 (1976).
4) D. L. Hammick, *J. Chem. Soc.*, **1926**, 1303.
5) E. König, *Coord. Chem. Rev.*, **3**, 471 (1968).
6) E. König, G. Ritter, H. Spiering, S. Kremer, K. Madeja, and A. Rosenkranz, *J. Chem. Phys.*, **56**, 3139 (1972).
7) W. M. Reiff and G. J. Long, *Inorg. Chem.*, **13**, 2150 (1974).
8) R. Ingalls, *Phys. Rev.*, **133**, A787 (1964).
9) R. H. Toeniskoetter and S. Solomon, *Inorg. Chem.*, **7**, 617 (1968); P. C. H. Mitchell and R. J. P. Williams, *J. Chem. Soc., A*, **1960**, 1912; J. Lewis, R. S. Nyholm, and P. W. Smith, *ibid., A*, **1961**, 4590.
10) E. König, K. Madeja, and K. J. Watson, *J. Am. Chem. Soc.*, **90**, 1146 (1968).
11) R. R. Berett and B. W. Fitzsimmons, *J. Chem. Soc., A*, **1967**, 525.
12) F. A. Cotton and M. D. Meyers, *J. Am. Chem. Soc.*, **82**, 5023 (1960).
13) M. A. Robinson, J. D. Curry, and D. H. Busch, *Inorg. Chem.*, **2**, 1178 (1963).

Gel Chromatography of β-Diketones and Their Metal Complexes. III. The Chromatographic Behavior of Metal(II, III) Chelates with Acetylacetone in Systems of a Poly(vinyl acetate) Gel and Various Eluting Solvents[1]

Nobuo SUZUKI and Koichi SAITOH

Department of Chemistry, Faculty of Science, Tohoku University, Sendai 980

(Received February 3, 1977)

Chelate compounds of acetylacetone (2,4-pentanedione) with metal ions (Al(III), Cr(III), Fe(III), Co(III), and Be(II)) were passed through a chromatograph in columns packed with a cross-linked poly(vinyl acetate) gel (Merckogel OR-2000). Various organic solvents (chloroform, benzene, toluene, 1,4-dioxane, ethyl acetate, butyl acetate, acetone, ethyl methyl ketone, and methanol) were used as the eluents. The distribution coefficient, K_{av}, for each chelate in a given column system was measured to within 0.7% of the relative standard deviation. The K_{av} values of a chelate were dependent on the solvent used. With most of the solvents, the K_{av} values of the metal(III)-chelates were close together and smaller than the K_{av} value of the Be(II)-chelate. The effective molar volume, V_{eff}, of the chelates thus determined, using calibration charts prepared on the basis of elution data for normal alkanes, depended strongly on the solvent used. With all the solvents except chloroform, the V_{eff} values of each chelate were smaller than the literature value of the molar volume for that chelate.

The uniqueness of gel chromatography can be found in its separation mechanism which is usually referred to as the molecular sieve effect resulting from the difference in the molecular dimensions of the solute species. This method is actively used in the fields of polymer and biological chemistry, not only as a method of separation, but also as a means of determining the molecular weight and size of solute molecules. Gel chromatography of neutral metal complexes has not yet been actively studied. Only a few papers have dealt with this subject.[2]

The program of the present study was initiated in an attempt to utilize the unique capabilities of gel chromatography in studying metal complexes in organic solvent media.[3] Acetylacetone (Hacac) and its metal chelates have been exclusively selected as model compounds and Merckogel OR-2000, a cross-linked poly(vinyl acetate) gel, has so far been used as the column-packing material. In the work dealing with metal(II, III) chelates with acac and normal alkanes in the column system, including tetrahydrofuran as an eluent, it was observed that these two sets of compounds are differ in their relationships between the distribution coefficient and the molar volume.[4] In an effort to elucidate this fact, the elution behavior of normal alkanes[5] and the degree of gel swelling[6] were investigated from a viewpoint of solvent effects.

In the present work, the distribution coefficients of some metal(II, III) chelates with acac were measured in various solvent systems, and determinations of the effective molar volume of these chelates were attempted.

Experimental

Metal Chelates. Tris(acetylacetonato)aluminum(III), -chromium(III), -iron(III), and -cobalt(III) (hereafter abbreviated to $[Al(acac)_3]$, $[Cr(acac)_3]$, $[Fe(acac)_3]$, and $[Co(acac)_3]$, respectively) were prepared and purified according to methods in the literature.[7-9] The results of elemental analysis are as follows. $[Al(acac)_3]$. Found: C, 55.19; H, 6.54%. Calcd: C, 55.56; H, 6.54%. $[Cr(acac)_3]$. Found: C, 51.87; H, 6.29%. Calcd: C, 51.56; H, 6.07%. $[Fe(acac)_3]$. Found: C, 51.02; H, 5.98%. Calcd: C, 51.00; H, 6.00%. $[Co(acac)_3]$. Found: C, 50.42; H, 5.99%. Calcd: C, 50.56; H, 5.95%. Bis(acetylacetonato)-beryllium(II) (hereafter abbreviated to $[Be(acac)_2]$) (Dojin Labs.) was further recrystallized from benzene and petroleum ether. Found: C, 57.99; H, 6.83%. Calcd: C, 57.77; H, 6.94%.

Solvents. Benzene, toluene, 1,4-dioxane, ethyl acetate, butyl acetate, acetone, ethyl methyl ketone and methanol were carefully distilled. Since the purified material was unstable, reagent-grade chloroform (Wako Chemicals) was used without further purification.

Columns and Apparatus. Most of the parts coming into contact with the liquids were made of PTFE or Pyrex, rather than metal, in order to avoid undesirable effects. The chromatographic column was a 100 cm long Pyrex tube with a 5-mm inside diameter packed with Merckogel OR-2000 (E. Merck) swollen by the solvent to be used. A Model FLC-350 syringe-type pump (JASCO) and a Model 1107L refractometric detector (L. D. C.) were used. The detection signal was fed into a JEC-5 computer (JEOL) for on-line data processing.

Procedure. A sample solution was prepared by dissolving 15 mg of a metal chelate and 5 mg of a mono-dispersed polystyrene standard (M_w=200 000, Pressure Chemical Co.) in 5 cm^3 of the solvent used as the eluent. With methanol, methylated blue dextran which had been prepared by methylation of Blue Dextran 2000 (Pharmacia)[5] was used in place of polystyrene. A 0.05-cm^3 portion of the sample solution was fed into the column with the aid of a loop injector, and elution was carried out at a solvent flow-rate of 0.20 cm^3 min^{-1} and at a column temperature of 25.0±0.02 °C. The UV and visible absorption spectra of the eluates were recorded in order to confirm the species eluted. Each experiment on a sample in a given column system was carried out at least three times.

Results and Discussion

Shape of Elution Curves. The chelates except for $[Fe(acac)_3]$ gave elution curves without excessive skewness in all solvent systems studied, with the values of the skew ratio[10] ranging from 0.9 to 1.0. $[Al(acac)_3]$ gave an exceptionally skewed elution curve with methanol. On the other hand, $[Fe(acac)_3]$ gave somewhat tailing elution curves in all solvent systems used.

Table 1. K_{av} values of metal chelates with acac in systems of Merckogel OR-2000 and various eluting solvents at 25.0 °C

No.	Eluting solvent	K_{av}[a]				
		$Al(acac)_3$	$Cr(acac)_3$	$Fe(acac)_3$	$Co(acac)_3$	$Be(acac)_2$
1	Chloroform	0.220	0.218	0.295	0.217	0.271
2	Benzene	0.326	0.342	0.439	0.335	0.542
3	Toluene	0.384	0.400	0.439	0.397	0.653
4	1,4-Dioxane	0.430	0.436	0.455	0.432	0.570
5	Tetrahydrofuran[b]	0.497	0.517	0.536	0.523	0.620
6	Ethyl acetate	0.565	0.609	0.618	0.623	0.702
7	Acetone	0.588	0.622	0.638	0.648	0.660
8	Ethyl methyl ketone	0.597	0.628	0.630	0.654	0.653
9	Butyl acetate	0.725	0.790	0.802	0.728	0.828
10	Methanol	—	0.677	—	0.608	1.02

a) The relative standard deviation in each instance is less than 0.7%.
b) Data from Ref. 4.

Table 2. K_d values of metal chelates with acac on Merckogel OR-2000 columns

No.	Eluting solvent	K_d[a]				
		$Al(acac)_3$	$Cr(acac)_3$	$Fe(acac)_3$	$Co(acac)_3$	$Be(acac)_2$
1	Chloroform	0.290	0.288	0.389	0.286	0.358
2	Benzene	0.479	0.503	0.645	0.492	1.20
3	Toluene	0.687	0.716	0.786	0.711	1.17
4	1,4-Dioxane	0.615	0.623	0.651	0.618	0.815
5	Tetrahydrofuran	0.726	0.755	0.783	0.764	0.905
6	Ethyl acetate	0.848	0.914	0.927	0.935	1.05
7	Acetone	0.858	0.908	0.931	0.946	0.964
8	Ethyl methyl kotone	0.895	0.942	0.945	0.981	0.980
9	Butyl acetate	1.23	1.34	1.36	1.24	1.41

a) Values converted from the K_{av} values.

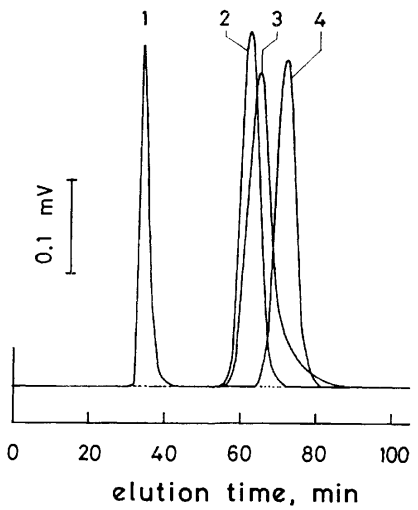

Fig. 1. Elution curves of (1) polystyrene (M_w= 200 000), (2) $[Cr(acac)_3]$, (3) $[Fe(acac)_3]$, and (4) $[Be(acac)_2]$.
Merckogel OR-2000 column, 100 cm×5 mm I. D., 25.0±0.02 °C; eluting solvent, 1,4-dioxane, 0.2 $cm^3 \cdot min^{-1}$; R. I. Detector, sens. 16 for (1), (2), and (4), sens, 8 for (3).

With methanol, both $[Al(acac)_3]$ and $[Fe(acac)_3]$ gave such skewed elution curves that no elution data with high reproducibility could be obtained for these two chelates. Typical elution curves obtained are shown in Fig. 1.

Distribution Coefficient. The elution volume, V_e, of a substance passed through a chromatograph in a given column system is expressed by

$$V_e = V_o + K_{av}V_x, \quad (1)$$

where V_o, V_x, and K_{av} are the column void volume, the volume of the gel phase, and the distribution coefficient, respectively.[11] In the present work, the K_{av} value of each chelate was calculated according to the relation,

$$K_{av} = (V_e - V_o)/(V_t - V_o), \quad (2)$$

where V_t is the total volume of the column ($V_t = V_o + V_x$). The V_t values of all columns used in this work were exactly 19.63 cm^3. The V_o value of the column was determined from a measurement of the V_e value of either a polystyrene standard or methylated blue dextran which are regarded as substances to be completely excluded from the Merckogel OR-2000 gel network. The dead volume related to that part of the tubing was corrected for in the calculation of the K_{av}

Table 3. Separation factor, α, for the $[Be(acac)_2]$-$[Cr(acac)_3]$ pair on Merckogel OR-2000 columns at 25.0 °C

No.	Eluting solvent	α
1	Chloroform	1.24
2	Benzene	1.58
3	Toluene	1.63
4	1,4-Dioxane	1.31
5	Tetrahydrofuran	1.20
6	Ethyl acetate	1.15
7	Acetone	1.06
8	Ethyl methyl ketone	1.04
9	Butyl acetate	1.05
10	Methanol	1.51

value.

The K_{av} values of the metal chelates were obtained with high reproducibility, the relative standard deviation in each instance being not more than 0.7%. However, precise data for $[Al(acac)_3]$ and $[Fe(acac)_3]$ could not be obtained in the systems with methanol. The results are given in Table 1 together with previous data on the system with tetrahydrofuran.

The gel chromatographic behavior of a solute substance is characterized also by the elution parameter K_d, derived from the relation,

$$V_e = V_o + K_d V_i, \quad (3)$$

where V_i is the volume of the internal solvent in the swollen gel beads. When V_x is assumed to be equal to the sum of V_i and the volume of the gel matrix, V_g, K_d can be obtained from K_{av} according to the following relation,

$$K_d = (V_x/V_i)K_{av} = [Q/(Q-1)]K_{av}, \quad (4)$$

where Q is the degree of gel swelling defined as the reciprocal of the volume fraction of the gel matrix in the swollen gel. The K_d values of metal chelates thus calculated from the available K_{av} and Q values[6] are given in Table 2.

It is obvious that both the K_{av} and K_d values of the chelates are strongly dependent on the solvent used. The solvents are arranged in Tables 1 and 2 in order of increasing K_{av} and K_d values for $[Al(acac)_3]$.

The K_{av} values of metal(III) chelates in a solvent are close together. This fact implies that separation of these chelates is not easy if a solvent is used as the eluent. The K_{av} value of $[Be(acac)_2]$ is larger than that of a metal(III) chelate in any solvent. The separation factor, α, defined as the ratio of the K_{av} values, for the $[Be(acac)_2]$-$[Cr(acac)_3]$ pair is given in Table 3. The α value for this solute pair depends on the solvent used, which reveals the importance of the choice of the solvent as the eluent for gel chromatographic separation.

Effective Molar Volume. For large molecules such as polymers, the molecular weight is frequently used as a size parameter for a compound in gel chromatography, whereas for small molecules having molecular weights less than 1000, the molar volume, V_m, is an effective size parameter.[12] The molar volume experimentally determined by means of gel chromatography

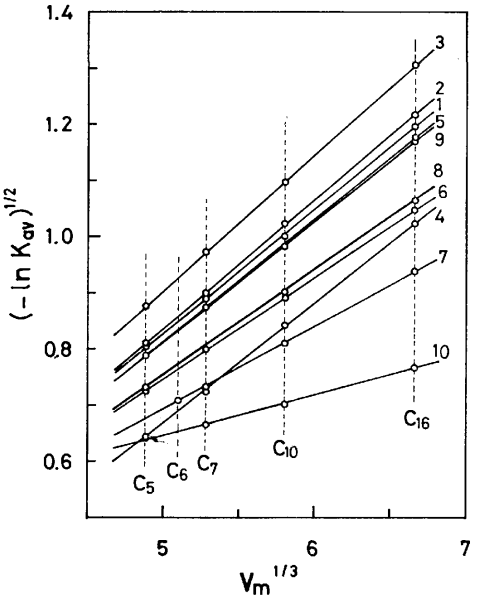

Fig. 2. Relationship between K_{av} and V_m for normal alkanes in the systems of Merckogel OR-2000 and various eluting solvents.
C_5, C_6, C_7, C_{10}, and C_{16} denote pentane, hexane, heptane, decane, and hexadecane, respectively. Numerals 1—10 denote solvents as in Table 1.

is termed the effective molar volume, V_{eff}, as distinct from V_m.[13,14] The V_{eff} values of the metal chelates were obtained in this work using the calibration charts based on the elution data for normal alkanes.

Laurent and Killander[11] have proposed the following equation,

$$K_{av} = \exp[-\pi L(r_r + r_s)^2], \quad (5)$$

where r_s is the radius of the solute molecule, and L and r_r are constant for a given combination of gel matrix and solvent. Assuming r_s to be proportional to the cube root of V_m, we can write

$$(-\ln K_{av})^{1/2} = k_1 + k_2 V_m^{1/3}, \quad (6)$$

where k_1 and k_2 are constants in a column system. The $(-\ln K_{av})^{1/2}$ *versus* $V_m^{1/3}$ plots in Fig. 2 are based on the K_{av} values for normal alkanes on Merckogel OR-2000[5] and the V_m values calculated from the molecular weight and density data for the respective compounds.[15] When these plots are used for calibration, the V_{eff} values of the chelates were obtained by comparing their K_{av} values with the plots. The results are given in Table 4. It is obvious that the V_{eff} values for each chelate is strongly dependent on the solvent used. The V_{eff} values of $[Cr(acac)_3]$, for example, range from 27 to 317 $cm^3\ mol^{-1}$.

Irving and Smith have shown that the partial molar volume of $[Cr(acac)_3]$ is nearly constant in different organic solvents[16] and Irving have reported V_m values of the chelates as follows: $[Al(acac)_3]$, 271; $[Cr(acac)_3]$, 267; $[Fe(acac)_3]$, 269; $[Co(acac)_3]$, 261 $cm^3 \cdot mol^{-1}$.[17] When the semi-empirical relation expressed by

$$V_{m,M(acac)_n} = 0.9\, n V_{m,Hacac}, \quad (7)$$

is used, the V_m value of $[Be(acac)_2]$ is estimated to be

Table 4. The V_{eff} values of metal chelates with acac determined using the calibration charts based on the gel chromatographic data for normal alkanes

No.	Eluting solvent	V_{eff}/cm^3 mol^{-1}				
		$Al(acac)_3$	$Cr(acac)_3$	$Fe(acac)_3$	$Co(acac)_3$	$Be(acac)_2$
1	Chloroform	315	317	245	317	266
2	Benzene	211	202	150	210	108
3	Toluene	150	143	126	144	56
4	1,4-Dioxane	234	230	217	232	155
5	Tetrahydrofuran	133	125	117	122	86
6	Ethyl acetate	128	106	102	99	65
7	Acetone	143	120	110	104	94
8	Ethyl methyl ketone	111	97	96	86	88
9	Butyl acetate	48	27	23	47	13
10	Methanol	—	95	—	216	—

184 cm^3 mol^{-1}, where $V_{m,Hacac}$ and $V_{m,M(acac)_n}$ are the molar volumes of Hacac (=102 cm^3 mol^{-1}) and of its metal chelate containing an integral number n of $(acac)^-$ anions, respectively.[18] Comparing the V_m value of a chelate with the V_{eff} values shown in Table 4, it is obvious that the latter values are different from the former value. The V_{eff} values of the chelates, except for $[Fe(acac)_3]$ in chloroform, are marked larger than the V_m values of the respective chelates. Considering that many metal chelates with acac form solvated species in chloroform,[19,20] the larger V_{eff} values observed in this solvent may refer to solvations. Despite the fact that the V_m values of the 4 metal(III) chelates studied are close together, the V_{eff} values of $[Fe(acac)_3]$ are smaller than those of other metal(III) chelates in many solvents. Recalling that $[Fe(acac)_3]$ gave elution curves with a tailing and larger K_{av} values relative to other metal(III) chelates, and considering that Fe(III)-chelate is known to be a labile complex, it is deduced that some partial dissociation of the chelate occured in the chromatographic process. It is reasonable to consider that the relatively smaller V_{eff} values for $[Fe(acac)_3]$ result from such anomalous chromatographic behavior.

The fact that the K_{av} value for $[Be(acac)_2]$ in a given solvent is larger than the K_{av} values of the metal(III) chelates indicates that one of the factors governing the chromatographic behavior of those compounds is the molecular sieve effect. Considering that V_{eff} values of the chelates are different from the expected values (V_m values) and also that the K_d values, in some instances, are larger than unity, it is reasonable to assume that gel chromatography of the chelates is based not only on the molecular sieve effect but also on some other effects caused by interactions among the solute, solvent and gel matrix.

The selection of an appropriate eluting solvent is quite important for the purpose of estimating the molar volume of a solute species. According to the available data, the V_{eff} value of a metal chelate with acac obtained using 1,4-dioxane as an eluent appears to be close to the V_m value.

The solvent dependence of the gel chromatographic behavior is an attractive problem to be further elucidated. The details of the solvent effects and the so-called secondary effect in gel chromatography will be treated in a subsequent paper.

References

1) For parts I and II of this series, see Refs. 3 and 4, respectively.

2) Y. Yamamoto, M. Yamamoto, S. Ebisui, T. Takagi, T. Hashimoto, and M. Izuhara, *Anal. Lett.*, **6**, 451 (1973).

3) K. Saitoh, M. Satoh, and N. Suzuki, *J. Chromatogr.*, **92**, 291 (1974).

4) K. Saitoh and N. Suzuki, *J. Chromatogr.*, **109**, 333 (1975).

5) K. Saitoh and N. Suzuki, *J. Chromatogr.*, **111**, 29 (1975).

6) K. Saitoh, T. Ozawa, and N. Suzuki, *J. Chromatogr.*, **124**, 231 (1976).

7) E. W. Berg and J. T. Treumper, *J. Phys. Chem.*, **64**, 478 (1960).

8) W. C. Fernerius and J. E. Blanch, "Inorganic Syntheses," Vol. V, ed by T. Moeller, McGraw-Hill, New York (1957), p. 130.

9) B. E. Bryant and W. C. Fernerius, "Inorganic Syntheses," Vol. V (1957), p. 188.

10) A. J. B. Cruickshank and D. H. Everett, *J. Chromatogr.*, **11**, 289 (1963).

11) T. C. Laurent and J. Killander, *J. Chromatogr.*, **14**, 317 (1964).

12) W. B. Smith and A. Kollmansberger, *J. Phys. Chem.*, **67**, 4157 (1965).

13) G. D. Edward and Q. Y. Ng, *J. Polym. Sci.*, **C21**, 105 (1968).

14) A. Lambert, *Anal. Chim. Acta*, **51**, 63 (1971).

15) J. A. Riddick and W. B. Bunger, "Organic Solvents," 3rd ed, Wiley-Interscience, New York (1970), pp. 70—138.

16) H. M. N. H. Irving and J. S. Smith, *J. Inorg. Nucl. Chem.*, **31**, 1212 (1969).

17) H. M. N. H. Irving, "Ion Exchange and Solvent Extraction," Vol. 6, ed by J. A. Marinsky and Y. Marcus, Dekker, New York (1970), p. 139.

18) T. Wakahayashi, S. Oki, T. Omori, and N. Suzuki, *J. Inorg. Nucl. Chem.*, **26**, 2255 (1964).

19) F. R. Clark, J. F. Steinbach, and W. F. Wagner, *J. Inorg. Nucl. Chem.*, **26**, 1311 (1964).

20) J. F. Steinbach and J. H. Burns, *J. Am. Chem. Soc.*, **80**, 1839 (1958).

A Method for the Analysis of Halogenated Organic Compounds in Tap Water by Means of Mass Fragmentography of GC-MS

Toshihiro FUJII

Division of Chemistry and Physics, National Institute for Environmental Studies, Yatabe, Tsukuba, Ibaraki 300-21

(Received February 17, 1977)

A simple, sensitive and practical method for the halogenated organic compound analysis of tap water is reported. A pentane extraction procedure using a ten fold increase in concentration by volume (without further concentration) followed by mass fragmentography of GC-MS was used. As little as 0.05 ppb concentration of each compound was detectable. Five simple halogenated organic compounds, including CCl_4 and $CHBr_3$ whose concentrations are relatively small, were determined for tap water in Japan.

Recent years have seen an increasing concern[1,2] for levels of trace organic contaminants in water ultimately used for human consumption. In some cases less than 1 μg/l (1ppb) of the minimum detectable limit is required for specific compounds. This concentration is significant and all methods should approach this sensitivity requirement. Until now, procedures used for obtaining the required sensitivity have involved some sort of extraction procedure. Solvent extraction,[3-5] followed by further concentration for extreme trace concentration samples, has been commonly used. Although this method meets the sensitivity requirement, it suffers from serious interferences due to accumulation of solvent impurities as well as the informative substances.

However, solvent extraction without further concentration can be successfully applied to even extreme trace concentrations, when very high sensitive and specific detection is possible. Mass fragmentography[6] of GC-MS is a useful technique to meet the high sensitive and specific detection requirement, which provides specific information at a sensitive level that often surpasses that of the electron capture detector. I wish to report here a method for the analysis of halogenated organic compounds in tap water, utilizing mass fragmentography of GC-MS. A pentane extraction procedure without further concentration followed by mass fragmentography of GC-MS does not seem to have been reported.

Experimental

Apparatus. Gas chromatographic separation and mass spectrometric analysis were performed on a Finnigan 3300F gas chromatograph-quadrupole mass spectrometer equipped with multiple ion detector (Finnigan, PROMIM), by which mass fragmentography can be carried out. A selected mass can be quickly set with the aid of a digital mass marker display. The GC-MS interface utilizes an all glass jet-type enrichment device. A 3 m × 2 mm (i.d.) glass column packed with 5% SE-30 on 60/80 mesh Chromosorb W. AW. DMCS. (Johns-Manville) was used. Other conditions were: flow rate of helium carrier gas 30 ml/min, temperature of gas chromatograph injection port 200 °C, temperature of interface and transfer line 200 °C, pressure in the mass spectrometer 6×10^{-6} Torr, electron energy 70 eV, emission current 0.45 mA, electron multiplier 1450 volts.

Standard Solutions. A series of $CHCl_3$ standard concentrations in the range 0.5—400 ppb were made by successive dilution into special grade pentane (Wako pure chemicals) starting with pure $CHCl_3$ (Dojin chemicals). Calibration standards were made from pure reagents for each organohalide, $CHCl_2Br$, $CHClBr_2$, $CHBr_3$, and CCl_4 (Tokyo Kasei chemicals). Water used for recovery works was prepared by double distillation of ground water.

Procedure. Pretreatment of water samples was performed as follows, using pentane extraction procedure as a concentration technique. 10 ml of pentane was floated on 100 ml of water samples in a tightly closed container and agitated rigorously for 10 min. 10 μl injection of the extract was then made with a 10-μl Hamilton syringe (701-RN). At the start of each run the column was maintained at 40 °C for 7 min and programmed from 40 to 70 °C at 4 °C/min. The mass spectrometer was set to unit resolution (10% valley between adjacent nominal masses). The mass spectrometer was then set to monitor a specific mass of the examined compounds. The resulting ion currents were recorded on a strip chart recorder.

Positive identification of the compounds is supported not only by known retention times of the standards but also by the selectivity afforded by specific ion detection. The ions chosen to be monitored[7] include the chlorine and (or) bromine of each compound. Comparison of the expected ratio of isotope clusters with the observed ratio gives the permissible limit for analyzing unknown substances and determining whether they are free of coeluting impurities. Quantitative information was obtained using peak areas.

Results and Discussion

Detection Limit. Detection response (peak area) was linear over the range of standard solutions for each organohalide. The range was chosen to cover the concentrations likely to be found in various tap water samples. The detection limit of each compound (concentration of substance producing a peak five times higher than noise level) was found to be 0.5 ppb. Thus, water samples of 0.05 ppb concentration compound were determined by the extraction procedure using a ten fold increase in concentration by volume (10 ml of pentane per 100ml of water).

Recovery. Recovery was tested with amounts of the examined compounds similar to those which would be present in samples. A testing solution for recovery was prepared by mixing standard solutions of the compounds in treated and pretested water. The extraction was carried out as mentioned above. Recovery of each compound is given in Table 1. It is seen that efficient recovery was obtained for all tested substances, although a decrease in precision was observed at low concentration levels.

Table 1. Recovery of the halogenated organic compounds spiked into water

Compounds	Concentration added to water (μg/l)	Average[a] recovery (%)
$CHCl_3$	20	96±4
$CHCl_2Br$	1	94±8
$CHClBr_2$	1	93±7
$CHBr_3$	0.1	95±15
CCl_4	0.1	109±18

a) Average of five recovery works.

Table 2. Halogenated organic compounds in tap water

Compounds	Retention time (min)	Mass monitored (*m/e*)
$CHCl_3$	3.9	83,[a] 85
$CHCl_2Br$	7.2	83, 85, 127,[a] 129
$CHClBr_2$	10.8	127,[a] 129
$CHBr_3$	14.5	171, 173,[a] 175
CCl_4	4.9	117, 119[a]

a) Specific ions chosen for quantitative information of each compound.

Table 3. Halogenated organic compound concentrations (ppb) in tap water sample (July 8, 1976)

Location	$CHCl_3$	$CHCl_2Br$	$CHClBr_2$	$CHBr_3$	CCl_4
Hanamuro[a]	22.5	0.6	0.24	undetectable	0.1
Kanamachi[b]	17.5	2.6	1.7	0.06	0.08
Hamura[c]	18.8	1.0	0.53	undetectable	0.05

a) Tsukuba Research Center. b) West Tokyo. c) East Tokyo.

Solvent. The pentane used as the diluent of the standard solutions and the solvent of the extraction was found to contain no detectable $CHCl_2Br$, $CHClBr_2$ and $CHBr_3$ with the exception of $CHCl_3$ and CCl_4. The presence of $CHCl_3$ (0.06 ppb to be estimated with exploration) and CCl_4 (0.05 ppb) as a trace contaminant in pentane limited the accuracy. However, there is no trouble with $CHCl_3$ since its amount is negligibly small to affect the signal. There is a much wider choice of solvents, such as the higher alkanes. However, these solvents obscure the volatile extraction components. It is more difficult to obtain them in sufficient purity. Pentane was found to be the most suitable solvent.

Tap Water Analysis. Many halogenated organic compounds have been found in tap water in the U. S.,[1,2,5,8-10] considerable interest in their determination being aroused. Analyses were made in an attempt to survey the amounts of five halogenated organic compounds in tap water in Japan. Table 2 summarizes their retention times and masses monitored. These compounds were major components of the halogenated organic compounds discovered in the U.S. water supplies. Figure 1 shows typical mass fragmentograms (*m/e* 83, 119, 127, 173), results of the analysis of tap water

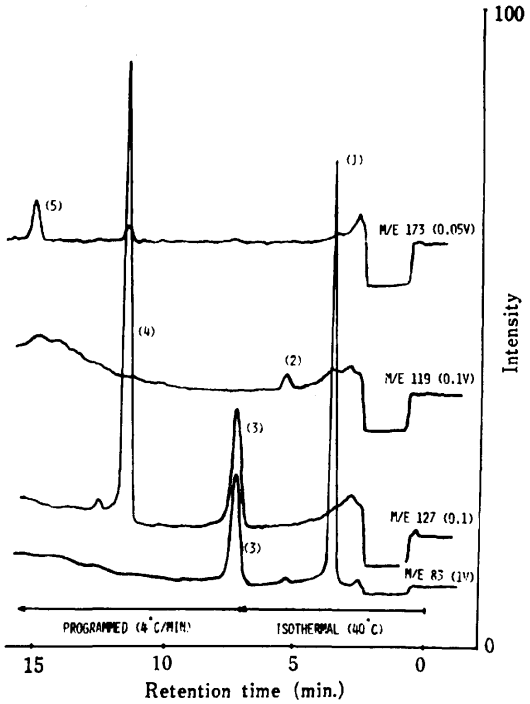

Fig. 1. Typical analysis of halogenated organic compounds in the tap water by mass fragmentography. A 10 μl injection.
Peaks are: (1) $CHCl_3$, (2) CCl_4, (3) $CHCl_2Br$, (4) $CHClBr_2$, (5) $CHBr_3$.

taken at Kanamachi in Tokyo. The results of measurements are given in Table 3. The $CHCl_2Br$ and $CHClBr_2$ concentrations were remarkably invariant. The related compound $CHBr_3$ was found in very low concentrations (0.06 ppb). The CCl_4 levels were very low. Individual samples of CCl_4 produced the same or a slightly higher peak than that of the trace contaminants in pentane. Quantitative values of CCl_4 were obtained by subtracting the amount of CCl_4 trace contaminants in pentane.

References

1) B. Dowty, D. Carlisle, J. L. Laseter, and J. Storer, *Science*, **187**, 75 (1975).
2) T. A. Bellar, J. J. Lichtenberg, and J. J. Kroner, *J. Am. Water Works Ass.*, **66**, 703 (1974).
3) M. Ahnoff and B. Josefsson, *Anal. Chem.*, **46**, 658 (1974).
4) A. J. Murray and J. P. Riley, *Anal. Chim. Acta*, **65**, 261 (1973).
5) K. Grob, K. Grob, Jr., and G. Grob, *J. Chromatogr.*, **106**, 299 (1975).
6) C. G. Hammer, B. Holmstedt, and R. Ryhage, *Anal. Biochem.*, **25**, 532 (1968).
7) E. Stenhagen, S. Abrahamson, and F. W. Mclafferty, "Registry of Mass Spectral Data," John Wiley & Sons, New York (1974).
8) W. Bertsh, G. Anderson, and G. Holzer, *J. Chromatogr.*, **112**, 701 (1975).
9) R. D. Kleopfer and B. J. Fairless, *Environ. Sci. Technol.*, **6**, 1036 (1972).
10) J. Novak, J. Zlutickey, V. Kubelka, and J. Mostecky, *J. Chromatogr.*, **76**, 45 (1973).

The Mutual Separation of ^{227}Ac, ^{227}Th, ^{223}Ra, and ^{223}Fr by the Solvent Extraction Technique Using Bis(2-ethylhexyl)phosphoric Acid as an Extractant

Toshiaki MITSUGASHIRA, Hajimu YAMANA, and Shin SUZUKI

The Research Institute for Iron, Steel and Other Metals, Tohoku University, Katahira 2-chome, Sendai 980

(Received March 11, 1977)

The separation and purification of ^{227}Ac, ^{227}Th, ^{223}Ra, and ^{223}Fr were studied by the solvent extraction method using HDEHP (bis(2-ethylhexyl)phosphoric acid) as an extractant. The mutual separation of Ac, Th, and Ra was achieved, and new milking processes for ^{223}Fr and ^{228}Ac are presented.

The cyclic relation between ^{227}Ac, ^{227}Th, ^{223}Fr, and ^{223}Ra in natural actinium decay series is shown in Fig. 1. These nuclides are important as radioactive tracers, and interesting from the viewpoint of investigation of natural radioactive substances. Measurement of the radioactivity of ^{227}Ac is especially difficult, since its γ-activity and α-activity are very weak and the energy of β-rays are too low for quantitative detection. Many authors have reported on the application of radiation of its daughter nuclides to the detection and determination of ^{227}Ac. The separation of these nuclides is very important for the chemistry of natural radioactive substances.

The separation of Ac and Ra has been attempted by the cation exchange[1] and solvent extraction methods utilizing the TTA-TBP synergistic effect,[2] but these methods have certain drawbacks.

The cation exchange method,[1] because of its rather prolonged elution time, is not suitable for the separation of short-lived tracers such as ^{228}Ac ($t_{1/2}$=6.13 h)[3] and ^{223}Fr ($t_{1/2}$=21 min)[3] from each other. In the solvent extraction method using TTA as an extractant, it is necessary for the aqueous solution to have acidity of 4—5 pH, in spite of the remarkable tendency of Ac and Th toward hydrolysis in such a low acidic solution. The separation coefficient of Ac and Ra is expected to increase with the decrease in acidity of the aqueous solution, and there is a possibility of the hydrolysis of Ac also increasing in such a low acidic solution. Once the hydrolysis of Ac occurs, the separation coefficient should decrease because of the decrease in the proportion of the native ion Ac^{3+} in aqueous solution. It would be better to extract Ac from the solution whose acidity is as high as possible. Since HDEHP can extract some multivalent metal elements selectively from a highly acidic solution,[4] it is expected that Ac, Ra, and Th can be effectively separated from each other by HDEHP extraction. We have studied the application of HDEHP as an extractant to the separation of ^{227}Ac, ^{227}Th, ^{223}Ra, and ^{223}Fr.

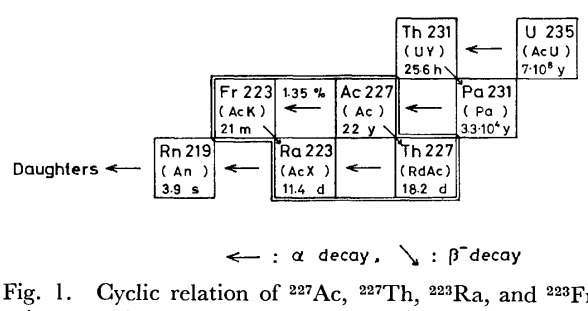

Fig. 1. Cyclic relation of ^{227}Ac, ^{227}Th, ^{223}Ra, and ^{223}Fr in natural actinium decay series.

It is well known that Th is quantitatively extracted by 1 M HDEHP–benzene solution from 0.2—0.5 M HCl solution. However, the extraction behavior of Ac, Ra, and Fr in the HDEHP extraction system is not known as yet. From the difference in the charge of the native ions Ac^{3+}, Ra^{2+}, and Fr^{+}, we can expect that Ac can most easily be extracted. Thus, the extraction conditions of Ac in the HDEHP extraction system were investigated first. It was found that Th is much more extractable than Ac and the separation of Ac and Th is easy. Thus the main problem was to separate Ac and Ra or Fr, and we tried to find the exact conditions for the separation of Ac and Ra. Fr goes to the Ra-fraction in our separation method, and there remains the problem of separating ^{223}Ra and ^{223}Fr. However, the difference in their half-lives is too large, and makes our procedures feasible. It is rather worthwhile to establish a new milking method of ^{223}Fr by which we can easily get ^{223}Fr grown from ^{227}Ac.

Experimental

Reagents. All the chemicals used were of analytical grade. HDEHP was purified by the procedures reported previously.[5]

Radioisotopes and Their Detection. *Ac*: ^{228}Ac was used as a tracer of Ac, whose γ-activity is very easy to detect,[3] and was prepared by the cation exchange chromatography method from ^{228}Ra isolated from ^{232}Th. When a sample of ^{228}Ac contains any amount of ^{228}Ra that is a parent nuclide of ^{228}Ac, the γ-activity of the sample does not vanish because of the radio-equilibrium between ^{228}Ac and ^{228}Ra. Thus, the purity of the sample of ^{228}Ac could be confirmed by checking the decay out of the γ-activity of the sample in each experiment.

Ra and Th: ^{223}Ra and ^{227}Th isolated from ^{227}Ac in their radio-equilibrium by cation exchange chromatography were used as the tracers. These two nuclides were determined by measuring their γ-spectra by Ge(Li) detector and calculating the peak area of their characteristic γ-ray peaks.

pH Buffer Solution. Considering the fact that the distribution ratios of multivalent metal ions in HDEHP extraction system are expected to be a sensitive function of the acidity of the solution, the pH value of the aqueous phase must be fixed in order to keep the reproducibility of the extraction. Thus, we used "Clark-Lubbs pH buffer solution"[6] which consists of KCl and HCl in the range of pH$\leq$ 2.2, and KH phthalate and HCl in the range of pH$\geq$2.2, where the concentration of both salts in each solution is 0.05 M. Solutions, the pH values of which were 1.0—3.6 were prepared using this buffer solution in this work. Since there might be difference in their behavior between KCl-system and KH phthalate-system, two kinds of solutions made from two different salts were prepared in the range of 2.1$\leq$pH$\leq$

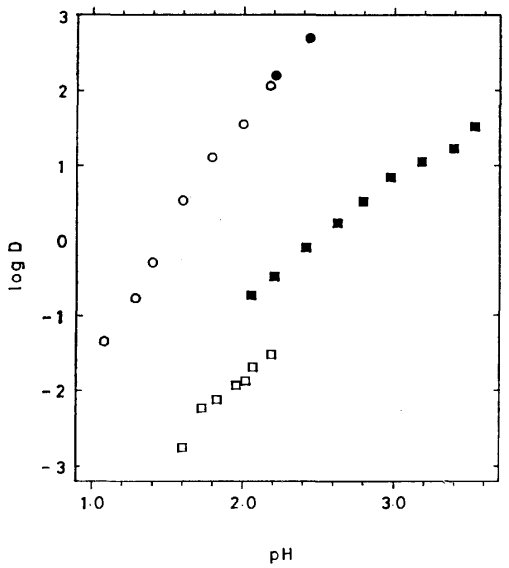

Fig. 2. Relations between D_{Ac}, D_{Ra} and the acidity of the aqueous phase.
○● : D_{Ac} when KCl (○) and KH phthalate (●) buffer solution was used. □■ : D_{Ra} when KCl (□) and KH phthalate (■) buffer solution was used.

2.2, and the data were compared with each other.

Apparatus. The apparatus used are as follows. *Separatory Funnel Shaker*: IWAKI KM type (200—400 rpm), *Ge(Li) Detector*: ORTEC model number 8101-1820 (the effective volume is about 60 ml), *Multichannel Pulse Height Analyser*: TOSHIBA USC-1 4096 ch (controlled by a mini-computer TOSBAC-40 A), *NaI Scintillation Counter*: HITACHI well type $1^3/_4'' \times 2''$, *Digital pH Meter*: ORION 801-A type.

Procedures. The back extraction behavior of Ac was investigated according to the following procedures. The pH value of the ^{228}Ac solution was adjusted to 3.0 and ^{228}Ac was extracted with a 1M HDEHP-benzene solution. Then a 5 ml portion of the organic phase containing ^{228}Ac was poured to the another separatory funnel and shaken for 20 min with 5 ml of buffer solution.

The forward extraction of ^{223}Ra was investigated with the shaking time of 20 min.

In both cases of Ac and Ra, the pH value of the aqueous phase was checked after extraction with a digital pH meter. A 2 ml portion of each phase was taken into a polyethylene test tube and their γ-rays were measured. The calculation of the peak area of the characteristic γ-rays of ^{223}Ra and ^{227}Th were carried out with a mini-computer system[7] connected to the multichannel pulse height analyzer.

For the final experiment to check the separation method, a mixed solution of ^{227}Ac, ^{227}Th, and ^{223}Ra in radio-equilibrium was used. A radio-equilibrium mixture of ^{227}Ac and ^{223}Fr was used for the check of the milking of ^{223}Fr.

The distribution ratio of each element is defined by

$$D_M = C_{M.org}/C_{M.aq}$$

where M denotes metal element, $C_{M.org}$ the concentration of M in the organic phase and $C_{M.aq}$ that in the aqueous phase. The separation coefficient is defined by

$$\alpha_{Ac,Ra} = D_{Ac}/D_{Ra}.$$

Results and Discussion

Dependence of D_{Ac} and D_{Ra} on the pH in 1 M HDEHP–Benzene Extraction System. Figure 2 shows the relation between the logarithm of D_{Ac} or D_{Ra} and the pH value of the aqueous phase. They show linearity with different slopes. The slope for Ac is *ca.* 3.0 and that for Ra, 1.9. In the data of D_{Ra}, there is a large difference between the two kinds of buffer solutions containing KCl and KH phthalate. Two explanations are possible. One is the difference of the stability of the complex ion of Ra with Cl^- or $C_6H_4(COO)_2^{2-}$; the other is the synergistic effect caused by the coordination of the neutral phthalic acid molecules to the extracted compound of Ra. However, we could not decide which explanation is feasible, while it is clear that D_{Ra} shows a larger value when KH phthalate is used than when KCl is used. Considering that there is no difference between the two kinds of buffer solution in the data of D_{Ac}, it is obvious that the separation coefficient of Ac and Ra ($\alpha_{Ac,Ra}$) becomes larger when KCl is used and the KCl-buffer solution is more suitable for the separation of Ac and Ra. The calculated values of $\alpha_{Ac,Ra}$ using the above-mentioned data, are given in Table 1. These values were calculated from the two straight lines drawn by the method of linear least square fitting. There is the tendency that $\log(\alpha_{Ac,Ra})$ increases in proportion to the pH value. The maximum of $\alpha_{Ac,Ra}$ is 4.1×10^3 at pH=2.2 where over 99.4% of Ac is extracted into the orgaic phase and over 99.9% of Ra remains in aqueous phase. Thus, the separation of Ac from Ra can be made by adjusting the pH of the aqueous solution to 2.2 and then shaking it with 1 M HDEHP–benzene solution, as described in the following. Th which is more extractable than Ac can be

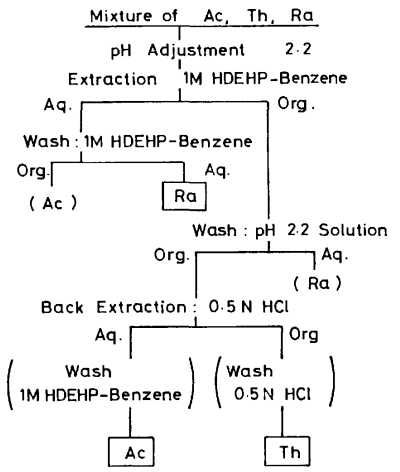

Fig. 3. Separation procedures for Ac, Th, and Ra system.

TABLE 1. SEPARATION COEFFICIENT OF Ac AND Ra IN THE 1 M HDEHP–BENZENE EXTRACTION SYSTEM

pH	D_{Ac}	D_{Ra}	$\alpha_{Ac,Ra}$	$\log \alpha_{Ac,Ra}$
1.6	1.914	0.0024	778.0	2.891
1.7	3.917	0.0038	1025.4	3.001
1.8	8.017	0.00593	1351.9	3.131
1.9	16.405	0.00920	1783.2	3.251
2.0	33.574	0.01429	2349.5	3.371
2.1	68.707	0.02220	3094.9	3.491
2.2	140.61	0.03450	4075.5	3.610

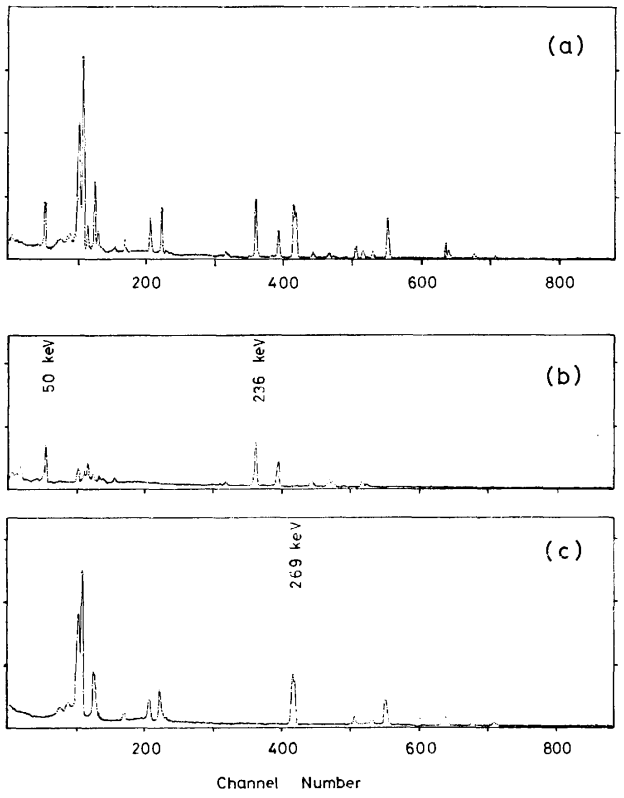

Fig. 4. γ-Spectra of fractions separated.
(a) Starting mixture of ^{227}Ac, ^{227}Th, and ^{223}Ra, (b) ^{227}Th-fraction separated, (c) ^{223}Ra-fraction separated.

separated from Ra and goes to the Ac-fraction.

The Mutual Separation of Ac, Ra, and Th. From the above result, and the fact that Th is quantitatively extracted by 1 M HDEHP–benzene solution from 0.1—0.5 M HCl solution, we propose the following separation method for Ac, Th, and Ra system (Fig. 3).

The acidity of the mixed solution of Ac, Th, and Ra is adjusted to pH=2.2 and the solution is shaken with 1 M HDEHP–benzene solution. Ac and Th are quantitatively extracted to the organic phase while Ra remains in the aqueous phase. Pure Ra solution can be easily prepared by washing the aqueous phase with the same organic solution. The organic phase is washed by the solution of pH 2.2 and shaken with 0.5 M HCl solution. Ac is back-extracted to the aqueous phase while Th remains in the aqueous phase.

Ra is recovered as HCl solution whose pH is equal to 2.2, Ac, as 0.5 M HCl solution, and Th, as 1 M HDEHP–benzene solution. The yield of each element is over 99%.

Figure 4 shows the γ-spectrum of each fraction after the separation of ^{227}Ac, ^{227}Th, and ^{223}Ra which were in radio-equilibrium. Comparing the spectrum of each fraction with that of the original mixed solution, we see that these elements are isolated and purified. No characteristic γ-peaks could be found in the ^{227}Ac-fraction. However, when a sample of ^{227}Ac having a much higher specific activity is used, the growth of the γ-peaks of ^{223}Fr will be detected in a period of about 40 min after purification of ^{227}Ac.

Milking Method for ^{223}Fr Using HDEHP–Solvent Extraction. We can easily carry out the milking of ^{223}Fr from ^{227}Ac by utilizing the principle of the above-mentioned separation method. The procedure is shown in Fig. 5. After recovering ^{227}Ac as 0.5 M HCl solution (Fig. 3), the pH is adjusted again to 2.2 and shaken with 1 M HDEHP–benzene solution to prepare the organic solution of ^{227}Ac to be used as a milking source. Extraction of ^{227}Ac is carried out twice because ^{223}Fr has γ-rays very similar to those of ^{227}Th and it is better to completely eliminate the contamination of ^{227}Th. By shaking the milking source with the solution of pH 2.2 once, ^{223}Fr and a small amount of ^{223}Ra that have grown in the organic phase is back-extracted to the aqueous phase. In a period of 2.5—3.0 h after the first back-extraction, ^{223}Fr whose half-life is 21 min grows and attains radio-equilibrium with ^{227}Ac in the organic phase. Thus, after standing for 2.5—3.0 h, ^{223}Fr should be back-extracted to the aqueous phase by shaking with the same buffer solution. ^{223}Ra also grows in this period. However, because the half-life of ^{223}Ra is 11.4 days and too long compared with that of ^{223}Fr, the growth of ^{223}Ra in this period does not need to be considered, unless the amount of ^{227}Th in the organic phase is not too large. ^{223}Fr is easily isolated from ^{227}Ac by carrying out the same extraction twice. Figure 6 shows the γ-spectrum of ^{223}Fr purified by this milking method. In the second measurement,

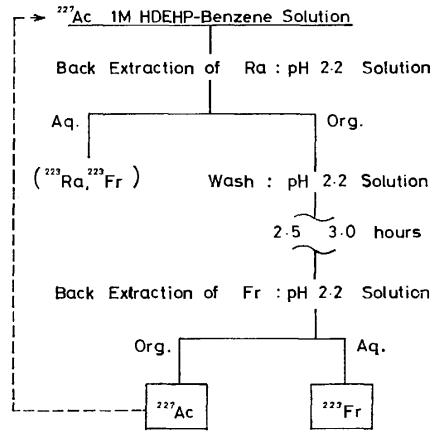

Fig. 5. Milking procedures for ^{223}Fr.

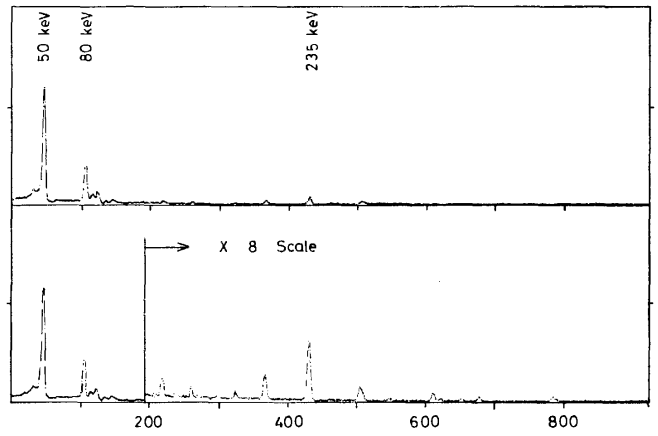

Fig. 6. γ-Spectrum of ^{223}Fr obtained by the proposed milking method.

almost all of the γ-peaks disappeared and a slight growth of the characteristic γ-peaks of ^{223}Ra and the Kx-rays of Rn were observed.

Possibility of the Determination of ^{227}Ac Utilizing the γ-Activity Measurement of ^{223}Fr. It is impossible to detect and determine ^{227}Ac by its γ-activity since it has no characteristic γ-rays that have intensity sufficient for measurement. Thus, the only way to detect and determine ^{227}Ac by the γ-ray measurement is to measure the γ-activity of its daughter nuclides (^{223}Ra, ^{223}Fr, and ^{227}Th). However, for ^{223}Ra and ^{227}Th, because of their long half-lives of 11.4 and 18.2 days respectively, we must wait more than 3 months for the attainment of radio-equilibrium for the determination of ^{227}Ac. For ^{223}Fr, since its γ-rays are similar to those of ^{227}Th, correct measurement of its γ-activity is difficult. However, the proposed separation method can eliminate the contamination of ^{227}Th which prevents accurate measurement of ^{223}Fr, and we can expect a new method to determine ^{227}Ac by measuring the γ-activity of ^{223}Fr in radio-equilibrium with ^{227}Ac. As shown in Fig. 6, the peak of 50 keV of ^{223}Fr has sufficient intensity to be measured and ^{227}Ac can be easily determined by correct measurement of this peak. It is also possible to determine the absolute amount of ^{227}Ac by this γ-ray, if we know the absolute abundance ratio of this γ-transition and its relation with the absolute disintegration rate of ^{227}Ac. The proposed method for the determination of ^{227}Ac is very attractive. However, we must be careful no to allow even a slight contamination of ^{227}Th in ^{223}Fr fraction, since ^{227}Th also has intense γ-ray of 50 keV. Elimination of ^{227}Th is completely done by the separation method, and check of contamination of ^{227}Th could be easily made by checking the relative ratio of the intensity of each γ-peak.

Separation of ^{228}Ac and ^{228}Ra in Natural Thorium Decay Series. The separation method using HDEHP extraction can be applied to the ^{232}Th-^{228}Ra-^{228}Ac chain in the natural thorium decay series. ^{228}Ac is the most useful radioactive tracer of Ac, and is convenient for obtaining ^{228}Ac from ^{228}Ra by applying the simple milking method. The separation of ^{228}Ra and ^{228}Ac can be easily made by HDEHP extraction, and a new milking method for ^{228}Ac utilizing HDEHP extraction was proposed as shown in Fig. 7.

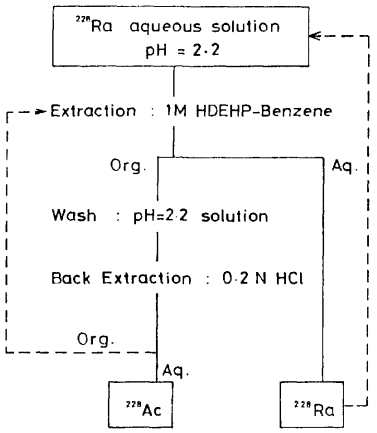

Fig. 7. Milking procedures for ^{228}Ac from ^{228}Ra.

References

1) M. J. Cabell, *Can. J. Chem.*, **37**, 1094 (1959).
2) T. Sekine, Y. Koike, and M. Sakairi, *J. Nucl. Sci. Technol.*, **4** (6), 308 (1967).
3) C. M. Lederer, J. M. Hollander, and I. Perlman, "Table of Isotopes," 6th ed, John Wiley & Sons, New York (1967).
4) D. F. Pepard, G. W. Marson, J. L. Maier, and W. J. Driscoll, *J. Inorg. Nucl. Chem.*, **4**, 334 (1957).
5) T. Mitsugashira and S. Suzuki, *J. Radioanal. Chem.*, **34** (2), 309 (1976).
6) J. A. Dean, "Lange's Handbook of Chemistry," 11th ed, McGraw-Hill Book Company, New York (1973).
7) T. Mitsugashira, Y. Shiokawa, and S. Suzuki, *Kagaku No Ryoiki*, **29** (6), 32 (1975).

Linear-sweep Voltammetry and the Simultaneous Determination of Purine Bases and Their Nucleosides in the Glassy Carbon Electrode

Toshio YAO, Tamotsu WASA, and Soichiro MUSHA
Department of Applied Chemistry, College of Engineering, University of Osaka Prefecture, Mozuumemachi, Sakai 591
(Received March 12, 1977)

Adenine, adenosine, guanine, and guanosine were voltammetrically oxidized in a glassy carbon electrode in aqueous solutions, but at different potentials. In general, the nucleosides were oxidized at more positive potentials than their bases. The bases and their nucleosides were strongly adsorbed on the surface of the glassy carbon electrode at the pH values around neutrality, so that the concentration *vs.* anodic peak current curves were not linear. The adsorption on the electrode was very dependent on the pH, and at pH values below 4 good linear relationships were observed between the anodic peak current and the concentration. The differences between the peak potentials of each of the purine bases and their nucleosides were most pronounced at pH 2—4. Consequently, it was possible to determine simultaneously both in mixtures of the purine bases and their nucleosides by using Britton-Robinson buffer as a supporting electrolyte in the pH range of 2—4. The proposed method is simple and rapid, since no prior treatment or separation procedure is required.

The electrochemical reduction and oxidation of biologically-important compounds have been investigated with much interest. The electrochemical reduction of purine bases, which are important components of nucleic acids, has been investigated in both aqueous[1-3] and nonaqueous solutions.[4] It is known that adenine is reduced and guanine is not at a dropping mercury electrode(DME). Adenosine appears to be reduced by the same mechanism, but, as the half-wave potentials are very close, the polarographic analysis of mixtures of adenine and adenosine is not possible. Also, the ultraviolet absorption spectra of these bases are very similar, so it is very difficult to work out a simple method for the analysis of such mixtures. A paper chromatographic method[5] for the quantitative determination of purine bases and their nucleosides involves extracting the paper chromatogram after separation and determining the amount of each species by UV spectrophotometry. Apart from being time-consuming, this method can be applied only to samples containing relatively high concentrations of the bases and their nucleosides.

A few studies[6-8] on the electrochemical oxidation of the purine bases were done at the pyrolytic graphite electrode(PGE) in aqueous solutions. Dryhurst[9] determined adenine in the presence of fairly large amounts of adenosine by taking advantage of the competitive adsorption of the two compounds on the PGE. However, this method cannot be applied to the simultaneous determination of adenine and adenosine in mixtures of the two compounds, because large amounts of adenosine must be added to test solutions.

In the present work, the oxidation behavior of purine bases and their nucleosides was investigated by linear-sweep voltammetry using a stationary, planar glassy carbon electrode (GCE). Also, in order to develop a satisfactory analytical method it was found necessary to investigate in some detail the adsorption of the purine bases on the GCE. This paper will describe a method whereby adenine, adenosine, guanine, and guanosine in mixtures of these bases can be determined simultaneously by utilizing the voltammetric oxidation peak of each of these bases at the GCE.

Experimental

Chemicals. The adenine, adenosine, guanine, and guanosine were all obtained from the Wako Pure Chemical Co. and were recrystallized two times from distilled water before drying *in vacuo* at 60 °C. The Britton-Robinson buffer used throughout this work was prepared from reagent-grade chemicals.

Apparatus. The polarograms and anodic voltammograms were recorded using a Yanagimoto P-8 type Polarograph at a scan rate of 3.3 mV/s. The three-electrode voltammetric cell maintained at (25±0.1)°C was used for all the experiments. An aqueous saturated calomel electrode(SCE) was used as the reference electrode, and a platinum wire served as the counter electrode.

The DME used had the following characteristics: mercury flow rate, $m=2.28$ mg/s and drop time, $t=3.35$ s at an open circuit with a mercury head of 70 cm in 1 M $HClO_4$.

The working electrode for anodic voltammetry was constructed from a 3-mm glassy carbon rod (Grade GC-20, Tokai Electrode Co.). The rod was cut into a length of 10 mm and was sealed in one end of a glass tube 3 mm in diameter with epoxy cement. The end of the glass tube-carbon rod assembly was polished with 400-grade emery paper until it was quite smooth. Then, by polishing with 1500-grade emery paper and a paste of sedimented calcium carbonate, the surface of the electrode was brought to a mirror finish.

Voltammetric Procedure. In order to obtain reproducible results, a standard pretreatment procedure was applied before recording each voltammogram. The GCE was polished for 60 s with 1500-grade emery paper and then for 30 s with a paste of sedimented calcium carbonate. The surface of the electrode was then washed for about 10 s with a fine spray of water. Any water remaining on the electrode surface and the shaft of the electrode was removed by touching the surface very gently with a piece of soft absorbent paper. Test solutions were not deaerated. The voltage scan was commenced after quiescency for 20 s at the starting potential (always 0.0 V *vs.* SCE). At least three replicate voltammograms were recorded for each test solution. A voltammogram of the background solution was recorded in the same way, while the peak current was obtained by arithmetrically subtracting the observed background current at the peak potential from that of the test solution.

Results and Discussion

Effect of pH. The half-wave potentials for the polarographic reduction of adenine and adenosine at the DME shifted linearly towards negative potentials with the increase in the pH. The wave-heights for both compounds were relatively constant at pH values below 5, but began to decrease sharply with a further increase in the pH. Adenine and adenosine also had practically identical $E_{1/2}$ values at all the pH values where the polarographic waves were observed, *e.g.*, at the pH 4.0 $E_{1/2}=-1.31$ V for adenine and -1.32 V for adenosine, so that the polarographic analysis of mixtures of the two compounds was not possible. Also, since the polarographic waves of both guanine and guanosine occurred close to the background-discharge potential, it was difficult to measure the limiting current accurately.

Each of the purine bases and their nucleosides gave a well-defined oxidation peak at a stationary GCE. The effect of the pH on the voltammetric peaks was investigated by recording the voltammograms of 0.05 mM purine bases and their nucleosides in Britton-Robinson buffer solutions. Adenine and adenosine both gave the single voltammetric oxidation peaks over the pH range of 2—12. The half-peak potentials($E_{p/2}$) of the voltammetric oxidation peaks of adenine and adenosine shifted linearly towards negative potentials with the increase in the pH; $E_{p/2}$(V *vs.* SCE)$=1.45-0.064$ pH for adenine and $E_{p/2}$(V *vs.* SCE)$=1.49-0.032$ pH for adenosine (Fig. 1). Both guanine and guanosine also gave single voltammetric oxidation peaks at the GCE. The half-peak potential shifted linearly towards negative potentials with the increase in the pH according to the following equations: $E_{p/2}$(V *vs.* SCE)$=1.13-0.059$ pH for guanine and $E_{p/2}$(V *vs.* SCE)$=1.25-0.046$ pH for guanosine. The analytical significance of these experimental results lies in the facts that the voltammetric oxidation peak-potential for each of the purine bases and their nucleosides is quite different in the pH range of 2—4, and that the oxidation potential for each of the purine bases is more negative than that for each of their nucleosides at all the pH values studied.

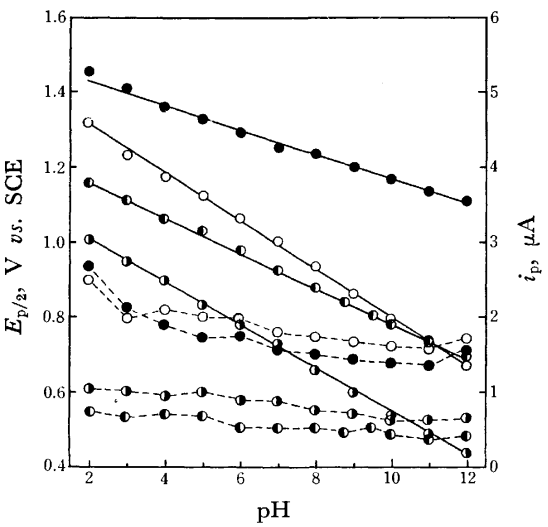

Fig. 1. The effect of pH on the peak current and the half-peak potential of the voltammetric oxidation peaks of 0.05 mM adenine(○), adenosine(●), guanine(◑), and guanosine(◐) in the Britton-Robinson's buffer solutions.
GCE geometric area; 7.1 mm², scan rate; 3.3 mV/s.
i_p, (----); $E_{p/2}$, (——).

Table 1. The effect of the pH on the peak current of the voltammetric oxidation peak of 1.0 mM bases
GCE geometric area, 7.1 mm²; scan rate, 3.3 mV/s.

	Britton-Robinson buffer					0.5 M H_3PO_4
	pH 10	pH 7	pH 4	pH 3	pH 2	
Adenine	4.9[a)]	7.9	14.5	14.9	14.9	15.6
Adenosine	6.9	10.5	14.4	14.0	14.2	14.8
Guanine	4.4	7.1	10.0	9.8	10.2	10.5
Guanosine	3.8	6.2	8.5	8.8	9.2	9.1

a) Peak current (μA).

The peak current of the voltammetric oxidation peaks of purine bases and their nucleosides increased gradually with the decrease in the pH, as is shown in Fig. 1. This experiment was undertaken at a very low concentration (0.05 mM) of the purine bases. When the depolarizer concentration was fairly high (1.0 mM), the pH values were found to have a pronounced effect on the peak current of the purine bases and their nucleosides. This result is shown in Table 1. The peak current increased sharply with the decrease in the pH and remained almost constant at pH values below 4. The same result was obtained in other buffers (acetate buffers and chloride buffers) and acid solutions (1 M HCl, H_2SO_4, $HClO_4$, and H_3PO_4) as supporting electrolytes; in electrolytes containing chloride ions the oxidation peaks of both adenine and adenosine were masked by the oxidation of the chloride ion in the background electrolytes. Also, in the acid solutions the oxidation peak of adenosine occurred close to the background discharge potential, so that the accurate measurement of the peak current was impossible.

Effect of the Scan Rate. In order to study the adsorption of the purine bases and their nucleosides on the stationary GCE, the effect of the voltage scan rate on the peak current of these compounds was examined.

The electrochemical oxidation of the purine bases and their nucleosides was irreversible, as was shown by cyclic voltammetric experiments in which no cathodic peak corresponding to the reduction of the oxidation product was observed at any scan rate.

For a linear diffusion-controlled irreversible peak, the peak current function, $i_p/ACV^{1/2}$, shoud be a constant,[10] and a plot of this function *vs.* $V^{1/2}$ should be a straight line parallel to the $V^{1/2}$ axis, where A is the area of the electrode surface; C, the bulk concentration of depolarizer; and V, the scan rate. At pH values below 4, the peak current functions of both adenine and adenosine were almost independent of the scan rate. At pH values above 4, however, the peak current functions increased markedly with the increase in the scan rate. This behavior is typical of an electrode process where the

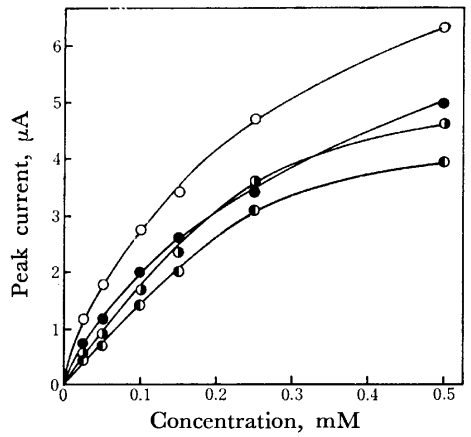

Fig. 2. Peak current-concentration curves for the voltammetric oxidation of the purine bases at the stationary GCE in the Britton-Robinson's buffer (pH 7.0).
○, Adenine; ●, adenosine; ◑, guanine; ◐, guanosine.
GCE geometric area; 7.1 mm², scan rate; 3.3 mV/s.

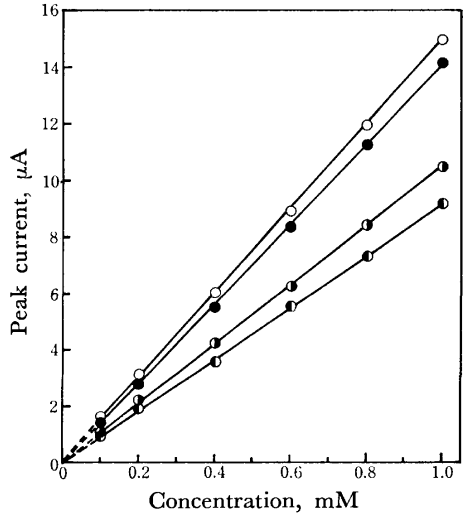

Fig. 3. The relationships between peak current and concentration for the purine bases in the Britton-Robinson's buffer at pH 3.0.
○, Adenine; ●, adenosine; ◑, guanine; ◐, guanosine.
GCE geometric area; 7.1 mm², scan rate; 3.3 mV/s.

reactant is adsorbed on the electrode.[11] In the cases of both guanine and guanosine, also, similar effects of the pH and the scan rate on the peak current function were observed.

Effect of the Concentration. In the Britton-Robinson buffer with pH values above 4, each of the purine bases studied showed a non-linear relationship between the peak current and the concentration, as is shown in Fig. 2. Such curves clearly indicate that the adsorption of the depolarizer takes place on the surface of the GCE. Also, the peak potential of the voltammetric oxidation peak for each of the purine bases and their nucleosides was dependent on the concentration and slightly shifted to more positive values with an increase in the concentration. Over the concentration range of 0.05—0.5 mM this shift was about 30—50 mV for all the purine bases.

In equimolar solutions (pH 7.0) of adenine and guanine, guanine showed a non-linear relationship between the peak current and the concentration similar to that shown in Fig. 2, but the peak current of adenine decreased in concentrations more than 0.25 mM in spite of the increase in the adenine concentration. However, in the Britton-Robinson buffer at pH 3 these purine bases showed a linear relationship between the peak current and the concentration, as is shown in Fig. 3.

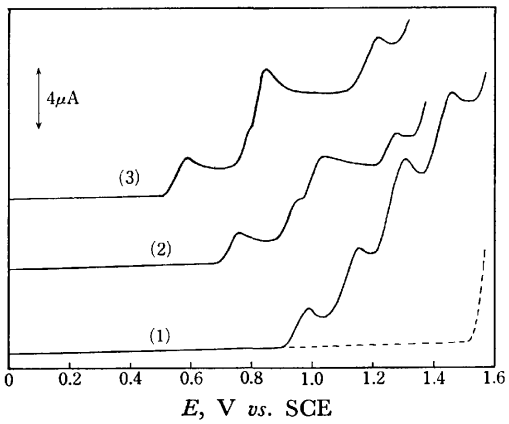

Fig. 4. Anodic voltammograms for the mixtures of adenine, adenosine, guanine, and guanosine.
Concn of each of adenine, adenosine, and guanosine : 0.4 mM, Concn of guanine : 0.2 mM. pH(Britton-Robinson's buffer); (1): 3.0, (2): 7.0, (3): 10.0.

Table 2. Voltammetric results for the determination of each component in mixtures of purine bases and their nucleosides

Taken (mM)				Found (mM)			
A	B	C	D	A	B	C	D
0.20	0.20	0.20	0.20	0.18	0.18	0.20	0.22
0.20	0.40	0.20	0.40	0.19	0.38	0.22	0.44
0.20	0.80	0.20	0.80	0.21	0.83	0.20	0.86
0.40	0.20	0.40	0.20	0.37	0.19	0.40	0.21
0.40	0.40	0.40	0.40	0.42	0.42	0.36	0.41
0.40	0.80	0.40	0.80	0.41	0.85	0.38	0.77
0.80	0.20	0.80	0.20	0.77	0.19	0.75	0.18

A, Guanine; B, guanosine; C, adenine; D, adenosine.
Supporting electrolyte; Britton-Robinson's buffer pH 3.0. GCE geometric area, 7.1 mm²; scan rate, 3.1 mV/s.

These effects of the concentration and the pH and the scan rate on the peak current imply that the adsorption of the depolarizer on the GCE is very dependent on the pH, but in the electrolytes at pH values below 4 the voltammetric oxidation is a diffusion-controlled process.

The Simultaneous Determination of the Purine Bases and Their Nucleosides. The anodic voltammograms for the mixtures of adenine, adenosine, guanine, and guanosine were recorded in Britton-Robinson buffer solutions of various pH values (Fig. 4). At pH values below 4 four successive well-defined oxidation peaks were observed, but a further increase in the pH made the voltammetric peaks sensitive to the adsorption of

depolarizer on the GCE. Also, the differences between the peak potentials of each of the purine bases and their nucleosides were most pronounced at pH 2—4. Accordingly, for the quantitative determination of the purine bases and their nucleosides a Britton-Robinson buffer in the pH range of 2—4 is suitable.

In order to test the quantitative method developed here, the voltammograms for some mixtures of four purine bases were recorded in the Britton-Robinson buffer of pH 3.0 at a stationary GCE. The concentration of each of the purine bases was determined by the calibration-curves method from the respective heights of the resulting voltammetric oxidation peaks. Some typical analytical results are shown in Table 2. Clearly this method is readily capable of determining simultaneously each component in mixtures of the purine bases and their nucleosides.

The principal advantage of the proposed method is the rapidity of analysis. The speed of analysis is aided by the fact that no prior treatment or separation procedure is needed. Furthermore, as dissolved oxygen does not interfere with the anodic voltammetry, no deaeration is required. One disadvantage is that the electrode must be pretreated before every voltammogram in order to ensure reproducibility. In addition, the method is of only moderate sensitivity, and traces (sub ppm) of the purine bases cannot be detected. It would be possible to improve the sensitivity by utilizing a pulse voltammetric method.

References

1) D. L. Smith and P. J. Elving, *J. Am. Chem. Soc.*, **84**, 1412 (1962).
2) G. Dryhurst and P. J. Elving, *Talanta*, **16**, 855 (1969).
3) B. Janik and P. J. Elving, *J. Electrochem. Soc.*, **116**, 1087 (1969).
4) T. Yao and S. Musha, *Bull. Chem. Soc. Jpn.*, **47**, 2650 (1974).
5) E. Gerlach, R. H. Dreisbach, and B. Deuticke, *J. Chromatogr.*, **18**, 76 (1965).
6) G. Dryhurst and P. J. Elving, *J. Electrochem. Soc.*, **115**, 1014 (1968).
7) G. Dryhurst and G. F. Pace, *J. Electrochem. Soc.*, **117**, 1259 (1970).
8) G. Dryhurst, *Anal. Chim. Acta*, **57**, 137 (1971).
9) G. Dryhurst, *Talanta*, **19**, 769 (1972).
10) R. S. Nicholson and I. Shain, *Anal. Chem.*, **36**, 706 (1964).
11) R. H. Wopschall and I. Shain, *Anal. Chem.*, **39**, 1514 (1967).

Reaction of Ru(II)-EDTA in Sodium Formate–Formic Acid Solutions*

Kunio SHIMIZU

Department of Chemistry, Faculty of Science and Technology, Sophia University, Chiyoda-ku, Tokyo 102

(Received May 2, 1977)

When $[Ru^{III}(Hedta)(H_2O)]$ was reduced at mercury electrode in sodium formate–formic acid solutions, the reduced species gradually became polarographically inactive. The final product of the deactivation reaction was isolated and identified as $Na_2[Ru^{II}(edta)(CO)]$. The kinetics follows the second-order rate equation, $-dc_1/dt=k_{obsd}\,c_1\,c_2$, where $c_1=[[Ru^{II}(Hedta)(H_2O)]^-]+[[Ru^{II}(edta)(H_2O)]^{2-}]$ and $c_2=[HCOO^-]+[HCOOH]$. The k_{obsd} value was found to be expressed by $k\,[H^+]/(K_A+[H^+])(K_R+[H^+])$, where $K_A(=3.28\times10^{-4}$ mol dm$^{-3})$ and $K_R(=6.92\times10^{-4}$ mol dm$^{-3})$ are the acid-dissociation constants of formic acid and $[Ru^{II}(Hedta)(H_2O)]^-$, respectively, with $k=1.01\times10^{-5}$ s^{-1} at 25 °C (ionic strength=0.5 mol dm^{-3}). Several possible mechanisms for the reaction were discussed. Probably the reaction proceeds through the formation of an intermediate involving one formate anion followed by dehydration and rearrangement.

Formation of carbonyls through decarbonylation of organic compounds by metal complexes has attracted considerable interest in recent years and a number of such reactions have been reported.[1–8] Halpern and Kemp studied the decarbonylation of formic acid by ruthenium(II) chloride in strongly acid solutions (about 3 mol dm^{-3} HCl) and obtained $(NH_4)[Ru^{II}(CO)Cl_4(H_2O)]$.[3] They also examined the kinetics of the decarbonylation and claimed that the reaction is of the second-order with respect to the ruthenium(II) species and *formic acid*. However, their results may be equally well explained by postulating formate anion as a reactant.

It has been pointed out[9] that electrolytically generated $[Ru^{II}(Hedta)(H_2O)]^-$ or $[Ru^{II}(edta)(H_2O)]^{2-}$ ** undergoes a deactivation process in formate–formic acid buffer solutions.

In the present work the final reaction product of this process has been identified as a carbonyl–edta-complex of ruthenium(II), the kinetics of its formation being examined in detail.

Experimental

Materials. Aqua(hydrogenethylenediaminetetraacetato)ruthenium(III) tetrahydrate, $[Ru(Hedta)(H_2O)]\cdot4H_2O$, was prepared according to the procedure of Mukaida *et al.*[10] with some modifications. An intensely blue ruthenium(II) cluster complex[11] was prepared by evaporating a mixture of 200 cm^3 of ethanol and 150 cm^3 of 3 mol dm^{-3} HCl solution containing 1.05 g of ruthenium(III) on a water bath. It was dissolved in a small portion of water, and a solution of 2.4 g of disodium ethylenediaminetetraacetate was added. The mixture, after being acidified by the addition of 1 cm^3 of concentrated hydrochloric acid, was evaporated nearly to dryness. The residue was dissolved in a small amount of water and evaporated again. The procedure was repeated several times until an orange solution was obtained on dissolving the residue. The pH of solution was then adjusted to *ca.* 2 with a sodium hydroxide solution. Ethanol was solwly added to the solution with stirring until a yellow precipitate appeared, and the mixture was left to stand overnight in a refrigerator. The yellow precipitate was filtered, washed several times with ethanol, and then dried *in vacuo* at 40 °C (yield, 2.4 g). Found: Ru, 20.57; C, 24.61; N, 5.60; H, 4.48%. Calcd for $[Ru(Hedta)(H_2O)]\cdot4H_2O$: Ru, 21.04; C, 25.00; N, 5.83; H, 4.28%. The IR spectrum of the product agreed with that reported by Mukaida *et al.* Its purity as determined by alkalimetric titration was 99.3%.

Deionized water distilled in an all-glass apparatus was used for the electrochemical experiments. The oxygen dissolved in the electrolytic solutions was removed by bubbling nitrogen gas which had been passed through acid vanadium(II) sulfate solution and then distilled water. The other chemicals used were of guaranteed reagent grade.

Measurements. All the electrochemical measurements were carried out at (25.0±0.1) °C under nitrogen atmosphere. All the potentials were measured against a saturated calomel electrode (SCE).

The electrolysis for the preparation of the final reaction product was performed with a Yanagimoto Controlled Potential Electrolyzer CE-3. The geometry of the electrolytic cell is illustrated in Fig. 1.

Controlled potential coulometry was carried out as described earlier[9] except that the integration of the electrolytic current was carried out on a digital counter (Takedariken, Universal Counter TR-5104) by converting the current signal into pulses with a voltage-frequency converter (Aiko VF 500).[12]

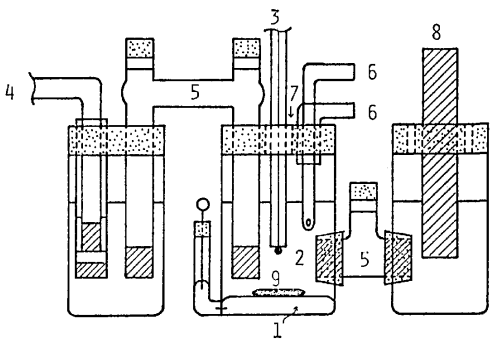

Fig. 1. Electrolytic cell for recorvery of the final reaction product.
1. Mercury pool working electrode (*ca.* 7.2 cm^2); 2. electrolytic solution; 3. DME; 4. to SCE; 5. salt bridge (1 mol dm^{-3} sodium formate) with filter paper plugs; 6. gas inlets; 7. gas outlet; 8. carbon anode immersed in 1 mol dm^{-3} sodium formate solution; 9. magnetic stirrer.

* Partly presented at the 22nd Annual Meeting on Ploarography and Electroanalytical Chemistry, October, 1976 in Nagano.

** The following abbreviations will be used: Ru(II)-Hedta$^-$ for $[Ru^{II}(Hedta)(H_2O)]^-$, Ru(III)-Hedta for $[Ru^{III}(Hedta)(H_2O)]$, Ru(II)-edta^{2-} for $[Ru^{II}(edta)(H_2O)]^{2-}$, and Ru(III)-edta$^-$ for $[Ru^{III}(edta)(H_2O)]^-$.

All the polarograms were recorded with a potentiostat-type dc-ac polarograph constructed in this laboratory. The drop time of the DME was controlled by an electronic drop-dislodger.[13,14] The device incorporated a relay which cuts off the polarographic current signal to the recorder at the moment of drop dislodging in order to suppress the noise accompanying the drop fall and to enhance the S/N ratio.[15] The polarographic current signal was sampled at 3.50 s after dislodgement. The flow rate of mercury from the DME was 1.78 mg s^{-1} under a mercury head of 50 cm. All the polarographic currents were corrected for the residual currents.

Infrared spectra were recorded with a Hitachi EPI-G2 IR spectrophotometer by the potassium bromide disk technique. Visible spectra were measured with a Hitachi 124 spectrophotometer. Conductivity was measured in distilled water with a TOA Electronics Conduct Meter CM-6A. Magnetic properties were measured by the Gouy method.

All the pH_c† values of the solutions were determined with a Radiometer pH meter 25E equipped with a glass electrode Type G202B and an SCE Type K401, whose meter readings were calibrated against standard hydrochloric acid solutions adjusted to 0.5 mol dm^{-3} of ionic strength by the addition of NaCl.

Analysis. Elemental analysis of C, H, and N was carried out by means of a Yanagimoto MT2 CHN Corder.

Spectrophotometric determination of ruthenium in the complexes was carried out according to the ruthenate method.[16] A weighed sample (*ca.* 10 mg) was decomposed in a nickel crucible by heating, and then fused with 0.1 g of potassium hydroxide and 0.3 g of potassium nitrate. The melt was dissolved in 50 cm^3 of a solution containing 10 g of potassium hydroxide, the solution volume then being adjusted to 100 cm^3 with water. The absorbance of the solution was measured at 465 nm.

The content of sodium ions in the final reaction product was determined by the cation-exchange method. A weighed sample (*ca.* 0.1 g) dissolved in 10 cm^3 of water was passed through a column of an H-form cation exchanger (Dowex 50-X8, 100—200 mesh), the column was washed with water and the combined eluate was titrated with a standard sodium hydroxide solution.

The content of water of crystallization was estimated by thermal gravimetric analysis with a Rigakudenki TG-DTA M8075.

Procedure. Isolation of the Final Reaction Product: A 20 cm^3 portion of sodium formate–formic acid (0.5 mol dm^{-3} each) containing 1.0 g of Ru(III)-Hedta was placed in the electrolytic cell and deoxygenated. Electrolysis was carried out at −0.5 V with stirring until more than 99% of the Ru(III)-Hedta was reduced. After the cell solution had been left to stand for 2 h under a nitrogen atmosphere, it was transferred into a flask and concentrated to one-fourth the initial volume under a reduced pressure at 40 °C. Ethanol was slowly added to the resulting solution until fine, pale yellow crystals precipitated; the mixture was allowed to stand in a refrigerator overnight. The precipitate, after being filtered, was recrystallized from methanol. The product was washed several times with ethanol and then dried *in vacuo* at 40 °C.

Measurement of Acid-dissociation Constants: The acid-dissociation constants of formic acid and Ru(III)-Hedta in 0.5 mol dm^{-3} NaCl solution were determined from the respective pH-titration curves.[17] The constnat of Ru(II)-Hedta$^-$ was calculated from the pH_c dependence of the reversible half-wave potential of the Ru(III)-Hedta reduction step in acid buffer solutions (sodium chloride–hydrochloric acid–0.001% Triton X-100 for $pH_c<2$, sodium formate–formic acid for $2<pH_c<4$, sodium acetate–acetic acid for $pH_c>4$; ionic strength = 0.5 mol dm^{-3} (NaCl)). The method was essentially the same as that described earlier;[9] but in the present case the data for $pH_c = 1.8$—5.5 were used so as to secure a higher precision for K_R. The values are given in Table 1.

TABLE 1. ACID-DISSOCIATION CONSTANTS
(Ionic strength = 0.5 mol dm^{-3}, 25 °C), $K = [H^+][X]/[HX]$.

Symbol	X	K/mol dm^{-3}
K_A	$HCOO^-$	3.28×10^{-4}
K_O	$[Ru^{III}(edta)(H_2O)]^-$	2.22×10^{-3}
K_R	$[Ru^{II}(edta)(H_2O)]^{2-}$	6.92×10^{-4}

Kinetic Measurements: For the kinetic measurements, sodium formate was used as the supporting electrolyte and the ionic strength of the solution was adjusted to 0.5 mol dm^{-3} by the addition of sodium *p*-toluenesulfonate. A 12 cm^3 portion of the supporting electrolyte solution was placed in the cell and deoxygenated. The solution was pre-electrolyzed at −0.5 V unitl a constant electrolytic current (usually about 3 μA) was reached. A known amount of Ru(III)-Hedta (*ca.* 20 μmol) was dissolved in the pre-electrolyzed solution, and the polarogram was recorded. When *ca.* 80% of Ru(III)-Hedta was reduced at −0.5 V to the bivalent state, a known amount of concentrated formic acid was injected into the solution from a microsyringe. After bubbling the nitrogen for 2—3 min, the decreasing anodic diffusion current at 0 V was recorded (chart speed, 2.5×10^{-2} cm s^{-1}) until it reached one-tenth the initial current.

Results and Discussion

Final Reaction Product. Elemental analyses of the final reaction product gave Ru, 19.48; C, 26.09; N, 5.59; H, 3.30%. The thermal gravimetric analysis showed that the water content in the product is 6.5%. These results indicate that the product contains 11 carbon, 2 nitrogen and 16—17 hydrogen atoms, and 2 molecules of water per ruthenium atom. The presence of protonated carboxyl groups and coordinated water is excluded by the fact that the final reaction product had no dissociable hydrogen. The cation-exchange experiment showed the complex ion in the product to be an anion, the number of sodium ions per ruthenium atom being 1.92.

The IR spectrum of the product is similar to that of the Ru(III)-Hedta. Two points, the presence of a very strong absorption at 1940 cm^{-1} and the absence of the >C=O stretching band which would be expected for a protonated carboxyl group (1730 cm^{-1} for Ru(III)-Hedta), were noted. The former strongly suggests the existence of a carbonyl group coordinated to ruthenium (II).[2,3,18] The latter indicates that each of the four carboxyl groups is either ionized or coordinated; in this event the >C=O absorption band should appear at 1590—1650 cm^{-1}.[19] In fact, a band was observed at 1630 cm^{-1}.

The oxidation state of the ruthenium in the final reaction product is considered to be II (t_{2g}^6) since the substance is diamagnetic. This view is supported by the fact that the product in acetate–acetic acid buffer solutions shows no polarographic step in the potential

† pH_c represents $-\log([H^+]/\text{mol dm}^{-3})$.

range +0.2——1.2 V. The effect of the coordinating carbonyl in ruthenium(II) complexes has been discussed in terms of the strong back-bonding with the metal orbitals of d_π-symmetry.[20] Coordination of carbonyl to ruthenium(II) renders the complex much less oxidizable. The frequency of the CO band also leads to the same conclusion: if the oxidation state of ruthenium were higher than II, the frequency would be higher because of the increase in positive charge on the central atom; for example, the ν(CO) is 1950 cm^{-1} in $(NH_4)_2[Ru^{II}Cl_4(CO)(H_2O)]$ and 2059 cm^{-1} in $(NH_4)_2[Ru^{III}Cl_5(CO)]$.[2] We infer $Na_2[Ru^{II}(edta)(CO)]\cdot 2H_2O$ as the formula of the final reaction product. The elemental composition calculated on the basis of the formula is in line with the experimental values: Ru, 20.24; C, 26.46; N, 5.61; H, 3.23%.

The molar conductivity of the product at 8.01×10^{-4} mol dm^{-3} in aqueous solution was 250 S mol^{-1} cm^2 at 25 °C, which is reasonable for a 1 : 2 type electrolyte.

The absorption peak in the visible region was at 428 nm at which the molar absorption coefficent was 9.06×10^4 mol^{-1} cm^2.

Results of Kinetic Studies. When Ru(III)-Hedta was partially electrolyzed in solutions containing sodium formate and sodium *p*-toluenesulfonate at a potential on the diffusion-current plateau of its reduction step, a single oxidation-reduction polarographic step appeared at about −0.25 V. The anodic limiting current, I_a, was proved to be diffusion-controlled, being proportional to the quantity of electricity consumed for the reduction, *i.e.*, to the total concentration of the Ru(II) species (in such weakly alkaline solutions, $[Ru^{II}(edta)(OH)]^{3-}$ is also present together with Ru(II)-$edta^{2-}$). No change in the polarogram was observed at least for a few hours at 25 °C.

When formic acid was present, however, the anodic current decreased with time as shown in Fig. 2, while the cathodic current remained constant. In the presence of excess formic acid–formate ion (at least 50-fold the concentration of Ru(II) species), the rate of decrease of the anodic diffusion current always obeyed the pseudo-first-order rate expression (Eq. 1) until the reaction had proceeded at least 80% to completion (Fig. 3):

$$-\ln\frac{I_a(t)}{I_a(0)} = k'_{obsd}\,t, \qquad (1)$$

where $I_a(t)$ and $I_a(0)$ are the anodic diffusion current at time t and $t=0$, respectively. The values of k'_{obsd} determined from the slopes of the first-order rate plots were substantially independent of the concentrations of initially present ruthenium(II) and coexisting ruthenium(III) species.

At a given hydrogen ion concentration, k'_{obsd} was proportional to the sum of the concentrations of formate ion and formic acid (Fig. 4). Hence Eq. 1 becomes

$$-\ln\frac{I_a(t)}{I_a(0)} = k_{obsd}\,c_2\,t, \qquad (2)$$

where $c_2=[HCOO^-]+[HCOOH]$ and k_{obsd} is the second-order rate constant. As seen from Fig. 5, k_{obsd} is a function of the hydrogen ion concentration, increasing almost linearly up to a maximum at $[H^+]=5\times10^{-4}$ mol dm^{-3}, after which it decreased slowly. The kinetic data are summarized in Table 2.

Interpretation of Kinetic Results. Under the experimental conditions there may be four reactant species participating in the deactivation reaction: Ru(II)-$Hedta^-$, Ru(II)-$edta^{2-}$, $HCOO^-$, and HCOOH. Here, $[Ru^{II}(edta)(OH)]^{3-}$ is ignored because the acid-dissociation constant for

$$[Ru^{II}(edta)(H_2O)]^{2-} \rightleftharpoons [Ru^{II}(edta)(OH)]^{3-} + H^+$$

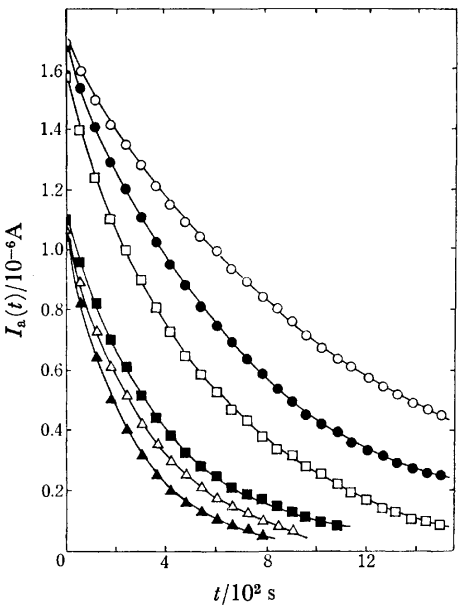

Fig. 2. Typical decay curves (ionic strength=0.5 mol dm^{-3}, 25 °C) with reference to Table 2.
○, No. 10; ●, No. 11; □, No. 9; ■, No. 14; △, No. 12; ▲ No. 13.

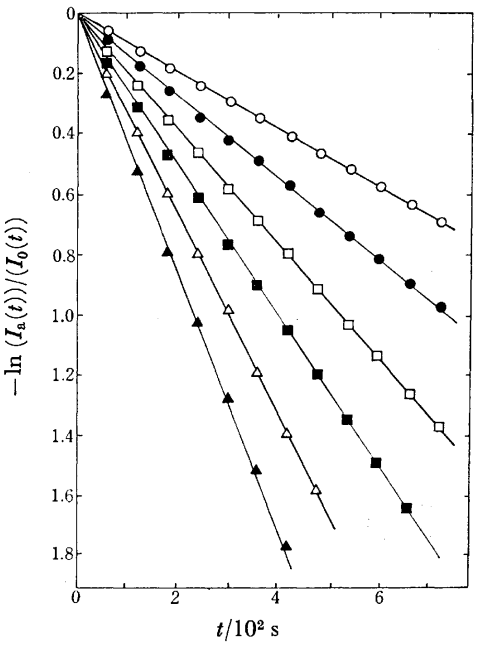

Fig. 3. Typical pseudo-first-order rate plots for the deactivation reaction (ionic strength=0.5 mol dm^{-3}, 25 °C) with reference to Table 2.
○, No. 10; ●, No. 11; □, No. 9; ■, No. 14; △, No. 12; ▲, No. 13.

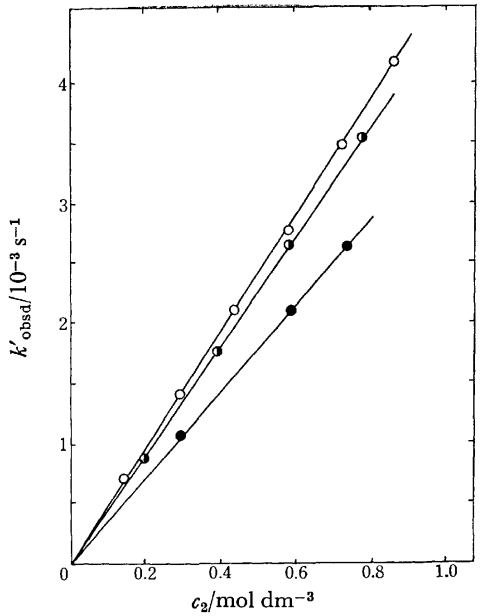

Fig. 4. Dependence of k'_{obsd} on c_2 at given hydrogen concentrations (ionic strength=0.5 mol dm^{-3}, 25 °C) with reference to Table 2.
c_2=[HCOO$^-$]+[HCOOH]; ○, No. 18—23; ◑, No. 9—14; ●, No. 3—5.

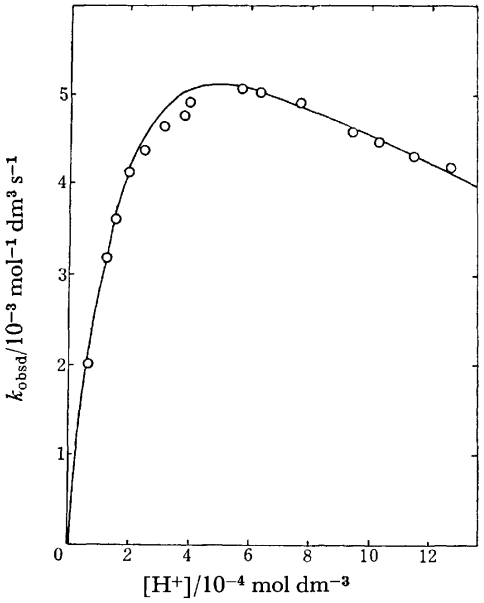

Fig. 5. Dependence of k_{obsd} on hydrogen ion concentration (ionic strength=0.5 mol dm^{-3}, 25 °C). The curve is calculated from Eq. 8 with $k=1.01\times10^{-5}$ s^{-1}.

should be appreciably smaller than that of the corresponding Ru(III)-edta$^-$ (pK=7.63)[9] so that its concentration is negligible in formic acid–formate buffer solutions.

There are several mechanisms involving these four reactants that can explain the experimental data. Most probably, the reaction will proceed through some intermediate(s) which contains formate ion or formic acid:

$$\text{Reactants} \xrightarrow{\text{(I)}} \text{Intermediate(s)} \xrightarrow{\text{(II)}} \text{Product}$$

Either step (I) or step (II) may be rate-determining.
Case I: step (I) rate-determining.

Table 2. Kinetic data for deactivation rate
(ionic strength=0.5 mol dm^{-3}, 25 °C)

No.	[H$^+$] / 10^{-4} mol dm^{-3}	c_2 / mol dm^{-3}	k'_{obsd} / 10^{-3} s^{-1}	k_{obsd} / 10^{-3} mol^{-1} dm^3 s^{-1}
1	0.164	0.596	1.20	2.01
2	1.26	0.347	1.10	3.17
3	1.51	0.297	1.06	3.57
4	1.55	0.591	2.11	3.57
5	1.55	0.737	2.63	3.57
6	2.00	0.247	1.02	4.13
7	2.44	0.442	1.92	4.34
8	2.51	0.442	1.91	4.32
9	3.09	0.392	1.80	4.59
10	3.16	0.198	0.914	4.62
11	3.16	0.295	1.36	4.61
12	3.16	0.779	3.53	4.53
13	3.16	0.970	4.35	4.48
14	3.24	0.586	2.67	4.56
15	3.86	0.178	0.835	4.69
16	3.98	0.344	1.69	4.91
17	5.62	0.313	1.58	5.05
18	6.31	0.294	1.45	4.93
19	6.46	0.148	0.708	4.78
20	6.46	0.438	2.09	4.77
21	6.61	0.582	2.77	4.76
22	6.61	0.725	3.48	4.80
23	6.66	0.866	4.17	4.82
24	7.64	0.273	1.36	4.98
25	9.33	0.263	1.21	4.60
26	10.3	0.256	1.15	4.49
27	11.4	0.251	1.09	4.34
28	12.7	0.244	1.05	4.30

c_2=[HCOO$^-$]+[HCOOH]

Mechanism Ia

$$\text{Ru(II)-Hedta}^- + \text{HCOOH} \xrightarrow{k_1} \text{intermediate}, \quad \text{(R1)}$$

$$\text{Ru(II)-Hedta}^- + \text{HCOO}^- \xrightarrow{k_2} \text{intermediate}, \quad \text{(R2)}$$

$$\text{Ru(II)-edta}^{2-} + \text{HCOOH} \xrightarrow{k_3} \text{intermediate}, \quad \text{(R3)}$$

$$\text{Ru(II)-edta}^{2-} + \text{HCOO}^- \xrightarrow{k_4} \text{intermediate}, \quad \text{(R4)}$$

where k_1, k_2, k_3, and k_4 are the corresponding second-order rate constants. If these reactions proceed in parallel, the rate of decrease of the total concentration of the Ru(II) species (c_1=[Ru(II)-Hedta$^-$]+[Ru(II)-edta^{2-}]), is given by

$$-\frac{dc_1}{dt} = k_1[\text{Ru(II)-Hedta}^-][\text{HCOOH}] + k_2[\text{Ru(II)-Hedta}^-][\text{HCOO}^-] + k_3[\text{Ru(II)-edta}^{2-}][\text{HCOOH}] + k_4[\text{Ru(II)-edta}^{2-}][\text{HCOO}^-]. \quad (3)$$

Since the proton transfer reactions between Ru(II)-Hedta$^-$ and Ru(II)-edta^{2-} and between HCOOH and HCOO$^-$ must be very fast and remain in a quasi-equilibrium state so that (R2) and (R3) are kinetically indistinguishable, the above expression is reduced to

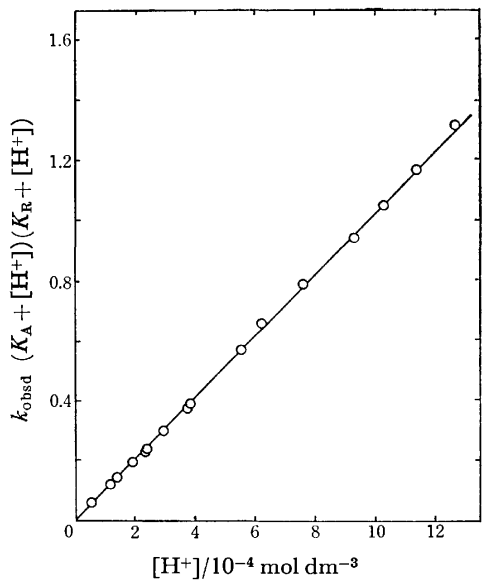

Fig. 6. Plot of k_{obsd} $(K_A+[H^+])(K_R+[H^+])$ against hydrogen ion concentration (ionic strength=0.5 mol dm^{-3}, 25 °C).

$$-\frac{dc_1}{dt}=\frac{k_1[H^+]^2+(k_2K_A+k_3K_R)[H^+]+k_4K_AK_R}{(K_A+[H^+])(K_R+[H^+])}c_1c_2. \quad (4)$$

Equation 4 is integrated with $c_1=c_2(0)$ at $t=0$ and c_2=constant. Since I_a is proportional to c_1, by comparing the resulting expression with Eq. 2, we obtain

$$k_{obsd}=\frac{k_1[H^+]^2+(k_2K_A+k_3K_R)[H^+]+k_4K_AK_R}{(K_A+[H^+])(K_R+[H^+])}. \quad (5)$$

Thus the plot of $k_{obsd}(K_A+[H^+])(K_R+[H^+])$ against hydrogen ion concentration generally should be a parabola.

The plot gives a straight line with zero intercept (Fig. 6). Hence, k_1 and k_4 must be negligibly small with respect to k_2 and/or k_3, since $[H^+]$, $K_A[H^+]$, $K_R\cdot[H^+]$, and K_AK_R are of the same order of magnitude under the experimental conditions.

Mechanism 1b

The termoleclar rate determining step,

$$Ru(II)\text{-}edta^{2-}+HCOO^-+H^+ \xrightarrow{k_5} \text{intermediate}, \quad (R5)$$

is also possible but seems unlikely on statistical grounds.

Case II: step (II) is rate determining. In this case step (I) is in quasi-equilibrium state.

Mechanism 2a

$$Ru(II)\text{-}Hedta^-+HCOOH \underset{k_6}{\overset{K_6}{\rightleftharpoons}} \text{intermediate(6)} \xrightarrow{} \text{product}, \quad (R6)$$

$$Ru(II)\text{-}Hedta^-+HCOO^- \underset{k_7}{\overset{K_7}{\rightleftharpoons}} \text{intermediate(7)} \xrightarrow{} \text{product}, \quad (R7)$$

$$Ru(II)\text{-}edta^{2-}+HCOOH \underset{k_8}{\overset{K_8}{\rightleftharpoons}} \text{intermediate(8)} \xrightarrow{} \text{product}, \quad (R8)$$

$$Ru(II)\text{-}edta^{2-}+HCOO^- \underset{k_9}{\overset{K_9}{\rightleftharpoons}} \text{intermediate(9)} \xrightarrow{} \text{product}, \quad (R9)$$

where K_6, K_7, K_8, and K_9 are the equilibrium constants for respective reactions, and k_6, k_7, k_8, and k_9 are the first-order rate constants for the respective intermediate. Here, intermediates(6)—(9) are not necessarily different.

If the intermediates are also oxidized at the potential where I_a is measured and their diffusion coefficients are the same or nearly the same as that of Ru(II) species, $-dI_a(t)/dt$ is proportional to

$$-d([Ru(II)\text{-}Hedta^-]+[Ru(II)\text{-}edta^{2-}]+\sum_{i=6}[\text{intermediate}(i)])/dt.$$

If these reactions proceed in parallel, a simple calculation similar to that in the preceeding section leads to

$$k_{obsd}=\frac{k_6K_6[H^+]^2+(k_7K_7K_A+k_8K_8K_R)[H^+]+k_9K_9K_AK_R}{(K_A+[H^+])(K_R+[H^+])}. \quad (6)$$

For the same reason as in the case of Mechanism 1a, the reaction paths (R6) and (R9) are neglected.

If the intermediates are electro-inactive at the potential concerned and hence I_a is proportional to Ru(II) species only, the resulting expression becomes consistent with the experimental results only when the concentrations of the intermediates are very small. In such a case k_{obsd} is obtained by Eq. 6.

Mechanism 2b

$$Ru(II)\text{-}edta^{2-}+HCOO^- \underset{k_{10}}{\overset{K_{10}}{\rightleftharpoons}} \text{intermediate} \xrightarrow{} \text{product} \quad (R10)$$

If the intermediate is electro-active, we get

$$k_{obsd}=\frac{k_{10}K_{10}K_AK_R[H^+]}{(K_A+[H^+])(K_R+[H^+])}, \quad (7)$$

which is compatible with the experimental results.

On the other hand, if the intermediates is electro-inactive, the resulting expression is reduced to Eq. 7 only when the intermediate concentration is very small.

The probable mechanisms 1a, 1b, 2a, and 2b are kinetically indistinguishable and their discrimination requires further information.

At present, the rate constant is expressed by

$$k_{obsd}=\frac{k[H^+]}{(K_A+[H^+])(K_R+[H^+])}, \quad (8)$$

where k is a constant equal to 1.01×10^{-5} s^{-1} at 25 °C (ionic strength=0.5 mol dm^{-3}).

Conclusion

Cleare and Griffith[8] in their study of the formation of halogeno-carbonyl complexes of the platinum metals identified formato-intermediates from the formic acid-hexahalogenorhodate(2—) reactions by IR spectroscopy. Although no such intermediate was identified in the case of ruthenium, they noted "indications that the reactions proceed *via* formato- and formato-halogeno-carbonyl intermediates (the use of hydrochloric acid in the reactions appears to inhibit the formation of formato complexes)."

Most probably, the present reaction also will proceed through such formato-intermediates. The reaction path that involves Ru(II)-Hedta$^-$ and HCOOH (R1

or R6) is not compatible with the experimental results. Since HCOOH does not react with Ru(II)-Hedta$^-$, it will not react with Ru(II)-edta^{2-} because it is improbable that HCOOH, being an uncharged species, behaves in an essentially different way depending on the charge of the bulky reaction partner: (R3) and (R8) are excluded. A reaction path involving no hydrogen ion such as (R4) and (R9) has been excluded on the basis of the kinetic data.

The formato-intermediate requires one proton to undergo the subsequent dehydration process to [Ru^{II}-(edta)(CO)]$^{2-}$. The proton is involved in the rate determining step as indicated by the kinetic data. In (R2) or (R7) the proton is supplied from Ru(II)-Hedta$^-$, the concentration of which is much larger than the free hydrogen ion concentration in the solution.

The above discussion and the kinetic analysis lead to three probable mechanisms:

Mechanism 1a

$$\text{Ru(II)-Hedta}^- + \text{HCOO}^- \xrightarrow[\text{slow}]{k_2} \text{Ru(II)-Hedta-HCOO}^{2+}$$

$$\text{Ru(II)-Hedta-HCOO}^{2-} \xrightarrow[\text{fast}]{} \text{Ru}^{II}\text{(edta)(CO)}^{2-} + \text{H}_2\text{O}$$

Mechanism 2a

$$\text{Ru(II)-Hedta}^- + \text{HCOO}^- \overset{K_7}{\rightleftharpoons} \text{Ru(II)-Hedta-HCOO}^{2-}$$

$$\text{Ru(II)-Hedta-HCOO}^{2-} \xrightarrow[\text{slow}]{k_7} \text{Ru}^{II}\text{(edta)(CO)}^{2-} + \text{H}_2\text{O}$$

Mechanism 2b

$$\text{Ru(II)-edta}^{2-} + \text{HCOO}^- \overset{K_{10}}{\rightleftharpoons} \text{Ru(II)-edta-HCOO}^{3-}$$

$$\text{Ru(II)-edta-HCOO}^{3-} + \text{H}^+ \xrightarrow[\text{slow}]{k_{10}} \text{Ru}^{II}\text{(edta)(CO)}^{2-} + \text{H}_2\text{O}$$

The second steps of these mechanisms involve dehydration and rearrangement of the formato ligand. Direct evidence for the formato-intermediate is yet to be sought, but information on the kinetics of acetylacetonato-ruthenium(II)–formate reactions[21] suggests that it may be formed through substitution of the aqua ligand by formate ion. At present, the experimental data available are insufficient to establish the most probable mechanism. The numerical values for the rate constants as interpreted according to the three mechanisms are given in Table 3.

Equation 8 implies that the rate is maximum when $[H^+]=(K_AK_R)^{1/2}$, in this case, 4.76×10^{-4} mol dm^{-3}. It should be noted that a mild acidic condition is favorable for preparing carbonyl complexes when the reaction mechanism is similar to the present one.

The author would like to express grateful appreciation to Prof. Gen P. Satô, Sophia University, for his continuous guidance and encouragenent. Thanks are also due to Profs. Kunio Nakano and Tatsujiro Ishimori, St. Paul's (Rikkyo) University, for their valuable suggestions; to Mr. Kenji Hirose and Mr. Misao Hayashi for their assistance in the preliminary experiments; and to Sr. Jean Michalce for correcting the manuscript.

The present work was partially supported by a Grant-in-Aid for Scientific Research from the Ministry of Education in 1973.

TABLE 3. RATE CONSTANT FOR PROBABLE MECHANISMS

Mechanism	k	Experimental value
1a	k_2k_R	$k_2=3.08\times10^{-2}$ mol^{-1} dm^3 s^{-1}
2a	k_7K_7	$k_7K_7=3.08\times10^{-2}$ mol^{-1} dm^3 s^{-1}
2b	$k_{10}K_{10}K_AK_R$	$k_{10}K_{10}=44.5$ mol^{-2} dm^6 s^{-1}

References

1) J. Halpern, B. R. James, and A. L. W. Kemp, *J. Am. Chem. Soc.*, **83**, 4097 (1961).
2) J. Halpern, B. R. James, and A. L. W. Kemp, *J. Am. Chem. Soc.*, **88**, 5141 (1966).
3) J. Halpern and A. L. W. Kemp, *J. Am. Chem. Soc.*, **88**, 5147 (1966).
4) R. H. Prince and K. A. Raspin, *Chem. Commun*, **1966**, 156.
5) J. Chatt, B. L. Shaw, and A. E. Field, *J. Chem. Soc.*, **1964**, 3466.
6) A. Rusina and A. A. Vlček, *Nature*, **206**, 295 (1965).
7) L. Vaska, *J. Am. Chem. Soc.*, **86**, 1943 (1964).
8) M. J. Cleare and W. P. Griffith, *J. Chem. Soc., A*, **1969**, 372.
9) K. Shimizu, T. Matsubara, and G. P. Satô, *Bull. Chem. Soc. Jpn.*, **47**, 1651 (1974).
10) M. Mukaida, H. Okuno, and T. Ishimori, *Nippon Kagaku Zasshi*, **86**, 598 (1965).
11) J. D. Gilbert, D. Rose, and G. Wilkinson, *J. Chem. Soc., A*, **1970**, 2765.
12) S. Hayashi, K. Shimizu, and G. P. Satô, *Rev. Polarogr. (Kyoto)*, **21**, 13 (1975).
13) K. Shimizu, M. Kobayashi, and G. P. Satô, *Bunseki Kagaku*, **23**, 1537 (1974).
14) K. Shimizu and M. Kobayashi, *Bunseki Kiki*, **12**, 687 (1974).
15) G. P. Satô and K. Shimizu, *Bunseki Kagaku*, **26**, 77 (1977).
16) G. A. Stoner, *Anal. Chem.*, **27**, 1186 (1955).
17) G. M. Fleck, "Equilibria in Solution," Japanese Ed translated by K. Mizumachi, Maruzen (1968), Chap. 4.
18) G. M. Brown, F. R. Hopf, J. A. Ferguson, T. J. Meyer, and D. G. Whitten, *J. Am. Chem. Soc.*, **95**, 5939 (1973).
19) K. Nakamoto, "Infrared Spectra of Inorganic and Coordination Compounds," 2nd ed, John Wiley & Sons, New York (1970), p. 238.
20) G. M. Brown, F. R. Hopf, T. J. Meyer, and D. G. Whitten, *J. Am. Chem. Soc.*, **97**, 5385 (1975).
21) K. Shimizu and G. P. Satô, unpublished work.

Hydrolytic Behavior of Oxovanadium(IV) Ions

Akitoshi KOMURA, Mutsuo HAYASHI, and Hiroto IMANAGA

Faculty of Technology, Kanazawa University, Kanazawa 920

(Received March 18, 1977)

The hydrolysis of VO^{2+} was investigated in 0.1 M $LiClO_4$ by potentiometric, conductometric and turbidimetric measurements. The following values of the equilibrium constants were obtained: $\beta_{11}=[VOOH^+][H^+]/[VO^{2+}]=9.0\times10^{-6}$ M (M=mol dm^{-3}); $\beta_{22}=[(VO)_2(OH)_2{}^{2+}][H^+]^2/[VO^{2+}]^2=1.9\times10^{-7}$ M. The solubility product of $VO(OH)_2$ given by $K_{sp1}=[VO^{2+}][OH^-]^2$ was found to be 6.6×10^{-23} M^3 from the pH values at which precipitation occurs. Only one species with a stoichiometric ratio VO/OH=2.5 is present in basic solutions in the pH range 9—12. The solubility product of $VO(OH)_2$ given by $K_{sp2}=[H^+][(VO)_2(OH)_5{}^-]$ is $\log K_{sp2}=-11.1$. A less soluble salt $Na(VO)_2(OH)_5$ or $NaHV_2O_5$ was isolated from strongly basic solutions. Measurements of Na^+ concentration at which the solid phase first appears give $\log K_{sp3}=-3.74$ as its solubility product, $K_{sp3}=[Na^+][(VO)_2(OH)_5{}^-]$.

The species with metal-oxygen multiple bonds are of particular interest in connection with their reactivities and structures.[1,2] The oxovanadium(IV) ion seems to be the most stable diatomic ion known, forming a wide variety of stable complexes and persisting in VO^{2+} entity.[3] The susceptibility of the VO^{2+} ion to hydrolysis, however, may greatly complicate the coordinative behavior of vanadium(IV) in aqueous solution. Investigations[4-6] on the hydrolysis of VO^{2+} in acidic solutions have provided strong evidence for the existence of a simple monohydroxo species accompanied by the formation of a dinuclear species. On the other hand, only a few quantitative studies have been made on the nature of vanadium(IV) in neutral or basic solutions. Titration curves obtained by Britton and Welford[7] showed the presence of the $V_4O_9{}^{2-}$ species in basic solutions. The polarographic data by Lingane and Meites[8] were interpreted in terms of the formation of two ions $V_2O_5{}^{2-}$ and $V_4O_9{}^{2-}$. A recent ESR study[9] showed that the vanadium(IV) species in basic solutions was monomeric $VO(OH)_3{}^-$. Various vanadate(IV) compounds, often called either vanadites or hypovanadates, were isolated from strongly basic solutions of vanadium(IV).[10,11] The present authors have examined the hydrolysis of VO^{2+} over a wide range of pH, using potentiometric, conductometric and turbidimetric techniques, in order to identify the hydrolysis species of vanadium(IV) and clarify their formation equilibria.

Experimental

Materials. Chemicals of guaranteed quality were used without further purification. Stock solutions of oxovanadium perchlorate in dilute perchloric acid (*ca.* 0.1 M) were prepared by dissolving vanadium(IV) hydroxide in a perchloric acid solution, and standardized by permanganate titration. The free acid in the oxovanadium perchlorate solution was determined by passing an aliquot portion of the stock solution through a cation-exchange resin, and titrating the effluent with a standard base. Lithium perchlorate was prepared from perchloric acid and lithium carbonate, and recrystallized twice from water. A standard carbonate-free sodium hydroxide solution was prepared by the usual procedure from a saturated NaOH solution, and stored in a polyethylene bottle under a CO_2-free atmosphere. Perchloric acid solutions were prepared by dilution of concentrated perchloric acid (Wako Super Special Grade).

Apparatus and Procedures. Potentiometric titration was carried out by means of a Horiba F-7SS pH meter with a Horiba glass electrode and an asbestos fiber-junction calomel electrode in a gas-tight cell under a stream of purified nitrogen. All the pH measurements were made in $LiClO_4$ solutions at a constant ionic strength (I=0.1 M) and at 25±0.05 °C. The electrode system was calibrated in terms of free hydrogen ion concentration, h, with standard $HClO_4$ and NaOH solutions. The liquid junction potential of the cell was independent of h within the limit of experimental error (0.5 mV) in the range $h\leq0.001$ M. The value of h in the vanadium solutions was determined by comparing the cell potential of the solutions with that of a standard solution of 0.001 M $HClO_4$ in 0.1 M $LiClO_4$. In order to remove the oxygen dissolved, nitrogen was bubbled through sample solutions for 1 h before titration. Small increments of a standardized NaOH or $HClO_4$ solution were added to the titration cell with a microburet and the pH was read every 2—3 min after each addition of the titrant. The decrease in concentration of ions due to dilution in the course of titration was below 2% of initial concentration over the pH range studied. The concentrations of ions were corrected for the dilution effect on the basis of the added amount of titrant.

Conductometric titration was carried out under purified nitrogen at 25±0.01 °C with the use of a Yokogawa conductance bridge (1000 Hz) and a conductometric cell with platinized platinum black electrodes. Precipitation boundaries were determined by measuring the concentration of H^+ or Na^+ at which a solid phase first appeared in vanadium(IV) solutions. The experimental procedure was similar to that for the potentiometric titration, except that titrants were added very slowly to the cell. The turbidity of the vanadium solutions was observed either visually under irradiation with a beam of light or by means of a Hitachi 124 spectrophotometer. The formation of a solid phase was detected as a sudden development of turbidity. Electronic spectra of solutions were recorded on a Hitachi 124 spectrophotometer with the use of matched 10 mm quartz cells fitted with ground-glass stoppers. All solutions for spectral measurements were prepared under anaerobic conditions. In basic solutions, extreme care was required to prevent oxidation of vanadium(IV).

Results and Discussion

Hydrolysis in Acidic Solution. The average number of hydroxide ions bound per vanadium, $\bar{n}$, is calculated at any point of titration from the following relationship:

$$\bar{n}=\frac{h-C_H}{C_m}, \quad (1)$$

where C_H and C_m are the total analytical concentrations of H^+ and vanadium(IV). The hydrolysis of VO^{2+}

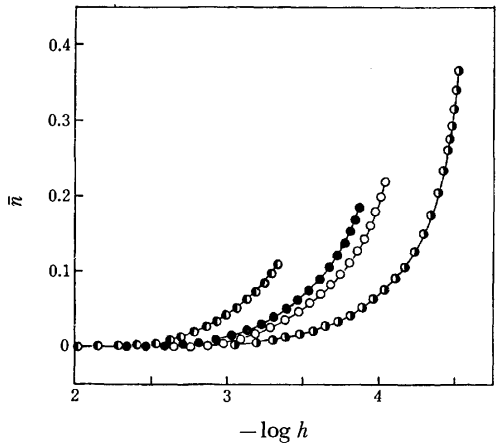

Fig. 1. Average number, $\bar{n}$, of hydroxide ions bound per vanadium as a function of log h.
The total concentrations of vanadium: ◐, 5×10^{-2} M; ●, 10^{-2} M; ○, 5×10^{-3} M; ◑, 10^{-3} M.

can be expressed by

$$pVO^{2+} + qH_2O \rightleftharpoons (VO)_p(OH)_q^{2p-q} + qH^+, \quad (2)$$

where p and q are positive integral numbers. Equilibrium constants β_{pq} and $\bar{n}$ are defined as follows:

$$\beta_{pq} = [(VO)_p(OH)_q^{2p-q}][VO^{2+}]^{-p}h^q, \quad (3)$$

$$\bar{n} = \frac{\Sigma q[(VO)_p(OH)_q^{2p-q}]}{C_m}. \quad (4)$$

The total concentration of vanadium is given by

$$C_m = [VO^{2+}] + \Sigma p[(VO]_p(OH)_q^{2p-q}]. \quad (5)$$

Precipitation of vanadium hydroxide at a low value of $\bar{n}$ restricts the region of measurements accessible to the study of solution equilibrium. As shown in Fig. 1, $\bar{n}$ *vs.* log h curves in the region without precipitation are parallel to each other over the range C_m=0.001—0.05 M. The treatment for the general 'core-links' complexes[12] was applied. Analysis of the data in the range C_m=0.001—0.05 M strongly indicates the species with p=2 and q=2 to be the predominant hydrolysis product of VO^{2+}, in agreement with Rossotti and Rossotti.[4] A value of β_{22} of 1.9×10^{-7} M was obtained on the assumption that only the $(VO)_2(OH)_2^{2+}$ species was formed. The assumption could not, however, explain satisfactorily the experimental data for C_m below 0.001 M. The possible presence of hydrolysis species other than $(VO)_2(OH)_2^{2+}$ was tested by a curve-fitting procedure. The potentiometric data over a wide range of C_m could best be interpreted in terms of the additional formation of the mononuclear $VOOH^+$ species at lower C_m values. The β values evaluated by the procedure were β_{11}=$(9\pm1)\times10^{-6}$ M and β_{22}=$(1.9\pm0.5)\times10^{-7}$ M. If the species $(VO)_2(OH)_2^{2+}$ and $VOOH^+$ are the only two complexes formed, the following relation can also be derived from Eqs. 3, 4, and 5.

$$h\bar{n}(1-\bar{n})^{-1} = \beta_{11} + 2\beta_{22}C_m h^{-1}(1-\bar{n}). \quad (6)$$

A plot of $h\bar{n}(1-\bar{n})^{-1}$ *vs.* $C_m h^{-1}(1-\bar{n})$ should give a straight line with a slope equal to $2\beta_{22}$ and an intercept equal to β_{11} (Fig. 2). The straight line gives the same values of β as those obtained above. The β_{22} value we obtained is in good agreement with that of $10^{-6.88}$ M in 3 M $NaClO_4$ reported by Rossotti and Rossotti,[4] whereas our β_{11} value is 8—9 times as large as that[4] in 3 M $NaClO_4$. A noticeable difference is also observed between the β_{11} values in literature.[4,13-15]

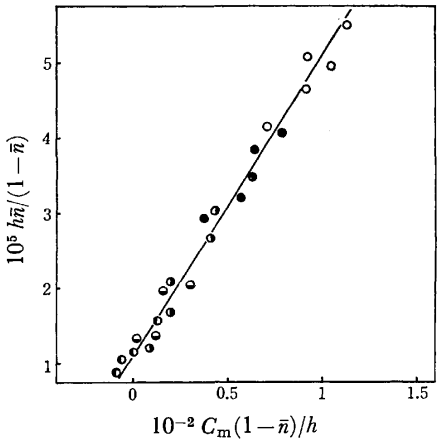

Fig. 2. A plot of $h\bar{n}/(1-\bar{n})$ as a function of $C_m(1-\bar{n})/h$.
The total concentrations of vanadium: ○, 5×10^{-2} M; ●, 10^{-2} M; ◑, 10^{-3} M; ◒, 5×10^{-4} M; ◐, 10^{-4} M.

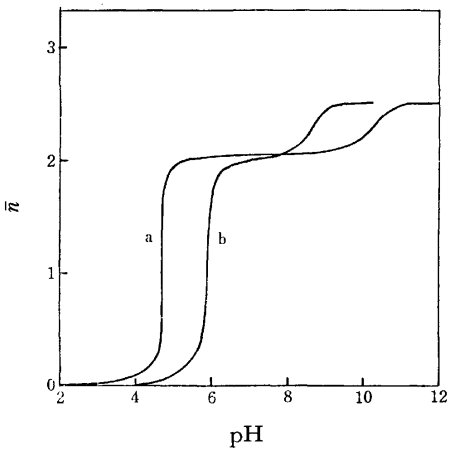

Fig. 3. The $\bar{n}$ *vs.* pH curves over a wide range of $\bar{n}$.
The total concentrations of vanadium: a, 10^{-3} M; b, 5×10^{-5} M.

Figure 3 shows $\bar{n}$ *vs.* pH curves over a wide range of $\bar{n}$. The curves exhibit a plateau at $\bar{n}$=2 corresponding to the precipitation of vanadium(IV) hydroxide. The IR spectrum of the hydroxide isolated (found: V, 50.2%) has a strong band at *ca.* 970 cm^{-1} assigned to the V=O stretching vibration. According to Selbin[3], a very strong band at 985 ± 50 cm^{-1} indicates the presence of the V=O bond. Thus the vanadium hydroxide appears to have the formula $VO(OH)_2$ or $VO_2\cdot H_2O$ (calcd: V, 50.5%). The solubility product, K_{sp_1}, of $VO(OH)_2$ given by Eq. 8 was determined as follows:

$$VO^{2+} + 2OH^- \rightleftharpoons VO(OH)_2(s) \quad (7)$$

$$K_{sp_1} = [VO^{2+}][OH^-]^2 \quad (8)$$

In the pH range where no precipitation of $VO(OH)_2$ occurs, the concentration of unhydrolyzed oxovanadium(IV) ions is given by

$$[VO^{2+}] = (1-\bar{n})C_m. \quad (9)$$

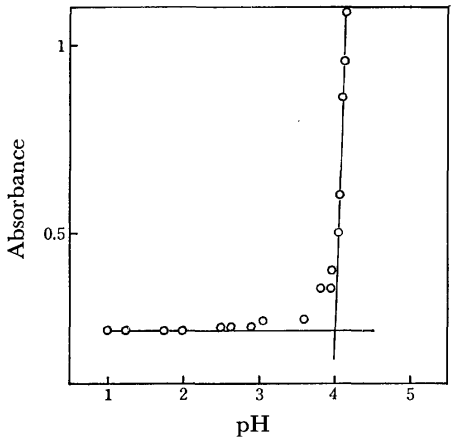

Fig. 4. The absorbance of vanadium(IV) solution as a function of pH.
The concentration of vanadium is 10^{-3} M. Wavelength, 240 nm.

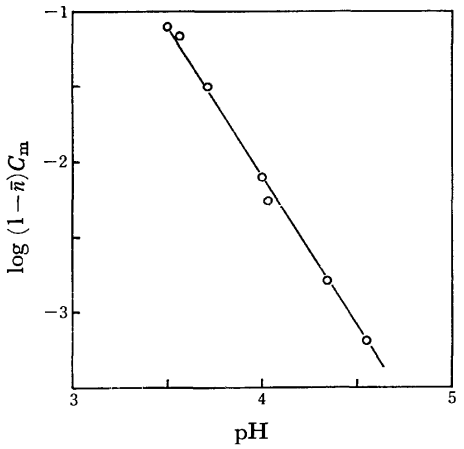

Fig. 5. The relation between the total concentration of vanadium and the pH at which vanadium hydroxide first appeared in acidic solutions.

Equation 9 can be derived from Eqs. 4 and 5, since only the $VOOH^+$ and $(VO)_2(OH)_2^{2+}$ species are the hydrolysis products of VO^{2+}. If Eq. 9 holds at the pH at which precipitation first takes place, the following relation can be derived from Eqs. 8 and 9:

$$\log K_{spl} = \log (1-\bar{n})C_m + 2\log K_w + 2pH, \quad (10)$$

where K_w is the ionic product of water. The pH at which precipitation first takes place was determined by measuring the absorbance of vanadium(IV) solutions at a given C_m as a function of pH. Figure 4 shows the plot at $C_m=0.001$ M. Extrapolation of the linear portion in the plot gave the critical pH at which solid phase first appeared at the given C_m. Figure 5 shows a plot of the critical pH *vs.* $\log (1-\bar{n})C_m$, giving a straight line with a slope −2 which corresponds to the value given by Eq. 10. If we use $\log K_w=-13.78$ in 0.1 M $NaClO_4$,[16] the K_{spl} value of 6.6×10^{-23} M^3 is obtained from the intercept.

Species of Vanadium(IV) in Basic Solution. The $VO(OH)_2$ precipitate dissolves in alkali to give a golden brown solution indicative of the formation of a new species. The electronic spectra of vanadium(IV) in basic solutions are given in Table 1, together with those of VO^{2+} for comparison. The spectrum of the vanadium species in basic solutions differs from that of VO^{2+} in the appearance of the third d-d band which is hidden under the strong charge-transfer band at 240 nm in the spectrum of VO^{2+}. The same spectrum of vanadium(IV) in a basic solution has also been obtained by Iannuzzi and Rieger.[9] They indicated that the Raman spectrum of vanadium(IV) in 1 M NaOH has a strong band at 987 cm^{-1} indicating the presence of the V=O group in the vanadium species. Basic solutions of vanadium(IV) may contain any species of the general formula $(VO)_p(OH)_q^{2p-q}$. The vanadium species in a basic solution were formulated in the following way. A solution of NaOH in 0.1 M $LiClO_4$ was titrated with a vanadium-containing solution of $HClO_4$ and a vanadium-free solution of $HClO_4$, respectively. The values of $\bar{n}$ are then given by

Table 1. Electronic spectra (λ_{max}/nm) of vanadium(IV)[a]

0.1 M $HClO_4$	0.5 M NaOH
764 (17.4)	790 (14)
620sh (7.50)	525 (15)
240 (242)	418 (25)

a) Molar absorption coefficients (M^{-1} cm^{-1}) are given in parentheses.

$$\bar{n} = \frac{C_{OH}-C_{OH}'}{C_m}, \quad (11)$$

where C_{OH} and C_{OH}' are the total analytical concentrations of OH^- added to reach the same pH in the presence and in the absence, respectively, of vanadium. Addition of VO^{2+} to NaOH solutions gave the soluble species in the basic pH region followed by precipitation of a vanadium compound in the region of nearly neutral pH. Table 2 gives the $\bar{n}$ values obtained in the pH region where no precipitation occurs. The potentiometric data indicate that $\bar{n}$ is 2.5 over the range of C_m and pH studied. A constant value of $\bar{n}=2.5$ suggests that only one species with a stoichiometric ratio $q/p=2.5$ is present in basic solutions in the pH range 9—12. The formation of this species is also seen as the second plateau of the potentiometric titration curves (Fig. 3), for which low C_m values were used in order to cause rapid redissolution of the oxovanadium hydroxide precipitated. Further evidence of the above stoichiometry was obtained by means of conductometric titration, in which an acid solution of $VO(ClO_4)_2$ was added incrementally to a NaOH solution. The titration was carried out at low C_m value so as to effect no precipitation up to neutral pH. From the electroneutrality condition on the titration system, we have

$$C_b + [H^+] = C_a + [OH^-] + \Sigma q[(VO)_p(OH)_q^{2p-q}], \quad (12)$$

where C_a and C_b are the analytical concentrations of $HClO_4$ and NaOH, respectively, in the system. At $[H^+]=[OH^-]$, $\bar{n}$ is given as follows from Eqs. 4 and 12:

$$\bar{n} = \frac{C_b-C_a}{C_m}. \quad (13)$$

The point of minimum conductivity in titration curves

Table 2. The $\bar{n}$ values evaluated potentiometrically in basic solutions of vanadium(IV)

pH	a) (10^4 C/M)				pH	b) (10^3 C/M)			
	C_{OH}'	C_{OH}	C_m	$\bar{n}$		C_{OH}'	C_{OH}	C_m	$\bar{n}$
11.8	25.9	36.0	3.98	2.54	12.0	5.80	8.81	1.23	2.45
11.4	16.4	33.2	6.70	2.51	11.6	3.08	8.02	2.01	2.46
11.0	11.1	31.7	8.20	2.52	11.2	1.90	7.69	2.31	2.51
10.6	8.41	31.0	9.01	2.51	10.8	1.37	7.55	2.45	2.52
10.0	6.21	30.4	9.59	2.52	10.4	1.10	7.47	2.53	2.52
9.60	5.12	30.1	9.89	2.53	9.80	0.88	7.39	2.61	2.49
9.00	4.05	29.7	10.4	2.47	9.40	0.79	7.36	2.64	2.49
8.60	3.45	29.4	10.6	2.45	9.00	0.69	7.32	2.68	2.47

a) A solution of 0.004 M NaOH in 0.1 M $LiClO_4$ was titrated with a solution 0.1 M in $VO(ClO_4)_2$ and 0.1 M in $HClO_4$, and a 0.1 M $HClO_4$ solution, respectively. b) A solution of 0.01 M NaOH in 0.1 M $LiClO_4$ was titrated with a solution 0.2 M in $VO(ClO_4)_2$ and 0.2 M in $HClO_4$, and a 0.2 M $HClO_4$ solution, respectively.

Table 3. The $\bar{n}$ values of basic vanadium species determined by conductometric titrations[a)]

C_b	C_a	C_m	$\bar{n}$
7.84	3.08	1.87	2.55
7.56	1.35	2.48	2.50
3.87	0.650	1.28	2.52
1.94	0.316	0.639	2.54

a) Each C (10^{-3} M) is the concentration at $[H^+]=[OH^-]$.

was taken as that corresponding to the relation $[H^+]=[OH^-]$. The conductometric data (Table 3) indicate that the $\bar{n}$ values obtained are practically 2.5, regardless of C_m. This is in line with the potentiometric measurements. At low C_m, the occurrence of precipitation in the neutral pH region, if any, probably leads to no significant error in the estimation of $\bar{n}$. Attempts were made to determine ionic charge (z) of the vanadium species in basic solutions by use of an anion-exchange resin. However, the results are not decisive, although the ion-exchange behavior of the species suggests that $|z|$ is not greater than 2. The experiments were accompanied with a great difficulty due to the fact that the species is highly sensitive to oxygen. If the smallest integers giving the above stoichiometric ratio are taken as the values of p and q, the dinuclear, probably monohydroxo-bridged ion $(VO)_2(OH)_5^-$ or $HV_2O_5^-$ should be presented as the vanadium species in basic solutions. In the range of pH below 12, no evidence was found for the monomeric $VO(OH)_3^-$ species proposed by Iannuzzi and Rieger[9] corresponding to the stoichiometric ratio $q/p=3$. They obtained an indication of the $VO(OH)_3^-$ ion from experiments in more basic solutions, in which potentiometric measurements seemed impracticable.

A dark brown precipitate of vanadium is obtained on addition of acid to its basic solution, and a gray precipitate on neutralization of its acidic solution. Britton and Welford[7] state that oxovanadium hydroxide, on first precipitation, is grayish-white, turning dark brown as precipitation proceeds. The color change results from the formation of a sparingly soluble sodium vanadite. Stoichiometry of the formation of the dark brown precipitate might be expressed as follows;

$$(VO)_2(OH)_5^- + mH^+ + yM^+ \rightleftharpoons M_y(VO)_2(OH)_{2n}(s) + mH_2O, \quad (14)$$

where M^+ is a +1 charged ion, $n=(5-m)/2$, and $y=1-m$. The solubility product, K_{sp2}, of the solid is defined by

$$K_{sp2} = [(VO)_2(OH)_5^-][H^+]^m[M^+]^y. \quad (15)$$

If the concentration of $(VO)_2(OH)_5^-$ is still equal to $C_m/2$ at the pH where precipitation first occurs, the following relation is obtained:

$$\log K_{sp2} = \log C_m/2 - m\mathrm{pH} + y \log [M^+]. \quad (16)$$

The pH at which the solid phase first appears was determined at a given ionic strength (0.1 M). Figure 6 represents a plot of the critical pH *vs.* $\log C_m/2$ giving a straight line. The slope $m=1$ of the line indicates that $n=2$ and $y=0$. Thus the dark brown precipitate also has the formula $VO(OH)_2$. The dark brown color of the precipitate might be due to co-precipitation of the $(VO)_2(OH)_5^-$ ion, as presumed from its formation reaction,

$$(VO)_2(OH)_5^- + H^+ \rightleftharpoons 2VO(OH)_2(s) + H_2O. \quad (17)$$

The solubility product of $VO(OH)_2$ in basic solutions is found to be $\log K_{sp2}=-11.1$ from the intercept of the line in Fig. 6. From the values of K_{sp1} and K_{sp2}, we can estimate the equilibrium constant, β_{25}^b, for the reaction,

$$2VO^{2+} + 5OH^- \rightleftharpoons (VO)_2(OH)_5^-, \quad (18)$$

$$\beta_{25}^b = \frac{[(VO)_2(OH)_5^-]}{[VO^{2+}]^2[OH^-]^5} = \frac{K_{sp2}}{K_w K_{sp1}^2} = 1.8\times10^{47}\ M^{-6}. \quad (19)$$

Vanadium(IV) is less soluble even in strongly basic solutions, as noticed by Iannuzzi and Rieger.[9] Various vanadates(IV) compounds have been isolated from basic solutions of vanadium, *e.g.*, $M_2^{IV}V_4O_9\cdot xH_2O$,[10,11] $M_2^{IV}V_2O_5\cdot xH_2O$[10] and $K_2V_3O_7\cdot 2H_2O$.[9] When a large excess of Na^+ is added to a basic solution containing $(VO)_2(OH)_5^-$ ion, a solid is precipitated owing to the common ion effect. The formula of the compound was determined on the basis of stoichiometry of its precipitation. Figure 7 shows the concentration of Na^+ at which the solid phase first appears at given C_m and basicity. A plot of $\log[Na^+]$ *vs.* $\log C_m/2$ gives a straight line with

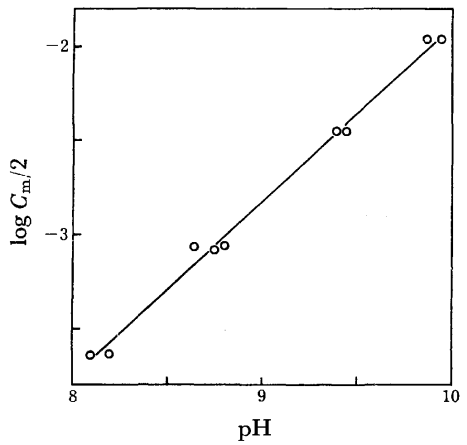

Fig. 6. The relation between the total concentration of vanadium and the pH at which the vanadium hydroxide first appeared in basic solutions.

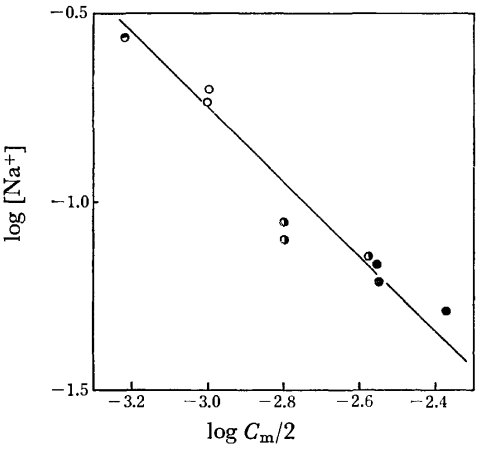

Fig. 7. The concentrations of sodium ion at which less soluble vanadium salt first appeared in NaOH solutions. The concentrations of NaOH: ◓, 0.01 M; ○, 0.015 M; ●, 0.03 M, ◑, 0.05 M.

a slope of −1. Thus the value of y in Eq. 16 is 1, and the values of m and n in reaction 14 are 0 and 2.5, respectively. The results of the measurements indicate that the less soluble compound may have the stoichiometric formula $Na(VO)_2(OH)_5$ or $NaHV_2O_5$ apart from the hydration water. The formula corresponds to sodium vanadate(IV) $Na_2V_4O_9 \cdot xH_2O$ which has occasionally appeared in literature.[7,10,11] The intercept of the straight line gives $\log K_{sp3} = -3.74$ as the solubility product of the compounds defined by Eq. 21.

$$Na^+ + (VO)_2(OH)_5^- \rightleftharpoons Na(VO)_2(OH)_5\ (s), \quad (20)$$

$$K_{sp3} = [Na^+][(VO)_2(OH)_5^-]. \quad (21)$$

Under the experimental conditions, the present work gave no indication of such salts as $M_2^IV_2O_5$ and $K_2V_3O_7$ formulated by Crow[10] and by Iannuzzi and Rieger,[9] respectively.

References

1) W. P. Griffith, *Coor. Chem. Rev.*, **5**, 459 (1970).
2) J. Selbin, *Angew. Chem. Int. Ed. Engl.*, **5**, 712 (1966).
3) a) J. Selbin, *Chem. Rev.*, **65**, 153 (1965); b) J. Selbin, L. H. Holmes, Jr., and S. P. McGlynn, *J. Inorg. Nucl. Chem.*, **25**, 1359 (1963).
4) F. J. C. Rossotti and H. S. Rossotti, *Acta Chem. Scand.*, **9**, 1177 (1955).
5) B. Lutz and H. Wendt, *Ber. Bunsenges. Phys. Chem.*, **74**, 372 (1970).
6) J. Francavilla and N. D. Chasteen, *Inorg. Chem.*, **14**, 2860 (1975).
7) H. T. S. Britton and G. Welford, *J. Chem. Soc.*, **1940**, 758.
8) J. J. Lingane and L. Meites, *J. Am. Chem. Soc.*, **69**, 1882 (1947).
9) M. M. Iannuzzi and P. H. Rieger, *Inorg. Chem.*, **14**, 2895 (1975).
10) J. K. Crow, *J. Chem. Soc.*, **30**, 453 (1876).
11) J. Koppel and R. Goldman, *Z. Anorg. Chem.*, **36**, 281 (1903).
12) L. G. Sillén, *Acta Chem. Scand.*, **8**, 299, 318 (1954).
13) M. M. T. Khan and A. E. Martell, *J. Am. Chem. Soc.*, **90**, 6011 (1968).
14) R. P. Henry, P. C. H. Mitchell, and J. E. Prue, *J. Chem. Soc., Dalton Trans.*, **1973**, 1156.
15) L. Meites, *J. Am. Chem. Soc.*, **75**, 6059 (1953).
16) R. Fischer and J. Bye, *Bull. Soc. Chim. Fr.*, **1964**, 2920.

Processes in the Reaction of Y_2O_3 with WO_3

Kiyoshi KURIBAYASHI and Toshiyuki SATA

Research Laboratory of Engineering Materials, Tokyo Institute of Technology, Ookayama, Meguro-ku, Tokyo 152

(Received April 2, 1977)

The processes of the solid state reaction of Y_2O_3 with WO_3 were studied for samples mixed in the molar ratios of $Y_2O_3 : WO_3 = 1 : 3$, $1 : 1$, $7 : 4$, $5 : 2$, and $3 : 1$. It was found that all the reactions except $Y_2O_3 : WO_3 = 5 : 2$ from the powders of both Y_2O_3 and WO_3 in air proceeded according to the following order step reactions: $Y_2O_3 \cdot 3WO_3 \rightarrow Y_2O_3 \cdot WO_3 \rightarrow 7Y_2O_3 \cdot 4WO_3 \rightarrow 5Y_2O_3 \cdot 2WO_3$ and $5Y_2O_3 \cdot 2WO_3 \rightarrow 3Y_2O_3 \cdot WO_3$, with temperatures rising from 600 to 1300 °C and with an unknown compound, X, always first formed below 700 °C. In a reaction couple in contact with both Y_2O_3 and WO_3 pellets, WO_3 components preferentially diffused to the Y_2O_3 side to form $Y_2O_3 \cdot 3WO_3$ (orthorhombic form) on the boundary between them at 1000 °C.

The compounds formed in the reaction of the sesquioxides of the rare earth elements (R_2O_3) with WO_3 are attracting the attention of research workers because of the possibility of using them as engineering materials: refractory materials, dielectrics, laser materials, and luminescents materials. They are also interesting from a crystallographical point of view and from the point of view of reaction kinetics.

H. J. Borchardt[1] studied a phase relation in the Y_2O_3–WO_3 system and reported that there were six compounds: $Y_2O_3 \cdot 3WO_3$, $Y_2O_3 \cdot WO_3$, $3Y_2O_3 \cdot 2WO_3$ (metastable phase), $15Y_2O_3 \cdot 8WO_3$, $9Y_2O_3 \cdot 4WO_3$, and $3Y_2O_3 \cdot WO_3$. Recently, G. H. McCarthy *et al.*[2] reported that five compounds existed in the system: $Y_2O_3 \cdot 3WO_3$ (YW_3), $Y_2O_3 \cdot WO_3$(YW), $7Y_2O_3 \cdot 4WO_3$-(Y_7W_4), $5Y_2O_3 \cdot 2WO_3$(Y_5W_2), and $3Y_2O_3 \cdot WO_3$(Y_3W). However, the Y_2O_3-rich region of the system has not yet been made clear.

In the present study, the processes of the solid state reaction between Y_2O_3 and WO_3 were studied. Also, we tried to determine what the diffusion component was through an interface where the two oxides came in contact using an electron-probe microanalyzer (EPMA).

Experimental

Both dried Y_2O_3(Rare-Metallic Co., 99.99%) and WO_3 (Mitsuwa Chemical Co., 99.9%), calcined at 800 °C for 3h, were weighed in the appropriate oxide ratio and were mixed thoroughly in an agate mortar. These oxide mixtures were then pressed into pellets at 800 kg cm^{-2}. The pellets were then heated in air on an alumina boat for 48 h at temperatures from 600 °C up to 1300 °C in a mullite tube in a silicon carbide furnace. The temperature was controlled within ±10 °C. After heating, the products were identified by the X-ray powder diffraction methods.

Y_2O_3 was pressed into a pellet at 3200 kg cm^{-2} and sintered in air at 1400 °C for 48 h; the apparent porosity of the pellet was 19%. The surface of the pellet was polished with diamond paste. A 0.2 mmϕ platinum wire was fixed as a marker on the Y_2O_3 pellet and was then pressed into a larger pellet, with WO_3 powder covering the pellet, at 3200 kg cm^{-2}. It was heated on an alumina boat in air for 72 h at 1000 °C. After cooling, the pellet was cut off perpendicular to the interface between the Y_2O_3 and WO_3 layers, as is shown in Fig. 1a. The cut surface was polished and measured by means of an EPMA.

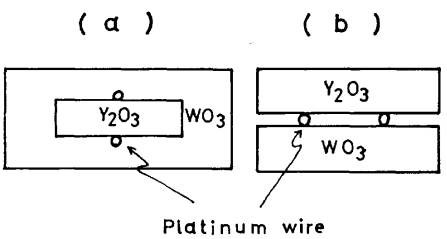

Fig. 1. Schematic diagrams of specimen to study diffusion components.

Each portion of Y_2O_3 or WO_3 was pressed into a pellet at 3200 kg cm^{-2}. The Y_2O_3 pellet was sintered at 1400 °C, while the WO_3 was sintered at 1000 °C for 48 h. After cooling, both the pellets were placed with a 0.2 mmϕ platinum wire sandwiched between, in order to give a clearance of 0.2 mm between them, as is shown in Fig. 1b. The above sandwich-type specimen, wrapped up by a platinum plate, was covered with WO_3 powder in order to confirm the occurrence of a reaction of solid-state Y_2O_3 with WO_3 vapor and was heated on an alumina boat in air at 1000 °C for 72 h.

Results

The relative amounts of phases present in the products after Y_2O_3–WO_3 reactions for 48 h in air at each temperature are shown in Fig. 2a—e. The relative amounts were obtained from the intensities of the peaks on the X-ray diffraction pattern from each compound. It was found that all the reactions except $Y_2O_3 : WO_3 = 5 : 2$ from both Y_2O_3 and WO_3 in air proceeded according to the following order: $YW_3 \rightarrow YW \rightarrow Y_7W_4 \rightarrow Y_5W_2$ and $Y_5W_2 \rightarrow Y_3W$, with temperatures increasing from 600 °C up to 1300 °C, though for the reaction of $5Y_2O_3 + 2WO_3$, Y_3W was formed by the reaction of Y_2O_3 with a part of the Y_7W_4 and the reaction of $6(Y_3W) + Y_7W_4 \rightarrow 5(Y_5W_2)$ yielded the Y_5W_2 compound. The unknown compound, X, was first formed for all the reactions; its X-ray diffraction diagram, shown in Table 1, has not been indexed. Oxide mixtures weighed in the molar ratios of $Y_2O_3 : WO_3 = 1 : 2$, $1 : 3$, or $1 : 4$ were heated in air at temperatures from 600 °C up to 800 °C for 5 days in order that Compound X could be studied in detail. The pellets were reground twice during the heating schedule and then pelletized again in order to insure homogeneity. The products are shown in Table 2. It was impossible to obtain Compound X alone for each composition because of the incomplete reactions. The same results were obtained from 10 days' heating.

A microscopical photograph of the EPMA specimen

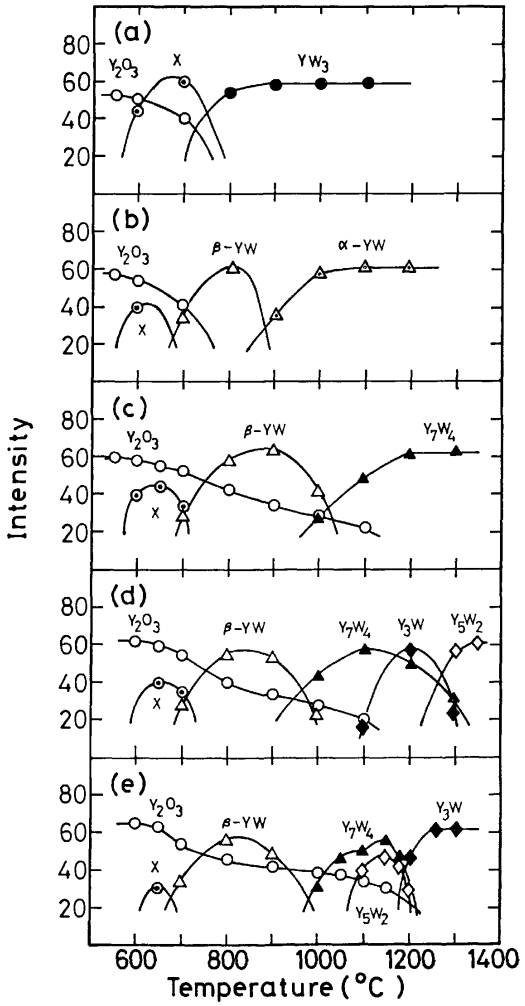

Fig. 2. Relative amounts of phases present in the products from Y_2O_3–WO_3 reactions for 48 h in air at each temperature. (a) Y_2O_3–$3WO_3$, (b) Y_2O_3–WO_3, (c) $7Y_2O_3$–$4WO_3$, (d) $5Y_2O_3$–$2WO_3$, (e) $3Y_2O_3$–WO_3. Y_2O_3, (662), (○); X, 2θ=18.8, (⊙); YW_3, 2θ=20.3, (●); α-YW, 2θ=33.6, (△); β-YW, (112), (△); Y_7W_4, (003), (▲); Y_5W_2, (113), (◇); Y_3W, (003), (◆).

(Fig. 1a) and the results of the EPMA measuremnts are shown in Fig. 3. The WO_3 layer was detached from the reaction layer because of a difference in thermal expansion between WO_3 and the reaction product. A reaction layer 120μm thick was produced as a single layer in the Y_2O_3 layer. The diffusion of Y_2O_3 component to WO_3 side was negligible. The reaction layer was found to be YW_3(orthorhombic form) using the X-ray powder diffraction methods and the EPMA.

On the other hand, no reaction layer was found by the X-ray powder diffraction methods or microscopic observation of the specimen shown in Fig. 1b and heated for 72h at 1000 °C.

Discussion

The Sample Mixed in the Ratio of Y_2O_3 : WO_3=1 : 3. Compound X began to form at about 600 °C, and YW_3 (orthorhombic from) was produced above 800 °C. It

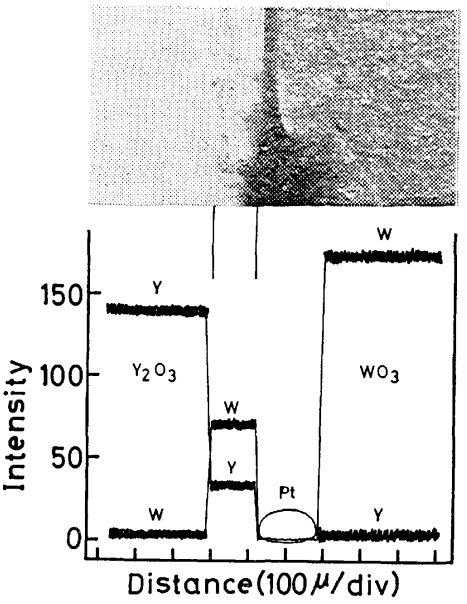

Fig. 3. A microscopical photograph and a result of a EPMA measurement for a reaction couple contacted both Y_2O_3 and WO_3 pellets.

Table 1. X-Ray powder data for compound X

Line No.	d	I/I_0
1	6.0619	5
2	5.3358	20
3	4.7111	80
4	3.5319	15
5	3.1475	90
6	3.0024	100
7	2.8289	30
8	2.5902	50
9	2.3272	15
10	2.2097	10
11	1.9087	60
12	1.9049	60
13	1.8974	30
14	1.6876	20

Table 2. Products from Y_2O_3–WO_3 reaction heated in air for 5 days

Temp	$Y_2O_3+2WO_3$	$Y_2O_3+3WO_3$	Y_2O_3+4WO
600 °C	$X+Y_2O_3$	$X+Y_2O_3+WO_3$	$X+WO_3+Y_2O_3$[a]
700 °C	$X+Y_2O_3$	$X+Y_2O_3+WO_3$	$X+WO_3+Y_2O_3$[a]
800 °C	$YW_3+Y_2O_3$	YW_3	YW_3+WO_3

a) Trace of Y_2O_3.

was impossible to obtain Compound X alone because of the slow reaction rate at low temperatures, as is shown in Table 2; *i.e.*, oxide mixtures with this bulk composition, when subjected to the usual heat treatment at 600 or 700 °C, yielded products which consisted of Compound X and unreacted Y_2O_3 and WO_3. The phase changes for $R_2O_3 \cdot 3WO_3$ (R=Dy and Ho) were reported by V. E. Plyuschev and V. M. Amosov[3] and those for R=La—Dy, by K. Nassau *et al.*[4] M. Yoshimura *et al.*[5-7] synthesized $2R_2O_3 \cdot 9WO_3$ (R=La,

Ce, Pr, and Nd) and pointed out that rare earths which are heavier than Sm would be too small to form this type of compound. Considering the above reports and the present results, Compound X can be assumed to be a high-temperature form of YW_3 or a compound near to YW_3. This compound may exist as a metastable phase between 600 and 700 °C.

The Sample Mixed in the Ratio of Y_2O_3 : WO_3=1 : 1. Compound X began to form at about 600 °C, and the Y_3W_2 (metastable phase) reported by H. J. Borchardt[1] was yielded about 700 °C. Recently, M. Yoshimura *et al.*[8] reported that this metastable phase was a high-temperature form(β-phase) of YW plus Y_2O_3. A low-temperature form(α-phase) of YW was produced above 900 °C through the process of Compound X→β-YW→α-YW. YW_3 (orthorhombic form) was not observed in this process.

The Sample Mixed in the Ratio of Y_2O_3 : WO_3=7 : 4. The compound of Y_7W_4 was produced above 960 °C through the process of Compound X→β-YW→Y_7W_4. YW_3 and α-YW(low-temperature form) were not formed, as is the case of the sample mixed in the ratio of Y_2O_3 : WO_3=1 : 1. Similar results were obtained for the formation of Y_5W_2 and Y_3W.

The Sample Mixed in the Ratio of Y_2O_3 : WO_3=5 : 2. After passing through the process of Compound X→β-YW→Y_7W_4, the reaction of Y_2O_3 with a part of Y_7W_4 yielded Y_3W. The Y_5W_2 compound was produced by the reaction of Y_7W_4 with Y_3W at temperatures higher than 1300 °C.

G. J. McCarthy *et al.*[2] reported that $5R_2O_3 \cdot 2WO_3$ was found only for the rare earths, R=Gd—Ho and Y. The reaction products from mixtures with their bulk compositions, after usual heat treatment at 1400 °C, consisted of $3R_2O_3 \cdot WO_3$, plus $7R_2O_3 \cdot 4WO_3$ for other rare earths. $5R_2O_3 \cdot 2WO_3$ may be also yielded by heating at temperatures higher than 1400 °C for the other rare earths, because the reactions proceeding at 1400 °C for them correspond to that of the mixture of $5Y_2O_3$ and $2WO_3$ heated at 1200 °C.

The Sample Mixed in the Ratio of Y_2O_3 : WO_3=3 : 1. After passing through the process of Compound X→β-YW→Y_7W_4, the compound of Y_3W(low-temperature form) was produced by a reaction of Y_2O_3 with Y_7W_4 and Y_5W_2 above 1200 °C. The high-temperature form of Y_3W was not yielded before the production of the low-temperature form from this oxide mixture. It is different from the other samples because the reaction temperature is sufficiently high to enhance the mobilities of the reactant ions, and transition temperature of Y_3W is about 1800 °C too high compared to this reaction temperature.

Reaction of Pellets of Y_2O_3 and WO_3. Considering that the vapor pressure of WO_3 was as low as 10^{-5} Torr[9] at 1000 °C and that the reaction layer did not form in the specimen shown in Fig. 1b, it can be said that the solid state reaction of pellets of both Y_2O_3 and WO_3 occurred in the specimen shown in Fig. 1a. Flor Giorgio *et al.*[10] reported that the $WO_3+SrCO_3 \rightarrow SrWO_4+CO_2$ solid state reaction was controlled by the counterdiffusion of cations involving W^{6+} and Sr^{2+}. E. V. Tkachenko *et al.*[11] reported that the elements of the tungsten sublattice in $CuWO_4$ and Cr_3WO_6 had a higher mobility than that of the copper sublattice. It is possible to consider the diffusion of W^{6+}, so W^{6+} and O^{2-} may be preferentially diffused to the Y_2O_3 side in the reaction of the pellets of both Y_2O_3 and WO_3. The reaction process of Y_2O_3 with WO_3 is similar to that of boron with tungsten metal reported earlier by one of the present authors;[12] the reaction from both BN and W proceeded thus: $WB_4 \rightarrow WB_2 \rightarrow WB$ and $WB \rightarrow W_3B$ with an increase in the temperature because the diffusibility of B is higher than that of W. Such a reaction is due to the significant difference in mobilities between the reactant ions. The diffusion species, W^{6+}, or any W–O complex ions must be confirmed by a more detailed examination of the reaction kinetics.

Conclusion

(1) All the reactions of the powders of both Y_2O_3 and WO_3 in air proceeded according step-by-step in the following order: $YW_3 \rightarrow YW \rightarrow Y_7W_4 \rightarrow Y_5W_2$ and $Y_5W_2 \rightarrow Y_3W$ with the elevation of the temperature from 600 °C up to 1300 °C, and an unknown compound, X, was always first formed below 700 °C.

(2) In a reaction couple bringing Y_2O_3 and WO_3 pellets in contact with each other, WO_3 components preferentially diffused to the Y_2O_3 side to form YW_3 (orthorhombic form) on the boundary between them at 1000 °C.

The authors wish to thank Dr. Masahiro Yoshimura of this laboratory for his helpful advice and discussions.

References

1) H. J. Borchardt, *Inorg. Chem.*, **2**, 170 (1963).
2) G. J. McCarthy, R. D. Fisher, and G. C. Johonon, NBS special publication, **364**, 397 (1972).
3) V. E. Plyuschev and V. M., Amosov *Dokl. Akad. Nauk SSSR*, **157**, 131 (1964).
4) K. Nassau, H. J. Levinstein, and G. M. Loiacono, *J. Phys. Chem. Solids*, **26**, 1805 (1965).
5) M. Yoshimura, T. Sata, and T. Nakamura, *Nippon Kagaku Kaishi*, **6**, 914 (9170).
6) M. Yoshimura, F. Sibieude, A. Rouanet, and M. Foex, *J. Solid State Chem.*, **16**, 219 (1976)
7) M. Yoshimura, H. Morikawa, and M. Miyake, *Mater. Res. Bull.*, **10**, 1221 (1975).
8) M. Yoshimura, F. Sibieude, A. Rouanet, and M. Foex, *Rev. Int. Htes. Temp. et Refract*, **12**, 215 (1975).
9) J. L. Margrave, "The Characterization of High-Temperature Vapors," John Wiley & Sons, New York (1967), p. 497.
10) F. Giorgio, M. Vincenzo, and R. Riccardo, *Z. Naturforsch., Teil A*, **29**, (3) 503 (1974).
11) E. V. Tkachenko, T. F. Telnykh, V. M. Zhukovskii, and A. S. Zhukovskaya, *Russ. J. Phys. Chem.*, **50**, 969 (1976).
12) T. Sata and T. Urano, *Yogyo Kyokai Shi*, **78**, 21 (1970).

Ion-Pair Effect on the Rate of the Base Hydrolysis of the Pentaamminechlorocobalt(III) Complex

Masayasu IIDA* and Hideo YAMATERA

Department of Chemistry, Faculty of Science, Nagoya University, Chikusa-ku, Nagoya 464

(Received May 16, 1977)

The rate of the base hydrolysis of pentaamminechlorocobalt(III) ions was measured in the presence of multivalent anions at a constant ionic strength. The results were analyzed in view of the S_N1 C.B. mechanism considering the formation of ion-pairs. The ion-pairing has the effect of suppressing the acid dissociation of the complex or the formation of its conjugate base, which acts as the intermediate of the reaction. This effect out-weighs the adverse effect of the probable acceleration of the rate-determining step of the base hydrolysis. The association constants obtained for $[CoCl(NH_3)_5]^{2+}\cdot SO_4^{2-}$ and $[CoCl(NH_3)_5]^{2+}\cdot P_3O_9^{3-}$ were 40±5, and 82±5, respectively (I=0.1, 25 °C).

The effect of multivalent anions on the rates of the acid and base hydrolyses of pentaamminechlorocobalt-(III) ions has been studied by Monk *et al.*, who found that ion-pairing accelerated the acid hydrolysis[1] and retarded the base hydrolysis.[2,3] If the latter is assumed to be a simple bimolecular reaction, the retardation can be explained on electrostatic grounds by the reduced positive charge of the ion-pair. However, among several possible mechanisms[4] thus far proposed for this base hydrolysis, the most widely accepted is the S_N1 C.B. mechanism, with which Monk *et al.*[3] failed to explain the retardation effect.

In this paper, the effect of multivalent anions on the rate of the base hydrolysis of pentaamminechlorocobalt-(III) cations at a constant ionic strength is analyzed in view of the S_N1 C.B. mechanism and is explained by considering the formation of the ion-pairs of the ammine and the amido complexes with the multivalent anions.

Experimental

Materials. *Pentaamminechlorocobalt(III) Perchlorate*: The chloride of the complex, prepared by the method of Hynes *et al.*,[5] was dissolved in hot water and was then converted to the perchlorate by treating it with concentrated perchloric acid and by then cooling the solution in ice. The complex was identified spectrophotometrically.

Sodium Perchlorate: Sodium perchlorate was prepared from a saturated sodium hydroxide solution and perchloric acid. Heavy metal impurities in the sodium perchlorate were precipitated as hydroxides at pH 9, and the removal of heavy metals was confirmed by means of PAN(= 1-(2-pyridylazo)-2-naphthol).

Sodium Acetate: Anhydrous sodium acetate, a guaranteed reagent of Wako Pure Chemical Co, was used after dried at 110 °C.

Sodium Sulfate: Anhydrous sodium sulfate, a guaranteed reagent of Wako Pure Chemical Co, was recrystallized from water at 80 °C and dried at 100 °C.

Sodium Trimetaphosphate:[6] Disodium hydrogenphosphate was heated at about 800 °C for 200 h, after which the product was cooled very slowly. Then the sodium trimetaphosphate thus produced was extracted with a small amount of water and recrystallized by the addition of alcohol and cooling in a refrigerator. The purity of the twice-recrystallized salt was confirmed by paper chromatography.

Kinetic Runs. The rate was measured spectrophotometrically by following the change in the absorbance of solutions containing the complex (2.0×10^{-4} M (= mol dm^{-3})), an ammonia (2×10^{-3} M)-ammonium perchlorate (2×10^{-4} M) buffer, added salts (in appropriate concentrations), and sodium perchlorate, the last being added so as to adjust the ionic strength to 0.1. The reaction mixture, contained in a 1-cm quartz cell, was placed in the cell compartment of a Carl-Zeiss spectrophotometer, PMQ II, maintained at 25± 0.05 °C by circulating water from a thermostat.

pH Measurement. After the reaction had reached completion, the pH value of the sample solution was measured with a Beckman Research pH meter standardized with a buffer solution of Na_2CO_3–$NaHCO_3$ (pH 10.02 at 25 °C). As the internal solution of the reference electrode, a saturated NaCl solution was used so as to avoid the precipitation of $KClO_4$. The change in the liquid junction potential due to the displacement of the added salts was assumed to be negligible.

Results and Discussion

The experimental conditions and the rate constant observed for each run are shown in Fig. 1 and Tables 1—5. The rates were determined by plotting $\ln(D_\infty - D_t)$ against the time t, where D_∞ and D_t are the absorbances at an infinite time and at the time t respectively. The pseudo-first-order rate constant, k_{obsd} was thus

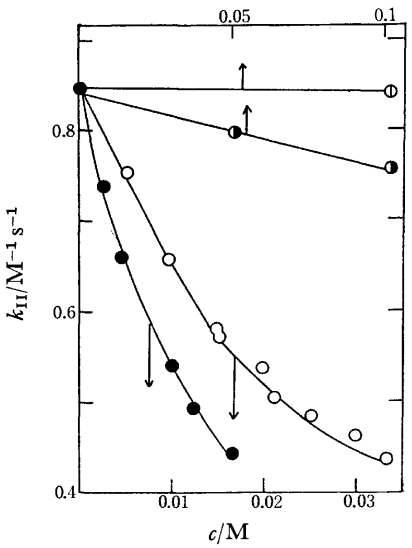

Fig. 1. Effects of added salts on the rate of base hydrolysis of $[CoCl(NH_3)_5]^{2+}$. I=0.1. KCl: ◑, CH_3CO_2Na: ◑, Na_2SO_4: ○, $Na_3P_3O_9$: ●.

*Present address: Department of Chemistry, Faculty of Science, Nara Women's University, Nara 630.

TABLE 1. EFFECT OF ACETATE IONS ON THE RATE OF THE BASE HYDROLYSIS OF $[CoCl(NH_3)_5]^{2+}$

Run	$[NaClO_4]$ M	$[CH_3CO_2Na]$ M	pH	$10^4 k_{obsd}$ s^{-1}	k_{II} $M^{-1}s^{-1}$
1	0.10	0	10.25	1.46	0.839
2	0.05	0.05	10.26	1.42	0.780
3	0	0.10	10.27	1.40	0.752

TABLE 2. EFFECT OF SULFATE IONS ON THE RATE OF THE BASE HYDROLYSIS OF $[CoCl(NH_3)_5]^{2+}$ (Ionic strength=0.1)

Run	$[NaClO_4]$ M	$[Na_2SO_4]$ M	pH	$10^4 k_{obsd}$ s^{-1}	k_{II} $M^{-1}s^{-1}$
1	1.000	0	10.28	1.658	0.870
			10.28	1.604	0.842
			10.22[a]	1.397	0.842
2	0.085	0.005	10.29	1.462	0.750
3	0.070	0.010	10.29	1.262	0.650
4	0.055	0.015	10.30	1.155	0.585
5	0.050	0.016	10.29[a]	1.117	0.573
6	0.040	0.020	10.32	1.132	0.542
7	0.025	0.025	10.33	1.044	0.488
8	0.010	0.030	10.31[a]	0.948	0.464
9	0	0.033	10.34	0.963	0.440
			10.23[a]	0.734	0.432

a) The buffer solutions used in these runs were not identical with those used in the other runs.

TABLE 3. CONCENTRATIONS OF EACH ION IN THE $NaClO_4$-Na_2SO_4 SYSTEMS

Run	$[ClO_4^-]$ M	$[SO_4^{2-}]$ M	$[Na^+\cdot SO_4^{2-}]$ M	$[Na^+]$ M	I
1	0.1	0	0	0.1	0.1
2	0.085	0.00424	0.000765	0.0942	0.0985
3	0.070	0.00852	0.00148	0.0885	0.0970
4	0.055	0.0129	0.00209	0.0820	0.0958
5	0.050	0.0144	0.00230	0.0810	0.0955
6	0.040	0.0173	0.00265	0.0774	0.0947
7	0.025	0.0219	0.00309	0.0719	0.0938
8	0.010	0.0265	0.00347	0.0665	0.0931
9	0	0.0297	0.00362	0.0631	0.0928

TABLE 4. EFFECT OF TRIMETAPHOSPHATE IONS ON THE RATE OF THE BASE HYDROLYSIS OF $[CoCl(NH_3)_5]^{2+}$ (Ionic strength=0.1)

Run	$[NaClO_4]$ M	$[Na_3P_3O_9]$ M	pH	$10^4 k_{obsd}$ s^{-1}	k_{II} $M^{-1}s^{-1}$
1	0.085	0.0035	10.19	1.14	0.737
2	0.070	0.0050	10.19	1.02	0.657
			10.19	1.04	0.672
3	0.040	0.0100	10.20	0.859	0.542
			10.20	0.864	0.545
4	0.025	0.0125	10.24	0.868	0.500
			10.24	0.894	0.515
5	0	0.0167	10.26	0.806	0.443

TABLE 5. CONCENTRATIONS OF EACH ION IN THE $NaClO_4$-$Na_3P_3O_9$ SYSTEMS

Run	$[ClO_4^-]$ M	$[P_3O_9^{3-}]$ M	$[Na^+\cdot P_3O_9^{3-}]$ M	$[Na^+]$ M	I
1	0.1	0	0	0.1	0.1
2	0.085	0.00164	0.00086	0.0916	0.0974
3	0.070	0.00339	0.00161	0.0834	0.0951
4	0.040	0.00723	0.00277	0.0672	0.0917
5	0.025	0.00934	0.00316	0.0592	0.0905
6	0	0.0132	0.00349	0.0465	0.0897

obtained as the slope of this plot. Therefore, the rate of the reaction measured in the buffer solution is:

$$\text{Rate} = k_{obsd}[CoCl(NH_3)_5^{2+}]_0, \quad (1)$$

where $[CoCl(NH_3)_5^{2+}]_0$ is the total concentration of the complex.

On the other hand, according to the S_N1 C.B. mechanism, the following reaction scheme has been proposed:

$$[CoCl(NH_3)_5]^{2+} + OH^- \underset{\text{fast}}{\overset{K}{\rightleftharpoons}} [CoCl(NH_2)(NH_3)_4]^+ + H_2O, \quad (2)$$

$$[CoCl(NH_2)(NH_3)_4]^+ \underset{\text{slow}}{\overset{k}{\longrightarrow}} [Co(NH_2)(NH_3)_4]^{2+} + Cl^-, \quad (3)$$

$$[Co(NH_2)(NH_3)_4]^{2+} + H_2O \underset{\text{fast}}{\longrightarrow} [Co(OH)(NH_3)_5]^{2+}, \quad (4)$$

where K is the equilibrium constant and k is the rate constant of the rate-determining step (3). Unless otherwise stated, the equilibrium constants appearing in this paper are the concentration equilibrium constants under the present experimental conditions (I= 0.1, 25 °C).[7] In such a case, the rate equation for the hydrolysis would be:

$$\begin{aligned}\text{Rate} &= k[CoCl(NH_2)(NH_3)_4^+] \\ &= kK[CoCl(NH_3)_5^{2+}][OH^-] \\ &= k\frac{K_a}{K_w}[CoCl(NH_3)_5^{2+}][OH^-], \end{aligned} \quad (5)$$

where K_a represents the acid dissociation constant of the ammine complex, and K_w, the ionic product of water.

Considering $[CoCl(NH_3)_5^{2+}] \gg [CoCl(NH_2)(NH_3)_4^+]$ under the present experimental conditions, a comparison of Eqs. 1 and 5 would give:

$$k_{obsd} = k\frac{K_a}{K_w}[OH^-]. \quad (6)$$

The concentration of hydroxide ions can be related to the measured pH by:

$$\log[OH^-] = \text{pH} - 14 - \log y_{OH}.$$

Under the condition of a constant ionic strength, y_{OH} is almost kept constant, and the observed differences in the pH among the different solutions can be attributed to the effects of the added salts on the $NH_3+H_2O \rightleftharpoons NH_4^+ + OH^-$ equilibrium. To allow for the pH change, the second-order rate constant, k_{II}, defined by Eq. 7 will be used in the following discussion.

$$k_{II} = k_{obsd}/y_{OH}[OH^-]. \quad (7)$$

Figure 1 shows that k_{II} changed with the change in the amount of salt added at the constant ionic strength of 0.1. Thus, the simple reaction scheme (Eqs. 2, 3, and 4) is not adequate in the presence of multivalent anions. However, the scheme given below is considered to relate the observed change in the reaction rate to the ion-pairing between the complex cations and the added anions:

$$\begin{array}{ccc} [CoCl(NH_3)_5]^{2+} & \overset{K_{22}}{\rightleftharpoons} & [CoCl(NH_3)_5]^{2+}\cdot X^{n-} \\ \Big\downarrow{\scriptstyle K_a} & & \Big\downarrow{\scriptstyle K_a^{IP}} \\ [CoCl(NH_2)(NH_3)_4]^{+} & \overset{K_{12}}{\rightleftharpoons} & [CoCl(NH_2)(NH_3)_4]^{+}\cdot X^{n-} \\ \searrow{\scriptstyle k^\circ} & & \swarrow{\scriptstyle k^{IP}} \\ & [Co(NH_2)(NH_3)_4]^{2+} & \\ & \Big\downarrow{\scriptstyle \text{fast}} & \\ & [Co(OH)(NH_3)_5]^{2+} & \end{array} \quad (8)$$

where X^{n-} represents the added multivalent anions, K_{22} and K_{12} are the ion association constants; K_a and K_a^{IP}, the acid dissociation constants, and k° and k^{IP}, the rate constants of the rate-determining steps. In this reaction scheme, the rate expression is:

$$\begin{aligned} \text{Rate} &= k^\circ[CoCl(NH_2)(NH_3)_4^+] \\ &\quad + k^{IP}[CoCl(NH_2)(NH_3)_4^+\cdot X^{n-}] \\ &= \frac{k^\circ K_a}{K_w}[CoCl(NH_3)_5^{2+}][OH^-] \\ &\quad + \frac{k^{IP}K_a^{IP}}{K_w}[CoCl(NH_3)_5^{2+}\cdot X^{n-}][OH^-] \end{aligned} \quad (9)$$

For a weakly basic solution where $[CoCl(NH_3)_5^{2+}] \gg [CoCl(NH_2)(NH_3)_4^+]$, Eq. 9 becomes:

$$\text{Rate} = \frac{(k^\circ K_a + k^{IP}K_a^{IP}K_{22}[X^{n-}])[OH^-]}{K_w(1+K_{22}[X^{n-}])}[CoCl(NH_3)_5^{2+}]_0$$

Relating this equation to Eq. 1, one obtains:

$$k_{obsd} = \frac{(k^\circ K_a + k^{IP}K_a^{IP}K_{22}[X^{n-}])[OH^-]}{K_w(1+K_{22}[X^{n-}])}$$

Then Eq. 7 leads to:

$$k_{II} = \frac{k^\circ K_a + k^{IP}K_a^{IP}K_{22}[X^{n-}]}{K_w y_{OH}(1+K_{22}[X^{n-}])} \quad (10)$$

Substituting k_{II}° for $(k^\circ K_a)/(K_w y_{OH})$ in Eq. 10 and using the relation:

$$K_a^{IP}/K_a = K_{12}/K_{22} \quad (11)$$

one obtains:

$$k_{II} = k_{II}^\circ \frac{1+(k^{IP}/k^\circ)K_{12}[X^{n-}]}{1+K_{22}[X^{n-}]} \quad (12)$$

This equation will be used below for the explanation of the change in k_{II} shown in Fig. 1.

Monk *et al.*[2] observed little change in the rate when sodium perchlorate was replaced by potassium chloride. On the other hand, our experiments have shown that acetate ions have the effect of decreasing the reaction rate (Table 1). Thus, the substitution of acetate for perchlorate resulted in a slight decrease in k_{obsd} in spite of the increased pH of the solution; therefore, the second-order rate constant, k_{II}, showed an unmistakable decrease. Since electrostatic theories[8] of ion association predict only a slight difference between perchlorate and acetate ions in the tendency to form ion-pairs, the observed reaction rates seem to suggest some interaction such as hydrogen-bonding operating between the acetate and the complex ion.

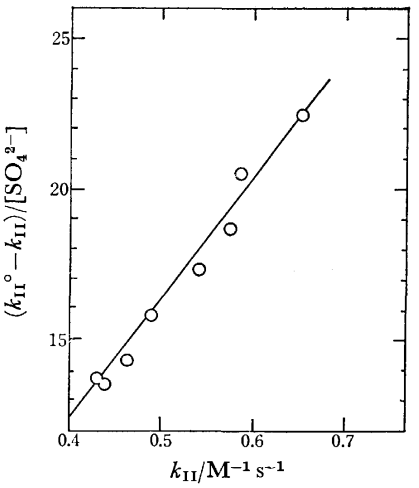

Fig. 2. Determination of the formation constant of the $[CoCl(NH_3)_5]^{2+}\cdot SO_4^{2-}$, ion-pair. (slope$=K_{22}$)

The substitution of sodium sulfate for sodium perchlorate caused a remarkable decrease in k_{obsd} (Table 2). For a quantitative treatment of the effect of the ion-pair formation between the bivalent complex cations and sulfate ions, the net concentration of free sulfate ions must be known. The decrease in the concentration of free sulfate ions due to the formation of hydrogensulfate ions and of the ion-pairs with the complex cations was estimated to be negligible at very low concentrations of hydrogen ions ($\approx 10^{-10}$ M) and the complex cations (2×10^{-4} M). On the other hand, the formation of the $Na^+\cdot SO_4^{-2}$ ion-pairs cannot be neglected.[9] The third column of Table 3 gives the concentrations of free sulfate ions, which were calculated by using the value of 2.0 (at $I=0.1$) for the formation constant of the $Na^+\cdot SO_4^{2-}$ ion-pairs. The last column of the table shows how the ionic strength decreases as a result of the ion-pair formation. According to the Brønsted-Bjerrum equation,[10] this decrease in the ionic strength will cause a decrease in the reaction rate of only 3% at most, a magnitude of the same order as the experimental error. This Brønsted-Bjerrum neutral-salt effect was, therefore, disregarded. For the analysis of the experimental results, Eq. 12 was transformed to:

$$(k_{II}^\circ - k_{II})/[X^{n-}] = K_{22}k_{II} - (k^{IP}/k^\circ)K_{12}k_{II}^\circ. \quad (13)$$

By taking X^{n-} as free sulfate ions, $(k_{II}^\circ - k_{II})/[X^{n-}]$ was plotted against k_{II}. As Fig. 2 shows, a linear relationship was observed, and the slope gives the K_{22} value of 40±5. Then, in order to avoid mathematical difficulty at $[X^{n-}]=0$, Eq. 13 was transformed to:

$$k_{II}(1+K_{22}[X^{n-}]) = k_{II}^\circ + (k^{IP}/k^\circ)K_{12}[X^{n-}]k_{II}^\circ.$$

With the K_{22} value determined above, the left-hand side of this equation was plotted against $[X^{n-}]$ $(=[SO_4^{2-}])$. This plot gave the values of k_{II}° and $(k^{IP}/k^\circ)K_{12}k_{II}^\circ$, from which $(k^{IP}/k^\circ)K_{12}$ was found to be 6±1.

TABLE 6. ASSOCIATION CONSTANTS OF $[CoCl(NH_3)_5]^{2+}\cdot X^{n-}$ ($X^{n-}=SO_4^{2-}$, $NaP_3O_9^{2-}$, and $P_3O_9^{3-}$)

	(i) $\log K_{22}(I=0)$	
$[CoCl(NH_3)_5]^{2+}\cdot SO_4^{2-}$	2.40±0.05	This work
	2.48	Ref. 11 (solubilities)
	2.49	Ref. 1 (kinetic data)
$[CoCl(NH_3)_5]^{2+}\cdot(NaP_3O_9)^{2-}$	2.4 ±0.1	This work
Theoretical ($a=6$ Å)[a]	1.98	Ref. 8 (Yokoyama-Yamatera Eq.)
	1.80	Ref. 8 (Fuoss Eq.)
($a=7$ Å)	1.87	Ref. 8 (Yokoyama-Yamatera Eq.)
	1.71	Ref. 8 (Fuoss Eq.)
	(ii) $\log K_{23}$ ($I=0$)	
$[CoCl(NH_3)_5]^{2+}\cdot P_3O_9^{3-}$	3.20±0.03	This work
$Mg^{2+}\cdot P_3O_9^{3-}$	3.31	Ref. 13
$Ca^{2+}\cdot P_3O_9^{3-}$	3.45	Ref. 13
$Sr^{2+}\cdot P_3O_9^{3-}$	3.35	Ref. 13
Theoretical ($a=7$ Å)	2.70	Ref. 8 (Yokoyama-Yamatera Eq.)
	2.60	Ref. 8 (Fuoss Eq.)

a) The notation a represents the closest distance of the approach of ions.

In Table 6, the K_{22} value here obtained is compared with other experimental and theoretical values. Our K_{22} value is in good agreement with those obtained by Monk *et al.* in a solubility study[11] and in a kinetic study of acid hydrolysis,[1] but it is about three times greater than the theoretical values. This difference can be attributed to the fact that the complex ion is not spherical but has an electric dipole moment in addition to the electric charge.

The value of K_{12} for the 1—2 ion-pair can be estimated with the Yokoyama-Yamatera equation[12] to be 4.7 ($I=0$), which is in reasonable agreement with the experimental K_{12} values for alkali metal sulfates, 5—10 ($I=0$).[13] Then, with K_{12} ($I=0.1$)$=2$, one obtains $k^{IP}/k^{\circ}=3\pm0.5$. This value can be compared with the corresponding value of 2.35 experimentally obtained by Monk *et al.* for the acid hydrolysis,[1] if allowance is made for the probable overestimate in the present k^{IP}/k° value. This overestimate is due to the neglect of the polarity of the complex ion, leading to an underestimated K_{12} value.

In a system with added sodium trimetaphosphate, the reaction scheme is more complicated. The decrease in free trimetaphosphate ions by the formation of hydrogentrimetaphosphate ions ($pK_{a1}=2.05$)[14] as well as by the ion-pair formation with the complex cations can be ignored, as in the case of sulfate. The formation of ion-pairs between sodium and trimetaphosphate ions, $Na^+ + P_3O_9^{3-} \rightleftharpoons Na^+\cdot P_3O_9^{3-}$, was studied by Gardner *et al.*,[15] who found the ion-association constant to be 25.1 at an infinite dilution. Then, the ion-association constant at $I=0.1$ would be 5.7. This value was used in the calculation of the net concentrations of the ions derived from the added sodium trimetaphosphate (Table 5). Although the decrease in the ionic strength is larger in this case than in the case of the sulfate ions, its effect on the reaction rate was estimated to be still of a magnitude within the limits of experimental error. Ignoring the formation of the ion-pairs with univalent anions, as in the case of the sulfate ions, the reaction scheme is:

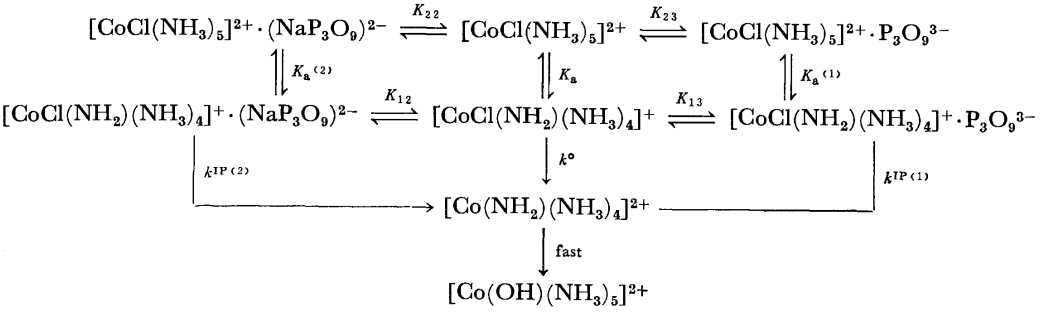

(14)

where the definitions of the parameters are similar to those in the case of Eq. 8. In this scheme, the rate expression is:

$$k_{II} = k_{II}^{\circ}\frac{1+(k^{IP(1)}/k^{\circ})K_{13}[P_3O_9^{3-}]+(k^{IP(2)}/k^{\circ})K_{12}[Na^+\cdot P_3O_9^{3-}]}{1+K_{23}[P_3O_9^{3-}]+K_{22}[Na^+\cdot P_3O_9^{3-}]}. \quad (15)$$

As a first approximation, ignoring the formation of the $Na^+\cdot P_3O_9^{3-}$ ion-pairs, one can simplify Eq. 15 to obtain:

$$k_{II} = k_{II}^{\circ}\frac{1+(k^{IP(1)}/k^{\circ})K_{13}[P_3O_9^{3-}]_0}{1+K_{23}[P_3O_9^{3-}]_0}, \quad (16)$$

where $[P_3O_9^{3-}]_0$ is the total concentration of sodium trimetaphosphate. With Eq. 16, the experimental results were analyzed in a manner similar to that used in the case of sulfate; the values $K_{23}=75\pm5$ and $(k^{IP(1)}/k^{\circ})K_{13}=9\pm2$ were thus obtained. Since Eq. 15 involves too many parameters, all the parameters except for K_{23} and K_{22} were estimated by theory or by analogy. The K_{13} and K_{12} values were calculated by means of the Yokoyama-Yamatera theory of ion-association,[8] which gave $K_{13}=5.1$ and $K_{12}=1.5$ under the present experimental condition (or 22.3 and 4.0 respectively at $I=0$), assuming the closest distance of approach of ions to be 7 Å (=0.7 nm). The values for $k^{IP(1)}/k^{\circ}$ and $k^{IP(2)}/k^{\circ}$ were estimated at 2.5[16] and 2.0[1] respectively from the values for analogous acid hydrolyses. Using these parameter values and starting with the $K_{23}=75$ obtained with Eq. 16, successive approximations with Eq. 15 resulted in the final values, $K_{23}=82\pm5$ and $K_{22}=40\pm10$. Since no experimental results on the same system are found in the literature,

the constants are compared with those for the systems of similar charge types, such as bivalent metal ions–trimetaphosphate ions and pentaamminechlorocobalt-(III) ions–sulfate ions. The comparison in Table 6 shows that the values obtained are of reasonable magnitude.

It has been shown above that the experimental results can be explained on the basis of the scheme shown in Eqs. 8 and 14 giving ion-association constants of an acceptable magnitude. The discussion also shows that the retardation of the base hydrolysis of pentaamminechlorocobalt(III) ions by multivalent anions can be attributed mainly to the multivalent anions preferring the ammine complex rather than the amido complex (the reaction intermediate) in the ion association or, in other words (using Eq. 11), to the suppression of the acid dissociation of the ammine complex by the ion-pairing. The probable acceleration effect at the rate-determining step, represented by the k^{IP}/k° term is relatively small, so that the net effect of ion-pairing is the retardation of the rate of hydrolysis.

The present work was partially supported by a Grant-in-Aid for Scientific Research from the Ministry of Education.

References

1) S. H. Laurie and C. B. Monk, *J. Chem. Soc.*, **1965**, 724.

2) M. R. Wendt and C. B. Monk, *J. Chem. Soc., A*, **1969**, 1624.

3) M. B. M. Campbell, M. R. Wendt, and C. B. Monk, *J. Chem. Soc., Dalton Trans.*, **1972**, 1714.

4) F. Basolo and R. G. Pearson, "Mechanisms of Inorganic Reactions," 2 nd ed, John Wiley & Sons, New York (1967), p. 183.

5) W. A. Hynes, L. K. Yanowski, and M. Shiller, *J. Am. Chem. Soc.*, **60**, 3053 (1938).

6) S. Ohashi, private communication; *cf.* R. N. Bell, *Inorg. Syn.*, **3**, 103 (1950).

7) The thermodynamical equilibrium constant or the equilibrium constant at $I=0$ can be calculated by the use of the Davies equation for activity coefficients:

$$\log y_i = -0.5115 z_i^2 \left(\frac{\sqrt{I}}{1+\sqrt{I}} - 0.3I \right)$$

where y_i is the activity coefficient of the i ion, z_i is the charge number of the i ion, and I is the ionic strength.

8) H. Yokoyama and H. Yamatera, *Bull. Chem. Soc. Jpn.*, **48**, 1770 (1975); N. Bjerrum, *Kgl. Danske Videnskab. Selskab.*, **7**, No. 9 (1926); R. M. Fuoss, *J. Am. Chem. Soc.*, **80**, 5059 (1958); W. Ebeling, *Z. Phys. Chem. (Leipzig)*, **238**, 400 (1968).

9) I. L. Jenkins and C. B. Monk, *J. Am. Chem. Soc.*, **72**, 2695 (1950).

10) A. A. Frost and R. G. Pearson, "Kinetics and Mechanism," John Wiley & Sons, New York (1961), p. 150.

11) D. W. Archer, D. A. East, and C. B. Monk, *J. Chem. Soc.*, **1965**, 720.

12) Although the Yokoyama-Yamatera equation[8] was derived for symmetrical electrolytes, its application to unsymmetrical electrolytes is permitted as an approximation.

13) L. G. Sillén and A. E. Martell, "Stability Constants of Metal-Ion Complexes," The Chemical Society, London (1964), pp. 194, 235.

14) C. W. Davies and C. B. Monk, *J. Chem. Soc.*, **1949**, 413.

15) G. L. Gardner and G. H. Nancollas, *Anal. Chem.*, **41**, 202 (1969).

16) This estimation resulted from the experiments measuring the effect of trimetaphosphate anions on the rate of acid hydrolysis of the complex (unpublished results).

Formation and Properties of Strontium Uranates

Hiroaki TAGAWA, Takeo FUJINO, and Jun TATENO

Division of Chemistry, Japan Atomic Energy Research Institute, Tokai-mura, Ibaraki 319-11

(Received May 28, 1977)

The formation and nonstoichiometry of strontium uranates, especially those with the Sr/U atom ratio around unity, were examined by means of thermogravimetry and X-ray diffraction. The reaction of $SrCO_3$ with U_3O_8 in air, where Sr/U=1, produced the stoichiometric β-$SrUO_4$, which had an orthorhombic structure. The reactions in vacuum and in hydrogen yielded the products of the composition $SrUO_{3.563}$ and $SrUO_{3.175}$, respectively. On the other hand, the reduction of β-$SrUO_4$ in vacuum and in hydrogen gave $SrUO_{3.48}$ and $SrUO_{3.65}$, respectively. Stoichiometric $SrUO_3$ was prepared by the reaction of SrO with UO_2. The reduction product of β-$SrUO_4$, $SrUO_{4-x}$, was oxidized in air below 500 °C to α-$SrUO_4$ which was rhombohedral. During the phase transition to β-$SrUO_4$, α-$SrUO_4$ exhibited anomalous behavior; that is, α-$SrUO_4$ was first reduced and then reoxidized to nearly the initial composition with the formation of β-$SrUO_4$. Of the uranates with $Sr/U \neq 1$, the formations of SrU_4O_{13}, SrU_2O_7, and Sr_2UO_5 were examined; the single phase SrU_2O_7 was not obtained. Thermograms for their reduction, followed by the oxidation of the resultants, suggest the existence of the compounds SrU_4O_{11} and $SrU_2O_{6.0-6.6}$. No uranates containing only U(IV) were obtained by hydrogen reduction of the uranates containing U(VI) formed in air at high temperatures.

It is widely known that so-called uranates[1] are formed by the reaction of uranium oxides with alkali or alkaline earth oxides, carbonates, nitrates, chlorides, *etc.* There have been many reports concerning the preparation, properties, and crystal structures of these uranates. However, the literature data on their composition and crystal structure often seem to be incomplete or conflicting. Interest in these uranates, which are possibly produced in the reactions of the matrix oxide with the alkali and alkaline earth metals as fission products in nuclear fuel, has given the stimulus to investigate systematically the compound systems.

Strontium uranates can be, according to Keller,[2] classified into the following three groups of compounds: $SrUO_3$,[3,4] Sr_2UO_4(?),[3] and Sr_3UO_5[5,6] in the system SrO–UO_2 containing uranium in tetravalent state; SrU_2O_6[5,7,8] in the system SrO–U_2O_5 containing U(V); and SrU_4O_{13},[6,9] SrU_2O_7(?),[5,6,10] $Sr_2U_3O_{11}$,[6] (α and β) $SrUO_4$,[6,9,11-17] Sr_2UO_5,[4,6,9,16-19] and Sr_3UO_6[3,6,15,20-22] in the system SrO–UO_3 containing U(VI). However, the physical and chemical properties as well as the phase relations of these strontium uranates have not been well investigated. In the present paper, we examine the formation, reactivity, and nonstoichiometry of the uranates; our interst was centered on the compounds with the Sr/U atom ratio around unity as determined by means of thermogravimetry.

Experimental

Materials. Strontium carbonate, $SrCO_3$, uranium dioxide, UO_2, and triuranium octoxide, U_3O_8, were used as starting materials. $SrCO_3$ was prepared by adding strontium nitrate aqueous solution into ammonium carbonate ammoniacal solution, similar to the procedure for producing the precipitated calcium carbonate.[23] U_3O_8 was prepared by heating ammonium diuranate in air at 900 °C for one day. UO_2 was obtained by reducing U_3O_8 at 1000 °C in a stream of hydrogen for 10 h.

Almost all reactions were performed with samples in the form of pressed pellets. The compounds of $SrCO_3$ and UO_2 or U_3O_8 were thoroughly mixed in an agate mortar and compacted at 3 ton/cm^2 into cylindrical pellets of 10 mm in diameter and of about 2 mm in thickness. The weight of each pellet was usually about 800 mg.

Apparatus and Procedures. The experimental apparatus for thermogravimetry was similar to that described in an earlier paper, where the equilibrium nitrogen pressure was measured in the UN–U_2N_3 system.[24] It consists of a Cahn RH-type automatic electrobalance, a Kanthal resistance furnace, a pressure measurement system, and vacuum pumps. The balance was adjusted so as to have a maximum weight change of 500 mg, and a sensitivity of 0.01 mg. A fused quartz crucible, 20 mm in height and 18 mm in outer diameter, was suspended from the balance, and then a quartz tube of 26 mm in inner diameter was connected to the vessel containing the balance. After being connected, the system was evacuated to 1×10^{-5} mmHg or below.

The temperature of the specimen was measured by means of a Pt/Pt+13%Rh thermocouple placed close to the crucible inside the reaction tube. Most of the experiments were made at the heating rate of 2 °C/min unless otherwise specified.

X-Ray Analysis. The samples were finely ground and loaded into capillaries, and then vacuum-sealed. The X-ray powder photographs were obtained with a Nerelco 114.6 mm camera using the nickel-filtered Cu$K\alpha$ radiation.

Results and Discussion

Reaction of $SrCO_3$ with U_3O_8 ($Sr/U=1$). Strontium monouranate, $SrUO_4$, is known to be dimorphic: one is rhombohedral[11] and the other is orthorhombic.[13,20] They are conventionally named α- and β-$SrUO_4$ respectively. The reaction of $SrCO_3$ with U_3O_8 in air, where the Sr/U atom ratio is unity, yielded yellow colored β-$SrUO_4$. The equiatomic mixture was heated in air from room temperature to 1100 °C, and then it was kept at 1100 °C for 3 h. A typical thermogravimetric curve is shown in Fig. 1, together with the results obtained in other atmospheres, and also with the decomposition curve of $SrCO_3$. The weight loss of $SrCO_3$ due to decomposition should be 29.1%, but in this figure it was normalized to the $SrCO_3+1/3U_3O_8$ mixture for the sake of convenience, where the value was to be 10.27%. This was attained at 1100 °C. As seen in the figure, the reaction of $SrCO_3$ with U_3O_8 in air began at 470 °C and then it proceeded stepwise. When the thermogravimetric curve of the reaction is compared with the decomposition curve of $SrCO_3$, it may be deduced that the first step is the reaction

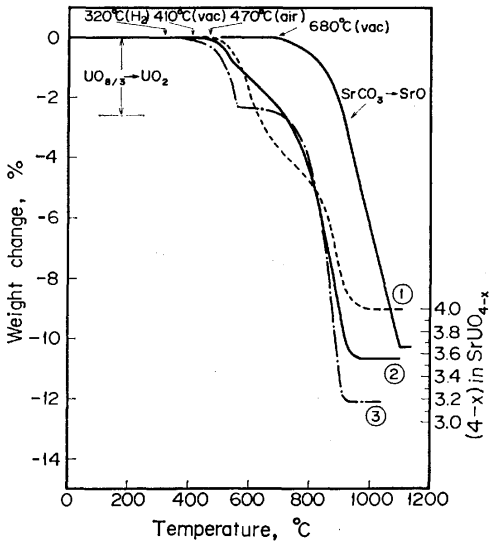

Fig. 1. Thermograms for the reaction of $SrCO_3$ with U_3O_8 in various atmospheres: ① in air; ② in vacuum; ③ in hydrogen; heating rate, 2 °C/min.

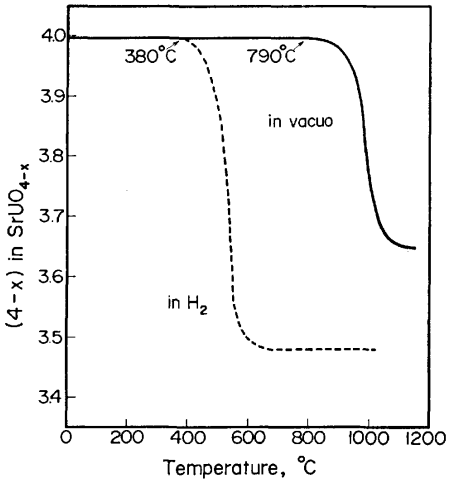

Fig. 2. Thermograms for reduction of β-$SrUO_4$ in vacuum and in hydrogen atmosphere: heating rate, 2 °C/min.

of $SrCO_3$ with U_3O_8, and that the second is the reaction of the decomposition product of $SrCO_3$ with U_3O_8. The X-ray pattern of the product was identical with that of the β-$SrUO_4$, which is orthorhombic and isomorphous with $BaUO_4$ with space group Pbcm, $z=4$.[13,17] The composition of the product was $SrUO_{3.997}$. Therefore, the overall weight change consists of weight loss due to the thermal decomposition of $SrCO_3$ plus weight gain due to oxidation in forming the uranate. The average valency of uranium in the compound is seen to increase from +5.33 to +5.99 during the reaction.

In vacuum, the reaction occurred at 410 °C and finished at about 950 °C. The composition of the product was $SrUO_{3.563}$ under the condition that the sample was heated to 1100 °C and then kept at that temperature for 1 h. Because the formal valency of uranium in this compound is +5.13, the U_3O_8 is regarded as losing a part of the combined oxygen. In a strict sense, the oxygen content varies as functions of oxygen pressure, temperature, and holding time; the number of oxygen atoms per formula can be changed in the range between 3.55 and 3.65 at 1100—900 °C in vacuum. According to X-ray analysis, the crystal was rhombohedral with space group $R\bar{3}m$, $z=1$, which is isomorphous with $CaUO_4$.[11] Although the structure of oxygen deficient $SrUO_{4-x}$ is basically the same as that of the α-$SrUO_4$, it has vacant O(II) sites due to nonstoichiometry.[25] The product was dark green.

In a hydrogen atmosphere, the reaction of $SrCO_3$ with U_3O_8 started at 320 °C. The reaction obviously proceeded stepwise, as seen in Fig. 1. The first is the reduction of U_3O_8 to UO_2 in the reaction mixture, because the same curve is obtained when U_3O_8 is reduced to UO_2 in hydrogen. The second step proceeds at temperatures above 700 °C, and probably corresponds to the reaction of $SrCO_3$ with UO_2. The overall composition of the product heated to 1000 °C was $SrUO_{3.175}$. The product was dark gray. No stoichiometric $SrUO_3$ was obtained by the reaction under the following conditions: maximum temperature, 1000 °C; holding time at 1000 °C, 1 h; atmosphere, hydrogen; and heating rate, 2 °C/min. The bulk composition of the products obtained under the conditions was $SrUO_{3.18-3.20}$.

The products, obtained by the reactions in vacuum or in hydrogen, gradually took up oxygen into the crystal even at room temperature when exposed to air, and the color changed from dark green or dark gray to red over 3 months. According to X-ray analysis, the red product was rhombohedral with nearly the same lattice parameters as those of the stoichiometric α-$SrUO_4$.[26]

Reaction of $SrCO_3$ with UO_2 ($Sr/U=1$). Behavior of the reaction in a vacuum was similar to that of the second step of the reaction of $SrCO_3$ with U_3O_8 in a hydrogen atmosphere. The reaction began at about 580 °C and finished at 950 °C. The composition of the product heated to 1100 °C was $SrUO_{3.21}$; the stoichiometric $SrUO_3$ was not obtained.

Reduction of β-$SrUO_4$. Thermograms of β-$SrUO_4$ heated in vacuum and in a hydrogen atmosphere are in Fig. 2. When the reaction was performed in a vacuum of 10^{-6} mmHg, the dissociation began at 790 °C and continued at a slow rate even at 1100 °C. The composition of the product kept at 1100 °C for 3 h was $SrUO_{3.65}$; its oxygen amount was slightly larger than that obtained by the reaction of $SrCO_3$ and U_3O_8 in vacuum, *i.e.* $SrUO_{3.56}$. As already mentioned, the oxygen content of the product is not only a function of temperature and of oxygen pressure, but tends to decrease with time at temperatures as high as 1100 °C. If the sample is heated for a longer time, the oxygen content must be smaller than that in $SrUO_{3.65}$. The equilibrium oxygen pressure over $SrUO_{4-x}$ at the given temperatures has not been measured.

The reduction in hydrogen began at 380 °C and finished at about 650 °C. The composition of the product heated to 1000 °C and kept at that temperature for 1 h was $SrUO_{3.48}$. Its oxygen content was much larger than that obtained by the reaction of $SrCO_3$ with U_3O_8 in hydrogen, *i.e.* $SrUO_{3.18}$. It was very dif-

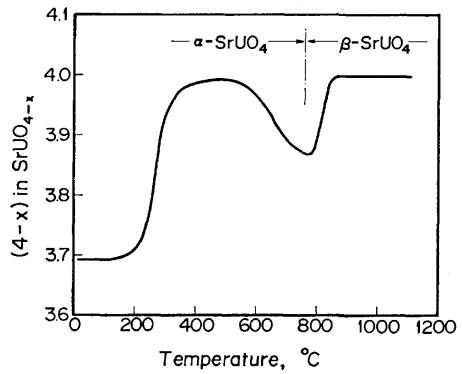

Fig. 3. Thermogram for oxidation of α-$SrUO_{4-x}$ in air: sample weight, 0.86476 g; heating rate, 2 °C/min.

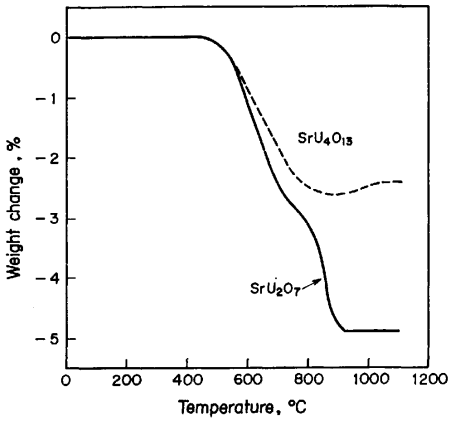

Fig. 4. Thermograms for formation of SrU_4O_{13} and SrU_2O_7 by the reaction of $SrCO_3$ with U_3O_8 in air at a heating rate of 2 °C/min.

ficult to get a lower oxygen content than that for $SrUO_{3.48}$, even if β-$SrUO_4$ was heated in a hydrogen atmosphere at 1000 °C for more than 3 h.

Preparation of $SrUO_3$. As already mentioned, the attempts to prepare $SrUO_3$ in a hydrogen atmosphere at temperatures below 1000 °C by the reaction of $SrCO_3$ with U_3O_8 and by the reduction of $SrUO_4$ were unsuccessful. Thus, as a next step, an equimolar mixture of SrO and UO_2 was heated in a vacuum at 1100 °C for 3 h. The product had the composition $SrUO_{3.04}$ and was yellowish-brown. When the compound was heated in air at a rate of 2 °C/min, it ignited at about 60 °C and changed into yellow β-$SrUO_4$, passing through a red-heated state for a short time of about 10 min.

In another experiment, an equimolar mixture of SrO and UO_2 was heated in a vacuum at 1650 °C for 5 h by using a tantalum-resistor high temperature vacuum furnace. For comparison, in one further experiment β-$SrUO_4$ was reduced in a hydrogen stream at 1500 °C for 3 h by using a high frequency-induced furnace. Both the products had the composition $SrUO_3$ and their X-ray diffraction lines were in the same pattern. However, these patterns were not consistent with the reported data, which have been assigned to the orthorhombic perovskite structure.[2] The structure analysis of $SrUO_{3.00}$ by X-ray and neutron diffraction will be reported elsewhere.

Oxidation of α-$SrUO_{4-x}$. The nonstoichiometric $SrUO_{4-x}$, which was prepared by the reaction of $SrCO_3$ with U_3O_8 or by the reduction of $SrUO_4$ in a vacuum or in hydrogen, had the rhombohedral structure. Here this uranate is designated as α-$SrUO_{4-x}$. Although the compound is oxidized at a very slow rate in air even at room temperature, the oxidation is accelerated by heating. Figure 3 shows a thermogram for the oxidation of α-$SrUO_{4-x}$ in air, where the initial composition of the sample is $SrUO_{3.688}$. As seen in Fig. 3, the α-$SrUO_{3.688}$ began to be oxidized at about 150 °C, and attained to its maximum oxygen content, $SrUO_{3.991}$, around 500 °C. This oxidation process is not reversible. Above 500 °C the compound with the composition $SrUO_{3.991}$ began to lose its oxygen. The weight loss continued till 770 °C, at which the minimum oxygen content, $SrUO_{3.867}$, was observed. The compound was still in the α phase region, and if it was cooled from 770 °C, the oxygen content again increased on the same line with that of the heating process up to the maximum point at 500 °C, and the oxygen content remained unchanged on further cooling of the temperature. On the other hand, if the sample was heated above the temperature giving the minimum oxygen content, the α phase transformed into the β phase, along with oxidation. The transition was finished at 870 °C. The product was a mixture of α-$SrUO_4$ and β-$SrUO_4$ at temperatures between 770 and 870 °C. The oxidation process in this region was not reversible.

The temperature and the composition at the minimum point varied with oxygen pressure and heating rate. When α-$SrUO_{4-x}$ was heated in oxygen at different pressures, the composition and the transition temperature were as follows: $SrUO_{3.867}$ at 770 °C in air (160 mmHg O_2), $SrUO_{3.839}$ at 790 °C in 50 mmHg O_2, and $SrUO_{3.805}$ at 800 °C in 10 mmHg O_2.[26] When the heating rate of the sample was varied from 2 to 5 °C/min, the composition at the minimum point in air was changed from $SrUO_{3.867}$ at 770 °C to $SrUO_{3.838}$ at 800 °C.

The weight loss of α-$SrUO_4$ at temperatures from 500 to 770 °C in air is due to oxygen nonstoichiometry, because the weight loss is enhanced with temperature and also with decreasing oxygen pressure. Therefore, the minimum point of oxygen content in Fig. 3 seems to have resulted from the competitive reactions between the weight loss due to the reduction of the α-$SrUO_4$ and the weight gain due to the formation of the β-$SrUO_4$.

Formation of Strontium Uranates with $Sr/U<1$. Strontium uranates SrU_4O_{13} and SrU_2O_7 were prepared by the reactions between $SrCO_3$ and U_3O_8 in air. Figure 4 shows thermograms for the formation of these compounds. The shape of the curves for the formation of SrU_4O_{13} is different from that for SrU_2O_7. In the case of SrU_4O_{13}, the minimum oxygen content appeared at about 900 °C. The shape of the curve and the initiation temperature of the reaction for SrU_2O_7 were similar to those obtained by the reaction of the equiatomic mixture of $SrCO_3$ and U_3O_8. The reactions proceeded stepwise. The compositions of the products were $SrU_4O_{12.741}$ for Sr : U=1 : 4 and $SrU_2O_{6.933}$ for Sr : U=1 : 2. They were not in the stoichiometric compositions.

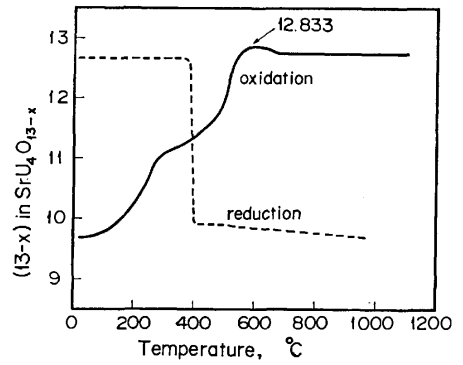

Fig. 5. Thermograms for reduction of SrU_4O_{13} in hydrogen and for oxidation of the resultant uranate in air at a heating rate of 2 °C/min.

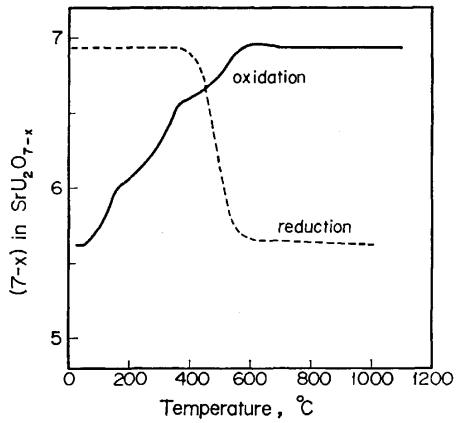

Fig. 6. Thermograms for reduction of SrU_2O_7 in hydrogen and for oxidation of the resultant uranate in air at a heating rate of 2 °C/min.

The SrU_4O_{13} obtained here was reduced in a hydrogen atmosphere by heating from room temperature to 1000 °C. The result is shown in Fig. 5. As seen in the figure, the composition was changed from $SrU_4O_{12.741}$ to $SrU_4O_{9.668}$ by reduction. The latter was found to be a mixture of UO_2 and α-$SrUO_{4-x}$. When the resultant product was oxidized in air to 1100 °C, the thermogram showed a bend near the composition SrU_4O_{11}. The existence of the compound SrU_4O_{11} has not been reported so far, and we did not examine further whether there was a compound or not at this composition. The compound SrU_4O_{13} has been prepared by using the reaction of $Sr(NO_3)_2$ with U_3O_8.[6] Cordfunke and Loopstra[6] have pointed out that it shows nonstoichiometry; $SrU_4O_{12.8}$. Our results were in good agreement with theirs.

Figure 6 shows thermograms of the reduction of the compound with Sr : U=1 : 2, followed by the oxidation of the product obtained in the reduction process. The compound obtained in air showed a nearly stoichiometric bulk composition $SrU_2O_{6.933}$, but it was seen not to be a single phase compound from the X-ray pattern, as Cordfunke and Loopstra[6] stated. When heated in a hydrogen atmosphere, it was reduced to $SrU_2O_{5.572}$. Next, the resultant product was oxidized by heating in air. As shown in the thermogram in Fig. 6, the curve bends near the compositions of $SrU_2O_{6.0}$ and $SrU_2O_{6.6}$.

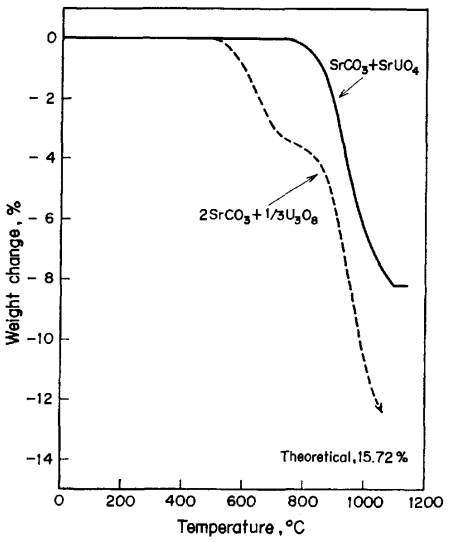

Fig. 7. Thermograms for formation of Sr_2UO_5 by the reaction of $SrCO_3$ with U_3O_8 and by the reaction of $SrCO_3$ with $SrUO_4$ in air at a heating rate of 2 °C/min.

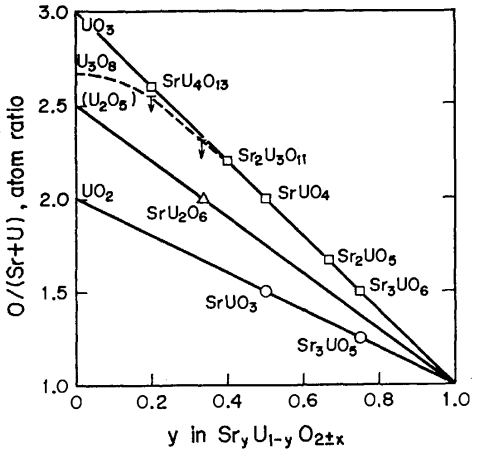

Fig. 8. Summary for compounds in the system Sr–U–O.

According to Hoekstra and Katz,[5] there exists a nonstoichiometric compound $SrU_2O_{6\pm x}$ with CaF_2-type f.c.c. structure. The anomalies in our curve may be interpreted to correlate with the lower and the upper limits of this nonstoichiometric $SrU_2O_{6\pm x}$.

Formation of Sr_2UO_5. For preparing the compound Sr_2UO_5, the reaction of $SrCO_3$ with U_3O_8 was first examined. A thermogram for this reaction is shown in Fig. 7. The shape of the curve was similar to that observed in the formation reaction of the other uranates mentioned above, for example $SrUO_4$. The theoretical weight loss of this reaction was 15.72%, but the reaction did not finish when the sample was heated to 1060 °C and kept at that temperature for 3 h. Next, the reaction of $SrCO_3$ with $SrUO_4$ was studied as a way to obtain Sr_2UO_5. Its thermogram is also shown in Fig. 7. The reaction started at about 750 °C and finished at 1100 °C. The product was the stoichiometric Sr_2UO_5, which was pale yellow. To prepare Sr_3UO_6, a mixture of $SrCO_3$ with $SrUO_4$ was heated under the same conditions as in the formation of Sr_2UO_5, but the

reaction did not terminate. It seems that the chemical reactivity in the formation reaction of the uranates tends to be lowered as the content of strontium increases.

Reduction of Sr_2UO_5 by hydrogen at 1000 °C did not yield Sr_2UO_4, but the product with the composition of $Sr_2UO_{4.618}$. When heated in air, the reduction product was again oxidized in a manner similar to the case where the α-$SrUO_{4-x}$ was oxidized in air. From the curve, it could not be distinguished whether the reduction product is a new compound or a mixture containing α-$SrUO_{4-x}$.

Summary for Strontium Uranates. All of the strontium uranates are shown in Fig. 8. In the system SrO–UO_3, five uranates are known. The valence state of uranium in the uranates formed in air is nearly or exactly +6. This value is higher than +5.33 of uranium in U_3O_8, which is the most stable compound in the uranium–oxygen system in air. However, the compound SrU_4O_{13} is not stoichiometric, the valence state of uranium being +5.87. The dashed line in Fig. 8 shows the bulk composition when a mixture of $SrCO_3$ and U_3O_8 is heated in air. In the system SrO–U_2O_5, there is only one compound SrU_2O_6 which shows a rather wide range of oxygen nonstoichiometry. Although it was reported that the uranate has the homogeneity range between 5.95 and 6.4 in the number of oxygen atoms per formula,[5] there is another report in which the SrU_2O_6 is described to be a mixture of CaF_2-type f.c.c. uranate, $Sr_yU_{1-y}O_{2\pm x}$, and a solid solution containing β-$SrUO_4$.[10] Our results show that the nonstoichiometry range is 6.0 to 6.6 in air. In the system SrO–UO_2, two uranates are known. When reduced in hydrogen at 1000 °C, U_3O_8 is readily converted into the stoichiometric UO_2. However, strontium uranates containing U(VI) are not reduced to the uranates containing U(IV) under the same condition; *i.e.* $SrU_4O_{9.69}$ for SrU_4O_{13}, $SrU_2O_{5.57}$ for SrU_2O_7, and $SrUO_{3.48}$ for $SrUO_4$. In addition to this, when exposed to air at room temperature, these uranates, which are prepared by vacuum or hydrogen reduction, are gradually oxidized by accommodating oxygen into the crystal, whereas UO_2 is scarcely oxidized. The uranates containing U(IV) can be produced only by the reactions of SrO with UO_2.

References

1) F. A. Cotton and G. Wilkinson, "Advanced Inorganic Chemistry," 2nd ed, Interscience Publishers, New York (1966), p. 1097.

2) C. Keller, "Gmelins Handbuch der anorganischen Chemie," System-Nr.55, U Erg. -Bd. Teil C3 (1975), p. 102.

3) R. Scholder and L. Brixner, *Z. Naturforsch., Teil B*, **10**, 178 (1955).

4) C. Keller, KFK-225 (1964).

5) H. R. Hoekstra and J. J. Katz, *J. Am. Chem. Soc.*, **74**, 1683 (1952).

6) E. H. P. Cordfunke and B. O. Loopstra, *J. Inorg. Nucl. Chem.*, **29**, 51 (1967).

7) H. Hoekstra and S. Siegel, Proc. International Conf. on "Peaceful Uses of Atomic Energy," Vol. 7, United Nations, New York (1956), p. 394.

8) R. Brochu and J. Lucas, *Bull. Soc. Chim. Fr.*, **1967**, 4764.

9) C. Brisi, M. Montorsi, and G. Acquarone Burlando, *Rev. Int. Hautes Temper. et Refract.*, **8**, 37 (1971).

10) N. M. Voronov and R. M. Sofronova, "Physical Chemistry of Alloys and Refractory Compounds of Thorium and Uranium," ed by O. S. Ivanov, Israel Program for Sci. Trans., Jerusalem (1972), p. 215.

11) W. H. Zachariasen, *Acta Crystallogr.*, **1**, 281 (1948).

12) E. A. Ippolitova, Yu. P. Simanov, L. M. Kovba, G. P. Polunina, and I. A. Bereznikova, *Radiokhimiya*, **1**, 660 (1959).

13) E. A. Ippokitova, I. A. Bereznikova, V. D. Kosynkin, Yu. P. Simanov, and L. M. Kovba, ANL-Trans-33 (1961), p. 180.

14) C. Keller, *Nukleonik*, **4**, 271 (1962).

15) J. Klima, D. Jakes, and J. Moravec, *J. Inorg. Nucl. Chem.*, **28**, 1861 (1966).

16) B. O. Loopstra and H. M. Rietveld, *Acta Crystallogr., Sect. B*, **25**, 787 (1969).

17) J. O. Sawyer, *J. Inorg. Nucl. Chem.*, **34**, 3268 (1972).

18) N. M. Voronov, R. M. Sofronova, and E. A. Voitekhova, "Physical Chemistry of Alloys and Refractory Compounds of Thorium and Uranium," ed by O. S. Ivanov, Israel Program for Sci, Trans., Jersalem (1972), p. 222.

19) J. O. Sawyer, *J. Inorg. Nucl. Chem.*, **25**, 899 (1963).

20) W. Rudorff and F. Pfitzer, *Z. Naturforsch., Teil B*, **9**, 568 (1954).

21) A. W. Sleight and R. Ward, *Inorg. Chem.*, **1**, 790 (1962).

22) H. M. Rietveld *Acta Crystallogr*, **20**, 508 (1966).

23) "Experimental Chemistry," Vol. 9, ed by Chem. Soc. Japan, Maruzen Co., Tokyo (1958), p. 176.

24) H. Tagawa, *J. Nucl. Mater.*, **41**, 313 (1971).

25) T. Fujino, N. Masaki, and H. Tagawa, *Z. Krist.*, in press.

26) H. Tagawa and T. Fujino, *Inorg. Nucl. Chem. Lett.*, in press.

The Liquid-Phase Oxidation of Aldehydes with Metal Tetra(*p*-tolyl)porphyrins

Yasukazu OHKATSU and Tetsuo OSA

Department of Synthetic Chemistry, Faculty of Engineering, University of Tokyo, Bunkyo-ku, Tokyo 113

(Received October 1, 1975)

The effects of the kind of metal of metal porphyrins and the substituent of the phenyl group of porphynato plane were discussed, using them as catalysts in the autoxidation of aldehydes. The effect of the solvent and the additive on the above-mentioned catalytic activity of the porphyrins was put into order by means of their $pK_a(BH^+)$ and $pK_a(H^+)$ values; the increased $pK_a(BH^+)$, namely, the electron-donating power of solvents, seemed to lead to their strong coordination, followed by the initiation of the coordination of oxygen. On the other hand, the oxygen which had been activated on the porphyrins was estimated to react with or be stabilized by a solvent with a low $pK_a(H^+)$; it could not initiate the autoxidation with ease.

The interaction of molecular oxygen with hemoproteins is important in respiratory and metabolic processes. Many investigators have studied this interaction using a metal porphyrin as a model of such hemoproteins as hemoglobin and myoglobin. It has been one of their most important aims to ioslate a so-called dioxygen complex, such as the "picket fence porphyrin" obtained by Collman *et al.*[1] On the other hand, there have been reported[2,3] a number of studies of Fe(II) dioxygen complexes in terms of the effect of the environmental conditions of dioxygen complexes on their stability or instability—the concept of axial bases and hydrophobic circumstances.

Welscher and Anderson[4] reported the *trans* effect of axial bases on the dissociation of Fe(TPP)(base)(O_2), namely, the reversible liberation of the oxygen of the dioxygen complex, to be in the order of pyridine> piperidine≫ 1-methylimidazole, and concluded that π-donating ability of an axial base was responsible for the instability of the dioxygen complex. Bringer, Chang, and Traylor[5] showed the effect of the basicity of the media on the oxygenation of porphyrin.

The above-mentioned papers, however, offer no detailed information about whether axial bases help the stabilization of the oxygen of the dioxygen complex, or whether they act as activating agents of such an oxygen molecule for a substrate approaching from the outside. We have tried to make it clear, in the autoxidation of organic compounds, how oxygen molecule behaves on complexes such as metal polyphthalocyanines and cobalt tetra(*p*-tolyl)porphyrin in its interaction with cumene,[6] and aldehydes[7–10] as proton donors. In these studies, it has been found that the interactions among all chemical species including an oxygen molecule, a substrate to be oxidized, and a solvent are of importance.[10] However, there remain a few points to be clarified, because Taft's equation, which is considered in these experiments to show, only incompletely, the direct correlation with the electron-donating and electron-accepting natures of chemical species, has been used in the measurements.

In this paper, the interactions among all of chemical species are more distinctly discussed using the acidity and basicity of the chemical species in place of the σ^* and ρ^* values of Taft's equation. It is also discussed how the concentrations of chemical species are important in addition to their electron-donating and electron-accepting properties.

Experimental

Materials. Metal tetra(*p*-substituted phenyl)porphyrins used for this study were metal tetra-(*p*-methoxyphenyl)-, -(*p*-tolyl)-, -phenyl-, and -(*p*-chlorophenyl)-porphyrins, which were prepared according to the procedure described in an earlier paper.[11] As metals, nickel, copper, manganese, and cobalt were introduced.[12]

Aldehydes, such as acetaldehyde and benzaldehyde, were purified under nitrogen by the conventional methods just before use in order to avoid the formation of the corresponding peracids.

Solvents, such as ethyl acetate and ethyl isobutyrate, and additives as a part of the solvents, such as pyridine, *N,N*-dimethylformamide, water, acetone, ethanol, trichloroethanol, nitroethane, succinic acid, benzoic acid, trichloroacetic acid, benzamide, urea, quinoline, benzylamine, piperidine, and acridine, were purified by standard methods.

Procedure. The oxidation of aldehydes with a porphyrin complex catalyst and the titration of peracids and hydrogen peroxide were carried out as has been described in a previous paper.[10]

Results and Discussion

General Aspect of Oxidation. The liquid-phase oxidation of aldehyde with a porphyrin complex catalyst proceeds according to the autoxidation mechanism represented by the rate equation,

$$-d[O_2]/dt = k[RCHO]^{3/2}[porphyrin]^{1/2}[O_2]^{1/2}, \quad (I)$$

as has been described before.[10] The rate of initiation can be written as

$$R_i = k'[RCHO][porphyrin][O_2]. \quad (II)$$

According to the ESR study by many investigators[13,14] and by us,[15] porphyrins can activate molecular oxygen as superoxide ions, which abstract hydrogen atom from a substrate to be oxidized, initiating autoxidation as follows:[16,17]

$$Co(II)TPP + O_2 \rightleftharpoons Co(III)TPP\cdots O_2^-, \quad (1)$$

$$Co(III)TPP\cdots O_2^- + RCHO \rightarrow Co(III)TPP\cdots O_2H^- + R\dot{C}O. \quad (2)*$$

The nature of the central metal of a porphyrin

* Step (2) may be followed by

$$Co(III)TPP\cdots O_2H^- \rightarrow Co(II)TPP + {}^{\cdot}O_2H, \quad (3)$$

$$RCHO + {}^{\cdot}O_2H \rightarrow R\dot{C}O + H_2O_2. \quad (4)$$

Table 1. Effect of the metal ion of tetraphenylporphyrins on the oxidation rate

Metal ion ($\times 10^3$ M)		Acetaldehyde (M)	$-d[O_2]/dt$ ($\times 10^5$ M s^{-1})
Ni(II)	5.0	0.5	3.1
Cu(II)	5.0	0.5	3.4
Mn(II)	5.0	0.5	3.5
Co(II)	5.0	0.5	2.6
Co(II)	6.7	0.1	3.6

Reaction conditions: solvent, ethyl acetate; temperature, 10 °C; $[O_2]$, 1 atm.

Table 2. Effect of the substituent of the phenyl group of cobalt tetraphenylporphyrins on the oxidation rate

Substituent	$-d[O_2]/dt$ ($\times 10^6$ M s^{-1})	Relative activity for oxidative dehydrogenation[a]
p-OCH_3	4.2	1.18
p-CH_3	81	1.44
H	2.6	1.00
p-Cl	1.2	—
p-NO_2	—	0.82

Reaction conditions: Acetaldehyde, 0.5 M; catalyst, 5.0×10^{-3} M; solvent, ethyl acetate; temperature, 10 °C; (O_2), 1 atm.
a) Details of the reaction are unknown.

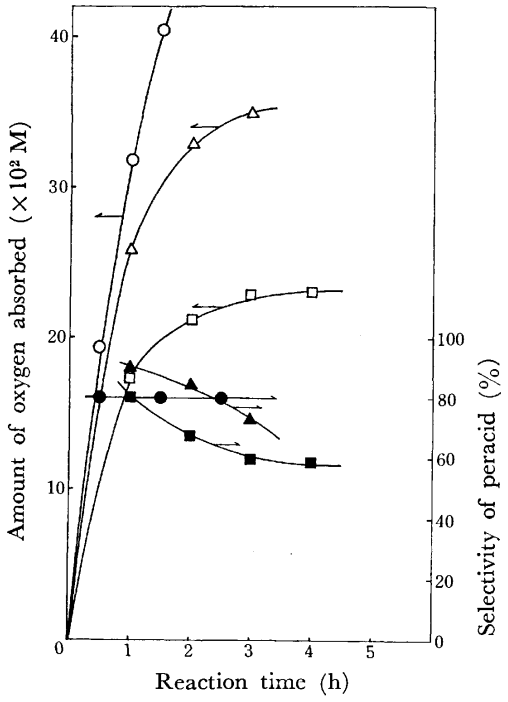

Fig. 1. Amount of oxygen absorbed and selectivity of peracid.

Catalyst	Solvent	AcH	Temp	Ref.
○, ● Co tetra(*p*-tolyl)-porphyrin, 5×10^{-3} M	ethyl acetate	1.0 M	10 °C	This work
□, ■, Fe,Cu-polyphth-alocyanine 5×10^{-3} M	ethyl acetate	0.45 M	10 °C	9
△, ▲, Fe,Cu-polyphth-alocyanine 5×10^{-3} M	bromo-benzene	0.45 M	10 °C	9

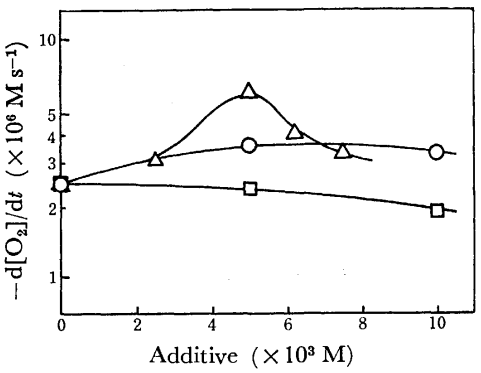

Fig. 2. Effective of some additives on oxidation rate. Reaction conditions: Co tetra(*p*-tolyl)porphyrin, 5.0×10^{-3} M; acetaldehyde, 0.5 M; solvent, ethyl acetate; temperature, 10 °C; (O_2), 1 atm.
△: Pyridine, ○: *N*,*N*-dimethylformamide, □: water.

affected its activity little, compared with the case of metal polyphthalocyanine (Table 1), but the substituents of the phenyl group in the porphynato plane had a considerable effect (Table 2); the effects of substituents on the rate of oxidation were in the order of $CH_3 \gg CH_3O > H > Cl$. This order, though it cannot be easily explained by only the electron-donating and electron-attracting properties of the substituent, coincides with that of the influence of chemical substituents on the catalytic activity for oxidative dehydrogenation, as studied for tetra(*p*-substituted phenyl)porphyrins by Manassen (see Column 3 in Table 2).[18]

A metal porphyrin had little activity to decompose a peracetic acid as one of oxidation products and produced the peracid quantitatively, as is in the case of a metal polyphthalocyanine (Fig. 1). Hydrogen peroxide was also considerably stable in the presence of the porphyrin at 10 °C. This result suggests that the formation of free radicals by the redox decomposition of peracid with a metal porphyrin, if any, is less important as an initiation reaction in this oxidation.

The addition of a small amount of pyridine, *N*,*N*-dimethylformamide, or water to a main solvent such as ethyl acetate used in the reaction system affected the activity of the catalyst, as is observed in the case of a metal polyphthalocyanine (Fig. 2). Water did not affect, or was apt to decrease the oxidation rate upon addition, whereas pyridine or *N*,*N*-dimethylformamide gave the maximum rate when the catalytic amount was added. A small addition of such an electron-donating additive is likely to increase the catalytic activity, which depends on the characteristic donating power of the additive. The effect of additives was of the order of pyridine > *N*,*N*-dimethylformamide > water.

The increase in the catalytic activity of a metal porphyrin can be well explained by the coordination of an additive to the metal, resulting in the activation of oxygen molecule at the trans-position, as has been reported with respect to a metal polyphthalocyanine.[6] The decrease upon the addition of more than a catalytic amount of the additive, on the contrary, may be ascribed to the occupation of both axial positions by the additive. The effect of the additive on the decrease mentioned

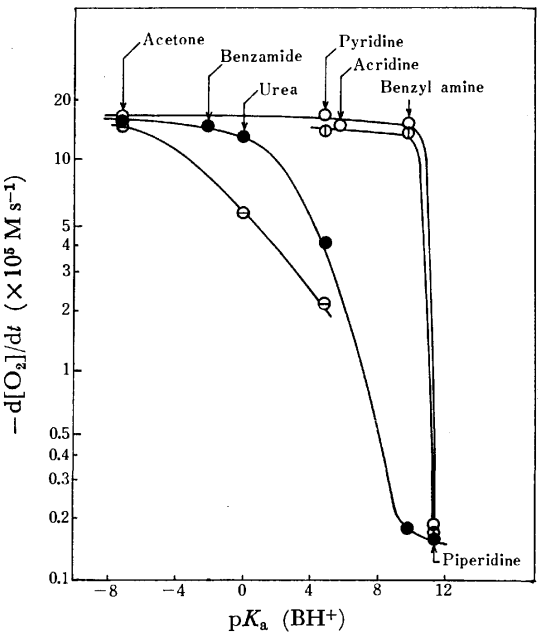

Fig. 3. Effect of pK_a(BH$^+$) of basic additive on oxidation rate. Reaction conditions: Co tetra(*p*-tolyl)porphyrin, 2.5×10^{-3} M; benzaldehyde, 0.4 M; solvent, ethyl isobutyrate; temp, 10 °C; (O_2), 1 atm; additive ○: 2.5×10^{-3} M, ⊕: 6.0×10^{-3} M, ●: 2.5×10^{-2} M, ⊖: 4.0×10^{-2} M.

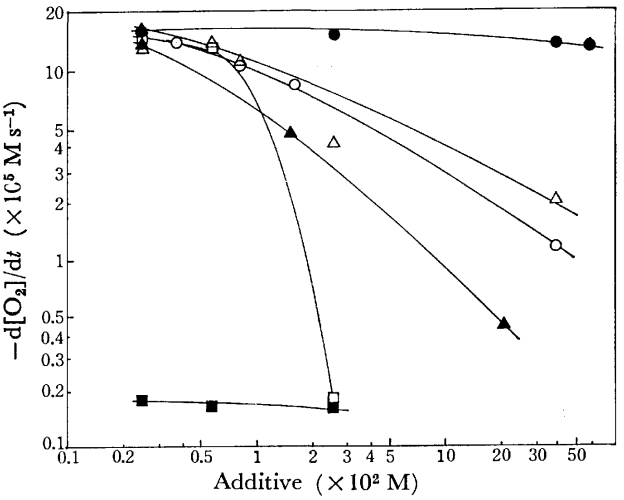

Fig. 4. Effect of the amount of basic additive on oxidation rate. Reaction conditions: Cobalt tetra(*p*-tolyl)-porphyrin, 2.5×10^{-3} M; benzaldehyde, 0.4 M; solvent ethyl isobutyrate; temperature, 10 °C; (O_2), 1 atm; additive, ●: acetone (pK_a(BH$^+$)$=-7.2$), ○: quinoline (4.83), △: pyridine (5.21), ▲: acridine (5.50), □: benzylamine (9.33), ■: piperidine (11.12).

above will be discussed in the next paragraph.

Effect of Additives. *Effect of Bases*: An additive with an elctron-donating or electron-accepting ability was added to the oxidation system consisting of cobalt tetra(*p*-tolyl)porphyrin as a catalyst, benzaldehyde, and oxygen, with ethyl isobutyrate as the main solvent. Figure 3 shows the relation of the pK_a(BH$^+$) of an additive as a conjugated acid to the oxidation rate under same concentrations of acetaldehyde and a catalyst, and oxygen pressure. The additive with a higher pK_a(BH$^+$) value—that is, a stronger electron-donating ability, suppressed the oxidation by preventing the oxygen from coordinating, depending on the amount present. Based on the mole of the catalyst, the catalytic and 2.4 times as much of the additive gave the point of the abrupt suppression of the rate near pK_a(BH$^+$)$=10$; 10 times, near pK_a(BH$^+$)$=-2$, and 160 times, pK_a(BH$^+$)$=-8$. In addition, it is very surprising that a small change in the pK_a(BH$^+$) values near 10 brought about a sudden decrease in the oxidation rate, even in the presence of a catalytic amount of the additive.

The effect of the additive concentration on the rate is illustrated in Fig. 4. The pK_a(BH$^+$) of the oxygen molecule is not known. However, it is considered to be under about 5, because the pK_a(BH$^+$) of the superoxide ion has been reported as 4.8.[19] Acetone with a pK_a(BH$^+$) of -7.2 did not affect the rate even if it was present in an amount 100 times that of the moles of the catalyst. The additive of a relatively high pK_a(BH$^+$), such as quinoline (4.83), pyridine (5.21), or acridine (5.50), reduced the rate gradually when the concentration went over a certain amount. However, an additive such as benzylamine of pK_a(BH$^+$)$=$ 9.33 lowered the oxidation rate abruptly, and piperidine (11.12) inhibited the oxidation almost completely even if there was only a little more than the catalytic amount. In other words, as the pK_a(BH$^+$) of the additive became higher, the degree of competitive coordination between an additive and the molecular oxygen increased. In the case of piperidine, almost all substances added seem to occupy the coordination sites of the catalyst because of its high pK_a(BH$^+$) value.

The competitive reaction can be successfully explained by the above-mentioned results and discussion. However, a minor effect, namely, the steric effect of an additive, may be observed. On quinoline, pyridine, and acridine, the respective pK_a's are 4.81, 5.21, and 5.50. These additives, accordingly, would lead to the lowering of the oxidation rate in the order of: quinoline $>$ pyridine $>$ acridine when present in inhibitive amounts. However, the experimental order was reversed in quinoline and pyridine. This may be due to the difference in steric bulkiness on gaining access to the central metal of catalyst: quinoline$>$pyridine.

Effect of Acids. For the start of oxidation, it is essential for the substrate to be oxidized to approach and react with the activated oxygen. The ease of approach will be discussed using the electron-attracting, namely, the proton-giving, property of the chemical species in the reaction system, such as an aldehyde, a solvent, and an additive. Such a point of view with respect to aldehydes has been previously reported.[12] The role of the last additive is shown in Fig. 5. The figure shows that a decrease in the oxidation rate was observed below pK_a(H$^+$) of 4 on the addition of a proton-donating substrate corresponding to the amount of a catalyst, below pK_a(H$^+$)$=6$ on the addition of 10 times the amount, and below pK_a(H$^+$)$=10$ on the addition of 100 times the amount. It is also well known in the field of electrochemistry that the superoxide ion, which is fairly stable under an alkaline condition,

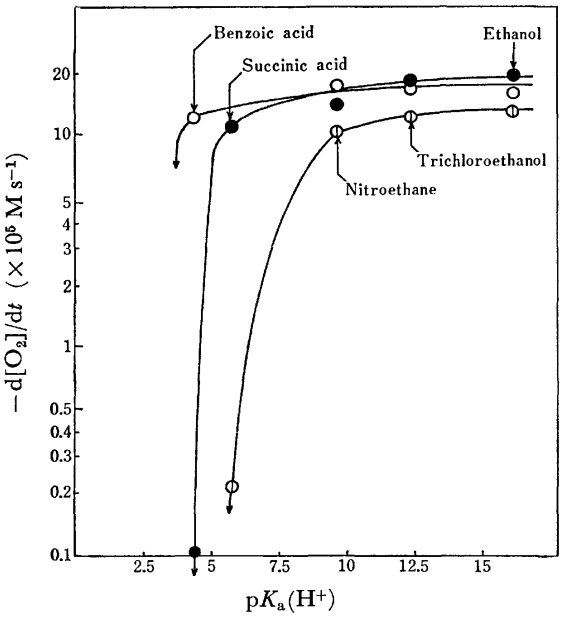

Fig. 5. Effect of $pK_a(H^+)$ of protic additive on oxidation rate. Reaction conditions: Co tetra(*p*-tolyl)-porphyrin, 2.5×10^{-3} M; benzaldehyde, 0.4 M; solvent, ethyl isobutyrate; temp, 10 °C; (O_2), 1 atm; additive, ○ 2.5×10^{-3} M, ● 2.5×10^{-2} M, ⓘ 2.5×10^{-1} M. Arrow (↓) means no absorption of oxygen in trichloroacetic acid ($pK_a(H^+)=0.65$).

reacts easily with a proton-giving substrate thus:

$$O_2 + e + H^+ \rightarrow HO_2^{\cdot}, \quad (5)$$

$$HO_2^{\cdot} + e + H^+ \rightarrow H_2O_2. \quad (6)^{20)}$$

These facts imply that the oxygen activated on porphyrin is deactivated by a protic substrate. If its acidity is stronger than that of benzaldehyde, it obstructs the hydrogen abstraction of benzaldehyde and converts the activated oxygen into the other form which interacts with the aldehyde only with difficulty.

This may be explained by plotting the oxidation rate against the amount of an additive added (Fig. 6). In the presence of ethanol ($pK_a(H^+)=15.9$) or trichloroethanol ($pK_a(H^+)=12.24$), the oxidation rate begins to be suppressed only after the addition of approximately the same amount of the additive as benzaldehyde. This means that the solvent with a $pK_a(H^+)$ over about 12 has no power to compete with benzaldehyde in approaching to the activated oxygen because of its lower electrophilic property: the $pK_a(H^+)$ of aldehyde is from about 10 to about 13.5; that of formaldehyde, 13.29, and that of chloralaldehyde, 10.93. On the other hand, benzoic acid ($pK_a(H^+)=4.20$) inhibited the oxidation considerably even if only 2.5×10^{-2} M was present, corresponding to 10 times the catalytic amount. Trichloroacetic acid ($pK_a(H^+)=0.65$) prevented the oxidation almost completely in the presence of the catalytic amount.

These experimental facts coincide well with the curve of oxygen absorption (Fig. 1). The oxidation of acetaldehyde and benzaldehyde produces acetic and benzoic acids respectively as follows:

$$RCOOOH + RCHO \rightarrow 2RCOOH. \quad (7)$$

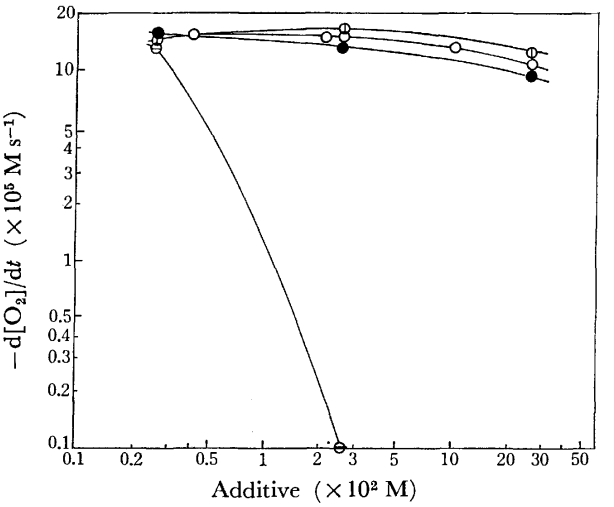

Fig. 6. Effect of the amount of protic additive on oxidation rate. Reaction conditions: Cobalt tetra(*p*-tolyl)-porphyrin, 2.5×10^{-3} M; benzaldehyde, 0.4 M; solvent ethyl isobutyrate; temperature, 10 °C; (O_2), 1 atm; additive, ⓘ: ethanol, ○: trichroloethane, ●: nitroethane, ○: benzoic acid.

These acids may deactivate the activated oxygen; the $pK_a(H^+)$ values of these acids are 4.76 and 4.20 respectively.**

Conclusion

As an additive included in a solvent has some parallel interaction with a porphyrin and its active intermediate, its pK_a plays an important role in the initiation reaction in terms of change of the rate. The concentration of the solvent relative to other chemical species is also important. These results and this dicussion can considerably clarify the questionable aspects proposed by other investigators.

F. A. Walkner, for example, studied the thermodynamics of the reaction of molecular oxygen with a cobalt porphyrin.[21] The thermodynamics data of the reaction,

$$CoP\cdot B + O_2 \rightleftarrows CoP\cdot B\cdot O_2, \quad (8)$$

in which B represents an axial base, probably corresponding to the activation of the oxygen molecule, were measured at −65 °C for bases such as pyridine, 4-picoline, 3,4-lutidine, 4-methylimidazole, and piperidine. He could not find any direct relationship between the pK_a of the coujugated acids of amines and the equilibrium constants of Scheme 8 or the ΔH of the formation of the Co–O bond. In this paper, moreover, there remain a few questions with respect to the following points: (A) The stabilization of coordinated oxygen by the base $CoP\cdot O_2\cdot B$ was not taken into account in the kinetical treatment of formation of oxygen complexes. This action of the amine cannot always be neglected, though; Pauling[22] and others[23,24] suggest that a more distinct imidazole from

** The sudden decrease in the oxidation rate after a certain amount of oxygen has been absorbed (Fig. 1) may be attributed to the formation of such an acid.

the histidine residue (E-7) projecting into the oxygen-binding pocket in the oxygen-carrying protein may somehow stabilize the coordinated dioxygen by hydrogen bonding. (B) The sample used in his experiments contained cobalt tetra(*p*-tolyl)porphyrin in a concentration of $(8-9)\times10^{-4}$ M and the above-mentioned amine in a concentration of $1\times10^{-2}-1\times10^{-1}$ M. In other words, the ratio of the amine to porphyrin was from about ten to one hundred. This ratio is considered to be in the range of concentration ratios in which some bases can stop the oxidation completely (see Fig. 4) and the formation of dioxygen complex may be suppressed, and in which only 0.8% of the cobalt would be in the form of the oxygen adduct under an atmosphere in the presence of 4-dimethylaminopyridine or *N*-methylimidazole as an axial base. The ratio seems to be too high for us to dicuss the formation of the oxygen complex kinetically. In autoxidation under such a ratio, a difference in the slopes of the straight parts of the graphs in relation with pK_a was observed, namely, the equilibrium constants, as shown in Figs. 4 and 6, and the straight parts sometimes crossed each other. A discussion based on the special ratio may, therefore, misunderstand the actual phenomena. The results reported by Stynes and Ibers[25] for the similar cobalt protoporphyrin IX dimethyl ester·B system, including pyridine, 4-butylpyridine, *N*-methylimidazole, and several others as axial bases, showed a direct relationship between the $pK_a(BH^+)$ of the base and the formation of the Co–O bond. The ratio of 2—3 which they used will be suitable for a discussion of the interaction of porphyrin with the oxygen molecule. (C) Though the steric hindrance of bases is probably small, it should also be considered.

We wish to express many thanks to Professor Teiji Tsuruta for giving us fruitful advice and discussion through this work.

References

1) J. P. Collman, R. R. Gagne, C. A. Reed, T. R. Halbert, G. Lang, and W. T. Robinson, *J. Am. Chem. Soc.*, **97**, 1427 (1975).
2) J. H. Wang, *J. Am. Chem. Soc.*, **80**, 3168 (1958).
3) J. E. Baldwin and J. Huff, *J. Am. Chem. Soc.*, **95**, 5757 (1975).
4) C. J. Welscher and D. L. Anderson, *J. Chem. Soc., Chem. Commun.*, **1974**, 757.
5) W. S. Bringer, C. K. Chang, and T. G. Traylor, *J. Am. Chem. Soc.*, **96**, 5597 (1974).
6) T. Hara, Y. Ohkatsu, and T. Osa, *Chem. Lett.*, **1973**, 103.
7) T. Hara, Y. Ohkatsu, and T. Osa, *Chem. Lett.*, **1973**, 953.
8) T. Hara, Y. Ohkatsu, and T. Osa, *Bull. Chem. Soc. Jpn.*, **48**, 85 (1975).
9) Y. Ohkatsu, T. Hara, and T. Osa, *Bull. Chem. Soc. Jpn.*, **50**, 696 (1977).
10) Y. Ohkatsu, O. Sekiguchi, and T. Osa, *Bull. Chem. Soc. Jpn.*, **50**, 701 (1977).
11) J. E. Falk, "Porphyrins and Metalloporphyrins," Elsevier, Amsterdam (1964).
12) P. Rothemund and A. R. Menotti, *J. Am. Chem. Soc.*, **70**, 1808 (1948).
13) K. Tamamoto and T. Kwan, *J. Catal.*, **18**, 354 (1970).
14) B. B. Wayland, J. V. Minkiewcz, and M. E. Abd-Elmageed, *J. Am. Chem. Soc.*, **96**, 2795 (1974).
15) M. Tezuka, Y. Ohkatsu, and T. Osa, *Bull. Chem. Soc. Jpn.*, **49**, 2765 (1976).
16) M. Tezuka, Y. Ohkatsu, and T. Osa, *Chem. Lett.*, **1973**, 99.
17) M. Tezuka, Y. Ohkatsu, and T. Osa, *Bull. Chem. Soc. Jpn.*, **48**, 1471 (1975).
18) J. Manassen, *J. Catal. Rev.*, **1974**, 223.
19) D. Bahar, G. Czapski, L. M. Dorfman, J. Rabani, and H. A. Schwarz, *J. Phys. Chem.*, **74**, 3209 (1970).
20) J. M. McCord and I. Fridovich, *J. Biol. Chem.*, **244**, 6049 (1969).
21) F. A. Walkner, *J. Am. Chem. Soc.*, **95**, 1154 (1973).
22) L. Pauling, *Nature (London)*, **203**, 182 (1964).
23) C. L. Nobbs, H. C. Watson, and J. C. Kendrew, *Nature (London)*, **209**, 339 (1966).
24) H. C. Watson, *Prog. Stereochem.*, **1968**, 4.
25) H. C. Stynes and J. A. Ibers, *J. Am. Chem. Soc.*, **94**, 1559 (1972).

The Kinetics and Mechanism of the Radical Addition of Hydrogensulfite Ions to 1-Dodecene in a Micellar Solution of Sodium 1-Dodecanesulfonate

Teijiro MIYATA, Akihisa SAKUMOTO, and Masamitsu WASHINO

Japan Atomic Energy Research Institute, Takasaki, Gunma 370-12

(Received September 16, 1976)

The addition reaction induced by Co-60 gamma-rays proceeded without any detectable induction period under homogeneous conditions in the presence of sodium 1-dodecanesulfonate. The consumption rate of 1-dodecene was equal to that of sodium hydrogensulfite and proportional to the square roots of the hydrogensulfite-ion and 1-dodecene concentrations. The *g*-value of 1-dodecene consumption was 860 at the concentrations of 0.260 mol/l of sodium hydrogensulfite, 0.0966 mol/l of 1-dodecene, and 0.11 mol/l of sodium 1-dodecanesulfonate at the dose rate of 2.70×10^{15} eV/g·s and the dose of 1.62×10^{18} eV/g. The apparent rate constant was 2.6×10^{-4} s^{-1} under these reaction conditions. The reaction of $CH_3(CH_2)_9\dot{C}HCH_2SO_3^-$ with the sulfite radical ion was proposed as the termination step of the reaction.

It is well known that the addition of hydrogensulfite ions to olefins initiated by oxidizing agents,[1-4] by ultraviolet light[5] or gamma irradiation[6] proceeds by a radical process, but the reaction is still not sufficiently understood. Investigations in this area have recently been stimulated by the interest in converting 1-alkenes with 8 to 18 carbon atoms into 1-alkanesulfonates, but to date no kinetic study has been made, probably because of the low solubilities of these olefins in water.

1-Alkanesulfonates with 8 to 18 carbon atoms have good surfactant properties.[7] Surfactants have been utilized extensively for the enhancement and the inhibition of industrially and biologically important radical processes.[8] Emulsion polymerization[9] is perhaps the prime example of this application of surfactants. Similarly, micellar amphiphiles affect the rate of the oxidation of dispersed or emulsified hydrocarbons,[10] aldehydes,[11] and unsaturated esters.[12] In the present study, some preliminary experiments showed that the addition reaction started at a significant rate and without any detectable induction period in the presence of sodium 1-dodecanesulfonate, though hardly no reaction occurred in its absence.

The present study was undertaken in order to throw some light on the kinetics and mechanism of the radiation-induced addition of hydrogensulfite ions to 1-dodecene in micellar solutions of sodium 1-dodecanesulfonate. In this study an aqueous *t*-butyl alcohol solution, which has been reported to be the most appropriate solvent for the similar photo-reaction,[5] was used as the solvent, and the reaction was carried out under homogeneous conditions.

Experimental

Materials. The sodium hydrogensulfite was of a guaranteed grade and was used without further purification. The 1-dodecene (97.8%) was distilled under a reduced pressure of nitrogen. The water and *t*-butyl alcohol were distilled. The sodium 1-dodecanesulfonate was prepared from sodium hydrogensulfite and 1-dodecene as follows. Sodium hydrogensulfite (0.25 mol/l), 1-dodecene (0.25 mol/l), water (200 ml), and *t*-butyl alcohol (200 ml) were added to a flask (1000 ml) fitted with a stirrer. The rapidly stirred mixture was irradiated with Co-60 gamma-rays (3.47×10^{15} eV/g·s) for about 2 h at room temperature and then neutralized with dilute hydrochloric acid. After the neutralization, the mixture was irradiated again for 1 h to complete the reaction. The irradiated mixture was then dried under reduced pressure overnight to give a white powder as the product. Neither sodium hydrogensulfite nor 1-dodecene was observed in the product.

Procedure and Irradiation. A reaction mixture was prepared by dissolving sodium hydrogensulfite, 1-dodecene, and sodium 1-dodecanesulfonate (0.11 mol/l) in a *t*-butyl alcohol–water (50 vol%) mixture. In order to keep the starting reaction mixture a single liquid phase, it is necessary that the initial concentrations of sodium hydrogensulfite and 1-dodecene be in the ranges of 0.04—0.30 mol/l and 0.03—0.20 mol/l respectively. The reaction mixture was placed in a glass tube (50 ml) and irradiated with Co-60 gamma-rays at room temperature after the tube had been deaerated under reduced pressure. The dose rate was determined by means of a Fricke dosimeter, taking $G(Fe^{3+})=15.6$. No correction was introduced (<1%) for the electronic density difference between the dosimetric solutions and those studied. The pH of the reaction mixture was measured before and after irradiation using a Tōa Denpa HM-5A pH meter; no significant differences in the pH values (about 4.1) were found.

Analytical Procedure. The determination of unreacted 1-dodecene was made on a gas chromatograph (Yanagimoto model G-80) equipped with a flame-ionization detector and a 1.5 m stainless steel column packed with 60—80 mesh Celite 545 and coated with 30% Silicone DC 550, where aqueous samples were directly injected into the gas chromatograph without pretreatment.

Unreacted sodium hydrogensulfite was determined by titration: after the oxidations of sulfite and hydrogensulfite ions into the sulfate ion with hydrogen peroxide, the sulfate ion was titrated with barium perchlorate using 4,5-dihydroxy-3,6-[(2-sulfo-4-methylphenyl)azo]-2,7-naphthalenedisulfonic acid, Na_2 salt (*m,m'*-dimethyl sulfonazo III[13]) as the indicator.

The product was identified as sodium 1-dodecanesulfonate by a comparison of its infrared spectrum [721, 798 (νC–S), 1063 (νS–O), 1175, 2855, 2924 cm^{-1} (νC–H)] with the spectra of the alkanesulfonates in the literature.[14] The spectrum was obtained by the use of an infrared spectrophotometer, Hitachi EPI-S_2, using a potassium bromide disk method.

Results and Discussion

Hydrogensulfite-ion Concentration. The hydrogensulfite-ion concentration in an aqueous solution is given by[15]

$$[HSO_3^-] = \left\{1+\left(\frac{[a_{H^+}]}{K_1}\right)\left(\frac{f_{HSO_3^-}}{f_{H_2SO_3}}\right)+\left(\frac{K_2}{[a_{H^+}]}\right)\left(\frac{f_{HSO_3^-}}{f_{SO_3^{2-}}}\right)\right\}^{-1}\cdot[NaHSO_3], \quad (1)$$

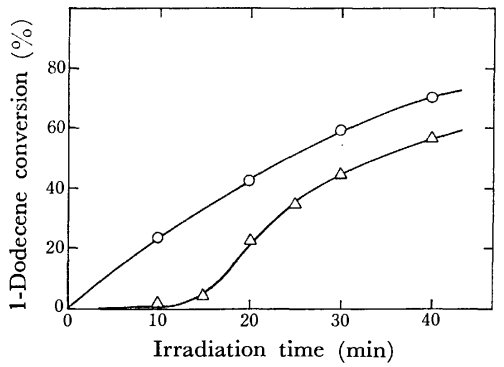

Fig. 1. The conversion of 1-dodecene as a function of irradiation time.
○—$NaHSO_3$: 0.260 mol/l, 1-dodecene: 0.0966 mol/l, $1\text{-}C_{12}H_{25}SO_3Na$: 0.11 mol/l, dose rate: 2.70×10^{15} eV/g·s. △—$NaHSO_3$: 0.46 mol/l, 1-dodecene: 0.47 mol/l, dose rate: 1.11×10^{16} eV/g·s.

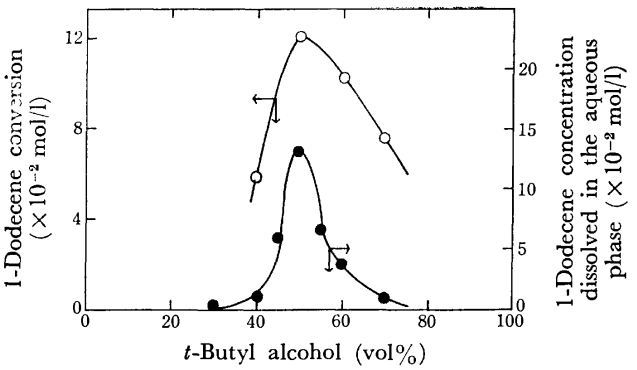

Fig. 2. The conversion of 1-dodecene and the concentration of 1-dodecene dissolved in the aqueous phase as a function of the content of *t*-butyl alcohol.
○—$NaHSO_3$: 0.458 mol/l, 1-dodecene: 0.214 mol/l, dose: 1.42×10^{17} eV/g at the dose rate of 2.37×10^{15} eV/g·s. ●—$NaHSO_3$: 0.229 mol/l, 1-dodecene: 0.225 mol/l, $1\text{-}C_{12}H_{25}SO_3Na$: 0.055 mol/l.

where K_1 and K_2 are the dissociation constants of H_2SO_3 and HSO_3^- respectively; $f_{H_2SO_3}$, $f_{HSO_3^-}$, and $f_{SO_3^{2-}}$, the activity coefficients of H_2SO_3, HSO_3^-, and SO_3^{2-} respectively; $[a_{H^+}]$, the activity of the hydrogen ion, and $[NaHSO_3]$, the concentration of the sodium hydrogensulfite initially dissolved in the solution.

The pH values of sodium hydrogensulfite solutions in water and in a *t*-butyl alcohol–water (50 vol%) mixture were roughly independent of the sodium hydrogensulfite concentration. The pH value observed in the *t*-butyl alcohol–water mixture was only about 0.2 pH-units higher[16] than that (about 3.9) in water. Therefore, the pa_{H^+}, $-\log[a_{H^+}]$, value in the mixture was roughly estimated to be equal to the pH value in water, by analogy with the pa_{H^+}-determination of succinate buffer solutions in alcohol–water mixtures.[17] Accordingly, $[a_{H^+}]$ in Eq. 1 is 1.3×10^{-4} mol/l. Since K_1 and K_2 are 1.54×10^{-2} and 1.02×10^{-7} [18] respectively at 18 °C, and since the activity coefficient ratios of $f_{HSO_3^-}/f_{H_2SO_3}$ and $f_{HSO_3^-}/f_{SO_3^{2-}}$ do not differ greatly from unity,[15,19] the substitution of these values into Eq. 1 gives,

$$[HSO_3^-] \approx [NaHSO_3].$$

Reaction in Micellar Solution. Alkanesulfonates with a straight-chain alkyl group of from 8 to 18 carbon atoms are usually capable of forming micelles and solubilizing olefins in aqueous solutions above their critical micelle concentrations.[20] The critical micelle concentration of sodium 1-dodecanesulfonate in an aqueous solution is 9.8×10^{-3} mol/l at 31 °C[21], and the addition of alcohols except methyl alcohol to the solution causes a decrease in the critical micelle concentration.[22–25] In the present work, 0.11 mol/l of sodium 1-dodecanesulfonate was added to the reaction solution so that the reaction might be carried out under homogeneous conditions. It follows, then, that the micelles must be formed in this solution. Accordingly, it may be noted that the solution, though it is seemingly a single liquid phase under the homogeneous conditions, comprises both a micellar phase and a bulk phase in the presence of the surfactant. In such a solution, it is necessary to consider that the rate of the addition reaction is subject to the influence of the solubilization of 1-dodecene by the micelles, since this olefin is hardly soluble in water.

Figure 1 shows two typical plots of the 1-dodecene conversion against the absorbed dose. The reaction began without any detectable induction period in the presence of the surfactant, while hardly no reaction occurred for up to 10 min in its absence. In this case, at the beginning of the reaction, the reaction solution was apparently homogeneous in the former case, while it comprised both an organic (olefin) phase and an aqueous (hydrogensulfite ion) phase in the latter case. The 1-dodecene concentration in the aqueous phase was only 0.014 mol/l, less than that in the former solution by a factor of about 10. Figure 2 shows the plots of the 1-dodecene conversion and of the 1-dodecene concentration in the aqueous phase as functions of the vol% of *t*-butyl alcohol under such heterogeneous conditions that this solution comprises both the organic and aqueous phases in the presence of 0.055 mol/l of sodium 1-dodecanesulfonate. The 1-dodecene concentration in the aqueous phase decreased with the decrease in the *t*-butyl alcohol content below 50 vol% of *t*-butyl alcohol. It follows, then, that the 1-dodecene concentration in the organic phase must increase with the decrease in the *t*-butyl alcohol content below 50 vol% of *t*-butyl alcohol. In addition, the organic-phase portion of the solution increased with the decrease in the *t*-butyl alcohol content. If the reaction takes place predominantly in the organic phase, the 1-dodecene conversion will increase with the decrease in the *t*-butyl alcohol content below 50 vol% of *t*-butyl alcohol. On the contrary, if the reaction takes place predominantly in the aqueous phase, the rate of 1-dodecene consumption will depend on the 1-dodecene concentration in the aqueous phase. As is evident from Fig. 2, the 1-dodecene conversion did not increase with the decrease in the *t*-butyl alcohol content below 50 vol% of *t*-butyl alcohol; rather a nearly close correlation was found between the 1-dodecene conversion and the 1-dodecene concentration in the aqueous phase. From the facts described above, it appears more likely that

TABLE 1. CONVERSIONS OF 1-DODECENE UNDER VARIOUS REACTION CONDITIONS

$[NaHSO_3]$ ($\times 10^{-2}$ mol/l)	[1-Dedecene] ($\times 10^{-2}$ mol/l)	$[1\text{-}C_{12}H_{25}SO_3Na]$ ($\times 10^{-2}$ mol/l)	1-Dodecene conv. ($\times 10^{-2}$ mol/l)
9.61	6.75	1.8	2.01
9.61	6.75	3.7	2.03
9.61	6.75	7.3	2.08
9.61	6.75	11.0	1.97
14.4	6.75	1.8	2.46
14.4	6.75	3.7	2.59
14.4	6.75	7.3	2.54
14.4	4.50	11.0	1.86
26.0	9.66	11.0	4.10

Dose: 3.24×10^{18} eV/g at the dose rate of 2.70×10^{15} eV/g·s.

the reaction takes place predominantly in the aqueous phase in the presence of the surfactant.

1-Dodecene was hardly soluble in the aqueous phase in the absence of the surfactant. As can be seen in Fig. 2, however, the 1-dodecene concentration in the aqueous phase was 0.255 mol/l at 50 vol% of *t*-butyl alcohol in the presence of 0.055 mol/l of sodium 1-dodecanesulfonate. Since this surfactant can solubilize 1-dodecene in aqueous solutions above its critical micelle concentration, most of this olefin dissolved in the aqueous phase can be considered to be solubilized by the surfactant. Table 1 shows the 1-dodecene conversion at various surfactant concentrations under the homogeneous conditions. This conversion was independent of the surfactant concentration in the range studied. It can, therefore, be considered that most of the olefin is solubilized by the surfactant under the homogeneous conditions, because the distribution of the olefin between the micellar and the bulk phases, which is responsible for the alteration of the reaction rate, will vary with the surfactant concentration if the olefin is present in these two phases. From this result and from the experimental findings described above, it can be concluded that solubilized 1-dodecene predominantly takes part in the addition reaction in the presence of the surfactant.

Reaction Mechanism. The addition of the hydrogensulfite ion to 1-dodecene is known to proceed by a radical chain process involving the chain-carrying steps given by[1]

$$\dot{S}O_3^- + CH_3(CH_2)_9CH{=}CH_2 \rightarrow CH_3(CH_2)_9\dot{C}HCH_2SO_3^-, \quad (2)$$

$$CH_3(CH_2)_9\dot{C}HCH_2SO_3^- + HSO_3^- \rightarrow CH_3(CH_2)_9CH_2CH_2SO_3^- + \dot{S}O_3^-. \quad (3)$$

In general, the action of ionization radiation upon dilute solutions results in the degradation of the solvent.[26]

The degradation of water by radiation is expressed as[27]

$$H_2O \rightsquigarrow \cdot OH, \cdot H, e_{aq}^-, H_2, H_2O_2$$

and the radiolysis of *t*-butyl alcohol gives such species as $\cdot H$, $\dot{C}H_2(CH_3)_2COH$, and $e_{sol.}^-$.[28] Of these species, $\cdot H$, $\cdot OH$, and e_{aq}^- or e_{sol}^- react with the hydrogensulfite ion to give the sulfite radical ion.[29,30]

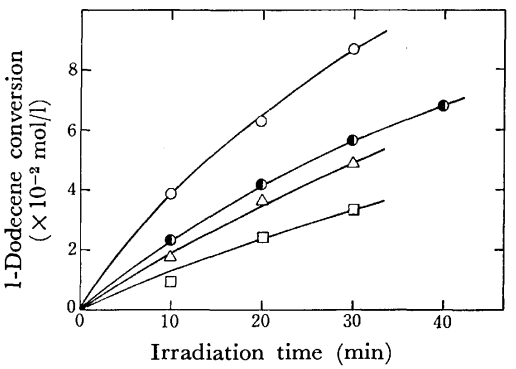

Fig. 3. The conversion of 1-dodecene as a function of irradiation time with various dose rates and concentrations.
○, △, □—$NaSHO_3$: 0.252 mol/l, 1-dodecene: 0.144 mol/l, $1\text{-}C_{12}H_{25}SO_3Na$: 0.11 mol/l, dose rate (eV/g·s): 4.75×10^{15} for ○, 1.68×10^{15} for △, 8.19×10^{14} for □.
◐—$NaSHO_3$: 0.260 mol/l, 1-dodecene: 0.0966 mol/l, $1\text{-}C_{12}H_{25}SO_3Na$: 0.11 mol/l, dose rate: 2.70×10^{15} eV/g·s.

TABLE 2. THE CONVERSION RATIO OF 1-DODECENE TO $NaHSO_3$ IN THE ADDITION OF HSO_3^- TO 1-DODECENE

Dose rate $\times 10^{-15}$ (eV/g·s)	Dose $\times 10^{-18}$ (eV/g)	Conversion(mol/l) 1-Dodecene	Conversion(mol/l) $NaHSO_3$	Conv. ratio $\left(\frac{\text{1-Dodecene}}{NaHSO_3}\right)$
0.81	2.43	0.048	0.044	1.09
1.68	2.02	0.040	0.043	0.93
1.68	2.43	0.035	0.032	1.09
2.70	3.24	0.053	0.053	1.00
2.70	3.53	0.058	0.057	1.02
2.70	4.86	0.069	0.070	0.99
4.57	5.48	0.061	0.063	0.97

Figure 3 shows the plots of the 1-dodecene conversion as a function of the irradiation time at various dose rates and at various concentrations of the hydrogensulfite ion and of 1-dodecene. The reaction began without any detectable induction period under these reaction conditions. Table 2 shows that a 1 : 1 product is formed independently of the dose and the dose rate. Most of the product obtained was identified as sodium 1-dodecansulfonate.

The termination of the addition reaction may result mostly from processes such as the dimerization of the chain-carrying radicals given in Eqs. 2 and 3 or a coupling reaction of these radicals. If the dimerization of the sulfite radical ion takes place as the termination, the rate of 1-dodecene disappearance should be proportional to the 1-dodecene concentration, by analogy with kinetic analysis in general.[31] Similarly, if the dimerization of the alkanesulfonate radical takes place, the rate should be proportional to the hydrogensulfite ion concentration. On the other hand, if the alkanesulfonate radical couples with the sulfite radical ion to terminate the addition reaction, the rate should be proportional to the square roots of both the 1-dodecene

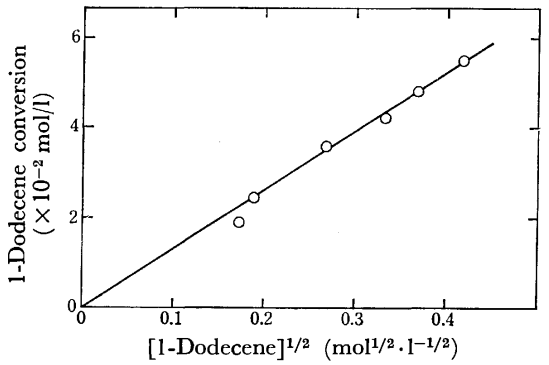

Fig. 4. The conversion of 1-dodecene as a function of the square root of the initial concentration of 1-dodecene.
$NaHSO_3$: 0.260 mol/l, 1-$C_{12}H_{25}SO_3Na$: 0.11 mol/l, dose: 2.43×10^{18} eV/g at the dose rate of 2.70×10^{15} eV/g·s.

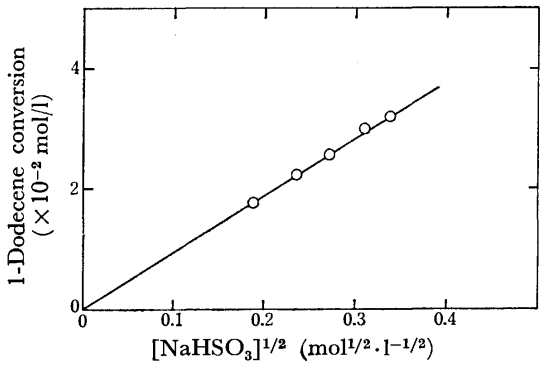

Fig. 5. The conversion of 1-dodecene as a function of the square root of the initial concentration of sodium hydrogensulfite.
1-Dodecene: 0.0902 mol/l, 1-$C_{12}H_{25}SO_3Na$: 0.11 mol/l, dose: 4.05×10^{18} eV/g at the dose rate of 2.70×10^{15} eV/g·s.

and hydrogensulfite ion concentrations. The conversion was independent of the surfactant concentration in the range studied, as can be seen in Table 1. Figures 4 and 5 show the plot of the 1-dodecene conversion against the square root of the initial 1-dodecene concentration, and that against the square root of the initial hydrogensulfite ion concentration, respectively. These results indicate that the rate of 1-dodecene disappearance is proportional to the square roots of both the 1-dodecene and hydrogensulfite ion concentrations. Consequently, the termination can be deduced to be the coupling reaction of the alkanesulfonate radical with the sulfite radical ion to give dodecanedisulfonate. In fact, substantial amounts of dodecanedisulfonate were identified in a similar radical-addition initiated by nitrate salts.[1)]

On the basis of the above experimental findings and the chain-carrying steps cited above, the basic reaction mechanism of the addition reaction may be deduced to be as follows:

$$\text{Solvent} \sim\!\!\sim\!\!\sim\!\!\rightarrow \text{A}, \tag{4}$$

$$\text{A} + HSO_3^- \longrightarrow \text{AH} + \dot{S}O_3^-, \tag{5}$$

$$\dot{S}O_3^- + CH_3(CH_2)_9CH{=}CH_2 \longrightarrow CH_3(CH_2)_9\dot{C}HCH_2SO_3^-, \tag{6}$$

$$CH_3(CH_2)_9\dot{C}HCH_2SO_3^- + HSO_3^- \longrightarrow CH_3(CH_2)_9CH_2CH_2SO_3^- + \dot{S}O_3^-, \tag{7}$$

$$CH_3(CH_2)_9\dot{C}HCH_2SO_3^- + \dot{S}O_3^- \longrightarrow CH_3(CH_2)_9CH(SO_3^-)CH_2SO_3^-, \tag{8}$$

where A represents the above-mentioned radiolytic species which participate in the initiation of the addition reaction.

Rate Equation. According to Eqs. 4 to 8, and assuming the usual steady-state approximation for each radical we obtain the over-all rate equation of the 1-dodecene consumption in the micellar solution as follows:

$$-\frac{d[RCH{=}CH_2]}{dt} = \frac{g_oI_o}{4}\left\{1+\left(1+\frac{8k_6k_7}{g_oI_ok_8}[RCH{=}CH_2][HSO_3^-]\right)^{1/2}\right\}, \tag{9}$$

where g_o is the number of A per absorbed dose of one eV; I_o, the dose rate (eV/g·s); k_6, k_7, and k_8, the rate constants of Eqs. 6, 7, and 8 in the micellar solution respectively, and $[RCH{=}CH_2]$, the 1-dodecene concentration.

From Fig. 1, the g-value (the number of molecules reacted per 100 eV of radiation energy absorbed) of 1-dodecene consumption was calculated to be 860 at the absorbed dose of 1.62×10^{18} eV/g (in irradiation time of 10 min) and at the concentrations of 0.0966 mol/l of 1-dodecene, 0.260 mol/l of sodium hydrogensulfite, and 0.11 mol/l of sodium 1-dodecanesulfonate. This g-value is very large compared to the primary yields of the active species produced from the radiolysis of water and organic compounds,[32,33)] so it may be assumed that, in Eq. 9, $8k_6k_7[RCH{=}CH_2][HSO_3^-]/g_oI_ok_8 \gg 1$. Consequently, Eq. 9 can be simplified to

$$-\frac{d[RCH{=}CH_2]}{dt} = k[RCH{=}CH_2]^{1/2}[HSO_3^-]^{1/2}, \tag{10}$$

where,

$$k = \left(\frac{g_oI_ok_6k_7}{2k_8}\right)^{1/2}. \tag{11}$$

The expression of Eq. 10 agrees well with the experimental findings shown in Figs. 4 and 5.

Since the conversion of 1-dodecene was equal to that of sodium hydrogensulfite, Eq. 10 becomes

$$\frac{dx}{dt} = k(a-x)^{1/2}(b-x)^{1/2}, \tag{12}$$

where x is a variable representing the decrease in the concentrations of the reactants in the given time and where a and b are the initial concentrations of 1-dodecene and the hydrogensulfite ion respectively. On integrating Eq. 12 with the boundary condition, $x=0$ at $t=0$, the apparent rate constant of the 1-dodecene consumption can be derived as

$$k = \frac{2}{t}\ln\left\{\frac{(a-x)^{1/2}-(b-x)^{1/2}}{a^{1/2}-b^{1/2}}\right\}. \tag{13}$$

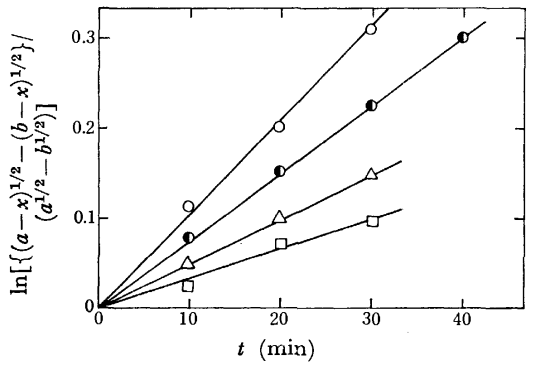

Fig. 6. Plots of $\ln[\{(a-x)^{1/2}-(b-x)^{1/2}\}/(a^{1/2}-b^{1/2})]$ against t.
○, ◐, △, □: See Fig. 4.

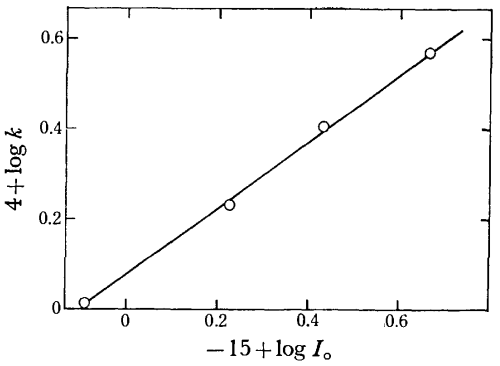

Fig. 7. Plot of log k against log I_0.

TABLE 3. THE APPARENT RATE CONSTANTS FOR THE ADDITION OF HSO_3^- TO 1-DODECENE UNDER VARIOUS REACTION CONDITIONS IN MICELLAR SOLUTIONS AT ROOM TEMPERATURE

$[NaHSO_3]$ $\times 10^2$ (mol/l)	[1-Dodecene] $\times 10^2$ (mol/l)	$[1\text{-}C_{12}H_{25}SO_3Na]$ $\times 10^2$ (mol/l)	Dose rate $\times 10^{-15}$ (eV/g·s)	k $\times 10^4$ (s^{-1})
9.61	6.75	1.8	2.70	2.4
9.61	6.75	3.7	2.70	2.4
9.61	6.75	7.3	2.70	2.5
9.61	6.75	11.0	2.70	2.4
14.4 Table 1	6.75	1.8	2.70	2.4
14.4	6.75	3.7	2.70	2.6
14.4	6.75	7.3	2.70	2.5
14.4	4.50	11.0	2.70	2.3
26.0	9.66	11.0	2.70	2.6
25.2	14.4	11.0	4.57	3.6
25.2 Fig. 6	14.4	11.0	1.68	1.7
25.2	14.4	11.0	0.819	1.0

Apparent Rate Constant. According to Eq. 13, a plot of $\ln[\{(a-x)^{1/2}-(b-x)^{1/2}\}/(a^{1/2}-b^{1/2})]$ against the time, t, should be a straight line, passing through the point of origin, with a slope equal to $k/2$. As is shown in Fig. 6, a good straight line was obtained for each dose rate by using the same data as those given in Fig. 3. The apparent rate constants can be calculated from the slopes of these straight lines; they are summarized in Table 3, together with those calculated from the values given in Table 1.

Dose-rate Dependence of the Apparent Rate Constant. According to Eq. 11, a plot of the logarithm of k against the logarithm of I_0 should be a straight line with a slope of 0.5. The plot of the experimental data gave a straight line with a slope of 0.73, as is shown in Fig. 7. This value is somewhat different from 0.5. This difference may be attributable to the termination steps other than Eq. 8, a part of which is presumably the reactions of the alkanesulfonate radical with radicals from the irradiated solvent.

Surfactant Effects. Although the coupling reaction of the alkanesulfonate radical with the sulfite radical ion was proposed as the termination of the addition reaction, it is possible to postulate another coupling reaction, the dimerization of the alkanesulfonate radical, by analogy with radical reactions in general. According to the accepted model[34] for ionic micelles, the hydrophobic part of the aggregated surfactants forms the core of the micelles, which is liquid-paraffin-like in character, while the polar-head groups are located at the micelle-water interface in contact with, and hydrated by, a number of water molecules. The unpaired electron of the alkanesulfonate radical is assumed, on this basis, to be located at the micelle-water interface. On the contrary, the charged species, such as the sulfite, hydrogensulfite or sulfite radical ions, are generally in the bulk phase.[20] However, water molecules very probably penetrate beyond the polar-head groups at the micellar exterior.[35] Accordingly, it is assumed that solutes in the bulk phase may interact with the alkanesulfonate radical solubilized in the micelle, without penetrating into the nonpolar micellar core. Since there are a great number of micelles in the reaction solution, two or more alkanesulfonate radicals are scarcely ever produced in the micelle at the same time. Therefore, the rate of the dimerization of this radical may be very slow because there is electrostatic repulsion between the micelles. Consequently, the coupling reaction of the alkanesulfonate radical with the sulfite radical ion may be more predominant than the dimerization of the alkanesulfonate radical as the termination of the addition reaction.

The authors wish to thank Dr. Akira Mitsui for his valuable discussions.

References

1) C. J. Norton, N. F. Seppi, and M. J. Reuter, *J. Org. Chem.*, **33**, 4158 (1968).
2) C. J. Norton and D. E. Drayer, *Hydrocarbon Process.*, **49**, 140 (1970).
3) D. E. Drayer and C. J. Norton, *Hydrocarbon Process.*, **49**, 163 (1970).
4) E. Clippinger, *Ind. Eng. Chem. Prod. Res. Dev.*, **3**, 3 (1964).
5) C. L. Furrow and C. E. Stoops, *Ind. Eng. Chem. Prod. Res. Dev.*, **7**, 26 (1968).
6) E. L. Stogryn and P. A. Argabright, *Ger.*, 1090198 (1960).
7) J. Rubinfeld and H. D. Cross, *Soap. Chem. Res.*, **43**, 41 (1967).
8) P. H. Elworthy, A. T. Florence, and C. B. Macfarlance, "Solubilization by Surface Active Agents and Its Applications

in Chemistry and Biological Science," Chapman and Hall, London (1968).
9) F. A. Bovey, I. M. Kolthoff, A. I. Medalia, and E. J. Meehan, "Emulsion Polymerization," Interscience, New York (1966).
10) G. P. Armstrong, R. H. Hall, and D. C. Quin, *J. Chem. Soc.*, **1950**, 666.
11) J. Swarbrick and J. E. Carless, *J. Pharm. Pharmacol.*, **16**, 670 (1964).
12) J. E. Carless and J. R. Nixon, *J. Pharm. Pharmacol.*, **12**, 348 (1960).
13) B. Budesinsky, D. Vrazalova, and Bezdekova, *Acta Chim. Acad. Sci. Hung.*, **52**, 37 (1967).
14) K. Fujimori, *Bull. Chem. Soc. Jpn.*, **32**, 850 (1959).
15) T. Miyata, A. Sakumoto, M. Washino, and T. Abe, *Nippon Kagaku Kaishi*, **1976**, 15.
16) No correction was made of the pH values, which were determined by the use of a pH meter calibrated with aqueous standard buffer solutions.
17) W. J. Gelsema, C. L. De Ligny, A. G. Remijinse, and H. A. Blijleven, *Recl. Trav. Chim., Pays-Bas*, **85**, 647 (1966).
18) Landolt-Börnstein, "Zahlenwerte und Funktionen," Springer (1960), IIB., 7 teil, p. 842.
19) J. Kielland, *J. Am. Chem. Soc.*, **59**, 1675 (1937).
20) E. H. Cordes and R. B. Dunlap, *Acc. Chem. Res.*, **2**, 329 (1969).
21) H. V. Tartar and K. A. Wright, *J. Am. Chem. Soc.*, **61**, 539 (1939).
22) S. H. Herzfeld, M. L. Corrin, and W. D. Harkins, *J. Phys. Colloid Chem.*, **54**, 271 (1950).
23) K. Shimada, *J. Phys. Chem.*, **58**, 1136 (1936).
24) A. W. Raison and D. N. Eggenbergen, *J. Am. Chem. Soc.*, **70**, 983 (1948).
25) B. D. Flockhart, *J. Colloid Sci.*, **12**, 557 (1957).
26) M Anbar, "Fundamental Processes in Radiation Chemistry," ed by P. Ausloos, Interscience, New York (1968), p. 677.
27) A. O. Allen, *Radiat. Res., Suppl.*, **4**, 54 (1964).
28) D. Verdin, *Int. J. Rad. Phys. Chem.*, **2**, 201 (1970).
29) T. E. Eriksen, *J. Chem. Soc., Faraday Trans. 1*, **70**, 208 (1974).
30) E. Hayon, A. Treinin, and J. Wilf, *J. Am. Chem. Soc.*, **94**, 47 (1972).
31) K. J. Laider, "Chemical Kinetics," McGraw Hill, New York (1950), p. 233.
32) B. H. J. Bielsky and A. O. Allen, *Int. J. Rad. Phys. Chem.*, **1**, 153 (1969).
33) A. J. Swallow, "Radiation Chemistry of Organic Compounds," Int. Series of Monographs on Radiation Effects in Materials, Vol. 2, Pergamon Press (1960).
34) E. J. Fendler and J. H. Fendler, *Adv. Phys. Org. Chem.*, **8**, 271 (1970).
35) N. Muller, "Reaction Kinetics in Micelles," ed by E. H. Cordes, Plenum Press, New York (1973), p. 1.

The Synthesis of α-Aminonitriles Starting from the Corresponding Amino Acids. I. Use of *o*-Nitrophenylsulfenyl as an N-Protecting Group[1)]

Katsuhiro KAWASHIRO, Hideyuki YOSHIDA, and Shiro MORIMOTO

Department of Chemical Engineering, Faculty of Engineering, Tokushima University, Minamijosanjima, Tokushima 770

(Received October 25, 1976)

N-*o*-Nitrophenylsulfenylamino acid amides of glycine, alanine (DL and L), leucine (DL and L), methionine (DL), phenylalanine (DL and L), and proline (L) were dehydrated in $POCl_3$–pyridine. The N-protected α-aminonitriles obtained were treated with anhydrous HCl affording the corresponding α-aminonitrile hydrochlorides. The optical purity of the L-α-aminonitriles was well retained.

α-Aminonitriles can be synthesized by reactions of ammonium cyanide with carbonyl compounds, which is known as Zelinsky-Stadnikoff synthesis[2)] and which always yields racemic products. It may be more convenient to prepare α-aminonitriles from the corresponding amino acids on a laboratory scale. The purpose of this study is to obtain some racemic and enantiomerically pure α-aminonitriles from the corresponding amino acids, and also to establish a procedure applicable to the enantiomeric analysis of α-aminonitriles.

Several investigators[3–7)] have reported the preparation of N-protected α-aminonitriles by dehydrating the corresponding amino acid amides. They employed benzyloxycarbonyl, phthaloyl, or acetyl as an N-protecting group. These N-protecting groups have not been removed. Recently, Ojima *et al.*[8)] have reported the asymmetric synthesis of some α-aminonitriles *via* cyanosilylation of the Schiff bases.

Alanyl-α-aminopropiononitriles have been obtained as hydrochlorides by the dehydration of the corresponding *N*-*o*-nitrophenylsulfenyl(NPS)-dipeptide amides, followed by treatment with anhydrous HCl.[9)] The present paper is concerned with the preparation of α-aminonitriles, which includes the dehydration of NPS-amino acid amides and the subsequent removal of the N-protecting groups.

As model compounds, NPS derivatives[10)] of α-aminonitriles (aminoacetonitrile and DL-α-aminoglutaronitrile) were prepared. Their NPS groups were easily removed by treatment with anhydrous HCl, and ion-exchange chromatography of each α-aminonitrile obtained gave a single peak. On the basis of this work, the nine α-aminonitrile hydrochlorides were synthesized as shown in Scheme 1.

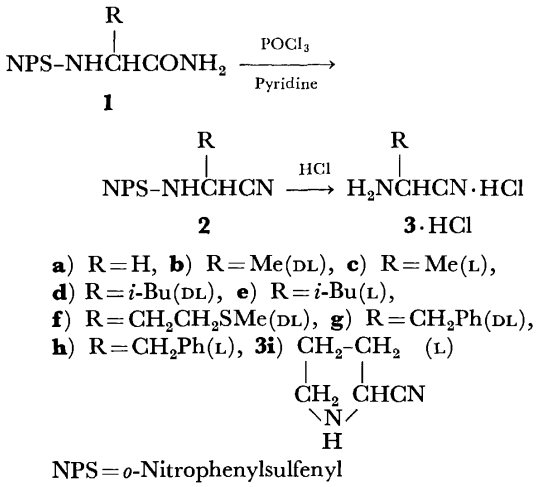

Scheme 1.

The methyl esters of NPS-glycine and alanine (DL and L) were easily converted into the corresponding amides (**1a—c**) by ammonolysis at room temperature for several days in methanol saturated with NH_3. The other NPS-amino acid amides (**1d—i**) were not obtained by ammonolysis of the corresponding NPS-amino acid methyl esters but were prepared by the reaction of the amino acid amides with *o*-nitrobenzensulfenyl chloride. The NPS-amino acid amides (**1a—i**) were dehydrated in cold $POCl_3$–pyridine according to the method of Liberek *et al.*[4)] to afford the corresponding nitriles (**2a—i**), among which the N-protected nitrile derivatives of glycine, alanine (DL and L), and DL-leucine (**2a—d**) were obtained as crystalline products and those of the other amino acids (**2e—i**) as oily products. When the NPS-α-aminonitriles (**2a—i**) dissolved in ethyl acetate or diethyl ether were treated with anhydrous HCl, the α-aminonitrile hydrochlorides (**3a—i**·HCl) shown in Table 1, were obtained. The yields of the products based on the corresponding NPS-amino acid amides (**1a—i**) were poor (10—40%). The IR spectra of the products had absorption bands at 2250—2260 cm^{-1} corresponding to the C≡N stretching vibration.

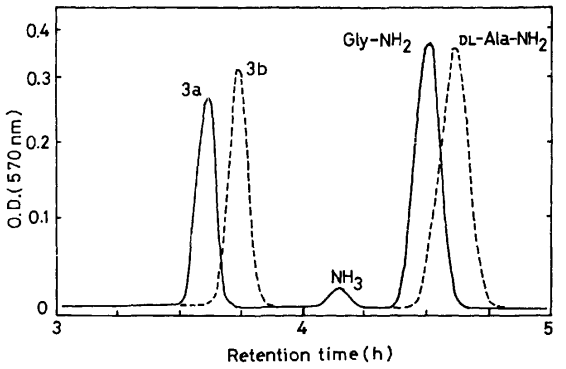

Fig. 1. Ion-exchange chromatograms of α-aminonitriles.
——: **3a**(0.305 μmol)+Gly-NH_2(0.229 μmol).
----: **3b**(0.118 μmol)+DL-Ala-NH_2(0.204 μmol).
Column: 0.25ϕ×50 cm. Thirty min after the elution began, the eluent was changed from a pH 3.25 buffer to a pH 5.28 buffer.

Table 1. α-Aminonitrile hydrochlorides

α-Amino-nitrile·HCl	Molecular formura	Mp (°C) (dec)	Yield (%)[a]	$\nu_{C\equiv N}$[b] (cm^{-1})	$[\alpha]_D^{22}$ (deg)	Found (Calcd) (%) C	H	N
3a	$C_2H_4N_2$·HCl	164—166[c]	9	2260		26.30 (25.96)	5.47 5.45	30.21 30.28)
3b	$C_3H_6N_2$·HCl	135—137[d]	17	2260		34.16 (33.82)	6.62 6.62	26.28 26.29)
3c	$C_3H_6N_2$·HCl	156—158	13	2260	−15.3 (*c* 0.708, H_2O)	33.77 (33.82	6.69 6.62	26.37 26.29)
3d	$C_6H_{12}N_2$·HCl	203—208[e]	9	2260		48.33 (48.49	8.66 8.82	18.60 18.85)
3e	$C_6H_{12}N_2$·HCl	173—176	13	2260	+16.8 (*c* 0.80, H_2O)	48.28 (48.49	8.86 8.82	18.90 18.85)
3f	$C_5H_{10}N_2S$·HCl	112—115	40	2260		35.91 (36.03	6.59 6.65	17.15 16.81)
3g	$C_9H_{10}N_2$·HCl	166—168	35	2250		59.09 (59.18	6.21 6.07	15.26 15.34)
3h	$C_9H_{10}N_2$·HCl	176—178	30	2250	+5.8 (*c* 0.79, H_2O)	58.88 (59.18	6.14 6.07	15.29 15.34)
3i[f]	$C_5H_8N_2$·HCl	128—130	34	2250	−25.5 (*c* 0.80, H_2O)	44.86 (45.29	6.94 6.84	20.05 21.13)

a) Calculated on the basis of **1**. b) IR spectra were measured in KBr pellets. c) Lit, mp (dec) 165 °C: Ref. 16. d) Lit, mp (dec) 125—128 °C: Ref. 3 and lit, mp 115—117 °C: Ref. 17. e) Lit, mp (dec) 175—180 °C: Ref. 18. f) Hygroscopic and contaminated with impurities.

Table 2. Chromatographic data of α-aminonitriles

α-Amino-nitrile	Ion-exchange retention time (h)[a]		Paper[b] R_f[a]
3a	3.6 (4.5)	c)	0.25 (0.29)
3b, **3c**	3.7 (4.6)	c)	0.55 (0.49)
3d, **3e**	4.0 (3.7)	d)	0.86 (0.69)
3f	2.5 (4.4)	d)	0.70 (0.63)
3g, **3h**	5.2 (6.9)[e]	d)	0.80 (0.63)
3i	1.8 (2.4)	d)	0.43 (0.53)

a) Values in parentheses are those of the corresponding amino acid amides. b) Carried out with Toyo filter paper No. 50 using a *n*-BuOH–AcOH–H_2O (4 : 1 : 2 v/v) solvent system. c) 0.25ϕ × 50 cm column. Thirty min after the elution began, the eluent was changed from a pH 3.25 buffer to a pH 5.28 buffer. d) 0.25ϕ × 15 cm column, eluent: pH 5.28 buffer. e) Eluent: pH 5.28 buffer-*t*-BuOH (8 : 2 v/v).

The results of ion-exchange chromatography of the α-aminonitriles (**3a—i**) are summarized in Table 2. Only the small peaks of NH_3 were observed in the chromatograms, in addition to the α-aminonitriles. These α-aminonitriles were eluted more rapidly than the corresponding amides with the exception of the α-aminoisocapronitriles (**3d** and **e**), which were not separated from leucine amide when a 0.25ϕ × 15 cm column and a pH 5.28 buffer were used. The chromatograms presented in Fig. 1 show that the chromatographic method is available for quantitative analysis of the α-aminonitriles. Aminoacetonitrile (**3a**) and DL-α-aminopropiononitrile (**3b**) were identified by comparing their retention times on the chromatograms with those of authentic samples. The results of paper chromatography of the α-aminonitriles (**3a—i**) are also summarized in Table 2. In this case, **3d** and **3e** were separated from the corresponding amides.

Configuration retention for the L-α-aminonitriles (**3c**, **e**, **h**, and **i**) was confirmed using a gas chromatographic method.[11] These compounds were transformed into the corresponding *N*-trifluoroacetyl(TFA)-amino acid (+)-2-butyl esters as shown in Scheme 2.

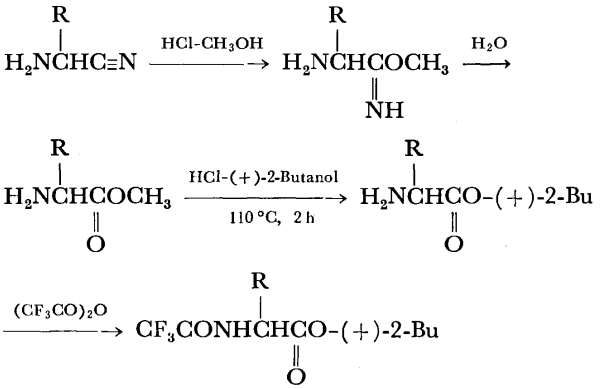

Scheme 2.

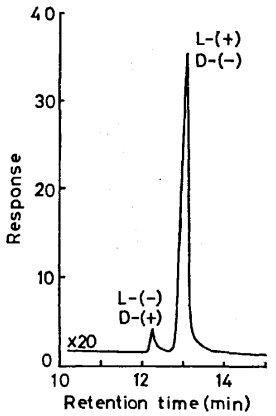

Fig. 2. Gas chromatogram of *N*-TFA-analine (+)-2-butyl ester derived from **3c**.

TABLE 3. A COMPARISON OF THE GAS CHROMATOGRAMS OF *N*-TFA-AMINO ACID (+)-2-BUTYL ESTERS DERIVED FROM BOTH L-AMINO ACIDS AND L-α-AMINONITRILES

Derivative	Retention time (min)		Fraction of peak height[c]	
	I[a]	II[b]	Derivative of L-amino acid	Derivative of L-α-aminonitrile
Ala	12.2	13.0	0.93	0.93 (**3c**)
Leu	21.8	22.8	0.93	0.93 (**3e**)
Phe	64.0	64.8	0.92	0.94 (**3h**)
Pro	44.4	45.2	0.94	0.93 (**3i**)

a) D-(+), L-(−) Diastereomer, b) L-(+), D-(−) Diasteromer. c) Peak height of II/sum of peak heights of I and II.

Each of the *N*-TFA-amino acid (+)-2-butyl esters was analyzed by gas chromatography on a capillary column coated with LB 550X. The *N*-TFA-L-amino acid (+)-2-butyl esters derived from L-amino acids (alanine, leucine, phenylalanine, and proline) were also analyzed. The chromatogram of the sample derived from **3c** is presented in Fig. 2. The sample from L-alanine also gave a similar chromatogram, which shows that the (+)-2-butanol[12] used in this work contains a small amount of the (−)-isomer. The gas chromatographic data are summarized in Table 3, which shows that the fraction of observed peak heights of the sample for each L-α-aminonitrile is approximately equal to that of the sample for the corresponding standard L-amino acid. These results indicate that the enantiomeric purity of the L-α-aminonitriles (**3c**, **e**, **h**, and **i**) is well retained and also that the procedure described in Scheme 2 is available for the enantiomeric analysis of α-aminonitriles.

The poor yields of **2a**—**d** may be due to the unfavorable elimination of the NPS group during the dehydration of the corresponding amides (**1a**—**d**) in $POCl_3$–pyridine. Although the overall yields of **3a**—**i** are also poor, the method described in Scheme 1 may be useful for preparing racemic and enantiomeric α-aminonitriles of as high a purity as possible.

Experimental

All the melting points were determined with a Yanagimoto micro-melting point apparatus and are uncorrected. IR spectra were taken with a Hitachi EPI-G2 spectrometer. The optical rotations were measured with a Yanaco OR-50 polarimeter. Ion-exchange chromatography was carried out with a Sibata amino acid analyzer, AA-600, under the following conditions: column size, $0.25\phi \times 50$ cm or $0.25\phi \times 15$ cm (Aminex A-4); eluent, citrate buffer of pH 3.25 (0.2 M Na) and pH 5.28 (0.35 M Na); flow rate, 6 ml/h; jacket temperature, 30 °C. Gas chromatography was carried out with a Hitachi gas chromatograph 063 provided with a flame ionization detector; column, 0.01ϕ in $\times$ 150 ft stainless steel capillary column coated with LB 550X (Perkin Elmer); temperature 100—170 °C, 1 °C/min; carrier gas He, 6 ml/min. Amino acid methyl ester hydrochlorides were prepared by the thionyl chloride method.[13] *o*-Nitrobenzenesulfenyl chloride was prepared from bis(*o*-nitrophenyl) disulfide and chlorine.[14] Amino acid amides were prepared according to the method of Yang and Rising.[15]

NPS-α-aminonitriles. The neutral sulfate of the α-aminonitrile (aminoacetonitrile or DL-α-aminoglutaronitrile) (0.04 mol) was dissolved in a mixture of 2 M aq NaOH (20 ml) and dioxane (25 ml). Into the solution, *o*-nitrobenzenesulfenyl chloride (0.04 mol) was added in small portions as 2 M aq NaOH (24 ml) were added dropwise, with vigorous stirring during a period of 20 min. The reaction mixture was filtered and diluted with water (400 ml). A yellow product precipitated out, which was recrystallized from ethyl acetate–petroleum ether.

NPS-aminoacetonitrile: Yield, 80%; mp 112—114 °C. Found: C, 46.12; H, 3.50; N, 20.09%. Calcd for $C_8H_7N_3O_2S$: C, 45.93; H, 3.37; N, 20.08%.

NPS-DL-α-aminoglutaronitrile: Yield, 73%; mp 100—102 °C. Found: C, 50.50; H, 3.70; N, 21.21%. Calcd for $C_{11}H_{10}N_4O_2S$: C, 50.37; H, 3.84; N, 21.36%.

Removal of the NPS from the Model NPS-α-aminonitriles. When 5 ml of diethyl ether including anhydrous HCl (3 M) was added to the solution of the NPS-α-aminonitrile (aminoacetonitrile or DL-α-aminoglutaronitrile) (5 mmol) in a minimum amount of ethyl acetate, the α-aminonitrile hydrochloride precipitated out. The precipitates collected were washed with diethyl ether and dried in a vacuum without further purification. The recovery yields of aminoacetonitrile and DL-α-aminoglutaronitrile were 58 and 69%, respectively. The results of ion-exchange chromatography of the products showed that the samples included no impurities such as the corresponding amino acids or amino acid amides.

NPS-amino Acid Methyl Esters. These compounds were prepared according to the method of Zervas *et al.*[10]

NPS-DL-alanine Methyl Ester: Yield, 60% mp 79—81 °C. Found: C, 46.94; H, 4.65; N, 10.76%. Calcd for $C_{10}H_{12}N_2O_4S$: C, 46.87; H, 4.72; N, 10.93%.

Ammonolysis of NPS-amino Acid Methyl Esters. The NPS-amino acid methyl esters of glycine, DL-alanine, and L-alanine were dissolved in small amounts of ethanol and then large excess amounts of methanol saturated with NH_3 were added. The solutions were allowed to stand at room temperature for 2—3 d. The crystals precipitated were collected and recrystallized from hot ethanol. The experimental results for the NPS-amino acid amides (**1a**—**c**) are shown in Table 4.

*NPS-amino Acid Amides (**1d**—**i**).* These compounds were prepared by reactions of the amino acid amides with *o*-nitrobenzenesulfenyl chloride in chloroform in the presence of triethylamine and recrystallized from hot ethanol. In the case of **1d**, the reaction was carried out in chloroform–ethanol (1 : 1 v/v). The experimental results for the NPS-amino acid amides (**1d**—**i**) are shown in Table 4.

*NPS-α-aminonitriles (**2a**—**i**).* An NPS-amino acid amide dissolved in a minimum amount of pyridine or pyridine–dimethylformamide (2 : 1 v/v) was cooled on an ice salt bath below −5 °C and a slight excess of $POCl_3$ was added dropwise to the solution. After the mixture had been allowed to stand at room temperature for 30 min, ice was added to it in order to decompose the excess $POCl_3$ and then the solution was treated with ethyl acetate to extract the product. The extract was washed successively with water, dilute aq HCl, and water, and then dried over anhydrous Na_2SO_4. After evaporation of the ethyl acetate from the extract, the product was separated out as a solid (**2a**—**d**) or an oil (**2e**—**i**) by the addition of petroleum ether. Recrystallization was performed from ethyl acetate–petroleum ether. The crystalline products (**2a**—**d**) obtained are shown in Table 5.

*α-Aminonitrile Hydrochlorides (**3a**—**i**·HCl).* Into a solution of an NPS-α-aminonitrile in a minimum amount of ethyl acetate or diethyl ether were added two equivalents of anhydrous HCl in diethyl ether to afford the α-aminonitrile

Table 4. NPS-amino acid amides

NPS-amino acid amide[a]	Molecular formula	Mp (°C)	Yield (%)	$[\alpha]_D^{30}$ (deg)	Found (Calcd) (%) C	H	N
1a	$C_8H_9N_3O_3S$	166—168	83		42.40 (42.28	4.03 3.99	18.27 18.49)
1b	$C_9H_{11}N_3O_3S$	182—184	78		45.02 (44.80	4.65 4.60	17.27 17.42)
1c	$C_9H_{11}N_3O_3S$	199—201	53	−49.0 (*c* 1.0, DMF)	45.02 (44.80	4.72 4.60	17.62 17.42)
1d	$C_{12}H_{17}N_3O_3S$	206—210	60		51.08 (50.87	6.09 6.05	14.56 14.83)
1e	$C_{12}H_{17}N_3O_3S$	95—98	32	−24.8 (*c* 1.0, DMF)	50.70 (50.87	6.16 6.05	14.57 14.83)
1f	$C_{11}H_{15}N_3O_3S_2$	135—139	41		43.69 (43.84	5.08 5.02	14.04 13.94)
1g	$C_{15}H_{15}N_3O_3S$	122—124	57		56.46 (56.77	4.90 4.76	13.16 13.24)
1h	$C_{15}H_{15}N_3O_3S$	120—122	50	+36.6 (*c* 1.0, DMF)	57.04 (56.77	4.82 4.76	13.10 13.24)
1i	$C_{11}H_{13}N_3O_3S$	192—194	45	−23.4 (*c* 1.0, DMF)	49.17 (49.43	4.89 4.90	15.58 15.72)

a) **1a—c** were obtained by ammonolysis of the NPS-amino acid methyl esters. The others were obtained by reactions of the amino acid amides with *o*-nitrobenzensulfenyl chloride.

Table 5. NPS-α-aminonitriles

NPS-α-amino-nitrile	Molecular formula	Mp (°C)	Yield (%)	$\nu_{C\equiv N}$[a] (cm^{-1})	$[\alpha]_D^{30}$ (deg)	Found (Calcd) (%) C	H	N
2a	$C_8H_7N_3O_2S$	114—116	22	2240		45.88 (45.93	3.38 3.37	20.04 20.08)
2b	$C_9H_9N_3O_2S$	98—100	30	2230		48.14 (48.42	3.77 4.06	18.50 18.82)
2c	$C_9H_9N_3O_2S$	108—110	32	2230	−28.6 (*c* 1.0, DMF)	48.40 (48.42	4.11 4.06	18.48 18.82)
2d	$C_{12}H_{15}N_3O_2S$	53—54	37	2230		54.26 (54.32	5.72 5.70	15.78 15.84)

a) IR spectra were measured in KBr pellets.

hydrochloride. After a large amount of diethyl ether had been added to it, the precipitated crystals were collected and recrystallized from ethanol–diethyl ether.

Derivation of L-α-*Aminonitriles for Gas Chromatographic Analysis.* About 10 mg of each L-α-aminonitrile hydrochloride were dissolved in 9 M HCl in methanol (10 ml) and then water (0.05 ml) was added to the solution. After 2 d, the solution was evaporated to dryness to remove the excess methanol and the residue (amino acid methyl ester hydrochloride) was heated to 100—110 °C for 2 h in (+)-2-butanol (1 ml) saturated with anhydrous HCl. After transesterification, the solution was evaporated to dryness in a vacuum to remove the excess (+)-2-butanol. Trifluoroacetic anhydride (1 ml) was added to the residue and then a clear solution was obtained. Methylene dichloride (5 ml) was added to the solution and it was allowed to stand overnight at room temperature. After trifluoroacetylation, the solution was evaporated to dryness carefully and the residue was taken up in nitromethane for direct injection into the gas chromatographic column.

Preparation of N-*TFA*-DL- *and* L-*amino Acid (+)-2-Butyl Esters.* About 10 mg of the amino acid were suspended in (+)-2-butanol (1 ml) saturated with anhydrous HCl. The suspension was heated to 100—110 °C for 3 h and then a clear solution was obtained. After esterification, the solution was evaporated to dryness in a vacuum and trifluoroacetylation was carried out in a manner similar to that described above.

References

1) A preliminary communication of the present paper has appeared: K. Kawashiro, H. Yoshida, and S. Morimoto, *Chem. Lett.*, **1976**, 417.

2) N. Zelinsky and G. Stadnikoff, *Ber.*, **39**, 1722 (1906).

3) J. Jenni, H. Kühne, and B. Prijs, *Helv. Chim. Acta*, **45**, 1163 (1962).

4) B. Liberek, A. Nowicka, and J. Szrek, *Rocz. Chem.*, **39**, 369 (1965).

5) J. S. Morley, *J. Chem. Soc., C*, **1969**, 809.

6) D. W. Woolley, J. W. B. Hershey, and H. A. Jodlowsky, *J. Org. Chem.*, **28**, 2012 (1963).

7) Y. Hirotsu, T. Shiba, and T. Kaneko, *Bull. Chem. Soc. Jpn.*, **40**, 2945 (1967).

8) I. Ojima, S, Inaba, and Y. Nagai, *Chem. Lett.*, **1975**, 737.

9) K. Kawashiro, H. Yoshida, and S. Morimoto, *Chem. Lett.*, **1975**, 323.

10) L. Zervas, D. Borovas, and E. Gazis, *J. Am. Chem.*

Soc., **85**, 3660 (1963).
11) E. Gil-Av, R. Charles-Sigler, G. Fischer, and D. Nurok, *J. Gas Chromatogr.*, **4**, 51 (1966).
12) The (+)-2-butanol was obtained from Norse Laboratories, Inc., U.S.A.
13) M. Brenner and W. Huber, *Helv. Chim. Acta*, **36**, 1109 (1953).
14) M. H. Hubacher, *Org. Synth.* Coll. Vol. I. 455 (1943).
15) P. S. Yang and M. M. Rising, *J. Am. Chem. Soc.*, **53**, 3183 (1931).
16) A. Klages, *J. Prakt. Chem.*, [2], **65**, 188 (1902).
17) N. Zelinsky and G. Stadnikoff, *Ber.*, **41**, 2061 (1908).
18) G. T. Newbold, W. Sharp, and F. S. Spring, *J. Chem. Soc.*, **1951**, 2679.

Proton Magnetic Resonance Studies of *cis-trans* Equilibria of Some *N*-(2,5-Dichlorophenyl)-3-aminocrotonamides

Michio KONDO

Central Research Laboratories, Sankyo Co., Ltd., Hiromachi 1-2-58, Shinagawa-ku, Tokyo 140

(Received November 16, 1976)

The ^{1}H NMR spectra of 3-(alkylamino)crotonamides indicate that these substances exist in solution as a mixture of the geometric isomers, *cis* and *trans*, in which the chelated *cis* form is predominant. Unsubstituted 3-aminocrotonamide appears to exist in the *cis* form only, and *N*,*N*-disubstituted derivatives in the *trans* form. In the case of 3-(alkylamino)crotonamide it is found that the *cis-trans* equilibrium is solvent dependent and that the apparent rate of interconversion between the isomers is very slow in chloroform-*d*, fast in dimethyl-d_6 sulfoxide, and intermediate in acetone-d_6 and methanol-d_4. It seems that the *cis-trans* equilibrium is almost independent of both temperature and concentration, and that the replacement of the olefinic H by D proceeds through enamine⇌imine tautomerization.

^{1}H NMR spectroscopy has proved to be a powerful method for studying structural problems such as tautomeric equilibrium and proton-deuteron exchange. The previous paper reported the ^{1}H NMR spectroscopic study of *N*-(2,5-dichlorophenyl)acetoacetamide (**7**), in which the *enol* form was found to be a minor component in any solvent used.[1] The ^{1}H NMR spectral study of the title compounds, easily prepared from **7** and appropriate amines, will give further information about their conformations.

From the ^{1}H NMR spectral studies of 3-aminocrotonic esters it has been found that *N*-monosubstituted derivatives exist as mixtures of two geometric isomers, *cis* (**A**) and *trans* (**B**).[2,3] In the case of the title compounds there is another problem, the *cis-trans* isomerism about the amide bond, but its conformation can be confined to *trans* on the basis of the diagnostic acylation-deshielding shifts of the ring proton-6.[4] Hereafter the terms *cis* and *trans* will refer to the conformation about the olefinic bond, C_2–C_3, unless otherwise noted.

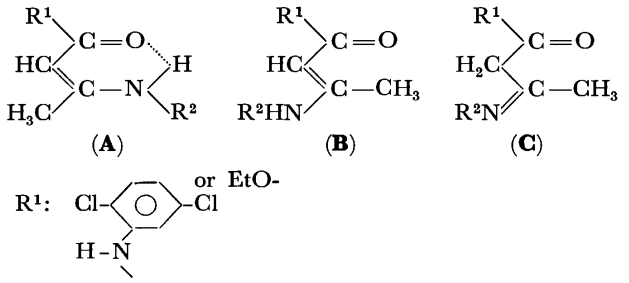

Another point of interest is that the shift direction of the olefinic proton signals of the title compounds was opposite to that for ethyl 3-(alkylamino)crotonate when the solvent was changed from $CDCl_3$ to DMSO.

Experimental

Materials. To 2,5-dichloroacetoacetanilide (1/20 mol) suspended in ethanol (50 ml) was added an appropriate amine in slight excess. The reaction mixture was gently warmed to give a pale yellow solution and then concentrated to near dryness at room temperature. Repeated crystallizations of the precipitates from ethanol or aqueous ethanol gave the pure compounds, as proved by the satisfactory results of elemental analyses. This indicates that the condensation reaction occurred at either the acetyl-carbonyl or the amide-carbonyl group. However, the latter position may be ruled out from the constancy of the chemical shifts of the ring protons of these six compounds. Therefore, it is concluded that the reaction products are 3-aminocrotonamides (**A** and **B**) or their imino-tautomer (**C**). The structure **C** can be ruled out on the basis of the absence of signals assignable to methylene protons.

(2,5)$Cl_2C_6H_3NHCOCH$=$C(CH_3)X$

	1	**2**	**3**
X	NH_2	$NHCH_3$	$NHCH_2CH_3$
mp(°C)	130.5	72.5	85.0
	4	**5**	**6**
X	$N(CH_3)_2$	$N(CH_2CH_2)_2O$	$N(CH_3)CH_2C_6H_5$
mp(°C)	141(dec)	195.5	157

The ^{1}H NMR spectra were recorded on a Varian T-60A spectrometer. Sample concentrations were 20 mg/ml unless otherwise noted. The concentration dependence of the chemical shifts of **2** was examined in DMSO and found to be negligible. The temperature dependence of the spectra of **2** was tested in DMSO at higher temperatures, using a Varian A-60D spectrometer.

Results and Discussion

Signal Assignment. A single set of signals was observed for $CDCl_3$ solution of **2** and **3**, whereas two sets of signals were observed for DMSO solutions of **2** and **3**; one set of the two corresponded well to the signals observed for the $CDCl_3$ solution. The amino proton signals of **2** and **3** in $CDCl_3$ are located at δ 9.17 and 9.21 respectively, suggesting a molecular conformation containing an intramolecular hydrogen bond between the amino proton and the amide carbonyl, *i.e.*, the *cis* conformation (**A**). The other set of signals of the DMSO solutions of **2** and **3** can be attributed to the *trans* conformation. The chemical shifts thus assigned to the *cis*- and *trans*-C–CH_3, N–CH_3, and =CH protons of **2** in DMSO, for example, are in fair agreement with those reported for the corresponding protons of ethyl 3-(methylamino)crotonate (**8**) in DMSO.[3]

Each of the ^{1}H NMR spectra of **1**, **4**, **5**, and **6** consists of only a single set of signals in both $CDCl_3$ and DMSO solutions. The chemical shifts of various kinds of protons of **1**, except for the amino protons, are close to those of **2** in the *cis* form, leading to the conclusion that the molecular conformation of **1** in the solutions is *cis*. A similar comparison of the chemical shifts of

TABLE 1. THE CHEMICAL SHIFTS OF VARIOUS KINDS OF PROTONS IN SOME *N*-(2,5-DICHLOROPHENYL)-3-(ALKYLAMINO)CROTONAMIDES IN $CDCl_3$ AND DMSO

Compd	Solvent		CCH_3	NCH_3	=CH	NH	NHCO	H-3	H-4	H-6
1	$CDCl_3$	c[a]	1.95	—	4.58	6.60	7.20	7.26	6.93	8.56
	DMSO	c	1.84	—	4.80	7.50	8.44	7.44	7.03	8.20
2	$CDCl_3$	c	1.93	2.93	4.51	9.17	7.07	7.24	6.88	8.52
		t	(not detected)							
	DMSO	c	1.92	2.88	4.87	9.05	8.38	7.43	7.03	8.26
		t	2.26	2.65	4.95	6.60	8.26	7.42	7.01	8.34
3	$CDCl_3$	c	1.95	b)	4.48	9.21	7.03	7.24	6.88	8.52
		t	(not detected)							
	DMSO	c	1.91	b)	4.83	9.07	8.43	7.44	7.03	8.18
		t	2.23	b)	4.97	6.53	8.30	7.41	7.00	8.26
4	$CDCl_3$	t	2.53	2.98	4.56	—	7.23	7.25	6.88	8.61
	DMSO	t	2.42	2.93	5.02	—	8.43	7.43	7.01	8.25
5	$CDCl_3$	t	2.49	c)	4.80	—	7.3	7.25	6.92	8.58
	DMSO	t	2.40	c)	5.36	—	8.64	7.45	7.07	8.23
6	$CDCl_3$	t	2.61	2.96	4.71	—	d)	d)	6.89	8.58
	DMSO	t	2.50	2.93	5.20	—	8.50	7.41	7.02	8.23

a) c and t mean *cis* and *trans*, respectively. b) *N*-Ethyl signals are omitted. c) Signals of the morpholine moiety are omitted. d) Not identified because of overlapping of the benzyl signals.

TABLE 2. DMSO-INDUCED SHIFTS ($\delta_{DMSO}-\delta_{CDCl_3}$)

Compd	CCH_3	NCH_3	=CH	NH	NHCO	H-3	H-4	H-6
1 (*cis*)	−0.09	—	0.22	0.90	1.24	0.18	0.10	−0.36
2 (*cis*)	−0.01	0.05	0.36	−0.12	1.31	0.19	0.15	−0.26
3 (*cis*)	−0.04	—	0.35	−0.14	1.40	0.20	0.15	−0.34
4 (*trans*)	−0.09	−0.05	0.46	—	1.20	0.18	0.13	−0.36
5 (*trans*)	−0.09	—	0.56	—	1.34	0.20	0.15	−0.35
6 (*trans*)	−0.09	−0.03	0.49	—	—	—	0.13	−0.35

various kinds of protons of **4**, **5**, and **6**, with those of **2** leads to the conclusion that these three amides have *trans* conformation in the solutions.

The chemical shifts thus determined are collected in Table 1.

DMSO-induced Shifts. The changes ($\delta_{DMSO}-\delta_{CDCl_3}$) in the chemical shifts of various protons are summarized in Table 2.

The chemical shifts of the ring protons show characteristic changes upon changing solvents from $CDCl_3$ to DMSO: proton 3 and 4 show downfield shifts of about 0.1—0.2 ppm and proton 6 an upfield shift of about 0.33 ppm. Similar observations were reported for a number of acetanilides having an electronegative ortho substituent capable of forming an intramolecular hydrogen bond with the amide proton.[4]

The same solvent change caused slight upfield shifts of the C–CH_3 and N–CH_3 signals (<0.1 ppm), but remarkable downfield shifts of the olefinic proton (0.22—0.56 ppm) and the amide proton signals (1.20—1.40 ppm). This DMSO-induced downfield shift of the olefinic proton signal may be explained in terms of the deshielding effect[5] of a DMSO molecule intermolecularly hydrogen bonded with the amide proton (**D**), because DMSO is known as a powerful solvent for disrupting the intermolecular association among amide molecules through forming intermolecular hydrogen bonds with the amide proton.[6] This kind of deshielding effect is not expected for *N*,*N*-dimethylamide or the ethyl ester of 3-aminocrotonic acid, because each of them can be supposed to have no specific interactions with DMSO molecules. In fact, the olefinic proton signals for these compounds remained at almost the same field for the solvent change described above.[3,7]

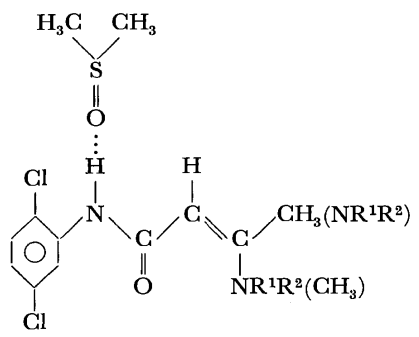

(**D**)

The fact that the *cis* form was observed for **1**, **2**, and **3** only is indicative of the important role of the intramolecular hydrogen bond between the amino proton and the carbonyl oxygen in stabilizing the *cis* form.

As for the amino protons of **1**, the DMSO-induced deshielding shift is 0.90 ppm. The deshielding shift for the amino proton not involved in the intramolecular hydrogen bond could be calculated as 1.92 ppm (see next section). This value is a little larger than the deshielding shift of about 1.3 ppm for the amide proton, probably reflecting stronger interactions with DMSO molecules.

Intramolecular Hydrogen Bonds. The amino protons of **2** and **3** in the *cis* form resonate at very low fields (δ 9.17 and 9.21, respectively) even in $CDCl_3$. The concentration dependence of these resonances was found to be negligible. This means that the *cis*-amino proton is involved in the intramolecular hydrogen bond with the carbonyl oxygen. With the change of solvents from $CDCl_3$ to DMSO, this amino-signal showed only a trivial upfield shift which may be a reflection of the persistence of the intramolecular hydrogen bond with almost the same strength even in DMSO. The UV absorption spectrum of **2** in DMSO is very similar to that in cyclohexane; this supports the above argument about the intramolecular hydrogen bond.

The amino protons of **1** resonate at δ 6.60 in $CDCl_3$ and at δ 7.50 in DMSO. These values are smaller by as much as about 2.59 and 1.56 ppm than those for the *cis*-amino protons of **2** and **3** in $CDCl_3$ and those in DMSO, respectively, mainly because of time averaging through a rapid internal exchange on the NMR time scale between the two amino protons (one is involved and the other is not involved in the intramolecular hydrogen bond) and partly because of the difference between NH_2 and NHR (R=CH_3 or C_2H_5).

It is reasonable to assume that the inductive effect due to the alkyl group is common and has the same magnitude for both the *cis* and *trans* amino protons. In this approximation, the hydrogen bonded and free amino protons of **1** in DMSO are expected to resonate at $\delta_{h.b.}=9.06-\Delta I$ and $\delta_{free}=6.57-\Delta I$, where ΔI stands for the inductive effect. From these two values and the observed chemical shift (δ 7.50), the inductive effect is evaluated as $\Delta I=0.32$ ppm. Since the inductive effect can be assumed to be solvent independent, the hydrogen bonded amino proton of **1** dissolved in

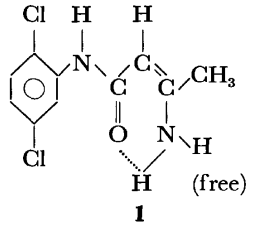

1

$CDCl_3$ is expected to resonate at δ 8.87. Therefore, the free amino proton of **1** in $CDCl_3$ would resonate at δ 4.33. The free amino proton of ethyl 3-(methylamino)crotonate in $CDCl_3$ was reported to resonate at δ 5.18 at −30 °C.[8] This difference could be ascribed to the difference in intermolecular interactions under different temperatures as well as the difference between the ester and the amide. The DMSO-induced shift for the free amino proton would be calculated as 1.92 ppm.

The splitting of about 5 Hz in the N–CH_3 signal of **2** and the N–CH_2 signal of **3** suggests that the intramolecular hydrogen bond is not the RH_2C=N···HO–C type but the RH_2CNH···O=C type. Dudek *et al.* discussed a similar problem for some ^{15}N enriched anilides.[9]

Population Equilibrium between the two Isomers and the H/D Exchange of the Olefinic Proton. In this section the isomeric equilibrium of **2** will be discussed in some detail. The equilibrium is solvent dependent; the percentage of the *trans* isomer is negligible in $CDCl_3$ even after two days, 7% in acetone, 22% in methanol-d_4, and 32% in DMSO at the sample concentration of 100 mg/ml at room temperature, respectively.

In a $CDCl_3$ solution of **2**, the ^{1}H NMR spectrum consists of only the *cis*-signal; the *trans*-signals were not observed even after two days. In the case of a methanol-d_4 solution of **2**, on the other hand, the ^{1}H NMR spectrum recorded just after dissolution consists of almost only the *cis*-signals and then the *trans*-signals for the C–CH_3 and the N–CH_3 grew gradually on repeated recording at the expense of the *cis*-signals until the *cis-trans* equilibrium was attained after about 30 min. These observations can be explained by assuming the *cis* conformation of **2** in the crystalline state.

During the *cis-trans* equilibration in the methanol solution of **2** described above, the *cis*-signal for the olefinic proton disappeared.

In acetone solution of **2** the *cis-trans* equilibrium is established in one and a half hours. An addition of D_2O of about 10% v/v to this acetone solution induced the disappearance of the olefinic proton signal without any change in the intensity ratio of *trans*/*cis*. Each of the doublet signals due to the N–CH_3 protons for both the *cis* and *trans* forms collapsed more rapidly because of the remarkable reduction in the spin-spin coupling constant by the deuteration of the amino proton. However, the C–CH_3 signals did not show any change in either their signal positions or their relative intensities.

Almost the same behavior was observed for a DMSO solution of **2**, with the addition of D_2O (5% v/v). The H/D replacement at the olefinic site attained equilibrium in about 40 min (Fig. 1).

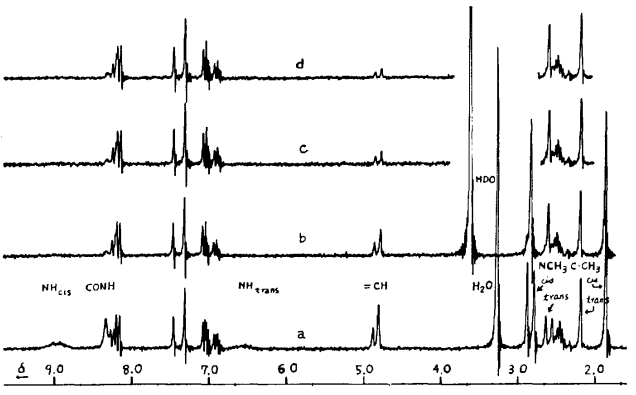

Fig. 1. The time dependent ^{1}H NMR spectrum of *N*-(2,5-dichlorophenyl)-3-(methylamino)crotonamide (**2**) in DMSO-D_2O (20 : 1) (*ca.* 80 mg/ml!): a) no D_2O; b) just after the addition of D_2O; c) after 25 min; d) after 43 min.

From these observations, the H/D replacement at the olefinic site seems to proceed through a transient state which is also involved in the *cis*⇌*trans* isomerization process.

In order to clarify whether or not the *cis*-amino proton plays an important role in the H/D exchange, the ^{1}H NMR spectrum of **6** in DMSO–D_2O was recorded. The addition of D_2O of about 5% v/v to a DMSO solution of **6** induced a very slow reduction in the intensity of the olefinic proton signal and the amide one, without any changes in the other signals. The plot of the log-value of the ratio, I/I_0, of the intensity of the olefinic proton signal to the initial intensity *vs.* time yielded a straight line. This suggests that a unimolecular mechanism is operative in the H/D exchange at the olefinic site. The exchange rate is much slower for **6** than for **2**, suggesting that the olefinic proton exchange in **2** may occur mainly through enamine⇌imine tautomerization (*E*), but there must be some other mechanism concurrently contributing to the H/D exchange.

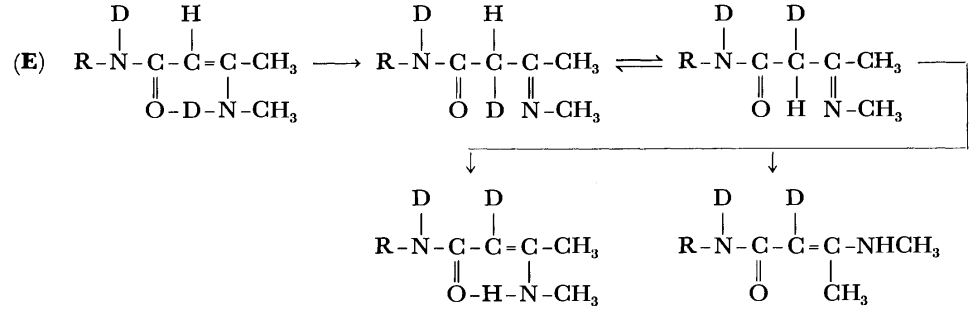

The deuteration of the vinyl proton of some enamino ketones was detected by means of the ^{1}H NMR spectroscopy; the imine tautomer has been proposed as an intermediate in the *cis-trans* isomerization.[10] The replacement of the olefinic proton by a deuteron was found to be rapid (<10 min) for *N*,*N*-dimethyl-3-(methylamino)crotonamide, but much slower for methyl 3-(1-pyrrolidinyl)crotonate, upon addition of D_2O to the DMSO solutions. These results are consistent with the above argument about the exchange mechanism.

The concentration dependence of the *cis-trans* equilibrium was tested for DMSO solutions of **2** and found to be negligible over the concentration range from 10 to 140 mg/ml, reflecting the relative importance of the intramolecular mechanism for the isomerization.

The temperature variation of the ^{1}H NMR spectrum of **2** in DMSO was found to be negligible for all protons except for the amide proton and the *trans* amino proton; their signals shifted upfield with raising the temperature, probably because of reduced intermolecular interactions both between the solute-solute and the solute-solvent molecules. The population ratio of the *trans* to the *cis* isomer seemed to be constant within the experimental accuracy over the temperature range from room temperature to about 90 °C. This fact may be ascribed to an occasional cancellation between two counteracting factors: (i) increased thermal motions at the elevated temperatures would break the intramolecular hydrogen bond and shift the equilibrium to the *trans* preference, and (ii) weaker intermolecular interactions at elevated temperatures would destabilize the *trans* form.

References

1) M. Kondo, *Bull. Chem. Soc. Jpn.*, **49**, 1719 (1976).
2) G. O. Dudek and G. P. Volpp, *J. Am. Chem. Soc.*, **85**, 2697 (1963).
3) A. G. Sanchez, M. T. Aldave, and U. Scheideggar, *J. Chem. Soc., C*, **1968**, 2570.
4) I. D. Rae, *Can. J. Chem.*, **46**, 2589 (1968) and references cited therein.
5) W. Lin and S. Tsay, *J. Phys. Chem.*, **74**, 1037 (1970).
6) a) L. A. LaPlanche and M. T. Rogers, *J. Am. Chem. Soc.*, **86**, 337 (1964); b) R. H. Barker and G. J. Boudreaux, *Spectrochim. Acta, Part A*, **23**, 727 (1967).
7) M. Kondo, unpublished data.
8) J. Ulrich and P. Vay, *Chim. Anal. (Paris)*, **48**, 549 (1966).
9) G. O. Dudek and E. P. Dudek, *J. Am. Chem. Soc.*, **88**, 3407 (1966).
10) a) J. Dabrowski and J. Terpinski, *Tetrahedron Lett.*, **1965**, 1363; b) J. Dabrowski and J. Terpinski, *Rocz. Chem.*, **41**, 697 (1967); *cf. Chem. Abstr.*, **67**, 53498 h (1967).

Stereochemical Studies of the Electrolytic Reactions of Organic Compounds. IV.* Electrolytic Reduction of Optically-active 1-Pyridylalkanols to the Corresponding Substituted-alkyl Pyridines

Tsutomu NONAKA, Tetsuro OTA,** and Toshio FUCHIGAMI

Department of Electronic Chemistry, The Graduate School, Tokyo Institute of Technology, Nagatsuta, Midori-ku, Yokohama 227

(Received January 12, 1977)

The mechanism of electrolytic reduction of 1-pyridylalkanol to the corresponding substituted-alkyl pyridine was examined by electrolyzing several optically-active 1-pyridylalkanols in an aqueous sulfuric acid solution in the vicinity of a mercury cathode. The alkyl pyridine from 1-(2-pyridyl)alkanol showed optical rotation, while that from 1-(4-pyridyl)alkanol was almost racemized.

Alcoholic hydroxyl groups are generally difficult to reduce electrolytically.[1-3] In a previous work,[4] it was found that 1-(2-pyridyl)- and (4-pyridyl)alkanols are electrolytically reduced to the corresponding substituted-alkyl pyridines in high yields and current efficiencies with a mercury cathode in an aqueous sulfuric acid solution. Also a tentative mechanism for the reductive elimination of the hydroxyl group of 1-pyridylalkanols was proposed on the basis of their adsorption on a cathode surface and the steric hindrance effect of their substituents. Namely, the two electrons required for the reduction were supposed to be introduced from the cathode to a carbon atom adjacent to the hydroxyl group following the route of the conjugated π-electron system of a pyridine nucleus.

In order to discuss the stereochemical aspects of the reaction mechanism, the starting 1-pyridylalkanol and the alkyl pyridine formed must be chiral. In this work, the three kinds of optically-active 1-pyridylalkanols (**1**, **2**, and **3**) studied are electrolytically reduced to the corresponding substituted-alkyl pyridines.

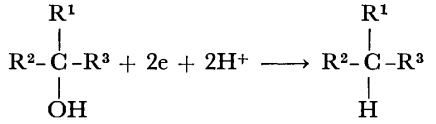

1 : R^1=4-Pyridyl, R^2=Methyl, R^3=Ethyl
2 : R^1=4-Pyridyl, R^2=Methyl, R^3=Phenyl
3 : R^1=2-Pyridyl, R^2=Ethyl, R^3=Phenyl

Results and Discussion

Although a number of racemic 1-pyridylalkanols were synthesized, only 2-(4-pyridyl)-2-butanol (**1**), 1-(4-pyridyl)-1-phenylethanol (**2**), and 1-(2-pyridyl)-1-phenyl-1-propanol (**3**) could be optically resolved by fractional recrystallization of their salts with optically-active acids, such as (+)-camphor-10-sulfonic acid or (+)-tartaric acid.

Electrolysis was carried out at a constant cathodic potential, for which the initial cathodic current density was 6 A/dm^2 and no hydrogen evolution was observed. The electrolytic results are summarized in Table 1.

Optically-active 1-(4-pyridyl)alkanols (**1** and **2**) were reduced to the corresponding alkylpyridines, which were almost racemized, in high yields. On the other hand, the reduction of optically-active 1-(2-pyridyl)alkanol (**3**) afforded the optically-active alkylpyridine in a low yield, and two by-products were detected by gas chromatograph. The amount of these by-products increased steadily with increasing electric charge passed, while the amount of alkylpyridine reached a maximum of 3 to 4×10^5 C/mol of electric charge passed.[5] This fact indicates that the alkylpyridine formed was further reduced to the by-products. Although the by-products could not be isolated, their molecular weights were both determined to be 201 using a gas chromatograph-mass spectrometer. Therefore, they may be two isomers of 2-(1-phenylpropyl)tetrahydropyridine, though the position of the double bond was undetermined. Polymeric substances insoluble in ether were also formed upon the reduction of **3**.

No optical yield of the alkylpyridines could be estimated because the attempt to determine the optical purities of both the starting 1-pyridylalkanols and the alkylpyridines formed using an optically-active NMR shift reagent, such as europium tris[3-(trifluoromethylhydroxymethylene)-*d*-camphorate,[6] was unsuccessful.

The absolute steric configurations of the 1-pyridylalkanols and the alkylpyridines are unknown. Therefore, the change in relative configuration in the course of the reduction was investigated on the basis of an empirical rule, the so-called Freudenberg displacement rule.[7] The rule states that, when two similarly constituted dissymmetric compounds are chemically changed in the same way and the change produces a considerable shift in optical rotation in the same direction, then the two compounds probably have the same configuration. In order to apply the rule to determining the relative configuration of the 1-pyridylalkanols and the corresponding alkylpyridines, their derivatives were prepared by the same way. As shown in Table 2, for 1-substituted pyridinium halides from **3** and the corresponding alkylpyridine, the shifts were in the same direction. This fact suggests that the configurations of **3** and the alkylpyridine are the same, *i.g.*, in the reduction of **3** to the alkylpyridine, retention of the configuration is predominant over inversion. On the other hand, the free base and N-oxide of either **3** or the alkylpyridine may not fall in the category of the displacement rule, since the intramolecular hydrogen bonding in these compounds should give a rather different contribution

* Part III: *Chem. Lett.*, **1977**, 47.

** Present address: Chemical Administration, Asahi Chemical Industry Co., Ltd., 1-3-1 Yakoo, Kawasaki-ku, Kawasaki 210.

TABLE 1. RESULTS OF THE ELECTROLYSIS OF OPTICALLY-ACTIVE 1-PYRIDYLALKANOLS

	1-Pyridylalkanol	Cathodic potential	Charge passed	Alkylpyridine	
	$[\alpha]_D^{20}$ (degree)	(V *vs.* SCE)	($\times 10^5$ C/mol)	Yield (%)	$[\alpha]_D^{20}$ (degree)
1	-1.7 ± 0.4[a]	-1.22	1.88	92	-0.1 ± 0.1[a]
2	$+2.4\pm0.4$[b]	-1.25	1.96	94	$+0.1\pm0.1$[b]
3	$+8.8\pm0.2$[b]	-1.36	3.09	62	-5.0 ± 0.2[b]

a) Measured in ethanol. b) Measured in methanol.

TABLE 2. MOLECULAR OPTICAL ROTATIONS OF THE DERIVATIVES OF 1-PYRIDYLALKANOLS AND ALKYLPYRIDINES

	$[M]_D^{20}$ (degree)						
	Original base	Hydrochloride	Hydroiodide	1-Phenacylpyridinium bromide	1-Methylpyridinium iodide	1-Benzylpyridinium bromide	1-Oxide
1	-2.6 ± 0.6[a]	-0.6 ± 0.2[a]	-1.8 ± 0.5[b]				
Alkylpyridine from **1**	-0.1 ± 0.1[a]	-0.2 ± 0.2[a]	-0.1 ± 0.2[b]				
2	$+4.3\pm0.2$[c]	$+10.5\pm0.5$[c]	$+11.0\pm0.5$[b]	$+1.0\pm0.1$[c]			
Alkylpyridine from **1**	$+0.2\pm0.2$[c]	-0.2 ± 0.5[c]	-0.2 ± 0.5[b]	-0.0 ± 0.1[c]			
3	$+18.8\pm0.4$[c]	$+248.8\pm1.6$[c]	$+258.8\pm1.4$[d]		-205.9 ± 1.6[d]	-38.4 ± 0.3[d]	-14.4 ± 0.1[c]
Alkylpyridine from **3**	-9.9 ± 0.5[c]	$+19.9\pm0.5$[c]	$+35.8\pm0.5$[d]		-11.9 ± 0.1[d]	$+7.4\pm0.2$[d]	$+12.1\pm0.1$[c]

a) Measured in ethanol. b) Measured in water. c) Measured in methanol. d) Measured in acetone.

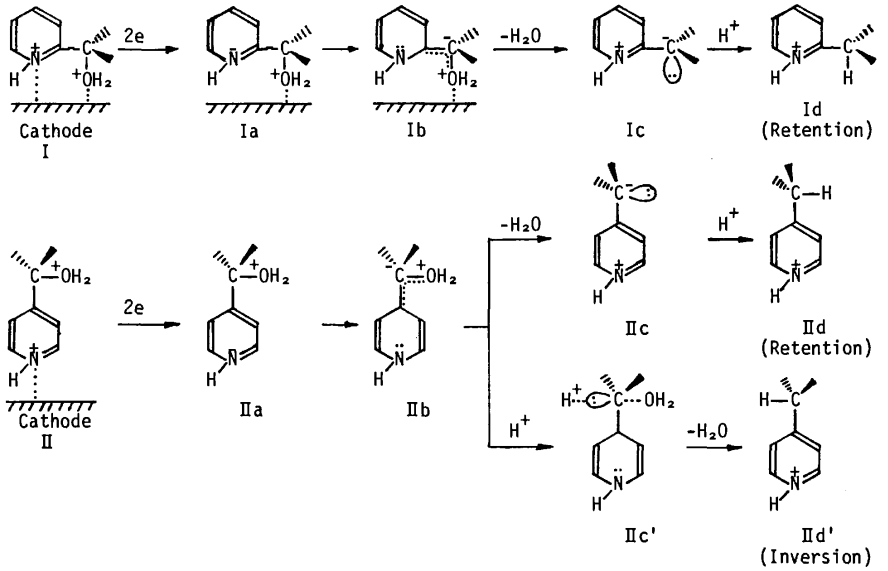

Scheme.

to their optical activities. Such an exception to the displacement rule is acceptable.[7]

In the cases of **1** and **2**, the optical rotations of not only the original alkylpyridines, but also their derivatives, were so small that the displacement rule could not be applied.[8] Such small optical rotations may indicate that racemization occurs almost exclusively in the reduction of **1** and **2**.

Although the reductive elimination of the hydroxyl group of a 1-pyridylalkanol is formally similar to that of the halo group of an alkyl halide, it is doubtful that these eliminations proceed *via* similar mechanisms. If the reduction of a 1-pyridylalkanol proceeds *via* a mechanism similar to that for the reduction of an optically-active alkyl halide,[9] the formation of configurationally inverted alkylpyridine is expected, since an intermediate radical formed by the first one-electron transfer appears to be sufficiently planar in its steric form to result in an inverted carbanion as a result of the second electron transfer. The planarity of a pyridylmethyl radical is thought to be due to the interaction between an unpaired electron and the π-electrons of a pyridine nucleus.

The electrolytic results, however, indicate that the reduction involves configurational retention and racemization in the cases of 1-(2-pyridyl)- and (4-pyridyl)-

alkanols, respectively. A mechanism involving the pyridylmethyl radical as an important intermediate should also be inadequate to explain such a difference between the electrolytic results of 1-(2-pyridyl)- and (4-pyridyl)alkanols.

According to the mechanism proposed in a previous paper[4] two electrons are supplied to a pyridine nucleus *via* a pyridinium nitrogen atom adsorbed on the cathode surface and then migrate to an asymmetric carbon atom through the π-electron system of the pyridine nucleus. As is shown in the scheme, a protonated 1-(2-pyridyl)-alkanol molecule (I) promotes adsorption at a pyridinium nitrogen, on which a positive charge would be localized to some degree, and at a hydroxonium oxygen. The orientation perpendicular to the cathode surface of the adsorbed pyridine nucleus may contribute to relaxing the steric hindrance between the cathode and I. Two electrons are transferred to the pyridine nucleus from the cathode. Excess electrons in the resulting intermediate (Ia), which should be substantially regarded as an unstable dihydropyridine such as Ib, are sequentially introduced into the bonding σ orbital of the C–O bond lengthened by the attachment of a positive hydroxonium group, and then water is eleminated from the asymmetric carbon. Consequently, a carbanion (Ic), the configuration of which is retained, is formed by the restoration of the completely conjugated system of the pyridine nucleus. The sequence of processes from I to Ic may be regarded as a multi-centered reaction involving two adsorption sites on the cathode.

On the other hand, a protonated 1-(4-pyridyl)-alkanol molecule (II) should promote adsorption only at its pyridinium nitrogen, which has an electron density lower than that of the hydroxonium oxygen, because of the rigidity of the molecule. In the course of the formation of the carbanion from IIb, an electron should be introduced not only into the bonding σ orbital of the C–O bond but also into the antibonding σ^* orbital. The latter process may be accelerated by a proton approaching to the asymmetric carbon from the opposite side of the hydroxonium group. Racemization in the reduction of 1-(4-pyridyl)alkanols should be rationalized as being due to the almost even competition between the above two processes, one of which results in configurational inversion and the other of which results in retention. In the above discussion, it is tacitly assumed that the configurations of the carbanions (Ic and IIc) are stable enough not to be racemized before undergoing protonation. Such an assumption should be acceptable, especially in a strongly acidic medium, since it is known that no recemization occurs in the reduction of optically-active alkyl halides to the corresponding alkanes in neutral media,[9,11,12] which involves a carbanion as an intermediate.[10]

In conclusion, the mechanism proposed in a previous paper[4] is consistent with the stereochemical data obtained in this work.

Experimental

Materials. *Optically-active 2-(4-Pyridyl)-2-butanol (**1**)*: Racemic **1** was prepared from 4-cyanopyridine using the method of Nakajima.[13] Yield 12%, mp 103—104 °C (lit,[13] 113—114 °C), and *m/e* 151 (M^+). Found: C, 71.46; H, 9.01; N, 8.94%. Calcd for $C_9H_{13}NO$: C, 71.49; H, 8.64; N, 9.25%. After 30 g (0.2 mol) of racemic **1** and 46 g (0.2 mol) of (+)-camphor-10-sulfonic acid ($[\alpha]_D^{20}$ +22.1° in water) were dissolved in 90 ml of absolute ethanol at 60 °C, the mixture was slowly cooled to room temperature. The resulting crystals were repeatedly recrystallized (three times) from ethanol. Optically-active **1** was finally obtained: Yield 6.4 g with $[\alpha]_D^{20}$ −1.7° (in ethanol).

*Optically-active 1-(4-Pyridyl)-1-phenylethanol (**2**)*: Racemic **2** was synthesized from 4-pyridyl pheny ketone and methylmagnesium iodide in benzene. Yield 80 g, mp 146—148 °C (lit,[14] 148—150 °C), and *m/e* 199 (M^+). Found: C, 77.76; H, 6.48; N, 6.82%. Calcd for $C_{13}H_{13}NO$: C, 78.46; H, 6.58; N, 7.03%. The compound, **2**, was optically resolved using the method of Thakar and Pathak.[11] $[\alpha]_D^{20}$ +2.4° (in methanol) (lit,[14] $[\alpha]_D^{31}$ +1.567°).

*Optically-active 1-(2-Pyridyl)-1-phenyl-1-propanol (**3**)*: The synthesis and optical resolution of **3** were carried out by the method of Davies.[15] Mp 84—85 °C (lit,[15] 80—81 °C) and *m/e* 213 (M^+). Found: C, 78.61; H, 7.33; N, 6.42%. Calcd for $C_{14}H_{15}NO$: C, 78.84; H, 7.09; N, 6.57%. $[\alpha]_D^{20}$ +80.0° (in chloroform) (lit,[12] $[\alpha]_D^{23}$ +65.9°).

Electrolytic Procedure. Electrolysis was carried out using a method similar to that used in previous work.[4] The products were analyzed by a gas chromatograph (OV-1 column at 150 °C) and were isolated by fractional distillation.

Alkylpyridines. *4-(2-Butyl)pyridine*: Bp 36—37 °C/1.5 Torr (lit,[13] 93—97 °C/15 Torr) and *m/e* 135 (M^+). Picrate: Mp 145—146 °C. Found: C, 49.37; H, 4.42; N, 15.07%. Calcd for $C_{15}H_{16}N_4O_7$: C, 49.45; H, 4.43; N, 15.38%.

4-(α-Methylbenzyl)pyridine: Bp 96—98 °C/1 Torr and *m/e* 183 (M^+). Picrate: Mp 153—154 °C. Found: C, 55.32; H, 3.93; N, 13.29%. Calcd for $C_{19}H_{16}N_4O_7$: C, 55.34; H, 3.91; N, 13.59%.

2-(1-Phenylpropyl)pyridine: Bp 89—90 °C/1 Torr (lit,[16] 104—106 °C/0.01 Torr) and *m/e* 197 (M^+). Picrate: Mp 144—145 °C. Found: C, 56.53; H, 4.38; N, 12.78%. Calcd for $C_{20}H_{18}N_4O_7$: C, 56.34; H, 4.26; N, 13.14%.

N-Substituted Derivatives of 1-Pyridylalkanols and Alkylpyridines. *4-(1-Hydroxy-1-phenylethyl)-1-phenacylpyridinium Bromide*: Compound **1** was heated at 70 °C in an excess amount of phenacyl bromide for 2.5 h. Yield 45% and mp 220—222 °C. Found: C, 63.16; H, 5.15; N, 3.22%. Calcd for $C_{21}H_{20}NO_2Br$: C, 63.33; H, 5.06; N, 3.52%.

4-(α-Methylbenzyl)-1-phenacylpyridinium Bromide: This compound was prepared by a method similar to that described above. Yield 70% and mp 228—229 °C. Found: C, 65.86; H, 5.36; N, 3.43%. Calcd for $C_{21}H_{20}NOBr$: C, 65.98; H, 5.27; N, 3.66%.

2-(1-Hydroxy-1-phenylpropyl)-1-methylpyridinium Iodide: Compound **3** was heated with an excess amount of methyl iodide at 50—60 °C for 3 days in a sealed tube. Yield 40% and mp 119—120 °C. Found: C, 50.57; H, 5.40; N, 3.56%. Calcd for $C_{15}H_{18}NOI$: C, 50.72; H, 5.11; N, 3.94%.

2-(1-Phenylpropyl)-1-methylpyridinium Iodide: 4-(1-Phenylpropyl)pyridine was reflexed in an excess amount of methyl iodide for 5 h and the separated oil was solidified by treatment with diethyl ketone. The titled compound was obtained in a form including three molecules of diethyl ketone as a solvent of crystallization. Yield 36%, mp 100 °C, and $\nu_{C=O}$ 1690 cm^{-1} Found: C, 60.41; H, 7.75; N, 1.97%. Calcd for $C_{15}H_{18}NI \cdot 3C_5H_{10}O$: C, 60.30; H, 8.09; N, 2.34%.

2-(1-Hydroxy-1-phenylpropyl)-1-benzylpyridinium Bromide: An equimolar mixture of **3** and acetic acid was heated at 90 °C in an excess amount of benzyl bromide for 12 h. Yield 70% and mp 97—100 °C. Found: C, 65.70; H, 5.58; N, 3.50%.

Calcd for $C_{21}H_{22}NOBr$: C, 65.63; H, 5.77; N, 3.64%.

2-(1-Phenylpropyl)-1-benzylpyridinium Bromide: 2-(1-Phenylpropyl)pyridine was heated in an excess amount of benzyl bromide at 90 °C for 4 h. Yield 60% and mp 121—123 °C. Found: C, 68.30; H, 6.18; N, 3.61%. Calcd for $C_{21}H_{22}NBr$: C, 68.48; H, 6.21; N, 3.80%.

2-(1-Hydroxy-1-phenylpropyl)pyridine 1-Oxide: Two grams of **3** and 4 ml of 30% hydrogen peroxide were heated in 10 ml of acetic acid at 80 °C for 24 h. Yield 74%, mp 119—120 °C, and *m/e* 229 (M^+). Found: C, 73.02; H, 6.59; N, 5.83%. Calcd for $C_{14}H_{15}NO_2$: C, 73.34; H, 6.59; N, 6.11%.

2-(1-Phenylpropyl)pyridine 1-Oxide: This compound was prepared by a method similar to that described above. Yield 78%, mp 99—101 °C, and *m/e* 213 (M^+). Found: C, 78.48; H, 7.17; N, 6.37%. Calcd for $C_{14}H_{15}NO$: C, 78.84; H, 7.17; N, 6.59%.

This work was supported by a grant from the Kawakami Memorial Foundation, to which the authors wish to express their deep appreciation.

References

1) A benzoylated hydroxyl group is electrolytically reducible.[2,3]

2) S. Wawzonek and J. D. Fredericksen, *J. Electrochem. Soc.*, **106**, 325 (1959).

3) R. E. Erickson and C. M. Fischer, *J. Org. Chem.*, **35**, 1604 (1970).

4) T. Nonaka, T. Amakawa, and K. Odo, *Denki Kagaku*, **40**, 100 (1972).

5) The current decay rate for the electrolysis of **3** was less than that for the electrolysis of **1** and **2**,

6) G. M. Whitesides and D. M. Lewis, *J. Am. Chem. Soc.*, **92**, 6979 (1970).

7) K. Freufenberg, J. Todd, and R. Seidler, *Justus Liebigs Ann. Chem.*, **501** 199, (1933): E. L. Eliel, "Stereochemistry of Carbon Compounds," McGraw-Hill Book Co. Inc. (1962), p. 110.

8) In order to apply the displacement rule, the shift in the molecular optical rotation should be rather large.[7]

9) T. Nonaka, T. Ota, and K. Odo, *Bull. Chem. Soc. Jpn.*, **49**, 419 (1977).

10) P. J. Elcing and B. Pullman, *Adv. Chem. Phys.*, **3**, 1 (1961).

11) B. Czochralska, *Chem. Phys. Lett.*, **1**, 239 (1967).

12) R. Annino, R. E. Erickson, J. Michalovic, and B. McKay, *J. Am. Chem. Soc.*, **88**, 4424 (1966).

13) T. Nakajima, *J. Pharm. Soc. Jpn.*, **77**, 698 (1957).

14) K. A. Thakar and U. S. Pathak, *J. Indian Chem. Soc.*, **41**, 555 (1964).

15) A. G. Davies, *J. Chem. Soc.*, **1956**, 659.

16) E. Sury and K Hoffman, *Helv. Chem. Acta*, **37**, 2133 (1954).

The Reaction of *N*-(Phenylsulfonyl)benzohydrazonoyl Chloride with *N*-Substituted Benzamidines, with Benzimidates, and with 2-Aminopyridines*

Suketaka Ito, Yumo Tanaka, Akikazu Kakehi, and Hirotaka Miyazawa

Department of Industrial Chemistry, Faculty of Engineering, Shinshu University, Wakasato, Nagano 380

(Received December 9, 1976)

4-Alkyl or aryl-3,5-diphenyl-4*H*-1,2,4-triazoles, 3-phenyl-1,2,4-triazolo[4,3-*a*]pyridine, and -pyrimidine are obtained by the title reactions. The reaction may proceed *via* the nucleophilic attack of amidine or imidate on the imidoyl carbon of hydrazonoyl chloride and the subsequent intramolecular cyclization of the intermediate formed in the initial step, with the removal of the amino or alkoxyl and phenylsulfonyl groups.

N-(Phenylsulfonyl)benzohydrazonoyl chloride(**1**) does not function as a 1,3-dipole source for the cyclo-addition reaction because of the strong electron-withdrawing nature of the phenylsulfonyl group.[1] However, since the arylsulfonyl group can be eliminated as an arenesulfinate anion or -sulfonyl cation, and since the imidoyl carbon and amino nitrogen of **1** possess electrophilic and nucleophilic[2] characters respectively, **1** may serve for synthesizing heterocycles.

In the previous paper,[3] we reported the synthesis of 2,5-diaryltetrazoles by the reaction of **1** with arylhydrazine, in which the elimination of the benzenesulfinate ion was observed.

The present paper will deal with the formation of 1,2,4-triazoles from **1** and *N*-substituted benzamidines, benzimidates, or 2-aminopyridines. In this reaction, the phenylsulfonyl group may be removed cationically.

Fusco and Musante[4] reported the preparation of 1-substituted 1*H*-1,2,4-triazoles using *N*-phenylbenzohydrazonoyl chloride and unsubstituted benzamidines. Similarly, Huisgen *et al.*[5] obtained 1,2,4-triazole by the reaction of ethyl acetimidate with *N*-phenylbenzohydrazonoyl chloride in the presence of triethylamine. In these methods, however, *N*-substituted benzamidines or imidates cannot be used, and the resulting triazole bears the *N*-substituent of the starting hydrazonoyl chloride, virtually the phenyl group only, as its 1-substituent.

In contrast, the present method, using various amidines and imidates, gives 4-aryl or alkyl substituted 4*H*-1,2,4-triazoles as well as 1-phenylsulfonyl-1*H*-1,2,4-triazole.

Results and Discussion

Reaction with Benzamidines. The reaction of **1** with benzamidines was carried out in a 1 : 2 mole ratio in THF at room temperature, giving 4-substituted 3,5-diphenyl-4*H*-1,2,4-triazole (**4** or **4'**), and/or 1-phenylsulfonyl-3,5-diphenyl-1*H*-1,2,4-triazole(**5**), and 1,4-dihydro-3,6-diphenyl-1,4-bis(phenylsulfonyl)-1,2,4,5-tetrazine(**2**), together with a trace amount of 3,6-diphenyl-1,2,4,5-tetrazine.[6] The results are summarized in Scheme 1 and Table 1.

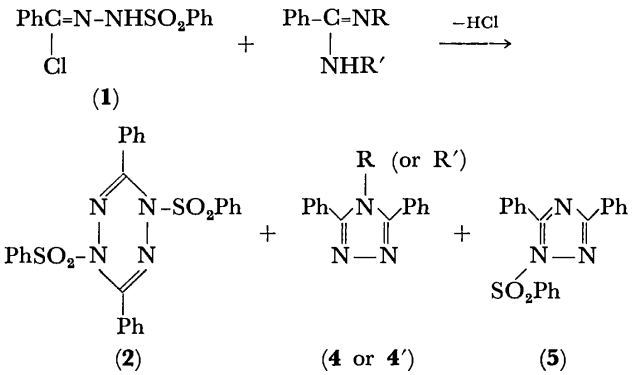

Scheme 1.

Benzenesulfonamides and *N*-phenylsulfonylated amidine were also obtained. Interestingly, the formation of benzenesulfonyl chloride was observed in the reaction with *N*,*N*-disubstituted benzamidines.[7]

As is shown in Table 1, *N*-arylbenzamidines gave **4** predominantly, and the reaction with benzamidine and its *N*-alkylated derivatives resulted in an increase in the yield of **2**. Aliphatic amidines such as *N*-ethylacetamidine, a stronger base than benzamidines, gave **2** primarily, and a small amount of *N*-(phenylsulfonyl)-*N*-[*N*-(phenylsulfonyl)benzohydrazonoyl]benzohydrazonoyl chloride(**2'**)[8] was isolated in this case.

Since the phenylsulfonyl group is a strong electron-withdrawing group, the amino hydrogen of **1** may be acidic and may be abstracted easily by amidine, a base, and the resulting *N*-(phenylsulfonyl)benzohydrazonoyl chloride anion(**1'**) may be also stable. Considering the isolation of **2'** in the reaction with *N*-ethylacetamidine, the following mechanism involving the nucleophilic attack of **1'** on **1** may be possible for the formation of **2** (Scheme 2).[9] The increased formation of **2** observed in the reaction with benzamidine and its *N*-alkylated derivatives may be attributed to their basicity being stronger than that of *N*-arylbenzamidines.

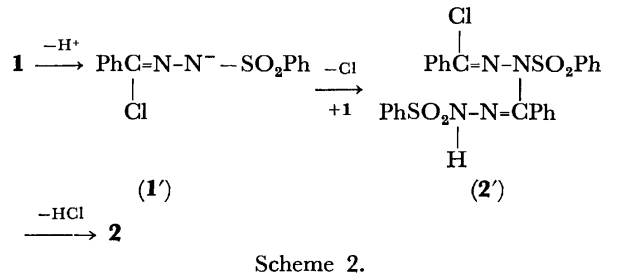

Scheme 2.

* Presented in part at the Autumnal Joint Meeting of the Tokai Branch of the Chemical Society of Japan and the Chubu Branches of the related Societies, Nagoya, October, 1975.

Table 1. The reactions of *N*-(phenylsulfonyl)-benzohydrazonoyl chloride with benzamidines

Ph-C=N-R (NHR′) R	R′	Yields(%) of products[a] 2	5[b]	4[c]	Mp of 4 (°C)
Ph	H	trace	4	82	
Ph	Ph	trace	—	90	291—292[e]
Ph	Me	7	—	70 9(4′, R′=Me)[d]	
p-ClC_6H_4	H	4	6	80	266—267[f]
p-MeC_6H_4	H	trace	8	69	291—292[g]
$PhCH_2$	H	10	58	26	223—224[h]
Et	H	22	40	12	159—160[i]
Me	H	16	37	16	248—250[j]
H	H	20	49	—	
Ph-C=NH | N=CHPh		12	72	—	

a) Yields(isolated) as mole per cent based on **1** used. Satisfactory analytical data (±0.3% for C,H,N) were obtained for all the known products in the table. b) Colorless needles. Mp 145—147 °C (EtOH). Found: C, 66.56; H, 4.10; N, 11.72%. Calcd for $C_{20}H_{15}N_3O_2S$: C, 66.46; H, 4.19; N, 11.63%. c) The 4-substituent corresponds to the N^2-substituent of the starting amidine shown in the table. d) Identical with 4(R=Me). e) Lit, mp 291—292 °C: Y. A. Levin and M. S. Skorobagotova, *Khim. Geterotsikl. Soedin*, **1967**, 339; *Chem. Abstr.*, **67**, 100076f(1967). f) Lit, mp 252.5—254 °C: *idem.*, *ibid.* g) Lit, mp 291—292 °C: *idem.*, *ibid.* h) Lit, mp 229 °C: T. Curtius and G. Ehrhart, *Ber.*, **55**, 1559 (1922); "Beilsteins Handbuch der Organischen Chemie," E2, Bd. XXVI (1954), p. 49. i) Lit, mp 163.5—164.5 °C: L. A. Lee, R. Evans, and J. W. Wheeler, *J. Org. Chem.*, **37**, 343 (1972). j) Lit, mp 242—243 °C: L. A. Lee and J. W. Wheeler, *ibid.*, **37**, 348 (1972).

The attempted reactions of **1** with a number of dipolarophiles in the presence of a base *via* the 1,3-dipolar cyclo-addition were unsuccessful, but resulted in the formation of **2** in all cases. The reactivity of **1** different from that of *N*-phenylbenzohydrazonoyl chloride is probably due to the fact that the negative-charge delocalizability of the phenylsulfonyl group is superior to that of the phenyl group: the charge on the amino nitrogen of **1′** is delocalized by the phenylsulfonyl group, so **1′** does not release the chloride anion to form a 1,3-dipole.

Thus, the 1,3-dipolar cyclo-addition mechanism may not be applicable to the reaction of **1** with amidines, and a step-by-step mechanism involving the nucleophilic attack of amidine on **1**, followed by the intramolecular cyclization of the resultant *N*-hydrazonoylbenzamidine (**3** or **3′**)[10] *via* the nucleophilic attack of amino group on the imino carbonyl carbon of the original amidine moiety, can be postulated as more probable (Schemes 3 and 4):

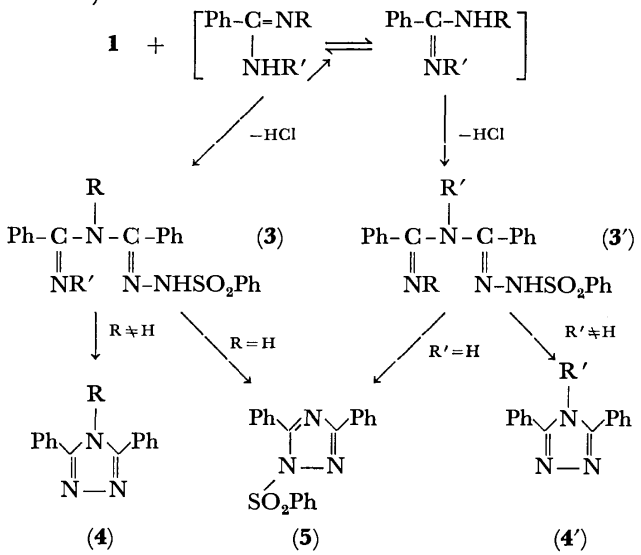

Scheme 3.

Amidines are a tautomeric compound, so that the nucleophilic attack of amidine on the imidoyl carbon of **1** may take place in two ways. Since the nucleophilicity of imino nitrogen of amidine is stronger than that of amino nitrogen, the predominant formation of **4** in the reaction with *N*-arylbenzamidines indicates that the amidines exist preferentially as arylimino tautomers. This preference is probably a result of the

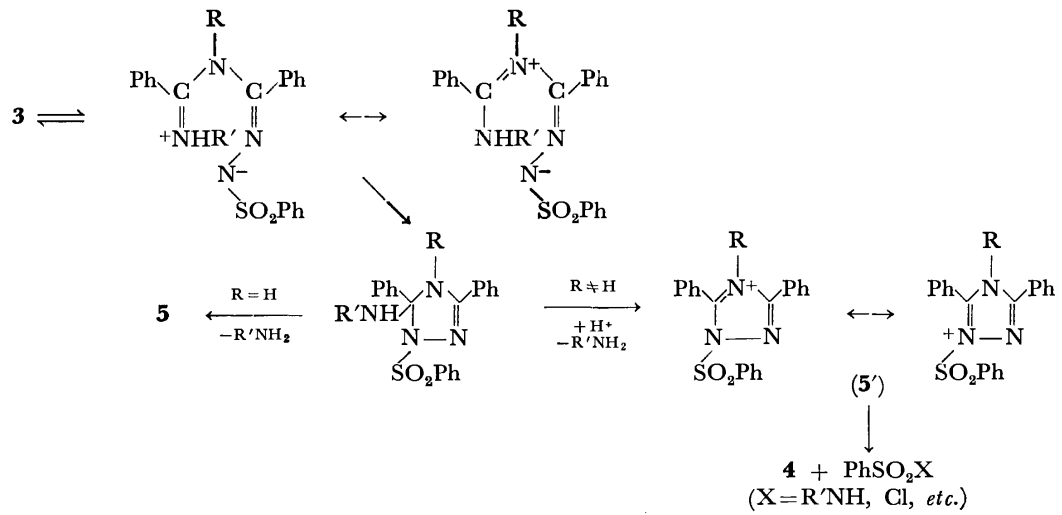

Scheme 4.

conjugation between the aryl and imino groups.[11] On the other hand, *N*-alkylbenzamidines gave **5** as the major product: presumably, this result is due to the steric hindrance of the *N*-alkyl group.

Since the arylsulfonamido group is also workable as a leaving group, as may be seen in the diazo-transfer reaction with tosyl azide,[12] an alternative process involving the direct replacement of the sulfonamido group, given in Scheme 5, is conceivable for the cyclization of **3** or **3'**; in such a case, R'=H in **3** or R=H in **3'**.

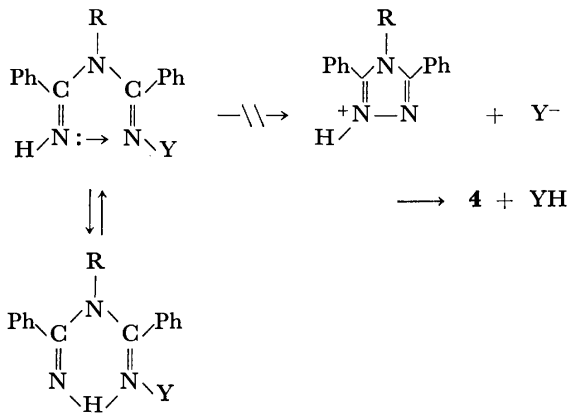

(**3**, R'=H) : Y=$PhSO_2NH$
(**7**) : Y=$PhSO_2$

Scheme 5.

In this route, benzenesulfonamide should be the only product carrying a phenylsulfonyl group. Actually, however, *N*-phenylsulfonylated amidine and amine were mainly obtained, and benzenesulfonamide was a minor product. Consequently, this reaction route is improbable.[13]

Stirring the reaction mixture obtained in the first step of the reaction of **1** with amidine with potassium carbonate after the removal of the precipitates led to the formation of 3,5-diphenyl-4*H*-1,2,4-triazole(**6**) in part, which must have been derived from 1-phenylsulfonyl-3,5-diphenyl-1*H*-1,2,4-triazole(**5**). The combined yield of the two products were almost invariable.

The transformation of **5** to **6** proceeded excellently when the ethanolic solution of **5** was refluxed in the presence of a catalytic amount of *p*-toluensulfonic acid.

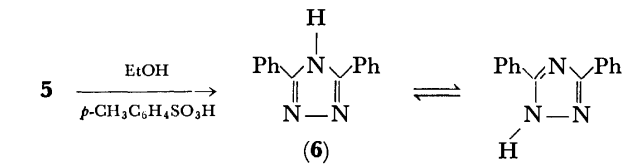

Attempts to derive **5** to **4** by alkylation with alkyl halide were, however, unsuccessful.

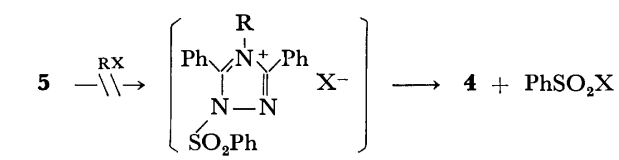

N-Benzylidenebenzamidine gave **5** upon the removal of the benzylideneamine moiety, and the elimination of benzenesulfinic acid from the primary intermediate could not be observed in the presence of alkali.

Table 2. 3,5-diphenyl-1,2,4-triazoles from benzimidates(Ph-C(=NR)-OR')

Benzimidate R	Benzimidate R'	Triazole (Yield, %)	
H	Et	**5**	(95)
Ph	Et	**4**(R=Ph)	(25)
Me	Me	**4**(R=Me)	(33)

Reaction with Benzimidates. The reaction of **1** with benzimidates took place analogously with the removal of the alkoxyl group to give triazoles (Table 2). With a slight modification of Schemes **3** and **4** by replacing R'NH by R'O, the reaction route can be represented. In the case of *N*-substituted benzimidates, the reaction proceeded slowly and gave **2** as the main product; this may be due to the uneasy formation of an intermediate because of the lack of a hydrogen atom to be removed as a proton in the imidates.

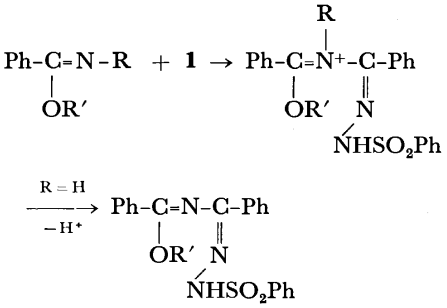

Reaction with 2-Aminopyridine and -Pyrimidine. 2-Aminopyridine(**8a**) and -pyrimidine(**8b**), cyclic amidines known to exist as amino tautomers, reacted with **1** in a manner similar to that above to give 3-phenyl-1,2,4-triazolo[4,3-*a*]pyridine and -pyrimidine(**9**) respectively in fairly good yields (Table 3).

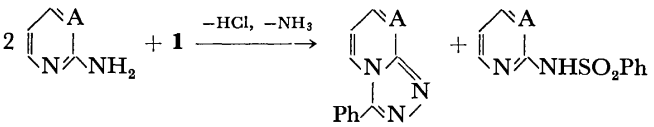

(**8a**: A=CH, **8b**: A=N) (**9**)

The main phenylsulfonylated products were 2-(phenylsulfonylamino)pyridine and -pyrimidine. These results indicate that the initial hydrazonoylation took place at the ring nitrogen, and that the 2-amino group was removed. No product *via* the alternative process could be isolated.

Since several methods for preparing 4-substituted 3,5-diaryl-4*H*-1,2,4-triazoles are available,[14] the present method is not always useful from the synthetic point of view. On the other hand, for preparing 1,2,4-triazolopyridines, known to be useful anti-convulsants and tranquilizers, the reaction of 2-hydrazinopyridine with carboxylic acid[15] may be the only available method. Thus, because of the ready availability of starting materials, the simplicity of procedure, and the comparatively higher yield of products, this reaction might be useful in obtaining this type of compound.

Table 3. Preparation of 3-phenyl-1,2,4-triazolo[4,3-*a*]pyridines(**9**)

9 A	Yield (%)	Mp (°C)	IR (ν_{max}^{KBr}, cm^{-1})	^{1}H-NMR(δ, ppm, $CDCl_3$)[a] C-4	C-5	C-6	C-7	Ph
CH	54	174—177[b] (EtOH)	1630, 1495, 1461, 1375, 1309, 1176, 1135, 1163, 1010, 751	8.32 brd	6.86 dt	7.28 brt	[d]	7.50—8.00 m
				$J_{4,5}=J_{5,6}=7.0$, $J_{5,7}=1.5$, $J_{6,7}=8.0$ Hz				
N[c]	42	190—193 (EtOH)	1616, 1507, 1442, 1417, 1379, 1347, 1293, 1226, 1172, 1123, 766	8.92 dd	7.09 q	8.86 dd	—	8.30—8.50 m (2H) 7.40—7.70 m (3H)
				$J_{4,5}=6.0$, $J_{4,6}=1.5$, $J_{5,6}=4.5$ Hz				

a) Abbreviations of the NMR spectral patterns are as follows: d, doublet; t, triplet; q, quartet; m, multiplet; dd, double doublet; dt, double triplet; br, broad. b) Lit, mp 173—174 °C: S. Takase and T. Demura, *Kogyo Kagaku Zasshi*, **69**, 1417 (1966). Found: C, 75.32; H, 4.60; N, 21.45%. c) Almost colorless leaflets. Found: C, 67.02; H, 4.12; N, 28.27%. Calcd for $C_{11}H_8N_4$: C, 67.33; H, 4.11; N, 28.56%. d) Overlapped with C-3 phenyl-proton.

Experimental

The melting points were determined with a Yanagimoto micromelting point apparatus, Model MP-S3, and are uncorrected. The microanalysis was performed on a Perkin-Elmer elemental analyzer, Model 240. The IR and NMR spectra were recorded with a JASCO DS-301 spectrometer and a JEOL C60-HL spectrometer respectively.

The *N*-(phenylsulfonyl)benzohydrazonoyl chloride(**1**) was prepared by the previously reported method,[3] while the benzamidines were obtained from ethyl benzimidate hydrochloride or *N*-substituted benzimidoyl chlorides according to methods described in the literature. The products were identified by means of their analytical and spectral data and by comparison with authentic specimens prepared by other synthetic methods.

*Reaction of **1** with Amidines.* *General Procedure*: A solution of amidine(0.01 mol) in THF(15 ml) was added, drop by drop, to a solution of **1**(0.005 mol) in THF(15 ml) at room temperature. Within a few minutes, precipitates began to separate. The reaction mixture was stirred for 2 h and then allowed to stand overnight. The separated precipitates were filtered and washed with THF. The filtrate combined with the washings was concentrated and then chromatographed on a silica gel(20 g) column, using benzene as the eluent, to give dihydrotetrazine, benzenesulfonamides, *N*-phenylsulfonylamidine, and 1,2,4-triazole. Benzenesulfonyl chloride, when formed, was obtained as the first eluate. Most of the 4-substituted 3,5-diphenyl-4*H*-1,2,4-triazole was obtained in a fairly pure state by washing the precipitates above separated with water, followed by cold ethanol. The results are summarized in Tables 1 and 3.

*Reaction of **1** with Benzimidates.* The reaction was conducted in a manner similar to that used with amidines. The results are summarized in Table 2.

References

1) S. Ito, Y. Tanaka, and K. Yoshida, Abstracts of the Meeting of the Tokai Branch of the Chemical Society of Japan, Matsumoto, November 1972, p. 1; Abstracts of the 28th Annual Meeting of the Chemical Society of Japan, Tokyo, April 1973, Vol. III, p. 1371.

2) Phenylsulfonylamino nitrogen may function also as an electrophilic center with the elimination of the benzenesulfinate ion; see Ref. 3.

3) S. Ito, Y. Tanaka, and A. Kakehi, *Bull. Chem. Soc. Jpn.*, **49**, 762 (1976).

4) R. Fusco and C. Musante, *Gazz. Chim. Ital.*, **68**, 147 (1938).

5) R. Huisgen, R. Grashey, E. Aufderhaar, and R. Kunz, *Chem. Ber.*, **98**, 642 (1965).

6) Amine and amidine hydrochloride separated as precipitates in the reaction.

7) This fact might support the possible and potential intermediacy of **5′**(Scheme 4), which may be a strong phenylsulfonylating agent.

8) Compound **2′**: mp 160—162 °C(dec), IR(KBr, cm^{-1}), 3190(ν_{NH}), 1370; 1350; 1170(ν_{SO_2}). Found: C, 56.79; H, 3.79; N, 10.12%. Calcd for $C_{26}H_{21}N_4S_2O_4Cl$: C, 56.47; H, 3.83; N, 10.13%.

9) Wawzonek and Kellen obtained 1,4-dihydro-3,6-diphenyl-1,4-bis(*p*-tolylsulfonyl)-1,2,4,5-tetrazine by treating *N*-(*p*-tolylsulfonyl)benzohydrazonoyl chloride with triethylamine, and suggested the same reaction route for this dehydrochlorodimerization(S. Wawzonek and J. N. Kellen, *J. Org. Chem.*, **38**, 3627 (1973)).

10) The overall reaction generally proceeded easily at room temperature, and the primary product or intermediate, **3** or **3′**, could not be isolated. However, **1** is able to function as a hydrazonoylating agent: for example, the formation of **2′** should be ascribed to the hydrazonoylation of **1′** with **1**, and the reaction of **1** with arylhydrazines[3] proceeds *via* the *N*-hydrazonoylation of hydrazine with **1**. Therefore, the postulation of **3** or **3′** is reasonable.

11) P. A. S. Smith, "The Chemistry of Open-Chain Organic Nitrogen Compounds," Vol. I, W. A. Benjamin, New York (1965), p. 178.

12) M. Regitz, *Angew. Chem.*, **79**, 786 (1967).

13) In order to obtain some mechanistic information, the ring closure of N^1-phenyl-N^1-benzimidoyl-N^2-(phenylsulfonyl)-benzamidine(**7**, prepared from *N*-(phenylsulfonyl)benzimidoyl chloride and *N*-phenylbenzamidine, mp 222—225 °C) to **4** was examined. However, even under reflux in xylene in the presence of alkali, no remarkable change was observed, and most of the **7** was recovered. The concerted 1,5-*cis* elimination of benzenesulfinic acid should not be possible because of the anti-aromaticity of the transition state; in the intramolecular S_N2-type route(Scheme 5), the separation of an unlike charge is required for the activation process; the most stable configuration of **7** may be the U-shaped form with hydrogen-bonding. These seem to be the reasons for the unreactivity of **7**.

14) *E.g.*, R. Stolle, *J. Prakt. Chem.*, **73**, 288(1906); G. Scheuing and B. Walach, German Patent 543026; *Chem. Abstr.*, **26**, 3263 (1932).

15) J. B. Bicking, U. S. Patent 2917511; *Chem. Abstr.*, **54**, 8854e (1960).

The Photochemical Reaction of 1,2-Naphthoquinones with Aldehydes. III.[1] The Reactions with Aromatic Aldehydes and α,β-Unsaturated Aliphatic Aldehydes

Akio TAKUWA

Department of Chemistry, Faculty of Literature and Science, Shimane University, Nishikawatsu-cho, Matsue 690

(Received December 24, 1976)

Photochemical reactions of 1,2-naphthoquinone and the substituted derivatives with a variety of aldehydes in the liquid phase have been investigated. The reaction with saturated aliphatic aldehydes gives a mixture of 3-acyl-1,2-naphthalenediol and 1,2-naphthalenediol monoacyl esters. On the other hand, the irradiation of the benzene solution of a 1,2-naphthoquinone derivative and an aromatic aldehyde gives, in general, 1,2-naphthalenediol monoaroyl esters, together with small amounts of other products. Unlike saturated aliphatic aldehydes, α,β-unsaturated aldehydes; *i.e.*, propenal, 2-butenal, *trans*-2-hexenal, 1-cyclopentenecarbaldehyde, and 1-cyclohexenecarbaldehyde, behave similary to the aromatic aldehydes in the photochemical reaction, giving only 1,2-naphthalenediol monoesters. However, 10-undecenal, 3-phenylpropanal, cyclopentanecarbaldehyde, cyclohexanecarbaldehyde, and 3-cyclohexenecarbaldehyde give mixtures of 3-acyl-1,2-naphthalenediols and 1,2-naphthalenediol monoacyl esters similar to those from saturated aliphatic aldehydes. The origin of these significant differences is discussed.

Light-induced reactions between quinone and aldehyde have been extensively studied by several workers,[2] but there have been few studies of those of 1,2-naphthoquinone derivatives, probably because of their instability.[3] Awad and Hafez, for example, failed to isolate photo-adducts by the photolysis of 1,2-naphthoquinone in the presence of acetaldehyde.[4] The successful isolation of photo-adducts in the photochemical reactions of 1,2-naphthoquinone with saturated aliphatic aldehydes was first reported by the present author.[1] Thus, 3-acyl-1,2-naphthalenediols, **1**, (C-attacking product) and 1,2-naphthalenediol monoacyl esters, **2**, (O-attacking product) were isolated as the reaction products.

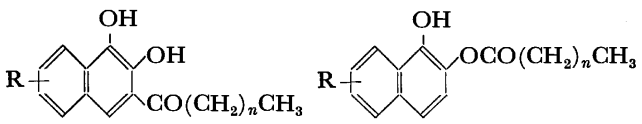

1 (C-attacking product) **2** (O-attacking product)

R=H, 4-CN, 6-Br, 6-CH_3; n=0—8

On the contrary, a preliminary investigation of the photochemical reactions of aromatic or α,β-unsaturated aliphatic aldehydes with 1,2-naphthoquinones revealed that the reaction products consisted exclusively of 1,2-naphthalenediol monoesters. On the other hand, *p*-quinones, in general, give C-attacking products as their major products in photochemical reactions with aliphatic or aromatic aldehydes.[2] In this paper, a detailed investigation of the reaction products, as well as of the effect of the structure of aldehydes and the substituent effect of 1,2-naphthoquinones on the product distributions, will be described.

Results and Discussion

The quinones examined in this work are 1,2-naphthoquinone and its 3-chloro-, 3-bromo-, 4-cyano-, 4-methyl-, 4-methoxy-, 6-bromo-, 6-chloro-, and 6-methyl derivatives. Benzaldehyde, and its *p*-nitro-, *m*-nitro-, *p*-methyl-, *p*-methoxy-, 2,4-dimethoxy-, 3,4,5-trimethoxy-, 2,4,6-trimethyl-, and 2,4,6-triisopropyl derivatives are examined as typical aromatic aldehydes. As representative α,β-unsaturated aliphatic aldehydes, propenal, 2-butenal, *trans*-2-hexenal, 1-cyclopentenecarbaldehyde, 1-cyclohexenecarbaldehyde, and cinnamaldehyde are used in this work. In addition, 10-undecenal, 3-phenylpropanal, cyclopentanecarbaldehyde, cyclohexanecarbaldehyde, 3-cyclohexenecarbaldehyde, and 3-chlorobutanal are also examined.

A benzene solution of a 1,2-naphthoquinone derivative and an aldehyde was irradiated by means of a 300-W high-pressure Hg arc lamp for a suitable time. The reaction mixture was then concentrated and chromatographed on silica gel. The products are summarized in Tables 1, 2, and 3.

In the reaction of 1,2-naphthoquinone with benzaldehyde, only 1,2-naphthalenediol monobenzoate, **3a**, is obtained. The other aromatic aldehydes used here behave much like benzaldehyde, giving the corresponding 1,2-naphthalenediol monoaroyl esters (O-attacking products), together with no ring-substituted derivatives (C-attacking products). Other substituted 1,2-naphthoquinone derivatives give O-attacking products exclusively in photochemical reactions with aromatic aldehydes (see Table 1).

These results are surprising because, in the photochemical reactions of 1,2-naphthoquinones with saturated aliphatic aldehydes, acetaldehyde, for example, gives 3-acetyl-1,2-naphthalenediols in a yield comparable to that of 1,2-naphthalenediol monoacetates. In addition, it is well known that *p*-benzoquinones and 1,4-naphthoquinones, in general, give C-attacking products predominantly, along with minor O-attacking products, in photochemical reactions with both aliphatic and aromatic aldehydes.[2]

In the photochemical reactions of 1,2-naphthoquinones with aromatic aldehydes, the larger steric requirement of the phenyl than of the alkyl group might be the cause of the absence of the C-attacking product. Cyclopentanecarbaldehyde and cyclohexanecarbaldehyde, however, give both C-attacking products and O-

Table 1. The photo-addition compounds from the photochemical reaction of 1,2-naphthoquinone derivatives with aromatic aldehydes

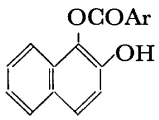

3

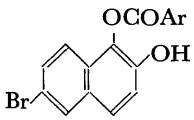

4

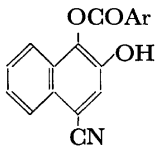

5

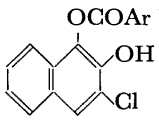

6

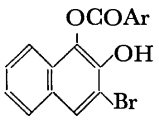

7

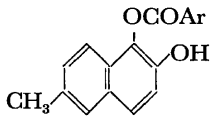

8

and/or isomer

Quinone[a]	Aldehyde	Ar	Compound No	Yield[b,c] (%)	Mp (°C)
1,2-NQ	Benzaldehyde	C_6H_5	**3a**	29	162—166
1,2-NQ	*p*-Nitrobenzaldehyde	*p*-$NO_2C_6H_4$	**3b**	39	182—183
1,2-NQ	*m*-Nitrobenzaldehyde	*m*-$NO_2C_6H_4$	**3c**	31	159—161
1,2-NQ	*p*-Methylbenzaldehyde	*p*-$CH_3C_6H_4$	**3d**	23	158—160
1,2-NQ	*p*-Methoxybenzaldehyde	*p*-$CH_3OC_6H_4$	**3e**	26	184—185
1,2-NQ	3,4,5-Trimethoxybenzaldehyde	3,4,5-$(CH_3O)_3C_6H_2$	**3f**	14	195—198
6-Br-1,2-NQ	Benzaldehyde[d]	C_6H_5	**4a**	47	173—174
6-Br-1,2-NQ	*p*-Nitrobenzaldehyde	*p*-$NO_2C_6H_4$	**4b**	49	201—202
6-Br-1,2-NQ	*m*-Nitrobenzaldehyde	*m*-$NO_2C_6H_4$	**4c**	39	177—178
6-Br-1,2-NQ	*p*-Methylbenzaldehyde[d]	*p*-$CH_3C_6H_4$	**4d**	35	189—190
6-Br-1,2-NQ	*p*-Methoxybenzaldehyde[d]	*p*-$CH_3OC_6H_4$	**4e**	54	193—194
6-Br-1,2-NQ	2,5-Dimethoxybenzaldehyde	2,5-$(CH_3O)_2C_6H_3$	**4f**	65	145—149
6-Br-1,2-NQ	3,4,5-Trimethoxybenzaldehyde	3,4,5-$(CH_3O)_3C_6H_2$	**4g**	15	211—214
6-Br-1,2-NQ	2,4,6-Trimethylbenzaldehyde	2,4,6-$(CH_3)_3C_6H_2$	**4h**	41	292—293
6-Br-1,2-NQ	2,4,6-Triisopropylbenzaldehyde	2,4,6-$[(CH_3)_2CH]_3C_6H_2$	**4i**	19	190—192
4-CN-1,2-NQ	Benzaldehyde	C_6H_5	**5a**	21	177—178
4-CN-1,2-NQ	*p*-Nitrobenzaldehyde[e]	*p*-$NO_2C_6H_4$	**5b**	39	253—255
4-CN-1,2-NQ	*m*-Nitrobenzaldehyde	*m*-$NO_2C_6H_4$	**5c**	35	225—227
4-CN-1,2-NQ	*p*-Methylbenzaldehyde	*p*-$CH_3C_6H_4$	**5d**	16	186—188
4-CN-1,2-NQ	*p*-Methoxybenzaldehyde[e]	*p*-$CH_3OC_6H_4$	**5e**	26	215—217
4-CN-1,2-NQ	3,4,5-Trimethoxybenzaldehyde	3,4,5-$(CH_3O)_3C_6H_2$	**5f**	27	151—152
4-CN-1,2-NQ	2,4,6-Trimethylbenzaldehyde	2,4,6-$(CH_3)_3C_6H_2$	**5g**	55	217—219
3-Cl-1,2-NQ	Benzaldehyde	C_6H_5	**6a**	26	141—144
3-Cl-1,2-NQ	Cinnamaldehyde	$C_6H_5CH{=}CH$	**6b**	25	180—181
3-Cl-1,2-NQ	*p*-Nitrobenzaldehyde	*p*-$NO_2C_6H_4$	**6c**	44	203—205
3-Cl-1,2-NQ	*m*-Nitrobenzaldehyde	*m*-$NO_2C_6H_4$	**6d**	26	194—196
3-Cl-1,2-NQ	*p*-Methylbenzaldehyde	*p*-$CH_3C_6H_4$	**6e**	40	164—166
3-Cl-1,2-NQ	*p*-Methoxybenzaldehyde	*p*-$CH_3OC_6H_4$	**6f**	26	184—186
3-Br-1,2-NQ	Benzaldehyde	C_6H_5	**7a**	21	150—153
3-Br-1,2-NQ	Cinnamaldehyde	$C_6H_5CH{=}CH$	**7b**	20	189—190
3-Br-1,2-NQ	*p*-Nitrobenzaldehyde	*p*-$NO_2C_6H_4$	**7c**	17	202—205
3-Br-1,2-NQ	*m*-Nitrobenzaldehyde	*m*-$NO_2C_6H_4$	**7d**	15	188—190
3-Br-1,2-NQ	*p*-Methylbenzaldehyde	*p*-$CH_3C_6H_4$	**7e**	22	176—178
3-Br-1,2-NQ	*p*-Methoxybenzaldehyde	*p*-$CH_3OC_6H_4$	**7f**	20	196—198
6-Me-1,2-NQ	Benzaldehyde	C_6H_5	**8a**	38	172—174
6-Me-1,2-NQ	Cinnamaldehyde	$C_6H_5CH{=}CH$	**8b**	35	145—146
6-Me-1,2-NQ	*p*-Nitrobenzaldehyde	*p*-$NO_2C_6H_4$	**8c**	23	187—189
6-Me-1,2-NQ	*m*-Nitrobenzaldehyde	*m*-$NO_2C_6H_4$	**8d**	24	172—175
6-Me-1,2-NQ	*p*-Methylbenzaldehyde	*p*-$CH_3C_6H_4$	**8e**	41	185—186
6-Me-1,2-NQ	*p*-Methoxybenzaldehyde	*p*-$CH_3OC_6H_4$	**8f**	53	184—185

a) 1,2-NQ: 1,2-naphthoquinone, 6-Br-1,2-NQ: 6-bromo-1,2-naphthoquinone, 4-CN-1,2-NQ: 4-cyano-1,2-naphthoquinone, 3-Cl-1,2-NQ: 3-chloro-1,2-naphthoquinone, 3-Br-1,2-NQ: 3-bromo-1,2-naphthoquinone, 6-Me-1,2-NQ: 6-methyl-1,2-naphthoquinone. b) The yield was calculated on the basis of the amount of quinone used. c) The relatively low yields may be due to the instability of 1,2-naphthoquinone and its derivatives, because they were not recovered from the reaction mixture. d) *Cf.* A. Mustafa *et al.*, *J. Am. Chem. Soc.*, **78**, 4306 (1956). e) *Cf.* A. Schönberg *et al.*, *J. Am. Chem. Soc.*, **77**, 3850 (1955).

TABLE 2. THE PHOTO-ADDITION COMPOUNDS FROM THE PHOTOCHEMICAL REACTION OF 1,2-NAPHTHOQUINONE DERIVATIVES WITH α,β-UNSATURATED ALIPHATIC ALDEHYDES

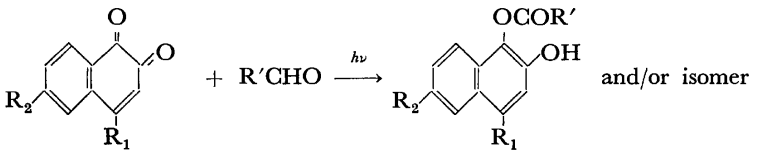

9

Quinone[a]	Aldehyde	Product			Compound No	Yield[b,c] (%)	Mp (°C)
		R_1	R_2	R'			
1,2-NQ	Propenal	H	H	CH_2=CH-	**9a**	47	111—113
6-Br-1,2-NQ	Propenal	H	Br	CH_2=CH-	**9b**	72	150—151
4-CN-1,2-NQ	Propenal	CN	H	CH_2=CH-	**9c**	51	165—166
1,2-NQ	2-Butenal	H	H	CH_3CH=CH-	**9d**	42	99—101
4-CN-1,2-NQ	2-Butenal	CN	H	CH_3CH=CH-	**9e**	28	153—154
1,2-NQ	*trans*-2-Hexenal	H	H	$CH_3(CH_2)_2CH$=CH-	**9f**	16	80— 81
6-Br-1,2-NQ	*trans*-2-Hexenal	H	Br	$CH_3(CH_2)_2CH$=CH-	**9g**	43	129—131
4-CN-1,2-NQ	*trans*-2-Hexenal	CN	H	$CH_3(CH_2)_2CH$=CH-	**9h**	20	135—137
1,2-NQ	1-Cyclopentenecarbaldehyde	H	H		**9i**	37	130—132
6-Br-1,2-NQ	1-Cyclopentenecarbaldehyde	H	Br		**9j**	30	176—177
4-CN-1,2-NQ	1-Cyclopentenecarbaldehyde	CN	H		**9k**	8	145—146
1,2-NQ	1-Cyclohexenecarbaldehyde	H	H		**9l**	28	140—142
6-Br-1,2-NQ	1-Cyclohexenecarbaldehyde	H	Br		**9m**	41	156—157
1,2-NQ	Cinnamaldehyde	H	H	C_6H_5CH=CH-	**9n**	57	179—180
6-Br-1,2-NQ	Cinnamaldehyde	H	Br	C_6H_5CH=CH-	**9o**	39	190—191
4-CN-1,2-NQ	Cinnamaldehyde[d]	CN	H	C_6H_5CH=CH-	**9p**	58	178—180

a, b), c) See the footnotes in Table 1. d) *Cf.* A. Schönberg *et al.*, *J. Am. Chem. Soc.*, **77**, 3850 (1955).

attacking products in reactions with 1,2-naphthoquinone. 4-Cyano-1,2-naphthoquinone behaves similarly to give both C-attacking and O-attacking products. In addition, α,β-unsaturated aliphatic aldehydes also give 1,2-naphthalenediol monoesters exclusively (see Table 2). Therefore, there is no reason to consider that the higher steric factor of the phenyl group could be the controlling factor of the product distribution.

What is, then, the controlling factor for the C-attacking or O-attacking products in these reactions? Since these photochemical reactions are undoubtedly initiated by hydrogen abstraction from aldehyde by the photo-excited 1,2-naphthoquinone molecule,[5] giving an acyl radical and a 1,2-naphthosemiquinone radical,[6] the structure of the combination product of the two resulting radicals must depend on the electronic character of the radical concerned. It has been reported that both the acetyl radical and the benzoyl radical have a nucleophilic character.[7] However, considering the photochemical reactions of 1,2-naphthoqinone with acetaldehyde, propenal, and benzaldehyde, the present author could arrange the decreasing nucleophilic character of the acyl radicals concerned in the following order: $CH_3\dot{C}$=O>CH_2=CH–$\dot{C}$=O>$C_6H_5\dot{C}$=O, on the basis of the inductive effect of the methyl, vinyl, and phenyl groups. Acyl radicals are, in general, of a strong σ-radical character and most of the free spin localizes on the acyl carbon. This was confirmed by the ESR measurement of the benzoyl radical.[8]

p-Methyl- and *p*-methoxybenzaldehyde, in reaction with *p*-benzoquinone, give 2-aroylhydroquinones as the predominant products.[9] However, as is shown in Table 1, the introduction of three methyl or three methoxyl groups on the phenyl ring has no appreciable effects on the product distributions, giving 1,2-naphthalenediol monoesters exclusively. Thus, α,β-unsaturated aldehydes, including aromatic aldehydes, are characteristic in giving the O-attacking products selectively.

As for the reactions with 10-undecenal, 3-phenylpropanal, and 3-cyclohexenecarbaldehyde, which have no olefinic π-system conjugated to carbonyl, we obtained the C-attacking product together with the O-attacking product in the reaction with 1,2-naphthoquinone derivatives, as is shown in Table 3. Whereas the carbonyl carbon of the acyl radical derived from α,β-unsaturated aldehydes attaches to the sp^2 carbon, the carbonyl carbon derived from these three aldehydes attaches to the sp^3 carbon. Therefore, it is reasonable to consider that the former acyl radical is more electrophilic than the latter. Thus, the inherent polarity of an acyl radical could exert the controlling influence on determining the attacking position on the 1,2-naphthosemiquinone radical. To support the

Table 3. The photo-addition compounds from the photochemical reaction of 1,2-naphthoquinone derivatives with aldehydes which have no conjugated olefinic π-system to carbonyl

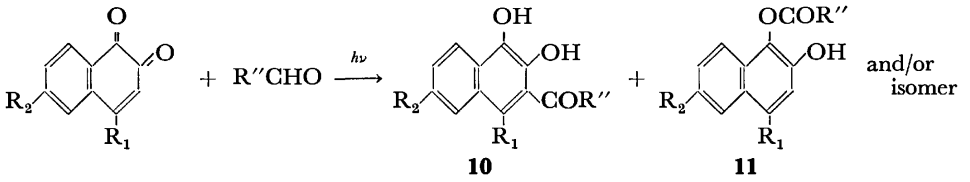

Quinone[a]	Aldehyde	Product R_1	Product R_2	Product R″	Compound No	Yield[b,c] (%)	Mp (°C)
1,2-NQ	Cyclopentanecarbaldehyde	H	H		**10a**	8	148—149
					11a	25	107—109
6-Br-1,2-NQ	Cyclopentanecarbaldehyde	H	Br		**10b**	14	133—134
					11b	37	156—158
4-CN-1,2-NQ	Cyclopentanecarbaldehyde	CN	H		**10c**	21	181—182
					11c	6	130—131
1,2-NQ	Cyclohexanecarbaldehyde	H	H		**10d**	9	186—187
					11d	34	104—105
6-Br-1,2-NQ	Cyclohexanecarbaldehyde	H	Br		**10e**	20	138—139
					11e	36	180—181
4-CN-1,2-NQ	Cyclohexanecarbaldehyde	CN	H		**10f**	17	149—150
					11f	8	165—167
1,2-NQ	10-Undecenal	H	H	CH_2=CH$(CH_2)_8$-	**10g**	8	65— 67
					11g	11	68— 69
6-Br-1,2-NQ	10-Undecenal	H	Br	CH_2=CH$(CH_2)_8$-	**10h**	12	65— 66
					11h	32	84— 87
4-CN-1,2-NQ	10-Undecenal	CN	H	CH_2=CH$(CH_2)_8$-	**10i**	25	84— 85
					11i	6	82— 83
1,2-NQ	3-Phenylpropanal	H	H	$C_6H_5CH_2CH_2$-	**10j**	5	128—129
					11j	33	103—104
6-Br-1,2-NQ	3-Phenylpropanal	H	Br	$C_6H_5CH_2CH_2$-	**10k**	18	125—126
					11k	43	120—122
4-CN-1,2-NQ	3-Phenylpropanal	CN	H	$C_6H_5CH_2CH_2$-	**10l**	32	165—166
					11l	8	149—150
1,2-NQ	3-Cyclohexenecarbaldehyde	H	H		**10m**	5	109—110
					11m	34	139—140
6-Br-1,2-NQ	3-Cyclohexenecarbaldehyde	H	Br		**10n**	12	143—144
					11n	42	163—165
4-CN-1,2-NQ	3-Cyclohexenecarbaldehyde	CN	H		**10o**	10	157—158
					11o	17	147—148

a), b), c) See the footnotes in Table 1.

above consideration it was confirmed that, in the reactions of 6-bromo-1,2-naphthoquinone with butyraldehyde[1] and with 3-chlorobutanal, the ratios of C-attacking to O-attacking products were 47 : 53 and 9 : 91 respectively.

On the other hand, the introduction of an electron-attracting group, such as halogen or cyano groups, into the quinone ring should facilitate the C-attacking on the basis of the same considerations. Since the electron densities on the C_3-carbon of the 1,2-naphthosemiquinone radical, of the 6-bromo-1,2-naphthosemiquinone radical, and of the 4-cyano-1,2-naphthosemiquinone radical may decrease in this order, the C-attacking product would increase in the same order. The results of the photochemical reactions of 1,2-naphthoquinone, 6-bromo-1,2-naphthoquinone, and 4-cyano-1,2-naphthoquinone with acetaldehyde, propanal and 3-phenylpropanal are compared in Table 4. In actual, the amounts of the C-attacking product relative to the amounts of the O-attacking product change regularly. That is, the relative yields of the C-attacking products are 13—27, 30—57, and 80—85 % respectively. In the cases of the reaction with other aliphatic aldehydes, as has been described in a previous paper[1] and as is shown in Table 3, these tendencies can also be recognized.

Contrary to the effect of introducing some electron-attracting groups into the quinone ring, the introduction of an electron-donating group, such as methyl or methoxyl group, should exert the opposite influences on the product distributions. Actually, 4-methyl- or 4-methoxy-1,2-naphthoquinone gives only O-attacking products, without any C-attacking product, as is shown in Table 4.

The 2-butenoyl radical is also of an O-attacking character for the 1,2-naphthosemiquinone radical, but it shows a somewhat C-attacking character for the 6-halo-1,2-naphthosemiquinone radical. This might be due to the fact that the introduction of the halogen atom at the 6-position of the 1,2-naphthosemiquinone

Table 4. The relative yields of the photo-addition compounds obtained in the reaction of 1,2-naphthoquinone derivatives with several aldehydes

Quinone[a]	Aldehyde	Relative yields C-product (%)[e]	Relative yields O-product (%)[f]
1,2-NQ	CH_3CHO[b]	24	76
6-Br-1,2-NQ	CH_3CHO[b]	46	54
4-CN-1,2-NQ	CH_3CHO[b]	82	18
4-Me-1,2-NQ	CH_3CHO[c]	0	100
4-MeO-1,2-NQ	CH_3CHO[c]	0	100
1,2-NQ	CH_3CH_2CHO[d]	27	73
6-Br-1,2-NQ	CH_3CH_2CHO[d]	57	43
4-CN-1,2-NQ	CH_3CH_2CHO[d]	83	17
4-Me-1,2-NQ	CH_3CH_2CHO[c]	0	100
4-MeO-1,2-NQ	CH_3CH_2CHO[c]	0	100
1,2-NQ	$C_6H_5(CH_2)_2CHO$[c]	12	88
6-Br-1,2-NQ	$C_6H_5(CH_2)_2CHO$[c]	29	71
4-CN-1,2-NQ	$C_6H_5(CH_2)_2CHO$[c]	80	20

a) 4-MeO-1,2-NQ: 4-Methoxy-1,2-naphthoquinone. The other quinones are shown in Table 1. The relative yields were determined by b) the integration of the ^{1}H-NMR signals of the concentrated reaction mixture, c) the weights of the isolated products, and d) the integration of the ^{1}H-NMR signals of the isolated products with TLC. e) 3-Acyl-1,2-naphthalenediol. f) 1,2-Napthalenediol monoacyl esters.

Table 5. The relative yields of the photo-addition compounds obtained in the reaction of 6-bromo- and 6-chloro-1,2-naphthoquinone with 2-butenal and 3-methyl-2-butenal

Quinone[a]	Aldehyde	Relative yields (%)[b] C-product[c]	Relative yields (%)[b] O-product[d]
6-Br-1,2-NQ	$CH_3CH{=}CHCHO$	2.6	97.4
6-Cl-1,2-NQ	$CH_3CH{=}CHCHO$	4.9	95.1
6-Br-1,2-NQ	$(CH_3)_2C{=}CHCHO$	6.3	93.7

a) 6-Br-1,2-NQ: 6-bromo-1,2-naphthoquinone, 6-Cl-1,2-NQ: 6-chloro-1,2-naphthoqinone. b) Average of three experiments. c) C-attacking product. d) O-attacking product.

radical induces a change in the electron density of the radical. Thus, the relative ratio of the C-attacking product to the O-attakcing product in the photochemical reaction of 6-chloro-1,2-naphthoquinone with 2-butenal increases slightly compared with the case of 6-bromo-1,2-naphthoquinone(see Table 5).

The reaction of 6-bromo-1,2-naphthoquinone with propenal yields the O-attacking product exclusively, but with 2-butenal a minor C-attacking product arises along with the major O-attacking product, suggesting that the methyl group somewhat enhances the nucleophilic character of the derived acyl radical.[10] However, as compared with 2-butenal, 3-methyl-2-butenal gives a slightly larger C-attacking product in the reaction with 6-bromo-1,2-naphthoquinone (Table 5).

Experimental

The melting points are uncorrected. The infrared spectra were obtained on a Hitachi 215 spectrometer, using a KBr disc. The ^{1}H-NMR spectra were taken with a JEOL MH-100 spectrometer, using TMS as the internal standard. Elemental analyses were carried out using a Yanaco MT-2 CHN corder.

Materials. *Quinones*: The 1,2-naphthoquinone (mp 121—122 °C),[11] 3-chloro-(mp 171 °C),[12] 3-bromo-(mp 164 °C),[13] 4-cyano-(mp 175—176 °C),[14] 4-methoxy-(mp 191—192 °C),[15] 6-bromo-(mp 156 °C),[16] and 6-chloro-1,2-naphthoquinone (mp 160—161 °C)[16] were prepared according to the methods described in the literature. 6-Methyl-1,2-naphthoquinone(mp 126—127 °C)[17] and 4-methyl-1,2-naphthoquinone(mp 77—80 °C)[18] were prepared by the oxidation of 6-methyl-2-naphthol and 4-methyl-1-naphthol respectively with Fremy's salt.

Aldehydes: The *p*-nitro-, *m*-nitro-, *p*-methyl-, *p*-methoxy-, 2,4-dimethoxy-, and 3,4,5-trimethoxybenzaldehyde, and cinnamaldehyde were commercially available and were used without further purification. The acetaldehyde, propanal, propenal, 2-butenal, *trans*-2-hexenal, 10-undecenal, 3-phenylpropanal, and benzaldehyde were commercially available and were further purified by distillation before use. The 2,4,6-trimethylbenzaldehyde(bp 94—95 °C/5 mmHg),[19] 2,4,6-triisopropylbenzaldehyde(bp 110—114 °C/3 mmHg),[19] cyclohexanecarbaldehyde(bp 75—77 °C/21 mmHg),[20] 1-cyclohexenecarbaldehyde(bp 82 °C/24 mmHg),[20] 3-cyclohexenecarbaldehyde(bp 70—73 °C/20 mmHg),[21] cyclopentenecarbaldehyde(bp 57—59 °C/28 mmHg),[22] 1-cyclopentenecarbaldehyde(bp 49 °C/20 mmHg),[23] 3-methyl-2-butenal(bp 67 °C/81 mmHg),[24] and 3-chlorobutanal(bp 65 °C/64 mmHg),[25] were prepared according to the methods given in the literature.

General Procedures. A 1,2-naphthoquinone derivative (1—2.5 mmol) and an aldehyde(1—10 mmol) were dissolved in benzene(25—80 ml), and the solution was irradiated for an appropriate time from outside in an ordinary glass tube by means of 300-W high-pressure mercury arc lamp through a 5-cm-thick layer of flowing water(15—20 °C) or of cold water (0—5 °C). After the removal of the solvent under reduced pressure, the residue was chromatographed on silica gel 60 (Merck, Art 7734, 0.063—0.200 mm), using benzene as the eluent. The photo-adducts thus obtained were further purified by recrystallization from benzene or benzene-light petroleum, or by TLC.

Structure Determination of Photo-adducts. 3-Acyl-1,2-naphthalenediols have characteristic IR bands at 3300—3500 (OH) and 1620—1650 (C=O) cm^{-1}. The 2-hydroxyl proton of them appeared at δ: 11—12 as a result of intramolecularly bonded hydrogen bonding with the carbonyl of the 3-acyl group. The 1,2-naphthalenediol monoesters show IR bands corresponding to carbonyl(1700—1740 cm^{-1}) and hydroxyl(3300—3400 cm^{-1}) groups. The existence of two isomers in these esters was confirmed by ^{1}H-NMR analyses. The yields and melting points of the adducts are listed in Tables 1, 2, and 3. Their physical properties and elemental analyses are shown in Table 6.

Detection of C-attacking Products. The presence of 3-acyl-1,2-naphthalenediol in a reacting system has been confirmed by inspecting the ^{1}H-NMR signal at δ: 11—12 in the concentrated reaction mixture. Thin-layer chromatography has been also used to detect the C-attacking products.

Irradiation of 6-Bromo-1,2-naphthoquinone with 2-Butenal: A benzene solution of the quinone (355.5 mg, 1.5 mmol) and

Table 6. Spectral properties and analytical data of the photo-addition compounds obtained in the reaction of 1,2-naphthoquinone derivatives with aldehydes

Compound No	IR(KBr, cm^{-1})			PMR ($CDCl_3$, δ)[a,b]	Found (%)			Calcd (%)			Molecular formula
	OH	CN	C=O		C	H	N	C	H	N	
3a	3410	—	1720	—	77.35	4.61		77.26	4.58		$C_{17}H_{12}O_3$
3b	3400	—	1740 1720	—	65.88	3.40	4.61	66.02	3.58	4.53	$C_{17}H_{11}NO_5$
3c	3430	—	1740 1718	—	65.92	3.63	4.51	66.02	3.58	4.53	$C_{17}H_{11}NO_5$
3d	3380	—	1710	2.44(s), 2.47(s)	77.62	5.17		77.68	5.07		$C_{18}H_{14}O_3$
3e	3380	—	1728 1700	3.89(s), 3.91(s)[c]	73.60	4.71		73.46	4.79		$C_{18}H_{14}O_4$
3f	3425	—	1725	4.02(s), 4.05(s)	67.62	5.00		67.79	5.12		$C_{20}H_{18}O_6$
4a	3375	—	1720	—	59.21	3.28		59.50	3.23		$C_{17}H_{11}BrO_3$
4b	3380	—	1715	—	52.23	2.64	3.81	52.58	2.58	3.61	$C_{17}H_{10}NBrO_5$
4c	3330	—	1715	—[c]	52.67	2.52	3.69	52.58	2.58	3.61	$C_{17}H_{10}NBrO_5$
4d	3350	—	1705	2.43(s), 2.54(s)[c]	60.55	3.52		60.53	3.67		$C_{18}H_{13}BrO_3$
4e	3320	—	1700	3.89(s), 3.92(s)[c]	57.80	3.42		57.73	3.51		$C_{18}H_{13}BrO_4$
4f	3350	—	1710	3.75(s), 3.78(s), 3.90(s), 3.93(s)	56.79	3.77		56.60	3.75		$C_{19}H_{15}BrO_3$
4g	3420	—	1735	3.72(s), 8.81(s)[c]	55.27	3.77		55.45	3.96		$C_{20}H_{17}BrO_6$
4h	3320	—	1720	2.29(s), 2.42(s), 2.48(s)	62.30	4.53		62.35	4.45		$C_{20}H_{17}BrO_3$
4i	3380	—	1720	1.26(t), 1.29(t), 2.82—3.27(m)	66.30	6.48		66.53	6.23		$C_{26}H_{29}BrO_3$
5a	3325	2220	1735	—	74.71	3.88	4.69	74.73	3.83	4.84	$C_{18}H_{11}NO_3$
5b	3255	2240	1745	—[c]	64.77	2.95	8.46	64.67	3.02	8.38	$C_{18}H_{10}N_2O_5$
5c	3274	2237	1745	—[c]	64.51	3.14	8.45	64.67	3.02	8.38	$C_{18}H_{10}N_2O_5$
5d	3345	2238	1735	2.51(s)	75.34	4.33	4.58	75.24	4.32	4.62	$C_{19}H_{13}NO_3$
5e	3275	2250	1725	3.80(s), 3.83(s)	71.40	4.00	4.46	71.47	4.10	4.39	$C_{19}H_{13}NO_4$
5f	3420	2225	1683	3.66(s), 3.75(s)	66.53	4.50	3.52	66.49	4.52	3.69	$C_{21}H_{17}NO_6$
5g	3325	2230	1720	2.40(s), 2.53(s)	76.18	5.06	4.19	76.12	5.17	4.23	$C_{21}H_{17}NO_3$
6a	3330	—	1722	—	68.30	3.77		68.35	3.71		$C_{17}H_{11}ClO_3$
6b	3350	—	1715	6.81(d), 6.90(d), 7.89(d), 7.97(d)[c]	70.14	4.08		70.27	4.03		$C_{19}H_{13}ClO_3$
6c	3375	—	1720	—	59.40	2.85	4.11	59.39	2.91	4.08	$C_{17}H_{10}NClO_5$
6d	3345	—	1718	—[c]	59.27	2.88	3.93	59.39	2.91	4.08	$C_{17}H_{10}NClO_5$
6e	3360	—	1717	2.43(s)	69.22	4.15		69.13	4.19		$C_{18}H_{13}ClO_3$
6f	3310	—	1710	8.89(s), 3.91(s)[c]	65.67	4.01		65.76	3.99		$C_{18}H_{13}ClO_4$
7a	3340	—	1720	—[c]	59.47	3.23		59.50	3.23		$C_{17}H_{11}BrO_3$
7b	3300	—	1700	6.83(d), 6.89(d), 7.89(d), 7.92(d)[c]	61.78	3.61		61.81	3.55		$C_{19}H_{13}BrO_3$
7c	3375	—	1720	—	52.55	2.52	3.68	52.58	2.58	3.61	$C_{17}H_{10}NBrO_5$
7d	3370	—	1720	—	52.44	2.59	3.56	52.58	2.58	3.61	$C_{17}H_{10}NBrO_5$
7e	3325	—	1715	2.44(s)	60.50	3.69		60.53	3.67		$C_{18}H_{13}BrO_3$
7f	3320	—	1710	3.90(s), 3.91(s)[c]	57.77	3.44		57.73	3.51		$C_{18}H_{13}BrO_4$
8a	3380	—	1705	2.46(s)[d]	77.77	5.13		77.67	5.07		$C_{18}H_{14}O_3$
8b	3490	—	1705	2.53(s), 6.07(d)	78.85	5.21		78.93	5.30		$C_{20}H_{16}O_3$
8c	3420	—	1719	2.50(s), 2.54(s)	66.63	4.09	4.44	66.87	4.05	4.33	$C_{18}H_{13}NO_5$
8d	3360	—	1710	2.51(s)	66.85	3.96	4.41	66.87	4.05	4.33	$C_{18}H_{13}NO_5$
8e	3375	—	1710	2.44(s), 2.46(s), 2.50(s)	77.98	5.56		78.06	5.52		$C_{19}H_{16}O_3$
8f	3450	—	1739 1707	2.45(s), 2.50(s) 3.90(s), 3.91(s)	74.05	5.30		74.01	5.23		$C_{19}H_{16}O_4$
9a	3410	—	1725	—[d]	72.89	4.61		72.89	4.71		$C_{13}H_{10}O_3$
9b	3340	—	1710	—	53.24	3.12		53.27	3.09		$C_{13}H_9BrO_3$
9c	3250	2226	1738	—	70.14	3.73	5.80	70.29	3.79	5.85	$C_{14}H_9NO_3$
9d	3375	—	1910	1.90(dd), 1.95(dd)	73.57	5.31		73.67	5.30		$C_{14}H_{12}O_3$
9e	3300	2230	1740	2.04(dd), 6.25(m)	71.11	4.40	5.22	71.14	4.38	5.53	$C_{15}H_{11}NO_3$
9d	3390	—	1710	1.03(t), 1.50—1.75(m), 2.33(q), 6.15(d)	74.99	6.25		74.98	6.29		$C_{16}H_{16}O_3$
9g	3340	—	1700	0.97(t), 1.37—1.67(m), 2.24(q), 5.98(d)	57.42	4.56		57.33	4.51		$C_{16}H_{15}BrO_3$
9h	3330	2240	1745	1.03(t), 1.50—1.75(m), 2.37(q), 6.22(d)	72.56	5.32	4.89	72.58	5.37	4.89	$C_{17}H_{15}NO_3$

TABLE 6. (Continued)

Compound No	IR(KBr, cm^{-1}) OH	CN	C=O	PMR ($CDCl_3$, δ)[a,b]	Found (%) C	H	N	Calcd (%) C	H	N	Molecular formula
9i	3300	—	1700	1.91—2.28, 2.46—2.85(m)	75.33	5.58		75.58	5.55		$C_{16}H_{14}O_3$
9j	3360	—	1700	1.94—2.20, 2.49—2.84(m)	57.77	3.90		57.68	3.93		$C_{16}H_{13}BrO_3$
9k	3240	2220	1700	1.92—2.16, 2.49—2.84(m)	73.16	4.66	5.01	73.11	4.69	5.01	$C_{17}H_{13}NO_3$
9l	3350	—	1690	1.56—1.87, 2.15—2.56(m)	76.24	6.04		76.10	6.01		$C_{17}H_{16}O_3$
9m	3360	—	1700	1.48—1.82, 2.17—2.47(m)	58.75	4.31		58.81	4.35		$C_{17}H_{15}BrO_3$
9n	3330	—	1708	6.76(d), 6.88(d)[c]	78.39	4.95		78.61	4.86		$C_{19}H_{14}O_3$
9o	3380	—	1705	6.76(d), 6.88(d), 8.03(d), 8.13(d)[c]	62.00	3.62		61.81	3.55		$C_{19}H_{13}BrO_3$
9p	3275	2236	1740	6.75(d)[c]	76.01	4.32	4.47	76.18	4.16	4.44	$C_{20}H_{13}NO_3$
10a	3480	—	1650	1.48—2.14(m), 3.78—4.03(m), 11.78(s)[d]	74.90	6.31		74.98	6.29		$C_{16}H_{16}O_3$
11a	3320	—	1720	1.48—2.20(m), 2.89—3.24(m)	75.11	6.26		74.98	6.29		$C_{16}H_{16}O_3$
10b	3450	—	1640	1.63—2.16(m), 3.70—4.01(m), 11.69(s)[d]	57.33	4.44		57.33	4.51		$C_{16}H_{15}BrO_3$
11b	3420	—	1720	1.60—2.21(m), 2.90—3.33(m)	57.28	4.62		57.33	4.51		$C_{16}H_{15}BrO_3$
10c	3310	2220	1640	1.55—2.30(m), 4.40—4.62(m), 11.51(s)	72.47	5.35	4.79	72.58	5.37	4.98	$C_{17}H_{15}NO_3$
11c	3220	2235	1755	1.53—2.20(m), 2.90—3.29(m)	72.58	5.30	4.99	72.58	5.37	4.98	$C_{17}H_{15}NO_3$
10d	3460	—	1635	1.20—2.20(m), 3.28—3.68(m), 11.87(s)[d]	75·51	6.60		75.53	6.71		$C_{17}H_{18}O_3$
11d	3310	—	1710	1.20—2.20(m), 2.37—2.64(m)[d]	75.60	6.78		75.53	6.71		$C_{17}H_{18}O_3$
10e	3440	—	1645	1.20—2.07(m), 3.23—3.57(m), 11.87(s)[d]	58.28	4.96		58.47	4.91		$C_{17}H_{17}BrO_3$
11e	3400	—	1720	1.18—2.18(m), 2.58—2.82(m)	58.48	4.83		58.47	4.91		$C_{17}H_{17}BrO_3$
10f	3370	2210	1625	1.20—2.15(m), 3.95—4.22(m), 11.60(s)	73.28	5.86	4.65	73.20	5.80	4.74	$C_{18}H_{17}NO_3$
11f	3250	2220	1745	1.20—2.20(m), 2.54—2.80(m)	73.19	5.86	4.71	73.20	5.80	4.74	$C_{18}H_{17}NO_3$
10g	3470	—	1650	1.17—2.12(m), 3.06(t), 4.70—5.01(m), 11.55(s)[d]	77.07	8.03		77.27	8.03		$C_{21}H_{26}O_3$
11g	3430	—	1735	1.17—2.14(m), 2.48—2.80(m), 4.72—4.97(m)[d]	77.25	7.94		77.27	8.03		$C_{21}H_{26}O_3$
10h	3440	—	1650	1.16—2.13(m), 2.97(t), 4.73—4.98(m), 5.50—5.80(m), 11.84(s)[d]	62.02	6.27		62.23	6.22		$C_{21}H_{25}BrO_3$
11h	3400	—	1735	1.30—2.20(m), 2.70(t), 4.95—5.18(m), 5.76—6.25(m)	62.28	6.16		62.23	6.22		$C_{21}H_{25}BrO_3$
10i	3300	2220	1630	1.20—2.10(m), 3.42(t), 4.70—4.96(m), 5.44—5.84(m), 12.01(s)[d]	75.15	7.15	3.95	75.19	7.17	3.99	$C_{22}H_{25}NO_3$
11i	3370	2230	1745	1.10—2.20(m), 2.63(t), 4.80—4.98(m), 5.60—5.90(m)	75.23	7.01	4.04	75.19	7.17	3.99	$C_{22}H_{25}NO_3$
10j	3450	—	1660	3.02(t), 3.39(t), 11.36(s)	78.02	5.54		78.06	5.52		$C_{19}H_{16}O_3$
11j	3320	—	1725	2.92—3.10(m)	78.16	5.50		78.06	5.52		$C_{19}H_{16}O_3$
10k	3450	—	1660	2.96(t), 3.27(t), 11.31(s)[d]	61.47	4.13		61.47	4.07		$C_{19}H_{15}BrO_3$
11k	3320	—	1730	2.83—3.02(m)[d]	61.35	3.98		61.47	3.98		$C_{19}H_{15}BrO_3$
10l	3280	2225	1638	3.07(t), 3.76(t), 11.57(s)	75.61	4.80	4.44	75.70	4.76	4.41	$C_{20}H_{15}NO_3$
11l	3275	2230	1760	3.00(m)	75.72	4.70	4.33	75.70	4.76	4.41	$C_{20}H_{15}NO_3$
10m	3470	—	1630	1.78—2.43(m), 3.68(m), 5.68(m), 11.68(s)[d]	76.00	6.05		76.10	6.01		$C_{17}H_{16}O_3$
11m	3380	—	1720	1.77—2.67(m), 2.91(m), 5.67(m)[d]	75.99	5.87		76.10	6.01		$C_{17}H_{16}O_3$
10n	3450	—	1640	1.63—2.45(m), 3.65(m), 5.69(m), 11.66(s)[d]	58.84	4.30		58.81	4.35		$C_{17}H_{15}BrO_3$
11n	3400	—	1720	1.80—2.54(m), 1.96(m), 5.75(m)	58.88	4.26		58.81	4.35		$C_{17}H_{15}BrO_3$
10o	3450	2215	1630	1.95—2.52(m), 4.22(m), 5.68(m), 11.58(s)[d]	73.76	5.01	4.78	73.71	5.15	4.78	$C_{18}H_{15}NO_3$
11o	3250	2230	1750	1.97—2.53(m), 2.96(m), 5.77(m)	73.81	5.03	4.87	73.71	5.15	4.78	$C_{18}H_{15}NO_3$

a) The protons appeared in the aromatic region, and the hydroxyl protons, except for the 2-hydroxyl proton which shifted to the low field of 3-acyl-1,2-naphthalenediols, are not listed. b) s: singlet, d: doublet, t: triplet, q: quartet, m: multiplet, dd: double doublet. c) The solvent is acetone-d_6. d) The solvent is carbon tetrachloride.

the aldehyde (350 mg, 5 mmol) was irradiated for 2 days. The reaction mixture was then worked-up as usual. 3-(2-Butenoyl)-6-bromo-1,2-naphthalenediol: orange-red needles (7.5 mg, 1.6%), mp 185—186.5 °C. IR: 3450(OH), 1655 (C=O) cm^{-1}. PMR($CDCl_3$), δ: 2.02(dd, 3H, J=1.5, 7.0 Hz), 5.96(s, 1H, removed by D_2O), 7.05—7.97(m, 6H), 11.37 (s, 1H, removed by D_2O). 6-Bromo-1,2-naphthalenediol mono-2-butenoate: white crystals (283 mg, 61.6%), mp 173.5—175 °C. IR: 3340(OH), 1710(C=O) cm^{-1}. PMR ($CDCl_3$), δ: 1.94 (dd, 3H, J=1.5, 7.0 Hz), 1.99 (dd, 3H, J=1.5, 7.0 Hz), 5.82—6.10 (m, 4H), 7.04—8.06 (m, 14H).

Irradiation of 6-Chloro-1,2-naphthoquinone with 2-Butenal: A benzene solution of the quinone (192.5 mg, 1 mmol) and the aldehyde (350 mg, 5 mmol) was irradiated for 3 days. The reaction mixture was then worked-up as usual. 3-(2-Butenoyl)-6-chloro-1,2-naphthalenediol: red crystals (6.5 mg, 2.5 %), mp 151—154 °C. IR: 3460(OH), 1655 (C=O) cm^{-1}. PMR (CCl_4), δ: 2.08 (dd, 3H, J=1.5, 7.0 Hz), 6.13 (s, 1H, removed by D_2O), 7.07—8.13 (m, 6H), 11.93 (s, 1H, removed by D_2O). 6-Chloro-1,2-naphthalenediol mono-2-butenoate: white crystals (125 mg, 47.6%), mp 179—180 °C. IR: 3340 (OH), 1708 (C=O) cm^{-1}. PMR ($CDCl_3$), δ: 2.00 (dd, 3H, J=1.5, 7.0 Hz), 2.05 (dd, 3H, J=1.5, 7.0 Hz), 6.21 (s, 2H, removed by D_2O), 7.25—8.24 (m, 14H).

Irradiation of 6-Bromo-1,2-naphthoquinone with 3-Methyl-2-butenal: A benzene solution of the quinone (476 mg, 2 mmol) and the aldehyde (504 mg, 6 mmol) was irradiated for 3 days. The reaction mixture was then worked-up as usual. 3-(3-Methyl-2-butenoyl)-6-bromo-1,2-naphthalenediol: red crystals (22 mg, 3.4%), mp 148—150 °C. IR: 3400 (OH), 1635 (C=O) cm^{-1}. PMR (CCl_4), δ: 2.10 (s, 3H), 2.27 (s, 3H), 5.94 (s, 1H, removed by D_2O), 6.93—8.00 (m, 5H), 12.04 (s, 1H, removed by D_2O). 6-Bromo-1,2-naphthalenediol mono(3-methyl-2-butenoate): white crystals, mp 147—148 °C. IR: 3345 (OH), 1700 (C=O) cm^{-1}. PMR ($CDCl_3$), δ: 2.02 (s, 3H), 2.27 (s, 3H), 6.02 (br, 1H), 6.24 (s, 1H, removed by D_2O), 7.23—8.15 (m, 5H).

Irradiation of 4-Methyl-1,2-naphthoquinone with Acetaldehyde: A benzene solution (80 ml) of the quinone (258 mg, 1.5 mmol) and the aldehyde (660 mg, 15 mmol) was irradiated for 42 h. No C-attacking product was detected by ^1H-NMR or TLC in the concentrated reaction mixture. The reaction mixture was then worked-up as usual. 4-Methyl-1,2-naphthalenediol monoacetate: white needles (165 mg, 51%), mp 174 °C (dec). IR: 3410 (OH), 1740 (C=O) cm^{-1}. PMR ($CDCl_3$), δ: 2.40 (s, 3H), 2.52 (s, 3H), 5.45 (br, 1H), 7.14—7.74 (m, 4H). Found: C, 72.01; H, 6.04%. Calcd for $C_{13}H_{12}O_3$: C, 72.21; H, 5.59%.

Irradiation of 4-Methyl-1,2-naphthoquinone with Propanal: A benzene solution (25 ml) of the quinone (86 mg, 0.5 mmol) and the aldehyde (87 mg, 1.5 mmol) was irradiated for 24 h. The reaction mixture was then worked-up as usual. 4-Methyl-1,2-naphthalenediol monopropanoate: white needles (52 mg, 45%), mp 112 °C. IR: 3400 (OH), 1730 (C=O) cm^{-1}. PMR ($CDCl_3$), δ: 1.25 (t, 3H), 1.32 (t, 3H), 2.51 (s, 6H), 2.64 (q, 2H), 2.67 (q, 2H), 5.46 (bs, 1H), 5.63 (br, 1H), 6.85 (s, 2H), 7.16—7.75 (m, 8H). The ratio of the isomer contents was 1 : 1, as estimated on the basis of the integration of the ^1H-NMR signals of the mixture. Found: C, 73.12; H, 6.08%. Calcd for $C_{14}H_{14}O_3$: C, 73.03; H, 6.13%.

Irradiation of 4-Methoxy-1,2-naphthoquinone with Acetaldehyde: A benzene solution (25 ml) of the quinone (200 mg, 1.06 mmol) and the aldehyde (500 mg, 11.4 mmol) was irradiated for 2 days at 0—5 °C. The reaction mixture was then worked-up as usual. 4-Methoxy-1,2-naphthalenediol monoacetate: white needles (186 mg, 76%), mp 105—106 °C (dec). IR: 3360 (OH), 1728 (C=O) cm^{-1}. PMR ($CDCl_3$), δ: 2.30 (s, 18%), 2.38 (s, 82%), 3.66 (s, 82%), 3.81 (s, 18%), 5.81 (br, removed by D_2O), 6.32 (s, 82%), 6.35 (s, 18%), 7.09—7.96 (m). Found: C, 67.22; H, 5.10%. Calcd for $C_{13}H_{12}O_4$: C, 67.23; H, 5.21%.

Irradiation of 4-Methoxy-1,2-naphthoqinone with Propanal: A benzene solution of the quinone (188 mg, 1 mmol) and the aldehyde (87 mg, 1.5 mmol) was irradiated for 2 days. The reaction mixture was then chromatographed on silica gel, using benzene–ether (8 : 2) as the eluent. 4-Methoxy-1,2-naphthalenediol monopropanoate: white needles (200 mg, 81%), mp 90—91 °C (dec). IR: 3320 (OH), 1725 (C=O) cm^{-1}. PMR ($CDCl_3$), δ: 1.33 (t, 21%), 1.40 (t, 79%), 2.73 (q, 21%), 2.83 (q, 79%), 3.82 (s, 79%), 3.99 (s, 21%), 6.47 (s, 79%), 6.58 (s, 21%), 7.36—8.20 (m). Found: C, 68.09; H, 5.71%. Calcd for $C_{14}H_{14}O_4$: C, 68.23; H, 5.73%.

Irradiation of 6-Bromo-1,2-naphthoquinone with 3-Chlorobutanal: A benzene solution (25 ml) of the quinone (237 mg, 1 mmol) and the aldehyde (211 mg, 2 mmol) was irradiated for 2 days. The concentrated reaction mixture was then chromatographed on silica gel, using benzene as the eluent. 3-(3-Chlorobutanoyl)-6-bromo-1,2-naphthalenediol: orange yellow needles (22.3 mg), mp 138—141 °C. IR: 3420 (OH), 1642 (C=O) cm^{-1}. PMR ($CDCl_3$), δ: 1.70 (d, 3H), 3.58 (m, 2H), 4.72 (m, 1H), 6.11 (s, 1H), 7.55—8.03 (m, 4H), 11.40 (s, 1H). 6-Bromo-1,2-naphthalenediol mono (3-chlorobutanoate): white needles (203.3 mg), mp 135—137.5 °C. IR: 3410 (OH), 1725 (C=O) cm^{-1}. PMR ($CDCl_3$), δ: 1.66 (d, 3H), 1.69 (d, 3H), 3.03 (m, 4H), 4.75 (m, 2H), 5.62 (br. 1H), 5.92 (s, 1H), 7.20—7.93 (m, 10H).

The author wishes to express his deep gratitude to Professor Kazuhiro Maruyama, Kyoto University, and Professor Osamu Soga, Shimane University, for their fruitful suggestions and invaluable encouragement. He also wishes to thank the Ministry of Education for its financial support for this research.

References

1) a) K. Maruyama and A. Takuwa, *Chem. Lett.*, **1974**, 471. b) A. Takuwa, *Bull. Chem. Soc. Jpn.*, **49**, 2790 (1976).

2) L. M. Bruce, *Quart. Rev.*, **21**, 405 (1967), and the references cited therein.

3) A. Mustafa, A. H. E. Harhash, A. K. E. Mansour, and S. M. A. E. Omuran, *J. Am. Chem. Soc.*, **78**, 4306 (1956).

4) W. I. Awad and M. S. Hafez, *J. Am. Chem. Soc.*, **80**, 6057 (1957).

5) 9,9′-Bixanthenyl was obtained as one of the reaction products from the photochemical reaction of 1,2-naphthoquinone with xanthene. By means of the photo-CIDNP study of the reaction of 1,2-naphthoquinone with hydroquinone, the polarized signals of both *p*-benzoquinone (emission signal) and hydroquinone itself (enhanced absorption) were observed. On the basis of these results, it may safely be concluded that the photo-excited 1,2-naphthoquinone molecule, which is probably in its n-π^* triplet state, acts as a hydrogen abstractor.

6) Bruce and Cutts reported on the mechanism of the formation of 2-acetylhydroquinone in the photochemical reaction of *p*-benzoquinone with acetaldehyde. In their paper they considered the attack of the acetyl radical on the quinone in its ground state, followed by the subsequent enolization of the primary adduct. However, the present author confirmed that 3-acetyl-1,2-naphthalenediols were not obtained in the reaction of the acetyl radical with 1,2-naphthoquinone

derivatives in their ground state. The experimental conditions were as follows: a mixture of a 1,2-naphthoquinone (200 mg) and di-*t*-butyl peroxyoxalate (200 mg) in acetaldehyde (20 ml) was kept in the dark at room temperature for 7 days. Furthermore, CIDNP signals were observed in the photochemical reaction of 1,2-naphthoquinone with acetaldehyde in hexadeuteriobenzene. In addition, the photoinduced Fries rearrangement of the O-attacking product to C-attacking product did not occur under the experimental conditions used in this work. *Cf.* a) J. M. Bruce and E. Cutts, *J. Chem. Soc., C*, **1966**, 449; b) K. Maruyama and Y. Miyagi, *Bull. Chem. Soc. Jpn.*, **47**, 1303 (1974).

7) T. Carona, G. Fronza, F. Minisci, and O. Porta, *J. Chem. Soc., Perkin Trans. 2*, **1972**, 1477.
8) J. Krusic and T. A. Rettig, *J. Am. Chem. Soc.*, **92**, 722 (1970).
9) J. M. Bruce, D. Creed, and J. N. Ellis, *J. Chem. Soc., C*, **1967**, 1486.
10) J. M. Bruce and K. Dawes, *J. Chem. Soc., C*, **1970**, 645.
11) A. H. Blatt, *Org. Synth.*, Coll. Vol. II, 430 (1948).
12) T. Zincke, *Ber.*, **19**, 2497 (1886).
13) T. Zincke, *Ber.*, **19**, 2495 (1886).
14) W. Bradley and R. Robinson, *J. Chem. Soc.*, **1934**, 1484.
15) H. J. Teuber and N. Göts, *Chem. Ber.*, **87**, 1249 (1954).
16) R. W. A. Oliver, R. M. Rashman, and A. W. Somerville, *Tetrahedron*, **24**, 1211 (1968).
17) K. Dzieqonsky, J. Schoenowna, and E. Waldmann, *Ber.*, **58**, 1211 (1925).
18) L. F. Fieser and C. K. Bradsher, *J. Am. Chem. Soc.*, **61**, 417 (1939).
19) E. C. Horning, *Org. Synth.*, Coll. Vol. III, 549 (1967).
20) S. I. Heilbron, E. R. H. Jones, R. W. Richardson, and F. Sondheimer, *J. Chem. Soc.*, **1949**, 737.
21) O. Diels and K. Alder, *Ann. Chem.*, **460**, 121 (1928).
22) H. E. Baumgarten, *Org. Synth.*, Coll. Vol. V, 320 (1973).
23) J. B. Brown, H. B. Henbest, and E. R. H. Jones, *J. Chem. Soc.*, **1950**, 3634.
24) W. G. Young and S. L. Linden, *J. Am. Chem. Soc.*, **69**, 2912 (1947).
25) F. A. Kekulé, *Ann. Chim.*, **162**, 100 (1872).

The Ullmann Condensation Reaction of Haloanthraquinone Derivatives with Amines in Aprotic Solvents. II.[1] The Presence of an Induction Period in the Condensation with 2-Aminoethanol

Sadao ARAI, Mitsuhiko HIDA, Takamichi YAMAGISHI, and Satoshi OTOTAKE

Department of Industrial Chemistry, Faculty of Technology, Tokyo Metropolitan University, Fukazawa, Setagaya-ku, Tokyo 158

(Received February 7, 1977)

An induction period was present in the Ullmann condensation reactions of 1-bromoanthraquinone(AQBr) with 2-aminoethanol(AE) in the presence of CuBr or CuI in aprotic solvents under a nitrogen atmosphere, while there was no induction period in the reaction systems of 1-iodoanthraquinone(AQI)–AE–CuBr, AQI–AE–CuI, and AQBr–AE–$[Cu(CH_3CN)_4]ClO_4$. In the condensation system with a copper(I) catalyst, the Cu(I) species was oxidized to the Cu(II) species by means of an electron transfer from Cu(I) to haloanthraquinone as the reaction proceeded. By adding copper(II) bromide, the induction period vanished in the reaction system of AQBr–AE–CuBr. The copper(II) species increased the catalytic activity of the copper(I) species. The formation of the copper(II) species was responsible for the presence of an induction period and played an important role in the Ullmann condensation reaction of haloanthraquinones with amines in the presence of copper(I) salt as a catalyst.

The Ullmann condensation reaction, the nucleophilic substitution of aryl halides by amines or phenols in the presence of copper catalyst, is widely used for the synthesis of diaryl amines or diaryl ethers. Although many studies of the condensation of phenols with aryl bromides have been described, and although aryloxycopper(I) has been proposed as a nucleophile,[2,3] only a few mechanistic studies of the condensation with amines have been reported. We reported previously on the catalysis of copper(II) species in the reaction of sodium 1-amino-4-bromoanthraquinone-2-sulfonate with aniline in an aqueous alkaline solution.[4–7] Kurdyumova investigated the reaction of haloanthraquinones with aromatic and aliphatic amines in the presence of copper salts as catalysts.[8] However, scarcely no systematic studies of the Ullmann condensation reaction of haloanthraquinone derivatives with amines in aprotic solvents have been reported.

In our preceding paper,[1] we discussed the reactivities of haloanthraquinones, amines, and catalysts in the reaction of haloanthraquinones with amines by copper catalysts in aprotic solvents under a nitrogen atmosphere.

In this paper we will report that an induction period is observed under some reaction conditions in the reaction of 1-haloanthraquinones with 2-aminoethanol in the presence of copper(I) halides in aprotic solvents, and we will propose that the formation of the copper(II) species plays an important role in determining the presence of an induction period and the catalytic activity of copper salts.

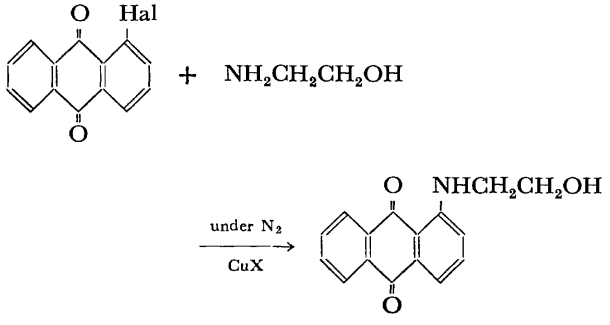

Results and Discussion

The plot of the yield of the reaction product against the reaction time shows that the copper(I) catalyst is more effective than the copper(II) catalyst, that the catalytic activity of copper(I) salts decreases in this order: CuBr>CuI, and that 1-iodoanthraquinone (AQI) is more reactive than 1-bromoanthraquinone (AQBr) (Fig. 1). An induction period is observed in the condensation systems of AQBr–2-aminoethanol (AE)–CuBr and AQBr–AE–CuI, while an induction period is absent in the condensation systems using AQI. In explaining the presence of an induction period, the following several factors were discussed: the autocatalytic reaction, the halogen-exchange reaction between AQBr and CuI, the depolymerization of the polymeric copper(I) complex to monomeric species, and the formation and catalytic action of the copper(II) species.

Autocatalytic Reaction. When the catalytic activity of copper salt is increased by the coordination of a condensation product, the reaction rate will increase as the reaction proceeds, and there will be an induction period. If this is the case, the addition of the condensation product [1-(2-hydroxyethylamino)-anthraquinone] will enhance the reaction rate and the induction period will vanish. However, the yield of the condensation product decreased and the induction period did not vanish upon the addition of the condensation product(Fig. 2). This result probably indicates that the catalytic action of the copper(I) species diminishes by means of the coordination of the condensation product. Therefore, autocatalysis does not seem to be responsible for the presence of the induction period.

Halogen-exchange Reaction between 1-Bromoanthraquinone and Copper(I) Iodide. It has been established that the halogen atoms of haloaromatics are replaced by halogens or other groups of copper(I) salts in aprotic solvents.[9–12] In the case of the reaction of 1-bromoanthraquinone with 2-aminoethanol by the CuI catalyst, 1-iodoanthraquinone was indeed produced along

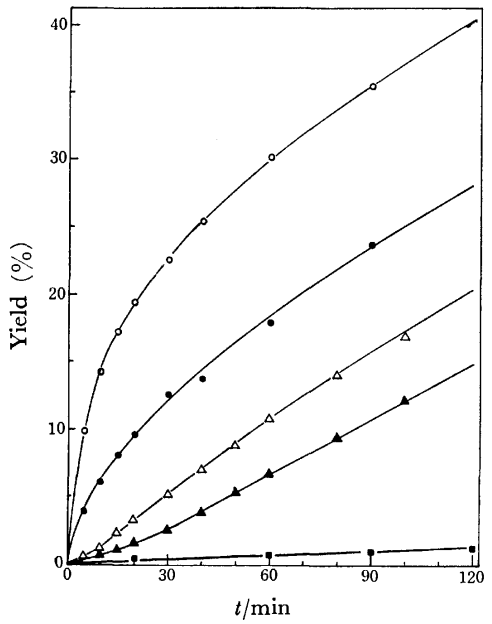

Fig. 1. Plots of the yields of products *vs.* reaction time in the reaction of 1-haloanthraquinone(AQHal) with 2-aminoethanol(AE) by copper salt(CuX) catalyst at 70 °C; $[AQHal]_0=5.00\times10^{-3}$ mol/l, $[AE]_0=0.50$ mol/l, $[CuX]_0=2.00\times10^{-3}$ mol/l, solvent 1,2-dimethoxyethane–methyl cellosolve 4 : 1. ○: AQI–CuBr, ●: AQI–CuI, △: AQBr–CuBr, ▲: AQBr–CuI, ■: AQBr–$CuBr_2$.

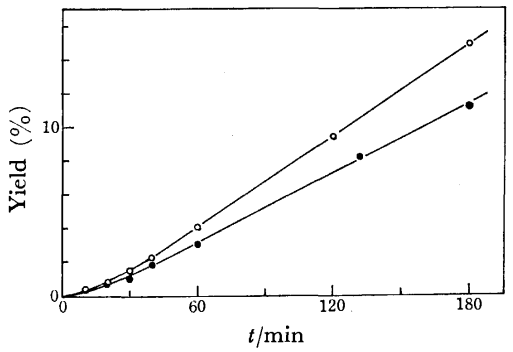

Fig. 2. Effect of the addition of condensation product; $[AQBr]_0=5.00\times10^{-3}$ mol/l, $[AE]_0=0.50$ mol/l, $[CuI]_0=2.00\times10^{-3}$ mol/l, temp 60 °C, solvent THF–ethanol 4 : 1. ○: control, ●: [1-(2-hydroxyethylamino)anthraquinone]$_0=1.30\times10^{-3}$ mol/l.

with the condensation product (Fig. 3). This result suggests that the bromine atom of 1-bromoanthraquinone is replaced by the iodine atom in the course of the condensation reaction,

$$AQBr + CuI \rightarrow AQI + CuBr.$$

Since more reactive 1-iodoanthraquinone is produced with the lapse of time, the rate of the condensation reaction will increase as the reaction proceeds, then an induction period will be observed.

If the rate law is supposed to be first-order in both concentrations of the substrate and catalyst,[10] the reaction rate can be written by

$$v = (k_1[CuBr]+k_1'[CuI])[AQBr] + (k_2[CuBr]+k_2'[CuI])[AQI]. \quad (1)$$

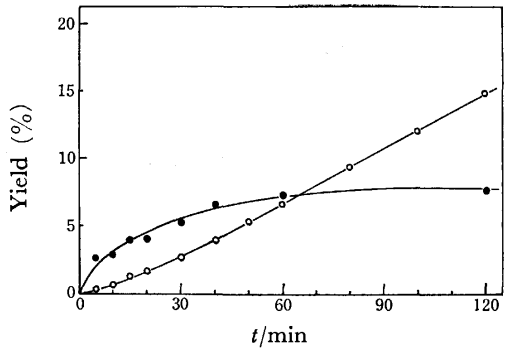

Fig. 3. Reaction of 1-bromoanthraquinone with 2-aminoethanol by CuI catalyst; $[AQBr]_0=5.00\times10^{-3}$ mol/l, $[AE]_0=0.50$ mol/l, $[CuI]_0=2.00\times10^{-3}$ mol/l, temp 70 °C, solvent 1,2-dimethoxyethane–methyl cellosolve 4 : 1.
○: 1-(2-Hydroxyethylamino)anthraquinone,
●: 1-iodoanthraquinone.

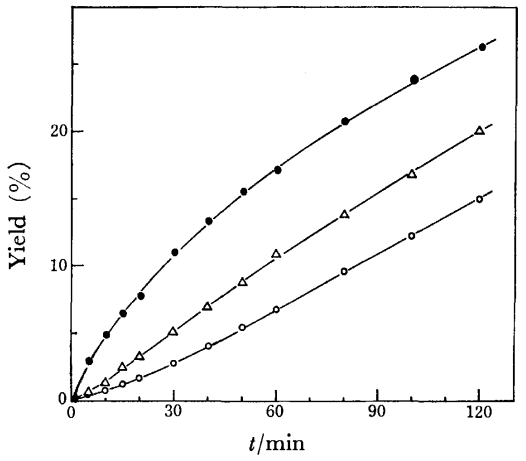

Fig. 4. Effect of anionic ligand of CuX; $[AQBr]_0=5.00\times10^{-3}$ mol/l, $[AE]_0=0.50$ mol/l, $[CuX]_0=2.00\times10^{-3}$ mol/l, temp 70 °C, solvent 1,2-dimethoxyethane–methyl cellosolve 4 : 1. ●: $[Cu(CH_3CN)_4]ClO_4$, △: CuBr, ○: CuI.

The values of k_1/k_1', k_2/k_1', and k_2'/k_1', estimated from the initial rate of each, were 2.4, 45.4, and 17.2 respectively. AQI was formed in a yield of about 7% after 60 min (Fig. 3). Since the resulting AQI is consumed in the reaction with 2-aminoethanol, the concentration of the resulting CuBr may be supposed to be higher than that of the observed AQI. Consequently, the rate after 60 min was estimated to be larger than the initial rate by a factor of more than 2.7. On the other hand, Fig. 3 shows that the rate after 60 min rises to about two times the initial rate. These values may indicate some effects of the halogen exchange on the reaction rate. However, it cannot be considered as the main reason for the presence of the induction period even in the reaction of AQBr with 2-aminoethanol caused by the CuI catalyst, for the induction period was also present in the condensation system of AQBr–AE–CuBr and it could not result from an increase in the rate by the halogen-exchange reaction.

Consequently, the presence of the induction period cannot be understood on the basis only of the halogen-

exchange mechanism.

Depolymerization of the Polymeric Copper(I) Complex to Monomeric Species. As is shown in Fig. 4, the induction period was observed in the reaction systems of AQBr–AE–CuBr and AQBr–AE–CuI, while it was not present in the system of AQBr–AE–tetrakis(acetonitrile)copper(I) perchlorate ($[Cu(CH_3CN)_4]ClO_4$). Copper perchlorate complexes are known to be present as monomeric species in solution because the perchlorate ligand cannot act as a bridging group between copper(I) species.[13-14] The structures of copper(I) halide–amine complexes were proposed to be the halogen-bridged dimer(A)[15-17] or the tetramer(B)[15,16,18] on the basis of the cryoscopic data on solution and an X-ray examination of the crystalline state.

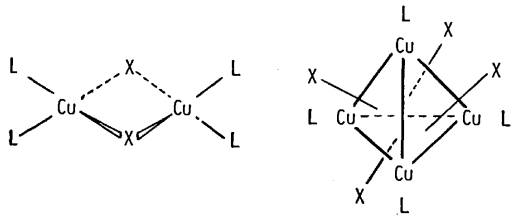

(A) L=RNH_2, R_2NH. X=Cl, Br, I.

(B) L=RNH_2; X=Cl, Br, I. L=R_2NH; X=Cl.

The $[Cu(CH_3CN)_4]ClO_4$ catalyst, which did not exhibit the induction period, was more effective catalyst than CuBr and CuI, which did exhibit the induction period(Fig. 4). These facts seem to indicate that the monomeric copper(I) species is a rather more effective catalyst than the polymeric one in the Ullmann condensation and that the induction period may be ascribed to the change from the polymeric copper(I) species to the active monomeric species. The polymeric copper(I) species will be depolymerized by the coordination of amine as follows:

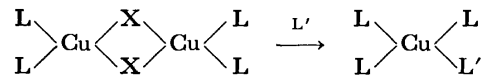

X=Halogen; L=Halogen, Amine, AQBr; L′=Amine.

As is shown in Fig. 5, the induction period was shortened with the increase in the concentration of amine, and it was not observed at a high concentration of amine. This result seems to support the above consideration. The Cu(I)–amine solution was allowed to stand for a long time, either at room temperature or at 70 °C, and then the solution was added to a solution containing 1-bromoanthraquinone. If the induction period was caused by the depolymerization of the polymeric copper(I) species in the course of the reaction, the induction period would vanish under the above condition, but no change of the induction period was observed. This finding may enable us to exclude the idea that the change in copper(I) species from a polymeric complex to a monomeric one was responsible for the presence of the induction period.

Formation and Catalytic Action of the Copper(II) Species. Figure 6 shows that the plots of $-\log(1-x)$ against the time, where x denotes the yield of the reaction product, are independent of the initial concentration of AQBr. This result suggests that the reaction rate is first-order

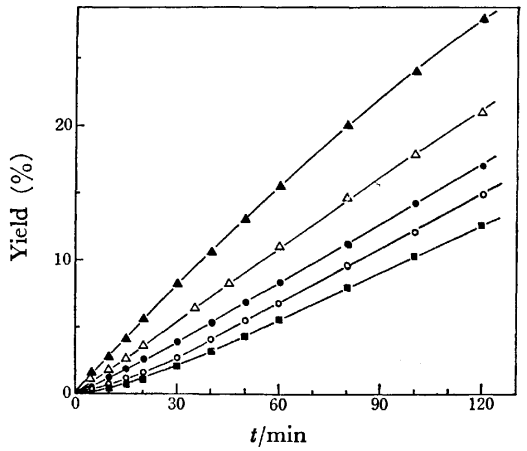

Fig. 5. Effect of the concentration of 2-aminoethanol; $[AQBr]_0=5.00\times10^{-3}$ mol/l, $[CuI]_0=2.00\times10^{-3}$ mol/l, temp 70 °C, solvent 1,2-dimethoxyethane–methyl cellosolve 4 : 1. $[AE]_0$; ▲: 2.00, △: 1.50, ●: 1.00, ○: 0.50, ■: 0.25 mol/l.

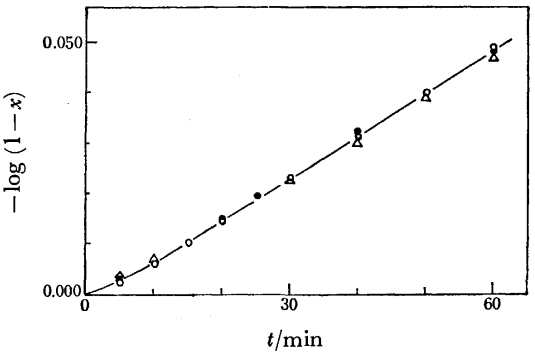

Fig. 6. Effect of the concentration of 1-bromoanthraquinone; $[AE]_0=0.50$ mol/l, $[CuBr]_0=2.00\times10^{-3}$ mol/l, temp 70 °C, solvent 1,2-dimethoxyethane–methyl cellosolve 4 : 1. $[AQBr]_0$; ●: 7.00×10^{-3}, ○: 5.00×10^{-3}, △: 3.00×10^{-3} mol/l.

in the concentration of AQBr. Since the concentration of amine used in a large excess may reasonably be supposed to be kept constant, the presence of the induction period is considered to reflect the change in the catalytic activity. We reported previously that the copper(I) species was oxidized to the copper(II) species by means of an electron transfer from copper(I) to haloanthraquinone as the reaction proceeded, but the reaction rate did not decrease in accordance with the formation of the copper(II) species, which was less active than the copper(I) species.[1] Figures 4 and 7 suggest that the induction period is observed in the case of the slow formation of the copper(II) species. As has been mentioned above, the induction period was absent at high concentrations of amine. The ESR spectra of the reaction system indicated that the formation of copper(II) species increased with the increase in the concentration of amine. The ESR spectra showed also that the formation of the copper(II) species in the reaction of 1-iodoanthraquinone with 2-aminoethanol was much faster than that in the reaction using 1-bromoanthraquinone. The reaction with 1-iodoanthraquinone did not reveal any induction period, but the

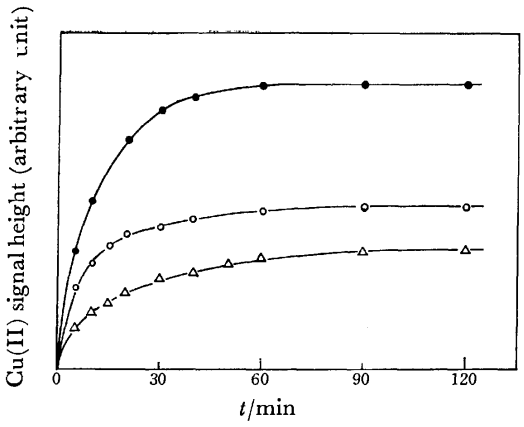

Fig. 7. Time dependence of Cu(II) signal height; $[AQBr]_0=5.00\times10^{-3}$ mol/l, $[AE]_0=0.50$ mol/l, $[CuX]_0=2.00\times10^{-3}$ mol/l, temp 70 °C, solvent 1,2-dimethoxyethane–methyl cellosolve 4 : 1. ●: $[Cu(CH_3CN)_4]ClO_4$, ○: CuBr, △: CuI.

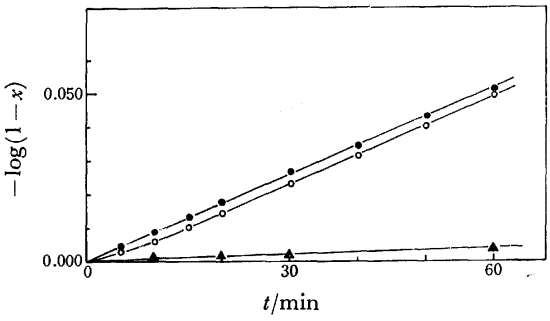

Fig. 8. Pseudo-first order plots of the condensation catalyzed by CuBr, $CuBr_2$, or CuBr+$CuBr_2$; $[AQBr]_0=5.00\times10^{-3}$ mol/l, $[AE]_0=0.50$ mol/l, temp 70 °C, solvent 1,2-dimethoxyethane–methyl cellosolve 4 : 1. ●: $[CuBr]_0=1.70\times10^{-3}+[CuBr_2]_0=0.30\times10^{-3}$ mol/l, ○: $[CuBr]_0=2.00\times10^{-3}$ mol/l, ▲: $[CuBr_2]_0=2.00\times10^{-3}$ mol/l.

reaction using 1-bromoanthraquinone revealed a marked induction period(Fig. 1).

Thus, the formation of the copper(II) species seems to be related to the presence of the induction period. If this is the case, the induction period will vanish upon the addition of copper(II) bromide to copper(I) bromide. The experimental results fit in with this expectation(Fig. 8). Although the yield of the condensation product was strikingly low when the $CuBr_2$ catalyst was used, it is noteworthy that the copper(II) species increased the catalytic activity of the copper(I) species.

All of the results support the idea that the formation of copper(II) species is closely correlated with the induction period. Thus, the presence of an induction period can be understood to be due to the effect of the formation of the copper(II) species on the catalytic activity of the copper(I) species.

Further detailed studies are in progress to elucidate the formation and role of the copper(II) species.

Experimental

Materials. The 1-bromoanthraquinone, 1-(2-hydroxyethylamino)anthraquinone, and copper(I) halides were prepared as has been reported previously.[1] The 1-iodoanthraquinone was prepared by the reaction of anthraquinone-1-diazonium salt and potassium iodide and purified by column chromatography on silica gel (using benzene as the developing solvent), followed by recrystallization from acetic acid: mp 205.3—205.5 °C (cor) (lit, mp 204—205 °C[19]) (Found: C, 50.32; H, 1.94%). Copper(II) bromide was purified by washing with ethyl acetate and anhydrous ethanol and then dried *in vacuo*. Tetrakis(acetonitrile)copper(I) perchlorate was prepared as has been described in the literature,[20] recrystallized several times from acetonitrile, and dried under a nitrogen atmosphere. The 2-aminoethanol was purified by the method described previously.[1] All the solvents were dried by the usual methods, distilled, and stored under a nitrogen atmosphere.

Kinetic Measurements. The kinetic measurements were conducted by the method described in the previous paper.[1] The 1-iodoanthraquinone formed by the halogen-exchange reaction was analyzed as follows: sample(0.5 ml) were withdrawn and diluted in ethanol. The solution was analyzed by the use of a Shimadzu Du Pont LC-1 high-speed liquid chromatograph(column: Zorbax ODS; eluent: methanol–water 67 : 33), with 1-amino-2-bromoanthraquinone as the internal standard.

ESR Measurement. The ESR spectra were measured at 70 °C by means of a JEOL-PE-3X ESR spectrometer. A single sample tube was used throughout the measurement, and the conditions of the ESR spectrometer were kept constant as far as possible.

References

1) Part I of this series: S. Arai, T. Yamagishi, S. Ototake, and M. Hida, *Bull. Chem. Soc. Jpn.*, **50**, 547 (1977).
2) H. Weingarten, *J. Org. Chem.*, **29**, 3524 (1964).
3) T. Kawaki and H. Hashimoto, *Bull. Chem. Soc. Jpn.*, **45**, 1499 (1972).
4) T. D. Tuong and M. Hida, *Bull. Chem. Soc. Jpn.*, **43**, 1763 (1970).
5) T. D. Tuong and M. Hida, *Bull. Chem. Soc. Jpn.*, **44** 756 (1971).
6) T. D. Tuong and M. Hida, *Chem. Lett.*, **1973**, 363.
7) T. D. Tuong and M. Hida, *J. Chem. Soc., Perkin Trans. 2*, **1974**, 676.
8) T. N. Kurdyumova, *Org. Poluprod. Krasiteli*, **1969**, 94; *Chem. Abstr.*, **72**, 90134k (1970).
9) W. H. Hardy and R. B. Fortenbaugh, *J. Am. Chem. Soc.*, **80**, 1716 (1958).
10) R. G. R. Bacon and H. A. O. Hill, *J. Chem. Soc.*, **1964**, 1037.
11) T. Cohen, J. Wood, and A. G. Dietz, Jr., *Tetrahedron Lett.*, **1974**, 3555.
12) J. Burdon, P. L. Coe, C. R. Marsh, and J. C. Tatlow, *J. Chem. Soc., Perkin Trans., 1*, **1972**, 763.
13) J. B. Mine, *Can. J. Chem.*, **48**, 75 (1970).
14) C. L. Jenkins and J. K. Kochi, *J. Am. Chem. Soc.*, **94**, 843 (1972).
15) R. G. Wilkins and A. R. Burkin, *J. Chem. Soc.*, **1950**, 127.
16) J. G. Clifton and J. T. Yoke, *Inorg. Chem.*, **5**, 1630 (1966).
17) P. Murray-Rust, P. Day, and C. K. Prout, *Chem. Commum.*, **1966**, 277.
18) J. R. Clifton and J. T. Yoke, *Inorg. Chem.*, **7**, 39 (1968).
19) J. Mindl, J. Slosar, and M. Vecera, *Colloct. Czech. Chem. Commun.*, **33**, 2895 (1968).
20) B. J. Hathaway, D. G. Holah, and J. D. Postlethwaite, *J. Chem. Soc.*, **1961**, 3215.

Restricted Rotation Involving the Tetrahedral Carbon. XX. Barriers to Rotation and ^{13}C NMR Spectra of 9-(2-Alkylphenyl)fluorene Derivatives[1,2]

Mikio NAKAMURA,[3] Nobuo NAKAMURA, and Michinori ŌKI*

Department of Chemistry, Faculty of Science, The University of Tokyo, Hongo, Bunkyo-ku, Tokyo 113

(Received June 22, 1977)

A series of 9-(2-alkylphenyl)fluorene derivatives are prepared and their internal rotation about the C_9–C_{ar} bond is examined. Those which have a methyl, an ethyl, or an isopropyl group in 2′ position exist as a mixture of sp and ap forms, showing coalescence phenomena in the NMR spectra at high temperatures. The barriers to rotation of these compounds are obtained by the usual DNMR method. 9-(2-*t*-Butylphenyl)fluorene, in contrast, is found to exsist exclusively as an sp form and thus the barrier to rotation must be determined by measuring the rates of conversion from the unstable ap form which is successfully obtained by the protonation of the corresponding lithium fluorenide at low temperatures. The barriers to rotation of the compounds are alike except for the *t*-butyl compound. The difference is explained in terms of the conformation of the alkyl group in the ground and the transition state for rotation. The ^{13}C NMR data also exhibit a large steric interaction between the alkyl group and the fluorene ring.

Barriers to rotation about C_9–C_{ar} bond are known to be extremely high in 9-arylfluorenes, especially when the aryl group is a 2,6-disubstituted phenyl.[4] For example, the barrier to rotation of 9-(2,6-dimethylphenyl)fluorene (**1**) was reported to be larger than 23 kcal/mol and, as expected from the barrier, we could isolate the two rotamers of structurally anologous 9-(2-bromomethyl-6-methylphenyl)fluorene (**2**). When one of the substi-

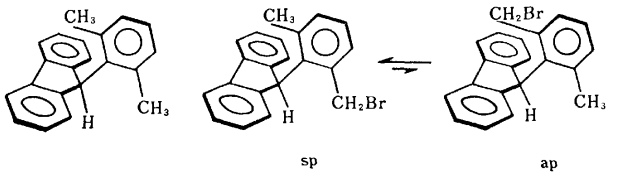

(**1**) (**2**)

tuents in 2 and 6 positions of the aryl group is replaced by hydrogen, the barrier to rotation decreases to a great extent and the rotamer is no longer isolable at room temperature. In such a case DNMR method may become a powerful tool for deciding the barriers to rotation. The barrier to rotation of 9-(*o*-tolyl)-fluorene was measured to be *ca.* 16 kcal/mol by this method.[5]

As for the equilibrium constant between rotamers, it depends mainly on the relative bulkiness of the substituents in 2 and 6 positions of the aryl, though in some cases electronic effect such as charge transfer stabilization controls the population.[1] Judging from the results on equilibrium constants, so far reported, in this series, a bulkier substituent is apt to take the position in proximity of 9-H. Thus, in the case of **2** the sp form is favored over the ap form as the bromomethyl is larger than the methyl group. If one of the substituents is exceedingly large, the populations of two rotamers must be one-sided. In such a case, information on the barrier to rotation cannot be obtained by the DNMR method. Signals due to the unfavorable ap forms of 9-(2-alkylphenyl)fluorene derivatives **4**, **5**, and **6** could be observed in the ^1H NMR spectra, whereas none of the signals attributable to the ap form could be detected when the substituent was *t*-butyl.[2] Thus compounds **4**, **5**, and **6** belong to a category which gives barriers to rotation by the DNMR method, whereas compound **7** needs a device

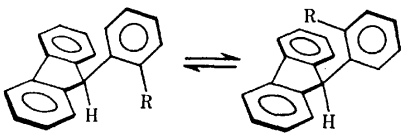

(**3**) R=H
(**4**) R=Me
(**5**) R=Et
(**6**) R=^{i}Pr
(**7**) R=^{t}Bu

for measuring the barrier. We could solve the latter problem by finding a method for preparing unstable isomer and by measuring the rates of isomerization.

In this paper we wish to describe the method for obtaining the barrier to rotation of 9-(2-*t*-butylphenyl)-fluorene (**7**) together with the substituent effects on the rotational barriers in the 9-(2-alkylphenyl)fluorene series. To identify the substituent, the positions are referred to by numbers with primes when they are carried in the 9-aryl group.

Experimental

Materials. The syntheses of 9-aryl-9-fluorenol were carried out by the Grignard reaction of fluorenone with the corresponding arylmagnesium halide followed by treatment with dilute hydrochloric acid. 9-Arylfluorenes were obtained by reducing the corresponding fluorenol with hydriodic acid. Details of the syntheses were described in a previous paper, taking **6** and **7** as examples.[6]

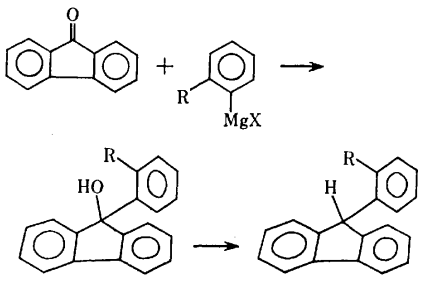

9-(2-Ethylphenyl)-2-fluorenol (***10***), mp 133—134 °C. Yield 75%. ^1H NMR ($CDCl_3$, δ): 0.43 (CH_3CH_2), 1.72 (CH_3-CH_2), 8.2 (6′-H). Found: C, 88.10; H, 6.36%. Calcd for $C_{21}H_{18}O$: C, 88.08; H, 6.34%.

9-(2-Ethylphenyl)fluorene (***4***), mp 65—66 °C. Yield 84%. ^1H NMR ($CDCl_3$, δ): 1.42 (sp-CH_3CH_2), 0.40 (ap-CH_3CH_2), 3.07 (sp-CH_3CH_2), 1.4 (ap-CH_3CH_2), 5.37 (sp-9-H), 4.95 (ap-9-H), 6.33 (sp-6′-H). Found: C, 93.45; H, 6.65%. Calcd for $C_{21}H_{18}$: C, 93.29; H, 6.71%.

Table 1. Activation parameters for rotation and equilibrium constants at 0 °C

	sp→ap			ap→sp			
	$\Delta H^{\ddagger}$ (kcal/mol)	$\Delta S^{\ddagger}$ (eu)	$\Delta G^{\ddagger}$ (kcal/mol)	$\Delta H^{\ddagger}$ (kcal/mol)	$\Delta S^{\ddagger}$ (eu)	$\Delta G^{\ddagger}$ (kcal/mol)	K(ap/sp)
H[a]	—	—	<9	—	—	<9	—
Me	15.9	−2.4	16.6	15.9	−1.5	16.3	1/1.6
Et	18.2	1.1	17.9	18.2	3.3	17.3	1/3.3
^{i}Pr	16.0	−8.6	18.3	16.0	−7.3	18.0	1/2.4
^{t}Bu	—	—	>23	21.8	5.6	20.3	<1/100

a) Data reported by Siddall *et al.*[5] for 9-(*m*-tolyl)fluorene.

Synthesis of ap Form of **7**. The synthesis of thermodynamically unstable ap form of **7** was carried out by the following procedure.

To an NMR sample tube containing *ca.* 20 mg of **7** was added *ca.* 0.2 ml of ether–THF solution of butyllithium which contained about 0.15 mmol of net butyllithium. The solution gradually changed red as lithium salt was produced. When the 9-H signal disappeared completely, the sample was cooled to *ca.* −50 °C and a small amount of pre-cooled trifluoroacetic acid in THF was added in small portions with stirring until the solution turned colorless. The ^{1}H NMR spectra of the colorless solution showed the presence of only ap form at this temperature.

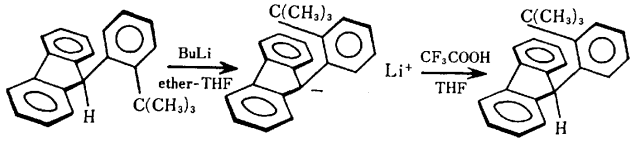

sp ap

Kinetics. Although the ap form of **7** was stable at −50 °C, new signals assigned to the sp form appeared gradually when the temperature was raised up to *ca.* −10 °C. The rate of isomerization was followed by comparison of the signal height of 9-H's of two rotamers. The temperature was calibrated by the peak separation of methyl alcohol. Plots of log $(1-x/a)$ *vs.* time gave a straight line and the first order rate constants were obtained by the usual way. The rate constants were 3.9×10^{-4} s^{-1} (−1 °C), 1.2×10^{-4} s^{-1} (−9 °C), and 4.1×10^{-5} s^{-1} (−15 °C). Putting these rate constants into Eyring's equation, we could obtain the activation parameters for rotation.

As for compounds **4**, **5**, and **6**, barriers to rotation were obtained by the usual DMNR method since the signals of these compounds broadened and showed coalescence phenomena when the temperature was changed. Thus the rate constant at each temperature was obtained by the computer simulation of the observed curves. Free energies, enthalpies, and entropies of activation for rotation are given in Table 1 together with the equilibrium constants between rotamers.

NMR Measurement. ^{1}H NMR spectra were determined on a Hitachi R-20B spectrometer operating at 60 MHz. ^{13}C NMR spectra were measured on a JNM-FX 60 spectrometer operating at 15.04 MHz and ^{13}C-^{1}H coupling constants were obtained from all proton undecoupled spectra. The estimated error in reading the coupling constants was ±0.5 Hz. In every compound except **7** the chemical shifts and the coupling constants of 9-C's of two rotamers were easily obtained since these compounds existed as a mixture of sp and ap form at the equilibrium. The ^{13}C NMR parameters of the ap form of compound **7**, on the other hand, was difficult to obtain as it was prepared by the protonation of the corresponding fluorenide anion at low temperature in ether–THF solution: These solvents interfered the measurement of the 9-C signal. Thus the solvent had to be replaced by $CDCl_3$. The replacement of the solvent was easily attained, since the 9-lithio derivative crystallized when the solution was maintained at −5 °C for a day. The solvents were decanted and the red crystals of the lithium salt were dried under reduced pressure. A $CDCl_3$ solution containing a small amount of trifluoroacetic acid was added slowly at −50 °C to the crystals placed in a ^{13}C NMR sample tube. After the solution was stirred vigorously, the ^{13}C NMR spectra were measured at −40 °C to exhibit a clear 9-C signal. These data are listed in Table 2.

Results and Discussion

Barriers to Rotation. In Table 1, kinetic parameters for rotation of compounds **4**, **5**, and **6** at 0 °C are listed for both sp→ap and ap→sp processes. We limit our discussion here on free energies of activation, since values of entropies of activation obtained by the DNMR method are often controversial.

The free energy of activation for the process sp→ap of compound **7** was not possible to obtain, since no *t*-butyl signal of the ap form could be detected at the equilibrium state. Although the extremely concentrated solution of **7** was prepared in order to observe the *t*-butyl signal of the ap form, if any, in ^{1}H NMR spectrum, no signal could be detected at the expected position. Thus we concluded that the equilibrium constant at 0 °C is less than 1/100 which corresponds to the free energy difference of *ca.* 2.5 kcal/mol. Since the barrier to rotation was estimated at 20.3 kcal/mol for the ap→sp process, that for sp→ ap must be larger than 23 kcal/mol from the above discussion. The measurement of the ^{1}H NMR spectrum at high temperature may be another possible method for detecting the ap form, since, in general, the population of a less stable isomer increases as the temperature is raised. But neither broadening of the *t*-butyl signal due to exchange nor the change of its chemical shift was observed up to 180 °C, indicating that the sp form is more stable than the ap form at least by *ca.* 2.5 kcal/mol even at 180 °C.

To start, let us compare the barriers to rotation for the process from the sp to the ap form. Data in Table 1 indicate that a considerably large increase in energy is observed when a methyl group is introduced in 2′ position in place of a hydrogen (more than 7 kcal/mol) and when an isopropyl group is replaced by a *t*-butyl group (more than 5 kcal/mol). In contrast to these the

replacement of the methyl group by a bulkier ethyl or isopropyl group results in a small increase in activation energy. The substituent effect on the rotational barriers observed in this system is somewhat similar to that of neopentyl derivatives (**8**) reported by Dahlberg *et al.*;[7] barriers to rotation at the coalescence temperature are 10.6 (T_c=−56 °C), 10.7 (−53 °C), and 12.7 (−15 °C) kcal/mol for **8a**, **8b**, and **8c**, respectively, whereas it becomes as high as 17.6 kcal/mol (+82 °C) when R is a *t*-butyl.

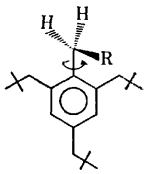

8 **a** R=Me
b R=Et
c R=^{i}Pr
d R=^{t}Bu

In principle, the barriers to rotation are relative values: even if the absolute value of a barrier is very high, the barrier may be low if the ground state is rich in energy. We must, therefore, discuss both the transition state and the ground state, if we compare the barriers.

The transition state for rotation may be considered as a conformation which gives rise to most repulsive interaction between the alkyl group in 2′-position and 1 (or 8)-position of the fluorene ring, whereas the ground state involves the interaction of the alkyl group with 9-H. The fact that substitution of 2′-hydrogen by a methyl group causes great enhancement of the barrier is interpreted as such that the destabilization of the ground state due to 2′-CH_3–9-H interaction is relatively small and that of the transition state due to 2′-CH_3–1(or 8)-H is large.

Ground state of compounds **4**, **5**, and **6** may not differ to a great extent, because they can take a conformation in which the smallest group comes to a most crowded site. This type of consideration is well documented in explaining the free energy difference of axial-equatorial alkylcyclohexanes. Likewise the destabilization of the transition state will be also comparable for compounds **4**, **5**, and **6** (Fig. 1a). Thus the similar free energies of activation for rotation is reasonable, if the substituent in 2′-position has at least a hydrogen in α-position of the alkyl group, although the entropy factor may be unfavorable for those which have smaller number of hydrogens.

The *t*-butyl compound has no hydrogen to lessen the repulsion by taking a conformation of the least strain. Thus both the ground state and the transition state are greatly destabilized relative to the lower homologs.

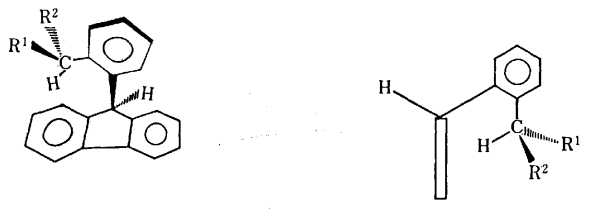

(a) Transition state (b) Ground state

Fig. 1. Possible conformations of the compound, the substituent of which has an α hydrogen.

Again the effect seems to be larger in the transition state than in the ground state. Thus the barrier is increased to a great extent, compared to that of the isopropyl compound.

The barriers to rotation of the ap→sp processes show a quite different aspect in a sense that only a 2 kcal/mol increase in energy is observed by the introduction of a *t*-butyl group instead of an isopropyl group. This clearly means that, in compound **7**, a remarkable amount of energy increase in the transition state for rotation is compensated by nearly the same degree of increase in energy in the ground state. The destabilization of the ap form of compound **7** can again be explained by taking the conformation of the alkyl group into account. In methyl, ethyl, and isopropyl derivatives the repulsive interaction between the substituent and the fluorene ring may not become so large if the α-hydrogen of the substituent faces the fluorene ring. Whereas in the *t*-butyl derivative severe repulsion inevitably occurs (Fig. 1b).

The large repulsion between the *t*-butyl group and the fluorene ring is more clearly demonstrated in 9-(2-alkylphenyl)-9-fluorenols **9**, **10**, **11**, and **12**. The ^{1}H NMR spectrum of compound **9** showed a characteristic feature of the ap form: a methyl signal appeared at a high field (δ 1.27) and 6′-H multiplet at a low field (δ 8.2). The ^{1}H NMR spectra of **10** and **11** showed the same trends as that of **9**, indicating that these compounds also existed as ap forms probably because of a large repulsion between the alkyl and the 9-hydroxyl groups compared with that between the alkyl group and the fluorene ring. The *t*-butyl derivative (**12**), on the other hand, was concluded to exist exclusively as the sp form, since the *t*-butyl signal appeared at a low field (δ 1.79) as a little broad singlet and signals due to 6′-H was observed at quite a high field (δ 6.4) also as a broad doublet. When the temperature was raised, the *t*-butyl

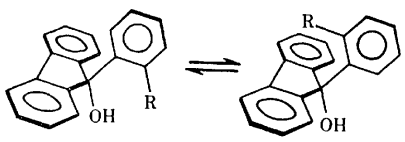

(**9**) R=Me
(**10**) R=Et
(**11**) R=^{i}Pr
(**12**) R=^{t}Bu

signal showed further broadening and at 50 °C its half band width amounted to 2.9 Hz. The signals of 6′-H changed more appreciably in the same temperature range: the doublet broadened with the increase in temperature and at 60 °C the fine structure of the signals almost disappeared. Both signals sharpened on further raising of the temperature. When the temperature was lowered, there appeared a trace of a signal at δ 0.7 which was assigned to the *t*-butyl group of the ap form because structurally analogous **11** gave isopropyl signals of the ap form at δ 0.5. While it was difficult to obtain an accurate equilibrium constant from the spectra, it was roughly estimated to be 1/80 at −30 °C from the integration of the two signals. These results again suggest the existence of considerably large repulsion between the *t*-butyl group and the fluorene ring.

^{13}C NMR Spectra. Above discussion implies that the deformation of molecular structure may exsist in

Table 2. ^{13}C NMR data of rotameric 9-arylfluorenes in $CDCl_3$ at room temperature (δ from TMS)

R	δ of 9-C		$^1J_{^{13}C-^1H}$ of 9-C	
	sp	ap	sp	ap
H[a)]	53.93	53.93	128.8	128.8
Me	49.79	55.96	127.7	125.1
Et	49.26	56.28	126.7	124.8
^{i}Pr	48.90	56.33	127.6	122.7
^{t}Bu	50.97	59.66	127.2	115.4

a) The compound carries a methyl group in *p*-position.

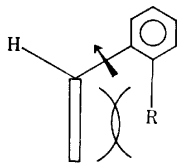

Fig. 2. Molecular deformation of the sp form.

the ap form of compound **7**, since it is less stable than the sp form by at least *ca.* 2.5 kcal/mol. Several deformations are expected for the relief of the strain which is originated by the repulsion between the bulky *t*-butyl and the fluorene ring. Of those, bending of the C_9–C_{ar} bond outwards from the fluorene ring will be of most importance (Fig. 2). If such a deformation really exists, it will affect the chemical shift and the coupling constant (^{13}C–^1H) of 9-C, making them quite different from those of other normal 9-arylfluorenes. In Table 2 ^{13}C and ^1H NMR spectral data of rotameric 9-arylfluorenes are listed. In each case, 9-C gave two distinct signals corresponding to the sp and ap form. As for the chemical shifts of the ap forms, they tend to increase as the size of the alkyl group increases: this tendency is in accordance with the above assumption of molecular deformation, because bending of the C_9–C_{ar} bond outwards from the fluorene ring is expected to change the hybridization of 9-C sp^2-like to cause the low field shift of the signal due to 9-C of the ap form. The degree of the low-field shift of the 9-C signals of the ap forms parallels somewhat with the increase in free energy difference between rotamers as the size of the alkyl group increases. In methyl, ethyl, and isopropyl derivatives the chemical shifts of 9-C lie within a small range of 0.4 ppm. Correspondingly free energy differences between rotamers are 0.3, 0.6, and 0.4 kcal/mol for the methyl, the ethyl, and the isopropyl compound. In the *t*-butyl derivative, however, the low field shift by about 3.3 ppm and the large free energy difference of more than 2.5 kcal/mol are observed. The correlation may be an indication that the population of 9-(2-alkylphenyl)fluorene is mainly regulated by the nonbonded interaction between the alkyl group and the fluorene ring. It may mean in turn that repulsion between the alkyl group and 9-H is relatively small.

Another method to check the presence of the molecular deformation, shown in Fig. 2, is the measurement of the ^{13}C–^1H coupling constant of 9-C. Inspection of Table 2 reveals that the coupling constants of the ap forms decrease as the size of the alkyl group increases. Since the magnitude of the ^{13}C–^1H coupling constant is correlated to s-character of the C-H bonding orbital, the decrease can be taken as an indication of the increase in p-character of the C–H bonding orbital.[8] This may most reasonably be caused by bending of the C_9–C_{ar} bond as shown in Fig. 2, though it may also be caused by widening any of the C–C–C angles at 9-C. As was seen in the chemical shifts of this series, the coupling constant of **7** showed a striking difference from those of other compounds. The value of 115.4 Hz may be one of the smallest C–H coupling constants ever reported for neutral molecules.[8]

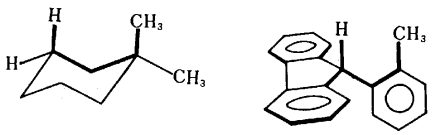

Fig. 3. The spacial arrangement of groups in 1,1-dimethylcyclohexane and **4**.

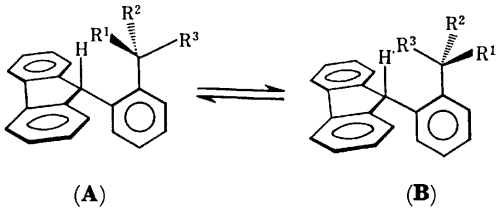

(**A**) (**B**)

Fig. 4. Conformation of the *o*-alkyl group in 9-arylfluorenes.

As for the chemical shifts of 9-C of the sp-forms, they showed rather a complicated tendency as the size of the substituents increases: a large high field shift (4.1 ppm) was observed when a methyl group was introduced in 2′ position, whereas the shift was affected to only a small extent (0.9 ppm or less) on change of the methyl group by an ethyl or an isopropyl group. In contrast, a low field shift of *ca.* 2 ppm was observed when the alkyl changed from isopropyl to *t*-butyl. A large high field shift observed in the methyl compound may be attributed to the well-known γ effect, because the spacial arrangement of the 2′-methyl and 9-C in **4** is quite similar to that of an axial-methyl and 3-C in 1,1-dimethylcyclohexane (Fig. 3).[9] In both compounds the high field shift caused by the introduction of a methyl group amounted to *ca.* 4 ppm.

The most difficult point to explain is why the chemical shift of 9-C of compound **7** showed a relatively large low field shift. We tentatively consider that the difference in the prefered conformation of the alkyl group plays some role in determining the chemical shift of the sp form. Two stable conformations are possible for the alkyl group in position 2′. One is a conformation where 9-H squeezes in R^1 and R^2 (Conformer **A**) and the other is the one where 3′-H is situated between R^1 and R^2 (Conformer **B**) as shown in Fig. 4. In each conformation R^3 opposes either 3′-H or 9-H. Thus the stability of two conformations must be decided by the relative bulkiness of R^1, R^2, and R^3. In compound **6** where R^1 and R^2 are methyl and R^3 is hydrogen, conformer **B** must be more stable than conformer **A**,

because two methyl groups are placed within a repulsive region of 9-H in the latter, whereas the repulsive force between two hydrogens in the conformation **B** will be less. There is another possibility in conformation **A**: that is, the conformation where R^1 and R^3 are methyls and R^2 is hydrogen. Contribution of this conformation will be minor because the opposing effect of R^3 (CH_3) with 3'-H is large. Likewise, conformation **B** where R^1 and R^3 are methyls and R^2 is a hydrogen may contribute to only a small extent becuase of the opposing effect between R^3 and 9-H. Similarly the stable conformation of **5** is expected to be the one where an α hydrogen of the substituent is in proximity of 9-H. In this sense ethyl and isopropyl groups give similar steric effects on carbon at position 9 and thus the chemical shift of 9-C is almost invariable for the methyl, the ethyl, and the isopropyl compounds. In the case of compound **7**, R^1, R^2, and R^3 are all methyl groups and therefore **A** must be more stable than **B**: in **B** the distance between the methyl (R^3) and 9-H is quite small and a large repulsion is expected.

Then the spacial relation between 9-C and methyl carbon of this compound is quite similar to that between the methyl and the hydroxyl group of 4a-methyl-*trans*-1-decalol (**13**) (Fig. 5).[10] In **13** a downfield shift of *ca.* 3.4 ppm was observed and was attributed to the syn-axial arrangement of two interacting groups separated by four bonds. Thus the observed downfield shift of *ca.* 2 ppm may become a support for the δ effect originally described by Stothers *et al.*

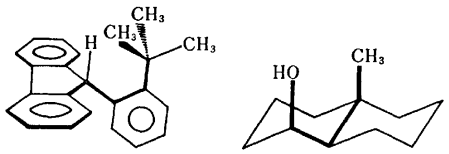

(**7**) (**13**)

Fig. 5. The spacial arrangement of groups in **7** and **13**.

References

1) The preceding paper: M. Nakamura and M. Ōki, *Chem. Lett.*, 651 (1976)

2) Presented in part as a preliminarly form: M. Nakamura, N. Nakamura and M. Ōki, *Chem. Lett.*, **1977**, 17.

3) Present address: Department of Chemistry, School of Medicine, Toho University, Omorinishi, Otaku, Tokyo 143.

4) M. Ōki, *Angew. Chem. Int. Ed. Engl.*, **15**, 87 (1976).

5) T. H. Siddall, and W. E. Stewart, *J. Org. Chem.*, **34**, 233 (1969).

6) M. Nakamura, N. Nakamura, and M. Ōki, *Bull. Chem. Soc. Jpn.*, **50**, 1097 (1977).

7) E. Dahlberg, B. Nilsson, K. Olsson, and P. Martinson, *Acta Chem. Scand.*, **B29**, 300 (1975).

8) Although the correlation between the s-character and the C-H coupling constant is questionable in highly straingd molecules (see, for example, L. S. Bartell and H. B. Bürgi, *J. Am. Chem. Soc.*, **94**, 5239 (1972)), the correlation holds to many compounds: J. H. Goldstein, V. S. Watts, and L. S. Rattet, *Prog. Nucl. Magn. Resonance Spectrosc.*, **8**, 103 (1971); T. L. Marshall, D. E. Miller, S. A. Conn, A. Seiwell, and A. M. Ihrig, *Acc. Chem. Res.*, **7**, 333 (1974).

9) D. K. Dalling and D. M. Grant, *J. Am. Chem. Soc.*, **89**, 6612 (1967).

10) S. H. Grover and J. B. Stothers, *Can. J. Chem.*, **52**, 870 (1974).

Studies of Heterocyclic Compouds. XII.[1] Structures of Acetylated Products of 5-Hydroxy-4-(2-hydroxyethyl)-3-methylpyrazole

Hisao Ochi, Tadashi Miyasaka, and Kiichi Arakawa

School of Pharmaceutical Sciences, Showa University, Hatanodai, Shinagawa-ku, Tokyo 142

(Received March 18, 1977)

Acetylation of 5-hydroxy-4-(2-hydroxyethyl)-3-methylpyrazole (**1**) produced five acetyl derivatives: 4-(2-acetoxyethyl)-5-hydroxy-3-methylpyrazole (**2**), 4-(2-acetoxyethyl)-2-acetyl-5-hydroxy-3-methylpyrazole (**3**), 4-(2-acetoxyethyl)-1-acetyl-5-hydroxy-3-methylpyrazole (**4**), 5-acetoxy-4-(2-acetoxyethyl)-2-acetyl-3-methylpyrazole (**5**), and 1-acetyl-5-hydroxy-4-(2-hydroxyethyl)-3-methylpyrazole (**6**). The partial hydrolysis of **3** and **5** in aq acetic acid gave the monoacetate (**2**). The triacetate (**5**) afforded **3** by heating in a mixture of pyridine and methanol. Migration of the acetyl group from the N_1-position to the C_5-O- and to the side chain-O-position is suggested. It is also suggested that the triacetate (**5**) may be effective for acetylation of amines.

In previous papers we have shown that five mono- and diacetyl derivatives could be prepared from 5-hydroxy-3-methylpyrazole by acetylation with acetic anhydride.[2,3] We have also shown that the acetyl derivatives were useful as mild acetylating reagents.[3]

In order to improve the usefulness of this type of acetylating reagent we have prepared vinylpyrazole derivatives as a monomeric source of acetyl group-exchange resins.

In this paper we deal with the acetylation of 5-hydroxy-4-(2-hydroxyethyl)-3-methylpyrazole (**1**),[4] which is readily prepared from α-acetyl-γ-butyrolactone.[5]

The pyrazole (**1**) can be expected to give a very complicated mixture of mono-, di- and triacetyl derivatives, because, as Katritzky and Lagowski have predicted, **1** has eight possible tautomers[6] (Scheme 1), and the first attack of the acetylating reagent may occur either at N_1-, N_2-, C_5-O-, or the side chain-O-position. The structures of the reaction products were determined based on the IR, the NMR, and the UV spectra and the ferric chloride coloration test.[7]

By heating in refluxing acetic acid, **1** gave a monoacetate (**2**), whose UV spectrum was almost superimposable with that of the starting material. The IR spectrum (1750 cm^{-1}) and the NMR spectrum (1.98, 2.08 ppm) indicated that the acetyl group bonded to the oxygen atom on the side chain to furnish 4-(2-acetoxyethyl)-5-hydroxy-3-methylpyrazole.

When **1** was heated with two molar equivalents of acetic anhydride in pyridine under reflux, diacetate (**3**) was formed in good yield; this was identical in every respect with the specimen prepared by acetylation of **2** with an equimolar amount of acetic anhydride in pyridine. Hydrolysis of **3** in aq acetic acid afforded **2**. The diacetate (**3**) gave a reddish brown coloration with methanolic ferric chloride; there was one absorption maximum (257.5 nm) in the UV spectrum and a chemical shift of C_3–CH_3 at 2.50 (or 2.52) ppm.

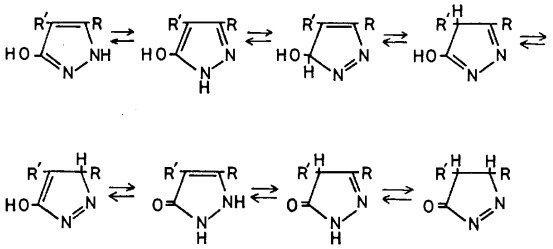

Scheme 1.

By heating **2** in acetic anhydride at 110 °C for 1.5 min the diacetate (**4**) separated; its UV spectrum displayed two absorption maxima (224 and 295.5 nm) and the NMR spectrum displayed the C_3–CH_3 peak at 2.21 ppm. According to the empirical rule that N_2-acetyl groups bring about low field shifts of a C_3–CH_3 signal,[2] the diacetate (**3**) which showed a C_3–CH_3 signal at the lower field of 2.50 (or 2.52) ppm has the N_2-acetyl group, which is 4-(2-acetoxyethyl)-2-acetyl-5-hydroxy-3-methylpyrazole, while the diacetate (**4**) is 4-(2-acetoxyethyl)-1-acetyl-5-hydroxy-3-methylpyrazole.

Heating a suspension of **1** in acetic anhydride under reflux for 4 h afforded triacetate (**5**), which did not show any coloration with ferric chloride. The IR spectrum showed a phenol ester band at 1785 cm^{-1}, and the NMR spectrum displayed a C_3–CH_3 signal at 2.53 ppm. Since the C_3–CH_3 signal shifted to the lower field of 2.53 ppm compared with that of the parent compound (**1**), the structure of **5** corresponds to 5-acetoxy-4-(2-acetoxyethyl)-2-acetyl-3-methylpyrazole.

Further acetylation of the diacetate (**3**) and monoacetate (**2**) with acetic anhydride produced the triacetate (**5**). The partial hydrolysis of **5** in aq acetic acid afforded the monoacetate (**2**) and milder hydrolysis of **5** in a mixture of methanol and pyridine afforded the diacetate (**3**). These results further supported the similarity of the structures of the triacetate (**5**), the diacetate (**3**), and the monoacetate (**2**).

Heating of **1** in acetic anhydride at 110 °C for 1.5 min gave monoacetate (**6**). In contrast to the other

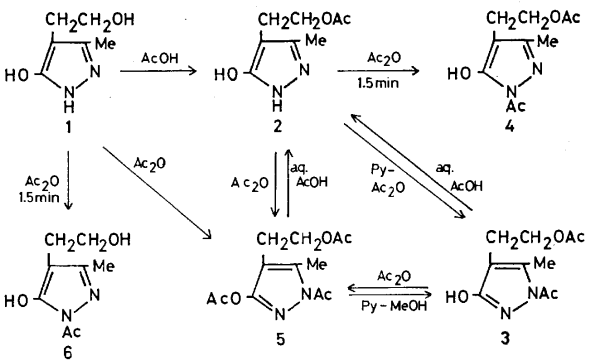

Scheme 2.

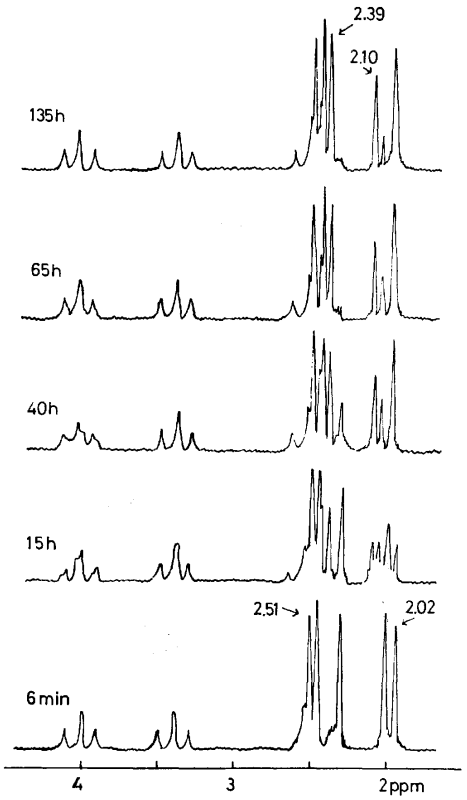

Fig. 1. NMR spectra of the time-course of the conversion of a mixture of **1** and **5** at 35 °C in DMSO-d_6 into a mixture of **3** and **6**.

monoacetate (**2**), **6** gave bluish green coloration with ferric chloride and had two distinct absorption maxima (225.5, 296.5 nm) in the UV spectrum. The methyl signal of C_3-position (2.10 ppm) is not so much lowered in contrast to the parent compound (**1**) which has its methyl signal at 2.02 ppm; the carbonyl band shifted to the lower wave number of 1715 cm^{-1} as a result of hydrogen bonding with C_5–OH. So **6** has the N_1-acetyl group and its structure corresponds to 1-acetyl-5-hydroxy-4-(2-hydroxyethyl)-3-methylpyrazole.

Next we examined the mode of acetyl-transfer reaction during the formation of the acetyl derivatives.

Heating a solution of **5** and an equimolar amount of **1** in benzene under reflux for 28 h afforded a mixture of **1**, **2**, **3**, **5**, and **6**. Fig. 1 shows the time dependence of the NMR signals of the reaction mixture in DMSO-d_6. The chemical shifts of the methyl proton and ethylene proton signals of a mixture of **1** and **5** in DMSO-d_6 were changed at 35 °C and finally the NMR spectrum turned into that of a mixture of diacetate (**3**) and monoacetate (**6**) after 135 h. These results suggest that the acetyl group at the C_5-O-position of **5** migrates to the N_1- or N_2-position of the other pyrazole molecule.

A solution of monoacetate (**6**) in chlorobenzene was heated at 130 °C for 1 h; colorless crystals separated after cooling, and their IR and NMR spectra indicated that the product was monoacetate (**2**). On the other hand 5-hydroxy-4-(2-hydroxyethyl)-1,3-dimethylpyrazole (**7**) was heated with acetic acid under reflux to afford 4-(2-acetoxyethyl)-5-hydroxy-1,3-dimethylpyrazole (**8**). A mixture of an equivalent amount of **5** and **7** was converted by heating under reflux in benzene into four components; **2**, **3**, **4**, and **8**. This result suggests that the acetyl group at the C_5-O-position of the triacetate (**5**) was transferred to the alcoholic group at the side chain of **7** to form **3** and **8**. The fact that the two isomeric diacetates **3** and **4** were isolated from the reaction mixture suggests the existence of an equilibrium between **3** and **4**. Indeed, heating of **4** in chlorobenzene under reflux for 8 h afforded a mixture of **3** (53%) and **4** (47%). A mixture of **3** and **4** in almost the same ratio was also formed from **3**.

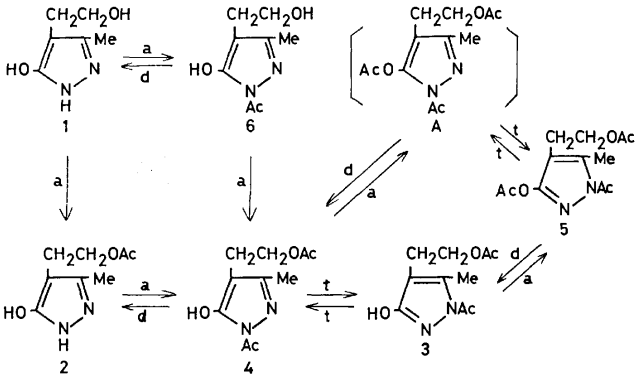

Scheme 3. a: acetylation t: acetyl transfer d: deacetylation

The reaction path of these conversions can be formulated as shown in Scheme 3. In the acetylation of **1**, the kinetically controlled product (**6**) was formed at the first stage. The acetyl group of 1-acetyl-5-hydroxypyrazole was formed, which easily migrates to a position like N_2- or C_5-O-.[3] By heating **6**, therefore, acetyl group at N_1-position migrated either intermolecularly or intramolecularly to the side chain-oxygen to form **2**. The formation of **2** was promptly followed by acetylation at N_1-position to give diacetate (**4**), which was rearranged by heating into the thermally more stable isomer (**3**), and the hydroxyl group at C_5-position of **3** was finally acetylated to form the stable triacetate (**5**). At this stage acetylation of **4** may promptly rearrange into **5** under the present reaction conditions.

The acetoxyl group of the compound **5** was considered to be effective as an acetylating reagent of amines, as shown in the case of 5-acetoxy-2-acetyl-3-methylpyrazole.[3,8] When **5** was treated with an equimolar amounr of aniline, acetanilide was separated in quantitative yield. Further investigation concerning the application of this reagent to other materials is proceeding in this laboratory and will be reported elswhere.

Experimental

All the melting points were measured in capillary tubes and were uncorrected. NMR spectra were measured on Hitachi R-20 60 MHz and Hitachi R-22 90 MHz spectrophotometers, using tetramethylsilane as an internal reference. IR and UV spectra were measured on a JASCO IRA-1 spectrophotometer and a Hitachi EPS-3 spectrophotometer, respectively. Column chromatography was carried out through silica gel (Merck, art. 7734, 70—230 mesh) using chloroform containing 5% methanol as the eluting solvent,

*4-(2-Acetoxyethyl)-5-hydroxy-3-methylpyrazole (**2**).* After 4-(2-hydroxyethyl)-5-hydroxy-3-methylpyrazole (**1**) (1.00 g) was heated in acetic acid (10 ml) under reflux for 1 h, the reaction mixture was evaporated to dryness *in vacuo*. The residual mass was recrystallized from methanol to give colorless plates (995 mg, 76.9% yield), mp 186—188 °C, which gave reddish brown coloration with methanolic ferric chloride. Found: C, 52.11; H, 6.38; N, 15.38%. Calcd for $C_8H_{12}O_3N_2$: C, 52.16; H, 6.57; N, 15.21%. IR (KBr): 1750 cm^{-1}. UV λ_{max}^{MeOH} nm (log ε): 227 (3.72), 239 (3.77). NMR δ ppm (DMSO-d_6): 1.98 (3H), 2.08 (3H), 3.99 (t, 2H, J= 7.5 Hz), 4.29 (t, 2H, J=7.5 Hz).

*4-(2-Acetoxyethyl)-2-acetyl-5-hydroxy-3-methylpyrazole (**3**).* A solution of **1** (284 mg) and acetic anhydride (420 mg) in pyridine (3 ml) was heated under reflux for 3 h. After pyridine was evaporated *in vacuo*, the residue was added onto ice-water. The colorless powder was collected by filtration, and recrystallized from ethyl acetate to give colorless needdles (396 mg, 88.6%), mp 113—114 °C. The material showed reddish brown coloration with methanolic ferric chloride. Found: C, 53.10; H, 6.30; N, 12.11%. Calcd for $C_{10}H_{14}O_4N_2$: C, 53.09: H, 6.24; N, 12.38%. IR (KBr): 1740, 1720, 1640 cm^{-1}. UV λ_{max}^{MeOH} nm (log ε): 257.5 (4.28). NMR δ ppm ($CDCl_3$): 2.02 (3H), 2.50 (3H), 2.52 (3H), 2.68 (t, 2H, J=7 Hz), 4.19 (t, 2H, J=7 Hz).

*4-(2-Acetoxyethyl)-1-acetyl-5-hydroxy-3-methylpyrazole (**4**).* A suspension of **2** (300 mg) in acetic anhydride (3 ml) was heated at 110 °C for 1.5 min with vigorous agitation. After cooling in an ice-salt bath crystals separated; these were collected by filtration and washed with cold ether to give a colorless powder (192 mg, 52%), mp 115—117 °C. The compound was too unstable to be purified by recrystallization from an ordinary organic solvent. The material showed bluish green coloration wtih methanolic ferric chloride. IR (KBr): 1740, 1720, 1650 cm^{-1}. UV λ_{max}^{MeOH} nm (log ε): 224 (4.00), 295.5 (3.75). NMR δ ppm ($CDCl_3$) 2.03 (3H), 2.21 (3H), 2.60 (t, 2H, J=7 Hz), 2.62 (3H), 4.18 (t, 2H, J=7 Hz).

*5-Acetoxy-4-(2-acetoxyethyl)-2-acetyl-3-methylpyrazole (**5**).* After **1** (1.00 g) was heated in acetic anhydride (20 ml) under reflux for 4 h, the acetic anhydride was evaporated *in vacuo*. The residual oil was distilled under reduced pressure to give a colorless oil (1.55 g, 81.6%), bp 178 °C (6 mmHg). The material did not show any coloration with ferric chloride. Found: C, 53.62; H, 6.04; N, 10.35%. Calcd for $C_{12}H_{16}O_5N_2$: C, 53.72; H, 6.01; N, 10.44%. IR ($CHCl_3$): 1785, 1750, 1730 cm^{-1}. UV λ_{max}^{MeOH} nm (log ε): 247 (4.06). NMR δ ppm ($CDCl_3$): 2.02 (3H), 2.33 (3H), 2.53 (3H), 2.59 (m, 5H), 4.09 (t, 2H, J=7.5 Hz).

*1-Acetyl-5-hydroxy-4-(2-hydroxyethyl)-3-methylpyrazole (**6**).* A mixture of **1** (300 mg) and acetic anhydride (3 ml) was heated at 110 °C for 1.5 min with vigorous agitation. After cooling in an ice-salt bath crystals separated; these were collected by filtration and washed with cold ether to give a colorless powder (132 mg, 33.8%), mp 115—118 °C. The compound was too unstable to be purified by recrystallization from an ordinary organic solvent. The material showed bluish green coloration with methanolic ferric chloride. IR (KBr): 1715, 1675 cm^{-1}. UV λ_{max}^{MeOH} nm (log ε): 225.5 (4.31), 296.5 (3.76). NMR δ ppm (DMSO-d_6): 2.10 (3H), 2.28 (t, 2H, J=7 Hz), 2.50 (3H), 3.43 (t, 2H, J=7 Hz).

*4-(2-Acetoxyethyl)-5-hydroxy-1,3-dimethylpyrazole (**8**).* 5-Hydroxy-4-(2-hydroxyethyl)-1,3-dimethylpyrazole (**7**) (1.00 g) was heated in acetic acid (30 ml) under reflex for 5 h. After the acetic acid was evaporated, the residue was separated by column chromatography to give colorless crystals (1.71 g) and the starting material (**7**) (78 mg). The former was recrystallized from benzene to give colorless needles (900 mg, 72%), mp 64—65 °C. Found: C, 54.43; H, 7.22; N, 14.32%. Calcd for $C_9H_{14}O_3N_2$: C, 54.53; H, 7.12; N, 14.13%. IR (KBr): 1755, 1750 cm^{-1}. UV λ_{max}^{MeOH} nm (log ε): 221 (3.72). NMR δ ppm ($CDCl_3$): 2.00 (3H), 2.12 (3H), 2.58 (t, 2H, J=7.5 Hz) 3.39 (3H), 4.10 (t, 2H, J=7.5 Hz).

*Partial Hydrolysis of the Triacetate (**5**) in 60% Aq Acetic Acid.* After **5** (500 mg) was heated in 60% aq acetic acid (10 ml) under reflux for 3 h, the solvent was evaporated under reduced pressure to give a colorless powder (270 mg, 78.7%), mp 186—188 °C. The mixed melting point and the IR spectrum showed that the material was identical with the monoacetate (**2**).

*Partial Hydrolysis of the Diacetate (**3**) in 60% Aq Acetic Acid.* The diacetate (**3**) (100 mg) was treated as described above to give colorless powder (79 mg, 96%). The IR and the NMR spectra were completely identical with those of the monoacetate (**2**).

*Partial Deacetylation of the Triacetate (**5**) with Methanolic Pyridine.* A solution of **5** (200 mg) and pyridine (0.3 ml) in methanol (3 ml) was heated under reflux for 1 h. After evaporation of the solvent *in vacuo* the residue was washed with cold ether to afford colorless crystals (155 mg, 92%), mp 112—114 °C. The IR and the NMR spectra were completely identical with those of the diacetate (**3**).

*Treatment of the Monoacetate (**2**) with an Equimolar Amount of Acetic Anhydride in Pyridine.* A mixture of **2** (368 mg), pyridine (3 ml), and acetic anhydride (210 mg) was heated at 100 °C for 1.5 h. After the pyridine was evaporated *in vacuo*, the reaction mixture was poured onto ice-water. The separated crystals (298 mg, 65.8%) were collected by filtration. The filtrate was extracted with chloroform. The organic layer was dried over magnesium sulfate and the solvent was removed to give colorless crystals (130 mg, 28.7%). The IR and the NMR spectra of each sample indicated that both of them were identical with the authentic specimen of the diacetate (**3**).

*Treatment of the Monoacetate (**2**) with Excess Acetic Anhydride.* After **2** (300 mg) was heated in acetic anhydride (6 ml) under reflux for 2 h, the acetic anhydride was evaporated *in vacuo*. The residual oil was distilled *in vacuo* to give a colorless oil (353 mg), 84.8%), bp 176—178 °C (6 mmHg). The IR and the NMR spectra were completely identical with those of the triacetate (**5**).

*Treatment of the Diacetate (**3**) with Excess Acetic Anhydride.* Diacetate (**3**) (300 mg) was treated as described above to give the triacetate (**5**) (293 mg, 82.4%), bp 176—178 °C (6 mmHg), after distillation.

*Treatment of the Pyrazole (**1**) with the Triacetate (**5**) at 80 °C in Benzene.* Into a solution of **5** (140 mg) in benzene (20 ml) was added finely powdered **1** (70 mg), after being heated under reflux for 28 h, the benzene was evaporated *in vacuo*. The residue was separated by column chromatography to give **5** (32 mg), **3** (90 mg), **6** (5 mg) **2** (958 mg), and **1** (16 mg). These materials were identical with the authentic samples by comparing the IR spectra.

*Treatment of the Pyrazole (**1**) with the Triacetate (**5**) at 35 °C in DMSO-*d_6. A sample tube for the NMR measurement which contained **5** (27 mg), **1** (14 mg), and DMSO-d_6 (0.3 ml) was sealed under a nitrogen stream. The sample tube was warmed to 35 °C and the NMR spectra were measured (TMS as an internal reference). The results are shown in Fig. 1.

*Thermal Treatment of the Monoacetate (**6**) in Chlorobenzene.* After a solution of **6** (100 mg) in chlorobenzene (8 ml) was heated under reflux for 4 h, it was cooled in an ice-salt bath.

The separated crystals were collected by filtration to give colorless leaflets (85 mg, 85%), mp 185—188 °C. The IR spectrum showed that it was identical with the monoacetate (**2**).

*Treatment of the Pyrazole (**7**) with the Triacetate (**5**) at 80 °C in Benzene.* A mixture of **7** (156 mg) and **5** (270 mg) in bezene (5 ml) was heated under reflux for 5 h. After the benzene was evaporated *in vacuo*, the residual solid was separated by column chromatography to give **4** (23 mg), **3** (157 mg), **8** (190 mg), and **2** (30 mg). These materials were found to be identical with the authentic samples by comparing the IR and the NMR spectra.

*Thermal Treatment of the Diacetate (**4**) in Chlorobenzene.* After **4** (100 mg) was heated in chlorobenzene (5 ml) under reflux for 8 h, the solvent was evaporated *in vacuo* to give a colorless powder (98 mg, 98%). The NMR spectrum indicated that the substance was a mixture of **3** and **4** (17 : 15).

*Thermal Treatment of the Diacetate (**3**) in Chlorobenzene.* The diacetate (**3**) (100 mg) was treated in the same manner as described in the case of the diacetate (**4**). After 8 hours' heating the NMR spectrum became identical with that of the compound **4**.

*Acetylation of Aniline with the Triacetate (**5**).* The triacetate (**5**) (270 mg) was added into a solution of aniline (93 mg) in benzene (7 ml) and the mixture was heated under reflux for 2 h. After the solvent was evaporated, the residue was separated by column chromatography to give diacetate (**3**) (215 mg) and acetanilide (131 mg, 97%), which was recrystallized from water to give colorless plates, mp 112—114 °C. The material was proved to be identical with the authentic sample of acetanilide by comparing the IR spectra.

The authers are grateful to the member of the Central Analysis Division of this school for the elemental analyses and the measurement of NMR spectra.

References

1) Part XI: K. Satoh, T. Miyasaka, and K. Arakawa, *Yakugaku Zasshi*, **97**, 422 (1977)

2) K. Arakawa, T. Miyasaka, and H. Ochi, *Chem. Pharm. Bull.*, **22**, 207 (1974)

3) K. Arakawa, T. Miyasaka, and H. Ochi, *Chem. Pharm. Bull.*, **22**, 214 (1974)

4) The nomenclature and structure form of this compound series are represented by enol form, which have some possible tautomers as shown in Scheme 1.

5) a) G. B. Bachman and L. V. Heisey, *J. Am. Chem. Soc.*, **71**, 1985 (1949)
b) H. Wamhoff and E. Korte, *Chem. Ber.*, **99**, 2962 (1966)
c) E. Magien and W. Tom, *J. Org. Chem.*, **1967**, 1229

6) A. R. Katritzky and J. M. Lagowski, "Advances in Heterocyclic Compounds," Vol. 2, Academic Press, New York and London (1963), p. 44.

7) The chemical shift of C_3–CH_3 is lowered in the case that it is adjacent to the *N*-acetyl group. 1-Acetyl-3-methyl-5-hydroxypyrazole showed two absorption maxima at 227 and 289 nm in the UV spectrum and deep purple coloration with methanolic ferric chloride. 2-Acetyl-3-methyl-5-hydroxypyrazole showed one absorption maximum at 253 nm in the UV spectrum and reddish brown coloration with ferric chloride.[2)]

8) M. Irie, T. Miyasaka, and K. Arakawa, *J. Biochem.*, **72**, 65 (1972)

Light-induced Conformational Changes of Polypeptides. Random Copolymers of γ-Benzyl-L-glutamate with *m*- and *p*-Phenylazobenzyl-L-aspartates

Akihiko UENO, Jun-ichi ANZAI, Tetsuo OSA, and Yoshinori KADOMA*

Pharmaceutical Institute, Tohoku University, Aobayama, Sendai 980

**Institute for Medical and Dental Engineering, Tokyo Medical and Dental University, Kanda Surugadai, Chiyoda-ku, Tokyo 101*

(Received March 22, 1977)

Copolymers of γ-benzyl-L-glutamate with *m*- and *p*-phenylazobenzyl-L-aspartates were prepared for investigating the effect of side-chain photoisomerization on their conformations. A study was made of the circular dichroism associated with the n,π* transition of the amide group, as well as the extrinsic bands associated with the azo chromophore. The intensity of the 222-nm amide band seems unaffected by the interaction with the side-chain chromophore. The circular dichroism spectra before irradiation indicate that poly[β-(*m*-phenylazobenzyl)-L-aspartate] (mPALA) adopts a left-handed α-helical form and the other copolymers a right-handed form in 1,2-dichloroethane. After irradiation, remarkable changes of the 222-nm band were observed for the meta copolymer with 89.3% azo residues and mPALA. The increased absolute ellipticity for the former indicates that photoisomerization enhances the helicity of the polymer. Decrease in ellipticity for the latter indicates that photoisomerization induces significant instability of the left-handed α-helical conformation. In the course of subsequent relaxation of mPALA, an abrupt change in the CD spectra was found above 50% of cis followed by a gradual change with decreasing cis%.

The conformation of ester derivatives of poly(L-aspartic acid) has been shown to depend on the nature of the side chain. Left- and right-handed α-helical conformations are usually identified by the circular dichroism (CD), IR or NMR spectra. Poly(β-benzyl-L-aspartate) (PBLA) was shown to adopt a left-handed α-helical conformation,[1,2] but the para substitution of the benzene ring with a methyl, chloro, cyano, or nitro group induces a reversal of the helical sense to a right-handed α-helical conformation.[3–11] The chloro substituted PBLAs assume different handed helices depending on the position of the chlorine atom attached to the benzene ring.[12] These observations indicate that the balance of forces is so delicate that a small change in the side-chain conformation could reverse the helix sense. This prompted us to realize conformational changes of polyaspartates by inducing a configurational change of their side chains. From this view point we prepared some copolymer series containing azobenzene groups in their side chains. We report here the results of copolymers of γ-benzyl-L-glutamate with *m*- and *p*-phenylazobenzyl-L-aspartate. The side-chain azo chromophore undergoes trans-to-cis photoisomerization and subsequent relaxation back to the original trans form. The energy balance of the polymers might be perturbed by the configurational change, and the conformational changes as exemplified below might be possible.

$$\text{left-handed helix} \underset{\Delta}{\overset{h\nu}{\rightleftharpoons}} \text{right-handed helix} \quad (1)$$

$$\text{left-handed helix} \underset{\Delta}{\overset{h\nu}{\rightleftharpoons}} \text{random coil} \quad (2)$$

$$\text{random coil} \underset{\Delta}{\overset{h\nu}{\rightleftharpoons}} \text{right-handed helix} \quad (3)$$

Process 1 has been confirmed to occur for a copolymer of β-benzyl-L-aspartate and β-(*p*-phenylazobenzyl)-L-aspartate (41 : 59).[13] In this report, Processes 2 and 3 are discussed. Photoisomerization of polypeptide side chains itself has been reported for the copolymers of L-*p*-(phenylazo)phenylalanine[14] and also for poly(γ-cinnamyl-L-glutamate).[15] However, no conformational change could be induced by irradiation probably due to their conformational stability.

Experimental

Materials. The solvents used for recrystallization of *N*-carboxy anhydries (NCA) and for polymerization were purified shortly before use, dioxane and hexane by distillation over sodium, ethyl acetate by distillation over CaH_2, and triethylamine by drying and distillation over KOH. For the measurements of optical properties in solution, "Dotite Spectrosol" grade 1,2-dichloroethane was used without further purification.

p-*Aminobenzyl Alcohol (**1**).* A mixture of *p*-nitrobenzyl alcohol (30 g), dry methanol (50 ml) and palladium carbon (5 weight%) (1.5 g) was agitated in an autoclave under an atmosphere of hydrogen (initial pressure was 100 kg/cm²). After the catalyst had been removed by suction filtration, the filtrate was evaporated to dryness under reduced pressure. The crude product was recrystallized from ethanol. Yield, 18.5 g (77%); mp 58—60 °C (lit,[16] 63—64 °C). Found: C, 67.71; H, 7.22; N, 11.30%. Calcd for C_7H_9NO: C, 68.27; H, 7.37; N, 11.37%.

m-*Aminobenzyl Alcohol (**2**).* *m*-Nitrobenzyl alcohol (30 g) was reduced, as described above, to *m*-aminobenzyl alcohol. Yield, 15.9 g (66%); mp 91—93 °C (lit,[17] 95—96 °C). Found: C, 68.29; H, 7.47; N, 11.15%. Calcd for C_7H_9NO: C, 68.27; H, 7.37; N, 11.37%.

p-*Phenylazobenzyl Alcohol (**3**).* A mixture of alcohol **1** (12 g) and ethanol (40 ml) was added with stirring to a mixture of nitrosobenzene (12 g), ethanol (120 ml) and glacial acetic acid (12 ml). After the mixture had been stirred for 2 h, the product was crystallized upon cooling. The crude solid was recrystallized from ethanol. Yield, 9.9 g (48%); mp 142—143.5 °C (lit,[18] 142.5—143 °C). Found: C, 72.78; H, 5.72; N, 13.16%. Calcd for $C_{13}H_{12}N_2O$: C, 73.56; H, 5.70; N, 13.20%.

m-*Phenylazobenzyl Alcohol (**4**).* This alcohol was prepared from **2** (12 g) and nitrosobenzene (12 g) in the same way as for **3**. The crude product was purified by distillation (177 °C/3 mmHg). Yield, 18.8 g (91%); mp 36 °C (lit,[19] 34.5—36 °C). Found: C, 73.50; H, 5.68; N, 13.10 %. Calcd for $C_{13}H_{12}N_2O$: C, 73.56; H, 5.70; N, 13.20%.

p-*Phenylazobenzyl-L-aspartate (**5**).* A mixture of L-

Table 1. Yields, viscosities, and cis percentage in the photostationary state

Copolymer series[a]	Mol% azo NCA[b]	Mol% azo content[c]	Yield mg	Yield %	η_{sp}/c[d]	Cis%
p	50	46.5	19	18	0.04	69
p	70	74.0	22	22	—	74
p	90	85.9	27	26	0.16	68
p	100	100	63	61	—	70
m	30	26.2	62	63	0.51	88
m	50	45.9	46	44	0.37	75
m	70	78.0	5	4	—	68
m	90	89.3	64	53	0.28	62
m	100	100	218	75	0.23	68

a) p: para-copolymer. m; meta-copolymer. b) Mol% of *m*- or *p*-phenylazobenzyl-L-aspartate NCA reacted with γ-benzyl-L-glutamate NCA. c) Determined from the nitrogen content of elemental analysis. d) 0.1% 1,2-dichloroethane solution.

aspartic acid (5.8 g), alcohol **3** (10 g), *p*-toluenesulfonic acid (9.2 g), and dioxane (60 ml) was heated with stirring at 80 °C for 24 h. The reaction mixture was evaporated to dryness, and the residue was neutralized with a sodium hydrogencarbonate solution. The precipitated crystalline product was filtered, and washed with acetone. This was recrystallized from a mixed solution of dioxane and water (1 : 1 by volume). Yield, 1.3 g (8.4%); mp 229—229.5 °C; $[\alpha]_D = +0.63$ ($c=3.1$, dichloroacetic acid). IR: 1735, 1585 cm^{-1}. Found: C, 62.26; H, 5.38; N, 12.33%. Calcd for $C_{17}H_{17}N_3O_4$: C, 62.38; H, 5.23; N, 12.84%.

m-*Phenylazobenzyl*-L-*aspartate* (**6**). Ester **6** was prepared from alcohol **4** (10 g) and L-aspartic acid (5.8 g) in the same way as for **5**. Yield, 0.86 g (5.8%); mp 218—218.5 °C; $[\alpha]_D = +0.93°$ ($c=1.5$, acetic acid). IR: 1720, 1585 cm^{-1}. Found: C, 62.41; H, 5.45; N, 12.38%. Calcd for $C_{18}H_{15}N_3O_5$: C, 62.38; H, 5.23; N, 12.84%.

p-*Phenylazobenzyl*-L-*aspartate NCA* (**7**). This NCA was prepared from amino acid **5** (2.5 g) and phosgene using the reported procedure.[20] Yield, 1.3 g (48%); mp 240—240.5 °C. IR: 1860, 1788, 1725 cm^{-1}. Found: C, 61.41; H, 4.42; N, 12.02%. Calcd for $C_{18}H_{15}N_3O_5$: C, 61.19; H, 4.28; N, 11.89%.

m-*Phenylazobenzyl*-L-*aspartate NCA* (**8**). This NCA was prepared from amino acid **6** (2 g) and phosgene using the reported procedure.[20] Yield, 1.2 g (56%), mp 133.5—134.5 °C. IR: 1850, 1800, 1735 cm^{-1}. Found: C, 61.27; H, 4.27; N, 11.86%. Calcd for $C_{18}H_{15}N_3O_5$: C, 61.19; H, 4.28; N, 11.89%.

Poly[β-(p-*phenylazobenzyl*)-L-*aspartate*] (*pPALA*). NCA **7** was dissolved in dioxane (0.1 M), and a 0.004-M solution of triethylamine in dioxane (monomer/initiator=40) was added. Polymerizatiom was carried out at room temperature for 5 days. The reaction mixture was added to vigorously stirred ethanol. The precipitate was collected on a filter, washed with several portions of ethanol and dried *in vacuo* at 40 °C. Found: C, 65.79; H, 4.83; N, 13.03%. Calcd for $(C_{17}H_{15}N_3O_3)_n$: C, 66.01; H, 4.89; N, 13.58%.

Poly[β-(m-*phenylazobenzyl*)-L-*aspartate*] (*mPALA*). mPALA was prepared from NCA **8** in the same way as for pPALA. Found: C, 66.24; H, 4.91; N, 13.73%. Calcd for $(C_{17}H_{15}N_3O_3)_n$: C, 66.01; H, 4.89; 13.58%.

Polymers. Copolymers were prepared in an analogous way to that for homopolymers by using varing ratios of γ-benzyl-L-glutamate NCA and *m*- or *p*-phenylazobenzyl-L-aspartate NCA. Mole percentage of azo residue in the copolymers was estimated from their nitrogen contents obtained by elemental analyses. The reduced specific viscosity, η_{sp}/c, of each polymer was measured for a 0.1% 1,2-dichloroethane solution at 25 °C. Viscosity measurement could not be carried out for pPALA because of its insoluble character, or for the copolymers containing 74.0% *p*-phenylazobenzyl residue and 78.0% *m*-phenylazobenzyl residue because of low yields of the samples. Data on the homopolymers and copolymers are summerized in Table 1.

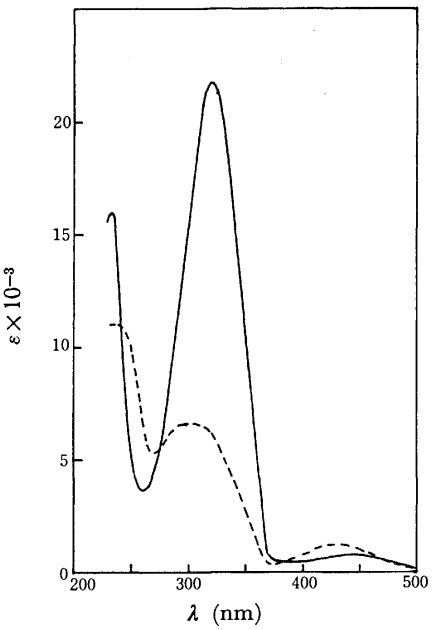

Fig. 1. Ultraviolet spectra of mPALA before (——) and after (---) irradiation.

Photoisomerization. Photoirradiation was carried out on solutions with concentration of 1-mg/ml using a Corning 7—37 filter which permits the light of 310—380 nm to pass. The cis percentage was calculated from the absorbance at 320 nm assuming that the absorbance is substantially proportional to the concentration of the trans isomer in view of the low extinction of the cis isomer at the wavelength.[21]

Measurements. CD spectra were recorded on a JASCO J-20 circular dichrograph apparatus with cell thickness of 0.1 and 0.01 cm. Due to the absorption of the solvent no spectra could be obtained below 210 nm. Molar ellipticities were calculated for the supposedly intrinsic band around 222 nm using the molar concentration of amide groups, while the molar concentration of the azo groups was used for the calculation of the ellipticities associated with the extrinsic bands. Ultraviolet (UV) spectra were measured with a JASCO UVIDEC-1 spectrophotometer.

Results and Discussion

Photoisomerization. The UV spectra of mPALA before and after irradiation are shown in Fig. 1. The major electronic transitions of this polymer are essentially those of azobenzene.[22] The band for mPALA before irradiation in the 320 nm region ($\varepsilon=22000$) is attributed to π,π^* transition and the band in the 430 nm region ($\varepsilon=700$) to n,π^* transition.[23] The spectrum after irradiation resembles the spectrum of *cis*-azobenzene reported by Gerson and co-workers.[22] The spectra

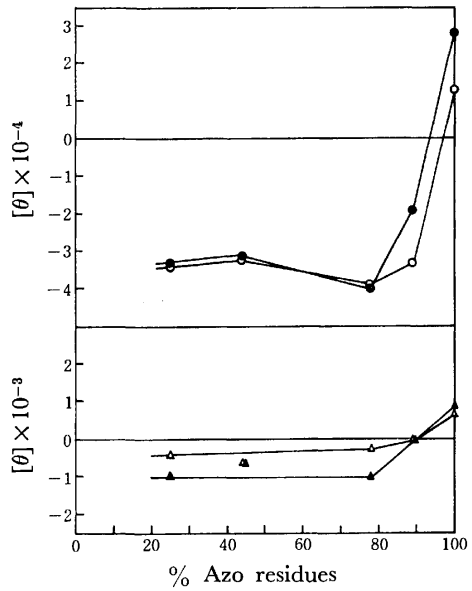

Fig. 2. Variation of the maximum or minimum ellipticities associated with the side-chain n,π^* (▲,△) and the amide n,π^* (●,○) transitions before (▲,●) and after (△,○) irradiation for the meta-copolymers as a functions of the azo content.

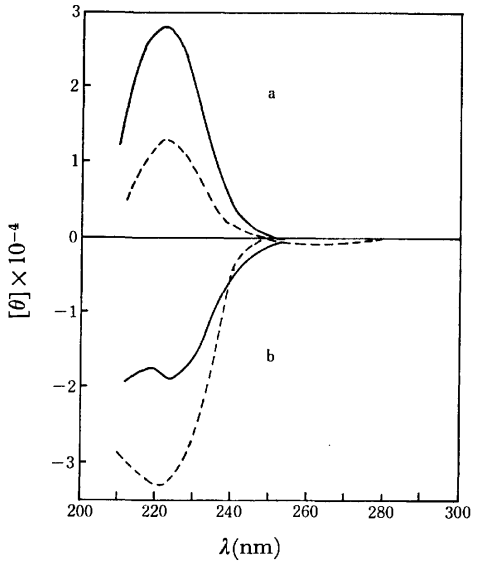

Fig. 3. CD spectra of mPALA (a) and the meta-copolymer with the azo content of 89.3% (b) before (——) and after (---) irradiation.

of the other polymers before and after irradiation are similar to those of mPALA in the regions of the azo π,π^* and n,π^* transitions.

The cis percentages of all the polymers at the photostationary state are given in Table 1. The values of the para copolymer series are almost the same and close to 70%. On the other hand, a considerable decrease in cis percentage is observed for the meta copolymer series on proceeding from the copolymer with the least azo residue to the copolymer which contains 89.3% azo residue. The decreased cis conversion for the meta-copolymers may result from steric restrictions between the side-chain meta-azobenzene groups.

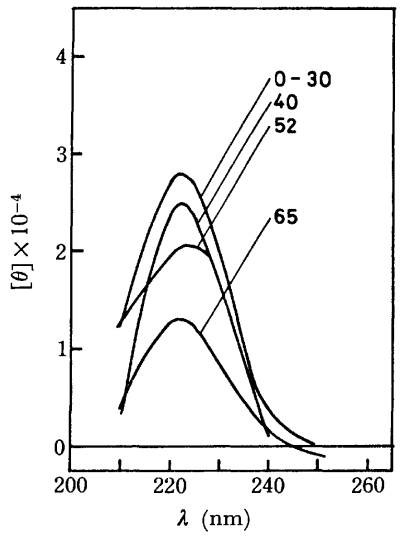

Fig. 4. CD spectra of mPALA at different cis per cents in the course of relaxation.

The cis percentage of mPALA seems slightly higher as a polymer with side-chains of maximal steric restrictions. This might be due to the conformational difference.

CD Spectra of meta-Copolymers. The maximum or minimum ellipticities associated with the amide n,π^* transition at 222 nm before and after irradiation are plotted against the mole percentage of azo residue (Fig. 2). The values are almost independent of the copolymer composition for the copolymers with less than 80% azo residue. These observations suggest that the overlapping of allowed transitions of the side-chain chromophore with those from the peptide main chain is either small or absent in the polymers. This is in contrast to that for other azoaromatic copolypeptides which contain *p*-(*p*-hydroxyphenylazo)phenylalanine residue.[24] For these polymers, decreasing intensity of the peptide main-chain band was observed with increase in mole percentage of the azo residue. If one takes $[\theta]_{222}=-40000\pm10\%$ for 100% right-handed α-helix,[25] the meta-copolymers are all confirmed to exist as right-handed α-helices. On the other hand, the CD spectrum of mPALA before irradiation shows a maximum with the value of $[\theta]_{222}=28000$ (Fig. 3), confirming the conclusion together with the results of its IR spectrum that the helix of mPALA is left-handed in 1,2-dichloroethane. The ellipticities at 222 nm seem unaffected by irradiation for the copolymers with less than 80% azo residue. However, irradiation causes significant changes in the ellipticity values of the copolymers with more azo residue. The absolute ellipticity of 89.3% azo copolymer increases from 19000 to 33000 by irradiation, confirming the increased percentage of helicity. This enhanced helix content might be due to the release of steric restrictions between the trans side chains by the formation of cis isomers. The ellipticity of mPALA decreases from 28000 to 13000 by irradiation, confirming the induced instability for its left-handed α-helical conformation. This observation could be due to the partial transition from the left-handed α-helix to a random coil or a right-handed

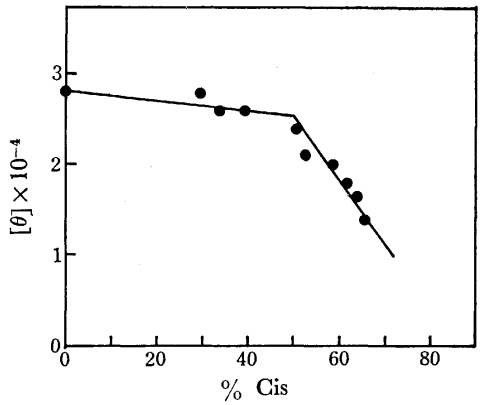

Fig. 5. Variation of the maximum ellipticities around 222 nm for mPALA as a function of the cis per cent.

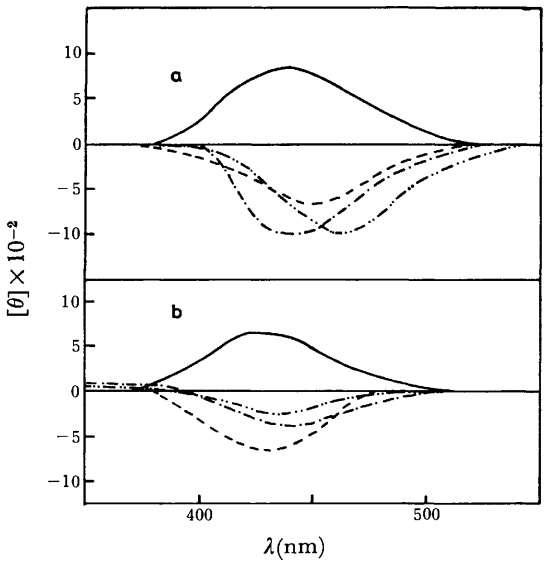

Fig. 6. CD spectra associated with the side-chain n,π^* transition before (a) and after (b) irradiation for the meta-copolymers. Azo%: 100(——); 78.0(—·—); 45.9 (---); 26.2 (—·—).

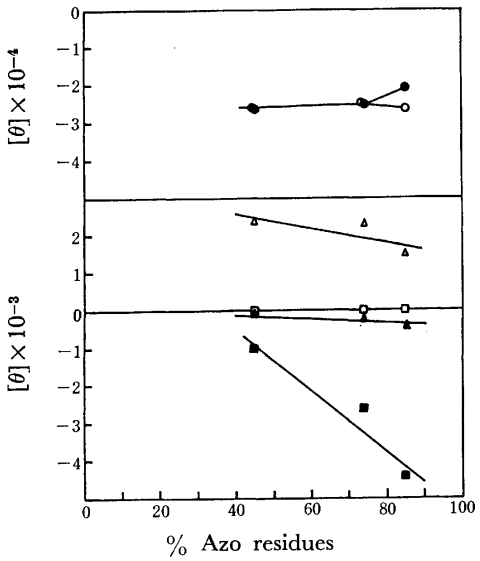

Fig. 7. Variation of the maximum or minimum ellipticities associated with the side-chain n,π^* (▲,△), π,π^* (■,□) and the amide n,π^* (●,○) transitions before (▲,■,●) and after (△,□,○) irradiation for the para-copolymers as a function of the azo content.

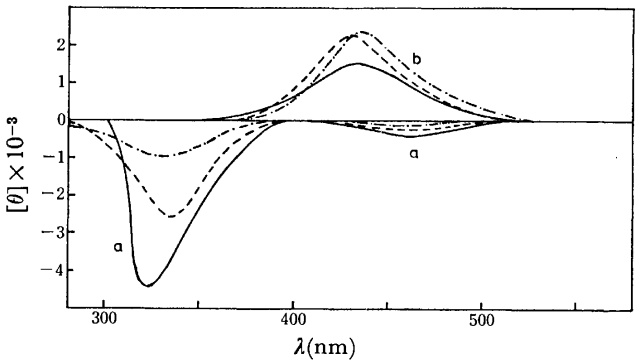

Fig. 8. CD spectra associated with the side-chain n,π^* and π,π^* transitions before (a) and after (b) irradiation for the para-copolymers. Azo%: 85.9 (——); 74.0 (---); 46.5 (—·—).

α-helix. We reported that the copolymer of *p*-phenylazobenzyl-L-aspartate and β-benzyl-L-aspartate (59 : 41) undergoes a light-induced conformational change from left- to right-handed helix.[13] The CD band associated with the peptide n,π^* transition of this copolymer changes its sign from positive to negative by irradiation, giving clear evidence for inversion of its helix sense. In the case of mPALA, however, it is difficult only by the CD spectrum to determine which of the conformational transformations is responsible for the observation. NMR spectra could, in principle, give some information.

Subsequent relaxation of mPALA back to the original conformation was followed by its CD spectra (Fig. 4). Maximum ellipticities at 222 nm are plotted as a function of cis percentage (Fig. 5). It shows an abrupt change of $[\theta]_{222}$ at over 50% followed by a gradual change with decrease. The result demonstrates that the energy required for the conformational change comes from cis forms in the side chain, *viz.*, ultimately from light energy.

The CD spectra associated with the n,π^* transition of the side-chain chromophore before and after irradiation are given in Fig. 6, maximum or minimum ellipticities being plotted against mole percentage of azo residue (Fig. 2). The copolymers show no dichroic band in the region of the π,π^* transition of the side-chain chromophore. One important aspect is the relation between the sign of the side-chain CD band and the backbone helix sense. There is a possibility that the sign of a side-chain band is opposite corresponding to the left- and right-handed helices.[20] The CD spectra of the meta copolymer series provide one example of the corresponding behavior since mPALA shows a positive band while the right-handed copolymers show negative bands. Usually the origin of induced dichroic bands are discussed in the terms of side chain-side chain and side chain-main chain interactions. In the case of the former interactions, the induced circular dichroism is expected to be dependent on the concentration of the side-chain chromophores in the copoly-

mers. No such dependency was observed for the polymers we studied. The ellipticities of the side-chain CD bands before and after irradiation are almost independent of mole percentage of azo residue in the copolymers unless conformational changes are induced. Thus the side-chain n,π^* CD band should be attributed to the coupling between the backbone and the side chain.

CD Spectra of para-Copolymers. The minimum ellipticities associated with the amide n,π^* transition are plotted against mole percentage of azo residue in Fig. 7. The CD spectrum of pPALA could not be measured since it is insoluble in 1,2-dichloroethane. The spectra of the copolymers show that they assume a right-handed α-helical conformation. Photoirradiation did not change the minimum ellipticities of the copolymers in the region of the amide n,π^* transition except for the azo 85.9% copolymer. This copolymer shows increase in absolute ellipticity after irradiation, which indicates an increase of helicity though not so remarkable as observed for the 89.3% meta-azo copolymer.

The CD spectra before and after irradiation associated with the side-chain n,π^* and π,π^* transitions are given in Fig. 8. Their maximum or minimum ellipticities are plotted against the mole percentage of azo residue in Fig. 7. The side-chain transitions are affected remarkably by irradiation. The ellipticity for the n,π^* transition increases a great deal with inversion of its sign, whereas the circular dichroism for the π,π^* transition vanishes. Similarly to the case for the meta-copolymers, the ellipticities of the side-chain n,π^* CD bands before and after irradiation seem to be almost independent of the mole percentage of azo residue. This confirms the fact that the origin of the CD bands resides in side chain-main chain interactions. However, the absolute ellipticity of the side-chain π,π^* band observed only before irradiation increases with increasing azo residue, which suggests side chain-side chain interactions as the origin of the CD band.

Conclusion

The effect of irradiation on the backbone conformation is remarkable for the two polymers of the meta copolymer series, the 89.3% azo copolymer and mPALA For the former, stability of the right-handed α-helical conformation is promoted. On the other hand, significant instability is induced for the left-handed α-helical conformation of the latter. The conformational change of mPALA occurs abruptly at greater than 50% cis. Thus, the light-induced conformational change can be compared with visual purple, rhodopsin, where its retinal component undergoes photoisomerization accompanied by a change in conformation of opsin.

The authors wish to express their appreciation for permission to use the JASCO J-20 circular dichrograph apparatus at the National Industrial Research Institute, Tohoku.

References

1) E. M. Bradbury, A. R. Downie, A. Elliott, and W. E. Hanby, *Pro. R. Soc. London, Ser. A*, **259**, 110 (1960).
2) R. H. Karlson, K. S. Norland, G. D. Fasman, and E. R. Blout, *J. Am. Chem. Soc.*, **82**, 2268 (1960).
3) M. Hashimoto and J. Aritomi, *Bull. Chem. Soc. Jpn.*, **39**, 2707 (1966).
4) M. Hashimoto, *Bull. Chem. Soc. Jpn.*, **39**, 2713 (1966).
5) M. Hashimoto and S. Arakawa, *Bull. Chem. Soc. Jpn.*, **40**, 1698 (1967).
6) C. Toniolo, M. L. Falxa, and M. Goodman, *Biopolymers*, **6**, 1579 (1968).
7) M. Goodman, C. M. Deber, and A. M. Felix, *J. Am. Chem. Soc.*, **84**, 3773 (1962).
8) J. B. Aragao and M. H. Loucheux, *J. Chim. Phys.*, 1578 (1974).
9) D. F. Bradley, M. Goodman, A. Felix, and R. Records, *Biopolymers*, **4**, 607 (1966).
10) M. Goodman, A. M. Felix, C. M. Deber, A. R. Brause, and G. Schwartz, *Biopolymers*, **1**, 371 (1963).
11) M. H. Loucheux and C. Duflot, *Biopolymers*, **14**, 469 (1975).
12) E. H. Erenrich, R. H. Andreatta, and H. A. Sheraga, *J. Am. Chem. Soc.*, **92**, 1116 (1970).
13) A. Ueno, J. Anzai, T. Osa, and Y. Kadoma, *J. Polym. Sci. Polym. Lett. Ed.*, **15**, 407 (1977).
14) M. Goodman and M. L. Falxa, *J. Am. Chem. Soc.*, **89**, 3863 (1967).
15) Y. Kadoma, A. Ueno, K. Takeda, K. Uno, and Y. Iwakura, *J. Polym. Sci. Polym. Chem. Ed.*, **13**, 1545 (1975).
16) P. Phillips and A. Maggiolo, *J. Org. Chem.*, **15**, 659 (1950).
17) L. H. Conover and D. S. Tarbell, *J. Am. Chem. Soc.*, **72**, 3586 (1950).
18) R. Schwyzer, K. Zatsko, P. Sieber, and H. Kappeler, Ger. Patent 1087128 (1960); *Chem. Abstr.*, **57**, 13883b (1962).
19) D. N. Kursanov and P. A. Solodkov, *J. Appl. Chem. (USSR)*, **16**, 351 (1943).
20) A. Ueno, T. Ishiguro, F. Toda, K. Uno, and Y. Iwakura, *Biopolymers*, **14**, 353 (1975).
21) C. S. Paik and H. Morawetz, *Macromolecules*, **5**, 171 (1972).
22) F. Gerson, E. Heibronner, A. van Ween, and B. M. Wepster, *Helv. Chim. Acta*, **43**, 1889 (1960).
23) H. H. Jaffe, Y. Si-Jung, and R. W. Gardner, *J. Mol. Spectrosc.*, **2**, 120 (1958).
24) M. Goodman and E. Benedetti, *Biochemistry*, **7**, 4226 (1968).
25) G. Holzwarth and P. Doty, *J. Am. Chem. Soc.*, **87**, 218 (1965).

The Photocyclization of 3,3′-Diphenyl-2,2′-bi-1*H*-indene-1,1′-dione

Fumio TODA and Yozo TODO

Department of Industrial Chemistry, Faculty of Engineering, Ehime University, Matsuyama 790

(Received March 28, 1977)

The photocyclization of the title compound afforded 14-hydroxy-4b-phenylbenz[*c*]indeno[2,1-*a*]fluoren-13-(4b*H*)-one, which is easily isomerized to 4b,13b-dihydro-4b-phenylbenz[*c*]indeno[2,1-*a*]fluorene-13,14-dione. The hydrogenation of both compounds gave *anti*-4b,8b,13a,13b-tetrahydro-4b-phenylbenz[*c*]indeno[2,1-*a*]fluorene-13,14-dione.

Although the photooxidative cyclizations of stilbenes[1] and 2-styrylthiophenes[2] to phenanthrenes and naphtho-[2,1-*b*]thiophenes respectively have been proposed to proceed *via* 4a,4b-dihydrophenanthrene and 9a,9b-dihydronaphtho[2,1-*b*]thiophene intermediates, such intermediates have not yet been isolated because of their extreme instability. Recently, though, Doyle *et al.*[3] have isolated the keto-form of the 4a,4b-dihydrophenanthrene intermediate in the photocyclization of 3,4-bis-(*p*-hydroxyphenyl)-3-hexene, and Cuppen and Laarhoven[4] have clarified that this photocyclization proceeds in the first excited state and then in a conrotatory manner.

The hypothetical photocyclization product (**2**) of 3,3′-diphenyl-2,2′-bi-1*H*-indene-1,1′-dione (**1**) is expected to be isolable, because **2** has a highly conjugated enone structure, and because the conditions are unfavorable for the elimination of benzene from **2**.

The photolysis of **1**, however, gave a proton-migrated isomer of **2**, 14-hydroxy-4b-phenylbenz[*c*]indeno[2,1-*a*]fluoren-13(4b*H*)-one (**3**). We will report on this photocyclization and an some reactions of **3**.

The irradiation of **1** in benzene for 20 h afforded **3**[5] as blue-black prisms in a 70% yield. Although the νOH band of **3** was not observed, presumably because of a strong intramolecular hydrogen bond, an OH proton signal appeared at δ 9.93. The UV spectral data of **3** (604 nm (ε 2800)) were comparable to those of the analogous compound, **6** (626 nm (ε 4000)).[6,7] The UV spectral data of the acetate of **3** (513 nm (ε 2700)) were also comparable to those of the acetate of **6** (535 nm (ε 3250)).[6] It has previously been reported that the heating of 3,3′,4,4′,5,5′-hexaphenyl-2,2′-bi-2,4-cyclopentadiene-1,1′-dione in boiling benzophenone affords **6** in a 70% yield.[7] However, the heating of **1** under these conditions did not give **3**, and **1** was recovered unchanged. In contrast to the thermal stability of **6**, **3** was easily converted into 4b,13b-dihydro-4b-phenylbenz[*c*]indeno[2,1-*a*]-fluorene-13,14-dione (**4**) by heating in boiling toluene. This ketonization of **3** was performed more easily by treating it with acid. The phenyl group and the hydrogen atom marked in **4** probably bear a *syn* relationship to each other, because the signal due to this hydrogen atom was at a higher magnetic field (δ 4.25), and because the spectral data of **4** were comparable to those of **7** of the *syn*-form.[8]

The treatment of **3** and **4** with Br_2 afforded 4b,8b-dihydro-8b-bromo-4b-phenylbenz[*c*]indeno[2,1-*a*]fluorene-13,14-dione (**5a**) both in 93% yields, on treatment with $AgClO_4$ in MeOH this substance was converted into its methoxy derivative (**5b**). The spectral data of **5a** and **5b** were comparable to those of **5c**.[9] The hydrogenation of **3** and **4** over Pd–C gave *anti*-4b,8b,13a,13b-tetrahydro-4b-phenylbenz[*c*]indeno[2,1-*a*]fluorene-13,14-dione (**8**) in 50 and 25% yields respectively. These hydrogenations of **3** and **4** were performed more easily in 55 and 69% yields respectively, using the recently reported reagent, Zn–$ZnCl_2$–EtOH.[10] Interestingly, this reagent was also effective for the conversion of **5b** and the acetate of **3** into **8** in 48 and 44% yields respectively.

The *anti*-relationship between the indanone rings of **8** was determined by comparing its NMR spectral data with those of **9** of the *syn*-configuration[11] and of **10** of the *anti*-configuration, which had been prepared by the hydrogenation of **7**. The NMR spectral data of **8** (δ 4.01 (d, J_{BC}=8 Hz, H_B), 4.07 (s, H_A), 4.92 (d, H_C)) were comparable to those of **10** (δ 4.12 (d, J_{BC}= 6.5 Hz, H_C), 4.61 (s, H_A), and 4.67 (d, H_B)), but not to those of **9**, which shows complex signals of an ABX pattern.[11] The absence of spin-spin coupling between H_A and H_B in **8** and **10** is probably due to the fact that the dihedral angle between the hydrogen bonds is nearly 90°. The examination of the molecular models supports this idea.

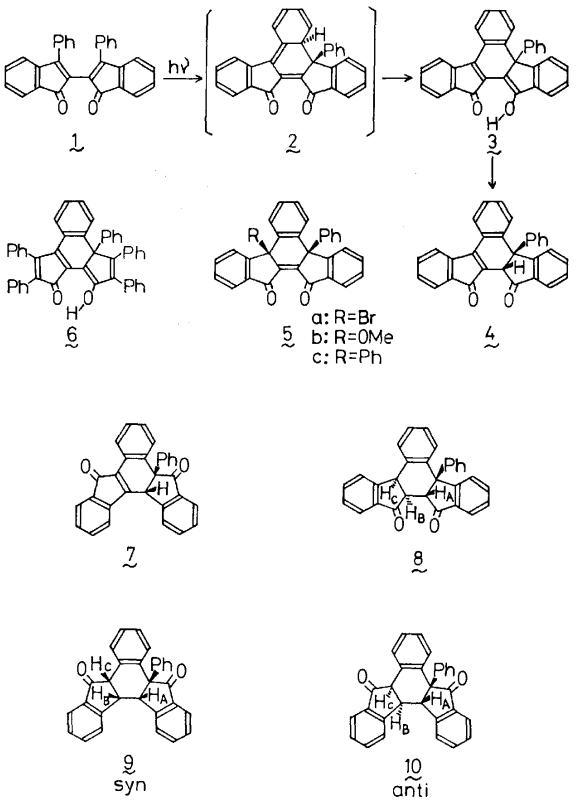

Experimental

All the melting points are uncorrected. The IR, UV, and NMR spectra were measured in Nujol mull, $CHCl_3$, and $CDCl_3$ respectively. The mass spectra were measured with an ionization energy of 75 eV.

Photocyclization of ***1***. A solution of **1** (2 g) in benzene (400 ml) was irradiated with light from a 400-W high-pressure mercury lamp, filtered through Pyrex glass, at room temperature under N_2 for 20 h. The crude crystals after the evaporation of the solvent were recrystallized from AcOEt to afford **3** as blue-black prisms; 1.4 g (70%); mp 194 °C (dec). IR: 1670, 1615, 1590, 1560, and 1520 cm^{-1}; λ_{max}: 297 (35700), 373 (13800), and 604 nm (ε 2800); NMR δ: 7.0—8.4 (m, Ar, 17H) and 9.93 (s, OH, 1H); MS *m/e* (rel intensity): 410 (M^+, 100), 333 (M^+-Ph, 70), and 305 (333−CO, 21).

Found: C, 87.51; H, 4.35%. Calcd for $C_{30}H_{18}O_2$: C, 87.78; H, 4.42%.

The keeping of a solution of **3** (0.1 g) in Ac_2O (0.5 ml)-pyridine (2 ml) at room temperature for 12 h afforded, after recrystallization from CCl_4, the acetate of **3** as purple prisms; 0.105 g (95%); mp 254—256 °C; IR: 1760, 1695, and 1190 cm^{-1}; λ_{max}: 285 (30500), 307 (18800), and 513 nm (ε 2700); NMR δ: 2.58 (s, AcO, 3H) and 7.1—8.2 (m, Ar, 17H).

Found: C, 84.74; H, 4.30%. Calcd for $C_{32}H_{20}O_3$: C, 84.94; H, 4.46%.

Conversion of ***3*** *into* ***4***. HCl gas was bubbled through a solution of **3** (0.5 g) in $CHCl_3$ (50 ml) at 0 °C for 10 min. Recrystallization from AcOEt afforded **4** as orange prisms; 0.45 g (90%); mp 245—247 °C (dec); IR: 1710 and 1695 cm^{-1}; λ_{max}: 292 (11300), 332 sh (4700), and 430 nm (ε 1700); NMR δ: 4.25 (s, CH, 1H) and 6.9—8.5 (m, Ar, 17H); MS *m/e* (rel intensity): 410 (M^+, 100), 333 (M^+-Ph, 98), and 305 (333−CO, 28).

Found: C, 87.55; H, 4.52%. Calcd for $C_{30}H_{18}O_2$: C, 87.78; H, 4.42%.

The heating under reflux of a solution of **3** (0.1 g) in toluene (10 ml) under N_2 for 24 h afforded, after recrystallization from AcOEt, **4**; 0.06 g (60%).

Preparation of ***5a*** *and* ***5b***. To a solution of **3** (0.69 g) in $CHCl_3$ (25 ml), Br_2 (0.4 g) was added, and then the mixture was stirred for 10 min. Recrystallization from AcOEt-$CHCl_3$ afforded **5a** as yellow prisms; 0.764 g (93%); mp 209—210 °C; IR: 1740 and 1700 cm^{-1}; λ_{max} 301 nm (ε 15600); MS *m/e* (rel intensity): 490 and 488 (M^+, 5) and 409 (M^+-Br, 100).

Found: C, 73.35; H, 3.41%. Calcd for $C_{30}H_{17}O_2Br$: C, 73.63; H, 3.50%.

The treatment of **4** (0.18 g) in $CHCl_3$ (10 ml) with Br_2 (0.1 g) as above afforded **5a**; 0.2 g (93%).

The treatment of a solution of **5a** (0.27 g) in MeOH (10 ml)-tetrahydrofuran (10 ml) with $AgClO_4$ (0.5 g) afforded, after recrystallization from AcOEt, **5b** as yellow needles; 0.22 g (91%); mp 258—260 °C; IR: 1710 and 1640 cm^{-1}; λ_{max}: 302 nm (ε 17400); NMR δ: 2.29 (s, OMe, 3H) and 6.9—8.3 (m, Ar, 17H); MS *m/e* (rel intensity): 440 (M^+, 20) and 409 (M^+-OMe, 100).

Found: C, 84.27; H, 4.44%. Calcd for $C_{31}H_{20}O_3$: C, 84.53; H, 4.58%.

Hydrogenation of ***3***, ***4***, *and* ***7***. A mixture of **3** (0.2 g), tetrahydrofuran (30 ml), and a catalytic amount of Pd-C was stirred under H_2 at room temperature for 12 h. The filtrate after the filtration of Pd-C was evaporated to dryness to leave crude crystals. The recrystallization of the crude crystals from AcOEt afforded **8** as colorless prisms; 0.11 g (50%); mp 233 °C; IR: 1720 cm^{-1}; λ_{max} 247 (23200) and 295 nm (ε 4200); NMR δ: 4.01 (d, J_{BC}=8 Hz, H_B, 1H), 4.07 (s, H_A, 1H), 4.92 (d, J_{BC}=8 Hz, H_C, 1H), and 6.5—8.0 (m, Ar, 17H); MS *m/e* (rel intensity): 412 (M^+, 100), 335 (M^+-Ph, 16), and 307 (335−CO, 15).

Found: C, 87.63; H, 4.66%. Calcd for $C_{30}H_{20}O_2$: C, 87.35; H, 4.89%.

The same treatment of **4** as described above afforded **8** in a 25% yield.

The same treatment of **7** as described above afforded **10** as pale yellow needles in a 58% yield; mp 263—265 °C; IR: 1700 cm^{-1}; λ_{max}: 249 (23800), 290 (4600), 326 (800), and 340 nm (ε 800); NMR δ: 4.12 (d, J_{BC}=6.5 Hz, H_C, 1H), 4.61 (s, H_A, 1H), and 4.67 (d, J_{BC}=6.5 Hz, H_B, 1H).

Found: C, 87.55; H, 4.68%. Calcd for $C_{30}H_{20}O_2$: C, 87.35; H, 4.89%.

The treatment of **3**, **4**, and **7** with Zn-$ZnCl_2$-EtOH by the previously reported procedure[10] afforded **8** (55), **8** (69), and **10** (69%) respectively.

The authors wish to thank to Dr. R. S. Atkinson, The University of Leicester for his valuable suggestion as to the structure of the photocyclization product of **1** (**3**).

References

1) F. B. Mallory, C. S. Wood, J. T. Gordon, L. C. Lindquist, and M. L. Savitz, *J. Am. Chem. Soc.*, **84**, 4361 (1962).

2) W. Carruthers and H. N. Stewart, *Tetrahedron Lett.*, **1965**, 301.

3) T. D. Doyle, N. Filipescu, W. R. Benson, and D. Banes, *J. Am. Chem. Soc.*, **92**, 6371 (1970); T. D. Doyle, W. R. Benson, and N. Filipesucu, *ibid.*, **98**, 3262 (1976).

4) Th. J. H. M. Cuppen and W. H. Laarhoven, *J. Am. Chem. Soc.*, **94**, 5914 (1972).

5) In a preliminary communication, we have incorrectly reported that the photocyclization product is **2**; F. Toda and Y. Todo, *J. Chem. Soc., Chem. Commun.*, **1976**, 848. However, the structure of the product should be corrected to read like that depicted as **3**.

6) R. S. Atkinson, *J. Chem. Soc., C*, **1971**, 3524.

7) M. K. Conner, J. M. Dunston, E. LeGoff, and P. Yates, *Tetrahedron*, **27**, 1813 (1971).

8) A. L. Bednowitz, R. G. Brown, and L. G. Donaruma, *J. Org. Chem.*, **39**, 537 (1974).

9) F. Toda and Y. Todo, *Bull. Chem. Soc. Jpn.*, **50**, 273 (1977).

10) F. Toda and K. Iida, *Chem. Lett.*, **1976**, 695.

11) P. H. Lacy and D. C. C. Smith, *J. Chem. Soc. Perkin 1*, **1974**, 2617.

The Photosensitized Oxygenation of Furanoeremophilanes. II.[1] The Preparation and Stereochemistry of the Isomeric Hydroperoxides and the Corresponding Lactones from Furanofukinin and Furanoeremophilane

Keizo NAYA, Noboru NOGI, Yasuo MAKIYAMA, Hideo TAKASHINA, and Takashi IMAGAWA

Department of Chemistry, Faculty of Science, Kwansei Gakuin University, Uegahara, Nishinomiya, Hyogo 662

(Received March 30, 1977)

The dye-sensitized oxygenation of furanofukinin, and furanoeremophilane, in methanol gave, quantitatively, crystalline mixtures of two isomeric hydroperoxides each consisting of a pair of 8α-methoxy-12β-hydroperoxy and 8β-methoxy-12α-hydroperoxy derivatives respectively. The hydroperoxides were readily transformed to the corresponding lactones with acetic anhydride–pyridine through dehydration. The stereochemistry of the hydroperoxides and the corresponding lactones has been elucidated by spectral and chemical methods according to a previously outlined generalization. Further, furanofukinin, furanoeremophilane, and 8β-hydroxyeremophilenolide, have been synthesized from petasalbin, fukinone, and an epimeric mixture of 8α- and 8β-methoxy lactones, respectively.

In our previous paper,[1] we reported on the photosensitized oxygenation of petasalbin (**1**) to yield, quantitatively, a mixture of two isomeric hydroperoxides, (**2a**) and (**2b**), both of which were then transformed quantitatively to the corresponding lactones, (**3a**) and (**3b**), by treatment with acetic anhydride–pyridine. Their configurational assignments were ascertained by a comparison of the chemical and spectral properties between sets of the two isomeric substances. In the present paper, we will describe the photosensitized oxygenation of furanofukinin (**4**)[2] and furanoeremophilane (**5**),[3] performed in order to examine the utility of the generalization outlined in the preceding paper[1] for the configurational assignments to hydroperoxides, **2a,b**, and the corresponding lactones, **3a,b**, converted from petasalbin, **1**. Thus, a pair of 8α- and 8β-methoxy isomers have been estimated to exist in non-steroidal and steroidal A/B *cis* chair/chair conformations respectively.

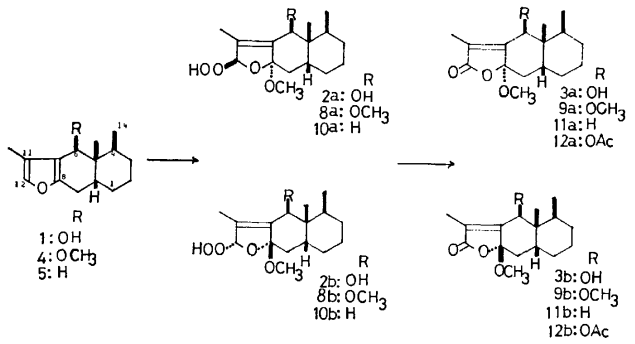

Both furanofukinin, **4**, and furanoeremophilane, **5**, were isolated from the rhizomes of a wild plant,[2] *Petasites japonicus* Maxim. and its subspecies, subsp. *gigantus* Kitam. These substances, **4** and **5**, were also synthesized in good yields by the methylation of petasalbin, **1**, with methanol in the presence of acetic acid, and by Treibs' method[4,5] *via* sultone (**7**) from fukinone (**6**), respectively.

The dye-sensitized oxygenation of furanofukinin, **4**, in methanol gave a crystalline product, which showed

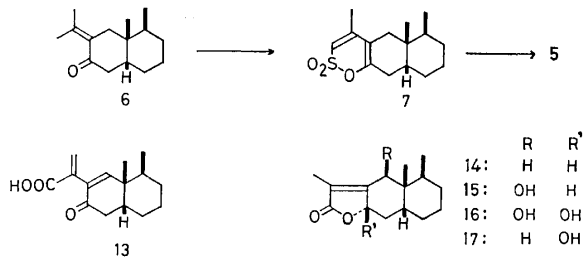

two spots on TLC (R_f, 0.40 and 0.20; benzene–ethyl acetate, 10 : 1) and which was then separated by fractional recrystallization from benzene to afford two hydroperoxides, (**8a**) (mp 116.0—117.0 °C (dec)) and (**8b**) (mp 136.0—137.0 °C (dec)). Both hydroperoxides have the same molecular formula, $C_{17}H_{28}O_5$, and both are positive to a peroxide test (KI–AcOH). They showed similar spectra characteristic of hydrperoxide groups: δ 11.30 (s) and 11.29 (s); IR(KBr): 3380 and 3350 cm^{-1}. Upon treatment with acetic anhydride–pyridine, the mixture of hydroperoxides, **8a,b**, gave, quantitatively, an epimeric mixture of 6β,8α-dimethoxyepieremophilenolide[6] (**9a**) (mp 132.5—133.5 °C) and 6β,8β-dimethoxyeremophilenolide (**9b**) (mp 123.0—123.5 °C) through dehydration. Subsequently each lactone was isolated by fractional recrystallization from benzene.

The stereochemistry of the hydroperoxides, **8a,b**, and the corresponding lactones, **9a,b**, can be readily determined as follows according to the previously outlined generalization.[1] The formation and the stereochemistry of the hydroperoxides, **8a,b**, can be well demonstrated by the use of the approved mechanism on the basis of the known oxygenation mode[1,7] of a furan moiety in methanol. Then, with the aid of the Dreiding model, it is evident that the introduced 8α- and 8β-methoxyl groups force the molecules to adopt exclusively non-steroidal (**A**) and steroidal (**B**) A/B *cis* chair/chair configurations respectively (*cf.* Fig. 1). Therefore, the non-steroidal 8α- (**A**) and steroidal 8β-isomers (**B**) have *cis-anti-cis* and *cis-syn-cis*-type ring-fusion systems, and they will tend to possess *trans* and

Table 1. Comparison of the chemical shifts (δ), specific rotations, and R_f values of the corresponding isomers

Compound [mp]°C	Solvent[a]	15-Me	14-Me	13-Me	6-H	$[\alpha]_D^\circ$ c) MeOH d) CHCl	R_f d) $CHCl_3$
8a [116—117]	A	0.78 s	0.96 d J=7.5	1.87 d J=1.5	4.20 q J=1.5	−54[c]	0.40[b]
8b [136—137]	A	1.02 s	0.78 d J=5.3	1.85 s	3.88 s	+13.4[c]	0.20[b]
9a [132.5—133.5]	B	0.75 s	0.96 d J=7.5	1.90 d J=1.8	4.28 q J=1.8	−185[d]	0.80[b]
9b [123—123.5]	B	0.99 s	0.75 d	1.81 s	3.89 s	+170[d]	0.70[b]
10a [123.5—124]	A	0.80 s	0.98 d J=6.0	1.71 d J=1.2		−15.2[c]	0.40[b]
10b [120.5—121]	A	0.98 s	0.80 d J=6.0	1.74 d J=1.2		+2.9[c]	0.40[b]
11a [110.5—111.5]	B	0.77 s	0.98 d J=7.0	1.76 d J=1.5		−168[d]	0.78[d]
11b [98.5—99.5]	B	0.98 s	0.74 d J=6.0	1.76 d J=1.2		+164[d]	0.70[d]
17 [212—213.5]	A	1.04 s	0.80 d J=5.5	1.73 d J=1.6		+157[d]	

a) A: acetone-d_6; B: CCl_4. b) C_6H_6: AcOEt, 10 : 1. c) MeOH. d) $CHCl_3$.

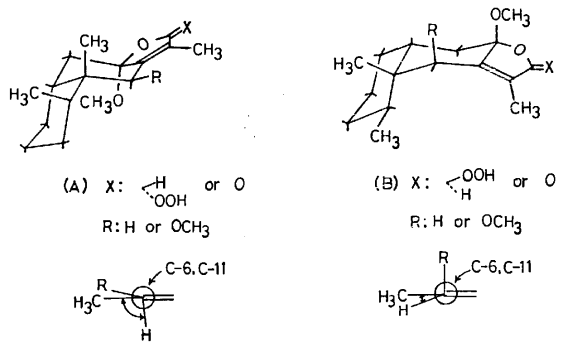

Fig. 1. Conformations of 8α- and 8β-methoxyl isomers, and the angles between 6-H and 13-CH_3.

cis characters respectively, depending on the molecular volume and the symmetric factor.[8]

Next, furanoeremophilane, **5**, lacking a C-6 substituent, was photooxygenated by a method similar to that described above to yield a single spot on TLC; it was nevertheless separated to furnish two hydroperoxides, (**10a**) (mp 123.5—124.0 °C (dec)) and (**10b**) (mp 120.5—121.0 °C (dec)), by careful recrystallization from light petroleum. Subsequently, the correspoding lactones, (**11a**) (mp 110.5—111.5 °C) and (**11b**) (mp 98.5—99.5 °C), were obtained from each hydrperoxide, **10a** or **10b**, by dehydration with acetic anhydride–pyridine, and also from the **10a,b** mixture by lactonization, followed by column chromatography and fractional recrystallization respectively. The stereochemistry of **10a,b** and **11a,b** can be settled in a similar manner; that is, the 8α- and 8β-isomers have non-steroidal (**A**) and steroidal (**B**) conformations (*cf.* Fig. 1).

Finally, the specified assignments to the 8α-(**A**) and 8β-(**B**) configurations between the two isomers were drawn by a comparison of the melting points, solubilities, adsorptive properties, specific rotations, and NMR spectra. In Table 1, the *cis*-like 8β-methoxy derivatives generally have lower melting points, higher solubilities, and stronger adsorptive properties than those of the *trans*-like 8α-isomers, in agreement with the well-known "von Auwers-Skita rule"[8] (*cf.* Experimental). There are, however, a few exceptions in which the 8β-methoxyl isomer, **8b**, has a higher melting point, together with a lower solubility, than the corresponding 8α-isomer, **8a**, much as in the relation between 6β-acetoxy-8α- and 6β-acetoxy-8β-methoxy lactones, **12a** and **12b**, described in the earlier work.[1]

In addition, in the NMR spectra of the hydroperoxides, **8a,b**, and the lactones, **9a,b**, only the 8α-methoxyl derivatives, **8a** and **9a**, exhibit homoallylic couplings[9] (1.0—1.8 Hz) between 6α-H and 13-CH_3, because the dihedral angle between the plane of the double bond—C-6–C-13— and the 6α-H is around 90°, as shown by an inspection of the configuration (**A**) with the Dreiding model (Fig. 1), whereas 8β-isomers do not show these couplings between 6α-H and 13-CH_3, all lying around 20° (*cf.* Fig. 1 and Table 1). Furthermore, the 8α-methoxy compounds showed the chemical shifts due to 14-methyls at a lower field than those due to 15-methyls; this relation of the chemical shifts between 14- and 15-methyls is reversed in the 8β-series (*cf.* Table 1). These variations in the chemical shifts may be explained similarly in terms of the effect due to the alteration in the geometry of the skeleton observed in the steroid field— by bending rings away from the angular methyl group, or by blocking the angular methyl's view over the remaining skeleton the methyl signal may cause a downfield shift.[10] On the other hand, 8β-methoxyl compounds have stronger positive rotations than the corresponding isomers. This can be expected from the helicities[1] derived from dihydrofuran/ring A fusion. The helicity was clarified by ORD-CD study in the 6-oxo derivatives of **3a** and **3b**.

All the derivatives, **10a,b** and **11a,b**, transformed

from furanoeremophilane, **5**, showed the signals due to 13-methyls with homoallylic couplings in their NMR spectra: δ 1.71 and 1.74 (each d, J=1.2 Hz) in **10a** and **10b**, and 1.76 and 1.76 (each d, J=1.2 and 1.5 Hz) in **11a** and **11b**. These couplings are obviously the expected ones between 6α-protons and 13-methyls in 8α-methoxyl compounds, and between 6β-protons and 13-methyls in 8β-isomers, as a consideration of the angles with the Dreiding model shows (Fig. 1).

Thus, summarizing the above results, the generalization outlined in the previous paper[1] was found also to be applicable to the configurational assignments of the hydroperoxides, **8a,b** and **10a,b**, and the lactones, **9a,b** and **11a,b**, prepared from furanofukinin, **4**, and furanoeremophilane, **5**.

On alkaline hydrolysis, a mixture of dimethoxy lactones, **9a,b**, gave a sole product, $C_{15}H_{20}O_3$ (mp 95.0—96.0 °C), which was identical with the expected unsaturated acid (**13**)[1] previously prepared by alkaline hydrolysis from a mixture of 6β-acetoxy-8(α and β)-methoxy lactones **12a,b**. On the other hand, a mixture of **11a,b** was treated with 1.5 M potassium hydroxide–methanol to yield also a sole product, $C_{15}H_{22}O_3$ (mp 212.0—213.5 °C), in a good yield: this product showed spectra suggesting the presence of a hydroxyl group and an α,β-unsaturated γ-lactone group: 3565, 3330 (OH), and 1745, 1697 cm^{-1} (unsaturated γ-lactone C=O), and an UV maximum at 222 nm. The structure of this lactone was easily inferred from its NMR spectrum, closely similar to that of the natural eremophilenolide (**14**)[11] except for the absence of the signal due to 8-H. Moreover, the lactone revealed a steroidal character—the chemical shift due to 14-methyl is higher than that due to 15-methyl in the NMR spectrum, and it showed a strong positive rotation (Table 1). The above conclusion can be further supported by the similar feature observed in the known natural eremophilenolides with 8β-substituents (a hydrogen or a hydroxyl) other than a methoxyl group. The specific rotations and the chemical shifts of 15- and 14-methyls in the spectra of eremophilenolide, **14**, 6β-hydroxyeremophilenolide (**15**), and 6β,8β-dihydroxyeremophilenolide (**16**) are as follows; **14**: $[\alpha]_D^{20}$+16.6° (c, 3.67, $CHCl_3$),[12,13] δ 1.01 (s) and 0.78 (br d);[11] **15**: $[\alpha]_D^{24}$+205.8° (c, 1.021, $CHCl_3$), δ 1.11 (s) and 0.78 (non-resolved methyl signal);[14] **16**: $[\alpha]_D^{16}$+169° (c, 0.985, $CHCl_3$), δ 1.11 (s) and 0.78 (non-resolved methyl signal).[1] Thus, the lactone can be represented as in the formula (**17**) with a steroidal configuration (**B**). Compound **17** has previously been derived as the by-product from the autoxidation of furanoeremophilane, **5**, by Šorm *et al.*[15]

Experimental

The IR, UV, and mass spectra were taken with Hitachi EPI-G3, Cary 14, and Hitachi RMU-6 spectrophotometers respectively. The NMR spectra were recorded with a Hitachi R-20B (60 MHz) spectrophotometer, and the chemical shifts are reported in δ-values (with TMS as the internal reference). The optical rotations were measured with a Perkin-Elmer 141 polarimeter. The TLC were run on Kieselgel G (Merck).

Synthesis of Furanofukinin (4). Petasalbin, **1** (492 mg), was dissolved in a solution of methanol (10 ml) and acetic acid (0.5 ml), and then left for three days at room temperature. After the removal of the solvent *in vacuo* and dilution with water, the reaction product was extracted with ether. Subsequent working-up as usual gave a crude product as a yellow oil (477 mg), which was purified by column chromatography on alumina (10 g, grade IV), with light petroleum–ether (100 : 1) as the eluent, and by vacuum-distillation to give furanofukinin (**4**) as a colorless oil; bp 96.0—106.0 °C (bath temperature)/6×10^{-3} mmHg. This was identical in all respects with the natural specimen.[2]

Synthesis of Furanoeremophilane (5) via Sultone (7) from Fukinone (6). *Sultone (7)*: Concentrated sulfuric acid (d= 1.84, 1.91 g) was stirred, drop by drop, into acetic anhydride (5.15 g) under ice-cooling below −10 °C, and then fukinone, **6** (3.34 g) ,was added to the stirred solution over a period of 15 min under continued cooling. After stirring for a further 1.5 h, the mixture was left for 38 h at −8 °C—−4 °C and for 1 h at room temperature. The subsequent addition to the reaction mixture of cracked ice (*ca.* 1 g) and a solution of sodium hydroxide (0.89 g) in water (1.6 ml) deposited yellowish brown crystals, which were filtered and washed with water. The crude product (3.0 g, 70%) was recrystallized from ethyl acetate to afford a sultone (**7**) as colorless prisms; mp 187.5—188.0 °C; UV: λ_{max}^{MeOH} 275.2 nm (ε, 4330); IR (KBr): 1653, 1578, 1195, 1085, 865 cm^{-1}; NMR ($CDCl_3$): 6.24 (m, 12-H), 1.96 (d, J=1.0 Hz, 13-CH_3), 0.89 (s, 15-CH_3), 0.87 (d, J=6.3 Hz, 14-CH_3).

Found: C, 63.59; H, 7.90; S, 11.38%. Calcd for $C_{15}H_{22}O_3S$: C, 63.80; H, 7.85; S, 11.35%.

Furanoeremophilane (5): A mixture of the sultone, **7** (497 mg), and zinc oxide (500 mg) was subjected to pyrolytic distillation. The distillate was collected in a 10% potassium hydroxide aqueous solution (0.3 ml) and then extracted with ether. The ethereal extract was washed with a saturated sodium hydrogencarbonate solution and then with water, and dried over anhydrous sodium sulfate. The subsequent evaporation of the solvent gave crude furanoeremophilane (**5**) as an oil (360 mg, 94%), which was purified by vacuum-distillation (bp 67—100 °C (bath temperature)/0.15 mmHg) to furnish a pure specimen (297 mg, 77%) and subsequently by GLC to obtain an analytical sample (PEG 20 M, 2.6 m; column temperature, 175 °C; H_2-flow rate, 60 ml/min; retention time, 8.8 min); IR (film): 1641, 1560, 1145, 1087, 985 cm^{-1}; $[\alpha]_D^{23}$ −13.2 °C (c, 1.0, $CHCl_3$).

Found: C, 82.35; H, 10.21%. Calcd for $C_{15}H_{22}O$: C, 82.51; H, 10.16%. This compound was identical in all respects (IR, NMR, GLC, and specific rotation) with the natural specimen.[2]

Photosensitized Oxygenation of Furanofukinin (4). A solution of furanofukinin, **4** (770 mg), and Rose Bengal (30 mg) in methanol (300 ml) was irradiated with a circular fluorescent lamp (30 watt) for 1 h under the bubbling of air. After the subsequent removal of the solvent *in vacuo*, the residue was taken up with benzene. The benzene extract was washed with water and then passed through a filter filled with anhydrous sodium sulfate for drying and taking off the dye-stuff. The removal of the solvent *in vacuo* gave a colorless solid, which showed two spots on TLC (R_f, 0.40 and 0.20; benzene–ethyl acetate, 10 : 1) and which was separated into two hydroperoxides, (**8a**) and (**8b**), by careful fractional crystallization from benzene. The **8b** compound was less soluble than **8a** in benzene.

Hydroperoxide (8a): Mp 116.0—117.0 °C (dec) as colorless prisms, $[\alpha]_D^{24}$ −54 °C (c, 1.0, MeOH); IR(KBr): 3380, 1300, 1140, 1090, 960 cm^{-1}; NMR (acetone-d_6): 11.30 (s, OOH), 5.68 (s, 12-H), 4.20 (q, J=1.5 Hz, 6-H) 3.43 and 3.17 (each s, 6- and 8-OCH_3), 1.87 (d, J=1.5 Hz, 13-CH_3),

0.96 (d, J=7.5 Hz, 14-CH_3), 0.78 (s, 15-CH_3).

Found: C, 65.43; H, 9.05%. Calcd for $C_{17}H_{28}O_5$: C, 65.36; H, 9.03%.

*Hydroperoxide (**8b**)*: Mp 136.0—137.0 °C (dec) as colorless needles, $[\alpha]_D^{24}$ +13.4° (*c*, 1.12, MeOH); MS: *m/e* 294 (M^+-H_2O), 154 (base peak); IR(KBr): 3350, 1280, 1200, 1080, 1050, 970 cm^{-1}; NMR (acetone-d_6): 11.29 (s, OOH), 5.73 (s, 12-H), 3.88 (s, 6-H), 3.27 and 3.11 (each s, 6- and 8-OCH_3), 1.85 (s, 13-CH_3), 1.02 (s, 15-CH_3), 0.78 (d, J= 5.3 Hz, 14-CH_3).

Found: C, 65.34; H, 8.97%. Calcd for $C_{17}H_{28}O_5$: C, 65.36; H, 9.03%.

*6β,8α-Dimethoxyepieremophilenolide (**9a**) and 6β,8β-Dimethoxyeremophilenolide (**9b**)*. A mixture of hydroperoxides **8a**, **b** (527 mg) was dissolved in pyridine (4 ml) and acetic anhydride (1 ml) and then left overnight at room temperature. Subsequent working-up as usual gave a colorless solid (480 mg), which was subjected to fractional crystallization from light petroleum to deposit a less soluble isomer (**9a**) (143 mg) and then an epimer (**9b**) (48 mg). In addition, the two hydroperoxides, **8a** (9 mg) and **8b** (15 mg), were transformed into the corresponding lactones, **9a** (6 mg) and **9b** (10 mg).

*6β,8α-Dimethoxyepieremophilenolide (**9a**)*: Mp 132.5—133.5 °C, colorless needles, $[\alpha]_D^{25}$ −185° (*c*, 0.80, $CHCl_3$); UV: λ_{max}^{MeOH} 224 nm (ε, 13700); IR ($CHCl_3$): 1750, 1300, 1100, 960, 920, 900 cm^{-1}; NMR (CCl_4): 4.28 (q, J=1.8 Hz, 6-H), 3.40 and 3.13 (each s, 6- and 8-OCH_3), 1.90 (d, J= 1.8 Hz, 13-CH_3), 0.96 (d, J=7.5 Hz, 14-CH_3), 0.75 (s, 15-CH_3).

Found: C, 69.39; H, 8.85%. Calcd for $C_{17}H_{26}O_4$: C, 69.36; H, 8.90%.

*6β,8β-Dimethoxyeremophilenolide (**9b**)*: Mp 123.0—123.5 °C, colorless prisms, $[\alpha]_D^{25}$ +170° (*c*, 1.0, $CHCl_3$); UV: λ_{max}^{MeOH} 220.5 nm (ε, 7600); IR($CHCl_3$): 1760, 1320, 1100, 1085, 995, 975, 920 cm^{-1}; NMR(CCl_4): 3.89 (s, 6-H), 3.25 and 3.06 (each s, 6- and 8-OCH_3), 1.81 (s, 13-CH_3), 0.99 (s, 15-CH_3), 0.75 (d, J=5.5 Hz, 14-CH_3).

Found: C, 69.44; H, 8.78%. Calcd for $C_{17}H_{26}O_4$: C, 69.36; H, 8.90%.

*Photosensitized Oxygenation of Furanoeremophilane (**5**)*. A stirred solution of furanoeremophilane, **5** (560 mg), and Rose Bengal (30 mg) in methanol (300 ml) was irradiated with a circular fluorescent lamp (30 watt) for 1 h under the bubbling of air. A subsequent working-up as has been described above gave a colorless crystalline mixture of hydroperoxides, which showed a single spot on TLC (R_f, 0.40, benzene-ethyl acetate, 10 : 1). The mixture was separated by fractional crystallization from benzene to deposit the less soluble 8α-epimer (**10a**) (181 mg) first, and then the 8β-epimer (**10b**) (167 mg) from the mother liquors.

*Hydroperoxide (**10a**)*: Mp 123.5—124.0 °C (dec) as colorless needles, $[\alpha]_D^{24}$ −15.2° (*c*, 1.0, MeOH); MS: *m/e* 264 (M^+-H_2O), 109 (base peak); IR(KBr): 3300, 1700, 1130, 1040, 960, 860 cm^{-1}; NMR (acetone-d_6): 11.20 (s, OOH), 5.70 (s, 12-H), 3.07 (s, OCH_3), 1.71 (d, J=1.2 Hz, 13-CH_3), 0.98 (d, J=6.0 Hz, 14-CH_3), 0.80 (s, 15-CH_3).

Found: C, 68.03; H, 9.24%. Calcd for $C_{16}H_{26}O_4$: C, 68.05; H, 9.28%.

*Hydroperoxide (**10b**)*: Mp 120.5—121.0 °C (dec) as colorless prisms, $[\alpha]_D^{24}$ +2.9° (*c*, 1.01, MeOH); MS: *m/e* 264 (M^+-H_2O), 109 (base peak); IR(KBr): 3300, 1710, 1160, 1070, 970, 920 cm^{-1} ;NMR (acetone-d_6): 11.21 (s, OOH), 5.73 (s, 12-H), 3.06 (s, OCH_3), 1.74 (d, J=1.2 Hz, 13-CH_3), 0.98 (s, 15-CH_3), 0.80 (d, J=6.0 Hz, 14-CH_3).

Found: C, 68.03; H, 9.30%. Calcd for $C_{16}H_{26}O_4$: C, 68.05; H, 9.28%.

*8α- and 8β-Methoxy Lactones, (**11a**) and (**11b**)*. A colorless crystalline mixture of hydroperoxides, **10a,b**, prepared from furanoeremophilane, **5** (455 mg), was dissolved in pyridine (1 ml) and acetic anhydride (2 ml) and then left overnight at room temperature. A subsequent working-up in the usual manner gave an oil (524 mg) which showed two spots on TLC (R_f, 0.78 and 0.70, $CHCl_3$) and which was then chromatographed over silica gel (12 g). Elution with light petroleum–ether (50 : 1) and subsequent fractional recrystallization from light petroleum gave 8α-methoxy lactone (**11a**) (130 mg) at first, and the 8β-epimer (**11b**) was obtained from the mother liquors.

*8α-Methoxyepieremophilenolide (**11a**)*: Mp 110.5—111.5 °C, colorless prisms, $[\alpha]_D^{24}$ −168° (*c*, 0.95, $CHCl_3$); UV: λ_{max}^{MeOH} 227 nm (ε, 12500); IR(KBr): 1750, 1690, 1310, 940 cm^{-1}; NMR(CCl_4): 3.05 (s, OCH_3), 1.76 (d, J=1.5 Hz, 13-CH_3), 0.98 (d, J=7.0 Hz, 14-CH_3), 0.77 (s, 15-CH_3).

Found: C, 72.59; H, 9.20%. Calcd for $C_{16}H_{24}O_3$: C, 72.69; H, 9.15%.

*8β-Methoxyeremophilenolide (**11b**)*: Mp 98.5—99.5 °C, colorless needles, $[\alpha]_D^{24}$ +164° (*c*, 1.08, $CHCl_3$); UV: λ_{max}^{MeOH} 225 nm (ε, 11500); IR(KBr): 1750, 1690, 1170, 990 cm^{-1}; NMR (CCl_4): 2.99 (s, OCH_3), 1.76 (d, J=1.2 Hz, 13-CH_3), 0.98 (s, 15-CH_3), 0.74 (d, J=6.0 Hz, 14-CH_3).

Found: C, 72.65; H, 9.27%. Calcd for $C_{16}H_{24}O_3$: C, 72.69; H, 9.15%.

*Unsaturated Acid (8-Oxo-eremophila-6,11-dien-12-oic Acid) (**13**)*.[1] A mixture of dimethoxy lactones, **9a,b** (200 mg), was dissolved in methanol (10 ml) and 1.84 M potassium hydroxide–methanol (8 ml) and then left for 36 h. After the removal of the solvent and dilution with water, the solution was acidified with 10% sulfuric acid and then extracted with ether. A subsequent working-up as usual gave an acid (198 mg) as a colorless oil, which was recrystallized from diisopropyl ether–light petroleum to afford the pure acid (**13**) (mp 95.0—96.0 °C). The acid, **13**, was found by a mixed-melting point determination and a comparison of the IR spectra to be identical with the 8-oxo-eremophila-6,11-dien-12-oic acid prepared from a mixture of 6β-acetoxy-8(α and β)-methoxy lactones, **12a,b**.[1]

*8β-Hydroxyeremophilenolide (**17**)*. A mixture of 8α- and 8β-methoxy lactones, **11a,b** (53 mg), was dissolved in a 1.5 M potassium hydroxide–methanol solution (1.3 ml) and then left for 3 h at room temperature. After the evaporation of the solvent *in vacuo* and acidification with 10% sulfuric acid, the reaction mixture was extracted with ether, washed with water, and dried. The removal of the solvent gave a semi-crystalline product (59 mg), which was subsequently recrystallized from methanol–diisopropyl ether to afford 8β-hydroxyeremophilenolide (**17**) (25 mg) as colorless prisms; mp 212.0—213.5 °C, $[\alpha]_D^{20}$ +157° (*c*, 0.69, $CHCl_3$); UV: λ_{max}^{MeOH} 222 nm (ε, 9200); MS: *m/e* 250 (M^+), 91 (base peak); IR($CHCl_3$): 3565, 3330, 1745, 1697 cm^{-1}; NMR (acetone-d_6): 5.90 (br s, OH), 2.83 (d, J=13.5 Hz, 6-CH_2), 1.73 (*d*, J=1.6 Hz, 13-CH_3), 1.04 (s, 15-CH_3), 0.80 (d, J=5.5 Hz, 14-CH_3).

Found: C, 71.93; H, 8.70%. Calcd for $C_{15}H_{22}O_3$: C, 71.97; H, 8.86%.

References

1) Part I: K. Naya, R. Kanazawa, and M. Sawada, *Bull. Chem. Soc. Jpn.*, **48**, 3220 (1975).

2) K. Naya, M. Nakagawa, M. Hayashi, K. Tsuji, and M. Naito, *Tetrahedron Lett.*, **1971**, 2961.

3) J. Hochmannová, L. Novotný, and V. Herout, *Collect. Czech. Chem. Commun.*, **27**, 1870 (1962).

4) W. Treibs, *Ber.*, **70**, 85 (1937).

5) F. Bohlmann and Ch. Fischer, *Chem. Ber.*, **107**, 1767 (1974): they reported the synthesis of the recamic furanoeremophilane.

6) The 8α-epimers corresponding to the 8β-substituted eremophilenolides were designated as epieremophilenolides (*cf.* Ref. 1).

7) C. S. Foote, M. T. Wuesthoff, S. Wexler, I. G. Burstain, R. Denny, G. O. Schenck, and K. H. Schulte-Elte, *Tetrahedron*, **23**, 2583 (1967).

8) E. L. Eliel, "Stereochemistry of Carbon Compounds," McGraw-Hill (1962), pp. 216, 326.

9) N. S. Bhacca and D. H. Williams, "Application of NMR Spectroscopy in Organic Chemistry," Holden-Day, San Francisco (1964), p. 110.

10) Ref. 9), p. 16.

11) L. Novotný, Z. Samek, and F. Šorm, *Collect. Czech. Chem. Commun.*, **31**, 371 (1966).

12) L. Novotný, J. Jizba, V. Herout, and F. Šorm, *Collect. Czech. Chem. Commun.*, **27**, 1398 (1962).

13) K. Naya and M. Tsumura: the synthetic eremophilenolide, **14**, converted from 6β-hydroxyeremophilenolide, **15**, showed the following spectra; $[\alpha]_D^{21}$ +163° (*c*, 1.0, $CHCl_3$), δ 1.02 (s) and 0.78 (d, J=5.5 Hz). The details will be published soon.

14) H. Ishii, T. Tozyo, H. Minato, *J. Chem. Soc.*, **1966**, 1545; L. Novotný and V. Herout, *Collect. Czech. Chem. Commun.*, **30**, 3580 (1955).

15) L. Novotný, V. Herout, and F. Šorm, *Collect. Czech. Chem. Commun.*, **29**, 2182 (1964).

The Synthesis and Properties of Diacyl Selenides

Hideharu ISHIHARA, Shigeyuki SATO and Yoshio HIRABAYASHI
Faculty of Engineering, Gifu University, Nakamonzen-cho, Kakamihara, Gifu 504
(Received April 12, 1977)

Diacyl selenides were synthesized in good yields by the deselenization of diacyl diselenides, which have conveniently been prepared from acyl chlorides and sodium hydroselenide. The reaction of dibenzoyl selenide with piperidine at 0 °C formed a fairly stable piperidinium salt. The methanolysis of distearoyl selenide gave selenostearic acid as an unstable intermediate.

Although the reactions of diacyl sulfides with various reagents have been investigated extensively, few studies of diacyl selenides have been known. In 1932, dibenzoyl selenide was obtained by Szperl and Wiorogoski[1] by the treatment of benzoyl chloride with dry hydrogen selenide in the presence of aluminium chloride. Recently, Jensen *et al.*[2] prepared dipropionyl selenide, not selenopropionic acid, by the reaction of propionyl chloride with hydrogen selenide in the presence of an equimolar amount of pyridine, but the yield was poor. In this paper, we will describe a convenient method for synthesizing diacyl selenides, which are important as the starting material for preparations of potassium selenocarboxylates,[3] by the deselenization of diacyl diselenides with triphenylphosphine and will discuss the reactions of diacyl selenides with amines and methanol.

Results and Discussion

The reaction sequence used in the synthesis of diacyl selenides is outlined in Scheme 1.

$$\mathrm{RCOCl} \xrightarrow{\mathrm{NaHSe}} [\mathrm{RCOSeH} \xrightarrow{\mathrm{NaHSe}} \mathrm{RCOSeNa}]$$
$$\downarrow \mathrm{O_2\ and\ I_2}$$
$$\mathrm{RCOSeSeCOR}\ \ (\mathbf{2})$$
$$\downarrow \mathrm{Ph_3P}$$
$$\mathrm{RCOSeCOR}\ \ (\mathbf{1})$$

R=C_6H_5– (**a**), *p*-$CH_3C_6H_4$– (**b**), *p*-ClC_6H_4– (**c**), *p*-$CH_3OC_6H_4$– (**d**), *n*-$C_{17}H_{35}$– (**e**).

Scheme 1.

First, diacyl diselenides were prepared by a new, convenient method. The oxidation of a mixture of selenocarboxylic acid and sodium selenocarboxylate, which had been prepared by the reaction of acyl chlorides and sodium hydrogen selenide in ethanol, gave diacyl diselenides in good yields, as is shown in Table 1.[4] Next, diacyl selenides were obtained in good yields by the deselenization of diacyl diselenides. That is, the diacyl diselenides readily reacted with an equimolar amount of triphenylphosphine in benzene to give diacyl selenides and triphenylphosphine selenide. Diacyl selenides were isolated in good yields by the recrystallization of the resulting mixture from hexane–ether. The results and some properties are summarized in Table 2.

Distearoyl selenide was also prepared by the one-step reaction of stearoyl chloride with sodium selenide in benzene. The recrystallization of the crude product from benzene gave distearoyl selenide in a 67% yield, while small amounts of distearoyl diselenide and octadecylidene bis(selenostearate) were obtained as by-products. On the other hand, attempts to use the same method for the preparation of dibenzoyl selenide were unsuccessful, though some of the dibenzoyl diselenide was isolated.

Reactions of Dibenzoyl Selenide with Amines. Jensen *et al.*[2] have described that dipropionyl selenide reacted with aniline to form 2 mol of propionanilide. However, when dibenzoyl selenide was treated with 2 mol of piperidine at 0 °C, piperidinium selenobenzoate (**3**) was isolated in a 79% yield. The piperidinium salt (**3**) was fairly stable in the solid state and did not change when left standing for a day under nitrogen. However, the salt (**3**) decomposed in ether at ordinary temperatures to give 1-benzoylpiperidine, with the concurrent evolution of hydrogen selenide (Scheme 2). The salt

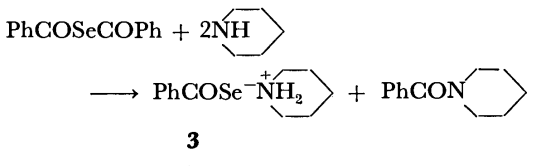

Scheme 2.

was confirmed by elemental analysis and by a study of its IR and NMR spectra. That is, in the IR spectrum the characteristic multiple absorption bands (νNH) at 2500—3000 cm^{-1} and a carbonyl absorption band at 1550 cm^{-1} were observed. The NMR spectrum showed peaks at 1.14 (6H, piperidine), 3.22 (4H, piperidine), 7.48, 8.28 (5H, C_6H_5), and near 9.4 ppm (about 2H, NH_2). Furthermore, the structure of the salt was chemically suported by the formation of methyl selenolbenzoate in a 90% yield by the reaction of the salt with methyl iodide in dry ether.

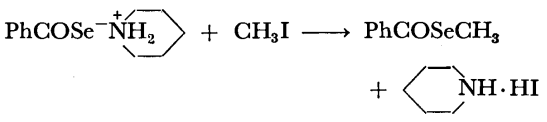

In a similar way, the reactions of bis(*p*-chlorobenzoyl) selenide and bis(*p*-methylbenzoyl) selenide with piperidine gave the corresponding piperidinium salts in 79 and 82% yields, respectively. Though, attempts to isolate the analogous adducts of dibenzoyl selenide with morpholine or dibutylamine failed, the infrared spectra of the oily substances, obtained by evaporating the solvent from the reaction mixture, showed multiple

Table 1. Synthesis and properties of diacyl diselenides (RCOSeSeCOR)

Compound	R	Yield %	Mp °C	Selenium Found(Calcd) %	IR, cm^{-1} (CCl_4) $\nu_{C=O}$	UV, nm (cyclohexane) λ_{max} (log ε)
2a	C_6H_5	77	131.0—132.0	42.55 (42.90)	1741 1700	242 (4.47) 281 (3.97)
2b	p-$CH_3C_6H_4$	80	110.0—111.5	39.41 (39.86)	1744 1704	253 (4.51) 280 (4.12)
2c	p-ClC_6H_4	81	122.0—124.0	35.75 (36.13)	1739 1700	253 (4.53) 285 (4.10)
2d	p-$CH_3OC_6H_4$	65	106.0—107.0	36.20 (36.88)	1746 1703	276 (4.53) 285[a]
2e	n-$C_{17}H_{35}$	86	79.8— 80.3	22.73 (22.79)	1732	244 (3.56)

a) Shoulder.

Table 2. Synthesis and properties of diacyl selenides (RCOSeCOR)

Compound	R	Yield %	Mp °C	Selenium Found(Calcd) %	IR, cm^{-1} (CCl_4) $\nu_{C=O}$	UV, nm (cyclohexane) λ_{max} (log ε)
1a	C_6H_5	88	61.5— 62.3	27.08 (27.30)	1737 1685	252 (4.34) 285 (3.86)
1b	p-$CH_3C_6H_4$	93	90.0— 91.0	24.72 (24.89)	1738 1690	263 (4.47) 303 (3.85)
1c	p-ClC_6H_4	91	118.5—120.0	21.88 (22.05)	1737 1686	263 (4.53) 304 (3.89)
1d	p-$CH_3OC_6H_4$	77	77.8— 80.2	22.33 (22.61)	1735 1687	282 (4.51) 305[a]
1e	n-$C_{17}H_{35}$	98	75.3— 75.8	12.74 (12.86)	1775 1715	 261 (3.15)

a) Shoulder.

Table 3. Methanolysis of distearoyl selenide at 50 °C

Reaction conditions			Yield[a] Mole ratio(%)		
Selenide	Gas	Time h	**1e**	**2e**	Ester[b]
1e	N_2	10	—	—	100
1e	N_2	0.5	22	12	66
1e	air	0.5	5	27	67
2e	N_2	0.5	10	71	19

a) The yields of these products were obtained by the UV method (Ref. 8). b) Methyl stearate.

bands(νNH) at 2500—3000 cm^{-1} and a carbonyl absorption band at 1550 cm^{-1}. These results may show that the reaction of diacyl selenide with amine gives, at first, the amine salt and amide, and that then the salt decomposes to give amide, with the evolution of hydrogen selenide.

Methanolysis of Distearoyl Selenide. It is known that the alcoholysis of diacyl sulfides gives the thio acid and the ester.[5] On the other hand, a methanolysis of distearoyl selenide (**1e**) in both a stream of nitrogen and air gave methyl stearate, distearoyl diselenide (**2e**), and **1e**, with the concurrent evolution of hydrogen selenide, but selenostearic acid was not obtained. On the other hand, as is shown in Table 3, in case of the reaction in a stream of air, the yield of **2e** was 27%, and in case of the reaction in a stream of nitrogen, that of **2e** was 12%, whereas the yields of **1e** were 5 and 22%, respectively. Furthermore, the reaction mixtures comsumed iodine in methanol. These results show that **2e** may be produced by the oxidation of selenostearic acid. That is, selenostearic acid may be formed by the methanolysis of **1e**, and the acid may change to **1e** with the evolution hydrogen selenide or may be oxidized to give **2e**, as is shown in the following equations:

$$RCOSeCOR + CH_3OH \longrightarrow [RCOSeH] + RCOOCH_3, \quad (1)$$

$$2[RCOSeH] \longrightarrow RCOSeCOR + H_2Se, \quad (2)$$

$$2[RCOSeH] \xrightarrow{(O)} RCOSeSeCOR + H_2O, \quad (3)$$

$$RCOSeSeCOR + CH_3OH \longrightarrow [RCOSeH] + RCOOCH_3 + Se + H_2Se. \quad (4)$$

These equations are supported by the reaction of **2e** with methanol in a stream of nitrogen to give **1e**, methylstearate and elemental selenium, with the concurrent evolution hydrogen selenide (Eq. 4).

Experimental

Synthesis of Dibenzoyl Diselenide. Hydrogen selenide, generated from Al_2Se_3 (0.80 mol)[7] and dilute hydrogen chloride and dried by being passed through a $CaCl_2$-tube, was led into a solution of sodium ethoxide (0.60 mol) in 400 ml of ethanol at 0 °C. Then, 71 g (0.50 mol) of benzoyl chloride was slowly added to the solution at 0 °C. After the stirring had continued for another 3 h, the mixture was treated with 100 g of iodine in ethanol and 5% aqueous

K_2CO_3. The organic layer was extracted with benzene, and the benzene solution was washed with aqueous $Na_2S_2O_3$ and then water, and dried over Na_2SO_4. The solvent was evaporated, and the residue was recrystallized from benzene–ether. Yield, 70.8 g (77%); mp 131—132 °C (lit,[1] 129—130 °C).

Synthesis of Dibenzoyl Selenide. A mixture of equimolar amounts of dibenzoyl diselenide (11.0 g; 0.03 mol) and triphenylphosphine (7.9 g; 0.03 mol) in benzene (150 ml) was stirred at room temperature for 1 h. After the benzene had then been evaporated under reduced pressure, ether was added to the residue. The resulting insoluble part (Ph_3PSe; mp 179—181 °C) was filtered off. After the ether had been removed from the filtrate, recrystallizations of the residue solid from hexane–ether gave 7.6 g (88%) of dibenzoyl selenide as white crystals; mp 60—61 °C (lit,[1] 61—62 °C).

Synthesis of Distearoyl Selenide by the Reaction of Stearoyl Chloride with Sodium Selenide. In a four-necked flask, 300 ml of ammonia dried by being passed through CaO-tube was liquefied, and then metal sodium (2.3 g; 0.10 mol) was added. Thereafter, elemental selenium (3.95 g; 0.05 mol) was slowly added to the solution at −40 °C under vigorous stirring. After the stirring had been continued for another 2 h, a small portion of selenium or sodium was added, as required. (If the solution become orange, a small quantity of sodium was added, or if it showed blue, a small quantity of selenium was added). Then, the solution turned white. After the solvent had been completely removed, to the residue in dry benzene (200 ml) stearoyl chloride (30.3 g; 0.10 mol) was added, drop by drop, at 50 °C and the stirring was continued for another 3 h. After the removal of the insoluble part from the reacting mixture by filtration, the solvent was removed. Recrystallizations of the residue from benzene gave 20.5 g (67%) of distearoyl selenide; mp 75.3—75.8 °C; Se 12.78% (Calcd for $C_{36}H_{70}O_2Se$: 12.86%), 1.5 g of distearoyl diselenide; mp 79.8—80.3 °C; Se 22.73% (Calcd for $C_{36}H_{70}O_2Se_2$: 22.79%), and 0.8 g of $(C_{17}H_{35}COSe)_2CHC_{17}H_{35}$; mp 58—59 °C; Se 16.67% (Calcd for $C_{54}H_{106}O_2Se_2$: 16.70%) νC=O 1709 cm^{-1}, νC–Se 945 cm^{-1}; NMR peaks 4.82 (–CH–, 1H, T,) 2.59 ($-CH_2CO-$, 4H, T), 1.25 ($-CH_2-$, about 92H, S) and 0.83 ppm ($-CH_3$, 9H, T).

Reaction of Dibenzoyl Selenide with Piperidine. A mixture of dibenzoyl selenide (2.90 g; 10 mmol) and piperidine (1.70 g; 20 mmol) in 50 ml of anhydrous ether was stirred at 0 °C for 30 min. The resulting precipitated were collected from the reaction mixture, and recrystallizations of the precipitate from dichloromethane–hexane gave 2.13 g (79%) of piperidinium selenobenzoate. The filtrate was concentrated under reduced pressure, giving 2.28 g (128%) of 1-benzoylpiperidine and a small amount of elemental selenium.

Reaction of Piperidinium Selenobenzoate with Methyl Iodide. The reaction of piperidinium selenobenzoate (1.0 g; 3.7 mmol) with methyl iodide (2.6 g) in 20 ml of dry ether at room temperature gave methyl selenolbenzoate (0.66 g, 90%; bp 105—106 °C/6 mmHg). The ester was identified by a comparison of its IR spectrum with that of an authentic sample.

Reaction of Distearoyl Selenide with Methanol. Methanol (15 ml) was added to a solution of 615 mg of distearoyl selenide in benzene (30 ml). The mixture was heated at 50 °C by means of N_2 gas. After 30 min, the reaction mixture was cooled and extracted with ether. The ether solution was washed with water, dried, and concentrated, giving a crystalline residue. Distearoyl selenide, distearoyl diselenide, and methyl stearate were obtained by the recrystallization of the residue, while the hydrogen selenide was evaporated during the reaction. We found nothing else. The yields (Table 3) of these products in the residue were calculated by fitting a equation[8] to extinction at 244 and 261 nm.

References

1) L. Szperl and W. Wiorogorski, *Rocz. Chem.*, **12**, 71 (1932)
2) K. A. Jensen, L. Bøje, and L. Henriksen, *Acta Chem. Scand.*, **26**, 1465 (1972).
3) H. Ishihara and Y. Hirabayashi, *Chem. Lett.*, **1976**, 203.
4) Diacyl diselenides were also obtained by the reaction of acyl chlorides with sodium diselenide in benzene; yields: **2a**, 64%; **2b**, 44%; **2e**, 58%.
5) Y. Hirabayashi, M. Mizuta, and T. Mazume, *Bull. Chem. Soc. Jpn.*, **38**, 1099 (1965).
6) All the melting points are uncollected. The IR, UV, and NMR spectra were determined on Jasco IR A-2, Shimadzu UV-200, and Hitachi-Perkin Elmer R-22 (90 MHz) spectrometers, respectively.
7) H. S. Booth, *Inorg. Synth.*, Vol. 2, 184 (1939).
8) D. T. Englis and D. A. Skoog, *Ind. Eng. Chem., Anal. Ed.*, **15**, 748 (1943).

On the Mechanism of the Formation of Steroidal Cyclic Hydroxamic Acids in the Photolysis of Steroidal 17β-ol Nitrite[1)]

Hiroshi SUGINOME, Norihisa YONEKURA, Terutoshi MIZUGUCHI, and Tadashi MASAMUNE

Department of Chemistry, Faculty of Science, Hokkaido University, Sapporo 060

(Received April 18, 1977)

The Photolysis of 5α-androstane-3α,17β-diol 3-acetate 17-nitrite (**1**) in benzene with monochromatic light (372 ±4 nm) afforded two rearranged products, 17a-aza-D-homo-5α-androstane-3α,17a-diol-17-one 3-acetate (**2**) and the C-13 epimer (**8**). This result confirmed that the cyclization of the nitroso aldehyde intermediate (**C**) to the two products **2** and **8** proceeds without the involvement of excited species of the nitroso aldehyde intermediate **C**. This conclusion differs from that obtained for bornyl and isobornyl nitrites by Kabasakalian and Townley. The results of photolysis in carbon tetrachloride are also compared with that in benzene. The photolysis of the nitrite **1** in an EPA matrix at 77 K showed that essentially no β-cleavage of the 17β-oxyl radical takes place at the temperature of liquid nitrogen.

In previous papers, the formations of steroidal cyclic nitrones and spiroisoxazolines *via* the photochemical rearrangement of steroidal cyclopentyl and cyclopentenyl nitrites were reported.[2a-2e)] The reaction pathways of these photoinduced rearrangements were confirmed to involve nitroso aldehyde intermediates formed *via* the β-cleavage of the oxyl radical to afford the allyl radical, followed by the combination of NO and the allyl radical.[2b,2c)] The cyclization of the nitroso aldehyde to the products is a thermal process and proceeds without any involvement of excited species.[2c,2d)]

In connection with these investigations, we were interested in the formation of a steroidal cyclic hydroxamic acid (**2**) *via* the photochemical rearrangement of a steroidal 17-nitrite (**1**) reported by Barton and his collaborators,[3)] since the proposed pathway for this photoinduced rearrangement, which is illustrated in Scheme 1, involved also the formation of a nitroso aldehyde intermediate (**C**) and its cyclization to the product **2**.[3)] Although the proposed pathway is quite reasonable, no experimental evidence for the intermediacy of the nitroso aldehyde **C** has been available and the problem of whether the cyclization of the nitroso aldehyde **C** is a thermal process or a photochemical one seemed also to remain to be clarified.

Subsequent to this work,[3)] Kabasakalian and Townley[4)] and Nakazaki and Naemura[5)] reported an analogous photorearrangement of bornyl and isobornyl nitrites. These two groups of investigators found that the photolysis of bornyl and isobornyl nitrites (*e.g.*, **3**) in benzene or in trichlorotrifluoroethane with black light or ultraviolet light led to the formation of 1,8,8-trimethyl-2-hydroxy-2-azabicyclo[3.2.1]octan-3-one (**4**) in a 27—30% yield, together with several products derived from a β-cleavage of the corresponding oxyl radical, as is depicted in Scheme 2. Moreover,

Scheme 2.

Kabasakalian and Townley were able to isolate a nitroso aldehyde intermediate (**5**), although none of its physical constants were given in the paper.[4)] They also reported that they succeeded in converting the nitroso aldehyde **5** into the hydroxamic acid **4** on exposure to sunlight or a neon lamp (585—660 nm), but failed to transform the aldehyde **5** into the hydroxamic acid **4** by heat at 60 °C (Scheme 3). On the basis of these results, they concluded that the cyclization of the nitroso aldehyde **5** to the hydroxamic acid **4** took place from an excited species of the nitroso aldehyde **5**.

Scheme 3.

It would not be unreasonable to extrapolate these results to the pathway of the analogous rearrangement of the steroidal 17-nitrite. In order to obtain independent evidence for the intermediacy of the nitroso aldehyde **C** and the mode of cyclization in the steroidal rearrangement, however, we carried out the photolysis of the nitrite **1** with a monochromatic light and the photolysis of the nitrite **1** in an EPA matrix at 77 K. Thus, if the hydroxamic acid **2** is formed from the assumed nitroso aldehyde **C**, we can readily ascertain whether this process is thermal or photochemical by the photolysis of the nitrite **1** with monochromatic light, which will be able to excite only the O–NO group of

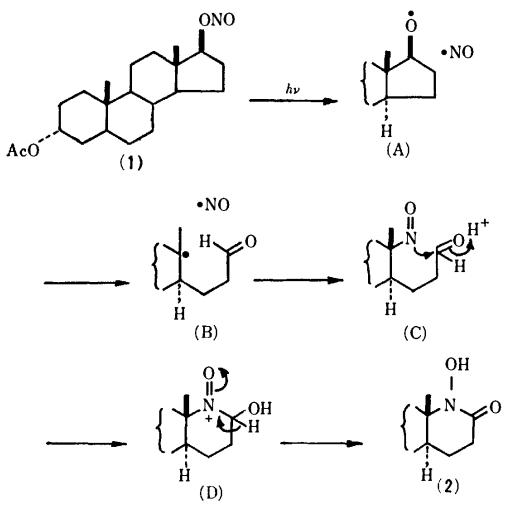

Scheme 1.

the nitrite **1**, not the C–NO group or the CHO group of the assumed nitroso aldehyde intermediate(s) **C** in Scheme 1.

Results and Discussion

The O–NO group generally has a characteristic structured band centred at *ca.* 370 nm due to the n→π^* transition.[6] The stronger absorption at the shorter wave length was ascribed to the intramolecular charge-transfer band.[7] The UV spectrum of 5α-androstane-3α-17β-diol 3-acetate 17-nitrite (**1**) in benzene or in THF exhibited a characteristic structured absorption due to the n→π^* of the ONO group centred at *ca.* 372 nm (ε; 112 in benzene). On the other hand, the nitroso aldehyde (**1**) would have one weak absorption at *ca.* 290 nm[8] due to an n→π^* transition of the aldehyde group, and another at 670 nm due to the n→π^* transition of the C-nitroso group.[9] Therefore, the nitrite **1** in dry benzene was photolyzed with 372±4 nm monochromatic light generated by a CRM-FA grating spectroirradiator in order to excite only the ONO chromophore. A careful separation of the products by preparative TLC afforded 5α-androstan-3α-ol-17-one 3-acetate (**6**) (8%), 5α- androstane-3α, 17β-diol 3-acetate (**7**) (12%), a new compound (**8**) (mp 118—120 °C), (21%), and 17a-aza-D-homo-5α-androstane-3α,17a-diol-17-one 3-acetate (**2**)[3] (20%), in the order of decreasing mobilities in TLC (Scheme 4). The electron-

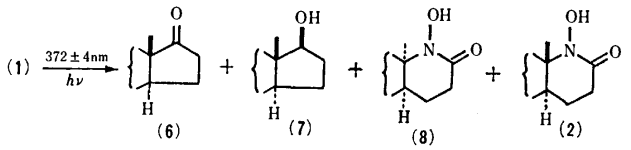

Scheme 4.

impact mass spectrum of the new compound **8** revealed a fragmentation pattern very similar to that of the hydroxamic acid **2**. They both show a molecular ion at *m/e* 363 and the principal fragment ions at *m/e* 348, 332, 272 and 150. The relative intensities of the principal ions in the mass spectra of the two compounds **2** and **8** are shown in Table 1. This mass spectrum, together with the IR and NMR spectra, suggest that the structure of the new compound is 17a-aza-D-homo-5α, 13α-androstane-3α, 17a-diol-17-one 3-acetate.

Table 1. Relative intensities (%) of the principal ions in the mass spectra of compounds **2** and **8**

Compd	$M^{+\cdot}$	*m/e*			
		348	332	272	150
2	1	12	100	10	24
8	4	48	100	16	10

The base peak of the two compounds **2** and **8** is the fragment ion 332 corresponding to $[M-CH_3, O]^+$. The (a) in Scheme 5 is a possible representation of this fragment. The intense fragment ion at *m/e* 348 involves the elimination of CH_3, and this ion may possess the structure (b) in Scheme 6. The intense peak at *m/e* 150 is most probably formed *via* an ion (c)[10] identical

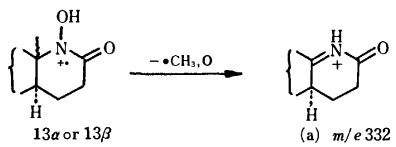

Scheme 5.

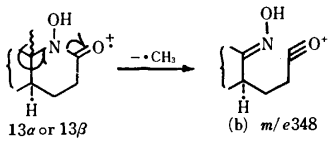

Scheme 6.

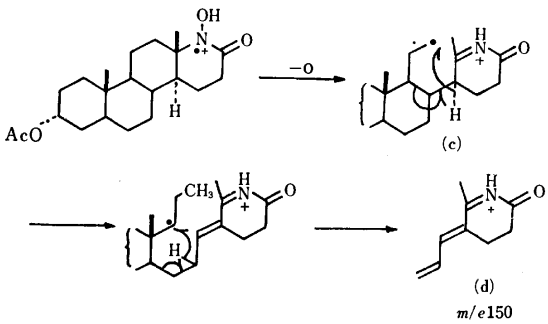

Scheme 7.

with the ion postulated for the mass spectral fragmentation[11] of 17a-aza-5α-androstan-17-one and is represented as having a structure (d). The pathway for the formation of the ion (d) from the ion (c) suggested by Budzikiewicz and his collaborators[11] is illustrated in Scheme 7.

This structure for the hydroxamic acid **8** was confirmed by its conversion into 17a-aza-D-homo-5α,13α-androstan-3α-ol-17-one 3-acetate: the reduction of the product **8** with zinc and acetic acid under reflux[3] afforded the corresponding known lactam identical with an authentic sample[12] prepared by the Beckmann rearrangement of an oxime of 5α,13α-androstan-3α-ol-17-one acetate. Very similar results were obtained in the photolysis of the nitrite **1** with Pyrex-filtered light, as is shown in Table 2.

Since the monochromatic light of 372±4 nm is unable to excite the formyl group or the nitroso group of the hypothetical intermediate **C**, it may be concluded that the cyclization of the nitroso aldehyde **C** to the observed hydroxamic acids **2** and **8** is a thermal process. This conclusion differs from the one obtained for bornyl and isobornyl nitrites by Kabasakalian and Townley.[4]

Table 2. Yields (%) of the products in the photolysis of the nitrite **1** with monochromatic light in various solvents

	6	**7**	**8**	**2**
Benzene[a]	10	9	20	20
Benzene	8	12	21	20
THF	trace[b]	52	13	12
CCl_4	21	52	8	8

a) Results with Pyrex-filtered light.
b) Detected by TLC.

The mode of the transfer of the 17-hydrogen of the nitrite **1** remains to be clarified.

In order to examine the effects of solvents, the photolysis of the nitrite **1** in two aprotic solvents, THF and carbon tetrachloride, was studied. Thus, it was found that the four products, **6**, **7**, **8**, and **2**, are also formed in two solvents under conditions comparable to the case in benzene and with light of a 372±4 nm wave length. However, the ratios of the four products are different, as is shown in Table 2.

Thus, it is apparent that the hydroxamic acids are generally produced in aprotic solvents.[13] However, the main product in THF and in carbon tetrachloride is the parent alcohol **7**. Needless to say, THF is a better hydrogen-donating solvent than benzene, and hydrogen abstraction by the 17β-oxyl radical from a hydrogen attached to the oxygen-bearing carbon of THF may take place readily to produce the parent alcohol. In the photolysis in carbon tetrachloride, the ketone **6** is formed in a considerable amount, together with the parent alcohol. Some of these compounds, **6** and **7**, may perhaps be formed *via* the disproportionation of the 17β-oxyl radical (**A**).

We also carried out the photolysis of bornyl nitrite **3** in benzene. Let us discuss the results briefly. The photolysis of the nitrite **3** in benzene with monochromatic light (358±8 nm) gave the hydroxamic acid **4**,[4,5] although the yield was only 3% and the major product was the parent borneol, as was confirmed by TLC. A repetition of the photolysis with Pyrex-filtered light also afforded the hydroxamic acid **4** in an equally poor yield (*ca.* 2%) and borneol as the major product (TLC).[14] These results indicate that the hydroxamic acid **4** may also be formed by a thermal cyclization of the nitroso aldehyde **5**.

Finally, an experiment aimed at proving the intermediacy of the nitroso aldehyde **C** will be described. In a previous publication[2c] we described the photolysis of a nitrite carried out in an EPA matrix at 77 K. This technique successfully proved the intervention of a nitroso aldehyde in the photorearrangement of the nitrite to nitrone. In the present case, the nitrite **1** in an EPA matrix (8.3×10^{-3} M) was photolyzed at 77 K through a Pyrex glass filter in the hope that we might be able to trap the nitroso aldehyde intermediate **C**. The reaction was monitored by UV spectroscopy in the 250—800 nm region, as in the previous case.[2c] However, in contrast to the case of the nitrite-nitrone transformation,[2c] the increase in the absorption maximum at *ca.* 670 nm in the matrix due to the C-nitroso compound **C** was not signifcant, even after a prolonged irradiation. This is due to the fact that the β-cleavage of the 17β- oxyl radical (**A**) at 77 K took place to only a small extent, as was proved by the presence of the hydroxamic acids on the thin-layer chromatogram of the EPA solution after irradiation.

Experimental

For the instruments and general procedures, see Part 30[2d] in this series.

5α-Androstane-3α,17β-diol 3-Acetate 17-Nitrite (1). This nitrite was prepared by the procedure of Barton and his colleagues.[3] Mp 183—184 °C (lit,[3] 177—180 °C) NMR: τ 9.26 (18-H), 9.20 (19-H), 7.94 (OAc), 5.00 (bs. $W_{1/2}$=7.5 Hz) (3β-H), 4.78 (t, J=8.4 Hz) (17α-H). UV: $\lambda_{max}^{benzene}$ (nm) 372 (112), 360 (116), 348 (96), 336 (72). λ_{max}^{THF} (nm) 372 (93), 360 (96), 348 (81), 336 (64).

Photolysis of the 17-Nitrite 1 with Pyrex-filtered Light. A solution of the nitrite **1** (300 mg) in dry benzene (30 ml) was irradiated for 1.5 h under an argon atmosphere with a 100-W high pressure Hg arc at room temperature. After the removal of the solvent by means of rotatory evaporator at 30 °C, the residue was subjected to preparative TLC. Four fractions, A, B, C, and D, were obtained in order of decreasing mobilities. The most mobile fraction, A (26 mg, 10%), was 5α-androstan-3α-ol-17-one acetate (**6**). The second most mobile fraction, B (26 mg, 9%), was 5α-androstane-3α,17β-diol 3-acetate **7**. The fraction C was recrystallized from aq ethanol to afford a new compound (**8**) (60 mg, 20%); mp 118—120 °C. Found: C, 69.11; H, 9.19; N, 3.70%. Calcd for $C_{21}H_{33}O_4N$: C, 69.39; H, 9.15; N, 3.85%. IR: 1742 (OAc), 1628 (amide C=O), 3127 cm^{-1} (hydrogen bonded hydroxyl). NMR: τ 9.28 (19-H), 8.64 (18-H), 7.06 (OAc), 4.99 (bs. $W_{1/2}$=7.5 Hz) (3β-H) 7.44—7.62 (m, 2H, 16α- and 16β-H).

The fraction D was recrystallized from ether to afford 17α-aza-D-homo-5α-androstane-3α,17a-diol-17-one 3-acetate (**2**) (59 mg, 20%). Mp 230—234 °C. (Lit,[3] mp 229—233 °C). NMR: τ 9.21 (19-H), 8.74 (18-H), 7.95 (OAc), 4.99 (b.s. $W_{1/2}$=7.5 Hz) (3β-H), 7.46—7.62 (m, 2H, 16α- and 16β-H).

Photolysis of the 17-Nitrite 1 with Monochromatic Light (372±4 nm). a) Photolysis in Benzene: A solution of the nitrite (200 mg) in dry benzene (3 ml) in a quartz cell (10×10×45 mm) was flushed with argon and then placed in the chamber of a JASCO CRM-FA grating spectroirradiator. Irradiation was carried out with light of 372±4 nm. The progress of the reaction was monitored by means of TLC. After the completion of the photolysis (33.3 h), the solution was evaporated *in vacuo*. The TLC of the residue exhibited 4 spots (benzene/ether=1/5); the residue was subjected to preparative TLC (benzene/ether=1/1) as has been described above. The yields of the four products were as follows: ketone **6** (15 mg, 8%); 17β-ol **7** (22 mg, 12%); hydroxamic acid **8** (41 mg, 21%); isomeric hydroxamic acid **2** (40 mg, 20%). *b) Photolysis in THF*: A solution of the nitrite **1** (200 mg) in dry THF (3 ml) in a quartz cell was flushed with nitrogen and then photolyzed as in the photolysis in benzene. Eleven hours was required for the completion of the photolysis. The yields of the four products were as follows; ketone **6** (trace); 17β-ol **7** (96 mg, 52%); hydroxamic acid **8** (26 mg, 13%); isomeric hydroxamic acid (**2**) (23 mg, 12%). *c) Photolysis in Carbon Tetrachloride*: A solution of the nitrite (200 mg) in dry carbon tetrachloride (luminazol, dotite, Wako) (3 ml) in a quartz cell was flushed with argon and then photolyzed as has been described above. Forty hours were required for the completion of the photolysis. The yields of the four products were as follows: ketone **6** (37 mg, 21%); 17β-ol **7** (95 mg, 52%); hydroxamic acid **8** (16 mg, 8%); isomeric hydroxamic acid (**2**) (15 mg, 8%).

17a-Aza-D-homo-5α,13α-androstan-3α-ol-17-one 3-Acetate by Reduction of the Hydroxamic Acid 8. Into a solution of the hydroxamic acid **8** (14 mg) in glacial acetic acid (2.8 ml), we stirred Zn dust (70 mg). After solution has then been heated under reflux for 3 h, the reaction mixture was filtered and the filtrate poured into ice water. The solution was neutralized with saturated sodium hydrogencarbonate solution and extracted with methylene chloride. The dichloromethane solution was worked up in the usual way. The residue

(12 mg) was purified by preparative TLC to afford the lactam, **8**, R=H, (4 mg) (mp 192.5—193.5 °C), identical with an authentic specimen.[12]

Photolysis of dl-*Bornyl Nitrite* ***3*** *with Monochromatic Light 385 ±8 nm.* A solution of the nitrite (1.5 g) in dry benzene (2 ml) in a quartz cell was flushed with argon and then photolyzed as in the photolysis of steroidal nitrites. Eighty-five hours were required for the completion of the photolysis. The yellowish green solution was evaporated *in vacuo*, and the residue was subjected to preparative TLC (benzene/ether; 4/1). The polar fraction containing the hydroxamic acid was then again subjected to preparative TLC (ether). The least mobile fraction (46 mg, 3%) was the hydroxamic acid **4**. The analytical results of a specimen obtained by chromatographic purification were in agreement with the $C_{10}H_{17}NO_2$ formula. (Found: C, 65.80, H, 9.21, N, 7.48%) MS, *m/e* 183 (M^+); NMR: τ 8.65 (1-methyl), 8.95, 8.99 (8.8-gem dimethyl) IR: 1637 (amide C=O), 3131 and 3411 cm^{-1} (hydrogen-bonded hydroxyl).

Photolysis of d-*Bornyl Nitrite* ***3*** *in Benzene with Pyrex-filtered Light.* Bornyl nitrite **3** (2 g) in dry benzene (200 ml) was photolyzed for 12 h. A brownish solution was evaporated, and the residue was recrystallized from hexane to yield the crude hydroxamic acid. The compound was again recrystallized from benzene–hexane to yield 37 mg (2%) of the hydroxamic acid **4**.

Irradiation of the Nitrite ***1*** *in an EPA Matrix at 77 K.* The matrix was prepared by dissolving the nitrite **1** (30 mg) in EPA (diethyl ether–isopentane–ethanol 1 : 1 : 2 in volume) 10 ml (8.3×10^{-3} M) and by then freezing the solution with liquid nitrogen. The matrix was degassed by freeze-thaw cycles. This matrix was irradiated through a Pyrex-filter with a 250-W super high-pressure Hg arc (USHIO UI 501C). The change in the spectrum was monitored at appropriate time intervals by means of a Carry ultraviolet spectrometer. After a 30-min irradiation, a very weak broad absorption at 695 nm due to the C-nitroso compound appeared, although the banded absorption due to the O–NO (385, 372, 358, 348, and 336 nm) nearly vanished. After the matrix had been brought to room temperature, a TLC examination of the solution revealed that the major product was the 11β-ol **7**, though traces of the hydroxamic acids **2** and **8** were also present.

We thank Professor Katsumi Kimura of the Research Institute of Applied Electricity of Hokkaido University for his help in the matrix experiment. We also thank Tomoko Okayama of this laboratory for the ^1H NMR measurements.

References

1) Photoinduced Transformations, Part 37, Part 36: H. Suginome and F. Yagihashi, *J. Chem. Soc., Perkin Trans. 1*, in press.

2) a) H. Suginome, N. Sato, and T. Masamune, *Tetrahedron*, **27**, 4863 (1971); b) H. Suginome, T. Mizuguchi, and T. Masamune, *J. Chem. Soc., Perkin Trans. 1*, **1976**, 2365; c) H. Suginome T. Mizuguchi, S. Honda, and T. Masamune, *ibid.*, **1977**, 927; d) H. Suginome, T. Tsuneno, N. Sato, N. Maeda, T. Masamune, H. Shimanouchi, Y. Tsuchida, and Y. Sasada, *ibid.*, **1976**, 1297; e) H. Suginome, N. Maeda, and T. Masamune, *ibid.*, **1976**, 1312.

3) C. H. Robinson, O. Gnoj, A. Mitchell, E. P. Oliveto, and D. H. R. Barton, *Tetrahedron*, **21**, 743 (1965).

4) P. Kabasakalian and E. R. Townley, *J. Org. Chem.*, **27**, 3562 (1962).

5) M. Nakazaki and K. Naemura, *Bull. Chem. Soc. Jpn.*, **37**, 532 (1964).

6) J. G. Calvert and J. N. Pitts, Jr., "Photochemistry," John Wiley, New York (1967), p. 450.

7) M. Tanaka, J. Tanaka, and S. Nagakura, *Bull. Chem. Soc. Jpn.*, **39**, 776 (1966).

8) H. H. Jaffé and M. Orchin, "Theory and Applications of Ultraviolet Spectroscopy," John Wiley, New York (1966), p. 178.

9) L. E. Orgel, *J. Chem. Soc.*, **1953**, 1276; J. Mason, *ibid.*, **1957**, 3904.

10) The loss of oxygen to form the ion (c) through the *N*-oxide tautomer of **2** or **8** is another possibility.

11) H. Budzikiewicz, F. Compernolle, K. V. Cauwenberghe K. Schulze, H. Wolf, and G. Quinkert, *Tetrahedron*, **24**, 6797 (1968).

12) H. Suginome and T. Uchida, *Bull. Chem. Soc. Jpn.*, **47**, 687 (1974).

13) Because of the solubility problem, the photolysis of the nitrite **1** in protic solvents such as alcohol has not been studied.

14) We could not achieve the yield described in the literature in spite of repeated experiments under various concentrations. The reason for the low yield is obscure.

Competitive Cyclization in the Reaction of Hexafluoropropene with 2-Aminobenzamide

Takeshi NAKAI, Nabil M. HASSAN,* and Nobuo ISHIKAWA

Department of Chemical Engineering, Tokyo Institute of Technology, Ookayama, Meguro-ku, Tokyo 152

(Received April 25, 1977)

The reaction of hexafluoropropene (HFP) with 2-aminobenzamide afforded 2-(1,2,2,2-tetrafluoroethyl)-4(3*H*)-quinazolinone (**4**) and *N*-(2-cyanophenyl)-2,3,3,3-tetrafluoropropionamide (**5**) in *ca.*1 : 1 ratio, which is essentially independent of the reaction temperatures ranging from room temperature to 100 °C. The formation of the two products is explained in terms of the competitive cyclization of the imidoyl fluoride intermediate, the N-6 and O-6 ring closures ultimately yielding **4** and **5**, respectively. In contrast to the HFP reaction, 2-(trifluoromethyl)pentafluoropropene (OFIB) and 2-aminobenzamide gave only the O-6 cyclized product, *N*-(2-cyanophenyl)-2-trifluoromethyl-3,3,3-trifluoropropionamide. The difference in reactivity between HFP and OFIB is discussed.

It is well-known that amines undergo nucleophilic addition to perfluoroolefins affording acetamidine derivatives *via* reactive imidoyl fluoride intermediates (**1**)[1,2] (Eq. 1).

$$RNH_2 + CF_2{=}CFR_f \longrightarrow [R{-}N{=}CF{-}CHFR_f] \xrightarrow{RNH_2} \underset{\mathbf{1}}{R{-}N{=}C{-}CHFR_f} \quad (1)$$
$$\qquad\qquad\qquad\qquad\qquad\qquad\qquad\qquad\qquad\qquad\qquad\quad \underset{}{NHR}$$

R_f=F, CF_3, *etc.*

The reaction of hexafluoropropene (HFP) with 2-substituted anilines afforded the heterocyclic compounds (**2**) in good yields[3] (Eq. 2). The formation of the heterocyclic products has been explained by the X-5[4] ring closure of the imidoyl fluoride (**3**).

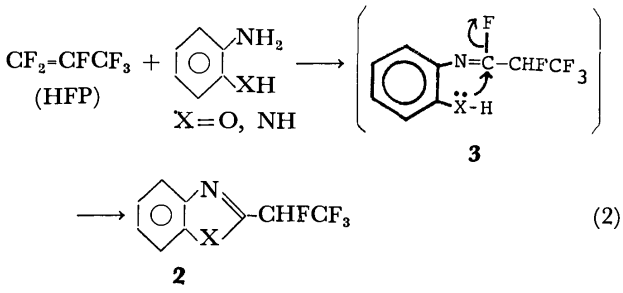

(2)

The reaction of perfluoroolefins with 2-aminobenzamide is of particular interest since the carbamoyl group is expected to act as "an ambident internal nucleophile"[5] affording the N-6 and/or O-6 cyclized products. Thus we have studied the reactions of HFP and 2-(trifluoromethyl)pentafluoropropene (OFIB, octafluoroisobutylene) with 2-aminobenzamide. This paper deals with the reaction mechanisms involving the competitive cyclization of the imidoyl fluoride intermediates.

Results and Discussion

Product Determinations. The reactions of HFP with 2-aminobenzamide were carried out in *N*,*N*-dimethylformamide (DMF) under various conditions in pressure vessels. As an example, a mixture of HFP and the benzamide in DMF was stirred overnight at room temperature and then at 60 °C for 6 h. Removal of DMF *in vacuo* gave a solid residue. Its ^{19}F NMR spectrum indicates that the residue consists of two compounds in nearly 1 : 1 ratio. The two compounds were then successfully separated by utilizing the great difference in solubility in hot water. On the basis of the spectral data, the water-soluble and insoluble parts were assigned to 2-(1,2,2,2-tetrafluoroethyl)-4(3*H*)-quinazolinone (**4**) and *N*-(2-cyanophenyl)-2,3,3,3-tetrafluoropropionamide (**5**), respectively. The formation of **4** was easily anticipated but that of **5** was somewhat surprising, and it is suggested that a dehydration process permitting the conversion of the carbamoyl to the cyano group was involved in the reaction.

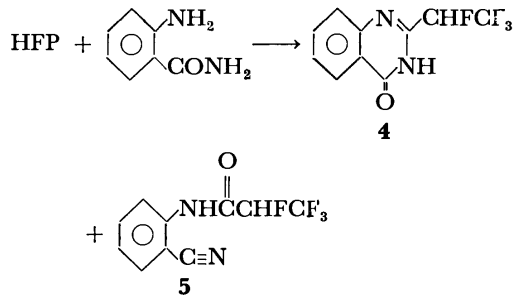

Table 1 gives the results of the reactions carried out under various conditions. The product ratio is seen to be independent of the reaction conditions.

TABLE 1. REACTIONS OF HFP WITH 2-AMINOBENZAMIDE

Run	Temp (°C)	Time (h)	Total yield (%)	Product ratio[a] **4** : **5**
1	50	10	41	1.0 : 1.06
2	60	6	63	1.0 : 1.02
3	70	5	33	1.0 : 1.19
4[b]	70	7	7.5	1.0 : 1.13
5	80	8	84	1.0 : 1.14
6	100	6	77	1.0 : 1.05
7	R. T.	5 day	28	1.0 : 1.37

a) Determined by ^{19}F NMR analysis of the reaction mixtures. The values are essentially the same as those obtained from weights of each compound separated from the reaction mixtures. b) The reaction was carried out in an open system in which which HFP was bubbled to a solution of the benzamide in DMF.

The structure proofs for **4** and **5** are as follows. Both mass spectral and elemental analytical data for **4** and **5** gave the same formula $C_{10}H_6F_4N_2O$.

For the quinazolinone **4**, the IR spectrum shows bands at 2900—3005 (NH), 1680 (C=O), and 1615 cm^{-1} (C=N). Both ^{19}F and ^{1}H NMR spectra un-

* UNESCO Post-graduate Fellow on leave from the Department of Chemistry, Cairo University, Cairo, A. R. Egypt.

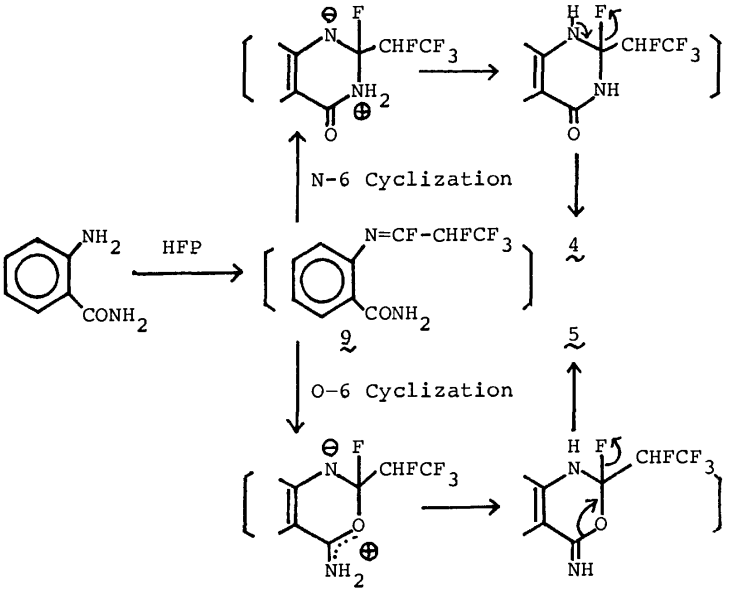

Scheme 1.

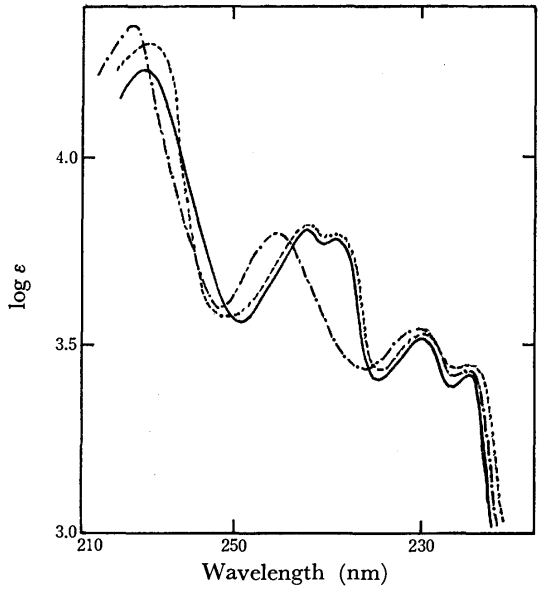

Fig. 1. UV spectra of the quinazolinone **4** and reference compounds in 95% ethanol.
—— **4**; —·—·— **6**; —— **7**.

equivocally indicate the presence of the grouping of $-CHF-CF_3$ (see Experimental). Comparison of its UV spectrum with reported spectra[6] for 4(3*H*)-quinazolinone (**6**) and 3-methyl-4(3*H*)-quinazolinone (**7**) (Fig. 1) supports the quinazolinone structure for **4**. It has been established that the parent compound **6** exists mainly in the hydroxy tautomeric form (**6a**).[6,7] Although the three tautomeric forms, **4a**, **4b**, and **4c**, are possible for the product **4**, the spectrum of **4** is more similar to that of **7** than that of **6**, suggesting that **4** exists mainly in the tautomeric form **4a**.

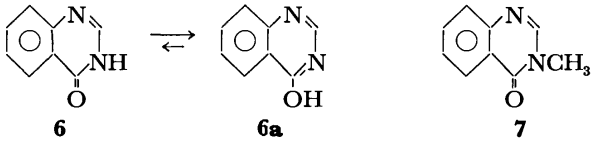

6 **6a** **7**

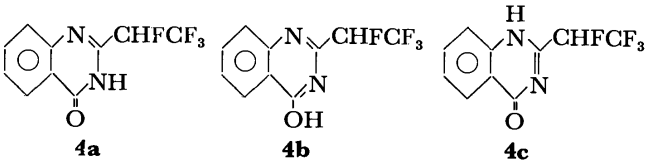

4a **4b** **4c**

Quinazolinone **4** fluoresces a light green color and is soluble in concentrated aqueous sodium carbonate solutions to give a salt stable even in the boiling solutions. On acidification **4** was recovered unchanged. Methylation of **4** with diazomethane in a mixture of ethanol and ether afforded a single product assigned to the 3-methylquinazolinone **8** based on the following spectral data. The IR spectrum of **8** showed bands at 1600 (C=O) and 1605 cm^{-1} (C=N), no absorption due to the NH being observed. The ^1H NMR spectrum showed not only a slightly split singlet at 3.4 ppm for the $N-CH_3$ protons but also the presence of the grouping of $-CHF-CF_3$. The finding supports the tautomeric structure **4a** for **4**. Although **6** (mainly **6a**) reacts with hydrazine hydrate giving 3-amino-4(3*H*)-quinazolinone *via* a ring-opening,[8] no similar reaction of **4** takes place under the same conditions.

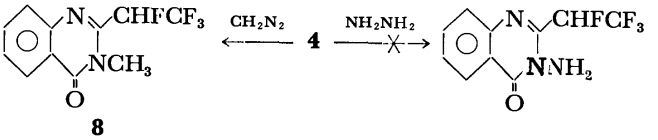

8

On the other hand, the structure of another product **5** was elucidated as follows. The IR spectrum of **5** showed bands at 3226 (NH), 2230 (C≡N), and 1684 cm^{-1} (C=O). Both the ^{19}F and ^1H NMR spectra indicated the presence of the grouping of $-CHF-CF_3$. The structure was confirmed by an independent synthesis of an authentic sample (Eq. 3). The authentic sample thus obtained was identical with **5**.

(3)

Reaction Mechanisms The formation of **4** and **5** can be explained in terms of the competitive N-6 *vs.* O-6 cyclization of the imidoyl fluoride intermediate (**9**) formed *via* addition of the amino group to HFP followed by elimination of HF (Scheme 1).

Imidoyl fluoride **9** thus formed undergoes the N-6 cyclization *via* the attack of the carbamoyl nitrogen at the imidoyl carbon atom followed by proton transfer and elimination of HF to give the quinazolinone **4**. Alternatively **8** undergoes the O-6 cyclization by the attack of the carbamoyl oxygen followed by elimination of HF accompanied by the cleavage of the carbon-oxygen bond, finally yielding the cyanoanilide **5**. The O-6 ring closure is of mechanistic and synthetic interest since it can be considered as an intramolecular dehydration reacion accomplishing the conversion of the amido into cyano groups.

Reaction of OFIB with 2-Aminobenzamide. The reaction of OFIB with 2-aminobenzamide was studied. The benzamide was allowed to react with OFIB in DMF at 60 °C for 4 h to afford only *N*-(2-cyanophenyl)-2-trifluoromethyl-3,3,3-trifluoropropioamide (**10**) in 82 % yield; no quinazolinone **11** was found in the resulting mixture. The IR spectrum of **10** showed a strong band at 2240 cm^{-1} due to the cyano group, and the ^{19}F NMR spectrum exhibited a doublet at −15 ppm for $CH(CF_3)_2$

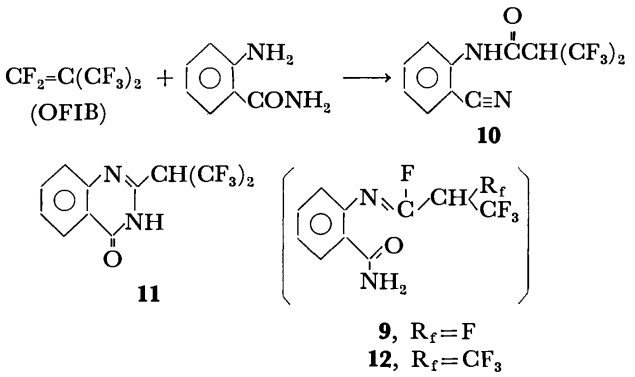

It should be noted that the OFIB reaction proceeds more rapidly than the HFP reaction. Such a difference between HFP and OFIB can be interpreted by assuming the difference in the electrophilicity of the imidoyl carbon atoms in **9** and **12**; the carbon atom in **12** is more electron-deficient and might combine only with the more highly electron-donating carbamoyl oxygen rather than the carbamoyl nitrogen leading to the exclusive O-6 cyclization process.

Experimental

All melting points are uncorrected. IR and UV spectra were recorded on Hitachi 215 and EPS-3T spectrometers, respectively. ^{19}F NMR spectra were taken with a Hitachi R-24F spectrometer using trifluoroacetic acid (TFA) as an external standard, the chemical shifts being given in δ ppm upfield from TFA. ^1H NMR spectra were measured with a Hitachi R-24 and a Varian EM 360 spectrometer using tetramethylsilane (TMS) as an internal standard, the chemical shifts being given in δ ppm downfield from TMS. Mass spectra (MS) were recorded on a JEOL JMS-D100 spectrometer.

Reactions of HFP with 2-Aminobenzamide. A typical procedure is as follows. HFP (3 ml, 25 mmol) was transferred from the bomb to a trap tube cooled in a dry ice–acetone bath, and then put into a cooled pressure vessel equipped with a magnetic stirrer in which 2-aminobenzamide (2.0 g, 12 mmol) and 30 ml of DMF were placed. The vessel was then closed and brought to room temperature (internal pressure, 3.1 kg/cm^2). The mixture was stirred overnight at room temperature and then heated at 60 °C for 6 h. The vessel was carefully opened after being cooled and the resulting mixture was transferred to a distillation apparatus. The solvent was completely distilled under reduced pressure and the residual solid was cooled and collected to give a solid mixture (2.26 g, 63%). The solid mixture was separated by recrystallization from hot water (10 ml). The water-insoluble solid was filtered and recrystallized from methanol to give colorless plates of **4**; mp 210—212 °C; IR (KBr), 2900—3005 (NH), 1680 (C=O), and 1605 cm^{-1} (C=N); ^{19}F NMR (DMSO), δ −2.0 (d of d, $J_{vic\text{-}HF}$=10.8 and $J_{vic\text{-}FF}$=10.8 Hz, CHF-CF_3) and +126 (d of q, $J_{vic\text{-}FF}$=10.8 and $J_{gem\text{-}HF}$=36.2 Hz, CHF-CF_3); ^1H NMR ($CDCl_3$), δ 6.4 (d of q, CHF-CF_3) and 7.5—8.3 (m, 4H, aromatic protons); UV (ethanol) (Fig. 1), λ_{max} (log ε), 313.5 (3.47), 301 (3.57), 277.5 (3.80), 269 (3.81), and 227 nm (4.23); MS, *m/e* 246 (M^+, 100%).

Found: C, 48.41; H, 2.37; N, 11.37%. Calcd for $C_{10}H_6F_4N_2O$: C, 48.79; H, 2.46; N, 11.38%.

The filtrate was cooled in an ice box to give colorless needles of **5**; mp and mixed mp 95—96 °C; IR (KBr), 3226 (NH), 2230 (C≡N), and 1680 cm^{-1} (C=O); ^{19}F NMR (DMSO), δ −4.0 (d of d, $J_{vic\text{-}HF}$=9.9 and $J_{vic\text{-}FF}$=9.9 Hz, CHF-CF_3) and +125 (d of q, $J_{gem\text{-}HF}$=36.2 Hz, CHF-CF_3); ^1H NMR ($CDCl_3$), δ 3.3 (br s, 1H, NH), 6.08 (d of q, 1H, CHF-CF_3) and 7.2—8.0 (m, 4H, aromatic protons); MS, *m/e* 246 (M^+, 100%).

Found: C, 49.02; H, 2.66; N, 11.47%. Calcd for $C_{10}H_6F_4N_2O$: C, 48.79; H, 2.46; N, 11.38%.

Yields and product ratios are given in Table 1.

Preparation of an Authentic Sample of ***5***. 2,3,3,3-Tetrafluoropropionyl chloride (bp 48—49 °C) was prepared from phosphorus pentachloride and the tetrafluoropropionic acid[9] (7.3 g). The acid chloride (10 mmol) was added dropwise to a solution of 2-cyanoaniline (10 mmol) in 10 ml of benzene and the mixture was then refluxed for 15 min and allowed to stand overnight at room temperature. Crystals formed were filtered and recrystallized from hot water giving colorless needles; mp 95—96 °C.

Reaction of ***4*** *with Diazomethane.* Quinazolinone **4** (0.3 g) was dissolved in a mixture of ethanol (20 ml) and ether (20 ml) and diazomethane generated from Diazad (7 g) and potassium hydroxide (1.3 g) was bubbled into the mixture with stirring. The resulting mixture was stirred overnight at room temperature and the solvent was evaporated to give colorless plates (0.55 g, 84%) of the crude **8** (recrystallized from hexane); mp 132—133 °C; IR (KBr), 1660 cm^{-1} (C=O); ^1H NMR ($CDCl_3$), δ 3.4 (slightly split s, 3H, NCH_3), 5.9 (d of q, 1H, CHFCF$_3$) and 7.3—8.4 (m, 4H, aromatic protons).

Found: C, 50.70; H, 3.10; N, 10.49%. Calcd for $C_{11}H_8F_4N_2O$: C, 50.78; H, 3.09; N, 10.76%.

Reaction of OFIB with 2-Aminobenzamide. The reaction was carried out in the same way for the HFP reaction. A mixture of OFIB (2.5 ml) and 2-aminobenzamide (1.0 g) in DMF (7.5 ml) was stirred at room temperature for 2 h and then heated at 60 °C for 4 h with stirring. The resulting mixture was cooled and the vessel was opened carefully. The solvent was distilled *in vacuo* to give a solid residue (1.78 g, 82%). Recrystallization from benzene afforded colorless

needles; mp 185—186 °C; IR(KBr), 3270 (NH), 2240 (C≡N), and 1670 cm^{-1} (C=O); ^{19}F NMR (DMSO), δ −15 (d, $CH(CF_3)_2$).

Found: C, 44.89; H, 2.18; N, 9.50%. Calcd for $C_{11}H_6F_6N_2O$: C, 44.61; H, 2.04; N, 9.46%.

References

1) Review: R. D. Chambers and R. H. Mobbs, "Advances in Fluorine Chemistry," Vol. 4, ed by M. Stacey, *et al.*, Butterworth Sci. Publ., London (1965), p. 62.

2) D. C. England, L. R. Melby, M. A. Dietsich, and R. V. Lindsey, Jr., *J. Am. Chem. Soc.*, **82**, 5116 (1960); I. L. Knunyants, L. S. German, and B. L. Dyatkin, *Izv. Akad. Nauk SSSR, Ser. Khim.*, **1956**, 1353; N. Ishikawa and T. Muramatsu, *Bull. Chem. Soc. Jpn.*, **44**, 1699 (1971).

3) N. Ishikawa and T. Muramatsu, *Nippon Kagaku Kaishi*, **1973**, 563.

4) For the terminology of X-n ring closure, see F. L. Scott, R. E. Click, and S. Winstein, *Experientia*, **13**, 183 (1957).

5) *Cf.* F. L. Scott and D. F. Fenton, *Tetrahedron Lett.*, **1964**, 1681.

6) J. M. Hearn, R. A. Morton, and J. C. E. Simpson, *J. Chem. Soc.*, **1951**, 3318.

7) W. L. F. Armarego, "Advances in Heterocyclic Chemistry," Vol, 1. ed by A. R. Katrizky, Academic Press, New York, N. Y. (1963), p. 266.

8) N. L. Leonard, W. V. Rigle, and L. C. Bannister, *J. Org. Chem.*, **13**, 617, 903 (1948).

9) M. D. Bargamova and Yu. A. Cheburkov, *Izv. Akad. Nauk SSSR, Ser. Khim.*, **1966**, 377.

Nuclear Magnetic Resonance Study of Exchanging Systems. IX.[1] The Slow Rotation of the Methyl Group in Sterically Overcrowded Compounds

Hiroshi NAKANISHI and Osamu YAMAMOTO

National Chemical Laboratory for Industry, Honmachi, Shibuya-ku, Tokyo 151

(Received April 27, 1977)

In order to obtain information about the slow rotation of methyl groups, the ^{1}H NMR spectra of 9-*t*-butylethenoanthracene and 9-*t*-butyltriptycene derivatives were measured at very low temperatures. It was found that the signals of the two methyls of the *t*-butyl group in these compounds show a considerable line broadening at low temperatures, and it was made clear that the rotation of the methyl groups in these compounds is strongly restricted.

A rotation about the sp_3–sp_3 carbon-carbon single bond has for a long time been considered to be free, but recently it was reported[2] that, in some sterically overcrowded molecules, the rotation about the sp_3–sp_3 carbon-carbon single bond in bulky groups, such as *t*-butyl and isopropyl groups, is strongly restricted. On the other hand, the rotation of the methyl group, the smallest alkyl group, is especially rapid, and it is well known that the rotation of the methyl group in a quite overcrowded compound, for example, hexamethylbenzene, is not frozen on the NMR time scale at a temperature as low as −150 °C, even in the solid state.[3]

Most recently, however, the first example of a strongly restricted rotation of a methyl group on the NMR time scale was found in 1-*t*-butyl-1,4-dihydro-1,4-epoxynaphthalene derivatives (**1**).[4,5] Then, in 9-methyltriptycene derivatives (**2**), the methyl rotations were also found to be sufficiently slow and the activation parameters of the rotation were determined from the NMR complete line-shape analyses.[6,7] The rotation of a methyl group in the Diels-Alder adduct (**3**) of 9-methylanthracene with *p*-benzoquinone was also analysed.[8]

In this paper, we will present new examples of the slow rotation of methyl groups in two sterically overcrowded compounds.

Experimental

Materials. Dimethyl 9-*t*-butyl-9,10-ethenoanthracene-11,12-dicarboxylate (**4**) was prepared by a Diels-Alder reaction between 9-*t*-butylanthracene and dimethyl acetylenedicarboxylate, heating at 180—200 °C for 10 h in a sealed Pyrex tube. The purification was made by Al_2O_3 column chromatography and three recrystalizations from ethanol. mp 146—148 °C (lit,[9] mp 182—183 °C).

1,2,3,4-Tetrachloro-9-*t*-butyltriptycene (**5**) was prepared by the benzyne reaction of 9-*t*-butylanthracene and 1,2,3,4-tetrachloroanthranilic acid by a method similar to that described in the literature.[7,10] mp 277—278 °C. The purification of **5** was done similarly as has been described above.

The purity of these compounds was checked by studying the ^{1}H NMR spectra.

Measurements. The ^{1}H NMR spectra of **4** and **5** were recorded on Varian HA-100 D (100.0 MHz) and XL-100-15 A FT (100.1 MHz) spectrometers. The spectra of **4** at 155 and 199 °C were measured by the former spectrometer, using a 5-mmϕ sample tube. The solvent was hexachloro-1,3-butadiene. The measurements at low temperatures were made by means of the latter spectrometer. As the solubility of **4** and **5** is very poor at low temperatures, a 12-mmϕ sample tube was used and a one hundred-fold accumulation was made by means of a pulsed FT method

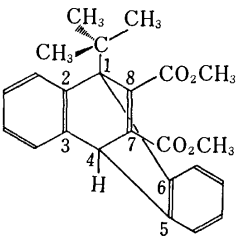

4

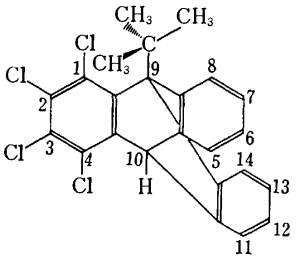

5

at very low temperatures. The sample concentration was 0.013 mol/l for **4** and 0.011 mol/l for **5** in the (CS_2+$CDCl_3$+CD_2Cl_2+CD_3COCD_3+$CD_3C_6D_5$, 5 : 1 : 2 : 1 : 2) solvent system. The temperature was read by means of a calibrated copper-constantan thermocouple.

Results and Discussion

The ^{1}H NMR signal of the *t*-butyl group of **4** at room temperature consists of two sharp peaks (δ: 1.733 and 1.874 from TMS), whose intensities are in a 2 : 1 ratio, as is shown in Fig. 1. The higher field peak is assigned to methyl A protons, and the lower to methyl B protons, judging from the line intensities (see the Newman projection **6**). This spectrum shows that the rotation of the *t*-butyl group is frozen at this temperature on the NMR time scale. This line shape remains unchanged at temperatures as high as 155 and 199 °C, and no line broadening occurs.* This means that the rotation of the *t*-butyl group of **4** is sufficiently slow at these temperatures.**

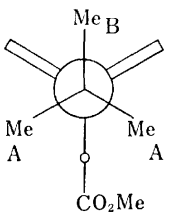

6

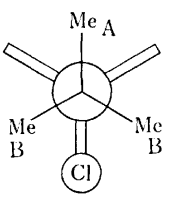

7

In order to obtain information about the rotation of a methyl group, the spectra of **4** were measured at low temperatures, since the methyl rotation is expected to be strongly restricted by the bulky phenyl and meth-

* Ōki and Suda reported the same result for the spectrum of **4** at 132 °C.[9]

** The activation free energy, ΔG^*, of the rotation of the *t*-butyl group in **4** is roughly estimated to be much larger than 30 kcal/mol.

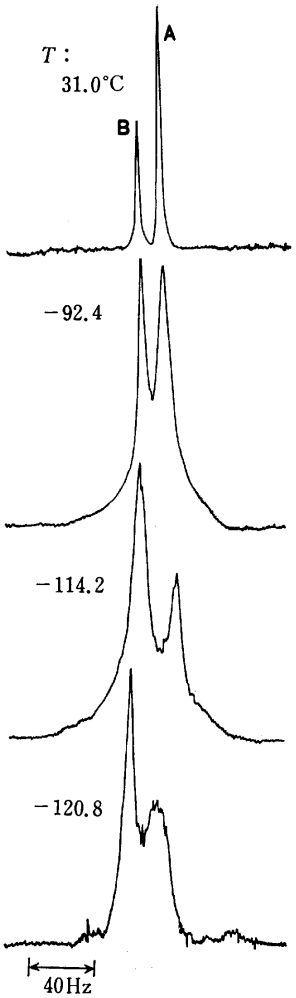

Fig. 1. ^{1}H NMR spectra of *t*-butyl group in **4** at low temperatures.

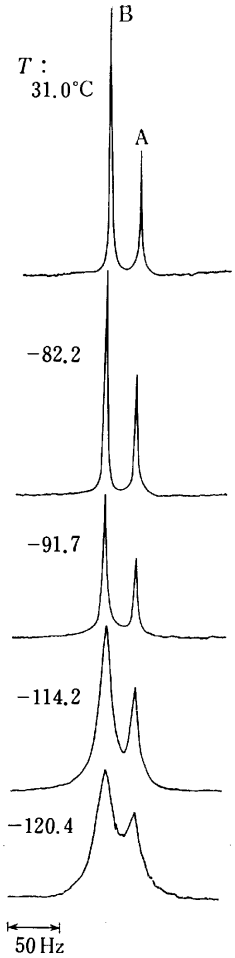

Fig. 2. Temperature-dependent ^{1}H NMR spectra of *t*-butyl group in **5**.

oxycarbonyl groups, and since the bicyclo[2.2.2]octatriene skeleton is very rigid. The spectra obtained are given in Fig. 1. Figure 1 clearly shows that the peak height of the higher field signal of methyl A protons is conspicuously reduced as the temperature is decreased. The peak hieght of the higher field signal of methyl A, which is twice that of the methyl B at room temperature, is almost the same as that of the methyl B at −92.4 °C and becomes a half of it at −114.2 °C. At −120.4 °C, the line width of the A peak is 18 Hz and that of the B peak is 8 Hz. The exceeding peak-height reduction in the signal of the methyl A protons of **4** with the decrease in the temperature clearly shows that the rotation of the methyl A group is strongly restricted at these low temperatures, and that the line-broadening occurs because of the chemical exchange among three *non-equivalent* protons of the methyl group. Figure 1 also shows that the line-broadening in the signal of the methyl B protons occurs to a small extent at such low temperatures. Nevertheless, this fact does not directly indicate a slow rotation of the methyl B group, because the line-broadening in the methoxy protons also occurs and the peak height ratio between the signals of the methyl B and methoxy methyl protons are almost the same at all temperatures. The small line-broadening in the methyl B protons may be due to the high viscosity of the sample and the poor resolution of the NMR measurements at these very low temperatures. The anomalous slow rotation of the methyl A group in **4** indicates that the bis(methoxycarbonyl)etheno bridge is more bulky than the benzo bridge, which is the same conclusion as in the ^{13}C NMR study of the isopropyl analogue.[1]

As an extension of the study of the slow rotation of the methyl groups in **4**, the 9-*t*-butyltriptycene derivatives (**5**) was also investigated, because the steric hindrance in **5** is expected to be large in the triptycene (tribenzo[b,e,h]bicyclo[2.2.2]octatriene) skeleton.[6,7,11] The spectra at low temperatures are shown in Fig. 2. The peak height ratio of the lower-field peak, B, to the higher-field peak, A (the chemical shift δ: 2.296 for B and 2.005 for A from TMS), is 2.0 at 31.0 °C, 1.8 at −91.7 °C, and 1.4 at −120.4 °C. The peak height ratios of the methyl A peak to the bridgehead methine peak (δ: 5.986 from TMS) are almost the same throughout the temperature range from 31.0 °C to −114.2 °C. These facts mean that the line-broadening due to the chemical exchange occurs at the lower-field methyl signal, which is assigned to the methyl B group surrounded by a phenyl ring and a tetrachloro-substituted phenyl ring, as is shown in the Newman projection sheme **7**, on the basis of the line intensities.

This result indicates that the rotation of the methyl B group in **5** is also strongly restricted at the low temperatures, although the degree of the restriction seems to be smaller than in the case of **4**, judging from the apparent line shapes.***

Thus, it was made clear that the rotations of the two methyl groups in the *t*-butyl group in **4** and **5** are strongly restricted at low temperatures. It is worth pointing out, from the results in this study, that, in **4** and **5**, the rotation of the methyl groups β-positioned to the bicyclo[2.2.2]octatriene skeleton is severely restricted by the bulky *peri*-substituents, while in the previously reported compounds **2** (*e.g.*, 1,2,3,4-tetrachloro-9-methyltriptycene) and **3**, the rotation of the α-positioned methyl group is restricted also by the *peri*-substituents.[6-8] In the case of **1** (*e.g.*, 1-*t*-butyl-5,6,7,8-tetrachloro-1,4-dihydro-1,4-epoxynaphthalene), the rotation of the β-positioned methyl group is restricted by the *oxide bridge* instead of the *peri*-substituent in the 1,4-dihydro-1,4-epoxynaphthalene skeleton.[5] This interesting difference may be caused by the variety in the geometries of their different skeletons and the bonded alkyl groups.

*** Strictly speaking, the comparison between the activation parameters of the rotations of the methyl groups in **4** and **5** is impossible at the present time, because we do not know the exact chemical shifts of the three protons of the methyl groups in question, and so no line-shape analyses can be made.

The authors wish to express their hearty thanks to Prof. Michinori Ōki of the University of Tokyo for his helpful discussions.

References

1) The preceding paper: H. Nakanishi, Y. Kitagawa, O. Yamamoto, and M. Ōki, *Org. Magn. Reson.*, **9**, 118 (1977).
2) M. Oki, *Angew. Chem.*, **88**, 67 (1976).
3) P. S. Allen and A. Cowking, *J. Chem. Phys.*, **47**, 4286 (1967).
4) H. Nakanishi, O. Yamamoto, M. Nakamura, and M. Ōki, *Tetrahedron Lett.*, **1973**, 727.
5) M. Nakamura, M. Ōki, and H. Nakanishi, *Tetrahedron*, **30**, 543 (1974).
6) M. Nakamura, M. Ōki, and H. Nakanishi, *J. Am. Chem. Soc.*, **95**, 7169 (1973).
7) M. Nakamura, M. Ōki, H. Nakanishi, and O. Yamamoto, *Bull. Chem. Soc. Jpn.*, **47**, 2415 (1974).
8) J. E. Anderson and D. I. Rawson, *J. Chem. Soc., Chem. Commun.*, **1973**, 830.
9) M. Ōki and M. Suda, *Bull. Chem. Soc. Jpn.*, **44**, 1876 (1971).
10) H. Heaney and J. M. Jablonski, *J. Chem. Soc. C*, **1968**, 1895.
11) F. Suzuki, M. Ōki, and H. Nakanishi, *Bull. Chem. Soc. Jpn.*, **47**, 3114 (1974).

The Ethylation of Nucleic Acid-Bases with Triethyl Phosphate

Toshizumi TANABE, Kiyoshi YAMAUCHI, and Masayoshi KINOSHITA
Department of Applied Chemistry, Osaka City University, Sumiyoshi-ku, Osaka 558
(Received April 30, 1977)

Uracil, thymine, cytosine, adenine, and guanine were alkylated by triethyl phosphate in a homogeneous aqueous phase at 60—80 °C, giving the corresponding ethyl derivatives in considerable yields. The reactivity order on the ethylating site in each base was found to be as follows; uracil, thymine, and cytosine: N-1>N-3; adenine: N-9≈N-3>N-7, N-1; guanine: N-1>N-7>N-3, N-9.

It has been known that the structural deformation of nucleic acids caused by such alkylating agents as mustards may be relevant to their mutagenic and carcinogenic effects on many living systems. Therefore, the action of various alkylating agents, such as dialkyl sulfates,[1-5] alkyl alkanesulfonates,[3-6] alkyl halides,[5-8] diazoalkanes,[9] and mustards,[10] on nucleic acids and their components has been studied actively.

In previous papers, we reported that trialkyl phosphates were very useful for the *N*-alkylation of nitrogen heterocycles, such as imidazoles,[11,12] pyrimidines,[13] and purines.[14,15] Especially, trimethyl and triethyl phosphates are suited for the alkylation of many natural products because of their moderate reactivity and high solubility in water. In practice, the methylations of nucleic acid-bases with trimethyl phosphate have been carried out successfully in a homogeneous aqueous phase.[16]

While many methylation studies of nucleic acids and their components have been reported, little is known about ethylation. The ethylating reaction has though been reported to show mutagenic effects in some biological systems, and Singer *et al.* indicated that ethyl ethanesulfonate and ethyl methanesulfonate were good mutagenes.[17] Furthermore, Kononova and Gumanov reported that triethyl phosphate (TEP) inactivated phage T4V more readily than did trimethyl phosphate (TMP), although TMP was more mutagenic.[18] Industrially, TEP has been employed as a gasoline additive and a flame retardant for polymers and paints; in addition, TEP has even been proposed as a food additive.

In this regard, we have investigated the ethylation of nucleic acid-bases, such as uracil (**1**), thymine (**2**), cytosine (**3**), adenine (**11**), and guanine (**12**) with TEP in an aqueous phase.

Below we will characterize the products from these reactions. The reaction sites on ethylation will also be compared with those on methylation.

Results and Discussion

The reactions were carried out at 60—80 °C by stirring a mixture of a base and a 2—5 molar excess of TEP in water. (The pH values were 10—10.5 for **1**, **2**, **3**, and **11** and pH 12 for **12**. A relatively high pH value was used for the reaction of **12** in order to obtain a homogeneous solution.) The yields of the products were determined by means of the UV spectra. The products were isolated through extraction and column chromatography and were identified conveniently by means of their UV and NMR spectra. The results are summarized in Tables 1 and 2.

Uracil (1), Thymine (2), and Cytosine (3). Compounds **1** and **2** are generally alkylated with alkyl halide to give 1-alkyl and 1,3-dialkyl derivatives.[19,20] Diazomethane also alkylated **1** to give the corresponding *N*-methyl and *O*-methyl derivatives.[21] We reported previously that trimethyl phosphate (TMP) alkylated these pyrimidines at the N-1 and N-3 positions in almost equal amounts to give 1-methyl, 3-methyl, and 1,3-dimethyl derivatives.[16]

On the other hand, the present reactions of **1** and **2** with TEP gave results different from those of methylations, showing ethylation to take place mainly at the N-1 position. Thus, the reactions of **1** and **2** with TEP afforded the corresponding 1-ethyl derivatives (**4** and **7**) chiefly, along with 3-ethyl derivatives (**5** and **8**) in small yields. When the reaction temperature was raised to 80 °C, 1,3-diethyl derivatives (**6** and **9**) were also produced.

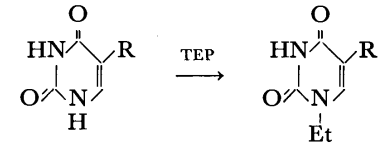

1: R=H
2: R=Me

4: R=H
7: R=Me

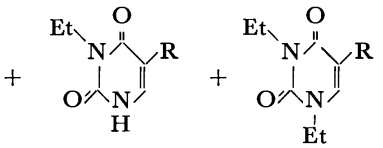

5: R=H
8: R=Me

6: R=H
9: R=Me

In cytosine (**3**), dimethyl sulfate in DMF has been reported to methylate **3** at the N-3 position mainly to give 3-methylcytosine,[1] while TMP has been shown to methylate **3** at the N-1 position predominantly to give 1-methylcytosine.[16]

The present reaction of **3** with TEP at 80 °C afforded six UV absorbing products (**6**, **10**, and four unknown products). Compound **10** was produced mainly and

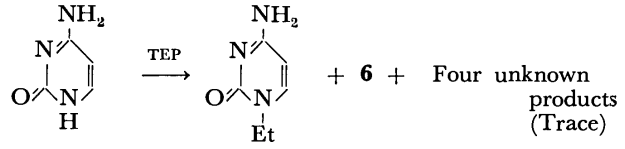

3 **10**

was identified as 1-ethylcytosine through its physical constants. Compound **6** was produced in a small yield and was identified as 1,3-diethyluracil through its UV

TABLE 1. REACTIONS OF NUCLEIC ACID-BASES WITH TRIETHYL PHOSPHATE (TEP)[a]

Base	pH	Product	Yield (%)			UV Spectra λ_{max}		
			60 °C, 48 h	80 °C, 24 h	80 °C, 48 h	pH 1	pH 7	pH 13
Uracil (U)	10—10.5	1-Ethyl-U	15	23	34	267.0	268.0	268.0
		3-Ethyl-U	6	8	10	260.0	261.0	284.0
		1,3-Diethyl-U	0	5	7	267.0	268.0	268.0
Thymine (T)	10—10.5	1-Ethyl-T	14	24	34	273.0	273.0	271.0
		3-Ethyl-T	6	9	12	260.0	267.0	290.0
		1,3-Diethyl-T	0	4	6	273.0	272.0	273.0
Cytosine (C)	10—10.5	1-Ethyl-C	13[b]	15	17	284.0	276.0	276.0
		1,3-Diethyl-U	0	2	3			
		Unknown A	0	Tr[c]	Tr	261.0	271.0	271.0
		Unknown B	0	Tr	Tr	267.0	265.0	269.0
		Unknown C	0	0	Tr		270.0	
		Unknown D	0	0	Tr		277.0	
Adenine (A)	10—10.5	9-Ethyl-A	26[b]	33	39	261.0	263.0	263.0
		3-Ethyl-A	15[b]	22	29	275.0	275.0	274.0
		7-Ethyl-A	0	4	6	273.0	269.0	269.0
		N^6,9-Diethyl-A	0	1	3	265.0	268.0	267.0
		Unknown E	0	Tr	Tr	268.0	268.0	270.0
		Unknown F	0	0	Tr	263.0	263.0	268.0
Guanine (G)	11—12	1-Ethyl-G	0	37	28	249.5 273.5s)	248.0 272.0s)	
		7-Ethyl-G	5[b]	12	17	251.0 275.0s)	250.0s) 282.5	280.0
		Other minor products	—	Tr	Tr		[d]	

a) The ratio of TEP to base was 6 : 1 at 80 °C and 3 : 1 at 60 °C. b) Isolated yield. c) Tr refers to a trace yield. d) The yields of these minor products were too small for the UV spectra to be measured. s) Shoulder.

TABLE 2. REACTIONS OF ALKYLATED NUCLEIC ACID-BASES WITH TRIETHYL PHOSPHATE (TEP)

Base	pH	TEP/Base	Temp (°C)	Product	Yield (%)[a]	
					24 h	48 h
1-Ethyluracil	10	6	80	1,3-Diethyluracil	23	28
1-Ethylthymine	10	6	80	1,3-Diethylthymine	16	22
1-Methylcytosine	10	6	80	3-Ethyl-1-methyluracil	8	13
9-Ethyladenine	10	6	80	N^6,9-Diethyladenine	4	10

a) Spectroscopic yields.

spectrum. Although 1,3-diethylcytosine was not observed in the reaction mixture, the formation of **6** may be attributed to the rapid alkaline hydrolysis of 1,3-diethylcytosine. In practice, the analogous compound, 1,3-dimethylcytosine, was converted to 1,3-dimethyluracil under similar conditions. The UV spectra of all possible alkyl derivatives of **3** were compared with those of the four unknown products (A-D), but only one compound showed an UV spectrum similar to that of O^2-methylcytosine. Although the alkylation of the cytosine ring at the O^2-atom has not been reported, Singer *et al.* have suggested the possibility of the formation of O^2-ethylcytidine from the reaction of cytidine with ethyl iodide.[5] When the reaction temperature was lowered to 37—60 °C, **10** was formed as the sole product.

The difficulty of ethylation at the N-3 position of these three pyrimidine bases (**1**, **2**, and **3**) with TEP might be attributed to the steric hindrance on the approach of TEP to the N-3 position by two adjacent carbonyl groups of **1** and **2** and amino and carbonyl groups of **3**. Similar results were shown in the alkylation of xanthine and its derivatives.[15] However, when the reactions were performed at 80 °C, 1-alkylpyrimidines (**4**, **7**, and 1-methylcytosine) reacted with TEP to afford the corresponding 3-ethyl derivatives.

Since the rates of the reactions of **1**, **2**, and **3** were enhanced with the increase in the pH value of the reaction mixture, **1**, **2**, and **3** may react in the anionic form with TEP. The slower reaction of **3** than **1** and **2** may, therefore, be originated by the larger pK_a value of **3** (12.15) than those of **1** (9.46) and **2** (9.90).

Adenine (11) and Guanine (12). These purine bases of nucleic acids have been known to be reactive towards alkylating agents. The alkylations of **11** with various alkylating agents have been studied actively,

and, thanks to these works, **11** has been shown to be alkylated at the N-3 position under neutral conditions,[2,4,22] while under basic conditions the N-9 position was alkylated mainly, with the co-formation of N-3 substituted adenine.[8] However, a reaction of **11** with TMP in a homogeneous alkaline aqueous phase afforded 3-methyl- and 9-methyladenines chiefly in almost equal yields, with the co-formation of small amounts of N^6-methyl- and 7-methyladenines.[16]

The present reaction of **11** with TEP at 80 °C gave six UV absorbing products. Two main products (**13** and **14**) were isolated and identified as 9-ethyl- and 3-ethyladenines respectively through their physical properties. The yield of **13** was a little more than that of **14**. Compounds **15** and **16** were produced in low yields and were identified as 7-ethyl- and N^6,9-diethyladenines through their UV spectra which corresponded excellently to those of 7-methyl- and N^6,9-dimethyladenines. N^6,9-Dialkyladenine was established to be formed by the Dimroth rearrangement of 1,9-dialkyladenine under alkaline conditions.[16] When the reaction temperature was lowered to 37—60 °C, only two products, **13** and **14**, were formed. These results show that the reactivity order of the four nitrogens of **11** is similar to that in the methylation, that is, N-9≈N-3>N-7, N-1.

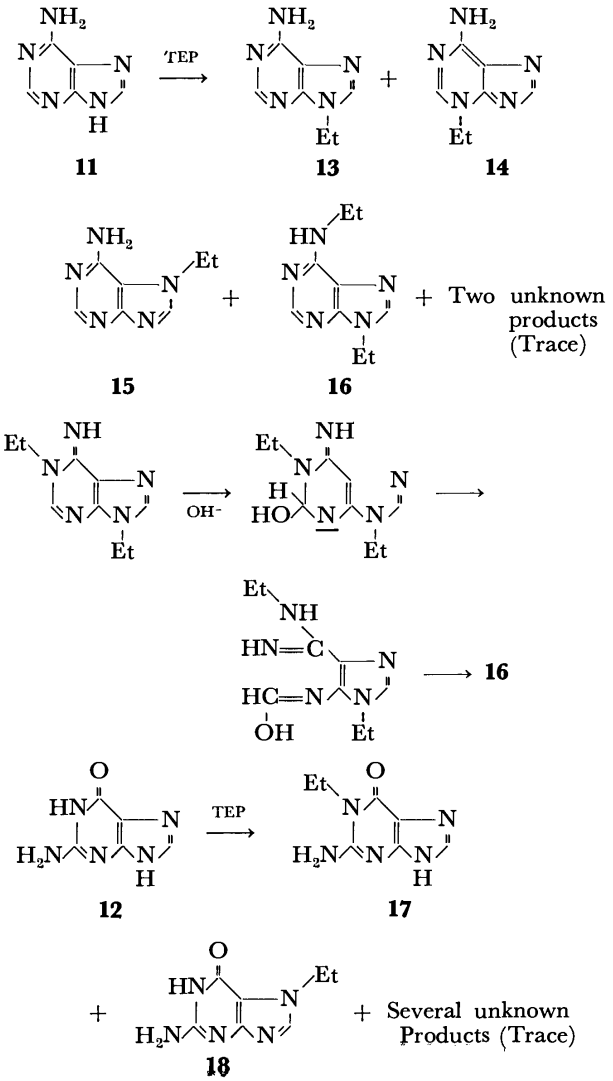

Although **13**, which is considered as the model of adenosine, was not as reactive as adenine itself, **13** was ethylated with TEP at 80 °C at the N-1 position, which has been established as the most nucleophilic and basic site in 9-alkyladenine. Resulting 1,9-diethyladenine was rearranged *in situ* to give N^6,9-diethyladenine.

On the other hand, only a few studies have been carried out on the alkylation of guanine (**12**); with ethyl ethanesulfonate[4] and dimethyl sulfate,[2] the formation of 7-ethyl- and 7,9-dimethylguanines has been reported. Recently, we reported that **12** was successfully methylated with TMP in water at pH 11—12 to give 1-methylguanine mainly, with the co-formation of 3-methyl-, 7-methyl-, and O^6-methylguanines.[16]

The present reaction of **12** with TEP at 80 °C afforded several UV-absorbing products; the two main products could be identified as 1-ethyl- and 7-ethylguanines (**17** and **18**) through their UV spectra. Compound **17** was produced chiefly at 80 °C, but, at 60 °C, **18** was given as the sole product. Since **12** was consumed for the ethylation reaction in a rate similar to that in the ethylation of **11**, the reactivity of **12** towards TEP may be considered to be almost the same as that of **11**. Compound **17** gradually decreased in quantity with the progress of reaction time; probably it was subsequently ethylated to diethylguanine, which, however, could not be isolated.

Conclusion

TEP was found to react with five nucleic acid-bases in a homogeneous aqueous phase because of its solubility in water. Although TEP was not so reactive as TMP, which reacted with five nucleic acid-bases at 25—37 °C very well, at 60—80 °C five nucleic acid-bases were ethylated with TEP, giving the corresponding ethyl derivatives in yields comparable with those obtained by the use of other ethylating agents.

The reactivity order of five nucleic acid-bases towards TEP was found to be as follows, based on the consumption of the starting materials of the reaction with TEP: adenine (**11**)≈guanine (**12**)>uracil (**1**)≈thymine (**2**)>cytosine (**3**). In each base, ethylation occured in the following order: uracil, thymine, and cytosine: N-1>N-3; adenine: N-9≈N-3>N-7, N-1; guanine: N-1>N-7>N-3, N-9. This reactivity order of bases and sites in each base was almost the same as in the methylation. However, the sterically hindered sites, the N-3 positions of **1**, **2**, and **3**, were less reactive in ethylation than in methylation.

The alkylated bases shown in Table 2, which have alkyl groups in the same position as nucleosides have ribose or deoxyribose, also reacted with TEP to afford the dialkyl derivatives. The reactivity order of these alkylated bases was different from that of the parent bases: 1-ethyluracil (**4**)>1-ethylthymine (**6**)>1-methylcytosine>9-ethyladenine (**13**).

Thus, TEP has a considerable ethylating ability of the base moiety of nucleic acids, therefore, it seems reasonable to pay attention to the use of TEP as an additive for commercial products.

Experimental

The UV and IR spectra were measured with Hitachi EPS-3T and Jasco IR-G spectrometers respectively. The

NMR spectra were recorded on a Hitachi-Perkin Elmer R-20 spectrometer, with a dilute solution in deuterioxide, deuteriochloroform, or trifluoroacetic acid and tetramethylsilane as an internal or an outside standard. Thin-layer chromatography was performed on silica gel [GF_{254} (type 60), Merck] or aluminium oxide [PF_{254} (type 150), Merck] or cellulose [13254, Eastman] using a mixture of chloroform and methanol in the following volume ratio. Solvent A: 10 : 1, B: 5 : 1, C: 5 : 2, or Solvent D: 1-propanol-concentrated ammonium hydroxide–water, 9 : 1 : 3. Column chromatography was carried out using silica gel (Merck, Art. 7734, 70—230 mesh) or cellulose (CF 11, Whatman).

Commercially available uracil (**1**), thymine (**2**), cytosine (**3**), adenine (**11**), and guanine (**12**) as well as TEP were used without further purification.

Ethylation of Uracil (1). *A*: A mixture of **1** (112 mg, 1.0 mmol) and TEP (1.07 g, 6.0 mmol) in water (2.0 ml) was stirred at 80 °C. The solution was maintained at pH 10—10.5 throughout the reaction by the occasional addition of 4M sodium hydroxide. After stirring for 48 h, 3 μl of the reaction mixture was spotted in aluminum oxide thin-layer chromatography. The plate was developed immediately using Solvent A. Three UV-absorbing products (**4**, **5**, and **6**) were observed. (R_f value; **1**: 0.03, **4**: 0.35, **5**: 0.56, **6**: 0.95). Each spot was then scraped individually from the plate to extract the substance on the spot with 4 ml of water. The yield of each product was calculated, by means of a procedure similar to that described in a previous paper,[16] from the absorbancy of the solution; we thus found the yields of **4**, **5**, and **6** were 34, 10, and 7% respectively.

B: A similar reaction of **1** (1.21 g, 10.8 mmol) and TEP (5.35 g, 2.90 mmol) at 60 °C was carried out. After stirring for 48 h, the reaction mixture was neutralized with concentrated hydrochloric acid to give a precipitate of **1**. The mother liquor was then extracted with chloroform. After the solvent had then been removed from the organic layer, the addition of hexane to the residue afforded the crystals of 1-ethyluracil (**4**, 0.05 g, 4%); mp 146—147.5 °C (from THF–ether) (lit,[19] mp 147.5 °C); NMR ($CDCl_3$): 1.28 (t, 3H, $-CH_2CH_3$, J=7 Hz), 3.77 (q, 1H, $-CH_2CH_3$, J=7 Hz), 5.67 (d, 1H, **H**^{5}, J=8 Hz), 7.18 (d, 1H, **H**^{6}, J=8 Hz), and 10.17 ppm (δ) (bs, 1H, N^3–**H**).

Ethylation of Thymine (2). *A*: The treatment of **2** (126 mg, 1.0 mmol) with TEP (1.07 g, 6.0 mmol) in water (2.0 ml) at 80 °C for 48 h gave 1-ethylthymine (**7**, 34%), 3-ethylthymine (**8**, 12%), and 1,3-diethylthymine (**9**, 6%), whose yields were calculated in a way similar to that used in the ethylation of **1**. (R_f value on aluminumn TLC using Solvent A; **2**: 0.06, **7**: 0.49, **8**: 0.65, **9**: 0.98)

B: The isolation of 1-ethylthymine (0.08 g, 5%) was carried out in a manner similar to that used for 1-ethyluracil after a mixture of **2** (1.30 g, 10.30 mmol) and TEP (5.35 g, 29.0 mmol) in water (10 ml) had been stirred for 48 h at 60 °C; mp 220—222 °C (from THF–ether) (lit,[23] mp 223 °C); NMR ($CDCl_3$) 1.42 (t, 3H, $-CH_2CH_3$, J=7 Hz), 2.02 (d, 3H, $-CH_3$, J=1.2 Hz), 3.88 (q, 2H, $-CH_2CH_3$, J=7 Hz), 7.09 (d, 1H, **H**^{6}, J=1.2 Hz), and 9.90 ppm (δ) (bs, 1H, N^3–**H**).

Ethylation of Cytosine (3). *A*: A mixture of **3**(111 mg, 1 mmol) and TEP (1.07 g, 6.0 mmol) in water (2 ml, pH 10—10.5, NaOH) was stirred at 80 °C for 48 h. The reaction mixture (4 μl) was then developed on a silica gel TLC using Solvent C, giving the following spots. R_f value; **3**: 0.18, **6**: 0.76, **10**: 0.45, unknown A: 0.73, B: 0.57, C: 0.49, D: 0.23. A treatment similar to that used in the ethylation of **1** showed that the yields of **10** and **6** were 17 and 3% respectively.

B: A mixture of **3** (1.0 g, 9.0 mmol) and TEP (5.25 g, 29.0 mmol) in water (15 ml, pH 10, NaOH) was stirred at 60 °C for 48 h. The subsequent neutralization of the reaction mixture with concentrated hydrochloric acid gave the precipitate of **3**. After the precipitate had been filtered out, the mother liquor was extracted with chloroform to remove the unreacted TEP. The water layer was concentrated to give a residue, which was subsequently mixed with ethanol to remove any undissolved substances. The residue which was obtained after concentrating the alcoholic solution was treated by silica gel column chromatography (1.5×60 cm). Elution with Solvent C provided the salt of 1-ethylcytosine with diethyl hydrogen phosphate (0.54 g). The salt was subsequently treated with an anionic exchange resin (Dowex 1×8, 200—400 mesh, OH form). Elution with water gave the free form of 1-ethylcytosine (**8**, 0.16 g, 13%); mp 236—238 °C (sublime) (lit,[24] 245—246 °C); NMR (D_2O): 1.22 (t, 3H, $-CH_2CH_3$, J=7 Hz), 3.76 (q, 2H, $-CH_2CH_3$, J=7 Hz), 5.95 (d, 1H, **H**^{5}, J=8 Hz), and 7.58 ppm (δ) (d, 1H, **H**^{6}, J=8 Hz); Found: C, 51.75; H, 6.31; N, 30.51%, Calcd for $C_6H_9N_3O_1$: C, 51.78; H, 6.52; N, 30.20%.

Ethylation of Adenine (11). A: Compound **11** (135 mg, 1 mmol) and TEP (1.07 g, 6.0 mmol) were stirred in water (2 ml, pH 10—10.5, NaOH) for 48 h at 80 °C. The reaction mixture (4 μl) was then developed on silica gel TLC, using Solvent B, to give the following spots. R_f value; **11**: 0.32, **13**: 0.57, **14**: 0.42, **15**: 0.23, **16**: 0.66, unknown E: 0.10, F: 0.14. Calculations from the absorbancy of the solution of each spot similar to that described above showed the yields of **13**, **14**, **15**, and **16** to be 39, 29, 6, and 3% respectively.

B: A mixture of **11** (1.35 g, 10.0 mmol) and TEP (5.25 g, 29.0 mmol) was stirred in water (10 ml, pH 10, NaOH) at 60 °C for 48 h. The reaction mixture was then neutralized with concentrated hydrochloric acid and extracted with hexane to remove any unreacted TEP. The water layer was concentrated to give a residue, which was subsequently mixed with ethanol to remove any undissolved substances. The residue which was obtained after concentrating the alcoholic solution was then treated by silica gel column chromatography (1.5×60 cm). Elution with Solvent B provided 9-ethyladenine (**12**, 0.42 g, 26%) and then 3-ethyladenine (**13**, 0.24 g, 15%); **12**: mp 202—203 °C (from ethanol) (lit,[25] mp 194—195 °C); NMR ($CDCl_3$): 1.58 (t, 3H, $-CH_2CH_3$, J=7 Hz), 4.25 (q, 2H, $-CH_2CH_3$, J=7 Hz), 6.39 (bs, 2H, $-NH_2$), 7.79 (s, 1H, **H**^{2}), and 8.32 ppm (δ) (s, 1H, **H**^{8}); **13**: mp 233—234 °C (from ethanol) (lit,[26] mp 233 °C); NMR (D_2O): 1.34 (t, 3H, $-CH_2CH_3$, J=7 Hz), 4.13 (q, 2H, $-CH_2CH_3$, J=7 Hz), 7.67 (s, 1H, **H**^{2}), and 7.95 ppm (δ) (s, 1H, **H**^{8}).

Ethylation of Guanine (12). *A*: After **12** (151 mg, 1 mmol) had been dissolved in water (2 ml, pH 13) at 80 °C, TEP (1.07 g, 6.0 mmol) was added. Soon after the reaction began, the pH of solution dropped to 11—12; this value was maintained by the occasional addition of 4M sodium hydroxide. The reaction mixture (4 μl) was developed on silica gel TLC, using Solvent A, to give the following spots: R_f value; **12**: 0.00, **17**: 0.21, **18**: 0.24, six minor unknown products: 0.03, 0.12, 0.32, 0.35, 0.45, 0.74. After a treatment similar to that described above, the yields of **17** and **18** were found to be 28 and 17% respectively.

B: A mixture of **12** (1.25 g, 8.30 mmol) and TEP (5.25 g, 29 mmol) in water (50 ml, pH 11—12, NaOH) was stirred for 48 h at 60 °C. The reaction mixture was then extracted with chloroform to remove any unreacted TEP. The water layer was concentrated to give a residue, which was subsequently treated by a cellulose column chromatography (2.5×60 cm).

Elution with Solvent D provided a viscous liquid which was crystalized by the addition of a small amount of water and identified as 7-ethylguanine through its UV spectra (**18**, 0.075 g, 5%); mp>300 °C dec; NMR (CF_3CO_2H): 1.14 (t, 3H, $-CH_2CH_3$, J=7 Hz), 4.15 (q, 2H, $-CH_2CH_3$, J=7 Hz), and 8.34 ppm (δ) (s, 1H, H^8).

References

1) P. Brookes and P. D. Lawley, *J. Chem. Soc.*, **1962**, 1348.
2) J. W. Jones and R. K. Robins, *J. Am. Chem. Soc.*, **84**, 1914 (1962).
3) B. Singer, L. Sun, and H. Fraenkel-Conrat, *Biochemistry*, **13**, 1913 (1974).
4) C. B. Pal, *Biochemistry*, **1**, 558 (1962).
5) L. Sun and B. Singer. *Biochemistry*, **13**, 1905 (1974).
6) B. Singer, *Biochemistry*, **11**, 3939 (1972).
7) J. W. Jones and R. K. Robins, *J. Am. Chem., Soc.* **85**, 193 (1963).
8) M. Rasmussen and J. H. -S. Chan, *Aust. J. Chem.*, **28**, 1031 (1975).
9) J. A. Hains, C. B. Reese, and L. Todd, *J. Chem. Soc.*, **1962**, 5281.
10) C. C. Price, G. M. Gaucher, P. Koneru, R. Shibakawa, J. R. Sowa, and M. Yamaguchi, *Biochem. Biophys. Acta*, **166**, 327 (1968).
11) K. Yamauchi and M. Kinoshita, *J. Chem. Soc., Perkin Trans. 1*, **1973**, 2506.
12) M. Hayashi, K. Yamauchi, and M. Kinoshita, *Bull. Chem. Soc. Jpn.*, **49**, 283 (1976).
13) K. Yamauchi and M. Kinoshita, *J. Chem. Soc., Perkin Trans. 1*, **1973**, 391.
14) K. Yamauchi, M. Hayashi, and M. Kinoshita, *J. Org. Chem.*, **40**, 385 (1975).
15) T. Tanabe, K. Yamauchi, and M. Kinoshita, *Bull. Chem. Soc. Jpn.*, **49**, 3224 (1976).
16) K. Yamauchi, T. Tanabe, and M. Kinoshita, *J. Org. Chem.*, **41**, 3691 (1976).
17) B. Singer and H. Fraenkel-Conrat, *Virology*, **39**, 395 (1969).
18) S. D. Kononova and L. L. Gumanov, *Dokl. Akad. Nauk SSSR*, **198**, 1442 (1971).
19) G. E. Hilbert and T. B. Johnson, *J. Am. Chem. Soc.*, **52**, 2001 (1930).
20) E. Wittenburg, *Chem. Ber.*, **99**, 2380 (1966).
21) J. L. Wong and D. S. Fuchs, *J. Org. Chem.*, **36**, 848 (1971).
22) N. J. Leonard and R. A. Laursen, *J. Am. Chem. Soc.*, **85**, 2026 (1963).
23) J. B. Johnson and S. H. Clapp, *J. Biol. Chem.*, **5**, 56 (1908).
24) L. Doub and U. Krolls, *J. Heterocycl. Chem.*, **7**, 527 (1970).
25) J. A. Montgomery and C. Temple, Jr., *J. Am. Chem. Soc.*, **79**, 5238 (1957).
26) R. Denayer, *Bull. Soc. Chim. Fr.*, **1962**, 1358.

The Sensitized Photooxygenation of 2-Vinylbenzofurans

Masakatsu MATSUMOTO, Satoshi DOBASHI, and Kiyosi KONDO
Sagami Chemical Research Center, Nishi-Ohnuma, Sagamihara, Kanagawa 229

(Received May 4, 1977)

The sensitized photooxygenation of benzofuran, 2-methylbenzofuran, and six 2-vinylbenzofurans was investigated. Benzofuran and 2-methylbenzofuran were stable toward singlet oxygen. On the other hand, the vinylbenzofurans were easily photooxygenated to give the 1,4-endoperoxides. The 1,4-cycloaddition of singlet oxygen to the 2-benzofurans was confirmed to proceed with stereospecificity.

Recently, it has been found that, for some styrene derivatives[1] and vinyl-substituted polynuclear aromatic hydrocarbons,[2] an aromatic double bond in conjugation with extranuclear unsaturation produces an active diene system capable of undergoing the 1,4-cycloaddition of singlet oxygen. Vinyl-substituted heteroaromatics such as 2-vinylthiophene[3] and 1-methyl-3-vinylindoles,[4] have also been found to undergo the 1,4-cycloaddition of singlet oxygen. On the other hand, such aromatics as benzene, naphthalene, phenanthrene, and thiophene are themselves known to be stable to singlet oxygen.[5] Of the heteroaromatics, furans have been most intensively studied in connection with their photooxygenation, though their benzo analogs, *i. e.*, benzofurans, have scarcely been known to undergo any sensitized photooxygenation.[5] We have studied here the sensitized photooxygenation of **1** benzofurans and 2-vinylbenzofurans, **2**, in order to investigate the reactivities of the 2,3-double bond of the ring and a conjugated system composed of the 2-vinyl group and the 2,3-double bond of these aromatics.

Results and Discussion

Preparation of 2-Vinylbenzofurans. Of six vinylbenzofurans, **2**, used in this work, 2-(2-methyl-1-propenyl)- (**2a**), *trans*-2-styryl- (**2c**), *cis*-2-styryl- (**2d**), and 2-isopropenylbenzofuran (**2f**) were prepared by the Witting reaction of 2-formylbenzofuran or 2-acetylbenzofuran and the corresponding methylenetriphenylphosphoranes. The other two, 2-vinyl- (**2b**) and 2-(1-phenylvinyl)benzofuran (**2e**) were obtained by the dehydration of the corresponding alcohols which themselves had been prepared from 2-acetylbenzofuran. The preparations of these vinylbenzofurans were described in detail in the Experimental Section.

Sensitized Photooxygenation of 2-Vinylbenzofurans

First, the sensitized photooxygenation of benzofuran (**1a**) and 2-methylbenzofuran (**1b**) as typical examples of 2- and 3-alkyl-substituted benzofurans were examined. When 2-methylbenzofuran (**1b**) was photooxygenated for 3 h as in the cases of the vinylbenzofurans **2** described below, scarcely no oxygen was consumed and the starting material was recovered. Benzofuran (**1a**) itself was also fairly stable under similar irradiation conditions. These results showed that, for benzofurans, the 2,3- double bond is more stable than for indoles,[6] though 2,3-dimethylbenzofuran (**1c**) has been known to be the only substance to undergo the 1,2-addition of singlet oxygen to give *o*-acetoxyacetophenone.[7]

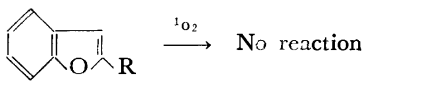

1a: R=H
1b: R=CH_3

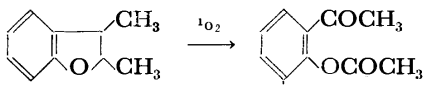

1c

Second, the sensitized photooxygenation of 2-vinylbenzofurans **2** was carried out. A solution of 2-(2-methyl-1-propenyl)benzofuran (**2a**) and tetraphenylporphine (TPP) (used as a sensitizer) in carbon tetrachloride was irradiated externally with low-pressure sodium vapor lamps under an oxygen atmosphere at 5 °C. After the irradiation, the photolysate was condensed and purified by chromatography on silica gel to give a 1,4-endoperoxide **3a** as colorless plates in a 90% yield. The structure of **3a** was assigned on the basis of spectral evidence and combustion analyses. In this examination, scarcely no 1,2-cycloaddition of singlet oxygen to the 2,3-double bond of the side chain or the "ene" reaction was observed. The similar photooxygenation of 2-vinylbenzofuran (**2b**) afforded the corresponding 1,4-endoperoxide **3b** as an oil in a 41% yield. Then, in order to investigate the stereochemical features of the 1,4-cycloaddition of singlet oxygen to 2-vinylbenzofurans **2**, *trans*-2-styrylbenzofuran (**2c**) and its *cis*-isomer **2d** were individually photooxygenated under similar conditions. The *trans*-isomer **2c** gave the corresponding 1,4-endoperoxide **3c** in a 70% yield. On the other hand, the peroxide **3d** was obtained from the *cis*-isomer in a 75% yield. The olefin **2c** gave no **3d**, whereas the isomer **2d** gave no **3c**. Consequently the results obtained here confirm that the 1,4-cycloaddition of singlet oxygen to 2-vinylbenzofurans **2** proceeds with stereospecificity.

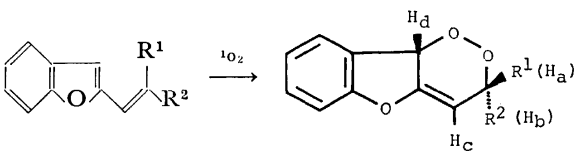

2a: R^1, R^2=CH_3
2b: R^2, R^2=H
2c: R^1=H, R^2=C_6H_5
2d: R^1=C_6H_5, R^2=H

3a: R^1, R^2=CH_3
3b: R^1, R^2=H
3c: R^1=H, R^2=C_6H_5
3d: R^1=C_6H_5, R_2=H

The endoperoxides **2a**—**d** were thermally stable, but were easily changed under basic conditions. When the peroxide **3c** was treated with a catalytic amount of triethylamine in ether at an ambient temperature, 2-benzoylmethyl-3(2*H*)-benzofuranone (**4**) was obtained in a 58% yield.

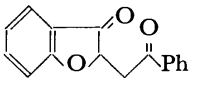

4

The 1,4-cycloaddition of singlet oxygen has been found to take place with 1-vinylnaphthalenes,[2a] 9-vinylphenanthrenes,[2b] and 2-vinylthiophenes[3] bearing no substituent and a β-substituent on the side chain. An α-substituent of these aromatics has been known to cause significantly different results; for the naphthalene or the phenanthrene derivatives, no 1,4-cycloaddition but "ene" reaction of singlet oxygen occurs,[2] hereas, for the vinylthiophenes, both the 1,4-cycloaddition and the "ene" reaction occur competitively.[3] The 2-vinylbenzofurans **2** seemed to behave much like the 2-vinylthiophenes in the reaction with singlet oxygen. When 2-(1-phenylvinyl)benzofuran **2e** was photooxygenated as in the cases described above, the corresponding peroxide **3e** was formed. A similar irradiation of 2-isopropenylbenzofuran (**2f**) also gave the expected peroxide **3f**. Neither peroxide **3e** or **3f** could be isolated in a pure form because of their instabilities. In particular, the former, **3e**, was highly explosive. These differences between a pair of 2-vinylthiophenes and 2-vinylbenzofurans **2**, and a pair of 1-vinylnaphthalenes and 9-vinylphenanthrenes may be due to steric and electronic factors. For the vinylnaphthalenes and vinylphenanthrenes with an α-substituent on the side chain, a steric repulsion between the 8-hydrogen and the α-substituent may hinder the favorable conformation of the side chain for 1,4-cycloaddition, though this hindrance seems to be overcome at higher temperatures.[8] On the other hand, in the cases of 2-vinylthiophenes and 2-vinylbenzofurans **2** such steric repulsion need not be considered and carbons in both the β-position of the side chain and the 3-position of the aromatic nucleus may be activated toward electrophiles, such as singlet oxygen, more than the corresponding carbons in the naphthalene or phenanthrene analogs, by the sulfur or the oxygen atom. These suggestion may be supported by the fact that maleic anhydride reacts more easily with **2e** and **2f** (in refluxing benzene)[9b] than with naphthalene and phenanthrene analogs (in refluxing xylene).[8]

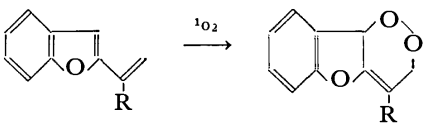

2e: R=C_6H_5 **3e**: R=C_6H_5
2f: R=CH_3 **3f**: R=CH_3

In summary, we have found that, for 2-vinylbenzofurans **2**, the 2,3-double bond, which is scarcely active itself in response to singlet oxygen, in conjugation with 2-ethylenic double bond produces an active diene system capable of undergoing the 1,4-cycloaddition of singlet oxygen.

Experimental

All the melting points and boiling points are uncorrected. The NMR spectra were recorded with a Varian HA-100 spectrometer, with TMS as the internal standard. The

Table 1. NMR spectral data of the peroxides **3**[a]

Chemical shifts (ppm).

	H_a	H_b	H_c	H_d	R^1	R^2
3a	—	—	6.10	5.06	1.28[b]	1.38[b]
3b	4.50	4.91	6.15	5.17	—	—
3c	5.48	—	6.24	5.30	—	7.1—7.4[c]
3d	—	5.90	6.37	5.36	7.1—7.5[c]	—

Coupling Constants (Hz).

	J_{ab}	J_{ac}	J_{ad}	J_{bc}	J_{bd}	J_{cd}
3a	—	—	—	—	—	2.5
3b	15.0	2.5	2.5	3.0	2.5	2.5
3c	—	3.0	2.0	—	—	3.0
3d	—	—	—	2.5	2.0	2.5

a) Measured in CCl_4. b) Methyl group. c) Phenyl group.

NMR spectral data of the peroxide **3** are summarized in Table 1. The mass spectra were obtained with a Hitachi RMU-6E spectrometer. The light source was consisted of eight 60-W low pressure sodium-vapor lamps (National SOI-60).

*Preparation of 2-Methylbenzofuran (**1b**).* To a solution of coumarone (1.18 g, 10 mmol) in tetrahydrofuran (THF) (30 ml) was added 10 mmol of *n*-butyllithium (6.4 ml of a 10% hexane solution) under an argon atmosphere at room temperature. After 30 min, methyl iodide (1.42 g, 10 mmol) in THF (5 ml) was added to the solution of the carbanion of coumarone, and the mixture was stirred for 1 h. After the usual work-up, the crude product was purified by chromatography on silica gel. The furan **1b** was obtained as a colorless oil [bp 195 °C (lit,[10] bp 192 °C/744 mmHg)] in an 81% yield (1.07 g)

*Preparation of 2-(2-Methyl-1-propenyl)benzofuran (**2a**).* Under an argon atmosphere, to a solution of isopropylidenetriphenylphosphorane (prepared from 10 mmol of isopropyltriphenylphosphonium bromide and an equimolar amount of *n*-butyllithium) in THF (20 ml) was added 2-formylbenzofuran (1.46 g, 10 mmol) at an ambient temperature. After 1 h, the reaction mixture was poured into brine and extracted with hexane. The hexane solution was dried over $MgSO_4$ and condensed. The residue was chromatographed on silica gel and eluted with hexane to yield 1.35 g of the furan **2a** (78%) (colorless needles; mp 48—49.5 °C, from hexane); IR (KBr): 3027, 1660, 1455, 1258, 1194, 940, 750 cm^{-1}; NMR (CCl_4): δ 1.92 (s, 3H), 2.08 (s, 3H), 6.07 (m, 1H), 6.34 (s, 1H), 6.9—7.5 (m, 4H) ppm.

*Preparation of 2-Vinylbenzofuran (**2b**).* 2-Acetylbenzofuran[11] (3.6 g, 23 mmol) was reduced as usual with lithium aluminium hydride (0.4 g, 10 mmol) in dried ether (15 ml) overnight at room temperature to give 2-(1-hydroxyethyl)-benzofuran. The crude alcohol was dehydrated with alumina (Woelm neutral, for column chromatography) at 140 °C (bath temperature). Thus, **2b** was obtained as a colorless oil [bp 52 °C/2 mmHg (lit,[9b] 50 °C/0.1 mmHg)] in a 62% yield; IR (liquid film): 3050, 1548, 1452, 1255, 980, 910 cm^{-1}; NMR (CCl_4): δ 5.22 (d of d, J=11.0 and 2.0 Hz, 1H) 5.84 (d of d, J=18.0 and 2.0 Hz, 1H), 6.38 (s, 1H), 6.47 (d of d, J=18.0 and 11.0 Hz, 1H), 6.9—7.5 (m, 4H) ppm

Preparation of trans-*2-Styrylbenzofuran (**2c**) and* cis-*2-Styrylbenzofuran (**2d**).* To a solution of benzylidenetriphenylphosphorane (prepared from 10 mmol of benzyltriphenylphosphonium bromide and an equimolar amount of *n*-butyllithium in THF was added 2-formylbenzofuran (1.46 g, 10 mmol) under an argon atmosphere at room temperature. The reac-

tion mixture was then treated as in the case of **2a** to give a mixture of **2c** and **2d** (**2c**/**2d**=71/29, 1.30 g). The separation of the mixture was performed by chromatography on silica gel in hexane.

2c: Colorless crystals (mp 123 °C) from ethanol; IR (KBr): 3050, 1444, 1255, 960, 945, 805 cm^{-1}, NMR (CCl_4): δ 6.49 (s, 1H), 6.82 (d, J=16.0 Hz, 1H), 6.9—7.5 (m, 10H) ppm.

2d: A colorless viscous oil; IR (liquid film): 3050, 1452, 1260, 945, 810 cm^{-1}; NMR (CCl_4): δ 6.42 (s, 1H), 6.46 (q_{AB}, J_{AB}=13.0 Hz, 2H), 6.9—7.5 (m, 9H) ppm.

Preparation of 2-(1-Phenylvinyl)benzofuran (2e). To a solution of phenylmagnesium bromide (prepared from 25 mmol of bromobenzene and an equimolar amount of magnesium) in ether was added 2-acetylbenzofuran 3.0 g, 19 mmol) under an argon atmosphere. The usual work-up afforded the crude 2-(α-hydroxy-α-methylbenzyl)benzofuran, which was subsequently dehydrated with phosphorus pentaoxide in ether at room temperature for 2 h. The ether solution was then washed with water and dried over $MgSO_4$. After the evaporation of ether, the crude product was chromatographed on silica gel in hexane to give **2e** as a pale yellow oil in a 43% yield: the spectral data were identical with those in the literature.[9b]

2-Isopropenylbenzofuran (2f) was prepared by a Witting reaction of 2-acetylbenzofuran and methyltriphenylphosphonium bromide in accord with the method described in the literature,[9a]

Irradiation of Benzofuran (1a) and 2-Methylbenzofuran (1b). A solution of 1.00 g of **1a** and 5 mg of TPP in CCl_4 (60 ml) was irradiated under an oxygen atmosphere at 5 °C for 3h. Scarcely no oxygen was consumed, and no products were observed by TLC. The furan (**1b**) was also stable under similar irradiation conditions.

Photooxygenation of 2-(2-Methyl-1-propenyl)benzofuran (2a). A solution of 1.35 g (8 mmol) of **2a** was photooxygenated in 60 ml of CCl_4 until 158 ml of oxygen has been consumed (30 min). After the removal of the solvent, the photolysate was chromatographed on silica gel and eluted with a hexane $-CH_2Cl_2$ (1 : 1) mixture to give 1.42 g of the endoperoxide **3a** (colorless plates (mp 107.5—109.0 °C) from ether) (90% yield); IR (KBr): 3070, 2973, 1610, 1460, 1088, 1043, 760 cm^{-1}; MS *m/e*: 204 (M^+, 15), 172 (100), 161 (55), 157 (33), 131 (24), 77 (25), 43 (61).

Found: C, 70.53; H, 5.93%. Calcd for $C_{12}H_{12}O_3$: C, 70.58; H, 5.92%.

Photooxygenation of 2-Vinylbenzofuran (2b). A solution of 1.0 g (7 mmol) of **2b** and 5 mg of TPP in 60 ml of CCl_4 was irradiated for 3.5 h (O_2 uptake=129 ml). The photolysate was then condensed and chromatographed on alumina (Woelm neutral) previously treated with 20% water. Elution with hexane gave 0.50 g (41%) of the peroxide **3b** as an oil: IR (liquid film): 3050, 1610, 1460, 1095, 1050, 750, 740 cm^{-1}; MS *m/e*: 176 (M^+, 18), 147 (100), 146 (51), 134(85).

Photooxygenation of trans-*2-Styrylbenzofuran (2c).* A solution of 0.93 g (4 mmol) of **2c** and TPP in 60 ml of CCl_4 was irradiated for 3 h (O_2 uptake=91 ml). The chromatographic purification of the photolysate on silica gel in a hexane $-CH_2Cl_2$ (1 : 1) mixture afforded 0.74 g (70%) of the peroxide **3c** (colorless needles (mp 75.5—76.5 °C) from ether); IR (KBr): 3050, 1610, 1460, 1092, 1050, 755, 739, 695 cm^{-1}; MS *m/e*: 252 (M^+, 15), 220 (100), 147 (24), 105 (45), 77 (54), 51 (26).

Found: C, 76.58; H, 4.63%. Calcd for $C_{16}H_{12}O_3$: C, 76.18; H, 4.79%.

Photooxygenation of cis-*2-Styrylbenzofuran (2d).* A solution of 0.24 g (1 mmol) of **2d** and TPP in 60 ml of CCl_4 was photooxygenated for 2.5 h. After the irradiation, the photolysate was treated as in the case of **2c** to give 0.19 g (75%) of the peroxide **3d** (colorless granules, mp 115.0—116.5 °C) from ether; IR (KBr): 3040, 1622, 1465, 1095, 1045, 750, 700 cm^{-1}; MS *m/e*: 252 (M^+, 9), 220 (100), 105 (27), 77 (49), 51 (26).

Found: C, 75.83; H, 4.96%. Calcd for $C_{16}H_{12}O_3$: C, 76.18; H, 4.79%.

Photooxygenation of 2-(1-Phenylvinyl)benzofuran (2e). A solution of 1.10 g (5 mmol) and TPP in CCl_4 (70 ml) was oxygenated for 1 h. After the removal of CCl_4, the reaction mixture was chromatographed on silica gel and eluted with CH_2Cl_2 to give a viscous oil of the peroxide **3e** (10% yield), which crystallized on standing and exploded when subjected to weak friction; NMR (CCl_4): δ 4.29 (q_{AB}, J=15.0 Hz, 2H), 6.22 (s, 1H), 6.7—7.6 (m, 9H) ppm.

Photooxygenation of 2-Isopropenylbenzofuran (2f). A solution of 1.0 g (6 mmol) of **2f** and TPP in CCl_4 (60 ml) was irradiated for 3.5 h. The NMR spectrum (CCl_4) of the crude photolysate revealed the formation of the corresponding endoperoxide **3f**; δ 1.70 (s with fine coupling, 3H, CH_3), 4.56 (q_{AB} with fine coupling, J=15 Hz, 2H, $-CH_2O-$), and 6.20 (m, 1H, $-CHO-$)ppm. All the efforts to purify **3f** by chromatography on silica or alumina were unsuccessful; when the photolysate was adsorbed on the absorbent, immediately an exothermic reaction was occurred to give complex products.

Isomerization of the Peroxide 3c. Triethylamine (100 mg) was added to a solution of 350 mg of the peroxide **3c** in 10 ml of ether and the mixture was stirred for 20 min at an ambient temperature. Then, the mixture was condensed and chromatographed on silica gel. Elution with CH_2Cl_2 gave 200 mg of 2-benzoylmethyl-3(2*H*)-benzofuranone (**4**) as pale yellow granules (mp 113 °C, from ether); IR (KBr): 3070, 2930, 2900, 1725, 1710, 1687, 1615 cm^{-1}; MS *m/e*: 252 (M^+, 25), 147 (38), 105 (100), 77 (45); NMR ($CDCl_3$): δ 3.55 (m, 2H), 5.08 (m, 1H), 6.9—8.0 (m, 9H) ppm.

Found: C, 76.07; H, 4.96%. Calcd for $C_{16}H_{12}O_3$: C, 76.18; H, 4.79%.

References

1) a) C. S. Foote, S. Mazur, P. A. Burns, and D. Lerdal, *J. Am. Chem. Soc.*, **95**, 586 (1973); G, Rio, D. Bricout, and L. Lacomb, *Tetrahedron*, **29**, 3553 (1973); c) P. A. Burns, C. S. Foote, and S. Mazur, *J. Org. Chem.*, **41**, 899 (1976); P. A. Burns and C. S. Foote, *ibid.*, **41**, 908 (1976).

2) a) M. Matsumoto and K. Kondo, *Tetrahedron Lett.*, **1975**, 3935; b) M. Matsumoto, S. Dobashi, and K. Kondo, *Bull. Chem. Soc. Jpn.*, in press. c) A. P. Schaap, P. A. Burns, and K. A. Zaklika, *J. Am. Chem. Soc.*, **99**, 1270 (1977).

3) M. Matsumoto, S. Dobashi, and K. Kondo, *Tetrahedron Lett.*, **1975**, 4471.

4) M. Matsumoto and K. Kondo, *J. Am. Chem. Soc.*, **99**, 2393 (1977).

5) For a review, see R. W. Denny and A. Nickon, "Organic Reaction," Vol. 20, John Wiley & Sons, New York, N. Y. (1973), p. 133.

6) I. Saito, M. Imuta, and T. Matsuura, *Chemistry Lett.*, **1972**, 1173, 1197.

7) C. Mumford, *Chemistry in Britain*, **1975**, 402.

8) a) E. Bergmann and F. Bergmann, *J. Am. Chem. Soc.*, **59**, 1443 (1937); b) F. Bergmann and A. Weizmann, *J. Org. Chem.*, **11**, 592 (1946).

9) a) W. J. Davidson and J. A. Elix, *Aust. J. Chem.*, **23**, 2119 (1970); b) J. D. Brewer and J. A. Elix, *ibid.*, **28**, 1059 (1975).

10) B. B. Corson, H. E. Tiefenthal, J. E. Nickels, and W. J. Heintzelman, *J. Am. Chem. Soc.*, **77**, 5428 (1955).

11) R. Störmer, *Ber.*, **30**, 1711 (1897).

Odor and Volatile Compounds in Liquid Swine Manure. II. Steam-distillable Substances

Akio YASUHARA* and Keiichiro FUWA**

Division of Chemistry and Physics, National Institute For Environmental Studies, Yatabe, Tsukuba, Ibaraki 300-21

***Faculty of Science, University of Tokyo, Hongo, Bunkyo, Tokyo 113*

(Received May 18, 1977)

Many aliphatic hydrocarbons, nitrogen-containing compounds, and other substances were isolated from neutral or alkaline liquid swine manure by steam distillation and column chromatography, and identified by means of gas chromatography-mass spectrometry. Aliphatic hydrocarbons have an oily odor, and nitrogen-containing substances, particularly indole, skatole, and *o*-aminoacetophenone, have a strong malodor. Sulfur-containing substances which have a strong malodor have been detected in a trace quantity.

Malodor has been the most frequent nuisance except noise in Japan. Swine buildings are among the most important sources of this malodor. Liquid swine manure evolves a very strong and offensive odor, mainly by means of an anaerobically microbial decomposition. Only a little knowledge has been obtained about the chemical nature of the odor of liquid swine manure. Seventeen carboxylic acids and four phenols in acidic liquid swine manure have been reported in a previous paper.[1] The odor of neutral or slightly alkaline swine manure is different from that of acidic swine manure. Anaerobically decomposed liquid swine manure shows a neutral or slightly alkaline nature. It has been thought that amines and sulfur-containing compounds play an important role with regard to malodor.[2,3] Steam distillation is a useful method to isolate volatile compounds containing odorous substances, although it is apt to lose very volatile compounds such as lower amines, or to decompose unstable substances such as sulfur-containing material.

This paper will deal with the separation by steam distillation and column chromatography of odorous components in neutral or slightly alkaline liquid swine manure, and with the results of the application of gas chromatography-mass spectrometry and the organoleptic technique to the determination of the compounds most responsible for the malodor.

Experimental

Gas Chromatography. A Shimadzu Model GC-5A gas chromatograph was equipped with dual-flame ionization detectors, a matrix temperature programmer, a dual-pen recorder, and a Takeda Riken *-tr-*2215 A digital integrator. The flame detectors were operated at a hydrogen-flow rate of 50 ml/min and an air-flow rate of 0.5 l/min. Some apparatus was also used for the organoleptic tests, as will be described below. The gas-chromatographic conditions were as follows: injector and detector temperatures, 300 °C; column temperatures for Fraction **A**, 80 °C for a minute, followed by an increase to 280 °C at a rate of 2 °C/min, and then held at 280 °C for 30 min; column temperatures for the other fractions, 70 °C for 3 min, followed by an increase to 270 °C at a rate of 8 °C/min, and then held at 270 °C until the completion of the analysis; carrier-gas (nitrogen) flow rate, 43 ml/min at 5 kg/cm² for Fraction **A** or 20 ml/min at 5 kg/cm² for the other fractions. A 3 m×3 mm i.d. glass column packed with 5% Silicone SE-30 on 60- to 80-mesh, acid-washed, DMCS-treated Chromosorb W was used.

Mass Spectrometry. A JEOL Model JMS-D 100 mass spectrometer was connected with a JEOL JGC-20 K gas chromatograph and a JEOL JMA-2000 data-treatment system. The gas-chromatographic conditions were the same as above except for the size of the column. A 3 m×2 mm i.d. glass column packed with 5% Silicone SE-30 on 60- to 80-mesh, acid-washed, DMCS-treated Chromosorb W was used. The mass-spectrometric conditions were as follows: ion-source temperature, 135 °C; ionizing current, 3×10^{-4} A; ionizing voltage, 25 V; accelerating voltage, 3 kV; scan range, *m/e* 35 to 400; scan time, 2.1 s; scan interval, 5 s. The data-treatment procedures were the addition of the mass spectra on several scans, the subtraction of the integrated background-mass spectra from the added mass spectra, and normalization by means of the most intense peak.

Organoleptic Test. This test was carried out by smelling the odor of compounds progressively eluted from the outlet of the gas chromatograph, which was modified as follows in order to study the quality of odors: the gas eluted from the end of the column was divided into two streams in a 10 : 1 ratio, a eleventh of the gas was led into the flame-ionization detector, and ten elevenths of the gas was emitted from the outlet of gas chromatograph for smelling. A 3 m× 3 mm i.d. stainless column was used for this test.

Sampling Procedure and Fractionation. The experiments reported here were performed using accumulated liquid swine manure collected from pits under confinement swine buildings near Takezono, Tsukuba New Town, Ibaraki, Japan The liquid manure (52 l) was steam-distilled. The distillate was saturated with sodium chloride and extracted two times with

Table 1. Fractionation of the extract by liquid chromatography

First chromatography[a]		Second chromatography[b]		Fraction
Solvent	V/ml	Solvent	V/ml	
Hexane	150	Hexane	150	**A**
		Hexane	300	**B**
Benzene	350	Benzene	100	**C**
		Benzene	100	**D**
Ether	650	Benzene	100	**E**
		Benzene	50	**F**
		Benzene	100	**G**

a) Silica gel was used as an adsorbent. b) Alumina was used as an adsorbent.

* Author to whom correspondence should be addressed.

dichloromethane. The extract was evaporated by means of a Kvrderna-Danish concentrator under atmospheric pressure. The concentrated residue was dissolved in ether (50 ml), and the solution was washed with an aqueous solution of sodium hydroxide in order to eliminate the phenol compounds. The solution was then concentrated and chromatographed over silica gel (60 g) (Wako Gel obtained from Wako Pure Chemicals Industries). As elution solvents, hexane, benzene, and ether were used. Each fraction was chromatographed again over neutral alumina (90 g), obtained from the Merck Co., Ltd. The details of the first and second chromatographies are shown in Table 1.

Results and Discussion

The steam-distillate had a malodor, but it was relatively different from the odor of neutral or slightly alkaline liquid swine manure. It is considered that lower aliphatic amines might be lost and some sulfur-containing compounds might decompose during steam distillation. Fractions **A**, **C**, **D**, **F**, and **G** have a malodor. Figures 1 to 7 show gas chromatograms of Fractions **A**, **B**, **C**, **D**, **E**, **F**, and **G** respectively. A large quantity of extracted matter was contained in Fractions **A** and **C**.

The components included in each fraction were identified by gas chromatography-mass spectrometry. No other identification method such as IR, NMR, and UV, has been practical because of the small quantity of extracted matter and the difficulty of separating components of a similar chemical nature. Fraction **A** had a roasted rubber-like or oily odor, and it consisted mainly of alkanes whose origins were unknown. Table 2 shows the results of the identification of Fraction **A** and the content ratio of each component, which was calculated from the areas of the peaks on the gas chromatogram, corrected by the relative sensitivity of each normal alkane against the gas-chromatographic detector. 2,6-Di-*t*-butyl-*p*-cresol, only a little of which was present in Fraction **A**, was the main component in Fraction **B**; its presence in liquid swine manure has already been reported in a previous paper.[1] From the mass spec-

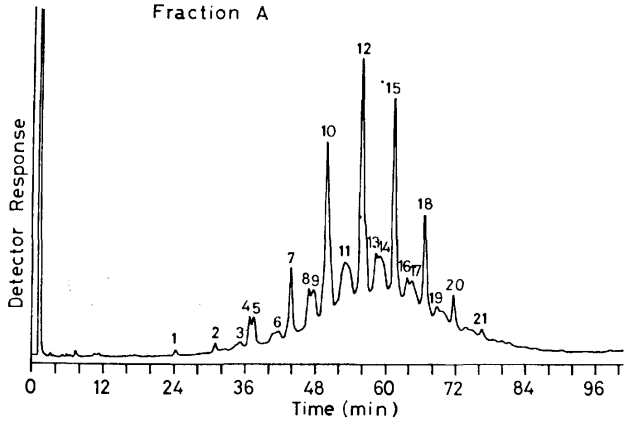

Fig. 1. Gas chromatogram of fraction **A**.

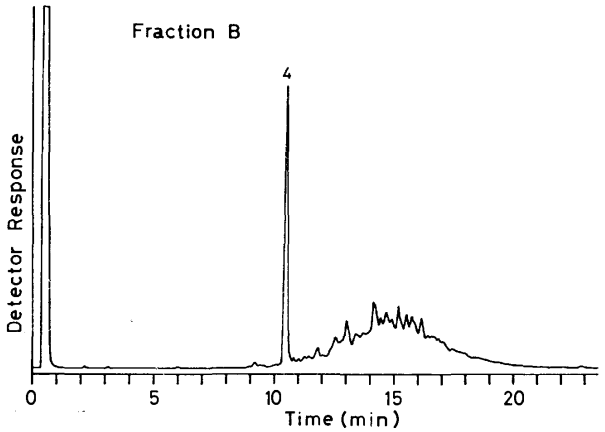

Fig. 2. Gas chromatogram of fraction **B**.

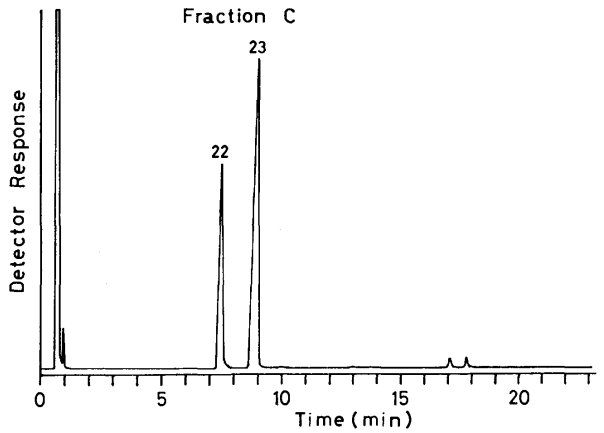

Fig. 3. Gas chromatogram of fraction **C**.

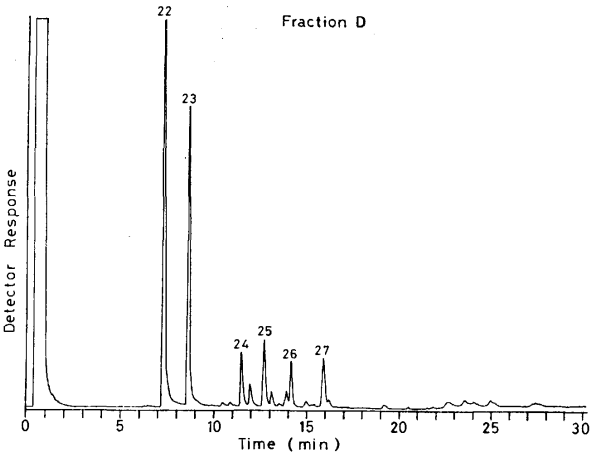

Fig. 4. Gas chromatogram of fraction **D**.

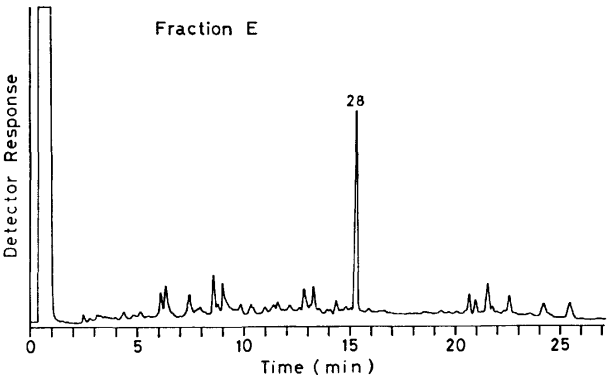

Fig. 5. Gas chromatogram of fraction **E**.

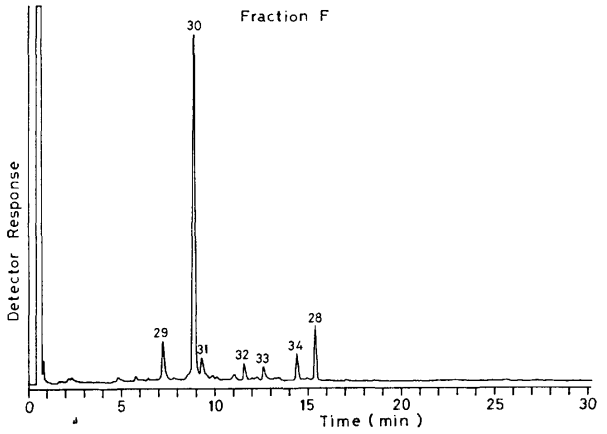

Fig. 6. Gas chromatogram of fraction **F**.

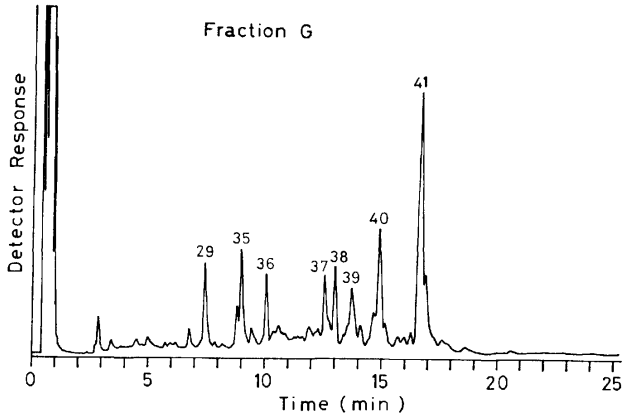

Fig. 7. Gas chromatogram of fraction **G**.

trum normal alkanes can be distinguished from isoalkanes, but structure determinations of the isoalkanes are almost impossible using only the mass spectra.

Table 3 shows the results of the identification of Fractions **C** to **G**. Fraction **C** consisted almost entirely of indole and skatole, which are well-known to have a fecal odor and which had already been detected in liquid animal manure.[4] However, the odors of indole and skatole are quite different from that of the swine manure, although they are thought to contribute to the total odor of the swine manure. Fraction **D** contained some aldehydes besides indole and skatole. However, the aldehydes did not play any role in the odor of swine manure. Fraction **E** consisted exclusively of dibutyl phthalate (DBP), which was also confirmed, with a peak enhancement, by the co-injection of an authentic substance into the gas chromatograph. DBP is an odorless compound and a well-known pollutant; thus, its origin in liquid swine manure may not be a metabolic process, but, rather, it may be a pollution from the synthetic polymers.

Fractions **F** and **G** had a characteristic and tenacious malodor. The organoleptic test showed that a compound with a peak number of 29 had the odor. It was concluded from its mass spectrum to be aminoacetophenone. Further, it was confirmed to be *o*-aminoacetophenone by means of a comparison with an authentic substance using gas chromatography. As the odor of this compound has been recognized for the first time by column chromatography, it must fuse with odors of other odoriferous substances to become a new malodor. Many components in Fractions **F** and **G** could not be identified by mass spectrometry alone.

Trace components which did not appear as peaks in the gas chromatograms with the detector's gain,

Table 2. Components of fraction **A**

Peak number	Name	Content ratio (%)
1	Tridecane	0.1
2	Tetradecane	0.2
3	Pentadecane isomer	0.4
4	2,6-Di-*t*-butyl-*p*-cresol	2.0
5	Pentadecane	
6	$C_{16}H_{30}$	0.7
7	Hexadecane	2.4
8	Octadecane isomer	6.2
9	Heptadecane isomer	
10	Heptadecane	8.7
11	Nonadecane isomer	12.4
12	Octadecane	14.7
13	Nonadecane isomer	11.5
14	Nonadecane isomer	
15	Nonadecane	12.3
16	Eicosane isomer	8.2
17	Eicosane isomer	
18	Eicosane	7.6
19	Heneicosane isomer	1.8
20	Heneicosane	6.9
21	Docosane	0.2

Table 3. Results of identification of fractions, **C**, **D**, **E**, **F**, and **G**

Peak number	Name
22	Indole
23	Skatole
24	Tetradecanal
25	Pentadecanal
26	Hexadecanal
27	$C_{18}H_{34}O$
28	Dibutyl phthalate
29	*o*-Aminoacetophenone
30	Unknown
31	Unknown
32	Unknown
33	Unknown
34	Unknown
35	2-(1-Propenyl)-6-methoxyphenol
36	3,4-Dimethoxyacetophenone
37	2-(Butylamino)benzoxazole
38	2-Tridecanol
39	Unknown
40	Unknown
41	Unknown

shown in Figs, 1, 3, 5, and 6, were also identified by gas chromatography-mass spectrometry; most of them were odoriferous. They are trithiapentane and terathiahexane in Fraction **A**; ethylindole, 2-pentadecanone, and 2-hexadecanone in Fraction **C**; 3,3-dimethyl-2-thiapentane and benzothiazole in Fraction **E**, and quinazoline in Fraction **F**.

The authors wish to thank Mr. Minoru Kuriyama, a hog raiser near Tsukuba New Town of Ibaraki, for his offer of liquid swine manure.

Refer nces

1) A. Yasuhara and K. Fuwa, *Bull. Chem. Soc. Jpn.*, **50**, 731 (1977).
2) J. R. Miner and T. E. Hazen, *Trans. Am. Soc. Agr. Eng.*, **12**, 772 (1969).
3) J. Ronald Miner, "Odors from Confined Livestock Production," Office of Research and Development, U. S. Environmental Protection Agency, Washington, D.C., 1974.
4) W. E. Burnett, *Environ. Sci. Technol.*, **3**, 744 (1969).

Effects of Neighboring Functional Groups in the Asymmetric Reduction of ω-Substituted Alkyl Phenyl Ketones with Lithium Tri-*l*-Menthoxyaluminum Hydride[1]

Shozo YAMAGUCHI and Kuninobu KABUTO

Department of Chemistry, College of General Education, Tohoku University, Kawauchi, Sendai 980

(Received May 25, 1977)

In the enantioselective reduction of ω-substituted alkyl phenyl ketones, $PhCO(CH_2)_nY$, with lithium tri-*l*-menthoxyaluminum hydride, the effect of the functional groups, $Y(NR_2$, OMe, and SMe) on the stereoselectivity was examined in comparison with that of the alkyl group. Of the functional groups tested, the MeO group is more effective in enhancing the stereoselectivity than the NMe_2 or SMe group except in the case of $n=1$. The optical yields are also affected by the number of the methylene group (n) in the substrates. These results strongly suggest that the coordination of the Y group with the reducing reagent is one of the essential factors in the stereoselectivity. The absolute configurations of the resulting alcohols are correlated with the relative magnitudes of the lanthanide-induced shifts(LIS) of their (+)-MTPA esters.

There have been many studies[2] of the asymmetric reduction of achiral ketones with lithium aluminum hydride modified by chiral reagents. Although some systematic studies[3] have been done in exploring effective chiral ligands, attention has so far been mostly focused on the steric effects of the substituents around the chiral center on the asymmetric bias. Mosher and his co-workers have developed the LAH–chiral amino alcohol complexes,[4] which give excellent asymmetric yields of as much as 75% in the reduction of acetophenone. They explained this high stereoselectivity in terms of a rigid conformation of the chiral hidride reagent as a result of the coordination of such functional groups as NMe_2 in the chiral ligand with Li^+. A similar coordinating effect has also been reported[5] in the asymmetric reduction with LAH–*N*-(*o*-substituted benzyl)-α-methylbenzylamine complexes.

On the other hand, in order to conduct the asymmetric reduction of the substrates with functional groups effectively, it is necessary to get information on the effect of the functional group on asymmetric induction. Such investigation has, however, been limited to the diastereoselective reductions[6] of the carbonyl group, and little is known about the role of the groups[7] in substrates on enantioselective reduction.

For the purpose of clarifying the stereoselectivity enhancement by the functional group in substrates in the case of enantioselective reductions, it is desirable that a chiral ligand not have any additional group other than the one essential for complex formation with a reducing reagent, and that the asymmetric yield not be high when the functional group is absent in the substrates.[8]

On the basis of these considerations, the asymmetric reduction of ω-substituted alkyl phenyl ketones, $PhCO(CH_2)_nY$ ($Y=NR_2$, OMe, SMe, and alkyl; $n=1-4$), with $LiAlH(O\text{-Menthyl})_3$ was carried out in order to find the most profitable group(Y) and number of the methylene group(*n*).

The reduction of ketones was conducted in ether under a nitrogen atmosphere. The synthetic yields were 80—100%, and the resulting secondary alcohols were purified by preparative GLC. The results are shown in Table 1.

Of the absolute configurations of the alcohols obtained by this reduction, those of 2-methoxy-1-phenylethanol(**2**) and 2-methylthio-1-phenylethanol(**3**) were assigned as *S*(+) by correlating them chemically to (*S*)-(+)-mandelic acid according to the procedure outlined in Scheme 1, while that of 4-dimethylamino-1-phenyl-1-butanol(**12**) was determined to be *R*(+) by correlation to 1-phenyl-1-butanol(**6**) (Scheme 2).

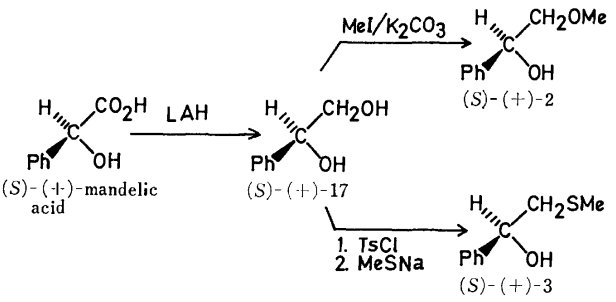

Scheme 1.

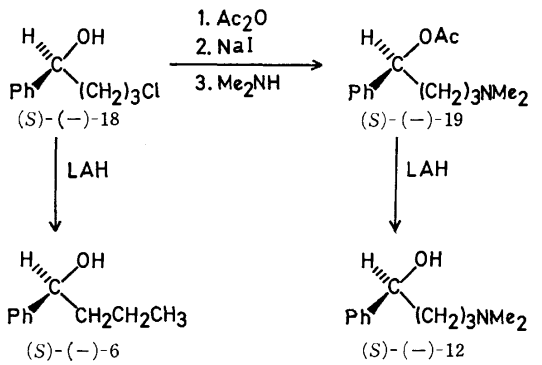

Scheme 2.

The absolute configurations of the other alcohols with functional groups were assigned[9] by means of the (*R*)-(+)-MTPA*/$Eu(fod)_3$ method[10] previously reported by the present authors, since it has been confirmed that this method is also applicable to 1-phenylethanols with the functional groups [$Y=NMe_2$ (**1**); OMe(**2**); SMe(**3**)] at the C-2 position.

The (*R*)-(+)-MTPA/$Eu(fod)_3$ method correlates the

* (*R*)-(+)-α-Methoxy-α-trifluoromethylphenylacetic acid (Mosher's Reagent).

TABLE 1. ASYMMETRIC REDUCTION OF ω-SUBSTITUTED ALKYL PHENYL KETONES WITH $LiAlH(O\text{-}l\text{-Menthyl})_3$ AND THE ABSOLUTE CONFIGURATION OF THE RESULTING ALCOHOLS

$PhCO(CH_2)_nY$ (1′—16′) —$LiAlH(O\text{-Menthyl})_3$, Ether, 0 °C→ $PhCH(OH)(CH_2)_nY$ (1—16)

Entry	Alcohol		LIS_{OMe}			Config[a]	%ee[b]
		Functional group(Y)	LIS_A	LIS_B	ΔLIS		
1	$n=1$	NMe_2 (**1**)	4.4	4.2	0.2	$S(-)$[c,d]	7
2		OMe (**2**)	7.1	4.9	2.2	$R(-)$[c]	4
3		SMe (**3**)	8.4	6.4	2.0	$S(+)$[c]	12
4		H (**4**)	12.6	8.6	4.0	$R(+)$[c]	3
5		Me (**5**)	9.6	7.5	2.1	$R(+)$[c]	7
6		Et (**6**)	9.8	7.8	2.0	$R(+)$	15
7	$n=2$	NMe_2 (**7**)				$R(+)$[f]	25[g]
8		OMe (**8**)	10.0	8.2	1.8	$R(+)$	35
9		SMe (**9**)	10.0	9.3	0.7	$R(+)$	17
10		Et (**10**)	9.3	8.3	1.0	$R(+)$	19
11		N⟨ ⟩ (**11**)				$R(+)$[f]	37[g]
12	$n=3$	NMe_2 (**12**)				$R(+)$	3[h]
13		OMe (**13**)	9.5	7.4	2.1	$R(+)$	38
14		SMe (**14**)	8.7	7.9	0.8	$R(+)$	14
15		Et (**15**)	11.5	10.0	1.5	$R(+)$	13
16	$n=4$	OMe (**16**)	11.3	9.6	1.7	$R(+)$	16

a) The optical rotations, $[\alpha]_D$, were taken in cyclopentane unless otherwise specified. b) All the data are the averages of 2—3 runs. The enentiomeric excesses were determined based on the relative peak area of the MeO signals of the (*R*)-(+)-MTPA acid moiety in the presence of $Eu(fod)_3$. c) In these three alcohols, the $-CH_2Y$ group takes nomenclatural precedence over that of the Ph group; therefore, the *S* configuration in these alcohols corresponds to the *R* of the others. d) Sign for the hydrochloride of **1** in water; H. Yoshimura, *Yakugaku Zasshi*, **84**, 305 (1963). e) Ref. 10. f) Sign for a methanol solution; Ref. 7. g) Based on the absolute rotations: **7**, $[\alpha]_D$ +27.6° (*c* 1.61, MeOH); **11**, $[\alpha]_D$ +29.3° (*c* 1.9, MeOH). Refs. 7 and 14. h) Determined on the basis of the relative peak area of carbinyl protons in the ^1H NMR spectrum of **12** in the presence of the chiral shift reagent, $Eu(hfc)_3$, since (*R*)-(+)-MTPA esters of **12** were not obtained under ordinary conditions.

relative magnitude of LIS_{OMe} (the lanthanide-induced shift by $Eu(fod)_3$ of the MeO signal of the MTPA acid moiety in (*R*)-(+)-MTPA esters of secondary alcohols) with their absolute configurations; the diastereomeric ester with the larger LIS value has Structure A, while the other ester, with the smaller LIS value, has Structure B. The results are also summarized in Table 1.

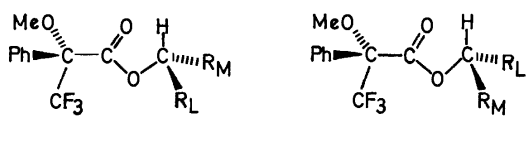

A B

$R_L > R_M$

The most pertinent observations in the asymmetric reduction are as follows: (1) When the Y group is alkyl or H, the preferential attack of the hydride ion occurs on the *si*-face of the carbonyl group, and the presence of the functional group does not alter the sense of the asymmetric induction except in the case of 2-methoxyacetophenone(Table 1, Entry 2); (2) The stereoselectivity in the reduction dependes on the functional group. Among the functional groups examined, OMe(when $n=2$ and 3) and NR_2 (when $n=2$) functioned effectively to increase the stereoselectivity (Table 1, Entries 7, 8, 11, and 13) while the SMe group did not give any higher asymmetric induction, in comparison with the non-polar ethyl group. The ethyl group was chosen as a standard, since its steric requirement, including the extention effect,[11] was considered to be similar to those of OMe and SMe, and its steric effect would be the sole controlling factor in the stereoselectivity; (3) As can be seen from Fig. 1, the stereoselectivity also depends on the number of the methylene group(n) in the case of Y=OMe or NMe_2; even the sense of asymmetric induction was reversed when Y=OMe($n=1$). The highest selectivity was observed at $n=2$(Y=NMe_2, 25%ee) or $n=3$(Y=OMe, 38%ee). On the other hand, when Y=SMe or Et, there was no distinct dependence.

It is apparent that these results could not be elucidated by an exclusive consideration of the steric effects of the functional group Y, because the similar steric requirements of the group (OMe, SMe, and Et) re-

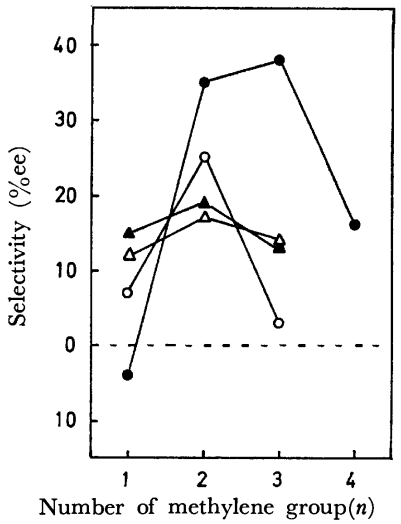

Fig. 1. Selectivity dependence on the number of methylene groups.
●: Y=OMe, ○: Y=NMe_2, ▲: Y=Et, △: Y=SMe.

Table 2. Asymmetric reduction of **11′** in the presence of TMEDA

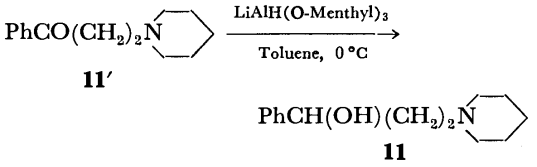

11′ **11**

TMEDA/LAH (mol/mol)	0	1.0	2.0	4.0
Optical yield[a] (%)	23	13	12	12

a) Based on the reported absolute rotation; $[\alpha]_D$ +29.3° (*c* 1.9, MeOH). Ref. 7.

sulted in two different patterns of stereoselectivity dependence (Fig. 1, Y=OMe; SMe and Et). These observations strongly suggest that the coordination of the Y group (OMe or NR_2) with the reducing reagent also plays an important role in the stereoselectivity.

The coordination of the Y group with the reducing reagent can be substantiated by the asymmetric reduction of 3-piperidinopropiophenone (**11**) in the presence of the additive, *N,N,N′,N′*-tetramethylethylenediamine(TMEDA), which can strongly coordinate with Li^+. The reduction was conducted in toluene in order to eliminate the effect of ether oxygen, which may act as a coordinating functionality. The results are shown in Table 2. Although the change in the stereoselectivity was not very remarkable because of the rather low asymmetric induction in the absence of the additive, it can be seen that the stereoselectivity was immediately decreased by the addition of TMEDA in a 1 molar ratio and did not change upon the further addition of TMEDA. This can be interpreted as a result of the interference of the coordination of piperidino nitrogen with the reducing reagent caused by TMEDA.

The oxygen and nitrogen atoms in the functional group Y are hard bases, and they can strongly coordinate with Li^+ or Al^{3+} of hard acids, while the sulfur atom is a soft base which can hardly coordinate at all with the light metal cations. Therefore, the SMe group can be considered to act as a functionality with a poor coordinating capability in the present case. The observations that the effects of the SMe group on the stereoselectivity are almost the same as those of the non-polar Et group (see Fig. 1) is consistent with this expectation.

Experimental support for the coordination of OMe being stronger than that of SMe with Li^+ has been found in the asymmetric reduction[5] of propiophenone with LAH modified by (*S*)-(−)-*N*-(*o*-dimethylaminobenzyl)-α-methylbenzylamine, where the addition of 1,2-dimethoxyethane to the reaction mixture caused a dramatic decrease in the stereoselectivity, while that of 1,2-bis(methylthio)ethane did not.

The stereoselectivity was greatly affected by the position of the carbonyl group relative to the functional group Y (OMe, NR_2) in the present case, indicating that the reduction proceeded *via* a cyclic transition state. Concerning the mechanism of the metal hydride reduction of the carbonyl group, Pierre and Handel demonstrated that the alkali metal cation is indispensable[12] and that it also plays very important role in the stereoselectivity.[6b]

They examined the diastereomeric reduction of N-substituted 2-aziridinyl ketones and proposed a cyclic model where the alkali metal cation (not the metal hydride anion) is incorporated in the chelate ring. On the basis of this model, it can be considered that a similar coordination (C) of the carbonyl and the Y group with Li^+ occurs in the present asymmetric reduction:

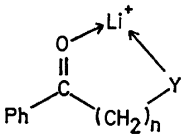

C

The number of the methylene group(*n*) determines the size of the chelate ring and thus affects the rigidity of the transition state, being responsible for the stereoselectivity. As can be seen from the low stereoselectivity in the reduction of 2-methoxyacetophenone (Table 1, Entry 2), however, the ease of the chelate-ring formation, predicted from both the ring size[13] and the nature of the heteroatoms, does not always afford a high asymmetric induction.

Experimental

Instruments. The NMR spectra were taken on a Hitachi R-22 (90 MHz) spectrometer, with TMS as the internal standard. The gas-liquid chromatographic (GLC) determination was performed on a Shimadzu GC-5A apparatus, using a PEG 20 M or PDEG succinate column (3 mm × 1.5 m). The preparative GLC was carried out on a Varian Aerograph 700 using the same stationary phases (1/4″ × 1.5 m). The optical rotations were tekan on a Perkin Elmer 241 polarimeter, using a 1-dm thermostated microcell.

Reagents. The ether was distilled over sodium hydride and stored over Linde molecular sieves 3A. The toluene was dried over the same molecular sieves. A stock $LiAlH_4$

solution in ether was passed through a glass filter under nitrogen and stored in a flask closed with a rubber septem. It was analysed by iodometry just before use. Aliquots were taken up by syringe as needed. A commercially available *l*-menthol [Tokyo Kasei, $[\alpha]_D^{20}$ −50° (*c* 10, EtOH)] was used without further purification.

Materials. 2-Dimethylaminoacetophenone(**1'**),[15] 2-methoxyacetophenone(**2'**),[16] 3-dimethylaminopropiophenone (**7'**),[7] 3-methoxypropiophenone(**8'**),[17] 3-(methylthio)propiophenone(**9'**),[18] and 3-piperidinopropiophenone(**11'**)[7] were prepared according to the reported procedures.

*2-(Methylthio)acetophenone(**3'**)*: A solution of phenacyl bromide (30 g, 0.15 mol) in ethanol (120 ml) was cooled with ice, and then a 20% aq solution of sodium methyl sulfide (36 ml) was added over a period of 10 min under stirring. The reaction mixture gradually turned red, and stirring was continued for 1 h. The reaction mixture was then poured into 600 ml of ice water. After being salted out, it was extracted with ether and the extract was washed with water, dried(Na_2SO_4), concentrated, and distilled, giving 17.5 g (70%) of **3'** as a pale yellow oil: bp 118—119 °C/3 Torr; NMR(CCl_4) δ=2.02 (3H, s, SCH_3), 3.60 (2H, s, $-CH_2S$); Found: C, 65.06; H, 6.05%. Calcd for $C_9H_{10}OS$: C, 65.02; H, 6.06%.

*4-Dimethylaminobutyrophenone(**12'**)*: To a 100 ml portion of a cold ether solution of dimethylamine (25 g, 0.056 mol), was added, little by little, crude 4-iodobutyrophenone (7.35 g, 0.027 mol, prepared from 4-chlorobutyrophenone and sodium iodide, and heated at 90 °C for 18 h in ethyl methyl ketone). After standing for a day at room temperature, the reaction mixture was warmed at 30—40 °C for 1 h. The precipitates were filtered off, and then the filtrate was concentrated to yield a pale yellow oil, which was subsequently dissolved in ether. The ether solution was extracted with 2M HCl.

After the acid layer had been made alkaline with dilute sodium hydroxide solution, it was extracted with ether. The extract was washed with water, dried (Na_2SO_4), concentrated, and distilled *in vacuo*, yielding 2.6 g (50%) of **12'** as a colorless oil: bp 122—124 °C/0.5 Torr; NMR (CCl_4) δ= 1.80 (2H, quintet, $-CH_2\underline{CH_2}CH_2-N$), 2.13 (6H, s, $-N(CH_3)_2$), 2.27 (2H, t, $-CH_2-N$), 2.93 (2H, t, $-CO-CH_2-$); Found: N, 7.43%. Calcd for $C_{12}H_{17}ON$: N, 7.32%.

*4-Methoxybutyrophenone(**13'**)*: To a solution of sodium methoxide, prepared from 1.38 g (0.06 mol) of sodium and 60 ml of methanol, was added, by portions, 4-chlorobutyrophenone ethylene acetal (11.4 g, 0.05 mol; mp 55—57 °C; Found: C, 63.60; H, 6.83%. Calcd for $C_{12}H_{15}ClO_2$: C, 63.58; H, 6.67%, prepared from 4-chlorobutyrophenone, ethylene glycol, and a catalytic amount of *p*-toluenesulfonic acid, refluxed in benzene for 48 h with a Dean-Stark water separator; yield, 69%). The reaction mixture was subsequently stirred for 45 min at 50 °C and then cooled to room temperature. After the addition of a saturated sodium chloride solution, the reaction mixture was extracted with benzene and the extract was washed with water, dried (Na_2SO_4), and concentrated, yielding 10.2 g of a pale yellow oil. It was dissolved in 50 ml of methanol, and, after the addition of 10 ml of concd HCl, the methanol solution was stirred for 1 h at room temperature. The solvent was then removed, and the residue was extracted with ether. The extract was washed with a sodium hydrogencarbonate solution and brine successively, dried (Na_2SO_4), concentrated, and distilled, yielding 5.0 g (56%) of **13'** as a colorless oil: bp 93 °C/0.5 Torr; NMR (CCl_4) δ=1.96 (2H, quintet, $-CH_2\underline{CH_2}CH_2-O$), 3.01 (2H, t, $-CO-CH_2-$), 3.41 (2H, t, $-CH_2OMe$), 3.29 (3H, s, OMe); Found: C, 74.23; H, 8.01%. Calcd for $C_{11}H_{14}O_2$: C, 74.13; H, 7.92%.

*4-(Methylthio)butyrophenone(**14'**)*: To a solution of a 20% aq solution of sodium methyl sulfide (16 ml) was added, drop by drop, 4-chlorobutyrophenone ethylene acetal (9.08 g, 40 mmol) in 120 ml of ethanol, after which the reaction mixture was warmed at 60 °C for 1 h. After concentration *in vacuo*, the mixture was poured into water and extracted with ether. The extract was washed with a saturated sodium chloride solution. After the removal of the ether, the pale yellow residue was dissolved in 50 ml of methanol and stirred for 1 h with 10 ml of concd HCl at room temperature. The methanol was then removed under reduced pressure, and the residue was dissolved in ether, washed with saturated sodium hydrogencarbonate and brine successively, dried (Na_2SO_4), concentrated, and distilled, giving a pale yellow oil, which was subsequently distilled *in vacuo* to yield 5.6 g (72%) of **14'**: bp 118 °C/1 Torr; NMR (CCl_4) δ=1.8—2.1 (2H. m, $-CH_2\underline{CH_2}CH_2-S$), 2.07 (s, SMe), 2.56 (2H, t, $-CH_2-S$), 3.07 (2H, t, $-CO-CH_2-$); Found: C, 68.07; H, 7.40%. Calcd for $C_{11}H_{14}OS$: C, 68.00; H, 7.26%.

*5-Methoxyvalerophenone(**16'**)*: To a Grignard reagent prepared from 1-chloro-4-methoxybutane (12.3 g, 0.1 mol), magnesium turnings (2.6 g, 0.11 mol), and ether (35 ml) was added, drop by drop, benzonitrile (10.3 g, 0.1 mol) in toluene (50 ml). After the moderately exothermic reaction had subsided, about 50 ml of the solvent was distilled off. Reflux was continued for 4 h, and then the mixture was stood overnight at room temperature. It was subsequently poured into water containing concd HCl, extracted with ether, washed with dil NaOH and water successively, dried ($MgSO_4$), concentrated and distilled *in vacuo* to yield 16.3 g (85%) of **16'** as a colorless oil: bp 119—120 °C/0.2 Torr; NMR (CCl_4) δ=1.7 (4H, m, $-CO-CH_2\underline{CH_2}\underline{CH_2}CH_2$), 2.96 (2H, t, $-CO-CH_2-$), 3.29 (s, $-OCH_3$), 3.38 (t, $-CH_2-O$); Found: C, 74.96; H, 8.56%. Calcd for $C_{12}H_{16}O_2$: C, 74.97; H, 8.39 %.

*ω-Substituted 1-Phenyl-1-alkanols (**9**, **12**, **13**, **14**, and **16**)*: These new carbinols were obtained as a colorless oil by the $LiAlH_4$ reduction of the corresponding ketones in ether. (±)-**9**: NMR (CCl_4) δ=1.75—2.1 (m, $-CH(OH)-\underline{CH_2}$), 2.01 (s, SMe), 2.47 (2H, t, $-CH_2-S$), 4.67 (1H, dd, $-\underline{CH}-(OH)-$); Found: C, 65.85; H, 7.77%. Calcd for $C_{10}H_{14}OS$: C, 65.89; H, 7.74%. (±)-**12**: NMR (CCl_4) δ=1.65 (4H, m, $-CH(OH)-\underline{CH_2}\underline{CH_2}-$), 2.17—2.2 (8H, NMe_2 and $-CH_2-N$), 4.47 (1H, dd, $-\underline{CH}(OH)-CH_2-$); Found: C, 74.53; H, 9.95; N, 7.00%. Calcd for $C_{12}H_{19}ON$: C, 74.57; H, 9.91; N, 7.25%. (±)-**13**: NMR (CCl_4) δ=1.6 (4H, m, $-CH(OH)-\underline{CH_2}\underline{CH_2}-$), 3.21—3.28 (5H, OMe and $-CH_2-O$), 4.49 (1H, t, $-\underline{CH}(OH)-$); Found: C, 73.36; H, 9.04%. Calcd for $C_{11}H_{16}O_2$: C, 73.30; H, 8.95%. (±)-**14**: NMR (CCl_4) δ=1.6 (4H, m, $-CH(OH)-\underline{CH_2}\underline{CH_2}-$), 1.96 (3H, s, SMe), 2.36 (2H, t, $-CH_2-S$), 4.49 (1H, t, $-CH(OH)-$); Found: C, 67.25; H, 8.26%. Calcd for $C_{11}H_{16}OS$: C, 67.25; H, 8.28%. (±)-**16**: NMR (CCl_4) δ=1.6 (6H, m, $-CH(OH)-\underline{CH_2}\underline{CH_2}\underline{CH_2}-$), 3.20—3.26 (5H, OMe and $-CH_2-O$), 4.51 (1H, t, $-CH(OH)-$); Found: C, 74.18; H, 9.44%. Calcd for $C_{12}H_{18}O_2$: C, 74.19; H, 9.34%.

*Determination of Absolute Configurations by Chemical Correlation. (S)-(+)-2-Methoxy-1-phenylethanol(**2**)*: A mixture of (*S*)-(+)-1-phenyl-1,2-ethanediol(**17**) [1.38 g, 10 mmol, $[\alpha]_D^{29}$ +39.2° (*c* 2.62, EtOH)],[19] potassium carbonate (2.38 g), and methyl iodide (0.75 ml, 12 mmol) in acetone (15 ml) was refluxed for 15 h. The reaction mixture was then filtered, and the filtrate was concentrated, after which the residue was dissolved in ether. The ether solution was washed with water, dried (Na_2SO_4), and concentrated to give 1.24 g of a pale yellow oil containing about 50% of **2**. The monomethyl ether was concentrated by silica gel column chromatography,

using benzene-ether (10 : 1) as the eluent, purified by preparative GLC(PDEGS 1/4″×1.5 m, 170 °C, He 60 ml/min), and distilled *in vacuo* [115 °C (bath)/1 Torr]. 197 mg; NMR (CCl_4) δ=3.1—3.6 (AB part of ABX, $-CH_2-O$), 3.36 (3H, s, OMe), 4.73 (1H, dd, -CH(OH)-); $[\alpha]_D^{20}$+44.6° (*c* 4.54, cyclopentane).

(S)-(+)-*2-Methylthio-1-phenylethanol* (**3**): Tosyl chloride (3.14 g, 16 mmol) was added, portion by portion ,to a solution of (*S*)-(+)-**17** (2.07 g, 15 mmol, $[\alpha]_D^{20}$ +39.2° in EtOH) in pyridine (20 ml) at 0 °C. After the addition was completed, the reaction mixture was allowed to stand overnight in a refrigerator, poured into water (200 ml), and extracted with benzene. The extract was washed with 2M HCl and saturated sodium hydrogencarbonate successively, dried (Na_2SO_4), and concentrated to yield crude (*S*)-(+)-1-phenyl-1,2-ethanediol 2-tosylate (4.1 g), which was then recrystallized from benzene-hexane to give fine needles (2.6 g, 59%); mp 72—73 °C; $[\alpha]_D^{20}$ +30.3° (*c* 3.35, MeOH); Found: C, 61.75; H, 5.52%. Calcd for $C_{15}H_{16}O_4S$: C, 61.63; H, 5.52%. To a stirred solution of the tosylate (584 mg, 2 mmol) in ethanol (10 ml) was added, drop by drop 20% aq sodium methyl sulfide (0.8 ml, *ca.* 3 mmol) at room temperature. Stirring was continued for 2 h. After water had been added to the mixture, it was extracted with ether. The subsequent evaporation of the solvent afforded a pale yellow oil (290 mg), which was chromatographed on silica gel using benzene–ether (20 : 1) as the eluent and distilled [120 °C(bath)/1 Torr] to yield 150 mg (45%) of **3** as a pale yellow oil: NMR (CCl_4) δ=2.02 (3H, s, SMe), 2.4—2.9 (AB part of ABX, $-CH_2-S$), 4.6 (1H, dd, -CH(OH)-); $[\alpha]_D^{20}$ +63.8° (*c* 5.63, cyclopentane).

(S)-(−)-*4-Chloro-1-phenyl-1-butanol* (**18**): This alcohol was prepared by the asymmetric reduction of 4-chlorobutyrophenone by $LiAlH_4$ modified by (−)-(2*R*, 3*S*)-4-dimethylamino-3-methyl-1,2-diphenyl-2-butanol (LAH : R*OH=1 : 2.3) according to the reported procedure.[4b] The absolute configuration was determined to be *S*(−) by (*R*)-(+)-MTPA/$Eu(fod)_3$ method;[10] LIS_A 8.64, LIS_B 8.08, ΔLIS 0.56; 54 %ee, $[\alpha]_D^{20}$ −27.3° (*c* 2.83, cyclopentane); NMR (CCl_4) δ= 1.73 (4H, m, -CH(OH)-CH_2CH_2-), 3.42 (2H, bt, $-CH_2Cl$), 4.50 (1H, bt, -CH(OH)-). Acetate of **18**; $[\alpha]_D^{20}$ −49.3° (*c* 5.88, cyclopentane). The absolute configuration of **18** was confirmed by hydrogenolysis to (*S*)-(−)-1-phenyl-1-butanol (**6**) (see Table 1, Entry 6) as follows. A THF solution (8 ml) of $LiAlH_4$ (160 mg, 4 mmol) and **18** (277 mg, 1.5 mmol, $[\alpha]_D^{20}$ −27.3°) was refluxed at 95 °C for 3 h. The reaction mixture was then worked-up in a usual way, and the resulting colorless oil (198 mg) was submitted to preparative TLC (silica gel, 20% ethyl acetate in hexane) to yield 48 mg of (*S*)-(−)-**6** as colorless crystals; $[\alpha]_D^{20}$−31.0° (*c* 3.08, cyclopentane).

(S)-(−)-*4-Dimethylamino-1-phenyl-1-butanol* (**12**): The acetate (412 mg, $[\alpha]_D^{20}$−49.3° in cyclopentane) of **18** was refluxed for 6 h with sodium iodide (600 mg) in ethyl methyl ketone and then transformed to 493 mg of crude 4-iodo-1-phenyl-1-butanol as a colorless oil: $[\alpha]_D^{20}$ −33.6° (*c* 3.21, cyclopentane). This was used without further purification. To a solution of dimethylamine (5 g) in ether (10 ml) was added crude 4-iodo-1-phenyl-1-butanol (480 mg) in dry ether (5 ml), and the mixture was stood overnight at room temperature. The precipitates were filtered off, and the filtrate was concentrated *in vacuo*. The residue was dissolved in ether and extracted with 2M HCl. After having been washed with ether, the acid layer was made alkaline and extracted with ether, washed with water, dried (Na_2SO_4), concentrated, and distilled [120 °C (bath)/0.4 Torr], yielding 225 mg of **19**: NMR (CCl_4) δ=1.2—1.9 (4H, m, -CH(OAc)-CH_2CH_2-), 2.0 (3H, s, OAc), 2.09 (6H, s, NMe_2), 2.22 (2H, t, $-CH_2-N$), 5.67 (1H, t, -CH(OAc)-); $[\alpha]_D^{20}$ −42.5° (*c* 3.30, cyclopentane). The reduction of **19** (200 mg) with $LiAlH_4$ (150 mg) in ether (4 ml) at room temperature for 4 h afforded **12** (125 mg) as a colorless oil, which was distilled *in vacuo* [90 °C (bath)/0.2 Torr]; $[\alpha]_D^{20}$ −28.6° (*c* 3.40, cyclopentane).

Asymmetric Reduction of ω-Substituted Alkyl Phenyl Ketones with Lithium Tri-l-menthoxyaluminum Hydride. Under a nitrogen atmosphere, to a stirred solution of $LiAlH_4$ (1.2 mmol) in ether (2.5 ml) was added *l*-menthol (562 mg, 3.6 mmol) in 2 ml of the same solvent at 0 °C. The container of *l*-menthol was washed with 1 ml of ether, and the washing was added to the $LiAlH_4$ solution. Three minutes after the initial addition of menthol, ketone (1 mmol) in 0.5 ml of ether was added, drop by drop, to the LAH–menthol complex and the container of ketone was also washed with 0.5 ml of ether. The reaction mixture was stirred for 3 h at 0 °C to give a transparent solution. The excess hydride was decomposed with a small amount of water. After the addition of excess dil HCl, the mixture was extracted with ether. The extract was washed with saturated sodium hydrogencarbonate and water successively and dried (Na_2SO_4). The product was purified by preparative GLC and finally distilled *in vacuo*. In the case of the reduction of amino ketones, the products were extracted with dil HCl from the reaction mixture. After the extract had then been made alkaline, the amino alcohol liberated was extracted with ether and purified by preparative GLC and distilled *in vacuo*.

The enantiomeric purities of the resulting alcohols were determined according to a method previously reported.[10]

Optical rotations, $[\alpha]_D^{20}$ in cyclopentane, of the new optically active alcohols are as follows. (*S*)-**2**, +44.6° (*c* 4.54) optically pure; (*S*)-**3**, +63.8° (*c* 5.63) optically pure; (*R*)-**8**, +11.1° (*c* 3.78) 34%ee; (*R*)-**9**, +3.63° (*c* 3.94) 18%ee; (*R*)-**12**, +1.65° (*c* 4.67) 3%ee; (*R*)-**13**, +15.2° (*c* 4.72) 38 %ee; (*R*)-**14**, +1.43° (*c* 4.44) 12%ee; (*R*)-**15**, +2.86° (*c* 5.71) 13%ee; (*R*)-**16**, +0.322° (*c* 8.73) 16%ee.

Asymmetric Reduction of 3-Piperidinopropiophenone (**11′**) *in the Presence of TMEDA.* To a solution of $LiAlH_4$ (2.0 mmol) in 5 ml of ether was added *l*-menthol (938 mg, 6 mmol) in 4 ml of ether at 0 °C. The ether was subsequently removed *in vacuo*, and the residue was dissolved in 9 ml of dry toluene. *N,N,N′,N′*-Tetramethylethylenediamine (TMEDA) [Run 1, 0.3 ml (2 mmol); 2, 0.6 ml (4 mmol); 3, 1.2 ml (8 mmol); 4, none] was added to the solution, and the resulting solution was cooled to 0 °C. After 3 min, **11′** (217 mg, 1 mmol) in 1 ml of toluene was added. The reaction mixture was kept overnight at 0 °C. After the cautious addition of water, the reaction mixture was extracted with dil HCl. The acid layer was made alkaline with dil NaOH and extracted with ether. The solvent and TMEDA were removed *in vacuo*, and the product was purified by distillation [120 °C(bath)/0.5 Torr]. No starting ketone was detected on GLC. The results are shown in Table 2.

The authors wish to express their deep gratitude to Professor Harry S. Mosher, Stanford University, for his helpful suggestions throughout this work. The authors also wish to thank Mrs. Fujiko Yasuhara for the measurement of the NMR spectra.

References

1) A part of this work was presented at 31st Annual Meeting of the Chemical Society of Japan, Sendai, October 1974.

2) J. D. Morrison and H. S. Mosher, "Asymmetric Organic Reactions," Prentice-Hall, Englewood Cliffs, New Jersey

(1971), p. 202.

3) (a) O. Cěrvinka and O. Belovsky, *Coll. Czech. Chem. Commun.*, **32**, 3897 (1967); (b) O. Cěrvinka, *ibid.*, **30**, 1684 (1965); (c) O. Cěrvinka and O. Belovsky, *ibid.*, **30**, 2487 (1965).

4) (a) S. Yamaguchi, H. S. Mosher, and A. Pohland, *J. Am. Chem., Soc.* **94**, 9254 (1972); (b) S. Yamaguchi and H. S. Mosher, *J. Org. Chem.*, **38**, 1870 (1973); (c) C. J. Reich, Ph. D. Thesis, Stanford University, 1976.

5) S. Yamaguchi, F. Yasuhara, and K. Kabuto, *J. Org. Chem.*, **42**, 1578 (1977).

6) S. Yamada and K. Koga, *Chem. Pharm. Bull.*, **20**, 526 (1972) and the references therein; (b) H. Handel and J. L. Pierre, *Tetrahedron*, **31**, 997 (1975).

7) R. Andrisano, A. S. Angeloni, and S. Marzocchi, *Tetrahedron*, **29**, 913 (1973).

8) (a) A. Horeau, H. B. Kagan, and J. P. Vigneron, *Bull. Soc. Chim. Fr.*, **1968**, 3795; (b) R. J. Evans, S. R. Landor and J. P. Regan, *J. Chem. Soc., Pekin Trans. 1*, **1974**, 552.

9) The same results were obtained by means of Mosher's method based on the chemical-shift difference of the MeO signals of the (*R*)-(+)-MTPA acid moiety, except in the case of Y=OMe (**2**, **8**, **13**, and **16**), where a partial overlapping between the MeO(MTPA) and the methylene($-CH_2-$OMe) signals made the configurational determination difficult. The chemical-shift differences of the OMe, SMe, and NMe_2 of the carbinyl moiety can also be utilized for the configurational determination; J. A. Dale and H. S. Mosher, *J. Am. Chem. Soc.*, **95**, 512 (1973).

10) S. Yamaguchi, F. Yasuhara, and K. Kabuto, *Tetrahedron*, **32**, 1363 (1976).

11) (a) G. R. Sullivan, J. A. Dale, and H. S. Mosher, *J. Org. Chem.*, **38**, 2143 (1973); (b) S. Yamaguchi, J. A. Dale, and H. S. Mosher, *ibid.*, **37**, 3174 (1972).

12) J. L. Pierre and H. Handel, *Tetrahedron Lett.*, **1974**, 2317.

13) R. W. Parry in "Chemistry of the Coordination Compounds," ed by J. C. Bailar, Reinhold Publishing Cooporation, New York (1956), p. 220.

14) While this study was in progress, higher optical yields (**7**, 77%ee; **11**, 66%ee) were reported by Andrisano *et al.*[7] under similar reaction conditions. In spite of the repeated reinvestigation of the various reaction conditions which are considered to be important factors in regulating the optical yields (the aging factor of the reagent;[4a,20] the concentration and composition of the reagent; the purities of the substrates, ligand, and LAH), the results reported in the literature were not duplicated.

15) N. B. Chapman, *J. Chem. Soc.*, **1963**, 1387.

16) R. B. Moffett and R. L. Schriner, *Org. Synth.* **21**, 79 (1941).

17) R. E. Lesile and H. R. Henze, *J. Am. Chem. Soc.*, **71**, 3480 (1949).

18) M. J. Weiss and M. D. O'Donoghue, *J. Am. Chem. Soc.*, **79**, 4774 (1957).

19) V. Prelog, M. Wilhelm, and D. B. Bright, *Helv. Chim. Acta*, **37**, 221 (1954).

20) (a) L. J. Altman and Y. Li, *Tetrahedron Lett.*, **1976**, 2493; (b) D. J. Sandman, K. Mislow, W. P. Giddings, J. Dirlam, and G. C. Hanson, *J. Am. Chem. Soc.*, **90**, 4877 (1968).

Chemical Transformation of Seldomycin 5 into 3′-Episeldomycin 5 and Its Antibacterial Activity

Hideo MATSUSHIMA,* Kozo KITAURA,** and Yasuki MORI

Tokyo Research Laboratory, Kyowa Hakko, Asahimachi, Machida, Tokyo 194

***Pharmaceuticals Research Laboratory, Kyowa Hakko, Shimotokari, Suntogun, Shizuoka 411*

(Received June 6, 1977)

3′-Episeldomycin 5 (**7**) was synthesized from seldomycin 5. Reaction of hexa-*N*-ethoxycarbonylseldomycin 5 (**2**) with *o*-nitrobenzenesulfonyl chloride gave penta-*N*-ethoxycarbonylseldomycin 5-2′,3′-epicyclic carbamate (**3**) in one step. Hexa-*N*-ethoxycarbonyl-3′-*O*-tosylseldomycin 5 or hexa-*N*-ethoxycarbonyl-3′-*O*-mesylseldomycin 5, prepared from **2**, was also converted into **3** by being heated in weakly basic solvents such as *N,N*-dimethylformamide or pyridine. Compound **3** was hydrolyzed to give **7**. Structure of **7** was confirmed by PMR, CMR, MS, and Δ[M] values. Compound **7** was found to be active against resistant bacteria which carry 3′-*O*-phosphorylating enzymes. Δ[M] values for vicinal amino groups were shortly discussed.

Seldomycins are new aminoglycoside antibiotic complex produced by *Streptomyces hofuensis* and five factors are known among which factor 5 is the most active component.[1] Structure of seldomycin 5 has been shown to be 4-*O*-[2,6-diamino-2,4,6-trideoxy-α-D-*xylo*-hexopyranosyl]-6-*O*-[2,3-diamino-2,3-dideoxy-4-*O*-methyl-α-D-xylopyranosyl]-2-deoxystreptamine (**1**).[2] Seldomycin 5 has been shown to exhibit strong antibacterial activity against both gram-positive and gram-negative bacteria, but to be inactivated, similarly to other aminoglycoside antibiotics having 3′-hydroxyl group,[3] by resistant strains carrying 3′-*O*-phosphorylating enzymes.[1] Consideration of spatial specifity manifested by most enzymes led us to transform **1** into 3′-episeldomycin 5 (**7**) which has an axial hydroxyl group at 3′ position and expect it to be active against resistant strains carrying those enzymes. Hanessian *et al.* had transformed paromamine into 3′-epiparomamine by oxidation of the 3′-hydroxyl group to a carbonyl group and reducing it by sodium borohydride, but the antibacterial activity of the product had not been reported.[4]

Results and Discussion

Compound **1** was converted into hexa-*N*-ethoxycarbonyl(ecb)-seldomycin 5 (**2**) as an *N*-protected derivative. Reaction of **2** with *o*-nitrobenzenesulfonyl chloride in pyridine at 60—65 °C for 45 h surprisingly gave penta-*N*-*ecb*-seldomycin 5-2′,3′-epicyclic carbamate (**3**) in 57.9% yield. When this reaction was run at 13.5 °C for 20 h, hexa-*N*-*ecb*-seldomycin 5-3′-*O*-(*o*-nitrobenzenesulfonate) (**4**) was isolated in 70.3% yield and **4** was then converted into **3** by being heated in pyridine at 65 °C for 43 h in 80.4% yield. These results indicate that direct formation of **3** from **2** at higher temperature occurs by way of the formation of **4** *in situ*. The critical temperature above which the direct formation of **3** mainly occurs within 45 h was determined to be about 55 °C. Although the anchimeric ability of a benzyloxycarbonylamino group to a vicinal carbon atom which has an eliminating group such as halogen, mesyloxy, and epoxide is well known,[5] direct conversion of **2** into **3** may be, to our best knowledge, the first instance of epimerization of a free hydroxyl group in one step. On the other hand, reaction of **2** with *p*-toluenesulfonyl chloride or methanesulfonyl chloride in pyridine at 55—65 °C for 23 h gave hexa-*N*-*ecb*-3′-*O*-tosylseldomycin 5 (**5**) or hexa-*N*-*ecb*-3′-*O*-mesylseldomycin 5 (**6**) in 96.0 or 90.6% yield, respectively. Conversion of **5** or **6** into **3** was achieved by heating them in weakly basic solvents such as pyridine, *N,N*-dimethylformamide, at 80—110 °C for 18—19.5 h in 75.8 or 38.6% yield, respectively.

The structure of **3** was elucidated by the following evidences. (i) elemental analysis, (ii) disappearance of the signals due to the sulfonate residues in PMR and IR, (see experimental section), (iii) appearance of a new peak at 1760 cm^{-1} in IR due to a carbonyl group of a five-membered cyclic carbamate, (iv) In the CMR spectrum of **3** (Table 1), a new signal appeared at 158.8 ppm which is attributable to the carbonyl carbon of the newly formed cyclic carbamate. There were 6.5 and 9.8 ppm upfield shifts in the C-2′ and C-4′ signals, respectively, relative to the corresponding signals in the spectrum of **2**, while 7.2 ppm downfield shift in the C-3′ signal was observed resulting from the transformation of **2** into **3**. (v) hydrolysis to **7**. The reactions described above are summarized in Scheme 1 and possible mechanism for the formation of the epicyclic carbamate ring is shown in Scheme 2. This mechanism requires water for the formation of **3**, which is supposed to be contained in the solvents used. In fact both the pyridine and DMF that we used were revealed (Karl Fisher method) to contain about 650 ppm water, which is stoichiometrically enough for the

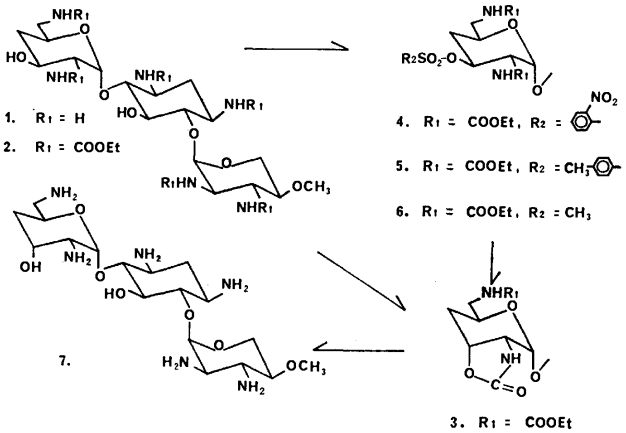

Scheme 1.

* To whom correspondence should be addressed.

TABLE 1. CMR CHEMICAL SHIFTS OF COMPOUNDS **1**, **2**, **3**, AND **7**

Compound	**2**[a]	**3**[a]	Δ	**1**[b,c]	**7**[b]	Δ
C-1′	99.3	96.5	−2.8	101.9	102.6	0.7
C-2′	57.6	51.1	−6.5	57.6	51.8	−5.8
C-3′	64.4	71.6	7.2	69.0	67.9	−1.1
C-4′	37.0	27.2	−9.8	37.0	35.3	−1.7
C-5′	66.6	65.2	−1.4	70.8	66.0	−4.8
C-6′	44.4	44.0	−0.4	45.6	45.6	0.0
C-1	50.7	51.1	0.4	51.1	51.0	−0.1
C-2	35.0	34.7	−0.3	36.5	36.5	0.0
C-3	49.9	49.5	−0.4	50.1	49.9	−0.2
C-4	82.3	81.7	−0.6	87.6	88.7	1.1
C-5	74.6	74.6	0.0	75.1	75.1	0.0
C-6	79.4	78.7	−0.7	86.8	86.9	0.1
C-1″	96.7	96.5	−0.2	99.9	100.0	0.1
C-2″	54.4	54.3	−0.1	56.2	56.2	0.0
C-3″	53.1	53.2	0.1	54.8	54.7	−0.1
C-4″	76.1	76.2	0.1	80.1	80.2	0.1
C-5″	59.5	59.6	0.1	60.8	60.8	0.0
OCH_3	57.6	57.7	0.1	58.7	58.7	0.0
$COOCH_2\underline{CH_3}$[d]	14.6	14.6	0.0	—	—	—
$COO\underline{CH_2}CH_3$[d]	59.5	59.6	0.1	—	—	—
$\underline{COO}CH_2CH_3$[e]	155.4	155.2	—	—	—	—
	156.0	155.3	—	—	—	—
	—	156.0	—	—	—	—
new CO	—	158.8	—	—	—	—

a) Measured in DMSO-d_6 solution with DMSO-d_6 as internal reference and shown by ppm from TMS, using $\delta_{TMS}=39.5-\delta_{DMSO}$. b) Measured in D_2O solution with dioxane as internal reference and shown by ppm from TMS, using $\delta_{TMS}=67.4-\delta_{dioxane}$. c) CMR data of this compound had been reported in Ref. 2. Each chemical shifts obtained here are consistent with those reported in Ref. 2 within 0.5 ppm deviation. d) All the methyls or methylenes of the ecb residues showed the single chemical shift. e) The carbonyls of the ecb residues in **2** or **3** showed the two or three chemical shifts, respectively.

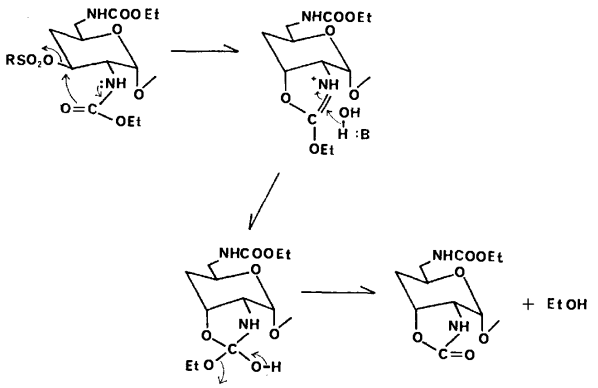

Scheme 2. Possible mechanism for the formation of the epicyclic carbamate ring.

reactions.

Alkaline hydrolysis of **3** caused simaltaneous deethoxycarbonylation and fission of the epicyclic carbamate ring to give **7**. The structure of **7** was supported by the following evidences. (i) High resolution mass spectrum gave the (M+1) peak at 451.2912 (*m/e*), which means **7** is an isomer of **1**. Its fragmentation pattern is quite similar to that of **1**.[2] (ii) In the CMR spectrum of **7** (Table 1), the four signals due to the C-2′—C-5′ carbons appeared in the range of 1.1—5.8 ppm upfield compared with the corresponding signals in the spectrum of **1**. These upfield shifts resulting from epimerization of the 3′-hydroxyl group are consistent with those reported by Roberts and Dorman[6] or Perlin *et al.*[7] (iii) In the PMR spectrum of **7** (Table 2), the signals due to the H-2′, H-3′, and H-4′ax showed 0.3—0.4 ppm downfield shifts, respectively, from the corresponding shifts in the spectrum of **1**. These downfield shifts are well compared with the empirical rule proposed by Lemiuex and Stevens.[8] (iv) Optical rotatory behavior (Δ[M] value) in copper-ammonium solutions[9,10] also supported the structure of **7**. Compound **1** or **7** has two sites where the formation of copper complex are possible, *i.e.*, a pair of adjacent 2′-amino and 3′-hydroxyl groups (site A) and a pair of adjacent 2″- and 3″-amino groups (site B). Supposing that the complex formation occurs equally at site A and site B, contributions of each site to the apparently observed Δ[M] values could be calculated as shown in Table 3. These results indicate that the projected angle[9] at site A in **7** is +60° (counter-clockwise), while it is −60° (clockwise) in **1**. It seems to be noteworthy that the sign of $\Delta[M]_{cupra\ B}$ for the vicinal amino groups at site B (the projected angle: clockwise) is minus. That is in accord with the sign conventionally observed for vicinal amino and hydroxyl groups or vicinal hydroxyl groups in a chair-formed pyranose or cyclitol. On the other hand the $\Delta[M]_{CuAm}$ value for the vicinal amino groups is nearly zero.

Table 2. Selected PMR chemical shifts (τ value) of compounds **1** and **7**[a]

	H-1′	H-2′	H-3′	H-4′$_{ax}$	H-4′$_{eq}$	H-5′
Compound **1**	4.70	7.4	6.3	8.72	8.1	6.0
Compound **7**	4.86	7.1	6.0	8.3	8.1	5.9

a) Measured in D_2O solution with DSS as internal standard (100 MHz). Each chemical shifts were confirmed by spin decoupled method.

Table 3. Δ[M] value of compounds **1** and **7**

	CuAm		Cupra B	
	1	**7**	**1**	**7**
$\Delta[M]_{observed}$	−950	+780	−1100	+620
Contribution of the site A[a]	−870	+870	−860	+860
Contribution of the site B[b]	−90	−90	−240	−240

a) $(\Delta[M]_{\text{observed with 7}}-\Delta[M]_{\text{observed with 1}})/2$.
b) $(\Delta]M]_{\text{observed with 7}}+\Delta[M]_{\text{observed with 1}})/2$.

Table 4. The minimum inhibitory concentrations of compounds **7** and **1** (mcg/ml)

Strain	Inactivating enzyme[a]	**7**	**1**
Staphylococcus aureus 209-P		1.56	0.78
Staphylococcus aureus Smith		1.56	0.78
Escherichia coli NIHJC-2		12.5	6.25
Escherichia coli GN-2411-5		25	12.5
Escherichia coli R-5	APH(3′)-I	25	>100
Escherichia coli R-12	ANT(2″)	25	6.25
Escherichia coli R-16	APH(3′)-I	6.25	>100
Escherichia coli R-17	AAC(6′)-I	25	25
Escherichia coli R-18	APH(3′)-II	12.5	12.5
Escherichia coli R-19	AAC(3)-I	>100	>100
Escherichia coli R-20	APH(3′)-I	12.5	>100
Proteus vulgaris JJ		50	6.25
Pseudomonas aeruginosa BmH♯1		12.5	12.5
Pseudomonas aeruginosa TI-13a	APH(3′)-I	50	>100
Klebsiella pneumoniae KY4274		12.5	>100
Klebsiella pneumoniae Y-58	ANT(2″)	12.5	50
Providencia 164	AAC(2′)-I	>100	>100
Serratia marcescens 1065	AAC(6′)-IV	>100	>100

a) APH: aminoglycoside antibiotic phosphotransferase, ANT: aminoglycoside antibiotic nucleotidyltransferase, AAC: aminoglycoside antibiotic acetyltransferase. The figure in parenthesis indicates the position where the antibiotic is enzymatically modified.

No Δ[M] values for vicinal amino groups has been hitherto reported.

Table 4 shows *in vitro* antibacterial activities of **7** and **1**. It is obvious that epimerization of the 3′-hydroxyl group of **1** improves, as expected, its antibacterial activity against these resistant strains carrying 3′-*O*-phosphorylating enzyme [APH(3′)-I],[11] but does not improve its activity against other kinds of resistant strains and sensitive strains. LD_{50} value of **7** was estimated to be 183 mg/kg (mice, intravenously), while that of **1** was 667 mg/kg, namely, **7** is unexpectedly more toxic than **1** in acute toxicity.

After we had completed this work, Mallams *et al.* reported the synthesis of 3′-epigentamicin X_2, starting from 3,4,6-tri-*O*-acetyl-D-allal, with similar objective in mind.[12]

Experimental

General. Mps were determined with Yanaco micro melting point apparatus and uncorrected. IR spectra (with KBr pellet) were taken with Shimazu IR-27G or Perkin-Elmer 125 model. Varian T-60 or JEOL PS-100 was employed for NMR measurements with TMS as internal reference or in D_2O with DSS as internal reference. Samples of **1** and **7** were decarbonated by the usual manner[13] just before the NMR measurements. Optical rotations were measured with Hitachi-Perkin-Elmer 141 polarimeter at ambient temperature. Mass spectra were obtained with JEOL JMS-01SG-2 model at 75 eV using direct insertion probe. Thin layer chromatography (tlc) was carried out with Merck TLC plate and spots were visualized with iodine vapor and or UV light and or ninhydrin. Water content of solvent was measured with Tsutsui Rikagaku Kikai's Karl-Fisher automatic titrator. Evaporation of solvents was done *in vacuo* at bath temps of below 45 °C. The solutions of CuAm and Cupra B were prepared according to the literatures.[10,11] Antibacterial activity was determined with the agar dilution method at pH 7.2 specified by the Japan Society of Chemotherapy.

Hexa-N-ecb-*seldomycin 5 (2).* To an ice-cooled solution of **1** (13.5 g) in water (195 ml) and acetone (195 ml) containing sodium carbonate (anhydrous, 45.6 g), was added with vigorous stirring ethyl chroloformate (43.2 g) in ten minutes. After all the ethyl chloroformate was added, the reaction mixture was stirred for 20 h at 19 °C. The white ppt formed was filtered, washed with water (800 ml) and ether (500 ml), successively. The ppt was suspended again in water (600 ml) and stirred for 1 h at room temp. The undissolved material was filtered, washed with water (1000 ml) and dried *in vacuo* over phosphorus pentaoxide overnight to give a white powder of **2**, 18.9 g. Mp>300 °C, $[\alpha]_D^{17}$ +76.1° (*c* 0.315, DMF), R_f value on TLC (chloroform–methanol 12 : 1); 0.55.

Found: C, 48.50; H, 7.20; N, 9.36%. Calcd for $C_{36}H_{62}N_6O_{19}$: C, 48.96; H, 7.09; N, 9.52%.

Hexa-N-ecb-*3′*-O-*tosylseldomycin 5 (5).* To a solution of **2** (3.00 g) in pyridine (150 ml), *p*-toluenesulfonyl chloride (9.90 g) was added and the solution was allowed to stand at 55—65 °C for 23 h. A single spot appeared on TLC (R_f= 0.67, chloroform–methanol 12 : 1). After addition of water (10 ml), the solution was evaporated and the residue was treated with water (150 ml), the water-insoluble material was filtered, washed with water (200 ml) and then with ether (150 ml), dried *in vacuo* overnight to give a white powder, 3.42 g. Analytical sample was recrystallized from aq ethanol. Mp 193—197 °C, $[\alpha]_D^{19}$ +72.3° (*c* 0.361, DMF);

Found: C, 49.51; H, 6.65; N, 8.08; S, 2.98%. Calcd for $C_{43}H_{68}N_6O_{21}S$: C, 49.79; H, 6.62; N, 8.10; S, 3.09%. IR: 1175 cm^{-1}, PMR (in DMSO-d_6): τ 2.50 (4H, q), 7.60 (3H,s).

Hexa-N-ecb-*3′*-O-*mesylseldomycin 5 (6).* To a solution of **2** (5.20 g) in pyridine (500 ml), methanesulfonyl chloride (11.8 g) was added and the solution was allowed to stand at 24 °C for 3.5 h. On TLC with chloroform–methanol 9 : 1 a spot (R_f=0.80) appeared. After addition of water (10 ml), the solution was concentrated to *ca.* 20 ml. Water (150 ml) was added to the concentrate and the ppt formed was filtered, washed with water (80 ml) and dried *in vacuo* overnight

to give a white powder, 5.14 g. Analytical sample was recrystallized from aq ethanol. Mp 242—243 °C, $[\alpha]_D^{24}$ +118° (*c* 0.347, DMF).

Found: C, 46.30; H, 6.81; N, 8.68; S, 3.62%. Calcd for $C_{37}H_{64}N_6O_{21}S$: C, 46.23; H, 6.73; N, 8.75; S, 3.34%. IR: 1170 cm^{-1}. PMR (in DMSO-d_6): τ 6.87 (3H, s).

Hexa-N-ecb-*3'*-O-*(o-nitrophenylsulfonyl)seldomycin 5 (4).* To a solution of **2** (1.00 g) in pyridine (50 ml), *o*-nitrobenzenesulfonyl chloride (3.02 g) was added and the solution was kept at 13 °C for 20 h. Similar processing as described above gave a solid of crude **4**, which showed a major spot (R_f=0.36, chloroform–methanol 18 : 1) and two faster moving spots on TLC. Recrystallization of the crude **4** from aq ethanol gave a pure product which showed a single spot on tlc. mp 169—171 °C, $[\alpha]_D^{14}$ +34.6 ° (*c* 0.327, DMF).

Found: C, 47.08; H, 6.07; N, 8.91, S, 3.49%. Calcd for $C_{42}H_{65}N_7O_{23}S$: C, 47.22; H, 6.15; N, 9.18; S, 3.00%. PMR (in DMSO-d_6): τ 2.0 (4H, m).

Penta-N-ecb-*seldomycin 5-2',3'-Epicyclic Carbamate (3).*
i) *form 2*: To a solution of **2** (2.78 g) in pyridine (150 ml) *o*-nitrobenzenesulfonyl chloride (7.50 g) was added and the solution was kept at 60—65 °C for 45 h. On TLC with chloroform–methanol 12 : 1 a major spot of **3** (R_f=0.24) and a small spot of **4** (R_f=0.54) appeared. After a small amount of water (1.5 ml) was added, the solution was evaporated to dryness. The residue was chromatographed on a column of silica gel (Merck, 170 g) with chloroform–methanol 30 : 1—25 : 1. The portion containing **3** was evaporated to give a white powder which showed a single spot on TLC, 1.53 g. Mp 247—248 °C, $[\alpha]_D^{16}$ +47.8 ° (*c* 0.320, DMF).

Found: C, 48.37; H, 6.73; N, 9.91%. Calcd for $C_{34}H_{56}N_6O_{18}$: C, 48.79; H, 6.76; N, 10.04%. IR: 1760 cm^{-1}.

ii) *from 5*: The compound **5** (2.90 g) was dissolved in DMF (58 ml) and the solution was heated at 110 °C for 19.5 h. A small amount of ppt was filtered off and the filtrate was evaporated to dryness. The residue was chromatographed on a column of silica gel (180 g) with chloroform–methanol 30 : 1—20 : 1. From earlier fractions 0.445 g of unreacted **5** was recovered. The portion containing **3** was evaporated to give 1.49 g of a white solid. Mp 249—250 °C. IR spectrum was identical with that of **3** obtained in i).

iii) *from 6*: The solution of **6** (1.00 g) in a mixture of DMF (18 ml) and water (2ml) was kept at 110 °C for 18 h. Recovered **6** (0.47 g) and a white powder of **3** (0.18 g) was respectively isolated after similar processing and chromatography as described in ii). mp 248—249 °C IR spectrum was identical with that of **3** obtained in i).

iv) *from 4*: The solution of **4** (0.72 g) in pyridine (40 ml) was kept at 65—70 °C for 43 h. The solvent was evaporated to dryness and the residue was chromatographed as described in i). Pure **3** was obtained as a white powder, 0.45 g. Mp 248—251 °C. IR spectrum was identical with that of **3** obtained in i).

Experiment Concerning Temperature Dependence of the Reaction of 2 with o-Nitrobenzenesulfonyl Chloride. Eleven solutions of **2** (18—20 mg each) and *o*-nitrobenzenesulfonyl chloride (48—53 mg each) in pyridine (1.00 ml each) were kept at 11 different temps between 67 and 9.5 °C, respectively, using Toyo Kagaku Sangyo's Temperature Gradient Incubator TN-3. After 44 h the solutions were inspected by TLC (chloroform–methanol 12 : 1). The samples reacted at 9.5, 14.5, 20, and 26 °C showed a single spot of **4** on TLC and even a trace spot of **3** was not detected. At 31.5, 37.5, and 41.5 °C a major spot of **4** and a trace spot of **3** were visible. At 49.5 and 53 °C the spots of **4** and **3** appeared in apparently 1 : 1 ratio. At 57 and 67 °C a major spot of **3** and a tiny spot of **4** appeared.

3'-Episeldomycin 5 Free Base (7). The compound **3** (1.15 g) was suspended in a mixture of 2N-aq sodium hydroxide (25.5 ml) and methanol (25.5 ml) and heated at 110 °C in a sealed glass tube. After 15 minutes **3** dissolved completely and heating was continued for 100 minutes. A white ppt formed was filtered off, washed with aq methanol. The filtrate and washings combined were neutralized with concd hydrochloric acid and evaporated to dryness. The residue was dissolved in water (10 ml) and adjusted to pH 4.80 by hydrochloric acid. A small amount of ppt formed was filtered off and the filtrate was charged on a column of Amberlite CG-50 (ammonium cycle, 50 ml). After washing the column with water (370 ml), it was eluted stepwisely by 0.1- and 0.2 M aqueous ammonia. From a portion eluted by 0.1 M-ammonia a white powder (0.13 g) was obtained which showed no antibacterial activity. $[\alpha]_D^{18}$ +126° (*c* 0.300, water). This compound was supposed to be 1*N*,3*N*-carbonyl-3'-episeldomycin 5.[14] Fractions eluted by 0.2 M -ammonia gave a white powder of pure **7** (0.14 g) after evaporation. Mp 189—194 °C, $[\alpha]_D^{20}$ +95.1° (*c* 0.377, water). PMR (in D_2O): τ 4.86 (d, J=4 Hz, H-1'), 5.00 (d, J=3 Hz, H-1").

Found: C, 45.52; H, 7.75; N, 16.82%. Calcd for $C_{18}H_{38}N_6O_7$ 1/2 H_2CO_3: C, 46.13; H, 8.18; N, 17.45%.

The authors wish to thank Mrs. Mayumi Yoshida for the CMR measurements, Mrs. Kazuko Yamaguchi for the elemental analysis, and MissYuriko Adachi for obtaining the mass spectra. The authors are also indebted to Sagami Central Research Institute for the elemental analysis of sulfur and the IR measurements with a Perkin-Elmer 125 model.

References

1) T. Nara, M. Yamamoto, S. Takasawa, S. Sato, T. Sato, I. Kawamoto, R. Okachi, I. Takahashi, and A Morikawa, *J. Antibiot.*, **30**, 17 (1977).

2) J. B. McAlpine, A. C. Sinclair, R. S. Egan, R. L. DeVault, R. S. Stanaszek, M. Cirovic, S. L. Mueller, P. C. Goodley, R. J. Mauritz, N. E. Wideburg, L. A. Mitcsher, K. Shirahata, H. Matsushima, S. Sato, and T. Iida, *J. Antibiot.*, **30**, 39 (1977).

3) H. Umezawa, *Adv. Carbohydr. Chem. Biochem.*, **30**, 183 (1974).

4) S. Hanessian, R. F. Butterworth, and T. Nakagawa, *Carbohydr. Res.*, **26**, 261 (1973).

5) i) L. Goodman, *Adv. Carbohydr. Chem. Biochem.*, **22**, 139 (1967); ii) H. E. Khadem, *ibid.*, **25**, 375 (1970).

6) D. E. Dorman and J. D. Roberts, *J. Am. Chem. Soc.*, **92**, 1355 (1970).

7) A. S. Perlin, B. Casu, and H. J. Koch, *Can. J. Chem.*, **48**, 2596 (1970).

8) R. U. Lemieux and J. D. Stevens, *Can. J. Chem.*, **44**, 249 (1966).

9) R. E. Reeves, *J. Am. Chem. Soc.* **71**, 2116 (1949).

10) S. Umezawa, T. Tsuchiya, and K. Tatsuta, *Bull. Chem. Soc. Jpn.*, **39**, 1235 (1966).

11) S. Mitsuhashi, L. Rosival, and V. Krcmery, Ed., "Drug Inactivating Enzymes and Antibiotic Resistance," Springer-Verlag, Berlin (1975), p. 115.

12) M. Kugelman, A. K. Mallams, and H. F. Vernay, *J. Chem. Soc. Perkin Trans.*, *1*, **1976**, 1113.

13) J. B. Morton, R. C. Long, P. J. L. Daniels, R. W. Tkach, and J. H. Goldstein, *J. Am. Chem. Soc.* **95**, 7464 (1973).

14) Private communication from Dr. J. McAlpine, Abbott Laboratories.

NOTES

BULLETIN OF THE CHEMICAL SOCIETY OF JAPAN, VOL. 50 (11), 3043—3044 (1977)

Colloid Titration Behavior of the Maleic Acid–Methyl Vinyl Ether Copolymer

Etsuo KOKUFUTA* and Shinji IWAI

College of Industrial Technology, Nihon University, Izumi-cho, Narashino, Chiba 275

(Received March 4, 1977)

Synopsis. The colloid titration of the maleic acid–methyl vinyl ether (MA–MVE) copolymer with trimethylammonium glycol chitosan iodide (MGCH) was carried out at various pH values. The mechanism of the formation of the polyion complex between the MA–MVE copolymer and the MGCH ions was discussed.

The colloid titration, which was originated by Terayama,[1] is based on the stoichiometric complex formation between polyacidic and polybasic titrants. Strong polyelectrolytes, such as potassium poly(vinyl alcohol) sulfate (PVSK),[1] trimethylammonium glycol chitosan iodide (MGCH),[1] and poly(diallyldimethylammonium chloride),[2] are frequently used as standard titrants.

In previous studies,[3,4] the effects of the pH on the dissociation of the above-mentioned three polyelectrolytes were investigated by using colloid titration and electrophoresis. From the results obtained, the mechanism of the formation of the polyion complex between polyacidic and polybasic titrants was discussed.

In the present study, the colloid titration with MGCH was carried out for the maleic acid–methyl vinyl ether (MA–MVE) copolymer, which is a representative polydibasic acid. The colloid titration curves were compared with the results of electrophoresis and potentiometric titration reported previously,[5] and the mechanism of the formation of the polyion complex between the MA–MVE copolymer and the MGCH ions was discussed.

Experimental

Materials. The MA–MVE copolymer and the sodium salt of the copolymer (NaMA–MVE copolymer) used were prepared in the manner described in previous paper.[5] The MA–MVE copolymer was prepared by the hydrolysis of the maleic anhydride–MVE copolymer manufactured by the General Aniline & Film Co. On the other hand, the NaMA–MVE copolymer was prepared by the neutralization of the MA–MVE copolymer with sodium hydroxide. The molecular weight of the repeating unit for the MA–MVE copolymer, as estimated by elemental analysis and by potentiometric titration, was 176. This value agrees with that calculated on the assumption that this copolymer is an alternating copolymer. The intrinsic viscosity of the NaMA–MVE copolymer was 1.57 dl/g, as established by viscometric measurement in a 1M NaCl solution at 25 °C. The PVSK and MGCH were obtained from Wako Pure Chemical Industries, Ltd. These properties were characterized in previous papers.[3,4]

Colloid Titration. The sample solution (0.005 N) was titrated indirectly with MGCH (0.005 N) by the method of Terayama.[1] An excess of MGCH was added to the sample solution to precipitate a polyion complex, and then the excess of MGCH was back-titrated with PVSK (0.0025 N). A blank titration was also carried out. The titrant volume was determined by means of the difference in these titration results. The end point was indicated by the metachromatic color change of toluidine blue[1] and the turbidity measurements. The pH of the titration system was adjusted with 0.1—1M HCl, NaOH, $Ba(OH)_2$, and tetrabutylammonium hydroxide (TBAH).

Results and Discussion

The colloid titration curve was obtained by plotting the reciprocal of the equivalent weight (E_w) of the sample copolymer against the pH. A titration curve of the NaMA–MVE copolymer is shown in Fig. 1. In contrast to the results for poly(sodium acrylate) (NaPAA) and carboxymethylcellulose (CMC),[2] the titration curve shows an inflection point at about pH 6.5. From this result, it can be estimated that one of the two carboxylic groups in a monomer residue of the copolymer dissociates at first in the pH region below the inflection point, while the other dissociates in the pH region above the inflection point. This agrees with the result of the potentiometric titration.[5] The values of E_w (219) and pH (*ca.* 6.5) at the inflection point are equal to the molecular weight of the repeating unit for the NaMA–MVE copolymer and to the pH value at a half-neutralization point of the potentiometric titration curve, respectively. Therefore, this inflection point can be considered to be the half-neutralization point.

On the other hand, it is observed from the colloid titration curve that E_w^{-1} reaches a constant value above pH 9. This suggests that the two carboxylic groups in a monomer residue are completely dissociated in this pH region. However, the value of E_w (145) is not equal to one-half of the molecular weight of the repeating unit for the NaMA–MVE copolymer. The electrophoretic studies of polycarboxylic acids in previous papers[5,6] showed that the binding effect of the counterion on the MA–MVE copolymer ion is larger than that of the counterion on the NaPAA and CMC ions in the pH region from 7 to 10. The disagreement mentioned above can be explained on the basis of the assumption that the complex formation of the MA–MVE copolymer with MGCH is not stoichiometric

* Present address: Department of Chemistry, The University of Tsukuba, Sakura-mura, Niihari-gun, Ibaraki 300-31.

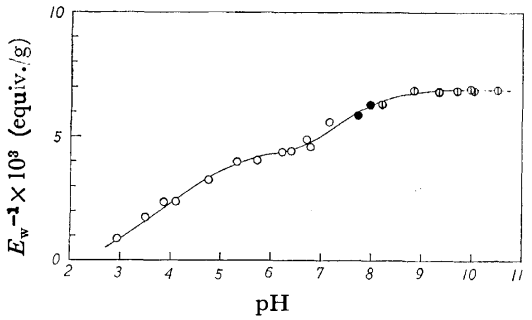

Fig. 1. Colloid titration curve of NaMA–MVE copolymer with MGCH.
pH-adjuster: ○, HCl; ⓘ, NaOH; ●, non.

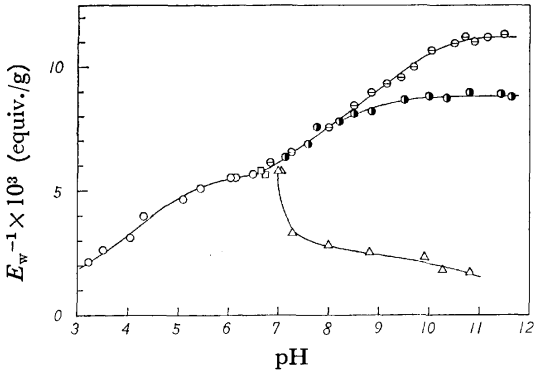

Fig. 2. Effects of pH-adjusters on the colloid titration curve of MA–MVE copolymer with MGCH.
pH-adjuster: ○, HCl; ⊖, TBAH; ◑, NaOH; △, $Ba(OH)_2$; □, non.

because of the inhibitory effect of the counterion.

In order to confirm this assumption, a colloid titration with MGCH was carried out for the MA–MVE copolymer, using NaOH, $Ba(OH)_2$, and TBAH as pH-adjusters. The results are shown in Fig. 2. When the sample solution was titrated in the absence of any pH-adjuster, the pH of the titration system at the end point was about 6.5. Hence, the titration was carried out with adjustment of the pH with HCl in the pH region below 7 and with the bases in the pH region above 7. It is generally believed that the binding effect of a counterion on a polyacidic ion does not need to be considered if the counterion is a tetraalkylammonium ion.[7] In the case of a bivalent metal ion such as the Ba^{2+} ion, however, this effect on a polydibasic acid seems to be important, since a stable ring structure will be formed between the metal cation and the two carboxylate ions in a monomer residue. In Fig. 2, from the titration curve for which the pH was adjusted with NaOH, it is observed that E_w^{-1} is independent of the pH in the pH region above 9. The value of E_w (115) in this pH region is not equal to one-half of the molecular weight of the repeating unit for the MA–MVE copolymer. In contrast to this result, in the case of the titration curve for which the pH was adjusted with TBAH, E_w^{-1} increases in the pH region from 7 to 10, and reaches a constant value above pH 10.5. In the pH region above 10.5, the value of E_w (89) is comparable with one-half of the molecular weight of the repeating unit for the MA–MVE copolymer. On the other hand, when the pH was adjusted with $Ba(OH)_2$, E_w^{-1} rapidly decreased with the increase in the pH, since Ba^{2+} ions are bound to the MA–MVE copolymer ion. From these facts, it may be concluded that the binding effect of the counterion on the MA–MVE copolymer ion plays an important role in the complex formation of this copolymer with MGCH.

The authors wish to express their thanks to Professor Kyoji Toei, Okayama University, for his valuable guidance and encouragement in the colloid titration.

References

1) H. Terayama, *J. Polym. Sci.*, **8**, 243 (1952).
2) K. Toei and T. Kohara, *Anal. Chim. Acta*, **83**, 59 (1976).
3) E. Kokufuta, S. Kokubo, M. Hirata, and S. Iwai, *Kobunshi Ronbunshu*, **32**, 665 (1975).
4) E. Kokufuta, S. Kokubo, and S. Iwai, *Nippon Kagaku Kaishi*, **1976**, 1335.
5) E. Kokufuta, M. Ito, M. Hirata, and S. Iwai, *Kobunshi Ronbunshu*, **31**, 688 (1974).
6) E. Kokufuta, M. Hirata, and S. Iwai, *Kobunshi Ronbunshu*, **32**, 235 (1975).
7) H. P. Gregor, D. H. Gold, and M. Frederik, *J. Polym. Sci.*, **23**, 467 (1957).

BULLETIN OF THE CHEMICAL SOCIETY OF JAPAN, VOL. 50 (11), 3045—3046 (1977)

Phosphorescence Spectra of $[Cr(NH_3)_6][Co(CN)_6]$ and $[Cr(NH_3)_6][CdCl_5]$. Splitting of Their 0–0 Bands

Yusuke YAMAMOTO

Department of Chemistry, Faculty of Science, Rikkyo University, Nishi-ikebukuro, Toshima-ku, Tokyo 171

(Received May 19, 1977)

Synopsis. High resolution $^2E \rightarrow {}^4A_2$ phosphorescence spectra of $[Cr(NH_3)_6][Co(CN)_6]$ and $[Cr(NH_3)_6][CdCl_5]$ were measured. The 0–0 bands split into two components separated by 3.7 and 3.4 cm^{-1} for $[Cr(NH_3)_6][Co(CN)_6]$ and $[Cr(NH_3)_6][CdCl_5]$, respectively. The same spacings were also resolved in the ν_8 bands. The splitting in both cases is assigned as that of the ^2E phosphorescent electronic level.

There have been many studies of $^2E \rightarrow {}^4A_2$ phosphorescence spectra of hexaamminechromium(III) salts.[1–5] The phosphorescence spectrum of $[Cr(NH_3)_6][Co(CN)_6]$ was studied by Kataoka[1] in our laboratory, and by Cervone *et al.*[2] from the viewpoint of energy transfer from $[Co(CN)_6]^{3-}$ to $[Cr(NH_3)_6]^{3+}$, but no assignment of the vibronic bands was made. Flint *et al.*[3] investigated the phosphorescence spectra of $[Cr(NH_3)_6][CdCl_5]$, $[Cr(NH_3)_6][Co(CN)_6]$, and $[Cr(NH_3)_6](N_3)_3$, where the complex cation is in non-cubic environment, and they have given an assignment of vibronically active fundamentals. On the other hand, X-ray studies of $[Cr(NH_3)_6][Co(CN)_6]$[6] and $[Cr(NH_3)_6][CdCl_5]$[7] showed that the $[Cr(NH_3)_6]^{3+}$ ion occupies $\bar{3}$ site symmetry in the lattice. A ^2E level does not split by the sole action of the trigonal field or the spin orbit interaction, but splits into two Kramers doublets through the interplay of the two. Hence a splitting of the 0–0 band would be expected, but to date no splitting has been observed in $[Cr(NH_3)_6][Co(CN)_6]$ and $[Cr(NH_3)_6][CdCl_5]$.

Experimental

The materials were prepared according to the published methods[1,7] from carefully recrystallized $[Cr(NH_3)_6](NO_3)_3$, $K_3[Co(CN)_6]$, and $CdCl_2 \cdot 2.5H_2O$.

Phosphorescence spectra were recorded using excitation from a mercury lamp, the line being isolated by a Spex Michromate (f 2.5, 10 cm). The detection monochromator was a Jasco CT-100 (f 8.5, 100 cm) equipped with a cooled Hamamatsu R-649S (S-20) photomultiplier connected with Hamamatsu C-767 photon counter. Spectral slit width was 0.8 cm^{-1} for this measurement.

Results and Discussion

$[Cr(NH_3)_6][Co(CN)_6]$. The 20 K, 365 nm excited phosphorescence spectrum measured on a powdered sample ranging from the 0–0 to ν_7 band is shown in Fig. 1 together with the assignment of the vibronic bands observed. Down to 77 K, the 0–0 band clearly split into two components separated by 3.7 cm^{-1}, and the same spacing was also observed in the $\nu_8(e_u)$ band. The two components of each of these bands at 77 and 20 K are shown in Fig. 2. In the 0–0 band,

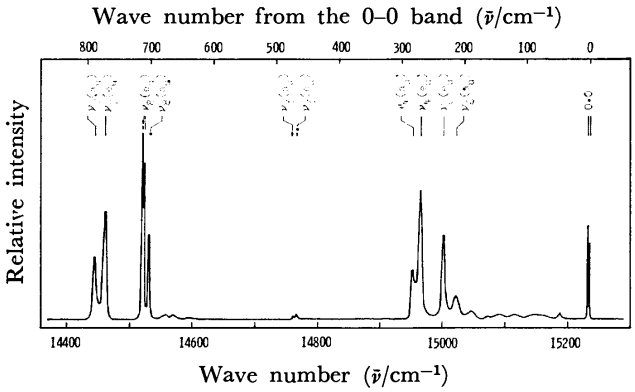

Fig. 1. Phosphorescence spectrum of $[Cr(NH_3)_6][Co(CN)_6]$ at 20 K.

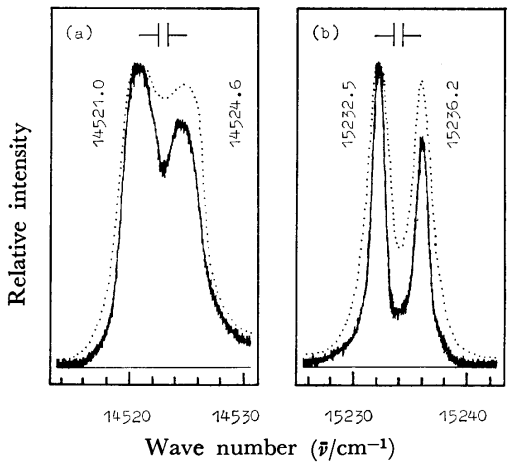

Fig. 2. Phosphorescence spectra of $[Cr(NH_3)_6][Co(CN)_6]$ at 20 K. (a) $\nu_8(e_u)$ band, (b) 0–0 band. Dotted line indicates outline of the spectra at 77 K. Lower energy component of each band is normalized.

these components, completely separated, had comparable intensities and their intensity ratios at 77 and 20 K are given by $\exp(-\Delta E/kT)$. Hence, the splitting of both the 0–0 band and the $\nu_8(e_u)$ band can be assigned as that of the ^2E phosphorescent electronic level, and can be interpreted as being due to the combined effect of the trigonal distortion of the $[Cr(NH_3)_6]^{3+}$ ion in the lattice and the spin orbit interaction. Splitting of the $^4A_2$ ground state is expected to be much smaller than that of the ^2E state.[8] In other vibronic bands, the splitting of the ^2E level could not be resolved because of their broadness.

$[Cr(NH_3)_6][CdCl_5]$. This complex salt is photosensitive even in a solid state. During a few minutes exposure to the excitation source, the original bands decreased in intensity and new bands appeared. For

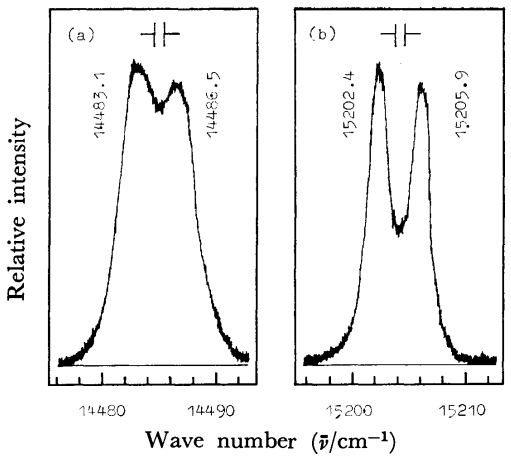

Fig. 3. Phosphorescence spectra of $[Cr(NH_3)_6][CdCl_5]$ at 77 K. (a) ν_8 band, (b) 0–0 band.

this reason, an excitation wavelength less susceptible to decomposing was selected, and measurement was done as quickly as possible, changing the sample for measuring each band. The 77 K, 313 nm excited phosphorescence spectra of a powdered sample of the 0–0 and ν_8 bands are shown in Fig. 3. Splitting of the 0–0 and ν_8 bands with a spacing of 3.4 cm^{-1} was also observed as in $[Cr(NH_3)_6][Co(CN)_6]$. The two components of these bands can be reasonably assigned as the transition from two levels, originated from the ^2E state, to the $^4A_2$ ground state, but neither of them can be a constituent band of a photodecomposition product, because long exposure gave no shift of the 0–0 and ν_8 bands, and intensity ratios of the two were constant.

The 0–0 band splitting observed is very small compared with 27 cm^{-1} for $[Cr(NH_3)_6](N_3)_3$,[3] 48 cm^{-1} for $[Cr(en)_3](ClO_4)_3$,[9] and 18 cm^{-1} for $2[Cr(en)_3]Cl_3 \cdot KCl \cdot 6H_2O$.[8,9] This indicates that the deviation from cubic symmetry is very small as expected from the X-ray studies. Since the structural studies were done at room temperature, it can be considered that phase transition might occur at low temperature, although observation of the bands while the sample was being cooled indicated no change in the spectral pattern in detail other than sharpening of the bands. This suggests that no phase transition occurred, or if it did occur, the structural difference should be little.

The author is grateful to Professor Yukio Kondo and Professor Masayoshi Nakahara for their encouragement throughout this work. He also wishes to thank Professor Gene S. Leheman for his kindness in reading the original manuscript.

References

1) H. Kataoka, *Bull. Chem. Soc. Jpn.*, **46**, 2078 (1973).
2) E. Cervone, C. Conti, and G. Sartori, *Gazz. Chim. Ital.*, **103**, 923 (1973).
3) C. D. Flint, P. Greenough, and A. P. Matthews, *J. Chem. Soc., Faraday Trans. 2*, **69**, 23 (1973).
4) C. D. Flint and P. Greenough, *J. Chem. Soc., Faraday Trans. 2*, **69**, 897 (1972).
5) T. V. Long and D. J. B. Penrose, *J. Am. Chem. Soc.*, **93**, 632 (1970).
6) H. Steinmetz, *Z. Krystallogr.*, **57**, 233 (1922).
7) W. E. Estes, D. Y. Jeter, J. C. Hempel, and W. E. Hatfield, *Inorg. Chem.*, **10**, 2074 (1971).
8) P. J. McCarthy and M. T. Vala, *Mol. Phys.*, **25**, 17 (1973).
9) C. D. Flint and A. P. Matthews, *J. Chem. Soc., Faraday Trans. 2*, **72**, 579 (1976).

BULLETIN OF THE CHEMICAL SOCIETY OF JAPAN, VOL. 50 (11), 3047—3048 (1977)

The Effects of Sodium Chloride on the Ultrasonic Properties of an Aqueous Solution of Isopropyl Alcohol

Sadakatsu NISHIKAWA, Mitsuo MASHIMA, and Tatsuya YASUNAGA*

Department of Chemistry, Faculty of Science and Engineering, Saga University, Honjo-machi Saga 840

**Department of Chemistry, Faculty of Science, Hiroshima University, Higashisenda-machi, Hiroshima 730*

(Received May 19, 1977)

Synopsis. The ultrasonic absorptions in an aqueous solution of isopropyl alcohol with sodium chloride (NaCl) were measured in the frequency range from 2.5 to 220 MHz at 25 °C. The ultrasonic properties were remarkably affected by the addition of NaCl, and a new absorption was found around 7 MHz in addition to that observed in the solution without NaCl. The results were discussed in terms of the forming effects of NaCl on the water structure.

As has been reported in previous papers,[1,2] ultrasonic absorptions in aqueous solutions of alcohols have been characterized by two kinds of relaxations. One is associated with the interaction between alcohol and water molecules, and the other, with aggregation reaction of alcohols having a relatively high hydrophobicity. However, the latter absorption was not observed in the aqueous solution of isopropyl alcohol over all the concentration range studied.[3]

In order to investigate further the properties of the aqueous solutions of alcohols and the structure of water, the ultrasonic absorption measurements were performed in the aqueous solution of isopropyl alcohol with sodium chloride (NaCl) added.

Experimental

The isopropyl alcohol and water used in this study were the same as those described in a previous paper.[3] The NaCl was the purest grade obtainable and was used without further purification. The ultrasonic absorption was measured in the manner described in previous work.[1] All the measurements were made at 25 °C.

Results and Discussion

The ultrasonic absorptions were measured under various concentrations of NaCl at a constant concentration of isopropyl alcohol (5.20 mol dm^{-3}), because the ultrasonic parameters for the aqueous solution could be determined with a relatively high accuracy at this concentration. Figure 1 shows the representative ultrasonic absorption spectra in the mixed solution. In general, the spectra associated with several relaxation processes can be expressed by the following equation:

$$\alpha/f^2 = \sum_i A_i/[1+(f/f_{ri})^2] + B, \quad (1)$$

where α is the absorption coefficient; f, the frequency; A_i, the amplitude of the excess absorption for the i-th process; f_{ri}, the relaxation frequency, and B, the constant. The absorption data in the concentration range of NaCl below 0.50 mol dm^{-3} were represented by a single relaxation formula and were analyzed graphically from the plot of α/f^2 *vs.* $[1+(f/f_r)^2]^{-1}$ so as to obtain a straight line. However, with an increase in the NaCl concentration, a new absorption appeared in the low frequency range (around 7 MHz); the absorption data were analyzed by means of a nonlinear least-squares routine. Figure 2 shows the variation in the relaxation frequencies with the NaCl concentration. The amplitudes of the excess absorptions are also shown in Fig. 3.

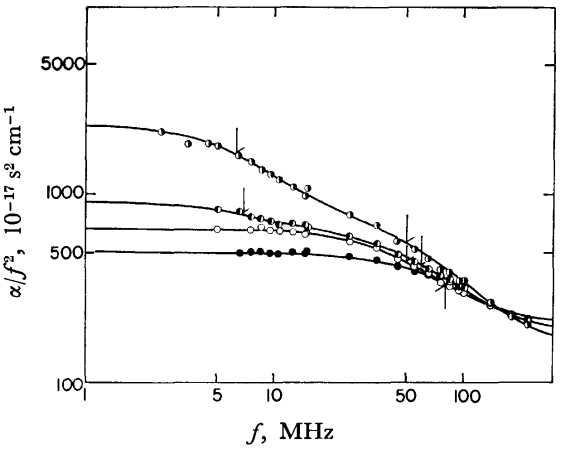

Fig. 1. Ultrasonic absorption spectra in 5.20 mol dm^{-3} solution of isopropyl alcohol with various NaCl concentrations at 25 °C. The arrow indicates the relaxation frequency. ●: without NaCl, ○: 0.40 mol dm^{-3} (NaCl), ◐: 0.60 mol dm^{-3} (NaCl), ◑: 1.20 mol dm^{-3} (NaCl).

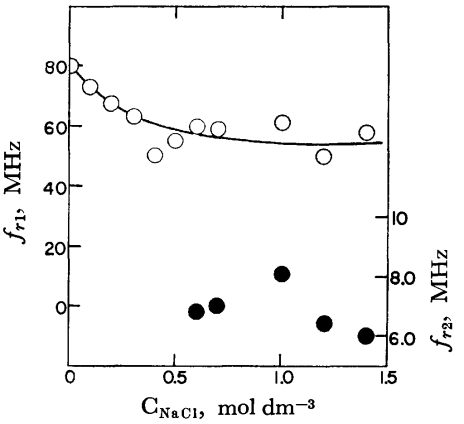

Fig. 2. Dependences of the relaxation frequencies in 5.20 mol dm^{-3} solution of isopropyl alcohol on the concentration of NaCl at 25 °C. ○: f_{r1}, ●: f_{r2}.

As has been reported in a previous study,[3] only a single relaxational absorption was observed over all the concentration range of isopropyl alcohol and the ab-

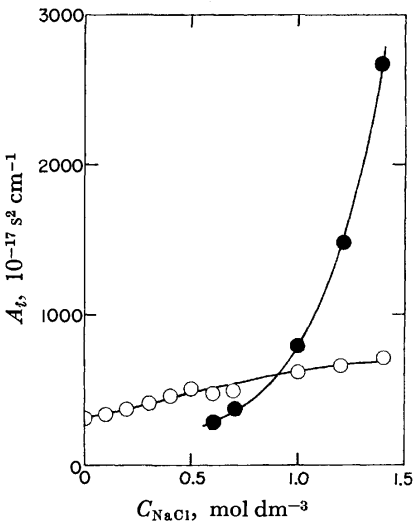

Fig. 3. Dependences of the amplitudes of the excess absorption in 5.20 mol dm^{-3} solution of isopropyl alcohol on the concentration of NaCl at 25 °C. ○: A_1. ●: A_2.

sorption mechanism was interpreted quantitatively in terms of a solute-solvent interaction as follows:

$$A + B \underset{k_b}{\overset{k_f}{\longleftrightarrow}} AB, \quad (2)$$

where A and B are the monomers of alcohol and water, and where k_f and k_b are the forward and backward rate constants respectively. The relaxation frequency for this process was related by the following equation:

$$2\pi f_r = k_f([A]+[B]) + k_b. \quad (3)$$

In this analysis, water molecules are assumed to be in two states; that is, there exists an equilibrium between hydrogen bonded and non-hydrogen bonded water, and only non-hydrogen bonded water molecules participate in the reaction with alcohol molecules. If the addition of NaCl disturbs the equilibrium in water, the ultrasonic parameters associated with the reaction of Eq. 2 will be affected. Considering that NaCl acts as the former of the water structure,[4] the relaxation frequency, f_{r1}, should be decreased through Eq. 3 by the decrease in the monomer concentration of water with an increase in the NaCl concentration. The experimental results are in agreement with this expectation, as is shown in Fig. 2.

Another important and interesting feature of the ultrasonic absorption in the mixed solution is the appearance of a new absorption in the low frequency range at concentrations of NaCl more than 0.50 mol dm^{-3}, as may be seen in Fig. 1. The frequency range in which the new absorption was found is near that in which the relaxational absorption associated with the hydrophobic effects were observed in aqueous solutions of *n*-propyl and *t*-butyl alcohols.[1,2] This shows that even the molecules with relatively low hydrophobicities can interact with each other by means of the hydrophobic effect when the enviroments of the molecules are changed by added substances.

Finally, urea is well known to be a breaker of the water structure, and its effect on the ultrasonic properties of the aqueous solution might be expected. However, no effective changes in the relaxation parameters were observed when urea was added to the aqueous solution of isopropyl alcohol.

References

1) S. Nishikawa, M. Mashima, and T. Yasunaga, *Bull. Chem. Soc. Jpn.*, **48**, 661 (1975).
2) Nishikawa, M. Mashima, M. Maekawa, and T. Yasunaga, *Bull. Chem. Soc. Jpn.*, **48**, 2353 (1975).
3) S. Nishikawa, M. Mashima, and T. Yasunaga, *Bull. Chem. Soc. Jpn.*, **49**, 1413 (1976).
4) M. Gross, J. Azoulay, and D. Gerlich, *J. Chem. Phys.*, **58**, 5812 (1973).

BULLETIN OF THE CHEMICAL SOCIETY OF JAPAN, VOL. 50 (11), 3049—3050 (1977)

The Silver(I) Ion-catalyzed Oxidation of Ethylenediaminetetraacetatocobaltate(II) by the Peroxodisulfate Ion

Kousaburo OHASHI and Katsumi YAMAMOTO

Department of Chemistry, Faculty of Science, Ibaraki University, Mito 310

(Received March 3, 1977)

Synopsis. A spectrophotometric study of the silver(I) ion-catalyzed oxidation of the ethylenediaminetetraacetatocobaltate(II) (Co^{II}-edta) peroxodisulfate ion ($S_2O_8^{2-}$) was carried out in acidic media. The rate is independent of the concentration of Co^{II}-edta, but first-order-dependent with respect to the concentrations of $S_2O_8^{2-}$ and Ag(I) in the 1.67×10^{-2}—7.25×10^{-2} M and 2.00×10^{-3}—2.26×10^{-2} M ranges respectively.

Recently, kinetic studies of the oxidation reaction of nitrilopolyacetatocobaltate(II) with various oxidants have been carried out.[1-4] The present authors found that the rate of the oxidation of Co^{II}-edta by $S_2O_8^{2-}$ is first-order-dependent on the concentration of $S_2O_8^{2-}$, but is independent of the Co^{II}-edta concentration for $Co^{II}(bpy)_3^{2+}$ oxidation; however, the rate is dependent on the concentrations of both $Co^{II}(bpy)_3^{2+}$ and $S_2O_8^{2-}$. Such a difference in rate law between Co^{II}-edta and $Co(bpy)_3^{2+}$ must come from the difference in charge on the cobalt(II) complexes.[5] In this note, the mechanism of the silver(I) ion-catalyzed oxidation of Co^{II}-edta[6] by $S_2O_8^{2-}$ and also the effect of other ions on the rate will be reported.

Experimental

Materials. A cobalt(II) perchlorate solution was prepared by dissolving cobalt carbonate into a slight excess of perchloric acid. This cobalt(II) solution was standardized by titration with a disodium dihydrogenethylenediaminetetraacetate (Na_2H_2edta) solution. The working solution was prepared by dilution with redistilled water.

Standard solutions of Na_2H_2 edta were prepared by dissolving known quantities of disodium dihydrogenethylenediaminetetraacetate dihydrate into redistilled water. Standard solutions of potassium peroxodisulfate were prepared by dissolving known quantities of the reagent into redistilled water. The peroxodisulfate ion solution was prepared just before use to avoid any decomposition. The standard solutions of silver(I) nitrate were prepared by dissolving silver nitrate into 0.01 M perchloric acid. These silver(I) solutions were standardized by the Volhard method. The adjustment of the pH of the solution was made by adding an acetate buffer solution. The ionic strengths of the solutions of Co^{II}-edta were adjusted to 0.50 by the addition of sodium perchlorate.

Procedure for the Measurement of the Reaction Rate. For the preparation of Co^{II}-edta solutions, the concentration of Na_2H_2edta was kept at three times that of the cobalt(II) ion. The solutions of $S_2O_8^{2-}$, the acetate buffer, Co^{II}-edta, and the silver(I) ion were each thermostated at 25 °C. In each experiment, $S_2O_8^{2-}$, acetate buffer, and Co^{II}-edta solutions were pipetted into a 50-ml measuring flask. Then the silver(I) ion solution was added to the solution. A portion of the solution was transferred into a 1-cm cell placed in a thermostated cell compartment of a Hitachi EPS-3-type spectrophotometer. The time dependence on the variation in the absorbance of the solution was measured at 540 nm. All the kinetic measurements were carried out in a large excess of the $S_2O_8^{2-}$ concentration to that of Co^{II}-edta.

Results and Discussion

Kinetics of the Silver(I) Ion-catalyzed Oxidation of Co^{II}-edta by $S_2O_8^{2-}$. The rate of the oxidation of Co^{II}-edta by $S_2O_8^{2-}$ in the absence of silver(I) ions was slow, as was shown in a previous paper.[5] In the present work, however, it was found that the silver(I) ions catalyze the oxidation of Co^{II}-edta by $S_2O_8^{2-}$. The oxidation product was characterized spectrophotometrically as $Co^{III}(edta)^-$. It was confirmed spectrophotometrically that one mole of $S_2O_8^{2-}$ oxidizes two moles of Co^{II}-edta in the presence of silver(I) ions when there is a large excess of Co^{II}-edta relative to the concentration of $S_2O_8^{2-}$. However, the attempt to confirm the stoichiometry in the presence of a large excess of $S_2O_8^{2-}$ to Co^{II}-edta was unsuccessful.

As is shown in Fig. 1, the plot of the absorbance vs. the time shows a straight line up to a 95% reaction. This behavior indicates that the oxidation rate is zero-order with respect to the Co^{II}-edta concentration. It was ascertained that no oxidation rate changes with the variation in the Co^{II}-edta concentration (Table 1).

In order to examine the effect of the $S_2O_8^{2-}$ concentration on the rate, the reaction was carried out at five different initial concentrations of $S_2O_8^{2-}$. As is shown in Fig. 2, the plot of the apparent rate *vs.* the $S_2O_8^{2-}$ concentration shows a straight line. Furthermore, it was confirmed that the oxidation rates were first-order with respect to the silver(I) ion concentration (Fig. 3). The rate law for this reaction is represented by Eq. 1:

$$\frac{d[Co^{III}(edta)^-]}{dt} = k_{obsd}[Ag(I)][S_2O_8^{2-}], \qquad (1)$$

where k_{obsd} is the second-order rate constant at a given pH value.

The effect of the pH on the oxidation rate was investigated over the pH range from 3.50 to 5.00 (Fig.

TABLE 1. THE KINETIC DATA FOR THE SILVER(I) ION-CATALYZED OXIDATION OF Co^{II}-edta BY PEROXODISULFATE

Concentration of Co^{II}-edta (10^{-3} M)	Rate[a] (10^{-6} M s^{-1})
1.5	6.4
2.5	6.3
4.0	6.4
7.5	6.4
10.0	6.3

a) $[Ag(I)]=8.0\times10^{-3}$ M, $[S_2O_8^{2-}]=8.57\times10^{-2}$ M, pH 3.60, $I=0.50$, 25 °C.

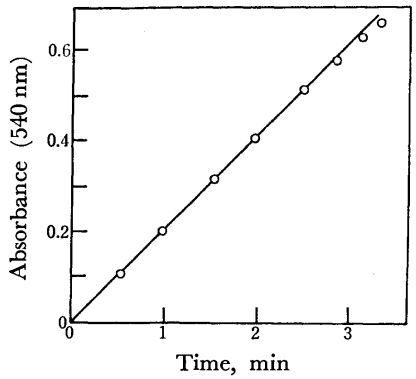

Fig. 1. A typical kinetic run of the reaction between Co^{II}-edta and peroxodisulfate ions in the presence of silver(I) ions at pH 3.60, 25 °C, and $I=0.50$ ($NaClO_4$). $[Co^{II}\text{-edta}]=2.08\times10^{-3}$ M, $[S_2O_8^{2-}]=8.57\times10^{-2}$ M, $[Ag(I)]=1.35\times10^{-2}$ M.

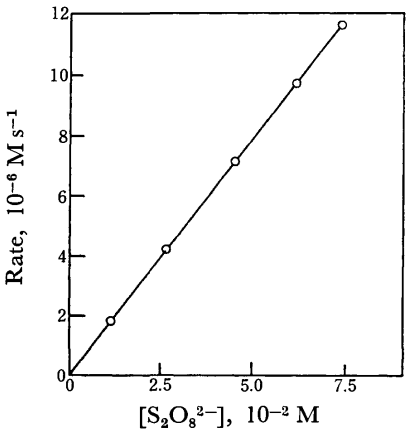

Fig. 2. Apparent rate *vs.* $[S_2O_8^{2-}]$ at pH 3.60, 25 °C, and $I=0.50$($NaClO_4$). $[Co^{II}\text{-edta}]=2.08\times10^{-3}$ M, $[Ag(I)]=1.67\times10^{-2}$ M.

4). The rate constant increases with an increase in the pH. No detailed explanations of the effect of the hydrogen ions on the rate could be given. The effect of the Na_2H_2edta concentration on the rate was not observed over the range of $1.40\times10^{-3}-7.54\times10^{-3}$ M.

The rate-determining step in the silver(I) ion-catalyzed oxidation reaction of Co^{II}-edta by $S_2O_8^{2-}$ must be the reaction between the silver(I) ion and $S_2O_8^{2-}$, since the oxidation rate is first-order with respect to the concentrations of both $S_2O_8^{2-}$ and silver(I) ions. The path for the oxidation of Co^{II}-edta may be represented by Eqs. 2, 3, 4, and 5:

$$Ag(I) + S_2O_8^{2-} \xrightarrow{\text{slow}} Ag(II) + SO_4^{2-} + SO_4^{\cdot-}, \quad (2)$$

$$Ag(I) + SO_4^{\cdot-} \xrightarrow{\text{fast}} Ag(II) + SO_4^{2-}, \quad (3)$$

$$Co^{II}\text{-edta} + SO_4^{\cdot-} \xrightarrow{\text{fast}} Co^{III}(edta)^- + SO_4^{2-}, \quad (4)$$

$$Co^{II}\text{-edta} + Ag(II) \xrightarrow{\text{fast}} Co^{III}(edta)^- + Ag(I). \quad (5)$$

The effects of the other ions on the silver(I) ion-catalyzed oxidation of Co^{II}-edta by $S_2O_8^{2-}$ were also examined. In the presence of 250 ppm Ag(I), the Zn^{2+}, Cd^{2+}, Pb^{2+}, Fe^{3+}, Mo(VI), and W(VI) metal

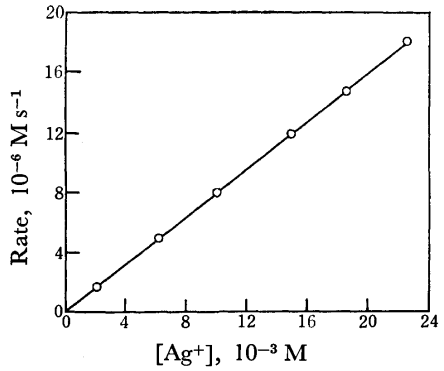

Fig. 3. Apparent rate *vs.* [Ag(I)] at pH 3.60, 25 °C, and $I=0.50$ ($NaClO_4$). $[Co^{II}\text{-edta}]=2.08\times10^{-3}$ M, $[S_2O_8^{2-}]=8.57\times10^{-2}$ M.

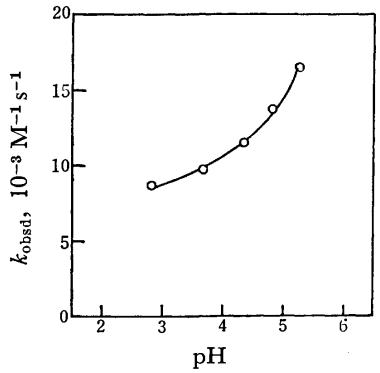

Fig. 4. The relation between the observed second-order rate constant and pH. $[Co^{II}\text{-edta}]=2.08\times10^{-3}$ M, $[S_2O_8^{2-}]=8.57\times10^{-2}$ M, $[Ag(I)]=1.67\times10^{-2}$ M, 25 °C, and $I=0.50$ ($NaClO_4$).

ions did not affect the rate at a concentration of 200 ppm, but at the same concentration the Ni^{2+}, Mn^{2+}, and Cu^{2+} metal ions increase the rate by more than 40% of the rate in the presence of the silver(I) ions.

This reaction may be applied to the determination of the concentration of the silver(I) ions, since the rate of the oxidation reaction of Co^{II}-edta is first-order-dependent on the silver(I) ions over the range of 108 to 400 ppm (Fig. 3).

References

1) D. H. Huchital and R. G. Hodges, *Inorg. Chem.*, **12**, 998, 1004 (1973).

2) H. Ogino, M. Takahashi, and N. Tanaka, *Bull. Chem. Soc. Jpn.*, **47**, 1426 (1974).

3) R. G. Wilkins and R. E. Yelin, *J. Am. Chem. Soc.*, **92**, 1191 (1970).

4) K. Ohashi, A. Onuma, K. Yamamoto, and Y. Kurimura, *Nippon Kagaku Zasshi*, **92**, 51 (1971).

5) K. Ohashi, M. Matsuzawa, E. Hamano, and K. Yamamoto, *Bull. Chem. Soc. Jpn.*, **49**, 2440 (1976).

6) The equilibrium constant ($K=[Co^{II}(Hedta)(H_2O)^-]/[Co^{II}(edta)^{2-}][H^+]$) is $10^{3.1}$ M^{-1} at 20 °C and $I=0.10$.[7] The Co^{II}-edta complex exists as $Co^{II}(Hedta)(H_2O)^-$ and $Co^{II}(edta)^{2-}$ in the pH range from 3.50 to 5.36. The formula of Co^{II}-edta used in this paper represents a mixture of $Co^{II}(edta)^{2-}$ and $Co^{II}(Hedta)(H_2O)^-$.

7) G. Anderegg, *Helv. Chim. Acta*, **47**, 1801 (1964).

BULLETIN OF THE CHEMICAL SOCIETY OF JAPAN, VOL. 50 (11), 3051—3052 (1977)

The Separation of Aluminium(III) and Chromium(III) as Their AcAc(acetylacetone)-Complexes, and of Cobalt(II), Copper(II), Magnesium(II), Manganese(II), Nickel(II), and Lead(II) as Their TTA(thenoyltrifluoroacetone)-Complexes, by Extraction Chromatography

Takaharu Honjo, Yoshio Honda, Tetsu Matsumoto, Ryumon Honda, and Toshiyasu Kiba

Department of Chemistry, Faculty of Science, Kanazawa University, Marunouchi, Kanazawa 920

(Received April 25, 1977)

Synopsis. The liquid-liquid extraction behavior of the Al(III) and Cr(III)–AcAc(acetylacetone)–$CHCl_3$ system and of the Mg(II), Pb(II), Mn(II), Co(II), Ni(II), and Cu(II)–TTA(thenoyltrifluoroacetone)–MIBK (isobutyl methyl ketone) system have been studied, and the results have been applied to the separation of these metals as their AcAc- and TTA-complexes by extraction chromatography.

The systematic and quantitative group separation of nineteen common cations by extraction chromatography has been devised in the authors' laboratory using the following six columns, in which the organic solvents were adsorbed on Kel-F(poly(chlorotrifluoroethylene)):[1]

	Stationary phase (5.5 g Kel-F)	Mobile phase (HCl(M) or pH)	Metal ions retained (each 0.5 mg)
1	100% TBP(1)	2M HCl	Fe(III), Hg(II), Sn(IV)
2	20% TOA–CCl_4	2M HCl	Ag(I), Bi(III), Cd(II), Zn(II)
3	100% TBP(2)	6M HCl	Sb(III)
4	50% AcAc–$CHCl_3$	pH 5.0	Al(III), Cr(III)
5	1.5M TTA(1)–MIBK	pH 5.0	Co(II), Cu(II), Mg(II), Mn(II), Ni(II), Pb(II)
6	1.5M TTA(2)–MIBK	pH 7.0	Ca(II), Ba(II), Sr(II)

The mutual separation of the metal ions retained on each column has already been attempted by passing a suitable eluting solution through columns of TBP (tributyl phosphate) (1),[2] TOA(trioctylamine)–CCl_4,[3] and TTA(2)–MIBK(isobutyl methyl ketone).[4] In this investigation, the extraction behavior of the Al(III) and Cr(III)–50% AcAc–$CHCl_3$ system and of the Co(II) Cu(II), Mg(II), Mn(II), Ni(II), and Pb(II)–0.2 M TTA–MIBK system have been examined, and the results have been applied to the mutual separation by extraction chromatography of the metals retained on the columns of the 50% AcAc–$CHCl_3$ system, and the 1.5 M TTA (1)–MIBK system.

Experimental

The experimental procedures were almost the same as those previously described.[1-6] Into a 50-ml centrifuge tube, 50% AcAc in chloroform(10-ml) and an aqueous solution (10-ml) containing 0.5 mg each of Al(III) and Cr(III), 10-ml of 0.2 M TTA in MIBK, and 10-ml of an aqueous solution containing 10 ppm each of Co(II), Cu(II), Mg(II), Mn(II), Ni(II), and Pb(II) were put together, and the contents for each of the metal ions were agitated with a mechanical shaker for 30—40 min at room temperature (20—23 °C). The pH of the solution was adjusted to a desired value by using 0.5 M acetic acid or an aqueous ammonia solution. The pH was checked again after every extraction by means of the pH meter. In the case of Cr(III), the mixture was heated gently for 1 h until the completion of the formation of the AcAc-chelate of Cr(III) with or without Al(III), because the quantitative extraction of Cr(III) with 50% AcAc in chloroform was impossible at room temperature.[1,7] The back extraction was carried out by shaking a 5-ml or 10-ml portion of the organic phase containing the extracted metal chelates with an aqueous solution of the desired acidity. The distribution ratios of the metals were determined radiometrically with Co-60, Cr-51, Mn-54, Ni-63, and Pb-210, colorimetrically for Al oxinate at 390 nm, or atomic absorptiometrically for Cu(II) and Mg(II). The extraction chromatography was carried out by using a glass chromatographic column (10 mm in diameter and 30 cm long, with a course frit at the bottom) containing a 5.5 g portion of Kel-F(40—80 mesh), a definite volume of 50% AcAc in chloroform (5.0-ml) and 1.5 M TTA in MIBK (6.5-ml) which had been pre-equilibrated with the eluting solution of pH 5.0, and a definite volume of the eluting solution(5.0—6.5 ml). A 50-ml sample solution containing 0.5 mg each of Co(II), Cu(II), Mg(II), Mn(II), Ni(II), and Pb(II), adjusted to pH 5.0, was passed through the column at the rate of 0.03—0.3 ml per minute, and then an eluting solution of a suitable pH, which had previously been pre-equilibrated with the organic solution of the stationary phase, was passed through at the flow rate of 0.4—0.5 ml per minute. The effluent was taken up in a fraction collector. In the case of the Al(III) and Cr(III)–50% AcAc–$CHCl_3$ system, a 100-ml sample solution of pH 5.0 containing acetylacetonates of Al(III) and Cr(III)(each 0.5 mg), which had been prepared by heating for an hour, was percolated through the column at the rate of 0.2-ml per minute, and then an eluting solution of a definite acidity was passed through at the flow rate of 0.5-ml per minute, as has previously been reported.[1]

Theoretical

The percentage of extraction, % E, and the percentage of back extraction, % E_{back}, can be calculated by means of the following equations: % $E=D/(1+D)\cdot 100$, % $E_{back}=D^*/(1+D^*)\cdot 100$, where D and D^* are the net distribution ratios of a metal in the extraction and in the back extraction respectively. The % E and the % E_{back} of metals in the column can be expressed by the following equation[5]: % $E=(1-V^*/V_m)\cdot 100$, where V^* is the volume of the mobile phase and where V_m is the volume of the eluate relative to the maximum of the eluted metal concentration.

Results and Discussion

The symbols in Fig. 1 A→O and O→A denote the extraction and the back extraction of chemical species

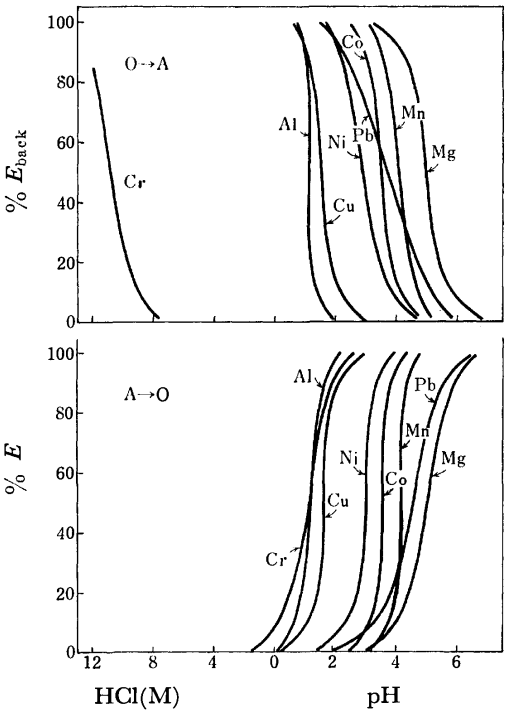

Fig. 1. The effect of pH or HCl(M) on the extraction and the back extraction of Al(III) and Cr(III)–50% AcAc–$CHCl_3$ system, and Co(II), Cu(II), Mg(II), Mn(II), Ni(II), and Pb(II)–0.2 M TTA–MIBK system.

respectively. The extraction and the back extraction are repeated in the column many times during the process of the extraction chromatography, which is closely related to the batch extraction; therefore, the optimum pH or acidity of the eluting solution can be predicted from the distribution ratios of the metals obtained by the ordinary extraction.[1-6] When the results of the batch extraction of metals with 0.2 M TTA in MIBK are applied by extraction chromatography to the mutual separation of metals retained on

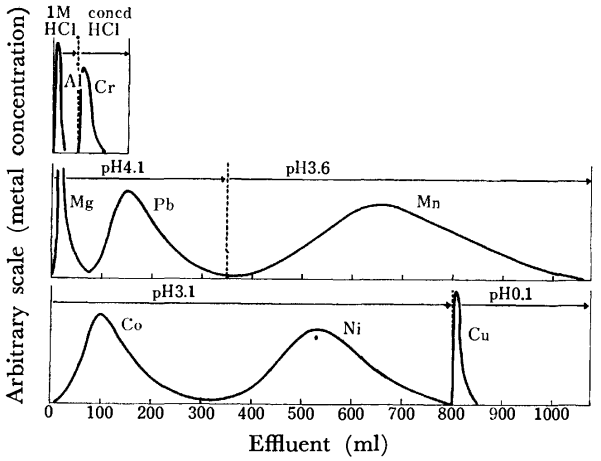

Fig. 2. The mutual separation of Al(III) and Cr(III) on a 50% AcAc–$CHCl_3$–Kel-F column, and Co(II), Cu(II), Mg(II), Mn(II), Ni(II), and Pb(II) on a 1.5 M TTA–MIBK–Kel-F column from a mixed solution.

Table 1. % E and % E_{back} of Al(III), Cr(III), Mg(II), Pb(II), Mn(II), Co(II), Ni(II), and Cu(II) obtained from the extraction and elution curves

Metal	Acidity	Liquid-liquid extraction[a] % E	% E_{back} Found	% E_{back} Calcd	Extraction chromatography[b] Acidity	%
Al(III)	1M HCl	0	90	100	1M HCl	58
Cr(III)	concd HCl	0	85	100	concd HCl	55
Mg(II)	pH 5.0	50	50	50	pH 4.1	62
Pb(II)	pH 5.0	74	13	26	pH 4.1	96
Mn(II)	pH 4.5	94	18	6	pH 3.6	98
Co(II)	pH 4.0	94	13	6	pH 3.1	94
Ni(II)	pH 4.0	100	8	0	pH 3.1	99
Cu(II)	pH 1.0	8	90	92	pH 0.1	7

a) Al(III) and Cr(III) (each 0.5 mg)–50% AcAc–$CHCl_3$, Mg(II), Pb(II), Mn(II), Co(II), Ni(II), and Cu(II) (each 10 ppm)–0.2M TTA–MIBK systems. b) Al(III) and Cr(III) (each 0.5 mg)–50% AcAc–$CHCl_3$, Mg(II), Pb(II), Mn(II), Co(II), Ni(II), and Cu(II) (each 0.5 mg)–1.5 M TTA–MIBK systems.

the column of the 1.5 M TTA–MIBK system, the eluting solution with every pH lower by 0.88 than that predicted from the batch extraction with the 0.2 M TTA–MIBK system was adopted, because the shift of the pH of the extraction curves to the lower pH region was assumed to be 0.87 when the concentration of TTA was changed from 0.2 M to 1.5 M. An optimum mutual separation of Al(III) and Cr(III) in the 50% AcAc–$CHCl_3$ system and of Co(II), Cu(II), Mg(II), Mn(II), Ni(II), and Pb(II) in the 1.5 M TTA–MIBK system was established by using the eluting solutions given in Fig. 2. The recovery of the metals was about 70—100 %. The deposit of some chelate in the column due to the loss of the stationary solvent phase was observed during the course of loading; this phenomenon may cause the lower recovery. The values of the distribution ratios of the metals obtained by the batch extraction and the extraction chromatography are summarized in Table 1. The main discrepancy between the two values may be caused by the differences in the contact times of the two phases and/or by the time-lag in the complex formation in the extraction and the back extraction, as has previously been pointed out by the present authors.[3-6]

The authors wish to thank Dr. Ikuko Akaza of Kanazawa Women's College for her helpful advice and discussion.

References

1) I. Akaza, T. Tajima, and T. Kiba, *Bull. Chem. Soc. Jpn.*, **46**, 1199 (1973).
2) I. Akaza, M. Nomura, and T. Kiba, unpublished results.
3) T. Honjo, S. Ushijima, and T. Kiba, *Bull. Chem. Soc. Jpn.*, **46**, 3764 (1973).
4) I. Akaza, *Bull. Chem. Soc. Jpn.*, **39**, 980 (1966).
5) T. Honjo and T. Kiba, *Bull. Chem. Soc. Jpn.*, **46**, 1706 (1973).
6) T. Honjo, M. Horiuchi, and T. Kiba, *Bull. Chem. Soc. Jpn.*, **47**, 1176 (1974).
7) J. P. Mckaveney and H. Freiser, *Anal. Chem.*, **30**, 1965 (1958).

BULLETIN OF THE CHEMICAL SOCIETY OF JAPAN, VOL. 50 (11), 3053—3054 (1977)

The Formation of the N-bound Hydroxyiminoacetylacetonato Ligand by the Reaction of Nitrosyl in Bis(2,2'-bipyridine)chloronitrosylruthenium(II) with Acetylacetone

Masao MUKAIDA, Masakazu YONEDA, and Terunosuke NOMURA

Department of Chemistry, Faculty of Science and Technology, Sophia University, Kioicho, Chiyoda-ku, Tokyo 102

(Received May 16, 1977)

Synopsis. Nitrosyl in $[RuCl(bpy)_2NO]^{2+}$ reacts with Hacac, giving the N-bound hydroxyiminoacetylacetonato ligand(hia, $CH_3COC(NO)COCH_3^-$) under mild conditions. The reaction product, $[Ru(hia)(bpy)_2(H_2O)]X$ ($X=ClO_4$, PF_6), was characterized on the basis of its IR spectra, including those of the ^{15}N-complex.

Although the reactivities of coordinated nitrosyl in transition metal complexes have been widely studied, little work has been reported on the formation of N–C bonding *via* nitrosyl complexes.[1-4] These reactions are, however, thought to be useful for the nitrosation of some organic compounds.[5] We wish now to report on the complex, $[Ru(hia)(bpy)_2(H_2O)]X$ ($X=ClO_4$, PF_6), which was formed by the reaction of $[RuCl(bpy)_2NO]^{2+}$ with Hacac. The hia ligand in this complex functions as an unidentate ligand coordinating through the nitrogen atom, as is shown in Fig. 1.

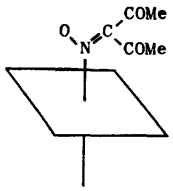

Fig. 1. N-bound hia ligand.

Experimental

Materials. The nitrosyl complex, $[RuCl(bpy)_2NO](ClO_4)_2$, was prepared by the procedure described by Meyer *et al.*, but $[RuCl_2(bpy)_2]Cl$ was used as a starting material instead of $[RuCl_2(bpy)_2]$. $[RuCl_2(bpy)_2]Cl$ was prepared by a new method using a "ruthenium blue" solution which was formed by the reaction of Ru(III) chloride with formic acid.[7]

Formation of Aquabis(2,2'-bipyridine)hydroxyiminoacetylacetonatoruthenium(II), $[Ru(C_5H_6NO_3)(C_{10}H_8N_2)_2(H_2O)]X$ ($X=ClO_4$, PF_6). The nitrosyl complex(200 mg, 0.295 mmol) was dissolved in a mixed solution of EtOH–H_2O(20 ml–10 ml), and then Hacac(1 ml) was added. After 10—15 days, a dark brown precipitate was collected, washed with water, and air-dried. The crude product(200 mg) was dissolved in water(300 ml). The resultant solution was charged on the top of a column containing SP sephadex C25 in the Na form (diameter, 12 mm; column height, 150 mm). When an aqueous solution of NH_4OAc(0.06 M) was then poured into the column at the rate of *ca.* 1—2 ml/min, a brown band appeared. Brown crystals were isolated as ClO_4 or PF_6 salt from the eluate of the band. A few further bands can be observed by the addition of an eluent containing KNO_3. The characterization of the products obtained from these bands is now under investigation. The present complex was filtered off, washed with water, and dried *in vacuo* over silica gel. Yield: about 30 mg. Found: N, 10.83; C, 45.76; H, 3.39; ClO_4, 14.70; H_2O, 2.38%. Calcd for $C_{25}H_{24}N_5O_8ClRu$: N, 10.62; C, 45.53; H, 3.64; ClO_4, 15.10; H_2O, 2.73%. Found: N, 10.23; C, 42.83; H, 3.13; PF_6, 21.01%. Calcd for $C_{25}H_{24}N_5O_4PF_6Ru$: N, 9.94; C, 42.59; H, 3.41; PF_6, 20.58%. The complex was soluble in common organic solvents. The crude product was diamagnetic. This suggests that the reaction product is a Ru(II) complex.

Results and Discussion

The complex formed by the reaction of $[RuCl(bpy)_2NO]^{2+}$ with Hacac gave the analytical data corresponding to the formula of $[Ru(hia)(bpy)_2](X\cdot H_2O)$. The complex containing the bidentate hia, $[Ru(acac)_2(hia)]$, has been found in the reaction of $[RuCl(acac)_2NO]$ with Hacac.[3] The IR spectra of the present complex, however, indicate the formula of $[Ru(hia)(bpy)_2(H_2O)]X$ containing the unidentada hia. By a comparison between the spectra of the ^{14}N-complex and the ^{15}N-complex in the 700—4000 cm^{-1} region, the isotopic effects were found two bands at 1350 and 806 cm^{-1}. In contrast, the ^{15}N substitution effects for $[Ru(acac)_2(hia)]$ have been found in three bands—at about 1400, 1160, and 800 cm^{-1}.[3] This finding can be explained by assuming the presence of different types of hia ligand in the two complexes. The bands in the present complex and its related complexes in which the ^{15}N substitution effects were observed are listed in Table 1.

Recently Mayer *et al.* reported that the nitrosyl in $[RuCl(bpy)_2NO]^{2+}$ reacts with aromatic amines to give *N*-bound *p*-nitrosoarene complexes.[2] They identified those products on the basis of the IR spectra. Armor

Table 1. Data of ^{15}N substitution shifts for the hia complexes and relevant complexes

Complex	Tentative assignments ν(N=C)	ν(N–O)	
$[Ru(hia)(bpy)_2(H_2O)]ClO_4$		1342(1327)	
$[Ru(hia)(bpy)_2(H_2O)]PF_6$		1350(1340)	806(793)
$[Ru(hia)(acac)_2]$	(1387)*	1162(1148)	807(796) 782(782) (771)
$[Ru(N(O)C_6H_4RCH_3)(bpy)_2Cl]PF_6$ [a]			
R=H		1286(1261)	875(860)
R=CH_3		1284(1276)	875(860)
$[Ru(NH_3)_5\{(NO)CH_2C(CH_3)_2OH\}]B(C_6H_5)_4$ [b]		1365(~1355)	

* New band. The bands based on ^{15}N complexes are shown in parentheses. a) Ref. 2. b) Ref. 4.

et al. also obtained an alkylnitrosoruthenium(II) complex by the radiolysis of $[Ru(NH_3)_5NO]^{3+}$ in *t*-butyl alcohol.[4] The isotopic shifts observed for the present complex are in almost the same regions and in almost the same magnitude as those of the complexes in Refs. 2 and 4, indicating the presence of the unidentate hia. The bands at 1350 and 806 cm^{-1} in the present complex can be assigned tentatively to the stretching and the rocking vibrations of the N–O and N–C respectively of the unidentate hia, according to the assignments in Ref. 2. The band characteristic of uncoordinated carbonyl in the hia ligand was found in 1660 cm^{-1}. As is shown in Table 1, the band due to the N–O stretching vibration of the unidentate hia was found in a higher region than that of the chelating hia. In addition, the stretching vibration band due to the oxime-type C=N bonding in chelating hia has also been found in a lower region than that expected.[8] No explanation for why the stretching bivrations of both N=C and N–O become lower in $[Ru(acac)_2(hia)]$ can be offered at the present time.

Bottomley *et al.* proposed that coordinated NO^+ with $\nu(NO) > 1886$ cm^{-1} behaves as an electrophile.[9] According to their criterion, $[RuCl(acac)_2NO]$(ν(NO); 1884 cm^{-1}) in Ref. 3 exists on the borderline between complexes reactive and unreactive toward nucleophiles. On the other hand, $[RuCl(bpy)_2NO](ClO_4)_2$(ν(NO); 1927 cm^{-1}) has been known to be very reactive.[2] It was found in the present work that $[RuCl(bpy)_2NO]^{2+}$ reacts with Hacac to give a Ru(II) complex containing the unidentate hia, while $[RuCl(acac)_2NO]$ gives a Ru(III) complex containing the bidentate hia under the same conditions.[3] The formation of the two types of hia seems to be connected with the difference in the reactivities of coordinated nitrosyl between $[RuCl(bpy)_2NO](ClO_4)_2$ and $[RuCl(acac)_2NO]$.

The authors wish to express their thanks to Professor Thomas J. Meyer, the University of North Carolina, for his kind consent for us to investigate the nitrosyl complex prepared by himself. The present work was partially supported by a Grant-in-Aid for Scientific Research from the Ministry of Education.

References

1) J. H. Swinehart, *Coord. Chem. Rev.*, **2**, 385 (1967).
2) T. J. Meyer, W. F. Little, and W. L. Bowdon, *J. Am. Chem. Soc.*, **96**, 5605 (1974); *ibid.*, **98**, 444 (1976).
3) M. Mukaida, T. Nomura, and T. Ishimori, *Bull. Chem. Soc., Jpn.*, **48**, 1443 (1975). $[Ru(acac)_2(hia)]$ can also be obtained by the reaction of $[Ru(acac)_2Cl(H_2O)]$ with Hhia. The identity was checked by means of the elemental analyses, magnetic moments, and IR and UV spectra. *Cf.* M. Mukaida Y. Nakamura, and T. Nomura, Abstr. No. 3I12, 34th Natioanl Meeting of the Chemical Society of Japan, Tokyo, April 1976.
4) J. N. Armor, R. Furman, and M. Z. Hoffman, *J. Am. Chem. Soc.*, **97**, 1737 (1975).
5) J. A. McCleverty, C. W. Ninnes, and I. Wolochowicz, *J. Chem. Soc., Chem. Commun.*, **1976**, 1061.
6) T. J. Meyer and J. B. Godwin, *Inorg. Chem.*, **10**, 471 (1971).
7) M. Mukaida, M. Hatano, E. Kondo, T. Nomura, and T. Ishimori, Abstr. No. 2M18, 32nd National Meeting of the Chemical Society of Japan, Tokyo, April 1975.
8) I. Masuda, M. Tamaki, and K. Shinra, *Bull. Chem. Soc. Jpn.*, **42**, 157 (1969).
9) F. Bottomley, W. V. F. Brooks, S. G. Clarkson, and S. Tong, *J. Chem. Soc., Chem. Commun.*, **1973**, 919.

BULLETIN OF THE CHEMICAL SOCIETY OF JAPAN, VOL. 50 (11), 3055—3056 (1977)

^{1}H and ^{13}C NMR of 2,2′-Bipyridine Adducts with Butyltin(IV) Trichloride and Tin(IV) Tetrachloride, and Tetrabromide

Gen-etsu MATSUBAYASHI and Jun IYODA*

Department of Applied Chemistry, Faculty of Engineering, Osaka University, Yamadakami, Suita, Osaka 565

**Government Industrial Research Institute, Midorigaoka, Ikeda, Osaka 566*

(Received June 13, 1977)

Synopsis. ^{1}H and ^{13}C NMR spectra of 2,2′-bipyridine adducts of butyltin(IV) trichloride and tin(IV) tetrachloride and -bromide have been measured in *N,N*-dimethylacetamide. On the basis of the chemical shifts of the ^{13}C nucleus and spin-spin coupling constants of the $^{117/119}Sn$ with the ligand ^{1}H and ^{13}C nuclei the configuration of the adducts and the nitrogen-tin coordination bond are discussed.

Spin-spin coupling constants between the ligand atoms and the metal nucleus of complexes give important informations about the metal-ligand bond. To date, however, there have been only a few reports[1-3] on the coupling constants between $^{117/119}Sn$ nuclei and ligand protons measured in tin(IV) halide adducts of organic ligands, and tin couplings with ligand ^{13}C nuclei of the adducts have never been measured. Recently we have observed the couplings between the tin nuclei and the protons attached to the carbons adjacent to the coordinating nitrogen atoms in the 2,2′-bipyridine (bpy) adduct of butyltin trichloride.[2] This paper reports ^{1}H and ^{13}C NMR data of bpy adducts of butyltin trichloride and tin tetrachloride and tetrabromide in *N,N*-dimethylacetamide.

As described previously,[2] the bpy adduct of $BuSnCl_3$ is monomeric and a non-electrolyte in acetonitrile. Essentially the same situation is expected in *N,N*-dimethylacetamide, because the adduct in this solvent shows quite similar ^{1}H NMR spectral behavior to the observations in acetonitrile solution both in the absence and in the presence of excess bpy. The figure indicates the ^{13}C NMR spectrum of the bpy adduct of $BuSnCl_3$ in *N,N*-dimethylacetamide. Signal assignment is facilitated by the ^{13}C NMR measurement with selective $\{^{1}H\}$–^{13}C decoupling of each bpy proton signal. This assignment is consistent with that of platinum(II)–bpy complexes.[4,5] The occurrence of the doubly separated C(2,2′) and C(5,5′) signals is in agreement with the previously suggested configuration A, where the butyl group lies on the N–Sn–N plane of the hexa-coordinated complex.[2]

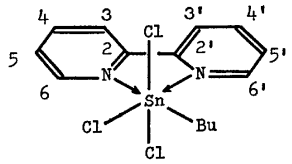

(A)

In the spectra of the hexa-coordinated bpy–SnX_4 (X=Cl or Br) adducts the signals were also unchanged by the addition of excess bpy, indicating no significant exchange between the complexed and free ligands on the NMR time scale in this solvent.

The ^{13}C signal assignment of the adducts, as well as their ^{1}H NMR data, is summarized in the table.

The C(2,2′) and C(6,6′) signals of free bpy move upfield and the others move downfield in the complexes. Although the same behavior concerning the direction of signal shift upon complexation was also detected in the platinum(II)-bpy complexes,[4,5] the large upfield shift of C(2,2′) and C(6,6′) signals is noticeable in the present tin halide adducts (see Table). This is rather analogous to the signal shift in the protonation of pyridine (C(2,6), +7.8 ppm; C(3,5), −5.0 ppm; C(4), −12.4 ppm).[6]

As is apparent from the figure, each ^{13}C signal has satellites due to the spin-spin coupling with the tin nuclei, while the ligand proton coupling with the tin atom is detected only at the H(6,6′) signal.[2] In the platinum(II)–bpy complexes all bpy ^{13}C signals also give satellites due to the coupling with the ^{195}Pt nucleus.[4,5] However, a marked difference in the relative magnitudes of the coupling constants in these complexes can be noticed; the C(4,4′)–platinum coupling is extremely small (≈6 Hz) compared with the platinum couplings of the other ring carbons (26—32 Hz), while the C(4,4′)–tin coupling is rather larger than the C(3,3′) and C(5,5′) couplings. This larger C(4,4′) coupling observed in the tin halide adducts may be indicative of a

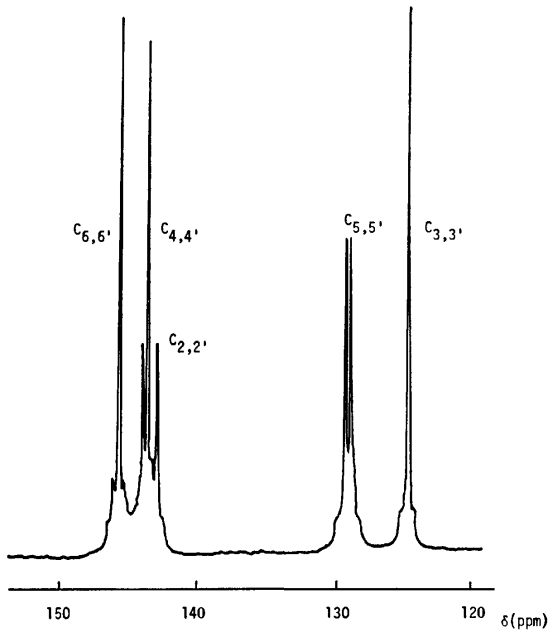

Figure. The ^{13}C NMR spectrum of $BuSnCl_3$·bpy in *N,N*-dimethylacetamide at 32 °C.

TABLE. ^{1}H AND ^{13}C NMR CHEMICAL SHIFTS (ppm) AND COUPLING CONSTANTS ($^{117/119}Sn$–^{1}H AND $^{117/119}Sn$–^{13}C) (Hz)[a] FOR 2,2′-BIPYRIDINE ADDUCTS OF Tin(IV) HALIDES IN *N,N*-DIMETHYLACETAMIDE

	^{1}H Resonances[b]					^{13}C Resonances[c]						
	$H_{3,3'}$	$H_{4,4'}$	$H_{5,5'}$	$H_{6,6'}$		$C_{2,2'}$		$C_{3,3'}$	$C_{4,4'}$	$C_{5,5'}$		$C_{6,6'}$
bpy	8.48	7.94	7.44	8.72		156.2		121.0	137.5	124.5		149.8
$SnCl_4$·bpy	9.35	8.84	8.38	9.66 (34)		142.1 (36)		125.3 (15)	145.0 (22)	129.7 (18)		145.0 (22)
$SnBr_4$·bpy	9.39	8.87	8.46	9.81 (38)		141.1 (e)		125.4 (16)	144.1 (25)	129.5 (18)		145.3 (23)
$BuSnCl_3$·bpy[d]	9.13	8.63	8.18	9.84 (38)	9.21 (11)	142.8 (15)	144.1 (e)	124.5 (20)	143.6 (22)	128.4 (24)	128.9 (e)	145.5 (22)

a) Shown in parentheses. b) Measured at 24 °C. c) Measured at 32 °C. d) For ^{1}H NMR data in Ref. (2). e) Could not be obtained since the signals were obscured by other signals.

significant π-interaction of bpy with the tin atom. This is in contrast with the fact that in trimethylphenyltin having a covalent aryl–tin bond the coupling between the tin and para-carbon nuclei is small;[7] here the phenyl-metal π-interaction may be small, as deduced in phenylplatinum derivatives.[8]

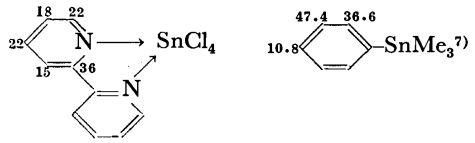

The tin–H(6,6′) or –carbon coupling constants of the $SnBr_4$ adduct are larger than those of the $SnCl_4$ adduct, indicating stronger Lewis acidity of $SnBr_4$. This is consistent with the result that stability constants of the $(CH_3)_2SnX_2$–bpy complexes increase in the order of X=Cl<Br<I.[9]

Directly bonded ^{13}C–^{1}H coupling constants of bpy obtained from the measurements without proton decoupling are larger in the adduct compared with those of the free ligand as follows.

	$^{1}J(^{13}C$–$^{1}H)$ (Hz)			
	$C_{3,3'}$–H	$C_{4,4'}$–H	$C_{5,5'}$–H	$C_{6,6'}$–H
Free bpy	170	163	163	178
$BuSnCl_3$·bpy	172	171	174	188

This is explainable as due to an increase of s-character in the C–H bond upon the adduct formation. The same behavior was reported in the directly bonded ^{13}C–^{1}H couplings on protonation of nicotinamide.[10]

Experimental

Materials. The preparation of $BuSnCl_3$·bpy was described previously.[2] SnX_4·bpy (X=Cl and Br) were prepared as white needles by mixing SnX_4 with an equimolar amount of bpy in acetonitrile. $SnCl_4$·bpy. Mp>300 °C. Found: C, 29.07; H, 2.00; N, 7.00%. Calcd for $C_{10}H_8N_2Cl_4Sn$: C, 28.82; H, 1.93; N, 6.72%. $SnBr_4$·bpy. Mp >300 °C. Found: C, 20.34; H, 1.34; N, 4.88%. Calcd for $C_{10}H_8N_2Br_4Sn$: C, 20.20; H, 1.36; N, 4.71%.

NMR Measurements. The ^{1}H NMR spectra were measured at 24 °C as described elsewhere.[1] The ^{13}C NMR spectra were obtained at 25.15 MHz using the pulse Fourier transform technique with a JEOL PS 100 spectrometer, an FT-100 FT unit, a DP-1 pulse programmer, and an EC-100 computer. ^{13}C chemical chifts in ppm were measured relative to TMS as an internal standard at 32 °C.

We wish to express our hearty thanks to Professor Toshio Tanaka for his continuous encouragement through this study.

References

1) G. Matsubayashi, M. Okunaka, and T. Tanaka, *J. Organomet. Chem.*, **56**, 215 (1973).
2) G. Matsubayashi and T. Tanaka, *J. Organomet. Chem.*, **120**, 347 (1976).
3) G. Matsubayashi and T. Tanaka, to be published.
4) S. T. Chow and R. B. Martin, *Inorg. Nucl. Chem. Lett.*, **10**, 1131 (1974).
5) L. E. Erickson, J. E. Sarneski, and C. N. Reilley, *Inorg. Chem.*, **14**, 3007 (1975).
6) R. J. Pugmire and D. M. Grant, *J. Am. Chem. Soc.*, **90**, 697 (1968).
7) C. D. Schaeffer, Jr., and J. J. Zuckerman, *J. Organomet. Chem.*, **55**, 97 (1973).
8) H. C. Clark and J. E. H. Ward, *J. Am. Chem. Soc.*, **96**, 1741 (1974).
9) T. Tanaka, G. Matsubayashi, A. Shimizu, and S. Matsuo, *Inorg. Chim. Acta*, **3**, 187 (1969).
10) B. Birdsall, J. Feeney, and P. Partington, *J. Chem. Soc., Perkin 2*, **1973**, 2145.

BULLETIN OF THE CHEMICAL SOCIETY OF JAPAN, VOL. 50 (11), 3057—3058 (1977)

A New Measure of Aromatic Stabilization: Resonance Energy per π Bond (REPB)

Jun-ichi AIHARA

Department of Chemistry, Faculty of Science, Hokkaido University, Sapporo 060

(Received October 18, 1976)

Synopsis. A concept of resonance energy per π electron appears unsuitable for representing the aromatic stabilization of a conjugated compound. If the resonance energy is divided by the number of π bonds constituting π rings in the conjugated system, though, a reasonable index is obtained for the same purpose.

In 1971, Hess and Schaad[1] interpreted Dewar's theory of aromaticity[2] by means of the HMO theory. They defined the aromatic resonance energy of a conjugated compound as the difference between the HMO π energy and the π energy of a "localized structure" obtained in an additive manner using the empirical π bond energies. Here, a "localized structure" signifies an olefinic reference structure which is hypothetically free from aromaticity. They further showed that if the resonance energy is divided by the number of π electrons in the compound, a quantity is obtained which correlates well with the experimental stability.[1] This was termed "resonance energy per π electron (REPE)". In previous papers,[3] we succeeded in formulating a characteristic polynomial for a "localized structure" of a conjugated compound, and analytically reproduced the resonance energies of Hess and Schaad without any parametrization. Of course, our resonance energies are Dewar-type.[1-3] In this note, we wish to point out that the definition of REPE should be modified in line with our exact resonance energies.

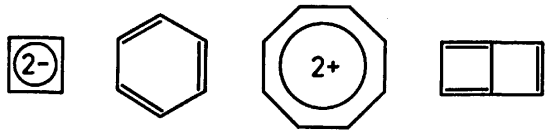

(I) (II) (III) (IV)

First, one should remember that Hess and Schaad defined REPE in order to overcome the wide variation in the size of conjugated systems usually compared.[1] This means that the REPE was presented as a better way of comparing resonance energies of various compounds. However, one finds that when the concept of REPE is extended to ionic conjugated systems, a serious ambiguity arises. For example, the resonance energies of the cyclobutadiene dianion(I), benzene(II), and the cyclooctatetraene dication(III) must be divided by the same number of π electrons, *i.e.*, six, to obtain their REPE values. This procedure is obviously in contradiction to the original intention of Hess and Schaad.[1] As has been suggested above, they intended to reflect the size of a conjugated system in the resonance energy by defining REPE. Therefore, the divisor should be changed if the size of a conjugated system is changed. Logically it should not depend upon the ionicity of a conjugated system.

According to the same definition of REPE, the resonance energies of benzene(II) and butalene(IV) must also be divided by the same number of π electrons, *i.e.*, six, in order to obtain their REPE values. Although butalene has one more π bond than benzene, the sizes of their conjugated systems have been tacitly considered to be identical.[1] We might say that the number of π electrons does not always reflect the size of a conjugated system, even if it is a neutral compound. Such an aspect of REPE is found among many sets of conjugated compounds.

We verified previously that aromaticity arises exclusively from a set of π rings in a conjugated system.[3] It is obvious that even if side chains and the like are conjugated with the main part of a cyclic conjugated system, they are absolutely olefinic. We might say that these side chains are neither stabilized or destabilized by the overall resonance energy. The role of the side chains is to somewhat modify the resonance energy of a π ring system (*i.e.*, a set of π rings in the conjugated system). The resonance energy obtained should, therefore, be attributed exclusively to the π rings or their constituents (*i.e.*, π bonds constituting these π rings). This fact is also inconsistent with the previous definition of REPE.

In order to avoid such REPE-based difficulties, we propose a new quantity which supposedly represents the actual stability of a conjugated system. It is defined as the Dewar-type resonance energy, divided by the number of π bonds which form a π ring system of a conjugated compound, and is termed "resonance energy per π bond" or REPB for short. As is indicated in this definition, the π bonds involved here are limited to those constituting cyclic components of Sachs graphs (*i.e.*, subgraphs of a molecular graph originally introduced by Sachs[4]).

It is noteworthy to see that, as an index of the size of a π ring system, the number of π bonds in it is preferable to the number of π electrons. It is nothing other than all the π bonds in the π ring system which must be sustained by the overall resonance energy. In this sense, the REPB reflects the size of a π ring system. The resonance energy has thus been assigned to individual π bonds forming a π ring system. Such a consideration appears to support our definition of REPB.

Table 1 contains 18 examples of conjugated compounds, shown with their values for REPE and REPB. When a conjugated system is neutral and monocyclic, REPE exactly agrees with REPB. However, when a conjugated system is ionic or polycyclic, the two quantities generally disagree. The deviation of REPE from REPB is never small for most conjugated compounds. One can see by using REPB that substituents such as a vinyl group do not stabilize a cyclobutadiene ring so

Table 1. REPE and REPB values in units of β for 18 conjugated systems

Compound	Resonance energy[a]	REPE$\times 10^3$	REPB$\times 10^3$	$100\times\frac{(\text{REPE}-\text{REPB})}{\text{REPB}}$
Cyclobutadiene	−1.226	−306.6	−306.6	0.0
Tetravinylcyclobutadiene	−0.703	−58.6	−175.7	−66.6
Cyclobutadiene dianion	0.305	50.8	76.1	−50.0
Cyclopentadienyl anion	0.317	52.8	63.3	−16.7
Benzene	0.273	45.4	45.4	0.0
Styrene	0.249	31.2	41.5	−24.8
Cycloheptatrienyl cation	0.225	37.6	32.2	16.7
Cyclooctatetraene dication	0.186	30.9	23.2	33.3
Butalene	−0.604	−100.7	−86.3	16.7
Pentalene	−0.215	−26.9	−23.9	12.5
Calicene	0.433	54.2	54.2	0.0
Fulvalene	−0.299	−29.9	−29.9	0.0
Azulene	0.151	15.1	13.7	10.0
s-Indacene	0.055	4.6	3.9	16.7
Naphthalene	0.389	38.9	35.3	10.0
Anthracene	0.475	33.9	29.7	14.3
Pyrene	0.598	37.4	31.5	18.8
Coronene	0.947	39.5	31.6	25.0

a) Ref. 3.

dramatically. This is in marked contrast to the prediction based on the REPE values.[5]

So far, such a discrepancy has not been noticed, partly because the degree of aromaticity cannot be measured quantitatively, and partly because scarcely no resonance energies have been estimated for ionic species.[6] Furthermore, the resonance energies published for neutral species are all empirical ones, in the sense that they are based on empirical π bond energies.[1,2] Now the situation has been totally changed. We have shown that Dewar-type resonance energies can be exactly calculated for any conjugated systems, including ions, as long as the HMO theory is used.[3] Accordingly, a measure of the aromatic stabilization should also be refined in harmony with the exactness of these resonance energies. This is exactly why REPE must be replaced by REPB. If a more detailed discussion of aromaticity is made in the future, it should be based on the values for REPB. The same definition of REPB can be applied to any Dewar-type resonance energies.[1–3]

References

1) B. A. Hess, Jr., and L. J. Schaad, *J. Am. Chem. Soc.*, **93**, 305, 2413 (1971); *ibid.*, **95**, 3907 (1973); *J. Org. Chem.*, **36**, 3418 (1971); B. A. Hess, Jr., L. J. Schaad, and C. W. Holyoke, Jr., *Tetrahedron*, **28**, 3657, 5299 (1972); *ibid.*, **31**, 295 (1975).

2) M. J. S. Dewar and G. J. Gleicher, *J. Am. Chem. Soc.*, **87**, 685, 692 (1965); M. J. S. Dewar and C. de Llano, *ibid.*, **91**, 789 (1969); M. J. S. Dewar, A. J. Harget, and N. Trinajstić *ibid.*, **91**, 6321 (1969); M. J. S. Dewar and N. N. Trinajstić, *Tetrahedron*, **26**, 4269 (1970); M. J. S. Dewar, A. J. Harget, N. Trinajstić, and S. D. Worley, *ibid.*, **26**, 4505 (1970).

3) J. Aihara, *J. Am. Chem. Soc.*, **98**, 2750 (1976); *ibid.*, **99**, 2048 (1977); *J. Org. Chem.*, **41**, 2488 (1976); *Kagaku No Ryôiki*, **30**, 379 (1976).

4) H. Sachs, *Publ. Math. (Debrecen)*, **11**, 119 (1963); A. Graovac, I. Gutman, N. Trinajstić, and T. Živković, *Theor. Chim. Acta*, **26**, 67 (1972); J. Aihara, *J. Am. Chem. Soc.*, **98**, 6840 (1976).

5) B. A. Hess, Jr., and L. J. Schaad, *J. Org. Chem.*, **41**, 3058 (1976).

6) Here, the resonance energies are restricted to those of the Dewar type. The only previous attempt to estimate the resonance energies of ionic species was made by the present author [J. Aihara, *Bull. Chem. Soc. Jpn.*, **49**, 1427 (1976)].

BULLETIN OF THE CHEMICAL SOCIETY OF JAPAN, VOL. 50 (11), 3059—3060 (1977)

The Acid-catalyzed Reaction of Alicyclic Ketones with Formaldehyde. II.[1] The Reaction of Cycloheptanone and Cyclooctanone with Formaldehyde

Fukumi HIRANO and Shoji WAKABAYASHI

Department of Chemistry, Faculty of Science, Okayama College of Science, Ridai-cho, Okayama 700

(Received January 29, 1977)

Synopsis. The acid-catalyzed reaction of cycloheptanone and cyclooctanone with formaldehyde gave predominantly 2,4-dioxaspiro[5.6]dodecan-7-one and 2,4-dioxaspiro[5.7]tridecan-7-one respectively.

In the previous paper,[1] we reported the reactions of cyclopentanone, cyclohexanone, and the alkyl-substituted cycloalkanones with formaldehyde in the presence of acid catalysts. The reactions produced hydroxymethyl derivatives, spiromono- and bis(1,3-dioxanes). The distribution of these products was markedly affected by both the skeletal structure and the substituent of the cycloalkanones. In this paper, we wish to report on the reactions of cycloheptanone (**1a**) and cyclooctanone (**1b**), together with the ring-size effect of cycloalkanones on the acid-catalyzed reaction.

The reaction of **1a** or **1b** with formaldehyde was carried out in a mixture of acetic acid and acetic anhydride in the presence of phosphoric acid at 60 °C. After the distillation of the resulting mixture, the products were isolated by preparative GLPC and were characterized on the basis of their chemical behavior and by spectroscopic methods.

The reaction of **1a** gave 2-acetoxymethylcycloheptanone (**2a**) and 2,4-dioxaspiro[5.6]dodecan-7-one (**4a**) in 21.4 and 43.8% yields respectively on the basis of the **1a** used. Similarly, the reaction of **1b** gave 2-acetoxymethylcyclooctanone (**2b**), 2,2-diacetoxymethylcyclooctanone (**3b**), and 2,4-dioxaspiro[5.7]tridecan-7-one (**4b**) in 8.7, 13.5, and 36.5% yields respectively.

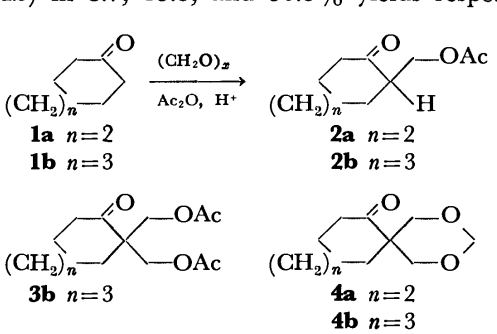

Scheme 1.

The PMR spectra of **4a** and **4b** showed a methylenedioxy proton at δ 4.53 (a characteristic quartet in the AB-type) in both compounds, and their IR spectra showed an absorption due to a methylenedioxy group at 2775 cm^{-1} in **4a** and at 2745 cm^{-1} in **4b** respectively. From these results, the structure of **4a** and **4b** was assigned to spiromono(1,3-dioxane) derivatives. The structure of **3b** was confirmed by the fact that the identical diacetate was obtained by the acetolysis of **4b** in the presence of phosphoric acid.

The acid-catalyzed reaction of **1a** and **1b** was compared with that of cyclopentanone and cyclohexanone. The reactivity might decrease in the order of C_6->C_5->C_7->C_8-cycloalkanones, judging from the experiments undertaken. The product distribution was quite sensitive to the ring-size of the cyclic ketones. The reaction of C_7- and C_8-cycloalkanones afforded mainly spiromono(1,3-dioxanes), but not bis(1,3-dioxanes), which were yielded largely in the reaction of cyclohexanone. These facts seem to be explained by the increased transannular repulsions arising from the formation of bis(1,3-dioxanes) in C_7- and C_8-cycloalkanones.

Experimental

All the boiling and melting points are uncorrected. The IR spectra were measured using a JASCO model IR-A spectrophotometer. The PMR spectra were obtained on a JEOL MH-60 II spectrometer (60 MHz), using tetramethylsilane as the internal standard. The mass spectra were taken with a Hitachi Model RMU-6GC mass spectrometer at 70 eV.

Materials. The cycloheptanone (**1a**) and cyclooctanone (**1b**) were prepared by the reported method;[2] **1a**: bp 65—67 °C/2 mmHg; **1b**: mp 32—33 °C.

Reaction of Cycloheptanone (1a) with Formaldehyde. To a stirred solution of paraformaldehyde (9.0 g, 0.3 mol), acetic anhydride (10.2 g, 0.1 mol), and 85% phosphoric acid (5.7 g, 0.05 mol) in glacial acetic acid (30 ml), **1a** (11.2 g, 0.1 mol) in glacial acetic acid (20 ml) was added over a 3-h period at 60 °C, after which the mixture was stirred at the same temperature for 7 h. The usual work-up gave 15.9 g of an oily product. The oil was then distilled under reduced pressure to give an unreacted **1a** (4.2 g, 37.1% yield, based on the **1a** used) and a colorless liquid (9.5 g, bp 67—113 °C/2 mmHg; GLPC analysis showed **2a**, **4a**, and the self-condensates of formaldehyde with peak area ratios of 31, 56, and 13% respectively). The latter distillate was separated by preparative GLPC (Apparatus: Yanaco G-80. Column, 30% Diethylene Glycol Succinate Polyester on Chamelite CK, 14 mm × 3 m. Temp, 170 °C. Carrier gas, H_2 at 280 ml/min) to afford **2a** (2.4 g, 21.4%) and **4a** (4.9 g, 43.8%), each as a colorless liquid; *2-acetoxymethylcycloheptanone (2a)*: d_4^{25} 1.0682, n_D^{25} 1.4640. PMR (CCl_4): δ 1.12—2.19 (br, 8H), 1.96 (s, 3H), 2.40 (m, 2H), 2.82 (m, 1H), and 3.98 (ABX, J_{AB}=11 Hz, J_{AX}=J_{BX}=6.0 Hz, $\Delta\nu_{AB}$=19.5 Hz, 2H). IR (neat): 1732 (vs), 1692 (vs), 1236 (vs), 1040 (s), and 1024 (s) cm^{-1}. Found: C, 65.42; H, 8.73%. Calcd for $C_{10}H_{16}O_3$: C, 65.19; H, 8.75%. *2,4-Dioxaspiro[5.6]dodecan-7-one (4a)*: Bp 112—113 °C/2 mmHg, d_4^{25} 1.1217, n_D^{25} 1.4880. MS: *m/e* 184 (M^+). PMR (CCl_4): δ 1.60 (br s, 6H), 1.94 (m, 2H), 2.36 (m, 2H), 3.63 (AB-q, J=12 Hz, 4H), and 4.53 (AB-q, J=5.7 Hz, 2H). IR (neat): 2775 (w), 1684 (vs), 1160 (vs), 1152 (vs), 1028 (s), 1004 (s), and 920 (s) cm^{-1}. Found: C, 65.37; H, 8.68%. Calcd for $C_{10}H_{16}O_3$: C, 65.19; H, 8.75%.

*Reaction of Cyclooctanone (**1b**) with Formaldehyde.* In a way similar to that in the reaction of **1a**, the reaction of **1b** (12.6 g, 0.1 mol) with paraformaldehyde (9.0 g, 0.3 mol) and acetic anhydride (10.2 g, 0.1 mol) gave 17.5 g of an oily product. The oil was distilled under reduced pressure to give an unreacted **1b** (5.2 g, 41.3%) and two colorless fractions (A: 8.2 g, bp 59—132 °C/0.1 mmHg; B: 1.8 g, bp 132—134 °C/0.1 mmHg). The A fraction (GLPC analysis indicated **2b**, **4b**, and the self-condensates of formaldehyde with peak area ratios of 15, 73, and 12% respectively) was then separated by preparative GLPC to afford **2b** (1.1 g, 8.7%) and **4b** (4.6 g, 36.5%), each as a colorless liquid; *2-Acetoxymethylcyclooctanone (**2b**)*: d_4^{25} 1.0565, n_D^{25} 1.4689. PMR (CCl_4): δ 0.82—2.10 (br, 10H), 1.95 (s, 3H), 2.23 (m, 2H), 2.87 (m, 1H), and 3.93 (ABX, J_{AB}=11 Hz, J_{AX}=6.0 Hz, J_{BX}=8.7 Hz, $\Delta\nu_{AB}$=15 Hz, 2H). IR (neat): 1732 (vs), 1696 (vs), 1232 (vs), 1044 (s), and 1028 (s) cm^{-1}. Found: C, 66.90; H, 9.13%. Calcd for $C_{11}H_{18}O_3$: C, 66.64; H, 9.15%. *2,4-Doixaspiro[5.7]tridecan-7-one (**4b**)*: bp 104—105 °C/0.1 mmHg. d_4^{25} 1.1076, n_D^{25} 1.4927. MS: *m/e* 198 (M^+). PMR (CCl_4): δ 1.48 (m, 8H), 2.17 (m, 4H), 3.72 (s, 4H), and 4.53 (AB-q, J=6.0 Hz, 2H). IR (neat): 2745 (w), 1682 (vs), 1170 (vs), 1154 (vs), 1134 (vs), 1064 (vs), 1040 (s), 1028 (vs), 921 (s) cm^{-1}. Found: C, 66.91; H, 9.13%. Calcd for $C_{11}H_{18}O_3$: C, 66.64; H, 9.15%.

On the other hand, the B fraction crystallized directly on standing and was recrystallized from cyclohexane to yield *2,2-diacetoxymethylcyclooctanone (**3b**)* (1.7 g, 13.5%) as white crystals; mp 65—66 °C; PMR (CCl_4): δ 1.16—2.10 (br, 10H), 1.98 (s, 6H), 2.42 (m, 2H), and 4.05 (AB-q, J=12 Hz, 4H). IR (CCl_4): 1740 (vs), 1693 (s), 1233 (s). 1219 (s), 1040 (s), and 1021 (s) cm^{-1}. Found: C, 62.28; H, 8.23%. Calcd for $C_{14}H_{22}O_5$: C, 62.20; H, 8.20%.

*Acetolysis of Spiromono(1,3-dioxane) (**4b**).* A solution of **4b** (198 mg, 1 mmol), acetic anhydride (204 mg, 2 mmol), and 85% phosphoric acid (57 mg, 0.5 mmol) in glacial acetic acid (1 ml) was stirred at 60 °C for 10 h. After a subsequent work-up, 190 mg of an oily mixture were obtained. The PMR analysis revealed that the reaction mixture consisted of an acetolysis product (12%) and unreacted **4b** (88%), which were isolated by preparative GLPC to give 22 mg (11.1% yield, based on the **4b** used) of the acetolysis product and 158 mg (79.8%) of **4b**. The IR spectrum of the acetolysis product was completely identical with that of **3b** obtained from **1b**.

References

1) Part I; F, Hirano and S. Wakabayashi, *Bull. Chem. Soc. Jpn.*, **48**, 2579 (1975).

2) E. P. Kohler, M. Tishler, H. Potter, and H. T. Thompson, *J. Am. Chem. Soc.*, **61**, 1059 (1939); R. Adams, *Org. Synth.*, **34**, 24 (1954).

BULLETIN OF THE CHEMICAL SOCIETY OF JAPAN, VOL. 50 (11), 3061—3062 (1977)

The Photochemical Sulfenylation of Hindered Phenols with Diaryl Disulfides

Tamotsu FUJISAWA and Takakazu KOJIMA

Sagami Chemical Research Center, Nishi-Ohnuma, Sagamihara, Kanagawa 229

(Received March 16, 1977)

Synopsis. The photochemical reaction of diaryl disulfides with 2,6-disubstituted phenols was investigated. The reaction with highly hindered phenols proceeded appreciably upon irradiation with a high-pressure mercury lamp, giving rise to 4-arylthio-2,6-disubstituted phenols. The reaction was initiated by the homolytic scission of the disulfides.

A previous report[1] concerning hindered phenols has demonstrated the synthesis of 4-arylthio-2,6-disubstituted phenols in basic media using diaryl disulfides as sulfenylating agents. We wish to report here another simple method of preparing the same sulfides by a photochemical sulfenylation of hindered phenols. The reaction proceeds smoothly and mildly upon the simple irradiation of a solution of diaryl disulfides and hindered phenols in an inert solvent with an ultraviolet lamp.

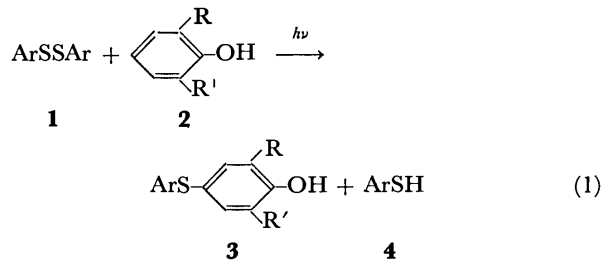

1 **2** **3** **4** (1)

Thus, a solution of diphenyl disulfide (**1**, Ar=C_6H_5) and 2,6-di-*t*-butylphenol (**2**, R=R′=*t*-C_4H_9) in cyclohexane was irradiated with a high-pressure mercury lamp through a Pyrex filter at room temperature for 20 h. 2,6-Di-*t*-butyl-4-(phenylthio)phenol (**3**, Ar=C_6H_5, R=R′=*t*-C_4H_9) was obtained in a 65% yield based on the phenol **2** consumed (GLC). Table 1 summarizes the results of the application of this method to several disulfides and substituted phenols.

In this reaction, solvents with no hydrogen active towards abstraction, such as cyclohexane and benzene, are suitable. Carbon tetrachloride, well-known chain-transfer reagents,[2] showed itself a good solvent, perhaps by reason of the formation of arenesulfenyl chloride, which subsequently acted as a sulfenylating agent.[3,4] The yields of **3** were significantly influenced by the substituents (R and R′). A less hindered phenol, 2,6-dimethylphenol, did not afford the corresponding arylthiolated phenol and was recovered quantitatively. The reaction of 2,6-di-*t*-butylphenol with aqueous hexacyanoferrate(III) in the presence of diphenyl disulfide or thiophenol leads to the exclusive formation of a diphenoquinone derivative, **5**,[5] yielded from the dimerization of the phenoxyl radical, without forming the expected **3**. The radical reaction of **1** and **2** initiated with α,α'-azodiisobutyronitrile also failed.

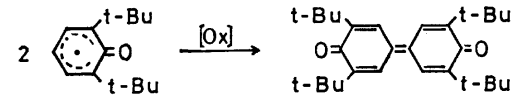

5 (2)

Unlike the photochemical reaction of disulfide with the aryl radical generated from aryl halide,[6] the present reaction proceeds *via* the aryl thiyl radical formed by the homolytic scission of aryl disulfide. This radical species, then, attacks the phenol, **2**, followed by the abstraction of hydrogen by another thiyl radical to give an intermediate dienone; it subsequently rearranges to (arylthio)phenol, **3**.

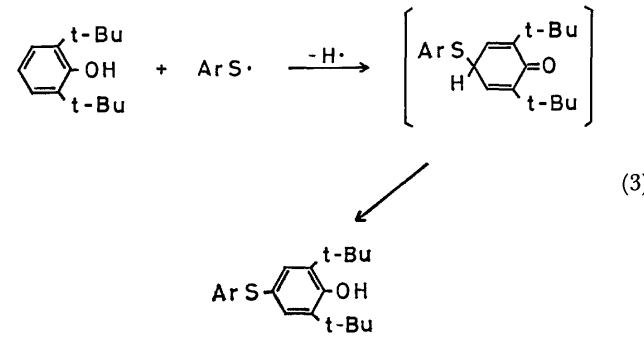

(3)

Table 1. Arylthiophenols from disulfides and phenols

Disulfide (**1**) Ar	Phenol (**2**) R	R′	Solvent	Yield of (Arylthio)phenol (**3**) (%)
C_6H_5	*t*-Bu	*t*-Bu	*c*-C_6H_{12}	29 (61)
C_6H_5	*t*-Bu	*t*-Bu	C_6H_6	25 (54)
C_6H_5	*t*-Bu	*t*-Bu	CCl_4	24 (65)
p-$CH_3C_6H_4$	*t*-Bu	*t*-Bu	*c*-C_6H_{12}	28 (61)
p-$CH_3OC_6H_4$	*t*-Bu	*t*-Bu	*c*-C_6H_{12}	10 (69)
p-ClC_6H_4	*t*-Bu	*t*-Bu	C_6H_6	23 (39)
C_6H_5	*t*-Bu	Me	*c*-C_6H_{12}	13 (36)
C_6H_5	*i*-Pr	*i*-Pr	*c*-C_6H_{12}	24 (48)
C_6H_5	Me	Me	*c*-C_6H_{12}	0 (0)

Irradiated for 24 h. The yields are based on the phenols. The yields based on the phenols consumed are shown in parentheses.

The ultraviolet spectrum of 2,6-di-*t*-butylphenol shows no notable absorption in the Pyrex-filtered region (>300 nm), and diphenyl disulfide is known to have an n-π^* transition at 320 nm (ε=783)[7] in the skirt of the strong π-π^* transition (243 nm). Two or three times as much disulfide was consumed under irradiation as was expected in the stoichiometry shown by Eq. 1. Consequently, arenethiols, **4**, were formed in greater amounts than (arylthio)phenols, **3**. One of the by-products formed in this reaction was bis[4-(2-phenylthio)phenyl] disulfide (**6**), which was isolated in an 18% yield when equimolar amounts of diphenyl disulfide and 2,6-di-*t*-

butylphenol were irradiated in cyclohexane for 50 h. This disulfide, **6**, is considered to be formed *via* 2-(phenylthio)benzenethiol, a rearranged dimer of the phenylthiyl radical.[8]

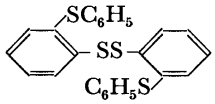

6

Experimental

Preparation of 4-Arylthio-2,6-dialkylphenol (3). The following procedure is representative of the preparation of **3**. Diphenyl disulfide (**1**, Ar=C_6H_5, 371 mg) and 2,6-di-*t*-butylphenol (**2**, R=R′=*t*-C_4H_9, 175 mg) were dissolved in cyclohexane (5 ml) and were then, after degassing, irradiated in a Pyrex ampoule with a high-pressure mercury lamp (450 W) for 20 h. The products were analyzed by GLC. Then, the solvent was removed from the reaction mixture under reduced pressure; subsequent column chromatography of the residue on silica gel (eluted by hexane) gave 2,6-di-*t*-butyl-4-(phenylthio)phenol (**3**, Ar=C_6H_5, R=R′=*t*-C_4H_9) in a 57% yield (58 mg) based on the phenol consumed. The conversion of **2** was 38%.

All of the products, (arylthio)phenols (**3**), were identified by a comparison of the mp, GLC, and IR and NMR spectra with those of the authentic sample.[1]

Bis[4-(2-phenylthio)phenyl] Disulfide (6). When diphenyl disulfide (110 mg) and 2,6-di-*t*-butylphenol (105 mg) in cyclohexane (3 ml) were irradiated using the above procedure, bis[4-(2-phenylthio)phenyl] disulfide (20 mg, 18% based on the **1**) was obtained after column chromatographic separation, along with **3** (Ar=C_6H_5, R=R′=*t*-C_4H_9, 18 mg) and **4** (Ar=C_6H_5, 8 mg). Recrystallization with aqueous ethanol gave pale yellow crystals; mp 118.5—120 °C. MS *m/e*: 434(M^+). IR (Nujol) 1582, 1440, 758, and 693 cm^{-1}. UV (cyclohexane) max: 254 nm (ε 8.2×10^4). Found: C, 66.15; H, 4.38; S, 29.59%. Calcd for $C_{24}H_{18}S_4$: C, 66.31; H, 4.18; S, 29.50%.

References

1) T. Fujisawa and T. Kojima, *J. Org. Chem.*, **38**, 687 (1973).
2) W. A. Pryor, "Free Radicals," McGraw-Hill, New York (1966), p. 214.
3) E. Müller, Ed., "Methoden der Organischen Chemie," Vol. IX, Georg Thieme Verlag, Stuttgart (1955), p. 136.
4) T. Fujisawa, M. Yamamoto, and G. Tsuchihashi, *Synthesis*, **1972**, 624.
5) C. D. Cook, E. S. English, and B. J. Wilson, *J. Org. Chem.*, **23**, 755 (1958).
6) T. Fujisawa and H. Ohta, *Bull. Chem. Soc. Jpn.*, **49**, 2341 (1976).
7) H. J. Backer and H. Kloosterziel, *Recl. Trav. Chim. Pay-Bas*, **73**, 129 (1954).
8) Y. Schaafsma, A. F. Bickel, and E. C. Kooyman, *Tetrahedron*, **10**, 76 (1960).

BULLETIN OF THE CHEMICAL SOCIETY OF JAPAN, VOL. 50 (11), 3063—3064 (1977)

Photo-acylamination on Anthracene with Use of Acyl Azides

Kunihiro ICHIMURA

Research Institute for Polymers and Textiles, Sawatari 4, Kanagawa-ku, Yokohama 221

(Received April 22, 1977)

Synopsis. Irradiation of anthracene in the presence of acyl azide gives isocyanate and 9-acylaminoanthracene. The photolysis of aromatic hydrocarbon–acyl azide was followed by UV spectrophotometry and analyzed by the EDQ (quotients of extinction differences) diagram method.

Although direct photolysis of acyl azide has been extensively investigated,[1] its sensitized decomposition is scarcely known. In relation to the photolysis of acyl azide–zinc porphyrin system,[2] studies have been extended to the interaction of excited aromatic hydrocarbons with the ground state of acyl azides. In this paper a report is given on the decomposition of benzoyl azides sensitized by anthracene affording isocyanates and 9-acylaminoanthracenes. This seems to be the first example of sensitized photo-Curtius rearrangement;[3] benzophenon-sensitization has been reported to involve the free radical chain reaction initiated by benzophenone triplet which affords no isocyanate.[4]

A solution of anthracene (**1**) and excess benzoyl azide (**2a**) was irradiated in dichloromethane under nitrogen with light of >320 nm absorbed specifically by the hydrocarbon. The IR spectral change indicated the formation of phenyl isocyanate accompanied by the disappearance of **2a**. TLC revealed the formation of a non-fluorescent product. The pale yellow crystals of mp 250—251 °C were separated by means of column chromatography. The IR bands at 3250 and 1648 cm^{-1} are assignable to the amide band. The structure of the product was unequivocally confirmed by identification with 9-benzoylaminoanthracene (**3a**). In a similar way, 9-(*p*-chlorobenzoylamino)- (**3b**) and 9-(*p*-cyanobenzoylamino)anthracene (**3c**) were obtained. The formation of the corresponding isocyanates was confirmed by the presence of the characteristic IR band. The results are summarized in Tables 1 and 2.

In order to extend the sensitization to the other aromatics, the photolysis of aromatic hydrocarbon–benzoyl azide was followed UV-spectrophotometrically and analyzed by the ED (extinction differences)- and EDQ (quotients of extinction differences)-diagram methods.[5] As shown in Fig. 1-a, the family of absorption curves of **1–2a** system irradiated with light of wavelength >320 nm intersect at the early stage of photolysis, the absorption spectrum of the photoproduct being almost the same as that of **3a**. Linearity was observed in the EDQ-diagram, but not in the ED-diagram. This implies that the photolysis contains two successive reactions: the formation and subsequent slower disappearance of **3a**. It was confirmed that the irradiation of **3a** in the presence of **2a** causes the disappearance of **3a** and that the rate of photolysis of the **3a–2a** system is much slower than that of the **1–2a** system. The

TABLE 1. 9-ACYLAMINOANTHRACENES (**3**)

Acyl	Mp (°C)	Yield (%)	Elementary analyses Found C	Found H	Found N	Calcd C	Calcd H	Calcd N
C_6H_5	250—251	37	84.34	4.83	4.69	84.81	5.09	4.72
p-ClC_6H_4	266—268	30	75.82	4.18	4.34	76.02	4.25	4.23
p-CNC_6H_4	297—300	20	81.21	4.32	8.50	81.99	4.38	8.70

TABLE 2. ULTRAVIOLET AND INFRARED SPECTRA OF 9-ACYLAMINOANTHRACENES

Acyl	λ_{max} nm ($\times 10^{-3}$)[a]	$\bar{\nu}_{max}$ cm^{-1} [b]
C_6H_5	258 (117), 335 (3.04), 350 (5.91), 367 (8.50), 386 (7.74).	3250, 1648
p-ClC_6H_4	258.5 (124), 335 (3.10), 351 (5.94), 368 (8.05), 387 (7.68).	3250, 1648
p-CNC_6H_4	258.5 (103), 335 (3.01), 351 (5.54), 368 (8.05), 387 (7.68).	3250, 2225, 1646

a) In chloroform. b) In KBr.

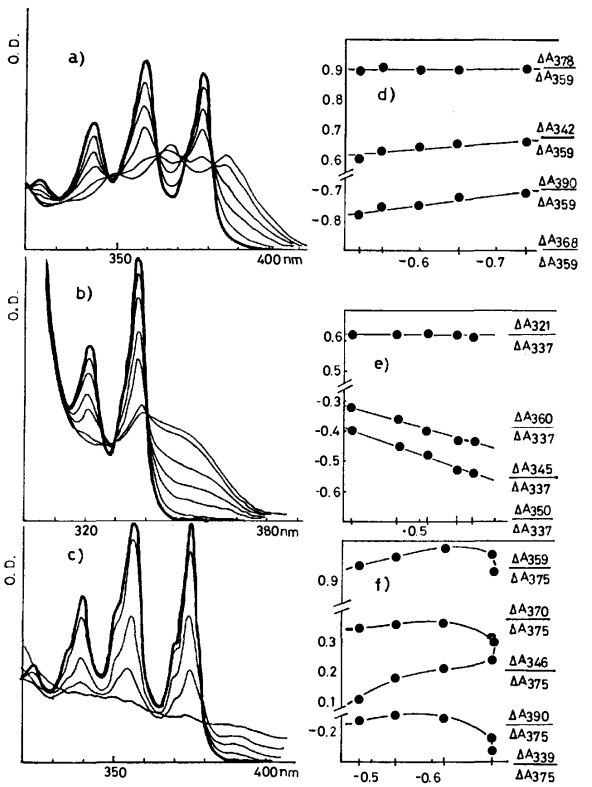

Fig. 1. The electronic absorption spectra recorded at intervals for the UV irradiation of aromatic hydrocarbon–acyl azide system ((a): anthracene–benzoyl azide in toluene, (b): pyrene–benzoyl azide in toluene, (c): anthracene–*p*-toluenesulfonyl azide in methylcyclohexane) and the corresponding EDQ diagrams ((d)—(f)).

spectral change of **3a–2a** shows a linear ED-diagram, in line with the linearity of EDQ-diagram for the photolysis of **1–2a**.

When a solution containing pyrene and **2a** was irradiated with light of wavelength >320 nm, the peaks due to the hydrocarbon decreased in intensity along with the increase of peaks at 338 nm (Fig. 1-b). The EDQ-diagram was linear in this case (Fig. 1-e). Although the photoproducts are yet to be isolated because of the difficulty of product separation, the appearance of the absorption maxima at greater wavelengths suggests that the photo-induced acylamination may take place on pyrene nucleus as in the case of **1**.

In the cases of 9,10-dimethyl- and 9,10-diphenylanthracene, the absorption peaks decreased on UV irradiation. No new absorption maximum was observed, while the linear EDQ-diagram was obtained.

It was found that anthracene is photolysed in the presence of *p*-toluenesulfonyl azide (**4**). The spectral change during the course of irradiation, however, differs from that of the **1–2a** system (Fig. 1–c). A weak absorption maximum appeared at *ca.* 390 nm at an early stage of photolysis and disappeared completely on prolonged irradiation. The absorption may be due to 9-(*p*-tolylsulfonylamino)anthracene (**5**) having λ_{max} at 337.5, 354, 371, and 391.5 nm. In contrast to the **1–2a** system, linear EDQ-diagram was no longer observed in this case (Fig. 1-f), indicating the involvement of more than three elementary photoreactions. 9-Sulfonylaminoanthracene (**5**) was found to be photolysed in the presence of acyl azide including **4**, the EDQ-diagram for the photolysis being non-linear, which demonstrates the difference in photolytic behavior between **3a** and **5**. The photolysis rate of **5** was found to be *ca.* 15 times greater than that of **3a** when benzoyl azide coexists. The difference in the mode of spectral change between **1–2a** and **1–4** systems reflects the difference in the photoreactivity of the products initially formed, *i.e.*, **3** and possibly **5**. As for the effect of acylamino group on the photoreactivity of anthracene nucleus toward acyl azide, it should be mentioned that 9-acylaminoanthracenes are non-fluorescent whilst 9-sulfonylamino derivative (**5**) gives the blue fluorescence. This implies that the introduction of the acylamino group to anthracene shortens the singlet lifetime so that the photoreactivity may be reduced, whereas the sulfonylamino group shows no remarkable influence on the fluorescence behavior and the photoreactivity of anthracene nucleus.

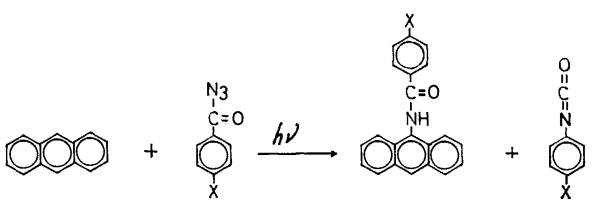

1 2 3

The photoinduced acylamination on anthracene using acyl azide appears to closely resemble that of zinc octaethylporphin.[2] A distinct difference between both reactions should be stressed: the photolysis of acyl azide-zinc porphyrin affords no isocyanate. This suggests that the sensitization mechanism is quite different from each other.

Experimental

All melting points were not corrected. Ultraviolet and infrared spectra were recorded on a Hitachi type 323 spectrophotometer and a Hitachi EPI-3G spectrophotometer, respectively.

Photolysis of Anthracene in the Presence of Benzoyl Azide. A solution of anthracene (180 mg) and benzoyl azide (1.42 g) in dichloromethane (20 ml) was irradiated under nitrogen gas with a 450 W high pressure mercury arc passed through a Corning 0-54 filter (>320 nm). The photolysis was followed by TLC and IR- and UV-spectrophotometry. The IR band assignable to phenyl isocyanate appeared in proportion to the disappearance of anthracene. After removal of the solvent, the residue was dissolved in dichloromethane and chromatographed on a silica gel column with use of dichloromethane as an eluent. After eluting the fluorescent fraction of anthracene, a pale yellow fraction was collected and evaporated to dryness. The residue was recrystallized from acetonitrile to give 67.4 mg yellow needles of 250—251 °C which was identified with 9-benzoylaminoanthracene by the mixture melting point and IR spectra. The amount of recovered anthracene was estimated to be 72.4 mg with the aid of UV spectroscopy. The yield of 9-benzoylaminoanthracene was therefore 37% based on consumed anthracene.

In a similar way, 9-(*p*-chlorobenzoylamino)- and 9-(*p*-cyanobenzoylamino)anthracene were obtained, starting from *p*-chlorobenzoyl azide and *p*-cyanobenzoyl azide, respectively. The results are summarized in Tables 1 and 2.

EDQ-Diagram Examination of Photolysis.[5] A three ml solution of anthracene (*ca.* 10^{-5} M/l) and benzoyl azide (*ca.* 10^{-2} M/l) in toluene was irradiated with light of wavelength >320 nm, and the UV spectra were recorded at intervals. The final spectrum was essentially the same as that of 9-benzoylaminoanthracene, the yield being estimated to be 56% (Fig. 1-a).

Similarly, the photolysis of the following combinations were determined by the EDQ-diagrams; pyrene–benzoyl azide in toluene, anthracene–*p*-toluenesulfonyl azide in methyl-cyclohexane, 9,10-dimethylanthracene–benzoyl azide in toluene, and 9,10-diphenylanthracene–benzoyl azide in toluene. Typical examples are shown in Fig. 1.

References

1) a) G. L'abbe, *Chem. Rev.*, **68**, 345 (1968); b) G. R. Felt and W. Lwowski, *J. Org. Chem.*, **41**, 96 (1976), and references cited therein.

2) K. Ichimura, *Chem. Lett.*, **1976**, 641.

3) Horner and coworkers have described the slow evolution of nitrogen gas on irradiation of a solution of naphthalene or triphenylene in the presence of benzoyl azide,[4a] but no product was characterized.

4) a) L. Horner, G. Bauer, and J. Doerges, *Chem. Ber.*, **98**, 2631 (1965); b) M. Sukigara, Y. Ito, K. Honda, and S. Kikuchi, *Nippon Shashin Gakukaishi*, **35**, 94 (1972).

5) G. Quinkert, *Angew. Chem.*, **84**, 1157 (1972).

BULLETIN OF THE CHEMICAL SOCIETY OF JAPAN, VOL. 50 (11), 3065—3066 (1977)

The Aromatic Thiocyanation of 1-Alkoxynaphthalene by the Copper(II) Thiocyanate Method

Kiyoko FUJIKI

Department of Agricultural Chemistry, Faculty of Agriculture, Meiji University, Ikuta, Tama-ku, Kawasaki 214

(Received May 20, 1977)

Synopsis. A facile thiocyanation of 1-alkoxynaphthalene using copper(II) thiocyanate afforded 4-thiocyanato compound. The reaction proceeded at a moderate temperature (80—90 °C) even for 1-alkoxynaphthalene with higher alkyl groups (C_6, C_8, and C_{12}).

During the course of an investigation of the pesticidal activities of aryl ethers it became desirable to prepare thiocyanato compounds of 1-alkoxynaphthalene because of their effected insecticidal and fungicidal activities.[1]

As a means of introducing a thiocyanato group into the aromatic nucleus, thiocyanogen is useful as a reagent for such reactive substrates as amines and phenols.[2] Less reactive substrates, such as phenolic ethers, naphthalene derivatives, and anillides, which are unreactive towards thiocyanogen, give thiocyanates in high yields when treated with thiocyanogen chloride in acetic acid;[3] however, 2-methoxynaphthalene reacts with not only thiocyanogen chloride[3] but also thiocyanogen[2,4] to give the 1-thiocyanato compound. As to the thiocyanation of 1-methoxynaphthalene, it has been thiocyanated at the 4-position in a 10.7% yield by a mixture of KSCN and *N*-chlorourea in acetone.[5] The 4-thiocyanato compounds of 1-ethoxy, 1-propoxy, 1-butoxy, and 1-isopentyloxy naphthalene have also been synthesized in a liquid state in a similar manner.[6] Other methods for the thiocyanation of aryl ethers involve the reaction of arylthallium(III) compounds with copper(II) and (I) thiocyanate[7] or with KSCN under the irradiation of light.[8]

The present paper will deal with the preparation of 1-alkoxy-4-thiocyanatonaphthalene by the copper(II) thiocyanate method[9], which was previously applied to the thiocyanation of 1-naphthol.[2] It is considered that the copper(II) thiocyanate method shows promise of being effective for the thiocyanation of higher alkyl naphthyl ethers, since copper(II) thiocyanate releases thiocyanogen merely by the dissociation of the cupric to cuprous salt (Eq. 1). Moreover, the procedure has the advantage over the others previously described of permitting a higher temperature for thiocyanation.

$$2Cu(SCN)_2 \rightarrow 2CuSCN + (SCN)_2 \quad (1)$$

Thiocyanation with $(SCN)_2$ was less reactive in higher alkyl (C_6–C_{12}) naphthyl ethers due to an electrophilic attack of SCN^+.

To a solution of 1-alkoxynaphthalene in acetic acid we added copper(II) thiocyanate, freshly prepared[10] in advance; the mixture was then warmed while being stirred for 2.0 to 2.5 h. The reaction is accompanied by a color change from black to white[2] (actually from black to a yellowish green or yellow color) due to the formation of copper(I) thiocyanate.

$$ArH + 2Cu(SCN)_2 \rightarrow ArSCN + 2CuSCN + HSCN \quad (2)$$

Usually the 4-thiocyanato compound of 1-alkoxynaphthalene was obtained in a good yield when the molar ratio of $Cu(SCN)_2$ to the 1-alkoxynaphthalene was 4 to 1. The IR and NMR spectra[11] revealed no isomeric naphthyl isothiocyanate or 2-thiocyanato compound in the reaction product. When the molar ratio of $Cu(SCN)_2$ to 1-ethoxynaphthalene was 2 to 1, and when the reaction temperature was raised to the range from 115 to 118 °C, no thiocyanate was produced, but a small amount of the disulfide of 4-ethoxynaphthalene was obtained. The experimental results are summerized in Table 1.

Experimental

The method used in the preparation of 1-alkoxynaphthalene was a modification of the method of Yokoyama *et al.*[12] The IR spectra were recorded on a Hitachi EPI G3 spectrophotometer. The NMR spectra were taken on a Varian A-60 or on a Japan Electron JNM-G-60 or 100 spectrometer in $CDCl_3$, using TMS as the internal standard.

The following is a typical method for the thiocyanation.

Thiocyanation of 1-Methoxynaphthalene. Copper(II) thiocyanate (100 mmol), which has been prepared according to the directions of Jenkins and Kochi,[10] was suspended in a solution of 1-methoxyanphthalene (25 mmol) in glacial acetic acid (30 ml). The mixture was then warmed while being stirred until the solid of copper(II) thiocyanate turned brownish yellow. After cooling, the solid, which was extracted with ether if necessary, was filtered off. The filtrate was cooled or poured into 300 ml of ice water, and the resulting solid was extracted with ether. The ether solution was washed with water, dried over anhydrous sodium sulfate, and concentrated under reduced pressure, thus giving a crystalline residue. In the course of a number of preparations, both low-melting (95—97 °C; yellow plates) and high-melting (102—102.5 °C; colorless plates) forms were obtained. (The reported value is 105—105.5 °C.[5]) The former was converted to the high-melting variety upon numerous recrystallizations from methanol. The IR and NMR spectra of the yellow plates were exactly the same as those of the colorless ones. IR ($CHCl_3$) 2145 cm^{-1} (SCN). NMR ($CDCl_3$) δ=3.91 (3H, s, OCH_3), 6.72 (1H, d, J=7.5 Hz, aromatic proton of the 2-position[11]), 7.74 (1H, d, J=7.5 Hz), 7.4—7.7 (2H, m), 8.1—8.4 (2H, m, aromatic proton of the 5 and 8 positions[11]) Found: C, 67.13; H, 3.91; N, 6.55; S, 14.91%; M^+, 215. Calcd for $C_{12}H_9NOS$: C, 66.95; H, 4.21; N, 6.51; S, 14.89%; M, 215.

The characterization of other alkoxynaphthyl thiocyanates is as follows. R=C_2H_5, mp 73.5—75 °C). (recrystallization solvent; ethanol. Lit,[6] bp/7 Torr 105 °C). IR ($CHCl_3$) 2140 cm^{-1}. NMR ($CDCl_3$) δ=1.52 (3H, t, J=7 Hz), 4.16 (2H, q, J=7 Hz), 6.64 (1H, d, J=8 Hz), 7.69 (1H, d, J=8 Hz), 7.3—7.7 (2H, m), 8.1—8.3 (2H, m). Found: C, 67.95; H, 4.68; N, 6.23; S, 13.92%: M^+, 229. Calcd for $C_{13}H_{11}NOS$; C, 68.10; H, 4.84; N, 6.11; S, 13.98%; M, 229. R=*n*-C_3H_7, mp 82.2—83.5 °C (isopropanol, lit,[6] bp/4 Torr

Table 1. Thiocyanation of 1-alkoxynaphthalene

R	Alkoxynaphthalene : $Cu(SCN)_2$ (molar ratio)		Temp (°C)	Time (h)	Yield (%)
CH_3	1	4	67—70	2.5	79.2
C_2H_5	1	4	64—69	2.0	80.8
C_2H_5[a)]	1	2	115—118	5.0	—
n-C_3H_7	1	4	70—76	2.8	67.8
n-C_4H_9	1	4	65—70	2.5	60.3
i-C_5H_{11}	1	4	72—76	6.0	50.8
	1	4	75—79	0.8	32.6
	1	3	70—76	2.0	35.9
n-C_6H_{13}	1	4	77—79	2.5	38.5
n-C_8H_{17}	1	4	90—92	1.5	19.1
n-$C_{12}H_{25}$	1	4	77	2.4	24.2

a) The product is bis(1-ethoxynaphthyl) disulfide.

109—110 °C). IR ($CHCl_3$) 2145 cm^{-1}. NMR ($CDCl_3$) δ= 1.08 (3H, t, J=7 Hz), 1.90 (2H, sex, J=7 Hz), 4.00 (2H, t, J=7 Hz, OCH_2), 6.65 (1H, d, J=8 Hz), 7.72 (1H, d, J=8 Hz), 7.3—7.8 (2H, m) 8.1—8.5 (2H, m). Found: S, 13.55%; M^+, 243. Calcd for $C_{14}H_{13}NOS$: S, 13.18%; M, 243. R=n-C_4H_9, mp 50—51.5 °C (methanol, lit,[6)] bp/6 Torr 127—130 °C). IR ($CHCl_3$) 2140 cm^{-1}. NMR ($CDCl_3$) δ=1.01 (3H, t, J=7 Hz), 1.3—2.1 (4H, m), 4.07 (2H, t, J=7 Hz), 6.66 (1H, d, J=8 Hz), 7.69 (1H, d, J=8 Hz), 7.3—7.7 (2H, m), 8.1—8.3 (2H, m). Found: C, 70.01; H, 5.87; N, 5.44; S, 12.46%; M^+, 257. Calcd for $C_{15}H_{15}NOS$: C, 70.30; H, 5.90; N, 5.65; S, 12.42%; M, 257. R=iso-C_5H_{11}, mp 40—41 °C (methanol, lit,[6)] bp/5 Torr 113—116 °C). IR (KBr) 2140 cm^{-1}. NMR ($CDCl_3$) δ=1.01 (6H, d, J=6 Hz, $(CH_3)_2$-C), 1.5—2.0 (3H, m), 4.18 (2H, t, J=6 Hz), 6.88 (1H, d, J=8.5 Hz), 7.91 (1H, d, J=8.5 Hz), 7.3—7.9 (2H, m), 8.2—8.6 (2H, m). Found: C, 70.58; H, 6.49; N, 5.22; S, 11.80%; M^+, 271. Calcd for $C_{16}H_{17}NOS$: C, 70.82; H, 6.31; N, 5.16; S, 11.81%; M, 271. R=n-C_6H_{13}, mp 41 °C (methanol–water). IR ($CHCl_3$) 2140 cm^{-1}. NMR ($CDCl_3$) δ=0.91 (3H, deformed t), 1.40 (8H, m), 4.08 (2H, t, J= 6 Hz), 6.70 (1H, d, J=8 Hz), 7.75 (1H, d, J=8 Hz), 7.2—7.9 (2H, m), 8.1—8.5 (2H, m). Found: C, 71.45; H, 6.65; N, 4.90%; M^+, 285. Calcd for $C_{17}H_{19}NOS$: C, 71.54; H, 6.71; N, 4.91%; M, 285. R=n-C_8H_{17}, mp 44 °C (methanol). IR (KBr) 2140 cm^{-1}. NMR ($CDCl_3$) δ=0.91 (3H, deformed t), 1.36 (12 H, m), 4.16 (2H, t, J=6 Hz), 6.82 (1H, d, J= 8 Hz), 7.87 (1H, d, J=8 Hz), 7.5—8.0 (2H, m), 8.2—8.5 (2H, m). Found: C, 72.31; H, 7.41; N, 4.52; S, 10.18%; M^+, 313. Calcd for $C_{19}H_{23}NOS$: C, 72.80; H, 7.40; N, 4.47; S, 10.22%; M, 313. R=n-$C_{12}H_{25}$, mp 44.5—45 °C (acetone–methanol). IR (KBr) 2125 cm^{-1}. NMR ($CDCl_3$) δ=0.88 (3H, deformed t), 1.1—2.3 (20H, m), 4.16 (2H, t, J=6 Hz), 6.81 (1H, d, J=8 Hz), 7.86 (1H, d, J=8 Hz), 7.5—8.0 (2H, m), 8.2—8.5 (2H, m), Found: C, 74.90; H, 8.46; N, 3.65; S, 8.41%, M^+, 369. Calcd for $C_{23}H_{31}NOS$: C, 74.75; H, 8.45; N, 3.79; S, 8.68%; M, 369.

Bis(1-ethoxynaphthyl) disulfide, mp 144.5—145 °C (ethyl acetate). IR ($CHCl_3$) No characteristic band of νSCN. NMR ($CDCl_3$) δ=1.47 (3H, t, J=7 Hz), 4.07 (2H, q, J= 7 Hz), 6.46 (1H, d, J=8 Hz), 7.40 (1H, d, J=8 Hz), 7.2—7.6 (2H, m), 8.1—8.4 (2H, m). Found: C, 70.94; H, 5.57; S, 15.75%; M^+, 406. Calcd for $C_{24}H_{22}O_2S_2$: C, 70.90, H, 5.46; S, 15.77%; M, 406.

The author is indebted to the Research Laboratories, Tanabe Pharmaceutical Co., Ltd., for the elemental analyses and the obtaining the mass and NMR spectra.

References

1) a) Y. Hamada, H. Matsuoka, and H. Fukatsu, *Yakugaku Zasshi*, **91**, 565 (1971); b) A. A. Newman, Ed., "Chemistry and Biochemistry of Thiocyanic Acid and Its Derivatives," Academic Press, London (1975), Chap. 4.
2) J. L. Wood, *Org. React.*, **3**, 240 (1946).
3) R. G. R. Bacon and R. G. Guy, *J. Chem. Soc*, **1960**, 318.
4) N. Kharasch, ed., "Organic Sulfur Compounds," Pergamon Press, Vol. 1, New York (1961), Chap. 27.
5) A. Kaji, *Nippon Kagaku Zasshi*, **82**, 382 (1961).
6) A. Kaji and S. Kano, Japan Patent 1722 (1962); *Chem. Abstr.*, **58**, 7886g.
7) S. Uemura, S. Uchida, M. Okano, and K. Ichikawa, *Bull. Chem. Soc. Jpn.*, **46**, 3254 (1973).
8) E. C. Taylor, F. Kienzle, and A. McKillop, *Synthesis* **1972**, 38.
9) H. P. Kaufmann, "Newer Methods of Preparative Organic Chimistry," Interscience, Vol. 1, New York (1948), pp. 377—379.
10) C. L. Jenkins and J. K. Kochi, *J. Org. Chem.*, **36**, 3095 (1971).
11) G. O. Dudek, *Spectrochim. Acta*, **19**, 691 (1963).
12) M. Yokoyama, K. Iwata, and S. Toyoshima, *Yakugaku Zasshi*, **78**, 428 (1958).

BULLETIN OF THE CHEMICAL SOCIETY OF JAPAN, VOL. 50 (11), 3067—3068 (1977)

Formation of Indan and 2,3-Dihydrobenzofuran *via* Intramolecular Insertion of Phenylcarbene

Akira SEKIGUCHI and Wataru ANDO

Department of Chemistry, The University of Tsukuba, Niiharigun, Ibaraki 300-31

(Received June 4, 1977)

Synopsis. Pyrolysis of *p-t*-butyl- and *p*-trimethylsilylbenzaldehyde tosylhydrazone sodium salts gave indans *via* intramolecular C-H insertions of *o*-substituted phenylcarbenes through carbene-carbene rearrangements. Pyrolysis of *o*- and *p*-alkoxybenzaldehyde tosylhydrazone sodium salts afforded 2,3-dihydrobenzofurans.

Alkylcarbenes react predominantly by insertion into β- and γ-C–H bonds to give olefins and cyclopropanes, respectively.[1] In contrast to the number of studies on the intermolecular reactions of phenylcarbenes,[2] seems to have been little reported on the intramolecular insertion reactions of phenylcarbenes[3] which are expected to be convenient for the syntheses of cyclic compounds. In this paper, we would like to report on the formation of indan and 2,3-dihydrobenzofuran by insertion of phenylcarbenes.

(*p-t*-Butylphenyl)carbene was generated by the pyrolysis of *p-t*-butylbenzaldehyde tosylhydrazone sodium salt (**1**) at 500 °C *in vacuo*, the volatile product being trapped in a dry ice acetone trap. 1,1-Dimethylindan (**2**) was obtained in 23% yield by separation of GLC. 1,1-Dimethyl-1-silaindan (**4**)[4] was also produced in 15 % yield by the pyrolysis of *p*-trimethylsilylbenzaldehyde tosylhydrazone sodium salt (**3**) under the above reaction conditions.

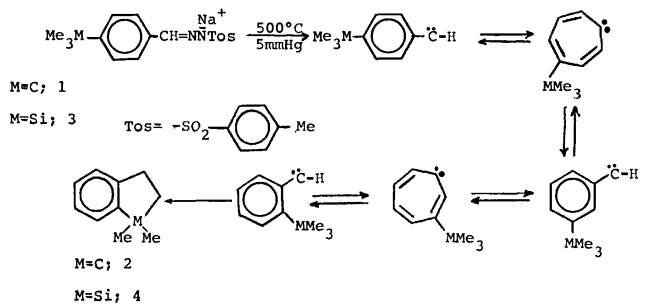

Scheme 1.

A reasonable mechanism probably involves intramolecular insertion of (*o-t*-butyl- and *o*-trimethylsilyl-)phenylcarbenes into C–H bonds of *ortho t*-butyl and trimethylsilyl groups *via* carbene-carbene rearrangements[5] of (*p-t*-butyl- and *p*-trimethylsilyl-)phenylcarbenes, giving products (**2**) and (**4**) as shown in Scheme 1. This is the first example of the formation of indans from the intramolecular reactions through the carbene-carbene rearrangements of the *p*-substituted phenylcarbenes. The yield is low, but it is a simple and handy method for the synthesis of *o*-substituted cyclic compounds from *p*-substituted phenylcarbenes since the corresponding *p*-substituted benzaldehydes can be easily obtained.

The intramolecular reaction of phenylcarbene containing a hetero atom is important as means for the synthesis of a hetero cyclic compound. The pyrolysis of *o*- and *p*- anisaldehyde tosylhydrazone sodium salts, (**5**) and (**6**), under the above conditions gave 2,3-dihydrobenzofuran (**7**) in 30 and 7% yields, respectively. The formation of (**7**) from (*p*-methoxyphenyl)carbene might involve the carbene-carbene rearrangement to (*o*-methoxyphenyl)carbene.

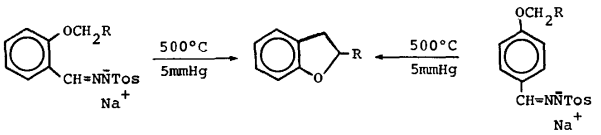

5: R=H **7**: R=H **6**: R=H
8: R=Me **9**: R=Me **10**: R=Me

In the pyrolysis of *o*-ethoxybenzaldyhyde tosylhydrazone sodium salt (**8**), 2-methyl-2,3-dihydrobenzofuran (**9**) was obtained in 69% yield *via* regiospecific intramolecular C-H insertion, without any formation of benzopyran *via* intramolecular β-C–H insertion of (*o*-ethoxyphenyl)-carbene. On the other hand, the pyrolysis of *p*-ethoxybenzaldehyde tosylhydrazone sodium salt (**10**) gave *p*-methylphenetole in 2—3% yield in hydrogen abstraction of (*p*-ethoxyphenyl)carbene. The major part is non-volatile substance which might be produced during the cource of carbene-carbene rearrangement. In contrast to the carbene-carbene rearrangements of (*p*-alkylphenyl)carbenes, the reason for the unfavorable carbene-carbene rearrangements of (*p*-alkoxyphenyl)-carbenes remains unclarifed.

Experimental

General. The IR and NMR data were recorded on Hitachi 215 and Hitachi R-24A spectrometers, respectively. Gas chromatographic analyses were made on an Ohkura 802 gas chromatograph with use of a 1.5 m × 5 mm stainless column packed with 15% SF-96 on Celite 545. All melting points are uncorrected.

Pyrolysis Procedure. Pyrolysis was performed with a vertical tube oven (inside diameter, 3 cm; length, 33 cm). The pyrolysis apparatus consists of a Pyrex tube, diam. 1 cm, length 18 cm. The powdered tosylhydrazone sodium salts were dropped into the pyrolysis apparatus heated at 500 °C *in vacuo*, and the product was trapped in a dry ice acetone trap.

Reagents. Tosylhydrazones were prepared in the conventional way. *p-t*-Butylbenzaldehyde tosylhydrazone was prepared in 71% yield by dissolving *p-t*-butylbenzaldehyde (14 g, 86 mmol) in MeOH, adding an equivalent of tosylhydrazine (16 g, 86 mmol) and refluxing for 30 min. Recrystallization from MeOH gave pure *p-t*-butylbenzaldehyde tosylhydrazone; mp 143.5—144.5 °C. Found: C, 65.68; H, 6.72; N, 8.78%. Calcd for $C_{18}H_{22}N_2SO_2$: C, 65.43; H, 6.71; N, 8.48%. *p*-Trimethylsilylbenzaldehyde tosylhydrazone; mp 155—156 °C. Found: C, 58.49; H, 5.96%. Calcd for $C_{17}H_{22}N_2SO_2Si$:

C, 58.93; H, 6.40%. *p*-Anisaldehyde tosylhydrazone; mp 114—115 °C. Found: C, 59.42; H, 5.25; N, 9.51%. Calcd for $C_{15}H_{16}N_2SO_3$: C, 59.19; H, 5.30; N, 9.20%. *o*-Anisaldehyde tosylhydrazone; mp 169.5—172 °C. Found: C, 59.07; H, 5.27; N, 9.47%. Calcd for $C_{15}H_{16}N_2SO_3$: C, 59.19; H, 5.30; N, 9.20%. *p*-Ethoxybenzaldehyde tosylhydrazone; mp 157—158 °C. Found: C, 60.23; H, 5.66; N, 9.07%. Calcd for $C_{16}H_{18}N_2SO_3$: C, 60.36; H, 5.70; N, 8.80%. *o*-Ethoxybenzaldehyde tosylhydrazone; mp 142—144 °C. Found: C, 60.44; H, 5.70; N, 9.15%. Calcd for $C_{16}H_{18}N_2SO_3$: C, 60.36; H, 5.70; N, 8.80%. Sodium salt (**1**) was obtained in 87% yield by dissolving the *p*-*t*-butylbenzaldehyde tosylhydrazone (6.0 g, 18 mmol) in dry THF and adding an equivalent of sodium hydride (0.88 g, 50% in mineral oil) slowly with stirring. Petroleum ether was added, and the resulting precipitate filtered. The sodium salts, (**3**), (**5**), (**8**), and (**10**) were also prepared from the above tosylhydrazones and sodium hydride in THF.

Pyrolysis of Tosylhydrazone Sodium Salts. Tosylhydrazone sodium salt (**1**, 1.61 mmol) was pyrolyzed by means of the pyrolysis apparatus at 500 °C, 5 mmHg. Dimethylindan (**2**)[6] was obtained in 23% yield by GLC analysis. The pyrolysis of (**3**, 0.99 mmol) afforded silaindan (**4**)[4] in 15% yield under the above reaction conditions. 2,3-Dihydrobenzofuran (**7**)[7] was formed by the pyrolysis of (**5**, 1.04 mmol) and (**6**, 1.01 mmol) in 30 and 7% yields, respectively. The pyrolysis of (**8**, 1.18 mmol) gave 2-methyl-2,3-dihydrobenzofuran (**9**)[7] in 69% yield, while that of (**10**) gave *p*-methylphenetole.

References

1) W. Kirmse, "Carbene Chemistry," 2 nd ed, Academic Press, New York (1971), pp. 236—260.

2) R. A. Moss and M. Jones, Jr., "Carbenes," Vol. 1, John Wiley & Sons (1973), pp. 63—73.

3) a) C. D. Gutsche, G. L. Bachman, and R. S. Coffey, *Tetrahedron*, **18**, 617 (1962); b) H. E. Zimmerman and R. H. Paskovich, *J. Am. Chem. Soc.*, **86**, 2149 (1964); c) R. Garner, *Tetrahedron Lett.*, **1968**, 221; d) T. A. Baer and C. D. Gutsche, *J. Am. Chem. Soc.*, **93**, 5180 (1971); e) W. Kirmse and H. Dietrich, *Chem. Ber.*, **100**, 2710 (1967).

4) W. Ando, A. Sekiguchi, T. Hagiwara, and T. Migita, *J. Chem. Soc., Chem. Commun.*, **1974**, 372.

5) M. Jones, Jr., *Acc. Chem. Res.*, **7**, 415 (1974).

6) M. T. Bogert and D. Davidson, *J. Am. Chem. Soc.*, **56**, 185 (1934).

7) a) R. Adams and R. E. Rindfusz, *J. Am. Chem. Soc.*, **41**, 648 (1919); b) K. v. Auwers, *Ann.*, **415**, 98 (1918).

BULLETIN OF THE CHEMICAL SOCIETY OF JAPAN, VOL. 50 (11), 3069—3070 (1977)

A Convenient Preparation of Arylthioynamines

Takeshi NAKAI, Kiyoshi TANAKA, Hiroyuki SETOI, and Nobuo ISHIKAWA
Department of Chemical Technology, Tokyo Institute of Technology, Meguro, Tokyo 152

(Received June 6, 1977)

Synopsis. (2,2,2-Trifluoroethylthio)benzenes prepared from sodium thiolates and 2,2,2-trifluoroethyl *p*-toluenesulfonate reacted with 3 equiv of lithium dialkylamides in diethyl ether to give arylthioynamines in good yields. The present procedure gives good results with aliphatic sulfide.

Ynamines have received current interest as a versatile tool in organic synthesis.[1] Of particular interest are arylthioynamines{(arylthioethynyl)amines} which we call in short "thioynamines" since the arylthio groups can be utilized for further synthetic elaboration. However, little information has been available concerning the preparation and reactions of thioynamines.[2,3] In our previous paper, it has been shown that the equimolar reaction of (2,2,2-trifluoroethylthio)benzene with lithium diisopropylamide afforded the phenylthioynamine along with the difluorovinyl sulfide(**1**). This is in contrast to the exclusive formation of the difluorovinyl ether(**2**) with (2,2,2-trifluoroethoxy)benzene.[4]

$$PhX\text{–}CH{=}CF_2$$

1, X=S
2, X=O

Herein we wish to report a convenient preparation of various thioynamines **5** by the reactions of trifluoroethyl sulfides **4** with 3 equiv of various lithium dialkylamides.

$$\underset{\mathbf{3}}{TsOCH_2CF_3} \xrightarrow{NaSR} \underset{\mathbf{4}}{RSCH_2CF_3} \xrightarrow{LiNR'_2} \underset{\mathbf{5}}{RS\text{–}C{\equiv}C\text{–}NR'_2}$$

Sulfides **4** were obtained in 73—80% yields by the reactions of trifluoroethyl *p*-toluenesufonate(**3**)[5] with the corresponding sodium thiolate. The reactions of sulfides **4** with 3 equiv of lithium dialkylamides generated *in situ* from butyllithium and dialkylamines in diethyl ether at −78 °C for 3 h afforded thioynamines **5** in good yields except for **5c** (see Table); **5c** was obtained in 12% yield due to the partial decomposition during distillation. All thioynamines **5** were identified by their ^{1}H NMR and IR data (see Experimental part). The IR spectra show strong bands at 2120—2130 cm^{-1} due to the carbon-carbon triple bonds.

These thioynamines are stable on storage free from moisture for several weeks; however, they are quite susceptible to hydration affording the corresponding arylthio- or alkylthioacetamides.[6]

The present procedure gives good results both with aromatic and aliphatic sulfides and is more advantageous than the reported one[2] in the points of the easy availability of the starting materials and the simplicity of the procedures. The synthetic utility of the thioynamines is now under study.[7]

Experimental

All boiling points are uncorrected. NMR and IR spectra were recorded on a Varian EM390 spectrometer and a Hitachi 215 spectrometer, respectively.

Preparation of Trifluoroethyl Sulfides **4**. The reaction was carried out in the dark. Thiol (36 mmol) was added to a stirred suspension of sodium hydride (36 mmol) in DMF (40 ml). After the mixture was stirred at room temperature for 30 min, tosylate **3** (30 mmol) was added to the thiolate solution over a 10-min period and the mixture was stirred for an additional 1 h at room temperature. The mixture was then poured into water, and the aqueous solution was extracted twice with ether. The combined ethereal extracts were washed with a 5% aqueous NaOH and brine, dried over magnesium sulfate, and evaporated to leave crude **4**. Purification were effected by distillation under reduced pressure. Yields and boiling points are as follows; phenyl sulfide, 73%, 82—84 °C/25 mmHg (lit,[8] 62—63 °C/5.5 mmHg); *p*-tolyl sulfide, 80%, 95—97 °C/20 mmHg (lit,[9] 87 °C/12 mmHg); ethyl sulfide, 75%. 88—91 °C (lit,[10] 90 °C).

Preparation of Thioynamines **5**; *General Procedure*. The reaction was carried out under nitrogen. A 2.0 M solution of butyllithium (22.5 ml) in hexane was added to a mixture of sulfide **4** (15 mmol) and dialkylamine (45 mmol) in diethyl ether (30 ml) cooled in a dry ice–acetone bath. The mixture was then stirred for 3 h, and allowed to stand at room temperature. The mixture was poured into a 5% aqueous sodium hydrogencarbonate solution, and the aqueous mixture

TABLE. PREPARATION OF THIOYNAMINES **5**

	Thioynamine[a]	Yield (%)	Bp (°C/mmHg) lit[c]
5a	$C_6H_5S\text{–}C{\equiv}C\text{–}N(C_2H_5)_2$	91	108—113/2 (110—115/0.01)
5b	$C_6H_5S\text{–}C{\equiv}C\text{–}N(i\text{-}C_3H_7)_2$	70	154—156/5
5c	$C_6H_5S\text{–}C{\equiv}C\text{–}N(CH_2)_5$	12[d]	128—132/1
5d	$p\text{-}H_3C\text{–}C_6H_4S\text{–}C{\equiv}C\text{–}N(C_2H_5)_2$	78	124—127/0.04 (80—83/0.01)
5e	$p\text{-}H_3C\text{–}C_6H_4S\text{–}C{\equiv}C\text{–}N(i\text{-}C_3H_7)_2$	87	140—142/3
5f	$C_2H_5S\text{–}C{\equiv}C\text{–}N(C_2H_5)_2$	83	110—112/20 (65—70/0.1)

a) Hydration occurred too readily to give reliable elemental analyses. The purities could be checked by IR and NMR spectra (Ref. 6) since the hydration product was the only contaminant. b) Yields refer to the isolated thioynamine after distillation. c) See Ref. 2. d) See the text. The ^{1}H NMR spectrum of crude **5c** showed that it was practically pure.

was extracted twice with ether. The combined ethereal extracts were washed with brine, dried over potassium carbonate, and evaporated to leave crude **5**. Purification was done by distillation under reduced pressure. Yields and boiling points are given in Table and $\nu_{C\equiv C}$ in IR (liq film) and ^1H NMR (CCl_4) data are as follows; **5a**, 2130 cm^{-1}, $\delta=1.0$—1.3 (2t, 6H), 2.8—3.2 (2q, 4H), 6.8—7.3 ppm (m, 5H); **5b**, 2120 cm^{-1}, $\delta=1.2$ (d, 12H), 3.1 (sep, 2H), 6.9—7.4 ppm (m, 5H); **5c**, 2125 cm^{-1}, $\delta=1.3$—1.8 (m, 6H), 2.8—3.3 (m, 4H), 6.7—7.4 ppm (m, 5H), **5d**, 2120 cm^{-1}, $\delta=1,2$ (t, 6H), 2.3 (s, 3H), 3.0 (q, 4H), 7.0—7.3 ppm (m, 4H); **5e**, 2120 cm^{-1}, $\delta=1.2$ (d, 12H), 2.3 (s, 3H), 2.8 (sep, 2H), 6.8—7.2 ppm (m, 4H); **5f**, 2125 cm^{-1}, $\delta=1.2$ (t, 6H), 1.3 (t, 3H), 2.4 (q, 2H), 2.9 ppm (q, 4H),

References

1) J. Ficini, *Tetrahedron* **32**, 1449 (1976); H. G. Viehe, *Angew. Chem. Int. Ed. Engl.*, **6**, 767 (1967).

2) S. Y. Delavarenne, H. G. Viehe, *Tetrahedron Lett.*, **1969**, 4761.

3) R. Gompper, S. Mentsch, G. Seybolt, *Angew. Chem. Int. Ed. Engl.*, **14**, 704 (1975).

4) T. Nakai, K. Tanaka, N. Ishikawa, *Chem. Lett.*, **1976**, 1263.

5) F. G. Bordwell, W. T. Brannen, Jr., *J. Am. Chem. Soc.*, **86**, 4645 (1964). Available from Aldrich Chem. Co., Inc., Milwaukee, Wisconsin 53233, U.S.A.

6) The IR spectra of the acetamides showed strong carbonyl absorptions at 1640 cm^{-1} and the NMR exhibited sharp singlets around δ 3.6 ppm due to the *S*-methylene protons.

7) Recently we developed a new method for the stereospecific synthesis of conjugated dienamides via additions of allylic alcohols to thioynamines **5** followed by the [3,3] sigmatropic rearrangement; T. Nakai and H. Setoi, Abst. No. 1T03, 36th Annual Meeting of the Chemical Society of Japan, Osaka, April, 1977.

8) J. Hine, R. G. Ghirardell, *J. Org. Chem.*, **23**, 1550 (1958).

9) T. Nakai, K. Tanaka, N. Ishikawa, *Nippon Kagaku Kaishi*, **1976**, 1888.

10) R. C. Terrell, T. Veciardi, J. F. Vitcha, *J. Org. Chem.*, **30**, 4011 (1965).

BULLETIN OF THE CHEMICAL SOCIETY OF JAPAN, VOL. 50 (11), 3071—3072 (1977)

Convenient Synthesis of α-Mercaptoalkanoic Acid Esters Using *S*-Cyanomethyl Thiocarbamates

Yoshiro MASUYAMA, Yoshio UENO, and Makoto OKAWARA

Research Laboratory of Resources Utilization, Tokyo Institute of Technology, Nagatsuta-cho, Midori-ku, Yokohama 227

(Received June 18, 1977)

Synopsis. The reaction of cyanomethyl dithiocarbamate and *S*-cyanomethyl thiocarbamate with alkyl halides in aqueous medium selectively gave mono- and di-alkylated products. The treatment of the alkylated products with concd sulfuric acid gave α-mercaptoalkanoic acid esters.

Organic synthesis using phase-transfer catalyst in aqueous medium is one of the attractive subjects for effecting the C–C bond formation.[1] We previously reported the selective alkylation of cyanomethyl dithiocarbamate **1a** to give mono- (**2**) and di-alkylated cyanomethyl dithiocarbamates (**4**) and the subsequent ketone formation in aqueous medium.[2] On the other hand, it is well known that α-mercaptoalkanoic acids are useful as reducing and chelating agents in organic synthesis and medical fields.[3] Recently, α,α-diphenylmercaptoacetic acid was used effectively for the preparation of some hindered olefins.[4] α-Mercaptoalkanoic acids and their derivatives, however, have not been so easily accessible.

We wish to report here a convenient synthesis of α-mercaptoalkanoic acid esters **7** *via* stepwise alkylation and alcoholysis of cyanomethyl dithiocarbamate **1a** and *S*-cyanomethyl thiocarbamate **1b** in aqueous media.

Selective alkylation of **1a** with alkyl halides in the presence of catalytic amount of tetrabutylammonium iodide (TBA) in 50% aqueous sodium hydroxide has been previously reported.[2] Stepwise alkylation of **1b** was similarly achieved to give mono- (**3**) and di-alkylated thiocarbamates (**5**) in high yields. Dialkylated cyclic product **5d** was also obtained quantitatively by using 1,4-dibromobutane as an alkylating agent.

Alkaline hydrolysis of **4** in refluxing ethanol gave the corresponding ketones **6** in good yields.[2] On the other hand, α-mercaptoalkanoic acid esters **7** were obtained in good yields by the reaction of **4** with excess concd sulfuric acid (10 equiv) in refluxing ethanol for 20 h. The hydrolysis of **4** using lesser amounts of sulfuric acid (5 equiv) gave mainly (dimethylcarbamoylthio)acetic acid esters **9** (IR: ester C=O at 1725 and carbamoyl C=O at 1640 cm^{-1}). Meanwhile, treatment of thiocarbamates **3** and **5** with lesser amounts of concd sulfuric acid (5 equiv) gave **7** in good yields. Thus, *S*-cyanomethyl thiocarbamate **1b** seems to be a better starting material than dithiocarbamate **1a** for the preparation of α-mercaptoalkanoic acid esters **7**. Facile cleavage of the S–C bond with ethanolic sulfuric acid would be performed simultaneously with the conversion of nitrile into ester. Thiols **7** (IR: SH at 2550 cm^{-1}) were further converted to the corresponding disulfides **8** by air oxidation. The results are summarized in Scheme 1 and Table 1. The structures of all new compounds were confirmed by elemental analyses and spectral data.

TABLE 1. ALKYLATION OF **1b** AND HYDROLYSIS OF **3**, **4**, AND **5**

	R^1	R^2	Yield(%)		Yield(%)
3a	CH_3	H	86		
3b	$CH_3(CH_2)_4$	H	95	**7b**	61
5c	CH_3	$CH_3(CH_2)_5$	77	**7c**	66 (60)[a]
5d		$(CH_2)_4$	≈100	**7d**	75 (69)[a]

a) Figures in parentheses are yields *via* dithiocarbamates **4**.

Experimental

*Dithiocarbamates **1a**, **2**, and **4**.* These compounds were prepared by the procedures described in our earlier paper.[2]

*S-Cyanomethyl Diethylthiocarbamate **1b**.* To 42 g (0.1 mol, 1.16 equiv) of 38% aq sodium diethylthiocarbamate in 25 ml of dimethylformamide was added dropwise 6.5 g (86 mmol) of chloroacetonitrile at 0—5 °C. The solution was stirred for 3 h at 25 °C, diluted with 50 ml of water, and extracted with two 50 ml portions of ether. The ether solutions were washed successively with three 30 ml portions of water and 50 ml of brine and dried over anhydrous sodium sulfate. Evaporation of the ether and distillation gave 14 g (95%) of **1b**; bp 135—136 °C/2.5 mmHg; IR (neat) 2270 (C≡N) and 1650 cm^{-1} (C=O); NMR (CCl_4) δ=1.20 (6H, t, J=7 Hz, CH_3), 3.40 (4H, q, J=7 Hz, N–CH_2), and 3.80 ppm (2H, s, S–CH_2); Found: C, 48.62; H, 7.07; N, 16.43%. Calcd for $C_7H_{12}N_2OS$: C, 48.83; H, 7.03; N, 16.27%.

*Alkylation of **1b**. 2-Diethylcarbamoylthioheptanenitrile **3b**:* To 0.86 g (5 mmol) of **1b** and 92 mg (0.25 mmol, 0.05 equiv) of TBA in 5 ml of 50% aq sodium hydroxide was added 0.62 ml (5 mmol) of 1-bromopentane. The solution was vigorously stirred for 10 h, diluted with 20 ml of water, and extracted with two 20 ml portions of ether. The ether solutions were washed successively with three 20 ml portions of water and 20 ml of brine and dried over anhydrous sodium sulfate. The crude product was purified by alumina column chromatography eluting with 4 : 1 hexane–chloroform to afford 1.16 g (95%) of **3b**; IR (neat) 2270 (C≡N) and 1655 cm^{-1} (C=O); NMR (CCl_4) δ=0.66—2.00 (11H, m), 1.17 (6H, t, J=7 Hz, N–C–CH_3), 3.35 (4H, q, J=7 Hz, N–CH_2), and 4.30 ppm (1H, t, J=7 Hz, S–CH); Found: C, 59.36; H, 9.44; N, 11.39%. Calcd for $C_{12}H_{22}N_2OS$: C, 59.48; H, 9.15; N, 11.56%.

*2-Diethylcarbamoylthiopropanenitrile **3a**:* As described above, 0.86 g (5 mmol) of **1b**, 92 mg (0.25 mmol) of TBA, and 0.62 ml (10 mmol, 2 equiv) of iodomethane were allowed to react for 8 h in 5 ml of 50% aq sodium hydroxide. After work-up, 0.80 g (86%) of **3a** was obtained; IR (neat) 2280 (C≡N) and 1660 cm^{-1} (C=O); NMR (CCl_4) δ=1.18 (6H, t, J=7 Hz, N–C–CH_3), 1.65 (3H, d, J=7.5 Hz, S–C–CH_3), 3.38 (4H, q, J=7 Hz, N–CH_2), and 4.33 ppm (1H, q, J=7.5 Hz, S–CH); Found: C, 51.67; H, 7.91; N, 15.09%. Calcd for

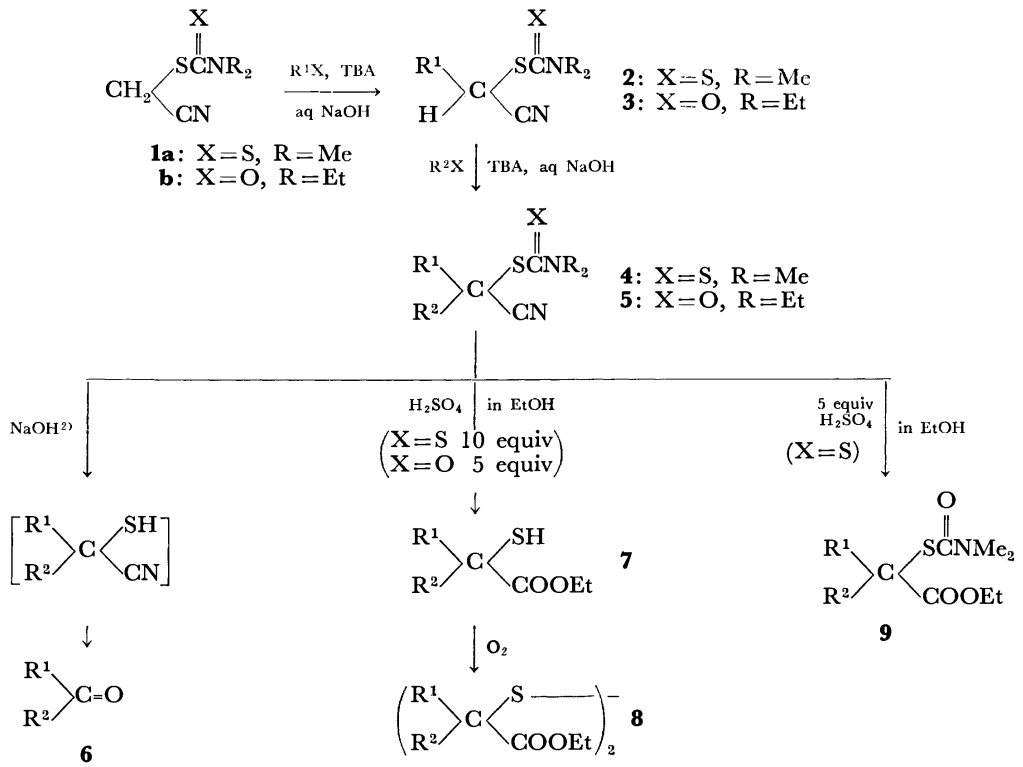

Scheme 1.

$C_8H_{14}N_2OS$: C, 51.58; H, 7.58; N, 15.04%.

2-Diethylcarbamoylthio-2-methyloctanenitrile **5c**: As described above, 0.93 g (5 mmol) of **3a**, 92 mg (0.25 mmol) of TBA, and 0.70 ml (5 mmol) of 1-bromohexane were allowed to react for 25 h in 5 ml of 50% aq sodium hydroxide. After work-up, 1.04 g (77%) of **5c** was obtained; IR (neat) 2270 (C≡N) and 1660 cm^{-1} (C=O); NMR (CCl_4) δ=1.15 (6H, t, J=7 Hz, N-C-CH_3), 0.77—2.00 (13H, m), 1.77 (3H, s, S-C-CH_3), and 3.33 ppm (4H, q, J=7 Hz, N-CH_2); Found: C, 62.21; H, 9.58; N, 10.34%. Calcd for $C_{14}H_{26}N_2OS$: C, 62.19; H, 9.69; N, 10.36%.

1-Diethylcarbamoylthiocyclopentanecarbonitrile **5d**: As described above, 0.86 g (5 mmol) of **1b**, 92 mg (0.25 mmol) of TBA, and 0.60 ml (5 mmol) of 1,4-dibromobutane were allowed to react for 20 h in 5 ml of 50% aq sodium hydroxide. After work-up, 1.12 g (≈100%) of **5d** was obtained; IR (neat) 2270 (C≡N) and 1655 cm^{-1} (C=O); NMR (CCl_4) δ=1.20 (6H, t, J=7 Hz, N-C-CH_3), 1.63—2.67 (8H, m), and 3.35 ppm (4H, q, J=7 Hz, N-CH_2); Found: C, 58.27; H, 8.27; N, 12.25%. Calcd for $C_{11}H_{18}N_2OS$: C, 58.39; H, 8.02; N, 12.38%.

Hydrolysis of **3b**, **4**, *and* **5**. *Ethyl 2-Mercaptoheptanoate* **7b**: To 486 mg (2 mmol) of **3b** in 5 ml of ethanol was added 1.2 ml (ca. 5 equiv) of concd sulfuric acid. The mixture was refluxed for 20 h, cooled, diluted with 10 ml of water, and extracted with two 20 ml portions of ether. The combined ether solutions were washed successively with three 20 ml portions of water and 20 ml of brine and dried over anhydrous sodium sulfate. The solvent was evaporated to yield 232 mg (61%) of **7b**; IR (neat) 2550 (SH) and 1735 cm^{-1} (C=O). **7b** was confirmed as the corresponding disulfide **8b** by allowing to stand for 2 days in contact with air; IR (neat) 1735 cm^{-1} (C=O); NMR (CCl_4) δ=0.67—2.00 (11H, m), 1.27 (3H, t, J=7 Hz, O-C-CH_3), 3.47 (1H, t, J=7 Hz, S-CH), and 4.22 ppm (2H, q, J=7 Hz, O-CH_2). An analytical sample was prepared by silica gel column Chromatography eluting with 1 : 1 hexane–chloroform; Found: C, 57.05; H, 9.12%. Calcd for $C_{18}H_{34}O_4S_2$: C, 57.12; H, 9.06%.

Ethyl 2-Mercapto-2-methyloctanoate **7c**: As described above, 540 mg (2 mmol) of **5c** and 1.2 ml (ca. 5 equiv) of concd sulfuric acid were allowed to react for 30 h in 5 ml of refluxing ethanol. After work-up, 288 mg (66%) of **7c** was obtained. **7c** was confirmed as the corresponding disulfide **8c** by air oxidation; IR (neat) 1730 cm^{-1} (C=O); NMR (CCl_4) δ= 0.70—1.93 (13H, m), 1.27 (3H, t, J=7 Hz, O-C-CH_3), 1.40 (3H, s, S-C-CH_3), and 4.20 ppm (2H, q, J=7 Hz, O-CH_2); Found: C, 60.46; H, 9.92%. Calcd for $C_{22}H_{42}O_4S_2$: C, 60.80; H, 9.74%.

Ethyl 1-Mercaptocyclopentanecarboxylate **7d**: As described above, 452 mg (2 mmol) of **5d** and 1.2 ml (ca. 5 equiv) of concd sulfuric acid were allowed to react for 25 h in 5 ml of refluxing ethanol. After work-up, 261 mg (75%) of **7d** was obtained. **7d** was confirmed as the corresponding disulfide **8d** by air oxidation; IR (neat) 1735 cm^{-1} (C=O); NMR ($CDCl_3$) δ=1.28 (3H, t, J=7 Hz, O-C-CH_3), 1.48—2.35 (8H, m), and 4.22 ppm (2H, q, J=7 Hz, O-CH_2); Found: C, 55.57; H, 7.90%. Calcd for $C_{16}H_{26}O_4S_2$: C, 55.48; H, 7.57%.

The hydrolysis of dithiocarbamates **4** was carried out similarly to the hydrolysis of thiocarbamates **5** except using 10 equiv of concd sulfuric acid. These products were identified by comparison of physical properties with those of disulfides **8** obtained from thiocarbamates **5**.

References

1) E. V. Dehmlow, *Angew. Chem. Int. Ed. Engl.*, **13**, 170 (1974); M. Makosza, *Pure Appl. Chem.*, **43**, 439 (1975).

2) Y. Masuyama, Y. Ueno, and M. Okawara, *Tetrahedron Lett.*, **1976**, 2967.

3) Kirk-Othmer, "Encyclopedia of Chemical Technology," 2nd ed., Intersceience Publishers, Vol. 20, New York (1969), p. 198.

4) D. H. R. Barton and B. J. Willis, *J. Chem. Soc. Perkin Trans. 1*, **1972**, 305.

BULLETIN OF THE CHEMICAL SOCIETY OF JAPAN, VOL. 50 (11), 3073—3074 (1977)

Chemical Synthesis of Antigenic Determinants of Hen Egg-White Lysozyme. II. Tetradecapeptide Corresponding to Positions 1—14 in the Primary Structure but with Ala^{6} and Met(O)^{12} *

Shin-ichiro KUMAGAE and Yasutsugu SHIMONISHI

Institute for Protein Research, Osaka University, Yamada-kami, Suita, Osaka 565

(Received August 1, 1977)

Synopsis. For characterizing one of the antigenic determinants of hen egg-white lysozyme in delayed hypersensitivity, the tetradecapaptide, H–Lys–Val–Phe–Gly–Arg–Ala–Glu–Leu–Ala–Ala–Ala–Met(O)–Lys–Arg–OH, was synthesized by the solid phase method using ultrasonic waves. This peptide corresponds to positions 1—14 of the amino acid sequence of hen egg-white lysozyme but with alanine and methionine *S*-oxide residues at positions 6 and 12, respectively.

The antigenic determinant on a macromolecule recognized by immunocytes for circulating antibody is topographically distinct from that for cellular immunity or delayed hypersensitivity induced with glucagon[1,2] as an immunogen. Recently, Miyagawa *et al.*[3,4] investigated the structural relations between the antigenic determinants of hen egg-white lysozyme for circulating antibody and those for delayed hypersensitivity, induced by hen egg-white lysozyme as an immunogen. They found that the peptide [sequence[5,6] Lys^{1} to Hse^{12} and Trp^{123} to Leu^{129} linked by a disulfide (Cys^{6} and Cys^{127})], named here peptide A, obtained by treatment of the peptide [sequence Lys^{1} to Asn^{27} and Trp^{123} to Leu^{129} linked by a single disulfide (Cys^{6} and Cys^{127})], named here peptide B, with cyanogen bromide, reacted both with circulating antibody to hen egg-white lysozyme and with cells sensitized with hen egg-white lysozyme in delayed hypersensitivity. However, when peptide A was reductively alkylated, the resulting N-terminal peptide [Lys^{1} to Hse^{12}] showed no reactivity with circulating antibody of hen egg-white lysozyme elicited to peptide B,[7] but retained its ability to induce delayed hypersensitivity in cells sensitized with hen egg-white lysozyme. These results show that the specificity of the antigenic determinant elicited to peptide B for circulating antibody is distinct from that for delayed hypersensitivity, induced with hen egg-white lysozyme as an immunogen.

For characterizing this determinant, we synthesized the N-terminal fragment of hen egg-white lysozyme, H–Lys–Val–Phe–Gly–Arg–Ala–Glu–Leu–Ala–Ala–Ala–Met(O)–Lys–Arg–OH, by the solid phase methode using ultrasonic waves.[8] The sequence contained alanine and methionine *S*-oxide residues instead of cysteine and methionine residues at positions 6 and 12 of hen egg-white lysozyme, respectively, because it seemed unlikely that a disulfide linkage between positions 6 and 127 and the methionine residue at position 12 were essential for reactivity. The crude peptide cleaved from resin with hydrogen fluoride was purified on a column of carboxymethylcellulose, as shown in Fig. 1. The tetradecapeptide thus synthesized inhibited migration of macrophages from a peritoreal exudate from guinea pigs immunized with hen egg-white lysozyme.[9] Furthermore, this peptide was found to be immunogenic in guinea pigs.[9]

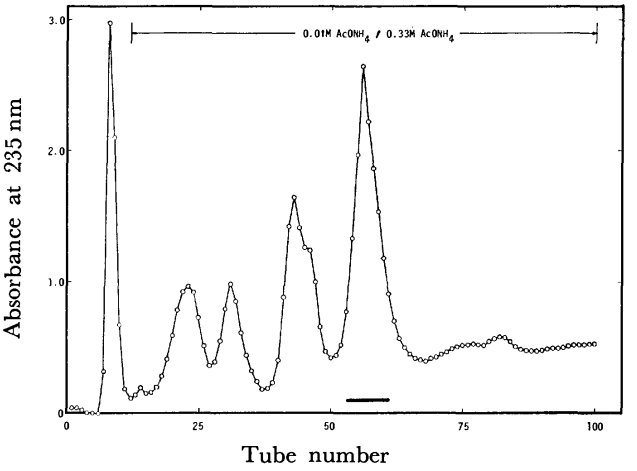

Fig. 1. Chromatogram of the crude product on carboxymethylcellulose (ammonium cycle). The column was eluted with a linear gradient of 0.01 M to 0.33 M ammonium acetate, pH 7.0, at a flow rate of 25—30 ml per h. Fractions of 3 g were collected.

Experimental

Boc–Arg(NO_2)–resin (2.00 g; 0.18 mmol of arginine per g of resin) prepared by the method of Kishida *et al.*[10] was used as starting material. The peptide was synthesized on the solid support using ultrasonic waves, as reported previously,[8] except that a mixture of trifluoracetic acid and dichloromethane (v/v, 1/1) was used instead of 1M HCl in acetic acid for removing the Boc group. The Boc amino acid derivatives were coupled in the following order: Lys(Z), Met(O), Ala, Ala, Ala, Leu, Glu(OBzl), Ala, Arg(Tos), Gly, Phe, Val, and Lys(Boc). After introductions of the Boc derivatives of Lys(Z), Met(O), and Arg(Tos), respectively, the resin was treated with acetic anhydride.[11] Peptide resin (520 mg) was weighed with anisole (0.6 ml) in the Daiflon cylinder of the HF-reaction apparatus.[12] HF (10 ml) was distilled into the cylinder previously cooled to −78 °C in a Dry-Ice–methanol bath. The sample was transfered from the bath at −78 °C to that at 0 °C and stirred for 60 min. Then the HF was evaporated off from the reaction mixture as fast as possible. The free peptide cleaved from the resin was extracted into 0.1 M acetic acid by treatment with ultrasonic waves for 3 min. The extract was passed through a column of IR-45 (acetate cycle). The eluate was lyophilized; 100 mg (*ca.* 75 %). This material (80 mg) was dissolved in 0.01 M am-

* All the amino acids used except glycine were of the L-configuration. The abbreviations used are those recommended by IUPAC-IUB: *J. Biol. Chem.*, **247**, 977 (1972).

monium acetate and charged on a column of carboxymethylcellulose (ammonium cycle, 1×33 cm). The column was eluted with 700 ml of a linear gradient of 0.01 M to 0.33 M ammonium acetate at pH 7.0. The fractions shown by a bar in Fig. 1 were collected and lyophilized; yield 30 mg; R_f (TLC) 0.34 in 1-butanol : acetic acid : pyridine : water (15 : 3 : 10 : 12, by volume); $R_{f,arg}$ (paper electrophoresis) 0.67 (0.2 M pyridinium acetate, 30 V/cm). The amino acid ratio after hydrolysis in 6M HCl for 24 h at 105 °C was Lys, 1.99 (2): Arg, 2.01 (2): Glu, 1.02 (1): Gly, 1.00 (1): Ala, 3.85 (4); Val, 0.92 (1): Met, 0.82 (1): Leu, 1.00 (1): Phe, 1.06 (1).

References

1) G. Senyk, D. Nitecki, and J. W. Goodman, *Science*, **171**, 407 (1971).
2) G. Senyk, E. B. Williams, D. Nitecki, and J. W. Goodman, *J. Exp. Med.*, **133**, 1294 (1971).
3) N. Miyagawa, T. Ashizawa, S. Kashiba, S. Miyagawa, H. Fujio, Y. Ha, and T. Amano, *Biken J.*, **18**, 215 (1975).
4) N. Miyagawa, T. Ashizawa, S. Kashiba, S. Miyagawa, H. Fujio, Y. Ha, and T. Amano, *Biken J.*, **18**, 229 (1975).
5) J. Jauregui-Adell, J. Jolles, and P. Jolles, *Biochim. Biophys. Acta*, **107**, 97 (1965).
6) R. E. Canfield and A. K. Liu, *J. Biol. Chem.*, **240**, 1997 (1965).
7) Y. Ha, H. Fujio, N. Sakato, and T. Amano, *Biken J.*, **18**, 47 (1975).
8) S. Takahashi and Y. Shimonishi, *Chem. Lett.*, **1974**, 51.
9) H. Fujio and T. Amano, to be published.
10) Y. Kishida, S. Sakakibara, and Y. Kikuchi, Proc. 5th Symposium on Peptide Chemistry, ed by Izumiya, Fukuoka (1967), p. 30.
11) D. Yamashiro and C. H. Li, *J. Am. Chem. Soc.*, **95**, 1310 (1973).
12) S. Sakakibara, Y. Shimonishi, Y. Kishida, M. Okada, and H. Sugihara, *Bull. Chem. Soc. Jpn.*, **40**, 2164 (1967).

BULLETIN OF THE CHEMICAL SOCIETY OF JAPAN, VOL. 50 (11), 3075 (1977)

A Simple Method for the Synthesis of 5-Methyloxazolo-[4,5-*c*]quinolin-4(5*H*)-ones

J. R. MERCHANT and S. S. SHIRALI

Organic Chemistry Department, Institute of Science, Madame Cama Road, Bombay 400032, India

(Received January 10, 1977)

Synopsis. A general and simple method for the synthesis of oxazolo[4,5-*c*]quinoline-4(5*H*)-ones by heating 3-amino-4-hydroxy-2-quinolone hydrochloride with aromatic acids in the presence of PPA has been described. The structures are based on spectral and analytical data.

In recent years, a number of 1-methyl-2-quinolone derivatives have been synthesised since many of them have been reported to show antiseptic properties and also exhibit fungicidal activity.[1] Also, 4-hydroxy-3-nitro-2-quinolone derivatives have been reported[2] to possess antihistaminic action. The work on 1-methyl-2-quinolone also has received importance due to the isolation of 1-methyl-4,7,8-trimethoxy-2-quinolone from the plant *Spathelia sorbifolia* L and its subsequent synthesis.[3] Further, the antibiotics nybomycin and deoxynybomycin which have also been synthesised[4] possess an oxazolo[4,5-*c*]quinoline-2-one structure.

In view of this interesting data it was thought of interest to prepare 5-methyloxazolo[4,5-*c*]quinolin-4-(5*H*)-ones (III) since the latter would also be related to the antibiotic novobiocin.[5] We describe here a simple method to synthesise these compounds by heating 3-amino-4-hydroxy-1-methyl-2-quinolone hydrochloride (II), prepared from 4-hydroxy-1-methyl-3-phenylazo-2-quinolone[6] (I), with aromatic acids in the presence of PPA at 170—180 °C for 4 h. The required new oxazole derivatives were obtained as crystalline solids from ethyl acetate in 40—50% yields.

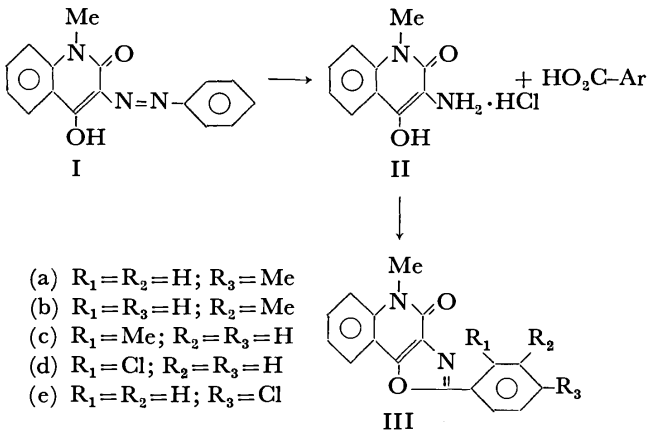

It is evident that in the reaction first an amide is formed which then cyclizes to an oxazole derivative.

TABLE 1. 5-METHYLOXAZOLO[4,5-*c*]QUINOLIN-4(5*H*)-ONES

Compound No.	Formula	Mp (°C)	Found (%) (Calcd) (%) C	H	N
IIIa	$C_{18}H_{14}N_2O_2$	235—236	74.6 (74.5)	5.0 (4.8)	9.7 (9.6)
IIIb	$C_{18}H_{14}N_2O_2$	189—191	74.5 (74.5)	5.0 (4.8)	9.8 (9.6)
IIIc	$C_{18}H_{14}N_2O_2$	205—206	74.4 (74.5)	4.5 (4.8)	9.9 (9.6)
IIId	$C_{17}H_{11}N_2O_2Cl$	196—198	65.6 (65.8)	3.7 (3.5)	9.4 (9.1)
IIIe	$C_{17}H_{11}N_2O_2Cl$	264—266	65.7 (65.8)	3.4 (3.5)	9.3 (9.1)

Experimental

All the meltng points are uncorrected. IR spectra were recorded by means of a Perkin Elmer spectrometer, while NMR spectra were obtained by Varian NMR spectrometer at 60 MHz, using tetramethylsilane as an internal standard.

Preparation of IIIa. A typical procedure is shown for IIIa. 3-Amino-4-hydroxy-1-methyl-2-quinolone (550 mg) and *p*-toluic acid (350 mg) were added to a mixture of phosphorus pentaoxide (5.5 g) and phosphoric acid (2.5 ml) preheated at 100 °C for 30 min. The heating was continued for 4 h at 170—180 °C. The mixture was cooled and decomposed with ice. The solid which separated was filtered, treated with aq sodium hydrogencarbonate solution and washed with water. It was crystallised from ethyl acetate in colourless needles, mp 235—236 °C (IIIa).

The spectral data of a typical compound (IIIa) are as follows: λ_{max}^{MeOH} nm (log ε): 210 (4.74), 255 (4.59), 310 (4.64), and 340 (4.53); IR (KBr): 1700 (C=O), 1625, 1590, and 1570 (heteroaromatic system) cm^{-1}. The position of the carbonyl band rules out the alternate 4-quinolone structure; NMR ($CDCl_3$): δ 2.43 (3H, s, Ar-$\underline{CH_3}$), 3.8 (3H, s, N-$\underline{CH_3}$), 7.0 and 8.3 (8H, m, aromatic protons). MS: *m/e* 290 (M^+).

References

1) J. C. Sharp, U. S. Patent, 3836657; *Chem. Abstr.*, **82**, 81689z (1975).

2) D. R. Buckle, Cantello, C. C. Barrie, and H. Smith, Ger. Patent, 2424676; *Chem Abstr.*, **82**, 139976j (1975).

3) R. Storer, D. W. Young, D. R. Taylor, and J. M. Warner, *Tetrahedron*, **29**, 1721 (1973).

4) R. M. Forbis and K. L. Rinehart, Jr., *J. Am. Chem. Soc.*, **95**, 5003 (1973).

5) a) J. W. Hinman, E. L. Caron, and H. Hoeksema, *J. Am. Chem. Soc.*, **79**, 3789 (1957); b) C. H. Stammer, E. Walton, A. N. Wilson, R. W. Walker, N. R. Trenner, F. W. Holly, and K. Folkers, *J. Am. Chem. Soc.*, **80**, 137 (1958).

6) H. Waldmann, *J. Prakt. Chem.*, **147**, 321 (1937).

BULLETIN OF THE CHEMICAL SOCIETY OF JAPAN, VOL. 50 (11), 3076 (1977)

Oxidation of Biphenylene with Ammonium Cerium(IV) Nitrate. A Convenient Route to Biphenylene-2,3-dione

Masaru SATO, Harutoshi FUJINO, Seiji EBINE, and Josuke TSUNETSUGU

Department of Chemistry, Faculty of Science, Saitama University, Urawa, Saitama 338

(Received June 18, 1977)

Synopsis. Biphenylene was directly oxidized with ammonium cerium(IV) nitrate to give biphenylene-2,3-dione in moderate yield, along with 2-nitrobiphenylene and 3-nitrobiphenylen-2-ol.

Biphenylene-2,3-dione (**2**)[1] is considered to be a peripheral $(4n+2)\pi$-annulenoquinone containing a fused four-membered ring. The physical properties of quinones containing a fused four-membered ring were recently examined from the viewpoint of aromaticity.[2] We have payed attention to the synthesis and chemical properties of **2**, because 6,4,7-ring compounds in which we are interested[3] may be conveniently prepared by ring enlargement of **2**.[4] Thus, development of a convenient procedure to obtain **2** is necessary since the previous method is a tedious multi-step synthesis. The direct oxidation of polynuclear arenes to corresponding quinones is a convenient and valuable synthetic procedure. Various oxidizing agents were used in recent years, cerium(IV) salt being a strong and suitable reagent.[5] We have examined the oxidation of biphenylene (**1**) with cerium(IV) salt to give **2**.

Biphenylene (**1**) was treated with ammonium cerium(IV) nitrate at 0 °C and the resulting reaction mixture was separated by chromatography on silica gel to give three crystalline products.

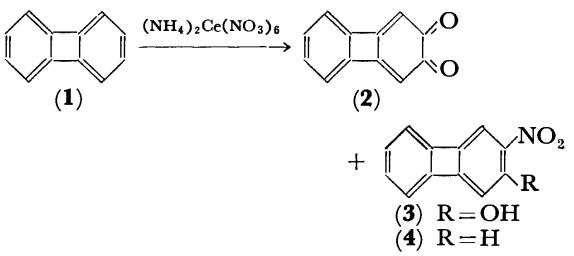

(**1**) (**2**) + (**3**) R=OH (**4**) R=H

The first product (yellow needles, mp 137—138 °C) was identified as 2-nitrobiphenylene (**4**)[6] by the following spectral data: IR(KBr) 1500 and 1320 cm^{-1}, NMR ($CDCl_3$) δ 6.71 (d, 1H, $J_{3,4}$=8.0 Hz), 6.85 (m, 4H, aromatic protons), 7.38 (d, 1H, $J_{1,3}$=2.0 Hz), and 7.81 (dd, 1H). The second product (red-orange needles, mp 142—143 °C) was identified as 3-nitrobiphenylen-2-ol (**3**) by its NMR spectrum in line with the result of Blatchly *et al.*[7] The last product (red-orange needles, mp 213.5—214.5 °C) was identified to be biphenylene-2,3-dione (**2**)[1] by the following spectral data: IR(KBr) 1655 and 1635 cm^{-1}, NMR($CDCl_3$) δ 6.60 (s, 2H, H-1,4) and 7.78 (s, 4H, H-5,6,7,8). This was further confirmed by the fact that no depression was observed on admixture with an authentic sample.[1] The preparation of of **2** through the direct oxidation of **1** with cerium(IV) salt results in somewhat low yield but the tedius multi-step method[1] is considerably simplified. Attempt to oxidize 2-methoxybiphenylene under similar conditions was unsuccesful, no crystalline product being obtained.

Biphenylene (**1**), like benzene, was predicted to resist free-radical attack, this being confirmed experimentally.[8] However, this is in disagreement with the result described here, since all the isolable products from the direct oxidation of **1** with ammonium cerium(IV) nitrate (a one-electron oxidant)[9] seem to be formed by free-radical reaction although the pathway is unknown.

Experimental

A Typical Procedure. To a solution of biphenylene (**1**) (3.18 g, 0.02 mol) in 300 ml of tetrahydrofuran was added aqueous ammonium cerium(IV) nitrate (46.8 g, 0.08 mol in 100 ml of water) drop by drop at 0 °C on an ice-salt bath. The solution was then poured into water and the resulting mixture was extracted with dichloromethane. The extract was washed with water and dried over sodium sulfate. After evaporation, the residue was chromatographed on silica gel with dried dichloromethane to give succesively the recovered **1** (0.6%), 2-nitrobiphenylene (**4**) (0.26 g, 6.7%), 3-nitrobiphenylen-2-ol (**3**) (0.076 g, 1.8%), and biphenylene-2,3-dione (**2**) (0.78 g, 21%).

References

1) J. M. Blatchly, J. F. W. McOmie, and S. D. Thatte, *J. Chem. Soc.*, **1962**, 5090.

2) R. Breslow, D. R. Murahashi, and R. Grubbs, *J. Am. Chem. Soc.*, **95**, 6688 (1973); H. N. C. Wong, F. Sondheimer, R. Goodin, and R. Breslow, *Tetrahedron Lett.*, **1976**, 2715.

3) M. Sato, S. Ebine, and J. Tsunetsugu, *Tetrahedron Lett.*, **1977**, 855; *J. Chem. Soc., Chem. Commun.*, **1974**, 846.

4) M. Sato, J. Tsunetsugu, and S. Ebine, *Bull. Chem. Soc. Jpn.*, **45**, 638 (1972).

5) T. L. Ho, T. W. Hall, and C. M. Wong, *Synthesis*, **1973**, 206.

6) W. Baker, J. W. Barton, and J. F. W. McOmie, *J. Chem. Soc.*, **1958**, 2666.

7) J. M. Blatchly, D. V. Gardner, J. F. W. McOmie, and M. L. Watts, *J. Chem. Soc., C*, **1968**, 1545.

8) M. P. Cava and M. J. Mitchell, "Cyclobutadiene and Related Compounds," Academic Press, New York and London (1967), p. 282.

9) W. H. Richardson, "Oxidation in Organic Chemistry," ed by K. B. Wiberg, Academic Press, New York and London (1965), p. 243.

COMMENTS

BULLETIN OF THE CHEMICAL SOCIETY OF JAPAN, VOL. 50 (11), 3077 (1977)

On the Conductometric Determination of the Formation Constants of the Alkali Metal Complexes of "Crown" Polyethers

Joseph JAGUR-GRODZINSKI*
Weizman Institute of Science, Rehovot, Israel
(Received March 3, 1977)

Matsuura *et al.*[1] recently published data on the formation constants of the alkali metal complexes of dibenzo-18-crown-6 (DBC). Their results are, however, at variance with the values of the formation constants in DMF of the sodium and lithium thiocyanate complexes of DBC previously reported by Shchori *et al.*[2] Both investigations were based on conductometric measurements. The discrepancy certainly calls for comment. The experimental set-ups applied in the two investigations differ. Accordingly, a different mathematical treatment should be adopted to calculate the formation constants from the experimentally determined conductances.

Shchori *et al.* performed experiments at a constant concentration of a salt, while changing the concentrations of DBC. The opposite has been done by Matsuura *et al.* In the latter case, the calculation of formation constants was based on small differences in the values of equivalent conductances due to their concentration dependence and to the differences in the degree of complexation[1].

This makes the method extremely sensitive to minor experimental errors. Moreover, the concentration dependence of the equivalent conductance of the complex differs from that of the uncomplexed salt, since the respective Λ_0 values differ.[3] An appropriate mathematical treatment should be applied taking this fact into account. Unfortunately, it has been neglected by Matsuura *et al.*

* Temporarily with Ciba-Geigy Ltd., CH-4002 Basel, Switzerland (On Sabbatical leave)

References

1) N. Matsuura, K. Umemoto, Y. Takeda and A. Sasaki, *Bull. Chem. Soc. Jpn.*, **49**, 1246 (1976).

2) a) E. Shchori, J. Jagur-Grodzinski, Z. Luz, and M. Shporer, *J. Am. Chem. Soc.*, **93**, 7133 (1971); b) E. Shchori, J. Jagur-Grodzinski and M. Shporer, *ibid.*, **95**, 3842 (1973).

3) E. Shchori and J. Jagur-Grodzinski, *Israel J. Chem.*, **11**, 243 (1973).

BULLETIN OF THE CHEMICAL SOCIETY OF JAPAN, VOL. 50 (11), 3078 (1977)

Formation Constants of Dibenzo-18-crown-6 Complexes with Alkali Metal Ions in Dimethyl Sulfoxide, *N,N'*-Dimethyl Formamide, and Propylene Carbonate at 25 °C

Niro MATSUURA, Kisaburo UMEMOTO, Yasuyuki TAKEDA, and Atsuko SASAKI

Department of Pure and Applied Sciences, College of General Education, The University of Tokyo, Komaba, Meguro-ku, Tokyo 153

(Received May 19, 1977)

In a previous paper[1] we reported formation constants for 1 : 1 complexes of dibenzo-18-crown-6 (DBC) with Li^+, Na^+, K^+, Rb^+, and Cs^+ measured in DMSO (dimethyl sulfoxide), DMF (*N,N'*-dimethyl formamide), and PC (propylene carbonate). The fraction (α) of the cation in the 1 : 1 complex $M(DBC)^+$ is given by

$$\alpha=\frac{\Lambda^1-\Lambda^2}{\Lambda^1-\Lambda^3},$$

where Λ^1, Λ^2, and Λ^3 denote the corresponding phoreograms (1, 2, and 3, Figs. 1—5).[1]

Since α is equal to 0 for complete dissociation, the phoreograms 1 and 2 should coincide at zero concentration. Actually in PC as well as in DMF the curves apparently converge. However, no such trend is found between the phoreograms 1 and 3. A well defined Λ_0^3 value will be obtained at extreme dilution, if extrapolation is made. However, a straightforward extrapolation is not good for a complexed salt in the presence of excess DBC, and we must be satisfied with the values of K_f (formation constant of a 1 : 1 complex) obtained in a concentration range in which an accurate conductance measurement can be carried out.

According to the definition of K_f (Eq. 2 of the previous paper)[1], the value of K_f is approximately equal to α/C when α is much smaller than unity, where α is the fraction of the cation in the 1 : 1 complex and C is the initial molar concentration of the alkali metal ion and DBC.

This condition, however, is not easily satisfied because α has a value of the order of 0.1 or greater as is shown in phoreogram 3.

The value of K_f for $Na(DBC)^+$ at 1.44×10^{-3} M of $NaClO_4$[1] is about three times larger than that given by Shchori *et al.* at 1.0×10^{-3} M of NaSCN.[2] At this stage no prediction can be made for the discrepancy between them, since it is likely that Na^+ and ClO^-_4 dissociate completely in DMF, whereas Na^+ and SCN^- associate slightly in DMF. Moreover the K_f values in Table 1[1] are practically constant within these concentration ranges.

References

1) N. Matsuura, K. Umemoto, Y. Takeda, and A. Sasaki, *Bull. Chem. Soc. Jpn.*, **49**, 1246 (1976).

2) E. Shchori, J. Jagur-Grodzinski, Z. Luz, and M. Shporer, *J. Am. Chem. Soc.*, **93**, 7133 (1971).

Interactions of Calcium Ions with Carbohydrates: X-Ray Diffraction and NMR Spectroscopic Studies on the Potassium Salt and the Calcium Salt of D-Glucaric Acid

Tooru TAGA, Yoshihiro KURODA, and Kenji OSAKI

Faculty of Pharmaceutical Sciences, Kyoto University, Sakyo-ku, Kyoto 606

(Received December 27, 1976)

The crystal structure of potassium D-glucarate was determined by X-ray analysis. The conformation of the glucaric anion in the potassium salt differs from that of the dianion in the crystal of the calcium salt. The proton magnetic resonance spectra of the solutions of the potassium salt and the calcium salt show that the glucarate solution is an equilibrium mixture of the two conformers observed in the crystals. Studies on the induced shifts by adding europium nitrate to the acidic solution indicate that the europium ions are selectively bound to the potassium type conformer. Calcium sequestant by the glucaric acid in alkaline solutions should occur when calcium ions bind the calcium type conformers in a dianionic state.

D-Glucaric acid is known to have high calcium sequestering effect in alkaline solutions. The calcium affinity of the glucaric acid was supposed to be due to the increased ionization of the hydrogen of the hydroxyl groups in the glucaric acid in aqueous alkaline solution, the calcium–glucaric acid complex in chelating form being expected in the solution.[1] In relation to this subject, a report was given on the crystal structure of calcium D-glucarate tetrahydrate.[2] In the crystal structure, a stable chelating structure of the glucaric dianions binding to the calcium ion was observed. However, the structural evidence for such a calcium binding or a calcium–sugar complex in the solution is still not known. We have therefore studied the crystal structure of potassium D-glucarate and the NMR spectra of several glucarate salt solutions. The relationship between the structures of the crystals and the solutions was discussed. We were particularly interested in the structure of the metal ion–glucaric acid complex, which is elucidated by NMR spectroscopy using the shift reagent.

Experimental

X-Ray Analysis of the Potassium D-Glucarate. The single crystals of potassium D-glucarate, $K^+ C_6H_9O_8^-$, were obtained by the evaporation method. Preliminary X-ray diffraction experiments showed that the crystals are monoclinic, space group $P2_1$, $Z=2$, $D_x=1.807$ g/cm^3, with cell dimensions $a=8.55$, $b=10.9$, $c=4.85$ Å and $\beta=90.0°$. The intensity data of 675 independent reflections were collected from the equi-inclination Weissenberg photographs taken by rotating the crystals about the b- and c-axes, using Cu $K\alpha$ radiation. The intensities on the films were measured on a SYNTEX AD-1 densitometer controlled by a NOVA 1200 computer. Absorption correction for a cylindrical crystal was applied ($\mu R=2.0$). The structure was solved by the direct method using the program MULTAN,[3] and refined by the block diagonal least-squares method. The hydrogens bonded to the carbons were located from the difference Fourier maps and included in the structure factor calculations. Successive cycles of the anisotropic least-squares refinement gave an R-value of 0.123. Scattering factors for all atoms were obtained from the International Table for X-Ray Crystallography IV.[4] The final structural parameters are given in Table 1.

NMR Studies on the Solution. The 100 MHz proton magnetic resonance spectra of the solutions were measured on a VARIAN HA-100D spectrometer, using an internal lock signal of tetramethylsilane sealed in a capillary tube. The deuterium oxide solutions of 0.1 mol potassium glucarate and 0.1 mol calcium glucarate were prepared and adjusted to predominantly diprotonated (LH_2), monoanionic (LH^-)

TABLE 1. ATOMIC PARAMETERS AND THEIR STANDARD DEVIATIONS IN POTASSIUM D-GLUCARATE

The values have been multiplied by 10^4. Temperature factors are in the form, $T^{-1}=\exp(\beta_{11}h^2+\beta_{22}k^2+\beta_{33}l^2+2\beta_{12}hk+2\beta_{13}hl+2\beta_{23}kl)$.

Atom	x	y	z	β_{11}	β_{22}	β_{33}	β_{12}	β_{13}	β_{23}
K	2155 (6)	0	3430 (14)	67	32	577	25	30	95
C (1)	1316 (21)	7284 (17)	7661 (47)	27	15	296	6	−41	20
C (2)	2051 (20)	6342 (15)	9653 (42)	26	4	206	4	−39	4
C (3)	3008 (21)	5435 (16)	7964 (43)	22	11	197	11	−2	3
C (4)	3826 (20)	4451 (16)	9672 (44)	17	11	211	13	−11	−3
C (5)	2719 (22)	3549 (17)	11050 (43)	47	20	126	−1	−14	−1
C (6)	1890 (21)	2705 (17)	9018 (47)	23	17	284	−5	−34	−23
O (1)	1790 (17)	8394 (12)	7658 (36)	76	13	380	−17	−17	17
O (1′)	217 (15)	6840 (12)	6103 (32)	45	12	291	1	−37	25
O (2)	3002 (16)	6893 (13)	11744 (31)	65	27	211	−7	−35	11
O (3)	4266 (15)	6088 (12)	6584 (31)	29	21	273	−15	−6	2
O (4)	4935 (15)	3735 (13)	8002 (32)	34	25	252	16	−10	−11
O (5)	3549 (16)	2863 (12)	13147 (31)	66	24	156	10	−28	15
O (6)	2295 (17)	1559 (12)	8826 (34)	88	10	324	2	−19	0
O (6′)	804 (16)	3216 (12)	7491 (32)	40	21	256	−4	−46	5

and dianionic (L^{2-}) states by adding an equimolar amount of KOH and DCl. The pH values corresponding to each state were approximately 1.5, 3.8, and 9.8 in the pH-meter readings for the potassium salts, and 0.7, 1.4, and 6.1 for the calcium salts, respectively. The concentration of calcium glucarate in the solution at pH 6.1 was extremely low, since the calcium salt was insoluble in neutral deuterium oxide. The induced shifts of protons H(2)—H(5) by europium ions were measured by adding europium nitrate to the 0.1 mol potassium salt solution at pH 1.5. The shift ratios of H(2)/H(4), H(3)/H(4) and H(5)/H(4) at null concentration of the europium ions were derived from the induced shifts observed in various ionic strengths of the solutions. The water in the commercial $Eu(NO_3)_3 6H_2O$ was removed by drying the sample solved in the deuterium oxide. All the experiments were performed at room temperature (23 °C).

Calculations of the Europium–Glucarate Complex Model. The shift ratios of ligand protons for an axially symmetric complex can be calculated by the following McConnell-Robertson equation:

$$\Delta\nu/\nu_0 = K\cdot(3\cos^2\theta - 1)/r^3,$$

where K is the constant related to the magnetic field, r is the distance between the europium ion and the proton, and θ is the angle between the principal magnetic axis of the complex and the vector r.[5] A number of europium–glucarate complex models were generated on a FACOM 230-75 high-speed computer in the Data Processing Center, Kyoto University. The most reasonable model was selected by minimizing the sum of the square errors between the calculated and observed shift ratios.[6–8] In consideration of several stereochemical situations of the present complex, the following assumptions were made. (i) The complex has a symmetric axis which coincides with the principal magnetic axis; (ii) the symmetric axis is coincident with one of the principal axes of the inertia tensor of the complex in the time average; (iii) the ligand has the rigid conformation observed in the crystals; (iv) there are no abnormally short contacts between the europium ion and the ligand oxygens, nor between the neighboring ligand atoms, and (v) each ligand has at least two oxygens bonded to the europium ion. The stoichiometric component of the europium–glucarate complex was not determined by the experiments. However, the europium ion observed in the crystal structure determined hitherto[9–12] is usually bonded to seven to nine oxygens, a similar coordination number being expected for the europium ions in the solution. A certain number of water molecules can be inculuded in this coordination. For the stable complex formation, two or three oxygens of each ligand should be bonded to the europium ion (assumption v). Hence, the stoichiometric component of the present complex was limited in the three cases of 1 : 1, 1 : 2, and 1 : 3. Since the principal axis of the inertia tensor of the complex coincides with the symmetric axis (assumption ii) and all the ligand anions are limited in the D-isomer, two-fold and three-fold axes were assigned to the symmetric axes of the 1 : 2 and 1 : 3 complexes, respectively. If such an axial symmetry of the complex is assumed and the internal freedom of the ligand is forbidden by fixing the atomic parameters of the ligand to those of the crystal structures (assumption iii), the structure of the complex can be determined by the three positional parameters of the ligand relative to the europium ion and by the three orientational parameters of the symmetric axis through the central europium ion. In the actual calculation, the positional parameters in the first place changed step by step. The atomic distance between the europium ion and ligand atoms was inspected at each position, from the criterion that an abnormally short distance less than 2.2 Å is unallowable and that at least two oxygens have Eu–O proximity in the range 2.2—3.4 Å. After fixing the position of the ligand, the directions of the principal axes of the inertia tensor and the mean direction of the Eu–O bonds were calculated, one of them being selected as the direction of the magnetic axis of the complex. The symmetric axes of the 1 : 2 and 1 : 3 complexes were determined according to the following procedure. The minimum of the sum of the square errors between the calculated and observed shift ratios was found by changing three Eulerian angles of the axis at suitable intervals. The second and third ligands corresponding to the 1 : 2 and 1 : 3 complexes were generated by the symmetric operation around this axis, and the atomic contacts between the adjacent ligands were checked. The two cases of the ligand forms, TGG and GTT, observed in the crystal state were examined by iterative application of the procedure described above. The 1 : 2 complex composed of the TGG conformers gave the best fit between the calculated and observed shift ratios.

Although the complex model derived here is based upon the assumption that the ligand has the fixed conformation observed in the crystals, the glucaric acid in the actual solution might have a flexibility and many different types of ligand conformers might interact with the europium ions. The observed shifts would result from an averaging of these various conformations. Thus, the complex models including further different conformers should be taken into account for the model calculations, and the shift ratios calculated as a mixture of these complex models. However, the large conformational change of the ligand by the complex formation was unexpected, since the J values did not change much on adding the europium ions. The mixture model of the TGG and GTT conformers also seemed impossible since the GTT conformer complex models gave a very large discrepancy between the calculated and observed shift in any assignment of the ligand positions and of the directions of the magnetic axis. The TGG conformer complex proposed here is, therefore, the most probable form in spite of the large flexibility of the ligand, and should be the main component in various complexes in the equilibrium solution.

Results and Discussion

The Crystal Structure of Potassium D-*Glucarate.* Figure 1 shows a perspective view of the crystal structure of potassium glucarate. The crystal structure is stabilized by the attractive forces between the potassium ions and the oxygen atoms of the glucaric anions. The potassium ions are surrounded by four carboxyl oxygens and four hydroxyl oxygens in a distorted cubic-prism arrangement, and one cation binds six ligand anions. The K–O distances range from 2.43 to 3.32 Å, the average value being 2.97 Å. This chelating structure differs from that of the calcium ion observed in the crystal of calcium glucarate tetrahydrate, in which the cations are surrounded by two carboxyl oxygens, three hydroxygens and three water molecules, and the central cation binds only two ligand dianions.[2] The hydrogen bonds also stabilize the crystal structure of the potassium salt. The hydrogen bond linkage –O(3)–O(2)–O(4)–O(5)– binds four hydroxyl groups of the adjacent glucaric anions. Another O(1′)–O(6′) hydrogen bond binds the carboxyl groups of the adjacent glucaric anions at the head and the tail along the molecular axis. Although the positions of the hydrogen in the O(1′)–O(6′) hydrogen bond are of interest in relation to the

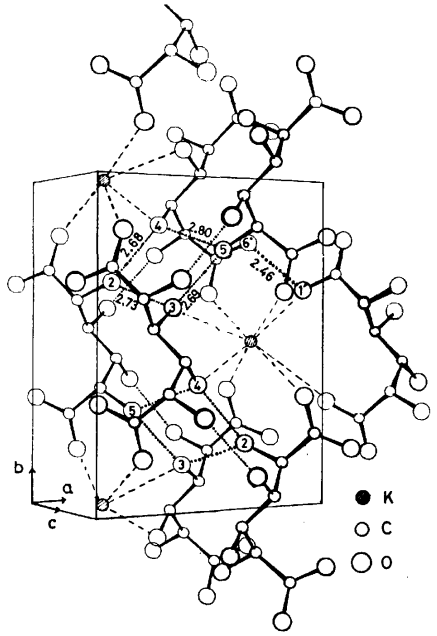

Fig. 1. A perspective view of the crystal structure of potassium glucarate. The dotted lines show the hydrogen bonds. Their distances are given in Å unit.

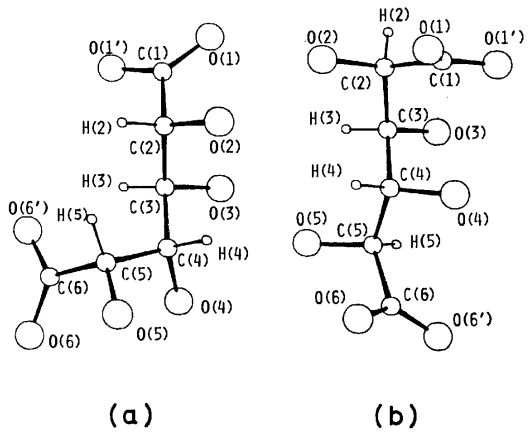

(a) (b)

Fig. 2. Conformations of the glucaric acid, (a) in the crystal of the potassium salt and (b) in the crystal of the calcium salt.

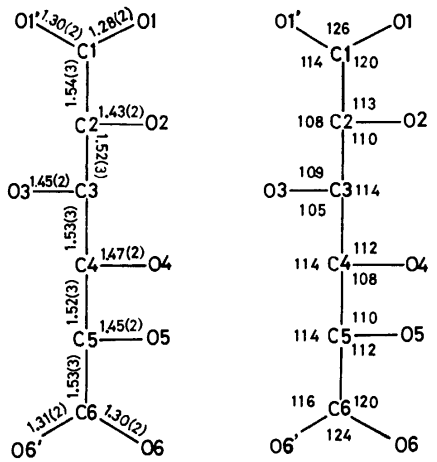

Fig. 3. Bond lengths (Å) and angles (°) of the glucaric acid in the crystal of the potassium glucarate.

dissociation state of the protons of the carboxyl groups at C(1) and C(6), they were not determined accurately because of the poor resolution of the difference Fourier maps.

Figure 2(a) shows a perspective view of the glucaric anion in the crystal of the potassium salt. The bond lengths and angles are given in Fig. 3. The carbon chain has a bent conformation. The structure differs from that of the calcium salt given in Fig. 2(b). The torsional angles about the C–C bonds in each case are given in Table 2. In the case of the potassium salt, C(1) and C(4) are located in trans positions with respective to the C(2)–C(3) bond. C(2) and C(5) are gauche for C(3)–C(4), and C(3) and C(6) are gauche for C(4)–C(5). Thus, the structure for the potassium salt can be represented in terms of "TGG form," while that for the calcium salt will be of "GTT form." In these structures, unfavorable parallel interaction between the C(2)–O(2) and C(4)–O(4) bonds,[13,14] as would occur in a fully extended structure, is avoided, both structures being more stable than other possible structures.

Table 2. Torsional angles ϕ (°) in D-glucaric acid

Bond	Crystal		Solution	
	K salt	Ca salt	$0 \leqq \phi \leqq 90$	$90 \leqq \phi \leqq 180$
H(2)-C(2)-C(3)-H(3)	57.6	−67.6	62	122
H(3)-C(3)-C(4)-H(4)	−168.2	−71.3	51	136
H(4)-C(4)-C(5)-H(5)	68.3	167.8	54	133
O(1)-C(1)-C(2)-C(3)	−110.5	−124.2		
O(1')-C(1)-C(2)-C(3)	70.1	56.1		
C(1)-C(2)-C(3)-C(4)	179.3	55.7		
C(2)-C(3)-C(4)-C(5)	67.4	162.4		
C(3)-C(4)-C(5)-C(6)	68.7	168.0		
C(4)-C(5)-C(6)-O(6)	106.1	67.3		
C(4)-C(5)-C(6)-O(6')	−71.5	−109.9		

Solutions of the Potassium Salt and the Calcium Salt. The 100 MHz NMR spectra of the potassium salt and the calcium salt consist of twelve peaks in the most separated case and each peak can be assigned to four protons H(2), H(3), H(4), and H(5) in the glucaric acid (Fig. 4). The assignments agree with those given for the sodium salt by Sawyer and Brannan.[15] When the pH value of the solution decreases, the H(2) and H(5) peaks shift lowfield to a greater extent than the H(3) and H(4) peaks. There is no significant difference between the chemical shifts in the potassium salt and the calcium salt (Table 3). The coupling constants J for both salts are also similar, the J values for each pair of protons remaining almost the same even when the dissociation states of the glucaric acid change (Table 4). The H–C–C–H torsional angles calculated from the average J values for each pair of protons by application of the modified Karplus equation[16] of Lemieux and Lown[17] are also given in Table 2. When the J values were calculated from the torsional angles observed in the two crystal structures, their arithmetic average values are given as 3.0, 5.9, and 6.2 Hz for $J_{2,3}$, $J_{3,4}$, and $J_{4,5}$, respectively. These values are close to the

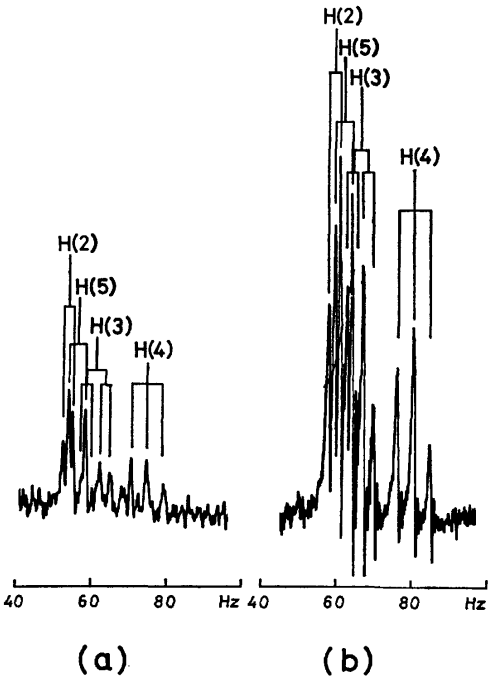

Fig. 4. The 100 MHz proton magnetic resonance spectra of D-glucaric acid. (a) For the saturated solution of the calcium salt at pH 6.1. (b) For the solution of 0.1 mol potassium salt at pH 9.8. The chemical shifts (Hz) are measured from internal HDO in upfield.

TABLE 3. CHEMICAL SHIFTS (Hz) OF D-GLUCARIC ACID UPFIELD FROM INTERNAL HDO

Proton	LH_2	LH^-	L_2^-
		Potassium salt	
H(2)	23	43	59
H(3)	56	62	66
H(4)	75	78	80
H(5)	34	49	61
		Calcium salt	
H(2)	26		55
H(3)	59		61
H(4)	77		75
H(5)	37		57

TABLE 4. PROTON COUPLING CONSTANTS (Hz) OF D-GLUCARIC ACID FOR K, Ca, AND Eu SALTS

Coupling constants	K salt			Ca salt		Eu salt
	LH_2	LH^-	L^{2-}	LH_2,LH^-	L^{2-}	LH_2
$J_{2,3}$	3.0	3.0	2.8	3.0	2.5	3.0
$J_{3,4}$	5.5	5.0	4.3	5.5	4.3	5.5
$J_{4,5}$	4.8	4.8	4.5	5.0	4.5	4.8

corresponding observed values of 3.0, 5.5, and 5.0 Hz. The glucaric acid in the solution is thus supposed to be an equilibrium mixture of the TGG and GTT conformers found in the crystals, although other conformers may be more or less mixed.

The Europium–Glucarate Complex in the Solution. When europium nitrate is added to an acidic solution of potassium glucarate, the H(2), H(3), and H(5) peaks shift highfield and the H(4) peak shifts lowfield (Fig. 5). The shift ratios, H(2)/H(4), H(3)/H(4), and H(5)/H(4), induced by the europium ion are linear for the relative concentration of the europium ions [Eu]/[S], and the values of the shift ratios extrapolated to the null concentration of europium ions are −2.89, −1.56, and

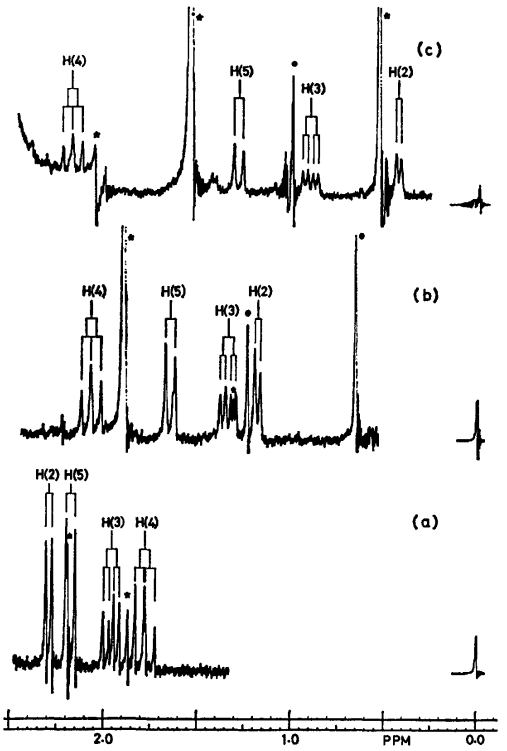

Fig. 5. Change of the 100 MHz proton magnetic resonance spectra of D-glucaric acid by adding europium nitrate to the solution of 0.1 mol potassium salt at pH 1.5.
(a) Eu was not included. (b) [Eu]: [S]=2: 3. (c) [Eu]: [S]=4: 3.
The chemical shifts were measured in relative values to the internal acetone. The peaks noted by asterisks (*) indicate the side band by the sample spinning.

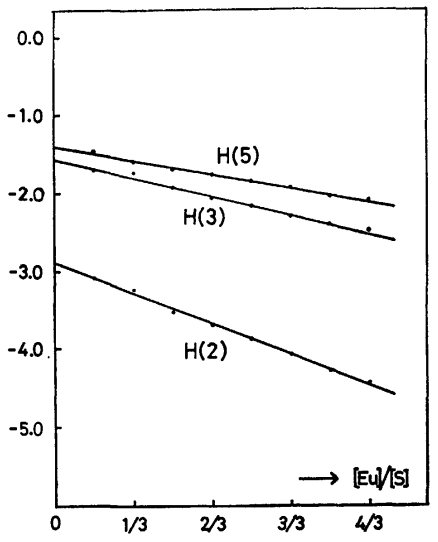

Fig. 6. Shift ratios of the protons of the glucaric acid *vs.* ionic strength [Eu]/[S]. The shift of proton H(4) was chosen as the reference.

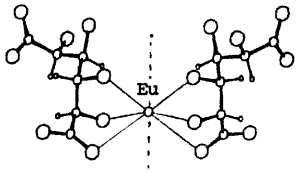

Fig. 7. Structure of Eu–glucaric acid complex. The assumed direction of the magnetic axis is indicated by the broken line through the center of the Eu ion.

−1.40, respectively (Fig. 6). The observed values were compared with the calculated shift ratios, and the best fit was obtained in the case of the 1 : 2 complex composed of the TGG conformers (see Experimental). The calculated shift ratios were −2.90, −1.57, and −1.10 for H(2)/H(4), H(3)/H(4), and H(5)/H(4), respectively. Figure 7 shows a perspective view of the obtained complex model. The three oxygens of the glucaric acid bind to the europium ion. The Eu–O distances are 3.17 Å for Eu–O(1′), 2.21 Å for Eu–O(2) and 2.64 Å for Eu–O(3). The europium–glucarate binding feature agrees with the calcium chelating form of gluconic acid found in lactobionic acid CaBr crystal, in which the gluconic acid moiety has the same TGG conformation.[18]

The Calcium Sequestering Effect by Glucaric Acid in Alkaline Solutions. Quite a large amount of the calcium salt of glucaric acid is precipitated in alkaline solutions. This can be explained as follows. The ionic radius of the calcium ion (0.99 Å) is close to that of the europium ion (1.11 Å), and in spite of their different charges, both ions show a similar behavior in glucaric acid solutions. From this analogy between the calcium and europium ions, the calcium ion should form a complex with the TGG conformers of glucaric acid as well as the europium ion did, the complex being stable in the solution over a wide pH range. The assumption of the calcium–glucarate complex is also supported by the fact that the calcium salt of glucaric acid is more easily dissolved in a high concentrated solution of calcium chloride than pure water, since the increased solubility of glucaric acid may be due to the complex formation between calcium ions and glucaric acid. Although the TGG conformers form such a calcium complex, the GTT conformers in an equilibrium state weakly interact with the calcium ions, not forming the calcium complex in the acidic solution. However, the calcium affinity of the glucaric acid is increased in the alkaline solution since the hydrogens of the carboxyl groups and probably of the hydroxyl groups in the glucaric acid are ionized in the aqueous alkaline solution. In this state, the calcium ions will bind not only to the TGG conformers but also to the GTT conformers. Once the GTT conformers bind to the calcium ions, they will form insoluble calcium salt and will be precipitated. Since the equilibrium ratio between the TGG and GTT conformers in the solution is unchangeable during the course of precipitation, the GTT conformers lost by precipitation should be supplied by the conformational change of the TGG conformers to the GTT form. Precipitation of the calcium salt would proceed until the solution attains an equilibrium state of low limited concentration of the glucaric acid in the last stage.

In conclusion, glucaric acid has two stable conformations found in the two salt crystals. The glucarate solutions are an equilibrium mixture of these two conformers. Their equilibrium ratio is not affected by the ionization states of glucaric acid or by the kind of cation in the solution. The TGG conformers form the 1 : 2 calcium complex in a wide pH range. The precipitation of the calcium salt occurs when the GTT conformers in the dianionic state bind to the calcium ions.

All the computations were performed on a FACOM 230-75 in the Data Processing Center, Kyoto University. The program system KPAX for the X-ray crystallography was used for the structure analysis of potassium glucarate crystal. The FORTRAN programs for the computations of complex models and of the chemical shifts were written by one of the authors (T.T).

References

1) C. L. Mehltretter, B. H. Alexander, and C. E. Rist, *Ind. Eng. Chem.*, **45**, 2782 (1958).
2) T. Taga and K. Osaki, *Bull. Chem. Soc. Jpn.*, **49**, 1517 (1976).
3) G. Germain, P. Main, and M. M. Woolfson, *Acta Crystallogr., Sect. A*, **27**, 368 (1971).
4) "International Table for X-Ray Crystallography IV," Kynoch Press, Birmingham (1974), p. 71.
5) H. M. McConnell and R. E. Robertson, *J. Chem. Phys.*, **29**, 1361 (1958).
6) G. N. La Mar, W. DeW. Horrocks, Jr., and L. C. Allen, *J. Chem. Phys.*, **41**, 2126 (1964).
7) J. J. Uebel and R. M. Wing, *J. Am. Chem. Soc.*, **94**, 8910 (1972).
8) T. Anthonsen, B. Larsen, and O. Smidsrod, *Acta Chem. Scand.*, **27**, 2671 (1973).
9) I. Grenthe, *Acta Chem. Scand.*, **25**, 3347 (1971).
10) E. Hansson, *Acta Chem. Scand.*, **27**, 2827 (1973).
11) R. E. Cramer and K. Seff, *Acta Crystallogr., Sect B*, **28**, 3281 (1972).
12) R. M. Wing, J. J. Uebel, and K. K. Anderson, *J. Am. Chem. Soc.*, **95**, 6046 (1973).
13) G. A. Jeffrey and H. S. Kim, *Carbohydr. Res.*, **14**, 207 (1970).
14) G. A. Jeffrey and E. J. Fasiska, *Carbohydr. Res.*, **21**, 187 (1972).
15) D. T. Sawyer and J. R. Brannan, *Anal. Chem.*, **38**, 192 (1966).
16) M. Karplus, *J. Chem. Phys.*, **30**, 11 (1959).
17) R. U. Lemieux and J. W. Lown, *Can. J. Chem.*, **42**, 893 (1964).
18) W. J. Cook and C. E. Bugg, *Acta Crystallogr., Sect. B*, **29**, 215 (1973).

A Phenomenological Description of Electron Paramagnetic Double-Resonance Relaxation of Organic Free Radicals in Solution. I. Theory of ENDOR Based on the Spin-Population Number Method

Hideo SHIKATA

Laboratory of Chemistry, Faculty of General Education, Ehime University, Bunkyo-cho, Matsuyama 790

(Received July 21, 1976)

ENDOR enhancement is phenomenologically described, applying the method of Lloyde and Pake. Emphasis is placed on the effect of incomplete hf separation. It is shown that fractional ENDOR enhancement can approximately be expressed as the product of that which Freed has formulated when the effect is absent, and an modified Allendoerfer-Maki type correlation, $T_{2e}^2\Delta\omega^2/(c+T_{2e}^2\Delta\omega^2)$, where c is a constant dependent on the microwave power. Also, a simplified method is proposed for calculating the fractional ENDOR enhancement for a multi-level system consisting of several sets of equivalent protons, when $W_n \ll W_e$, and it is proven that the week rf power irradiated leads to an ENDOR enhancement proportional to the number of equivalent protons, in the absence of the effect of incomplete hf separation.

The ENDOR measurements for an organic radical in solution give, in general, very simple spectra. The spacing among the ENDOR lines easily results in an accurate value of the hfs constant even for a proton having its hfs hidden within the ESR linewidth. On the other hand, the intensity of ENDOR lines (ENDOR enhancement) conspicuously varies with temperature (viscosity), concentration, microwave (mw) power and radiofrequency (rf) power. Thus, under the usual conditions of measurement, ENDOR enhancement does not directly reflect the number of equivalent protons which considerably helps in the assignment of the proton. Such a complicated behavior of ENDOR enhancement has stimulated some experimental and theoretical investigations for the purpose of extracting the relaxational characteristics of an observed proton. This paper covers the theoretical part of those investigations.

It has been established that the relaxation matrix theory developed by Freed and coworkers[1-5] describes ENDOR phenomena quite satisfactorily.[4-7] However, it is not easy to obtain an exact solution to the Freed equations for a simple system consisting of only a few sets of equivalent protons, even with the aid of a computer. Therefore, a simplification based on a phenomenological theory is still of value in spite of its lack of rigor, as long as it can explain, to some extent, the experimental results for complex molecules.

The Freed theory assumes that all the hfs are completely separated. However, one often encounters cases for which the hfs is of the order of the ESR linewidth (and for which ENDOR exhibits its full capability). In this situation, when one of the spin packets is saturated by mw irradiation, other packets are partially saturated because of the overlapping of the packets, which consequently reduces the ENDOR enhancement. This effect of incomplete hf separation, or the self-ELDOR effect, was first treated by Allendoerfer and Maki,[8] who have proposed the following formula,

$$I = I_{\max}\frac{T_{2e}^2\Delta\omega^2}{2.5+T_{2e}^2\Delta\omega^2}, \tag{1}$$

where $I_{\max}$ is the ENDOR enhancement in the absence of the effect, $\Delta\omega$ is a hfs constant and T_{2e} is the spin-spin relaxation time of an electron spin corresponding to the ESR linewidth. The applicability of the formula has been discussed by several authors.[9-14] The beauty of the formula is its simplicity, although it has inevitable defects. A difficult point is that it does not contain any relaxation term, except for T_{2e}, and therefore it is not clear under which conditions it is applicable. Indeed, it is known that the ratio of the ENDOR enhancement corresponding to each proton in a molecule also varies markedly with the measurement conditions mentioned above.

The present work is a direct extention of the idea of Allendoerfer and Maki. Here, the method for the spin population number of Lloyd and Pake[15] and Stephan[16] is applied. Introducing a coefficient of incomplete hf separation, we can express the ENDOR enhancement in terms of this coefficient and various kinds of transition probabilities, and thus we wish to examine the role of the effect of incomplete hf separation. In addition, a simplified method is proposed for calculating the ENDOR enhancement for a multi-level system consisting of several sets of equivalent protons, under the condition that $W_n \ll W_e$.

Theory

(a) Outline. We assume first-order formalism for the transition velocity of the spin population number in a stationary state, thus

$$\dot{\mathbf{N}} = \mathbf{CN} = 0. \tag{2}$$

$\mathbf{N}=\{N_i\}$ is the spin population number of each spin level, in which case the total spin population number should be conserved, thus

$$\sum_i N_i = N. \tag{3}$$

$\mathbf{C}$ is a conduction matrix composed of various kinds of transition probabilities. For the lattice-induced transition probabilities, we assume that

$$\frac{W_{\uparrow}^{(e)}}{W_{\downarrow}^{(e)}} = \varepsilon = \exp\left(\frac{-\gamma_e\hbar H_0}{kT}\right) \tag{4}$$

and

$$\frac{W_{\uparrow}^{(n)}}{W_{\downarrow}^{(n)}} = 1, \tag{5}$$

where $W^{(e)}$ and $W^{(n)}$ are the transition probabilities satisfying $\Delta M_s=\pm 1$, and $\Delta M_s=0$, $\Delta M_J=\pm 1$, respectively. The latter equation is assumed because the nuclear Zeeman and hf interactions are too small to bear a net population difference among electron spin levels. Also, we assume a Lorentzian shape function for the transition probabilities induced by the mw and rf fields. When the mw field, $2H_1\cos\omega_e t$, is applied, we have

$$P_e=\frac{1}{2}\gamma_e^2H_1^2T_{2e}|\langle\frac{1}{2}|S_+|-\frac{1}{2}\rangle|^2\frac{1}{1+T_{2e}^2(\omega_e-\omega_{e0})^2}, \quad (6)$$

and when the rf field, $2H_2\cos\omega_n t$, is applied,

$$P_n=\frac{1}{2}\gamma_n^2H_2^2T_{2n}|\langle M_J|J_+|M_J-1\rangle|^2\frac{1}{1+T_{2n}^2(\omega_n-\omega_{n0})^2}. \quad (7)$$

It is well known that only weak ENDOR enhancement is observed for a proton whose hfs is equal to or smaller than the ESR linewidth. In order to treat such cases, one must explicitly take into account the effect of incomplete hf separation. Now, mw excitation induces a transition between the observed spin levels at the ESR resonance, with probability,

$$P_e=\frac{1}{2}\gamma_e^2H_1^2T_{2e}. \quad (8)$$

At the same time, another transition is induced between the neighboring spin levels (Fig. 1), with probability,

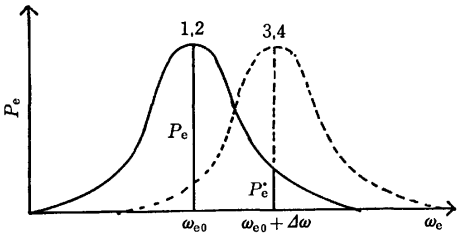

Fig. 1. Schematic diagram of the effect of the incomplete hf separation.

$$P_e'=\frac{1}{2}\gamma_e^2H_1^2T_{2e}\frac{1}{1+T_{2e}^2\Delta\omega^2}. \quad (9)$$

Therefore, a coefficient of incomplete hf separation is introduced as follows:

$$\alpha=\frac{1}{1+T_{2e}^2\Delta\omega^2}. \quad (10)$$

α takes any value between 0 and 1 which correspond to complete hf separation ($\Delta\omega=\infty$) and complete overlap ($\Delta\omega=0$), respectively. Then,

$$P_e'=\alpha P_e. \quad (11)$$

The alternating field-induced transition probabilities have inherent reversibility in contrast to the lattice-induced transition probabilities. Therefore, the role of the field-induced probabilities is thought to be that of making a partial short-circuit over the relaxation pathways, which decreases the difference in the spin population numbers among the spin levels, whereas that of the lattice-induced probabilities is to be that of keeping the Boltzmann distribution. Thus, the presence of P_e' causes the ELDOR-like effect to decrease the ENDOR enhancement.

Equations 2 and 3 result in the difference in the spin population numbers, n, between the two spin levels at which ESR is observed. Then, using the mw energy absorbed per unit time, which is given by

$$A=2\omega_e\chi''H_1^2=nP_e\hbar\omega_e, \quad (12)$$

the integral intensity of the ESR absorption line (I), the peak intensity of the first derivative (I_{ESR}), the ENDOR enhancement (I_{ENDOR}) and the fractional ENDOR enhancement (E) are defined as follows:

$$I=\chi''H_1, \quad (13)$$

$$I_{ESR}=\left(\frac{\partial I}{\partial\omega_e}\right)_{max}, \quad (14)$$

$$I_{ENDOR}=I_{ESR}(ON)-I_{ESR}(OFF), \quad (15)$$

$$E=\frac{I_{ENDOR}}{I_{ESR}(OFF)}, \quad (16)$$

where ON denotes rf irradiation and OFF the absence of rf power. As a whole, the present approach to ENDOR enhancement may be regarded as a simplified version[17] of the relaxation matrix formulation developed by Freed.

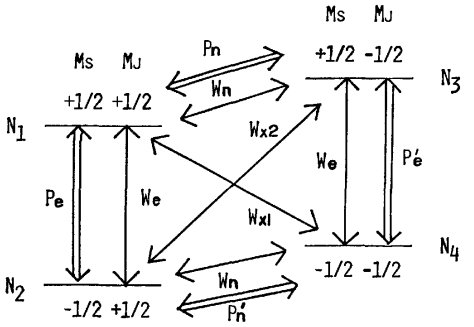

Fig. 2. Schematic diagram of the energy levels and the transition probabilities for a four-spin-level system.

(b) Four-level System (J=1/2). We first treat the four-level system shown in Fig. 2 in order to illustrate the main feature of double resonance relaxation. In the following treatment, we neglect the effects of exchange processes. It is convenient to represent transition probabilities in units of W_e, thus

$$b=\frac{W_n}{W_e},\quad b_{x1}=\frac{W_{x1}}{W_e},\quad b_{x2}=\frac{W_{x2}}{W_e},$$

$$p_e=\frac{P_e}{W_e},\quad p_n=\frac{P_n}{W_e}. \quad (17)$$

Table 1. Conduction matrix for a four-level system

For ENDOR enhancement, either p_n or p_n' is set to 0.
For ELDOR reduction, both p_n and p_n' are set to 0.

$$\begin{pmatrix} -(1+b+b_{x1}+p_e+p_n) & (\varepsilon+p_e) & (b+p_n) & b_{x1}\varepsilon \\ (1+p_e) & -(\varepsilon+b+b_{x2}+p_e+p_n') & b_{x2} & (b+p_n') \\ (b+p_n) & b_{x2} & -(1+b+b_{x2}+p_n+p_e') & (\varepsilon+p_e') \end{pmatrix}$$

TABLE 2. COEFFICIENTS IN Eq. 19

A_0, E_0: $1+2b+(1+b)(b_{x1}+b_{x2})+b_{x1}b_{x2}+(2+b_{x1}+b_{x2})p_n'$;
A_1: $1+b_{x2}$; B_0, F_0: $(1+b)\{2b+(1+b)(b_{x1}+b_{x2})+2b_{x1}b_{x2}\}$ $+\{1+2b+(1+b)(b_{x1}+b_{x2})+b_{x1}b_{x2}\}p_n'$; B_1: $2b+(1+b)(b_{x1}$ $+b_{x2})+2b_{x1}b_{x2}+(1+b_{x1})p_n'$; C_0: $1+b+b_{x1}+p_n$; C_1: 1;
D_0: $b(2+b)+(1+b)(b_{x1}+b_{x2})+b_{x1}b_{x2}+(1+b+b_{x2})p_n'$;
D_1: $2b+b_{x1}+b_{x2}+p_n'$; E_1: $1+b+b_{x2}+p_n'$;
F_1: $b(2+b)+(1+b)(b_{x1}+b_{x2})+b_{x1}b_{x2}+(1+b+b_{x1})p_n'$.

Note that $p_e=\gamma_e^2H_1^2T_{2e}/2W_e\approx\gamma_e^2H_1^2T_{1e}T_{2e}$ at the ESR resonance. Then, using the conduction matrix listed in Table 1, we obtain the difference in the spin population numbers between the 1 and 2 spin levels in the form

$$n = n_0\frac{Ap_n+B}{(Cp_n+D)p_e+Ep_n+F}\frac{F}{B}, \tag{18}$$

with

$$A = A_0+A_1p_e', B = B_0+B_1p_e', \cdots, F = F_0+E_1p_e', \tag{19}$$

A_0, A_1,……, F_0, F_1 being listed in Table 2. n_0, the difference in the spin population numbers in the absence of alternating fields, is related by $n_0=(1-\varepsilon)N/4$ and by

$$M_0 = \chi_0H_0 = \frac{1}{2}\gamma_e\hbar n_0 = \frac{N'\gamma_e^2\hbar^2}{4kT} \qquad \left(N' = \frac{N}{2}\right). \tag{20}$$

Complete hf Separation ($P_e'=0$ or $\Delta\omega=\infty$). Using Eqs. 6 and 18, Eq. 13 can be expressed as a saturated Lorentzian, thus

$$I = \frac{1}{2}\chi_0H_0\frac{\gamma_eH_1T_{2e}}{1+T_{2e}^2(\omega_e-\omega_{e0})^2+\gamma_e^2H_1^2T_{1e}(\mathrm{ON})T_{2e}}, \tag{21}$$

where $T_{1e}(\mathrm{ON})$ is the effective longitudinal relaxation time of an electron spin under NMR excitation:

$$T_{1e}(\mathrm{ON}) = \frac{1}{2W_e}\frac{C_0p_n+D_0}{A_0p_n+B_0}. \tag{22}$$

Note that when $W_n=W_{x1}=W_{x2}=0$, $T_{1e}(\mathrm{ON})=1/2W_e$. Then,

$$I_{\mathrm{ESR}} = \frac{3\sqrt{3}}{16}\chi_0H_0\frac{\gamma_eH_1T_{2e}^2}{\{1+\gamma_e^2H_1^2T_{1e}(\mathrm{ON})T_{2e}\}^{3/2}}, \tag{23}$$

$$I_{\mathrm{ENDOR}} = \frac{9\sqrt{3}}{32}\chi_0H_0\frac{\gamma_e^3H_1^3T_{2e}^3\Delta T_{1e}}{\{1+\gamma_e^2H_1^2T_{1e}(\mathrm{ON})T_{2e}\}^{5/2}}, \tag{24}$$

and

$$E = \frac{3}{2}\frac{\gamma_e^2H_1^2\Delta T_{1e}T_{2e}}{1+\gamma_e^2H_1^2T_{1e}(\mathrm{ON})T_{2e}}, \tag{25}$$

where $\Delta T_{1e}=T_{1e}(\mathrm{OFF})-T_{1e}(\mathrm{ON})$ and Eq. 23 is expanded to the first order in ΔT_{1e} to give Eq. 24. If $\gamma_e^2H_1^2T_{1e}T_{2e}\gg1$, then

$$E_\infty = \frac{3}{2}\frac{\Delta T_{1e}}{T_{1e}} = E_{\infty\infty}\frac{p_n}{p_n+D_0/C_0}, \tag{26}$$

where

$$E_{\infty\infty} = \frac{3}{2}\frac{\{b(1+b_{x2})+b_{x2}(1+b_{x1})\}^2}{(1+b)(1+b+b_{x1})\{2b+(1+b)(b_{x1}+b_{x2})+2b_{x1}b_{x2}\}}. \tag{27}$$

Equation 26 also justifies the conventional interpretation that ENDOR measures the variation in the longitudinal electron spin relaxation time by NMR excitation. Substitution of Eq. 7 into Eq. 26 again gives a saturated Lorentzian for the NMR transition, thus

$$E_\infty = E_{\infty\infty}\frac{\gamma_n^2H_2^2T_{1n}T_{2n}}{1+T_{2n}^2(\omega_n-\omega_{n0})^2+\gamma_n^2H_2^2T_{1n}T_{2n}}, \tag{28}$$

with the effective nuclear spin longitudinal relaxation time

$$T_{1n} = \frac{1}{2W_n}\frac{C_0}{D_0}. \tag{29}$$

Note that if $W_e=W_{x1}=W_{x2}=0$, then $T_{1n}=1/2W_n$.

Incomplete hf Separation. In this case, the ESR absorption line is neither expressed by a simple Lorentzian curve nor by superposition of such curves. Therefore, it is more convenient to define the fractional ENDOR enhancement by the following equation, using Eq. 12 at the ESR resonance:

$$E = \frac{n(\mathrm{ON})-n(\mathrm{OFF})}{n(\mathrm{OFF})}. \tag{30}$$

In addition, we restrict our discussion to the case of an electron-nuclear dipolar (END) mechanism and we neglect the cross relaxations to avoid complexity. Such an approximation may well be satisfied for protons in most of the organic radicals in solution except for some cases in which isotopic hf modulation may be effective.[9,13] A straight forward calculation of Eq. 30 gives

$$E=(1-\alpha)b(1+\alpha p_e)p_np_e[2(1+b+\alpha p_e)[\{2(1+b)+(1+\alpha)(2+b)p_e+2\alpha p_e^2\}b+\{1+2b+(1+\alpha)(1+b)p_e+\alpha p_e^2\}p_n]]^{-1}. \tag{31}$$

For further analysis, the reciprocal of the above equation is expanded to the first order in p_e, thus

$$\frac{1}{E} = \frac{2}{(1-\alpha)bp_np_e}[(1+b)\{2b(1+b)+p_n(1+2b)\} + (b\{(1+b)(2+b)+\alpha(2+b-b^2)\} + p_n\{(1+b)^2+\alpha(1+b-b^2)\})p_e+\alpha O(p_e^2)]. \tag{32}$$

Hence, we obtain a straight line in plotting E^{-1} *vs.* p_e^{-1}, in the region where we can neglect the quadratic terms for p_e which can be proven to be proportional to α. The reciprocal of the intercept in this plot is thus expressed as

$$E_\infty=(1-\alpha)bp_n/2[\{(1+b)(2+b)+\alpha(2+b-b^2)\}b+\{(1+b)^2+\alpha(1+b-b^2)\}p_n]^{-1}. \tag{33}$$

Also, the intercept divided the slope become proportional to the product of T_{2e} and T_{1e}, the latter being expressed, in this case, as

$$T_{1e} = \left(\frac{1}{2W_e}\right)b\{(1+b)(2+b)+\alpha(2+b-b^2)\} + p_n\{(1+b)^2+\alpha(1+b-b^2)\} [(1+b)\{2b(1+b)+p_n(1+2b)\}]^{-1}. \tag{34}$$

Substitution of Eq. 7 into Eq. 33 again gives a saturated Lorentzian for the NMR transition, with

$$T_{1n} = \frac{1}{2W_n}\frac{(1+b)^2+\alpha(2+b-b^2)}{(1+b)(2+b)+\alpha(2+b-b^2)}. \tag{35}$$

Then, we obtain a straight line in plotting E^{-1} *vs.* p_n^{-1}.

Equation 31, as well as Eq. 33, is still of too complicated a form for practical use. One may generally consider that a proton with a small hfs (or large α) has a small END term (or small b) and *vice versa*, as deduced from the McConnell-Strathdee formula.[18] If $b\ll1$, the linear part of Eq. 32 can be written as

$$E=\frac{(1-\alpha)p_e}{1+(1+\alpha)p_e}\frac{bp_n}{2(2b+p_n)}. \tag{36}$$

Hence, the effect of incomplete hf separation reduces the fractional ENDOR enhancement by the following factors, depending on p_e:

(i) for small p_e by $T_{2e}^2\Delta\omega^2/(1+T_{2e}^2\Delta\omega^2)$
(ii) at the ESR maximum ($p_e=1/2$) by $T_{2e}^2\Delta\omega^2/\{(4/3)+T_{2e}^2\Delta\omega^2\}$
(iii) at the ENDOR maximum ($p_e=3/2$) by $T_{2e}^2\Delta\omega^2/\{(8/5)+T_{2e}^2\Delta\omega^2\}$
(iv) and at infinite p_e by $T_{2e}^2\Delta\omega^2/(2+T_{2e}^2\Delta\omega^2)$.

On the other hand, if $\alpha=0$, Eq. 33 becomes

$$E_\infty^{(0)}=\frac{1}{2}\frac{bp_n}{b(1+b)(1+2b)+p_n(1+b)^2}, \tag{37}$$

which coincides with the Freed equation. Note that Eq. 37 also coincides with Eq. 27, except for a trival numerical factor, if p_n is set to infinity. Therefore, an inspection of the above two equations allows us to express approximately the fractional ENDOR enhancement as a formula including correlation of the modified Allendoerfer-Maki type and the Freed formula for $b\lesssim 1$, thus

$$E=\frac{(1-\alpha)p_e}{1+(1+\alpha)p_e}E_\infty^{(0)}. \tag{38}$$

From an experimental point of view, it is desirable to use the mw power at the ESR maximum for ENDOR signals with good S/N ratios. The maximum deviation of Eq. 38 from the linear part of Eq. 32 under these conditions is 6%, for $\alpha=1$ and $b=1$.

(c) Multi-level System—a Simplified Method. The ESR absorption line of an actual molecule is formed by the superposition of its component lines, designated by the various quantum numbers of the total nuclear spin angular momentum.[19] Therefore, for quantitative discussions of the ENDOR relaxation, we must proceed to a multi-level system consisting of several sets of equivalent protons. Treatment of this system along same lines as the scheme in (*b*) may be possible, in principle, but is too complicated and deviates from the purpose of the present work. Instead, a simplified method for calculating the fractional ENDOR enhancement for such a system is proposed with the following approximations and derivations.

In this system, the spin state is represented by

$$|\gamma\pm\rangle=|\pm\frac{1}{2}\rangle\prod_u|J_u^{(\kappa)}M_u\rangle, \tag{39}$$

where J_u and M_u are the quantum numbers of the total nuclear angular momentum for the u'th set of equivalent protons and κ denotes the different degenerate states with the same value of J_u. Now, we assume that T_{2e} is independent of J_u and M_u, so that the ESR absorption is expressed as a superposition of component lines with the same linewidth, corresponding to the transitions from $|\gamma-\rangle$ to $|\gamma+\rangle$. On the other hand the nuclear spin transition probabilities are dependent on the nuclear spin quantum numbers, as follows:[5]

$$1/T_{2n}(J_n, M_u\leftrightarrow J_u, M_u-1)=W_e\left[1+\left\{2f(J_u, M_u)+\frac{1}{3}\right\}b_u\right], \tag{40}$$

$$W_n(J_u, M_u\leftrightarrow J_u, M_u-1)=f(J_u, M_u)W_n^{(u)}, \tag{41}$$

and

$$P_n(J_u, M_u\leftrightarrow J_u, M_u-1)=f(J_u, M_u)P_n^{(u)}, \tag{42}$$

where $W_n^{(u)}$ and $P_n^{(u)}$ are the nuclear spin transition probabilities for a four-level system consisting of a single u'th proton, and with

$$f(J_u, M_u)=J_u(J_u+1)-M_u(M_u-1), \tag{43a}$$

and

$$f\left(J_u, 0 \text{ or } \frac{1}{2}\right)\equiv f_{J_u}. \tag{43b}$$

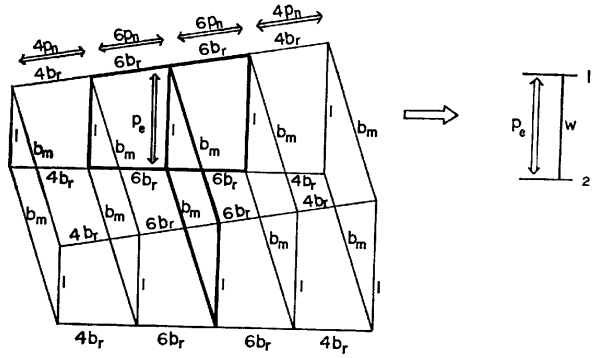

Fig. 3. Schematic diagram of the energy levels and the transition probabilities for a system with $J_m=1/2$ and $J_r=2$. The cetral line of the each quintet of the ESR absorption is observed, and the rf power corresponding to the hfs of the r'th equivalent protons is irradiated. Left side diagram draws an equivalent two-spin-level system corresponding to the relaxation pathways with thick line.

Next, we neglect the relaxation pathways passing more than twice through the W_n's, under the assumption that $b\ll 1$. For example, for the system with $J_m=1/2$ and $J_r=2$ illustrated in Fig. 3, only the relaxation pathways with thick lines are considered. Then, all of the multi-level systems are reduced to a superposition of the maximum six-level systems. This can further be reduced to the two-level system illustrated in the right side of Fig. 3, using a summing method for the electric conduction. The energy of the ESR absorption for this system is easily obtained as

$$A=\frac{n_0\hbar\omega_e WP_e}{2(W+P_e)}, \tag{44}$$

so that the spin lattice relaxation becomes the rate-determining step of the energy absorption, if P_e is set to infinity. Therefore, the fractional ENDOR enhancement, corresponding to Eq. 37, is expressed as

$$E^{(0)}=\frac{w(\text{ON})-w(\text{OFF})}{w(\text{OFF})}, \quad \left(w=\frac{W}{W_e}\right). \tag{45}$$

For actual application it is sufficient only to treat the central line of the ESR absorption. In this case, the summing method leads to the following resultant transition probability for an electron spin:

$$w=1+\sum_u\sum_{J_u}\frac{D_{J_u}}{D_u}\frac{2f_{J_u}(b_u+p_n^{(u)})}{(f_{J_u}+2)b_u+(f_{J_u}+1)p_n^{(u)}}$$

$$+\sum_{u'}\sum_{J_{u'}}\frac{D_{J_{u'}}}{D_{u'}}\left[\frac{(f_{J_{u'}}-1)b_{u'}(b_{u'}+p_n^{(u')})}{\{2+(f_{J_{u'}}-1)b_{u'}\}b_{u'}+\{1+(f_{J_{u'}}-1)b_{u'}\}p_n^{(u')}}\right.$$
$$\left.+\frac{f_{J_{u'}}b_{u'}(b_{u'}+p_n^{(u')})}{(2+f_{J_{u'}}b_{u'})b_{u'}+(1+f_{J_{u'}}b_{u'})p_n^{(u')}}\right], \quad (46)*$$

where u and u′ denote even and odd numbers equivalent protons, respectively, D_u is the total degeneracy of the central absorption line of the u'th set of equivalent protons, and D_{J_u} is the degeneracy of the state with the same value of J_u. These are given by

$$D_{J_u}=\frac{n_u(n_u-1)\cdots\{(n_u/2)-J_u+1\}(2J_u+1)}{\{(n_u/2)+J_u+1\}!}, \quad (47)$$

$$D_u=\sum_{J_u}D_{J_u}=\binom{n_u}{[n_u/2]}, \quad (48)$$

where n_u is the number of u'th equivalent protons.

It can also be proven that for a six-level system for which the hfs is incompletely separated, a calculation similar to Eq. 30 leads to the same form of the fractional ENDOR enhancement as Eq. 38. Therefore, it is considered that Eq. 38 is still valid for general multi-level systems, as long as the above approximation of treating them as the superposition of maximum six-level systems is valid. Hence, we obtain the following limiting expressions for the fractional ENDOR enhancement of the u'th proton, corresponding to Eq. 38. If p_n is set to infinity, then

$$E_{\infty}^{(u)}=\frac{(1-\alpha)p_e}{1+(1+\alpha)p_e}\sum_{J_u}\frac{D_{J_u}}{D_u}\frac{2f_{J_u}b_u}{(1+f_{J_u}b_u)(2+f_{J_u}b_u)}/w(\mathrm{OFF}) \quad (49)$$

for an even number of equivalent protons. Also, if p_n approaches 0, then

$$E_{0}^{(u)}=\frac{(1-\alpha)p_e}{1+(1+\alpha)p_e}\sum_{J_u}\frac{D_{J_u}}{D_u}\frac{2f_{J_u}p_n^{(u)}}{(2+f_{J_u}b_u)^2}/w(\mathrm{OFF}). \quad (50)$$

For an odd number of equivalent protons,

$$E_{\infty}^{(u')}=\frac{(1-\alpha)p_e}{1+(1+\alpha)p_e}\sum_{J_{u'}}\frac{D_{J_{u'}}}{D_{u'}}\left[\frac{f_{J_{u'}}}{(1+f_{J_{u'}}b_{u'})(2+f_{J_{u'}}b_{u'})}\right.$$
$$\left.+\frac{f_{J_{u'}}-1}{\{1+(f_{J_{u'}}-1)b_{u'}\}\{2+(f_{J_{u'}}-1)b_{u'}\}}\right]b_{u'}/w(\mathrm{OFF}). \quad (51)$$

$$E_{0}^{(u')}=\frac{(1-\alpha)p_e}{1+(1+\alpha)p_e}\sum_{J_{u'}}\frac{D_{J_{u'}}}{D_{u'}}\left[\frac{f_{J_{u'}}}{(2+f_{J_{u'}}b_{u'})^2}\right.$$
$$\left.+\frac{f_{J_{u'}}-1}{\{2+(f_{J_{u'}}-1)b_{u'}\}^2}\right]p_n^{(u')}/w(\mathrm{OFF}). \quad (52)$$

Equations 49 and 51 and Eqs. 50 and 52 correspond approximately to the reciprocal of the intercept and that of the slope of the plot of E^{-1} *vs.* p_n^{-1}, respectively. The linearity of this plot is approximately assured, because, in general, if $x\ll r_i/q_i$,

$$y=\sum_i\frac{p_ix}{q_ix+r_i}\simeq\frac{\sum_i(p_i/q_i)^2x}{\sum_i(p_i/q_i)x+\sum_i(p_ir_i/q_i^2)}. \quad (53)$$

Application of Eqs. 47 and 48 to a four-level system leads, of cource, to the same result as Eq. 38 with Eq. 37. Because $\sum_{J_u}f_{J_u}D_{J_u}/D_u=n_u/2$, the above equations can further be reduced to more simplified forms, if we can neglect the quadratic terms for b_u, thus

$$E_{\infty}^{(u)}\simeq\frac{(1-\alpha)p_e}{1+(1+\alpha)p_e}\frac{n_ub_u}{2}, \quad (54)**$$

$$E_{0}^{(u)}\simeq\frac{(1-\alpha)p_e}{1+(1+\alpha)p_e}\frac{n_up_n^{(u)}}{4}. \quad (55)**$$

Considering that from Eq. 36, $p_n^{(u)}$ is independent of u under this condition, Eq. 55 indicates that the fractional ENDOR enhancement is proportional to the number of equivalent protons, if $\alpha=0$ and enough weak rf power is irradiated. This conclusion is the same as the result of the "average ENDOR" proposed by Freed *et al.*[3]

Although ENDOR experiments have been reported in the literature for many radicals in solution since the first successful observation by Hyde and Maki,[20] ENDOR detection for many radicals remains impossible or at least difficult, in spite of the ease of ESR observation. Perhaps, Heisenberg and chemical exchange may be the reason. However, Eqs. 49—52 may offer an additional reason. In these equations, all the END terms of atoms with nuclear spins make contributions to the denominator, w(OFF), whereas only that of the observed proton makes a contribution to the numerator. Therefore, if a radical contains atoms with nuclear spins on which the electron spin density is moderately localized resulting in a large END term, one may observe only weak ENDOR enhancement. This may be a possible reason why ENDOR enhancement for hydrocarbon radicals is, in general, more easily observed than that for nitroxide radicals.

Summary

A simple theory has been formulated to calculate the fractional ENDOR enhancement (E) in the presence of the effect of incomplete hf separation, using the conduction matrix composed of the lattice-induced transtition probabilities and the alternating field-induced transition probabilities, the latter being assumed to be a Lorentzian. The coefficient of incomplete hf separation, α, has been introduced and it is shown that a plot of E^{-1} *vs.* H_1^2 results in a straight line even in the presence of this effect, if $\alpha p_e\ll 1$, where p_e is the mw-induced transition probability in units of W_e. Also, it is shown that the effect of incomplete hf separation reduces the fractional ENDOR enhancement formulated by Freed, by an Allendoerfer-Maki type factor. However, this factor should be modified to $T_{2e}^2\Delta\omega^2/\{(4/3)+T_{2e}^2\Delta\omega^2\}$ at the mw power corresponding to the ESR maximum.

The theory has been extended to a multi-level system consisting of several sets of equivalent protons and it is shown that the plot of E^{-1} *vs.* H_2^{-2} also results in a straight line and that the reciprocal of the slope in this plot is proportional to the number of equivalent protons, if $\alpha=0$ and $b\ll 1$. Thus, the effect of incomplete hf separation should be examined by the following procedure. The H_2 dependence of the ENDOR enhance-

* $\sum_{J_u}$ denotes the single summation over the u'th set of equivalent protons.

** In this case, u denotes odd and even numbers of equivalent protons.

ment is measured at high temperatures of which $b \ll 1$ is satisfied for all protons. E^{-1} is plotted against H_2^{-2}, and the reciprocal of the slope divided by the number of equivalent protons is compared with the proton species.

The author wishes to express his gratitude to Professors K. Ishizu of Ehime University and K. Kuwata of Osaka University for fruitful discussions and encouragement throughout the cource of this work. He also would like to express his appreciation to Professor Y. Deguchi of Kyoto University.

Appendix

TRIPLE Enhancement. Recently, Möbius and coworkers were the first to succeed in observing electron-nuclear triple resonance (TRIPLE) in solution.[12] The most attractive results of their experiments are that TRIPLE enhancement has a better S/N ratio than does ENDOR enhancement and that TRIPLE enhancement is proportional to the number of equivalent protons.

It is worthwhile to interpret TRIPLE enhancement from the standpoint of the present theory. The fractional TRIPLE enhancement is defined by Eq. 30, where OFF means, in this case, that P_e is present but P_n and P_n' are absent, and ON means that P_e, P_n and P_n' are all present. Straightforward calculation gives the following expression for the fractional TRIPLE enhancement for a four-level system, where hf is incompletely separated and $P_n = P_n'$, thus

$$E_t = (1-\alpha)p_e p_n (1+\alpha p_e)(b+p_n)[(1+b+\alpha p_e)[\{p_n^2 + 2(1+b+\alpha p_e)p_n + b(2+b+2\alpha p_e)\}p_e + (2+\alpha p_e)p_n^2 + 2\{1+2b+(1+b)\alpha p_e\}p_n + b\{2+2b+(2+b)\alpha p_e\}]]^{-1}. \quad \text{(A1)}$$

The above equation indicates that the effect of incomplete hf separation also reduces TRIPLE enhancement and that if $\alpha = 0$, TRIPLE enhancement has a S/N ratio eight times larger than does ENDOR enhancement, when Eq. A1 is compared with Eq. 37 at their optimum conditions. Indeed, the TRIPLE enhancement for 2,6-*di-t*-butyl protons in the 2,4,6-*tri-t*-butylphenoxyl radical[12] appears to support the presence of this effect.

For a multi-level system, we start with Eq. 45 as the basis of discussion. However, because P_n and P_n' are simultaneously excited, even the previous approximation to reduce a multi-level system to a superposition of the maximum six-level system is not valid. Instead, we consider the entire system in the extreme cases that $P_n = P_n' = 0$ (OFF) and that $P_n = P_n' = \infty$ (ON), under the condition that $b \ll 1$. In the former case, all the relaxation pathways are cut off except for the original two-level system (W_e). In the latter case, all the W_n pathways are completely short-circuited by P_n and P_n', so that all the W_e pathways are gathered to form a net twe-level system. Thus,

$$w(\mathrm{ON}) = \sum_{J_u} \frac{D_{J_u}}{D_u}(2J_u+1), \quad \text{(A2)}$$

with $w(\mathrm{OFF}) = 1$. Hence, the fractional TRIPLE enhancement is given by

$$E_t^{(u)} = \sum_{J_u} \frac{D_{J_u}}{D_u} 2J_u. \quad \text{(A3)}$$

Such a simple formula appears to explain fairly well the experimental results demonstrated by Möbius *et al.* For example, the ratio of the TRIPLE enhancement for 4,5,9,10-protons to that for 1,7-protons in the pyrene negative ion is obtained from Eq. A3 as 1.67, whereas the experimental ratio is 1.3 and the ratio of the number of equivalent protons is 2.

References

1) J. H. Freed, "Electron Spin Relaxation in Liquids," ed by L. T. Muus and P. W. Atkins, Plenum Press, New York (1972), p 503.
2) J. H. Freed, *J. Chem. Phys.*, **43**, 2312 (1965).
3) J. H. Freed, D. S. Leniart, and H. D. Connor, *J. Chem. Phys.*, **58**, 3089 (1973).
4) J. H. Freed, *J. Phys. Chem.*, **71**, 38 (1967).
5) J. H. Freed, D. S. Leniart, and J. S. Hyde, *J. Chem. Phys.*, **47**, 2762 (1967).
6) D. S. Leniart, H. D. Connor, and J. H. Freed, *J. Chem. Phys.*, **63**, 165 (1975).
7) N. M. Atherton and B. Day, *Mol. Phys.*, **29**, 325 (1975).
8) R. D. Allendoerfer and A. H. Maki, *J. Magn. Reson.*, **3**, 396 (1970).
9) N. M. Atherton and B. Day, *Mol. Phys.*, **27**, 145 (1974).
10) R. D. Allendoerfer and D. J. Eustace, *J. Chem. Phys.*, **75**, 2765 (1971).
11) R. D. Allendoerfer and J. H. Engelman, *Mol. Phys.*, **20**, 569 (1971).
12) K. Ishizu, T. Yamamoto, M. Kono, A. Nakajima, and Y. Deguchi, *Tetrahedron Lett.*, **1974**, 1537.
13) K. P. Dinse, R. Biehl, and K. Möbius, *J. Chem. Phys.*, **61**, 4335 (1974).
14) N. S. Dalal, D. E. Kennedy, and C. A. McDowell, *J. Chem. Phys.*, **61**, 1689 (1974).
15) J. P. Lloyde and G. E. Pake, *Phys. Rev.*, **94**, 579 (1954).
16) M. J. Stephan, *J. Chem. Phys.*, **34**, 484 (1961).
17) According to the Freed theory presented in Ref. 3, $Z''_{a'a}$, which determines the energy of the ESR absorption and the line shape, is obtained by solving the system of simultaneous equations 4.5a—4.6e of that paper. Then, the fractional ENDOR enhancement is given by $E = \{Z''_{a'a}(\mathrm{ON}) - Z''_{a'a}(\mathrm{OFF})\}/Z''_{a'a}(\mathrm{OFF})$. It is possible to calculate $Z''_{a'a}$ using an approximate method instead of the exact solution of the complicated equations. First, the coherence effect is neglected, so that Eq. 4.5c and the third term on the left-hand side of Eq. 4.5a and b are neglected. Next, the second terms on the left-hand sides of both equations are tentatively neglected. Then, both $Z''_{a'a}$ and $Z''_{a'b'}$ become Lorentzian, and both are substituted into Eq. 4.6. $\chi_a - \chi_{a'}$, thus obtained, is again substituted into Eq. 4.5a in exact form, and finally $Z''_{a'a}$ is calculated. This procedure certainly corresponds to the present approach.
18) H. M. McConnel and J. Strathdee, *Mol. Phys.*, **2**, 129 (1959).
19) J. H. Freed and G. K. Fraenkel, *J. Chem. Phys.*, **39**, 326 (1963).
20) J. S. Hyde and A. H. Maki, *J. Chem. Phys.*, **40**, 3117 (1964).

A Phenomenological Description of Electron Paramagnetic Double-Resonance Relaxation of Organic Free Radicals in Solution. II. ENDOR Relaxation of Galvinoxyl

Hideo SHIKATA and Kazuhiko ISHIZU*

Laboratory of Chemistry, Faculty of General Education, Ehime University, Bunkyo-cho, Matsuyama 790
**Department of Chemistry, Faculty of Science, Ehime University, Bunkyo-cho, Matsuyama 790*

(Received September 6, 1976)

The ratio of the ENDOR enhancement to the ESR intensity (E) of galvinoxyl in toluene was measured under various conditions of microwave power, rf power and temperature. The results are discussed in comparison with a phenomenological theory in part I. It is proven that the apparent longitudinal electron spin relaxation time for a *t*-butyl proton under NMR excitation is about twice as long as those for methylidyne and ring protons, which is explained by the effect of incomplete hf separation. Also, it is shown that the reciprocal of the slope of the plot of E^{-1} *vs.* (rf power)$^{-1}$ for methylidyne and ring protons is approximately proportional to the number of equivalent protons, whereas that for a *t*-butyl proton can be explained only if the effect of incomplete hf separation is taken into consideration. The value of $b=W_n/W_e$ for methylidyne and ring protons, simulated from the temperature dependence of E based on a previous theory, can be closely correlated to the spin distribution in galvinoxyl.

A phenomenological theory has been described in part I. The purpose of the present paper is to report the results of an experimental examination of the applicability and the limits of the theory.

Because the pulse technique[1,2] is not widespread in the field of ESR spectroscopy, experimental information about the relaxational behavior of a radical can usually be extracted from an analysis of the ESR saturation curve, as well as from that of the linewidth.[3] The same procedure should be applied to ENDOR, by measuring the microwave(mw)- and rf-power dependence of ENDOR enhancement. More abundant information is expected from ENDOR, because two parameters can be varied independently. Recently, Leniart *et al.*[4] have applied such a method to the study of some semiquinones. However, to the present authors' knowledge, there has been no attempt to compare this dependence for different proton species in a molecule over a wide temperature range.

In the present study, the ratio of the ENDOR enhancement to the ESR intensity was measured for different protons, as functions of the mw and rf powers at temperatures from −20 to −95 °C. The sample used in the experiments is the galvinoxyl radical which has one methylidyne proton, four ring protons and thirty-six *t*-butyl protons. It was selected because its ENDOR spectra is one of the most easily observable and because the purity of this very stable radical can be precisely determined from a measurement of the magnetic susceptibility, so that a solution of known concentration can be easily obtained. It is one of materials for which the liquid phase ENDOR was first successfully observed.[5] The results are discussed with reference to the theory in part I, forcussing our attention on a comparison of the proton species.

Experimental

The ENDOR spectra were measured using a JEOL EDX-1 ENDOR unit with a frequency modulation of 6.5 kHz, attached to a JEOL ME-X ESR spectrometer with a field modulation of 80 Hz. The rf amplifier employed can provide maximum rf power of 1 kW. The mw power was calibrated using the ESR intensity of a powdered DPPH radical. The rf power was measured using a level meter connected to a tunk circuit which was calibrated by a 100-MHz oscilloscope, using a search coil. No attempt was made to determine the absolute value of either magnetic field. The intensity of the 80-Hz field modulation was set to a value 3 db lower than that for optimum ENDOR enhancement, because overmodulation reduces the relative enhancement for a *t*-butyl proton with respect the enhancement of other protons.[6]

A toluene solution of galvinoxyl in a quartz tube was degassed using the usual method. The purity of the compound synthesized in this laboratory in the past has been determined to be 85%. The viscosity of toluene was estimated using the empirical formula reported by Barlow *et al.*[7] In most of cases, the ENDOR enhancement was observed at concentration a little more dilute than optimum. The ESR and ENDOR intensity were measured as the peak-to-peak heights of the first derivatives of lines. However, because the ENDOR enhancement for the *t*-butyl proton was not resolved completely at high temperatures, it was measured as the distance from the highest to the lowest peak of the doublet enhancement.

Results and Discussion

An example of an ESR spectrum and an ENDOR spectrum of galvinoxyl (Fig. 1) at −80 °C are shown in Fig. 2. For the latter measurement, the ESR field was adjusted to the highest peak of the low-field part of the doublet of the methylidyne proton. The ESR spectrum completely splits the doublet of quintets of methylidyne and ring protons, but does not resolve any

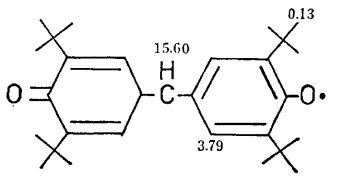

Fig. 1. Structure of galvinoxyl. The numbers indicate the hfs constant in MHz.

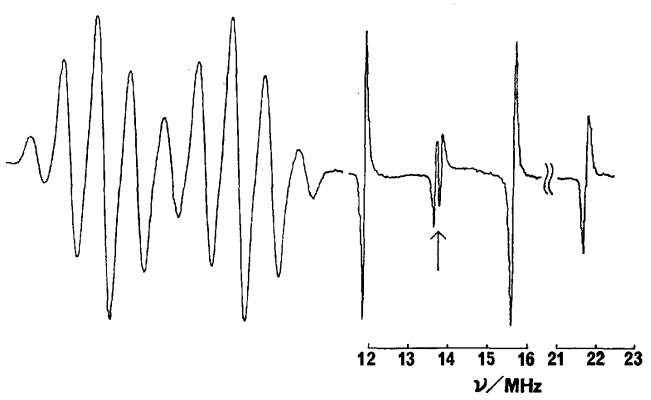

Fig. 2. ESR and ENDOR spectra of galvinoxyl in toluene at −80 °C. The arrow indicates the free proton frequency.

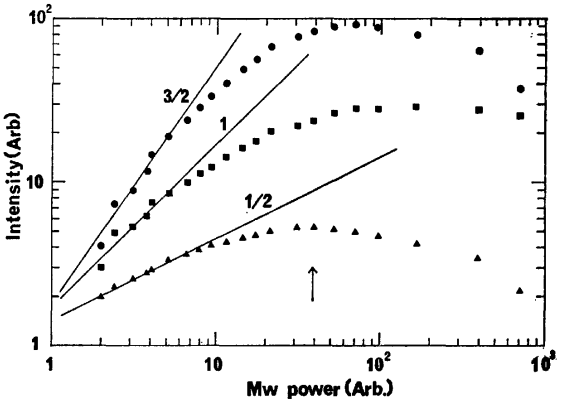

Fig. 3. Dependence of ESR intensity I_{ESR} (▲), ENDOR enhancement I_{ENDOR} (●) and ENDOR quotient I_{ENDOR}/I_{ESR} (■) of ring protons on mw power. The arrow indicates the mw power used for the measurement in Figs. 5—8. The numbers on the lines indicate the order in the low mw-power region.

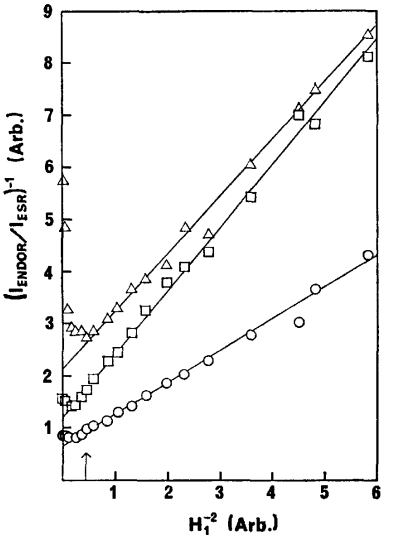

Fig. 4. Reciprocal of the ENDOR quotient as a function of the reciprocal of the mw power. The triangles are for *t*-butyl protons, circles for ring protons and square for a methylidyne proton. The arrow indicates the same mw power as in Fig. 3.

t-butyl proton splitting. From the ENDOR spectrum, however, the hfs constants are found to be 15.60, 3.79, and 0.13 MHz at −80 °C, corresponding to methylidyne, ring and *t*-butyl protons, respectively. No marked dependence of the hfs constants on temperature was observed. In the following discussion, the proton species in galvinoxyl are denoted by the subscripts, m, r, and tb, respectively.

In the present work, the ENDOR enhancement is always divided by the ESR intensity of the peak for which the ENDOR was observed. The quantity, which we tentatively call the ENDOR quotient, is taken to be proportional to the fractional ENDOR enhancement. This procedure will remove experimental errors which may result from, for example, a change in Q value of the cavity during the measurement of the mw-power, rf-power and the temperature dependence. Moreover, the ENDOR quotient is more favorable from the viewpoint of theoretical analysis.

Regarding variation of concentration, the ENDOR enhancement is optimized at about 3×10^{-4} M, and is sharply decreased for other concentrations. On the other hand, as the concentration decreases, the ENDOR quotient monotonically increases and appears to approach to a limiting value. More detailed results will be discussed in a subsequent paper, and it is merely noted that the ratio of the ENDOR enhancement for different protons at the concentration used here is almost the same as the limiting ratio. Thus, we temporarily neglect the Heisenberg exchange effect, as well as the chemical exchange effect, because the addition of another ambiguous parameter would not aid in understanding the essential features of the present system.

(a) Dependence on mw Power. Figure 3 shows the dependence of the ESR intensity, the ENDOR enhancement and the ENDOR quotient on the mw power, measured for ring protons at −75 °C. The rf power employed is indicated by the arrowed in Fig. 5. This figure shows that for sufficiently weak mw powers, the ESR intensity is proportional to the square root of the mw power, the ENDOR enhancement to the 3/2 power of the mw power, so that the ENDOR quotient is proportional simply to the mw power, as is predicted by Eqs. 23—25 in part I. Also, interesting features are found in Fig. 4, in which the reciprocal of the ENDOR quotient for different protons is plotted against the reciprocal of the mw power. As the mw power is increased over a moderately wide range, all the plots go down linearly, but they start to turn up as the mw power is further increased. This means that the ENDOR enhancement decreases more rapidly than does the ESR intensity with a further increase of the mw power. Such a tendency is most marked for *t*-butyl protons, and a more detailed examination reveals that the mw power corresponding to the point at which the plot deviates from a straight line for this proton is about one-half of those for methylidyne and ring protons.

From the theory of part I, the effect of incomplete hf separation is parametrized by a coefficient, α, defined by

$$\alpha = \frac{1}{1+T_{2e}^2\Delta\omega^2}, \quad (1)$$

where $\Delta\omega$ is the hfs constant. Considering that the ESR resolves no splitting for *t*-butyl protons in contrast to the case for methylidyne and ring protons and that T_{2e} ordinarily has a value of 10^{-6}—10^{-7} s, the α for galvinoxyl will be $0 \leq \alpha_m$ and $\alpha_r \ll \alpha_{tb} \leq 1$. It was shown in part I that the plot of E^{-1} *vs.* p_e^{-1} forms a straight line in the weak mw-power region and that the deviation from linearity at higher mw powers is due to the quadratic terms for p_e, which are proportional to α (Eq. 32 in part I). Thus, the theory explains well the experimental features mentioned above taking account of the difference in the α values.

Furthermore, the effective longitudinal electron spin relaxation time, T_{1e}, under rf-power excitation is given by Eq. 34 in part I. Since $b \ll 1$ at temperatures normally used for ENDOR (as shown in (*c*)), this equation is reduced to

$$T_{1e} \simeq \begin{cases} \dfrac{1}{2W_e} & (\alpha=0) \\ \dfrac{1}{W_e} & (\alpha=1). \end{cases} \quad (2)$$

On the other hand, the slope divided by the intercept of the linear part of the plot in Fig. 4 is interpreted as being proportional to $T_{1e}T_{2e}$. The experimental ratio was 1 : 1.0 : 1.9 for methylidyne, ring and *t*-butyl protons, respectively. The good agreement between the experimental and theoretical results suggests the validity of the treatment for the effect of incomplete hf separation given in part I, although coherence effects[8] may also be involved in the upward-turning tendency of the curve in the high mw-power region in Fig. 4. This is beyond of the limits of the theory in part I.

A similar situation for the mw-power saturation of ENDOR enhancement is also found for the 2,4,6-tri-*t*-butylphenoxyl radical in mineral oil,[6] where the values of the mw power for optimum ENDOR enhancement decreases in the order, 2,6-di-*t*-butyl, 4-*t*-butyl and 3,5-ring protons. Such a result suggests the importance of the effect of incomplete hf separation for the former two types of protons.

(b) Dependence on rf Power. During the analysis of ENDOR enhancement as a function of rf power, the effect of hf enhancement must be kept in mind.[9] In addition to the external rf field, the nuclear spin is affected by another field, caused by the rf modulation of the hf coupling with the electron spin, so that if $|\Delta\omega|/2 < \omega_p$, the effective rf field is given by

$$H_{2eff} = \left(1 \pm \frac{|\Delta\omega|}{2\omega_p}\right) H_2 = \frac{\omega_{n0}}{\omega_p} H_2, \quad (3)$$

where the plus and minus signs correspond to the high- and low-frequency ENDOR lines, respectively, and ω_p is the free proton frequency. However, since the rf power is usually monitored by a search coil having an ω-dependent induced voltage $V = -\partial\Phi/\partial t \propto \omega_{n0}H_2$, no correction was made for this effect in the present work.

Figure 5 shows the rf-power dependence of the high-frequency ENDOR lines measured for different protons at —80 °C, using the values of the mw power indicated

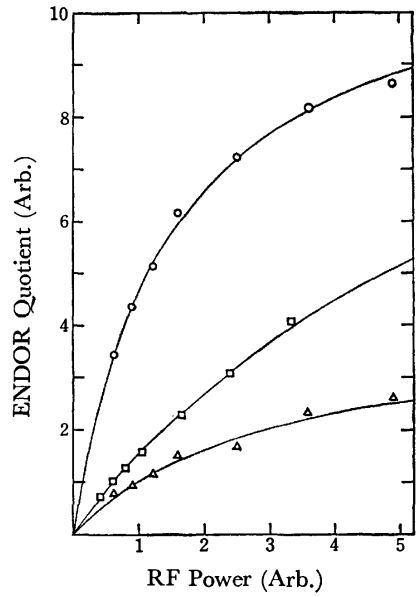

Fig. 5. ENDOR quotient as a function of rf power. The arrow indicates the rf power used for measurements of Figs. 3 and 4.

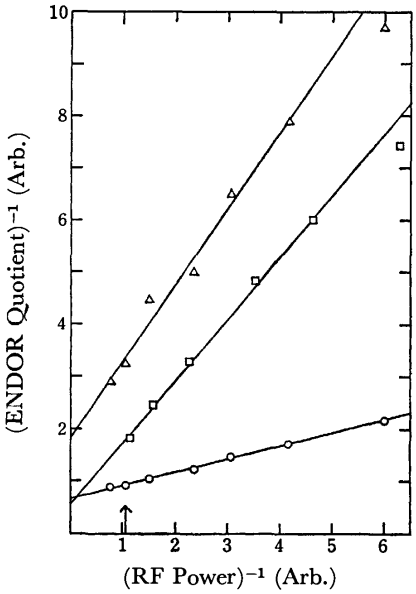

Fig. 6. Reciprocal of the ENDOR quotient as a fuction of the reciprocal of the rf power. The triangles are for *t*-butyl protons, circles for ring protons and squares for a methylidyne proton.

by arrows in Figs. 3 and 4. Figure 6, which shows a reciprocal plot of Fig. 5, indicates that the data fall well along a straight line.[10] Equation 28 in part I predicts this linearity. Also, this equation indicates that the linewidth of the ENDOR enhancement increases as the rf power increases, which agrees with what is found experimentally. On the other hand, it is found that this linewidth decreases with temperature. This is qualitatively explained using the same equation, considering that the T_{2n} of a radical is mainly composed of W_e (see Eq. 9).

(c) Dependence on Temperature. The ENDOR enhancement is known to vary with temperature in a

rather interesting fashion: it sharply increases to a maximum at a specific value of the ratio of the viscosity to the temperature, $(\eta/T)_{opt}$, independent of the kind of solvent.[11] $(\eta/T)_{opt}$ increases as the size of the molecule decreases[12] and as the spin density on the carbon atom, to which an observed proton is bonded, decreases.[11,12] All this appears to be due to the fact that the fractional ENDOR enhancement is maximum at the temperature for which $b=W_n/W_e$ has a certain value characteristic of the observed proton. Accordingly, from an analysis of the temperature dependence, it should be possible to obtain the ratio of the values of b for different protons in a molecule or even information about its spin distribution. However, because an actual molecule contains several sets of equivalent protons, it is preferable for a quantitative discussion to use a theory for a multi-level system rather than the simple theory for a four-level system. Such a theory was presented in part I and is seen to predict that the ENDOR enhancement is proportional to the number of equivalent protons,[13] if a weak rf power is irradiated with $b \ll 1$ and the effect of incomplete hf separation can be neglected. This has sufficient value for use as an analytical tool such that its applicability should be examined experimentally over the whole temperature range used in ENDOR measurements.

For the above reasons, the ENDOR quotients for different protons in galvinoxyl were measured at temperatures from −20 to −95 °C, by varying the rf power at five points for each temperature. Such measurements and a comparison of the results with theory requires specification of both the mw and rf powers. It was shown in (*a*) that the slope divided by the intercept for a methylidyne proton in the plot in Fig. 4 is identical to that for ring protons. This means the ratio of the ENDOR quotients for both protons at any

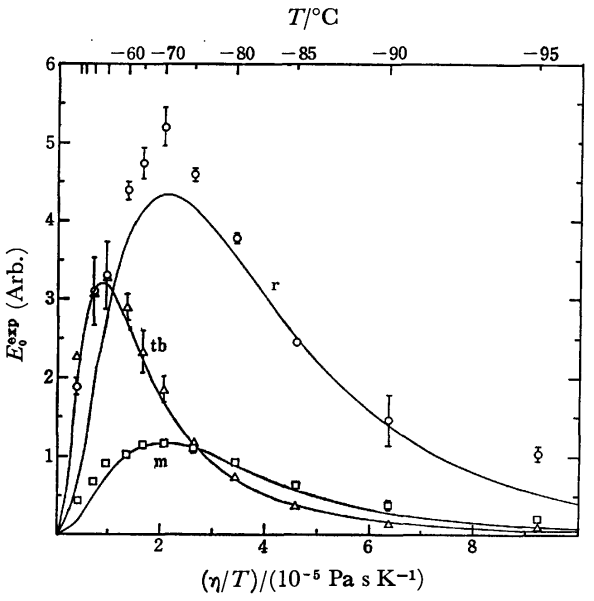

Fig. 7. E_0^{exp} as a function of η/T. The vertical lines indicate the probable error, as determined by the least-squares method. The solid lines are theoretical results. The triangles are for *t*-butyl protons, circles for ring protons and squares for a methylidyne proton.

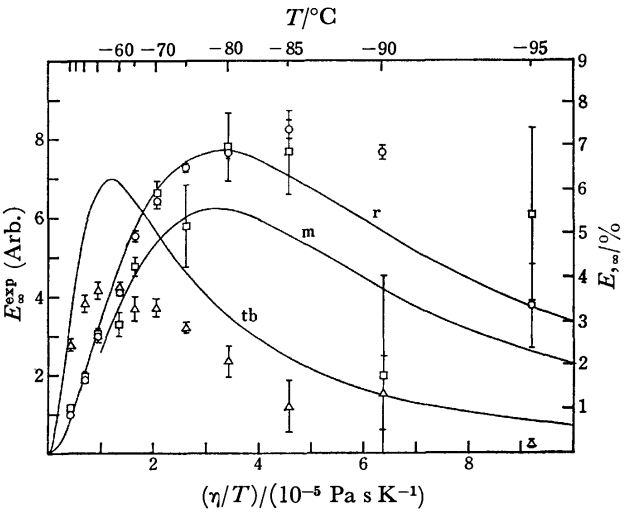

Fig. 8. E_∞^{exp} as a function of η/T. The vertical lines indicate the probable error, as determined by the least-squares method. The solid lines are theoretical results. The triangles are for *t*-butyl protons, circles for ring protons and squares for methylidyne proton.

mw power is identical to that at infinite mw power. The mw power employed in this experiment corresponds to the maximum ESR intensity. Also, the rf power can be specified if the reciprocals of the slope and the intercept are determined from a similar plot shown in Fig. 6, because they correspond to the ENDOR quotients at infinitesimal and infinite rf powers, E_0^{exp} and E_∞^{exp}, respectively. E_0^{exp} and E_∞^{exp} thus determined are shown in Figs. 7 and 8 as a function of η/T. These are analyzed using the following procedure.

Simulation. According to the theory of part I for a multi-level system consisting of several sets of equivalent protons, the fractional ENDOR enhancement at infinitesimal and infinite rf powers are approximately given by Eqs. 50 and 52 and by Eqs. 49 and 51, respectively, with Eqs. 46—48 in part I. The transition probabilities in these equations have been formulated by Freed and Fraenkel[14] and by Freed.[15] Accordingly, if we have information about the g tensor, hf tensor and the other molecular parameters of this radical, we can in principle calculate these values and thus the fractional ENDOR enhancement. Atherton and Day[16] have performed such an estimation for a methylidyne proton in galvinoxyl. However, this involves considerable ambiguities at the present stage. For instance, the rotational correlation time of a molecule, τ_R, is expressed by the extended Debye relationship as

$$\tau_R = \frac{4\pi\kappa r^3\eta}{3kT}. \quad (4)$$

The hydrodynamic radius, r, and a constant, κ, are both dependent on the molecular structures of the radical and the solvent, and consequently, involve unavoidable ambiguities.

For this reason, here, only the η/T dependence of each transition probability is assigned under the following assumptions in an attempt to examine how the fractional ENDOR enhancement varie with temperature. A moderately slow tumbling molecular motion is

assumed so that the following conditions are satisfied:

$$\omega_{e0}^2\tau_R^2 \gg 1, \quad \omega_{n0}^2\tau_R^2 \ll 1. \tag{5}$$

For W_e, we neglect the contribution from the END interaction, as well as the spin rotational interaction, and thus it is assumed to be independent of the nuclear spin quantum numbers. Then, denoting the spectral density by $j(\omega)$, the η/T dependence of the transition probabilities can be written as

$$W_e \approx 2j_{G_s}(\omega_{e0})H_0^2 \approx \frac{1}{\tau_R} \approx \frac{T}{\eta}, \tag{6}$$

and

$$W_n^{(u)} \approx \frac{1}{2}j_D^{(u)}(0) \approx \tau_R \approx \frac{\eta}{T}, \tag{7}$$

so that

$$b_u \approx \frac{j_D^{(u)}(0)}{4j_{G_s}(\omega_{e0})} \approx \tau_R^2 \approx \left(\frac{\eta}{T}\right)^2. \tag{8}$$

Also, the η/T dependence of T_{2n} is derived from

$$\frac{1}{T_{2n}(J_u)} = W_e\left\{1+\left(2f_{J_u}+\frac{1}{3}\right)b_u\right\}. \tag{9}$$

We assume p_e and T_{2e} to have constant values of 1/2 and 1.2 μs, respectively, independent of the temperature. (The choice of the latter value is discussed below.)

If we choose given values of b_m, b_r, and b_{tb} at any temperature and apply these equations to Eqs. 50 and 52 in part I, the relative values of $E_{,0}$ for each proton in galvinoxyl are readily evaluated for all temperatures. Thus, the values of b_m, b_r, and b_{tb} are determined in such a way that the experimental and theoretical T_{opt} for $E_{,0}$ are in complete agreement, since the T_{opt} for $E_{,0}^{exp}$ are known precisely for each proton. Then, using the values of b thus determined, the values of $E_{,\infty}$ are calculated for each proton from Eqs. 49 and 51 in part I. The results are shown by solid lines in Figs. 7 and 8. In Fig. 7, the values of $E_{,0}$ are normalized to that of E_0^{exp} for a methylidyne proton at the optimum temperature for this proton.

Comparison of Experimental and Theoretical Results. Because the determination of the E_0^{exp} involves much smaller errors than that of the E_∞^{exp}, the T_{opt} in Fig. 7 are unambiguously obtained to be −70, −70, and −50 °C for the methylidyne, ring and *t*-butyl protons, respectively. On the other hand, these temperatures are not clear in Fig. 8. However, repeated experiments indicate the T_{opt} to be about −55 °C for the *t*-butyl protons and in the neighborhood of −80——85 °C for the methylidyne and ring protons. Thus, E_0^{exp} has a maximum at a value of η/T of about one-half of that for E_∞^{exp}. In addition, E_0^{exp} decreases more rapidly than does E_∞^{exp} for temperatures below the T_{opt}. The theoretical curves describe these features well. However, at very low temperatures, the theoretical curves tend to be below the experimental points in both figures, as was more evidently confirmed from repeated experiments. This is believed to arise from the $b_u \ll 1$ assumption which is invalid at these temperatures. In Eqs. 49—52 in part I, the relaxation pathways for the END terms of protons other than that observed contribute only to the denominator, so that the fractional ENDOR enhancement tends to be underestimated when $b_u \gtrsim 1$.

Regarding the relative intensity, E_0^{exp} for the methylidyne proton in Fig. 7 is about four times smaller than that for the ring protons. This is more clearly indicated in Fig. 9, in which the ratios of the values of $E_{,0}$ for the ring and *t*-butyl protons to that for the methylidyne proton are plotted against η/T. It is encouraging that the experimental and theoretical values of $E_{,0}$ for the methylidyne and ring protons are approximately proportional to the number of equivalent protons even at temperatures for which the condition, $b_u \ll 1$, is not necessarily valid. On the other hand, in Fig. 8, the E_0^{exp} for a methylidyne proton agrees with that for ring protons (see also Fig. 6), whereas the theoretical counterparts at optimum temperatures, −79 °C (b_m=0.84 and b_r=0.29), are 5.6 and 6.9% for methylidyne and ring protons, respectively, with a ratio of 1.26. The quantitative justification of these values is left until absolute measurements of fractional ENDOR enhancement are performed. However, it should be noted that the calculated values are much smaller than the value, 12.5%, expected from the simple theory for a four-level system.

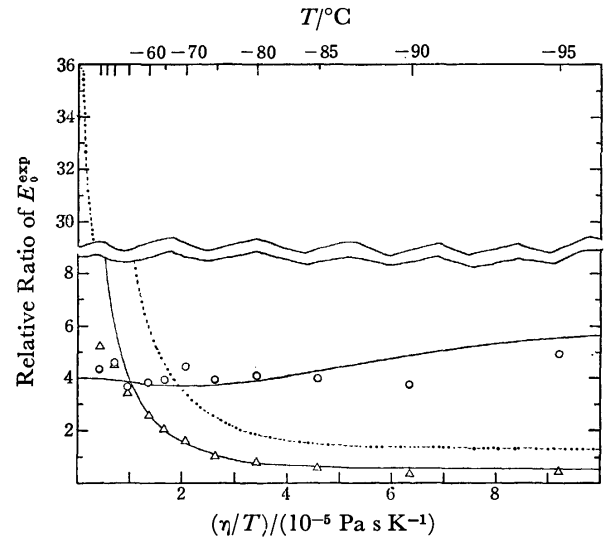

Fig. 9. Ratio of E_0^{exp} values for *t*-butyl protons (△) and ring protons (○) to E_0^{exp} for a methylidyne proton as a function of η/T. The solid lines are theoretical results.

It is worthwhile to discuss the correlation of the values of b estimated from Fig. 7 with the spin distribution in galvinoxyl. The value of b obtained at −70 °C (η/T= 2.05×10^{-5} Pa s K^{-1}) are b_m=0.32 and b_r=0.11 with b_m/b_r=2.9. Luckhurst[17] has studied in detail the structure and the spin distribution of galvinoxyl, and has found ρ_m=−0.0748 and ρ_r=−0.0448. It is considered that $W_n^{(u)}$ is proportional to the square of the spin density on the carbon atom to which the u'th proton is bonded.[11,18] Thus, the above ratio of b values should be 2.79. The good agreement between both values shows the close correlation between the spin density and the ENDOR relaxation. Also, the agreement seen at high temperatures between the E_∞^{exp} values for the methylidyne and ring protons in Fig. 8 leads to a ratio in the neighborhood of 2, using Eq. 54 in part I.

Now the ENDOR quotient for *t*-butyl protons will be considered. The experimental results show two peculiar features, (1) the high optimum temperature, as seen in both Figs. 7 and 8, in spite of the fact that a

proton with a smaller END term should have a lower optimum temperature, and (2) the much smaller ratio of E_0^{exp} for this proton to that for the methylidyne proton than would be expected from the number of equivalent protons (see Fig. 9).

Such a high optimum temperature for this proton is also found for 2,4,6-tri-*t*-butylphenoxyl,[6] 2,5-di-*t*-butyl-*p*-benzosemiquinone[11] and *m,m,m'm'*-tetra-*t*-butylbiphenyl[12] and appears to be characteristic of *t*-butyl protons. Allendoerfer and Maki[6] have suggested that this is attributable to the effect of incomplete hf separation. Considering only the secular terms for the same assumption under which Eq. 6 is based, T_{2e} may decrease with temperature as follows:

$$\frac{1}{T_{2e}} \approx \frac{8}{3} j_{G_s}(0) H_0^2 \approx \tau_R \approx \frac{\eta}{T}, \tag{10}$$

so that this effect is more prominent at lower temperatures and results in a higher optimum temperature. However, simulation shows that this effect requires a T_{2e} as short as 10 ns at −50 °C in order to produce such a high temperature with the result that the ENDOR enhancement becomes negligibly small. In addition, the apparent ESR linewidth for galvinoxyl was found to decrease with temperature down to −20 °C, is constant as a whole from −20 to −70 °C, and increases rapidly at lower temperatures. This implies that nonsecular and pseudosecular terms, as well as the contribution from the spin-rotational interaction, compete with secular terms in Eq. 10 at high temperatures.

It is believed that the high optimum temperature is attributable rather to the large average total nuclear-spin quantum number of the *t*-butyl protons. Let us assume a crude four-level system for *t*-butyl protons whose relaxation pathways involve only the W_e and the $\langle f_{Ju} \rangle W_n^{(u)}$, the average nulear-spin transition probability, which is given by

$$\langle f_{Jn} \rangle W_n^{(u)} = \sum_{Jn} \frac{D_{Jn}}{D_u} J_u(J_u+1) W_n^{(u)} = \frac{1}{2} n_u W_n^{(u)}. \tag{11}$$

Then the fractional ENDOR enhancement is optimized when

$$\frac{1}{2} n_u b_u \approx 1. \tag{12}$$

Therefore, the fractional ENDOR enhancement for a proton species with many equivalent protons has a high optimum temperature.

The much smaller value of E_0^{exp} for *t*-butyl protons than for other protons evidently results from the effect of incomplete hf separation. However, the choice of the value of T_{2e} involves ambiguities, because inhomogeneous broadening unfortunately prevents an estimate of T_{2e} from the unsaturated ESR linewidth. The T_{1e} of galvinoxyl in *s*-butylbenzene, determined by Huisjen and Hyde[19] from saturation recovery, has a value in the range of 1—10 μs at −30 °C. If the extreme narrowing condition is satisfied at this temperature, T_{2e} may also be of the same order of magnitude. Here, T_{2e} was taken as a constant with a value of 1.2 μs, from consideration of the behavior of the ESR linewidth mentioned above. Then, the optimization process for *t*-butyl protons gave $b_{tb}=0.13$ at −70 °C, whereas $b_{tb}=1/18$ at −55 °C or $b_{tb}=0.19$ at −70 °C, from Eq. 12. It is felt that these values of b_{tb} are rather large compared with those for other protons. A possible explanation may be the closeness of the location of *t*-butyl protons to oxygen atom which has large spin density, resulting in large END terms. The theoretical solid curves, calculated from Eqs. 49—52 in part I, are close the experimental curves in Figs. 7 and 8. Also, Fig. 9 shows that the ratio of E_0^{exp} for *t*-butyl protons to that for a methylidyne proton decreases monotonically with temperature, in contrast to the ratio for ring protons. Such a feature is again described by the theoretical solid lines. It is to be noted that the dotted line, calculated from Eq. 50 in part I in which the first factor is omitted, has a value much smaller than 36, except at extremely high temperatures. The above discussion should not be taken too seriously since the present lack of information about the internal motion of the *t*-butyl group prevents further considerations, such as of the isotopic hf modulation. Nevertheless, it is felt that the essential features of the ENDOR quotient for *t*-butyl protons can be explained by the effect of incomplete hf separation and the large average multiplicity for this proton discussed above.

In conclusion, it may be said that the theory in part I describes fairly well the ENDOR relaxation of galvinoxyl.

The authors wish to express their gratitude to Professor K. Kuwata of Osaka University for stimulating and helpful discussions throughout the course of this work.

References

1) W. B. Mims, *Rev. Sci. Instrum.*, **36**, 1472 (1965).
2) M. Huisjen and J. S. Hyde, *Rev. Sci. Instrum.*, **45**, 669 (1974).
3) R. G. Kooser, W. V. Volland, and J. H. Freed, *J. Chem. Phys.*, **50**, 5243 (1969).
4) D. S. Leniart, H. D. Connor, and J. H. Freed, *J. Chem. Phys.*, **63**, 165 (1975).
5) J. S. Hyde and A. H. Maki, *J. Chem. Phys.*, **40**, 3117 (1964).
6) R. D. Allendoerfer and A. H. Maki, *J. Magn. Reson.*, **3**, 396 (1970).
7) A. J. Barlow, J. Lamb, and A. J. Matheson, *Proc. R. Soc.*, **292**, 322 (1966).
8) J. H. Freed, D. S. Leniart, and J. S. Hyde, *J. Chem. Phys.*, **47**, 2762 (1967).
9) D. H. Whiffen, *Mol. Phys.*, **10**, 595 (1966).
10) The plot for *t*-butyl protons appears to be curve downward. This fact is explained by the theory in part I for a multi-level system, *i. e.*, a plot of y^{-1} *vs.* x^{-1} in Eq. 53 of part I is, strictly saying, curve downward.
11) Y. Kotake and K. Kuwata, *Bull. Chem. Soc. Jpn.*, **47**, 45 (1974).
12) K. Ishizu, M. Ohnishi, and H. Shikata, *Bull. Chem. Soc. Jpn.*, **50**, 76 (1977).
13) J. H. Freed, D. S. Leniart, and H. D. Connor, *J. Chem. Phys.*, **58**, 3089 (1973).
14) J. H. Freed and G. K. Fraenkel, *J. Chem. Phys.*, **39**, 326 (1963).
15) J. H. Freed, *J. Chem. Phys.*, **43**, 2312 (1965).
16) N. M. Atherton and B. Day, *Mol. Phys.*, **27**, 145 (1974).
17) G. R. Luckhurst, *Mol. Phys.*, **11**, 205 (1966).
18) J. H. Freed, *J. Phys. Chem.*, **71**, 38 (1967).
19) M. Huisjen and J. S. Hyde, *J. Chem. Phys.*, **60**, 1682 (1974).

Electronic Absorption Spectra of Pyrene and Hydropyrenes

Tetsutaro YOSHINAGA, Hiroshi HIRATSUKA, and Yoshie TANIZAKI

Department of Chemistry, Tokyo Institute of Technology, Meguro-ku, Tokyo 152

(Received August 31, 1976)

Vibronic π-π^* transition bands of pyrene, 4,5-dihydropyrene (DHP), and 4,5,9,10-tetrahydropyrene (THP) were assigned by means of dichroism analysis using stretched poly(vinyl alcohol) films. The absorption spectra of the samples in the non-stretched films were divided into two component spectra polarized along the long (x) and short (z) axes of the molecular plane. For pyrene, in addition to the four conventionally-assigned band systems (^1L_b, ^1L_a, ^1B_b, and ^1B_a), some forbidden bands were found in the respective band regions. Most of the vibronic DHP and THP bands were also reasonably well assigned from comparisons with the calculated results for phenanthrene and biphenyl, respectively.

Three fundamental factors, the transition energy (wavelength), the transition moment (polarization), and the transition probability (intensity) must be considered in making assignments of electronic absorption spectra. Generally speaking, it is almost impossible to determine exactly all of these three factors for solution spectra, except in special cases where well-separated band systems are observed. Apparent bands observed in most cases are considered as consisting of more than two different kinds of transition bands. Accordingly, in order to precisely determine the three factors experimentally, we must separate or resolve the overlapped bands from one another, using methods such as photoselection techniques,[1] an external electric field,[2,3] a single or mixed crystal[4,5] and stretching of the polymer film.[6-8]

The stretching film method can be applied to various kinds of compounds and has the merit that the substrate of the film is transparent to the very short wavelengths of 220 nm for the poly(vinyl alcohol) [PVA] film, for example. If we choose planar molecules with proper symmetries, the π electronic spectra can be divided into components polarized parallel and perpendicular to a symmetry axis in the molecular plane.

The experience of the dichroism investigation tells us that the orientation direction of the sample molecule in the stretched PVA film depends mainly on molecular geometry. And it is expected that the three compounds, pyrene, 4,5-dihydro- and 4,5,9,10-tetrahydropyrene, in the stretched PVA films have the same orientation state since their skeletal structures are similar to one another (see Fig. 1).

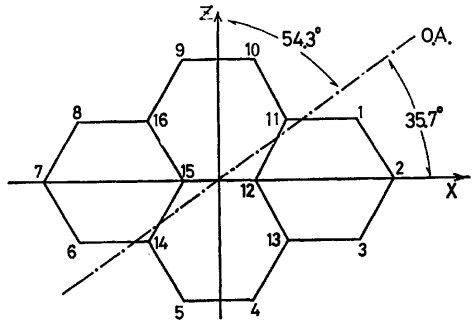

Fig. 1. Co-ordinates of the pyrene molecule. The orientation axis of the molecule in the streched PVA film is represented by O. A. which is determined by the orientation angle (54.3°) for the third band of pyrene [Fig. 2(a)].

The purpose of this paper is to make assignments of the π-π^* electronic spectra of pyrene, 4,5-dihydropyrene(abbreviation, DHP) and 4,5,9,10-tetrahydropyrene (THP). Pyrene shows well separated band systems and, therefore, its orientation direction is precisely determined by dichroism analysis with this orientation direction necessary in obtaining the divided spectra. On the other hand, the absorption spectra of DHP and THP do not show any isolated bands. Therefore, in order to divide these spectra into components, it is assumed here that the orientation direction determined for the pyrene molecule can be applied to the DHP and THP molecules.

Experimental

Commercially-available pyrene (ultra pure reagent, zone refined; Tokyo Kasei Kogyo Co., Ltd.) was used. The guaranteed reagents, 4,5-dihydropyrene (abbreviation:DHP) and 4,5,9,10-tetrahydropyrene (THP) were used with furtherpurification made at our request by the Tokyo Kasei Kogyo Co., Ltd.

Poly(vinyl alcohol) [PVA] having a mean polymerization of 1400 was obtained commercially (Koso Chemical Co., Ltd.) and used without further purification for making the PVA films.

Dichroism Analysis. The dichroic spectra were determined with a Shimadzu QV-50 Spectrophotometer equipped with a Glan-Thompson type calcite polarizer. Both the sample and reference films were stretched at 70—80 °C. The stretching ratio, R_s, was limited to 6.0 throughout the experiments.

The optical density ratio, R_d, is defined as $D_{//}/D_{\perp}$, where $D_{//}$ and $D_{\perp}$ are optical densities measured with light polarized parallel and perpendicular to the stretched direction of the film, respectively. The R_d values are plotted in the figures showing the dichroic spectra.

From the dichroism analysis,[9] the orientation angle of any absorption band is defined as the angle between the transition moment and the orientation direction of the molecule, and it is obtained using the experimental values of R_s and R_d. The orientation angles thus obtained are indicated at the maxima and minima of the R_d curves of the dichroic spectra.

It is necessary to make a few remarks concerning the "orientation direction," which is a direction peculiar to molecular geometry. It is empirically known that, upon stretching, a sample molecule in the PVA substrate is longitudinally inclined in the stretched direction. In this case, the longitudinal direction does not, in general, coincide with the geometrically-defined long axis, say, the x-axis of the molecule (see Fig. 1).

It is a natural consequence of the inclination of the molecule, as mentioned above, that the absorption band having the

greater R_d value (or smaller orientation angle) must be polarized principally along the long (x) axis. Accordingly, if a planar molecule has at least one C_2-symmetry axis in the molecuar plane (xz-plane) and if one or more bands are found to be pure in the transition directions (x or z), we can divide the absorption spectrum (D) in the non-stretched PVA film into two component spectra (D_x, D_z) that are polarized parallel and perpendicular to the axis of symmetry.[9] In the present case, the relative errors in the absorbance of the component spectra were less than 10% and the oscillator strength of the relatively strong band was reproduced to within a relative error of 4—7%.

Calculation

The sample molecules, DHP and THP, have π-electron systems equivalent to those of phenanthrene and biphenyl, respectively. Therefore, for convenience, the latter were calculated instead of the former.

The MO calculations were carried out using the Pariser-Parr-Pople method.[10,11] The one-center repulsion integrals were evaluated in the Pariser-Parr approximation,[10] in which the ionization potential and the electron affinity were taken, respectively, as $I_p(C)=11.16$ eV and $E_a(C)=0.03$ eV for the carbon atom. The two-center repulsion integrals were evaluated using the Nishimoto-Mataga equation.[12] All the singly-excited configurations associated with the transitions between the occupied and vacant MO levels were included in the CI calculation.

The co-ordinates of the molecular framework of pyrene were taken as shown in Fig. 1. All the bond lengths and bond angles were assumed to be 1.395 Å and 120°, respectively. The framework of the π-electron system of DHP(4,5-dihydropyrene) was considered excluding the Nos. 4 and 5 carbon atoms in Fig. 1. Similarly, for THP(4,5,9,10-tetrahydropyrene), the Nos. 4, 5, 9, and 10 carbon atoms were excluded, and the C^{12}–C^{15} bond length (inter-ring distance) was assumed to be 1.48 Å. The x and z axes denote the long and short axes, respectively, in the molecular plane for the case of both the D_{2h} (pyrene and THP) and C_{2v} (DHP) point groups.

Results and Assignment

Dichroic Spectra. Figures 2(a)—(c) show the dichroic spectra and R_d curves of pyrene, DHP and THP, respectively.

The dichroic spectra of pyrene in Fig. 2(a) exhibits four well-separated absorption bands. The shape of the R_d curve clearly shows that these four bands are distinguished by transition directions; that is, the R_d values for the first (350—380 nm) and third (250—280 nm) bands are small, while those for the second (340 nm) and fourth (*ca.* 245 nm) are great. This indicates that the transition vectors of the former are in the same direction as the short axis of the molecule and the latter in that of the long axis. It is concluded, therefore, that the directions of the electronic transition moments of pyrene are z-, x-, z-,and x- polarized, in order of decreasing wavelength. Since the symmetry of the pyrene molecule is D_{2h}, the four corresponding excited

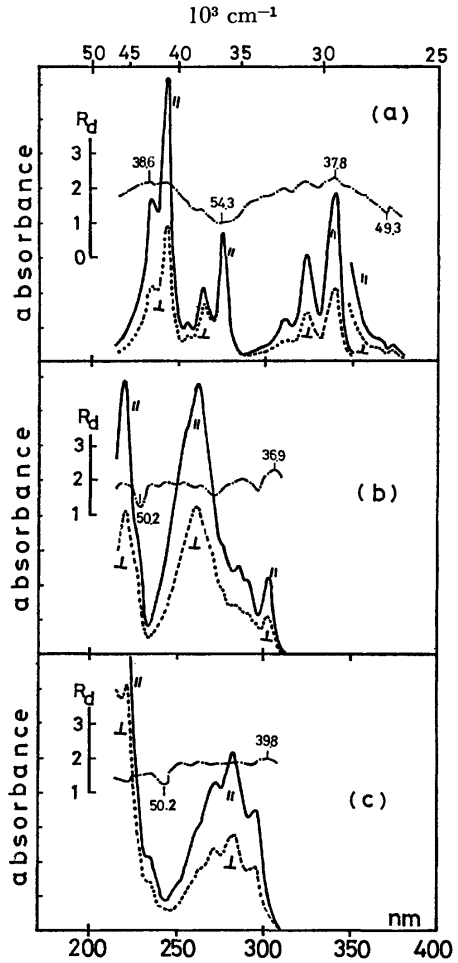

Fig. 2. Dichroic spectra and R_d curves for (a) pyrene, (b) DHP (4,5-dihydropyrene) and (c) THP (4,5,9,10-tetrahydropyrene). $R_s=6.0$. The numerals at the maxima and minima of R_d curves indicate the orientation angle (in degree) of the polarizations at those wavelengths.

states are assigned to B_{2u}, B_{1u}, B_{2u} and B_{1u}, respectively. According to the Platt notation, these are L_b, L_a, and B_b and B_a, respectively (see Fig. 3). In Figs. 2(b) and (c), no remarkable variations of the R_d curves similar to those in Fig. 1(a) are found. Only for a couple of bands, however, are the polarizations distinguishable by the relative R_d values; for example, for DHP (C_{2v}) in Fig. 2(b), the R_d value at 305 nm is the greatest and that at 228 nm (shoulder) the smallest in the region observed. This suggests that the 305-nm band and the shoulder consist mainly of bands with long- and short-axis transitions, respectively. Indeed, the sum (87.1°) of the orientation angles of these bands becomes nearly 90°. Thus, we can conclude that the 305-and 230-nm bands are polarized along the molecular long (x, B_2) and short (z, A_1) axes, respectively. It must be noted here that in the DHP spectra in Fig. 2(b), the 305-nm band is not first but is second. The first band at 343 nm, which corresponds to the ^1L_b of phenanthrene at the longest wavelength, could not be determined in the present work owing to experimental difficulties.

For the THP(D_{2h}) spectra in Fig. 2(c), polarizations of at least two absorption bands were also observed;

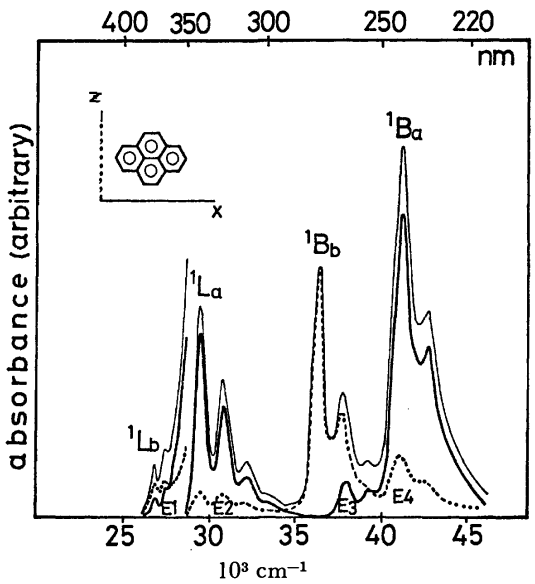

Fig. 3. Divided spectra of pyrene. The fine line means the absorption spectrum (D) of pyrene in the non-stretched PVA film. The conventional assignment is indicated by ^1L_b, ^1L_a, ^1B_b and ^1B_a. The solid line is the x-component spectrum (D_x) and the dotted line the z-component (D_z). Extra band systems are temporarily marked with E_1 to E_4.

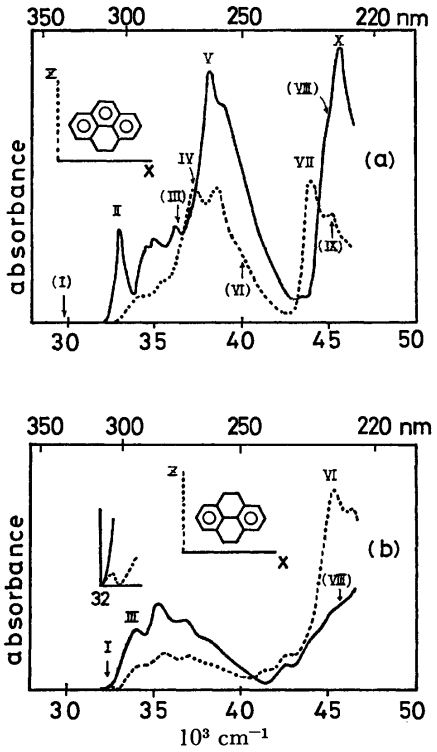

Fig. 4. Divided spectra of (a) DHP (4,5-dihydropyrene) and (b) THP (4,5,9,10-tetrahydropyrene). The solid lines are the x-component spectra (D_x) and the dotted lines the z-components (D_z). Roman numerals are the transition numbers calculated for (a) phenanthrene and (b) biphenyl.

main absorption at 300 nm being due to the long-axis transition (x, B_{1u}) and that at 240 nm to the short-axis transition (z, B_{2u}).

Divided Spectra. In order to make more precise assignments of the electronic bands, especially for DHP and THP, the absorption curves in the non-stretched PVA films were divided into two component spectra (D_x and D_z).[9] To divide the spectra, it was necessary to determine a standard direction relative to the geometry of the molecule. A standard direction, namely, in general, an orientation direction, can be determined for a symmetrical molecule provided that at least two electronic bands with polarizations orthogonal to each other can be observed separately. Fortunately, the pyrene molecule satisfies such a condition.

It has already been mentioned that the second and third bands of pyrene [Fig. 2(a)] are due to the electronic transitions along the x (long) and z (short) axes of the molecule, respectively, and that the sum of the orientation angles for the second (37.8°) and third (54.3°) bands becomes 92.1°. This value is somewhat greater than 90°. This fact indicates that the degree of mixing of the z-polarized absorption in the x band (second) is greater than that of the x-polarized absorption in the z band (third band). Considering that the absolute deviation from 90° is small, let us assume here that the transition direction at 276 nm, for the third band, is exactly in accord with the transition direction of the z axis of the pyrene molecule. Then, the orientation direction of the molecule relative to the coordinates is determined as shown in Fig. 1, that is, the orientation axis (O.A.) is 35.7° with respect to the x axis.

The skeletal structure of the other molecules are very similar to that of the pyrene molecule. It was assumed, therefore, that the other molecules have the same orientation direction as pyrene. Thus, by taking the standard angles of other sample molecules to be 35.7°, the component spectra are obtained from the spectra of the non-stretched sample film.

The divided spectrum of pyrene is shown in Fig. 3, and those of DHP and THP in Fig. 4. It is seen that every band is more or less composed of overlapping of the x and z bands. For this reason, it is expected that some additional absorptions will be found from a comparison with the calculated results. These extra absorption bands may be explained in terms of vibronic interactions or intensity borrowing, neglecting the so-called hot absorptions.

Assignments for Pyrene Spectrum. The results of an MO calculation for pyrene, which is shown in Table 1, indicate four symmetry-allowed transitions below 46×10^3 cm^{-1}, which is the limit of the spectral region observed. These allowed transitions may correspond to the divided component bands shown in Fig. 3, as follows.

The peak at 26.8×10^3 cm^{-1} is considered to be the 0-0 transition of the very weak first band system. Since the intensity at the peak is stronger for the z component than for the x component, the former is regarded as the first band. Therefore, the I transition calculated as $B_{2u}\leftarrow A_g$ for pyrene must be compared with the first band which is z-polarized. The other three allowed transitions, II, V, and IX, correspond to the three strong band systems in Fig. 3, respectively. The II

Table 1. Calculated and experimental results for pyrene (D_{2h})

Transition No.	Transition energy		Oscillator strength f		Polarization		Symmetry
	Calcd 10^3 cm^{-1} (nm)	Obsd 10^3 cm^{-1} (nm)	Calcd[a]	Obsd[b]	Calcd	Obsd	
I	27.05 (370)	26.8 (373)	0.005	0.0014	z	z	B_{2u}
II	28.00 (357)	29.4 (340)	0.764	0.326	x	x	B_{1u}
III	34.24 (292)		forb.				B_{3g}
IV	34.51 (290)		forb.				B_{3g}
V	38.17 (262)	36.4 (275)	0.954	0.418	z	z	B_{2u}
VI	38.58 (259)	[37.9]	forb.		[$\times b_{1u}$]	x	A_g
VII	39.79 (251)		forb.				B_{3g}
VIII	42.76 (234)	[41.0]	forb.		[$\times b_{2u}$]	z	A_g
IX	43.57 (230)	41.2 (243)	1.468	0.750	x	x	B_{1u}
X	43.64 (229)		forb.				A_g
XI	47.91 (209)		0.004		z		B_{2u}
XII	48.60 (206)		forb.				A_g

a) Calculated using the dipole-length method with off-diagonal (adjacent) terms included in the calculation of the oscillator strength. R. S. Mulliken, *J. Chem. Phys.*, **7**, 14 (1939). b) Determined using $f=4.32\times10^{-9}\int\varepsilon d\sigma$, assuming that the molar extinction coefficient ε at the band maximum in the non-stretched PVA film is equivalent to that of the corresponding band in an ethanol solution.

transition ($B_{1u}\leftarrow A_g$) corresponds to the second band system starting at 29.4×10^3 cm^{-1}, which is x-polarized and reveals a progression of five vibrational bands reaching as far as 35×10^3 cm^{-1}. The V transition ($B_{2u}\leftarrow A_g$) corresponds to the third band system which is z-polarized and has its 0-0 peak at 36.4×10^3 cm^{-1}. Finally, the IX transition corresponds to the fourth band with x-polarization, which has its 0-0 peak at 41.2×10^3 cm^{-1}. The bands thus assigned are designated in the Platt notation as ^1L_b, ^1L_a, ^1B_b, and ^1B_a, respectively, as shown in Fig. 3.

For the oscillator strengths, a very good correlation is observed between the calculated and observed results; the calculated values are nearly twice as large as the corresponding observed values.

According to the above correspondence between the band systems and the calculated transitions, the other four absorption bands remain as extra bands which are temporarily designated as E_1 to E_4, as is shown in Fig. 3. In order to discuss the extra absorption bands, it will be necessary to determine some basis for making assignments. Fortunately, it was found that the calculated and experimental transition energies (in wavenumbers) correspond well to each other. That is to say, when the calculated (abscissa) and experimental wavenumbers (ordinate) are plotted on a graph, a straight line is obtained as shown in Fig. 5, in which the wavenumbers at the 0-0 peaks are taken from the experimental values and the white circles represent the allowed transitions. The fact that almost all the white circles lie on a straight line shows that the semi-empirical calculations employed here lead to quite reliable results for making assignments. Accordingly, utilizing this linear relation as a basis, the extra absorption bands are assigned.

First of all, from the point of view of the linearity between the calculated and experimental results, only the experimental value for ^1L_a is unexpected. If we

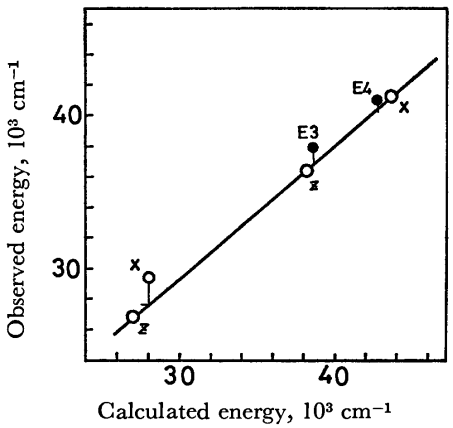

Fig. 5. Correlation between the observed (ordinate) and calculated wave numbers (abscissa) of pyrene. White circles represent the 0-0 peaks of band systems and the corresponding transitions calculated, where x and z mean the polarizations along the long and short axes of the molecule, respectively.

take the linearity seriously, the peak at 29.4×10^3 cm^{-1} may not be a 0-0 but a 1-0 transition. In this case, if we regard the shoulder of the x component band at 27.8×10^3 cm^{-1} in Fig. 3 to be the 0-0 peak of ^1L_a, linearity for all the allowed transitions, including ^1L_a, is nearly satisfied.

Now, utilizing the linear relation, the extra bands are assigned as follows. According to Fig. 3, the E_1 band, which is x-polarized and has fine structure, starts at about 26.8×10^3 cm^{-1}, but, strictly speaking, this is slightly lower than 26.8×10^3 cm^{-1}. It is clear from Table 1 that no excited state relevant to E_1 exists. Therefore, the E_1 band may be induced by intensity borrowing from the second (^1L_a, x) band. The E_2 band, which is z-polarized, has its first peak at 29.5×10^{-3} cm^{-1}. In Table 1, no transition corresponding to

Table 2. Comparison of calculated results for phenanthrene and experimental results for DHP (C_{2v})

Transition No.	Transition energy: Calcd 10^3 cm^{-1} (nm)	Transition energy: Obsd 10^3 cm^{-1} (nm)	Oscillator strength: Calcd[a]	Oscillator strength: Obsd[b]	Polarization: Calcd	Polarization: Obsd	Symmetry
I	29.00 (345)	[29.2] [343][c]	0.001	—	z		A_1
II	32.96 (303)	33.1 (302)	0.372	0.149	x	x	B_2
III	37.40 (267)		0.002		x		B_2
IV	39.85 (251)	37.3 (268)	0.526	0.279	z	z	A_1
V	39.87 (251)	38.2 (262)	1.440	0.396	x	x	B_2
VI	41.81 (239)		3.0×10^{-5}		z		A_1
VII	45.25 (221)	44.0 (227)	0.348	0.167	z	z	A_1
VIII	46.94 (213)		7.0×10^{-5}		x		B_2
IX	47.80 (209)		2.4×10^{-4}		z		A_1
X	48.85 (205)	45.7 (219)	0.086	0.317	x	x	B_2
XI	49.56 (202)		0.464		x		B_2

a), b) See footnote in Table 1. c) See Ref. 18.

29.5×10^3 cm^{-1} is found, because, according to the linear relation of Fig. 5, the calculated energy corresponding to the E_2 band must be less than 30.0×10^3 cm^{-1}. Therfore, the E_2 band may also be attributed to an intensity-borrowing absorption from the $^1B_b(z)$ band.

The E_3 band of which the first peak occurs at 37.9×10^3 cm^{-1} is polarized in the x direction. According to the linear relation of Fig. 5, the calculated transition energy corresponding to 37.9×10^3 cm^{-1} is 39.8×10^3 cm^{-1}. If the E_3 band is electronically forbidden, E_3 must vibronically be allowed. Then the calculated energy should be less than 39.8×10^3 cm^{-1}, at least by one vibrational quantum number. The only relevant transition in Table 1 is the VI transition, which has A_g symmetry. Consequently, the vibration to be coupled with the A_g electronically excited state must have a mode of b_{1u} symmetry. The vibrational energy of b_{1u} for the present case is estimated to be about 1×10^3 cm^{-1} from the linear relation of Fig. 5.

Similarly, it is considered that the E_4 band, which has its first peak at 41.0×10^3 cm^{-1}, is a vibronically-induced transition of VIII (A_g) resulting from the coupling of a b_{2u}-type vibration because of the z-polarized absorption. From the linear relation of Fig. 5, the coupled vibrational energy is estimated to be about 0.6×10^3 cm^{-1}.

Assignment of DHP and THP Spectra. The DHP and THP component spectra are shown in Figs. 4(a) and (b), respectively. In Fig. 4(a), the first band, which is observed at 343 nm (29.15×10^3 cm^{-1}) in an ethanol solution, is not shown here as explained above. Therefore, the first peak at 33.1×10^3 cm^{-1} is the 0-0 peak of the second band which is evidently x-polarized. Generally speaking, when both the x and z component spectra are complicated, the band shape can not be easily determined. For this reason, let us first examine only the prominent band peaks and compare them with the calculated results for phenanthrene. The prominent band peaks are found at 33.1 (x), 37.3 (z), 38.2 (x), 44.0 (z), and 45.7×10^3 cm^{-1} (x).

On the other hand, the calculated results for phenanthrene (C_{2v}) are shown in Table 2: The transitions with oscillator strengths stronger than 0.01 are the II (B_2), IV (A_1), V (B_2), VII (A_1) and X (B_2) transitions. These transitions and the above-mentioned band peaks are compared in Table 2. The calculated and experimental polarizations are in complete agreement. Furthermore, the correspondence between the transition energies, as well as the intensities, is fairly good.

In order to observe the correlation between the calculated and experimental transition energies for DHP, the wavenumbers were plotted in the same way

Table 3. Comparison of calculated results for biphenyl and experimental results for THP

Transition No.	Transition energy: Calcd 10^3 cm^{-1} (nm)	Transition energy: Obsd 10^3 cm^{-1} (nm)	Oscillator strength: Calcd[a]	Oscillator strength: Obsd[b]	polarization: Calcd	polarization: Obsd	Symmetry
I	34.63 (289)	32.6 (307)	3.1×10^{-4}	4.4×10^{-4}	z	z	B_{2u}
II	35.09 (285)		forb.				B_{3g}
III	36.40 (275)	33.9 (295)	0.847	0.24	x	x	B_{1u}
IV	46.50 (215)		forb.				B_{3g}
V	47.82 (209)		forb.				A_g
VI	48.85 (205)	45.3 (221)	0.887	0.53	z	z	B_{2u}
VII	48.87 (205)		forb.				A_g
VIII	49.66 (201)	[46] [217]	1.083		x	x	B_{1u}

a), b) See footnote in Table 1.

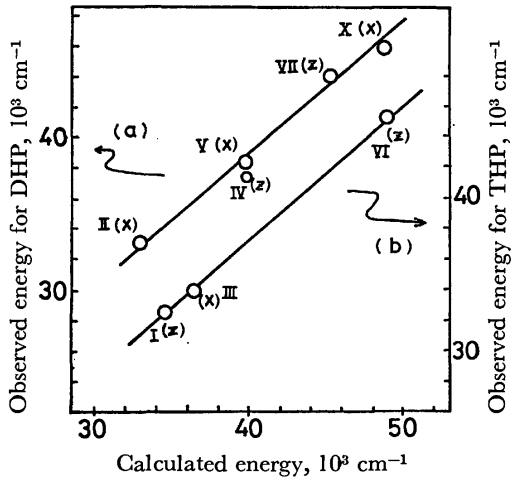

Fig. 6. Correlation between the observed (ordinate) and calculated wave numbers (abscissa) of (a) DHP (4,5-dihydropyrene) and (b) THP (4,5,9,10-tetrahydropyrene), where the calculated values are taken for (a) phenanthrene and (b) biphenyl. Roman numerals represent the transition numbers calculated.

as in the case of pyrene. In this case, however, on the abscissa are plotted the calculated wavenumbers for phenanthrene instead of DHP. The result is illustrated in Fig. 6(a), in which the Roman numerals represent the calculated transition numbers. The linearity is not as good as that shown in Fig. 5 for pyrene. This may be interpreted as resulting from the fact that the calculation for phenanthrene is used instead of that of DHP itself, with the result that the effect of the methylene groups at the 4 and 5 positions of DHP was neglected (see Fig. 1). At any rate, let us use the straight line shown in Fig. 6(a) as a basis for discussing the DHP spectrum.

According to Table 2, transition III (37.4×10^3 cm^{-1}) is of weak intensity and x (B_2) polarization. The linear relation in Fig. 6(a) indicates that the calculated value of 37.4×10^3 cm^{-1} corresponds to the experimental value of 36.3×10^3 cm^{-1} on the x-component curve of Fig. 4(a). For this reason, the peak may be attributed to transition III. The z-polarized band in Fig. 4(a), which extends from 32×10^3 cm^{-1} to about 36×10^3 cm^{-1}, could not be assigned, since no relevant transition is listed in Table 2. Other calculated transitions, transitions VI (41.8×10^3 cm^{-1}, A_1), VIII (46.9×10^3 cm^{-1}, B_2), and IX (47.8×10^3 cm^{-1}, A_1), which are of very weak intensity, correspond respectively to the experimental wavenumbers of 40.2×10^3 cm^{-1} (z), 44.8×10^3 cm^{-1} (x) and 45.4×10^3 cm^{-1} (z). They may appear as shoulders at the corresponding positions which are indicated respectively by the Roman numerals in parenthesis in Fig. 4(a), VI, VIII, IX.

Figure 4(b) illustrates the component spectra of THP (D_{2h}). Table 3 shows that the calculation for biphenyl (D_{2h}) produces four allowed transitions. Transition I (z, B_{2u}) is of very weak intensity and the other three transitions, transitions III (x, B_{1u}), VI (z, B_{2u}) and VIII (x, B_{1u}) are strong. Accordingly, the first three transitions can easily be assigned as indicated in Fig. 4(b) by the Roman numerals. Again, a linearity similar to the case of DHP is found [Fig. 6(b)]. Using the linear relation in Fig. 6(b), the experimental wavenumber corresponding to the fourth allowed transition, transition VIII (49.66×10^3 cm^{-1}), becomes 45.7×10^3 cm^{-1}. However, no prominent band peak appears although a very slight shoulder appears, as indicated by VIII in Fig. 4(b).

Figure 4(b) shows that an additional z absorption, the first peak of which is at 33.9×10^3 cm^{-1}, occurs together with the x band indicated by III. This z absorption can be interpreted in two ways. One possible interpretation is that the band is vibronically induced by the coupling of transition II (35.09×10^3 cm^{-1}, B_{3g}) with a b_{1u} type vibration. In this case, the experimental band origin must be located at 33.7×10^3 cm^{-1} as estimated from the linear relation in Fig. 6(b). The other interpretation is to consider the additional z absorption as a progression of the first z band starting at 32.6×10^3 cm^{-1}, which is assigned to the very weak allowed transition I.

Discussion

The first four allowed π-π^* transitions of pyrene have been established theoretically to have z-, x-, z-, and x-polarizations.[13–15] Experimental studies on the polarization of pyrene have been carried out for the crystalline state[16] using the photoselection method[17] and the stretched polyethylene sheet technique.[8] These experimental results agree quite well with one another and also with the theoretical values. Thulstrup, Michl and Eggers[8] have obtained a reduced spectrum of pyrene from a dichroic spectrum in a stretched polyethylene sheet. Their reduced spectrum for pyrene is very similar as a whole to the separated spectra shown in Fig. 3. However, the weak first band and some of the extra bands are not found in their reduced spectra.

A few spectroscopic studies have been carried out on DHP[18] and THP.[19] On the other hand, many descriptions[20–30] have been given for phenanthrene and biphenyl, which are iso-electronic with DHP and THP, with respect to the π-electron systems, respectively. For instance, according to Zimmermann and Joop[28] and other workers,[30] the third and fourth transition bands of phenanthrene occur close together, but with different polarization directions. Regarding the polarization directions, however, most of the experimental studies reported were only qualitative and were not effective in analyzing overlapping bands, such as the third band of phenanthrene, without aid of theoretical calculations, while the component spectra presented here give quantitative information.

The separated spectra of DHP shown in Fig. 4(a) are in agreement with the case of phenanthrene.[7,8] But in Fig. 4(a), the z-polarized absorption in the 32—36 $\times10^3$ cm^{-1} region, which should be distinguishable from the third band (transition IV, z), could not be clearly assigned. Even in phenanthrene itself, this third (z-polarized) band shows anomalous width in the component spectra. Thulstrup *et al.*[8] have considered this band to be the result of vibronic coupling.

For THP, as is shown in Fig. 4(b), a very weak hidden band at 33.9×10^3 cm^{-1} is revealed as a z-polarized band.

The presence of such an extraordinarily weak absorption in the case of biphenyl has been confirmed by Berlman *et al.*[23] from an investigation of the fluorescence lifetimes of biphenyls. However, there are some ambiguities in the number of allowed transitions in the first band region of biphenyl.[26] On the other hand, the results of the present work for THP show that there are an extremely weak (hidden) z band, a relatively strong x band and an additional intensity-borrowing or vibronically-induced z band in the first-band region, though THP has a structured band shape and a considerable red shift relative to biphenyl. The oscillator strength for the very weak first band of THP was determined from the component spectra, even though the estimated value may contain a large error because of the extreme weakness of the intensity.

There are few experimental studies on the oscillator strengths. Furthermore, in most cases, the conventional value has been determined from a band which is composed of overlapping bands of different polarizations. In order to make a more precise comparison with theory, the experimental values should be determined using the component spectra. The experimental oscillator strengths in Tables 1—3 are determined from the component spectra. The values calculated using the dipole length method are about twice as large as the experimental results. In the calculations of the oscillator strengths, it should be noted that, when only diagonal matrix elements are considered, the oscillator strengths for the allowed L_b bands become zero, while those including the off-diagonal elements give non-zero values in agreement with the experimental results. It must be emphasized, therefore, that the off-diagonal elements of the transition density matrix become very important in the calculation of the allowed L_b band, especially when using the dipole-length method.

References

1) A. C. Albrecht, *J. Mol. Spectrosc.*, **6**, 84 (1961).
2) J. Czekalla, *Chimica*, **15**, 26 (1961); *Z. Elektrochem.*, **64**, 1221 (1960).
3) H. Labhart, *Chimica*, **15**, 20 (1961); *Helv. Chim. Acta*, **44**, 447 (1961); *Tetrahedron*, **19**, 223 (1963).
4) A. C. Albrecht and W. T. Simpson, *J. Chem. Phys.*, **23**, 1480 (1955).
5) D. S. McClure, *J. Chem. Phys.*, **22**, 1668 (1954); *ibid.*, **24**, 1 (1956).
6) K. R. Popov, L. V. Smirnov, L. A. Nakhimovskaya, and V. L. Grebneva, *Opt. Spektrosk.*, **31**, 363 (1971); *Opt. Spectrosc.*, **31**, 195 (1971).
7) T. Hoshi, H. Inoue, J. Yoshino, T. Masamoto, and Y. Tanizaki, *Z. Phys. Chem. N. F.*, **81**, 23 (1972).
8) E. W. Thulstrup, J. Michl, and J. H. E. Eggers, *J. Phys. Chem.*, **74**, 3868 (1970).
9) Y. Tanizaki and S. Kubodera, *J. Mol. Spectrosc.*, **24**, 1 (1967); H. Hiratsuka, Y. Tanizaki, and T. Hoshi, *Spectrochim. Acta, Part A*, **28**, 2375 (1972).
10) R. Pariser and R. G. Parr, *J. Chem. Phys.*, **21**, 466, 767 (1953).
11) J. A. Pople, *Proc. R. Soc. London, Ser A*, **68**, 81 (1955).
12) N. Mataga and K. Nishimoto, *Z. Physik. Chem. N. F.*, **13**, 13 (1957).
13) N. Ham and K. Ruedenberg, *J. Chem. Phys.*, **25**, 1, 13 (1956).
14) K. Nishimoto and L. S. Forster, *Theor. Chim. Acta (Berl.)*, **3**, 407 (1965).
15) J. Pancir and R. Zahradnik, *J. Phys. Chem.*, **77**, 121 (1973).
16) R. Hochstrasser, *J. Chem. Phys.*, **33**, 459 (1960).
17) A. C. Albrecht, *J. Mol. Spectrosc.*, **6**, 84 (1961).
18) A. P. Marchetti and D. R. Kearns, *J. Am. Chem. Soc.*, **89**, 768 (1967).
19) K. Mislow, M. A. W. Glass, H. B. Hopps, E. Simon, and G. H. Wahl, *J. Am. Chem. Soc.*, **86**, 1710 (1964).
20) H. Suzuki, *Bull. Chem. Soc. Jpn.*, **27**, 597 (1954).
21) A. Unaue and P. Bothorel, *Bull. Soc. Chim.*, **1963**, 1640.
22) Y. Gondo, *J. Chem. Phys.*, **41**, 3928 (1964).
23) I. B. Berlman and O. J. Steingraber, *J. Chem. Phys.*, **43**, 2140 (1965).
24) A. Gamba, G. F. Tantardini, and M. Simonetta, *Spectrochim. Acta, Part A*, **28**, 1877 (1972).
25) L. O. Edward and W. T. Simpson, *J. Chem. Phys.*, **53**, 4237 (1970).
26) I. B. Berlman, *J. Chem. Phys.*, **52**, 5616 (1970).
27) B. Norden, R. Hakansson, and M. Sundbom, *Acta Chem. Scand.*, **26**, 429 (1972).
28) H. Zimmermann and N. Joop, *Z. Elektrochem.*, **65**, 66 (1961).
29) T. Azumi and S. P. McGlynn, *J. Chem. Phys.*, **37**, 2413 (1962).
30) F. Dörr, G. Hohlneicher, and S. Schneider, *Ber. Bunsenges.*, **70**, 803 (1966).

The Effect of Temperature on the Mass Spectra of 1-Alkenes. II

The late Hiroko HOSHINO, Susumu TAJIMA, Fusako ISOGAI, and Toshikazu TSUCHIYA
National Chemical Laboratory for Industry, Honmachi, Shibuya-ku, Tokyo 151

(Received January 20, 1977)

The mass spectra of 1-alkenes ranging from C_5 to C_{10} were measured at temperatures of the ion source 120—250 °C. Fragmentation $M^+ \xrightarrow{m_{28}} (M-28)^+$ and $M^+ \xrightarrow{m_{29}} (M-29)^+$, where m_{28} and m_{29} denote the metastable peaks of the fragmentations, were studied. The behavior of the curve of the intensity ratios $R'_{28}=m_{28}/F_{28}$ and $R'_{29}=m_{29}/F_{29}$ (F_{28} and F_{29} denote the intensities of the $(M-28)^+$ ion and the $(M-29)^+$ ions, respectively), *versus* temperature T of the ion source of the mass spectrometer is explained by the quasi-equilibrium theory (QET).

Many theoretical studies have been carried out[1-7] on the mechanism of fragmentation of ions produced by elecron impact from various organic compounds. These works can be divided roughly into two categories, one using QET and the other based on the molecular orbital calculation (MOT).[2,4] So far nothing definite has been given on a comparison of the two methods. It seems difficult to interpret the mechanism of each fragmentation by either one of the methods. It was shown[2] that the intensities of some peak in the mass spectra of a few derivatives of aromatic compounds can be interpreted by MOT. Subsequently, QET was applied to explain some experimental results for a series of primary alcohols and of 1-alkenes,[6] and found to give satisfactory results. QET was also successfully applied to the elucidation of the behavior of common ions, such as $C_5H_5^+$,[8] $C_6H_5CO^+$,[9] and $C_7H_7^+$ [10] from various precursors.

For 1-hexene, the slope of the curve R'_{28} *versus* T becomes positive though it is expected to take a negative value according to QET, when a simple form is assumed for the internal energy distribution function, $P(E)$, for M^+. The behavior of the curve can be explained by using the measured photoelectron spectrum as $P(E)$ instead of a simple function.[6]

We have obtained the curves R'_{29} *versus* T for C_5—C_{10} 1-alkenes and a curve R'_{28} *versus* T for 1-pentene, and studied the behavior of these curves and the R'_{28} curves for C_6—C_{10} 1-alkenes. The slopes of a few curves for smaller compounds take a negative sign as expected with QET having a simple $P(E)$ function. In contrast, the tangents of most of the curves for larger compounds are found to take a positive sign. The behavior of these curves can be elucidated on the same basis as in the case of R'_{28} for 1-hexene.

Experimental

A CEC 21-103C mass spectrometer was used to obtain the mass spectra. $R'_{28}=m_{28}/F_{28}$ and $R'_{29}=m_{29}/F_{29}$ were measured in the temperature range 120—250 °C. The results for R'_{28}, including those for C_6—C_{10}, and for R'_{29} are given in Figs. 1 and 2, respectively, the curves being given in Table 1. The result was investigated by QET. For the investigation, curve log k *versus* E, where k is the rate constant for the decomposition of M^+ into F^+, and E is the internal energy of M^+, should be drawn in order to estimate the location,* of the "metastable window" on the E axis. The corresponding curve for 1-hexene is given in Fig. 11 in a previous report.[6] In order to construct curve log k *versus* E, the ionization potential, I, of M^+ and the appearance potential, A, of F^+ were measured at the ion source temperature 250 °C using the EDD technique[11] (Table 1).

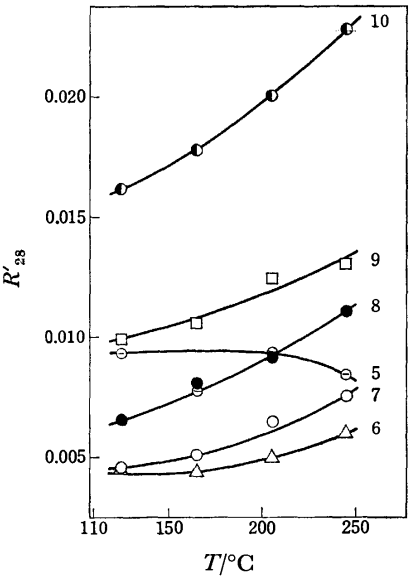

Fig. 1.

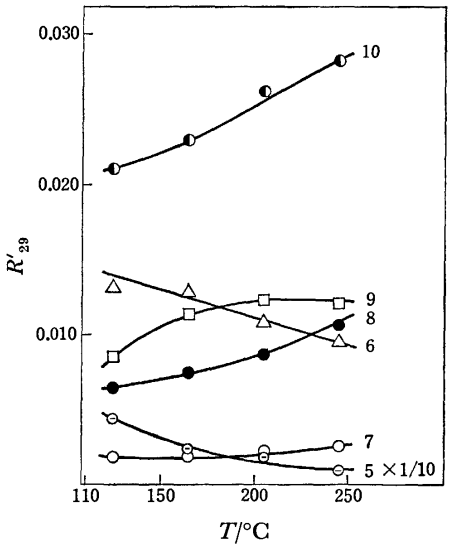

Fig. 2.

Figs. 1 and 2. The relation of intensity ratios of ions, R'_2 and R'_{29}, *versus* the temperature, T, of the ion source. The numbers on the curves are those of the carbon atoms of the 1-alkenes.

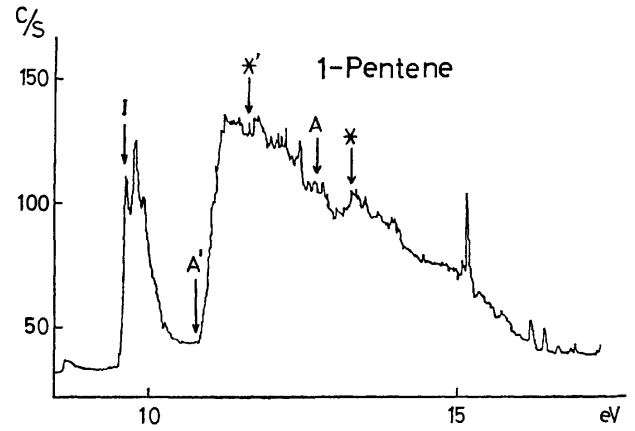

Fig. 3.

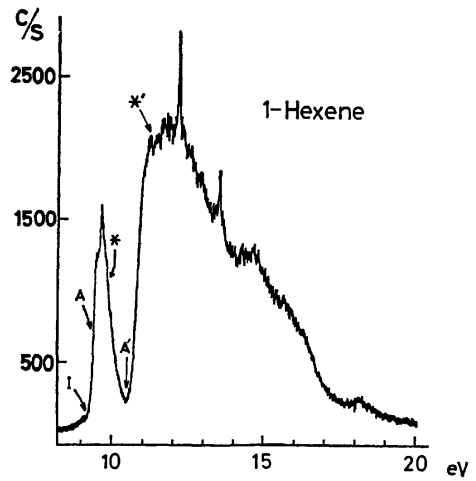

Fig. 4.

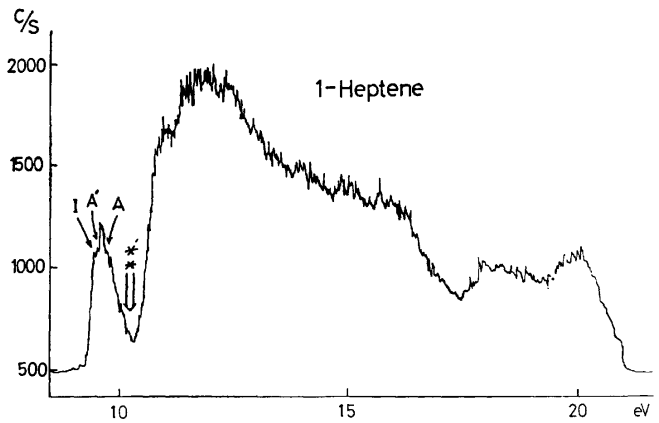

Fig. 5.

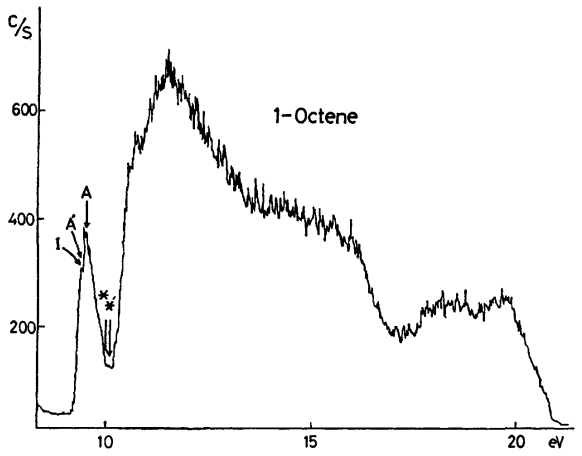

Fig. 6.

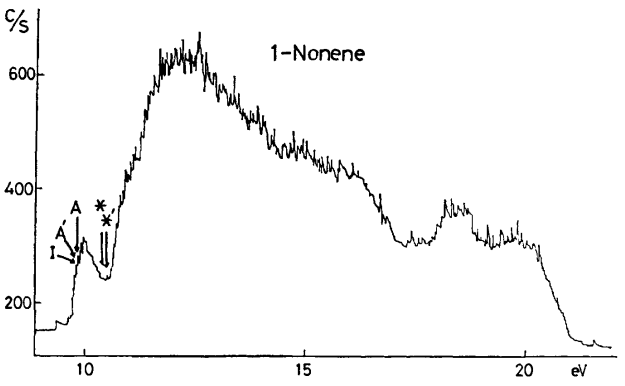

Fig. 7.

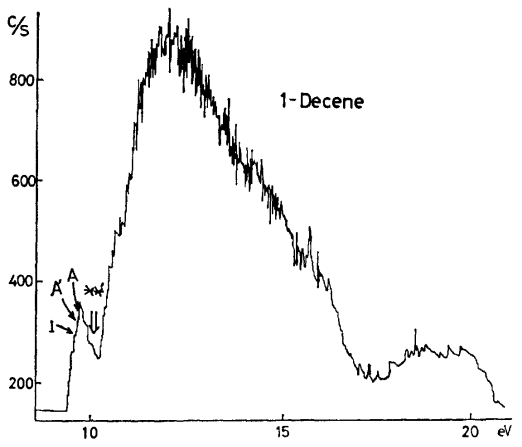

Fig. 8.

Figs. 3—8. The photoelectron spectra of 1-alkenes. The meanings of the notations are given in the text.

A JASCO PE-1 photoelectron spectrometer was used to obtain photoelectron spectra with HeI as a light source. The photoelectron spectra measured were used as $P(E)$. The spectra for each compound are shown in Figs. 3—8. The conditions of measurement are the same as already described.[6]

The olefins used were API standard samples, the purity being greater than 99.7%. All the reagents were mass-spectroscopically confirmed to be pure.

Results and Discussion

The relation between the temperature of the ion source, T, and the intensities, [M$^+$], [m], and [F$^+$], of the ions in the following fragmentation was investigated by QET.

$$M^+ \xrightarrow{m} F^+$$

Though more sophisticated expressions are proposed for

Table 1. Ionization potential, I, activation energies, ε_{28} and ε_{29}, in eV, and the schematic curves of the behavior of R' *versus* T (Figs. 1 and 2)
$\varepsilon_n = A(M-n)^+ - I$, where $A(M-n)^+$ is the appearance potential of the fragment ion $(M-n)^+$. Errors in the measured I and A values are estimated to be ± 0.1 eV.

Number of C atom	I a)	I Present result	ε_{28}	ε_{29}	R'_{28}	R'_{29}
5	9.66	9.76	1.25	2.92	⟍	⟍
6	9.59	9.54	0.11	1.18	⟋	⟍
7	9.54	9.53	0.10	0.26	⟋	⟋
8	9.52	9.54	0.06	0.21	⟋	⟋
9	—	9.56	0.02	0.10	⟋	⟋
10	9.51	9.52	0.03	0.08	⟋	⟋

a) F. H. Field and J. L. Franklin, "Electron Impact Phenomena and the Properties of Gaseous Ions," Academic Press Inc. (1957), p. 108.

the rate constant and intensities of ions, the rate constant for the fragmentation was assumed to be given by

$$k = \nu(1-\varepsilon/E)^{n-1}$$

where the notations have their usual meanings.[6] The intensities of the ions were assumed to be given by[12]

$$[M^+] = \int_0^{\varepsilon} P(E)dE + \int_{\varepsilon}^{\infty} P(E)\exp[-k(E)t_4]dE, \quad (4)$$

$$[F^+] = \int_{\varepsilon}^{\infty} P(E)[1-\exp\{-k(E)t_1\}]dE, \quad (5)$$

$$[m] = \int_{\varepsilon}^{\infty} P(E)[\exp\{-k(E)t_2\} - \exp\{-k(E)t_3\}]dE. \quad (6)$$

The mean time spent by a newly-formed ion in the ionization chamber is t_1. After being accelerated, the ions dissociated between the times t_2 and t_3 are observed as a metastable peak, and the M^+ ions which do not dissociate until t_4 are observed as the parent ion, M^+. The internal energy distribution function, $P(E)$, was assumed to be

$$P(E) = \exp[-E/kT]E/(kT)^2. \quad (7)$$

The values of t were estimated from the dimensions of the mass spectrometer and the conditions of measurement. Substituting these values in Eqs. 4—7, graphs showing the relationship between $R=[F^+]/[M^+]$, $R^*=[m]/[M^+]$ and $R'=[m]/[F^+]$ *versus* T were obtained and compared with the experimental results. The graphs for R and R^* obtained by calculation increased, and the graph for R' decreased with rise in temperature. Comparing the behavior of these curves with those obtained by experiments for M^+, $F^+=(M-28)^+$, R_{28}, R^*_{28} and R'_{28} *versus* T, it was found that while values of R_{28} and R^*_{28} for 1-alkenes of C_5—C_{10} increase with rise in temperature in line with the theoretical prediction, those of R'_{28} for 1-alkenes for C_6—C_{10} also increase, contrary to the prediction based on the assumption mentioned above. Taking R'_{28} for 1-hexene as an example, this anomaly was shown[6] to be adequately explained if the photoelectron spectrum for the compound was used as $P(E)$, instead of Eq. 7.

In the present study, R_{29}, R^*_{29}, and R'_{29} for 1-alkenes of C_5—C_{10} are measured in addition to R'_{28} for 1-pentene, and their behavior, when the temperature of the ion source is increased, is compared with that expected by QET using Eq. 7 as $P(E)$. As the result, the behavior of the curves for R' is found to be inconsistent with the expectation by QET with Eq. 7, except for R'_{28}, R'_{29} for 1-pentene and R'_{29} for 1-hexene, while the behavior of R'_{29} and R^*_{29} is found to be consistent with the prediction, *i.e.*, both the ratios increase with rise in temperature. Namely, the schematic curves shown in the 6 and 7th columns of Table 1, (*cf.* Figs. 1 and 2) increase with the temperature increase, except for R'_{28}, R'_{29} for 1-pentene and R'_{29} for 1-hexene.

The experimentally obtained ionization potential, I, appearance potentials, A and A', of $(M-28)^+$ and $(M-29)^+$ ions, respectively, and approximate positions of the metastable windows, * and *', of the $(M-28)^+$ and $(M-29)^+$ ions, respectively, estimated by the same procedure as described,[6] are shown by arrows in Figs. 3—8. In calculating the location of * and *', ν was assumed to be 10^7 for $(M-28)^+$, the rearrangement ion, and 10^{13} for $(M-29)^+$, the ion considered to be produced by simple cleavage of a bond.

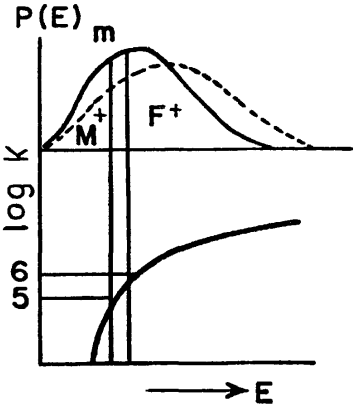

Fig. 9. Relationship of $P(E)$ and k (E) for unimolecular ion decompositions in the mass spectrometer; see text for definitions.

Using the positions * and *', of the metastable windows, the behavior of curves of R, R^*, and R' *versus* T can be explained as follows. For the sake of simplicity, the internal energy distribution function, $P(E)$, is assumed to be given by Eq. 7 for the moment. Figure 9 shows the relation between $P(E)$ and the internal energy, E, and the position, m, of metastable window schematically. The positions of the origin and the onset of the curve in the lower diagram are located by the measured I and A, respectively. The dotted curve in the upper diagram shows the behavior of the $P(E)$ curve schematically when the temperature T increases.[14] The intensities of molecular ion, $[M^+]$, metastable ion, [m], and fragment ion, $[F^+]$, are assumed to be proportional to the area under the $P(E)$ curve (upper diagram) denoted by M^+, m, and F^+, respectively. As the temperature rises and the $P(E)$ takes a flatter shape, shown by the dotted curve in Fig. 9, the areas for both M^+ and m decrease and that for F^+ increases and consequently $R=[F^+]/[M^+]$ increases and $R'=[m]/[F^+]$ decreases. As for R,* the calculated result based on Eqs. 4—7, and

shown in Fig. 9 of the previous report,[6] suggests its increase with the temperature increase.

First, R' curves obtained by experiments are compared with those predicted by the theory. In the following investigation, the photoelectron spectrum for each compound is assumed to represent the internal energy distribution function, $P(E)$, for the compound instead of Eq. 7. In the case of 1-pentene given in Fig. 3, since the metastable windows * and *′ are both situated near the shoulder of the wider band of its photoelectron spectrum (*cf.* the $P(E)$ curve in Fig. 9), the behavior of R'_{28} and R'_{29}, with the temperature increase is consistent with that expected from the simple consideration mentioned above. The behavior of R'_{29} in the case of 1-hexene (Fig. 1 and Table 1) can be explained in exactly the same manner from the location of *′ given in Fig. 4.

The values of * and *′ for all other compounds studied including * for hexene[6] are located on the higher energy side of the narrower band of the photoelectron spectrum of each compound. This band is considered to originate from the π electron. When T increases and the band takes a flatter shape, the area corresponding to the metastable peak increases, while the fractional increase of the area for F^+ is very small, resulting in the increase in R'_{28} or in R'_{29}, in contrast to the theoretical expectation based on Eq. 7.

The values of $R=[F^+]/[M^+]$ and $R^*=[m]/[M^+]$ show no "anomaly," *i.e.*, they both increase with temperature. This can easily be explained by the consideration for R'.

As far as these phenomena are concerned, they can be qualitatively elucidated by QET with photoelectron spectra used as the internal energy distribution functions. Various investigations[13-18] have been made of possible methods for the evaluation of the internal energy distribution functions resulting in ions from the impact of energetic electrons. Meisels *et al.*[19] postulate that the photoelectron spectrum of a compound gives a reasonable representation of the actual function under certain conditions. Innorta *et al.*[20] report that it is too crude an approximation to use photoelectron spectra as a representation of the internal energy distribution function for some compounds in interpreting their mass spectra. The former idea receives support from the present investigation for a series of 1-alkenes ranging from C_5 to C_{10}.

The diagrams of the measured appearance potentials of $(M-28)^+$ and $(M-29)^+$ ions *versus* the number of carbon atoms were found to be smooth curves which decrease at first and then approach gradually nearly constant values as the carbon number increases. The behavior of these curves deserves further investigation.

It is not clear whether the reactions producing $(M-28)^+$ and $(M-29)^+$ are competing reactions or reactions starting from different electronic states, into which the sample molecules are excited with certain probabilities. Judging from the present result, the effect of the reaction mechanism on the result is not so large that it influences the qualitative elucidation based on QET, aside from whether the reactions compete with each other or not.

In conclusion the "anomaly" in the mass spectra of 1-alkenes ranging from C_5 to C_{10} is explained qualitatively by QET using photoelectron spectra of the compounds as the internal energy distribution functions, $P(E)$.

The authors are indebted to Mr. Hiroshi Matsumoto and Mr. Tadashi Miyazaki for carrying out the photoelectron spectrometry experiment.

References

1) H. M. Rosenstock and M. Krauss, *Adv. Mass Spectrom.*, **2**, 251 (1962).
2) S. Tajima, N. Wasada, and T. Tsuchiya, *Bull. Chem. Soc. Jpn.*, **44**, 884 (1971); S. Tajima, Y. Niwa, N. Wasada, and T. Tsuchiya, *ibid.*, **45**, 1250 (1972).
3) For instance, D. H. Williams and I. Howe, "Principles of Organic Mass Spectrometry," McGraw-Hill (1972).
4) K. Hirota and Y. Niwa, *Tetrahedron Lett.*, **1966**, 5757.
5) M. V. Gur'ev and M. V. Tikhomirov, *Zh. Fiz. Khim.*, **32**, 2731 (1958); M. V. Gur'ev, *ibid.*, **34**, 475 (1960).
6) H. Hoshino, S. Tajima, and T. Tsuchiya, *Bull. Chem. Soc. Jpn.*, **46**, 3043 (1973). *Cf.* Fig. 11.
7) S. Tajima, Y. Niwa, M. Nakajima, and T. Tsuchiya, *Bull. Chem. Soc. Jpn.*, **44**, 2340 (1971).
8) S. Tajima and T. Tsuchiya, *Bull. Chem. Soc. Jpn.*, **46**, 3291 (1973).
9) S. Tajima, N. Wasada, and T. Tsuchiya, *Bull. Chem. Soc. Jpn.*, **46**, 3687 (1973).
10) S. Tajima and T. Tsuchiya, *Org. Mass Spectrom.*, **9**, 265 (1974).
11) R. E. Winters, J. H. Collins, and W. L. Courchene, *J. Chem. Phys.*, **45**, 1931 (1966).
12) I. Howe and D. H. Williams, *J. Chem. Soc.*, **91**, 7137 (1960).
13) A. N. H. Yeo and D. H. Williams, *J. Chem. Soc.*, **92**, 3984 (1970).
14) H. Ehrhardt and O. Osberghaus, *Z. Naturforschg.*, **15a**, 575 (1960).
15) H. Ehrhardt, F. Linder, and T. Tekaat, *Adv. Mass Spectrometry*, **4**, 705 (1968).
16) B. Steiner, C. F. Giese, and M. G. Inghram, *J. Chem. Phys.*, **34**, 189 (1961).
17) J. D. Morrison, *J. Chem. Phys.*, **21**, 1767 (1953).
18) H. von Koch, *Arkiv Fysik*, **28**, 559 (1963).
19) G. G. Meisels, C. T. Chen, B. G. Giessner, and R. H. Emmel, *J. Chem. Phys.*, **56**, 793 (1972).
20) G. Innorta, S. Torroni, and S. Pignataro, *Org. Mass Spectrom.*, **6**, 113 (1972).

Spin-Probe Study of Aqueous Soap and Polysoap Solutions

Masayuki AIZAWA, Tsuyoshi KOMATSU, and Tsurutaro NAKAGAWA
Department of Polymer Science, Faculty of Science, Hokkaido University, Sapporo 060
(Received January 29, 1977)

Poly(2-vinylpyridine) partially quaternized with 1-dodecylbromide, a "polysoap," sodium dodecyl sulfate (SDS), and dodecylpyridinium bromide (DPBr) in their micellar solutions were investigated by the spin-probe technique. It was found that the alkyl side chains in polysoap micelles associate more rigidly than in low-molecular surfactant micelles. This fact is attributed to the surface active groups covalently connected to long polymer chains in the polysoap molecule. By a recently developed method, the rotational correlation times of 2,2,6,6-tetramethyl-4-benzoyloxypiperidin-1-oxyl radical in SDS and DPBr micelles were found to be 5.9×10^{-10} and 3.5×10^{-10} s/rad, respectively. From the values of the isotropic hyperfine splitting constants, it was estimated that the DPBr micelle solubilizes the probe molecule at a more inner site of the hydrophobic portion than does the SDS micelle.

In the aqueous solutions of amphiphile substances, some intermolecular and/or intramolecular structures are formed by the "hydrophobic interaction." Surfactant molecules form the ordered aggregates known as micelles, so that their aqueous solutions manifest such properties as solubilization of hydrophobic compounds and hydrolysis of ester bonds. In the case of amphiphile macromolecules, their hydrophobic portions tend to an intramolecular association which contributes to stabilize the conformation of the macromolecules.

Strauss and coworkers[1] have studied polysoap, which is defined as an amphiphile macromolecule with a surface active side chain. According to the results of the measurement of viscosity, solubilization of hydrophobic compounds, scattering of light, and surface tension, the polysoap molecules dissolve with a relatively compact structure and can solubilize more hydrophobic compounds than low-molecular surfactant molecules corresponding to the monomer units of the polysoap molecule can. These properties, which differ from those of ordinary polyelectrolytes, result from the formation of polysoap micelle, as in the case of low-molecular surfactant micelles.

Thus the hydrophobic interaction plays an important role in the properties of such aqueous amphiphile solutions. But details of the interaction have not yet been sufficiently clarified with respect to energy and structure.

Recently, the spin-probe or spin-label technique developed by McConnell and coworkers[2] has become available for the study of various systems[3] such as polymeric materials, aqueous micellar solutions, and natural or artificial membranes. In these studies one could obtain information about the microscopic environment of the stable radical molecules; the molecular motion and structure of the host materials can thus be uncovered.

In this paper, the authors present some results obtained from the application of the spin-probe technique to aqueous polysoap solutions. Some results about the structure of the inner hydrophobic portion of polysoap micelles, by comparison with that of low-molecular surfactant micelles are also given. The authors finally examine the manner in which the hydrophobic probe is solubilized in micelles.

Experimental

Polysoap (Fig. 1(a)) derived from poly(2-vinylpyridine) (PVP) was synthesized according to the method of Inoue.[4] PVP was obtained by radical polymerization and its elemental analysis was as follows. Found: C, 80.01; H, 6.73; N, 13.22%. Calcd for $(C_7H_7N)_n$: C, 79.97; H, 6.71; N, 13.32%. From viscosity measurements in 95% ethanol solution the molecular weight and the degree of polymerization of PVP were found to be 3.0×10^5 and 2.8×10^3, respectively. Polysoap was prepared by heating a DMF solution of PVP with excess (*ca.* 2 mol) 1-dodecylbromide in an ampoule at 100 °C for 41.5 h. The partially quaternized PVP was precipitated with ether and dried under vacuum. Then the product was dissolved into water and purified by dialysis using a cellophane tubing. The degree of quaternization was estimated to be 32.2% from elemental analysis.

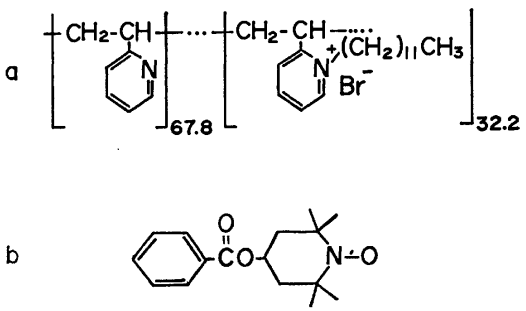

Fig. 1. (a) Polysoap, (b) BzONO.

Sodium dodecyl sulfate (SDS) was supplied from Nakarai Chemicals Ltd., and dodecylpyridinium bromide (DPBr) was obtained by ion-exchange of guaranteed grade dodecylpyridinium chloride.

The hydrophobic nitroxide radical used as the spin probe, 2,2,6,6-tetramethyl-4-benzoyloxypiperidin-1-oxyl(BzONO, Fig. 1(b)) was synthesized by Rozantzev's method.[5] Its melting point was 105.6 °C (lit, 105 °C) and its elemental analysis was as follows. Found: C, 69.63; H, 8.13; N, 4.91%. Calcd for $C_{16}H_{22}NO_3$: C, 69.53; H, 8.02; N, 5.07%; mol wt 276.4.

The concentration of the spin probe, BzONO, was 1.06×10^{-4} mol/dm^3 in all sample solutions. Besides these solutions, those saturated with BzONO were also prepared for comparison.

ESR spectra were recorded on a JEOLCO model ME-3X spectrometer equipped with a variable temperature accessory.

Results and Discussion

ESR spectra of BzONO in water are shown in Fig. 2. The three main lines of the spectra result from the contact hyperfine interaction between electron spin ($S=1/2$) and ^{14}N nuclear spin ($I=1$), corresponding to nitrogen nuclear spin quantum numbers $M_I=+1$, 0, and -1, respectively, toward the high field direction. One finds out that a less resolved hyperfine structure appears in each line, due to some protons in the BzONO molecule. In Fig. 2(b) (full line), the magnified spectrum of the central line ($M_I=0$), the proton hyperfine structure is observed clearly. Thus, the previous analysis[6] which neglected the proton hyperfine structure of nitroxide radicals cannot be applicable to our systems.

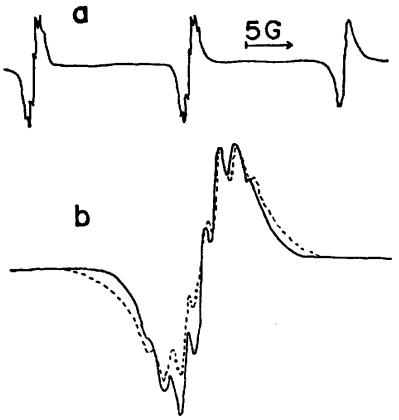

Fig. 2. (a) ESR spectrum of 1.06×10^{-4} mol/dm^3 BzONO in water at 30 °C. (b) The magnified spectrum of central line ($M_I=0$) (full line) and the simulated spectrum (dashed line).

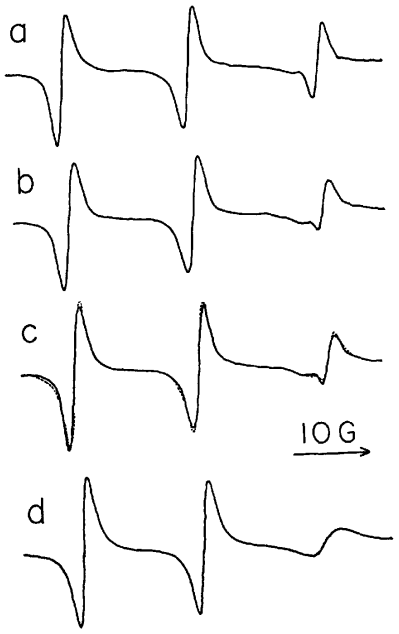

Fig. 3. ESR spectra of 1.06×10^{-4} mol/dm^3 BzONO in aqueous polysoap solutions at 30 °C and the simulated spectrum of BzONO in polysoap micelle. Polysoap concentration: (a) 1.02%, (b) 2.99%, (c) 3.94%. (d) The simulated spectrum in polysoap micelle.

ESR spectra of the aqueous polysoap solutions are shown in Fig. 3. The resolved hyperfine structure in Fig. 2 disappears here, owing to a broadening of each proton hyperfine line. From the shape of the high field line ($M_I=-1$), however, it is clear that two different components are superposed. The changes in line shape with increase in polysoap concentration indicate that the broad component is due to BzONO in the polysoap micellar environment and that the sharp one is due to BzONO in bulk water. The fact that the two different components of BzONO from two media are simultaneously observed indicates that the exchange rate of BzONO molecules between the two media is relatively low. In order to separate the broad component from the sharp one, the experimental spectra were simulated by two sets of three Lorentzian lines. As a sharp component, a spectrum with $T_2^{-1}(M_I)$ of 1.06×10^{-4} mol/dm^3 BzONO in water is used after wiping out the proton hyperfine structure. The dashed line in Fig. 3(c) is a simulated spectrum and Fig. 3(d) is the broad component used in the simulated spectrum.

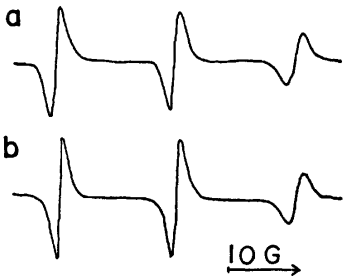

Fig. 4. ESR spectra of 1.06×10^{-4} mol/dm^3 BzONO in (a) 6.3% aqueous SDS solution and (b) 3.0% aqueous DPBr solution at 30 °C.

Figures 4(a) and 4(b) show the spectra of BzONO in the SDS and DPBr solutions, respectively. In the low-molecular surfactant solutions, above CMC which is 0.22 wt% for SDS aqueous solution and 0.37 wt% for DPBr aqueous solution, the spectra are almost independent of surfactant concentration. All over the concentration range of these solutions, the authors cannot distinguish the two different components associated with two media, that is, the micelle and the bulk water. According to the previous studies[7,8] of similar systems, the above finding does not imply that the exchange rate of the probe is too high to be resolved by ESR method, but implies that the g- and A-tensors of the probe radical are only slightly different between the two media, and that the probe is isotropically tumbling in the low-molecular surfactant micelle. By computer simulation employing the modified Bloch equations which take account of both the micelle-water exchange and the spin exchange in the micelle, the exchange rate of BzONO between SDS micelle and bulk water is estimated to be $(2.5—5.0)\times10^4$/s. This value supports the previous interpretation of spectra of probes in low-molecular surfactant micellar solutions.

Comparing the line width of these spectra, one notices that the line width of spectra of BzONO is broader in the polysoap micellar environment than in either the low-molecular surfactant micellar environment or bulk

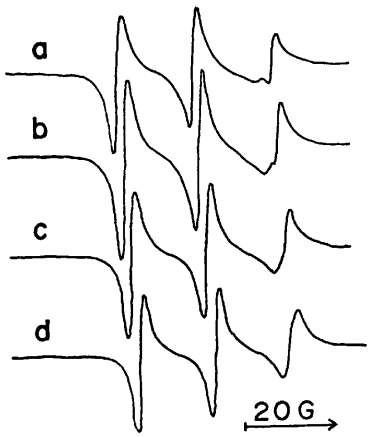

Fig. 5. ESR spectra at various temperatures of BzONO saturated at 30 °C in 4.45% aqueous polysoap solution. Temperature: (a) 30, (b) 40, (c) 50, (d) 60 °C.

water. As the causes of the line width broadening in polysoap micelle, two assumptions are possible; one is the appearance of anisotropy of g- and A-tensors and the other is Heisenberg spin exchange interaction between probe radicals solubilized in polysoap micelle where the local concentration of radicals is extremely high. Here, if the latter occurs, the broadening must decrease with the increase in polysoap concentration at the constant radical concentration, and, on the other hand, it must be intensified with an increase in radical concentration or in temperature. But the present results are not consistent with these suppositions, as shown in Figs. 3 and 5. Therefore, it is quite reasonable that the broadening of the line width in the polysoap micelle results from anisotropy of g- and A-tensors, which depends on nitrogen spin quantum number M_I and is remarkable especially in the high field line ($M_I=-1$). Thus, it is concluded that the probe molecule tumbles more slowly in polysoap micelle than in low-molecular surfactant micelles. From another point of view, the result may reflect the fact that the inner alkyl chains in polysoap micelle form more rigid structures than those in low-molecular surfactant micelles.

Recently, in the measurement of NMR relaxation times of poly(4-vinylpyridine) partially quaternized with 1-octylbromide in methanol, Ghesquire and coworkers[9] have found that the spin-lattice relaxation times T_1 of ^{13}C in the octyl group decrease with the increase in degree of quaternization. This result partly supports the present supposition about the structure of alkyl chains in polysoap micelle, since in a system with dipole-dipole interaction T_1 is inversely proportional to mobility about the spin under consideration. The authors suppose that surface active groups connected covalently into long polymer chains are mainly responsible for the mobility reduction of alkyl chains. Moreover, if the hydrophobic portion of amphiphile macromolecules used as synthetic enzymes has a rigid structure similar to that of the polysoap micelle, the rigidity may partly contribute to the rate of enzyme reactions such as hydrolysis of esters.[10]

For quantitative discussion, the authors determined the rotational correlation time τ_c of probe molecule, BzONO, in SDS and DPBr micelles, respectively, and roughly estimated it in the polysoap micelle. According to the Debye and BPP theory,[11] the rotational correlation time τ_c of a molecule in solution has the following relation to the environmental viscosity η:

$$\tau_c = 4\pi a^3\eta/3kT, \tag{1}$$

where a is the spherical radius of the molecule, k the Boltzmann constant, and T is the absolute temperature.

The spectra are analyzed by Poggi and Johnson's method[12] taking into account the unresolved proton hyperfine structure of ESR spectra of nitroxide radicals. The main assumptions required for the spectra analysis are as follows:

(1) Each spectra line consists of unresolved hyperfine splitting lines from 12 equivalent methyl protons of a BzONO molecule.

(2) Proton hyperfine lines have Lorentzian shape and an equal splitting constant. Their line widths are equal in the same M_I line.

(3) The g- and A-tensors of ^{14}N are axially symmetric, that is, $A_X=A_Y$ and $g_X=g_Y$.

By a spectral simulation using these assumptions, each line width, $W_H(M_I)$, of the proton hyperfine lines in the three lines is obtained. The dashed line in Fig. 2(b) is the simulated spectrum for the experimental spectrum (full line) of the central line ($M_I=0$) of BzONO in water. The agreement between the two spectra is satisfactory except for the unsymmetry of the experimental spectrum. These $W_H(M_I)$ are substituted into the following equation derived from Kivelson's theory:[13]

$$\tau_c = \frac{T_2^{-1}(-1)+T_2^{-1}(+1)-2T_2^{-1}(0)}{0.25b} = \frac{\frac{\sqrt{3}}{2}\{W_H(-1)+W_H(+1)-2W_H(0)\}}{0.25b}, \tag{2}$$

$$b = \frac{2}{3}\left\{A_z-\frac{1}{2}(A_x+A_y)\right\},$$

where A_X, A_Y, and A_Z are the three components of the A-tensor.

The obtained rotational correlation times for SDS and DPBr micelles are 5.9×10^{-10} and 3.5×10^{-10} s/rad, respectively. The values of the nitrogen hyperfine splitting constants a_N in SDS and DPBr micelles are 16.7 and 16.3 G, respectively. It should be noted that the values of both τ_c and a_N in SDS micelle are greater than those in DPBr micelle. From the previous study,[14] the nitrogen hyperfine splitting constant a_N is in a proportional relationship to the polarity of environment. By considering that the values of a_N in water and dodecane are 17.1 and 15.4 G, respectively, and that τ_c is proportional to environmental viscosity η, the above findings are interpreted as follows. The SDS micelle solubilizes BzONO in the vicinity of the polar surface of micelle, whereas the DPBr micelle solubilizes in the internal hydrophobic portion where the BzONO molecule is more mobile. The order of τ_c of the present results also indicates that the state of the internal hydrophobic portion in the low-molecular surfactant micelles is not solid-like, but liquid-like, as was reported

in the previous papers.[15,16]

The rotational correlation time τ_c of BzONO in the polysoap micelle is roughly estimated to be 9.8×10^{-10} s/rad by a similar procedure, except for employing $T_2^{-1}(M_I)$ evaluated by the peak-to-peak width of the above spectrum (Fig. 3(d)) instead of $T_2^{-1}(M_I)$ obtained by the spectra simulation taking account of the proton hyperfine structure. If τ_c in the low-molecular surfactant micelles are also estimated by the same rough estimation, the values in SDS and DPBr micelles are 4.3×10^{-10} and 2.1×10^{-10} s/rad, respectively. The result confirms quantitatively the preceding suggestion that BzONO tumbles more slowly in the polysoap micelle than in the low-molecular surfactant micelles.

References

1) a) U. P. Strauss and E. G. Jackson, *J. Polym. Sci.*, **6**, 649 (1951); b) U. P. Strauss and N. L. Gershfeld, *J. Phys. Chem.*, **58**, 747 (1954); c) U. P. Strauss and B. L. Williams, *ibid.*, **65**, 1390 (1961); d) H. E. Jorgensen and U. P. Strauss, *ibid.*, **65**, 1873 (1961).

2) S. Ohnishi and H. M. McConnell, *J. Am. Chem. Soc.*, **87**, 2293 (1965).

3) "Spin Labeling," ed by L. J. Berliner, Academic Press Inc., New York (1976).

4) H. Inoue, *Kolloid-Z. Z. Polym.*, **195**, 102 (1964).

5) E. G. Rozantzev, V. A. Golubev, and M. B. Neiman, *Bull. Acad. Sci. USSR*, **1965**, 379.

6) T. T. Stone, T. Buckman, P. L. Nordio, and H. M. McConnell, *Proc. Natl. Acad. Sci. U.S.A.*, **54**, 1010 (1965).

7) S. Ohnishi, T. J. R. Cyr, and H. Fukushima, *Bull. Chem. Soc. Jpn.*, **43**, 673 (1970).

8) N. M. Atherton and S. J. Strach, *J. Chem. Soc., Faraday Trans. 2*, **68**, 374 (1972).

9) D. Ghesquire, C. Chachaty, B. Ban, and C. Loucheux, *Makromol. Chem.*, **177**, 1601 (1976).

10) T. Rodulfo, J. A. Hamilton, and E. H. Cordes, *J. Org. Chem.*, **39**, 2281 (1974).

11) N. Bloembergen, E. M. Purcell, and R. V. Pound, *Phys. Rev.*, **73**, 679 (1948).

12) G. Poggi and C. S. Johnson, Jr., *J. Magn. Reson.*, **3**, 436 (1970).

13) D. Kivelson, *J. Chem. Phys.*, **33**, 1094 (1960).

14) C. Jolicoeur and H. L. Friedman, *J. Solution Chem.*, **3**, 15 (1974).

15) G. P. Rabold, *J. Polym. Sci., A-1*, **7**, 1187 (1969).

16) A. S. Waggoner, O. H. Griffith, and C. R. Christensen, *Proc. Natl. Acad. Sci. U.S.A.*, **57**, 1198 (1967).

"Molecular Orbital Analysis" of Naphthalene Derivatives. An Application of Configuration Analysis to the Assignment of Photoelectron Spectra

Tsuneo FUJII and Satoshi SUZUKI

Department of Industrial Chemistry, Faculty of Engineering, Shinshu University, Wakasato, Nagano 380

(Received February 4, 1977)

Molecular orbital analysis, which is an application of configuration analysis proposed by Baba *et al.*, has been applied to the interpretation of the photoelectron spectra of substituted naphthalenes, with particular attention paid to the dependence of the spectra on the position of substitution and on the character of the substituents. The results of MO calculations based on the Pariser-Parr-Pople method have been analyzed in terms of the π-MO's of naphthalene and the π-AO or π-MO's of a substituent. The results of the molecular orbital analysis for naphthalene derivatives with an electron-donating group are compared with the results for those with an electron-accepting group.

Since Turner first succeeded in measuring high resolution photoelectron (PE) spectra,[1] the PE spectra of many compounds have been reported. The PE spectra give precise data on the vertical ionization potentials (I_v) of atoms and molecules. Assuming Koopmans' theorem,[2] one may also easily obtain information on the orbital energies. Recently Kimura *et al.* have found a sum rule—that the sum of the experimental ionization energies may be reproduced by the sum of the calculated orbital energies of the localized orbitals.[3] Heilbronner *et al.* have calculated the π-orbital energies of naphthalene by three different approximations and compared them with experimental data.[4] Marschner and Goetz could reproduce the experimental values of the PE spectra of naphthalene by using modified Pariser-Parr-Pople (PPP) parameters.[5]

The PE spectra of substituted naphthalenes have been observed by several authors.[6-8] The changes in the π-MO energies of naphthalene caused by the introduction of a substituent depend on the position and properties of the substituent. Although the change in the energy and character of MO's due to the introduction of a substituent into the parent naphthalene is a very interesting problem for chemists, the origin of such a change in the π-MO character and energy has not been fully understood. From the experimental results on monosubstituted naphthalenes with an electron-donating group,[6-8] it has been found that the individual bands are apparently shifted to a higher energy compared with those of naphthalene. In contrast to this, the PE spectra of monosubstituted naphthalenes with an electron-accepting group are apparently shifted to a lower energy compared with that of naphthalene.

The method of configuration analysis proposed by Baba *et al.* has enabled us to give a quantitative interpretation of the electronic absorption spectra of the derivatives of aromatic hydrocarbons in terms of locally excited and charge-transfer states.[9] In the calculation process of configuration analysis, the matrix which transforms the set of MO's of a derivative into a set of reference MO's, that is, the MO's of a corresponding parent compound and a substituent, is obtained. This matrix gives us information on the correlation between the MO's of a derivative and the MO's of a parent compound and a substituent. This procedure will be called "Molecular Orbital Analysis" (MOA), by analogy with configuration analysis. The quantitative assignments of the MO's of the derivatives to their reference MO's can be made by the application of MOA.

This paper will present the assignments of the MO's of monosubstituted naphthalenes in terms of the MO's of naphthalene and a substituent and will make a comparison between the electron-donating and electron-accepting cases. In the present paper, naphthalene and its derivatives, *i.e.*, 1- and 2-naphthols, 1- and 2-naphthylamines, 1- and 2-naphthonitriles, and 1- and 2-naphthaldehydes, will be considered. The LCAO-SCF-MO calculations of the PPP type have been performed, and the results subjected to the MOA.

Procedure and Calculation

The semiempirical MO's of substituted compounds may be obtained by the PPP procedure. Although the quantitative correlation between the MO's of substituted compounds and those of the corresponding parent compounds is an interesting problem in such fields of chemistry as PE spectroscopy, such information cannot be obtained by means of the usual MO calculations. It can, though, be derived in the course of the calculation of configuration analysis. This procedure will be outlined below.

The MO's of a substituted compound, ϕ_i's, which are obtained by the usual procedure, can be written in a matrix form as

$$\boldsymbol{\phi} = \boldsymbol{\chi}\mathbf{C}, \tag{1}$$

where $\boldsymbol{\chi}$ represents the row vector of n orthonormal AO's, χ_p, and where $\mathbf{C}$ is an $n \times n$ unitary matrix, the elements of which are AO coefficients of ϕ_i's. In the present study, systems composed of naphthalene and a substituent are employed as the reference systems; therefore, the reference MO's used are the LCAO-SCF-MO's of naphthalene and the π-AO or π-MO's of a substituent. The MO's of the reference system, $\boldsymbol{\phi}^\circ$, are expressed in terms of the same basis set, $\boldsymbol{\chi}$, as well as ϕ_j's

$$\boldsymbol{\phi}^\circ = \boldsymbol{\chi}\mathbf{C}^\circ. \tag{2}$$

It follows, then, that

$$\boldsymbol{\phi} = \boldsymbol{\phi}^\circ\mathbf{B}, \tag{3}$$

with

$$\mathbf{B} = (\mathbf{C}^{\circ})^{\dagger}\mathbf{C}, \quad (4)$$

where $(\mathbf{C}^{\circ})^{\dagger}$ is the Hermitian conjugate of the $\mathbf{C}^{\circ}$ matrix. The **B** matrix represents the correlation between $\boldsymbol{\phi}$ and $\boldsymbol{\phi}^{\circ}$. This matrix is used in the calculation of the configuration analysis. When the configuration analysis of a certain compound has been completed, the **B** matrix of the compound has also been obtained as a matter of course.

Calculations have been made for the π-electron systems of naphthalene, naphthols, naphthylamines, naphthonitriles, and naphthaldehydes by the semiempirical LCAO-SCF-MO method. The parameters used in this study have been given elsewhere.[10,11]

Results

Tables 1 and 2 give the calculated π-MO energies, ε_i, and the I_v's for ϕ_i° and ϕ_j in the first and third rows for individual compounds; the values of I_v's were obtained from the PE spectroscopy. The MO's of the compounds are numbered in the order of increasing energy. The corrected MO energies, $\varepsilon_i^{corrd}=\varepsilon_i+1.65$ eV, are also included in the second row of Tables 1 and 2. The correction factor of 1.65 eV is taken to give a general agreement between the experimental and theoretical data.

The results of MOA are shown in Tables 3—10. The reference MO's consist of ϕ_1°, ϕ_2°,$\cdots$, ϕ_{10}°, which are the SCF-MO's of naphthalene, and ϕ_X°'s, which represent the π-AO or the π-MO of the substituents, X being

Table 1. SCF MO energies(ε), corrected SCF MO energies (ε^{corrd}), and vertical ionization potentials (I_v) in eV for naphthalene

	Photoelectron band (upper) and orbital function (lower)				
	V ϕ_1°	IV ϕ_2°	III ϕ_3°	II ϕ_4°	I ϕ_5°
ε	−14.56	−12.79	−11.86	−10.78	−9.79
ε^{corrd}	−12.91	−11.14	−10.21	−9.13	−8.14
I_v[a]	12.36	11.00	10.10	8.88	8.15

a) Ref. 14.

Table 2. SCF MO energies(ε), corrected SCF MO energies (ε^{corrd}), and vertical ionization potentials (I_v) in eV for naphthols, naphthylamines, naphthonitriles, and naphthaldehydes

Compound	Photoelectron band (upper) and orbital function (lower)					
	VI ϕ_1	V ϕ_2	IV ϕ_3	III ϕ_4	II ϕ_5	I ϕ_6
1-Naphthol						
ε	−15.06	−13.72	−12.44	−11.29	−10.66	−9.26
ε^{corrd}	−13.41	−12.07	−10.79	−9.64	−9.01	−7.61
I_v[a]				9.57	8.89	7.78
2-Naphthol						
ε	−14.91	−13.89	−12.12	−11.55	−10.24	−9.42
ε^{corrd}	−13.28	−12.24	−10.47	−9.90	−8.61	−7.77
I_v[a]			10.54	9.91	8.63	7.90
1-Naphthylamine						
ε	−14.57	−12.95	−12.15	−10.82	−10.62	−8.99
ε^{corrd}	−12.92	−11.30	−10.50	−9.17	−8.97	−7.34
I_v[a,b]	12.70	11.40	10.49	9.26	8.66	7.46
2-Naphthylamine						
ε	−14.44	−13.14	−11.78	−11.26	−9.99	−9.16
ε^{corrd}	−12.79	−11.49	−10.13	−9.61	−8.34	−7.51
I_v[a,b]	12.50	11.70	10.14	9.65	8.32	7.56
1-Naphthonitrile						
ε	−15.02	−13.65	−12.85	−11.82	−11.04	−9.94
ε^{corrd}	−13.37	−12.00	−11.20	−10.17	−9.39	−8.29
I_v[a]				10.31	9.35	8.61
2-Naphthonitrile						
ε	−14.97	−13.87	−12.58	−12.05	−10.89	−10.01
ε^{corrd}	−13.32	−12.22	−10.93	−10.40	−9.24	−8.36
I_v[a]			11.18	10.51	9.33	8.64
1-Naphthaldehyde[c]						
ε	−15.06	−13.76	−12.99	−12.08	−11.11	−10.11
ε^{corrd}	−13.41	−12.11	−11.34	−10.43	−9.46	−8.46
2-Naphthaldehyde[c]						
ε	−15.06	−13.97	−12.83	−12.22	−11.09	−10.16
ε^{corrd}	−13.41	−12.32	−11.18	−10.57	−9.44	−8.51

a) Ref. 8. b) Ref. 7. c) The observed data are not available.

Table 3. Elements of **B** matrix of 1-naphthol[a)]

Reference MO	Symmetry type	Band notation	Photoelectron band (upper) and orbital function (lower)					
						III	II	I
			ϕ_1	ϕ_2	ϕ_3	ϕ_4	ϕ_5	ϕ_6
ϕ_1°	b_{1u}	B_5	0.7594	0.6327	0.1279	−0.0696	−0.0030	0.0391
ϕ_2°	b_{2g}	B_4	−0.1656	0.4008	−0.8791	0.1919	0.0131	−0.0436
ϕ_3°	b_{3g}	B_3	−0.2152	0.2875	0.3642	0.8468	0.0092	−0.1428
ϕ_o°		B_o	0.5629	−0.5557	−0.2562	0.3794	0.0053	−0.3261
ϕ_4°	b_{1u}	B_2	0.0045	−0.0044	0.0093	−0.0102	0.9997	0.0108
ϕ_5°	a_u	B_1	−0.1399	0.1760	0.0896	−0.2910	0.0077	−0.9249
ϕ_6°	b_{2g}		−0.0763	0.0901	0.0456	−0.0847	0.0026	0.0870
ϕ_7°	b_{3g}		−0.0041	0.0009	0.0033	−0.0027	−0.0119	−0.0011
ϕ_8°	b_{1u}		−0.0629	0.0685	0.0371	−0.0529	−0.0021	0.0634
ϕ_9°	a_u		−0.0405	0.0444	0.0224	−0.0378	−0.0026	0.0365
ϕ_{10}°	b_{3g}		0.0412	−0.0430	−0.0218	0.0338	−0.0013	−0.0364
Assignment[a)]			ϕ_1°		ϕ_2°	$\phi_3^\circ(B_3)$	$\phi_4^\circ(B_2)$	$\phi_5^\circ(B_1)$

a) See text for definition.

Table 4. Elements of **B** matrix of 2-naphthol[a)]

Reference MO	Symmetry type	Band notation	Photoelectron band (upper) and orbital function (lower)					
					IV	III	II	I
			ϕ_1	ϕ_2	ϕ_3	ϕ_4	ϕ_5	ϕ_6
ϕ_1°	b_{1u}	B_5	0.7100	0.6956	−0.0865	0.0516	0.0310	0.0286
ϕ_2°	b_{2g}	B_4	−0.3215	0.4522	0.7850	−0.2343	−0.1125	−0.0885
ϕ_3°	b_{3g}	B_3	−0.0921	0.1182	−0.3946	−0.8990	−0.1089	−0.0399
ϕ_o°		B_o	0.5774	−0.4971	0.3703	−0.2353	−0.3025	−0.2826
ϕ_4°	b_{1u}	B_2	−0.1719	0.1746	−0.2450	0.2642	−0.8640	−0.2506
ϕ_5°	a_u	B_1	−0.0862	0.0901	−0.1188	0.0705	0.3567	−0.9152
ϕ_6°	b_{2g}		0.0506	−0.0478	0.0390	−0.0322	−0.0406	−0.0514
ϕ_7°	b_{3g}		0.0677	−0.0634	0.0594	−0.0342	−0.0627	−0.0570
ϕ_8°	b_{1u}		0.0317	−0.0310	0.0269	−0.0182	−0.0204	−0.0272
ϕ_9°	a_u		0.0655	−0.0614	0.0539	−0.0351	−0.0526	−0.0478
ϕ_{10}°	b_{3g}		−0.0345	0.0305	−0.0261	0.0180	0.0239	0.0232
Assignment[a)]			ϕ_1°		$\phi_2^\circ(B_4)$	$\phi_3^\circ(B_3)$	$\phi_4^\circ(B_2)$	$\phi_5^\circ(B_1)$

a) See text for definition.

Table 5. Elements of **B** matrix of 1-naphthylamine[a)]

Reference MO	Symmetry type	Band notation	Photoelectron band (upper) and orbital function (lower)					
			VI	V	IV	III	II	I
			ϕ_1	ϕ_2	ϕ_3	ϕ_4	ϕ_5	ϕ_6
ϕ_1°	b_{1u}	B_5	0.9635	−0.1943	0.1498	−0.0920	−0.0028	−0.0526
ϕ_2°	b_{2g}	B_4	−0.0587	−0.8164	−0.5332	0.2038	−0.0163	0.0615
ϕ_3°	b_{3g}	B_3	−0.1127	−0.3134	0.7309	0.5684	0.0120	0.1757
ϕ_4°	b_{1u}	B_2	0.0036	0.0144	0.0023	−0.0111	0.9996	−0.0131
ϕ_5°	a_u	B_1	−0.0579	−0.1537	0.1361	−0.5270	0.0072	0.8220
ϕ_N°		B_N	0.2243	0.4063	−0.3639	0.5777	0.0078	0.5051
ϕ_6°	b_{2g}		−0.0265	−0.0651	0.0613	−0.1235	0.0032	−0.1332
ϕ_7°	b_{3g}		−0.0036	−0.0006	0.0038	−0.0056	−0.0132	−0.0004
ϕ_8°	b_{1u}		−0.0244	−0.0491	0.0507	−0.0782	−0.0034	−0.0912
ϕ_9°	a_u		−0.0154	−0.0322	0.0304	−0.0552	−0.0030	−0.0550
ϕ_{10}°	b_{3g}		0.0162	0.0308	−0.0295	0.0482	−0.0012	0.0521
Assignment[a)]			$\phi_1^\circ(B_5)$	$\phi_2^\circ(B_4)$	$\phi_3^\circ(B_3)$		$\phi_4^\circ(B_2)$	$\phi_5^\circ(B_1)$

a) See text for definition.

Table 6. Elements of **B** matrix of 2-naphthylamine[a)]

Reference MO	Symmetry type	Band notation	Photoelectron band (upper) and orbital function (lower)					
			VI ϕ_1	V ϕ_2	IV ϕ_3	III ϕ_4	II ϕ_5	I ϕ_6
ϕ_1°	b_{1u}	B_5	0.9662	−0.2309	0.0566	0.0813	0.0356	−0.0437
ϕ_2°	b_{2g}	B_4	−0.1392	−0.8360	−0.0369	−0.3349	−0.1231	0.1330
ϕ_3°	b_{3g}	B_3	−0.0298	−0.1314	0.8374	−0.5127	−0.1129	0.0705
ϕ_4°	b_{1u}	B_2	−0.0704	−0.1866	0.2299	0.6159	−0.6373	0.3479
ϕ_5°	a_u	B_1	−0.0289	−0.0818	0.1077	0.1627	0.6309	0.7456
ϕ_N°		B_N	0.1973	0.4251	−0.2988	−0.4464	−0.3906	0.5191
ϕ_6°	b_{2g}		0.0171	0.0419	−0.0282	−0.0543	−0.0504	0.0869
ϕ_7°	b_{3g}		0.0217	0.0517	−0.0476	−0.0645	−0.0756	0.1019
ϕ_8°	b_{1u}		0.0096	0.0263	−0.0215	−0.0345	−0.0263	0.0459
ϕ_9°	a_u		0.0206	0.0505	−0.0414	−0.0634	−0.0649	0.0857
ϕ_{10}°	b_{3g}		−0.0119	−0.0256	0.0195	0.0319	0.0296	−0.0406
Assignment[a)]			$\phi_1^\circ(B_5)$	$\phi_2^\circ(B_4)$	$\phi_3^\circ(B_3)$			$\phi_5^\circ(B_1)$

a) See text for definition.

Table 7. Elements of **B** matrix of 1-naphthonitrile[a)]

Reference MO	Symmetry type	Band notation	Photoelectron band (upper) and orbital function (lower)					
			ϕ_1	ϕ_2	ϕ_3	III ϕ_4	II ϕ_5	I ϕ_6
ϕ_1°	b_{1u}	B_5	0.9398	−0.3218	0.0784	−0.0584	−0.0061	0.0082
ϕ_{CN1}°		B_{CN}	0.3005	0.6938	−0.3925	0.4482	0.0023	−0.2431
ϕ_2°	b_{2g}	B_4	−0.0955	−0.5174	−0.8385	0.1247	−0.0224	−0.0115
ϕ_3°	b_{3g}	B_3	−0.0825	−0.3316	0.3503	0.8662	0.0087	−0.0182
ϕ_4°	b_{1u}	B_2	0.0042	−0.0110	−0.0211	−0.0054	0.9996	0.0088
ϕ_5°	a_u	B_1	−0.0544	−0.1573	0.1052	−0.1442	0.0081	−0.9595
ϕ_6°	b_{2g}		−0.0284	−0.0637	0.0350	−0.0344	−0.0054	0.0062
ϕ_7°	b_{3g}		−0.0007	−0.0008	0.0025	0.0032	−0.0007	0.0063
ϕ_{CN2}°			0.0771	0.0655	0.0103	−0.0808	−0.0038	0.1401
ϕ_8°	b_{1u}		−0.0204	−0.0489	0.0264	−0.0267	0.0021	0.0035
ϕ_9°	a_u		−0.0133	−0.0304	0.0169	−0.0171	−0.0011	0.0030
ϕ_{10}°	b_{3g}		0.0129	0.0301	−0.0158	0.0170	0.0000	−0.0019
Assignment[a)]			ϕ_1°		ϕ_2°	$\phi_3^\circ(B_3)$	$\phi_4^\circ(B_2)$	$\phi_5^\circ(B_1)$

a) See text for definition.

Table 8. Elements of **B** matrix of 2-naphthonitrile[a)]

Reference MO	Symmetry type	Band notation	Photoelectron band (upper) and orbital function (lower)					
			ϕ_1	ϕ_2	IV ϕ_3	III ϕ_4	II ϕ_5	I ϕ_6
ϕ_1°	b_{1u}	B_5	0.9466	0.3081	0.0745	0.0255	0.0209	−0.0027
ϕ_{CN1}°		B_{CN}	0.2733	−0.6684	−0.5208	−0.2766	−0.3010	0.1634
ϕ_2°	b_{2g}	B_4	−0.1330	0.6217	−0.7447	−0.1697	−0.0506	0.0121
ϕ_3°	b_{3g}	B_3	−0.0399	0.1293	0.3370	−0.9288	−0.0559	−0.0052
ϕ_4°	b_{1u}	B_2	−0.0541	0.1840	0.2051	0.1643	−0.9375	0.0544
ϕ_5°	a_u	B_1	−0.0323	0.0881	0.0901	0.0386	0.1127	0.9806
ϕ_6°	b_{2g}		0.0139	−0.0376	−0.0282	−0.0164	−0.0076	0.0057
ϕ_7°	b_{3g}		0.0206	−0.0515	−0.0369	−0.0197	−0.0142	−0.0018
ϕ_{CN2}°			0.0688	−0.0787	0.0334	0.0441	0.1060	−0.0923
ϕ_8°	b_{1u}		0.0098	−0.0224	−0.0151	−0.0093	−0.0079	0.0033
ϕ_9°	a_u		0.0194	−0.0474	−0.0338	−0.0156	−0.0128	0.0042
ϕ_{10}°	b_{3g}		−0.0095	0.0235	0.0166	0.0072	0.0068	−0.0034
Assignment[a)]			ϕ_1°		$\phi_2^\circ(B_4)$	$\phi_3^\circ(B_3)$	$\phi_4^\circ(B_2)$	$\phi_5^\circ(B_1)$

a) See text for definition.

Table 9. Elements of **B** matrix of 1-naphthaldehyde[a)]

Reference MO	Symmetry type	Band notation	Orbital function					
			ϕ_1	ϕ_2	ϕ_3	ϕ_4	ϕ_5	ϕ_6
ϕ_1°	b_{1u}	B_5	0.9585	−0.2692	−0.0648	−0.0266	0.0139	0.0042
ϕ_{CHO1}°		B_{CHO}	0.2605	0.8046	0.3533	0.3469	0.0029	−0.1758
ϕ_2°	b_{2g}	B_4	−0.0497	−0.4182	0.8994	0.0950	−0.0002	0.0046
ϕ_3°	b_{3g}	B_3	−0.0610	−0.2758	−0.2368	0.9237	−0.0178	−0.0068
ϕ_4°	b_{1u}	B_2	0.0163	0.0048	0.0039	−0.0169	−0.9996	−0.0001
ϕ_5°	a_u	B_1	−0.0316	−0.1371	−0.0630	−0.0827	0.0018	−0.9732
ϕ_6°	b_{2g}		−0.0021	−0.0604	−0.0176	−0.0190	−0.0042	−0.0129
ϕ_{CHO2}°			−0.0716	0.0551	−0.0343	−0.0945	0.0126	0.1475
ϕ_7°	b_{3g}		−0.0036	−0.0052	−0.0010	0.0060	−0.0003	0.0023
ϕ_8°	b_{1u}		−0.0147	−0.0446	−0.0162	−0.0114	−0.0084	−0.0018
ϕ_9°	a_u		−0.0102	−0.0298	−0.0098	−0.0090	−0.0032	−0.0061
ϕ_{10}°	b_{3g}		0.0088	0.0274	0.0100	0.0086	0.0029	0.0020
Assignment[a)]			ϕ_1°	ϕ_{CHO1}°	ϕ_2°	ϕ_3°	ϕ_4°	ϕ_5°

a) See text for definition.

Table 10. Elements of **B** matrix of 2-naphthaldehyde[a)]

Reference MO	Symmetry type	Band notation	Orbital function					
			ϕ_1	ϕ_2	ϕ_3	ϕ_4	ϕ_5	ϕ_6
ϕ_1°	b_{1u}	B_5	0.9577	−0.2786	−0.0525	0.0023	−0.0125	0.0055
ϕ_{CHO1}°		B_{CHO}	0.2479	0.7426	0.5254	−0.1980	0.2271	0.1115
ϕ_2°	b_{2g}	B_4	−0.1127	−0.5580	0.8128	−0.0746	0.0080	−0.0093
ϕ_3°	b_{3g}	B_3	−0.0402	−0.1211	−0.1842	−0.9727	0.0286	−0.0237
ϕ_4°	b_{1u}	B_2	−0.0377	−0.1655	−0.1344	0.0812	0.9663	0.0065
ϕ_5°	a_u	B_1	−0.0297	−0.0833	−0.0595	0.0015	−0.0402	0.9900
ϕ_6°	b_{2g}		0.0082	0.0314	0.0205	−0.0110	−0.0041	0.0053
ϕ_{CHO2}°			0.0641	0.0697	−0.0570	0.0458	−0.1099	−0.0819
ϕ_7°	b_{3g}		0.0159	0.0462	0.0250	−0.0110	−0.0005	−0.0087
ϕ_8°	b_{1u}		0.0067	0.0182	0.0101	−0.0072	0.0036	0.0030
ϕ_9°	a_u		0.0144	0.0415	0.0233	−0.0076	0.0012	0.0010
ϕ_{10}°	b_{3g}		−0.0067	−0.0202	−0.0117	0.0033	−0.0019	−0.0025
Assignment[a)]			ϕ_1°	ϕ_{CHO1}°	ϕ_2°	ϕ_3°	ϕ_4°	ϕ_5°

a) See text for definition.

O, N, CN, and CHO, corresponding to naphthols, naphthylamines, naphthonitriles, and naphthaldehydes respectively. The symmetry types shown in the tables are those for the naphthalene SCF-MO's, where the X- and Y-axes are chosen as the long and short axes of the naphthalene ring respectively. The band notations for the PE bands of naphthalene and the substituents, B_1, B_2,···, B_X, are also given in the tables. In columns of these tables, the elements of **B** matrix defined by Eq. 4 are given. The square of the element represents the weight of the individual ϕ_i°'s. When a reference MO, ϕ_i°, makes a contribution of more than 50% to ϕ_j, the ϕ_j is assigned to the ϕ_i°; the band notation for the ϕ_i° is given in the assignment column.

Figures 1 and 2 show the energy diagrams for the occupied π-orbitals of the compounds studied. When ϕ_i° makes a contribution of more than 50% to ϕ_j, the level of the ϕ_i° is connected to that of the ϕ_j by —·—. When the ϕ_i° makes a contribution of between 30 to 50% to the ϕ_j, the level of the ϕ_i° is connected to that of the ϕ_j by ·····. The MO energy levels of monosubstituted naphthalenes with an electron-donating group look as if they are shifted toward a higher energy

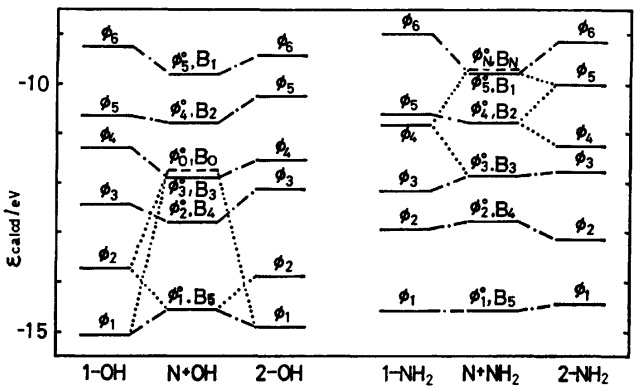

Fig. 1. Orbital energy diagram for the occupied π-orbitals of naphthalene(N), 1- and 2-naphthols(1-OH and 2-OH), and 1- and 2-naphthylamine(1-NH_2 and 2-NH_2). OH and NH_2: the π-AO of the substituents; ——: SCF-MO energies of the compounds; ——: π-AO of the substituents. A semibroken line(—·—) indicates that ϕ_i° makes a contribution higher than 50% to ϕ_j and a dotted line (·····)a contribution ranging from 30% to 50%. B_1, B_2, ···, correspond to the band notation (see text).

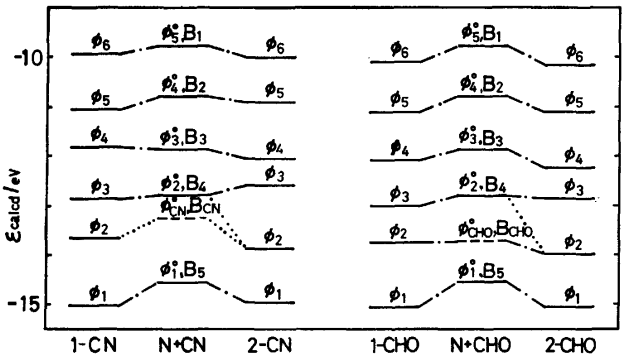

Fig. 2. Orbital energy diagram for the occupied π-orbitals of naphthalene(N), 1- and 2-naphthonitriles(1-CN and 2-CN), and 1- and 2-naphthaldehydes(1-CHO and 2-CHO). CN and CHO: the occupied π-MO of the substituents; ——: π-MO of the substituents. Other symbols are the same as in Fig. 1.

compared with those of naphthalene, although the case of naphthylamines is somewhat complicated. On the other hand, the MO energy levels of naphthonitriles and naphthaldehydes are apparently shifted toward a lower energy.

Discussion

Usually the ionization potentials are evaluated from the SCF molecular wavefunction by the use of Koopmans' theorem,[2] according to which the energy required to remove an electron from the ith orbital of a molecule, leaving the nuclei fixed and the orbital unaltered, is given by

$$I_i = -\varepsilon_i. \tag{5}$$

Tables 1 and 2 show that the $\varepsilon_i^{\text{corrd}}$'s for the compounds studied in the present paper are in good agreement with the observed I_v's. The $\varepsilon_i^{\text{corrd}}$ of the unoccupied orbital ϕ_6° of naphthalene is equal to 0.25 eV. The reported value of the electron affinity is 0.16 eV[12] or 0.20 eV.[13] Hence, $\varepsilon_i^{\text{corrd}}$ is found to be a reasonable value for both the I_v and the electron affinity. Below, discussion will be limited to the occupied orbitals.

Orbital Assignment. Let us now proceed to discuss the results of the MOA, beginning with naphthols.

Tables 3 and 4 show that the ϕ_1, ϕ_3, ϕ_4, ϕ_5, and ϕ_6 of naphthols are assigned to the ϕ_1°, ϕ_2°, ϕ_3°, ϕ_4°, and ϕ_5° of naphthalene respectively. There is a relatively strong interaction among the ϕ_1°, ϕ_2°, and ϕ_0° of which the ϕ_2 of naphthols is composed. The most important reference MO's in the ϕ_2 of naphthols are the ϕ_1° and ϕ_0°. There is a splitting of the reference MO's. For example, the ϕ_1° splits into the ϕ_1 and ϕ_2 of nearly equal weights, the ϕ_1 lying on the lower-energy side, and the ϕ_2 on the higher-energy side, relative to ϕ_1°. The ϕ_5 of 1-naphthol has almost the same property as the ϕ_4°. The ϕ_0° makes an important contribution to the ϕ_1, ϕ_2, ϕ_4, and ϕ_6 by weights of 31.7, 30.9, 14.4 and 10.6% in 1-naphthol and to the ϕ_1, ϕ_2, and ϕ_3 by weights of 33.3, 24.7, and 13.7% in 2-naphthol, respectively.

With reference to the results shown in Tables 5 and 6, the ϕ_1, ϕ_2, ϕ_3, and ϕ_6 of naphthylamines can reasonably be assigned to the ϕ_1°, ϕ_2°, ϕ_3°, and ϕ_5° respectively. The ϕ_5° of 1-naphthylamine has almost the same property as the ϕ_4°, the situation being the same as in 1-naphthol. There is a relatively strong interaction among the ϕ_3°, ϕ_5°, and ϕ_N° of which the ϕ_4 of 1-naphthylamine is composed. They make nearly equal contributions to the ϕ_4. However, in the case of 2-naphthylamine, the interaction among the ϕ_2°, ϕ_3°, ϕ_4°, ϕ_5°, and ϕ_N° is large, yielding the ϕ_4 and ϕ_5. A splitting of the reference MO's is also found, as in the case of naphthols. For example, ϕ_4° splits into the ϕ_4 and ϕ_5 with nearly equal weights. The ϕ_4° is the most important reference MO in the ϕ_4 and ϕ_5 of 2-naphthylamine. The weight of the ϕ_4° to the ϕ_4 is larger than that of the ϕ_3°. The ϕ_4 lies on the higher-energy side, and the ϕ_5 lies on the lower-energy side, relative to the ϕ_4°. The ϕ_N° makes an important contribution to the ϕ_2, ϕ_3, ϕ_4, and ϕ_6 by weights of 16.5, 13.2, 32.2, and 25.5% in 1-naphthylamine, and to the ϕ_2, ϕ_4, ϕ_5, and ϕ_6 by weights of 18.1, 19.9, 15.3, and 27.0% in 2-naphthylamine, respectively.

It may be seen in Tables 7 and 8 that the ϕ_1, ϕ_3, ϕ_4, ϕ_5, and ϕ_6 of naphthonitriles can reasonably be assigned to the ϕ_1°, ϕ_2°, ϕ_3°, ϕ_4°, and ϕ_5° respectively and that the ϕ_5 of 1-naphthonitrile has the same property as the ϕ_4°, just as in 1-naphthol and 1-naphthylamine. The ϕ_2 of naphthonitriles is mainly composed of the ϕ_{CN1}° and ϕ_2°. The ϕ_{CN1}° makes an important contribution to the ϕ_2, ϕ_3, and ϕ_4 by weights of 48.1, 15.4, and 20.1% in 1-naphthonitrile and to the ϕ_2 and ϕ_3 by weights of 44.7 and 27.1% in 2-naphthonitrile respectively. The splitting of the reference MO's is also found, as in the case of electron-donating.

Tables 9 and 10 show that the ϕ_1, ϕ_2, ϕ_3, ϕ_4, ϕ_5, and ϕ_6 of naphthaldehydes are assigned to the ϕ_1°, ϕ_{CHO1}°, ϕ_2°, ϕ_3°, ϕ_4°, and ϕ_5°, respectively, irrespective of the substitution at the 1- or 2-position. The ϕ_{CHO1}° mixes mainly with the ϕ_2°. It is also found that the reference MO's split into several MO's of naphthaldehydes. The ϕ_5 of 1-naphthaldehyde also has the same property as the ϕ_4°. The ϕ_{CHO1}° makes an important contribution to the ϕ_3 and ϕ_4 by weights of 12.5 and 12.0% respectively in 1-naphthaldehyde and to the ϕ_3 by a weight of 27.6% in 2-naphthaldehyde.

As may be seen from Tables 3, 5, 7, and 9, the weight of the ϕ_4° in the ϕ_5 is always 99.9% in the case of the naphthalene derivatives with a substitution at the 1-position. The ϕ_4° of naphthalene is little affected by the substitution at the 1-position. This situation can be well interpreted in terms of the property of the orbital. Since the ϕ_4° orbital of naphthalene has a node at the 1-position, its energy is little changed by the ϕ_0°, ϕ_N°, ϕ_{CN}°'s, and ϕ_{CHO}°'s in the cases of 1-naphthol,[8] 1-naphthylamine,[8] 1-naphthonitrile,[8] and 1-naphthaldehyde.

Assignment of the Photoelectron Spectra. The results of the orbital assignment will now be related to the PE spectra. The PE spectra of naphthalene have five bands in the region from 8 to 13 eV.[4,6,7,14] Table 1 shows that Bands I, II, III, IV, and V are assigned to the ionization corresponding to taking an electron away from the ϕ_5°, ϕ_4°, ϕ_3°, ϕ_2°, and ϕ_1° respectively. The PE bands corresponding to these ionization processes are con-

veniently indicated by the B_1, B_2, B_3, B_4, and B_5 notations respectively. The B_O, B_N, B_{CN}, and B_{CHO} notations indicate taking an electron away from the $\phi_O°$, $\phi_N°$, $\phi_{CN1}°$, and $\phi_{CHO1}°$ respectively (see Tables 3—10).

The PE spectra of naphthalene derivatives have been reported by several authors.[6-8] 1-Naphthol[8] has three bands, I, II, and III, in the region from 7 to 10 eV, while 2-naphthol has four bands, I, II, III, and IV, in the region from 7 to 11 eV. From Table 3, Bands I, II, and III of 1-naphthol are assigned to the B_1, B_2, and B_3 of naphthalene, while from Table 4 Bands I, II, III, and IV of 2-naphthol are assigned to the B_1, B_2, B_3, and B_4 of naphthalene respectively.

In the cases of 1- and 2-naphthylamines, there are six bands in the region from 7 to 13 eV.[7,8] Bands I, II, IV, V, and VI of 1-naphthylamine are assigned to the B_1, B_2, B_3, B_4, and B_5, while Bands I, IV, V, and VI of 2-naphthylamine are assigned to the B_1, B_3, B_4, and B_5 respectively. Band III of 1-naphthylamine is composed of the B_N, B_1, and B_3. Bands II and III of 2-naphthylamine are composed of the B_1 and B_2 and of the B_2 and B_3 respectively.

The PE bands of naphthonitriles have been reported by the same authors.[8] Bands I, II, and III for 1-naphthonitrile and Bands I, II, III, and IV for 2-naphthonitrile have been found. It may be seen from Tables 7 and 8 that they are assigned to the B_1, B_2, and B_3 for 1-naphthonitrile and to the B_1, B_2, B_3, and B_4 for 2-naphthonitrile.

Effects of the Electron-donating and Electron-accepting Properties on the Photoelectron Spectra. It is well known that the amino and hydroxyl groups have an electron-donating property, while the formyl and cyano groups have an electron-accepting property. In this subsection we will discuss the effect of these properties of the substituent on the PE spectra.

The PE spectra of naphthylamine, on the whole, are similar in appearance to the PE spectra of the corresponding naphthols. However, in passing from naphthols to naphthylamines, the individual bands undergo considerable changes in location.

The weight of the most important reference orbitals in naphthylamines is considerably smaller than that of the corresponding orbitals in naphthols. This suggests that amino substitution has a greater influence on the PE bands of naphthalene than does hydroxyl substitution. Since the calculated orbital energy is −9.7 eV for an amino group and −11.7 eV for a hydroxyl group, the higher the energy of the orbital of the substituent, the greater the mixing among the reference orbitals in the case of electron-donating substitution.

There may also be a similarity of the PE spectra between naphthonitriles and naphthaldehydes, as in the case between naphthols and naphthylamines.

It may be seen from Tables 7—10 that the weight of the most important reference orbitals in the individual orbitals of naphthaldehydes and the mixing among the local π-MO's of naphthalene and the orbital of the formyl group in naphthaldehydes are smaller than those in naphthonitriles. This suggests that the cyano substitution has a greater influence on the lower-energy PE bands of naphthalene than does the formyl substitution. The cyano and formyl groups have one occupied MO and one unoccupied MO. The calculated π-MO energies for the cyano group are $\varepsilon_{CN1} = -13.2209$ eV and $\varepsilon_{CN2} = -0.1855$ eV, while those for the formyl group are $\varepsilon_{CHO1} = -13.7252$ eV and $\varepsilon_{CHO2} = -0.7651$ eV. The energy difference between the unoccupied orbital of the formyl group and the occupied π-MO's of naphthalene is smaller than that between the unoccupied orbital of the cyano group and the occupied π-MO's of naphthalene. Therefore, the smaller the energy difference between the unoccupied orbital of the substituent and the occupied π-MO's of naphthalene, the smaller the mixing among the reference orbitals, this is in contrast with the electron-donating case.

The individual electronic absorption bands of naphthalene derivatives shift to the red relative to the corresponding bands of naphthalene whether the substituents are electron-donating or electron-accepting. The behavior of the individual electronic absorption bands of naphthalene derivatives can now be satisfactorily interpreted by the method of configuration analysis.[10,11,15] On the other hand, the PE spectra of naphthonitriles and naphthaldehydes shift to the lower energy of the corresponding bands of naphthalene. The PE spectra of naphthols and naphthylamines seem to shift to the higher energy relative to the corresponding bands of naphthalene. No simple explanation of the relationships observed in the PE spectra of naphthalene derivatives can be offered at the present time.

References

1) D. W. Turner, C. Baker, A. D. Baker, and C. R. Brundle, "Molecular Photoelectron Spectroscopy," John Wiley & Sons, New York, N. Y. (1969).
2) T. Koopmans, *Physica*, **1**, 104 (1934).
3) K. Kimura, S. Katsumata, Y. Achiba, H. Matsumoto, and S. Nagakura, *Bull. Chem. Soc. Jpn.*, **46**, 373 (1973).
4) P. A. Clark, F. Brogli, and E. Heilbronner, *Helv. Chim. Acta*, **55**, 1415 (1972).
5) F. Marschner and H. Goetz, *Tetrahedron*, **30**, 3159 (1974).
6) H. Bock, G. Wagner, and J. Krener, *Chem. Ber.*, **105**, 3850 (1972).
7) J. P. Maier, *Helv. Chim. Acta*, **57**, 994 (1974).
8) C. Utsunomiya, T. Kobayashi, and S. Nagakura, *Bull. Chem. Soc. Jpn.*, **48**, 1852 (1975).
9) H. Baba, S. Suzuki, and T. Takemura, *J. Chem. Phys.*, **50**, 2078 (1969).
10) S. Suzuki, T. Fujii, and H. Baba, *J. Mol. Spectrosc.*, **47**, 243 (1973).
11) S. Suzuki, T. Fujii, and T. Ishikawa, *J. Mol. Spectrosc.*, **57**, 490 (1975).
12) R. S. Becker and E. Chen, *J. Chem. Phys.*, **45**, 2403 (1966).
13) M. Bathey, Ph. D. Thesis, University of Queensland, Australia, 1966.
14) F. Brogli, E. Heilbronner, and T. Kobayashi, *Helv. Chim. Acta*, **55**, 274 (1972).
15) S. Suzuki and T. Fujii, *J. Mol. Spectrosc.*, **61**, 350 (1976).

Application of INDOR Method to a Relatively Slow Exchange System. OH Protons of the 1,3-Dihydroxyacetone Dimer in Dimethyl-d_6 Sulfoxide

Yoshihiro KURODA

Faculty of Pharmaceutical Sciences, Kyoto University, Sakyo-ku, Kyoto 606

(Received February 21, 1977)

The nuclear magnetic multiple-resonance method developed by Forsén and Hoffman for the study of exchange rates has been applied to the two different types of OH protons of the 1,3-dihydroxyacetone dimer in dimethyl-d_6 sulfoxide, *i.e.*, OH (α) and CH_2OH (β). Here, "decay" and "recovery" curves were obtained using the so-called "INDOR" method, instead of a rapid repetitive scan method. Since the INDOR method continuously monitors a peak height, decay and recovery curves as fast as 1 s can be drawn by storing them in a computer after a single scan. The concentration dependence was examined as a two-site exchange system by neglecting the small amount of water (γ) contained in the dimethyl sulfoxide solvent. Both the lifetime, τ, and the longitudinal relaxation time, T_1, obtained from this assumption correlate well with the concentration variation of the 1,3-dihydroxyacetone dimer. The difference in the types of OH protons on the concentration dependence is clearly seen for the latter parameter, T_1. From the triple-resonance experiments including γ, it was found that the β proton is more "labile" than the α.

One of the most powerful uses of nuclear magnetic resonance spectroscopy in physical chemistry is its application to rate processes, such as chemical exchange reactions, restricted internal rotations and ring inversions. Two types of experimental and analysis methods have been developed so far for studies using a continuous wave (cw) NMR spectrometer, one is the line-shape analysis method originated by Gutowsky, McCall, and Slichter[1,2] and further extended and widely applied by many investigators[3] and the other is the double- or multiple-resonance method presented by Forsén and Hoffman,[4,5] which will hereafter be referred to as the FH method. This latter method is somewhat specific, since it can be applied for relatively slow-rate processes and in a narrower range than the former, *i.e.*, in the 0.01—1 s^{-1} range of a first-order rate constant. Therefore, examples of investigations using the FH method have been relatively few up to now.[6] These limitations arise for theoretical and technical reasons, *i.e.*, the lifetime of an exchanging nucleus must be comparable with its spin-lattice relaxation time, T_1, and the "decay" of the signal intensity upon sudden irradiation to another signal must be accurately followed. This latter gives the upper limit of the rate process which can be followed. Forsén and Hoffman have employed the rapid repetitive scan method in a state of no spin and misadjustment of the field homogeneity which prevents signal distortion due to wiggling and maintains slow passage conditions. Anet and Bourn have devised their equipment to continuously receive the intensity of a sharp signal with the sample spining and with the help of a field-frequency lock system.[7] This method can handle somewhat more rapid processes and closer signals of exchanging nucleus than the rapid repetitive scan method.

In the present work, an attempt was made to deal with relatively fast rate processes for the FH method, *i.e.*, processes with lifetimes less than about one second. This fills the gap between the fast limit of the FH method and the slow limit of the line-shape analysis method and extends the rate constant range over which the FH method can be applied. For this purpose, continuous observation of the signal height, a method similar to that of Anet and Bourn was adopted although the necessary decay curves were obtained differently. The so-called "INDOR" technique, first described and applied by Baker,[8] was employed in this work. In order to follow and record fast changes in the signal height, CAT (time-averaging computer) was used. For a preliminary examination, a dimethyl sulfoxide solution of a 1,3-dihydroxyacetone dimer was chosen as an example and it was examined to what extent this INDOR technique could follow a fast rate process within the framework of the FH method.

Experimental

Materials. The highest purity 1,3-dihydroxyacetone dimer (hereafter abbreviated as DAD) was obtained from the Tokyo Kasei Kogyo Co., Ltd, and dimethyl-d_6 sulfoxide (DMSO-d_6) was obtained from the Stohler Isotope Chemicals (SIC) Co., Ltd. These were used without further purification including in the deoxygenation and drying procedures, since from the preliminary experiment the magnitude of the lifetimes, τ, and spin-lattice relaxation times, T_1, of the OH protons of DAD were appropriately suited to this purpose. The balancing of the magnitudes of these two parameters is a very important point of the FH method.[4,5]

NMR Measurements. All measurements were performed at 26 °C with a Varian HA-100 D spectrometer operating in the frequency sweep mode at 100 MHz and with a 20-dB RF-field attenuation. Tetramethylsilane was used as an internal lock signal. The leakage from the transmitter coil to the receiver coil was minimized as much as possible with probe tuning paddles to avoid receiver overload when perturbing H_2 and H_3 fields were switched on. The "INDOR" experiments were performed using a Hewlett-Packard Model 4204 A oscillator as an additional oscillator for observing the H_1 field. Attention was paid to the amplitude of the H_1 field so as not to reduce the observing signal height by saturation. For triple-resonance experiments, a Wavetek Model 111 oscillator was employed. The perturbing field strengths of H_2 and H_3 used were determined to sufficiently saturate the signals but not to cause receiver overload. A Varian C-1024 time-averaging computer (CAT) operating in the internal trigger mode was used to follow and to store the fast changes in the signal intensity and then to read out the data on the recorder of the HA-100 D spectrometer. The sweep time of the C-1024 was

arbitrarily set in the range from 2.5 to 10 s depending on the duration of the decay and recovery curves. A pen response time of 5 Hz was used for filtering.

Results and Discussion

1,3-Dihydroxyacetone (I) is known to be present as a dimer having a 1,4-dioxane structure (II) in the crystalline state. This form is maintained as the main species in a dimethyl sulfoxide solution, at least for a few hours after dissolution.[9] Figure 1 shows a typical proton magnetic resonance spectrum of DAD in a DMSO-d_6 solution (2.0 M) together with assignments using the notation and numbering shown in II. The weak signal at about 3.65 ppm is due to water protons and is also designated as γ. As is seen in Fig. 1, since the

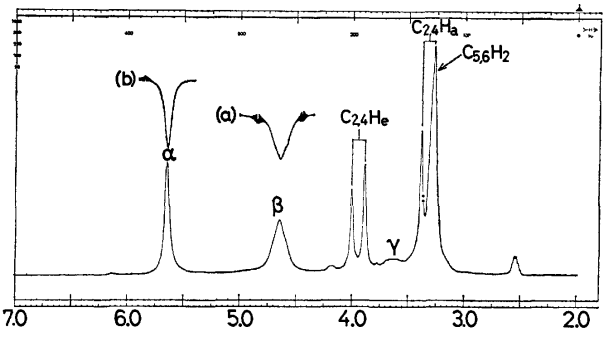

Fig. 1. The proton magnetic resonance spectrum of DAD observed in 2.0 M solution in DMSO-d_6, together with the assignments and INDOR spectra for α and β resonances. (a) INDOR spectrum for $\alpha(\beta)$, (b) INDOR spectrum for $\beta(\alpha)$.

two types of OH protons, α and β, are well separated from each other and also from the other signals, DAD can be irradiated safely by the strong rf fields inherent to the FH method. The concentration dependence of the features of the α and β signals is shown in Fig. 2, in which the α and β signals for 2.0, 1.0, 0.5, and 0.25 M solutions are presented. When the concentration was lowered, both the α and β signals became sharp. This was particularly clear for the β signals. This sharpening implies a slowdown in the exchange rate, although an increase in the spin-spin relaxation time, T_2, may also contribute to this sharpening. Accordingly, the sharpening of the α and β signals cannot be explained simply. It was difficult to monitor the γ signal for 2.0 M by the INDOR technique due to its weakness. When the solutions were diluted from 2.0 M, the γ signal shifted to higher field with concomitant narrowing of the line

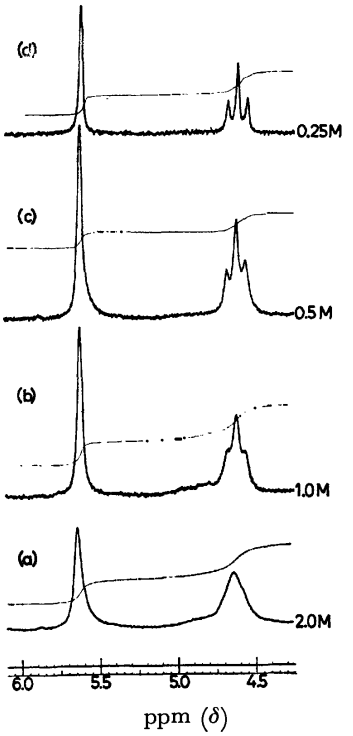

Fig. 2. The α and β resonances of DAD, showing the effect of concentration.
(a) 2.0 M, (b) 1.0 M, (c) 0.5 M, and (d) 0.25 M in DMSO-d_6.

width and at 0.25 M it overlapped the low-field signal of the $C_{2,4}H_a$ doublet. For these reasons, the exchange reactions of the α and β protons were first investigated using the INDOR technique over the 2—0.25 M range neglecting the presence of the γ proton. The elimination of the γ proton from the exchange pathway in the experiment gives an apparent lifetime, τ, and a spin-lattice relaxation time, T_1, which may be useful as relative parameters to observe trends. Subsequently, a three-site exchange system, which includes γ as an exchangeable site, was investigated for 1.0 and 0.5 M and compared with the results of the two-site exchange approximation.

Two-site Exchange System between α and β Protons. Figures 1 (a) and (b) show examples of INDOR spectra in cases where the α and β signals were monitored and the β and α signals were perturbed, respectively. Only one negative INDOR signal is obtainable in each case, since the spin transferred by chemical exchange from the saturating site simply reduces the monitoring signal intensity. Here, an abbreviation for the formal description of the multiple resonance experiment, is used with the nucleus under study outside the parenthesis and the nucleus being irradiated inside the parenthesis, *e.g.*, $\alpha(\beta)$ for case (a) and $\beta(\alpha)$ for case (b). If a recorder pen is set at the frequency of the bottom position of the INDOR spectrum and then if the irradiation field is switched on, the decay curve of the monitoring signal can be obtained by sweeping the CAT at a constant speed. Similarly, a recovery curve can be obtained when the radiation is switched off after the transient decay reaches a steady state. Figures 3 and 4 show the decay and recovery curves obtained at 2.0 and 0.25 M

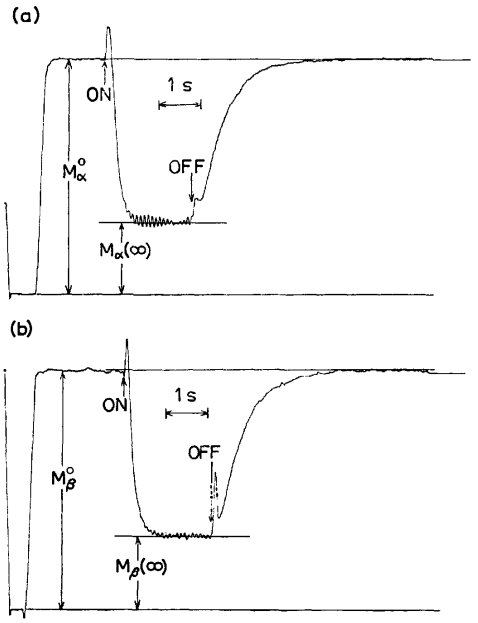

Fig. 3. The decay and recovery of the magnetization of DAD, 2.0 M in DMSO-d_6 solution for (a) $\alpha(\beta)$ and (b) $\beta(\alpha)$ arrangements. "ON" and "OFF" indicate the start and the removal of the irradiation, respectively.

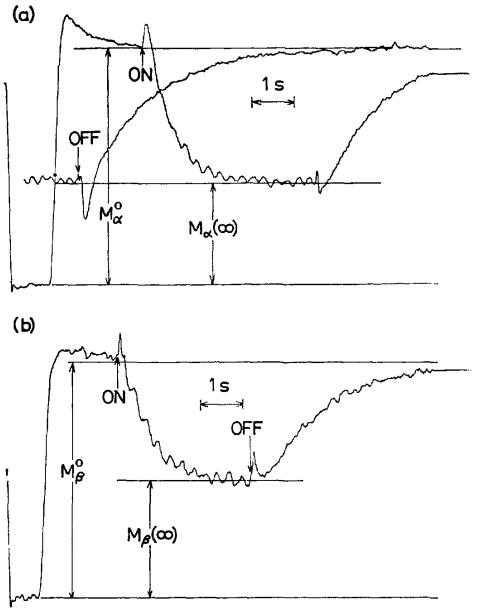

Fig. 4. As for legend to Fig. 3, except that 0.25 M in DMSO-d_6 solution was used.

for both $\alpha(\beta)$ and $\beta(\alpha)$ experimental arrangements. In analyzing the decay curves, the following three points were taken into account:

(a) There is a time lag until complete saturation after the irradiation power is switched on.

(b) A time lag due to pen response may be present. For example, in this experiment, a response frequency of 5 Hz was used, which causes a time lag of at most 0.2 s for the decay curve as a whole.

(c) "Shock noise" appears when the irradiation rf power is switched on or off, as Figs. 3 and 4 show. This noise also causes a lag in the recovery curve.

These three points introduce errors in the analysis of the decay curves. However, in practice, the scale of the decay curves is less than 10 cm, so that the time lag due to (b) may be less than 0.1 s. This time lag may have some effect in the case of the decay of a 2.0 M solution, but may not be as large for the case of the slow decay of a 0.25 M solution. The time lag due to (a) is inevitable, in principle, but due to (c), the decay curves were analyzed after the decay had passed through its initial value, *i.e.*, $M_\alpha{}^0$ or $M_\beta{}^0$. This delay may compensate the time lags due to (a) and (b) to approximately the same extent. Figure 5 shows the logarithmic plots $(\ln[M_1(t)-M_1(\infty)]$ *versus* $t)$ of the magnetization decay for 2.0, 1.0, 0.5 and 0.25 M solutions. The slopes of the lines give $\tau_{1\alpha}$=0.14, 0.21, 0.38, and 0.55 s and $\tau_{1\beta}$= 0.15, 0.31, 0.47, and 0.62 s from 2.0 to 0.25 M, respectively. From these τ_1, τ, and T_1 for each concentration can be calculated using Eqs. 2 and 10 of Ref. 4 and are plotted in Figs. 6(a) and (b), respectively. The results of two series of experimental trials are shown. In

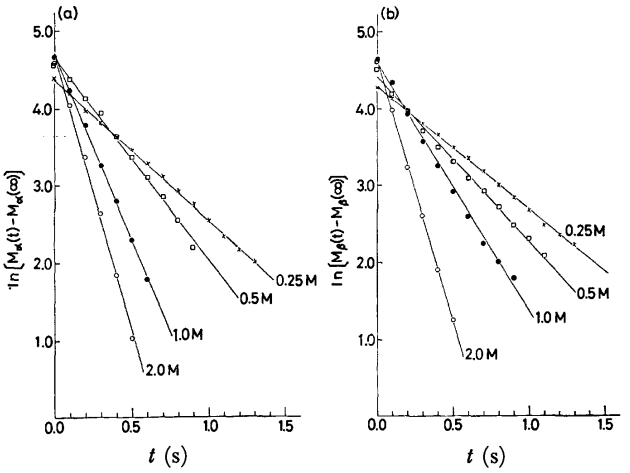

Fig. 5. Logarithmic plots (base e) of the decay of magnetization for (a) $\alpha(\beta)$ and (b) $\beta(\alpha)$ arrangements at various concentrations. The experimental points are taken from a smooth curve drawn through the decay curve "by-eye".

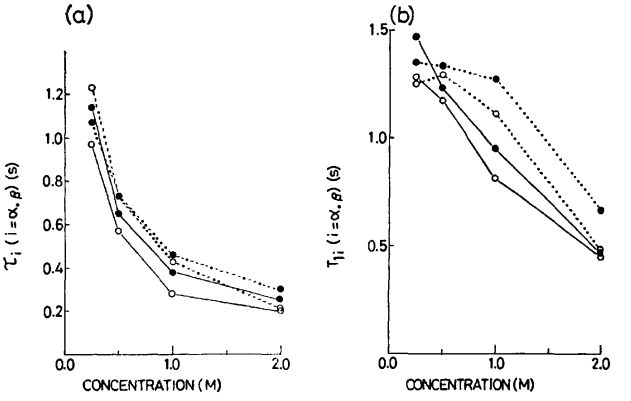

Fig. 6. The effect of concentration on (a) τ_i and (b) T_{1i} (i=α,β). ○: Experiment 1, ●: Experiment 2. ——: α, ------: β.

Experiment 1, sample solutions of 1.0, 0.5, and 0.25 M were prepared by successive dilution from a 2.0 M solution, whereas in Experiment 2, each sample solution was prepared by weighing the corresponding amount of DAD individually. These two series were made to see the extent of scatter of τ and T_1 by the sampling method. However, as shown in Figs. 6(a) and (b), both Experiments 1 and 2 give similar trends. This indicates that τ and T_1 are not appreciably influenced by a small difference in the water content arising from the difference in sampling methods.

As shown in Fig. 6(a), when the concentration is lowered, both τ_α and τ_β increase steeply. This trend clearly shows the slowing down of the exchange rate between the α and β protons which was implied by sharpening of the signals upon dilution, as seen in Fig. 2. The steep increase in τ indicates that the exchange reaction may be controlled by the collision probability which depends on the concentration. On the other hand, with regard to T_1, $T_{1\alpha}$, and $T_{1\beta}$ show different tendencies with $T_{1\alpha}$ increasing monotonically and $T_{1\beta}$ reaching a maximum at about 1.0 M. This difference may be caused by the difference in the magnetic environments of the α and β protons, namely, the β proton has neighboring methylene protons while the α proton does not.

For both Experiments 1 and 2, τ_β was slightly larger than τ_α. This is reasonable since $M_\beta{}^0$ is 1.1—1.2 times larger than $M_\alpha{}^0$. Another important point for checking

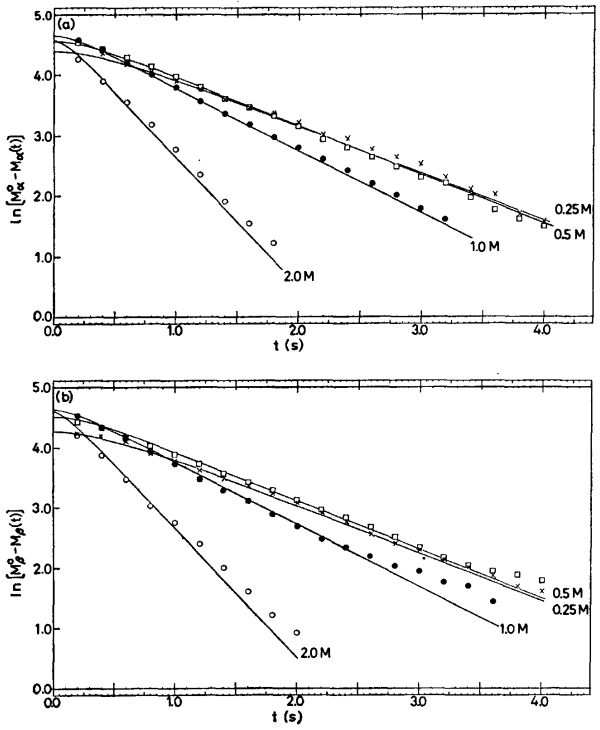

Fig. 7. Logarithmic plots (base e) of the recovery of magnetization for (a) α and (b) β nuclei at various concentrations. The full curves represent the theoretically predicted recoveries. The experimental points are taken from a smooth curve drawn through the recovery curve and are shown by the following symbols for each concentration: ○, 2.0 M; ●, 1.0 M; □, 0.5 M; ×, 0.25 M.

Table 1. Calculated parameters used to draw the recovery curves in Fig. 7

Concentration	type of proton	C_1(mm)	C_2(mm)	$\lambda_1(s^{-1})$	$\lambda_2(s^{-1})$
2.0 M	α	21.8	−119.8	11.8	2.1
	β	21.9	−120.3		
1.0 M	α	18.9	−124.4	7.0	1.0
	β	18.4	−120.9		
0.5 M	α	24.7	−120.2	3.9	0.8
	β	23.4	−113.9		
0.25 M	α	34.7	−115.7	2.6	0.8
	β	30.7	−102.2		

the reliability of τ and T_1 is to observe the degree of fitness between the recovery curve calculated using these parameters and the experimental recovery points. Since the recovery process is slower than the decay process and also is free from apprehension for receiver overload, a more precise curve than the decay curve is obtainable. Figure 7 shows the calculated recovery curves and the experimental points, with $\ln[M_i{}^0 - M_i(t)]$ plotted *versus* t. The necessary parameters for drawing the theoretically-determined full curves were calculated from Eqs. 15, 19, and 20 of Ref. 4 and are shown in Table 1. The scales of C_1 and C_2 are adjusted to the present experimental size in terms of $M_i{}^0$. All the theoretically-predicted curves are nearly straight on the whole and, since λ_1 is much larger than λ_2, the exponential part of λ_1 decays quickly to zero. In order to obtain the best fit, the experimental points were read off by delaying the null-point time by about 0.1—0.2 s from the actual moment that the irradiating field was removed. This type of time lag has also been reported by Forsén and Hoffman.[4] The resulting fit between the theoretically-predicted curves and the experimental points is satisfactory for all cases. These results show clearly that the two-site exchange approximation is justifiable for determining the relative tendencies and that the INDOR technique used here can follow the fast rate processes which is impossible by the rapid repetitive-scan method used up to now.

Three-site Exchange System for α, β, and γ Protons. In the case of a three-site exchange system, including γ which originates from the water protons, exactly the same procedures as those for the two-site exchange system can be utilized, except that a triple resonance is considered. The triple resonance is rather difficult to carry out, since it causes more beating than does double resonance. However, fortunately, this was not such a serious problem in the present experiments. Figure 8 shows, in level-diagram form, the concentration dependence of the steady-state ratios necessary for calculating τ_1 and λ_{ij}. Ratios for a 0.25-M solution are included for reference, although the measurement of the γ signal at this concentration is somewhat questionable because of overlapping with other signals. The parameter λ_{ij} is the probability per unit time for a nucleus at site i to be transferred to site j and is generally related to the life time τ_i by

$$1/\tau_i = \sum_{j \neq 1} \lambda_{ij}. \quad (1)$$

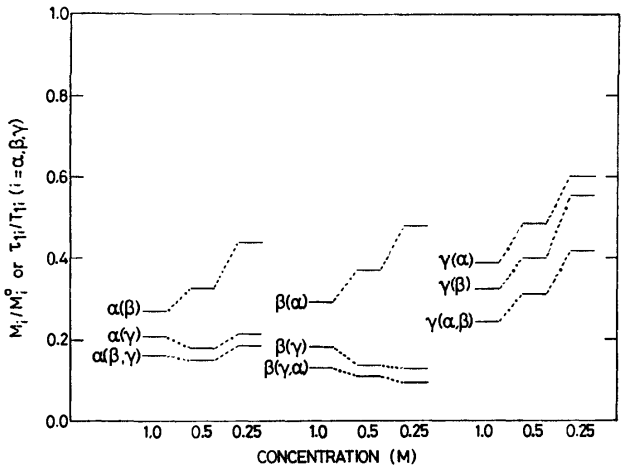

Fig. 8. The schematic illustration of the intensity ratios M_i/M_i^0 and τ_{1i}/T_{1i} for various experimental arrangements. Experiment 1 series of samples were used. Double resonance experiments ($\alpha(\beta)$ *etc.*) give ratios M_i/M_i^0 and triple resonance experiments ($\alpha(\beta,\gamma)$ *etc.*) give ratios τ_{1i}/T_{1i}.

TABLE 2. TIME CONSTANTS OBTAINED FROM THE DECAY CURVES TREATED AS THREE-SITE EXCHANGE SYSTEMS

Concentration	Type of proton i	τ_{1i}(s)	T_{1i}(s)	τ_i(s)	τ_i(s) from Eq. 1
1.0 M	α	0.13	0.85	0.16	0.18
	β	0.11	0.91	0.12	0.16
	γ	0.14	0.58	0.18	0.21
0.5 M	α	0.17	1.05	0.20	0.23
	β	0.14	1.32	0.16	0.18
	γ	0.26	0.84	0.39	0.41

Table 2 shows the time constants which were obtained from an analysis of the triple-resonance decay curves. In the triple-resonance experiment, when the γ site was included as the irradiation site, the transient decay rate increased above that of the double-resonance case. This effect results in a smaller value of τ_1 than that of the corresponding two-site exchange approximation. However, it is interesting to note that it only affects the magnitude of τ leaving that of T_1 almost unchanged.

TABLE 3. CALCULATED λ_{ij} IN s^{-1} FOR 1.0 M (LEFT) AND 0.5 M (RIGHT) SOLUTIONS

i \ j	α	β	γ
α	—	2.5, 1.2	3.0, 3.0
β	1.9, 1.1	—	4.6, 4.3
γ	1.8, 0.9	3.0, 1.6	—

Table 3 shows the values of λ_{ij} calculated from Eqs. 7 and 8 of Ref. 5, using the necessary values given in Table 2 and Fig. 8. The following ratios were also utilized: $M_\alpha^0 : M_\beta^0 : M_\gamma^0 = 1 : 1.1 : 1.4$ for 1.0-M and 1 : 1.2 : 3.0 for 0.5 M-solutions. These were obtained by integrating the corresponding band of the single-resonance spectrum. Before using the values of λ_{ij} to attempt to obtain significant information, the reliability

TABLE 4. THE RATIO OF THE MAGNETIZATION WHICH FLOWS IN A SITE TO THAT WHICH EFFUSES FROM THE SITE PER UNIT TIME

Type of proton	Concentration 1.0 M	0.5 M
α	0.8	1.0
β	0.9	0.9
γ	1.2	1.1

of these values must be checked. Since λ_{ij} depends on the difference between two asymptotic intensity ratios of similar magnitude, they may include large errors.[5] One way of checking the reliability of λ_{ij} is to test the agreement between the τ_i calculated from λ_{ij} using Eq. 1 and those calculated from the decay curves. In the last column of Table 2, the values of the τ_i calculated from λ_{ij} are given. As can be seen from this table, the agreement is satisfactory for all cases. The another important check is to test whether or not these λ_{ij} satisfy the balance equations of Ref. 5, namely, the magnetization which flows into a site must be equal to that which effuse from the site per unit time. This is shown in Table 4 as the ratio of the former to the latter for each site. All the calculated ratios are nearly equal to unity, so that the balance equations can be said to be well satisfied. Based on these checks, it can be said that the probability of proton transfer is in the following order of magnitude: $\beta\rightarrow\gamma > \alpha\rightarrow\gamma > \gamma\rightarrow\beta > \alpha\rightarrow\beta > \beta\rightarrow\alpha > \gamma\rightarrow\alpha$. This order indicates that:

(a) The probability of proton transfer is larger in the direction of the β and α protons to the γ proton than is the direct exchange between α and β protons. This implies that proton exchange between α and β sites is accelerated by the presence of water protons.

(b) The β proton is more "labile" than is the α proton. This is consistent with the well-known fact that primary alcohols are more acidic than tertiary alcohols and that the extent of esterification of the former is larger than that of the latter *etc.*,[10] although for DAD, the β nucleus is the hydrogen of the hydroxyl of a hemiacetal, which can be thought of as a fairly labile hydrogen.

Presently, the INDOR technique is a very popular method for analyzing spin-coupled spectra, with an appropriate attachment often being installed in commercially-available CW NMR spectrometers. This work was undertaken with the intention of applying this technique to the investigation of rate processes. It was shown that with the aid of CAT, the INDOR technique is more suitable and easier to use for following fast changes in magnetization than is the rapid repetitive-scan method. This will enable relatively fast rate processes to be investigated using the elegant multiple-resonance method presented by Forsén and Hoffman for the study of rate processes together with relaxation processes.

References

1) H. S. Gutowsky, D. W. McCall, and C. P. Slichter, *J. Chem. Phys.*, **21**, 279 (1953).

2) J. A. Pople, W. G. Schneider, and H. J. Bernstein, "High-resolution Nuclear Magnetic Resonance," McGraw-Hill, New York (1959), Chap. 10.
3) L. M. Jackman and F. A. Cotton, Ed, "Dynamic Nuclear Magnetic Resonance Spectroscopy," Academic Press, New York (1975).
4) S. Forsén and R. A. Hoffman, *J. Chem. Phys.*, **39**, 2892 (1963).
5) S. Forsén and R. A. Hoffman, *J. Chem. Phys.*, **40**, 1189 (1964).
6) J. H. Noggle and R. E. Schirmer, "The Nuclear Overhauser Effect, Chemical Applications," Academic Press, New York (1971), Chap. 7.
7) F. A. L. Anet and A. J. R. Bourn, *J. Am. Chem. Soc.*, **89**, 760 (1967).
8) E. B. Baker, *J. Chem. Phys.*, **37**, 911 (1962); E. B. Baker and L. W. Burd, *Rev. Sci. Instrum.* **34**, 234 (1963).
9) L. Davis, *Bioorg. Chem.*, **2**, 197 (1973).
10) R. T. Morrison and R. N. Boyd, "Organic Chemistry," 2nd ed, Allyn and Bacon, Inc., Boston (1966), Chap. 16.

Pentamethylnitrosobenzene as a Spin-trapping Agent

Takahisa DOBA, Tsuneki ICHIKAWA, and Hiroshi YOSHIDA
Faculty of Engineering, Hokkaido University, Kita-ku, Sapporo 060
(Received March 3, 1977)

Pentamethylnitrosobenzene synthesized readily from pentamethylbenzene was studied for utilization in a spin-trapping technique. In a benzene solution it forms a dimer with a dissociation constant of $10^{5.26}\exp(-50/RT)$ in units of kJ/mol. It traps the *t*-butyl radical with the trapping rate constant of 1.4×10^{8} mol^{-1} dm^{3} s^{-1} at 299 K. It is thus an efficient spin-trapping agent, even though only a fraction of it is reactive with the short-lived free radicals because the equilibrium lies more on the side of the dimeric form. Electron spin resonance parameters were determined for the spin-adduct radicals derived from alkyl, alkoxyl, and phenyl radicals with this trapping agent. These free radicals were found to attach exclusively to the nitrogen atom of the nitroso compound.

Aliphatic and aromatic nitroso compounds have been widely used as spin-trapping agents for the spin-trapping technique, whereby short-lived free radicals in a reaction system attach to the trapping agents to form stable nitroxide (or anilino-type) radicals and are indirectly identified by means of conventional electron spin resonance (ESR) measurements.[1,2] Although available rate constant is very scanty for reactions between a trapping agent and a short-lived free radical,[3-5] nitrosobenzene appears more reactive compared with its alkyl-substituted derivatives. A drawback of this trapping agent is that its spin-adduct radicals generally show complex hyperfine structures in ESR spectra because of the ring protons, which renders difficult the identification of the trapped radicals.[6] On the other hand, 2,4,6-tri-*t*-butylnitrosobenzene (BNB) yield well-resolved hyperfine structures of its adduct radicals, but is much less reactive with short-lived free radicals.[7] Pentamethylnitrosobenzene (PMNB) is expcted to give a simpler hyperfine structure and to be moderately reactive, as is nitrosodurene,[8] thus being a useful spin-trapping agent. However, PMNB has not been studied as yet. This particular nitroso compound has one advantage as a spin-trapping agent in that it can be synthesized very readily from commercially-available pentamethylbenzene.[9,10] The present report will present several aspects of PMNB as a spin-trapping agent.

Results and Discussion

ESR Spectra of Spin-adduct Radicals. A typical ESR spectrum of spin-adduct radicals is shown in Fig. 1A. When a methyl radical generated in a benzene solution of methyl iodide and tributylstannane is trapped with PMNB, an adduct radical of the nitroxide type is formed and can be identified from the hyperfine splittings due to one nitrogen nucleus and three protons at the β-position with respect to the oxygen atom of the nitroxyl group (see the observed hyperfine splitting constants given in Table 1). Figure 1 also shows methyl-radical adducts from nitrosobenzene and BNB, for comparison. The adduct from PMNB shows broader

TABLE 1. HYPERFINE SPLITTING CONSTANTS AND *g*-VALUES AT 299 K FOR SEVERAL NITROXIDE-TYPE SPIN ADDUCT RADICALS FORMED FROM PENTAMETHYLNITROSOBENZENE AS A SPIN-TRAPPING AGENT IN BENZENE SOLUTIONS. PREVIOUS RESULTS FOR TRI-*t*-BUTYLNITROSOBENZENE ARE ALSO SHOWN FOR COMPARISON

Trapped radical	Radical source	PMNB, Present results			BNB, by Terabe *et al.*[a]		
		g-Value	Splitting const		*g*-Value	Splitting const[b]	
			a_N	$a_{\beta\text{-H}}$		a_N	$a_{\beta\text{-H}}$
$\cdot CH_3$	$CH_3I+(n\text{-}C_4H_9)_3SnH$	2.0058	1.38	1.23	2.0060	1.303	1.233
$\cdot CH_2CH_2CH_3$	$n\text{-}C_3H_7Cl+\gamma$	2.0058	1.42	1.12	2.0060	1.339	1.783
$\cdot CH_2CH_2CH_2CH_3$	$(n\text{-}C_4H_9)_3SnH+h\nu$	2.0060	1.37	1.13	2.0061	1.344	1.797
$\cdot CH(CH_3)_2$	$CHCl(CH_3)_2+\gamma$	2.0059	1.39	0.97	2.0060[c]	1.329	2.219
$\cdot CH(CH_3)CH_2CH_3$	$CHCl(CH_3)C_2H_5+\gamma$	2.0058	1.37	0.78	2.0061[c]	1.333	2.225
$\cdot C(CH_3)_3$	$t\text{-}C_4H_9NO+h\nu$	2.0060	1.36	—	Anilino-type		
$c\text{-}\dot{C}_6H_{11}$	$c\text{-}C_6H_{12}+\gamma$	2.0058	1.40	0.76	Anilino-type		
$\cdot CH(CH_3)C_6H_5$	$CH_3CHClC_6H_5+\gamma$	2.0060	1.39	0.85	Anilino-type		
$\cdot C_6H_5$	$[C_6H_5C(O)O:]_2+h\nu$	2.0057	1.00	0.28[d] 0.09[d]	2.0057	0.988	0.286[d] 0.261[d] 0.092[d]
$\cdot CH(CH_3)OC_2H_5$	$(C_2H_5)_2O+\gamma$	2.0058	1.40	0.46	—		
$\cdot C(CH_3)O$	$(CH_3CO)_2+h\nu$	2.0058	1.32	—	—		
$\cdot C(CN)(CH_3)_2$	$[(CH_3)_2C(CN)N:]_2+h\nu$	2.0063	1.30	—	Anilino-type		

a) Ref. 11. b) Other small coupling constants are omitted. c) Anilino-type adduct is also generated. d) Splitting constants due to ring protons.

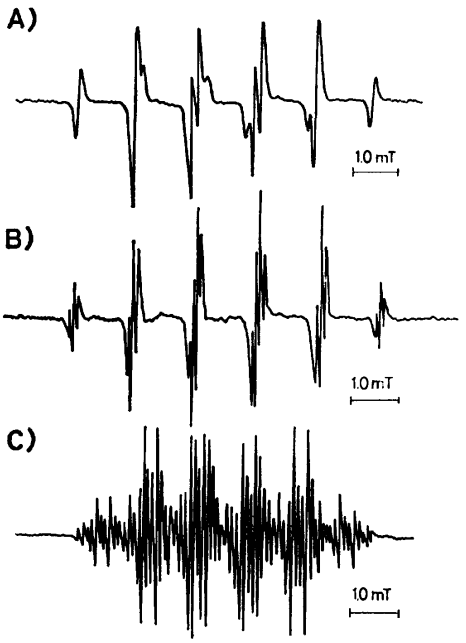

Fig. 1. ESR spectra of the spin adduct radicals generated by trapping methyl radical with (A) PMNB, (B) BNB, or (C) nitrosobenzene in benzene solution. The methyl radical was generated by the photolysis of tributylstannane in the presence of methyliodide.

hyperfine lines than do the adducts from nitrosobenzene and BNB, but it gives a much simpler hyperfine structure facilitating the identification of the trapped radical.

Table 1 summarizes the observed ESR parameters at 299 K for a number of adduct radicals generated from short-lived free radicals with PMNB in benzene. The short-lived free radicals were in turn generated by the photolysis or γ-radiolysis of appropriate radical sources. The observed ESR parameters are similar to those reported for nitrosodurene.[8] The hyperfine splitting due to the nitrogen atom lies in the range 1.42—1.30 mT, except for the phenyl radical adduct. Hyperfine splitting due to the β-proton(s) of the alkyl-radical adducts tends to decrease with the number of hydrogen (or with an increasing number of carbon) atoms attached to the β-carbon atom (the α-carbon in the trapped alkyl radicals). This trend is similar to that for nitrosobenzene and nitrosodurene,[8] being opposite to that for BNB[11] as shown in Table 1.

All the short-lived free radicals examined were found to attach to the nitrogen atom rather than to the oxygen atom of the nitroso compound, thereby giving nitroxide radicals. No formation of anilino-type adduct radicals was observed.

Monomer-Dimer Equilibrium. As in the case of aliphatic nitroso compounds[12] and nitrosodurene,[8] PMNB is present in solution mostly as a dimer, which is inactive in trapping short-lived free radicals. PMNB shows a weak optical absorption band with a maximum at 790 nm and an intense band with a maximum at 324 nm. The former band is due to the $n\pi^*$ transition of the monomeric form, and the latter to the dimeric form. Changing the temperature causes complementary change in the intensity of both the bands, higher temperature favoring the monomeric form. According

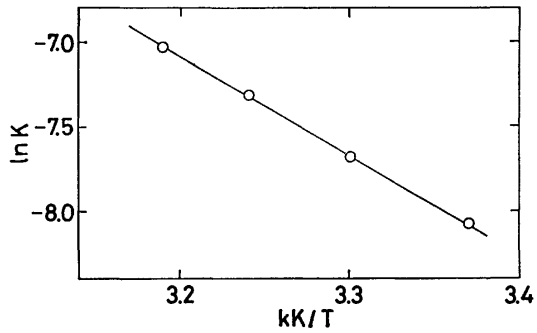

Fig. 2. Dependence of the dimer-monomer equilibrium constant for PMNB in benzene on reciprocal temperature.

to the well-known relationship, $c/OD = 1/2\varepsilon + 1/K\varepsilon^2 OD$, where OD represents the optical density at 790 nm and c represents the total concentration of PMNB based on its dimeric form, the dissociation constant K was determined at several temperatures, as shown in Fig. 2. The extinction coefficient ε was also determined to be 83.3 $mol^{-1}\ dm^3\ cm^{-1}$, almost independent of temperature.

The temperature dependence of the equilibrium constant is expressed by the equation, $K = 10^{5.26}\exp(\Delta H/RT)$, where the heat of dissociation is -50 kJ/mol. This means that only 12% of the 10 mmol dm^{-3} PMNB in a benzene solution is in monomeric form and is effective in the trapping reaction at 300 K. This behavior is very similar to that of nitrosodurene.[8]

Rate Constant for the Spin-trapping Reaction. In a separate investigation, the rate constant for the spin-trapping reaction of 2-methyl-2-nitrosopropane with the *t*-butyl radical, being $3.3 \times 10^6\ mol^{-1}\ dm^3\ s^{-1}$ at 299 K in benzene solution, was investigated.[7] Based on this figure, the rate constant for PMNB was determined by studying the competition between PMNB and 2-methyl-2-nitrosopropane in trapping the *t*-butyl radical generated by the photolysis of the latter. Figure 3 shows the linear increase in the concentration of the

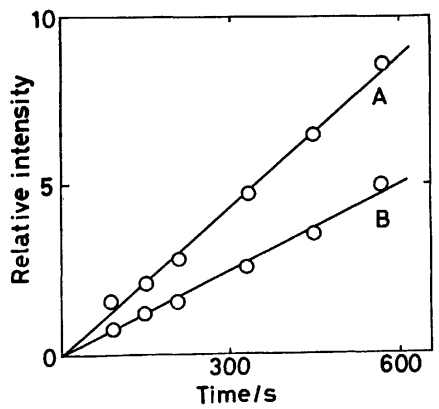

Fig. 3. Yield of the *t*-butyl radical adducts formed from (A) PMNB and (B) 2-methyl-2-nitrosopropane in benzene at 299 K as a function of photolysis time. The *t*-butyl radical was generated by the photolysis of the latter spin trapping agent 0.0276 mol dm^{-3} in benzene solution, where the former trapping agent (0.0012 mol·dm^{-3}) was coexisting.

t-butyl adducts with both the trapping agents coexisting in the benzene solution during the early period of photolysis. From the observed slopes and the concentration of the trapping agents present, the rate constant for PMNB was determined to be 1.4×10^8 mol^{-1} dm^3 s^{-1}, based on the concentration of PMNB in monomeric form, in the reaction with the *t*-butyl radical at 299 K.

Although very little has been reported on spin-trapping rate constants, the data so far available indicate that trapping reactions proceed with rate constants of 10^5—10^8 mol^{-1} dm^3 s^{-1}, depending on the spin-trapping agent used and the radical trapped.[3-5] PMNB appears to be a comparatively reactive spin-trapping agent. It was also found to be a more efficient trapping agent than BNB, even when the monomer-dimer equilibrium of PMNB is taken into account.

Experimental

Synthesis. According to McKillop *et al.*,[9] pentamethylbenzene is converted to $C_6(CH_3)_5Tl(OCOCF_3)_2$, with the yield of this organothallium compound being *ca.* 60%. It was then converted into PMNB upon treatment with nitrosyl chloride with a yield of almost 100% by applying the method reported by Taylor and Danforth for the general synthesis of aromatic nitroso compounds.[10] The PMNB thus obtained was purified by recrystallization from an acetone solution three times. Its observed melting point of 427 K was unchanged by further purification. This value is in agreement with the previously-reported melting point of 425—428 K.[13] Elementary analysis gave the following results. Found: C, 74.51; H, 8.56; N, 7.8%. Calcd for $C_{11}H_{15}NO$: C, 74.52; H, 8.54; N, 7.9%.

PMNB was synthesized much more easily than nitrosodurene. This is an advantage of PMNB as a spin-trapping agent over nitrosodurene, although PMNB shows similar behavior in spin-trapping reactions and gives similar features of the hyperfine structures of the adduct radicals as does nitrosodurene.

Photolysis and Radiolysis. The short-lived free radicals trapped were generated by photolysis or radiolysis at room temperature from appropriate radical sources present in a benzene solution of 10 mmol dm^{-3} PMNB sealed in a quartz ESR tube after degassing by the freeze-pump-thaw technique. The solvent and the radical sources were of the highest purity commercially available and were used as received. The photolysis was carried out with light from an ultra-high pressure Hg lamp using a wavelength selected by a set of filters, so that only the radical sources were excited. The radio ysis was carried out with ^{60}Co γ-rays to a dose of approximately 0.1 Mrad.

ESR Measurements. Spin-adduct radicals were observed using a conventional X-band ESR spectrometer (JEOL, Model 2X) at 299 K. Their *g*-value was determined with reference to that of polycrystalline DPPH, 2.0036.[14] The hyperfine splittings were corrected with reference to that of Fremy's salt in aqueous solution, 1.300 mT.[15]

Optical-absorption Measurements. The optical absorption of PMNB in benzene was recorded with a recording spectrophotometer (Hitachi, Model EPS-3T). The sample solutions in a quartz cell having an optical path length of 1.0 cm were examined without degassing. Temperature was controlled in a water bath using a Dewar vessel with quartz windows.

This work was supported by the Science Fund of the Japanese Ministry of Education (No. 0.85010, 1975).

References

1) C. Lagercrantz, *J. Phys. Chem.*, **75**, 3466 (1971).
2) E. G. Janzen, *Acc. Chem. Res.*, **4**, 31 (1971).
3) E. G. Janzen, C. A. Evans, and Y. Nishi, *J. Am. Chem. Soc.*, **94**, 8236 (1972); E. G. Janzen and C. A. Evans, *ibid.*, **95**, 8205 (1973); E. G. Janzen and C. A. Evans, *ibid.*, **97**, 205 (1975).
4) F. P. Sargent, *J. Phys. Chem.*, **81**, 89 (1977).
5) M. J. Perkins and B. P. Roberts, *J. Chem. Soc., Chem. Commun.*, **1973**, 173.
6) S. Terabe and R. Konaka, *J. Chem. Soc., Perkin Trans. 2*, **1972**, 2163.
7) T. Doba, T. Ichikawa, and H. Yoshida, *Bull. Chem. Soc. Jpn.*, **50**, 3158 (1977).
8) S. Terabe, K. Kuruma, and R. Konaka, *J. Chem. Soc., Perkin Trans. 2*, **1972**, 1252.
9) A. McKillop, J. S. Fowler, M. J. Zesko, and J. D. Hunt *Tetrahedron Lett.*, **29**, 2423 (1969).
10) E. C. Taylor and R. H. Danforth, *J. Org. Chem.*, **38**, 2088 (1973).
11) S. Terabe and R. Konaka, *J. Chem. Soc., Perkin Trans. 2*, **1973**, 369.
12) J. C. Stowell, *J. Org. Chem.*, **36**, 3055 (1971).
13) L. I. Smith and F. L. Taylor, *J. Am. Chem. Soc.*, **57**, 2460 (1935).
14) R. G. Bennett and A. Henglein, *J. Chem. Phys.*, **30**, 1117 (1959).
15) S. I. Weissman and D. Banfill, *J. Am. Chem. Soc.*, **75**, 2534 (1953).

Crystal Structure and Electrical Conductivity of Tetrathiafulvalene Thiocyanate (TTF)(SCN)$_{0.57}$

Hayao KOBAYASHI and Keiji KOBAYASHI*

Department of Chemistry, Faculty of Science, Toho University, Chiba 274

**Department of Chemistry, College of General Education, The University of Tokyo, Komaba, Meguroku, Tokyo 153*

(Received March 8, 1977)

The organic conductor, (TTF) (SCN)$_{0.57}$, is a quasi-one-dimensional non-stoichiometric compound, which crystallizes in a tetragonal system having a $P4_2/mnm$ space group. The lattice constants are $a=11.154$ (3) and $c=3.607$ (2) Å. TTF molecules form segregate eclipsed stacks with thiocyanate ions occupying the channels between the stacks. The intermolecular distance between adjacent TTF molecules is 3.607 Å. The room-temperature electrical conductivity is 85—310 $(\Omega\,cm)^{-1}$. A series of *resistance jumps* are observed in the temperature-dependent resistivity curves.

Considerable work has recently been focussed on attempting to understand the unusual physical properties of the quasi-one-dimensional salts of organic radicals. Unlike a crystal of (TTF)(TCNQ) composed of segregated stacks of TTF and TCNQ, crystals of (TTF)(X) (X=I, Br, Cl) contain only TTF columns. The large room-temperature conductivities of (TTF)(X) (200—500 $(\Omega\,cm)^{-1}$), comparable to that of (TTF)-(TCNQ), are attributed to the characteristic columnar structures.[1-4]

In this paper, the crystal structure and the elctrical conductivity of 1,4,5,8-tetrathiafulvalene thiocyanate, (TTF)(SCN)$_{0.57}$, are reported.

Experimental

Tetrathiafulvalene was synthesized according to the published procedure.[5] After recrystallization twice from a cyclohexane–hexane solution, TTF was converted to tetrafluoroborate $(TTF)_3(BF_4)_2$. Tetrathiafulvalene thiocyanate crystals having the approximate composition, $(TTF)_{11}(SCN)_6$ (or (TTF)(SCN)$_{0.545}$),[6] were easily prepared from $(TTF)_3(BF_4)_3$ and tetrabutylammonium thiocyanate[7] *via* methathesis in hot acetonitrile.

Oscillation and Weissenberg photographs show the crystals to be tetragonal. The systematic absence of $h0l$ with $h+l=2n+1$ and of $0k0$ with $k=2n+1$ indicate that the space group is $P4_2/mnm$, $P4_2nm$ or $P\bar{4}n2$. The unit-cell dimensions, as determined by means of a diffractometer using Mo $K\alpha$ radiation, are $a=11.154(3)$ and $c=3.607(2)$ Å. The density measured using the flotation method was 1.756 ± 0.015 g cm^{-3} and the corresponding composition of the complex was calculated to be (TTF) (SCN)$_{0.57\pm0.03}$. No additional weak satellite-type reflections[1,2] indicating the existence of two distorted sublattice cations and anions were observed (see note added in proof). The intensity data were collected with a Rigaku automated four-circle diffractometer. Owing to the small size of the specimen, only 120 independent reflections of 461 accessible reflections ($2\theta\leqq55°$) were recorded sufficiently accurately ($|F|>3\sigma$).

Structure Determination and Discussion

The trial structure was easily deduced from the Patterson syntheses and refined by the block-diagonal least-squares method. In view of the planar structure of TTF, the space group was assumed to be $P4_2/mnm$ which was confirmed by the reasonable convergence of the structure at a later stage of refinement. Fourier calculations based on the atomic parameters of TTF showed a columnar distribution of the electron densities at $(0,1/2,z)$ $(0\leqq z<1)$ and that the magnitude of the electron density is almost constant along the crystallographic c axis, indicating one-dimensional disorder of the atomic positions of the S, C, and N atoms. Therefore, the scattering factors of the S, C, and N atoms were evaluated by assuming a one-dimensionally random distribution and a common isotropic thermal parameter. The R value was reduced smoothly to 0.045. The final atomic parameters are given in Table 1.

The structure viewed along the c axis is shown in Fig. 1. TTF has D_{2h}(mmm) symmetry and is stacked in an eclipsed column. Similar eclipsed stacks have been found in the crystals of TTF–halogen systems. The c axis is perpendicular to the molecular plane. The interplanar distance of 3.607 Å is comparable to those in (TTF)(Br)$_{0.71-0.76}$ (3.57 Å[1]) and (TTF)(I)$_{0.71}$ (3.55 Å[2]) crystals, but is much larger than the interplanar distances of TCNQ in the "ring-external bond type" columns of the high-conductive TCNQ salts (3.17—3.26 Å[8]). Considering the large intermolecular distances, the "metallic" conductivities[1,3,4] are undoubtedly due

Table 1. The final atomic parameters ($\times10^4$)

The standard deviations are in parenthesis. The temperature factors are of the form $\exp[-2\pi^2(h^2U_{11}a^{*2}+k^2U_{22}b^{*2}+l^2U_{33}c^{*2}+2hkU_{12}a^*b^*+2hlU_{13}a^*c^*+2klU_{23}b^*c^*)]$.

	x	y	z	U_{11}	U_{22}	U_{33}	U_{12}	U_{13}	U_{23}
S	3054 (2)	4902 (3)	0	433 (12)	598 (17)	625 (14)	2 (8)	0	0
C(1)	4580 (15)	4580	0	347 (95)	347	707 (112)	24 (20)	0	0
C(2)	2558 (10)	3423 (10)	0	555 (65)	739 (75)	831 (89)	−47 (22)	0	0
H	1669 (102)	3452 (105)	0	6.9[a]					
(SCN)[b]	0	5000	(0—1.0)	3.5					

a) Isotropic temperature factor (Å^2). b) The atomic position of the SCN anion is disordered along the c axis.

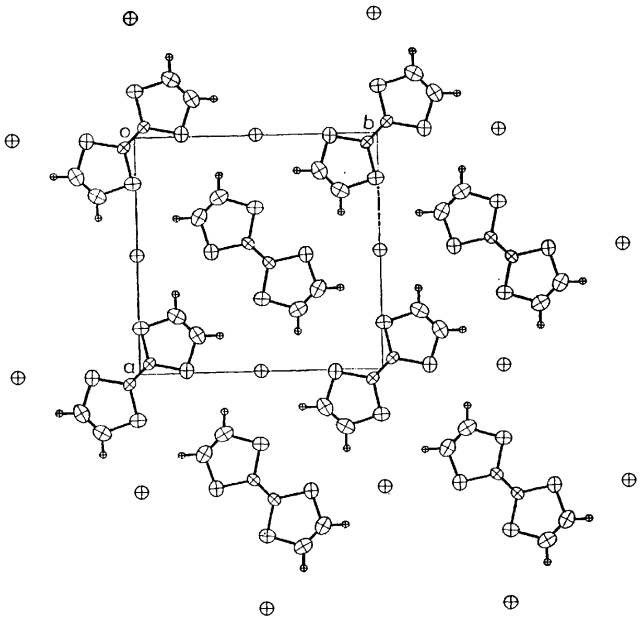

Fig. 1. The (001) projection of the $(TTF)(SCN)_{0.57}$.

to the intermolecular overlap of the atomic orbitals of the sulfur atoms. As observed in the TTF-halogen crystals, the TTF columns form tunnels. Like $(TTF)(SCN)_{0.57}$, $(TTF)(Cl)_{0.92}$ has a tetragonal structure and the tunnels are occupied by the disordered chlorine anions.[2] (see note added in proof). However in $(TTF)(Br)_{0.71-0.76}$ and $(TTF)(I)_{0.71}$, there are separate cation and anion sublattices.[1,2] This incommensurability produces additional "satellite-type" reflections[1,2] due to the periodically-modulated superstructure. As originally pointed out by Johnson and Watson,[2] the general features of the crystal structure of these salts can be summarized as follows:

(1) If the radius of the cation is small enough to enter the tunnel formed by the TTF columns ($r \leqq 1.8$ Å (the Cl ionic radius)), the crystal is tetragonal. Owing to loose packing, the atomic positions of the anions tend to be disordered in the tunnels.

(2) If $r \geqq 1.96$ Å (the Br ionic radius), the anions cannot enter the tunnel without distortion of the "TTF sublattice" so that a modulated superlattice is formed. Due to compact packing, the atoms are regularly arranged.

Consequently, it may be said that the repulsive force between anions and cations plays an important role in the appearance of the modulated superlattices of the TTF-halogen systems.

The tunnel structure of $(TTF)(SCN)_{0.57}$ appears to indicate the non-stoichiometric nature of the crystal. Considering that monoclinic $(TTF)(Br)_x$ can exist over the range of compositions, $0.71 \leqq x \leqq 0.76$, the number of anions stacked in a tunnel does not appear to be necessarily constant. Therefore, the composition obtained by Wudl *et al.*, $(TTF)_{11}(SCN)_6$, may be regarded as approximate. Since the distance between the adjacent atoms (ions) must be larger than the sum of the two van der Waals (ionic) radii, the value of x for the $(TTF)(X)_x$ system must be smaller than $R/2r$, where $R(\approx 3.60$ Å) is the intermolecular distance between neighboring TTF molecules and r is the ionic radius of the anion. The calculated maximum values (with observed values in parenthesis) are 0.83 (0.71), 0.92 (0.71—0.76), 1.0 (0.92), and 0.59 (0.583) (see note added in proof) for the iodide, bromide, chloride and thiocyanate, respectively. In this connection, it may be worthwhile to point out that 1 : 1 bromide ($x=1.0$) is stacked quite differently.[1]

The bond lengths and angles are given in Table 2. Considering the fairly large standard deviations, the values for $(TTF)(SCN)_{0.57}$ appear to be in good agreement with those for other TTF salts.

Electrical Conductivity

The room-temperature conductivities of $(TTF)(I)_{0.71}$ and $(TTF)(Br)_{0.71-0.76}$ are continuous in the range from 200—500 $(\Omega\,cm)^{-1}$. [1,3,4] For the iodide, a transition occurs between 200 and 230 K, which is similar to that which occurs near 180 K for the bromide. Unlike $(TTF)(Br)_{0.71-0.76}$, $(TTF)(I)_{0.71}$ displays a hysteresis in its conductivity curve upon temperature cycling. Although these systems are considered to undergo metal-insulator transitions at about 200 K, no

Table 2. Dimensions of TTF molecule

	$(TTF)(SCN)_{0.57}$ 295 K	TTF[a] 295 K	$(TTF)(TCNQ)$[b] 295 K	$(TTF)(TCNQ)$[b] 45 K	$(TTF)_7(I)_5$[c] 295K	$(TTF)(Cl)_{0.92}$[c] 295 K
a(Å)	1.324(24)	1.349(3)	1.372(4)	1.370(4)	1.350	1.329
b	1.739(17)	1.757(2)	1.745(3)	1.743(2)	1.732	1.734
c	1.730(12)	1.726(2)	1.739(3)	1.733(2)	1.721	1.723
d	1.317(15)	1.314(3)	1.326(4)	1.349(2)	1.336	1.315
α(°)	123.1(1.1)	122.8(1)	122.6(2)	122.4(2)	122.9	123.0
β	113.8(1.6)	114.5(2)	114.7(3)	115.1(1)	114.3	113.9
γ	95.6(0.7)	94.4(1)	95.0(1)	95.0(1)	95.7	95.5
δ	117.5(0.9)	118.3(1)	117.4(1)	117.4(2)	117.2	117.4
e	1.02(12)					
ε	106(7)					

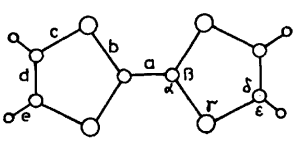

a) Ref. 9. b) Ref. 10. c) Ref. 2.

direct evidence has been obtained from the temperature dependence of the conductivities.

The conductivity measurements of (TTF)(SCN)$_{0.57}$ were performed along the crystallographic c axis (needle axis of the crystal) using the standard four-probe method with a 25 μm diameter gold wire bonded to the crystal by *duPont* 4817 conductivity paint and/or colloidal graphite (aquadag). The crystals became less conductive after they had been stored for a long time in contact with air. In addition, they are very fragile and are frequently broken by a rapid change in temperature, especially when the temperature change passes through *ca.* 0 °C. Thus, measurements of the temperature-dependent conductivities (300—120 K) were performed for only a few specimens. The room-temperature conductivities for the five samples are 85, 100, 200, and 310 $(\Omega\,\mathrm{cm})^{-1}$, respectively which agree with the value $(250\ (\Omega\,\mathrm{cm})^{-1})$ of Wudl. The discrepancies between the conductivities for the various specimens is not as large as those reported for many one-dimensional conductors.[11] Figure 2 shows the d.c. resistivity of (TTF)(SCN)$_{0.57}$ ($R(\Omega\,\mathrm{cm})=1/\sigma$). For most of the specimens, the resistivity does not decrease with temperature. Curve IIa is a typical result and is similar to those for (TTF)(Br)$_{0.71-0.76}$ and (TTF)(I)$_{0.71}$;[3,4] the conductivities decrease slightly with temperature in the high-temperature region ($T>230$ K) and decrease sharply with temperature in the low-temperature region ($T<200$ K). However, for one specimen (σ(R.T.)$=100$ $(\Omega\,\mathrm{cm})^{-1}$), a minimum point, indicative of the possible existence of a metal-insulator transition, is observed in temperature-dependent resistivity curve Ia. This result appears to be consistent with the conductivities reported by wudl who showed that (TTF)(SCN)$_{0.57}$ becomes more conductive over certain low-temperature regions (σ(R.T.)$=250$ $(\Omega\,\mathrm{cm})^{-1}$ and $\sigma(200\ \mathrm{K})=310$ $(\Omega\,\mathrm{cm})^{-1}$).[6] Considering that the disorder and defects in a crystal have great influence on the electrical conductivity and frequently smear out the metal-insulator transition,[12] the difference between the curves can be attributed to a difference in the quality of the samples.

As the temperature was changed, a series of *resistance jumps* were observed. Similar *jumps* observed for (TTF)-(I)$_{0.71}$ have been attributed to separate occurrences of the transition in different portions or domains of the crystal. A similar explanation appears to be probable, since a microscopic examination revealed that a (TTF)-(SCN)$_{0.57}$ crystal is composed of many *blocks*. At first, it appeared that a *resistance jump* accompanied a *break*

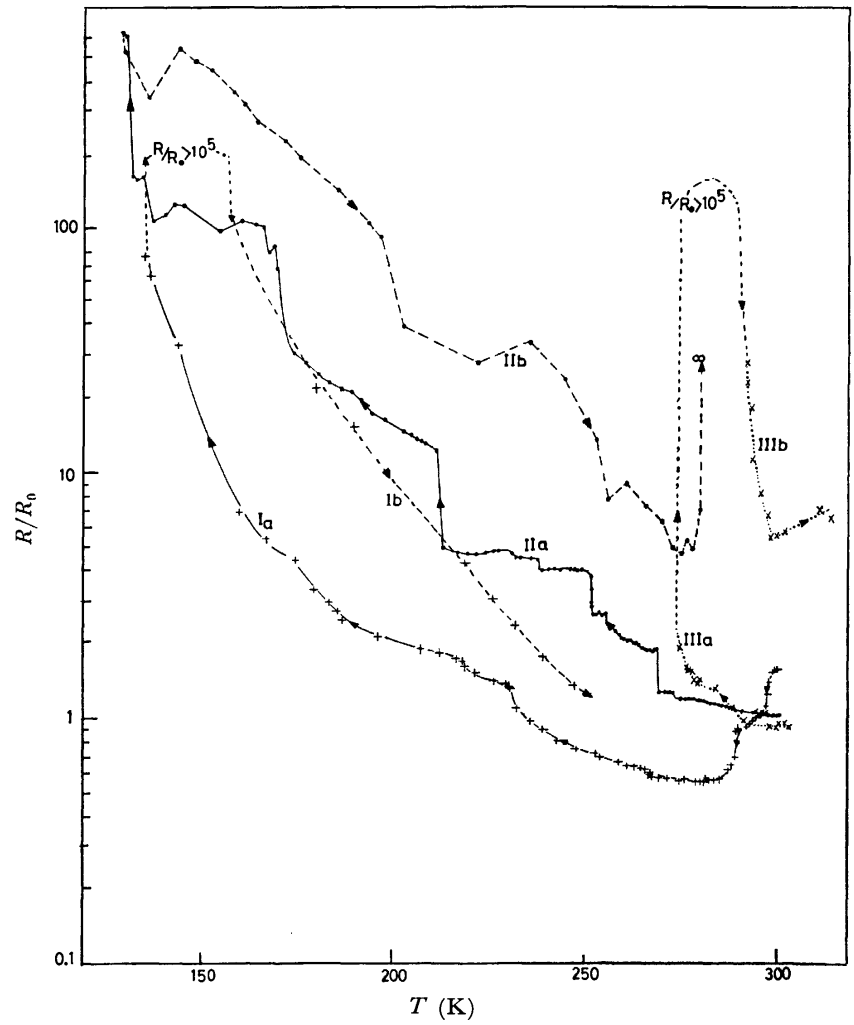

Fig. 2. Temperature dependence of the conductivity along the c axis for three samples. Arrows indicate the direction of temperature change.

TABLE 3. COMPARISON OF THE CRYSTAL STRUCTURE DETERMINATIONS

		$(TTF)(SCN)_x$ x	System	Space group	a (Å)	c	D(g cm^{-3}) Obsd	D(g cm^{-3}) Calcd
i.	This work	0.57±0.03	tetragonal	$P4_2/mnm$	11.154	3.607	1.756±0.015	—
ii.	Wudl *et al.*	0.545 (=6/11)	tetragonal	P4n2[a]	11.205	3.633	—	1.700
iii.	Somoano *et al.*	0.583 (=7/12)	tetragonal (or pseudotetragonal)	—	$\sqrt{2}\times 11.11$	3.61[b] 6.15	—	1.76

a) This space group[13] is probably incorrect and the correct one is P$\bar{4}$n2. b) The *C*-centered lattice is used to facilitate comparisons with the $(TTF)_7(I)_5$ structure. 3.61 and 6.15 Å are the lattice constants of the TTF and the SCN sublattices, respectively.

in the *blocks*, because the crystals are very fragile. According to this conjecture, many blocks can be considered to be broken during the cooling process and then the electric conduction paths would become very limited. However, in fact, upon heating to room temperature after cooling to about 130 K, the resistivities again decrease. In addition, the observation of the stepwise decrease in resistivity (curve Ia (for 270—300 K) appears to be inconsistent with the above explanation based on the *breaks* in the *blocks*. Probably, the resistivity jumps are associated with crystal blocks passing through the transition between a high-conductive state and a low-conductive state separately.[2] The series of transitions appears to indicate that the phase transition is affected by the shape and size of each *block*.

Note Added in Proof. After the completion of this paper, investigations of the electronic and structural properties of $(TTF)(SCN)_x$ and $(TTF)(SeCN)_x$ were reported by Wudl *et al.*[13] and Somoano *et al.*[14] As shown in Table 3, the crystallographic data given in their papers do not agree with those reported here. It is therefore, appropriate to briefly mention the reason for these discrepancies.

(1) Repeated elemental analysis by Wudl *et al.* results in the formula, $(TTF)_{11}(SCN)_6$ (*i.e.*, $(TTF)(SCN)_{0.545}$), whereas the formula of Somoano *et al.* is $(TTF)_{12}(SCN)_7$ (*i.e.*, $(TTF)(SCN)_{0.583}$), which was determined on the basis of the ratio of the TTF sublattice spacing to the SCN sublattice spacing. Although, in the present work, the samples were prepared according to the method of Wudl, the formula, $(TTF)(SCN)_{0.57\pm0.03}$, obtained on the basis of the measured density (1.756±0.015) agrees rather well with that of Somoano *et al.* The crystal structure of $(TTF)(SCN)_x$ was refined for several x-values. For $0.50<x<0.70$, the final structures as well as the temperature factor for SCN, are essentially identical to each other. For $x=0.60$, the lowest R-value, 0.045, and the corresponding final atomic parameters listed in Table 1 were obtained.

(2) The lattice constants of the TTF sublattice of Somoano *et al.* agree well with those presented here, whereas the values of Wudl *et al.* appear to differ from the other two, by more than the experimental error.

(3) For the crystals used here, the atomic positions of the S, C, and N atoms are one-dimensionally disordered along the c direction and no indication of the existence of the two sublattices of the TTF and SCN compound were obtained from X-ray diffraction. However, the X-ray examination of Somoano *et al.* revealed the existence of the two spacings, 3.61 Å for TTF and 6.15 Å for SCN, *i.e.*, in their crystals, the translational symmetry of the SCN arrangement is different from that for TTF. Considering that the crystals of Somoano *et al.* were grown by the diffusion method from $(CH_3)_4N(SCN)$ and $(TTF)_3(BF_4)_2$, this disagreement appears to be due to the difference in the sample preparation procedures. Some details of the crystal structure of $(TTF)_{11}(SCN)_6$ were reported by Wudl *et al.* The arrangement of TTF is very similar to that determined here, whereas their conclusion of the regular arrangement of SCN is inconsistent with their c-axis lattice constant, because this constant should be larger than the SCN spacing (c/0.545).

In conclusion, the crystals used here appear to be identical with those of Somoano *et al.* except for the orderliness of SCN. The degree of disorder may change according to differences in the procedure of preparation of the crystals. Such disorder has been observed for crystals of *N*-methylphenazinium-TCNQ.[15,16] It is not clear how the crystals of Wudl *et al.* differ from those of Somoano *et al.* and those used in the present experiments.

References

1) S. J. LaPlaca, P. W. R. Corfield, R. Thomas, and B. A. Scott, *Solid State Commun*, **17**, 635 (1975).
2) C. K. Johnson and C. R. Watson, Jr., *J. Chem. Phys.*, **64**, 2271 (1976).
3) R. B. Somoano, A. Gupta, and V. Hadek, *J. Chem. Phys.*, **63**, 4970 (1975).
4) R. J. Warmack, T. A. Callcott, and C. R. Watson, *Phys. Rev. B*, **12**, 3336 (1975).
5) F. Wudl, M. L. Kaplan, E. J. Hufnagel, and E. W. Southwick, Jr., *J. Org. Chem.*, **39**, 3608 (1974).
6) F. Wudl, *J. Am. Chem. Soc.*, **97**, 1962 (1975).
7) Tetrabutylammonium thiocyanate was prepared according to a procedure analogous to that for the preparation of tetraisoamylammonium thiocyanate (C. A. Kraus and R. M. Fuoss, *J. Am. Chem. Soc.*, **55**, 22 (1933)).
8) H. Kobayashi, *Bull. Chem. Soc. Jpn.*, **47**, 1346 (1974).
9) W. F. Cooper, N. C. Kenney, J. W. Edmonds, A. Nagel, F. Wudl, and P. Coppens, *Chem. Commun.*, **1971**, 889.
10) A. J. Schultz, G. D. Stucky, R. H. Blessing, and P. Coppens, *J. Am. Chem. Soc.*, **98**, 3194 (1976).
11) For example, G. A. Thomas, D. E. Schafer, F. Wudl, P. M. Horn, D. Rimai, J. W. Cook, D. A. Glocker, M. J. Skove, C. W. Chu, R. P. Groff, J. L. Gillson, R. C. Wheland, L. R. Melby, M. B. Salamon, R. A. Craven, G. De Pasquali, A. N. Bloch, D. O. Cowan, V. V. Walatka, R. E. Pyle, R. Gemmer, T. O. Poehler, G. R. Johnson, M. G. Miles, J. D. Wilson, J. P. Ferraris, T. F. Finnegan, R. J. Warmack, V. F. Raaen, and D. Jerome, *Phys. Rev. B*, **13**, 5105 (1976).
12) S. Etemad, *Phys. Rev. B*, **13**, 2254 (1976).
13) F. Wudl, D. E. Schafer, W. M. Walsh, Jr., L. W. Rupp, F. J. DiSalvo, J. V. Waszczak, M. L. Kaplan, and G. A. Thomas, *J. Chem. Phys.*, **66**, 377 (1977).
14) R. B. Somoano, A. Gupta, V. Hadek, M. Novotny, M. Jones, T. Datta, R. Deck, and A. M. Hermann, *Phys. Rev. B*, **15**, 595 (1977).
15) H. Kobayashi, *Bull. Chem. Soc. Jpn.*, **48**, 1373 (1975).
16) B. Morosin, *Phys. Lett. A*, **53**, 455 (1975).

Conformational Study of Glutathione by NMR

Shizuo FUJIWARA, Grazyna FORMICKA-KOZLOWSKA,* and Henryk KOZLOWSKI*
Department of Chemistry, Faculty of Science, The University of Tokyo, Bunkyo-ku, Tokyo 113
**Institute of Chemistry, University of Wrocław, Wrocław, Poland*
(Received March 29, 1977)

Proton NMR spectra of glutathione have been analyzed over the whole pH region. The spectra of the glutamic acid residue are of the ABCDX type at pHs below 2.5, of the AA'BB'X types in the pH region 2.5—9, and of the ABCC'X type at pHs higher than 9. For the cysteine part, spectra of the ABC type have been observed at pHs higher than 8, which change to spectra of the A_2B type at pHs lower than 7. On the basis of these results the conformation of the glutathione molecule in solution has been discussed in detail.

The NMR technique has been successfully used in the conformational study of various amino acids.[1-9] A similar study of more complex molecules like polypeptides is usually complicated by poorly resolved spectra and a large number of coupled protons.

A fundamental and manifold interest in the recognition of the chemical, physical, and biological properties of peptides has occasioned our attempts to establish the structure of glutathione in solution by means of NMR.[10-14] Knowledge of the conformation of glutathione should help us in better understanding some metal-glutathione interaction, which is the further aim of our study.

Experimental

Materials. The glutathione was purchased from Wako Pure Chemical Industries, and the D_2O, from E. Merck. The pHs of the solutions were controlled by adding a concentrated DCl or NaOH solution in D_2O, and measured with a Toa Dempa pH-meter, model HM-5A. The concentration of glutathione in the solutions was 0.1 M. The chemical shifts are reported in Hz relative to internal tetramethylammonium (TMA). The NMR spectra were recorded with a JNM PS-100 spectrometer operating at 100 MHz.

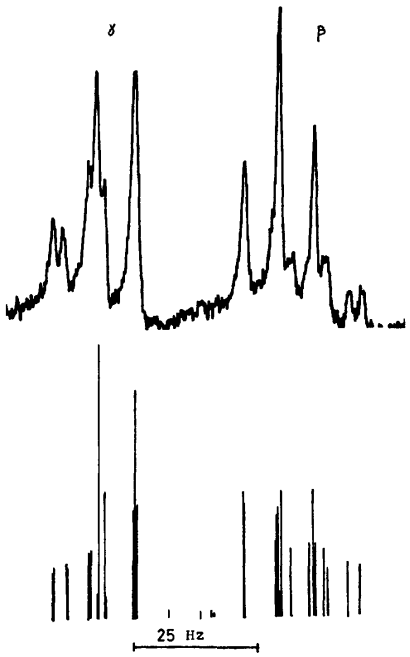

Fig. 1. Experimental and calculated spectra of γ and β protons of the glutamic acid residue at pH 0.7.

Analysis of Spectra. Glutamic Acid Residue Spectra: Five protons of the glutamic-acid part give spectra of the ABCDX type at pH lower than 2 (Fig. 1), of the AA'BB'X type in the pH range of 2.51—8.05 (Fig. 2), and of the ABCC'X type at pH higher than 9 (Fig. 3). Here ABCDX, AA'BB'X, or ABCC'X refers to the β, β', γ, γ', α protons (Fig. 4). In the pH region of 2.5—8.05 the AA'BB' pattern for the β and γ protons was confirmed by the decoupling of the α proton. An analysis of the spectra observed at a certain pH was carefully carried out with a set of input data which had been obtained in the analysis of spectra observed at a slightly different pH. It has been found that, in order to reproduce a calculated spectrum which is in good agreement with the

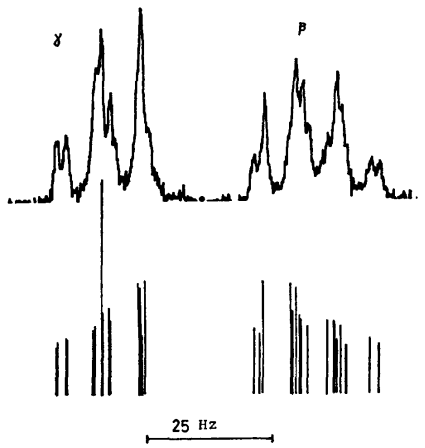

Fig. 2. Experimental and calculated spectra of γ and β protons of the glutamic acid residue at pH 4.5.

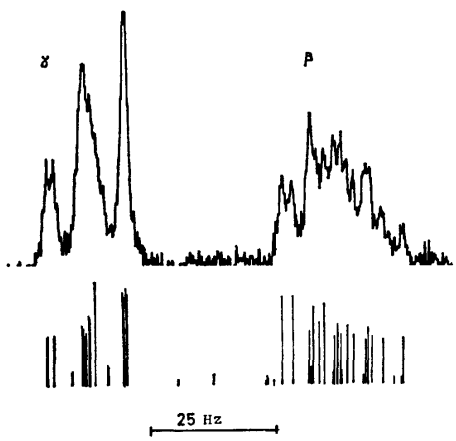

Fig. 3. Experimental and calculated spectra of γ and β protons of the glutamic acid residue in 2 M NaOH.

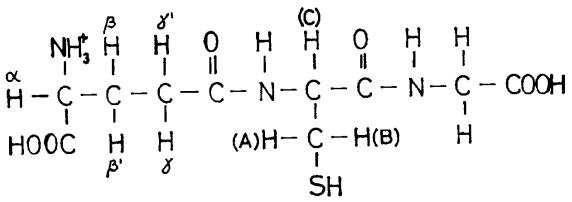

Fig. 4. Glutathione molecule and notation of the protons.

Table 1. NMR parameters of the glutamic acid residue

pH	$\Delta\nu_{\beta\beta'}$	$\Delta\nu_{\gamma\gamma'}$	$J'=J_{\beta\gamma}=J_{\beta'\gamma'}$	$J=J_{\beta\gamma'}=J_{\beta'\gamma}$	$J_{\beta\alpha}$
2 M NaOH	9.75	0	10.5	5.55	6.56
12.8	9.8	0	10.5	5.6	6.6
9.58	3.8	0	9.2	6.45	6.4
9.1	1.6	0	8.8	6.9	6.4
8.05	0	0	8.5	7.15	6.34
7.75	0	0	8.5	7.05	6.30
4.5	0	0	8.4	7.1	6.34
2.95	0	0	8.5	7.2	6.3
2.51	0	0	8.3	7.15	6.39
2.02	2.7	2.55	7.95	7.3	6.55
1.2	5.2	4.65	7.55	7.35	6.52
0.7	5.4	4.9	7.45	7.35	6.55
6 M DCl	6.2	5.1	7.6	7.4	6.54

All the NMR parameters are given in Hz.

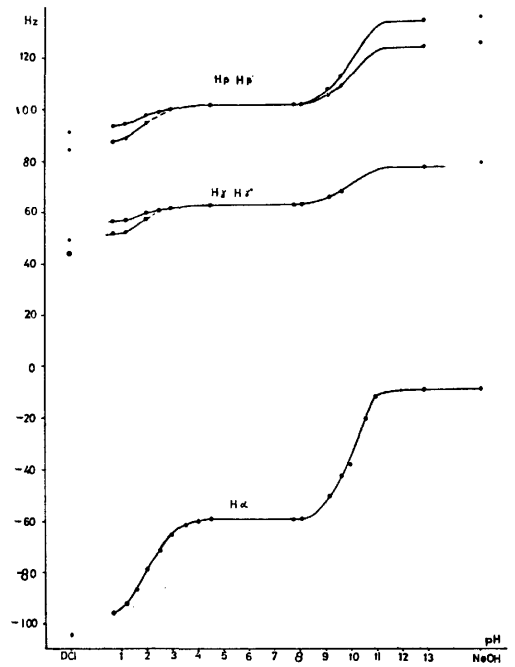

Fig. 5. pH dependence of the protons of glutamic acid residue relative to TMA.

observed one, the chemical shifts and spin-coupling constants have to be correct within ± 0.2 Hz. J_{gem} was assumed to be -15.0 Hz, and $J_{\alpha\gamma}=J_{\alpha\gamma'}=0$, which was confirmed by the decoupling of the β protons. All the NMR parameters for the glutamic acid residue over the whole pH region are given in Table 1 and Fig. 5.

Cysteine and Glycine Residues. The NMR spectra of the cysteine residue are of the ABC type. Below pH=8, however,

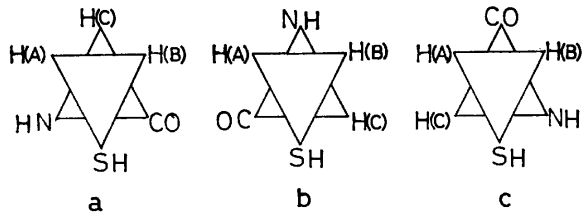

Fig. 6. Three rotational isomers of cysteine.

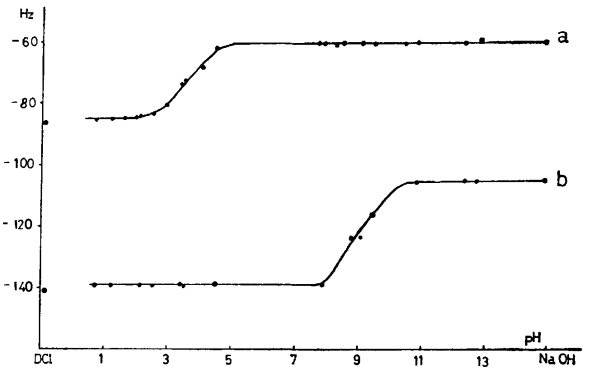

Fig. 7. pH dependence of the glycine protons (a) and C proton of cysteine (b) relative to TMA.

Table 2. NMR parameters of the cysteine residue

pH	$\Delta\nu_{C-TMA}$	J_{AB}	J_{AC}	J_{BC}	$\Delta\nu_{AB}$
2 M NaOH	105.4	−13.2	7.88	5.12	11.1
12.95	103.3	−13.0	8.1	4.85	11.4
12.8	105.0	−13.1	7.9	5.00	11.0
12.4	105.1	−13.0	8.1	4.9	11.5
10.9	105.9	−13.1	8.05	4.85	11.2
9.5	116.6	−13.5	7.96	4.9	10.7
9.1	123.7	−13.8	7.8	4.9	8.2
8.8	123.9	−14.1	7.6	5.0	9.0

All the NMR parameters are given in Hz.

the spectra are very poorly resolved and have to be analysed as the A_2B type. In this pH region, $J_{AC}=J_{BC}=6.3$ Hz. Using the notation "ABC" given in Fig. 6, the NMR parameters are given in Table 2, where the chemical shift of the A proton is taken to be in a higher field than that of the B proton. The pH dependence of the chemical shifts of the C proton of the cysteine and CH_2 protons of the glycine are shown in Fig. 7. The CH_2 protons of the glycine give a singlet line due to the exchange by deuterium of the NH proton of the neighboring peptide nitrogen,** and there is a small difference in the chemical shifts of the two protons. To confirm the pH dependence of the chemical shifts, the microscopic ionization constant (Fig. 8) were calculated using a method described by Rabenstein[10] (Table 3).

Rotational Isomerism. In order to discuss the conformation of the entire glutathione molecule, the populations of the rotamers for cysteine and glutamic acid residues were calculated separately.***

** In the case of the H_2O solution, above pH 7.5 the CH_2 protons of glycine also give a singlet as a result of the averaging of conformations due to the fast exchange of peptide protons.

*** The population of rotational isomers was obtained by following the procedure originally used by Pachler.[1] The scope and limitations of this method, especially in the case of simple amino acids, have been discussed previously.[2]

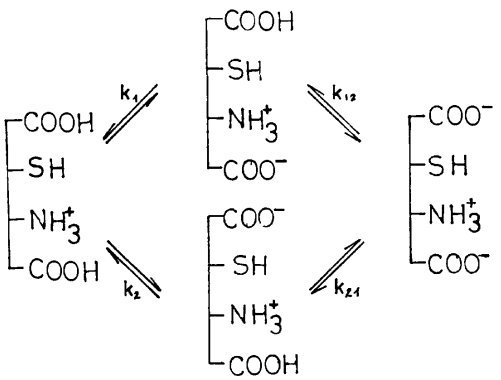

Fig. 8. Microscopic ionization scheme for carboxyl groups of the glutathione.

Table 3. Microscopic ionization constants for the dissociation of the carbonyl group

	This work	Ref. 10
pk_1	2.05±0.1	2.09±0.05
pk_2	3.14±0.05	3.12±0.05
pk_{21}	2.33±0.05	2.33±0.01
pk_{12}	3.42±0.1	3.36±0.1

Rotamers for Glutamic Acid Residue. In this part of glutathione, nine rotamers have to be considered (Fig. 9). From the experimental data, $J_{\alpha\gamma}\cong 0$. Thus, it is not possible to find the relative conformations of the α and γ protons from the J value. We will calculate the populations of the I, II, and III rotamers (Fig. 10a) and, independently, the populations of 1, 2, and 3 rotamers (Fig. 10b).

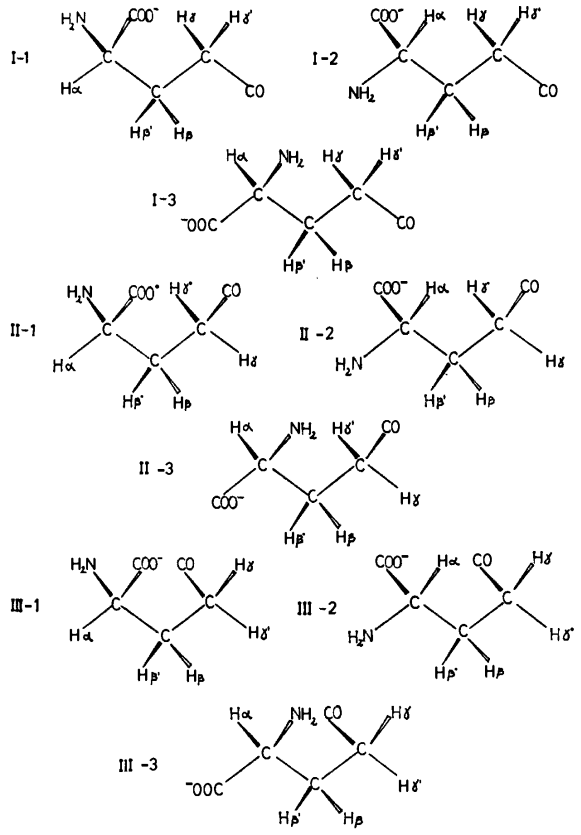

Fig. 9. Nine rotational isomers of the glutamic acid residue.

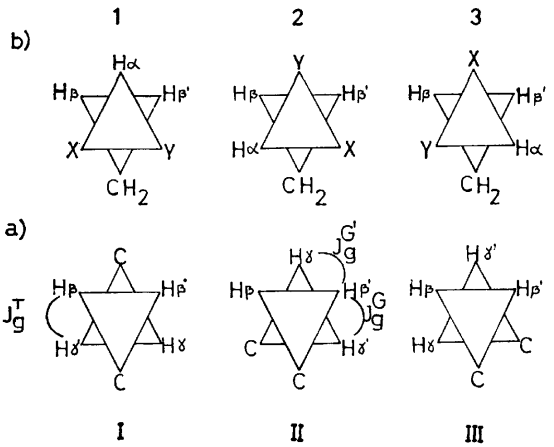

Fig. 10. The partial rotamers of glutamic acid:
a) for β and γ carbons
b) for α and β carbons.
X and Y are the carboxyl and amino groups, respectively.

Rotamers I, II, and III. We will approximate this unit in the glutamic residue as a substituted ethane. For the estimation of an average vicinal coupling constant, it may be possible to use the Abraham and Pachler empirical equation;[16]

$$J_{av} = 17.96 - 0.796 \sum_{i=1}^{6} E_i \qquad (1)$$

where E_i is the Huggins electronegativity of atoms attached to the ethyl carbons. From this equation, $J_{av}\cong 7.1$. Equation 1, however, is only a general expression for the relation between the electronegativity and J_{vic}, and it seems more reasonable to use the experimental data for the estimation of J_{av}. At pH 0.7, all four J values are almost equal to each other within the limits of experimental error, and $J_{av}=7.41$. Because there are two different sets of J values, we rewrite: $J_{\beta\gamma}=J_{\beta'\gamma'}=J'$ and $J_{\beta\gamma'}=J_{\beta'\gamma}=J$, and, if $N=J+J'$ and $L=J-J'$, we obtain another expression for the J_{av};

$$\begin{aligned} J_{av} &= 1/3(3/2N+1/2L) \\ &= 1/3(2J+J') \\ &= 1/3(J_t+2J_g) \end{aligned} \qquad (1')$$

and $J_{av}=7.43$ Hz if $(3/2N+1/2L)=22.3$. For further discussion, $J_{av}=7.4$ Hz will be used. The vicinal coupling constants, $J_{\beta\gamma}$, $J_{\beta\gamma'}$, $J_{\beta'\gamma}$, and $J_{\beta'\gamma'}$ for this system (Fig. 10a) are given by the following equations:

$$\begin{aligned} J_{\beta\gamma} &= p_I J_t + p_{II} J_g^{\,G} + p_{III} J_g^{\,G} \\ J_{\beta'\gamma'} &= p_I J_t + p_{II} J_g^{\,G} + p_{III} J_g^{\,G} \\ J_{\beta\gamma'} &= p_I J_g^{\,T} + p_{II} J_t + p_{III} J_g^{\,G'} \\ J_{\beta'\gamma} &= p_I J_g^{\,T} + p_{II} J_g^{\,G'} + p_{III} J_t, \end{aligned} \qquad (2)$$

where p_I, p_{II}, and p_{III} are the populations of the I, II, and III rotamers and $J_g^{\,T}$, $J_g^{\,G}$, and $J_g^{\,G'}$ are as defined in Fig. 10a. From the Eq. 2 one can see directly that, for any values of p_I, p_{II}, and p_{III}, $J_{\beta\gamma}=J_{\beta'\gamma'}$. This results is in agreement with the results of the analysis. Also from these results, $J_{\beta\gamma'}=J_{\beta'\gamma}$; hence, $p_{II}=p_{III}$. The fact that the populations of both rotamers of the gauche form are equal to each other agrees with the results obtained for simple 1,2-disubstituted ethanes.[17,18] This appears to justify our assumption that the $-CH_2-CH_2-$ unit in glutamic acid can be considered as a substituted ethane.

Equation 2 may be simplified to this form:

$$J' = J_{\beta\gamma} = J_{\beta'\gamma'} = p_{\mathrm{I}}J_{\mathrm{t}} + 2p_{\mathrm{II}}J_{\mathrm{g}}^{\mathrm{G}}$$
$$J = J_{\beta\gamma'} = J_{\beta'\gamma} = p_{\mathrm{I}}J_{\mathrm{g}}^{\mathrm{T}} + p_{\mathrm{II}}(J_{\mathrm{g}}^{\mathrm{G}'} + J_{\mathrm{t}}) \quad (2')$$

To estimate populations, it is necessary to have the values of $J_{\mathrm{g}}^{\mathrm{T}}$, $J_{\mathrm{g}'}^{\mathrm{G}}$ and $J_{\mathrm{g}}^{\mathrm{G}'}$ ($J_{\mathrm{g}}^{\mathrm{T}} > J_{\mathrm{g}}^{\mathrm{G}} > J_{\mathrm{g}}^{\mathrm{G}'}$ [17]).

Table 4. Populations of the I, II, and III rotamers of the glutamic acid residue

pH	$\bar{p}_{\mathrm{I}}$	$\bar{p}_{\mathrm{II}}$	Δp_{II}	$3/2N+1/2L$
2 M NaOH	0.60	0.20	0.01	21.60
12.8	0.59	0.20	0.01	21.77
9.58	0.48	0.26	0	22.11
9.1	0.42	0.29	0	22.56
8.05	0.40	0.30	0.01	22.78
7.75	0.40	0.30	0	22.53
4.5	0.40	0.30	0.01	22.58
2.95	0.39	0.30	0.01	22.86
2.51	0.39	0.30	0.01	22.58
2.02	0.36	0.32	0.01	22.64
1.2	0.34	0.33	0	22.25
0.7	0.34	0.33	0	22.20
6 M DCl	0.34	0.33	0	22.32

From Table 4 it can be seen that, with an increase in pH, the J' value also increases. According to Equations 2', this result implies that there is an increase in the population of a trans isomers (p_{I}). Thus, if the $J_{\mathrm{g}}^{\mathrm{T}}$ values is sufficiently higher than that of $J_{\mathrm{g}}^{\mathrm{G}}$ and $J_{\mathrm{g}'}^{\mathrm{G}'}$ the values $(3/2N+1/2L)=(J'+2J)$ should steadily increase with an increase in p_{I}. In the present case, these values are almost constant at all pH values, equal to 22.2 ± 0.6 Hz. The deviation may be attributed to the experimental error. However, the deviation of this range may be caused by a small cahnge in the nature of the medium, such as the dielectric field in the solution, or the dissociation of functional groups of the glutathione. $J_{\mathrm{g}'}^{\mathrm{T}}$, $J_{\mathrm{g}'}^{\mathrm{G}}$, or $J_{\mathrm{g}}^{\mathrm{G}}$ should be constant throughout the pH rang examined. Therefore, it seems reasonable to put one J_{g} value into Eq. 2'. By combining Eqs. 2' and 3:

$$p_{\mathrm{I}} + 2p_{\mathrm{II}} = 1 \quad (3)$$

the following expressions can be obtained:

$$\text{from } J': \quad p_{\mathrm{I}} = (J'-J_{\mathrm{g}})/(J_{\mathrm{t}}-J_{\mathrm{g}}), \quad p_{\mathrm{II}} = 1/2(J_{\mathrm{t}}-J')/(J_{\mathrm{t}}-J_{\mathrm{g}}), \quad (4)$$

$$\text{from } J': \quad p_{\mathrm{I}} = (J_{\mathrm{t}}+J_{\mathrm{g}}-2J)/(J_{\mathrm{t}}-J_{\mathrm{g}}), \quad p_{\mathrm{II}} = (J-J_{\mathrm{g}})/(J_{\mathrm{t}}-J_{\mathrm{g}}). \quad (4')$$

In order to determine J_{t} and J_{g} in addition to J_{av}, it is necessary to assume the $J_{\mathrm{t}}/J_{\mathrm{g}}$ ratio, for which we will take a common value of 5.2[1,2,9,20] ($J_{\mathrm{t}}/J_{\mathrm{g}}=5.6$ for pure ethane[19]) for all α-amino acids. The result is that $J_{\mathrm{t}}=16.03$ Hz and $J_{\mathrm{g}}=3.08$ Hz. From Eqs. 4 and 4' we can determine two sets of p_{I} and p_{II} values, using the J' or J spin-coupling constant. The very good agreement between the two sets of p_{I} and p_{II} populations confirms that, at least for a qualitative discussion, the present assumptions are sufficiently correct. The average values, $\bar{p}_{\mathrm{I}}$ and $\bar{p}_{\mathrm{II}}$, and the deviation of $\bar{p}_{\mathrm{II}}$ from the values obtained using Figs. 4 and 4' are given in Table 4.† $J_{\alpha\beta}$ changes only slightly from about 6.3 Hz in the pH range 2.9—8.05 to about 6.6 Hz for pH values lower than 0.7 and higher than 11. Using the J_{t} and J_{g} values estimated for simple amino acids,[1,2,9] it is easy to find that, in the region of pH 2.9—8.05, all three rotamers, 1, 2, and 3 (Fig. 10b), have the same population. In other pH regions there is some excess of the 2 and 3 rotamers over the 1 rotamer, the populations being 0.36, 0.36, and 0.28. The 2 and 3 rotamers cannot be distinguished from one another because the observed spectrum is of the A_2X type. (We can determine only the average value of $J_{\alpha\beta}$).

Cysteine Residue. Using $J_{\mathrm{g}}=2.6$ Hz, $J_{\mathrm{t}}=13.6$ Hz, and $J_{\mathrm{av}}=6.3$ Hz, the populations of the three *a*, *b*, and *c* rotamers (Fig. 6) can be obtained (Table 5). However, it is not possible to distinguish the A and B protons in this experiment. Furthermore it is not certain which rotamer, *b* or *c*, is more stable. In the pH region where poorly resolved spectra are observed, $J_{\mathrm{AC}}=J_{\mathrm{BC}}=6.3$ Hz and $a=b=c=1/3$.

Discussion

Glutamic Acid Residue. The I-1, 2, and 3 rotamers appear to be stable with respect to the interaction of the two terminal functional groups of this residue with the peptide linkage between glutamic and cysteine parts. In gauche isomers (II, III), the II-1 rotamer appears to be the least stable because of the electrostatic interaction of the carboxyl and ammonium group with the peptide backbone, especially with the carbonyl group. For a similar reason, the III-2 isomer seems to be less stable. At pH<2, the total population of the gauche form is large in comparison to the trans one (I), and this interaction with the peptide-bond group induces an observable difference in the populations of the 1, and 2, and 3 rotamers. It is also likely that there exists some difference in population of the II-2 and II-3 rotamers, and so on, but the fast interconversion between the two isomers of the gauche form (II and III) (*e.g.*, II-2—III-2) makes it impossible to distinguish them.††

The dissociation of the COOH group to COO^- which occurs between pH 0.7—2.95 makes this interaction stronger because of the excessive negative charge on the carboxyl group, and some increase in the population of the trans (I) form has been observed. In the pH range of 8—11, where the dissociation of the NH_3^+ group occurs, an additional negative charge on the glutamic terminal causes an other increase in the population of the trans (I) isomer, for the same reason. The rotamers stable at pH values higher than 11 are I-1, 2, and 3, and the gauche forms, II-2 and III-3. The least stable should be II-1 and III-1.

At pHs below 2.5 and pHs higher than 9, the unequal populations of the 1, 2, and 3 rotamers distinguish the chemical shifts of β and β', while at pHs below 2.5 the chemical shifts for γ and γ' protons can be differentiated. The interaction of the carboxyl and the ammonium groups with the γ and γ' protons is more effective in the gauche form of the unit considered, and at high pHs probably a smaller population of this form causes $\Delta_{\gamma\gamma'}$, to equal 0. To explain this, more accurate populations of the particular rotamers, II-1—III-3, have to be known.

Cysteine. Below pH 8, $a=b=c=1/3$. When the

† The $\bar{p}$ values are the average values of the populations obtained from Eqs. 4 and 4'.

†† In this case, a more complex intercoversion between the 1, 2, 3 and I, II, III rotamers should be considered.

Table 5. Populations of the cysteine residue rotamers

pH	a	b(or c)	c (or b)
2 M NaOH	0.29	0.48	0.23
12.95	0.29	0.50	0.21
12.8	0.30	0.48	0.22
12.4	0.29	0.50	0.21
10.9	0.30	0.49	0.21
9.5	0.30	0.49	0.21
9.1	0.31	0.48	0.21
8.8	0.32	0.46	0.22
<8	$a \cong b \cong c \cong 0.33$		

SH group dissociates to S^-, the spectra are better resolved (ABC type) and a more detailed population of the three rotamers (a, b, and c) can be found (Table 5, Fig. 6). The smallest change of the population is observed for the a rotamer, where the population is decreased from 0.33 to about 0.29. This result means that the most stable rotamer after the dissociation of the SH group is the one in which the position of S is trans to the cysteine peptide nitrogen or the carbonyl peptide group.

From all these considerations it seems that a peptide linkage between glutamic acid and cysteine, and the interaction of the carbonyl group in the peptide linkage with the changes in the functional groups of the glutamic residue are important for the conformational equilibrium in solution. Thus, the most stable conformer after the complete dissociation of the peptide molecule is the one in which the COO^- and NH_2 groups of the glutamic acid residue are far from the peptide backbone of the glutathione.

We wish to thank Dr. Yoji Arata, Dr. Hidehiro Ishizuka and Dr. Akira Yamasaki for their helpful discussion and help during the analysis of the NMR spectra.

References

1) K. G. R. Pachler, *Spectrochim. Acta*, **19**, 2085 (1963); **20**, 581 (1964).
2) H. Ogura, Y. Arata, and S. Fujiwara, *J. Mol. Spectrosc.*, **23**, 76 (1967).
3) S. Fujiwara and Y. Arata, *Bull. Chem. Soc. Jpn.*, **36**, 578 (1963).
4) S. Fujiwara and Y. Arata, *Bull. Chem. Soc. Jpn.*, **37**, 344 (1964).
5) K. G. R. Pachler, *Z. Anal. Chem.*, **224**, 211 (1967).
6) F. Tadei and L. Pratt, *J. Chem. Soc.*, **1964**, 1553 (1964).
7) J. R. Cavanauch, *J. Am. Chem. Soc.*, **89**, 1558 (1967).
8) H. Ishizuka, Doctoral Thesis, Tokyo University (1973).
9) H. Ishizuka, T. Yamamoto, Y. Arata, and S. Fujiwara, *Bull. Chem. Soc. Jpn.*, **46**, 468 (1973).
10) D. L. Rabenstein, *J. Am. Chem. Soc.*, **95**, 2797 (1973).
11) B. J. Fuhr and D. L. Rabenstein, *J. Am. Chem. Soc.*, **95**, 6944 (1973).
12) J. Feeney, P. Patington, and G. C. K. Robers, *J. Magn. Reson.*, **13**, 268 (1974).
13) J. P. Casey and R. B. Martin, *J. Am. Chem. Soc.*, **94**, 6141 (1972).
14) G. Jung, E. Breitmaier, and W. Voelter, *Eur. J. Biochem.*, **24**, 438 (1972).
15) S. M. Castellano, "Computer Program for Chemistry," Vol. 1, ed by D. F. Detar, Benjamin, New York (1968), p. 10.
16) R. J. Abraham and K. G. R. Pachler, *Mol. Phys.*, **7**, 165 (1963).
17) R. J. Abraham, L. Cavalli, and K. G. R. Pachler, *Mol. Phys.*, **11**, 471 (1966).
18) N. Sheppard and J. J. Turner, *Proc. R. Soc. London, Ser. A*, **252**, 506 (1959).
19) R. M. Lynden-Bell and N. Sheppard, *Proc. R. Soc. London, Ser. A*, **269**, 385 (1962).
20) R. J. Abraham and K. A. McLauchlan, *Mol. Phys.*, **5**, 513 (1962).

Nuclear Quadrupole Resonances of $AlBr_3 \cdot SbBr_3$, $AlI_3 \cdot SbI_3$, and $AlBr_3 \cdot BiBr_3$

Tsutomu OKUDA, Koji YAMADA, Hideta ISHIHARA, and Hisao NEGITA

Department of Chemistry, Faculty of Science, Hiroshima University, Hiroshima 730

(Received May 30, 1977)

The quadrupole coupling constants (e^2Qq/h) and the principal axes of electric field gradient (efg) at ^{81}Br, ^{127}I, ^{27}Al, ^{121}Sb, and ^{209}Bi in $AlBr_3 \cdot SbBr_3$, $AlI_3 \cdot SbI_3$, and $AlBr_3 \cdot BiBr_3$ were determined by means of NQR or NMR, in order to clarify the structures and chemical bonds of these compounds. The NQR spectra of $AlBr_3 \cdot SbBr_3$ and $AlI_3 \cdot SbI_3$ resemble each other and these two compounds consist of V-shaped SbX_2^+ and distorted tetrahedral AlX_4^- ions (X=Br and I). However, there are weak bonds between the Sb atom in SbX_2^+ and the halogens in AlX_4^- ion. The V-shaped SbX_2^+ has the bond angle 97.3° for the bromide and 99.0° for the iodide. The orientation of the efg axes at the ^{121}Sb atom suggests that the antimony atom has a lone pair of electrons in the opposite direction to the bisector of the two Sb–X bonds. On the other hand, only one terminal bromine atom bonded to the Bi atom was found for $AlBr_3 \cdot BiBr_3$.

The formation of the 1:1 adducts between trihalides of the metals of group III and V such as $AlX_3 \cdot SbX_3$ or $GaX_3 \cdot SbX_3$ (X=Cl, Br, or I) has been reported in the literature.[1-3] According to the electron diffraction study, $AlBr_3 \cdot SbBr_3$ has an ethane-like structure (Br_3Sb–$AlBr_3$) in the gaseous state.[4] In the solid state, however, no crystal structure for these compounds has been reported so far. Recently, Chemouni and Potier studied vibrational spectra of the $GaX_3 \cdot SbX_3$ (X=Cl, Br, or I) compounds in the solid state and concluded that the bridging structure (X_2Sb–X–GaX_3) is more probable than the ethane-like structure (X_3Sb–GaX_3).[5]

In the present investigation we discuss the structure and chemical bonds for the adducts $AlBr_3 \cdot SbBr_3$, $AlI_3 \cdot SbI_3$, and $AlBr_3 \cdot BiBr_3$, on the basis of the quadrupole coupling constants and the orientation of the principal axes of the electric field gradient (efg). A part of this work has already been reported elsewhere.[6]

Experimental

Adducts $AlBr_3 \cdot SbBr_3$, $AlI_3 \cdot SbI_3$, and $AlBr_3 \cdot BiBr_3$ were prepared from the stoichiometric mixture of the relevant halides in a sealed tube and crystallized slowly from the melt. The single crystals of these compounds were grown by the Bridgman-Stockbarger method. The NQR spectrometer was a super-regenerative type, and signals were observed on an oscilloscope. The Zeeman effect on the NQR was examined by means of the zero-splitting cone method.[7] The quadrupole coupling constants of ^{27}Al were determined by use of a broad line NMR spectrometer operated at 13.000 MHz. Using single crystals of these compounds, the shift of the central line ($-1/2 \leftrightarrow +1/2$) due to the second order quadrupole effect were observed and analyzed by the Volkoff method.[8,9]

TABLE 1. NQR PARAMETERS OF $AlBr_3 \cdot SbBr_3$, $AlI_3 \cdot SbI_3$, AND $AlBr_3 \cdot BiBr_3$ (296 K)

Compound		ν_1/MHz	ν_2/MHz	ν_3/MHz	ν_4/MHz	$\eta^{a)}$	$\eta^{b)}$	e^2Qq/h/MHz
	^{121}Sb	97.406	113.30			0.817	0.821	415.9
	$^{81}Br(1)$	76.637				0.543		146.6
	Br(2)	79.088				0.477		152.5
$AlBr_3 \cdot SbBr_3$	Br(3)	81.930				0.307		161.3
	Br(4)	82.689				0.141		164.8
	Br(5)	143.63				0.024		287.2
	Br(6)	149.99				0.011		300.0
	^{121}Sb	75.681	94.832			0.742	0.736	343.2
	$^{127}I(1)$	118.18	200.48			0.371	0.382	686.6
	I(2)	118.86	232.68			0.129	0.130	778.2
$AlI_3 \cdot SbI_3$	I(3)	123.04	201.73			0.428	0.426	694.9
	I(4)	123.19	214.40			0.347	0.347	731.1
	I(5)	186.88	373.79			0.014	0.00	1246
	I(6)	207.39	414.40			0.029	0.027	1382
	^{209}Bi	36.941	46.126	72.422	97.364		0.271	587.2
	$^{81}Br(1)$	75.691				0.204		150.3
	Br(2)	76.760				0.868		137.2
$AlBr_3 \cdot BiBr_3$	Br(3)	81.003				0.526		155.0
	Br(4)	83.937				0.426		163.0
	Br(5)	95.316				0.539		182.0
	Br(6)	148.30				0.027		296.6

a) These values were determined by Zeeman effect experiments.

b) These values were determined by the use of frequency ratios, ν_1/ν_2.

Results and Discussion

Tables 1 and 2 show the quadrupole coupling constants (e^2Qq/h) and the asymmetry parameter (η) of the efg tensors observed for ^{81}Br, ^{121}Sb, ^{127}I, ^{209}Bi, and ^{27}Al. These parameters were determined by NQR or NMR experiments using single crystals. The NQR lines of ^{79}Br and ^{123}Sb were also observed at the frequencies expected from the quadrupole moment ratios, $Q(^{79}Br)/Q(^{81}Br)=1.1971$ and $Q(^{123}Sb)/Q(^{121}Sb)=1.2748$.

Table 2. Quadrupole coupling constants for ^{27}Al

Compound	e^2Qq/h/MHz	η	Temp/K
$AlBr_3 \cdot SbBr_3$	7.2±0.1	0.56±0.03	295
$AlI_3 \cdot SbI_3$	5.7±0.1	0.55±0.03	285
$AlBr_3 \cdot BiBr_3$	4.0±0.1	0.32±0.03	295
Al_2Br_6[a]	13.5635	0.7476	298.2
KAl_2Br_7[b]	10.4±0.1	0.19±0.03	284
	8.7±0.1	0.09±0.02	

a) Ref. 19. b) Ref. 9.

$AlBr_3 \cdot SbBr_3$. It is apparent from Table 1 that the bromine atoms are divided into two groups. The first group contains Br(1), Br(2), Br(3), and Br(4), and the second group Br(5) and Br(6). Bromine atoms in the first group have large η values and their e^2Qq/h values are approximately the same as those of $AlBr_4^-$ in $MAlBr_4$ (M=Li, Na, or Cs).[9] These four Br atoms can be assigned to $AlBr_4^-$ ions in the present compound, although most of them have strong interactions with neighboring atoms. Bromine atoms in the second group have very small η values and slightly higher quadrupole coupling constants than those due to the bromines in $SbBr_3$.[10] On the basis of these parameters, Br(5) and Br(6) are considered to form bonds with an antimony atom and they have no interactions with other neighboring atoms, thus differing from the Br atoms in the $SbBr_3$ crystal. Figure 1 shows the zero-splitting patterns which are considered to arise from the Sb and Br atoms in one $SbBr_2$ unit. In practice, however, a pair of zero-splitting patterns was observed for each resonance line; these patterns were symmetrical with respect to the b-axis because of the monoclinic system. It is reasonable to assume that the efg z-axis of the Br(5) or Br(6) atom lies along its Br–Sb bond because of the small η. The bond angle $\angle$BrSbBr determined in this way is 97.3°, which is nearly equal to that of the $SbBr_3$ crystal. In the case of ^{121}Sb ($I=5/2$), the locus of the zero-splitting for ν_1 is formed around

Table 3. NQR parameters of $SbBr_3$, SbI_3, and $BiBr_3$

Compound		η/%	e^2Qq/h/MHz	Temp/K	Ref.
$SbBr_3$	^{81}Br	6.8—8.0	273.6[a]	292.5	10
	^{121}Sb	8.3	319.9	304	20
SbI_3	^{127}I	56.5	895.8	77	20
	^{121}Sb	0	169.4	77	20
$BiBr_3$	^{81}Br	7.7—42.4	223.5[a]	298	18
	^{209}Bi	82.8	266.6	289	18

a) Averaged values of three resonance lines.

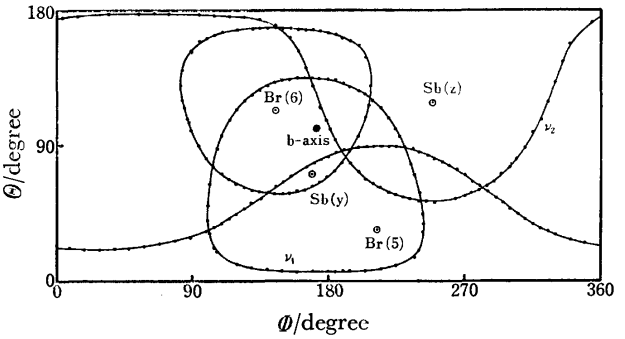

Fig. 1. Zero-splitting loci for the $^{81}Br(5)$, $^{81}Br(6)$, $^{121}Sb(\pm1/2\leftrightarrow\pm3/2)$, and $^{121}Sb(\pm3/2\leftrightarrow\pm5/2)$ lines in the $AlBr_3 \cdot SbBr_3$ crystal at room tempreature. In practice a pair of zero-splitting patterns was observed for each resonance line symmetrically with respect to the b-axis because of the monoclinic system. ⊙: efg axis.

the y-axis of the efg tensor and that of ν_2 is formed around the z-axis when η is greater than 41.2%.[11,12] Therefore, it is apparent from Fig. 1 that the z-axis of this antimony atom is almost perpendicular to the Br–Sb–Br plane and the y-axis is parallel to the bisector of the two Sb–Br bonds. Table 4 shows the angles between their efg axes determined by the Zeeman effect of NQR. Furthermore, the large values of η and e^2Qq/h of the antimony atom also support the existence of the V-shaped $SbBr_2$ unit. Figure 2 shows the orientation of the efg axes of this antimony atom as compared with that of the bridging Br atom existing in Al_2Br_6[13] or KAl_2Br_7.[9] This figure shows that the x-axis and y-axis of these two bridging atoms are reversed, although their bond angles are nearly equal to each other. The efg axes for the bridging Br atom have been explained by assuming that the Br atom forms sp^3 hybridized orbitals with two lone pair orbitals.[14,15] On the other hand, in order to explain the reversed orientation of the x- and y-axes at the Sb atom, sp^2 hybridized orbitals

Table 4. The angles between efg principal axes for the SbX_2^+ ion[a] (1) $SbBr_2^+$ (2) SbI_2^+

(1) $SbBr_2^+$	Sb z-axis	Sb y-axis	Br(5) z-axis
Sb y-axis	90.0°		
Br(5) z-axis	90.0°	48.6°	
Br(6) z-axis	90.0°	48.8°	97.3°
(2) SbI_2^+	Sb z-axis	Sb y-axis	I(5) z-axis
Sb y-axis	90.0°		
I(5) z-axis	90.1°	56.4°	
I(6) z-axis	89.9°	42.7°	99.0°

a) Experimental error was estimated to be ±0.2°.

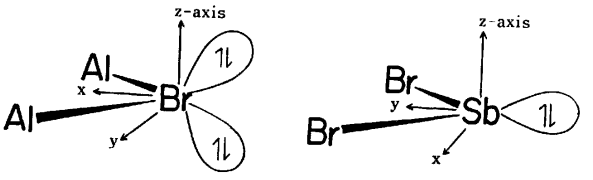

Fig. 2. efg axes with respect to the bridging plane. (a) Bridging Br atom in the Al_2Br_6 crystal and (b) antimony in the $SbBr_2^+$ ion.

with C_{2v} symmetry are adopted by assuming no hybridization of the d orbitals. The orthonormal orbitals at the Sb atom are expressed as follows:

$$\phi_1 = \psi_z,$$
$$\phi_2 = \alpha\psi_s - (1-\alpha^2)^{1/2}\psi_y,$$
$$\phi_3 = (2)^{-1/2}\{(1-\alpha^2)\psi_s + \alpha\psi_y - \psi_x\},$$
$$\phi_4 = (2)^{-1/2}\{(1-\alpha^2)\psi_s + \alpha\psi_y + \psi_x\},$$

with $$\alpha = \cot 2\gamma,$$

where ψ_s, ψ_x, ψ_y, and ψ_z are the 5s, $5p_x$, $5p_y$, and $5p_z$ orbitals of the antimony atom and 2γ is the bond angle ∠BrSbBr. The ∠BrSbBr angle was determined to be 97.3° by measuring the ^{81}Br Zeeman effect. The lone pair orbital ϕ_2 contains two electrons and has a large portion of s orbital; the electrons can be regarded as an inert pair of the Sb atom. The sigma-bonding orbitals ϕ_3 and ϕ_4 are used to form bonds with two Br atoms. The populations of these orbitals are roughly estimated to be 0.55 from the ionic character of the Sb–Br bond, which was determined by the NQR parameters of ^{81}Br by assuming 15% s-electron character for the bonding orbital of the Br atom. Then, the populations of the orbitals ϕ_1, ϕ_2, and ϕ_3 $(=\phi_4)$ are

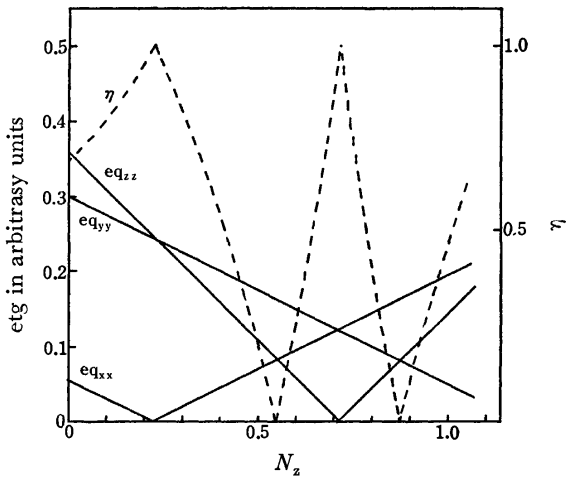

Fig. 3. Dependence of the efg at the Sb site on the population of the ϕ_1 orbital. If the population is smaller than 0.23, the observed orientation of the efg axes is consistent with this calculation.

assumed to be N_z, 2, and 0.55, respectively. Using the Townes-Dailey theory, the efg at the Sb site can be expressed as a function of N_z, where x-, y-, and z-axes are chosen as shown in Fig. 2. At N_z=0.11, the observed asymmetry parameter and the orientation of the efg tensor could be explained satisfactorily. This electronic configuration is consistent with that expected from the $SbBr_2^+$ ion, because the outer electron configuration of the Sb^+ ion is $5s^25p^2$. Further calculation is obstracted because of the lack of accurate information on the crystal structure and the quadrupole coupling constant for a 5p electron of antimony.

Figure 4 shows the zero-splitting patterns of the Br(1)—Br(4). The angles between their z-axes are distributed from 103.9 to 118.1°. This fact suggests the existence of a distorted tetrahedral $AlBr_4^-$ ion, although their efg z-axes somewhat deviate from the Br–Al bond axes because of the large η value. Figure 5

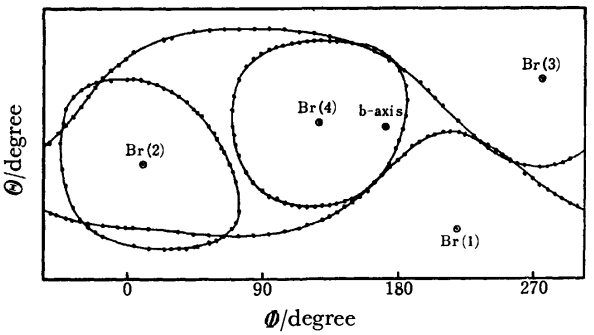

Fig. 4. Zero-splitting loci for the ^{81}Br(1)—Br(4) lines in the $AlBr_3 \cdot SbBr_3$ crystal. In practice a pair of zero-splitting patterns was observed for each resonance line symmetrically with respect to the b-axis. ⊙: efg axis.

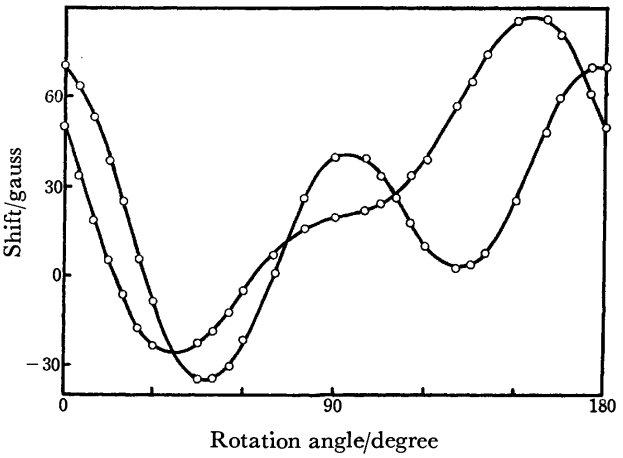

Fig. 5. The second order quadrupole effect in ^{27}Al NMR for the $AlBr_3 \cdot SbBr_3$ crystal.

shows the ^{27}Al NMR rotation pattern of the central line $(-1/2 \leftrightarrow +1/2)$, and in this case the rotation axis was arbitrarily chosen. Because of the monoclinic system, two central lines corresponding to different orientations of their efg tensors were observed. The e^2Qq/h and η thus obtained also support the distortion of the $AlBr_4^-$ ion from the regular tetrahedron, but the e^2Qq/h value is smaller than that of tetrahedrally bonded aluminum in the Al_2Br_6[14] or KAl_2Br_7[9] crystal.

From these findings it seems reasonable to propose that the $AlBr_3 \cdot SbBr_3$ crystal consists of the $SbBr_2^+$ and $AlBr_4^-$ ions and these ions are linked together by weak bonds between the Sb atom in $SbBr_2^+$ and the Br atom in $AlBr_4^-$. The lower population for the ϕ_1 orbital than ϕ_3 or ϕ_4 may suggest the existence of a weak bond between the Sb atom and the Br atom of the $AlBr_4^-$ ion. According to X-ray crystal analysis, similar structures are reported for $AlCl_3 \cdot ICl_3$,[16] $SbCl_5 \cdot ICl_3$,[16] and $AlCl_3 \cdot TeCl_4$.[17] These crystals consist of ion pairs, $AlCl_4^-ICl_2^+$, $SbCl_6^-ICl_2^+$, and $AlCl_4^-TeCl_3^+$, in which cations and anions are linked by weak bonds through the Cl atoms of the anions.

$AlI_3 \cdot SbI_3$. In the case of ^{127}I and ^{121}Sb (both I=5/2), a pair of NQR lines, $\nu_1(\pm 1/2 \leftrightarrow \pm 3/2)$ and $\nu_2(\pm 3/2 \leftrightarrow \pm 5/2)$, were observed. Zero-splitting patterns were observed for the six ν_1 transitions of the ^{127}I nuclei and for the ν_1 and ν_2 transitions of the ^{121}Sb nuclei.

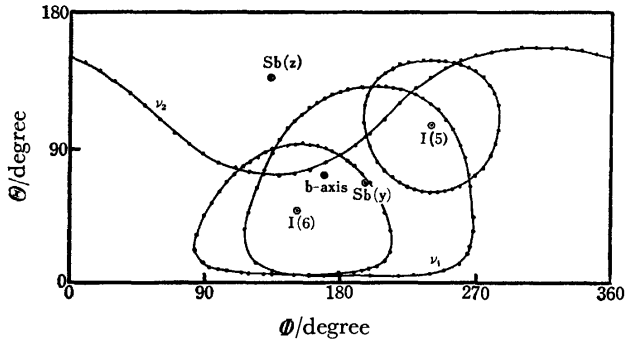

Fig. 6. Zero-splitting loci for the $^{127}I(5)$, $^{127}I(6)$, $^{121}Sb(\pm 1/2 \leftrightarrow \pm 3/2)$, and $^{121}Sb(\pm 3/2 \leftrightarrow \pm 5/2)$ lines in the $AlI_3 \cdot SbI_3$ crystal at room temperature. In practice a pair of zero-splitting patterns was observed for each resonance line symmetrically with respect to the b-axis because of the monoclinic system. ⊙: efg axis.

Therefore, the assignment of the pair ν_1 and ν_2 can be determined on the basis of the asymmetry parameter from the zero-splitting pattern. For the ^{127}I and ^{121}Sb nuclei the two values of the asymmetry parameter were independently calculated from the results of the Zeeman effect and from the frequency ratio of the pair, as shown in Table 1. The NQR parameters of this compounds are similar to that of the $AlBr_3 \cdot SbBr_3$ crystal, *i.e.*, this compound is expected to consist of the ion pair of SbI_2^+ and AlI_4^-. Figure 6 shows the zero-splitting patterns of $^{121}Sb(\pm 1/2 \leftrightarrow \pm 3/2)$, $^{121}Sb(\pm 3/2 \leftrightarrow \pm 5/2)$, $^{127}I(5)(\pm 1/2 \leftrightarrow \pm 3/2)$, and $^{127}I(6)(\pm 1/2 \leftrightarrow \pm 3/2)$, which arise from one SbI_2 unit. From the orientations of the efg tensors, the V-shaped SbI_2 unit has the geometry shown in Table 4. The z-axis of the Sb atom is almost perpendicular to the I–Sb–I plane, whereas the y-axis deviates about 7 degrees from the bisector of the two Sb–I bonds to the z-axis of the I(6) atom within the ISbI plane. This may be due to the fact that the two Sb–I bonds somewhat differ from each other, as is obvious from the e^2Qq/h of the I(5) and I(6) atoms.

$AlBr_3 \cdot BiBr_3$. The NQR spectra for this compound are different from those of the former compounds in the following points. (1) The asymmetry parameter of the ^{209}Bi atom is relatively small. (2) Only the Br(6) atom can be regarded as a terminal atom bonded to the Bi atom. (3) The Br(5) atom yields a somewhat smaller

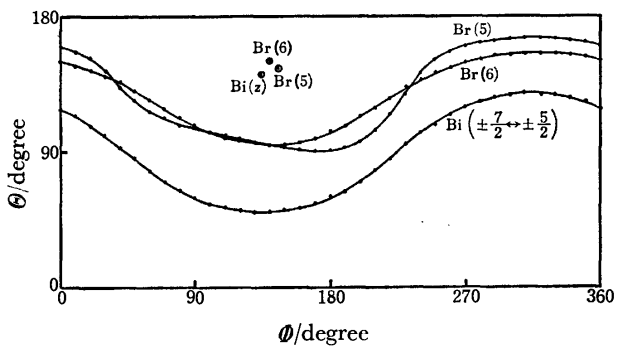

Fig. 7. Zero-splitting loci for the $^{81}Br(5)$, $^{81}Br(6)$, and ^{209}Bi $(\pm 5/2 \leftrightarrow \pm 7/2)$ lines in the $AlBr_3 \cdot BiBr_3$ crystal. ⊙: efg axis.

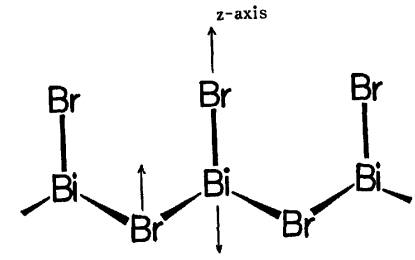

Fig. 8. Proposed structure for the $BiBr_2^+$ ion. The arrows indicate efg z-axes.

e^2Qq/h value compared with that of $BiBr_3$,[18] so that it must form a bridging bond of the type Bi–Br–Bi because of its large η.

Figure 7 shows the zero-splitting patterns of the ^{209}Bi $(\pm 7/2 \leftrightarrow \pm 9/2)$, $^{81}Br(5)$, and $^{81}Br(6)$ resonance lines. Each resonance line yields only one zero-splitting pattern. This fact suggests that the crystal belongs to a triclinic system. As is obvious from this figure, the z-axes of the three atoms are nearly parallel, within 9 degrees. On the basis of these findings, it is supposed that the $BiBr_2^+$ ions form a chain-like structure such as is shown in Fig. 8.

References

1) J. Kendall, E. D. Crittenden, and H. K. Miller, *J. Am. Chem. Soc.*, **45**, 963 (1923).
2) A. T. Nizhnik, *J. Gen. Chem.*, **7**, 1935 (1937).
3) E. Chemouni, M. H. Maglione, and A. Potier, *Bull. Soc. Chim. Fr.*, **1970**, 489.
4) V. P. Spiridonov and A. S. Malkova, *Zh. Strukt. Khim.*, **10**, 332 (1969).
5) E. Chemouni and A. Potier, *J. Inorg. Nucl. Chem.*, **33**, 2353 (1971).
6) T. Okuda, K. Yamada, H. Ishihara, and H. Negita, *Chem. Lett.*, **1975**, 785.
7) T. P. Das and E. L. Hahn, "Nuclear Quadrupole Resonance Spectroscopy," Solid State Physics, Suppl. 1, Academic Press, New York (1957).
8) G. M. Volkoff, *Can. J. Phys.*, **31**, 820 (1953).
9) K. Yamada, *J. Sci. Hiroshima Univ., Ser. A*, **41**, 77 (1977).
10) T. Okuda, H. Terao, O. Ege, and H. Negita, *Bull. Chem. Soc. Jpn.*, **43**, 2398 (1970).
11) K. Shimomura and N. Inoue, *J. Phys. Soc. Jpn.*, **14**, 86 (1959).
12) T. Okuda, K. Yamada, Y. Furukawa, and H. Negita, *Bull. Chem. Soc. Jpn.*, **48**, 3480 (1975).
13) T. Okuda, H. Terao, O. Ege, and H. Negita, *J. Chem. Phys.*, **52**, 5489 (1970).
14) P. A. Casabella, P. J. Bray, and R. G. Barnes, *J. Chem. Phys.*, **30**, 1393 (1959).
15) E. A. C. Lucken, "Nuclear Quadrupole Coupling Constants," Academic Press, New York (1969).
16) C. G. Vonk and E. H. Wiebenga, *Acta Crystallogr.*, **12**, 859 (1959).
17) B. Krebs, B. Buss, and D. Altena, *Z. Anorg. Allg. Chem.*, **386**, 257 (1971).
18) Y. Furukawa, *J. Sci. Hiroshima Univ., Ser. A*, **37**, 357 (1973).
19) N. Weiden and A. Weiss, *J. Magn. Reson.*, **20**, 334 (1975).
20) S. Ogawa, *J. Phys. Soc. Jpn.*, **13**, 618 (1958).

Polarized Absorption Spectra and Configuration Analyses of Xanthene and Xanthone

Tsuneyuki MINEGISHI, Toshihiko HOSHI,* Hiroshi HIRATSUKA, and Yoshie TANIZAKI

Department of Chemistry, Tokyo Institute of Technology, Meguro-ku, Tokyo 152
** Department of Chemistry, College of Science and Engineering, Aoyama Gakuin University, Chitosedai, Setagaya-ku, Tokyo 157*

(Received April 1, 1977)

The polarized absorption sepctra of xanthene and xanthone were measured in stretched poly(vinyl alcohol) films, and the polarization direction of each electronic transition was determined. It was confirmed that xanthone has the short molecular-axis polarized bands ($^1A_1 \leftarrow {}^1A_1$) at 343, 260, and 226 nm, and the long molecular-axis polarized ones ($^1B_2 \leftarrow {}^1A_1$) at 290, 266, and 242 nm. The electronic transitions of xanthone are discussed in connection with those of xanthene by use of the configuration analysis. For the 266 and 260 nm bands, the contributions of the intramolecular charge transfer character from the xanthene skeleton to the carbonyl group are considerable.

Derivatives of xanthone have been found as plant pigments and have received considerable attention because of their anomalous emission behavior. From lifetime and polarization measurements, it has been indicated that the configuration of the lowest triplet state of xanthone is $^3(n, \pi^*)$ type in a nonpolar solvent (3-methylpentane) but $^3(\pi, \pi^*)$ in a polar solvent.[1] The electronic absorption spectra of xanthone and its derivatives have been studied by several investigators,[1-3] but their assignments of the individual bands are different. For instance, Pownall and Huber[1] measured absorption and polarized phosphorescence spectra of xanthone, and they found five electronic bands at 364, 335, 282, 256, and 234 nm. The five bands were assigned to $^1A_2(n, \pi^*) \leftarrow {}^1A_1$, $^1A_1 \leftarrow {}^1A_1$, $^1B_2 \leftarrow {}^1A_1$, $^1A_1$-(CT)$\leftarrow {}^1A_1$, and $^1A_1 \leftarrow {}^1A_1$ transitions in order of increasing energy. From the measurements of absorption and fluorescence spectra and PPP calculations, Mizutani *et al.*[2] have also discussed the electronic structure of xanthone and its hydroxy and methoxy derivatives, and reported that there are a few discrepancies between their results and the above-mentioned ones.[1]

In this paper, measurements of polarized absorption spectra using stretched poly(vinyl alcohol) films and PPP calculations for xanthene and xanthone have been performed, and the electronic spectrum of xanthone is analyzed in connection with that of xanthene by use of the method of configuration analysis developed by Baba *et al.*[4]

Experimental

Materials. Commercially available (Tokyo Kasei Co., Ltd.) xanthene and xanthone were purified by repeated recrystallizations from ethanol. The melting point of xanthene was 99—100.2 °C (lit,[9] 99 °C) and that of xanthone 173.6 °C (lit,[9] 174 °C).

Measurements and Notations Used. The polarized absorption spectra were measured with a Shimadzu QV-50 spectrophotometer.[5-7]

The notations used in the figures of the polarized absorption spectra are as follows: R_s is a ratio of stretching,[5] $D_{//}$ and $D_\perp$ are absorbances for the light polarized parallel to and perpendicular to the stretched direction of the film, respectively, and R_d is the ratio of the optical densities ($R_d = D_{//}/D_\perp$).

In the case of planar molecules belonging to the point group C_{2v}, D_2, D_{2h} *etc.*, we can obtain a reduced polarization spectrum using the above-mentioned R_s and R_d values, *i.e.*, the absorption spectrum in a non-stretched polymer film can be reduced into two component spectra which are polarized parallel (D_z) to and perpendicular (D_y) to the principal symmetry axis (z).

Calculations

In the MO calculations, a modified PPP method developed by Nishimoto and Förster[8] was employed. The valence state ionization potentials ($I_p(r)$) and electron affinities ($E_a(r)$) used are as follows: $I_p(C) = 11.42$, $E_a(C) = 0.58$, $I_p(-O-) = 32.9$, $E_a(-O-) = 13.37$, $I_p(=O) = 23.7$, and $E_a(=O) = 2.47$ eV. The resonance integrals (β_{rs}) were adjusted at every iteration of the SCF calculations by the equations[8]

$$\beta_{CC} = -0.51 p_{CC} - 1.84,$$
$$\beta_{CO} = -0.56 p_{CO} - 2.20.$$

Here, p_{rs} is a π-bond order between the atoms r and s. In the CI calculations, all the one-electron excited configurations among the upper five occupied and lower five unoccupied SCF orbitals were taken into account.

It is very interesting for chemists to know the origin of the elctronic transitions more quantitatively. The configuration analysis developed by Baba and his coworkers[4] may be one of the most useful methods for this purpose. According to their method, any state function Ψ can be developed in terms of reference wavefunctions (Ψ°) appropriately chosen,

$$\Psi = \Psi^\circ M,$$

where M is a transformation matrix and the square of the matrix element (M_{ji}) of M represents the degree of contribution of a reference wavefunction Ψ_i° to the resultant wavefunction Ψ_j under consideration.

Results and Discussion

Figure 1 shows the polarized absorption spectrum of xanthene in the stretched poly(vinyl alcohol) film. The absorption spectrum ($D_{//}$ or $D_\perp$ curve) of this compound consists of three apparent bands at 294, 252, and ≈215 nm. The R_d values for the 252 nm band are large compared with those of the 294 nm band. This indicates that the relatively intense 252 nm band is polarized along the long molecular-axis (y-axis) and 294 nm

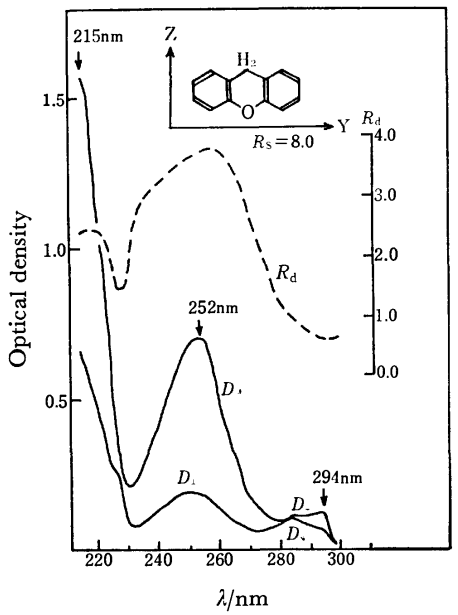

Fig. 1. The polarized absorption spectrum of xanthene in the stretched poly(vinyl alcohol) film.

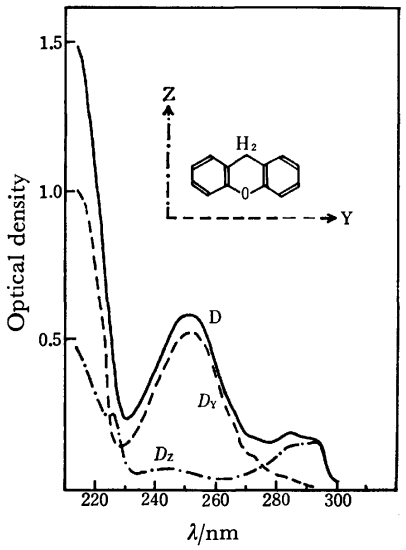

Fig. 2. The reduced polarized absorption spectrum of xanthene. D: The absorption spectrum in the non-stretched poly(vinyl alcohol) film. D_y and D_z: The reduced polarization spectrum.

band along the short-axis (z). The behavior of the R_d curve suggests the presence of additional weak bands at 285 and 226 nm, that is, the R_d values are steeply increased with decreasing wavelength around 285 nm and a distinct minimum is found at 226 nm. To determine in more detail the locations of these hidden bands, we obtained the reduced polarization spectrum, which is shown in Fig. 2. From this figure, it is clearly seen that the z-axis polarized bands are at 294 and 226 nm and the y-axis polarized ones are at 285, 252, and around 215 nm.

The above experimental results are compared with calculated ones in Table 1. From this table, it is clear that the observed 294 and 226 nm bands can be assigned

Table 1. Comparison of the observed and calculated transition energies, intensities, and polarizations for xanthene

Symmetry	Transition energy (nm) Calcd	Obsd[a]	Intensity Calcd(f)	Obsd(ε)[b]	Polarization Calcd	Obsd
I A_1	287	294	0.016	1900	z	z
II B_2	287	285	0.008		y	y
III B_2	254	252	0.500	8000	y	y
IV A_1	222	226	0.001	*ca.* 6000	z	z
V B_2	211	≈215	0.226	14700	y	y
VI B_2	207		0.855		y	
VII A_1	206		0.323		z	—

a) In poly(vinyl alcohol) film. b) In ethanol.

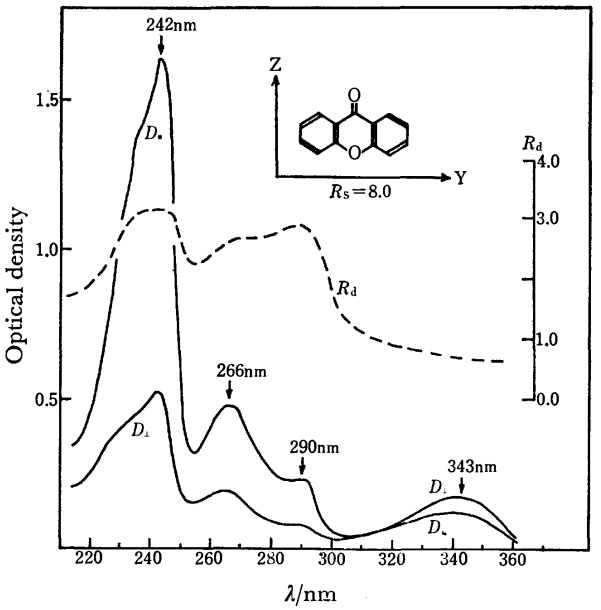

Fig. 3. The polarized absorption spectrum of xanthone in the stretched poly(vinyl alcohol) film.

to $^1A_1 \leftarrow {}^1A_1$ transitions and the observed 285 and 252 nm bands to $^1B_2 \leftarrow {}^1A_1$.

Figure 3 shows the polarized absorption spectrum of xanthone. The spectrum of this compound is very complex, *i.e.*, four apparent peaks are found at 343, 290, 266, and 242 nm besides a shoulder around 235 nm. The R_d curve shows clear maxima at 290 and 242 nm and a shoulder at 266 nm, indicating that the 290, 266, and 242 nm bands are polarized along the long molecular-axis (y). On the other hand, the 343 nm band is polarized along the short molecular-axis (z), because the R_d values for this band are the smallest in the observed wavelength region. The R_d values decrease steeply on both sides of the intense 242 nm band and a clear minimum is found around 254 nm. This indicates that weak bands polarized along the short molecular-axis are hidden at about 254 and 220 nm.

Figure 4 shows the reduced polarization spectrum of xanthone. From this figure the location of each band including above-mentioned hidden bands can be clearly seen. That is, the long molecular-axis polarized bands

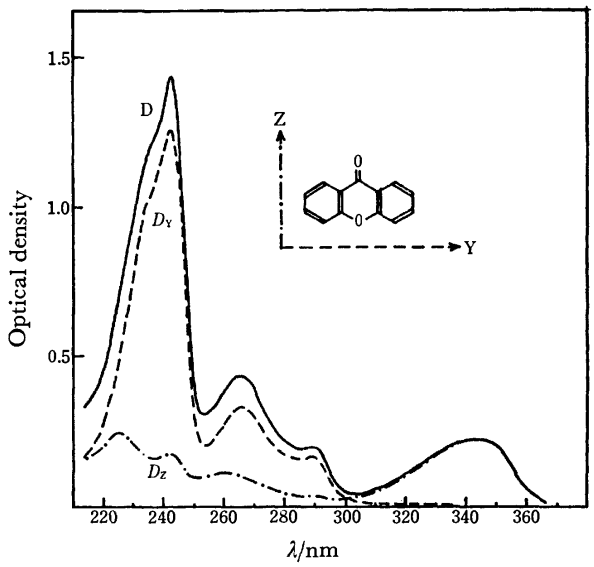

Fig. 4. The reduced polarized absorption spectrum of xanthone. Notations used: *cf.* Fig. 2.

are found at 290, 266, and 242 nm, and the short molecular-axis polarized ones at 343, 260, and 226 nm. From the above experimental results, the z-axis polarized 343 and 260 nm bands can be assigned to the $^1A_1 \leftarrow {}^1A_1$ transitions, and the y-axis polarized 290, 266, and 242 nm bands to $^1B_2 \leftarrow {}^1A_1$, as shown in Table 2. This assignment is not always consistent with the previously reported assignments.[1] For instance, the relatively intense 266 and 242 nm bands were earlier assigned to $^1A_1 \leftarrow {}^1A_1$ transitions.[1]

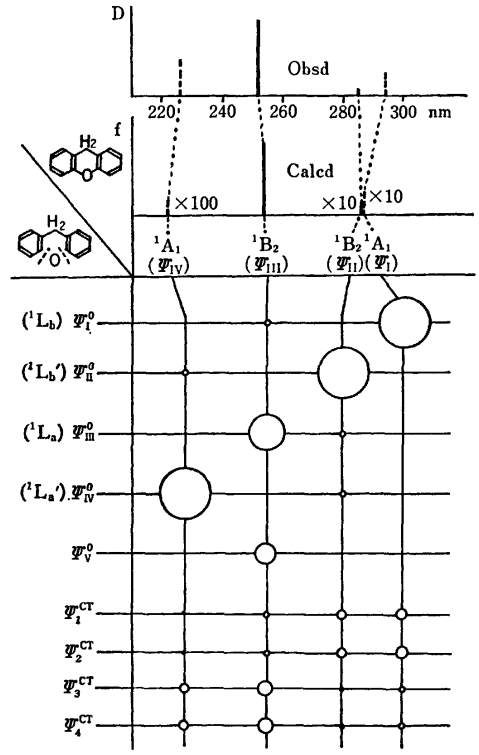

Fig. 5. Results of the configuration analysis of xanthene. The radius of the circle is proportional to the magnitude of M_{ji}, *i.e.* the area of the circle represents the degree of the contribution of Ψ_i° to Ψ_j.
D: Observed relative intensity.
f : Calculated oscillator strength.
Ψ_i° and Ψ_j: See text.
Ψ_i^{CT}: Wavefunction for the charge transfer state from oxygen to the two benzene rings.

TABLE 2. COMPARISON OF THE OBSERVED AND CALCULATED TRANSITION ENERGIES, INTENSITIES, AND POLARIZATIONS FOR XANTHONE

Sym-metry		Transition energy (nm)		Intensity		Polarization	
		Calcd	Obsd[a]	Calcd(f)	Obsd(ε)[b]	Calcd	Obsd
I	A_1	316	343	0.114	7200	z	z
II	B_2	293	290	0.003	4200	y	y
III	B_2	266	266	0.162	13000	y	y
IV	A_1	243	260	0.146		z	z
V	B_2	241	242	1.363	42800	y	y
VI	A_1	230	226	0.135		z	z
VII	B_2	228	—	0.027		y	—

a) In poly(vinyl alcohol) film. b) In ethanol.

Configuration Analysis. State wavefunctions of a molecule can be developed in terms of wavefunctions of an appropriately chosen reference molecule. In the case of xanthene, we have chosen the structure of the reference molecule as

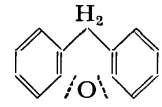

The results of the configuration analysis are shown in Fig. 5. From this figure, it is clear that the state wave-

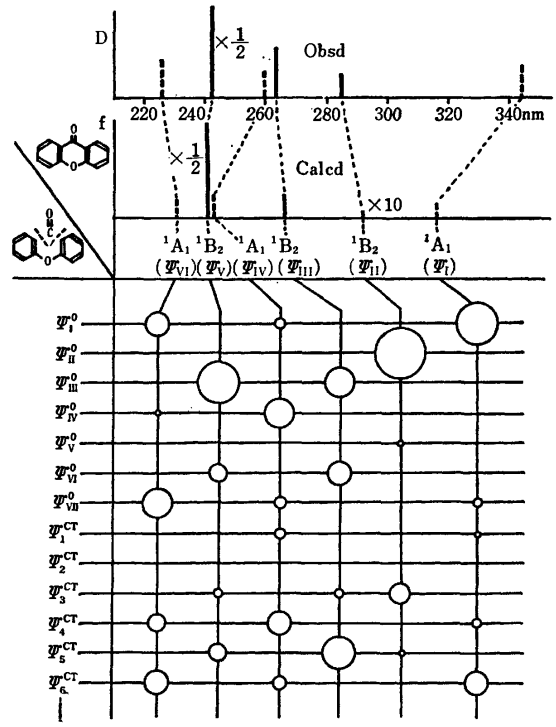

Fig. 6. Results of the configuration analysis of xanthone. See the explanation of Fig. 5, where Ψ_i^{CT} stands for wavefunction for the charge transfer state from xanthene skeleton to the carbonyl group.

functions Ψ_{I}, Ψ_{II}, Ψ_{III}, and Ψ_{IV} are approximately represented by the state functions Ψ_{I}°, Ψ_{II}°, Ψ_{III}°, and Ψ_{IV}° of the reference molecule, respectively. That is, it may be considered that the first two transitions ($\Psi_{I}\leftarrow\Psi_{0}$ and $\Psi_{II}\leftarrow\Psi_{0}$) arise from the interaction between the $^{1}L_{b}$ states of the two benzene rings and the next two transitions ($\Psi_{III}\leftarrow\Psi_{0}$ and $\Psi_{IV}\leftarrow\Psi_{0}$) from the two $^{1}L_{a}$ states.

As for xanthone, the excited state wavefunctions were developed in terms of the wavefunctions of xanthene (reference molecule) as shown in Fig. 6. The transitions I(Ψ_{I}), II(Ψ_{II}), and V(Ψ_{V}) of xanthone are approximately represented by the transitions I(Ψ_{I}°), II(Ψ_{II}°), and III(Ψ_{III}°), respectively. Transition III(Ψ_{III}) is considered to be due to the interaction of Ψ_{III}°, Ψ_{VI}°, and Ψ_{CT5}°, and transition IV(Ψ_{IV}) due to the interaction of Ψ_{IV}° and Ψ_{CT4}°, where Ψ_{CT}°'s represent the charge transfer configuration from the xanthene skeleton to the carbonyl group. Transitions III and IV of xanthone observed at 266 and 260 nm may be considered to be charge transfer bands. As for this molecule, charge transfer configurations from the C=O group to the xanthene skeleton can also be considered, but the contributions of these configurations are negligibly small.

References

1) H. J. Pownall and J. R. Huber, *J. Am. Chem. Soc.*, **93**, 6429 (1971).
2) K. Mizutani, K. Miyazaki, K. Ishigaki, and H. Hosoya, *Bull. Chem. Soc. Jpn.*, **47**, 1596 (1974).
3) A. A. Efimov, R. N. Nurmukhametov, I. L. Belaits, and A. I. Tolmachev, *Opt. Spectrosc.*, **30**, 337 (1971).
4) H. Baba, S. Suzuki, and T. Takemura, *J. Chem. Phys.*, **50**, 2078 (1969).
5) Y. Tanizaki, *Bull. Chem. Soc. Jpn.*, **38**, 1798 (1965).
6) T. Hoshi and Y. Tanizaki, *Z. Phys. Chem. (Frankfurt)*, **71**, 230 (1970).
7) T. Hoshi, H. Inoue, J. Shiraishi, and Y. Tanizaki, *Bull. Chem. Soc. Jpn.*, **44**, 1743 (1971).
8) K. Nishimoto and L. S. Förster, *Theor. Chim. Acta*, **3**, 407 (1969).
9) A. Albert, "Heterocyclic Chemistry," Athlone Press, London (1959), pp. 276—281.

Kinetic Studies on Double Relaxation of Surfactant Solutions Using a Capillary Wave Method

Minoru SASAKI, Tatsuya YASUNAGA, Shigemi SATAKE, and Minoru ASHIDA

Department of Chemistry, Faculty of Science, Hiroshima University, Higashisenda-machi, Hiroshima 730

(Received May 4, 1977)

The frequency dependence of the damping coefficient of a capillary wave was measured in decylamine hydrochloride solutions. The observed relaxations were well expressed by the double-relaxation equations. From the concentration dependence of the relaxation parameters obtained, the relaxations at low and high frequencies were attributed to the adsorption-desorption and ion-pair formation reactions on the surface, respectively. Furthermore, the adsorption rate constants are related to the hydrophobic and hydrophilic properties of the surfactants.

Very recently, adsorption-desorption phenomena on the surface of sodium dodecyl sulfate (SDS), dodecylamine hydrochloride (DAC), and octylamine hydrochloride (OAC) solutions have been investigated theoretically and experimentally by means of the capillary wave method.[1,2] Similar studies on a homologous series of alkylamine hydrochloride solutions would give valuable information about the relationship between the dynamic behavior and the structure of the surfactant molecules.

The purpose of this paper is to study the adsorption-desorption phenomena by measuring the frequency dependence of the damping coefficient of the capillary wave on the surface of decylamine hydrochloride (DeAC) solutions as an extension of previous studies.

Theoretical

Let us consider the following scheme, which is a combination of adsorption-desorption and ion-pair formation reactions on the surface of a surfactant solution:[1]

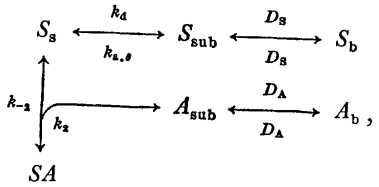

where

$$K = \frac{k_2}{k_{-2}},$$

S, A, and SA are the surfactant ion, counter ion, and ion-pair on the surface, subscripts s, sub, and b refer to the surface, subsurface and bulk phase, $k_{a,\theta}$ and k_d are the adsorption and desorption rate constants defined in a previous paper,[1] k_2 and k_{-2} are the association and dissociation rate constants, D_S and D_A are the diffusion coefficients for S and A, respectively, and K is the equilibrium constant.

The following rate and diffusion equations are given for the two processes:[1]

For the diffusion processes ($y \leqslant -d_{sub}$),

$$\frac{dc_i}{dt} = D_i\left(\frac{\partial^2 c_i}{\partial x^2} + \frac{\partial^2 c_i}{\partial y^2}\right)$$

$$(c_i = c_{S,b},\ c_{A,b} \text{ and } D_i = D_S,\ D_A), \qquad (1)$$

and for the (Langmuir-type) adsorption-desorption and ion-pair formation processes ($0 \geqslant y \geqslant -d_{sub}$),

$$\frac{d\theta_1}{dt} = k_{a,\theta}(1-\theta_1-\theta_2)c_{S,sub} - k_d\theta_1 - k_2\theta_1 c_{A,sub} + k_{-2}\theta_2 \qquad (2)$$

and

$$\frac{d\theta_2}{dt} = k_2\theta_1 c_{A,sub} - k_{-2}\theta_2,$$

where x and y are the rectangular coordinates normal and tangent to the surface at rest, $c_{S,sub}$, $c_{A,sub}$, $c_{S,b}$, and $c_{A,b}$ are the molar concentrations of S_{sub}, A_{sub}, S_b, and A_b, t is the time, d_{sub} is the thickness of the subsurface layer, and θ_1 and θ_2 are the fractions of sites occupied by S and SA, respectively. The changes in the concentrations are given by:

$$c_j = \bar{c}_j + \Delta c_j \exp\{i(\omega' t + \kappa x)\}$$

$$(c_j = c_i,\ c_{S,sub},\ c_{A,sub}) \qquad (3)$$

and

$$\theta_k = \bar{\theta}_k + \Delta\theta_k \exp\{i(\omega' t + \kappa x)\} \quad (k = 1, 2),$$

where

$$\omega' = 4\pi f, \quad \kappa = 2k,$$

with ω' and κ being the angular frequency and wavenumber of the perturbed variables, f and k the frequency and wavenumber, respectively, and with the bar denoting the equilibrium state. The solution of Eq. 1 gives:[1,3,4]

$$\Delta c_i = E_i \exp(n_i y)$$

$$(E_i = E_S,\ E_A \text{ and } n_i = n_S,\ n_A), \qquad (4)$$

where

$$n_i = \left(\kappa^2 + \frac{i\omega'}{D_i}\right)^{1/2} = \beta_{11} + i\omega'\beta_{12},$$

E_i is a constant and n_i are the parameters related to the thickness of the bulk phase concerned with the diffusion process. On the other hand, the laws of conservation of mass give two independent relations for the concentration changes of the surfactant and counter ions:[1]

$$F(\Delta\theta_1 + \Delta\theta_2) + \int_{-\infty}^{-d_{sub}} E_S \exp(n_S y)dy = F(\Delta\theta_1 + \Delta\theta_2) + \frac{\Delta c_{S,sub}}{n_S} = 0 \qquad (5)$$

and

$$F\Delta\theta_2 + \int_{-\infty}^{-d_{sub}} E_A \exp(n_A y)dy = F\Delta\theta_2 + \frac{\Delta c_{A,sub}}{n_A} = 0,$$

where

$$F = 10^3\Gamma_{max},$$

and Γ_{max} is the maximum value of the surface excess. A combination of Eqs. 2—5 gives:

$$\begin{aligned} i\omega'\{1+k_{a,\theta}(1-\bar{\theta}_1-\bar{\theta}_2)F\beta_{S2}\}\Delta\theta_1 \\ +i\omega'F\{k_{a,\theta}(1-\bar{\theta}_1-\bar{\theta}_2)\beta_{S2}+k_2\bar{\theta}_1\beta_{A2}\}\Delta\theta_2 \\ = -[k_{a,\theta}\{\bar{c}_{S,sub}+(1-\bar{\theta}_1-\bar{\theta}_2)F\beta_{S1} \\ +k_d+k_2\bar{c}_{A,sub}]\Delta\theta_1-[k_{a,\theta}\{\bar{c}_{S,sub} \\ +(1-\bar{\theta}_1-\bar{\theta}_2)F\beta_{S1}\}+Fk_2\bar{\theta}_1\beta_{A1}-k_{-2}]\Delta\theta_2 \end{aligned} \quad (6)$$

and

$$\begin{aligned} i\omega'(1+k_2F\bar{\theta}_1\beta_{A2})\Delta\theta_2 \\ = k_2\bar{c}_{A,sub}\Delta\theta_1-(k_2F\bar{\theta}_1\beta_{A1}+k_{-2})\Delta\theta_2. \end{aligned}$$

For relatively concentrated surfactant solutions near the CMC, these equations are simplified in the cases of c_0 (the initial concentration)$>10^{-3}$ mol dm^{-3}, $k_2<5\times10^4$ mol^{-1} dm^3 s^{-1}, and $K<10^4$ mol^{-1} dm^3 (with $D_S\approx10^{-6}$ cm^2 s^{-1}, $D_A\approx10^{-5}$ cm^2 s^{-1}, and $\bar{c}_{S,sub},\approx\bar{c}_{A,sub}\approx c_0$)[1] to

$$\begin{aligned} i\omega'\Delta\theta_1 &= -a_{11}-a_{12} \\ \text{and} \\ i\omega'\Delta\theta_2 &= -a_{21}-a_{22}, \end{aligned} \quad (7)$$

where

$$a_{11} = k_{a,\theta}c_0+k_d+k_2c_0, \quad a_{12} = k_{a,\theta}c_0-k_{-2},$$
$$a_{21} = -k_2c_0, \quad a_{22} = k_{-2}.$$

Solving Eq. 7, one obtains the following equation for the relaxation times, τ:[5]

$$\tau_{I,II}^{-1} = \frac{1}{2}(a_{11}+a_{22})\left[1\pm\left\{1-\frac{4(a_{11}a_{22}-a_{12}a_{21})}{(a_{11}-a_{22})^2}\right\}^{1/2}\right]. \quad (8)$$

This equation is easily simplified by the conditions $a_{11}\gg a_{22}$ and $a_{22}\gg a_{11}$ to the following forms:[5]

For $a_{11}\gg a_{22}$ ($\tau_I^{-1}\gg\tau_{II}^{-1}$),

$$\begin{aligned} \tau_I^{-1} &= a_{11} = k_{a,\theta}c_0 + k_d + k_2c_0 \\ \text{and} \\ \tau_{II}^{-1} &= a_{22} - \frac{a_{12}a_{21}}{a_{11}} = k_{-2} + \frac{k_2c_0(k_{a,\theta}c_0-k_{-2})}{k_{a,\theta}c_0+k_d+k_2c_0}, \end{aligned} \quad (9a)$$

and for $a_{22}\gg a_{11}$ ($\tau_{II}^{-1}\gg\tau_I^{-1}$),

$$\begin{aligned} \tau_I^{-1} &= a_{11} - \frac{a_{12}a_{21}}{a_{22}} = k_{a,\theta}(1+Kc_0)c_0 + k_d \\ \text{and} \\ \tau_{II}^{-1} &= a_{22} = k_{-2}. \end{aligned} \quad (9b)$$

The apparent relaxation strengths, δ', for two-step reactions on the surface are given by the following equations on the basis of two-dimensional relaxation theory[1] and of the theory for ultrasonic absorption[5] at constant activity:

$$\delta_I' = \frac{(W\Delta\gamma_1+X\Delta\gamma_2)^2}{\gamma RT}\left(W^2\Sigma\frac{\nu_{i1}^2}{c_i}+2XW\Sigma\frac{\nu_{i1}\nu_{i2}}{c_i}+X^2\Sigma\frac{\nu_{i2}^2}{c_i}\right)^{-1}$$

and

$$\delta_{II}' = \frac{(Y\Delta\gamma_1+Z\Delta\gamma_2)^2}{\gamma RT}\left(Y^2\Sigma\frac{\nu_{i1}^2}{c_i}+2YZ\Sigma\frac{\nu_{i1}\nu_{i2}}{c_i}+Z^2\Sigma\frac{\nu_{i2}^2}{c_i}\right)^{-1},$$

where

$$\begin{pmatrix} W & Y \\ X & Z \end{pmatrix} = \begin{pmatrix} 1 & a_{12}/(a_{22}-\tau_I^{-1}) \\ a_{21}/(a_{11}-\tau_{II}^{-1}) & 1 \end{pmatrix},$$

γ is the surface tension, $\Delta\gamma$ is the standard surface tension change defined in a previous paper,[1] R is the universal gas constant, T is the temperature, ν is the stoichiometric coefficient, and subscripts 1 and 2 denote the adsorption-desorption and ion-pair formation processes, respectively. The conditions $a_{11}\gg a_{22}$ and $a_{22}\gg a_{11}$ then lead to:[1,5] for $a_{11}\gg a_{22}$:

$$\delta_I' = \frac{(\Delta\gamma_1)^2}{\gamma RT}\left(\frac{1}{\Gamma_{max}\bar{\theta}_1}+\frac{3}{2}\times10^2N^{1/3}c_0^{-2/3}\right)^{-1}$$

and

$$\begin{aligned} \delta_{II}' = \frac{(Y\Delta\gamma_1+\Delta\gamma_2)^2}{\gamma RT}\left\{\frac{1-2Y-Y^2}{\Gamma_{max}\bar{\theta}_2}+\frac{1}{\Gamma_{max}\bar{\theta}_2}\right. \\ \left.+\frac{3}{2}\times10^2(1+Y^2)N^{1/3}c_0^{-2/3}\right\}^{-1}, \end{aligned} \quad (10a)$$

where

$$\begin{pmatrix} W & Y \\ X & Z \end{pmatrix} = \begin{pmatrix} 1 & -a_{12}/a_{11} \\ 0 & 1 \end{pmatrix},$$

and for $a_{22}\gg a_{11}$,

$$\begin{aligned} \delta_I' = \frac{(\Delta\gamma_1+X\Delta\gamma_2)^2}{\gamma RT}\left\{\frac{1-2X+X^2}{\Gamma_{max}\bar{\theta}_1}+\frac{X^2}{\Gamma_{max}\bar{\theta}_2}\right. \\ \left.+\frac{3}{2}\times10^2(1+X^2)N^{1/3}c_0^{-2/3}\right\}^{-1} \end{aligned}$$

and

$$\delta_{II}' = \frac{(\Delta\gamma_2)^2}{\gamma RT}\left(\frac{1}{\Gamma_{max}\bar{\theta}_1}+\frac{1}{\Gamma_{max}\bar{\theta}_2}+\frac{3}{2}\times10^2N^{1/3}c_0^{-2/3}\right)^{-1}, \quad (10b)$$

where

$$\begin{pmatrix} W & Y \\ X & Z \end{pmatrix} = \begin{pmatrix} 1 & 0 \\ -a_{21}/a_{22} & 1 \end{pmatrix}.$$

Experimental

The apparatus employed was the same as that reported in a previous paper.[2]

Decylamine (Schuchardt, purity; 90%) was distilled twice and the purity of the distillate was confirmed to be 99.8% using gas chromatography. Decylamine was neutralized by hydrochloric acid in a butanol solution and was then recrystallized four times from the butanol solution and finally washed with petroleum ether. The value of the CMC was determined to be 62.5 mM* using the electric conductivity method at 25 °C.

The measurements of the damping coefficient of the capillary wave were carried out from 40 to 700 Hz on the surface of concentrated DeAC solutions below the CMC at 25± 0.4 °C.

Results and Discussion

The frequency dependence of the damping coefficient, α, is shown in Fig. 1. As seen from this figure, the experimental values of α/f are greater than the theoretical results of α_d/f, where α_d refers to the damping coefficient resulting only from diffusion between the surface and the bulk phase.[1,3,4] This difference cannot be expressed by a single relaxation equation as was done in a previous paper.[2] In order to interpret the experimental results, let us consider multiple-step reactions on the surface. The equation for the damping coefficient derived in previously[2] is generalized to the mutiple relaxations, as follows:

$$\frac{3\rho c^3}{2\pi\gamma k}\left(\frac{\alpha}{f}-\frac{\alpha_d}{f}\right) = \sum_{i=1}^{N}\frac{\omega'\tau_i\delta_i'}{1+\omega'^2\tau_i^2}, \quad (11)$$

* Throughout this paper, 1 M=1 mol dm^{-3}.

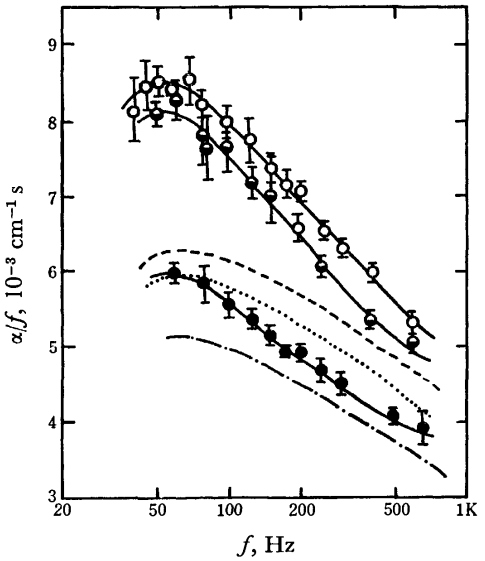

Fig. 1. The plots of α/f *vs.* f in the DeAC solutions. The theoretical curves of α_d/f are shown; ------: 50 mM, ·····: 40 mM, —·—: 25 mM. ○: 50 mM, ◒: 40 mM, ●: 25 mM.

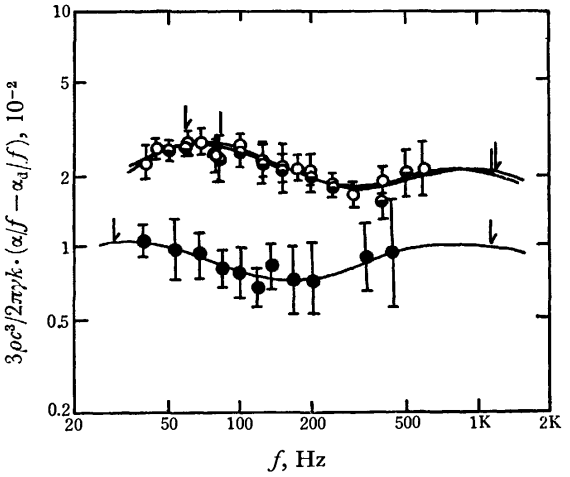

Fig. 2. The relaxation absorption spectra in the DeAC solutions. The solid lines show the theoretical curves calculated by right hand side of Eq. 11 with the relaxation parameters listed in Table 1. The arrows show the relaxation frequency $f_r=(4\pi\tau)^{-1}$.
○: 50 mM, ◒: 40 mM, ●: 25 mM.

Table 1. Relaxation parameters in DeAC and OAC solutions at 25 °C

	c_0 (mM)	τ_1^{-1} (10^2 s^{-1})	τ_2^{-1} (10^4 s^{-1})	δ'_1 (10^{-2})	δ'_2 (10^{-2})
DeAC	25.0	5.6±0.4	1.5±0.2	2.0±0.5	1.9±0.5
	40.0	7.5±1.1	1.5±0.2	4.9±0.5	3.7±0.5
	50.0	10.5±0.6	1.5±0.5	4.8±1.0	2.7±0.5
	60.0	11.1±1.8	1.6±0.5	2.5±0.3	1.0±0.3
OAC	34.6	4.1±0.5	—	1.3±0.5	—
	46.1	3.6±0.5	—	2.5±0.3	—
	57.7	4.7±0.7	0.9±0.2	3.9±0.7	2.6±0.7
	76.9	6.1±0.8	1.1±0.3	5.2±0.7	2.9±0.7
	115.3	8.2±0.5	1.3±0.4	7.7±0.8	2.9±0.8

where ρ is the density, c is the propagation velocity, and N is the number of reaction steps. The frequency dependence of the left hand side of Eq. 11 is shown in Fig. 2. The experimental results can be satisfactorily represented by the right hand side of Eq. 11 in the case of $N=2$; thus, the existance of double relaxations was confirmed. The relaxation parameters obtained are listed in Table 1, where subscripts 1 and 2 refer to the relaxations at lower and higher frequencies, respectively.

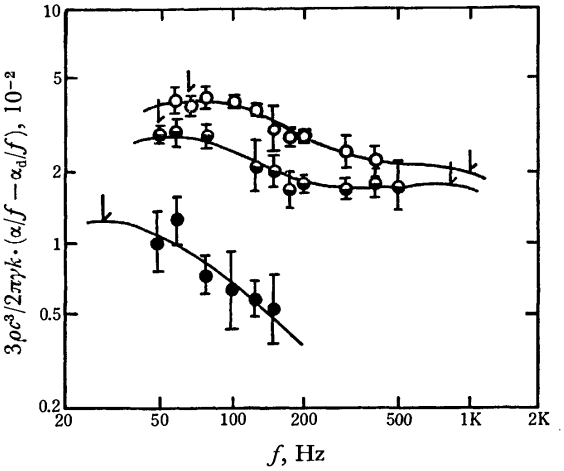

Fig. 3. The relaxation absorption spectra in the purified OAC solutions.
○: 115 mM, ◒: 76.9 mM, ●: 46.1 mM.

These facts lead to a new problem: why was only a single relaxation observed for the SDS, DAC, and OAC solutions reported in Ref. 2. Before this problem could be clarified, the experimental results for the OAC solutions stimulated a reexamination of the purified OAC solutions, since the OAC contained a minute amount of DeAC (content; 2.3%). The OAC was prepared by neutralizing octylamine (the purity of which was verified to be 99.9% using gas chromatography) with hydrochloric acid. The experimental results for the purified OAC solutions are shown in Fig. 3. As seen from this figure, double relaxations are observed and the relaxation parameters obtained are listed in Table 1 together with those for the DeAC solutions. The concentration dependence of the relaxation parameters is the same as that for the DeAC solutions. This suggests that the relaxation phenomena in both solutions are caused by perturbation of the same process. In a series of studies on relaxation phenomena on the surface of surfactant solutions,[2] double relaxations were observed in the DeAC and OAC solutions but were not observed in the SDS and DAC solutions. The concentration dependence of τ_2^{-1} for the former solutions differs from that of the reciprocal relaxation time for the latter solutions. Moreover, the τ_2^{-1} for the DeAC solution is larger than that for the OAC solution. Since the SDS and DAC hydrocarbon chain lengths are longer than those for DeAC and OAC, the above-mentioned facts suggest that the relaxations at the higher frequency in the SDS and DAC solutions may be located outside the measured frequency range.

Table 2. Kinetic parameters in various surfactant solutions at 25 °C

	purity (%)	CMC (mM)	$k_{a,\theta}$ (10^4 M^{-1} s^{-1})	k_a (10^5 s^{-1})	k_d (10^2 s^{-1})	k_2 (10^4 M^{-1} s^{-1})	k_{-2} (10^4 s^{-1})	K (M^{-1})
SDS[a]	99.5	8.3	11±5	4±2	9±1	—	—	—
DAC[a]	99.7	15.8	6±3	3±1	8±2	—	—	—
DeAC	99.8	62.5	1.3±0.4	0.5±0.2	3±1	6±1	1.5±0.3	4
OAC	97.7[a]	175	1.0±0.3	0.6±0.2	—	—	—	—
	99.9	180	0.32±0.09	0.2±0.05	2.5±0.5	7±1	1.1±0.2	5

a) Ref. 2.

The new experimental results described above prompted a modification of the adsorption-desorption mechanism model proposed in a previous paper.[1] The concentration dependence of τ_1^{-1} listed in Table 1 is similar to that for the relaxation times reported previously.[2] This fact suggests that the relaxation at lower frequency may be due to the adsorption-desorption process of the surfactants. On the other hand, the τ_2^{-1} values were independent of the surfactant concentration as seen from Table 1. Various reactions on the surface are considered, *e.g.*, an ion-pair formation reaction, a monomer-dimer reaction, and a conformational change reaction. Of these, the ion-pair formation reactions between halide and dodecylpyridinium ions and between the various anions and polysoap on the surface have been studied under static conditions by Parreira[6] and Plaisance and Ter-Minassian-Saraga,[7] respectively. Thus, the model of the adsorption-desorption mechanism presented in a previous paper[1] was modified in the manner expressed by the scheme given in the theoretical section. Since the τ_1^{-1} values are an order of magnitude smaller than the τ_2^{-1} values, *i.e.*, $a_{22} \gg a_{11}$ (see Eq. 9b), the equations for the relaxation times and the apparent relaxation strengths are given by Eq. 9b ($\tau_I=\tau_1$ and $\tau_{II}=\tau_2$) and by the following equation, respectively:

$$\delta'_{1,2} = \frac{(\Delta\gamma)^2}{\gamma RT} \cdot f_{1,2}(\gamma, c_1), \tag{12}$$

where

$$f_1(\gamma, c_1) = (1+Kc_0)^2 \left\{ \frac{1-2Kc_0+K^2c_0^2}{\Gamma_{max}\bar{\theta}_1} + \frac{K^2c_0^2}{\Gamma_{max}\bar{\theta}_2} + \frac{3}{2} \times 10^2 (1+K^2c_0^2) N^{1/3} c_0^{-2/3} \right\}^{-1},$$

$$f_2(\gamma, c_1) = \left(\frac{1}{\Gamma_{max}\bar{\theta}_1} + \frac{1}{\Gamma_{max}\bar{\theta}_2} + \frac{3}{2} \times 10^2 N^{1/3} c_0^{-2/3} \right)^{-1},$$

under the assumption that $\Delta\gamma_1$ in Eqs. 10a and 10b is approximately equal to $\Delta\gamma_2$, since the counter ion may associate in the immediate proximity of the surface.

The K values in Eq. 12 were determined so as to give straight lines for the plots of $\delta'_{1,2}$ *vs.* $f_{1,2}$ (γ, c_1). As is shown in Fig. 4, the experimental values fall on the theoretical straight lines in the cases of $K=4$ and 5 for the DeAC and OAC solutions, respectively. With the K values obtained, the equations for the relaxation times were applied to the experimental results listed in Table 1. As seen from Figs. 5 and 6, the experimental values fall on the straight lines. The linearities of these plots confirm the validity of the scheme. The values of $\Delta\gamma$, $k_{a,\theta}$ k_d, and k_{-2} were obtained from the slopes and intercepts in Figs. 4, 5, and 6, respectively and are listed in Tables 2 and 3. The k_2 values listed in Table 2 were calculated using the values of K and k_{-2}. The values of the adsorption rate constant, k_a,[1] and the adsorption energy, ΔG,[2] were calculated and are also listed in Tables 2 and 3. The K and k_2 values listed in Table 2 satisfy the conditions for the simplification of Eq. 6. In the present work, other plausible processes, a monomer-dimer reaction and a conformational change reaction on the surface, were also examined, but no results were obtained.

Table 3. Thermodynamic parameters in various surfactant solutions at 25 °C

	ΔG ($-RT$)		$\Delta\gamma$ (10^{10} dyn cm mol^{-1})[d]	
SDS[a]	6.1	6.8[b]	10	6[c]
DAC[a]	5.9	6.3[b]	8	7[c]
DeAC	5.1	4.6[b]	2	7[c]
OAC	4.4	4.5[b]	2	7[c]

a) Ref. 2. b) These values were calculated using the Szyszkowski equation. c) These values were estimated using $(\gamma_{water}-\gamma_{CMC})/\Gamma_{max}$. d) 1 dyn=$10^{-5}$ N.

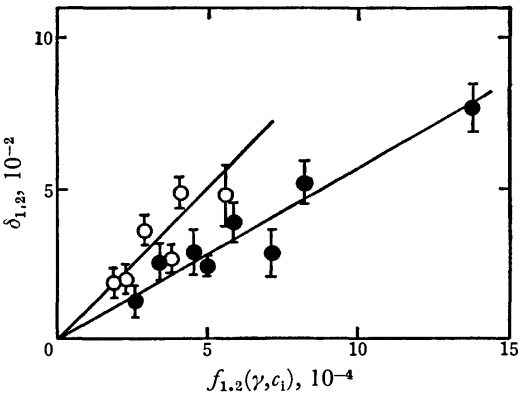

Fig. 4. The plots of $\delta'_{1,2}$ *vs.* $f_{1,2}$ (γ,c_1) in the DeAC (open circles) and OAC (closed circles) solutions. The values of $f_{1,2}$ (γ,c_1) were calculated using $K=4$ and 5 in the DeAC and OAC solutions, respectively.

Among the kinetic parameters concerned with the adsorption-desorption process listed in Table 2, $k_{a,\theta}$ and k_a are inversely proportional to the CMC, as seen in Fig. 7 but k_a is independent of the CMC. Since the logarithm of the CMC bears a linear relation to the hydrophile-liophile balance (HLB) value,[8,9] $k_{a,\theta}$ and k_a can be related to the HLB values as follows:

$$\log k_{a,\theta} = (0.30\pm0.06)HLB + (0.5\pm0.6)$$

and

$$\log k_a = (0.25\pm0.05)HLB + (1.8\pm0.6). \tag{14}$$

These relations indicate that the adsorption rate

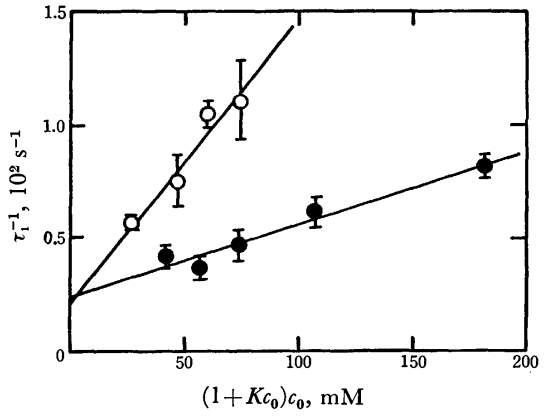

Fig. 5. The plots of τ_1^{-1} *vs.* $(1+Kc_0)c_0$ in the DeAC (open circles) and OAC (closed circles) solutions.

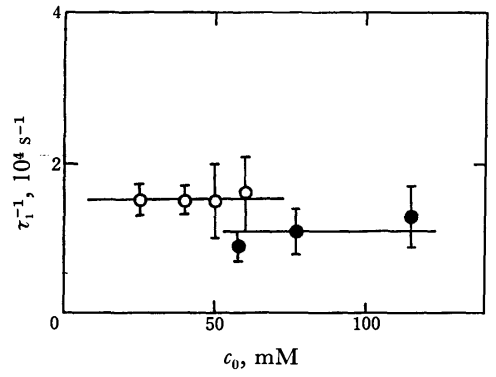

Fig. 6. The plots of τ_2^{-1} *vs.* c_0 in the DeAC (open circles) and OAC (closed circles) solutions.

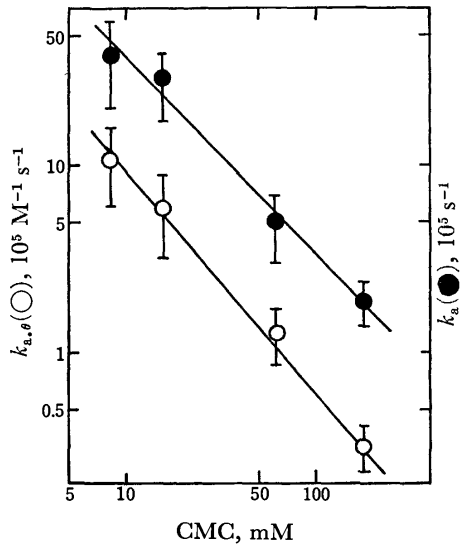

Fig. 7. The plots of $k_{a,\theta}$ (open circles) and k_a (closed circles) *vs.* CMC.

constants are influenced considerably by the instability of the surfactants in the bulk phase. In the alkylamine hydrochloride solutions, moreover, k_a also involves the number of $-CH_2-$ groups, n, as follows:

$$\ln k_a = (0.7\pm0.1)n + (4\pm1). \quad (15)$$

This equation indicates that the activation adsorption energy per $-CH_2-$ group is 0.4 kcal at 25 °C. On the other hand, the ΔG values are in good agreement with the theoretical results calculated using the Szyszkowski equation, as can be seen from Table 3. The $\Delta\gamma$ values are also in orderly agreement with those estimated using $(\gamma_{water}-\gamma_{CMC})/\Gamma_{max}$.[2]

As seen in Table 2, the kinetic parameters involving the ion-pair formation process are appreciably independent of the hydrocarbon chain length. This suggests that the interaction between the surfactant and counter ions may be governed by that between a hydrophilic group and Cl^- ions. Since the interaction energy between Na^+ and the anionic surfactant is smaller than that between Cl^- and the cationic surfactant,[10] however, SDS will scarcely associate on the surface and the relaxation concerned with the ion-pair formation should not be observed even outside the measured frequency range.

The remarkable difference between the relaxations observed for the OAC solutions in the present work and those of previous work[2] implies that the relaxation phenomena on the surface of surfactant solutions are sensitive to impurities in the surfactants. In a subsequent paper, the experimental results for the effect of additives on the relaxation of DeAC solutions, which are homologous to the OAC solutions, will be reported.

Finally, it can now be asserted that the capillary wave method is a powerful tool for analyzing reactions at the gas-liquid interface.

References

1) M. Sasaki, T. Yasunaga, and N. Tatsumoto, *Bull. Chem. Soc, Jpn.*, **50**, 852 (1977).
2) M. Sasaki, T. Yasunaga, and N. Tatsumoto, *Bull. Chem. Soc. Jpn.*, **50**, 858 (1977).
3) M. van den Tempel and R. P. van de Riet, *J. Chem. Phys.*, **42**, 2769 (1965).
4) R. S. Hansen and J. A. Mann, *J. Appl. Phys.*, **35**, 152 (1964).
5) L. G. Jackopin and E. Yeager, Technical Report 35, ONR Contract Nonr 1439 (04) Project NR 384-305, Western Reserve University (1969).
6) H. C. Parreira, *J. Colloid Interface Sci.*, **29**, 235 (1969).
7) M. Plaisance and L. Ter-Minassian-Saraga, *J. Colloid Interface Sci.*, **56**, 33 (1976).
8) I. J. Lin, J. P. Friend, and Y. Zimmels, *J. Colloid Interface Sci.*, **45**, 378 (1973).
9) I. Nishi, T. Imai, and M. Kasai, "Handbook of Surfactants," Sangyo Tosyo Co., Tokyo (1960), p. 316.
10) J. T. Davies and E. K. Rideal, "Interfacial Phenomena," Academic Press, New York and London (1961), p. 86.

Crystal and Molecular Structure of α-Form of 2,4,6-Trimethyl-1,3,5-trithiane*

Kiyotane SEKIDO, Haruaki ONO,** Teruo NOGUCHI,** and Sakutaro HIROKAWA

Department of Chemistry, The National Defense Academy, Hashirimizu, Yokosuka 239

***Koa Oil Co., Ltd., Ōtemachi, Tokyo 100*

(Received May 10, 1977)

The crystal structure of α-form of 2,4,6-trimethyl-1,3,5-trithiane (α-TTA) has been determined by the X-ray method. The crystal data are $a=9.768$, $b=12.306$, $c=8.521$ Å, and $\beta=116.33$ °. The space group is Cc with four molecules in a unit cell. The structure was deduced from interpretation of the 3D-Patterson series, and refined by 3D-Fourier and least-squares method to the final R factor of 0.040 for 1371 reflections. The molecule has a six-membered ring where three sulfur atoms and three carbon atoms are linked alternatively, forming a chair-form. Two methyl groups are in the equatorial positions and one methyl group in the axial. The mean values of the bond distances are 1.818 Å for S–C and 1.519 Å for C–C_{eq}. The distance is 1.541 Å for C–C_{ax}. The mean values of the bond angles are 101.89° for C–S–C, 107.60° for S–C–C_{eq}, 113.25° for S–C–C_{ax}, and 112.92° for S–C–S.

Studies on organic synthesis show that TTA has two isomers. One isomer is called the α-form (mp 102 °C), where two methyl groups are in the equatorial positions and a third one is axial. The other is called the β-form (mp 126 °C), where all the methyl groups are equatorial.

The crystal structure of the β-form has been reported by Valle *et al.*[1] and Hirokawa *et al.*,[2] but not that of the α-form. We have determined the crystal and molecular structure of the α-form from the viewpoint of molecular geometry or the packing of molecules in the crystal. The results are given below.

Experimental

Colorless prisms elongated along the a-axis were obtained by slow evaporation of α-TTA from acetone solution. The crystals are built upon a monoclinic unit cell.

Crystal Data. The cell dimensions were determined by the least-squares method using various sets of high angle reflections on a diffractometer. Systematic absence, $h+k$ odd in hkl and l odd in $h0l$, restricted the possible space group to either Cc or C2/c. Consideration on the number of molecules in the unit cell and the symmetric feature of the molecule favored the former. This was supported by the statistical test of intensity-distribution, and confirmed by the packing of the molecules. The crystal data are given in Table 1.

TABLE 1. CRYSTAL DATA
The experimental errors, given in parentheses, refer to the last figures.

Molecular formula	$C_6H_{12}S_3$
Formula weight	180.4
Mp	102 °C
Crystal system	Monoclinic
a	9.768 (4) Å
b	12.306 (7)
c	8.521 (4)
β	116.33(3)°
Systematic absences	hkl, $h+k=2n$
	$h0l$, $l=2n$
Space group	Cc
V	918.0(3) Å^3
Z	4
D_m	1.299 g cm^{-3}
D_x	1.305
μ (Mo $K\alpha$)	7.31 cm^{-1}
Crystal dimension	0.5 mm $\phi\times$0.8 mm
λ (Mo $K\alpha$)	0.7107 Å

Intensity Data. A prismatic crystal was ground to a cylinder of 0.5 mm in diameter and 0.8 mm in length. It was mounted on a four-circle diffractometer (Rigaku AFC-III) with Mo $K\alpha$ from a graphite monochrometer, and intensities were collected for the independent 1403 reflections within $2\theta<60°$, using the ω-2θ scan technique with a scanning speed of 4° min^{-1} in 2θ. Thirty-two reflections whose $|F|$'s were less than $2\sigma(|F|)$ were designated unobserved, where $\sigma(|F|)$ is the standard deviation of $|F|$ due to counting statistics. After corrections for background and Lorentz-polarization factor, the intensities were reduced to structure amplitudes. No corrections were made for absorption or extinction.

Structure Determination

The location of three sulfur atoms in the general positions was derived from synthesized 3D-Patterson series. The first 3D-Fourier series were synthesized, using phases determined by the atomic coordinates of the three sulfur atoms. The synthesized electron-density maps showed extra peaks in addition to the peaks due to the three sulfur atoms. Some of these extra peaks were considered to be significant as the constituent-atoms of the molecule. These were added to the successive Fourier-works. After three cycles of the procedure, the location of all the carbon atoms was determined. The possibility of centrosymmetric arrangement was discarded because of the mode of the packing of the molecules in the unit cell.

The structure was refined by syntheses of 3D-Fourier and 3D-difference series, where structure factors were calculated with isotropic B values for all the atoms. Location of the hydrogen atoms was roughly obtained from the 3D-difference maps. They were refined after the heavier atoms were fixed, assuming the tetrahedral angle for each carbon atom and a bond length of 1.09 Å for each C–H bond. Further refinements were made with a block-diagonal least-squares program on a computer CDC-6600 in Century Research Center Co.,

* A preliminary report was presented at the 30th National Meeting of the Chemical Society of Japan, Osaka, April 1974.

TABLE 2. ATOMIC COORDINATES ($\times 10^4$) AND ANISOTROPIC THERMAL PARAMETERS ($\times 10^4$) OF THE NON-HYDROGEN ATOMS
The estimated standard deviations given in parentheses, refer to the last decimal position. The anisotropic temperature factor is of the form $\exp[-2\pi^2(h^2a^{*2}U_{11}+k^2b^{*2}U_{22}+l^2c^{*2}U_{33}+2hka^*b^*U_{12}+2hla^*c^*U_{13}+2klb^*c^*U_{23})]$.

	x	y	z	U_{11}	U_{22}	U_{33}	U_{12}	U_{13}	U_{23}
S(1)	42(2)	1881(1)	−30(2)	129(1)	65(1)	120(1)	−6(1)	52(1)	−9(1)
S(2)	189(2)	3584(1)	2601(2)	208(2)	48(1)	211(2)	0(1)	129(2)	−9(1)
S(3)	−859(2)	1304(1)	2850(2)	140(2)	63(1)	189(2)	−18(1)	94(2)	−6(1)
C(4)	1127(6)	2985(4)	1373(6)	116(6)	56(3)	156(8)	−8(4)	65(6)	2(4)
C(5)	302(6)	2461(4)	4029(6)	148(7)	69(3)	135(7)	−6(4)	73(6)	−5(4)
C(6)	72(6)	858(4)	1529(7)	162(8)	48(3)	182(9)	−15(4)	91(7)	−18(4)
C(7)	1282(8)	3873(5)	232(9)	209(11)	73(4)	246(12)	−14(6)	146(10)	31(6)
C(8)	−300(9)	2870(5)	5295(9)	283(14)	93(5)	231(13)	−13(7)	190(12)	−27(7)
C(9)	1673(8)	373(5)	2607(9)	201(11)	70(4)	234(15)	35(6)	116(11)	22(7)

TABLE 3. ATOMIC COORDINATES ($\times 10^3$) OF THE HYDROGEN ATOMS
The average refined values for the isotropic temperature factor are 2.5 Å^2.

	x	y	z	Bonding atom
H(10)	224	270	226	C(4)
H(11)	147	221	474	C(5)
H(12)	−63	24	72	C(6)
H(13)	140	353	−87	C(7)
H(14)	33	443	−18	C(7)
H(15)	233	434	100	C(7)
H(16)	−151	272	478	C(8)
H(17)	25	225	638	C(8)
H(18)	22	364	585	C(8)
H(19)	158	−22	349	C(9)
H(20)	212	10	171	C(9)
H(21)	238	105	338	C(9)

Tokyo, using anisotropic thermal parameters for the non-hydrogen atoms with B values of the hydrogen atoms fixed at isotropic values. After six cycles of this procedure convergence was attained with R=0.040. The final parameters with standard deviations resulting from the procedure are given in Tables 2 and 3.***

Discussion

Molecular Geometry and Conformation. The structural and conformational features are shown in Fig. 1, together with atomic numbering and thermal vibration ellipsoids[3] scaled to 50% probability, excluding the hydrogen atoms. Intramolecular interatomic distances and angles involving the non-hydrogen atoms are given in Table 4, being also shown in Fig. 2(a) and (b). The standard deviations of these measurements are 0.001 Å for distances and 0.01—0.05° for angles. S–C lengths are in the range 1.810—1.824 Å with a mean of 1.818 Å, showing a slight alternative shortening along the sides of the six-membered ring. These values together with the bond angles of the sulfur atoms (101.89° as a mean) are comparable to those for organic compounds which have ring-membered sulfur atoms.[1,2,4-7]

*** The complete F_o-F_c data are deposited as Document No. 7722 at the Office of the Editor of the Bulletin of the Chemical Society of Japan.

A significant difference can be seen between the lengths of C–C_{eq} (from a ring-membered carbon to a methyl carbon in the equatorial position) and C–C_{ax} (axial); a mean of 1.519 Å is given to C–C_{eq} and 1.541 Å to C–C_{ax}. This might correspond to the difference in the bond angles for the ring-membered carbon atoms; a mean of 107.60° for S–C–C_{eq} and a mean of 113.25° for S–C–C_{ax}. A similar difference can be seen in the distance from a sulfur atom to a ring-membered carbon atom which is in a diagonal position of the ring; a mean of 3.431 Å for S···C whose carbon atom is linked with the equatorial methyl group, and 3.466 Å for S···C where the carbon atom is linked with the axial methyl group. The conformation of a methyl group may affect the molecular dimensions of a ring-membered carbon atom linked with it.

TABLE 4. INTRAMOLECULAR INTERATOMIC DISTANCES (l) AND ANGLES (ϕ) INVOLVING THE NON-HYDROGEN ATOMS
Estimated standard deviations are given in parentheses.

	l/Å		ϕ/°
S(1)–C(4)	1.810(1)	C(6)–S(1)–C(4)	102.81(3)
S(2)–C(4)	1.824(1)	C(4)–S(2)–C(5)	100.31(3)
S(2)–C(5)	1.812(1)	C(5)–S(3)–C(6)	102.54(3)
S(3)–C(5)	1.821(1)	C–S–C(mean)	101.89
S(3)–C(6)	1.817(1)	S(1)–C(4)–S(2)	112.77(3)
S(1)–C(6)	1.821(1)	S(2)–C(5)–S(3)	112.90(3)
S–C(mean)	1.818	S(3)–C(6)–S(1)	113.09(3)
C(4)–C(7)	1.514(1)	S–C–S(mean)	112.92
C(5)–C(8)	1.524(1)	S(1)–C(4)–C(7)	108.27(5)
C–C_{eq}(mean)	1.519	S(2)–C(4)–C(7)	107.12(5)
C(6)–C(9)	1.541	S(2)–C(5)–C(8)	107.16(5)
		S(3)–C(5)–C(8)	107.86(5)
S(1)···S(2)	3.026(0)	S–C–C_{eq}(mean)	107.60
S(2)···S(3)	3.027(0)	S(3)–C(6)–C(9)	113.76(5)
S(3)···S(1)	3.035(0)	S(1)–C(6)–C(9)	112.73(5)
S···S(mean)	3.029	S–C–C_{ax}(mean)	113.25
C(4)···C(5)	2.791(1)	S(1)···S(2)···S(3)	60.20(1)
C(5)···C(6)	2.837(1)	S(2)···S(3)···S(1)	59.88(1)
C(6)···C(4)	2.838(1)	S(3)···S(1)···S(2)	59.93(1)
C···C(mean)	2.822	S···S···S(mean)	60.00
S(1)···C(5)	3.428(1)	C(4)···C(5)···C(6)	60.52(2)
S(3)···C(4)	3.433(1)	C(6)···C(4)···C(5)	60.53(2)
S···C(mean)	3.431	C(5)···C(6)···C(4)	58.93(2)
S(2)···C(6)	3.466(1)	C···C···C(mean)	60.00

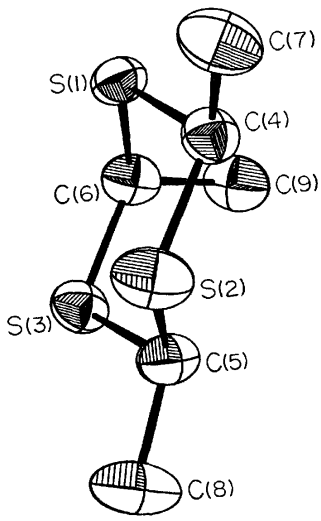

Fig. 1. The thermal vibration ellipsoids of non-hydrogen atoms drawn by ORTEP.[3]

Table 5. Torsion angles (ϕ)
Torsion angle A(i)–A(j)–A(k)–A(l) is viewed down A(j)–A(k) with a clockwise rotation of A(i) to A(l) taken to be positive.

Ring torsion angles	ϕ/°
C(6)–S(1)–C(4)–S(2)	−65.4
C(5)–S(2)–C(4)–S(1)	67.0
C(4)–S(2)–C(5)–S(3)	−67.0
C(6)–S(3)–C(5)–S(2)	65.6
C(5)–S(3)–C(6)–S(1)	−62.2
C(4)–S(1)–C(6)–S(3)	62.4
Mean (absolute value)	64.9
Exocyclic torsion angles	
C(6)–S(1)–C(4)–C(7)	176.3
C(5)–S(2)–C(4)–C(7)	−174.0
C(4)–S(2)–C(5)–C(8)	174.4
C(6)–S(3)–C(5)–C(8)	−176.2
Mean (absolute value)	175.2
C(5)–S(3)–C(6)–C(9)	68.2
C(4)–S(1)–C(6)–C(9)	−68.5
Mean (absolute value)	68.3

The triangle formed by these three sulfur atoms is regular, the averaged length being 3.029 (±0.006) Å and the averaged apex angle 60.00 (±0.12)°. Another triangle formed by three ring-membered carbon atoms is also regular, with length 2.822 (±0.031) Å and angle 60.00 (±1.07)°. These triangles are approximately parallel to each other, showing that the ring has a chair-form. Shifts of three sulfur atoms from the plane containing three ring-membered carbon atoms are −0.635 Å for S(1), −0.712 Å for S(2), and −0.637 Å for S(3), where signs indicate whether or not the atoms are on the same side of the plane.

A torsion angle of these two triangles is calculated to be 60.4° (from S(1) to C(6)), which is given as a dihedral

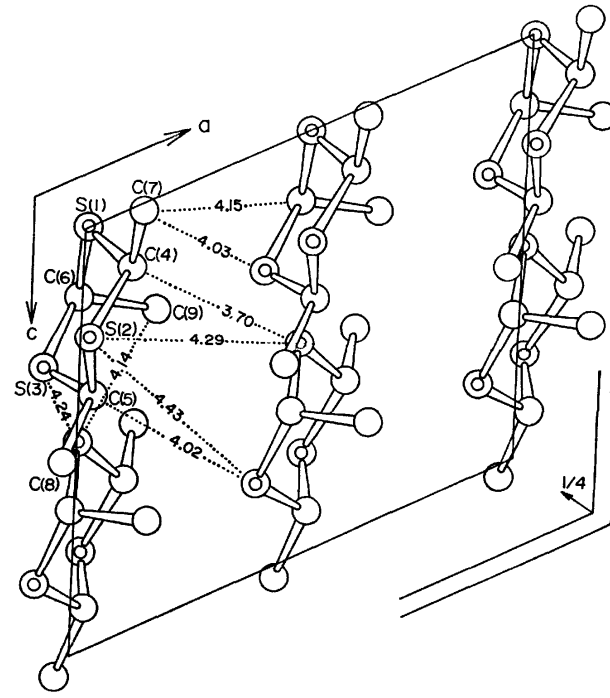

Fig. 3. The molecular packing viewed down b, showing all intermolecular distances (the non-hydrogen atoms) of less than 4.50 Å.

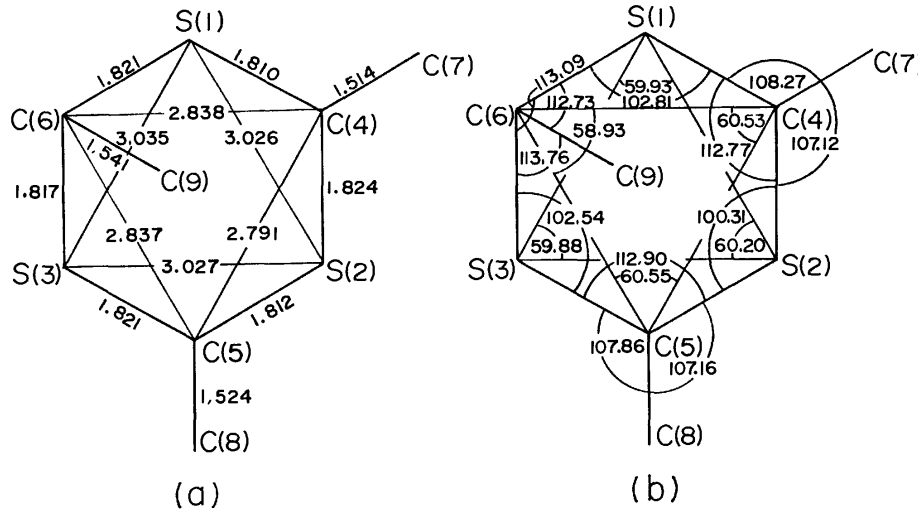

Fig. 2. Intramolecular interatomic distances (a) and angles (b).

angle around the line connecting the centers of the triangles.

Shifts of the three methyl carbon atoms from the plane formed by the three ring-membered carbon atoms are −0.283 Å for C(7), −0.389 Å for C(8), and +1.531 Å for C(9), showing that C(7) and C(8) are equatorial and C(9) is axial.

Torsion angles in the molecule are given in Table 5, where an angle for A(i)–A(j)–A(k)–A(l) is viewed down A(j)–A(k) with a clockwise rotation of A(i) to A(l) to be positive. The conformation of the chair-form is clearly seen from the alternative change of sign assigned to each torsion angle. The averaged value of the endocyclic torsion angles is 64.9° in absolute value.

The conformation of each methyl group is also clear; a mean of 175.2° for C···C_{eq} and a mean of 68.3° for C···C_{ax} rotation.

Molecular Packing. The molecular packing in the unit cell together with intermolecular interatomic distances less than 4.50 Å are shown in Fig. 3. The shortest contact of 3.70 Å is seen between C(4) and S(1) operated by the n-glide plane. No significant contact other than this can be seen. The molecules are held together in the crystal by the weak van der Waals contacts, corresponding to a low melting point.

References

1) G. Valle, V. Busetti, and M. Mammi, *Acta Crystallogr., Sect B*, **25**, 1631 (1969).
2) S. Hirokawa, K. Sekido, A. Suzuki, and T. Noguchi, *Memoirs of the Defense Academy, Jpn.*, XIV, No. 3, 89 (1974).
3) C. K. Johnson, *ORTEP*, **ORNL-3794**, Oak Ridge National Laboratory, Tennessee (1965).
4) H. T. Kalff and C. Romers, *Acta Crystallogr.*, **18**, 164 (1965).
5) G. Y. Chao and J. D. McCullough, *Acta Crystallogr.*, **13**, 727 (1960).
6) H. Montgomery, *Acta Crystallogr.*, **13**, 381 (1960).
7) W. A. Dollase, *J. Am. Chem. Soc.*, **87**, 979 (1965).

Solid-State Anodic Oxidation of Aluminum with Organic-Conductor Counterelectrode

Susumu YOSHIMURA and Mutsuaki MURAKAMI
Matsushita Research Institute Tokyo, Inc., Ikuta, Tama-ku, Kawasaki 214
(Received May 18, 1977)

Solid-state anodic oxidation of aluminum contacted to a pellet of various organic conductors based on 7,7,8,8-tetracyanoquinodimethane was observed. A typical passivation curve was observed in the current-voltage characteristics for the anodic polarization of the metal. Along with impedance measurements on the electrode system, it was proved that the passivation is due partly to a thermal transformation in the organic conductor and partly to a solid-state anodization of aluminum, the latter being conditioned by the former through the formation of an electrolyte layer *in situ*. The current efficiency of anodization was estimated by a linear voltage sweep method to be as high as 2%, depending on the ambient moisture. The high efficiency explains the prominent self-healing action of a new type of solid electrolytic capacitor in which manganese dioxide is replaced by an organic-conductor counterelectrode.

The solid electrolytic capacitor was developed in 1956,[1] but little experimental information on the anodic oxidation of valve metals with a solid electrolyte has been given since then. Smith[2] studied the electrical properties of a tantalum electrode pressed on a surface of manganese dioxide, MnO_2, and claimed that the tantalum oxide is anodically formed at the expense of the local oxygen content of MnO_2. There is, however, another theory according to which the counterelectrode functions in the capacitor self healing; a thermally induced transition of the oxide to insulating lower oxides.[3] Smith did not exclude the thermal reduction of MnO_2 but rather credited it with the appearance of a high electric field appropriate to the ionic conduction.[2]

Recently a new type of aluminum solid electrolytic capacitor, in which MnO_2 is replaced by organic conductor, OC, was developed.[4] Highly conductive organic salts based on 7,7,8,8-tetracyanoquinodimethane, TCNQ,[5] were adopted, because of their prominent effect on the capacitor self healing. The capacitor was featured by stable high frequency characteristics[6] and a very low leakage current density. In this paper we wish to report on the electrical properties of an Al/OC electrode system, showing that the solid state anodic oxidation proceeds at an efficiency of up to 2%, considerably higher than that with MnO_2. The current-voltage and impedance characteristics of the electrode system, are presented with a discussion on the mechanism of anodic oxidation.

Experimental

Materials. Typical molecular compounds of TCNQ, including non-ionic change transfer complexes and less conductive ion-radical salts with metallic cations were examined. We report herewith on highly conductive salts which might have significance in capacitor application. The effects of resistivity, thermal stability and stoichiometry on the solid state reaction were studied for the compounds, quinolinium-$(TCNQ)_2$, $Q(TCNQ)_2$, *N*-methylquinolinium$(TCNQ)_{2.2}$, $(NMQ)(TCNQ)_{2.2}$, *N*-propylquinolinium$(TCNQ)_2$, $(NPQ)(TCNQ)_2$, *N*-methylacridinium$(TCNQ)_2$, $(NMA)(TCNQ)_2$, and *N*-methylphenazinium(TCNQ), (NMP)(TCNQ). $(NMQ)(TCNQ)_{2.2}$ and (NMP)(TCNQ) were a metastable, highly conductive modification,[7] the former sample being used to examine the contribution of the thermal transformation of the solid counterelectrode. Results on the salts with metallic cations will be referred to as regards the discussion of the reaction mechanism.

Electrode System. The TCNQ compounds were compressed under a pressure of *ca.* 2000 kg/cm^2 into a pellet of 13 mm in diameter and *ca.* 0.8 mm in thickness. A 99.999% hard aluminum bar, 0.5 mm diam., was used as an electrode metal. This was degreased with 10% NaOH and rinsed with deionized water and acetone. The bar was truncated immediately before measurement and the fresh surface was pressed on the OC pellet. It was extremely difficult to obtain a reproducible contact between Al and OC. The dominant factors for the reproducibility were the nature of the surfaces of both solids, contact pressure and the water content of the pellet. Figure 1 shows a test jig for the Al/OC electrode system, with which a pressure as high as 100 kg/cm^2 could be applied to the contact without any deformation of the bar. Since the glossy surface of the OC pellet did not give a reproducible result, it was rubbed with emery paper and lapped with cotton gauze.

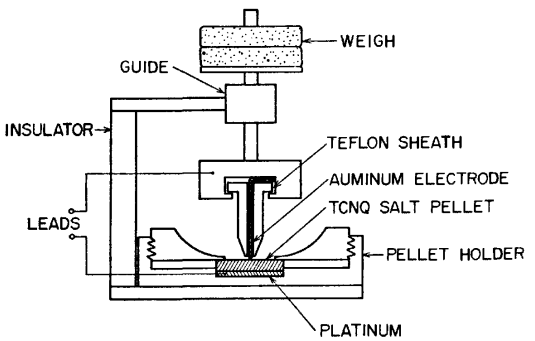

Fig. 1. Sketch of a constant-pressure, point-contact electrode system.

Apparatus. The current-voltage characteristics were measured by the constant-rate-of-voltage-increase (CRVI) method first adopted by Dignam[8] for the anodic oxidation of Al in a liquid electrolyte. Since a very low rate of voltage increase with a very low noise level is required to meet the supposed low efficiency of the solid state reaction,[2] we constructed a Miller integrator with operational amplifiers and a 500 μF slug tantalum electrolytic capacitor. Measurements with stepwise application of constant voltage were found to be inappropriate for the OC system, for it was not possible to distinguish between the anodic and the cathodic reactions especially

when the thermal transformation of OC took part in the reaction. The impedance of the Al/OC system was measured as a function of the applied voltage with a Yokogawa BV-Z 13A universal bridge at a frequency of 1 kHz. Measurements of the equivalent series capacitance, C_s, and resistance, R_s, were made after the current had reached a steady state for each applied voltage.

Results

Current-Voltage Characteristics. The *I-V* characteristics measured by the CRVI method for three Al/OC systems, shown in Fig. 2, are typical data for a humidity of 50% RH and a voltage rise rate of 1/24 V/s. For the anodic polarization (*e.g.* when Al was anodically polarized), all the electrode systems exhibited a well-known passivation curve with a current peak, V_p^+, between 2.5 and 4.7 V, the current following as low as 10^{-5} A for higher voltages. The curves are very smooth with no discontinuity below *ca.* 15 V, at which the current suddenly diverges resulting in decomposition in OC at the contact point. For the cathodic polarization, there are more than one current peaks, the current making an oscillatory growth. The first peak appears, in all cases, at a lower voltage than the anodic peak. The anodic and cathodic peak voltages and powers ($W_p^+ = V_p^+ I_p^+$) along with the specific resistivity of compactions[9] for the OC's examined are summarized in Table 1. The superlinear curve in the anodic direction results from a contact resistance at voltages lower than 1 V and the Joule heat above 1 V. In the underlinear and decreasing regions, the change in the electrode resistance is irreversible; the resistance is not restored by the application of cathodic voltage. In the cathodic direction, however, an reversible increase in the electrode resistance takes place from *ca.* 0.1 V, for the resistance is restored by the anodic polarization, provided that the cathodic electrification does not exceed the voltage of the first peak. The difference in the *I-V* characteristics between the anodic and cathodic directions strongly suggests that the passivations are due to electrochemical reactions.

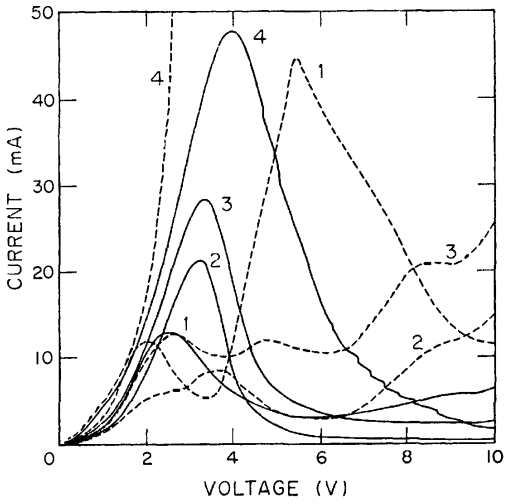

Fig. 2. Current-voltage characteristics at 1/24 V/s and 50% RH of an Al electrode system for anodic (solid lines) and cathodic (dotted lines) polarizations. 1. Q-(TCNQ)$_2$, 2. (NPQ)(TCNQ)$_2$, 3. (NMA)(TCNQ)$_2$, 4. MnO_2.

Table 1. Peak voltage $V_p^{\pm}$ and power $W_p^{\pm}$ of passivation curves

Compound	V_p^+ (V)	W_p^+ (mW)	V_p^- (V)	W_p^- (mW)	ρ (Ω cm)
Q(TCNQ)$_2$	2.5	32.5	2.0	23.6	0.6
(NMQ)(TCNQ)$_{2.2}$	3.3	64.4	2.5	20.0	1.0
(NPQ)(TCNQ)$_2$	3.0—3.2	74.5	2.3	12.7	3.6
(NMA)(TCNQ)$_2$	3.1—3.3	89.1	2.6	33.3	1.3
(NMP)(TCNQ)	4.7	91.2	4.2	52.5	7.8
MnO_2	3.8—4.0	568	—	—	5

The results for an Al/MnO_2 systems are also shown in Fig. 2. MnO_2 was obtained by thermal decomposition of a 50% $Mn(NO_3)_2$ solution in the form of a block which was cut and lapped into nearly the same shape as that of the OC pellet. The MnO_2 system exhibited essentially the same anodic curves as the OC system, though there were a number of discontinuous falls in current at $V > V_p^+$, indicating thermal transformation in MnO_2. The cathodic current, however, increased to infinity (over 200 mA) at *ca.* 2.5 V.

Thermal Transformation in OC. We measured the *I-V* characteristics using Ta and noble metals, Pt and Au. All the electrodes exhibited a large passivation peak similar to those shown in Fig. 2. However, in the case of the noble metal, there was no difference in the *I-V* curves between the anodic and cathodic polarizations. This indicates that, although the anodic passivation in the Al/OC system is peculiar to the valve metal and is of electrochemical nature, it was initiated by some kind of thermal transformation in OC. Figure 3 shows the current and temperature-voltage characteristics of a chromel-almel, Al/OC system, where the current was passed through the thermocouple, 0.5 mm in diameter (Omega Engineering, Inc.), which was pressed on the OC pellet with a Pt bar. The figure illustrates not only the existence of the passivation peak for the non-valve metal system but also the correspondence of the current to the electrode temperature. A current peak appeared at 2.5 and 4.7 V for Q(TCNQ)$_2$

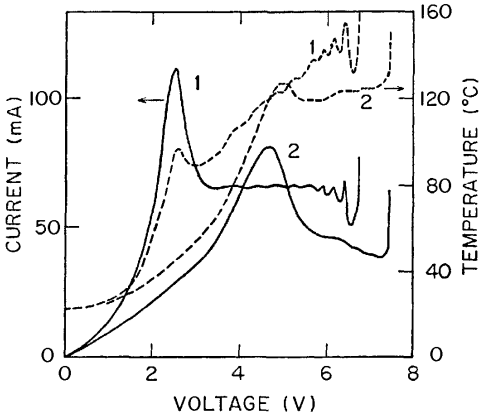

Fig. 3. Current (solid lines)- and temperature (dotted lines)- voltage characteristics at 1/24 V/s and 50% RH of chromel-almel/organic systems.
1. Q(TCNQ)$_2$, 2. (NPQ)(TCNQ)$_2$.

and $(NPQ)(TCNQ)_2$, respectively, and the corresponding temperature peak appeared at 95.7 and 126.4 °C for the former and the latter, respectively. The peak temperatures are considerably lower than the decomposition temperatures of these compounds.[5,10] However, the resistivity of the highly conductive TCNQ salts frequently increases irreversibly at these temperatures.[11] This seems to be due to the dissociation of the neutral TCNQ from the salts.[12] The difference in the position of the current peak or the electric power of the peak (Table 1) between compounds is understandable on the basis of the thermal stability against the dissociation of the compounds.

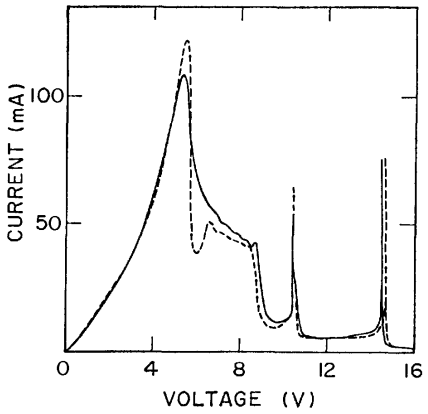

Fig. 4. Current-voltage characteristics at 1/24 V/s of a $Pt/(NMQ)(TCNQ)_{2.2}$ system. —anodic, ···cathodic.

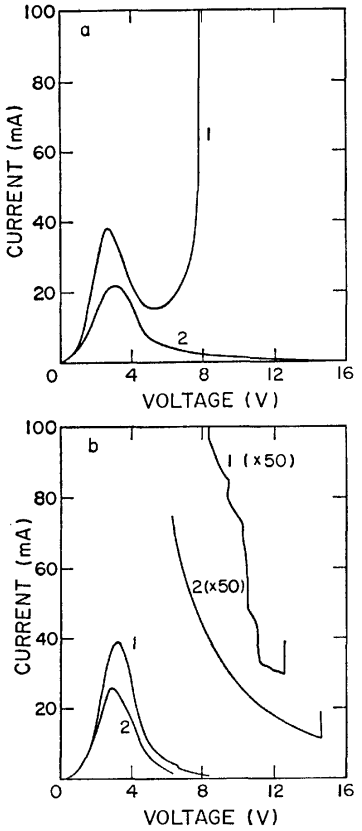

Fig. 5. Effect of humidity on the current-voltage characteristics of $Al/Q(TCNQ)_2$ (a) and $Al/(NMA)(TCNQ)_2$ (b) systems. 1: 20%RH, 2: 98%RH.

Figure 4 shows the *I-V* curves of a $Pt/(NMQ)(TCNQ)_{2.2}$ system forming a single exception in the non-valve metal system. This system displayed drastic decay and spikes in the current starting from *ca.* 8.5 V in addition to the above mentioned passivation at 5.3 V. The metastable modification of $(NMQ)(TCNQ)_{2.2}$ undergoes a monotropic phase transition and the resistivity increases by a factor of 80.[13] The drastic decay (Fig. 4) is undoubtedly due to the phase transition in the bulk of the OC. That the *I-V* curves of $Al/(NMQ)(TCNQ)_{2.2}$ showed no discontinuity implies that the thermal transformation does not dominate at higher voltage ($V \gg V_p^+$).

Effect of Ambient Moisture. The *I-V* characteristics measured at various relative humidities are shown in Fig. 5. The *I-V* curves in the higher voltage region are severely altered by the ambient moisture. At a relative humidity of 98%RH, the current declines to about an order of magnitude lower than those at 50%RH. In dry air, on the contrary, it increases to infinity with $Q(TCNQ)_2$ or shows lots of jumps with $(NMA)(TCNQ)_2$ at higher anodic voltages. The discontinuous falls for the $(NMA)(TCNQ)_2$ system are strikingly similar to those for the MnO_2 system (Fig. 2), indicating that a thermal transformation proceeds locally in the OC. In the case of $Q(TCNQ)_2$, however,

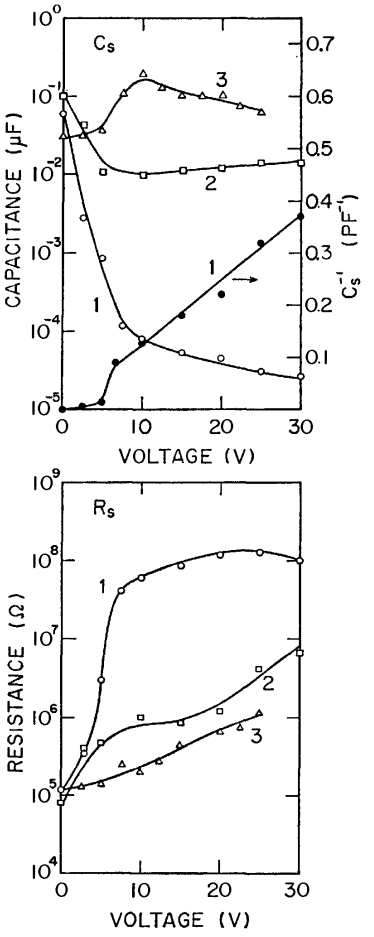

Fig. 6. Equivalent series capacitance and resistance of an $Al/Q(TCNQ)_2$ system. 1: Anodic polarization in the room air (about 70 %RH), 2: anodic polarization in dry oxygen, 3: cathodic polarization in the room air.

the *I-V* curve and the appearance of the Al contact indicate carbonization in the OC. This seems to be due to the low thermal stability of $Q(TCNQ)_2$. In any case, the results confirm that the anodic passivation should be ascribed to two mechanisms, each being replaced by the other at a voltage of *ca.* $2V_p^+$ in the presence of water. The cathodic *I-V* curves and the curves obtained using the non-valve metal electrodes are not largely altered by the relative humidity.

Impedance Characteristics. Figure 6 shows C_s and R_s at 1 kHz of the Al/$Q(TCNQ)_2$ system measured under three typical conditions. For the anodic polarization in humid air (about 70%RH), C_s decreases and R_s increases markedly with increasing voltage. The inverse of C_s shows a linear dependence on the voltage at voltages in excess of *ca.* 6 V, the voltage roughly corresponding to that at which the CRVI curve reaches a steady state (Fig. 2). This strongly indicates the formation of the anodic oxide on Al. The very high electrode resistance, R_s, may also be evidence for the anodization, since the thermal transformation alone cannot yield such a high resistance as suggested by curve 2. Curves marked 2 give the result of measurements in dry oxygen. They have almost the same features as those of the non-valve metal systems, so that the measured impedance is thought to be that of the transformed OC alone. It should be noted that the R_s measured at higher RH decreased again at higher voltages; in the case of $(NMQ)(TCNQ)_{2.2}$, for example, R_s decreased to the same value as the initial R_s. The decrease can be explained by the formation of a very high resistance connected in parallel with the anodic capacitor. The cathodic reaction causes an increase in C_s with a slight increase in R_s, indicating that the cathodic passivation is not dominated by the thermal transformation of OC either.

Discussion

Anodic Oxidation. The experimental results on the electrical properties of the Al/OC electrode system as a whole confirm the solid-state anodic oxidation of Al, though no direct evidence for the material transport or the existence of Al_2O_3 was found. One possible objection may be that there might be an electrochemical reaction of the TCNQ salts followed by a disproportionation reaction with water or *vice versa* at high electric fields. However, if such reaction could take place, the strict relation C_sV=constant (Fig. 6) would be too accidental, since the electrification period was not made constant for each applied voltage. Assuming the electrode area as 2×10^{-3} cm^2, we obtain C_sV=0.44 μF·V/cm^2, which is to be compared with $C\cdot V$=6.45 μF·V/cm^2 for the ideal anodization in a boric acid-borate solution.[14] Coincidence between experiment and theory is considered to be good in view of various factors through which the capacitance is lowered; namely, 1) reduction of the contact area arising from the roughness of the surface, 2) a series capacitance due to the thermally transformed OC, and 3) a low efficiency of the solid-state reaction.

The CRVI method, which was originally introduced for the analysis of the anodic oxidation in the liquid electrolyte,[8] is useful and powerful for the solid state reaction. The anodic and the cathodic reactions are discriminated and different reactions depending upon the voltage are manifested. Let us calculate the current efficiency of the anodic oxidation using the CRVI results.[15] When the ionic current I_i flows through the oxide of thickness x, the equation for an oxide growth rate dx/dt is given by Faraday's law,

$$dx/dt = \Omega I_i \quad (1)$$

where Ω is 5.55 A s^{-1} mA^{-1} cm^2 for Al_2O_3. Then the potential across the oxide V_{ox} increases as follows,

$$dV_{ox}/dt = E_v dx/dt \quad (2)$$

where E_v is the Maxwell field strength which depends on the rate of voltage increase v. If we assume

$$dV_{ox}/dt = dV_a/dt = v \quad (3)$$

where V_a is the applied voltage and define the ionic current efficiency η with respect to the total current I through the electrode system as

$$I_i = \eta I, \quad (4)$$

then we obtain from Eqs. 1 through 4,

$$\eta = v/\Omega E_v I. \quad (5)$$

Since Eq. 3 holds for $V_a \gg V_p^+$ or for I_i=constant, η can be calculated using the experimental data on I in Fig. 2. The results for a relative humidity of 50%RH are shown in Table 2, where E_v was obtained by Dunn[15]

Table 2. Current efficiency of anodic oxidation, η (%), at 50% RH

Compound	η (Voltage, V)
$Q(TCNQ)_2$	0.053 (6)
$(NMQ)(TCNQ)_{2.2}$	1.68 (13)
$(NPQ)(TCNQ)_2$	0.62 (13)
$(NMA)(TCNQ)_2$	0.10 (13)
(NMP)(TCNQ)	0.21 (16)

as $E_v=8\times10^6$ V/cm for v=1/24 V/s. The efficiency was found to be 0.05 to 1.7%, considerably higher than the published data on the Ta/MnO_2 system (0.01 to 0.001%).[2] At higher relative humidities, the efficiency was higher; 2.1% for $Q(TCNQ)_2$ and 1.5% for (NMA)-$(TCNQ)_2$ at 98%RH. The efficiency for the MnO_2 system cannot be obtained, since the discontinuous falls in the *I-V* curves do not allow us to assume Eq. 3. An apparent efficiency was calculated to be 0.93% at 14 V, which is thought to be an overestimate by about two orders of magnitude over a true value if we take the amount of the discrete jumps in current into account.

Reaction Mechanism. The anodic oxidation necessitates both an ionically conducting layer which prevents the short circuiting of the electrode system and ionogens which may serve as an oxygen source of Al_2O_3. The TCNQ salts are known as an electronic conductor. The idea of Gutmann *et al.*[16] that $Mg(TCNQ)_2$ behaves as a solid electrolyte has been vitiated by Friedel[17] and Weidenthaler and Pelinka.[18] We postulate that the initial passivation at relatively low voltages (V_p^+) produces an ionically conducting layer between Al and OC. Since the transformed layer has a higher resistivity, the applied voltage may be absorbed by this thin layer,

resulting in a high electric field effective to the ionic conduction. The TCNQ salts we examined meet the requirement for the anodizing electrolyte postulated by Smith.[2] The transformed OC was dissolved in acetonitrile and the composition was determined spectroscopically.[7] It was shown that the layer contains an excess of neutral TCNQ molecules over a stoichiometric composition; *e.g.*, TCNQ/cation=2.11 for the transformed NPQ salt. The resulting nonstoichiometric compound is very advantageous for anodic oxidation. First, the disordered structure may give a good chance for the ionic conduction as in the case of inorganic materials.[19,20] Second, the OC layer with excess TCNQ molecules may behave as a p-type conductor,[21] to facilitate rectification of a junction $Al/Al_2O_3/OC$.[22]

It was assumed in the above discussion that the existence of neutral TCNQ is essential for anodization. For the sake of comparison simple salts with metallic cations, such as Li, Na, K, Mg, Ca, Ba, Mn(II), Fe(II), Ni(II), and Cu(I) were examined. However, they were not anodizing electrolytes for the valve metals. The only metallic salt which exhibits both a passivation curve in the CRVI experiment and a remarkable decrease in C_s in the impedance measurement is $Cu(TCNQ)_2$. An X-ray photoemission study[23] and IR study have shown that $Cu(TCNQ)_2$ is not a simple salt but is composed of Cu(I)(TCNQ) and $TCNQ^0$ as a formulation of $Cu^+(TCNQ^-)(TCNQ^0)$ or $(Cu^+)_2(TCNQ^-)_2(TCNQ^0)_2$,[5] providing another support for our model. The anodizing ability of the simple salt (NMP)(TCNQ) is not counterevidence either. A recent examination has revealed a partial charge transfer between NMP and TCNQ,[24] suggesting the existence of $TCNQ^0$. This may explain the striking difference in the anodizing ability between (NMP)(TCNQ) and alkali-TCNQ's, the charge transfer being complete in the latter.[24] The results and those with $(NMQ)(TCNQ)_{2.2}$ suggest that nonstoichiometric salts having higher contents of TCNQ[25] may be a more efficient anodizing electrolyte.

Since the TCNQ salts we examined have no oxygen in their composition, water should be the oxygen source. It is not unreasonable because water is, with a few exceptions,[26] the oxygen source in most of the anodic oxidation in liquid electrolyte. The findings of Weidenthaler and Pelinka[18] that the presence of water is essential for the electromotive force to be observed in a cell, metal/TCNQ-salt solution/Pt, should also be considered. Smith's claim that water is a catalyst in the anodic oxidation of the Ta/MnO_2 system cannot be accepted. The major electrochemical reactions are the dissociation of water and/or the oxidation of Al, and the efficiency may vary with the catalytic activity of $TCNQ^0$ in the electron transfer processes. In fact, the formation of an ion pair Al···TCNQ with the aid of water has been known[27] and a slowly decreasing electromotive force was generated in a cell Al/OC/Pt with Al negative.

Conclusion

The experimental results as a whole support the anodic oxidation of Al with the OC functioning as a solid electrolyte *in situ*. The material criteria for the anodizing electrolyte are that the existence of neutral TCNQ molecules in the salt is essential and the disordered structure is favored. The high efficiency of anodization explains the prominent self-healing action of a new type of solid electrolytic capacitor in which MnO_2 is replaced by an OC counterelectrode.[4]

The authors wish to express their sincere gratitude to Dr. Katsue Hasegawa for his continuous encouragement. They are also indebted to Shirow Asakawa and Dr. Shigeo Kondo for various valuable discussions on the electrochemical properties of the TCNQ salts and water.

References

1) D. A. McLean and F. S. Power, *Proc. IRE*, **44**, 872 (1956).
2) D. M. Smith, *J. Electrochem. Soc.*, **113**, 19 (1966).
3) G. I. Parisi, *IEEE Trans. Parts Hybrids Packag.*, **PHP-8**, 33 (1972).
4) S. Yoshimura, Y. Itoh, M. Yasuda, M. Murakami, S. Takahashi, and K. Hasegawa, *IEEE Trans. Parts Hybrids Packag.*, **PHP-11**, 315 (1975).
5) L. R. Melby, R. J. Harder, W. R. Hertler, W. Mahler, R. E. Benson, and W. E. Mockel, *J. Am. Chem. Soc.*, **84**, 3374 (1962).
6) Y. Itoh and S. Yoshimura, *J. Electrochem. Soc.*, **124**, 1128 (1977).
7) M. Murakami and S. Yoshimura, *Bull. Chem. Soc. Jpn.*, **48**, 157 (1975).
8) M. J. Dignam, *J. Electrochem. Soc.*, **109**, 184 (1962).
9) The specific resistivity was measured by a four probe method on a pressed disc, 13 mm diam. The higher resistivity of (NMP)(TCNQ) with respect to a published value may be due to the inclusion of a less-conductive modification.
10) L. R. Melby, *Can. J. Phys.*, **43**, 1448 (1963).
11) V. Walatka, Jr. and J. H. Perlstein, *Mol. Cryst. Liq. Cryst.*, **15**, 269 (1971).
12) S. Yoshimura, M. Murakami, Y. Itoh, and K. Hasegawa, *Chem. Lett.*, **1972**, 835.
13) M. Murakami and S. Yoshimura, *J. Phys. Soc. Jpn.*, **38**, 488 (1975).
14) W. J. Bernard and J. W. Cook, *J. Electrochem. Soc.*, **106**, 643 (1959).
15) C. G. Dunn, *J. Electrochem. Soc.*, **115**, 219 (1968).
16) F. Gutmann, A. M. Hermann, and A. Rembaum, *J. Electrochem. Soc.*, **114**, 323 (1967).
17) R. A. Friedel, *J. Electrochem. Soc.*, **115**, 614 (1968).
18) P. W. Weidenthaler and E. Pelinka, *Collect. Czech. Chem. Commun.*, **34**, 1482 (1969).
19) A. B. Lidiard, "Encyclopedia of Physics," Vol. 20, ed by S. Fliigge, Springer-Verlag, Berlin (1957), p 246.
20) Yu. Ya. Gurevich and Yu. I. Kharkats, *Phys. Lett. A*, **57**, 382 (1976).
21) E. Krikorian and R. J. Sneed, *J. Appl. Phys.*, **40**, 2306 (1969).
22) Y. Sasaki, *J. Phys. Chem. Solids*, **13**, 177 (1960).
23) I. Ikemoto, J. M. Thomas, and H. Kuroda, *Bull. Chem. Soc. Jpn.*, **46**, 2237 (1973).
24) S. Flandrois and D. Chasseau, *Acta Crystallogr., Sect. B*, **33** (1977), in press.
25) M. Murakami and S. Yoshimura, *Chem. Lett.*, **1977**, 929.
26) G. Amsel, C. Cherki, G. Feuillade, and J. P. Nadai, *J. Phys. Chem. Solids*, **30**, 2117 (1969).
27) T. Takeda, T. Kobayashi, N. Ueda, and E. Suito, Proc. Symp. Molecular Structure, Fukuoka, Japan, Oct. (1970), p. 237.

Kinetic Studies of Spin-trapping Reactions. I. The Trapping of the *t*-Butyl Radical Generated by the Photodissociation of 2-Methyl-2-nitrosopropane by Several Spin-trapping Agents

Takahisa DOBA, Tsuneki ICHIKAWA, and Hiroshi YOSHIDA
Faculty of Engineering, Hokkaido University, Kita-ku, Sapporo 060
(Received May 20, 1977)

The photochemical reaction of 2-methyl-2-nitrosopropane (a spin-trapping agent) in benzene was studied at 299 K by monitoring the optical absorption intensity of the spin-trapping agent and the ESR signal intensity of the spin-adduct radical (di-*t*-butyl nitroxide). The observed kinetic feature was interpreted in terms of three elementary processes; the photodissociation of the spin-trapping agent giving a *t*-butyl radical, the spin trapping of the *t*-butyl radical by the trapping agent giving the spin adduct radical, and the reaction of the spin-adduct radical with the *t*-butyl radical giving diamagnetic products. The rate constant of the last process was found to be 10 times as large as that of the spin-trapping process, which was determined to be 3.3×10^{6} mol^{-1} dm^{3} s^{-1} based on the reported rate constant for the scavenging of the *t*-butyl radical by tributylstannane. The relative spin-trapping rate constants toward the *t*-butyl radical were also determined to be 0.07, 1.0, 41, 63, and much higher than 50 for 2,4,6-tri-*t*-butylnitrosobenzene, 2-methyl-2-nitrosopropane, pentamethylnitrosobenzene, nitrosodurene and nitrosobenzene, respectively. *C*-phenyl-*N*-*t*-butylnitrone was found to be much less reactive by a factor of less than 0.003.

The reaction of several nitroso compounds with short-lived free radicals giving stable nitroxide radicals (or anilino-type radicals) provides an indirect but convenient technique for detecting the short-lived free radicals by the conventional electron spin resonance (ESR) method.[1,2] This spin-trapping technique has been widely used in recent years to study radical intermediates in photochemical, radiation chemical, and even thermal reaction systems.[3–5] 2-Methyl-2-nitrosopropane, like nitrosobenzene derivatives, has been used very often as a spin-trapping agent because it gives an ESR spectrum of spin-adduct radicals (products of spin-trapping reactions) with a better-resolved hyperfine structure, facilitating the identification of the trapped radicals. However, one drawback of this spin-trapping agent is that it decomposes readily to give a *t*-butyl radical when irradiated by light.[2,6]

Naturally the observed yield of the spin-adduct radicals depends not only on the concentration of the trapped radicals in the reaction systems, but also on the rate constant of the spin-trapping process. The stability of the spin-adduct radicals is another factor determining the observed yield if they are unstable either in decomposing by themselves or in reacting with other radical entities. No quantitative information can, therefore, be drawn from spin-trapping experiments without knowing the kinetic features involved. However, there have been only a limited number of reports on the kinetic study of spin-trapping reaction systems. Although the figures available for the spin-trapping rate constant of the nitroso compounds have been very scanty,[7,8] it appears that the spin trapping is a comparatively slow process, and that it cannot always be the main reaction pathway of the short-lived free radicals. The accumulation of rate data on the spin-trapping is, therefore, desirable in order to extend the utility of this technique and to correlate more firmly the spin-adduct radicals with the actual reaction intermediates.

In the present study, the photochemical processes of 2-methyl-2-nitrosopropane in benzene were investigated mechanistically and kinetically. This photochemical reaction system was then used to determine the reaction rate constants of several spin trapping agents toward the *t*-butyl radical.

Experimental

Benzene and tributylstannane of analytical grade were used as received, without further purification. The benzene solvent was degassed by the freeze-pump-thaw technique, mixed with a spin-trapping agent (or agents) through a break seal under a vacuum of about 10^{-5} Torr in the dark, and sealed in a glass tube with a quartz-tip portion for ESR measurements at one end and a quartz optical-absorption cell at the other. The concentration of spin-trapping agents were usually from 0.01 to 0.1 mol dm^{-3}.

The trapping agents used were 2-methyl-2-nitrosopropane (BNO), nitrosobenzene, nitrosodurene, pentamethylnitrosobenzene, 2,4,6-tri-*t*-butylnitrosobenzene, and *C*-phenyl-*N*-*t*-butylnitrone (*N*-*t*-butyl-α-toluenimine *N*-oxide). The BNO and nitrosobenzene were commercially purchased from the Aldrich Chem. Co., Inc., and Nakarai Chem., Ltd., and were used without further purification. The pentamethylnitrosobenzene was synthesized[9–11] and recrystallized from an acetone solution. The nitrosodurene, tri-*t*-butylnitrosobenzene, and *C*-phenyl-*N*-*t*-butylnitrone were kindly supplied by R. Konaka of Shionogi Pharm. Co., Ltd., M. Tabata of Hokkaido University, and K. Kuwata of Osaka University.

The solution was photolyzed with light from a Xe lamp through a band-pass filter (transmission maximum at 690 nm). The concentration of the spin-adduct radicals was monitored by means of an X-band ESR spectrometer (JEOL, JES-ME-2X), and that of BNO, by measuring its absorption at 680 nm by means of a recording spectrophotometer (Hitachi, EPS-3T). The photolysis and measurements were carried out 299 K.

Results and Discussion

Optical Absorption and Photodecomposition of BNO. The BNO solution in benzene shows, immediately after its preparation, an intense optical-absorption band with a maximum at 295 nm and a weak absorption band with a maximum at 680 nm, as is shown in Fig. 1. The latter band is attributed to the $\pi^{*}\leftarrow$n transition of

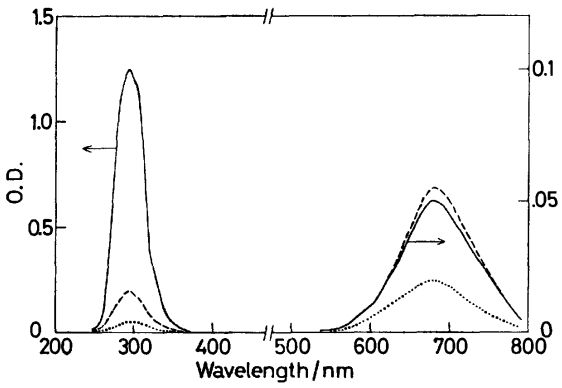

Fig. 1. The optical absorption spectra of BNO at 299 K (solid curves) immediately after dissolving it in benzene, (dashed curves) after 90 minutes when the monomer-dimer equilibrium was reached, and (dotted curves) after the photolysis for 200 minutes.

monomeric BNO, which is red-shifted by 15 nm compared with the band observed in the polar solvent of acetone.[12] The former band was found to decrease gradually in its intensity concomitantly with the increase in the band of monomeric BNO in the dark, as is shown in Fig. 1. Therefore, it is attributable to dimeric BNO. The monomer-dimer equilibrium was reached very slowly (in an hour) and was found to be shifted almost completely over to the monomer. Photoirradiation at the dimer band enhanced the dissociation of the dimer into the monomer.

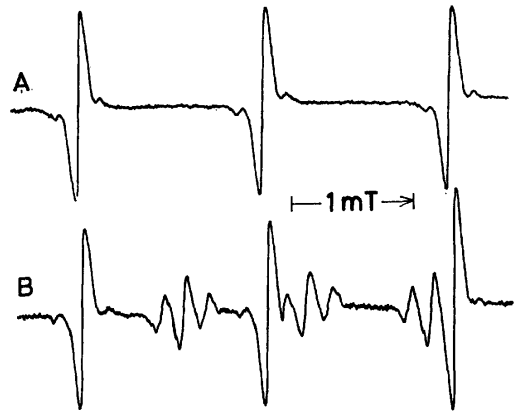

Fig. 2. The ESR spectra observed after the photolysis of BNO at 299 K. The upper spectrum was recorded from the benzene solution of BNO and is due to the di-*t*-butyl nitroxide formed by the spin trapping of *t*-butyl radical by BNO, and the bottom spectrum recorded from the benzene solution containing BNO and 2,4,6-tri-*t*-butylnitrosobenzene is due to both the di-*t*-butyl nitroxide and *N*-*t*-butoxy-2,4,6-tri-*t*-butylanilino radical formed from these two spin trapping agents.

On irradiating the solution at the monomer band, the BNO disappeared gradually, while an ESR spectrum with the hyperfine splitting due to a nitrogen nucleus (1.57 mT) developed, as is shown in Fig. 2. The ESR spectrum is attributed to the di-*t*-butyl nitroxide radical, the spin-adduct radical of the *t*-butyl radical resulting from the photodissociation of the spin-trapping agent itself,[1,2]

$$(t\text{-Bu})\text{NO} \xrightarrow{h\nu} t\text{-Bu}\cdot + \text{NO} \quad (1)$$

$$t\text{-Bu}\cdot + (t\text{-Bu})\text{NO} \xrightarrow{k_2} (t\text{-Bu})_2\text{NO}\cdot \quad (2)$$

No other ESR spectrum was observed. No optical absorption other than that of the BNO was recorded down to 260 nm, either. The spin-adduct radical was found stable in the dark at room temperature.

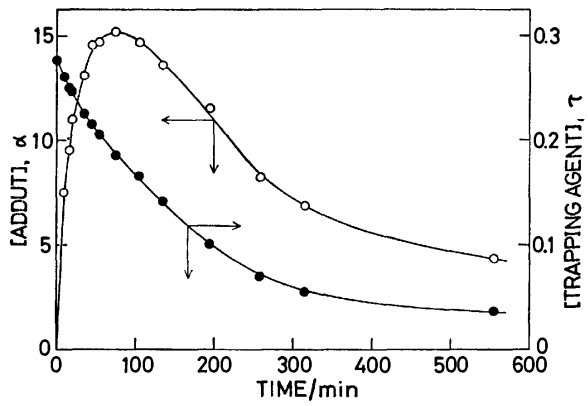

Fig. 3. The change in (●) the concentration of the spin trapping agent, BNO and (○) that of the spin adduct radical, di-*t*-butyl nitroxide, during the photolysis of BNO (2.7×10^{-2} mol dm^{-3}) in benzene at 299 K. The arbitrary units, α and τ are given in the text.

The change in the concentrations of the BNO and the spin adduct radical were followed by means of optical absorption and ESR measurements during the photolysis. The results are shown in Fig. 3. The spin-adduct radical initially increased in its intensity, reached a maximum, and then decreased gradually. By examining the effect of the initial BNO concentration, no indication was observed of the involvement of a second-order process with respect to the short-lived intermediates, such as a combination between the *t*-butyl radicals. The decay of the spin-adduct radical is, therefore, attributed to its reaction with the *t*-butyl radical, giving a diamagnetic product (or products) as:

$$(t\text{-Bu})_2\text{NO}\cdot + t\text{-Bu}\cdot \xrightarrow{k_3} (t\text{-Bu})_2\text{NO}(t\text{-Bu}). \quad (3)$$

The reaction between di-*t*-butyl nitroxide and the *t*-butyl radical was inferred to occur in the gas-phase reaction in pyrolyzing BNO.[13] The photodecomposition of the spin-adduct radical is not expected to occur, because the photolysis was carried out with light of selected wavelengths. The adduct radicals do not combine with themselves,[14] and so such a combination reaction cannot be a reason for their decay either.

Kinetic Features of the Photochemical Reaction of BNO. Based on the three elementary processes, Reactions 1 to 3, the photochemical reaction of the BNO can be totally described by the following rate equations:

$$\frac{d[T]}{dt} = -I\phi - k_2[T][R] \quad (4)$$

$$\frac{d[R]}{dt} = I\phi - k_2[T][R] - k_3[A][R] \quad (5)$$

$$\frac{d[A]}{dt} = k_2[T][R] - k_3[A][R] \quad (6)$$

where T, R, and A stand for the spin trapping-agent (BNO), the *t*-butyl radical, and the spin adduct radical (di-*t*-butyl nitroxide) respectively. In principle, the ratio of the rate constants, k_3/k_2, can readily be determined as $k_3/k_2=[T]/[A]$ at the time when [A] reaches the maximum. The assumption of the steady-state for [R] leads to:

$$\frac{d[A]}{d[T]} = \frac{(k_3/k_2)[A]-[T]}{(k_3/k_2)[A]+2[T]}, \quad (7)$$

which tests the validity of the presumed reaction mechanism by using the observed changes of [A] and [T] and the determined value of k_3/k_2.

However, it is a difficult task to determine precisely enough the absolute values of [A] by means of the ESR method. Therefore, the values were determined only relatively in the present experiment. Using the instrumental constants of a and b, [A] and [T] are expressed as $[A]=a\alpha$ and $[T]=b\tau$ respectively, α and τ being the recorded intensity of the ESR spectra of the spin-adduct radical and that of the optical-absorption spectra of the spin-trapping agent. Then, at the maximum α, this relationship:

$$(\tau/\alpha) = (k_3/k_2)(a/b) \quad (8)$$

is obtained. The results shown in Fig. 3 gave the value of 0.0123 for $(k_3/k_2)(a/b)$. Equation 7 is transformed as:

$$\frac{d\alpha}{d\tau} = \frac{b}{a}\cdot\frac{(k_3/k_2)(a/b)\alpha-\tau}{(k_3/k_2)(a/b)\alpha+2\tau}. \quad (9)$$

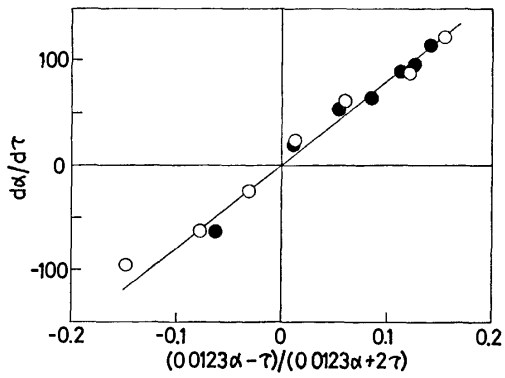

Fig. 4. The relationship between the ratio of the changing rate of the concentration of the spin trapping agent to that of the concentration of the spin adduct radical, $d\alpha/d\tau$, and the concentrations of the spin trapping agent and the spin adduct radical, $(0.0123\alpha-\tau)/(0.0123\alpha+2\tau)$, during the photolysis of (○) 2.7×10^{-2} mol dm^{-3} or (●) 1.2×10^{-2} mol dm^{-3} of BNO in benzene. The slope gives the value of 820 for b/a and, in turn, the value of 10 for k_3/k_2. See also the text.

The results in Fig. 3 are replotted in Fig. 4, where the expected linear relationship is observed between $d\alpha/d\tau$ and $(0.0123\alpha-\tau)/(0.0123\alpha+2\tau)$, and the slope gives the value of 820 for b/a. It turns out that $k_3/k_2=10$. The observed linear relationship gives a support to the presumed reaction mechanism comprised of Reactions 1, 2, and 3. Using the reported extinction coefficient of the monomer band[12] and the determined value of b/a, the concentration of the spin-adduct radical is found to have reached its maximum value of 1.8×10^{-3} mol dm^{-3} when the BNO concentration decreased to 1.9×10^{-2} mol dm^{-3} from its initial value of 2.7×10^{-2} mol dm^{-3} (*cf.* Fig. 3).

Equation 7 shows that d[A]/d[T] (or $d\alpha/d\tau$) is independent of the initial concentration of the spin-trapping agent. As a matter of fact, the data obtained for the initial BNO concentration half as much fall on the same straight line in Fig. 4. This result gives evidence that the second-order reaction with respect to the *t*-butyl radical concentration is effectively absent.

Although the available data on the rate constant of radical scavengers against the *t*-butyl radical has been very little, tributylstannane has been reported to react with the *t*-butyl radical at the constant of 7.4×10^5 mol^{-1} dm^3 s^{-1} in cyclohexane at 298 K.[15] If the radical scavenger is present in the solution, the radical-scavenging reaction:

$$t\text{-Bu}\cdot + (t\text{-Bu})_3\text{SnH} \xrightarrow{k_{10}} t\text{-BuH} + (t\text{-Bu})_3\text{Sn}\cdot \quad (10)$$

competes with Reaction 2 in the early period of the photolysis when Reaction 3 is effectively absent. An example of the observed scavenger effect is shown in Fig. 5. The linear increase of [A] is reduced in the presence of the radical scavenger. The reduction of the spin-adduct formation depends on the concentration of the radical scavenger, [S], as is shown in Fig. 6, and agrees with the normal competition kinetics:

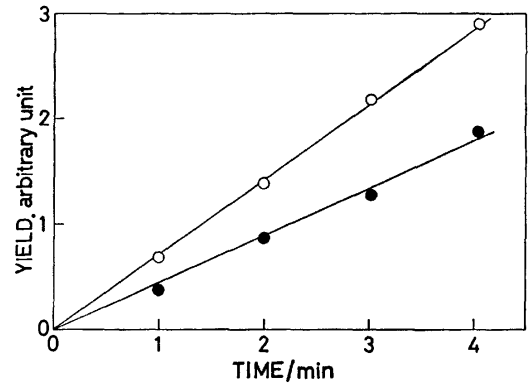

Fig. 5. The yield of the spin adduct radical in the benzene solution at 299 K as a function of the photolysis time, (○) in the presence of only 0.19 mol dm^{-3} BNO and (●) in the presence of 0.19 mol dm^{-3} BNO and 0.56 mol dm^{-3} tributylstannane.

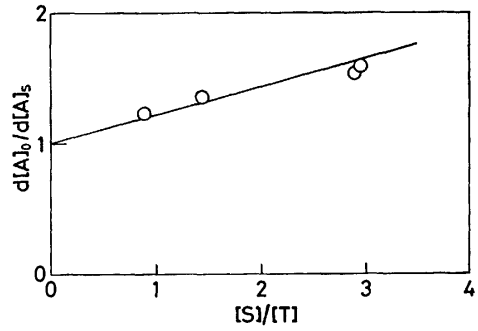

Fig. 6. The dependence of the rate of the spin adduct formation on the concentration of radical scavenger, tributylstannane, during the photolysis of BNO in benzene at 299 K.

$$\frac{d[A]_0}{d[A]_s} = 1 + \frac{k_{10}[S]}{k_2[T]}. \quad (11)$$

On the basis of the reported k_{10},[15] k_2 is determined to be 3.3×10^6 mol^{-1} dm^3 s^{-1}.

Spin-trapping Rate Constants of Several Spin-trapping Agents. When BNO and another spin trapping agent (RNO) are present in the solution, and when the former is selectively photolyzed to generate the *t*-butyl radical, the spin-trapping rate constant of the latter can be determined relative to that of the former by the conventional treatment of competition reactions. As has been shown in the preceeding section, only the reaction:

$$t\text{-Bu}\cdot + \text{RNO} \xrightarrow{k_{12}} \text{RN}(t\text{-Bu})\text{O}\cdot \text{ or } \text{R}\dot{\text{N}}\text{O}(t\text{-Bu}) \quad (12)$$

competes with Reaction 2 against the *t*-butyl radical in the initial period of the photolysis. The rate constant, k_{12}, can readily be determined from this relationship:

$$\frac{d[A']}{d[A]} = \frac{k_{12}[T']}{k_2[T]}, \quad (13)$$

and the observed intensities of ESR spectra due to two kinds of spin-adduct radicals in the short photolysis time when they are increasing linearly. T′ stands for the second spin trapping-agent, from which the spin-adduct radical, A′, is generated.

Figure 2B shows the ESR signal observed from the solution of BNO and 2,4,6-tri-*t*-butylnitrosobenzene. The *t*-butyl radical is added to the oxygen atom of tri-*t*-butylnitrosobenzene to form an anilino-type spin-adduct radical,[16] whose ESR spectrum is distinguished from that of the spin-adduct radical from BNO. Even when the nitroxide-type spin-adduct radical was generated from either the nitrosobenzene, nitrosodurene, or

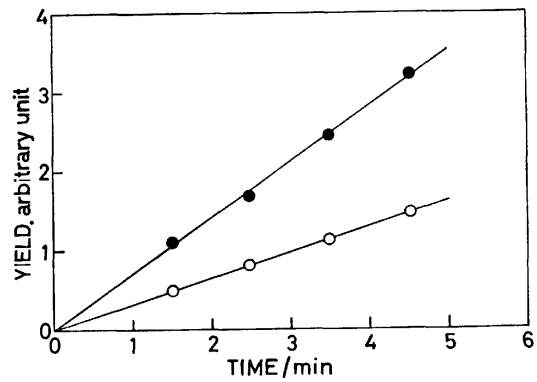

Fig. 7. The yields of the *t*-butyl radical adducts competitively formed (○) from 2.3×10^{-2} mol dm^{-3} BNO and (●) from 1.0×10^{-2} mol dm^{-3} nitrosodurene during the photolysis of BNO in the benzene solution at 299 K.

pentamethylnitrosobenzene coexisting with BNO in the solution, the ESR spectra of the two kinds of nitroxide radicals could readily be distinguished and their intensities determined relative to each other. In the presence of BNO and nitrosodurene in the solution, for instance, the concentration of the spin-adduct radicals increased linearly, as is shown in Fig. 7. The relative spin-trapping efficiency, k_{12}/k_2, was determined to be 63 from the observed slopes of the linear increases and the concentrations of the two spin-trapping agents dissolved in the solution. This shows that the spin-trapping rate constant of nitrosodurene is 2.0×10^8 mol^{-1} dm^3 s^{-1} toward the *t*-butyl radical. The spin-trapping rate constants were determined in the same manner for pentamethylnitrosobenzene,[11] tri-*t*-butylnitrosobenzene,

Table 1. The rate constants of the trapping *t*-butyl radical and the dimerization equilibrium constants of several spin-trapping agents at 299 K in benzene

		Relative rate constant k_{12}/k_2	Rate constant[a] (mol^{-1} dm^3 s^{-1})	Equilibrium constant, K (mol dm^{-3})	Monomer fraction[c]
2-Methyl-2-nitroso-propane		1.0	3.3×10^6	1.92[b]	0.99
Nitrosobenzene		>50	$>2.0\times10^8$	—	1.0
Nitrosodurene	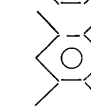	63	2.0×10^8	1.6×10^{-4}	0.086
Pentamethylnitroso-benzene	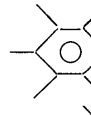	41	1.4×10^8	3.6×10^{-4}	0.13
2,4,6-Tri-*t*-butyl-nitrosobenzene	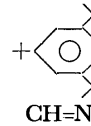	0.07	2.3×10^5	—	1.0
Phenyl-*N*-*t*-butyl-nitrone	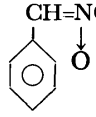	<0.003	$<1.0\times10^4$	—	1.0

a) The absolute values were determined with an experimental uncertainty of ±10%. b) From Ref. 21, the value determined at 299.5 K. c) The monomer fraction for 0.01 mol dm^{-3} of the total concentration based on the monomeric form.

and nitrosodurene, as is shown in Table 1. Nitrosobenzene was found to be too reactive toward the *t*-butyl radical for the rate constant to be determined precisely. The rate constants in Table 1 may include an experimental uncertainty, at the most, of 10% caused mainly in measuring the ESR intensities and in weighing the small amounts of spin-trapping agents.

The only data available to be compared with these results are those for BNO: the spin-trapping rate constant is 1.1×10^{6} mol^{-1} dm^{3} s^{-1} at 317 K toward the *t*-butoxycarbonyl radical[7] and 1.3×10^{8} mol^{-1} dm^{3} s^{-1} at 228 K toward the methoxyl radical.[8] The reactivity of BNO depends very much on the free radicals trapped, and the rate constant toward the *t*-butyl radical reasonably falls in between. The rate constant depends also very much on the spin-trapping agents used. Although tri-*t*-butylnitrosobenzene is exceptionally unreactive toward the *t*-butyl radical (it gives an anilino-type spin-adduct radical) because of the steric hindrance due to the ring substitution with bulky *t*-butyl groups, aromatic nitroso compounds are generally more reactive than BNO, the nitrosoalkane examined.

C-phenyl-*N*-*t*-butylnitrone, one of the most commonly used spin-trapping agents, was also examined in the same way. However, its concentration 30 times as high as the BNO concentration gave no detectable ESR spectrum of the spin-adduct radical from it in the competition reaction experiment. Thus, *C*-phenyl-*N*-*t*-butylnitrone was found to be less reactive than BNO by a factor of less than 0.003 toward the *t*-butyl radical. It turns out that the spin-trapping rate constant is as small as 1×10^{4} mol^{-1} dm^{3} s^{-1} or less. This is much smaller than the spin-trapping rate constants previously reported for *C*-phenyl-*N*-*t*-butylnitrone: 4×10^{5} mol^{-1} dm^{3} s^{-1} toward the benzyloxyl radical at room temperature,[17] 5.5×10^{6} mol^{-1} dm^{3} s^{-1} toward the *t*-butoxyl radical at 298 K,[18] and 1.2×10^{7} mol^{-1} dm^{3} s^{-1} toward the phenyl radical at 298 K.[19] This trapping agent seems to be exceptionally unreactive toward the *t*-butyl radical.

Monomer-Dimer Equilibrium of Spin-trapping Agents. Nitroso compounds are often present in solutions in the dimeric form, which is inactive in trapping free radicals. Therefore, the dissociation constant, K (=[monomer]^2/[dimer]), of the spin-trapping agent used is an important parameter in the quantitative application of the spin-trapping technique.

Nitrosodurene showed optical absorption bands at 800 and 320 nm, the former being due to the monomer, and the latter, to the dimer. According to the well-known relationship between the total concentration of nitrosodurene, c, and the optical density of the monomer band:

$$\frac{c}{\mathrm{OD}}=\frac{1}{2\varepsilon}+\frac{1}{K\varepsilon^{2}}\mathrm{OD}, \qquad (14)$$

the dissociation constant was determined to be 7.5×10^{-5} mol dm^{-3} at 298 K in benzene. It turns out that only 8% of the nitrosodurene is present in the monomeric form at the total concentration usually occurring in the spin-trapping experiments, 10 mmol dm^{-3}. The temperature dependence of K was also studied in the 293—313 K range, as is shown in Fig. 8, which gives the

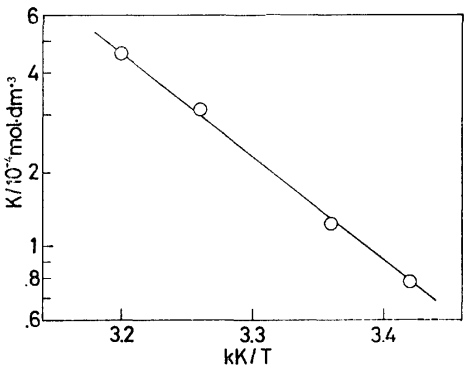

Fig. 8. The dependence of the monomer-dimer equilibrium constant of nitrosodurene in benzene on the reciprocal temperature.

Arrhenius expression of $K=10^{6.80}\exp(-61/RT)$ in kJ/mol unit. The molar extinction coefficient, ε, was found to be 91 mol^{-1} dm^{3} cm^{-1}, almost unchanged in the temperature range examined.

For pentamethylnitrosobenzene, K was determined in the same way to be $10^{5.26}\exp(-50/RT)$, as has been reported previously.[11] Stowell reported the monomer-dimer equilibria for BNO at 288 and 298 K,[20] which were confirmed by the present observation that K is 1.31 at 290 K. Nitrosobenzene and tri-*t*-butylnitrosobenzene are already known to be totally monomeric in solutions.[21,22] *C*-phenyl-*N*-*t*-butylnitrone does not form the dimer at all, either.

The spin-trapping rate constants, k_{12}, shown in the preceeding section were determined on the basis of the monomer concentration calculated by using the dissociation constants obtained here. The dissociation constants used in the calculation and the monomer fractions for the total concentration of 10^{-2} mol dm^{-3} are also shown in Table 1.

In a practical sense, the efficiency of spin-trapping agents may be given by the product of the spin-trapping rate constant and the monomer fraction. Even though nitrosodurene and pentamethylnitrosobenzene are mostly in the dimeric form in benzene, they are more efficient in trapping the *t*-butyl radical than are BNO and tri-*t*-butylnitrosobenzene. Nitrosobenzene is an extremely efficient spin-trapping agent, though it gives a complicated hyperfine structure of the ESR spectrum of the spin-adduct radical.

Summary and Conclusion

The most significant results in the present investigation may be summarized as follows: (1) The *t*-butyl radical reacts with its spin-adduct radical formed from BNO more readily than with BNO itself, so that the yield of the spin-adduct radical cannot go above a certain level. (2) The spin-trapping rate constant depends very much on the nitroso compounds used as the spin-trapping agents; it varies from 2.3×10^{5} to 2.0×10^{7} or more toward the *t*-butyl radical in benzene at 299 K. Aromatic nitroso compounds are generally more efficient in trapping the *t*-butyl radical than the nitrosoalkane. *C*-phenyl-*N*-*t*-butylnitrone is less efficient

in trapping the *t*-butyl radical than the nitroso compounds. (3) In some cases, the monomer-dimer equilibrium shifts well over to the dimer and reduces the practical effectiveness of the spin-trapping agents. Furthermore, the equilibrium was found to be reached extremely slowly (in about an hour) after mixing the spin-trapping agents with a benzene solvent.

These results are believed to give a clue to developing a quantitative utilization of the spin-trapping technique in the study of free radical reaction intermediates.

The authors wish to express their thanks to Professor Keiji Kuwata of Osaka University, Dr. Ryusei Konaka of Shionogi Pharm. Co., Ltd., and Dr. Masayoshi Tabata of Hokkaido University for kindly supplying some of the spin-trapping agents used here. This work was supported by a Science Grant from the Japanese Ministry of Education (No. 085010, 1975).

References

1) E. G. Janzen, *Acc. Chem. Res.*, **4**, 31 (1971).
2) C. Lagercrantz, *J. Phys. Chem.*, **75**, 3466 (1971).
3) C. Lagercrantz, *J. Am. Chem. Soc.*, **95**, 220 (1973); J. R. Harbour, V. Chow and J. R. Bolton, *Can. J. Chem.*, **52**, 3549 (1974); K. A. Mclauchlan and R. C. Sealy, *J. Chem. Soc., Chem. Commun.*, **1976**, 115.
4) M. Shiotani, S. Murabayashi, and J. Sohma, *Int. J. Radiat. Phys. Chem.*, **8**, 483 (1976); F. P. Sargent and E. M. Gardy, *Can. J. Chem.*, **54**, 275 (1976).
5) T. Kunitake and S. Murakami, *J. Poly. Sci.*, **12**, 67 (1974); M. Ko, T. Sato, and T. Otsu, *Macromol. Chem.*, **176**, 643 (1975).
6) M. Mackor, Th. A. J. W. Wajer, and Th. J. de Boer, *Tetrahedron Lett.*, **19**, 2115 (1966).
7) M. J. Perkins and B. P. Roberts, *J. Chem. Soc., Chem. Commun.*, **1973**, 173.
8) F. P. Sargent, *J. Phys. Chem.*, **81**, 89 (1977).
9) A. McKillop, J. S. Fowler, M. J. Zelesko, J. D. Hunt, E. C. Taylor, and G. McGillivary, *Tetrahedron Lett.*, **29**, 2423 (1969).
10) E. C. Taylor and R. H. Danforth, *J. Org. Chem.*, **38**, 2089 (1973).
11) T. Doba, T. Ichikawa, and H. Yoshida, *Bull. Chem. Soc. Jpn.*, **50**, 3124 (1977).
12) E. C. C. Baly and H. Desch, *J. Chem. Soc.*, **1908**, 1747.
13) B. G. Gowenlock and M. J. Healey, *J. Chem. Soc., B*, **1968**, 1014.
14) K. Adamic, D. F. Bowman, T. Gillan, and K. U. Ingold, *J. Am. Chem. Soc.*, **93**, 6551 (1971).
15) D. J. Carlsson and K. U. Ingold, *J. Am. Chem. Soc.*, **90**, 7047 (1968).
16) S. Terabe and R. Konaka, *J. Chem. Soc., Perkin Trans. 2*, 369 (1973).
17) E. G. Janzen, C. A. Evans, and Y. Nishi, *J. Am. Chem. Soc.*, **94**, 8236 (1972).
18) E. G. Janzen and C. A. Evans, *J. Am. Chem. Soc.*, **95**, 8205 (1973).
19) E. G. Janzen and C. A. Evans, *J. Am. Chem. Soc.*, **97**, 205 (1975).
20) J. C. Stowell, *J. Org. Chem.*, **36**, 3055 (1971).
21) S. Terabe and R. Konaka, *J. Chem. Soc., Perkin Trans. 2*, 2163 (1972).
22) R. Okazaki, T. Hosogai, E. Iwamoto, M. Hashimoto, and N. Inamoto, *Bull. Chem. Soc. Jpn.*, **42**, 3611 (1969).

NMR Study of Spontaneous Degradation of Penicillin G in Aqueous Solution

Fumiyuki MITSUMORI, Yoji ARATA, Shizuo FUJIWARA, Masaharu MURANAKA,* and Yoshihiko HORIUCHI*

Department of Chemistry, Faculty of Science, The University of Tokyo, Hongo, Tokyo 113
** School of Medicine, The University of Tokyo, Hongo, Tokyo 113*

(Received June 20, 1977)

The spontaneous degradation of penicillin G in aqueous solution has been studied using NMR and thin layer chromatography. Correlation NMR spectroscopy was used to follow products which appear at the early stage of degradation. It has been found that in 0.3 M phosphate buffer (pH 7.0, 30 °C) a successive first order degradation

$$\text{penicillin G} \xrightarrow{k_1} \text{penicilloic acid} \xrightarrow{k_2} \text{secondary product}$$

is dominant with kinetic constants of $k_1 = 0.7 \times 10^{-2}$ h^{-1} and $k_2 = 6 \times 10^{-2}$ h^{-1}.

It is well known that penicillin G is labile in aqueous solution, and degraded to give a number of products. Several pathways of degradations have already been proposed.[1] However, until now kinetic studies of the degradation of penicillin G[2-4] have been based on the observation of a decreasing time-course of undegraded penicillin G, and information from a number of degradation products has never been used quantitatively; only an overall rate of degradation of penicillin G was reported, which actually consists of several consecutive steps.

In the present work, in order to clarify the elementary process of degradation of penicillin G, a degradation product such as penicilloic acid has been followed quantitatively using NMR spectroscopy. Correlation NMR spectroscopy[5] was employed to follow products which appear at the early stage of degradation.

Experimental

Penicillin G potassium salt for injection (Takeda Chemical Industries, Lot No. 0021) and penicillinase (Calbiochem., Lot No. 400960) were used without further purification. All other reagents are of analytical grade. The concentration of penicillin G is 10 mg/ml which is approximately equal to that used for intramuscular injection. Penicillin G was dissolved in 0.3 M deuterated phosphate buffer (pH 7.0). The sample temperature was maintained at 30 °C throughout the experiments.

NMR measurements were performed using a JEOL PS-100 spectrometer. Chemical shift values reported are from external TMS (10% (v/v) in CCl_4). The concentrations of penicillin G and its degradation products were determined by comparing the peak height of each signal with that of TMS sealed in a coaxial tube. Correlation NMR technique was employed to follow degradation products which give small signals near the strong HDO peak.[5]

Degradation of penicillin G was also monitored by thin layer chromatography (TLC), the procedure of Vandamme and Voets[1] being followed with a slight modification. TLC plates are Merck $60F_{254}$ (5×20 cm with a thickness of 250 μ). 5—6 μl of penicillin G solution (4 mg/ml, 10 mg/ml) was applied and developed at 21 °C using an 85% aqueous solution of acetone. The solvent was allowed to rise to a height of 17 cm. Each TLC plate was sprayed consecutively with 2 M NaOH, 1% starch gel and iodine azide reagent. The R_f values of degradation products were standardized by that of penicillin G.

Results and Discussion

First, a decreasing time-course of degradation of penicillin G was followed using NMR spectroscopy. Figure 1 shows a time change in the NMR peak intensity of α-methyl, $-CH_2-$ and 3-H of penicillin G dissolved in 0.3 M phosphate buffer (pH 7.0). This result indicates that the overall degradation process of penicillin G is of a pseudo-first order reaction with a half life of 85 h. From this result the kinetic constant of overall degradation process, $k_{overall}$, can be estimated at 0.8×10^{-2} h^{-1} at 30 °C in the phosphate buffer solution. A kinetic constant of 1.4×10^{-3} h^{-1} has been reported at 35 °C, pH 7.0 using UV spectroscopy and other methods.[2,3] The phosphate buffer solution used in the present experiment is known to accelerate the degradation of penicillin G.[4] In view of this, the kinetic constant obtained using NMR is consistent with the previously known value.

However, the result of TLC indicates that the process of spontaneous degradation of penicillin G is actually not so simple as described above. The R_f values of degradation products at several different stages are

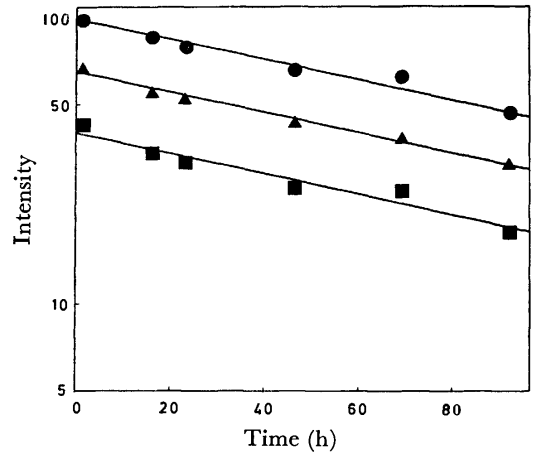

Fig. 1. Semilog plots of intensity of α-CH_3 ●, $-CH_2-$ ▲ and 3-H ■ of penicillin G *vs.* time at 30 °C in the phosphate buffer solution (pH 7.0). Initial value of α-CH_3 intensity of penicillin G is arbitrarily taken to 100.

Table 1. R_f values ($\times 100$) of degradation products of penicillin G at several different stages in the phosphate buffer solution

Penicillin G was used as a standard.

Time(h)	0	2.5	7	17	30	70	118	240	Product
	56	56	56	56	56	56	56	56	Penicillin G
						49			
					37	40	43	40	
R_f values $\times 100$			31	32	27	31	33	32	Secondary product
		16	17	17	15	15	17	14	Penicilloic acid

summarized in Table 1. Only one species of degradation products can be observed at 2.5 h after penicillin G is dissolved. After 7 h, the second species becomes observable, and more than three species can be observed after 17 h. This result indicates that from the observation of the decreasing time-course of penicillin G, only an overall degradation rate of penicillin G can be obtained. Therefore, in order to study the actual complicated process of degradation of penicillin G, the formation process of the degradation products was followed quantitatively.

In order to identify the initial product of spontaneous degradation using NMR, the chemical shift values of the initial product were compared with those of penicillinase-degraded products.[6] This result clearly indicates that the initial product is penicilloic acid.

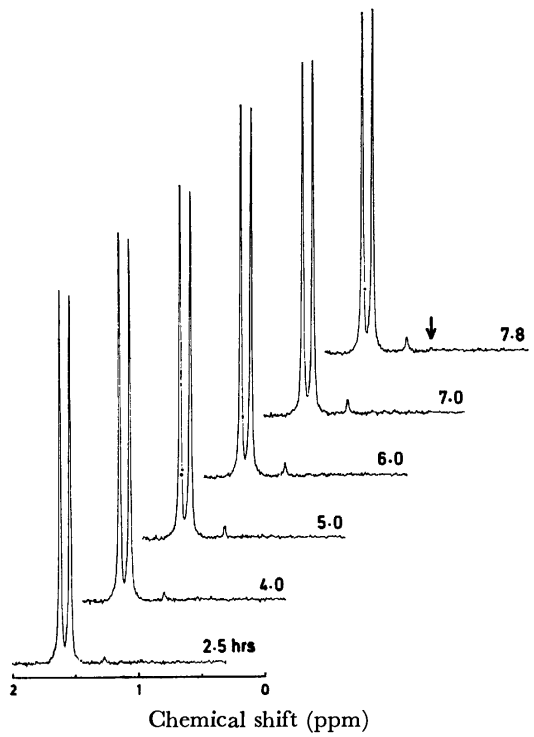

Fig. 2. Correlation NMR spectra of methyl region of penicillin G and penicilloic acid at early stages of degradation. Number of accumulations: 128. Two large peaks at $\delta=1.54$ and 1.62 ppm result from penicillin G and a small peak at $\delta=1.27$ ppm results from penicilloic acid. The signal due to the secondary product ($\delta=1.07$ ppm) is marked by an arrow.

In order to follow the formation of penicilloic acid at the early stage, 32—128 accumulations were performed in the correlation mode. Each accumulation was completed within 10 min. Figure 2 gives NMR spectra of the methyl region of penicillin G and penicilloic acid at the early stage of degradation. The α-methyl peak of penicilloic acid appears at $\delta=1.27$ ppm. Although NMR is less sensitive than TLC, a signal due to the secondary product ($\delta=1.07$ ppm) can be clearly seen in Fig. 2, where the signal is marked by an arrow. This signal becomes much stronger at a later stage of degradation. An aqueous solution containing only penicilloic acid also gives a product which is identical with this secondary product. This result demonstrates that the secondary product is produced from penicillin G through penicilloic acid, *i.e.* the process of formation of penicilloic acid and the secondary product is a successive degradation reaction. When pH is not regulated, penicilloic acid is known to undergo degradation forming penilloic acid by decarboxylation.[1] In the present experiment, the secondary product is presumably penilloic acid, judging from the formation of bubbles in the solution during the course of incubation. No attempt has been made to identify this product. The order of appearance of the degradation products observed by the correlation NMR method is consistent with that observed by TLC; as shown in Table 1, penicilloic acid with an R_f value of 0.15 appears first, followed by the secondary product which gives an R_f value of 0.3. Products whose R_f values are 0.4 and 0.49 cannot be assigned to any distinct NMR peaks due to a low concentration of these products.

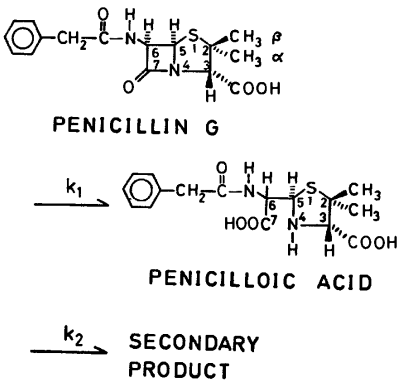

Fig. 3. A degradation process of penicillin G.

A computer simulation of the process of formation of penicilloic acid and the secondary product was performed by assuming that the reaction is successive first order reaction. The result is illustrated in Fig. 3. For the simulation, the yields for these products observed within 17 h after the addition of penicillin G were used; no other products exist during this period judging from the TLC result. The computer simulation gives kinetic constants of $k_1=0.7\times10^{-2}\,h^{-1}$ and $k_2=6\times10^{-2}\,h^{-1}$. Figure 4 illustrates observed and calculated formation processes for penicilloic acid and the secondary product. In the case of penicilloic acid the calculated curve is in good agreement with the observed yield over the entire range of the reaction. On the other hand, the observed

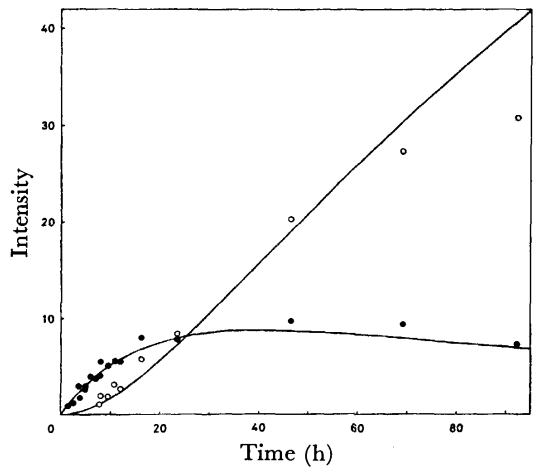

Fig. 4. Plots of intensity of the methyl group of penicilloic acid ● and the secondary product ○ *vs.* time at 30 °C in the phosphate buffer solution. Solid lines indicate the calculated values. Initial value of α-CH_3 intensity of penicillin G is arbitrarily taken to 100.

value for the secondary product does not agree well with the calculated value at a later stage of the reaction. This suggests that the secondary product is labile and further degraded.

A kinetic constant of the first step, k_1 obtained here is in good agreement with $k_{overall}$ which is obtained from the decreasing time-course of penicillin G. From this result it was found that the successive first order reaction given in Fig. 3 is dominant in 0.3 M phosphate buffer solution (pH 7.0) at 30 °C with kinetic constants of $k_1=0.7\times10^{-2}$ h^{-1}, $k_2=6\times10^{-2}$ h^{-1}.

The authors gratefully acknowledge a support from the Ministry of Health and Welfare (Special Research Grant #160).

References

1) E. J. Vandamme and J. P. Voets, *J. Chromatogr.*, **71**, 141 (1971).
2) T. Yamana, A. Tsuji, and Y. Mizukami, *Chem. Pharm. Bull.*, **22**, 1186 (1974).
3) J. T. H. Ong and H. B. Kostenbauder, *J. Pharm. Sci.*, **64**, 1378 (1975).
4) P. Finholf, G. Jürgensen, and H. Kristiansen, *J. Pharm. Sci.*, **54**, 387 (1965).
5) Y. Arata and H. Ozawa, *J. Magn. Reson.*, **21**, 67 (1976).
6) J. H. Hash, Ed, "Methods in Enzymology, XLIII, Antibiotics," Academic Press (1972), p. 640.

The Crystal Structures of Tin(II) Chloride Dihydrate in High- and Low-Temperature Phases as Studied by Neutron and X-Ray Diffractions

Katsuki KITAHAMA and Hideko KIRIYAMA

The Institute of Scientific and Industrial Research, Osaka University, Yamadakami, Suita, Osaka 565

(Received June 27, 1977)

The neutron-diffraction results for deuterated single crystals have shown definitely that the phase transition is ascribable to the ordering of the hydrogen atoms. The ordered arrangement below the transition temperature (T_t= 234 K) agrees well with the NMR results. No doubling of the unit cell or loss of the center of symmetry can be detected. In the disordered phase above T_t, four deuterons of two non-equivalent water molecules are distributed into seven sites. The occupancy factors of the individual sites have been refined by least-squares methods under different constraints. Bernal and Fowler's ice rule is obeyed in the H-bonded water layers, and the water molecules of crystallization scarcely dissociate at all. The crystal structure has been redetermined by the X-ray diffraction method at 209 and 223 K, using an $SnCl_2 \cdot 2H_2O$ single crystal. No distinct change in the structure of non-hydrogen atoms has been disclosed on passing through the transition point (T_t=218 K). However, in the close vicinity of T_t, the *a* and *c* lattice parameters and the three H-bonded O···O distances steeply change in association with the ordering of the hydrogen atoms.

Crystals of $SnCl_2 \cdot 2H_2O$ exhibit a phase transition accompanied by a characteristic dielectric anomaly at 218 K (at 234 K for its deuterated analogue).[1] Successive studies of proton (PMR) and deuteron (DMR) magnetic resonance,[2,3] X-ray diffraction,[4] and Raman scattering[5] have shown that the phase transition should be ascribed to the ordering of hydrogen atoms in H-bonded water layers without another distinct change in the crystal structure. Furthermore, the critical phenomena of the phase transition have been studied by other approaches, such as specific heat,[6,7] and dielectric measurements.[8] On the other hand, the theory of the phase transition[9] and the explanation of the dielectric behavior[10] have been developed in cooperation with these experiments.

This study was performed to elucidate more directly the hydrogen arrangement in the H-bonded network below and above the phase-transition temperature, T_t. Some of the neutron-diffraction (ND) results have been given previously.[11] Additionally, the crystal structures at 209 and 223 K as well as the lattice parameters in the 93—293 K range were determined by X-rays in order to make sure whether or not the hydrogen-ordering is associated with structural changes in other atoms.

Neutron-diffraction Experiments

Samples. Deuterated single crystals, $SnCl_2 \cdot 2D_2O$, were used for the present ND study, because X-ray photographs taken at both 293 and 93 K had shown no change in the crystal structure on deuteration. Single crystals were grown from a deuterated hydrochloric acid solution saturated with anhydrous tin(II) chloride. A large single crystal was cut into three cylindrical pieces, weighing 0.8957, 0.9282, and 1.2361 g. The smallest one has dimensions of 5.5, 6.0, and 7.5 mm along the a, c, and b axes respectively, and it was mainly used. Another crystal, weighing 12.3 g, was also used at the initial stage of the experiment. These four crystals are labeled S1, S2, S3, and S4 in increasing order of weight. Since this compound is sensitive to moisture, many sorts of organic adhesives, and metals, each single-crystal sample was wrapped with Teflon tape and then placed in an aluminium capsule.

Intensity Data Collection. All the ND measurements were carried out with the KUR-1 reactor of the Research Reactor Institute, Kyoto University. The intensity data of Bragg reflections were collected on a Rigaku neutron four-circle diffractometer at 297 and 88 K. The neutron flux had a density of 7×10^4 n cm^{-2}·s^{-1} at the specimen and a wavelength of 0.994 Å. The reflections were measured within $\sin\theta/\lambda$ of 0.72 Å^{-1}. The 2θ-ω step-scan technique was used with the step size of $\Delta 2\theta = 0.1°$. The scan range for each reflection was adjusted so as to include at least five background points on both sides of the peak. The counting time was controlled by monitoring the intensity of an incident neutron beam. A graphical method was used for integrating the observed intensity and for correcting the background. No correction for absorption was made because of the small linear absorption coefficient (μ= 0.255 cm^{-1}). The standard intensity was monitored every 25 reflections. There was no significant change in the intensity of the standard reflection throughout the data collection.

At room temperature (297 K) the *hk*0 and 0*kl* intensity data were collected with the biggest crystal, S4, while 0*kl*, *h*0*l*, and *hkh̄* were measured with the smallest, S1. For the measurement at 88 K, a ten-liter Dewar vessel containing liquid nitrogen was attached on the ϕ table of the four-circle diffractometer to cool the specimen down to 88 K by a conduction method. Because this arrangement limited the tilting angle of the χ-circle to the range of $-20° < \chi < 20°$, three crystals, S1, S2, and S3, were mounted with b, a, and c axes respectively along the ϕ-axis of the goniostat.

Some forbidden reflections for the $P2_1/c$ space group, as determined by X-rays, were carefully checked, but their intensities did not exceed more than one half of the background level. Thus, no evidence was found to suggest that the low-temperature phase is either antiferroelectric or ferroelectric.

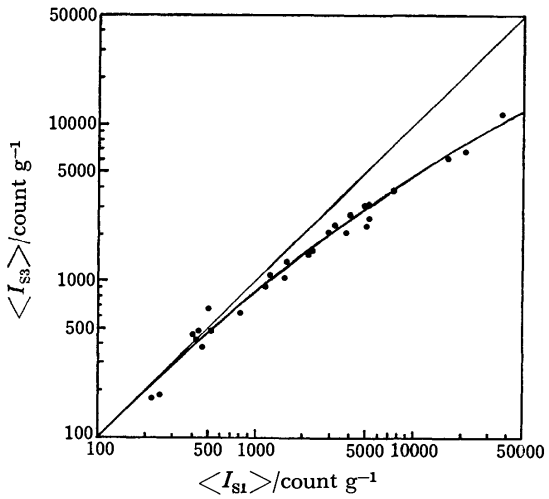

Fig. 1. The extinction effect observed in the ND experiment of $SnCl_2 \cdot 2D_2O$. The reduced intensity of a bigger crystal S3 is plotted against that of a smaller crystal S1, both on logarithm scale. Deviation from the line with a slope of unity reflects the extinction effect.

Extinction Correction. In the early stage of least-squares refinements, it became apparent that the intensities were affected by severe extinction and that the data required adequate corrections. Two kinds of isotropic corrections were attempted, for simplicity neglecting the dependence of the extinction on the Bragg angles. One was an exponential type with a single parameter, such as $I_o = I_c \exp(-kI_c)$. This type of correction was unsuccessful, probably because the I_o/I_c ratio was less than 0.7, as was suggested by Hamilton.[12] The other was based on the reduced intensity, $\langle I \rangle$, which was a quotient of the observed intensity divided by the crystal weight. The reduced intensity of a bigger crystal, $\langle I_b \rangle$ was plotted against that of a smaller crystal, $\langle I_s \rangle$, both on the logarithm scale. The difference in these reduced intensities, $\Delta\langle I \rangle$ $(=\langle I_s \rangle - \langle I_b \rangle)$, was evaluated from the smoothed curve shown in Fig. 1. Thus, the intensity data were corrected by extrapolating the $\langle I \rangle$ to an infinitesimally small weight, using either of the following two equations:

$$\langle I_{corr} \rangle = \langle I_b \rangle + \frac{W_b}{W_b - W_s} \Delta\langle I \rangle$$
$$= \langle I_s \rangle + \frac{W_s}{W_b - W_s} \Delta\langle I \rangle$$

where W_b and W_s are the weights of a bigger and a smaller crystal, respectively. This type of correction was effective in avoiding negative temperature factors and in lowering the R-value by more than 2%. However, this correction seemed to be not enough for the biggest crystal, S4; therefore its intensity data were excluded from the final least-squares refinement.

X-Ray-diffraction Experiments

A single crystal of $SnCl_2 \cdot 2H_2O$, with dimensions of $0.08 \times 0.1 \times 0.32$ mm^3 and sealed in a Lindemann-glass capilary, was used throughout the X-ray work. This crystal was mounted on a Rigaku four-circle diffractometer, with its c-axis along the ϕ-axis of the goniostat. The crystal was cooled by blowing a stream of cold nitrogen, using an X-ray low-temperature device manufactured by the Rigaku Denki Co. The reflection intensities at 209 and 223 K, and monoclinic cell dimensions (space group; $P2_1/c$) from 93 to 293 K were measured with an Mo $K\alpha$ radiation monochromatized by pyrolytic graphite. The temperatures were controlled within ± 0.5 K during each measurement of the lattice parameters, and within ± 1.0 K throughout each collection of the intensity data. The cell dimensions at a given temperature were refined by a least-squares method using 21 reflections with 2θ between 40 and 65°. They are summarized in Table 1. All the intensity data were collected by means of the 2θ-ω scan technique. No correction was made for absorption ($\mu = 54.9$ cm^{-1}).

Table 1. Lattice parameters at various temperatures

T/K	a/Å	b/Å	c/Å	β/°	V/Å^3
93	9.140(3)	7.150(2)	8.914(4)	114.32(3)	532.5(3)
125	9.153(2)	7.156(2)	8.958(3)	114.35(2)	534.5(2)
153	9.167(3)	7.165(2)	8.961(3)	114.33(2)	536.2(3)
173	9.178(2)	7.172(2)	8.970(3)	114.36(2)	537.9(3)
195	9.200(3)	7.184(2)	8.975(3)	114.44(2)	540.0(3)
209	9.213(2)	7.189(2)	8.969(3)	114.50(2)	540.6(3)
223	9.244(3)	7.202(2)	8.963(3)	114.64(2)	542.6(3)
233	9.262(3)	7.212(2)	8.953(4)	114.73(3)	543.2(4)
243	9.272(3)	7.217(2)	8.949(3)	114.79(2)	543.6(3)
253	9.283(3)	7.227(2)	8.955(4)	114.82(3)	545 3(4)
268	9.299(4)	7.237(3)	8·961(4)	114.89(3)	547.1(4)
293	9.320(8)	7.255(4)	8.970(7)	114.91(5)	550.1(8)

Space group; $P2_1/c$ (throught the temperature range), $Z=4$, F.W. 225.63 g mol^{-1}, $\rho_{obsd}=2.710$,[19] $\rho_{calcd\,(293\ K)} = 2.724$ g cm^{-3}, μ(Mo $K\alpha$)$=54.85$ cm^{-1}. E.s.d.'s are given in parentheses.

Structure Analyses and Refinements

Structure at 88 K by Neutron Diffraction. The approximate positions of deuterons were easily determined from the Fourier projections of nuclear-scattering density along the a and c axes; the signs were based on the heavy-atom coordinates from a previous X-ray study.[4] No evidence was found for any disordering of the deuteron positions. The extinction correction described above was made prior to the refinement. In order to check whether or not the deuterium substitution was complete, the neutron-scattering length of deuteron was refined, as well as the positional and isotropic thermal parameters for all the atoms and a scale factor, in the full-matrix least-squares refinement. The obtained scattering length was $b_D = (0.605 \pm 0.018) \times 10^{-12}$ cm, indicating that the unsubstituted hydrogen was negligibly small. The scattering lengths used were $b_{Sn}=0.610$, $b_{Cl}=0.961$, $b_O=0.577$, and $b_D=0.612$ in units of 10^{-12} cm from Neutron Diffraction Commission, 1969.[13]

The refinement was performed by a block-diagonal least-squares method with 814 reflections, in which positional and anisotropic thermal parameters for all the atoms, an overall temperature factor, and a scale factor (a total of 65 parameters) were varied until the maximum shift in any parameter was less than one-fourth of its e.s.d. The quantity minimized in this

TABLE 2. OBSERVED AND CALCULATED STRUCTURE AMPLITUDES($10F$) FOR $SnCl_2 \cdot 2D_2O$ AT 88 K BY NEUTRON DIFFRACTION[a,b]

H	FO	FC	H	FO	FC	H	FO	FC	H	FO	FC	H	FO	FC	H	FO	FC	H	FO	FC	H	FO	FC
K= 0 L= 0			1	50	-54	2	23	-21	1	3	-2	K= 1 L= 3			-7	36	36	-2	47	-46	K= 4 L= 6			-1	62	59	1	3	-7
1	59	81	2	49	-54	3	15	-13				-12	34	35	-6	57	56	-1	35	-34	-2	56	-51	0	80	-82			
2	4	-1	3	68	69	4	0	-1	K= 0 L= 2			-11	24	27	-5	21	21	0	57	56	-1	19	-17	1	43	-42	K= 6 L= 9		
3	70	72	4	29	29	5	24	25	-12	16	14	-10	16	-16	-4	75	70	1	9	-10	0	52	47	2	47	50	-1	18	-19
4	30	-26	5	6	-7	6	24	26	-11	0	0	-9	0	2	-1	35	38				1	16	-16	3	84	-82	0	11	-12
5	81	-81	6	31	33	7	8	-7	-10	97	-93	-8	9	4	0	6	0	K= 4 L= 5						4	62	-64			
6	11	-9	7	51	49	8	13	-13	-9	8	3	-7	64	-60	1	25	26	-2	21	21	K= 5 L= 6			5	36	44	K= 0 L=10		
7	38	37							-8	70	65	-6	27	-26	2	40	41	-1	34	34	-2	14	-14				-11	18	20
8	13	-10	K= 9 L= 0			K= 5 L= 1			-7	85	-80	-5	56	52	3	13	-7	0	33	32	-1	10	-8	K= 1 L= 8			-10	61	67
9	47	-45	1	42	-45	-10	32	-32	-6	18	-16	-1	45	46	4	7	6	1	7	-7	0	53	-51	-12	10	14	-9	7	5
10	47	47	2	0	0	-9	0	-2	-5	35	32	0	60	-63	5	44	-39				1	16	-19	-11	33	-37	-8	104	-104
11	17	18	3	19	-19	-8	17	18	-4	126	-132	1	9	-8	6	50	-46	K= 5 L= 5						-10	18	-21	-7	21	-19
			4	12	-10	-7	22	19	-3	120	-128	2	29	26	7	16	17	-2	47	-46	K= 6 L= 6			-9	0	0	-6	6	-4
K= 1 L= 0			5	17	17	-6	52	51	-2	36	-28	3	97	-90	8	9	9	-1	17	-9	-2	7	-4	-8	39	-35	-5	117	-116
1	13	-11				-5	50	46	-1	5	3	4	76	-70	9	48	49	0	87	91	-1	47	-46	-7	27	17	-4	19	19
2	30	29	K=10 L= 0			-4	19	17	0	26	21	5	60	56				1	13	14	0	6	6	-6	11	16	-3	99	102
3	28	-25	0	48	48	-3	10	9	1	65	72	6	11	12	K= 2 L= 4						1	6	-4	-5	14	18	-2	0	5
4	24	-18	1	9	8	-2	35	-34	2	121	123	7	32	-31	-1	15	-13	K= 6 L= 5						-4	73	73	-1	52	49
5	3	2	2	35	-37	-1	41	-41	3	17	13	8	65	62	0	50	-42	-2	22	-19	K= 7 L= 6			-3	37	39	0	85	90
6	15	-11				0	12	-8	4	41	-42	9	53	51	1	19	-17	-1	8	-5	-2	6	6	-2	45	47	1	41	42
7	49	47	K= 1 L= 1			1	56	-57	5	29	24	10	43	-47	5	6	-4	0	19	-18	-1	11	-10	-1	35	36	2	0	2
8	22	23	-12	40	41	2	83	-84	6	45	-47				6	10	6	1	16	-16	0	21	19	0	14	-12			
9	18	-8	-11	5	-2	3	22	-19	7	56	-57	K= 2 L= 3			7	55	-50				1	7	9	1	30	31	K= 1 L=10		
10	2	1	-10	38	-38	4	6	-5	8	7	-7	-1	32	-32	8	11	-11	K= 7 L= 5						2	21	21	-11	24	-26
11	55	-56	-9	13	-12	5	25	-24	9	49	-53	0	30	-27	9	45	48	-2	28	-28	K= 8 L= 6			3	18	20	-10	8	-7
			-8	8	-7	6	46	44	10	13	-18	1	4	-6				-1	18	-19	-2	31	-29	4	45	49	-9	17	-18
K= 2 L= 0			-7	12	-10	7	88	93				5	22	23	K= 3 L= 4			0	54	51	-1	0	2	5	10	-11	-8	52	-52
0	29	-21	-6	23	20	8	8	9	K= 1 L= 2			6	0	4	-1	30	-33	1	10	-12	0	56	54				-7	10	-11
1	60	-66	-5	36	33	9	22	-23	-12	0	6	7	0	0	0	35	31				1	6	-6	K= 2 L= 8			-6	39	-40
2	88	-102	-4	35	34				-11	38	41	8	10	-8	1	5	1	K= 8 L= 5						-1	43	38	-5	18	-21
3	17	17	-3	31	30	K= 6 L= 1			-10	18	22	9	16	-17				-2	34	31	K= 1 L= 7			0	45	-46	-4	30	29
4	35	37	0	10	-7	-9	12	-13	-9	55	58				K= 4 L= 4			-1	31	30	-12	40	42	1	16	15	-3	0	1
5	87	-105	3	10	10	-8	20	-20	-8	0	7	K= 3 L= 3			-2	38	-38	0	13	14	-11	17	18	2	42	37	-2	30	31
6	14	-11	4	24	25	-7	18	-28	-7	15	-9	-1	33	33	-1	6	-6	1	43	-46	-10	42	-44	3	8	-11	-1	15	16
7	57	60	5	21	-20	-6	10	10	-6	26	29	0	63	-60	0	29	26				-9	49	51	4	26	-28	0	18	-20
8	45	-43	6	42	40	-5	28	26	-5	11	-7	1	28	26	1	10	-7	K= 9 L= 5			-8	84	80	5	59	57	1	8	9
9	24	22	7	86	79	-4	8	7	0	34	-30							-2	57	-57	-7	27	-26				2	10	-11
10	69	68	8	19	-18	-3	21	-17	1	16	-18	K= 4 L= 3			K= 5 L= 4			-1	37	-37	-6	16	-16	K= 3 L= 8					
11	0	-1	9	41	-40	-2	29	-23	2	17	7	-1	6	5	-2	18	-13	0	46	42	-5	42	39	-1	54	-58	K= 2 L=10		
			10	31	33	-1	20	-16	3	59	-57	0	10	7	-1	29	26				-4	39	-37	0	9	-11	-2	43	-41
K= 3 L= 0			11	11	-10	0	24	-21	4	40	-40	1	14	-15	0	0	3	K= 0 L= 6			-3	80	-74	1	32	-36	-1	76	-75
1	16	-15				1	14	15	5	47	-45				1	14	13	-12	7	-4	-2	8	3				0	31	34
2	49	-55	K= 2 L= 1			2	53	52	6	56	-53	K= 5 L= 3						-11	9	-3	-1	16	16	K= 4 L= 8			1	17	-15
3	4	0	-11	18	-18	3	17	19	7	23	20	-2	50	51	K= 6 L= 4			-10	75	-76	0	14	-14	-1	42	43	2	89	-84
4	7	-9	-10	29	-29	4	0	-2	8	14	13	-1	32	30	-2	27	-27	-9	60	-56	1	30	28	0	70	-70			
5	10	-9	-9	19	-19	5	0	0	9	18	18	0	58	-59	-1	32	-31	-8	53	-51	2	52	49	1	18	-20	K= 3 L=10		
6	40	37	-8	12	-12	6	11	-12	10	12	16	1	16	-13	0	14	-27	-7	35	-31	3	8	2				-1	9	-8
7	18	-15	-7	3	-3	7	11	-11							1	18	20	-6	60	57	4	11	-13	K= 5 L= 8			0	17	16
8	7	-5	-6	36	19	8	0	-2	K= 2 L= 2			K= 6 L= 3						-5	24	27	5	12	-13	-1	22	24	1	27	-35
9	16	16	-5	25	24	9	14	11	-1	30	27	-2	16	-18	K= 7 L= 4			-4	57	54	6	22	-24	0	11	-11			
10	8	-8	-4	5	5				0	84	-98	-1	31	-31	-2	21	-20	-3	77	75				1	26	29	K= 4 L=10		
11	23	23	-3	24	-19	K= 7 L= 1			1	15	7	0	16	-17	-1	29	-28	-2	68	-65	K= 2 L= 7						-1	10	7
			-2	35	-33	-8	25	-27	6	0	0	1	15	13	0	43	39	-1	56	-49	-1	4	1	K= 6 L= 8			0	59	53
K= 4 L= 0			0	21	-18	-7	44	-44	7	22	-17				1	10	9	0	15	14	0	16	-14	-1	36	36	1	20	23
0	120	150	1	14	14	-6	36	-35	8	6	-1	K= 7 L= 3						1	41	-39	1	11	-10	0	49	-49			
1	14	11	2	44	42	-5	23	-22	9	54	53	-2	56	61	K= 8 L= 4			2	12	-20	2	11	-11	1	5	2	K= 5 L=10		
2	28	-28	3	33	32	-4	15	13	10	19	23	-1	35	34	-2	4	2	3	43	42	3	15	-14				-1	12	15
3	79	82	4	15	16	-3	33	31				0	62	-60	-1	22	21	4	62	59	4	0	-1	K= 7 L= 8			0	0	0
4	15	14	5	0	2	-2	19	17	K= 3 L= 2			1	11	11	0	25	21	5	7	4	5	9	9	-1	48	-46			
5	36	-35	6	15	-14	-1	10	7	-1	21	23				1	30	-32	6	14	14	6	12	14	0	12	-10	K= 1 L=11		
6	19	16	7	17	-19	0	23	21	0	48	47	K= 8 L= 3						7	89	102							-10	0	-1
7	42	40	8	11	-13	1	12	10	1	33	38	-2	5	6	K= 9 L= 4						K= 3 L= 7			K= 1 L= 9			-9	15	-17
8	18	-17	9	0	0	2	6	-5				-1	40	-37	-2	34	-36	K= 1 L= 6			-1	24	24	-11	21	-25	-8	24	-28
9	50	-50	10	0	5	3	63	58	K= 4 L= 2			0	29	-25	-1	32	29	-12	40	-37	0	38	-34	-10	20	22	-7	32	33
10	41	41	11	5	6	4	61	58	-1	5	-2	1	32	-32	0	36	35	-11	66	-65	1	12	-11	-9	6	1	-6	48	45
						5	33	-32	0	28	=26				1	33	33	-10	57	-54				-8	0	3	-5	6	-5
K= 5 L= 0			K= 3 L= 1			6	8	-9	1	5	0	K= 9 L= 3						-9	8	0	K= 4 L= 7			-7	44	45	-4	42	30
1	20	-17	-11	11	-12	7	15	15				-2	6	4	K= 1 L= 5			-8	35	-33	-1	30	32	-6	38	38	-3	56	55
2	35	35	-10	22	-23	8	59	-60	K= 5 L= 2			-1	6	4	-12	31	-33	-7	5	1	0	35	34	-5	11	11	-2	32	-35
3	5	-3	-9	11	9				-2	25	-23	0	43	-42	-11	17	16	-6	12	13	1	29	33	-4	3	0	-1	53	-54
4	8	-6	-8	9	-10	K= 8 L= 1			-1	5	-2	1	11	12	-10	91	88	-5	5	-2				-3	24	-23	0	17	17
5	8	7	-7	37	-36	-7	35	37	0	34	-32				-9	6	-3	-4	53	46	K= 5 L= 7			-2	29	-29	1	12	-14
6	11	-8	-6	36	-32	-6	32	31	1	5	-5	K= 0 L= 4			-8	48	-46	-3	9	5	-1	9	6	-1	26	-24			
7	30	29	-5	27	-23	-5	35	35				-12	67	-68	-7	47	44	-2	7	-6	0	17	-17	0	33	-35	K= 2 L=11		
8	0	1	-4	6	2	-4	17	-17	K= 6 L= 2			-11	6	4	-6	6	0	-1	8	5	1	25	28	1	0	0	-2	15	-13
9	0	-1	-3	25	22	-3	38	-42	-2	53	51	-10	10	8	-5	102	-100	0	44	-45				2	40	42	-1	6	-5
10	37	34	-2	12	9	-2	8	-11	-1	38	39	-9	39	-38	-4	6	-1	1	6	-2	K= 6 L= 7			3	7	7	0	2	-2
			-1	16	14	-1	21	-24	0	36	-35	-8	6	-2	-3	67	60	2	11	8	-1	18	-17	4	6	-5			
K= 6 L= 0			0	45	44	0	33	-35	1	67	74	-7	59	54	-2	43	-40	3	21	-19	0	44	-42				K= 3 L=11		
0	57	61	1	21	19	1	7	-8				-6	98	90	-1	6	-3	4	0	0	1	8	-9				-1	6	-5
1	8	7	2	0	0	2	20	19	K= 7 L= 2			-5	28	21	0	94	99	5	63	-59				K= 2 L= 9			0	71	76
2	60	-59	3	64	61	3	34	31	-2	59	61	-4	8	0	1	16	14	6	67	-67	K= 7 L= 7			-2	8	-8			
3	9	10	4	48	44	4	25	25	-1	12	12	-3	10	4	2	62	-56	7	41	-40	-1	24	25	-1	5	-1	K= 0 L=12		
4	7	7	5	48	-51	5	38	36	0	35	31	-2	95	-90	3	12	12				0	19	-17	0	2	4	-8	14	15
5	121	-117	6	16	-18	6	17	17	1	38	38	-1	50	-49	4	7	-4	K= 2 L= 6			1	0	2	1	3	2	-7	62	-63
6	24	-22	7	19	20							0	21	17	5	81	-78	-2	17	12				2	6	-8	-6	66	-70
7	45	46	8	53	-55	K= 9 L= 1			K= 8 L= 2			1	21	18	6	18	-19	-1	22	-20	K= 8 L= 7			3	5	-6	-5	61	-64
8	50	-48				-5	4	3	-2	30	31	2	99	90	7	40	41	0	31	29	-1	51	49	4	6	-5	-4	48	-46
9	9	5	K= 4 L= 1			-4	28	-29	-1	14	-14	3	57	53	8	0	0	1	11	-7	0	39	37				-3	70	-69
			-11	4	-4	-3	11	-11	0	62	-63	4	23	22				2	109	-97				K= 3 L= 9			-2	25	-21
K= 7 L= 0			-10	14	13	-2	26	-27	1	52	-54	5	74	71	K= 2 L= 5			3	23	23	K= 0 L= 8			-1	35	32			
1	20	-20	-9	38	36	-1	13	-12				6	0	-1	-1	7	-5	4	34	34	-12	43	45	0	0	1	K= 1 L=12		
2	48	-50	-8	42	44	0	41	42	K= 9 L= 2			7	21	-24	0	23	-20	5	75	-69	-11	35	37	1	0	-1	-8	14	-11
3	9	-9	-7	23	23	1	6	6	-2	11	12	8	7	9	1	23	-23	6	0	5	-10	84	-88				-7	5	10
4	36	-34	-6	5	5	2	27	-24	-1	35	35	9	25	-30	3	13	11	7	17	20	-9	23	-25	K= 4 L= 9			-6	34	-33
5	27	-26	-5	7	4	3	4	4	0	5	2				4	23	21				-8	33	-33	-1	5	5	-5	12	-10
6	45	41	-4	16	-15	4	11	-12	1	14	15	K= 1 L= 4			5	23	21	K= 3 L= 6			-7	127	-130	0	32	32	-4	6	8
7	7	7	-3	9	-10							-12	28	-30	6	29	27	-2	10	-10	-6	36	-37	1	18	25	-3	10	-12
8	8	8	-2	28	22	K=10 L= 1			K=10 L= 2			-11	6	-9	7	23	23	-1	20	-18	-5	58	53				-2	30	35
			-1	20	13	-2	6	6	-1	38	40	-10	0	0	8	5	6	0	32	31	-4	34	34	K= 5 L= 9					
K= 8 L= 0			0	9	-12	-1	13	14	0	26	-24	-9	59	55				1	7	9	-3	4	3	-1	34	-33			
0	52	49	1	19	-21	0	20	-18				-8	19	19	K= 3 L= 5						-2	54	52	0	48	-46			

a) $F_{ND}(000) = 24.683$ cm^{-12} cell^{-1}. b) Extinction corrections have been applied.

TABLE 3. FINAL POSITIONAL PARAMETERS (10^4x_j) AND THERMAL PARAMETERS ($10^2B_{ij}/Å^2$) IN THE LOW-TEMPERATURE PHASE OF $SnCl_2 \cdot 2D_2O$

Estimated standard deviations are given in parentheses. The anisotropic thermal factors are of the form: $T=\exp[-1/4(h^2a^{*2}B_{11}+\cdots+2klb^*c^*B_{23})]$.

	x	y	z	B_{11}	B_{22}	B_{33}	B_{12}	B_{13}	B_{23}
Sn	3773 (3)	2565 (4)	5335 (3)	16 (8)	54 (9)	36 (7)	3 (9)	23 (6)	13 (9)
Cl (1)	2830 (2)	4899 (3)	6836 (2)	73 (6)	62 (6)	53 (5)	2 (7)	39 (5)	−6 (6)
Cl (2)	3071 (2)	5008 (3)	3043 (2)	50 (5)	59 (6)	58 (5)	−2 (6)	34 (5)	12 (6)
O (1)	1096 (4)	1685 (5)	4156 (4)	54 (9)	78 (10)	41 (8)	−27 (11)	26 (8)	8 (11)
O (2)	−683 (4)	2058 (5)	5931 (4)	56 (9)	62 (9)	59 (9)	0 (12)	35 (8)	−7 (10)
D (1)	—	—	—	—	—	—	—	—	—
D (2)	1014 (4)	331 (5)	4056 (4)	120 (11)	81 (10)	149 (11)	−9 (12)	82 (9)	−21 (12)
D (3)	—	—	—	—	—	—	—	—	—
D (4)	502 (4)	2004 (6)	4847 (4)	131 (11)	147 (12)	141 (11)	−26 (14)	95 (10)	−10 (13)
D (5)	−117 (5)	2509 (7)	7022 (5)	198 (14)	199 (15)	134 (11)	8 (15)	67 (11)	−39 (14)
D (6)	—	—	—	—	—	—	—	—	—
D (7)	−1550 (5)	2907 (7)	5399 (5)	106 (11)	154 (13)	218 (13)	63 (15)	8 (11)	2 (15)

refinement was $\Sigma w(|F_o|-|F_c|)^2$, with a unit weight for all reflections. The final $R[=\Sigma||F_o|-|F_c||/\Sigma|F_o|]$ was 0.081 for all reflections and 0.078 for non-zero reflections. The final F_c and F_o, with the extinction corrections, are given in Table 2. The final positional and thermal parameters are listed in Table 3, where the anisotropic temperature factors are shown in Å^2 for comparison with the isotropic ones at 297 K.

Structure at 297 K by ND. The difference Fourier projections of the nuclear-scattering density along the a and c axes and [101] direction were calculated using the heavy-atom positions from the X-ray study.[4] The maps revealed that the four deuterons scatter in seven sites of the asymmetric unit, providing direct evidence for the disordering of deuteron positions in the high-temperature phase. Moreover, the heights of the deuteron peaks were considerably different from one another. Accordingly, the occupancy factors of the individual deuteron sites should be adjusted as well as the positional and thermal parameters in the least-squares refinement.

A full-matrix least-squares refinement based on 311

TABLE 4. OBSERVED AND CALCULATED STRUCTURE AMPLITUDES(10^2F) FOR $SnCl_2 \cdot 2D_2O$ AT 297 K BY NEUTRON DIFFRACTION[a,b]

H	K	L	FO	FC	H	K	L	FO	FC	H	K	L	FO	FC	H	K	L	FO	FC	H	K	L	FO	FC	H	K	L	FO	FC
0	1	1	71	-64	0	5	8	82	-124	-9	0	2	157	171	-5	0	6	60	81	-3	0	12	394	-367	6	4	-6	118	102
0	1	2	223	-169	0	5	9	170	-152	-8	0	2	570	605	-4	0	6	362	366	-2	0	12	112	-121	6	5	-6	0	101
0	1	3	531	-532	0	5	10	0	-21	-7	0	2	438	-447	-3	0	6	526	526	1	1	-1	266	-251	6	6	-6	0	-8
0	1	4	410	-375	0	6	0	295	314	-6	0	2	0	-48	-2	0	6	537	-517	1	2	-1	179	204	6	7	-6	127	-142
0	1	5	800	806	0	6	1	213	-185	-5	0	2	328	319	-1	0	6	379	-347	1	3	-1	146	152	6	8	-6	0	23
0	1	6	98	-101	0	6	2	388	-360	-4	0	2	963	-1141	0	0	6	50	41	1	4	-1	220	-232	7	1	-7	173	-184
0	1	7	136	-132	0	6	3	70	-37	-3	0	2	978	-1207	1	0	6	370	-350	1	5	-1	292	-308	7	2	-7	0	-25
0	1	8	201	-195	0	6	4	109	-141	-2	0	2	366	-327	2	0	6	92	-80	1	6	-1	147	127	7	3	-7	306	-284
0	1	9	152	-161	0	6	5	120	-128	-1	0	2	49	-26	3	0	6	402	334	1	7	-1	108	111	7	4	-7	120	95
0	1	10	102	-91	0	6	6	81	39	0	0	2	183	158	4	0	6	420	387	1	8	-1	107	94	7	5	-7	175	-186
0	1	11	67	48	0	6	7	175	-177	1	0	2	714	746	5	0	6	124	130	1	9	-1	78	-108	7	6	-7	0	-50
0	2	0	307	-270	0	6	8	220	-186	2	0	2	1044	1257	6	0	6	117	164	1	10	-1	52	-59	7	7	-7	88	-126
0	2	1	154	-151	0	6	9	0	3	3	0	2	246	252	7	0	6	411	414	2	1	-2	351	323	8	1	-8	300	328
0	2	2	811	-944	0	7	1	213	248	4	0	2	167	-146	-12	0	8	180	185	2	2	-2	725	822	8	2	-8	330	321
0	2	3	54	-113	0	7	2	179	169	5	0	2	441	414	-11	0	8	129	170	2	3	-2	388	-396	8	3	-8	168	-142
0	2	4	235	-230	0	7	3	438	-426	6	0	2	185	-180	-10	0	8	331	-323	2	4	-2	123	121	8	4	-8	142	161
0	2	5	132	-155	0	7	4	283	303	7	0	2	162	-232	-9	0	8	0	5	2	5	-2	154	190	8	5	-8	87	133
0	2	6	165	234	0	7	5	281	283	8	0	2	170	179	-8	0	8	97	-94	2	6	-2	368	351	8	6	-8	71	110
0	2	7	107	-132	0	7	6	62	73	9	0	2	56	-56	-7	0	8	666	-638	2	7	-2	311	-328	8	7	-8	0	57
0	2	8	229	-229	0	7	7	159	-169	10	0	2	56	32	-6	0	8	134	-142	2	8	-2	205	240	9	1	-9	0	-12
0	2	9	0	17	0	7	8	0	43	11	0	2	0	73	-5	0	8	312	341	2	9	-2	0	-31	9	2	-9	67	-78
0	2	10	157	178	0	8	0	223	256	-13	0	4	0	97	-4	0	8	183	243	2	10	-2	123	130	9	3	-9	141	-148
0	2	11	0	7	0	8	1	105	-99	-12	0	4	260	-280	-3	0	8	0	92	3	1	-3	191	-173	9	4	-9	157	139
0	3	1	461	458	0	8	2	260	-267	-11	0	4	0	-28	-2	0	8	409	404	3	2	-3	125	-171	9	5	-9	68	55
0	3	2	202	181	0	8	3	125	-160	-10	0	4	73	12	-1	0	8	414	363	3	3	-3	519	-534	10	1	-10	50	-76
0	3	3	630	-624	0	8	4	172	185	-9	0	4	177	-175	0	0	8	580	-528	3	4	-3	73	41	10	2	-10	370	390
0	3	4	437	438	0	8	5	86	61	-8	0	4	0	-6	1	0	8	281	-247	3	5	-3	153	-145	10	3	-10	0	20
0	3	5	482	436	0	8	6	247	270	-7	0	4	397	416	2	0	8	168	170	3	6	-3	190	-217	10	4	-10	79	64
0	3	6	55	91	0	8	7	168	149	-6	0	4	773	779	3	0	8	564	-517	3	7	-3	324	-339	8	1	0	75	31
0	3	7	365	-305	0	9	1	152	128	-5	0	4	261	255	4	0	8	260	-266	3	8	-3	40	-70	9	1	0	113	-119
0	3	8	116	157	0	9	2	0	9	-4	0	4	149	141	5	0	8	187	200	3	9	-3	148	-150	7	1	1	475	427
0	3	9	58	71	0	9	3	143	-127	-3	0	4	157	143	-11	0	10	0	-12	4	1	-4	405	-439	8	1	1	87	-152
0	3	10	105	71	0	9	4	60	36	-2	0	4	734	-796	-10	0	10	185	190	4	2	-4	85	106	7	1	2	268	277
0	3	11	271	268	0	9	5	134	113	-1	0	4	457	-463	-9	0	10	47	-40	4	3	-4	299	340	8	1	2	163	136
0	4	0	951	1263	0	10	0	196	225	0	0	4	96	89	-8	0	10	565	-522	4	4	-4	35	82	6	1	3	0	5
0	4	1	78	51	0	10	1	0	-70	1	0	4	0	29	-7	0	10	80	-126	4	5	-4	246	-247	7	1	3	159	-201
0	4	2	190	-201	0	10	2	141	-129	2	0	4	664	601	-6	0	10	133	-152	4	6	-4	66	81	5	1	4	367	-342
0	4	3	99	82	1	0	0	621	803	3	0	4	419	369	-5	0	10	763	-713	4	7	-4	125	141	6	1	4	351	-305
0	4	4	242	254	2	0	0	0	-21	4	0	4	95	138	-4	0	10	57	53	4	8	-4	52	50	4	1	5	48	-42
0	4	5	224	211	3	0	0	658	681	5	0	4	374	362	-3	0	10	409	412	4	9	-4	0	34	5	1	5	510	-479
0	4	6	338	321	4	0	0	357	-324	6	0	4	61	-121	-2	0	10	0	-41	5	1	-5	758	-779	3	1	6	81	-74
0	4	7	136	139	5	0	0	781	-802	7	0	4	132	-174	-1	0	10	305	294	5	2	-5	152	206	4	1	6	71	29
0	4	8	416	-401	6	0	0	156	-142	8	0	4	0	12	0	0	10	502	452	5	3	-5	455	-484	1	1	7	232	223
0	4	9	0	41	7	0	0	139	140	9	0	4	120	-141	1	0	10	168	156	5	4	-5	226	-242	2	1	7	350	335
0	4	10	228	188	8	0	0	172	-184	-13	0	6	0	-53	2	0	10	0	-2	5	5	-5	447	-460	3	1	7	0	-11
0	5	1	28	-67	9	0	0	290	-281	-12	0	6	0	-6	3	0	10	0	22	5	6	-5	215	239	-2	1	8	36	75
0	5	2	193	-184	10	0	0	155	179	-11	0	6	0	-8	-9	0	12	203	215	5	7	-5	270	-286	-1	1	-8	-0	42
0	5	3	337	-331	11	0	0	0	-19	-10	0	6	376	-371	-8	0	12	66	96	5	8	-5	147	-161	1	1	8	127	102
0	5	4	205	-220	12	0	0	217	-252	-9	0	6	293	-307	-7	0	12	148	-179	5	9	-5	107	-144	2	1	8	55	26
0	5	5	505	485	-12	0	2	100	143	-8	0	6	391	-383	-6	0	12	209	-229	6	1	-6	92	-64	-2	1	9	193	-194
0	5	6	161	-169	-11	0	2	145	147	-7	0	6	237	-289	-5	0	12	215	-246	6	2	-6	79	-77	-1	1	9	126	-158
0	5	7	70	-92	-10	0	2	315	-369	-6	0	6	295	294	-4	0	12	234	-254	6	3	-6	0	-22					

a) $F_{ND}(000)=24.683$ cm^{-12} cell^{-1}. b) Extinction corrections have been applied.

independent reflections (obtained by use of the S1 sample) was initiated with the heavy-atom positions from the X-ray study[4] and the deuteron positions postulated just above. In the early stage of the refinement, the occupancy factors of the deuteron positions were fixed at values of 1/3, 2/3, 1/3, 2/3, 1/3, 2/3, and 1.0 for D(1), D(2),···, D(7) in the same order, according to the suggestion from the DMR study.[2,3] After the stage of $R=0.121$, several kinds of full-matrix least-squares refinements were carried out under appropriate constraints, because of the occupancy factors strongly correlate with the temperature factors; these were labeled A, B, C, D, and E as follows.

Refinement A: All the occupancy and temperature factors for the deuteron positions were refined at the same time with no constraint.

Refinement B: The sum of the occupancy factors of the two deuteron positions in each H-bond was fixed at unity.

Refinement C: The occupancy and temperature factors of deuteron were refined alternately every four cycles. This procedure yielded the lowest R_0 (R for non-zero reflections), the minimum standard deviation of observation, and the uniform temperature factors.

Refinement D: The occupancy and temperature factors were varied in alternate cycles. All the occupancy factors were adjusted after every cycle of their refinement

Table 5. Final positional parameters (10^4x_j), thermal parameters ($10^2B/Å^2$), and site occupancy factors (W) in the high-temperature phase at 297 K
Estimated standard deviations are given in parentheses. The isotropic temperature factors are of the form: $T=\exp(-B\sin^2\theta/\lambda^2)$.

	W	x	y	z	B
Sn	1.0	3756(7)	2591(14)	5353(7)	224(12)
Cl(1)	1.0	2870(5)	4906(11)	6887(5)	277(9)
Cl(2)	1.0	3076(6)	4986(15)	3051(5)	267(8)
O(1)	1.0	1129(17)	1764(13)	4134(12)	263(16)
O(2)	1.0	−665(12)	2042(14)	5978(10)	228(15)
D(1)	0.38(3)	−913(46)	887(33)	5959(35)	301(46)
D(2)	0.66(4)	1084(32)	349(21)	4062(22)	345(27)
D(3)	0.34(3)	−136(26)	2342(41)	5344(24)	264(36)
D(4)	0.70(3)	544(15)	2024(20)	4819(14)	325(21)
D(5)	0.21(3)	−250(44)	2409(51)	6893(38)	195(47)
D(6)	0.79(4)	477(12)	2246(17)	2982(12)	298(20)
D(7)	0.93(4)	−1494(18)	2882(25)	5457(16)	496(27)

Table 6. Occupancy(W_j) and isotropic temperature factors ($B_j/Å^2$) in $SnCl_2 \cdot 2D_2O$ at 297 K, obtained by various least-squares refinements[a]

Refinement	A	B	C	D	E
Conditions of least-squares refinement	No constraint	Sum of deueron occupancies on each H-bond is constrained to unity	Refinements of occupancy and thermal factor for each deuteron position alternate every four cycles	Adjusted in every cycle, as each oxygen atoms has a total of two deuterons (B and W are refined alternately)	Constrained as each H-bond has one deuteron and each oxygen has two deuterons (B+D)
W_1	0.38(6)	0.29 [$=1.0-W_2$]	0.38(3)	0.44(4)	0.57 [$=W_4+W_6-1.0$]
W_2	0.64(6)	0.71(5)	0.66(4)	0.60(3)	0.43 [$=2.0-W_4-W_6$]
W_3	0.32(6)	0.25 [$=1.0-W_4$]	0.34(3)	0.36(3)	0.27 [$=1.0-W_4$]
W_4	0.65(6)	0.75(5)	0.70(3)	0.65(3)	0.73(5)
W_5	0.12(4)	0.18 [$=1.0-W_6$]	0.21(3)	0.22(3)	0.16 [$=1.0-W_6$]
W_6	0.81(6)	0.82(4)	0.79(4)	0.75(4)	0.84(5)
W_7	1.01(8)	1.0	0.93(4)	0.98(5)	1.0
B_1	2.7(9)	1.7(4)	3.0(5)	4.6(6)	6.0(6)
B_2	3.3(5)	3.8(4)	3.5(3)	2.9(3)	1.5(3)
B_3	2.8(8)	1.7(4)	2.6(4)	3.0(4)	2.1(4)
B_4	2.9(4)	3.5(3)	3.3(2)	3.0(2)	3.4(4)
B_5	0.5(12)	1.5(5)	2.0(5)	2.3(5)	1.3(6)
B_6	2.7(3)	3.2(3)	3.0(2)	2.9(2)	3.3(3)
B_7	5.1(5)	5.3(3)	5.0(3)	5.3(3)	5.3(3)
W_1+W_2	1.02(9)	1.0	1.04(5)	1.04(5)	1.0
W_3+W_4	0.97(9)	1.0	1.04(5)	1.01(5)	1.0
W_5+W_6	0.93(9)	1.0	1.00(5)	0.97(5)	1.0
$W_1+W_3+W_5+W_7$	1.83(12)	1.72(8)	1.86(7)	2.0	2.0
$W_2+W_4+W_6$	2.10(10)	2.28(9)	2.15(6)	2.0	2.0
Total of W_j	3.93(16)	4.0	4.01(9)	4.0	4.0
R_0-value	0.108	0.097	0.096	0.096	0.099
STD of obs.[b]	2.25	1.54	1.51	1.52	1.58
NV[c]	56	52	50	50	51
Overall B	not refined	not refined	refined	refined	not refined

a) E.s.d.'s in parentheses are in units of the last significant digit. b) Standard deviation of observation as defined by $\sqrt{w(F_o-F_c)^2/(NO-NV)}$ (NO: Number of observations). c) NV: Number of variable parameters.

TABLE 7. POSITIONAL PARAMETERS (10^4x_j) AND THERMAL PARAMETERS (10^2B_{ij}/Å^2) AT VARIOUS TEMPERATURES[a)]

Temp (Method)		88 K (N.D.)	209 K (X-Ray)	223 K (X-Ray)	293 K (X-Ray)
Sn	x	3773(3)	3763(1)	3754(1)	3744(1)
	y	2565(4)	2568(1)	2575(1)	2599(1)
	z	5335(3)	5347(1)	5347(1)	5359(1)
	B_{11}	16(8)	182(2)	198(1)	232(2)
	B_{22}	54(9)	124(2)	151(1)	204(2)
	B_{33}	36(7)	168(2)	181(1)	218(2)
	B_{12}	3(9)	9(2)	10(1)	15(1)
	B_{13}	23(6)	77(2)	69(1)	79(1)
	B_{23}	13(9)	6(2)	10(1)	14(1)
Cl(1)	x	2830(2)	2841(3)	2849(2)	2864(2)
	y	4899(3)	4899(3)	4907(2)	4915(3)
	z	6836(2)	6857(3)	6859(2)	6874(2)
	B_{11}	73(6)	270(8)	291(6)	359(8)
	B_{22}	62(6)	158(7)	191(5)	272(7)
	B_{33}	53(5)	215(7)	230(5)	278(7)
	B_{12}	2(7)	−3(6)	−3(4)	−7(6)
	B_{13}	39(5)	124(6)	121(5)	148(6)
	B_{23}	−6(6)	−33(6)	−29(4)	−41(6)
Cl(2)	x	3071(2)	3067(2)	3063(2)	3062(2)
	y	5008(3)	4999(3)	4996(2)	4992(3)
	z	3043(2)	3053(3)	3045(2)	3051(2)
	B_{11}	50(5)	226(7)	237(5)	277(6)
	B_{22}	59(6)	148(6)	188(5)	256(6)
	B_{33}	58(5)	170(7)	200(5)	242(6)
	B_{12}	−2(6)	−4(6)	−4(4)	−5(5)
	B_{13}	34(5)	86(6)	81(4)	88(5)
	B_{23}	12(6)	33(5)	35(4)	50(5)
O(1)	x	1096(4)	1091(7)	1091(5)	1095(6)
	y	1685(5)	1713(8)	1741(4)	1757(7)
	z	4156(4)	4148(9)	4139(6)	4129(6)
	B_{11}	54(9)	212(22)	219(15)	242(19)
	B_{22}	78(10)	135(20)	176(15)	234(19)
	B_{33}	41(8)	165(21)	177(14)	217(18)
	B_{12}	−27(11)	−21(17)	−22(12)	−39(16)
	B_{13}	26(8)	86(17)	73(12)	78(15)
	B_{23}	8(11)	−14(16)	−2(12)	−9(15)
O(2)	x	−683(4)	−678(7)	−671(5)	−674(6)
	y	2058(5)	2053(8)	2065(5)	2067(8)
	z	5931(4)	5956(10)	5960(7)	5984(7)
	B_{11}	56(9)	207(22)	229(16)	278(21)
	B_{22}	62(9)	143(21)	173(15)	250(21)
	B_{33}	59(9)	246(24)	249(16)	300(22)
	B_{12}	0(12)	16(18)	24(13)	37(17)
	B_{13}	35(8)	95(19)	87(14)	92(18)
	B_{23}	−7(10)	3(18)	−1(13)	2(18)

a) Estimated standard deviations are given in parentheses. The anisotropic thermal factors are given by the same expression as in Table 3.

in such a way that an oxygen atom always has a total of two nearest deuterons to constitute a water molecule.

Refinement E: The strong constraint of so-called ice rules was imposed on the refinement. Since each oxygen has a total of two nearest deuterons, and since each H-bond involves one deuteron, only two occupancy factors, such as D(4)'s and D(6)'s, need to be refined. This refinement converged only slightly, and it was far from satisfactory (see Table 6).

No positional parameters of any of the atoms differed by more than their associated e.s.d.'s among these refinements. Therefore, only the final F_c, the F_o after the extinction correction, and the final positional parameters in the C refinement are presented in Tables 4 and 5. The occupancy factor, W_j, and the isotropic temperature factor, B_j, for the j-th deuteron position are compared in Table 6. The extinction correction described above was made before any refinement, and the weighting scheme used throughout the refinement was

$$w = I_o/I_e, \quad \text{if } I_o > 4I_{min},$$
$$w = (I_o+I_{min})/5I_{min}, \quad \text{if } I_o < 4I_{min},$$

where I_o and I_e were the integrated intensities before and after the extinction correction respectively, and where I_{min} was the averaged background intensity. The quantity minimized in all least-squares refinements was $\Sigma w(|F_o|-|F_c|)^2$.

Structure at 209 and 223 K by X-Ray Diffraction. The procedure used was almost the same as in the previous study.[4] The structure was refined by a block-diagonal least-squares method, with 1582 and 1589 independent reflections at 209 and 223 K respectively. For comparison, the structure at 293 K was refined again including anomalous dispersion corrections for Sn and Cl. In these calculations, the atomic scattering factors for Sn^{2+}, Cl^-, and O^- and anomalous dispersion corrections, f' and f'' for Sn and Cl were taken from the International Tables for X-Ray Crystallography, Vol. IV.[14] The values of R and R_0 at each temperature are [given as T/K, R, R_0]: 209, 0.053, 0.047; 223, 0.045, 0.038; and 293, 0.045, 0.043. The final positional and thermal parameters at 209, 223, and 293 K are summarized in Table 7, together with those at 88 K obtained from the neutron study. A list of the observed and calculated structure factors at 209 and 223 K has been deposited with the Chemical Society of Japan (Document No. 7723).

Computation. All the computations in this study were made on the NEAC 2200/700 at the Computer Center, Osaka University, using local modifications of the RSFLS, RSSFR-5, HBLS-V, and RSDA-4 in the UNICS program system[15] and the stereoscopic drawing program ORTEP.[16]

Results and Discussion

Crystal Structure Except for Hydrogens. The crystal contains two kinds of water molecules. The first, $H_2O(1)$, is coordinated to a tin atom to form a trigonal pyramidal dichloroaquatin(II) comples, $SnCl_2 \cdot OH_2$, whereas the second, $H_2O(2)$, does not. These two are H-bonded to each other to construct a puckered water-layer, which extends along the (100) plane. Tin and Cl atoms form double layers parallel to (100), also. Between these Cl/Sn double layers, the water layer intervenes (Fig. 2).

The Sn–Cl(2) bond length is significantly longer (by 0.06 Å) than Sn–Cl(1). This is consistent with the facts that Cl(2) is close to two Sn atoms of different pyramids

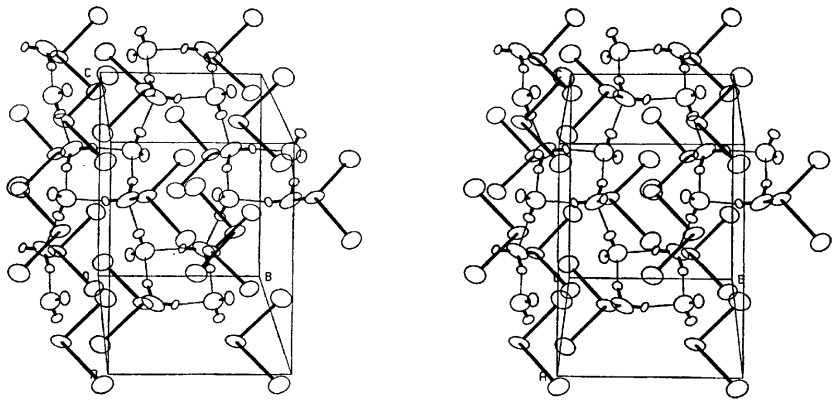

Fig. 2. View of the whole cell in $SnCl_2 \cdot 2D_2O$ determined by ND at 88 K. The c axis is vertical and the b axis is horizontal on the page.

at distances of 3.22 and 3.33 Å, while Cl(1) has two Sn neighbors with much longer separations of 3.41 and 3.65 Å. Such a difference in the nature of the chemical bonds should reflect on the quadrupole resonance (NQR) frequences of the ^{35}Cl nuclei. Recently Trontelj and Pirnat have detected two NQR frequencies of 8.656 and 8.511 MHz at 300 K.[17] The former can be assigned to Cl(1), and the latter, to Cl(2), because Cl(1) is less ionic than Cl(2) in view of the interatomic distances. Further details with regard to the arrangement of non-hydrogen atoms have already been described in a previous paper.[4]

Hydrogen-ordered Structure at 88 K. The positions and site-occupancy factors of hydrogen atoms are of much interest, because they play a dominant role in the phase transition. The unit cell of the hydrogen-ordered structure is shown in Fig. 2; it was determined by neutron diffraction at 88 K. It was confirmed from these results that the configuration of $D_2O(1)$ is Type H, while that of $D_2O(2)$ is Type E, according to the classification of Chidambaram *et al.*[18] In the former, one of the lone pairs of oxygen O(1) is directed toward a tin atom, and the other, toward an H-bond-donor oxygen O(2). On the other hand, two lone pairs of oxygen O(2) are directed toward two H-bond-donor oxygens, O(1) and $O(1^{iii})$. Thus, the three deuterons, D(2) and D(4) of the coordinated water molecule and D(5) of the non-coordinated one, form three normal O–D···O hydrogen bonds. The remaining one, D(7), of $D_2O(2)$ does not participate in any H-bond, but is directed toward one Cl atom rather than two; the separations of $D(7)\cdots Cl(1^{iv})$ and $D(7)\cdots Cl(2^{iv})$ are 2.43 and 2.78 Å respectively at 88 K. These ordered, non-centric hydrogen positions are consistent with our PMR and DMR results.[2,3]

Mognaschi *et al.* have revealed, from their dielectric measurement, that a weak but significant, antiferroelectric interaction develops between the H-bonded

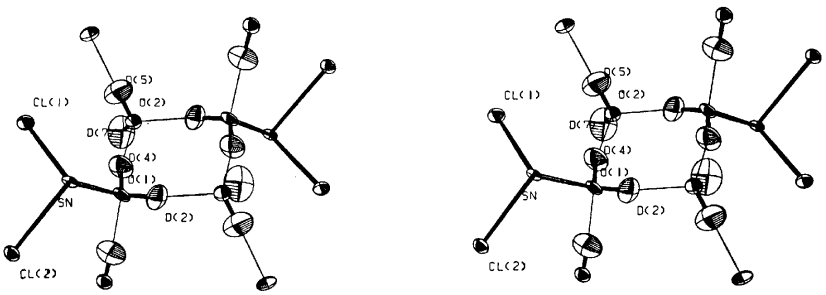

Fig. 3. Stereoscopic drawings of the ordered-arrangement of deuterons with thermal ellipsoids at 50% probability.

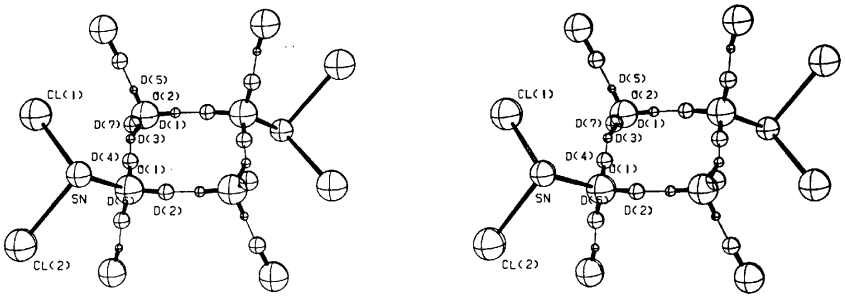

Fig. 4. Stereoscopic view of the disordered-arrangement of deuterons at 297 K. Each occupancy factor given in Table 5 is represented by a size of sphere.

water layers, in addition to the ferroelectric interaction within the layer, as the temperature approaches T_t very closely.[8] They explained the anomalous behavior of the dielectric constant and of the spin-lattice relaxation rate of protons near T_t in terms of a "critical slowing down" of the electric polarization, as in many ferroelectric and antiferroelectric substances. However, as has been described earlier, our examinations by both X-ray and neutron-diffraction methods showed that no superstructure reflection indicating the doubling of [100] or any lowering of the crystal symmetry appears in the low-temperature phase.

Hydrogen-disordered Structure at 297 K. This compound undergoes the phase transition at 218 K (the deuterated analogue does at 234 K), above which the reorientation rates of both water molecules are high enough to affect the NMR spectra. The deuteron arrangements in the H-bonded layer at 88 and 297 K are compared in Figs. 3 and 4.

In the high-temperature phase, two deuterons of $D_2O(1)$ are distributed among three sites, D(2), D(4), and D(6). In contrast with this, only one deuteron of $D_2O(2)$ is dispersed among the D(1), D(3), and D(5) sites, while the other remains at the fixed position of D(7). This striking feature, together with the DMR results,[3] suggests that $D_2O(1)$ and $D_2O(2)$ reorient about Sn–O(1) and O(2)–D(7) bonds respectively, with a nearly three-fold symmetry. If this is the case, the deuteron occupancy factors, W_j, would be 2/3 for D(2), D(4), D(6), and 1/3 for D(1), D(3), D(5). The ND results of the various least-squares refinements given in Table 6 are in fair agreement with the above picture, at least in regard to W_1, W_2, W_3, W_4, and W_7.

It is noteworthy, however, that the occupancy factors, W_5 and W_6, deviate from the expected values by more than three times their e.s.d.'s in all the refinements. This indicates that the H-bond involving D(5) and D(6) is closely associated with the phase transition, as was suggested in a previous paper.[11] Salinas and Nagle have calculated, using statistical mechanics, the site occupancy of D(5) as a function of the temperature and have pointed out that its value should be less than 1/3 at high temperatures ($\lim_{T\to\infty} W_5=0.119$).[9] At room temperature, the theoretical value of W_5 is 0.34, which is larger by 0.1 than the experimental one (0.21 in the C refinement). However, in view of the approximation of the theory and the uncertainty in the experimental occupancy factor, the agreement between these values seems satisfactory. In summary, it may be said that the ND results support the mechanism of the phase transition proposed by Salinas and Nagle.

The results of the least-squares refinements show that each oxygen atom has a total of approximately two deuteron neighbors and that the sum of the two occupancy factors on each H-bond amounts to unity. It can, therefore, be concluded that Bernal and Fowler's ice rules are obeyed in this two-dimensional H-bonded network; hence, scarcely no partial dossociation water molecules occurs.[11]

The bond angle of $D_2O(1)$ in the low-temperature phase is typical of a water molecule of crystallization, in spite of a considerably narrow acceptor-angle, O(2)···

TABLE 8. BOND DISTANCES (l/Å) AND ANGLES (θ/°) DETERMINED BY NEUTRON DIFFRACTION

	88 K	297 K
(a) Water molecules		
O(1)–D(2)	0.973(5)	1.036(18)
O(1)–D(4)	1.004(6)	1.005(22)
O(1)–D(6)		1.011(13)
O(2)–D(1)		0.860(26)
O(2)–D(3)		0.929(32)
O(2)–D(5)	0.952(5)	0.790(35)
O(2)–D(7)	0.955(5)	0.925(19)
Sn–O(1)–D(2)	109.8(3)	106.5(17)
Sn–O(1)–D(4)	113.5(3)	114.2(9)
Sn–O(1)–D(6)		117.0(13)
D(2)–O(1)–D(4)	104.0(5)	102.7(22)
D(2)–O(1)–D(6)		107.5(14)
D(4)–O(1)–D(6)		107.8(16)
D(1)–O(2)–D(3)		115.0(35)
D(1)–O(2)–D(5)		110.1(36)
D(1)–O(2)–D(7)		119.7(27)
D(3)–O(2)–D(5)		113.7(39)
D(3)–O(2)–D(7)		94.6(22)
D(5)–O(2)–D(7)	106.4(5)	102.6(33)
(b) Aquacomplex $SnCl_2\cdot OH_2$		
Sn–Cl(1)	2.510(4)	2.530(11)
Sn–Cl(2)	2.565(4)	2.559(12)
Sn–O(1)	2.318(4)	2.323(16)
Cl(1)–Sn–Cl(2)	86.9(1)	87.8(4)
Cl(1)–Sn–O(1)	83.7(1)	84.0(4)
Cl(2)–Sn–O(1)	87.4(1)	86.4(4)
(c) Hydrogen bonds		
O(1)···O(2^{i}) ($=d_{12}$)	2.702(5)	2.781(14)
O(1)···O(2) ($=d_{34}$)	2.718(6)	2.805(20)
O(1)···O(2^{ii}) ($=d_{56}$)	2.808(4)	2.751(13)
O(2)···O(1)···O(2^{i})	90.2(2)	88.2(5)
O(2)···O(1)···O(2^{ii})	109.6(2)	109.4(6)
O(2^{i})···O(1)···O(2^{ii})	105.9(1)	105.1(4)
O(1)···O(2)···O(1^{i})	89.8(2)	91.8(5)
O(1)···O(2)···O(1^{iii})	113.5(2)	112.1(6)
O(1^{i})···O(2)···O(1^{iii})	111.2(2)	111.5(4)
D(1)···O(1)		1.928(24)
D(2)···O(2)	1.737(5)	1.763(19)
D(3)···O(1^{i})		1.949(34)
D(4)···O(2^{i})	1.730(6)	1.816(20)
D(5)···O(1^{iii})	1.857(5)	1.972(33)
D(6)···O(2^{ii})		1.741(13)
(d) Some interatomic distances		
D(7)···Cl(1^{iv})	2.427(5)	2.543(16)
D(7)···Cl(2^{iv})	2.777(5)	2.844(20)
O(2)···Cl(1^{iv})	3.271(4)	3.364(18)
O(2)···Cl(2^{iv})	3.420(5)	3.487(15)
Sn···Cl(2^{v})	3.162(4)	3.198(11)
Sn···Cl(1^{ii})	3.377(4)	3.384(10)
Sn···Cl(2^{iii})	3.310(4)	3.336(11)
Cl(1)···Cl(2^{v})	3.712(3)	3.761(8)

Symmetry code

none	x,	y,	z	iii	x, 1/2−y, 1/2+z
i	−x,	−y,	1−z	iv	−x, 1−y, 1−z
ii	x, 1/2−y,	−1/2+z		v	1−x, 1−y, 1−z

O(1)···O(2^{ii}) (90.2°). On the other hand, some H–O–H angles in the high-temperature phase deviate from the tetrahedral angle or the typical value of 105°, but these deviations are of no significance, because of the large number of refined parameters relative to the number of the intensity data. Some interatomic distances and angles based on the neutron data at 88 and 297 K are compared in Table 8.

Change in the Crystal Structure with the Temperature. In order to make clear whether or not the ordering of the hydrogen atoms is accompanied by any displacement of other atoms, especially in the vicinity of the transition point, T_t, the crystal structure was analyzed by means of X-ray diffraction at 209 and 223 K, a little below and above T_t.

The structures obtained at both temperatures were almost the same as those previously determined by X-rays at 293 K and by neutron diffraction at 88 K (Table 7), except, of course, for the hydrogen atoms. Only a slight, but, significant change was found in the H-bonded net work. The O···O distances of the three non-equivalent H-bonds vary with the temperature in complicated ways (Fig. 5). In Fig. 5 the H-bonds are designated as d_{12}, d_{34}, and d_{56}, according to the numbering of the deuterons (or protons) involved; the temperature dependence of an Sn···Cl separation between adjacent layers is also included for comparison. It is noteworthy again that the H-bond d_{56} differs from the other two in their features; the former distance decreases with an increase in the temperature, whereas those of the other two increase normally. As the temperature approaches T_t from below, these H-bond distances change drastically; one of them contracts and the others elongate, and then just above T_t all three become nearly equal. As a result, the volume change of the unit cell occurring at T_t is quite small, and the single crystal does not shatter nor become opaque on passing through the phase transition.

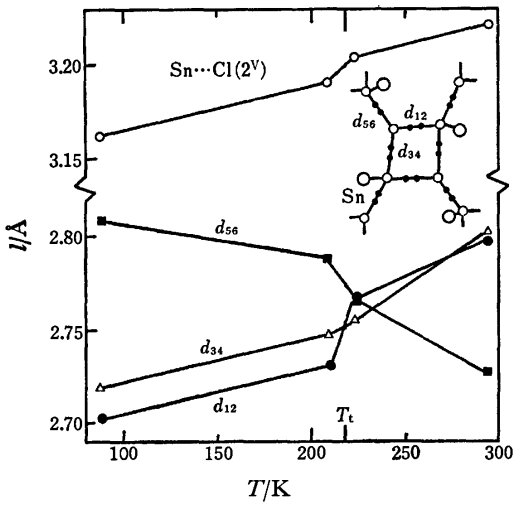

Fig. 5. Plot of three H-bonded O···O distances and an Sn···O distance against temperature. The results at 88 K come from ND, and the others from X-ray diffraction.

Thermal Expansion. The high-resolution heat-capacity measurements by Matsuo *et al.* showed that the phase transition is of a quasi-first-order type.[7] No hysteresis was detected on the curve of any lattice parameter or of the unit-cell volume near T_t, within ±0.5 K. The anomaly of the linear and volume expansion-coefficients extends over a much wider temperature range than that of the heat capacity. In particular, the volume expansion-coefficient swings in a complicated manner around the phase transition. Figure 6 shows the results deduced by numeric point-by-point differentiation from the lattice parameters at various temperatures. The remarkable elongation of the a-axis about T_t corresponds to an abrupt expansion of the separation between adjacent double layers of Cl and Sn atoms. The anomalous expansion-coefficient along the c-axis reflects the change in the $d_{34}+d_{56}$ with the temperature. On the other hand, the elongation of d_{12} is partly canceled by the contraction of d_{56}, resulting in a monotonic elongation along the b direction. A steep variation near T_t was also found in the monoclinic β angle.

The line profiles of all (h00) reflections checked by X-rays are often broadened in both 2θ-ω and ω scans in the low-temperature phase; their half-widths are more than twice the corresponding ones in the high-temperature phase. They can, however, be sharpened by annealing for 24 h 20 K below T_t.

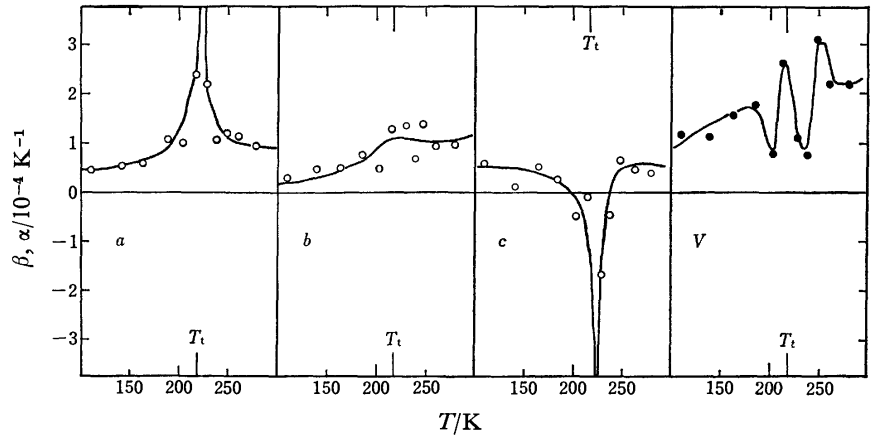

Fig. 6. Temperature dependences of thermal expansion-coefficents. Linear and volume expansion-coefficients are defined as $\beta = 1/l \cdot dl/dT$ and $\alpha = 1/V \cdot dV/dT$, respectively.

The authors are greatly indebted to Professor Iwao Shibuya for his guidance and assistance in this ND work at the Research Reactor Institute, Kyoto University. The authors are also grateful to Professor Emeritus Ryôiti Kiriyama for his continued interest and encouragement throughout the present study and to Dr. Takeshi Asai for his careful reading of the manuscript.

References

1) H. Kiriyama and R. Kiriyama, *J. Phys. Soc. Jpn.*, **28**, S114 (1970).
2) H. Kiriyama, O. Nakamura, and R. Kiriyama, *Acta Crystallogr., Sect. A*, **28**, S240 (1972).
3) H. Kiriyama, O. Nakamura, and R. Kiriyama, *Chem. Lett.*, **1976**, 689.
4) H. Kiriyama, K. Kitahama, O. Nakamura, and R. Kiriyama, *Bull. Chem. Soc. Jpn.*, **46**, 1389 (1973).
5) H. Morisaki, H. Kiriyama, and R. Kiriyama, *Chem. Lett.*, **1973**, 1061.
6) T. Matsuo, M. Oguni, H. Suga, and S. Seki, *Proc. Jpn. Acad.*, **48**, 237 (1972); T. Matsuo, M. Oguni, H. Suga, and S. Seki, *Bull. Chem. Soc. Jpn.*, **47**, 57 (1974).
7) T. Matsuo, M. Tatsumi, H. Suga, and S. Seki, *Solid State Commun.*, **13**, 1829 (1973).
8) E. Mognaschi, A. Rigamonti, and L. Menafra, *Phys. Rev. B*, **14**, 2005 (1976).
9) S. R. Salinas and J. F. Nagle, *Phys. Rev. B*, **9**, 4920 (1974).
10) S. R. Salinas and J. F. Nagle, *J. Phys. Soc. Jpn.*, **41**, 1643 (1976).
11) R. Kiriyama, H. Kiriyama, K. Kitahama, and O. Nakamura, *Chem. Lett.*, **1973**, 1105.
12) W. C. Hamilton, *Acta Crystallogr.*, **10**, 629 (1957).
13) Neutron Diffraction Commission, *Acta Crystallogr., Sect. A*, **25**, 391 (1969).
14) "International Tables for X-Ray Crystallography," Vol. IV, Kynoch Press, Birmingham (1974), pp. 71—98, 148—150.
15) T. Sakurai, Ed., "UNICS Program System," Crystallographic Society of Japan (1967).
16) C. K. Johnson, ORTEP, Oak Ridge National Laboratory Report ORNL-3794 (1965).
17) Z. Trontelj and J. Pirnat, *Proc. 2nd Intern. Symposium on NQR Spectroscopy*, Sept. 3—6 (1973), Viareggiv, Italy, ed by A. Colligiani, A Vallerini Publ., Pisa, pp. 191—205.
18) R. Chidambaram, A. Sequeira, and S. Sikka, *J. Chem. Phys.*, **41**, 3616 (1964).
19) B. Kamenar and D. Grdenić, *J. Chem. Soc.*, **1961**, 3954.

The Crystal and Molecular Structure of Dichloro [*N*, *N*-dimethyl-*α*-methyl-*o*-(butylphenylphosphino)benzylamine] palladium(II)

Akio TAKENAKA, Yoshio SASADA, Keiji YAMAMOTO, and Jiro TSUJI

Tokyo Institute of Technology, Ookayama, Meguro-ku, Tokyo 152

(Received June 30, 1977)

The crystal structure of dichloro[*N*,*N*-dimethyl-α-methyl-*o*-(butylphenylphosphino)benzylamine]palladium-(II) has been determined from Mo*K*α diffraction data. The space group is $P2_1$ with $Z=2$, $a=9.255(2)$, $b=14.372$ (3), $c=8.584(1)$ Å, and $\beta=105.99(1)°$. The final R became 0.034 by least-squares refinement. The Pd atom has a square planar coordination of N, P, and two Cl atoms, which is considerably distorted by the intramolecular atomic repulsions. The Pd–N distance, 2.134(4) Å, which is longer than those found so far, is accompanied by a short distance 2.285(1) Å of trans Pd–Cl. A plot of Pd–Cl distance *versus* trans Pd–N distance in several Pd complexes, in which the nitrogen atom is not π-acceptor, shows a linear relationship with the correlation factor of −0.28(4).

N,*N*-Dimethyl-α-methyl-*o*-(butylphenylphosphino)-benzylamine, $(C_6H_5)P(C_4H_9)C_6H_4CH(CH_3)N(CH_3)_2$, prepared from (*S*)-α-methylbenzylamine, is a diastereomeric bidentate ligand. The rhodium complexes with the optically resolved ligand catalyze hydrogenation of certain olefins; the preferred configuration of the products depends primarily upon the chirality of the ligand.[1] To determine the absolute configuration of the ligand, the title Pd complex was synthesized and its crystal structure was analyzed by the X-ray diffraction method.

Experimental

$Pd(C_6H_5CN)_2Cl_2$ (156 mg, 0.4 mmol) and $C_6H_5P(C_4H_9)C_6H_4CH(CH_3)N(CH_3)_2$ (124 mg, 0.4 mmol), a pure epimer, were dissolved in 15 ml of dry benzene. After 2 h stirring in N_2 atmosphere, deep yellow precipitates, 150 mg, were collected by filtration and recrystallized from a hexane–CH_2Cl_2 (1:2) solution. Calcd for $C_{20}H_{28}Cl_2NPPd$: C, 48.95; H, 5.75; N, 2.85%. Found: C, 48.41; H, 5.86; N, 2.84%; mp 196—197 °C (dec); $[\alpha]_D^{20}$ −202° (in CH_2Cl_2).

Table 1. Crystal data

$Pd[C_6H_5P(C_4H_9)C_6H_4CH(CH_3)N(CH_3)_2]Cl_2$	
F.W. 490.7	
Monoclinic, $P2_1$ (systematic absence $0k0$ $k=2n+1$)	
$a=9.255(2)$ Å	$Z=2$
$b=14.372(3)$	$D_m=1.48$ g cm^{-3} (by flotation)
$c=8.584(1)$	$D_x=1.485$ g cm^{-3}
$\beta=105.99(1)°$	μ (Mo*K*α) $=12.4$ cm^{-1}

A crystal, 0.15×0.3×0.5 mm in size, was used for data collection on a Rigaku computer-controlled four-circle diffractometer, using graphite-monochromated Mo*K*α radiation ($\lambda=0.71069$ Å). The cell parameters were obtained by least-squares calculation with 22 high-angle reflexions. The crystal data are summarized in Table 1. Intensities were measured in ω-2θ scan mode with scan width of 1.5° (in 2θ) plus α_1-α_2 divergence at scan speed 4° (in 2θ) min^{-1}, using a large receiving slit 5.5×5.5 mm. By this scan technique, intensity profile of each reflexion showed a single peak, although the specimen gave twinned spots on Weissenberg photographs owing to a crack within it. Five reference reflexions, monitored after every 50 reflexions, indicated no significant intensity variations throughout the experiment. Out of 2616 independent reflexions in the range $2\leq 2\theta\leq 55°$, 88 weak reflexions which gave the counts under background were considered as zero-reflexions. The data were corrected for Lorentz and polarization factors but not for absorption effects. Bijvoet pairs of reflexions were collected on Weissenberg photographs using Cu*K*α radiation.

Structure Determination

The structure was solved by the heavy-atom method and its atomic parameters were refined by block-diagonal least-squares technique. All the hydrogen atoms, found on a difference map, were included. The quantity minimized was $\Sigma w(|F_o|-|F_c|)^2$, with $w=1/(\sigma_p^2+qF_o^2)$, where σ_p is due to counting statistics and q is 1.02×10^{-5} derived from the variation of the monitored reflexions.[2] The zero-reflexions were included in least-squares calculation by assuming $F_o=F_{lim}$ and $w=w(F_{lim})$, where F_{lim} is 3.198, an observational threshold value, but those for which $|F_c|<F_{lim}$ were omitted. The final R value was 0.034; the maximum shift of coordinates in the last cycle was 0.10σ for Pd, Cl, and P, 0.15σ for N, 0.44σ for C, and 1σ for H atoms. The absolute configuration was determined from a comparison of intensities of 22 Bijvoet pairs. Atomic parameters are listed in Table 2.[3] A stereoscopic view of the molecule is shown in Fig. 1, and bond distances and angles in Fig. 2. Atomic scattering factors used were taken from International Tables for X-Ray Crystallography.[4]

Results and Discussion

As shown in Fig. 1, the Pd atom has a considerably distorted square planar coordination of the N, P, and two Cl atoms. The chlorine atoms are cis as required by the geometry of the bidentate chelating ligand. The absolute configuration of C(7) is sinister (*S*) and that of P is rectus (*R*). The methyl group C(9) and the butyl group are located above the coordination plane, while the methyl group C(8) lies below it. If the rhodium complexes[1] take the same structure, such an arrangement might furnish the structural basis for the mechanism of the asymmetric hydrogenation. When the prochiral substrate approaches Rh above or below the coordination plane to form a π-complex, the steric constraint could determine the preferable enantiotropic face of the substrate.

The two Pd–Cl bond distances differ significantly to

Table 2. Fractional coordinates ($\times 10^5$ except for H and $\times 10^4$ for H) and thermal parameters ($\times 10^5$ except for H)

The anisotropic temperature factor has the form: $\exp[-(\beta_{11}h^2+\beta_{22}k^2+\beta_{33}l^2+\beta_{12}hk+\beta_{13}hl+\beta_{23}kl)]$.

Standard deviations are given in parentheses.

	x	y	z	β_{11}	β_{22}	β_{33}	β_{12}	β_{13}	β_{23}
Pd	99449(4)	25000(5)	16950(3)	801(3)	520(2)	702(3)	112(8)	231(5)	−192(8)
Cl(1)	124579(13)	30288(12)	20426(15)	759(16)	861(11)	1260(20)	−139(22)	303(29)	−149(25)
Cl(2)	102713(14)	27693(10)	43939(12)	1181(17)	849(14)	593(14)	−87(22)	141(25)	−449(21)
P	75005(12)	23074(10)	15126(12)	758(14)	356(9)	598(13)	29(18)	185(22)	−87(18)
N	96901(39)	21581(29)	−7859(41)	871(52)	625(34)	984(57)	−13(62)	744(90)	−385(65)
C(1)	69109(49)	19602(35)	−18214(49)	973(67)	437(30)	747(65)	−135(75)	81(107)	−295(74)
C(2)	63386(44)	23003(35)	−5771(44)	866(55)	401(37)	685(54)	−157(73)	52(89)	72(72)
C(3)	48952(48)	26622(39)	−9506(50)	908(59)	447(41)	1105(64)	−60(79)	251(100)	222(86)
C(4)	39903(51)	27006(37)	−25415(58)	908(64)	470(44)	1547(79)	−248(77)	−622(113)	442(90)
C(5)	45535(53)	23563(50)	−37679(51)	1610(77)	508(40)	940(63)	−631(107)	−677(109)	148(98)
C(6)	59599(57)	20084(39)	−34239(52)	1477(84)	546(34)	754(68)	−321(88)	−107(122)	−304(81)
C(7)	84047(57)	15235(40)	−15367(52)	1429(84)	666(40)	694(69)	48(94)	544(123)	−639(86)
C(8)	85044(67)	5845(44)	−7573(69)	1935(109)	585(41)	1740(107)	353(112)	379(170)	−688(110)
C(9)	95094(67)	30608(49)	−16651(55)	2104(107)	973(49)	843(76)	−1146(120)	1254(150)	−109(104)
C(10)	110990(63)	16860(56)	−9063(69)	1338(94)	1304(64)	1673(105)	416(127)	1056(165)	−1365(139)
C(11)	69819(53)	12867(34)	24871(51)	1234(75)	319(28)	834(68)	−79(75)	470(116)	−271(72)
C(12)	80743(65)	7578(39)	35680(63)	1808(98)	408(34)	1450(94)	311(94)	645(154)	251(92)
C(13)	76495(76)	222(44)	43787(70)	2944(142)	458(38)	1866(114)	513(122)	1915(208)	347(113)
C(14)	61718(86)	−1653(44)	41526(75)	3944(179)	420(37)	1848(117)	−518(133)	2902(245)	−82(108)
C(15)	50856(70)	3288(47)	30864(68)	2515(128)	634(41)	1855(111)	−1180(130)	1847(196)	−377(118)
C(16)	54883(62)	10662(41)	22585(62)	1532(90)	541(38)	1293(88)	−241(95)	596(142)	172(94)
C(17)	67935(49)	32689(35)	24650(50)	881(65)	412(30)	882(67)	−16(73)	547(108)	−159(75)
C(18)	69954(60)	42268(37)	17770(63)	1440(85)	386(32)	1522(92)	−42(85)	1228(146)	−100(90)
C(19)	65642(64)	50198(41)	27250(74)	1753(104)	413(35)	2520(128)	302(100)	1529(187)	−120(117)
C(20)	76730(83)	51316(53)	43495(82)	3116(163)	804(56)	2594(148)	247(154)	1096(249)	−1619(158)

/Å²	x	y	z	B/Å²		x	y	z	B/Å²
H(3)	4470(44)	2924(29)	−122(49)	1.4(1.0)	H(19B)	5454(48)	4946(34)	2691(53)	1.9(1.1)
H(4)	3051(45)	2971(30)	−2747(47)	1.1(1.0)	H(7)	8519(56)	1423(40)	−2382(64)	4.0(1.4)
H(5)	4012(44)	2368(42)	−4809(48)	3.1(1.2)	H(20A)	7444(52)	4644(36)	5131(58)	3.1(1.3)
H(6)	6417(46)	1795(33)	−4171(51)	1.6(1.1)	H(20B)	7541(53)	5628(39)	4653(59)	3.9(1.4)
H(12)	9085(43)	905(29)	3766(48)	0.8(1.0)	H(20C)	8672(61)	5015(42)	4346(66)	5.1(1.6)
H(13)	8448(55)	−297(36)	5155(60)	3.2(1.3)	H(8A)	9372(56)	264(41)	−762(61)	4.7(1.5)
H(14)	5900(56)	−583(41)	4608(62)	4.3(1.5)	H(8B)	7798(48)	232(34)	−1099(52)	2.4(1.2)
H(15)	3988(54)	296(41)	2902(58)	3.8(1.4)	H(8C)	8415(48)	659(33)	199(51)	1.9(1.1)
H(16)	4818(44)	1459(31)	1632(47)	1.1(1.0)	H(9A)	10421(67)	3474(50)	−1050(75)	6.6(1.8)
H(17A)	5665(44)	3145(31)	2379(46)	0.7(0.9)	H(9B)	8396(52)	3537(36)	−1768(55)	2.7(1.2)
H(17B)	7219(41)	3240(30)	3372(44)	0.4(0.9)	H(9C)	9362(52)	2903(33)	−2883(54)	2.6(1.2)
H(18A)	8002(41)	4238(28)	1895(45)	0.0(0.8)	H(10A)	11934(48)	2094(33)	−454(53)	2.6(1.2)
H(18B)	6372(44)	4271(31)	615(49)	1.0(1.0)	H(10B)	11058(63)	1636(44)	−2028(67)	5.2(1.6)
H(19A)	6489(52)	5548(38)	2144(57)	3.3(1.3)	H(10C)	11276(55)	1140(37)	−191(60)	3.7(1.4)

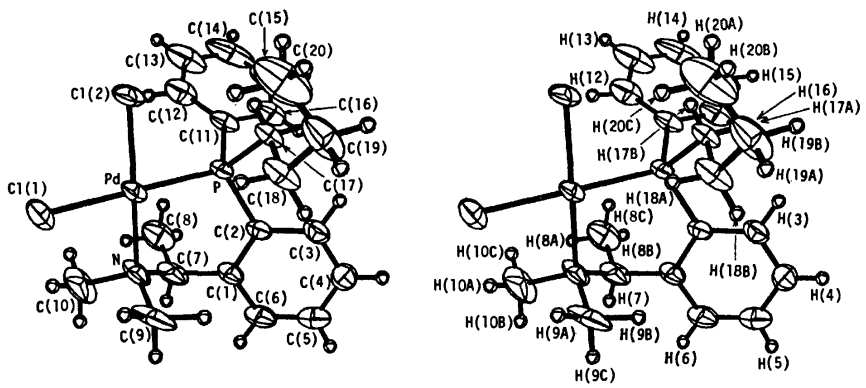

Fig. 1. Stereoscopic drawing of the molecule of dichloro[*N*,*N*-dimethyl-α-methyl-*o*-(butylphenylphosphino)benzylamine]palladium(II). The non-hydrogen atoms are represented by their thermal ellipsoids with 50% probability, while the hydrogen atoms are represented by arbitrary spheres.

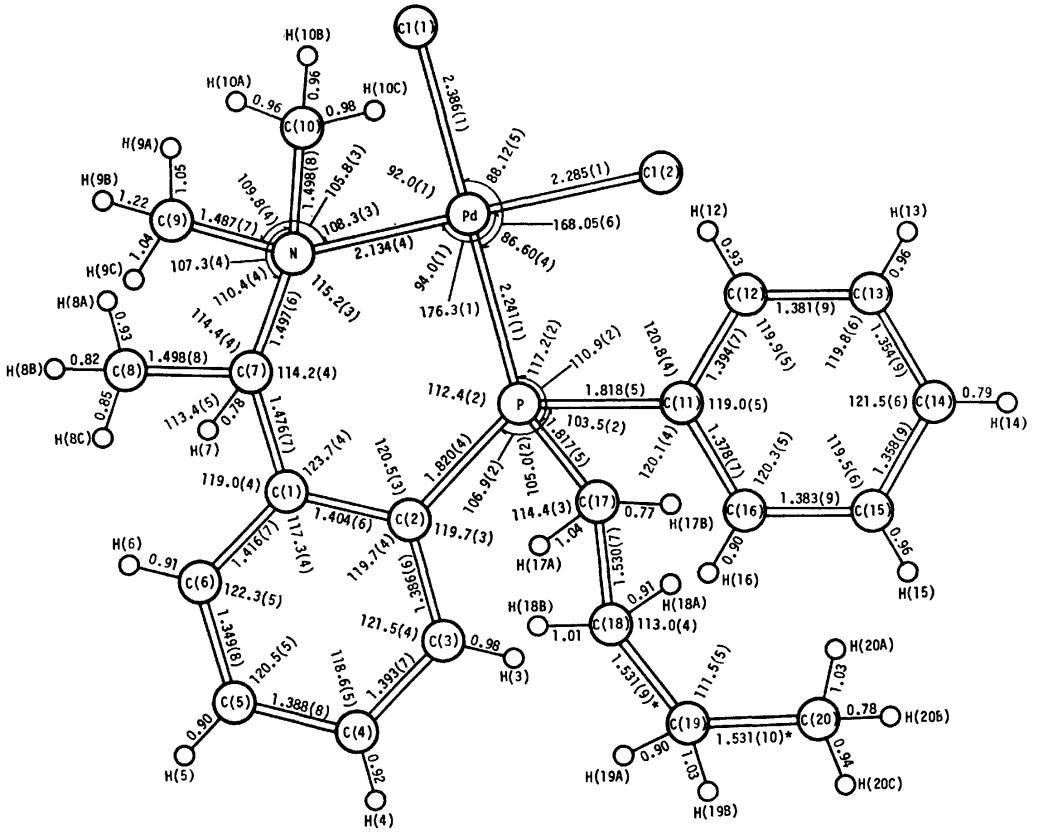

Fig. 2. Bond distances (l/Å) and bond angles (ϕ/°), with their e.s.d.'s in parentheses. Starred values are corrected for riding motion. Standard deviations of C–H bonds are 0.06 Å, and bond angles involving hydrogen atom are nearly tetrahedral or trigonal angle.

each other. The greater length of Pd–Cl(1) (trans to Pd–P) than Pd–Cl(2) (trans to Pd–N) is consistent with the observation that the Pd–Cl bond length decreases as the electronegativity of the trans atom increases.[5] The Pd–Cl(1) distance, 2.386(1) Å, is in the range expected for a Pd–Cl bond trans to Pd–P. On the other hand, the Pd–Cl(2) distance, 2.285(1) Å, is shorter and the Pd–N distance, 2.134(4) Å, is longer than those found so far in Cl–Pd–N systems. Figure 3 shows a plot of Pd–Cl distance *versus* trans Pd–N distance for several Pd complexes, in which the nitrogen atom is not a π-acceptor. Except for $Pd(NH_2CH_2CH_2NH_2)Cl_2$, a linear relationship is observed, the correlation factor is −0.28(4). This observation could be explained in terms of electrostatic interaction, as proposed for Cl–Pt–C system by Manojlović-Muir and Muir.[11] The present Pd–N bond is lengthened by the geometrical constraints mentioned later. The "bend" deformation of the metal d_π orbital by electrostatic repulsion from the σ orbital of Pd–N bond would be small, so that the trans Cl(2) could approach the metal. The value of the correlation factor may be reasonable, since the repulsions from the deformed d_π is mitigated at a long distance of Pd–Cl(2).

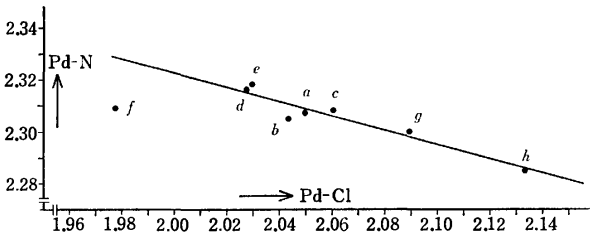

Fig. 3. A plot of Pd–Cl distance *versus* trans Pd–N distance. *a*: $PdCl_2$(*S*-methyl-L-cysteine)H_2O Ref. 6, *b*: *idem*, *c*: $PdCl_2$(D,L-methionine) Ref. 7, *d*: $PdCl_2$(*meso*-2,3-diaminobutane) Ref. 8, *e*: *idem*, *f*: $PdCl_2$(ethylenediamine) Ref. 9, *g*: $PdCl_2$(tetrahydrogen-ethylenediaminetetraacetate)$5H_2O$ Ref. 10, *h*: present work.

The geometrical constaint is indicated by the deviations of atoms from the mean plane through the four coordinating atoms, Pd −0.172, P 0.044, Cl(1) 0.056, Cl(2) −0.050, and N −0.423 Å. The deviation of P is due to repulsions from C(7) and C(8), and that of Cl(1) is caused by C(10); the close contacts are given in Fig. 4. At the same time these repulsions make the N–Pd–Cl(1) and N–Pd–P angles expand, so that P–Pd–Cl(1) deviates from a line. In addition the bond angles involving C(8), C(8)–C(7)–N and C(8)–C(7)–C(1), expand owing to the close contact between P and C(8). The 6-membered chelate ring is also constrained to enlarge the angles, P–Pd–N, Pd–N–C(7), N–C(7)–C(1), C(7)–C(1)–C(2), and Pd–P–C(2), from their normal values. The torsion angles about the C(17)–C(18) and C(18)–C(19) bonds are 186.8(4) and 70.8(6)°, respectively. The three P–C bond distances are 1.817—1.820 Å. The C–N bond distance is 1.494 Å in average. The bond lengths are apparently shortened.

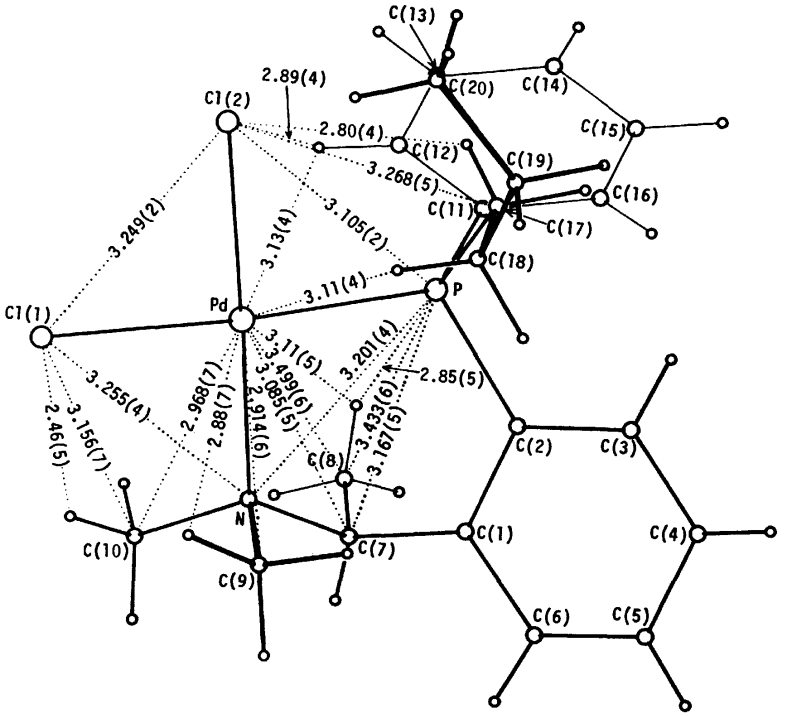

Fig. 4. Close contacts (in Å) around the palladium atom.

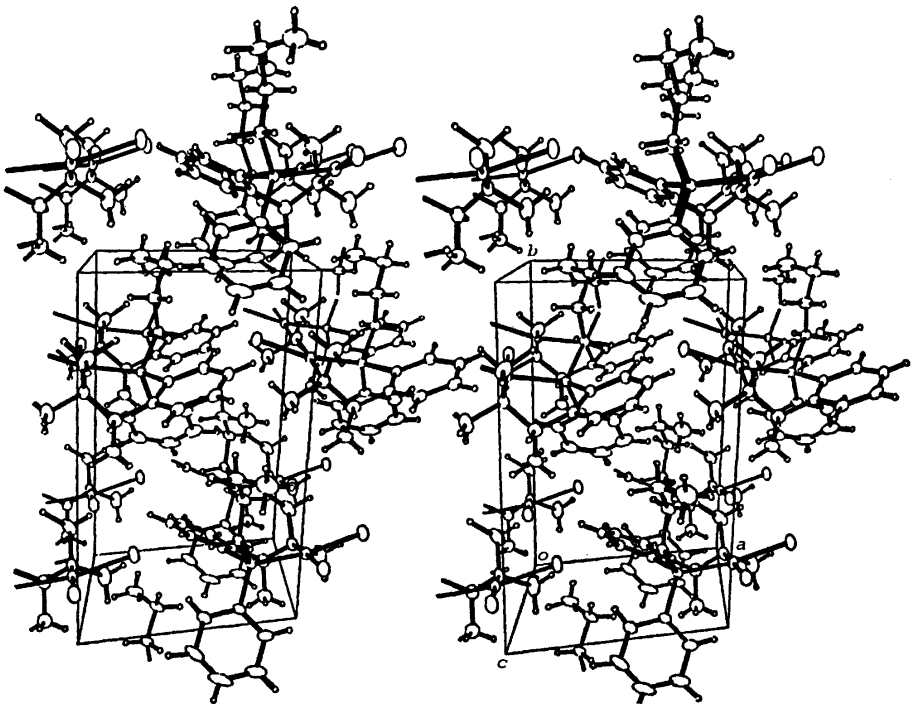

Fig. 5. Stereoscopic diagram showing the molecular packing.

at the periphery of the molecule by the large thermal motions.

As shown in Fig. 5, the complex molecules are packed by van der Waals interactions. A survey of the intermolecular distances indicates no abnormal contacts.

The authors thank Prof. T. Shimanouchi for permitting the use of the TOOL-IR system, by which the data of palladium complexes were looked up in the Cambridge Crystallographic Files.

References

1) K. Yamamoto, A. Tomita, and J. Tsuji, presented at the 36 th JCS Meeting (1977), Abstr. 3E38.

2) L. E. McCandlish and G. H. Stout, *Acta Crystallogr.*,

Sect. A, **31**, 245 (1975).

3) A list of structure factors has been deposited at the Chemical Society of Japan (Document No. 7724).

4) "International Tables for X-Ray Crystallography," Vol. IV, The Kynoch Press, Birmingham (1974), p. 71.

5) W. L. Steffen and G. J. Palenik, *Inorg. Chem.*, **15**, 2432 (1976).

6) L. P. Battaglia, A. B. Corradi, C. G. Palmieri, M. Nardelli, and M. E. V. Tani, *Acta Crystallogr., Sect. B*, **29**, 762 (1973).

7) R. C. Warren, J. F. McConnell, and N. C. Stephenson, *Acta Crystallogr., Sect. B*, **26**, 1402 (1970).

8) T. Ito, F. Marumo, and Y. Saito, *Acta Crystallogr., Sect. B*, **27**, 1695 (1971).

9) J. Iball, M. MacDougall, and S. Scrimgeour, *Acta Crystallogr., Sect. B*, **31**, 1672 (1975).

10) D. J. Robinson and C. H. L. Kennard, *J. Chem. Soc., Sect. A*, **1970**, 1008 (1970).

11) L. Manojlović-Muir and K. W. Muir, *Inorg. Chim. Acta*, **10**, 47 (1974).

The Crystal and Molecular Structure of Dimethyl *m*-Phenylenediacrylate

Hachiro NAKANISHI and Yoshio SASADA*

Research Institute for Polymers and Textiles, Sawatari, Kanagawa-ku, Yokohama 221
**Faculty of Science, Tokyo Institute of Technology, O-okayama, Meguro-ku, Tokyo 152*

(Received June 30, 1977)

Photooligomerizable crystals of dimethyl *m*-phenylenediacrylate are orthorhombic, $Pmn2_1$, with $a=26.419(8)$, $b=3.960(1)$, $c=5.935(2)$ Å, and $Z=2$. The structure was solved by the direct method and refined by the block-diagonal least-squares calculation to the R value of 0.042 for 617 observed reflections. The molecule is nearly planar and V-shaped with a mirror symmetry. A parallel plane-to-plane stack is found along the short b-axis. The molecules in the stack overlap completely, in contrast with the half-molecule overlap in the photopolymerizable crystals of this kind. The length of the b-axis is just the shortest intermolecular distance between reactive double bonds, indicating that the double bonds related by the b-translation would react to form a cyclobutane ring with a mirror symmetry.

Many diolefinic compounds undergo the four-center type photopolymerization in the crystalline state.[1] In the serial studies on the photopolymerizable crystals,[2] we have shown that all the photopolymerizable diolefins with *p*-phenylene moiety change, under the strict control of monomer crystal lattice, into crystalline polymers containing cyclobutane rings with the center of symmetry.

In contrast, dimethyl *m*-phenylenediacrylate (*m*-PDAMe) has been found to give amorphous oligomer having more than two kinds of cyclobutane rings with respect to steric configuration, by prolonged irradiation. At the lower reaction temperature, the dimer with a regular conformation of cyclobutane ring is formed in better yield.[3] From such results, a two-step reaction mechanism, *i.e.*, topochemical dimer formation in a regular crystal lattice and subsequent random cycloaddition in a disordered crystal lattice, was proposed previously.[3] The present crystal structure analysis has been undertaken in order to clarify the mechanism of such characteristic oligomer formation.

Experimental

m-PDAMe was synthesized according to the method described in the previous paper.[4] Plate-shaped crystals were grown from a methanol solution by slow evaporation. The specimen used was a fragment of a plate, $0.15\times0.15\times0.10$ mm in size. The space group was determined from photographs. The precise lattice constants and intensity data were obtained from measurements on a Rigaku computer-controlled four-circle diffractometer, with graphite-monochromatized Cu $K\alpha$ radiation. All reflections within the range of $2\theta<150°$ were collected by use of 2θ-ω scan mode with the scanning rate of 4° min^{-1}. Stationary background counts were accumulated for 10 s before and after each scan. Out of 681 reflections, 617 were greater than $3\sigma(|F_o|)$ and were used for structure determination. No correction was made for absorption. Crystallographic data of *m*-PDAMe are: $C_{14}H_{14}O_4$, *M. W.* 246.3. Orthorhombic, $Pmn2_1$, $a=26.419(8)$, $b=3.960(1)$, $c=5.935(2)$ Å, $U=620.9$ Å^3. $Z=2$, $Dx=1.318$, $Dm=1.320$ g cm^{-3}. μ(Cu $K\alpha$)$=9.30$ cm^{-1}.

* A list of structure factors is deposited as Document No. 7725 at the Office of the Editor of the Bulletin of the Chemical Society of Japan, 1-5, Kanda-Surugadai, Chiyoda-ku, Tokyo 101.

Determination and Refinement of the Structure

The space group and Z indicated that the molecule has a mirror symmetry. The structure was solved by the direct method with MULTAN.[5] All the non-hydrogen atoms were clearly located in the E map computed with the best set of phases. The parameters were refined by the block-diagonal least-squares method using $\omega=0.5$ for $|F_o|\leq1.0$, 1.0 for $|F_o|>1.0$. Isotropic hydrogen atoms were first located geometrically and then refined. The final R value was 0.042.* Atomic scattering factors were taken from International Tables for X-Ray Crystallography (1962). Final atomic coordinates and thermal parameters are given in Table 1.

Results and Discussion

Bond Lengths and Angles. The molecular structure and the numbering system used are shown in Fig. 1. The structure is compared with those of related compounds[6–10] in Table 2, where abbreviations of the compounds are also given.

Close resemblance is found among the molecular dimensions of *m*-PDAMe, *p*-phenylenediacrylic acid (*p*-PDA) derivatives and the corresponding half of

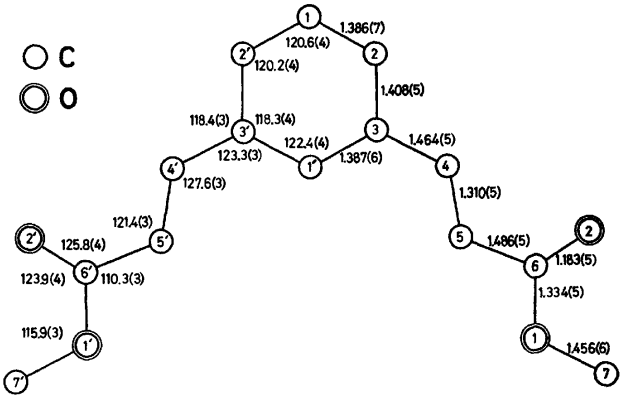

Fig. 1. Bond lengths (Å) and angles (°). The estimated standard deviations are in parentheses.

TABLE 1. ATOMIC PARAMETERS

(a) Fractional atomic coordinates ($\times 10^4$) for non-hydrogen atoms.

	x	y	z		x	y	z
C(1′)	0(0)	4733(11)	5694(8)	C(5)	1034(1)	6243(9)	3736(6)
C(1)	0(0)	1446(14)	9801(9)	C(6)	1557(1)	6958(9)	2944(6)
C(2)	456(1)	2293(8)	8791(6)	O(1)	1547(1)	8239(7)	865(5)
C(3)	460(1)	3937(8)	6687(6)	O(2)	1933(1)	6437(8)	3968(6)
C(4)	950(1)	4812(9)	5691(6)	C(7)	2036(2)	9125(11)	−98(8)

(b) Thermal parameters for non-hydrogen atoms ($\times 10^3$). The anisotropic thermal parameters are described by $\exp(-\beta_{11}h^2-\beta_{22}k^2-\beta_{33}l^2-\beta_{12}hk-\beta_{13}hl-\beta_{23}kl)$.

	β_{11}	β_{22}	β_{33}	β_{12}	β_{13}	β_{23}
C(1′)	1.33(6)	47(3)	21.0(13)	−0.0(0)	−0.0(0)	5(4)
C(1)	1.66(8)	70(4)	25.1(15)	−0.0(0)	−0.0(0)	17(5)
C(2)	1.67(5)	55(2)	24.5(10)	1.0(6)	−2.2(4)	6(3)
C(3)	1.26(4)	47(2)	22.2(9)	0.3(5)	−0.2(4)	0(3)
C(4)	1.11(4)	63(2)	28.5(11)	1.4(6)	−1.4(4)	1(3)
C(5)	1.08(4)	69(2)	25.8(10)	0.7(6)	−0.9(4)	1(3)
C(6)	1.19(4)	67(2)	30.6(11)	0.4(6)	0.6(4)	−0(3)
O(1)	1.13(3)	112(2)	29.6(8)	−0.9(5)	1.5(3)	20(3)
O(2)	1.09(3)	147(3)	42.2(10)	−0.6(6)	−1.9(3)	34(4)
C(7)	1.53(6)	113(4)	40.9(15)	−2.5(9)	4.8(5)	27(5)

(c) Fractional atomic coordinates ($\times 10^3$) and isotropic thermal parameters for hydrogen atoms. The bond lengths to the attached carbons are also given.

	x	y	z	B (Å^2)	C–H (Å)
H(C1′)	0(0)	622(13)	442(10)	3.2(13)	0.96(6)
H(C1)	0(0)	−22(16)	1118(11)	4.5(15)	1.05(6)
H(C2)	80(1)	173(8)	951(5)	1.3(7)	1.03(3)
H(C4)	124(1)	431(10)	654(7)	4.1(10)	0.93(4)
H(C5)	77(1)	670(10)	271(7)	3.6(10)	0.95(4)
H(C7)1	198(2)	1038(12)	−149(8)	6.8(13)	0.98(5)
H(C7)2	227(1)	709(9)	−15(7)	2.8(8)	1.02(4)
H(C7)3	219(1)	1114(11)	113(7)	5.4(12)	1.16(4)

TABLE 2. BOND LENGTHS (Å) AND ANGLES (°) OF *m*-PDAMe AND RELATED COMPOUNDS

	p-PDAMe[a]	*p*-PDAEt[b]	*p*-PDAPh[c]	HNCMe[d]	CVCCMe[e]	*m*-PDAMe[f]
C1′–C3	1.385(4)	1.388(3)	1.399(9)	1.386(3)	1.397(8)	1.387(6)
C2–C3	1.391(4)	1.388(3)	1.387(9)	1.398(3)	1.419(9)	1.408(5)
C3–C4	1.463(4)	1.466(3)	1.468(9)	1.468(3)	1.478(8)	1.464(5)
C4–C5	1.330(4)	1.316(3)	1.325(3)	1.308(4)	1.306(9)	1.310(5)
C5–C6	1.476(4)	1.479(3)	1.468(9)	1.471(3)	1.476(9)	1.486(5)
C6–O2	1.194(4)	1.197(3)	1.182(8)	1.188(3)	1.207(8)	1.183(5)
C6–O1	1.335(4)	1.332(3)	1.368(8)	1.341(3)	1.329(8)	1.334(5)
O1–C7	1.443(4)	1.461(3)	1.412(8)	1.442(4)	1.443(9)	1.456(6)
C1′–C3–C2	117.9(3)	118.0(2)	117.4(6)	117.6(2)	118.0(5)	118.3(4)
C2–C3–C4	118.8(2)	118.7(2)	119.7(6)	119.6(2)	119.1(5)	118.4(3)
C1′–C3–C4	123.3(3)	123.3(2)	122.9(6)	122.8(2)	122.9(5)	123.3(3)
C3–C4–C5	127.2(3)	127.2(2)	125.9(6)	126.4(2)	127.5(6)	127.6(3)
C4–C5–C6	119.3(3)	120.4(2)	119.6(6)	121.6(2)	120.0(6)	121.4(3)
C5–C6–O1	110.8(2)	110.9(2)	108.8(5)	111.0(2)	110.9(5)	110.3(3)
C5–C6–O2	126.0(3)	125.2(2)	127.3(6)	126.4(2)	125.7(6)	125.8(4)
O1–C6–O2	123.2(3)	123.9(2)	123.9(6)	122.6(2)	123.4(6)	123.9(4)
C6–O1–C7	115.0(2)	115.5(2)	117.6(5)	116.4(2)	116.6(5)	115.9(3)
θ_1[g]	2.2	6.0	−15.9	1.4	5.1	3.4
θ_2[h]	7.2	10.9	10.8	1.5	3.3	3.5
θ_3[i]	1.0	5.0	65.0	0.9	2.0	1.3
Ref.	6	7	8	9	10	This work

a) *p*-Phenylenediacrylic acid dimethyl ester. b) *p*-Phenylenediacrylic acid diethyl ester. c) *p*-Phenylenediacrylic acid diphenyl ester. d) Methyl 4-hydroxy-3-nitrocinnamate. e) 4-(β-Carboxyvinyl)-α-cyanocinnamic acid dimethyl ester. f) *m*-Phenylenediacrylic acid dimethyl ester. g) The internal rotation (°) around the bond C(3)–C(4). h) The internal rotation around C(5)–C(6). i) The rotation around C(6)–O(1).

TABLE 3. DEVIATIONS (Å, $\times 10^3$) OF ATOMS FROM SOME LEAST-SQUARES PLANES

The equation of the plane is expressed in the form of $AX+BY+CZ+D=0$, where X, Y, and Z are in Å referred to orthogonal axes, a, b, and c*.

	P(I)[a]	P(II)	P(III)	P(IV)[a]	P(V)[a]
A	0	40	52	0	0
B	−884	−900	−921	−888	−890
C	−468	−433	−386	−460	−456
D	3238	3077	2991	3252	3215
C(1′)	−0	−74[b]		8	6
C(1)	9	42[b]		43	52
C(2)	−7			21	27
C(3)	2	2		16	17
C(4)		−2	65[b]	−19	−21
C(5)		−2	2	11	4
C(6)		2	−5	−25	−34
O(1)		79[b]	2	92	78
O(2)		−36[b]	2	−121	−127
C(7)			−33[b]		26

a) For these planes, the equivalent atoms which are related by the mirror symmetry have also been included in the plane evaluation. b) The atoms are not included in the plane evaluation.

CVCCMe: all the bond lengths and angles other than the double bond lengths of six esters in Table 2 are nearly identical within 3σ.

Planarity and Conformation. The equations of mean planes and the displacements of atoms from each plane are given in Table 3. The benzene ring, ethylene and carbonyl groups are planar. Referring to the benzene ring, the ethylenic plane rotates by 3.4° (θ_1 in Table 2) about C(3)–C(4), and the carbonyl by 3.5° (θ_2) about C(5)–C(6) in the same direction. The methyl group rotates by only 1.5° (θ_3) about O(1)–C(7). Thus, the molecule as a whole is nearly planar within the deviation of 0.127 Å from the mean plane; the maximum deviation is found at O(2).

The carbonyl oxygen atom with lone pair electrons is situated at the same side as the ethylenic double bond with respect to the intervening single bond C(5)–C(6), so that the lone pair electrons extend parallel to the double bond. This is also the case of photopolymerizable diolefins,[7] and suggests that the electronic interaction between lone pair and π electrons (especially of ethylenic double bond) is operative for taking the present conformation in preference to the alternative one where the carbonyl group is at the opposite side.

According to the discussion in the previous paper,[7] the internal rotation (θ_2) around C(5)–C(6) should be near 10° in this type of conjugated system. However, θ_2 of *m*-PDAMe is considerably small compared with those of the photopolymerizable diolefins. Such small θ_2 is also found in CVCCMe and HNCMe (Table 2). This may be due to intermolecular repulsion, since molecules in these three crystals are piled up along the short crystal axis as will be described below.

Crystal Structure and Reaction Mechanism. The crystal structure viewed along the b-axis is shown in Fig. 2. The molecules are piled up along the shortest

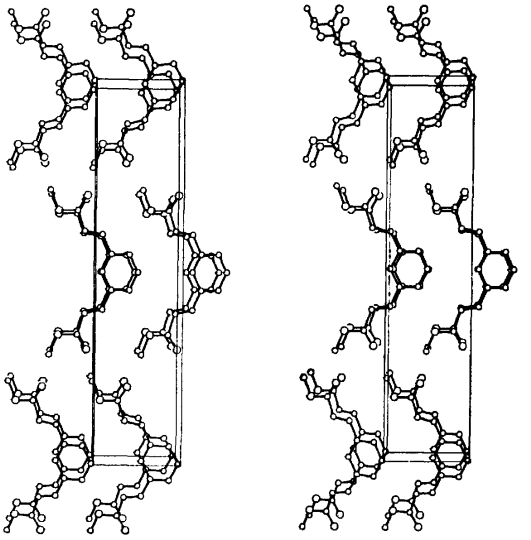

Fig. 2. A stereoview of the crystal structure viewed along the b-axis.

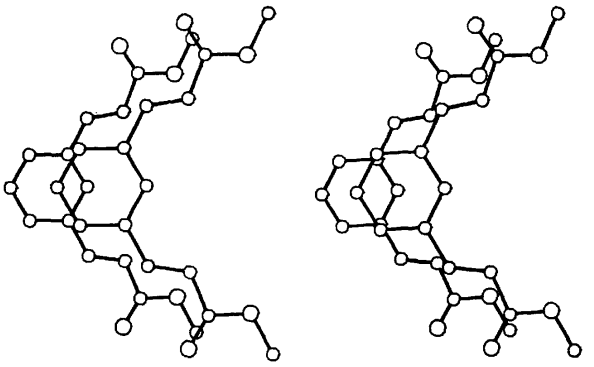

Fig. 3. A stereoview of the overlapping of molecules to react, viewed along the normal of the mean plane of the molecule.

crystal axis (b-axis) to form a parallel plane-to-plane stack. As seen from Fig. 3, the adjacent molecules in the stack overlap completely to each other. The same type of stack is also found in CVCCMe, another photo-oligomerizable crystal having the shortest crystal axis of 3.956 Å.[10] This stack is quite different from that in the photopolymerizable crystals where molecules are piled up along about 7 Å axis, displaced by half a molecule in the direction of the molecular long axis,[7] and also from the layer-type packing of the photostable modification of 2,5-distyrylpyrazine where molecules in the adjacent layers do not overlap at all.[11]

The length of the b-axis is just the shortest intermolecular distance between reactive double bonds, which is very close to those found in the photopolymerizable crystals (3.94 Å on the average). The second shortest distance, longer than 5 Å, is found between the molecules in different stacks (related by the two-fold screw axis) (Table 4).

The most plausible explanation for the reaction behavior,[3] on the basis of the crystal structure, is as follows. At the initial stage of photoirradiation, the molecules related by the b-translation react topo-

Table 4. Intermolecular distance (Å) between double bonds

$C(4^{i})\cdots C(4^{ii})$	3.960	$C(5^{i})\cdots C(4'^{iv})$	9.986
$C(4^{i})\cdots C(5^{ii})$	4.679	$C(5^{i})\cdots C(5'^{iv})$	9.657
$C(5^{i})\cdots C(4^{ii})$	3.593	$C(4^{i})\cdots C(4'^{v})$	9.510
$C(5^{i})\cdots C(5^{ii})$	3.960	$C(4^{i})\cdots C(5'^{v})$	9.986
$C(4^{i})\cdots C(4'^{ii})$	6.392	$C(5^{i})\cdots C(4'^{v})$	9.270
$C(4^{i})\cdots C(5'^{ii})$	7.021	$C(5^{i})\cdots C(5'^{v})$	9.657
$C(5^{i})\cdots C(4'^{ii})$	6.350	$C(4^{i})\cdots C(4'^{vi})$	8.714
$C(5^{i})\cdots C(5'^{ii})$	6.747	$C(4^{i})\cdots C(5'^{vi})$	8.182
$C(4^{i})\cdots C(4^{iii})$	7.135	$C(5^{i})\cdots C(4'^{vi})$	8.984
$C(4^{i})\cdots C(5^{iii})$	8.419	$C(5^{i})\cdots C(5'^{vi})$	8.354
$C(5^{i})\cdots C(4^{iii})$	5.862	$C(4^{i})\cdots C(4'^{vii})$	8.714
$C(5^{i})\cdots C(5^{iii})$	7.135	$C(4^{i})\cdots C(5'^{vii})$	8.984
$C(4^{i})\cdots C(4'^{iv})$	9.510	$C(5^{i})\cdots C(4'^{vii})$	8.182
$C(4^{i})\cdots C(5'^{iv})$	9.270	$C(5^{i})\cdots C(5'^{vii})$	8.354

Symmetry code:

Superscript			
i	x	y	z
ii	x	$1+y$	z
iii	x	y	$-1+z$
iv	$1/2-x$	$-y$	$1/2+z$
v	$1/2-x$	$-y$	$-1/2+z$
vi	$1/2-x$	$1-y$	$1/2+z$
vii	$1/2-x$	$1-y$	$-1/2+z$

chemically to form the dimer having a cyclobutane ring with a mirror symmetry. The cyclobutane ring formation in one wing of the molecular pair makes large the distance between the double bonds in the other wing. The dimerization of this type probably destroys the regular arrangement of surrounding monomers. The subsequent reaction between the dimer and its neighbor in the disordered crystal lattice results in amorphous oligomer having more than two kinds of cyclobutane rings. The rate of the reaction should be smaller than that of the initial dimerization with topochemical assistance. Such reaction in the disordered lattice will be more favorable at higher temperature. Thus, the reaction mechanism proposed previously[3] is supported by the present structural study.

The authors are grateful to Dr. Masaki Hasegawa and Dr. Fusae Nakanishi of the Research Institute for Polymers and Textiles for their valuable suggestion and encouragement. The authors also thank Messrs. Katsuhiko Ueno and Kazuaki Harata for their assistance through this work.

References

1) For a review, M. Hasegawa, Y. Suzuki, H. Nakanishi, and F. Nakanishi, *Prog. Polym. Sci. Jpn.*, **5**, 143 (1973).
2) (a) H. Nakanishi, M. Hasegawa, and Y. Sasada, *J. Polym. Sci., A-2*, **10**, 1537 (1972); (b) H. Nakanishi, M. Hasegawa, and Y. Sasada, *ibid., Polym. Phys. Ed.*, **15**, 173 (1977).
3) F. Nakanishi, H. Nakanishi, M. Hasegawa, and Y. Yamada, *J. Polym. Sci., Polym. Chem. Ed.*, **13**, 2499 (1975).
4) F. Suzuki, Y. Suzuki, H. Nakanishi, and M. Hasegawa, *J. Polym. Sci., A-1*, **7**, 2319 (1969).
5) G. Cermain, P. Main, and M. M. Woolfson, *Acta Crystallogr., Sect. A*, **27**, 368 (1971).
6) K. Ueno, H. Nakanishi, M. Hasegawa, and Y. Sasada, *Acta Crystallogr., Sect. B*, to be published.
7) H. Nakanishi, K. Ueno, and Y. Sasada, *Acta Crystallogr., Sect. B*, to be published.
8) H. Nakanishi, K. Ueno, and Y. Sasada, *Acta Crystallogr., Sect. B*, to be published.
9) A. W. Hanson, *Acta Crystallogr., Sect. B*, **31**, 1963 (1975).
10) H. Nakanishi and Y. Sasada, *Acta Crytallogr., Sect. B*, to be published.
11) H. Nakanishi, K. Ueno, and Y. Sasada, *Acta Crystallogr., Sect. B*, **32**, 3352 (1976).

Infrared and Mössbauer Spectra of Synthetic Garnets $A_3Fe_2Si_3O_{12}$ (A: Mn, Cd, Ca)

Hitoshi NISHIZAWA, Masahiko SHIMADA,* Kiyoshi MATSUOKA, and Mitsue KOIZUMI*

Department of Chemistry, Faculty of Science, The University of Kochi, Asakura, Kochi 780

**The Institute of Scientific and Industrial Research, Osaka University, Yamadakami, Suita, Osaka 565*

(Received July 4, 1977)

The garnet $Mn_3Fe_2Si_3O_{12}$ with $a_0=11.821$ Å was synthesized at high pressure and temperature. Infrared and Mössbauer spectra of the synthetic garnets $A_3Fe_2Si_3O_{12}$ (A: Mn, Cd, Ca) suggest that the distortion of SiO_4 tetrahedra in these garnets increases and that of FeO_6 octahedra decreases with increase in the radius of eight fold coordinated cation.

The garnets, general formula $A_3B_2C_3O_{12}$, contain metal ions in eight, six and four coordinated sites, affording a fruitful field for investigation of the influence of ionic substitution and excellent models for crystal chemical studies.

Infrared absorption spectra of garnet group minerals $A_3B_2Si_3O_{12}$ were studied by Wickersheim and Tarte.[1-4] They found that the major absorption bands for 800 to 1100 cm^{-1} arise from the site group splitting of ν_3 due to the distortion of the isolated SiO_4 tetrahedron. Moor and White[5] explained the distortion of tetrahedra in the crystal lattice of natural garnet series by using group theory.

Recently considerable attention has been paid to the chemical application of the Mössbauer effect. The two parameters, the chemical shift and the electric quadrupole splitting obtained from Mössbauer spectra, vary not only with oxidation state and electronic configuration and coordination number of iron atoms in crystal structure, but also with marked changes in geometry of the ligand environment.

We have measured infrared and Mössbauer spectra for synthetic garnet series $A_3Fe_2Si_3O_{12}$ (A: Mn, Cd, Ca). The effects of the substitution of ions in the eight coordinated site on the geometry of SiO_4 tetrahedra and FeO_6 octahedra are discussed.

Experimental

For the synthesis of $A_3Fe_2Si_3O_{12}$ (A: Mn, Cd, Ca), starting materials were prepared by mixing oxides, nitrates or carbonates of the cations with colloidal silica in stoichiometric proportions. They were then dried and heated at 750 °C in most cases for at least four hours. The temperature was varied somewhat with material since it had to be high enough to decompose the starting material without causing any volatilization. After the heating, the starting materials were ground and mixed.

Piston-cylinder type and cubic type apparatus were used for high temperature and pressure experiments. The starting materials were packed into a platinum capsule and compressed. After treatment at 10—60 kbar and 1000—1200 °C for one hour, the samples were rapidly cooled to room temperature and the pressure was released. The product was identified by X-ray powder diffraction and optical microscopy.

The Mössbauer spectra were measured at room temperature using radiation from ^{57}Co in Pd, with a 400 channel multichannel analyzer. Velocity scale was calibrated with iron foil as a standard absorber. Infrared spectra were obtained using a Hitachi Model 225 Spectrophotometer and the Nujol mull technique.

Results

Single phases of garnets $Ca_3Fe_2Si_3O_{12}$ and $Cd_3Fe_2Si_3O_{12}$ were synthesized at 15 kbar and 1000 °C. They have a cubic structure with $a_0=12.06$ and 12.01 Å, respectively. Geller and Miller[6] attempted to synthesize the solid solution of $Mn_3(Al_{1-x}Fe_x)_2Si_3O_{12}$ in air and succeeded in synthesizing garnets containing up to 20 per cent of Fe^{3+}. High pressure was necessary to synthesize the single phase of garnet $Mn_3Fe_2Si_3O_{12}$ which is the last member in the above solid solution series. The products synthesized below 35 kbar at 1000 °C consist of mixtures of two or more phases such as $(Mn, Fe)_2O_3$, spinel phases and SiO_2 (quartz or coesite). Even under high pressure conditions of 40 kbar, traces of these phases were found when the temperature was above 1100 °C. The single phase garnet $Mn_3Fe_2Si_3O_{12}$ was synthesized under the conditions of 1000 °C and 60 kbar. No evidence was found for the other phases mentioned above by means of X-ray data. The garnet $Mn_3Fe_2Si_3O_{12}$ obtained has a cubic structure with $a_0=11.821$ Å. X-Ray diffraction data are given in Table 1.

TABLE 1. X-RAY POWDER DATA OF $Mn_3Fe_2Si_3O_{12}$

h	k	l [a]	d_{obsd}	I_{obsd}
4	0	0	2.96	45
4	2	0	2.65	100
3	3	2	2.52	25
4	2	2	2.416	65
5	1	0	2.320	15
5	2	1	2.160	10
6	1	1	1.918	25
6	2	0	1.870	5
4	4	4	1.707	10
6	4	0	1.640	25
7	2	1	1.608	5
6	4	2	1.580	60
8	0	0	1.478	15

a) Indexed on the basis of $a_0=11.821$ Å.

The relation between lattice constants and the ionic radii of eight fold coordinated cations in the synthetic garnets are shown in Fig. 1 on the basis of Shannon and Prewitt's effective radii.[7] The same relationship for the pyralspite series $A_3Al_2Si_3O_{12}$ was also found.[8] Parallelism was found in both garnet series.

The infrared spectra for the synthetic garnets are

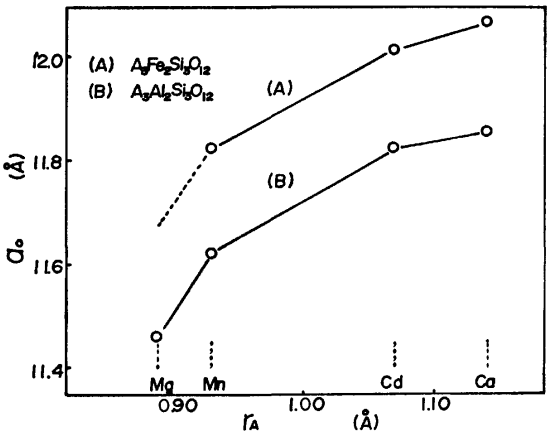

Fig. 1. Lattice constants a_0 *vs.* ionic radii of divalent dodecahedrally coordinated cations.

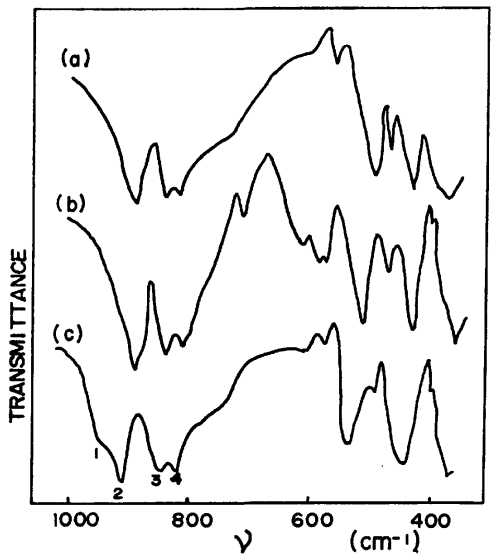

Fig. 2. Infrared spectra of synthetic garnets (a)—(c): $A_3Fe_2Si_3O_{12}$ (A: Ca, Cd, Mn).

Table 2. Infrared data for synthetic garnets

	ν/cm^{-1}			
	1	2	3	4
$Ca_3Fe_2Si_3O_{12}$		889	833	814
$Cd_3Fe_2Si_3O_{12}$		889	835	810
$Mn_3Fe_2Si_3O_{12}$	949	913	848	822

qualitatively similar in the region 800—1000 cm^{-1}. There are three strong and sharp bands (2, 3, 4 in curve c) with almost equal intensity (Fig. 2). The band frequencies decrease almost linearly with increase of a_0. They are assigned to the ν_3 vibration of SiO_4. Splitting of ν_3 vibration into three bands due to the distortion of SiO_4 tetrahedron in the garnet structure is in line with the results of site group and factor group analyses.[5] The origin of band 1 is not clear but it may result from a combination of internal and/or external mode.[10] The magnitude of band splitting of ν_3, Band 2—(Band 3—Band 4)/2, is known to be correlated with the distortion of SiO_4 tetrahedron.[11] From the band splitting of

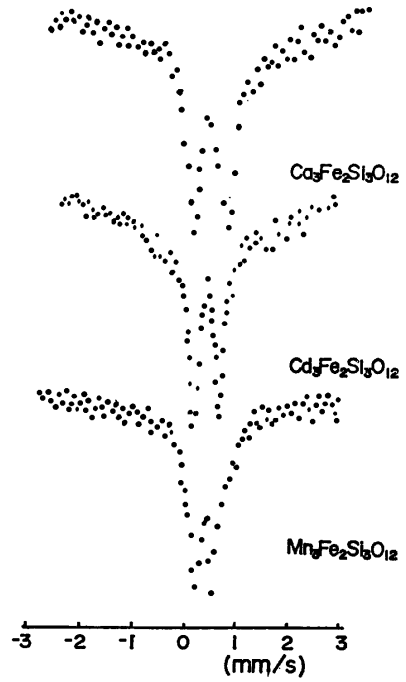

Fig. 3. Mössbauer spectra of synthetic garnets.

Table 3. Parameters of the Mössbauer spectra of ^{57}Fe nuclei for synthetic garnets

	Q.S. mm/s	I.S. mm/s
$Ca_3Fe_2Si_3O_{12}$	0.585	0.414
$Cd_3Fe_2Si_3O_{12}$	0.573	0.384
$Mn_3Fe_2Si_3O_{12}$	0.344	0.385

ν_3, the distortion of SiO_4 tetrahedron seems to increase with decrease in the radius of eight fold coordinated cation.

Figure 3 shows the Mössbauer spectra of synthetic garnets at room temperature. All the spectra are resolved symmetric doublets. The garnets are paramagnetic at room temperature and there is no hyperfine magnetic splitting. The doublet lines arise from the quadrupole interaction of the ^{57}Fe nuclei with the inhomogeneous electric field in the crystal. Table 3 shows the Mössbauer parameters for all the garnets synthesized. The values of the isomer shifts for all the garnets lie in the range characteristic of the trivalent high spin state of iron ion. The parameters indicate little contribution of covalent forces to the ionic chemical bond of iron with oxygen in the octahedral coordination. The quadrupole splitting due to the electric field gradient decrease with decrease in the radius of eight fold coordinated cation. This shows that the trivalent high spin state of iron ions in the garnet $Mn_3Fe_2Si_3O_{12}$ is in the most symmetrical octahedral environment.

Discussion

$Mn_3Fe_2Si_3O_{12}$ with a cubic garnet structure was synthesized under high temperature and high pressure conditions. The reason for the synthetic conditions under high pressure for $Mn_3Fe_2Si_3O_{12}$ being influenced

by temperature thought to be due to the instability of Mn^{2+} ions in a high pressure vessel at elevated temperature. The parameter values of Mössbauer spectra for iron ions are typical for the trivalent high spin state of iron ions in an octahedral site. It is concluded that all manganese ions are divalent in the dodecahedral site and all iron ions are trivalent in the octahedral site. Although Mason reported the natural occurrence of a garnet with a probable composition of $Mg_3Fe_2Si_3O_{12}$, this compound could not be prepared under the experimental conditions employed in this study. From the similarity of both curves in Fig. 1, the lattice constant of $Mg_3Fe_2Si_3O_{12}$ is predicted to be 11.656 Å, which is a little higher than 11.515 Å reported by Mason.[9] Some of the Si^{4+} ions are presumed to be substituted for Fe^{3+} ions in the octahedral site of natural garnet $Mg_3Fe_2Si_3O_{12}$.

Usually, but not always, increase in the regularity of SiO_4 tetrahedron should allow the sp^3 hybrid orbitals on oxygen to be in a position for a more favorable overlap with those of Si, suggesting a decrease in the Si–O bond length. Novak showed by comparison of the refined structures of eight natural garnets that the Si–O bond length actually increases, as SiO_4 tetrahedron in pyralspite garnet series $A_3Al_2Si_3O_{12}$ (A: Ca, Mn, Fe, Mg) becomes more regular.[12] From the infrared spectra of synthetic garnets $A_3Fe_2Si_3O_{12}$, it seems that the regularity of SiO_4 tetrahedron also increases as the Si–O bond length increases due to a simple stretching of the $Fe_2Si_3O_{12}$ framework in response to the increase of radius of eight fold coordinated cation.

In pyralspite $A_3Al_2Si_3O_{12}$, the octahedral edge shared with triangular dodecahedron AO_8 is longer than the octahedron's unshared edge in A^{2+} ion's radius longer than 1.01 Å by weakening repulsive forces between A^{2+} and Al^{3+} (0.53 Å) cations. In the garnets $A_3Fe_2Si_3O_{12}$ with Fe^{3+} (0.645 Å) cations in octahedral site, the effect appears when the radius of A^{2+} ion is smaller than 1.01 Å. When the radius of the ion is near that of Mn^{2+} ion, shared and unshared octahedral edge lengths are statistically identical. $Mn_3Fe_2Si_3O_{12}$ garnet is thus considered to have an almost regular octahedron in line with the result of Mössbauer spectra.

The authors express their thanks to Drs. Nobukazu Kinomura, and Shoichi Kume, Osaka University. The study was partly defrayed by a Scientific Grant from the Ministry of Education.

References

1) K. A. Wickersheim, *J. Appl. Phys.*, **32**, 2055 (1961).
2) K. A. Wickersheim, R. A. Lefever, and B. M. Hanking, *J. Chem. Phys.*, **22**, 271 (1960).
3) P. Tarte, *Spectrochim. Acta*, **18**, 467 (1962).
4) P. Tarte, *Acad. Roy. Belg. Cl. Sci. Mem.*, **35**, 103 (1965).
5) R. K. Moor and W. B. White, *Am. Mineral.*, **56**, 54 (1971).
6) S. Geller and C. E. Miller, *Am. Mineral.*, **44**, 665 (1959).
7) R. D. Shannon and C. T. Prewitt, *Acta Crystallogr., Sect. B*, **25**, 925 (1969).
8) S. Geller, *Z. Kristallogr.*, **125**, 1 (1967).
9) B. Mason, J. Nelen, and J. S. White, Jr., *Science*, **160**, 66 (1968).
10) Y. Suwa and S. Naka, *Am. Mineral.*, **60**, 1125 (1975).
11) Y. Suwa and S. Naka, *Nippon Kagaku Kaishi*, **1972**, 1643.
12) G. A. Novak and G. V. Gibbs, *Am. Mineral.*, **56**, 791 (1971).

A Selectivity Study on Liquid Anion Exchange Membranes*

Nobuo YOSHIDA** and Nobuhiko ISHIBASHI

Department of Applied Analytical Chemistry, Faculty of Engineering, Kyushu University, Fukuoka 812

(Received July 7, 1977)

The selectivity of liquid anion exchange membranes consisting of a perchlorate, thiocyanate, or iodide salt of Crystal Violet dissolved in nitrobenzene was studied by measuring membrane potentials. In bi-ionic systems the selectivity coefficient was observed to vary with the concentrations of aqueous solutions and of the ion exchanger in the membrane. This was attributed mainly to the ionic composition at the membrane-solution interface differing from that in the bulk solution. However, when the concentration of the aqueous solutions was sufficiently high in comparison with that of the ion exchanger, a selectivity coefficient intrinsic to a pair of counter ions was obtained. This selectivity coefficient was also applicable to mixed electrolyte systems and was shown to be consistent with the Conti-Eisenman theory on the relation between the selectivity coefficient and ionic parameters.

The potentials measured with liquid membrane electrodes in solutions containing a number of species of univalent ions to which the electrode responds, have been found to obey the following empirical equation:[1,2]

$$E = \text{const} - \frac{RT}{F} \ln (a_i + \sum_j K_{i,j}^{pot} a_j). \quad (1)$$

Here a_i and a_j are activities of the primary ion i and any other ion j. $K_{i,j}^{pot}$ is the potentiometric selectivity coefficient of ion j over the primary ion. The selectivity coefficient calculated by means of Eq. 1, however, has generally been observed to vary with solution concentration, composition, and ion exchanger concentration in the membrane. Such variations of the selectivity coefficient have been considered to be due to the changes of the ion-exchange selectivity coefficient with solution concentration[2,3] and of the physical properties of the membrane with ion exchanger concentration.[4]

In the present work, the selectivity of liquid anion exchange membranes consisting of a perchlorate, thiocyanate, or iodide salt of Crystal Violet dissolved in nitrobenzene was studied. The variation of the selectivity coefficient is explained in terms of the change of ionic composition at the membrane-solution interface and a selectivity coefficient intrinsic to a pair of counter ions is introduced. This selectivity coefficient is compared with that expected from a theory of a liquid ion exchange membrane.

Experimental

Reagents and Liquid Membranes. All reagents used in this study were of analytical reagent grade. A Crystal Violet salt of anion X (CV-X, where X=ClO_4^-, SCN^-, or I^-) was prepared by dissolving Crystal Violet (obtained as a chloride salt from Kishida Kagaku Co.) in hot water and precipitation with aqueous NaX at the same temperature. The precipitate was washed with demineralized water and dried in vacuum. Liquid membranes were prepared by dissolving a known amount of the Crystal Violet salt in nitrobenzene.

Measurement of Membrane Potentials. Membrane potentials were measured by means of the cell

SCE/KCl-agar bridge/Solution(′)/Liquid membrane/Solution(″)/KCl-agar bridge/SCE. (2)

Here the symbols (′) and (″) are used to designate the solutions on both sides of the membrane. In cells with solutions containing perchlorate ion, NH_4Cl-agar bridges were used in place of KCl-agar bridges. The experimental cell used was a U-shaped glass tube with 12 cm^3 of the membrane phase at the bottom and 10 cm^3 of each aqueous solution above. The aqueous and the membrane phases were not stirred unless differently indicated. In most experiments, the concentration ranges of the aqueous solutions and of the ion exchanger (the Crystal Violet salt) in the membrane were chosen so as not to cause the elution of the ion exchanger into the adjacent aqueous solutions. All membrane potentials were measured with a Takeda Riken Electrometer TR 8651 at room temperature (23±3 °C), after the cells had been constructed.

Determination of Composition Changes in Aqueous Solutions. Cells of the type: 0.1 M† NaI (′)/CV-I in nitrobenzene/0.1 M NaX (″) (where X=NO_3^- or ClO_4^-) were used to examine composition changes in aqueous solutions which may be caused by ion exchange during the measurement of membrane potentials. About 30 min after the construction of the cell, the concentration of iodide ion in solution (″) was determined by using an iodide ion-selective electrode (Toa Denpa Kogyo Co., Model I-125).

Determination of Distribution Coefficients. A nitrobenzene solution of a Fuchsine Basic salt of anion X (X=ClO_4^-, SCN^-, or I^-) was prepared by extraction from a mixture of Fuchsine Basic (obtained as a chloride salt from Kishida Kagaku Co.) and NaX in water. The concentration of the Fuchsine Basic salt in the nitrobenzene solution was of the order of 10^{-4} M. Ten cm^3 of the solution was vigorously agitated with 10 cm^3 of water. The system was maintained overnight in a thermostated water bath (25.0±0.1 °C). After complete separation of the phases the salt concentration in the aqueous phase was determined by measuring the absorbance at 542 nm. Next, the distribution coefficient of the salt was calculated.

Results and Discussion

In order to evaluate the ratios of the activity coefficients (concentration basis) of thiocyanate and perchlorate ions, $y(SCN^-)/y(ClO_4^-)$, at high concentrations (necessary in the following calculation of the selectivity coefficient), concentration potentials were first measured for aqueous NaSCN and $NaClO_4$ solutions. Figure 1 shows the observed potentials as a function of the ion exchanger concentration. In this figure the concentration potentials which are independent of the exchanger concentration (horizontal parts of the curves) may be

* A preliminary report has been published: N. Yoshida and N. Ishibashi, *Chem. Lett.*, **1974**, 493.

** Present address: Department of Chemistry, Faculty of Science, Kyushu University, Fukuoka 812.

† Throughout this paper 1 M=1 mol dm^{-3}.

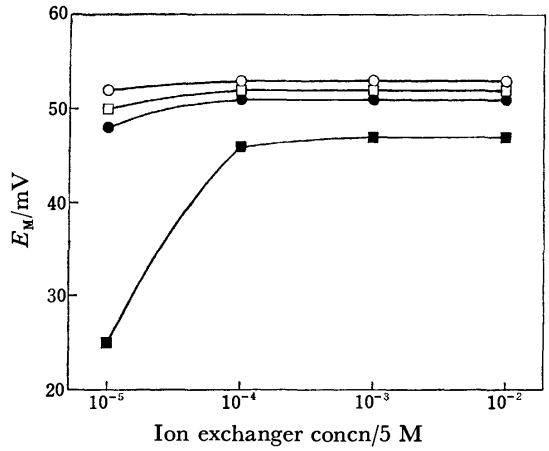

Fig. 1. Concentration potential, E_M, *vs.* concentration of ion exchanger. Systems: ○, 0.01 M NaSCN (′)–0.1 M NaSCN (″); □, 0.01 M $NaClO_4$ (′)–0.1 M $NaClO_4$ (″); ●, 0.1 M NaSCN (′)–1 M NaSCN (″); ■, 0.1 M $NaClO_4$ (′)–1 M $NaClO_4$ (″). Membrane solvent: nitrobenzene. Ion exchangers: ○, ●, CV–SCN; □, ■, CV–ClO_4.

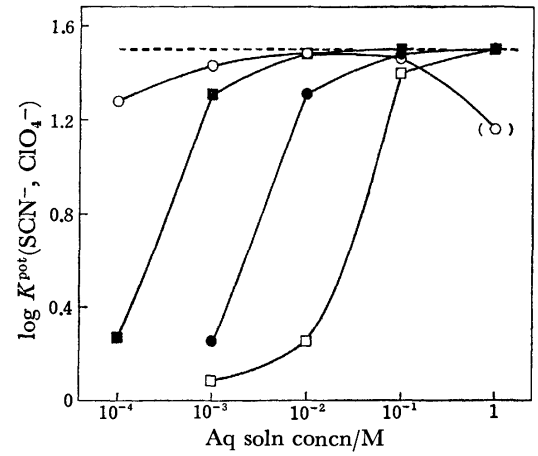

Fig. 2. Variation of the selectivity coefficient with concentrations of aqueous solution and of ion exchanger in the bi-ionic system NaSCN–$NaClO_4$. Membrane solvent: nitrobenzene. Concentrations of ion exchanger (CV–SCN): ○, 5×10^{-5} M; ■, 5×10^{-4} M; ●, 5×10^{-3} M; □, 5×10^{-2} M.

considered to be ideal; the decrement of the potentials at the low exchanger concentrations is presumably due to the incomplete exclusion of the co-ion (sodium ion) from the membrane. By application of the Nernst equation to the former potentials, the values of $\log\{y(SCN^-)/y(ClO_4^-)\}$ in 0.1- and 1-M solutions were estimated to be 0.02 and 0.09, respectively, where the ratio $y(SCN^-)/y(ClO_4^-)$ was assumed to be unity below 10^{-2} M. These results were used for the calculation of the selectivity coefficient in the bi-ionic system NaSCN–$NaClO_4$ presented below.[5]

In the case of two univalent counter ions (anions) X and Y, the membrane potential, E_M, in cell (2) may be expressed by

$$E_M = \frac{RT}{F}\ln\frac{a''_X + K^{pot}_{X,Y}a''_Y}{a'_X + K^{pot}_{X,Y}a'_Y}. \quad (3)$$

Here the sign of the potential refers to solution (″). For cells in which solution (′) contains only ion X and solution (″) only ion Y, Eq. 3 reduces to

$$E_M = \frac{RT}{F}\ln\frac{K^{pot}_{X,Y}a''_Y}{a'_X}. \quad (4)$$

Figure 2 shows the selectivity coefficient $K^{pot}(SCN^-, ClO_4^-)$ for the bi-ionic system NaSCN–$NaClO_4$ in which the membrane (CV–SCN in nitrobenzene) is interposed between solutions of NaSCN (′) and of $NaClO_4$ (″) of the same concentration. The selectivity coefficient was calculated from the measured potential by the use of Eq. 4. (Such a selectivity coefficient is an "apparent" one described below). It is observed that the selectivity coefficient varies with the concentrations of the ion exchanger in the membrane and of the aqueous solutions. However, with membranes having a given concentration of the exchanger, the selectivity coefficient approaches a limiting value (indicated by the dashed line in the figure) with the increasing concentration of the aqueous solutions. With solutions having a given concentration of the electrolytes, the selectivity coefficient also tends toward the same limiting value as the exchanger concentration decreases. As in the case of the concentration potentials described above, the deviation of the parenthesized value from the limiting one is attributed to the incomplete exclusion of the co-ion (sodium ion) from the membrane. Similar results were obtained with the bi-ionic systems NaI–$NaClO_4$ and NaI–NaSCN by the use of nitrobenzene solutions of CV–I as the liquid membranes.[6]

The variation of the selectivity coefficient may be understood from the following argument. In the bi-ionic cell used here, before the aqueous solutions and the liquid membrane are in contact with each other, solution (′) and the membrane contain the same counter ion X, whereas solution (″) contains a different counter ion Y. When the cell is assembled, an exchange of the counter ions occurs between solution (″) and the membrane. Therefore, the ionic composition at the membrane-solution (″) interface is generally different from that in the bulk of solution (″) since a diffusion layer (through which the transport of ions can occur by diffusion only) exists adjacent to the interface. (In experiments of short duration, such a change of ionic composition would be negligible at the membrane-solution (′) interface).

Such a cell is not a true bi-ionic cell and, taking account of the composition change at the interface, we must express the membrane potential of the cell as

$$E_M = \frac{RT}{F}\ln\frac{a^*_X + K^{pot}_{X,Y}a^*_Y}{a'_X} + (\phi'' - \phi^*), \quad (5)$$

where the asterisks refer to the interface inside solution (″) and ϕ is the electric potential. As shown in Appendix, since the mobilities of the counter ions used (ClO_4^-, SCN^-, and I^-) are nearly equal in the aqueous solution,[7] the second term in Eq. 5 becomes negligible and $c^*_X + c^*_Y \approx c''_Y \approx c'_X$ (c: concentration). We then obtain (assuming, for simplicity, activities to be equal to concentrations)

$$E_M \approx \frac{RT}{F}\ln\left\{K^{pot}_{X,Y} + (1 - K^{pot}_{X,Y})\frac{c^*_X}{c'_X}\right\}, \quad (6)$$

from which an "apparent" selectivity coefficient, $K^{pot}_{X,Y}$(app), (obtained from the straightforward application of Eq. 4 to the cell) is given by

$$K^{pot}_{X,Y}(app) \approx K^{pot}_{X,Y} + (1-K^{pot}_{X,Y})\frac{c^*_X}{c'_X}. \quad (7)$$

The higher the exchanger concentration compared with the solution concentration, the larger will be the value of c^*_X/c'_X. Hence $K^{pot}_{X,Y}$(app) becomes correspondingly smaller when $K^{pot}_{X,Y}>1$ and larger when $K^{pot}_{X,Y}<1$. This indeed the case for the bi-ionic system NaSCN–$NaClO_4$ presented above, where $K^{pot}(SCN^-, ClO_4^-)$ (which is considered to be the limiting value of the selectivity coefficient in this system as described below) is 1.5 on logarithmic scale.

However, in cases where the solution concentration is sufficiently high in comparison with the exchanger concentration, the influence of the composition change at the interface will be negligibly small. The above-mentioned limiting value of the selectivity coefficient (limiting selectivity coefficient) corresponds to such situations of the cell and is considered to be a parameter correctly describing the properties of the membrane.[8]

Table 1. Changes in composition of aqueous solutions in the cell

0.1 M NaI (′)/CV–I in nitrobenzene/0.1 M NaX (″).

Concn of CV–I / M	X	$c''(I^-)$ / M	log $K^{pot}(I^-, X)$ Apparent	Corrected
5×10^{-4}	NO_3^-	4.7×10^{-5}	−1.3	−1.3
5×10^{-3}	NO_3^-	2.6×10^{-4}	−1.2	−1.2
5×10^{-2}	NO_3^-	8.5×10^{-4}	−0.95	−0.98
5×10^{-4}	ClO_4^-	1.1×10^{-4}	1.97	1.97
5×10^{-3}	ClO_4^-	2.9×10^{-4}	1.96	1.96
5×10^{-2}	ClO_4^-	2.0×10^{-3}	1.86	1.86

The variation of the selectivity coefficient may also be attributed partly to the contamination of the bulk solution itself caused by the counter-ion exchange mentioned above. Table 1 shows the composition changes in bulk solutions observed with some bi-ionic cells, together with the apparent selectivity coefficients obtained as before from the measured potentials. In this table $c''(I^-)$ represents the molarity of iodide ions (in solution (″)) which were exchanged for nitrate or perchlorate ions (initially present in solution (″)) during the potential measurement. The selectivity coefficients corrected for the composition change in solution (″) (*i.e.*, calculated by use of Eq. 3 with $a'(NO_3^-)=0$ or $a'(ClO_4^-)=0$) are presented in the last column. As can be seen from the table, however, this correction is small and the selectivity coefficient still shows the variation with the ion exchanger concentration. (Incidentally, the limiting selectivity coefficients $K^{pot}(I^-, NO_3^-)$ and $K^{pot}(I^-, ClO_4^-)$ were found to be −1.3 and 1.97, respectively, on logarithmic scale). The variation of the selectivity coefficient is thus ascribed mainly to the change of ionic composition at the membrane-solution interface.

The limiting selectivity coefficient is also applied to cells in which the two solutions each contain only one of two species of counter ions but at different concentrations, as long as the composition change at the interface is expected to be small. Figures 3 and 4

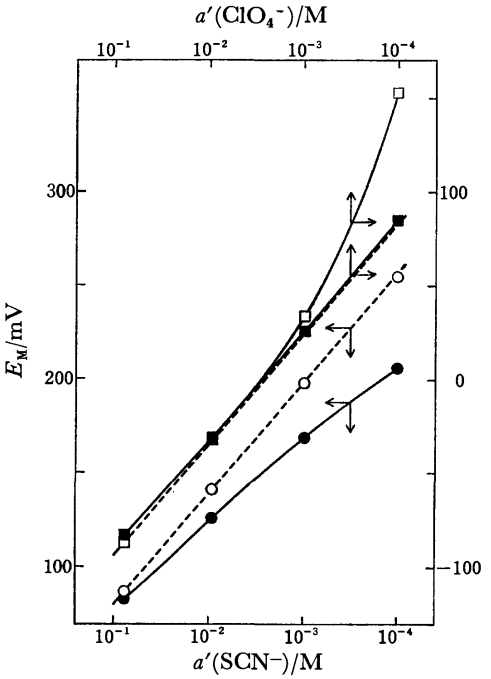

Fig. 3. Membrane potential *vs.* anion activity. Systems: ○, ●, NaSCN with molarity variable (′)–0.1 M $NaClO_4$ (″); □, ■, $NaClO_4$ with molarity variable (′)–0.1 M NaSCN (″). Membrane solvent: nitrobenzene. Ion exchangers: ○, □, 5×10^{-4} M CV-SCN; ●, ■, 5×10^{-4} M CV-ClO_4.

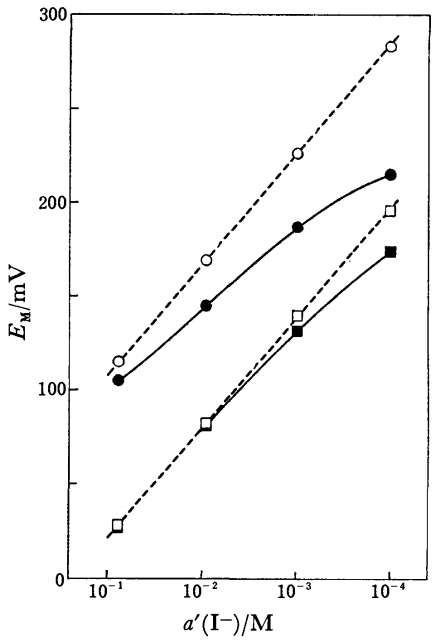

Fig. 4. Membrane potential *vs.* activity of iodide ion. Systems: ○, ●, NaI with molarity variable (′)–0.1 M $NaClO_4$ (″); □, ■, NaI with molarity variable (′)–0.1 M NaSCN (″). Membrane solvent: nitrobenzene. Ion exchangers: ○, □, 5×10^{-4} M CV–I; ●, 5×10^{-4} M CV-ClO_4; ■, 5×10^{-4} M CV-SCN.

show membrane potentials measured with such cells, where ClO_4^-, SCN^-, and I^- are paired against each other. The observed potentials are indicated by points; the dashed lines represent the values calculated from Eq. 4 with the values of the limiting selectivity coefficient obtained in the corresponding bi-ionic systems (see Table 2). (The solid curves merely connect the experimental points). The experimental points can be seen to agree with the calculated lines in cells of the type: NaX with molarity variable (′)/5×10^{-4} M CV–X in nitrobenzene/0.1 M NaY (″) where X=SCN^-, Y=ClO_4^-; X=I^-, Y=ClO_4^-; or X=I^-, Y=SCN^-. Figures 3 and 4 also illustrate the effect on the membrane potential of varying the counter ion species initially present in the membrane. When in the above cells CV–Y is used, instead of CV–X, as the ion exchanger, the measured potentials become lower than the calculated, which is due to the composition change at the membrane-solution (′) interface. In the cell: $NaClO_4$ with molarity variable (′)/5×10^{-4} M CV–ClO_4 in nitrobenzene/0.1 M NaSCN (″), although solution (′) and the membrane contain the same counter ion, perchlorate ion, the experimental points lie slightly above the corresponding calculated line (dashed). This is probably because the concentration of NaSCN in solution (″) (0.1 M) is not high enough to eliminate completely the effect of the composition change at the membrane-solution (″) interface.

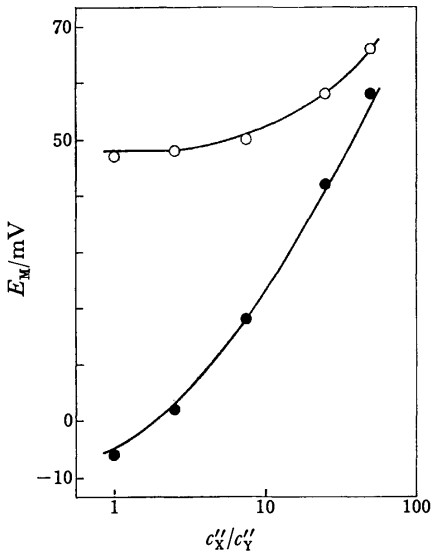

Fig. 5. Comparison of experimental and calculated potentials in the mixed electrolyte system NaX (′)/10^{-4} M CV–X in nitrobenzene/NaX+NaY (″) where $c'_X=10^{-2}$ M, c''_X=variable, and $c''_Y=2\times10^{-3}$ M. ○: X=SCN^-, Y=ClO_4^-; ●: X=I^-, Y=SCN^-.

The limiting selectivity coefficient is further applicable to mixed electrolyte systems. Typical data for such systems are shown in Fig. 5. Circles represent the experimentally observed potentials for mixed solutions containing a pair of counter ions, either SCN^-–ClO_4^- or I^-–SCN^-. The curves were drawn according to Eq. 3 with the values of the limiting selectivity coefficient obtained in the corresponding bi-ionic systems. The agreement between the experimental and calculated potentials is seen to be excellent.

As judged from the association constants of ion pairs in nitrobenzene,[9–11] the degree of ion association in the membrane used here is small and virtually negligible at the low exchanger concentrations. For the case of a liquid ion exchange membrane with negligible association, Conti and Eisenman[12] have shown theoretically that the selectivity coefficient between counter ions X and Y is given by

$$K^{pot}_{X,Y}=\frac{\bar{u}_Y k_Y}{\bar{u}_X k_X}, \tag{8}$$

where $\bar{u}_X$ and $\bar{u}_Y$ are the mobilities of ions X and Y in the membrane, and k_X and k_Y are the single-ion distribution coefficients between the membrane solvent and water. The selectivity coefficient is therefore expected to be nearly independent of solution concentration, composition, and exchanger concentration, which is consistent with the experimental observations described above.

Table 2. Comparison of limiting selectivity coefficients with calculated values

X	Y	$\log K^{pot}_{X,Y}$	
		Limiting	Calcd
I^-	ClO_4^-	1.97	1.94
SCN^-	ClO_4^-	1.5	1.39
I^-	SCN^-	0.47	0.546

For a direct comparison of the limiting selectivity coefficient with that expected from Eq. 8, the parameters controlling the selectivity were evaluated. The distribution coefficients of perchlorate, thiocyanate, and iodide salts of Fuchsine Basic between nitrobenzene and water were found to be 68.1, 13.1, and 7.40, respectively. Here the distribution coefficient is given as the ratio of the salt concentration in the organic phase to that in the aqueous phase. The value of k_Y/k_X was calculated from the square of the ratio of these distribution coefficients. The corresponding value of $\bar{u}_Y/\bar{u}_X$ was obtained from the ratio of the limiting ionic conductances.[11,13] The selectivity coefficients calculated by Eq. 8 from these values are compared with limiting selectivity coefficients[14] in Table 2. The limiting selectivity coefficients can be seen to be in good agreement with the calculated values.

Appendix

The ionic fluxes in the diffusion layer (at the solution side of the membrane-solution interface) may be expressed by the following Nernst-Planck equations:

$$J_X=-u_X c_X\frac{d}{dx}(RT\ln c_X-F\phi), \tag{A-1}$$

$$J_Y=-u_Y c_Y\frac{d}{dx}(RT\ln c_Y-F\phi), \tag{A-2}$$

$$J_{Na}=-u_{Na} c_{Na}\frac{d}{dx}(RT\ln c_{Na}+F\phi), \tag{A-3}$$

where J_X, J_Y, and J_{Na} are the fluxes of counter ions (univalent anions) X and Y and sodium ion (co-ion); u_X, u_Y, and u_{Na}, and c_X, c_Y, and c_{Na} are the corresponding mobilities and concentrations (u_X, u_Y, and u_{Na} are assumed to be constants); ϕ is the electric potential; and x is the space coordinate perpendicular to the membrane-solution interface. The conditions of electroneutrality and absence of electric current lead to

$$c_X + c_Y = c_{Na}, \quad \text{(A-4)}$$

$$J_X + J_Y = J_{Na} = 0, \quad \text{(A-5)}$$

where it has been assumed that the membrane is impermeable to sodium ion. Inserting Eqs. A-1—A-3 into Eq. A-5 and eliminating $d\phi/dx$, we have

$$\frac{d\{c_{Na}(u_X c_X + u_Y c_Y)\}}{dx} = 0. \quad \text{(A-6)}$$

For the case where $u_X = u_Y$, Eq. A-6 becomes with the help of Eq. A-4

$$\frac{dc_{Na}}{dx} = \frac{d(c_X + c_Y)}{dx} = 0. \quad \text{(A-7)}$$

Inserting this result into Eq. A-3 and taking into account Eq. A-5, we obtain

$$\frac{d\phi}{dx} = 0. \quad \text{(A-8)}$$

Thus the total counter-ion concentration and the electric potential are constant throughout the diffusion layer.

References

1) J. W. Ross, Jr., "Ion-Selective Electrodes," National Bureau of Standards Special Publication, No. 314, ed by R. A. Durst, U. S. Government Printing Office, Washington, D. C. (1969), Chap. 2.

2) K. Srinivasan and G. A. Rechnitz, *Anal. Chem.*, **41**, 1203 (1969).

3) S. Bäck, *Anal. Chem.*, **44**, 1696 (1972).

4) P. R. Danesi, G. Scibona, and B. Scuppa, *Anal. Chem.*, **43**, 1892 (1971).

5) Except in this system, activity coefficients were obtained from Kielland's table since solution concentrations were all below 0.1 M. J. Kielland, *J. Am. Chem. Soc.*, **59**, 1675 (1937).

6) The limiting value of the selectivity coefficient was found to be more easily obtained in cases where the counter ion less extractable into the membrane was initially present in the membrane. In order to determine the limiting value of K^{pot} (SCN^-, ClO_4^-), for example, the membrane containing the less extractable thiocyanate ion was preferable to the membrane containing perchlorate ion.

7) For these ions, the ratio of the limiting ionic conductances does not exceed 1.2 in water. "Landolt-Börnstein Tabellen," Vol. II, Part 7, 6th ed, Springer-Verlag, Berlin, Göttingen, and Heidelberg (1960), pp. 259, 261.

8) G. Shean and K. Sollner [*J. Membr. Biol.*, **9**, 297 (1972)] have also found that bi-ionic potentials are essentially independent of solution concentration and exchanger concentration, although their experimental conditions are somewhat different from ours.

9) N. Ishibashi, H. Kohara, and K. Horinouchi, *Talanta*, **20**, 867 (1973).

10) E. Hirsch and R. M. Fuoss, *J. Am. Chem. Soc.*, **82**, 1018 (1960).

11) F. R. Longo, J. D. Kerstetter, T. F. Kumosinski, and E. C. Evers, *J. Phys. Chem.*, **70**, 431 (1966).

12) F. Conti and G. Eisenman, *Biophys. J.*, **6**, 227 (1966); J. Sandblom, G. Eisenman, and J. L. Walker, Jr., *J. Phys. Chem.*, **71**, 3862 (1967).

13) C. R. Witschonke and C. A. Kraus, *J. Am. Chem. Soc.*, **69**, 2472 (1947).

14) In this case, strictly speaking, the limiting selectivity coefficient must be evaluated under conditions in which a steady state is established across the membrane, since the Conti-Eisenman theory applies only to such experimental conditions. For this purpose membrane potentials were measured by using a cell with a stirred membrane. When the membrane phase is stirred, no concentration gradient of ions exists inside the bulk membrane and a stable concentration gradient will be established in the (unstirred) diffusion layers just internal to each membrane-solution interface. Hence, as far as the membrane potential is concerned, the membrane phase may be regarded as consisting of the two diffusion layers alone where the steady state required by the theory is attained. However, in cells in which the influence of the composition change at the interface (discussed in the text) is negligible, the stirring of the membrane interior had little effect on the membrane potential. Thus the value of the limiting selectivity coefficient was the same with stirred and unstirred membranes.

Electronic States of the Picric Acid Complexes with 1-Methylnicotinamide, Tryptamine, DL-Tryptophan, and Serotonin

Masashi TANAKA

Department of Chemistry, Faculty of Science, Nagoya University, Chikusa, Nagoya 464

(Received July 25, 1977)

The polarized reflection spectra of the crystals of the picric acid complexes with 1-methylnicotinamide, tryptamine, DL-tryptophan and serotonin have been measured from 15000 to 40000 cm^{-1} and the molar extinction coefficient of these crystals has been obtained by the Kramers-Kronig transformation. Furthermore, the theoretical calculation of the electronic states of these complexes has been made and compared with the experimental results. This analysis shows that the appearance of the new band in the region of 20000 cm^{-1} is the origin of the reddish color of the crystals of tryptamine picrate, DL-tryptophan picrate, and serotonin picrate; the new band can be assigned to the charge-transfer band from the picrate anion to the indole nucleus.

Indole derivatives are widely distributed through biological systems and form donor-acceptor complexes with a variety of aromatic acceptors. Szent-Gyorgyi and Isenberg[1] reported the formation of colors on mixing electron donors such as indole with certain electron acceptors and further showed that the new band, not present in either component alone, can be assigned to the charge-transfer band.

The charge-transfer interactions were shown to play an important part in such biological processes as the binding of nicotinamide[2-3] and flavin coenzymes[4] to tryptophan residues of enzymes, the interactions of indoles with nucleotides and with nucleic acid,[5] and the binding of serotonin and hallucinogenic tryptamines to synaptic receptor sites.[6]

The simplest of the substituted nicotinamides, 1-methylnicotinamide, forms donor-acceptor complexes with iodide ions.[7] Freeman and Bugg[8] determined the crystal structure of the iodide of 1-methylnicotinamide and compared the interactions and structural features in this iodide salt with the crystal structures of the chloride and picrate salts of 1-methylnicotinamide, where charge-transfer forces are expected to be of little or no importance.

Tryptamine picrate is obtained as a reddish orange salt; DL-tryptophan picrate is prepared as a reddish brown crystal; and serotonin crystallized as a dark red picric salt. Since these amino acids are colorless and the picrate ion is pale yellow, the red color of the picrate salts is unexpected and suggests the formation of a donor-acceptor complex. Thewalt and Buug[9] determined the crystal structure of serotonin picrate monohydrate in order to examine the solid state interactions between serotonin and the picrate ion. Gartland, Freeman, and Bugg[10] described the crystal structures of the picrate complexes of tryptamine and DL-tryptophan in order to obtain information about the structural factors involved in the indole interactions with aromatic acceptors.

The complexes of picric acid with amines revealed that a proton is transferred from picric acid to amine and the interaction between the picrate ion and the amine molecule is capable of producing a charge-transfer absorption band. Matsunaga[11] reported that the picrate anion is as strong as picric acid as an electron acceptor and the indole derivatives are the electron donors and the color of the tryptophan picrate complex aries from the charge-transfer interaction between the nucleus and the picrate anion.

The author undertook the spectroscopic examination of the crystals of the picrate complexes with 1-methylnicotinamide, tryptamine, DL-tryptophan, and serotonin molecules by measuring the microscopic polarized reflection spectra. Furthermore, we studied theoretically the electronic states of these complexes and showed that the new band in the region of 20000 cm^{-1} is the charge-transfer band from the picrate anion to the indole nucleus.

Experimental and Theoretical

Single crystals of the picrate complex with 1-methylnicotinamide, tryptamine, DL-tryptophan, and serotonin were crystallized by the slow evaporation of the solution of the salt.

Reflection spectra at the normal incidence have been measured over a range of 15000—40000 cm^{-1} with a reflection spectrophotometer made in our laboratory and the absorption spectra have been obtained by the Kramers-Kronig transformation.

The electronic states of the molecules are calculated by the Pariser-Parr-Pople[12] SCF method in order to obtain the molecular orbitals and the orbital energies.

The two-center coulomb integrals γ_{pq} are estimated by Nishimoto-Mataga's method.[13] The one-center core coulomb integrals α_p and the two-center core resonance integrals β_{pq} are approximated in the following equations:

$$\alpha_p = -I_p - (n_p-1)\gamma_{pp} - \sum_{r\neq p} n_r\gamma_{pr},$$

$$\beta_{pq} = -K(I_p+I_q)S_{pq},$$

where the constant K is taken to be 0.39. The overlap integrals S_{pq} are calculated between the nearest neighbor atoms by using the Slater type AO's and neglected in other cases. Then, the overlap integrals S_{CN} between the 2pπ AO's of the carbon atom on the benzene ring and the nitrogen atom on the nitro group are estimated by the equation

$$S_{CN} = S^{\circ}_{CN}\cos\theta,$$

where θ is the dihedral angle between the two 2pπ AO's χ_C and χ_N. The overlap integrals S°_{CN} are determined by using the 2pπ AO's χ°_C and χ°_N on the same plane. The values of the first ionization potentials I_P are taken from Pilcher and Skinner's[14] table and the one-center coulomb integrals γ_{PP} are given by the relation $\gamma_{pp}=I_p-A$. These parameters (I_p, γ_{pp}, and n_p) are given in Table 1.

The intermolecular overlap integrals are written as follows:

Table 1. The values of the ionization potentials (I_p in eV), the one-center intergrals (γ_{pp} in eV), and the core charge (n_p) used in the SCF calculation

Atom		I_p	r_{pp}	n_p	Bonding type
Carbon	$t_1t_2t_3z$	−11.22	10.60	1	-CH=CH-
Nitrogen	$t_1^2t_2t_3z$	−14.51	13.31	1	-N=CH-
	$t_1t_2t_3z^2$	−12.26	13.31	2	-NH-, $-NO_2$
Oxygen	sx^2y^2z	−17.76	13.89	1	$-NO_2$
	$t_1^2t_2t_3z^2$	−14.97	14.89	2	-OH
	$t_1^2t_2^2t_3z^2$	−14.97	14.89	1	$-O^-$

$$S_{at,bf} = \int \phi_a^t(1)^* \phi_b^f(1) d\tau = \sum_{p,q} C_{at,p} C_{bf,q} (\chi_p^a | \chi_q^b)$$

where ϕ_a^t is the t-th molecular orbital on the molecule a and ϕ_b^f the f-th molecular orbital on the molecule b. χ_p^a is the $2p\pi$ AO of the p-th atom on the molecule a and χ_q^b the $2p\pi$ AO of the q-th atom on the molecule b. Then, the intermolecular overlap integrals involve the integrals between two $2p\pi$ AO's χ_p^a and χ_q^b at orientations determined by the crystal structure. The line joining the atoms p and q defines the z axis and the y axis may be chosen to be perpendicular to one orbital, defining

$$A = \boldsymbol{n}\cdot\boldsymbol{x}_p, \quad B = \boldsymbol{n}\cdot\boldsymbol{y}_p = 0, \quad C = \boldsymbol{n}\cdot\boldsymbol{z}_p,$$
$$D = \boldsymbol{m}\cdot\boldsymbol{x}_q, \quad E = \boldsymbol{m}\cdot\boldsymbol{y}_q, \quad F = \boldsymbol{m}\cdot\boldsymbol{z}_q,$$

when $\boldsymbol{n}$ and $\boldsymbol{m}$ are unit vectors in the direction of the $2p\pi$ orbitals located on the centers p and q, respectively. Then, the atomic overlap integrals may be expressed as

$$(\chi_p^a | \chi_q^b) = AD(2p\pi_p^a | 2p\pi_q^b) + CF(2p\sigma_p^a | 2p\sigma_q^b).$$

The calculation of the excitation energy of the charge-transfer complex is carried out by the composite molecule method. That is, the matrix elements between the ground configuration Φ_0, the locally excited configuration $\Phi_{at\to af}$, and the charge-transfer configuration $\Phi_{at\to bf}$ are given in the zero-differential overlap approximation as follows.

$$(\Phi_{at\to af}|H|\Phi_{at\to af}) = E_0 + \varepsilon_{af} - \varepsilon_{at} - (\phi_a^t\phi_a^t|\phi_a^f\phi_a^f) + 2(\phi_a^t\phi_a^f|\phi_a^t\phi_a^f)$$
$$(\Phi_{at\to bf}|H|\Phi_{at\to bf}) = E_0 + \varepsilon_{bf} - \varepsilon_{at} - (\phi_a^t\phi_a^t|\phi_b^f\phi_b^f) + P$$
$$(\Phi_{at\to af}|H|\Phi_{ak\to al}) = 2(\phi_a^t\phi_a^f|\phi_a^k\phi_a^l) - (\phi_a^t\phi_a^k|\phi_a^f\phi_a^l)$$
$$(\Phi_{at\to af}|H|\Phi_{bk\to bl}) = 2(\phi_a^t\phi_a^f|\phi_b^k\phi_b^l)$$
$$(\Phi_{at\to bf}|H|\Phi_{ak\to bl}) = -(\phi_a^t\phi_a^k|\phi_b^f\phi_b^l)$$
$$(\Phi_{at\to bf}|H|\Phi_0) = \sqrt{2}K'S_{at,bf}$$
$$(\Phi_{at\to bf}|H|\Phi_{at\to bl}) = K'S_{bf,ql}$$
$$(\Phi_{at\to bf}|H|\Phi_{bk\to bf}) = -K'S_{at,bk}$$
$$(\Phi_0|H|\Phi_{at\to af}) = (\Phi_{at\to af}|H|\Phi_{ak\to bl}) = (\Phi_{at\to bf}|H|\Phi_{bk\to al}) = 0$$

Here P is the term which takes into account the polarization effect and K' is a constant. ε_{at} is the orbital energy of the t-th MO on the molecule a and ε_{bf} the orbital energy of the f-th MO on the molecule b.

In the calculation of the picrate complexes, P is taken to be 0.8 eV and K' given as −15.0 eV. All of the above-mentioned computations were carried out on a FACOM 230-75 computer at the Nagoya University computation center.

Results and Discussion

1-Methylnicotinamide Picrate. The picrate salt of 1-methylnicotinamide was crystallized as yellow prisms by slowly cooling a hot, saturated aqueous solution containing approximately equimolar quantities of 1-methylnicotinamide chloride and of picric acid.[8] The projection onto the ab plane of the picrate salt is shown in Fig. 1. The amino group of 1-methylnicotinamide is hydrogen bonded to the oxygen atom of the C–O^- bond in the picrate anion. The picrate and 1-methylnicotinamide moieties do not overlap and there are no unusually short intermolecular contacts except for the hydrogen-bonded interactions. Therefore, the charge-transfer interactions are probably of little importance in the crystals of 1-methylnicotinamide picrate.

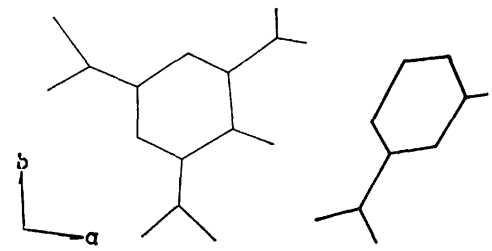

Fig. 1. Projection onto the ab plane of the crystal of 1-methylnicotinamide picrate.

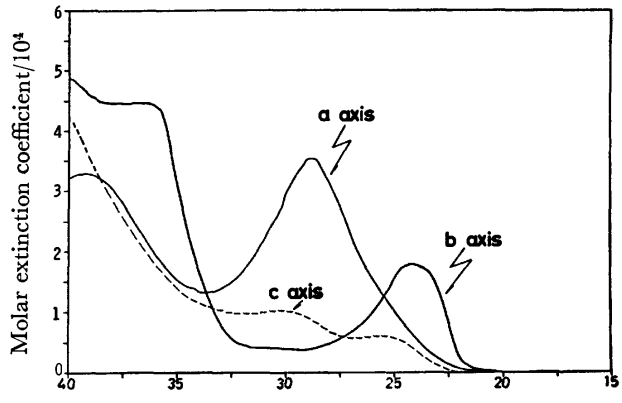

Fig. 2. The polarized absorption spectra of the crystal of 1-methylnicotinamide picrate obtained by the K-K transformation of the reflection spectra.

The absorption spectra transformed from the reflection spectra of the crystal of this salt are depicted in Fig. 2. The 23400 (LE_1) and 28800 (LE_2) cm^{-1} bands can be assigned to the local excitation band of the picrate anion. The LE_1 band is observed in the b axis spectrum and the LE_2 band in the a axis. Therefore, the LE_1 band is allowed for the light polarized perpendicular to the C–O^- bond of the picrate anion and the LE_2 band is active for the light polarized parallel to the C–O^- bond.

Tryptamine Picrate. Tryptamine picrate was obtained as a reddish orange crystal upon mixing aqueous solutions of tryptamine and picric acid. The

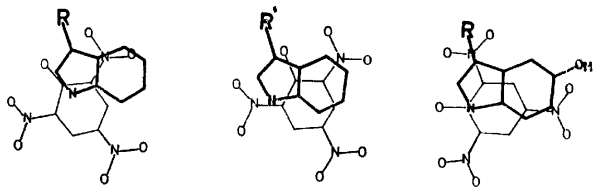

Fig. 3. Stacking patterns in the crystals of tryptamine picrate, DL-tryptophan picrate-methanol and serotonin picrate monohydrorate.

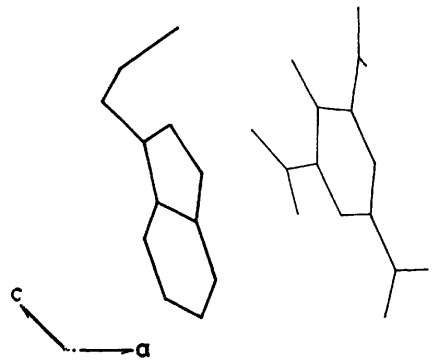

Fig. 4. Projection onto the ac plane of the crystal of tryptamine picrate.

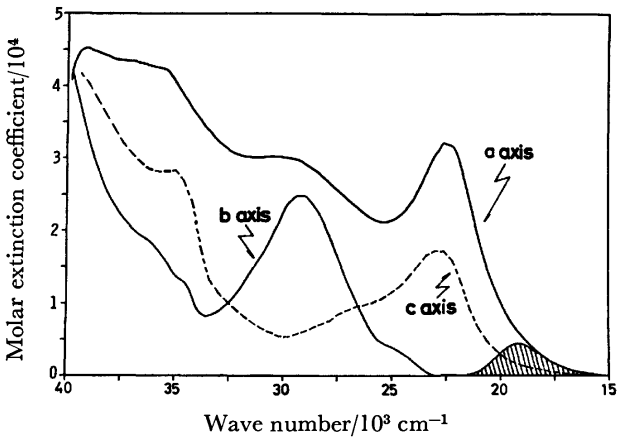

Fig. 5. The polarized absorption spectra of the crystal of tryptamine picrate obtained by the K-K transformation of the reflection spectra.

crystal packing scheme for the tryptamine picrate is described in Fig. 3 and the projection onto the ac plane in Fig. 4.[10]

The absorption spectra transformed from the reflection spectra of the crystal of this complex are shown in Fig. 5. The LE_1 band is observed at 22500 cm^{-1} in the both the a and c axes spectra and the LE_2 band at 28200 cm^{-1} mainly in the b axis spectra, as predicted from the directions of the transition moments of the LE_1 and LE_2 bands. Furthermore, the new, quite diffuse band appears as a long extension on the side of the longer wave length of the LE_1 band in the a axis spectrum. Because of this overlap, the position of the maximum of the new band cannot be known, and so the shaded region may be thought to be a new absorption band which has its peak at 19200 cm^{-1}.

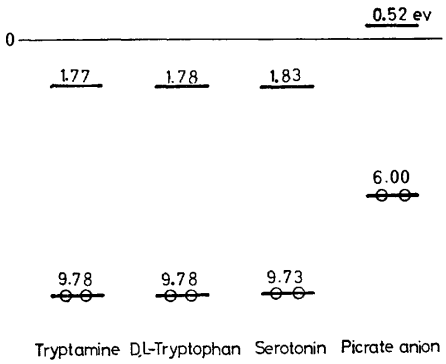

Fig. 6. The orbital energy diagram of the donor and acceptor molecules in the picrate salt system.

In the theoretical calculation, the overlap integral between the HOMO of the indole ring in the tryptamine cation and the LUMO of the picrate anion is 0.0084; the orbital energy diagram of the donor and acceptor molecules is shown in Fig. 6. The calculated excitation energy (E_{CT}) and the wavefunction (Ψ_{CT}) of the lowest excited state are shown as follows.

$$E_{CT} = 20250\ cm^{-1},$$

$$\Psi_{CT} = 0.9769\Phi(\phi_2^{10}\rightarrow\phi_1^6) - 0.1231\Phi(\phi_2^9\rightarrow\phi_1^6) + 0.1019\Phi(\phi_2^{10}\rightarrow\phi_2^{11}) + 0.0929\Phi(\phi_1^5\rightarrow\phi_1^6) + 0.0755\Phi_0.$$

The stabilization energy (ΔE) and the wave function (Ψ_0) of the ground state are written in the following equations:

$$\Delta E = 0.019\ eV,$$

$$\Psi_0 = 0.9966\Phi_0 - 0.0721\Phi(\phi_2^{10}\rightarrow\phi_1^6),$$

where ϕ_1^i is the i-th molecular orbital of the tryptamine molecule and ϕ_2^j the j-th molecular orbital of the picrate anion.

Therefore, the new band at 19200 cm^{-1} can be assigned to the chrage-transfer band from the picrate anion to the indole nucleus.

DL-Tryptophan Picrate–Methanol. Reddish brown crystals of the DL-tryptophan picrate–methanol complex were obtained by slowly evaporating a methanol solution that contained an equimolar mixture of DL-tryptophan and picric acid. The crystal packing scheme for the DL-tryptophan picrtate–methanol is depicted in Fig. 3 and the projection onto the bc plane in Fig. 7.[10]

The absorption spectra transformed from the reflection spectra of the crystal of this complex are shown in Fig. 8. The LE_1 band is observed at 23400 cm^{-1} in the

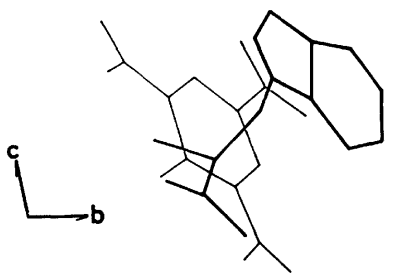

Fig. 7. Projection onto the bc plane of the crystal of DL-tryptophan picrate–methanol.

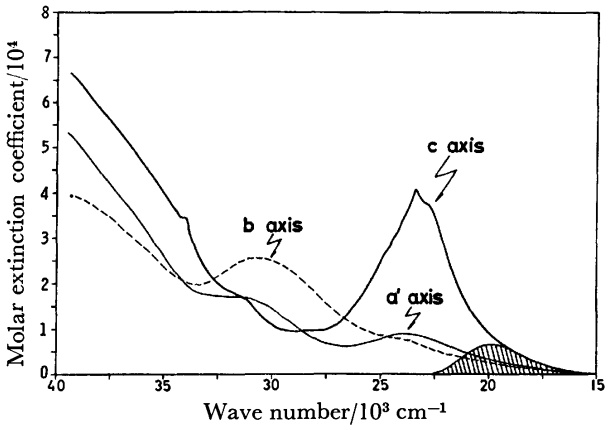

Fig. 8. The polarized absorption spectra of the crystal of DL-tryptophan picrate obtained by the K-K transformation of the reflection spectra.

c axis spectrum and the LE_2 band at 30600 cm^{-1} in the b axis spectrum, as predicted from the directions of the transition moments of the LE_1 and LE_2 bands. Furthermore, the new diffuse band appears as a long extension on the side of the longer wavelength of the LE_1 band in the c, b, and a′ axes spectra. The maximum of the new band cannot be located but the shaded region may be thought to be a new band which has its peak at 19600 cm^{-1}.

In the theoretical calculation, the overlap integral between the HOMO of the indole ring in the tryptophan cation and the LUMO of the picrate anion is 0.0077 and the relation of the orbital energies of the donor and acceptor molecules is shown in Fig. 6. The calculated excitation energy (E_{CT}) and the wavefunction (Ψ_{CT}) of the lowest excited state are expressed as follows:

$$E_{CT} = 19020\,cm^{-1},$$
$$\Psi_{CT} = 0.9918\Phi(\phi_2^{10}\rightarrow\phi_1^6) + 0.0502\Phi(\phi_1^4\rightarrow\phi_1^6) + 0.0443\Phi(\phi_1^5\rightarrow\phi_1^6) + 0.0679\Phi_0.$$

The stabilization energy (ΔE) and the wavefunction (Ψ_0) of the ground state are written in the next equations:

$$\Delta E = 0.024\,eV,$$
$$\Psi_0 = 0.9959\Phi_0 - 0.0692\Phi(\phi_2^{10}\rightarrow\phi_1^6) + 0.0444\Phi(\phi_2^9\rightarrow\phi_1^6),$$

where ϕ_1^i is the i-th molecular orbital of the tryptophan molecule and ϕ_2^j the j-th molecular orbital of the picrate anion.

Accordingly, the new band at 19600 cm^{-1} can be assigned to the charge-transfer band from the picrate anion to the indole nucleus.

Serotonin Picrate Monohydrate. Serotonin picrate monohydrate was crystallized as dark red prisms by slowly evaporating a saturated aqueous solution containing approximately equimolar quantities of serotonin creatinine sulphate and picric acid. The crystal packing for the serotonin picrate monohydrate is shown in Fig. 3 and the projection onto the bc plane in Fig. 9.[9]

The absorption spectra transformed from the reflection spectra of the crystal of this complex are shown in Fig. 10. The LE_1 band is not observed in the b and c axes spectra but the LE_2 band is observed at 27200

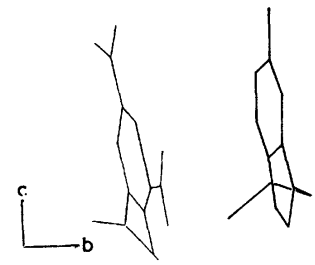

Fig. 9. Projection onto the bc plane of the crystal of serotonin picrate monohydrate.

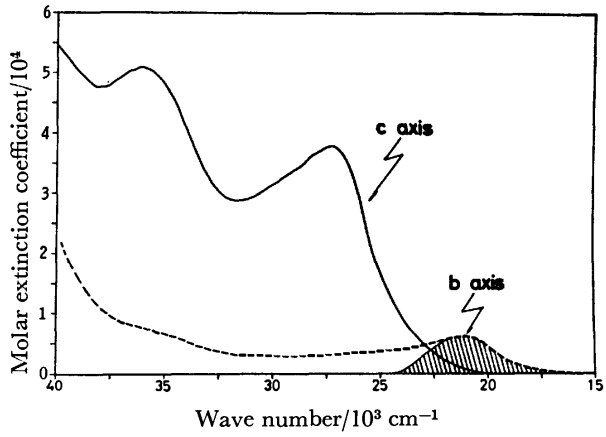

Fig. 10. The polarized absorption spectra of the crystal of serotonin picrate monohydrate.

cm^{-1} in the c axis spectrum, as expected from the direction of the transition moments of the LE_1 and LE_2 bands. Furthermore, the new band appears at 21000 cm^{-1} in the b axis spectrum and the observed transition moment is directed along the intermolecular vector between the hydroxyindole and picrate molecules.

In the theoretical calculation, the overlap integral between the HOMO of the hydroxyindole ring in the serotonin cation and the LUMO of the picrate anion is 0.0059; the diagram of the orbital energies of the donor and acceptor molecules is shown in Fig. 6. The calculated excitation energy (E_{CT}) and the wavefunction (Ψ_{CT}) of the lowest excited state are written as follows.

$$E_{CT} = 20770\,cm^{-1},$$
$$\Psi_{CT} = 0.9678\Phi(\phi_2^{10}\rightarrow\phi_1^7) - 0.1735\Phi(\phi_2^9\rightarrow\phi_1^7) + 0.0640\Phi(\phi_2^{10}\rightarrow\phi_1^8) - 0.0623\Phi(\phi_2^{10}\rightarrow\phi_2^{11}) + 0.1289\Phi(\phi_1^5\rightarrow\phi_1^7) + 0.0533\Phi_0.$$

The stabilization energy (ΔE) and the wavefunction (Ψ_0) of the ground state are given in the following equations:

$$\Delta E = 0.013\,eV,$$
$$\Psi_0 = 0.9978\Phi_0 - 0.0491\Phi(\phi_2^{10}\rightarrow\phi_1^7),$$

where ϕ_1^i is the i-th molecular orbital of the serotonin molecule and ϕ_2^j the j-th molecular orbital of the picrate anion.

Therefore, the new band at 21000 cm^{-1} can be assigned to the charge-transfer band from the picrate anion to the hydroxyindole nucleus.

References

1) A. Szent-Gyorgyi and I. Isenberg, *Proc. Natl. Acad. Sci.*, **46**, 1334 (1960).
2) S. G. Alivisatos, F. Ungar, A. Jibril, and G. A. Mourkides, *Biochim. Biophys. Acta*, **51**, 361 (1961).
3) G. Cilento and P. Tedeschi, *J. Biol. Chem.*, **236**, 907 (1961).
4) J. E. Wilson, *Biochemistry*, **5**, 1351 (1966).
5) T. Montenay-Garestier and C. Helene, *Biochemistry*, **10**, 300 (1971).
6) A. Szent-Gyorgyi, "Introduction to a Submolecular Biology," Academic Press, New York (1960), p. 107.
7) E. M. Kosower, "The Enzymes," Vol III, Acedamic Press, New York (1960), p. 171.
8) G. R. Freeman and C. E. Bugg, *Acta Crystallogr., Sect B*, **30**, 431 (1974).
9) U. Thewalt and C. E. Bugg, *Acta Crystallogr., Sect. B*, **28**, 82 (1972).
10) G. L. Gartland, G. R. Freeman, and C. E. Bugg, *Acta Crystallogr., Sect. B*, **30**, 1841 (1974).
11) Y. Matsunaga, *Bull. Chem. Soc. Jpn.*, **46**, 998 (1973).
12) R. Pariser and R. G. Parr, *J. Chem. Phys.*, **21**, 466, 767 (1953); J. A. Pople, *Trans. Faraday Soc.*, **49**, 1375 (1953).
13) K. Nishimoto and N. Mataga, *Z. Phys. Chem. (NF)*., **12**, 335 (1957).
14) G. Pilcher and H. A. Skinner, *J. Inorg. Nucl. Chem.*, **24**, 937 (1962).

Studies of Electrode Processes of Oxovanadium(IV). IV. Catalytic Reduction of Acetylacetone Coupled with Cathodic Reduction of Bis(acetylacetonato)oxovanadium(IV)

Mitsutaka KITAMURA, Kazuo SASAKI,* and Hideo IMAI

Faculty of Integrated Arts and Sciences, Hiroshima University, Hiroshima 730
**Faculty of Engineering, Hiroshima University, Hiroshima 730*

(Received February 24, 1977)

Acetylacetone was catalytically reduced in the course of the electrolytic reduction of bis(acetylacetonato)-oxovanadium(IV) at a mercury cathode. In acetonitrile solutions the catalytic reduction proceeded at −2.1 V *vs.* Ag/0.01 mol dm^{-3} $AgClO_4$ electrode and the reduction products were hydrogen and acetylacetonate anion, while by the direct electrolysis of acetylacetone at −2.5 V a product with vicinal hydroxyl groups was formed. A steady-state current was observed in the controlled potential electrolysis. A reaction mechanism involving the regeneration of trivalent vanadium by the coupled chemical reaction of divalent vanadium with acetylacetone is proposed.

The electrochemical or photochemical behavior of oxovanadium(IV) complexes has been reported in previous papers.[1-3] Although in acetonitrile solution containing a large excess of acetylacetone (Hacac) a well-defined polarographic cathodic wave of bis-(acetylacetonato)oxovanadium(IV), $[VO(acac)_2]$, was developed in a single step with two-electron transfer, only trivalent vanadium was detected in the solution subjected to controlled potential electrolysis at −2.1 V *vs.* Ag/0.01 M $AgClO_4$ electrode (M=mol dm^{-3}). The processes involved therein were postulated as follows:

(1) One-electron transfer to break a V-O bond;

$$[VO(acac)_2] + e^- + \text{Hacac} \longrightarrow [V(acac)_3] + OH^-. \quad (1)$$

(2) Further one-electron transfer to form divalent vanadium;

$$[V(acac)_3] + e^- \longrightarrow [V(acac)_3]^-. \quad (2)$$

Reaction 1 proceeded at a more negative potential ($E_1/_2$=−1.93 V) than Reaction 2 ($E_1/_2$=−1.78 V) owing to the strong V-O bond and ligand rearrangement. Reactions 1 and 2 may be followed by the reaction of OH^- with Hacac or of $[V(acac)_3]^-$ with $[VO(acac)_2]$, thus forming $acac^-$ or $[V(acac)_3]$. But, the concentration of $acac^-$ was found to increase even after the vanadyl species was depleted completely in the solution, suggesting another route in the reaction sequence.

The evidence for catalytic regeneration of trivalent vanadium by a coupled chemical reaction of divalent vanadium with Hacac is presented in this paper, and the reaction mechanism is discussed.

Experimental

An ordinary polarograph and a potentiostat were used, and the UV and visible absorption spectroscopy and vapor phase chromatography were employed for subsidiary purposes.

For the controlled potential electrolysis a three-compartment cell separated by sintered glass diaphragms was used. A mercury pool cathode was stirred by a magnetic bar, and the solution was agitated by bubbling purified nitrogen through it. For measurements of steady-state current, vigorous agitation was essential in order to obtain reproducible data. The reference electrode was Ag/0.01 M $AgClO_4$ electrode.

Solutions were prepared by using purified acetonitrile, which contained a trace of water. The supporting electrolyte was tetraethylammonium perchlorate (TEAP). The prepared solution was deaerated carefully by bubbling purified nitrogen through it. Experiments were carried out at room temperature.

Results and Discussion

Reduction Mechanism of Acetylacetone. Acetylacetone in an acetonitrile solution containing 0.1 M TEAP developed an irreversible polarographic cathodic wave at about −2.3——2.4 V, the reduction potential being largely shifted with the concentration of Hacac. After the reduction of Hacac by the controlled potential electrolysis at −2.5 V, the polarogram showed an anodic wave at −0.45 V corresponding to the anodic process of $acac^-$. The absorption spectra before and after the electrolysis are shown in Fig. 1. The wavelengths of the absorption maximum, 273 nm for Hacac and 293 nm for $acac^-$, coincide well with Neal and Murray's data.[4] The difference between our results and Neal and Murray's data can be attributed to the difference in reaction mechanisms, as will be described later. Neal and Murray used a thin layer cell for the electrolysis of Hacac in acetonitrile, and confirmed $acac^-$ (I) to be the main reduction product. In addition to $acac^-$, in our case where an ordinary electrolysis cell was used, the existence of vicinal hydroxyl groups was confirmed in the reduction products by means of the periodate titration. It is highly likely that the

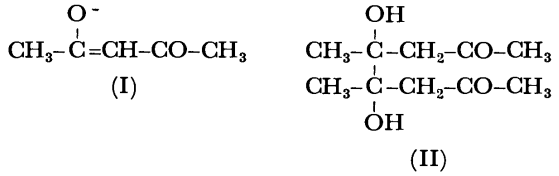

(I) (II)

product is 4,5-dihydroxy-4,5-dimethyl-2,7-octanedione (II). This estimate is supported by the formation of pinacol as a dimeric product of the reduction of 1,3-diphenyl-1,3-propanedione in DMSO as reported by Buchta and Evans.[5] Vapor phase chromatography indicated that an ether extract from the electrolyzed solution contained two dominant species which appeared

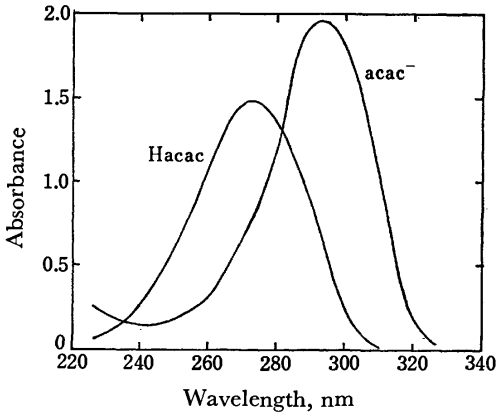

Fig. 1. Absorption spectra of 0.22 mM Hacac in acetonitrile solution before and after controlled potential electrolysis at −2.5 V.

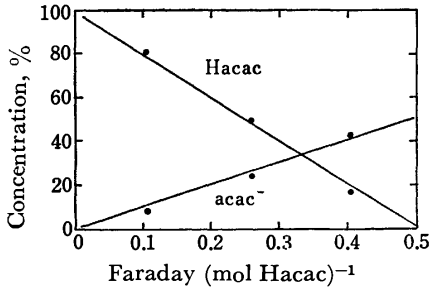

Fig. 2. Relative change in concentrations of Hacac and acac⁻ in the course of controlled potential electrolysis of Hacac at −2.5 V. Solution: 1 mM Hacac in acetonitrile solution containing 0.1 M TEAP.

at far later stages compared with the retention time of pinacol derived from acetone. Unfortunately, the direct confirmation of these compounds was unsuccessful, owing to their extreme instability and rapid decomposition during the isolation procedure.

The relative concentration changes in both Hacac and acac⁻ during the course of the controlled potential electrolysis were monitored by using an ordinary polarograph. The result is shown in Fig. 2, where the ordinate and abscissa are expressed in terms of the concentration ratio in % and electricity consumed in Faraday mol^{-1}, respectively. As is seen in Fig. 2, the descending line intersects the abscissa at about 0.5 Faraday mol^{-1}. This indicates that the number of electrons transferred per molecule (n) is equal to 0.5. The increase of the concentration of acac⁻ was no longer observed after 0.5 Faraday mol^{-1} was consumed. Since the increment of acac⁻ is exactly one half of the decrement of Hacac, it is concluded that one mol of acac⁻ is produced from two mol of Hacac. Taking the product with vicinal hydroxyl groups into consideration, the reaction scheme can be expressed as follows:

$$4\ \text{enol–Hacac} + 2e^- \longrightarrow \text{Dimer} + 2\text{acac}^-. \quad (3)$$

In reaction 3 a proton abstraction by an acetylacetone anion radical from an acetylacetone molecule is assumed to be involved.

This reaction mechanism is consistent with the observed facts, but inconsistent with the result obtained by Neal and Murray,[3] who concluded that the reaction proceeded as follows:

$$\text{Hacac} + e^- \longrightarrow \text{Hacac}^{\cdot} \longrightarrow \frac{1}{2}H_2 + \text{acac}^{\cdot}. \quad (4)$$

According to the reaction mechanism of Eq. 4, the stoichiometric molar ratio of Hacac and acac⁻ is 1 : 1. The difference between Reactions 3 and 4 is clearly shown when we compare the ratio of absorbance of Hacac and acac⁻ in Fig. 1 of this report and Fig. 1 of Ref. 4. The difference in the reaction mechanisms seems to be attributed to the experimental techniques employed. In the thin layer cell used by Neal and Murray, most of the depolarizer undergoes the electrode reaction without any complication such as proton abstraction or dimer formation, and the reaction intermediate seems to decompose directly to hydrogen and acac⁻.

Bis(acetylacetonato)oxovanadium(IV) dissolved in the acetonitrile solution containing an amount of Hacac 20 times excess in molar ratio was reduced at a dropping mercury electrode with the half-wave potential of −2.00 V; the reduction product was divalent vanadium, as shown in Eqs. 1 and 2. In polarograms observed *in situ* in solutions subjected to the controlled potential electrolysis at −2.1 V the same anodic wave was observed at −0.45 V as in the case of the direct electrolytic reduction of Hacac. But in this case no dimeric product with vicinal hydroxyl groups could be detected. The relative concentration changes of Hacac and acac⁻ during the course of the controlled potential electrolysis are shown in Fig. 3. The concentration change of oxovanadium(IV) ions in Fig. 3 was separately measured spectrophotometrically at the wavelength of 700 nm by using 3 mM bis(acetylacetonato)oxovanadium(IV) solution. As shown in Fig. 3, oxovanadium(IV) ions are quickly depleted with a coulombic efficiency of about 1 faraday mol^{-1}. The concentration of acac⁻ increased steadily even after the oxovanadium(IV) ions were depleted completely. The increment of acac⁻ at each quantity of electricity consumed was exactly equal to the decrement of Hacac, as shown in Fig. 3, so that the stoichiometric molar ratio of acac⁻ and Hacac was 1 : 1. The extrapolation of the descending line gives an

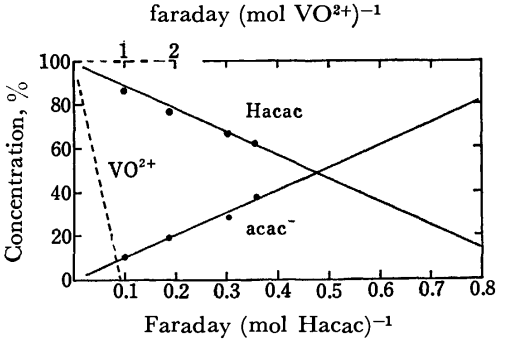

Fig. 3. Relative change in concentrations of VO^{2+}, Hacac and acac⁻ in the course of controlled potential electrolysis of VO^{2+} at −2.1 V. Solution: 1 mM [VO(acac)$_2$] and 20 mM Hacac in acetonitrile solution containing 0.1 M TEAP. (Refer to the text in relation to the concentration change of VO^{2+}.)

intercept at about 1 F mol^{-1}. This result indicates that the value of n is unity. It is noteworthy that this result coincides well with Neal and Murray's result. In view of these findings the following reaction mechanism is deduced:

$$[V(acac)_3]^- + Hacac \longrightarrow [V(acac)_3] + Hacac^{\cdot}, \quad (5)$$

$$Hacac^{\cdot} \longrightarrow \frac{1}{2}H_2 + acac^-. \quad (6)$$

Reaction 2 is coupled with Reaction 5, so that Hacac is catalytically reduced by a regenerative cycle of vanadium(II). This mechanism is also supported by the fact that the limiting current of oxovanadium(IV) ion shows the characteristics of kinetic current, as shown previously in Ref. 2. The formation of a dimeric product by Reaction 3 does not seem to be involved in this case.

Steady-state Current in Controlled Potential Electrolysis. When a solution containing a known quantity of oxovanadium(IV) ion and 20 times excess of Hacac was electrolyzed at −2.1 V, the electrolytic current decreased gradually and attained a steady-state value in a few minutes. The plot of the steady-state current, i_{st}, *versus* the concentration of oxovanadium(IV), C_y, is shown in Fig. 4, where i_{st} is linearly proportional to C_y up to the concentration of 0.6 mM. As described in the previous paper,[2] the color of the electrolyzed solution turned to greenish yellow and finally to dark green. The dark green color indicates the existence of divalent vanadium in the solution bulk, but it promptly fades to yellow on being left to stand in a nitrogen atmosphere. The yellow solution was cathodically reduced to form divalent vanadium at −1.78 V. Therefore, it is concluded that the oxidation of divalent vanadium by Hacac proceeds fairly rapidly, and thus the concentration of trivalent vanadium in the bulk solution is kept practically constant. Under this condition, the electrolytic current flowing through the cell can be expressed by the following equation:

$$i_{st} = nFADC_y/\delta, \quad (7)$$

where A is the surface area of the mercury cathode, the concentration of trivalent vanadium in the bulk solution is practically equal to C_y, δ is the thickness of the diffusion layer, C_y/δ the concentration gradient of trivalent vanadium in the diffusion layer, and the other symbols have their usual meanings. It is noteworthy that in the ordinary case C_y is time deptendent, but in this special case C_y can be treated as a constant.

By introducing numerical data in Eq. 7 ($i_{st}/C_y = 3.5\times10^3$ amp mol^{-1} cm^3, $n=1$, $A=12.6$ cm^2, and $D=6\times10^{-6}$ cm^2 s^{-1}), we obtain the value of δ to be about 3×10^{-3} cm. This value seems to be reasonable in view of the controlled potential electrolysis with vigorous stirring of the solution.

At the final stage of the controlled potential electrolysis at −2.1 V the steady-state current decreased, and the electrolyzed solution gave no more cathodic wave. This indicates that the regenerative cycle of trivalent vanadium by the coupled chemical reaction ceases owing to the depletion of Hacac.

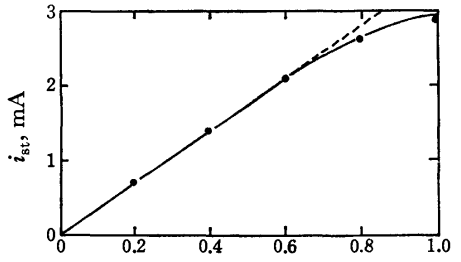

Fig. 4. Dependence of steady-state current on concentration of oxovanadium(IV) ion.

References

1) M. Kitamura and H. Imai, *Bull. Chem. Soc. Jpn.*, **48**, 1459 (1975).
2) M. Kitamura, K. Yamashita, and H. Imai, *Bull. Chem. Soc. Jpn.*, **49**, 97 (1976).
3) M. Kitamura, K. Yamashita, and H. Imai, *Chem. Lett.*, **1975**, 1071.
4) T. E. Neal and R. W. Murray, *Anal. Chem.*, **42**, 1654 (1970).
5) R. C. Buchta and D. H. Evans, *Anal. Chem.*, **40**, 2181 (1968).

A Spectrophotometric Study of Phosphomolybdenum Blue Formed by the Reaction of Phosphate with a Mixture of Molybdenum(V) ($Mo_2O_4^{2+}$) and Molybdenum(VI) and Application to the Spectrophotometric Determination of Small Amounts of Phosphates

Kousaburo Ohashi, Kumiko Yasu, Choutaro Suzuki, and Katsumi Yamamoto

Department of Chemistry, Faculty of Science, Ibaraki University, Mito 310

(Received March 3, 1977)

The spectrophotometric determination of trace amounts of phosphates, based on the color development of phosphomolybdenum blue formed by the reaction of phosphate with a mixture of molybdenum(V) ($Mo_2O_4^{2+}$) and molybdenum(VI), is described. The rates of formation of phosphomolybdenum blue were measured at 25 °C in a perchloric acid medium. The maximum constant color development was obtained in the perchloric-acid range from 0.20 to 0.41 M under given conditions by warming the solution for 10 min at 80 °C. The method obeys Beer's law in the phosphate-concentration range from 0.08 to 1.16 μg/ml. The molar absorptivity at 840 nm was calculated to be 2.4×10^4 l mol^{-1} cm^{-1}. The rate is inverse fifth-order with respect to the perchloric-acid concentration in the range from 0.20 to 0.41 M and is first-order with respect to the molybdenum(V) concentration. The formation rates increase with the phosphate and molybdenum(VI) concentrations, although the rate dependence on the concentrations of these reactants is complicated. The ratio of P: Mo(V) for phosphomolybdenum blue was determined to be 1: 1 using the molar-ratio method.

Analytical methods for the determination of phosphates are usually based on the formation of molybdophosphoric acid from the reaction between molybdenum(VI) and the phosphate in an acidic solution,[1] and the subsequent reduction to phosphomolybdenum blue.[2-5] Extensive investigations of the analytical methods and their numerous modifications have been carried out.

Lucena-Conde and Prat[6] developed a spectrophotometric determination method for phosphates based on the blue color development of phosphomolybdenum blue formed by the reaction of the phosphate with a mixture of molybdenum(VI) and molybdenum(V). They examined the effect of the ratio Mo(VI): Mo(V) on the color development.

Hosokawa and Ohshima[7] have modified the method established by Lucena-Code and Prat and applied it to the determination of phosphate in sea water. They also examined the effect of hydrogen-ion concentration on the color development.

The present authors found that the rate of formation of phosphomolybdenum blue formed by the reaction of phosphate with a mixture of molybdenum(VI) and molybdenum(V) is notably dependent on the perchloric-acid concentration. Therefore, the phosphomolybdenum blue formation and the spectrophotometric determination of phosphate, based on the color development of phosphomolybdenum blue, were investigated in perchloric-acid media. The effects of various ions on the color development are described. The composition of molybdenum blue was also studied using the molar-ratio method.

Experimental

Materials. A 1.00×10^{-1} M molybdenum(VI) solution was prepared by dissolving 24.196 g of sodium molybdate dihydrate into 1 litre of redistilled water. Working solutions were prepared by dilution with redistilled water to the desired concentrations. A molybdenum(V) ($Mo_2O_4^{2+}$) perchlorate solution was prepared using a method similar to that reported in Ref. 8. The concentration of this molybdenum(V) solution was determined spectrophotometrically at 384 nm (ε= 103).[9] The hydrogen-ion concentration of the molybdenum(V) solution was determined using a cation-exchange resin of hydrogen form. Thus, the hydrogen-ion concentration was established at 2.0 M. The stock solution of molybdenum(V) perchlorate was stored in a refrigerator. A 1.00×10^{-2} M phosphate solution was prepared by dissolving known quantities of sodium dihydrogenphosphate dihydrate or disodium hydrogenphosphate dodecahydrate into redistilled water. All the other chemicals were of analytical grade.

Apparatus. All the absorption spectra and absorbance at the given wavelengths were measured using a Hitachi EPS-3 type automatic recording spectrophotometer. The measurements of absorbances at a fixed wavelength were made on a Hitachi 101 manual spectrophotometer. Cells having a light path length of 1 cm were used in all cases. A Yamato BS-44 type water bath was used for warming the solution.

General Procedure for the Spectrophotometric Determination of Phosphate Content. In each experiment, 5 ml of 1.60×10^{-2} M molybdenum(VI), 2 ml of 2.20×10^{-2} M molybdenum (V), and a given quantity of a phosphate at 4.00×10^{-4} M were pipetted into a 25-ml measuring flask. 3 ml of 1.0 M perchloric acid was added to adjust the final hydrogen-ion concentration to 0.28 M. The final volume was brought to 25 ml by the addition of redistilled water. The solution was warmed for at least 10 min at 80 °C in a thermostatically-controlled water bath. A portion of the solution was then transferred into a cell. The measurements of absorbances were made at 840 nm.

Measurements of the Formation Rate of Phosphomolybdenum Blue. The solutions of molybdenum(VI), molybdenum(V), and sodium dihydrogen phosphate were maintained at 25 °C. In each experiment, portions of these solutions were pipetted into a 25-ml measuring flask, the molybdenum(V) perchlorate solution was added last to the solution containing molybdenum(VI) and phosphate, and the time was measured from its addition. A portion of the solution was transferred into a cell, which was placed in a thermostatically-controlled cell compartment. The kinetic measurements were carried out by recording the change in absorbance at 840 nm as a function of the time. The plots of the absorbance at 840 nm *vs.* time

were linear for at least 15% of the entire reaction. Therefore, the zeroth-order rate constants of the formation of phosphomolybdenum blue were determined from the initial slope of the absorbance *vs.* time plots.

Results and Discussion

Absorption Spectra of Phosphomolybdenum Blue Formed by the Reaction of Molybdenum(V) with Molybdenum(VI). The absorption spectra of a product formed by the reaction of a given concentration of phosphate with a mixture of 1.76×10^{-3} M molybdenum(V) and 3.20×10^{-3} M molybdenum(VI) in 0.28 M perchloric acid are shown in Fig. 1. The absorption spectra coincide with that of phosphomolybdenum blue formed by the reduction of molybdenum(VI) by hydrazinium sulfate in the presence of a phosphate.

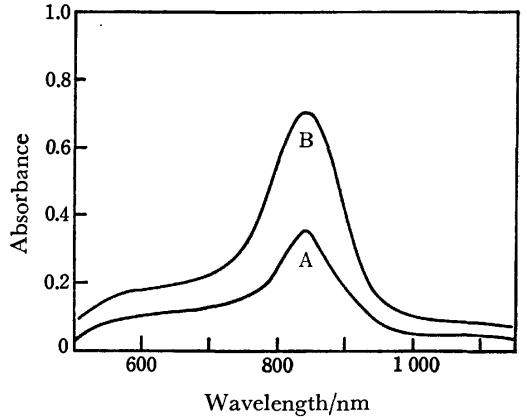

Fig. 1. The absorption spectra of phosphomolybdenum blue formed from the reaction of 1.76×10^{-3} M molybdenum(V) with 3.20×10^{-3} M molybdenum(VI) in the presence of phosphate at 0.28 M perchloric acid. (A): $[NaH_2PO_4]=1.45\times10^{-5}$ M, (B): $[NaH_2PO_4]=2.90\times10^{-5}$ M.

Effects of the Reaction Time and Temperature on the Color Development. The effects of the reaction time at 25 and 80 °C on the color development were examined with 1.76×10^{-3} M Mo(V), 3.20×10^{-3} M Mo(VI), 2.90×10^{-5} M NaH_2PO_4, and 0.28 M $HClO_4$. The results are shown in Fig. 2. The rate at 25 °C is very small, but the formation rate at 80 °C is relatively large. It requires at least 3 min for the color development to proceed completely at 80 °C. The color is quite stable even after standing for 6 h at 80 °C.

Effect of Perchloric-acid Concentration on the Color Development and the Formation Rate of Phosphomolybdenum Blue. The effect of the perchloric-acid concentration on the color development was studied with 2.90×10^{-5} M phosphate, 1.76×10^{-3} M Mo(V), and 3.20×10^{-3} M Mo(VI). The absorbances were measured after warming the solution for 10 min at 80 °C. The results are shown in Fig. 3. The maximum constant absorbance was obtained in the range for perchloric-acid concentration from 0.20 to 0.41 M. Above 0.43 M perchloric acid, the absorbances decrease with increasing perchloric-acid concentration. Below 0.20 M perchloric acid, the reaction of molybdenum(V) with molybdenum(VI)

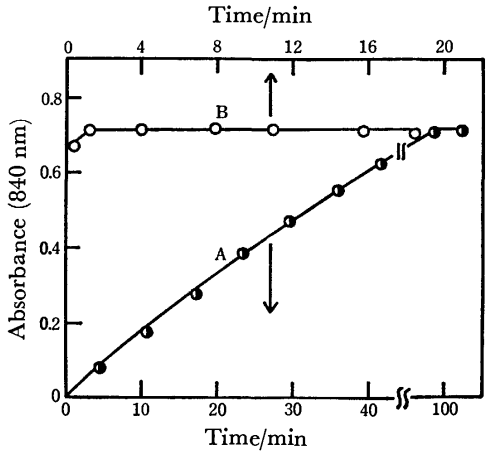

Fig. 2. The Effect of the heating time on the color development. $[Mo(VI)]=3.20\times10^{-3}$ M, $[Mo(V)]=1.76\times10^{-3}$ M, $[NaH_2PO_4]=2.90\times10^{-5}$ M, $[HClO_4]=0.28$ M. (A): 20 °C, (B): 80 °C.

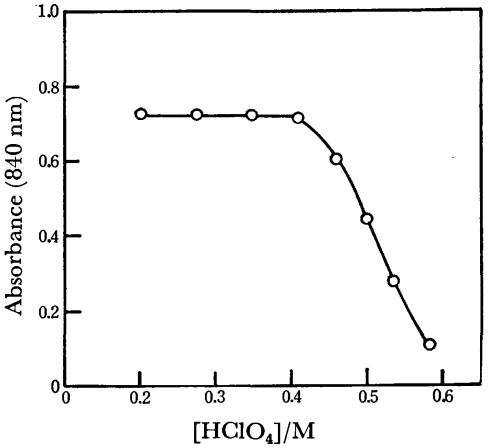

Fig. 3. The effect of the concentration of perchloric acid on the color development. $[Mo(VI)]=3.20\times10^{-3}$ M, $[Mo(V)]=1.76\times10^{-3}$ M, $[NaH_2PO_4]=2.90\times10^{-5}$ M, 10 min, 80 °C.

gives a blue precipitation.

The effect of the perchloric-acid concentration on the rate of formation of phosphomolybdenum blue was examined in the range from 0.20 to 0.55 M for 1.01×10^{-3} M Mo(V), 1.60×10^{-3} M Mo(VI), and 5.80×10^{-5} M NaH_2PO_4 (Fig. 4). The result that the slope of the logarithm of the rate *vs.* pH plot is −5 indicates that the rate of the formation is inversely fifth order with respect to the perchloric-acid concentration in the range from 0.20 to 0.40 M.

Effects of Molybdenum(VI) and Molybdenum(V) Concentrations on the Color Development and the Formation Rate of Phosphomolybdenum Blue. The effect of molybdenum(VI) concentration on the formation of phosphomolybdenum blue was examined under given conditions. The results are shown in Fig. 5. Constant maximum color development was obtained in the range for molybdenum(VI) from 2.30×10^{-3} to 6.40×10^{-3} M with 1.76×10^{-3} M Mo(V), 2.90×10^{-5} M phosphate, and 0.28 M $HClO_4$. In the case of 1.00×10^{-3} M Mo(V), any concentration of molybdenum(VI) greater than 1.50×10^{-3} M results in constant maximum color

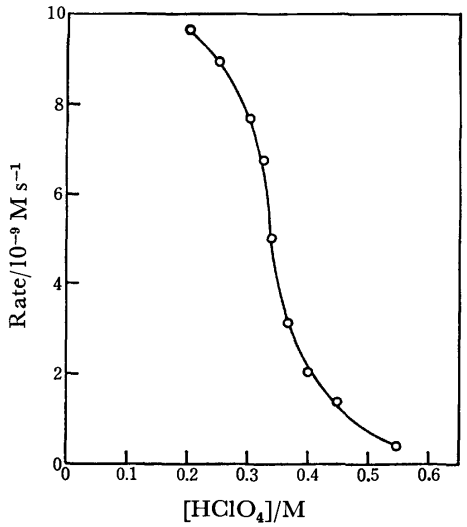

Fig. 4. The relation between the formation rate of phosphomolybdenum blue and the concentration of perchloric acid.
$[Mo(VI)]=1.60\times10^{-3}$ M, $[Mo(V)]=1.01\times10^{-3}$ M, $[NaH_2PO_4]=5.80\times10^{-5}$ M, $I=0.70$ M ($NaClO_4$), 25 °C.

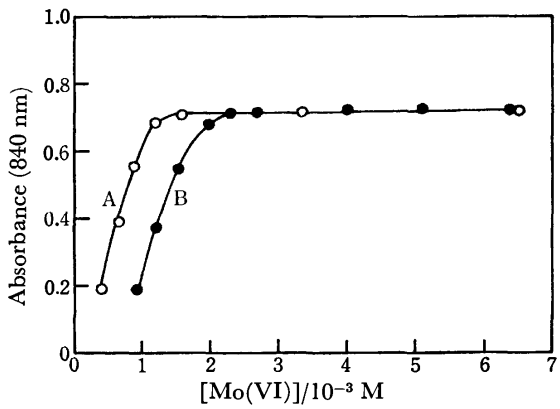

Fig. 5. The effect of the concentrations of molybdenum(VI) on the color development.
$[NaH_2PO_4]=2.90\times10^{-5}$ M, $[HClO_4]=0.28$ M.
(A): $[Mo(V)]=1.00\times10^{-3}$ M, (B): $[Mo(V)]=1.76\times10^{-3}$ M.

development. These results indicate that the color development is significantly affected by the Mo(VI): Mo(V) ratio.

The effect of the molybdenum(VI) concentration on the formation rate of phosphomolybdenum blue was examined for 0.36 M $HClO_4$, 6.76×10^{-4} M Mo(V), and 4.36×10^{-5} M NaH_2PO_4. The results are shown in Fig. 6. At low concentrations of molybdenum(VI), the formation rate is greatly affected by the molybdenum(VI) concentration, but at high concentrations the effect is small.

The effect of molybdenum(V) concentration on the formation of phosphomolybdenum blue was also examined. The rate has a first-order dependence on the molybdenum(V) concentration in the range from 2.00×10^{-4} to 1.76×10^{-3} M for 2.40×10^{-3} M Mo(VI), 5.80×10^{-5} M NaH_2PO_4, and 0.28 M $HClO_4$.

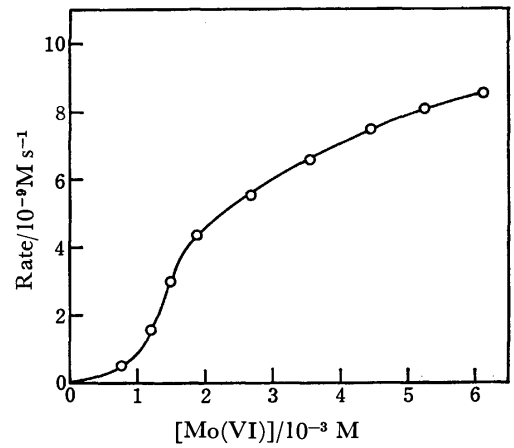

Fig. 6. The relation between the formation rate of phosphomolybdenum blue and the concentration of molybdenum (VI).
$[Mo(V)]=6.76\times10^{-4}$ M, $[NaH_2PO_4]=4.36\times10^{-5}$ M, $[HClO_4]=0.36$ M, $I=0.70$ M ($NaClO_4$), 25 °C.

Determination of Phosphate Concentration. The calibration curve was obtained by the general procedure for the determination of phosphate concentrations. The phosphomolybdenum blue color system obeys Beer's law in the phosphate range from 0.08 to 1.16 μg/ml. Based on the phosphate concentration, the molar absorptivity at 840 nm can be calculated to be 2.4×10^4 l mol^{-1} cm^{-1}. The sensitivity is very high. Standard solutions prepared from Na_2HPO_4 and NaH_2PO_4 give the same result.

Precision and Accuracy. The accuracy of the results is represented in Table 1. An estimate of the

Table 1. Accuracy of the results

Measured absorbance[a] (840 nm)	Amount of phosphate in 25 ml (μg)		
	Taken	Found	Error (%)
0.780	21.7	21.3	−1.84
0.610	15.9	16.4	+3.14
0.453	12.6	12.4	−1.59
0.309	8.0	8.3	+3.75
0.150	4.4	4.3	−2.27

a) $[Mo(VI)]=3.20\times10^{-3}$ M, $[Mo(V)]=1.76\times10^{-3}$ M, $[HClO_4]=0.28$ M.

Table 2. Precision of the results

0.8 μg/ml phosphate Measured absorbance (840 nm)[a]	0.4 μg/ml phosphate
0.696	0.345
0.710	0.342
0.693	0.361
0.701	0.357
0.717	0.359
0.720	0.363
Av. 0.706	0.355
Std. dev. 0.011	0.0029

a) $[Mo(VI)]=3.30\times10^{-3}$ M, $[Mo(V)]=1.76\times10^{-3}$ M, $[HClO_4]=0.28$ M.

precision was obtained for the results of replicate samples at two different phosphate concentrations. These results are listed in Table 2.

Effect of Various Ions. The effect of many different ions was examined by the proposed procedure for the determination of 0.8 μg/ml of phosphate. The metal ions, such as Mg^{2+}, Al^{3+}, Ca^{2+}, Cr^{3+}, Mn^{2+}, Fe^{3+}, Co^{2+}, Ni^{2+}, Zn^{2+}, Cd^{2+}, Hg^{2+}, Pb^{2+}, UO_2^{2+}, and SiO_3^{2-} in moderate amounts (4 μg/ml) do not interfere with this determination.

Determination of the P: Mo(V) Molar Ratio in Phosphomolybdenum Blue. There are a few investigations of the formation mechanism and composition of phosphomolybdenum blue. Arnold and Wacker,[10] Baman *et al.*,[11] and Hahn and Schmidt[12] have investigated the composition of phosphomolybdenum blue formed by the reduction of 12-molybdophosphoric acid by reducing agents. Assuming that phosphomolybdenum blue contains the same number of molybdenum atoms as the unreduced 12-molybdophosphoric acid, they proposed that the Mo(VI): Mo(V) ratios in phosphomolybdenum blue are 2: 1 or 5: 1, depending on the type of reducing agents and reduction time.

Recently, Meiklejohn *et al.*[13] isolated $(Bu_4N)_4PMo^{V}Mo^{VI}_{11}O_{40}$, which was prepared by the interaction of $PMo_{11}O_{39}^{7-}$ and $Bu_4N[MoOCl_4]$ in acetonitrile or propylenecarbonate, where Bu_4N represents the tetrabutyl ammonium ion.

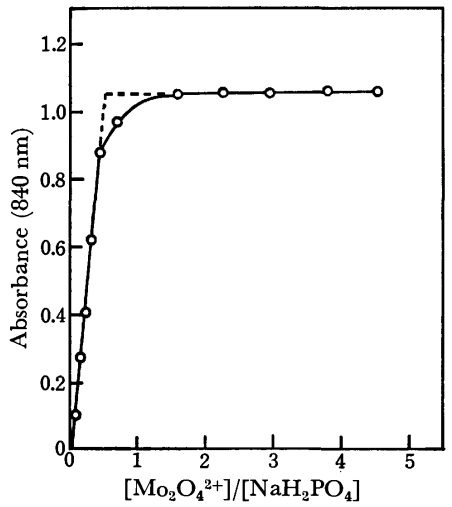

Fig. 7. The determination of molar ratio of P: Mo(V) in phosphomolybdenum blue.
$[Mo(VI)]=2.40\times10^{-3}M$, $[NaH_2PO_4]=4.36\times10^{-5}M$, $[HClO_4]=0.28$ M,

In this work, the P: Mo(V) molar ratio in phosphomolybdenum blue, which was formed by the reaction of molybdenum(V) with molybdenum(VI), was determined by means of the molar-ratio method, under the condition of the presence of amounts of molybdenum(V) small with respect to that of molybdenum(VI). The results are shown in Fig. 7. Since the formation rate of phosphomolybdenum blue is markedly small for these experimental conditions, it requires at least 300 min at 80 °C for the color to completely develop. The results shown in Fig. 7 illustrate that the P: Mo(V) molar ratio (as a monomer) is 1: 1 for 0.28 M $HClO_4$. The same result was obtained with 0.36 M $HClO_4$. A determination of the P: Mo(VI) molar ratio based on the molar-ratio method was unsuccessful.

The formation mechanism of phosphomolybdenum blue determined from this work has not yet been ascertained. The present authors are planning a detailed kinetic treatment of the formation of phosphomolybdenum blue.

References

1) D. F. Boltz and M. G. Mellon, *Anal. Chem.*, **20**, 749 (1948).
2) D. F. Boltz and M. G. Mellon, *Anal. Chem.*, **19**, 873 (1947).
3) H. Levin, J. J. Rowe, and F. S. Grimaldi, *Anal. Chem.*, **27**, 258 (1955).
4) J. T. Woods and M. G. Mellon, *Ind. Eng. Chem. Anal. Ed.*, **13**, 760 (1941).
5) S. Maekawa and K. Kato, *Bunseki Kagaku*, **15**, 969 (1966).
6) F. Lucena-Conde and L. Prat, *Anal. Chim. Acta*, **16**, 473 (1957).
7) I. Hosokawa and F. Ohshima, *Water Res.*, **7**, 283 (1973).
8) The molybdenum(V) used in this work is of dimeric form, $Mo_2O_4^{2+}$, which was prepared by a method similar to that described in Ref. 9.
9) Y. Sasaki, R. S. Taylor, and A. G. Sykes, *J. Chem. Soc., Dalton Trans.*, **1975**, 396.
10) R. Arnold and S. M. Wacker, *J. S. African Chem. Inst.*, **9**, 80 (1956).
11) E. Bamann, K. Schriever, A. Freytag, and R. Toussaint, *Ann. Chem. Liebigs*, **605**, 65.
12) H. Hahn and G. Schmidt, *Naturwissenschaften*, **49**, 513 (1962).
13) P. T. Meiklejohn, M. T. Pope, and R. A. Prados *J. Am. Chem. Soc.*, **96**, 6779 (1974).

Catalytic Decomposition of the Excess Reagent in the Spectrophotometric Determination of Copper(II) with *o,o'*-Dihydroxyazo Compounds

Masao SUGAWARA, Yuh'ichi ROKUGAWA, and Tomihito KAMBARA

Department of Chemistry, Faculty of Science, Hokkaido University, Sapporo 060

(Received April 16, 1977)

A simple and sensitive spectrophotometric method for determination of copper(II) is described. It is based on the reaction of copper(II) with Hydroxynaphthol Blue in the weakly alkaline medium and the decomposition of the unconsumed reagent which shows an intense absorption at the wavelength, 555 nm, of the maximum absorbance of the copper(II) complex. Beer's law is obeyed over the range 0.13—1.27 ppm copper with the molar absorption coefficient of $\varepsilon_{555}=3.01\times10^4$ dm^3 mol^{-1} cm^{-1} (Sandell's sensitivity 2.11×10^{-3} μg/cm^2). A fairly large number of common ions except for nickel(II) do not interfere.

Several *o,o'*-dihydroxyazo reagents have been employed in spectrophotometric determination of metal ions,[1] but in some cases the use of the azo reagent as a spectrophotometric reagent is prevented by similarity in absorption spectrum of the metal complex and the reagent itself. In addition, the color reaction is poor in selectivity. For improving the sensitivity and selectivity of the reaction, extraction of the complex anion formed between a sulfonated azo-dye and a metal ion as an ion-pair with a quaternary ammonium cation has been investigated[2] and applied to the spectrophotometric determination of aluminium,[3] magnesium,[4] and rare earth elements.[5]

In the present paper, a new method for spectrophotometric determination of copper(II) with *o,o'*-dihydroxyazo compounds is described, in which the excess reagent and some of the colored chelates formed by interfering metal ions are decomposed by the use of the manganese(II)-catalysed discoloration reaction.[6,7] The reaction is also utilized in the catalymetric microdetermination of manganese(II) by Yamane and Fukasawa.[8]

Experimental

Reagents. Commercially available 1-(2-hydroxy-4-sulfo-1-naphthylazo)-2-naphthol-3,6-disulfonic acid, trisodium salt (Hydroxynaphthol Blue, abbreviated as HNB), 1-(1-hydroxy-2-naphthylazo)-6-nitro-2-naphthol-4-sulfonic acid, sodium salt (Eriochrome Black T), 1-(2-hydroxy-1-naphthylazo)-2-naphthol-4-sulfonic acid, sodium salt (Calcon) and 1-(2-hydroxy-5-methylphenylazo)-2-naphthol-4-sulfonic acid (Calmagite) were obtained from Dojindo Laboratories Ltd. and used without further purification. The purity of the reagents was checked by the method described below. The solution was daily prepared by dissolving the reagent in water and concentration was corrected.

A 0.01 mol dm^{-3} standard solution of copper(II) was prepared from its sulfate and standardized by the method of the conventional chelatometric titration.

A mixture of 3 (w/w)% hydrogen peroxide and 0.2 mmol·dm^{-3} manganese(II) was freshly prepared before use by mixing the appropriate amounts of 30 (w/w)% hydrogen peroxide and 0.01 mol dm^{-3} manganese(II) chloride solutions and diluting with water.

Sörensen's buffer solution (pH 8.0—11.0), Kolthoff's buffer solution (pH 6.0—7.4) and deionized water were used.

All the chemicals except for the azo reagents used were of analytical grade.

Apparatus. A Hitachi two-wavelength and double-beam spectrophotometer 356 and a Shimadzu spectrophotometer, Model QV-50, with 10-mm glass cells were used for spectrophotometric measurements. A Hitachi-Horiba glass electrode pH-meter, Model F-5, was used for pH measurements.

The Purity of Azo Reagents. The purity of the reagent was evaluated by applying the familiar mole-ratio method to the copper(II)–dye system, where excess reagent is decomposed in the similar manner as described below. After correcting the reagent concentration, a continuous variation method was applied to the calcium(II)- or magnesium(II)–dye system to check the estimated value of the purity. It was found that the molar ratio of the dye to the metal ion is 1:1, in accordance with the results reported by several authors.[9,10] The purity was found to be *ca.* 40% for HNB, 46.5% for Eriochrome Black T, 64% for Calmagite and 45% for Calcon, and the concentration of the reagent was therefore corrected in a suitable manner.

Procedure. In a 50-cm^3 volumetric flask are taken an appropriate volume up to 20 cm^3 of the solution containing less than 63.6 μg of copper(II), 5 cm^3 of 0.4 mmol dm^{-3} HNB solution and 20 cm^3 of the buffer solution (pH 10). The solution is mixed well. After addition of 2 cm^3 of a 3% hydrogen peroxide-0.2 mmol dm^{-3} manganese(II) solution, the mixture is diluted with water to the volume and allowed to stand for 15 min. The absorbance of the solution is measured at 555 nm against water.

The similar procedure is available for preparing the calibration graph with other dyes.

Results and Discussion

Absorption Spectra. The absorption spectra of HNB and its copper(II) complex are shown in Fig. 1. On adding hydrogen peroxide and manganese(II) after the full development of color of copper(II)–HNB complex, the HNB present in excess is rapidly decomposed by the catalytic effect of manganese(II), whereas the red-purple copper(II)–HNB complex, the absorption maximum being 555 nm, remains stable. The addition of hydrogen peroxide alone is not effective for the discoloration of the HNB solution. After standing the solution for 15 min, only approx. 5% decrease in absorbance is observed. Of the azo-dyes used, the decomposition rate of HNB is most rapid and the absorbance of the resulting solution at the wavelength of the maximum absorption of the copper(II) complex is the lowest.

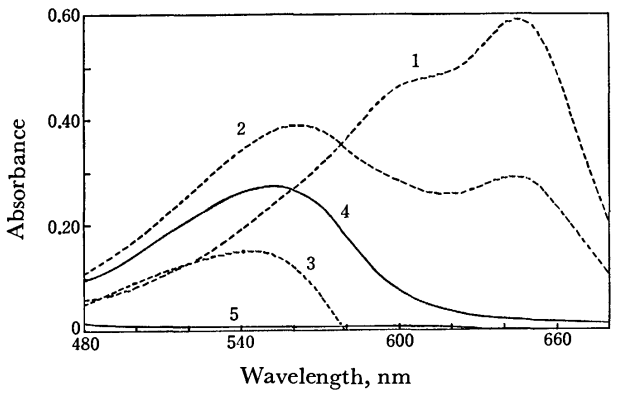

Fig. 1. Absorption spectra of copper-(II)HNB complex and HNB at pH 9.1 in the presence (——) and absence (------) of 0.12% hydrogen peroxide and 4 μmol dm^{-3} manganese (II).
1: HNB 20 μmol dm^{-3}. 2: Cu(II) 10 μmol dm^{-3}, HNB 20 μmol dm^{-3}. 3: Cu(II)-HNB complex measured against the reagent blank solution. 4: Cu(II) 10 μmol dm^{-3}, HNB 20 μmol dm^{-3}, after decomposition of excess reagent by H_2O_2 and Mn(II). 5: The reagent blank solution corresponding to 4. The measurements were carried out after standing for 15 min.

Effect of pH. The extent of the decomposition of azo reagents is dependent on the pH of solution as shown in Fig. 2. In the pH range from 9.3 to 10.5, the reagents are almost completely decomposed after standing the solution longer than 10 min. The absorbance of the copper(II) complexes is constant in the pH range where the decomposition is almost complete.

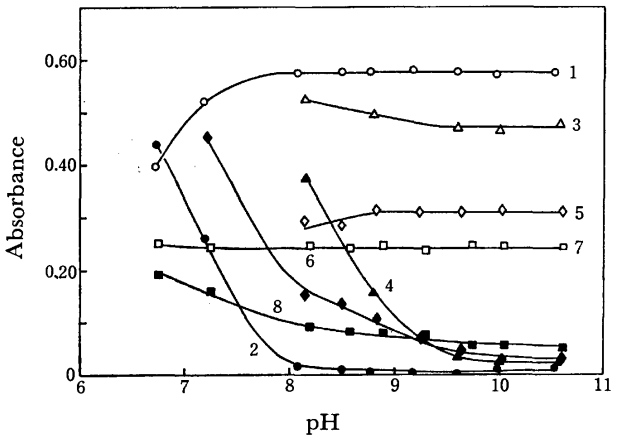

Fig. 2. Effect of pH on the absorbance of the copper(II) complexes and the reagent blank solutions after standing for 15 min in the presence of 0.12% hydrogen peroxide and 16 μmol dm^{-3} manganese (II).
1: HNB 40 μmol dm^{-3}, Cu(II) 20 μmol dm^{-3}, 555 nm. 2: The reagent blank solution corresponding to 1. 3: Calcon 44.5 μmol dm^{-3}, Cu(II) 20 μmol dm^{-3}, 545 nm. 4: The reagent blank solution corresponding to 3. 5: Eriochrome Black T 46.5 μmol dm^{-3}, Cu(II) 20 μmol dm^{-3}, 540 nm. 6: The reagent blank solution corresponding to 5. 7: Calmagite 64.5 μmol dm^{-3}, Cu(II) 12 μmol dm^{-3}, 530 nm. 8: The reagent blank solution corresponding to 7. The absorbance of the complexes was measured against the reagent blank solution.

Effect of Reagent Concentration. It was found that a small excess of the reagent more than the stoichiometrically necessary amount was sufficient to develop fully the color of the copper(II) complex with each dye except for Eriochrome Black T as shown in Fig. 3. The absorbance of the copper(II)-Eriochrome Black T complex was observed to increase notably with increasing concentration of the reagent more than the equivalent amount to copper(II). The composition of the complex formed between copper(II) and the azo-dye is estimated to be 1 : 1 molar ratio for each copper(II)-dye system except for the Eriochrome Black T complex.

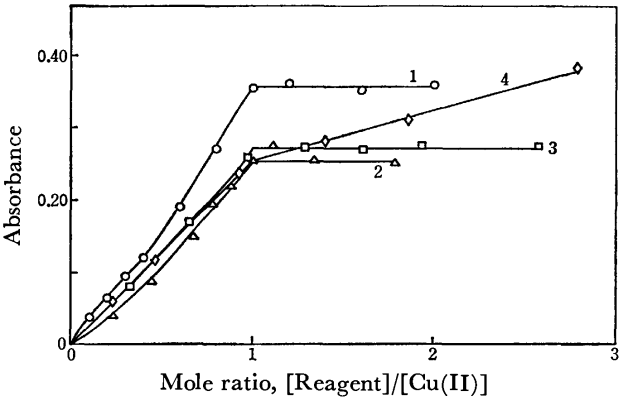

Fig. 3. Effect of the reagent concentration on the absorbance of copper(II) complex measured against water after standing for 15 min. Hydrogen peroxide 0.12%, manganese(II) 16 μmol dm^{-3}.
1: HNB, Cu(II) 12 μmol dm^{-3}, 555 nm, pH 9.1.
2: Calcon, Cu(II) 10 μmol dm^{-3}, 545 nm, pH 10.
3: Calmagite, Cu(II) 12 μmol dm^{-3}, 530 nm, pH 9.9.
4: Eriochrome Black T, Cu(II) 20 μmol dm^{-3}, 540 nm, pH 9.9.

Stability of Copper(II) Complex. The copper(II)-HNB complex after decomposing the excess reagent is sufficiently stable for practical use and the absorbance of the complex is constant at least for one hour as shown in Table 1. The addition of the hydrogen peroxide-manganese(II) solution more than 4 cm^3 is undesirable because the optical measurements are prevented by the occurrence of bubble which is adsorbed onto the wall of cell. The copper(II) complex with Calcon, Calmagite or Eriochrome Black T is somewhat unstable as compared with that of the HNB complex and the absorbance of the complexes at 12 μmol dm^{-3} copper(II) level decreases by 3—7% between 15 and 60 min.

Table 1. Stability of the copper(II)-HNB complex

Cu(II) taken μg/50 cm^3	Amount of {1.5% H_2O_2–0.2 mmol dm^{-3} $MnCl_2$} added cm^3	Absorbance at 555 nm *vs.* water after 15 min	30 min	45 min	60 min
19.0	1.0	0.174	0.173	0.173	0.172
	2.0	0.174	0.173	0.173	0.172
	4.0	0.176	0.176	0.175	0.175
38.1	1.0	0.349	0.349	0.349	0.349
	2.0	0.346	0.347	0.347	0.347
	4.0	0.350	0.350	0.350	0.350

HNB concentration 40 μmol dm^{-3}, pH 9.2.

Calibration Curve and Sensitivity. The copper(II)-HNB system conforms to Beer's law in the range of 0.13 to 1.27 ppm copper with the molar absorption coefficient of 3.01×10^4 dm^3 mol^{-1} cm^{-1} at 555 nm. The molar absorption coefficient of copper(II)-Calcon and -Calmagite system is 2.59×10^4 at 545 nm and 2.04×10^4 at 530 nm, respectively. The copper(II)-Eriochrome Black T system does not obey the Beer's law. The sensitivity of the HNB method is higher than those of cuprizone method (molar absorption coefficient 1.6×10^4),[1] zincon method (2.2×10^4),[11] *N*-[2-(2-pyridylmethyleneamino)ethyl]-*N*-(2-aminoethyl)dithiocarbamic acid method (1.75×10^4),[12] Calcichrome method (8×10^3),[13] Xylenol Orange method (1.25×10^4)[14] and Sarcosine Cresol Red method (2.09×10^4),[15] but lower than those of tetraphenylporphine-trisulfate method (4.8×10^5),[16] Chromazurol S-zephiramine method (4.76×10^4)[17] and 2-bromo-4,5-dihydroxyazobenzene-4'-sulfonate-hexadecyltrimethylammonium chloride method (4.8×10^4).[18]

Effect of Foreign Ions. From the viewpoint of sensitivity and simplicity in the procedure, it seems that the HNB is most preferable among the four reagents examined in the present work. Therefore, the effect of diverse ions on the determination of copper(II) according to the above-mentioned HNB procedure was examined, as tabulated in Table 2. The cations were added as nitrates, chlorides or sulfates and anions as sodium, potassium or ammonium salts. The major interference arises from nickel(II) which reacts with HNB and produces an intense coloration. Magnesium(II), zinc(II), cadmium(II) and thorium(IV) form the similarly colored complexes, but these complexes, being unstable under the given conditions, decompose on the addition of hydrogen peroxide and manganese(II). Aluminium(III) at the 2-fold excess amount and iron(III) at the 4-fold excess amount over copper(II) are easily masked by adding a 20-fold excess amount of fluoride. The four-fold excess amount of cobalt(II) over copper(II) is masked by previously oxidizing it to cobalt(III) with hydrogen peroxide in ammoniacal buffer solution. In Table 3 are given the analytical results of copper(II) in the synthetic sample. Almost satisfactory results were obtained.

TABLE 2. EFFECT OF VARIOUS IONS

Ion added (X)	Amount μg	Copper(II) found μg	Error %	Tolerance limit X: Cu(II)
Al(III)	32	38.5	+20.3	interfere
	64	32.3[a]	+1.0	2
Ba(II)	3200	31.7	−0.9	100
Bi(III)	160	32.2	+0.6	5
Ca(II)	3200	32.1	+0.3	100
Cd(II)	960	32.6[b]	+1.9	30
Cr(III)	160	32.4	+1.3	5
Co(II)	32	62.0	+93.8	interfere
	128	32.3[c]	+0.9	4
Fe(III)	160	26.8	−16.3	interfere
	128	32.7[a]	+2.2	4
Mg(II)	3200	31.9	−0.3	100
Mn(II)	64	32.4	+1.3	2
Mo(VI)	960	31.8	−0.6	30
Ni(II)	32	54.5	+70.3	interfere
Pb(II)	320	32.4	+1.3	10
Sr(II)	1600	32.4	+1.3	50
Th(IV)	1600	33.0	+3.1	50
V(V)	64	38.1	+19.1	interfere
	320	32.8[d]	+2.5	10
Zn(II)	640	32.9	+2.8	20
Br^-	3200	31.8	−0.6	100
Cl^-	3200	32.0	0	100
F^-	320	31.1	−2.8	10
PO_4^{3-}	3200	32.3	+0.9	100

Copper(II) taken: 32.0 μg. Each results are the mean of three separate analyses. a) With 1.2 mg of NH_4F. b) With 80 μmol dm^{-3} of HNB. c) With 3 cm^3 of 3% H_2O_2 in ammoniacal buffer solution. d) With 3 cm^3 of 3% H_2O_2, measured after 40 min.

TABLE 3. THE ANALYTICAL RESULTS OF COPPER(II) IN A SYNTHETIC SAMPLE[a]

Copper(II) taken μg/50 cm^3	Copper(II) found[b] μg/50 cm^3	Error %	Relative standard deviation %	Number of determinations
16.0	15.9[c]	−0.6	2.5	4
	16.4	+2.5	3.2	4
32.0	31.6[c]	−1.2	1.5	4
	32.1	+0.3	2.0	4
48.0	47.2[c]	−1.7	1.5	4
	47.1	−1.9	1.0	4

a) Amount of foreign ions: Al(III) 16, Cd(II) 1.6, Cr(III) 3.5, Fe(III) 9.6, Pb(II) 2.2, Mn (II) 1.6, Zn(II) 20.8 μg in 50 cm^3. b) With 624 μg NH_4F. c) Without foreign ions.

References

1) Z. Marczenko, "Spectrophotometric Determination of Elements," Ellis Horwood Ltd., Chichester, England (1976).
2) C. Woodward and H. Freiser, *Talanta*, **20**, 417 (1973).
3) C. Woodward and H. Freiser, *Talanta*, **15**, 321 (1968).
4) K. Fukamachi, H. Kohara, and N. Ishibashi, *Bunseki Kagaku*, **19**, 1529 (1970).
5) M. K. Akmedli, P. B. Granovskaya, and R. A. Neimatova, *Zh. Analit. Khim.*, **28**, 278 (1973).
6) M. Sugawara, Y. Ozawa, and T. Kambara, *Bunseki Kagaku*, **23**, 1058 (1974).
7) M. Sugawara, Y. Sato, and T. Kambara, *Bunseki Kagaku*, **26**, 346 (1977).
8) T. Yamane and T. Fukasawa, *Bunseki Kagaku*, **26**, 300 (1977).
9) A. Itoh and K. Ueno, *Analyst*, **95**, 583 (1970).
10) K. Ueno, "Kirêto Tekiteihô (Chelatometric Titration)," Nankodo, Tokyo (1972), p. 97.
11) R. M. Rush and J. H. Yoe, *Anal. Chem.*, **26**, 1345 (1954).
12) Y. Itoh, M. Sugawara, and T. Kambara, *Bunseki Kagaku*, **24**, 571 (1975).
13) H. Ishii and H. Einaga, *Bull. Chem. Soc. Jpn.*, **39**, 1154 (1966).
14) M. Otomo, *Bunseki Kagaku*, **14**, 45 (1965).
15) T. Matsuo, J. Shida, and S. Sato, *Bunseki Kagaku*, **20**, 693 (1971).
16) J. Itoh, T. Yotsuyanagi, and K. Aomura, *Anal. Chim. Acta*, **74**, 53 (1975).
17) Y. Shijo and T. Takeuchi, *Bunseki Kagaku*, **16**, 51 (1967).
18) Y. Wakamatsu, *Bunseki Kagaku*, **25**, 671 (1976).

Four Isomers of the Bis(ethylenediamine)sarcosinatocobalt(III) Ion: Separation, Identification, and Characterization

Miho FUJITA,* Yuzo YOSHIKAWA, and Hideo YAMATERA

Department of Chemistry, Faculty of Science, Nagoya University, Chikusa, Nagoya 464
**Department of Chemistry, Nagoya City University, Mizuho, Nagoya 467*

(Received April 18, 1977)

All four possible isomers of the bis(ethylenediamine)sarcosinatocobalt(III) ion, $[Co(sar)(en)_2]^{2+}$, were separated chromatographically on the column of an SP-Sephadex cation exchanger, and their absorption, circular dichroism, and ^{13}C NMR spectra were measured. The more stable pair of isomers were identified as Λ-$[Co(S\text{-sar})(en)_2]^{2+}$ and Λ-$[Co(R\text{-sar})(en)_2]^{2+}$, while the less stable pair were Λ-$[Co(R\text{-sar})(en)_2]^{2+}$ and Λ-$[Co(S\text{-sar})(en)_2]^{2+}$. The Λ-$[Co(S\text{-sar})(en)_2]^{2+}$ isomer in an aqueous solution showed mutarotation which can be ascribed to a change in configuration (epimerization) about the sarcosinato nitrogen atom. In equiribrium at 25 °C, the mixture consisted of 84.8% of the $\Lambda(S)$ isomer and 15.2% of the $\Lambda(R)$ isomer. From this result, the free-energy difference between the isomers was estimated to be 4.2_6 kJ mol^{-1}. The presence of the less stable isomers, which were not found by Buckingham *et al.*, was also confirmed by the ^{13}C NMR measurements.

The bis(ethylenediamine)sarcosinatocobalt(III) ion possesses four possible isomers arising from two asymmetric centers, one at the cobalt and the other at the sarcosinato nitrogen atom. Figure 1 shows two of the isomers, $\Lambda(S)$ and $\Lambda(R)$, which are different from each other only with respect to their configurations about the nitrogen atom. The $\Lambda(R)$ configuration appears to be less stable than $\Lambda(S)$ due to nonbonded repulsive interactions between the hydrogen atoms on the methyl group and those on the adjacent ethylenediamine chelate ring.

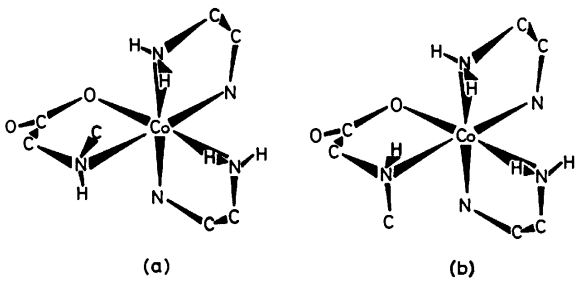

Fig. 1. Structures of Λ-$[Co(S\text{-sar})(en)_2]^{2+}$ (a) and Λ-$[Co(R\text{-sar})(en)_2]^{2+}$ (b) viewed along the pseudo-C_3 axis. Some of hydrogen atoms attached to carbon and nitrogen atoms are omitted.

The first attempt to separate the four isomers was made by Meisenheimer *et al.*,[1] who claimed to have obtained one isomer having high positive rotatory power in the pure state and two having lower rotatory powers of positive and negative signs, at least in an impure state. However, their results have not been reproduced by other investigators.[2]

In a previous paper,[3] the present authors briefly reported that the four isomers were present as a mixture in an aqueous solution and that their less stable enantiomers were completely resolved into optical isomers by a chromatographic technique using an SP-Sephadex column.

The present study was undertaken to obtain all four isomers of the complex in optically pure form, and to characterize them from measurements of the absorption, circular dichroism (CD), and ^{13}C NMR spectra, the mutarotation rate, and the isomer distribution. The results will be discussed from the structural point of view with reference to the available data on X-ray structural analysis[6] and conformational analysis.[9]

Experimental

Synthesis of the Racemic Complex. Bis(ethylenediamine)-sarcosinatocobalt(III) iodide was prepared from *trans*-$[CoCl_2(en)_2]Cl$ and sarcosine according to the procedure described by Liu and Douglas.[4] The iodide obtained was recrystallized twice from slightly alcoholic water and was dried under reduced pressure. Found: C, 16.14; H, 4.26; N, 13.44%. Calcd for $[Co(CH_3NHCH_2COO)(C_2H_8N_2)_2]I_2$: C, 16.55; H, 4.18; N, 13.52%.

Resolution. The method of Buckingham *et al.*[5] for the resolution of $[Co(sar)(en)_2]I_2$ was used with slight modification. A very slight excess of silver (+)-bromocamphorsulfonate,† Ag (+)-BCS, suspended in water was added to a solution of the complex at about 40 °C. After stirring of the mixture for 30 min, the precipitated silver iodide was filtered off and washed with water. The filtrate and washings were combined and evaporated to dryness on a water bath. The resulting (+)-bromocamphorsulfonate, $[Co(sar)(en)_2]\{(+)\text{-BCS}\}_2$, was recrystallized from aqueous ethanol. The crystals showed a negative CD peak in the vicinity of 518 nm and the filtrate showed a positive CD peak in the same region. After repeated fractional recrystallizations, the least soluble fraction gave a $\Delta\varepsilon_{518}/\varepsilon_{495}$ value of -0.014 and the most soluble fraction a value of $+0.015$. The isomers of the complex showing CD signs of $\{-\}_{518}$ and $\{+\}_{518}$ will hereafter be represented by M and P, respectively (see Table 1).

Chromatographic Separation. An aqueous solution containing about 0.2 g of the (+)-bromocamphorsulfonate of the M-complex was poured onto a small column of SP-Sephadex (volume of 5 cm^3) to collect the complex ions. The SP-Sephadex carrying the complex was transferred to the top of another SP-Sephadex column (2.7 diam × 137 cm). Chromatographic elution with 0.12 M (=mol dm^{-3}) sodium (+)-tartratoantimonate(III), $Na_2[Sb_2((+)\text{-}C_4H_2O_6)_2]$, (pH 3.5) gave two bands, denoted by M-I and M-II in order of effluence (Fig. 2). Similar experiments were also made on the P-complex, which gave two bands, P-I and P-II, and,

† In the present paper, (+)-bromocamphorsulfonate denotes (+)-3-bromocamphor-8-sulfonate.

Table 1. Assignments and abbreviations of the isomers

Isomer	Assignment	CD sign[a)]	Abbrev.	Relative stability
P-I	$\Lambda(+)_{589}$[Co(*S*-sar)$(en)_2]^{2+}$	$\{+\}_{518}$	$\Lambda(S)$	less stable
P-II	$\Lambda(+)_{589}$[Co(*R*-sar)$(en)_2]^{2+}$	$\{+\}_{518}$	$\Lambda(R)$	stable
M-I	$\Delta(-)_{589}$[Co(*R*-sar)$(en)_2]^{2+}$	$\{-\}_{518}$	$\Delta(R)$	less stable
M-II	$\Delta(-)_{589}$[Co(*S*-sar)$(en)_2]^{2+}$	$\{-\}_{518}$	$\Delta(S)$	stable

a)The $\{+\}_\lambda$ and $\{-\}_\lambda$ symbols represent the CD sign at λ nm.[7)]

on the racemic complex, which gave three bands, A, B, and C (Fig. 2). The notations, M-I, M-II, P-I, and P-II, will hereafter also be used to designate the isomer contained in each band.

Conversion to the Chloride. The combined eluate of the M-I bands from several elutions was diluted twenty times with water, acidified by a small amount of HCl (pH≈3), to prevent isomerization.†† The complex in the diluted eluate from the M-I band was again collected on a separate SP-Sephadex column. After washing the column with 0.005 M HCl to remove sodium ions, if any, the M-I isomer sorbed was eluted with 0.5 M HCl. The eluate containing the chloride of the M-I isomer was evaporated almost to dryness under reduced pressure. Ethanol, and subsequently ether, were added to precipitate the chloride. The chloride of the M-I isomer obtained was dried under reduced pressure. The chlorides of the M-II, P-I, and P-II isomers were also obtained from the eluates of the corresponding bands by means of similar procedures. M-I (P-I). Found: C, 20.47 (20.51); H, 6.55 (6.33); N, 16.57 (16.57)%. Calcd for [Co(CH_3-$NHCH_2COO$)$(C_2H_8N_2)_2$]$Cl_2\cdot 2H_2O\cdot HCl$: C, 20.47; H, 6.63; N, 17.06%. M-II (P-II). Found: C, 22.24 (22.40); H, 6.33 (5.88); N, 18.15 (18.38)%. Calcd for [Co(CH_3NHCH_2COO) $(C_2H_8N_2)_2$]$Cl_2\cdot 2H_2O$: C, 22.47; H, 5.93; N, 18.72%.

Physical Measurements. Absorption spectra were recorded on a Shimadzu UV 200S spectrophotometer equipped with a 1-cm quartz cell at room temperature. The sample solutions contained complex ions at approximately 4×10^{-3} M in 0.5 M HCl. CD curves were measured for a *ca.* 10^{-3} M solution of each isomer in 0.5 M HCl with a JASCO J-20 CD recorder using a 1-cm cell. The ^{13}C NMR spectra were obtained with a JEOL JNM FX-60 spectrometer at a probe temperature of 35 °C. Dioxane in D_2O in a coaxial inner tube was used as an external reference for all samples. The concentrations of the samples were approximately 0.1 M. Usually, 40000—50000 pulses were accumulated to produce a very clear spectrum.

Equilibration. About 0.02 g of each isomer was dissolved in 10 cm^3 of each solution listed in the first column of Table 4. The slightly alkaline or neutral solution (with added NaOH, if necessary) was allowed to stand at 25 °C for three days and then acidified with 0.5 M HCl. The complex was collected from the solution on a small amount of SP-Sephadex. The collected equilibrium mixture of the complex was subjected to chromatographic separation on an SP-Sephadex column (1.5 diam×87 cm) using 0.12 M $Na_2[Sb_2((+)\text{-}C_4H_2O_6)_2]$ as the eluent. The isomer ratio was obtained from the ratio of the areas of the bands in the elution curve.

Mutarotation. The rate of CD change was measured for a 0.1 M acetate buffer solution (pH 5.66) of each isomer (3.0×10^{-3} M) at 30.0 °C. The change in the CD intensity was observed at 465 nm, the wavelength at which the CD spectra showed a marked difference between the I and II isomers. The reaction was followed for at least three half-lives.

†† Although the elutions were carried out at room temperature (15—20 °C), the eluates were stored in a refrigerator (≈5 °C) to inhibit isomerization.

Results and Discussion

Chromatographic Behavior and Identification. Figure 2 shows the results of chromatographic elutions of the M-, P-, and racemic complexes with 0.12 M sodium (+)-tartratoantimonate(III). The ratios of the areas under the peaks are approximately 1 : 4.5 for (a) and (b), and 1 : 1 : 9 for (c) in Fig. 2. Comparisons of the band positions identified the A, B, and C bands of the racemic complex as the M-I, P-I, and combined P-II and M-II bands, respectively. For the C band, the CD sign at 518 nm was positive at the head of the band and negative at the tail, in agreement with the observation that the P-II isomer was eluted slightly faster than M-II.

The CD spectrum of the M-II isomer (Fig. 4) closely resembles that of $(-)_{589}$[Co(sar)$(en)_2]^{2+}$ obtained by Buckingham *et al.*[5)] On the basis of an X-ray analysis of $(-)_{589}$[Co(sar)$(en)_2]I_2\cdot 2H_2O$,[6)] the M-II isomer is identified as Δ-[Co(*S*-sar)$(en)_2]^{2+}$ (Fig. 1(a)). The P-II isomer can be identified as Λ-[Co(*R*-sar)$(en)_2]^{2+}$ from its enantiomeric relationship to the M-II isomer. Taking account of the isomerization behavior, which is described below, the M-I and P-I isomers are identified as the less stable isomers, Δ-[Co(*R*-sar)$(en)_2]^{2+}$ (Fig.

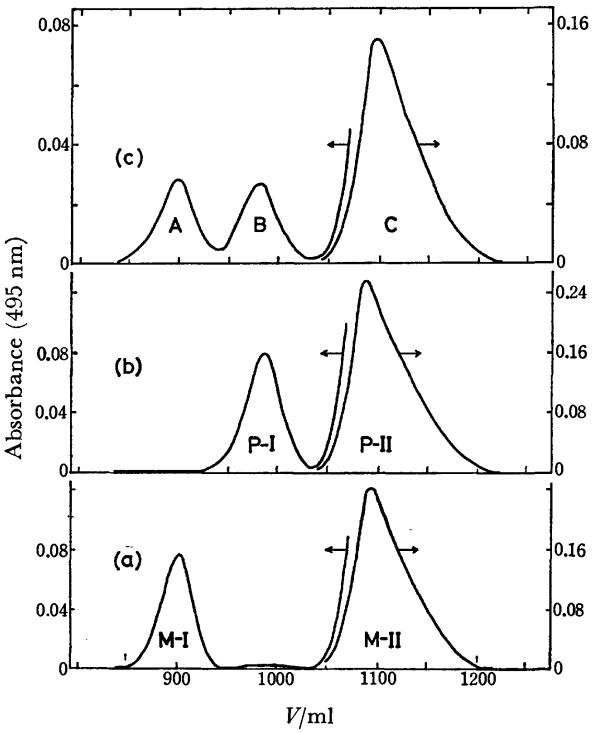

Fig. 2. Elution curves for $\{-\}_{518}$[Co(sar)$(en)_2]^{2+}$ (a), $\{+\}_{518}$[Co(sar)$(en)_2]^{2+}$ (b), and *rac*-[Co(sar)$(en)_2]^{2+}$(c).

1(b)) and *Λ*-$[Co(S\text{-sar})(en)_2]^{2+}$, respectively. The assignments are summarized in Table 1.

The P-I isomer showed no measurable CD change either in 0.12 M $Na_2[Sb_2((+)\text{-}C_4H_2O_6)_2]$ or in acidified water at room temperature over one week. This indicates that epimerization (configuration change) at the nitrogen center of the sarcosinato ligand is very slow in acidic solutions. The (+)-bromocamphorsulfonate of M-complex was dissolved in acidified water (pH≈3), and was subjected to chromatographic separation, as described in the experimental section. The elution curve showed a very small peak corresponding to M-I and a large peak corresponding to M-II, with the area ratio being 1 : 23. This suggests that the recrystallized (+)-bromocamphorsulfonate of the M-complex consists almost solely of the M-II isomer. On the other hand, in a neutral or alkaline solution, epimerization at the nitrogen center occurred to give an equilibrium mixture of M-I and M-II (Fig. 2(a)).

The fact that the less stable isomers, M-I and P-I, are eluted faster than the more stable M-II and P-II (Fig. 2) can be taken as an indication of the former being favored in the interaction with the eluting agent, sodium (+)-tartratoantimonate(III). The stereoselectivity is ascribed to the structural feature of the less stable isomers that each has a set of three N–H hydrogens directed nearly parallel to the pseudo-C_3 axis of the complex (Fig. 1). Further discussion in this connection can be found below.

Absorption (AB) and Circular Dichroism (CD) Spectra. Figures 3 and 4 show the AB and CD spectra of the four isomers, and Table 2 summarizes the numerical data for the M-I and M-II isomers. For the less stable isomer, M-I, both the first and second absorption bands appeared at slightly lower wave numbers than for the more stable isomer, M-II, indicating a slightly weaker ligand field in the M-I isomer. The CD spectra of M-I and P-I (Fig. 3) were mirror images of each other, confirming the enantiomeric relationship deduced from their chromatographic behavior. A similar relationship was observed between M-II and P-II (Fig. 4). The CD spectra of M-I and M-II are similar in that they have a main CD band of negative sign in the $^1T_{1g} \leftarrow {}^1A_{1g}$ (O_h) region, but are different from each other in other respects, as depicted in Figs. 3 and 4.

In Fig. 5, the halved sum of CD curves for P-I and P-II, showing the contribution of the *Λ*-configuration about the cobalt center, is compared with the CD curve for $\Lambda(+)_{546}[Co(gly)(en)_2]I_2$;[4] the latter has a configura-

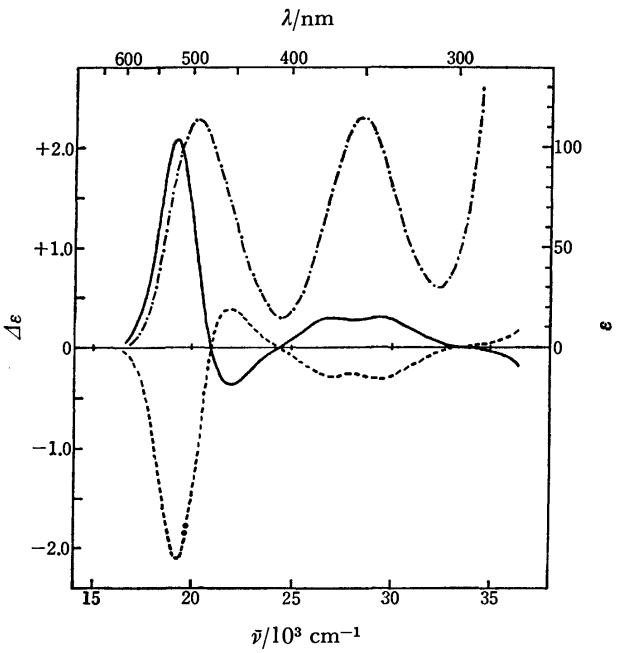

Fig. 3. Absorption spectrum (– · –) of P-I and circular dichroism spectra of P-I (——) and M-I (------) in 0.5 M HCl solutions.

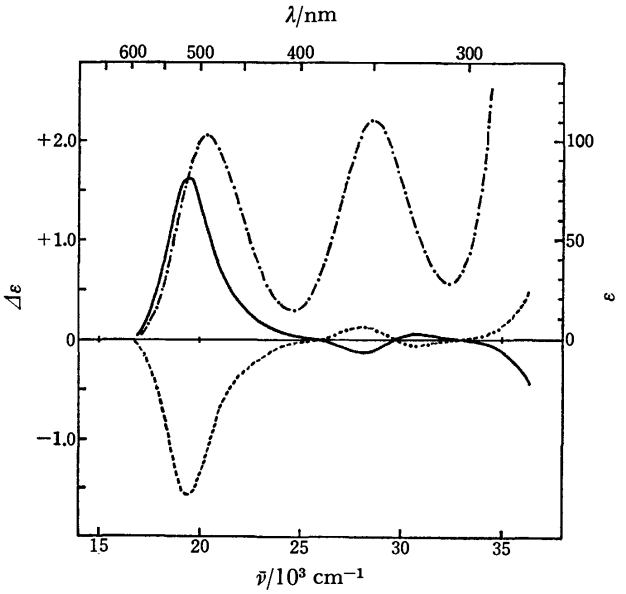

Fig. 4. Absorption spectrum (– · –) of P-II and circular dichroism spectra of P-II (——) and M-II (------) in 0.5 M HCl solutions.

Table 2. Absorption (AB) and circular dichroism (CD) spectral data

Complex		AB peak		CD peak	
		$\bar{\nu}/10^3$ cm^{-1}	ε	$\bar{\nu}/10^3$ cm^{-1}	$\Delta\varepsilon$
Λ{−}$_{518}[Co(R\text{-sar})(en)_2]Cl_2\cdot 2H_2O\cdot HCl$ (M-I)	1st band	20.3	114	19.2	−2.10
				21.9	+0.38
	2nd band	28.4	115	27.1	−0.29
				29.4	−0.31
Λ{−}$_{518}[Co(S\text{-sar})(en)_2]Cl_2\cdot 2H_2O$ (M-II)	1st band	20.4	103	19.5	−1.59
	2nd band	28.6	111	28.1	+0.13
				30.8	−0.04

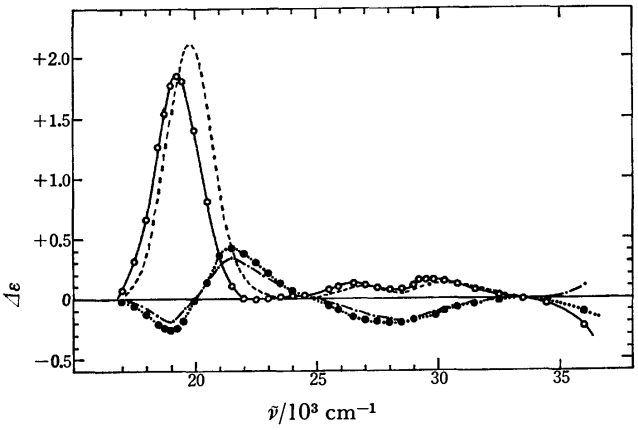

Fig. 5. Configurational and vicinal CD curves of $[Co(sar)(en)_2]^{2+}$: $1/2\times\{(P\text{-}I)+(P\text{-}II)\}$ (-○-) and $1/2\times\{(M\text{-}I)-(M\text{-}II)\}$ (···●···), respectively, compared with the CD spectra of Λ-$[Co(gly)(en)_2]^{2+}$ (------) and $(-)_{436}$-$[Co(R\text{-}sar)(NH_3)_4]^{2+}$ (- · -).

tion similar to that of the P-isomers, but has no asymmetric center at the aminoacidato nitrogen. Figure 5 also shows the halved difference of the CD spectra for M-I and M-II, showing *R*-vicinal contribution of the asymmetric nitrogen. This difference was compared with the CD spectrum for $(-)_{436}[Co(R\text{-}sar)(NH_3)_4](NO_3)_2$,[8] which makes only a vicinal contribution of the sarcosinato nitrogen to the CD spectrum. The similarity of the halved-sum and -difference spectra to those of the reference complexes can be taken as additional evidence for our assignment of the absolute configurations of the isomers; the small difference in the position of the main peak between the halved-sum CD spectrum and the reference spectrum may result from some conformational effect of the ethylenediamine rings.

In an X-ray study of the Λ-$[Co(S\text{-}sar)(en)_2]I_2\cdot 2H_2O$ crystal, the conformation of the ethylenediamine rings was found to be $\delta\lambda$.[6] On the other hand, Buckingham and his coworkers[9] have shown in their strain-energy

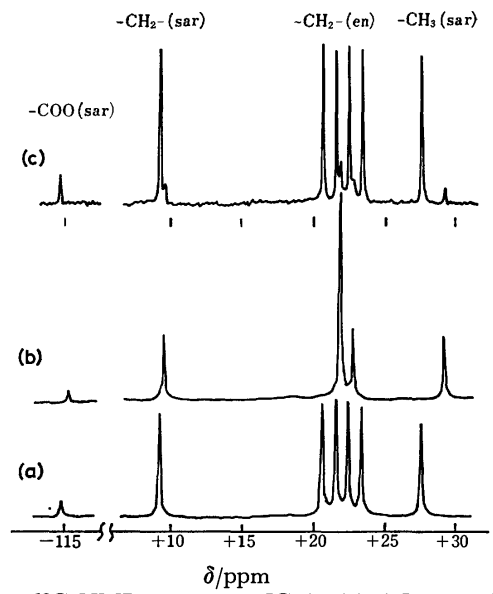

Fig. 6. ^{13}C NMR spectra of $[Co(sar)(en)_2]^{2+}$ in 0.5 M HCl solutions using dioxane as an external standard: P-II, (a); P-I, (b); racemic complex, (c).

calculations that the $\delta\lambda$ and $\lambda\lambda$ conformations would have the same minimum energy for the $\Delta(S)$ ion and that the $\lambda\lambda$ conformation is most stable for the $\Delta(R)$ ion. Thus, it is very probable that the $\Delta(S)$ and $\Delta(R)$ ions have different ring conformations and, therefore, that the halved-sum spectrum of these ions shows a conformational effect in addition to the Δ-configurational effect.

Carbon-13 NMR Spectra. Figure 6 shows the ^{13}C NMR spectra (^1H "noise" decoupled) of P-II, P-I, and the racemic mixture, which was equilibrated in an aqueous solution. All measurements were made in 0.5 M hydrochloric acid solutions to prevent isomerization. A comparison of the spectra shows that the racemic mixture contains II isomers as the major component and I isomers as the minor component.

The $[Co(sar)(en)_2]^{2+}$ ion has seven carbon atoms:

Table 3. Carbon-13 NMR Spectral data

Compound	Chemical shifts, δ[a]							
	$-CH_3$(sar)		$-CH_2$-(en)		$-CH_2$-(sar)		-COO (sar)	
$[Co(sar)(en)_2]^{2+}$								
P-II		+27.3		+23.2 (1)[b]		+9.14		−116.4
				+22.3 (1)				
				+21.4 (1)				
				+20.4 (1)				
P-I	+28.9		+22.6 (1)[b]		+9.40		−116.0	
			+21.7 (3)					
Racemic	+28.7	+27.2	+22.5[c]	+23.2	+9.33[c]	+9.06	—[d]	−116.4
			+21.7	+22.3				
				+21.4				
				+20.4				
$[Co(gly)(en)_2]^{2+}$			+22.9		+20.5[e]		−118.4[f]	
			+21.8					
			+21.6					
			+21.0					

a) Shifts in ppm from dioxane: positive values, upfield; negative values, downfield. b) Figures in parentheses are relative intensities. c) Shoulders. d) Peak not detected. e) Glycinato methylene carbon. f) Glycinato carboxyl carbon.

four methylene carbon atoms in the two ethylenediamine ligands, and single methyl, methylene, and carboxyl carbon atoms in the sarcosinato ligand. Correspondingly, the spectrum for P-II shows seven resonance peaks of nearly equal intensity except for the lowest-field peak of low intensity (Fig. 6(a)). The latter was assigned to the carboxyl carbon, which is known to relax slowly and to show a weak resonance peak.[10] Further information was obtained by allowing the ^{13}C nuclei to couple with protons. The resonance peak at the highest field split into a quartet and was readily assigned to the methyl carbon atom of the sarcosinato ligand. The signal of the methylene carbon atom in the sarcosinato ligand was distinguished from those of the methylene carbon atoms in the ethylenediamine ligands, because each of the triplet signals of the latter carbon atoms was broadened due to long-range coupling with the protons of the adjacent methylene and amino groups. However, the resonances of the ethylenediamine carbon atoms were difficult to assign to the individual atoms. The chemical shift data and assignments are summarized in Table 3. The table also gives the data for *rac*-$[Co(gly)(en)_2]Cl_2$ measured under the same conditions.

All the resonance peaks for the carbon atoms in the sarcosinato ligand appeared at a higher field for P-I than P-II. Since the chemical shift difference was the greatest between the methyl carbon signals of the two isomers, the high-field shifts observed for P-I can be ascribed to a distortion of the chelate ring brought about by an increase in the nonbonded repulsive interactions of the methyl group with an adjacent ethylenediamine ring. Such a distortion was also inferred from the low wave-number shift of the absorption spectrum of P-I relative to that of P-II. Concerning the resonance pattern of the four carbon atoms in ethylenediamine ligands, a marked difference was observed between P-I and P-II. Whereas P-II gave four nearly equally spaced peaks (Fig. 6(a)), P-I resulted in a pattern in which three of the four carbon atoms were apparently equivalent (Fig. 6(b)). The reasons for the incidental degeneracy in this nonsymmetric complex are not immediately evident. The ethylenediamine carbon atoms of the corresponding glycinato complex gave four distinct resonance peaks similar to those of P-II, although slight chemical-shift differences were observed among them. Therefore, nonbonded repulsive interactions of methyl group are responsible for the incidental degeneracy of the ethylenediamine carbon signals of P-I.

Mutarotation Rate (Rate of Epimerization at the Nitrogen Center). Figure 7 shows a typical set of CD spectra (480—380 nm) obtained at intervals after the P-I isomer had been dissolved in the acetate buffer solution at 28 °C. The spectra gave an isosbestic point at 403 nm and showed the greatest intensity change at 465 nm. From these observations, it is inferred that the CD change resulted from only one reaction which is epimerization at the nitrogen center yielding the P-II isomer.

The CD change measurements were carried out starting from the P-I and P-II isomers. In each kinetic run, the plot of $\ln|(\Delta\varepsilon)_t-(\Delta\varepsilon)_\infty|$ *vs.* time gave a straight line for at least three half-lives, where $(\Delta\varepsilon)_t$ and $(\Delta\varepsilon)_\infty$ represent the CD intensities at time t and at infinite

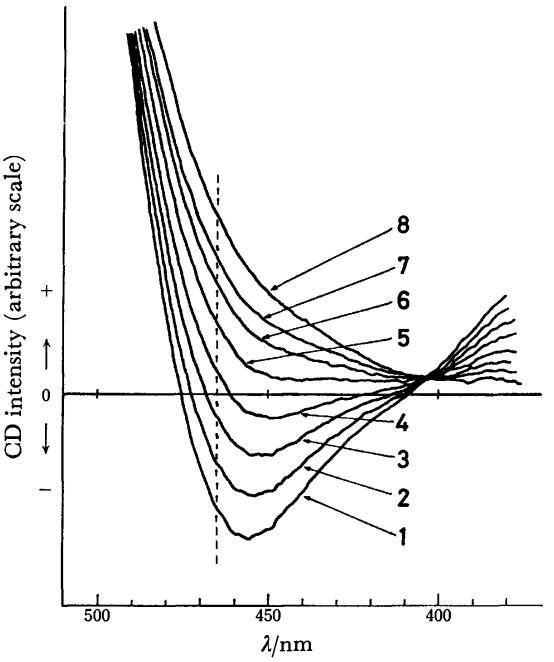

Fig. 7. Change of the CD spectrum with time for the P-I isomer in a 0.1 M acetate buffer at 28 °C. The curves 1—8 show the spectra measured at 5, 30, 60, 90, 130, 170, 215, and >1400 minutes, respectively.

time, respectively, at 465 nm. The slope gave the pseudo first-order rate constant, k_{obsd}. The runs using P-I and P-II as the starting isomers in a 0.1 M acetate buffer solution (pH 5.66) at 30.0 °C gave k_{obsd} values of 3.32×10^{-4} and 3.37×10^{-4} s^{-1}, respectively. They are in good agreement with each other.

For reversible isomerization (epimerization):

$$\text{P-II}(\Lambda(R)) \underset{k_r}{\overset{k_f}{\rightleftharpoons}} \text{P-I}(\Lambda(S))$$

the forward and reverse rate constants, k_f, and k_r, are related to the observed rate constant, k_{obsd}, and to the equilibrium constant, K, as follows:

$$k_{obsd} = k_f + k_r$$
$$K = k_f/k_r.$$

The K values was found to be 0.177 in chromatographic experiments on the equilibrium mixture (Table 4). This leads to k_f and k_r values of 0.50×10^{-4} and 2.85×10^{-4} s^{-1}, respectively. The rate of epimerization is known to be proportional to the hydroxide ion concentration,[8] and the second-order rate constants, k, k_1, and k_2, can be obtained from the corresponding first-order rate constants, k_{obsd}, k_f, and k_r, in terms of the equations:

$$k = k_{obsd}/[OH^-],\ k_1 = k_f/[OH^-],\ \text{and}\ k_2 = k_r/[OH^-].$$

The resulting values are 7.32×10^4, 1.1×10^4, and 6.2×10^4 M^{-1} s^{-1}, respectively. On the other hand, Halpern *et al.*[8] obtained a corresponding rate constant, $k=1.9\times10^4$ M^{-1} s^{-1}, for the racemization of $[Co(sar)(NH_3)_4](NO_3)_2$ dissolved in a 0.1 M acetate buffer at 30.0 °C. This gives $k_1=k_2=1.0\times10^4$ M^{-1} s^{-1}, which can be compared with the k_1 value for $[Co(sar)(en)_2]^{2+}$ of the present study. The several times greater value of k_2 for $[Co(sar)(en)_2]^{2+}$ suggests that some steric

TABLE 4. EQUILIBRIUM ISOMER DISTRIBUTIONS FOR $[Co(sar)(en)_2]^{+2}$ IN VARIOUS SOLUTIONS AT 25.0 °C

Solution	Isomer[a]	Isomer proportion(%)		Isomer ratio I/II
		I	II	
H_2O	M-I	15.4	84.6	0.182
	M-II	15.1	84.9	0.177
	P-II	15.1	84.9	0.178
0.1 M $NaCH_3COO$[b]	P-II	15.1	84.9	0.177
0.3 M $NaCH_3COO$	M-II	15.3	84.7	0.181
	P-II	15.7	84.3	0.187
	racemic	7.90+7.61	84.5	0.184
0.1 M Na_2SO_4	M-II	18.1	81.9	0.221
	P-II	17.7	82.3	0.215
0.1 M $Na_2(+)$-$C_4H_4O_6$	M-II	16.3	83.7	0.195
	P-II	16.3	83.7	0.195
0.3 M $Na_2(+)$-$C_4H_4O_6$	M-II	17.0	83.0	0.205
	P-II	17.8	82.2	0.217

a) Starting substance for equilibration. b) Kinetic run in an acetate buffer at 30.0 °C (see text).

repulsion exists in the $\Lambda(S)$ isomer to result in the acceleration of the $\Lambda(S)$ to $\Lambda(R)$ epimerization.

Equilibrium Isomer Distribution. The complex was equilibrated in various solutions at 25 °C and chromatographically analyzed for the isomer distribution. The results are given in Table 4. No indication was observed of the formation of other isomers and decomposition products in the column-chromatographic procedure.

The runs starting from M-I and from M-II in water gave essentially the same I to II ratios within the experimental error ($\approx\pm3\%$), consistent with the mutarotation experiments. Therefore, other runs were performed with either of the stable isomers (M-II and P-II) as the starting substance. At equilibrium in an aqueous solution, the I to II ratio was 15.2: 84.8 on the average, which gave the equilibrium constant, $K=0.177$, and the free energy difference, $\Delta G=4.2_6$ kJ mol^{-1}, between the I and II isomers. This ΔG value is close to the strain energy difference of 0.9 kcal mol^{-1} (=3.8 kJ mol^{-1}) calculated by Buckingham and his coworkers,[9] who gave minimized strain energies of 3.8 kcal mol^{-1} for the $\delta\lambda$-*S* and $\lambda\lambda$-*S* isomers of the Δ-complex and 4.7 kcal mol^{-1} for the $\lambda\lambda$-*R* isomer of the Δ-complex.†††

The addition of oxo anions effected an increase in the proportion of I isomer. Whereas, in 0.3 M CH_3COONa, this effect was not clearly observable due to the experimental error, a marked effect was found in 0.1 M Na_2SO_4. Sodium (+)-tartrate also showed the effect of increasing the proportion of I isomer, although the abundance of I isomer in 0.1 M $Na_2((+)$-$C_4H_4O_6)$ was not as high as that in 0.1 M Na_2SO_4 (Table 4). It is to be noted that, in 0.3 M $Na_2((+)$-$C_4H_4O_6)$, the M-and P-isomers showed different I/II ratios (Table 4), which is suggestive of stereoselective interactions of the isomers with the (+)-tartrate ion.

Such stereoselectivity was confirmed by the following chromatographic experiment. A slightly acidic (with HCl) aqueous solution of the P-I and M-I isomers mixed in equal amounts was allowed to flow through an SP-Sephadex column (1.5 dia. × 90 cm) and the complex sorbed by the column was eluted with 0.24 M $NaH((+)$-$C_4H_4O_6)$ (pH 3.4). Although the elution curve showed only one band, CD measurements revealed partial resolution of the enantiomers with an elution order P-I ($\Lambda(S)$) and M-I ($\Delta(R)$). This order can be compared with the Λ-Δ order of $[Co(en)_3]^{3+}$ when eluted with a sodium (+)-tartrate solution[11] and also when eluted with a sodium hydrogen-(+)-tartrate solution,[12] although the stereoselectivity was much higher in the $[Co(en)_3]^{3+}$ cases.

The behavior of the I isomer is understandable from the structural point of view. Both P-I and M-I isomers have a set of three N–H bonds (one sarcosinato and two ethylenediamine N–H bonds) aligned approximately parallel to the pseudo-C_3 axis of the complex, if the ethylenediamine ligands assume the *lel* conformation (Fig. 1). In the P-II and M-II isomers, on the other hand, the N–CH_3 bond of the sarcosinato ligand is nearly parallel to the pseudo-C_3 axis. Therefore, I isomers will more favorably interact with sulfate, (+)-tartrate, and hydrogen-(+)-tartrate ions than will II isomers and, thus, the proportion of I isomers in the equilibrated mixture will increase. The greatest effect shown by sulfate ions (Table 4) can be taken as suggesting that sulfate ions have the greatest tendency to form ion pairs with I isomers. This is consistent with the fact that the formation constant for the $[Co(en)_3]^{3+}$–SO_4^{2-} ion pair is approximately twice as large as that for the ion pair with the (+)-tartrate.[13]

The stereoselectivity of the (+)-tartrate ion for the P-I and M-I isomers can be explained in a manner similar to that for the case of stereoselective ion-pair formation between the (+)-tartrate ion and the $[Co(en)_3]^{3+}$ isomers.[14] The lower stereoselectivity for the $[Co(sar)(en)_2]^{2+}$ isomers appears to result mainly from the lower charge of this complex than for $[Co(en)_3]^{3+}$. For $[Co(gly)(en)_2]^{2+}$, (+)-tartrate ions showed little stereoselectivity.

The stereoselectivity shown by (+)-tartratoanti-

††† However, they assumed that the actual ΔG value probably exceeds $\approx$2 kcal mol^{-1}, since their careful ion-exchange chromatographic studies failed to show any isomeric separation.

monate(III) ions is very different from that of (+)-tartrate ions. As illustrated in Fig. 2(c), (+)-tartratoantimonate(III) ions show a high stereoselectivity for $[Co(sar)(en)_2]^{2+}$; however, this selectivity is the reverse of that shown by (+)-tartrate ions. This is in contrast to the case of $[Co(en)_3]^{3+}$, for which (+)-tartratoantimonate(III) ions show a stereoselectivity of the same preference as that shown by (+)-tartrate ions. The formation of the $[Co(sar)(en)_2]^{2+}$–$[Sb_2((+)\text{-}C_4H_2O_6)_2]^{2-}$ ion pair may occur through a mechanism different from that in the ion-pair formation involving (+)- tartrate or hydrogen-(+)-tartrate ions, since the tartrato hydroxyl groups in the (+)-tartratoantimonate(III) ion are bound to antimon(III) ions[15] and not readily available for ion pairing.

References

1) J. Meisenheimer, L. Angermann, and H. Holsten, *Justus Liebigs Ann. Chem.*, **438**, 261 (1924).

2) D. A. Buckingham, S. F. Mason, A. M. Sargeson, and K. R. Turnbull, *Inorg. Chem.*, **5**, 1649 (1966), and references cited therein.

3) M. Fujita, Y. Yoshikawa, and H. Yamatera, *Chem. Lett.*, **1976**, 959.

4) C. T. Liu and B. E. Douglas, *Inorg. Chem.*, **3**, 1356 (1964).

5) D. A. Buckingham, S. F. Mason, A. M. Sargeson, and K. R. Turnbull, *Inorg. Chem.*, **5**, 1649 (1966).

6) J. F. Blount, H. C. Freeman, A. M. Sargeson, and K. R. Turnbull, *J. Chem. Soc., Chem. Commun.*, **1967**, 324.

7) Y. Yoshikawa, *Bull. Chem. Soc. Jpn.*, **49**, 159 (1976).

8) B. Halpern, A. M. Sargeson, and K. R. Turnbull, *J. Am. Chem. Soc.*, **88**, 4630 (1966).

9) B. F. Anderson, D. A. Buckingham, G. J. Gainsford, G. B. Robertson, and A. M. Sargeson, *Inorg. Chem.*, **14**, 1658 (1975).

10) K. D. Gailey, K. Igi, and B. E. Douglas, *Inorg. Chem.*, **12**, 2956 (1972); O. W. Howarth, P. Moore, and N. Winterton, *J. Chem. Soc., Dalton Trans.*, **1974**, 2271.

11) Y. Yoshikawa and K. Yamasaki, *Inorg. Nucl. Chem. Lett.*, **6**, 523 (1970).

12) M. Fujita, Y. Yoshikawa, and H. Yamatera, unpublished work.

13) K. Ogino, *Bull. Chem. Soc. Jpn.*, **42**, 447 (1969).

14) M. Fujita and H. Yamatera, *Bull. Chem. Soc. Jpn.*, **49**, 1301 (1976).

15) B. Kamenar, D. Grdenic, and C. K. Prout, *Acta Crystallogr., Sect. B*, **26**, 181 (1970).

Preparation and Stereochemistry of Cobalt(III) Complexes Containing *N*-Methylbis(2-aminoethyl)amine

Masaaki KOJIMA, Masaru IWAGAKI, Yuzo YOSHIKAWA, and Junnosuke FUJITA

Department of Chemistry, Faculty of Science, Nagoya University, Chikusa, Nagoya 464

(Received May 10, 1977)

Seven new cobalt(III) complexes containing *N*-methylbis(2-aminoethyl)amine (4-methyldiethylenetriamine, abbreviated as dema) were prepared and their structures were determined by electronic, circular dichroism, and PMR spectroscopy. For the mixed $[Co(dien)(dema)]^{3+}$ complex(dien=diethylenetriamine), three geometric isomers, *s-fac*, *u-fac*, and *mer* were isolated. The $[Co(dema)_2]^{3+}$ complex formed only *s-fac* isomer. A conformational analysis was carried out to compare the stability of these geometric isomers.

Recently three geometric isomers of $[Co(dien)_2]^{3+}$ (dien=diethylenetriamine) were isolated, and the *u-fac* and the *mer* isomers were resolved into optical antipodes.[1,2] The formation ratio in an equilibrium mixture of the bromides (25 °C),[1] *s-fac*: *u-fac*: *mer*= 7: 30: 63 indicates that the *mer* arrangement is preferred over the *fac* one. The absolute configuration of the $(+)_{589}$-*u-fac* isomer assigned on the basis of the circular dichroism spectrum agreed with that determined by X-ray work.[3] For the *mer* isomer, however, the relationship between the circular dichroism spectrum and the absolute configuration is not clear yet.

The same isomerism is expected for the complex ions, $[Co(dien)(dema)]^{3+}$ (dema=*N*-methylbis(2-aminoethyl)amine, 4-methyldiethylenetriamine) and $[Co(dema)_2]^{3+}$. Molecular model studies indicate that the *mer* and the *u-fac* isomers of these complexes involve considerable steric interactions between the methyl group and its surroundings. Accordingly, the distribution of isomers in these complexes will differ from that in $[Co(dien)_2]^{3+}$. It will also be interesting to see how such steric interactions are reflected on the absorption and circular dichroism spectra.

Experimental

Ligands. *N*-Methylbis(2-aminoethyl)amine (dema) and its hydrochloride(dema·3HCl) were prepared by the method of Nakajima *et al.*[4] Diethylenetriamine(dien) was obtained from Tokyo Kasei Co., and used without further purification.

$[Co(NO_2)_3(dema)]$ and $[CoCl_2(H_2O)(dema)]Cl\cdot 0.5H_2O$. $[Co(NO_2)_3(dema)]$ was prepared from $Co(NO_3)_2\cdot 6H_2O$, $NaNO_2$, and dema by a method similar to that for $[Co(NO_2)_3(dien)]$,[5] and recrystallized from water containing a small amount of $NaNO_2$ and a few drops of acetic acid . Orange needle crystals were filtered off, washed with water and air dried, 60% yield. Found: C, 18.93; H, 4.64; N, 26.71%. Calcd for $CoC_5H_{15}N_6O_6=[Co(NO_2)_3(dema)]$: C, 19.12; H, 4.81; N, 26.75%.

$[Co(NO_2)_3(dema)]$(6.8 g, 22 mmol) was gently heated with 70 cm³ of concd HCl until the evolution of nitrogen dioxide ceased. Fine blue crystals which formed on standing the resulting solution overnight at room temperature were filtered off and washed with acetone, 75% yield. Found: C, 19.22; H, 6.13; N, 13.08; H_2O, 8.92%. Calcd for $CoC_5H_{18}N_3O_{0.5}Cl_3=[CoCl_2(H_2O)(dema)]Cl\cdot 0.5H_2O$: C, 19.39; H, 5.86; N, 13.58; H_2O, 8.74%.

s-fac-$[Co(dien)(dema)]Cl_3\cdot H_2O$(Isomer A). To a solution of $CoCl_2\cdot 6H_2O$(0.6 g, 2.5 mmol) in 10 cm³ of water were added a solution of dema (0.4 g, 3.5 mmol) and dien (0.35 g, 3.5 mmol) in 10 cm³ of water, and active charcoal (0.3 g). The mixture was aerated for 6 h at room temperature, and filtered to remove the charcoal. The resulting orange filtrate was diluted with about 1 dm³ of water and passed through an SP-Sephadex column ($\phi 2.5\times 4$ cm). A small portion of the SP-Sephadex charged with the product was poured on the top of the adsorbent layer of an SP-Sephadex column ($\phi 2.7\times 120$ cm) and the adsorbed complexes were eluted with a 0.2 M aqueous solution of Na_2SO_4. Three separate bands were obtained. The first band was *s-fac*-$[Co(dien)_2]^{3+}$, but the second and the third bands were mixtures of *u-fac*-$[Co(dien)_2]^{3+}$ and *s-fac*-$[Co(dien)(dema)]^{3+}$, and *mer*-$[Co(dien)_2]^{3+}$ and *s-fac*-$[Co(dema)_2]^{3+}$, respectively. The effluent of the second band was diluted with water and reloaded on an SP-Sephadex column, and the adsorbed band was eluted with a 0.15 M sodium $(+)_{589}$-tartratoantimonate(III) solution. Three separate bands, II_A, II_B, and II_C which eluted in this order were $(+)_{589}$-*u-fac*-$[Co(dien)_2]^{3+}$, $(-)_{589}$-*u-fac*-$[Co(dien)_2]^{3+}$, and *s-fac*-$[Co(dien)(dema)]^{3+}$, respectively. The third band was rechromatographed by a method similar to that for the second band. The column gave three separate bands, III_A, III_B, and III_C in the order of elution, which were $(+)_{589}$-*mer*-$[Co(dien)_2]^{3+}$, $(-)_{589}$-*mer*-$[Co(dien)_2]^{3+}$, and *s-fac*-$[Co(dema)_2]^{3+}$, respectively. The formation ratio, *s-fac*-$[Co(dien)_2]^{3+}$: *u-fac*-$[Co(dien)_2]^{3+}$: *mer*-$[Co(dien)_2]^{3+}$: *s-fac*-$[Co(dien)(dema)]^{3+}$: *s-fac*-$[Co(dema)_2]^{3+}$ was about 1: 4: 15: 6: 5. The effluent containing *s-fac*-$[Co(dien)(dema)]^{3+}$ was diluted with water and poured again on an SP-Sephadex column ($\phi 1.5\times 3$ cm), the column was washed with a large amount of 10^{-2} M HCl, and then the adsorbed complex was eluted with 1.0 M HCl. Orange crystals were obtained by evaporating the effluent to almost dryness in a vacuum desiccator over NaOH and P_2O_5. Found: C, 26.41; H, 7.40; N, 20.98%. Calcd for $CoC_9H_{30}N_6OCl_3$=*s-fac*-$[Co(dien)(dema)]Cl_3\cdot H_2O$: C, 26.78; H, 7.49; N, 20.82%.

u-fac-*$[Co(dien)(dema)]^{3+}$(Isomer B).* An aqueous solution (50 cm³) of dien·3HCl(0.63 g, 3 mmol) neutralized with $NaHCO_3$ (0.75 g, 9 mmol) was added to a solution of $[CoCl_2(H_2O)(dema)]Cl\cdot 0.5H_2O$(0.9 g, 3 mmol) in 50 cm³ of water. The solution was heated at 50 °C for 40 h, and then diluted with 1 dm³ of water. The solution was poured on an SP-Sephadex column ($\phi 2.5\times 4$ cm), and the adsorbed product was chromatographed by a method similar to that for *s-fac*-$[Co(dien)(dema)]^{3+}$ with a 0.2 M aqueous aolution of Na_2SO_4. The column gave orange, red-violet, and violet bands in the order of elution. The effluent of the first orange band was diluted with water and reloaded on an SP-Sephadex column, and the adsorbed band was eluted with a 0.2 M sodium $(+)_{589}$-tartrate solution. The column showed three yellow-orange bands. The first, the second, and the third bands in the order of elution were *u-fac*-$[Co(dien)(dema)]^{3+}$, *s-fac*-$[Co(dien)(dema)]^{3+}$, and *u-fac*-$[Co(dien)_2]^{3+}$, respectively. The

effluent of *u-fac*-[Co(dien)(dema)]$^{3+}$ was diluted with water and poured again on an SP-Sephadex column (ϕ1.5×3 cm), and the adsorbed complex was eluted with a 1.0 M NaCl solution. The complex was isolated as hexacyanocobaltate(III) salt by adding a $K_3[Co(CN)_6]$ solution to the effluent. Found: C, 33.26; H, 6.28; N, 30.74%. Calcd for $Co_2C_{15}H_{34}N_{12}O_3$= *u-fac*-[Co(dien)(dema)][$Co(CN)_6$]·3H_2O: C, 32.85; H, 6.25; N, 30.64%. The complex hexacyanocobaltate(III) was converted into chloride by use of the anion exchanger, Dowex 1×8 in the chloride form. The complex chloride did not crystallize on the addition of common organic solvents to a concentrate of the chloride solution. Thus, the orange residue obtained by evaporation in a vacuum desiccator was used for measurement.

The complex was resolved by SP-Sephadex column chromatography with a 0.15 M sodium $(+)_{589}$-tartratoantimonate-(III) solution as the eluent. The optically active chloride salt was isolated as an orange residue by a method similar to that for the racemic complex chloride.

mer-[*Co(dien)(dema)*]$^{3+}$*(Isomer C)*. To a suspension of *mer*-[$CoCl_3$(dien)][6] (2.2 g, 8.2 mmol) in 10 cm^3 of *N,N*-dimethylformamide (DMF) was added dema (1.0 g, 8.5 mmol), and the mixture was stirred for 1 h at 50 °C. The resulting orange solution was diluted to 1 dm^3 with water, and poured on SP-Sephadex. The product adsorbed on SP-Sephadex was similarly chromatographed. By elution with 0.15 M sodium $(+)_{589}$-tartratoantimonate (III), the column gave two pairs of enantiomers, the fast-(very small amount) and the slow-moving bands being $(+)_{589}$- and $(-)_{589}$-*mer*-[Co(dien)$_2$]$^{3+}$ and $(-)_{490}$- and $(+)_{490}$-*mer*-[Co(dien)(dema)]$^{3+}$, respectively. The optically active *mer*-[Co(dien)(dema)]$^{3+}$ was isolated as hexacyanocobaltate(III) salt by a method similar to that for *u-fac*-[Co(dien)(dema)]$^{3+}$, and the isolated salt was converted into bromide with the anion exchanger, Dowex 1X 8 in the bromide form. The solution of the complex bromide was evaporated to dryness in a vacuum desiccator to give orange crystals. Found: C, 19.30; H, 5.74; N, 14.82%. Calcd for $CoC_9H_{33}N_6Br_3O_{2.5}$=$(+)_{490}$-*mer*-[Co(dien)(dema)]$Br_3$·2.5-$H_2O$: C, 19.17; H, 5.90; N, 14.89%. The racemic complex was isolated as perchlorate salt by the following method; the effluents containing $(-)_{490}$- and $(+)_{490}$- isomers were combined, diluted with water, and poured on SP-Sephadex. The adsorbed complex was eluted with a 1.5 M $NaClO_4$ solution and the effluent was concentrated in a vacuum desiccator over P_2O_5 to give orange crystals. Found: C, 17.74; H, 5.21; N, 13.70%. Calcd for $CoC_9H_{32}N_6O_{14}Cl_3$=*mer*-[Co(dien)(dema)]$(ClO_4)_3$·2H_2O: C, 17.62; H, 5.26; N, 13.69%.

s-fac-[*Co(dema)*$_2$]$^{3+}$. *Method 1*: A solution of dema·3HCl(5.0 g, 22 mmol) in water (20 cm^3) was neutralized with an aqueous solution (10 cm^3) of NaOH (2.4 g, 60 mmol) or Na_2CO_3(3.2 g, 30 mmol). The solution was added to a solution of $CoCl_2$·6H_2O (2.38 g, 10 mmol) in water (30 cm^3), and then mixed with active charcoal (0.5 g). The mixture was aerated for 12—120 h at room temperature.

Method 2: To a solution of $CoCl_2$·6H_2O (0.24 g, 1 mmol) in 50 cm^3 of water were added a solution of Na_3PO_4·12H_2O (1.9 g, 5 mmol) and dema·3HCl (0.46 g, 2 mmol) in water (10 cm^3), and active charcoal (0.2 g). The cobalt ions were oxidized by bubbling a stream of air through the solution at room temperature for 22 h. The addition of phosphate is known to change the distribution of isomers in the complex formation of [Co(dien)$_2$]$^{3+}$.[7]

Method 3: To a dimethyl sulfoxide (DMSO) solution (20 cm^3) containing $Co(NO_3)_2$·6H_2O(0.29 g, 1 mmol) and dema·3HCl(0.23 g, 1 mmol) were added a solution of dema(0.29 g, 2.5 mmol) in DMSO (10 cm^3), and active charcoal (0.2 g). The oxidation of cobalt ions was carried out under the same conditions as that for Method 2.

Method 4: A solution of dema·3HCl (0.91 g, 4 mmol) in 10 cm^3 of water was neutralized with Na_2CO_3 (0.64 g, 6 mmol). To this solution were added a solution of [$Co(H_2O)$-$(NH_3)_5$]$(ClO_4)_3$(0.46 g, 1 mmol) in water (20 cm^3), and active charcoal (0.2 g). The mixture was heated at 70—80 °C for 2 h.

Method 5: To a solution of [$Co(H_2O)(NH_3)_5$]$(ClO_4)_3$(0.92 g, 2 mmol) in 20 cm^3 of DMSO was added a DMSO solution (10 cm^3) of dema (0.8 g, 7 mmol). The solution was heated at 85 °C for 15 min.

Method 6: To a solution of dema·3HCl (0.68 g, 3 mmol) and sodium methoxide (0.41 g, 7.5 mmol) in methanol (12 cm^3) was added a solution of *trans*-[$CoCl_2(py)_4$]Cl·6H_2O[8] (0.59 g, 1 mmol) in methanol (8 cm^3). The reaction took place immediately to give orange precipitate.

Method 8: This method was the same as Method 7 except that pyridine was used as the solvent instead of methanol.

Method 9: To an ice-cold, stirred solution of $K_3[Co(CO_3)_3]$[9] (2.1 mmol) in water (5 cm^3) was added dropwise a solution of dema·3HCl (1.0 g, 4.4 mmol) in water (5 cm^3). The mixture was heated at 70—80 °C for 6 h until the color of the solution became red. The solution was mixted with acetic acid (50%, 15 cm^3) and heated further 2 h.

Method 10: To a solution of dema (2 g, 17 mmol) in 10 cm^3 of DMF was added [$CoCl_2(H_2O)$(dema)]Cl·0.5H_2O (0.8 g, 2.7 mmol). The mixture was heated at 50 °C for 2 h.

Method 11: This method was the same as Method 1 except that the aeration was carried out at 80 °C for 7 h.

The reaction mixtures were filtered to remove the charcoal if necessary, diluted with water, and then the pH of the solutions were adjusted to 4—6 with HCl. A small amount of each solution was applied to SP-Sephadex column (ϕ2.7 ×120 cm) chromatography. The eluents used were 0.2 M sodium sulfate, 0.2 M sodium $(+)_{589}$-tartrate, or 0.15 M sodium $(+)_{589}$-tartratoantimonate(III) solutions. All the preparative methods except for Method 11 gave only one isomer, *s-fac*-[Co(dema)$_2$]$^{3+}$. No indication for the formation of other isomers was found. The complex was isolated as perchlorate salt by a method similar to that for *mer*-[Co(dien)-(dema)]$(ClO_4)_3$·2H_2O. Found: C, 20.04; H, 5.00; N, 14.12%. Calcd for $CoC_{10}H_{31}N_6O_{12.5}Cl_3$=*s-fac*-[Co(dema)$_2$]$(ClO_4)_3$·0.5 H_2O: C, 20.00; H, 5.20; N, 13.99%. The solution obtained from Method 11 was chromatographed in a manner similar to those for Method 1—10. By elution with a 0.2 M Na_2SO_4 solution, the column gave four yellow-orange bands. The first small band was *s-fac*-[Co(dien)(dema)]$^{3+}$ which may be a demethylated product of *s-fac*-[Co(dema)$_2$]$^{3+}$, and the second main band was *s-fac*-[Co(dema)$_2$]$^{3+}$. Complexes obtained from the third and the fourth bands gave analytical results which do not correspond to the dien or dema complexes, and were not characterized.

Measurements. Absorption and diffuse reflectance spectra were recorded on a Hitachi 323 spectrophotometer, and circular dichroism spectra on a JASCO model J-20 spectropolarimeter. PMR spectra were recorded on a JEOL PMX-60 spectrometer at 60 MHz in DMSO-d_6 with TMS as the internal reference.

Results and Discussion

Preparation and Characterization of the Isomers. (i) [*Co(NO$_2$)$_3$(dema)*], [*CoCl$_2$(H$_2$O)(dema)*]$^+$, *and* [*CoCl$_3$-(dema)*]: The [$Co(NO_2)_3$(dien)] complex has been determined to be *mer* configuration by X-ray analysis.[10] By heating this complex with concd hydrochloric acid,

brown crystals of $[CoCl_3(dien)]$ are obtained.[7] It gives only *mer* isomer of $[Co(dien)(dema)]^{3+}$ by reacting with dema in DMF. On the other hand, the reaction of $[Co(NO_2)_3(dema)]$ with concd hydrochloric acid yields blue crystals of $[CoCl_2(H_2O)(dema)]Cl\cdot 0.5H_2O$, which turn green $[CoCl_3(dema)]$ by heating at 110 °C for 1 h *in vacuo*. These chlorodema complexes give only *s-fac*-$[Co(dema)_2]^{3+}$ by the reaction with dema. These results and the diffuse reflectance spectra of the tri-chloro complexes (*vide post*) indicate that the dien and the dema ligands in the present nitro and chloro complexes have *mer* and *fac* configurations, respectively. Two geometric isomers are possible for *fac*-$[CoCl_2(H_2O)(dema)]^+$. However, the structure of the present blue complex could not be assigned by PMR and absorption spectroscopy.

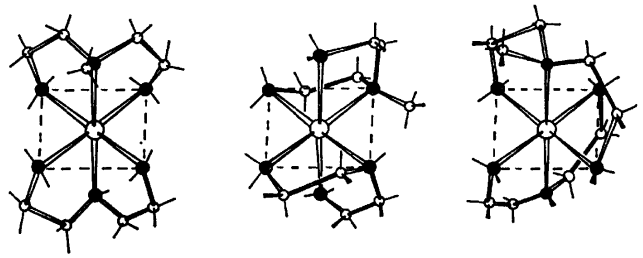

(a) *s-fac* (b) *u-fac* (c) *mer*

Fig. 1. Three geometric isomers of $[Co(dien)(dema)]^{3+}$.

(ii) $[Co(dien)(dema)]^{3+}$: As Fig. 1 shows, the *s-fac* isomer is achiral, while both the *u-fac* and the *mer* isomers are chiral and exist each in a pair of enantiomers. The *mer* isomer is expected to be optically stable only in acidic solution as has been observed for *mer*-$[Co(dien)_2]^{3+}$.[1,2] The isomer A can be assigned to the *s-fac* isomer, since it is not resolved, while the other two isomers (the isomers B and C) are completely resolved. The resolved isomer C loses rapidly its optical activity in alkaline solution, but the isomer B is optically stable under the same condition. Thus the isomers B and C are assigned to the *u-fac* and the *mer* isomers, respectively. As described in Experimental part, only the *s-fac* isomer of $[Co(dien)(dema)]^{3+}$ was isolated from the product obtained by the reaction in the presence of active charcoal, although the product contained three isomers of $[Co(dien)_2]^{3+}$ and *s-fac*-$[Co(dema)_2]^{3+}$. Strain energy minimization calculation reveals that the *u-fac* and the *mer* isomers are less stable than the *s-fac* isomer by 22.1 and 6.1 $kJ\cdot mol^{-1}$, respectively (*vide post*).

The *u-fac* isomer was obtained by the reaction of *fac*-$[CoCl_2(H_2O)(dema)]Cl\cdot 0.5H_2O$ with dien in water without the addition of active charcoal. The *mer* isomer was prepared similarly from *mer*-$[CoCl_3(dien)]$ and dema in DMF, as stated previously. The triamine ligands in the starting complexes seem to retain the arrangement in these substitution reactions.

(iii) $[Co(dema)_2]^{3+}$: All the preparative methods give a single geometric isomer as evidenced by column chromatography. The PMR spectrum of $[Co(dema)_2](ClO_4)_3\cdot 0.5H_2O$ in DMSO-d_6 exhibits only one kind of the NH_2 group, (δ=5.1 ppm). In the *s-fac* isomer, the NH_2 groups should be equivalent, while the other two isomers have two nonequivalent sets of NH_2 groups (Fig. 1). Thus, the complex can be assigned to the *s-fac* isomer. Conformational analysis also indicates that the *s-fac* isomer is the most stable (*vide post*).

Very recently, Searle and Larsen[11] reported the PMR data for the *u-fac* isomer, but did not describe the preparative method.

Absorption and Circular Dichroism Spectra. Figure 2 and Table 1 compare the absorption spectra of the *s-fac* isomers of $[Co(dema)_2]^{3+}$, $[Co(dien)(dema)]^{3+}$, and $[Co(dien)_2]^{3+}$. All of the absorption bands shift to longer wavelengths as the number of the dema ligand increases. A similar shift is observed for a series of complexes of the type $[Co(en)_x(N\text{-meen})_{3-x}]^{3+}$ (x= 0—3, N-meen=N-methylethylenediamine).[12] The differences in the absorption maxima of the first absorption bands amount to 480 cm^{-1} between $[Co(dien)_2]^{3+}$ and $[Co(dien)(dema)]^{3+}$ and 490 cm^{-1} between $[Co(dien)(dema)]^{3+}$ and $[Co(dema)_2]^{3+}$. Therefore, it is concluded that dema is located at a lower position than dien in the spectrochemical series. Both *s-fac*-[Co-

Table 1. Absorption and CD spectral data

Complex	Absorption		CD	
	$\bar{\nu}$/cm^{-1}	log ε	$\bar{\nu}$/cm^{-1}	$\Delta\varepsilon$
s-fac-$[Co(dien)_2]^+$	21760	1.84		
	29900	1.80		
	47200	4.35		
$(+)_{589}$-*u-fac*-$[Co(dien))_2]^{3+}$	21370	1.99	19900	+0.98
			22500	−0.84
	29500	1.97	29900	+0.37
	46200	4.35	44400	−9.0
			50700	+7.4
$(+)_{589}$-*mer*-$[Co(dien)_2]^{3+}$	21460	2.17	19500	+0.096
			21900	−0.18
	29200	2.05	27800	−0.014
			30700	+0.057
	44400	4.32	45500	+0.26
s-fac-$[Co(dien)(dema)]^{3+}$	21280	1.90		
	29600	1.86		
	45500	4.32		
$(+)_{589}$-*u-fac*-$[Co(dien)(dema)]^{3+}$	20750	2.06	19840	+1.02
			22270	−0.023
	29100	1.99	27200	+0.30
	44500	4.32	38600	+1.0
			43500	−6.7
			48500	+6.6
$(-)_{490}$-*mer*-$[Co(dien)(dema)]^{3+}$	20790	2.17	19120	+0.083
			21410	−0.19
	28700	2.13	29000	+0.080
	43300	4.25	43000	+0.36
			49000	−0.86
s-fac-$[Co(dema)_2]^{3+}$	20790	1.90		
	29400	1.89		
	44600	4.25		
mer-$[Co(NO_2)_3(dien)]$	23300	2.56		
	29700	3.80		
	39700	4.41		
fac-$[Co(NO_2)_3(dema)]$	22600	2.54		
	29500	3.83		
	39200	4.39		

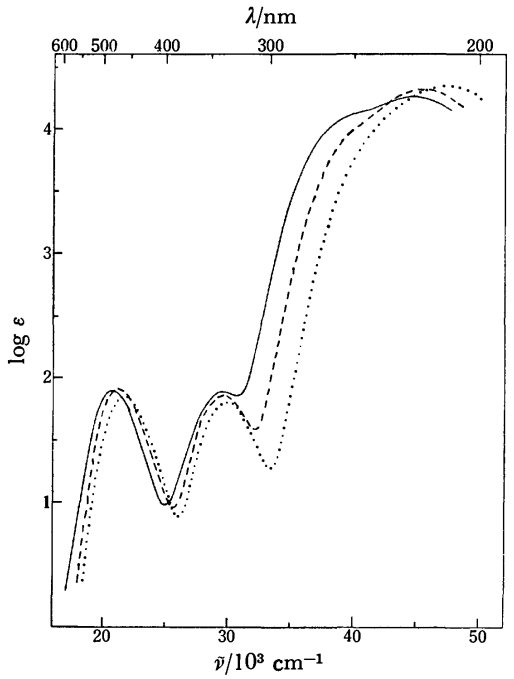

Fig. 2. Absorption spectra of the *s-fac* isomers of [Co(dema)$_2$]$^{3+}$ (——), [Co(dien)(dema)]$^{3+}$ (——), and [Co(dien)$_2$]$^{3+}$ (·····) in water.

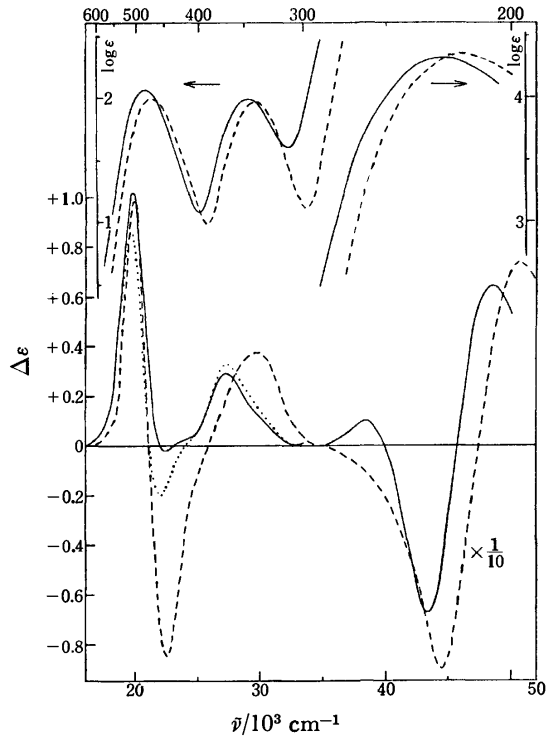

Fig. 3. Absorption and CD spectra of (+)$_{589}$-*u-fac*-[Co(dien)(dema)]$^{3+}$ in water (——) and CD spectrum in 0.2 M Na_2SO_4 (·····). Absorption and CD spectra of (+)$_{589}$-*u-fac*-[Co(dien)$_2$]$^{3+}$ in water (——).

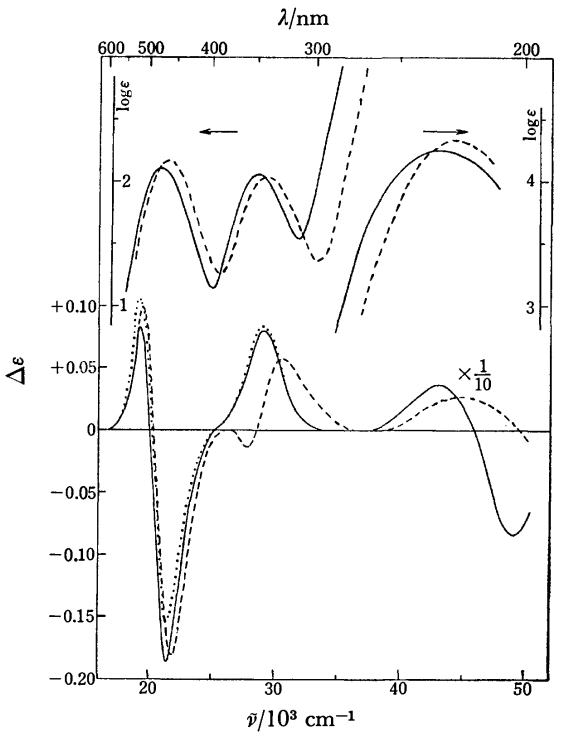

Fig. 4. Absorption and CD spectra of (−)$_{490}$-*mer*-[Co(dien)(dema)]$^{3+}$ in 10^{-2} M HCl (——) and CD spectrum in 0.2 M Na_2SO_4–10^{-2} M HCl (·····). Absorption and CD spectra of (+)$_{589}$-*mer*-[Co(dien)$_2$]$^{3+}$ in 10^{-2} M HCl (——).

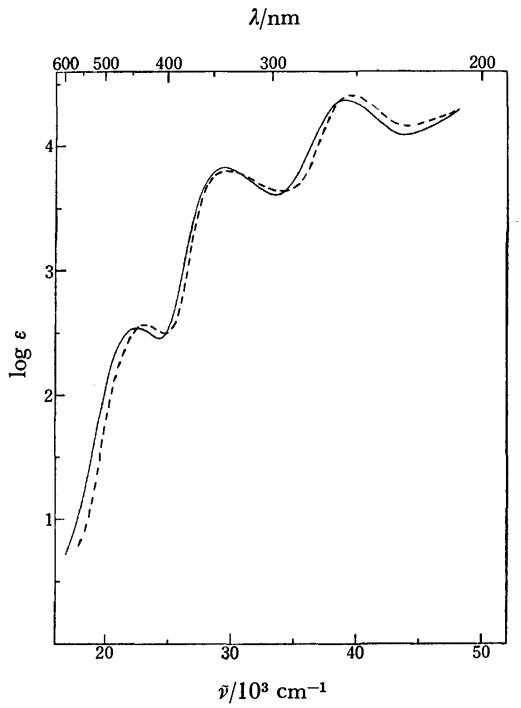

Fig. 5. Absorption spectra of *mer*-[Co(NO$_2$)$_3$(dien)](——) and *fac*-[Co(NO$_2$)$_3$(dema)](——) in water.

(dien)(dema)]$^{3+}$ and *s-fac*-[Co(dema)$_2$]$^{3+}$ exhibit shoulders at a longer wavelength side of the charge transfer bands. These shoulders may correspond to the charge transfer transitions from the tertiary nitrogen atom of the dema ligand to the central cobalt ion. The absorption bands of the *u-fac* and the *mer* isomers of [Co(dien)(dema)]$^{3+}$ are also at a longer wavelength side than those of the corresponding isomers of [Co(dien)$_2$]$^{3+}$

(Figs. 3 and 4, and Table 1). The first absorption bands of the isomers of $[Co(dien)(dema)]^{3+}$ shift to longer wavelengths in the order of *s-fac*, *mer*, and *u-fac* isomers, the same order being observed in the isomers of $[Co(dien)_2]^{3+}$.[1]

Figure 5 shows the absorption spectra of *mer*-$[Co(NO_2)_3(dien)]$ and $[Co(NO_2)_3(dema)]$ which was assigned to the *fac* configuration as stated previously. The former has a pair of nitrite ions in the *trans* positions. It is known that the so-called nitro specific band ($\approx$30000 cm^{-1}) of a *trans*-dinitrocobalt(III) complex is located at a longer wavelength than that of the corresponding *cis* complex. However, the present nitro complexes give their nitro specific bands at nearly the same position.

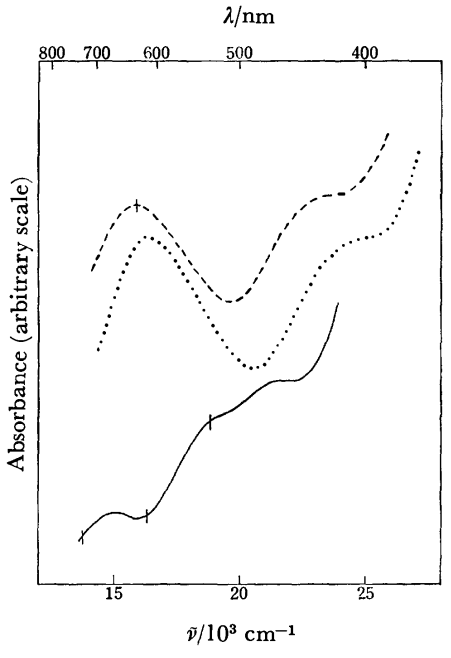

Fig. 6. Diffuse reflectance spectra of *mer*-$[CoCl_3(dien)]$ (——), *fac*-$[CoCl_3(dema)]$(——), and *fac*-$[CoCl_2(H_2O)(dema)]Cl\cdot 0.5H_2O$ (……). Short vertical lines show the calculated band positions.

Figure 6 compares the diffuse reflectance spectra of $[CoCl_3(dien)]$ and $[CoCl_3(dema)]$, which have been assigned previously to the *mer* and the *fac* configurations, respectively. These tri-chloro complexes are hardly soluble in common organic solvents and aquate rapidly in water. From Yamatera's theory,[13] the first absorption band of *mer*-$[CoCl_3(dien)]$ is expected to split into three components, and their positions can also be predicted. Since the first absorption maximum (21.5×10^3 cm^{-1}) of *mer*-$[Co(dien)_2]^{3+}$ is at nearly the same position as that of $[Co(en)_3]^{3+}$ (21.4×10^3 cm^{-1}), the values of parameters, δ(N) and δ(Cl) for *mer*-$[CoCl_3(dien)]$ may be approximated to those obtained from $[Co(en)_3]^{3+}$ and *trans*-$[CoCl_2(en)_2]^{+}$[14] (21.6, 16.2×10^3 cm^{-1}). The predicted positions of the three components of *mer*-$[CoCl_3(dien)]$ are 18.85, 16.3, and 13.75×10^3 cm^{-1}. On the other hand, no splitting is expected for the first absorption band of *fac*-$[CoCl_3(dema)]$. The first absorption band of *s-fac*-$[Co(dema)_2]^{3+}$ (20.8×10^3 cm^{-1}) is at nearly the same position as that of $[Co(NH_3)_6]^{3+}$ (21.0×10^3 cm^{-1}). Thus, the first absorption band of *fac*-$[CoCl_3(dema)]$ is similarly predicted at *ca.* 15.9×10^3 cm^{-1} with reference to the maximum positions of *trans*-$[CoCl_2(NH_3)_4]^{+}$[15] (21.0 and 15.9×10^3 cm^{-1}). The predicted values for both the tri-chloro complexes satisfy the observed spectra as marked on the curves in Fig. 6. These results will support the previous assignment for the structures of *mer*-$[CoCl_3(dien)]$ and *fac*-$[CoCl_3(dema)]$. The first absorption band of *fac*-$[CoCl_2(H_2O)(dema)]Cl\cdot 0.5H_2O$ is at a shorter wavelength (610 nm) than that of *fac*-$[CoCl_3(dema)]$ (630 nm) in accordance with the order of the spectrochemical series of H_2O and Cl^-, indicating that the water molecule coordinates to the cobalt ion.

In Fig. 3 the absorption and CD spectra of $(+)_{589}$-*u-fac*-$[Co(dien)(dema)]^{3+}$ are shown. It exhibits a CD spectrum similar to that of Λ-$(+)_{589}$-*u-fac*-$[Co(dien)_2]^{3+}$[3] over the entire region. The effect of sulfate ions on the CD spectrum of $(+)_{589}$-*u-fac*-$[Co(dien)(dema)]^{3+}$ is also similar to that of the corresponding bis-dien complex. Thus, the absolute configuration of $(+)_{589}$-*u-fac*-$[Co(dien)(dema)]^{3+}$ can be assingned to Λ.

As Fig. 1 shows, *mer*-$[Co(dien)(dema)]^{3+}$ has an equal number of Δ and Λ ring-pairs, and of δ and λ conformers. Hence, the chiral contributions from the configurational and the conformational effects may be canceled out as in the case of *mer*-$[Co(dien)_2]^{3+}$. The chirality in the *mer*-$[Co(dien)(dema)]^{3+}$ isomer should come from the stereochemical relationship between the N–H bond of the secondary nitrogen atom in the dien ligand and the N-CH_3 bond in the dema ligand. The CD spectrum of $(-)_{490}$-*mer*-$[Co(dien)(dema)]^{3+}$ is shown in Fig. 4. The pattern and magnitude of the CD spectrum of this isomer, and the changes in the CD band area on the addition of sulfate are all similar to those of $(+)_{589}$-*mer*-$[Co(dien)_2]^{3+}$. Therefore, it can be concluded that these two isomers have the same absolute configuration. However, the relationship between the CD sign and the absolute configuration for complexes of this type still remains unknown.

The active *mer*-$[Co(dien)(dema)]^{3+}$ isomer is optically stable over one year in acidic water (*ca.* pH 2) at room temperature (*ca.* 25 °C), but racemizes immediately on raising the pH to 12 by adding a NaOH solution.

Conformational Analysis. The strain energies of the isomers of $[Co(dien)(dema)]^{3+}$ and $[Co(dema)_2]^{3+}$ were calculated by the previously reported method,[16] the force field in which includes the contributions from bond stretching, nonbonded interactions, angle bending, and tortional potentials. The initial molecular structures of the isomers were the same as those of the final results obtained previously for the corresponding $[Co(dien)_2]^{3+}$ isomers,[16] except that the N–C(H_3) bond of 1.5 Å was taken for the dema ligand instead of the N–H (secondary amine) bond of dien. When the dema ligand coordinates to the Co(III) ion, the Co–N(CH_3) (tertiary amine) distance lengthens (1.99—2.02 Å) compared with the Co–N(H) (secondary amine) distance (1.94—1.97 Å), and the $\angle$CoNC (of the methyl group) angle becomes much larger (117—120°) than the normal tetrahedral angle. Similar results are also obtained for the

TABLE 2. FINAL ENERGY TERMS FOR THE ISOMERS OF $[Co(dien)(dema)]^{3+}$ AND $[Co(dema)_2]^{3+}$

Isomer	Bond	Nonbond	Angle	Torsion	Total
$[Co(dien)(dema)]^{3+}$					
s-fac	6.42	34.10	16.28	31.17	89.58 kJ·mol^{-1}
u-fac[a]	8.74	41.29	20.22	41.39	111.64
mer	7.62	35.64	25.77	26.63	95.65
$[Co(dema)_2]^{3+}$					
s-fac	11.16	47.08	23.91	31.37	113.53
u-fac[a]	14.06	51.86	36.90	32.55	134.38
mer	11.97	53.09	27.71	30.79	123.56

a) This isomer corresponds to the *u-fac*-1 isomer in the preceding paper.[16] The *u-fac*-2 isomer has the more strained structure.

N-methylethylenediamine[17] and sarcosinato[18] complexes of Co(III). Table 2 shows the minimized energy terms of all the isomers of $[Co(dien)(dema)]^{3+}$ and $[Co(dema)_2]^{3+}$. In contrast to the case of $[Co(dien)_2]^{3+}$, of which the energies of the isomers are calculated to be *mer*≲*s-fac*≲*u-fac*,[16] both the dema complexes have the lowest and the highest energies in the *s-fac* and the *u-fac* isomers, respectively. As stated in Experimental part, the reaction of $CoCl_2 \cdot 6H_2O$ with a mixture of dien and dema (1 : 1) in the presence of active charcoal produced only the *s-fac* isomers of $[Co(dien)(dema)]^{3+}$ and $[Co(dema)_2]^{3+}$, together with the three isomers of the bis-dien complex. The other isomers of $[Co(dien)(dema)]^{3+}$ were not detected in SP-Sephadex column chromatography, although the energy difference between the *s-fac* and the *mer* isomers was calculated to be 6.1 kJ·mol^{-1}. The *u-fac* and the *mer* isomers of $[Co(dien)(dema)]^{3+}$ were prepared from *fac*-$[CoCl_2(H_2O)(dema)]^+$ and *mer*-$[CoCl_3(dien)]$, respectively in the absence of active charcoal. All the preparative methods for $[Co(dema)_2]^{3+}$ gave always only the *s-fac* isomer. If the calculated energy differences among the isomers of this complex were correct, the formation of other isomers than the *s-fac* would almost be zero. Thus, the experimental results agree with those obtained by the energy minimization calculation; each complex of $[Co(dien)(dema)]^{3+}$ and $[Co(dema)_2]^{3+}$ is the most stable in the *s-fac* isomer.

References

1) Y. Yoshikawa and K. Yamasaki, *Bull. Chem. Soc. Jpn.*, **45**, 179 (1972).
2) F. R. Keene and G. H. Searle, *Inorg. Chem.*, **11**, 148 (1972).
3) M. Konno, F. Marumo, and Y. Saito, *Acta Crystallogr., Sect. B*, **29**, 739 (1973).
4) K. Nakajima, T. Shin-uchi, and M. Tauchi, *Nippon Kagaku Zasshi*, **89**, 408 (1968).
5) B. Bosnich and F. P. Dwyer, *Aust. J. Chem.*, **19**, 2045 (1966).
6) P. H. Crayton, *Inorg. Synth.*, **7**, 207 (1963).
7) F. R. Keene and G. H. Searle, *Inorg. Chem.*, **13**, 2173 (1974).
8) A. Werner and R. Feenstra, *Ber.*, **39**, 154 (1906).
9) M. Shibata, *Nippon Kagaku Zasshi*, **87**, 771 (1966).
10) Y. Kushi, K. Watanabe, and H. Kuroya, *Bull. Chem. Soc. Jpn.*, **40**, 2985 (1967).
11) G. H. Searle and E. Larsen, *Acta Chem. Scand.*, **A30**, 143 (1976).
12) M. Kojima, Y. Yoshikawa, and K. Yamasaki, Presented at the 23rd Symposium on Coordination Chemistry, Fukuoka, Oct., 1973.
13) H. Yamatera, *Bull. Chem. Soc. Jpn.*, **31**, 95 (1958).
14) Y. Shimura and R. Tsuchida, *Bull. Chem. Soc. Jpn.*, **28**, 572 (1955).
15) R. Tsuchida, *Bull. Chem. Soc. Jpn.*, **11**, 721 (1936).
16) Y. Yoshikawa, *Bull. Chem. Soc. Jpn.*, **49**, 156 (1976). In this paper, the unit of energy is erroneously used, and all the values of the energy should be multiplied by $(4.184)^2 = 17.5$.
17) Y. Yoshikawa, M. Kojima, and K. Yamasaki, Presented at the annual meeting of the Chemical Society of Japan, April, 1975.
18) B. F. Anderson, D. A. Buckingham, G. J. Gainsford, G. B. Robertson, and A. M. Sargeson, *Inorg. Chem.*, **14**, 1658 (1975).

The Crystal and Molecular Structure of the Aquabis(cyclo-L-histidyl-L-histidylato)dicopper(II) Perchlorate Hydrate $[H_2O\ Cu_2(C_{12}H_{13}N_6O_2)_2](ClO_4)_2 \cdot 3.5H_2O$

Yoshitane KOJIMA, Ken HIROTSU, and Keiji MATSUMOTO

Department of Chemistry, Faculty of Science, Osaka City University, Sumiyoshi-ku, Osaka 558

(Received May 28, 1977)

The crystal structure of the title compound has been determined by a three-dimensional X-ray structure analysis, using 4563 counter intensity data. The crystals are monoclinic, with $a=22.97(2)$, $b=15.89(1)$, $c=10.00(1)$ Å, $\beta=100.1(1)°$, space group $P2_1$, and $Z=4$. The structure was solved by the Patterson and Fourier technique and was refined by the block-diagonal least-squares method to $R=0.061$. The unit cell contains two crystallographically independent complex cations, the structure of which are very similar to each other. The complex cation is dimeric; there are two Cu atoms, and each of the two cyclo-L-histidyl-L-histidylato ligands bridges two metal atoms. Except for the aqua ligand, the main body of the complex has an approximate twofold axis which passes through the two metal atoms and relates the ligands to each other. The two Cu atoms have different coordination geometries. One Cu atom has a flattened tetrahedral coordination by 4N atoms, whereas the other is surrounded by 2N and 3O atoms and is intermediate between the square pyramid and the trigonal bipyramid.

There has been considerable interest in the structures of the metal chelates of amino acid anhydride as simple model compounds for the biomolecules.[1] Although some infrared and visible spectral studies have been made of these complexes,[2] the stereochemical details of the complexes have not yet been elucidated. Since no X-ray structure has been reported as yet, we wish to report here the preparation and X-ray structure of the title compound. A preliminary communication on the structure of the complex has already been published.[3]

Experimental

Preparation of the Complex. $HISH_2$[$HISH_2$=cyclo(L-histidyl-L-histidyl)] was prepared following the procedure of Abderhalden *et al.*[4] A suspension of equimolar amounts of $HISH_2$(0.585g, 2 mmol) and copper(II) perchlorate hexahydrate (0.741 g, 2 mmol) in hot methanol was stirred until both substances had been completely dissolved. Lithium hydroxide monohydrate (0.084 g, 2 mmol) was then added, and the resultant solution was allowed to stand for one day at room temperature. The blue crystals were separated out. The square prisms were obtained upon recrystallization from a hot aqueous solution. Yield, 0.393 g (41.2%).

Found: C, 30.26; H, 3.63; N, 17.68%. Calcd for $[H_2O\ Cu_2(C_{12}H_{13}N_6O_2)_2](ClO_4)_2 \cdot 3.5H_2O$: C, 30.23; H, 3.70; N, 17.63%.

X-Ray Data Collection. The specimen employed for data collection had dimensions of $0.22 \times 0.25 \times 0.28$mm. Preliminary X-ray photographic studies, using oscillation, Weissenberg, and precession techniques, revealed the approximate unit-cell dimensions, the Laue symmetry of $2/m$, and the systematic absences of $0k0$ for $k=2n+1$. These extinctions indicate that the space group is $P2_1$, since the compound is optically active.

Crystal Data: $Cu_2(C_{12}H_{13}N_6O_2)_2(ClO_4)_2(H_2O)_{4.5}$, $a=22.97(2)$, $b=15.89(1)$, $c=10.00(1)$Å, $\beta=100.1(1)°$, $U=3596.3$Å^3, $Z=4$, $D_x=1.76$, $D_m=1.74$ g cm^{-3}, space group $P2_1$, λ(Mo$K\alpha$)$=0.7107$Å, μ(Mo$K\alpha$)$=78.0$ cm^{-1}.

The cell dimensions were determined by the least-squares treatment using 48 θ values measured accurately on a Philips PW1100 diffractometer. Intensity data with $3° \leqq 2\theta \leqq 50°$ were collected at room temperature by the use of graphite-monochromated Mo$K\alpha$ radiation. The ω-2θ scan technique was employed. The scan range was $(0.9+0.3\tan\theta)°$, and the scan speed, 2°/min; the background was counted for 15 s at each end of the scan. The three standard reflections, 080, 900, and 004, measured every 150 min, showed no appreciable decay. A total of 4563 intensities with $I_{top} - 2\sqrt{I_{top}} > I_{back}$ were classified as observed, where I_{top} is the intensity (count/s) measured at the top of the peak and I_{back} is the mean background intensity (count/s), obtained from the preliminary background measurements for 5 s on each side of the peak. The Lorentz-poralization corrections were made, and relative structure factors were derived.[5] No absorption correction was applied.

Structure Determination and Refinement. The four copper stoms were located from a three-dimensional Patterson map, and the positions of the remaining non-hydrogen atoms were determined by successive Fourier syntheses. The structure was initially refined by the isotropic block-diagonal least-squares method. In the course of refinement, it was found that the 15O atoms of perchlorate ions and all the water molecules of crystallization were somewhat disordered. Therefore, isotropic temperature factors were assigned to them throughout the refinement. Six cycles of the anisotropic least-squares refinement resulted in convergence at $R=0.061$. No parameter was observed to shift by $>0.1\,\sigma$. The function minimized was $\sum w(F_o - |F_c|)^2$, with $w=1/\sigma(F_o)^2$ being used. The scattering factors for the neutral Cu, Cl, O, N, and C atoms were taken from Ref. 6. No attempt was made to locate the hydrogen atoms. The absolute crystal structure was determined on the basis of the known configuration of the cyclo-L-histidyl-L-histidilato ligand. The final atomic coordinates which give the absolute crystal structure are presented in Table 1, along with their temperature factors. The observed and calculated structure factors have been deposited at the Chemical Society of Japan (Document No. 7721). All the calculations were performed on a FACOM 270-30 computer at Osaka City University. The programs used included a local version of the UNICS.[7]

Results and Discussion

The structural formula of cyclo-L-histidyl-L-histidyl ($HISH_2$) is shown in Fig. 1. The middle 2,5-piperadinedione moiety ($DKPH_2$) takes a planar structure. Since the C(5) and C(7) atoms have an S absolute configuration, both the C(4) and C(9) atoms lie on one side of the ring plane of the $DKPH_2$. The $HISH_2$ molecule

TABLE 1. FRACTIONAL POSITIONAL PARAMETERS ($\times 10^4$) AND ANISOTROPIC TEMPERATURE FACTORS ($\times 10^4$), WITH e.s.d.'s IN PARENTHESES

The temperature factors are of the form: $\exp[-(h^2B_{11}+k^2B_{22}+l^2B_{33}+hkB_{12}+hlB_{13}+klB_{23})]$.

Atom	x	y	z	B_{11}	B_{22}	B_{33}	B_{12}	B_{13}	B_{23}
Cu(A)	3870(1)	6565(1)	6382(2)	10(0)	31(1)	88(2)	−1(1)	14(1)	−1(2)
Cu(B)	3752(1)	4382(1)	5687(2)	8(0)	29(1)	71(2)	0(1)	6(1)	3(2)
Cu′(A)	8482(1)	4020(1)	11101(2)	11(0)	25(1)	58(2)	−8(1)	12(1)	−24(2)
Cu′(B)	9240(1)	5000(1)	8651(2)	9(0)	21(1)	55(2)	−2(1)	0(1)	−6(2)
Cl	8070(2)	9384(3)	8932(4)	16(1)	39(2)	95(5)	−7(3)	7(3)	−1(6)
Cl′	611(2)	6600(3)	6797(4)	16(1)	40(2)	83(4)	7(2)	15(3)	10(6)
Cl″	7168(2)	6660(4)	5639(6)	20(1)	55(3)	215(8)	9(3)	23(5)	81(9)
Cl‴	4266(3)	8217(7)	9916(9)	35(2)	176(8)	323(14)	64(7)	33(9)	−192(19)
C(1)	3376(7)	6160(12)	8802(15)	20(4)	53(10)	70(19)	−16(11)	11(14)	4(23)
C(2)	2414(7)	6320(11)	8279(15)	20(4)	46(10)	66(18)	11(10)	14(13)	10(20)
C(3)	2651(6)	6515(9)	7176(14)	9(3)	16(6)	108(19)	0(8)	10(11)	1(20)
C(4)	2380(6)	6750(10)	5747(14)	9(3)	33(8)	70(16)	9(8)	−6(11)	−10(19)
C(5)	2285(6)	5983(9)	4843(14)	10(3)	27(7)	90(19)	−1(8)	13(12)	30(20)
C(6)	2853(6)	5520(10)	4925(13)	17(4)	29(7)	37(15)	−2(9)	−22(12)	−5(17)
C(7)	2432(6)	4197(10)	5663(14)	7(3)	39(9)	79(16)	−2(8)	2(10)	18(19)
C(8)	1827(6)	4624(10)	5344(14)	11(3)	42(9)	60(16)	−16(8)	−16(11)	2(19)
C(9)	2550(6)	4031(10)	7263(13)	15(3)	33(7)	67(16)	26(9)	3(12)	42(20)
C(10)	3114(6)	3534(10)	7685(15)	12(3)	32(8)	84(18)	−6(8)	10(12)	6(20)
C(11)	3155(7)	2835(11)	8481(15)	17(4)	36(9)	95(20)	−7(9)	−12(14)	19(22)
C(12)	4047(8)	3155(12)	7980(17)	19(4)	38(9)	128(23)	−2(10)	0(16)	−5(24)
C′(1)	4351(7)	6810(11)	3910(17)	16(4)	37(9)	146(24)	−12(9)	31(15)	7(24)
C′(2)	5326(7)	6707(11)	4442(15)	18(4)	45(9)	99(20)	−15(10)	28(14)	19(23)
C′(3)	5096(6)	6657(10)	5593(16)	14(3)	21(7)	139(22)	2(9)	35(14)	−24(22)
C′(4)	5382(7)	6501(11)	7058(16)	18(4)	33(8)	114(21)	−14(10)	−4(14)	−17(23)
C′(5)	5366(6)	5543(11)	7404(17)	11(3)	32(8)	140(24)	1(9)	21(14)	−43(23)
C′(6)	4735(6)	5207(9)	6964(13)	14(3)	27(8)	57(16)	6(8)	−3(12)	3(18)
C′(7)	5033(6)	4148(10)	5488(13)	9(3)	37(8)	77(17)	−2(8)	21(11)	−11(20)
C′(8)	5679(5)	4400(10)	6007(15)	4(3)	34(7)	119(20)	6(8)	5(11)	−16(22)
C′(9)	4922(6)	4358(12)	3915(14)	13(3)	48(9)	81(17)	1(10)	21(12)	22(23)
C′(10)	4320(6)	4024(12)	3232(14)	15(3)	54(9)	69(17)	0(10)	15(12)	−54(23)
C′(11)	4187(8)	3731(15)	1902(21)	22(5)	83(15)	182(31)	10(14)	−9(19)	−99(36)
C′(12)	3374(7)	3794(12)	2863(15)	19(4)	56(11)	77(19)	−6(11)	5(14)	−13(23)
C″(1)	8496(7)	2430(10)	9613(14)	20(4)	27(7)	57(16)	−5(9)	27(13)	−13(18)
C″(2)	7655(7)	2286(10)	8251(15)	16(4)	27(8)	97(19)	−12(8)	22(14)	−24(20)
C″(3)	7669(6)	3023(9)	8942(13)	13(3)	25(7)	57(16)	−17(8)	16(11)	−21(17)
C″(4)	7231(5)	3743(9)	8747(15)	5(3)	24(7)	113(19)	6(7)	15(12)	10(19)
C″(5)	7417(5)	4447(10)	7850(13)	9(3)	28(7)	61(15)	−2(8)	3(10)	3(18)
C″(6)	8058(5)	4737(8)	8367(13)	9(3)	12(6)	68(16)	4(6)	−6(10)	4(15)
C″(7)	8371(5)	4309(10)	6282(13)	8(3)	27(7)	81(17)	−4(7)	5(11)	−11(19)
C″(8)	7718(5)	4149(9)	5645(12)	10(3)	24(7)	54(14)	−11(7)	12(10)	−25(16)
C″(9)	8675(6)	3435(9)	6387(15)	13(3)	21(7)	106(20)	10(8)	−1(13)	−24(19)
C″(10)	9359(6)	3506(9)	6810(13)	13(3)	21(7)	56(15)	2(7)	31(11)	5(17)
C″(11)	9773(7)	2993(11)	6391(15)	20(4)	42(9)	62(17)	10(10)	9(13)	−23(21)
C″(12)	10207(6)	4006(11)	7775(14)	15(3)	34(7)	82(17)	20(9)	31(12)	−11(21)
C‴(1)	8431(7)	5581(11)	12620(18)	19(4)	30(8)	150(25)	−1(10)	50(17)	−18(24)
C‴(2)	9249(7)	5585(11)	14199(14)	17(4)	38(8)	62(17)	−21(9)	14(3)	−1(20)
C‴(3)	9249(6)	4865(10)	13473(12)	16(3)	41(8)	30(14)	−24(9)	14(11)	−12(18)
C‴(4)	9675(6)	4161(10)	13593(14)	19(4)	27(8)	67(16)	−1(8)	−2(12)	2(18)
C‴(5)	10089(6)	4178(8)	12510(13)	14(3)	14(7)	68(16)	−2(7)	−6(11)	11(16)
C‴(6)	9727(5)	4342(10)	11117(13)	7(3)	32(7)	66(15)	8(8)	11(10)	−20(19)
C‴(7)	10225(6)	5643(9)	10771(14)	9(3)	26(7)	75(18)	−7(8)	−22(11)	12(19)
C‴(8)	10646(6)	5465(10)	12164(15)	13(3)	33(8)	89(20)	−11(9)	14(13)	−21(20)
C‴(9)	9867(6)	6454(10)	11019(14)	14(3)	31(8)	61(16)	1(8)	−19(12)	−23(19)
C‴(10)	9462(6)	6748(9)	9757(13)	11(3)	29(8)	63(16)	−7(8)	4(11)	−3(18)
C‴(11)	9304(8)	7550(11)	9444(16)	23(4)	41(9)	88(20)	−5(10)	19(15)	13(23)
C‴(12)	8793(7)	6685(10)	7865(15)	17(4)	23(7)	111(21)	−3(9)	22(14)	8(21)
N(1)	3266(5)	6408(8)	7532(11)	11(3)	28(6)	79(14)	2(6)	7(10)	−39(5)
N(2)	2859(6)	6093(10)	9312(12)	21(4)	58(8)	71(16)	4(9)	24(12)	17(20)
N(3)	1795(5)	5462(8)	5119(12)	16(3)	22(6)	80(16)	−4(7)	−8(11)	8(15)
N(4)	2922(5)	4719(7)	5350(11)	8(2)	25(6)	70(14)	−1(6)	7(9)	−9(14)
N(5)	3647(5)	3734(8)	7358(12)	13(3)	37(7)	73(14)	17(7)	−2(10)	12(16)
N(6)	3769(7)	2606(10)	8672(14)	28(4)	48(8)	110(19)	4(10)	15(14)	18(21)
N′(1)	4472(5)	6692(9)	5175(13)	11(3)	35(7)	124(17)	−7(7)	36(11)	2(19)
N′(2)	4862(6)	6793(9)	3393(14)	24(4)	43(8)	129(19)	−13(9)	45(14)	−10(20)

TABLE 1. (Continued)

Atom	x	y	z	B_{11}	B_{22}	B_{33}	B_{12}	B_{13}	B_{23}
N′(3)	5794(5)	5050(9)	6800(13)	10(3)	37(7)	138(18)	17(8)	−20(11)	−65(20)
N′(4)	4602(5)	4562(8)	6146(11)	9(2)	39(7)	67(13)	2(7)	5(9)	9(16)
N′(5)	3824(5)	4084(9)	3799(12)	10(3)	47(7)	86(15)	1(8)	−2(10)	−15(19)
N′(6)	3569(6)	3562(12)	1729(14)	14(3)	104(13)	117(19)	−7(11)	−2(13)	−97(26)
N″(1)	8215(5)	3126(7)	9787(11)	9(2)	24(6)	61(13)	−9(6)	−2(9)	−21(14)
N″(2)	8192(6)	1926(8)	8740(12)	23(4)	26(6)	79(16)	−1(8)	21(12)	−35(16)
N″(3)	7322(5)	4204(7)	6438(10)	14(3)	21(6)	57(12)	1(6)	9(9)	−30(14)
N″(4)	8450(5)	4694(7)	7650(10)	8(2)	22(5)	53(13)	−9(5)	5(9)	−20(13)
N″(5)	9626(5)	4125(8)	7665(11)	14(3)	29(6)	65(13)	3(7)	25(9)	−12(15)
N″(6)	10302(6)	3331(9)	7053(13)	18(3)	36(7)	96(17)	4(7)	11(12)	4(18)
N‴(1)	8726(5)	4876(8)	12484(12)	9(3)	33(6)	98(15)	−7(7)	20(10)	−29(17)
N‴(2)	8745(6)	6027(9)	13688(13)	27(4)	28(7)	99(17)	−14(8)	30(13)	−26(18)
N‴(3)	10547(5)	4807(9)	12866(12)	8(2)	49(8)	81(15)	−8(7)	−11(9)	52(17)
N‴(4)	9819(4)	4961(8)	10333(10)	10(2)	25(5)	40(11)	−3(7)	4(8)	−1(15)
N‴(5)	9138(5)	6210(7)	8783(12)	9(3)	18(5)	100(16)	−5(6)	6(10)	−15(15)
N‴(6)	8871(6)	7498(8)	8236(13)	22(3)	23(6)	111(18)	1(7)	8(12)	15(17)
O(1)	3305(4)	5922(6)	4679(9)	11(2)	34(5)	77(12)	−12(5)	31(8)	12(13)
O(2)	1393(4)	4197(6)	5330(11)	7(2)	26(6)	180(16)	−3(5)	5(9)	2(15)
O(3W)	3648(6)	7796(8)	6152(13)	28(4)	36(6)	168(18)	8(8)	34(13)	2(18)
O(4)	8610(6)	9534(11)	9785(13)	30(4)	109(12)	136(18)	−43(11)	−36(13)	44(24)
O(5)	7723(6)	8798(10)	9560(12)	32(4)	92(11)	115(16)	−32(10)	20(13)	43(22)
O(6)	8157(5)	9046(8)	7662(11)	25(3)	42(6)	126(15)	11(8)	22(11)	−8(17)
O(7)	7757(6)	10145(9)	8701(14)	35(4)	44(7)	197(21)	21(9)	32(14)	−24(21)
O′(1)	4339(4)	5607(7)	7461(10)	13(2)	31(5)	105(14)	5(6)	20(9)	3(14)
O′(2)	6079(4)	3996(8)	5612(12)	6(2)	52(7)	206(19)	0(7)	6(10)	−66(20)
O′(3W)	7801(6)	3656(9)	12086(12)	31(4)	80(9)	109(15)	−55(9)	69(12)	−73(19)
O′(4)	50(5)	7001(9)	6710(14)	21(3)	61(8)	230(23)	3(8)	49(14)	−11(23)
O′(5)	617(5)	6176(10)	5550(13)	19(3)	86(10)	161(19)	28(9)	17(12)	−92(22)
O′(6)	760(7)	6087(12)	7990(14)	51(5)	100(12)	137(20)	2(3)	−41(17)	104(26)
O′(7)	1069(6)	7251(9)	6943(15)	21(3)	68(9)	233(23)	1(9)	17(14)	66(24)
O″(1)	8140(4)	4994(6)	9603(8)	10(2)	23(4)	60(10)	4(5)	6(7)	5(13)
O″(2)	7594(4)	3985(8)	4431(9)	17(2)	65(7)	65(11)	−13(7)	3(8)	−48(16)
O″(4)	7509(10)	7303(16)	6481(22)	a)					
O″(5)	6850(9)	6226(14)	6495(19)	a)					
O″(6)	7608(9)	6160(15)	5229(20)	a)					
O″(7)	6829(9)	7129(14)	4719(19)	a)					
O‴(1)	9302(4)	3814(6)	10731(9)	12(2)	24(5)	73(11)	−9(5)	9(8)	−13(12)
O‴(2)	11047(4)	5962(7)	12514(10)	13(2)	52(7)	89(13)	−23(6)	−14(9)	−6(16)
O‴(4)	4603(11)	8952(18)	10363(24)	a)					
O‴(5)	4531(8)	7730(13)	9019(18)	a)					
O‴(6)	3699(9)	8424(14)	8981(20)	a)					
O‴(7)	4170(11)	7748(18)	11077(25)	a)					
O(8W)	7716(6)	6624(10)	9775(14)	a)					
O(9W)	6513(7)	6015(12)	9585(16)	a)					
O(10W)	1097(7)	2574(11)	5121(16)	a)					
O(11W)	4809(9)	1477(14)	9188(19)	a)					
O(12W)	8512(10)	7715(17)	11708(23)	a)					
O(13W)	6503(11)	654(18)	8160(24)	a)					
O(14W)	3205(12)	321(19)	7490(26)	a)					

Atom	B(Å^2)	Atom	B(Å^2)	Atom	B(Å^2)	Atom	B(Å^2)
O″(4)	1330(68)	O″(5)	1154(59)	O″(6)	1200(61)	O″(7)	1116(56)
O‴(4)	1530(81)	O‴(5)	1064(53)	O‴(6)	1152(58)	O‴(7)	1585(84)
O(8W)	702(35)	O(9W)	905(46)	O(10W)	843(42)	O(11W)	1182(59)
O(12W)	1420(73)	O(13W)	1510(78)	O(14W)	1668(89)		

a) Isotropic temperature factors ($\times 10^2$) with e.s.d.'s in parentheses.

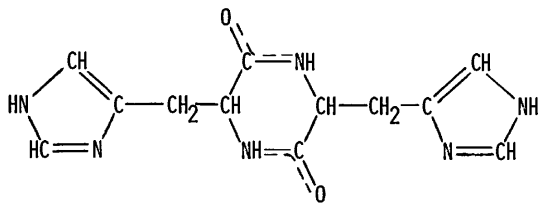

Fig. 1. The schematic drawing of cyclo(L-histidyl-L-histidyl)

has four donor atoms: two N atoms of the respective imidazole groups (Im) and two O atoms in the $DKPH_2$. In the cyclo-L-histidyl-L-histidylato ligand ($HISH^-$) of the present complex, one of the NH groups in the $DKPH_2$ is deprotonated; the resulting "anionic" N atom also coordinates to the Cu atom.

There are two crystallographically independent complex cations in the unit cell; a stereoscopic view of them is given in Fig. 2, where the atom numbering

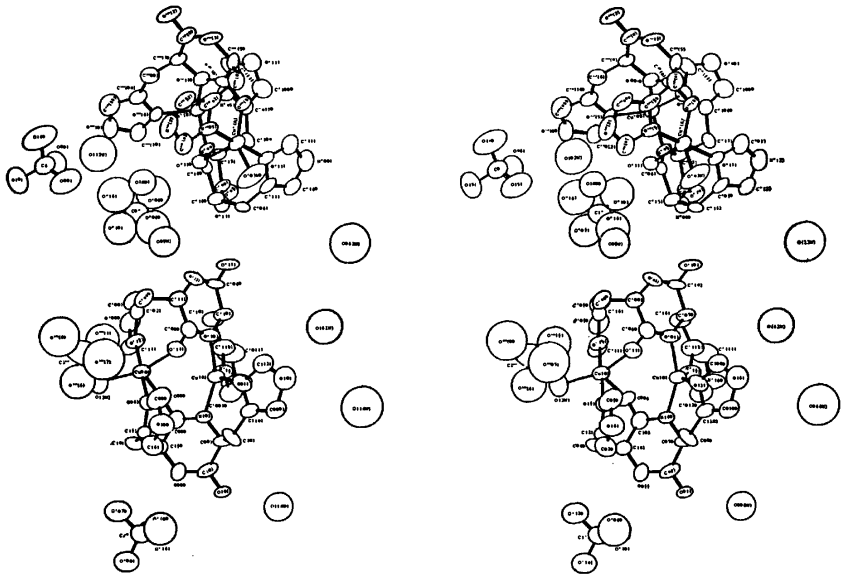

Fig. 2. Stereoscopic view of aquabis(cyclo-L-histidyl-L-histidylato)dicopper(II) perchlorate hydrate, looking down along the c axis.

TABLE 2. BOND DISTANCES (d/Å), WITH e.s.d.'s IN PARENTHESES

Cu(A)–N(1)	1.97(1)	Cu(A)–N′(1)	2.00(1)	Cu′(A)–N″(1)	1.96(1)	Cu′(A)–N‴(1)	1.95(1)
Cu(A)–O(1)	2.21(1)	Cu(A)–O′(1)	2.06(1)	Cu′(A)–O″(1)	2.20(1)	Cu′(A)–O‴(1)	2.01(1)
Cu(A)–O(3W)	2.02(1)			Cu′(A)–O′(3W)	2.07(1)		
Cu(B)–N(4)	1.95(1)	Cu(B)–N′(4)	1.95(1)	Cu′(B)–N″(4)	1.97(1)	Cu′(B)–N‴(4)	1.96(1)
Cu(B)–N(5)	2.01(1)	Cu(B)–N′(5)	1.98(1)	Cu′(B)–N″(5)	2.00(1)	Cu′(B)–N‴(5)	1.95(1)
C(1)–N(1)	1.31(2)	C′(1)–N′(1)	1.26(2)	C″(1)–N″(1)	1.31(2)	C‴(1)–N‴(1)	1.33(2)
C(1)–N(2)	1.38(2)	C′(1)–N′(2)	1.36(2)	C″(1)–N″(2)	1.30(2)	C‴(1)–N‴(2)	1.38(2)
C(2)–C(3)	1.35(2)	C′(2)–C′(3)	1.35(2)	C″(2)–C″(3)	1.36(2)	C‴(2)–C‴(3)	1.36(2)
C(2)–N(2)	1.37(2)	C′(2)–N′(2)	1.37(2)	C″(2)–N″(2)	1.37(2)	C‴(2)–N‴(2)	1.38(2)
C(3)–C(4)	1.50(2)	C′(3)–C′(4)	1.52(2)	C″(3)–C″(4)	1.51(2)	C‴(3)–C‴(4)	1.48(2)
C(3)–N(1)	1.41(2)	C′(3)–N′(1)	1.42(2)	C″(3)–N″(1)	1.40(2)	C‴(3)–N‴(1)	1.42(2)
C(4)–C(5)	1.51(2)	C′(4)–C′(5)	1.56(3)	C″(4)–C″(5)	1.54(2)	C‴(4)–C‴(5)	1.56(2)
C(5)–C(6)	1.49(2)	C′(5)–C′(6)	1.54(2)	C″(5)–C″(6)	1.54(2)	C‴(5)–C‴(6)	1.52(2)
C(5)–N(3)	1.46(2)	C′(5)–N′(3)	1.47(2)	C″(5)–N″(3)	1.44(2)	C‴(5)–N‴(3)	1.45(2)
C(6)–N(4)	1.34(2)	C′(6)–N′(4)	1.31(2)	C″(6)–N″(4)	1.25(2)	C‴(6)–N‴(4)	1.30(2)
C(6)–O(1)	1.28(2)	C′(6)–O′(1)	1.28(2)	C″(6)–O″(1)	1.29(2)	C‴(6)–O‴(1)	1.29(2)
C(7)–C(8)	1.53(2)	C′(7)–C′(8)	1.54(2)	C″(7)–C″(8)	1.54(2)	C‴(7)–C‴(8)	1.58(2)
C(7)–C(9)	1.60(2)	C′(7)–C′(9)	1.58(2)	C″(7)–C″(9)	1.55(2)	C‴(7)–C‴(9)	1.57(2)
C(7)–N(4)	1.48(2)	C′(7)–N′(4)	1.44(2)	C″(7)–N″(4)	1.48(2)	C‴(7)–N‴(4)	1.45(2)
C(8)–N(3)	1.35(2)	C′(8)–N′(3)	1.30(2)	C″(8)–N″(3)	1.31(2)	C‴(8)–N‴(3)	1.30(2)
C(8)–O(2)	1.20(2)	C′(8)–O′(2)	1.24(2)	C″(8)–O″(2)	1.23(2)	C‴(8)–O‴(2)	1.22(2)
C(9)–C(10)	1.51(2)	C′(9)–C′(10)	1.53(2)	C″(9)–C″(10)	1.56(2)	C‴(9)–C‴(10)	1.51(2)
C(10)–C(11)	1.36(2)	C′(10)–C′(11)	1.39(3)	C″(10)–C″(11)	1.37(2)	C‴(10)–C‴(11)	1.35(2)
C(10)–N(5)	1.36(2)	C′(10)–N′(5)	1.36(2)	C″(10)–N″(5)	1.38(2)	C‴(10)–N‴(5)	1.41(2)
C(11)–N(6)	1.44(2)	C′(11)–N′(6)	1.43(2)	C″(11)–N″(6)	1.39(2)	C‴(11)–N‴(6)	1.43(2)
C(12)–N(5)	1.37(2)	C′(12)–N′(5)	1.35(2)	C″(12)–N″(5)	1.33(2)	C‴(12)–N‴(5)	1.34(2)
C(12)–N(6)	1.34(2)	C′(12)–N′(6)	1.34(2)	C″(12)–N″(6)	1.33(2)	C‴(12)–N‴(6)	1.35(2)
Cl–O(4)	1.40(1)	Cl′–O′(4)	1.43(1)	Cl″–O″(4)	1.46(2)	Cl‴–O‴(4)	1.43(3)
Cl–O(5)	1.44(2)	Cl′–O′(5)	1.42(1)	Cl″–O″(5)	1.40(2)	Cl‴–O‴(5)	1.40(2)
Cl–O(6)	1.43(1)	Cl′–O′(6)	1.44(2)	Cl″–O″(6)	1.40(2)	Cl‴–O‴(6)	1.50(2)
Cl–O(7)	1.41(1)	Cl′–O′(7)	1.47(2)	Cl″–O″(7)	1.33(2)	Cl‴–O‴(7)	1.43(3)

scheme is also given. Both of the complex cations can be represented by the same formula, $[Cu(HISH)_2Cu(H_2O)]^{2+}$. The four $HISH^-$ ligands in the two complex cations are crystallographically independent of each other. The atom-numbering scheme for the $HISH^-$ is shown in Fig. 2; the same numbering was used for these four ligands, but primes are utilized in order to distinguish between these ligands. The bond lengths and angles are listed in Tables 2 and 3 respectively.

The two complexes have a close resemblance in

Table 3. Bond angles (ϕ/°)

N(1)–Cu(A)–O(1)	90.7(4)	N″(1)–Cu′(A)–O″(1)	91.2(4)
N(1)–Cu(A)–O(3W)	90.0(5)	N″(1)–Cu′(A)–O′(3W)	86.8(5)
N(1)–Cu(A)–O′(1)	87.5(5)	N″(1)–Cu′(A)–O‴(1)	87.2(4)
N′(1)–Cu(A)–O(1)	87.5(4)	N‴(1)–Cu′(A)–O″(1)	90.9(4)
N′(1)–Cu(A)–O(3W)	91.2(6)	N‴(1)–Cu′(A)–O′(3W)	90.3(5)
N′(1)–Cu(A)–O′(1)	92.1(5)	N‴(1)–Cu′(A)–O‴(1)	94.6(4)
O(1)–Cu(A)–O(3W)	104.9(4)	O″(1)–Cu′(A)–O′(3W)	108.1(4)
O(1)–Cu(A)–O′(1)	104.2(4)	O″(1)–Cu′(A)–O‴(1)	102.9(4)
O(3W)–Cu(A)–O′(1)	150.8(4)	O′(3W)–Cu′(A)–O‴(1)	148.5(5)
N(1)–Cu(A)–N′(1)	178.1(5)	N″(1)–Cu′(A)–N‴(1)	176.8(5)
N(4)–Cu(B)–N(5)	91.6(5)	N″(4)–Cu′(B)–N″(5)	91.5(5)
N(4)–Cu(B)–N′(4)	155.4(5)	N″(4)–Cu′(B)–N‴(4)	148.8(5)
N(4)–Cu(B)–N′(5)	98.2(5)	N″(4)–Cu′(B)–N‴(5)	99.6(5)
N(5)–Cu(B)–N′(4)	98.0(5)	N″(5)–Cu′(B)–N‴(4)	96.2(5)
N(5)–Cu(B)–N′(5)	135.3(6)	N″(5)–Cu′(B)–N‴(5)	142.2(5)
N′(4)–Cu(B)–N′(5)	90.7(5)	N‴(4)–Cu′(B)–N‴(5)	92.6(5)
C(1)–N(1)–C(3)	107.3(13)	C′(1)–N′(1)–C′(3)	109.6(14)
C″(1)–N″(1)–C″(3)	103.5(11)	C‴(1)–N‴(1)–C‴(3)	109.0(12)
Cu(A)–N(1)–C(1)	124.6(10)	Cu(A)–N′(1)–C′(1)	124.5(11)
Cu′(A)–N″(1)–C″(1)	126.8(9)	Cu′(A)–N‴(1)–C‴(1)	124.8(10)
Cu(A)–N(1)–C(3)	128.1(9)	Cu(A)–N′(1)–C′(3)	125.9(10)
Cu′(A)–N″(1)–C″(3)	129.4(10)	Cu′(A)–N‴(1)–C‴(3)	126.2(10)
N(1)–C(1)–N(2)	110.5(13)	N′(1)–C′(1)–N′(2)	108.9(13)
N″(1)–C″(1)–N″(2)	113.0(13)	N‴(1)–C‴(1)–N‴(2)	107.8(13)
C(1)–N(2)–C(2)	106.2(13)	C′(1)–N′(2)–C′(2)	108.6(14)
C″(1)–N″(2)–C″(2)	109.2(13)	C‴(1)–N‴(2)–C‴(2)	108.6(13)
C(3)–C(2)–N(2)	108.9(14)	C′(3)–C′(2)–N′(2)	107.0(14)
C″(3)–C″(2)–N″(2)	103.8(12)	C‴(3)–C‴(2)–N‴(2)	108.1(12)
C(2)–C(3)–N(1)	107.2(12)	C′(2)–C′(3)–N′(1)	105.7(12)
C″(2)–C″(3)–N″(1)	110.4(12)	C‴(2)–C‴(3)–N‴(1)	106.5(13)
C(2)–C(3)–C(4)	132.5(13)	C′(2)–C′(3)–C′(4)	131.7(14)
C″(2)–C″(3)–C″(4)	129.1(12)	C‴(2)–C‴(3)–C‴(4)	131.1(12)
C(4)–C(3)–N(1)	120.2(13)	C′(4)–C′(3)–N′(1)	122.3(14)
C″(4)–C″(3)–N″(1)	119.8(12)	C‴(4)–C‴(3)–N‴(1)	122.4(13)
C(3)–C(4)–C(5)	111.2(12)	C′(3)–C′(4)–C′(5)	110.5(13)
C″(3)–C″(4)–C″(5)	112.2(12)	C‴(3)–C‴(4)–C‴(5)	113.9(12)
C(4)–C(5)–C(6)	109.4(11)	C′(4)–C′(5)–C′(6)	109.4(12)
C″(4)–C″(5)–C″(16)	111.5(10)	C‴(4)–C‴(5)–C‴(6)	109.7(11)
C(4)–C(5)–N(3)	112.3(12)	C′(4)–C′(5)–N′(3)	112.6(14)
C″(4)–C″(5)–N″(3)	111.4(12)	C‴(4)–C‴(5)–N‴(3)	110.2(11)
C(6)–C(5)–N(3)	114.1(12)	C′(6)–C′(5)–N′(3)	111.4(13)
C″(6)–C″(5)–N″(3)	112.4(11)	C‴(6)–C‴(5)–N‴(3)	111.5(11)
C(5)–C(6)–N(4)	122.7(13)	C′(5)–C′(6)–N′(4)	123.6(13)
C″(5)–C″(6)–N″(4)	122.3(11)	C‴(5)–C‴(6)–N‴(4)	124.3(12)
C(5)–C(6)–O(1)	118.5(13)	C′(5)–C′(6)–O′(1)	114.7(12)
C″(5)–C″(6)–O″(1)	112.9(12)	C‴(5)–C‴(6)–O‴(1)	115.3(12)
N(4)–C(6)–O(1)	118.6(13)	N′(4)–C′(6)–O′(1)	121.7(13)
N″(4)–C″(6)–O″(1)	124.8(11)	N‴(4)–C‴(6)–O‴(1)	120.4(11)
C(6)–O(1)–Cu(A)	118.1(8)	C′(6)–O′(1)–Cu(A)	120.4(9)
C″(6)–O″(1)–Cu′(A)	113.9(8)	C‴(6)–O‴(1)–Cu′(A)	121.5(9)
C(5)–N(3)–C(8)	124.6(12)	C′(5)–N′(3)–C′(8)	126.5(12)
C″(5)–N″(3)–C″(8)	127.4(11)	C‴(5)–N‴(3)–C‴(8)	127.5(11)
C(6)–N(4)–C(7)	123.1(11)	C′(6)–N′(4)–C′(7)	122.6(12)
C″(6)–N″(4)–C″(7)	124.7(11)	C‴(6)–N‴(4)–C‴(7)	123.3(10)
C(6)–N(4)–Cu(B)	111.9(9)	C′(6)–N′(4)–Cu(B)	112.0(10)
C″(6)–N″(4)–Cu′(B)	112.8(8)	C‴(6)–N‴(4)–Cu′(B)	112.7(8)
C(7)–N(4)–Cu(B)	124.6(9)	C′(7)–N′(4)–Cu(B)	124.5(9)
C″(7)–N″(4)–Cu′(B)	121.6(8)	C‴(7)–N‴(4)–Cu′(B)	122.9(9)
C(8)–C(7)–C(9)	105.8(11)	C′(8)–C′(7)–C′(9)	105.0(12)
C″(8)–C″(7)–C″(9)	106.0(11)	C‴(8)–C‴(7)–C‴(9)	105.4(11)
C(8)–C(7)–N(4)	114.0(12)	C′(8)–C′(7)–N′(4)	115.2(12)

TABLE 3. (Continued)

C″(8)–C″(7)–N″(4)	113.8(11)	C‴(8)–C‴(7)–N‴(4)	113 4(12)
C(9)–C(7)–N(4)	107.6(10)	C′(9)–C′(7)–N′(4)	110.7(11)
C″(9)–C″(7)–N″(4)	109.0(10)	C‴(9)–C‴(7)–N‴(4)	109.5(11)
C(7)–C(8)–N(3)	119.6(13)	C′(7)–C′(8)–N′(3)	119.7(13)
C″(7)–C″(8)–N″(3)	117.8(11)	C‴(7)–C‴(8)–N‴(3)	118.9(12)
C(7)–C(8)–O(2)	118.3(14)	C′(7)–C′(8)–O′(2)	118.9(13)
C″(7)–C″(8)–O″(2)	119.0(12)	C‴(7)–C‴(8)–O‴(2)	117.0(14)
N(3)–C(8)–O(2)	122.2(13)	N′(3)–C′(8)–O′(2)	121.4(12)
N″(3)–C″(8)–O″(2)	123.2(12)	N‴(3)–C‴(8)–O‴(2)	124.1(13)
C(7)–C(9)–C(10)	110.7(12)	C′(7)–C′(9)–C′(10)	110.3(12)
C″(7)–C″(9)–C″(10)	112.1(11)	C‴(7)–C‴(9)–C‴(10)	112.7(11)
C(9)–C(10)–C(11)	123.9(14)	C′(9)–C′(10)–C′(11)	125.0(15)
C″(9)–C″(10)–C″(11)	126.4(13)	C‴(9)–C‴(10)–C‴(11)	126.2(13)
C(9)–C(10)–N(5)	125.0(14)	C′(9)–C′(10)–N′(5)	123.2(13)
C″(9)–C″(10)–N″(5)	122.7(12)	C‴(9)–C‴(10)–N‴(5)	124.5(13)
C(11)–C(10)–N(5)	111.1(13)	C′(11)–C′(10)–N′(5)	111.3(14)
C″(11)–C″(10)–N″(5)	110.9(12)	C‴(11)–C‴(10)–N‴(5)	109.0(12)
C(10)–C(11)–N(6)	104.5(14)	C′(10)–C′(11)–N′(6)	103.0(17)
C″(10)–C″(11)–N″(6)	102.7(13)	C‴(10)–C‴(11)–N‴(6)	105.2(14)
C(10)–N(5)–C(12)	107.1(13)	C′(10)–N′(5)–C′(12)	106.4(13)
C″(10)–N″(5)–C″(12)	106.3(12)	C‴(10)–N‴(5)–C‴(12)	108.2(12)
C(10)–N(5)–Cu(B)	124.3(9)	C′(10)–N′(5)–Cu(B)	120.0(9)
C″(10)–N″(5)–Cu′(B)	128.0(9)	C‴(10)–N‴(5)–Cu′(B)	126.3(9)
C(12)–N(5)–Cu(B)	123.5(11)	C′(12)–N′(5)–Cu(B)	124.2(11)
C″(12)–N″(5)–Cu′(B)	125.6(10)	C‴(12)–N‴(5)–Cu′(B)	125.1(10)
N(5)–C(12)–N(6)	109.2(15)	N′(5)–C′(12)–N′(6)	110.6(14)
N″(5)–C″(12)–N″(6)	109.0(12)	N‴(5)–C‴(12)–N‴(6)	108.5(12)
C(11)–N(6)–C(12)	108.2(14)	C′(11)–N′(6)–C′(12)	108.6(15)
C″(11)–N″(6)–C″(12)	111.0(13)	C‴(11)–N‴(6)–C‴(12)	109.2(13)
O(4)–Cl–O(5)	110.1(8)	O′(4)–Cl′–O′(5)	107.8(8)
O″(4)–Cl″–O″(5)	106.0(13)	O‴(4)–Cl‴–O‴(5)	112.3(14)
O(4)–Cl–O(6)	111.1(8)	O′(4)–Cl′–O′(6)	112.6(10)
O″(4)–Cl″–O″(6)	103.0(13)	O‴(4)–Cl‴–O‴(6)	112.3(14)
O(4)–Cl–O(7)	109.2(9)	O′(4)–Cl′–O′(7)	108.4(8)
O″(4)–Cl″–O″(7)	101.4(13)	O‴(4)–Cl‴–O‴(7)	108.9(15)
O(5)–Cl–O(6)	108.6(8)	O′(5)–Cl′–O′(6)	115.1(10)
O″(5)–Cl″–O″(6)	112.3(14)	O‴(5)–Cl‴–O‴(6)	98.5(12)
O(5)–Cl–O(7)	108.8(9)	O′(5)–Cl′–O′(7)	107.9(9)
O″(5)–Cl″–O″(7)	113.3(13)	O‴(5)–Cl‴–O‴(7)	112.3(15)
O(6)–Cl–O(7)	109.0(8)	O′(6)–Cl′–O′(7)	104.8(9)
O″(6)–Cl″–O″(7)	118.7(13)	O‴(6)–Cl‴–O‴(7)	112.3(13)

structure, but the values of a number of bond angles in one complex are somewhat different from those of the corresponding ones in the other. Furthermore, some of the corresponding bonds show a slight but, in view of a statistical significant test, significant differences in length. However, the "significant differences" may be ascribed to the underestimation of standard deviation. On the other hand, the bond angle will vary with the packing. Therefore, the two complex cations should be considered to be chemically identical. Since the difference between the equivalent structural parameters including the equivalent bond angles is small, we will use the mean values of the respective parameters in the following description, unless we state otherwise, and make use of one of the two complex cations for illustration.

Figures 3(a) and (b) show the elevation perpendicular to a plane through Cu(A), Cu(B), N(1), and N′(1), and the projection along the Cu(A)···Cu(B) axis, respectively. The complex cation is dimeric, with two Cu atoms of different coordination modes. In case the ligating water molecule [O(3W)] is excluded from the complex, the remaining part has a pseudo twofold axis which passes through the two Cu atoms. The structural parameters related by this axis are almost identical except for the Cu(A)–O(1) and Cu(A)–O′(1) bond lengths. The average bond lengths are shown in Fig. 4.

The Cu(B) atom has a flattened tetrahedral coordination by the N(5) atom of the Im group and the anionic N(4) atom of the $DKPH^-$ moiety of one ligand, and the chemically equivalent N′(5) and N′(4) atoms of the other [Cu–N=1.97 Å]. The average value of the chelate bite angles at the Cu(B) is 91.7°. The dihedral angle between the N(4), Cu(B), and N(5) plane and the N′(4), Cu(B), N′(5) plane is 50.0°, which is comparable to the value (53.6°) in bis(*N*-*t*-butylsalicylideneaminato)copper(II).[8] The tetrahedral coordination of bivalent copper is rather unusual. The dimerization

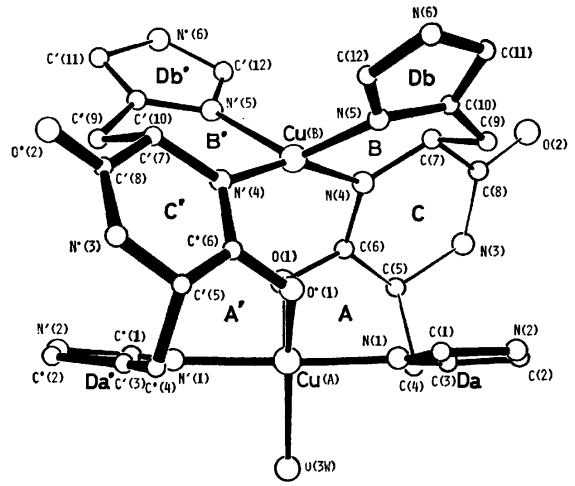

(a)

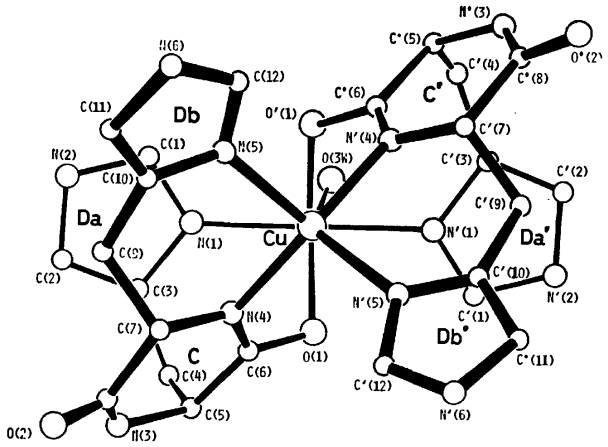

(b)

Fig. 3. Projection of aquabis(cyclo-L-histidyl-L-histidyl-ato)dicopper(II).
(a) On the plane through Cu(A), Cu(B), N(1), and N'(1), (b) along the Cu(A)···Cu(B) axis.

and strong affinity of Cu(II) for N atoms may be responsible for such a coordination in the present complex.

The coordination geometry of Cu(A) atom seems to be intermediate between the square pyramid and the trigonal bipyramid (Fig. 3). From the square-pyramidal viewpoint, the apical position is occupied by the O(1) atom, whereas the basal plane is defined by the O(3W) (oxygen of ligating water molecule), N(1), O'(1), and N'(1) atoms. The disposition of the four basal atoms is not planar, the maximum deviation of the atom from the plane being 0.38 Å. The Cu–O(1) apical bond is longer than the four basal bonds ($Cu–O(1)_{apex}=2.21$, $Cu–O_{base}=2.04$, $Cu–N_{base}=1.97$ Å). The N(1)–Cu(A)–N'(1) angle is close to 180°, which is suggestive of the trigonal-bipyramidal coordination. In the trigonal bipyramidal approximation, the N(1) and N'(1) atoms occupy the axial positions. The Cu(A) atom is displaced 0.13 Å toward N'(1) from the equatorial

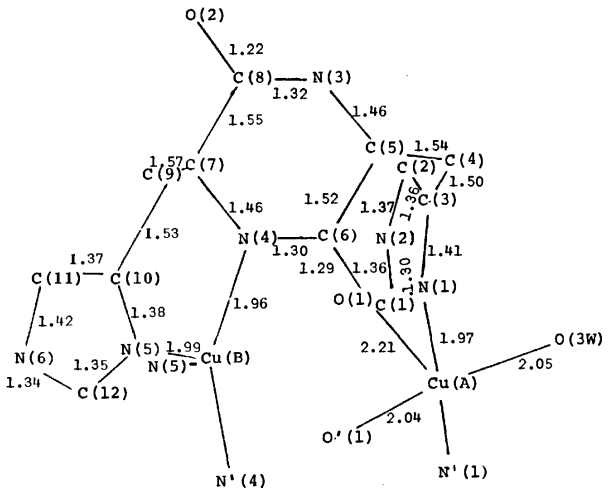

Fig. 4. The average bond lengths of aquabis(cyclo-L-histidyl-L-histidylato)dicopper(II).

Table 4. Deviations of the atoms from least-squares planes (d/Å) and the dihedral angles between them

(B) plane through C(9), C(10), N(4), N(5), and Cu(B) (Plane B)							
C(7)	−0.65	C(9)	0.08	C(10)	−0.13	N(4)	−0.03
N(5)	0.09	Cu(B)	−0.01				
(B') plane through C'(9), C'(10),N'(4), N'(5), and Cu(B) (Palne B')							
C'(7)	−0.66	C'(9)	0.08	C'(10)	−0.08	N'(4)	−0.06
N'(5)	0.02	Cu(B)	0.04				
(B'') plane through C''(9), C''(10), N''(4), N''(5), and Cu'(B) (Plane B'')							
C''(7)	0.74	C''(9)	−0.05	C''(10)	0.01	N''(4)	0.06
N''(5)	0.05	Cu'(B)	−0.07				
(B''') plane through C'''(9), C'''(10), N'''(4), N'''(5), and Cu'(B) (Plane B''')							
C'''(7)	0.66	C'''(9)	−0.04	C'''(10)	0.06	N'''(4)	0.02
N'''(5)	−0.04	Cu'(B)	0.00				
(C) plane through C(5), C(6), C(7), C(8), N(3), and N(4) (Plane C)							
C(4)	−1.22	C(5)	−0.03	C(6)	0.05	C(7)	−0.06
C(8)	0.10	C(9)	−1.50	N(3)	−0.05	N(4)	−0.01
O(1)	0.09	O(2)	0.31	Cu(B)	−0.23		
(C') plane through C'(5), C'(6), C'(7), C'(8), N'(3), and N'(4) (Plane C')							
C'(4)	1.12	C'(5)	−0.05	C'(6)	0.02	C'(7)	0.15
C'(8)	−0.07	C'(9)	1.59	N'(3)	−0.08	N'(4)	−0.06
O'(1)	0.04	O'(2)	−0.17	Cu(B)	0.31		

TABLE 4. (Continued)

(C″) plane through C″(5), C″(6), C″(7), C″(8), N″(3), and N″(4) (Plane C″)							
C″(4)	1.35	C″(5)	0.08	C″(6)	−0.04	C″(7)	0.08
C″(8)	−0.04	C″(9)	1.49	N″(3)	0.01	N″(4)	−0.08
O″(1)	−0.04	O″(2)	−0.18	Cu′(B)	−0.05		
(C‴) plane through C‴ (5), C‴(6), C‴(7), C‴(8), N‴(3), and N‴ (4) (Plane C‴)							
C‴(4)	1.32	C‴(5)	0.03	C‴(6)	0.02	C‴(7)	0.06
C‴(8)	−0.03	C‴(9)	1.48	N‴(3)	−0.03	N‴(4)	−0.05
O‴(1)	0.09	O‴(2)	−0.11	Cu′(B)	0.04		
(Da) plane through C(1), C(2), C(3), N(1), and N(2) (Plane Da)							
C(1)	0.00	C(2)	0.00	C(3)	0.00	C(4)	−0.08
N(1)	0.00	N(2)	0.00	Cu(A)	−0.04		
(Db) plane through C(10), C(11), C(12), N(5), and N(6) (Plane Db)							
C(9)	0.07	C(10)	0.01	C(11)	−0.01	C(12)	0.00
N(5)	0.00	N(6)	0.01	Cu(B)	−0.71		
(Da′) plane through C′(1), C′(2), C′(3), N′(1), and N′(2) (Plane Da′)							
C′(1)	0.02	C′(2)	0.00	C′(3)	0.02	C′(4)	−0.06
N′(1)	−0.02	N′(2)	−0.01	Cu(A)	−0.15		
(Db′) plane througA C′(10), C′(11), C′(12), N′(5), and N′(6) (Plane Db′)							
C′(9)	0.10	C′(10)	−0.02	C′(11)	0.02	C′(12)	0.00
N′(5)	0.01	N′(6)	−0.02	Cu(B)	−0.15		
(Da″) plane through C″(1), C″(2), C″(3), N″(1), and N″(2) (Plane Da″)							
C″(1)	0.00	C″(2)	0.01	C″(3)	−0.02	C″(4)	0.13
N″(1)	0.01	N″(2)	−0.01	Cu′(A)	−0.12		
(Db″) plane through C″(10), C″(11), C″(12), N″(5), and N″(6) (Plane Db″)							
C″(9)	0.02	C″(10)	0.00	C″(11)	0.01	C″(12)	0.01
N″(5)	−0.01	N″(6)	−0.01	Cu′(B)	−0.12		
(Da‴) plane through C‴(1), C‴(2), C‴(3), N‴(1), and N‴(2) (Plane Da‴)							
C‴(1)	0.00	C‴(2)	0.00	C‴(3)	0.00	C‴(4)	−0.01
N‴(1)	0.00	N‴(2)	0.00	Cu′(A)	0.03		
(Db‴) plane through C‴ (10), C‴(11), C‴(12), N‴(5), and N‴(6) (Plane Db‴)							
C‴(9)	−0.12	C‴(10)	0.01	C‴(11)	0.00	C‴(12)	0.01
N‴(5)	−0.01	N‴(6)	−0.01	Cu′(B)	0.15		

Dihedral angles between the planes (ϕ/°):

B and B′	54.9	B″ and B‴	49.7	Da and Da′	11.2
Db and Db′	75.6	Da″ and Da‴	8.3	Db″ and Db‴	52.7

Equations of planes:

(B)	$0.131X+0.790Y+0.599Z-\ 9.868=0$	(Da)	$0.041X+0.953Y+0.300Z-12.190=0$
(B′)	$0.131X-0.954Y+0.269Z+\ 4.098=0$	(Db)	$0.052X+0.582Y+0.811Z-\ 9.708=0$
(B″)	$0.204X+0.607Y-0.768Z-\ 2.373=0$	(Da′)	$0.037X+0.993Y+0.109Z-11.494=0$
(B‴)	$0.847X+0.127Y-0.516Z-13.310=0$	(Db′)	$0.111X-0.929Y+0.354Z+\ 3.794=0$
(C)	$-0.024X-0.267Y-0.963Z+\ 7.206=0$	(Da″)	$0.513X+0.443Y-0.736Z-\ 3.889=0$
(C′)	$-0.032X+0.596Y-0.802Z+\ 0.892=0$	(Db″)	$0.162X+0.594Y-0.788Z-\ 1.312=0$
(C″)	$-0.112X-0.942Y+0.315Z+\ 2.557=0$	(Da‴)	$0.614X+0.468Y-0.636Z-\ 6.769=0$
(C‴)	$-0.739X+0.522Y+0.426Z+\ 6.810=0$	(Db‴)	$0.835X+0.068Y-0.547Z-12.185=0$

where X, Y, and Z are coordinates in Å units relative to the a, b, and c^* axes respectively.

plane defined by the O(1), O′(1), and O(3W) atoms. One of the equatorial bonds is longer than the other two, and the O–Cu–O angles in the equatorial plane are 103.6, 106.5, and 149.7°. The Cu(B) atom is distant from O(1) and O′(1) by 2.81(1) and 2.80(1) Å respectively, and the interatomic distance, Cu(A)··· Cu(B), is 3.570(3) Å.

All the $HISH^-$ ligands assume a similar, asymmetric conformation; the C(4)–Im and C(9)–Im fragments are rotated respectively about the C(4)–C(5) and C(7)–C(9) bonds in such a way that the donor atoms in the Im groups are favorably located for coordination to the Cu(A) and Cu(B) atoms. The average bond lengths in the $HISH^-$ ligand are also shown in Fig. 4. Each Im group is planar within 0.02 Å, and the bond lengths and angles are in agreement with the corresponding ones in the bis(histidino)-nickel(II) and -cobalt(II).[9] The leastsquares planes of various parts of the complex and the dihedral angles between them are listed in Table 4. The $DKPH^-$ ring is nearly planar, and the torsional angles in the ring (IUPAC-IUB conventions)[10] are presented in Table 5. In the two C=O bonds, the one whose O atom participates in the coordination is longer than the other. In the peptide-bondings, N(4)–C(6)–O(1) and N(3)–C(8)–O(2), a short N–C bond length indicated the delocalization of π electrons over this bonding.

The $DKPH_2$ can be regarded as a kind of secondary

TABLE 5. TORSIONAL ANGLES (deg.) IN DKPH$^-$ [a]

Angle		Angle	
ϕ[C(5), N(3)]	−4.2	ϕ[C(7), N(4)]	5.1
ϕ[C(6), C(5)]	−6.5	ϕ[C(8), C(7)]	−14.9
ω[N(4), C(6)]	5.4	ω[N(3), C(8)]	14.9
ϕ[C′(5), N′(3)]	−1.1	ϕ[C′(7), N′(4)]	11.0
ϕ[C′(6), C′(5)]	0.2	ϕ[C′(8), C′(7)]	−11.9
ω[N′(4), C′(6)]	−5.4	ω[N′(3), C′(8)]	7.3
ϕ[C″(5), N″(3)]	5.4	ϕ[C″(7), N″(4)]	14.1
ϕ[C″(6), C″(5)]	−5.2	ϕ[C″(8), C″(7)]	−13.2
ω[N″(4), C″(6)]	−5.0	ω[N″(3), C″(8)]	4.0
ϕ[C‴(5), N‴(3)]	2.9	ϕ[C‴(7), N‴(4)]	12.8
ϕ[C‴(6), C‴(5)]	0.7	ϕ[C‴(8), C‴(7)]	−9.0
ω[N‴(4), C‴(6)]	−9.2	ω[N‴(3), C‴(8)]	1.5
χ[C(4), C(5)]	73.1	χ[C(9), C(7)]	−63.1
χ[C′(4), C′(5)]	74.1	χ[C′(9), C′(7)]	−62.9
χ[C″(4), C″(5)]	74.4	χ[C″(9), C″(7)]	−65.8
χ[C‴(4), C‴(5)]	76.5	χ[C‴(9), C‴(7)]	−61.0

a) The conventions of the IUPAC-IVB Commission are followed.[b] b) See also Ref. 10.

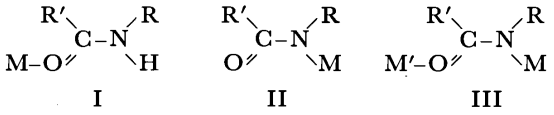

I II III

amide group which is capable of ligating in three ways:[11] I is most usual, whereas II and III are uncommon and deprotonation is necessary prior to complex formation. The coordination mode of the "amide group" in the present DKPH$^-$ group can be classified as III. In μ-formamide-bis[pentaamminecobalt(III)] pentachloride monohydrate, which is known as the sole example of III, the M′–O bond is nearly coplanar with the plane of the amide group, the M′–O–C bond angle being 126°.[12] However, in the present complex the Cu(A)–O′(1) bond is not coplanar with the [N′(4), C′(6), O′(1)] "amide plane," but makes an angle of 59.3° with this plane. Similarly, the Cu(A)–O(1) bond intersects the [N(4), C(6), O(1)] "amide plane" in an angles of 61.7°.

TABLE 6. DATA OF THE HYDROGEN BONDS

A–H–B		A–B	Positions[a] of A	Positions[a] of B
N(3)	O′(5)	3.03	1	1
N(6)	O(11W)	2.96	1	1
N′(3)	O″(5)	3.12	1	1
N″(3)	O′(2)	2.85	1	1
N‴(6)	O(6)	2.96	1	1
O(10W)	O(2)	2.67	1	1
O‴(6)	O(3)	2.98	1	1
O(8W)	O″(1)	2.78	1	1
O(8W)	O(9W)	2.90	1	1
O(12W)	O(8W)	2.98	1	1
O(12W)	O(5)	3.08	1	1
O′(3)	O″(2)	2.53	2	1
N(3)	O‴(2)	2.97	1	3
N‴(3)	O(2)	3.02	3	1
O(3)	O′(2)	2.74	4	1
N′(2)	O(11W)	2.86	4	1
O(13W)	O(1)	2.98	1	4
N(2)	O(7)	3.03	1	5
N‴(2)	O(10W)	2.73	5	1
O(11W)	O‴(5)	2.92	1	5
O(13W)	N(2)	2.78	1	5
N″(2)	O‴(2)	2.78	1	6

a) Numerals refer to the following equivalent positions: 1 (x,y,z), 2 $(x,y,-1+z)$, 3 $(-1+x,y,-1+z)$, 4 $(1-x,-1/2+y,1-z)$, 5 $(1-x,-1/2+y,2-z)$, 6 $(2-x,-1/2+y,2-z)$.

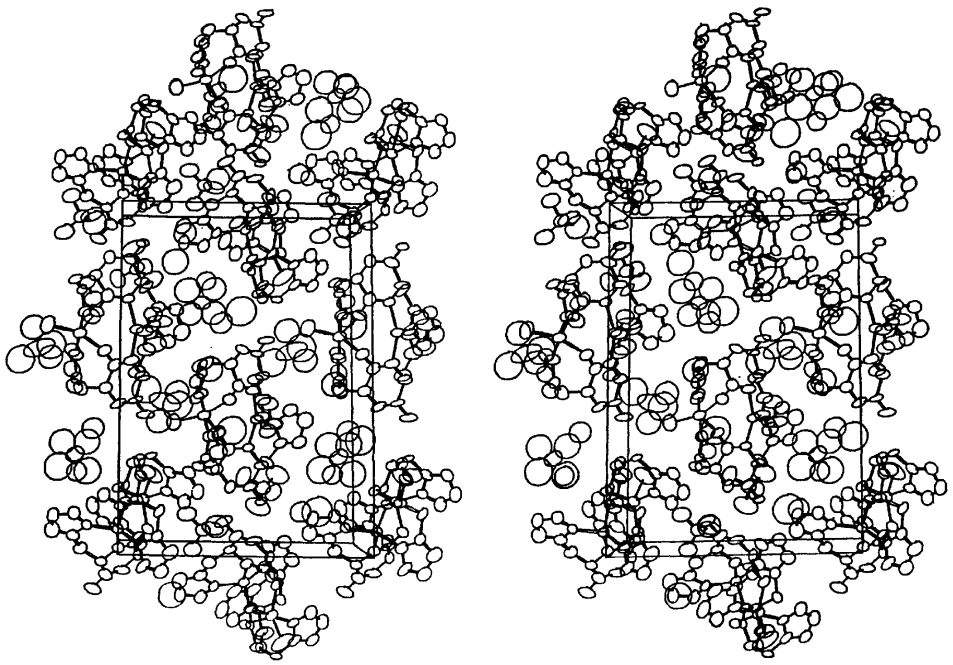

Fig. 5. Stereoview of crystal structure of aquabis(cyclo-L-histidyl-L-histidylato)dicopper(II) perchlorate hydrate along the c axis.

Both of the 6-membered chelate rings, B[N(4), Cu(B), N(5), C(10), C(9), C(7)] and B'[N'(4), Cu(B), N'(5), C'(10), C'(9), C'(7)], which are related mutually by the pseudo twofold axis, assume an envelope form; the five atoms in each chelate ring are planar within 0.13 Å, whereas C(7) in B and C'(7) in B' deviate by 0.65 and 0.66 Å from the respective least-squares planes defined by the five atoms. The 7-membered ring A[Cu(A), O(1), C(6), C(5), C(3), C(4), N(1)] and the A' related with A by the pseudo twofold axis have a boat form. Although the 7-membered ring has been thought generally to be unstable compared with 5- and 6- membered ones, and although, moreover, the ligating ability of the oxygen in an amide group toward metal is not strong, the formation of the 7-membered ring in the present complex presumably results from the dimerization and migration of the negative charge to the O atom from the adjacent "anionic" N atom.

Figure 5 shows the stereoview of the crystal structure along the c axis. The data concerning hydrogen bonds are presented in Table 6. The perchlorate anions and uncoordinated water molecules participate in the O–H···O, N–H···O, and O–H···N hydrogen bonds. The N(3) atom in the complex which involves unprimed Cu atoms has short contacts of N(3)···O'(5) (3.03 Å) and N(3)—O''(2)(2.97 Å). These contacts suggest that the H atom linked to N(3) takes part in the bifurcated hydrogen bonding.

References

1) For instance, T. Sugihara, Y. Imanishi, and T. Higashimura, *Biopolymers*, **12**, 2823 (1973).

2) A. Nakahara, K. Sakurai, and Y. Nakao, *Bull. Chem. Soc. Jpn.*, **38**, 1051 (1965); J. C. Prado and G. Vincentini, *Inorg. Nucl. Chem. Lett.*, **9**, 693 (1973).

3) Y. Kojima, K. Hirotsu, and K. Matsumoto, *Chem. Lett.*, **1976**, 809.

4) E. Abderhalden and W. Geidel, *Fermentforschung*, **12**, 518 (1930).

5) J. Hornstra and B. Stubbe, PW1100 Data Processing Program, Philips Research Laboratories, Eindhoven, Holland.

6) "International Tables for X-Ray Crystallography," Vol. 3, Kynoch Press, Birmingham (1962), pp. 215, 202.

7) T. Sakurai, Ed, The Universal Crystallographic Computation Program System (UNICS), The Cystallographic Society of Japan (1967).

8) T. P. Cheeseman, D. Hall, and T. N. Waters, *J. Chem. Soc., A*, **1966**, 685.

9) K. A. Fraser and M. M. Harding, *J. Chem. Soc., A*, **1967**, 415; M. M. Harding and H. A. Long, *ibid.*, **1968**, 2554; R. Candlin and M. M. Harding, *ibid.*, **1970**, 384.

10) IUPAC-IUB Commision of Biological Nomenclature, *Biochemistry*, **9**, 3471 (1970); C.-F. Lin and L. E. Webb, *J. Am. Chem. Soc.*, **95**, 6803 (1973).

11) M. Nonoyama and K. Nonoyama, *Kagaku No Ryoiki*, **31**, 136 (1977).

12) R. J. Balahura, G. Ferguson, and M. L. Schneider, *J. Chem. Soc. Dalton Trans.*, **1975**, 603.

A Re-investigation of the Dimer ESR Spectra in Several Quadridentate Schiff Base Complexes of Copper(II)

Makoto CHIKIRA and Hiroshi YOKOI

Chemical Research Institute of Non-aqueous Solutions, Tohoku University, Katahira, Sendai 980

(Received June 1, 1977)

The angle between the $g_{//}$ axis and the copper-copper axis in most parallel planar dimers of the quadridentate salicylaldehyde Schiff base complexes of copper(II) in toluene or xylene has been reconfirmed to be not $\approx$35°, but $\approx$17°, by a computer simulation of the dimer ESR spectra at both the K and X-bands. In order to remedy the shortcomings of the so-called point-dipole approximation generally used in the simulation, a delocalization model, in which the delocalization of each unpaired electron on the copper atom and its surrounding four ligand atoms is explicitly taken into consideration, has been discussed in some detail. The delocalization effect has been proven to be highly significant in estimating dimeric structures reliably. An application of this model to the structural estimation of several dimers in solutions has also been made.

A number of mono-nuclear planar copper(II) complexes have been found to exist as dimers in crystals[1–4] and in solutions.[5–11] The structures of dimers in solutions have been estimated by the computer simulation of the dimer ESR spectra.[6–11,13–16] We have previously reported that many quadridentate salicylaldehyde Schiff base complexes of copper(II) (hereafter abbreviated as Cu(nX-SalB), Fig. 1) in toluene form dimers with almost coaxial g and fine-structure tensors,[12] together with the fact that the dimeric structures of Cu(SalB) in solution are markedly different from those of Cu(3NO$_2$-SalB).[13]

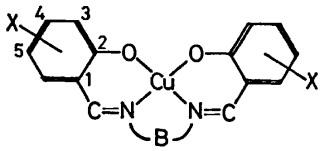

Cu(nX-SalB)

Fig. 1. Quadridentate salicylaldehyde Schiff base complexes of copper(II).
Abbreviations: Me=$-CH_3$, en=$-CH_2CH_2-$, pn=$-CH(CH_3)CH_2-$, ibn=$-C(CH_3)_2CH_2-$, MeO=$-OCH_3$, tn=$-CH_2CH_2CH_2-$.

Recently, Cookson *et al.* have reported that the angle, ξ, between the $g_{//}$ axis and the copper-copper axis in the dimers of Cu(nX-SalB) (nX=H or 3MeO and B=pn or tn) in frozen xylene is estimated to be 35° by the computer simulation of the X-band ESR spectra, suggesting that these dimers are similar in structure to that of Cu(Salen) in crystals.[2,14] This value, however, is very different from the value (15°) we ourselves previously estimated for similar systems.[12] More reliable information on the mutual orientation of these axes can often be obtained by investigating simultaneously the dimer ESR spectra at different microwave frequencies. In this study, therefore, the dimeric structures for Cu(3Me-Salpn) in toluene, Cu(Salpn) in xylene, and Cu(3NO$_2$-Salibn) in nitroethane were examined by the computer simulation of the K-band ESR spectra as well as the X-band ones.

In most studies so far reported on the computer simulation of dimer ESR spectra, the magnetic dipole interaction has been calculated using the so-called point-dipole approximation.[6,15,16] Actually, however, each unpaired electron in a dimer is delocalized on the copper atom and its surrounding ligand atoms. It has been suggested that there is a tendency for the Cu–Cu distance, r, and the ξ value in the dimer to be over- and under-estimated respectively by the use of the point-dipole approximation.[17,18] A notable example of the delocalization effect has recently been presented for the dimer of bis(dialkyldithiocarbamato)copper(II) (Cu(dtc)$_2$) by Van Rens and De Boer.[19] By calculating the fine-structure tensor of the dimer from the results of extended Hückel molecular orbital calculations, they have indicated that the delocalization reduces the dipolar interaction by a factor of two, and that one of the principal axes of the fine-structure tensor bisects the angle between the $g_{//}$ and Cu–Cu axes.

Although the metal-ligand bondings of Cu(dtc)$_2$ are strongly covalent,[20] the question still comes to our minds whether or not the delocalization effect can be neglected in many other cases. In order to obtain detailed information on errors inherent in the point-dipole approximation, a delocalization model was discussed and checked by applying the model to two dimeric systems of known structures in the title complexes. Using the results, an attempt was made to reestimate the structures of several dimers in solution more reliably.

Experimental

All the quadridentate salicylaldehyde Schiff base complexes of copper(II) used here had been prepared and purified in previous works.[12,13] The Cu(Salen)·$CHCl_3$ was prepared by the recrystallization of Cu(Salen) from chloroform.[21] The sample of Cu(Salen) diluted in the nickel complex was prepared by the recrystallization of a 5:1 mixture of Ni(Salen) and Cu(Salen) from nitrobenzene, and the Ni(Salen) was prepared by the same method. All the solvents used were purified by the usual methods.[22]

The ESR spectra at 77 K were recorded on Hitachi 771 X-band and MES-4001 K-band ESR spectrometers and analyzed by computer simulation. All the calculations in the simulation were carried out at the Computer Center of Tohoku University on a NEAC 2200 computer, using fundamentally the same program as in previous works,[7,13] except that the delocalization of each unpaired electron was taken into consideration, as will be described later. The co-ordinate system for the present dimers is shown in Fig. 2.

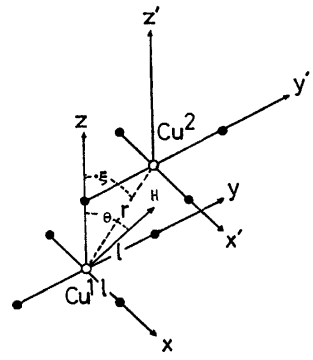

Fig. 2. Co-ordinate system for the dimers.

Results and Discussion

Combined Use of K and X-Band ESR Spectral Simulations. The observed ESR spectra of Cu(3Me-Salpn) in toluene at X and K-bands and of Cu(Salpn) in xylene at K-band are shown in Figs. 3, 4, and 5 respectively, together with the calculated spectra. The $\Delta M=2$ transition probability is inversely proportional to the square of microwave frequency,[15] so that, unfortunately, we have not observed any well-defined $\Delta M=2$ spectra at K-band with our spectrometer because of the low signal-to-noise ratios. The observed X-band and K-band dimer ESR spectra of Cu(3Me-Salpn) in toluene were almost the same as those of Cu(Salpn) in xylene, so their dimeric structures are similar. In this section, only the magnetic and structural parameters estimated by the computer simulation of the dimer ESR spectra using the point-dipole approximation will be discussed.

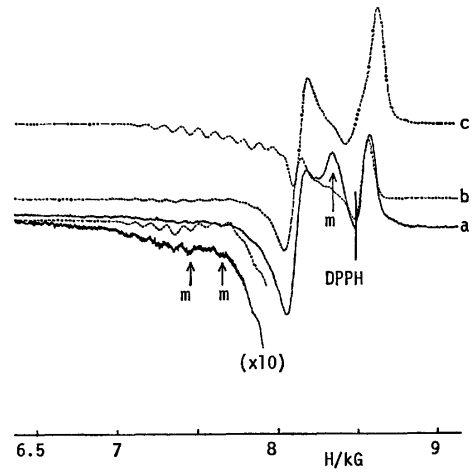

Fig. 5. K-Band ESR spectra of Cu(Salpn): a (solid lines), observed in xylene at 77 K; b and c, computer simulated with the parameters, (b) $g_{//}=2.19$, $g_{\perp}=2.045$, $|A_{//}|=0.0100$ cm^{-1}, $|A_{\perp}|=0.0015$ cm^{-1}, $r=4.05$ Å, $\xi=15°$, $\Delta H=25$ Gauss, and (c) $g_{//}=2.18$, $g_{\perp}=2.03$, $|2A_{//}|=0.0225$ cm^{-1}, $|2A_{\perp}|=0.0010$ cm^{-1}, $r=3.95$ Å, $\xi=35°$, $\Delta H=30$ G m represents absorption line due to monomers.

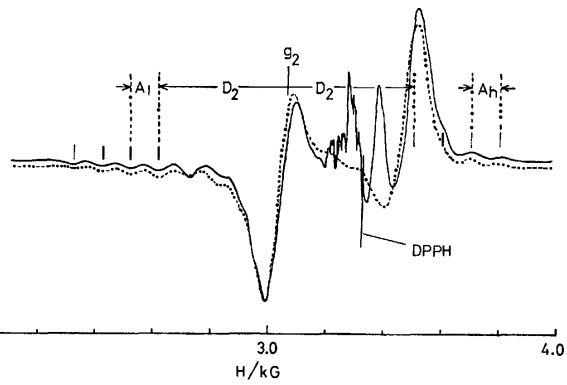

Fig. 3. X-Band ESR spectra of Cu(3Me-Salpn): (——), observed in toluene at 77K; (------), computer simulated with the parameters, $g_{//}=2.19$, $g_{\perp}=2.045$, $|A_{//}|=0.0100$ cm^{-1}, $|A_{\perp}|=0.0015$ cm^{-1}, $r=4.04$ Å, $\xi=15°$, and $\Delta H=25$ G (Gaussian linewidth).

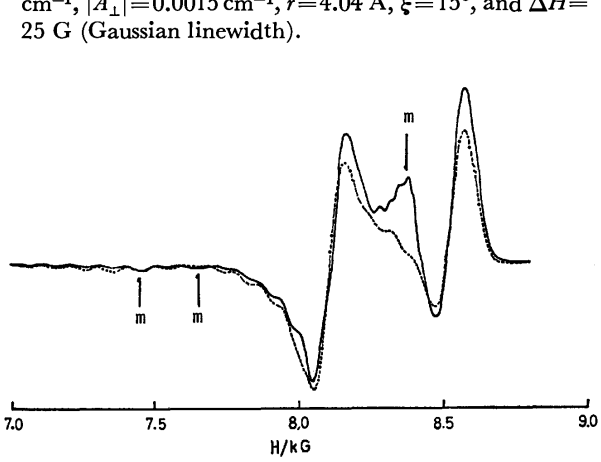

Fig. 4. K-Band ESR spectra of Cu(3M-Salpn): (——), observed in toluene at 77 K; (------), computer simulated with the parameters, $g_{//}=2.19$, $g_{\perp}=2.045$, $|A_{//}|=0.0100$ cm^{-1}, $|A_{\perp}|=0.0015$ cm^{-1}, $r=4.04$ Å, $\xi=15°$, and $\Delta H=30$ G. m represents absorption line due to monomers.

The parameters of (b) and (c) in Fig. 5, which have been estimated from the X-band spectra by us and by Cookson *et al.* respectively for the dimer of Cu(Salpn), are considerably different, especially in ξ. On the basis of the fact that both the A_1 and A_h values and the g_2 value are almost equal to the monomer's $A_{//}/2$ and $g_{//}$ values respectively in many quadridentate Schiff base complexes, we have previously concluded that the $g_{//}$ and Cu–Cu axes in these complexes almost coincide; namely, the ξ value is close to 0°,[6,12,13] where the parameters of A_1, A_h, and g_2 are as defined in Fig. 3. Two calculated $\Delta M=1$ spectra (b and c) of Cu(Salpn) at K-band, which we obtained with their respective sets of parameters, are shown in Fig. 5, together with the observed one. It should be noted that no complicated progression of the hyperfine structure in the 7.5—8 kG range (1 G=10^{-4} T) can be seen in the observed K-band spectra of either Cu(3Me-Salpn) in toluene or of Cu(Salpn) in xylene, but such a progression can be seen in the calculated spectrum of c. The appearance of such a hyperfine structure, therefore, was found to be characteristic of non-coaxial g and fine-structure tensors. In addition, the calculated spectrum of c as a whole is shifted to a little higher magnetic field than the observed one. As one can see in Fig. 5, a much better fit between the calculated and observed spectva at K-band is obtained with the parameters of (b) than with those of (c). We may conclude, therefore, that the ξ value of

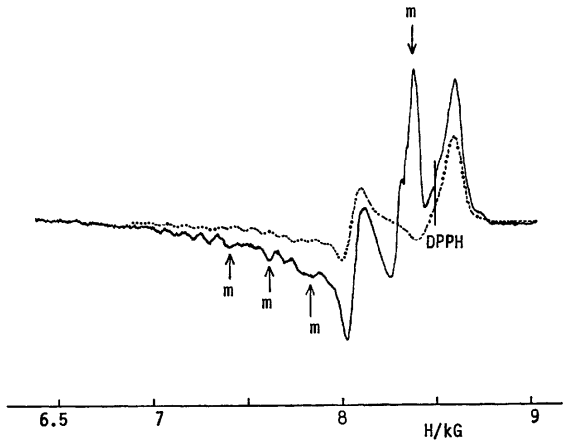

Fig. 6. K-Band ESR spectra of Cu(3NO$_2$-Salibn): (——), observed in nitroethane at 77 K; (------), computer simulated with the parameters, $g_{//}=2.20$, $g_{\perp}=2.045$, $|A_{//}|=0.0100$ cm^{-1}, $|A_{\perp}|=0.0010$ cm^{-1}, $r=3.8$ Å, $\xi=35°$, $\Delta H=30$ G. m represents absorption line due to monomers.

35° is too large for the present dimer, as far as the point-dipole approximation is concerned.

On the other hand, the dimer of Cu(3NO$_2$-Salibn) in nitroethane is a typical dimer with a larger ξ value. The observed and calculated K-band spectra of this dimer are shown in Fig. 6, in which the parameters used in the calculation were the same as those previously chosen for the X-band spectrum ($\xi=35°$).[13] Although the hyperfine structures due to the monomer were also simultaneously observed in the 7—8 kG range, every peak in the range can be well assigned by comparison with the simulated spectrum. Accordingly, we are led to the conclusion that the dimeric structure of Cu(3NO$_2$-Salibn) in nitroethane is remarkably different from those of many other quadridentate salicylaldehyde Schiff base complexes in toluene.

Errors Inherent in the Point-dipole Approximation. In order to obtain information on errors inherent in the point-dipole approximation, we first simulated the ESR spectra for the dimers of a known structure. The observed X-band spectrum of Cu(Salen)·CHCl$_3$ in the powder state at 77 K is shown in Fig. 7. This spectrum is obviously due to typical $\Delta M=1$ transitions in copper(II) pairs, although no hyperfine structure was observed in it. According to Baker *et al.*,[21] the molecules of Cu(Salen) in Cu(Salen)·CHCl$_3$ crystals exist as dimers with $r=3.37$ Å and $\xi=34°$. The best calculated spectrum, which is also shown in Fig. 7, was obtained with the parameters listed there, in which the g and A values were taken from the monomer spectrum of Cu(Salen) in chloroform and in which the ξ value mentioned above was adopted. The difference of 0.28 Å between the true and estimated r values is probably responsible for the point-dipole approximation used.[17,18]

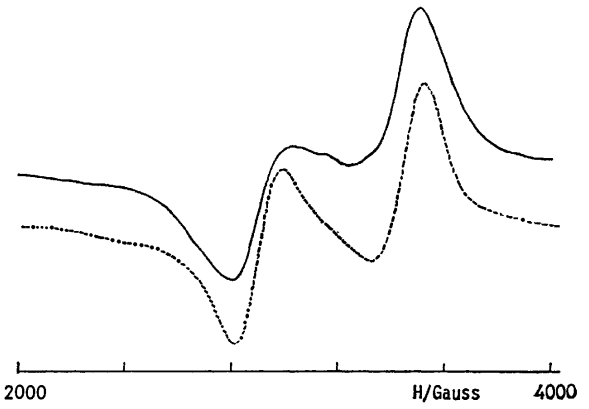

Fig. 7. X-Band powder ESR spectra of Cu(Salen)·CHCl$_3$: (——), observed at 77 K; (------), computer simulated with the parameters, $g_{//}=2.19$, $g_{\perp}=2.04$, $|A_{//}|=0.0100$ cm^{-1}, $|A_{\perp}|=0.0010$ cm^{-1}, $r=3.65$ Å, $\xi=34°$, and $\Delta H=60$ G.

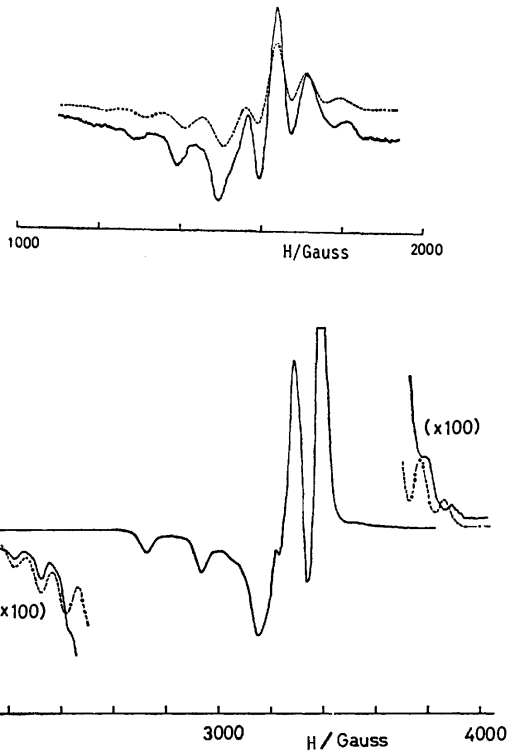

Fig. 8. X-Band powder ESR spectra of Cu(Salen) in Ni(Salen) crystals: (——), observed at 77 K; (------), computer simulated with the parameters, $g_{//}=2.19$, $g_{\perp}=2.04$, $|A_{//}|=0.0100$ cm^{-1}, $|A_{\perp}|=0.0010$ cm^{-1}, $r=3.8$ Å, $\xi=15°$, and $\Delta H=25$ G.

The powder X-band ESR spectra of Cu(Salen) doped in a high concentration in Ni(Salen) crystals are shown in Fig. 8. According to Shkol'nikova *et al.*,[23] the Ni(Salen) molecules in crystals are also present as dimers with $r=3.22$ Å and $\xi=15°$. This ξ value is much closer to those estimated for the dimers of Cu(Salpn) and Cu(3Me-Salpn) in frozen solutions than those for Cu(Salen) in crystals of Cu(Salen) itself ($\xi=40°$) and Cu(Salen)·CHCl$_3$. In the $\Delta M=1$ spectrum shown in Fig. 8, it is noteworthy that the hyperfine splittings at both edges are equal ($\approx$100 G), being the same as one half of the monomer's $|A_{//}|$ value. This fact indicates that the principal axes of the g and fine-structure tensors are almost coincident and, therefore, that the dimeric structure of Cu(Salen) in Ni(Salen) crystals is similar to that of the host nickel complex. The best fit for the $\Delta M=1$ spectrum at both sides and for the $\Delta M=2$

spectrum was obtained with the same g and A values as in Fig. 7 and with $r=3.80$ Å and $\xi=15°$. The difference of 0.58 Å between the true and estimated r values for the dimer of Cu(Salen) in Ni(Salen) crystals is larger than that in Cu(Salen)·$CHCl_3$ crystals. This fact suggests that the error in r inherent in the point-dipole approximation depends upon both r and ξ. Such might also be the case with the error in ξ.

In order to check these errors more systematically, we calculated the fine-structure splittings in the $\Delta M=1$ spectra, assuming that, in each of the monomeric halves in the dimers, the fractions of the unpaired electron on the copper atom and on each of its four coordinating ligand atoms are given by α^2 and $(1-\alpha^2)/4$ respectively, where α^2 is a covalency parameter which has its usual meaning in the metal-ligand bondings.[24,25] As may be seen in Fig. 2, the x′ and y′ axes are parallel to the x and y axes respectively, and the Cu^2 atom is located on the xz plane. It is obvious from a symmetry consideration of the dimer that the maximum principal value axis of the fine-structure tensor is on the xz plane. We calculated the fine-structure splitting D, setting the static magnetic field on the xz plane and changing θ from 0 to 90° at intervals of 1°. The maximum principal value, D_H, and the direction, θ_{max}, of the D tensor were determined graphically from the plots of D against θ.[26]

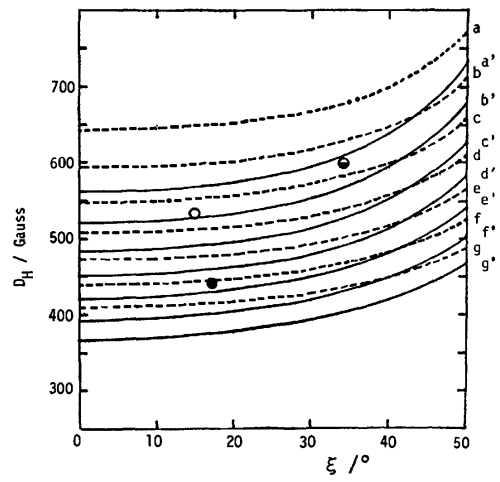

Fig. 9. Dependence of D_H on ξ and r: (——), $\alpha^2=0.65$; (------), $\alpha^2=0.75$.
a and a′, $r=3.2$ Å, b and b′, $r=3.3$ Å; c and c′, $r=3.4$ Å; d and d′, $r=3.5$ Å; e and e′, $r=3.6$ Å; f and f′, $r=3.7$ Å; g and g′, $r=3.8$ Å. D_H was calculated for $g_{//}=2.19$, $g_\perp=2.045$, and microwave frequency=9.23 GHz. ○, Cu(Salen) in Ni(Salen) crystals; ◒, Cu(Salen) in Cu(Salen)·$CHCl_3$ crystals; ●, Cu(3Me-Salpn) in toluene.

Figure 9 shows the dependence of D_H on ξ and r for $\alpha^2=0.65$ and 0.75. This figure clearly indicates that D_H increases with ξ and α^2, and that the increment of D_H *vs.* α^2 decreases with an increase of r. These results are in agreement with the intuitively acceptable fact that the point-dipole approximation becomes a better one as α^2 or r increases. This figure also explains why the error in r inherent in the point-dipole approximation is smaller for the dimer of Cu(Salen) in Cu(Salen)·$CHCl_3$ crystals than for the one in Ni(Salen) crystals.

The open and half-darkened circles shown in Fig. 9 are for the dimers of Cu(Salen) in Ni(Salen) and Cu(Salen)·$CHCl_3$, to which the D_H values estimated and the ξ values taken from the crystal data were assigned, respectively. A closer inspection of these circles with regard to r indicates that the above-mentioned dimers can have their actual r value when $\alpha^2=\approx0.65$ and 0.75 respectively are assumed for them. Both of the α^2 values are smaller than 0.82,[27] which was calculated from the monomer's ESR parameters by the usual method.[25] These small inconsistencies in α^2, however, do not seem significant because all the procedures involved are originally rough. We would like to emphasize here that, in order to get more fruitful results from the dimer ESR spectra, an explicit consideration of the delocalization effect in the simulation is necessary.

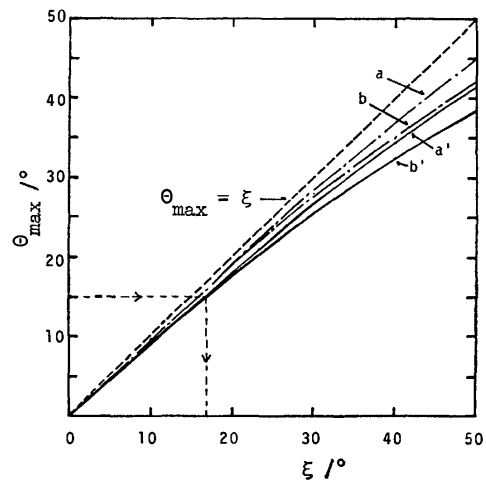

Fig. 10. Dependence of θ_{max} on ξ for $g_{//}=2.19$ and $g_\perp=2.045$.
a, $r=3.8$ Å and $\alpha^2=0.75$; b, $r=3.2$ Å and $\alpha^2=0.75$; a′, $r=3.8$ Å and $\alpha^2=0.65$; b′, $r=3.2$ Å and $\alpha^2=0.65$.

Figure 10 shows the dependence of θ_{max} on ξ, r, and α^2. Apparently, the value of $\Delta\xi=\xi-\theta_{max}$ increases with ξ and decreases with increases in α^2 and r. When each unpaired electron is completely localized on the copper nucleus, θ_{max} is equal to ξ. For a dimer with a considerable delocalization of the unpaired electron, therefore, the ξ value estimated by the use of the point-dipole approximation should approach the θ_{max} value rather than the actual ξ one. As has been described above, the ξ ($\simeq\theta_{max}$) values for the dimers of Cu(Salpn) in xylene and of Cu(3Me-Salpn) in toluene have been estimated to be 15° using the point-dipole approximation. These results suggest that their dimeric structures are similar to that of Cu(Salen) in Ni(Salen) crystals, in which the D_H value has been satisfactorily explained on the assumption of $\alpha^2=0.65$. By applying the case of $\theta_{max}=15°$ and $\alpha^2=0.65$ to Fig. 10, we can estimate $\xi=17°$ for these dimers in solution. Furthermore, by re-plotting their estimated D_H values at $\xi=17°$ as darkened circles in Fig. 9, we can estimate their r values more reliably as ≈3.55 Å. In the same way, $r=\approx3.50$ Å and $\xi=\approx38.5°$ have been estimated for the dimer of Cu(3NO_2-Salibn) in nitroethane. The result of $\xi=17°$ thus re-estimated for the dimers of Cu(Salpn) in xylene

and of Cu(3Me-Salpn) in toluene supports our previous conclusion that these dimers are remarkably different in structure from that of Cu(Salen) in crystals.

The authors are grateful to Professor Masamoto Iwaizumi for his encouragement throughout this work.

References

1) D. Hall, S. V. Sheat, and T. N. Waters, *J. Chem. Soc.*, *A*, **1968**, 460.
2) D. Hall and T. N. Waters, *J. Chem. Soc.*, **1960**, 2644.
3) E. Frasson, R. Bardi, and S. Bezzi, *Acta Crystallogr.*, **12**, 201 (1959).
4) G. J. Palenik, *Acta Crystallogr.*, **17**, 687 (1964).
5) H. Yokoi and T. Isobe, *Bull. Chem. Soc. Jpn.*, **44**, 1446 (1971); *ibid.*, **46**, 447 (1973); H. Yokoi, *ibid.*, **47**, 497 (1974).
6) M. Chikira and T. Isobe, *Bull. Chem. Soc. Jpn.*, **45**, 3006 (1972).
7) M. Chikira and T. Isobe, *Chem. Lett.*, **1974**, 865.
8) H. Yokoi and M. Chikira, *J. Chem. Soc., Dalton Trans.*, **1975**, 2101.
9) J. R. Pilbrow, A. D. Toy, and T. D. Smith, *J. Chem. Soc.*, *A*, **1969**, 1029.
10) P. D. W. Boyd, T. D. Smith, J. H. Price, and J. R. Pilbrow, *J. Chem. Phys.*, **56**, 1253 (1972).
11) A. D. Toy, M. D. Hobday, P. D. W. Boyd, and T. D. Smith, *J. Chem. Soc.*, *A*, **1973**, 1259.
12) M. Chikira, H. Yokoi, and T. Isobe, *Bull. Chem. Soc. Jpn.*, **47**, 2208 (1974).
13) M. Chikira and T. Isobe, *Bull. Chem. Soc. Jpn.*, **48**, 2052 (1975).
14) D. J. Cookson, T. D. Smith, and J. R. Pilbrow, *Bull. Chem. Soc. Jpn.*, **48**, 2832 (1975).
15) T. D. Smith and J. R. Pilbrow, *Coord. Chem. Rev.*, **13**, 174 (1974), and references sited therein.
16) T. Lund and W. E. Hatfield, *J. Chem. Phys.*, **59**, 885 (1973).
17) R. L. Belford, N. D. Chasteen, H. So, and R. E. Tapscott, *J. Am. Chem. Soc.*, **91**, 4675 (1969).
18) J. Owen and E. A. Harris, "Electron Paramagnetic Resonance," ed by S. Geschwind, Plenum Press, New York (1972), p. 436.
19) J. G. M. Van Rens and E. De Boer, *Chem. Phys. Lett.*, **31**, 377 (1975).
20) H. R. Gersmann and J. D. Swalen, *J. Chem. Phys.*, **36**, 3221 (1962).
21) E. N. Baker, D. Hall, and T. N. Waters, *J. Chem. Soc.*, *A*, **1970**, 406.
22) J. A. Riddick and W. B. Bunger, "Organic Solvents," Wiley, New York (1970).
23) L. M. Shkol'nikova, E. M. Yumal', E. A. Shugam, and V. A. Voblikova, *Zh. Strukt. Khim.*, **11**, 886 (1970).
24) A. H. Maki and B. R. McGarvey, *J. Chem. Phys.*, **29**, 31 (1958).
25) D. Kivelson and R. Neiman, *J. Chem. Phys.*, **35**, 149 (1961).
26) The approximate determination of D_H begins by plotting the resonance magnetic field for $\Delta M=1$ transitions against θ. Since $2D_H$ is defined as the maximum difference between two resonance fields at the same θ value, θ_{max}, D_H is graphically determined from the plot. D_2 is generally different from D_H, because $2D_2$ is defined as the difference between the maximum and minimum magnetic fields at different θ values (see Ref. 6).
27) The value of 0.82 is likely to decrease slightly if we regard the α^2 value as the metal orbital population in the anti-bonding molecular orbital occupied by an unpaired electron. See R. S. Mulliken, *J. Chem. Phys.*, **23**, 1833 (1955).

Preparation and Spectroscopic Studies of Four Stereoisomers of Tris[(*S*)-1,3-butanediamine]cobalt(III) Complex

Masaaki KOJIMA and Junnosuke FUJITA

Department of Chemistry, Faculty of Science, Nagoya University, Chikusa, Nagoya 464

(Received June 3, 1977)

Four stereoisomers, *mer*-Δ, *mer*-Λ, *fac*-Δ, and *fac*-Λ, of the tris[(*S*)-1,3-butanediamine]cobalt(III) complex were obtained, and their absorption and circular dichroism spectra were recorded in water in the absence or presence of sulfate ions. The shift of absorption bands and the variation of circular dichroism spectra caused by the addition of sulfate ions seem to be correlated with the conformational instability of six-membered (*S*)-1,3-butanediamine chelate rings in the complexes.

Experimental observations[1-4] indicate that the most stable conformation of the (*S*)(or (*R*))-1,3-butanediamine(*S*(or *R*)-bn) chelate ring is the chair form with an equatorially disposed methyl group. However, a six-membered chelate ring is known to be conformationally flexible and to interchange easily its conformation between two forms, the chair and the skew depending on environment. The *S*(or *R*)-bn chelate ring in the δ(or λ)-skew conformation also has the methyl group in equatorial orientation (see Fig. 2). In a previous paper,[5] we have suggested that the variation of circular dichroism spectra of some cobalt(III) complexes containing (*R*,*R*)-2,4-pentanediamine (*RR*-ptn) in various solvents is closely related with such conformational instability of the six-membered *RR*-ptn chelate ring. The most stable conformation of the *RR*-ptn chelate ring is the λ-skew form in which the two methyl groups are equatorially disposed. In order to compare the effects of a methyl group on the conformational instability of six-membered chelate rings, this paper reports the preparation of four stereoisomers of the $[Co(S\text{-bn})_3]^{3+}$ complex and their absorption and circular dichroism spectra in the absence or presence of sulfate ions. The circular dichroism spectrum of $[Co(NH_3)_4(S\text{-bn})]^{3+}$ is also recorded.

Experimental

Ligand. 1,3-Butanediamine (bn) was prepared by the method of Strack *et al.*[6] and resolved by the method of Balieu *et al.*[7] The $(+)_{589}$-isomer is known to have the *S*-configuration,[7] and its dihydrochloride salt (*S*-bn·2HCl) was used to prepare cobalt(III) complexes.

[Co(NH$_3$)$_4$(S-bn)](ClO$_4$)$_3$. This complex was prepared from $[Co(H_2O)(NH_3)_5](ClO_4)_3$ and *S*-bn·2HCl by a method similar to that for the corresponding (*R*,*R*)-2,4-pentanediamine (*RR*-ptn) complex.[5]

trans-[CoCl$_2$(S-bn)$_2$]Cl. An aqueous solution (50 cm^3) of *S*-bn·2HCl (4.8 g, 30 mmol) was neutralized with Na_2CO_3 (3.1 g, 30 mmol). To this solution was added a solution of $Na_3[Co(NO_2)_6]$ (6.1 g, 15 mmol) in water (40 cm^3), and the mixture was heated at 70 °C for 3 h. The resulting yellow solution was mixed with concd HCl (50 cm^3), and heated at 70 °C for 2 h with occasional stirring to give a reddish violet solution. Green crystals which formed by concentrating the solution to a small volume in a rotary evaporator were filtered off and washed with ethanol. Yield: *ca.* 30%.

Tris(S-bn)cobalt(III) Complex. A suspension of *S*-bn·2HCl (0.4 g, 2.5 mmol) and sodium methoxide (0.22 g, 4 mmol) in methanol (3 cm^3) was added to a solution of *trans*-$[CoCl_2(S\text{-bn})_2]Cl$ (0.69 g, 2 mmol) in DMSO (30 cm^3). The mixture was stirred for a day at room temperature, then diluted with 1 dm^3 of water and passed through an SP-Sephadex column (ϕ 2.7×5 cm). A small portion of the Sephadex charged with the product was loaded on the top of adsorbent layer of an SP-Sephadex column (ϕ 2.7×120 cm), and the adsorbed complexes were developed with a 0.2 M aqueous solution of sodium $(+)_{589}$-tartratoantimonate(III). The column gave three separate bands, I, II, and III in the order of elution, which were *mer*-Δ, *fac*-Δ, and a mixture of *mer*-Λ and *fac*-Λ isomers, respectively. The effluent of the band III was diluted with water and loaded again on an SP-Sephadex column, and the adsorbed band was eluted with a 0.2 M sodium sulfate solution. Two isomers, *fac*-Λ(IIIA) and *mer*-Λ(IIIB) were eluted separately from the column in this order. The formation ratio, *mer*-Δ(I): *fac*-Δ(II): *fac*-Λ(IIIA): *mer*-Λ(IIIB) was 2:1:1:2. Each effluent was reloaded on SP-Sephadex and the isomers were isolated by the following methods.

$(-)_{546}$-mer-Δ-[Co(S-bn)$_3$]Cl$_3$·3H$_2$O and $(-)_{470}$-fac-Λ-[Co(Sbn)$_3$]Cl$_3$·2H$_2$O. The complex adsorbed on SP-Sephadex was eluted with 1.0 M HCl. The effluent was evaporated to

TABLE 1. ANALYTICAL DATA OF THE NEW COMPLEXES

Complex	C/%		H/%		N/%	
	Found	Calcd	Found	Calcd	Found	Calcd
mer-Δ-$[Co(S\text{-bn})_3](ClO_4)_3\cdot 2H_2O$	21.90	21.91	5.90	6.13	12.69	12.78
mer-Δ-$[Co(S\text{-bn})_3]Cl_3\cdot 3H_2O$	29.48	29.79	8.52	8.75	17.39	17.37
fac-Δ-$[Co(S\text{-bn})_3](ClO_4)_3\cdot 2H_2O$	22.12	21.91	5.61	6.13	12.72	12.78
fac-Δ-$[Co(S\text{-bn})_3]Cl_3\cdot 3.5H_2O$	29.16	29.25	8.47	8.79	17.33	17.05
fac-Λ-$[Co(S\text{-bn})_3](ClO_4)_3\cdot H_2O$	22.87	22.53	5.82	5.99	13.23	13.14
fac-Λ-$[Co(S\text{-bn})_3]Cl_3\cdot 2H_2O$	30.66	30.94	8.47	8.66	18.06	18.04
mer-Λ-$[Co(S\text{-bn})_3](ClO_4)_3\cdot 2H_2O$	21.66	21.91	5.86	6.13	12.82	12.78
mer-Λ-$[Co(S\text{-bn})_3]Cl_3\cdot 2H_2O$	31.02	30.94	8.78	8.66	18.27	18.04
$[Co(NH_3)_4(S\text{-bn})](ClO_4)_3$	9.25	9.35	4.67	4.71	16.51	16.36

almost dryness in a vacuum desiccator over P_2O_5 and NaOH. Orange crystals which formed by the addition of ethanol were filtered off and washed with ethanol.

(+)$_{546}$-mer-Λ-[*Co(*S-*bn)*$_3$]$Cl_3 \cdot 2H_2O$. This complex was obtained in a similar way to that for the *mer-Δ* or the *fac-Λ* isomer except that methanol was used for crystallization instead of ethanol.

(+)$_{470}$-fac-Δ-[*Co(*S-*bn)*$_3$]$Cl_3 \cdot 3.5H_2O$. This complex did not crystallize on the addition of common organic solvents to a concentrate of the effluent. Thus the orange residue obtained by evaporating the effluent in a vacuum desiccator was used for measurements.

mer-Δ-, fac-Δ-, *and* mer-Λ-[*Co(*S-*bn)*$_3$]$(ClO_4)_3 \cdot 2H_2O$ *and* fac-Λ-[*Co(*S-*bn)*$_3$]$(ClO_4)_3 \cdot H_2O$. The adsorbed complex was eluted with a 1.5 M sodium perchlorate solution and the effluent was concentrated to a small volume in a rotary evaporator. Orange crystals which formed on cooling the concentrate were filtered off and washed with ethanol.

Other complexes, *mer-* and *fac-*[Co(*meso*-ptn)$_3$]$^{3+}$ were prepared and resolved by the method reported previously.[8]

Table 1 shows the results of chemical analysis.

Measurements. Absorption and circular dichroism spectra were recorded on a Hitachi 323 spectrophotometer, and a JASCO model J-20 spectropolarimeter, respectively. PMR spectra were recorded on a JEOL C-60H spectrometer in D_2O–DCl with DSS (sodium 2,2-dimethyl-2-silapentane-5-sulfonate) as the internal reference.

Results and Discussion

*1. Tetraammine(*S-*bn)cobalt(III) Complex.* As Fig. 1 shows, [Co$(NH_3)_4$(*S*-bn)]$(ClO_4)_3$ in water exhibits extremely weak CD in the region of the d-d absorption bands. Hawkins and Lawrance[2] reported that [Co$(NH_3)_4$(*S*-bn)]$(NO_3)_3 \cdot H_2O$ shows no measurable CD in this region. In general, a tetraammine complex containing an optically active diamine chelate exhibits CD much stronger than that of the *S*-bn complex in the region of the first absorption band, and the sign of a main CD band depends on the conformational chirality of a diamine chelate ring. For example, [Co$(NH_3)_4$(*R*-pn)]$^{3+}$ (*R*-pn=*R*-propylenediamine) gives a positive CD band ($\Delta\varepsilon = +0.33$) at 461 nm, and the *R*-pn chelate ring is assigned to the λ-gauche conformation.[9] The main CD band of [Co$(NH_3)_4$(*RR*-ptn)]$^{3+}$ is rather weak ($\Delta\varepsilon = +0.10$, 490 nm), and the *RR*-ptn chelate ring is suggested to be in equilibrium between the λ-skew and the chair conformations.[5] Accordingly, the weak CD of the *S*-bn complex in water may indicate that the *S*-bn chelate ring exists predominantly in the achiral chair conformation with the equatorial methyl group as suggested by Hawkins and Lawrance.[2] Energy minimization calculation on a hypothetical complex, [$CoCl_4$(*S*-bn)]$^-$ shows that the predominant conformer of the *S*-bn chelate ring is the same chair form.[10]

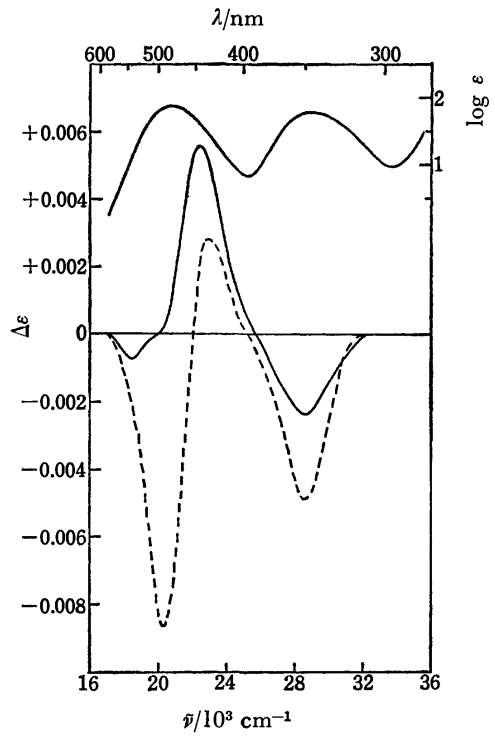

Fig. 1. Absorption and CD spectra of [Co$(NH_3)_4$(*S*-bn)]$(ClO_4)_3$ in water (——) and CD spectrum in 0.2 M Na_2SO_4 (------).

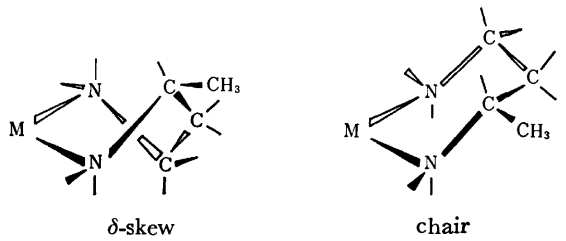

Fig. 2. Possible conformations of six-membered *S*-bn chelate.

The CD spectrum of [Co$(NH_3)_4$(*S*-bn)]$^{3+}$ in water changes remarkably on the addition of Na_2SO_4, as shown in Fig. 1. The sign of the main CD band in the region of the first absorption band is reversed, and the spectral pattern is almost mirror image of that of [Co$(NH_3)_4$(*RR*-ptn)]$^{3+}$ in which the *RR*-ptn chelate ring will be in equilibrium between the λ-skew and the chair conformations as stated previously. Thus, it is suggested that the δ-skew conformation of the *S*-bn chelate ring is stabilized by the addition of Na_2SO_4. Both the chair and the δ-skew conformations have the equatorially disposed methyl group, as shown in Fig. 2. However, the strength of the CD bands is still very weak in the presence of Na_2SO_4. The *S*-bn chelate ring will also exist predominantly in the chair conformation in this solution.

*2. Tris(*S-*bn)cobalt(III) Complexes. a) Characterization of the Isomers*: The tris(*S*-bn)cobalt(III) complex exists in four stereoisomers, *mer-Δ*, *mer-Λ*, *fac-Δ*, and *fac-Λ* (Fig. 3). As Fig. 4 shows, the PMR spectra of the isomers, II and IIIA show only one kind of doublet signal due to the methyl protons, while those of the isomers, I and IIIB give signals indicating the presence of nonequivalent methyl groups. From symmetry argument (*fac*(C_3), *mer*(C_1)), therefore, the isomers, I, II, IIIA, and IIIB can be assigned to *mer*, *fac*, *fac*, and *mer* configurations, respectively.

Figures 5—8 show the CD spectra of all the isomers in water and in 0.2 M Na_2SO_4 solutions. In the region of

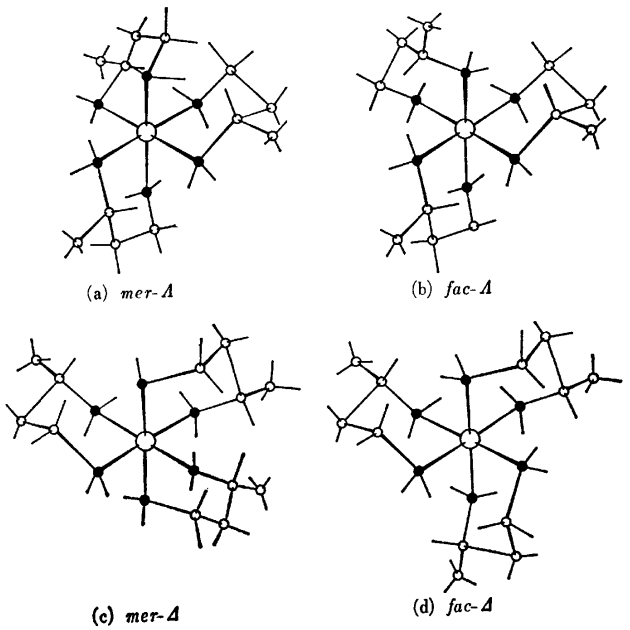

Fig. 3. Schematic structure of tris(*S*-bn)cobalt(III) ions in the chair$_3$ conformer.

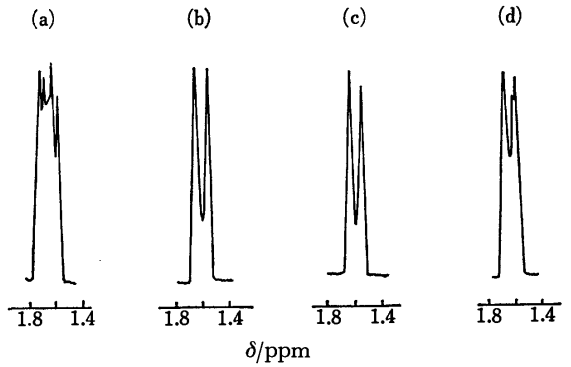

Fig. 4. PMR spectra of the isomers, (a) I(*mer*-Δ), (b) II(*fac*-Δ), (c) IIIA(*fac*-Λ), and (d) IIIB(*mer*-Λ).

the first absorption band, the main CD bands of the isomers, I(*mer*) and II(*fac*) in water have negative sign, while those of the isomers, IIIA(*fac*) and IIIB(*mer*) positive sign. Thus, the former two and the latter two are suggested to have the Δ and Λ configurations, respectively. In the charge transfer region, the isomers, I(*mer*) and II(*fac*) exhibit three CD bands with positive, negative, and positive signs from longer to shorter wavelengths. This pattern coincides with that of Δ-$[Co(tn)_3]^{3+}$ (tn=trimethylenediamine), whose absolute configuration has been determined by X-ray work[11] (Fig. 9). The other isomers, IIIA(*fac*) and IIIB(*mer*) show the same CD pattern in this region, but the signs are reversed. These results lead to the conclusion that the isomers, I, II, IIIA, and IIIB are *mer*-Δ, *fac*-Δ, *fac*-Λ, and *mer*-Λ configurations, respectively. The effect of sulfate ions on the CD spectra will be described later.

b) Absorption Spectra: Table 2 shows that the maxima of the first absorption bands of the four isomers are in the range of 489.5 (20430) to 491 nm (20370

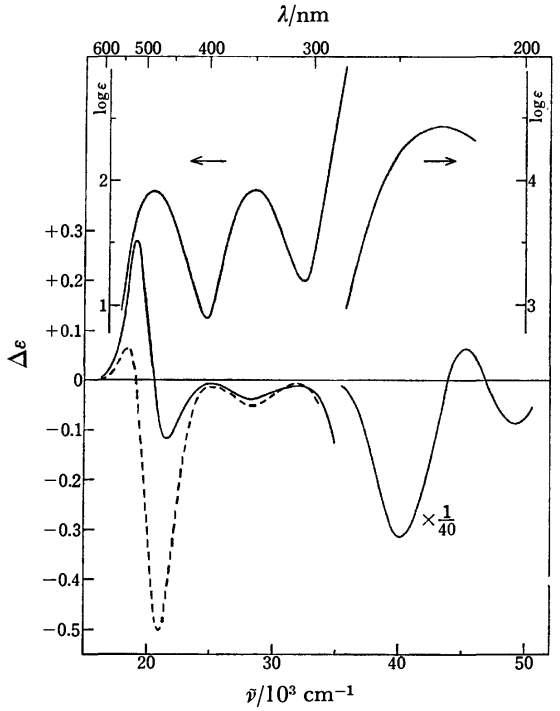

Fig. 5. Absorption and CD spectra of IIIA: *fac*-Λ-[Co(*S*-bn)$_3$]$(ClO_4)_3 \cdot H_2O$; 3.06×10^{-3} M in visible region and 1.88×10^{-4} M in UV region in water (——), and 3.06×10^{-3} M in 0.2 M Na_2SO_4 (------).

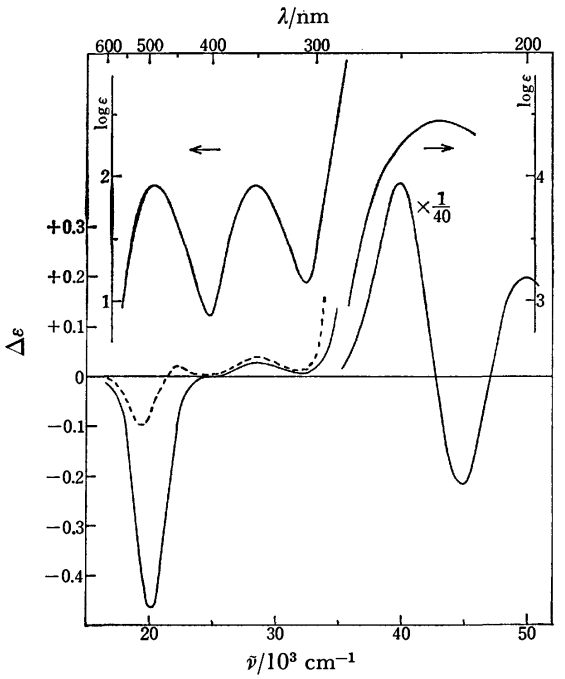

Fig. 6. Absorption and CD spectra of II: *fac*-Δ-[Co(*S*-bn)$_3$]$(ClO_4)_3 \cdot 2H_2O$; 4.02×10^{-3} M in visible region and 1.90×10^{-4} M in UV region in water (——), and 4.02×10^{-3} M in 0.2 M Na_2SO_4 (------).

cm^{-1}). For a complex of six-membered 1,3-diamine, maximum position of the first absorption band seems to depend on the conformation of the diamine; a diamine complex in the skew conformation gives the first absorp-

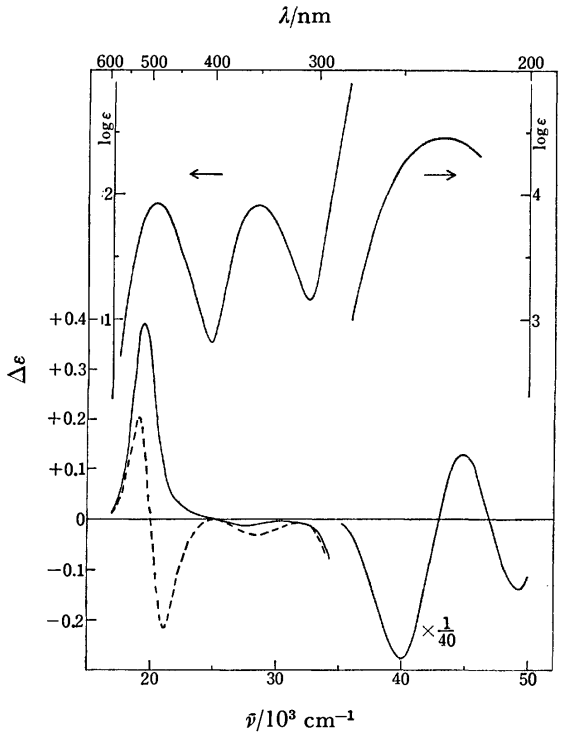

Fig. 7. Absorption and CD spectra of IIIB: *mer*-*Λ*-[Co(*S*-bn)$_3$](ClO$_4$)$_3$·2H$_2$O; 3.08×10^{-3} M in visible region and 1.23×10^{-4} M in UV region in water (——), and 3.08×10^{-3} M in 0.2 M Na_2SO_4 (------).

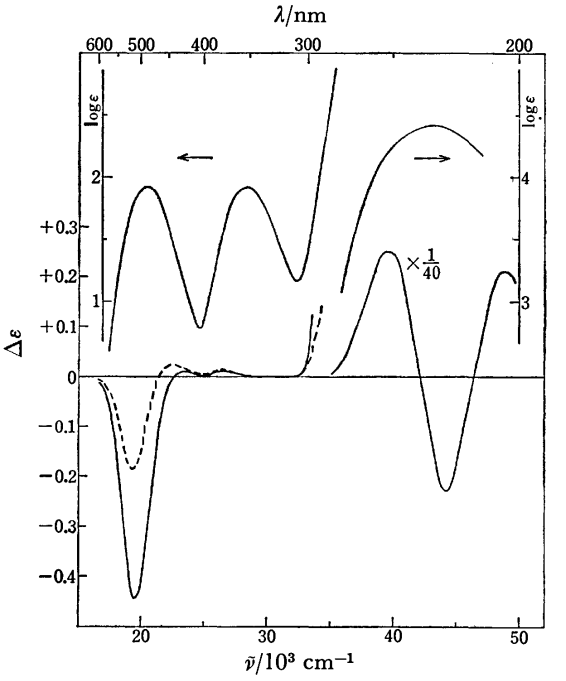

Fig. 8. Absorption and CD spectra of I: *mer*-*Λ*-[Co(*S*-bn)$_3$](ClO$_4$)$_3$·2H$_2$O; 2.82×10^{-3} M in visible region and 1.13×10^{-4} M in UV region in water (——), and 2.82×10^{-3} M in 0.2 M Na_2SO_4 (------).

tion band at a shorter wavelength than that in the chair conformation. For example, *Λ*-[Co(*RR*-ptn)$_3$]$^{3+}$ of which the most stable conformation is the *λ*-skew form exhibits the first absorption band at 482 nm (20750

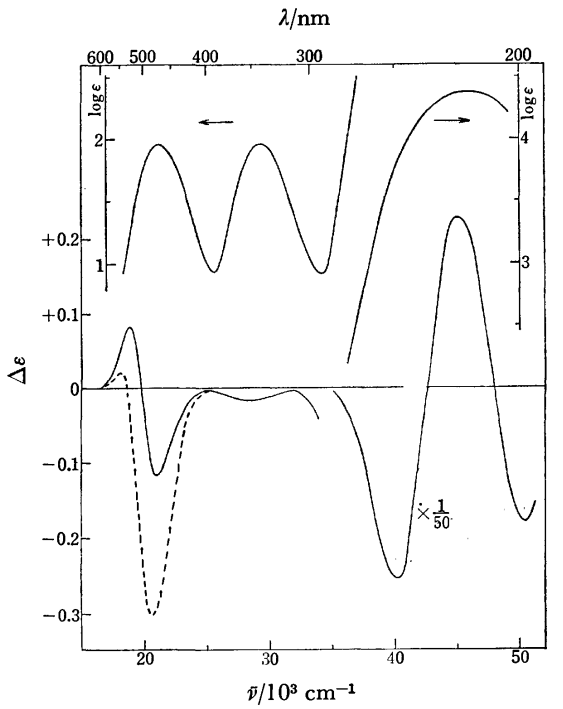

Fig. 9. Absorption and CD spectra of *Λ*-[Co(tn)$_3$](ClO$_4$)$_3$; 5.68×10^{-3} M in visible region and 2.27×10^{-4} M in UV region in water (——), and 5.68×10^{-3} M in 0.2 M Na_2SO_4 (------).

cm^{-1}), while those of *fac*-[Co(*meso*-ptn)$_3$]$^{3+}$ and [Co(tn)$_3$]$^{3+}$ in which the chelate ligands take predominantly the chair conformation are at 491(20370) and 490 nm (20410 cm^{-1}), respectively. Therefore, it is suggested that the *S*-bn chelate rings in all the [Co(*S*-bn)$_3$]$^{3+}$ isomers are intrinsically the most stable in the chair conformation.

The first absorption band of the *fac*-*Λ* isomer (489.5 nm, 20430 cm^{-1}) is a little at a shorter wavelength than that of the *fac*-*Δ* isomer (490.5 nm, 20390 cm^{-1}). It is observed that for a pair of diastereomers, the d-d absorption bands of the one involving more steric interactions lie at longer wavelengths than those of the other.[12] In contrast to such observations, molecular models show that the structure of the *fac*-*Λ* isomer (489.5 nm) seems to be a little more crowded than that of the *fac*-*Δ* isomer (490.5 nm), because the three methyl groups of the former in the chair conformation are disposed so as to concentrate around the C_3 axis of the complex ion (Fig. 3). The observed difference in the peak positions between the two *fac* isomers may be related with conformational instability of the chelate rings in solution. As stated previously, the *δ*-skew conformation of a *S*-bn chelate ring also has the equatorially disposed methyl group. When the *S*-bn chelate ring forms the *δ*-skew conformation, the *fac*-*Λ* isomer results in the *lel*$_3$(*Λ*(*δδδ*)) structure, while the *fac*-*Δ* isomer the *ob*$_3$(*Δ*(*δδδ*)) one. Since the *ob*$_3$ conformer has been calculated by conformational analysis to have a substantially higher energy,[13] the chelate rings in only the *fac*-*Λ* isomer could interchange between the chair and the *δ*-skew conformations, and the complex would be in equilibrium between these two conformers.

TABLE 2. ABSORPTION AND CD SPECTRAL DATA

Complex	Absorption log ε ($\bar{\nu}_{max}$/cm^{-1})	CD $\Delta\varepsilon$ ($\bar{\nu}$/cm^{-1})	Concentration C/M
mer-*Λ*-$[Co(S\text{-bn})_3](ClO_4)_3\cdot 2H_2O$	1.92 (20370)	−0.446 (19530)	2.82×10^{-3}
		+0.012 (23310)	
	1.92 (28400)	+0.011 (26670)	
	4.41 (42900)	+10 (39500)	1.13×10^{-4}
		−9.3 (44100)	
		+8.3 (48800)	
mer-*Λ*-$[Co(S\text{-bn})_3]Cl_3\cdot 3H_2O$	1.92 (20370)	−0.411 (21530)	4.18×10^{-3}
		+0.014 (23260)	
	1.92 (28400)	+0.014 (26300)	
	4.42 (42900)	+10 (39500)	1.67×10^{-4}
		−8.9 (44600)	
		+8.7 (49800)	
fac-*Λ*-$[Co(S\text{-bn})_3](ClO_4)_3\cdot 2H_2O$	1.93 (20390)	−0.461 (19900)	4.02×10^{-3}
	1.93 (28400)	+0.040 (28600)	
	4.45 (43000)	+12 (39700)	1.90×10^{-4}
		−7.6 (44800)	
		+6.1 (50000)	
fac-*Λ*-$[Co(S\text{-bn})_3]Cl_3\cdot 3.5H_2O$	1.93 (20390)	−0.374 (19840)	3.51×10^{-3}
	1.93 (28400)	+0.021 (28500)	
	4.46 (43000)	+12 (39700)	1.82×10^{-4}
		−7.4 (44800)	
		+6.4 (50000)	
fac-*Λ*-$[Co(S\text{-bn})_3](ClO_4)_3\cdot 2H_2O$	1.93 (20430)	+0.266 (19080)	3.06×10^{-3}
		−0.105 (21510)	
	1.94 (28400)	−0.037 (28300)	
	4.43 (43100)	−12 (40200)	1.88×10^{-4}
		+1.6 (45200)	
		−4.1 (49300)	
fac-*Λ*-$[Co(S\text{-bn})_3]Cl_3\cdot 2H_2O$	1.93 (20430)	+0.216 (19050)	4.18×10^{-3}
		−0.220 (21280)	
	1.92 (28400)	−0.040 (28600)	
	4.41 (43100)	−12 (40200)	1.68×10^{-4}
		+1.8 (45200)	
		−3.9 (49300)	
mer-*Λ*-$[Co(S\text{-bn})_3](ClO_4)_3\cdot 2H_2O$	1.92 (20430)	+0.394 (19380)	3.08×10^{-3}
	1.91 (28410)	−0.013 (27800)	
	4.45 (43100)	−11 (39800)	1.23×10^{-4}
		+5.0 (44600)	
		−5.5 (49500)	
mer-*Λ*-$[Co(S\text{-bn})_3]Cl_3\cdot 2H_2O$	1.92 (20430)	+0.361 (19340)	4.45×10^{-3}
	1.91 (28410)	−0.011 (28200)	
	4.45 (43100)	−11 (40000)	1.71×10
		+4.2 (44600)	
		−5.9 (49500)	
$[Co(NH_3)_4(S\text{-bn})](ClO_4)_3$	1.83 (20860)	−0.00071 (18520)	1.76×10^{-2}
		+0.0056 (22520)	
	1.78 (29200)	−0.0024 (28400)	
	4.35 (48300)	not detected	

The formation of the skew conformer causes shift in the first absorption band to a shorter wavelength as stated previously. The fact that the first absorption band of the more crowded *fac*-*Λ* isomer is at a shorter wavelength than that of the less crowded *fac*-*Δ* isomer may be accounted for by such a conformational equilibrium of the *S*-bn chelate ring.

In the presence of Na_2SO_4 (0.5 M), the first absorption band of the *fac*-*Λ* isomer shifts a little, but more than 1 nm to a shorter wavelength. The *fac*-*Δ* isomer also shows such a band shift toward a shorter wavelength under the same condition, but the magnitude of shift is very small (less than 0.5 nm). In the presence of sulfate ions, the $lel_3(\Lambda(\delta\delta\delta))$ conformer may be stabilized by ion-pair formation between the complex cation and the sulfate ion, and the first absorption band shifts further to a shorter wavelength owing to the increasing amount of the δ-skew conformer. For a tris-diamine

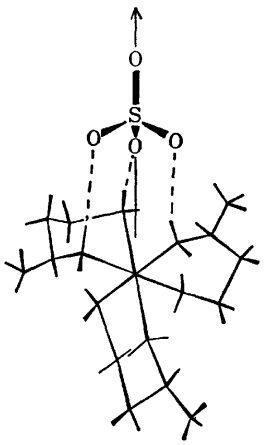

Fig. 10. A proposed structure of the ion-pair between *fac*-Δ(chair$_2\delta$(*ob*))-[Co(*S*-bn)$_3$]$^{3+}$ and SO_4^{2-}.

complex, the *lel*$_3$ conformer is known to have the most effective structure in forming an ion-pair through hydrogen bonding between the amino protons and the sulfate ion.[5] The [Co(tn)$_3$]$^{3+}$ complex of which the conformational behavior is expected to resemble that of the *fac*-Λ isomer also shows a similar shift (*ca.* 1 nm) in the first absorption band on the addition of sulfate ions. The *fac*-Δ isomer could not form the *lel*$_3$(Δ($\lambda\lambda\lambda$)) conformer without difficulty, because the λ-skew conformation has the axial methyl group. However, the first absorption band of this isomer also shifts a little to a shorter wavelength in the presence of sulfate ions. If it is assumed that such a shift is caused by the formation of a certain conformer involving the δ-skew form stabilized by an ion-pair with the sulfate ion, the most probable conformer will be of *fac*-Δ(chair$_2\delta$(*ob*)) form as shown in Fig. 10. This conformer has a set of three N–H bonds provided by two *S*-bn chelate ligands, one being in the chair and the other in the δ-skew conformation. These N–H bonds are parallel to an axis as shown in Fig. 10, and the complex may form an ion-pair in a similar way with the oxoanions such as sulfate ion through hydrogen bonding. The increase in the amount of the *fac*-Δ(chair$_2\delta$(*ob*)) conformer in the presence of sulfate ions may cause shift similarly to a shorter wavelength in the first absorption band of the *fac*-Δ isomer.

The first absorption bands of the *mer*-Δ (491 nm, 20370 cm^{-1}) and the *mer*-Λ (489.5 nm, 20430 cm^{-1}) isomers are at nearly the same wavelengths as those of the corresponding *fac* isomers, respectively (Table 2). If all of the *S*-bn chelate rings adopt the chair conformation, these *mer* isomers will be more crowded and strained than the *fac* isomers, since the two chelate rings in each *mer* isomer approach very close to each other. For [Co(*meso*-ptn)$_3$]$^{3+}$ in which the *meso*-ptn chelate rings are expected to be very stable in the chair conformation, the first absorption band of the more crowded *mer* isomer is at longer wavelengths by 2 nm than that of the less crowded *fac* isomer.[8] The fact that both Δ- and Λ-isomers of the *mer*-[Co(*S*-bn)$_3$]$^{3+}$ complex exhibit the first absorption bands at nearly the same wavelengths as those of the *fac* isomers may indicate that one of the two close *S*-bn chelate ligands in each *mer* isomer prefers to take the δ-skew conformation to reduce interactions between the ligands. The chair$_2\delta$ conformer will give the first absorption band at a shorter wavelength than that expected for the chair$_3$ conformer. The difference in the absorption maxima of the two *mer* isomers may be interpreted by the difference in the structures of the isomers. In the *mer*-Λ isomer, two methyl groups on the two close *S*-bn chelate rings are disposed away from each other (*exo* form), while those in the *mer*-Δ isomer come near to each other (*endo* form) (Fig. 3). The *endo-mer*-Δ isomer should be more crowded, and gives the first absorption band (491 nm) at a longer wavelength compared with that of the other *exo- mer*-Λ isomer (489.5 nm). Furthermore, the latter isomer can also form the *lel*$_3$(Λ($\delta\delta\delta$)) conformer, the first absorption band of which will be at a shorter wavelength than those of the other conformers involving the chair conformation.

On the addition of sulfate ions, the first absorption bands of both the *mer*-Δ and -Λ isomers shift to a shorter wavelength, the latter (*ca.* 1 nm) showing larger shift than the former (*ca.* 0.5 nm). These band shifts may be caused by a mechanism similar to that described for the *fac* isomers. The *mer*-Λ isomer can form the *lel*$_3$(Λ($\delta\delta\delta$)) conformer suitable for ion-pair formation with the sulfate ion. On the other hand, the *mer*-Δ isomer in the Δ(chair$_2\delta$(*ob*)) conformation can provide a set of three N–H bonds in a similar manner to that of the *fac*-Δ isomer in the same conformation. These conformers will be stabilized by ion-pair formation with sulfate ions, and give the first absorption bands at shorter wavelengths than those in the absence of sulfate ions.

c) Circular Dichroism Spectra. The CD patterns of all the isomers of [Co(*S*-bn)$_3$]$^{3+}$ in water satisfy the known relationship between the absolute configuration and the CD sign, if our assignments were correct. However, the additive law for the configurational and the vicinal effects does not hold for the present diastereomeric isomers. For example, the CD spectra of the *fac*-Δ and -Λ isomers are not mirror image of each other, although the CD spectrum of [Co(NH$_3$)$_4$(*S*-bn)]$^{3+}$ shows that the vicinal effect of the *S*-bn chelate ligand is negligible. This result also indicates that the complexes are in equilibrium among some conformers and that the conformational equilibrium of one complex is different from those of the other complexes. In a previous paper,[5] we have reported that the CD spectra of conformationally flexible complexes such as Δ-[Co(*RR*-ptn)$_3$]$^{3+}$ or Δ(or Λ)-[Co(tn)$_3$]$^{3+}$ are remarkably affected by the vicinal effect of chelate rings in a certain conformation stabilized by ion-pair formation between a complex ion and its counter ion. The *fac*-Λ-[Co(*S*-bn)$_3$]$^{3+}$ isomer seems to be the case. In the region of the first absorption band, the CD spectrum of the complex chloride in water shows a clear dependence on the concentration, as shown in Fig. 11. The complex perchlorate exhibits no such dependence in the concentration range of 3.25×10^{-2} to 3.15×10^{-4} M. In the presence of sulfate ions, the negative CD component at a shorter wavelength is considerably enhanced (Fig. 5). Such features quite resemble those observed for Λ-[Co(tn)$_3$]$^{3+}$, indicating that the CD variation is brought about by the vicinal effect of the δ-skew conformer of the *S*-bn chelate ring

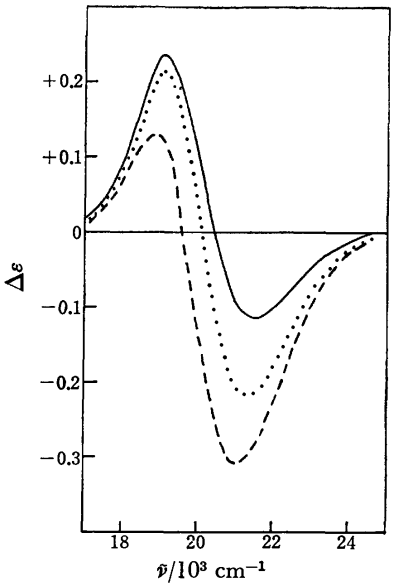

Fig. 11. Dependence of CD of *fac*-*Λ*-[Co(*S*-bn)$_3$]Cl$_3$·2H$_2$O on its concentration in water: 4.21×10^{-4} M (——), 4.18×10^{-3} M (……), and 4.17×10^{-2} M (-----).

stabilized by ion-pair formation. The vicinal effect of the *δ*-skew conformation is known to exhibit negative CD in this region. Therefore, it can be concluded that the *fac*-*Λ* isomer is conformationally flexible and is in equilibrium between the chair$_3$ and the *lel*$_3$(*Λ*(*δδδ*)) conformers. This conclusion coincides with that obtained from the study of absorption spectra.

In contrast to the *fac*-*Λ* isomer, the other three complex chlorides show little dependence on the concentration, the CD patterns in the region of the first absorption band remaining unchanged; *fac*-*Δ*$=-0.37$ (3.54×10^{-4} M)——0.30 (3.66×10^{-2} M): *mer*-*Λ*$=0.38$ (3.13×10^{-4} M)—0.34 (3.12×10^{-2} M): *mer*-*Δ*$=-0.42$ (4.00×10^{-4} M)——0.39 (2.72×10^{-2} M). Since the ability of these isomers to form ion-pairs with chloride ions will not differ greatly from that of the *fac*-*Λ* isomer, the result indicates that these isomers are not stabilized in particular conformers by ion-pair formation with chloride ions. The isomers may be less conformationally flexible than the *fac*-*Λ* isomer as claimed in the previous discussion. In the presence of sulfate ions, however, these three isomers change the CD patterns remarkably (Figs. 6—8). Of these CD changes, that of the *mer*-*Λ* isomer is similar to the CD change of the *fac*-*Λ* isomer. Each of these *Λ* isomers in the presence of sulfate ions gives a strong negative CD band at the expense of the positive CD band. As stated previously, the *mer*-*Λ* isomer could also form the *lel*$_3$(*Λ*(*δδδ*)) conformer. The oxoanions such as sulfate ion may induce the conformational change of rather crowded, rigid chelate rings by forming strong hydrogen bonds with the amino protons of the complex. Thus, the *mer*-*Λ* isomer in the presence of sulfate ions may be stabilized in the *lel*$_3$(*Λ*(*δδδ*)) conformer.

On the other hand, both *mer*- and *fac*-isomers of the *Δ* configuration in the presence of sulfate ions diminish considerably the strength of the main CD bands, but show no marked increase in the CD bands with the reversed sign as observed in the *Λ*-isomers (Figs. 6 and 8). According to the previous discussion, the decrease in the negative CD strength indicates the formation of chelate rings with the *λ*-skew conformation. However, this indication seems to be unlikely, since the *λ*-skew conformer has the axial methyl group. A similar CD variation is seen in the spectra of *mer*- and *fac*-*Λ*(or *Δ*)-[Co(*meso*-ptn)$_3$]$^{3+}$ on the addition of sulfate ions, as shown in Figs. 12 and 13. The conformation of the *meso*-

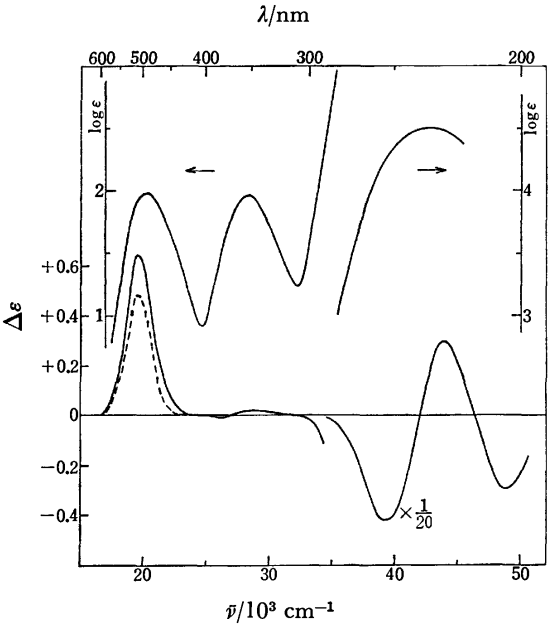

Fig. 12. Absorption and CD spectra of *mer*-*Λ*-[Co(*meso*-ptn)$_3$](ClO$_4$)$_3$·2H$_2$O; 2.89×10^{-3} M in visible region and 1.16×10^{-4} M in UV region in water (——), and 2.89×10^{-3} M in 0.2 M Na$_2$SO$_4$ (------).

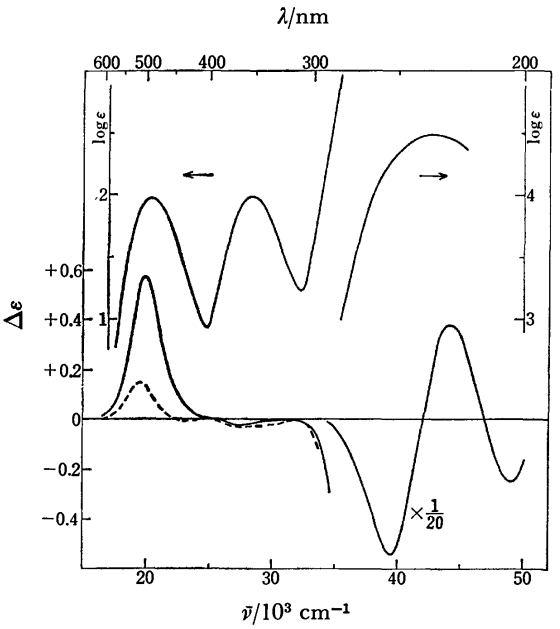

Fig. 13. Absorption and CD spectra of *fac*-*Λ*-[Co(*meso*-ptn)$_3$](ClO$_4$)$_3$·2H$_2$O; 3.11×10^{-3} M in visible region and 3.46×10^{-4} M in UV region in water (——), and 3.11×10^{-3} M in 0.2 M Na$_2$SO$_4$ (------).

ptn chelate ring is expected to be very stable in the chair form. The CD patterns of these *S*-bn and *meso*-ptn complexes in the presence of sulfate ions somewhat differ from those of the *Λ* isomers of *S*-bn and tn complexes in the same condition. In the latter two *Λ* isomers, the enhancement of one CD component seems to be accompanied with the diminution of the other CD component, and the total strength of the two CD components does not seem to change greatly. On the other hand, the former *S*-bn and *meso*-ptn complexes diminish the total CD strength. Such a difference in the CD variations can not be explained at present, but may also be related with the conformational instability of chelate rings in the complexes. The complexes, *mer-Δ*, *fac-Δ*-$[Co(S\text{-bn})_3]^{3+}$, *mer-Λ*-, and *fac-Λ*-$[Co(meso\text{-ptn})_3]^{3+}$ which diminish the total CD strength in the presence of sulfate ions will have more crowded, rigid structures compared with those of *fac-Λ*-$[Co(S\text{-bn})_3]^{3+}$ and *Λ*-$[Co(tn)_3]^{3+}$. For these crowded complexes, the CD variation of the more crowded *mer-Λ*-$[Co(meso\text{-ptn})_3]^{3+}$ is smaller than that of the corresponding less crowded *fac-Λ* isomer. A similar relation is seen between the *mer-Δ* and the *fac-Δ* isomers. The crowded, rigid $\Lambda(ob_3)$-$[Co(RR\text{-ptn})_3]^{3+}$ complex shows little variation in the CD spectra in various solvents.[5] These observations strongly suggest that the CD variations observed for both *Δ*-$[Co(S\text{-bn})_3]^{3+}$ and $[Co(meso\text{-ptn})_3]^{3+}$ are also closely related to the conformational instability of the six-membered chelate rings.

References

1) A. Pajunen, K. Smolander, and I. Belinskij, *Suom. Kemistil. B*, **45**, 317 (1972).
2) C. J. Hawkins and G. A. Lawrance, *Aust. J. Chem.*, **26**, 2401 (1973).
3) M. Parris, L. J. DeHayes, and D. H. Busch, *Can. J. Chem.*, **50**, 3569 (1972).
4) T. G. Appleton and J. R. Hall, *Inorg. Chem.*, **10**, 1717 (1971).
5) M. Kojima, M. Fujita, and J. Fujita, *Bull. Chem. Soc. Jpn.*, **50**, 898 (1977).
6) E. Strack and H. Schwaneberg, *Ber.*, **67**, 39 (1934).
7) E. Balieu, P. M. Boll, and E. Larsen, *Acta Chem. Scand.*, **23**, 2191 (1969).
8) M. Kojima and J. Fujita, *Chem. Lett.*, **1976**, 429.
9) K. Ogino, K. Murano, and J. Fujita, *Inorg. Nucl. Chem. Lett.*, **4**, 351 (1968).
10) L. J. DeHayes and D. H. Busch, *Inorg. Chem.*, **12**, 1505 (1973).
11) R. Nagao, F. Marumo, and Y. Saito, *Acta Crystallogr., Sect. B*, **29**, 2438 (1973).
12) F. Mizukami, H. Ito, J. Fujita, and K. Saito, *Bull. Chem. Soc. Jpn.*, **45**, 2129 (1972).
13) S. R. Niketic and F. Woldbye, *Acta Chem. Scand.*, **27**, 621 (1973).

Preparation and Properties of Pd(II) and Pt(II) Complexes of *N*-Picolinoyl-*S*,*S*-tetramethylenesulfilimine, *N*-Trimethylammoniopicolinamidate, and Related Ylides

Hideo KISE, Hiroyuki ENDŌ, and Manabu SENŌ

Institute of Industrial Science, The University of Tokyo, Roppongi, Minato-ku, Tokyo 106

(Received June 11, 1977)

The reactions of *N*-picolinoyl-*S*,*S*-tetramethylenesulfilimine and *N*-trimethylammoniopicolinamidate with dichlorobis(benzonitrile)palladium(II) and dipotassium tetrachloroplatinate(II) afforded chelate complexes of formula MCl_2[Ylide]. The structures of the complexes were examined by IR and NMR spectroscopy, and determined as mononuclear complexes with ligands coordinated through two nitrogen atoms. A reverse relationship between pK_a values of the ylides and C=O stretching band frequency shifts on complex formation was found, and the nature of the coordination *via* ylidic nitrogen was discussed in terms of σ- and π-character of the ligands in the chelate complexes and several related bis-ylide complexes.

Carboxylic acid amides are anbidentate ligands and have potential coordination sites of nitrogen and carbonyl oxygen atoms. In most cases, they form complexes with a variety of Lewis acids *via* carbonyl oxygen in neutral media.[1] In alkaline media, however, amides liberate the hydrogen and form neutral complexes through anionic nitrogen atoms.[2] In the case of picolinamides, both cationic and neutral chelate complexes with transition metals were prepared and characterized;[3] the former has coordination through nitrogen and oxygen atoms, while the latter has coordination through two nitrogen atoms (**1** and **2**).

In this paper we describe a novel type of Pd(II) and Pt(II) complexes of sulfilimine (S–N ylide) and aminimide (N–N ylide) with picolinoyl group on ylidic nitrogen (**3** and **8**). These ylides have a close similarity to picolinamide anions in that they are bidentate *via* nitrogen atom in pyridine ring and anionic nitrogen with charge delocalized over adjacent carbonyl group. In contrast to amide anions, they are stable enough to be prepared and isolated by known procedures, and this would make it possible to elucidate directly the change in electronic state of the ligands upon complex formation. In addition, while each of the ylides has an anionic center, it has ammonium or sulfonium moiety adjacent to the ylidic nitrogen, and hence is a neutral molecule as a whole. The effect of the positively charged group on complex formation would be an interesting problem to examine.

An increasing number of reports have been published on metal–ylide complexes.[4] Many of them describe reactions of metal carbonyl with ylides,[5] and direct formation of metal–carbon bonds by reactions of metal salts with stable[6] and unstable[7] phosphorus and sulfur ylides. Several papers also describe the formation of metal complexes of sulfilimines and aminimides,[8] but chelate complexes of these ylides have not been reported so far except *ortho*-metallated *N*-(1-pyridinio)benzamidate complexes of transition metals.[9]

Results and Discussion

Preparation of Complexes. The complex formation of the ylides **3** and **8** occurred smoothly with dichlorobis(benzonitrile)palladium(II) in ethanol and with dipotassium tetrachloroplatinate(II) in water at room temperature. In all cases, the complexes were isolated as yellow or orange-yellow precipitates. The Pd(II) complexes were also prepared by reactions with disodium tetrachloropalladate(II) in ethanol or with dichloro(1,5-cyclooctadiene)palladium(II) in acetone, giving the same products as described above. The elemental analyses revealed that the complexes have equimolar compositions of MCl_2 (M=Pd or Pt) and ylides (Table 1), suggesting chelate structures for these complexes. *N*-Benzoyl- and *N*-acetylsulfilimines and aminimides formed complexes with two ylide molecules per metal atom (bis-ylide complexes). The thermal stability of the bis-ylide complexes is somewhat lower than that of the chelate complexes.

In the case of bidentate ligands, **3** and **8**, the reactions were carried out at the mole ratio of metal salt to ligand of 1 : 1 and 1 : 2, but no differences in the yield and spectroscopic properties of the products were observed. This indicates that the coordinating nitrogen atoms in the chelate complexes are not replaced by another ligand molecules, suggesting that the chelate formation is favored not only entropically but also energetically, resulting in the formation of stronger coordination bonds than those of bis-ylide complexes.

Structure of Complexes. The sulfilimines and aminimides used as ligands have an ambidentate character with resonance structures such as shown in **3a**—**c** and **8a**—**b**. The difference between a sulfilimine and an aminimide is that the former has dπ-pπ interaction between sulfur and ylide nitrogen, making the S–N bond length shorter than ordinary single bond length,[10] while the latter does not have such interaction; the single bond character of N–N linkage and shortening of N–C(carbonyl) bond have been proved by X-ray analysis.[11] These ylides form stable sulfonium and ammonium salts by treatment with aqueous HCl in acetone except for **3** and **8**, whose HCl salts were not isolated. The IR spectral data of these ylides and salts are collected in Table 2. It is evident that the ylides have large contribution from the enolate form structures such as **3c** and **8b**, as manifested by low carbonyl stretching frequencies similar to those of carboxylate ions. The C=O bands shift as much as 105—160 cm^{-1} to higher frequencies, while the C=N stretching bands shift down from 1290—1350 to 1220—1274 cm^{-1} in going from ylides to their salts,[12] indicating that

Table 1. Melting points and elemental analyses of complexes

Complex		Mp(°C)	Found %			Calcd %		
			C	H	N	C	H	N
$PdCl_2[(CH_2)_4S{=}NCOC_5H_4N]$	**14**	216—217(d)	30.66	3.16	7.12	31.15	3.14	7.27
$PtCl_2[(CH_2)_4S{=}NCOC_5H_4N]$	**15**	185—188(d)	25.10	2.62	5.85	25.32	2.56	5.91
$PdCl_2[(CH_2)_4S{=}NCOC_6H_5]_2$	**16a**	168—170(d)	44.76	4.57	5.15	44.64	4.44	4.73
$PdCl_2[(CH_2)_4S{=}NCOC_6H_4CH_3$-*p*$]_2$	**16b**	181—182(d)	46.91	4.34	4.52	46.49	4.89	4.52
$PdCl_2[(CH_2)_4S{=}NCOC_6H_4Cl$-*p*$]_2$	**16c**	168—169(d)	40.91	3.58	5.04	40.00	3.67	4.24
$PdCl_2[(CH_2)_4S{=}NCOCH_3]_2$	**17**	198—200(d)	30.69	4.85	6.54	30.81	4.75	5.99
$PdCl_2[(CH_3)_3\overset{+}{N}\text{–}\bar{N}COC_5H_4N]$	**18**	219—220(d)	30.03	3.68	11.45	30.32	3.68	11.78
$PtCl_2[(CH_3)_3\overset{+}{N}\text{–}\bar{N}COC_5H_4N]$	**19**	196—197(d)	23.27	2.88	8.70	24.28	2.95	9.44
$PdCl_2[(CH_3)_3\overset{+}{N}\text{–}\bar{N}COC_6H_5]_2$	**20**	210—211(d)	44.25	5.13	10.22	45.00	5.30	10.50
$PdCl_2[(CH_3)_3\overset{+}{N}\text{–}\bar{N}COCH_3]_2$	**21**	207—208(d)	27.70	6.57	14.18	29.32	5.92	13.68
$Pd[(CH_3)_2N\bar{N}COC_5H_4N]_2$	**22**	262—263	44.16	4.71	19.94	44.19	4.65	19.33
$PdCl_2[(CH_2)_4S{=}NCOC_6H_5]PPh_3$	**24**	193—195	53.82	4.28	2.13	53.84	4.37	2.17
$PdCl_2[(CH_2)_4S{=}NCOCH_3]PPh_3$	**25**	208—210	49.35	4.44	2.31	49.29	4.49	2.40

Table 2. IR data of sulfilimines, aminimides, and their salts (cm^{-1})

Compound		C=O st.	Aromatic ring st.	C–N st.	S–N st.	Aromatic C–H def.
$(CH_2)_4S{=}NCOC_5H_4N$	**3**	1547	1587	1330	785	750
$(CH_2)_4S{=}NCOC_6H_5$	**4a**	1527	1590	1335	780	780, 720
$(CH_2)_4\overset{+}{S}\text{–}NHCOC_6H_5$ Cl^-	**5a**	1674	1595	1246	—	784, 690
$(CH_2)_4S{=}NCOC_6H_4CH_3$-*p*	**4b**	1540	1590	1335	800	843
$(CH_2)_4\overset{+}{S}\text{–}NHCOC_6H_4CH_3$-*p* Cl^-	**5b**	1645	1609	1260	—	840
$(CH_2)_4S{=}NCOC_6H_4Cl$-*p*	**4c**	1536	1587	1336	795	846
$(CH_2)_4\overset{+}{S}\text{–}NHCOC_6H_4Cl$-*p* Cl^-	**5c**	1683	1594	1253	—	846
$(CH_2)_4S{=}NCOCH_3$	**6**	1540	—	1290	788	—
$(CH_2)_4\overset{+}{S}\text{–}NHCOCH_3$ Br^-	**7**	1700	—	1220	—	—
$(CH_3)_3\overset{+}{N}\text{–}\bar{N}COC_5H_4N$	**8**	1560	1605	1350	—	750
$(CH_3)_3\overset{+}{N}\text{–}\bar{N}COC_6H_5$	**9**	1560	1600	1334	—	726
$(CH_3)_3\overset{+}{N}\text{–}NHCOC_6H_5Cl^-$	**10**	1692	1598	1272	—	705
$(CH_3)_3\overset{+}{N}\text{–}\bar{N}COCH_3$	**11**	1575	—	1335	—	—
$(CH_3)_3\overset{+}{N}\text{–}NHCOCH_3$ Cl^-	**12**	1695	—	1274	—	—
$(CH_3)_2N\text{–}NHCOC_5H_4N$	**13**	1675	1587	1306	—	740

protonation occurred at ylidic nitrogen to form salts such as **5** and **10**.

As shown in Table 3, the C=O bands of the ylides shift to higher frequencies on complex formation, and this seems to indicate that coordination to metal occurs through ylidic nitrogen. In view of the Pd–Cl stretching bands of Pd(II) complexes, there seems to be two groups of complexes; one includes **16a—c, 24,** and **25** which have only one Pd–Cl absorption band at 323—345 cm^{-1}, and another one includes **14, 17, 18, 20,** and **21** which have two Pd–Cl bands at 327—331 and 346—368 cm^{-1}. The former is considered to have *trans*-configuration and the latter has *cis*-configuration around the Pd atom.

In the case of picolinoyl ylides **3** and **8**, the absorption bands due to in-plane deformation of pyridine ring[3f] appear at 615 and 623 cm^{-1} respectively, and these bands shift to higher frequencies (655—665 cm^{-1}) on complex formation. Furthermore, the lack of IR bands characteristic of the bridging M–Cl–M stretching mode that would be expected below 300 cm^{-1} rules out binuclear structures.[13] These and analogous considerations on the Pt(II) complexes, **15** and **19**, lead to the conclusion that the structures of **14, 15, 18,** and **19** are best represented by **A** and **B** in Fig. 1. In the NMR spectrum of **18**, protons of the pyridine ring, as well as protons of methyl groups, show down field shift in comparison with the free ligand **8**, and this also implies the chelate ring formation through two nitrogen atoms.

One of the structurally related Pd(II) complexes of picolinamides is shown in Fig. 1 (**C**).[3f] In this case, the amide groups coordinate to metal *via* anionic nitrogens, forming a 1 : 2 metal-amide complex. The C=O band of the complex **C** appears at 1625 cm^{-1} which

TABLE 3. IR DATA OF COMPLEXES (cm^{-1})[a]

Complexe	C=O st.	Aromatic ring st.	C–N st.	Aromatic C–H def.	Pyridine[b] def.	M–Cl	Δ_1	Δ_2	Δ%	pK_a
14[c]	1665	1605	1316	762	655	346, 329	29	118	80	(2.62)
15[c]	1665	1605	1310	752	665	342, 327	29	118	80	(2.62)
16a	1625	1578	1282	776, 712	—	323, 300	49	100	67	2.62
16b	1595	1606	1320	835	—	325	50	55	52	2.72
16c	1595		1310	843	—	328	88	59	40	
17	1594	—	1316	—	—	368, 328	106	54	34	3.45
18[d]	1655	1600	1326	762	656	356, 328	37	95	72	4.42
19[d]	1656	1610		757	656	308, 302	36	96	73	4.42
20	1610	1596	1340	755, 696	—	362, 327	82	50	38	4.40
21	1600	—	1327	—	—	361, 331	95	25	21	5.48
22	1626, 1598[e]		1345	762	—	—				
24	1605	1574	1322	724, 687	—	340	69	78	53	2.62
25	1604	1585	1298	—	—	345	96	64	38	3.45
f)	1625		—				35	101	74	7.75
g)	1630	1580	—	750, 695	—	330	50	122	71	8.10

a) Δ_1 and Δ_2 are C=O frequency differences between salts and complexes, and between complexes and ylides, respectively. Δ% is $\Delta_2/(\Delta_1+\Delta_2)\times 100$. b) Pyridine in plane deformation band.[3f] In free ligands this bands appear near 615 cm^{-1}. c) Values of Δ were calculated using $\nu_{C=O}=1694\ cm^{-1}$ for the salt of **3**. d) Values of Δ were calculated using $\nu_{C=O}=1692\ cm^{-1}$ for the salt of **8**. e) Two absorption bands of almost equal intensities were observed. f) $PdCl_2[(C_6H_5)_3P{=}CHCOC_6H_5]_2$, Ref. 6a. g) $PdCl_2[(CH_3)_2S{=}CHCOC_6H_5]_2$, Ref. 6c.

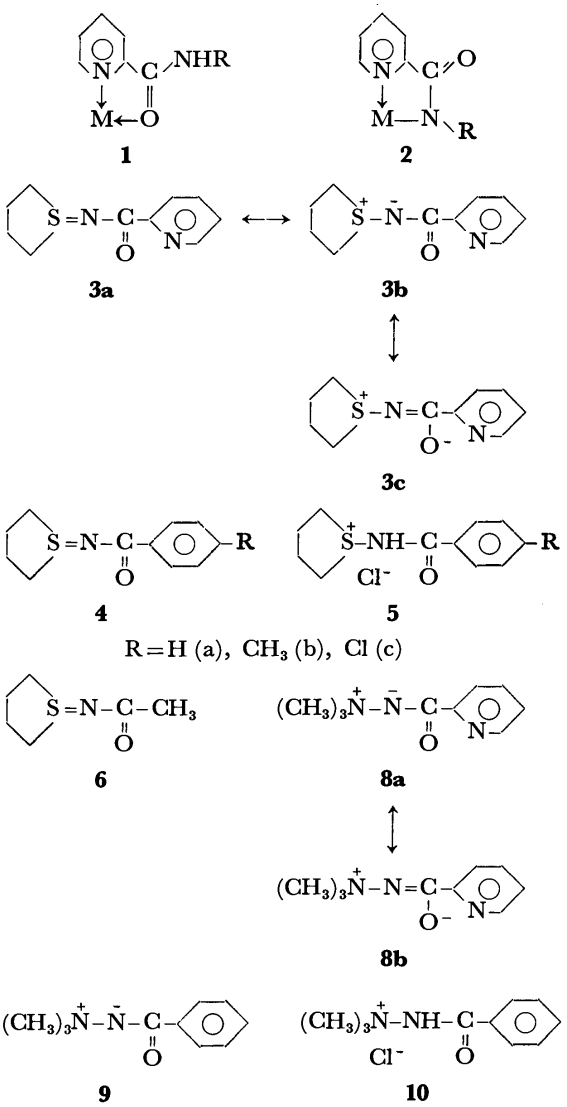

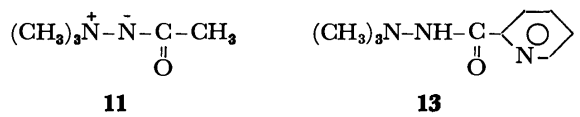

is the same frequency as the C=O band of **16a**. Considering that the basicity of the anionic ligand and hence the strength of metal–ligand bonding is thought to be much higher in the former complex than the latter, it is obvious that the metal–ligand bond strength can not be estimated by the observed C=O band shift. In fact, including a hydrazide complex **D** (*vide infra*), the order of basicity (pK_a of the corresponding amide hydrogens) of the anionic nitrogens is expected to be **C>D>B>A**, while the C=O frequency is in the order **C<D<B<A.**

The degree of higher shift of C=O band on complex

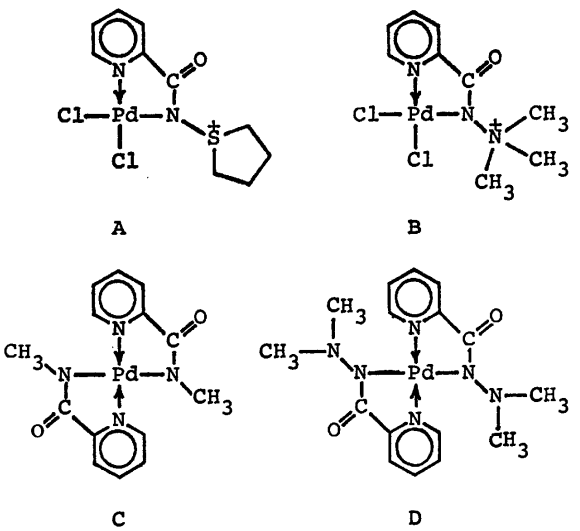

Fig. 1. Structures of chelate complexes.

formation is quite different between the aminimides and the sulfilimines, and among the ylides with different substituents on the carbonyl group. In order to visualize these structural effects, the C=O frequency differences between the salts and the complexes (Δ_1), and those between the complexes and the ylides (Δ_2) are summerized in Table 3, together with the percentages of $\Delta\% = \Delta_2/(\Delta_1+\Delta_2)$ ($\Delta_1+\Delta_2$ equal to the frequency differences between the ylides and the salts). Since the attempted preparations of the salts of the picolonoyl ylides, **3** and **8**, were unsuccessful, the values of Δ_1 and $\Delta\%$ of **14**, **15**, **18**, and **19** were calculated using hypothetical values of 1694 and 1692 cm^{-1} for the salts of **3** and **8**, respectively. These values were calculated on assumption that the values of $\Delta_1+\Delta_2$ of the *N*-picolinoyl compounds are equal to those of *N*-benzoyl compounds. Table 3 also includes the values for the P–C and S–C ylides calculated from the reported data and the pK_a values of the salts of the ylides. The value of $\Delta\%$ is considered to be a measure of degree of σ-bonding between dsp^2 hybridized orbital of the metal ion and sp^2 orbital of the ylidic nitrogen.

There is a tendency that the sulfilimine complexes have somewhat higher values of $\Delta\%$ than the aminimide complexes with the same substituents on the carbonyl carbon. This may indicate that the latter has smaller σ-bond character than the former. In the case of carboxylate complexes such as metal complexes of amino acids, the stretching frequency of the coordinated carboxyl group becomes higher as the metal–oxygen bond becomes stronger.[14] Therefore, it may be considered that the coordination in the sulfilimine complexes is stronger than that in the aminimide analogs. However, the conclusion is somewhat dubious, because the observed basicity of the sulfilimines is lower than the aminimides, and hence the latter is expected to have stronger electrostatic interactions with metal ions.

An alternative explanation for these results is that the metal-ylide coordination is appreciably of ionic character with π-electron delocalized over N–C–O atoms (**E**).

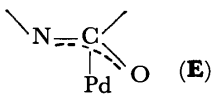

(**E**)

Chelate complexes cannot have a coordination like **E**. A similar complex of an anionic ligand, acetamidopentaamminecobalt(III) perchlorate $[Co(NHCOCH_3)(NH_3)_5](ClO_4)_2$, has been reported by Schneider *et al.*[2b] The complex has C=O stretching band at 1560 cm^{-1}, and X-ray analysis revealed that C=O bond length is longer than ordinary double bonds, indicating electron delocalization over N–C–O atoms.

It should be noted that the chelate complexes have larger σ-bond character than the bis-ylide complexes as seen in Table 3, and that the complexes of *N*-acetyl ylides have remarkably larger ionic character; the C=O bands appear closer to those of free ylides rather than salts.

One of the distinguishable characteristics of ylide ligands is that they have a positively charged group adjacent to the coordination site. In order to evaluate the effect of the charged group, a complex of 2′, 2′-dimethylpicolinohydrazide (**13**) was prepared by the reaction with disodium tetrachloropalladate(II) in an alkaline medium. The proposed structure of the complex (**22**) is shown in Fig. 1 (**D**), and the comparison of C=O bands of **B** and **D** (Table 3) suggests that the latter has a little larger ionic character. It is interesting that by complex formation the NMR bands of methyl and pyridine-6-CH protons of 2′,2′-dimethylpicolinohydrazide show down field shift by 0.25 and 1.36 ppm, respectively. The magnitude of the shift of pyridine-6-CH protons is larger than that expected from the electronic deshielding by coordination of pyridine N atom, and this was ascribed to the van der Waal's interaction with methyl groups of another ligand in the complex.

Ligand Exchange Reactions. The complexes prepared in the present study have relatively low solubilities in water and ordinary organic solvents, making it difficult to study the reactions in solution. However, it was found that the NMR spectra of bis-ylide complexes **16** in DMSO-d_6 were essentially the same with those of free ligands, suggesting that the ligands in these complexes were readily replaced by the solvent molecules. On the contrary, the spectra of the chelate complexes **18** and **22** observed under the same condition were unchanged for more than one week.

The heterogeneous reaction of the complexes with equimolar triphenylphosphine were carried out in refluxing acetonitrile. The bis-sulfilimine Pd(II) complexes **16a** and **17** afforded monosubstituted complexes $PdCl_2(Ylide)PPh_3$ in 76 and 60% yields, respectively, while the chelate complexes did not give monsubstituted complexes, but mixtures of $PdCl_2(PPh_3)_2$ and unreacted complexes were obtained together with small amounts of unidentified products.

Experimental

Melting points are uncorrected. IR spectra were taken on JASCO IRA-2 and DS-403G spectrometer, and NMR spectra were recorded on a Hitachi R-20A spectrometer (60 MHz) using TMS as an internal standard. Elemental analyses were performed on a Perkin Elmer 240 analyzer.

Preparation of Sulfilimines, Aminimides, and Their Salts.

N-Picolinoyl-S,S-tetramethylenesulfilimine (3): To a solution of 4.59 ml (0.052 mol) of tetrahydrothiophen in 30 ml of methanol was added dropwise 5.62 ml (0.050 mol) of *t*-butyl hypochlorite at −50—−45 °C. To the resulting mixture a solution of 6.10 g (0.050 mol) of picolinamide and 1.20 g (0.054 mol) of sodium in 40 ml of methanol was added dropwise keeping the temperature between −55 and −45 °C.[15] After 3 h reaction, the mixture was allowed to warm up to room temperature, evaporated by a rotary evaporator under vacuum, and the residue was extracted by 60 ml of dichloromethane. By evaporation of dichloromethane, crude **3** was obtained in 90% yield. Pure **3** was obtained by recrystallization from a mixture of benzene and petroleum ether. Mp 78—80 °C. Found: C, 57.29; H, 5.97; N, 13.44%. Calcd for $C_{10}H_{12}N_2OS$: C, 57.66; H, 5.82; N, 13.45%. NMR ($CDCl_3$) δ=1.7—2.8 (4H, m, $C-CH_2-C$), 3.38 (4H, br. t, J=8 Hz, CH_2S), 7.15—7.50 (1H, m, Py-4-CH), 7.75 (1H, t, J=8 Hz, Py-5-CH), 8.12 (1H, d, J=8 Hz, Py-3-CH), 8.77 (1H, d, J=5 Hz, Py-6-CH).

N-Benzoyl- and N-(p-Substituted Benzoyl)-S,S-tetramethylenesul-

filimines (4a—c): These sulfilimines were prepared and purified by similar methods to that described above. Analytical and NMR data are shown: **4a**, mp 116—117 °C. Found: C, 64.03; H, 6.71; N, 6.71%. Calcd for $C_{11}H_{13}NOS$: C, 63.73; H, 6.33; N, 6.76%. NMR ($CDCl_3$) δ=1.7—2.7 (4H, m, C-CH_2-C), 3.25 (4H, br. t, J=8 Hz, CH_2S), 7.37 (3H, t, J=3 Hz, *m*- and *p*-CH), 7.9—8.2 (2H, m, *o*-CH). **4b**, mp 99—100 °C. Found: C, 65.61; H, 6.92; N, 6.40%. Calcd for $C_{12}H_{15}NOS$: C, 65.11; H, 6.85; N, 6.33%. NMR ($CDCl_3$) δ=1.7—2.5 (4H, m, C-CH_2-C), 2.35 (3H, s, CH_3), 3.25 (4H, br. t, J=8 Hz, CH_2S), 7.12 (2H, d, J=8 Hz, *m*-CH), 7.93 (2H, d, J=8 Hz, *o*-CH). **4c**, mp 106—108 °C. Found: C, 54.46; H, 5.14; N, 6.04%. Calcd for $C_{11}H_{12}NOSCl$: C, 54.65; H, 5.01; N, 5.80%. NMR ($CDCl_3$) δ=1.7—2.6 (4H, m, C-CH_2-C), 3.25 (4H, br. t, J=7 Hz, CH_2S), 7.28 (2H, d, J=8 Hz, *m*-CH), 7.97 (2H, d, J=8 Hz, *o*-CH).

1-(Benzoylamino and p-Substituted Benzoylamino)thiolanium Chlorides (5a—c): These sulfonium chlorides were prepared by the method reported previously.[16]

N-Acetyl-S,S-tetramethylenesulfilimine (6) and 1-Acetylaminothiolanium Bromide (7): These compounds were also reported in a literature.[17]

N-Trimethylammoniopicolinamidate (Trimethylamine-picolinimide) (8): A modified method of McKillip and Slagel[18] was employed for the syntheses of aminimides **8**, **9**, and **11**. Thus, a mixture of 10.43 g (0.0516 mol) of 1,1,1-trimethylhydrazinium iodide, 7.08 g (0.0516 mol) of methyl picolinate, and 6.02 g (0.0536 mol) of potassium *t*-butoxide in 60 ml of *t*-butyl alcohol was heated with stirring at 60—65 °C for 4.5 h. The precipitate was separated by filtration and the filtrate was evaporated to dryness under vacuum. The residue was recrystallized from ethyl acetate, and a hygroscopic solid was obtained which was identified as **8** by IR and NMR. Yield 70%, mp 148—149 °C. NMR ($CDCl_3$) δ=3.56 (9H, s, CH_3), 7.1—7.5 (1H, m, Py-4-CH), 7.75 (1H, t, J=7 Hz, Py-5-CH), 8.11 (1H, d, J=8 Hz, Py-3-CH), 8.66 (1H, d, J=5 Hz, Py-6-CH).

N-Trimethylammoniobenzamidate (**9**), mp 167—168 °C, (lit,[19] 168—169 °C), and *N*-trimethylammonioacetamidate (**11**), mp 124—126 °C (lit,[20] 122.5—123 °C), were prepared in similar manners and converted to hydrochloric acid salts. **9**; Found: C, 67.49; H, 7.93; N, 15.22%. Calcd for $C_{10}H_{14}N_2O$: C, 67.37; H, 7.93; N, 15.72%. NMR ($CDCl_3$) δ=3.42 (9H, s, CH_3), 7.2—7.5 (3H, m, *m*- and *p*-CH), 7.8—8.1 (2H, m, *o*-CH). **10**; mp 178—179 °C. Found: C, 56.32; H, 7.15; N, 13.11%. Calcd for $C_{10}H_{15}N_2OCl$: C, 55.93; H, 7.06; N, 13.05%. NMR (DMSO-d_6) δ=3.80 (9H, s, CH_3), 7.4—7.7 (3H, m, *m*- and *p*-CH), 7.8—8.1 (2H, m, *o*-CH). Ylide **11** was very hygroscopic and could not analyzed. NMR ($CDCl_3$) δ=1.79 (3H, s, C-CH_3), 3.36 (9H, s, N-CH_3). **12**, mp 198—199 °C. Found: C, 39.17; H, 8.54; N, 18.18%. Calcd for $C_5H_{13}N_2OCl$: C, 39.49; H, 8.60; N, 18.34%. NMR (DMSO-d_6) δ=2.02 (3H, s, C-CH_3), 3.63 (9H, s, N-CH_3).

2',2'-Dimethylpicolinohydrazide (13): This compound was prepared by the reaction of 1,1-dimethylhydrazine with picolinic acid in the presence of dicyclohexylcarbodiimide in dichloromethane.[21] Picolinic acid (4.9 g, 0.04 mol) was added to a solution of 8.2 g (0.04 mol) of dicyclohexylcarbodiimide and 2.4 g (0.04 mol) of 1,1-dimethylhydrazine in 160 ml of dichloromethane, and the solution was stirred at room temperature for 2 h. The precipitate was removed by filtration, and the filtrate was extracted by three portions of 50 ml of 3 M HCl. After the extract was neutralized by sodium carbonate, the product was extracted by chloroform and dried over anhydrous sodium sulfate. The evaporation of chloroform gave crude **13** in 78% yield. After several recrystallization from benzene-hexane or cyclohexane, pure **13** was obtained, mp 67—68 °C. Found: C, 57.79; H, 6.75; N, 24.92%. Calcd for $C_8H_{11}N_3O$: C, 58.15; H, 6.72; N, 25.44%. NMR ($CDCl_3$) δ=2.72 (6H, s, CH_3), 7.25—7.50 (1H, m, Py-4-CH), 7.80 (1H, t, J=7 Hz, Py-5-CH), 8.18 (1H, d, J=7 Hz, Py-3-CH), 8.45 (1H, d, J=4 Hz, Py-6-CH), 8.65 (1H, br. s, NH).

Preparation of Complexes. Dichloro(N-picolinoyl-S,S-tetramethylenesulfilimine)palladium(II) (14): To a solution of 0.763 g (3.66 mmol) of **3** in 60 ml of benzene 1.26 g (3.29 mmol) of dichlorobis(benzonitrile)palladium(II) was added. After overnight reaction with stirring, an orange-yellow precipitate was separated and dried *in vacuo*. Crude **14** (93% yield) was purified by recrystallization from DMSO. Alternative procedures for the preparation of **14** are the reaction of **3** with disodium tetrachloropalladate(II) in ethanol or with dichloro-(1,5-cyclooctadiene) palladium(II) in acetone. In both cases the products were obtained as precipitates and identified as **14**.

Dichloro(N-picolinoyl-S,S-tetramethylenesulfilimine)platinum(II) (15): A solution of 0.514 g (2.47 mmol) of **3** in 5 ml of water was added dropwise to a solution of 0.257 g (0.618 mmol) of dipotassium tetrachloroplatinate(II) in 5 ml of water. After 3 h reaction at room temperature, an orangered precipitate was separated, washed with water, and dried *in vacuo*; yield 66%.

Dichlorobis(N-benzoyl-S,S-tetramethylenesulfilimine)palladium(II) (16a): A solution of 0.447 g (2.15 mmol) of **4a** in 5 ml of ethanol was added dropwise at room temperature to a solution of 0.376 g (1.08 mmol) of disodium tetrachloropalladate (II) in 25 ml of ethanol. The orange precipitate formed was filtered, washed with ethanol-water, and dried *in vacuo*; yield 95%. *p*-Methyl- and *p*-chlorobenzoylsulfilimine complexes of palladium(II) were prepared by similar methods. The NMR spectra of **15a—c** in DMSO-d_6 were essentially the same with those of **4a—c** respectively, indicating that the ylide ligands were replaced by the solvent. The complex **17** was prepared in tha same way.

Dichloro(N-trimethylammoniopicolinamidate)palladium(II) (18): A solution of 0.555 g (3.09 mmol) of **8** in 5 ml of ethanol was added at room temperature to a solution of 0.598 g (1.56 mmol) of dichlorobis(benzonitrile)palladium(II) in 30 ml of ethanol. A brownish precipitate formed immediately. After 1 h reaction, the precipitate was separated, washed with ethanol, and dried *in vacuo*; yield 74%. NMR (DMSO-d_6) δ=3.68 (9H, s, CH_3), 7.4—8.4 (3H, m, Py-3,4,5-CH), 8.90 (1H, d, J=6 Hz, Py-6-CH). No significant change was observed in the spectrum of **18** in DMSO-d_6 after 1 week, indicating that the aminimide ligand was not displaced by the solvent. The reactions of **8** with disodium tetrachloropalladate(II) in ethanol and with dichloro(1,5-cyclooctadiene)-palladium(II) in acetone also gave **18** in almost quantitative yields.

Dichloro(N-trimethylammoniopicolinamidate)platinum(II) (19): A solution of 0.289 g (1.61 mmol) of **8** in 5 ml of water was added at room temperature to a solution of dipotassium tetrachloroplatinate(II) (0.666 g, 1.60 mmol) in 10 ml of water. After 6 h reaction, the precipitate was separated, washed with water, and dried *in vacuo*; yield 49%.

Dichlorobis(N-trimethylammoniobenzamidate)palladium(II) (20) and Dichlorobis(N-trimethylammonioacetamidate)palladium(II) (21): These complexes were prepared by the reactions of disodium tetrachloropalladate(II) with two equivalents of the aminimides **9** and **11** in ethanol. Yields were 95 and 73%, respectively.

Bis(2',2'-dimethyl-1'-picolinoyl-1'-hydrazino)palladium(II) (22): A solution of 0.712 g (4.31 mmol) of **13** and 0.172 g (4.31 mmol) of sodium hydroxide in 8 ml of ethanol was added dropwise to a solution of disodium tetrachloropalladate(II) (0.635 g, 2.16 mmol) in 30 ml of ethanol. After 2 h reaction

at room temperature, the precipitate was separated by filtration, the filtrate was concentrated, and the solution was poured into 200 ml of water. After standing in a refrigerator overnight, the yellow crystal was filtered and dried *in vacuo*. Yield 83%. NMR ($CDCl_3$) δ=2.97 (6H, s, CH_3), 7.40—7.65 (1H, m, Py-4-CH), 8.02 (2H, d, J=4 Hz, Py-3- and -5-CH), 9.84 (1H, d, J=5 Hz, Py-6-CH).

Reactions of Pd (II) Complexes with Triphenylphosphine. A mixture of 0.228 g (0.591 mmol) of **14** and equimolar amount of triphenylphosphine in 15 ml of acetonitrile was refluxed for 4 h. The precipitate was separated by filtration and it was found to be a mixture of **14** and dichlorobis(triphenylphosphine)palladium(II) (**23**). The reaction of **18** with triphenylphosphine was also carried out in a similar way, and **23** was isolated in 40% yield. In the case of bis-sulfilimine complexes, **16a** and **17**, monosubstituted complexes, $PdCl_2[(CH_2)_4S{=}NC{-}OC_6H_5](PPh_3)$ (**24**) and $PdCl_2[(CH_2)_4S{=}NCOCH_3](PPh_3)$ (**25**) were obtained as orange precipitates by cooling the reaction mixtures in 76 and 60% yields, respectively.

pK_a Measurement of Aminosulfonium and Aminoammonium Chlorides. pK_a values of the salts **5** and **7** were reported in a previous paper,[16] and those of **10** and **12** were measure by a similar method.

References

1) a) M. Nonoyama and K. Nonoyama, *Kagaku No Ryoiki*, **31**, 136 (1977); b) J. M. Giorio and B. P. Susz, *Helv. Chim. Acta*, **54**, 2251 (1971); c) M. E. Stone, B. E. Robertson, and E. Stanley, *J. Chem. Soc., A*, **1971**, 3632.

2) a) R. J. Balahura and R. B. Jordan, *J. Am. Chem. Soc.*, **92**, 1533 (1970); b) M. L. Schneider, G. Ferguson, and R. J. Balahura, *Can. J. Chem.*, **51**, 2180 (1973).

3) a) K. Yamasaki and M. Sekizaki, *Bull. Chem. Soc. Jpn.*, **38**, 2206 (1965); b) M. Sekizaki and K. Yamasaki, *Nippon Kagaku Zasshi*, **87**, 1053 (1966); c) M. Sekizaki, M. Tanase, and K. Yamasaki, *Bull. Chem. Soc. Jpn.*, **42**, 399 (1969); d) Y. Nawata, H. Iwasaki, and Y. Saito, *ibid*, **40**, 515 (1967); e) H. Ojima, *Nippon Kagaku Zasshi*, **88**, 333 (1967); f) M. Nonoyama and K. Yamasaki, *Inorg. Chim. Acta*, **3**, 585 (1969); g) M. Nonoyama and K. Yamasaki, *Nippon Kagaku Zasshi*, **92**, 719 (1971).

4) H. Schmidbaur, *Acc. Chem. Res.*, **8**, 62 (1975).

5) a) W. C. Kaska, D. K. Mitchell, R. F. Reichelderfer, and W. D. Korte, *J. Am. Chem. Soc.*, **96**, 2847 (1974); b) E. Lindner, *J. Organomet. Chem.*, **94**, 229 (1975).

6) a) P. A. Arnup and M. C. Baird, *Inorg. Nucl. Chem. Lett.*, **5**, 65 (1969); b) H. Koezuka, G. Matsubayashi, and T. Tanaka, *Inorg. Chem.*, **13**, 443 (1974); c) P. Bravo, G. Fronza, and C. Ticozzi, *J. Organomet. Chem.*, **74**, 143 (1974); d) E. T. Weleski, Jr., J. L. Silver, M. D. Jansson, and J. L. Burmeister, *ibid.*, **102**, 365 (1975); e) H. Nishiyama, K. Itoh, and Y. Ishii, *ibid.*, **87**, 129 (1975).

7) a) Y. Yamamoto and H. Schmidbaur, *J. Organomet. Chem.*, **96**, 133 (1975); b) Y. Yamamoto and H. Schmidbaur, *ibid.*, **97**, 479 (1975); c) P. Bravo, G. Fronza, and C. Ticozzi, *ibid.*, **118**, C78 (1976).

8) a) G. Matsubayashi, M. Toriuchi, and T. Tanaka, *Chem. Lett.*, **1973**, 985; b) M. Toriuchi, G. Matsubayashi, H. Koezuka, and T. Tanaka, *Inorg. Chim. Acta*, **17**, 253 (1976).

9) S. A. Dias, A. W. Downs, and W. R. McWhinnie, *J. Chem. Soc., Dalton Trans.*, **1975**, 162.

10) a) A. Kalman, *Acta Crystallogr.*, **22**, 501 (1967); b) A. Kalman, K. Sasvari, and A. Kucsman, *J. Chem. Soc., D*, **1971**, 1447.

11) A. F. Cameron, N. J. Hair, and D. G. Morris, *J. Chem. Soc., Perkin Trans. 2*, **1972**, 1071.

12) Dias *et al*[9] assigned the absorption band of *N*-(1-pyridino)benzamidate at 1335 cm^{-1} to N–N stretching vibration, but the present authors consider that the strong absorption bands at 1290—1350 cm^{-1} are more likely of C–N stretching, because the bands shift to lower frequencies on salt formation (amide III band), and because similar strong bands are also observed in carbonyl stabilized sulfilimines.

13) R. J. H. Clark and C. S. Williams, *Inorg. Chem.*, **4**, 350 (1965).

14) A. E. Martell Ed, "Coordination Chemistry," Vol. 1, Van Nostrand Reinhold Co., New York (1971), Chap. 3.

15) D. Swern, I. Ikeda, and G. F. Whitfield, *Tetrahedron Lett.*, **1972**, 2635.

16) H. Kise, Y. Sugiyama, and M. Seno, *J. Chem. Soc., Perkin Trans. 2*, **1976**, 1869.

17) H. Kise, G. F. Whitfield, and D. Swern, *J. Org. Chem.*, **37**, 1121 (1972).

18) W. J. McKillip and R. C. Slagel, *Can. J. Chem.*, **45**, 2619 (1967).

19) R. L. Hinman and M. C. Flores, *J. Org. Chem.*, **24**, 660 (1959).

20) R. Appel, H. Heinen, and R. Schoelhorn, *Chem. Ber.*, **99**, 3118 (1966).

21) R. F. Smith, A. C. Bates, A. J. Battisti, P. G. Byrnes, C. T. Mroz, T. J. Smearing, and F. X. Albrecht, *J. Org. Chem.*, **32**, 851 (1968).

The Consitution of $NaPO_3$-GeO_2 Melts

Makoto WATANABE, Masao ITO, Shoji SATO, and Tamotsu YAMADA

Department of Industrial Chemistry, Chubu Institute of Technology, Matsumoto-cho, Kasugai-shi, Aichi 487

(Received June 13, 1977)

The glassy and crystalline thermal products were prepared by heating a mixture of sodium phosphate glass and germanium dioxide with P/Ge ratios of 1.0—300 at 1000 °C for 3 h in a platinum crucible, and by then rapidly quenching the resulting melt. The thermal products with P/Ge ratios larger than 50 were glassy. The products with P/Ge ratios smaller than 30 were a mixture of glassy and crystalline substances, and the quantity of the glassy substance in the mixture increased with an increase in the P/Ge ratio. The crystalline substance was insoluble in water. From the results of the distribution and the average chain length of the condensed phosphates present in the glassy thermal products, it was concluded that the glass has P–O–Ge linkages and that the most reasonable chemical structure of the glass is $Ge\text{-}(\text{-}O\text{-}\underset{\underset{|}{O}}{P}\text{-})_4$. The colorimetric determination of the phosphorus and germanium contained in the crystalline thermal product showed that the P/Ge ratio of the crystalline substance is 1.3. The value of the P/Ge ratio corresponds to that of $Ge_3(PO_4)_4$.

Studies of the reaction of phosphate glass with the oxides or oxoacid salts of some elements other than phosphorus at moderately high temperatures have been carried out by several research workers. The systems studied were arsenate–phosphates,[1] silicate–phosphates,[2] vanadate–phosphates,[3] and borate–phosphates.[4,5] It was found, as a result, that the thermal products of these systems have P–O–As, P–O–Si, P–O–V, and P–O–B linkages respectively. The authors also studied the constitution of thermal products in the systems of antimonate–phosphates,[6–8] molybdate–phosphates,[9] tungstate–Phosphates,[9] aluminate–phosphates,[10] and chromate–phosphates.[11] It was concluded that they have P–O–Sb, P–O–Mo, P–O–W, P–O–Al, and P–O–Cr linkages respectively. In the present work, the glassy and crystalline thermal products in the system of $NaPO_3$–GeO_2 were investigated to obtain some information concerning the reactivity of $NaPO_3$ glass with germanium dioxide at a moderately high temperature and the structures of the thermal products.

Experimental

Preparation of the Thermal Products. A mixture of sodium phosphate glass (Graham's salt) and germanium dioxide with P/Ge ratios from 1.0 to 300 was heated in a platinum crucible at 1000 °C for 3 h. The resulting melts were quenched rapidly by placing the crucible in ice water. Sodium phosphate glass was made by heating sodium dihydrogenorthophosphate in a platinum crucible at 1000 °C for 3 h and by then quenching the melt by the same method described above.

The Solubility of the Products. About two grams of the thermal products were stirred in about 100 ml of water for 30 min at room temperature. The water-insoluble parts were then filtered off, dried, and weighed.

Paper Chromatography. The compositions of the phosphate species contained in the water-soluble part of the thermal product were determined by using one-dimensional paper chromatography. Acidic and basic developing solvents were used to separate chain phosphates (ortho-, pyro-, tri-, and high-polyphosphates) and small-ring phosphates (*cyclo*-tri- and *cyclo*-tetraphosphates) respectively.[12] About 5 μl of the mother liquor obtained by the measurement of the solubility of the thermal product was spotted onto a Toyo No. 51A filter paper (2 by 50 cm). The development was achieved at 5 °C for about 50 h. Then the filter paper was heated at 75 °C for more than 30 min in an air bath and a perchloric acid–molybdate solution was sprayed on. After drying, the paper was exposed to ultraviolet rays until blue spots appeared. The identification of each spots on the chromatograms was done by referring the spots to those of known phosphates. When the acidic developing solvent was used, the germanate ions contained in the water-soluble part of the thermal product were separated from the phosphate ions.

Colorimetric Measurement of Phosphates. Phosphates contained in the paper chromatograms were extracted with 0.1 M aqueous ammonia and determined colorimetrically by the method described in a previous paper.[6]

The Determination of the Phosphorus and Germanium Present in the Water-insoluble Thermal Product. About 0.5 g of the water-insoluble part of the thermal product was mixed with about 1.0 g of sodium carbonate, and the mixture was heated at 1000 °C for 1 h in a platinum crucible. The resulting melt was cooled rapidly in a desiccator and dissolved in 50 ml of water. About 5 μl of the sample solution was placed on a Toyo No. 51A filter paper (2 by 50 cm) and developed at room temperature for 2 days by using the acidic solvent described above. The paper was dried and sprayed a perchloric acid–molybdate solution. Then the paper was dried again and exposed to ultraviolet rays until blue spots appeared. The blue spots of phosphate and germanate were cut at the demarcation line and soaked in 10 ml of 0.1 M aqueous ammonia for 1 h. The determination of the phosphorus present in the extracting solution was made by the same method as that of a previous paper.[6] The germanium present in the extracting solution was determined colorimetrically (phenylfluorone method).

X-Ray Diffractometry. The samples were ground with an agate mortar until they could pass through a 150-mesh screen. Their X-ray diffraction diagrams were recorded on a Toshiba X-ray diffractometer, ADG-102, by means of a powder method.

Infrared Spectral Measurement. The IR spectra of the thermal products were measured with a JASCO infrared spectrophotometer, model IR-G, by using a KBr tablet method.

The Average Chain Length of Phosphates. The average chain length of phosphates present in the glassy thermal products was measured by the pH-titration method.[13,14] The effect of a germanate ion on the titration was nagligibly small.

Results and Discussion

Solubility and X-Ray Diffraction Diagrams of the Thermal Products. Table 1 shows the amount (%) of the

TABLE 1. AMOUNT OF WATER-SOLUBLE PARTS OF THE PRODUCTS AND IDENTIFICATION OF THE CRYSTALLINE PRODUCTS BY X-RAY DIFFRACTOMETRY

P/Ge	X-Ray diffraction	Water-soluble parts (%)
1.0	GeO_2, $Ge_3(PO_4)_4$	69
2.0—30	$Ge_3(PO_4)_4$	83—99
50—300	Glassy	100

water-soluble part of the thermal product and the results of the identification of crystalline thermal products by means of their X-ray diffraction patterns. The amount of the water-soluble part increased with an increase in the P/Ge ratio. The thermal products with P/Ge ratios larger than 50 were completely dissolved in water. The thermal products with P/Ge ratios from 1.0 to 30 contained crystalline substances. By referring the X-ray diffraction diagrams of the thermal products to those of ASTM cards, it was found that the thermal product with the P/Ge ratio of 1.0 contains germanium dioxide and an unknown crystalline substance, while those with the P/Ge ratios from 2.0 to 30 contain only an unknown crystalline substance. The intensity of the diffraction peaks of the products decreased with an increase in the P/Ge ratio, and the thermal products with P/Ge ratios of 20 and 30 showed only one or two weak peeks. The unknown crystalline substance was insoluble in water. According to the quantitative analysis of the phosphorus and germanium contained in the unknown crystalline substance, the P/Ge ratio of the crystal was 1.3. This value corresponds to the P/Ge ratio of germanium orthophosphate, $Ge_3(PO_4)_4$. This crystalline substance can be made by the method to be described below. The pH of an aqueous solution of sodium dihydrogenorthophosphate (30%) was adjusted to 5—7 with aqueous ammonia or aqueous sodium hydroxide, and then, under vigorous stirring, about 5 g of germanium tetrachloride was added to about 50 ml of the orthophosphate solution. The resulting precipitate was filtered off and heated at 1000 °C for 3 h in a platinum crucible. This substance gave the same X-ray diffraction diagram and P/Ge ratio as those of the unknown crystalline thermal product. Therefore, the crystalline substance may be germanium orthophosphate, $Ge_3(PO_4)_4$. The X-ray diffraction pattern of the crystalline substance is shown in Fig. 1.

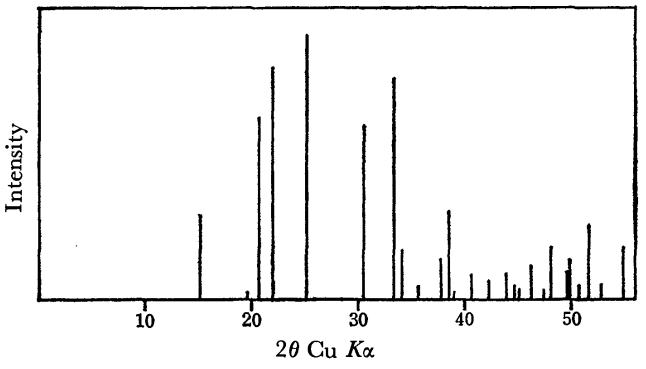

Fig. 1. X-Ray diffraction diagram of $Ge_3(PO_4)_4$.

TABLE 2. DISTRIBUTION OF PHOSPHATES OF WATER-SOLUBLE PARTS IN THE PRODUCTS

P/Ge	Ortho	Pyro	Tri	*cyclo*-Tri	*cyclo*-Tetra	Higher
1.0	42.3	45.1	9.4			3.2
2.0	44.1	45.8	7.1			3.0
3.0	19.3	61.3	10.9			8.4
5.0	3.1	47.2	3.6	2.4		43.7
7.0	1.4	30.4	6.8	2.2	1.1	58.1
10	0.4	17.8	5.0	2.8	2.1	71.9
15	0.9	11.8	3.4	3.3	2.5	78.1
20	0.3	9.1	2.6	3.3	2.4	82.3
30	0.4	6.6	2.0	3.1	2.3	85.6
50	0.6	3.7	1.4	3.4	2.6	88.3
80		2.1	1.1	3.6	2.9	90.3
100		0.8	0.9	3.6	2.4	92.3
150		0.8	0.8	3.9	3.3	91.2
200		0.4	0.4	4.2	2.7	92.3
300		0.1	0.1	4.5	2.9	92.4

Distribution of Phosphates. The results of the colorimetric determination of the phosphates (P%) contained in the water-soluble thermal products with P/Ge ratios from 1.0 to 300 are listed in Table 2. The orthophosphate content decreases with an increase in the P/Ge ratio. The pyro- and triphosphate contents show the largest value at the P/Ge ratio of 3.0 and decrease with an increase in the P/Ge ratio from 3.0 to 300. *cyclo*-Tri- and *cyclo*-tetraphosphates were usually not contained in the thermal products with P/Ge ratios of 1.0—3.0 and 1.0—5.0 respectively; if they were present, the contents of those phosphates amounted to a small percentage. The quantity of long-chain phosphates increased with an increase in the P/Ge ratio. The spot of germanate ion also appeared on the chromatograms of the sample solutions of P/Ge ratios from 1.0 to 300. The R_f value of a germanate ion was 0.50. Accordingly, the reaction of germanium dioxide with sodium phosphate glass at 1000 °C produces germanium orthophosphate and a glassy substance. In the glassy product, it could be concluded that germanium dioxide is a network-former and makes a P–O–Ge linkage. The P–O–Ge linkage may be readily hydrolyzed in a water solution to form phosphate and germanate ions, because the chain length of the phosphates contained in glassy products increases with an increase in the P/Ge ratio.

Average Chain Length of Phosphates and the Chemical Structure of Glassy Products. As is shown in Fig. 2, the average chain length of the polyphosphates of glassy products increased with an increase in the P/Ge ratio. The result is in good accordance with that of distribution of phosphates. Therefore, it can be said that the result also supports the presence of a P–O–Ge linkage in glassy products and the rapid hydrolysis of the P–O–Ge linkage in a water solution. According to the method described in previous papers,[2,6–11] the chemical structure of the glassy thermal products can be discussed by examining the relation between the average chain length of polyphosphates contained in the glassy products and the P/Ge ratio. The average chain length, $\bar{n}$, of the polyphosphates in the glass of the $NaPO_3$–GeO_2

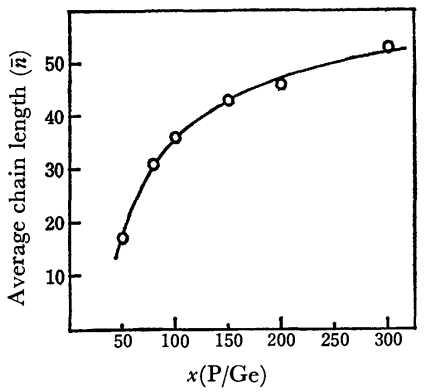

Fig. 2. Variation of average chain length of polyphosphates in the glassy thermal products with P/Ge ratios larger than 50.

system is given by the following equation:

$$(\bar{n}+2)/\bar{n} = (x+y-z+fx)/x, \quad (1)$$

where x, y, and z stand for, respectively, the number of phosphorus atoms, the P–O–Ge linkages, and the Ge–O^- linkages per atom of germanium and where f is the factor shortning the chain length of the polyphos phates, given with respect to an atom of phosphorus. The f value of sodium phosphate glass was given by the following equation:

$$(\bar{n}+2)/\bar{n} = (1+f)/1. \quad (2)$$

Since the average chain length of sodium phosphate glass was 77 under the experimental conditions employed, the f value is 0.026. These four chemical structures with P–O–Ge and Ge–O^- linkages may be considered:

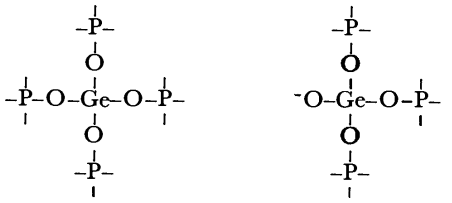
Structure A

Structure B

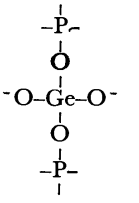
Structure C

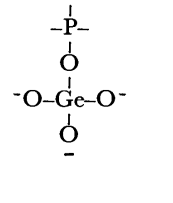
Structure D

For each chemical structure, one can calculate the average chain length of polyphosphates present in the glass of this system by using Eq. 1. The measured and calculated average chain lengths of polyphosphates contained in the glassy products are listed in Table 3. The most reasonable chemical structure of the glassy product is Structure A, because the measured $\bar{n}$ value agrees well with the calculated one throughout the P/Ge range of 50—300.

Infrared Spectral Measurement. The infrared spectra of the starting materials and the thermal products are shown in Fig. 3. The infrared spectra of the thermal products with P/Ge ratios larger than 20 are not shown because the spectra are the same as that of sodium phosphate glass. As the P/Ge ratio becomes larger, the infrared spectrum of the thermal product gradually becomes similar to that of sodium phosphate glass. The infrared spectra of the thermal products with P/Ge

Table 3. Average chain length of polyphosphates of the thermal products with P/Ge ratios larger than 50

x (P/Ge)	$\bar{n}$ Found	$\bar{n}$ calcd by Eq. 1 (f=0.026) Structure A (y=4, z=0)	B (y=3, z=1)	C (y=2, z=2)	D (y=1, z=3)
50	17	19	30	77	—
80	31	26	39	77	2000
100	36	30	43	77	333
150	43	38	51	77	158
200	46	43	56	77	125
300	53	51	61	77	103

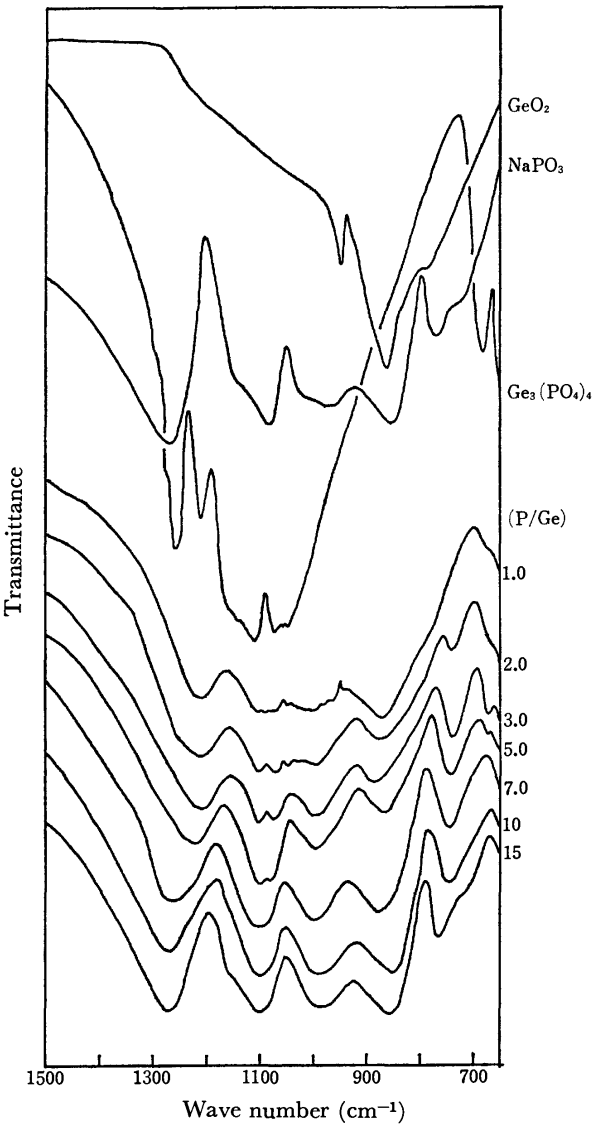

Fig. 3. IR spectra of GeO_2, $NaPO_3$, $Ge_3(PO_4)_4$, and the products with P/Ge ratios of 1.0—15.

ratios of 1.0—5.0 show absorptions (1110, 1070, and 680 cm^{-1}) attributable to germanium orthophosphate (water-insoluble part of thermal products); the absorptions are ambiguous because, as is shown in Table 1, the quantity of the water-insoluble part of the thermal products with P/Ge ratios of 1.0—5.0 is small. According to Corbridge and Lowe,[15] the absorption of sodium phosphate glass at 1270 cm^{-1} is due to P=O stretching. This absorption of thermal products gradually shifts to a lower wave number as the P/Ge ratio changes to a smaller value. It could be considered that the shift is caused by the decrease in the P=O bond strength. This could be explained as the P=O bond in sodium phosphate glass being transferred to the P⋯O⋯Ge bond by the coordination of a germanium atom. Therefore, it could be concluded that the glassy product has a four-way branching as follows:

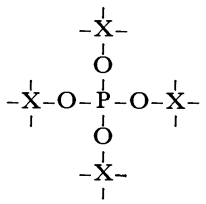

where X stands for phosphorus or germanium. This phenomenon was also observed in the infrared spectra of the thermal products of the $NaPO_3$–Al_2O_3 system.[10]

References

1) K-H. Jost, H. Worzalla, and E. Thilo, *Z. Anorg. Allg. Chem.*, **325**, 98 (1963).
2) S. Ohashi and F. Oshima, *Bull. Chem. Soc. Jpn.*, **36**, 1489 (1963).
3) S. Ohashi and T. Matsumura, *Bull. Chem. Soc. Jpn.*, **35**, 501 (1962).
4) T. Nakamura and S. Ohashi, *Bull. Chem. Soc. Jpn.*, **40**, 110 (1967).
5) K. Honma and K. Honma, *Nippon Kagaku Kaishi*, **1972**, 856.
6) M. Watanabe, K. Tanabe, T. Takahara, and T. Yamada, *Bull. Chem. Soc. Jpn.*, **44**, 712 (1971).
7) M. Watanabe and H. Kato, *Bull. Chem. Soc. Jpn.*, **45**, 1058 (1972).
8) M. Watanabe, *Bull. Chem. Soc. Jpn.*, **46**, 2468 (1973).
9) M. Watanabe, *Nippon Kagaku Kaishi*, **1974**, 1407, 1412.
10) M. Watanabe, S. Sato, and H. Saito, *Bull. Chem. Soc. Jpn.*, **48**, 893 (1975).
11) M. Watanabe, S. Sato, and H. Saito, *Bull. Chem. Soc. Jpn.*, **49**, 3265 (1976).
12) M. Watanabe, S. Sato, and H. Saito, *Bull. Chem. Soc. Jpn.*, **48**, 896 (1975).
13) J. R. Van Wazer, E. J. Griffith, and J. F. McCulough, *Anal. Chem.*, **26**, 1755 (1954).
14) E. J. Griffith, *Anal. Chem.*, **28**, 525 (1956).
15) D. E. C. Corbridge and E. J. Lowe, *J. Chem. Soc.*, **1954**, 493, 4555.

The Disproportionation Constants of Mercury(I) in Dilute Solutions

Isao SANEMASA and Tsutomu HIRATA

Department of Chemistry, Faculty of Science, Kumamoto University, Kurokami-machi, Kumamoto 860

(Received July 5, 1977)

The disproportionation constants for the $Hg_2^{2+} \rightleftarrows Hg(aq) + Hg^{2+}$ reaction have been measured in dilute mercury(I) perchlorate solutions over the temperature range from 15 to 30 °C. The technique was based on a simple kinetic method which made use of a characteristic property of the elemental mercury in aqueous solutions. The disproportionation constant at 25 °C and $\mu=0.1$ was found to be $1.1\pm0.1\times10^{-8}$ M, and the associated thermodynamic parameters were $\Delta H=13.2\pm0.2$ kcal/mol and $\Delta S=8.0\pm0.8$ e.u. The reliability of the method was discussed with relation to the reported values in the literature.

It is widely accepted that mercury(I) ions in aqueous solutions exist in the dimeric form and are in equilibrium with dissolved mercury atoms and mercury(II) ions, and that the equilibrium is rapidly established:[1,2]

$$Hg_2^{2+} \rightleftarrows Hg(aq) + Hg^{2+}. \quad (1)$$

The equilibrium constant, K_d, can be expressed by $K_d=[Hg^{2+}]f_2\cdot[Hg(aq)]f_0/[Hg_2^{2+}]f_1$, where the brackets indicate molarities and where the f values are activty coefficients for the corresponding species. It has been common practice to assume that $f_0=1$ and that $f_2=f_1$, an approximation which is reasonable at low ionic strengths. Therefore, the equilibrium constant can be expressed more conveniently by

$$K_d = [Hg^{2+}][Hg(aq)]/[Hg_2^{2+}]. \quad (2)$$

Kinetic and thermodynamic studies of the reactions concerned with mercury(I) require accurate knowledge of the disproportionation constant.[2-7] Potentiometric studies of $[Hg^{2+}]/[Hg_2^{2+}]$ ratios have been reported in the literature by many investigators.[8-11] However, there have been few studies of the equilibrium constant involving the [Hg(aq)] term, K_d. The first and the only attempt to determine the K_d was made by Moser and Voigt.[12] They made use of the extraction of free mercury into non-polar solvents to measure the extent of the disproportionation of mercury(I) and estimated K_d by using the solubilities of Hg^0 in an aqueous solution and organic solvents. The technique they used was, however, troublesome, and their data were limited to those at 25 °C.

This paper will describe a simple technique that might allow an estimation of the disproportionation constant of mercury(I) in dilute aqueous solutions. It makes use of the fact that elemental mercury in the aqueous phase is readily carried by an air-stream into the gaseous phase:

$$Hg(aq) \xrightarrow{k} Hg(gas), \quad (3)$$

where k is the rate constant associated with the Hg^0 phase-transfer. When a nitrogen gas is made to flow through a solution containing Hg_2^{2+}, the dispropotionation of mercury(I) may occur according to Reaction 1. Considering Process 3 to be a rate-controlling step, the rate of the disproportionation of mercury(I) can be expressed by:

$$-d[Hg_2^{2+}]/dt = kK_d[Hg_2^{2+}]/[Hg^{2+}]. \quad (4)$$

The initial concentration of Hg^{2+} in equilibrium with Hg_2^{2+} is sufficiently low, and $[Hg^{2+}]=[Hg^{2+}]_0+[Hg_2^{2+}]_0-[Hg_2^{2+}]=[Hg^{2+}]_0-[Hg_2^{2+}]$. Then, Eq. 4 becomes, on integration

$$[Hg_2^{2+}]_0 \log [Hg_2^{2+}] - [Hg_2^{2+}]/2.303 = -kK_dt/2.303 + [Hg_2^{2+}]_0 \log [Hg_2^{2+}]_0 - [Hg_2^{2+}]_0/2.303, \quad (5)$$

where the subscript 0 denotes the initial concentration. The rate constant, k, can be determined by a separate experiment. Nitrogen gas is passed through a solution containing a known concentration of elemental mercury, which can be prepared by saturating mercury vapor in an aqueous solution.[13] Then, Reaction 3 proceeds; its rate can be expressed by

$$-d[Hg(aq)]/dt = k[Hg(aq)], \quad (6)$$

which becomes, on integration

$$\log [Hg(aq)] - \log [Hg(aq)]_0 = -kt/2.303. \quad (7)$$

Eqs. 5 and 7 enable us to determine kK_d and k respectively, from which we can determine K_d.

Experimental

Reagents. Doubly distilled water was used throughout this work. All the chemicals were of an analytical reagent grade. The metallic mercury was purified in the usual manner.[13] The sodium perchlorate solutions to maitain a constant ionic strength were obtained by mixing sodium carbonate solutions and perchloric acid. The preparation and standardization of mercury(I) perchlorate solutions were all done in the way described in a previous paper.[3] Saturated solutions of elemental mercury of a constant ionic strength adjusted with $NaClO_4$ were prepared using a mercury-vapor solubility apparatus as has been described in a previous paper,[13] with a modification of its gas-inlet-type adaptor. A fritted disk was employed in place of the inlet glass tube in order to attain equilibrium within a shorter time. As a result of this modification, a time of 10 min was found to be sufficient to attain the solubility equilibrium.

Apparatus and Procedure. Two separate measurements were made: atomic absorption spectrophotometric measurements of elemental mercury, which lead to k values (*Procedure A*), and spectrophotometric measurements of mercury (I), which lead to kK_d values (*Procedure B*). Several Pyrex Erlenmeyer flasks of a 100-ml capacity and of the same size and form were used as reaction vessels in both *Procedures A* and *B*. The reaction vessel was connected at the ground-glass joint to a gas-washing-type adaptor. The adaptor was equipped with a fine tip of a glass tube *ca.* 1 mm i.d., and the front was positioned centrally 1 cm above the bottom of the reaction vessel. The reaction vessel containing the sample solution was immersed in a constant bath thermostated to within 0.05 °C.

Procedure A: A 40-ml portion of a saturated mercury solution was introduced into the reaction vessel. Then, nitrogen gas was immediately dispersed at a constant flow rate through the solution by means of the fine tip. The resulting mercury vapor was carried with the nitrogen stream through a 10-cm-path-length absorption cell with quartz windows, where it was detected by a Hitachi Model 508 atomic absorption spectrophotometer. In order to catch water droplets, an empty trap immersed in an ice-cooled bath was inserted between the reaction vessel and the cell. The absorption peaks of mercury were recorded on a Hitachi Model 108 recorder with a chart speed of 40 mm/min.

Procedure B: A 500-ml mercury(I) perchlorate solution was prepared by diluting a 10^{-3} M mercury(I) stock solution with 0.05 M $HClO_4$ and by adding a suitable volume of a 1 M $NaClO_4$ solution. This solution was then divided into 40-ml portions in separate reaction vessels which had been stoppered until used. Nitrogen gas was then passed through the solution under the same conditions as in *Procedure A*. After a fixed time, the reaction vassel was placed by another one. The solutions were measured by means of a Hitachi Model 181 spectrophotometer at 236.5 nm, and the concentrations of Hg_2^{2+} were determined based on a calibration curve.[14]

Results

Some typical results of atomic absorption monitoring of the elemental mercury carried with nitrogen gas at a constant flow rate are shown in Fig. 1. The ordinate is an arbitrary unit represented by the height on the recorder chart. The total peak area from zero to infinity time corresponds to the initial amount of mercury present in the solution, and is related to $[Hg(aq)]_0$, which can be predicted from the solubility study.[13] Then, we can estimate [Hg(aq)] at any time, t, by subtracting the peak area from zero to time t from the total peak area. As a matter of convenience, the summation of all the individual peak heights read every 1 mm on the abscissa is employed instead of the peak area. The plots of log[Hg(aq)] *vs.* t were found to be linear for at least 3 half-lives, as predicted from

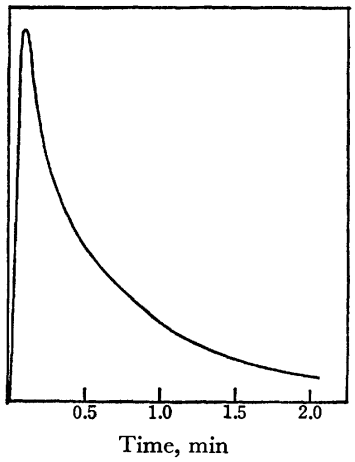

Fig. 1. Typical result of monitoring Hg° by atomic absorption spectrophotometry. The ordinate is an arbitrary unit represented by the recorder chart height. $[Hg(aq)]_0$; 1.75×10^{-7} M, temp; 15 °C, μ; 0.1, N_2 flow rate; 2.0 l/min.

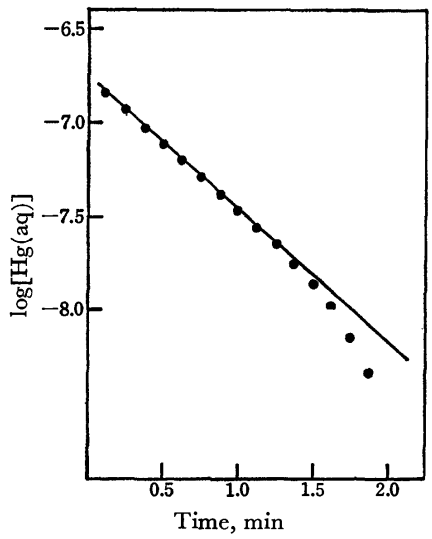

Fig. 2. Plot of Figure 1 according to Eq. 7.

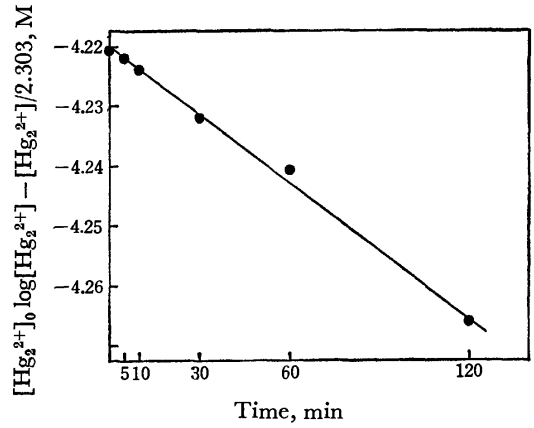

Fig. 3. Plot according to Eq. 5. $[Hg_2^{2+}]_0$; 0.76×10^{-5} M, temp; 15 °C, μ; 0.1, N_2 flow rate; 2.0 l/min.

Eq. 7 in the range of the nitrogen flow rate from 1.5 to 2.5 l/min. A typical result is shown in Fig. 2. From the slope of the straight line, k was obtained. According to Eq. 5, the concentrations of Hg_2^{2+} were plotted against time t. The results are shown in Fig. 3. From the slope of the straight line, we can estimate the kK_d value.

The conditions under which some typical runs were made and their results are given in Table 1. The disproportionation constants of mercury(I) over the temperature range of 15 to 35 °C were determined under such conditions that μ=0.1, nitrogen flow rate= 2.0 l/min, $[Hg_2^{2+}]_0=0.76\times10^{-5}$ M, and $[Hg(aq)]_0$= saturated at each temperature under study. The results are listed in Table 2. The thermodynamic parameters associated with K_d are calculated from Table 2 by the least-squares method, $\Delta H=13.2\pm0.2$ kcal/mol and $\Delta S=8.0\pm0.8$ e.u.

Discussion

The method described here to determine the disproportionation constant of mercury(I) is essentially the

Table 1. The effects of the ionic strength, the nitrogen flow rate, and the initial concentrations of Hg_2^+ and Hg(aq) on the estimations of k, kK_d, and K_d

	k, min^{-1}	kK_d, 10^{-9} M min^{-1}	K_d, 10^{-9} M
Ionic strength (μ)	(N_2 flow rate; 2.0 l/min, temp; 15 °C, $[Hg_2^{2+}]_0$; 0.76×10^{-5} M, $[Hg(aq)]_0$; 1.75×10^{-7} M)		
0.05	1.6±0.1	8.4±0.8	5.2±0.2
0.1	1.7±0.1	8.2±0.5	4.8±0.1
N_2 flow rate (l/min)	(μ; 0.1, temp; 15 °C, $[Hg_2^{2+}]$; 0.76×10^{-5} M, $[Hg(aq)]_0$; 1.75×10^{-7} M)		
2.5	1.8±0.1	9.2±0.4	5.1±0.1
2.0	1.7±0.1	8.2±0.5	4.8±0.1
1.5	1.5±0.1	8.4±0.2	5.6±0.2
$[Hg_2^{2+}]_0$, 10^{-5} M	(N_2 flow rate; 2.0 l/min, μ; 0.1, temp; 25 °C)		
1.52		21±1	
0.76		23±2	
0.38		22±1	
$[Hg(aq)]_0$, 10^{-7} M	(N_2 flow rate; 2.0 l/min, μ; 0.1, temp; 25 °C)		
3.2	2.2±0.1		
1.6	2.2±0.1		
1.1	2.1±0.1		

Table 2. Disproportionation constants determined at various temperatures[a)]

Temp, °C	k, min^{-1}	kK_d, 10^{-9} M min^{-1}	K_d, 10^{-9} M
15	1.7±0.1	8.2±0.5	4.8±0.1
20	2.0±0.1	16±1	7.9±0.1
25	2.2±0.1	23±2	11±1
30	2.3±0.1	36±1	16±1
35	2.5±0.1	55±1	22±1

a) N_2 flow rate; 2.0 l/min, μ; 0.1, $[Hg_2^{2+}]_0$; 0.76×10^{-5} M, $[Hg(aq)]_0$; saturated at each temperature.

same as those used in the kinetic studies of oxidation reactions of mercury(I) with inorganic oxidants.[5)] According to Sykes and his co-workers,[6,15)] for two-equivalent oxidants with relatively low oxidation potentials, the general rate law is expressed satisfactorily by

$$-d[Hg_2^{2+}]/dt = k_1K_d[Hg_2^{2+}][Oxidant]/[Hg^{2+}]. \quad (8)$$

The mechanism has been explained as involving the following paths:

$$Hg_2^{2+} \overset{K_d}{\rightleftharpoons} Hg(aq) + Hg^{2+}, \text{ fast}$$

$$Hg(aq) + Oxidant(2e^-) \overset{k_1}{\longrightarrow} Hg^{2+}$$

It is usually difficult to determine k_1 independently because of the limited solubility of elemental mercury in an aqueous solution. Therefore, the rate constant of the rate-controlling step, k_1, has been estimated by combining the observed rate constant and the K_d value.[5)] In the present study, Hg(aq), which is in equilibrium with Hg^{2+} and Hg_2^{2+}, was removed from the aqueous phase by the use of an inert gas instead of oxidants. In such a treatment, the reaction system is very much simplified, and, moreover, the rate constant in the rate-controlling step can be determined independently by the use of a highly sensitive atomic-absorption technique. The rate of Hg^0 transfer from the aqueous to the gaseous phase was taken to be the rate-controlling step because the disproportionation equilibrium is rapidly established. In such a heterogeneous system, the rate constant, k, must be a function of the surface area of the gaseous phase in contact with a solution, which depends on many factors, such as the shape of the nitrogen-inducing tube and the reaction vessel, the flow rate of the nitrogen gas, and the size of the sample solutions. However, the k required for the present purpose is not an inherent value, but a relative value sensitive only to the solution temperature. It is absolutely essential to carry out independent determinations of k under the same conditions as the determinations of kK_d. Under the present experimental conditions, N_2 flow rates in the range from 1.5 to 2.5 l/min were suitable for the determinations of k. Deviations from linear plots according to Eq. 7 were observed both at lower and higher flow rates than this range. These deviations are probably because a lower flow rate may result in an insufficient stirring of the aqueous phase, while a higher flow rate may result in the disturbance of a regular stream of the gaseous phase along the path from the reaction vessel and in the measuring cell. The variations in the initial concentrations of Hg_2^{2+}, 1.52×10^{-5} to 0.38×10^{-5} M, and Hg(aq), 3.2×10^{-7} to 1.1×10^{-7} M, have little effect on kK_d and k respectively, as may be seen from Table 1. This appears to support the rate laws expressed by Eqs. 4 and 6.

The present method is very similar to that by Moser and Voigt,[12)] though different experimental approaches are employed, that is, a kinetic and a static method respectively. The latter requires accurate solubility data of elemental mercury in water and organic solvents, while the present kinetic method does not require the absolute values of $[Hg_2^{2+}]$ and [Hg(aq)], since they have no effects on the slopes of the rate plots obtained by means of Eqs. 5 and 7. The K_d value at 25 °C determined in the present study is about two times larger than that reported by Moser and Voigt, 5.5×10^{-9} M. The discrepancy, however, seems to be small when we consider the different experimental approaches employed in the two studies.

The thermodynamic principles underlying the Hg(0)/Hg(I)/Hg(II) equilibria are quite well understood. The equilibrium constant, $K=[Hg^{2+}]/[Hg_2^{2+}]$, can be calculated from the formal potentials of the Hg(I)-Hg(0) and Hg(II)-Hg(I) couples reported in the literature, ranging from 0.006 to 0.012.[7,12,16] The product of K and the mercury solubility, 3.2×10^{-7} M,[13] comes to be from 1.9×10^{-9} to 3.8×10^{-9} M. The potentiometric method may give a reliable K value in the presence of liquid mercury. However, it appears extremely doubtful that the product of K and the mercury solubility should be taken as K_d. The solubility of mercury cited in the literature might be unsuitable for predicting [Hg(aq)] under relatively high mercury(I) concentrations and in the presence of liquid mercury because of the formation of the colloidal mercury.[17] If the colloidal mercury could take part in the disproportionation equilibrium, Reaction 1 should be shifted to the left, leading to a lower apparent K_d. In the studies of reactions concerned with dilute mercury(I) ions in which mercury atoms are present in equilibrium with Hg_2^{2+} and Hg^{2+} and are not in excess, the K_d value should be adopted as the equilibrium constant.

Schwarzenbach and Anderegg have reported that, for the $Hg(l)+Hg^{2+}\rightleftharpoons Hg_2^{2+}$ reaction, $\Delta H^\circ=-0.820$ kcal/mol, $\Delta S^\circ=6.0$ e.u., and $\Delta G^\circ=-2.62$ kcal/mol.[10] In the present study, $\Delta H^\circ=13.2$ kcal/mol, $\Delta S^\circ=8.0$ e.u., and $\Delta G^\circ=10.8$ kcal/mol were obtained for the $Hg_2^{2+}\rightleftharpoons Hg(aq)+Hg^{2+}$ reaction. When these two reactions are compared, it follows that $\Delta G^\circ=8.19$ kcal/mol for the $Hg(l)\rightleftharpoons Hg(aq)$ equilibrium. A termodynamic datum for this equilibrium has been published: $\Delta G^\circ=9.4$ kcal/mol.[18] The discrepancy between these two values may be partly due to the experimental errors.

In his spectrophotometric study Higginson suggested a homolytic dissociation, $Hg_2^{2+}\rightleftharpoons 2\,Hg^+$, in dilute mercury(I) solutions and reported a value of $k_{diss}=[Hg^+]^2/[Hg_2^{2+}]$ within the limits of 10^{-8} and 10^{-6} M.[14] However, such a dissociation constant was not taken into consideration in the present work for the following reasons, as suggested by other investigators: (1) a deviation from Beer's law in dilute mercury(I) solutions was not observed by another investigator;[19] (2) a K_{diss} value as large as 10^{-7} M is shown by the extraction technique to be highly unlikely[12] and (3) the evidence for a contribution from $[Hg_2^{2+}]^{1/2}$ instead of $[Hg_2^{2+}]$ has not been observed in kinetic studies of the reactions in which mercury(I) ions are concerned.[6]

The authors wish to express their thanks to Professor Hideo Nagai and Dr. Toshio Deguchi of Kumamoto University for their encouragement and discussions. They also wish to thank Dr. Kenzo Kitayama of the Tokyo Institute of Technology for his helpful discussions on the thermodynamic interpretation.

References

1) R. L. Wolfgang and R. W. Dodson, *J. Phys. Chem.*, **56**, 872 (1952).
2) I. Sanemasa, *Inorg. Chem.*, in press.
3) I. Sanemasa, *Inorg. Chem.*, **15**, 1973 (1976).
4) D. R. Rosseinsky, *J. Chem. Soc.*, **1963**, 1181.
5) A. M. Armstrong, J. Halpern, and W. C. E. Higginson, *J. Phys. Chem.*, **60**, 1661 (1956); A. M. Armstrong and J. Halpern, *Can. J. Chem.*, **35**, 1020 (1957).
6) R. Davies, B. Kipling, and A. G. Sykes, *J. Am. Chem. Soc.*, **95**, 7250 (1973).
7) M. J. Taylor, "Metal-to-Metal Bonded States of the Main Group Elements," Academic Press, N. Y. (1975), pp. 28—35.
8) A. Jonsson, I. Qvarfort, and L. G. Sillén, *Acta Chem. Scand.*, **1**, 461 (1947).
9) W. Forsling, S. Hietanen, and L. G. Sillén, *Acta Chem. Scand.*, **6**, 901 (1952).
10) G. Schwarzenbach and G. Anderegg, *Helv. Chim. Acta*, **37**, 1289 (1954).
11) T. H. Wirth and N. Davidson, *J. Am. Chem. Soc.*, **86**, 4314 (1964).
12) H. C. Moser and A. F. Voigt, *J. Am. Chem. Soc.*, **79**, 1837 (1959).
13) I. Sanemasa, *Bull. Chem. Soc. Jpn.*, **48**, 1795 (1975).
14) W. C. E. Higginson, *J. Chem. Soc.*, **1951**, 1438.
15) A. G. Sykes, "Kinetics of Inorganic Reaction," 1st ed, Pergamon Press, Elmsford, N. Y. (1966), pp. 170—172.
16) F. A. Cotton and G. Wilkinson, "Advanced Inorganic Chemistry," 3rd ed, John Wiley and Sons, N. Y. (1972), p. 509.
17) M. A. Thompson, J. C. Sullivan, and E. Deutch, *J. Am. Chem. Soc.*, **93**, 5667 (1971).
18) For instance, "JANAF Thermochemical Tables," 2nd ed, NSRDS-NBS 37 (1971).
19) E. Onat, *J. Inorg. Nucl. Chem.*, **36**, 2029 (1974).

Synthesis and Properties of Cobalt(II), Nickel(II), and Copper(II) Complexes with Acetaldehyde Oxime and Benzaldehyde Oxime

Hideaki TANAKA, Hiro KUMA, and Shoichiro YAMADA

Institute of Chemistry, College of General Education, Osaka University, Toyonaka, Osaka 560

(Received July 20, 1977)

Cobalt(II), nickel(II), and copper(II) complexes with acetaldehyde oxime and benzaldehyde oxime have been prepared and characterized by vibrational and electronic spectroscopy, magnetism, and other methods. The cobalt(II) and nickel(II) complexes isolated are of the general formulae: (A) $MX_2(oxime)_4$ (X=Cl, Br, I, NO_3, NCS and CH_3COO); (B) $M(NCS)_2(oxime)_2$; (C) $MSO_4(oxime)_3 \cdot 3H_2O$. They are all six-coordinate, and the complexes (B) are probably multinuclear. Copper(II) forms complexes of the formulae: (A) $CuX_2(oxime)_4$ (X=Cl, Br), (B) $CuX_2(oxime)_2$ (X=Cl, Br, NCS); (C) $CuSO_4(oxime)_4 \cdot H_2O$. Possible structures for these copper(II) complexes are also discussed. Acetaldehyde oxime and benzaldehyde oxime are unidentates in all these complexes, being coordinated through their nitrogen atom.

Some complexes of cobalt, nickel, and copper with acetaldehyde oxime and benzaldehyde oxime were prepared fifty years ago.[1] However, little work has been done on the more detailed examination of their stereochemistries based upon physicochemical measurements.[2,3] Such studies are thought to be highly desirable in order to elucidate the nature of interaction between the oximes and transition metal ions.

In the present work cobalt(II), nickel(II), and copper(II) complexes with acetaldehyde oxime and benzaldehyde oxime, including previously reported ones, have been synthesized and their stereochemistries have been examined on the basis of vibrational and electronic spectra, magnetism, conductivities, and powder X-ray diffraction patterns. Acetaldehyde oxime and benzaldehyde oxime are abbreviated in the present paper as acox and bzox, respectively.

Experimental

Materials. Acetaldehyde oxime and benzaldehyde oxime were obtained commercially and used as received.

Analytical data of the metal complexes prepared in the present work are given in Tables 1 and 2.

Dichloro- and Dibromotetrakis(acetaldehyde oxime)nickel(II), $NiX_2(acox)_4$ (X=Cl, Br) were prepared as reported previously.[1]

Diiodotetrakis(acetaldehyde oxime)nickel(II) Hydrate, $NiI_2(acox)_4 \cdot H_2O$. A suspension of $NiI_2 \cdot 6H_2O$ (0.01 mol) in chloroform (50 ml) was heated under stirring at 40 °C for 15 min and acetaldehyde oxime (0.04 mol) was added to the suspension. The mixture was heated at 40 °C for 1 h and filtered. The filtrate was concentrated to 10 ml with a rotary evaporator at 40 °C and allowed to stand in a refrigerator overnight. A crystalline precipitate was collected by filtration and recrystallized from chloroform to yield olive-green, prismatic crystals.

TABLE 1. ANALYTICAL DATA OF NICKEL(II) AND COBALT(II) COMPLEXES WITH ACETALDEHYDE OXIME AND BENZALDEHYDE OXIME

Compound	Found, %			Calcd, %			μ
	C	H	N	C	H	N	
$NiCl_2(acox)_4$	26.09	5.60	15.33	26.26	5.51	15.31	3.22
$NiBr_2(acox)_4$	20.72	4.65	12.37	21.13	4.43	12.32	3.18
$NiI_2(acox)_4 \cdot H_2O$	16.95	3.82	9.94	16.95	3.91	9.89	3.14
$Ni(NO_3)_2(acox)_4 \cdot H_2O$	21.77	4.95	19.14	21.99	5.07	19.23	3.16
$Ni(CH_3COO)_2(acox)_4$	34.62	6.25	13.32	34.90	6.34	13.57	3.13
$NiSO_4(acox)_3 \cdot 3H_2O$	18.43	5.16	10.74	18.67	5.48	10.89	3.17
$Ni(NCS)_2(acox)_4$	29.14	4.97	20.57	29.21	4.90	20.44	3.02
$Ni(NCS)_2(acox)_2$	24.90	3.60	19.58	24.59	3.44	19.12	3.23
$NiCl_2(bzox)_4$	54.76	4.68	9.13	54.30	4.60	13.43	3.17
$NiBr_2(bzox)_4$	47.83	4.16	7.95	47.83	4.01	7.97	3.08
$NiI_2(bzox)_4 \cdot H_2O$	41.26	3.65	6.78	41.26	3.71	6.87	3.07
$Ni(NCS)_2(bzox)_2$	45.90	3.53	13.42	46.07	3.38	13.43	3.17
$CoCl_2(acox)_4$	25.87	5.72	15.23	26.24	5.51	15.30	4.86
$CoBr_2(acox)_4$	21.04	4.59	12.40	21.12	4.43	12.31	4.93
$CoSO_4(acox)_3 \cdot 3H_2O$	19.01	5.13	11.06	18.66	5.48	10.88	5.15
$Co(NCS)_2(acox)_2$	24.30	3.63	19.19	24.57	3.44	19.11	4.85
$CoCl_2(bzox)_4$	54.62	4.66	9.22	54.73	4.59	9.12	5.11
$CoBr_2(bzox)_4$	47.81	4.01	8.02	47.81	4.01	7.97	5.04
$Co(NCS)_2(bzox)_2$	45.62	3.54	13.24	46.04	3.38	13.42	4.90

μ: BM at room temperature.

Table 2. Analytical data of copper(II) complexes with acetaldehyde oxime and benzaldehyde oxime

Compound	Found, %			Calcd, %			μ
	C	H	N	C	H	N	
$CuCl_2(acox)_4$	25.71	5.48	15.04	25.92	5.44	15.11	1.80
$CuBr_2(acox)_4$	20.62	4.44	12.18	21.03	4.39	12.19	1.88
$CuCl_2(acox)_2$	19.18	4.14	10.98	19.02	4.00	11.09	1.88
$CuBr_2(acox)_2$	13.69	3.06	8.03	14.07	2.95	8.20	1.82
$CuSO_4(acox)_4 \cdot H_2O$	23.62	5.13	13.82	23.21	5.36	13.54	1.92
$CuCl_2(bzox)_2$	44.32	3.88	7.43	44.63	3.75	7.44	1.99
$CuBr_2(bzox)_2$	36.11	3.03	6.06	36.11	3.03	6.02	1.87

μ: BM at room temperature.

Dinitratotetrakis(acetaldehyde oxime)nickel(II) Hydrate, $Ni(NO_3)_2(acex)_4 \cdot H_2O$, was prepared from $Ni(NO_3)_2 \cdot 6H_2O$ (0.01 mol) and acetaldehyde oxime (0.04 mol) in a manner analogous to the diiodo-complex.

$Ni(NCS)_2(acox)_4$ and $Ni(NCS)_2(acox)_2$. A suspension of $Ni(NCS)_2$ (0.01 mol) in ethanol (50 ml) was heated at 60 °C under stirring for 2 h, until the solution turned green, and filtered. To the filtrate was added acetaldehyde oxime (0.04 mol) and stirred for 1 h at room temperature. On evaporating the solution spontaneously, blue crystals of $Ni(NCS)_2(acox)_4$ appeared in the solution. They were collected by filtration and washed with ethanol. The filtrate was heated for 2 h at room temperature. A crystalline powder of $Ni(NCS)_2(acox)_2$ formed in the solution was filtered, washed with ethanol, and dried in a desiccator over silica gel.

$NiSO_4(acox)_3 \cdot 3H_2O$ was prepared as blue microcrystals from $NiSO_4 \cdot 7H_2O$ (0.01 mol) and acetaldehyde oxime (0.04 mol) in a manner analogous to the dinitrato-complex.

Dichloro- and Dibromotetrakis(benzaldehyde oxime)nickel(II), $NiX_2(bzox)_4$ (X=Cl, Br), were prepared by the literature method.[1]

Diiodotetrakis(benzaldehyde oxime)nickel(II) Hydrate, $NiI_2(bzox)_4 \cdot H_2O$, was prepared as olive-green crystals in a manner similar to the corresponding acetaldehyde oxime complex.

Dihalogenotetrakis(acetaldehyde oxime)- and Dihalogenotetrakis(benzaldehyde oxime)cobalt(II), $CoX_2(acox)_4$ and $CoX_2(bzox)_4$ (X=Cl, Br), were prepared as reported previously.[1]

$Co(NCS)_2(acox)_2$. To a suspension of $Co(NCS)_2 \cdot 4H_2O$ (0.01 mol) in chloroform (50 ml) was added acetaldehyde oxime (0.04 mol) at 60 °C, and the mixture was refluxed for 2 h. A pink crystalline precipitate was filtered and washed with chloroform several times.

$Co(NCS)_2(bzox)_2$ was prepared as red-brown crystals in a manner analogous to the corresponding complex with benzaldehyde oxime.

$CoSO_4(acox)_3 \cdot 3H_2O$ was prepared as wine-red crystals from $CoSO_4 \cdot 7H_2O$ (0.01 mol) and acetaldehyde oxime (0.04 mol) in a manner analogous to the corresponding nickel(II) complex.

$CuCl_2(acox)_2$. To a solution of $CuCl_2 \cdot 2H_2O$ (0.015 mol) in ethanol (50 ml) was added acetaldehyde oxime (0.02 mol), and the solution was stirred at room temperature for 3 h. Light-blue flaky crystals of $CuCl_2(acox)_2$ formed in the solution were filtered and washed with ether. The *filtrate* was used for preparing $CuCl_2(acox)_4$. The crystals thus obtained are highly hygroscopic. When left in a desiccator over silica gel for a long time, the blue form of $CuCl_2(acox)_2$ transformed into a green substance of the same composition.

Dichlorotetrakis(acetaldehyde oxime)copper(II), $CuCl_2(acox)_4$. Acetaldehyde oxime (0.05 mol) was added to the *filtrate* obtained in the preparation of $CuCl_2(acox)_2$. Stirring the solution at room temperature for 15 min yielded blue prismatic crystals. They are hygroscopic and are readily decomposed even in the solid state. When kept in a desiccator over silica gel, they gradually lose acetaldehyde oxime, turning green. The composition of the green final product was close to $CuCl_2(acox)_2$.

$CuBr_2(acox)_4$ and *$CuBr_2(acox)_2$* were prepared as blue and yellow-green crystals, respectively, by methods similar to the corresponding dichloro-complexes. They are hygroscopic. When left in a desiccator, $CuBr_2(acox)_4$ loses acetaldehyde oxime to yield $CuBr_2(acox)_2$.

$CuCl_2(bzox)_2$ was prepared as yellow-green crystals by the literature method.[1] Purification was carried out by recrystallization from chloroform or acetone.

$CuBr_2(bzox)_2$ was prepared as brown crystals from $CuBr_2$ and benzaldehyde oxime in a manner analogous to the corresponding dichloro-complex.

$CuSO_4(acox)_4 \cdot H_2O$. To a suspension of $CuSO_4 \cdot 5H_2O$ (0.01 mol) in chloroform was added acetaldehyde oxime (0.06 mol), and the mixture was stirred at room temperature for a few hours. The precipitate was recrystallized from chloroform to yield a blue crystalline powder.

Measurements. Electronic absorption spectra of the complexes in solution and in Nujol were recorded on a Shimadzu MPS-50L spectrophotometer. Infrared spectra were measured as Nujol mulls on a Hitachi EPI-S2 infrared spectrophotometer and a Hitachi 215 infrared spectrophotometer.

Magnetic measurements at room temperature were carried out by the Gouy method using $CoHg(SCN)_4$ as a calibrant.

Powder X-ray diffraction patterns were obtained with a Toshiba DX-103 X-ray diffractometer equipped with a Geiger-Müller counter, using Co $K\alpha$ radiation and an iron filter.

Conductivity measurements were carried out using a calibrated Toa-Electronics CG 201 PL conductivity cell and a Toa-Electronics Model CM-1DB conductivity bridge.

Results and Discussion

Nickel(II) Complexes. The following types of nickel(II) complexes were isolated, L being acox or bzox: (1) NiX_2L_4 (X=Cl, Br, I, NO_3, CH_3COO); (2) $Ni(NCS)_2L_2$; (3) $NiSO_4(acox)_3 \cdot 3H_2O$. All these nickel(II) complexes are paramagnetic with magnetic moments of 3.0—3.2 BM (Table 1). The dichloro- and dibromo-nickel(II) complexes were reported previously by Hieber and Leutert.[1]

All the dihalogeno-complexes are non-electrolytes in nitrobenzene, indicating that the halide ions are bound to the nickel(II) ion. According to a previous X-ray

study,[3] $NiCl_2(acox)_4$ in the crystalline state has a six-coordinate *trans*-dichloro-structure. The acetaldehyde oxime molecules are coordinated to the nickel(II) ion through their nitrogen atom, and the OH group is hydrogen-bonded to Cl. It is presumed that $NiX_2(acox)_4$ (X=Br, I) and $NiX_2(bzox)_4$ (X=Cl, Br, I) also have a six-coordinate *trans*-dihalogeno-structure, since their electronic absorption spectra are similar to that of *trans*-$NiCl_2(acox)_4$. They all show a significantly large tetragonal splitting in the d-d bands. This *trans*-structure is retained in chloroform, since the spectra of the chloroform solutions are essentially the same as the solid state spectra. On the contrary, they undergo decomposition in water, methanol, and ethanol. For instance, the spectra of the ethanolic solutions differ appreciably from the spectra of the chloroform solutions as well as from the solid state spectra.

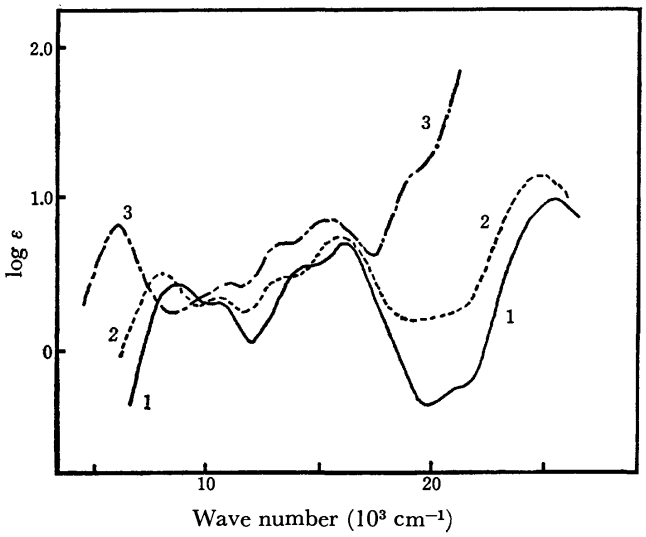

Fig. 1. Electronic absorption spectra of *trans*-dihalogeno-tetrakis(acetaldehyde oxime)nickel(II), *trans*-$NiX_2(acox)_4$, in chloroform: 1, X=Cl; 2, X=Br; 3, X=I.

As representative examples, the spectra of the acetaldehyde oxime complexes are shown in Fig. 1. It is predicted theoretically that regularly octahedral nickel(II) complexes show three spin-allowed d-d bands, each of which is split into two components as the symmetry of the complexes changes from O_h to D_{4h}. If the splitting is considerably large, the components are likely to be well resolved in the observed spectrum. The band splitting in the spectra of the present dihalogeno-complexes is large enough to enable us to resolve the three main d-d bands into their components with reasonable accuracy. The maxima of the components obtained are shown in Table 3. From these data and using expressions derived on the basis of the crystal field approximation,[4] the tetragonal splitting parameters were estimated. The results are shown in Table 3. For *trans*-$NiCl_2(acox)_4$ a similar analysis was made previously using solid state spectrum.[2] The results roughly agree with the present ones. Comparison of the present results with previous studies[4a] on $NiX_2(py)_4$, py being pyridine, gives the following order as to the in-plane crystal field parameter: bzox<acox<py. It is thus found that bzox and acox are close to, though slightly lower than, py in the spectrochemical series.

Table 3. Split components of d-d bands and crystal field parameters in 10^3 cm^{-1} of *trans*-NiX_2L_4

	L=acox (=bzox)		
	X=Cl	X=Br	X=I
$\nu(^3E_g{}^a \leftarrow {}^3B_{1g})$	8.7 (8.5	8.2 8.2	7.3 7.5)
$\nu(^3B_{2g} \leftarrow {}^3B_{1g})$	10.6 (10.4	10.6 10.5	10.4 10.4)
$\nu(^3A_{2g} \leftarrow {}^3B_{1g})$	14.2 (13.6	13.5 13.5	12.2 13.4)
$\nu(^3E_g{}^b \leftarrow {}^3B_{1g})$	16.3 (16.2	16.2 15.9	15.7 16.1)
Dq^{xy}	1.06 (1.04	1.06 1.04	1.04 1.05)
Dq^z	0.62 (0.62	0.57 0.59	0.42 0.46)
Dt	0.24 (0.24	0.27 0.26	0.35 0.33)
Ds	0.30 (0.48	0.51 0.46	0.66 0.55)

In $Ni(NO_3)_2(acox)_4$ the nitrate ions are not free but coordinated to the nickel(II) ion, since infared bands due to the nitrate ions occur at 1290, and 1495 cm^{-1}.[5] The complex is paramagnetic and its electronic spectrum is typical of the six-coordinate nickel(II) complex (Table 4). The broad d-d bands at about 10 and 17×10^3 cm^{-1} have a shoulder at higher frequencies in the former band and at lower frequencies in the latter, indicating

Table 4. Maxima of main d-d absorption bands of nickel(II) complexes with acetaldehyde oxime and benzaldehyde oxime

Compound	Medium	ν_1(log ε)	ν_2(log ε)	ν_3(log ε)
$Ni(CH_3COO)_2(acox)_4$	Nujol	9.9	16.7	27.1
	$CHCl_3$	9.8 (0.62)	16.6 (0.76)	26.3 (1.20)
$Ni(NO_3)_2(acox)_4\cdot H_2O$	Nujol	9.3	17.0	26.9
	$CHCl_3$	9.3 (0.59)	16.6 (0.85)	26.9 (1.17)
$NiSO_4(acox)_3\cdot 3HO_2$	Nujol	8.3, 10.7	16.7	26.7
$Ni(NCS)_2(acox)_4$	Nujol	9.9	16.9	26.9
	$CHCl_3$	10.1 (1.08)	16.6 (1.15)	26.7 (1.74)
$Ni(NCS)_2(acox)_2$	Nujol	8.6, 11.2 sh	16.6	27.1
$Ni(NCS)_2(bzox)_2$	Nujol	8.5, 10.9 sh	16.2	27.1

ν_1 $^3T_{2g} \leftarrow {}^3A_{2g}$; ν_2 $^3T_{1g} \leftarrow {}^3A_{2g}$; ν_3 $^3T_{1g}(P) \leftarrow {}^3A_{2g}$ or components thereof. sh: shoulder.

an apparent band splitting, in agreement with the model of the six-coordinate *trans*-dinitrato-complex.

The complex $Ni(CH_3COO)_2(acox)_4$ exhibits CO stretching vibrations at 1580 and 1340 cm^{-1}, showing that the acetate ions are not free but coordinated to the nickel(II) ion as unidentate ligands.[5] The complex is paramagnetic and shows an electronic absorption spectrum typical of the six-coordinate nickel(II) complex.

In $NiSO_4(acox)_3 \cdot 3H_2O$, the ν_1 stretching vibration due to the sulfate group appears at 993 cm^{-1} and ν_3 is split into three bands at 1040, 1085, and 1200 cm^{-1}. Based on the criteria proposed previously,[5] these results indicate that the sulfate group in this complex is coordinated as a bidentate ligand to the nickel(II) ion. Its electronic spectrum is typical of the six-coordinate nickel(II) complex (Table 4). It is, therefore, most likely that the nickel(II) ion forms a six-coordinate complex with three acetaldehyde oxime molecules, a bidentate sulfate ion and a water molecule coordinated. A multinuclear structure, however, may not be eliminated.

$Ni(NCS)_2(acox)_4$ is paramagnetic with a moment of about 3 BM, indicative of a six-coordinate structure for this complex. Its Nujol spectrum is similar to the spectrum of its chloroform solution, showing that the configuration in the solid state is retained in the chloroform solution. The spectra are typical of the six-coordinate nickel(II) complex, and resemble that of *trans*-$Ni(NCS)_2(NH_3)_4$,[6] although slightly displaced towards lower frequencies. It is highly probable that $Ni(NCS)_2(acox)_4$ has a similar structure to that of *trans*-$Ni(NCS)_2(NH_3)_4$ with the thiocyanate ions coordinated through their nitrogen atom to the nickel(II) ion. Any appreciable splitting was not observed in the d-d bands for $Ni(NCS)_2(NH_3)_4$ and $Ni(NCS)_2(acox)_4$, possibly because the N-coordinating thiocyanate stands comparatively close to acox and NH_3 in the spectrochemical series.

The complex $Ni(NCS)_2(acox)_4$ undergoes decomposition gradually. Infrared bands due to unidentate N-coordinating thiocyanate ions appear at 2090 and 820 cm^{-1}, but in addition to them another band, probably originating from the decomposition product, appears at 2020 cm^{-1}.

The complexes $Ni(NCS)_2L_2$, L being acox and bzox, are paramagnetic (Table 1) and show electronic absorption spectra typical of the six-coordinate nickel(II) complex (Table 4). They show infrared ν(C–N) and ν(C–S) vibrations at 2115 and 780 cm^{-1} for L=acox and at 2130 and 785 cm^{-1} for L=bzox. The values lie in the range expected for the bridging NCS group.[7] It is highly probable that $Ni(NCS)_2L_2$ are multinuclear with six-coordinate nickel(II) ions and bridging NCS ions, having a similar structure to that of $Ni(NCS)_2(py)_2$.[8]

All the nickel(II) complexes show hydrogen bonded OH stretching vibrations at about 3150—3200 cm^{-1}, except for $Ni(NCS)_2(acox)_2$ and $Ni(NCS)_2(bzox)_2$, which show a sharp band at a much higher frequency, indicative of the presence of the non-hydrogen-bonded NOH group (Table 6).

Cobalt(II) Complexes. The following types of cobalt(II) complexes were isolated, L being acox and bzox: (1) CoX_2L_4 (X=Cl, Br); (2) $Co(NCS)_2L_2$; (3) $CoSO_4(acox)_3 \cdot 3H_2O$. The dichloro- and dibromo-complexes were prepared previously.[1]

The complexes $CoX_2(acox)_4$ and $CoX_2(bzox)_4$ are paramagnetic with magnetic moments of 4.9—5.2 BM, which are in the range expected for six-coordinate cobalt(II) complexes. Their electronic absorption spectra (Table 5) are also typical of the six-coordinate cobalt(II) complexes. Conductivity measurements show that they are non-electrolytes in nitrobenzene. It is most likely that in these cobalt(II) complexes the six-coordination of the cobalt(II) ion is achieved by two halide ions and four oximes, which are unidentate ligands coordinating through the nitrogen atom. In agreement with this, their OH stretching vibrations appear at frequencies close to those of the dihalogeno-nickel(II) complexes, which have been concluded to have a *trans*-configuration. The powder X-ray diffraction patterns of the dichloro-cobalt(II) complexes are similar to those of the dibromo-cobalt(II) complexes. When dissolved in chloroform, the dichloro-cobalt(II) complexes retain the structure existing in the solid state, while the dibromo-cobalt(II) complexes tend to undergo decomposition gradually. Both the dichloro- and the dibromo-complexes are decomposed in methanol, ethanol, and water.

In $CoSO_4(acox)_3 \cdot 3H_2O$, the ν_1 stretching vibration due to the sulfate group appears at 940 cm^{-1} and ν_3 is split into three bands at 1030, 1080, and 1190 cm^{-1}. As discussed in the preceding section of the present paper,

TABLE 5. MAXIMA OF MAIN d-d ABSORPTION BANDS OF COBALT(II) COMPLEXES WITH ACETALDEHYDE OXIME AND BENZALDEHYDE OXIME

Compound	Medium	ν_1(log ε)	ν_2(log ε)	ν_3(log ε)
$CoCl_2(acox)_4$	Nujol	8.4	15.3 sh	18.4, 19.5
	$CHCl_3$	8.3 (0.33)	15.4 sh	18.1 (0.91), 19.3 (0.96)
$CoBr_2(acox)_4$	Nujol	8.4	15.1 sh	17.8, 18.9
$CoCl_2(bzox)_4$	Nujol	8.3	15.2 sh	18.3, 19.1
	$CHCl_3$	8.3 (0.52)	15.2 sh	18.1 (1.37), 19.0 (1.38)
$CoBr_2(bzox)_4$	Nujol	8.2	15.1 sh	17.8, 18.9
$CoSO_4(acox)_3 \cdot 3H_2O$	Nujol	8.8	16.3 sh	19.5, 20.9 sh
$Co(NCS)_2(acox)_2$	Nujol	9.6	15.8 sh	18.9
$Co(NCS)_2(bzox)_2$	Nujol	8.8	15.5 sh	19.1

ν_1 $^4T_{2g} \leftarrow {}^4T_{1g}$; ν_2 $^4A_{2g} \leftarrow {}^4T_{1g}$; ν_3 $^4T_{1g}(P) \leftarrow {}^4T_{1g}$ or components thereof. sh: shoulder.

Table 6. Main infrared bands of nickel(II) and cobalt(II) complexes with acetaldehyde oxime and bezaldehyde oxime

Compound	ν(OH)	ν(NO)
$NiCl_2(acox)_4$	3210	939, 953
$NiBr_2(acox)_4$	3215	939, 953
$Ni(NCS)_2(acox)_4$	3210	938
$Ni(NCS)_2(acox)_2$	3450	940
$Ni(NO_3)_2(acox)_2$	3210	940, 960
$NiSO_4(acox)_3\cdot 3H_2O$	3250	935, 950
$NiCl_2(bzox)_4$	3200	940, 967
$NiBr_2(bzox)_4$	3235	938, 962
$NiI_2(bzox)_4\cdot H_2O$	3203	936, 955
$Ni(NCS)_2(bzox)_2$	3415	940
$CoCl_2(acox)_4$	3215	945, 950
$CoBr_2(acox)_4$	3210	935, 950
$CoCl_2(bzox)_4$	3205	938, 950
$CoBr_2(bzox)_4$	3205	938, 957
$Co(NCS)_2(acox)_2$	3450	940
$Co(NCS)_2(bzox)_2$	3425	942
$CoSO_4(acox)_3\cdot 3H_2O$	3270	945

ν: cm^{-1}.

these results indicate that the sulfate group in this complex is coordinated as a bidentate ligand to the cobalt(II) ion. Its electronic spectrum (Table 5) is typical of the six-coordinate cobalt(II) complex, and its magnetic moment (5.15 BM) lies in the range expected for the six-coordinate cobalt(II) complex. The powder X-ray diffraction pattern is very similar to that of the corresponding nickel(II) complex, indicating that these cobalt(II) and nickel(II) complexes have a similar structure.

The complexes $Co(NCS)_2L_2$, L being acox and bzox, are paramagnetic with magnetic moments of 4.86 and 4.93 BM, which are in the range expected for the octahedral cobalt(II) complexes. Their electronic absorption spectra are also typical of the six-coordinate cobalt(II) complexes. They show infrared ν(C–N) and ν(C–S) vibrations at 2100 and 785 cm^{-1} for L=acox and at 2110 and 780 cm^{-1} for L=bzox. In the same way as in $Ni(NCS)_2(bzox)_2$, the infrared data indicate that the NCS groups function as bridging ligands. It is thus most likely that the complexes $Co(NCS)_2L_2$ have a similar multinuclear structure to that of $Ni(NCS)_2L_2$. The powder X-ray diffraction patterns of $Co(NCS)_2L_2$ are almost identical with those of $Ni(NCS)_2L_2$. Exactly like the corresponding nickel(II) compounds, they exhibit a sharp OH band at 3450 and 3425 cm^{-1} typical for the NOH group, which is not involved in hydrogen bonding.

The other cobalt(II) complexes show OH stretching vibrations at about 3150—3200 cm^{-1}.

Copper(II) Complexes. The copper(II) complexes obtained are of the following three types, X being Cl and Br: (1) $CuX_2(acox)_4$; (2) $CuX_2(acox)_2$ and $CuX_2(bzox)_2$; (3) $CuSO_4(acox)_4\cdot H_2O$. The complexes $CuCl_2(acox)_2$ and $CuCl_2(bzox)_2$ were prepared previously.[1]

Since $CuCl_2(acox)_4$ shows a powder X-ray diffraction pattern similar to that of *trans*-$NiCl_2(acox)_4$, it also has a six-coordinate *trans*-dichloro-structure, in which the molecules of acox are bound to the copper(II) ion through the nitrogen atom. The electronic absorption spectrum of $CuBr_2(acox)_4$ is very similar to that of $CuCl_2(acox)_4$. Their d-d band maxima lie at almost equal frequencies (Table 7). It is, therefore, very likely that $CuBr_2(acox)_4$ has a structure similar to that of $CuCl_2(acox)_4$, namely a six-coordinate *trans*-dihalogeno-structure.

Table 7. Maxima of main d-d absorption bands and of some infrared bands of copper(II) complexes with acetaldehyde oxime and benzaldehyde oxime

Compound	d-d band, 10^3 cm^{-1}	Infrared bands, cm^{-1}	
		ν(M-X)	ν(M-L)
$CuCl_2(acox)_2$	14.8	296, 235	272
$CuBr_2(acox)_2$	14.8	243, 208	259
$CuCl_2(bzox)_2$	14.3	295, 224	267
$CuBr_2(bzox)_2$	14.2	235, 210	261
$CuCl_2(acox)_4$	16.5	285	272
$CuBr_2(acox)_4$	16.6	238	271
$CuCl_2(py)_2$*	14.5	294, 235	268
$CuBr_2(py)_2$*	14.6	255, 202	269

* Multinuclear. The data are taken from references 9 and 10 in the text.

In view of the results on the corresponding cobalt(II) and nickel(II) complexes, it may be reasonable to assume that acox and bzox are coordinated through their nitrogen atom in the complexes of the types $CuX_2(acox)_2$ and $CuX_2(bzox)_2$. In agreement with this, they show OH-stretching vibrations at about 3150—3200 cm^{-1}, which lie close to those of $MX_2(acox)_4$ and $MX_2(bzox)_4$. Since acox and bzox lie close to pyridine in the spectrochemical series, it may be pertinent to remember previous studies on the copper(II) pyridine complexes of a similar composition. Billing and Underhill[9] examined correlation between electronic spectra and stereochemistries of complexes of the type CuX_2L_2, L being pyridine and its derivatives. They obtained two types of the complexes. The complexes of one type have a multinuclear structure, in which the copper(II) ion is in a six-coordinate, tetragonally distorted pseudo-octahedral environment, showing a broad d-d band with a maximum at $14—15\times10^3$ cm^{-1}. The d-d band maxima vary considerably, depending upon the extent of the tetragonal distortion. The complexes of the other type have a binuclear structure with square-pyramidal coordination about the copper(II) ion with bridging apical chloride ions and basal pyridine or substituted pyridine molecules. The spectra of the latter complexes have a d-d band at $16—19\times10^3$ cm^{-1} with a shoulder at 13.5×10^3 cm^{-1}. The uninuclear square-pyramidal copper(II) complex would show the corresponding d-d band at a higher frequency.

The complexes $CuX_2(acox)_2$ and $CuX_2(bzox)_2$ obtained in the present work show a broad d-d band at about $14.2—14.8\times10^3$ cm^{-1} (Table 7). According to the criteria derived previously,[9] these copper(II) complexes probably have a multinuclear structure similar to that of $CuX_2(py)_2$; $CuCl_2(py)_2$ and $CuBr_2(py)_2$ show a d-d band at about 14.5 and 14.6×10^3 cm^{-1}, respectively.

Their infrared ν(M-X) and ν(M-L) bands also seem to correspond well to those of multinuclear $CuCl_2(py)_2$ and $CuBr_2(py)_2$ (Table 7).[9,10]

When left in a desiccator for a long period, the blue form of $CuCl_2(acox)_2$ transformed into the green form of the same composition. The green form shows almost the same infrared spectrum as that of the blue form of $CuCl_2(acox)_2$ in the range from 200 to 3500 cm^{-1}. The electronic spectrum of the green substance is similar to that of the blue form, although the green form shows a d-d band at a slightly lower frequency than the blue form (Table 7). From the spectral criteria proposed previously,[9] both the two modifications probably have a similar multinuclear structure. The slight difference in the band maximum between the two may arise from the different extent of the tetragonal distortion.

In $CuSO_4(acox)_4 \cdot H_2O$, the ν_3 stretching vibration due to the sulfate group is split into two bands at 1035 and 1195 cm^{-1}, indicating that the sulfate group in this complex is coordinated as a unidentate ligand to the copper(II) ion.[5] The copper(II) ion probably takes five-coordination with four molecules of acetaldehyde oxime and a unidentate sulfate group.

Its electronic absorption spectrum has a broad d-d band with a maximum at 16.5×10^3 cm^{-1}, being in accordance with the five-coordinate structure.[11] A six-coordinate model with a water molecule as an additional ligand may not be eliminated.

The authors are grateful to Professor Masayoshi Obashi for powder X-ray diffraction patterns.

References

1) W. Hieber and F. Leutert, *Ber.*, **60**, 2296 (1927).
2) M. E. Stone and K. E. Johnson, *Can. J. Chem.*, **51**, 1260 (1973).
3) M. E. Stone, B. E. Robertson, and E. Stanley, *J. Chem. Soc. A*, **1971**, 3632.
4) (a) A. B. P. Lever, *Coord. Chem. Rev.*, **3**, 119 (1968); (b) C. R. Hare and C. J. Ballhausen, *J. Chem. Phys.*, **40**, 788 (1964).
5) K. Nakamoto, "Infrared Spectra of Inorganic and Coordination Compounds," Wiley-Interscience, New York (1970).
6) C. R. Hare and C. J. Ballhausen, *J. Chem. Phys.*, **40**, 792 (1964).
7) S. M. Nelson and T. M. Shepherd, *J. Inorg. Nucl. Chem.*, **27**, 2123 (1965); R. A. Bailey, S. L. Kozak, T. W. Michelsen, and W. N. Mills, *Coord. Chem. Rev.*, **6**, 407 (1971).
8) M. A. Porai-Koshits and G. N. Tishchenko, *Kristallografiya* **4**, 239 (1959); *Chem. Abstr.*, **55**, 12990a (1961).
9) D. E. Billing and A. E. Underhill, *J. Inorg. Nucl. Chem.*, **30**, 2147 (1968).
10) R. J. H. Clark and C. S. Williams, *Inorg. Chem.*, **4**, 350 (1965).
11) B. J. Hathaway and A. A, G. Tomlinson, *Coord. Chem. Rev.*, **5**, 1 (1970).

A Relationship between the Circular Dichroism and the Configuration of Asymmetric Nitrogen in *trans*(*N*,Ethylene)-chloro-L-aminocarboxylato-η^2-ethyleneplatinum(II)

Yoshiro TERAI, Hiroaki KIDO, and Kazuo SAITO

Chemistry Department, Faculty of Science, Tohoku University, Aramaki, Aoba, Sendai 980

(Received July 27, 1977)

The circular dichroism (CD) peaks of *trans*(*N*, ethylene)[PtCl(L-am)(C_2H_4)] (L-am, L-amino carboxylate) in acetonitrile (AN) at 33000 and 37000 cm^{-1} are characteristic of those complexes with asymmetric nitrogen. The CD sign depends on the substituents on the asymmetric nitrogen, and the additivity law holds for methyl and benzyl derivatives of L-prolinato, L-hydroxyprolinato, and L-valinato complexes. The quadrant rule is applicable to the contribution of the substituents on the nitrogen. On the preparation of the benzyl-L-valinato complex from Zeise's salt in a weakly acid medium the nitrogen exhibits a marked stereoselectivity to give *R* configuration.

Optical rotatory dispersion (ORD) and circular dichroism (CD) of asymmetric nitrogen on *N*-alkyl-L-amino carboxylate ligand have been mostly studied with cobalt(III) complexes. The absolute configuration of asymmetric nitrogen of $(+)_{589}$-[Co(sar)$(en)_2]^{2+}$ (sar, sarcosinate; en, ethylenediamine) was determined by X-ray diffraction to be *R*.[1] This complex gives a plus CD peak in 20000 to 25000 cm^{-1} region (first d-d transition band region), which was assigned to the asymmetric nitrogen.[2,3] Crystal structure[4] and CD spectra of copper(II) complexes containing asymmetric nitrogen[5,6] were studied but their relationship has not been discussed.

We have extended CD studies of square planar platinum(II) complexes containing amino carboxylates and η^2-olefins,[7] and synthesized various complexes of the type *trans*(*N*, ethylene)[PtCl(L-am)(C_2H_4)], where L-am stands for amino carboxylates having asymmetric nitrogens. This paper deals with the syntheses and the relationship between CD spectra and absolute configurations of the coordinated asymmetric nitrogens.

Experimental

Materials. Ligands: L-Allohydroxyproline (2*S*, 4*S*) (L-ahyp) was prepared from L-hydroxyproline (L-hyp) by the known method.[8,9] *N*-Methyl- and *N*-benzyl derivatives of L-proline (L-pro), L-hydroxyproline, L-valine (L-val), L-phenylalanine (L-phe), and L-alanine (L-ala) were synthesized by known methods.[10,11] Guaranteed grade L-proline, L-hydroxyproline, L-valine, L-phenylalanine, and L-alanine were used without further purification. (The abbreviations in parentheses indicate their deprotonated forms.)

Complexes. *trans*(*N*,Ethylene)-isomers of various [PtCl(L-am)(C_2H_4)] and *cis*(*N*,ethylene)[PtCl(L-pro)(C_2H_4)] were prepared by the reported methods.[7,12] New *trans*(*N*,ethylene) complexes containing L-hyp, L-ahyp, *N*-me-L-hyp, and *N*-bz-L-val were identified by elemental analysis of carbon, hydrogen, and nitrogen, and ultraviolet (UV) absorption spectra.

Measurements. The UV absorption and CD spectra were recorded in acetonitrile (AN) at room temperature with a Hitachi 323 and a JASCO J-40 Spectrophotometer, respectively.

Results and Discussion

CD Pattern. The UV absorption pattern of all the *trans*(*N*, ethylene) complexes is similar to one another and exemplified in Fig. 1A by *trans*(*N*, ethylene)-[PtCl(L-pro)(C_2H_4)]. The CD spectra of *trans*(*N*, ethylene) complexes containing L-pro, L-hyp, and L-

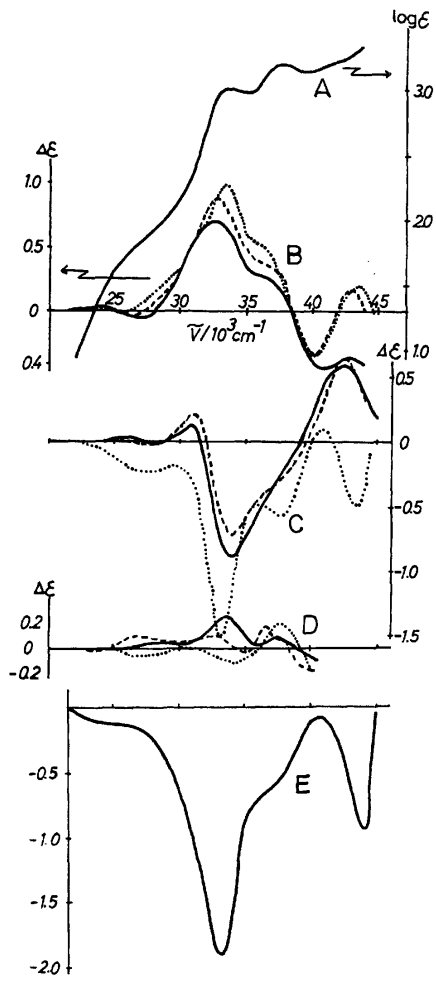

Fig. 1. Ultraviolet absorption and circular dichroism (CD) spectra of *trans*(*N*,ethylene)[PtCl(L-am)(C_2H_4)] in acetonitrile at room temperature. (L-am=L-amino carboxylate).
A: UV absorption of L-prolinato complex.
B: CD of — L-pro, --- L-hyp, and- -- L-ahyp complex.
C: CD of — *N*-me-L-pro, --- *N*-me-L-hyp, and --- *N*-bz-L-pro complex.
D: CD of — L-ala, --- L-phe, and --- L-val complex.
E: CD of *N*-bz-L-val complex.

ahyp have large plus components with $\Delta\varepsilon$ 0.7 to 1.0 in the 33000 cm^{-1} region. (Fig. 1B). In the same region, similar complexes containing substituted L-prolinate, *i.e* *N*-me-L-pro, *N*-me-L-hyp, and *N*-bz-L-pro, have large minus CD peaks with $\Delta\varepsilon$'s -1 to -2. (Fig. 1C). All these complexes have a fixed configuration of the coordinated asymmetric nitrogen. On the other hand, complexes without asymmetric nitrogen, *i.e.* L-ala, L-val, and L-phe complexes fail to show large CD peaks in this region. (Fig. 1D). Hence the characteristics of CD peaks in 33000 cm^{-1} region must depend on the configuration around coordinated asymmetric nitrogen.

These complexes have other absorption peaks in the regions *ca.* 25000, 37000, and 45000 cm^{-1}, and CD peaks are observable in these regions. However, the CD peaks corresponding to the first and the last absorption peak are irregular, and do not seem to be directly related to the coordinated asymmetric nitrogen. The CD peaks in the 37000 cm^{-1} region of the complexes with asymmetric nitrogens are large, and have the same sign as those in the 33000 cm^{-1} region. Hence we consider that these peaks are also related to the asymmetric nitrogen (*vide infra*).

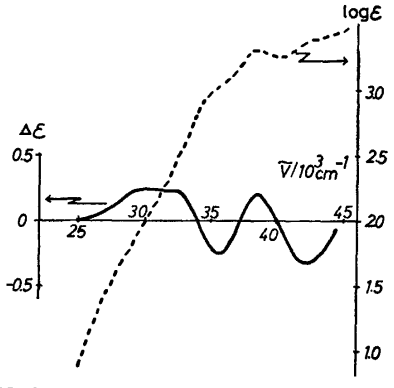

Fig. 2. UV absorption and CD spectra of *cis*(*N*,ethylene)-[PtCl(L-pro)(C_2H_4)] in acetonitrile.

The *cis*(*N*, ethylene) complex gives an absorption peak at *ca.* 38000 cm^{-1} and three shoulders at 28000, 35000, and 42000 cm^{-1}. CD peaks are observed in these regions corresponding to the absorption peak and shoulders. (Fig. 2). The absorption pattern is similar to that of the trans isomer. The CD peaks, however, are not very large and the signs are not equal to those of the *trans*(*N*, ethylene) complexes. Hence no further discussion will be made with the *cis* complex.

Stereoselectivity. The nitrogen of *N*-benzyl-L-valinate can coordinate to a metal ion in either *R* or *S* configuration, and its complex *trans*(*N*, ethylene)[PtCl(*N*-bz-L-val)(C_2H_4)] can exist as a pair of diastereoisomers, *S*(N)*S*(C) and *R*(N)*S*(C). Its CD spectrum is very similar both in location and intensity to that of the *N*-bz-L-pro complex, which can be only in *R*(*N*)*S*(C) configuration. It appears as if the *R*(N)*S*(C) diastereoisomer was obtained almost exclusively, when *N*-benzyl-L-valinate underwent substitution reaction with Zeise's salt in a very wealky acid aqueous solution of pH 5—6.[7] Saburi and Yoshikawa found that *N*-methyl-L-alaninate coordinates to cobalt(III) in a basic solution stereospecifically in *R* form, to give [Co(*R*(N)-*N*-me-L-ala)(NH_3)$_4$]$^{2+}$.[13]

The common preference of *R* configuration around coordinated nitrogen in these complexes may be understood by a molecular model study; *S*-configuration around coordinated nitrogen gives *N*-substituents in *cis* position to the substituents on the asymmetric α-carbon in *S* configuration, to result in large steric hindrance between the substitutents on *S*-nitrogen and *S*-carbon. Thus the *R*(N)*S*(C) configuration should be prefered regardless of the other moieties of the complex.

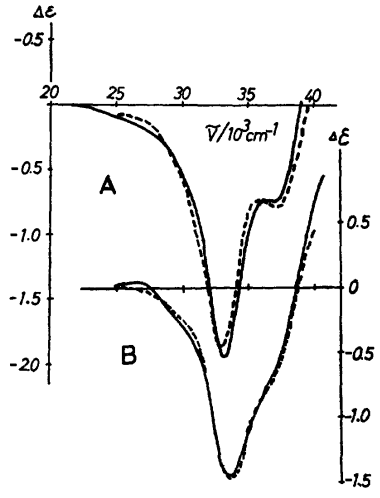

Fig. 3. Difference in CD between two complexes of the type *trans*(*N*,ethylene)[PtCl(L-am)(C_2H_4)] in AN.
A: $\delta\Delta\varepsilon$, — between *N*-bz-L-pro and L-pro, and --- between *N*-bz-L-val and L-val.
B: $\delta\Delta\varepsilon$, — between *N*-me-L-pro and L-pro, and --- between *N*-me-L-hyp and L-hyp.

Additivity of CD. Figure 1B and 1C indicate that the curves in 33000 and 37000 cm^{-1} regions show CD' of reverse signs. In Fig. 3A the differences of CD's between the *N*-benzyl-L-prolinato and L-prolinato, and between *N*-benzyl-L-valinato and L-valinato complexes are plotted against the wave number. Both $\delta\Delta\varepsilon$ curves are very similar to each other. In Fig. 3B similar plots of $\delta\Delta\varepsilon$'s between *N*-methyl-L-hydroxyprolinato and L-hydroxyprolinato, and between *N*-methyl-L-prolinato and L-prolinato complexes are shown. Again both curves are similar to each other. These curves should reflect the contribution of *N*-benzyl and *N*-methyl group upon the asymmetric nitrogen, the $\delta\Delta\varepsilon$ being -1.9 and -1.5, respectively. Hence additivity law should hold between the contribution of *N*-substituent and the L-prolinato moiety. The contribution of the former should be independent of the amino carboxylate framework.

Application of Quadrant Rule. Scott and Wrixon found an empirical rule between the absolute configuration of asymmetrically coordinated prochiral η^2-olefins and the CD sign of their platinum(II) complexes in 25000 cm^{-1} region, and interpreted the results on the basis of quadrant rule.[14] We have applied this rule to the interpretation of the CD spectra coming from asymmetric nitrogen. A projection of *trans*(*N*, ethylene)-

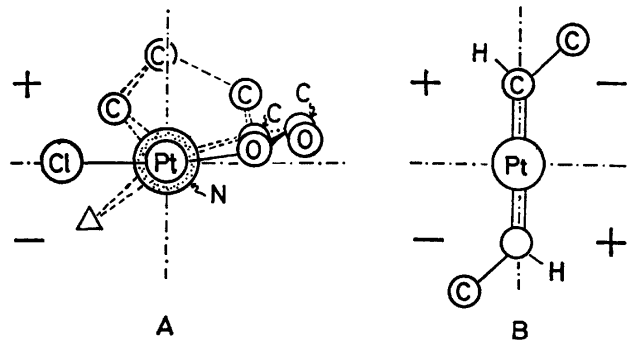

Fig. 4. Projection of the square planar complexes.
A: *N*-substituted-L-am moiety, the Pt–N bond is perpendicular to the paper and N is beneath Pt.
B: *trans*-2-butene moiety, the C–C axis is across the square plane of the Pt(II) complex behind the paper, and Pt-olefin bond is perpendicular to the paper.

[PtCl(*N*-alkyl-L-pro)(C_2H_4)] is shown in Fig. 4A. The square plane of the complex is represented by the horizontal line, and the Pt–N bond is perpendicular to the paper plane. The asymmetric nitrogen is beneath the platinum(II) and shown by a large dotted circle. When the quadrant rule is to be applied on the basis of this projection, the contribution of the minus quadrant at below left side behind the paper should depend on the size of the moiety, shown by a triangle on Fig. 4A. The larger the size of this substituent (benzyl, methyl, or hydrogen), the greater the contribution of the minus component. The substitution of benzyl or methyl for the hydrogen on the asymmetric nitrogen gives a large minus contribution. The apparently reverse CD sign in these regions in Fig. 1B and 1C and the additivity law are thus accounted for.

The UV absorption of all the present complexes shows peaks with log ε *ca.* 3 from 31000 to 45000 cm^{-1} region. Denning, Hartley, and Venanzi assigned the absorption bands of Zeise's salt in these regions to that d-π^* (ethylene) transition.[15] We have observed CD peaks at *ca.* 35000 and 39500 cm^{-1} with $\Delta\varepsilon$'s -1.3 and $+3.3$, respectively, for the tetraphenylphosphonium salt of [$PtCl_3$(${}^2S$,${}^3S$-*trans*-2-butene)]$^-$ in AN.[16] The absorption peak at 35000 cm^{-1} must correspond to the same transition to which the main CD of Fig. 3 owes.[17] In Fig. 4B a similar projection of this Zeise-type complex is shown, the C–C moiety being placed across the square plane of platinum(II) behind the paper surface. Application of the quadrant rule discloses that the contribution of the same minus regions behind the paper predominates for the Zeise- type complex, as it does to the present complexes with asymmetric nitrogens. It is thus suggested that the d-π^*(ethylene) transition is perturbed by the asymmetric nitrogen trans to the ethylene, so that a remarkable CD appears in this region.

References

1) J. F. Blount, H. C. Freeman, A. M. Sargeson, and K. R. Turnbull, *Chem. Commun.*, **1967**, 324.
2) B. Halpern, A. M. Sargeson, and K. R. Turnbull, *J. Am. Chem. Soc.*, **88**, 4630 (1966).
3) D. M. Buckingham, S. F. Mason, A. M. Sargeson, and K. R. Turnbll, *Inorg. Chem.*, **5**, 1649 (1966).
4) G. G. Aleksandrov, Y. T. Struchkov, S. V. Rogozhin, and V. A. Davankov, *Inorg. Nucl. Chem. Lett.*, **10**, 959 (1974).
5) T. Yasui, *Bull. Chem. Soc. Jpn.*, **38**, 1746 (1965).
6) T. Yasui, J. Hidaka, and Y. Shimura, *J. Am. Chem. Soc.*, **87**, 2762 (1965).
7) J. Fujita, K. Konya, and K. Nakamoto, *Inorg. Chem.*, **9**, 2794 (1970).
8) A. A. Patchett and B. Witkop, *J. Am. Chem. Soc.*, **79**, 185 (1957).
9) F. Irreverre, K. Morita, A. V. Robertson, and B. Witkop, *ibid.*, **85**, 2824 (1963).
10) P. Quitt, J. Hellerbach, and K. Vogler, *Helv. Chim. Acta*, **46**, 327 (1963).
11) A. B. Mauger and B. Witkop, *Chem. Rev.*, **66**, 48 (1966).
12) Y. Terai, H. Kido, K. Kashiwabara, J. Fujita, and K. Saito, *Bull. Chem. Soc. Jpn.*, **50**, 150 (1977).
13) M. Saburi and S. Yoshikawa, *Inorg. Chem.*, **7**, 1890 (1968).
14) A. I. Scott and A. D. Wrixon, *Tetrahedron*, **27**, 2339 (1971).
15) R. G. Denning, F. R. Hartley, and L. M. Venanzi, *J. Chem. Soc., A*, **1967**, 1322.
16) Y. Terai and K. Saito, *Bull. Chem. Soc. Jpn.*, in press.
17) I. Kinoshita, Y. Terai, K. Kashiwabara, H. Kido, and K. Saito, *J. Organomet. Chem.*, **127**, 237 (1977).

Sydnones. Synthesis and Photochromic Behavior of 3-(3-Pyridyl)sydnone Derivatives and a 4-Alkenyl-3-phenylsydnone

Shinichi INOUE, Nobuyoshi ASAI,* Gorou YASUDA, and Takuya HORI

Department of Applied Chemistry, Aichi Institute of Technology, Yagusa-cho, Toyoda-shi, Aichi 470-03

(Received January 18, 1977)

Six new sydnones [3-(3-pyridyl)-4-(*p*-chlorophenyl)sydnone (**1**), 3-(3-pyridyl)-4-(*p*-tolyl)sydnone (**2**), 3-(3-pyridyl)-4-(*p*-nitrophenyl)sydnone (**3**), 3-(3-pyridyl)-4-(*p*-aminophenyl)sydnone (**4**), 3-(3-pyridyl)-4-(*p*-acetamidophenyl)sydnone (**5**), and 3-phenyl-4-(α-phenylstyryl)sydnone (**6**)] were synthesized and examined for photochromic behavior. Sydnone **2** exhibited photochromism in the solid state upon UV irradiation (230—580 nm).

Photochromic 3-(3-pyridyl)sydnone was synthesized for the first time by Tien and Hunsberger. Later, several investigators prepared 3-(3-pyridyl)sydnone derivatives[1,2] and examined the effect of substituents on pyridylsydnone photochromism. However, none of the prepared sydnones exhibited photochromic behavior. Recently, several photochromic 4-alkenyl-3-phenylsydnones were synthesized by several groups[3-7] and investigated for photochromic properties. Here, the synthesis of new sydnones and their photochromic behavior is reported.

When *p*-chlorophenyl-(3-pyridylamino)acetonitrile (**7**) and *p*-tolyl-(3-pyridylamino)acetonitrile (**8**), which were easily obtained from the reaction of 3-aminopyridine with *p*-substituted benzaldehydes and potassium cyanide, were hydrolyzed with hydrochloric acid, *N*-(3-pyridyl)-*p*-chlorophenylglycine hydrochloride (**9**) and *N*-(3-pyridyl)-*p*-tolylglycine hydrochloride (**10**) were obtained. Compounds **9** and **10** easily reacted with sodium nitrite to afford *N*-nitroso-*N*-(3-pyridyl)-*p*-chlorophenylglycine (**11**) and *N*-nitroso-*N*-(3-pyridyl)-*p*-tolylglycine (**12**), which were then cyclized with acetic anhydride to give **1** and **2** in 50—70% yields.

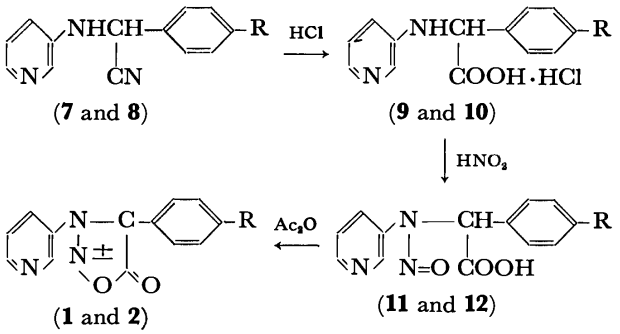

(**7** and **8**) (**9** and **10**) (**1** and **2**) (**11** and **12**)

(**1**), (**7**), (**9**), and (**11**): R=Cl;
(**2**), (**8**), (**10**), and (**12**): R=CH_3

In order to obtain 4-(*p*-nitrophenyl)derivative **3**, the nitration of 3-(3-pyridyl)-4-phenylsydnone was examined. The nitration was accomplished in the following manner. Treatment of 3-(3-pyridyl)-4-phenylsydnone with fuming nitric acid at −5 °C afforded **3** in a moderate yield (52%). Compound **3** was readily reduced with iron powder in acetic acid at 90 °C to give 4-(*p*-aminophenyl)derivative **4** in a 45% yield. **4** underwent acetylation to give 4-(*p*-acetamidophenyl)-derivative **5** in an excellent yield (82%).

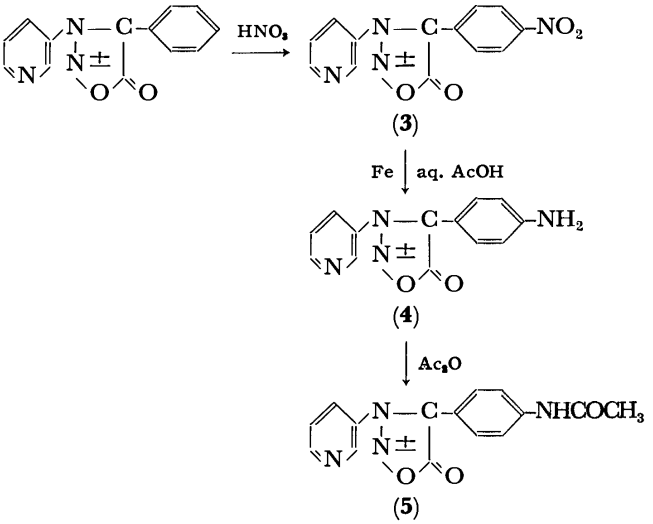

The reaction of 3-phenylsydnone with butylmagnesium bromide in THF at 2 °C gave the corresponding Grignard compound, which then reacted with deoxybenzoin to give 4-(1-hydroxy-1,2-diphenylethyl)-3-phenylsydnone (**13**) in a 54% yield. 3-Phenylsydnone derivative **13** was dehydrated by means of phosphoryl chloride and acetic anhydride to give 3-phenyl-4-(α-phenylstyryl)sydnone **6**, in an 88% yield.

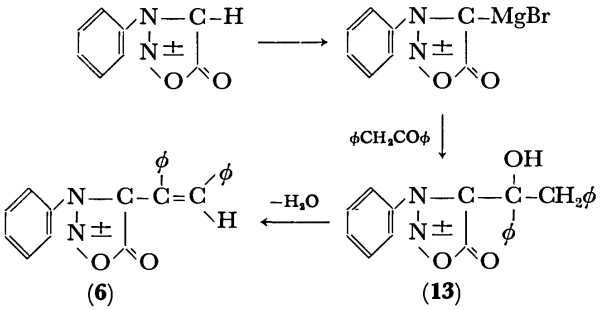

The structures of the new sydnones (**1**—**6**) were assigned on the basis of their IR, NMR, mass, and UV spectra, and elemental analysis.

In the solid state, each of the new sydnones was exposed to ultraviolet radiation (230—580 nm). Sydnone **2** exhibited photochromism, with no other sydnones, however, exhibiting this behavior.

Sydnone **2** is a pale yellow compound, stable in air at room temperature if stored in the dark. **2** turned blue upon irradiation with ultraviolet light for a period of 3 to 5 min. This photochromic change was reversible; **2** returned to its original state after storage in the dark for several days. A more rapid recovery of **2** can be

* Present address: Institute of Chemistry, The University of Tsukuba, Niihari-gun, Ibaraki 300-31.

induced by heating at 80 °C for 30 min. After repeated exposures to ultraviolet radiation, **2** showed a delay in returning to its original state. The photochromic change was restricted to the crystalline state at room temperature; no such phenomenon was observed in solution.

An infrared spectrum of **2** was obtained and compared with that taken after a 5 min irradiation with ultraviolet light. The two spectra were essentially identical. The similarity between the infrared spectra of **2** before and after ultraviolet irradiation is an indication that there is no structural alternation associated with the photochromic change.

A conclusion drawn from these observations gives support to the proposition of Greco and O'Reilly[4] that the mesoionic ring may be a necessary, but not a sufficient, structural feature for photochromism. At present, the effect of molecular modification on the photochromism of compound **2** is being examined in order to elucidate the photochromic mechanism.

Finally, it should be noted that the new sydnones are comparatively stable even at high temperature.

Experimental

The IR spectra were recorded with a Hitachi Model 215 spectrophotometer and the UV spectra with a Hitachi Model EPS-3T spectrophotometer. The NMR spectra were obtained on a JEOL JNM-C-60H spectrometer, with tetramethylsilane as the internal reference. The mass spectra were determined on a Hitachi RMU-6E spectrometer. The melting points are uncorrected.

Materials. *p*-Chlorophenyl- and *p*-tolyl(3-pyridyl)acetonitriles (**7** and **8**) were prepared by the reaction of 3-aminopyridine with *p*-substituted benzaldehydes and potassium cyanide. **7**, mp 152—153 °C. Found: C, 64.12; H, 4.10; N, 17.21%. Calcd for $C_{13}H_{10}N_3Cl$: C, 64.07; H, 4.14; N, 17.24 %. **8**, mp 145.5—146.5 °C. Found: C, 75.30; H, 5.81; N, 18.77%. Calcd for $C_{14}H_{13}N_3$: C, 75.31; H, 5.87; N, 18.82%.

3-(3-Pyridyl)-4-phenylsydnone was prepared using the method of Ohta and Masaki.[1]

3-Phenylsydnone was also prepared by cyclization of *N*-nitroso-*N*-phenylglycine using the usual procedure.[8]

Hydrolysis of p-*Substituted Phenyl(3-pyridylamino)acetonitrile. Preparation of* N-*(3-Pyridyl)*-p-*chlorophenylglycine Hydrochloride(**9**) and* N-*(3-Pyridyl)*-p-*tolylglycine Hydrochloride (**10**)*: A mixture of **7** (2.0 g, 8 mmol) and concentrated HCl (18 ml) was stirred for 2 h under reflux. After cooling for 3 h at 0 °C, the resulting ammonium chloride was filtered, the solvent was distilled and the residue was heated with concentrated HCl for 15 min. After washing with concentrated HCl and recrystallization from concentrated HCl, pure **9** (2.1 g, 85%) was obtained.

The same procedure starting with acetonitrile (**8**) gave product **10** in a yield of 88%.

*Glycine Hydrochloride (**9**)*, mp 223—227 °C. Found: C, 52.17; H, 4.01; N, 9.40%. Calcd for $C_{13}H_{12}N_2O_2Cl_2$: C, 52.19; H, 4.05; N, 9.37%.

*Glycine Hydrochloride (**10**)*, mp 224—228 °C. Found: C, 60.34; H, 5.40; N, 9.99%. Calcd for $C_{14}H_{15}N_2O_2Cl$: C, 60.32; H, 5.43; N, 10.05%.

Nitrosation of Glycine Hydrochloride. Preparation of N-*Nitroso*-N-*(3-pyridyl)*-p-*chlorophenylglycine (**11**) and* N-*Nitroso*-N-*(3-pyridyl)*-p-*tolylglycine (**12**)*: To a suspension of **9** (4.4 g, 15 mmol) in water (45 ml) was added a 20% aqueous sodium hydroxide solution until compound **9** was completely dissolved. Sodium nitrite (1.2 g, 17 mmol) was added and concentrated HCl was then added at 0 °C until the solution showed acidity (pH 2) and then the reaction mixture was stirred for 30 min. After standing overnight at −2 °C, the deposited crystals were collected by filtration. Upon washing with cold water, pure **11** (3.4 g, 79%) was obtained.

Application of the same procedure to glycine hydrochloride (**10**) led to product **12** in a yield of 89%.

*Nitrosoglycine (**11**)*, mp 140—141 °C (dec). Found: C, 53.51; H, 3.45; N, 14.42%. Calcd for $C_{13}H_{10}N_3O_3Cl$: C, 53.53; H,3.46; N, 14.41%.

*Nitrosoglycine (**12**)*, mp 145.5—146.5 °C (dec). Found: C, 61.96; H, 4.82; N, 15.45%. Calcd for $C_{14}H_{13}N_3O_3$: C, 61.99; H, 4.83; N, 15.49%.

*3-(3-Pyridyl)-4-(*p-*chlorophenyl)sydnone (**1**)*. A mixture of **11** (1.0 g, 3 mmol) and acetic anhydride (20 ml) was stirred for 2 h at room temperature. After heating for 5 min at 50 °C, the solvent was removed under reduced pressure in a nitrogen atmosphere. To the residual oil was added 50% ethanol and the mixture was then allowed to stand for a few minutes. The resulting crystals were filtered off and the residue was washed with ethanol and recrystallized from ethanol to give 0.6 g (64%) of sydnone **1** as pale yellow needles; mp 141—142 °C. IR (KBr): 1752 (C=O) and 1735 cm^{-1} (C=O); NMR ($CDCl_3$): δ 9.10—7.60 (4H, m, py) and 7.37 (4H, m, C_6H_4); UV (MeOH) max: 254 (ε 12400) and 340 nm (10500); MS *m/e* (%): 273 (M^+, 57), 215 (100), and 78 (58). Found: C, 57.25; H, 2.78; N, 15.13%. Calcd for $C_{13}H_8N_3O_2Cl$: C, 57.05; H, 2.95; N, 15.35%.

*3-(3-Pyridyl)-4-(*p-*tolyl)sydnone (**2**)*. A mixture of **12** (1.0 g, 4 mmol) and acetic anhydride (10 ml) was stirred for 3 h at room temperature. After heating for 5 min at 70 °C, the mixture was worked up using the same method as described above to give 0.52 g (56%) of sydnone **2** as pale yellow needles; mp 142—143 °C. IR (KBr): 1745 cm^{-1} (C=O); NMR ($CDCl_3$): δ 9.05—7.50 (4H, m, py), 7.22 (4H, m, C_6H_4), and 2.64 (3H, s, CH_3); UV (MeOH) max: 251 (ε 7950) and 341 nm (6170); MS *m/e* (%): 253 (M^+, 60), 195 (100), and 78 (26). Found: C, 66.34; H, 4.17; N, 16.59%. Calcd for $C_{14}H_{11}N_3O_2$: C, 66.39; H, 4.37; N, 16.59%.

*3-(3-Pyridyl)-4-(*p-*nitrophenyl)sydnone (**3**)*. To fuming nitric acid (10 ml) was slowly added 3-(3-pyridyl)-4-phenylsydnone (2.0 g, 8 mmol) at −5 °C which was then stirred for 20 min. The reaction mixture was poured into ice water. The resulting crystals were filtered off and washed several times with cold water and then crystallized from 60% ethanol to give 1.2 g (52%) of synone **3** as yellow needles; mp 162—163 °C. IR (KBr): 1770 (C=O), 1750 (C=O), 1520 (NO_2), 1353 (NO_2), and 856 cm^{-1}; NMR (DMSO-d_6): δ 9.10—7.84 (8H, m, py and C_6H_4); UV (MeOH) max: 262 (ε 7080) and 362 nm (17000); MS *m/e* (%): 284 (M^+, 63), 226 (100), 180 (38), and 78 (66). Found: C, 55.03; H, 2.67; N, 19.71%. Calcd for $C_{13}H_8N_4O_4$: C, 54.93; H, 2.83; N, 19.71%.

*3-(3-Pyridyl)-4-(*p-*aminophenyl)sydnone (**4**)*. To a suspension of **3** (3.5 g, 12 mmol) in hot water were added iron powder (8 g) and acetic acid (10 ml) and then the mixture was stirred for 20 min at 95 °C. After cooling, the reaction mixture was neutralized with $NaHCO_3$. The precipitate was filtered and washed several times with cold water. After drying, the residue was extracted with THF (100 ml) three times, and then the solvent was concentrated under reduced pressure in a nitrogen atmosphere. Petroleum ether (40 ml) was added and the mixture was coold. The resulting crystals were collected by filtration and then washed with petroleum ether. Recrystallization from absolute ethanol afforded 1.4 g (45%) of pure **4** as pale yellow needles; mp 194.5—196 °C. IR (KBr): 3425 (NH_2), 3342 (NH_2), and 1735 cm^{-1} (C=O); NMR (py-d_5): δ

9.02—7.40 (4H, m, py), 7.36—6.65 (4H, m, C_6H_4), and 5.35 (2H, s, NH_2); UV (MeOH) max: 266 (ε 13200) and 378 nm (6760); MS *m/e* (%): 254 (M^+, 27) and 196 (100). Found: C, 61.28; H, 3.80; N, 21.96%. Calcd for $C_{13}H_{10}N_4O_2$: C, 61.41; H, 3.96; N, 22.04%.

*3-(3-Pyridyl)-4-(*p*-acetamidophenyl)sydnone (**5**).* A mixture of **4** (0.20 g, 0.78 mmol), acetic anhydride (1.5 ml), and acetic acid (5 ml) was stirred for 20 min at 80 °C. The solvent was removed under reduced pressure in a nitrogen atmosphere. To the residual oil ethanol (2 ml) was added. The resulting crystals were collected by filtration. Recrystallization from 50% ethanol afforded 0.19 g (82%) of pure **5** as yellow needles; mp 242—244 °C. IR (KBr): 3300 (NH), 1720 (C=O), and 1678 cm^{-1} (CH_3C=O); NMR (DMSO-d_6): δ 9.00—7.80 (4H, m, py), 7.75—7.15 (4H, m, C_6H_4), 3.56 (1H, s, NHC=O), and 3.15 (3H, s, CH_3C=O); UV (MeOH) max: 269 (ε 8710) and 351 nm (6760). Found: C, 60.82; H, 4.01; N, 18.88%. Calcd for $C_{15}H_{12}N_4O_3$: C, 60.80; H, 4.09; N, 18.91%.

*Grignard Reaction. Preparation of 4-(1-Hydroxy-1,2-diphenylethyl)-3-phenylsydnone (**13**)*: To butylmagnesium bromide (30 ml, 50 mmol)[9] was added a solution of 3-phenylsydnone (3.2 g, 20 mmol) in THF (80 ml) at 2—3 °C which was then stirred for 1 h. To this was added a solution of deoxybenzoin (10.0 g, 50 mmol) in THF (10 ml) at 5 °C and this mixture was then stirred for 2 h and poured into dilute acetic acid. The reaction mixture was extracted with benzene (100 ml) three times. The extract, after washing with water (50 ml) three times and drying over anhydrous magnesium sulfate, was concentrated in a nitrogen atmosphere. The residue was purified by washing with benzene–hexane (1: 1) to give **13** (3.8 g, 54%).

*Sydnone (**13**)*; mp 130—131 °C. Found: C, 73.65; H, 5.12; N, 7.84%. Calcd for $C_{22}H_{18}N_2O_3$: C, 73.72; H, 5.07; N, 7.81%.

*Dehydration of 4-(1-Hydroxy-1,2-diphenylethyl)-3-phenylsydnone. Preparation of 3-Phenyl-4-(α-phenylstyryl)sydnone (**6**)*: To a solution of **13** (0.5 g, 0.14 mmol) in pyridine (10 ml) was added phosphoryl chloride (2 ml) at −5 °C. After standing for 12h at room temperature, the mixture was heated for 2 h and then poured into ice water. The resulting crystals were collected by filtration. Recrystallization from 50% ethanol afforded 0.22 g (47%) of pure **6** as pale yellow needles; mp 172—174 °C. IR (KBr): 1735 (C=O) and 818 cm^{-1} (C=CHR); NMR ($CDCl_3$): δ 7.56—7.12 (15H, m, C_6H_5) and 6.32 (1H, s, CHR); UV (MeOH) max: 231 (ε 11220) and 351 nm (8320); MS *m/e* (%): 330 (M^+, 18) and 272 (100). Found: C, 77.60; H, 4.76; N, 8.20%. Calcd for $C_{22}H_{16}N_2O_2$: C, 77.63; H, 4.74; N, 8.23%.

References

1) M. Ohta and M. Masaki, *Bull. Chem. Soc. Jpn.*, **33**, 649 (1960).

2) J. M. Tien and I. M. Hunsberger, *J. Am. Chem. Soc.*, **85**, 179 (1961).

3) C. V. Greco and I. M. Hunsberger, *J. Hetrocycl. Chem.*, **7**, 761 (1970).

4) C. V. Greco and B. P. O'Reilly, *J. Hetrocycl. Chem.*, **9**, 207 (1972).

5) M. Šorm and S. Nešpůrek, *Collect. Czech. Chem. Commun.*, **40**, 1537 (1975).

6) M. Šorm and S. Nešpůrek, *Collect. Czech. Chem. Commun.*, **40**, 3459 (1975).

7) S. Nešpůrek and M. Šorm, *Czech. J. Phys.*, B **25**, 1051 (1975).

8) J. Thoman and D. J. Voaden, *Org. Synth.*, Coll. Vol. V, 962 (1973).

9) J. M. Petersen, *Org. Synth.*, Coll. Vol. V, 763 (1973).

A New Type of Iminocarbonylaton of Diols, Mercaptoalkanol, and Dithiol *via* Their Dibutylstannyl Derivatives

Shizuyoshi SAKAI,* Hiroji NIIMI, Yoshihiro KOBAYASHI, and Yoshio ISHII

Department of Synthetic Chemistry, Faculty of Engineering, Nagoya University, Furo-cho, Chikusa-ku, Nagoya 464

(Received January 24, 1977)

Reactions of phenyl isothiocyanate with cyclic and acyclic dibutylstannyl dialkoxides derived from several alcohols, such as 1,2- and 1,3-diols and methanol, afforded quantitatively phenyliminocarbonate derivatives with the elimination of dibutylstannyl sulfide. Cyclic organostannyl sulfides, such as 2,2-dibutyl-1,3,2-oxathiastannolane and -dithiastannolane, reacted with phenyl or alkyl isothiocyanate to give 2-imino-oxathiolane (**10**) and -dithiolane (**14**), respectively. At higher reaction temperatures, rearrengment and decomposition of products **10** and **14** occurred.

The usual method for the preparation of iminocarbonates utilizes isocyanide dichloride, $RN{=}CCl_2$, as a reactant.[1] The major disadvantage of this method is that only a limited number of the reagent is available because of their toxicities. The present study is aimed at an application of organostannyl derivatives to the iminocarbonylation of alkanol and diols, mercaptoalkanols, and dithiols with various isothiocyanates (Reaction 1).

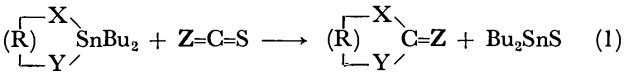

$$(R)\begin{matrix}X\\Y\end{matrix}SnBu_2 + Z{=}C{=}S \longrightarrow (R)\begin{matrix}X\\Y\end{matrix}C{=}Z + Bu_2SnS \quad (1)$$

X, Y=O, S; Z=NR

Reactions anologously to Reaction 1 using bis(tributylstannyl) derivatives of HX(R)YH have already been reported previously which dealt with the thiocarbonylation (X, Y=NMe or O; Z=S), iminocarbonylation (X, Y=NMe or O; Z=NPh),[2] and preparation of orthocarbonates.[3] However, this method appeares to be more suit for a new type of iminocarbonylation of diols, mercaptoalkanols and dithiols, because the corresponding dibutylstannyl compounds can be easily prepared from commercially available dibutylstannyl chloride or oxide, and are less toxic than tributylstannyl compounds.

Results and Discussion

The appropriate dibutylstannyl compounds were readily prepared and these starting materials were allowed to react with isothiocyanates is in a nitrogen atmosphere to afford cyclic iminocarbonylated products (X, Y=O or S in Reaction 1).

The reaction of some 2,2-dibutyl-1,3,2-dioxastannolanes (**1a**—**c**) with phenyl isothiocyanate for 2 h in 1,2-dichloroethane at 55 °C afforded the corresponding 2-phenylimino-1,3-dioxolanes (**3a**—**c**) and dibutylstannyl sulfide (**4**)[4] in quantitative yields (Reaction 2). However, a tetra-substituted derivative, dioxastannolane **1d** in Table 1, did not react with phenyl isothiocyanate under the same coditions, *i.e.*, more severe reaction conditions were required to complete the reaction, as is seen in Table 1. This fact suggests a large steric effect in the reactions with organostannyl compounds.

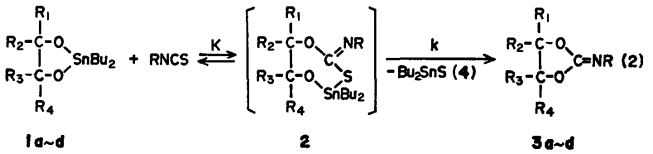

The intermediate (**2**) was not detected, even by IR and NMR measurements of the reaction mixture. However, it appears probable that the reaction proceeds *via* the addition of phenyl isothiocyanate to the tin-oxygen bond, followed by the elimination of a stable organostannyl sulfide (**4**), anologously to the case of the reactions of the compounds **5** and **8** mentioned below.

A six-membered ring compound, 2,2-dibutyl-1,3,2-dioxastannin (**1e**), was also allowed to react with phenyl isothiocyanate for 2 h at 55 °C to give 2-phenylimino-1,3-dioxane (**3e**) in a 60% yield (Reaction 3). On the other hand, the reaction of the seven-membered ring compound, 2,2-dibutyl-1,3,2-dioxoastannepane (**1f**), with phenyl isothiocyanate to form **3f** was unsuccessful, because of the instability of the product (**3f**). The instability is probably due to transfer polymerization of

TABLE 1. REACTIONS OF 2-DIBUTYLSTANNA-1,3-DIOXOLANES (**1**) WITH PHENYL ISOTHIOCYANATE

	1				Conditions		Iminocarbonate	
No.	R_1	R_2	R_3	R_4	Temp/°C	Time/h	Bp/°C/mmHg	Yield/%
1a	H	H	H	H	55	2	148—150/1.5 (72.0—72.5)[a]	98 (**3a**)
1b	H	Me	H	H	55	2	131—132/1.0	95 (**3a**)
1c	H	Me	H	Me	55	5	120—122/0.4	95 (**3c**)
1d	Me	Me	Me	Me	85	40	120—125 (79—81)[a]	95 (**3d**)

a) Melting point/°C.

* Present address: Department of Industrial Chemistry, Faculty of Engineering, Shizuoka University, Hamamatsu 432.

3f to give polyurethane: the C=O stretching band characteristic of urethane was observed at 1680 cm^{-1} in the IR spectrum of the reaction mixture.

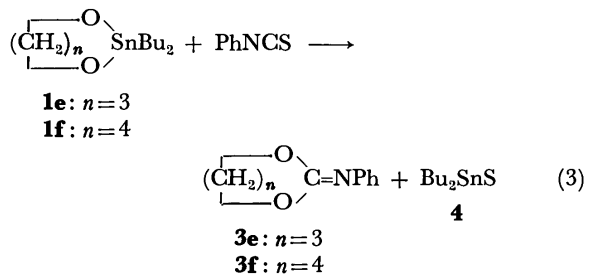

1e: $n=3$
1f: $n=4$

3e: $n=3$
3f: $n=4$

An acyclic organostannyl compound, **5**, was also submitted to the reaction with phenyl isothiocyanate in dichloroethane at 55 °C, affording only the 1 : 1 adduct (**6**) reported by Davies and Harrison.[5] However, under more severe conditions such as 70 °C for 16 h in 1,2-dichloroethane, the adduct (**6**) was converted to phenyl isocyanide dimethoxide (**7**) in a 96% yield (Reaction 4).

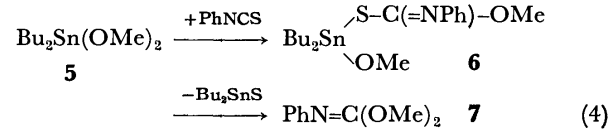

An aliphatic isothiocyanate, MeNCS, was also allowed to react with **1a**, and 2-methylimino-1,3-dioxolane was obtained in a moderate yield (70%).

In general, addition reactions of heterocumulenes to the tin-oxygen bond occur easily,[5] while heterocumulenes scarcely react with the tin-sulfur bond. Here, the reaction of an isothiocyanate with equimolar 2,2-dibutyl-1,2,3-oxathiastannolane (**8**), which was readily prepared from mercaptoethanol and dibutyltin oxide or chloride, was examined. For example, an equimolar mixture of phenyl isothiocyanate and **8** was heated for 2 h in dry 1,2-dichloroethane at 55 °C to afford 2-phenylimino-1,3-oxathiolane (**10**;R=Ph) and dibutylstannyl sulfide (Reaction 5). Alkyl isothiocyanates were also used in the reaction, the results of which are shown in Tables 2 and 3. The product (**10**) from the alkyl isothiocyanates were thermally unstable, and some parts decomposed to give alkyl isocyanates and thiirane.[6] Because of such thermal instability of the products, the reactions were carried out at relatively low temperatures such as 40 °C, even though alkyl isocyanates were less reactive than phenyl isothiocyanate.

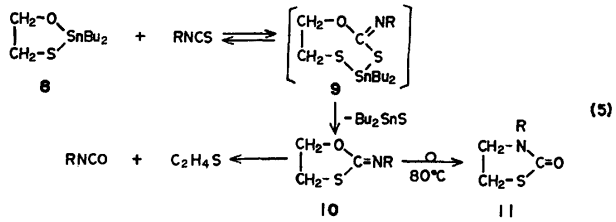

Table 2. Reactions of 2-dibutylstanna-1,3-oxathiolane (**8**) with isothiocyanates (RNCS) in dichloromethane

R	Conditions		Product yield %		
	Temp/°C	Time/d	**10**	RNCO	Others
Me	40	3	59	2	b,e
Et	40	4	64	4	b,e
Pr	40	5	79	6	b,e
Bu	40	5	70	trace	b,e
i-Pr	40	5	39	26	b,c,e
cyclo-C_6H_{11}	40	5	36	34	b,e
t-Bu	80[a]	4	0	0	d
Ph	55[a]	2(h)	95	0	b

a) In 1,2-dichloroethane. b) Dibutylstannyl sulfide was obtained in a quantitative yield. c) Accompanied by unreacted **8** (11%). d) The unreacted **8** was recovered in a quantitative yield. e) Ethylene sulfide and isocyanate were detected.

From the results in Table 2, the apparent order of the reactivities is as follows: PhNCS>MeNCS,EtNCS,PrNCS,BuNCS≫*i*-PrNCS,*cyclo*-C_6H_{11}≫Me_3CNCS. This order suggests that the reactivity of an isothiocyanate in the insertion across the tin-oxygen bond of **8** is affected by both the electronic nature and the bulkiness of the isothiocyanate substituent.

It is reasonable to assume that the reaction course forming **10** is an addition-elimination process (**8**→**9**→**10**): the formation of the intermediate (**9**) is strongly suggested on the basis of the fact that the C=N stretching band ascribable to **9** is observed at 1500—1530 cm^{-1} in

Table 3. Properties of 2-alkylimino-1,3-oxathiolanes (**10**) formed in reaction 5

R in **10**	Bp °C/mmHg	IR/cm^{-1}		NMR/ppm			Found (Calcd)	
		$\nu_{C=N}$	ν_{C-O}	δ_{CH_2O}	δ_{CH_2S}[b]	δ_{others}	C%	H%
Me	117—118/20	1668	1070, 1037	4.27	3.35	2.90	41.07[c] (40.94)	5.96 (6.09)
Et	68—70/0.6	1680	1047, 1037	4.25	3.35	3.00, 1.13	45.55 (45.79)	7.09 (6.91)
Pr	66.5—75.5	1680	1060, 1047	4.25	3.35	2.98, 2.5, 0.92	49.87 (49.62)	7.97 (7.64)
Bu	84—85/0.5	1676	1065, 1038	4.25	3.34	3.00, 0.92 2.1—2.7	53.09 (52.79)	8.54 (8.23)
i-Pr	63—64/0.4	1673	1100, 1033	4.24	3.42	2.95, 1.10	49.87 (49.62)	7.64 (7.64)
c-C_6H_{11}	98—99/0.3	1668	1067, 1026	4.16	3.28	2.7, 1.7—2.0	61.87 (61.80)	8.52 (8.54)

a) In carbon tetrachloride. b) Triplet, $J=6.8$ Hz. c) N% 11.96 (11.96).

the IR spectrum of the reaction mixture in the initial stage of the reaction at 40 °C. At elevated reaction temperatures (80 °C), **10** was partially rearranged to N-substituted thiazolidin-2-one (**11**). No such rearrangement was observed in the reaction of **8** with phenyl isothiocyanate.[7]

Finally, 2,2-dibutyl-1,3,2-dithiostannolane was allowed to react with sulfur-containing heterocumulene for several days at 40—80 °C to give a dithio-carbonate derivative (**14**) and dibutylstannyl sulfide. The results are tabulated in Table 4. Although no intermediate adduct (**13**) was detected, the reaction course may be depicted analogously to reaction scheme (5).

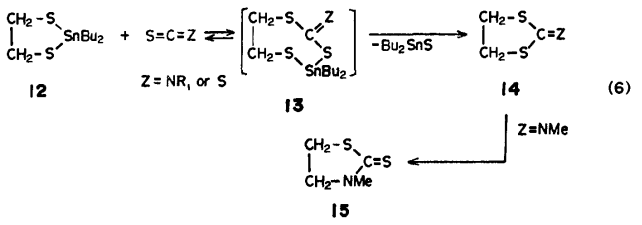

Table 4. Equimolar reactions of 2-dibutylstanna-1,3-dithiolane with heterocumulenes in dichloromethane

Hetrocumulene used	Conditions		Product yield/%[a]	
	Temp/°C	Time/d	**14**	Bu_2SnS
MeNCS	40	5	76(X=NMe)	91
MeNCS	80	4	64[b]	86
PhNCS	80[c]	5	65(X=NPh)	90
CS_2	40	9	39(X=S)	35

a) A trace amount of ethylene sulfide was detected by NMR measurements. b) Yield (%) of *N*-methylthiazolidin-2-thione. c) In 1,2-dichloroethane.

At elevated temperatures, 1-methylthiazolidine-2-thione (**15**) was obtained. Thus it is suggested that thermal rearrangement of **14** to **15** occured, as has been reported by Ueno *et al.*[6]

Organostannyl sulfides are known to be stable in ordinary reactions.[8] However, it is interesting to note that dibutylstannyl sulfide (**12**) is moderately reactive in reaction with methyl isothiocyanate. From a comparison of the result in Table 2 with that in Table 3, it is seen that methyl isothiocyanate is less reactive in reaction with **8** than is phenyl isothiocyanate, although the former is more reactive in reaction with **12** than is the latter. Moreover, carbon disulfide reacts with **12** to afford ethylene trithiocarbonate, but did not react with **8**, even in a mixture of **8** and carbon disulfide that was heated for nine days at 40 °C. These results cannot be explained by the usual rate order observed in reaction of simple organostannyl compounds, *i.e.*, Sn–N>Sn–O> Sn–S.[8,9] Therefore, the difference in the degree of association between **1a—d** or **8** (dimer) and **12** (monomer) and in the co-ordinating power of heterocumulene molecules to tin atom in these organostannyl compounds may affect their reactivities. A detailed discussion of the reaction rate and mechanism will be published elsewhere.[11]

Experimental

All melting and boiling points are uncorrected. The IR spectra were obtained on a Nippon-Binko DS-403G and IR-S spectrometers. The NMR spectra were recorded on a Japan Electron Optics Model C-60HL spectrometer with TMS as the internal standard. A Japan Electron Optics Model JMS-OISG mass spectrometer and a Yanagimoto Model GCG-220 gas chromatograph (Silicone DC-200, 25%) were also used. Analyses were performed in the laboratories of Professor Sasaki and of the Toa-gosei Co. All reactions and measurements were carried out using dry solvents.

All isothiocyanates (RNCS) were prepared using a reported method;[12] bp 117—119 (R=Me), 132—135 (Et), 153—154 (Pr), 170—175 (Bu), 137—142 (*i*-Pr), 120 (*cyclo*-C_6H_{11}) °C and 131—133 °C/10 mmHg (Me_3C). All solvents were dried over P_2O_5 and distilled before use. Mercaptoethanol and ethane-1,2-dithiol were obtained commercially and distilled in nitrogen; bp 55—58 °C/15 mmHg and 70—73 °C/50 mmHg, respectively. The dioxastannolanes (**1a—f**) were prepared from diol, Bu_2SnCl_2 and Na_2CO_3, or from diol and Bu_2SnO,[13] and stored in a dessicator containing blue silica gel.

Preparation of 2,2-Dibutyl-1,3,2-oxathiastannolane (8). (A) Mercaptoethanol (15.6 g, 200 mmol), dibutyltin dichloride (60.4 g, 200 mmol), and sodium carbonate (60 g) were heated under reflux in toluene (150 cm^3) in an atmosphere of nitrogen for 10 h in a flask equipped with a Dean-Stark water-separater, a condensor, and a stirrer. The hot reaction mixture was filtered, and evaporated to recover the toluene used. The residue was distilled in a vacuum to give crude **8** in a 90% yield (52.8 g). Redistillation afforded white solid **8**; bp 173—176 °C/0.4 mmHg; mp 92—93.5 °C (Ref.[10,14] 89—90 °C). The IR and NMR spectra coincided well with those previously reported.[1,14]

(B) Mercaptoethanol (15.6 g, 200 mmol) and Bu_2SnO (48 g, 200 mmol) were allowed to react under reflux in toluene and were treated as mentioned above, to afford **8** in a 92% (54 g) yield.

Preparation of 2,2-Dibutyl-1,3,2-dithiastannolane (12). A mixture of ethane-1,2-dithiol (18.2 g, 200 mmol), Bu_2SnCl_2 (60.4 g, 200 mmol), and Na_2CO_3 (65 g) was heated for 10 h in refluxing toluene (200 cm^{-1}) in an atmosphere of nitrogen, and treated as mentioned above to give **12** in a 77% yield; bp 127—129 °C/0.1 mmHg; mp 57—58 °C (Ref.[15] 59—60 °C); NMR (CCl_4) δ 2.93 (s, 4H, CH_2S) and 0.7—1.7 ppm (br., 18H, SnBu); IR (CCl_4) 1285, 1245, 925, and 845 cm^{-1}. The dithiastannolanes **12** was also prepared in a 86% yield (53 g) from Bu_2SnO instead of Bu_2SnCl_2 and Na_2CO_3.

The Reaction of 2,2-Dibutyl-1,2,3-dioxastannolane (1a) with PhNCS. To a solution of **1a** (5.8 g, 20 mmol) in dry 1,2-dichloroethane (40 cm^3) in a flask equipped with a condenser and a drying tube, PhNCS (2.8 g, 21 mmol) was added and the mixture was heated with stirring for 2 h at 55 °C. Then, the solvent was evaporated, and the residue was distilled in a vacuum to give 2-phenylimino-1,3-dioxolane (**3a**) in a 98% yield (3.2 g, 19.6 mmol); bp 148—150 °C/15mmHg; mp (recrystallized from toluene) 72—72.5 °C (Ref.[16] 74—75 °C); NMR δ 4.43 (s, 4H, CH_2O) and 6.8—7.3 ppm (m, 5H, Ph); IR ($CHCl_3$) 1721 ($\nu_{C=N}$) and 1056 cm^{-1}. The spectral data were the same as those of an authentic sample. The pot residue showed the same IR spectrum that of the authentic Bu_2SnS (ν_{SnSSn} at 360 cm^{-1}); yield 91% (4.9 g).

The Reaction of 2,2-Dibutyl-4-methyl-1,3,2-dioxastannolane (1b) with PhNCS. The stannolane **1b** was allowed to react with PhNCS for 2 h at 55 °C, and was treated as mentioned above; yield 95%; bp 131—132 °C/1 mmHg; NMR (CCl_4)

δ 1.23 (d, J=5.1 Hz, 3H, CH_3), 3.5—4.8 ($ABCX_3$-pattern, 3H,CH_2CH), and 6.8—7.3 ppm (m, 5H, Ph); IR ($CHCl_3$) 1708 ($\nu_{C=N}$) and 1040 (ν_{C-O}) cm^{-1}; Found C, 67.55; H, 6.37; N, 7.88%. Calcd for $C_{10}H_{11}ON$: C, 67.78; H, 6.29; N, 7.90%.

Dibutylstannyl sulfide was obtained as a pot residue in a 95% yield.

The Reaction of 2,2-Dibutyl-4,5-dimethyl-1,3,2-dioxastannolane (1c) with PhNCS. This compound (**1c**) was allowed to react with PhNCS for 5 h in 1,2-dichloroethane at 55 °C and was treated as described above to give **3c** (95% yield; bp 120—122 °C/0.4 mmHg). The IR and NMR spectra coincided well with those of an authentic sample.[16]

Reaction of Dimethoxydibutylstannane (5) with PhNCS. To a solution of **5** (5.9 g, 20 mmol) in 1,2-dichloroethane, PhNCS (2.7 g, 20 mmol) was added dropwise and the reaction mixture showed δ_{CH_3-O} at 3.93 and 3.51 ppm in the NMR spectrum and $\nu_{C=N}$ band at 1630 cm^{-1} in the IR spectrum, which are the same as those reported for the 1:1 adduct (**6**).[5] This adduct (**6**) was heated for 16 h at 70 °C, and distilled to give phenyl isocyanide dimethoxide **7** in a 96% yield; bp 60—62 °C/0.3 mmHg; NMR ($CDCl_3$) δ 3.17 (s, 6H, CH_3) and 6.7—7.3 ppm (m, 5H, Ph); IR ($CHCl_3$) 1677 ($\nu_{C=N}$) cm^{-1}. Those spectral data coincided well with those of a commercial sample.

The Reaction of 2,2-Dibutyl-1,3,2-dioxastannoxane (1e) with PhNCS. Compound **1e** was allowed to react with PhNCS in 1,2-dichloroethane as in the case of **1a**. The reaction mixture was fractionally distilled to afford 2-phenylimino-1,3-dioxacyclohexane **3e** in a 60% yield; bp 136—139 °C/0.2 mmHg; NMR ($CDCl_3$) δ 4.25 (t, J=5.5 Hz, 4H, CH_2O), $\approx$1.9 (m, 2H, CCH_2C), and 6.8—7.3 ppm (m, 5H, Ph); IR ($CHCl_3$) 1690 and 1100 cm^{-1}. Found: C, 67.48; H, 5.98; N, 7.75%. Calcd for $C_{10}H_{11}O_2N$: C, 67.78; H, 6.26; N, 7.90%.

The Reaction of 2,2-Dibutyl-1,3,2-dioxastannaepane (1f) with PhNCS. Compound **1f** was allowed to react with an equimolar amount of PhNCS for 20 h in 1,2-dichloroethane at 70 °C, to give a mixture which showed the characteristic $\nu_{C=N}$ band ascribable to 2-phenylimino-1,3-dioxepane (**3f**) at 1690 cm^{-1}, but distillation gave a resinous product having an IR band at 1680 cm^{-1}.

The Reaction of 1a with MeNCS. This compound (**1a**) was allowed to react with MeNCS for 16 h in dry 1,2-dichloroethane at 70 °C, to give 2-methylimino-1,3-dioxolane in a 70% yield; bp 98—100 °C/25 mmHg, NMR ($CDCl_3$) δ 2.99 (s, 3H, CH_3) and 4.38 ppm (s, 4H, CH_2); IR ($CHCl_3$) 1740 cm^{-1}. Found: C, 47.83; H, 7.12; N, 13.59%. Calcd for $C_4H_4O_2N$; C, 47.52; H, 6.98; N, 13.86%.

Reaction of 2,2-Dibutyl-1,3,2-oxathiostannolane (8) with PhNCS. An equimolar mixture of **8** and PhNCS was heated for 2 h in dry 1,2-dichloroethane at 55 °C. The reaction mixture was concentrated in vacuum and cooled to precipitate crude crystal of 2-phenylimino-1,3-oxathiolane (**10**, R=Ph) in a 95% yield; mp (recrystallized from a toluene–hexane (1:1) mixture) 65.0—65.5 °C; NMR ($CDCl_3$) δ 3.35 (t, J=6.3 Hz, 2H, CH_2S), 4.66 (t, J=6.3 Hz, 2H, CH_2O), and 6.8—7.3 ppm (m, 5H, Ph); IR ($CHCl_3$) 1658 ($\nu_{C=N}$) 1113, and 1038 (ν_{C-O}) cm^{-1}. Found: C, 60.10; H, 5.11; N, 7.80%. Calcd for C_9H_9ONS: C, 60.31; H, 5.06; N, 7.81%. The parent solution contained Bu_2SnS (97% yield).

Reaction of 8 with Some Alkyl Isothiocyanates. A typical example is as follows: the oxathiostannolane **8** and MeNCS (each 25 mmol) were heated for three days at 40 °C in dry dichloromethane in a flask equipped with a condensor and a drying tube. During the course of the reaction, the mixture showed the $\nu_{C=N}$ band of the 1:1 adduct at 1610 cm^{-1} in the IR spectrum. After the reaction, the solvent and the low boiling by-product were recovered in a cold trap by distillation at atmospheric pressure, and the residue was distilled in a vacuum, to afford 2-methylimino-1,3-oxathiolane (**10**;R=Me) in a 59% yield; bp 117—118 °C/20 mmHg. The identification of **10** was performed using IR and NMR spectroscopies and elemental analysis. It was confirmed by VPC and NMR measurements that the trapped mixture comprised the solvent, thiirane (3%), MeNCO (2%), and MeNCS (1%).

Bu_2SnS was obtained as a residue in an almost quantitative yield.

The results of the reactions of **8** with other alkyl isothiocyanates are summerized in Tables 2 and 3.

Picrate Formation of 10. Compound **10** (R=Me and Et) was added to a solution of picric acid in EtOH at room temperature, and cooled at 0 °C to precipitate the picrate crystals. The picrate of **10** (R=Me): mp (EtOH) 143—144 °C; IR (KBr) 1628, 1609, 1551, 1367, and 1268 cm^{1-}; Found: C, 34.69; H, 2.91; N, 16.18%. Calcd for $C_{10}H_{10}O_8S$: C, 34.57; H, 3.14; N, 16.26%. The picrate of **10** (R=Et): mp (EtOH) 80—82 °C; IR (KBr) 1660, 1615 (br.), 1368, and 1275 cm^{-1}; Found: C, 36.34; H, 3.64; N, 15.15%. Calcd for $C_{11}H_{12}O_8N_4S$: C, 36.67; H, 3.36; N, 15.15%.

The Rearrangement of 10 to 11 (R=Me). Compound **10** prepared *in situ* from **8** and MeNCS (25 mmol each) was heated under reflux for four days in 1,2-dichloroethane, and the reaction mixture was distilled to afford **11** (R=Me) in a 46% yield; bp 73—75 °C/0.2 mmHg (Ref.[6] 84—86 °C/0.2 mmHg); IR ($CHCl_3$) 1689 cm^{-1} (Ref.[6] 1685 cm^{-1}). Under the same reaction conditions, **10** (R=Ph) was not rearranged and recovered by distillation in an almost quantitative yield.

The Reactions of 2,2-Dibutyl-1,3,2-dithiostannolane (12) with MeNCS and PhNCS. This compound (**12**) was allowed to react with an equimolar amount of MeNCS for five days in dry dichloromethane under reflux, and was distilled to give 2-methylimino-1,3-dithiolane (**14**; Z=NMe) in a 76% yield; bp 64—68 °C/0.3 mmHg (Ref.[6] 79—81 °C/0.45 mmHg); the IR and NMR spectra coincided well with those prepared by a published method.[16] The trapped distillate contained only a trace amount of thiirane.

The reaction of **8** with MeNCS was carried out for one day in refluxing 1,2-dichloroethane, and the reaction mixture showed the characteristic C=N stretching band of **14** (Z=NMe) at 1614 cm^{-1}. The reaction was further continued for three days at 80 °C. Then, the solvent was evaporated, and the residual solid was recrystallized from CCl_4 to give 1-methylthiazolidine-2-thione (**15**) in a 64% yield; mp 68—69 °C (Ref.[6] 68—69 °C); NMR (CCl_4) δ 2.37 (t, J=7.3 Hz, 2H, CH_2N) and 4.08 (t, J=7.3 Hz, 2H, CH_2S); IR (CCl_4) 1308 cm^{-1}. These spectral data are the same as those prepared by a published method.[16]

The Reaction of the Dithiostannolane (12) with CS_2. An equimolar mixture of **12** and CS_2 was allowed to react for nine days in 1,2-dichloroethane at 40 °C, and the reaction mixture was submitted to column chromatography on silica gel (Wakogel C-100; CCl_4–$CHCl_3$) to give ethylene trithiocarbonate **14** (Z=S, 39% yield), dibutylstannyl sulfide (35%), and the unreacted **12** (65%). The IR ($\nu_{C=S}$ 1080 cm^{-1}) and NMR (δ_{CH_2} 3.92 ppm) spectra coincided well with those of a commercial sample.

References

1) T. Fujisawa, Y. Tamaru, I. Kuwajima, H. Nohira, Y. Nishikawa, and T. Mukaiyama, *Bull. Chem. Soc. Jpn.*, **37**, 797 (1963); *J. Org. Chem.*, **31**, 32 (1966).

2) S. Sakai, Y. Fujimura, and Y. Ishii, *J. Organomet. Chem.*, **50**, 113 (1973).

3) S. Sakai, U. Asai, Y. Kiyohara, K. Itoh, and Y. Ishii,

J. Organomet. Chem. Synth., **1**, 45 (1970).
4) Organostannyl sulfide (**4**) exists as a trimer, but is shown in monomeric form for a simplified description.
5) A. Davies and P. G. Harrison, *J. Chem. Soc., C*, **1967**, 1313.
6) Y. Ueno, T. Nakai, and M. Okawara, *Bull. Chem. Soc. Jpn.*, **43**, 162 (1970).
7) J. Burkhardt, R. Feinauer, E. Gulbins, and K. Haman, *Chem. Ber.*, **99**, 1912 (1966).
8) H. Schumann and Max Schmidt, "Organotin Compounds," Vol. II, ed by A. K. Sawyer, Mercel Decker, Inc., N. Y. (1970), p. 297.
9) S. Sakai, K. Itoh, and Y. Ishii, *J. Synth. Org. Chem. Jpn.*, **28**, 1109 (1970).
10) The compounds **1** and **8** have been reported to exist as dimers in solution, while **12** is monomeric; see M. Wada, S. Sato, M. Aritomi, M. Harakawa, and R. Okawara, *J. Organomet. Chem.*, **39**, 99 (1972), and J. Pommier and J. Valade, *ibid.*, **12**, 433 (1968).
11) S. Sakai, H. Matsunaga, and T. Fujinami, *Nippon Kagaku Kaishi*, **1977**, 1688.
12) M. L. Moore, *Org. Synth.*, Col. Vol. 3, 599 (1955).
13) S. Sakai, Y. Kobayashi, and Y. Ishii, *J. Org. Chem.*, **36**, 1176 (1971).
14) S. Sakai, Y. Fujimura, and Y. Ishii, *J. Org. Chem.*, **35**, 2344 (1970).
15) R. C. Poller, *Proc. Chem. Soc.*, **1963**, 312.
16) T. Mukaiyama, Y. Fujisawa, H. Nohira, and T. Hyugaji, *J. Org. Chem.*, **27**, 2337 (1962).

Synthesis and Hydrolysis of 4-Acetoxymethylbenzimidazoles. Effects of Freezing an Internal Rotation on Intramolecular Catalysis by a Benzimidazolyl Group

Masanori UTAKA, Masahisa TAKATSU,* and Akira TAKEDA

Department of Synthetics Chemistry, School of Engineering, Okayama University, Tsushima, Okayama 700

(Received January 24, 1977)

As models for acetyl-α-chymotrypsin, 4-acetoxymethylbenzimidazole (**2**), its 5-methyl derivative **3** and 2,5-dimethyl derivative **4** were synthesized from *o*-toluidine in moderate yields. Their hydrolytic reactivities were determined in water at 50 °C in comparison with their open-chain analog, 4-(acetoxyethyl)imidazole(**1**). The rate constant (k_1) for intramolecular general base catalysis by the imidazolyl group of **2** was 1.6 times larger than k_1 for **1**. A corrected relative rate of 4.1 is obtained by correcting the basicity difference and the polar substituent effect. The value of 4.1 is an expected magnitude of the effect of freezing an internal rotation as reported for 4,5-(1-acetoxymethyltetramethylene)imidazole. The 5-methyl group of **3** enhances the k_1 value 1.4 times as large as that for **2**. The enhancement can be attributed to restriction of the second internal rotation. The hydrolytic reactivity of **4** is discussed.

In a previous paper[1] we reported that intramolecular general base catalysis in the hydrolysis of acetate **5** by its imidazolyl group is 2.6 times more effective than the catalysis in acetate **1**. It was concluded that this enhancement of 2.6 can be rationalized from the entropy effect of freezing an internal rotation. This suggests that, even if the three remaining internal rotations in the acetoxymethyl group were frozen in **5**, the total enhancement would be a factor of about 50 at the highest, and that there remains a factor of about 500 to attain the deacylation rate constant of acetyl-α-chymotrypsin. This deficiency might possibly be provided by the presence of a carboxylate group which affords the so-called "charger-relay" system[2] in the enzyme, but such a large factor using a model system[3] has never been realized. Thus it is important to estimate the rate enhancement caused by freezing an internal rotation. In order to examine further the enhancement caused by the freezing, we have synthesized three new models **2**—**4** and compared their hydrolytic reactivities with the reactivity of **1** or **5**.

Acetate **2** is an unsaturated analog of acetate **5**. The former has a planar skeleton of benzene which is more rigid than that of cyclohexene in the latter.

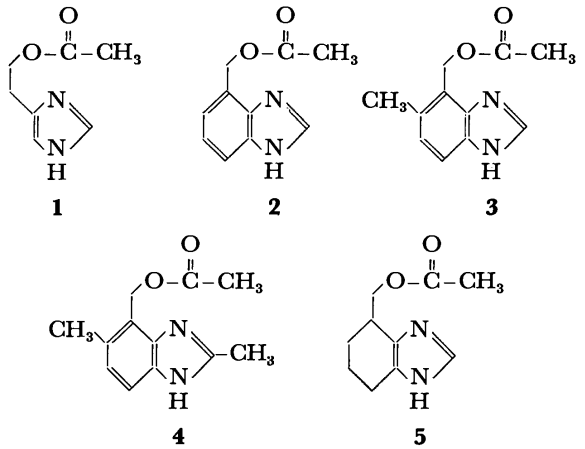

1 **2** **3** **4** **5**

* Present address: Nissei Kagaku Kogyo Co., Ltd., Fukumachi, Nishiyodogawa-ku, Osaka 555.

Moreover, **2** has a slightly shorter distance between the carbonyl carbon and the imidazolyl nitrogen than **5**. It seems interesting to show the effect of these factors on the reactivity. The 5-methyl derivative **3** was designed to investigate the rate enhancement caused by restricting the second internal rotation by the methyl group. The dimethyl derivative **4** was prepared as a modification of **3**.

Results and Discussion

Synthesis. Acetate **2** was obtained by reduction and subsequent acetylation of methyl 4-benzimidazolecarboxylate prepared from *o*-toluidine according to the method of Williams and Salvadori.[4]

The 5-methyl derivative **3** was prepared as outlined in Scheme 1. Reduction of 2-amino-6-methylbenzoic acid with lithium aluminum hydride gave **8** in 73% yield, which, after acetylation, was nitrated with 70% nitric acid in acetic anhydride to give a 2:1 to 3:1 mixture of **10** and **11** in 79% yield. The isomer **10** crystallized with ease from the oily layer in the aqueous reaction mixture. Another isomer **11** was isolated by column chromatography. From their NMR spectra showing an AX pattern in the aromatic region with an intensity of two protons, 1,2,3,4-tetrasubstitution was evident for their benzene rings. Although it was not possible to distinguish **10** from **11** using their NMR and IR spectra, the former was distinguishable from the latter since only **10** could provide the benzimidazole derivative **14**.

Reduction of **12** with Urushibara nickel A[5] gave the expected diamino derivative **13** in 99% yield. To prevent coloration of **13**, the reaction mixture was worked up in a nitrogen atmosphere and the product was used immediately for formation of the benzimidazole ring. Use of tin and concd hydrochloric acid reduced not only the nitro group but also the hydroxyl group in 74% yield. The product was confirmed by the formation of 4,5-dimethylbenzimidazole.[6] Reduction with tin(II) chloride and hydrochloric acid[7] gave **13** in a yield of less than 10%.

The benzimidazole derivative **14** was prepared

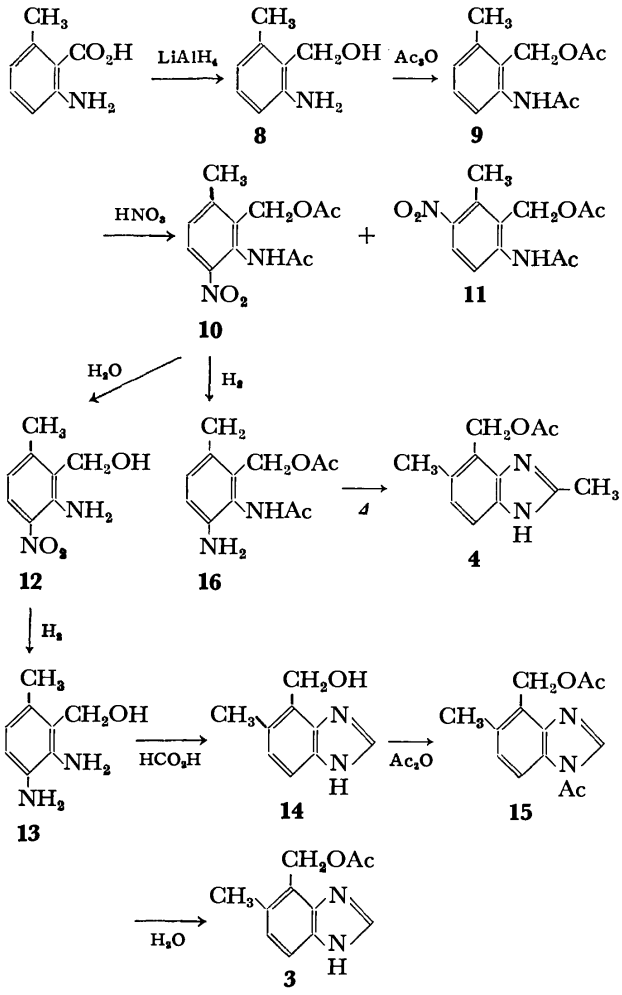

Scheme 1.

conveniently by heating **13** with 80% formic acid[8] in an about 40% yield. Although acetylation of **14** was accompanied by unavoidable *N*-acetylation, model **3** was obtained in a good yield after selective hydrolysis of the *N*-acetyl group.

Reduction of **10** with Urushibara nickel A also gave the corresponding amine quantitatively. By refluxing **16** in xylene[9] and cooling for deposition, model **4** was obtained in 87% yield. Its NMR spectrum showed no signal near δ 8.0 for the hydrogen attached to the C-2 carbon, but indicated the presence of the 2-methyl group by a singlet at δ 2.55.

Kinetics. In Table 1 are given k_1 (min^{-1}) for intramolecular catalysis of the acetate hydrolysis by an imidazolyl or a benzimidazolyl group and k_{OH} (M^{-1} min^{-1}) for bimolecular hydroxide ion attack for **1**—**5**. These rate constants were derived from the observed pseudo-first-order rate constant k_{obsd} using the equation

$$k_{obsd} = \alpha k_1 + k_{OH}[OH^-],$$

where α is the mole fraction of the neutral imidazole. To calculate the concentration of OH^-, the ionization constant of water was taken as $10^{-13.2617}$ at 50 °C.[10] The plots of log k_{obsd} *vs.* pH for acetates **2** and **3** are given in Fig. 1. The curves in Fig. 1 were drawn using the above equation and the rate constants and pK_a values given in Table 1. For comparison the rate constants for **1** and **5** taken from the previous paper[1] are included in Table 1 and the relative rates corrected for the basicity and the polar substituent effect are also given.

Table 1. Hydrolytic rate constants of acetates **1**—**5** and pK_a values of their benzimidazolyl or imidazolyl groups in water[a]

	1[b]	**2**	**3**	**4**	**5**[b]
pK_a[c]	6.50	4.57	4.85	5.62	6.90
$k_{OH}\times10^{-2}$ (M^{-1} min^{-1})	0.63	2.0	1.95	1.8	0.54
Rel rate	1	3.2 (1)	(0.97)	(0.90)	0.86
$k_1\times10^4$ (min^{-1})	1.00	1.6	3.1	2.9	2.6
Rel rate	1	1.6 (1)	(1.9)	(1.8)	2.6
Corrected rel k_1					
For basicity[d]	1	13 (1)	(1.4)	(0.58)	1.7
For polarity[e]	1	4.1			

a) At 50±0.1 °C, 0.1 M KCl. k_1 and k_{OH}, ±5%; pK_a, ±0.02. b) Taken from Ref. 1. c) For comparison the pK_a value for benzimidazole was determined to be 5.16 under the same conditions. d) Corrected for ΔpK_a using the Brönsted exponent β=0.47. e) Corrected for polar effects using the relative rate for k_{OH}.

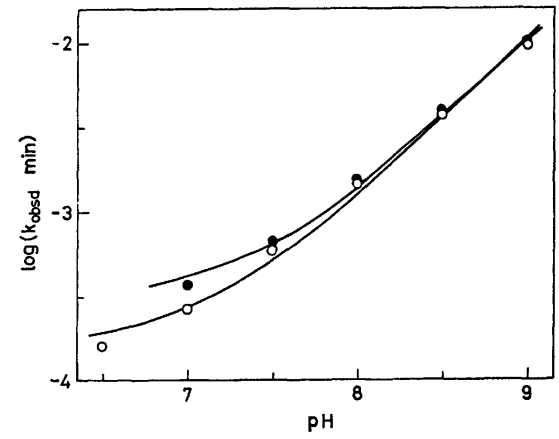

Fig. 1. Plots of log k_{obsd} *vs.* pH for the hydrolyses of **2** (○) and **3** (●) in water at 50 °C, 0.1 M KCl. The points are experimental and the lines theoretical using the equation $k_{obsd}=\alpha k_1+k_{OH}[OH^-]$ and the constants listed in Table 1.

pK_a *Values.* As seen from Table 1 the pK_a value (4.57) for **2** is 0.59 pK_a units smaller than that (5.16) for benzimidazole. This magnitude of a base-weakening effect of an acetoxymethyl group attached to the C-4 position coincides with that for the saturated analog **5** (pK_a 6.90) and 4,5-tetramethyleneimidazole (pK_a 7.50).[1] This suggests that the acetoxymethyl group exerts its effect on the imidazolyl nitrogen through space or sterically. The pK_a value for **3** is 0.28 pK_a units larger than that for **2** and this increment is comparable to 0.33 pK_a units reported for 5-methylbenzimidazole (pK_a 5.81) and benzimidazole (pK_a 5.48) in water at 25 °C.[11] We find an additivity of the substituent effect on the pK_a value (5.62) for **4** as shown by the fact that

the increment (1.05) for the two methyl groups in **4** is equal to the sum of the increments (0.33 and 0.71) for the 5- and 2-methyl[11] groups, no anomaly being found in the pK_a values for **2**, **3**, and **4**.

Effects of Freezing an Internal Rotation. Acetate **2** can be characterized by the rigidity of its structure. It has one internal rotation frozen between the imidazolyl nitrogen and the carbonyl carbon in comparison with acetate **1**. As reported the hydrolysis of **1** is catalyzed by its intramolecular imidazolyl group as general base.[1] The catalytic activity is enhanced in the acetate **5** by a factor of 2.6 mainly because of the rigidity in structure. Thus we can except acetate **2** to show a similar enhancement in the catalysis.

The catalytic rate constant k_1 for **2** was found to be 1.6 times as large as that for **1** (Table 1). This rate factor of 1.6 must be corrected for the basicity and polarity differences between **1** and **2**. Since **2** is less basic than **1** by 1.93 pK_a units, the general base catalysis in **2** is expected to decrease by a factor of 8.07 when we use the Brönsted exponent $\beta=0.47$ for the general base-catalyzed hydrolysis of ethyl dichloroacetate.[1,12] The correction gives a rate factor of 13 for **2**. A correction factor of 3.2 for the polarity difference was adopted from the relative rate for the hydroxide-ion hydrolysis. Although the polar substituent constants (σ^*) for the two alkoxyl groups in **1** and **2** have not been estimated, the observed rate factor of 3.2 seems reasonable as judged from the polar effect of ethyl and benzyl groups.[13]

Thus we obtain a rate factor of 4.1 for freezing an internal rotation in **2**. The value is about twice as large as the factor of 1.7 for **5**. However, the doubled factor is what had been expected previously.[1] In the imidazolyl group-catalyzed hydrolysis of **1** or **2**, two transition states, which are mirror images of each other and identical energetically, may take place during the imidazolyl residue rotation about the methylene-imidazolyl residue bond. But for **5**, since the acetoxymethyl group is expected to take a preferred pseudo-equatorial position, only one transition state can be realized.

We can thus concluded that the rigid structure of benzene in **2** gives rise to almost the same rate factor by freezing an internal rotation as the flexible structure of cyclohexene in **5**, and that the difference in the spatial alignments of the imidazolyl nitrogen and the carbonyl carbon between **2** and **5** is not critical for the intramolecular catalysis. These two conclusions are consistent with the looseness of the transition state in general base catalysis.[1]

Restriction of the Second Internal Rotation. The rate enhancement in k_1 by the 4-methyl group seems to be properly estimated using the concept of rotamer population.

Figure 2 shows the Newman projection for **2** and **3**, in which the horizontal line represents the benzimidazole plane. The projection formula indicates the existence of four rotamers **a**, **b**, **c**, and **d** with the acetoxyl group in a, b, c, and d regions, respectively. Rotamers **a** and **b** are considered to be active catalytically; rotamer **c** is thought to be inactive owing to the crowded and less

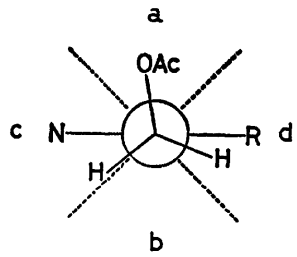

2 R=H
3 R=CH_3

Fig. 2. The projection formula for **2** and **3**. The horizontal line represents the benzimidazole plane.

favorable alignment of the acetoxyl group and rotamer **d** to be inactive because of the incorrect orientation of the acetoxyl group. Since the rotation about the carbon-carbon bond is expected to be essentially free for **2**, the four rotamer populations can be taken to be roughly equal to each other if the active region is accepted as shown in Fig. 2. Then the fraction of the active rotamer population is 2/4. If rotamer **c** is negligible owing to the steric repulsion between the nitrogen and the oxygen, the fraction will be 2/3.

On the other hand, rotamer **d** must be absent for the 4-methyl derivative **3**, whereas the remaining three rotamers are similar to the corresponding ones for **2**. Then the fraction of the active rotamer population is 2/3 or 2/2 for **3**. Thus we obtain a relative rate of 1.33—1.5 for the expected enhancement in k_1. Actually, the value of 1.4 was obtained for **3** after the correction for basicity (Table 1).

Effects of the 2-Methyl Group. Acetate **4** shows deceleration of the hydrolyses. A larger deceleration factor of 2.4 (=1.4/0.58) is obtained for k_1 in comparison with the small factor of 1.1 for k_{OH}, but the deceleration is not so large when compared with the deceleration factor of 92 reported for the intramolecular nucleophilic catalysis by 2-methylbenzimidazole of the hydrolysis of *p*-nitrophenyl acetate.[14]

Experimental

All melting points are uncorrected. Elemental analyses were carried out by Mr. E. Amano of our laboratory. ^1H NMR spectra were recorded at 60 MHz on a Hitachi Model R-24 spectrometer. Tetramethylsilane was used as internal standard unless otherwise noted.

Materials. Potassium chloride and benzimidazole of reagent grade were used after recrystallization. Hydrochloric acid, sodium hydroxide, and standard buffer solutions were obtained from Nakarai Chemicals (Kyoto). Deionized water was used in all kinetic runs.

4-Hydroxymethylbenzimidazole (6). Reduction of methyl 4-benzimidazolecarboxylate with lithium aluminum hydride in THF, prepared according to the method of Williams and Salvadori[4] from *o*-toluidine, gave crude yellow crystals of **6** in 74% yield. The crude crystals were recrystallized from hot water after treating with carbon, giving colorless needles: mp 140—144 °C; IR (KBr) 3400—2200 (OH and NH), 1620 (benzimidazole ring), and 1005 cm^{-1} (C–O); NMR (DMSO-d_6) δ (solvent peak as internal standard, δ 2.50) 8.22 (s, 1, N–CH=N), 7.7—7.1 (m, 3, benzene ring), 6.5 (s, NH and OH), and 4.92 ppm (s, 2, CH_2–O).

N-Acetyl-4-acetoxymethylbenzimidazole (7). In acetic anhydride **6** was heated at 70 °C for 1 h with stirring. The excess anhydride was distilled under reduced pressure, leaving white crystals of **7**. Recrystallization from carbon tetrachloride gave pure crystals in 95% yield: mp 96.0—97.5 °C; IR (KBr) 1730, 1725 (ester and amide C=O), 1600 (benzimidazole ring), and 1235 cm^{-1} (C–O); NMR ($CDCl_3$) δ 8.33 (s, 1, N–CH=N), 8.2—7.2 (m, 3, benzene ring), 5.53 (s, 2, CH_2–O), 2.71 (s, 3, N–$COCH_3$), and 2.10 ppm (s, 3, O–$COCH_3$).

4-Acetoxymethylbenzimidazole (2). In dil hydrochloric acid **7** was dissolved at 50 °C with stirring over a 50-min period. The solution was filtered and neutralized with aq potassium hydrogen carbonate. The neutral solution was extracted with chloroform, and the solvent was evaporated after drying over magnesium sulfate to leave white crystals of **2** in 94% yield. Recrystalliztion from chloroform gave a pure sample: mp 169.5—170.5 °C; IR (KBr) 3200—2200 (NH), 1723 (C=O), 1620—1605 (benzimidazole ring), 1242 (C–O), and 754, 715 cm^{-1} (1,2,3-trisubstituted benzene); NMR ($CDCl_3$) δ 8.06 (s, 1, N–CH=N), 7.9—7.1 (m, 3, benzene ring), 7.1 (s, 1, NH), 5.45 (s, 2, CH_2–O), and 2.08 ppm (s, 3, $COCH_3$). Found: C, 63.47; H, 5.50; N, 14.78%. Calcd for $C_{10}H_{10}N_2O_2$: C, 63.15; 5.30; N, 14.73%.

2-Amino-6-methylbenzyl Alcohol (8). 2-Amino-6-methylbenzoic acid[15] prepared from *o*-toluidine was reduced with lithium aluminum hydride in ether at room temperature. The excess hydride was decomposed with water and the resulting mixture was filtered. The white solid was washed with ether repeatedly. The filtrate and washings were combined, the solvent being removed to leave white crystals of **8** in 73% yield. Recrystallization from carbon tetrachloride gave white needless: IR (KBr) 3400—2400 (NH_2 and OH), 1600 (NH_2), 1000 (C–O), and 785, 745 cm^{-1} (1,2,3-trisubstituted benzene).

2-Acetylamino-6-methylbenzyl Acetate (9). In excess acetic anhydride **8** was heated at 70 °C for 2 h with stirring. The excess anhydride was removed under reduced pressure to leave **9** in a quantitative yield. Recrystallization from carbon tetrachloride gave colorless needles: mp 118—118.5 °C; IR (KBr) 3250 (NH), 1735 (ester C=O), 1650 (amide C=O), and 790, 750 cm^{-1} (1,2,3-trisubstituted benzene); NMR ($CDCl_3$) δ 9.05 (s, 1, NH), 7.8—6.8 (m, 3, benzene ring), 5.12 (s, 2, CH_2–O), 2.41 (s, 3, CH_3), 2.19 (s, 3, N–$COCH_3$), and 2.05 ppm (s, 3, O–$COCH_3$). Found: C, 64.87; H, 6.59%. Calcd for $C_{12}H_{15}NO_3$: C, 65.14; H, 6.83%.

2-Acetylamino-3-nitro-6-methylbenzyl Acetate (10). To a solution of 5.0 g (21.6 mmol) of **9** in 25 ml of acetic anhydride was added 4 ml of 70% nitric acid dropwise with stirring at 19—20 °C. After the addition was completed, the mixture was stirred for 1 h at the same temperature. The mixture was poured into 300 ml of cold water with stirring. Colorless needles separated were collected and recrystallized from ethanol to give pure **10** in 38% yield: mp 147—148 °C; IR (KBr) 3250 (NH), 1740 (ester C=O), 1655 (amide C=O), and 1510, 1355 cm^{-1} (NO_2); NMR ($CDCl_3$) δ 8.9 (s, 1, NH), 7.81 (d, 1, J=9 Hz, H_4), 7.19 (d, 1, J=9 Hz, H_5), 5.15 (s, 2, CH_2–O), 2.50 (s, 3, CH_3), 2.19 (s, 3, N–$COCH_3$), and 2.08 ppm (s, 3, O–$COCH_3$). Found: C, 53.86; H, 5.07%. Calcd for $C_{12}H_{14}N_2O_5$: C, 54.13; H, 5.30%.

From the mother liquor a mixture of **10** and **11** was recovered, giving a 79% yield for the nitration. The isomer **11** was separated by column chromatography using silica gel (Wakogel C-200) and dichloromethane, and recrystallized from carbon tetrachloride: mp 227—230 °C; IR (KBr) 3350 (NH), 1712 (ester C=O), 1688 (amide C=O), and 1520, 1350 cm^{-1} (NO_2); NMR ($CDCl_3$) δ 9.5 (s, 1, NH), 8.03 (d, 1, J=9 Hz, H_4), 7.78 (d, 1, J=9 Hz, H_3), 5.20 (s, 2, CH_2–O), 2.58 (s, 3, CH_3), 2.25 (s, 3, N–$COCH_3$), and 2.12 ppm (s, 3, O–$COCH_3$).

2-Amino-3-nitro-6-methylbenzyl Alcohol (12). In aq methanol **10** was dissolved and hydrolyzed for 3 h at 60 °C after addition of aq sodium hydroxide. The solution was neutralized with hydrochloric acid and extracted four times with chloroform. After drying over magnesium sulfate, the solvent was removed to give orange crystals of **12** in 99% yield. Recrystallization from ethanol gave a pure sample: mp 135—136 °C; IR (KBr) 3460, 3350 (NH_2 and OH), 1636 (NH_2), 1498, 1321 (NO_2), and 816 cm^{-1} (1,2,3,4-tetrasubstituted benzene); NMR ($CDCl_3$) δ 7.89 (d, 1, J=9 Hz, H_4), 6.48 (d, 1, J=9 Hz, H_5), 4.76 (s, NH_2 and OH), 4.70 (s, 2, CH_2–O), and 2.35 ppm (s, 3, CH_3). Found: C, 52.45; H, 5.41%. Calcd for $C_8H_{10}N_2O_3$: C, 52.74; H, 5.53%.

2,3-Diamino-6-methylbenzyl Alcohol (13). One hundred mg of **12** was dissolved in 5 ml of ethanol and reduced with hydrogen (1 atm) using about 20 mg of Urushibara nickel A.[5] Absorption of hydrogen ceased after the theoretical volume of hydrogen was taken up. The yellow solution was gradually decolorized as the hydrogen was absorbed. To dissolve a white precipitate 10 ml of hot ethanol was added and the reaction mixture was filtered with a glass filter with suction. Removal of ethanol gave 88 mg (99%) of white needles of **13**. The reaction mixture was worked up in a nitrogen atmosphere and **13** thus prepared was used immediately for the next step: mp 181—182 °C; IR (KBr) 3450—2400 (NH_2 and OH), 1660—1550 (NH_2), and 802 cm^{-1} (1,2,3,4-tetrasubstituted benzene); NMR (DMSO-d_6) δ 6.44 (d, 1, J=8 Hz, H_4 or H_5), 6.24 (d, 1, J=8 Hz, H_5 or H_4), 4.46 (s, 2, CH_2–O), and 2.16 ppm (s, 3, CH_3).

4-Hydroxymethyl-5-methylbenzimidazole (14). In 15 ml of 80% formic acid was dissolved 428 mg of freshly prepared **13**, and the solution was heated at 100 °C for 1 h with stirring. The resulting red solution was neutralized with concd aq sodium hydroxide to separate a red oil on the bottom. The decolorized supernatant solution was decanted and concentrated under reduced pressure to precipitate white needles. The needles were collected, washed with cold water, and dried, giving 171 mg (37%) of **14**: mp 205—205.5 °C; IR (KBr) 3300—2200 (NH and OH), 1590 (benzimidazole ring), and 811 cm^{-1} (1,2,3,4-tetrasubstituted benzene); NMR ($CDCl_3$) δ 8.00 (N–CH=N), 7.42 (d, 1, J=8 Hz, $H_{7(4)}$), 7.03 (d, 1, J=8 Hz, $H_{4(7)}$), 4.97 (s, 2, CH_2–O), and 2.45 ppm (s, 3, CH_3).

N-Acetyl-4-acetoxymethyl-5-methylbenzimidazole (15). Acetylation of **14** in the same way as for **6** gave crude **15**, which was recrystallized from carbon tetrachloride to give white needles in 80% yield: mp 156—157 °C; IR (KBr) 1725 (ester and amide C=O), 1595 (benzimidazole ring), and 817 cm^{-1} (1,2,3,4-tetrasubstituted benzene); NMR ($CDCl_3$) δ 8.32 (s, 1, N–CH=N), 8.06 (d, 1, J=9 Hz, H_7), 7.24 (d, 1, J=9 Hz, H_6), 5.59 (s, 2, CH_2–O), 2.71 (s, 3, N–$COCH_3$), 2.48 (s, 3, CH_3), and 2.07 ppm (s, 3, O–$COCH_3$).

4-Acetoxymethyl-5-methylbenzimidazole (3). Partial hydrolysis of **15** in the same way as for **7** gave white crystals of **3** in 83% yield after recrystallization from chloroform. The analytical and kinetic sample was purified further by sublimation *in vacuo*: mp 229—229.5 °C; IR (KBr) 3200—2400 (NH) 1720 (C=O), 1625, 1595 (benzimidazole ring), 1240 (C–O), and 820 cm^{-1} (1,2,3,4-tetrasubstituted benzene); NMR (CD_3OD) δ 8.02 (s, 1, N–CH=N), 7.46 (d, 1, J=9 Hz, $H_{7(4)}$), 7.05 (d, 1, J=9 Hz, $H_{6(5)}$), 5.42 (s, 2, CH_2–O), 4.74 (s, NH), 2.44 (s, 3, CH_3), and 2.02 ppm (s, 3, $COCH_3$). Found: C, 64.88; H, 5.98; N, 13.78%. Calcd for $C_{11}H_{12}N_2O_2$: C, 64.69; H, 5.92; N, 13.72%.

2-Acetylamino-3-amino-6-methylbenzyl Acetate (16). Using

the Urushibara nickel catalyst **10** was reduced with hydrogen in the same way as for **12**. White crystals of **16** were obtained in 100% yield: mp 149—151 °C; IR (KBr) 3390, 3230 (NH_2 and NH), 1732 (ester C=O), and 1650 cm^{-1} (amide C=O); NMR ($CDCl_3$) δ 8.8 (s, 1, NH), 6.90 (d, 1, J=8 Hz), 6.60 (d, 1, J=8 Hz), 5.07 (s, 2, CH_2-O), 2.30 (s, 3, CH_3), 2.20 (s, 3, N-$COCH_3$), and 2.01 ppm (s, 3, O-$COCH_3$).

4-Acetoxymethyl-2,5-dimethylbenzimidazole (4). A mixture of 2 ml of dry xylene and 50 mg of **16** was heated at 135 °C for 5 h with stirring. The reaction mixture was cooled to precipitate colorless needles, which were collected and washed with ether to give 40 mg (87%) of **4**. This was purified by recrystallization from carbon tetrachloride–chloroform and subsequent sublimation *in vacuo*: mp 220—221 °C; IR (KBr) 3500—2300 (NH), 1725 (C=O), 1625, 1595 (benzimidazole ring), 1235 (C-O), and 820 cm^{-1} (1,2,3,4-tetrasubstituted benzene); NMR (CD_3OD) δ 7.37 (d, 1, J=9 Hz, $H_{7(4)}$), 7.02 (d, 1, J=9 Hz, $H_{6(5)}$), 5.42 (s, 2, CH_2-O), 4.8 (s, NH), 2.55 (s, 3, CH_3), 2.44 (s, 3, CH_3), and 2.04 ppm (s, 3, $COCH_3$). Found: C, 65.94; H, 6.67; N, 13.12%. Calcd for $C_{12}H_{14}N_2O_4$: C, 66.04; H, 6.47; N, 12.84%.

Reduction of 12 with Tin and Hydrochloric Acid. To a mixture of 102 mg of **12** and 400 mg of tin was added 2.5 ml of concd hydrochloric acid, and the mixture was heated at 70 °C for 30 min. Then it was made basic (pH 11) by addition of 5 ml of 5 M sodium hydroxide and heated at 100 °C for a while. Extraction with chloroform gave 56 mg of white needles in 74% yield, which was identified as 3,4-*o*-xylenediamine: IR (KBr) 3400—3150 (NH_2), 1625 cm^{-1} (NH_2); NMR (CD_3OD) δ 6.45 (t, 2, CH=CH), 4.63 (s, 4, NH_2), 2.14 (s, 3, CH_3), and 2.03 ppm (s, 3, CH_3).

Kinetics. All kinetic measurements for hydrolysis were made at 50±0.1 °C (0.1 M KCl) in water by the titration of liberated acid with the titration assembly.[1] The initial concentration of acetate **2** was 0.0025 and 0.005 M. However, only 0.0025 M was used for **3** and **4** owing to their solbilities. Hydrolysis of the acetates were followed to 3 (at pH 6.5)—50 % (at pH 9.0) completion for **2**, to 2.4 (at pH 7.0)—47% (at pH 9.0) for **3**, and to 6.9 (at pH 6.5)—15% (at pH 9.0) for **4**. Deposition of **3** from the kinetic solution after 1 h or so from the start of kinetic run allowed only 2—3% completion for **3** at pH 6.5—7.0, although **3** could be dissolved initially in the acidic solution. All runs followed first-order kinetics. Values of k_{obsd} were reproduced within±5%.

pK_a *Determinations.* Values of pK_a were determined according to the method of Albert and Serjeant[16] using the apparatus for kinetics under the same conditions as for kinetics.

References

1) M. Utaka, J. Koyama, and A. Takeda, *J. Am. Chem. Soc.*, **98**, 984 (1976).

2) D. M. Blow, J. J. Birktoff, and B. S. Hartley, *Nature (London)*, **221**, 337 (1969); M. W. Hunkapiller, S. H. Smallcombe, D. R. Whitaker, and J. H. Richards, *Biochemistry*, **12**, 4732 (1973).

3) G. A. Rogers and T. C. Bruice, *J. Am. Chem. Soc.*, **96**, 2473 (1974).

4) A. Williams and G. Salvadori, *J. Chem. Soc., B*, **1972**, 883.

5) Y. Urushibara, S. Nishimura, and H. Uehara, *Bull. Chem. Soc. Jpn.*, **28**, 446 (1955).

6) NMR (CD_3OD) δ 8.07 (s, 1, NH), 7.33 (d, 1, $H_{6(5)}$), 7.03 (d, 1, $H_{7(4)}$), 2.48 (s, 3, CH_3), and 2.36 ppm (s, 3, CH_3).

7) F. H. S. Curd, D. G. Davey, and G. J. Staley, *J. Chem. Soc.*, **1949**, 1271.

8) L. F. Fieser and M. Fieser, "Reagents for Organic Synthesis," Vol. 1, Wiley, New York (1967), p. 405.

9) C. M. Roeder and A. R. Day, *J. Org Chem.*, **6**, 25 (1941).

10) R. C. Weast, Ed., "CRC Handbook of Chemistry and Physics," 50 th ed, Chemical Rubber Publishing Co., Cleveland, Ohio (1969), p. D120.

11) K. Hofmann, "Imidazole and Its Derivatives," Part I, Interscience, New York (1953), p. 251.

12) W. P. Jencks and J. Carriuolo, *J. Am. Chem. Soc.*, **83**, 1743 (1961).

13) R. W. Taft, Jr., "Steric Effects in Organic Chemistry," ed by M. S. Newman, Wiley, New York (1965), Chap. 13, pp. 619, 644—645. For the alkaline hydrolysis of ethyl and benzyl acetates, a rate factor of 2.93 can be calculated using σ^* values −0.100 and 0.215 for C_2H_5 and $C_6H_5CH_2$, respectively, and a ρ^* value of 1.465. The steric effect of the two substituents is calculated to give a factor of 1.09 using E_s values −0.09 and −0.22 for C_2H_5 and i-C_4H_9, respectively, and a δ value 0.301 for the alkaline hydrolysis of $ROCOCH_3$. Here the value for i-C_4H_9 is used instead of that for $C_6H_5CH_2$ since the latter is not known yet. The E_s values for C_2H_5 and $C_6H_5CH_2$ in the acyl component, however, are reported to be −0.07 and −0.38, respectively. With these we obtain the factor of 1.24. The steric effect on the relative rate is very small as compared with the polar effect.

14) T. C. Bruice and G. L. Schmir, *J. Am. Chem. Soc.*, **80**, 148 (1958); M. L. Bender, "Mechanisms of Homogeneous Catalysis from Protons to Proteins," Wiley-Interscience, New York (1971), pp. 162—163.

15) D. F. Detar and J. C. Howard, *J. Am. Chem. Soc.*, **77**, 4393 (1955); S. Gabriel and A. Thieme, *Chem. Ber.*, **52**, 1081 (1919); Y. Asahina and Y. Kondo, *Yakugaku Zasshi*, **1922**, No. 482, 264.

16) A. Albert and E. P. Serjeant, "The Determination of Ionization Constants," Chapman and Hall, London (1971), Chap. 2.

Photochemistry of Heterocyclic Compounds. VII.[1] Photochemical Reaction of 2,5-Diphenyl-1,3,4-oxadiazole with Benzo[*b*]thiophenes

Kōji Oe, Masashi Tashiro, and Otohiko Tsuge*

Research Institute of Industrial Science, Kyushu University 86, Hakozaki, Higashi-ku, Fukuoka 812

(Received February 19, 1977)

Irradiation of 2,5-diphenyloxadiazole **1** with benzothiophene **6a** gives 3-benzoylbenzothiophene **7**, its benzoylhydrazone **8**, and/or the oxadiazepine **9**; the yields depended on the nature of solvents. With benzophenone as a sensitizer, the photochemical reaction of **1** with **6a** forms the [2+2] cycloadduct **12**. It is found that **9** is photochemically dissociated to **1** and **6a**. In the case of 2-methylbenzothiophene **6b**, 3-benzoyl-2-methylbenzothiophene benzoylhydrazone **18** is formed, and with benzophenone as a sensitizer the [2+2] cycloadduct **19** is obtained. In the absence or presence of benzophenone, however, irradiation of **1** with 3-methylbenzothiophene **6c** gives the [2+2] cycloadduct **20**. The photochemical reaction of **1** with **6a** or **6b** in the presence of iodine gives the corresponding 3-benzoylbenzothiophene, **7** or **21**, and benzoylhydrazone, **8** or **18**, respectively. In the case of **6c**, however, the [2+2] cycloadduct **23** is formed, together with 2-benzoyl-3-methylbenzothiophene **22**. Mechanistic considerations of these reactions are also described.

Although [2+2] photocycloadditions of olefins to other olefins[2] and to ketones[3] are well characterized, only a few examples of similar photocycloadditions to the carbon-nitrogen double bonds appeared in the literature.[4-8] Previously, we reported some novel photoproducts from the photochemical reactions of 2,5-diphenyl-1,3,4-oxadiazole (**1**) with furan[4] and indene[5] in the absence or presence of iodine as depicted in Scheme 1. The [2+2] cycloadduct **2** is formed *via* the interation between a triplet excited state of **1** and furan, and the formation of the benzoylhydrazone **3** is attributable to the reaction of **1** with cyclobutadiene oxide (probably its iodine complex) produced from the photochemical interaction between furan and iodine. On the other hand, the reaction to afford the oxadiazepine **4** starts with a singlet excited state of indene, and the [2+2] cycloadduct **5** is produced *via* the photochemical reaction of **1** with σ-complex between indene and iodine.

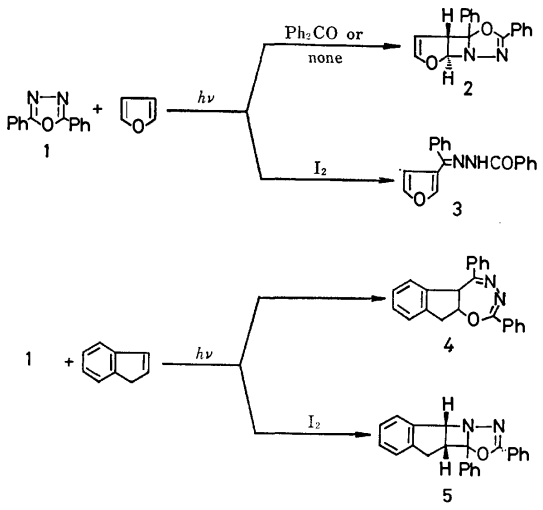

Scheme 1.

It has been reported that upon irradiation with olefins[9] and acetylenes[10] benzo[*b*]thiophene gave the cycloadducts. Thus we were interested in the photochemical reaction of **1** with benzo[*b*]thiophene. We now report here on the photochemical reactions of **1** with benzo[*b*]thiophene and its methyl derivatives under various conditions.

* To whom correspondences should be addressed.

Results and Discussion

Photochemical Reaction in the Absence of Iodine. Irradiation of a solution of the oxadiazole **1** and benzo[*b*]thiophene (**6a**) in benzene below 15 °C afforded 3-benzoylbenzo[*b*]thiophene (**7**), its benzoylhydrazone **8**, and the 1 : 1 cycloadduct **9**. The results in various solvents are shown in Table 1; the yields of the products depended on the nature of solvent. Structural elucidation of **7** and **8** was accomplished on the basis of their spectral data as well as of identification with authentic samples prepared by the routes depicted in Scheme 2.

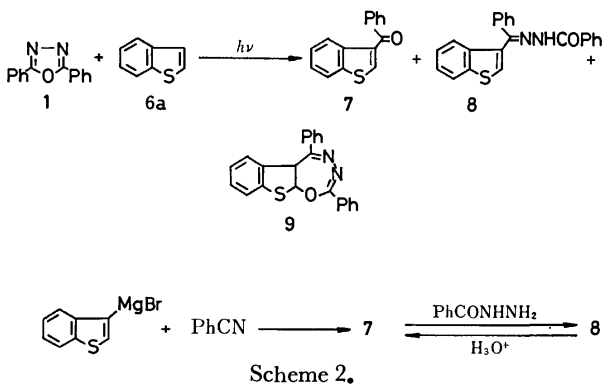

Scheme 2.

From the following evidence, the 1 : 1 adduct **9** was assigned to be 2,5-diphenyl-5a,10a-dihydro[1]benzothieno[3,2-*f*][1,3,4]oxadiazepine whose ring system is the same as that of **4**. The IR spectrum and chemical behavior of **9** are similar to those of the oxadiazepine **4**. The 1 : 1 adduct **9** is thermally labile and on being heated readily isomerized to the benzoylhydrazone **8** in benzene. Reduction of **9** with sodium borohydride afforded the dihydro compound whose structure was assigned to be 2,5-diphenyl-4,5,5a,10a-tetrahydro[1]-benzothieno[3,2-*f*][1,3,4]oxadiazepine (**10**), but not the 2,3,5a,10a-tetrahydro compound **10'**. The NMR spectrum of **10** exhibits methine proton signals at δ 4.67

(H_a, t, J=8 Hz), 6.23 (H_b, d, J=8 Hz) and 6.32 (H_c, d, J=8 Hz), besides aromatic and NH proton signals. In the NMR spectrum of **10**-d_1 which was prepared by reduction of **9** with sodium borohydride-d_4, the doublet at δ 6.32 does not appear, and two doubles (J=8 Hz) are displayed at δ 4.67 and 6.25. On treatment with hydrochloric acid in methanol at room temperature, **10** was converted into 1-benzoyl-2-[α-(3-benzo[*b*]thienyl)-benzyl]hydrazine (**11**), which was identical with an authentic sample (Scheme 3).

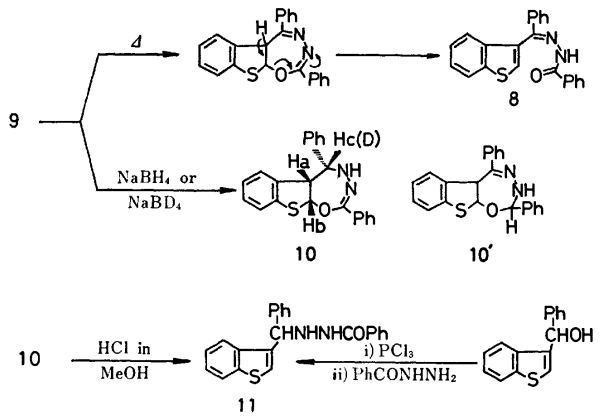

Scheme 3.

Previously,[5] we have reported that the oxadiazepine **4** is the *cis*-fused adduct, and that three methine hydrogens in the dihydro compound of **4** are situated *cis* each other. Although the NMR spectrum of **9** could not be measured owing to its insolubility in solvents and to its lability, it was deduced that **9** would be also the *cis*-fused adduct on the basis of stereochemistry of **10**. In analogy with the dihydro compound of **4**, we assumed that the moiety –N–N=C(O)Ph in the seven-membered cyclic ring of **10** is coplanar. An inspection of the Dreiding models of **10** indicates that the dihedral angles, θ_{ab} between H_a and H_b, and θ_{ac} between H_a and H_c, are *ca.* 25° respectively, when the hydrogens H_a, H_b, and H_c are situated *cis* each other. The observed J_{ab} and J_{ac} values are 8 Hz which is compatible with the calculated value (6.7 Hz) when θ is 25°.[11]

Table 1. Photochemical reaction of **1** with **6a** in various solvents

Solvent	Irradiation time, h	Products, %		
		7	**8**	**9**
Hexane	1	trace	—	69
Dioxane	1	6	—	21
Benzene	1	5	trace	24
Diethyl ether	1	2	—	47
Tetrahydrofuran	1	4	—	21
Acetonitrile	1	1	3	—
Acetonitrile	10	2	5	—

Irradiation of **1** with **6a** in benzene for 10 h did not give the oxadiazepine **9**, but instead a new 1 : 1 adduct **12** was obtained in 8% yield, together with small quantities of **7** and **8** and with recovery of **1** and **6a**. Photolysis of the oxadiazepine **9** in benzene or acetonitrile afforded the oxadiazole **1**, benzothiophene **6a**, benzoylbenzothiophene **7**, and 1 : 1 adduct **12** (Scheme 4). Thus, it can be concluded that the oxadiazepine **9** is photochemically dissociated to the starting materials **1** and **6a**, along with a partial isomerization to **8**. On treatment with ethanolic potassium hydroxide, the 1 : 1 adduct **12** isomerized to **8**. On the basis of the above fact and spectral data, **12** was assigned to be the *trans* [2+2] cycloadduct, 4,4a,9b,9c-tetrahydro-2,9c-diphenyl[1]benzothieno[3',2': 3,4]azetidino[2,1-*b*][1,3,4]oxadiazole.

In the benzophenone photosensitized reaction of **1** with **6a**, the [2+2] cycloadduct **12** was formed as the sole product. Both electronic absorption spectra of **1** and **6a** show absorptions around 310 nm, while that of benzo[*b*]furan displays no appreciable absorption above 290 nm. When a solution of **1** and benzo[*b*]-furan in benzene was irradiated with a high-pressure mercury lamp or with monochromatic light (313 nm), the *trans* [2+2] cycloadduct **13** was obtained. Thus, it may concluded that the reaction for the formation of **12** starts with a triplet excited state of **1**.

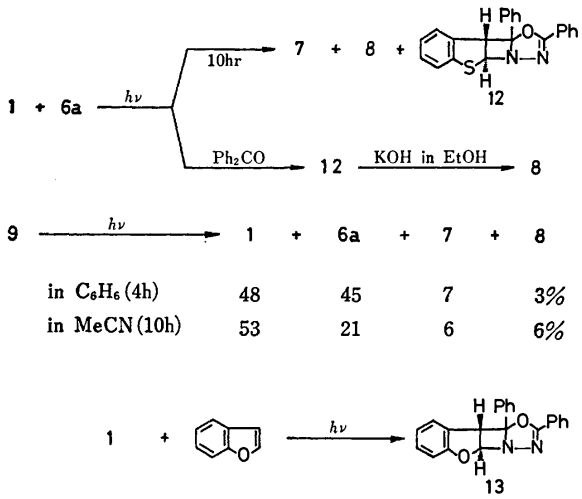

Scheme 4.

In a previous paper[5] we suggested that the reaction producing the oxadiazepine **4** starts with a singlet state of indene, and the subsequent interaction with **1** forms the betaine intermediate **A** which gives **4**. The plausible

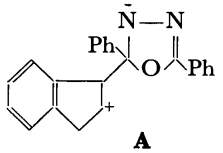

A

pathway for the formation of **9** is outlined in Scheme 5. By the absorption of light **6a** is excited to the polar species **B** proposed in the photochemical reaction of **6a**.[10] This is followed by interaction with **1** to give the betaine intermediate **C** like **A**, and subsequent ring opening of **C** with concurrent ring closure affords **9**.

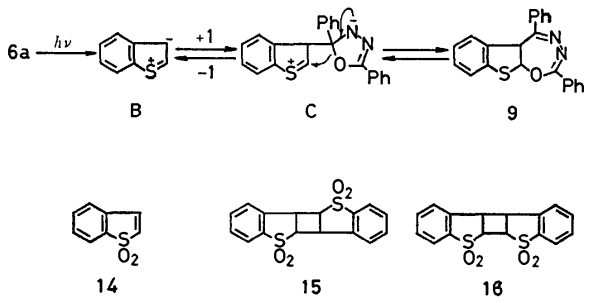

Scheme 5.

The following result suggests a significant contribution of **B** to the formation of **9**. Benzo[*b*]thiophene 1,1-dioxide (**14**) cannot form an excited species such as **B**. The 1,1-dioxide **14** failed to add **1**, but instead underwent a cinnamic acid type dimerization to give a mixture of two isomeric dimers **15** and **16**.

Although the photochemical reaction of **1** with **6a** in acetonitrile did not give the oxadiazepine **9** (Table 1), irradiation in ethyl ether containing acetonitrile (5 mol to **6a**) afforded the oxadiazepine **9** in 38% yield; this fact indicates that acetonitrile does not act as an inhibitor for the formation of **9**. Thus it may be viewed that the primary photoadduct **9** is readily dissociated to the starting materials in a polar solvent such as acetonitrile.

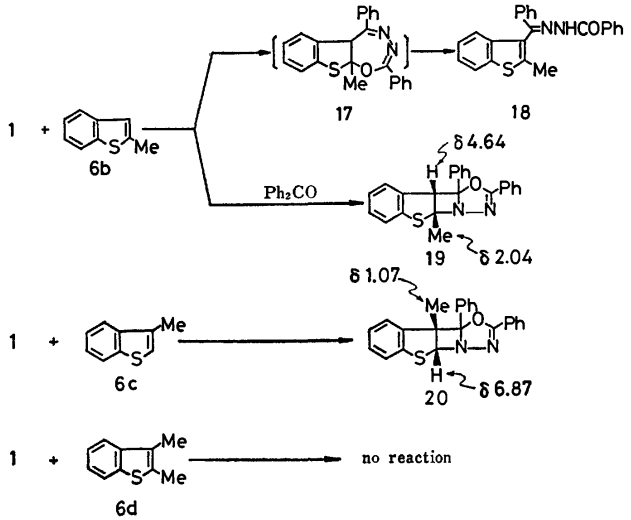

Scheme 6.

Next, we investigated the photochemical reaction between **1** and methylbenzo[*b*]thiophenes. Without or with benzophenone as the sesitizer, irradiation of **1** with 2-methylbenzo[*b*]thiophene (**6b**) afforded 3-benzoyl-2-methylbenzo[*b*]thiophene benzoylhydrazone (**18**) or [2+2] cycloadduct **19**, respectively. The benzoylhydrazone **18** might be interpreted as arising *via* the oxadiazepine **17**, but no **17** was detected in the reaction mixture. On the other hand, the photochemical reaction of **1** with 3-methylbenzo[*b*]thiophene (**6c**) did not give the corresponding oxadiazepine nor benzoylhydrazone, but instead the [2+2] cycloadduct **20** was formed in 13% yield; this fact means that the polarized species of **6c** such as **B** does not contribute to the reaction, because of the electron-donating 3-methyl group. With benzophenone as the sesitizer, the [2+2] cycloadduct **20** was obtained in 33% yield. Upon irradiation, however, 2,3-dimethylbenzo[*b*]thiophene (**6d**) did not react with **1** (Scheme 6). Structures of the photoproducts, **18**—**20**, were established by the spectral data. The stereochemistry of **19** and **20** will be described later.

It is reasonable to conclude that the reactions producing the [2+2] cycloadducts **19** and **20**, as well as the [2+2] cycloadduct **12**, start with a triplet excited state of **1**.

Photochemical Reaction in the Presence of Iodine. Irradiation of **1** with **6a** or **6b** in the presence of iodine (20 mol % to **1**) in benzene afforded the corresponding 3-benzoylbenzothiophene **7** (16%) or **21** (1%), and benzoylhydrazone **8** (50%) or **18** (15%), respectively. These results appear to be similar to that of the reaction with furan in the presence of iodine (Scheme 1). In the reaction of **1** with **6c** under similar conditions, however, a new [2+2] cycloadduct **23** was obtained, together with 2-benzoyl-3-methylbenzo[*b*]thiophene (**22**) (Scheme 7). The benzoyl compounds **21** and **22** were identical with the respective authentic samples prepared from the Friedel-Crafts benzoylation of **6b** and **6c**.

On the basis of the following spectral data, **23** was assigned to be 4,4a,9a,9b-tetrahydro-2,9b-diphenyl-4a-methyl[1]benzothieno[2′,3′: 3,4]azetidino[2,1-*b*][1,3,4]-oxadiazole, whose structure corresponds to the reversed adduct of **20**. The IR spectrum of **23** is very similar to that of **20**. The chemical shift of methine proton in **23** is comparable to that (δ 6.45) of the methine adjacent to the nitrogen atom in the [2+2] cycloadduct **5**, but not compatible with that in **20**. The methyl proton signal in **23** appears at a higher field than that in **19**, but at a lower field than that in **20**. The stereochemistry of **23** will be also described later.

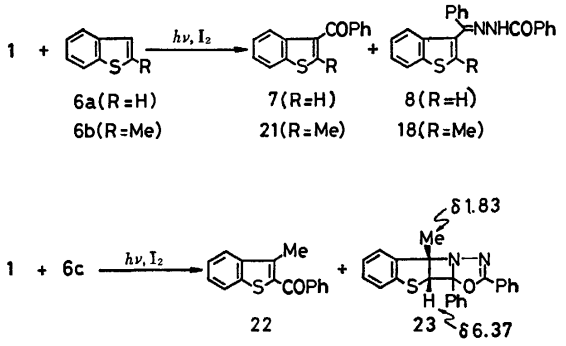

Scheme 7

It is known that **6a** undergoes electrophilic substitution with bromine to yield 3-bromobenzo[*b*]thiophene.[12] Thus, we investigated the possibility of the formation of **8** from the photochemical reaction of **1** with 3-iodobenzo[*b*]thiophene (**24**). As shown in Scheme 8, irradiation of **1** with **24** in benzene gave 2-benzoyl-3-phenylbenzo[*b*]thiophene (**25**), its benzoylhydrazone **26**, 2-phenylbenzo[*b*]thiophene (**27**), and 3-benzoyl-2-phenylbenzo[*b*]thiophene (**28**); no **7** and **8** were formed. The benzoylhydrazone **26** may be interpreted as arising *via* interaction between **1** and 3-phenylbenzo[*b*]thiophene which formed from the pho-

tochemical reaction of **24** with the solvent (benzene). It has been reported that the treatment of 3-phenylbenzothiophene with iodine does not give the 2-isomer **27**,[13] but with hydrogen fluoride 3-phenyl derivative isomerizes to **27**.[14] The formation of **27** seems to be attributable to the isomerization of 3-phenyl derivative with hydrogen iodide generated *in situ*.

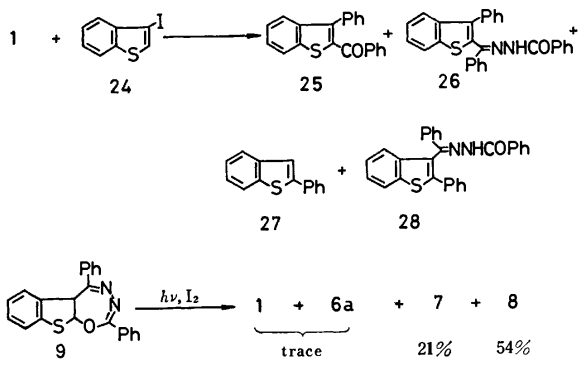

Scheme 8.

As mentioned above, the oxadiazepine **9** is photochemically dissociated to the starting materials. However, we found that iodine inhibited the photochemical dissociation of **9**. Irradiation of **9** in the presence of iodine afforded 3-benzoylbenzothiophene **7** and its benzoylhydrazone **8**, together with traces of **1** and **6a** (Scheme 8). It is noteworthy that the yields of **7** and **8** are almost equal to those in the direct irradiation of **1** with **6a** in the presence of iodine. In addition, upon irradiation of **9** in the presence of 2,5-di(*p*-tolyl)-1,3,4-oxadiazole **7** and **8** were formed in 18 and 50% yields respectively, but no 3-(*p*-toluoyl)benzothiophene and its *p*-toluoylhydrazone were formed. Thus, the formation of **8** in the direct irradiation of **1** with **6a** in the presence of iodine may be interpreted as arising *via* isomerization of the primary adduct **9** with iodine.[15]

The photochemical reaction of **1** with **6c** in the presence of iodine is comparable to that of **1** with indene producing the [2+2] cycloadduct **5**. Although mechanistic considerations are still speculative, a potential pathway for the formation of **23** is outlined in Scheme 9, which is similar to that previously proposed for the formation of **5**.[5] The photochemical reaction of **6c** with iodine yields the complex **E** *via* **D**. Subsequent interaction between **E** and **1** forms the intermediate **F**, which undergoes ring closure with loss of iodine to produce the [2+2] cycloadduct **23**.

*Stereochemistry of [2+2] Cycloadducts **19**, **20**, and **23**.* It is difficult to learn the stereochemistry of [2+2] cycloadducts **19**, **20**, and **23** from inspection of their NMR spectra. We have inadvertently found that the reduction of [2+2] cycloadducts with sodium borohydride can be used to distinguish between the *cis*- and *trans*-adducts.

Reduction of the *trans* [2+2] cycloadduct **2** with sodium borohydride in boiling methanol gave the corresponding dihydro compound, 2-(2,3-dihydro-3-furyl)-2,5-diphenyl-2,3-dihydro-1,3,4-oxadiazole (**29**).

Similarly, *trans* [2+2] cycloadducts, **12** and **13**, afforded the corresponding dihydro compounds, **30** and **31**, respectively. However, the *cis* [2+2] cycloadduct **5** remarkably resisted toward reduction under similar conditions; **5** was recovered quantitatively.

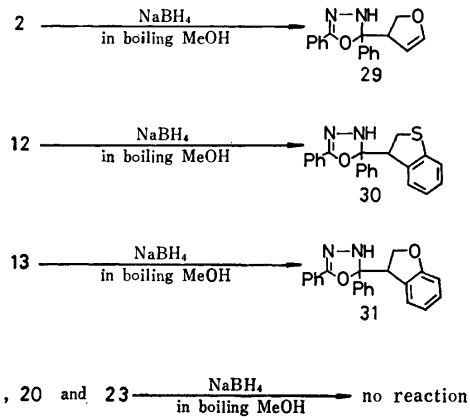

Scheme 10.

The above facts indicate that *trans* [2+2] cycloadducts, **2**, **12**, and **13**, are susceptible to reductive cleavage with sodium borohydride owing to their ring strain, and that this method can be used to diagnose the stereochemistry of [2+2] cycloadducts, **19**, **20**, and **23**. The cycloadducts, **19**, **20**, and **23**, as well as **5**, did not undergo reductive cleavage with sodium borohydride (Scheme 10). Thus, **19**, **20**, and **23** may be assigned to the corresponding *cis*-adducts respectively.

Experimental

All melting and boiling points are uncorrected. The IR spectra were measured in KBr disks, and NMR spectra were determined at 60 MHz with a Hitachi R-20 NMR spectrometer with TMS as an internal reference. The mass spectra were obtained on a Hitachi RMS-4 mass spectrometer, using a direct inlet and an ionization energy of 70 eV. Unless otherwise stated, irradiations were performed with Pyrex-filtered light from a 300-W high-pressure mercury lamp (Taika HLV-B) below 15 °C in a nitrogen atmosphere. Irradiation with monochromatic light (313 nm) was performed with a 100-W high-pressure mercury lamp (Riko UVL-100P) utilizing the potassium biphthalate aqueous solution[16] as a filter.

*Photochemical Reaction of 2,5-Diphenyl-1,3,4-oxadiazole (**1**) with Benzo[b]thiophene (**6a**).* A solution of 1.11 g (5×10^{-3} mol) of **1** and 2.01 g (1.5×10^{-2} mol) of **6a**[17] in 250 ml of benzene was irradiated for 1 h. The solvent from the

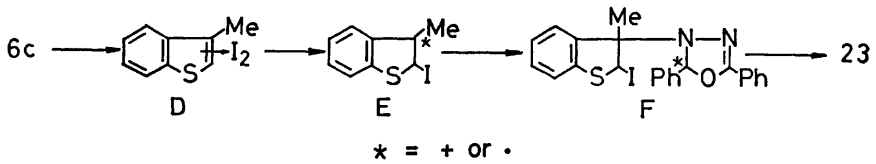

Scheme 9.

mixture was removed *in vacuo* to afford a residue, which was triturated with 30 ml of diethyl ether giving pale yellow needles. Filtration gave 0.43 g (24%) of oxadiazepine **9**, mp 172—173 °C, which was subjected to microanalysis without further purification. IR 1607, 1560 cm^{-1} ($\nu_{C=N}$); mass spectrum *m/e* 356 (M^+), 253 (M^+-PhCN), 251 (M^+-PhCO), 236 ($M^+-PhCONH$), 223, 222, 221, 189, 121, 105, 77. Found: C, 73.88; H, 4.43; N, 7.70%. Calcd for $C_{22}H_{16}N_2OS$: C, 74.14; H, 4.53; N, 7.86%.

The ether filtrate was evaporated *in vacuo*, and the residue was chromatographed on alumina using hexane and benzene as eluents. From the hexane elution 1.76 g (88%) of **6a**, and from the hexane–benzene (1: 1) elution 60 mg (5%) of 3-benzoylbenzo[*b*]thiophene (**7**) and traces of the benzoylhydrazone **8** were obtained respectively. The benzene elution gave 0.48 g (43%) of **1**.

7: yellow oil; IR (neat) 1645 cm^{-1} ($\nu_{C=O}$). This compound was identical with an authentic sample prepared by the reaction described below.

8: colorless needles, mp 172—173 °C; IR 3340 (ν_{NH}), 1640 cm^{-1} ($\nu_{C=O}$); NMR ($CDCl_3$) δ 7—8 (15H, m, aromatic protons), 9.05 (1H, br, N**H**); mass spectrum *m/e* 356 (M^+), 251 (M^+-PhCO), 236 ($M^+-PhCONH$), 233 ($PhO{\equiv}\overset{+}{N}NH-COPh$), 222, 221, 181, 121 ($[PhCO-NH_2]^+$), 105, 77. Found: C, 74.18; H, 4.36; N, 7.73%. Calcd for $C_{22}H_{16}N_2OS$: C, 74.14; H, 4.53; N, 7.86%. This compound was identical with an authentic sample prepared from **7** and benzoylhydrazine.

Similar photochemical reactions were carried out in various solvents, and the results are given in Table 1.

3-Benzoylbenzo[b]*thiophene (7).* A solution of 2.0 g of benzonitrile in 20 ml of diethyl ether was added to a solution of 3-benzo[*b*]thienylmagnesium bromide which was prepared *in situ* from 3-bromobenzo[*b*]thiophene[12] (3.3 g) and metallic magnesium (0.55 g) in 20 ml of diethyl ether, at 0 °C. The reaction mixture was stirred at room temperature for 1 h, and then refluxed for 30 min. After the mixture was stirred with 1 ml of concd hydrochloric acid, the ether layer was evaporated *in vacuo*, and the residue was chromatographed on alumina using benzene as an eluent to give 0.4 g (11%) of **7**.

Isomerization of Oxadiazepine 9. A suspension of 0.3 g of **9** in 30 ml of benzene was refluxed for 3 h. The solvent from the mixture was removed *in vacuo*, and the residue was triturated with small amounts of diethyl ether to give 0.29 g (97%) of benzoylhydrazone **8**.

Reduction of Oxadiazepine 9 with Sodium Borohydride. A suspension of 0.2 g of **9** in 40 ml of methanol was stirred with 0.1 g of sodium borohydride at room temperature for 1 h. The reaction mixture was poured into 100 ml of water, giving 0.2 g (*ca.* 100%) of crystals. Recrystallization from methanol afforded the dihydro compound **10**, mp 187—188 °C, as colorless needles. IR 3320 (ν_{NH}), 1650 cm^{-1} ($\nu_{C=N}$); NMR ($CDCl_3$) δ 4.67 (1H, t, >C**H**, J=8 Hz), 6.23, 6.32 (each 1H, d, >C**H**, J=8 Hz), 6.5—7.8 (14H, m, aromatic protons), 8.0 (1H, br, N**H**); mass spectrum *m/e* 358 (M^+), 356 (M^+-H_2), 224 ($[PhCH{=}NNHCOPh]^+$), 223, 147 (224—Ph), 134, 121 ($[PhCONH_2]^+$), 105, 91, 89, 77. Found: C, 73.75; H, 4.86; N, 7.80%. Calcd for $C_{22}H_{18}N_2OS$: C, 73.77; H, 5.06; N, 7.82%.

Similarly, reduction of **9** with sodium borohydride-d_4 in methanol-d_1, and recrystallization of the product from methanol afforded the dihydro compound **10**-d_1, mp 184—185 °C, as colorless needles. NMR ($CDCl_3$) δ 4.67, 6.25 (each 1H, d, >C**H**, J=8 Hz), 6.5—7.8 (14H, m, aromatic protons), 8.1 (1H, br, N**H**); mass spectrum *m/e* 359 (M^+), 358, 357 (M^+-H_2), 356, 225 ($[PhCD{=}NNHCOPh]^+$), 224, 148 (225^+-Ph), 134, 121, 105, 92, 90.

1-Benzoyl-2-[α-(3-benzo[b]*thienyl)benzyl]hydrazine (11).*

i) A solution of 1.35 g of **10** in 20 ml of methanol was stirred with 2 ml of concd hydrochloric acid at room temperature for 10 h. The reaction mixture was evaporated *in vacuo*, and the residue was triturated with 20 ml of diethyl ether, giving 0.95 g (70%) of crystals. Recrystallization from methanol afforded the hydrazine **11**, mp 165—166 °C, as colorless prisms. IR 3300, 3240 (ν_{NH}), 1650 cm^{-1} ($\nu_{C=O}$); NMR ($CDCl_3$) δ 4.74, 8.0 (each 1H, br, N**H**), 5.75 (1H, s, >C**H**), 7.0—8.0 (15H, m, aromatic protons); mass spectrum *m/e* 358 (M^+), 237 ($M^+-PhCONH_2$), 208 ($[PhCH{=}N{-}N{=}CH-Ph]^+$), 189, 178, 134, 121, 105, 91, 89, 77. Found: C, 73.60; H, 4.87; N, 7.87%. Calcd for $C_{22}H_{18}N_2OS$: C, 73.77; H, 5.06; N, 7.82%.

A similar treatment of the dihydro compound **10**-d_1 afforded the hydrazine **11**-d_1, mp 164—166 °C, in 80% yield. NMR ($CDCl_3$) δ 4.74, 8.0 (each 1H, br, N**H**), 7.0—8.0 (15H, m, aromatic protons); mass spectrum *m/e* 359 (M^+), 237, 236, 225, 224, 209, 190, 180, 178, 148, 134, 122, 105, 92, 77.

ii) A solution of 0.14 g of 3-benzoylbenzothiophene **7** in 20 ml of methanol was stirred with 50 mg of sodium borohydride at room temperature for 30 min. The reaction mixture was poured into 50 ml of water, and the aqueous solution was acidified with hydrochloric acid, and then extracted with chloroform. The extract was concentrated *in vacuo*, and the residue was chromatographed on silica gel using chloroform as an eluent to give 90 mg (64%) of 3-benzo[*b*]thienylphenylmethanol as pale yellow oil. IR (neat) 3300—3400 cm^{-1} (ν_{OH}); NMR (CCl_4) δ 3.75 (1H, br, O**H**), 5.62 (1H, s, >C**H**), 6.9—7.8 (10H, m, aromatic protons); mass spectrum *m/e* 240 (M^+), 233 (M^+-OH), 221, 163 (M^+-Ph), 161, 135, 105, 77.

After 70 mg of the alcohol was heated with 2 ml of phosphorus trichloride under reflux for 1 h, excess phosphorus trichloride from the mixture was removed *in vacuo*. The residue was treated with 0.1 g of benzoylhydrazine to give crystals, which on recrystallization from methanol gave 10 mg of the hydrazine **11**, mp 165—166 °C.

Irradiation of Oxadiazepine 9. A suspension of 1.0 g of **9** in 250 ml of benzene was irradiated for 4 h. The solvent from the mixture was removed *in vacuo*, and the residue was chromatographed on alumina. From the hexane elution 0.17 g (45%) of benzothiophene **6a**, and from the hexane–benzene (1: 1) 50 mg (7%) of benzoylbenzothiophene **7** were obtained respectively. Finally, 30 mg (3%) of the [2+2] cycloadduct **12** and 0.3 g (48%) of oxadiazole **1** were separated from the benzene elution.

12: colorless prisms, mp 187—188 °C. IR 1645 cm^{-1} ($\nu_{C=N}$); NMR ($CDCl_3$) δ 4.85, 6.97 (each $1H^2$ d, >C**H**, J= 2.5 Hz), 7.1—8.0 (14H, m, aromatic protons); mass spectrum *m/e* 356 (M^+), 253 (M^+-PhCN), 251 (M^+-PhCO), 237 ($M^+-PhCNO$), 210, 164, 134, 121, 105, 77. Found: C, 74.05; H, 4.31; N, 7.71%. Calcd for $C_{22}H_{16}N_2OS$: C, 74.14; H, 4.53; N, 7.86%.

A similar irradiation of **9** was performed in acetonitrile for 10 h, and the yields of products are given in Scheme 4.

Isomerization of the [2+2] Cycloadduct 12. A solution of 0.2 g of **12** in 30 ml of ethanol was stirred with 0.1 g of potassium hydroxide at 60—70 °C for 1 h. The reaction mixture was poured into 50 ml of water, and neutralized with 10% hydrochloric acid to give crystals. Recrystallization from methanol afforded 20 mg (10%) of the benzoylhydrazone **8**.

Photochemical Reaction of Oxadiazole 1 with Benzothiophene 6a in the Presence of Benzophenone. A solution of 1.11 g (5×10^{-3} mol) of **1**, 2.01 g (1.5×10^{-2} mol) of **6a**, and 0.45 g (2.5×10^{-3} mol) of benzophenone in 250 ml of benzene was irradiated for 10 h. The solvent from the mixture was removed *in*

vacuo, and the residue was chromatographed on silica gel using benzene and then chloroform as eluents. The first elution gave 1.25 g of a mixture of **6a** and benzophenone. From the second and third elutions, 0.25 g (14%) of the [2+2] cycloadduct **12**, and 0.65 g (59%) of 1 were isolated respectively.

*Photochemical Reaction of Oxadiazole **1** with Benzo*[b]*furan.* *i)* A solution of 1.11 g (5×10^{-3} mol) of **1** and 1.77 g (1.5×10^{-2} mol) of benzofuran[18] in 250 ml of benzene was irradiated for 10 h. The solvent from the mixture was removed *in vacuo*, and the residue was chromatographed on alumina using benzene as an eluent, giving 0.93 g (53%) of benzofuran, 0.22 g (13%) of the [2+2] cycloadduct **13**, and 0.85 g (77%) of **1**.

13: colorless prisms, mp 216—218 °C. IR 1670 cm^{-1} ($\nu_{C=N}$); NMR ($CDCl_3$) δ 4.68 (1H, m, >C**H**), 7.03 (1H, d, >C**H**, J=1.0 Hz), 6.8—7.9 (14H, m, aromatic protons); mass spectrum *m/e* 340 (M^+), 312 (M^+-CO), 311, 237 ($M^+-PhCNO$), 207 (312^+-PhCO), 194, 178, 118, 105, 77. Found: C, 77.63; H, 4.67; N, 8.26%. Calcd for $C_{22}H_{16}N_2O$: C, 77.63; H, 4.74; N, 8.23%.

A similar photochemical reaction in diethyl ether for 10 h afforded 0.15 g (9%) of **13**, together with recovery of **1** (47%) and benzofuran (56%).

ii) A solution of 1.11 g of **1** and 1.77 g of benzofuran in 600 ml of benzene was irradiated with monochromatic light (313 nm) for 30 h. A similar treatment afforded 50 mg (3%) of **13**, together with 0.82 g (74%) of **1** and 1.2 g (68%) of benzofuran.

Irradiation of Benzo[b]*thiophene 1,1-Dioxide (**14**) in the Presence of Oxadiazole **1**.* A solution of 1.9 g (1.1×10^{-2} mol) of **14**[19] and 1.11 g (5×10^{-3} mol) of **1** in 250 ml of diethyl ether was irradiated for 10 h. Filtration gave 0.74 g (39%) of crystals. Recrystallization from chloroform gave colorless needles, mp>300 °C, which were a mixture of the head to tail dimer **15**[20] and head to head dimer **16**[20] by inspection of the IR spectrum.

The filtrate was evaporated *in vacuo* to afford 1.92 g of a mixture of **1** and the dimers.

*Photochemical Reaction of Oxadiazole **1** with 2-Methylbenzo*[b]*thiophene (**6b**).* *i) Without Benzophenone*: A solution of 1.11 g (5×10^{-3} mol) of **1** and 2.22 g (1.5×10^{-2} mol) of **6b**[21] in 250 ml of diethyl ether was irradiated for 10 h. The solvent from the mixture was removed *in vacuo*, and the residue was chromatographed on alumina using benzene and then chloroform. From the benzene elution, 0.97 g (44%) of **6b**, and 0.61 g (55%) of **1** were recovered. The benzene–chloroform elution afforded 0.29 g (16%) of 3-benzoyl-2-methylbenzo[*b*]thiophene benzoylhydrazone (**18**), mp 125—126 °C, as colorless prisms. IR 3240 (ν_{NH}), 1675 cm^{-1} ($\nu_{C=O}$), NMR ($CDCl_3$) δ 2.40 (3H, s, C**H**$_3$), 7.0—8.2 (14H, m, aromatic protons), 9.0 (1H, br, N**H**); mass spectrum *m/e* 370 (M^+), 265 (M^+-PhCO), 250 ($M^+-PhCONH$), 249, 235 ($M^+-PhCONHNH$), 234, 223 ($PhC\equiv\overset{+}{N}NHCOPh$), 221, 147, 105, 77. Found: C, 74.47; H, 5.01; N, 7.33%. Calcd for $C_{23}H_{18}N_2OS$: C, 74.58; H, 4.90; N, 7.56%.

ii) With Benzophenone: A solution of 1.11 g of **1**, 2.22 g of **6b**, and 0.275 g (1.5×10^{-3} mol) of benzophenone in 250 ml of benzene was irradiated for 10 h. The solvent from the mixture was removed *in vacuo*, and the residue was chromatographed on alumina. From the benzene elution, 1.40 g of a mixture of **6b** and benzophenone, and 0.1 g (5%) of the [2+2] cycloadduct **19** were isolated, and the chloroform elution gave 0.67 g (60%) of **1**.

19: colorless prisms, mp 204—205 °C. IR 1645 cm^{-1} ($\nu_{C=N}$); NMR ($CDCl_3$) δ 2.04 (3H, s, C**H**$_3$), 4.64 (1H, s, >C**H**), 7.0—8.0 (14H, m, aromatic protons); mass spectrum *m/e* 370 (M^+), 267 (M^+-PhCN), 265 (M^+-PhCO), 237 (265^+-N_2), 235, 223, 221, 148, 105, 77. Found: C, 74.52; H, 4.75; N, 7.71%. Calcd for $C_{23}H_{18}N_2OS$: C, 74.58; H, 4.90; N, 7.56%.

*Photochemical Reaction of Oxadiazole **1** with 3-Methylbenzo*[b]*thiophene (**6c**).* *i) Without Benzophenone*: A solution of 2.22 g (10^{-2} mol) of **1** and 4.44 g (3×10^{-2} mol) of **6c**[22] in 250 ml of diethyl ether was irradiated for 10 h. The reaction mixture was concentrated *in vacuo*, and the residue was chromatographed on alumina using benzene and benzene–chloroform as eluents. From the benzene elution, 2.7 g (61%) of **6c** and 65 mg (2%) of the [2+2] cycloadduct **20** were isolated, and the benzene–chloroform elution gave 0.68 g (31%) of **1**.

20: colorless prisms, mp 267—268 °C. IR 1645 cm^{-1} ($\nu_{C=N}$); NMR ($CDCl_3$) δ 1.07 (3H, s, C**H**$_3$), 6.87 (1H, s, >C**H**), 7.0—8.1 (14H, m, aromatic protons); mass spectrum *m/e* 370 (M^+), 267 (M^+-PhCN), 265 (M^+-PhCO), 237 (265^+-N_2), 224, 221, 147, 105, 77. Found: C, 74.43; H, 4.87; N, 7.57%. Calcd for $C_{23}H_{18}N_2OS$: C, 74.58; H, 4.90; N, 7.56%.

A similar photochemical reaction in benzene affords the [2+2] cycloadduct **20** in 13% yield.

ii) With Benzophenone: A solution of 1.11 g (5×10^{-3} mol) of **1**, 2.22 g (1.5×10^{-2} mol) of **6c**, and 0.28 g (1.5×10^{-3} mol) of benzophenone in 250 ml of benzene was irradiated for 10 h. A similar work-up afforded 1.17 g of a mixture of **6c** and benzophenone, 0.61 g (33%) of **20**, and 0.52 g (47%) of **1**.

Photochemical Reaction in the Presence of Iodine. *i) Reaction with Benzothiophene **6a***: A solution of 2.0 g (9×10^{-3} mol) of oxadiazole **1**, 4.0 (3×10^{-2} mol) of **6a**, and 0.46 g (1.8×10^{-3} mol) of iodine in 500 ml of benzene was irradiated for 20 h. The solvent from the mixture was removed *in vacuo*, and chromatographic separation of the residue on alumina using benzene and then chloroform as eluents afforded 2.9 g (73%) of **6a**, 0.35 g (16%) of 3-benzoylbenzothiophene **7**, 0.21 g (11%) of **1** (from the benzene elution), and 1.59 g (50%) of the benzoylhydrazone **8** (from the benzene–chloroform elution).

*ii) Reaction with 2-Methylbenzothiophene **6b***: A solution of 1.11 g (5×10^{-3} mol) of **1**, 2.22 g (1.5×10^{-2} mol) of **6b**, and 0.25 g (10^{-3} mol) of iodine in 250 ml of benzene was irradiated for 10 h. A similar work-up afforded 15 mg (1%) of 3-benzoyl-2-methylbenzo[*b*]thiophene (**21**) and 0.28 g (15%) of the benzoylhydrazone **18**, together with recovery of 0.6 g (54%) of **1** and 1.05 g (47%) of **6b**.

The compound **21**, mp 73—74 °C, was identical with an authentic sample prepared from the Friedel-Crafts benzoylation of **6b**.

*iii) Reaction with 3-Methylbenzothiophene **6c***: A solution of 1.11 g of **1**, 2.22 g of **6c**, and 0.25 g of iodine in 250 ml of benzene irradiated for 10 h. A similar work-up afforded 75 mg (6%) of 2-benzoyl-3-methylbenzo[*b*]thiophene (**22**) and 0.15 g (8%) of the [2+2] cycloadduct **23**, together with recovery of 0.98 g (44%) of **6c** and 0.21 g (19%) of **1**. The compound **22**, mp 67—68 °C, was identical with an authentic sample prepared from the Friedel-Crafts benzoylation of **6c**.

23: colorless prisms, mp 152—153 °C; IR 1640 cm^{-1} ($\nu_{C=N}$); NMR ($CDCl_3$) δ 1.83 (3H, s, C**H**$_3$), 6.37 (1H, s, >C**H**), 6.9—8.1 (14H, m, aromatic protons); mass spectrum *m/e* 370 (M^+), 267 (M^+-PhCN), 265 (M^+-PhCO), 237 (265^+-N_2), 224, 223, 222, 165, 149, 148, 105, 77. Found C, 74.23; H, 4.56; N, 7.36%. Calcd for $C_{23}H_{18}N_2OS$: C: 74.58; H, 4.90; N, 7.56%.

*Photochemical Reaction of Oxadiazole **1** with 3-Iodobenzo*[b]*thiophene (**24**).* A solution of 1.11 g (5×10^{-3} mol) of **1** and 0.73 g (2.8×10^{-3} mol) of **24**[23] in 250 ml of benzene was irradiated for 10 h. The solvent from the mixture was removed *in vacuo*, and the residue was chromatographed on alumina using hexane, benzene, and then chloroform as eluents. From the hexane elution, 0.15 g (21%) of **24** and

40 mg (7%) of 2-phenylbenzo[*b*]thiophene (**27**) were obtained. From the benzene elution, 65 mg (7%) of 2-benzoyl-3-phenylbenzo[*b*]thiophene (**25**) and 0.59 g (53%) of **1** were isolated, and finally the chloroform elution gave 15 mg (1%) of 3-benzoyl-2-phenylbenzo[*b*]thiophene benzoylhydrazone (**28**) and 0.22 g (18%) of 2-benzoyl-3-phenylbenzo[*b*]thiophene benzoylhydrazone (**26**).

25: colorless prisms, mp 105—106 °C; IR 1630 cm^{-1} ($\nu_{C=O}$); mass spectrum *m/e* 314 (M^+), 286 (M^+-CO), 237 (M^+-Ph), 209 (M^+-PhCO), 165 ($M^+-PhCOS$), 105, 77. Found: C, 80.20; H, 4.50%. Calcd for $C_{21}H_{14}OS$: C, 80.24; H, 4.49%. This compound was identical with an authentic sample prepared from the Friedel-Crafts benzoylation of 3-phenylbenzo[*b*]thiophene.[14]

26: colorless prisms, mp 177—178 °C; IR 3160 (ν_{NH}), 1660 cm^{-1} ($\nu_{C=O}$); NMR ($CDCl_3$) δ 7.0—8.2 (19H, m, aromatic protons), 8.5 (1H, br, N**H**); mass spectrum *m/e* 432 (M^+), 327 (M^+-PhCO), 311 ($M^+-PhCONH_2$), 297 ($M^+-PhCONHNH$), 223 ($PhC{\equiv}\overset{+}{N}NHCOPh$), 105, 77. Found: C, 77.62; H, 4.63; N, 6.42%. Calcd for $C_{28}H_{20}N_2OS$: C, 77.76; H, 4.66; N, 6.48%. Hydrolysis of **26** with hydrochloric acid in boiling ethanol for 1 h afforded **25** in 28% yield.

27: colorless needles, mp 177—178 °C (lit,[14] mp 174—175 °C); IR 1600, 1480, 1440, 1420 cm^{-1}; mass spectrum *m/e* 178 (M^+-S), 176, 165 (M^+-CHS), 134, 92, 77.

28: colorless needles, mp 183—184 °C; IR 3360 (ν_{NH}), 1690 cm^{-1} ($\nu_{C=O}$); mass spectrum *m/e* 432 (M^+), 327 (M^+-PhCO), 311 ($M^+-PhCONH_2$), 297 ($M^+-PhCONHNH$), 223, 105, 77. Found: C, 77.29; H, 4.59; N, 6.49%. Calcd for $C_{28}H_{20}N_2OS$: C, 77.76; H, 4.66; N, 6.48%.

*Irradiation of Oxadiazepine **9** in the Presence of Iodine.* *i)* A suspension of 0.5 g (1.4×10^{-3} mol) of **9** in 250 ml of benzene was irradiated with 0.107 g (30 mol% to **9**) for 3 h. The solvent from the mixture was removed *in vacuo*, and chromatographic separation afforded traces of **6a**, 70 mg (21%) of **7** (from the benzene elution), traces of **1** and 0.27 g (54%) of **8** (from the chloroform elution).

ii) A suspension of 0.5 g of **9** in 250 ml of benzene irradiated in the presence of 0.107 g of iodine and 0.7 g (2.8×10^{-3} mol) of 2,5-di(*p*-tolyl)-1,3,4-oxadiazole for 3 h. A similar work-up afforded 60 mg (18%) of **7** and 0.25 g (50%) of **8**, together with recovery of 0.62 g (89%) of ditolyloxadiazole.

Reduction of the [2+2] Cycloadducts with Sodium Borohydride. A solution of 0.2 g of the [2+2] cycloadduct **2** in 20 ml of methanol was refluxed with 0.1 g of sodium borohydride for 3 h. The solvent from the mixture was removed *in vacuo*, and 30 ml of water was added to the residue to give crystals, which on recrystallization from methanol afforded 30 mg (15%) of the dihydro compound **29**, mp 142—143 °C, as colorless prisms. IR 3240 (ν_{NH}), 1620 cm^{-1} ($\nu_{C=N}$); NMR ($CDCl_3$) δ 2.9—3.9 (3H, m, C**H**$_2$ and N**H**), 4.8, 6.7 (each 1H, m, =C**H**), 5.1 (1H, m, $\rangle$C**H**), 6.9—7.9 (10H m, aromatic protons); mass spectrum *m/e* 292 (M^+), 290, 263 (M^+-CHO), 261, 187 (M^+-PhCO), 185, 170, 159, 157, 145, 128, 115, 105, 77. Found: C, 74.11; H, 5.48; N, 9.30%. Calcd for $C_{18}H_{16}N_2O_2$: C, 73.95; H, 5.52; N, 9.58%.

Similar reductions of the [2+2] cycloadducts **12** and **13** with sodium borohydride in boiling methanol for 1 h afforded the corresponding dihydro compounds **30** and **31** in 28 and 40% yields respectively.

30: colorless prisms, mp 152—153 °C; IR 3260 (ν_{NH}), 1620 cm^{-1} ($\nu_{C=N}$); NMR ($CDCl_3$) δ 3.20 (1H, dd, H**C**H, J=6, 12 Hz), 3.6 (1H, br, N**H**), 3.70 (1H, dd, HC**H**, J=7, 12 Hz), 4.18 (1H, dd, $\rangle$C**H**, J=6, 7 Hz), 7.0—8.0 (14H, m, aromatic protons); mass spectrum *m/e* 358 (M^+), 356, 253 (M^+-PhCO), 212, 211, 210, 165, 121, 105, 77. Found: C, 73.76; H, 5.04; N, 7.93%. Calcd for $C_{22}H_{18}N_2OS$: C, 73.73; H, 5.06; N, 7.82%.

31: colorless prisms, mp 182—183 °C; IR 3220 (ν_{NH}), 1660 cm^{-1} ($\nu_{C=O}$); NMR ($CDCl_3$) δ 3.25 (1H, dd, **H**CH, J=4, 12 Hz, when exchanged with D_2O, this signal changed to a doublet with J=12 Hz), 3.74 (1H, dd, HC**H**, J=6, 12 Hz), 4.10 (1H, d, $\rangle$C**H**, J=6 Hz), 4.6 (1H, m, N**H**), 6.7—7.9 (14H, m, aromatic protons); mass spectrum *m/e* 342 (M^+), 340, 237 (M^+-PhCO), 222, 220, 207, 194, 165, 105, 77. Found: C, 77.13; H, 5.17; N, 8.16%. Calcd for $C_{22}H_{18}N_2O_2$: C, 77.17; H, 5.30; N, 8.18%.

The [2+2] cycloadducts, **5**, **19**, **20**, and **23**, were inert with similar reduction.

References

1) Part VI of this series: O. Tsuge, K. Oe, and Y. Ueyama, *Chem. Lett.*, **1976**, 425,

2) O. L. Chapman and G. Lenz, "Organic Photochemistry," Vol. 1, ed by O. L. Chapman, Marcel Dekker, Inc., New York, N. Y. (1967), p. 283.

3) D. R. Arnold, "Advances in Photochemistry," Vol. 6, ed by W. A. Noyer, Jr., G. S. Hammond, and J. N. Pitts, Jr., John Wiley & Sons, Inc., New York, N. Y. (1966), p. 310.

4) O. Tsuge, M. Tashiro, and K. Oe, *Tetrahedron*, **29**, 41 (1973).

5) K. Oe, M. Tashiro, and O. Tsuge, *J. Org. Chem.*, **42**, 1496 (1977).

6) T. H. Koch and K. H. Howard, *Tetrahedron Lett.*, **1973**, 4035.

7) T. H. Koch and R. M. Rodehorst, *Tetrahedron Lett.*, **1972**, 4039.

8) J. S. Swenton and J. A. Hyatt, *J. Am. Chem. Soc.*, **96**, 4879 (1974).

9) D. C. Neckers, J. H. Dopper, and H. Wynberg, *J. Org. Chem.*, **35**, 1582 (1970).

10) J. H. Dopper and D. C. Neckers, *J. Org. Chem.*, **36**, 3755 (1971).

11) The calculated values of J_{ab} and J_{ac} were obtained by the Karplus' equation: $J=8.5\cos^2\theta-0.28$ ($0°\leq\theta\leq90°$) (M. Karplus, *J. Chem. Phys.*, **30**, 11 (1959)).

12) G. M. Badger, P. Cheuychit, and W. H. F. Sasse, *Aust. J. Chem.*, **17**, 371 (1964).

13) S. H. Groen, R. M. Kellogg, J. Buter, and H. Wynberg, *J. Org. Chem.*, **33**, 2218 (1968).

14) O. Dann and M. Kokorudz, *Chem. Ber.*, **91**, 172 (1958).

15) Although the interaction between iodine and the double bond of indene was observed by the NMR spectrum of a mixture of indene and iodine,[5] such a phenomenon was not observed in the NMR spectrum of a mixture of **6a** and iodine.

16) J. G. Calvert and J. N. Pitts, Jr., "Photochemistry," John Wiley & Sons, Inc., New York, N. Y. (1967), p. 732.

17) K. Rabindran and B. D. Tilak, *Current Sci.*, **20**, 205 (1951).

18) A. W. Burgstahler and L. R. Worden, *Org. Synth.*, Col. Vol. V, 251 (1973).

19) E. N. Karaulova, D. Sh. Meilanova, and G. D. Gal'pern, *Akad. Nauk. SSSR, Bashkirsk, Filial*, **3**, 25 (1960).

20) D. N. Harpp and C. Heitner, *J. Org. Chem.*, **35**, 3256 (1970).

21) E. N. Karaulova, D. Sh. Meilanova, and G. D. Gal'pern, *Zhur. Obshchei. Khim.*, **30**, 3292 (1960).

22) E. Campaigne and E. S. Neiss, *J. Heterocyclic Chem.*, **2**, 231 (1965).

23) R. Gaertner, *J. Am. Chem. Soc.*, **74**, 4950 (1952).

Stereoselective Monoalkylation of α-Halocyclopropyllithiums. A Versatile Method for the Synthesis of α-Alkylcyclopropyl Acetates and Alkylidenecyclopropanes

Katuzi KITATANI, Tamejiro HIYAMA, and Hitosi NOZAKI
Department of Industrial Chemistry, Kyoto University, Yoshida, Kyoto 606
(Received March 10, 1977)

The title carbenoids (**7** and **8**) prepared by the action of butyllithium on dihalocyclopropanes are smoothly methylated with methyl iodide. The product ratio of *cis*-methylated product (**3**)/*trans*-methylated one (**4**) (or *endo*-methylated product (**5**)/*exo*-methylated one (**6**) is found to depend on the aging period of the carbenoids; thermodynamic equilibration gives almost **3** or **5**. This procedure has been extended to general alkylation by utilizing HMPA co-solvent. The resulting α-alkylated cyclopropyl halides are converted into allylic acetates or cyclopropyl acetates upon acetolysis and also into alkylidenecyclopropanes upon base treatment. The protonolysis of **8** gives *trans*- or *exo*-bromocyclopropanes stereoselectively.

Halogen-metal exchange of *gem*-dihalo compounds with alkyllithium occurs easily to give lithium carbenoids which are generally nucleophilic enough to react with various electrophiles at low temperatures.[1] The title carbenoids derived from olefin-dihalocarbene adducts are thermally labile and decompose above −50 °C.[2] This instability has restricted their synthetic use only to such intramolecular process leading to allene and/or bicyclobutane formation.[3] As lithiation of *gem*-dihalocyclopropanes proceeds rapidly even at sufficiently low temperature (*e.g.* −110 °C) and the resulting carbenoids are stable for several hours to exist as such at −95 °C,[4] we have studied to utilize the reactive intermediates for synthetic purpose and found these species can actually add to carbonyl compounds, affording cyclopropyl ketones, cyclobutanones or 1,1-cyclopropanedicarboxylates.[5] This article describes alkylation of the carbenoids and several transformations of the resulting α-alkylcyclopropyl halides.[6]

Alkylation of α-Halocycloprophyllithiums. The carbenoids generated by lithiation of *gem*-dibromocyclopropanes (**1** or **2**) at −95 °C with butyllithium were converted into α-alkylcyclopropyl bromides in good yields upon treatment with excess alkyl halides. Methylation was scrutinized first in the hope that the present reaction would provide a short-cut methodology to construct a methyl substituted cyclopropane moiety commonly found among various natural products.[7] The results are summarized in Table 1. Addition of methyl iodide after 10 minutes' aging of the carbenoids (conditions A) resulted in the exclusive or at least predominant formation of *cis*-methylated products **3** or *endo*-methylated ones **5**. This might be ascribed to the thermodynamically preferred configuration of the carbenoid. When methyl iodide is present at the stage of lithium-halogen exchange, the resulting carbenoid should be methylated spontaneously before the configurational isomerization of the carbenoid (conditions B). The experiments showed a little increase of *trans*-methylated isomers **4** or *exo*-methylated ones **6**. Furthermore, the use of hexamethylphosphoric triamide (HMPA) co-solvent is expected to prompt the alkylation (conditions C). These conditions may reflect to some extent the susceptibility of each geminal bromine atom to the lithium-bromine exchange. The products were obtained in better yields with almost the same isomer ratio as conditions B, in general, with the exception of the reaction of **1a**, which yielded the otherwise less favored isomer **4a** now predominantly.

These observations can be understood by the Scheme 1. Less hindered bromine atom is preferentially lithiated to give a carbenoid **7** which isomerizes to thermodynamically more stable isomer **8**.[8] Subsequent methylation of **8** and **7** proceeds with retention of configuration to yield **3** (or **5**) and **4** (or **6**) respectively. The exclusive formation of **3** or **5** under the conditions A may be attributed to complete isomerization of **7** to **8**. The exclusive formation of **3c** from **1c** is particularly attributable to the ethereal substituent.[9]

In contrast, however, methylation of 1,1-dichloro-2-phenylcyclopropane (**1d**) afforded **3f** and **4f** with 12: 88 ratio under the conditions A, possibly due to slow configurational isomerization of the intermediary car-

Table 1. Yield (%) of the products in the methylation of 1,1-dibromocyclopropanes and the product ratios (**3**: **4** or **5**: **6**)

Dibromocyclopropane	Products	Conditions[a] A	B	C
1a	**3a**+**4a**	70(100: 0)	92(75: 25)	90(38: 62)
1b	**3b**+**4b**	66(88: 12)	80(77: 23)	72(78: 22)
1c	**3c**+**4c**	89(100: 0)	73(63: 37)	92(77: 23)
2a	**5a**+**6a**	60(100: 0)	67(81: 19)	86(80: 20)
2b	**5b**+**6b**	55(100: 0)	59(89: 11)	99(78: 22)

a) Details given in the Experimental part.

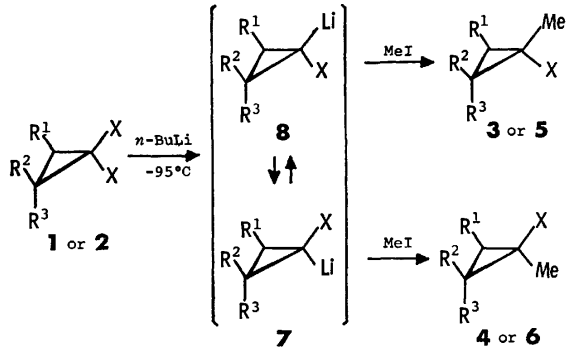

Scheme 1.

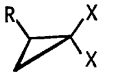

1

a, R=Ph, X=Br
b, R=*n*-C_6H_{13}, X=Br
c, R=$PhCH_2OCH_2$, X=Br
d, R=Ph, X=Cl

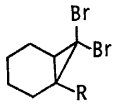

2

a, R=H
b, R=Me

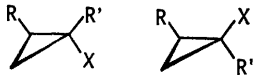

3 4

a, R=Ph, R′=Me, X=Br
b, R=*n*-C_6H_{13}, R′=Me, X=Br
c, R=$PhCH_2OCH_2$, R′=Me, X=Br
d, R=Ph, R′=CH_2=$CHCH_2$, X=Br
e, R=Ph, R′=Et, X=Br
f, R=Ph, R′=Me, X=Cl
g, R=Ph, R′=H, X=Br
h, R=*n*-C_6H_{13}, R′=H, X=Br
i, R=$PhCH_2OCH_2$, R′=H, X=Br
j, R=Ph, R′=H, X=Cl

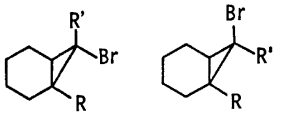

5 6

a, R=H, R′=Me
b, R=Me, R′=Me
c, R=H, R′=CH_2=$CHCH_2$
d, R=H, R′=Me_2C=$CHCH_2$
e, R=H, R′=H
f, R=Me, R′=H

benoids.[10]

Alkylation with ethyl iodide or allyl bromide required modification of the reaction conditions. Both halides turned out to react sluggishly. The use of HMPA co-solvent was found indispensable in order to eliminate the possible decomposition of carbenoids during the long reaction time. Another complicating side reaction was elimination of hydrogen halide from alkyl halides having β-hydrogen. This was, however, successfully suppressed by the addition of copper(I) salt such as copper(I) iodide or phenylacetylide.[11] Thus, **1a** was converted to **3d** and **4d** (89: 11, 59% yield) and to **3e** and **4e** (94: 6, 54% yield) respectively in the presence of Cu(I). Noteworthy is the alkylation of 7,7-dibromonorcarane with allyl bromide or 3-methyl-2-butenyl bromide; *endo*-alkylated product **5c** (87%) or **5d** (77%) was obtained exclusively. It should be noted that the coupling of 3-methyl-2-butenyl bromide with the carbenoid occurred at the α-position and no trace of S_N2' product was detected.

Stereoselective Reduction of gem-*Dihalocyclopropanes.* Protonolysis of the carbenoids, prepared as above, is expected to give monohalocyclopropanes[12] with high degree of stereoselectivity. Thus, production of the carbenoids according to the conditions A and the successive workup with ethanol at low temperature afforded monohalocyclopropanes (Table 2), the stereoselectivity being comparable with the above alkylation.

Table 2. Stereoselective reduction of 1,1-dihalocyclopropanes

Dihalocyclopropane	Products (yield, %)[a]	Product ratio[b] (**3**: **4** or **5**: **6**)
1a	**3g**(87)	100: 0
1b	**3h**+**4h**(75)	81:19
1c	**3i**(83)	100: 0
1d	**3j**+**4j**(82)	26:74
2a	**5e**(90)	100: 0
2b	**5f**+**6f**(74)	92: 8

a) Isolated yield after short-path distillation. b) The isomer ratio was calculated by GLC or NMR assay.

Acetolysis of α-Alkylcyclopropyl Bromides. The well-known conversion of monohalocyclopropanes into allyl cations obeys the orbital symmetry rule.[13] Therefore, α-alkylcyclopropyl halides obtained selectively should be utilized for selective olefin synthesis. We have attempted the acetolysis of **3** and **5** by heating in acetic acid in the presence of silver acetate and a catalytic amount of silver tetrafluoroborate. The bromocyclopropane **3a** gave 2-methyl-3-phenyl-2-propen-1-yl acetate (**9a**) in 74% yield and no regioisomer **10a**. In contrast **3b** produced two isomeric acetates **9b** (32%) and **10b** (43%), while **3c** gave **9c** (30%) and **10c** (28%). The trisubstituted ethylenes **9a**—**c** were found to have E configuration and this was attributed to the energetically favorable W-form of cations **11**.

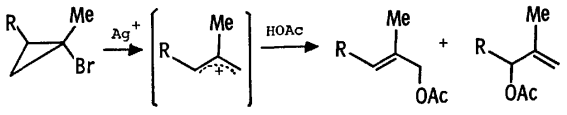

3 11 9 10

a, R=Ph **b**, R=*n*-C_6H_{13} **c**, R=$PhCH_2OCH_2$

The *endo*-alkylated bromonorcaranes **5** unexpectedly underwent acetolysis and the products were proved to be 7-acetoxy-7-alkylnorcaranes **12**. The *exo* configuration of 7-acetoxyl group is based on the assumed S_N1 type reaction involving **13**, which is stabilized by 7-alkyl group and do not rearrange into the strained cycloheptenyl cation **14**, and also based on the approach control. Similar stabilization has been recorded by Ledlie *et al.*[14]

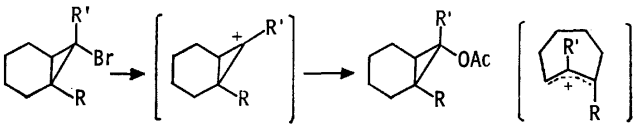

5 13 12 14

a, R=H, R′=Me 63%
b, R=Me, R′=Me 53%
c, R=H, R′=CH_2=$CHCH_2$ 47%
d, R=H, R′=Me_2C=$CHCH_2$ 48%

Alkylidenecyclopropane Synthesis. The 1-alkyl-1-bromocyclopropanes **3a**—**c**, **5a** and **5c** were easily

transformed into alkylidenecyclopropanes **15a—c** and **16a, b** in good yields by means of potassium *t*-butoxide in dimethyl sulfoxide. The rather mild reaction conditions prevent the subsequent thermal isomerization of the products. Consequently the alkylation of carbenoids **7** and **8** followed by dehydrobromination provides a variety of alkylidenecyclopropanes[15] which are otherwise difficultly accessible.

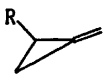

15

a, R=Ph 87%
b, R=*n*-C_6H_{13} 62%
c, R=$PhCH_2OCH_2$ 68%

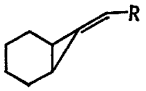

16

a, R=H 48%
b, R=CH_2=CH 66%

Stereochemistry of 3, 4, 5 and 6. The configurational assignment of monoalkylated products was based on PMR spectra (see the Experimental). Methyl substituent *cis* to phenyl group on cyclopropane ring (*e.g.* **3a**, δ 1.43) appeared at higher field than its *trans* isomer (**4a**, δ 1.93).[16] This applies to other isomers **3d**, **4d**; **3f**, **4f**. The bridge head protons of **5a** *cis* to halogen atom and *trans* to alkyl group on cyclopropane ring appeared at lower field than that of its isomer **6a**. The latter criterion is principally based on the deshielding effect[17] of the *trans* alkyl group and of the vicinal bromine atom as well. This assignment is also ascertained by the reactivity of each isomer under solvolytic conditions. Thus, 7-*exo*-bromo isomer **5a** was solvolyzed into **12a**, while the isomer **6a** was susceptible to ring opening.

Experimental

All the temperatures are uncorrected. The IR spectra were obtained on a Shimadzu spectrometer 27-G, MS on a Hitachi RMU-6L, and PMR on JEOL JNM-PMX 60, Varian EM-360, or Varian HA-100D spectrometers. Butyllithium was purchased from Aldrich Co., Ltd. Commercial copper(I) iodide was purified according to the literature.[18] Copper(I) phenylacetylide was prepared by the Castro's method[19] and vacuum dried before use. Tetrahydrofuran (THF) was dried on lithium aluminum hydride and freshly distilled before use. HMPA was dried on calcium hydride and distilled. The cold bath of −95 °C was prepared by mixing liquid nitrogen and toluene (freezing point of toluene). All the reactions were carried out under a nitrogen atmosphere.

gem-Dihalocyclopropanes. Dibromocarbene adducts were prepared by the reaction of bromoform and *t*-BuOK with the corresponding olefins. 1,1-Dichloro-2-phenylcyclopropane was obtained by the phase transfer method ($CHCl_3$/NaOH, hexadecyltrimethylammonium bromide). A typical procedure is given for the synthesis of **1c**.

1,1-Dibromo-2-(benzyloxymethyl)cyclopropane (1c). A suspension of *t*-BuOK (60 g, 0.45 mol, containing 26% of *t*-BuOH) in dry hexane (100 ml) was cooled to 0 °C and mixed with benzyl allyl ether (43 g, 0.36 mol). A solution of $CHBr_3$ (91 g, 0.36 mol) in hexane (50 ml) was added at such a rate as to maintain the temp. below 10 °C (*ca.* 2 h). After the addition was complete, stirring was continued for 14 h at room temp. The reaction mixture was then treated with water (100 ml) and extracted with four 200 ml portions of hexane. The combined organic layer was washed with three 100 ml portions of brine, dried (Na_2SO_4) and concentrated. The oily residue was fractionated through a 15 cm Vigreux column under reduced pressure. The product **1c** was collected at 120—129 °C/0.28 mmHg (18 g, 20% yield). Analytically pure sample was obtained by preparative TLC (silica gel, hexane–ether 10: 1, R_f 0.6—0.7). IR (neat): 3090, 3060, 3030, 2850, 1495, 1455, 1366, 1108, 730, 691, 676 cm^{-1}; MS: *m/e* (%), 322 (M^++4, 0.08), 320 (M^++2, 0.16), 318 (M^+, 0.08), 91 (100); PMR (CCl_4): δ 1.1—2.1 (m, 3H), 3.50 (d, J=6 Hz, 2H, $OC\underline{H}_2C$), 4.46 (s, 2H, $PhC\underline{H}_2$), 7.1—7.5 (m, 5H, Ph). Found: C, 41.5; H, 3.7%. Calcd for $C_{11}H_{12}Br_2O$: C, 41.3; H, 3.8%.

1-Bromo-1-methyl-2-phenylcyclopropanes (3a and 4a). The procedure exemplifies the preparation and alkylation of α-halocyclopropyllithiums.

Conditions A. A magnetically stirred solution containing 1.4 g (5.0 mmol) of **1a** in 10 ml of THF was cooled to −95 °C and maintained approximately at this temp. during the addition (5 min) of a solution of *n*-BuLi in hexane (4.3 ml of 1.17 M solution, 5.0 mmol). The reaction mixture was stirred at −95 °C for 10 min, treated with MeI (1.0 ml, *ca.* 3 eq) over 5 min, allowed to warm to room temp. in 2 h and quenched with water. Workup and distillation at 70—80 °C/4 mmHg of the oily residue gave 0.74 g (70% yield) of *r*-1-bromo-1-methyl-*t*-2-phenylcyclopropane (**3a**): bp 70—71 °C/4 mmHg; IR (neat): 1608, 1583, 1500, 1451, 1387, 1157, 1090, 770, 735, 700, 605 cm^{-1}; MS: *m/e* (%), 212 (M^++2, 2), 210 (M^+, 2), 131 (100), 117 (8), 91 (42); PMR (CCl_4): δ 1.17 (t, J=7 Hz, 1H), 1.43 (s, 3H, Me), 1.55 (dd, J=7, 10 Hz, 1H), 2.74 (dd, J=7, 10 Hz, 1H, $PhC\underline{H}$), 6.8—7.5 (m, 5H, Ph). Found: C, 56.9; H, 5.4%. Calcd for $C_{10}H_{11}Br$: C, 56.9; H, 5.3%.

Conditions B. A magnetically stirred solution containing 0.28 g (1.0 mmol) of **1a** and 0.5 ml of MeI in 5 ml of THF was cooled to −95 °C and maintained approximately at this temp. during the addition of *n*-BuLi (1.1 mmol, 1.00 M in hexane) over a 5 min period. Stirring was continued at −95 °C for 30 min and the temp. was raised gradually to room temp. in 2 h. After aqueous workup short-path distillation at 72—82 °C/4 mmHg gave an isomeric mixture of 1-bromo-1-methyl-2-phenylcyclopropanes (see Table 1). Each isomer was separated by preparative GLC on a 1 m stainless steel column packed with 20% Silicone HV grease coated Celite 545 (column temp 150 °C; carrier gas, He; 1.0 kg/cm^2; R_t 20 min for *trans* isomer and 21 min for *cis* one).

r-1-Bromo-1-methyl-c-2-phenylcyclopropane (4a): bp 58—61 °C/3 mmHg; IR (neat): 1605, 1582, 1499, 1450, 1260, 1167, 760, 730, 695 cm^{-1}; MS: *m/e* (%), 212 (M^++2, 2), 210 (M^+, 2), 131 (100), 117 (21), 91 (41); PMR (CCl_4): δ 1.25 (dd, J=7, 10 Hz, 1H), 1.50 (t, J=7 Hz, 1H), 1.93 (s, 3H, Me), 1.96 (dd, J=7, 10 Hz, 1H, $PhC\underline{H}$), 7.0—7.4 (m, 5H, Ph). Found: C, 56.7; H, 5.3%. Calcd for $C_{10}H_{11}Br$: C, 56.9; H, 5.3%.

Conditions C. A magnetically stirred solution containing 0.28 g (1.0 mmol) of **1a**, 1 ml of HMPA, and 0.5 ml of MeI in THF (10 ml) was cooled to −95 °C. The same operation as the conditions B, followed by short-path distillation at 70—80 °C/4 mmHg, gave a mixture of **3a** and **4a** (Table 1).

r-1-Bromo-1-methyl-t-2-hexylcyclopropane (3b): bp 50—51 °C/3 mmHg; IR (neat): 3080, 1470, 1380, 1154, 1032, 729 cm^{-1}; MS: *m/e* (%), 220 (M^+ 2, 0,9), 218 (M^+, 0.9), 139 (3), 97 (25), 83 (58), 69 (61), 55 (100), 41 (100); PMR (CCl_4): δ 0.2—0.5 (m, 1H), 0.7—1.7 (m, 15H), 1.70 (s, 3H, Me). Found: C, 54.6; H, 8.9%. Calcd for $C_{10}H_{19}Br$: C, 54.8; H,

8.7%.

r-*1-Bromo-1-methyl*-c-*2-hexylcyclopropane* (**4b**): bp 55—65 °C (bath temp)/3 mmHg; IR (neat): 3060, 1440, 1369, 1165, 1020 cm^{-1}; MS: *m/e* (%), 220 (M^++2, 0.9), 218 (M^+, 0.9), 139 (3), 97 (28), 83 (63), 69 (65), 55 (98), 41 (100); PMR (CCl_4): δ 0.6—0.8 (m, 2H), 0.8—1.7 (m, 14H), 1.73 (s, 3H, Me). Found: C, 55.0; H, 8.7%. Calcd for $C_{10}H_{19}Br$: C, 54.8; H, 8.7%.

r-*1-Bromo-1-methyl*-t-*2-(benzyloxymethyl)cyclopropane* (**3c**): bp 87—93 °C (bath temp)/0.1 mmHg; IR (neat): 3080, 3050, 1605, 1585, 1496, 1451, 1375, 1165, 1145, 1095, 1025, 733, 695 cm^{-1}; MS: *m/e* (%), 256 (M^++2, 0.07), 254 (M^+, 0.07), 145 (7), 105 (5), 91 (100), 77 (5); PMR (CCl_4): δ 0.58 (t, J= 6 Hz, 1H), 1.0—1.5 (m, 2H), 1.72 (s, 3H, Me), 3.1—3.7 (m, 2H, OCH_2), 4.43 (s, 2H, $PhC\underline{H}_2$), 7.1—7.5 (m, 5H, Ph). Found: C, 56.4; H, 5.9%. Calcd for $C_{12}H_{15}BrO$: C, 56.5; H, 5.9%.

r-*1-Bromo-1-methyl*-c-*2-(benzyloxymethyl)cyclopropane* (**4c**): bp 95—105 °C (bath temp)/0.06 mmHg; IR (neat): 3030, 1494, 1451, 1370, 1168, 1090, 1026, 739, 700 cm^{-1}; MS: *m/e* (%), 256 (M^++2, 0.1), 254 (M^+, 0.1), 91 (100); PMR (CCl_4): δ 0.8—1.4 (m, 3H), 1.77 (s, 3H, Me), 3.2—3.8 (m, 2H, OCH_2), 4.49 (s, 2H, $PhC\underline{H}_2$), 7.1—7.6 (m, 5H, Ph). Found: C, 56.4; H, 6.0%. Calcd for $C_{12}H_{15}BrO$: C, 56.5; H, 5.9%.

r-*1-Chloro-1-methyl*-t-*2-phenylcyclopropane* (**3f**): bp 40—50 °C (bath temp)/3 mmHg, IR (neat): 3040, 1604, 1500, 1450, 1382, 1165, 1090, 779, 703 cm^{-1}; MS: *m/e* (%), 168 (M^++2, 1), 166 (M^+, 3), 131 (100), 115 (19), 103 (5), 91 (38); PMR (CCl_4): δ 1.0—1.7 (m, 2H), 1.30 (s, 3H, Me), 2.65 (dd, J=7, 10 Hz, 1H, PhC$\underline{H}$), 7.1—7.4 (m, 5H, Ph). Found: C, 71.8; H, 6.6%. Calcd for $C_{10}H_{11}Cl$: C, 72.1; H, 6.7%.

r-*1-Chloro-1-methyl*-c-*2-phenylcyclopropane* (**4f**): bp 55—65 °C (bath temp)/20 mmHg; IR (neat): 3040, 1600, 1500, 1450, 1170, 880, 764, 730, 700 cm^{-1}; MS: *m/e* (%), 168 (M^++2, 1.4), 166 (M^+, 4.5), 131 (100), 115 (20), 103 (6), 91 (38); PMR (CCl_4): δ 1.1—1.6 (m, 2H), 1.77 (s, 3H, Me), 2.12 (dd, J=7, 10 Hz, 1H, PhC$\underline{H}$), 7.1—7.3 (m, 5H, Ph). Found: C, 72.0; H, 6.7%. Calcd for $C_{10}H_{11}Cl$: C, 72.1; H, 6.7%.

exo-*7-Bromo-7-methylnorcarane* (**5a**): bp 70—90 °C (bath temp)/22 mmHg; IR (neat): 3040, 1470, 1450, 1440, 1382, 1171, 1075, 832, 799, 750 cm^{-1}; MS: *m/e* (%), 190 (M^++2, 3), 188 (M^+, 3), 146 (10), 109 (91), 67 (100); PMR (CCl_4): δ 1.70 (s, 3H, Me), 1.0—2.3 (m, 10H). Found: C, 50.8; H, 6.7%. Calcd for $C_8H_{13}Br$; C, 50.8; H, 6.9%.

endo-*7-Bromo-7-methylnorcarane* (**6a**): bp 50—55 °C (bath temp)/2 mmHg; IR (neat): 3000, 1463, 1445, 1382, 1247, 1175, 1105, 867, 810 cm^{-1}; MS: *m/e* (%), 190 (M^++2, 4), 188 (M^+, 4), 146 (13), 109 (93), 67 (100); PMR (CCl_4): δ 1.76 (s, 3H, Me), 0.8—1.0 (m, 2H), 1.1—2.5 (m, 8H). Found: C, 51.0; H, 7.1%. Calcd for $C_8H_{13}Br$: C, 50.8; H, 6.9%.

exo-*7-Bromo-1,7-dimethylnorcarane* (**5b**): bp 42 °C/1 mmHg; IR (neat): 1447, 1375, 1229, 1069 cm^{-1}; MS: *m/e* (%), 204 (M^++2, 3), 202 (M^+, 3), 187 (5), 146 (5), 123 (100), 81 (89), 67 (54); PMR (CCl_4): δ 0.8—2.3 (m, 9H), 1.40 (s, 3H, Me), 1.76 (s, 3H, Me). Found: C, 53.1; H, 7.3%. Calcd for $C_9H_{15}Br$: C, 53.2; H, 7.4%.

endo-*7-Bromo-1,7-dimethylnorcarane* (**6b**): bp 65—70 °C (bath temp)/16 mmHg; IR (neat): 1440, 1250, 1095, 787 cm^{-1}; MS: *m/e* (%), 204 (M^++2, 3), 202 (M^+, 3), 187 (4), 146 (5), 123 (79), 81 (85), 67 (100); PMR (CCl_4): δ 0.5—0.7 (m, 1H), 1.15 (s, 3H, Me), 1.1—2.1 (m, 8H), 1.83 (s, 3H, Me). Found: C, 53.3; H, 7.5%. Calcd for $C_9H_{15}Br$: C, 53.2; H, 7.4%.

1-Allyl-1-bromo-2-phenylcyclopropanes. A solution of *n*-BuLi in hexane (1.7 ml of 1.17 M solution, 2.0 mmol) was added to a cooled (−95 °C) solution of **1a** (0.55 g, 2.0 mmol) in THF (10 ml) over a 5 min period. After 30 min copper(I) iodide (0.19 g, 1.0 mmol) was added and 30 min thereafter allyl bromide (0.26 g, 2.0 mmol) diluted with HMPA (1 ml) was added. Stirring for 4 h and subsequent workup gave a mixture of **3d** and **4d** (0.28 g, 59% yield, bp 85—95 °C/4 mmHg). Each isomer was separated by preparative GLC (Silicone HV grease, similar condition as described in conditions B).

1-Allyl-r-*1-bromo*-t-*2-phenylcyclopropane* (**3d**): bp 90—95 °C/4 mmHg; IR (neat): 1644, 1606, 1500, 1452, 1429, 1238, 1202, 1150, 918, 772, 738, 700 cm^{-1}; MS: *m/e* (%), 238 (M^++2, 1), 236 (M^+, 1), 157 (48), 129 (52), 115 (95), 91 (100); PMR (CCl_4): δ 1.2—2.4 (m, 4H), 2.81 (dd, J=7, 10 Hz, 1H, PhC$\underline{H}$), 4.7—5.9 (m, 3H), 7.1—7.3 (m, 5H, Ph). Found: C, 60.5; H, 5.4%. Calcd for $C_{12}H_{13}Br$: C, 60.8; H, 5.5%.

1-Allyl-r-*1-bromo*-c-*2-phenylcyclopropane* (**4d**): bp 84—94 °C (bath temp)/4 mmHg; IR (neat): 1640, 1603, 1582, 1499, 1450, 1430, 1266, 1150, 1043, 998, 920, 764, 732, 698 cm^{-1}; MS: *m/e* (%), 238 (M^++2, 1), 236 (M^+, 1), 157 (55), 129 (55), 115 (100), 91 (95); PMR (CCl_4): δ 1.2—1.6 (m, 2H), 2.01 (dd, J=7, 10 Hz, 1H, PhC$\underline{H}$), 2.2—3.0 (m, 2H), 4.9—6.3 (m, 3H), 6.8—7.3 (m, 5H, Ph). Found: C, 60.7; H, 5.5%. Calcd for $C_{12}H_{13}Br$: C, 60.8; H, 5.5%.

1-Bromo-1-ethyl-2-phenylcyclopropanes (**3e** *and* **4e**). A magnetically stirred suspension of copper(I) phenylacetylide (0.17 g, 1.0 mmol) in THF (5 ml) containing **1a** (0.28 g, 1.0 mmol) was cooled to −95 °C and the whole was maintained approximately at this temperature during the addition of *n*-BuLi in hexane (0.8 ml of 1.25 M solution, 1.0 mmol) over 5 min. Five min after the addition ethyl iodide (0.10 ml, *ca.* 1.2 mmol) and 15 min thereafter HMPA (1 ml) were added. The mixture was maintained at −95 °C for successive 5 h and warmed gradually to room temp (14 h). Workup and short-path distillation of the crude product at 60—80 °C/3 mmHg gave an isomeric mixture of **3e** and **4e** (0.12 g, 54% yield). Each isomer was separated by preparative GLC (Silicone HV grease, see conditions B).

r-*1-Bromo-1-ethyl*-t-*2-phenylcyclopropane* (**3e**): R_t 23 min; bp 72—74 °C/4 mmHg; IR (neat): 1603, 1580, 1497, 1454, 1140, 804, 770, 733, 699 cm^{-1}; MS: *m/e* (%), 226 (M^++2, 0.8), 224 (M^+, 0.8), 145 (100), 130 (14), 117 (31). 91 (32); PMR (CCl_4): δ 0.7—1.7 (m, 7H), 2.78 (dd, J=7, 10 Hz, 1H, PhC$\underline{H}$), 7.0—7.3 (m, 5H, Ph). Found: C, 58.6; H, 5.7%. Calcd for $C_{11}H_{13}Br$: C, 58.7; H, 5.8%.

r-*1-Bromo-1-ethyl*-c-*2-phenylcyclopropane* (**4e**): R_t 25 min; bp 99—103 °C (bath temp)/4 mmHg; IR (neat): 1602, 1580, 1496, 1450, 1370, 1157, 1025, 824, 752, 730, 694 cm^{-1}; MS: *m/e* (%), 226 (M^++2, 0.7), 224 (M^+, 0.7), 145 (100), 130 (14), 117 (50), 91 (42); PMR (CCl_4): δ 1.0—2.1 (m, 8H), 7.0—7.3 (m, 5H, Ph). Found: C, 58.6; H, 5.9%. Calcd for $C_{11}H_{13}Br$: C, 58.7; H, 5.8%.

endo-*7-Allyl-7-bromonorcarane* (**5c**). A suspension of copper(I) iodide (0.48 g, 2.5 mmol) in THF (15 ml) containing **2a** (1.3 g, 5.0 mmol) was cooled to −95 °C and a solution of *n*-BuLi in hexane (2.7 ml of 2.0 M solution, 5.5 mmol) was added to this suspension during the period of 5 min. After 10 min allyl bromide (1.0 ml) was added and stirring was continued for 4 h. The mixture was gradually warmed up to room temp in 2 h and quenched with water. Workup and extraction with ether followed by distillation at 80—90 °C/2 mmHg gave **5c** (0.94 g, 87% yield). Preparative GLC (Silicone HV grease, 120 °C, 1.0 kg/cm^2, R_t 15 min) gave the analytically pure sample. Bp 77—80 °C/2 mmHg; IR (neat): 3090, 3010, 1643, 1470, 1452, 1426, 1224, 1168, 1115, 1049, 980, 910, 835 cm^{-1}; MS *m/e*: (%), 216 (M^++2, 2), 214 (M^+, 2), 172 (2), 135 (77), 93 (78), 79 (66), 67 (100); PMR (CCl_4): δ 0.9—2.2 (m, 10H), 2.57 (dt, J=6.2, 1 Hz, 2H, CH_2=

$CHC\underline{H}_2$), 4.9—6.3 (m, 3H). Found: C, 55.8; H, 7.2%. Calcd for $C_{10}H_{15}Br$: C, 55.8; H, 7.0%.

exo-7-Bromo-7-(3-methyl-2-butenyl)norcarane (5d). A magnetically stirred solution containing **2a** (0.51 g, 2.0 mmol) in THF (10 ml) was cooled to −95 °C and maintained at this temp during the dropwise addition of a solution of *n*-BuLi (1.0 ml of 2.1 M hexane solution, 2.2 mmol) over a 5 min period. The reaction mixture was stirred at −95 °C for 10 min and 3-methyl-2-butenyl bromide (0.35 g, 2.4 mmol) diluted with HMPA (1 ml) was added at −95 °C over 5 min. The reaction mixture was allowed to warm to −78 °C in 2 h and quenched with ethanol (1 ml). Workup and preparative TLC (silica gel, hexane, R_f 0.7) gave pure **5d** (0.37 g, 77% yield). Bp 100—103 °C/4 mmHg; IR (neat): 3030, 1670, 1470, 1445, 1370, 1170, 1115, 1095, 1045, 805 cm^{-1}; MS: *m/e* (%), 244 (M^++2, 0.9), 242 (M^+, 0.9), 227 (0.5), 199 (12), 186 (24), 163 (54), 107 (99), 41 (100); PMR (CCl_4): δ 0.9—2.3 (m, 16H), 2.47 (d, J=6 Hz, 2H), 5.0—5.5 (m, 1H). Found: C, 59.1; H, 8.0%. Calcd for $C_{12}H_{19}Br$: C, 59.3; H, 7.9%.

trans-1-Bromo-2-phenylcyclopropane (3g).[12a] According to the procedure of conditions A the carbenoids were generated and quenched with ethanol (2 ml) instead of MeI, and the reaction mixture was warmed up to room temp. Workup and distillation at 109—113 °C/19 mmHg gave 87% yield of **3g**. IR (neat): 3030, 1600, 1498, 1229, 758, 700, 620 cm^{-1}; MS: *m/e* (%), 198 (M^++2, 0.5), 196 (M^+, 0.5), 195 (0.5), 117 (100), 115 (47), 91 (23); PMR: (CCl_4) δ 1.2—1.6 (m, 2H), 2.1—2.5 (m, 1H), 2.7—3.1 (m, 1H), 6.7—7.5 (m, 5H, Ph).

trans-1-Bromo-2-hexylcyclopropane (3h)[12g] *with Concomitant 4h (19%):* Bp 77—80 °C/19 mmHg; IR (neat): 3060, 1470, 1375, 1236, 1034, 920 cm^{-1}; MS: *m/e* (%), 206 (M^++2, 0.3), 204 (M^+, 0.3), 162 (2), 148 (4), 83 (49), 69 (100), 55 (88); PMR (CCl_4): δ 0.6—1.8 (m, 16H), 2.4—2.7 (m, 1H, CHBr).

trans-2-(Benzyloxymethyl)-1-bromocyclopropane (3i): Bp 90—98 °C (bath temp)/0.07 mmHg; IR (neat): 3040, 1600, 1493, 1450, 1090, 740, 700 cm^{-1}; MS: *m/e* (%), 242 (M^++2, 0.9), 240 (M^+, 0.9), 210 (0.8), 161 (1.5), 131 (11), 91 (100); PMR (CCl_4): δ 0.8—1.8 (m, 3H), 2.5—2.9 (m, 1H, CHBr), 3.1—3.6 (m, 2H, OCH_2), 4.42 (s, 2H, $PhC\underline{H}_2$), 7.1—7.4 (m, 5H, Ph). Found: C, 55.1; H, 5.3%. Calcd for $C_{11}H_{13}BrO$: C, 54.8; H, 5.4%.

trans-1-Chloro-2-phenylcyclopropane (3j):[20] bp 90—100 °C (bath temp)/19 mmHg; IR (neat): 3040, 1605, 1499, 1450, 1253, 940, 888, 760, 700, 680 cm^{-1}; MS: *m/e* (%), 154 (M^++2, 3), 152 (M^+, 8), 117 (100), 115 (43), 91 (18); PMR (CCl_4): δ 1.2—1.6 (m, 2H), 2.1—2.5 (m, 1H), 2.9—3.3 (m, 1H, CHCl), 6.9—7.5 (m, 5H, Ph).

cis-1-Chloro-2-phenylcyclopropane (4j):[20] Bp 89—95 °C (bath temp)/19 mmHg; IR (neat): 3030, 1600, 1495, 1450, 1278, 1078, 917, 812, 767, 730, 700, 658, 591 cm^{-1}; MS: *m/e* (%), 154 (M^++2, 3), 152 (M^+, 8), 117 (100), 115 (46), 91 (9); PMR (CCl_4): δ 1.0—1.6 (m, 2H), 2.0—2.5 (m, 1H), 3.1—3.4 (m, 1H, CHCl), 7.0—7.5 (m, 5H, Ph).

exo-7-Bromonorcarane (5e):[12a] Bp 63—68 °C (bath temp)/18 mmHg; IR (neat): 3010 1448 1330 1215 1006 760 685 cm^{-1}; MS: *m/e* (%) 176 (M^++2, 7) 174 (M^+, 7) 132 (16) 95 (100), 67 (54); PMR (CCl_4): δ 0.7—2.3 (m, 10H), 2.50 (t, J=3.5 Hz, CHBr).

exo-7-Bromo-1-methylnorcarane (5f):[21] Bp 55—59 °C (bath temp)/1 mmHg; IR (neat): 1450, 1375, 1231, 700 cm^{-1}; MS: *m/e* (%), 190 (M^++2, 0.4), 188 (M^+, 0.4), 173 (0.8), 109 (100), 93 (12), 81 (24), 67 (96), 55 (36); PMR (CCl_4): δ 0.8—2.2 (m, 9H), 1.25 (s, 3H, Me), 2.70 (d, J=4 Hz, CHBr). (Found: C, 51.1; H, 7.1%).

(E)-β-Methylcinnamyl Acetate (9a). A suspension of silver acetate (87 mg, 0.52 mmol) and silver tetrafluoroborate (15 mg, 0.07 mmol) in a solution of **3a** (0.11 g, 0.52 mmol) and acetic acid (1.0 ml) was stirred at 75 °C for 22 h. Workup, followed by preparative TLC (silica gel, benzene, R_f 0.6), gave **9a** (74 mg, 74% yield). Bp 70—77 °C (bath temp)/3 mmHg; IR (neat): 3080, 3050, 1740, 1660, 1600, 1580, 1493, 1445, 1370, 1230, 1120, 745, 700 cm^{-1}; MS: *m/e* (%), 190 (M^+, 21), 148 (37), 130 (74), 115 (59), 77 (13), 43 (100); PMR (CCl_4): δ 1.87 (s, 3H, Me), 2.04 (s, 3H, OAc), 4.57 (s, 2H, CH_2O), 6.47 (s, 1H, $PhC\underline{H}$), 7.1—7.4 (m, 5H, Ph). Found: C, 75.6; H, 7.5%. Calcd for $C_{12}H_{14}O_2$: C, 75.8; H, 7.4%.

Solvolysis of 3b. A mixture of **9b** and **10b** was obtained and each isomer was separated by preparative GLC (Silicone HV grease, 130 °C, 1.0 kg/cm^2).

(E)-2-Methyl-2-nonen-1-yl Acetate (9b): R_t 10 min; bp 64—72 °C (bath temp)/3 mmHg; IR (neat): 1736, 1464, 1370, 1225, 1015 cm^{-1}; MS: *m/e* (%), 198 (M^+, 0.3), 156 (6), 138 (14), 95 (23), 68 (41), 43 (100),; PMR (CCl_4): δ 0.7—1.5 (m, 13H), 1.63 (s, 3H, Me), 1.98 (s, 3H, OAc), 4.37 (s, 2H), 5.42 (t, J=7 Hz, 1H). Found: C, 72.8; H, 11.4%. Calcd for $C_{12}H_{22}O_2$: C, 72.7; H, 11.2%.

2-Methyl-1-nonen-3-yl acetate (10b): R_t 8 min; bp 53—64 °C (bath temp)/1.5 mmHg; IR (neat): 3080, 1730, 1650, 1235, 1020, 900 cm^{-1}; MS: *m/e* (%), 156 (M^+−42, 8), 138 (8), 113 (8), 95 (16), 82 (15), 68 (25), 43 (100); PMR (CCl_4): δ 0.7—2.3 (m, 13H), 1.68 (s, 3H, Me), 1.95 (s, 3H, OAc), 4.7—5.2 (m, 3H); Found: C, 72.4; H, 11.1%. Calcd for $C_{12}H_{22}O_2$: C, 72.7; H, 11.2%.

Solvolysis of 3c. A mixture of 4-benzyloxy-2-methyl-2-buten-1-yl acetate (**9c**) and 1-benzyloxy-3-methyl-3-buten-2-yl acetate (**10c**) was obtained and separated by preparative TLC (silica gel, hexane–ether 5: 1).

9c: R_f 0.3—0.4; bp 87—93 °C (bath temp)/1 mmHg; IR (neat): 3050, 3020, 1730, 1490, 1450, 1360, 1220, 1065, 1020, 737, 700 cm^{-1}; MS: *m/e* (%), 174 (M^+−60, 3), 159 (3), 105 (11), 91 (100), 43 (72); PMR (CCl_4): δ 1.63 (s, 3H, Me), 2.00 (s, 3H, OAc), 4.00 (d, J=6.5 Hz, 2H), 4.41 (s, 4H), 5.4—5.9 (m, 1H), 7.0—7.5 (m, 5H). Found: C, 72.0; H, 7.7%. Calcd for $C_{14}H_{18}O_3$: C, 71.8; H, 7.7%. The geometry of double bond is assumed to be (E) on the analogy of the solvolysis of **3a** to **9a**.

10c: R_f 0.4—0.5; bp 85—95 °C (bath temp)/1 mmHg; IR (neat): 3030, 1732, 1650, 1494, 1450, 1362, 1230, 1095, 1025, 905, 740, 700 cm^{-1}; MS: *m/e* (%), 234 (M^+, 0.01), 174 (2), 91 (78), 65 (43), 43 (100); PMR (CCl_4): δ 1.73 (s, 3H, Me), 2.00 (s, 3H, OAc), 3.45 (d, J=6 Hz, 2H), 4.45 (s, 2H), 4.8—5.1 (m, 2H), 5.31 (t, J=6 Hz, 1H), 7.0—7.5 (m, 5H, Ph). Found: C, 72.0; H, 8.0%. Calcd for $C_{14}H_{18}O_3$: C, 71.8; H, 7.7%.

Hydrolysis of 9b. One drop of sodium methoxide in methanol (1 M) was added to a solution of **9b** (7.5 mg, 0.04 mmol) in CH_2Cl_2 (1 ml). After stirring at room temp for 1 h the reaction mixture was worked up. Preparative TLC (silica gel, hexane–ether (2: 1. R_f 0.4—0.5) afforded *(E)*-2-methyl-2-nonen-1-ol (5.4 mg, quantitative yield). Bp 93—100 °C (bath temp)/20 mmHg; IR (neat): 3360, 1640, 1480, 1380, 1265, 1010 cm^{-1}; MS: *m/e* (%), 156 (M^+, 6), 138 (4), 109 (4), 95 (9), 83 (12), 71 (46), 55 (27), 40 (100); PMR (CCl_4): δ 0.6—2.2 (m, 14H), 1.63 (s, 3H, Me), 3.88 (s, 2H, CH_2O), 5.2—5.5 (m, 1H). The methyl signal of this alcohol is strictly different from that of (*Z*) isomer (δ 1.71).[22]

Hydrolysis of 9a. This reaction afforded *(E)*-β-methylcinnamyl alcohol in 65% yield. Bp 88—95 °C (bath temp)/3 mmHg; IR (neat): 3300, 3070, 3050, 3020, 1664, 1600, 1575, 1493, 1443, 1074, 1008, 739, 695 cm^{-1}; MS: *m/e* (%), 148 (M^+, 51), 133 (28), 115 (49), 105 (46), 91 (100); PMR (CCl_4): δ 1.84 (br s, 4H, Me and OH), 4.08 (br s, 2H, CH_2O),

6.4—6.6 (m, 1H), 7.0—7.5 (m, 5H, Ph). The product was identical in all respects with the authentic sample prepared from lithium aluminum hydride reduction of (*E*)-β-methylcinnamaldehyde.[23]

exo-*7-Acetoxy-7-methylnorcarane (**12a**)*. A solution of **5a** (0.15 g, 0.80 mmol) in acetic acid (1 ml) was added to a suspension of silver acetate (0.13 g, 0.80 mmol) and silver tetrafluoroborate (16 mg, 0.08 mmol) in acetic acid (2 ml). After stirring for 2 h at 75 °C the reaction mixture was neutralized by the addition of saturated sodium hydrogencarbonate aq solution and extracted with ether. The organic layer was dried over sodium sulfate and evaporated *in vacuo*. The crude product was purified by preparative TLC (silica gel, hexane–ether 4: 1, R_f 0.5). **12a** was obtained in 63% yield (85 mg). Bp 62—72 °C (bath temp)/4 mmHg; IR (neat): 3050, 1745, 1450, 1370, 1240, 1189, 1113, 1020, 893 cm^{-1}; MS: *m/e* (%), 126 (M^+−42, 13), 111 (15), 44 (85), 43 (100); PMR (CCl_4): δ 0.9—2.2 (m, 10H), 1.38 (s, 3H, Me), 1.85 (s, 3H, OAc). Found: C, 71.2; H, 9.9%. Calcd for $C_{10}H_{16}O_2$: C, 71.4; H, 9.6%.

exo-*7-Acetoxy-7-allylnorcarane (**12c**)*: Bp 72—82 °C (bath temp)/3 mmHg; IR (neat): 3070, 3000, 1735,1637, 1449, 1361, 1220, 1175, 910, 790 cm^{-1}; MS: *m/e* (%), 194 (M^+, 0.2), 153 (14), 111 (17), 67 (23), 43 (100), 41 (41); PMR (CCl_4): δ 0.6—2.4 (m, 10H), 1.85 (s, 3H, Me), 2.57 (d, J= 6 Hz, 2H), 4.9—6.2 (m, 3H). Found: C, 73.9; H, 9.4%. Calcd for $C_{12}H_{18}O_2$: C, 74.2; H, 9.3%.

exo-*7-Acetoxy-7-(3-methyl-2-butenyl)norcarane (**12d**)*: Bp 66—76 °C (bath temp)/2 mmHg; IR (neat): 3000, 1735, 1460, 1445, 1360, 1230, 1063, 1048 cm^{-1}; MS: *m/e* (%), 222 (M^+, 0.1), 180 (10), 162 (21), 147 (62), 43 (100); PMR (CCl_4): δ 0.5—2.3 (m, 12H), 0.83 (s, 6H, Me_2C), 1.98 (s, 3H, OAc), 4.67 (t, J=7 Hz, 1H). Found: C, 75.7; H 10.1%. Calcd for $C_{14}H_{22}O_2$: C, 75.6; H, 10.0%.

exo-*7-Acetoxy-1,7-dimethylnorcarane (**12b**)*: Bp 61—69 °C (bath temp)/4 mmHg; IR (neat): 1740, 1445, 1369, 1250, 1232, 1190, 1120, 1020, 790 cm^{-1}; MS: *m/e* (%), 182 (M^+, 0.2), 167 (0.3), 140 (12), 125 (26), 95 (10), 43 (100); PMR (CCl_4): δ 0.5—0.8 (m, 1H), 0.9—2.2 (m, 8H), 1.07 (s, 3H, Me), 1.38 (s, 3H, Me), 1.90 (s, 3H, OAc). Found: C, 72.2; H, 10.1%. Calcd for $C_{11}H_{18}O_2$: C, 72.5; H, 10.0%.

*Acetolysis of a Mixture of **5a** and **6a**.* A mixture of **5a** and **6a** (36: 64) (0.19 g, 1.0 mmol) dissolved in acetic acid (1 ml) was treated with silver salts as above affording an inseparable mixture of **12a** and 2-methyl-2-cyclohepten-1-yl acetate (93 mg, **12a**/ring opened isomer 59: 41) in 55% yield. The ratio was estimated by its PMR (δ 1.37 (s, Me), 1.85 (s, OAc) for **12a**; δ 1.98 (s, AOc), 5.2—5.8 (m, CHOAc and olefinic proton) for its isomer).

*2-Phenyl-1-methylenecyclopropane (**15a**)*.[24] A solution of **3a** (50 mg, 0.24 mmol) in dimethyl sulfoxide (0.5 ml) was added to a solution of *t*-BuOK (42 mg, containing 26% of *t*-BuOH, 0.30 mmol) in DMSO (3 ml) at room temp. After stirring for 1 h the reaction mixture was quenched with water and extracted with pentane. The yield was estimated by GLC (Silicone SE-30, indane as an internal standard). The pure sample was obtained by short-path distillation (50—58 °C/10 mmHg). IR (neat): 3080, 1745, 1603, 1496, 1452, 1198, 1118, 1014, 890, 743, 695 cm^{-1}; MS: *m/e* (%), 130 (M^+, 70), 129 (100), 128 (60), 115 (66); PMR (CCl_4): δ 1.0—1.9 (m, 2H), 2.4—2.8 (m, 1H), 5.5—5.8 (m, 2H), 7.0—7.5 (m, 5H, Ph).

*2-Hexyl-1-methylenecyclopropane (**15b**)*:[24] Bp 53—63 °C (bath temp)/20 mmHg; IR (neat): 3060, 3040, 1740, 1460, 1016, 885 cm^{-1}; MS: *m/e* (%), 138 (M^+, 3), 123 (16), 109 (18), 95 (37), 81 (100), 67 (88), 55 (80), 41 (70); PMR (CCl_4): δ 0.6—2.0 (m, 16H), 5.2—5.6 (m, 2H).

*2-(Benzyloxymethyl)-1-methylenecyclopropane (**15c**)*: Bp 65—75 °C (bath temp)/3 mmHg; IR (neat): 3060, 3040, 1735, 1600, 1580, 1492, 1450, 1350, 1080, 1021, 885, 735, 700 cm^{-1}; MS: *m/e* (%), 174 (M^+, 0.05), 129 (4), 107 (6), 91 (100), 65 (10); PMR (CCl_4): δ 0.7—2.0 (m, 3H), 3.0—3.6 (m, 2H), 4.45 (s, 2H), 5.3—5.6 (m, 2H), 7.1—7.5 (m, 5H). Found: C, 82.6; H, 8.3%. Calcd for $C_{12}H_{14}O$: C, 82.7; H, 8.1%.

*7-Methylenenorcarane (**16a**)*:[15f] Bp 65—75 °C (bath temp)/130 mmHg; IR (neat): 3060, 2970, 2700, 1749, 1452, 1351, 1331, 1140, 882, 848, 710 cm^{-1}; MS: *m/e* (%), 108 (M^+, 15), 107 (25), 93 (77), 91 (83), 79 (100), 55 (56); PMR (CCl_4): δ 0.8—2.1 (m, 10H), 5.2—5.4 (m, 2H).

*7-Allylidenenorcarane (**16b**)*: Bp 66—70 °C (bath temp)/4 mmHg; IR (neat): 3100, 2680, 1790, 1612. 1450 990 890 cm^{-1}; MS: *m/e* (%), 134 (M^+, 14), 119 (34), 105 (48), 91 (100), 80 (45), 79 (51), 77 (46), 67 (24); PMR (CCl_4): δ 1.1—2.5 (m, 10H), 4.8—5.5 (m, 2H), 6.0—6.9 (m, 2H). Exact mass : *m/e* 134.112 (M^+). Calcd for $C_{10}H_{14}$: *m/e* 134.110.

Financial aid by the Ministry of Education, Japanese Government (Grant-in-Aid 011010, 110309) is acknowledged.

References

1) a) G. Köbrich *Angew. Chem. Int. Ed. Engl.*, **11**, 473 (1972); see also b) H. Taguchi, H. Yamamoto, and H. Nozaki, *J. Am. Chem. Soc.*, **96**, 3010 (1974).

2) D. Seyferth, R. L. Lambert, Jr., and M. Massol, *J. Organomet. Chem.*, **88**, 255 (1975).

3) a) W. Kirmse, "Carbene Chemistry," 2nd ed, Academic Press, New York, N. Y. (1971), pp. 254, 462; b) R. Barlet and Y. VoQuange, *Bull. Soc. Chim. Fr.*, **1969**, 3729; c) K. J. Drachenberg and H. Hopf, *Tetrahedron Lett.*, **1974**, 3267; d) R. B. Reinarz and G. J. Fonken, *ibid.*, **1973**, 4591, 4595; **1974**, 441; e) D. W. Brown, M. E. Hendrick, and M. Jones, Jr., *ibid.*, **1973**, 3951; f) L. A. Paquette, G. Zon, and R. T. Taylor, *J. Org. Chem.*, **39**, 2677 (1974); g) L. Sydnes and L. Skattebøl, *Tetrahedron Lett.*, **1975**, 4603; h) J. C. Damiano, J. L. Luche, and P. Crabbe, *ibid.*, **1976**, 779.

4) G. Köbrich and W. Goyert, *Tetrahedron*, **24**, 4327 (1968).

5) a) M. Braun, R. Demmann, and D. Seebach, *Chem. Ber.*, **108**, 2368 (1975); b) T. Hiyama, S. Takehara, K. Kitatani, and H. Nozaki, *Tetrahedron Lett.*, **1974**, 3295.

6) A part of this study was published in K. Kitatani, T. Hiyama, and H. Nozaki, *J. Am. Chem. Soc.*, **97**, 949 (1975).

7) T. K. Devon and A. I. Scott, "Handbook of Naturally Occurring Compounds," Vol II, Academic Press, New York and London (1972), pp. 29—31, 51, 119, 151, 153, 171, 178, and 265.

8) Although it is not clear at present why **8** is preferred thermodynamically, one may understand it in terms of intramolecular hydrogen bonding between the carbanionic center and C–H moiety in the substituent. See M. Schlosser and J. Hartmann, *J. Am. Chem. Soc.*, **98**, 4674 (1976).

9) K. G. Taylor, W. E. Hobbs, and M. Saquet, *J. Org. Chem.*, **36**, 369 (1971); K. G. Taylor and J. Chaney, *J. Am. Chem. Soc.*, **98**, 4158 (1976).

10) Furthermore **1d** was recorvered completely unchanged under the conditions B. This result may imply the possible discrimination of dichloro- and dibromocyclopropane moiety in the same molecule. *Cf.* Y. M. Slobodin, I. Z. Egenburg, and A. S. Khachaturov, *J. Org. Chem. U.S.S.R.*, **10**, 18 (1974).

11) The reactive species is apparently neither a copper carbenoid nor a copper ate-complex, as the reagent thus prepared actually adds to cyclohexanone or crotonaldehyde at carbonyl carbon.

12) a) T. Ando, K. Wakabayashi, H. Yamanaka, and W. Funasaka, *Bull. Chem. Soc. Jpn.*, **45**, 1576 (1972). b) H. Nozaki, T. Aratani, and R. Noyori, *Tetrahedron*, **23**, 3645 (1967); c) T. Shirafuji, K. Oshima, Y. Yamamoto, and H. Nozaki, *Bull. Chem. Soc. Jpn.*, **44**, 3161 (1971) and references cited therein; d) L. Sydnes and L. Skattebøl, *Tetrahedron Lett.*, **1974**, 3703.

13) R. B. Woodward and R. Hoffmann, "The Conservation of Orbital Symmetry," Verlag Chemie GmbH and Academic Press Inc. (1970), p. 47.

14) D. B. Ledlie and E. A. Nelson, *Tetrahedron Lett.*,**1969**, 1175. **Note Added in Proof:** The configuration of the intermediary cyclopropyl cation of type **13** is recently found to be non-planar, and the overall substitution proceeds with retention of configuration. D. B. Ledlie, W. Barber, and F. Switzer, *Tetrahedron Lett.*, **1977**, 607; G. A. Olah, G. Liang, D. B. Ledlie, and M. G. Costopoulos, *J. Am. Chem. Soc.*, **99**, 4196 (1977).

15) Recent alkylidenecyclopropane syntheses: a) W. E. Billups, W. Y. Chow, K. E. Leavel, and E. S. Lewis, *J. Org. Chem.*, **39**, 274 (1974); b) S. Arora and P. Binger, *Synthesis*, **1974**, 801; c) M. S. Newman and G. M. Fraunfelder, *J. Org. Chem.*, **39**, 251 (1974); d) T. Sasaki, S. Eguchi, and T. Ogawa, *ibid.*, **39**, 1927 (1974); e) P. J. Stang, M. G. Mangum, D. P. Fox, and P. Haak, *J. Am. Chem. Soc.*, **96**, 4562 (1974); f) A. S. Kende and E. E. Riecke, *J. Chem. Soc., Chem. Commun.*, **1974**, 383.

16) C. H. Depuy, F. W. Breitbeil, and K. R. Debruin, *J. Am. Chem. Soc.*, **88**, 3347 (1966).

17) L. M. Jackman and S. Sternhell, "Applications of Nuclear Magnetic Resonance Spectroscopy in Organic Chemistry," 2nd ed, Pergamon Press, Oxford (1969), pp. 78, 80.

18) G. H. Posner, C. E. Whitten, and J. J. Sterling, *J. Am. Chem. Soc.*, **95**, 7788 (1973).

19) D. C. Qwsley and C. E. Castro, *Org. Synth.*, **52**, 128 (1972).

20) J. W. Hausser and N. J. Pinkowski, *J. Am. Chem. Soc.*, **89**, 6981 (1967).

21) J. Moreau and P. Caubere, *Tetrahedron*, **27**, 5741 (1971).

22) E. J. Corey and H. Yamamoto, *J. Am. Chem. Soc.*, **92**, 226 (1970).

23) N. E. Hoffman, A. T. Kanakkanatt, and R. F. Scheneider, *J. Org. Chem.*, **27**, 2687 (1962).

24) R. Noyori, H. Takaya, Y. Nakanisi, and H. Nozaki, *Can. J. Chem.*, **47**, 1242 (1969).

Substituent Effects on Tautomerism of 4-Pyridinethiones

Hiromichi BESSO,* Kimiaki IMAFUKU, and Hisashi MATSUMURA

Department of Chemistry, Faculty of Science, Kumamoto University, Kurokami, Kumamoto 860

(Received March 25, 1977)

The tautomeric constants K_t of several 4-pyridinethiones were determined by measurement of pK_a values. For 2-substituted 5-methoxy-4-pyridinethiones, the K_t values are correlated to the substituent constants σ, by the equation $\log K_t = 4.00 + 3.99\sigma_m - 7.33\sigma_o$.

Two tautomers, enethiol and thione forms, are possible for the tautomerism of 4-pyridinethiones. Ross[1] found by means of UV spectra that 4-pyridinethione exists predominantly in the thione form in ethanolic solution. Jones and Katritzky,[2] and Albert and Barlin[3] concluded by measurement of pK_a values that the thione form predominates in aqueous solution by factors of *ca.* 10^4 by comparative studies of 4-pyridinethione and both alkylated compounds. It was shown by means of IR,[4] NMR,[5] and UV[6] that polyhalogenated 4-pyridinethiones exist mostly in the enethiol form.

In the previous paper, we reported the substituent effects of 2-substituted 5-methoxy-4-pyridones in aqueous solution on tautomerism.[7] We hereby report the tautomerism of 2-substituted-5-methoxy-4-pyridinethiones by a similar treatment to that of 2-substituted 5-methoxy-4-pyridones.

Results and Discussion

Dissociation Constants. The dissociation constants of 4-pyridinethiones (I), *N*-methyl-4-pyridinethiones (II), and 4-methylthiopyridines (III) were determined spectrophotometrically in water at 25 °C. The results are summarized in Table 1, where pK_1 represents the first dissociation constants for 4-pyridinethiones (I), pK_{NCH_3} and pK_{SCH_3} corresponding to the dissociation constants for *N*-methyl-4-pyridinethiones (II) and 4-methylthiopyridines (III), respectively.

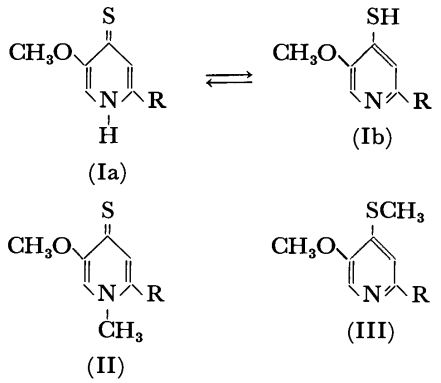

Since activity coefficients were not introduced into the calculation, the dissociation constants do not represent thermodynamic terms, giving only a relative measure of base strength.

The pK_a values of 4-pyridinethiones (I) and *N*-methyl-4-pyridinethiones (II) are smaller than those of 4-pyridones and *N*-methyl-4-pyridones, since electronegativity of sulfur atom is smaller than that of oxygen atom. The pK_a values of I, II, and III decrease by electron-withdrawing groups attached to 2-position similarly to those of 4-pyridones.

Table 1. Dissociation constants

Substituent	pK_1	pK_{NCH_3}	pK_{SCH_3}
CH_3	1.90	1.82	6.50
H	1.69		
CH_2OH	1.64	1.53	5.38
CH_2OCH_3		1.44	
CHO			3.86

Tautomeric Ratio. The tautomeric constants K_t which represent the ratio of NH-form (Ia) to SH-form (Ib), are given by the following equation:[8] (Table 2).

$$\log K_t = pK_{SCH_3} - pK_{NCH_3} \quad (1)$$

Table 2. Tautomeric constants

Substituent	$\log K_t$	
	4-Pyridinethiones	4-Pyridones
CH_3	4.7	3.7
CH_2OH	3.9	2.8

The K_t values for 4-pyridinethiones are affected by the substituents in the 2-position, decreasing by electron-withdrawing groups. It is concluded that the thione forms predominate in aqueous solution by factors of *ca.* 10^5 for 5-methoxy-2-methyl-4-pyridinethione and *ca.* 10^4 for 5-methoxy-2-hydroxymethyl-4-pyridinethione.

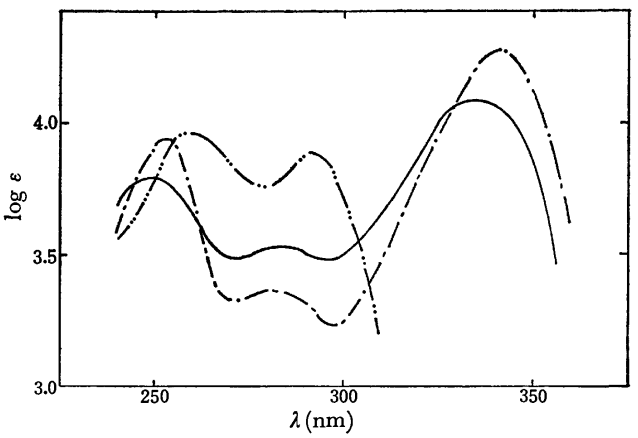

Fig. 1. The UV spectra of the neutral species of 5-methoxy-2-hydroxymethyl-4-pyridinethione series
—— 5-methoxy-2-hydroxymethyl-4-pyridinethione;
–·– 5-methoxy-2-hydroxymethyl-1-methyl-4-pyridinethione;–··– 5-methoxy-2-hydroxymethyl-4-methylthiopyridine.

* Present address: Wakunaga Pharmaceutical Co., Ltd., Koda-machi, Takata-gun, Hiroshima 729-64.

UV Spectra. The UV spectra of the neutral species of 5-methoxy-4-pyridinethiones (I) having the methyl and hydroxymethyl group in the 2-position are similar to those of their *N*-methyl derivatives (II), but differ a great deal from those of their *S*-methyl derivatives (III). Figure 1 shows the UV spectra of the neutral species of 5-methoxy-2-hydroxymethyl-4-pyridinethione series, the thione form being seen to exist predominantly.

Substituent Effects. Clark and Perrin[9] obtained the substituent constants σ_o for ortho-substituted pyridines from their dissociation constants. We also obtained the substituent constants σ_o and σ_m for the hydroxymethyl group.[7] When the pK_a values of 2-substituted 5-methoxy-4-pyridinethiones (I), pK_1, are plotted against the substituent constants σ_m,[10,11] a straight line is obtained, giving the following equation by the least-square methods:

$$pK_1 = 1.68 - 3.16\sigma_m \quad (r=0.998). \tag{2}$$

For the proton gain of 2-substituted 5-methoxy-1-methyl-4-pyridinethiones (II) and the proton loss of 2-substituted 5-methoxy-4-methylthiopyridines (III), Eqs. 3 and 4, respectively, are obtained.

$$pK_{NCH_3} = 1.54 - 3.99\sigma_m \quad (r=0.992), \tag{3}$$

$$pK_{SCH_3} = 5.54 - 7.33\sigma_o \quad (r=0.999). \tag{4}$$

When Eqs. 3 and 4 are substituted into Eq. 1, we have

$$\log K_t = 4.00 + 3.99\sigma_m - 7.33\sigma_o. \tag{5}$$

We have obtained a similar equation for 2-substituted 5-methoxy-4-pyridones:[7]

$$\log K_t = 2.98 + 2.93\sigma_m - 6.18\sigma_o. \tag{6}$$

The ρ-value 2.93 for the substituent constants σ_m indicates the decrease of the hydroxy form by electron-withdrawing groups in the 2-position. In contrast, the ρ-value -6.18 for the substituent constants σ_o shows that the ratio of the hydroxy form increases electron-withdrawing group in the 2-position. It is possible to explain the tautomerism of 2-substituted 5-methoxy-4-pyridinethiones in a similar manner to that above. In Eq. 5, the ρ-value 3.99 for σ_m indicates the decrease of the enethiol form (Ib) by the electron-withdrawing group in the 2-position. In contrast, the ρ-value -7.33 for σ_o shows that the ratio of (Ib) increases with electron-withdrawing group in the 2-position. The substituent effects on the tautomerism of 2-substituted 5-methoxy-4-pyridinethiones are similar to those of 2-substituted 5-methoxy-4-pyridones.

It is concluded that the thione forms for 4-pyridinethione-4-mercaptopyridine tautomerism predominate by factors of *ca.* 10 the keto forms for 4-pyridone-4-hydroxypyridine tautomerism.

Experimental

All the melting points were measured on a Yanagimoto micromelting point apparatus and are uncorrected. The IR spectra were taken on a JASCO IRA-1 spectrophotometer, and the NMR spectra on a Hitachi-Perkin-Elmer R-24 spectrometer (60 MHz) with tetramethylsilane as an internal reference.

The pK_a values of 4-pyridinethiones (I), *N*-methyl-4-pyridinethiones (II), and 4-(methylthio)pyridines (III) were measured spectrophotometrically in water at 25 °C by the method of Albert and Serjeant.[12] The absorption spectra were taken on a Hitachi EPS-3T spectrophotometer, while the pH values were measured with a Hitachi-Horiba F-7 pH meter.

Materials. 4-Pyridinethiones (I) and *N*-methyl-4-pyridinethiones (II) were obtained by the reaction of 4-pyranthiones with ammonia and methylamine. All 4-pyranthiones were prepared by the reaction of the corresponding 4-pyrones with phosphorus pentasulfide in dry benzene.

3-Methoxy-4-pyranthione: Yield, 36%; mp 110—114 °C (from carbon tetrachloride); IR (KBr) 1604 cm^{-1}; NMR ($CDCl_3$) δ: 7.45 (d, 1H, J=4.7 Hz), 7.45 (s, 1H), 7.26 (d, 1H, J=4.7 Hz), 3.83 (s, 3H). Found: C, 50.49; H, 4.26%. Calcd for $C_6H_6O_2S$: C, 50.71; H, 4.26%.

5-Methoxy-2-methyl-4-pyranthione: Yield, 40%; mp 98.5—100 °C (from carbon tetrachloride); IR (KBr) 1615 cm^{-1}; NMR ($CDCl_3$) δ: 7.43 (s, 1H), 7.22 (s, 1H), 3.82 (s, 3H), 2.24 (s, 3H). Found: C, 53.55; H, 5.06%. Calcd for $C_7H_8O_2S$: C, 53.82; H, 5.17%.

5-Methoxy-2-acetoxymethyl-4-pyranthione: Yield, 54%; mp 152.5—153.5 °C (from benzene); IR (KBr) 1750, 1630 cm^{-1}; NMR ($CDCl_3$) δ: 7.45 (s, 1H), 7.32 (s, 1H), 4.88 (s, 2H), 3.85 (s, 3H), 2.15 (s, 3H). Found: C, 50.40; H, 4.60%. Calcd for $C_9H_{10}O_4S$: C, 50.47; H, 4.67%.

5-Methoxy-2-methoxymethyl-4-pyranthione: Yield, 37%; mp 56—56.5 °C (from benzene–petroleum ether); IR (KBr) 1635 cm^{-1}; NMR ($CDCl_3$) δ: 7.43 (s, 1H), 7.36 (s, 1H), 4.24 (s, 2H), 3.86 (s, 3H), 3.46 (s, 3H). Found: C, 51.48; H, 5.33%. Calcd for $C_8H_{10}O_3S$: C, 51.59; H, 5.42%.

3-Methoxy-4-pyridinethione: Yield, 44%; mp 149—152 °C (from methanol); IR (KBr) 3160, 2800, 1602 cm^{-1}; NMR (CF_3COOH) δ: 8.3—7.7 (m, 3H), 4.20 (s, 3H). Found: C, 50.80; H, 5.02; N, 9.94%. Calcd for C_6H_7NOS: C, 51.06; H, 5.02; N, 9.93%.

5-Methoxy-2-methyl-4-pyridinethione: Yield, 66%; mp 156—158 °C (from ethyl acetate); IR (KBr) 3245, 2800, 1615 cm^{-1}; NMR (CF_3COOH) δ: 7.9—7.5 (m, 2H), 4.15 (s, 3H), 2.69 (s, 3H). Found: C, 54.04; H, 5.78; N, 8.90%. Calcd for C_7H_9NOS: C, 54.19; H, 5.81; N, 9.03%.

5-Methoxy-1,2-dimethyl-4-pyridinethione: Yield, 60%; mp 200—202 °C (dec) (from methanol); IR (KBr) 3450, 3370, 1615 cm^{-1}; NMR (CF_3COOH) δ: 7.92 (s, 1H), 7.64 (s, 1H), 4.17 (s, 3H), 4.12 (s, 3H), 2.69 (s, 3H). Found: C, 56.66; H, 6.53; N, 8.25%. Calcd for $C_8H_{11}NOS$: C, 56.79; H, 6.55; N, 8.28%.

5-Methoxy-2-hydroxymethyl-4-pyridinethione was obtained by the reaction of 5-methoxy-2-acetoxymethyl-4-pyranthione with ammonia: Yield, 41%; mp 154—156 °C (from methanol); IR (KBr) 3210, 1600, 1585 cm^{-1}; NMR (CF_3COOH) δ: 8.2—7.6 (m, 2H), 5.13 (s, 2H), 4.18 (s, 3H). Found: C, 48.78; H, 5.35; N, 8.08%. Calcd for $C_7H_9NO_2S$: C, 49.08; H, 5.30; N, 8.19%.

5-Methoxy-2-hydroxymethyl-1-methyl-4-pyridinethione was obtained by the reaction of 5-methoxy-2-acetoxymethyl-4-pyranthione with methylamine: Yield, 65%; mp 199.5—201.5 °C (from methanol); IR (KBr) 3300, 1615 cm^{-1}; NMR (CF_3COOH) δ: 7.99 (br, s, 2H), 5.14 (s, 2H), 4.27 (s, 3H), 4.16 (s, 3H). Found: C, 51.29; H, 6.07; N, 7.58%. Calcd for $C_8H_{11}NO_2S$: C, 51.85; H, 5.98; N, 7.57%.

5-Methoxy-2-methoxymethyl-1-methyl-4-pyridinethione: Yield, 70%; mp 166—168 °C (dec) (from methanol); IR (KBr) 1615 cm^{-1}; NMR (CF_3COOH) δ: 8.00 (s, 1H), 7.86 (s, 1H), 4.78 (s, 2H), 4.26 (s, 3H), 4.16 (s, 3H), 3.65 (s, 3H). Found: C, 54.08; H, 6.58; N, 7.01%. Calcd for $C_9H_{13}NO_2S$: C, 54.26; H, 6.58; N, 7.03%.

5-Methoxy-2-methyl-4-(methylthio)pyridine was obtained by the

methylation of 5-methoxy-2-methyl-4-pyridinethione with methyl iodide: Yield, 54%; mp 58—59 °C (from petroleum ether); IR (KBr) 1575 cm^{-1}; NMR (CCl_4) δ: 7.75 (s, 1H), 6.66 (s, 1H), 3.85 (s, 3H), 2.37 (s, 3H), 2.31 (s, 3H). Found: C, 56.79; H, 6.62; N, 8.30%. Calcd for $C_8H_{11}NOS$: C, 56.79; H, 6.55; N, 8.28%.

5-Methoxy-2-hydroxymethyl-4-methylthiopyridine was obtained by the methylation of 5-methoxy-2-hydroxymethyl-4-pyridinethione with methyl iodide: Yield, 53%; mp 108 °C (from carbon tetrachloride); IR (KBr) 3200, 1580 cm^{-1}; NMR ($CDCl_3$) δ: 7.97 (s, 1H), 7.02 (s, 1H), 4.69 (s, 2H), 3.95 (s, 3H), 2.43 (s, 3H), 4.3—3.3 (br, 1H). Found: C, 51.44; H, 5.95; N, 7.67%. Calcd for $C_8H_{11}NO_2S$: C, 51.85; H, 5.98; N, 7.57%.

5-Methoxy-2-formyl-4-(methylthio)pyridine was obtained by manganese dioxide oxidation of 5-methoxy-2-hydroxymethyl-4-methylthiopyridine: Yield, 62%; mp 116—117 °C (from petroleum ether); IR (KBr) 1720, 1550 cm^{-1}; NMR ($CDCl_3$) δ: 9.96 (s, 1H), 8.19 (s, 1H), 7.73 (s, 1H), 4.06 (s, 3H), 2.51 (s, 3H). Found: C, 52.35; H, 5.03; N, 7.55%. Calcd for $C_8H_9NO_2S$: C, 52.46; H, 4.95; N, 7.65%.

References

1) I. G. Ross, *J. Chem. Soc.*, **1951**, 1374.
2) R. A. Jones and A. R. Katritzky, *J. Chem. Soc.*, **1958**, 3610.
3) A. Albert and G. B. Barlin, *J. Chem. Soc.*, **1959**, 2384.
4) R. F. Banks, R. N. Haszeldine, D. R. Karsa, F. E. Rickett, and M. Young, *J. Chem. Soc., C*, **1969**, 1660.
5) E. Ager, B. Iddon, and H. Suschitzky, *Tetrahedron Lett.*, **1969**, 1507.
6) B. Iddon, H. Suschitzky, and A. W. Thompson, *J. Chem. Soc., Perkin Trans. 1*, **1974**, 2307.
7) H. Besso, K. Imafuku, and H. Matsumura, *Bull. Chem. Soc. Jpn.*, **50**, 710 (1977).
8) S. F. Mason, *J. Chem. Soc.*, **1958**, 674.
9) J. Clark and D. D. Perrin, *Quart. Revs.*, **18**, 295 (1964).
10) H. H. Jaffe, *Chem. Revs.*, **53**, 191 (1953).
11) O. Exner, *Collect. Czech. Chem. Commun.*, **31**, 65 (1966).
12) A. Albert and E. P. Serjeant, "Ionization Constants of Acids and Bases," 1st ed, Methuen & Co., Ltd., London (1962), Chap. 4.

A New Synthesis of Flavones by the Reaction of 2-Phenyl-2*H*-1-benzopyrans with Potassium Permanganate

Yoshihiro ASHIHARA, Yasuyuki NAGATA,* and Kazu KUROSAWA

Department of Chemistry, Faculty of Science, Kumamoto University, Kurokami, Kumamoto 860

(Received April 11, 1977)

The oxidation of ten 2-phenyl-2*H*-1-benzopyrans with potassium permanganate in acetone has been found to give the corresponding flavones in 8—73% yields. The reaction mechanism is discussed on the basis of the substituent effect and the oxidations of related compounds.

Flavones can be synthesized from 2'-hydroxychalcones[1] or from flavanones[2] or they can be synthesized from *o*-benzoyloxyacetophenones by the Baker-Venkataraman rearrangement followed by cyclization[3] or from *o*-hydroxyacetophenones and aromatic acids by the Allan-Robinson condensation.[4] We have investigated the possibility of transforming 2-phenyl-2*H*-1-benzopyrans into flavones; this could be accomplished by the oxidation of the former with potassium permanganate. The procedure is very simple and can be utilized as an easy preparation method for flavones when 2-phenyl-2*H*-1-benzopyrans are readily available.

The 2-phenyl-2*H*-1-benzopyrans (IIa—IIj) were prepared from the corresponding 2'-hydroxychalcones (Ia—Ij) by sodium borohydride reduction, followed by treatment with aqueous acetic acid. The structures of the new 2-phenyl-2*H*-1-benzopyrans were confirmed by examining their NMR spectra and by elemental analyses.

When the 2-phenyl-2*H*-1-benzopyrans (IIa—IIj) were oxidized with potassium permanganate in a molar ratio of 1 : 4 in acetone, flavones (IIIa—IIIj) were obtained in 8—73% yields; they were identified by comparing their melting points with those reported and by examining their NMR spectra. When the reaction was carried out with potassium permanganate as an oxidizing reagent in a molar ratio less than 1 : 4 (Table 1, entries 5 and 12) or more than 1 : 4 (entries 9 and 24), it gave a rather poor yield because of the presence of some unchanged II or of tarry products. The change in the reaction time did not alter the yield significantly (entries 6, 7, and 8). However, 2-phenyl-2*H*-1-benzopyran (IIa) and 7-methoxy-2-phenyl-2*H*-1-benzopyran (IIb) had longer reaction times, 16 h (entry 2) and 12 h (entry 4), respectively, and the yields after 4 h were much lower (entries 1 and 3). It is thus considered that the 4'-methoxyl group and two methoxyl groups in the ring A may accelerate the reaction rate. The yield of 2',3',4',7-tetramethoxyflavone (IIIe) is extremely low (entry 16). This may indicate that the 2'-methoxyl group has a steric hindrance towards potassium permanganate which attacks the hydrogen at C(2)-position. There were many unidentified products in this case. When the reaction was conducted in pyridine in place of acetone, the yields and the reaction times were not affected (entries 14 and 21). The reaction in acetic acid, on the other hand, gave the lowest figure (entry 22). The change of the oxidizing reagent from potassium permanganate to chromium trioxide-pyridine complex[5] caused a decrease in the yield of III (entry 11).

In order to explain the above observations, we assumed three probable reaction mechanisms. The reaction may proceed through a cyclic intermediate (V) which is known to be involved in the reaction of olefins with potassium permanganate to give α-diols or α-ketols[6] (pathway a). The reaction could be of an ionic nature and proceed *via* flavylium cation (VI) (pathway b). Or the reaction may proceed *via* radical intermediate (VII) (pathway c).

Pathway a is not attractive since it fails to explain the facts that the reaction rate was enhanced by the 4'-methoxyl group and that the steric hindrance was exercised by the 2'-methoxyl group which is located far from the ethylenic double bond in IIe. Pathway a is completely excluded for the case when 7-methoxy-2-(*p*-methoxyphenyl)-4*H*-1-benzopyran (IV) was readily oxidized to give IIId in a yield comparable to that obtained in the oxidation of IId. Isomerization of IId to IV is not likely to occur in the reaction conditions, as IId was stable in 0.75% potassium hydroxide-moist acetone-d_6 even after 24 h, as observed by NMR spectra. The fact that the reaction time of IV (2.5 h) was shorter than that of IId (4 h) also argues against the pathway IV→IId→V (R=CH_3O–, Ar=*p*-CH_3O-C_6H_4–)→IIId.

Pathway b seemed to be consistent with all our observations. The electron-donating group, such as the methoxyl group in the rings A and B, would make the hydrogen at C(2)-position easier to be removed by an oxidant, and the methoxyl group at C(2')-position would hinder the approach of the oxidant by steric reasons. The fact that the oxidation of IV also yielded IIId may indicate that 4',7-dimethoxyflavylium ion (VI; R=CH_3O–, Ar=*p*-CH_3O-C_6H_4–) could be an intermediate. However, when we examined the oxidation of VI (R=CH_3O–, Ar=*p*-CH_3O-C_6H_4–) under similar conditions, it gave a complex mixture of products in which IIId was not found. This suggests that pathway b should also be eliminated.

Pathway c will account for the substituent effects due to the methoxyl groups in rings A and B, and for the identical results of the oxidations of 2-phenyl-2*H*-1-benzopyrans (II) and 2-phenyl-4*H*-1-benzopyran. When the reaction was carried out in the presence of 2,6-di-*t*-butylphenol (entry 15) in the hope of trapping the radical intermediate (VII), whose presence has been successfully demonstrated in the reaction of 2'-hydroxychalcone with lead tetraacetate using 3,5-dimethoxy-

* Present address: Wakunaga Pharmaceutical Co., Ltd., 1624, Shimokotatsu, Koda-gun, Hiroshima 729-64.

TABLE 1. THE REACTIONS OF 2-PHENYL-2*H*-1-BENZOPYRANS(II) AND 7-METHOXY-2-(*p*-METHOXYPHENYL)-4*H*-1-BENZOPYRAN(IV)

Entry	Substrate	Reaction conditions				Flavone (yield, %)
		Oxidant	Molar ratio	Time(h)	Solvnt	
1	IIa[12]	$KMnO_4$	1 : 4	4	acetone	IIIa[15] (27)
2	IIa	$KMnO_4$	1 : 4	16	acetone	IIIa (44)
3	IIb	$KMnO_4$	1 : 4	4	acetone	IIIb[16] (31)
4	IIb	$KMnO_4$	1 : 4	12	acetone	IIIb (50)
5	IIc[10]	$KMnO_4$	1 : 3	4	acetone	IIIc[17] (53)
6	IIc	$KMnO_4$	1 : 4	4	acetone	IIIc (59)
7	IIc	$KMnO_4$	1 : 4	5	acetone	IIIc (60)
8	IIc	$KMnO_4$	1 : 4	8	acetone	IIIc (60)
9	IIc	$KMnO_4$	1 : 4.5	5	acetone	IIIc (29)
10	IIc	$KMnO_4$[a]	1 : 4	4	acetone	IIIc (55)
11	IIc	CrO_3py_2	1 : 8	24	CH_2Cl_2	IIIc (34)
12	IId[10]	$KMnO_4$	1 : 3	4	acetone	IIId[18] (48)
13	IId	$KMnO_4$	1 : 4	4	acetone	IIId (72)
14	IId	$KMnO_4$	1 : 4	4	pyridine	IIId (73)
15	IId b)	$KMnO_4$	1 : 6	2	acetone	IIId (34)
16	IIe	$KMnO_4$	1 : 4	2	acetone	IIIe (8)
17	IIf	$KMnO_4$	1 : 4	2	acetone	IIIf[18] (58)
18	IIg[8]	$KMnO_4$	1 : 4	4	acetone	IIIg[19] (42)
19	IIh	$KMnO_4$	1 : 4	4	acetone	IIIh[20] (39)
20	IIi[13]	$KMnO_4$	1 : 4	4	acetone	IIIi[21] (64)
21	IIi	$KMnO_4$	1 : 4	4	pyridine	IIIi (51)
22	IIi	$KMnO_4$	1 : 4	4	CH_3COOH	IIIi (5)
23	IIj[8]	$KMnO_4$	1 : 4	4	acetone	IIIj[21] (68)
24	IIj	$KMnO_4$	1 : 5	2.5	acetone	IIIj (49)
25	IV[14]	$KMnO_4$	1 : 3	2.5	acetone	IIId (74)
26	IV	$KMnO_4$	1 : 4	2.5	acetone	IIId (33)
27	IV	CrO_3py_2	1 : 8	24	CH_2Cl_2	IIId (14)

a) The reaction was carried out under nitrogen atmosphere. b) The reaction was carried out in the presence of 2,6-di-*t*-butylphenol (2 mmol).

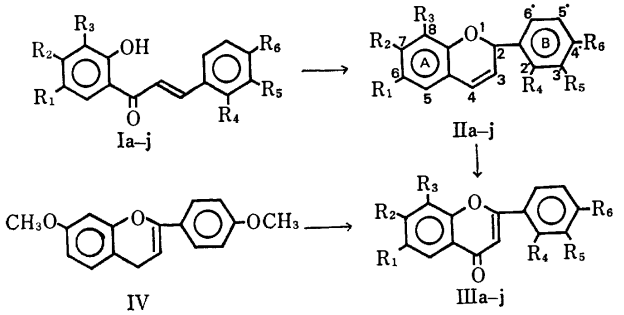

a $R_1=R_2=R_3=R_4=R_5=R_6=H$
b $R_1=R_3=R_4=R_5=R_6=H$, $R_2=OCH_3$
c $R_1=R_2=R_3=R_4=R_5=H$, $R_6=OCH_3$
d $R_1=R_3=R_4=R_5=H$, $R_2=R_6=OCH_3$
e $R_1=R_3=H$, $R_2=R_4=R_5=R_6=OCH_3$
f $R_3=R_4=R_5=R_6=H$, $R_1=R_2=OCH_3$
g $R_3=R_4=R_5=H$, $R_1=R_2=R_6=OCH_3$
h $R_1=R_4=R_5=R_6=H$, $R_2=R_3=OCH_3$
i $R_1=R_4=R_5=H$, $R_2=R_3=R_6=OCH_3$
j $R_1=R_4=H$, $R_2=R_3=R_5=R_6=OCH_3$

Scheme 1.

phenol,[7] it caused a decrease in the yield but no adduct was obtained. The reaction, carried out under nitrogen atmosphere, gave a flavone in a similar yield as well as in the same reaction time (entry 10).

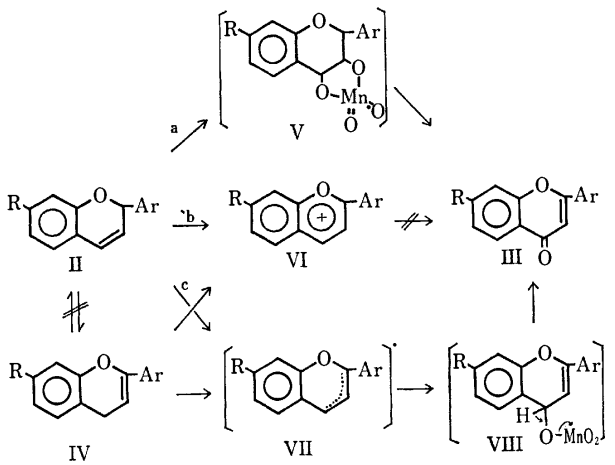

Scheme 2. The possible reaction pathways of the oxidations of 2-phenyl-2*H*-1-benzopyrans and 2-phenyl-4*H*-1-benzopyran.

Nevertheless, it is likely that the oxidation of II and IV may proceed through the hydrogen abstraction at the C(2)-position in the case of II and at the C(4)-position in the case of IV giving the identical radical (VII), and that the attack of the permanganate ion to VII at the C(4)-position gave VIII and the elimination of reduced manganese species in VIII would give III.

The oxidations of the 2-phenyl-2*H*-1-benzopyrans are also interesting in connection with their biogenetic transformations into 3-flavanols,[8,9] 4-flavanols,[10,11] 3,4-flavandiols,[9,10] and 3,4-epoxyflavans.[9]

Experimental

All ^{1}H NMR spectra were recorded with a Hitachi R 24 NMR spectrometer with TMS as an internal standard, while the IR spectrum was recorded with a JASCO IRA-1 grating spectrometer. Melting points were determined on a Yanagimoto micro hot-stage and were uncorrected.

*Preparations of 2-Phenyl-2*H*-1-benzopyrans (IIb, IIe, IIf, and IIh).* A mixture of 2'-hydroxychalcone (6 mmol), sodium borohydride (12 mmol), and ethanol (100 ml) was stirred for 3 h at room temperature. After the removal of the ethanol, the resulting solid was treated with 10% aqueous acetic acid (100 ml) and then extracted with benzene. The benzene solution was separated and evaporated under reduced pressure. The resulting liquid was purified on a silica gel column (Wakogel C 100, 100 g) by eluting with benzene and by recrystallization or by distillation.

*7-Methoxy-2-phenyl-2*H*-1-benzopyran (IIb)*: $Bp_{0.02}$ 180 °C (bath temp), 35% yield, NMR (CCl_4) δ=3.66 (3H, s, OCH_3), 5.57 (1H, dd, J=9.6, 3.6 Hz, $H_{(3)}$), 5.83 (1H, dd, J=3.6, 1.6 Hz, $H_{(2)}$), 6.3—6.6 (3H, m), 6.85 (1H, m, $H_{(5)}$), and 7.1—7.6 (5H, m, Ph). Found: C, 80.37; H, 5.81%. Calcd for $C_{16}H_{14}O_2$: C, 80.64; H, 5.92%.

*7-Methoxy-2-(2,3,4-trimethoxyphenyl)-2*H*-1-benzopyran (IIe)*: $Bp_{0.02}$ 200 °C (bath temp), 41% yield, NMR (CCl_4) δ= 3.65 (3H, s, OCH_3), 3.75 (3H, s, OCH_3), 3.75 (3H, s, OCH_3), 3.92 (3H, s, OCH_3), 5.48 (1H, dd, J=9.0, 3.3 Hz, $H_{(3)}$), 6.10 (1H, dd, J=3.3, 1.7 Hz, $H_{(2)}$), 6.22—6.5 (3H, m), 6.40 (1H, d, J=10.0 Hz, $H_{(5')}$), 6.78 (1H, m, $H_{(5)}$), and 7.02 (1H, d, J=10.0 Hz, $H_{(6')}$). Found: C, 69.35; H, 6.17%. Calcd for $C_{19}H_{20}O_5$: C, 69.50; H, 6.14%.

*6,7-Dimethoxy-2-phenyl-2*H*-1-benzopyran (IIf)*: Mp 79—80 °C (light petroleum), 67% yield, NMR (CCl_4) δ=3.62 (6H, s, 2×OCH_3), 5.47 (1H, dd, J=10.0, 3.5 Hz, $H_{(3)}$), 5.67 (1H, dd, J=3.5, 1.8 Hz, $H_{(2)}$), 6.30, (1H, dd, J=10.0, 1.8 Hz, $H_{(4)}$), 6.21 (1H, s, $H_{(8)}$), 6.37 (1H, s, $H_{(5)}$), and 7.20 (5H, m, Ph). Found: C, 75.95; H, 6.09%. Calcd for $C_{17}H_{16}O_3$: C, 76.10; H, 6.01%.

*7,8-Dimethoxy-2-phenyl-2*H*-1-benzopyran (IIh)*: Mp 60—61 °C (MeOH), 53% yield, NMR (CCl_4) δ=3.63 (3H, s, OCH_3), 3.77 (3H, s, OCH_3), 5.64 (1H, dd, J=9.7, 3.5 Hz, $H_{(3)}$), 5.81 (1H, dd, J=3.5, 1.8 Hz, $H_{(2)}$), 6.28 (1H, d, $H_{(6)}$), and 6.56 (1H, d, $H_{(5)}$) (AB system, J_{AB}=8.0 Hz), 6.40 (1H, $H_{(4)}$, coincided with a part of the AB system), and 7.2—7.5 (5H, m, Ph). Found: C, 75.93; H, 6.01%. Calcd for $C_{17}H_{16}O_3$: C, 76.10; H, 6.01%.

4',7-Dimethoxyflavylium Perchlorate (VI). Through a mixture of *p*-methoxyacetophenone (2.0 g), 2-hydroxy-4-methoxybenzaldehyde (2.5 g), and 85% formic acid (30 ml) was passed dry hydrogen chloride for 2.5 h at room temperature. 20% perchloric acid (27 ml) was added to the cooled reaction mixture, which was then left overnight. The precipitates were collected by filtration, giving a dark red powder, mp 265 °C (lit,[14] mp 270 °C) (3.05 g, 61%).

*7-Methoxy-2-(*p*-methoxyphenyl)-4*H*-1-benzopyran (IV).* 4',7-Dimethoxyflavylium perchlorate (1.83 g) in ethanol (50 ml) was reduced with sodium borohydride (51 mg) at 0 °C for 1 h. After the removal of the ethanol, the resulting solid was washed with ether. The ether was evaporated and the resulting substance was recrystallized to give colorless prisms, mp 137—139 °C (EtOH) (0.46 g, 35%).

*Oxidation of 2-Phenyl-2*H*-1-benzopyrans (IIa—IIj) with Potassium Permanganate.* A mixture of a 2-phenyl-2*H*-1-benzopyran (1 mmol), potassium permanganate (3—5 mmol), and a solvent (50 ml) was stirred at room temperature until all of II was consumed (the period of time is shown in the Table). The solvent was evaporated, and the resulting mixture was treated with 5% aqueous sodium hydrogen sulfite (20 ml) and acidified with concd sulfuric acid. The precipitates were collected and purified on a silica gel column by eluting with chloroform and by recrystallization to give II. In the case of IIe, the reaction mixture was filtered and the manganese dioxide was washed with chloroform. The combined filtrate was then evaporated, and the product was purified on TLC and by recrystallization. IIIa, mp 97 °C (MeOH) (lit,[15] mp 97 °C); IIIb, mp 107—108 °C (MeOH) (lit,[16] mp 110—111 °C); IIIc, mp 155—156 °C (MeOH) (lit,[17] mp 157—158 °C); IIId, mp 146—147 °C (MeOH) (lit,[18] mp 143—144 °C); IIIe. mp 164—165 °C (MeOH), IR ($CHCl_3$) 1635 cm^{-1} (C=O), NMR ($CDCl_3$) δ=3.87 (6H, s, 2×OCH_3), 3.88 (3H, s, OCH_3), 3.90 (3H, s, OCH_3), 6.78 (1H, d, J=8.1 Hz, $H_{(5')}$), 6.90 (1H, s, $H_{(3)}$), 6.85—7.05 (2H, m, $H_{(6)}$ and $H_{(8)}$), 7.49 (1H, d, J=8.1 Hz, $H_{(6')}$), and 8.09 (1H, m, $H_{(5)}$) [Found: C, 66.43; H, 5.36%. Calcd for $C_{19}H_{18}O_6$: C, 66.66; H, 5.30%.]; IIIf, mp 189—190 °C (MeOH) (lit,[18] mp 189 °C); IIIg, mp 181—182 °C (MeOH) (lit,[19] mp 184—185 °C); IIIh, mp 147—148 °C (MeOH) (lit,[20] mp 151 °C); IIIi, mp 192—194 °C (MeOH) (lit,[21] mp 189—190 °C); IIIj, mp 203—204 °C (MeOH) (lit,[21] mp 200 °C).

*Oxidation of 7-Methoxy-2-(*p*-methoxyphenyl)-4*H*-1-benzopyran (IV) with Potassium Permanganate.* The reaction was carried out in a manner similar to the above, giving IIId, mp 146—147 °C.

*Oxidation of 2-(*p*-Methoxyphenyl)-2*H*-1-benzopyran (IIc) with Chromium Trioxide–Pyridine Complex.* A mixture of IIc (1 mmol), chromium trioxide–pyridine complex[5] (8 mmol), and dichloromethane (30 ml) was stirred at room temperature under nitrogen atmosphere for 24 h. 5% aqueous sodium hydrogen sulfite (20 ml) and concd sulfuric acid (1 ml) were added to the reaction mixture, which was extracted with chloroform. The organic layer was separated, dried, and evaporated to dryness. The resulting solid was purified in a manner similar to the above, giving IIIc, mp 155—156 °C.

*Oxidation of 7-Methoxy-2-(*p*-methoxyphenyl)-4*H*-1-benzopyran (IV) with Chromium Trioxide–Pyridine Complex.* IV was oxidized with the reagent to give IIId, mp 146—147 °C.

References

1) H. S. Mahal and K. Venkataraman, *J. Chem. Soc.*, **1936**, 569.
2) A. Löwenbein, *Ber.*, **57**, 1515 (1924).
3) W. Baker, *J. Chem. Soc.*, **1933**, 1381.
4) J. Allan and R. Robinson, *J. Chem. Soc.*, **125**, 2192 (1924).
5) W. G. Dauben, M. Lorber, and D. S. Fullerton, *J. Org. Chem.*, **34**, 3587 (1969).
6) R. Stewart, "Oxidation in Organic Chemistry," Part A, ed by K. S. Wiberg, Academic Press, New York and London (1965), p. 1.
7) D. Ferreira, E. V. Brandt, F. du R. Volsteedt, and D. G. Roux, *J. Chem. Soc., Perkin Trans. 1*, **1975**, 1437.
8) J. W. Clark-Lewis and E. J. McGarry, *Aust. J. Chem.*, **26**, 809 (1973).
9) J. W. Clark-Lewis, E. J. McGarry, and A. H. Ilsley, *Aust. J. Chem.*, **27**, 865 (1974).
10) J. W. Clark-Lewis and E. J. McGarry, *Aust. J. Chem.*,

26, 2447 (1973).
11) J. W. Clark-Lewis and M. I. Baig, *Aust. J. Chem.*, **24**, 2581 (1971).
12) T. Hase, *Acta Chem. Scand.*, **22**, 2845 (1967).
13) J. W. Clark-Lewis, R. W. Jemison, D. C. Single, and L. R. Williams, *Chem. Ind. (London)*, **1967**, 1455.
14) L. Jurd, *Chem. Ind. (London)*, **1966**, 1683.
15) Beilsteins "Handbuch der Organischen Chemie," XVII, p. 373.
16) Beilsteins "Handbuch der Organischen Chemie," XVIII, p. 59.
17) Beilsteins "Handbuch der Organischen Chemie," XVIII, II p. 39.
18) Beilsteins "Handbuch der Organischen Chemie," XVIII, I p. 361.
19) Beilsteins "Handbuch der Organischen Chemie," XVIII, II p. 174.
20) Beilsteins "Handbuch der Organischen Chemie," XVIII, p. 126.
21) I. C. Badhwar, K. S. Kang, and K. Venkataraman, *J. Chem. Soc.*, **1932**, 1107.

The Reaction of *N*-Imidoylsulfimides with Carbon Disulfide

Hiroshi YOSHIDA, Tsuyoshi OGATA, and Saburo INOKAWA

Department of Synthetic Chemistry, Faculty of Engineering, Shizuoka University, Johoku, Hamamatsu 432

(Received April 15, 1977)

The reaction of *S,S*-diphenyl- and *S,S*-dimethyl-*N*-imidoylsulfimides (**1** and **2**) with carbon disulfide was studied. **1** yielded nitrile, isothiocyanate, diphenyl sulfide, and sulfur, whereas **2** gave *N*-thiocarbonyl-*S,S*-dimethylsulfimide together with isothiocyanate. Kinetic studies indicate that the reaction proceeds *via* a [2+2]cycloaddition mechnism, as is shown by the small effects of the solvents and the substitutent on the rate.

A number of recent works[1] on sulfimides have shown their importance in organic synthesis. Some interesting reactions of *N*-imidoyl-[2] and *N*-thiocarbonylsulfimides[3] have also been reported.

In continuation of our previous studies to explore the physical and chemical properties of *P*- and *S*-ylides and imides,[3] we have found an interesting reaction of the *S,S*-diphenyl- and *S,S*-dimethyl-*N*-imidoylsulfimides **1** and **2** with carbon disulfide.

Results and Discussion

Preparation. The *N*-imidoylsulfimides, **1a**—**c** and **2a**—**f** (Table 1), were prepared by the reaction of benzimidoyl chlorides with free *S,S*-diphenylsulfimide $Ph_2S{=}NH$ or *N*-haloamidines with dimethyl sulfide,

1 **2**

modifying the reported methods.[2a] The *N*-[(methythio)carbonimidoyl]sulfimides, **1d** and **e** were prepared by the reaction of the *N*-thiocarbamoylsulfimides, **3d** and **e** with methyl iodide, followed by treatment with a base.

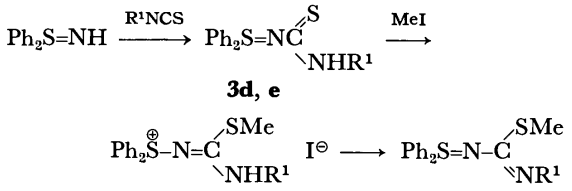

3d, e **4d, e** **1d, e**

d: R^1=Ph **e**: R^1=Me

The physical properties of **1** and **2** are collected in Table 1.

The Reaction of 1 and 2 with Carbon Disulfide. The **1b**, **2b**, and **c** sulfimides were shown to be stable up to 150 °C.[2a] On the other hand, the **1** and **2** sulfimides showed high reactivities with carbon disulfide even at room temperature. The products in the reaction of *S,S*-diphenylsulfimides **1a**—**e** with carbon disulfide were confirmed to be isothiocyanates, nitriles, diphenyl sulfide, and sulfur by comparing their IR and GLC with those of authentic samples.

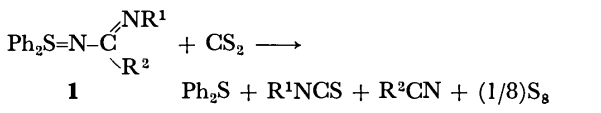

1 $Ph_2S + R^1NCS + R^2CN + (1/8)S_8$

Table 2. Products of the reaction of **1** or **2** with carbon disulfide

	Condition[a] (Time, day)	Products (%)
1a	1	R^1NCS(92), R^2CN(90), Ph_2S(96), S_8
1b	1	R^1NCS(90), R^2CN(93), Ph_2S(95), S_8
1c	1	R^1NCS(94), R^2CN(92), Ph_2S(96), S_8
1d	2	R^1NCS(87), R^2CN(81), Ph_2S(96), S_8
1e	1	R^1NCS(80), R^2CN(82), Ph_2S(97), S_8
2a	2	**5a**(93), R^1NCS
2b	2	**5a**(96), R^1NCS
2c	2	**5a**(91), R^1NCS
2d	2	**5d**(94), R^1NCS
2e	2	**5e**(91), R^1NCS
2f	2	**5f**(93), R^1NCS

a) **1** or **2** (1 mmol) with carbon disulfide(10 mmol) in chloroform (20 ml) at room temperature.

Table 1. Preparation and physical properties of **1** and **2**

	R^1	R^2	Yield(%)	Mp(°C)	NMR(δ in $CDCl_3$)[a]	Found(Calcd) (%) C	H	N
1a	*p*-Tol	Ph	76	140—141	2.113($CH_3C_6H_4$)	79.38(79.15)	5.73(5.62)	7.02(7.10)
1b	Ph	Ph	59	142—143[b]		78.76(78.91)	5.09(5.30)	7.44(7.36)
1c	Ph	*p*-Tol	73	150—151	2.25($CH_3C_6H_4$)	79.03(79.15)	5.44(5.62)	7.36(7.10)
1d	Ph	SMe	89	119—120	2.64(SMe)	68.23(68.54)	5.30(5.18)	7.75(7.99)
1e	Me	SMe	93	82—83	2.61(SMe), 2.96(NMe)	62.09(62.46)	5.37(5.59)	9.88(9.71)
2a	*p*-Tol	Ph	43	180—182	2.17($CH_3C_6H_4$), 2.73(Me_2S)	71.24(71.07)	6.52(6.71)	10.11(10.36)
2b	Ph	Ph	41	167—169[c]	2.70(Me_2S)	70.05(70.28)	6.41(6.29)	10.80(10.93)
2c	*p*-ClC_6H_4	Ph	36	185—187[d]	2.71(Me_2S)	61.83(61.95)	5.03(5.20)	9.76(9.63)
2d	Ph	*p*-Tol	48	155—156	2.16($CH_3C_6H_4$), 2.65(Me_2S)	70.91(71.07)	6.53(6.71)	10.15(10.36)
2e	Ph	*p*-ClC_6H_4	31	162—164	2.67(Me_2S)	61.77(61.95)	5.06(5.20)	9.52(9.63)
2f	Ph	*m*-Tol	47	169—171	2.20($CH_3C_6H_4$), 2.69(Me_2S)	71.20(71.07)	6.53(6.71)	10.15(10.36)

a) The phenyl-ring protons appeared at 6.5—8 as multiplets. b) Lit,[2a] mp 141—143 °C. c) Lit,[2a] mp 167—169 °C. d) Lit,[2a] mp180—182 °C.

Table 3. Physical properties of **5**

5	R^2	Mp(°C)	M^+	NMR(δ in $CDCl_3$)[a]	Found (Calcd)(%) C	H	N
5a	Ph	106—107	197	2.89($\underline{Me}_2S$)	54.53(54.78)	5.69(5.62)	6.93(7.10)
5d	*p*-Tol	107—108	211	2.36($C\underline{H}_3C_6H_4$), 2.93(Me_2S)	56.67(56.83)	6.32(6.20)	6.53(6.62)
5e	*p*-ClC_6H_4	156—158	231	2.82($\underline{Me}_2S$)	46.71(46.64)	4.51(4.35)	6.17(6.04)
5f	*m*-Tol	95—96	211	2.34($C\underline{H}_3C_6H_4$), 2.83(Me_2S)	56.58(56.83)	6.12(6.20)	6.48(6.62)

a) The phenyl-ring protons appeared at δ 7—8 as multiplets.

S,S-Dimethylsulfimides **2a—f** also reacted easily with carbon disulfide at room temperature yielding the *N*-thiocarbonyl-*S,S*-dimethylsulfimides together with the isothiocyanates.

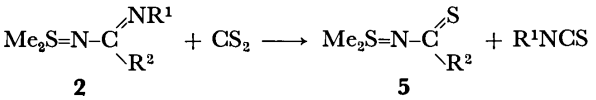

2 **5**

The structure of **5** was confirmed on the basis of their NMR, MS, and elemental analyses. These results are shown in Tables 2 and 3.

In a previous paper[3] we have shown that the thermal decomposition of *N*-thiocarbonyl-*S,S*-diphenylsulfimides **6**, proceeds *via*

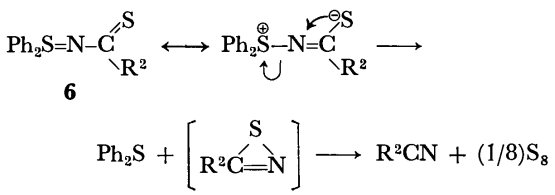

the nucleophilic attack of thiocarbonyl sulfur at the nitrogen atom, yielding thiazirine and diphenyl sulfide. On the other hand, **5** were stable under heating at 50 °C for a long time. We believe **6** to be the initial products of the reaction of **1** with carbon disulfide. The marked difference in thermal stability between **5** and **6** may be attributed to the electron-attracting power of the groups on the sulfide sulfur. The phenyl groups of **6** may facilitate the nucleophilic attack of the thiocarbonyl sulfur on the nitrogen in the transition state.

Table 4. Second-order rate constants(k_2) for the reaction of **1** or **2** with carbon disulfide

	Temp(°C)	Solvent	$k_2\times10^5$ l/mol s	E_a Cal/mol	ΔS e.u.
1a	50	$CDCl_3$	4.52		
	50	PhCN	44.5		
2a	45	$CDCl_3$	2.36		
	50	$CDCl_3$	3.48	15.0	−32.9
	55	$CDCl_3$	4.81		
	45	$PhNO_2$	37.3		
	50	$PhNO_2$	55.8	12.2	−36.2
	55	$PhNO_2$	75.1		
	50	CH_2Cl_2	9.03		
	50	PhCN	34.2		
2b	50	$CDCl_3$	2.18		
	50	$PhNO_2$	36.3		
2c	50	$CDCl_3$	1.21		
	50	$PhNO_2$	23.2		
2d	50	$CDCl_3$	2.73		
	50	$PhNO_2$	40.3		
2e	50	$CDCl_3$	1.34		
	50	$PhNO_2$	22.2		
2f	50	$CDCl_3$	2.47		
	50	$PhNO_2$	38.7		

Table 5. Hammett's constants for the reaction of **2** with carbon disulfide at 50°C

Solvent	$CDCl_3$	$PhNO_2$
ρ_{R^1}, R^2=Ph	−1.15	−0.94
ρ_{R^2}, R^1=Ph	−0.86	−0.80

The *N*-imidoylsulfimides **1** and **2** reacted easily with carbon disulfide under mild conditions. Meanwhile, the action of hydrogen sulfide on amidines represents a useful route to thioamides.[4] In an old article,[5] it was reported that *N,N'*-diphenylbenzamidine reacts with carbon disulfide under drastic conditions (130—140 °C) to yield thiobenzanilide and phenyl isothiocyanate. We have performed kinetic experiments in order to find a reasonable mechanism for the reaction of **1** and **2** with carbon disulfide. The reaction gave good second-order rate constants (k_2), which were first-order with **1** or **2** and carbon disulfide respectively, when the reaction was followed by NMR spectroscopy. The results are listed in Tables 4 and 5, which indicate small effects of solvents and substituents on rate and negative entropies for the reaction. These observations indicate that the mechanism for the formation of 1,3-thiazetidine-2-thione *via* a rate-determining electrophilic attack on iminonitrogen, followed by ring closure (Routes a' and b), can be ruled out. The reaction of **1** or **2** with carbon disulfide seems to be a typical [2+2]cycloaddition reaction.[6] The mechanism we suggest is shown is Scheme 1, which involves the initial formation of 1,3-

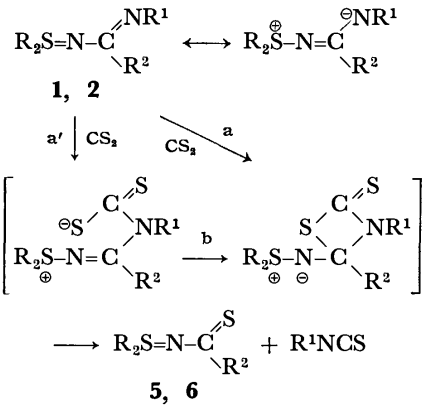

Scheme 1.

thiazetidine-2-thione *via* cycloaddition (Route a), followed by a rapid ring cleavage to yield **5** or **6** and isothiocyanate.

Experimental

Preparation of ***1a—c.*** Free *S,S*-diphenylsulfimide was prepared according to the literature.[7] The general procedure for the preparation of **1a—c** is as follows: to a solution of *S,S*-diphenylsulfimide (2.01 g, 0.01 mol) in 50 ml of dry benzene we added a solution of imidoyl chloride (5 mmol) in 10 ml of dry benzene in one portion. After 30 min the liquid layer was condensed *in vacuo* to give a crystalline mass, which afforded needles, **1a—c**, from chloroform–hexane. The results are shown in Table 1.

Preparation of ***1d and 1e.*** *N*-Thiocarbamoyl-*S,S*-diphenylsulfimides, **3d**, and **e** were prepared according to the literature.[3,8] To a solution of **3d** (0.01 mol) in chloroform we added methyl iodide (0.02 mol) in one portion. The resulting solution was kept standing at room temperature for 12 h. Then the solution was dried *in vacuo* to give a crystalline mass. We then added a solution of sodium ethoxide in ethanol [from sodium (0.015 mol) and ethanol (30 ml)] to the mass, portion by portion, under vigorous stirring. The mixture was stirred for 5 min and then poured into 100 ml of ice water. The product was extracted with chloroform, and crystallized from chloroform–hexane.

1e was prepared similarly; the results are shown in Table 1.

Preparation of ***2a—f.*** **2** were prepared according to the literature.[9] The yields (based on amidines used) and physical properties are shown in Table 1.

The Reaction of ***1a—e*** *with Carbon Disulfide.* A solution of **1a—e** (1 mmol) and carbon disulfide (10 mmol) in 20 ml of chloroform was kept standing for a day at room temperature. After the reaction, the mixture was dried *in vacuo* and separated into petroleum ether-soluble and insoluble parts. The former part was analyzed by GLC (silicone grease on celite) and found to be a mixture of diphenyl sulfide, isothiocyanate, and nitrile. The petroleum ether-insoluble part was sulfur. The results are shown in Table 2.

The Reaction of ***2a—f*** *with Carbon Disulfide.* A solution of **2a—f** (1 mmol) and carbon disulfide (10 mmol) in 20 ml of chloroform was kept standing at room temperature for 2 days. After drying the solvent *in vacuo*, the residue was separated into petroleum ether-soluble and insoluble parts. The former part was isothiocyanate, which was confirmed by comparing their IR and GLC with those of the known sample. The latter part was *N*-thiocarbonyl-*S,S*-dimethylsulfimide, **5**. The results are collected in Tables 2 and 3.

Kinetic Studies. A solution of **1** or **2** (0.05—0.3 mol/l) and carbon disulfide (0.4—0.8 mol/l) in chloroform-*d* (or other solvents) was sealed in an NMR sample tube; the rate was followed at suitable time intervals by analyzing the NMR signals of the methyl groups of **1a** or **2** and the products. The results are shown in Tables 4 and 5.

References

1) For example, Y. Tamura, H. Matsushima, M. Ikeda, and K. Sumoto, *Tetrahedron*, **32**, 431 (1976).

2) a) T. L. Gilchrist, C. J. Moody, and C. W. Rees, *J. Chem. Soc., Perkin Trans. 1*, **1975**, 1964; b) T. L. Gilchrist, C. J. Moody, and C. W. Rees, *ibid.*, **1975**, 1969; c) T. L. Gilchrist, C. J. Moody, and C. W. Rees, *J. Chem. Soc., Chem. Commun.*, **1976**, 414.

3) H. Yoshida, H. Taketani, T. Ogata, and S. Inokawa, *Bull. Chem. Soc. Jpn.*, **49**, 3124 (1976).

4) W. Walter and J. Voss, "The Chemistry of Amides," ed by J. Zabicky, Interscience Publishers, London (1970), p. 383.

5) A. Bernthsen, *Justus Liebigs Ann. Chem.*, **192**, 1 (1878).

6) For example, R. C. Kerber, T. J. Ryan, and S. D. Hsu, *J. Org. Chem.*, **39**, 1215 (1974).

7) N. Furukawa, T. Omata, T. Yoshimura, T. Aida, and S. Oae, *Tetrahedron Lett.*, **1972**, 1619.

8) N. Furukawa, T. Yoshimura, T. Omata, and S. Oae, *Chem. Ind. (London)*, **1974**, 702.

9) T. Fuchigami and K. Odo, *Chem. Lett.*, **1974**, 247.

Aminosugars. XXVIII. A Facile Synthesis of Benzyl α- and β-Kasugaminides *via* the Corresponding Abequosides[1]

Juji YOSHIMURA, Ken-ichi SATO, Hironobu HASHIMOTO, and Kuniaki SHIMIZU

Laboratory of Chemistry for Natural Products, Faculty of Science, Tokyo Institute of Technology, Meguro-ku, Tokyo 152

(Received April 19, 1977)

Synthesis of benzyl α- and β-kasugaminides (benzyl 2,4-diamino-2,3,4,6-tetradeoxy-α- and β-D-*arabino*-hexopyranosides) was carried out by the simultaneous substitution at 2,4-positions of 2,4-di-*O*-mesyl-abequosides (3,6-dideoxy-2,4-di-*O*-mesyl-α- and β-D-*xylo*-hexopyranosides) with sodium azide followed by hydrogenation. The substitution in *N,N*-dimethylformamide at higher temperature gave the elimination products (4-azido-2,3-unsaturated derivatives) and the subsequently rearranged products (3,4-unsaturated 2-azido derivatives), but, that in hexamethylphosphoric triamide at lower temperature gave the desired compounds in fairly good yields.

In connection with synthetic studies on kasugamycin[2,3] a few reports on the synthesis of racemic[4,5] and optically active[6] methyl α-kasugaminide (methyl 2,4-diamino-2,3,4,6-tetradeoxy-α-D-*arabino*-hexopyranoside) have been published. The necessity of the resolution of a racemate is a shortcoming in the former synthesis, whereas the stepwise conversion in the latter takes longer steps, and consequently gives a lower overall yield.

In order to study the relationship between the configuration of aminosugar moiety in kasugamycin and the biological activity, we intended to develope a better pathway for synthesis of optically active kasugaminide and its diastereomers. In this paper, a facile synthesis of benzyl α- and β-kasugaminides *via* the simultaneous S_N2-substitution at 2,4-positions of the corresponding abequosides (benzyl 3,6-dideoxy-α- and β-D-*xylo*-hexopyranosides) is descrided. As methyl α-abequoside[7-9] is known to be synthesized by the simultaneous deoxygenation of 3,6-positions of methyl 3,4-anhydro-6-*O*-*p*-tolylsulfonyl-α-D-galactopyranoside obtainable from D-glucose, the pathway offered here is advantageous.

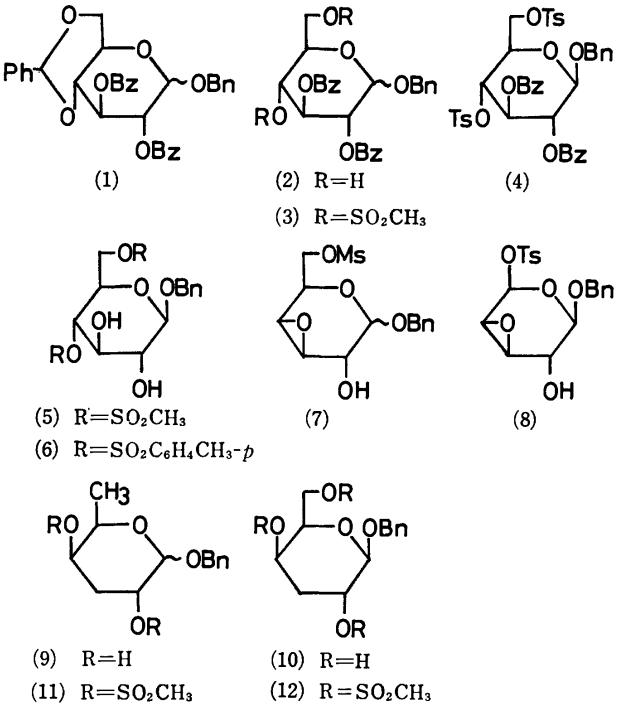

Results and Discussion

According to the method of Siewert and Westphal,[7] benzyl α- and β-abequosides were newly prepared. Benzoylation of benzyl 4,6-*O*-benzylidene-α-[10] and β-D-glucopyranosides[11] in the usual manner gave the 2,3-di-*O*-benzoates (**1α** and **1β**) in good yields, respectively. Partial hydrolysis of the 4,6-*O*-benzylidene group in **1α** and **1β** proceeded quantitatively in 70% acetic acid at 90—95 °C to give **2α** and **2β**, respectively. Mesylation of **2α** and **2β** in the usual manner gave the corresponding 4,6-di-*O*-mesylates (**3α** and **3β**) in good yields, respectively. Benzyl 2,3-di-*O*-benzoyl-4,6-di-*O*-*p*-tolylsulfonyl-β-D-glucopyranoside (**4**) was also prepared from **2β** in a similar manner.

Examination of the conversion of **3β** in dichloromethane or chloroform into the corresponding epoxide (**7β**) by treatment with sodium methoxide in methanol indicated that **3β** was once changed into an intermediate (**5**) within 6 h and then gradually converted into **7β**.

In fact, **5** deposited from the reaction mixture, when the amount of solvents (especially methanol) was not enough. This conversion proceeded slower than that of the corresponding methyl glucoside,[7] and the use of a little excess (1.3—1.4 mol) sodium methoxide gave a better result. Thus, **7α** and **7β** were obtained in 64 and 75% yields, respectively. In a similar way, tosylated intermediate (**6**) and tosylated epoxide (**8**) were obtained from **4**. It was characteristic that NMR spectra of these epoxides showed a coupling between OH and H_2 and a AB-quartet of H_3 and H_4. Reduction of **7α**, **7β**, and **8** in tetrahydrofuran (THF) with 3 mol of lithium aluminium hydride (LAH) gave sirupy benzyl abequosides (**9α** and **9β**), respectively. When 1.5 mol of LAH were used in one instance, crystalline benzyl 3-deoxy-β-D-*xylo*-hexopyranoside (**10**) was separated on a silica gel column in 22% yield, indicating that the epoxide ring was more reducible than the 6-*O*-sulfonate group. Excepting the last step in the synthesis of **9α** and **9β**, the purification of the product in each reaction was not always necessary, and both α- and β-abequosides could be actually obtained in *ca.* 20% overall yield from D-glucose. Mesylation of **9α** or **9β** and **10** gave the corresponding 2,4-di-*O*-mesylates (**11α** or **11β**) and 2,4,6-tri-*O*-mesylate (**12**) in good yields, respectively.

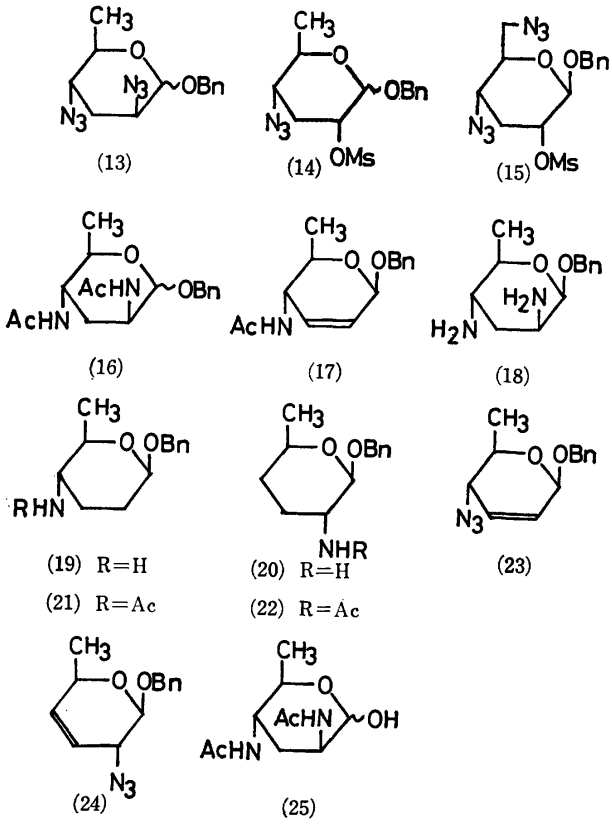

The simultaneous substitution at 2,4-positions of mesylates mentioned above with sodium azide was unexpectedly accompanied with the formation of unsaturated products. Reaction of **11**β in *N*,*N*-dimethylformamide (DMF) with 3 mol of sodium azide at 120 °C overnight was incomplete, and two spots other than a small amount of the starting material were detected on TLC. Separation of the products on a silica gel column gave one monoazide (**14**β) in pure state, but the NMR spectrum of another fraction indicated the presence of unsaturated compounds. Reaction of **12** under the same condition gave also the corresponding 4,6-diazide (**15**) in a low yield. Even after the reaction of **11**β was continued at 160—165 °C[6] until **14**β disappeared, the mixture of products could not be separated by repeating column chromatography. Therefore, the separation was tried after hydrogenation of the products with LAH in THF followed by *N*-acetylation. Thus, benzyl *N*,*N'*-diacetyl-β-kasugaminide (**16**β) and benzyl 4-acetamido-2,3,4,6-tetradeoxy-β-D-*erythro*-hex-2-enopyranoside (**17**) could be isolated in 12 and 19% yields, respectively. When the hydrogenation was carried out in the presence of Raney nickel, the corresponding saturated amino derivatives could be separated by column chromatography into three sirupy products (**19**, **20**, and **18**) in 8, 19, and 42% yields, respectively. These compounds were characterized after quantitative conversion into *N*-acetyl derivatives (**21**, **22**, and **16**β). The first-order analysis of the NMR spectrum of **16**β (*cf.* Experimental) completely proved the allocated structure, and $J_{1,2}$ values of **21** ($J_{1,2e}$=2.4, $J_{1,2a}$=8.0) and **22** ($J_{1,2}$=8.2) supported them. It will be noteworthy that **19** is a glycoside of the enantiomer of natural L-tolyposamine.[12,13]

The results mentioned above suggest that the second substitution at *C*-2 of the initial product (**14**β) gives 2,4-diazide (**13**β), but the substitution is followed by the elimination of axial C_2-azido group to give benzyl 4-azido-2,3,4,6-tetradeoxy-β-D-*erythro*-hex-2-enopyranoside (**23**), which subsequently rearranges to the corresponding 2-azido-3-enopyranoside (**24**). Recently, several papers have been published on the thermal rearrangement of 2,3-unsaturated 4-azido- and 4-thiocyanatoglycopyranosides to 3,4-unsaturated sugars having nitrogen function at *C*-2.[14–16] These conversions were explained as a [3,3]-sigmatropic rearrangement of cyclic allylic systems in which the asymmetry at the initial allylic centre is transmitted to the new centre by the suprafacial migration.[14] Although the formation of a small amount of unsaturated product in the substitution of equatorial C_4-sulfonyloxy group attached to 3-deoxy-hexopyranoside-ring with sodium azide in DMF has been reported,[10] the question whether the formation of **23** is initiated from the equatorial C_2-sulfonyloxy group of **14**β or from axial C_2-azido group of **13**β was remained ambiguous.

TABLE 1. SUBSTITUTION OF **11**α AND **11**β WITH SODIUM AZIDE IN HMPA

	Conditions		Products (%)		
	Temp (°C)	Time (h)	**14**	**13**	Unsaturated products
11α	80	20	86	—	—
11α	120	42	—	69	12[a]
11β	80	20	81	—	—
11β	100	5	78	—	—
11β	120	18	—	55	31[a]

a) Yields were estimated from the weight of crude products and the intensity ratio of olefinic proton and others in NMR spectra.

In order to prevent the formation of unsaturated compounds, the same substitution of **11**α and **11**β was examined at a lower temperature, using hexamethylphosphoric triamide (HMPA) as a solvent. As shown in Table 1, the reaction at 80 °C gave exclusively monosubstituted **14** in good yields. The continuation of the reaction at 120 °C until **14** disappeared also resulted in the formation of unsaturated compounds, but the yields of the desired diazides (**13**) were improved. Actually, **16**α and **16**β were obtained from the crude products in 60 and 46% yields, respectively, by subsequent hydrogenation and *N*-acetylation. The structure of **16**α and **16**β was further confirmed by respective hydrogenation into known *N*,*N'*-diacetyl-kasugamine (**25**).[17] It has been reported that the substitution of methyl 4,6-*O*-isopropylidene-3-*O*-methyl-2-*O*-methylsulfonyl-β-D-gluco- and D-mannopyranoside with potassium benzoate in DMF proceeded smoothly, whereas that of α-anomers did not occur.[18] Slower but steady substitution of the α-anomer in this experiment will be attributed to the absence of substituent at *C*-3 and to the flexibility of **11**α.

Experimental

All melting points are uncorrected. The solutions were evaporated under diminished pressure at a bath temperature not exceeding 45 °C. Specific rotations were measured in a 0.5-dm tube, with a Carl Zeiss LEP-Al polarimeter. The IR spectra were recorded with a Hitachi Model EPI-G2 spectrometer. The NMR spectra were taken with a JEOL-4H-100 MHz spectrometer using tetramethylsilane as an internal standard, in deuteriochloroform unless otherwise stated. Chemical shifts and coupling constants were recorded in δ and Hz units, and IR frequencies in cm^{-1}.

*Benzyl 2,3-Di-O-benzoyl-4,6-O-benzylidene-α- and β-D-glucopyranosides (**1α** and **1β**).* Benzyl 4,6-*O*-benzylidene-β-D-glucopyranoside[11] was benzoylated with benzoyl chloride in benzene. A usual work up and recrystallization of the product from ethanol gave pure **1β** in 90.5% yield. Mp 167—168.5 °C; $[\alpha]_D^{22}$ −19.9° (*c* 0.5, $CHCl_3$). IR: 1728 (ester), 1600 and 1490 (Ph); NMR: 7.90 and 7.60—7.00 (Ph; m), 5.73 (H_3: t, $J_{3,4}$=9.2), 5.52 (H_2: q, $J_{2,3}$=8.8), 5.51 (CH: s), 4.79 (H_1: d, $J_{1,2}$=7.4), 4.87 and 4.62 (CH_2: ABq, J_{AB}=12.5), 4.41 (H_{6e}: q, $J_{6e,6a}$=10.0), 3.93 (H_4: t, $J_{4,5}$=8.8), 3.87 (H_{6a}: t, $J_{5,6a}$=9.8), 3.72 (H_5: m, $J_{5,6e}$=5.0). Found: C, 72.02; H, 5.34%. Calcd for $C_{34}H_{30}O_8$: C, 72.07; H, 5.34%.

Similarly, benzoylation of benzyl 4,6-*O*-benzylidene-α-D-glucopyranoside[10] gave **1α** in 93% yield. Mp 134—136 °C; $[\alpha]_D^{22}$ +123.2° (*c* 0.35, $CHCl_3$). IR: 1700 (ester), 1600 (Ph); NMR: 7.95 and 7.50—7.10 (Ph; m), 6.10 (H_3: t, $J_{2,3}=J_{3,4}$=9.3), 5.51 (CH: s), 5.28 (H_1: broad s), 5.23 (H_2: q, $J_{1,2}$=3.3), 4.72 and 4.53 (CH_2: ABq, J_{AB}=13.0), 4.33—3.75 (H_4, H_5, H_6, and $H_{6'}$: m). Found: C, 72.34; H, 5.77%. Calcd for $C_{34}H_{30}O_8$: C, 72.07; H, 5.34%.

*Benzyl 2,3-Di-O-benzoyl-α- and β-D-glucopyranosides (**2α** and **2β**).* A suspension of **2β** (30 g) in 70% acetic acid–ethanol–acetone (300 ml, 150 ml, and 90 ml) was heated for 2 h at 90—95 °C until **2β** disappeared on TLC, and then evaporated to give a sirup which was crystallized from benzene. Yield, 24 g (94%); mp 157—158 °C; $[\alpha]_D^{22}$ +65.1° (*c* 1.2, $CHCl_3$); IR: 3460 (OH), 1725 and 1710 (ester), 1603 and 1495 (Ph). Found: C, 67.93; H, 5.56%. Calcd for $C_{27}H_{26}O_8$: C, 67.77; H, 5.48%.

In a similar manner, 4,6-*O*-benzylidene group of **1α** was hydrolyzed to give **2α** quantitatively. Mp 125—126 °C; $[\alpha]_D^{22}$ +175.2° (*c* 0.5, $CHCl_3$). IR: 3500 and 3380 (OH), 1730 and 1705 (ester), 1600 and 1490 (Ph). Found: C, 67.53; H, 5.57%. Calcd for $C_{27}H_{26}O_8$: C, 67.77; H, 5.48%.

*Benzyl 2,3-Di-O-benzoyl-4,6-di-O-methylsulfonyl-α- and β-D-glucopyranosides (**3α** and **3β**).* Mesylation of **2β** with methanesulfonyl chloride in the usual manner, and crystallization of the product from chloroform–ethanol (1: 1) gave pure **3β** in 90% yield. Mp 165—166 °C; $[\alpha]_D^{22}$ +43.7° (*c* 1.0, MeOH). IR: 1710 and 1733 (ester), 1595 and 1490 (Ph), 1345 and 1175 (sulfate); NMR: 8.02—7.08 (Ph: m), 5.70 (H_3: t, $J_{2,3}=J_{3,4}$=9.0), 5.46 (H_2: q), 4.98 (H_4: t, $J_{4,5}$=9.0), 4.83 and 4.69 (CH_2: ABq, J_{AB}=12.0), 4.70 (H_1: d, $J_{1,2}$=8.1), 4.63 (H_6: q, $J_{5,6}$=2.0), 4.44 ($H_{6'}$: q, $J_{5,6'}$=4.7, $J_{6,6'}$=10.8), 3.93 (H_5: m), 2.86 and 3.08 (OSO_2CH_3). Found: C, 55.10; H, 4.84; S, 9.72%. Calcd for $C_{29}H_{30}O_{12}S_2$: C, 54.88; H, 4.76; S, 10.10%.

Similarly, **2α** was mesylated to give the 4,6-di-*O*-mesylate in 93% yield. Mp 182—183 °C, $[\alpha]_D^{22}$ +137° (*c* 0.6, $CHCl_3$). IR: 1720 (ester), 1595 and 1490 (Ph), 1350 and 1180 (sulfate); NMR: 7.93 and 7.58—7.12 (Ph: m), 6.08 (H_3: t, $J_{2,3}=J_{3,4}$=10.0), 5.32 (H_1: d, $J_{1,2}$=3.8), 5.15 (H_2: q), 4.98 (H_4: t, $J_{4,5}$=9.5), 4.71 and 4.58 (CH_2: ABq, J_{AB}=11.5), 4.50—4.10 (H_5, H_6, and $H_{6'}$: m), 3.05 and 2.86 (OSO_2CH_3). Found: C, 54.62; H, 4.68; S, 10.00%. Calcd for $C_{29}H_{30}O_{12}S_2$: C, 54.88; H, 4.76; S, 10.10%.

*Benzyl 2,3-Di-O-benzoyl-4,6-O-p-tolylsulfonyl-β-D-glucopyranoside (**4**).* Reaction of **2β** and *p*-toluenesulfonyl chloride in pyridine in the usual manner gave **4** in 67% yield. Mp 125—126 °C; $[\alpha]_D^{22}$ +13.9° (*c* 1.0, $CHCl_3$). Found: C, 62.55; H, 4.81; S, 8.02%. Calcd for $C_{41}H_{38}O_{12}S_2$: C, 62.58; H, 4.87; S, 8.15%.

*Benzyl 3,4-Anhydro-6-O-methylsulfonyl-α- and β-D-glucopyranosides (**7α** and **7β**).* To a solution of **3β** (14.8 g, 124 mmol) in chloroform (150 ml) was added a methanol solution (100 ml) of sodium methoxide (0.56 g, 1.2 equivalent of sodium) and then kept in a refrigerator overnight. The reaction mixture was diluted with chloroform (100 ml), and then washed three times with water. The chloroform layer was dried and evaporated to give a sirup which was crystallized from benzene–petroleum ether. Yield 5.8 g (75%); mp 77—78 °C; $[\alpha]_D^{22}$ −108.3° (*c* 1.0, $CHCl_3$). IR: 3400 (OH), 1490 (Ph), 1350 and 1190 (sulfate), 930 (epoxide); NMR: 7.30 (Ph: s), 4.80 and 4.53 (CH_2: ABq, J_{AB}=11.5), 4.42—4.30 (H_6 and $H_{6'}$: m), 4.22 (H_1: d, $J_{1,2}$=7.0), 4.19 (H_5: t, $J_{5,6}=J_{5,6'}$=5.7), 3.68 (H_2: q, $J_{2,OH}$=3.8), 3.21 and 3.12 (H_3 and H_4: each d, $J_{3,4}$=3.8), 2.99 (OSO_2CH_3), 2.66 (OH: d). Found: C, 51.38; H, 5.42; S, 9.41%. Calcd for $C_{14}H_{18}O_7S$: C, 50.90; H, 5.49; S, 9.71%.

When the amount of solvents or the reaction time in the above reaction was not enough, the intermediate, benzyl 4,6-di-*O*-methylsulfonyl-β-D-glucopyranoside (**5**) deposited from the reaction mixture or from the chloroform layer during the washing with water. It was characterized as follows; mp 101—103 °C; $[\alpha]_D^{22}$ −41.8° (*c* 0.86, MeOH); IR: 3400 (OH), 1490 (Ph), 1350 and 1190 (sulfate). Found: C, 42.12; H, 5.39; S, 14.74%. Calcd for $C_{15}H_{22}O_{10}S_2$: C, 42.24; H, 5.20; S, 15.04%.

Similarly, **3α** was converted into **7α** in 64% yield. Mp 73—74 °C (from ethanol–hexane); $[\alpha]_D^{24}$ +42.4° (*c* 0.5, $CHCl_3$), IR: 3350 (OH), 1495 (Ph), 1350 and 1190 (sulfate); NMR: 7.40 (Ph, s), 4.94 (H_1: d, $J_{1,2}$=4.8), 4.84 and 4.60 (CH_2: ABq, J_{AB}=11.5), 4.45—4.30 (H_6 and $H_{6'}$: m), 3.85 (H_2: q, $J_{2,OH}$=10.5), 3.30 and 3.24 (H_3 and H_4: ABq, $J_{3,4}$=2.6), 3.07 (OSO_2CH_3), 2.50 (OH: d). Found: C, 50.62; H, 5.56; S, 9.53%. Calcd for $C_{14}H_{18}O_7S$: C, 50.90; H, 5.49; S, 9.71%.

*Benzyl 3,4-Anhydro-6-O-p-tolylsulfonyl-β-D-glucopyranoside (**8**) and Benzyl 4,6-Di-O-p-tolylsulfonyl-β-D-glucopyranoside (**6**).* Epoxidation of **4** in the same manner as above, and separation of the product on a silica gel column gave **8** (sirup) and **6** (mp 110—112 °C) in 48.4% and 25% yields, respectively.

8: $[\alpha]_D^{22}$ −93.4° (*c* 0.9, $CHCl_3$); NMR: 7.85—7.15 (Ph: m), 4.71 and 4.45 (CH_2: ABq, J_{AB}=14.0), 4.25—4.02 (H_5, H_6, and $H_{6'}$: m), 3.61 (H_2: broad d), 3.13 and 3.02 (H_3 and H_4: ABq, J_{AB}=4.4), 2.88 (OH: broad s), 2.37 (CH_3: s). Found: C, 59.26; H, 5.59; S, 7.76%. Calcd for $C_{20}H_{22}O_7S$: C, 59.10; H, 5.46; S, 7.89%.

6: $[\alpha]_D^{22}$ −37.7° (*c* 1.0, MeOH). Found: C, 57.21; H, 5.35; S, 10.51%. Calcd for $C_{28}H_{30}O_{10}S_2$: C, 56.93; H, 5.12; S, 10.86%.

*Benzyl 3,6-Dideoxy-α- and β-D-xylo-hexopyranosides (**9α** and **9β**).* To a suspension of lithium aluminium hydride (LAH, 2.4 g, 63 mmol) in tetrahydrofuran (THF, 100 ml) was added dropwise a solution of **7β** (8 g, 18 mmol) in THF (70 ml) with stirring. The reaction mixture was refluxed for 5 h, and a mixed solution of water and ethyl acetate was added to decompose excess LAH. After bubbling carbon dioxide into the reaction mixture, it was filtered, and the filtered mass was washed with methanol–water (1: 1). The filtrate and

washings were evaporated, and the residue was dissolved in water. Sodium periodate (2 g, 7.5 mmol) was added to the aqueous solution and kept in a refrigerator overnight. After addition of hydrogen peroxide (30%, 3 ml), the mixture was reduced with excess sodium thiosulfate, evaporated, and an aqueous solution of the residue was extracted with chloroform. Evaporation of the extracts gave a sirup (3.8 g) which was fractionated on a silica gel column (ethanol: benzene=1: 9) to give pure **9**β (3.0 g, 52%) as a sirup, $[\alpha]_D^{22}$ −107° (*c* 0.5, $CHCl_3$). Found: C, 65.81; H, 7.72%. Calcd for $C_{13}H_{18}O_4$: C, 65.53; H, 7.61%.

The same compound was also obtained from **8** in 48.5% yield. In a similar manner mentioned above, **9**α was obtained from **7**α in 53% yield as a sirup. $[\alpha]_D^{22}$ +119° (*c* 0.8, $CHCl_3$). Found: C, 64.98; H, 7.38%. Calcd for $C_{13}H_{18}O_4$: C, 65.53; H, 7.61%.

In case of 1.5 mol of LAH were used for hydrogenation of **7**β, fractionation of the product gave benzyl 3-deoxy-β-D-*xylo*-hexopyranoside (**10**) in 22% yield. Mp 95—95.5 °C; $[\alpha]_D^{22}$ −50.9° (*c* 1.1, MeOH). Found: C, 61.17; H, 7.08%. Calcd for $C_{13}H_{18}O_5$: C, 61.40; H, 7.14%.

*Benzyl 3,6-Dideoxy-2,4-di-O-methylsulfonyl-α- and β-D-xylo-hexopyranosides (**11**α and **11**β).* Mesylation of **9**β in the usual manner, and crystallization of the product from ethanol gave **11**β in 77% yield. Mp 104—105 °C; $[\alpha]_{22}^{D}$ −64° (*c* 1.0, $CHCl_3$). IR: 1360 and 1170 (sulfate); NMR: 7.32 (Ph, s), 4.92 and 4.58 (CH_2: ABq, J_{AB}=12.0), 4.23 (H_4: m), 4.68—4.50 (H_1 and H_2: m), 3.80 (H_5: octet, $J_{4,5}$=1.5), 2.91 and 3.08 (2×OSO_2CH_3), 2.71 (H_{3e}: m, J_{gem}=12.7), 2.04 (H_{3a}: m), 1.35 (CH_3: d, $J_{CH_3,5}$=6.3). Found: C, 45.91; H, 5.68; S, 16.28%. Calcd for $C_{15}H_{22}O_8S_2$: C, 45.67; H, 5.62; S, 16.26%.

Similarly, **9**α was mesylated to give **11**α quantitatively. Mp 92—93 °C (from ethanol–hexane); $[\alpha]_D^{22}$ +95.2° (*c* 0.6, $CHCl_3$); IR: 1340 and 1175 (sulfate). Found: C, 45.86; H, 5.69; S, 16.31%. Calcd for $C_{15}H_{22}O_8S_2$: C, 45.67; H, 5.62; S, 16.26%.

*Benzyl 3-Deoxy-2,3,6-tri-O-methylsulfonyl-β-O-xylo-hexopyranoside (**12**).* Mesylation of **10** in pyridine with methanesulfonyl chloride gave the tri-*O*-mesylate in 76% yield. Mp 123—126 °C; $[\alpha]_D^{22}$ −59.6° (*c* 1.0, $CHCl_3$); IR: 1350 and 1180 (sulfate); NMR: 7.32 (Ph: s), 4.97 (H_4: m), 4.90 and 4.65 (CH_2: ABq, J_{AB}=12.0), 4.67—4.56 (H_1 and H_2: m), 4.40—4.25 (H_6 and H_6': m), 4.00 (H_5: sex, $J_{4,5}$=1.0, $J_{CH_3,5}$=7.9), 3.11, 3.04 and 2.93 (3×OSO_2CH_3), 2.81 (H_{3e}: sex, J_{gem}=14.3, $J_{2,3e}$, $J_{3e,4}$=3.5), 2.04 (H_{3a}: m, $J_{2,3a}$=9.0, $J_{3a,4}$=4.0). Found: C, 39.61: H, 4.91; S, 19.63%. Calcd for $C_{16}H_{24}O_{11}S_3$: C, 39.33; H, 4.95; S, 19.69%.

*Benzyl 4-Azido-3,4,6-trideoxy-2-O-methylsulfonyl-α- and β-D-ribo-hexopyranosides (**14**α and **14**β).* i) Reaction in *N,N*-dimethylformamide (DMF). A suspension of **11**β (600 mg, 1.52 mmol) and sodium azide (500 mg, 7.69 mmol) in DMF (10 ml) was stirred at 120 °C overnight, filtered, and the filtrate was evaporated to give a sirup (450 mg) which showed two spots other than **11**β. The sirup was fractionated on a silica gel column (benzene: ethanol=10: 1). The first fraction (140 mg, 31.9%) was a mixture of **11**β and other products, and the second fraction was **14**β. Yield, 50 mg (9.6%); $[\alpha]_D^{22}$ −44.4° (*c* 0.4, $CHCl_3$); mp 76—78 °C (from ethanol). IR: 2120 (N_3), 1365 and 1180 (sulfate); NMR: 7.30 (Ph; s), 4.84 and 4.55 (CH_2: ABq, J_{AB}=11.5), 4.46 (H_1: d, $J_{1,2}$=7.0), 4.33 (H_2: dt, $J_{2,3a}$=8.0, $J_{2,3e}$=5.2), 3.27 (H_5: dq, $J_{4,5}$=9.6), 3.14 (H_4: sex, $J_{4,3a}$=9.6, $J_{4,3e}$=4.5), 2.87 (OSO_2CH_3), 2.58 (H_{3e}: dt, J_{gem}=12.0), 1.76 (H_{3a}: broad q), 1.31 (CH_3: d, J_{5,CH_3}=7,0). Found: C, 49.50; H, 5.61; N, 12.46; S, 9.21%. Calcd for $C_{14}H_{19}N_3O_5S$: C, 49.25; H, 5.61; N, 12.31; S, 9.39%. ii) Reaction in hexamethylphosphoric triamide (HMPA). A suspension of **11**β (1.2 g) and sodium azide (1 g) in HMPA (5 ml) was stirred at 80 °C for 20 h, and then poured into water (30 ml). The resulting solution was extracted with ether. The ether solution was washed with water, dried, and then evaporated to give a hard sirup (**14**β) which was crystallized from ethanol–hexane. Yield, 0.84 g (81%). The physical constants of this product were identical with those mentioned above.

The reaction of **11**α with sodium azide in the same manner gave sirupy **14**α in 86% yield. $[\alpha]_D^{22}$ +114.2° (*c* 0.76, $CHCl_3$); IR: 2100 (N_3), 1360 and 1180 (sulfate); NMR: 7.38 (Ph, s), 5.00 (H_1: d, $J_{1,2}$=3.4), 4.76 and 4.62 (CH_2: ABq, J_{AB}=12.0), 4.80—4.60 (H_2: m), 3.68 (H_5: dq, $J_{4,5}$=10.0, J_{5,CH_3}=6.3), 3.14 (H_4: sextet, $J_{3a,4}$=10.0, $J_{3e,4}$=5.3), 2.95 (OSO_2-CH_3), 2.35 (H_{3e}: $J_{2,3e}$=5.6, J_{gem}=11.6), 2.18 (H_{3a}: q, $J_{2,3a}$=11.0), 1.22 (CH_3: d). Found: C, 49.45; H, 5.51; N, 12.18; S, 9.45%. Calcd for $C_{14}H_{19}N_3O_5S$: C, 49.25; H, 5.61; N, 12.31; S, 9.39%.

*Benzyl 4,6-Diazido-3,4,6-trideoxy-2-O-methylsulfonyl-β-D-ribo-hexopyranoside (**15**).* A suspension of **12** (980 mg, 2 mmol) and sodium azide (780 mg, 12 mmol) in DMF (13 ml) was stirred at 120 °C overnight, filtered, and the filtrate was evaporated. A usual extraction gave a sirup which showed two spots other than **12** on TLC. Separation of the sirup on a silica gel column (benzene: ethanol=10: 1) gave two main fractions of which the first fraction (230 mg, 35%) showed no absorption of a sulfonyloxy group, but the second fraction (110 mg, 14.3%) showed the mesyl signal in the NMR spectrum. The former was rechromatographed, but it could not be purified. The latter fraction crystallized on standing, and recrystallized from benzene–petroleum ether. Mp 78—80 °C; $[\alpha]_D^{22}$ −25.2° (*c* 0.6, $CHCl_3$); IR: 2100 (N_3), 1365 and 1180 (sulfate); NMR: 7.30 (Ph, s), 4.88 and 4.58 (CH_2: ABq, J_{AB}=11.5), 4.51 (H_1: d, $J_{1,2}$=7.0), 4.37 (H_2: dt, $J_{2,3e}$=5.3), 3.41 (H_4, H_5, H_6, and H_6': broad s), 2.90 (OSO_2-CH_3), 2.67 (H_{3e}: dt, $J_{3e,4}$=4.2), 1.81 (H_{3a}: broad q, J_{gem}=$J_{3a,4}$=$J_{3a,2}$=11.0). Found: C, 44.26; H, 4.65; N, 22.33; S, 7.99%. Calcd for $C_{14}H_{18}N_6O_5S$: C, 43.97; H, 4.74; N, 21.98; S, 8.39%.

*Benzyl 2,4-Diacetamido-2,3,4,6-tetradeoxy-β-D-arabino-hexopyranoside (**16**β) and Benzyl 4-Acetamido-2,3,4,6-tetradeoxy-β-D-erythro-hex-2-enopyranoside (**17**).* A suspension of **11**β (800 mg, 2 mmol) and sodium azide (700 mg, 10.8 mmol) in DMF (15 ml) and water (1.5 ml) was stirred at 120 °C for one day, and then at 160—165 °C until the initial product **14**β disappeared (8 h). Treatment of the reaction mixture in the usual way and purified on a silica gel column gave a sirup (450 mg). A suspension of this sirup (350 mg) and LAH (380 mg, 10 mmol) in THF was refluxed on a oil-bath for 3 h, and a small amount of water containing ethyl acetate was added to decompose excess LAH, and then filtered. After neutralization of the filtrate, it was evaporated. The residue was dried, and then acetylated in the usual manner to give a sirup which contained two main components. The two products were isolated in pure state by column chromatography repeated twice. Thus, the first fraction **16**β and the second **17** were obtained in 50 mg (12%) and 80 mg (19.4%) yields, respectively.

16β: Mp 146—147.5 °C; $[\alpha]_D^{22}$ −45.2° (*c* 1.0, $CHCl_3$); IR: 3270 (NH); 1650 and 1550 (amide); NMR: 7.29 (Ph: s), 4.80 and 4.55 (CH_2: ABq, J_{AB}=12.0), 4.54 (H_1: d, $J_{1,2}$=2.5), 4.14 (H_2: broad s), 3.83 (H_4: m), 3.43 (H_5: dq, $J_{4,5}$=8.2), 2.18 (H_{3e}: dt, $J_{3e,4}$=$J_{3e,2}$=4.7, J_{gem}=13.5), 1.93 and 1.96 (2×NAc), 1.53 (H_{3a}: octet, $J_{3a,4}$=10.0, $J_{3a,2}$=4.0), 1.29 (CH_3: d, $J_{CH_3,5}$=7.0). Found: C, 64.03; H, 7.62; N, 8.73%.

Calcd for $C_{17}H_{24}N_2O_4$: C, 63.73; H, 7.55; N, 8.74%.

17: Mp 162—164 °C; $[\alpha]_D^{22}$ −249° (*c* 0.2, $CHCl_3$); IR: 3270 (NH), 1640 and 1550 (amide); NMR: 7.30 (Ph, s), *ca.* 5.7 (olefinic H, m), 4.83 and 4.57 (CH_2: ABq, J_{AB}=12.0), 4.63 (H_1: d, $J_{1,2}$=4.5), 4.5—4.2 (H_4 and H_5: m), 1.91 (NAc), 1.33 (CH_3: d, $J_{CH_3,5}$=7.0). Found: C, 69.23; H, 7.29; N, 5.52%. Calcd for $C_{15}H_{19}NO_3$: C, 68.94; H, 7.33; N, 5.36%.

*Preparation of Benzyl β-Kasugaminide (**18**), Benzyl 4-Amino-2,3,4,6-tetradeoxy-β-*D-erythro-*hexopyranoside (**19**), Benzyl 2-Amino-2,3,4,6-tetradeoxy-β-*D-erythro-*hexopyranoside (**20**), and Their Conversion into the Corresponding* N*-Acetates (**16β**, **21**, and **22**).*

In the same manner mentioned above, the reaction of **11β** (7.5 g) with sodium azide was carried out, and the crude product was hydrogenated in the presence of Raney nickel at 50 °C for 5 h under 50 atm hydrogen gas to give a sirup which showed three spots on TLC. The sirup on a silica gel (80 g Wakogel C-200) column was eluted with benzene–ethanol [in turn 7:1 (500 ml), 5:1 (500 ml), and 1:1 (300 ml)] to give **20** (0.8 g, 19.0%), **19** (0.34 g, 8.1%), and **18** (1.82 g, 41.9%) as a sirup, respectively. Each sirup was acetylated with acetic anhydride and pyridine. The reaction mixture was directly evaporated to dryness, and the product was purified by column chromatography if necessary. Each acetate obtained in almost quantitative yield was characterized with NMR spectrum, respectively.

Compound **20** was not characterized.

22: mp 161.5—162 °C; $[\alpha]_D^{22}$ −90.4° (*c* 0.6, $CHCl_3$); IR: 3280 (NH), 1635 and 1550 (amide); NMR: 7.35 (Ph, s), 4.88 and 4.58 (CH_2: ABq, J_{AB}=12.0), 4.36 (H_1: d, $J_{1,2}$=8.2), 3.82—3.40 (H_2 and H_5: m), 2.3—1.3 (H_{3a}, H_{3e}, H_{4a}, and H_{4e}: m), 1.90 (NAc), 1.26 (CH_3: d, $J_{CH_3,5}$=6.5). Found: C, 68.72; H, 8.30; N, 5.60%. Calcd for $C_{15}H_{21}NO_3$: C, 68.41; H, 8.04; N, 5.32%.

19: $[\alpha]_D^{22}$ −70.8° (*c* 1.1, $CHCl_3$). Found: C, 69.95; H, 8.88; N, 6.32%. Calcd for $C_{13}H_{20}NO_2$: C, 70.55; H, 8.65; N, 6.33%.

21: mp 165—167° (admixture with **22** showed mp of 137—146 °C); $[\alpha]_D^{22}$ −89.8° (*c* 0.5, $CHCl_3$); IR: 3270 (NH), 1635 and 1545 (amide); NMR: 7.35 (Ph, s), 4.90 and 4.58 (CH_2: ABq, J_{AB}=12.0), 4.51 (H_1: q, $J_{1,2e}$=2.4, $J_{1,2a}$=8.0), 3.70 (H_4: dt, $J_{4,5}$=$J_{3a,4}$=10.0, $J_{3e,4}$=4.4), 3.36 (H_5: dq, J_{5,CH_3}=6.0), 1.98 (NAc), 2.22—1.38 (H_{2a}, H_{2e}, H_{3a}, and H_{3e}: m), 1.28 (CH_3). Found: C, 68.82; H, 8.20; N, 5.37%. Calcd for $C_{15}H_{21}NO_3$: C, 68.41; H, 8.04; N, 5.32%.

18: $[\alpha]_D^{22}$ −92.4° (*c* 0.4, $CHCl_3$). Found: C, 65.76; H, 8.95; N, 11.58%. Calcd for $C_{13}H_{20}N_2O_2$: C, 66.07; H, 8.53; N, 11.86%.

Physical properties of *N,N'*-diacetate of **18** were identical with **16β**.

*Benzyl 2,4-Diacetamido-2,3,4,6-tetradeoxy-α-*D-arabino-*hexopyranoside (**16α**).* A suspension of **11α** (2.4 g, 6.08 mmol) and sodium azide (2 g, 28.8 mmol) in HMPA (10 ml) was stirred at 120 °C for 42 h until the initial product (**14α**) disappeared on TLC, and the subsequent hydrogenation with LAH and *N*-acetylation of the product were carried out as mentioned before to give a sirup which showed three spots on TLC. The main spot was separated by a silica gel column chromatography to give crystals which were recrystallized from ethanol–hexane. Yield, 1.17 g (60%); mp 95—98 °C; $[\alpha]_D^{22}$ +77.9° (*c* 0.6, $CHCl_3$). IR: 3260 (NH), 1645 and 1545 (amide); NMR (D_2O exchanged): 7.32 (Ph, s), 4.68 (H_1: broad s, $J_{1,2}$=<1.5), 4.66 and 4.52 (CH_2: ABq, J_{AB}=11.5), 4.18 (H_2: broad t), 3.95 (H_4: q, $J_{4,3a}$=8.0, $J_{4,5}$=10.0), 3.64 (H_5: dq, J_{5,CH_3}=6.0), 1.98 and 1.95 (2×NAc), 2.05—1.72 (H_{3e} and H_{3a}: m), 1.20 (CH_3: d). Found: C, 63.25; H, 7.31; N, 8.29%. Calcd for $C_{17}H_{24}N_2O_4$: C, 63.73; H, 7.55; N, 8.74%.

N,N'-*Diacetylkasugamine (**25**).* A solution of **16β** (0.84 g, 2.62 mmol) in methanol–50% acetic acid (1:1, 10 ml) was hydrogenolyzed in the presence of palladium–charcoal (5%, 0.5 g), filtered, and then the filtrate was evaporated to give a sirup which was crystallized from ethanol–hexane. Yield, 0.46 g (76%); mp 124—126 °C; $[\alpha]_D^{22}$ +65° (*c* 0.8, H_2O), [lit,[17] mp 123—125 °C; $[\alpha]_D^{20}$ +67° (*c* 1.0, H_2O)]. Found: C, 52.52; H, 8.02; N, 11.95%. Calcd for $C_{10}H_{18}N_2O_4$: C, 52.16; H, 7.88; N, 12.17%.

The same compound was also obtained from **16α** by hydrogenolysis in 80% yield.

The authors are indebted to the members of the Laboratory of Organic Analysis for microanalysis and to Mr. H. Matsumoto for NMR measurements.

References

1) Part XXVII: H. Hashimoto, T. Nishide, F. Chiba, and J. Yoshimura, *Carbohydr. Res.*, Vol. 60 in press.
2) H. Umezawa, Y. Okami, T. Hashimoto, Y. Suhara, M. Hamada, and T. Takeuchi, *J. Antibiot.*, **18A**, 101 (1965).
3) Y. Suhara, K. Maeda, H. Umezawa, and M. Ohno, *Tetrahedron Lett.*, **1966**, 1239.
4) Y. Suhara, J. Sasaki, G. Koyama, K. Maeda, H. Umezawa, and M. Ohno, *J. Am. Chem. Soc.*, **94**, 6501 (1972).
5) S. Yasuda, T. Ogasawara, S. Kawabata, I. Iwataki, and T. Matsumoto, *Tetrahedron*, **29**, 3141 (1973).
6) K. Kitahara, S. Takahashi, H. Shibata, N. Kurihara, and M. Nakajima, *Agric. Biol. Chem.*, **33**, 748 (1969).
7) G. Siewert and O. Westphal, *Ann. Chem.*, **720**, 171 (1968).
8) H. Zinner, B. Ernst, and F. Kreienbring, *Chem. Ber.*, **95**, 821 (1962).
9) K. Eklind, P. J. Garegg, and B. Gotthammar, *Acta Chem. Scand.*, **B29**, 633 (1975).
10) W. Meyer zu Reckendorf, U. Kamprath-Scholz, E. Bischof, and N. Wassiliadou-Micheli, *Chem. Ber.*, **108**, 3397 (1975).
11) E. Fischer and B. Helferich, *Ann. Chem.*, **383**, 71 (1911).
12) T. Kishi, S. Harada, M. Asai, M. Muroi, and K. Mizuno, *Tetrahedron Lett.*, **1969**, 97.
13) J. S. Brimacombe, L. W. Doner, A. J. Rollins, and A. K. Al-Radhi, *J. Chem. Soc., Perkin Trans. 1*, **1973**, 1295.
14) R. J. Ferrier and N. Vethaviyaser, *J. Chem. Soc., C*, **1971**, 1907.
15) R. D. Guthrie and G. J. Williams, *J. Chem. Soc., Perkin Trans. 1*, **1972**, 2619.
16) J. Cleophax, J. Leboul, A. Olesker, and S. D. Gero, *Tetrahedron Lett.*, **1973**, 4911.
17) Y. Suhara, K. Maeda, and H. Umezawa, *J. Antibiot.*, **18A**, 187 (1965).
18) M. Milikovic, M. Gligorijevic, and D. Glisin, *J. Org. Chem.*, **39**, 3223 (1974).

Layered Compounds. XLIV.[1] Transannular π-π Interactions in Tetracyanoethylene Complexes of [*m.n*]Paracyclophadiynes and the Related Cyclic Acetylenes

Takahiro KANEDA and Soichi MISUMI

The Institute of Scientific and Industrial Research, Osaka University, Suita, Osaka 565

(Received April 21, 1977)

The electronic spectra of TCNE complexes of acyclic and cyclic diacetylenes and cyclic tetraacetylenes were measured. They show a maximum in the narrow region 423—431 nm regardless of ring strain in the donor molecules and proximity of two diacetylene groups. Crystalline two-to-one TCNE complexes of [*m.n*]paracyclophadiynes were prepared, the formation of one-to-one TCNE complexes in solution being established by means of the Benesi-Hildebrand plots using various molar ratios of the two components. The electronic spectra of some 1 : 1 [*m.n*]paracyclophadiyne–TCNE complexes were measured. The spectra suggest that the complexes are equilibrium mixtures consisting of three isomeric complexes, *i.e.*, a diacetylene-site complex and two pseudo-conformers of benzene-site complex. The longer wavelength band of [*m.n*]paracyclophadiyne complexes shows a marked red-shift as compared with the other bands. This is interpreted in terms of transannular π-π interaction between the diacetylene group and the benzene ring fixed closely with each other by shortening of methylene bridges. The contribution of the three isomeric complexes on the red-shift is discussed.

In previous papers of this series[2,3] reports were given on the syntheses and spectra of [*n*]paracyclophadiynes or [*m.n*]paracyclophadiynes $\mathbf{1}_{mn}$ where *m* and *n* are the numbers of bridging methylenes inserted between a benzene ring and a diacetylene group. Thermal and photochemical cycloadditions[4] and ^{13}C-NMR spectra[5] of $\mathbf{1}_{mn}$ and related cyclic diacetylenes were also investigated. The unusual reactions and spectral properties have been interpreted in terms of proximity interactions between the diacetylene group and the aromatic ring placed close to each other in a molecule.

Tetracyanoethylene (TCNE) complexes have often been used in studies on the relative π-base strength of various methyl-substituted benzenes[6] and transannular π-π interactions in donor molecules, *e.g.*, [*m.n*]paracyclophanes,[7] [2.2]metacyclophanes,[8] multilayered [2.2]paracyclophanes,[9] and multilayered [2.2]paracycloheterophanes.[10] The π-basicity of the donor molecules increases with an increase in the number of substituted methyl groups and/or stacking benzene rings and an increase in the face-to-face overlapping between aromatic nuclei. In contrast to the cyclophanes having symmetric donor-sites, unsymmetric cyclophanes containing non-equivalent donor sites such as 4-acetyl- and 4-methoxy-[2.2]paracyclophanes[7b] can be expected to form two isomeric one-to-one complexes with TCNE, *i.e.*, pseudo-configurational isomers. An important factor for determining which isomeric complex is more predominant or exclusive is the magnitude of ionization potentials of the constituent donor moieties. The relative orientation between an acceptor and a donor, or pseudo-conformation, is the second factor to affect transition energy of charge transfer (CT) complexes. Two pseudo-conformers were assumed for one-to-one *p*-substituted benzene–TCNE complexes and were investigated experimentally and theoretically.[11]

Since dialkyldiacetylenes have also been proved to form CT complexes with TCNE in the present study, paracyclophadiynes $\mathbf{1}_{mn}$ can be regarded as unsymmetric donor molecules having two possible donor sites. In the present work the transannular π-π interactions in $\mathbf{1}_{mn}$ and cyclic tetraacetylenes $\mathbf{2}_n$, where a suffix *n* is the number of bridging methylenes, are discussed considering geometrical effect with the aid of their TCNE complexes.

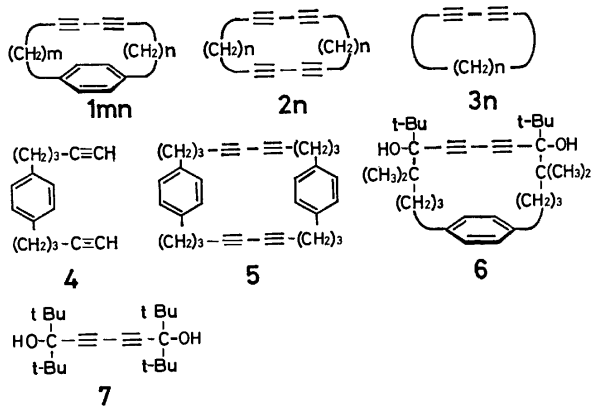

Results and Discussion

Charge Transfer Complexes of Alkadiyne and Alkynes with TCNE. The π-donation of triple bonds have been observed in some examples,[12] *e.g.*, in the formation of hydrogen bond with hydroxylic protons[13] and of molecular complex with hydrogen chloride,[14] but not in TCNE complex. Thus we first examined alkadiyne- and alkyne–TCNE complexes in connection with the study of paracyclophadiyne–TCNE complexes.

The equilibrium constants of 5-decyne- and 5,7-dodecadiyne–TCNE complexes were determined at 25°C in dichloromethane with the Benesi-Hildebrand equation[15]

$$\frac{(A)l}{\log I_0/I} = \frac{1}{K\varepsilon}\cdot\frac{1}{[D]} + \frac{1}{\varepsilon} \qquad (1)$$

where (A), *l*, [D], ε, and *K* are molar concentration of TCNE, light path length, mole fraction of the alkyne, apparent molar extinction coefficient, and the equilibrium constant, respectively. Plots of $(A)l/(\log I_0/I)$ against 1/[D] give straight lines for both complexes, demonstrating that a 1 : 1 complex is formed between

Table 1. Absorption maxima and equilibrium constants of alkyne–TCNE complexes (CH_2Cl_2, 25 °C)

Alkyne	λ (nm)	K (ε)
5,7-Dodecadiyne	424	7.0(1100)
5-Decyne	370	3.9(500)
3-Octyne	367	—

the alkyne and TCNE in the solution. The observed values of λ_{mn} and K given in Table 1 indicate 5,7-dodecadiyne to be a much stronger π-base to TCNE than 5-decyne.

Electronic Spectra of Cyclic Di- and Tetraacetylene–TCNE Complexes. The electronic spectra of $\mathbf{2}_n$– and $\mathbf{3}_n$–TCNE complexes exhibit absorption bands with a maximum in the narrow region 423—431 nm as well as the one-to-one 5,7-dodecadiyne–TCNE complex, suggesting that each spectrum is associated with the transition of one-to-one complex.

The TCNE complexes of two cyclic diacetylenes, strained $\mathbf{3}_9$ and $\mathbf{3}_{10}$, show the absorption maxima at the same position. This suggests a slight strain effect on the CT-transition of diacetylene–TCNE complexes. The cyclic tetraacetylene $\mathbf{2}_3$ in which a pair of diacetylene groups are closely fixed shows an abnormal spectrum[20b] due to transannular electronic interaction as compared with the other homologs $\mathbf{2}_n$. Thus, the $\mathbf{2}_3$–TCNE complex is also expected to exhibit transannular π-π electronic interaction differing from the other $\mathbf{2}_n$-TCNE complexes. However, it reveals a spectrum similar to those of the others, indicating that the proximity of the two diacetylene groups is not important for CT-transition energy of cyclic tetraacetylene–TCNE complexes.

Composition and Geometry of Paracyclophadiyne–TCNE Complexes. Crystalline TCNE complexes of both $\mathbf{1}_{34}$ and $\mathbf{1}_{44}$ were isolated and confirmed to consist of two moles of donors and one mole of TCNE. Harata *et al.* reported the crystal structure of the latter complex, where a TCNE molecule is sandwiched between the two benzene rings of two $\mathbf{1}_{44}$ molecules but not complexed with diacetylene group-site (Fig. 1).[16]

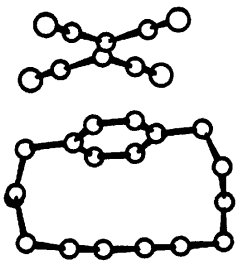

Fig. 1. Crystal structure of two-to-one [4.4]paracyclophadiyne–TCNE complex.[16]

In solution, on the other hand, [m.n]paracyclophadiynes $\mathbf{1}_{mn}$ are found to form one-to-one TCNE complex by the following experiments. When molar ratios of $\mathbf{1}_{33}$ and $\mathbf{1}_{44}$ *vs.* TCNE in dichloromethane are changed in the ranges 16—1/19 and 12—1/13, respectively, the position of absorption maximum and the shape of absorption curve remain unchanged for both

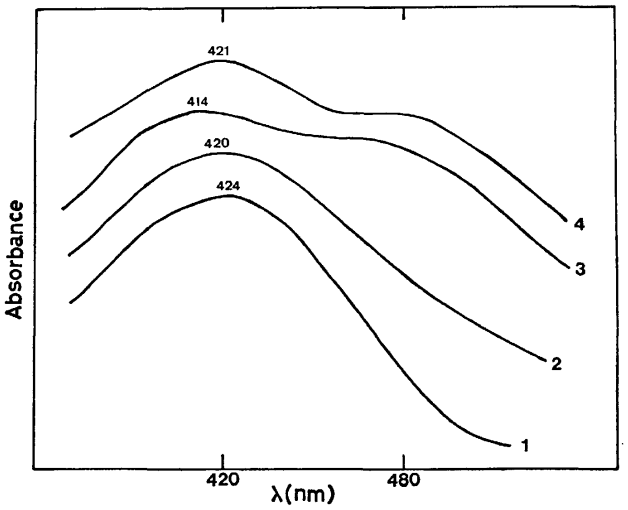

Fig. 2. Electronic spectra of TCNE complexes (CH_2Cl_2, room temp): curve 1, 5,7-dodecadiyne; 2, a 1:6:6 mixture of TCNE, **4**, and 5,7-dodecadiyne; 3, **4**; 4, **6**. * λ_{max} in nm.

the complex solution.

Two possible pseudo-configurational isomers are expected for the one-to-one complex of $\mathbf{1}_{mn}$, *viz.*, a diacetylene-site complex $\mathbf{10}_{mn}$ and a benzene-site complex for which two conformational isomers $\mathbf{11}_{mn}$ and $\mathbf{12}_{mn}$ are theoretically anticipated for *p*-xylene–TCNE complex.[11c,17]

In studying the electronic spectra of $\mathbf{1}_{mn}$–TCNE complexes, it is advantageous to examine those of TCNE complexes of *p*-di(4-pentynyl)benzene **4** and [5.5]-paracyclophadiyne derivative **6** bearing bulky groups at the propargyl positions. The spectra are shown in Fig. 2. A mixture of TCNE and 1-alkyne or 1,1,6,6-tetra-*t*-butyl-2,4-hexadiyne-1,6-diol **7** having similar bulky groups at the propargyl positions exhibits no band in the visible region. Complexing with TCNE is considered to be difficult owing to steric hindrance of the bulky groups in the latter case. Thus the observed CT-bands of **4**– and **6**–TCNE complexes should be attributed to the benzene-site complex, but not to the diacetylene-site one. The shorter- and longer-wavelength bands of these complexes are assigned to "perpendicular" and "parallel" complexes, respectively, according to the assignment (**8** and **9**)[11c] for *p*-xylene–

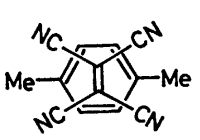

8

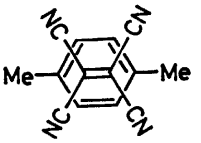

9

TCNE complex. As seen in Fig. 2, a mixture of TCNE, **4**, and 5,7-dodecadiyne of a 1:6:6 ratio shows a spectrum which is characterized as a superposition of the spectra due to the two independent complexes. It is quite reasonable that there are three isomeric complexes $\mathbf{10}_{mn}$—$\mathbf{12}_{mn}$ in the equilibrium mixture of $\mathbf{1}_{mn}$–TCNE complex (Scheme 1).

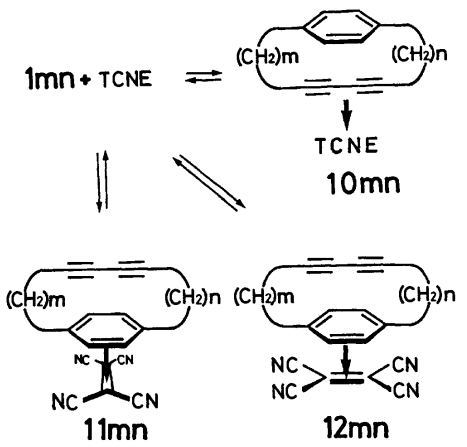

Scheme 1.

Electronic Spectra of Paracyclophadiyne–TCNE Complexes. The absorption curves and their apparent maxima of $\mathbf{1}_{mn}$– and **5**–TCNE complexes are given in Fig. 3 and Table 2. All the complexes show a maximum in the narrow region 425—431 nm, $\mathbf{1}_{33}$–TCNE complex exhibiting an additional, strong maximum at 555 nm. The other curves are unsymmetric, suggesting an additional band submerged in longer wavelength region. We have resolved the curves into two components on the assumption that they consist approximately of two CT-bands, since the shorter wavelength band (λ_{max} *p*-xylene 415 nm;[6] [*m.n*]paracyclophane 416—430 nm)[7a] of the two maxima of *p*-xylene derivative–TCNE complexes and the absorption band (421—431 nm) of diacetylene–TCNE complex appear at nearly the same position. The results of curve analyses are given in Table 2. The $\mathbf{1}_{24}$–, $\mathbf{1}_{44}$–, and $\mathbf{1}_{55}$–TCNE complexes exhibit a longer wavelength band at 470 or 480 nm in addition to a shorter wavelength band. From the fact that the absorption curves of these complexes are very similar to curve 2 in Fig. 2, one may reason as follows: the shorter wavelength band is possibly attributed both to the diacetylene-site complex $\mathbf{10}_{mn}$ and the benzene-site "perpendicular" complex $\mathbf{11}_{mn}$, and the longer wavelength band to the "parallel" complex $\mathbf{12}_{mn}$. It is also shown that in the cases of the three $\mathbf{1}_{mn}$–TCNE complexes, there is no appreciable transannular π-π interaction between the two chromophores in the donor molecules.

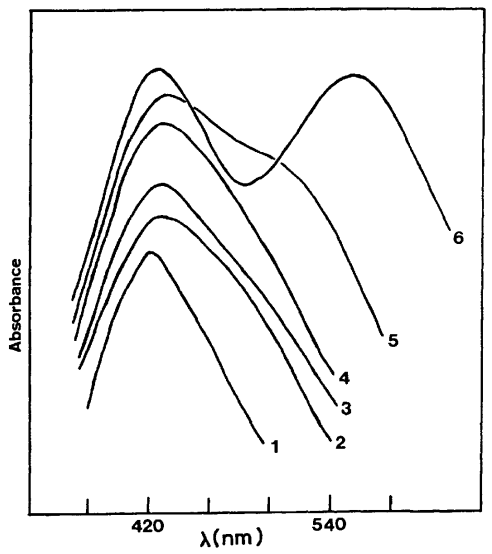

Fig. 3. Electronic spectra of [*m.n*]paracyclophadiyne–TCNE complexes (CH_2Cl_2, room temp): curve 1, **5**; 2, $\mathbf{1}_{24}$; 3, $\mathbf{1}_{55}$; 4, $\mathbf{1}_{44}$; 5, $\mathbf{1}_{34}$; 6, $\mathbf{1}_{33}$.

TABLE 2. CT-BAND POSITIONS OF CYCLOPHANE– AND *p*-XYLENE–TCNE COMPLEXES(CH_2Cl_2, ROOM TEMP)

Donor	λ_{max} (nm)[a]	
$\mathbf{1}_{33}$	427 (425)	555 (555)
$\mathbf{1}_{34}$	431 (415)	(510)
$\mathbf{1}_{24}$	430 (402)	(470)
$\mathbf{1}_{44}$	429 (410)	(480)
$\mathbf{1}_{55}$	426 (410)	(480)
5	425 (415)	(480)
p-xylene[b]	426 (408)	(490)
p-xylene[c]	415	460
[3.3] paracyclophane[d]	486	599
[3.4] paracyclophane[d]	470	538

a) Values in parentheses denote curve-resolved maximum. b) Ref. 11c ($CHCl_3$). c) Ref. 6. d) Ref. 7a.

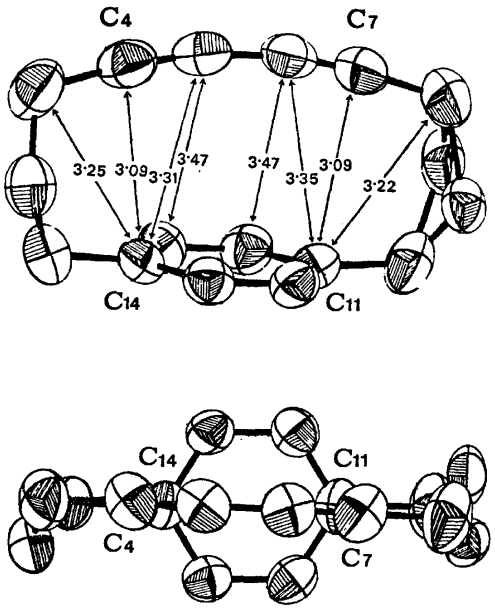

Fig. 4. Crystal structure of [3.3]paracyclophadiyne.[18]

The longer wavelength band of $\mathbf{1}_{33}$–TCNE complex appears with a red-shift of 75 nm as compared to those of complexes of $\mathbf{1}_{44}$ and $\mathbf{1}_{55}$. The crystal structure of $\mathbf{1}_{33}$ shows a remarkable distortion of the diacetylene group and a slight bending of the benzene ring from their normal arrangements as seen in Fig. 4.[18] Since the positions of CT-absorption maxima are little affected by such distortions of benzene ring[7a,b] and of diacetylene group as described for $\mathbf{3}_9$ and $\mathbf{3}_{10}$, the marked red-shift of $\mathbf{1}_{33}$–TCNE complex should be interpreted in terms of considerable transannular π-electron donation from the non-complexed diacetylene group to the complexed benzene ring in the parallel complex $\mathbf{12}_{33}$. On the other hand, the shorter wavelength band can be assigned

to the complex $\mathbf{10}_{33}$ and $\mathbf{11}_{33}$, provided that both complexes are in an equilibrium as shown in Scheme 1. Since the maximum of this band appears at nearly the same position as the corresponding maxima of the other complexes $\mathbf{10}_{mn}$ and $\mathbf{11}_{mn}$ having different number of bridged methylene, it is suggested that the transannular π-π interaction does not make a very important contribution to the CT-tansitions of both complexes $\mathbf{10}_{33}$ and $\mathbf{11}_{33}$.

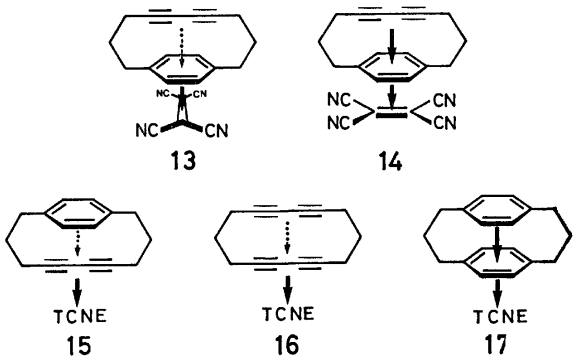

Fig. 5. Transannular π-π interaction in cyclic donor–TCNE complexes; thick and dotted arrows in the donor molecules indicate effective and unobserved interactions, respectively.

The complex of $\mathbf{1}_{34}$ shows an intermediate spectral feature between those of its homologs $\mathbf{1}_{33}$ and $\mathbf{1}_{m=n>3}$. The argument described for $\mathbf{1}_{33}$ seems to be also applicable to this complex.

Geometrical Effect of TCNE Complexes on Transannular π-π Interaction. A different π-donating character of the diacetylene group was observed between two pseudo-conformer $\mathbf{11}_{33}$ and $\mathbf{12}_{33}$ (or **13** and **14** in Fig. 5). The difference can be qualitatively accounted for according to the discussion for the spectra of two isomeric complexes of *p*-disubstituted benzenes.[11a,c] The molecular orbitals that take part in allowed CT-transitions are depicted as **18** for **13** and as **19** for **14**. In **19**, the large π-electron density at C_4, C_7, C_{11}, and C_{14} causes facile overlapping between the three chromophores as expected from the crystal structure in Fig. 4, making the charge delocalization favorable. In the alternative pseudo-conformer **18**, the π-π interaction is not favorable because of the existence of a nodal plane passing through C_4, C_7, C_{11}, and C_{14} (Fig. 6). Two bands of TCNE complexes of [3.4]paracyclophadiyne $\mathbf{1}_{34}$ and [3.3]paracyclophane[7a] are similarly explained in terms of two pseudo-conformers.

It is noteworthy that there is no appreciable transannular delocalization in the diacetylene-site complexes, **15** and **16**, and the benzene-site perpendicular complex **13** in contrast to marked delocalization in the parallel complex **14**. Unusual thermal cycloaddition reactions of [m.n]paracyclophadiynes with TCNE were observed to proceed *via* the complex $\mathbf{10}_{mn}$ and not *via* the more stable $\mathbf{12}_{mn}$.

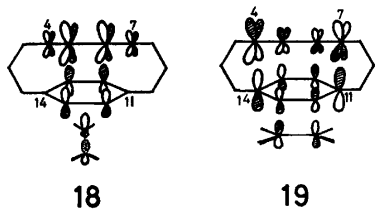

Fig. 6. Orbital sets of [3.3]paracyclophadiyne–TCNE complex.

Experimental

Materials. Five [m.n]paracyclophadiynes $\mathbf{1}_{mn}$, cyclic tetraacetylenes $\mathbf{2}_n$ (n=9 and 10), cyclic diacetylenes $\mathbf{3}_n$, diethynyl compound **4**, and paracyclophatetrayne **5** were prepared previously.[2] The diacetylene derivatives having bulky group at propargyl positions **6** and **7**,[19] cyclic tetraacetylenes $\mathbf{2}_n$ (n=3 and 4),[20] 5,7-dodecadiyne,[21] 5-decyne, and 3-octyne[22] were synthesized respectively according to the corresponding methods.

Tetracyanoethylene was recrystallized from chlorobenzene and sublimed twice at 125 °C/1 mmHg. TCNE was dissolved without coloration in dichloromethane (E. Merck Co. spectrograde) used as a solvent.

Electronic Spectra and Determination of Equilibrium Constants. All the spectra were measured on a Hitachi EPS-3T autorecording spectrophotometer using a 10 mm cell at room temperature within a few minutes after preparation of the solution.

Dichloromethane solutions of $\mathbf{1}_{mn}$- and **5**–TCNE complexes were prepared by a method similar to that for [m.n]paracyclophane–TCNE complexes.[7a] The observed maximum absorbances were 0.57—0.72 for $\mathbf{1}_{mn}$-complexes and 0.36 for **5**-complex. From the solutions of $\mathbf{1}_{33}$- and $\mathbf{1}_{44}$-complexes the donors were recovered by chromatography on alumina using hexane–ether (2: 1) as an eluent.

The spectra of $\mathbf{2}_n$- and $\mathbf{3}_n$–TCNE complexes were measured as follows: concentration of donor, 0.005—0.022 M; concentration of TCNE, 0.022—0.032 M; molar concentration ratio, 0.3—0.9. The observed maximum absorbances were in the range 0.20—0.42.

The Benesi-Hildebrand method[19] was used to determine the molar extinction coefficients and equilibrium constants for 5,7-dodecadiyne- and 5-decyne–TCNE complexes in dichloromethane at 25 °C. In these determinations the mole fraction of the donors was varied from 0.018 to 0.044, while the concentration of TCNE was held between 0.007 and 0.011 M. A straight line was obtained through the four measured points for each complex. The values of K and ε in Table 1 were calculated by the least-squares method.

Preparation of Crystalline Paracyclophadiyne–TCNE Complexes. The two-to-one complexes of [3.4]- and [4.4]-paracyclophadiynes over TCNE were prepared as follows.

A mixture of 0.1 g of $\mathbf{1}_{34}$ and 0.03 g of TCNE was dissolved in 0.5 ml of ethyl acetate, and then 3 ml of pentane was added. The solution was cooled to −20 °C to yield dark-red rhombic plates, which were collected and dried. $\mathbf{1}_{34}$–TCNE 2: 1 complex, mp 96—102 °C. Found: C, 83.84; H, 6.37; N, 9.69%. Calcd for $C_{40}H_{36}N_4$: C, 83.88; H, 6.34; N, 9.78%.

A solution of $\mathbf{1}_{44}$ (0.1 g) and TCNE (0.02 g) in 0.5 ml of ethyl acetate was cooled to −20 °C to give red crystals. The crystals were dissolved in a minimum amount of ethyl acetate, and the solution was allowed to stand overnight at room temperature. During this period the solvent was nearly completely evaporated to give reddish-orange rhombic plates, which were collected, washed quickly with petroleum ether containing a small amount of ethyl acetate, and dried. $\mathbf{1}_{44}$–TCNE 2: 1 complex, mp 117—128 °C. Found: C, 83.88; H, 6.71; N, 9.42%. Calcd for $C_{42}H_{40}N_4$: C, 83.96; H, 6.71;

N, 9.33%.

The infrared spectra of these crystalline complexes were illustrated as a superposition of those due to the two components.

The present work was partially supported by a Grant-in-Aid for Scientific Research from the Ministry of Education.

References

1) Part XLIII, T. Otsubo, S. Mizogami, N. Osaka, Y. Sakata, and S. Misumi, *Bull. Chem. Soc. Jpn.*, **50**, 1858 (1977).

2) a) T. Matsuoka, T. Negi, T. Otsubo, Y. Sakata, and S. Misumi, *Bull. Chem. Soc. Jpn.*, **45**, 1825 (1972); b) T. Matsuoka, T. Negi, and S. Misumi, *Synth. Commun.*, **2**, 87 (1972).

3) T. Takabe, M. Tanaka, and J. Tanaka, *Bull. Chem. Soc., Jpn.*, **47**, 1917 (1974).

4) T. Kaneda, T. Ogawa, and S. Misumi, *Tetrahedron Lett.*, **1973**, 3373; T. Inoue, T. Kaneda, and S. Misumi, *ibid.*, **1974**, 2969; T. Hayashi, N. Mataga, T. Inoue, T. Kaneda, M. Irie, and S. Misumi, *J. Am. Chem. Soc.*, **99**, 523 (1977); S. Inagaki, H. Fujimoto, and K. Fukui *ibid.*, **98**, 4693 (1976).

5) T. Kaneda, T. Inoue, Y. Yasufuku, and S. Misumi, *Tetrahedron Lett.*, **1975**, 1543.

6) R. E. Merrifield and W. D. Phillips, *J. Am. Chem. Soc.*, **80**, 2778 (1958).

7) a) D. J. Cram and R. H. Bauer, *J. Am. Chem. Soc.*, **81**, 5971 (1959); b) L. A. Singer and D. J. Cram., *ibid.*, **85**, 1080 (1963); c) M. Sheehan and D. J. Cram, *ibid.*, **91**, 3553 (1969).

8) D. J. Cram, R. C. Helgeson, D. Lock, and L. A. Singer, *J. Am. Chem. Soc.*, **88**, 1324 (1966); S. Hayashi and T. Sato, *Nippon Kagaku Zasshi*, **91**, 950 (1970).

9) a) D. T. Longone and H. S. Chow, *J. Am. Chem. Soc.*, **86**, 3898 (1964); *ibid.*, **92**, 994 (1970); b) A. J. Hubert, *J. Chem. Soc., C*, **1967**, 13; c) T. Otsubo, S. Mizogami, I. Otsubo, Z. Tozuka, A. Sakagami, Y. Sakata, and S. Misumi, *Bull. Chem. Soc. Jpn.*, **46**, 3519 (1973).

10) T. Otsubo, S. Mizogami, N. Osaka, Y. Sakata, and S. Misumi, *Bull. Chem. Soc. Jpn.*, **50**, 1841 (1977).

11) a) A. Zweig, *Tetrahedron Lett.*, **1964**, 89; b) E. M. Voigt, *J. Am. Chem. Soc.*, **86**, 3611 (1964); E. M. Voigt and C. Reid, *ibid.*, **86**, 3930 (1964); c) D. D. Holder and C. C. Thompson, *J. Chem. Soc., Chem. Commun.*, **1972**, 277.

12) T. F. Rutledge, "Acetylenic Compounds," Reinhold, New York (1968), p. 5.

13) For example, P. R. Schleyer, D. S. Trifan, and R. Bacskai, *J. Am. Chem. Soc.*, **80**, 6691 (1958).

14) D. Cook, Y. Lupien, and W. G. Schreiber, *Can. J. Chem.*, **34**, 957 (1956).

15) H. A. Benesi and J. H. Hildebrand, *J. Am. Chem. Soc.*, **71**, 2703 (1949).

16) K. Harata, T. Aono, K. Sakabe, N. Sakabe, and J. Tanaka, *Acta Crystallogr., Sect A*, **28**, S14 (1972).

17) J. L. Lippert, M. W. Hanna, and P. J. Trotter, *J. Am. Chem. Soc.*, **91**, 4035 (1969).

18) T. Aono, K. Sakabe, N. Sakabe, C. Katayama, and J. Tanaka, *Acta Crystallogr., Sect B*, **31**, 2389 (1975).

19) a) T. Negi, T. Kaneda, Y. Sakata, and S. Misumi, *Chem. Lett.*, **1972**, 703; b) T. Negi, T. Kaneda, H. Mizuno, T. Toyoda, Y. Sakata, and S. Misumi, *Bull. Chem. Soc. Jpn.*, **47**, 2398 (1974).

20) a) F. Sondheimer and Y. Amiel, *J. Am. Chem. Soc.*, **79**, 5817 (1957); b) F. Sondheimer, Y. Amiel, and R. Wolovsky, *ibid.*, **79**, 6263 (1957).

21) G. Zweifel and N. L. Polston, *J. Am. Chem. Soc.*, **92**, 4068 (1970).

22) E. A. Bried and G. F. Hennion, *J. Am. Chem. Soc.*, **59**, 1310 (1937).

The Structure and Reactions of Imidoyl Triphenylphosphonium Methylides

Hiroshi YOSHIDA, Tsuyoshi OGATA, and Saburo INOKAWA

Department of Synthetic Chemistry, Faculty of Engineering, Shizuoka University, Hamamatsu 432

(Received April 22, 1977)

Twenty-five imidoyl triphenylphosphonium methylides III were prepared from triphenylphosphonium methylide and imidoyl chlorides or imidates in moderate yields. The configration of these ylides was assigned on the basis of NMR spectroscopic studies. *N*-Tosyl substituted ylides showed no reactivity toward aldehydes, whereas *N*-aryl substituted ylides could be converted easily into α,β-unsaturated ketimines in good yields. The reaction of III with carbon disulfide was also studied.

In recent years a number of phosphonium ylides stabilized by adjacent groups, such as carbonyl, thiocarbonyl, sulfonyl, and cyano, have been isolated, and their physical and chemical properties have been documented.[1]

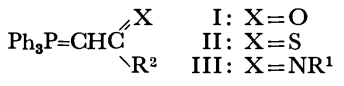

I: X=O
II: X=S
III: X=NR¹

In the course of our studies of *P*- and *S*-ylides and imides,[2,3] we have found a useful method for the preparation of imidoyl-stabilized phosphonium ylides, III. Here we will report on the structure and reactions of III.

Results and Discussion

Preparation of Imidoyl Triphenylphosphonium Methylides III. Some imidoyl-substituted ylides III have been reported.[4–6] The addition of phenylethynylphosphonium salt to aniline gives IIIp.[4] The thioimidate-type ylide IIIk is prepared by the alkylation of thiocarbamoyl triphenylphosphonium methylide with methyl iodide, followed by treatment with a base.[5] (This route seems to be a good method for the preparation of alkylthiocarbonimidoyl ylides). The addition of phosphinimine with dimethyl acetylenedicarboxylate gives α-imidoyl ylide IV.[6]

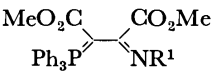

IV

These reported methods seems to have a limited application for the preparation of III with various substituents. We found that imidates, thioimidates, and imidoyl chlorides were good reagents for the preparation of imidoyl triphenylphosphonium methylides. The results are shown in Table 1.

Table 1. The preparation of III

III	V			III		Recryst solvent[a]	Found(Calcd)(%)		
	R^1	R^2	X	Yield(%)	Mp(°C)		C	H	N
IIIa	Ts	H	OEt	87	193—194	B–P	70.65(70.88)	5.17(5.29)	3.11(3.06)
IIIb	Ts	SMe	SMe	82	272—273	AcOH	66.89(66.78)	5.32(5.20)	2.70(2.78)
IIIc	Ts	SEt	SEt	78	235—238	C–P	67.11(67.29)	5.56(5.45)	2.85(2.71)
IIId	Ts	SPr-*i*	SPr-*i*	62	185—186	C–P	67.56(67.77)	5.79(5.69)	2.75(2.63)
IIIe	Ts	OMe	SMe	74	210—211	C–P	68.87(68.98)	5.24(5.38)	2.93(2.87)
IIIf	Ts	OEt	SMe	64	205—206	C–P	69.58(69.44)	5.57(5.63)	2.64(2.79)
IIIg	Ts	OPr-*i*	SMe	68	180—182	C-P	69.93(69.88)	5.75(5.86)	2.58(2.72)
IIIh	Ts	Ph	Cl	72	176—178	C–P	74.12(74.28)	5.03(5.29)	2.42(2.62)
IIIi	Ts	NMe_2	SMe	73	227—230	C–P	69.49(69.58)	5.96(5.84)	5.44(5.60)
IIIj	Bs	Me	Cl	51	125—127	C–P	70.97(70.88)	5.37(5.29)	3.16(3.06)
IIIk	Ph	SMe	SMe	67	164[5]	C–P	76.02(76.21)	5.51(5.68)	3.28(3.29)
IIIl	Ph	SEt	SEt	63	156—157	C–P	76.38(76.51)	5.89(5.96)	3.03(3.19)
IIIm	Ph	SPr-*i*	SPr-*i*	58	147—150	C–P	76.94(76.79)	6.10(6.22)	3.21(3.09)
IIIn	Ph	OMe	Cl	63	180—182	E–P	70.08(70.20)	5.83(5.91)	3.39(3.42)
IIIo	Ph	OEt	Cl	53	149—151	E–P	79.30(79.41)	6.04(6.19)	3.25(3.31)
IIIp	Ph	Ph	Cl	71	222—223[4]	C–P	84.27(84.37)	5.60(5.75)	3.19(3.07)
IIIq	Ph	*p*-$NO_2C_6H_4$	Cl	74	230—232	C	76.91(76.79)	5.23(5.03)	5.55(5.60)
IIIr	*p*-Tol	Ph	Cl	77	184—186	C–P	84.66(84.41)	6.14(6.01)	2.82(2.98)
IIIs	*p*-Anis	Ph	Cl	74	176—177	C–P	81.74(81.63)	5.72(5.81)	2.78(2.88)
IIIt	*p*-$NO_2C_6H_4$	*p*-$NO_2CC_6H_4$	Cl	68	244—246	C	70.20(70.45)	4.57(4.43)	7.75(7.70)
IIIu	2,4,6-$Me_3C_6H_2SO_2$	H	OEt	58	180—181	B–P	71.56(71.73)	5.61(5.81)	2.73(2.88)
IIIv	$EtSO_2$	H	OEt	63	167—169	B–P	66.71(66.82)	5.44(5.61)	3.46(3.54)
IIIw	2,4-$(NO_2)_2C_6H_3$	H	OEt	74	202—203	B	66.75(66.52)	4.53(4.29)	8.82(8.95)

a) B: benzene, C: chloroform, E:ethyl acetate, P: petroleum ether.

$$2Ph_3P{=}CH_2 + R^1N{=}C(R^2)X \longrightarrow Ph_3P{=}CHC(NR^1)R^2 + Ph_3\overset{\oplus}{P}Me\ \overset{\ominus}{X}$$

V III

The structure of the products were confirmed by the NMR, IR, and elemental analyses.

Although the reaction of V(R^1=Ph, R^2=H, X=OEt; R^1=Ph, R^2=Me, X=Cl; R^1=Me, R^2=Ph, X=Cl) with phosphonium methylide proceeded vigorously, the isolation of the corresponding ylides III(R^1=Ph, R^2=H; R^1=Ph, R^2=Me; R^1=Me, R^2=Ph) failed, yielding only a brown oil. This result suggests that strong electron-withdrawing groups, such as tosyl, *p*-nitrophenyl for the R^1 and/or R^2 of III, stabilize ylides III.

Table 2. IR and pK_a data for III

III	$\nu_{C=N}$[a] cm^{-1}	pK_a[b]
IIIa	1520	4.42
IIIb	1450	3.60
IIIf	1490	3.86
IIIh		4.35
IIIk	1490	10.7
IIIn	1470	10.9
IIIp		>12
IIIr	1510	>12
IIIs	1510	>12
IIIu	1520	4.45

a) Nujol mull. b) In 20% aqueous ethanol.

Structure of III Ylides. Evidence for the resonance interaction of the ylide carbanion with the imino group can be obtained by an examination of the infrared spectra of the imidoyl ylides, III. The C=N stretching frequencies of III occurred at around 1500 cm^{-1} (Table 2). Considering the frequencies of the model compounds[7] [ketimines (−1650 cm^{-1}), imidates (−1650 cm^{-1}), and thioimidates (−1610 cm^{-1})], the shifts of 100—150 cm^{-1} for III may be attributed to the increased single-bond character and to the delocalization of the carbanion electrons through the imino groups (*i.e.*, such betain forms as III_E and III_Z).

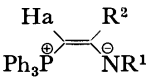

III_Z

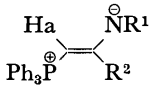

III_E

The structure of the ylide was confirmed on the basis of NMR spectroscopic studies.[10] The results obtained are collected in Tables 3 and 4.

The NMR spectra of ester-stabilized ylides, I and II(R^2=*O*-Alkyl), have been shown to be mixtures of *E* and *Z* isomers;[8] however, the carbonyl-stabilized ylides, I and II(R^2=Alkyl or Aryl), are only *Z* isomers.[9]

The aldimino-type ylides, IIIa, u, v, and w existed as mixtures of *E* and *Z* isomers in benzene, nitrobenzene, and chloroform, and the *E*/*Z* ratios increased in accordance with the solvent polarity (benzene–nitrobenzene). The hydrogen-bonding interaction between chloroform and a negative oxygen or sulfur atom[2,8] is not as important a factor for IIIa, u, v, and w (Table 3) as for II(R^2=H). This result reveals that the strong electron-withdrawing effect of the R^1 substituent would stabilize both betain forms, III_E and III_Z.

As is shown in Table 4, two kinds of methyl signals due to ethyl or isopropyl groups of alkoxycarbonimidoyl or alkylthiocarbonimidoyl ylides III(R^2=*O*-Alkyl or *S*-Alkyl) appeared at δ 0.5—0.8 and 1.2—1.4 respectively. The stereochemistry of these methyl groups was assigned on the assumptions that protons of the R^2 group, neighbouring *cis* to the phosphorus, are shielded by the phenyl groups and that they appear at a higher field than that of the *trans* isomer.[2] The IIIc, d, e, f, and g ylides were also considered to be mixtures of *E* and *Z* isomers. The *N*-phenyl-substituted ylides, IIIl, m and IIIn, o were only *Z* and/or *E* isomers respectively (Table 4).

The coupling constants, J_{PCH_a}, for the alkoxycarbonimidoyl, alkylthiocarbonimidoyl, and formimidoyl ylides III(R^2=*O*-Alkyl, *S*-Alkyl, and H) show that the constants for the *Z* isomers are larger than those for the

Table 3. NMR data for aldimino ylides, III

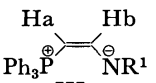

III_Z

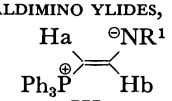

III_E

III	Structure (%)	Solvent			NMR Signals in $CDCl_3$				
		$CDCl_3$	PhH	$PhNO_2$	Ha(δ)	Hb(δ)	J_{HaHb}	J_{PCHa}	J_{PCCHb}
IIIa	*E*	50	18	35	4.72	a)	14	20	—
	Z	50	82	65	3.96	8.36	7	25	39
IIIu	*E*	47	16	39	4.51	a)	14	21	—
	Z	53	84	61	3.75	8.32	7	25	39
IIIv	*E*	51	—[b]	31	4.64	a)	13	20	—
	Z	49	—[b]	69	3.90	8.18	7	25	39
IIIw	*E*	28	—[b]	10	5.00	a)	13	20	—
	Z	72	—[b]	90	4.32	8.34	6	24	—
II(R=H)[c]	*E*	81	10	47	5.94	8.69	15	26	16
	Z	19	90	53	5.17	9.34	8	30	45

a) Signals appeared in the phenyl-proton region. b) The low solubility of IIIv, w inhibited precise studies.
c) Taken from Ref. 2.

Table 4. NMR spectroscopic studies of III in $CDCl_3$ [δ ppm (J Hz)]

III	Conf(%)	Ha(J_{PCHa})	Others[b]
IIIc	E(46)	4.83(18)	0.75(t, J=7, $CH_2C\underline{H}_3$), 2.44 (s, $C\underline{H}_3C_6H_4$), 2.86 (q, $C\underline{H}_2CH_3$)
	Z(54)	3.85(24)	1.39(t, J=7, $CH_2C\underline{H}_3$), 2.38 (s, $C\underline{H}_3C_6H_4$), 2.98 (q, $C\underline{H}_2CH_3$)
IIId	E(69)	4.76(20)	0.81(d, J=7, $CH\underline{Me}_2$), 2.36(s, $C\underline{H}_3C_6H_4$)
	Z(31)	3.83(24)	1.36(d, J=7, $CH\underline{Me}_2$), 2.28(s, $C\underline{H}_3C_6H_4$)
IIIe	E(96)	3.97(20)	2.39(s, $C\underline{H}_3C_6H_4$), 3.35(s, OMe)
	Z(4)	a)	2.29(s, $C\underline{H}_3C_6H_4$), 3.88(s, OMe)
IIIf	E(93)	3.89(20)	0.52(t, J=7, $CH_2C\underline{H}_3$), 2.36(s, $C\underline{H}_3C_6H_4$), 3.85(q, $C\underline{H}_2CH_3$)
	Z(7)	a)	1.23(t, J=7, $CH_2C\underline{H}_3$), 2.29(s, $C\underline{H}_3C_6H_4$)
IIIg	E(93)	3.90(19)	0.63(d, J=6, $CH\underline{Me}_2$), 2.38(s, $C\underline{H}_3C_6H_4$), 4.99(hept, $C\underline{H}Me_2$)
	Z(7)	a)	1.01(d, J=6, $CH\underline{Me}_2$), 2.26(s, $C\underline{H}_3C_6H_4$)
IIIh	Z	4.02(28)	2.34(s, $C\underline{H}_3C_6H_4$)
IIIi		a)	2.40(s, $C\underline{H}_3C_6H_4$), 3.41(s, NMe_2)
IIIj	Z	3.85(26)	2.39(d, J=1, Me)
IIIk	Z	3.05(24)	2.35(s, SMe).
IIIl	Z	3.13(24)	1.26(t, J=8, $CH_2C\underline{H}_3$), 2.90(q, $C\underline{H}_2CH_3$)
IIIm	Z	a)	1.26(d, J=7, $CH\underline{Me}_2$)
IIIn	E	2.46(20)	3.53(s, OMe)
IIIo	E	a)	0.69(t, J=7, $CH_2C\underline{H}_3$), 4.05(q, $C\underline{H}_2CH_3$)
IIIp	Z	a)	
IIIq	Z	3.21(23)	
IIIr	Z	3.27(27)	2.19(s, $C\underline{H}_3C_6H_4$)
IIIs	Z	a)	3.60(s, OMe)
IIIt	Z	3.92(24)	

a) Not observed. b) Phenyl-ring protons appeared at 6.5—8.0.

Table 5. The reaction of III with carbon disulfide in chloroform

III	Temp	Time(day)	Product(%)
IIIe	r.t	7	—
IIIh	r.t	7	—
IIIk	r.t.	1	IIb(82) PhNCS
IIIl	40 °C	1	IIc(85) PhNCS
IIIp	40 °C	1	IIa(66) PhNCS
IIIr	r.t.	1	IIa(71) p-TolNCS
IIIn	r.t.	1	VIII(76)

E isomers (24—25 and 18—20 Hz respectively). This result suggests that the structures of the ketimino-type ylides, IIIh, i, j, p, q, r, s, and t may be considered to be Z isomers on the basis of their coupling constants J_{PCHa} (23—28 Hz).

The Reaction of III with Carbon Disulfide. The electrophilic attack of carbon disulfide on phosphonium methylides[1] occurred at the ylide carbanions. The ylides III(R^1=Aryl) can react easily with carbon disulfide, as is shown in Table 5. The reaction of the alkylthiocarbonimidoyl ylides, IIIk and l with carbon disulfide gave the thiocarbonyl ylides, IIb and c (R^2= SMe and SEt), and phenyl isothiocyanate in good yields. The products were identified by comparing their NMR and mps with those of authentic samples.[2]

$Ph_3P{=}CHC(=S)R^2$ (II)

IIa: R^2=Ph
IIb: R^2=SMe
IIc: R^2=SEt
IId: R^2=OMe

The ketimino ylides, IIIp and r also showed a high reactivity toward carbon disulfide. The NMR spectroscopic study of this reaction seems to be interesting. To a solution of IIIr in chloroform-d we added a large excess amount of carbon disulfide in one portion, yielding a red solution within a minute. The NMR spectrum of this reaction mixture showed two new, nearly equivalent methyl signals of p-tolyl groups at δ 2.11 and 2.33, whose original signals appeared at 2.19. On standing at 40 °C for 2 days or heating at 70 °C for 12 h the higher-field signal disappeared almost entirely. The reaction products were triphenylphosphonium thiobenzoylmethylide, IIa, and p-tolyl isothiocyanate. To find the initial reaction products, controlled experiment was undertaken. IIIr (1 mmol) was dissolved in 3 ml of carbon disulfide. Three minutes later, to the resulting red mixture we added methyl iodide (0.66 mmol) in one portion and stirred the mixture well. Then all the liquid was removed *in vacuo*, and the benzene-soluble part was separated. Concentration and crystallization from chloroform–hexane yielded triphenylphosphonium[(methylthio)thiocarbonyl](*N*-p-tolylbenzimidoyl)methylide VIb (R^1=p-Tol, R^2=Ph) in a 19% yield. The structure of VIb was confirmed on the basis of NMR, MS, and a methylation reaction, yielding VIIb (R^1=p-Tol, R^2=Ph). A similar treatment of IIIp with carbon disulfide yielded VIa (R^1=R^2=Ph) in a 23% yield.

On the other hand, the reaction of IIIn with carbon disulfide proceeded slowly to give not IId,[2] but VIII, as an isolable product in a 76% yield (based on the methyl groups). The structure of VIII was confirmed on the basis of NMR (SMe and OMe groups), MS, and methylation with methyl iodide to yield IX.

The marked difference in the reactivity of these ylides III with carbon disulfide may be attributed to the pK_a values of the conjugate acids of the ylide carbanions.

Table 6. The reaction of III with aldehydes(X)

III	X R^3CHO	XI R^1	R^2	R^3	Yield(%)	Mp(°C)	M^+	NMR(δ in $CDCl_3$)[a]	Found(Calcd) (%) C	H	N
IIIk	PhCHO	Ph	SMe	Ph	91	90—91	235	2.51(s, SMe)	75.63 (75.85)	6.28 (6.42)	5.42 (5.53)
	MeCHO	Ph	SMe	Me	85	oil	191	1.70(dd, J=6 and 1, MeCH=), 2.32(s,SMe)	69.21 (69.07)	6.73 (6.85)	7.48 (7.32)
IIIl	PhCHO	Ph	SEt	Ph	90	50—51	267	1.37(t, J=7, CH_3), 3.08(q, CH_2)	76.49 (76.36)	6.23 (6.41)	5.16 (5.28)
IIIn	PhCHO	Ph	OMe	Ph	92	68—69	237	3.89(s, OMe)	80.74 (80.98)	6.28 (6.37)	6.02 (5.90)
	MeCHO	Ph	OMe	Me	82	oil	175	1.73 and 1.91 (d, J=6, 3:1, MeCH=), 3.80 and 3.83 (s, 3:1, OMe)	75.16 (75.40)	7.55 (7.48)	7.68 (7.99)
IIIp	PhCHO	Ph	Ph	Ph	94	108—109	283		89.17 (89.01)	6.18 (6.05)	4.98 (4.94)
IIIr	*p*-ClC_6H_4-CHO	*p*-Tol	Ph	*p*-ClC_6H_4	96	118—120	331	2.21 and 2.38 (s, 2:5, CH_3)	79.51 (79.63)	5.64 (5.47)	4.37 (4.22)
	PhCHO	*p*-Tol	Ph	Ph	91	94—95	297	2.20 and 2.38 (s, 1:3, CH_3)	88.67 (88.85)	6.23 (6.44)	4.39 (4.71)
	MeCHO	*p*-Tol	Ph	Me	87	oil	235	1.74 and 1.83 (d, J=6, 3:1, MeCH=), 2.15 and 2.31 (s, 1:3, $CH_3C_6H_4$)	86.84 (86.77)	7.13 (7.28)	5.84 (5.95)

a) Protons due to the phenyl and vinyl groups appeared at 6.5—8.0 as multiplets.

The reactivity decreases with the decrease in pK_a values (Tables 2 and 5). Considering the results obtained, we assumed equilibria between III, A, and B, followed by the kinetically controlled decomposition of A and B, depending on the nature of the substituents, R^1 and R^2 (Scheme 1). The A formed from IIIk, l, p, and r and carbon disulfide gave II and isothiocyanate, while the B from IIIp, r gave VIa and b in the presence of methyl iodide. On the other hand, IIIn reacted slowly with carbon disulfide to give the product, VIII, from B *via* the intermolecular nucleophilic attack of the thiolate anion on the methyl group of IIIn. The thiocarbonyl ylides, VI and VIII, can be easily identified because of their high reactivity with methyl iodide to yield two *S*-methylation products, VII and IX, as was observed for the II ylides.[2]

The Reaction of III with Aldehydes, X. The Wittig reaction of III with the aldehydes, X, gave α,β-unsaturated ketimines, XI, in fairly good yields (Table 6). The products were confirmed by MS, NMR, and acid hydrolysis. XI (R^1=R^2=R^3=Ph) and XI (R^1=*p*-Tol, R^2=R^3=Ph) gave chalcone on hydrolysis with 1M-HCl in 30% aqueous ethanol. Although the NMR spectra of XI (Table 6) showed the presence of stereo isomers, no effort was made to effect their isolation at this stage.

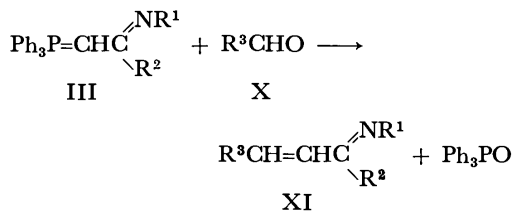

α,β-Unsaturated aldimines can be easily prepared by the condensation of unsaturated aldehydes and amines.[11] On the contrary, α,β-unsaturated ketones can react

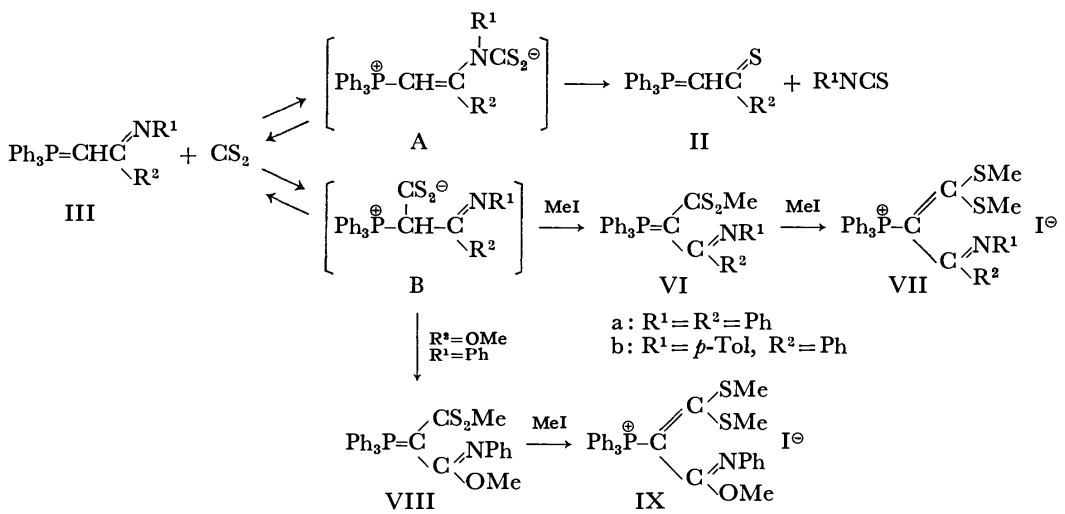

Scheme 1.

with amines to give not imines, but β-amino ketones.[12] The Wittig reaction of III seems to be a useful method for the preparation of α,β-unsaturated ketimines, XI.

N-Tosyl-substituted ylides IIIb and h showed no reactivity toward aldehydes even when heated at 80 °C for 10 h in benzene or chloroform.

Experimental

Preparation of Imidoyl Chlorides, Imidates, and Thioimidates. The formimidates, Va, u, v, and w were prepared by the condensation of ethyl orthoformate and amide or amine according to the literature.[13,14] The new compound, Vu, had a mp of 84—85 °C (ethanol); M^+, 255.

The other imidoyl chlorides and imidates were prepared by the known methods shown in the literature.[15] New compounds were checked by MS. Vd: mp 62—63 °C (ethanol); M^+, 363. Vf: mp 84—85 °C (ethanol); M^+, 273. Vg: mp 76 °C (ethanol); M^+, 287. Vi: mp 60—62 °C (ethanol); M^+, 272. Vl: bp 110—113 °C/3mmHg; M^+, 225. Vm: bp 136—138 °C/3 mmHg; M^+, 253.

Preparation of III. A suspension of triphenylmethylphosphonium bromide (5.0 g, 14 mmol) and sodium amide (1.5 g) in 50 ml of dry benzene was stirred for 12 h in a stoppered flask at room temperature. After the separation of the precipitate, the ammonia was removed *in vacuo* to give a yellow solution of triphenylphosphonium methylide. To the solution we added imidoyl chloride (6 mmol) in 10 ml of benzene in one portion. The mixture was then allowed to stand for 1 h at room temperature and subsequently treated with charcoal (phosphonium chloride also separated) and condensed *in vacuo* to give a crystalline mass. Crystallization from appropriate solvents yielded III. The results are shown in Table 1.

Determination of pK_a of Ylides, III. The pK_a values were measured in 20% aqueous ethanol according to the literature.[16] The results are given in Table 2.

The Reaction of III with Carbon Disulfide. To a solution of IIIk, l, p, and r (1 mmol) in 20 ml of chloroform we added 1 ml of carbon disulfide in one portion. The resulting solution was heated at 40 °C or at room temperature for 1—2 day, and condensed *in vacuo*, thus separating the petroleum ether-soluble and -insoluble parts. The latter part gave triphenylphosphonium thiocarbonylmethylides, IIa, b, and c, whose physical properties have been previously reported by the present authors.[2]

IIIp (1 mmol) was dissolved in 3 ml of carbon disulfide. Three minutes later methyl iodide (0.66 mmol) was added to the resulting red mixture. Then all the liquid was removed *in vacuo*, and a benzene-soluble product was separated. Crystallization from chloroform–hexane yielded VIa (R^1=R^2=Ph): mp 235—237 °C; NMR ($CDCl_3$) δ=2.64 (3H, s, SMe), 6.8—8.0 (25H, m, Harom). Found: C, 74.51; H, 5.42; N, 2.44%; M^+, 545. Calcd for $C_{34}H_{28}NPS_2$: C, 74.83; H, 5.17; N, 2.57%; M, 545. The methylation of VIa with methyl iodide in chloroform yielded VIIa (R^1=R^2=Ph) in a quantitative yield. VIIa: mp 162—164 °C; NMR ($CDCl_3$) δ=1.87 and 2.00 (3H, s, 1:2, SMe), 2.69 and 2.82 (3H, s, 1:2, SMe), and 6.9—8.2 (25H, m, Harom). In the similar treatment of IIIr with carbon disulfide, VIb (R^1=*p*-Tol, R^2=Ph) was obtained in a 19% yield. VIb: mp 228—229 °C; NMR ($CDCl_3$) δ=2.38 (3H, s, $C\underline{H}_3C_6H_4$), 2.58 (3H, s, SMe), and 6.8—8.0 (24H, m, Harom). Found: C, 75.28; H, 5.24; N, 2.39%; M^+, 559. Calcd for $C_{35}H_{30}NPS_2$: C, 75.10; H, 5.40; N, 2.50%; M, 559. VIIb (R^1=*p*-Tol, R^2=Ph): mp 193—194 °C; NMR ($CDCl_3$) δ=1.90 and 2.02 (3H, s, 1:2, SMe), 2.27 and 2.61 (3H, s, 1:2, $C\underline{H}_3C_6H_4$), 2.71 and 2.84 (3H, s, 1:2, SMe), and 6.8—8.0 (24H, m, Harom).

The reaction of IIIn with carbon disulfide was run similarly to give VIII in a 75% yield. VIII: mp 242—245 °C (ethyl acetate–hexane); NMR ($CDCl_3$) δ=2.62 (3H, s, SMe), 3.63 (3H, s, OMe), and 6.7—8.0 (20H, m, Harom). Found: C, 69.72; H, 5.33; N, 2.94%; M^+, 497. Calcd for $C_{29}H_{26}NOPS_2$: C, 70.00; H, 5.27; N, 2.81%; M, 497. IX: oil; NMR ($CDCl_3$) δ=1.82 (3H, s, SMe), 2.73 (3H, s, SMe), 3.56 (3H, s, OMe), and 6.7—8.0 (20H, m, Harom).

The Reaction of III with Aldehydes X. To a solution of III (1 mmol) in 10 ml of chloroform we added an equimolar amount of aldehyde, X. After 5 min the solution was condensed *in vacuo*, and the petroleum ether-soluble part (XI) and -insoluble part (phosphine oxide) were separated. By crystallization from ethanol XI substances were obtained in good yields (Table 6).

Hydrolysis of XI (R^1=R^2=R^3=Ph) and XI (R^1=p-Tol, R^2=R^3=Ph). A solution of XI (1 mmol) in 15 ml of 1M-HCl 30% aqueous ethanol was kept standing at room temperature for 12 h. The solution was quenched in 30 ml of water, yielding precipitates which, on crystallization from ethanol, gave chalcone in 70—80% yields.

References

1) a) H. J. Bestmann and R. Zimmerman, "Organic Phosphorus Compounds," ed by G. M. Kosolapoff and L. Maier, Vol. 3, Wiley-Intersciences, New York (1972), p. 1; b) A. W. Johnson, "Ylide Chemistry," Academic Press, New York and London (1966).

2) H. Yoshida, H. Matsuura, T. Ogata, and S. Inokawa, *Bull. Chem. Soc. Jpn.*, **48**, 2907 (1975).

3) H. Yoshida, H. Taketani, T. Ogata, and S. Inokawa, *Bull. Chem. Soc. Jpn.*, **49**, 3128 (1976).

4) H. Hoffman and H. Foerstar, *Tetrahedron Lett.*, **1964**, 983.

5) H. J. Bestmann and S. Pfohl, *Angew. Chem.*, **81**, 750 (1969).

6) G. W. Brown, R. C. Cookson, and I. D. R. Stevens, *Tetrahedron Lett.*, **1964**, 1263; G. W. Brown, R. C. Cookson, I. D. R. Stevens, T. C. W. Mak, and J. Trotter, *Proc. Chem. Soc.*, **1964**, 87.

7) C. Sandorfy, "The Chemistry of the Carbon-Nitrogen Double Bond," ed by S. Patai, Interscience Publishers, London (1970), p. 1.

8) J. P. Snyder, *Tetrahedron Lett.*, **1971**, 215.

9) H. I. Zeliger, J. P. Snyder, and H. J. Bestmann, *Tetrahedron Lett.*, **1969**, 2199.

10) L. M. Jackman and S. Sternhell, "Application of Nuclear Magnetic Resonance Spectroscopy in Organic Chemistry," 2nd ed, Pergamon Press, Oxford (1969).

11) S. R. Sandlar and W. Karo, "Organic Functional Group Preparations," Vol. II, Academic Press, New York and London (1971).

12) N. H. Cromwell, *Chem. Rev.*, **38**, 83 (1946).

13) H. Stetter and D. Theisen, *Chem. Ber.*, **102**, 1641 (1969).

14) T. Okuyama, T. C. Pletcher, D. J. Sahn, and G. L. Schmeier, *J. Am. Chem. Soc.*, **95**, 1253 (1973).

15) H. Ulrich, "The Chemistry of Imidoyl Halides," Plenum Press, New York (1968).

16) A. W. Speziale and K. W. Ratts, *J. Am. Chem. Soc.*, **85**, 2790 (1963).

The Components of *Petasites japonicus* Maxim. IV.[1] The Structure of Petasitin

Ichiro TAKAGI,* Yasuhito TAZUKE, and Keizo NAYA

Department of Chemistry, Faculty of Science, Kwansei Gakuin University, Uegahara, Nishinomiya, Hyogo 662

(Received April 30, 1977)

Petasitin, a component isolated from a wild variety of *Petasites japonicus* Maxim., has been shown to be 3α-[(*Z*)-2-methyl-2-butenoyloxy]-11-hydroxyeremophila-6,9-dien-8-one, and has been synthesized from the known isopetasin by photosensitized oxygenation.

In an earlier communication,[2] we reported the structural proof of petasitin (**1**) isolated from the wild plant of *Petasites japonicus* Maxim. ("Fuki" in Japanese). We wish now to describe its isolation and structural determination, and also the synthesis of **1** from a known isopetasin (**15**).[3]

A methanol extract of the dried flower stalks of the plant was chromatographed repeatedly on alumina and silica gel, and from the polar part a component named petasitin (**1**) was obtained.

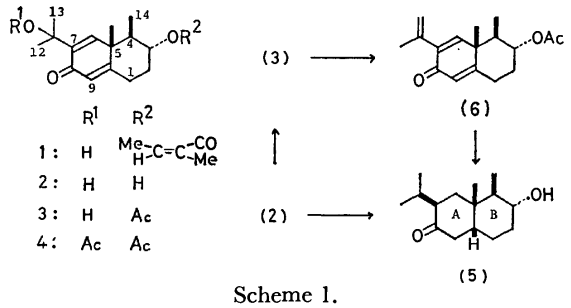

Scheme 1.

Petasitin (**1**), $C_{20}H_{28}O_4$ (bp 167.0—170 °C/2×10^{-4} mmHg, $[\alpha]_D$ −26.2°), is a colorless, highly viscous oil. Its IR and UV spectra show the presence of α,β-unsaturated carbonyl systems— a ketone (1665 cm^{-1} and λ_{max} 235 nm (ε, 14200)) and an ester (1710 and 1235 cm^{-1}). The spectral data also indicated that the fourth oxygen atom seemed to be a tertiary alcohol (3460 cm^{-1}) attached to the carbon atom bearing two methyls (δ 1.50, s, 6H). The existence of a (*Z*)-2-methyl-2-butenoate moiety as the ester group in petasitin, **1**, was inferred from the NMR signals, by analogy with those of the constituents[3-5] isolated from the same plant. In fact, the alkaline hydrolysis of **1** afforded (*Z*)-2-methyl-2-butenoic acid (angelic acid), accompanied by a small amount of the isomerization product, that is, the corresponding (*E*)-isomer (tiglic acid) and a diol, named petasitol (**2**), $C_{15}H_{22}O_3$ (mp 110.0—113.0 °C). In the UV spectrum of **2**, the intensity of the maximum at 244 nm (ε, 12700) suggests the presence of a cross-conjugated dienone system, and the IR spectrum exhibits bands at 3340 (hydroxyl), 1655 (α,β-unsaturated ketone), and 1610 cm^{-1} (double bond). In the NMR spectrum, petasitol, **2**, showed the signals due to four methyls, two vinyl protons (δ 6.12, t, J=1.0 Hz, 1H and 6.92, s, 1H), and a proton (δ 3.70, m, $W_{1/2}$=14 Hz) attached to a carbon atom carrying a newly appeared hydroxyl group. The acetylation of **2** with acetic anhydride–pyridine at room temperature gave a monoacetate (**3**) (mp 80.0—82.0 °C), which showed IR bands at 3420 (hydroxyl), 1735, 1240 (acetate), 1660 and 1610 cm^{-1} (α,β-unsaturated ketone), while acetylation with acetic anhydride–sodium acetate under reflux gave a mixture of monoacetate, **3**, and diacetate (**4**). The hydrogenation of **2** with 10% palladium charcoal in ethanol, followed by treatment with a catalytic amount of sodium methoxide in methanol, gave a dehydroxy-tetrahydro compound (**5**), $C_{15}H_{26}O_2$ (mp 103.0—103.5 °C), which was found to be identical with the known tetrahydroisopetasol (**5**)[3] (mp 103.0—104.0 °C), by a mixed-melting-point determination and a comparison of the spectral data. Thus, the one hydroxyl group lost by hydrogenolysis can be placed at an allylic position. This hydroxyl group in petasitol monoacetate, **3**, was readily dehydrated with phosphoryl chloride–pyridine to afford an anhydro derivative (**6**), whose spectra showed the NMR signals due to an *endo*-methylene group bearing a methyl (δ 5.11, d with allylic splittings, J=7.0 Hz, 2H and 1.97, d, J=1.0 Hz, 3H) and IR bands (3080, 920 cm^{-1}) attributable to the *exo*-methylene group. Tetrahydroisopetasol, **5**, was also obtained from the anhydro derivative, **6**, by hydrogenation with 10% palladium charcoal in ethanol, followed by stabilization in a basic medium. Thus, the **1** structure was assumed for petasitin on the basis of the above results.

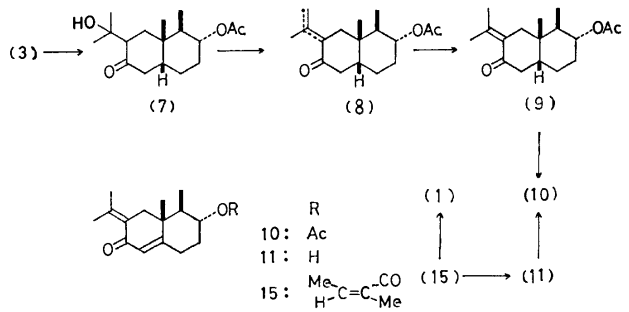

Scheme 2.

Furthermore, the location of a tertiary hydroxyl group was also confirmed by the following chemical reaction sequence— that is, by the conversion from petasitol monoacetate, **3**, to the known isopetasol acetate (**10**). The hydrogenation of **3** with Adams' catalyst in ethyl ether afforded a tetrahydroacetate (**7**),

* Present address: Department of Chemistry, Wakayama University, Masagocho, Wakayama 640.

$C_{17}H_{28}O_4$ (mp 92.0—95.0 °C), without the loss of a hydroxyl group. Compound **7** was dehydrated with phosphoryl chloride–pyridine to give a mixture of olefinic isomers (**8**), which were isomerized to an α,β-unsaturated ketone (**9**) by column chromatography over alumina. The dehydrogenation of **9** with DDQ afforded isopetasol acetate (**10**), $C_{17}H_{24}O_3$ (mp 82.0—85.0 °C), which was identified by a mixed-melting-point determination and by a comparison of the spectra.

The steric course of the hydrogenation for the cross-conjugated dienone system in isopetasol (**11**) has already been clarified by the stereochemical correlation between isopetasol, **11**, and fukinone (**12**).[3] Therefore, the hydrogenation of petasitol, **2**, and the monoacetate, **3**, with another type of dienone system also proceeds predominantly to furnish two steroidal A/B *cis*-fused compounds, **5** and **7**. The above results clearly indicate that the stereochemical course of the hydrogenation of the α,β-α',β'-unsaturated dienone system in a neutral medium must be influenced by the presence of the C-7 substituent; this must be compared with the earlier generalization, based on the hydrogenation of Δ^4-3-keto steroid-type compounds,[6] that the product compositions with *cis*- and *trans*-fused A/B rings were approximately equal.

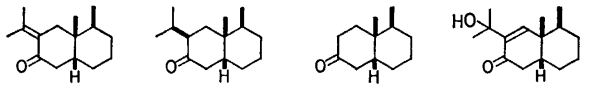

(12) (13) (14) (16)

In a previous paper,[2] we reported that tetrahydroisopetasol, **5** (mp 103.0—103.5 °C), derived from petasitol, **2**, showed a negative RD Cotton effect on the basis of the close resemblance to the RD curves of dihydro- (**13**) and desisopropylidene fukinone (**14**).[3] On the other hand, the pure tetrahydroisopetasol, **5**, has always been obtained as crystals after the crude hydrogenation product (**5a**) of isopetasol, **11**, has been subjected to isomerization with sodium methoxide–methanol or potassium hydroxide–methanol, that is, immediately after the hydrogenation product, **5a**, a viscous oil, showed a strong negative extreme, $[\theta]_{292}$ −1920, in the CD curve (Fig. 1). After all, the crystalline tetrahydroisopetasol, **5** (mp 103.0—104.0 °C), converted from isopetasol, **11**, has been found to show a weak positive Cotton effect, $[\theta]_{280}$ +460, by the reinvestigation of a part of the CD study of the eremophilan-8-one derivatives[7] (Fig. 1).

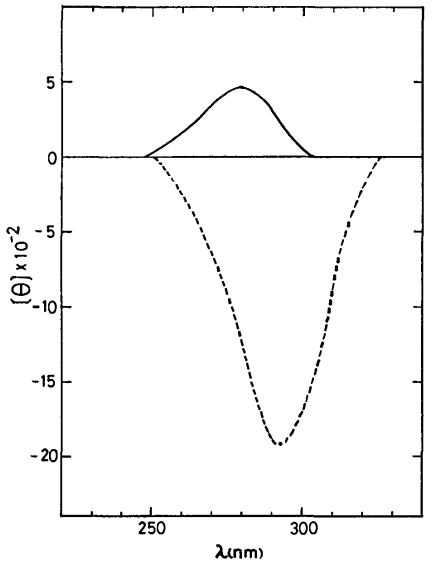

Fig. 1. CD curves of tetrahydroisopetasol: **5a** (an oily compd before isomerization; a dotted line) and **5** (a cryst compd after isomerization; a full line).

The final evidence for the stereochemistry of petasitin, **1**, was provided by the conversion of the known isopetasin (**15**) to **1** by means of photosensitized oxygenation in a manner similar to that in the case of the synthesis of petasitolone (**16**).[8]

Experimental

All the melting and boiling points are uncorrected. The IR, UV, ORD-CD, and mass spectra were taken with Jasco DS-402G, Cary Model 14, Jasco Model ORD-5, and Hitachi RMU-6 spectrophotometers respectively. The NMR spectra were recorded with JEOL C-60 and Hitachi R-20B (60 MHz) spectrophotometers, and the chemical shifts are reported in δ-values, with TMS as the internal reference. The optical rotations were measured with a Perkin-Elmer 141 polarimeter. The TLC were run on Kieselgel G (Merck). The analytical and preparative GLC were performed with a Shimadzu GC-1C apparatus on a stainless steel column (ϕ= 3 mm). The microanalyses were carried out in the microanalytical section of the Shionogi Research Laboratory, Shionogi and Co., Ltd.

Isolation of Petasitin (1). Dried flower stalks (34 kg) of *P. japonicus* Maxim. collected at Mt. Ioh in Ishikawa Prefecture, were extracted with methanol at room temperature. The extract was evaporated *in vacuo*, and the residue was dissolved in benzene. The benzene solution was washed with a saturated sodium hydrogencarbonate solution, dried over anhydrous sodium sulfate, and evaporated *in vacuo* to afford a dark green oil (2.4 kg). This oil was once chromatographed on alumina, and then repeatedly on silica gel. Subsequent elution with benzene–ethyl acetate (50: 1), gave petasitin (**1**) as a viscous oil (6.7 g) and almost a single spot on TLC (R_f, 0.2; benzene–ethyl acetate, 10: 1). This oil was purified by vacuum distillation and GLC for an analytical sample; bp 167.0—170.0 °C/2×10^{-4} mmHg; GLC: SF-96, 2 m, 60 ml/min H_2; column temperature, 240 °C; retention time, 16 min; $[\alpha]_D^{22}$ −26.2° (*c*, 1.0, MeOH); MS: *m/e* 332 M^+; IR (film): 3460, 1710, 1665, 1632, 1617, 1235 cm^{-1}; UV: λ_{max}^{EtOH} 235 nm (ε, 14200); NMR ($CDCl_3$): 6.93 (s, 6-H), 6.15 (t, J=1.0 Hz, 9-H), 6.13 (q, J=7.0 Hz, 3-H in an ester part), 4.95 (m, $W_{1/2}$=14 Hz, 3-H), 2.05 (d, J=7.0 Hz, 3-Me in an ester part), 1.90 (s, 2-Me in an ester part), 1.50 (s, 12- and 13-Me), 1.25 (s, 15-Me), 1.16 (d, J=7.0 Hz, 14-Me).

Found: C, 72.63; H, 8.56%. Calcd for $C_{20}H_{28}O_4$: C, 72.26; H, 8.56%.

Alkaline Hydrolysis of Petasitin (1). A solution of petasitin, **1** (1.26 g), in 5% ethanolic potassium hydroxide (20 ml) was allowed to stand at room temperature for 2 days. After the removal of the solvent, the aqueous solution of the residue was extracted with ether. The extract was washed with water and dried over anhydrous sodium sulfate. The evaporation of the solvent gave petasitol (**2**) (760 mg) as a semisolid, which was then crystallized from ethyl acetate–

light petroleum as colorless prisms; mp 110.0—113.0 °C, $[\alpha]_D^{21}$ −1.2 ° (*c*, 1.1, $CHCl_3$); $[\alpha]_D^{21}$ −5.5 ° (*c*, 1.0, MeOH); MS: *m/e* 250 M^+; IR (KBr): 3340, 1655, 1610 cm^{-1}; UV: λ_{max}^{EtOH} 244 nm (ε, 12700); NMR ($CDCl_3$): 6.92 (s, 6-H), 6.12 (t, J=1.0 Hz, 9-H), 3.70 (m, $W_{1/2}$=14 Hz, 3-H), 1.50 (s, 12- and 13-Me), 1.18—1.30 (partly superimposed two methyls).

Found: C, 67.01; H, 8.97%. Calcd for $C_{15}H_{22}O_3 \cdot H_2O$: C, 67.13; H, 9.09%.

The 2,4-dinitrophenylhydrazone was prepared as usual and crystallized from ethanol as red needles; mp 230.0—232.0 °C (dec).

Found: C, 58.71; H, 6.10; N, 13.24%. Calcd for $C_{21}H_{26}O_6N_4$: C, 58.59; H, 6.06; N, 13.02%.

The above alkaline solution was acidified with 3 M sulfuric acid and extracted with ether. The ethereal extract was washed with water and dried. The solvent was removed to give a crude acidic part (310 mg); IR (film): 3500—2400 (broad), 1685, 1655 cm^{-1}. The above residue was transformed to the *p*-phenylphenacyl ester in the usual manner, using *p*-phenylphenacyl bromide. The product (550 mg) was chromatographed with light petroleum–benzene (10: 1) on silica gel (10 g) to give *p*-phenylphenacyl (*Z*)-2-methyl-2-butenoate (220 mg), which was crystallized from methanol as colorless prisms; mp 88.0—89.5 °C.

Found: C, 77.54; H, 6.20%. Calcd for $C_{19}H_{18}O_3$: C, 77.53; H, 6.16%.

The subsequent elution on the above chromatography gave *p*-phenylphenacyl (*E*)-2-methyl-2-butenoate (30 mg), which was crystallized from methanol as colorless prisms (mp 104.5—106.5 °C). The two esters were identified by a mixed-melting-point determination with authentic samples.

Acetylation of Petasitol (2). a) A solution of petasitol, **2** (510 mg), in pyridine (2 ml) and acetic anhydride (2 ml) was left at room temperature for 20 h. The reaction mixture was then worked up in the usual manner to afford a crude monoacetate (**3**) as a solid, which was subsequently crystallized from acetone–light petroleum as prisms; mp 80.0—82.0 °C, $[\alpha]_D^{21}$ −17.9 ° (*c*, 1.0, $CHCl_3$), $[\alpha]_D^{21}$ −12.9 ° (*c*, 1.0, MeOH); MS: *m/e* 292 M^+; IR (KBr): 3420, 1735, 1660, 1616, 1240 cm^{-1}; UV: λ_{max}^{EtOH} 242 nm (ε, 14700); NMR ($CDCl_3$): 6.88 (s, 6-H), 6.10 (t, J=1.0 Hz, 9-H), 4.90 (m, $W_{1/2}$=14 Hz, 3-H), 2.06 (s, AcO), 1.48 (s, 12- and 13-Me), 1.20 (s, 15-Me), 1.10 (d, J=7.0 Hz, 14-Me).

Found: C, 65.79; H, 8.45%. Calcd for $C_{17}H_{24}O_4 \cdot H_2O$: C, 65.78; H, 8.44%.

b) A mixture of petasitol, **2** (44 mg), acetic anhydride (1.5 ml), and sodium acetate (70 mg) was refluxed for 8 h. Working-up as usual gave a crude product (63 mg), which was subsequently chromatographed on silica gel (5 g); elution with benzene–ethyl acetate (30: 1) then afforded diacetate (**4**) as a viscous oil (18 mg); MS: *m/e* 334 M^+, *m/e* 274 M^+ −60, *m/e* 214 M^+ −120, *m/e* 59 base peak; IR (film): 1735—1725, 1660, 1240 cm^{-1}.

Further elution with the same solvent gave monoacetate, **3** (20 mg), which was crystallized as has been described above and identified with the above monoacetate by a mixed-melting-point determination.

Hydrogenation of Petasitol (2). Petasitol, **2** (95 mg), was hydrogenated with 10% palladium charcoal (40 mg) in ethanol (3 ml). After the hydrogen-uptake (2 mol, 1 h) had ceased, the filtrate was evaporated *in vacuo* to furnish an oil (93 mg). The residue was chromatographed on silica gel (10 g), after which elution with benzene–ethyl acetate (15: 1) gave a viscous oil (74 mg) as a single spot on TLC (R_f, 0.56; benzene–ethyl acetate, 5: 1).

The above oil (60 mg) was refluxed with a catalytic amount of sodium under a nitrogen atmosphere in methanol for 2.5 h. After working-up as usual, the crystalline product (**5**) (63 mg) was crystallized from light petrolcum as leaflets; mp 103.0—103.5 °C, $[\alpha]_D^{22}$ +39.2 ° (*c*, 2.56, MeOH).

Found: C, 75.50; H, 11.05%. Calcd for $C_{15}H_{26}O_2$: C, 75.58; H, 11.00%.

The 2,4-dinitrophenylhydrazone was prepared in the usual manner and then crystallized from ethanol as yellow needles; mp 165.5—167.0 °C.

Found: C, 60.18; H, 7.14; N, 13.48%. Calcd for $C_{21}H_{30}O_5N_4$: C, 60.27; H, 7.23; N, 13.39%.

The semicarbazone was prepared in the usual manner and crystallized from methanol as needles; mp 188.0—189.5 °C.

Found: C, 65.06; H, 10.00; N, 13.95%. Calcd for $C_{16}H_{29}O_2N_3$: C, 65.05; H, 9.90; N, 14.23%.

The above substance and its derivatives were found by a mixed-melting-point determination and a comparison of the spectra, to be identical in all respects with those[3] of tetrahydroisopetasol (**5**) obtained from isopetasin (**12**).

Dehydration of Monoacetate (3). Monoacetate, **3** (550 mg), in pyridine (10 ml) was treated with phosphoryl chloride (10 ml) at room temperature for 44 h. The reaction mixture was then poured onto ice and extracted with ether. The extract was washed successively with a saturated sodium hydrogencarbonate solution and water. The dried solvent was removed to give a crude product (330 mg), which was then chromatographed on silica gel (30 g). Elution with benzene–ethyl acetate (50: 1) afforded the anhydro derivative (**6**) (145 mg) as an oil; MS: *m/e* 274 M^+, *m/e* 84 base peak; IR (film): 3080, 3040, 1737, 1664, 1637, 1242, 920 cm^{-1}; UV: λ_{max}^{EtOH} 240 nm (ε, 12500), ε, 9800/220 nm; NMR ($CDCl_3$): 6.82 (s, 6-H), 6.04 (t, J=1.0 Hz, 9-H), 5.11 (d, J=7.0 Hz, 12-C=CH_2), 4.87 (m, $W_{1/2}$=14 Hz, 3-H), 2.06 (s, AcO), 1.97 (d, J=1.0 Hz, 13-Me), 1.22 (s, 15-Me), 1.10 (d, J=7.0 Hz, 14-Me).

Hydrogenation of Anhydromonoacetate (6). Anhydroacetate, **6** (122 mg), in ethanol (3 ml) was hydrogenated with 10% palladium charcoal (23 mg). Hydrogen-uptake ceased after 10 h. The filtrate was evaporated *in vacuo* to leave an oil (137 mg). The residue (103 mg) was refluxed in methanol (4 ml) with sodium metal (28 mg) under a nitrogen atmosphere for 3 h. Working-up as usual gave a product (94 mg) which was chromatographed on silica gel (6 g) with benzene–ethyl acetate (5: 1) and then crystallized from aqueous ethanol as leaflets (mp 101.0—103.0 °C). This was found to be identical with tetrahydroisopetasol (**5**) by a mixed-melting-point determination and a comparison of the IR spectra.

Isomerization of Tetrahydroisopetasol (5) with a Base. Isopetasol, **11** (3.03 g), in ethanol (45 ml) was hydrogenated with 10% palladium charcoal (600 mg) at room temperature for 6 h. The subsequent working-up as usual gave a viscous oil, which was then chromatographed on silica gel (64 g). Elution with benzene–ethyl acetate (20: 1) gave tetrahydroisopetasol (**5a**) (3.01 g) as a colorless oil; $[\alpha]_D^{24}$ −19.1° (*c*, 1.26, MeOH); IR (film): 3380, 1695, 1380, 1360, 1020 cm^{-1}; ORD (*c*, 0.1025, MeOH): $[\phi]_{391}$ 0, $[\phi]_{325}$ −600, $[\phi]_{307}$ −1160 (trough), $[\phi]_{289}$ 0, $[\phi]_{265}$ +1330; CD (*c*, 0.1025, MeOH): Fig. 1; NMR ($CDCl_3$): 3.58 (m, $W_{1/2}$=18 Hz, 3-H), 1.08 (s, 15-Me), 0.98 and 0.88 (each d, J=7.0 Hz, 12- and 13-Me), 0.82 (d, J=6.5 Hz, 14-Me).

The above product (3.01 g) was dissolved in methanol (10 ml) and refluxed with 0.2 M potassium hydroxide–methanol (40 ml) under a nitrogen atmosphere for 5 h. The subsequent working-up as noted above gave a partially crystallized product, which was crystallized from ethyl acetate to afford tetrahydroisopetasol (**5**)[3] as leaflets; mp 103.0—104.0

°C, $[\alpha]_D^{25}$ +34.3° (*c*, 1.01, MeOH); IR (CCl_4): 3610, 3450, 1720, 1390, 1375, 1035 cm^{-1}; ORD (*c*, 0.0937, MeOH): $[\phi]_{375}$ +200, $[\phi]_{325}$ +330, $[\phi]_{288}$ +710, $[\phi]_{275}$ +530, $[\phi]_{258}$ +380, $[\phi]_{225}$ +1040; CD (*c*, 0.0937, MeOH): Fig. 1; NMR ($CDCl_3$): 3.53 (m, $W_{1/2}$=18 Hz, 3-H), 1.01 and 0.83 (each d, J=7.0 Hz, 12- and 13-Me), 0.93 (s, 15-Me), 0.91 (d, J=6.0 Hz, 14-Me).

Hydrogenation of Monoacetate (3). Monoacetate, **3** (1.03 g), was dissolved in ether (30 ml) and hydrogenated with Adams' catalyst (111 mg). Hydrogen-uptake (2.2 mol) ceased after 30 min. Working-up as usual gave a crude product, which was chromatographed on silica gel (22 g) with benzene–ethyl acetate (10: 1) to afford the tetrahydro compound (**7**) (687 mg) (mp 92.0—95.0 °C) as needles (from light petroleum); IR (KBr): 3490, 1710, 1263 cm^{-1}; IR (CCl_4): 3500, 1735, 1700, 1240 cm^{-1}; NMR ($CDCl_3$): 4.81 (m, 3-H), 4.28 (br s, OH), 2.05 (s, AcO), 1.23 (s, 12- and 13-Me), 1.18 (s, 15-Me), 0.95 (d, J=7.0 Hz, 14-Me).

Found: C, 68.89; H, 9.57%. Calcd for $C_{17}H_{28}O_4$: C, 68.89; H, 9.52%.

Dehydration of Tetrahydromonoacetate (7). The above product, **7** (565 mg), was treated with pyridine (8 ml) and phosphoryl chloride (6.5 ml) at room temperature for 20 h. Working-up as usual gave a mixture of a dehydration product (**8**) (438 mg); IR (film): 1735, 1717 (sh), 1687 (sh), 1645, 1633, 1245 cm^{-1}.

The above product, **8** (430 mg), was chromatographed on alumina (10 g); subsequent elution with light petroleum–ethyl acetate (50: 1) gave a sole product (**9**) (360 mg); IR (film): 1735, 1682, 1630, 1240 cm^{-1}; UV: λ_{max}^{EtOH} 251 nm (ε, 5160); NMR ($CDCl_3$): 4.80 (m, 3-H), 2.05 (s, AcO), 1.98 and 1.81 (each s, 12- and 13-Me), 1.04 (s, 15-Me), 0.90 (d, J=7.0 Hz, 14-Me).

The 2,4-dinitrophenylhydrazone was prepared as usual and crystallized from ethanol (mp 168 °C) as deep red needles.

Found: N, 12.54%. Calcd for $C_{23}H_{30}O_6N_4$: N, 12.22%.

Dehydrogenation of Unsaturated Monoacetate (9). Into a stirred solution of the acetate, **9** (320 mg), and DDQ (2,3-dichloro-5,6-dicyano-*p*-benzoquinone) (292 mg) in dry dioxane (4 ml) anhydrous hydrogen chloride was bubbled at room temperature over a 30-s period. After further stirring for 40 min, crystals were separated, after which the stirring was continued for 8 h. After subsequent filtration and concentration, the residue was diluted with ether, washed successively with a 1% aqueous sodium hydroxide solution and water, and dried over anhydrous sodium sulfate. The removal of the solvent gave a product (290 mg) which was later chromatographed on silica gel (8 g). Elution with benzene gave a fraction (R_f, 0.35; benzene–ethyl acetate, 10: 1) which was subsequently crystallized from aqueous methanol to afford a pure acetate (**10**) as prisms; mp 82.0—85.0 °C; IR (Nujol): 1735, 1662, 1630, 1245 cm^{-1}; IR (CCl_4): 1740, 1666, 1631, 1244 cm^{-1}; UV: λ_{max}^{EtOH} 242 nm (ε, 7550), 278 (sh) nm (ε, 2900). This was found to be identical with the isopetasol acetate (**10**) converted from isopetasol (**11**) by a mixed-melting-point determination and a comparison of the IR spectra.

Acetylation of Isopetasol (11).[3] Isopetasol, **11** (106 mg), was acetylated with pyridine (1 ml) and acetic anhydride (0.5 ml). A subsequent working-up in the usual manner afforded the acetate (**10**) (98 mg), which was subsequently crystallized from aqueous methanol as prisms; mp 86.0—87.0 °C, $[\alpha]_D^{25}$ +80° (*c*, 0.97, $CHCl_3$); IR (KBr): 1735, 1660, 1630, 1245 cm^{-1}; IR (CCl_4): 1740, 1660, 1630, 1245 cm^{-1}; UV: λ_{max}^{EtOH} 243 nm (ε, 8400), 278 (sh) nm (ε, 3100); NMR (CCl_4): 5.65 (d, J=1.0 Hz, 9-H), 4.76 (sex, J=12.0, 10.0, and 5.0 Hz, $W_{1/2}$=16 Hz, 3-H), 2.04 (s, 12-Me), 2.01 (s, AcO), 1.83 (s, 13-Me), 1.04 (s, 15-Me), 0.95 (d, J=6.0 Hz, 14-Me).

Found: C, 73.70; H, 8.79%. Calcd for $C_{17}H_{24}O_3$: C, 73.88; H, 8.75%.

Preparation of Petasitin (1). A stirred solution of isopetasin (**15**)[3] (1.0 g) and Rose Bengal (5 mg) in absolute methanol was irradiated with a circular fluorescent lamp (30 watt) for 36 h under the bubbling of air. The reaction mixture was then stirred with a solution of sodium sulfite (2.5 g) in water (15 ml) for 3 h. After the removal of the solvent, the residue was extracted with ether. The subsequent working-up in the usual manner gave a crude product, which was chromatographed over silica gel (20 g). Elution with benzene afforded petasitin (**1**) (430 mg), which was found to be identical with the natural specimen by a comparison of the spectral data (IR and NMR) and by GLC analysis under the conditions described above. The other products were not investigated further.

The authors wish to thank the staff of the Shionogi Research Laboratory, Shionogi and Co., Ltd., for the microanalysis and the Institute of Food Chemistry for the measurement of the MS and NMR spectra. The present work was partially supported by a Grant-in-Aid for Scientific Research from the Ministry of Education.

References

1) Parts I—III designate the following studies: I, Ref. 3; II, Ref. 8; III, Ref. 5.

2) K. Naya and I. Takagi, *Tetrahedron Lett.*, **1968**, 629.

3) K. Naya, I. Takagi, Y. Kawaguchi, Y. Asada, Y. Hirose, and N. Shinoda, *Tetrahedron*, **24**, 5871 (1968).

4) K. Naya, M. Nakagawa, M. Hayashi, K. Tsuji, and M. Naito, *Tetrahedron Lett.*, **1971**, 2963.

5) K. Naya, M. Hayashi, I. Takagi, S. Nakamura, and M. Kobayashi, *Bull. Chem. Soc. Jpn.*, **45**, 3673 (1972).

6) R. L. Augustin, *J. Org. Chem.*, **23**, 1853 (1958); R. L. Augustin and A. D. Broom, *ibid.*, **25**, 802 (1960); M. G. Combe, H. B. Henbest, and W. R. Jackson, *J. Chem. Soc.,C*, **1967**, 2467; H. B. Henbest, W. R. Jackson, and I. Malunowicz, *ibid.*, *C*, **1967**, 2469.

7) The Details of the CD study of the steroidal and non-steroidal isomers will be reported soon.

8) K. Naya, F. Yoshimura, and I. Takagi, *Bull. Chem. Soc. Jpn.*, **44**, 3165 (1971).

Nucleophilic Behavior of the Phenyl Radical in the Hydrogen Abstraction Reaction from Substituted Toluenes. A Contribution to the Study of the Phenyldiazenyl Radical

Tadashi SUEHIRO, Akira SUZUKI, Yasuyoshi TSUCHIDA, and Junji YAMAZAKI

Department of Chemistry, Faculty of Sciences, Gakushuin University, Mejiro, Toshimaku, Tokyo 171

(Received May 6, 1977)

Phenyl radicals derived from benzoyl peroxide (BPO) showed nucleophilic behavior, rho=+0.18 (meta-series) for the hydrogen abstraction reaction from substituted toluenes at 80 °C, and a kinetic deuterium isotope effect, $k_H/k_D=3.73\pm0.2$, was found for toluene. Comparison of these results with those for the phenyl radicals from phenylazotriphenylmethane (PAT) leads to the suggestion that the phenyldiazenyl radicals derived from PAT abstract hydrogen from toluene to yield benzene, which should amount to about 50% of the total benzene formed.

Phenyl radicals have been reported to be electrophilic in hydrogen abstraction reactions based on the results of investigations using phenylazotriphenylmethane (PAT) as the source of the phenyl radicals.[1,2] The phenyl radicals derived from PAT behave, however, differently from those generated from benzoyl peroxide (BPO), as revealed by the fact that the yields of benzene in the thermolysis of PAT in toluene at 60—70 °C, 50—58% per mole PAT,[3,4] are markedly larger than that of BPO, 32% per mole phenyl radicals,[4] in contrast to the very similar yields of methylbiphenyls in both cases, 25% for PAT and 23% for BPO.[4] Appreciable amounts of phenyl radicals from BPO are transformed into esters and quarterphenyls, which are not accounted for in the above measurements. This does not, however, affect the conclusion that the "phenyl" radicals from PAT produce much more benzene in toluene than do those from BPO.

In the thermolysis of PAT, the triphenylmethyl-nitrogen bond dissociates at first to give triphenylmethyl and phenyldiazenyl radicals in a cage.[5] Although the reaction of phenyldiazenyl radicals out of the "cage" is not clear as yet, the hydrogen abstraction reaction of the radicals from toluenes would lead to phenyldiazene, which is known to produce benzene in good yields upon thermal decomposition.[6] PAT could thus receive the cooperation of phenyldiazenyl radicals in the formation of benzene. When the reactions of phenyldiazenyl radicals proceed, the polarity of the "phenyl" radical deduced from the experiments on PAT should be different from that obtained from reactions using BPO, because in the latter studies the precursors of phenyl radicals, benzoyloxy radicals, are converted into benzoic acid upon hydrogen abstraction and can be separated completely from benzene. The intrinsic behavior of the phenyl radicals in the hydrogen abstraction reaction can only be determined using BPO as the radical source.

Results and Discussion

The polar nature of phenyl radicals was determined by the reactivities of substituted toluenes toward phenyl radicals. For the measurement of the reactivities of toluenes, competitive reactions of BPO (4.13 mmol) were carried out at 80 °C between each 100 mmol of a substituted toluene and carbon tetrachloride in a nitrogen atmosphere. Relative rate constants, k_H/k_{Cl}, of Reactions 1 and 2,

$$ArCH_3 + Ph\cdot \xrightarrow{k_H} PhH + ArCH_2\cdot, \quad (1)$$

$$CCl_4 + Ph\cdot \xrightarrow{k_{Cl}} PhCl + Cl_3C\cdot, \quad (2)$$

were calculated from the yields of benzene and chlorobenzene with proper corrections, as described below. Duplicate runs afforded the rate ratios listed in Table 1 and the Hammett plot shown in Fig. 1.

Table 1. Rates of hydrogen abstraction from toluenes relative to chlorine abstraction from carbon tetrachloride at 80 °C

$XC_6H_4CH_3$ X=	k_H/k_{Cl}	$XC_6H_4CH_3$ X=	k_H/k_{Cl}
m-$(CH_3)_2$	0.214±0.046	*p*-CH_3O	0.389±0.09
H	0.210±0.055	*p*-CH_3	0.270±0.035
m-Cl	0.288±0.055	*p*-Cl	0.277±0.054
m-CN	0.220±0.042	*p*-CN	0.265±0.051
m-NO_2	0.332±0.075	*p*-NO_2	0.646±0.11

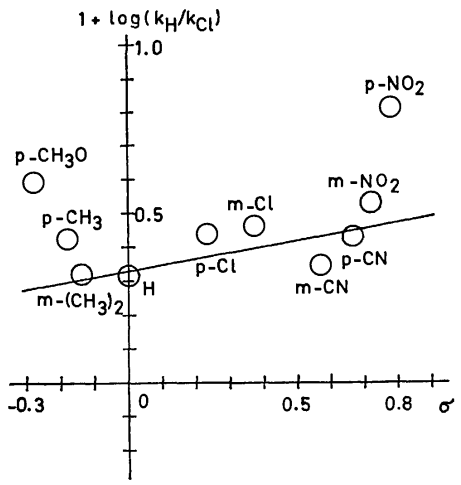

Fig. 1. Hammett plot of rates of hydrogen abstraction by phenyl radicals from toluenes relative to rates of chlorine abstraction from carbon tetrachloride.

The polar character of the phenyl radicals obtained from the results of meta-substituted toluenes was slightly nucleophilic, rho=+0.18, in contrast to the results of earlier reports, −0.1,[1] −0.4,[2] and −0.5.[7] The reactivities of para-substituted toluenes are larger than the values expected from the rates of the meta-series. Definite extra resonances are operative in the transition

state of the hydrogen abstraction reaction and they are especially effective in the cases of *p*-nitro- and *p*-methoxytoluenes. The effect of the extra resonances play an important role in the manifestation of B.

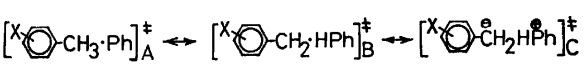

In the calculation of the rate ratios, the following were taken into consideration. Phenyl radicals from BPO can also take up hydrogen from the aromatic ring of a substrate molecule during the course of homolytic phenylation. Because the homolytic phenylation by BPO proceeds by means of the disproportionation reaction *via* substituted phenylcyclohexadienyl radicals,[8] and an appreciable amount of dihydrobiaryls are formed, phenyl radicals can abstract hydrogen from the cyclohexadienyl radicals and from dihydrobiaryls.

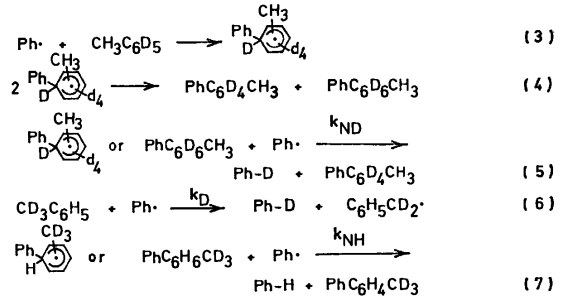

The extent of Reactions 5 and 7 can be estimated by examining benzene and deuteriobenzene formed from experiments using toluene-nuclear-d_5 and toluene-α-s_3 as the substrate, together with rate ratios ($k_{\text{total benzene}}/k_{\text{Cl}}$) for the toluene–carbon tetrachloride and toluene-α-d_3–carbon tetrachloride systems.[9]

From the reaction using toluene-d_5 (d_5-fraction 90.3 %), the ratio C_6H_6: C_6H_5D=93.8: 6.2 was obtained for the benzene formed. For the benzene formed from toluene-α-d_3 (d_3-fraction 90.0%), the ratio C_6H_6: C_6H_5D =54.5: 45.5 was found. The kinetic deuterium isotope effect for Reactions 7 and 5 ($k_{\text{NH}}/k_{\text{ND}}$) was calculated to be 2.97, and the hydrogen abstraction reaction at the nuclear positions (k_{NH}) contributes *ca.* 10% of the total formation of benzene.

It is tentatively assumed, that the participation of nuclear hydrogen in the formation of benzene in the system containing substituted toluenes is proportional to the rates of phenylation of the substituted toluenes, and that the rates of phenylation can be estimated using partial rate factors for phenylation.[10] The rates of phenylation of substituted toluenes (R_X) relative to that of toluene were calculated to be as follows:

R_X:	*p*-MeO	1.13	*p*-Me	1.01	*m*-Me 1.01
	p-Cl	1.19	*m*-Cl	1.03	*p*-CN 1.96
	m-CN	2.04	*p*-NO_2	2.02	*m*-NO_2 2.13

Measurements on benzene using GLPC for competitive reactions were corrected by substracting from them the amounts of benzene formed from the nuclear hydrogen by phenyl radicals:

$$(\text{benzene})_{\text{corr}} = (\text{benzene})_{\text{total}} \cdot (1 - \text{Corr})$$

$$\text{Corr}_{\text{toluene}} = 0.10.$$

Similarly, the corrections for X-substituted toluenes are

$$\text{Corr}_{\text{X-toluene}} = R_X \cdot \text{Corr}_{\text{toluene}} = 0.10 \cdot R_X.$$

The values in Table 1 have been corrected in this manner.

The effect of the methoxyl substituent of methoxytoluene in the formation of benzene was checked using the isotope tracer technique with *p*-deuteriomethoxytoluene as the substrate. For the benzene formed, a molar ratio C_6H_6: C_6H_5D of 92.3: 7.7 was found. The corrected value is listed in the table. The benzene from the methoxyl group amounts to about 33% of the total benzene formed.

The difference in the polar nature of the phenyl radical found here (+0.18) from that of Trosman and Bagdasar'yan[7] (−0.5) arises from different experimental conditions. The determination of benzene separately from one by-product, chloroform, is one of the key points in the present study. The column used by Bridger and Russell[1] was found to be unsuccessful in this laboratory. A 2-m column of ODPN (20% on C-22 AW), in combination with a 1-m column of Apiezon Grease L (25% on C-22 AW) was used at 80 °C with helium as the carrier gas. Much more chloroform was formed than benzene, when toluenes with electron-donating groups were used as the substrate. The rate ratios $k_{\text{H}}/k_{\text{Cl}}$ found for nitrotoluene by Trosman and Bagdasar'yan[7] 0.80 for para- and 0.475 for meta-compounds, gave 0.64 and 0.36 after the correction described above, which are in good accord with the present values of 0.646 and 0.332. Their values of the rate ratios for toluene and xylenes are by far larger than the present values.

The slightly nucleophilic nature of the phenyl radical for the hydrogen abstraction reaction in the present findings is in very good agreement with the results reported by Ito *et al.* for homolytic phenylation (rho= +0.05),[10] and with the results reported by Migita *et al.* for bromine abstraction from substituted benzyl bromides (rho=+0.15 for meta-series).[11] Thus, a parallel relationship in the polar nature of phenyl radicals was established between the addition reaction to benzene nuclei and the abstraction reaction from benzylic compounds.

The kinetic deuterium isotope effect was found to be 3.73±0.2. This is a little smaller than the value, 4.5± 0.5, found by Bridger and Russell.[1]

The nucleophilic nature of phenyl radicals from BPO for the hydrogen abstraction reaction contrary to the electrophilic radicals from PAT, suggests the coexistence of phenyldiazenyl radicals together with phenyl radicals in the thermolysis of PAT. In measuring the electrophilicity of phenyldiazenyl radicals, amino radicals should be taken as a reference. For example dimethylamino radicals are reported to be electrophilic for hydrogen abstraction from toluenes: rho=−1.08 (sigma plus) and $k_{\text{H}}/k_{\text{D}}$=4.0 at 130 °C.[12] Diphenylmethyleneamino radicals were also found to be electrophilic (rho=*ca.* −2.5).[13] Phenyldiazenyl radicals are, therefore, probably electrophilic in the abstraction of hydrogen from toluenes. Based on these assumptions, the results of Bridger and Russell[1] and Pryor *et al.*[2] appear to be explainable.

Another electrophilic property of particular radicals, X·, derived from PAT were also found for hydrogen abstraction from solvent molecule toluenes giving benzyl radicals during the thermolysis of PAT. The relative rates of formation of benzyl and substituted benzyl radicals, $k_{ArCH_2\cdot}/k_{PhCH_2\cdot}$, were measured by determining the amount of 1-aryl-2,2,2-triphenylethane, which was isolated by column chromatography in a 66% yield per mole of benzene as determined by GLPC. Because a fairly large amount of triphenylmethyl radicals were present in solution during the PAT thermolysis, it appears plausible to assume that the radical-scavenging step is effective, so that hydrogen abstraction is rate determining in the reaction,

$$ArCH_3 \xrightarrow{X\cdot} ArCH_2\cdot \xrightarrow{Ph_3C\cdot} ArCH_2CPh_3. \quad (8)$$

A mixture of aryltriphenylethanes from a competitive reaction mixture was obtained by column chromatography and analyzed using NMR or the ^{14}C-tracer technique. The rate ratios, $k_{ArCH_2\cdot}/k_{PhCH_2\cdot}$, are listed in Table 2. A Hammett plot is shown in Fig. 2. The polar nature of particular free radicals, X·, derived from PAT in the formation of benzyl radicals at 50 °C was electrophilic (rho=−0.49 (sigma plus)). The results are in good accord with those of Pryor *et al.* for the hydrogen abstraction reaction.[2)]

TABLE 2. RELATIVE RATE OF FORMATION OF SUBSTITUTED BENZYL RADICALS, $k_{ArCH_2\cdot}/k_{PhCH_2\cdot}$, BY PAT AT 50 °C

Substrate	Chemical shift of CH_2 in $ArCH_2CPh_3$ in pyridine (δ)	$k_{ArCH_2\cdot}/k_{PhCH_2\cdot}$
p-Methoxytoluene[a)]	4.05	3.52
p-Xylene	4.05	1.46[b)]
Toluene	4.05	1.00
p-Chlorotoluene	4.10	0.67
m-Chlorotoluene	3.98	0.79
p-Nitrotoluene	4.10	0.65

a) Measured by the ^{14}C-tracer technique. b) Corrected per methyl group.

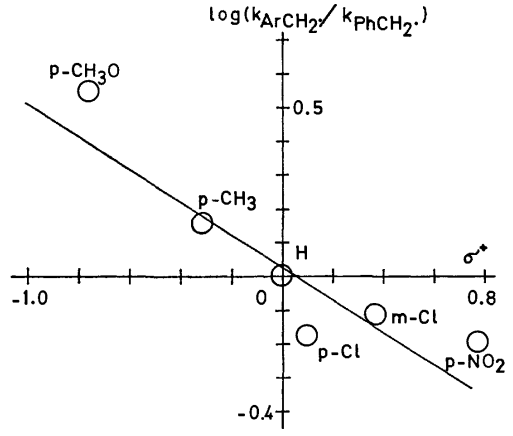

Fig. 2. Hammett plot (against sigma plus) of formation of substituted benzyl radicals from toluenes through hydrogen abstraction by particular radicals derived from PAT.

Assuming the phenyldiazenyl radical as the intermediate, the reaction scheme for thermolysis of PAT in toluene at 60 °C can be formulated as follows:

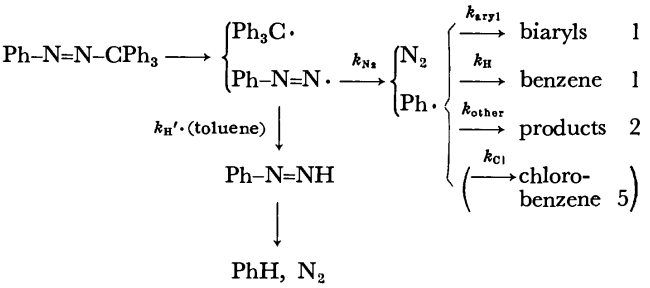

Scheme 1.

The reactions of phenyl radicals (k_{aryl}, k_H, and k_{other}) should be referred to the results of BPO, *i.e.*, the rate ratios with respect to each other are *ca.* 1 : 1 : 2 at 80 °C, and k_{N_2} is rate-determining. Because the benzene yield per mole of PAT is about twice that of BPO (Table 4), the rate, k_{N_2}, is about four times as large as the rate of hydrogen abstraction of phenyldiazenyl radicals, k_H'· (toluene). This gives $k_{N_2}=40\cdot k_H'$, using a toluene concentration of 10 M. When carbon tetrachloride is present as a co-solvent, k_{Cl} should also be taken into consideration and was about five times as large as k_H, because the k_H/k_{Cl} found was 0.210.

TABLE 3. CALCULATED RATE RATIOS, $k_{benzene}/k_{Cl}$ FOR THERMOLYSIS OF PAT IN TOLUENE–CARBON TETRACHLORIDE

Substrate	$k_{benzene}/k_{Cl}$
p-Methoxytoluene	2.80
p-Xylene	1.36
Toluene	1.00
p-Chlorotoluene	0.75
p-Cyanotoluene	0.68
p-Nitrotoluene	0.68

Based on this scheme, setting k_{N_2}, k_{Cl}, and k_{other} constant, the rho value for k_H to +0.18, the rho for k_H' to −2.5,[13)] and k_{aryl} proportional to R_x, as described previously, we can estimate the rate ratios, $k_{benzene}/k_{Cl}$, as shown in Table 3. These results are in very good agreement with the results shown in Table 2 and also with the results of Bridger and Russell[1)] and of Pryor *et al.*[2)] The data for PAT may thus be interpreted in terms of phenyldiazenyl and phenyl radicals.

Experimental

Gas Chromatographic Determination of Benzene and Chlorobenzene. Benzene and chlorobenzene were measured with apparatus of the KGL-2A (HITACHI) and JGC-1100 (JEOL) types using a 2-m column of ODPN (20% on C-22 AW) connected to a 1-m column of Apiezon Grease L (25% on C-22 AW), with the He carrier gas flowing at a rate of 90 ml/min at 80 °C. For the determination of chlorobenzene, only a 2-m column of ODPN was used with He at a flow rate of 150 ml/min at 80 °C. Their internal standard was selected from toluene, *p*-xylene, and *o*-xylene according to the reaction mixture.

TABLE 4.

Radical source	mmol	Toluene mmol	Temp (°C)	Benzoic acid mmol (%)	Benzene mmol (%/Ph·)	Methylbiphenyls mmol (%/Ph·)
PAT	4.017	760	50	—	1.515 (37.7)	—
PAT	2.04	200	60	—	—	0.514 (24.9)[a]
PAT	4.017	760	70	—	2.33 (58.0)	—
BPO	4.13	200	80	1.85 (43)	2.13 (33.2)	1.46 (22.6)[b]

a) *o*-: *m*-: *p*-=59.6: 25.6: 14.8. b) *o*-: *m*-: *p*-=46.5: 18.5: 34.7.

Yields of Benzene and Methylbiphenyls. The benzene and methylbiphenyls yields from the thermolysis of PAT and BPO in toluene were determined by GLPC (Table 4).

Competitive Reactions in the Substituted Toluene–Carbon Tetrachloride System. Benzoyl peroxide (4.13 mmol) was dissolved in a mixture of 100 mmol each of carbon tetrachloride and substituted toluene in a nitrogen atmosphere and heated for 42 h at 80±1.0 °C.

The reaction mixture was distilled with steam after a certain amount of mesitylene had been added to the mixture to assure the separation of chlorobenzene from high-boiling products. When nitrotoluenes were subjected to competitive reactions, the distillate was treated with a stannous chloride-concd. hydrochloric acid mixture to remove the nitro-compound. The purified distillates were subjected to GLPC determinations of benzene and chlorobenzene.

GC-MS Spectrometry. Mass spectrometric measurements were made on an apparatus of the LKB-9000 (SHIMADZU) type for a) the deuterated benzene formed, b) toluene-α-d_3, c) toluene-d_5, and d) *p*-deuteriomethoxytoluene.

a) The determination of the deuteriobenzene formed from the substrates, deuteriotoluene and deuteriomethoxytoluene, was made at 14 eV using a 3-m column of Apiezon Grease L on Chromosorb W (AW) at 42 °C. The He flow rate was 60 ml/min.

b) Toluene-α-d_3 was prepared by reduction of benzylidyne trichloride with a zinc dust–acetic acid-*d* solution according to the method of Renaud and Leitch.[14] The fraction of toluene-α-d_3 was found to be 90.0% at 12 eV.

c) Toluene-d_5 from Merk, Sharp and Dohme, Canada, Ltd., was used for the studies. The sample contained a 90.3% fraction of toluene-d_5 measured at 12 eV. Toluene-d_6 was present in a 2.3% fraction.

d) *p*-Methoxy-d_3-toluene was prepared from *p*-cresol and dimethyl-d_6 sulfate. Its boiling point was 80.5 °C at 37 Torr. The fraction of trideuteriomethoxytoluene was determined at 12 eV to be 98.1%.

Evaluation of Kinetic Deuterium Isotope Effects on Hydrogen Abstraction from the Methyl Group of Toluene, the Fraction of Hydrogen Abstraction from the Nuclear Position of Toluene, and the Fraction of Hydrogen Abstraction from the Methoxyl Group of p-*Methoxytoluene.* Kinetic deuterium isotope effect, (k_H/k_D), the relative rate of abstraction from the nuclear position, (k_{NH}/k_H) ((nuclear-H)/(toluene)), and the relative rate of abstraction from the methoxyl group of *p*-methoxytoluene, (k_{O-CH_3}/k_H), were evaluated using the following equations:

$$\frac{k_H(CH_3)+k_{NH}(n\text{-}H)}{k_D(CD_3)+k_{ND}(n\text{-}D)} = \frac{93.8}{6.2} \quad (9)$$

for benzene from toluene-d_5,

$$\frac{k_H(CH_3)+k_{NH}(n\text{-}H)}{k_D(CD_3)} = \frac{54.5}{45.5} \quad (10)$$

for benzene from toluene-d_3,

$$\frac{k_H(CH_3)+k_{NH}(n\text{-}H)}{k_D(CD_3)+k_{NH}(n\text{-}H)+k_H(CH_3)} = 2.91, \quad (11)$$

for the ratio of the rate ratios, $k_{toluene}/k_{Cl}$ and $k_{toluene\text{-}d_3}/k_{Cl}$,

$$\frac{k_H(CH_3)+k_{NH}(n\text{-}H)+k_{O\text{-}CH_3}(O\text{–}CH_3)}{k_{O\text{-}CD_3}(O\text{–}CD_3)} = \frac{92.3}{7.7}, \quad (12)$$

for benzene from methoxy-d_3-toluene, and

$$\frac{k_H(CH_3)+k_{NH}(n\text{-}H)+k_{O\text{-}CH_3}(O\text{–}CH_3)}{k_H(CH_3)+k_{NH}(n\text{-}H)+k_{O\text{-}CH_3}(O\text{–}CH_3)+k_{O\text{-}CD_3}(O\text{–}CD_3)} = 1.35, \quad (13)$$

for the ratio of the rate ratios, $k_{methoxytoluene}/k_{Cl}$ and $k_{methoxy\text{-}d_3\text{-}toluene}/k_{Cl}$,

here (CH_3), (CD_3), (n-H), (n-D), $(O\text{–}CH_3)$, and $(O\text{–}CD_3)$ denote the concentrations for the CH_3 and CD_3 groups of toluene or methoxytoluene, the nuclear-hydrogen and nuclear deuterium atoms of toluene or methoxytoluene, and the methoxyl group and deuteriomethoxyl groups of methoxytoluene, respectively. k_x represents the rate constants for hydrogen abstraction from the corresponding groups. The nuclear hydrogen concentrations were expressed by the yields of the biaryls formed during the thermolysis of BPO (4 mmol) in 200 mmol of toluene, *i.e.*, 1.43 mmol (n-H) in 200 mmol of toluene.

We obtain from Eqs. 9, 10, and 11, the following results:

$$k_H/k_D = 3.73\pm0.2, \quad k_{NH}/k_H = 17.6.$$

Using the same k_{NH} for Eqs. 12 and 13, as for Eqs. 9—11, we obtain

$$k_H/k_{O\text{-}CH_3} = 2.07\pm0.02.$$

The participation of the nuclear hydrogen of toluene in the hydrogen abstraction reaction was found from (k_{NH}/k_H) ((n-H)/(CH_3)) to be 0.125, *i.e.*, about 10% of the benzene was formed from nuclear hydrogen. The participation of the methoxyl group of methoxytoluene in the benzene formation is about 33%.

^{14}C-Tracer Experiments. Triphenylmethanol-α-^{14}C was prepared from benzoate-carbonyl-^{14}C by the Grignard reaction and its specific activity was measured. ^{14}C-PAT was derived from triphenylmethanol-^{14}C and used for thermolysis without dilution.

^{14}C-PAT (13.5 mmol) was heated to 50 °C in nitrogen in a mixture of toluene and *p*-methoxytoluene (a) 1: 1, b) 2: 1, total 3.0 mmol) and treated according to the standard dilution method.

a) The reaction mixture was divided into two equal parts and to each of them was added 1.00 g of unlabelled $PhCH_2CPh_3$ or $CH_3OC_6H_4CH_2CPh_3$.

b) The reaction mixture was divided into two parts in a 2: 1 volume ratio, and to each was added 1.00 g of unlabelled $PhCH_2CPh_3$ or $CH_3OC_6H_4CH_2CPh_3$. The results were as follows:

Radioactivity (dpm/mg)

	Starting Ph_3COH	Isolated $CH_3OC_6H_4$-CH_2CPh_3	Isolated $PhCH_2CPh_3$	k_{ArCH_3}/k_{PhCH_3}
a)	4080	559.5	191.8	3.48
b)	4080	313.3	357.8	3.56
			av.	3.52

The radioactivity was measured using a scintillation counter of the Beckman LS-200 type. The NMR spectra were recorded on Varian A-60 instrument, with TMS as the internal standard.

For the radio assay, we are grateful to Dr. N. Morikawa of the University of Tokyo.

References

1) R. Bridger and G. A. Russell, *J. Am. Chem. Soc.*, **85**, 3754 (1963).
2) W. A. Pryor, J. T. Echols, Jr., and K. Smith, *J. Am. Chem. Soc.*, **88**, 1189 (1966).
3) J. F. Garst and R. S. Cole, *Tetrahedron Lett.*, **1963**, 679.
4) The results in the present paper.
5) A. Tsolis, S. G. Mylonakis, M. T. Nieh, and S. Seltzer, *J. Am. Chem. Soc.*, **94**, 829 (1972); R. C. Neuman, Jr., G. D. Lockyer, Jr., and M. J. Amrich, *Tetrahedron Lett.*, **1972**, 1221; N. A. Porter, M. E. Landis, and L. J. Marnett, *J. Am. Chem. Soc.*, **93**, 795 (1971); W. A. Pryor and K. Smith, *ibid.*, **92**, 5403 (1970); **89**, 1741 (1967); K. Tagaki and R. J. Crawford, *ibid.*, **93**, 5910 (1971); S. Seltzer and F. T. Dunne, *ibid.*, **87**, 2628 (1965).
6) E. M. Kosower, *Acc. Chem. Res.*, **4**, 193 (1971); B. Kaiser, Dissertation of the University of Münster (1970).
7) E. A. Trosman and Kh. S. Bagdasar'yan, *Russ. J. Phys. Chem.*, **38**, 1466 (1964).
8) K. H. Pausacker, *Aust. J. Chem.*, **10**, 49 (1957); E. L. Eliel, S. Meyerson, Z. Welvart, and S. H. Wilen, *J. Am. Chem. Soc.*, **82** 2936 (1960).
9) The evaluation of the rate ratios is shown in the experimental section.
10) R. Ito, T. Migita, N. Morikawa, and O. Simamura, *Tetrahedron*, **21**, 955 (1965).
11) T. Migita, T. Nagai, and Y. Abe, *Chem. Lett.*, **1975**, 543.
12) C. J. Machejda and W. P. Hoss, *J. Am. Chem. Soc.*, **92**, 6298 (1970).
13) Diphenylmethyleneamino radicals have a rho value of *ca.* −2.5 for the hydrogen abstraction reaction from methyltoluenes at 70 °C. (T. Suehiro *et al.*, to be published)
14) R. Renaud and L. C. Leitch, *Can. J. Chem.*, **34**, 98 (1956).

Phenanthro[4,5-*bcd*]furan Derivatives. IV. A Synthesis of Phenanthro[4,5-*bcd*]furan

Takaaki HORAGUCHI

Department of Chemistry, Faculty of Science, Niigata University, Ikarashi, Niigata 950-21

(Received May 6, 1977)

Phenanthro[4,5-*bcd*]furan was synthesized from 1,2,3,8,9,9a-hexahydrophenanthro[4,5-*bcd*]furan-3-ol by dehydrogenation with palladium–charcoal. Some chemical reactivities and spectral properties of phenanthro[4,5-*bcd*]furan were investigated and compared with those of phenantherene and dibenzofuran. The results suggest that phenanthro[4,5-*bcd*]furan has the chemical properties of both phenanthrene and dibenzofuran, and does not have a large strain in the fused-ring system. Also, the reactivities of 1,2,3,8,9,9a-hexahydrophenanthro[4,5-*bcd*]furan-3-one were explored.

Compounds such as Formula **1** have bridged atoms (C, N, S, O) which link the 4 and 5-positions in phenanthrene. The synthetic methods of these compounds except for X=O were early reported in the literature.

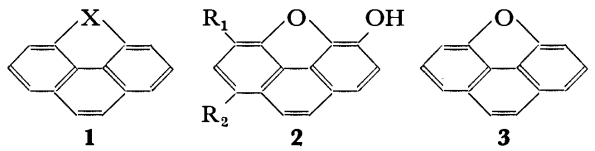

1 **2** **3**

1a: X=C
1b: X=N
1c: X=S
1d: X=O(**3**)

For example, phenanthro[4,5-*bcd*]thiophene (**1c**; X=S)[1] was prepared by heating phenanthrene with hydrogen sulfide at 630 °C in the presence of an alumina–chromia–magnesia catalyst. Also, phenanthro[4,5-*bcd*]-pyrrole (**1b**; X=N)[2] was similarly obtained from 4-phenanthrylamine. On the other hand, when X was a carbon atom 4*H*-cyclopenta[*def*]phenanthrene (**1a**; X=C)[3] was synthesized by the intramolecular cyclization of 3-(1-acenaphthenyl)propionic acid, followed by the reduction of the carbonyl group and then dehydrogenation. In the case of X=O, Compound **3** is termed phenanthro[4,5-*bcd*]furan and is a fundamental skeleton of morphine. Though the syntheses of **2** ($R_1=R_2=H$; $R_1=OCH_3$, $R_2=H$; $R_1=H$, $R_2=OCH_3$)[4-6] have already reported by us, the fundamental skeleton (**3**) has not yet been synthesized. It is said that the ring system of **3** has an inherent strain because of ether linkage between the 4 and 5-positions in phenanthrene. Therefore, we attempted to prepare phenanthro[4,5-*bcd*]furan (**3**) and discussed the strain in the phenanthro-[4,5-*bcd*]furan ring by comparing the chemical reactivities and physical properties of **3** with those of phenanthrene, dibenzofuran, and other related compounds.

Results and Discussion

The synthesis of phenanthro[4,5-*bcd*]furan (**3**) was attempted in three ways; the routes are shown in Scheme 1. For the synthesis of **3** 1,2,3,8,9,9a-hexahydrophenanthro[4,5-*bcd*]furan-3-one (**5**)[4] was employed as an important intermediate. When **5** was reduced with lithium aluminum hydride, only one product, 1,2,3,8,-9,9a-hexahydrophenanthro[4,5-*bcd*]furan-3-ol (**6**), was obtained. Although the formation of diastereoisomers is possible by the attack of lithium aluminum hydride on the carbonyl group from both sides, it seems that only one-sided attack from the less hindered face occurred preferentially because of steric requirements. A similar asymmetric synthesis has been reported[7] in the reduction of 1-bromocodeine to codeine with lithium aluminum hydride. It appears that the structure of the alcohol is as is shown in Formula **6** judging from the molecular model and the NMR spectrum. The methine proton on a carbon atom at the 3-position of **6** has absorptions (multiplet) at δ 4.85—5.06, and the coupling pattern is similar to that of the methine proton on a carbon atom at the 3-position of **16** (*vide infra*). This suggests that the configurations of the two methine protons of **6** and **16** are the same.

By the dehydrogenation of **6** with palladium–charcoal in *p*-cymene, the desired phenanthro[4,5-*bcd*]furan (**3**) was obtained in a 30% yield, along with 1,2,3,3a,8,9,-9a,9b-octahydrophenanthro[4,5-*bcd*]furan (**7**; 14% yield). The structure of **3** was confirmed by the elemental analysis and by its spectral properties (see Experimental). When **6** was heated with palladium-charcoal without a solvent at 270 °C, three kinds of products were obtained; phenanthro[4,5-*bcd*]furan (**3**; 9%), phenanthrene (**8**; 9%), and 4-phenanthrol (**9**; 22%). As the separation of **3** and **8** was fairly difficult, the ratio was determined by gas chromatography. This suggests that the ether bridge is easy to cleave at a high temperature. The reaction of **6** with *N*-bromosuccinimide gave a mixture of two products after the elimination of hydrogen bromide with potassium hydroxide. The NMR spectrum of the mixture showed that it consisted of phenanthro[4,5-*bcd*]furan (**3**; 13% yield) and 8,9-dihydrophenanthro[4,5-*bcd*]furan (**10**; 13% yield). Therefore, in all three methods the yield of the aromatization of **6** was the best when it was carried out in *p*-cymene.

Dendy *et al.*[8] attempted to cyclize **11** to a phenanthro-[4,5-*bcd*]furan derivative (**12**) by means of a Friedel-Crafts reaction. However, the yields was very low, and so they abandoned the subsequent synthesis of morphenol (**2**; $R_1=R_2=H$). In the case of naphtho[1,8-*bc*]furan derivatives (**4**), the cyclization occurred easily to give **5** in good yields.[4] The structure of **5** and **12** are similar to each other; therefore, the ring strains of the two compounds seem almost the same, if present at all. In the Friedel-Crafts reaction (**11**→**12**) an sp^2

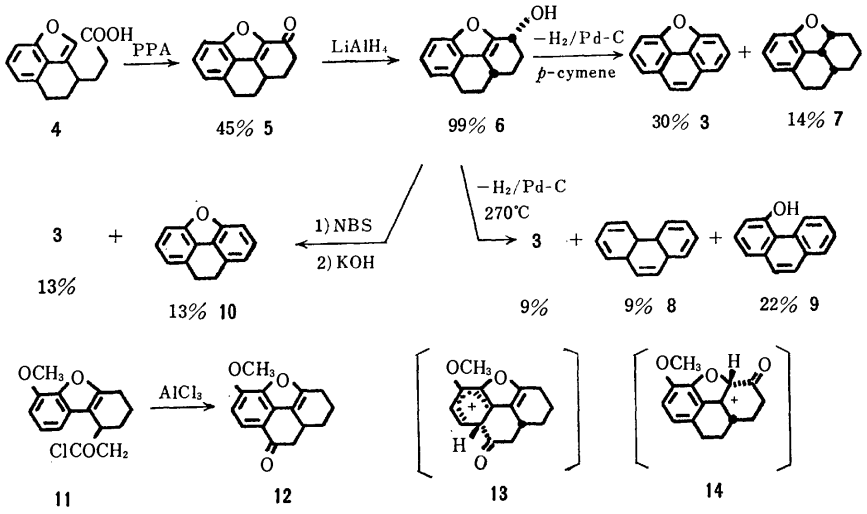

Scheme 1.

hybrid orbital of a carbon atom in the benzene ring must be changed to an sp^3 hybrid orbital in an intermediate, as is shown in Formula **13**. The consideration of a molecular model suggests that the conformation of the intermediate **13** must be cup-shaped and have a strain. On the other hand, in the case of **4** the cyclization occurs without a large deformation of the **4** molecule because the side chain of propionic acid is situated at a very favorable position for the cyclization reaction. From these consideration, it seems that the low yield of **12** is due to the strain in the intermediate, **13**, rather than to that in the product, **12**. If the carbon-carbon double bond in the furan ring of **11** is hydrogenated, the cyclization would become easy, for the side chain of acetic acid could closely approach the benzene ring.

Some chemical reactivities on **5** are shown in Scheme 2. Compound **6** dissolved in ethanol was converted to two products (**15** and **16**) by the action of sulfuric acid. The two products are diastereoisomers to each other, and the yields are 47 and 38% respectively. The structures of **15** and **16** were confirmed by comparing the NMR spectra with that of **6**. The catalytic hydrogenation of **5** with palladium–charcoal gave 1,2,3,3a,-8,9,9a,9b-octahydrophenanthro[4,5-*bcd*]furan-3-ol (**17**) in an 81% yield. The infrared spectrum of **17** shows an absorption due to a monomeric hydroxyl group at 3580 cm^{-1}. This suggests that a hydroxyl group is present in the cup-shaped molecule and that the juncture is all *cis*, as is shown in Formula **17**. By the Wolff-Kishner reduction of **5**, 1,2,3,8,9,9a-hexahydrophenanthro[4,5-*bcd*]furan (**18**) was obtained in a 50% yield. Compound **18** was hydrogenated with palladium–charcoal to give 1,2,3,3a,8,9,9a-octahydrophenanthro-[4,5-*bcd*]furan (**7**) in an 84% yield. The structure of **7** must be a *cis-cis* juncture, as is shown in Formula **7**, because **18** is easy to approach from the less-hindered face to the catalyst and the NMR spectrum of **7** is similar to that of **17**.

Some chemical reactivities of phenanthro[4,5-*bcd*]-furan (**3**) were investigated and compared with those of phenanthrene and dibenzofuran. The results are shown in Scheme 3. The catalytic hydrogenation of **3** with palladium–charcoal gave 8,9-dihydrophenanthro[4,5-*bcd*]furan (**10**) in a 74% yield. Under the same conditions, phenanthrene was not reduced, but it was hydrogenated to 9,10-dihydrophenanthrene under more drastic conditions (copper chromium oxide, 150—200 atm, 180 °C).[9] By the bromination of **3** with bromine, 8-bromophenanthro[4,5-*bcd*]furan (**20**) was obtained in a 67% yield. Also, phenanthrene was brominated to 9-bromophenanthrene.[12] However, the bromination of dibenzofuran gave 2-bromodibenzofuran.[13] These findings suggest that the 8,9-double bond of **3** has a considerable olefinic character and is more reactive than that in phenanthrene. When Compound **3** was heated with sodium and ethanol, 3,3a,8,9,9a,9b-hexahydrophenanthro[4,5-*bcd*]furan (**19**) was obtained in a 32% yield. Under these conditions dibenzofuran was reduced to 1,2,3,4-tetrahydrodibenzofuran,[10] but phenanthrene was not converted to 9,10-dihydro-

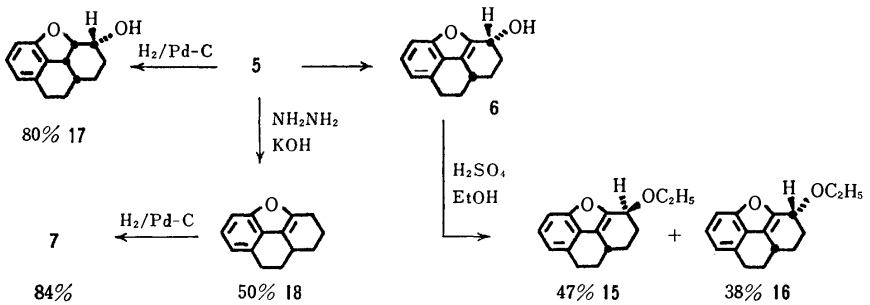

Scheme 2.

phenanthrene without the employment of sodium and 1-pentanol.[11] By the Friedel-Crafts reaction of **3** and benzoyl chloride with anhydrous aluminum chloride 1-benzoylphenanthro[4,5-*bcd*]furan (**21**) was obtained in an 84% yield. Under similar conditions, dibenzofuran also reacted with benzoyl chloride to give 2-benzoyldibenzofuran.[16] When **3** was treated with lithium aluminum hydride in dry ether, 4-phenanthrol (**9**) was obtained in an 80% yield. As the ether bridge in a five-membered ring is difficult to cleave with lithium aluminum hydride, the facile cleavage of the ether bridge may due to an inherent strain in the fused-ring system of **3**. In fact, dibenzofuran is not reduced under these conditions.

From these experimental results, it appears that phenanthro[4,5-*bcd*]furan has the character of both phenanthrene and dibenzofuran and is more reactive because of the ether bridge in the fused-ring system of **3**.

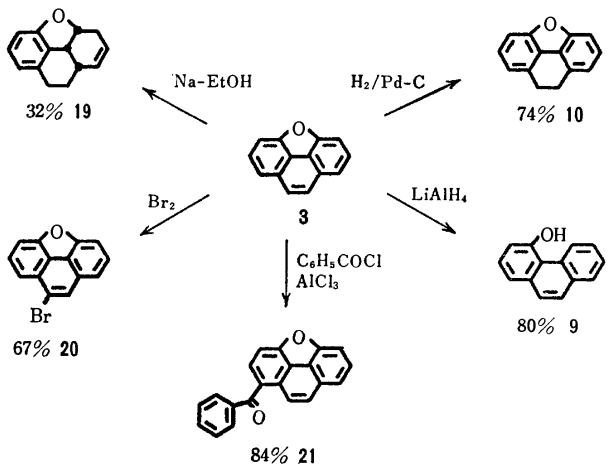

Scheme 3.

The ultraviolet spectrum of phenanthro[4,5-*bcd*]furan (**3**) is shown, along with that of pyrene[1] in Fig. 1. The shapes of the spectra of **3** and pyrene are very similar to each other, but the region of absorption for **3** is shifted to a shorter wavelength than that of pyrene. It is thus apparent that a non-bonding pair of electrons on the oxygen atom functions as part of the overall chromophoric π-system in phenanthro[4,5-*bcd*]furan. Also, the ultraviolet spectra of phenanthro[4,5-*bcd*]furan (**1d**; X=O), phenanthro[4,5-*bcd*]thiophene (**1c**; X=S),[1] and phenanthro[4,5-*bcd*]pyrrole (**1b**; X=N)[2,15] are shown in Fig. 2. The shapes of the three spectra are similar to one another, and in all the regions of absorptions shift to longer wavelengths as X changes from a oxygen atom to a sulfur or a nitrogen atom. This shows that interaction between the non-bonding pair of electrons on the oxygen atom and the π-electrons on the phenanthrene ring is weak in phenanthro[4,5-*bcd*]furan. In the case of X=N, the interaction is strong, while it is medium when X is a sulfur atom with *d*-orbitals. Moreover, the spectrum of pyrene is superimposable on that of phenanthro[4,5-*bcd*]thiophene.[1] The ultraviolet spectra of 8,9-dihydrophenanthro[4,5-*bcd*]furan and dibenzofuran are shown in Fig. 3. The shapes of the spectra of the corresponding pair of compounds are similar to each other. These spectral properties suggest that phenanthro[4,5-*bcd*]furan does not have a large strain in the fused-ring system.

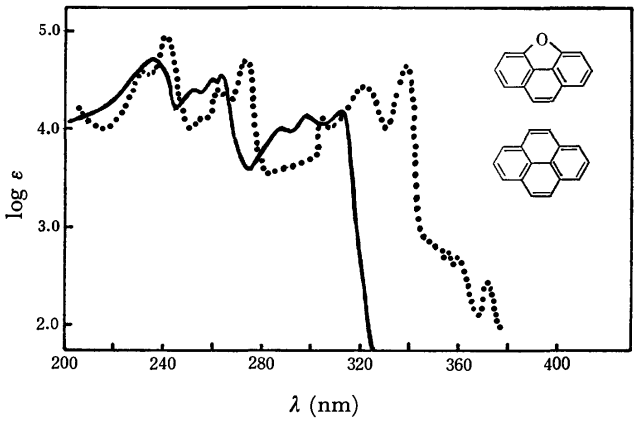

Fig. 1. Ultraviolet spectra for **3** (solid line) and pyrene (dotted line) in ethanol.

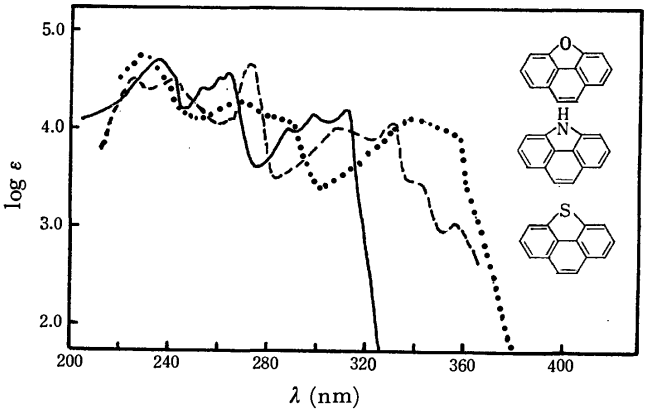

Fig. 2. Ultraviolet spectra for **3** (solid line), **1b** (X=N; dotted line), and **1c** (X=S; broken line) in ethanol.

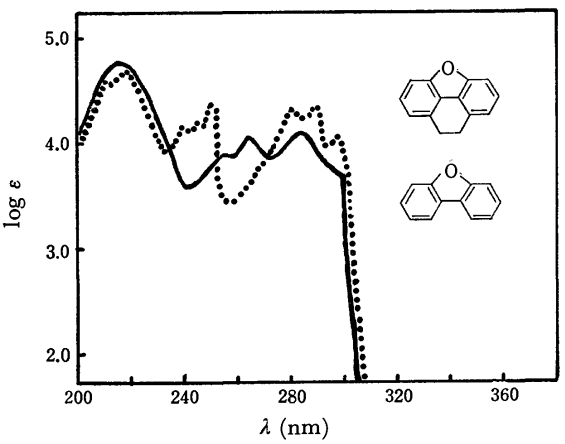

Fig. 3. Ultraviolet spectra for **10** (solid line) and dibenzofuran (dotted line) in ethanol.

Experimental

All the melting points are uncorrected. The column chromatography was performed on silica gel (WAKOGEL C-200).

Unless otherwise stated, anhydrous sodium sulfate was employed as the drying agent. The infrared absorption spectra were determined with a JASCO Model DS 402 G infrared spectrophotometer. The ultraviolet absorption spectra were determined with a Shimadzu Model UV-200 spectrophotometer. The nuclear magnetic resonance spectra were determined at 100 MHz with a JEOL Model 4H-100 NMR spectrometer, using tetramethylsilane as the internal standard.

*1,2,3,8,9,9a-Hexahydrophenanthro[4,5-*bcd*]furan-3-ol (6).* A mixture of **5** (2.0 g), lithium aluminum hydride (0.3 g), and dry ether (40 ml) was refluxed for 4 h. After the reaction, the excess lithium aluminum hydride was decomposed with ethyl acetate. The mixture was poured into ice water, acidified with 6 M hydrochloric acid, and extracted with ether. The ethereal layer was washed with water, dried, and then evaporated to give 2.0 g (99%) of **6** as crystals. Recrystallization from benzene gave colorless needles; mp 122—123 °C. IR (KBr): ν_{max} 746, 758, 775, 948, 996, 1023, 1052, 1075, 1240, 1350, 1635, 3300 cm^{-1}. NMR ($CDCl_3$): δ 1.02—1.43 (m, 2H, $-CH_2-$), 1.70—2.60 (m, 4H, $-CH_2-$ + $-CH_2-$), 2.46 (s, 1H, OH), 2.70—2.96 (m, 3H, $-CH_2-$ + =CH–), 4.85—5.06 (m, 1H, =CHO–), 6.90—7.23 (m, 3H, Ar–H). UV (EtOH): λ_{max} (ε) 210^{sh} (19500), 216 (21000), 257 (12700), 288 nm (900).

Found: C, 78.23; H, 6.71%. Calcd for $C_{14}H_{14}O_2$: C, 78.48; H, 6.59%.

*Phenanthro[4,5-*bcd*]furan (3) and 1,2,3,3a,8,9,9a,9b-Octahydrophenanthro[4,5-*bcd*]furan (7).* A mixture of **6** (3.6 g), 8% palladium–charcoal (1.0 g), and *p*-cymene (30 ml) was heated at 195 °C for 6 h under a nitrogen atmosphere. The initially produced water was removed at the first stage of the reaction. After the removal of the catalyst by filtration, the *p*-cymene was removed under reduced pressure to give an oil. The oil was chromatographed over silica gel and eluted with benzene(1)–hexane(9). From the first fraction we obtained 810 mg (30%) of **3** as crystals. Recrystallization from methanol gave colorless plates; mp 90—91 °C. IR (KBr): ν_{max} 709, 754, 816, 825, 993, 1030, 1218, 1240, 1312, 1355, 1420, 1440, 1500, 1590, 3080 cm^{-1}. NMR ($CDCl_3$): δ 7.53—7.77 (m, 6H, Ar–H), 7.92 (s, 2H, Ar–H). UV (EtOH): λ_{max} (ε) 236 (56700), 253 (26300), 260^{sh} (31000), 263 (34200), 288^{sh} (8100), 299 (12500), 313 nm (14500).

Found: C, 87.25; H, 4.27%. Calcd for $C_{11}H_8O$: C, 87.48; H, 4.20%.

By further elution with benzene(1)–hexane(1), 380 mg (14%) of **7** were obtained as crystals. Recrystallization from methanol gave colorless needles; mp 79.5—80.5 °C. IR (KBr): ν_{max} 743, 763, 855, 876, 915, 967, 1005, 1080, 1210, 1230, 1243, 1455, 1610, 1630, 2880, 2960, 3080 cm^{-1}. NMR ($CDCl_3$): δ 0.95—1.20 (m, 3H, $-CH_2-$ + $-CH_2-$), 1.35—1.70 (m, 2H, $-CH_2-$), 1.78—2.00 (m, 3H, $-CH_2-$ + $-CH_2-$), 2.05—2.39 (m, 1H, =CH–), 2.64 (d,d, J=6 and 10 Hz, 2H, $-CH_2-$), 3.35 (t, J=6 Hz, 1H, Ar–CH=), 4.91 (t, J=8 Hz, 1H, =CHO–), 6.56 (d, J=8 Hz, 1H, Ar–H), 6.62 (d, J=8 Hz, 1H, Ar–H), 7.00 (t, J=8 Hz, 1H, Ar–H). UV (EtOH): λ_{max} (ε) 208 (29200), 232^{sh} (4000), 275—285 nm (1600).

Found: C, 83.82; H, 8.06%. Calcd for $C_{14}H_{16}O$: C, 83.96; H, 8.05%.

Dehydrogenation of 6 without a Solvent. A mixture of **6** (1.0 g) and 8% palladium–charcoal (0.1 g) was heated at 275 °C for 1 h under a nitrogen atmosphere. After the reaction, benzene was added to the mixture and the catalyst was removed by filtration. The benzene was evaporated to give an oil. The oil was chromatographed over silica gel and eluted with benzene(1)–hexane(9). The first fraction gave 160 mg of crystals. It was composed of phenanthro[4,5-*bcd*]furan (**3**) and phenanthrene (**8**), and the **3**/**8** ratio was found to be 1 by gas chromatography. By the fractional recrystallization of the mixture from ethanol, a few of individual components were obtained in a pure state. However, the separation of **3** and **8** was generally difficult.

By further elution with benzene, 220 mg (22%) of 4-phenanthrol (**9**) were obtained as crystals. Recrystallization from benzene–hexane gave colorless needles; mp 112—113 °C. (lit,[14] mp 113 °C). IR (KBr): ν_{max} 716, 743, 800, 830, 1004, 1225, 1290, 1313, 1345, 1420, 1445, 1580, 3085, 3555 cm^{-1}. NMR ($CDCl_3$): δ 5.57 (s, 1H, OH), 6.81 (d,d, J=2 and 8 Hz, 1H, Ar–H), 7.17—7.90 (m, 6H, Ar–H), 7.65 (s, 2H, Ar–H). UV (EtOH): λ_{max} (ε) 213 (25000), 226 (23700), 244 (49500), 249^{sh} (44100), 275 (20900), 295^{sh} (9000), 302^{sh} (7700), 323 (2000), 338 (3300), 355 nm (4100).

Found: C, 86.32; H, 5.20%. Calcd for $C_{14}H_{10}O$: C, 86.57; H, 5.19%.

Reaction of 6 with N-Bromosuccinimide. A mixture of **6** (0.5 g), *N*-bromosuccinimide (1.0 g), and carbon tetrachloride (10 ml) was refluxed for 1 h. After the removal of the insoluble materials by filtration, the carbon tetrachloride was evaporated. To the residue potassium hydroxide (3.0 g) and ethanol (20 ml) was added, after which the mixture was refluxed for 3 h. The mixture was then poured into ice water, acidified with 6 M hydrochloric acid, and extracted with ether. The ethereal layer was washed with water, dried, and then evaporated. The resulting oil was chromatographed over silica gel and eluted with benzene(1)–hexane(9). The first fraction gave 120 mg (26%) of an oil which partially solidified. It consisted of phenanthro[4,5-*bcd*]furan (**3**) and 8,9-dihydrophenanthro[4,5-*bcd*]furan (**10**), and the **3**/**10** ratio was found to be 1 by a study of the NMR spectrum. The partially solidified oil was washed with methanol, and the resulting solid was recrystallized from methanol to give 10 mg (2%) of **3** as colorless plates; mp 90—91 °C.

*3-Ethoxy-1,2,3,8,9,9a-hexahydro[4,5-*bcd*]furan (15 and 16).* Sulfuric acid (3.0 g) was added, drop by drop, to **6** (1.5 g) in ethanol (15 ml) under cooling with ice water, after which the mixture was stirred for 3 h at 0 °C. The mixture was then poured into ice water and extracted with ether. The ethereal layer was washed with water, dried, and then evaporated to give an oil. The oil was chromatographed over silica gel and eluted with benzene. The first fraction gave 800 mg (47%) of **15** as a colorless oil. IR (neat); ν_{max} 753, 770, 780, 935, 995, 1015, 1070, 1090, 1120, 1150, 1205, 1235, 1340, 1360, 1405, 1435, 1450, 1465, 1635, 2890, 2960, 3005 cm^{-1}. NMR ($CDCl_3$): δ 1.07—1.63 (m, 2H, $-CH_2-$), 1.22 (t, J=7 Hz, 3H, $-CH_3$), 1.78—2.37 (m, 4H, $-CH_2-$ + $-CH_2-$), 2.56—3.00 (m, 3H, $-CH_2-$ + =CH–), 3.60—3.90 (m, 2H, $-OCH_2-$), 4.51—4.59 (m, 1H, –OCH=), 6.90—7.29 (m, 3H, Ar–H). UV (EtOH): λ_{max} (ε) 216 (23000), 256 (13100), 287 nm (1100).

Found: C, 79.10; H, 7.37%. Calcd for $C_{16}H_{18}O_2$: C, 79.31; H, 7.49%.

From the second fraction, 650 mg (38%) of **16** were obtained as crystals. Recrystallization from ethanol gave colorless needles; mp 85—86 °C. IR (KBr): ν_{max} 750, 760, 773, 1092, 1120, 1245, 1350, 1400, 1465, 2890, 2970, 3005 cm^{-1}. NMR ($CDCl_3$): δ 1.06—1.48 (m, 2H, $-CH_2-$), 3.31 (t, J= 8 Hz, 3H, $-CH_3$), 1.55—2.55 (m, 4H, $-CH_2-$ + $-CH_2-$), 2.67—3.07 (m, 3H, $-CH_2-$ + =CH–), 3.63—4.14 (m, 2H, $-OCH_2-$), 4.59—4.77 (m, 1H, –OCH=), 6.90—7.28 (m, 3H, Ar–H). UV (EtOH): λ_{max} (ε) 216 (21800), 257 (14200), 287 nm (1000).

Found: C, 79.06; H, 7.56%. Calcd for $C_{16}H_{18}O_2$: C, 79.31; H, 7.49%.

*1,2,3,3a,8,9,9a,9b-Octahydrophenanthro[4,5-*bcd*]furan-3-ol (17).* A mixture of **5** (1.0 g), 8% palladium–charcoal (0.3 g), and

ethanol (50 ml) was shaken for 10 h at room temperature under a hydrogen atmosphere. After the removal of the catalyst by filtration, the ethanol was evaporated under reduced pressure. The resulting oil was chromatographed over silica gel and eluted with benzene(8)–ether(2) to give 0.81 g (80%) of **17** as crystals. The crystals were dissolved in hexane and recrystallized after the removal of the insoluble materials to give colorless needles; mp 74.5—76 °C. IR (KBr): ν_{max} 534, 640, 765, 800, 838, 930, 956, 970, 1005, 1054, 1213, 1236, 1293, 1300, 1345, 1460, 1610, 1630, 2880, 2970, 3580 cm^{-1}. NMR ($CDCl_3$): δ 1.20—1.51 (m, 2H, $-CH_2-$), 1.63—2.03 (m, 2H, $-CH_2-$), 1.79 (s, 1H, OH), 2.66 (t, J=7 Hz, 2H, $-CH_2-$), 3.45 (t, J=7 Hz, 1H, Ar–CH=), 3.99—4.10 (m, 1H, –OCH=), 4.86 (d,d, J=6 and 8 Hz, 1H, –OCH=), 6.58 (d, J=8 Hz, 1H, Ar–H), 6.64 (d, J=8 Hz, 1H, Ar–H), 7.01 (t, J=8 Hz, 1H, Ar–H). UV (EtOH): λ_{max} (ε) 208 (28500), 276—286 nm (1600).

Found: C, 77.79; H, 7.45%. Calcd for $C_{14}H_{16}O_2$: C, 77.75; H, 7.46%.

*1,2,3,8,9,9a-Hexahydrophenanthro[4,5-*bcd*]furan (**18**).* A mixture of **5** (2.0 g), hydrazine hydrate (80%; 15 g), potassium hydroxide (28 g), and triethylene glycol (80 ml) was heated for 2 h at 140 °C and for 3.5 h at 190 °C. During the reaction, the distilled liquid was removed. After the reaction, the mixture was poured into ice water, acidified with 6 M hydrochloric acid, and extracted with ether. The ethereal layer was washed with water, dried, and then evaporated. The resulting oil was chromatographed over silica gel and eluted with benzene(1)–hexane(1) to give 0.93 g (50%) of **18** as crystals. Recrystallization from methanol gave colorless plates; mp 46—47 °C. IR (KBr): ν_{max} 758, 777, 822, 956, 1012, 1110, 1188, 1210, 1222, 1240, 1335, 1450, 1465, 1500, 1630, 1675, 2870, 2960, 3080 cm^{-1}. NMR ($CDCl_3$): δ 0.80—1.45 (m, 2H, $-CH_2-$), 1.70—2.34 (m, 4H, $-CH_2-$ + $-CH_2-$), 2.40—3.15 (m, 5H, $-CH_2-$ + $-CH_2-$ + =CH–), 6.85—7.20 (m, 3H, Ar–H). UV (EtOH): λ_{max} (ε) 217 (22900), 257 (12100), 288 nm (1000).

Found: C, 84.65; H, 7.15%. Calcd for $C_{14}H_{14}O$: C, 84.81; H, 7.12%.

*1,2,3,3a,8,9,9a,9b-Octahydrophenanthro[4,5-*bcd*]furan (**7**).* A mixture of **18** (0.4 g), 8% palladium–charcoal (0.3 g), and ethanol (20 ml) was shaken for 6 h at room temperature under a hydrogen atmosphere. After the removal of the catalyst by filtration, the ethanol was evaporated under reduced pressure. The resulting crystals were chromatographed over silica gel and eluted with benzene(6)–hexane(4) to give 0.34 g (84%) of **7** as crystals. Recrystallization from methanol gave colorless needles; mp 79.5—80.5 °C.

*8,9-Dihydrophenanthro[4,5-*bcd*]furan (**10**).* A mixture of **3** (0.35 g), 8% palladium–charcoal (0.3 g), and ethanol (30 ml) was shaken for 15 h at room temperature under a hydrogen atmosphere. After the removal of the catalyst by filtration, the ethanol was evaporated under reduced pressure. The resulting oil was chromatographed over silica gel and eluted with benzene(1)–hexane(9) to give 0.26 g (74%) of **10** as crystals. Recrystallization from methanol gave colorless leaflets; mp 41—42 °C. IR (KBr): ν_{max} 773, 982, 1015, 1194, 1238, 1435, 1450, 1595, 1630, 1660, 3065, 3090 cm^{-1}. NMR ($CDCl_3$): δ 3.28 (s, 4H, $-CH_2-$ + $-CH_2-$), 7.02—7.31 (m, 6H, Ar–H). UV (EtOH): λ_{max} (ε) 214 (49400), 227 (26300), 255^{sh} (8000), 264 (12000), 285 (11200), 294^{sh} (8600), 297^{sh} nm (8000).

Found: C, 86.38; H, 5.18%. Calcd for $C_{14}H_{10}O$: C, 86.57; H, 5.19%.

*4-Phenanthrol (**9**).* A mixture of **3** (0.1 g), lithium aluminum hydride (0.1 g), and dry ether (20 ml) was refluxed for 25 h. The excess lithium aluminum hydride was then decomposed with ethyl acetate, and the mixture was poured into ice water and acidified with 6 M hydrochloric acid. The mixture was subsequently extracted with ether. The ethereal layer was washed with water, dried, and then evaporated to give an oil. The oil was chromatographed over silica gel and eluted with benzene(1)–hexane(9). The first fraction gave 50 mg (50%) of the starting material (**3**). From the second fraction we obtained 40 mg (80%) of **9** as colorless leaflets. The IR spectrum of the product was in according with that of 4-phenanthrol (**9**) obtained by the dehydrogenation of **6** without a solvent.

*8-Bromophenanthro[4,5-*bcd*]furan (**20**).* To **3** (0.2 g) in carbon tetrachloride (10 ml) we added 1.2 mol of bromine in carbon tetrachloride (10 ml), after which the mixture was stirred for 2 h at room temperature. It was then heated at 70 °C for 30 min to eliminate the hydrogen bromide. After the evaporation of carbon tetrachloride, the resulting crystals were chromatographed over silica gel and eluted with benzene(1)–hexane(9) to give 0.21 g (67%) of **20** as crystals. Recrystallization from ethanol gave colorless needles; mp 144—145 °C. IR (KBr): ν_{max} 712, 770, 830, 866, 1036, 1188, 1235, 1300, 1345, 1420, 1465, 1505, 1590 cm^{-1}. NMR ($CDCl_3$): δ 7.53—7.88 (m, 6H, Ar–H), 8.16 (s, 1H, Ar–H). UV (EtOH): λ_{max} (ε) 222 (28100), 237 (45600), 258 (29600), 265 (34500), 308 (13100), 319 (13300), 337 (1900), 353 nm (200).

Found: C, 61.76; H, 2.73%. Calcd for $C_{14}H_7OBr$: C, 62.02; H, 2.60%.

*3,3a,8,9,9a,9b-Hexahydrophenanthro[4,5-*bcd*]furan (**19**).* Compound **3** (0.3 g) was dissolved in ethanol (20 ml), and the solution was heated under reflux. To the solution sodium (4.0 g) was added in limited amounts. When precipitates of sodium ethoxide were produced, additional ethanol (20 ml) was introduced into the solution and residual sodium was added. After the sodium had disappeared (1.5 h), the mixture was poured into ice water, acidified with 6 M hydrochloric acid, and extracted with ether. The ethereal layer was washed with water, dried, and then evaporated. The resulting oil was chromatographed over silica gel and eluted with benzene(1)–hexane(1) to give 0.1 g (32%) of **19** as a colorless oil. IR (neat): ν_{max} 740, 770, 810, 864, 880, 926, 1023, 1042, 1220, 1235, 1244, 1465, 1615, 1635, 2890, 2960, 3060 cm^{-1}. NMR ($CDCl_3$): δ 1.38—1.69 (m, 1H, $-CH_2-$), 1.80—2.12 (m, 2H, $-CH_2-$), 2.17—2.31 (m, 1H, $-CH_2-$), 2.39—2.65 (m, 2H, $-CH_2-$), 2.71—2.96 (m, 1H, =CH–), 3.56 (t, J= 8 Hz, 1H, Ar–CH=), 4.96—5.17 (m, 1H, –OCH=), 5.65 (s, 2H, CH=CH), 6.57 (d, J=8 Hz, 1H, Ar–H), 6.61 (d, J= 8 Hz, 1H, Ar–H), 6.98 (t, J=8 Hz, 1H, Ar–H). UV (EtOH): λ_{max} (ε) 207 (26800), 275—284 nm (1900).

Found: C, 84.56; H, 6.98%. Calcd for $C_{14}H_{14}O$: C, 84.81; H, 7.12%.

*1-Benzoylphenanthro[4,5-*bcd*]furan (**21**).* To a solution of **3** (100 mg) and benzoyl chloride (110 mg) dissolved in carbon disulfide (5 ml) we added anhydrous aluminum chloride (100 mg). The mixture was then stirred for 6 h at room temperature, decomposed with dilute hydrochloric acid, and extracted with ether. The ethereal layer was washed with water, dried, and then evaporated. The resulting oil was chromatographed over silica gel and eluted with benzene(8)–hexane(2). The first fraction gave 130 mg (84%) of **21** as crystals. Recrystallization from methanol gave colorless needles; mp 126—127 °C. IR (KBr): 660, 702, 733, 756, 792, 960, 1028, 1215, 1232, 1270, 1325, 1400, 1505, 1590, 1650 cm^{-1}. NMR ($CDCl_3$): δ 7.38—7.89 (m, 9H, Ar–H), 7.99 (d, J=9 Hz, 1H, Ar–H), 8.06 (d, J=8 Hz, 1H, Ar–H), 8.41 (d, J=9 Hz, 1H, Ar–H). UV (EtOH): λ_{max} (ε) 207 (36200), 238 (52500), 255 (40300), 278^{sh} (19500), 329 (19500).

Found: C, 84.89; H, 4.14%. Calcd for $C_{21}H_{12}O_2$: C, 85.12; H, 4.08%.

The author wishes to thank Mr. Yoshiaki Takahashi for the elemental analyses and Mr. Takao Oono for the nuclear magnetic resonance analyses.

References

1) L. H. Klemm, D. R. McCoy, and D. R. Olson, *J. Heterocycl. Chem.*, **7**, 1347 (1970).
2) O. Kruber and G. Grigoleit, *Chem. Ber.*, **87**, 1895 (1954).
3) W. E. Bachman and J. C. Sheehan, *J. Am. Chem. Soc.*, **63**, 204 (1941).
4) T. Horaguchi and T. Shimizu, *Bull. Chem. Soc. Jpn.*, **47**, 485 (1974).
5) T. Horaguchi and T. Shimizu, *Bull. Chem. Soc. Jpn.*, **48**, 488 (1975).
6) T. Shimizu, T. Horaguchi, and A. Watanabe, *Bull. Chem. Soc. Jpn.*, **46**, 1772 (1973).
7) M. Gates and G. Tschudi, *J. Am. Chem. Soc.*, **74**, 1109 (1952).
8) A. V. Dendy, J. H. P. Tyman, and W. B. Whalley, *J. Chem. Soc.*, **1963**, 4040.
9) J. R. Durland and H. Adkins, *J. Am. Chem. Soc.*, **59**, 135 (1937).
10) O. Hönigschmid, *Monatsh.*, **23**, 829 (1902).
11) G. Schroeter, H. Müller, and J. Y. S. Huang, *Chem. Ber.*, **62**, 645 (1929).
12) H. Henstock, *J. Chem. Soc.*, **119**, 55 (1921); H. Henstock, *ibid.*, **123**, 3097 (1923).
13) H. Gilman and S. Avakian, *J. Am. Chem. Soc.*, **68**, 580 (1946).
14) E. Mosettig and A. Burger, *J. Am. Chem. Soc.*, **57**, 2189 (1935).
15) M. Zander and W. H. Franke, *Chem. Ber.*, **99**, 1279 (1966).
16) R. G. Johnson, H. B. Willis, and H. Gilman, *J. Am. Chem. Soc.*, **76**, 6407 (1954); H. Gilman, P. T. Parker, J. C. Bailie, and G. E. Brown, *ibid.*, **61**, 2836 (1939).

1,3-Dipolar Cycloadditions to Bicyclic Olefins. II. The Effects of Non-aromatic Polar Solvents on the *exo/endo* Product Ratios in 1,3-Dipolar Cycloadditions to Norbornadienes[1,2]

Hisaji TANIGUCHI, Yoshihiro YOSHIDA, and Eiji IMOTO

Department of Applied Chemistry, College of Engineering, University of Osaka Prefecture, Mozu-Umemachi, Sakai, Osaka 591

(Received May 10, 1977)

The *exo/endo* product ratios for three types of 1,3-dipolar cycloadditions of phenylglyoxylonitrile oxide(**1**) to 2,3-bis(methoxycarbonyl)norbornadiene(**2a**), norbornadiene, and 2,3-dicyanonorbornadiene decrease with increasing E_T value of the non-aromatic polar solvent used. The *exo/endo* ratio in the reaction of **1** with **2a** is larger than unity, but the value of $\Delta H^{\ddagger}_{exo} - \Delta H^{\ddagger}_{endo}$ is nevertheless positive. This phenomenon is attributed to the relatively large positive value of $\Delta S^{\ddagger}_{exo} - \Delta S^{\ddagger}_{endo}$, that is, $\Delta G^{\ddagger}_{exo} - \Delta G^{\ddagger}_{endo} < 0$ at ordinary temperatures. On the basis of these results, the conditions, under which the *exo/endo* ratio in the reaction of **1** with **2a** is smaller than unity, were determined. The results can be reasonably explained by the assumption that the dipole moment of the *endo*-form in the transition state is greater than that of the *exo*-form.

In a previous paper, it was reported that various 1,3-dipolar cycloadditions to norbornadienes gave exo-adducts together with small amounts of endo-adducts.[2] Now, the *exo/endo* product ratios for the Diels-Alder reactions of cyclopentadiene with dienophiles, such as methyl acrylate, methyl methacrylate, and methyl *trans*-crotonate, decrease with increasing Ω value of the solvent used.[3] This fact suggests that the stereoselectivity of the 1,3-dipolar cycloadditions to norbornadienes may also depend on the solvent, because the 1,3-dipolar cycloadditions are mechanisms analogous to Diels-Alder reactions. Therefore, the effects of the solvents on the stereoselectivity of the cyloadditions of phenylglyoxylonitrile oxide (**1**) to 2,3-bis(methoxycarbonyl)norbornadiene (**2a**), norbornadiene (**2b**), and 2,3-dicyanonorbornadiene (**2c**), which have been shown to be kinetically controlled,[2] were studied and it was found that the *exo/endo* product ratios decrease with increasing E_T value[4] of the non-aromatic polar solvent. In addition, it was found that these ratios depend on the reaction temperature.

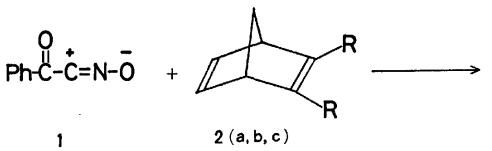

1 2 (a, b, c)

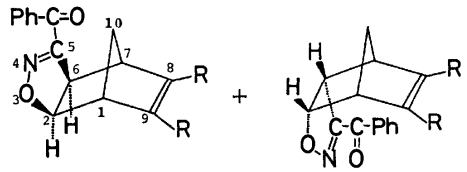

exo 3 (a, b, c) *endo* 4 (a, b, c)

a: R=CO_2CH_3, **b**: R=H, **c**: R=CN

Experimental

Solvents. THF was dried over NaOH for one week and distilled over $LiAlH_4$; bp 66 °C. Ethyl acetate was dried over $CaCl_2$ for a few days and distilled; 77 °C. Chloroform was shaken together with concd sufuric acid, washed with distilled water, dried over $CaCl_2$, and distilled; bp 61 °C. Dichloromethane was dried over $CaCl_2$ and distilled; bp 40 °C. Acetone was dried over $MgSO_4$ and distilled; 56.5 °C. 2-Propanol was dried over CaO and distilled; bp 82.5 °C. Ethanol was refluxed over CaO for 12 h and distilled; bp 78.5 °C. Methanol was prepared by distilling commercial methanol over CaO; bp 64.5 °C.

Materials. Dipolarophiles, **2a**[5] and **2c**,[2] were prepared by methods descrived in the literature. Norbornadiene was purchased and distilled before use. α-Chloro-α-hydroxyiminoacetophenone (**9**), which is a precursor of **1**, was prepared by a method described in the literature.[6] All of the cycloadducts (**3a**, **3b**, **3c**, **4a**, **4b**, and **4c**) produced by the cycloadditions of **1** to **2a**, **2b**, and **2c** have been characterized in previous work.[2]

General Procedure for 1,3-Dipolar Cycloadditions. a) The reaction of **1** with **2a**: A mixture of **9** (460 mg, 2.50 mmol) and **2a** (520 mg, 2.50 mmol) was dissolved in an appropriate solvent (40 cm^3). Then, the solution was maintained at a given temperature (Which was controlled to within ±0.1 °C). A solution of triethylamine (330 mg, 3.26 mmol) in the same solvent (10 cm^3) as that used above was added dropwise over 1 h. After additional stirring for 1 h, the triethylammonium chloride obtained was removed by filtration. The filtrate was evaporated under reduced pressure to give a mixture of the *exo*- and *endo*-adducts. This mixture was submitted to a measurement of the *exo/endo* product ratio by the NMR technique (*vide infra*). (When the ammonium salt was soluble in the solvent, the solvent was evaporated and then the cycloadducts were extracted with benzene.)

b) The reactions of **1** with **2b** and **2c**: Two molar equivalents of **2b** or **2c** with respect to **1** were taken. In the case of the reaction of **1** with **2b**, a small amount of bisadducts was produced in addition to a mixture of the *exo*- and *endo*-monoadducts. The monoadducts were separated from the bisadducts using column chromatography on silica gel.

Measurement of the exo/endo *Product Ratios.* Quantitative analysis of the *exo/endo* product ratios was carried out using NMR spectra (recorded on a Hitachi NMR R-24A spectrometer at 60 MHz.) The ratios were determined by measuring the area ratios of the signals of the *endo*- and *exo*-protons attached on each 2-carbon atom of the *exo*- and *endo*-adducts. These signals were well separated and, moreover, no other signals appeared in the vicinity of these signals.[2]

In order to minimize the error in the measurement of the area integrals, concentrated solutions containing the *exo*- and *endo*- adducts (in 40% $CDCl_3$ solutions) were prepared. The ratio values are subject to an uncertainty of ±0.02.

Results and Discussion

The Linear Relationship between the exo/endo *Product Ratios and the* E_T *Value of the Solvent.* The *exo/endo* product ratios in all three systems were dependent on the kind of the solvent, in the manner shown in Fig. 1. This figure indicates the following.

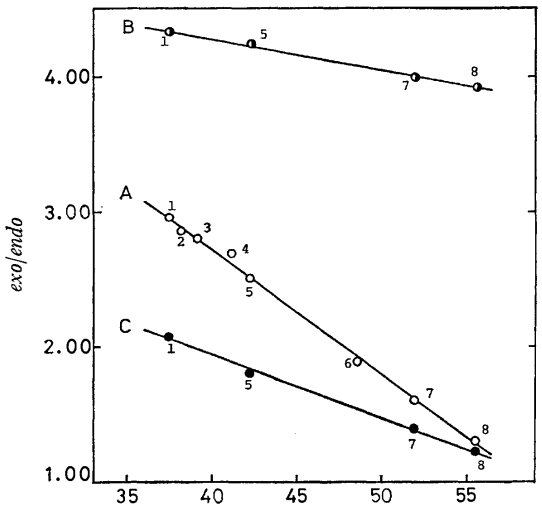

Fig. 1. The linear relationship between the *exo/endo* product ratios (at 0 °C) and $E_{T,30}$ value of the solvent.
A: Reaction of **1** with **2a**, B: reaction of **1** with **2b**, C: reaction of **1** with **2c**, 1; THF, 2; EtOAc, 3; $CHCl_3$, 4; CH_2Cl_2, 5; acetone 6; 2-propanol, 7; EtOH, 8; MeOH.

a) All the *exo/endo* product ratios are greater than unity.

b) The *exo/endo* ratios in each system decrease linearly with increasing E_T value[4] of the solvent.

c) The *exo/endo* ratios for the three systems are in decreasing order, **2b**, **2a**, and **2c**.

The Effect of Temperature on the exo/endo *Product Ratio.* A linear relationship between $1/T$ and the *exo/endo* ratio was observed for the reactions of **1** with **2a** and **2b** carried out in acetone, chloroform, or THF (Fig. 2).

From the results shown in Fig. 2, the differences in activation parameters were calculated (Table 1). Table 1 shows the following.

a) In the reaction of **1** with **2a**,

$$\Delta H^{\ddagger}_{exo} - \Delta H^{\ddagger}_{endo} > 0 \quad (1)$$

and

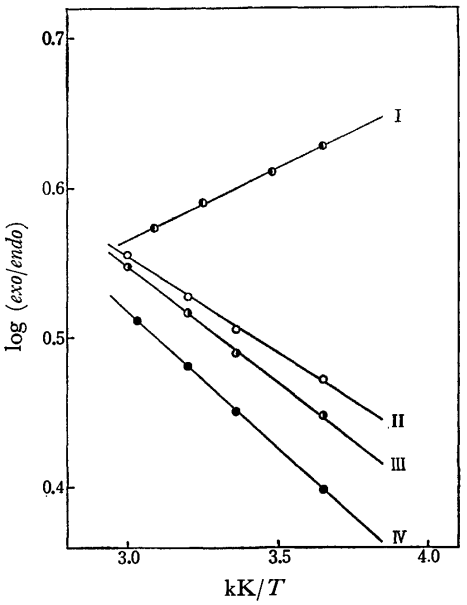

Fig. 2. The linear relationship between $1/T$ and the *exo/endo* product ratio.
I: Reaction of **1** with **2b** in acetone, II: reaction of **1** with **2a** in THF, III: reaction of **1** with **2a** in $CHCl_3$, IV: reaction of **1** with **2a** in acetone.

$$\Delta S^{\ddagger}_{exo} - \Delta S^{\ddagger}_{endo} > 0, \quad (2)$$

and in the reaction of **1** with **2b**,

$$\Delta H^{\ddagger}_{exo} - \Delta H^{\ddagger}_{endo} < 0 \quad (3)$$

and

$$\Delta S^{\ddagger}_{exo} - \Delta S^{\ddagger}_{endo} > 0. \quad (4)$$

If judged only from expression (1) without respect to expression (2), the *exo/endo* ratio should be smaller than unity. Actually, however, the ratio is greater than unity as shown in Fig. 1. This phenonmenon implies that the entropy term of the reaction greatly contributes to the difference in the free energies of activation, that is, the value of $\Delta G^{\ddagger}_{exo} - \Delta G^{\ddagger}_{endo}$ is negative at ordinary temperatures (Table 1).

Expressions of (3) and (4) explain the fact that the *exo/endo* ratio is greater than unity.

b) The value of $\Delta G^{\ddagger}_{exo} - \Delta G^{\ddagger}_{endo}$ for the reaction of **1** with **2a** decreases with increasing E_T value of the solvent.

Conditions Which Give an exo/endo *Product Ratio Smaller than Unity.* The results shown in Fig. 1 suggest that the yield of the *endo*-adduct of the reaction of **1** with **2a** should surpass that of the exo-adduct, if a solvent having a larger E_T value than 58.6 is used as the

TABLE 1. DIFFERENCES IN ACTIVATION PARAMETERS IN THE REACTION OF **1** WITH **2a** AND **2b***) (1 cal=4.184 J)

Diene	Solvent	$E_{T,30}$ / kcal mol^{-1}	$\Delta\Delta H^{\ddagger}$ / cal mol^{-1}	$\Delta\Delta S^{\ddagger}$ / cal K^{-1} mol^{-1}	$\Delta\Delta G^{\ddagger}$ / cal mol^{-1} (at 25 °C)
2a	CH_3COCH_3	42.2	+856	+4.88	−599
2a	$CHCl_3$	39.1	+703	+4.63	−677
2a	THF	37.4	+603	+4.34	−691
2b	CH_3COCH_3	42.2	−439	+1.26	−815

*) $\Delta\Delta H^{\ddagger} = \Delta H^{\ddagger}_{exo} - \Delta H^{\ddagger}_{endo}$, $\Delta\Delta S^{\ddagger} = \Delta S^{\ddagger}_{exo} - \Delta S^{\ddagger}_{endo}$, $\Delta\Delta G^{\ddagger} = \Delta G^{\ddagger}_{exo} - \Delta G^{\ddagger}_{endo}$.

Table 2. The *exo/endo* product ratio in the reaction of **1** with **2a**[a]

Medium	Solubility of **2a**	$E_{T_{30}}$ kcal mol^{-1}	*exo* / *endo*
MeOH	sol	55.5	1.31
MeOH–H_2O (7: 3)[b]	sol	—	1.04
MeOH–H_2O (5; 5)[b]	sol	—	0.725
water	insol	63.1	1.84
hexane	insol	30.9	1.88

a) Temp.: 0 °C, volume of medium: 40 cm^3, **1**: 2.50 mmol, **2a**: 2.50 mmol. b) Volume ratio.

reaction solvent. Such a solvent was prepared with the addition of water ($E_{T_{30}}$ value, 63.1) to mathanol ($E_{T_{30}}$ value, 55.5), since water does not dissolve **2a**.[7] In a medium consisting of methanol and water (1: 1, volume ratio), the yield of the *endo*-adduct in the reaction surpassed that of the *exo*-adduct (Table 2).

A Tentative Explanation for the Above Results. The explanation of Berson *et al.* for the *exo/endo* product ratio in the Diels-Alder reaction of cyclopentadiene with methyl acrylate[3] was adopted here.

The permanent dipole moments of the *exo*- and *endo*-forms in the transition states, **5** and **6**, were assumed to be given approximately by the vectorial sum of the dipole moments of the two components, **7** and **8**. The values of the dipole moments of **8a**, **8b**, and **8c** can be estimated using the bond angles and the bond moments shown in the figure (*vide infra*). The bond angles and the bond moments for the transition states were assumed to be equel to those for the cycloadducts produced. The bond angles for the cycloadducts were determined from their molecular models and the values of the bond moments were extracted from the literature.[8–10] The arrows shown for **5**—**8** are directed from the positive toward the negative end of each structure or component. The dihedral angles between the dipoles of the two components, **7** and **8**, were assumed to be 170° for the *exo*-form in the transition state and 55° for the *endo*-form using molecular models of the cycloadducts. The above estimate indicates that the resultant dipole moment of **6** is greater than that of **5**.

When the E_T value of the solvent becomes larger or the solute more polar, the free energy of solvation becomes smaller.[3,11] As described above, the dipole moment of the *endo*-form in the transition state is greater than that of the *exo*-form. Therefore, the change from a small E_T value for the solvent to a large value results in a larger decrease in the free energy of solvation for the *endo*-form in the transition state as compared with that for the *exo*-form. Thus, as the E_T value of the solvent becomes larger, the rate of formation of the *endo*-adduct increases more greatly as compared with that of the *exo*-adduct. This explanation is reasonable on the basis of the present results.

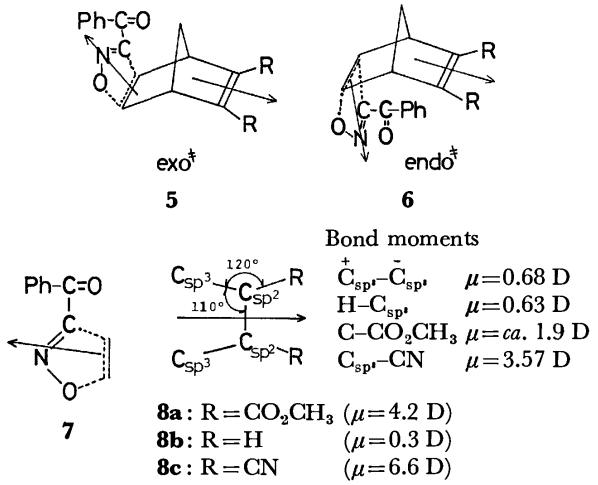

References

1) Presented at the 34th National Meeting of the Chemical Society of Japan, Hiratsuka, Japan, April 1976, Abstract, II. p. 615.

2) Preceding paper: H. Taniguchi, T. Ikeda, Y. Yoshida, and E. Imoto, *Chem. Lett.*, **1976**, 1139; *Bull. Chem. Soc. Jpn.*, **50**, 2694 (1977).

3) J. A. Berson, Z. Hamlet, and W. A. Mueller, *J. Am. Chem. Soc.*, **84**, 297 (1962).

4) K. Dimroth, C. Reichardt, T. Siepman, and F. Bohlmann, *Justus Liebigs Ann. Chem.*, **661**, 1 (1963).

5) O. Diels and K. Alder, *Justus Liebigs Ann. Chem.*, **490**, 236 (1931).

6) Y. Otsuji, Y. Tsujii, A. Yoshida, and E. Imoto, *Bull. Chem. Soc. Jpn.*, **44**, 223 (1971).

7) When this reaction was carried out in water, the *exo/endo* ratio was 1.84. This value resembles the value (1.88) of the *exo/endo* ratio for the reaction carried out in hexane which does not dissolve **2a**.

8) E. M. Kosower, *J. Am. Chem. Soc.*, **80**, 3253 (1958).

9) A. J. Petro, *J. Am. Chem. Soc.*, **80**, 4230 (1958).

10) R. L. Kelly, R. Rollefson, and B. S. Schurin, *J. Chem. Phys.*, **19**, 1595 (1951).

11) a) C. K. Ingold, "Structure and Mechanism in Organic Chemistry," 2nd ed, Cornell University Press, Ithaca, New York (1969), p. 457; b) R. F. Hudson, *J. Chem. Soc., B*, **1966**, 761; c) M. R. J. Dack, *J. Chem. Educ.*, **51**, 231 (1974).

Substituent Effects in the Diels-Alder Reaction of Substituted Benzynes with Hexamethylcyclohexa-2,4-dienone

Akira Oku and Akira Matsui

Department of Chemistry, Kyoto Institute of Technology, Matsugasaki, Sakyo-ku, Kyoto 606

(Received June 6, 1977)

The Diels-Alder reaction of unsymmetrically substituted benzynes that had been generated from 3-Me-, 4-Me-, 5-Me-, 6-Me-, 3,4-Me_2-, 3-NO_2-, 4-NO_2-, 5-NO_2-, and 3-Cl-benzenediazonium-2-carboxylates, with hexamethylcyclohexa-2,4-dienone gave a mixture of 5- or 6-substituted-1,2,3,4,10,10-hexamethyl-1,4-dihydro-1,4-ethanonaphthalene-9-one (Type **7**) and its 8- or 7-substituted isomer (Type **8**). The **7**/**8** isomer ratios varied from 1.0 to 2.0 depending substantially on the size and the position of substituents of the benzynes and also on the temperature and the solvent. The ratios were the same when two positionally isomeric acids, *i.e.*, 3- and 6-, or 4- and 5-substituted acids, were used as the precursors. Thus, the identity of the benzynes generated from these paired isomeric precursors was proved, ruling out the possibility of an inherent memory effect of the precursors. The factor that controls the isomer ratios is discussed in terms of the steric repulsive interaction between the substituents of benzynes and the *gem*-dimethyl groups of the dienone.

In view of the chemical interest in benzyne chemistry, the structure of benzyne does not seem to have been fully elucidated, particularly with regard to that in the transition state of chemical reactions. Triple-bond (**1a**), biradical (**1b**), and ion-pair (**1c**) structures have most often been proposed and discussed in numerous reactions.[1] Among them, the Diels-Alder-type reactions of benzyne with conjugated dienes, for example, have been considered to proceed mainly by means of the **1a** structure with symmetrical bonding, though there is some possibility of **1b** and **1c**.[2]

In our previous study of the synthesis of polymethylnaphthalenes, the reaction of hexamethylcyclohexa-2,4-dienone with unsymmetrically substituted benzynes that were generated from the corresponding benzenediazonium-2-carboxylates has been shown to give two isomeric adducts (Type **7** and Type **8**) in an unequal ratio.[3] Therefore, in the present study, our first interest was focussed on the characterization of the factors controlling the stereoselectivity in the formation of these adducts. We presumed, first of all, that when two different benzenediazonium-2-carboxylates, **2** and **4**, are used as the precursors of an identical benzyne, then the structure of the benzyne adducts may inherit the memory of the ionic structure of the diazonium carboxylates in certain reactions in which a substantial polar reactant interaction exists either prior to the benzyne generation or in the transition state, regardless of the substituent effect of the benzynes. Hexamethylcyclohexa-2,4-dienone (**6**),[4] for instance, seems to be a suitable dipolar diene for examining this memory effect. On the other hand, if this memory effect does not operate, then the reaction will be controlled by the benzyne structure, **1a** (or **1b**) or **1c**, only when there is a polar effect of the benzyne substituents. In this case, the isomer ratio, **7**/**8**, obtained from the reaction of **2** with **6** (Eq. 1) should be the same as that of **4** with **6** (Eq. 2), and the substituent effect that determines the **7**/**8** isomer ratio, will be either a steric effect, an inductive effect, or a dipole-dipole interaction between reactants.

In the present study, the reactions of hexamethylcyclohexa-2,4-dienone (**6**) with several unsymmetrically substituted benzynes that are generated from the corresponding arenediazonium-2-carboxylates (**2** and **4**, where X and Y are H, CH_3, Cl, or/and NO_2) are carried out under controlled conditions, and a qualitative diagnosis of the substituent effects in the transition state is deduced from the isomer ratios of the adducts.

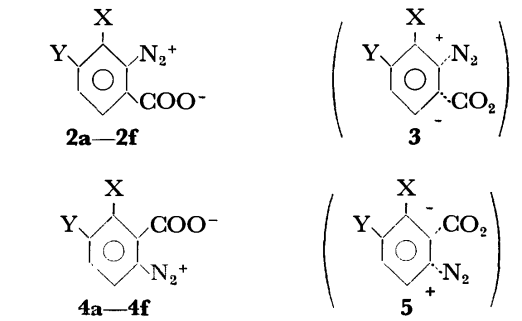

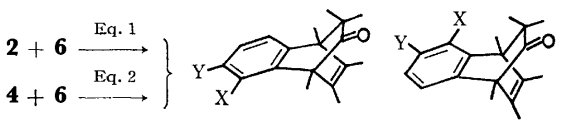

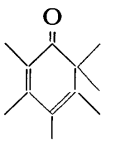

6

a: X=Me Y=H
b: X=H Y=Me
c: X=NO_2 Y=H
d: X=H Y=NO_2
e: X=Cl Y=H
f: X=Me Y=Me

Results and Discussion

Substituted benzenediazonium-2-carboxylates, as the aryne precursors, were prepared in the form of hydrochlorides from the corresponding anthranilic acids. They can be handled safely in the dried-powder state, except for the nitro derivatives, which are detonated by heat or impact. Most anthranilic acids were synthesized, after testing several procedures, *via* the corresponding isatines,[5] except in the case of nitroanthranilic acids, which were synthesized from the corresponding nitrophthalamic acids.

The reactions of unsymmetrically substituted benzenediazonium-2-carboxylate hydrochlorides (**2** and **4**) with hexamethylcyclohexa-2,4-dienone (**6**) were carried out under controlled conditions—constant rate of rising

TABLE 1. STRUCTURES AND NMR CHEMICAL SHIFTS OF THE BENZYNE-ADDUCTS

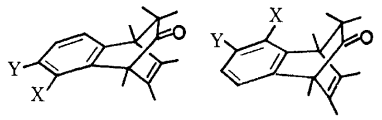

7a—7f **8a—8f**

Compd	Substituents X	Substituents Y	Chemical shifts of Me-groups (δ) 7 *syn*-Me	7 *anti*-Me	7 Ar-Me	8 *syn*-Me	8 *anti*-Me	8 Ar-Me
a	Me	H	0.54	1.02	2.47	0.61	0.99	2.52
b	H	Me	0.48	1.03	2.29	0.48	1.03	2.31
c	NO_2	H	0.68	1.04		0.57	1.08	
d	H	NO_2	0.52	1.10		0.53	1.10	
e	Cl	H	0.67	1.03		0.57	1.06	
f	Me	Me	0.56	1.00	2.21 2.37	0.62	0.97	2.23 2.41

temperatures and a constant concentration of reagents. The product analysis of these reactions, mainly by means of NMR, proved that the products were mixtures of two structurally isomeric adducts, **7** and **8**. Their NMR assignments were performed as follows (see Table 1).

The Assignment of Adduct Structures and the Determination of Isomer Ratios. The NMR spectrum of the adduct obtained from the reaction of **2a** with **6** was identical with that obtained from the reaction of **4a** with **6**, and it has been clarified that the adduct consisted of two structural isomers, **7a** and **8a**.[6,7] These isomers could not be separated, but their spectral assignment was achieved by a means analogous to that employed in the assignment of **7f** and **8f**, which was carried out with the aid of a lanthanoid shift reagent, $Eu(fod)_3$.[3] The **7a**/**8a** isomer ratio was determined mainly by the comparison of the NMR integration of the geminate methyl groups that are at the 9-position of the 1,4-dihydro-1,4-ethanonaphthalene ring and oriented *syn* to the benzene ring, since the difference in chemical shifts between the *syn*-methyls of **7a** and **8a** ($\Delta\delta$=0.07 ppm) is large enough to discriminate the two isomers. The ratios obtained from **2a** and **4a** are 1.73 and 1.75 respectively.

The same mixtures of isomeric adducts, **7b** and **8b**, were obtained from both benzyne precursors, **2b** and **4b**. The VPC separation of these two isomers was unsuccessful, and the NMR chemical shifts of the *syn-gem*-methyl groups were almost identical and undiscriminative. Fortunately, however, the chemical shifts of aryl methyl groups were slightly different between **7b** and **8b** ($\Delta\delta$= 0.02 ppm), and this difference could be enlarged clearly enough to distinguish the two isomers by the aid of the lanthanoid shift reagent, $Eu(fod)_3$ (0.30 mol equivalent). The isomer ratios obtained from **2b** and **4b** are 1.01 and 1.00 respectively. The assignment of NMR spectra to these isomers is based on the assumption that the aryl methyl group situated farther from the carbonyl group shows a lower field absorption than the one situated closer to the carbonyl group, which is analogous to the finding in the cases of **7a** and **8a**.

The reaction of 3-nitrobenzenediazonium-2-carboxylate hydrochloride (**4c**) with **6** gave a mixture of **7c** and **8c**. The NMR spectra of this mixture showed a clear difference in the chemical shift of the *syn* methyl group between the two isomers, **7c** and **8c** ($\Delta\delta$=0.11 ppm). The assignment of the chemical shifts to each isomer is based upon the assumption that the *syn* methyl group with the closer nitro substituent (isomer **8c**) will suffer a more shielding effect than that in the other isomer, **7c**. The ratio, thus determined by NMR, is 1.44 (by VPC, the ratio is 1.50). The same adducts were not obtained from the reaction of **2c**[8] because the diazotization of the corresponding 3-nitroanthranilic acid by isopentyl nitrite in the presence of hydrochloric acid caused an unusual nucleophilic substitution of the nitro group[9] by the chloride anion to produce 6-chlorobenzenediazonium-2-carboxylate (**2e**).

The assignment of the NMR spectra of the isomers, **7d** and **8d**, which were obtained as mixtures from both precursors, **2d** and **4d**, was carried out by the aid of the lanthanoid-shift reagent. The reagent facilitated the separation of the chemical shifts of the aromatic protons situated beta to the nitro substituent, *i.e.*, β_7-H in **7d** and β_8-H in **8d**. Here, the principal assumption is that β_8-H, that locates in closer proximity to the carbonyl group, is shifted to a lower field than β_7-H because of the complexation of the shift reagent with the carbonyl group.[10] The isomer ratio, **7d**/**8d**, determined therefrom, are 0.99 in the reaction of **2d** and 1.00 in that of **4d**. The ratios determined by a VPC analysis are 1.07 in both reactions. These two isomers, **7d** and **8d**, were separated by recrystallization from methanol; **7d**, with a less crowded structure, has a higher mp (158.5—159.5 °C) than that of **8d** (126—128 °C).

The two isomeric adducts, **7e** and **8e**, that were obtained from **2e**, can be separated; the isomer with a higher mp (107—108 °C) was assigned to **7e**, while the one with a lower mp (93—94 °C) to **8e**, on the basis of the mp as well as of the NMR chemical shift of the *syn-gem*-methyl groups. The isomer ratio (**7e**/**8e**) determined from the NMR integrations of *syn*-methyls ($\Delta\delta$=0.10 ppm) is 1.09, while it is 1.11 when determined by VPC.

In the adducts mentioned above, it is anticipated that the isomer with an intramolecularly more crowded

Table 2. Melting points of some benzyne-adducts (°C)

Substituents		Adducts	
o-	*m*-	Type **7**	Type **8**
H	NO_2	158.5—159.5	126—128
Cl	H	107—108	93—94
CH_3	CH_3	154—156.5	127—130

structure will have a lower mp than the one with a less crowded structure. In fact, some isomers which were separated and structurally assigned support this hypothesis (see Table 2). This finding must be useful for the structure assignment of isomeric benzyne-adducts by a comparison of their melting points.

Table 3. Substituent effects on the isomer ratios **7**/**8**[a)]

Run	Benzynes		Diazonium carboxylates	
	o-X	*m*-Y	**2**	**4**
1	CH_3	H	1.73 (2.03)	1.75 (2.11)
2	NO_2	H		1.44 (1.50)
3	Cl	H	1.09 (1.11)	
4	H	CH_3	1.01	1.00
5	H	NO_2	0.99 (1.07)	1.00 (1.07)
6	CH_3	CH_3		1.71

a) The numbers in parentheses are the ratios determined by VPC.

The Interrelation between Substituent Effects and the Structure of Arynes. The isomer ratios (**7**/**8**) in the addition products are listed in Table 3. There it is evident that the isomer ratios are the same in both adducts obtained from the precursors of Type **2** and Type **4**, though the dispositions of their ion-pairs are inverse to each other. Thus, the identity of the arynes generated from both precursors is established, ruling out any possibility of intervening ionic memory effect inheritable from the starting-diazonium salts. The reason for the predominant formation of the isomer of Type **7** over **8** will be presented below.

In the general reaction procedure, 1,2-dichloroethane was employed as the solvent. This solvent, however, is non-polar and shows a poor dissolving power to benzenediazonium-2-carboxylate hydrochlorides. In this solvent the polar interaction, if any, between dienone **6** and aryne precursors (**2** and **4**) in or prior to the transition state will be exerted less than that in polar solvents. Therefore, the effect of the increasing solubility of **2** and **4** in such polar solvents as acetonitrile, *N*-methylformamide, and dienone itself, in which all reactants are soluble, was examined. The results are shown in Table 4. No appreciable difference was observed in the **7a**/**8a** isomer ratio between the starting compounds **2** and **4**, although, in polar solvents, the ratios are inclined to increase somewhat more than those in less polar solvents. Thus again, the memory effect was not observed even in these polar solvents. The increased isomer ratio observed in polar solvents seems to be ascribable mainly to the lower temperature of the decomposition of the aryne precursors in these solvents.

Table 4. Isomer ratios **7a**/**8a** in various solvents

Solvent	Diazonium carboxylates	
	2a	**4a**
CH_2ClCH_2Cl	1.73	1.75
CH_2ClCH_2Cl[a)]	1.69	
CH_3CN	1.88	1.89
CH_3NHCHO	2.05	2.08
Dienone **6**[a)]	1.90	1.97

a) The diazonium salts, **2a′** and **4a′** were used without PO.

Table 5. Isomer ratios **7a**/**8a** at various temperatures[a)]

Temp (°C)	Diazonium carboxylates	
	2a	**4a**
80	1.72	1.70
70	1.71	1.72
60		1.70
50	1.77	1.79
40	1.76	1.80

a) Butene-1-oxide was used instead of PO.

The effect of the reaction temperature on the isomer ratios was also examined, especially in an attempt to know whether it is different between the two starting compounds (**2** and **4**). It has been calculated that the ion-pair structure, **1c**, has a higher free energy than that of **1a** or **1b**,[2)] hence, a temperature effect will be anticipated if any function of **1c** is involved in or prior to the transition state. The results in Table 5, however, give a negative evidence to this hypothesis, because no appreciable difference is observable in the isomer ratios obtained from the two aryne precursors, **2** and **4**. The slightly enhanced formation of the **7a** isomer over **8a** at lower temperatures, as shown in this table, seems to indicate that the energy of activation for the formation of **7** is slightly lower than that for **8**. This difference, $\Delta E_a = E_a(\mathbf{8a}) - E_a(\mathbf{7a})$, was determined by the Arrhenius plotting of the isomer ratios in Table 5. Thus, we found that $\Delta E_a = 0.26 \pm 0.04$ kcal/mol, and $A(\mathbf{7a})/A(\mathbf{8a}) = 1.18 \pm 0.07$.

Although the possibility of the participation of the memory effect was thus completely ruled out, the substituent effects that determine the isomer ratios in the benzyne adducts still remain unclarified. Table 3 clearly indicates that the steric interaction between the *gem*-dimethyl groups of **6** and the substituent, X, in the transition state seems to be the sole factor controlling the isomer ratios. Thus, the ratios decrease as the Van-der-Waals radius of the X substituent diminishes, and accordingly, the effect of the β-substituent, Y, is negligible.[11)] In the case of 3-methylbenzyne, that gave the largest isomer ratio (1.7—1.8) among those examined, the difference in kinetic parameters between the two sterically different transition states, *i.e.*, $\Delta E_a = 0.26$ kcal/mol, and especially the ratio of the frequency factors $A(\mathbf{7a})/A(\mathbf{8a}) = 1.18$, indicates that the steric course leading to the adduct of Type **7** is slightly, but apparently, favored over that of Type **8**. A framework diagnosis

of possible transition states (*e.g.*, **A** and **B**) also supports this. These framework are constructed on the supposition that benzyne approaches vertically to the 2- and 5-positions of the planar dienone, keeping the two bonding distances equal. Then, when Type **B** is concerned, the overlapping of Var-der-Waals radii between *gem*-dimethyl and aryne methyl groups becomes substantial in the range of bonding distances shorter than 2.8 Å, about twice the bond length in the adduct.

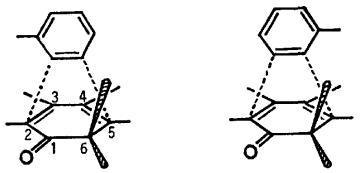

(The interaction between the aryne methyl and 5- methyl of the dienone in Type **B** is also substantial, but is cancelled out by the similar interaction in Type **A** between aryne methyl and 2-methyl of the dienone when **A**/**B** is considered).

Other substituent effects that seem to be involved in determining the isomer ratio are: *a*) the dipole-dipole interaction between the carbonyl group of the **6** dienone and the X substituent, or/and *b*) the inductive effect of X. In the case of nitrobenzynes, if the former effect operates between the nitro group and the carbonyl group, then the product, **8c** (or **8d**), should be the predominant product in Run 2 (or Run 5) in Table 3. However, the ratios are **7c**/**8c**=1.44 and **7d**/**8d**=1.00; thus, the possibility of *a* is ruled out. As for the latter effect, *b*, if it contributes to the polar structure of arynes, then the adduct of Type **8** should favorably be formed in Runs 1, 4, and 6, and Type **7**, in Runs 2, 3, and 5.

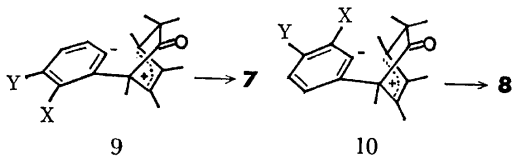

Alternatively, recent studies of aryne reactions[12] have led us to suspect that the inductive effect of the X substituent (or/and Y) operates in the transition state of a two-stage addition reaction, so that a zwitter-ion, **9** or **10**, can be stabilized. According to this hypothesis, the adduct of Type 7 should be obtained predominantly from methyl-substituted benzynes, and Type **8**, from nitro- or chloro-benzynes. However, this was not the case. Therefore, the inductive effect is not likely to be involved, and, even when be involved, its magnitude is too small to overcome the steric effects.

Recently, Newman and Kannan reported that, in the reaction of 2-substituted furans with the aryne precursors analogous to Types **2a** and **4a**, where the steric interaction was expected to be more substantial than in our system, the isomer ratios found were smaller than 1.8.[19] Comparing our results with those, it should be noticed that the interaction of the X substituent with the *gem*-methyl group of **6** that is located at the 5-position of a cyclic 1,3-diene is almost as large as that of X with the substituent at the 1- or 4-position.

Experimental

General. The NMR spectra were measured in CCl_4 solutions, and the chemical shifts are given in δ-units. The VPC analyses were performed on a chromatograph equipped with a FID. Below, the experimental description will be divided into three sections: 1) methylbenzynes, 2) nitrobenzynes, and 3) chlorobenzyne. The combustion analysis was performed by the Elemental Analysis Laboratory of the Institute for Chemical Research of Kyoto University. The analyses of isomeric mixtures of benzyne-adducts agreed well (within an error of 0.30%) with the corresponding calculated values for the methylbenzyne- and nitrobenzyne adducts, and fairly well (within an error of 0.80%) for the chlorobenzyne adduct.

1. Preparation and Reaction of Methylbenzynes. 1-a) 6-Methylbenzenediazonium-2-carboxylate Hydrochloride (2a): This compound, **2a**, was prepared from 3-methylanthranilic acid (**11**)[5] by a procedure analogous to that previously reported.[13] Yield, 97%; mp 112.5—113.5 °C (dec); IR ν(N≡N) 2230 cm^{-1} (Nujol).

1-a') Free 6-Methylbenzenediazonium-2-carboxylate (2a'): Compound *2a'* was prepared by a procedure analogous to that employed above (see *1-a*), except that HCl was not added to the initial ethanolic solution. Yield, 43%; mp 98—99 °C; IR ν(N≡N) 2230 cm^{-1}.

1-b) 1,2,3,4,6,10,10-Heptamethyl-1,4-dihydro-1,4-ethanonaphthalene-9-one (7a) and Its 1,2,3,4,7,10,10-Heptamethyl Isomer (8a) by the Reaction of 2a with 2,3,4,5,6,6-Hexamethylcyclohexa-2,4-dien-1-one (6): The experimental conditions of seven runs are tabulated below. The first three runs were carried out in order to examine the solvent effects, and the last four runs, to examine the temperature effects. For the isomer ratios, see Tables 3,4, and 5. The experimental procedure for Run 1 is described below as the standard procedure, which will be refered to in the procedures following.

Run	Base	Solvent	Temp (°C)	Time (min)	Yield (%)
1	PO	CH_2ClCH_2Cl	60	70	95
2	PO	CH_3CN	60	70	26
3	PO	CH_3NHCHO	60	70	17
4	EB	CH_2ClCH_2Cl	40	480	100
5	EB	CH_2ClCH_2Cl	50	180	100
6	EB	CH_2ClCH_2Cl	70	60	100
7	EB	CH_2ClCH_2Cl	80	60	100

EB: 1,2-epoxybutane.

Run 1. Into a suspension of **2a** (0.50 g, 2.5 mmol) in 1,2-dichloroethane (6.3 ml), **6** (0.45 g, 2.5 mmol) and propylene oxide (0.8 ml, abbreviated as PO) were added. The mixture was then immediately heated under the standard conditions; *i.e.*, the temperature was raised at the rate of 2.5 °C/min from 25 to 60 °C. After additional stirring at 60 °C for 70 min, the dark brown solution was cooled. (These conditions were employed in the other runs that were carried out with the purpose of obtaining the adduct-isomer ratios.) After a vacuum evaporation, the residue was redissolved in Et_2O, and the solution was washed four times with 5 ml of 5% aq NaOH and again four times with water, and then dried ($MgSO_4$). The subsequent evaporation of the solvent gave a mixture of **7a** and **8a**; 0.64 g (95%). These isomers could

not be separated satisfactorily by column chromatography ($CHCl_3$, silica gel). NMR **7a**: *gem*-Me 0.54 and 1.02 (3H each; Me's *syn* and *anti* to the benzene ring respectively), Ar–Me 2.47 (3H), allylic Me 1.65—1.75 (6H), bridge-head Me 1.55 and 1.78 (3H each), Ar–H 6.7—7.1 (3H) ppm. **8a**: *gem*-Me 0.61 and 0.99 (3H each; Me's *syn* and *anti* to the benzene ring respectively), Ar–Me 2.52 (3H), allylic Me 1.65—1.75 (6H), bridge-head Me 1.55 and 1.78 (3H each), Ar–H 6.7—7.1 (3H) ppm; $P^+(m/e)$ 268. The isomer ratio, **7a**/**8a**, determined by a comparison of the NMR-integration, was 1.73. A VPC analysis (PEG-succinate, 2 m at 175 °C), though not achieving a satisfactory isomer separation, also gave the isomer ratio of 2.03.

Runs 4—7. Instead of PO, 1,2-epoxybutane (0.44 ml; abbreviated as EB) was added to a mixture of **2a** and **6** in 1,2-dichloroethane; the mixture was immediately heated at 80-, 70-, 50-, or 40±0.2 °C for the periods listed in the table. For the work-up, see the details in Run 1. Yield (**7a**+**8a**), *ca.* 100% in all runs. For the isomer ratios, see Table 5.

1-c) 7a and 8a by the Reaction of 2a′ with 6: Two runs were performed in order to examine the effect of free diazonium carboxylate, **2a′**, on the isomer ratio: Run 1, without PO in CH_2ClCH_2Cl; yield, 37%; Run 2, without PO, but in an excess amount of **6**; yield, 54%. The other reaction conditions were the same as in *1-b*. For the isomer ratios, see Table 4.

1-d) 3-Methylbenzenediazonium-2-carboxylate Hydrochloride (4a). From 6-Mcthylanthranilic Acid (12): For the preparative procedure, see *1-a*. Yield, 84%; mp 110.5—111 °C (dec); IR ν(N≡N) 2210 cm^{-1} (Nujol).

1-e) 3-Methylbenzenediazonium-2-carboxylate (4a′): See the procedure *1-a′*. Yield 4%; mp 68—70 °C (dec); IR ν(N≡N) 2250 cm^{-1}.

1-f) 7a and 8a by the Reaction of 4a with 6: For the procedure, see *1-b*. The reaction conditions and the results of eight runs are tabulated below. The first three runs were carried out in order to examine the solvent effects, and the last five runs, to examine the temperature effects. For the isomer ratios, see Tables 3, 4, and 5.

Run	Base	Solvent	Temp (°C)	Time (min)	Yield (%)
1	PO	CH_2ClCH_2Cl	60	70	83
2	PO	CH_3CN	60	70	13
3	PO	CH_3NHCHO	60	70	13
4	EB	CH_2ClCH_2Cl	40	560	100
5	EB	CH_2ClCH_2Cl	50	180	98
6	EB	CH_2ClCH_2Cl	60	70	100
7	EB	CH_2ClCH_2Cl	70	60	98
8	EB	CH_2ClCH_2Cl	80	60	100

1-g) 7a and 8a by the Reaction of 4a′ with 6: Refer to the *1-c* procedure. See also Table 4. Yield (**7a**+**8a**), 36%.

1-h) 5- and 4-Methylbenzenediazonium-2-carboxylate Hydrochloride (2b and 4b): Diazonium salts, **2b** and **4b**, were prepared from the corresponding anthranilic acids by the same method as in *1-a*. Yields, 89% (**2b**) and 84% (**4b**).

1-i) 1,2,3,4,6,10,10-Heptamethyl-1,4-dihydro-1,4-ethanonaphthalen-9-one (7b) and Its 1,2,3,4,7,10,10-Heptamethyl Isomer (8b): See the *1-b* procedure, Run 1. The same mixture of the **7b**+**8b** adducts were obtained from either precursor **2b** or **4b**. Yields, 75—77%. The isomers could not be separated. $P^+(m/e)$ 268; NMR **7b**: *gem*-Me 0.48 and 1.03 (3H each, Me's *syn* and *anti* to the benzene ring respectively), Ar–Me 2.29 (3H), allylic Me 1.65—1.76 (6H), bridgehead Me 1.56 (6H), Ar–H 6.85—7.1 (3H) ppm. **8b**: all the chemical shifts, except that of Ar–Me at 2.31, are the same as those of **7b**. The **7b**/**8b** isomer ratios determined by the NMR integration (see the text) were 1.01 and 1.00 from **2b** and **4b** respectively.

2. Preparation and Reactions of Nitrobenzynes. The procedure reported in old literature[14–16] on the preparation of nitroanthranilic acids was insufficient to reproduce the same results reported therein. The present authors employed the following modified procedure, that gave the acids in better yields than those previously reported.

2-a) 6-Nitroanthranilic Acid (14) from 6-Nitrophthalamic Acid (13): Acid **13** (5.69 g, 27.1 mmol)[15] was slowly added to a NaOCl solution which had been prepared by mixing 17.6 g of a commercial grade NaOCl-solution containing 10% active Cl, 2.0 g of NaOH, and 10 ml water at 0 °C. The mixture was warmed at 82 °C for 30 min (gas evolution was observed), cooled, and acidified with HCl. "After removing the solids that precipitated at pH 4, the filtrate was evaporated. The residue was extracted with Et_2O to give **14**. The extraction residue was redissolved in dil NaOH, and the solution was acidified." The above procedure in quotation marks "—" was repeated three times. Yield, 1.68 g (34%); mp 185.5—189.5 °C.[17]

2-b) 3-Nitrobenzenediazonium-2-carboxylate Hydrochloride (4c) from 14: See the *1-a* procedure. **4c**: yellow-orange powder; yield, 69%; mp 110.5—111 °C (dec); IR ν(N≡N) 2190 cm^{-1} (Nujol). Avoid unnecessary impact by hammering or heating; otherwise, it detonates!

2-c) 1,2,3,4,10,10-Hexamethyl-5-nitro-1,4-dihydro-1,4-ethanonaphthalen-9-one (7c) and Its 8-Nitro Isomer (8c): See the *1-b* procedure. A mixture of **7c** and **8c** was obtained. They were purified through a silica gel column (benzene), but could not be separated. NMR **7c**: *gem*-Me 0.68 and 1.04 (3H each, Me's *syn* and *anti* to the benzene ring respectively), Ar–H 6.91—7.38 (3H), bridge-head Me 1.59 and 1.62 (3H each), allylic Me 1.71—1.84 (6H) ppm. **8c**: *gem*-Me 0.57 and 1.08 (3H each, Me's *syn* and *anti* to the benzene ring respectively), Ar–H 6.91—7.38 (3H), bridge-head Me 1.54 and 1.64 (3H each), allylic Me 1.71—1.84 (6H) ppm. **7c**/**8c** isomer ratio = 1.44 (NMR), 1.50 (VPC). $P^+(m/e)$ 299; IR ν(C=O) 1730 and (NO_2) 1355 cm^{-1} (for both isomers in CCl_4); yield, 1.69 g (44%) after column chromatography.

2-d) 4-Nitro- and 5-Nitroanthranilic Acid (17 and 18): A mixture of 4- and 5-nitrophthalamic acid (**15** and **16**)[14] was treated with the NaOCl solution by the same method as in *2-a*. Cooling the reaction mixture separated needle-like precipitates. They were dissolved in water and acidified with HCl to pH 3—4, and the separated solid was washed with water, dried, and extracted with xylene by means of a Soxhlet apparatus for two days. The insoluble residue was recrystallized from aq EtOH ($EtOH/H_2O$ = 1.0 v/v) to give glistening yellow-green needles of **18** (48%): mp 275—283 °C (dec). The xylene solution was then evaporated to give **17** (32%) contaminated by **18**.

2-e) 5-Nitrobenzenediazonium-2-carboxylate Hydrochloride (2d): See the *2-b* procedure. Commercially available acid **17** was used. Here also caution should be taken when handling the dried powder of **2d**: yield, 90%; mp 128—130 °C (dec); IR ν(N≡N) 2230 cm^{-1}.

2-f) 1,2,3,4,10,10-Hexamethyl-6-nitro-1,4-dihydro-1,4-ethanonaphthalen-9-one (7d) and Its 7-Nitro Isomer (8d): See the *1-b* procedure. Yield (**7d**+**8d**), 61% after recrystallization from MeOH. The two isomers were separated mannually by the aid of a magnifying glass and recrystallized independently. **7d**: mp 158.5—159.5 °C; NMR *gem* Me 0.52 and 1.10 (3H each, Me's *syn* and *anti* to the benzene ring respectively), Ar–H 7.90—8.12 (2H, α to NO_2) 7.29 (H, β to NO_2), other Me's 1.64—1.80 (12H) ppm; IR ν(C=O, NO_2) 1730

and 1355 cm^{-1} (CCl_4); $P^+(m/e)$ 299. **8d**: mp 126—128 °C; NMR *gem*-Me 0.53 and 1.10 (3H each, Me's *syn* and *anti* to the benzene ring respectively), Ar–H 7.90—8.12 (2H, α to NO_2), 7.26 (H, β to NO_2), other Me's 1.64—1.80 (12H) ppm; the IR and $P^+(m/e)$ were the same as those of **7d**. For the isomer ratio, see Table 3.

2-g) 4-Nitrobenzenediazonium-2-carboxylate Hydrochloride (4d): See *1-b*. Caution should be taken when handling *4d*. Yield, 67%; mp 119.5—120 °C (dec); IR ν(N≡N) 2210 cm^{-1}(Nujol).

2-h) 7d and 8d by the Reaction of 4d with 6: See *1-b*, Run 1. Yield (**7d**+**8d**), 69%. For the isomer ratio, see Table 3.

3. Preparation and Reaction of 3-Chlorobenzyne.

3-a) 6-Chlorobenzenediazonium-2-carboxylate Hydrochloride (2e) from 3-Chloroanthranilic Acid (19): Acid **19** was prepared from *o*-chloroaniline.[18,5] For the preparation of the diazonium salt **2e**, see *1-a*, Run 1. Yield, 92%; mp 146—148 °C; IR ν(N≡N) 2230 cm^{-1}.

3-b) 1,2,3,4,10,10-Hexamethyl-5-chloro-1,4-dihydro-1,4-ethanonaphthalen-9-one (7e) and Its 8-Chloro Isomer (8e): A mixture of **7e** and **8e** was obtained by the method described in *1-b*. The two isomers were separated by column chromatography (silica gel; cyclohexane for **7e** and benzene for **8e**). The separated isomers were recrystallized independently from MeOH (the rate of crystallization of **8e** was slower than that of **7e**). Yield (**7e**+**8e**), 89%; isomer ratio, see Table 3. **7e**: mp 107—108 °C; NMR *gem*-Me 0.67 and 1.03 (3H each, Me's *syn* and *anti* to the benzene ring respectively), Ar–H 7.00—7.15 (3H), allylic Me 1.7—1.9 (6H), bridge-head Me 1.59 and 1.98 (3H each) ppm; $P^+(m/e)$ 289; IR ν(C=O) 1725 cm^{-1} (CCl_4). **8e**: mp 93—94 °C; NMR *gem*-Me 0.57 and 1.06 (3H each, Me's *syn* and *anti* to the benzene ring respectively), Ar–H 7.0—7.15 (3H), allylic Me 1.77 (6H), bridge-head Me 1.59 and 1.91 (3H each) ppm; the $P^+(m/e)$ and IR were the same as those of **7e**.

References

1) For example: H. Heaney, *Chem. Rev.*, **62**, 81 (1962); M. Stiles, R. G. Miller, and U. Burckhardt, *J. Am. Chem. Soc.*, **85**, 1792 (1963); R. G. Miller and M. Stiles, *ibid.*, **85**, 1798 (1963); R. Hoffman, A. Imamura, and W. J. Hehre, *ibid.*, **90**, 1499 (1968); O. L. Chapman, C.-C. Chang, J. Kolc, N. R. Rosenquist, and H. Tomioka, *ibid.*, **97**, 6586 (1975).

2) For example: N. Inamoto, *Yuki Gosei Kagaku Kyokai Shi*, **19**, 809 (1961); I. Tabushi and H. Yamada, *ibid.*, **28**, 667 (1970); I. Tabushi, "Carbene, Ylide, Nitrene, and Benzyne," ed by T. Goto, Hirokawa Publishing Co., Tokyo (1976), p. 341.

3) A. Oku and Y. Yuzen, *J. Org. Chem.*, **40**, 3850 (1975).

4) H. Hart, P. M. Collins, and A. J. Waring, *J. Am. Chem. Soc.*, **88**, 1005 (1966).

5) B. R. Baker, R. E. Schaub, J. P. Joseph, F. J. McEvory, and J. H. Williams, *J. Org. Chem.*, **17**, 149 (1952).

6) A. Oku, T. Kakihana, and H. Hart, *J. Am. Chem. Soc.*, **89**, 4554 (1967).

7) A. Matsui, B. S. Thesis, Kyoto Institute of Tech., 1975.

8) L. Friedman and F. M. Logullo, *J. Org. Chem.*, **34**, 3089 (1969).

9) Unpublished results. A similar nucleophilic substitution has been reported for the diazotization of *o*-nitroaniline under more drastic conditions; see Z. J. Allan and J. Podstate, *Collect. Czech. Chem. Commun.*, **31** (8), 3418 (1966).

10) M. Kainosho and K. Ajisaka, *Yuki Gosei Kagaku Kyokai Shi*, **31**, 126 (1973).

11) A. Bondi, *J. Phys. Chem.*, **68**, 441 (1964); P-T. Leucy and D. Y. Curtin, *J. Am. Chem. Soc.*, **97**, 6790 (1975).

12) E. R. Biehl, *J. Org. Chem.*, **34**, 3595 (1965).

13) H. Hart and A. Oku, *J. Org. Chem.*, **37**, 4269 (1972).

14) E. Chapman and H. Stephan, *J. Chem. Soc.*, **127**, 1795 (1925).

15) M. T. Bogert and L. Boroschek, *J. Am. Chem. Soc.*, **23**, 740 (1901).

16) R. Kahn, *Ber.*, **35**, 3866 (1902).

17) H. Seidel, *Ber.*, **34**, 4352 (1901).

18) A. E. Senear, H. Sargent, J. F. Mead, and J. B. Koepfli, *J. Am. Chem. Soc.*, **68**, 2695 (1946).

19) M. S. Newman and R. Kannan, *J. Org. Chem.*, **41**, 3356 (1976).

Solid-Phase Syntheses of $Glu_{20}Ala_{20}Phe$ and $Ala_{20}Glu_{20}Phe$ by the Step-by-step Coupling of Dipeptide and Tetrapeptide[1]

Sho TAKAHASHI

Institute for Chemical Research, Kyoto University, Uji, Kyoto 611

(Received June 13, 1977)

$Glu_{20}Ala_{20}Phe$, (I), and $Ala_{20}Glu_{20}Phe$, (II), were synthesized by the step-by-step coupling of N^{α}-*t*-butoxycarbonyl (BOC-) derivatives of Ala–Ala and (γ-benzyl–Glu)$_4$ to phenylalanyl-1% crosslinked polystyrene resin using dicyclohexylcarbodiimide. The products were cleaved from the resin with hydrogen bromide in acetic acid and purified by gel filtration, followed by DEAE-cellulose chromatography, with yields of approximately 10% for both of the hentetracontapeptides. The optical purities of the glutamic acid and alanine incorporated in the peptides, I and II, were estimated as 1 and 5% respectively from the analysis of the diastereomeric mixture of dipeptides derived from the reaction between the total acid hydrolyzate of I or II with the *N*-hydroxysuccinimidyl ester of BOC–L-Leu.

The problem that an α-helix, one of the most important ordered secondary structure of a polypeptide chain, is uncoiled from one side, either the N- or the C-terminal, has not yet been studied experimentally. The available works on the problem have been limited to a few theoretical treatments.[2,3] The study of the effects exerted by the secondary structures of neighboring moieties in a polypeptide chain on a local α-helix has importance, especially in comprehending the stability of proteins, in which secondary structures are sequenced.

Block copolypeptides will serve as a good model to study the effects of a local conformation of a polypeptide chain on other parts of the chain. Previously we attempted to synthesize and to study the stability of the local α-helical conformation in two kinds of block copolypeptides, $Glu_{20}Ala_{20}$ and $Ala_{20}Glu_{20}$, in solution. The number of residues in a block, 20, was chosen as a compromise between the need for a stable α-helix and ease of syntheses. However, as has already been reported,[3] the attempted solid-phase peptide synthesis of these block copolypeptides by a step-by-step coupling of *t*-butoxycarbonyl-(BOC-)glutamic acid or -alanine was shown to be impractical due to the poor yield of the desired peptides. Furthermore, the difficulties in the solid-phase peptide synthesis of glutamyl peptides (including γ-peptides) have been well documented.[4–7] On the other hand, the coupling reactions of oligopeptides on a solid support have found their successful applications in syntheses of sequential peptides,[8,9] physiologically active peptides,[10–16] and some miscellaneous peptides.[17–19] We also tried a condensation of oligopeptides on a solid support as an alternative route to synthesizing $Glu_{20}Ala_{20}$ and $Ala_{20}Glu_{20}$ and obtained a satisfactory result, as will be described in this paper.

Results and Discussion

The synthesis of oligoglutamyl peptides by conventional solid-phase peptide synthesis has caused much trouble, as was initially documented by Bonora *et al.*[4] The yield of the desired peptide was drastically decreased with an increase in the number of residues, n, on their attempted synthesis of $(Glu)_n$, and the synthesis failed when n reached 5, where the desired peptide could not be isolated at all. As has also been reported previously,[3] we also attempted solid-phase syntheses of $(Glu)_n$ and $(Ala)_n$ by the step-by-step coupling of BOC-glutamic acid or -alanine. For both $(Glu)_n$ and $(Ala)_n$, it was observed that the elongation of a peptide chain proceeded smoothly with each cycle of the solid-phase synthesis if n was below about 5; then it became gradually sluggish and apparently stopped when n reached around 10. The failure of the syntheses might be ascribed to something other than the cleavage process of peptides from peptide-resin, because the yield of peptides was based on the incorporation of amino acids (glutamic acid or alanine), which was evaluated on the basis of the amino-acid analyses of hydrolyzates of peptide-resin. Some of the reasons for the failure of the synthesis by Bonora *et al.*[4] might be attributed to undesired side reactions of a glutamyl side chain which occurred during a cleavage reaction of peptides from peptide-resin, as has been reported by Sano and Kawanishi[5] and Feinberg and Merrifield,[6] but there seem to be other reasons inherent in the method itself in the case of solid-phase peptide syntheses of homologous peptides with enough residues to form a regular secondary structure.[3]

Although we are not yet aware of the exact reasons for the difficulties encountered in the solid-phase peptide synthetic approaches to some of the homologous peptides, one way devoid of difficulties would be a modification of the solid-phase method to incorporate a coupling reaction using oligopeptides instead of amino acids. The advantages would be as follows: (1) an improvement in the yield of the final product because of the smaller number of steps, (2) discrete distribution of the residues, which promises an easy purification of the reaction products, and (3) the possibility that the reactivity of a growing peptide chain on a solid matrix is critically dependent on the chain length due to interaction between the reactive center of a chain and a supporting matrix, especially if a stable secondary structure is present in that chain. Interactions of that kind seem likely for solid-phase syntheses of homologous peptides because a unique secondary structure is to be expected. The use of oligopeptides instead of amino acids as the unit in the syntheses may surpass the critical chain length.

Syntheses. Taking these points into account, we attempted solid-phase syntheses of $Glu_{20}Ala_{20}Phe$, (I), and $Ala_{20}Glu_{20}Phe$, (II), using oligopeptides as the

Table 1. A cycle of solid-phase peptide synthesis for the addition of one oligopeptide[a)]

	Function	Solvent or reagent	Time (min)	Number of applications
(1)	wash	CH_2Cl_2	2	3
(2)	deprotection	CF_3CO_2H–CH_2Cl_2 (1 : 1)	30	1
(3)	wash	CH_2Cl_2	2	4
(4)	neutralization	triethylamine (20 mmol) in CH_2Cl_2	5	2
(5)	wash	CH_2Cl_2	2	2
(6)	wash[b)]	CH_2Cl_2–DMF[c)] (1 : 1)	2	1
(7)	wash[b)]	DMF	2	1
(8)	peptide[d)]	BOC–(γ-Bzl–Glu)$_4$ in CH_2Cl_2 or BOC–Ala_2 in 30% DMF in CH_2Cl_2	2	1
(9)	coupling	DCC in CH_2Cl_2[e)]	240	1
(10)	wash	CH_2Cl_2	2	3

a) The amount was for 5 g of resin containing 0.825 mmol of a reactive amino group. Volume of solvent, 60 ml. b) In the case of glutamyl peptide, these procedures were omitted and Step (5) was repeated. c) *N*,*N*-dimethylformamide. d) 3.3 mmol of oligopeptide in 25 ml of the solvent. e) 3.3 mmol of DCC in 5 ml of the solvent.

condensing unit. First, phenylalanine was anchored to resin as an internal marker. 1% cross-linked polystyrene resin was used, for its porosity is higher than that of the usual 2% cross-linked resin. BOC–(γ-benzyl–Glu)$_4$, (III), and BOC–$(Ala)_2$, (IV), were used as units for the syntheses of a Glu_{20}– and an $(Ala)_{20}$–block respectively. We attempted to use BOC–Ala_4 as a condensing unit, but the poor solubility of the tetrapeptide in most solvents made the attempt impractical.

All the peptides used for solid-phase synthesis were synthesized by the method of Anderson *et al.*[20] The reaction of the BOC-alanine *N*-hydroxysuccinimidyl-(–OSu) ester with alanine gave IV. The optical purity of the purified IV which was used in the solid-phase syntheses was shown, by an analysis to be described in a later section, to be 97% in the L-configuration. The γ-benzyl(γ-Bzl–) ester of BOC–Glu–OSu, (V), was reacted with γ-Bzl-glutamate to give BOC–(γ-Bzl–Glu)$_2$, (VI), a half of which was then converted into its *N*-hydroxysuccinimidyl ester, (VII), and the other half to (γ-Bzl–Glu)$_2$, (VIII). A reaction between VII and VIII gave the desired tetrapeptide, III, and the peptide was purified *via* its salt with dicyclohexylamine (DCHA). The optical purity of I that was used in the following solid-phase synthesis was greater than 99% in the L-configuration.

Solid-phase peptide syntheses were carried out using a cycle summarized in Table 1. After each cycle had finished, an aliquot of peptide resin was hydrolyzed with acid and analyzed for its amino-acid composition. The results are shown in Fig. 1, where a tendency for the yield of peptide-chain elongation to decrease was observed when the number of residues reached about 10. Even under the assumption that the yield of a reaction needed to extend one oligopeptide unit is uniformly α, irrespective of the length of the peptide chain, there are two extreme possibilities. (1) At the one extreme, α is considered simply as the possibility of a reaction occurring at a reactive center, and the unreacted peptide fraction (1-α) remains reactive and will react with the same probability in the next reaction cycle (for instance, an incomplete removal of the BOC group, *etc.*). The total amount of alanine and glutamic acid incorporated

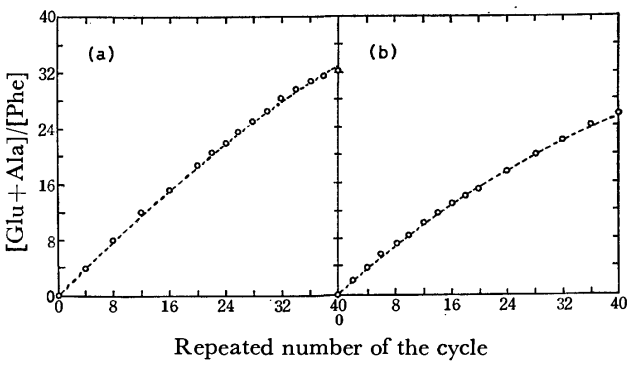

Fig. 1. The amount of amino acids incorporated with the progress of solid-phase peptide syntheses of: (a) $Ala_{20}Glu_{20}Phe$, and (b) $Glu_{20}Ala_{20}Phe$. The ordinate is the total amount of glutamic acid and alanine per mol of phenylalanine, and the abscissa is the repeated number of cycles of solid-phase synthesis. Circles represent the observed values and dotted curves for the calculation based on the dead-end products assumption. α(see text) was chosen as 0.97 for (a) and 0.95 for (b).

in the products will be linearly proportional to α. (2) At the other extreme, the peptide fraction, α, is considered living and reactive, and the fraction, (1-α), is a dead-end product which is no more reactive. In this case, if we start from 1 mol of phenylalanyl resin, the amount of such a dead-end product, $Glu_{4i}Ala_{2j}$, will be given by $\alpha^{i+j}(1-\alpha)$ moles, and the amounts of alanine and glutamic acid incorporated after m times coupling of IV and n times coupling of III are given by $2\sum_{i=1}^{m}\alpha^i$ and $4\sum_{i=1}^{n}\alpha^i$ moles respectively (after 10 times coupling of IV, followed by 5 times coupling of III, the number is $2\sum_{i=1}^{10}\alpha^i+4\alpha^{10}\sum_{i=1}^{5}\alpha^i$). The actual amounts of glutamic acid and alanine found in the acid-hydrolyzates of peptide resin with the progress of the number of coupling reactions (Fig. 1) deviate from a line, thus showing the (1) assumption to be unlikely. For a comparison, theoretical curves were calculated under the (2) assumption and for various values of α. α=0.97 and 0.95 for the

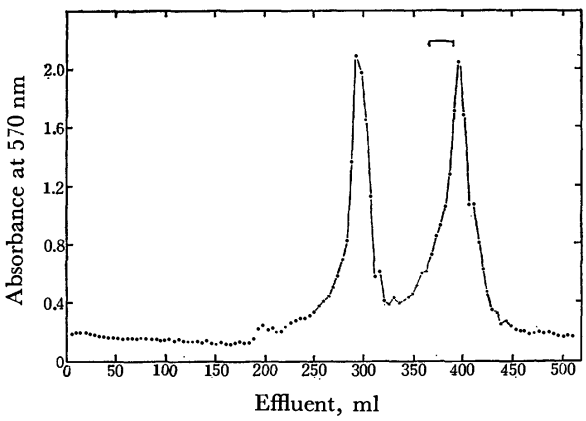

Fig. 2. Sephadex G-50 gel filtration of the product of solid-phase synthesis of $Glu_{20}Ala_{20}Phe$. The ordinate is absorption at 570 nm after the ninhydrin reaction of alkaline hydrolyzates of 0.01 ml aliquots from chromatographic fractions. The inserted bar shows the position of fractions which gave the amino acid composition was Glu: Ala: Phe= >19: >19: 1.

syntheses of Ala_mGlu_nPhe and Glu_mAla_nPhe respectively gave the best fit with the experimentally observed values, as shown in Fig. 1. Although the efficiency of a real peptide coupling reaction might depend on the length of the peptide chain, the comparison of the experimentally obtained plot and the theoretical ones for the extreme cases suggests that the experiments support, rather, the dead-end product assumption.

The peptides were cleaved from the resin by a conventional method, using hydrogen bromide in a mixture of acetic acid and trifluoroacetic acid. The products, (IX) and (X), obtained from the syntheses of I and II respectively were treated with aq. sodium hydrogencarbonate, and a fraction soluble in hydrogencarbonate solution was chromatographed on Sephadex G-50 (Figure 2 shows the results for IX). A fast eluting component appeared for both IX and X; it is considered to consist of peptide aggregates which are composed of alanine-rich peptides, as shown by their amino-acid analyses. All the chromatographic fractions were analyzed for their amino-acid compositions: the fractions containing Glu: Ala: phe=>19:>19: 1 were collected, desalted on a column Sephadex G-10, and lyophilized. The lyophilized material was chromatographed on DEAE-cellulose, and the fractions which gave the amino acid composition of: Glu: Ala: Phe= >19: >19: 1 were considered to be the final product, I or II (Fig. 3). These final products were analyzed by means of 2,4-dinitrophenylation for their free amino groups. The yield of 92—94% 2,4-dinitrophenylalanine or -glutamic acid suggested that only small amounts of pyroglutamate and/or other N-blocked products were present. The final yields of I and II were 9 and 11% respectively.

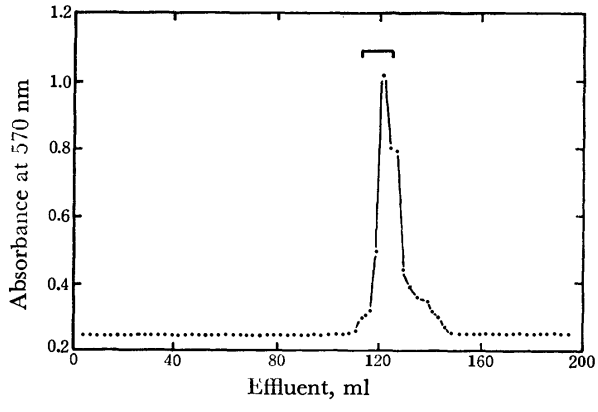

Fig. 3. DEAE-cellulose chromatography of $Glu_{20}Ala_{20}$-Phe. Aliquot of 0.025 ml from each fraction was alkaline hydrolyzed and absorbance at 570 nm was recorded after the ninhydrin reaction. The inserted bar has the same meaning as used in Fig. 2.

Degree of Racemization in the Products. The chromatographically purified products, I and II, were analyzed for their degrees of racemization caused by the peptide-coupling reactions. The racemization detection method by Manning[21] was modified and used. The peptide hydrolyzates, which were obtained by the treatment of the peptides with 6 M hydrochloric acid at 110 °C for 24 h, were reacted with BOC-L-Leu-OSu in the presence of sodium hydrogencarbonate. The products, after an acid treatment to remove the BOC group, were analyzed with an amino-acid analyzer. The authentic samples of D,L-glutamic acid and D,L-alanine were reacted with BOC-L-Leu-OSu under the same conditions and the ninhydrin colour value for each dipeptide separated on an amino-acid analyzer was used as the reference standard. The overall (because they included the difference in the reactivities of L- or D-amino acids towrd BOC-L-Leu-OSu) average ratio of ninhydrin colour values obtained from several experiments were: (L-Leu-D-Ala)/(L-Leu-L-Ala)=0.74, (L-Leu-D-Glu)/(L-Leu-L-Glu)=0.60, starting from a racemic mixture. The authentic samples of each dipeptide were also synthesized and used to identify the peaks in the chromatograms. These analyses showed the amounts of D-glutamic acid and D-alanine present in the hydrolyzate of the peptide I to be less than 1 and 5% respectively. The peptide II gave the same values.

The starting materials, III and IV, for the solid-phase syntheses were also tested for their degrees of racemization by the same method. The content of D-glutamic acid in III was shown to be less than 1%, and that of D-alanine in IV, to be 3%. Unfortunately, the original L-alanine used in the syntheses was found to contain 3% D-alanine. A comparison of the ORD curves of the hydrolyzate of IV and another sample of pure L-alanine confirmed the result ($[\alpha]_{230}$ were 1750° and 1860° (1%, 1 M HCl) for the hydrolyzate of IV and pure L-alanine respectively). Recrystallization seemed not to be able to separate a diastereomeric mixture, and the origin of a half of the D-alanine found in I and II was explained from the purity of the starting material. Therefore, the racemization accompanied by one step of the peptide-coupling reaction was about 0.3% or lower for the coupling of BOC-$(Ala)_2$ or BOC-$(\gamma$-Bzl-Glu$)_4$ respectively.

Experimental

The melting points were determined on a micro hot plate and are uncorrected. The elementary analyses were carried

out in the elementary analysis section in the Institute for Chemical Research, Kyoto University. The amino-acid analyses were carried out with a JEOL liquid chromatographic system under the conditions of Spackman *et al.*[22] A JASCO J-20 spectropolarimeter was used to measure the optical rotations. The BOC-hydrazide, trifluoroacetic acid, dicyclohexylcarbodiimide (DCC), and HOSu were purchased from the Protein Research Foundation, Osaka, Japan. The polystyrene beads (SX-1) were products of BioRad, Calif., U.S.A. The amino acids and other reagents were purchased from Nakarai Chemical Co., Kyoto, Japan. Reagent-grade dichloromethane was stored over sodium hydrogencarbonate, dried over molecular sieves (Type 4A, Linde), and distilled before use. The *N,N*-dimethylformamide was passed through a freshly packed column of silica gel G, dried over a molecular sieve (Type 4A, Linde), and distilled *in vacuo*. The trifluoroacetic acid was used after distillation over P_2O_5. The triethylamine was treated with 2,4-dinitrofluorobenzene and distilled over sodium.

N$^{\alpha}$-t-Butoxycarbonyl-L-alanyl-L-alanine, (IV). The dipeptide was synthesized from 143 g of BOC–Ala–OSu,[20] 53.5 g of alanine, and 50.5 g of $NaHCO_3$ in a mixture of 900 ml of tetrahydrofuran and 600 ml of water, according to the general method of Anderson *et al.*[20] Yield, 123 g (95%); mp 128—129 °C in a sealed tube (lit mp 85.5—87 °C,[23] 132—133 °C[24]). The compound could not be distinguished in melting point or infrared spectrum from the specimen obtained by the coupling of BOC-alanine with methyl alaninate employing isobutoxycarbonyl chloride, followed by saponification.[24] IV was hydrolyzed in 6M HCl at 110 °C for 24 h, and the hydrolyzate was submitted to measurements of the optical rotation and the racemization-detection reaction.

N$^{\alpha}$-t-Butoxycarbonyl-γ-benzyl-L-glutamic Acid, N-Hydroxysuccinimidyl Ester (V). 90 g of BOC–(γ-Bzl–Glu)[25] was allowed to react with 19.9 g of HOSu and 39.2 g of DCC at −8 °C in a mixture of 600 ml of ethyl acetate and 100 ml of tetrahydrofuran. Yield of V after recrystallization from 2-propanol, 68.3 g (91%); mp 106 °C (lit mp 100—101 °C[26]).

N$^{\alpha}$-t-Butoxycarbonyl-γ-benzyl-L-glutamyl-γ-benzyl-L-glutamic Acid (VI), and Its Dicyclohexylammonium Salt (VIa). 71.7 g of V, 59 g of γ-benzyl-L-glutamate, and 34.6 ml of triethylamine were stirred in 600 ml of *N,N*-dimethylformamide at room temperature for 10 h. Oily VI, obtained by the evaporation of the solvent *in vacuo*, was treated with 30 g of DCHA to give VIa, which was then recrystallized from ethyl acetate-cyclohexane. The VIa had a mp of 108—109 °C. Found: C, 66.65; H, 8.27; N, 5.72%. Calcd for $C_{41}H_{59}O_9N_3$ (VIa): C, 66.73; H, 8.06; N, 5.69%. VI has been known as oil.[26]

N-Hydroxysuccinimidyl Ester of VI(VII). 100 g of VIa was suspended in 400 ml of ethyl acetate and washed with 20% citric acid to convert the VIa into VI. The VI was reacted with 18.7 g of HOSu and 33.4 g of DCC at −8 °C for 10 h, and then at 5 °C for 25 h. The product, VII, was recrystallized from 2-propanol. Yield, 81 g (91%); mp 112—114 °C. Found: C, 60.88; H, 6.18; N, 6.42%. Calcd for $C_{33}H_{39}O_{11}N_3$: C, 60.63; H, 6.01; N, 6.43%.

γ-Benzyl-L-glutamyl-γ-benzyl-L-glutamic Acid(VIII). A 5.1-g portion of VIa was dissolved in 20 ml of dichloromethane and washed with 20% citric acid. The organic phase was washed with H_2O, dried over drierite, and then added to 10 ml of trifluoroacetic acid. The mixture was kept at room temperature for 1 h and then evaporated *in vacuo*. The residue was treated with 3% aq $NaHCO_3$ to crystallize the dipeptide acid VIII, which was subsequently recrystallized from ethanol. Yield, 2.1 g (65%); mp 124—125 °C. Found: C, 62.99; H, 6.22; N, 5.92%. Calcd for $C_{24}H_{28}O_7N_2$: C, 63.14; H, 6.18; N, 6.14%. The washing procedure with citric acid could be eliminated without any trouble. In that case, the amount of dichloromethane was reduced to 10 ml.

N$^{\alpha}$-t-Butoxycarbonyl-(γ-benzyl-L-glutamyl-)$_3$-γ-benzyl-L-glutamic-Acid, (III), and Its Dicyclohexylammonium Salt(IIIa). 52 g of VIII, 74 g of VII, 22.8 g of triethylamine, and 500 ml of *N,N*-dimethylformamide were mixed and stirred at room temperature for 24 h. The residues which were obtained after the evaporation of the solvent *in vacuo* were dissolved in ethyl acetate and washed thoroughly with 3% aq $NaHCO_3$. In the washing procedure, the sodium salt of tetrapeptide acid, III, was not transferred to the aqueous phase, but remained in the organic phase. The organic layer was washed with 5% citric acid and then with water, and dried over Na_2SO_4. A 20.4-g portion of DCHA was added to convert the III into IIIa, which was recrystallized several times from ethyl acetate. Yield, 105 g (79%); mp 129—130 °C. Found: 66.06; H, 7.24; N, 5.90%. Calcd for $C_{65}H_{85}O_{15}N_5$: C, 66.36; H, 7.28; N, 5.95%.

Solid-phase Peptide Synthesis. Polystyrene beads (BioBeads SX-1) which had been crosslinked with 1% divinylbenzene were chloromethylated[27] to a substitution level of 0.18 mmol Cl/g resin. The chloromethylated resin was reacted with BOC-phenylalanine to give the starting resin, BOC–Phe-resin. Acid hydrolysis, followed by amino-acid analysis, showed that 0.165 mmol of phenylalanine was incorporated per g of resin. 15 cycles of solid-phase peptide synthesis (the cycle is summarized in Table 1) were manually performed with a home-made shaker, starting with 5 g of BOC–Phe-resin for each block copolypeptide. After Step (11) in Table 1, an aliquot of peptide resin was removed, acid-hydrolyzed and analyzed for its amino-acid composition. Hydrolyses of the resin-bound peptides were carried out in a mixture of propionic acid and concd HCl (1: 1) or, for alanine-rich peptide-resin, in 95% trifluoroacetic acid, both in a sealed and evacuated tube at 110 °C for 24 h.

Cleavage of Peptide from Peptide-resin and Gel Chromatography of Peptides. A 20-ml portions of 20% HBr in acetic acid was added to 3 g of peptide-resin suspended in 10 ml of trifluoroacetic acid. The mixture was kept at room temperature for 1 h and then filtered to separate the resin. The resin was washed with a 1: 1 mixture of acetic acid and trifluoroacetic acid, and the combined filtrate was evaporated *in vacuo*. The residue was thoroughly washed with ether and dissolved in aq hydrogencarbonate solution. The peptides precipitated by acidification with HCl were redissolved in a small amount of aq $NaHCO_3$, and chromatographed on Sephadex G-50 (medium, 2.8×130 cm). Elution was achieved with 0.1 M NaCl–0.05M $NaHCO_3$–0.005M Na_2CO_3, and each fraction was analyzed for its peptide content by ninhydrin analysis after alkaline hydrolysis[28] or by UV absorption at 230—240 nm. An aliquot from each peptide-containing fraction was acid-hydrolyzed and analyzed for its amino-acid composition. Fractions containing a peptide whose amino acid composition was Glu: Ala: Phe= >19: >19: 1 were pooled and lyophilized. The lyophilized material was then dissolved in 2 ml of H_2O and placed on a column (1.5×130 cm) of Sephadex G-10. Elution was achieved with H_2O, and the peptide-containing fractions were combined and lyophilized.

$Glu_{20}Ala_{20}Phe$, (I). The yield of the material obtained after a gel filtration was 280 mg from 3 g of peptide-resin (14%). A 40-mg portion of the lyophilized sample was chromatographed on a DEAE-cellulose (Whatman DE-32) column (1.3×17 cm). The linear gradient of the concentration from 0M to 1M (in a 0.05M Na-phosphate buffer at pH 6.67) was applied for elution (total 200 ml). Each fraction was analyzed by ninhydrin analysis after alkaline hydrolysis,[28] and the peptide-containing fractions were analyzed for

their amino-acid compositions after total hydrolysis. Peptide-containing fractions, for which the amino-acid composition after total hydrolysis was given as Glu: Ala: Phe= >19: >19: 1, were pooled, desalted by Sephadex G-10, and lyophilized. Yield, 26 mg (the total yield was calculated as 306 mg (9%) starting from 5 g of BOC–Phe-resin).

$Ala_{20}Glu_{20}Phe$, (II). The gel-filtrated material was chromatographed on DEAE-cellulose and analyzed in a way similar to that described for I.

N-Terminal Analysis. Aliquots from I and II were 2,4-dinitrophenylated, hydrolyzed in 6M HCl at 110 °C for 18 h, and analyzed for the yield of 2,4-dinitrophenyl(DNP-)alanine or DNP-glutamic acid. After the necessary correction for the loss of DNP-amino acids during the acid hydrolysis, the yields of DNP-glutamic acid from I and DNP-alanine from II were found to be 92% and 94% respectively. No other DNP spots were detected on a TLC plate.

Detection of Racemization. The peptides in question (2 to 5 mg) were hydrolyzed in 2 ml of 6M HCl at 110 °C for 24 h. The hydrolyzates, which were completely free from acid by drying over KOH *in vacuo*, were dissolved in a mixture of 1 ml of H_2O and $NaHCO_3$ (5 equivalents for amino acids). 5 equivalents of BOC-L-Leu-OSu in 0.5 ml of acetonitrile were added to the mixture, and the reaction was carried out at room temperature for 1 h under shaking. The reaction mixture was then washed with ethyl acetate several times and evaporated to dryness. The residue was treated with a mixture of 1 ml of acetic acid and 1 ml of trifluoroacetic acid at room temperature 1 h, and then evaporated to afford a mixture of dipeptides, excess leucine, and some unreacted amino acids. The mixture was dissolved in a 0.2M sodium citrate buffer at pH 2.2 and placed in a 50-cm column of an amino-acid analyzer operated at 55 °C. A 0.2M sodium citrate buffer which had been adjusted to pH 3.10 by adding concd HCl to the regular pH 3.35 sodium citrate (0.2M) buffer[29] was used to separate L-Leu-D-Glu (425 min), L-Leu-L-Glu (488 min), and leucine (545 min), while the regular pH 4.25 buffer (0.2M sodium citrate)[29] was used to separete L-Leu-D-Ala (130 min) and L-Leu-L-Ala (157 min). The retention times are shown in parentheses. For the reference standard, authentic D,L-amino acids were treated under the same conditions. The product, the diastereomeric dipeptide mixture, was analyzed with an amino-acid analyzer to give the standard ratio of the ninhydrin colour values. The positions of the peptides were determined by the analysis of authentic peptides which had been synthesized from BOC-L-Leu-OSu and D- or L-amino acids. BOC-L-Leu-D-Ala (mp 166—168 °C from methanol. Found: C, 55.57; H, 8.67; N, 9.19%. Calcd for $C_{14}H_{26}O_5N_2$: C, 55.61; H, 8.67; N, 9.27%.) and BOC-L-Leu-L-Ala·DCHA (crystallized from ethyl acetate, mp 159—162 °C; the crystals turn unclear at 105—110 °C, presumably because of a loss of solvent for crystallization. Found: C, 63.71; H, 10.22; N, 7.78%. Calcd for $C_{26}H_{49}O_5N_3 \cdot 1/2CH_3CO_2C_2H_5$: C, 63.72; H, 10.12; N, 7.96%) were obtained as crystals, but the corresponding glutamyl peptides were oils.

References

1) All of the amino-acid residues in this communication have the L-configuration, unless especially noted.

2) S. Tanaka and H. A. Scheraga, *Macromolecules*, **9**, 142, 159, 168 (1976).

3) T. Kontani, K. Nishikawa, T. Iio, S. Takahashi, and T. Ooi, *Bull. Inst. Chem. Res., Kyoto Univ.*, **54**, 128 (1976).

4) G. M. Bonora, C. Toniolo, A. Fontana, C. D. Bello, and E. Scoffone, *Biopolymers*, **13**, 157 (1974).

5) S. Sano and S. Kawanishi, *J. Am. Chem. Soc.*, **97**, 3480 (1975).

6) R. S. Feinberg and R. B. Merrifield, *J. Am. Chem. Soc.*, **97**, 3485 (1975).

7) J. Meienhoffer, P. M. Jacobs, H. A. Godwin, and I. H. Rosenberg, *J. Org. Chem.*, **35**, 4137 (1970).

8) S. Sakakibara, Y. Kishida, Y. Kikuchi, R. Sakai, and K. Kakiuchi, *Bull. Chem. Soc. Jpn.*, **41**, 1273 (1968).

9) S. Sakakibara, K. Inouye, K. Shudo, Y. Kishida, Y. Kobayashi, and D. J. Prockop, *Biophys. Biochem. Acta*, **303**, 198 (1973).

10) K. Noda, S. Terada, N. Mitsuyasu, M. Waki, T. Kato, and N. Izumiya, *Mem. Fac. Sci. Kyushu Univ.*, **Ser. C7**, 189 (1970).

11) H. Yajima, H. Kawatani, and H. Watanabe, *Chem. Pharm. Bull.*, **18**, 1333 (1970).

12) H. Yajima and H. Kawatani, *Chem. Pharm. Bull.*, **19**, 1905 (1971).

13) H. Yajima, Y. Kiso, Y. Okada, and H. Watanabe, *J. Chem. Soc., Chem. Commun.*, **1974**, 106.

14) S. M. Karlsson and U. Ragnarsson, *Acta Chem. Scand.*, **B28**, 376 (1974).

15) U. Ragnarsson, S. M. Karlsson, and U. Hamberg, *Int. J. Peptide Protein Res.*, **7**, 307 (1975).

16) L.-E. Larsson, P. Melin, and U. Ragnarsson, *Int. J. Peptide Protein Res.*, **8**, 39 (1976).

17) G. S. Omenn and C. B. Anfinsen, *J. Am. Chem. Soc.*, **90**, 6571 (1968).

18) A. M. Felix and R. B. Merrifield, *J. Am. Chem. Soc.*, **92**, 1385 (1970).

19) M. A. Barton, R. U. Remieux, and J. Y. Savoie, *J. Am. Chem. Soc.*, **95**, 4501 (1973).

20) G. W. Anderson, J. E. Zimmerman, and F. M. Callahan, *J. Am. Chem. Soc.*, **86**, 1839 (1964).

21) J. M. Manning, *Methods in Enzymology*, **25**, 9 (1972).

22) D. H. Spackman, W. H. Stein, and S. Moore, *Anal. Chem.*, **30**, 1190 (1958).

23) B. B. Doyle, W. Traub, G. P. Lorenzi, F. R. Brown, III, and E. R. Blout, *J. Mol. Biol.*, **51**, 47 (1970).

24) V. A. Shibnev, L. I. Mar'yash, V. S. Grechishko, and K. T. Poroshin, *Izv. Akad. Nauk SSSR, Ser. Khim.*, 2820 (1970).

25) K. P. Polzhofer, *Tetrahedron Lett.*, **1969**, 2305.

26) W. Danho and C. H. Li, *Int. J. Protein Res.*, **3**, 81 (1971).

27) R. S. Feinberg and R. B. Merrifield, *Tetrahedron*, **30**, 3209 (1974).

28) C. H. W. Hirs, S. Moore, and W. H. Stein, *J. Biol. Chem.*, **219**, 623 (1956).

29) S. Moore, D. H. Spackman, and W. H. Stein, *Anal. Chem.*, **30**, 1185 (1958).

The Reaction of Dammarane Derivatives: Reactions Involving C-20 Carbonium Ions

Motoo Tori, Takahiko Tsuyuki, and Takeyoshi Takahashi

Department of Chemistry, Faculty of Science, The University of Tokyo, Bunkyo-ku, Tokyo 113

(Received June 23, 1977)

In order to investigate the reaction involving C-20 cation in dammarane derivatives, following reactions were examined: a) (20*S*)- and (20*R*)-dammaran-20-ols (**13** and **14**) with acids. b) dammar-20(22)-en-23-one (**15**) with hydrochloric acid, c) 20,21- and 20,22-epoxydammaranes (**16** and **17**) with boron trifluoride etherate, and d) hexanor- and pentanordammaran-20-ols (**18** and **19**) with phosphoryl chloride and with boron trifluoride etherate, *etc.*, and 20ξ-tosyloxyhexanordammarane (**46**) with silica gel. Either formation of a double bond in the framework or in the side chain (in the cases of **13**, **14**, **18**, **19**, and **46**), deconjugation of the double bond (in the case of **15**), or formation of a carbonyl group in the side chain (in the cases of **16** and **17**) was observed. However, D-homoannulation reaction was not observed in all cases.

The biogenetic pathway of triterpenes proposed by Ruzicka *et al.*[1] strongly suggests an intermediacy of a tetracyclic cation (**1**) with a dammarane-type skeleton as a primary cyclization product from squalene. The cation (**1**) is also suggested to be transformed into various triterpenes depending on characteristic enzyme action *in vivo*. For example, a $C_{(16)}$–$C_{(17)}$ bond migration to C-20 causes a formation of a baccharane skeleton (**2**) with the cation at C-20, which will be further derived into baccharis oxide (**3**) or shionone (**4**).

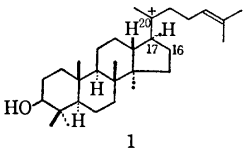

1

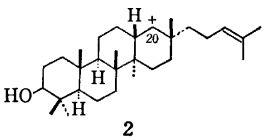

2

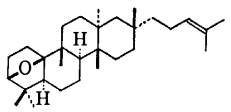

3

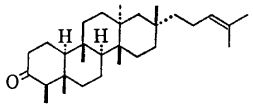

4

In the field of steroid chemistry, a number of investigations on backbone rearrangement and D-homoannulation reactions have been reported.[2] Among them, D-homoannulation of 20-tosylates has been shown to depend on the configuration at C-20 and also on the solvolytic conditions. For example, 3β-acetoxy-17α-hydroxy-5α-pregnan-20β-yl tosylate (**5**), on treatment with potassium acetate in aqueous acetone or with sodium iodide in acetone, gave 3β-acetoxy-17α-methyl-D-homo-5α-androstan-17a-one (**6**) as a principal product. While the epimeric 20α-tosylate (**7**) yielded 3β-acetoxy-17aα-methyl-D-homo-5α-androstan-17-one (**8**).[3] A solvolysis of 5α-pregnan-20β-yl tosylate (**9**) gave 17α-methyl-D-homo-5α-androstan-17aβ-yl tosylate (**10**) in a high yield.[4] The formolysis of 3β-acetoxy-5α-pregnan-20α-yl tosylate (**11**), however, proceeds predominantly without enlargement of the D-ring to afford 17β-methyl-18-nor-5α,17α-pregn-13-en-3β-yl acetate (**12**) as a main product.[2d]

Since Mills determined the structures of triterpenes of dammarane-type isolated from "Dammar Resin,"[5]

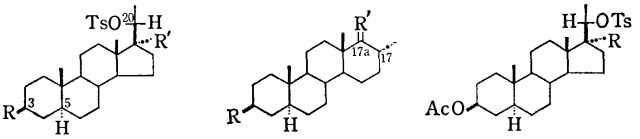

	R	R'
5	OAc	OH
9	H	H

	R	R'
6	OAc	O
10	H	β-OTs, α-H

	R
7	OH
11	H

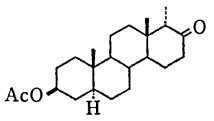

8

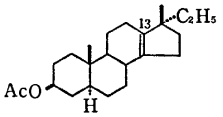

12

a variety of investigations on the reactions of dammarane derivatives have so far been carried out.[6,7] In order to examine the reaction of dammarane derivatives having a cationic center at C-20, following reactions have now been investigated: a) (20*S*)- and (20*R*)-dammaran-20-ols (**13** and **14**) with acids, b) dammar-20(22)-en-23-one (**15**) with hydrochloric acid, c) 20,21- and 20,22-epoxydammaranes (**16** and **17**) with boron trifluoride etherate, and d) hexanor- and pentanordammaran-20-ols (**18** and **19**) with phosphoryl chloride.

a) Reaction of (20S)- and (20R)-Dammaran-20-ols (13 and 14) with Acids. Although (20*S*)-dammaran-20-ol (**13**)[8] was easily prepared by Huang-Minlon reduction of (20*S*)-20-hydroxydammaran-3-one (**20**)[5b] derived from dipterocarpol (**21**),[5,6a–d] the epimeric (20*R*)-alcohol (**14**) was synthesized from **13** *via* hexanordammaran-20-one (**22**) or nordammaran-20-one (**23**).[9]

(20*S*)-Dammaran-20-ol (**13**) was treated with phosphoryl chloride in pyridine to afford an olefin mixture, which was subjected to separation by silver nitrate-impregnated silica gel TLC to give a mixture (*ca.* 1 : 1) of (20*R*)- and (20*S*)-dammar-13(17)-enes (**24a** and **24b**; yield 3%), a mixture of (*E*)- and (*Z*)-dammar-20(22)-enes (**25a** and **25b**; y. 65%), and dammar-20-ene (**26**; y. 25%). The structure of the former (**24**) was discussed below and those of the latter two (**25** and **26**) were determined by spectral data (*cf.* Experimental) and by their transformation into **22** and **23**, respectively. The olefin mixture, without separation, was subjected to ozonolysis and the resulting mixture was separated by chromatography to afford hexanordammaran-20-one

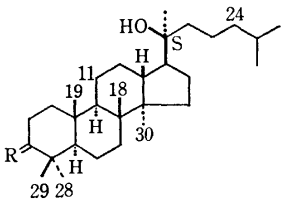

13 R = H_2
20 R = O
21 R = O; with Δ^{24}
34 R = β-OAc, α-H

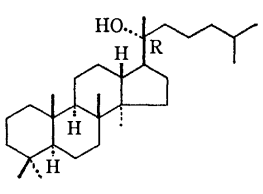

14

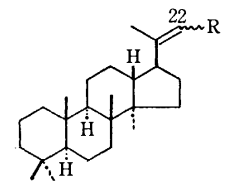

a: (E)-isomer
b: (Z)-isomer

15 R = $\overset{O}{\overset{\|}{C}}CH_2CH(CH_3)_2$
25 R = $(CH_2)_2CH(CH_3)_2$
37 R = CN
38 R = CO_2CH_3

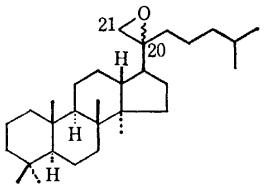

16

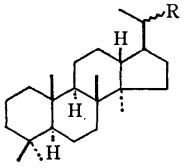

18 R = OH
42 R = $\overset{O}{\overset{\|}{C}}(CH_2)_2CH(CH_3)_2$
43 R = Cl
46 R = OTs

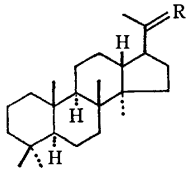

22 R = O
48 R = CH_2

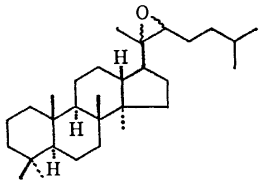

17

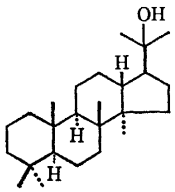

19

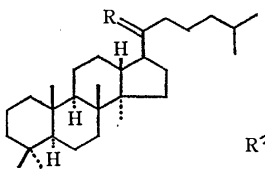

23 R = O
26 R = CH_2

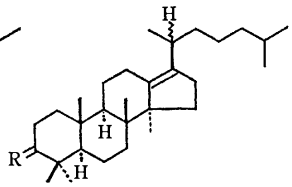

a: (20R)
b: (20S)
24 R = H_2
35 R = β-OAc, α-H

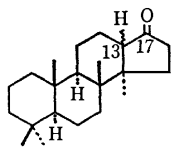

27 13α-H
28 13β-H

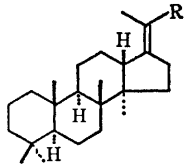

29a R = $(CH_2)_3CH(CH_3)_2$
47 R = CH_3

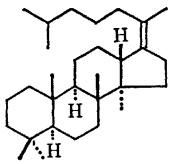

29b

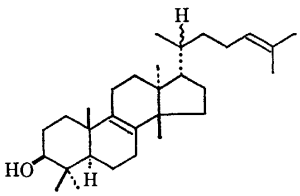

36 a: (20R)
b: (20S)

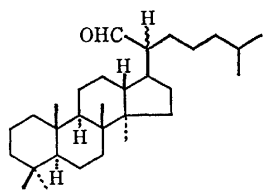

40

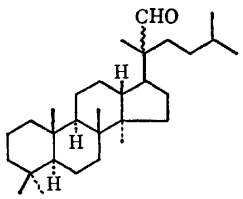

41

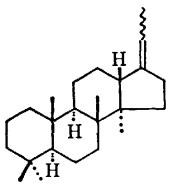

44

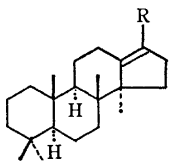

45 R = CH_2CH_3
49 R = $CH(CH_3)_2$

(**22**; 40%)[8,10] and nordammaran-20-one (**23**; 22%), together with 13α*H*-octanordammaran-17-one[11] (**27**; 0.4%) and octanordammaran-17-one[11] (**28**; 1.7%). It was therefore suggested that dammar-17(20)-enes (**29a** and/or **29b**) had also been present in a very small amount in the above olefin mixture.[7]

The structure of nordammaran-20-one (**23**) was confirmed by its conversion into dammaran-20-ols (**13** and **14**). Nordammaran-20-one (**23**) was treated with methylmagnesium iodide in ether to give a mixture of the epimeric alcohols (**13** and **14**) in a ratio of 1 : 2, while the Grignard reaction of hexanordammaran-20-one (**22**) with 1-bromo-4-methylpentane in tetrahydrofuran gave the same mixture in a ratio of 11 : 8.

The stereochemistry of the addition reaction of Grignard reagents to 20-keto steroids has been investigated. For example,[12] the addition of methylmagnesium bromide to 3β-acetoxy-21-nor-5α-cholestan-20-one (**30**) gave exclusively the corresponding (20*R*)-alcohol (**31**). On the contrary, the (20*S*)-epimeric alcohol (**32**) was obtained by addition of 4-methylpentylmagnesium bromide to 3β-acetoxy-5α-pregnan-20-one (**33**). The selectivity in these reactions seems to be attributable to the presence of the 13β-methyl group in the steroid skeleton. The lower selectivity to form the (20*S*)- or (20*R*)-alcohol in the case of the dammarane derivatives, compared with the reaction of 20-keto steroids, could be explained by the absence of the 13β-methyl group in the dammarane skeleton.[9]

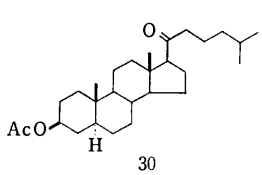

30

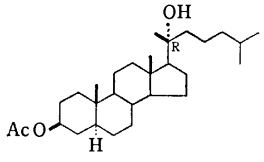

31

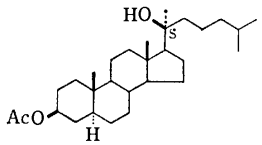

32

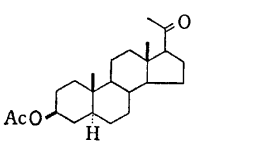

33

Mills showed that dammaranediol-II monoacetate (**34**) gave a mixture of isoeuphenyl acetate (**35a**) and isotirucallenyl acetate (**35b**) on treatment with 1 M sulfuric acid.[5b] Tanaka *et al.*[6e,13] reported acid treatments of (20*S*)-dammaran-20-ol (**13**), (20*S*)-dammar-24-en-20-ol, and of the corresponding 12-hydroxylated compounds to examine the epimerization at C-20.

Dehydration reaction of the epimeric (20*S*)- and (20*R*)-dammaran-20-ols (**13** and **14**) catalyzed by various acids has now been investigated under various conditions. i) Treatment of (20*S*)-dammaran-20-ol (**13**) in benzene with boron trifluoride etherate gave a hydrocarbon as a main product. This hydrocarbon was shown to be a mixture (*ca.* 1 : 1) of (20*R*)- and (20*S*)-dammar-13(17)-enes (**24a** and **24b**) by the following evidence. A mixture of euphol (**36a**) and tirucallol (**36b**), extracted from *Euphorbia kansui* Liou.,[14] was acetylated, hydrogenated, and then treated with hydrochloric acid in acetic acid according to the procedures described by Arigoni *et al.*,[15] to yield a mixture of isoeuphenyl acetate (**35a**) and isotirucallenyl acetate (**35b**).[15] This mixture (**35a** and **35b**) was subjected successively to alkaline hydrolysis, Jones oxidation, and Huang-Minlon reduction to afford a mixture of (20*R*)- and (20*S*)-dammar-13(17)-enes (**24a** and **24b**), which was found to be identical with the hydrocarbon obtained by boron trifluoride etherate treatment of **13**. The ratio (*ca.* 1 : 1) of **24a** and **24b** in the olefin mixture (**24**) was estimated from peak heights of the C-21 methyl signals (**24a**, δ 0.94; **24b**, δ 0.90)[16] and by gas chromatographic analysis. When (20*R*)-dammaran-20-ol (**14**) was treated with boron trifluoride etherate in benzene, the same mixture (**24a** and **24b**; *ca.* 1 : 1) was formed.

(20*S*)-Dammaran-20-ol (**13**) was then treated with the following conditions: ii) boron trifluoride etherate in dichloromethane at room temperature, iii) boron trifluoride etherate in acetic acid, iv) stannic chloride in benzene, v) picric acid in nitromethane,[17] vi) 1 M sulfuric acid in acetic acid under reflux according to Mills' procedure,[5b] and vii) formic acid in acetone under reflux. Treatment of (20*R*)-dammaran-20-ol (**14**) with i) boron trifluoride etherate in benzene, ii) boron trifluoride etherate in dichloromethane, or with iii) trifluoroacetic acid, was also examined. In each case, the same reaction products (**24a** and **24b**) were obtained. When protic acids were used, the formation of **25** and **26** was also observed. However, Lewis acid treatment afforded **24** as major products.

Removal of the hydroxyl group at C-20 of **13** or **14** by an acid catalyst may produce a cation at C-20. As this type of cation has rather a long life time, the hydrogen atom at C-17α can undergo 1,2-shift from both the back and the front sides of the cation, resulting in the formation of the epimeric mixtures at the C-20 carbon atom. A C-13β hydrogen atom is then removed to provide an unsaturated double bond $C_{(13)}$–$C_{(17)}$, the position of which is considered to be the most stable one in the dammarane skeleton.

b) Synthesis of Dammar-20(22)-en-23-one (15) and Reaction with Hydrochloric Acid. It was unsuccessful to build up the side chain of **15** directly by the Wittig reaction of hexanordammaran-20-one (**22**) with dimethyl 4-methyl-2-oxopentylphosphonate;[18] an anion derived from the phosphonate was unreactive with the ketone (**22**) in dimethyl sulfoxide or in dimethoxyethane under reflux. Hexanordammaran-20-one (**22**), however, reacted with diethyl cyanomethylphosphonate in dimethoxyethane using sodium hydride as a base. The reaction proceeded quantitatively to yield pentanordammar-20(22)-ene-22-carbonitrile (**37**). Recrystallization from petroleum ether-ether furnished a major isomer, mp 179—180 °C, which was shown to be an (*E*)-isomer (**37a**) from the proton NMR[19] (*cf.* Experimental) and the ^{13}C-NMR spectral data (Table 1). An examination of the mother liquor showed also the presence of the (*Z*)-isomer (**37b**).

The structure of the α,β-unsaturated carbonitrile (**37**) was also supported by its conversion into the α,β-unsaturated ester (**38**). The (*E*)-isomer of the carbonitrile (**37a**) was treated with potassium hydroxide in boiling ethylene glycol followed by methylation with diazomethane to give a mixture of methyl (*E*)- and (*Z*)-tetranordammar-20(22)-en-23-oates (**38a** and **38b**), which was separated by TLC into each isomer.

The residual C-4 unit was then introduced to the tetranordammarane skeleton (**37a**). Treatment of **37a** with isobutylmagnesium bromide gave an imine, which was hydrolyzed *in situ* with aqueous ammonium chloride.[20] The resulting products, consisting of (*E*)- and (*Z*)-dammar-20(22)-en-23-ones (**15a** and **15b**), were separated into each isomer by preparative TLC. Assignment of the geometry of the double bonds in **15a**

and **15b** was easily accomplished by NMR measurement.[21,22] The methyl group attached to an olefinic carbon atom at C-20 of the less polar (on TLC) isomer resonates at δ 1.79 (d, J=1.5 Hz) and that of the more polar one at δ 2.05 (d, J=1 Hz). The methyl group resonating in the lower field can be assigned as that of the (*E*)-isomer (**15a**).

The conformation of each enone (**15a** and **15b**) was also inferred by the solvent effect on the chemical shifts of the proton NMR spectrum.[21a,23] In benzene-d_6, the chemical shift of the $C_{(21)}$-Me of the (*E*)-isomer (**15a**) was observed in the lower field ($\delta_{CDCl_3}-\delta_{C_6D_6}=-0.14$), although the olefinic proton resonated in the higher field ($\delta_{CDCl_3}-\delta_{C_6D_6}=+0.03$). As for the (*Z*)-isomer (**15b**), both of the signals suffered appreciable upfield shifts ($\delta_{CDCl_3}-\delta_{C_6D_6}=+0.15$ for the methyl and +0.12 for the olefinic proton signals). These spectral data suggest the conformation depicted as in **15a**-1 and **15b**-1 (not as in **15a**-2 and **15b**-2) for **15a** and **15b**, respectively, in the solution.

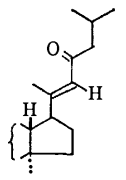

15a-1

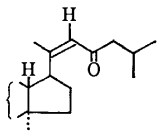

15b-1

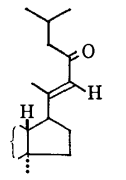

15a-2

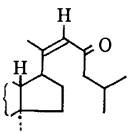

15b-2

Treatment of the (*E*)-isomer (**15a**) with *p*-toluenesulfonic acid in ether gave a mixture of the (*E*)- and (*Z*)-isomers (**15a** and **15b**). The (*Z*)-isomer (**15b**) also afforded the same mixture on the same treatment. Similar results were obtained upon treatment with boron trifluoride etherate.

The (*E*)-isomer (**15a**) was refluxed with concd hydrochloric acid in ethanol. Two products were obtained in about equal amounts. The IR spectrum of the less polar product (on TLC) shows bands at 1700 and 1600 cm^{-1} and that of the more polar one at 1705 cm^{-1}. Mass spectra of both compounds closely resemble each other. These observations suggest the similarity of the whole structure of both compounds having a deconjugated double bond. Since NMR spectra show no olefinic proton, the presence of a tetrasubstituted double bond is suggestive. A carbonyl function at C-23 is indicated by fragment peaks at *m/e* 369 and *m/e* 57 and also at *m/e* 341 and *m/e* 85. The location of the tetrasubstituted double bond is also suggested by the mass spectrum (*cf.* **39**). The structure of the two products are therefore considered to be ($20\xi_1$)- and ($20\xi_2$)-dammar-13(17)-en-23-ones (**39**).

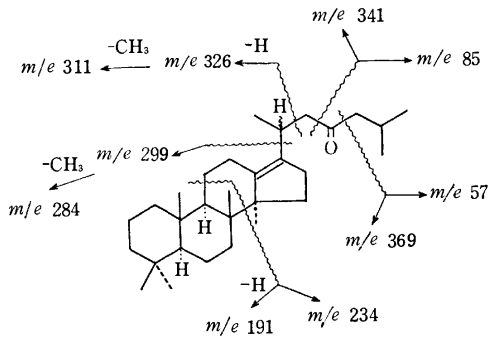

39

Protonation at $C_{(23)}$-O function of **15a** provokes of a generation of a cationic center at C-20. Successive 1,2-shift of a hydride from the C-17α to the C-20 carbon atom and deprotonation of $C_{(13\beta)}$-H, or a mechanism involving 1,3-shift, would give rise to a tetrasubstituted double bond between C-13 and C-17. Direct protonation at the double bond of **15a** could also illustrate the formation of the cationic center at C-20.

*c) Synthesis of 20,21- and 20,22-Epoxydammaranes (**16** and **17**) and Reaction with Boron Trifluoride Etherate.* Epoxidation of dammar-20-ene (**26**) with *m*-chloroperbenzoic acid in dichloromethane gave an epoxide (**16**). A signal due to two protons of the epoxide ring terminus appeared at δ 2.59 (br. s, $W_{1/2}$ 2 Hz). As this epoxide was thought to be a mixture of (20*S*)- and (20*R*)-configurations, it was reduced with lithium aluminium hydride in ether. (20*S*)-Dammaran-20-ol (**13**) and (20*R*)-dammaran-20-ol (**14**) were obtained in a ratio of 2: 3. No formation of other alcohols was detected. Consequently, the epoxide mixture was suggested to consist of the (20*S*)- and (20*R*)-20,21-epoxydammaranes (**16**) in a ratio of *ca.* 2: 3. Further separation was not attempted.

Treatment of this mixture of epoxide (**16**) with boron trifluoride etherate in benzene at room temperature for 10 min gave an aldehyde (**40**). Its IR (2680 and 1720 cm^{-1}) and NMR [δ 9.55 and 9.68 (each *ca.* 0.5H, d, J=3 Hz)] spectra suggested the presence of an aldehyde group attached to a secondary carbon atom. And the NMR spectrum also indicated the presence of a pair of C-20 isomeric aldehydes.

Epoxidation of the mixture of dammar-20(22)-enes (**25a** and **25b**) gave an epoxide mixture (**17**). An HPLC examination of **17** suggested the presence of four possible stereoisomers, one of which was the major. The mixture of the epoxides (**17**) including four stereoisomers was treated with boron trifluoride etherate in benzene at room temperature for 20 min. Three products were obtained after usual work-up. The least polar product (on TLC) showed bands at 2660 and 1720 cm^{-1} in its IR spectrum. Its mass spectrum showed peaks at *m/e* 428 (M^+), 399 (M−CHO), 357 ($M-C_5H_{11}$), and 301 ($M-C_8H_{15}O$). These observations suggest the presence of a tertiary aldehyde function and lead to the structure of ($20\xi_1$)-26,27-dinor-20,24-dimethyldammaran-21-al [($20\xi_1$)-**41**] for this product. The spectral data of the second product [($20\xi_2$)-**41**] were

very similar to those of the first one. This fact indicates that these two products are epimers at C-20 each other. However, the configuration of each compound has been left undetermined. The most polar product showed a band at 1710 cm^{-1} and peaks at *m/e* 428 (M^+), 357 ($M-C_5H_{11}$), and 329 ($M-C_6H_{11}O$). This product can be formulated as (20ξ)-dammaran-22-one (**42**) by these spectral data and mechanistic consideration.

An attack of boron trifluoride etherate to the oxygen atom of the epoxide and subsequent ring opening by the $C_{(20)}$–O bond cleavage may generate the cationic center at C-20. In the former (**16**) case, a hydride at C-21 migrates to the C-20 carbon atom to afford the aldehyde (**40**). The configuration at C-20 must be determined by the original configuration of the epoxide: *i.e.*, the hydride which migrates is considered to be introduced from the back side of the oxygen atom of the epoxide. In the latter (**17**) case, there are two possible migrating group, *i.e.*, a hydrogen atom and an isopentyl group on the C-22 carbon atom. When the hydrogen atom migrates to C-20, it may result in formation of the ketone (**42**), while the aldehyde (**41**) may be obtained when the isopentyl group undergoes a 1,2-shift to C-20. Neither hydride shift from C-17α to C-20 nor $C_{(17)}$–$C_{(13 \text{ or } 16)}$ bond migration was observed. A factor of stabilization for the formation of a carbonyl group seems to be larger than that for an en-ol structure. Recently, similar results using cholestane derivatives have been reported by Ikekawa et al.[24] and others.[25,26] All the isomers of the 20(22)-epoxides were synthesized independently and their chemical reactions were discussed.

d) *Reaction of Hexanor- and Pentanordammarane Derivatives.* Hexanordammaran-20-one (**22**) was reduced with sodium borohydride in ethanol to yield a mixture of alcohols (**18**) which could not be separated. This secondary alcohol (**18**) was dehydrated with phosphoryl chloride in pyridine to afford a mixture, which showed two spots on TLC of silica gel. The more polar product (on TLC) was shown to be a mixture of (20*S*)- and (20*R*)-20-chlorohexanordammarane (**43**) (*cf.* Experimental). The less polar part (hydrocarbon) showed one major peak along with two minor ones on GLC analysis. A signal due to an olefinic proton was observed around δ 5.0 ppm (diffused). In order to determine the exact position of the double bond, a solution of this hydrocarbon mixture in carbon tetrachloride was treated with ruthenium tetraoxide in the same solvent at room temperature. On separation by preparative TLC, octanordammaran-17-one (**28**) was obtained, which was identical with an authentic sample.[11] A solution of the hydrocarbon mixture in dry tetrahydrofuran was subjected to hydroboration-oxidation to yield hexanordammaran-20-ol (**18**). The formation of hexadammar-17(20)-enes (**44**) and of **43** from **18** was therefore shown.

Treatment of hexanordammaran-20-ol (**18**) with *p*-toluenesulfonyl chloride in pyridine gave a tosylate (**46**). The tosylate (**46**) was passed through a column of silica gel to give a single product (**45**), mp 104—106 °C, after recrystallization from methanol–chloroform. The elemental analysis and mass spectrum showed a molecular formula, $C_{24}H_{40}$, for this compound. The NMR spectrum showed the presence of an ethyl group and the absence of olefinic proton. In view of the above facts the most reasonable structure of this olefin is hexanordammar-13(17)-ene (**45**).

Hexanordammaran-20-one (**22**) was methylated with methylmagnesium iodide in ether to give a tertiary alcohol (**19**). The alcohol (**19**) was dehydrated with phosphoryl chloride in pyridine to afford two hydrocarbons, which were separated by preparative TLC on silver nitrate-impregnated silica gel. The less polar product could be formulated as pentanordammar-17(20)-ene (**47**) from its NMR spectrum showing the presence of an isopropylidene group. The NMR spectrum of the more polar product indicated the presence of an isopropenyl group; this led to the structure of pentanordammar-20-ene (**48**) for this hydrocarbon.

Treatment of the alcohol (**19**) with boron trifluoride etherate in benzene at room temperature for 1 h furnished two products. The more polar product (on TLC) was identical with **48**. The NMR spectrum of the less polar product showed the presence of an isopropyl group and the absence of olefinic proton; the structure of pentanordammar-13(17)-ene (**49**) was suggested for this product.

These characteristic dehydration reactions are mainly dependent on both of the acids and the solvents used. When a base such as pyridine is present in the reaction system, a proton adjacent to a hydroxyl group is easy to be abstracted. It is known that dammarane-type triterpenes having a normal side chain produce 20(22)- and 20-enes as major products[5] (*vide supra*). However, when the side chain is small, a base such as pyridine can abstract the hydrogen atom at C-17α to afford a 17(20)-ene. This is the remarkable difference between the two. In the case of boron trifluoride etherate, a hydride shift and a subsequent deprotonation can occur to yield the more stable 13(17)-ene, as the life time of the cationic center is longer.

Although all the reactions were attempted for aiming at the chemically induced rearrangements of the C-20 cation of the dammarane-type into baccharane-type skeleton, neither tertiary cation nor secondary cation at C-20 underwent such rearrangement.

^{13}C-NMR Spectra. Recently, O. Tanaka and his co-workers reported the assignments of carbon signals of dammarane-type triterpenes and discussed the chemical shift difference between (20*S*)- and (20*R*)-dammarane-12,20-diol derivatives.[27,28] Remarkable differences were observed owing to a hydrogen bonding between $C_{(12)}$–OH and $C_{(20)}$–OH groups.

We examined the ^{13}C-NMR spectra of some dammarane derivatives without $C_{(3)}$–oxygen function. The assignment of carbon signals of dipterocarpol (**21**) by O. Tanaka et al.[28] made it possible to assign the $C_{(24)}$ and $C_{(25)}$ carbon atoms of dihydrodipterocarpol (**20**; (20*S*)-20-hydroxydammaran-3-one). The accuracy of the assignment was confirmed by the hexanor derivative (**22**). Signals due to $C_{(1)}$—$C_{(6)}$, $C_{(28)}$, and $C_{(29)}$ of (20*S*)- and (20*R*)-dammaran-20-ols (**13** and **14**) were easily assigned by considering the additivity and the effects of substituents and also from comparison of the spectra from compound to compound.

Table 1. ^{13}C-NMR chemical shifts, δ_C, of some derivatives of dammarane-type in $CDCl_3$[1]

	21[2]	**20**	**13** 20(*S*)	**14** 20(*R*)	*S*–*R*[3]	**22**	**37a**
C-1	39.9	39.9[b]	40.6[c]	40.6[c]	0	40.7[c]	40.8[c]
2	34.0	34.0	18.7	18.6	+0.1	18.6	18.6
3	217.6	217.8	42.2[c]	42.1[c]	+0.1	42.1[c]	42.2[c]
4	47.3	47.3	33.4	33.4	0	33.4	33.4
5	55.3	55.4	57.0	57.0	0	57.0	57.0
6	19.6	19.7	18.7	18.6	+0.1	18.6	18.6
7	34.5	34.6	35.3	35.3	0	35.5	35.4
8	40.3	40.3	40.6	40.6	0	40.7	40.8
9	50.0	50.1	50.8	50.7	+0.1	50.8	50.9
10	36.8	36.8	37.5	37.4	+0.1	37.5	37.6
11	22.0	22.1	21.5	21.4	+0.1	21.1	21.1
12	25.4	25.6	25.6	25.3	+0.3	25.7[d]	24.9
13	42.3	42.4	42.2	42.1	+0.1	45.2	45.8
14	50.2	50.3	50.4	50.1	+0.3	50.1	49.9
15	31.2	31.2	31.2	31.0	+0.2	31.5	31.6
16	27.5	27.6	27.6	27.6	0	25.9[d]	27.9
17	49.7	49.7	49.8	49.6	+0.2	54.3	49.9
18	16.0[a]	16.0[a]	16.2[a]	16.2[a]	0	15.9[a]	15.9[a]
19	15.2[a]	15.2[a]	15.6[a]	15.6[a]	0	15.6[a]	15.7[a]
20	75.1	75.2	75.3	75.5	−0.2	211.9	168.3
21	24.8	24.8	24.8	23.9	+0.9	29.9	18.3
22	40.6	41.2	41.1	42.4	−1.3	—	94.5
23	22.6	21.5	21.5	21.1	+0.4	—	117.5
24	124.8	39.8[b]	39.8	39.7	+0.1	—	—
25	131.2	28.0	28.0	28.0	0	—	—
26	25.7	22.7	22.7	22.7	0	—	—
27	17.7	22.7	22.7	22.7	0	—	—
28	26.7	26.7	33.4	33.4	0	33.4	33.4
29	21.0	21.0	21.5	21.5	0	21.5	21.6
30	16.3	16.4	16.5	16.4	+0.1	16.2	16.3

a,b,c,d) Assignments may be reversed in each vertical column. 1) FT measurement conditions were as follows: spectral width, 4000 Hz; acquisition time, 1.0 s; number of data points, 8192; pulse width, 3 μs. 2) Ref. 28. 3) Difference of the chemical shift values (δ_C) between (20*S*)-dammaran-20-ol (**13**) and (20*R*)-dammaran-2-ol (**14**).

The unsaturated carbonitrile (**37a**) was deduced to be pure (*vide supra*), showing 26 peaks.

The chemical shift difference between the (20*S*)- and (20*R*)-isomers was very small except for $C_{(21)}$ and $C_{(22)}$ carbon atoms as described by O. Tanaka *et al.*[28] (Table 1).

Experimental

General Procedures. All melting points were measured on a Mel-temp capillary melting point apparatus (Laboratory Devices) and uncorrected. Optical rotations were determined in chloroform solutions on a JASCO polarimeter DIP-SL. Ultraviolet absorption (UV) spectra and infrared (IR) spectra were measured on a Hitachi EPS-2 and a Hitachi EPI-G2 spectrometer, respectively. Mass (MS) spectra were run on a Hitachi RMU-6-Tokugata mass spectrometer and high resolution mass spectra on a Hitachi RMH-2 mass spectrometer operating at 70 eV with a direct inlet system. The relative intensity was expressed in % in the parentheses. Proton nuclear magnetic resonance (NMR) spectra were taken in deuteriochloroform ($CDCl_3$) using a Hitachi R-20B (60 MHz), a JEOL JNM PS-100 (100 MHz), or a JEOL JNM FX-60 spectrometer. Chemical shifts were expressed in ppm downfield from tetramethylsilane (TMS) as an internal standard (δ value) and coupling constants in Hz. ^{13}C NMR spectra were recorded on a JEOL JNM FX-60 FT NMR spectrometer at 15.04 MHz in $CDCl_3$ with TMS as an internal reference (δ_C O) in 8-mm spinning tube. Gas chromatography (GLC) was carried out using Shimadzu 4A-PF or CG-2C equipped with a hydrogen flame ionization detector. Liquid Chromatograph Model ALC/GPC 202/401 (Waters Assoc.) was used for high performance liquid chromatography (HPLC); Column: μ-PORASIL 1/8 (inch) × 1 (foot); Solvent system: 1 or 10% ether–hexane; Flow rate: 1.0 or 1.2 ml/min; Pressure: *ca.* 500 psi; with an RI or UV detector at room temperature. Thin layer chromatography (TLC) was carried out on Kieselgel PF_{254} (E. Merck) or Wako Alumina B-10F (Wako) in 0.25 or 0.5 mm thickness. Wakogel C-200 (Wako) was used for column chromatography.

(20S)-Dammaran-20-ol (13). A mixture of (20*S*)-20-hydroxydammaran-3-one[5b] (**20**; 8 g), potassium hydroxide (4 g), hydrazine hydrate (*ca.* 100%; 3.5 g), and diethylene glycol (60 ml) was refluxed for 1.5 h. After removal of excess hydrazine and water, the reaction mixture was heated under reflux for 4 h. It was poured into water and extracted with chloroform five times. The extracts were combined, washed with water and brine, dried over magnesium sulfate, and evaporated to give a residue. The residue was crystallized from methanol to furnish *(20S)-dammaran-20-ol* (**13**; 5.5 g) as

white crystals; mp 86—87 °C (lit,[8] 85 °C); $[\alpha]_D$ +36° (*c* 1.4) (lit,[8] +34.6°); IR (KBr) 3570 and 3450 cm^{-1}; NMR δ 0.81—0.97 (7×Me) and 1.14 (3H, s, $C_{(20)}$-Me); MS *m/e* 415 (M−15; 2), 412 (M−18; 5), 397 (6), 345 (21), 327 (6), 302 (30), 287 (15), 231 (17), and 191 (100); Found: C, 83.39; H, 12.49%. Calcd for $C_{30}H_{54}O$: C, 83.65; H, 12.64%.

Dehydration of (20S)-Dammaran-20-ol (13). Phosphoryl chloride (2 ml) was added portionwise to a solution of (20*S*)-dammaran-20-ol (**13**; 574 mg) in pyridine (20 ml) at 0 °C. After standing overnight at room temperature, the reaction mixture was poured into ice–water and extracted with petroleum ether five times. The combined extracts were washed with 2M hydrochloric acid, water, and with brine, dried over magnesium sulfate, evaporated, and passed through a short column of silica gel to give a residue (511 mg; y. 93%); IR (film) 1630 and 885 cm^{-1}; NMR δ 1.52 (Me–C=CH–), 4.68 (H_2C=C–), and 5.10 (Me–C=CH–).

The residue was chromatographed on a column of silica gel (60 g) impregnated with silver nitrate (10 g) and eluted with petroleum ether (each 50 ml). Frs. 3—6 afforded a mixture (*ca.* 1:1) of (20*R*)- and (20*S*)-dammar-13(17)-enes (**24a** and **24b**; 17 mg, y. 3%; spectral data are registered later), frs. 8—20 a mixture of (*E*)- and (*Z*)-dammar-20(22)-enes (**25a** and **25b**; 357 mg, y. 65%, after crystallization from pentane), and frs. 26—61 gave dammar-20-ene (**26**; 135 mg, y. 25%). *Mixture of (E)- and (Z)-dammar-20(22)-enes (25)*: amorphous solid, IR (film) 1650 and 860 cm^{-1}; NMR δ 1.53 (3H, br. s, Me–C=CH–) and 5.10 (1H, t, J=*ca.* 6 Hz; Me–C=CH–); MS *m/e* 412 (M^+; 17), 397 (5), 380 (4), 328 (21), 313 (8), 299 (8), 286 (21), 273 (12), 259 (25), 231 (46), and 191 (100); MW Found: 412.4216. Calcd for $C_{30}H_{52}$: 412.4066. This mixture was inferred to consist of the (*E*)- and (*Z*)-isomers[29] by silver nitrate-impregnated silica gel TLC examination. However separation into each isomer was unsuccessful. *Dammar-20-ene (26)*: an oil, IR (film) 3060, 1635, and 885 cm^{-1}; NMR δ 0.84—1.00 (7×Me) and 4.70 (2H, br. s, $W_{1/2}$ 3 Hz; H_2C=C–); MS *m/e* 412 (M^+; 14), 397 (6), 380 (2), 342 (8), 327 (4), 300 (6), 299 (6), 286 (9), 259 (7), 239 (6), 231 (42), and 191 (100).

Nordammaran-20-one (23) and Hexanordammaran-20-one (22). The reaction mixture, obtained by dehydration of (20*S*)-dammaran-20-ol (**13**; 11.5 g) was dissolved in dichloromethane (300 ml) and a slow stream of ozone was bubbled through the solution kept at −78 °C for 2.5 h. After standing at room temperature for 1 h, acetic acid (200 ml) and zinc dust (5 g) were added under cooling. The solution was allowed to stand overnight at room temperature, concentrated to half volume, poured into water, and was extracted with ether. Usual work-up furnished a residue (*ca.* 10 g), which was chromatographed on a column of silica gel (950 g) and eluted with the following solvent system: frs. 1—29, petroleum ether; frs. 30—35, petroleum ether–benzene (20:1); frs. 36—69, (15:1); frs. 70—107, (5:1). From frs. 41—68 nordammaran-20-one (**23**; 2.4 g, y. 22%) was eluted and from frs. 72—94 hexanordammaran-20-one (**22**; 3.7 g, y. 40%, after crystallization from methanol) was obtained. 13α*H*-Octanordammaran-17-one[11] (**27**; 32 mg, y. 0.4%) and octanordammaran-17-one[11] (**28**; 155 mg, y. 1.7%) were eluted from frs. 95—100 and frs. 101—107, respectively. *Nordammaran-20-one (23)*: gum, $[\alpha]_D$ +65° (*c* 0.81); IR (film) 1700 cm^{-1}; NMR δ 0.81—1.00 (7×Me); MS *m/e* 414 (M^+; 8), 399 (6), 329 (3), 301 (42), and 191 (100); MW Found: 414.3739. Calcd for $C_{29}H_{50}O$: 414.3858. *Hexanordammaran-20-one (22)*: mp 130—131 °C (lit,[8] 110—130 °C; lit,[10] 121—132 °C); $[\alpha]_D$ +60° (*c* 1.3) (lit,[8] +61.7°; lit.[10] +60°); IR (KBr) 1705 and 1165 cm^{-1}: NMR δ 0.82, 0.87, 0.87, 0.90, and 1.00 (each 3H, s, *t*-Me) and 2.16 (3H, s, -COMe); MS *m/e* 344 (M^+; 7), 329 (9), 305 (60), 231 (4), 219 (9), 205 (13), and 191 (100); Found: C, 83.66; H, 11.90%. Calcd for $C_{24}H_{40}O$: C, 83.65; H, 11.70%.

Grignard Reaction of Nordammaran-20-one (23) with Methyl Iodide. An ethereal solution of methylmagnesium iodide was prepared from magnesium (300 mg) and methyl iodide (1.5 g) in dry ether under a nitrogen atmosphere. To this solution was added at room temperature a solution of nordammaran-20-one (**20**; 466 mg) in ether (8 ml). The mixture was stirred at reflux temperature for 1 h and then at room temperature for 2 h. After decomposition by addition of saturated ammonium chloride solution, the reaction product was extracted with ether. The organic solution was washed with water, 5% sodium hydrogencarbonate solution and then with brine and dried over magnesium sulfate. The solvent was removed to give a residue, which was chromatographed over silica gel. On elution with petroleum ether–benzene (5:1), (20*S*)-dammaran-20-ol (**13**; 106 mg) and (20*R*)-dammaran-20-ol (**14**; 233 mg) were obtained.

Grignard Reaction of Hexanordammaran-20-one (22) with 4-Methylpentyl Bromide. To the Grignard reagent prepared from 4-methylpentyl bromide (bp 146—149 °C; 1.5 g) and magnesium in dry tetrahydrofuran was added hexanordammaran-20-one (**22**; 340 mg) in tetrahydrofuran. The whole was heated under reflux for 30 min and stirred 3 h at room temperature. The same treatment as mentioned above afforded (20*S*)-dammaran-20-ol (**13**; 108 mg) and (20*R*)-dammaran-20-ol (**14**; 80 mg), together with the starting material (**22**; 13 mg) and an unidentified olfin mixture (114 mg). *(20S)-Dammaran-20-ol (13)*: mp 86—87 °C. Other physical and spectral data are given above. *(20R)-Dammaran-20-ol (14)*: Amorphous solid, $[\alpha]_D$ +32° (*c* 2.0); IR (KBr) 3600 and 3460 (br) cm^{-1}; NMR δ 0.80—0.96 (7×Me) and 1.11 (3H, s, $C_{(20)}$-Me); MS *m/e* 412 (M—18) and 191 (base peak); High resolution MS *m/e* 412.3978. Calcd for $C_{30}H_{52}$ ($M-H_2O$): 412.4066.

Acid-catalyzed Dehydration of (20S)-Dammaran-20-ol (13).

i) With Boron Trifluoride Etherate in Benzene: To a solution of (20*S*)-dammaran-20-ol (**13**; 10 mg) in anhydrous benzene (0.5 ml), boron trifluoride etherate (1 ml) was added at room temperature with stirring. After 15 min, 10% sodium hydrogencarbonate solution was added to the reaction mixture, which was extracted with benzene. The benzene extract was washed with 10% sodium carbonate solution, water, and then with brine and evaporated after drying over magnesium sulfate. The residue was subjected to separation by preparative TLC (SiO_2–$AgNO_3$; developed with petroleum ether) to give a mixture (10.3 mg; R_f *ca.* 0.7) of (20*R*)- and (20*S*)-dammar-13(17)-enes (**24a** and **24b**) as a main product. *(20R)- and (20S)-Dammar-13(17)-enes (24a and 24b)*: an oil; IR (film) 1460, 1380, and 1360 cm^{-1}; NMR δ 0.80—0.88 (6×Me), 0.90 (*ca.* 1.5H, d, J=7 Hz; $C_{(20)}$-Me of **24b**)[16], 0.94 (*ca.* 1.5H, d, J=7 Hz; $C_{(20)}$-Me of **24a**)[16], and 1.08 (3H, s, *t*-Me), neither olefinic proton nor olefinic methyl signal was observed; MS *m/e* 412 (M^+), 397, 327, 299, 220, 205, and 191 (base peak); and GLC examination showed that the mixture consisted of **24a** (R_t 4.8 min) and **24b** (R_t 5.2 min) in a ratio of *ca.* 1:1 [column: SE 30 (0.7 %), 1.5 m; column temperature: 250 °C; carrier gas flow rate: N_2, 27 ml/min].

ii) With Boron Trifluoride Etherate in Dichloromethane: A solution of **13** (19 mg) in dichloromethane (3 ml; purified by passing through a column of Al_2O_3) was treated with boron trifluoride etherate (1 ml) at room temperature for 15 min with agitation. Usual treatment gave the same mixture (**24a** and **24b**; 11 mg), whose IR and NMR spectra were identical with those of the specimen above obtained.

iii) With Boron Trifluoride Etherate in Acetic Acid: A solution of **13** (9.5 mg) in acetic acid (2 ml) was treated with boron trifiuoride etherate (0.7 ml) at room temperature for 15 min with stirring. The same reaction products (**24a** and **24b**) were obtained quantitatively after usual treatment.

iv) With Stannic Chloride in Benzene: To a solution of **13** (10.8 mg) in anhydrous benzene (1 ml) was added anhydrous stannic chloride (*ca.* 0.3 ml) with stirring at room temperature for 20 min. After the same treatment, the same reaction mixture (**24a** and **24b**; 9.7 mg) was obtained.

v) With Picric Acid in Nitromethane: To a solution of **13** (11 mg) in nitromethane (1 ml; dried over calcium chloride) containing 5 drops of dichloromethane, was added a solution of picric acid (12.8 mg) in nitromethane (1 ml) with stirring at room temperature for 8 days. Usual treatment gave a residue, which was chromatographed over silica gel. Fractions eluted with petroleum ether were combined and subjected to separation by preparative TLC (SiO_2–$AgNO_3$; developed with petroleum ether). As amain product the same hydrocarbon mixture (**24a** and **24b**; 5.1 mg) was obtained. The formation of dammar-20-ene (**26**) and dammar-20(22)-ene (**25**) was also shown by TLC.

vi) With Sulfuric Acid in Acetic Acid. A solution of **13** (13.1 mg) in glacial acetic acid (2 ml) containing sulfuric acid (1M; 0.2 ml) was heated under reflux for 2 h. After cooling, the reaction mixture was poured into ice–water and extracted with petroleum ether. The organic layer was worked up in a usual manner to yield the same reaction product (**24a** and **24b**). The formation of **25** and **26** was also observed.

vii) With Formic Acid in Acetone. A solution of **13** (6.1 mg) in acetone (3 ml) containing formic acid (99%, 0.5 ml) was heated under reflux for 17 h. The reaction mixture was treated as usual to give a residue, which was subjected to separation by preparative TLC (SiO_2–$AgNO_3$). A mixture of (20*R*)- and (20*S*)-dammar-13(17)-enes (**24a** and **24b**; 1.2 mg), dammar-20(22)-ene (**25**; 2.1 mg), and dammar-20-ene (**26**; 0.3 mg) were isolated.

Acid-catalized Dehydration of (20R)-Dammaran-20-ol (14). (20*R*)-Dammaran-20-ol (**14**) was treated with acids at room temperature under conditions described below and the reaction mixture was worked up as in the case of **13**. In each case, a mixture of (20*R*)- and (20*S*)-dammar-13(17)-enes (**24a** and **24b**) was obtained as a main product: i) A solution of **14** (15.7 mg) in anhydrous benzene (0.5 ml) with boron trifluoride etherate (1 ml) for 15 min; ii) A solution of **14** (12.2 mg) in dichloromethane (2 ml) with boron trifluoride etherate (1 ml) for 15 min; iii) **14** (7.7 mg) with trifluoroacetic acid (1 ml) for 20 min.

Mixture of (20R)- and (20S)-Dammar-13(17)-enes (24a and 24b). A mixture of isoeuphenyl acetate (**35a** and isotirucallenyl acetate (**35b**) was prepared from a mixture of euphol (**36a**) and tirucallol (**36b**) according to the known procedures.[15] Alkaline hydrolysis, Jones oxidation, and successive Huang-Minlon reduction of this mixture (**35a** and **35b**; 36 mg) by the usual manner gave a mixture (*ca.* 1: 1) of (20*R*)- and (20*S*)-dammar-13(17)-enes (**24a** and **24b**; 5.5 mg), which was identical (IR, MS, and TLC) with a specimen (*vide supra*) obtained by acid-catalyzed rearrangement of (20*S*)- and (20*R*)-dammaran-20-ols (**13** and **14**). The NMR spectra of these specimens (derived from **35**, **13**, and **14**) were virtually identical in respect to numbers of signals and their δ-values except their relative intensities.

Pentanordammar-20(22)-ene-22-carbonitrile (37). Sodium hydride (50%; 297 mg) and dry dimethoxyethane (*ca.* 10 ml) were placed in a flask and diethyl cyanomethylphosphonate (624 mg) was added with stirring at room temperature under a nitrogen atmosphere. After 30 min hexanordammaran-20-one (**22**; 493 mg) in dry dimethoxyethane (*ca.* 5 ml) was added to the solution of the anion and stirring was continued for 18 h. The reaction mixture was poured into water and extracted with ether five times. The organic layer was washed with 2M hydrochloric acid, water, and brine. After drying over magnesium sulfate, the solvent was removed to give a residue, which was crystallized from petroleum ether–ether to yield a white crystalline product (164 mg) of (*E*)-pentanordammar-20(22)-ene-22-carbonitrile (**37a**). The mother liquor was subjected to separation by column chromatography on silica gel (100 g; elution with benzene) and by preparative TLC to furnish the additional (*E*)-isomer (**37a**; 315 mg, recrystallized from petroleum ether; total 479 mg, y. 91%) and (*Z*)-isomer (**37b**). *(E)-Pentanordammar-20(22)-ene-22-carbonitrile (37a)*: mp 179—180 °C; IR (KBr) 2200, 1615, and 815 cm^{-1}; NMR δ 1.99 (3H, d, J=1 Hz; Me–C=CHCN) and 5.09 (1H, br. s, $W_{1/2}$ 3 Hz; Me–C=CHCN)[19]; MS *m/e* 367 (M^+; 68), 352 (45), 231 (37), 191 (100), and 137 (92); Found: C, 84.77; H, 11.04; N, 3.79%. Calcd for $C_{26}H_{41}N$: C, 84.95; H, 11.24; N, 3.81%. *(Z)-Pentanordammar-20(22)ene-22-carbonitrile (37b)*: amorphous solid; NMR δ 1.82 (3H, d, J=1 Hz, Me–C=CHCN) and 5.09 (1H, br. s, $W_{1/2}$ 3 Hz; Me–C=CHCN).[19]

Methyl (E)- and (Z)-Tetranordammar-20(22)-en-23-oates (38a and 38b). (*E*)-Pentanordammar-20(22)-ene-22-carbonitrile (**37a**; 315 mg) and potassium hydroxide (2 g) in ethylene glycol (80 ml) were refluxed under a nitrogen atmosphere for 6.5 h. The reaction mixture was poured into ice-water and extracted with chloroform four times. After usual work-up, a residue, without purification, was dissolved in ether and treated with diazomethane at 0 °C for 4 h. Usual work-up gave a residue, which was chromatographed on a column of silica gel (100 g). Solvent system (petroleum ether–benzene, 10: 1—10: 2) was used for elution (each 50 ml). Frs. 21—30 gave an (*E*)- and (*Z*)-mixture (195 mg) and frs. 31—40 afforded the (*E*)-isomer (16 mg). The mixture was further separated by preparative TLC into each isomer. The (*E*)-isomer was combined with the crops (16 mg) above obtained, and recrystallized from methanol to give *methyl (E)-tetranordammar-20(22)-en-23-oate* (**38a**; 41 mg), mp 87.5—88 °C; IR (film) 1720, 1635, and 860 cm^{-1}; NMR δ 2.10 (3H, d, J=1 Hz; Me–C=CH–), 3.68 (3H, s, –COOMe), and 5.67 (1H, br. s, $W_{1/2}$ 3H; Me–C=CH–); MS *m/e* 400 (M^+; 7), 385 (4), 369 (3), 231 (32), and 191 (100); Found: C, 80.75; H, 11.35%. Calcd for $C_{27}H_{44}O_2$: C, 80.94; H, 11.07%. The (*Z*)-isomer fraction was crystallized from methanol to afford 41 mg of *methyl (Z)-tetranordammar-20(22)-en-23-oate (38b)*; mp 174—174.5 °C; IR (KBr) 1720, 1630, and 855 cm^{-1}; NMR δ 1.82 (3H, d, J=1 Hz; Me–C=CH–), 3.66 (3H, s, –COOMe), and 5.69 (1H, q-like, J=1 Hz; Me–C=CH–); MS *m/e* 400 (M^+; 36), 385 (9), 369 (5), 368 (7), 231 (48), and 191 (100); Found: C, 81.00; H, 11.36%. Calcd for $C_{27}H_{44}O_2$: C, 80.94; H, 11.07%.

(E)- and (Z)-Dammar-20(22)-en-23-ones (15a and 15b). Magnesium powder (150 mg) and dry ether (*ca.* 1 ml) were placed in a flask under nitrogen atmosphere. Isobutyl bromide (809 mg) was added with stirring carefully so that the reaction proceeded smoothly at room temperature. After 1 h, ether was distilled off and anhydrous benzene (*ca.* 10 ml) was poured into the Grignard reagent. The (*E*)-α,β-unsaturated carbonitrile (**37a**; 24 mg) in anhydrous benzene (*ca.* 1 ml) was added portionwise to the Grignard solution and stirred at room temperature for 45 min. The solution was refluxed for 6 h and allowed to stand at room temperature overnight. The reaction mixture was poured into a mixture of ice and saturated aqueous ammonium chloride solution, and extracted

with ether three times. The organic layer was washed with water and brine, dried over magnesium sulfate, and evaporated to dryness. The residue was separated by preparative TLC to give (*Z*)-dammar-20(22)-en-23-one (**15b**; 4 mg, y. 14%) and (*E*)-dammar-20(22)-en-23-one (**15a**; 11 mg, y. 40%), respectively. *(Z)-Dammar-20(22)-en-23-one (15b)*: an oil, IR (film) 1685, 1610, and 980 cm^{-1}; NMR δ 1.79 (3H, d, J=1.5 Hz; Me–C=CH–), 2.22 (2H, d, J=2 Hz, –CO–CH_2–CH), and 6.03 (1H, q-like, J=1.5 Hz; Me–C=CH–CO–); MS *m/e* 426 (M^+; 95), 411 (5), 369 (9), 314 (6), 300 (11), 299 (11), 205 (51), 191 (63), 153 (51), and 95 (100); MW Found: 426.3808. Calcd for $C_{30}H_{50}O$: 426.2858. *(E)-Dammar-20(22)-en-23-one (15a)*: an oil, IR (film) 1680 and 1605 cm^{-1}; NMR δ 2.05 (3H, d, J=1 Hz; Me–C=CH–), 2.23 (2H, d, J=1.5 Hz; –CO–CH_2–CH–), and 6.02 (1H, br. s, $W_{1/2}$ 3 Hz; Me–C=CH–CO–); MS *m/e* 426 (M^+; 15), 411 (2), 369 (13), 341 (3), 326 (2), 274 (2), 259 (3), 191 (55), 153 (88), and 95 (100); *MW* Found: 426.3806. Calcd for $C_{30}H_{50}O$: 426.3858.

Acid Treatment of (E)-Dammar-20(22)-en-23-one (15a). To a solution of (*E*)-dammar-20(22)-en-23-one (**15a**; 23 mg) in ethanol (5 ml) was added 8M hydrochloric acid (0.5 ml) and the whole was refluxed for 18 h. The reaction mixture was poured into ice–water and extracted with ether three times. Usual work-up gave a residue, which was separated by preparative TLC to afford (20ξ_1)-dammar-13(17)-en-23-one [(20ξ_1)-**39**; 7 mg] and (20ξ_2)-dammar-13(17)-en-23-one [(20ξ_2)-**39**; 7 mg] as major products. *(20ξ_1)-Dammar-13(17)-en-23-one* [*(20ξ_1)-39*]: an oil, IR (film) 1700 and 1600 cm^{-1}; NMR δ 0.92 (3H, d, J=7 Hz) and 3.06 (1H, m); MS *m/e* 426 (M^+; 11), 411 (3), 341 (8), 326 (34), 311 (6), 299 (10), 297 (11), 284 (31), 245 (7), 234 (26), 221 (42), 191 (100), 121 (85), 85 (57), and 57 (63). *(20ξ_2)-Dammar-13(17)-en-23-one* [*(20ξ_2)-39*]: an oil, IR (film) 1705 cm^{-1}; NMR δ 0.96 (3H, d, J=7 Hz) and 3.03 (1H, m); MS *m/e* 426 (M^+; 9), 411 (2), 341 (9), 326 (26), 311 (5), 299 (6), 297 (8), 284 (21), 245 (6), 234 (28), 221 (42), 191 (100), 121 (82), 85 (64), and 57 (76).

20,21-Epoxydammarane (16). To a solution of dammar-20-ene (**26**; 163 mg) in dichloromathane (10 ml), *m*-chloroperbenzoic acid (214 mg) in dichloromethane (10 ml) was added at 0 °C and the reaction mixture was stirred for 1 h. After 10% aqueous sodium sulfite (3 ml) was added, the mixture was extracted with ether and the organic layer was washed with 10% aqueous sodium carbonate and brine, and dried over magnesium sulfate. The solvent was removed to afford an epoxide (178 mg). This epoxide is extraordinary labile and easily decomposed during storage. *20,21-Epoxydammarane (16)*: an oil, IR (film) 1080, 1040, and 855 cm^{-1}; NMR δ 0.82—0.97 (7×Me) and 2.59 (2H, br. s, $W_{1/2}$ 2 Hz; $C_{(21)}$–H); MS *m/e* 428 (M^+; 20), 413 (5), 410 (12), 395 (5), 380 (7), 343 (6), 300 (27), 205 (31), 192 (62), and 191 (100); MW Found: 428.3969. Calcd for $C_{30}H_{52}O$: 428.4015.

Reduction of 20,21-Epoxydammarane (16) with Lithium Aluminium Hydride. 20,21-Epoxydammarane (**16**; 3.1 mg) was reduced with lithium aluminium hydride in ether under reflux for 1.5 h and left at room temperature overnight. Usual work-up and preparative TLC furnished (20*R*)-dammaran-20-ol (**14**; 1.8 mg) and (20*S*)-dammaran-20-ol (**13**; 1.2 mg).

Dammaran-21-al (40). A solution of 20,21-epoxydammarane (**16**; 25 mg) in dry benzene (5 ml) was treated with boron trifluoride etherate (1 drop) at room temperature for 10 min. After addition of 10% aqueous sodium hydrogencarbonate, usual work-up furnished dammaran-21-al (**40**) as an oil. This aldehyde was also labile. *Dammaran-21-al (40)*: IR (film) 2680 and 1720 cm^{-1}; NMR δ 0.82—0.94 (7×Me), 9.55 and 9.68 (each *ca.* 0.5H, d, J=3 Hz); MS *m/e* 428 (M^+; 2), 413 (3), 300 (32), 285 (6), 205 (15), and 191 (100); *MW* Found: 428.4000. Calcd for $C_{30}H_{52}O$: 428.4015.

20,22-Epoxydammarane (17). To a solution of dammar-20(22)-ene (**25**; 74 mg) in dichloromethane (15 ml), *m*-chloroperbenzoic acid (81 mg) in dichloromethane (10 ml) was added at 0 °C. After stirring for 30 min at 0 °C, 10% aqueous sodium sulfite (10 ml) was added. Extraction with dichloromethane and usual work-up gave an epoxide (75 mg). *20,22-Epoxydammarane (17)*: an oil. IR (film) 980, 880, and 790 cm^{-1}; NMR δ 1.19 ($C_{(20)}$–Me) and *ca.* 2.6 (m, $C_{(22)}$–H); MS *m/e* 428 (M^+; 25), 413 (3), 410 (3), 399 (3), 395 (2), 385 (1), 357 (3), 325 (5), 311 (5), 300 (25), 299 (27), 285 (12), 231 (10), 205 (31), and 191 (100); *MW* Found: 428.4046. Calcd for $C_{30}H_{52}O$: 428.4016. An examination by HPLC revealed that this epoxide consisted of four isomers, one (t_R 11.8 min) of which was the major product (HPLC: μ-PORASIL, 1% ether–hexane, 1.0 ml/min; t_R 9.0, 10.8, 11.8, and 13.7 min).

Treatment of 20, 22-Epoxydammarane (17) with Boron Trifluoride Etherate. 20,22 Epoxydammarane (**17**; 73 mg) in dry benzen (7 ml) was treated with boron trifluoride etherate (0.5 ml) at room temperature for 20 min. The solution was poured into water and extracted with ether. After usual work-up a residue (65 mg) was obtained, which was separated by preparative TLC to afford (20ξ_1)-26,27-dinor-20,24-dimethyldammarane-21-al [(20ξ_1)-**41**; 6 mg], (20ξ_2)-26,27-dinor-20,24-dimethyldammaran-21-al [(20ξ_2)-**41**; 3 mg], and (20ξ)-dammaran-22-one (**42**; 25 mg), together with a small quantity of hydrocarbons. *(20ξ_1)-26,27-Dinor-20,24-dimethyldammaran-21-al* [*(20ξ_1)-41*]: an oil, IR (film) 2660 and 1720 cm^{-1}; NMR δ 9.41 (1H, s, –CHO); MS *m/e* 428 (M^+; 3), 413 (3), 399 (5), 385 (2), 357 (2), 329 (2), 301 (20), 300 (22), 285 (10), 205 (22), 192 (51), and 191 (100); *MW* Found: 428.3951. Calcd for $C_{30}H_{52}O$: 428.4014. *(20ξ_2)-26,27-Dinor-20,24-dimethyldammaran-21-al* [*(20ξ_2)-41*]: an oil, IR (film) 2660 and 1720 cm^{-1}; NMR δ 9.41 (1H, s, –CHO); MS *m/e* 428 (M^+). *(20ξ)-Dammaran-22-one (42)*: an oil, IR (film) 1710 cm^{-1}; NMR δ 0.82—0.95 (7×Me), 1.07 (3H, d, J=7 Hz), and 2.41 (3H, m); MS *m/e* 428 (M^+; 2), 413 (3), 357 (1), 329 (2), 300 (46), 285 (16), 205 (53), 192 (100), and 191 (76); *MW* Found: 428.3942. Calcd for $C_{30}H_{52}O$: 428.4015.

Hexanordammaran-20-ol (18). Hexanordammaran-20-one (**22**; 230 mg) in ethanol was treated with sodium borohydride (107 mg) and allowed to stand at room temperature for 4 h. The excess of the reagent was decomposed by addition of acetic acid, and the reaction mixture was extracted with ether. After usual work-up, the residue was crystallized from ethanol to furnish *a mixture of hexanordammaran-20-ols (18*; 207 mg), mp 116—118.5 °C; IR (film) 3350 (br) cm^{-1}; NMR δ 0.81—0.98 (5×Me), 1.11 and 1.21 (each *ca.* 1.5H, s; $C_{(20)}$-Me), and 3.70 (1H, m, $C_{(20)}$–H); MS *m/e* 346 (M^+; 8), 331 (5), 328 (4), 313 (6), 301 (35), 191 (88), and 109 (100); Found: C, 83.29; H, 12.02%. Calcd for $C_{24}H_{42}O$: C, 83.17; H, 12.22%. This mixture was inferred to consist of the (20*S*)- and (20*R*)-isomers from the NMR data. However, separation into each isomer was unsuccessful.

Dehydration of Hexanordammaran-20-ol (18) with Phosphoryl Chloride. To a solution of hexanordammaran-20-ol (**18**; 36 mg) in pyridine (3 ml), phosphoryl chloride (0.3 ml) was added portionwise at 0 °C. After stirring for 4 h, the solution was poured into ice–water and extracted with ether three times. Usual work-up and separation by preparative TLC gave crude hydrocarbon (**44**; 17 mg) and a chloride mixture (**43**; 10 mg). *Mixture of (20S)- and (20R)-20-Chlorohexanordammaranes (43)*: mp 114—115 °C (crystallized from CH_2Cl_2–MeOH), IR (KBr) 645 cm^{-1}; NMR δ 1.48 (3H, d,

J=7 Hz; $C_{(20)}$–Me) and 3.46 and 4.17 (each *ca.* 0.5H, q-like, J=7 Hz; $C_{(20)}$–H); *MW* Found: 364.3002 and 366.2898 (in a ratio of *ca.* 3:1). Calcd for $C_{24}H_{41}Cl$: 364.2895 and 366.2866. *Crude Hydrocarbon (44)*: an oil, IR (film) 1635, 840, 820, and 810 cm^{-1}; NMR δ *ca.* 5.0 (1H); MS *m/e* 328 (M^+; 28), 313 (13), 299 (8), 205 (44), 192 (77), and 191 (100). This crude hydrocarbon showed one major peak (R_t 4.1 min) accompanied by two minor peaks in GLC analysis (SE-30, 0.7%; 200 °C; N_2 flow rate: 55 ml/min). Crude **44**, without further separation, was subjected to the following reactions.

Oxidation of the Crude Hydrocarbon (44) with Ruthenium Tetraoxide. A solution of the crude hydrocarbon (**44**; 16 mg) in carbon tetrachloride was added to a solution of ruthenium tetraoxide (10 mg) in carbon tetrachloride with stirring and the stirring was continued for 2 h at room temperature. After addition of isopropyl alcohol (0.5 ml), ruthenium dioxide was filtered off and the filtrate was evaporated. The residue was separated by preparative TLC to afford octanordammaran-17-one[11] (**28**; 3.4 mg) as a major product.

Hydroboration of the Crude Hydrocarbon (44). A solution of the crude hydrocarbon (**44**; 7 mg) in dry tetrahydrofuran (2 ml) was treated with diborane in tetrahydrofuran at 0 °C for 40 min and then at room temperature for 30 min. After 10% aqueous sodium hydroxide solution (6 ml) and 30% hydrogen peroxide (3 ml) were added, the solution was allowed to stand at 60 °C for 1 h. Usual treatment gave hexanordammaran-20-ol (**18**) (*vide supra*).

Tosylation of Hexanordammaran-20-ol (18). A solution of hexanordammaran-20-ol (**18**; 422 mg) and *p*-toluenesulfonyl chloride (540 mg) in pyridine (10 ml) was stored in a refrigerator for 20 days. The solution was poured into ice–water and extracted with ether. Usual work-up furnished a residue, which was crystallized from pentane to give *a tosylate* (**46**) as an oil, IR (film) 1190, 1180, 900, 810, and 655 cm^{-1}; NMR δ 2.42 and 2.47 (total 3H, each s, $-OSO_2-C_6H_4Me$), *ca.* 4.26 (1H, dq, J=12 and 6 Hz; Me–CH–OTs), and 7.28 and 7.72; 7.34 and 7.86 (total 4H, each ABq, J=8 Hz; $-OSO_2-C_6H_4Me$).

Treatment of the Tosylate (46) with Silica Gel. The tosylate (**46**) prepared from hexanordammaran-20-ol (**18**; 84 mg) and *p*-toluenesulfonyl chloride (96 mg) in pyridine was passed through a column of silica gel (10 g). Elution with petroleum ether–benzene (10:1) and crystallization from methanol–chloroform gave *hexanordammar-13(17)-ene (45*; 40 mg*)* as a sole product; mp 104—106 °C, IR (KBr) 1630 cm^{-1}; NMR δ 0.93 (3H, t, J=7 Hz; $C_{(21)}$–H) and 1.08 (3H, s, $C_{(14\alpha)}$–Me); MS *m/e* 328 (M^+; 51), 313 (16), 299 (12), 273 (5), 260 (7), 205 (54), 192 (79), and 191 (100); Found: C, 87.66; H, 12.19%. Calcd for $C_{24}H_{40}$: C, 87.73; H, 12.27%.

Pentanordammaran-20-ol (19). To a solution of methylmagnesium iodide prepared from magnesium powder (94 mg) and methyl iodide (400 mg) in dry ether, hexanordammaran-20-one (**22**; 88 mg) was added at room temperature with stirring. After refluxing for 2 h, the reaction mixture was poured into a mixture of ice and saturated aqueous ammonium chloride, and extracted with ether three times. Washing with water and brine, drying over magnesium sulfate, and evaporation gave a residue (73 mg) of *pentanordammaran-20-ol (19)*, mp 138—138.5 °C (crystallized from MeOH), IR (KBr) 3450 cm^{-1}; NMR δ 0.83, 0.86, 0.86, 0.91, and 0.99 (each 3H, s, *t*-Me) and 1.19 (6H, s, Me_2C–OH); MS *m/e* 360 (M^+; trace), 345 (1), 342 (6), 327 (4), 302 (11), 287 (5), 191 (100), and 95 (93); Found: C, 81.08; H, 12.80%. Calcd for $C_{25}H_{44}O \cdot 1/2\ H_2O$: C, 81.23; H, 12.27%.

Dehydration of Pentanordammaran-20-ol (19) with Phosphoryl Chloride. To a solution of pentanordammaran-20-ol (**19**; 19 mg) in pyridine, phosphoryl chloride (27 drops) was added at 0 °C. After stirring at room temperature for 4 h, the solution was poured into ice–water and extracted with ether three times. Usual treatment and separation by preparative TLC (SiO_2–$AgNO_3$) furnished pentanordammar-17(20)-ene (**47**; 11 mg) and pentanordammar-20-ene (**48**; 8 mg). *Pentanordammar-17(20)-ene (47)*: amorphous solid, IR (KBr) 1630 cm^{-1}; NMR δ 0.83, 0.88 (each 6H, s, *t*-Me), 1.00 (3H, s, *t*-Me), and 1.58 (6H, br. s, $Me_2C{=}C-$); MS *m/e* 342 (M^+; 17), 327 (3), 299 (11), 273 (8), 192 (31), 191 (37), 121 (83), and 95 (100); *MW* Found: 342.3285. Calcd for $C_{25}H_{42}$: 342.3284. *Pentanordammar-20-ene (48)*: amorphous solid, IR (KBr) 3060, 1635, and 885 cm^{-1}; NMR δ 0.81, 0.89, 0.99 (each 3H, s, *t*-Me), 0.86 (6H, s, *t*-Me), 1.67 (3H, d, J=1 Hz; Me–C=CH_2), and 4.65 (2H, d, J=1 Hz; Me–C=CH_2); MS *m/e* 342 (M^+; 7), 327 (4), 299 (3), 231 (31), 191 (100), and 95 (65); *MW* Found: 342.3285. Calcd for $C_{25}H_{42}$: 342.3284.

Treatment of Pentanordammaran-20-ol (19) with Boron Trifluoride Etherate. A solution of pentanordammaran-20-ol (**19**: 22 mg) in benzene (3 ml) was treated with boron trifluoride etherate (0.6 ml) at room temperature for 1 h. To the solution was added 10% aqueous sodium hydrogencarbonate solution and the reaction mixture was extracted with ether three times. After usual treatment and separation by preparative TLC (SiO_2–$AgNO_3$), pentanordammar-13(17)-ene (**49**; 9 mg) and pentanordammar-20-ene (**48**; 11 mg) were obtained. *Pentanordammar-13(17)-ene (49)*: amorphous solid, IR (KBr) 1630 cm^{-1}; NMR δ 0.81 (6H, s, *t*-Me), 0.86, 0.87 (each 3H, s, *t*-Me), 0.93, 0.98 (each 3H, d, J=7 Hz; Me_2CH–C=C–), and 1.09 (3H, s, $C_{(14\alpha)}$–Me); MS *m/e* 341 (M^+; 32), 327 (5), 299 (23), 205 (41), 191 (67), 121 (89), and 95 (100); *MW* Found: 342.3432. Calcd for $C_{25}H_{42}$: 342.3284.

The authors wish to thank Professor G. Ourisson, Université Louis Pasteur, Strasbourg, for a generous gift of dipterocarpol, and Professor Y. Hirata and Dr. D. Uemura, Nagoya University, for a kind supply of extracts from *Euphorbia kansui* Liou. The authors are also grateful to Dr. N. Nakamura, the University of Tokyo, for ^{13}C-NMR measurement.

References

1) L. Ruzicka, A. Eschenmoser, and H. Heusser, *Experimentia*, **9**, 357 (1953); A. Eschenmoser, L. Ruzicka, O. Jeger, and D. Arigoni, *Helv. Chim. Acta*, **38**, 1890 (1955).

2) a) D. N. Kirk and M. P. Hartshorn, "Steroid Reaction Mechanisms," Elsevier, Amsterdam, London, New York (1968); b) R. T. Li and Y. Sato, *J. Org. Chem.*, **33**, 3632 (1968); c) M. Leboeuf, A. Cavé, and R. Goutarel, *Bull. Soc. Chim. Fr.*, **1969**, 1628; d) F. B. Hirschmann, D. M. Kautz, S. S. Deshmane, and H. Hirschmann, *Tetrahedron*, **27**, 2041 (1971); e) S. S. Deshmane and H. Hirschmann, *J. Org. Chem.*, **38**, 748 (1973); f) S. Aoyama, K. Kamata, and T. Komeno, *Chem. Pharm. Bull.*, **19**, 1329 (1971).

3) K. I. H. Williams, M. Smulowitz, and D. K. Fukushima *J. Org. Chem.*, **30**, 1447 (1965).

4) H. Hirschmann, F. B. Hirschmann, and A. P. Zala., *J. Org. Chem.*, **31**, 375 (1966).

5) a) J. S. Mills and A. E. A. Werner, *J. Chem. Soc.*, **1955**, 3132; b) J. S. Mills, *ibid.*, **1956**, 2196 and references cited therein.

6) *E.g.* a) J. F. Biellmann. *Tetrahedron Lett.*, **1966**, 4803; J. F. Biellmann, *Bull. Soc. Chim. Fr.*, **1967**, 3459; b) M. Nagai, O. Tanaka, and S. Shibata, *Tetrahedron Lett.*, **1966**, 4797; M. Nagai, O. Tanaka, and S. Shibata, *Chem. Pharm. Bull.*, **19**, 2349 (1971); c) P. Crabbé, G. Ourisson, and T. Takahashi,

Tetrahedron, **3**, 279 (1958); d) J. F. Biellmann, P. Crabbé, and G. Ourisson, *ibid.*, **3**, 303 (1958); e) O. Tanaka, M. Nagai, T. Ohsawa, N. Tanaka, K. Kawai, and S. Shibata, *Chem. Pharm. Bull.*, **20**, 1204 (1972). And references cited therein.

7) *Cf.* N. Iwasaki, K. Okaniwa, S. Okuda, The 94th Annual Meeting of Pharmaceutical Society of Japan, Sendai April, 1974 (Abstracts 5F2-2): 3ξ-Acetoxyoctanordammaran-17-one was derived from dipterocarpol. The formation of 3ξ-acetoxy-16(17→20)abeodammaran-17-one from 3ξ-acetoxy-dammarane-17,20-diol by pinacol rearrangement was announced. However, detailed data have not yet been published.

8) F. G. Fisher and N. Seiler, *Justus Liebigs Ann. Chem.*, **644**, 146 (1961); the alcohol (**13**) and the hexanorketone (**22**) were prepared from betulafolientriol.

9) *Cf.* a) Dammaramediol-II and -I were prepared from 3β-acetoxy-21-nordammaran-20-one: Ref. 6c; b) Dammaranediol-II was synthesized from 3β-acetoxyhexanordammaran-20-one: R. Kasai, K. Shinzo, O. Tanaka, and S. Shibata, *Chem. Pharm. Bull.*, **22**, 1213 (1974).

10) C. S. Barnes, M. N. Galbraith, E. Ritchie, and W. C. Taylor, *Aust. J. Chem.*, **18**, 1411 (1965); the hexanorketone (**22**) was derived from carnaubadiol.

11) O. Tanaka, M. Nagai, and S. Shibata, *Chem. Pharm. Bull.*, **14**, 1150 (1966).

12) N. K. Chaudhuri, J. G. Williams, R. Nickolson, and M. Gut, *J. Org. Chem.*, **34**, 3759 (1969).

13) M. Nagai, T. Ando, O. Tanaka, and S. Shibata, *Tetrahedron Lett.*, **1967**, 3579.

14) S. Murakami, T. Takemoto, and M. Inagaki, *Yakugaku Zasshi*, **75**, 1169 and 1171 (1955).

15) D. Arigoni, R. Viterbo, M. Dünnenberger, O. Jeger, and L. Ruzicka, *Helv. Chim. Acta*, **37**, 2306 (1954); D. Arigoni, O. Jeger, and L. Ruzicka, *ibid.*, **38**, 222 (1955); K. Christen, M. Dünnenberger, C. B. Roth, H. Heusser, and O. Jeger, *ibid.*, **35**, 1756 (1952).

16) D. N. Kirk and P. M. Shaw, *Chem. Commun.*, **1970**, 806.

17) K. B. Sharpless, *J. Am. Chem. Soc.*, **92**, 6999 (1970).

18) E. J. Corey and G. T. Kwaitkowski, *J. Am. Chem. Soc.*, **88**, 5654 (1966); E. J. Corey, I. Vlattas, N. H. Anderson, and K. Harding, *ibid.*, **90**, 3248 (1968).

19) N. K. Chaudhuri and M. Gut, *J. Am. Chem. Soc.*, **87**, 3737 (1965).

20) N. K. Chaudhuri, R. Nickolson, J. G. Williams, and M. Gut, *J. Org. Chem.*, **34**, 3767 (1969).

21) a) In the case of citral a and b, the chemical shift (in $CDCl_3$) of the methyl group in the *cis* position to the aldehyde group is δ 2.16 (d, $J=1.3$ Hz) and that in the *trans* δ 1.98 (d, $J=1.4$ Hz), respectively; M. Ohtsukru, M. Teraoka, K. Tori, and K. Takeda, *J. Chem. Soc. B*, **1967**, 1033; b) In the case of β,β-dimethylacrylic acid, each methyl group in the *cis* and the *trans* position to the carboxyl group resonates at δ 2.18 and δ 1.98, respectively; "High Resolution NMR Spectra Catalog," Varian Assoc. (1962), Vol. 1, 114; c) The proton in the *cis* to the carboxyl group of methyl methacrylate resonates at δ 6.10 and that in the *trans* at δ 5.57; *ibid.*, Vol. 1, 113.

22) D. J. Faulkner, *Synthesis*, **1971**, 175.

23) N. S. Bhacca and D. H. Williams, "Applications of NMR Spectroscopy in Organic Chemistry," Holden-Day, Inc., San Francisco, London, Amsterdam (1964), p. 159.

24) a) K. Bannai, S. Sato, M. Morisaki, and N. Ikekawa, The 96th Annual Meeting of the Pharmaceutical Society of Japan, April, 1976 (Abstracts 5F11-2); b) M. Morisaki, K. Bannai, S. Sato, N. Ikekawa, and M. Shikita, The 20th Symposium on the Chemistry of Natural Products, Sendai, October, 1976 (Symposium Papers, p. 312); c) K. Bannai, M. Morisaki, and N. Ikekawa, *J. Chem. Soc., Perkin Trans, 1*, **1976**, 2116.

25) C.-Y. Byon and M. Gut, *J. Org. Chem.*, **41**, 3716 (1976).

26) M. Koreeda, N. Koizumi, and B. A. Teicher, *Tetrahedron Lett.*, **1976**, 4565.

27) R. Kasai, J. Asakawa, and O. Tanaka, The Annual Meeting of the Pharmacognostical Society of Japan, Chiba, October, 1975 (Abstracts 11-4-3).

28) R. Kasai, M. Suzuo, K. Matsuura, J. Asakawa, K. Yamasaki, O. Tanaka, and S. Yahara, The 20th Symposium on the Chemistry of Natural Products, Sendai, October, 1976 (Symposium Papers, p. 280).

29) *Cf.* M. Koreeda, N. Koizumi, and B. A. Teicher, *J. Chem. Soc., Chem. Commun.*, **1976**, 1035: two stereospecific syntheses of (*Z*)-20(22)-didehydrocholesterol were described.

The Mechanism of NAD(P)H Reduction Reactions

Satoshi INAGAKI and Yoshio HIRABAYASHI

Department of Synthetic Chemistry, Faculty of Engineering, Gifu University, Kakamigahara, Gifu 504

(Received June 25, 1977)

The mechanism of reduction reactions by 1,4-dihydronicotinamides is investigated from the theoretical point of view of the electron configuration and orbital interactions for many systems. The following conclusions are drawn: (1) The reactions are situated near the one-electron-transfer region in the mechanistic spectra dependent on the donor-acceptor property of the reactants; (2) the hydride-equivalent transfers involved, whether concerted or not, proceed more or less in accordance with the nature of the sequential electron-proton-electron shift rather than *via* direct hydride-ion transfer; (3) the paradoxical frontier orbital interaction between the σ-LUMO of C_4–H of 1,4-dihydronicotinamides and the LUMO of substrates is significantly involved in the transfer of the protonic entity. Pseudoexcitation is classified into Type I, where the normal HOMO-LUMO interaction remains important in addition to the LUMO-LUMO and HOMO-HOMO interactions, and Type II, where the HOMO-LUMO interaction contributes little. The NAD(P)H reduction reactions are predicted to belong to Type II.

The roles of nicotinamide-adenine dinucleotide (NAD$^+$) and its phosphoric acid derivative (NADP$^+$), and their reduced form (NAD(P)H) in enzymic oxidation-reduction reactions have been interesting subjects not only in biochemistry, but also in organic chemistry.[1] These coenzymes catalyze similar reactions. Here they can be considered together. The enzymic reactions involve the transfer of a hydride equivalent between the pyridine nucleus in the coenzymes and substrates, generally formulated as in Eq. 1. The reduction reaction is regarded as a special case of further simplified process in which a hydride equivalent is transferred from an allylic position of one molecule to an unsaturated atom of another molecule (Eq. 2).

Theoretically of interest are the fact that no bonds form between the usually very reactive π bonds of 1,4-dihydronicotinamide groups and unsaturated substrates, and the nature of the hydride-equivalent shift. In this paper we shall present a qualitative molecular orbital argument to disclose underlying factors which differentiate the hydride-equivalent shift from the ene reaction (Eq. 3). The mechanism of NAD(P)H reduction reactions is inferred from the theoretical results.

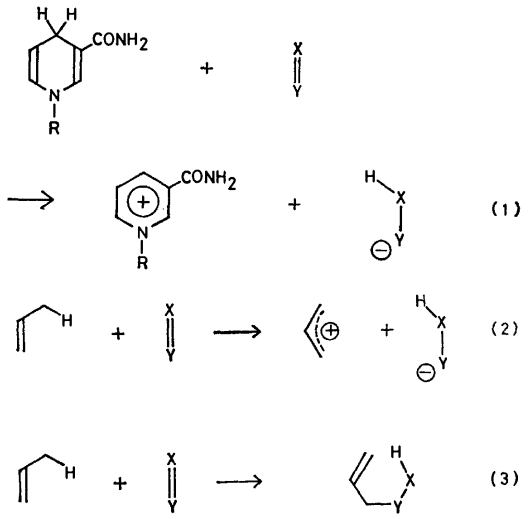

(1)

(2)

(3)

Theoretical

The reaction we are interested in is a bimolecular reaction between electron-donating unsaturated compounds with a reactive σ bond at the allylic position and electron-accepting unsaturated compounds. The weak interaction between the σ bond (M) and the π bond (D) in the donor allows us to suppose our reaction to be a termolecular interaction of M, D, and the acceptor π bond (A).[2,3]

Let the ground-state wavefunction, Ψ, be a linear combination of the electron configurations, Φ_K's, constructed by using the molecular orbitals of each system, *i.e.*,

$$\Psi = \sum_K C_K \Phi_K. \tag{4}$$

The electron density, $\rho(1)$, is then given by

$$\rho(1) = \sum_K C_K^2 \rho_{K,K}(1) + 2\sum_{K>L} C_K C_L \rho_{K,L}(1), \tag{5}$$

$$\rho_{K,K}(1) = n\int \Phi_K^2 dv_2 \cdots dv_n d\sigma_1 \cdots d\sigma_n,$$

$$\rho_{K,L}(1) = n\int \Phi_K \Phi_L dv_2 \cdots dv_n d\sigma_1 \cdots d\sigma_n.$$

Electron delocalization, responsible for the formation of covalent bonds, comes from the HOMO-LUMO interaction or from the mixing of the electron-transferred configuration, D^+A^-, into the initial configuration, DA.[4] The frontier orbital interaction contributes both to stabilizing the system and to accumulating electrons in the intermolecular region where bonds occur.[5] It may be a good approximation in our qualitative arguments to take into consideration the reorganization of the electronic structure due to electron transfer or promotion from HOMO to LUMO.

A further selection of configurations is possible from the point of view of intermolecular electron density. The density fraction, $\rho_{K,K}$, is approximated as the sum of the squares of the occupied orbitals in Φ_K. This term has little to do with the intermolecular electron density. Some $\rho_{K,L}$'s contain a product of two orbitals which belong to different molecules. These terms contribute significantly to the intermolecular density. Such a pair of configurations, K and L, should be obtained from each other by shifting an electron from one molecule to another. Figure 1 displays the configuration pairs (see Appendix).

Suppose that the donor-acceptor property of D and A is less significant. The ground-state wavefunction can then be approximated as a linear combination of

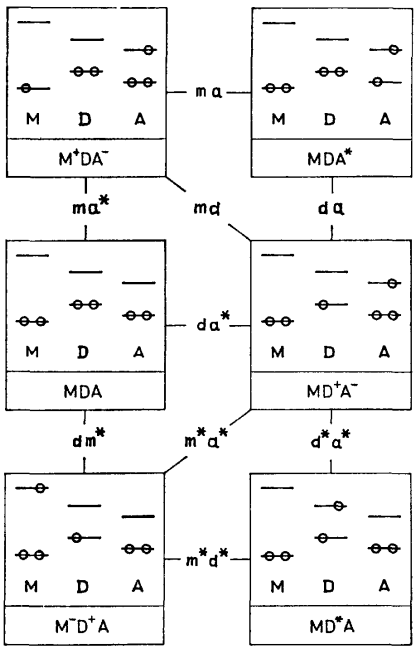

Fig. 1. Electron configuration pairs responsible for intermolecular electron density.

MDA and MD^+A^- (Eq. 6),

$$\Psi \simeq C_{MDA}\Phi_{MDA} + C_{MD^+A^-}\Phi_{MD^+A^-}, (C_{MDA} > C_{MD^+A^-}). \quad (6)$$

The intermolecular density is due to the orbital overlap between d and a*, *i.e.*, the first term in ρ_{MDA,MD^+A^-} (Eq. A7). For this donor-acceptor relation, bond formation neither between M and D nor between M and A is expected, while an attractive interaction gives rise to the association of D and A. The geometrical structure favoring the d-a* interaction was previously shown to be a three-centered interaction such as **1**.[6-8] No reactions of interest are likely to occur.

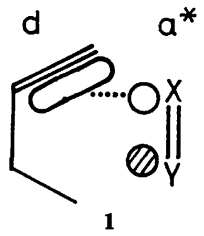

1

Second, let the power of A increase. The energy level of MD^+A^- then lowers and approaches that of MDA so closely that both configurations contribute comparably to the ground-state wavefunction. The comparable contribution of MD^+A^- accompanies an appreciable mixing-in of K's which have a large matrix element with MD^+A^-.[9] The M^+DA^-, M^-D^+A, MD*A, and MDA* configurations are here taken into consideration. The mixing-in of ditransferred configurations, $M^+D^+A^{--}$, $MD^{++}A^{--}$, and $M^-D^{++}A^-$, may be negligible because of the large energetical separation from MDA and MD^+A^-. The ground-state wavefunction is then approximated to be

$$\Psi \simeq C_{MDA}\Phi_{MDA} + C_{MD^+A^-}\Phi_{MD^+A^-} + C_{M^+DA^-}\Phi_{M^+DA^-} + C_{M^-D^+A}\Phi_{M^-D^+A} + C_{MD^*A}\Phi_{MD^*A} + C_{MDA^*}\Phi_{MDA^*}, \quad (7)$$
$$(C_{MDA} \simeq C_{MD^+A^-} > C_{M^+DA^-} \simeq C_{M^-D^+A} \simeq C_{MD^*A} \simeq C_{MDA^*}).$$

The coefficients, C_{MDA} and $C_{MD^+A^-}$, are larger than any others. Of primary concern are the configurations which contribute to the intermolecular density by means of the interactions with MDA or MD^+A^- (Eqs. A7—A13).

The most important interaction remains the one between MDA and MD^+A^- or between d and a*. A favorable geometry must resemble **1**, although the additional interactions singled out above may modify it. Most interesting is the interaction between MD^+A^- and M^+DA^-, since the weights of both configurations increase to a greater extent as the energy levels lower with an increase in the electron-acceptability of A. This interaction delocalizes the electrons from M to D through the m-d overlap (Eq. A10). The removal of the bonding electrons from m results in a weakening of the σ bond. The concurrent bond-lengthening lowers the m* level, increasing the ability of M to accept electrons

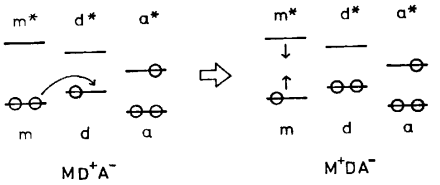

Scheme 1.

(Scheme 1). The M^-D^+A configuration is then allowed to mix effectively. The interaction of M^-D^+A with MD^+A^-, involving the m*-a* overlap (Eq. A11), leads to the structural change from **1** to a transient six-membered-ring state, **2**. As a result, the key orbital interaction occurs among d, a*, and m*. Ene reactions (Eq. 3) take place in this donor-acceptor region.[3]

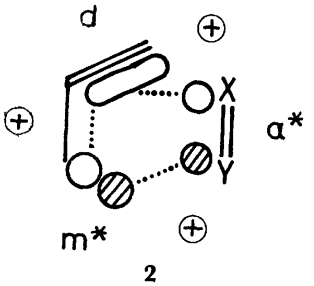

2

Finally, let us discuss the nature of the interaction with the more powerful A. The weights of MD^+A^- and M^+DA^- increase further while the weight of MDA decreases. Consequently, the M^-D^+A configuration contributes to a greater extent. The ground-state wavefunction is then approximated as

$$\Psi \simeq C_{MD^+A^-}\Phi_{MD^+A^-} + C_{M^+DA^-}\Phi_{M^+DA^-} + C_{M^-D^+A}\Phi_{M^-D^+A}, \quad (8)$$
$$(C_{MD^+A^-} > C_{M^+DA^-} \simeq C_{M^-D^+A}).$$

The main configuration is MD^+A^-. The significant interactions are those with MD^+A^-, *i.e.*, the MD^+A^--M^-D^+A and MD^+A^--M^+DA^- interactions. The m*-a* orbital overlap involved in the MD^+A^--

M^-D^+A interaction (Eq. A11) is responsible for the hydride-equivalent transfer, while the d-m orbital overlap involved in the MD^+A^--M^+DA^- interaction (Eq. A10) contributes to π-bond formation between D and M. It should be noted that the ρ_{MDA,MD^+A^-} term predominantly responsible for D-A bonding disappears, since $C_{MDA} \simeq 0$. The extreme stabilization of MD^+A^- disfavors the bond formation between D and A, although D and A are presumably bound through the Coulombic attraction. This difference from the preceding cases characterizes the reactions of powerful A's. The key orbital interaction is illustrated in **3**. The reactions for this donor-acceptor region take place *via* an almost one-electron transfer prior to the transfer of H as a protonic entity, with no σ-bond formation between the π bonds of the reactants.

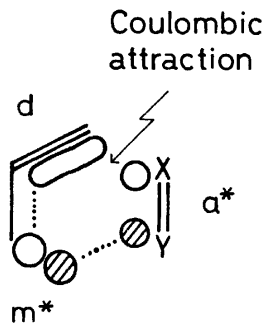

3

It was proposed that the chemical processes significantly involving the HOMO-HOMO (D^+A^--DA*) and/or LUMO-LUMO (D^+A^--D*A) interactions(s) even on the ground-state potential energy surface be termed "pseudoexcitation."[9] Attention was not paid to whether or not the HOMO-LUMO interaction remains important in addition to the HOMO-HOMO and LUMO-LUMO interactions. The pseudoexcitation is here proposed to be classified into Types I and II. Type I involves the HOMO-LUMO interaction significantly, while Type II does not (Fig. 2). The hydride-equivalent shift belongs to Type II (see **3**), while the ene reaction belongs to Type I (see **2**).

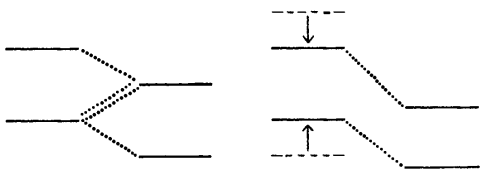

Fig. 2. Pseudoexcitation.

Discussion

From the preceding theoretical arguments on the prototype reaction, it can be suggested that the reduction of unsaturated bonds by 1,4-dihydronicotinamides occurs more or less in accordance with the nature of the sequential electron-proton-electron shift. The hydride-equivalent shift is likely to occur in a concerted manner if the reaction is favored by the donor-acceptor property and other properties. In the transition state, hydrogen migrates as a protonic entity from the cationic dihydronicotinamides to the anionic substrates (**4** and **5**), but not as a hydride anion, as was proposed by Westheimer *et al.*[10]

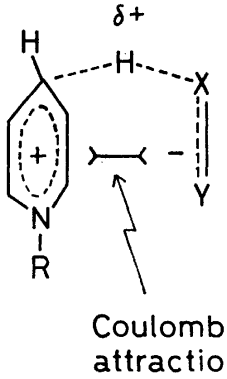

4

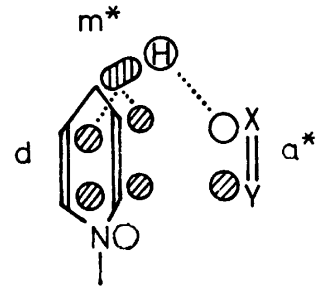

5

When substrates are not such powerful acceptors as to induce the Type II pseudoexcitation, the reactions fall in the Type I pseudoexcitation region. At least one bond forms between the π bonds of dihydronicotinamides and substrates. In fact, acrylonitrile reacts with 1,4-dihydropyridines to give the ene reaction product (Eq. 9),[11] while alkylidene- and arylmethylene-malononitriles are reduced.[12] Another example of the bond formation between the π bonds is the 2+2 cycloaddition reaction with dimethyl acetylenedicarboxylate (Eq. 10).[13]

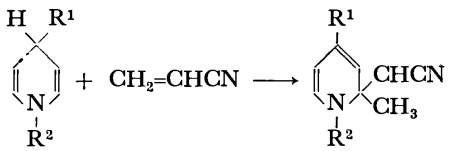

(9)

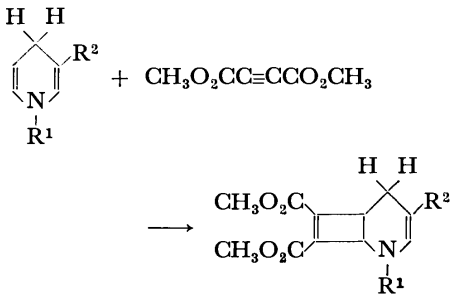

(10)

The hydride-equivalent shift may be intercepted or retarded by a radical ion-pair intermediate when more powerful acceptors are employed, or when reaction conditions—for example, the temperature and solvent, favor the formation and existence of the intermediate. Ohno and Kito[14] employed the ESR spectroscopic technique to demonstrate the nature of the sequential electron-proton-electron shift in the reduction of thiobenzophenone by 1,4-dihydronicotinamide. The ESR signal of the thiobenzophenone anion radical was detected at a low temperature (77K); the signal faded on warming to room temperature, giving rise to a new signal ascribable to the thiyl radical (Eq. 11). The competition between the reduction and the radical

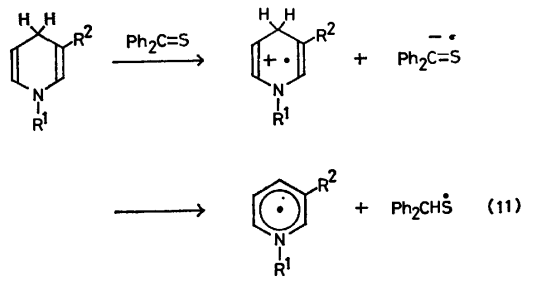

reaction observed by Dittmer and Fouty[15] is understood in terms of two mechanisms near the one-electron transfer region. At least one kinetically important intermediate suggested recently[16,17] is likely to be an ion-radical-pair complex.

Catalysts may affect the reaction course and the efficiency through changing the donor-acceptor property. For example, Lewis acids enhance the electron acceptability of carbonyl compounds by coordination to the carbonyl oxygen. Metal cations were found to assist the reduction of carbonyl compounds.[18-20] This may be explained in terms of the π^* orbital of the carbonyl function being energetically lowered by the positive charge of metal cations.[21] A similar positive-charge effect may also be responsible for the enhanced reactivity of carbonyl groups with an intramolecular hydrogen bond.[10,20,22] The phenolic proton involved provides the carbonyl oxygen with the electrostatic field. In contrast, 1-benzyl-1,4-dihydropyridines were found to be activated by an anionic group in the ortho position of the 1-benzyl substituent.[23] The negative charge may elevate the π-HOMO of the dihydropyridines.

Metal cations can catalyze the reduction reaction in another way, in which the cations are involved in cyclic interaction with dihydronicotinamides and substrates (**6**). In the cyclic interaction the lone-pair orbital on the nitrogen and the C=C bond of dihydronicotinamides are electron-donors, while the C_4–H bond, the unsaturated bond of substrates, and metal cations are acceptors. The orbital-phase requirements for stabilization[2,3] are satisfied if the metal cation provides the cyclic interaction with a low-lying vacant p- or d-orbital. The catalytic reduction should be carefully investigated with this possibility in mind.[24]

Other possible effects of catalysts should also be noted. Some reactions, favored by the donor-acceptor property under uncatalyzed conditions, may be retarded or inhibited if the optimum D-A relation is destroyed by added metal cations which coordinate onto 1,4-dihydronicotinamides or substrates.[25]

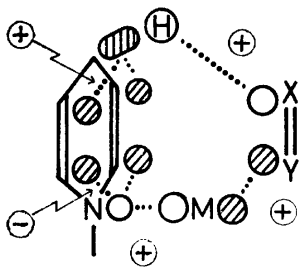

6

The theoretical results suggest that the mechanistic features of the reactions of dihydronicotinamides with unsaturated molecules change from one to another. The reduction mechanism can be predicted to be situated near the one-electron transfer region (Type II pseudo-excitation). Consequently, photochemical and catalytic reactions are expected to be of synthetic utility. A useful acceptor of hydride equivalents, 2,3-dichloro-5,6-dicyano-*p*-benzoquinone,[26] is now available to us. The reagents which are more electron-donating than 1,4-dihydronicotinamides and which are similar in structure are promissing candidates as effective donors of hydride equivalents.

The authors wish to express their thanks to Professor Kenichi Fukui of Kyoto University for his helpful discussion, and to Professor Atsuyoshi Ohno of Kyoto University for his stimulating discussion and for the personal communication of his results prior to publication. The present work was partially supported by a Grant-in-Aid from the Ministry of Education (No. 139012).

Appendix

The configuration functions in Fig. 1 and the electron-density fractions are as follows. The letters, m, d, and a, are used to denote the HOMO's of M, D, and A. The asterisk stand for the LUMO of each system.

$$\Phi_{MDA} = \frac{1}{\sqrt{6!}}|m(1)\bar{m}(2)d(3)d(4)a(5)\bar{a}(6)| \quad (A1)$$

$$\Phi_{MD^+A^-} = \frac{1}{\sqrt{2}\sqrt{6!}}\{|m(1)\bar{m}(2)a^*(3)d(4)a(5)\bar{a}(6)| + |m(1)\bar{m}(2)d(3)\bar{a}^*(4)a(5)\bar{a}(6)|\} \quad (A2)$$

$$\Phi_{M^+DA^-} = \frac{1}{\sqrt{2}\sqrt{6!}}\{|a^*(1)\bar{m}(2)d(3)d(4)a(5)\bar{a}(6)| + |m(1)\bar{a}^*(2)d(3)\bar{d}(4)a(5)\bar{a}(6)|\} \quad (A3)$$

$$\Phi_{M^-D^+A} = \frac{1}{\sqrt{2}\sqrt{6!}}\{|m(1)\bar{m}(2)m^*(3)d(4)a(5)\bar{a}(6)| + |m(1)\bar{m}(2)d(3)\bar{m}^*(4)a(5)\bar{a}(6)|\} \quad (A4)$$

$$\Phi_{MD^*A} = \frac{1}{\sqrt{2}\sqrt{6!}}\{|m(1)\bar{m}(2)d^*(3)d(4)a(5)\bar{a}(6)| + |m(1)\bar{m}(2)d(3)d^*(4)a(5)\bar{a}(6)|\} \quad (A5)$$

$$\Phi_{MDA^*} = \frac{1}{\sqrt{2}\sqrt{6!}}\{|m(1)\bar{m}(2)d(3)d(4)a^*(5)\bar{a}(6)| + |m(1)\bar{m}(2)d(3)d(4)a(5)\bar{a}^*(6)|\} \quad (A6)$$

$$\rho_{MDA,MD^+A^-} = \sqrt{2}\,[da^* + (2m^2+d^2+2a^2)s_{da^*} - ma^*s_{md} - mds_{ma^*} - aa^*s_{da}] + \quad (A7)$$

$$\rho_{MDA,M^+DA^-} = \sqrt{2}\,[ma^* + (m^2+2d^2+2a^2)s_{ma^*} - da^*s_{md} - mds_{da^*} - aa^*s_{ma}] + \quad (A8)$$

$$\rho_{MDA,M^-D^+A} = \sqrt{2}\,[m^*d + (2m^2+d^2+2a^2)s_{m^*d} - m^*as_{da} - das_{m^*a} - mm^*s_{md}] + \quad (A9)$$

$$\rho_{MD^+A^-,M^+DA^-} = -[md + (m^2+d^2+2a^2+a^{*2})s_{md} - 2ma^*s_{da^*} - 2da^*s_{ma^*} - mas_{da} - das_{ma}] + \quad (A10)$$

$$\rho_{MD^+A^-,M^-D^+A} = m^*a^* + (2m^2+d^2+2a^2)s_{m^*a^*} - mm^*s_{ma^*} - aa^*s_{m^*a} + m^*ds_{da^*} + da^*s_{m^*d} \quad (A11)$$

$$\rho_{MD^+A^-,MD^*A} = d^*a^* + (2m^2 + d^2 + 2a^2)s_{d^*a^*} - md^*s_{ma^*} - ma^*s_{md^*} + dd^*s_{da^*} - aa^*s_{d^*a} \quad \text{(A12)}$$

$$\rho_{MD^+A^-,MDA^*} = -[da + (2m^2 + d^2 + a^2 + a^{*2})s_{da} - mds_{ma} - mas_{md} - 2aa^*s_{da^*}] \quad \text{(A13)}$$

References

1) For example see T. C. Bruice and S. J. Benkovic, "Bioorganic Mechanism," Benjamin, Vol. 2, New York, N. Y. (1966), Chap. 9.

2) K. Fukui and S. Inagaki, *J. Am. Chem. Soc.*, **97**, 4445 (1975).

3) S. Inagaki, H. Fujimoto, and K. Fukui, *J. Am. Chem. Soc.*, **98**, 4693 (1976).

4) K. Fukui, *Fortschr. Chem. Forsch.*, **15**, 1 (1970).

5) a) H. Fujimoto, S. Yamabe, and K. Fukui, *Bull. Chem. Soc. Jpn.*, **44**, 2936 (1971); b) K. Fukui, 23rd Intern. Congress of Pure and Applied Chemistry, Butterworths, Vol. 1, London (1971), pp. 65—89.

6) a) S. Inagaki, S. Yamabe, H. Fujimoto, and K. Fukui, *Bull. Chem. Soc. Jpn.*, **45**, 3510 (1972); b) S. Inagaki and K. Fukui, *J. Am. Chem. Soc.*, **97**, 7480 (1975).

7) D. M. Hayes and R. Hoffmann, *J. Phys. Chem.*, **76**, 656 (1972); S. Inagaki and K. Fukui, *Bull. Chem. Soc. Jpn.*, **46**, 2240 (1973).

8) R. Sustman, A. Ansmann, and F. Vahrenholt, *J. Am. Chem. Soc.*, **94**, 8099 (1972).

9) S. Inagaki, H. Fujimoto, and K. Fukui, *J. Am. Chem. Soc.*, **97**, 6108 (1975).

10) R. H. Abeles, R. F. Hutton, and F. H. Westheimer, *J. Am. Chem. Soc.*, **79**, 712 (1957).

11) R. A. Sulzbach and A. F. M. Iqbal, *Angew. Chem.*, **83**, 758 (1971).

12) K. Wallenfels, W. Ertel, and K. Friedrich, *Justus Liebigs Ann. Chem.*, **1973**, 1663.

13) R. M. Acheson, N. D. Wright, and P. A. Tasker, *J. Chem. Soc., Perkin Trans. 1*, **1972**, 2918.

14) A. Ohno and N. Kito, *Chem. Lett.*, **1972**, 369.

15) D. C. Dittmer and R. A. Fouty, *J. Am. Chem. Soc.*, **86**, 91(1964).

16) J. J. Steffens and D. M. Chipman, *J. Am. Chem. Soc.*, **93**, 6694 (1971).

17) a) D. J. Creighton, J. Hajdu, G. Mooser, and D. S. Sigman, *J. Am. Chem. Soc.*, **95**, 6855 (1973); b) J. Hajdu and D. S. Sigman, *ibid.*, **98**, 6060 (1976).

18) a) D. J. Creighton and D. S. Sigman, *J. Am. Chem. Soc.*, **93**, 6314 (1971); b) D. J. Creighton, J. Hajdu, and D. S. Sigman, *ibid.*, **98**, 4619 (1976).

19) Y. Ohnishi, M. Kagami, and A. Ohno, *J. Am. Chem. Soc.*, **97**, 4766 (1975); *Tetrahedron Lett.*, **1975**, 2437.

20) S. Shinkai and T. C. Bruice, *J. Am. Chem. Soc.*, **94**, 8258 (1972); *Biochemistry*, **12**, 1750 (1973).

21) For example, the π-LUMO of acrolein was shown by a SCFMO calculation to be appreciably lowered through the protonation on a lone pair of the carbonyl oxygen [K. Fukui and H. Fujimoto, *Nippon Kagakuseni Koen-shu*, **29**, 27 (1972)]. See also the following papers about the electrostatic-field effects on the electronic structures of molecules: (a) H. Fujimoto and R. Hoffmann, *J. Phys. Chem.*, **78**, 1874 (1974); (b) A. Imamura and T. Hirano, *J. Am. Chem. Soc.*, **97**, 4192 (1975).

22) U. K. Pandit and F. R. Mas Cabre, *Chem. Commun.*, **1971**, 552.

23) J. Hajdu and D. S. Sigman, *J. Am. Chem. Soc.*, **97**, 3524 (1975).

24) A. Ohno, T. Kimura, H. Yamamoto, S. G. Kim, S. Oka, and Y. Ohnishi, *Bull. Chem. Soc. Jpn.*, **50**, 1535 (1977). Magnesium percholate, which accelerates the dihydronicotinamide reduction of methyl benzoylformate, appreciably affects the UV absorption spectra of dihydronicotinamides, but not those of the substrate. This result suggests the possibility that the metal cation does not always activate carbonyl compounds.

25) a) D. C. Dittmer, A. Lombardo, F. H. Batzold, and C. S. Greene, *J. Org. Chem.*, **41**, 2976 (1976); b) A. Ohno, private communication: magnesium percholate retards the reduction of phenyl *t*-butyl thioketone in contrast to that of methyl benzoylformate.[24]

26) H. O. House, "Modern Synthetic Reactions," 2nd ed, Benjamin, Menlo Park, California (1972), pp. 37—44.

A Macrocyclic Enzyme Model System. Deacylation of *p*-Nitrophenyl Carboxylates as Effected by a [20]Paracyclophane Bearing an Imidazole Group†

Yukito MURAKAMI,* Yasuhiro AOYAMA, Masaaki KIDA, and Akio NAKANO

Department of Organic Synthesis, Faculty of Engineering, Kyushu University, Hakozaki, Higashi-ku, Fukuoka 812

(Received July 5, 1977)

The kinetic effect of a [20]paracyclophane bearing an imidazole moiety (**1**) on the deacylation of various *p*-nitrophenyl carboxylates was investigated in 10.9%(v/v) ethanol–1.0%(v/v) dioxane–water of μ 0.10 (KCl) at 40.0±0.1 °C. The facile reaction of **1** with a hydrophobic ester resulted in the accumulation of the N^{Im}-acyl derivative of **1** along the progress of reaction, and the rate of regeneration of **1** (turnover) was negligibly small under present experimental conditions compared to the corresponding acylation rate. The overall feature for deacylation reactions of *p*-nitrophenyl carboxylates bearing a hydrophobic acyl moiety in the presence of **1** is consistent with the reaction scheme which involves the reactions of the monomeric and aggregated forms of **1** with substrate esters. The second-order rate constants for reactions of the monomeric species of **1** with relatively hydrophobic esters exceed considerably the corresponding second-order rate constants for imidazole-catalyzed reactions, suggesting the significant hydrophobic interaction between **1** and each hydrophobic ester. The binding constants (K) for complex formation of a micelle (aggregation number, N) with significantly hydrophobic substrates are greater than 10^5 M^{-1}. The second-order rate constants (k_mK/N) for reactions of the imidazole group of **1** with the long-chain carboxylates in micellar phase are the largest ever achieved for reactions of synthetic 4-substituted imidazoles with *p*-nitrophenyl esters.

Our recent studies have characterized the catalytic functions of [20]paracyclophanes bearing an oxime nucleophile in ester hydrolyses.[1-5] The novel and highly efficient catalysis played by those macrocycles have been attributed to their marked hydrophobic effect, which gives out the proximity effect through formation of a substrate-paracyclophane complex, and nucleophilic-electrostatic bifunctional character acted on the incorporated substrate. In this study, we have prepared an imidazole derivative of [20]paracyclophane (**1**) and investigated its esterase-like activity. Since the present paracyclophane is catalytically active in its neutral form, the aggregation behavior in a mixed aqueous-organic solvent system and its kinetic consequences in deacylation of various *p*-nitrophenyl carboxylates have been clarified.

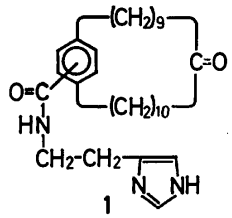

1

Experimental

Vibrational spectra were measured with a JASCO DS-403G grating spectrophotometer. ^{1}H NMR spectra were obtained with either a Varian A-60 or a Bruker WH-90 FT spectrometer and tetramethylsilane (TMS) was used as an internal reference. Fluorescence spectra were recorded on a Shimadzu spectrofluorophotometer RF-500. High speed liquid chromatography for preparative purpose was performed on a Hitachi 635 liquid chromatograph with Hitachi gel 3019. Gel filtration was carried out on a column packed with Sephadex LH-20. Methanol was used as eluant and components eluted were detected by UV absorption at either 254 or 265 nm for both chromatographic techniques.

N-*(Imidazol-4-ylethyl)-10(11)-oxo*[*20*]*paracyclophane-22-carboxamide (1)*. A mixture of 10(11)-oxo[20]paracyclophane-22-carboxylic acid[6] (70 mg) and thionyl chloride (3 ml) was stirred at room temperature for 2 h. Excess thionyl chloride was removed *in vacuo* from the reaction mixture, into which a small amount of dry tetrahydrofuran was added subsequently with stirring. The mixture was evaporated *in vacuo* to give the acid chloride. A tetrahydrofuran solution (15 ml) of the acid chloride was added at room temperature in a period of 1 h to a mixture of histamine dihydrochloride (300 mg) and sodium hydroxide (500 mg) in water (20 ml) with vigorous stirring, and stirring was continued for another 6.5 h. Then, the mixture was poured into water (50 ml) and extracted with ether (50 ml×6). The ether extract was washed with 50 ml of water, dried over sodium sulfate and evaporated. The crude product was extracted with methanol, and then purified by means of repeated preparative liquid chromatography and gel filtration chromatography to afford **1** as an oil; yield 25%. IR (neat): 1718 (ketone C=O str.), 1640 (amide C=O str.), and 1530 cm^{-1} (NH bend. and C–N str.). NMR (CD_3OD, TMS): δ 7.71 and 6.98 (both s, H's on imidazole ring), 7.18 (s, meta and para H's relative to the amide substituent on benzene ring), 7.13 (s, H ortho to the amide on benzene ring), 3.62 (t J=7 Hz, $C\underline{H}_2CH_2NHCO$ or $CH_2C\underline{H}_2NHCO$), 3.1—2.1 (complex m, CH_2CO, benzyl protons, and $CH_2C\underline{H}_2NHCO$ or $C\underline{H}_2CH_2NHCO$), and 1.8—1.2 (m, methylene protons). Found: C, 75.02; H, 9.64; N, 7.87%. Calcd for $C_{32}H_{48}N_3O_2$: C, 75.69; H, 9.73; N, 8.27%.

p-*Nitrophenyl Carboxylates*. *p*-Nitrophenyl acetate (**2**), hexanoate (**3**), decanoate (**4**), dodecanoate (**5**), hexadecanoate (**6**), phenylacetate (**12**), and α-naphthoate (**13**) were prepared by condensation of commercially available carboxylic acids or acid chlorides with *p*-nitrophenol. The esters were identified by elemental analyses and spectral measurements before use.

(a) p-*Nitrophenyl Cyclohexanecarboxylate (7)*: A mixture of cyclohexanecarbonyl chloride (6.5 g) and *p*-nitrophenol (5.0 g), magnesium ribbon (45 mg), and a small amount of iodine in dry benzene (20 ml) was refluxed for 4 h. After cooling down to room temperature, the organic layer was

† Contribution No. 440 from this Department.

* To whom correspondence should be addressed.

separated, washed successively with cold water, saturated aqueous sodium bicarbonate, and cold water, and dried over sodium sulfate. The organic layer was then evaporated *in vacuo* and the residue was distilled; bp 174 °C/0.7 mmHg, yield 6.8 g (62%). NMR ($CDCl_3$, TMS): δ 8.21 and 7.21 (ABq J=9 Hz, aromatic H's), and 2.85—1.00 (m, H's on cyclohexane ring). Found: C, 62.75; H, 6.16; N, 5.40%. Calcd for $C_{13}H_{15}NO_4$: C, 62.64; H, 6.06; N, 5.61%.

(b) p-*Nitrophenyl Cyclohexylacetate (8)*: The ester was prepared in a similar manner from cyclohexylacetyl chloride; yield 57%. NMR ($CDCl_3$, TMS): δ 8.23 and 7.23 (ABq J=9 Hz, aromatic H's), 2.46 (distorted d J=7 Hz, CH_2CO), and 1.70, 1.29, and 1.15 (m, H's on cyclohexane ring). Found: C, 63.77; H, 6.51; N, 5.34%. Calcd for $C_{14}H_{17}NO_4$: C, 63.86; H, 6.50; N, 5.32%.

(c) p-*Nitrophenyl α-Cyclohexylpropionate (9)*: The Reformatsky reaction of cyclohexanone (4.0 g) with methyl α-bromopropionate (6.0 g), which has been carried out under standard conditions,[7] gave *1-(1-methoxycarbonylethyl)cyclohexan-1-ol* (**14**; R^1=CH_3, R^2=H, n=6); bp 78—81 °C/2 mmHg, yield 52%. NMR ($CDCl_3$, TMS): δ 3.68 (s, OCH_3), 2.50 (q J=7 Hz, methine proton), 2.17—1.24 (broad s centered at 1.47, H's on cyclohexane ring and OH), and 1.17 (d J=7 Hz, $CHC\underline{H}_3$). The hydroxy ester was then dehydrated to give the unsaturated ester. The hydroxy ester (20 g) was added to a cold solution of thionyl chloride (30 ml) in benzene (50 ml) containing pyridine (15 ml) at 0 °C. The mixture was allowed to stand at room temperature for a half hour and poured into ice water (200 ml). The organic layer was separated, washed with water, dried over sodium sulfate, and evaporated *in vacuo*, and then the residue was distilled to afford *methyl α-(1-cyclohexenyl) propionate* (**15**; R^1=CH_3, R^2=H, n=6); bp 56.5 °C/1 mmHg, yield 80%. NMR ($CDCl_3$, TMS): δ 5.52 (broad s, CH=C), 3.62 (s, OCH_3), 3.01 (distorted q J=7 Hz, methine proton), 1.95 and 1.56 (m, H's on cyclohexane ring), and 1.22 (d J=7 Hz, $CHC\underline{H}_3$). Methyl α-(1-cyclohexenyl)propionate (14.6 g) in ethyl acetate (100 ml) was hydrogenated in an autoclave at 28 °C with 10% palladium carbon (2.0 g) as catalyst, initial hydrogen pressure being adjusted at 50 kg/cm². The catalyst was removed by filtration through celite 545 (Wako Pure Chemicals, Ltd.). The solvent was removed *in vacuo* and the residue was distilled to afford *methyl α-cyclohexylpropionate* (**17**; R^1=CH_3, R^2=H, n=6); bp 93—96 °C/15 mmHg, yield 69%. NMR ($CDCl_3$, TMS): δ 3.65 (s, OCH_3), 2.22 (distorted q J=7 Hz, methine proton), 1.65 and 1.11 (m, H's on cyclohexane ring), and 1.12 (d J=7 Hz, $CHC\underline{H}_3$). The methyl ester (10.0 g) was saponified with sodium hydroxide (15.0 g) in 50%(v/v) aqueous methanol (40 ml) to give *α-cyclohexylpropionic acid*, and recrystallized from ethyl acetate, mp 60.5—62.5 °C, yield 95%. Found: C, 69.14; H, 10.32%. Calcd for $C_9H_{16}O_2$: C, 69.19; H, 10.29%. The acid was treated with thionyl chloride to give the acid chloride (bp 84—86 °C/9 mmHg, yield 70%), which was converted to the corresponding *p*-nitrophenyl ester (**9**) in a manner as described above; bp 130 °C/0.05 mmHg, yield 57%. NMR ($CDCl_3$, TMS): δ 8.25 and 7.25 (ABq J=9 Hz, aromatic H's), 2.48 (distorted q J=7 Hz, $C\underline{H}CH_3$), 1.70 (m, H's on cyclohexane ring), and 1.26 (d J=7 Hz, $CHC\underline{H}_3$). Found: C, 65.13; H, 6.96; N, 4.96%. Calcd for $C_{15}H_{19}NO_4$: C, 64.96; H, 6.90; N, 5.05%.

(d) p-*Nitrophenyl 3,5-Dimethylcyclohexylacetate (10)*: The ester was obtained by a preparative procedure similar to that described for **9**. The Reformatsky reaction of ethyl bromoacetate with 3,5-dimethylcyclohexanone obtained by oxidation of 3,5-dimethylcyclohexanol with sodium dichromate afforded the corresponding hydroxy ester (**14**; R^1=H, R^2=CH_3, n=6); bp 92—95 °C/0.5 mmHg yield 32%. NMR (CCl_4, TMS): δ 4.12 (q J=7 Hz, $C\underline{H}_2CH_3$), 3.29 (s, OH), 2.45 and 2.33 (both s, CH_2CO), 1.76 and 1.59 (m, H's on cyclohexane ring), 1.27 (t J=7 Hz, $CH_2C\underline{H}_3$), and 0.86 (distorted d J=6.5 Hz, CH_3's on cyclohexane ring). Found: C, 67.22; H, 10.27%. Calcd for $C_{12}H_{20}O_3$: C, 67.24; H, 10.37%. The hydroxy ester was dehydrated to give *3,5-dimethyl-1-ethoxycarbonylmethyl-1-cyclohexene* (**15**; R^1=H, R^2=CH_3, n=6) and *ethyl 3,5-dimethylcyclohexylideneacetate* (**16**; R^1=H, R^2=CH_3, n=6) in a ratio of 1.6: 1 as judged by the NMR spectrum; bp 92—94 °C/4.5 mmHg, total yield 87%. NMR (CCl_4, TMS): δ 5.47 (s, C=CH–CO for **16**), 5.27 (broad s, CH=C for **15**), 4.06 (q J=7 Hz, $C\underline{H}_2CH)_3$, 2.80 (s, CH_2CO for **15**), 2.12 and 1.72 (m, H's on cyclohexane ring), 1.24 (t J=7 Hz, $CH_2C\underline{H}_3$), and 0.96 (distorted d J=6 Hz, CH_3's on cyclohexane ring). The mixture of unsaturated esters was hydrogenated in ethanol over either 10% palladium carbon or 5% rhodium carbon for 10 h at 80—100 °C and at the initial hydrogen pressure of 100 kg/cm² to give *ethyl 3,5-dimethylcyclohexylacetate* (**17**; R^1=H, R^2=CH_3, n=6), yield 85%. NMR (CCl_4, TMS): δ 4.07 (q J=7 Hz, $C\underline{H}_2CH_3$), 2.30 and 2.05 (both s, CH_2CO), 1.77 and 1.58 (m, H's on cyclohexane ring), 1.25 (t J=7 Hz, $CH_2C\underline{H}_3$), and 0.89 (double d J=2 and 7 Hz, CH_3's on cyclohexane ring). The ester was saponified and treated with thionyl chloride. The resulting acid chloride underwent reaction with *p*-nitrophenol to afford the *p*-nitrophenyl ester (**10**); bp 140 °C/0.2 mmHg, yield (from **17**) 42%. NMR (CCl_4, TMS): δ 8.21 and 7.21 (ABq J=9 Hz, aromatic H's), 2.34 with additional peaks at 2.43 and 2.55 (each s, CH_2CO), 1.97 and 1.63 (m, H's on cyclohexane ring), and 0.90 (d J=6 Hz, CH_3's on cyclohexane ring). Found: C, 65.89; H, 7.31; N, 4.75%. Calcd for $C_{16}H_{21}NO_4$: C, 65.95; H, 7.28; N, 4.80%.

(e) p-*Nitrophenyl Cyclodecylacetate (11)*: The ester was prepared from cyclodecanone[8] in a manner similar to those, described for **8**, **9**, and **10**. NMR (CCl_4, TMS): δ 8.20 and 7.20 (ABq J=9 Hz, aromatic H's), 2.38 (distorted s, CH_2CO), and 1.54 (s, H's on cyclodecane ring). Found: C, 67.43; H, 7.85; N, 4.42%. Calcd for $C_{18}H_{25}NO_4$: C, 67.67; H, 7.90; N, 4.38%. The intermediates obtained in this synthesis were identified as follows. *1-Ethoxycarbonylmethylcyclodecan-1-ol* (**14**; R^1=R^2=H, n=10); bp 125 °C/0.35 mmHg, yield 38%. NMR (CCl_4, TMS): δ 4.18 (q J=7 Hz, $C\underline{H}_2CH_3$), 3.15 (broad s, OH), 2.37 (s, CH_2CO), 1.58 (m, H's on cyclodecane ring), and 1.33 (t J=7 Hz, $CH_2C\underline{H}_3$). *1-Ethoxycarbonylmethyl-1-cyclodecene* (**15**; R^1= R^2=H, n=10) and *ethyl cyclodecylideneacetate* (**16**; R^1= R^2=H, n=10) in a ratio of 3: 1; bp 102—110 °C/7.5 mmHg, total yield 87%. NMR (CCl_4, TMS): δ 5.60 (broad s, C=CH–CO for **16**), 5.26 (t J=8 Hz, CH=C for **15**), 4.06 (q J=7 Hz, $C\underline{H}_2CH_3$), 2.87 (s, CH_2CO for **15**), 2.5—2.0 (m, H_2C–C=C), 1.40 (m, H's on cyclodecane ring), and 1.23 (t J=7 Hz, $CH_2C\underline{H}_3$). Found: C, 73.48; H, 11.54%. Calcd for $C_{14}H_{24}O_2$: C, 74.27; H, 11.60%. *Ethyl cyclodecylacetate* (**17**; R^1= R^2=H, n=10). NMR (CCl_4, TMS): δ 4.07 (q J=7 Hz, $C\underline{H}_2CH_3$), 2.12 (broad s, CH_2CO), 1.51 (s, H's on cyclodecane ring), and 1.23 (t J=7 Hz, $CH_2C\underline{H}_3$).

Kinetic Measurements. Rates of *p*-nitrophenol liberation from *p*-nitrophenyl esters were measured at 400 nm with a Union Giken high sensitive spectrophotometer SM-401 under instrumental conditions; response 2 s and sensitivity 0.02 OD/full scale. Each run was initiated by adding a dioxane solution (30 μl) of *p*-nitrophenyl ester (7.0×10^{-5} M) to a reaction medium (3.0 ml) which was pre-equilibrated at 40.0±0.1 °C in a thermostatted cell set in the spectrophotometer. The reaction medium was prepared by mixing a buffer solution (2.7 ml, buffer concentration 0.01 M) and ethanol (0.3 ml) containing an appropriate amount of **1**. The

ionic strength of kinetic solutions was maintained at 0.10 with KCl.

pH Measurements. pH Measurements were carried out with a Beckman expandomatic SS-2 pH meter equipped with a Metrohm EA-125 combined electrode after calibration with a combination of appropriate aqueous standard buffers.

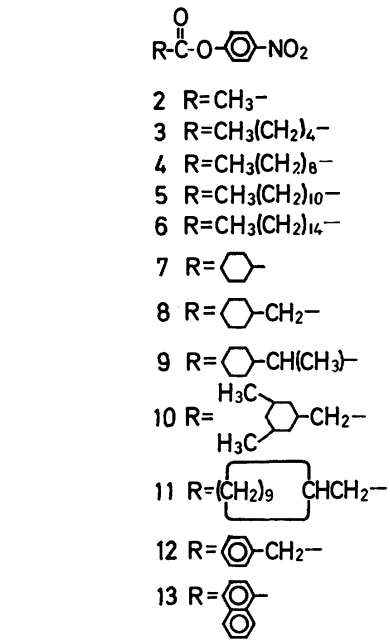

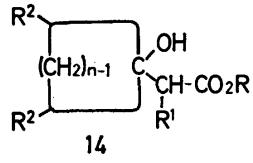

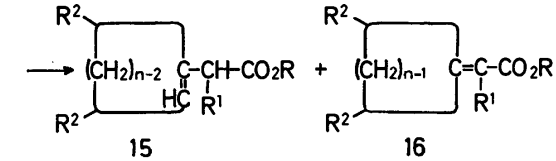

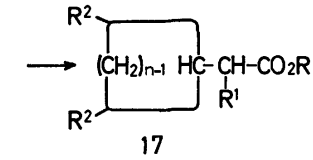

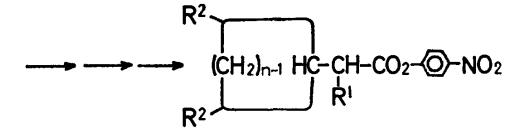

Results and Discussion

The kinetic effect of a [20]paracyclophane bearing an imidazole moiety (**1**) on the deacylation of various *p*-nitrophenyl carboxylates was investigated in 10.9%-(v/v)ethanol-1.0%(v/v)dioxane-water of μ 0.10 (KCl) at 40.0±0.1 °C. Since it is now well known that *p*-nitrophenyl carboxylates bearing a long alkyl chain tend to aggregate above the critical concentrations[9,10] (*e.g.*, 2.0×10^{-6} M for decanoate in 1.0%(v/v) aqueous dioxane at 40 °C),[10] the initial substrate concentrations were adjusted at 7.0×10^{-7} M for most kinetic runs. Although the present paracyclophane is not so much soluble in the above kinetic solvent system, the 5.0×10^{-6} M solution was confirmed to be completely homogeneous in the pH 7—10 range. *p*-Nitrophenyl esters of the present study may be classified into four categories in reference to the extent of rate acceleration brought about by **1** (5.0×10^{-6} M) at pH 8.33 (see Table 1):

Table 1. Pseudo-first-order rate constants for deacylation of *p*-nitrophenyl carboxylates in the absence (k_{hyd}) and presence (k_{obsd}) of **1**[a]

Substrate ester	$k_{hyd}\times10^5/s^{-1}$	$k_{obsd}\times10^4/s^{-1}$	k_{obsd}/k_{hyd}
2	7.8	8.2	1.0
3	3.2	20	6.2
4	2.0	480	240
5	1.4	590	420
6	0.73	680	930
7	1.5	8.3	5.5
8	2.1	9.7	4.6
9	0.18[b]	3.7	20
10	2.0	69	35
11	1.0	170	170
12	17.3	24	1.4
13	1.0	7.9	7.9

a) At 40.0±0.1 °C, pH 8.33 (6.3×10^{-3} M KH_2PO_4—3.7×10^{-3} M $Na_2B_4O_7$), and μ 0.10 (KCl) in 10.9%(v/v) ethanol–1.0%(v/v) dioxane–water; initial substrate concentration, 7.0×10^{-7} M unless otherwise stated; initial concentration of **1**, 5.0×10^{-6} M. b) Initial substrate concentration, 1.0×10^{-5} M.

those having a long alkyl chain (**4**, **5**, and **6**), more than 240-fold acceleration; those having a cyclodecyl moiety or a cyclohexyl moiety with an additional methyl substituent or substituents (**9**, **10**, and **11**), 20—170-fold acceleration; those having a less hydrophobic acyl portion (**3**, **7**, **8**, and**13**), 4—8-fold acceleration; acetate (**2**) and phenylacetate (**12**), the catalytic effect was fairly detected. Thus, the hydrophobic interaction of **1** with an acyl portion of each substrate ester seems to be responsible for the catalytic efficiency. This is evidenced by the effect of ethanol content on the catalytic activity of **1**. As the ethanol content is raised the hydrophobic interaction between **1** and the substrate would be progressively reduced, and consequently the catalytic efficiency of **1** would be lowered. This is what is observed in the deacylation of decanoate (7.0×10^{-7} M) as effected by 5.0×10^{-6} M of **1**: apparent second-order rate constants; 970 in 10%(v/v), 123 in 15%(v/v), 20 in 20%(v/v), and 11 $M^{-1}\,s^{-1}$ in 30%(v/v) aqueous ethanol. Similar effects have been noted elsewhere.[1,10]

The kinetic pK_a value for the deacylation of decanoate (1.0×10^{-6} M) as effected by **1** (5.0×10^{-6} M) was estimated graphically as 6.8 from the pH-rate profile (Fig. 1), which is referred to the acid dissociation of the catalytically active group, imidazole. The facile reaction of **1** with a hydrophobic ester resulted in the

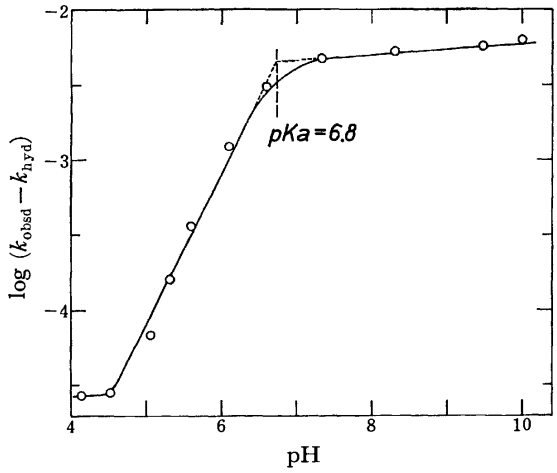

Fig. 1. pH-Rate profile for the deacylation of **4** in the presence of **1** (5.0×10^{-6} M) at 40.0±0.1 °C and μ 0.10 (KCl) in 10.9%(v/v) ethanol–1.0%(v/v) dioxane–water; initial concentration of **4**, 1.0×10^{-6} M. Both k_{obsd} and k_{hyd} are in s^{-1}.

accumulation of the N^{Im}-acyl derivative of **1** along the progress of reaction. The rate of regeneration of **1** (turnover) upon deacylation of the N^{Im}-acyl derivative was negligibly small under present experimental conditions compared to the corresponding acylation rate. With excess substrate ester, the amount of *p*-nitrophenol liberated in the course of reaction increased until it reached a maximal accumulation which exactly corresponds to the amount of **1** used.

Aggregation Behavior. The pseudo-first-order rate constants at pH 8.33 for deacylation of *active esters* are graphically shown in Figs. 2, 3, and 4 as a function of the initial concentration of **1**. In all cases the overall

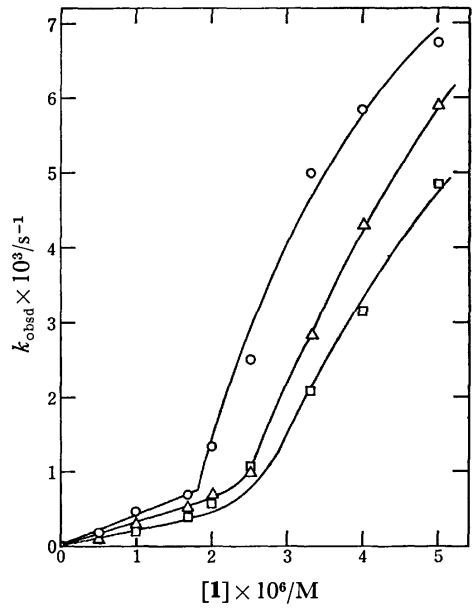

Fig. 2. Correlations of k_{obsd} with the initial concentration of **1** for the deacylation of **4** (□), **5** (△), and **6** (○) at 40.0±0.1 °C, pH 8.33, and μ 0.10 (KCl) in 10.9%-(v/v) ethanol–1.0%(v/v) dioxane–water; initial substrate concentration, 7.0×10^{-7} M.

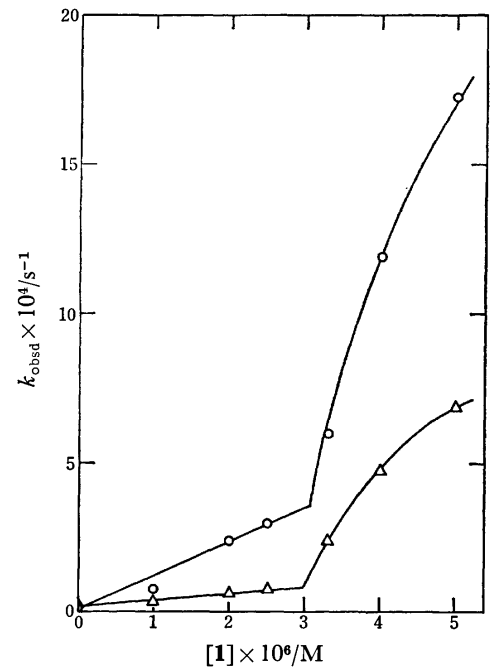

Fig. 3. Correlations of k_{obsd} with the initial concentration of **1** for the deacylation of **10** (△) and **11** (○) at 40.0±0.1 °C, pH 8.33, and μ 0.10 (KC) in 10.9%-(v/v) ethanol–1.0%(v/v) dioxane–water; initial substrate concentration, 7.0×10^{-7} M.

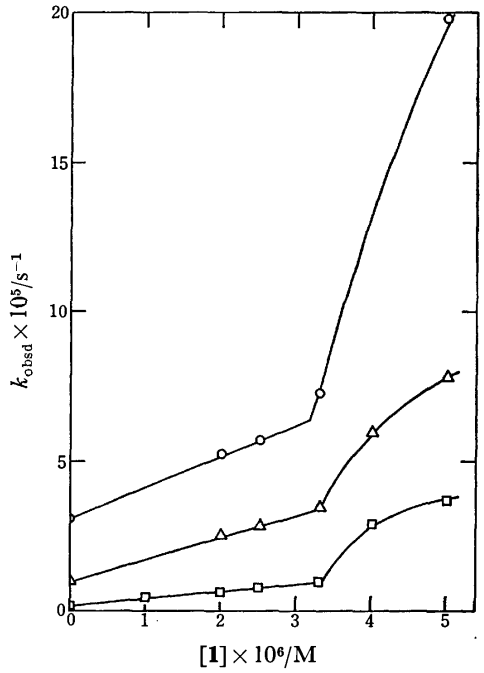

Fig. 4. Correlations of k_{obsd} with the initial concentration of **1** for the deacylation of **3** (○), **9** (□), and **13** (△) at 40.0±0.1 °C, pH 8.33, and μ 0.10 (KCl) in 10.9%(v/v) ethanol–1.0%(v/v) dioxane–water; initial substrate concentration, 7.0×10^{-7} M.

feature is similar to those observed for micelle-catalyzed reactions.[11] The linear portion in a rate-concentration correlation below the break point may correspond to the reaction of the monomeric species of **1**, and a sharp

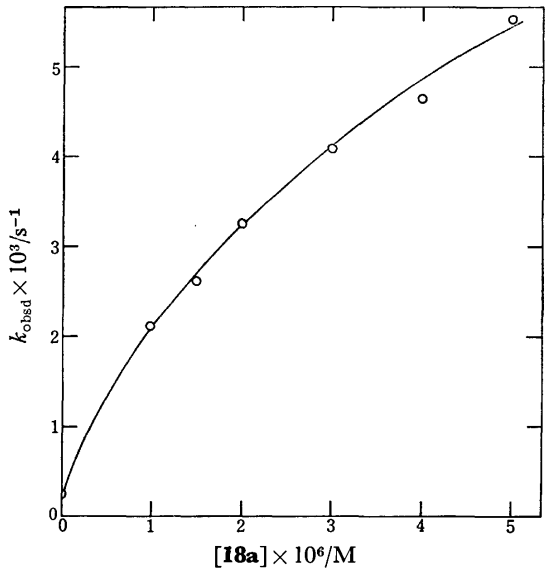

Fig. 5. Saturation-type kinetics for the deacylation of **6** in the presence of **18a** at 40.0±0.1 °C, pH 11.23, and μ 0.10 (KCl) in 10.9%(v/v) ethanol–1.0%(v/v) dioxane–water; initial substrate concentration, 7.0×10^{-7} M.

increase in rate above the break point may be due to aggregation or micellization of **1**. In marked contrast to [20]paracyclophane oximes which are believed to be monomeric under similar conditions,[1,2,4] such a kinetic behavior is rather surprising. Since the previous studies with paracyclophane oximes as catalysts in the deacylation reaction were carried out under conditions where the substrate esters were mostly in aggregated forms, we have re-examined the effect of 10-hydroxy-11-hydroxyimino[20]paracyclophane (**18a**) on the deacylation of *p*-nitrophenyl hexadecanoate at pH 11.23 under the same kinetic conditions as employed here; solvent system, temperature, and the initial substrate concentration (7.0×10^{-7} M) as shown in Fig. 5. The rate constant (k_{obsd}) is smoothly correlated with the initial concentration of **18a** without any break point in contrast to the **1**-catalyzed reaction shown in Fig. 2. Furthermore, the plot of $1/(k_{obsd}-k_{hyd})$ *vs.* 1/[**18a**] yielded a straight line in a manner as observed previously.[1,2,4] It may be concluded, therefore, that there is no abrupt change in physical state of **18a** in the concentration range investigated and its critical micelle concentration (CMC), if any, would be greater than 5.0×10^{-6} M. The difference in CMC between the imidazole and oxime derivatives of [20]paracyclophane may arise at least in part from charge difference between the two catalysts: the anionic hydroxyimino group placed in the catalytically active cyclophane raises CMC significantly relative to the imidazole group in neutral form (**1**). It is generally true that the CMC's of ionic surfactants are larger than those of nonionic ones, both types having similar apolar structures. Comparison of the CMC's of surfactants having a dodecyl or dodecanoyl moiety[12] reveals this point: dodecylammonium chloride (cationic), 1.5×10^{-2} M in water at 25 °C; dodecyltrimethylammonium bromide (cationic), 1.5×10^{-2} M in water at 25 °C; sodium dodecanoate

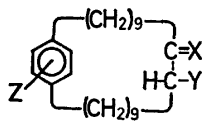

18a X=NOH, Y=OH, Z=H
18b X=O, Y=H, Z=$CH_2N^+(CH_3)_3$ Cl^-

(anionic), 2.4×10^{-2} M in water at 25 °C; polyoxyethylene(6) dodecanol (nonionic), 8.7×10^{-5} M in water at 25 °C; *N,N*-dimethyldodecylamine oxide (nonionic), 2.1×10^{-3} M in water at 27 °C; dodecyldimethylphosphine oxide (nonionic), 5.7×10^{-4} M in water at 30 °C; sucrose dodecanoate (nonionic), 1.9×10^{-4} M in water at 20 °C. Steroid micelles which bear a better resemblance to our paracyclophanes from the structural viewpoint are subject to a charge effect even to a pronounced extent: cholic acid derivatives (anionic), 10^{-3}—10^{-2} M in water at 25 °C;[13-16] and cholesterol (nonionic), $2—4 \times 10^{-8}$ M in water at 25 °C.[17]

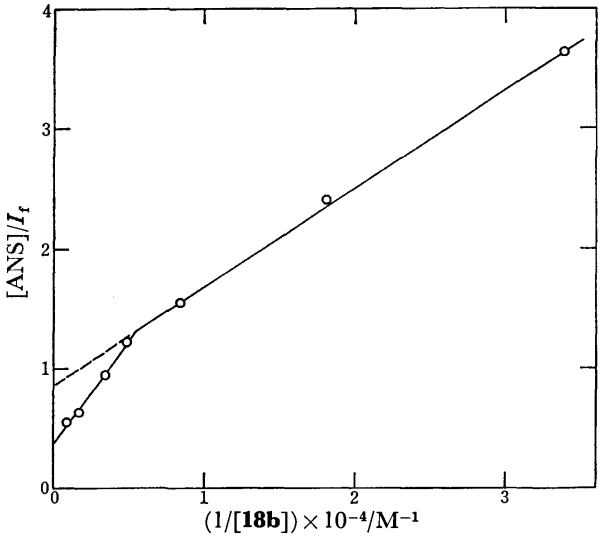

Fig. 6. Analysis of fluorescence spectral data for the interaction of **18b** with ANS (5.0×10^{-5} M) in a buffer solution of pH 8 at 20 °C by means of Eq. 1; I_f, in arbitrary scale.

The proposed charge effect on the CMC's of paracyclophanes is further exemplified by the micellization behavior of the cationic [20]paracyclophane bearing a quaternary ammonium group (**18b**) as investigated by the fluorescence dye technique with 1-anilinonaphthalene-8-sulfonate (ANS) as a probe: concentration of ANS, 5.0×10^{-5} M; excitation wavelength, 384 nm; fluorescence intensity, measured at 468 nm. The relative fluorescence intensity of ANS in a pH 8 buffer at 20 °C increased as the concentration of **18b** was raised in a concentration range of 2.95×10^{-5}—1.18×10^{-3} M. The reciprocal fluorescence intensity ($1/I_f$) is plotted in Fig. 6 as a function of reciprocal concentration of **18b** on the basis of the Benesi-Hildebrand type relationship[18] (Eq. 1) derived under the assumption that only the 1:1 interaction between **18b** and ANS takes place: I_f, observed fluorescence intensity; I_a, fluorescence intensity of ANS bound to the monomeric form of

Table 2. Kinetic parameters for deacylation of *p*-nitrophenyl carboxylates as catalyzed by **1** and imidazole[a)]

Substrate	k_2 ($M^{-1}s^{-1}$)	k_{1m} ($M^{-1}s^{-1}$)	k_2/k_{1m}[b)]	CMC[c)] (M)	k_m (s^{-1})	K/N (M^{-1})	k_mK/N ($M^{-1}s^{-1}$)	k_2(app)[d)] ($M^{-1}s^{-1}$)
2		0.79						0.8
3	10	0.57	18 (13)	3.1×10^{-6}			70	33
4	210	0.44	480 (270)	2.4×10^{-6}	≈0.02	1×10^{5}	2000	970
5	310	0.21	1500 (390)	2.3×10^{-6}	≈0.02	1.3×10^{5}	2600	1200
6	420	0.004	11000 (530)	1.8×10^{-6}	≈0.02	1.5×10^{5}	3000	1400
7		0.44						14
8		0.13						15
9	2.3	0.014	160	3.3×10^{-6}			30	7.0
10	22	0.093	240	3.0×10^{-6}	0.001	5×10^{5}	500	130
11	110	0.075	1500	3.0×10^{-6}	0.005	2×10^{5}	1000	340
12		1.6						14
13	7.5	0.033	230	3.3×10^{-6}			40	14

a) At 40.0±0.1 °C, pH 8.33 (6.3×10^{-3} M KH_2PO_4–3.7×10^{-3} M $Na_2B_4O_7$), and μ 0.10 (KCl) in 10.9%(v/v) ethanol–1.0%(v/v) dioxane–water; initial substrate concentration, 7.0×10^{-7} M. b) Values in parentheses, k_{Im} for acetate (**2**) was taken as the reference value. c) Critical micelle concentration of **1**. d) $k_2(\text{app})=(k_{obsd}-k_{hyd})/[\mathbf{1}]$, $[\mathbf{1}]=5.0\times10^{-6}$ M.

18b; K, binding constant for complex formation between the monomeric form of **18b** and ANS.

$$\frac{[\text{ANS}]}{I_f}=\frac{1}{I_a}+\frac{1}{I_aK[\mathbf{18b}]} \quad (1)$$

The break point, which corresponds to the CMC of **18b**, is observed at 1.8×10^{-4} M as shown in Fig. 6. This CMC value is 50—100 times as large as the substrate-dependent CMC's of **1** (Figs. 2, 3, and 4, and Table 2). The binding constant ($K=1.1\times10^{4}$ M^{-1}) is 190 and 7 times as large as those for β-cyclodextrin and a water-soluble heterocyclophane, respectively.[19)]

The overall feature of deacylation reactions of *p*-nitrophenyl carboxylates in the presence of **1** is consistent with reaction pathways shown in Scheme 1.

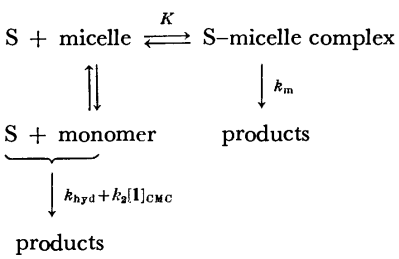

Scheme 1.

The kinetic parameters can be determined by Eq. 2:[11)] k_{hyd}, rate constant for spontaneous hydrolysis; k_2, second-order rate constant for reaction of an ester with the monomeric form of **1**; k_m, first-order rate constant for reaction of an ester in micellar phase; k_{obsd}, observed pseudo-first-order rate constant; K, association constant for formation of the ester–micelle complex; N, aggregation number of the micelle; [**1**], total concentration of **1**; $[\mathbf{1}]_{CMC}$, CMC of **1** which is dependent on the nature of a particular substrate used. The kinetic data for reactions of **4**, **5**, **6**, **10**, and **11** were analyzed by the aid of Eq. 2. Because of the limited solubilities of the reactants as well as relatively higher kinetic CMC's of **1**, the critical evaluation of k_m and K/N values were not performed for reactions of **3**, **9**, and **13** and the apparent second-order rate constants per mole of **1** forming micelles (k_mK/N) were obtained from the rate profiles shown in Fig. 4 by the aid of Eq. 2. For esters **2**, **7**, **8**, and **12** which showed the least affinity with **1**, the apparent second-order rate constants defined by $k_2(\text{app})=(k_{obsd}-k_{hyd})/[\mathbf{1}]$ were evaluated for the purpose of comparison of reactivity with other esters. All the kinetic parameters are summarized in Table 2 along with the second-order rate constants for reactions of the esters with imidazole as a reference.

$$\frac{1}{k_{obsd}-(k_{hyd}+k_2[\mathbf{1}]_{CMC})}=\frac{1}{k_m-(k_{hyd}+k_2[\mathbf{1}]_{CMC})}\times\left\{1+\frac{N}{K([\mathbf{1}]-[\mathbf{1}]_{CMC})}\right\} \quad (2)$$

Catalytic Efficiency. All the esters except acetate (**2**) are subject to profound catalysis by **1**. The second-order rate constants (k_2) for reactions of the monomeric species of **1** with relatively hydrophobic esters exceed considerably the corresponding second-order rate constants for imidazole-catalyzed reactions (k_{Im}), suggesting the significant hydrophobic interaction between **1** and each hydrophobic ester. The k_2/k_{Im} value may be referred to a measure of the extent of hydrophobic interaction. Care should be exercised for the long-chain esters. The hydrophobic coiling of the alkyl chain, which results in masking of the ester carbonyl against an attacking nucleophile,[10)] seems to be responsible for the decrease in k_{Im} in going from decanoate through hexadecanoate. The geometry of the hydrophobic interaction between each of these esters and the monomeric species of **1** is not known at present. If the intramolecular coiling were retained in the transition state of acyl transfer from the ester to **1**, the k_2/k_{Im} values would provide a meaningful comparison of relative catalytic efficiency. However, the esters most plausibly undergo decoiling or elongation before the transition state is reached.[1-5)] The k_{Im} value for acetate which

is free from the coiling effect may be cited as the plausible reference for the evaluation of catalytic efficiency of the monomeric form of **1** as shown in parentheses in Table 2. As expected from the viewpoint of hydrophobic affinity, the k_2/k_{1m} value increases as the alkyl chain of ester is lengthened (**3**<**4**<**5**<**6**). This value also increases in the order **9**<**10**<**11**. This fact may allow to draw the following conclusion; the extent of hydrophobic interaction between the monomeric species of **1** and an ester having an aliphatic ring moiety in its acyl portion may be primarily governed by the surface area[20] or more simply by the number of carbon atoms in the acyl portion of the ester concerned. The aromatic ester, α-naphthoate (**13**), seems less hydrophobic relative to **10** and **11** in the light of k_2/k_{1m} values even though all three esters have comparable number of carbon atoms.

The binding constants for micellar complex formation with **4**—**6**, **10**, and **11** are greater than $10^5\ M^{-1}$. It may be a surprise to see the decrease in K/N in going from **10** to **11** since **11** is expected to be more hydrophobic than **10** judging from the k_2/k_{1m} values for the two esters. This would be cited as an example of substrate selectivity for the binding process. However, we are not certain whether or not the micelle of **1** has the same aggregation number (N) for different substrates. It is reasonable to assume that N is relatively small for hydrophobic macrocycles in a manner as observed for cholic acid derivatives (N=5—22).[16] Under such circumstances, the aggregation number as well as CMC may be significantly dependent on the nature of a particular substrate employed.

The product of micellar reaction rate and binding constants (k_mK) is referred to the second-order rate constant for reaction of a substrate and a micelle, and consequently the k_mK/N value corresponds to the second-order rate constant for the same reaction as evaluated per mole of **1** forming micelles. There is indeed a wide variation in k_mK/N as can be seen in Table 2, and the long-chain carboxylates (**4**—**6**) show the highest values in the 2000—3000 $M^{-1}\ s^{-1}$ range. These values are the largest ever achieved for reactions of synthetic 4-substituted imidazoles with *p*-nitrophenyl esters,[21] and may be comparable to or greater than the second-order rate constant for the acylation of chymotrypsin with *p*-nitrophenyl acetate (410 $M^{-1}\ s^{-1}$ at 25 °C and pH 7.75).[22] The profound catalytic activity of **1** is due primarily to its large binding ability toward the substrates ($K>10^5\ M^{-1}$), since the micellar rate constant (k_m=0.02 s^{-1}) is less than one hundredth of the corresponding rate constant for acylation of the enzyme with the bound acetate (k_m=3.15 s^{-1} at 25 °C).

The authors are grateful to Professor Taku Matsuo and Mr. Satoru Mihara of our Department for measurements of the fluorescence spectra. This work was supported in part by a Scientific Research Grant (No. 147076) from the Ministry of Education.

References

1) Y. Murakami, J. Sunamoto, and K. Kano, *Bull. Chem. Soc. Jpn.*, **47**, 1238 (1974).
2) Y. Murakami, J. Sunamoto, H. Okamoto, and K. Kawanami, *Bull. Chem. Soc. Jpn.*, **48**, 1537 (1975).
3) Y. Murakami, Y. Aoyama, K. Dobashi, and M. Kida, *Bull. Chem. Soc. Jpn.*, **49**, 3633 (1976).
4) Y. Murakami, Y. Aoyama, and K. Dobashi, *J. Chem. Soc., Perkin Trans. 2*, **1977**, 24.
5) Y. Murakami, Y. Aoyama, and K. Dobashi, *J. Chem. Soc., Perkin, Trans. 2*, **1977**, 32.
6) Y. Murakami, Y. Aoyama, K. Ohno, K. Dobashi, T. Nakagawa, and J. Sunamoto, *J. Chem. Soc., Perkin, Trans. 1*, **1976**, 1320.
7) C. R. Hauser and D. S. Breslow, "*Org. Synth.*," Coll. Vol. III, 408 (1955).
8) W. Reusch and R. Lemahieu, *J. Am. Chem. Soc.*, **86**, 3068 (1964).
9) J. P. Guthrie, *J. Chem. Soc., Chem. Commun.*, **1972**, 897.
10) Y. Murakami, Y. Aoyama, and M. Kida, *J. Chem. Soc., Perkin Trans. 2*, in press.
11) J. H. Fendler and E. J. Fendler, "Catalysis in Micellar and Macromolecular Systems," Academic Press, New York, N. Y. (1975), Chap. 4.
12) Ref. 11, pp. 20—21.
13) A. F. Hofmann and D. M. Small, *Annu. Rev. Med.*, **18**, 333 (1967).
14) J. P. Kratohvil and H. T. DelliColli, *Can. J. Biochem.*, **46**, 945 (1968).
15) A. F. Hofmann, *Biochem. J.*, **89**, 57 (1963).
16) F. M. Menger and M. J. McCreery, *J. Am. Chem. Soc.*, **96**, 121 (1974).
17) M. E. Haberland and J. A. Reynolds, *Proc. Natl. Acad. Sci., U.S.A.*, **70**, 2313 (1973).
18) H. A. Benesi and H. Hildebrand, *J. Am. Chem. Soc.*, **71**, 2703 (1949).
19) I. Tabushi, H. Sasaki, and Y. Kuroda, *J. Am. Chem. Soc.*, **98**, 5727 (1976).
20) J. A. Reynolds, D. B. Gilbert, and C. Tanford, *Proc. Natl. Acad. Sci. U.S.A.*, **71**, 2925 (1974).
21) a) C. Gitler and A. Ochoa-Solano, *J. Am. Chem. Soc.*, **90**, 5004 (1968); b) W. Tagaki, M. Chigira, T. Ameda, and Y. Yano, *J. Chem. Soc., Chem. Commun.*, **1972**, 219; c) R. A. Moss, R. C. Nakas, and S. Ramaswami, *J. Am. Chem. Soc.*, **99**, 627 (1977); d) W. Tagaki, S. Kobayashi, and D. Fukushima, *J. Chem. Soc., Chem., Commun.*, **1977**, 29.
22) H. Gutereund and J. M. Sturtevant, *Biochem. J.*, **63**, 656 (1956).

Chemical Studies on Tuberactinomycin. XII.[1] Syntheses and Antimicrobial Activities of [Ala^3, Ala^4]-, [Ala^3]-, and [Ala^4]-Tuberactinomycin O[2]

Tadashi TESHIMA, Shinya NOMOTO, Tateaki WAKAMIYA, and Tetsuo SHIBA

Department of Chemistry, Faculty of Science, Osaka University, Toyonaka, Osaka 560

(Received July 8, 1977)

Total syntheses of [Ala^3, Ala^4]-, [Ala^3]-, and [Ala^4]-tuberactinomycin O corresponding to deoxy analogs of natural antibiotic tuberactinomycin O were achieved for the purpose of elucidation of relationship between chemical structure and biological activity. Cyclization of the pentapeptide intermediates at two different positions was investigated. Minimum inhibitory concentrations of the synthetic analogs against *Mycobacterium* or *Corynebacterium* indicated that both hydroxy groups of two serine residues of tuberactinomycins are not required for antibacterial activity, nor participated to drug-resistancy of bacilli. These analogs were found to have the same conformations in solution as those of natural antibiotic from the results of NMR, ORD, and CD measurements.

Chemical structures of tuberactinomycins (Tum),[3] antituberculous peptides isolated from *Streptomyces griseoverticillatus* var. *tuberacticus*,[4] were determined by X-ray analysis as well as chemical degradations in our previous investigations (Fig. 1).[5] Exhaustive study on proton magnetic resonance of tuberactinomycin family added one successful example to conformational analysis of cyclic peptides.[6] Total synthesis of one congener, Tum O, in our recent work contributed to unambiguous establishment of the structures of Tum.[7]

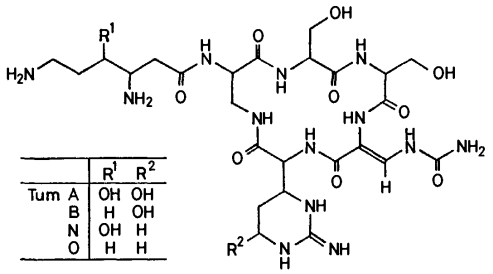

	R^1	R^2
Tum A	OH	OH
B	H	OH
N	OH	H
O	H	H

Fig. 1. Chemical structure of tuberactinomycins.

For the purpose of thorough elucidation of the structure-antibacterial activity relation of this antibiotic, we planned to exchange each amino acid residue in tuberactinomycins with others by full utilization of either semi-synthesis, total synthesis or chemical modification. In the first experiment, the branched part, *i.e.*, γ-Hy-β-Lys[3] in Tum N was replaced by many different acyl groups semi-synthetically.[1,8] From results of this study, it was concluded that the branched part is not necessarily required for the antibacterial activity but has an auxiliary role for enhancement of the activity.[1]

Therefore, in the present investigation, replacement of amino acid residues inside the cyclic moiety of Tum was so designed as to clarify the more significant site than branched part for the biological activity. Since two hydroxy groups of serine residues are common to all the Tum congeners, it seems to be important to see the effect of elimination of these functional groups from the molecule on antibacterial activity. Thus, we carried out the total syntheses of three deoxy analogs, *i.e.*, [Ala^3, Ala^4]-, [Ala^3]-, and [Ala^4]-Tum O.

In our synthetic strategy, prior to completion of the required amino acid sequence, the cyclic peptide moiety was first synthesized, and then β-Lys was introduced to the branched position as in the semi-synthesis of Tum O[8] from tuberactinamine (Tua) N.[3] In this synthetic plan, possible difficulties arising from extremely labile character of β-ureidodehydroalanine (Uda) residue must be overcome by some device. β,β-Diethoxyalanine (Dea) was chosen as a latent form of Uda,[3] so that Uda structure could be recovered at any synthetic step. A durability of Dea[3] residue during the entire course of this peptide synthesis was assured by preliminary experiments using model compounds.

In order to minimize a racemization at the C-terminal residue in the peptide cyclization reaction, Dea (route A) or A_2pr[3] (route B) was chosen as the C-terminal amino acid of the open chain pentapeptide, since Dea is to be converted to achiral Uda residue in the final synthetic step and α-amino group of A_2pr is not participated in the peptide linkage in the cyclic moiety but is able to be protected by Boc[3] group of urethane form.

In the preparations of [Ala^3, Ala^4]-Tum O, we compared both routes each other for relative advantages. However, the results showed no difference between them in respect of yield for the cyclization reaction. Therefore, route A was adopted for the syntheses of [Ala^3]- and [Ala^4]-Tum O.

Synthesis of [Ala^3, Ala^4]-Tum O. The Protected Cyclic Pentapeptide: *Route A*: H-Dea-OEt[9] and H-A_2pr(Z)-OH[10] were prepared according to the literatures. Capreomycidine (Cpd) was obtained from hydrolyzate of the natural Tum N. Whole synthetic scheme *via* route A was shown in Fig. 2. α-Amino group of Cpd was blocked by Nps[3] protecting group, since selective deprotection from Boc group is required prior to the cyclization. Nps-Cpd(NO_2)-OH (**6**) was coupled with a debenzyloxycarbonylated tetrapeptide, which was obtained by hydrogenolysis of **4**, to give a pentapeptide (**7a**). Saponification of **7a** followed by active esterification by means of DCC-HONSu[3] method to afford the pentapeptide active ester (**9a**). After removal of Nps group from **9a** by means of hydrogen chloride in THF, it was then cyclized under high-dilution conditions in pyridine to **10a** in 35% yield. Molecular weight of **10a** was measured to be 743

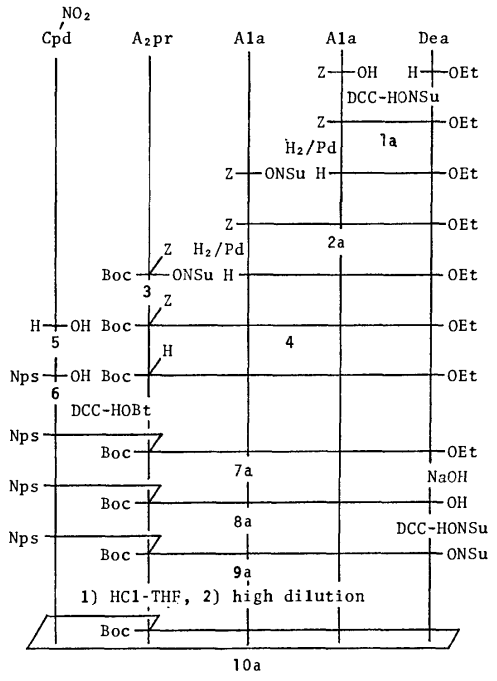

Fig. 2. Synthetic scheme for protected cyclic peptide (**10a**) *via* route A.

(Calcd for $C_{24}H_{46}O_{11}N_{10}\cdot 3/2H_2O$: 714) by means of vapor pressure osmometry, indicating formation of a cyclic monomer.

Route B: Synthetic scheme *via* route B was depicted in Fig. 3. The Nps group of the protected dipeptide (**12**) was selectively cleaved by hydrogen chloride in THF, and then coupled with the protected tripeptide (**14**) by DCC–HOBt[3] method to give the pentapeptide (**15**). This peptide (**15**) was converted into the 1-succinimidyl ester (**17**) after saponification. The active ester (**17**) was treated with hydrogen chloride in THF to remove the Nps group selectively, and then cyclized in pyridine under high-dilution condition in 38% yield. The cyclic peptide (**10a**) thus obtained was identical with the product *via* route A in thin-layer chromatography, high-pressure liquid chromatography, and NMR spectrum.

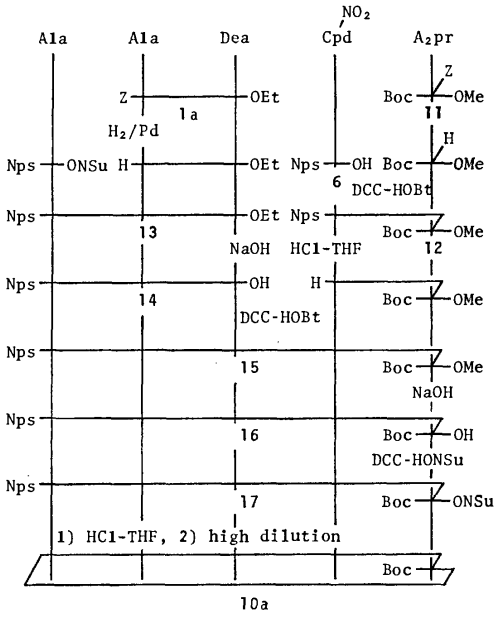

Fig. 3. Synthetic scheme for protected cyclic peptide (**10a**) *via* route B.

A Conversion to [Ala³, Ala⁴]-Tum O: A conversion of Dea residue in **10a** to Uda residue, being a key step throughout this synthesis, was carried out as follows. The deprotected product obtained by hydrogenolysis of **10a** was heated in acetone–1 M hydrochloric acid (1 : 1) under reflux for 8—10 min, and then excess of urea was added. By this procedure, the cyclic Uda peptide (**18a**) was obtained in a good yield, whose structure was confirmed by NMR (olefinic proton: δ 8.0(s) in D_2O) and UV spectra (λ_{max}: 268 nm (neutral or acidic medium), 286 (basic medium)). At the final step of the synthesis, introduction of Boc–β-Lys(Boc)–ONSu to the amino group of **18a** followed by deprotection gave the expected product, [Ala³, Ala⁴]-Tum O (**19a**) in a satisfactory yield (Fig. 4).

Synthesis of [Ala³]- and [Ala⁴]-Tum O. [Ala³]- and [Ala⁴]-Tum O were synthesized according to the route A for [Ala³, Ala⁴]-Tum O. Cyclization reaction

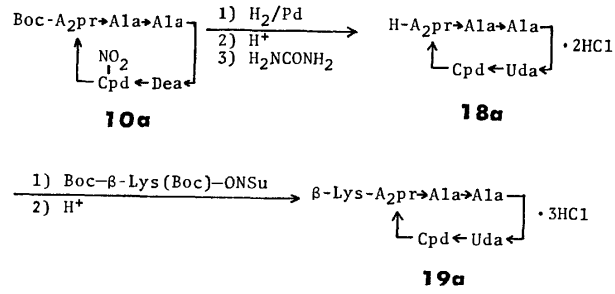

Fig. 4. Conversion of **10a** to **19a**.

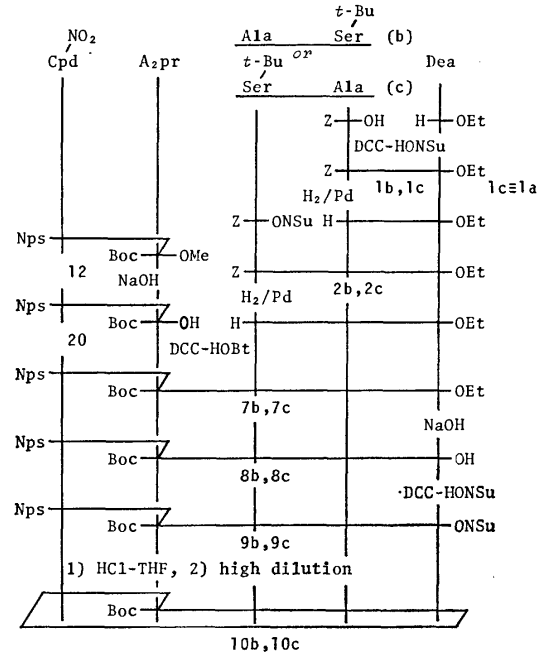

Fig. 5. Synthetic scheme for **19b** and **19c**. b: -Ala³–Ser⁴–, c: -Ser³–Ala⁴–.

Table 1. Chemical shifts of **18a**, **18b**, and **18c** in D_2O

		18a	**18b**	**18c**	Tua N
A_2pr	α-CH	4.4 (1H)	4.3 (1H)	4.4 (1H)	4.40 (1H,q)
	β-CH_2	3.3 (1H)	3.3 (1H)	3.30 (1H,dd)	3.30 (1H)
		4.1 (1H)	4.1 (1H)	4.15 (1H,dd)	4.12 (1H,q)
Ser^3	α-CH			4.82 (1H,t)	4.84 (1H,t)
	β-CH_2			3.92 (2H,d)	3.95 (2H,d)
Ala^3	α-CH	4.60 (1H,q)	4.70 (1H,q) [a]		
	β-CH_3	1.40 (3H,d)	1.50 (3H,d)		
Ser^4	α-CH		4.3 (1H)		4.32 (1H,q)
	β-CH_2		3.92 (1H,dd)		3.90 (1H,dd)
			4.10 (1H,dd)		4.20 (1H,dd)
Ala^4	α-CH	4.23 (1H,q)		4.32 (1H,q)	
	β-CH_3	1.40 (3H,d)		1.45 (3H,d)	
Uda	β-CH	8.00 (1H,s)	8.04 (1H,s)	8.03 (1H,s)	8.04 (1H,s)
Cpd	α-CH	4.95 (1H,d)	4.95 (1H,d)	5.01 (1H,d)	5.01 (1H,d)
	β-CH	4.4 (1H,m)	4.4 (1H,m)	4.4 (1H,m)	4.45 (1H,m)
	γ-CH_2	1.8 (1H,m)	1.8 (1H,m)	1.8 (1H,m)	1.8 (1H,m)
		2.1 (1H,m)	2.1 (1H,m)	2.1 (1H,m)	2.1 (1H,m)
	δ-CH_2	3.3 (2H,m)	3.3 (2H,m)	3.3 (2H,m)	3.32 (2H,m)

Abbreviations; s: singlet, d: doublet, dd: double doublet, t: triplet, q: quartet. a) Chemical shift in D_2O+TFA.

was carried out between the carboxyl group of Dea and the amino group of Cpd. The synthetic scheme for these analogs is shown in Fig. 5.

Tripeptides (**2b**, **c**) were prepared by stepwise elongation method from their C-terminal residue using the *t*-Bu group for protection of hydroxyl group of Ser. Dipeptide (**20**) was coupled with either of deprotected tripeptides obtained from **2b** and **2c** by DCC–HOBt method to give a pentapeptide (**7b**) or (**7c**). These ethyl esters (**7b**, **c**) were converted to their 1-succinimidyl esters (**9b**, **c**) *via* free carboxylic acids respectively. Each active ester was treated with hydrogen chloride in THF to remove Nps group selectively and then cyclized in pyridine under high dilution method to give **10b** in 32% or **10c** in 31% yield. Molecular weights of these peptides (**10b**, **c**) measured by means of vapour pressure osmometry (844 and 811 respectively, calcd for $C_{31}H_{54}N_{10}O_{12}\cdot H_2O$: 777) indicated that a cyclic monomer was formed in both cases. Removal of all protecting groups and conversion of Dea to Uda residue in cyclic peptides (**10b**, **c**) were performed. Resulting Uda peptides (**18b**, **c**) were coupled with Boc–β-Lys(Boc)–ONSu and the products were deblocked to give desired compounds, [Ala^3]- and [Ala^4]-Tum O (**19b**, **c**) (Fig. 6).

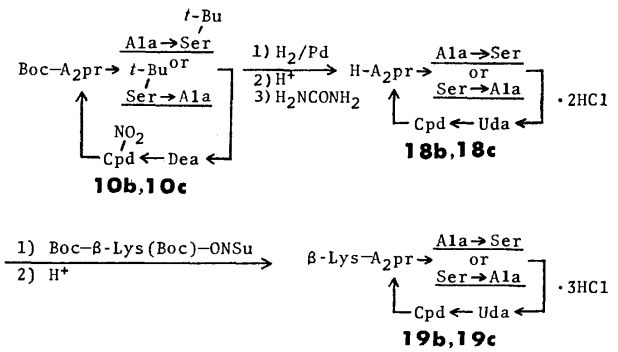

Fig. 6. Synthetic scheme for **19b** and **19c** (continued).
b: -Ala^3-Ser^4-, c: -Ser^3-Ala^4-.

Conformational Analyses. Conformational analyses of the compounds synthesized in this investigation were carried out by means of NMR, ORD, and CD studies. Each signal in NMR spectra of [Ala^3, Ala^4]-, [Ala^3]-, and [Ala^4]-Tua N[11] (**18a**—**c**) could be assigned by

Table 2. Chemical shifts of **18a**, **18b**, and **18c** in low-field region in H_2O at pH 2.5 (at 40 °C)

	18a	**18b**	**18c**	Tua N
1	9.17 (d)	9.28 (d)	9.27 (d)	9.33 (d)
2	9.13 (d)	9.25 (d)	9.24 (d)	9.24 (d)
3	8.68 (s)	8.82 (s)	8.81 (s)	8.83 (s)
4	8.63 (d)	8.78 (d)	8.72 (d)	8.67 (d)
5	—	—	—	—
6	7.69 (t)	8.09 (t)	8.22 (t)	8.15 (t)
7	8.00 (d)	8.03 (d)	8.03 (d)	8.00 (d)
8	7.69 (d)	7.74 (d)	7.86 (d)	7.72 (d)
9	7.43 (s)	7.45 (s)	7.41 (s)	7.37 (s)
10	7.28 (s)	7.25 (s)	7.37 (s)	7.31 (s)
11	6.44 (s)	6.46 (s)	6.39 (s)	6.34 (s)
12	6.30 (s)	6.31 (s)	6.29 (s)	6.24 (s)

Abbreviations; s: singlet, d: doublet, t: triplet.

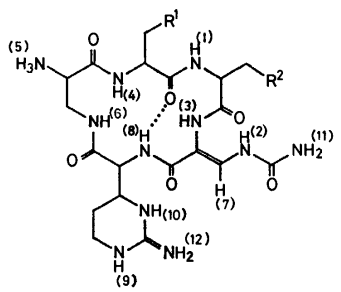

	R^1	R^2
[Ala^3,Ala^4]-Tua N	H	H
[Ala^3]-Tua N	H	OH
[Ala^4]-Tua N	OH	H
Tua N	OH	OH

Fig. 7.

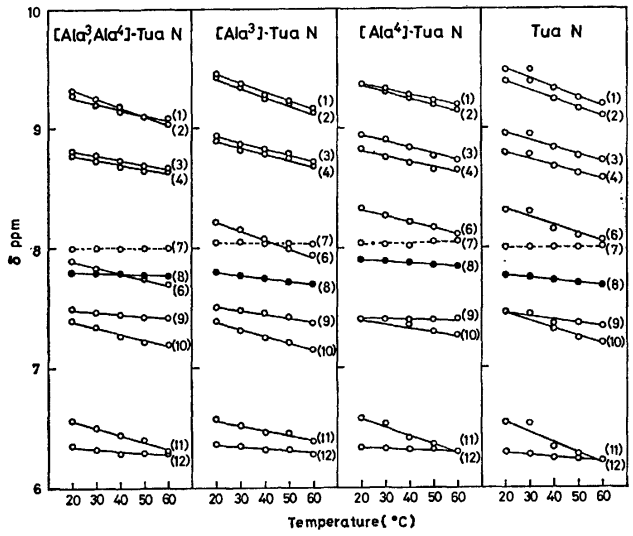

Fig. 8. Temperature dependence of chemical shifts in low-field region of NMR of **18a**, **18b**, and **18c**, as measured in H_2O at pH 2.5. o---o: olefinic proton, •—•: α-amide proton of Cpd, o—o: other NH protons.

decoupling method and comparison with natural ones[6] as shown in Table 1, 2, and Fig. 7. These assignments are very consistent with those for natural Tums, and rather abnormal differences in chemical shifts of α-CH or α-NH in Ser³ and Ser⁴ residues of natural sample were reconfirmed by this study.

Temperature dependence of chemical shifts as depicted in the Fig. 8 suggested that amide proton of Cpd may be participated to an intramolecular hydrogen bond as in natural tuberactinomycins.[6] Slower rate in deuterium exchange of the amide proton of Cpd compared to other protons, supported the existence of an intramolecular hydrogen bond mentioned above, too. Furthermore, for comparison between the synthetic and the natural peptides in terms of the conformation of whole molecules, ORD and CD curves were measured. Cyclic peptide moieties, *i.e.* **18a**—**c** which were synthesized in this study, showed principally the same patterns as that of Tua N. Similarly, ORD and CD curves of Tum O analogs resemble those of natural Tums as shown in Fig. 9. Therefore, it could be concluded that all cyclic peptides prepared here have the same conformations as the natural one including the intramolecular hydrogen bond.

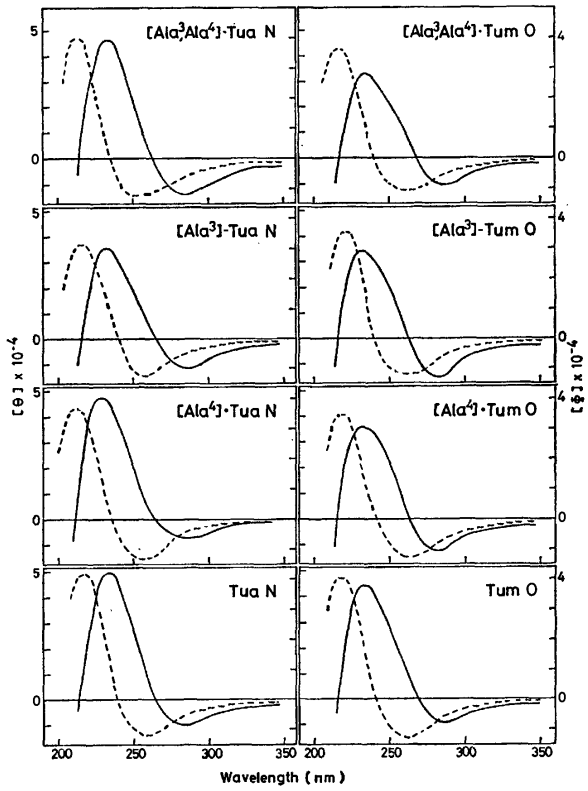

Fig. 9. ORD and CD curves of Tua N and O analogs. ——: ORD, ------: CD.

Antimicrobial Activities. Minimum inhibitory concentrations of [Ala³, Ala⁴]-, [Ala³]-, and [Ala⁴]-Tum O (**19a**—**c**) were listed in Table 3. Spectral patterns in their antibacterial activities of all these analogs were very similar to those of Tum N. It should be noted that [Ala⁴]-Tum O (**19c**) manifested even stronger activities than those of natural Tum N against some of test organisms, *i.e.*, *Bacillus subtilis*, *Salmonella paratyphi*, and *Salmonella enteritidis*, whereas [Ala³, Ala⁴]-Tum O (**19a**) was slightly weaker than natural antibiotics. Although

Table 3. Minimum inhibitory concentrations[a] of **19a**, **19b**, and **19c**

Test Organisms[b]	**19a**	**19b**	**19c**	Tum O	Tum N
Corynebacterium diphtheriae P.W. 8	12.5	6.3	6.3	6.3	6.3
Bacillus subtilis ATCC 6633	50	25	12.5	25	25
Escherichia coli NIHJ	100	50	12.5	12.5	12.5
Escherichia coli B	100	100	50	50	50
Salmonella typhosa H 901	100	100	25	25	25
Salmonella paratyphi PA 41-N-22	>100	>100	25	>100	>100
Salmonella enteritidis Gaertner	>100	>100	25	100	100
Shigella sonnei E33	>100	>100	100	50	50
Klebsiella pneumoniae ATCC 10031	100	100	25	25	25
Proteus vulgaris OX 19	>100	100	50	50	50
Mycobacterium ATCC 607	12.5	6.3	6.3	6.3	6.3

a) μg/ml. b) **19a**, **19b**, and **19c** were inactive to the following organisms: *Staphylococcus aureus* ATCC 6538P, *Staphylococcus epidermidis* sp-al-1, *Streptococcus pyogenes* N.Y. 5, *Sarcina lutea* ATCC 9341, *Micrococcus flavus* ATCC 10240, *Shigella flexineri* type 3a, *Serratia marcescens*, *Pseudomonas aeruginosa* IAM 1095.

Table 4. Minimum inhibitory concentrations[a] of **19a**, **19b**, and **19c** against human tubercule bacilli

	19a	**19b**	**19c**	Tum N
Human tubercule bacillus	12.5	<12.5	<12.5	<12.5
Human tubercule bacillus (100 μg-resistant to Tum B)	>100	>100	100	100
BCG (100 μg-resistant to Tum N)	>100	>100	>100	>100

a) μg/ml.

these synthetic analogs were also quite active against sensitive species of human tubercule bacillus, they showed no significant activity to Tum-resistant species of human tubercule bacillus and BCG. (Table 4).

Relationship between Structure and Activities. From all results of comparisons in biological activities of the synthetic peptides, it could be emphasized conclusively that both hydroxyl groups at Ser[3] and Ser[4] residues are not necessarily required for antibacterial activity of Tums, although the presence of these hydroxyl groups seemed to strengthen the activities, especially the hydroxyl group of Ser[3] playing more important role than that of Ser[4]. However, it is apparent that these hydroxyl groups may not be concerned with the drug resistancy of human tubercule bacilli.

Experimental

All melting points are uncorrected. NMR spectra were obtained with a Varian XL-100-15 spectrometer using sodium dimethylsilapentanesulfonate as an internal standard. ORD and CD spectra were obtained with a JASCO Model ORD/UV-5 in water. The specific rotations were obtained with a Perkin-Elmer 141 Polarimeter. Molecular weights were obtained with a Knauer vapor pressure osmometer using methanol as a solvent. UV spectra were recorded on a Hitachi 124 Spectrophotometer. TLC was carried out by the ascending method on silica gel G using a developing solvent chloroform–methanol (7: 1).

*Z–Ala–Dea–OEt (**1a**).* To a solution of Z–Ala–OH (14.6 g, 65.2 mmol) and H–Dea–OEt[9] (13.4 g, 65.2 mmol) in ethyl acetate (40 ml), a solution of HONSu[3] (9.01 g, 78.2 mmol) in dioxane (30 ml) and then DCC (14.8 g, 71.7 mmol) were added under stirring in an ice bath. Stirring was continued at 0 °C for 2 h, thereafter at room temperature overnight. After the addition of acetic acid (500 mg, 8.30 mmol), *N,N'*-dicyclohexylurea was filtered off and filtrate was concentrated *in vacuo*. A solution of the residue in ethyl acetate was washed with saturated aqueous sodium hydrogencarbonate and water. Organic layer was dried over anhydrous sodium sulfate and concentrated *in vacuo* to yield an oily product, yield 24.9 g (92.9%).

For characterization a portion of **1a** was converted into the crystalline hydrazide. Thus, to a solution of **1a** (1.40 g, 3.41 mmol) in DMF (20 ml), hydrazine hydrate (3.42 g, 68.3 mmol) was added. The mixture was allowed to stand for two days at room temperature and then concentrated *in vacuo*. The residue was triturated with water, and a crystalline product was filtered off, yield 0.920 g (68.1%). It was recrystallized from ethanol–ether–hexane, mp 208—209 °C (dec), $[\alpha]_D^{29}$ −1.2 °C (*c* 1.0, DMF).[12] Found: C, 54.21; H, 7.17; N, 14.19%. Calcd for $C_{18}H_{28}N_4O_6$: C, 54.53; H, 7.12; N, 14.13%.

*Z–Ala–Ala–Dea–OEt (**2a**).* Into a solution of **1a** (11.5 g, 28.0 mmol) and acetic acid (3.36 g, 56.0 mmol) in ethanol (200 ml), hydrogen was bubbled in the presence of palladium black. After debenzyloxycarbonylation had been completed, catalyst was filtered off and the filtrate was concentrated *in vacuo*. To a solution of the residue in ethyl acetate, triethylamine (3.30 g, 30.0 mmol) and Z–Ala–ONSu (8.96, 28.0 mmol) were added with stirring at 0 °C. The mixture was stirred at 0 °C for 1 h, thereafter at room temperature overnight. The reaction mixture was concentrated *in vacuo* and the residue was dissolved in chloroform. The organic solution was washed with saturated aqueous sodium hydrogencarbonate and water, and then dried over anhydrous sodium sulfate. A crystalline residue obtained after concentration *in vacuo* was recrystallized from chloroform–ethyl acetate, yield 11.7 g (86.8%), mp 186—188 °C. $[\alpha]_D^{28}$ −5.6 ° (*c* 0.9, DMF). Found: C, 57.32; H, 7.37; N, 8.94%. Calcd for $C_{23}H_{35}N_3O_8$: C, 57.37; H, 7.33; N, 8.73%.

*Boc–A$_2$pr(Z)–ONSu (**3**).* To a suspension of H–A$_2$pr(Z)–OH[10] (2.38 g, 10.0 mmol) in water (20 ml), triethylamine (2.1 ml, 15 mmol) and *t*-butyl 4,6-dimethylpyrimidyl-2-thiolcarbonate (2.64 g, 11.0 mmol)[13] in dioxane (6 ml) were added. The reaction mixture was stirred for 20 h. After addition of saturated aqueous sodium hydrogencarbonate, the solution was washed with ethyl acetate. The aqueous layer was acidified with citric acid and the product was transferred to ethyl acetate. The organic layer was washed with water, and then dried over anhydrous sodium sulfate, and then concentrated *in vacuo* to give an oily residue. To its solution in THF (30 ml), HONSu (1.15 g, 10.0 mmol) and DCC (2.06 g, 10.0 mmol) were added with stirring at 0 °C. The mixture was stirred at 0 °C for 2 h, and then at room temperature overnight. The *N,N'*-dicyclohexylurea formed was filtered off and the filtrate was concentrated *in vacuo*. Oily residue was triturated with hexane, and the crystalline product thus obtained (3.71 g, 85.2%) was recrye stallized from dioxane–hexane, yield 2.77 g (63.6%), mp 90—92 °C, $[\alpha]_D^{29}$ −30.7 ° (*c* 1.9, DMF). Found: C, 54.78; H, 5.80; N, 9.68%. Calcd for $C_{20}H_{25}N_3O_8$: C, 55.17; H, 5.79; N, 9.65%.

*Boc–A$_2$pr(Z)–Ala–Ala–Dea–OEt (**4**).* Hydrogenolysis of **2a** (7.00 g, 14.5 mmol) was carried out with addition of acetic acid (1.75 g, 29.1 mmol) in ethanol–dioxane (250 ml) as in the preparation of **2a** from **1a**. To a solution of the residual oil of $CH_3COOH \cdot$H–Ala–Dea–OEt and **3** (6.33 g, 14.5 mmol) in ethyl acetate (200 ml) *N*-methylmorpholine (2.94 g, 29.1 mmol) was added with stirring at 0 °C. The mixture was stirred at 0 °C for 2 h and then at room temperature overnight. The residue obtained after concentration *in vacuo* was dissolved in chloroform, and washed with 10% aqueous citric acid, saturated aqueous sodium hydrogencarbonate, and brine. The organic layer was dried over anhydrous sodium sulfate and concentrated *in vacuo*. The crystalline residue was recrystallized from chloroform–ethyl acetate–ether, yield 16.9 g (87.2%), mp 187—191 °C, $[\alpha]_D^{29}$ −9.2 ° (*c* 2.1, DMF). Found: C, 55.60; H, 7.41; N, 10.55%. Calcd for $C_{31}H_{49}N_5O_{11}$: C, 55.76; H, 7.40; N, 10.49%.

*H–Cpd(NO$_2$)–OH (**5**).* To a mixture of fuming nitric acid (*d*=1.52) (1.5 ml) and 50% fuming sulfuric acid (1.2 ml), H–Cpd–OH·HCl[14] (740 mg, 3.55 mmol) was added portionwise over 30 min with stirring at −20 °C, and then concentated

sulfuric acid (1 ml) was added. The mixture was stirred under the same conditions for 45 min, thereafter poured onto ice. On neutralization of the solution with sodium hydrogencarbonate, a crystalline product was separated out, yield 540 mg (70.0%). It was recrystallized from water, yield 535 mg (69.3%), mp 250 °C (dec), $[\alpha]_D^{29}$ +28.0° (*c* 1.0, 6 M HCl). Found: C, 32.82; H, 5.25; N, 32.22%. Calcd for $C_6H_{11}N_5O_4$: C, 33.18; H, 5.11; N, 32.25%.

Nps-Cpd(NO₂)-OH (6). To a solution of **5** (2.00 g, 9.21 mmol) in 1 M aqueous sodium hydroxide (10.1 ml) and dioxane (40 ml), Nps-Cl (1.92 g, 1.01 mmol) and 1 M aqueous sodium hydroxide (10.1 ml) were added over 15 min simultaneously. The solution was diluted with water, and acidified with citric acid. A yellow crystalline product separated out was filtered off. A small amount of the product was recovered from the filtrate by extraction with ethyl acetate. Both crops were combined and recrystallized from acetone–hexane, yield 2.55 g (74.7%), mp 180—181 °C (dec), $[\alpha]_D^{29}$ +31.3° (*c* 2.0, DMF). Found: C, 38.91; H, 3.94; N, 22.56; S, 8.56%. Calcd for $C_{12}H_{14}N_6O_6S$: C, 38.92; H, 3.81; N, 22.69; S, 8.66%.

Boc-A₂pr(Nps-Cpd(NO₂))-Ala-Ala-Dea-OEt (7a). To a solution of **4** (700 mg, 1.05 mmol) in DMF (10 ml), hydrogen was bubbled in the presence of palladium black. After completion of hydrogenolysis, the catalyst was filtered off. To the filtrate, **6** (383 mg, 1.05 mmol), HOBt (180 mg, 1.33 mmol) and then DCC (236 mg, 1.14 mmol) were added with stirring at 0 °C. The stirring was continued at 0 °C for 2 h and then at room temperature overnight. After addition of acetic acid (20 mg, 0.33 mmol), *N,N'*-dicyclohexylurea was filtered off. The filtrate was concentrated *in vacuo*, and a solution of the residue in ethyl acetate was washed with 10% aqueous citric acid, saturated aqueous sodium hydrogencarbonate and brine. The organic layer was dried over anhydrous sodium sulfate and concentrated *in vacuo*. The yellow solid obtained was reprecipitated from dioxane–ether, yield 760 mg (90.0%), mp 152—165 °C (dec), $[\alpha]_D^{27}$ +40.5° (*c* 2.2, DMF). Found: C, 47.80; H, 6.40; N, 16.80; S, 3.45%. Calcd for $C_{35}H_{55}N_{11}O_{14}S \cdot 1/2C_4H_8O_2$: C, 47.78; H, 6.39; N, 16.57; S, 3.45%.

Boc-A₂pr(Nps-Cpd(NO₂))-Ala-Ala-Dea-OH (8a). To a suspension of **7a** (1.73 g, 1.95 mmol) in ethanol (2 ml), 2 M aqueous sodium hydroxide (1.47 ml, 2.94 mmol) was added with stirring at room temperature and the stirring was continued for 1 h. After the solution was diluted with water (15 ml), it was washed with ethyl acetate, acidified with citric acid, and then extracted with ethyl acetate. The organic layer was washed with water, and dried over anhydrous sodium sulfate. The residue obtained after concentration *in vacuo* was reprecipitated with dioxane–ether, yield 1.46 g (87.0%), mp 154—166° (dec), $[\alpha]_D^{27}$ +39.4° (*c* 1.9, DMF). Found: C, 45.24; H, 5.86; N, 17.66; S, 3.88%. Calcd for $C_{33}H_{51}N_{11}O_{14}S \cdot H_2O$: C, 45.25; H, 6.10; N, 17.59; S, 3.66%.

Boc-A₂pr(Nps-Cpd(NO₂))-Ala-Ala-Dea-ONSu (9a). To a solution of **8a** (960 mg, 1.12 mmol) and HONSu (150 mg, 1.34 mmol) in dioxane (20 ml), DCC (280 mg, 1.34 mmol) was added with stirring at 0 °C. The mixture was stirred at 0 °C for 2 h and then at room temperature for 6 h. After addition of acetic acid (20 mg, 0.33 mmol), *N,N'*-dicyclohexylurea was filtered off. The filtrate was concentrated *in vacuo*, and the residue was reprecipitated from dioxane–ether, yield 920 mg (86.0%), mp 159—160 °C (dec), $[\alpha]_D^{27}$ +39.5° (*c* 2.0, DMF). Found: C, 45.63; H, 5.69; N, 17.39; S, 3.26%. Calcd for $C_{37}H_{54}N_{12}O_{16}S \cdot H_2O$: C, 45.67; H, 5.80; N, 17.27; S, 3.30%.

Cyclo[Boc-A₂pr-Ala-Ala-Dea-Cpd(NO₂)] (10a) via *Route A.* To a solution of **9a** (880 mg, 0.921 mmol) in THF (10 ml), 0.28 M hydrogen chloride in THF (9.86 ml, 2.76 mmol) was added dropwise over 15 min, and the stirring was continued for 30 min. Anhydrous ether was added to the mixture to obtain a precipitate of the free amino active ester, yield 730 mg (94.8%). It was immediately cyclized without purification. Thus, a solution of the product in DMF (100 ml) was added slowly into pyridine (800 ml) by use of high-dilution apparatus over 72 h at 55 °C with stirring. After stirring was continued for additional 24 h, the reaction mixture was concentrated *in vacuo*, and the residue was purified by silica gel chromatography. From the eluate with chloroform–methanol, a white solid was obtained [R_f 0.70 on TLC, ninhydrin negative], yield 212 mg (33.5%). For elemental analysis, the product thus obtained was reprecipitated from ethyl acetate, mp >250 °C, $[\alpha]_D^{19}$ −26.0° (*c* 0.94, DMF). Found: C, 45.81; H, 6.75; N, 19.52%, mol wt, 743. Calcd for $C_{27}H_{46}N_{10}O_{11} \cdot 3/2H_2O$: C, 45.43; H, 6.92; N, 19.63%, mol wt, 714.

Boc-A₂pr(Z)-OMe (11). To a solution of Boc-A₂pr-(Z)-OH, which was prepared from H-A₂pr(Z)-OH (13.77 g, 57.9 mmol) according to the method described for **3**, in ethyl acetate (100 ml), an ethereal solution of diazomethane was added, until yellow color remained. After excess diazomethane was decomposed with acetic acid, the mixture was concentrated *in vacuo*. The trituration of the oily residue with hexane in an ice–salt bath gave crystalline product, yield 18.47 g (90.5%). For elemental analysis, it was recrystallized from hexane. mp 50—52 °C $[\alpha]_D^{14}$ −8.8° (*c* 1.0, DMF). Found: C, 58.02; H, 6.92; N, 7.90%. Calcd for $C_{17}H_{24}N_2O_6$: C, 57.94; H, 6.87; N, 7.95%.

Boc-A₂pr(Nps-Cpd(NO₂))-OMe (12). Compound **11** (4.75 g, 13.5 mmol) was hydrogenolyzed over palladium black in DMF (30 ml). To the filtrate from the catalyst, **6** (5.00 g, 13.5 mmol), HOBt (2.03 g, 15.0 mmol), and then DCC (3.10 g, 15.0 mmol) were added with stirring at 0 °C. The stirring was continued at 0 °C for 2 h and then at room temperature overnight. The reaction mixture was concentrated *in vacuo*, and the residue was dissolved in ethyl acetate. Insoluble material was filtered off and the filtrate was washed with 10% aqueous citric acid, saturated aqueous sodium hydrogencarbonate and brine. The organic layer was dried over anhydrous sodium sulfate and concentrated *in vacuo*. The yellow solid was recrystallized from acetone–hexane, yield, 6.33 g (82.2%), mp 155—160 °C, $[\alpha]_D^{28}$ +89.8° (*c* 1.0, DMF). Found: C, 42.71; H, 5.37; N, 18.73; S, 5.47%. Calcd for $C_{21}H_{30}N_8O_9S \cdot H_2O$: C, 42.85; H, 5.48; N, 19.04; S, 5.45%.

Nps-Ala-Ala-Dea-OEt (13). As in the preparation of **2a**, **13** was synthesized from Z-Ala-Dea-OEt (1.00 g, 2.44 mmol) and Nps-Ala-ONSu (828 mg, 2.44 mmol). The yellow oily product was triturated with hexane to yield crystalline product (962 mg, 78.7%), which was recrystallized from ethyl acetate–hexane, yield 768 mg (62.7%). mp 128—131 °C, $[\alpha]_D^{29}$ −29.3° (*c* 1.0, DMF). Found: C, 50.33; H, 6.49; N, 11.08; S, 6.34%. Calcd for $C_{21}H_{32}N_4O_8S$: C, 50.39; H, 6.44; N, 11.19; S, 6.41%.

Nps-Ala-Ala-Dea-OH (14). To a suspension of **13** (750 mg, 1.50 mmol) in ethanol (5 ml), 1 M aqueous sodium hydroxide was added for saponification. The subsequent procedure was practically the same as that for **8a**. Trituration of the residual product with hexane gave a yellow solid, yield 699 mg, (98.7%). For elemental analysis, the solid was reprecipitated from ethyl acetate–hexane, mp 148—149 °C (dec), $[\alpha]_D^{28}$ −32.0° (*c* 1.0, DMF). Found: C, 47.93; H, 5.99; N, 11.51; S, 6.60%. Calcd for $C_{19}H_{28}N_4O_8S$: C, 48.29; H, 5.97; N, 11.86; S, 6.79%.

Boc-A₂pr(Nps-Ala-Ala-Dea-Cpd(NO₂))-OMe (15). To a suspension of **12** (500 mg, 0.876 mmol) in methanol (10

ml), 0.2 M hydrogen chloride in THF (4.5 ml, 0.90 mmol) was added with stirring at room temperature. After 45 min, additional 0.2 M hydrogen chloride in THF (1.0 ml, 0.20 mmol) was added, and the solution was stirred for additional 15 min. Addition of ether and hexane to the reaction mixture gave a white precipitate, yield 339 mg (85.3%). To a solution of this solid, **14** (353 mg, 0.747 mmol) and HOBt (111 mg, 0.822 mmol) in chloroform (25 ml), triethylamine (76 mg, 0.747 mmol) and DCC (170 mg, 0.822 mmol) were added with stirring at 0 °C. Afterwards, the reaction mixture was treated as in the preparation of **7a**. The solid obtained (565 mg, 74.0%) was reprecipitated from dioxane–ether, yield 382 mg (50.0%). mp 203—204 °C (dec), $[\alpha]_D^{28}$ −33.5° (*c* 1.0, DMF). Found: C, 47.02; H, 6.23; N, 16.77; S, 3.92%. Calcd for $C_{34}H_{53}N_{11}O_{14}S \cdot 1/2C_4H_8O_2$: C, 47.20; H, 6.27; N, 16.82; S, 3.50%.

*Boc–A_2pr(Nps–Ala–Ala–Dea–Cpd(NO_2))–OH (**16**).* The methyl ester **15** (900 mg, 1.03 mmol) was saponified with 1 M aqueous sodium hydroxide (1.13 ml, 1.13 mmol) in ethanol (9 ml) at room temperature for 2 h according to the usual procedure like in the preparation of **8a**. Yield 810 mg (93.9 %). For elemental analysis, it was recrystallized from dioxane–ether, mp 173—174 °C (dec), $[\alpha]_D^{28}$ −32.4° (*c* 1.0, DMF). Found: C, 46.37; H, 6.34; N, 16.72; S, 3.77%. Calcd for $C_{33}H_{51}N_{11}O_{14}S \cdot 1/2C_4H_8O_2$: C, 46.60; H, 6.15; N, 17.08; S, 3.56%.

*Boc–A_2pr(Nps–Ala–Ala–Dea–Cpd(NO_2))–ONSu (**17**).* The acid **16** (1.00 g, 1.17 mmol) was converted to **17** with HONSu (150 mg, 1.28 mmol) and DCC (260 mg, 1.28 mmol) in THF (50 ml) as in the synthesis of **9a**, A yellow solid was obtained, yield 960 mg (86.3%). For elemental analysis, this solid was reprecipitated from dioxane–hexane, mp 162—163 °C (dec), $[\alpha]_D^{23}$ −31.7° (*c* 1.0, DMF). Found: C, 46.90; H, 6.04; N, 16.81; S, 3.44%. Calcd for $C_{37}H_{54}N_{12}O_{16}S \cdot 1/2C_4H_8O_2$: C, 46.89; H, 5.85; N, 16.82; S, 3.21%.

*Cyclo[Boc–A_2pr–Ala–Ala–Dea–Cpd(NO_2)] (**10a**)* via *Route B.* To a solution of **17** (960 mg, 1.01 mmol) in THF (100 ml), 0.194 M hydrogen chloride in THF (11.4 ml, 2.21 mmol) was added with stirring at room temperature. After 1 h, the solution was concentrated *in vacuo* and trituration of the residue with anhydrous ether gave a solid, yield 810 mg (95.7%). The product thus obtained, was immediately cyclized without purification. The cyclization procedure was the same as that for **10a** *via* route A except for the use of the reaction conditions at 60 °C for 55 h. Purification by silica gel chromatography gave a white solid [R_f 0.70 on TLC ninhydrin negative], yield 251 mg (36.1%). For elemental analysis, the product thus obtained was reprecipitated from ethyl acetate, mp >250 °C, $[\alpha]_D^{29}$ −31.2° (*c* 0.94, DMF). Found: C, 45.49; H, 6.70; N, 19.67%. Calcd for $C_{27}H_{46}N_{10}O_{11} \cdot 3/2H_2O$: C, 45.43; H, 6.92; N, 19.63%.

*[Ala³, Ala⁴]-Tua N·2HCl (**18a**).* To a solution of **10a**, obtained either by route A or B (300 mg, 0.427 mmol) and acetic acid (0.2 ml) in a mixture of ethanol (50 ml) and water (15 ml), hydrogen was bubbled in the presence of palladium black for removal of the nitro group. The filtrate from catalyst was concentrated *in vacuo*, a solution of the residue in acetone–1 M hydrochloric acid (1: 1) (10 ml) was heated under reflux for 8 min. After cooling, the solution was allowed to stand with addition of urea (600 mg, 10.0 mmol) at room temperature overnight. The mixture was concentrated *in vacuo*, trituration of the residue with ethanol–ether gave a precipitate (207 mg, 81.3%). This precipitate was recrystallized from water–methanol, yield 126 mg (49.5%). mp >250 °C $[\alpha]_D^{28}$ −23.8° (*c* 1.0, H_2O). λ_{max}; 268 nm (H_2O, ε 25 700), 267 nm (0.1 M HCl, ε 25 400), 301 nm (1 M NaOH, ε 18 400). Found: C, 38.03; H, 5.97; N, 25.86; Cl, 11.68%. Calcd for $C_{19}H_{33}N_{11}O_6Cl_2 \cdot H_2O$: C, 38.00; H, 5.87; N, 25.66; Cl, 11.81%.

*[Ala³, Ala⁴]-Tum O·3HCl (**19a**).* To a suspension of **18a** (50 mg, 0.0858 mmol) in DMF (3 ml), Boc–β-Lys(Boc)–ONSu[8,15] (46 mg, 0.103 mmol) and triethylamine (10.4 mg, 0.103 mmol) were added with stirring at room temperature, and stirring was continued overnight. The solution was concentrated *in vacuo*. Trituration of the residue with THF gave a gelatinous solid, which was collected by centrifugation. The precipitate thus obtained was dissolved in water and washed with ethyl acetate. The aqueous layer was concentrated *in vacuo*. For deprotection, the residue was dissolved in 6 M hydrochloric acid (1 ml) and allowed to stand for 30 min. Addition of ethanol and ether to the mixture gave a white precipitate (58 mg, 91%), which was recrystallized from water–methanol, yield 40 mg (62.4%), mp 250 °C (dec), $[\alpha]_D^{22}$ −25.4° (*c* 0.52, H_2O), λ_{max}; 268 nm (H_2O, ε 23 400), 267 nm (0.1 M HCl, ε 22 500), 295 nm (1 M NaOH, ε 16 700). Found: C, 39.26; H, 6.29; N, 23.62; Cl, 13.72%. Calcd for $C_{25}H_{46}N_{13}O_7Cl_3 \cdot H_2O$: C, 39.24; H, 6.32; N, 23.80; Cl, 13.90%.

*Z–Ser(t-Bu)–Dea–OEt (**1b**).* Coupling of Z–Ser(*t*-Bu)–OH (13.2 g, 44.7 mmol) and H–Dea–OEt (9.17 g, 44.7 mmol) in a manner similar to that for **1a** gave an oily product **1b**, yield 20.8 g (96.5%).

For characterization a portion of **1b** was converted into the crystalline hydrazide as in the case of **1a**, mp 136—144 °C, $[\alpha]_D^{14}$ +10.3° (*c* 1.0, DMF).[12] Found: C, 56.31; H, 7.93; N, 12.00%. Calcd for $C_{22}H_{36}N_4O_7$: C, 56.39; H, 7.74; N, 11.96%.

*Z–Ala–Ser(t-Bu)–Dea–OEt (**2b**).* Hydrogenolysis of **1b** (10.0 g, 20.7 mmol) in DMF (40 ml), and coupling of its product with Z–Ala–OH (4.26 g, 20.7 mmol) by the succinimidyl ester method was performed in a similar manner to that for preparation of **2a**. Acetic acid (242 mg, 4.20 mmol) and *N*-(2-aminoethyl)-piperazine (1.00 g, 7.75 mmol) were used to destroy unreacted DCC and the succinimidyl ester respectively. Yield 8.90 g (77.4%). For elemental analysis, the product thus obtained was recrystallized from ethyl acetate–hexane, mp 104—109 °C, $[\alpha]_D^{19}$ +8.22° (*c* 2.13, DMF). Found: C, 58.16; H, 7.81; N, 7.55%. Calcd for $C_{27}H_{43}N_3O_9$: C, 58.57; H, 7.83; N, 7.59%.

*Z–Ser(t-Bu)–Ala–Dea–OEt (**2c**).* Z–Ser(*t*-Bu)–OH (10.0 g, 33.9 mmol) was coupled with $CH_3COOH \cdot$H–Ala–Dea–OEt prepared from **1c** (13.9 g, 33.9 mmol) by the succinimidyl ester method using *N*-methylmorpholine (6.85 g, 67.7 mmol). Yield 13.5 g (72.0%). For elemental analysis, the product thus obtained was recrystallized from ethyl acetate–hexane, mp 131—145 °C, $[\alpha]_D^{19}$ +5.55° (*c* 2.11, DMF). Found: C, 58.78; H, 7.95; N, 7.80%. Calcd for $C_{27}H_{43}N_3O_9$: C, 58.57; H, 7.83; N, 7.59%.

*Boc–A_2pr(Nps–Cpd(NO_2))–OH (**20**).* Saponification of **12** (3.00 g, 5.26 mmol) in a similar manner to that for **8a** gave a yellow solid, yield 2.49 g (85.0%). For elemental analysis, it was converted to a dicyclohexylammonium salt, and recrystallized from methanol–ether, mp 213—214 °C (dec), $[\alpha]_D^{23}$ +63.8° (*c* 1.0, DMF). Found: C, 51.57; H, 6.96; N, 16.79; S, 4.40%. Calcd for $C_{32}H_{51}N_9O_9S \cdot 1/2CH_3OH$: C, 51.77; H, 7.09; N, 16.72; S, 4.25%.

*Boc–A_2pr(Nps–Cpd(NO_2))–Ala–Ser(t-Bu)–Dea–OEt (**7b**).* Coupling of **20** (3.00 g, 5.39 mmol) and the debenzyloxycarbonylation product of **2b** (2.98 g, 5.39 mmol) in a similar manner as in the preparation of **7a** gave a yellow solid, yield 4.67 g (90.5%), mp 154—164°, $[\alpha]_D^{19}$ +48.6° (*c* 1.9, DMF). Found: C, 48.46; H, 6.58; N, 15.95; S, 3.28%. Calcd for $C_{39}H_{63}N_{11}O_{15}S$: C, 48.89; H, 6.63; N, 16.08; S, 3.35%.

*Boc–A_2pr(Nps–Cpd(NO_2))–Ser(t-Bu)–Ala–Dea–OEt (**7c**).*

Similarly, **20** (3.00 g, 5.39 mmol) was coupled with the deprotected product of **2c** (2.98 g, 5.39 mmol) to give a yellow solid, yield 4.63 g (89.7%), mp 143—153°, $[\alpha]_D^{19}$ +51.6° (*c* 1.9, DMF). Found: C, 48.14; H, 6.54; N, 15.81; S, 3.43%. Calcd for $C_{39}H_{63}N_{11}O_{15}S \cdot H_2O$: C, 47.99; H, 6.71; N, 15.79; S, 3.29%.

*Boc-A_2pr(Nps-Cpd(NO_2))-Ala-Ser(t-Bu)-Dea-OH (**8b**).* Saponification of **7b** (3.17 g, 3.31 mmol) gave a yellow solid in a similar manner as in the preparation of **8a**, yield 2.72 g (88.3%), mp 143 °C (dec), $[\alpha]_D^{19}$ +53.6° (*c* 1.6, DMF). Found: C, 46.74; H, 6.37; N, 16.17; S, 3.22%. Calcd for $C_{37}H_{59}N_{11}O_{15}S \cdot H_2O$: C, 46.88; H, 6.49; N, 16.25; S, 3.38%.

*Boc-A_2pr(Nps-Cpd(NO_2))-Ser(t-Bu)-Ala-Dea-OH (**8c**).* Similarly, saponification of **7c** (4.62 g, 4.82 mmol) gave a yellow solid, yield 3.98 g (88.8%), mp 140—141 °C (dec), $[\alpha]_D^{19}$ +49.2° (*c* 2.0, DMF). Found: C, 46.70; H, 6.40; N, 16.18; S, 3.33%. Calcd for $C_{37}H_{59}N_{11}O_{15}S \cdot H_2O$: C, 46.88; H, 6.49; N, 16.25; S, 3.38%.

*Boc-A_2pr-(Nps-Cpd(NO_2))-Ala-Ser(t-Bu)-Dea-ONSu (**9b**).* The free acid **8b** (2.98 g, 3.20 mmol) was converted to 1-succinimidyl ester as in the preparation of **9a**, yield 3.13 g (95.1%), mp 141—150 °C (dec), $[\alpha]_D^{19}$ +42.6° (*c* 1.1, DMF). Found: C, 46.84; H, 6.01; N, 15.90; S, 2.92%. Calcd for $C_{41}H_{62}N_{12}O_{17}S \cdot H_2O$: C, 47.12; H, 6.17; N, 16.08; S, 3.07%.

*Boc-A_2pr-(Nps-Cpd(NO_2))-Ser(t-Bu)-Ala-Dea-ONSu (**9c**).* Compound **8c** (4.30 g, 4.62 mmol) was changed to 1-succinimidyl ester as in the preparation of **9a**; yield 4.55 g (95.8 %), mp 145—155 °C (dec), $[\alpha]_D^{19}$ +49.5° (*c* 1.8, DMF). Found: C, 47.21; H, 6.10; N, 16.18; S, 3.02%. Calcd for $C_{41}H_{62}N_{12}O_{17}S \cdot H_2O$: C, 47.12; H, 6.17; N, 16.08; S, 3.07%.

*Cyclo[Boc-A_2pr-Ala-Ser(t-Bu)-Dea-Cpd(NO_2)] (**10b**).* Cleavage of the Nps group of **9b** (1.50 g, 1.46 mmol) and the subsequent cyclization were carried out like in the preparation of **10a**, yield 335 mg (30.2%), mp >250 °C, $[\alpha]_D^{17}$ −18.2° (*c* 1.2, DMF). Found: C, 48.21; H, 7.11; N, 18.01% mol wt, 844. Calcd for $C_{31}H_{54}N_{10}O_{12} \cdot H_2O$: C, 47.93; H, 7.27; N, 18.03%, mol wt, 777.

*Cyclo[Boc-A_2pr-Ser(t-Bu)-Ala-Dea-Cpd(NO_2)] (**10c**).* The cyclic peptide, **10c** was synthesized from **9c** (4.40 g, 4.28 mmol) as in the preparation of **10b**, yield 985 mg (30.3%), mp >250 °C, $[\alpha]_D^{17}$ −29.4° (*c* 1.1, DMF). Found: C, 48.13; H, 7.15; N, 18.17%, mol wt, 811. Calcd for $C_{31}H_{54}N_{10}O_{13} \cdot H_2O$: C, 47.93; H, 7.27; N, 18.03%, M. W., 777.

*[Ala³]—Tua N·2HCl (**18b**).* Deprotection of **10b** (370 mg, 0.488 mmol) and conversion of Dea to Uda residue were carried out as in the preparation of **18a**, yield 238 mg (81.5%), mp >250 °C, $[\alpha]_D^{14}$ −16.6° (*c* 0.56, H_2O). λ_{max}; 268 nm (H_2O, ε 20 600), 268 nm (0.1 M HCl, ε 22 100), 290 nm (1 M NaOH, ε 14 800). Found: C, 37.95; H, 5.64; N, 25.43; Cl, 11.62%. Calcd for $C_{19}H_{33}N_{11}O_7Cl_2 \cdot 1/2H_2O$: C, 37.57; H, 5.64; N, 25.37; Cl, 11.67%.

*[Ala⁴]—Tua N·2HCl (**18c**).* This crystalline compound was prepared from **10c** (300 mg, 0.395 mmol) was preapred in a manner similar to that for **18a**, yield 198 mg (83.5%), mp >250 °C, $[\alpha]_D^{14}$ +35.0° (*c* 0.59, H_2O). λ_{max}; 268 nm (H_2O, ε 23 300), 268 nm (0.1 M HCl, ε 24 700), 290 nm (1 M NaOH, ε 17 600). Found: C, 38.07; H, 5.62; N, 25.37; Cl, 11.78%. Calcd for $C_{19}H_{33}N_{11}O_7Cl_2$: C, 38.13; H, 5.56; N, 25.75; Cl, 11.85%.

*[Ala³]—Tum O·3HCl (**19b**).* Boc-β-Lys(Boc)-ONSu (267 mg, 0.602 mmol) was coupled with the free amino group of **18b** (240 mg, 0.401 mmol) followed by deprotection as in the preparation of **19a** to give colorless crystals, yield 250 mg, mp >250 °C, $[\alpha]_D^{14}$ −36.1° (*c* 0.52, H_2O). λ_{max}; 268 nm (H_2O, ε 23 800), 268 nm (0.1 M HCl, ε 24 100), 290 nm (1 M NaOH, ε 16 400). Found: C, 39.12; H, 6.36; N, 22.92; Cl, 13.47%. Calcd for $C_{25}H_{46}N_{13}O_8Cl_3 \cdot 1/2C_2H_5OH \cdot 1/2H_2O$: C, 39.27; H, 6.34; N, 22.90; Cl, 13.38%.

*[Ala⁴]—Tum O·3HCl (**19c**).* Similarly, coupling of Boc-β-Lys(Boc)-ONSu (130 mg, 0.293 mmol) with **18c** (117 mg, 0.196 mmol) and then deprotection gave colorless crystals, yield 124 mg (83.2%), mp 255 °C (dec), $[\alpha]_D^{14}$ −16.4° (*c* 0.53, H_2O). λ_{max}; 268 nm (H_2O, ε 20 300), 268 nm (0.1 M HCl, ε 21 600), 290 nm (1 M NaOH, ε 15 200). Found: C, 39.73; H, 6.39; N, 22.77; Cl, 13.31%. Calcd for $C_{25}H_{46}N_{13}O_8Cl_3 \cdot C_2H_5OH$: C, 40.08; H, 6.48; N, 22.50; Cl, 13.15%.

Authors are deeply indebted to the research laboratories, Toyo Jozo Co., Ltd. for supplying tuberactinomycins and measurements of antibacterial activities, and also to Dr. Masayasu Yamazaki, National Sanatorium, Toneyama Hospital for measurements of biological activities against human tubercule bacilli. We also wish to thank to Dr. Kenji Okawa and his coworkers to give a facility for the vapor pressure osmometer. This work was partially supported by a Grant-in-Aid for Scientific Research from Ministry of Education.

References

1) Part XI. T. Wakamiya, T. Teshima, H. Sakakibara, K. Fukukawa, and T. Shiba, *Bull. Chem. Soc. Jpn.*, **50**, 1984 (1977).

2) This study was presented at the 13th Symposium on Peptide Chemistry, Tokyo, November, 1975, p. 106 and the 14th Symposium on Peptide Chemistry, Hiroshima, November, 1976, p. 127.

3) Abbreviations according to IUPAC-IUB commission, *J. Biol. Chem.*, **247**, 977 (1972), are used. Tum: tuberactinomycin, Tua: tuberactinamine, γ-Hy-β-Lys: γ-hydroxy-β-lysine, Dea: β,β-diethoxyalanine, Uda: β-ureidodehydroalanine, A_2pr: α,β-diaminopropionic acid, Cpd: capreomycidine, Boc: *t*-butoxycarbonyl, Z: benzyloxycarbonyl, Nps: *o*-nitrophenylsulfenyl, DCC: dicyclohexylcarbodiimide, HONSu: *N*-hydroxysuccinimide, HOBt: 1-hydroxybenzotriazole, THF: tetrahydrofuran, DMF: *N,N*-dimethylformamide.

4) a) A. Nagata, T. Ando, R. Izumi, H. Sakakibara, T. Take, H. Hayano, and J. Abe, *J. Antibiot.*, **21**, 681 (1968); b) T. Ando, K. Matsuura, R. Izumi, T. Noda, T. Take, A. Nagata, and J. Abe, *ibid.*, **24**, 680 (1971); c) R. Izumi, T. Noda, T. Ando, T. Take, and A. Nagata, *ibid.*, **25**, 201 (1972).

5) H. Yoshioka, T. Aoki, H. Goko, K. Nakatsu, T. Noda, H. Sakakibara, T. Take, A. Nagata, J. Abe, T. Wakamiya, T. Shiba, and T. Kaneko, *Tetrahedron Lett.*, **1971**, 2043.

6) T. Wakamiya and T. Shiba, *Bull. Chem. Soc. Jpn.*, **48**, 2502 (1975).

7) T. Teshima, S. Nomoto, T. Wakamiya, and T. Shiba, *Tetrahedron Lett.*, **1976**, 2343.

8) T. Wakamiya and T. Shiba, *J. Antibiot.*, **28**, 292 (1975).

9) "The Chemistry of Penicillin," ed by Clarke, Johnson, and Robinson, Princeton University Press, Princeton, N. J. (1949), p. 512.

10) S. Takagi, H. Tsukatani, and K. Hayashi, *Chem. Parm. Bull.*, **7**, 616 (1959).

11) Convenient numbering for the positions of amino acid residues in the cyclic peptide moiety, *i.e.*, Tua N, corresponds to that of Tum as shown below.

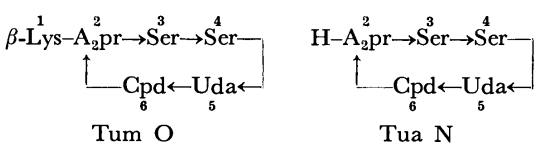

Tum O Tua N

12) DL-Dea was used in this study, while all the other amino acids were of the L-form. Therefore, specific optical rotations measured for Dea peptides may fluctuate to some extent depending on ratios of the diastereomers.
13) T. Nagasawa, K. Kuroiwa, K. Narita, and Y. Isowa, *Bull. Chem. Soc. Jpn.*, **46**, 1269 (1973).
14) Capreomycidine hydrochloride used in this study was obtained from a hydrolyzate of tuberactinomycin N.
15) T. Wakamiya, H. Uratani, T. Teshima, and T. Shiba, *Bull. Chem. Soc. Jpn.*, **48**, 2401 (1975).

Backbone Rearrangement of 3β,4β-Epoxyfriedelane. A Formation of Germanicol and Solvent Effects[1]

Motoo Tori, Takahiko Tsuyuki, and Takeyoshi Takahashi

Department of Chemistry, Faculty of Science, The University of Tokyo, Hongo, Bunkyo-ku, Tokyo 113

(Received July 12, 1977)

In the reaction of 3β,4β-epoxyfriedelane with boron trifluoride etherate in benzene, a backbone rearragement proceeds up to D/E rings, giving germanicol as the main product, together with D:B-friedo-olean-5(10)-en-3β-ol, D:B-friedo-olean-5-en-3β-ol, and β-amyrin. The reaction product ratio of this reaction in various solvents was examined by HPLC.

It has been reported that a treatment of 3α,4α-epoxyfriedelane with tin(IV) chloride[2a] or with boron trifluoride etherate[2b] gives D: B-friedo-olean-5(10)-en-3α-ol,[2] olean-12-en-3α-ol,[2b] 18αH-olean-12-en-3α-ol,[2b] olean-13(18)-en-3α-ol,[2b] and 18αH-A-neo-oleana-3(5), 12-diene.[2b] In connection with the synthesis of dendropanoxide (**1**), we previously investigated the boron trifluoride etherate-catalyzed backbone rearrangement of 3β,4β-epoxyfriedelane (**2**) in ether, and reported the formation of dendropanoxide (**1**), 4α-fluorofriedelan-3β-ol (**3**), D: B-friedo-olean-5(10)-en-3β-ol (**4**), D: B-friedo-olean-5-en-3β-ol (**5**), and β-amyrin (**6**), together with an unidentified alcohol in a minute quantity.[3] It has been also reported that the rearrangement reaction of 3β,4β-epoxyshionane with boron trifluoride etherate remarkably depends on the nature of solvents used.[4] The present paper describes the isolation and characterization of germanicol (**7**) in the reaction of 3β,4β-epoxyfriedelane (**2**) with boron trifluoride etherate in benzene and reports solvent effects on the reaction.

Treatment of 3β,4β-epoxyfriedelane (**2**) in benzene with boron trifluoride etherate at room temperature for 10 min gave a mixture of products, which proved by high performance liquid chromatography (HPLC) to consist of the unidentified alcohol[3] (45%), besides the known rearranged products:[3] D: B-friedo-olean-5(10)-en-3β-ol (**4**; 15%), D: B-friedo-olean-5-en-3β-ol (**5**; 15 %), and β-amyrin (**6**; 25%). This mixture was subjected to separation by column chromatography on silica gel and then by preparative HPLC to give the alcohol as crude crystals, which was recrystallized from chloroform–methanol. The alcohol was inferred to be germanicol (**7**)[5] by the following evidence. The alcohol showed mp 177—178.5 °C[5] and a molecular ion peak at *m/e* 426 together with prominent peaks at *m/e* 204, 189, and 177 typical of Δ^{18}-oleanenes.[6] The IR and NMR spectra indicated the presence of a secondary hydroxyl group, a trisubstituted double bond, and of eight tertiary methyl groups (*cf.* Experimental). In the NMR spectrum, the signal due to the olefinic proton resonating at δ 4.85 is characteristic of germanicol and its derivatives [*dl*-germanicol[5b] (δ 4.85, s), the acetate[7] (δ 4.88, d, J=2 Hz), and the butyrate[8] (δ 4.88, s)] and is different from those of taraxerol[9] (**8**; 5.54, 1H, dd, J=8 and 4 Hz, $C_{(15)}$–H), β-amyrin[3] (**6**; δ 5.20, 1H, t, J=4 Hz, $C_{(12)}$–H), 18αH-β-amyrin[10] (**9**; δ 5.15, 1H, m, $C_{(12)}$–H), D: B-friedo-olean-5-en-3β-ol[3] (**5**; δ 5.63, 1H, dd, J=4 and 1.8 Hz, $C_{(6)}$–H), walsurenol[11] (**10**; δ 5.62, 1H, m, $C_{(11)}$–H), or multiflorenol (**11**) derivatives[12] (δ 5.24—5.55, m, $C_{(7)}$–H). The structure (**7**) of this alcohol was confirmed by the following conversion. The alcohol (**7**) in anhydrous benzene was treated with potassium and methyl iodide.[13] Recrystallization of the product from acetone–benzene gave miliacin (**12**), which was found to be identical with an authentic specimen isolated from *Panicum miliaceum* L.[14]

Solvent effects on the formation of products in the reaction were then investigated. The small scale reaction using 3β,4β-epoxyfriedelane (1—3 mg) and boron trifluoride etherate in various solvents was carried out, and the products were examined by HPLC. The results are summarized in Table 1.

The attack of boron trifluoride etherate to the oxygen atom of the epoxide (**2**) gives rise to a cationic center at C-4 (or its equivalent species). A sequence of 1,2-shifts of methyl group(s) and hydride(s) would then be followed to give cations in various rearrangement stages, which after deprotonation afford the rearranged alcohols (**4**, **5**, **6**, and **7**). When the reaction was carried out in a solvent (such as DME, THF, or ether) apt to coordinate with a cation, the reaction was interrupted in early stages to give D: B-friedo-oleanene derivatives[3] (**1**, **4**, and **5**) together with the fluorohydrin[3] (**3**) and friedelin[3] (**13**). The rearrangement in solvents with low nucleophilicity (such as toluene, benzene, and

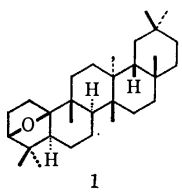

1

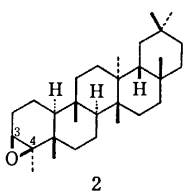

2

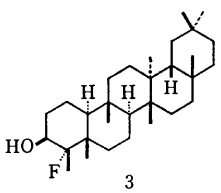

3

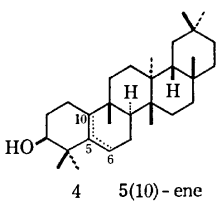

4 5(10)-ene
5 5-ene

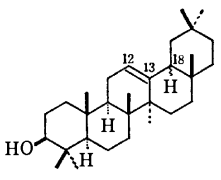

6 18β-H
9 18α-H

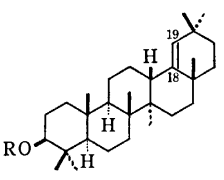

7 R=H
12 R=CH_3

Table 1. Relative amount ratios of the products in the reaction of **2** with boron trifluoride etherate[a]

Solvents	Temp (°C)	Time (min)	**2**	**12**	**3**	**1**	**5** (5-ene)	**4** 5(10)-ene	**6**[b] (12-ene)	**7**[b] (18-ene)
Toluene	r.t.[c]	10	0	5	0	0	10	15	25	45
Toluene	−5	10	0	5	0	0	10	10	30	45
Benzene	r.t.	10	0	5	0	0	15	15	25	40
CH_2Cl_2	r.t.	20	0	0	0	0	20	10	30	40
CH_2Cl_2	−5	20	0	0	0	0	30	5	25	40
Hexane	r.t.	20	0	5	0	0	15	10	30	40
Hexane	−5	20	0	5	0	25	20	15	15	20
Cyclohexane	r.t.	20	0	15	0	0	10	40	15	20
CH_3CN	r.t.	20	0	20	0	0	15	45	10	10
CH_3CN	−5	20	0	15	0	0	15	50	10	10
Ether	r.t.	20	0	5	60	15	5	15	trace	trace
Ether	−5	60	0	5	40	15	5	35	trace	trace
DME	r.t.	20	0	0	25	15	15	45	trace	trace
DME	−5	20	0	0	25	10	15	50	trace	trace
THF	r.t.	70	10	5	35	0	10	40	0	0
THF	−5	70	75	0	10	0	5	10	0	0

a) Relative yields were determined by HPLC. Measurements were carried out at room temperature using a Liquid Chromatograph Model ALC/GPC 202/401 (Waters Assoc.) with an RI detector; column: μ-PORASIL 1/8 (inch) × 1 (foot); solvent system: 10% ether–hexane; flow rate: 0.8 ml/min; pressure: *ca.* 450 psi. Even if HPLC analyses were carried out under these conditions, the retention times were variable. Mean values of their retention times were 5.1, 5.7, 6.9, 13.2, 14.5, 19.3, 21.2, and 21.8 min for **1**, **2**, **12**, **3**, **5**, **4**, **7**, and **6**, respectively. b) Errors are relatively large owing to the proximity of both retention times. c) Room temperature (r.t.) refers to a temperature range between 20 and 28 °C.

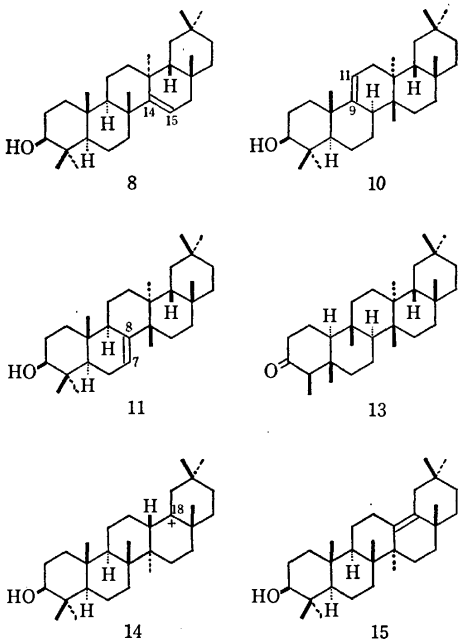

dichloromethane *etc.*) proceeded up to D/E rings to give germanicol (**7**; main product) and β-amyrin (**6**), besides **4** and **5**, as the cationic center survives longer in these solvents. Germanicol (**7**) could be derived from a cation (**14**; or its equivalent species);[15] olean-13(18)-en-3β-ol (**15**) which might be also derived from **14** was not detectable in the reaction mixture. These results (Table 1) shown above are parallel to those observed for the solvent effects on the reaction of 3β,4β-epoxyshionane.[4]

Driving force to provoke backbone rearrangement in the rigid polycyclic ring is considered to be a release[16] of intercyclic tension due to 1,3-diaxial interactions among the alkyl substituents (especially between the side chain and the 13α-methyl group in shionane series) and due to *cis*-fused D/E rings (in friedelane series). Thus, the acid-catalyzed backbone rearrangement of friedelane derivatives proceeds from ring A towards ring E, and constitutes a reversal of the biogenesis[17] of friedelin (**13**) from β-amyrin-type intermediate.[15] In the rearrangement of 3β,4β-epoxyshionane the formation of D: C-friedo-bacchar-7-en-3β-ol and D: C-friedo-bacchar-8-en-3β-ol was observed,[4] while the corresponding 7- and 8-enes were undetected in the product mixture from **2**. This is considered to be a structure difference between the two skeletons of friedelane and shionane. The acid-catalyzed backbone rearrangements hitherto reported for derivatives of friedelane,[2,3,18] alnusane (glutinane),[19] multiflorane,[20] and of taraxane[21] are limited to proceed up to C/D rings. Germanicol is the first example of product in which the backbone rearrangement of friedelane-oleanane-type effected up to E-ring.

Experimental

General procedures and preparation of 3β,4β-epoxyfriedelane (**2**) were the same as described in a previous paper.[3]

Isolation and Characterization of Germanicol (7). A solution of 3β,4β-epoxyfriedelane[3] (**2**; 175 mg) in anhydrous benzene (150 ml) was treated with boron trifluoride etherate (1 ml) at room temperature for 10 min and usual work-up gave a residue (*ca.* 170 mg). The residue was shown by HPLC examination to consist of germanicol[5] (**7**; 45%), D: B-friedo-

olean-5(10)-en-3β-ol[3,19] (**4**; 15%), D: B-friedo-olean-5-en-3β-ol[3,19] (**5**; 15%), and β-amyrin[3] (**6**; 25%). This residue was dissolved in benzene, passed through a column of silica gel (30 g), and eluted with the same solvent (each fraction 50 ml). Fractions 6—14, containing β-amyrin (**6**) and germanicol (**7**), were combined (*ca.* 133 mg) and subjected to preparative HPLC separation to afford about 30 mg of germanicol (**7**). The isolation yield of germanicol (**7**) was very poor, because the separation of **6** and **7** by HPLC was carried out with much difficulity owing to the proximity of their retention times (21.2 and 21.8 min for **7** and **6**, respectively). Recrystallization from chloroform–methanol gave pure germanicol (**7**; 10 mg), mp 177—178.5 °C, (lit, 176—177 °C,[5a] 173—175 °C,[5b] 179 °C,[5c] 176.5—177 °C,[5d] 180 °C,[5e] and synthetic *dl*-germanicol, 220—223 °C,[5f]); IR (KBr) 3450, 1630, and 840 cm^{-1}; NMR ($CDCl_3$) δ 0.74, 0.78, 0.89, 0.98, 1.02, 1.09 (each 3H, s, *t*-Me), 0.94 (6H, s, 2×*t*-Me), 3.20 (1H, dd, $J_{2\beta,3\alpha}=10$ and $J_{2\alpha,3\alpha}=5$ Hz, $C_{(3\alpha)}$–H), and 4.85 (1H, d, $J=1.5$ Hz, $C_{(19)}$–H); MS *m/e* (%) 426 (M^+; 50), 411 (31), 204 (100), 189 (83), and 177 (83).

Methylation of Germanicol (7). Potassium (100 mg) was added to a solution of germanicol (**7**; 5.7 mg) in anhydeous benzene (10 ml) and the mixture was refluxed for 2 h under a nitrogen atmosphere. A solution of methyl iodide (2 ml) in benzene (10 ml) was added and heating was continued for 4 h under reflux. After addition of methanol (2 ml) and benzene (10 ml), the organic solution was washed with water, 2M hydrochloric acid, and then with brine, dried over magnesium sulfate, and evaporated to afford a residue (7 mg). The residue was crystallized from acetone–benzene to give miliacin (**8**; 2.7 mg), mp 280—281.5 °C, (lit, 283 °C[14]); IR (KBr) 1635, 1180, 1110, 860, and 850 cm^{-1}; NMR ($CDCl_3$) δ 0.76 (6H, s, 2×*t*-Me), 0.89, 1.02, 1.08 (each 3H, s, *t*-Me), 0.95 (9H, s, 3×*t*-Me), 3.35 (3H, s, -OMe), and 4.85 (1H, d, $J=1.5$ Hz, $C_{(19)}$–H); MS *m/e* (%) 440 (M^+; 44), 425 (23), 393 (5), 204 (100), 189 (75), and 177 (63). Identification of this compound with an authentic sample (mp 282.5—283 °C) of miliacin[14] was effected on mixed mp (280—283 °C), TLC, IR, NMR, and on mass spectra.

Reaction of 3β,4β-Epoxyfriedelane (2) with Boron Trifluoride Etherate in Various Solvents. Examination of the Products by HPLC. 3β,4β-Epoxyfriedelane (**2**; 1—3 mg) dissolved in a solvent (2—10 ml) was treated with boron trifluoride etherate (2 drops) at −5 °C or at room temperature. After usual treatment, the reaction mixture was extracted with ether to give a residue on evaporation of the solvent. The residue was subjected to examination by HPLC. The results are listed in Table 1. Authentic samples (**1**, **3**—**6**, and **12**) used for an identification of the products are the compounds obtained in the previous work.[3]

References

1) A part of this work was reported in a preliminary form: M. Tori, T. Tsuyuki, and T. Takahashi, *Chem. Lett.*, **1977**, 699.

2) a) J. W. ApSimon, R. R. King, and J. J. Rosenfeld, *Can. J. Chem.*, **47**, 1989 (1969); b) P. Sengupta, B. Roy, S. Chakraborty, J. Mukherjee, and K. G. Das, *Indian J. Chem.*, **11**, 1249 (1973).

3) M. Tori, T. Torii, K. Tachibana, S. Yamada, T. Tsuyuki, and T. Takahashi, *Bull. Chem. Soc. Jpn.*, **50**, 469 (1977), and references cited therein.

4) M. Tori, K. Tachibana, Y. Moriyama, T. Tsuyuki, and T. Takahashi, *Chem. Lett.*, **1976**, 1359; K. Tachibana, M. Tori, Y. Moriyama, T. Tsuyuki, and T. Takahashi, *Bull. Chec. Soc. Jpn.*, **50**, 1552 (1977).

5) a) J. C. E. Simpson, *J. Chem. Soc.*, **1944**, 283; b) D. H. R. Barton and C. J. W. Brooks, *ibid.*, **1951**, 257; c) S. Nakamura, T. Yamada, H. Wada, Y. Inoue, T. Goto, and Y. Hirata, *Tetrahedron Lett.*, **1965**, 2017; d) T. Yamada, S. Nakamura, T. Goto, and Y. Hirata, *Nippon Kagaku Zasshi*, **86**, 1315 (1965); e) H. Wada, G. Goto, T. Goto, and Y. Hirata, *Tetrahedron Lett.*, **1966**, 3461; f) R. E. Ireland, S. W. Baldwin, D. J. Dawson, M. I. Dawson, J. E. Dolfini, J. Newbould, W. S. Johnson, M. Brown, R. J. Crawford, P. F. Hudrlik, G. H. Rasmussen, and K. K. Schmiegel, *J. Am. Chem. Soc.*, **92**, 5743 (1970).

6) H. Budzikiewicz, J. M. Wilson, and C. Djerassi, *J. Am. Chem. Soc.*, **85**, 3688 (1963).

7) D. Abramson, L. J. Goad, and T. W. Goodwin, *Phytochemistry*, **12**, 2211 (1973).

8) J. F. Keeton and M. Keogh, *Phytochemistry*, **14**, 290 (1975).

9) Taraxerol was isolated from the dry root of the common dandelion according to Burrows and Simpson's procedure (S. Burrows and J. C. E. Simpson, *J. Chem. Soc.*, **1938**, 2042).

10) 18αH-β-Amyrin was prepared from β-amyrin (**6**) according to a known method (R. Budziarek, W. Manson, and F. S. Spring, *J. Chem. Soc.*, **1951**, 3336).

11) A Chatterjee, A. B. Kundu, T. Chakrabortty, and S. Chandrasekharan, *Chem. Commun.*, **1968**, 418.

12) I. Agata, E. J. Corey, A. G. Hortmann, J. Klein, S. Proskow, and J. J. Ursprung, *J. Org. Chem.*, **30**, 1698 (1965).

13) K. Nishimoto, M. Ito, S. Natori, and T. Ohmoto, *Tetrahedron*, **24**, 735 (1968).

14) S. Abe, *Bull. Chem. Soc. Jpn.*, **33**, 271 (1960).

15) Germanicol (**7**) is considered to be derived biogenetically from an oleanane-type intermediate with a cationic center at C-19 (*cf.* Ref. 17).

16) *E.g.* D. N. Kirk and M. P. Hartshorn, "Steroid Reaction Mechamisms," Elsevier Publishing Company, Amsterdam (1968), pp. 290, 353; P. de Mayo, "Molecular Rearrangements," Vol. 2, John Wiley and Sons, Inc., New York (1964), p. 821; D. N. Kirk and P. M. Shaw, *Chem. Commun.*, **1971**, 948.

17) A. Eschenmoser, L. Ruzicka, O. Jeger, and D. Arigoni, *Helv. Chim. Acta*, **38**, 1890 (1955).

18) E. J. Corey and J. J. Ursprung, *J. Am. Chem. Soc.*, **78**, 5041 (1956); G. Brownlie, F. S. Spring, R. Stevenson, and W. S. Strachan, *J. Chem. Soc.*, **1956**, 2419; H. Dulter, O. Jeger, and L. Ruzicka, *Helv. Chim. Acta*, **38**, 1268 (1955); R. M. Coates, *Tetrahedron Lett.*, **1967**, 4143; H. W. Whitlock, Jr. and M. C. Smith, *ibid.*, **1968**, 821.

19) a) J. M. Beaton, F. S. Spring, R. Stevenson, and J. L. Stewart, *Tetrahedron*, **2**, 246 (1958); S. Chapon, *Bull. Soc. Chim. Fr.*, **1955**, 1076; b) J. H. Block and G. H. Contantine, Jr., *Phytochemistry*, **11**, 3279 (1972); G. H. Constantine, Jr. and J. H. Block, *ibid.*, **9**, 1659 (1970), and references cited therein.

20) H. N. Khastgir and P. Sengupta, *Chem. and Ind.*, **1961**, 1077; P. Sengupta and H. N. Khastgir, *Tetrahedron.*, **19**, 123 (1963).

21) J. M. Beaton, F. S. Spring, R. Stevenson, and J. L. Stewart, *J. Chem. Soc.*, **1955**, 2131.

Silyl Radicals. XV. Stereochemical Course of Chlorine Abstraction by 1-Methyl-4-*t*-butyl-1-silacyclohexyl Radicals from Polychloroalkane*

Hideki SAKURAI and Masashi MURAKAMI

Department of Chemistry, Faculty of Science, Tohoku University, Sendai 980

(Received July 11, 1977)

The isomerically pure *cis* and *trans* 1-methyl-4-*t*-butyl-1-silacyclohexane were subjected to the free radical chlorination with carbon tetrachloride in the presence of a catalytic amount of benzoyl peroxide under UV irradiation at 0 °C, affording the corresponding chlorosilanes with retention of configuration. With less reactive polyhalocarbons, however, less stereospecific products were obtained. A mechanism that inversion of silyl radicals competes with chlorine abstraction is proposed. Relative rates of each reaction were analyzed with a steady-state assumption.

During the course of the study on the Group IVB free radicals,[2] we have found that the silyl radical produced from an optically active hydrosilane undergoes chlorine-abstraction reaction mostly with retention of configuration.[3] The chiral silyl radical exists in a pyramidal form with considerable configurational stability, and retains the asymmetry prior to the abstraction of chloride from carbon tetrachloride.

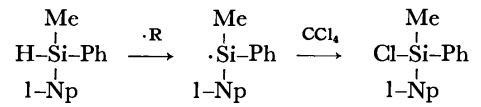

This observation has been amply supported by both other chemical[4-6] and ESR studies.[7-12] The inversion process must be slow, relative to the abstraction process, for retention of configuration to be observed.

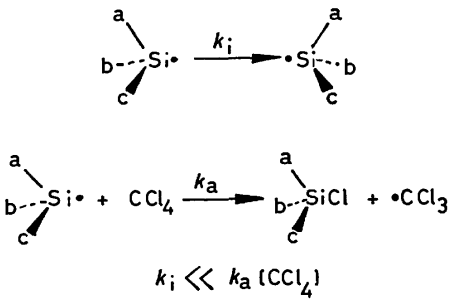

The reactivity of each enantiomeric radical generated from optically active compounds is energetically identical, because both steric and electronic environments around the radical center are equal in each enantiomeric radical. On the contrary, when a cyclic radical such as a silacyclohexyl radical is produced, it should exist as an equilibrium mixture of conformers and then reacts through energetically different pathways. Introduction of a *t*-butyl group on the ring prevents the ring inversion, then two steric courses of the reaction, *i.e.* axial and equatorial approaches to the radical become distinguishable if inversion around the radical center on silicon is slow enough for product-forming chlorine abstraction.

In this paper stereochemical course of the chlorine abstraction from polychloroalkanes by silyl radicals, which were generated from conformationally stable hydrosilanes, is discussed.

Results and Discussion

The reaction of *cis*- or *trans*-4-*t*-butyl-1-methyl-1-silacyclohexane** (Ia, Ib)[13,14] with carbon tetrachloride in the presence of dibenzoyl peroxide under UV irradiation at 0 °C proceeded stoichiometrically to give the corresponding chlorosilanes. Interestingly as observed in the chlorination of the optically active hydrosilane, the configuration of the hydrosilanes was retained in resulting 4-*t*-butyl-1-methyl-1-chloro-1-silacyclohexane

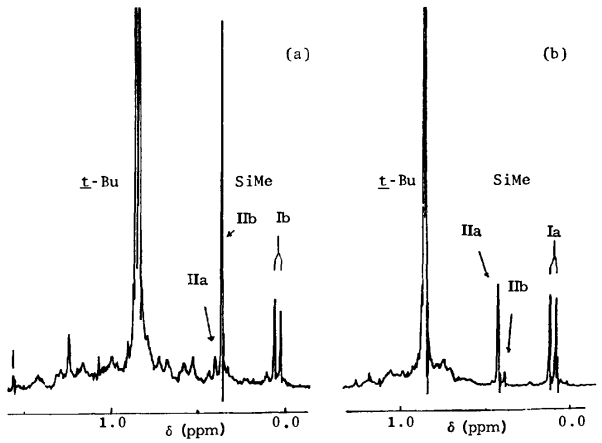

Fig. 1. NMR spectra of the reaction mixture of (a) the chlorination of (Ib) with CCl_4 and (b) the chlorination of (Ia) with CCl_4.

(II) as evidenced by NMR spectra. Figure 1 (a) shows the NMR spectra of the reaction mixture derived from the *trans*-hydrosilane (Ib). Thus, two methyl signals corresponding to *trans*- and *cis*-chlorosilane (IIb and IIa) appeared at δ 0.38 (singlet) and 0.42 (singlet), respectively, in a ratio of 94/6 in addition to the methyl signal of the unreacted *trans*-hydrosilane (Ib) at δ 0.07 (doublet). This means that the reaction proceeds with 94% retention of configuration. The *cis*-hydrosilane (Ia) gave a similar result but slightly less stereospecifically

* For part XIV, see Ref. 1.

** Throughout the paper, *cis* and *trans* are defined with respect to 4-*t*-butyl and 1-methyl groups. Suffix a is added to the *cis* compounds and b to the *trans*.

(87%), as seen in Fig. 1(b). Namely, the silyl radical obtained from (Ia) or (Ib) exists in pyramidal form and retains mostly its configuration prior to the abstraction of chlorine from carbon tetrachloride as in the case of the chiral silyl radical obtained from optically active hydrosilane[3,6] and acylsilane.[4]

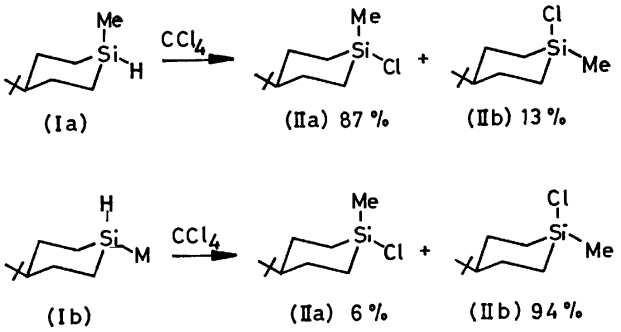

These results are in striking contrast to those observed for cyclohexyl radical.[15] Thus, *cis*- and *trans*-4-*t*-butylcyclohexane carbonyl peroxides, decomposed in carbon tetrachloride or bromotrichloromethane at 30 °C, give rise to the same products irrespective of the configuration of the starting materials.[16]

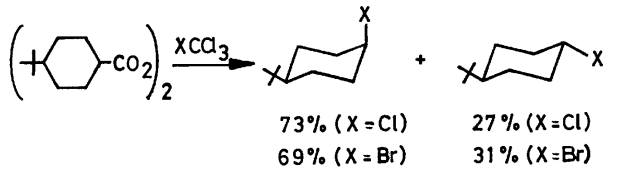

Similar results were reported in the decomposition of 1-(*cis* or *trans*-4-*t*-butylcyclohexyl)-1-methylethyl hypochlorite.[17]

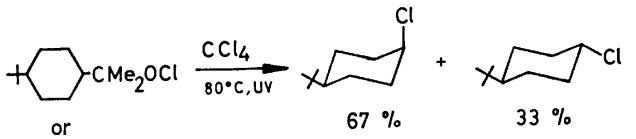

These facts requires the formation of a common intermediate from both starting substances. This is likely to be the 4-*t*-butylcyclohexyl radical which evidently reacts with a halogen donor from the two sides. The reason why the intermediate 4-*t*-butylcyclohexyl radical gives rise to the thermodynamically less favored product is ascribable either to a twist-boat conformation in the transition state[17] or, more likely, to a torsional effect at the product-forming process.[18] In any event, the intermediate cyclohexyl radicals are in a planar form or in a rapidly-equilibrated state.

Similar reactions of (I) were carried out with pentachloroethane ($CHCl_2$–CCl_3), 1,1,1,2-tetrachloroethane (CH_2Cl–CCl_3) and chloroform ($HCCl_3$). The resulting chlorosilane (II) systematically lost its configurational purity in the following order of solvent (reactants), $CCl_4 < CHCl_2CCl_3 < CH_2ClCCl_3 < HCCl_3$. In the case

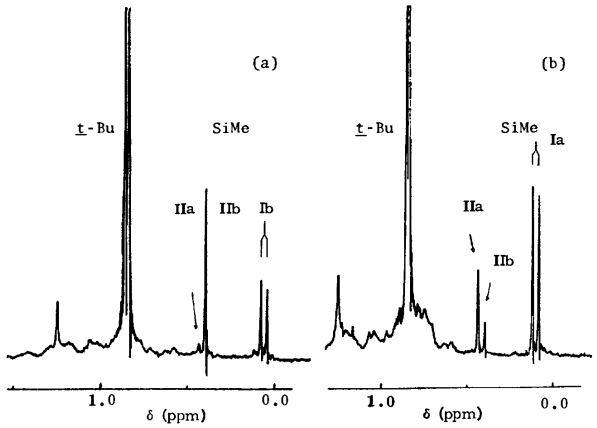

Fig. 2. NMR spectra of the reaction mixture of (a) the chlorination of (Ib) with $CHCl_2CCl_3$ and (b) the chlorination of (Ia) with $CHCl_2CCl_3$.

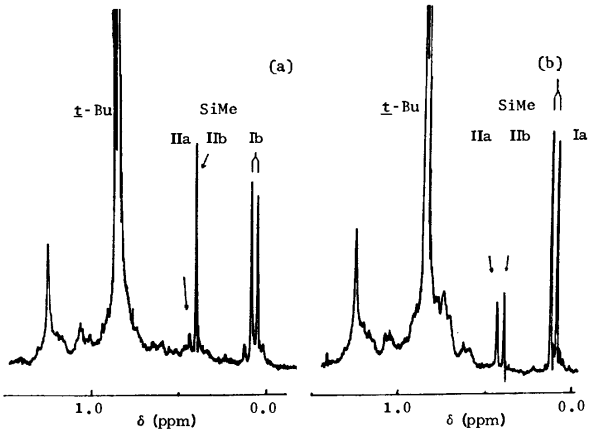

Fig. 3. NMR spectra of the reaction mixture of (a) the chlorination of (Ib) with CH_2ClCCl_3 and (b) chlorination of (Ia) with CH_2ClCCl_3.

Table 1. Reaction of (I) with polyhaloalkanes in the presence of benzoyl peroxide at 0°C

Starting material	Reactant	Reaction time (h)	Conversion (%)	Product(II) *cis*(IIa) : *trans*(IIb)
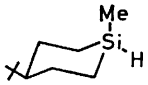 (Ia)	Cl–CCl_3	3	41	87 : 13
	$CHCl_2$–CCl_3	4	45	75 : 25
	CH_2Cl–CCl_3	4	23	57 : 43
	H–CCl_3	4.5	28	39 : 61
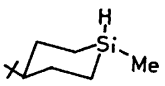 (Ib)	Cl–CCl_3	3	55	6 : 94
	$CHCl_2$–CCl_3	4	55	12 : 88
	CH_2Cl–CCl_3	6	24	18 : 82
	H–CCl_3	4	54	25 : 75

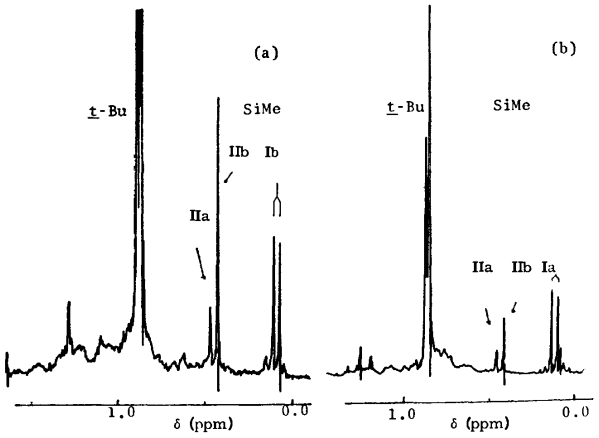

Fig. 4. NMR spectra of the reaction mixture of (a) the chlorination of (Ib) with $ZCHCl_3$ and (b) the chlorination of (Ia) with $CHCl_3$.

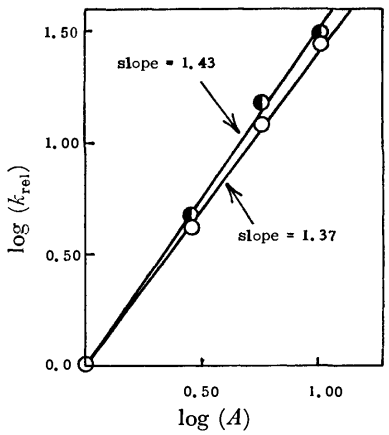

Fig. 5. Correlation between the logarithum of the relative reactivities of both *cis*- (◐) and *trans*- (○) silacyclohexyl radicals (vertical), and logarithum of the relative reactivities of triethylsiyl radicals (horizontal) in chlorine abstraction.

starting from the *cis*-hydrosilane (Ia), intensities of the methyl signal of the *cis*-chlorosilane (IIa) decrease gradually from in carbon tetrachloride to in chloroform. A similar trend can be seen for the case of *trans*-hydrosilane (Ib). These trends can be seen well qualitatively in Figs. 2—5. Quantitative determination of ratios of two isomeric chlorosilanes was performed by integrating the expanded NMR spectra. Generally, it is not easy to get precise integration for two near-by peaks on NMR, although fairly good reproducibility was observed in this particular case (Table 1). Therefore, care must be taken for detailed discussion, but the present data are still pertinent to an approximate kinetic analysis as shown in the next section.

The rate of abstraction of a chlorine atom from carbon tetrachloride is fast compared to the rate of inversion of silyl radicals.[6] On the contrary, the rate of abstraction of a chlorine atom from chloroform may be comparative to the rate of inversion of the same silyl radicals. There fore, net stereochemistry depends on both relative rates of chlorine abstraction and conformational stabilities of silacyclohexyl radicals as shown in the following scheme.

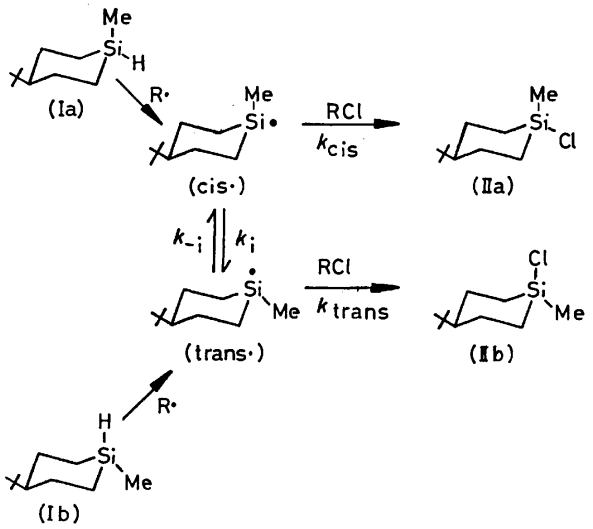

From this scheme using the relevant rate constants shown above, the *cis*/*trans* product ratio (*c*/*t*) can be expressed by the formula

$$(c/t) = (k_{cis}/k_{trans})([cis\cdot]/[trans\cdot]), \quad (1)$$

where [*cis*·] and [*trans*·] are the concentrations of *cis* and *trans* radicals, respectively. The *cis*/*trans* product ratio from *cis* hydrosilane (Ia), $(c/t)_{cis}$, can be derived as follows by assuming the steady-state concentration of the *trans* radical.

$$d[trans\cdot]/dt = k_i[cis\cdot] - k_{-i}[trans\cdot] - k_{trans}[trans\cdot][RCl] = 0, \quad (2)$$

$$[cis\cdot]/[trans\cdot] = (k_{-i}/k_i) + (k_{trans}/k_i)[RCl],$$

$$(c/t)_{cis} = (k_{cis}/k_{trans})(k_{-i}/k_i) + (k_{cis}/k_i)[RCl]. \quad (3)$$

Similarly one can obtain the *trans*/*cis* product ratio from *trans* hydrosilane (Ib), $(t/c)_{trans}$, by assuming the steady-state of the *cis* radical derived from *trans*-hydrosilane (Ib).

$$(t/c)_{trans} = (k_{trans}/k_{cis})(k_i/k_{-i}) + (k_{trans}/k_{-i})[RCl]. \quad (4)$$

Combination of Eqs. 3 and 4 yields

Table 2. Relative rate constants[a]

Reactant	concn (mol/l)	K	k_{trans}/k_{-i}	k_{cis}/k_i	A[b]
$Cl\text{-}CCl_3$	10.6	2.2	1.3(27)	0.59(33)	11.4
$CHCl_2\text{-}CCl_3$	8.31	2.1	0.63(13)	0.30(17)	6.18
$CH_2Cl\text{-}CCl_3$	9.45	2.4	0.23(4.8)	0.096(5.3)	3.07
$H\text{-}CCl_3$	12.4	2.4	0.048(1.0)	0.018(1.0)	1.00
			$\rho^*=0.46$[c]		$\rho^*=0.29$[c]

a) For definition of the symbols, see text. b) Relative reactivities of polyhaloalkanes in the chlorine abstraction by the triethylsilyl radical, see text. c) Reaction constants in the Taft equation.

$$K = (k_{trans}/k_{cis})(k_i/k_{-i}) = \frac{1+(t/c)_{trans}}{1+(c/t)_{cis}}.$$

Then values of $K=(k_{trans}/k_{cis})(k_i/k_{-i})$, (k_{trans}/k_{-i}) and (k_{cis}/k_i) can be calculated from the respective product ratios. These are listed in Table 2. Since it is reasonable to assume that the rate constants of inversion process are invariant regardless of the nature of the solvents used in this study, (k_{trans}/k_{-i}) and (k_{cis}/k_i) indicate the relative reactivities of both *trans* and *cis* radicals toward polyhalomethanes, respectively. These relative reactivities are also listed in parenthases in Table 2. Values of *cis* radicals agree with those of *trans* radicals within a possible experimental error.

Nagai and co-workers[19] reported that the reaction of the triethylsilyl radical with polychloroalkanes, X–CCl_3, where X stands CH_3, H, CH_2Cl, $CHCl_2$, CCl_3, and Cl, proceeded stoichiometrically to give X–CCl_2H, and that the relative reactivities increase in this order. For particular polyhaloalkanes such as $HCCl_3$, CH_2ClCCl_3, $CHCl_2CCl_3$, and CCl_4, they reported values of relative reactivity (k_{X-CCl_3}/k_{HCCl_3}) of chlorine abstraction toward the triethylsilyl radical at 80 °C to be 1.00, 3.07, 6.18 and 11.4, respectively. These relative reactivities derived from competitive experiments were treated by the Taft equation[20] with ρ^* values ranged from 0.26 to 0.29.[19]

The logarithms of relative reactivities toward silacyclohexyl radicals obtained in this study can be correlated strikingly well (correlation coefficient=0.999) with those toward triethylsilyl radicals as shown in Fig. 5. Higher selectivities of silacyclohexyl radicals than triethylsilyl radicals can be attributed to the temperature difference in the extent of 80 °C between two experiments which is reflected in a larger ρ^* value of the Taft equation of 0.46 in the present study.

The K $[K=(k_{trans}/k_{cis})(k_i/k_{-i})]$ values are almost constant irrespective of the solvents, as can be seen in Table 2. Since k_i and k_{-i} are unimolecular rate constants and must be invariant in a series of similar solvents, k_i/k_{-i} should be constant in the present case. Nagai *et al.* have also demonstrated that the reactivity of silyl radicals toward chlorine abstraction is rather insensitive to the structure of the radicals at the fixed condition.[19] Therefore, it seems to be reasonable to get constant K values.

As a conclusion, the remarkable configurational stability of silyl radicals is again demonstrated not only qualitatively but also semi-quantitatively.

Experimental

Materials. The required samples of *cis* and *trans*-4-*t*-butyl-1-methyl-1-silacyclohexane (Ia and Ib), and *cis*- and *trans*-4-*t*-butyl-1-methyl-1-chloro-1-silacyclohexane (IIa and IIb) were prepared as described in the previous paper.[13,14] Pentachloroethane ($CHCl_2$–CCl_3), 1,1,1,2-tetrachloroethane (CH_2Cl–CCl_3) and dibenzoyl peroxide were commercially available materials of the reagent grade.

Reaction of cis- *or* trans-*4-t-Butyl-1-methyl-1-silacyclohexane (Ia or Ib) with Polyhaloalkanes in the Presence of Dibenzoyl Peroxide (BPO).* Appropriate solutions (*ca.* 5%) of (Ia) or (Ib) in polyhaloalkanes (CCl_4, $CHCl_2CCl_3$, CH_2ClCCl_3, and $CHCl_3$) were prepared in NMR tubes. These were bubbled and filled with dry nitrogen and sealed with stoppers. These tubes were irradiated with a high-pressure mercury arc lamp (450 W, with a Pyrex filter) in an ice bath.

The color of the reaction mixtures changed to pale yellow. From the NMR spectra and GLC, the reaction mixture contained only 4-*t*-butyl-1-methyl-1-chloro-1-silacyclohexane (II) as a single product and the unchanged (I) as silicon-containing materials. The product and unchanged silane were identified by the way of NMR spectra and retention times of GLC by comparing with those of authentic samples.

The ratio of (II) and unchanged (I), and the conformational isomer ratio of each material were determined by means of NMR integration of Si–Me signals.

References

1) H. Sakurai, M. Kira, and M. Sato, *Chem. Lett.*, **1974**, 1323.
2) H. Sakurai, "Free Radicals," Vol. 2, ed by J. K. Kochi, John Wiley, New York, N. Y. (1973), Chap. 25.
3) H. Sakurai, M. Murakami, and M. Kumada, *J. Am. Chem. Soc.*, **91**, 519 (1969).
4) A. G. Brook and J. M. Duff, *J. Am. Chem. Soc.*, **91**, 2118 (1969).
5) H. Sakurai and M. Murakami, *Chem. Lett.*, **1972**, 7.
6) L. H. Sommer and L. A. Ulland, *J. Org. Chem.*., **37**, 3878 (1972).
7) P. J. Krusic and J. K. Kochi, *J. Am. Chem. Soc.*, **91**, 3938 (1969).
8) J. Cooper, A. Hudson, and R. A. Jackson, *Mol. Phys.*, **23**, 3938 (1972).
9) S. W. Bennet, C. Eaborn, A. Husdon, H. A. Hussain, and R. A. Jackson, *J. Organomet. Chem.*, **16**, 36 (1969).
10) S. W. Bennet, C. Eaborn, A. Hudson, R. A. Jacson, and K. D. Root, *J. Chem. Soc., A*, **1970**, 348.
11) H. Sakurai, K. Ogi, A. Hosomi, and M. Kira, *Chem. Lett.*, **1974**, 891.
12) J. H. Sharp and M. C. A. Symons, *J. Chem. Soc., A*, **1972**, 3084.
13) H. Sakurai and M. Murakami, *J. Am Chem. Soc.*, **94**, 5082 (1972).
14) H. Sakurai and M. Murakami, *Bull. Chem. Soc. Jpn.*, **49**, 3185 (1976).
15) O. Simamura, "Topics in Stereochemistry," Vol. 4, ed by E. L. Eliel and N. L. Allinger, John Wiley & Sons (1968), pp. 1—38.
16) F. D. Greene, C. -C. Chu, and J. Walia, *J. Org. Chem.*, **29**, 1285 (1964).
17) F. D. Greene, C. -C. Chu, and J. Walia, *J. Am. Chem. Soc.*, **84**, 2463 (1962).
18) F. R. Jensen, L. H. Gale, and J. E. Rodgers, *J. Am. Chem. Soc.*, **90**, 5793 (1968).
19) (a) Y. Nagai, I. Shiojima, K. Nishiyama, and H. Matsumoto, *Yuki Gosei Kagaku Kyokai Shi*, **26**, 999 (1968); (b) Y. Nagai, K. Yamazaki, I. Shiojima, M. Hayashi, and H. Matsumoto, *ibid.*, **26**, 1004 (1968).
20) R. W. Taft, Jr., "Steric Effects in Organic Chemistry," ed by M. S. Newman, Wiley (1956), p. 556.

Hetera-*p*-carbophanes. IX. Effect of the Chain-Length of Alkoxyl Groups on the Barrier to Internal Rotation of Dialkoxybenzene Rings in Dialkoxydioxodioxa[*n*]paracyclophanes[1]

Kazuhiko SAKAMOTO and Michinori ŌKI*

Department of Chemistry, Faculty of Science, The University of Tokyo, Hongo, Tokyo 113

(Received July 21, 1977)

Dioxodioxa[*n*]paracyclophanes which carry two methoxyl, ethoxyl, or propoxyl groups at the aromatic rings were prepared by condensation of α,ω-diols with corresponding 2,5-dialkoxy-1,4-phenylenediacetyl dichlorides under high dilution conditions. Dynamic ^{1}H NMR spectra of these compounds show that barriers to internal rotation of the dialkoxybenzene rings are affected by the chain-length of the alkoxyl groups; the longer the chain length, the higher the barrier.

It has been well documented that the steric hindrance of the alkyl group toward reactivities of organic compounds increases as the chain-length of the alkyl group increases. A typical example is the reactivity of carbonyl groups in alkyl methyl ketones (**1**) toward sodium hydrogen sulfite:[2] the reactivity decreases as the chain-length increases. Likewise, the chain-length of alkyl groups is known to play some role in the internal rotation of molecules. The rates of racemization of 2′-alkoxy-6-nitrobiphenyl-2-carboxylic acids (**2**) are affected by the chain-length of the alkyl group and the half-lives of **2** are 1 : 5 : 9 at *ca.* 18 °C for methyl, ethyl, and propyl compounds, respectively.[3] An apparently reverse

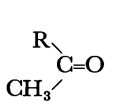

(**1**)

R = CH_3, CH_3CH_2, or $CH_3CH_2CH_2$

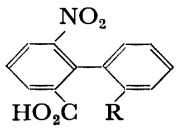

(**2**)

R = CH_3, CH_2CH_2, or $CH_3CH_2CH_2$

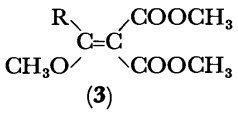

(**3**)

R = CH_3 or CH_3CH_2

phenomenon is observed in the internal rotation about the C_{sp^2}–R bond of dimethyl 1-methoxyalkylidenemalonates (**3**): the barrier lowers when R changes from methyl to ethyl.[4] This anomaly is, however, attributed to the steric effect which stabilizes the ground state to a greater extent than the transition state for rotation.

In any event, the change in barriers for internal rotation discussed above is 1 kcal/mol at the most. This small increase may be interpreted as such that the alkyl group takes a conformation, in which the steric effect is given by a first atom or group of the chain and the rest is located far from the site of direct interaction. Evidence for this consideration is found in ultraviolet spectral data which show that 2-alkylbiphenyls, where the alkyl is a straight chain, give absorption at almost the same wavelength.[5] This restriction of conformation, of course, causes the decrease in entropy in the transition state. Indeed, Hall and Harris found that the difference in the free energies of activation for rotation of compounds **2** is attributable to the difference in entropies of activation.[6]

We have briefly reported in a recent paper[7] that the barrier to internal rotation of cyclophanes is greatly influenced by the chain length of the alkoxyl groups which are attached to the benzene ring. The phenomenon was attributed to the fact that the steric hindrance is given not only by an atom or a group which is directly attached to the benzene ring in question but by the group as a whole. The group itself must pass a space provided by the ansa chain and the benzene ring for racemization of the compounds. Then a large difference in barriers is expected on elongating the chain length in contrast to the cases cited above. Our data presented before[7] give only the smallest limit (>1.0 kcal/mol) of difference and more work is needed to find the change in energies by lengthening the alkoxyl chain.

In this paper, we wish to describe the syntheses of dialkoxydioxodioxa[*n*]paracyclophanes, of which the alkoxyl groups are either methoxyl, ethoxyl, or propoxyl, and finding a large change in barriers due to the change in the alkoxyl group, as obtained by the ^{1}H DNMR method.

Experimental

The syntheses of dialkoxydioxodioxa[*n*]paracyclophanes (**4**$_n$, **5**$_n$, and **6**$_n$) were accomplished by condensation of α,ω-diols with 2,5-dialkoxy-1,4-phenylenediacetyl dichlorides under high dilution conditions as reported previously.[8]

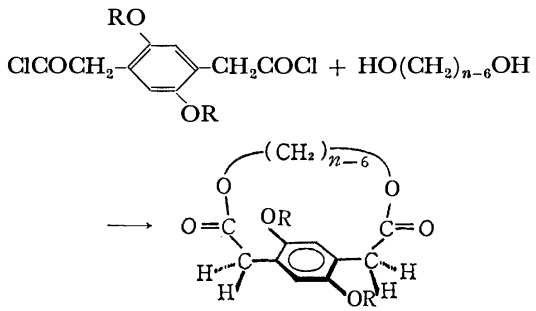

4: R = CH_3
5: R = CH_2CH_3
6: R = $CH_2CH_2CH_3$

The diols were of commercial origin except for 1,11-undecanediol which was prepared by lengthening the chain of 1,9-nonanediol. 1,9-Nonanediol was treated with hydrogen bromide followed by sodium cyanide in dimethyl sulfoxide to give undecanedinitrile which was hydrolyzed and esterified to

give the corresponding diester. Lithium aluminium hydride reduction of the ester gave 1,11-undecanediol, mp 57—60 °C (lit,[9] mp 62.0—62.5 °C). IR (KBr) 3300 cm^{-1} (ν_{OH}). Overall yield was *ca.* 50%.

2,5-Dialkoxy-1,4-phenylenediacetyl dichlorides were known compounds[7] except for the 2,5-dipropoxy compound of which synthesis is described below.

1,4-Dipropoxybenzene. To a solution of hydroquinone (11 g, 0.1 mol) and sodium hydroxide (8.8 g, 0.22 mol) in 200 ml of water was added 43 g of propyl tosylate, which was prepared from 1-propanol and *p*-toluenesulfonyl chloride,[10] in small portions. The mixture was heated under reflux for 20 h with stirring. The reaction mixture was extracted with ether and the extract was washed with 6 M hydrochloric acid and then with cold water. After drying over magnesium sulfate, the extract was evaporated to give a pale yellow residue. Recrystallization from CH_2Cl_2–CCl_4 gave 7.0 g (36%) of the desired material, mp 48.0—49.5 °C. IR (KBr) ν_{C-O} 1220, 1025 cm^{-1}. NMR ($CDCl_3$) δ=6.82 (s, 4H), 3.85 (t, J=6.5 Hz, 4H), 1.75 (sestet, J=*ca.* 6.5 Hz, 4H), 1.02 (t, J=*ca.* 6.5 Hz, 6H).

α^1,α^4-Dichloro-2,5-dipropoxy-1,4-xylene. A mixture of 1,4-dipropoxybenzene (7.0 g, 0.035 mol), 37% formalin (6.6 g), concentrated hydrochloric acid (40 ml), and glacial acetic acid (35 ml) was warmed at 50—60 °C for 1.5 h with stirring and introducing dry hydrogen chloride. The resulting solid was collected by filtration and was washed with water. Recrystallization from CH_2Cl_2–CCl_4 gave 8.0 g (78%) of the pure material, mp 79.5—81.0 °C. IR (KBr) ν_{C-O} 1230, 1030 or 1050 cm^{-1}. NMR ($CDCl_3$) δ=6.92 (s, 2H), 4.63 (s, 4H), 3.96 (t, J=6.5 Hz, 4H), 1.84 (sestet, J=*ca.* 6.5 Hz, 4H), 1.08 (t, J=*ca.* 6.5 Hz, 6H).

α^1,α^4-Dicyano-2,5-dipropoxy-1,4-xylene, mp 107.0—108.0 °C (recrystallized from ether–hexane), was prepared from the above dichloride by treatment with sodium cyanide[7] in *ca.* 90% yield. IR (KBr) $\nu_{C\equiv N}$ 2250, ν_{C-O} 1240 and 1030 cm^{-1}. NMR ($CDCl_3$) δ=6.92 (s, 2H), 3.95 (t, J=6.5 Hz, 4H), 3.70 (s, 4H), 1.84 (sestet, J=*ca.* 6.5 Hz, 4H), 1.06 (t, J=*ca.* 6.5 Hz, 6H). Found: C, 70.76; H, 7.52; N, 10.45%. Calcd for $C_{16}H_{20}N_2O_2$: C, 70.56; H, 7.40; N, 10.29%.

2,5-Dipropoxy-1,4-phenylenediacetic Acid. A mixture of the dicyanide (6.5 g, 0.24 mol), ethylene glycol monomethyl ether (50 ml), and sodium hydroxide (5.0 g) in 20 ml of water was refluxed until a homogeneous solution resulted. The reaction mixture was then diluted with 50 ml of cold water, cooled, and poured with stirring into 50 ml of concentrated hydrochloric acid to yield 5.0 g (67%) of a crude product. After purification, the product melted at 200.0—203.0 °C with decomposition. IR (KBr) $\nu_{C=O}$ 1710, ν_{C-O} 1240 and 1030 cm^{-1}.

2,5-Dipropoxy-1,4-phenylenediacetyl dichloride was obtained by a reaction of thionyl chloride with the diacid in dry ether. The yield was 70%. Mp 106.0—107.0 °C (recrystallized from ether). IR (KBr) $\nu_{C=O}$ 1810, ν_{C-O} 1230 and 1000 cm^{-1}. NMR ($CDCl_3$) δ=6.72 (s, 2H), 4.10 (s, 4H), 3.89 (t, J=6.5 Hz, 4H), 1.79 (sestet, J=*ca.* 6.5 Hz, 4H), 1.13 (t, J=*ca.* 6.5 Hz, 6H).

Syntheses of Dialkoxydioxodioxa[n]*paracyclophanes* (**4**$_n$, **5**$_n$, *and* **6**$_n$). The method of syntheses of the paracyclophanes was essentially the same as reported previously.[8] The products were purified by column chromatography on silica gel. Either hexane–benzene or hexane–ether was used for both chromatography and recrystallization. Melting points, analytical data, and solvents of recrystallyzation are summarized in Table 1.

Measurement of Spectra. The infrared spectra were recorded on a Hitachi EPI-G2 spectrometer as KBr discs or neat liquid. The ^1H NMR spectra were measured on a Hitachi R-20B spectrometer with a variable temperature accessory, operating at 60 MHz. The chemical shifts at lower temperatures than 34 °C were recorded with the use of TMS as an internal standard, whereas those at higher temperatures were recorded relative to internal $Cl_2CHCHCl_2$ and converted to the usual δ scale. The temperature reading was calibrated by measuring the chemical shift difference between methyl and hydroxyl protons of methanol at the lower temperatures, whereas the chemical shift difference between methylene and hydroxyl protons of ethylene glycol was used for the higher temperatures. The mass spectra were observed on a Hitachi RMU-6L spectrometer.

Table 1. Dialkoxydioxodioxa[*n*]paracyclophanes

Compound	Molecular formula	Mp(°C)	Analytical data[a] C(%)	Analytical data[a] H(%)	Mol wt[a] (M^+)	Solvent of recrystallization	Yield (%)
4$_{15}$	$C_{21}H_{30}O_6$	61.5—62.5	66.56	8.08	378	hexane	17
			66.64	7.99	378.5		
4$_{16}$	$C_{22}H_{32}O_6$	63.0—64.0	67.26	8.50	392	hexane	20
			67.32	8.22	392.5		
4$_{17}$	$C_{23}H_{34}O_6$	74.5—75.0	67.92	8.33	406	hexane–ether	
			67.96	8.43	406.5		
5$_{16}$	$C_{24}H_{36}O_6$	oil	68.31	8.82	420		
			68.55	8.63	420.5		
5$_{17}$	$C_{25}H_{38}O_6$	50.0—51.0	68.80	8.81	434	hexane–ether	
			69.10	8.81	434.6		
5$_{18}$	$C_{26}H_{40}O_6$	oil	69.91	9.25	448		
			69.61	8.99	448.3		
6$_{17}$	$C_{27}H_{42}O_6$	oil	69.82	9.39	462		
			70.09	9.15	462.3		
6$_{18}$	$C_{28}H_{44}O_6$	oil	70.86	9.60	476		
			70.56	9.30	476.3		

a) The upper numerical values are those found experimentally and the lower are the calculated.

Results and Discussion

For the convenience of discussion, compounds are denoted by bold face numbers with suffixes. The suffix corresponds to the length of the ansa chain.

Due to wide variety of coalescence temperatures and solubility, it was not possible to obtain spectra at appropriate temperatures with the use of a single solvent. Although this could cause, in principle, change in barriers, the barrier to rotation is known to be affected by solvent to a small extent expect special cases such as hydrogen bond formation.[11] Thus we discuss the barrier neglecting the solvent effect. Large differences shown below will allow such an approximation.

Heavy overlap of the signals handicapped the total line shape analysis and data so obtained are not expected to be highly reliable. Therefore we limited the investigation to obtaining the free energies. The discussion given below does have drawbacks due to comparison of free energies at different temperatures, yet it is valid because the difference in free energies are large enough to make the contribution of the entropy factor minor.

DNMR Spectra and Rotational Barriers. ^{1}H NMR spectral data of dialkoxydioxodioxa[*n*]paracyclophanes (**4**$_n$, **5**$_n$, and **6**$_n$) at 34 °C are summarized in Table 2. Geminal benzylic protons of **4**$_{15}$, **4**$_{16}$, **5**$_{16}$, **5**$_{17}$, **6**$_{17}$, and **6**$_{18}$ give AB type signals which suggest that the internal rotation of the dialkoxybenzene ring is slow on the NMR time scale. In contrast, those which carry longer ansa chains in the series of **4** and **5** give singlets for benzylic protons to indicate that the internal rotation in these compounds is fast. Thus the temperatures of measurement were varied to see possible coalescence phenomena. By observing coalescence temperature (T_c), difference ($\Delta\delta_{AB}$) in chemical shifts of the AB protons, and the coupling constant (J_{AB}), the barrier to rotation should be obtained by applying the following equation.[12]

$$\Delta G_c^{\neq} = 4.57T_c\{9.97+\log_{10}(T_c/\sqrt{\Delta\delta_{AB}^2+6J_{AB}^2})\}.$$

The line shape of the AB quartets due to benzylic protons of **4**$_{15}$, **5**$_{16}$, and **6**$_{17}$ does not show any essential change on raising the temperature up to 190 °C. The barriers to rotation in these compounds are estimated to be over 23 kcal/mol. In contrast, the AB quartets due to benzylic protons of **4**$_{16}$, **5**$_{17}$, and **6**$_{18}$ coalesce on raising the temperature, as is illustrated in Fig. 1. taking **5**$_{17}$ as an example.

The sharp singlet due to benzylic protons of **4**$_{17}$ broadened considerably on lowering the temperature and finally split into an AB quartet, although the downfield part of the quartet was masked by the signals due to CH_2's alpha to ether oxygens and by that of methoxyl groups. The coalescence temperature of the benzylic methylene signals of **4**$_{17}$ in CS_2–$CDCl_3$ (v/v 3:1) was −52 °C. Likewise the coalescence temperature of signals due to benzylic protons in **5**$_{18}$ was found to be −69 °C.

The AB signals due to benzylic protons of **4**$_{17}$ and **5**$_{18}$ were still dull at the lowest temperature attainable with the instrument. Thus exact values of $\Delta\delta_{AB}$ for both com-

Table 2. Spectral data of dialkoxydioxodioxa[*n*]paracyclophanes

Compound	^{1}H NMR (δ) Ar–H	OCH_3 or OCH_2 or OCH_2	CH_3 or CH_2	CH_3	$COOCH_2$	CH_2CO[a]	β-CH_2[b]	Other CH_2's	Solvent	IR(cm^{-1}) State	$\nu_{c=o}$	ν_{c-o}
4$_{15}$	6.69	3.79			4.03	3.48 (J=15.0, $\Delta\delta$=41.2)	1.50	1.11[c]	$CDCl_3$	KBr	1730	1220, 1055
4$_{16}$	6.69	3.78			4.09	3.48 (J=14.7, $\Delta\delta$=39.9)	1.50	1.15[c]	CCl_4	KBr	1725	1220, 1055
4$_{17}$	6.62	3.72			4.00	3.42 (singlet)	1.52	1.18[c]	CS_2	KBr	1730	1225, 1050
5$_{16}$	6.68	3.97	1.41		4.04	3.48 (J=14.8, $\Delta\delta$=41.7)	1.8—1.0[d]		CCl_4	neat	1735	1210, 1050
5$_{17}$	6.69	3.96	1.39		4.05	3.49 (J=14.9, $\Delta\delta$=39.0)	1.9—0.9[d]		CCl_4	KBr	1720, 1740	1220, 1060
5$_{18}$	6.58	3.87	1.33		3.97	3.42 (singlet)	1.8—0.9[d]		CS_2	neat	1735	1215, 1055
6$_{17}$	6.67	3.87	1.8	1.07	4.09	3.49 (J=15.0, $\Delta\delta$=39.7)	1.9—1.0[d]		CCl_4	neat	1735	1215, 1070
6$_{18}$	6.66	3.85	1.7	1.04	4.05	3.48 (J=15.1, $\Delta\delta$=39.9)	1.8—0.9[d]		CCl_4	neat	1735	1210, 1070

a) These signals are of AB type unless otherwise stated. Center of the chemical shifts, coupling constant, and difference in chemical shifts of two protons (in Hz) are shown. b) Relative to ether oxygen of the ester. c) Broad singlets. d) The signals are not resolved enough for identification.

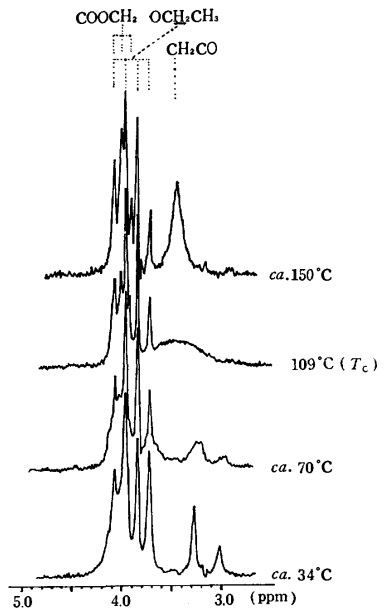

Fig. 1. DNMR Spectra of $\mathbf{5}_{17}$ in HCB.

pounds and that of J_{AB} for $\mathbf{5}_{18}$ could not be obtained. Then $\Delta\delta_{AB}$ and J_{AB} of $\mathbf{6}_{17}$ in CS_2 at 34 °C must be diverted to $\mathbf{4}_{17}$ and $\mathbf{5}_{18}$: this operation should not cause serious errors in barriers since the structures of these compounds are alike. The results are summarized in Tables 3 and 4. Data[7] of dialkoxydioxodiaza[*n*]-paracyclophanes (**7** and **8**) and dimethyldioxodioxa[*n*]-paracyclophanes (**9**) are also included for comparison.

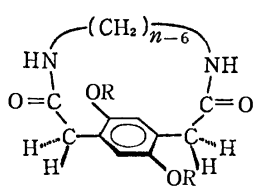

7: R=CH_3
8: R=CH_2CH_3

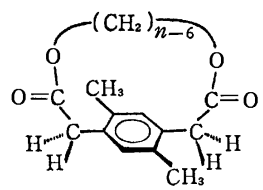

9

Table 3. ^{1}H NMR Data of geminal benzyl protons of substituted hetera-*p*-carbophanes[a]

Compound	$\Delta\delta_{AB}$(Hz)	J_{AB}(Hz)	T_c(°C)	Solvent[b]
$\mathbf{4}_{15}$	41.3	14.6	>190	HCB
$\mathbf{4}_{16}$	40.9	14.3	164	HCB
$\mathbf{4}_{17}$	(40.0)	15.0	−52	CS_2–$CDCl_3$(v/v 3:1)
$\mathbf{5}_{16}$	42.9	14.5	>190	HCB
$\mathbf{5}_{17}$	39.2	14.8	109	HCB
$\mathbf{5}_{18}$	(40.0)	(15.0)	−69	CS_2
$\mathbf{6}_{17}$	39.7	14.7	>190	HCB
$\mathbf{6}_{18}$	37.8	15.1	102	HCB
$\mathbf{7}_{16}$	36.8	14.4	>174	$CHCl_2CHCl_2$
$\mathbf{7}_{18}$	(39.8)	(14.4)	<−50	$CDCl_3$
$\mathbf{8}_{18}$	(39.8)	(14.4)	−30	$CDCl_3$
$\mathbf{9}_{15}$	16.7	13.6	189	HCB
$\mathbf{9}_{16}$	12.1	14.3	−50	CS_2–$CDCl_3$(v/v 3:1)

a) The values in parentheses are assumed ones. See the text and Ref. 7. b) HCB=hexachloro-1,3-butadiene.

Table 4. Free energies of activation for rotation of substituted benzene rings at coalescence temperatures (kcal/mol)

Diaza series				
Substituents at the aromatic ring		CH_3O (**7**)	CH_3CH_2O (**8**)	
Ansa-chain length	16	>22.2		
	18	<10.9	11.9	
Dioxa series				
Substituents at the aromatic ring		CH_3O (**4**)	CH_3CH_2O (**5**)	$CH_3CH_2CH_2O$ (**6**)
Ansa-chain length	15	>23.1		
	16	21.7	>23.0	
	17	10.7	18.9	>23.1
	18		9.8	18.5
Dioxa series				
Substituents at the aromatic ring		CH_3 (**9**)		
Ansa-chain length	15	23.3		
	16	11.0		

Effect of Rigidity of the Ansa Chain on the Rotational Barriers. It is well known that formal single bonds (C–N and C–O) of amides and ester groups often have considerable double bond character due to delocalization of the lone pair electrons as is visualized by the canonical forms:

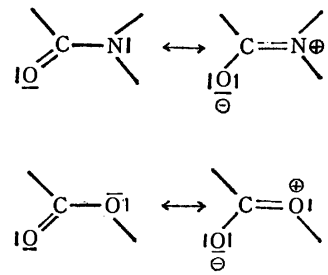

Contribution of these canonical forms with a double bond between C and N or between C and O raises the barrier to rotation about the bond in question by lowering the ground state and/or raising the transition state for rotation. Since contribution of the dipolar structure of amides is larger than that of esters, the barriers to internal rotation of amides[13] are usually higher than those of esters.[14] In other words, a chain containing amide groups is considered to be more rigid than that containing ester groups. The cyclophanes dealt with here and elsewhere[7] consitute a series to be compared from the stand point of the rigidity of the chain.

Inspection of Table 4 reveals that an amide with two ethoxyl groups ($\mathbf{8}_{18}$) has a higher barrier to rotation of the diethoxybenzene ring than an ester having the same groups ($\mathbf{5}_{18}$) by 2.1 kcal/mol. Since the coalescence temperature of $\mathbf{8}_{18}$ is higher than that of $\mathbf{5}_{18}$, the difference in enthalpies of activation may be still larger. Similar comparison is made between $\mathbf{7}_{16}$ and $\mathbf{4}_{16}$ to show that the amide gives a higher barrier by at least 0.5 kcal/mol. Thus if we compare the barriers to rotation of the dialkoxybenzene ring in diamides with that in

diesters with the same ansa-chain length, the barriers are always higher in amides. This must be a reflection of the fact that the higher mobility makes it easier for the ansa chain to take a suitable conformation to rotation of the substituted benzene ring.

Effect of the Chain Lengths of Alkoxyl Groups on Rotational Barriers. A recent report from this laboratory has revealed that $\mathbf{4}_{16}$ with two methoxyl groups at the aromatic ring possesses a higher barrier to rotation of the aromatic ring than $\mathbf{9}_{16}$ with two methyl groups by 10.7 kcal/mol.[15] This result was attributed to the steric hindrance of the methoxyl group, given not only by the oxygen atom but by the group as a whole: the methoxyl group must be bulkier than the methyl if the whole group is considered. The phenomenon makes a sharp contrast to the fact that the methoxyl group is generally considered to be of less effective bulkiness than the methyl as is shown by a typical example of barriers to rotation of 2'-substituted 5'-methyl-6-nitrobiphenyl-2-carboxylic acids.[16]

By finding an example of a methoxyl group giving its steric hindrance as a whole, comparison of the steric effect given by a series of straight chain alkyl groups becomes of interest. This is a reason why various dialkoxydioxodioxa[*n*]paracyclophanes were prepared to examine the barriers. Comparison of the data in Table 4 indicates that changing the alkoxyl group from methoxyl to ethoxyl causes the increase in the barrier to rotation by 8.2 kcal/mol in the series of 17-membered ansa chain. Similarly the barrier increases by at least 4.2 kcal/mol on going from ethoxyl to propoxyl in the same series. The same change in the series of 18-membered ansa chain causes the increase of 8.7 kcal/mol. The dramatic change in rotational barriers reflects a fact that the whole substituent must pass through a space, probably as a folded form, provided by the ansa-chain and the benzene ring. In sharp contrast to the fact that the chain-lengthening of the alkyl group usually affects the barriers to rotation to a small extent (1 kcal/mol or less), the steric effect presented here increases by 8—9 kcal/mol by lengthening the chain by but one carbon. This finding is a support for an assumption that the steric effect is often given by the first atom or group in the chain and gives a measure for the bulkiness of the alkoxyl group as a whole.

Effect of the Ansa-Chain Length on the Rotational Barriers. The difference ($\Delta\Delta G^{*}$) in free energies of activation for rotation of the aromatic rings in $\mathbf{9}_{15}$ and $\mathbf{9}_{16}$ with two methyl groups has been reported to be 12.3 kcal/mol.[8] $\Delta\Delta G^{*}$ between $\mathbf{4}_{16}$ and $\mathbf{4}_{17}$ of the dimethoxy series and that between $\mathbf{5}_{17}$ and $\mathbf{5}_{18}$ of the diethoxy series are 10.0 and 9.1 kcal/mol, respectively.

Although it is not possible to compare the whole series to investigate the effect of lengthening the ansa-chain on barriers to rotation, the effect of lengthening the ansa-chain by one on the barriers should become small, in principle, if the ansa-chain length is long enough. The present series represents a part of such tendency. Namely $\Delta\Delta G^{*}$ decreases as follows: $\Delta\Delta G^{*}$ ($\mathbf{9}_{15}$ and $\mathbf{9}_{16}$)$>\Delta\Delta G^{*}$ ($\mathbf{6}_{16}$ and $\mathbf{6}_{17}$)$>\Delta\Delta G^{*}$ ($\mathbf{7}_{17}$ and $\mathbf{7}_{18}$). Extending the chain of the alkoxyl group should provide a method of study on the effect of the ansa-chain length on the rotational barriers.

References

1) Hetera-*p*-carbophanes. VIII: K. Sakamoto and M. Ōki, *Bull. Chem. Soc. Jpn.*, **49**, 3159 (1976).
2) M. A. Gubareva, *Zh. Obshch. Khim.*, **17**, 2259 (1947); *Chem. Abstr.*, **42**, 4820a (1948).
3) C. C. Li and R. Adams, *J. Am. Chem. Soc.*, **57**, 1565 (1935).
4) Y. Shvo, *Tetrahedron Lett.*, **1968**, 5923.
5) H. Suzuki, *Bull. Chem. Soc. Jpn.*, **32**, 1350 (1959).
6) D. M. Hall and M. M. Harris, *J. Chem. Soc.*, **1960**, 490.
7) K. Sakamoto and M. Ōki, *Bull. Chem. Soc. Jpn.*, **48**, 497 (1975).
8) K. Sakamoto and M. Ōki, *Bull. Chem. Soc. Jpn.*, **47**, 2739 (1974).
9) P. Chuit, *Helv. Chim. Acta*, **9**, 264 (1926).
10) S. R. Sandler and W. Karo, "Organic Functional Group Preparation," Vol. 1, Academic Press, New York and London (1968), p. 57.
11) S. Forsén, W. E. Frankle, P. Laszlo, and Lubochinsky, *J. Mag. Resonance*, **1**, 327 (1967); C. Laruelle, *Tetrahedron Lett.*, **1970**, 2235; M. Ōki, A. Akashi, G. Yamamoto, and H. Iwamura, *Bull. Chem. Soc. Jpn.*, **44**, 1683 (1971); M. Nakamura, H. Kihara, and M. Ōki, *Tetrahedron Lett.*, **1976**, 1207.
12) J. A. Pople, W. G. Schneider, and H. J. Bernstein, "High Resolution Nuclear Magnetic Resonance," McGraw-Hill Book Co., Inc., New York (1958), p. 218; J. W. Emsley, J. E. Feeney, and C. H. Sutcliffe, "High Resolution Nuclear Magnetic Resonance Spectroscopy," Pergamon Press, Oxford (1965), p. 481.
13) W. E. Stewart and T. Siddall, III, *Chem. Rev.*, **70**, 517 (1970).
14) M. Ōki, and H. Nakanishi, *Bull. Chem. Soc. Jpn.*, **44**, 3148 (1971).
15) K. Sakamoto and M. Ōki, *Tetrahedron Lett.*, **1973**, 3989.
16) R. Adams and J. B. Hale, *J. Am. Chem. Soc.*, **61**, 2825 (1939).

Electrophilic Sulfides(II) as a Novel Catalyst. V.[1a-d] Structure, Nucleophilicity, and Steric Compression of Stabilized Sulfur Ylides as Observed by ^{13}C-NMR Spectroscopy[2]

Haruo MATSUYAMA,* Hiroshi MINATO, and Michio KOBAYASHI

Department of Chemistry, Faculty of Science, Tokyo Metropolitan University, Fukazawa, Setagaya, Tokyo 158

(Received July 23, 1977)

^{13}C chemical shifts and ^{13}C–H spin coupling constants (179.7 Hz) of the ylide carbons of two dialkylsulfonium phenacylides show that the ylide carbons are basically sp^2. Large upfield shifts (−9.5——11.8 ppm) of carbonyl carbon signals (δ_C 181.7 and 179.2) of the ylides from those of the corresponding salts (δ_C 191.2 and 191.0) suggest significant contribution of a betaine structure. The ^{13}C-NMR spectrum of methylisopropylsulfonium phenacylide showed two non-equivalent methyl signals (δ_C 17.9 and 18.4) for the isopropyl group. Steric γ-effects on ylide carbon chemical shifts were observed with several alkylsulfonium bis(methoxycarbonyl)methylides and trialkylsulfonium salts.

The sulfonium ylides containing such electron-withdrawing substituents as carbonyl groups on their negatively charged carbon atoms are described by the canonical structure **a**—**c**.[3] The carbonyl stretching

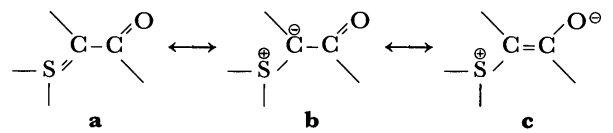

band of dimethylsulfonium phenacylide (**1a**) is observed at 1520 cm^{-1}, and this suggests that the contribution of **c** is important. In structure **c**, lone-pair electrons on the ylide carbon are considerably delocalized.[4] In fact, **1a** reacted as a zwitter ion and gave *O*-alkylation products.[5]

Recently, we studied the reactions of stable sulfonium ylides containing electron-withdrawing substituents on their ylide carbon atoms (COPh, COMe, COOMe, CN, *etc.*), and large differences were observed in the nucleophilic reactivity of ylide carbanions containing different electron-withdrawing substituents.

Carbon-13 chemical shifts provide some information on the electronic state of carbon atoms in molecules.[6] Some ^{13}C-NMR studies of phosphorus ylides have been reported,[7] but few ^{13}C-NMR studies have been reported on sulfonium ylides.

We measured the ^{13}C-NMR spectra of a series of sulfonium ylides containing electron-withdrawing substituents. The results are described in this paper and the nucleophilicity of these ylides is discussed.

Results and Discussion

sp^2-Carbanion and Betaine Structure. As is shown

Table 1. Carbon-13 NMR chemical shifts of dimethylsulfonium phenacylide (**1a**) and related compounds[a]

	Compound	$\overset{\ominus}{C}H$ or CH_2	C=O	CH_3–$S^{\oplus}$	1	2 and 3	4	5	6, 7, and 8	Solvent
1a	$(CH_3)_2\overset{\oplus}{S}$–$\overset{\ominus}{C}H$–CO–	53.2 [J_{CH} 179.7]	182.3	28.7 [J_{CH} 142.6]	140.9	126.2; 127.8	129.3			$CDCl_3$
		56.6	180.1	28.4	140.9	125.8; 127.4	128.7			CD_3CN
		60.6	181.7	31.8	143.8	129.0; 130.5	131.8			DMSO-d_6
1b	$(\overset{6}{C}H_3)_2\overset{5}{C}H$, CH_3, $\overset{\oplus}{S}$–$\overset{\ominus}{C}H$–CO–	51.8 [J_{CH} 179.7]	182.3	24.2 [J_{CH} 142.6]	140.9	126.4; 127.8	129.2	46.1 [J_{CH} 144.5]	17.9; 18.4 [J_{CH} 128.9]	$CDCl_3$
		53.4 [J_{CH} 175.8]	179.2	23.9 [J_{CH} 140.7]	141.2	126.0; 127.4 [J_{CH} 160.2]	128.7	46.6	16.5; 17.7	DMSO-d_6
1c	$(CH_3)_2\overset{\oplus}{S}$–$\overset{\ominus}{C}$, CO–, S–	65.1	189.5	27.4	142.2	127.4; 127.7	128.8	140.5	124.2; 125.1	$CDCl_3$
1d	$(CH_3)_2\overset{\oplus}{S}$–$\overset{\ominus}{C}$(CO–)$_2$	88.2	190.9	26.9	141.9	127.4; 128.6	129.7			$CDCl_3$
1a′	$(CH_3)_2\overset{\oplus}{S}$–$CH_2$–CO– $Br^{\ominus}$	52.6 [J_{CH} 146.5]	191.2	24.4 [J_{CH} 146.5]	134.8	128.4; 128.8 [J_{CH} 158.2]	133.8			DMSO-d_6
1b′	$(\overset{6}{C}H_3)_2\overset{5}{C}H$, CH_3, $\overset{\oplus}{S}$–CH_2–CO–, $Br^{\ominus}$	48.8 [J_{CH} 144.5]	191.0	19.7 [J_{CH} 146.5]	134.7	128.8 [J_{CH} 162.1]	133.9	45.2	17.1; 17.5 [J_{CH} 125]	DMSO-d_6
		b)	191.9	19.7 [J_{CH} 146.5]	135.8	129.0; 129.3 [J_{CH} 164.1]	133.5	46.2 [J_{CH} 146.5]	16.8; 17.5 [J_{CH} 123.1]	D_2O

a) δ_C, ppm from TMS(accurate to ±0.13 ppm); J_{CH}, Hz. b) Signal is not observable because of rapid H-D exchange in D_2O.

in Table 1, the ^{13}C–H coupling constant of the ylide carbon atom of dimethylsulfonium phenacylide (**1a**) as 179.7 Hz, and this shows that this carbon uses an sp^2 orbital in bonding with the hydrogen.[8] The coupling constant observed in **1a'** (146.5 Hz) is that expected for sp^3-hybridized carbon bound to a sulfonium sulfur atom.[9] X-Ray studies of various ylides have shown that ylide carbons are basically trigonal planar and therefore sp^2 hybridized.[10]

Large upfield shifts (−9.5—−11.8 ppm) were observed when the carbonyl carbon signals (δ_C 181.7 and 179.2 in DMSO-d_6) of the ylides were compared with those of the corresponding salts (δ_C 191.2 and 191.0 in DMSO-d_6). This suggests an important contribution of betaine structure **c**, since similar upfield shifts were observed when ketones were compared with α,β-unsaturated ketones.[11]

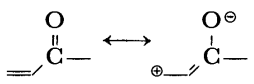

The chemical shifts of the ylide carbon of phenacylide (**1a**), which contains only one electron-withdrawing substituent, is dependent on kinds of solvent (δ_C 53.2 in $CDCl_3$ and 60.6 in DMSO-d_6). This suggests that the electrons are localized on its ylide carbon atom and that large nucleophilicity is expected.[12] The chemical shifts of ylides **1c** and **1d** containing two electron-withdrawing substituents (PhS and COPh) are found at fields lower than those of ylides **1a** and **1b**. Smaller nucleophilicity is expected for **1c** and **1d**.

Nucleophilicity of Disubstituted Sulfonium Ylides.

Nucleophilicity of these disubstituted sulfonium ylides was compared by determining the rates of transylidation[1b,1d] and olefin formation[1c] in the presence of dimethoxy disulfide. The results are shown in Table 2. Clearly, the presence of acetyl groups decreases the reactivity toward both transylidation and olefin formation.

Carbon-13 chemical shifts of acetyl and methoxycarbonyl ylides are listed in Table 3. These chemical shifts are not solvent dependent. When Tables 2 and 3 are compared, it is clear that these order of reactivity of sulfonium ylides are parallel with the order of the chemical shifts of ylide carbon atoms.

Asymmetric Environment about Sulfur of Ylides. The tetrahedral nature of sulfur in disubstituted sulfonium ylides has been shown on the basis of ^1H-NMR spectra.[13] The appearance of the methylene group of the benzyl and ethyl substituents, respectively, as AB patterns in their ^1H-NMR spectra requires an asymmetric environment about sulfur.

TABLE 2. TRANSYLIDATION[1b,1d] AND OLEFIN FORMATION[1c] OF SULFONIUM YLIDES IN THE PRESENCE OF DIMETHOXY DISULFIDE IN $CDCl_3$ AT 35 °C

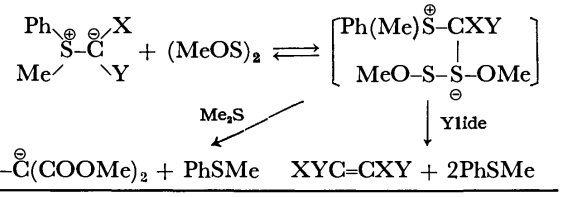

	Ylide X	Ylide Y	Transylidation[a] half life, $\tau_{1/2}$ (min)	Olefin formation[b] First-order rate constant calculated from $-d[Ylide]/dt = k[Ylide]$ $10^5 \times k$ (s^{-1})
2f	COOMe	COOMe	7	0.8
3b	COMe	COOMe	400	no reaction
4b	COMe	COMe	700[c]	no reaction

a) Mixture consists of ylide (0.5 mmol), Me_2S (0.6—0.8 mmol), and $(MeOS)_2$ (0.2—0.3 mmol), except in the case of **4b**. b) Mixture consists of ylide (0.85 mol/l) and $(MeOS)_2$ (1.36 mol/l). c) Mixture consists of ylide **4b** (0.5 mmol), Me_2S (6.5 mmol), and $(MeOS)_2$ (0.3 mmol).

We examined the ^1H-NMR spectrum of methylisopropylsulfonium penacylide (**1b**), since asymmetric environment of isopropylsulfonium ylides has not been reported in the literature. Two methyl signals were observed at δ_H 1.32 (d, J=6.6 Hz) and 1.36 (d, J=6.6 Hz). The ^{13}C-NMR spectrum of **1b** also showed two methyl signals at δ_C 17.9 and 18.4, and that of **2d** showed two methyl signals at δ_C 18.4 and 18.8 for the isopropyl group.

γ-Effect Observed in Sulfonium Compounds. In the system of sulfonium bis(methoxycarbonyl)methylides (**2a**—**2h**), effects of a bulky substituent on ^{13}C chemical shifts were investigated. The results are listed in Table 4. Clearly, the presence of a bulky substituent on the sulfur atom causes an upfield shift of the ylide carbon signal. This shift is not due to a simple inductive effect but due to steric compression through space (γ-effect).[14] It can be assumed that the inductive effect of the diethyl group of diethyl sulfonium ylide **2g** is similar to that of the pentamethylene group of pentamethylenesulfonium ylide **2h**. However, the chemical shift of the ylide carbon of **2g** was smaller than that of **2h** by −7.0

TABLE 3. CARBON-13 NMR CHEMICAL SHIFTS OF DISUBSTITUTED SULFONIUM YLIDES[a]

	Compound	C⊖	C=O ester	C=O keto	CH_3–S⊕	OCH_3	CH_3	Solvent
2a	$(CH_3)_2\overset{\oplus}{S}–\overset{\ominus}{C}(COOCH_3)_2$	58.6	166.6		27.6	50.7		$CDCl_3$
		58.4	165.6		27.1	49.7		DMSO-d_6
3a	$(CH_3)_2\overset{\oplus}{S}–\overset{\ominus}{C}(COOCH_3)(COCH_3)$	73.5	166.4	191.8	26.6	50.2	29.8	$CDCl_3$
		73.4	166.0	189.9	26.0	49.9	29.7	DMSO-d_6
4a	$(CH_3)_2\overset{\oplus}{S}–\overset{\ominus}{C}(COCH_3)_2$[b]	87.6		190.3	26.7		30.1	$CDCl_3$

a) δ_C, ppm from TMS (accurate to ±0.13). b) **4a** is insoluble in DMSO-d_6.

Table 4. ^{13}C Chemical shifts of ylide carbons of some sulfonium ylides[a]

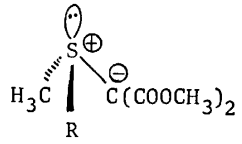

Compound	R	C⊖	$\Delta\delta$[b]	H_3C–S⊕	$\Delta\delta$[b]
2a	CH_3	58.6	0	27.7	0
2b	CH_3CH_2[c]	55.7	−2.9	25.9	−1.7
2c	$CH_3CH_2CH_2CH_2$[d]	56.2	−2.4	26.7	−1.0
2d	$(CH_3)_2CH$[e]	53.5	−5.1	24.4	−3.3
2e	$C_6H_5CH_2$[f]	57.4	−1.2	24.7	−3.0
2f	C_6H_5[g]	59.1	+0.5	27.1	−0.5

a) δ_C, ppm from TMS in $CDCl_3$ (accurate to ±0.13 ppm). b) ($\delta_C^R - \delta_C^{CH_3}$). c) CH_2 (α) 36.8, CH_3 (β) 9.53, C=O 167.1, and OCH_3 50.7. d) CH_2 (α) 42.6, CH_2 (β) 26.2, CH_2 (γ) 21.6, CH_3 (δ) 13.7, C=O 167.2, and OCH_3 51.0. e) CH (α) 46.0, CH_3 (β) 18.4 and 18.8, C=O 167.4, and OCH_3 50.9. f) CH_2 (α) 48.2, aromatic-C 129.3 and 130.3, C=O 167.1, and OCH_3 51.0. g) Aromatic-C 129.3, 130.5 and 132.3, C=O 166.4, and OCH_3 50.7.

ppm.

$(CH_3CH_2)_2\overset{\oplus}{S}-\overset{\ominus}{C}(COOCH_3)_2$

δ_C 52.0

2g

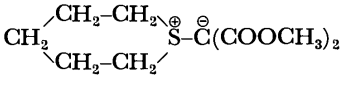

δ_C 59.0

2h

In the system of sulfonium phenacylides, **1a** and **1b**, a similar γ-effect was observed, which was shown in Table 1.

Table 5 shows the upfield shifts observed for some simple sulfonium salts possessing bulky substituents such as isopropyl and *t*-butyl groups. Such upfield shifts are found even in the sulfonium salts containing the electron-withdrawing phenacyl group (**1a′** and **1b′**), CH_2COPh.

As shown in Tables 4 and 5, large upfield shifts were observed for the ylide and methyl carbon signals when an isopropyl group was the substituent (**2d**, **5b**, **1b′**, and **5e**).

Experimental

Materials. The dimethylsulfonium ylides (**1a**,[4] **1d**,[15] **3a**,[16] and **4a**[16]) were prepared by the methods described in the literature. The phenylmethylsulfonium ylides (**2f**, **3b**, and **4b**) were synthesized by copper-catalyzed decomposition of diazo compounds in large excess sulfides.[17] **1c** was obtained by reaction between **1a** and methyl benzenesulfenate in chloroform at room temperature (75% yield, mp 136—137 °C (lit,[18] 136 °C)).[19] Sulfonium bis(methoxycarbonyl)methylides (**2a**—**c**, **2g**, and **2h**) were prepared by catalytic decomposition of methyl diazomalonate in excess sulfide in the presence of dialkoxy disulfide at room temperature.[1a] **2d** and **2e** were obtained by transylidation between **2f** and methyl isopropyl sulfide (or methyl benzyl sulfide) in chloroform in the presence of dimethoxy dusilfide at room temperature.[1b] **2d**: mp 76—77 °C; IR (KBr), 1640 and 1700 cm^{-1} (ν_{CO}); ^1H-NMR ($CDCl_3$), δ=1.33 (d, J=7.2 Hz), 1.45 (d, J=7.2 Hz) (6H, $(CH_3)_2C$), 2.86 (3H, s, $CH_3-\overset{\oplus}{S}$), 3.78 (6H, s, $COOCH_3$) and 3.90—4.35 (1H, m, CH). Found: C, 49.43; H, 7.34%. Calcd for $C_9H_{16}O_4S$: C, 49.08; H, 7.32%. Methylisopropylsulfonium phenacylide (**1b**) was prepared by deprotonation of salt (**1b′**) with 10% aqueous sodium hydroxide. **1b**: mp 108—109 °C; IR (KBr), 1520 cm^{-1} (ν_{CO}); ^1H-NMR ($CDCl_3$), δ=1.32 (d, J=6.6 Hz), 1.36 (d, J=6.6 Hz) (6H, $(CH_3)_2C$), 2.85 (3H, s, $CH_3-\overset{\oplus}{S}$), 3.8—4.3 (2H, m, CH and $\overset{\ominus}{C}H$) and 7.25—7.86 (5H, m, C_6H_5); ^1H-NMR (DMSO-d_6, δ=1.25 (d, J=6.6 Hz), 1.30 (d, J=6.6 Hz) (6H, $(CH_3)_2C$), 2.71 (3H, s, $CH_3-\overset{\oplus}{S}$), 3.20—3.60 (1H, m, CH), 4.30 (1H, s, $\overset{\ominus}{C}H$) and 7.25—7.80 (5H, m, C_6H_5). Found: C, 68.90; H, 7.77%. Calcd for $C_{12}H_{16}OS$: C, 69.21; H, 7.74%. The sulfonium

Table 5. ^{13}C Chemical shifts of methyl carbons of some sulfonium salts[a]

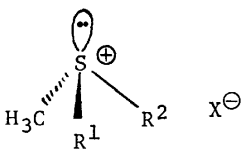

Compound	R^1	R^2	H_3C–S⊕	$\Delta\delta$[b]	C_α	C_β	X	Solvent
5a	CH_3	CH_3	27.7	0			I	D_2O
5b	CH_3	$(CH_3)_2CH$	22.0	−5.7	47.1	16.9	I	D_2O
5c	CH_3	$(CH_3)_3C$	24.4	−3.2	43.1	24.4	I	D_2O
5d	CH_3CH_2	CH_3CH_2	21.3	−6.4	35.6	8.4	I	D_2O
5e	$(CH_3)_2CH$	$(CH_3)_2CH$	15.6	−12.1	44.2	17.1; 18.9	I	D_2O
5f	CH_3CH_2	$(CH_3)_3C$	17.0	−10.6	32.1	9.5 (ethyl)	BF_4	D_2O
					43.5	24.8 (*t*-butyl)		
5a	CH_3	CH_3	26.1	0			I	DMSO-d_6
1a′	CH_3	$C_6H_5COCH_2$	24.4	−1.7	52.6 (phenacyl)		Br	DMSO-d_6
1b′	$(CH_3)_2CH$	$C_6H_5COCH_2$	19.7	−6.4	48.8 (phenacyl)		Br	DMSO-d_6
					45.2	17.1; 17.5 (isopropyl)		

a) δ_C, ppm from TMS as external standard in D_2O (accurate to ±0.08 ppm). b) ($\delta_C^{R^1,R^2} - \delta_C^{(CH_3)_2}$).

salts (**1a'** and **1b'**) were prepared by reaction between sulfides and phenacyl bromide in benzene at room temperature. **1b'**: mp 110—111 °C; IR (KBr), 1670 cm^{-1} (ν_{CO}); ^{1}H-NMR (DMSO-d_6), δ=1.55 (6H, d, J=6.6 Hz, $(CH_3)_2C$), 2.99 (3H, s, $CH_3-\overset{\oplus}{S}$), 4.09 (2H, s, CH_2) and 7.50—8.20 (5H, m, C_6H_5). The dialkylmethylsulfonium salts (**5a—e**) were obtained by direct reaction of the alkyl sulfides and methyl iodide. **5e**; ^{1}H-NMR (D_2O), δ=1.57 (d, J=6.6 Hz), 1.61 (d, J=6.6 Hz) (12H, $(CH_3)_2C$), 2.82 (3H, s, $CH_3-\overset{\oplus}{S}$) and 3.90 (2H, m, CH). **5f** was prepared by ethylation of methyl *t*-butyl sulfide with $(C_2H_5)_3O^{\oplus}\,BF_4^{\ominus}$).

Measurement. The ylides were dissolved in $CDCl_3$, CD_3CN and DMSO-d_6 (usually 100—150 mg/cm^3) containing 1—5% tetramethylsilane as reference. The sulfonium salts also were dissolved in D_2O (usually 100—150 mg/cm^3). Solutions were examined in 10-mm tubes using JEOL-FX-60 NMR spectrometer in the Fourier transform mode. Several hundred to several thousand transients were accumulated typically with acquisition times of 1.0 to 5 s, with 3.0 s being normal for coupling constant measurements. Line positions were determined automatically by computer software. The results are listed in Tables 1, 3, 4, and 5.

Transylidation and Olefin Formation. Transylidation and olefin formation of sulfonium ylides (**2f**, **3b**, and **4b**) in the presence of dimethoxy disulfide in $CDCl_3$ at 35 °C are described in the literature.[1b,c] The results are listed in Table 2.

References

1) a) Part I of this series: H. Matsuyama, H. Minato, and M. Kobayashi, *Bull. Chem. Soc. Jpn.*, **46**, 1512 (1973); b) Part II: H. Matsuyama, H. Minato, and M. Kobayashi, *ibid.*, **46**, 2845 (1973); c) Part III: H. Matsuyama, H. Minato, and M. Kobayashi, *ibid.*, **46**, 3158 (1973); d) Part IV: H. Matsuyama, H. Minato, and M. Kobayashi, *ibid.*, **46**, 3828 (1973).

2) Parts of this work were presented at the 34th National Meeting of the Chemical Society of Japan, April 4, 1976 (Abstracts of Papers, Vol. 2, p. 799).

3) B. M. Trost and L. S. Melvin, Jr., "Sulfur Ylides," Academic Press, New York (1975).

4) K. W. Ratts and A. N. Yao, *J. Org. Chem.*, **31**, 1185 (1966).

5) S. H. Smallcombe, R. J. Holland, R. H. Fish, and M. C. Caserio, *Tetrahedron Lett.*, **1968**, 5987.

6) J. B. Stothers, "Carbon-13 NMR Spectroscopy," Academic Press, Nrew Yok (1972).

7) K. A. O. Starzewski and H. Bock, *J. Am. Chem. Soc.*, **98**, 8486 (1976); G. A. Gray, *ibid.*, **95**, 5092, 7736 (1973).

8) J. B. Stothers, "Carbon-13 NMR Spectroscopy," Academic Press, New York (1972) p. 333; J_{CH}, 125 Hz for sp^3, 160 Hz for sp^2 and 250 Hz for sp.

9) P. Haake, W. B. Mitter, and D. A. Tyssee, *J. Am. Chem. Soc.*, **86**, 3577 (1964); J_{CH}, 146 Hz for $(CH_3)_3S^{\oplus}\ I^{\ominus}$ (in CF_3COOH).

10) A. T. Christensen and E. Thom, *Acta Crystallogr., Sect. B*, **27**, 581 (1971); A. T. Christensen and W. G. Witmore, *ibid.*, **25**, 73 (1969); J. P. Schaefer and L. L. Reed, *J. Am. Chem. Soc.*, **94**, 908 (1972).

11) J. B. Stothers, "Carbon-13 NMR Spectroscopy," Academic Press, New York (1972), p. 281.

12) The methylphenylsulfonium *p*-chlorophenacylide $CH_3(C_6H_5)\overset{\oplus}{S}\overset{\ominus}{C}HC(O)C_6H_4Cl$-*p* is reported (H. Koezuka, G. Matsubayashi, and T. Tanaka, *Inorg. Chem.*, **13**, 443 (1974)) to coordinate to $PtCl_2((CH_3)_2S)$ through the ylide carbon atom.

13) a) K. W. Ratts, *Tetrahedron Lett.*, **1966**, 4707; b) A. F. Cook and J. G. Moffatt, *J. Am. Chem. Soc.*, **90**, 740 (1968).

14) J. B. Stothers, "Carbon-13 NMR Spectroscopy," Academic Press, New York (1972), p. 134.

15) H. Nozaki, K. Nakamura, and T. Takaku, *Tetrahedron*, **25**, 3675 (1969); A. W. Johnson and R. T. Amel, *J. Org. Chem.*, **34**, 1240 (1969).

16) H. Nozaki, D. Tsunemoto, Z. Morita, K. Nakamura, K. Watanabe, M. Takaku, and K. Kondo, *Tetrahedron*, **23**, 4279 (1967).

17) W. Ando, T. Yagihara, S. Tozune, S. Nakaido, and T. Migita, *Tetrahedron Lett.*, **1969**, 1979.

18) Y. Hayashi, M. Takaku, and H. Nozaki, *Tetrahedron Lett.*, **1970**, 3179; T. Mukaiyama, K. Hosoi, S. Inokuma, and T. Kumamoto, *Bull. Chem. Soc. Jpn.*, **44**, 2453 (1971).

19) H. Matsuyama, M. Matsumoto, H. Minato, and M. Kobayashi, unpublished results (1977).

Photo-induced Electricity Generated by Thin-layer Photogalvanic Cells Containing Thionine and Iron(II) Salt

Kiyotaka SHIGEHARA, Masatoshi NISHIMURA, and Eishun TSUCHIDA
Department of Polymer Chemistry, Waseda University, Nishiohkubo, Tokyo 160
(Received March 1, 1977)

The photogalvanic effects of thionine and Fe(II) salt systems were studied by use of thin-layer photocells. Three systems of the cell components, *i.e.*, SnO_2/thionine–Fe(II) aq/Pt, SnO_2/thionine–Fe(II)-gelatinized reagent/Pt, and SnO_2/polymeric thionine membrane–Fe(II)/Pt, were compared. The photopotential ΔE and the photocurrent I were the largest in the third system. It was concluded that the excellent ability of the polymeric thionine system to generate the photo-induced electricity is due to the strong electrostatic repulsion between Fe^{3+} and the semi-species bound to the cationic polymers, since the repulsion diminished the short-circuit in a solution or the bulk-backward reaction with Fe^{3+}. The electron-recycling in a solution took place not only through the transportation of Fe^{3+} to the cathode, but also through the electron-exchange reaction between Fe^{2+} and Fe^{3+} *via* hydrogen bonds.

The mechanism of the photogalvanic effect in the photoredox reaction between thionine (thn) and Fe(II) has been studied by many investigators, especially in liquid-phase.[1–6] Few reports, however, describe photogalvanic cells composed of gel or membrane systems, although they are important from the viewpoint of application. We have prepared several types of photocell: (1) a double-Pt photocell containing thn–Fe(II) aq, (2) an SnO_2–Pt photocell of the same size as (1), and (3) a thin-layer type photocell containing thn–Fe(II) aq, thn–Fe(II)-gel (with a semi-permeable membrane), or polymeric thn–Fe(II). The following three points were examined :

(a) the electron-recycling mechanism in solution,
(b) the role of the SnO_2-electrode, and
(c) the factors which influence the photopotential ΔE and the photocurrent I.

Experimental

Reagents. Thionine (Tokyo Kasei Co., Ltd., reagent grade, Cl salt) was recrystallized from 50% aqueous ethanol solution before use. Its purity was confirmed by thin-layer chromatography after being eluted with a mixture of 2-propanol (5%) and chloroform. Analytical grade commercial reagents of acids, bases, and iron(II) sulfate containing 0.005% iron(III) were used without further purification. Soluble starch (Wakō Pure Chemical Co., Ltd., reagent grade for medical use) and poly(vinyl alcohol) (degree of polymerization=about 500) of commercial grade were purified by precipitating their hot aqueous solutions from excess methanol. Hydroquinone used as the reductant in the photoredox reaction was recrystallized twice. The formulas of the dyes and the polymers are given below. Thionine and its reduced species (Sthn=semi-thn, Lthn=leuco-thn) at pH 1—4[7,8] are as follows.

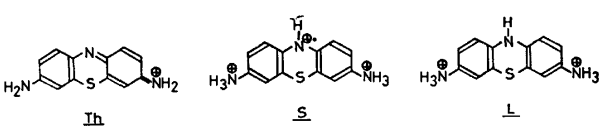

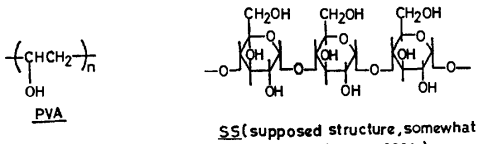

Preparation of Polymers. The ternary copolymer composed of hydroquinone, formaldehyde and piperazine residues was prepared by the Mannich-polyaddition-condensation-polymerization.[9] The thn-polymers were prepared by the reaction of poly(epichlorohydrin) (degree of polymerization=170, commercial reagent) with thn under the presence of triethylamine (HCl-remover). First, the prescribed amounts of the polymer and trimethylamine were reacted in an autoclave at 120 °C. The solvent, 50% aqueous *N,N*-dimethylformamide (DMF), was removed from the resulting solution. Solids were then dissolved in absolute methanol and reprecipitated with diethyl ether to yield copoly(epichlorohydrin-glycidyltrimethylammonium chloride) (QE). Next, QE and thn were reacted in absolute DMF at 60 °C in the dark. The solvent of the resulting solution was evaporated, and the product was washed with water until the filtrate showed no color of thn. The thn-polymers (BQEthns) thus obtained was to some extent cross-linked by thn nuclei, which are slightly soluble in methanol. When the reaction of QE and thn is carried out in the molar ratio, [thn]/[$-CH_2Cl$ of QE] $\gg$10, the resulting BQEthn is entirely soluble in water, since the cross-linking by thn nuclei can be avoided.[10] The experimental conditions and results are summarized in Table 1. The structures of the polymers are given below.

Apparatus. The over-all photobleaching rate constant k and the degree of photobleaching Δ% (=([Sthn]+[Lthn]) $\times 100/[\text{thn}]_0$) were measured with a stopped-flow rapid-scanning spectrophotometer (Union Giken Co., Ltd., RA-1300) modified into a cross-illumination system,[11] with a 100 W

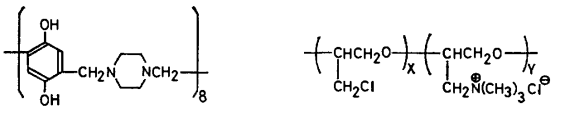

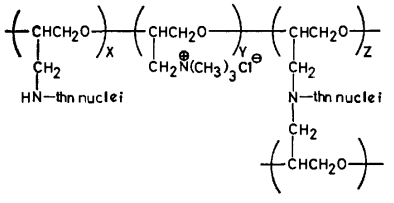

TABLE 1. PREPARATION AND CHARACTERISTICS OF POLYMERS

Polymer	Starting material g (mol)	Solvent (ml)	Time (h)	Products Y (%)	C% / N%	Cl (%)	Note
PH_2Q	H_2Q 11.0 (0.1) CH_2O 6.0 (0.2), Pip-2HCl 14.5 (0.1)	50% aqueous methanol (100)	12	98	5.143	24.2	2HCl salt
QE(1)	PEP 9.3 (0.1) TMA 30 (0.5)	50% aqueous DMF (60)	48	95	14.816	33.68	x=21%
QE(2)	PEP 9.3 (0.1) TMA 30 (0.5)	50% aqueous DMF (60)	60	95	12.462	32.77	x=26%
BQETh(1)	QE(1) 0.5 Th 5.0 (abt. 0.02)	absolute DMF (50)	48	94	4.763	18.91	x=19%, y=79%, z=2%
BQETh(2)	QE(2) 0.5 Th 7.5 (abt. 0.03)	absolute DMF (50)	48	97	4.703	18.10	x=23%, y=74%, z=3%

Pip-2HCl; piperazine·2HCl, TMA; trimethylamine. z% was estimated from the correlation of C%/N% with Cl%.

tungsten illumination light source and a 50 W measureing light source. The intensity of the latter was weakened to 0.03% of the former by use of neutral filters. It was confirmed that the illumination with the latter has little influence on the photoredox reaction. The photopotential ΔE and the photocurrent I of the thn-reductant systems were measured with the photocells illustrated in Figs. 1 (a)—(f), in which the SnO_2 electrode prepared by the usual chemical-vapor-depositing method (about 100 Ω/cm, transparent Nesa glass) was used, with a vibrating reed electrometer (Takeda Riken Co., Ltd., Model TR-84 BS).

Measurements. The prescribed amounts of thn and reductant solutions were bubbled with pure N_2 for 1 h before use, which was completely deoxygenated with use of the alkaline pyrogallol aq, sodium dithionite aq. and chromium-(II) perchlorate aq-zinc amalgam towers. The two reactant solutions were then taken into the syringes of the cross-illumination apparatus separately under N_2 and were rapidly mixed into a 2 mm-flow cell (dead time=450 μs). The rapid spectral changes with time due to the photobleaching of thn were measured. k was determined from the initial section of time-decay curve according to the pseudo-first order plots, and A from the final absorption intensity at a certain photo-equilibrium state. The values of ΔE and I were obtained by use of the photocells under pure N_2 atmosphere in a dry-box, their stationary values being recorded. Unless otherwise stated, the illumination light intensity was adjusted to 10 mW/cm² (>350 nm). The specific viscosity represented by η_{sp} was measured with an Ubbelohde viscometer at 25.0±0.04 °C.

Results and Discussion

Electron-recycling Mechanism. The photocells, one composed of double-Pt electrodes (a), and another of SnO_2–Pt electrodes (b) are shown in Figs. 1(a) and (b), respectively. The two photocells have similar size and surface area of electrodes (2.0 cm²) and also the same distance, 3.5 cm between the two electrodes. In the case of (b), visible light was cast onto both or one of the cell chambers, the light intensity being 10 mW/cm² on the surface of each electrode. The thin-layer photocells composed of a thn–Fe(II) aqueous solution, a gelatinized thn–Fe(II) aqueous system and a membrane-gel system are shown in Figs. 1(c)—(f). The surface area of SnO_2 and Pt electrodes is 3.0 cm² and the distance between the electrodes 2 mm. The visible light of the same intensity as in (a) and (b) was cast through the transparent SnO_2 electrode.

The electron-recycling mechanism proposed for the photogalvanic cells composed of thn–Fe(II) is as follows.[1-6]

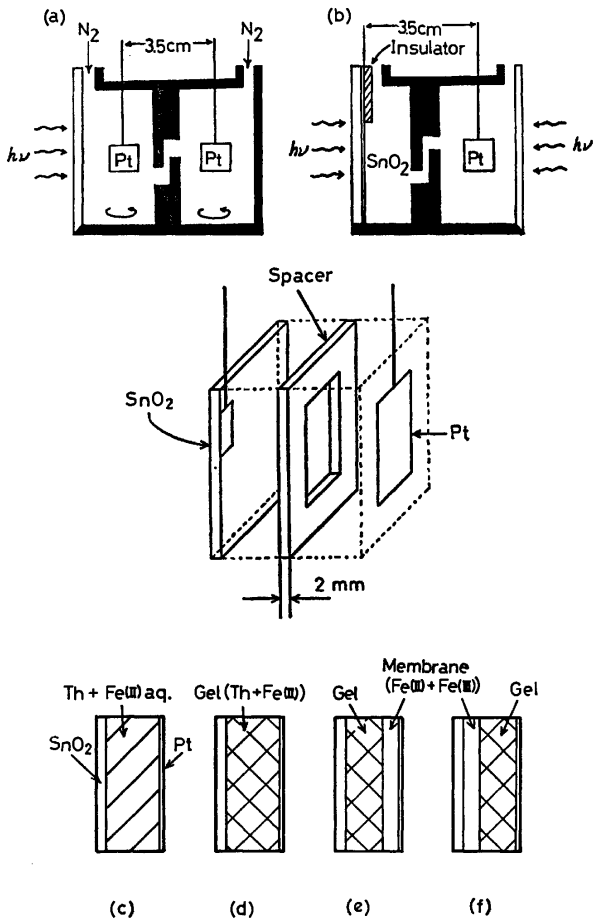

Fig. 1. Photogalvanic cells.
(a); d (distance between two electrodes) =3.5 cm, A (surface area of an electrode) =2.0 cm², (b); d=3.5 cm, A=2.0 cm², (c)—(f); d=2.0 mm adjusted by a spacer, A=3.0 cm². Visible light (>350 nm, 10 mW/cm²) was used, if no captions are given. Visible light can be illuminated onto both the cell-chambers of the photocell (b).

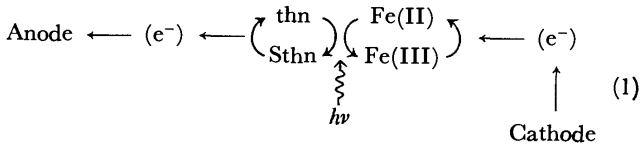

(1)

Only a few investigations have been carried out on the electron-recycling mechanism inside the cell despite its importance. It is doubtful that Fe(III) formed in an illuminated chamber is transported to the cathode *via* infinite pathway in a molecular scale due to diffusion, since the cathodic active species of Fe(III) would disappear by the possible bulk-backward reaction with Sthn or Lthn in the course of transportation. Therefore, another sufficiently fast mechanism should exist in order to cause the electron-recycling in solution.

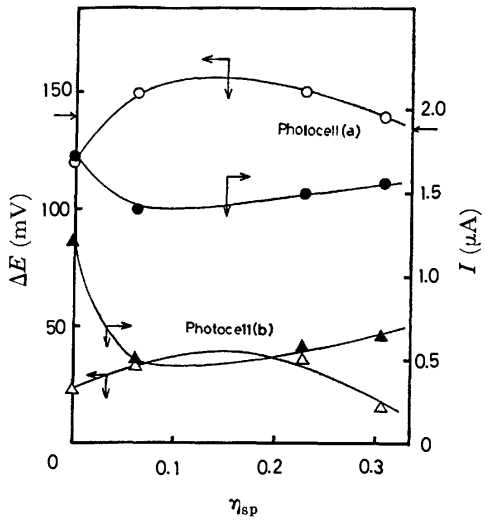

Fig. 2. Effect of added SS on ΔE and I of thn–Fe(II) systems. $[thn]_0=7.17\times10^{-5}$ mol/l, $[Fe(II)SO_4]_0=10^{-2}$ mol/l, $[Fe(III)]_0=5.0\times10^{-7}$ mol/l, pH 2.0-HCl, under N_2, without stirring.
(○,●); photocell (a), (△,▲); photocell (b). The arrows indicate ΔE and I without SS and with the most appropriate stirring of the solution, in photocell (a). η_{sp} indicates the specific viscosity of SS-added solution.

The effect of added SS (soluble starch) on ΔE and I in the thn–Fe(II) aq system is shown in Fig. 2, in which the abscissa indicate the specific viscosity of the solution (η_{sp}). Both ΔE and I measured without stirring of the solution remain almost unchanged with the increase of specific viscosity, which should decrease the transportation of Fe(III) from the illuminated cell-chamber to the cathode. They show the almost constant values of 150 mV and 1.5 μA, respectively, under the given conditions, whereas the effect of added PVA (poly(vinyl alcohol)) (Fig. 3) shows a bell-shaped curve. With increase in PVA concentration, ΔE and I become constant. The anomalous behavior in the PVA system cannot be understood from only the consideration that the electron-recycling in solution proceeds through the Fe(III) transportation.

It is well-kown that there is a very rapid electron-exchange reaction of 10^{-9}—10^{-12} s between Fe(II) and Fe(III) *via* hydrogen bonds in an aqueous solution:[12]

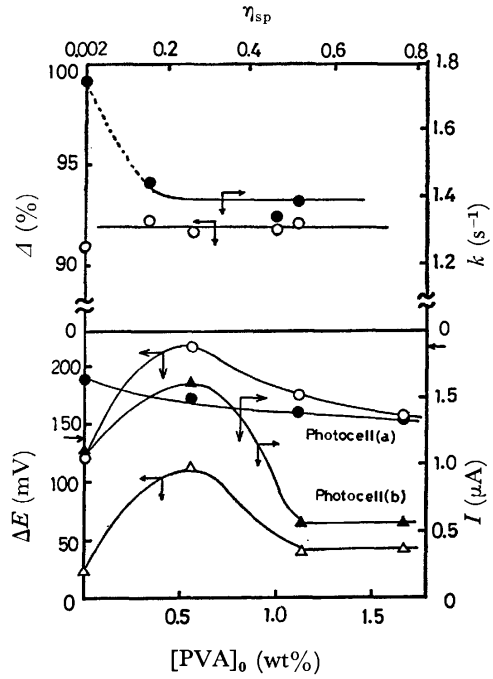

Fig. 3. Effect of added PVA on Δ, k, ΔE and I of thn–Fe(II) systems. The conditions are the same as in Fig. 2.

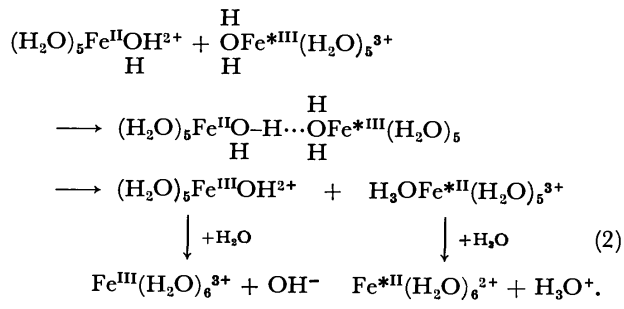

(2)

If this mechanism is valid, the reason for the increase of ΔE and I despite the fact that the values of k and Δ are constant when PVA was added in a small amount can be explained, since PVA forms the intramacromolecular hydrogen bonds which would enhance the electron-exchange reaction between Fe(II) and Fe(III) more easily:

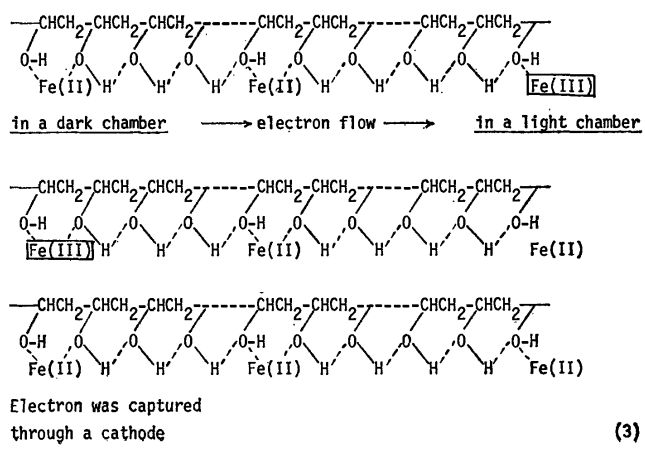

(3)

The value of ΔE and I given in Figs. 2 and 3 were obtained without stirring the solution. Values obtained under appropriate stirring are indicated by arrows at each axis in photocell (a), without addition of SS or PVA. The very small difference between these values and those indicated by circles suggests that stirring of the solution has no remarkable influence on ΔE and I. In other words, the transportation of Fe(III) from the illuminated cell-chamber to the cathode is not the main pathway for the electron-recycling in solution. Thus, the electron-recycling mechanism of the thn-Fe(II) photoredox systems in the aqueous media was considered to be as follows.

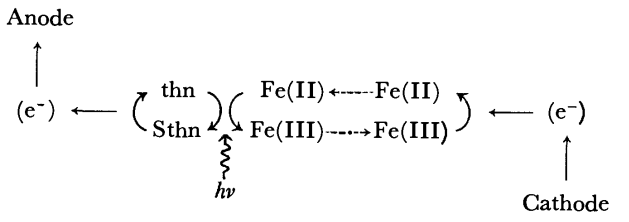

Electron-exchange *via* hydrogen bonds and/or ion-transport (4)

The side hydroxyl groups of SS are less effective than those of PVA, probably because they cannot form the polymeric hydrogen bonds intramacromolecularily due to their rigid chain-backbone.

Characteristics of SnO_2 Electrode. The circles and triangles in Figs. 2 and 3 are the values measured with photocells (a) and (b), respectively, where both cell chambers of photocell (b) were illuminated. The values of ΔE and I obtained by use of photocell (b) without stirring are much smaller than those obtained by use of photocell (a). The direction of electron-flow is Pt(L) →Pt(D) in photocell (a), and Pt(L)→SnO_2(L) in photocell (b), where L and D indicate illuminated and dark, respectively. If we consider that SnO_2 is an n-type semiconductor, the direction of electron-flow is irregular in the latter case. SnO_2 seems to select Fe(III) as the electrode-active species, although Sthn also exists (Table 2). Three illumination methods were examined for photocell (b), *i.e.*, visible light cast onto the Pt-camber, onto the SnO_2-chamber and onto both the chambers. As for I and the direction of electron-flow, the systems of Pt(L)–Pt(D) and Pt(L)–SnO_2(D) gave almost the same result. The I values was very small for the SnO_2(L)–Pt(D) in which the direction of electron-flow SnO_2(L)→Pt(D). The I values of SnO_2–Pt(L) system with stirring was the largest, the direction being Pt(L)→SnO_2(L). From the consideration that (1) the effect of stirring is remarkable, (2) the value of I is the largest when the solution is stirred, and (3) the direction is Pt(L)→SnO_2(L) in the SnO_2(L)–Pt(L) system in contrast to the n-type characteristics of SnO_2, there might be some other electrode-reaction differing from the mechanism generally proposed for the case of Pt(L)–Pt(D) systems as given by Eq. 1 or 4.

Clark and Eckert reported that the direction of electron-flow is SnO_2(L)→Pt(L).[14] This cannot explain the results we obtained by use of a thin-layer photocell (Figs. 1(c)—(f)). The distance between the SnO_2 and Pt electrodes is 0.1 mm in Clark and Eckert's cell, but in ours 2.0 mm. The effect of UV light, which might cause distortion of the energy band of SnO_2 as illustrated in Fig. 4(a), is summarized in Table 3. The results indicate that the additional UV-illumination brought about the anodic polarization of SnO_2 to decrease the electron-flow, Pt(L)→SnO_2(L). Hence it is considered that the SnO_2 illuminated by visible light

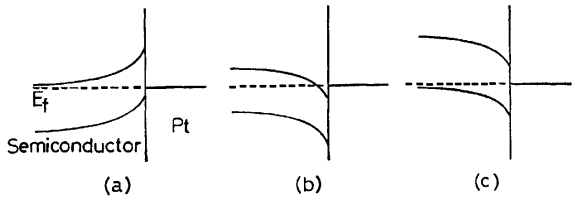

Fig. 4. Polarized state of semiconductors.
(a): Anodic polarization, (b): ohmic contact, (c): cathodic polarization.

TABLE 2. CORRELATION OF PHOTOCELLS (a) AND (b)

Photocell	Electrode	Illumd-electrode	ΔE (mV)	I (μA)	Stirring	Direction of e⁻
(a)	Pt(L)–Pt(D)	Pt(L)	120	1.6	o	Pt(L)→Pt(D)
		Pt(L)	100	1.5_2	x	Pt(L)→Pt(D)
(b)	Pt–SnO_2	Pt	190	1.5_0	x	Pt(L)→SnO_2(D)
		SnO_2	35	0.53	x	SnO_2(L)→Pt(D)
		Pt and SnO_2	80	2.7_5	o	Pt(L)→SnO_2(L)
		Pt and SnO_2	40	1.0	x	Pt(L)→SnO_2(L)

$[thn]_0=4.3\times10^{-5}$ mol/l, $[Fe(II)SO_4]_0=4.3\times10^{-3}$mol/l, $[Fe(III)]_0=2.15\times10^{-7}$ mol/l, pH 2.0-HCl aq, under N_2.

TABLE 3. EFFECT OF UV-LIGHT ON ΔE AND I IN THE PHOTOCELL (c)

Light source (mW/cm²)	ΔE (mV)	I (μA)	Direction of e⁻	Remark
Vis(0.267)	30	0.78	Pt(L)→SnO_2(L)	a)
Vis(0.267)+UV(0.01)	20	0.70	Pt(L)→SnO_2(L)	a)
UV(0.01)	1.5	0.02	Pt(L)→SnO_2(L)	a)
UV(0.01)	10	—	SnO_2(L)→Pt(L)	b)

a) $[thn]_0=1.0\times10^{-4}$ mol/l, $[Fe(II)SO_4]_0=5.0\times10^{-2}$ mol/l, $[Fe(III)]_0=2.5\times10^{-6}$ mol/l, pH 2.0-HCl aq, under N_2. b) pH 9.0-NaOH aq.

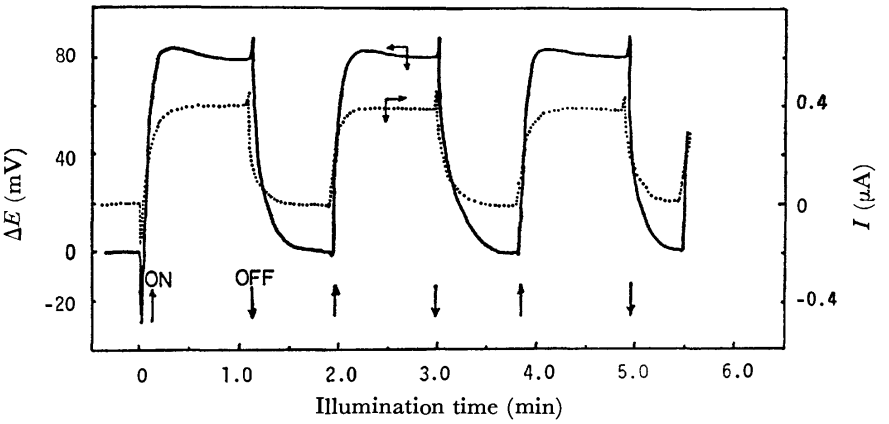

Fig. 5. On-off behavior of ΔE and I in photocell (c).
$[thn]_0=1.0\times10^{-4}$ mol/l, $[Fe(II)SO_4]_0=5.0\times10^{-2}$ mol/l, $[Fe(III)]_0=2.5\times10^{-6}$ mol/l, pH 2.0-HCl aq, under N_2. (+) values indicate the electron-flow Pt(L)→SnO_2(L).

has a distorted energy-band similar to the cathodic polarization. In order to let the electrons flow from Pt(L) to SnO_2(L), SnO_2, should have the ohmic contact or cathodic polarized state. The former is less probable, since the work-function of Pt is larger than that of SnO_2. There remains possible adsorption of some substances which bring about the cathodic polarization. Figure 5 shows the on-off behavior of ΔE and I in a thin-layer photocell. The electron-flow was SnO_2(L)→Pt(L), indicating that the discharged electrons from Sthn were captured by SnO_2 in the initial stage. The negative values in Fig. 5 represent the electron-flow of SnO_2(L)→Pt(L). The direction of electron-flow then reversed rapidly, *i.e.*, Pt(L)→SnO_2(L), ΔE and I reaching certain stationary values. By cutting off the illumination, ΔE and I increased temporarily toward (+)-side, showing the electron-flow to be Pt(L)→SnO_2(L), and then diminished rapidly. In this on-off behavior, the following should be noted:

1) the magnitude of temporary negative generation toward (−)-side of ΔE and I at on-illumination was larger than that of temporary positive generation toward (+)-side (Fig. 5) at off-illumination,

2) the temporary negative generation at on-illumination was scarecely observed after the second series of on-off recycles,

3) the temporary positive generation at off-illumination did not change with the repeated on-off recycles,

4) thn was strongly chemisorbed on the surface of SnO_2, which was almost constant at any off-illuminated state. The absorbed thn could be washed off with methanol, but not with water,

5) SnO_2 is activated only by UV-light (below 340 nm) to yield the anodic polarization, and is cathodic polarized state with the illumination of visible light, and

6) the SnO_2–Pt thin-layer photocell containing an aqueous solution of thn alone generated no dye-sensitized electricity under the illumination of visible light.

From the results, the reaction mechanism of the thn–Fe(II) system in these thin-layer photocells composed of SnO_2 and Pt is supposed to be as follows.
Firstly, a trivalent cation radical of Sthn at pH 1—4[7,8] encounters the surface of SnO_2, a real n-type semiconductor at this stage, and discharges. This may cause temporary negative generation at the on-illumination. The resulting monovalent cation of thn has smaller solubility than Sthn in water, and it will be adsorbed onto the SnO_2 electrode, which may cause the pseudo-cathodic polarization of SnO_2. However, further adsorption of thn, Sthn, and Lthn dissolved in the aqueous layer may occur on the surface of SnO_2 covered already with the dye (stuff). Thus we cannot determine which of the species thn, Sthn or Lthn covers the SnO_2

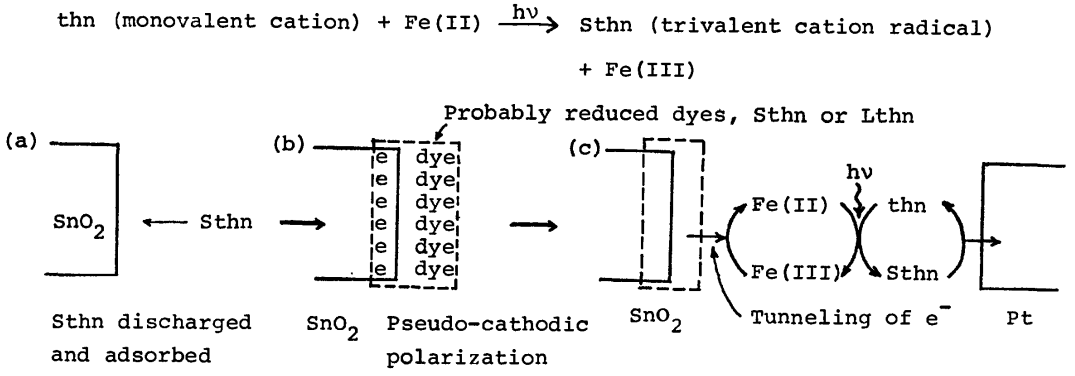

Fig. 6. Schematic representation of the role of SnO_2.

TABLE 4. CORRELATION OF THIN-LAYER PHOTOGALVANIC CELLS

Ref.	$[thn]_0$ (mol/l)	$[Fe(II)]_0$ (mol/l)	$[Fe(III)]_0$ (mol/l)	Vis-illumn (mW/cm²)	d[a] (mm)	ΔE (mV)	I (μA/cm)	Direction of e⁻
13)	10^{-3}—10^{-5}	10^{-2}	10^{-3}—10^{-5}	18.5	0.1	50—100	—	SnO_2(L)→Pt(L)
	10^{-3}—10^{-5}	10^{-2}	10^{-3}—10^{-5}	100	0.1	—	10—20	
This work	10^{-5}	5.0×10^{-2}	2.5×10^{-6}	10	2.0	80	0.07	Pt(L)→SnO_2(L)
	10^{-4}	5.0×10^{-2}	2.5×10^{-6}	10	2.0	80	0.4	

a) Distance between two electrodes.

electrode. When the solution was illuminated, the circuit closed and adsorption of dye (stuff) occurred, the species covering the SnO_2 electrode, formed by the photoredox reaction, was Sthn or Lthn rather than thn. Hence the direction of electron-flow was reversed as shown in Fig. 6(c). If this mechanism is valid, the experimental results 1)—4) and the effect of UV-light are understandable. The temporary negative generation of ΔE and I at the on-illumination in particular would be due to the initial stage of dye adsorption, which occurs only in the first on-off cycle, since the surface of SnO_2 is already covered with the dye (stuff) after the second cycle. The positive generation at off illumination was thus caused by the process of desorption of the dye (stuff) covering excessively the surface of SnO_2.

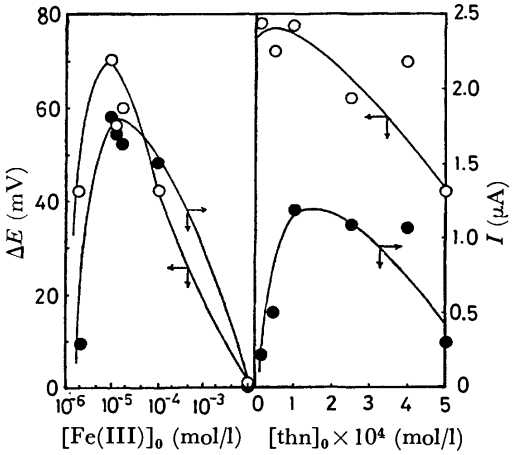

Fig. 7. Effect of $[Fe(III)]_0$ and $[thn]_0$ on ΔE and I of thn-Fe(II) systems. $[thn]_0=5.0\times10^{-4}$ mol/l in (a), $[Fe(OO)SO_4]_0=5.0\times10^{-2}$ mol/l, pH/l, pH 2.0-HCl aq, under N_2. (+) values indicate the electron-flow Pt(L)→SnO_2 (L).

Figure 7 illustrates the effect of $[Fe(III)]_0$ or $[thn]_0$ (subscript 0 indicates the initial concentration) on ΔE and I of the thn-Fe(II) aqueous systems studied by use of the thin-layer photocell (c). The dependence of ΔE and I on $[thn]_0$ is represented by a bell-shaped curve, the Δ values decreasing with $[thn]_0$. Under the conditions employed, $[thn]_0=5.0\times10^{-4}$ mol/l, $[Fe(II)]_0=5.0\times10^{-2}$ mol/l, the Δ value was almost 100%. The excess thn would decrease I due to the excessive adsorption of dye (stuff) onto SnO_2, and also decrease ΔE according to Nernst's equation:*

$$\Delta E = E_0 + 0.0592 \log \{([Sthn]/[thn][H^+])_A \times ([Fe(III)]/[Fe(II)])_C\}, \quad (5)$$

were A and C indicate the anodic and cathodic reactions, respectively. On addition of Fe(III), ΔE and I also showed the behavior represented by bell-shaped curves. At a low $[Fe(III)]_0$, the values increased due to the increased electron-exchange reaction and/or contribution of the $(\ )_C$ term in Eq. 6. The decrease in the values at high $[Fe(III)]_0$ was brought about by the increased short-circuit in solution or the increased bulk-backward reaction, which decreases the concentration of anode-active Sthn, and by the decrease of the dye-adsorption onto SnO_2. The direction of electron-flow reversed when the initial concentration of Fe(III) exceeded 10^{-2} mol/l. No quantitative discussions could be made due to the formation of thn-precipitates.

The experimental results of Clark and Eckert[13] and the present work are compared in Table 4. There is a large difference between the two I values if the direction of electron-flow is not taken into consideration. Since Clark and Eckert gave no details of the experimental procedure, it is difficult to find the reason for the difference. However, from the fact that (A) their I values are extraordinarily large for the thn-Fe(II) photogalvanic cells, and (B) we also observe a short-photocurrent of about 5 μA/cm² (or more) with the direction of SnO_2(L)→Pt(L) (under the conditions given in Table 4), the large I values they presented are considered to be short-photocurrent, or values obtained when the solution was pre-illuminated and the circuit then closed and I was measured. Especially, the phenomenon of (B) can be easily presumed from the on-off behavior shown in Fig. 5, in which the temporary negative generation, *i.e.*, the electron-flow SnO_2(L)→Pt(L), was observed at the on-illumination.

Thin-layer Photocells Composed of Gelatinized Thn-Fe(II) Systems. Since it was found that the electron-recycling in the thn-Fe(II) system mainly proceeds by the possible electron-exchange reaction between Fe(II)

TABLE 5. CORRELATION OF SEVERAL PHOTOGALVANIC CELLS

Systems of photocell	ΔE (mV)	I (μA)
(c) SnO_2/soln/Pt	70	1.82
(d) SnO_2/SS-gel/Pt	20	0.75
(e) SnO_2/SS-gel/membrane/Pt	29	0.30
(e) SnO_2/SS-gel/membrane×2/Pt*	32	0.53
(f) SnO_2/membrane/SS gel/Pt	6	0.23

$[thn]_0=5.0\times10^{-4}$ mol/l, $[Fe(II)SO_4]_0$ both in gel and membrane$=5.0\times10^{-2}$ mol/l, $[Fe(III)]_0$ both in gel and membrane$=2.5\times10^{-6}$ mol/l, *: $[Fe(III)]_0$ in membrane $=1.0\times10^{-5}$ mol/l. pH 2.0-HCl, under N_2. The direction of electron-flow was Pt(L)→SnO_2(L) in all cases.

* Nernst's equation is not correct in order to make quantitative discussions, since the equation does not take the formation of local cells into account. However, the equation is understandable for the qualitative discussions.

and Fe(III), the thin-layer photocells can be converted into some gel systems. Figures 1(c)—(f) illustrate the application of the thin-layer photocells. The results are summarized in Table 5. The semipermeable cellophane membrane having thickness 0.7—0.8 mm and porosity 24 Å was used for a diaphragm through which Fe(II) or Fe(III) permeates but not thn. In practice, thn permeated in a very small amount after 5 h. The most important facts are, (i) ΔE and I are very small in the SnO_2/wet membrane-[Fe(II)+Fe(III)]/gel-[thn+Fe(II)+Fe(III)]/Pt system, and (ii) in some extent larger ΔE and I were observed in the SnO_2/gel-[thn+Fe(II)+Fe(III)]/wet membrane-[Fe(II)+Fe(III)]/Pt system, in which the direction of electron-flow was Pt(L)→SnO_2(L). In the former system, there was no dye around SnO_2, since SnO_2 was attached to the membrane containing no dye. Hence SnO_2 is regarded as the real n-type semiconductor, which has an affinity for Sthn rather than for Fe(III). However, there existed only Fe(III) or Fe(II) around the SnO_2 electrode. Thus the former system is very disadvantageous as seen from the characteristics of SnO_2. In the latter system, SnO_2 can be converted into the pseudo-cathodic polarized state due to the adsorption of the dye (stuff), and consequently the cathodic reaction or the donation of electrons to Fe(III) is favorable on the SnO_2 electrode. However, it is very difficult to consider that Sthn, which cannot permeate to the Pt electrode through the cellophane membrane, discharges throughout the membrane. We consider the electron-recycling mechanism in the SnO_2/membrane/gel/Pt system to be as follows.

$$\underline{SnO_2} \longrightarrow (e^-) \longrightarrow$$

Pseudo-cathodic polarized by the adsorption of dyes.

$$\left(\begin{matrix}Fe(II)\\Fe(III)\end{matrix}\right)\left(\begin{matrix}thn\\Sthn\end{matrix}\right)\left(\begin{matrix}Fe(II)\longrightarrow Fe(II)\\Fe(III)\longleftarrow Fe(III)\end{matrix}\right)$$

$h\nu$ (photoexcitation); Electron-exchange

The reaction in a gel | The reaction in a wet membrane

$$\longrightarrow (e^-) \longrightarrow Pt \qquad (6)$$

As the use of membrane brought about the increase of internal resistivity to yield small ΔE and I values, a single-gel system was examined. Figure 8 illustrates the effect of $[Fe(III)]_0$ or $[thn]_0$ on ΔE and I observed by use of the thin-layer photocell (d) as in the SS (50 wt%)-gel systems. Although, the whole values were smaller than those in Fig. 7, similar bell-shaped curves were obtained. It is important that the dependency of $[Fe(III)]_0$ is more clearly recognized in Fig. 8 than in Fig. 7, *i.e.*, the direction of electron-flow reversed at high $[Fe(III)]_0$ as SnO_2(L)→Pt(L).

Figure 9 shows the effect of $[Fe(III)]_0$ on ΔE and I in the PVA (50 wt%)-gel systems. The values of ΔE and I showed similarly a maximum point of 82 mV at $[Fe(III)]_0=10^{-4}$ mol/l and of 0.85 μA at $[Fe(III)]_0=3.0\times10^{-5}$ mol/l, respectively, which were large enough

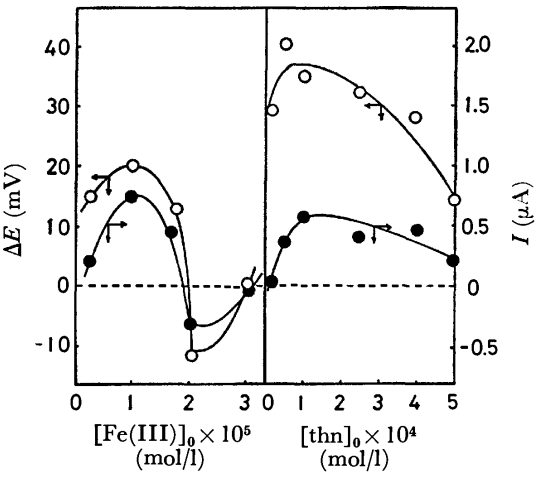

Fig. 8. Effect of $[Fe(III)]_0$ and $[thn]_0$ on ΔE and I of SS(thn-Fe(II))-gel systems. In SS 50 wt% gel, other conditions are the same as in Fig. 7.

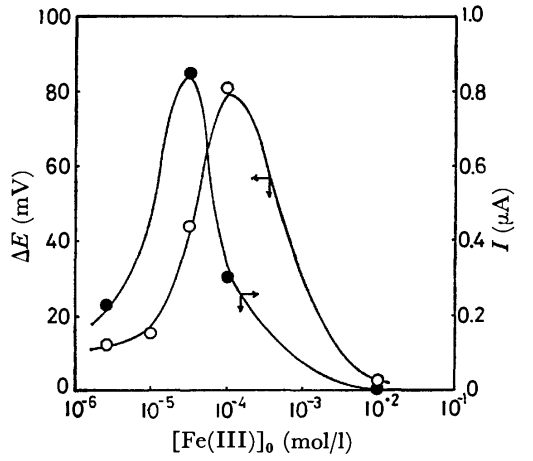

Fig. 9. Effect of $[Fe(III)]_0$ on ΔE and I of PVA(thn-Fe(II))-gel systems. In PVA 50 wt% gel, other conditions are the same as in Fig. 7.

as compared with the corresponding aqueous systems due to the excellent electron-recycling or electron-exchange reaction attributed to the role of the intra-macromolecular hydrogen bonds.

Hydroquinone (H_2Q) is a good reductant in the photoredox reaction with thn. The electrode active species are Sthn (anode) and benzoquinone (BQ) or semi-quinone radical (cathode) in this system. Vigorous stirring of the solution is necessary in order to keep the constant ΔE and I when the double-Pt type photocell as shown in Fig. 1(a) is used. This suggests that the electron-recycling in solution probably proceeds only by the transportation of the cathode active species. Figure 10 illustrates the effect of $[BQ]_0$ on ΔE and I in the SnO_2/thn-PH_2Q-gel/Pt system. The spontaneous decrease in ΔE and I indicates that there is no electron-exchange reaction between PH_2Q and BQ, while ΔE and I increase with $[BQ]_0$ in the SnO_2/thn-PH_2Q-SS-gel/Pt system, when a small amount of BQ is added (Fig. 11). The side hydroxyl groups of SS act the bridging reagent between H_2Q and BQ or semi-quinone residues to increase ΔE and I. PH_2Q is very easily oxidized by molecular oxygen, and the PVA-PH_2Q

TABLE 6. CORRELATION OF THIN-LAYER PHOTOGALVANIC CELLS UNDER THE MOST APPROPRIATE CONDITIONS

Photocell	$[thn]_0$(mol/l)	$[Reductant]_0$(mol/l)	$[Additive]_0$(mol/l)	ΔE (mV)	I (μA)	pH
(c)	1.0×10^{-4}	Fe(II), 5.0×10^{-2}	Fe(III), 2.5×10^{-6}	80	1.20	2.0
(c)	5.0×10^{-4}	Fe(II), 5.0×10^{-2}	Fe(III), 1.0×10^{-5}	70	1.82	2.0
(d), SS	1.0×10^{-4}	Fe(II), 5.0×10^{-2}	Fe(III), 2.5×10^{-6}	40,	0.50	2.0
(d), SS	5.0×10^{-4}	Fe(II), 5.0×10^{-2}	Fe(III), 1.0×10^{-5}	20	0.75	2.0
(d), PVA	5.0×10^{-4}	Fe(II), 5.0×10^{-2}	Fe(III), 1.0×10^{-4}	82	0.45	2.0
(d), PVA	5.0×10^{-4}	Fe(II), 5.0×10^{-2}	Fe(III), 3.0×10^{-5}	45,	0.85	2.0
(d), PH_2Q	5.0×10^{-2}	PH_2Q, 50 wt% gel	None	22	0.48	4.0
(d), SS	1.0×10^{-4}	PH_2Q, 5.0×10^{-2}	BQ, 1.0×10^{-4}	17	0.03	4.0
(d), SS	1.0×10^{-4}	PH_2Q, 5.0×10^{-2}	BQ, 1.0×10^{-3}	15	0.05	4.0
(e), SS	5.0×10^{-4}	Fe(II), 5.0×10^{-2}	Fe(III), 2.5×10^{-6} a) Fe(III), 1.0×10^{-5} b)	32	0.53	2.0
(f)	5.0×10^{-4}	Fe(II), 5.0×10^{-2}	Fe(III), 2.5×10^{-6}	6	0.23	2.0

a) in SS-gel. b) In membrane with double thickness, direction of electron-flow Pt(L)→SnO_2 (L).

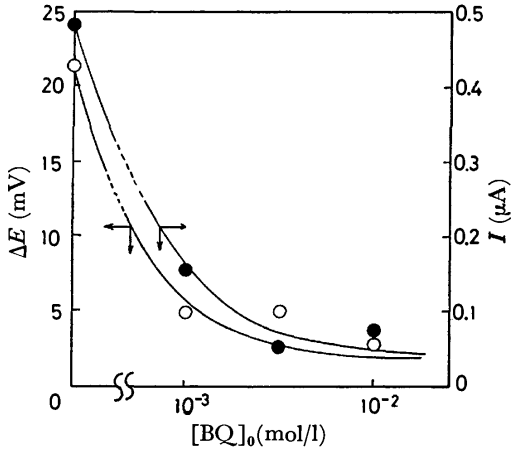

Fig. 10. Effect of $[BQ]_0$ on ΔE and I of PH_2Q(thn)-gel systems. $[thn]_0=5.0\times10^{-2}$ mol/l, PH_2Q 50 wt%-gel, pH 4.0-HCl aq under N_2. (+) values indicate the electron-flow Pt(L)→SnO_2(L).

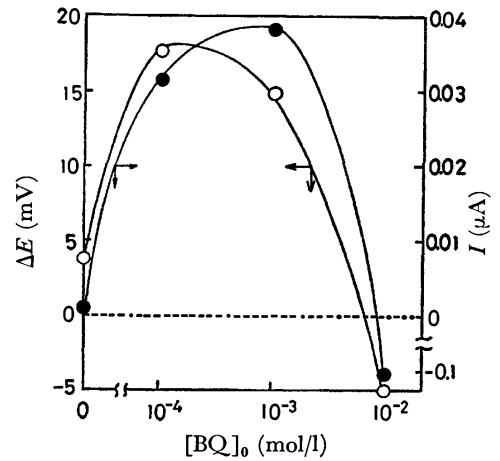

Fig. 11. Effect of $[BQ]_0$ on ΔE and I of SS(thn-PH_2Q)-gel systems. $[thn]_0=1.0\times10^{-4}$ mol/l, $[PH_2Q]_0=5.0\times10^{-2}$ mol/l, SS 50 wt%-gel, pH 4.0-HCl aq, under N_2. (+) values indicate the electron-flow Pt(L)→SnO_2(L).

system could not be examined.

The ΔE and I values under the most appropriate conditions in all the systems are summarized in Table 6. The ability to generate the photo-induced electricity in the PVA system is remarkable. It is noteworthy that the values and the direction of electron-flow in these thin-layer photocells composed of SnO_2 and Pt are very sensitive toward the experimental conditions, *i.e.*, the ration of $[thn]_0/[Reductant]_0$, or their absolute concentration, *etc.*, being balanced at the very critical and delicate situation.

Thin-layer Photocells Composed of Polymeric Thn-Membrane. A remarkable polymer effect in the photogalvanic property of the cationic thn-polymer-Fe(II) systems has been reported.[12] Large ΔE and I values were obtained due to the prohibition of the short-circuit in solution or the bulk-backward reaction between Sthn and Fe(III). The cationic thn-polymer in a gel or membrane state would generate much larger ΔE and I.

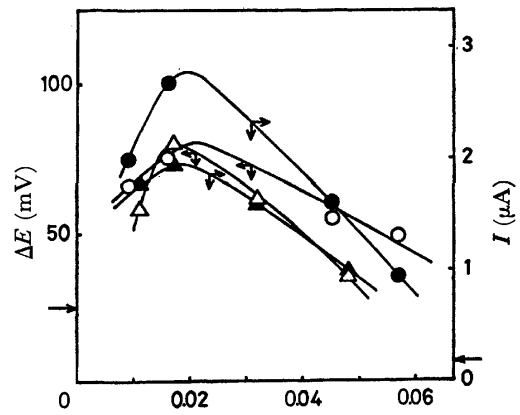

Fig. 12. Relationship between the thickness of BQEthn-film and ΔE, I in thin-layer photocell. (○,●); BQEthn 23%, (△,▲); BQEthn 19%. $[Fe(II)SO_4]_0=5.0\times10^{-2}$ mol/l, $[Fe(III)]_0=2.5\times10^{-6}$ mol/l, pH 2.0-HCl aq, under N_2.

BQEthn of the prescribed structure carrying cationic charges has been prepared, in which it is somewhat crosslinked with thn nuclei and is insoluble in water and soluble in methanol or *N,N*-dimethylformamide, and can thus be cast to a film from a methanol solution. Figure 12 illustrates ΔE and I of the BQEthn-Fe(II) systems cast between SnO_2 and Pt electrodes and swolled by the Fe(II) aqueous solution. Thus, the distance between two electrodes changes with the thickness of the film. The values ΔE and I show maxima at about 0.02 mm thickness of the film, and the direction of electron-flow is also $Pt(L) \rightarrow SnO_2(L)$. The decrease in the values with thicker films is probably due to the potential barrier formed by excess BQEthn. Hence the BQEthn of x (degree of incorporation of thn nuclie, see Experimental) $=23\%$ shows larger values than that of $x=19\%$, since the former requires a smaller amount of polymer than the latter, when the active thn concentration is kept constant. The BQEthn of $x=23\%$ shows absorpbance of about 0.3 at the 0.02 mm thickness, the influence of light-scattering being corrected in the measurement. The ΔE and I values of the thn-Fe(II) aqueous system possessing the same absorbance are also indicated by arrows in Fig. 12. The polymer systems shows much larger values than those of the monomeric solution system.

By utilizing the electron-exchange reaction and several polymer systems, the photogalvanic cells consisting of aqueous solutions could be converted into solid-phase cells without any remarkable decrease of the photo-induced electricity.

References

1) E. Rabinowitch, *J. Chem. Phys.*, **8**, 551, 560 (1940).
2) E. Rabinowitch and L. F. Epstein, *J. Am. Chem. Soc.*, **63**, 69 (1941).
3) S. Ainsworth, *J. Phys. Chem.*, **64**, 715 (1960).
4) R. Hardwick, *J. Am. Chem. Soc.*, **80**, 5667 (1958).
5) J. Schlag, *Z. Phys. Chem. N. F.*, **20**, 53 (1959).
6) P. Gomer, *Electrochimica Acta*, **20**, 13 (1975).
7) W. M. Clark, B. Cohen, and H. Gibbs, "Studies on Oxidation-Reduction," VIII, No. 1017, Pub. Health. Reps.
8) S. Granik, L. Michaelis, and M. P. Schubert, *Science*, **90**, 422 (1939); *J. Am. Chem. Soc.*, **62**, 204 (1940).
9) T. Tomono, E. Hasegawa, and E. Tsuchida, *J. Polym. Sci.*, **12**, 953 (1974).
10) K. Shigehara, H. Matsunaga, and E. Tsuchida, *J. Polym. Sci., Chem. Ed.*, submitted for publication.
11) K. Shigehara, and E. Tsuchida, *J. Phys. Chem.*, in press.
12) R. W. Dodson, and N. Davidson, *J. Phys. Chem.*, **56**, 866 (1952).
13) W. D. K. Clark and J. A. Eckert, *Solar Energy*, **17**, 147 (1975).

The Hydrocracking of a Heavy Anthracene Oil over Molten Salt Catalysts[1)]

Yohji NAKATSUJI, Shigeyuki FUJIOKA, Masakatsu NOMURA, and Shōichi KIKKAWA

Department of Applied Chemistry, Faculty of Engineering, Osaka University, Yamadakami, Suita, Osaka 565

(Received April 25, 1977)

The hydrocracking of a heavy anthracene oil over molten salt catalysts (zinc chloride or a binary mixture of zinc chloride and another metal chloride) at 400 °C for 3 h in a batch autoclave system was carried out, and the products were mainly identified by means of GC-MS. The effects of the hydrogen pressure (60 or 100 kg/cm^2), the quantity of the catalyst, and the addition of metal chloride (potassium chloride or copper(I) chloride) to zinc chloride on the product distribution were examined and discussed. Based on the detailed product analysis, it was found that *cata*-condensed polycyclic aromatic compounds were hydrocracked more efficiently than *peri*-condensed polycyclic aromatic compounds. The $CuCl/ZnCl_2$ molten salt displayed an excellent catalytic activity for the hydrocracking of the heavy anthracene oil.

The ring structures of the constituent units of bituminous coals are highly aromatic, and the average-sized configuration is considered to be three or four rings.[2,3)] In order to obtain a high yield of gasoline from coal, it is necessary to hydrocrack the constituent units to benzene and its derivatives. From this point of view, the hydrocracking of model compounds, which are supposed to be constituent units of coal, has been investigated.[3–12)] Zielke *et al.*[5)] had shown molten zinc chloride to be a superior catalyst for the hydrocracking of pyrene and coal extracts when used in high concentrations. Incidentally, intensive investigations have been under way in our laboratory on the catalytic action of molten salts in several organic reactions.[13)] As a part of this study, this paper will describe the hydrocracking of a heavy anthracene oil, which thus seems to be a kind of model substance. In addition, the change in the hydrocracking activity of zinc chloride by the addition of another metal chloride will be shown in this investigation.

Experimental

The NMR spectra were recorded by means of a JEOL JNM-PS-100 spectrometer, using tetramethylsilane as the internal standard. The GLC analyses were performed on a Shimadzu GC-3AH for gaseous products and on a GC-4BPTF for liquid and solid products. The GC-MS spectra were taken with a Hitachi RMU-6MG spectrometer at 20 eV connected with a Hitachi M 5201 apparatus using a 3 m× 3 mm column of 5% Silicone OV-1 on Uniport KS. The zinc chloride and potassium chloride were obtained from Wako Pure Chemical Industries, Ltd. The copper(I) chloride was obtained from Nakarai Chemicals, Ltd.

Characterization of Feed. A heavy anthracene oil (obtained from Osaka Gas Co., Ltd.; Specific gravity (50/4 °C) 1.142; moisture 0.5%; distillation test (dehydrated sample) 0—360 °C: 28.0%) was separated into three fractions and a residue by means of vacuum distillation. The characterization of these fractions is shown in Tables 1 and 2. Small amounts of heteroaromatics (indole, quinoline, carbazole, benzocarbazoles, and dibenzothiophene) were found in the feed and were identified using GC-MS. The type-analyses undertaken according to the Speight method[14)] (Table 3) gave results in good agreement with the results based on the information obtained from GC-MS.

Table 1. Characterization of feed

Fraction No.	Distillation conditions (°C/mmHg)	M.W.	Elemental analysis (wt%) C	H	N	S	O[a)]
I	—130/10	147	92.18	6.57	0.59	—	0.66
II	120—170/5	182	92.29	5.68	0.92	0.19	0.92
III	120—190/10^{-3}	203	92.21	4.86	1.07	0.25	1.61
IV	the residue	242	92.07	4.88	1.45	0.31	1.29

a) Difference

General Procedure. All the experiments were carried out in a stainless steel (Sus 32) autoclave with a capacity of 500 ml, shaken in a horizontal direction (70 strokes/min). A stainless steel vessel containing feed (about 20 g) and the catalyst were placed in the autoclave. The air in the autoclave was replaced by hydrogen, and then the system was filled with hydrogen to the determined pressure. The rate of the temperature rise was controlled to about 3 °C/min to 400 °C. The temperature was then held at the desired level for 3 h. After the system had been cooled to room temperature, gases were admitted into a gas holder and analyzed by GLC (60—80 mesh Silica gel column 3 m×3 mm). Solid samples from the reaction products were dissolved in a proper solvent and analyzed by GLC (4.5 m×3 mm column packed with 20% SE-30 on Uniport B 60—80 mesh). The liquid products were also analyzed by GLC. The mixture of coke and catalyst obtained after the extraction of the products was washed with water and refluxed in hydrochloric acid to remove the catalyst. The hydrogen sulfide evolved was trapped by the use of an iodine solution, and its quantity was determined by titrating the resulting solution with a sodium

Table 2. Main components in feed identified by means of GC-MS

Fraction No.	Main component (wt%)
I	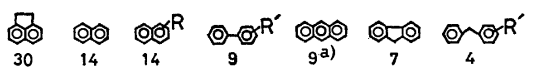 30 14 14 9 9[a)] 7 4
II	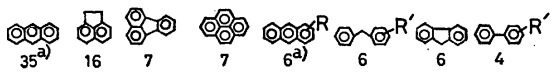 35[a)] 16 7 7 6[a)] 6 6 4
III	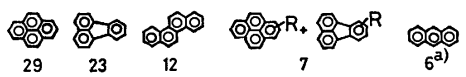 29 23 12 7 6[a)]
IV	Benzopyrenes 56  29 R = Me, Et; R′ = H, Me

a) Containing phenanthrene-type compounds.

Table 3. Type analysis by the Speight method

Fraction No.	Cs/Csα	Csα/Cp	Cp/Ca	Ra
I	1.2	0.17	0.79	2.0
II	1.1	0.10	0.70	2.9
III	1.1	0.07	0.61	3.9
IV	1.2	0.06	0.61	4.5

thiosulfate solution.

Analysis of Products. The products were mainly identified by using GC-MS; in order to characterize the activities of the molten salt catalysts, they were conveniently classified into fourteen groups as follows; **1**, C_1—C_4 gases; **2**, C_5—C_7 alkanes; **3**, cycloalkanes; **4**, monocyclic aromatics; **5**, indans and tetralins; **6**, bicyclic aromatics; **7**, partially hydrogenated compounds of tricyclic aromatics, fluorenes and benzindans; **8**, tricyclic aromatics; **9**, partially hydrogenated compounds of pyrenes and fluoranthenes; **10**, pyrenes and fluoranthenes; **11**, hydrochrysenes and its isomers; **12**, chrysenes; **13**, benzopyrenes and their hydrogenated compounds; and **14**, coke. Some representative constituents are shown in Table 4.

Table 4. Representative products identified by means of GC-MS

	Representative product
1	CH_4 C_2H_6 C_3H_8 n-and i-C_4H_{10} C_4H_8 C_3H_6
2	n-and i-C_5H_{12} 2,3-dimethylbutane 3-methylpentane
3	
4	
5	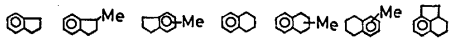
6	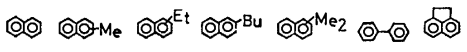
7[a]	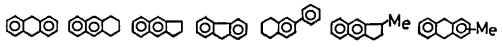
8[a]	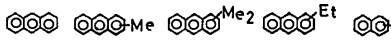
9	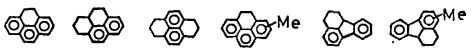
10	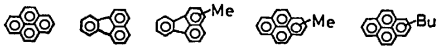
11	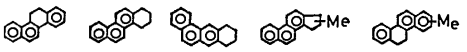
12	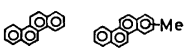

a) Phenanthrene-type compounds were not listed in this table.

Results and Discussion

Fractions II—IV are especially supposed to be better model substances for the hydrocracking of coals. The results of hydrocracking are shown in Table 5, along with the reaction conditions used. Table 6 describes the composition of the gaseous products (**1**: C_1—C_4 gases).

In the hydrocracking of Fraction II (Runs 1 and 2), the difference in the catalytic activity between zinc chloride and the binary mixture of zinc chloride and

Table 5. Reaction conditions and results

Run No.		1	2	3	4	5	6	7	8
Feed (Fraction No.)		II	II	III	III	III	III	IV	IV
Catalyst		$ZnCl_2$	$ZnCl_2$/CuCl[a]	—	$ZnCl_2$	$ZnCl_2$	$ZnCl_2$/KCl[b]	$ZnCl_2$	$ZnCl_2$
Cat. ratio[c]		1.0	1.0	—	1.0	1.0	1.0	1.8	0.7
Initial hydrogen pressure (kg/cm²)		100	100	100	60	100	100	100	100
Products (wt%)	**1**	16.4	21.9	5.9	23.7	17.4	9.7	49.4	22.9
	2	3.6	5.6	tr	1.0	1.2	0.5	0.9	0.9
	3	14.6	16.8	0.1	4.8	7.0	2.7	5.4	5.3
	4	14.6	23.3	0.3	10.3	6.6	3.2	10.9	5.5
	5	13.3	14.5	0.6	5.6	6.6	4.2	6.5	7.9
	6	8.6	4.4	1.1	5.0	3.6	4.1	6.0	5.3
	7	12.9	4.1	7.1	5.6	8.1	11.5	3.9	5.3
	8	10.7	1.7	8.7	5.5	9.5	11.4	5.0	4.8
	9	1.6	0.6	21.9	1.9	6.1	7.6	0.7	2.9
	10	3.1	2.2	38.0	18.7	25.6	34.4	8.1	13.8
	11	0.4	0.2	9.5	2.3	4.9	7.3	0.4	4.8
	12	—	—	6.8	3.0	2.1	3.1	0.8	8.3
	13	—	—	—	—	—	—	1.7	11.4
	14	0.2	4.7	tr	12.6	1.3	0.3	0.3	0.9

a) $ZnCl_2$: CuCl=60: 40 (mol%); $ZnCl_2$+CuCl/Feed=1.0. b) $ZnCl_2$: KCl=60: 40 (mol%); $ZnCl_2$/Feed=1.0. c) Catalyst/Feed (mol/mol) average molecular weights were used.

Table 6. Composition of gases in **1** (wt%)

	Run No.							
	1	2	3	4	5	6	7	8
CH_4	8.5	9.7	25.7	15.2	8.4	20.0	20.0	15.7
C_2H_6	18.6	14.1	68.4	18.9	31.1	48.1	30.7	31.4
C_2H_4	—	—	—	2.0	—	—	—	—
C_3H_8	23.1	23.2	5.9	24.8	26.6	16.4	22.5	22.9
C_3H_6	—	—	—	2.9	—	—	—	—
i-C_4H_{10}	37.1	39.3	tr	22.4	21.9	2.9	12.5	8.2
n-C_4H_{10}	7.8	9.3	tr	7.3	4.1	12.6	9.2	16.1
C_4H_8	4.9	4.4	—	6.5	7.9	tr	5.1	5.7

copper(I) chloride was examined. The yield of benzene and its derivatives (**4**) in Run 1 (14.6%) is lower than that in Run 2 (23.3%), and the combined yield of higher aromatics (**7**—**11**) in Run 2 (8.8%) is lower than that in Run 1 (28.7%). This result suggests that the catalytic activity of $ZnCl_2$/CuCl molten salt is superior to that of $ZnCl_2$. Since aromatic-type bonds are not expected to be thermally cleaved at 400 °C, the single C–C bonds of hydroaromatics are considered to be ruptured in the course of this hydrocracking. Therefore, it is necessary that aromatic rings be hydrogenated before they receive catalytic cracking by acidic molten salts. From this standpoint, the capabilities of both hydrogenation and cracking are demanded for the hydrocracking catalyst. On the basis of the product distribution, it is possible to estimate which acts predominantly in this hydrocracking. For example, the ratio of **5**/**6** is supposed to be a measure of the hydrogenating activity of the catalyst. The higher ratio of **5**/**6** in Run 2 than in Run 1 would demonstrate the improvement of its hydrogenating activity upon the addition of copper(I) chloride to zinc chloride. On the other hand, the ratio of isobutane to butane in the gaseous products was found to be not so changed by the addition of copper(I) chloride to zinc chloride. As the ratio of isobutane to butane is supposed to be a measure of the cracking activity of acidic molten salts, this finding shows that the intrinsic cracking activity of zinc chloride according to its Lewis acidity is not so much changed by this addition of copper(I) chloride. Kenney *et al.*[15] demonstrated that the catalytic activity of zinc chloride was lowered by

the addition of metal chlorides, such as KCl, NaCl, and AgCl, in the hydrogen chloride elimination of isopropyl chloride; the principal exception was copper(I) chloride. In addition to the results similar to their findings, an improvement in the hydrogenating activity was found in this investigation. This synergenic effect of the addition of copper(I) chloride to zinc chloride was also found in the hydrocracking of anthracene,[16] phenanthrene, pyrene, fluoranthene, and chrysene.[17]

In the hydrocracking of Fraction III (Runs 3—6), the change in the cracking activity of zinc chloride caused by the addition of potassium chloride and the effect of the initial hydrogen pressure on the hydrocracking were examined. By comparing the result of Run 5 with that of Run 6, the binary mixture of $ZnCl_2$ and KCl was found not to display any appreciable catalytic activity. In the hydrocracking of hydroaromatics in this temperature range, two different reactions can occur.[6] The first of them is thermal cracking under a hydrogen atmosphere, which proceeds by means of a free radical mechanism; the other is catalytic cracking, which proceeds by means of a carbonium ion mechanism. When the hydrocracking proceeds by means of the latter mechanism, the ratio of iso to normal isomers is higher than that in a thermodynamic equilibrium. From this standpoint, the low yield of branched alkanes found in the case of Run 6 describes the lowering of the cracking activity of zinc chloride by the addition of potassium chloride. As the catalytic action of $ZnCl_2$ is attributed to its own molecular character, the formation of ionic complexes (such as K_2ZnCl_4) lowers the intrinsic cracking activity of molten zinc chloride. This is consistent with the result of Kenney *et al.*[15] In the absence of an acidic metal chloride (Run 3), small amounts of gases (most of them are methane and ethane) are obtained, and so the hydrogenation of aromatics is considered to govern this reaction. The effect of the hydrogen pressure is also shown in Runs 4 and 5. At higher hydrogen pressures, the formation of coke is found to be suppressed to a significant extent. This result indicates that the formation of coke may proceed *via* intermolecular dehydrogenation, and that hydrogen may act to capture active intermediates, such as species leading to coke with lesser amounts of hydrogen. The reason for the lowering of cracked products at higher hydrogen pressures may also be attributed to this stabilization.

The quantity of the catalyst is one of the most important factors dominating this hydrocracking (Runs 7 and 8). For example, the change in the conversion according to the quantity of the catalyst is remarkable in the yields of gaseous products. From this finding, the lowering in the cracking activity upon the addition of potassium chloride to zinc chloride mentioned above is attributable to the decrease in the amounts of effective parts of the catalyst.

In all the runs, *cata*-condensed polycyclic aromatics (anthracenes, phenanthrenes and chrysenes) were hydrocracked more efficiently than *peri*-condensed polycyclic aromatics (pyrenes). Therefore, benzopyrenes were hydrocracked to pyrenes, which were relatively resistant to the hydrocracking in the molten salt catalyst. Also, the reactivity of fluoranthenes was found to be fairly high.

In the hydrocracking of Fraction IV with a higher S content, the behavior of S was examined. Most of the S was found in the form of zinc sulfide. Attention was not given to the behavior of N and O, but the contents of hetero atoms in the products were found to be lower than in the feed.

References

1) Organic Reaction in Fused Salts. XII. XI: S. Kikkawa, M. Nomura, and T. Ikeuchi, *Bull. Chem. Soc. Jpn.*, **50**, 1351 (1977); A part of this work was presented at the 34th National Meeting of the Chemical Society of Japan, Kanagawa, April 1976.

2) Y. Maekawa, K. Shimokawa, T. Ishii, and G. Takeya, *Nenryo Kyokaishi*, **46**, 927 (1967).

3) W. H. Wiser, S. Singh, S. A. Qader, and G. R. Hill, *Ind. Eng. Chem., Prod. Res. Dev.*, **9**, 350 (1970).

4) N. Choudhary and D. N. Saraf, *Ind. Eng. Chem., Prod. Res. Dev.*, **14**, 74 (1975), and references cited therein.

5) C. W. Zielke, R. T. Struck, J. M. Evans, C. P. Costanza, and E. Gorin, *Ind. Eng. Chem., Process Des. Rev.*, **5**, 151, 158 (1966).

6) R. A. Flinn, O. A. Larson, and H. Beuther,, *Ind. Eng. Chem.*, **52**, 153 (1960).

7) R. A. Sullivan, C. J. Egan, and G. E. Langlois, *J. Catal.*, **3**, 183 (1964).

8) S. A. Qader and G. R. Hill, *Am. Chem. Soc., Div. Fuel Chem., Prep.*, **16**, 93 (1972), and following articles.

9) C. Rumohr and G. Kölling, *Erdöl u. Kohle*, **25**, 309 (1972).

10) P. W. E. Blom, J. Dekker, L. Fourie, J. A. Kruger, and H. G. J. Potigieter, *J. S. Afr. Chem. Inst.*, **28**, 130 (1975).

11) M. Morita and K. Hirosawa, *Nippon Kagaku Kaishi*, **1976**, 1259. They also have reported the hydrocracking of destructive chemical disintegration extracts under the hydrogen pressure of Hokkaido coals; *Nenryo Kyokaishi*, **54**, 677 (1975).

12) S. Kikkawa, M. Nomura, and K. Murase, *Sekiyu Gakkaishi*, **19**, 863 (1976).

13) S. Kikkawa and M. Nomura, *Yuki Gosei Kagaku Kyokai Shi*, **33**, 593 (1975).

14) J. G. Speight, *Fuel*, **49**, 76 (1970).

15) C. N. Kenney and R. Takahashi, *J. Catal.*, **22**, 16 (1971).

16) S. Kikkawa, M. Nomura, T. Kubo, and Y. Nakatsuji, *Chem. Lett.*, **1976**, 1383.

17) Y. Nakatsuji, T. Kubo, M. Nomura, and S. Kikkawa, unpublished data.

NOTES

BULLETIN OF THE CHEMICAL SOCIETY OF JAPAN, VOL. 50 (12), 3409—3410 (1977)

Proton Spin Lattice Relaxation in Blends of Natural Rubber and Polyterpene

Masayoshi Ito and Koji Tanaka

Department of Chemistry, Faculty of Science, Science University of Tokyo, Kagurazaka, Shinjuku-ku, Tokyo 162

(Received May 12, 1977)

Synopsis. NMR measurements were carried out on blends of natural rubber (NR) and polyterpene (PT). The blends of NR and PT are perfectly mixed. The motion of NR chains play a dominant role in the glass transition of the blends. The mobility of NR segments in the blends are constrained by the presence of PT.

Rubbery mixtures of an elastomer and resin are tack, and the tackiness increases with increase in the concentration of resin. Hock[1] found by electron microscopy that the increase of tackiness is due to the development of a second phase, which probably consists of low molecular weight rubber dissolved in the resin. On the other hand, Fukuzawa[2] suggested that the compatibility of elastomer-resin is the most important factor in understanding the increase of tackiness. These different explanations imply that detailed information on the internal structure of the blend materials is necessary to understand the increase of tack.

The application of NMR method to the study of polymer blends is known to offer advantageous information on the microstructure of the blend materials.[3,4]

In the present study, the segmental mobility for the blends of natural rubber and polyterpene was investigated by the NMR method in order to further elucidate the mixing state of the blends.

Experimental

Samples. Unvulcanized natural rubber (Hevea rubber) and polyterpene which is a random copolymer of α-pinene and β-pinene (Sekisui Chemical Industry Co., Ltd.) were used. The number average molecular weight and softening point of polyterpene were 1200 and 100 °C, respectively. X-Ray diffraction patterns indicated that these materials are completely amorphous. The glass transition temperature of natural rubber and polyterpene was determined by DSC to be *ca.* −65 and 70 °C, respectively.

Films containing natural rubber and polyterpene were cast from carbon disulfide solution on glass at room temperature. The ratio of natural rubber to polyterpene is given on a weight basis. The films were dried in a vacuum at room temperature for a week.

Measurements. A pulsed NMR spectrometer similar to the one described by Clark[5] was used. The resonance frequency for protons was 30 MHz. Samples were packed in a glass tube in a vacuum.

Line width was obtained with a JNM W-40 type (resonance frequency for protons was 40 MHz) broad line NMR spectrometer.

Results and Discussion

The temperature dependence of spin-lattice relaxation times (T_1) for natural rubber (NR), polyterpene (PT), and their blends is shown in Fig. 1. T_1 for NR and the four blends shows one T_1 minimum, indicating the presence of a second minimum below the temperature accessible in this study. In NR, the high temperature minimum undoubtedly corresponds to the glass transition, while the low temperature process involves methyl group reorientation.[6] T_1 for PT shows one small minimum at around 150 °C, indicating the presence of two minima below and above the temperature accessible in this study. The low temperature process might be due to the methyl group reorientation as judged from

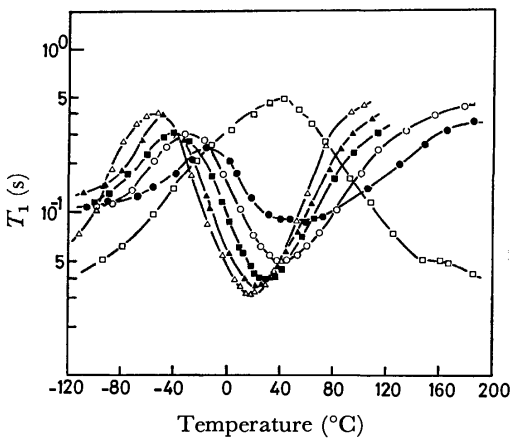

Fig. 1. Temperature dependence of T_1 for NR(△), PT(□), NR–PT=90: 10(▲), NR–PT=70: 30(■), NR–PT=50: 50(○), and NR–PT=30:70(●).

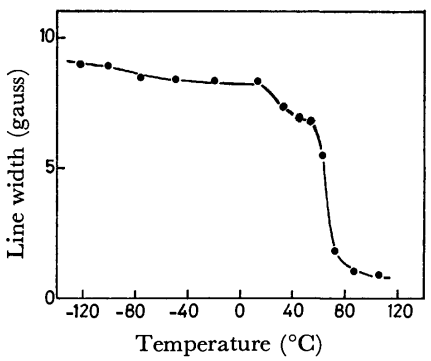

Fig. 2. Temperature dependence of NMR line width of polyterpene.

the very low T_1 minimum temperature and the chemical structure of polyterpene. The line widths for PT obtained from the derivatives of the broad line NMR absorption lines are plotted against temperature in Fig. 2. Two distinct transitions take place. At the first step the narrowing of line width starts at about 20 °C. After the first narrowing the curve enters into the second step of abrupt decrease at *ca.* 70 °C, followed by leveling off. The high temperature transition is consistent with the glass transition temperature of PT. A small decrease of line width at *ca.* 20 °C indicates a small scale segmental motion of PT. From a comparison of the line width data with the T_1 data (Fig. 1), it is postulated for the relaxation mechanisms of PT that the high temperature decrease of T_1 is due to the onset of micro-Brownian motions and the small T_1 minimum at around 150 °C corresponds to the local mode motions. On the basis of the characterization of T_1 minima for NR and PT, it is postulated for the relaxation mechanisms of the blends that the low temperature minimum is due to the reorientation of the methyl group and the high temperature process corresponds to the glass transition. As seen in Fig. 1, all the samples show only one T_1 value in the whole range of temperature. The fact that blends of natural rubber and polyterpene show only one glass transition and T_1 value over the whole range of composition and temperature demonstrates the excellent compatibility of NR and PT.

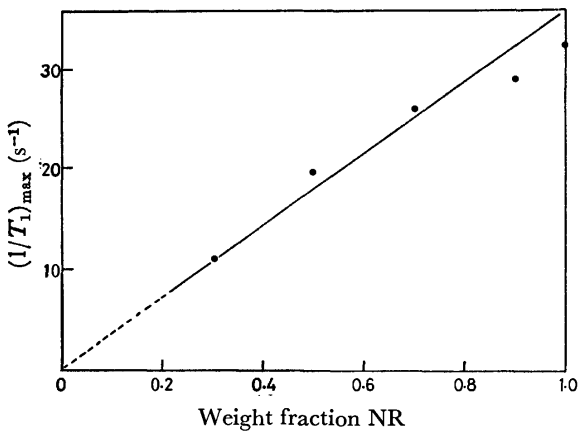

Fig. 3. Natural rubber weight fraction dependence of maximum relaxation rate at the glass transition.

Figure 3 shows the relation between the maximum relaxation rate $(1/T_1)_{max}$ of the blends at the glass transition and the weight fraction of NR. A linear dependence is found. This indicates that the motion of the natural rubber chain plays a dominant role in the mechanisms of glass transition of the blends.

The T_1-temperature curve is gradually broadened at the glass transition and the minimum temperature shifts to the higher temperature side with the increase of PT content (Fig. 1). The broadening of the T_1 minimum indicates that the distribution of correlation times related to the degree of the restriction imposed on the segments is broadened by addition of the PT resin. With the increase of PT content, the intermolecular interaction between NR and PT chains increases and the segmental motion of NR in the blends is constrained and the temperature of the T_1 minimum shifts to the higher temperature side.

In conclusion, blends of natural rubber and polyterpene are perfectly mixed over the whole range of composition. The motion of the natural rubber chain plays a dominant role in the mechanisms of glass transition of the blends and the segmental mobility of natural rubber chains in the blends are greatly constrained by the presence of polyterpene.

The authors wish to express their thanks to Professor M. Takeda for his continuing interest and encouragement during the course of this investigation.

References

1) C. W. Hock, *J. Polym. Sci., Part C*, **3**, 139 (1963).
2) K. Fukuzawa, Preprints of 9th Symposium on Adhesion and Adhesives, Tokyo, Japan (1971).
3) D. D. Davis and W. P. Slichter, *Macromolecules*, **6**, 728 (1973).
4) T. K. Kwei, T. Nishi, and R. F. Roberts, *Macromolecules*, **7**, 667 (1974).
5) W. G. Clark, *Rev. Sci. Instrum.*, **35**, 316 (1964).
6) W. P. Slichter and D. D. Davis, *J. Appl. Phys.*, **35**, 3103 (1964).

BULLETIN OF THE CHEMICAL SOCIETY OF JAPAN, VOL. 50 (12), 3411—3412 (1977)

Annihilation of the Catalytic Activity in Butene Isomerization of Porous Vycor Glass by Washing with EDTA Aqueous Solution

Shoji HIRAI,* Akira MORIKAWA, Yoshio ISHINAGA, Kiyoshi OTSUKA, and Yuji WADA

Department of Chemical Engineering, Tokyo Institute of Technology, O-okayama, Meguro-ku, Tokyo 152

* *Atomic Energy Research Laboratory, Musashi Institute of Technology, 971 Ozenji, Tama-ku, Kawasaki 215*

(Received June 13, 1977)

Synopsis. The catalytic activity of porous Vycor glass in the isomerization of butenes was eliminated by washing the glass with EDTA aqueous solution, though the contents of Al and Zr in the glass remained unchanged. Destruction by decationation of active sites of silica-alumina character has been suggested.

Porous Vycor glass is one of the most favourable materials for examining molecules bound to the surface by means of spectroscopy. The mechanism of the photoisomerization of butenes was investigated by sensitization of molecules adsorbed on the glass or of the Vycor glass itself.[1-3] However, the glass shows an appreciable thermal catalytic activity in the isomerization,[1,4] occasionally making the experimental results vague.

The minor components of the Vycor glass (96% SiO_2) are mainly alumina, boria, and zirconia. Aluminium forms acid surface sites of a silica-alumina character, with which butene molecules interact to isomerize.[5] Silica-zirconia is also a solid acid.[6] Thus, removal of aluminium or zirconium from the glass might cause annihilation of the thermal catalytic activity of the glass for isomerization. It has been reported that aluminium in zeolites is successfully removed by EDTA treatment.[7] We have applied this technique to porous Vycor glass and suppressed the activity. This paper deals with the results with respect to the change in the isomerization activity and the contents of aluminium and zirconium.

Experimental

A porous Vycor glass plate $30 \times 8 \times 0.9$ mm was calcined at 750 °C in the air for 3 h, washed with 0.01 M neutral aqueous solution of EDTA for an appropriate duration, washed twice with distilled water for 15 min each and dried for 2 h at 400 °C in the air. The glass plate was then placed in a coaxial tubular, quartz-made reactor, calcined at 500 °C for 2 h in a stream of oxygen gas with a pressure of 20 kPa, and degassed for 2 h under a pressure of 7×10^{-3} Pa at the same temperature. At 60 °C a reacting gas, *cis*-2-butene, of pressure 20 kPa was introduced into the reactor, the reaction then proceeding in a closed gas-circulation apparatus with a volume of 190 ml. The products were analyzed by gas chromatography at appropriate intervals. Elements other than Si, B, and O contained in the glass plate were analyzed by means of neutron activation analysis with the GAMA system at Atomic Energy Research Laboratory, Musashi Institute of Technology.

Results and Discussions

The elements present in appreciable amounts were Al, Zr, As, Ti, V, Mn, Fe, Na, and Mg among a large number of elements detected. The amounts of aluminium and zirconium were considerably greater than those of the others.

TABLE 1. *cis*-2-BUTENE ISOMERIZATION ACTIVITY AND CONTENTS OF ALUMINIUM AND ZIRCONIUM

Duration of EDTA washing (h)	0	0.5	1	2	3
Amount of Al (ppm)	2670	3070	2940	2550	3050
Amount of Zr (ppm)	962	960	978	938	852
Catalytic activity (mol s^{-1} g-cat^{-1})	5.1×10^{-9}	trace	none	a)	none

a) Transparency was measured.

The amounts of both aluminium and zirconium in the glass with various durations of EDTA washing are summarized in Table 1. The unwashed glass is denoted by zero duration. No effect of EDTA washing was detected on the contents of the two elements. On the other hand, the catalytic activity was drastically eliminated by only 30 min washing. For the unwashed glass the activities at 60 °C for the isomerization of *cis*-2-butene to 1-butene and *trans*-2-butene are 3.3×10^{-9} and 1.8×10^{-9} mol s^{-1} g-cat^{-1}, respectively, the corresponding apparent activation energies for the isomerization being *ca.* 71 and 83 kJ mol^{-1}, which may be reasonable values for isomerization on the acid sites of a silica-alumina character. For the washed glass, however, even at 80 °C, no activity could be measured.

The results lead us to the following conclusions. (1) Aluminium and zirconium atoms on the surface of the glass, contributing to formation of acid sites, can be removed by EDTA, resulting in annihilation of the catalytic activity for the butene isomerization. (2) Most of the aluminium and zirconium atoms probably entrapped in the silica network of the bulk of glass are resistant to the EDTA washing and inert for the reaction. (3) Such entrapped aluminium or zirconium atoms are immobile under heating at 500 °C for 4 h during the course of pretreatment. If mobile, they may diffuse from the bulk to the surface of the glass, forming acid sites during the course of pretreatment.

The transparency of the washed glass hardly decreased. Only 0.02 increase of absorbance to the light of wavelength 700—400 nm and 0.02—0.15 to 400—250 nm were observed for the 2 h washed glass.

Thus EDTA washing can be utilized for preparing catalytically inert supports of catalysts.

The present work was partially supported by the Visiting Researchers Program of Tokyo Institute of Technology and Atomic Energy Research Laboratory, Musashi Institute of Technology.

References

1) A. Morikawa, M. Hattori, K. Yagi, and K. Otsuka, *Z. Phys. Chem., Neue Folge*, **104**, 309 (1977).
2) K. Otsuka and A. Morikawa, *Bull. Chem. Soc. Jpn.*, **47**, 2335 (1974).
3) K. Otsuka and A. Morikawa, *Bull. Chem. Soc. Jpn.*, **48**, 3025 (1975).
4) N. F. Foster and R. J. Cvetanović, *J. Am. Chem. Soc.*, **82**, 4274 (1960).
5) G. A. Blomfield and L. H. Little, *J. Cat.*, **21**, 139 (1971).
6) V. A. Dzisko, *The 3rd International Congress on Catalysis (Amsterdam)*, *Preprint* I-19 (1964).
7) B. D. Flockhart, M. C. Megarry, and R. C. Pink, *Advan. Chem. Ser.*, **121**, 509 (1973).

BULLETIN OF THE CHEMICAL SOCIETY OF JAPAN, VOL. 50 (12), 3413—3414 (1977)

The Preparation of Trivalent Metal Chelates with Some N_3O_3-Type Ligands

Mariko TAKAHASHI and Susumu TAKAMOTO

Department of Chemistry, Faculty of Sciences, Gakushuin University, Mejiro, Toshima-ku, Tokyo 171

(Received June 6, 1977)

Synopsis. Iron(III), chromium(III), and cobalt(III) chelates with 1,4,7-triazacyclononane-*N,N',N''*-triacetate, 1,4,7-triazacyclodecane-*N,N',N''*-triacetate, and 2-(aminomethyl)-2-methyl-1,3-propanediamine-*N,N',N''*-triacetate were synthesized and characterized by means of the electronic absorption spectra in an aqueous solution. As they are non-charged chelates with a C_3 symmetry, their spectra resemble those of facial tris(glycinato) complexes.

One of the present authors reported earlier that 1,4,7-triazacyclononane formed extremely stable complexes with some hexa-coordinating metal ions,[1] and that the stability constants of divalent metal chelates with its triacetate derivative could be measured polarographically.[2] This complexane-type ligand includes three nitrogen and three oxygen atoms as donors; therefore, a trivalent metal ion can form a non-charged chelate which has a C_3 symmetry. This paper is concerned with the preparation of iron(III), chromium(III), and cobalt(III) chelates with similar tripodal ligands, 1,4,7-triazacyclononane-*N,N',N''*-triacetate (tnta), 1,4,7-triazacyclodecane-*N,N',N''*-triacetate (tdta), and 2-(aminomethyl)-2-methyl-1,3-propanediamine-*N,N',N''*-triacetate (apta).

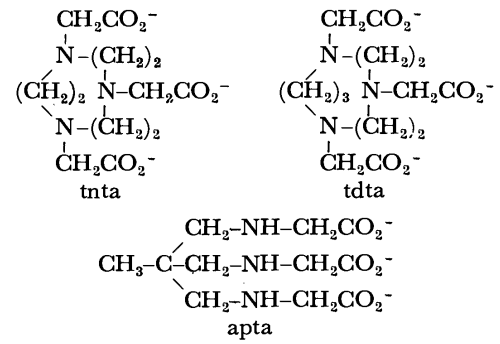

Experimental

Preparation of Ligands. Each ligand was synthesized by the carboxymethylation of the corresponding triamine, 1,4,7-triazacyclononane,[1,3,4] 1,4,7-triazacyclodecane,[3,4] or 2-(aminomethyl)-2-methyl-1,3-propanediamine,[5,6] which had all been prepared according to the methods in the literature. The procedures of all these carboxymethylations were like those to be described below. Triamine trihydrochloride (40 mmol) and excess chloroacetic acid (140 mmol) were dissolved in water (100 cm³). The mixture was heated to 45 °C, while the pH of the solution was maintained at 10 by adding lithium hydroxide intermittently. After consuming 400 mmol of alkali, the alkaline solution was refluxed for several hours. Then the pH of the solution was adjusted to about 2 with hydrochloric acid, and the mixture was evaporated almost to dryness. After having been washed throughly with methanol, the residue was twice recrystallized from aqueous ethanol. Yields: H_3tnta, 55%; H_3tdta, 35%; H_3apta·HCl, 30%.

Preparation of Chelates. *Iron(III) Chelates*: A solution of $Fe(NO_3)_3 \cdot 9H_2O$ (3.0 mmol in 5 cm³ of water) was added to a warm solution of the ligand (3.3 mmol in 5 cm³ of water). In the case of [Fe^{III}(tnta)], bright yellow needles were deposited almost quantitatively in a few minutes. The crystals were washed with water and ethanol. They were pure enough without further purification. Yield, 85%. [Fe^{III}(tdta)] and [Fe^{III}(apta)] were also obtained in a similar way, but the gentle evaporation of the mixture was needed to form the crystals. These were purified by recrystallization from aqueous ethanol. Yields, 30—50%.

Chromium Chelates: (A) Metallic chromium powder (10 mmol), water (10 cm³), and ligroin (40 cm³) were placed in a conical flask (100 cm³), into which concentrated HCl (3 cm³) was then slowly poured without stirring. After the bubbling reaction had then settled, the flask was put into a warm water bath (50 °C) for 15 min. A ligand solution (5 mmol in 25 cm³ of water) was degassed by boiling and added to the earlier bluish mixture. The excess acid was neutralized with solid $NaHCO_3$, and the ligroin was pipetted out. Then 30% H_2O_2 (2 cm³) was added to the bluish solution, which was heated several minutes. After the chromium hydroxide thus formed was filtered off, the filtrate was ice-cooled for several hours. Deep red crystals were slowly isolated in the case of [Cr^{III}(tnta)], but the tdta or apta chelate was obtained by evaporating the filtrate. The solid product was washed and recrystallized with aqueous ethanol. Yields, 30—50%.

(B) $[Cr^{III}(NH_3)_6]Cl_3$ (3.0 mmol) and the ligand (3.3 mmol) were dissolved in water (30 cm³), after which solution was refluxed for 8 h with stirring (if it did not turn wine red, a few drops of 5% NaOH were added and refluxing was continued). The little chromium hydroxide thus formed was filtered off while hot; then the filtrate was ice-cooled. Deep red crystals of [Cr^{III}(tnta)] were gradually formed, but the concentration of the solution was needed in the case of the tdta or the apta chelates. They were purified in a manner similar to the above. Yields, 30—50%.

Cobalt(III) Chelates: (A) $CoCl_2 \cdot 6H_2O$ (3.0 mmol) and H_3tnta (3.3 mmol) were dissolved in hot water (15 cm³), and 30% H_2O_2 (2 cm³) was added to the solution, which was then warmed for several minutes before being ice-cooled. Wine-red crystals of [Co^{III}(tnta)] were slowly deposited. By the evaporation of the filtrate, more chelate could be recovered. The crude complexes were recrystallized from hot water by adding ethanol and concentrating the solution. The product was washed thoroughly with aqueous ethanol. Yield, 70%. [Co^{III}(tdta)] and [Co^{III}(apta)] could also be prepared by the above procedure except for the addition of a little active charcoal, which had to be removed after the reaction. As these chelates were much more soluble in water than the tnta chelate, the filtrate was evaporated to solidify the complexes. They were recrystallized from aqueous ethanol. Yields, 30—50%.

(B) Cobalt chelates were prepared from the hexaamminecobalt(III) complex in the way that described in (B) for

Table 1. Elemental analyses and absorption spectral data

Substance	Elemental analyses Found, % (Calcd, %) C	H	N	Cl or M	Absorption bands $\tilde{\nu}/10^3$ cm^{-1} (log ε)		
H_3tnta	47.22	6.96	13.88				
($C_{12}H_{21}N_3O_6$)	(47.52)	(6.98)	(13.85)				
H_3tdta	48.79	7.23	13.05				
($C_{13}H_{23}N_3O_6$)	(49.20)	(7.31)	(13.24)				
H_3apta·HCl	40.16	6.83	12.94	10.71			
($C_{11}H_{22}N_3O_6Cl$)	(40.31)	(6.77)	(12.82)	(10.82)			
[Cr(tnta)]	40.30	5.10	11.77	14.62	19.5	25.7	
($CrC_{12}H_{18}N_3O_6$)	(40.91)	(5.15)	(11.93)	(14.76)	(2.39)	(2.18)	
[Cr(tdta)]	43.25	5.40	11.34	14.05	19.4	26.0	
($CrC_{13}H_{20}N_3O_6$)	(42.63)	(5.50)	(12.49)	(14.19)	(2.33)	(2.12)	
[Cr(apta)]	38.07	5.38	12.18	15.19	20.1	26.4	
($CrC_{11}H_{18}N_3O_6$)	(38.83)	(5.33)	(12.35)	(15.28)	(2.24)	(2.04)	
fac[Cr(gly)$_3$]	26.05	4.58	15.04	18.60	19.4	26.0	
($CrC_6H_{12}N_3O_6$)	(26.29)	(4.41)	(15.33)	(18.70)	(2.23)	(2.02)	
[Co(tnta)]	39.70	5.01	11.64	16.89	19.6	27.1	43.5
($CoC_{12}H_{18}N_3O_6$)	(40.12)	(5.05)	(11.70)	(16.40)	(2.54)	(2.34)	(4.26)
[Co(tdta)]	41.59	5.41	11.15	15.66	19.0	26.3	42.4
($CoC_{13}H_{20}N_3O_6$)	(41.83)	(5.40)	(11.26)	(15.79)	(2.46)	(2.31)	(4.35)
[Co(apta)]	37.79	5.20	11.84	17.10	19.6	27.0	46.0
($CoC_{11}H_{18}N_3O_6$)	(38.05)	(5.23)	(12.10)	(16.97)	(2.44)	(2.24)	(4.34)
fac[Co(gly)$_3$]	25.51	4.12	14.98	21.18	19.2	26.6	45.6
($CoC_6H_{12}N_3O_6$)	(25.64)	(4.30)	(14.95)	(21.20)	(2.24)	(2.17)	(4.30)
[Fe(tnta)]	40.36	5.08	11.84	15.73	20.0		38.8
($FeC_{12}H_{18}N_3O_6$)	(40.47)	(5.09)	(11.80)	(15.68)	(0.5)		(4.0)
[Fe(tdta)]	41.76	5.08	11.72	15.01	20.2		38.6
($FeC_{13}H_{20}N_3O_6$)	(42.18)	(5.45)	(11.35)	(15.09)	(0.5)		(4.2)
[Fe(apta)]	38.32	5.25	12.32	16.34	21.0		38.5
($FeC_{11}H_{18}N_3O_6$)	(38.39)	(5.27)	(12.21)	(16.23)	(shoulder)		(3.9)

chromium chelates, however, these reactions were relatively slow compared with that of the corresponding chromium complexes. Yields, 30—50%.

Facial Glycinato (gly) Complexes: [Cr^{III}(gly)$_3$]·3H_2O and [Co^{III}(gly)$_3$]·H_2O were prepared and purified according to the methods of Ley and Winkler[7] and Israily.[8] They were converted into anhydrous complexes by heating *in vacuo* at 130 °C.

Measurements. The electronic absorption spectra of metal chelates were measured on a Hitachi Model 124 recording spectrophotometer using a 10-mm cell. Sample cell of 50 mm or 100 mm was also used to measure the visible spectra of [Cr^{III}(gly)$_3$], [Co^{III}(gly)$_3$], and the iron(III) chelates, which were sparingly soluble in water. The absorption spectra of two glycinato complexes were measured anew under the same conditions, although they had already been reported.[8]

Results and Discussion

All these N_3O_3-type ligands could expel ammonia molecules from hexaamminechromium(III) or -cobalt(III) complexes. The replacement of ammonia with glycine also occurred in the chromium complex, but it was very difficult in the cobalt complex. Although the apta forms six-membered chelate rings upon coordination, it has great chelate effects. This ligand presumably has a very suitable structure for the octahedral coordination. Metal chelates of tnta seem to be the most stable and to have the smallest solubility in water. All these solid chelates were decomposed above 300 °C, leaving metal oxide. A tripodal ligand, apta, which contains three -NH-groups, did not react further with chloroacetate, and only this ligand was obtained as a monohydrochloride. Syntheses of similar triacetate derivatives of 1,4,8-triazacycloundecane and 1,5,9-triazacyclododecane were also attempted, but they failed to isolate any pure solids.

As expected, all the absorption spectra of the chromium(III) and cobalt(III) chelates with these tripodal ligands resemble those of the facial tris(glycinato) complexes. It is of interest that each apta chelate has the first absorption band of the highest energy.

The data of the elemental analysis and the absorption spectra are summarized in Table 1.

The present work was partially supported by a Grant-in-Aid for Scientific Research from the Ministry of Education.

References

1) T. Arishima, K. Hamada, and S. Takamoto, *Nippon Kagaku Kaishi*, **1973**, 1119.
2) H. Hama and S. Takamoto, *Nippon Kagaku Kaishi*, **1975**, 1182.
3) H. Koyama and T. Yoshino, *Bull. Chem. Soc. Jpn.*, **45**, 481 (1972).
4) J. E. Richman and T. J. Atkins, *J. Am. Chem. Soc.*, **96**, 2268 (1974).
5) H. Stetter and W. Böckmann, *Chem. Ber.*, **84**, 834 (1951).
6) N. Kitajiri, T. Arishima, and S. Takamoto, *Nippon Kagaku Zasshi*, **91**, 240 (1970).
7) H. Ley and H. Winkler, *Chem. Ber.*, **45**, 375 (1912).
8) M. N. Israily, *C. R. Acad. Sci., Ser. C*, **262**, 1426 (1966).

BULLETIN OF THE CHEMICAL SOCIETY OF JAPAN, VOL. 50 (12), 3415—3416 (1977)

The Formation and Extraction Equilibria of Several Manganese(II) β-Diketonates and Their Trioctyl-Phosphine Oxide Adducts

Tatsuya SEKINE, Ryokichi MURAI, Kazuhiko TAKAHASHI, and Shigehisa IWAHORI

Department of Chemistry, Science University of Tokyo, Kagurazaka, Shinjuku-ku, Tokyo 162

(Received July 6, 1977)

Synopsis. From the distribution ratio of manganese(II) between carbon tetrachloride containing various amounts of β-diketone (HA) and trioctylphosphine oxide (TOPO), and an aqueous 1 mol dm^{-3} perchlorate solution at 25 °C, the formation constants for the aqueous chelates and the TOPO adducts of the MnA_2, and the partition constants for the MnA_2 chelates were determined. The constants were then compared with those of other divalent metal ions.

Measurements have previously been made of the solvent extraction equilibria of four divalent metal ions with several β-diketones in carbon tetrachloride and also of the adduct formation equilibria of the extracted chelates with trioctylphosphine oxide (TOPO).[1-4] The present paper will report the results with manganese(II) under identical conditions and will compare the equilibrium constants thus obtained with those for the other divalent metal ions.

Experimental and Statistical

The experiments were performed at 25±0.3 °C in a manner similar to those used previously.[1-4] The initial organic phase was carbon tetrachloride containing various amounts of a certain β-diketone and TOPO, and the initial aqueous phase was a 1 mol dm^{-3} sodium perchlorate solution containing an acetate buffer (less than 0.01 mol dm^{-3}) or no buffer (when the β-diketone buffered) and 2×10^{-6} to 2×10^{-4} mol dm^{-3} of manganese(II). The two phases in a stoppered glass tube were placed on a rotating framework, agitated at 20 r.p.m., and then centrifuged. The metal content in each phase was determined by an atomic absorption method. The hydrogen-ion concentration was determined by potentiometry in stoichiometric units.

The distribution ratio was defined as

$$D = [\mathrm{Mn(II)}]_{\mathrm{org,total}}[\mathrm{Mn(II)}]_{\mathrm{total}}^{-1}, \quad (1)$$

where the subscript "org" and the lack of any subscript denoted those species in the organic and aqueous phases respectively. The β-diketones were denoted by HA and TOPO by L. The equilibrium constants employed were

$$K_a = [\mathrm{H^+}][\mathrm{A^-}][\mathrm{HA}]^{-1}, \quad (2)$$
$$K_d = [\mathrm{HA}]_{\mathrm{org}}[\mathrm{HA}]^{-1}, \quad (3)$$
$$\beta_n = [\mathrm{MnA}_n^{2-n}][\mathrm{Mn^{2+}}]^{-1}[\mathrm{A^-}]^{-n}, \quad (4)$$
$$K_{dm} = [\mathrm{MnA_2}]_{\mathrm{org}}[\mathrm{MnA_2}]^{-1}, \quad (5)$$
$$K_{ex} = [\mathrm{MnA_2}]_{\mathrm{org}}[\mathrm{H^+}]^2[\mathrm{Mn^{2+}}]^{-1}[\mathrm{HA}]_{\mathrm{org}}^{-2} \quad (6)$$
$$= (K_aK_d^{-1})^2K_{dm}\beta_2, \quad (7)$$
$$\beta_{n(\mathrm{org})} = [\mathrm{MnA_2L}_n]_{\mathrm{org}}[\mathrm{MnA_2}]_{\mathrm{org}}^{-1}[\mathrm{L}]_{\mathrm{org}}^{-n}. \quad (8)$$

The distribution ratio in the absence and in the presence of L can generally be written as

$$D_0 = [\mathrm{MnA_2}]_{\mathrm{org}}([\mathrm{Mn^{2+}}]+[\mathrm{MnA^+}]+[\mathrm{MnA_2}])^{-1}$$
$$= [\mathrm{MnA_2}]_{\mathrm{org}}[\mathrm{Mn^{2+}}]^{-1}(1+\sum\beta_n[\mathrm{A^-}]^n)^{-1}, \quad (9)$$
$$D = ([\mathrm{MnA_2}]_{\mathrm{org}}+[\mathrm{MnA_2L}]_{\mathrm{org}}+[\mathrm{MnA_2L_2}]_{\mathrm{org}})$$
$$\times([\mathrm{Mn^{2+}}]+[\mathrm{MnA^+}]+[\mathrm{MnA_2}])^{-1}$$
$$= D_0(1+\sum\beta_{n(\mathrm{org})}[\mathrm{L}]_{\mathrm{org}}^n). \quad (10)$$

The stability constants, β_n, were determined from the data obtained when the $[\mathrm{L}]_{\mathrm{org}}$ was zero or a certain constant value as a function of $[\mathrm{A^-}]$. The adduct formation constants were determined from the data obtained at a certain constant value of $[\mathrm{A^-}]$ as a function of $[\mathrm{L}]_{\mathrm{org}}$. The data were treated by a graphic method previously reported.[1-4] For the determination of the β_1 and β_2 of hexafluoroacetylacetonates, tributyl phosphate was used as the synergist instead of TOPO because TOPO was too effective to achieve suitable conditions.

Results and Discussion

The distribution ratio was measured at various pH values in the absence and in the presence of chromate ions. It was found that the distribution ratio reached a constant value in the absence of chromate if the −log $[\mathrm{H^+}]$ value was lower than 9 and if the agitation interval was shorter than 3 h. This D value was lower than that obtained in the presence of chromate. Thus, the D obtained after an agitation for less than 3 h at −log $[\mathrm{H^+}]$ values lower than 9 was concluded to show the distribution equilibrium of manganese(II) and no extraction of manganese(III).

The extraction curve with benzoylacetone was nearly a straight line with a slope of 2 when the distribution ratio was lower than 10^2; thus, only K_{ex} could be determined form these data. The curve with hexafluoroacetylacetone deviated only slightly from a straight line with a slope of 2 up to its maximum concentration, 0.1 mol dm^{-3}; thus, only K_{ex} and β_1 could be determined.

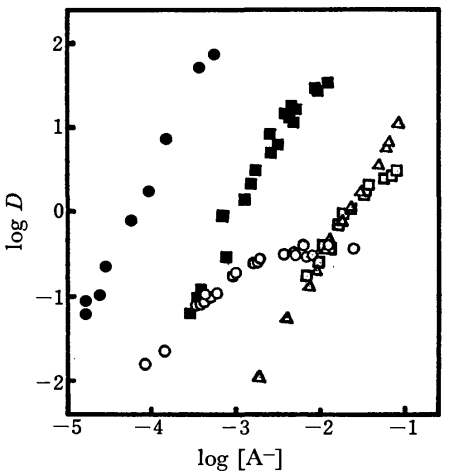

Fig. 1. Representative extraction curves. Org. phase: CCl_4 containing ○ acetylacetone+5×10^{-3} mol dm^{-3} of TOPO, ● benzoylacetone, □ trifluoroacetylacetone, ■ benzoyltrifluoroacetone, or △ hexafluoroacetylacetone+1×10^{-3} mol dm^{-3} of tributylphosphate. Aq. phase: 1 mol dm^{-3} $NaClO_4$.

Table 1. Summary of equilibrium constants

Aq. phase: 1 mol dm^{-3} $NaClO_4$. Org. phase: CCl_4. Adduct-forming ligand: trioctylphosphine oxide (TOPO). The data of Mn(II): present work. The other data: Refs. 1—4.

Extractant	Metal ion	log K_{ex}	log β_1	log β_2	log K_{dm}	log $\beta_{1\,(org)}$	log $\beta_{2\,(org)}$
Acetylacetone	Mn(II)	−11.8	4.09	6.98	−1.23	2.96	4.96
log K_a = −8.99	Co (II)	—	—	—	−0.94	1.46	nil
log K_d = 0.40	Ni (II)	—	—	—	−2.0 to −2.5	*ca.* 2	nil
	Cu (II)	−3.73	7.81	14.22	0.83	1.28	nil
	Zn (II)	−11.40	4.58	7.76	−0.38	3.07	4.66
Benzoylacetone	Mn(II)	−8.4	—	—	(>3)[a]	3.81	5.40
log K_a = −8.55	Co (II)	−13.05	4.55	8.14	1.37	3.40	nil
log K_d = 2.73	Ni (II)	−12.84	4.41	9.86	−0.14	3.50	nil
	Zn (II)	−11.36	4.15	7.70	3.50	3.76	nil
Trifluoroacetylacetone	Mn(II)	−10.28	0.94	2.96	−1.44	5.43	9.16
	Co (II)	−8.34	3.50	5.60	−2.14	5.36	7.76
logK_a = −6.90	Ni (II)	*ca.* −9	3.74	6.68	−3.0 to −3.5	*ca.* 5	*ca.* 8
log K_d = −0.19	Cu (II)	−1.26	4.80	9.14	1.40	2.96	nil
	Zn (II)	−8.76	2.72	4.48	−1.44	6.70	nil
Benzoyltrifluoroacetone	Mn(II)	−12.62	0.80	2.63	1.71	6.1	10.4
log K_a = −6.01	Co (II)	−9.66	3.40	5.24	2.06	6.15	9.34
log K_d = 2.47	Ni (II)	−9.52	3.60	6.68	0.76	5.19	8.98
	Zn (II)	−9.02	3.23	5.49	2.45	6.71	nil
Hexafluoroacetylacetone	Mn(II)	−5.0	1.04	—	(>−1)[a]	—[b]	—[b]
log K_a = −4.34	Co (II)	−3.90	1.56	2.32	−1.02	5.19	10.58
log K_d = −1.74	Ni (II)	−4.0	1.78	3.26	−2.1	5.8	10.5
	Cu (II)	−0.61	2.25	3.20	1.39	5.63	9.36
	Zn (II)	−5.2	1.0	—	(>−1)[a]	7.0	11.6

a) Since these values could not be determined, only the lower limit is assumed. b) Too high to be determined by the present experimental procedures; see text.

Figure 1 shows examples of representative extraction curves.

The extraction with these β-diketones was enhanced very much by TOPO. The adduct formation constants of the benzyltrifluoroacetonate were somewhat inaccurate, and those of the hexafluoroacetylacetonate could not be determined within the limits of experimental error. However, since the constants for the adducts with TBP determined instead of those with TOPO (log $\beta_{1(org)}$ =4.9 and log $\beta_{2(org)}$ =9.4) were rather similar to the corresponding zinc(II) TBP adducts (log $\beta_{1(org)}$ =5.5 and log $\beta_{2(org)}$ =8.5),[2] the values for the TOPO adducts of the manganese(II) hexafluoroacetylacetonate should be similar to those of the zinc(II) chelates.

The constants obtained are given in Table 1, together with the values previously obtained in our laboratory.[1-4]

From these data, it can be concluded that (i) the Irving-Williams natural order is well established among these β-diketonates, (ii) the K_{dm} values (showing the inverse of the aquophilic tendency when the molar volumes are similar[3]) of the manganese(II) chelates are much higher than those of the nickel(II) chelates and lower than those of the copper(II) chelates; they are approximately in the same order as the values of cobalt(II) and zinc(II) chelates, and (iii) the synergic enhancement with TOPO is similar to that of the zinc(II) chelates or greatest among the metal chelates in Table 1.

As is seen from the present results, these manganese(II) extractions, except for that with benzoylacetone, were poor for various practical purposes when the solvent was carbon tetrachloride. However, since the synergic enhancement was very great, the addition of a synergist such as TOPO and TBP or the use of oxygen-containing solvents such as 4-methyl-2-pentanone (MIBK), the extraction of this metal ion should become effective.

There have been reports on the extraction with these β-diketonates of manganese(II) that the extraction was partial with acetylacetone in benzene,[5] but that it was better when using butanol[6] or by the addition of hydrogen peroxide,[7] and that the extraction with benzoylacetone in benzene was more than 90% at pH values higher than 9.[5] Not much has been reported on the stability constants of manganese(II) β-diketonates which can be compared directly with the present results,[9] except that the log β_1 for the acetylacetonate in a 0.1 mol dm^{-3} medium was 4.01.[9]

References

1) R. Murai, T. Sekine, and M. Iguchi, *Nippon Kagaku Zasshi*, **92**, 967 (1971).

2) T. Sekine and N. Ihara, *Bull. Chem. Soc. Jpn.*, **44**, 2942 (1971).

3) T. Sekine, R. Murai, M. Niitsu, and N. Ihara, *J. Inorg. Nucl. Chem.*, **36**, 2569 (1974).

4) T. Sekine, S. Iwahori, and R. Murai, *J. Inorg. Nucl. Chem.*, **39**, 363 (1977).

5) J. Stary and E. Hladsky, *Anal. Chim. Acta*, **28**, 227 (1963).

6) N. K. Jatyanarayana and V. P. R. Rao, *Chem. Anal. (Warsaw)*, **53**, 78 (1964) (CA: 61, 11383).

7) T. Shigematsu and M. Tabushi, *Bull. Inst. Chem. Res., Kyoto Univ.*, **39**, 35 (1961).

8) A. E. Martelle and L. G. Sillén, "Stability Constants," Spec. Pub. No. 17 (1964), and Supplement No. 1, Spec. Pub. No. 25 (1971), The Chemical Society, London.

9) G. Gutnikov and H. Freiser, *Anal. Chem.*, **40**, 39 (1968).

BULLETIN OF THE CHEMICAL SOCIETY OF JAPAN, VOL. 50 (12), 3417—3418 (1977)

Reactions of 4-Acyl-2-phenyl-1,3,4-oxadiazoline-5-thiones with Alcohols in the Presence of Metal Ions

Hiroyuki FUKUDA, Takeshi ENDO, and Makoto OKAWARA

Research Laboratory of Resources Utilization, Tokyo Institute of Technology, Nagatsuda, Midori-ku, Yokohama 227

(Received February 7, 1977)

Synopsis. 4-Acetyl- and 4-benzoyl-2-phenyl-1,3,4-oxadiazoline-5-thiones reacted with alcohols in the presence of metal ions to give the corresponding esters in good yields.

It is known that metal ions promote some reactions, such as the hydrolysis of α-amino acid esters[1,2] and 8-acyloxy-quinolines,[3,4] the aminolysis of thiol esters,[5] and the alcoholysis of 8-acyloxyquinolines[6] and *S*-(2-pyridyl) thio carboxylates.[7]

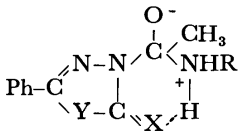

[I]

X=O, Y=O or S
X=S, Y=O or S

We have reported that 4-acetyl-2-phenyl-1,3,4-oxa-(thia)diazoline-5-ones(thiones) are 10^2—10^7 times more reactive than *p*-nitrophenyl acetate in the aminolysis by cyclohexylamine, unusually rapid aminolysis being due to the intramolecular base catalyzed reactions as illustrated in I.[8] However, the acetyl derivatives scarcely react with alcohols even under refluxing for several hours. This paper describes the reactions of 4-acyl-2-phenyl-1,3,4-oxadiazoline-5-thiones(IIIa, b) with alcohols in the presence of various metal ions, and with phenylmagnesium bromide.

2-Phenyl-1,3,4-oxadiazoline-5-thione(II), its 4-acetyl compound(IIIa) (yield 78%, mp 115—116 °C), and 4-benzoyl-2-phenyl-1,3,4-oxadiazoline-5-thione(IIIb) (yield 92%, mp 134.5—136 °C) were prepared by the method reported.[8]

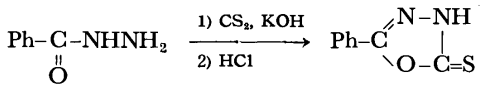

[II]

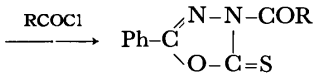

[IIIa]: R=CH_3 [IIIb]: R=Ph

When 4-acyl-2-phenyl-1,3,4-oxadiazoline-5-thiones-(III) is coordinated with metal ions as shown in IV, it might be subjected to nucleophilic attack on carbonyl carbon atom, as the consequence of activation of carbonyl group by such coordination. This reaction would also be remarkably accelerated if the final product (V) is mercaptide which is an excellent leaving group because of its high stability.

At first, the reactions of 2-phenyl-1,3,4-oxadiazoline-5-thione(II) with various metal ions were examined. Ag^+, Cu^{2+}, Hg^{2+}, and Pb^{2+} formed mercaptides (V) with II, but metal ions, such as Sn^{4+}, Mg^{2+}, Zn^{2+}, and Co^{2+}

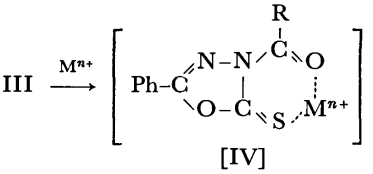

[IV]

[V]

gave no mercaptides in methanol or acetonitrile at room temperature. The results are given in Table 1. The mercaptides obtained were confirmed by IR spectra and elemental analyses.

TABLE 1. MERCAPTIDE FORMATION OF II WITH METAL IONS

Metal ions	Ag^+	Cu^{2+}	Hg^{2+}	Pb^{2+}
n	1	2	2	2
Yield (%)	99	98	91	95

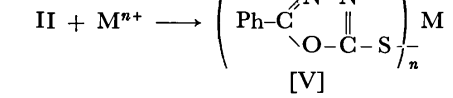

[V]

The reactions of III with alcohols in the presence of metal ions, which form mercaptides with II, were carried out at room temperature for 15 h. A white (mercury(II) salt) precipitate and a dark grey (silver salt) one were formed in a few minutes. In the case of copper(II) chloride, the reaction mixture was heterogeneous during the course of reaction because of the

TABLE 2. REACTIONS OF III WITH ALCOHOLS IN THE PRESENCE OF METAL IONS[a]

Compound	R′	Solvent	Metal salt	Yields of ester (%)[b]
IIIa	$PhCH_2$	CH_3CN	none	0
〃	〃	〃	$CuCl_2$	100
〃	〃	Acetone	〃	92
〃	〃	CH_3CN	$AgNO_3$	65
〃	〃	〃	$HgCl_2$	54
〃	〃	〃	$AgClO_4$	41
〃	〃	〃	$HgCl_2$[c]	36
〃	〃	〃	$Pb(NO_3)_2$	0
〃	C_6H_{13}	〃	$AgNO_3$	70
IIIb	$PhCH_2$	〃	$CuCl_2$	40
〃	C_6H_{13}	〃	〃	55

a) Equimolar reaction; reagents 4 mmol; solvent 30 ml; room temp, 15 h. b) Determined by NMR spectrum. c) Half molar of $HgCl_2$ used.

Table 3. Reactions of IIIa with benzyl alcohol in the presence of metal ions[a)]

Solvent	Metal salt	Yields of ester (%)[b)]
THF	Bu_2SnCl_2	75
CH_2Cl_2	$SnCl_4$	70
CH_3CN	$Mg(ClO_4)_2$	57
Acetone	$ZnCl_2$	14
CH_3CN	$CoCl_2$	6

a) Equimolar reaction; reagents 4 mmol; solvent 30 ml; room temp, 15 h. b) Determined by NMR spectrum.

low solubility of copper(II) chloride. As shown in Table 2, all the metal ions, except Pb^{2+}, capable of mercaptide formation, are effective for the acceleration of these reactions, copper(II) chloride being the most remarkable. Lead nitrate did not promote the reaction since it is insoluble in acetonitrile. The precipitates were confirmed to be mercaptides consisting of 1 : 1 molar ratio of II and metal ions by elemental analyses and IR spectra. It was observed that the reactions of IIIa with benzyl alcohol in the presence of metal ions, such as Sn^{4+}, Mg^{2+}, Zn^{2+}, and Co^{2+} which can not form mercaptides with II proceed homogeneously. The results given in Table 3 indicate that tin(IV) salt is very effective for activation of IIIa. Thus, in the deacylation of III with alcohols, the coordination effect of some metal ions on acyl function might be much more important than the increasing stability of the leaving group. If the coordination (IV) assumed above is strong, the shift of C=O and C=S absorption bands of IIIa would be observed in IR spectra. However, no shift of the absorption bands was noted even in the solution of IIIa and Bu_2SnCl_2 or $Mg(ClO_4)_2$. The results indicate that even the weak interaction which can not be observed in IR spectra is also effective for promotion of these reactions.

We have investigated the reactions of III with phenylmagnesium bromide. III was allowed to react with equimolar amount of phenylmagnesium bromide

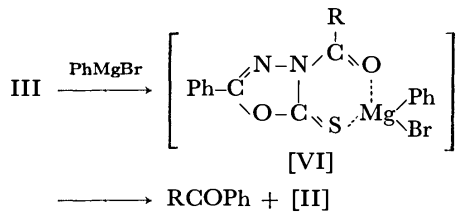

[VI]

⟶ RCOPh + [II]

in THF at *ca.* −20 °C for 4 h followed by hydrolysis to give the desired ketones. Thus, acetophenone and benzophenone were obtained from IIIa and IIIb in 76 and 78% yields, respectively. This is compatible with the above results.

Experimental

Mercaptides Formation of II with Metal Ions. A mixture of II (0.72 g, 4 mmol) and 4 mmol of metal ions in acetonitrile (30 ml) was stirred for 4 h at room temperature. The mercaptides obtained were filtrated and washed with dry acetonitrile three times, and dried at reduced pressure. The composition of mercaptides (Table 1) was determined by elemental analysis.

Reactions of III with Alcohols in the Presence of Metal Ions. Typical Procedure: A mixture of 0.88 g (4 mmol) of IIIa, 0.43 g (4 mmol) of benzyl alcohol, and 0.59 g (4 mmol) of copper(II) chloride in acetonitrile was stirred for 15 h at room temperature. The reaction mixture was poured into water, and the solution was extracted with ether. The extract was dried over anhydrous magnesium sulfate. After the solvent had been removed in a vacuum, the residue was distilled to afford 0.69 g of benzyl acetate quantitatively.

Reactions of III with Phenylmagnesium Bromide. Typical Procedure: To a solution of IIIa (1.76 g, 8 mmol) in dry THF (20 ml) was added a solution of phenylmagnesium bromide (1.45 g, 8 mmol) in dry THF (20 ml) over 30 min at −20 °C. After the mixture had been stirred at −20 °C for 4 h then at 25 °C for the same period, the reaction mixture was poured into water. The solution was extracted with ether, and the extract was dried over anhydrous magnesium sulfate. After removal of the solvent, the residue was distilled in a vacuum to afford 0.73 g (76%) of acetophenone.

References

1) H. Kroll, *J. Am. Chem. Soc.*, **74**, 2036 (1952).
2) M. L. Bender and B. W. Turnquest, *J. Am. Chem. Soc.*, **79**, 1889 (1957).
3) E. J. Corey and R. L. Dawson, *J. Am. Chem. Soc.*, **84**, 4899 (1962).
4) R. H. Barca and H. Freiser, *J. Am. Chem. Soc.*, **88**, 3744 (1966).
5) B. Boopsingh and D. N. Sctchell, *J. Chem. Soc., Perkin Trans. 2*, **1972**, 1288.
6) T. Sakan and Y. Mori, *Chem. Lett.*, **1972**, 793.
7) H. Gerlach and A. Thalman, *Helv. Chim. Acta*, **57**, 2661 (1974).
8) H. Fukuda, T. Endo, and M. Okawara, *Chem. Lett.*, **1973**, 1181; *Nippon Kagaku Kaishi*, **1976**, 315.

BULLETIN OF THE CHEMICAL SOCIETY OF JAPAN, VOL. 50 (12), 3419—3420 (1977)

Effect of a Polymer Ligand on Oxidation of Thiophenol Catalyzed by Cobaloximes

Hiroshi NISHIKAWA, Masanori KASAI, Ei-ichi TERADA, and Eishun TSUCHIDA

Department of Polymer Chemistry, Waseda University, Tokyo 160

(Received February 24, 1977)

Synopsis. The oxidation mechanism of thiophenol catalyzed by cobaloximes was deduced by spectroscopic measurement of the oxidation rate at various concentrations of the reactants, the reaction being a Michaelis-Menten type reaction. Addition of polymer ligands such as poly(4-vinylpyridine) and 4-vinylpyridine-styrene copolymer, stabilizing the intermediate similar to a Michaelis complex, resulted in an increase in the oxidation rate under low substrate concentration.

Studies have been reported on the catalytic action of polymer metal complexes,[1] but few detailed investigations have been carried out because of the complicated structure of the complexes and intermediates. Polymer ligands or substrates coordinate with cobaloximes, only in an axial position, making it easy to analyze the reaction mechanism since the structures of the complex coordinated with a polymer ligand or a substrate are confined.

The oxidation reaction of thiophenol catalyzed by cobaloximes is mild and enables us to apply spectroscopic analysis. This report deals with the reaction mechanism as deduced from kinetic studies, discussion being given on the effect of the polymer ligand on the catalytic action of cobaloximes.

Experimental

Materials. Commercial $CoCl_2 \cdot 6H_2O$, $Co(CH_3COO)_2 \cdot 4H_2O$, dimethylglyoxime ($dmgH_2$), pyridine (Py), thiophenol, and NaOH were used without further purification. Poly(4-vinylpyridine) (PVP) and 4-vinylpyridine-styrene copolymer (PPS) (styrene unit content 17%) were obtained by radical polymerization initiated by azobisisobutyronitrile purified by reprecipitation with ethyl acetate. The number-average molecular weights of PVP and PPS determined by the vapor pressure osmometry were 12800 and 18700, respectively. Methanol was distilled before use.

Preparation of Cobaloximes. $CoCl(dmgH)_2(Py)$ was prepared by the conventional method.[2] $CoCl(dmgH)_2(OH_2)$ was obtained through the reaction of 4.2 mmol NaOH in ethanol and aeration, and recrystallized from ethanol. Found: C, 28.0; N, 16.1; H, 4.8%. Calcd for $C_8H_{14}N_4O_4CoH_2OCl$: C, 28.0; N, 16.3; H, 4.7%.

Analysis of Oxidation Reaction. Air oxidation of thiophenol in alkaline methanol solution (containing 3×10^{-4} M NaOH) in the presence of cobaloximes gave diphenyl disulfide (DPS). An increase of absorbance at 310 nm, at which the difference of absorbance between the reactant and product (DPS) was large enough to detect a small change of the concentration of the product, gave the oxidation rate in a steady state under the addition of excess substrate using $CoCl(dmgH)_2(Py)$ as a catalyst. The rate was represented by the concentration of phenylthio radical produced per second. The formation of the Co(II) complex under an atmosphere of nitrogen accompanied by thiophenol oxidation and that of the air oxidation of the Co(II) complex were studied from a visible absorption spectral change. The relationsip between the oxidation rate and the added polymer ligand concentration was derived in a similar way using $CoCl(dmgH)_2(OH_2)$ as a catalyst and Py, PVP, and PPS as an axial ligand respectively. The concentration of the polymer ligand is indicated in 4VP unit mole per liter.

Results and Discussion

Reaction Mechanism of Thiophenol Oxidation. The following mechanisms were postulated for the thiol oxidation catalyzed by metals.[3]

$$M^{n+} + \text{thiophenol}^- \longrightarrow M^{(n-1)+} + \text{thiophenol}^*$$

$$M^{(n-1)+} \xrightarrow{O_2} M^{n+} \qquad 2\text{thiophenol}^* \longrightarrow \text{Pr} \qquad (1)$$

The oxidation rate determined by the measurement of oxygen uptake with Warburg's manometer was in agreement with that determined by spectroscopic measurement. This indicates that thiophenol was converted quantitatively into DPS in the present oxidation system.

The oxidation rate V is proportional to the catalyst concentration. The oxidation rate is proportional to the substrate concentration in the low substrate concentration range, approaching a certain value with increase in concentration (Fig. 1). This can be explained by assuming the existence of the intermediate complex consisting of a catalyst and a substrate. The linear relationship between the reciprocal of the oxidation rate, $1/V$, and that of the substrate concentration, $1/[S]$, suggests the following reaction mechanism, where $(Co)=Co(dmgH)_2XY$.

$$(Co^{III}) + C_6H_5\text{–}S^- \underset{k_{-1}}{\overset{k_1}{\rightleftharpoons}} (Co^{III})\,C_6H_5\text{–}S^- \xrightarrow{k_2}$$

$$(Co^{II}) + C_6H_5\text{–}S^*, \qquad (Co^{II}) \xrightarrow{k_3} (Co^{III}),$$

$$2C_6H_5\text{–}S^* \longrightarrow C_6H_5\text{–}S\text{–}S\text{–}C_6H_5 \qquad (2)$$

The change in visible spectra with time after the addition of the substrate to the solution containing $CoCl(dmgH)_2(Py)$ indicates the formation of the Co(II) complex with absorption maximum at 390 nm, reaching equilibrium after *ca.* 30 min. Reaction under nitrogen atmosphere is regarded to turn the Co(III) complex entirely into the Co(II) complex, causing an increase in the absorption at 390 nm about 1.5 times the equilibrium value in the air. The formation rate of Co(II) complex under nitrogen atmosphere at initial stage is proportional to the complex concentration. The decreasing rate in air of excess Co(II) complex formed by the thiophenol oxidation under a nitrogen atmosphere is also proportional to the complex concentration. These results strongly support the reaction mechanism describ-

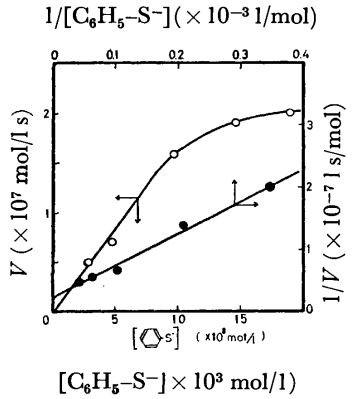

Fig. 1. Relationship between oxidation rate *(V)* and concentration of substrate ([C_6H_5–S^-]). [Co]=3.16×10^{-5} mol/l, [NaOH] =3×10^{-4} mol/l, solvent: methanol, at 22 °C.

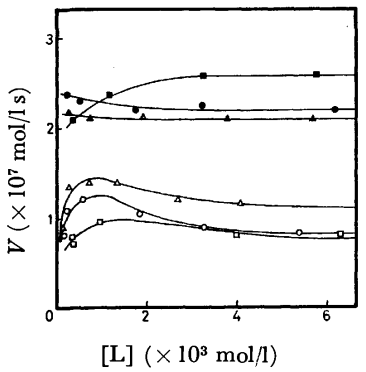

Fig. 2. Relationship between oxidation rate *(V)* and concentration of ligand ([L]). [Co]=3.16×10^{-5} mol/l, [NaOH] =3×10^{-4} mol/l, solvent: methanol, at 15 °C, [C_6H_5–S^-]=3.25×10^{-3} mol/l for ○, △, □, and 3.25×10^{-2} mol/l for ●, ▲, ■, L=Py: □, ■, PVP: △, ▲, and PPS: ○, ●.

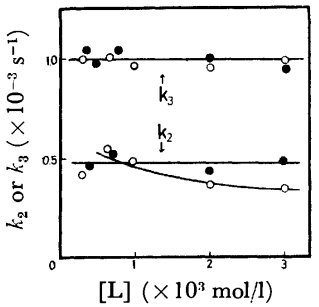

Fig. 3. Values of k_2 and k_3. [Co]=3.16×10^{-5} mol/l, [C_6H_5–S^-]=3.25×10^{-2} mol/l, [NaOH] =3×10^{-4} mol/l, solvent: methanol, at 15 °C, L=Py: ● or PVP: ○.

ed in Eq. 2. Equation 2 leads to the following equation for the oxidation rate at steady state.

$$1/V = [A + B/[C_6H_5\text{–}S^-]]/[Co]$$
$$A = (k_2+k_3)/k_2k_3, \quad B = (k_{-1}+k_2)/k_1k_2,$$
$$V = d[C_6H_5\text{–}S^*]/dt \qquad (3)$$

This equation represents the linear relationship between $1/V$ and $1/[C_6H_5\text{–}S^-]$ as shown in Fig. 1. The rate constants k_2 and k_3 can be determined by spectroscopic measurements of the Co(II) complex formation under nitrogen atmosphere and of the decrease of the Co(II) complex in air, respectively.

Effect of Polymer Ligand. Variations in the thiophenol oxidation rate with the ligand concentration, using $CoCl(dmgH)_2(OH_2)$ as a catalyst and Py, PVP, and PPS as an axial ligand are shown in Fig. 2.

The oxidation rate-ligand concentration curves obtained in lower thiophenol concentration have a maximum. The formation constant K of $CoCl(dmgH)_2(OH_2)$ with PPS is about 1×10^5 in *N,N*-dimethylformamide.[4] If we consider the formation constant in methanol to be almost the same as that in *N,N*-dimethylformamide, almost all the complexes have a ligand at the ligand concentration of the maximum point. The coordination of the axial ligand makes the complex more active as a oxidation catalyst.

The oxidation of thiophenol by $Co\cdot O_2$ complexes scarcely occurs in this system since one axial position of the catalyst,[5] where O_2 should coordinate, is occupied by a ligand such as Py or PVP.

In higher substrate concentration, for which the second term of Eq. 3 is negligible, only the value of A, *i.e.*, $(k_2+k_3)/k_2k_3$, determines the oxidation rate V. Figure 3 shows that the k_2 value of the Py system is larger than that of the polymer system, though k_3 value has almost the same value in both systems. This causes the Py system to have a larger oxidation rate than that of polymer systems. In the polymer system the k_2 value decreases with increase in ligand concentration. This can be explained in terms of steric hindrance by the polymer chain which prevents elimination of the substrates activated by the complex in polymer domain. The decrease in k_2 value with increase in the ligand concentration is in line with the decrease in the oxidation rate of the polymer system shown in Fig. 2.

Under conditions of the lower substrate concentration, where the second term in Eq. 3 is not negligible, the oxidation rate V is affected by the value of B. The faster oxidation rate in the polymer system under the lower substrate concentration indicates that B has a smaller value in the polymer systems than in the Py system. This is because the polymer domain stabilizes the reaction intermediate complex, and prevents the substrate from elimination, thus making k_{-1} value decrease.

It is concluded that the addition of polymer ligands can raise the oxidation activity of the catalyst at a lower substrate concentration region.

References

1) a) E. Tsuchida, H. Nishikawa, and E. Terada, *J. Polym. Sci., Polym. Chem. Ed.*, **14**, 825 (1976); b) H. Nishikawa and E. Tsuchida, *Eur. Polym. J.*, **13**, 269 (1977); c) E. Tsuchida, H. Nishide, and T. Nishiyama, *Makromol. Chem.*, **176**, 1349 (1975); d) I. Pecht, A. Levitzki, and M. Anbar, *J. Am. Chem. Soc.*, **89**, 1587 (1967); e) N. A. Vengerova, Yu. E. Kirshu, and V. A. Kabanov, *Vysokomol. Soedin., Ser. A*, **13**, 2509 (1971).

2) D. N. Hague and J. Halpern, *Inorg. Chem.*, **6**, 11, 2059 (1967).

3) G. Agnes, H. A. O. Hill, J. M. Pratt, S. C. Ridsdale, F. S. Kennedy, and R. J. P. Williams, *Biochim. Biophys. Acta*, **252**, 207 (1971).

4) H. Nishikawa, E. Terada, E. Tsuchida, and Y. Kurimura, *J. Polym. Sci.*, in press.

5) E. W. Abel, J. M. Pratt, R. Whelan, and P. J. Wilkinson, *J. Am. Chem. Soc.*, **96**, 7119 (1974).

BULLETIN OF THE CHEMICAL SOCIETY OF JAPAN, VOL. 50 (12), 3421—3422 (1977)

Reduction of Selenoxides with Thione Reagents

Seizo TAMAGAKI, Isao HATANAKA, and Seizi KOZUKA

Department of Applied Chemistry, Faculty of Engineering, Osaka City University, Sugimoto-cho, Sumiyoshi-ku, Osaka 558

(Received March 14, 1977)

Synopsis. The reaction of selenoxides with various thione compounds such as carbon disulfide, thioamides and thioureas was found to give selenides. The reaction mechanism was discussed.

It is widely known that sulfoxides are deoxygenated by various powerful reducing reagents.[1] Carbon disulfide, a weak reducing reagent, can never deoxygenate dialkyl and diaryl sulfoxides. Selenoxides are more basic and reactive as compared with analogous sulfur compounds due to the more polar nature of the Se=O bonding than the S=O bonding. Thus, diphenyl selenoxide is more basic and readily reducible by phosphines than the most basic sulfoxide, DMSO.[2,3]

However, few reports have been given so far on the chemical behavior of selenoxides toward weak reducing reagents. We report here the results of the reactions of diphenyl and dibenzyl selenoxides with various thione reagents.

Results and Discussion

Diphenyl and dibenzyl selenoxides (I) reacted at room temperature with equimolar amounts of thioamides such as 1-phenyl- and 1-methylpyrrolidine-2-thiones (II-Ph, -Me) and *N,N*-dimethylthioacetamide to give the selenides and the corresponding amides with extrusion of elemental sulfur (Table 1). The results indicate that, in marked contrast to sulfoxides, the oxides undergo a facile deoxygenation even with agents having weak reducing ability.

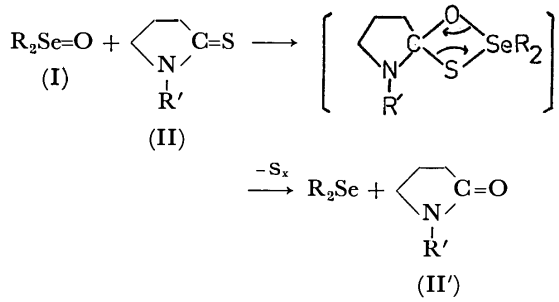

In a different way, selenoxides were readily reduced with carbon disulfide to give the corresponding selenides and chloroform-insoluble colorless precipitates without deposit of elemental sulfur. The results are summarized in Table 2. The reaction of dibenzyl selenoxide with small amounts of carbon disulfide or phosphorous pentasulfide in chloroform produced dibenzyl selenide

TABLE 1. REDUCTION OF DIPHENYL AND DIBENZYL SELENOXIDES (I) WITH THIONE REAGENTS (II and III) IN $CHCl_3$ AT ROOM TEMPERATURE

(I)	Thione reagent	Mole ratio[a]	Reaction time	Product (isolated%)
$Ph_2Se=O$	II-Ph	1	2 h	Ph_2Se(89), II′-Ph(83), S_x[b]
$Ph_2Se=O$	II-Me	1	2 h	Ph_2Se(73), II′-Me(73), S_x[b]
$Ph_2Se=O$	III	1	10 h	Ph_2Se(75), III′(0), III(78)
$Tol_2Se=O$	III	1	10 h	Tol_2Se(89), III′(12), III(48)
$(PhCH_2)_2Se=O$	II-Ph	1	5 min	$(PhCH_2)_2Se$(92), II′-Ph(82), II-Ph(3), S_x[b]
$(PhCH_2)_2Se=O$	II-Ph	0.1	5 min	$(PhCH_2)_2Se$(14), II′-Ph(75)[c]
$(PhCH_2)_2Se=O$	$MeC(S)NMe_2$	1	3 h	$(PhCH_2)_2Se$(93), MeC(O)NMe(93)
$(PhCH_2)_2Se=O$	III	1	4 h	$(PhCH_2)_2Se$(85), III′(21), III(63)
$(PhCH_2)_2Se=O$	$(Me_2N)_2CS$	1	2 h	$(PhCH_2)_2Se$(87), $(Me_2N)_2CO$(21), $(Me_2N)_2CS$(37)

a) [II or III]/[I]. b) Yields not determined. c) Based on the amount of the thione (II-Ph) used.

TABLE 2. REACTION OF DIPHENYL AND DIBENZYL SELENOXIDES (I) WITH CARBON DISULFIDE IN $CHCl_3$ AT ROOM TEMPERATURE

(I)	Mole ratio[a]	Reaction time	Product (isolated %)
$Ph_2Se=O$	10	10 h	Ph_2Se(47), oil(12),[c] Ph_2SeO(16)
$Ph_2Se=O$	b)	10 min	Ph_2Se(77), oil(21)[c]
$Tol_2Se=O$	b)	5 min	Tol_2Se(74), oil[c]
$(PhCH_2)_2Se=O$	3	12 h	$(PhCH_2)_2Se$(74), P(23)[d]
$(PhCH_2)_2Se=O$	0.1	24 h	$(PhCH_2)_2Se$(65), P(17)[d]
$(PhCH_2)_2Se=O$	1[e]	5 min	$(PhCH_2)_2Se$(96), P(0)[d]
$(PhCH_2)_2Se=O$	0.05[e]	3 h	$(PhCH_2)_2$(72), P(19)[d]

a) $[CS_2]/[I]$. b) CS_2 used as a solvent. c) Structure not identified. d) P denotes precipitate. e) The reaction with P_2S_5.

Table 3. The reaction of the precipitate (P) with thione reagents in $CHCl_3$ at room temperature

Thione	Mole ratio[a]	Reaction time	Products, isolated %		
			$(PhCH_2)_2Se$	II′ or III′	II or III
II-Ph	1	10 min	86	46	53
III	1	10 min	72	0	52[b]
$(Me_2N)_2C=S$	1	10 min	70	0	26[b]

a) [Thione]/[P]. b) Unidentified substances obtained.

and substantial amounts of precipitate, P (dec 115—117 °C). The elemental analysis of the precipitate gave no constant value, within analytical accuracy, with samples taken from different runs, but mostly agreed with a structure carrying five oxygen atoms per one dibenzyl selenide skeleton. This was further supported by the mass spectrum exhibiting the molecular peak at *m/e* 341 arising probably from $(PhCH_2)_2SeO_5$ (33% of base). The detailed structure is still not clear, but it involves $(PhCH_2)_2SeO_5$ as the most important species.

$$(PhCH_2)_2Se{=}O \xrightarrow[P_2S_5]{CS_2 \text{ or}} (PhCH_2)_2Se + \underset{(P)}{(PhCH_2)_2SeO_5}$$

The results given in Table 1 indicate that the reaction of dibenzyl selenoxide with an equimolar amount of thiourea, 1,3-dimethylimidazolidine-2-thione (III), gave only about 20% yield of the corresponding urea derivative (III′) together with the selenide, accompanied by considerable recovery of the starting thione compound (III). The same is true for tetramethylthiourea. The fact that considerable amounts of the thione compounds were recovered unchanged implies that two reactions

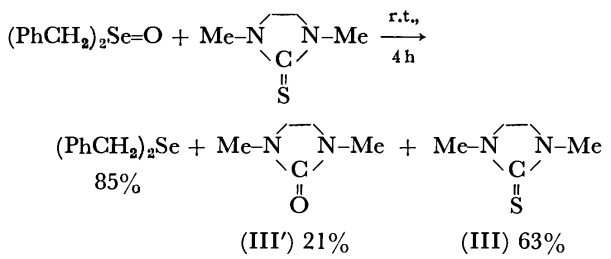

take place competitively: one producing dibenzyl selenide and the carbonyl compound, and the other catalytically affording the same selenide and, probably, the precipitate, which then reacts rapidly with the remaining thiourea to give the selenide. The fact, when the precipitate (P) itself was allowed to react with thioureas, dibenzyl selenide and a structure-unidentified product were obtained without being accompanied by the formation of the corresponding carbonyl compounds. The results are given in Table 3.

$$\underset{(P)}{(PhCH_2)_2SeO_5} + III \xrightarrow[10\,min.]{r.t.,} (PhCH_2)_2Se + \text{unidentified product}$$

It thus appears that, with thioamides having a labile thiocarbonyl group, Path a in Scheme 1 shown below is preferable for reduction and Path b, if operative, would be only minor, since the thioamides are almost completely consumed during the course of reaction. On the other hand, with carbon disulfide bearing stable C=S groups, the reaction proceeds mainly *via* Path b where no release of elemental sulfur is observed. The behavior of thioureas is intermediate between that of thioamides and carbon disulfide.

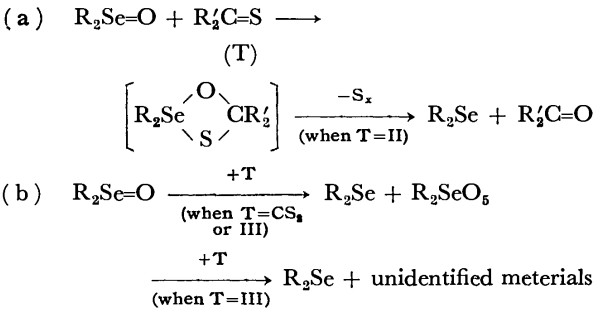

Scheme 1.

Experimental

Reaction of Diphenyl and Dibenzyl Selenoxides with Thione Compounds. A typical experimental procedure is as follows: 1-Phenylpyrrolidine-2-thione (177 mg, 1 mmol) was added at room temperature to a $CHCl_3$ (20 ml) solution of dibenzyl selenoxide (277 mg, 1 mmol). The reaction was followed by TLC. After the reaction was complete, evaporation of the solvent followed by preparative thin-layer chromatography of the residue gave dibenzyl selenide, 1-phenylpyrrolidone and the recovered thione in 92, 82 and 3% yields, respectively.

Some Physical Properties of the Precipitate (P). Mp: 115—117 °C; IR (KBr): 1100 (strong) cm^{-1}; NMR (d_6-DMSO): δ=7.27 (s, 10H), 4.22 (q, 4H) ppm from external TMS; Elemental analysis: Found: (1) C, 49.16; H, 4.58. (2) C, 48.70; H, 4.66. (3) C, 49.83; H, 4.73%. Calcd for $C_{14}H_{14}O_5Se$: C, 49.27; H, 4.13. MS: 342 (M^+), 262. Calcd M: 342 assuming Se=80.

Reaction of Dibenzyl Selenoxide with Carbon Disulfide. Dibenzyl selenoxide was added at room temperature to 20 ml of a $CHCl_3$ solution containing CS_2 (238 mg, 3 mmol). After 12 h, a colorless precipitate was filtered off. The filtrate was concentrated. Preparative TLC of the residue gave dibenzyl selenide in 74% yield.

References

1) R. G. Micelich, *Tetrahedron Lett.*, **1976**, 971; M. Miklajczyk, *Chem. Ind. (London)*, **1966**, 2059; S. Oae and S. Tamagaki, "Kangen Hanno," Maruzen Co., (Tokyo), 1974.

2) D. Hadzi, C. Klofature, and S. Oblak, *J. Chem. Soc.*, **1968**, 405; D. Hadzi, *Pure Appl. Chem.*, **11**, 435 (1965); *Chem Abstr.*, **65**, 16264e (1966).

3) S. Tamagaki, I. Hatanaka, and K. Tamura, *Chem. Lett.*, **1976**, 81.

BULLETIN OF THE CHEMICAL SOCIETY OF JAPAN, VOL. 50 (12), 3423—3424 (1977)

A Convenient Synthesis of 1-(2′,3′-Dideoxy-β-D-*erythro*-hex-2′-enopyranosyl)uracil

Tatsumi YAMAZAKI, Hiroshi SUGIYAMA,* Kazuo MATSUDA, and Shuichi SETO*

Department of Agricultural Chemistry, Tohoku University, Tsutsumidori-amamiya, Sendai 980

* *Chemical Research Institute of Non-Aqueous Solutions, Tohoku University, Katahira, Sendai 980*

(Received May 4, 1977)

Synopsis. 2,2′-Anhydro-1-(4′,6′-*O*-benzylidene-3′-*O*-methylsulfonyl-β-D-mannopyranosyl)urasil, prepared smoothly from β-D-glucopyranosyluracil in three steps, was converted into the corresponding unsaturated nucleoside in a good yield by the action of sodium iodide. The unsaturated nucleoside was then debenzylidenated with acid to afford the title compound.

Our recent attention has focussed on the synthesis of unsaturated sugars[1] and nucleosides.[2] In our previous publications,[2] a new synthetic route of the 2′,3′-unsaturation of thymine pyranoside *via* 2,2′-anhydronucleoside has been described, its reaction mechanism has also been discussed. We wish now to report an application of this reaction to the uracil nucleoside series, which can be considered as potent intermediates for the synthesis of such antibiotics[3] as blasticidin S and amicetin.

β-D-Glucopyranosyluracil (I)[4] was converted into the benzylidene derivative (II) in a 68% yield by treatment with benzaldehyde in the presence of zinc chloride. The subsequent sulfonylation of II with methanesulfonyl chloride in pyridine proceeded smoothly to afford a new crystalline product, the 2′,3′-di-*O*-mesyl derivative (III) (89%). Anhydronucleoside (IV) was prepared in an 89% yield by the treatment of III with an equivalent amount of sodium benzoate in *N,N*-dimethylformamide (DMF) at an elevated temperature.

The refluxing of IV with a 20-fold excess of sodium iodide and zinc dust in DMF for 2 h gave the unsaturated nucleoside (V) in a 33% yield. The treatment of IV with a 20-fold excess of sodium iodide in DMF for 1 h under reflux gave V in a 37% yield, along with about a 40% recovery of the starting material. When the reaction time of this reaction was prolonged until 4 h, the unsaturated nucleoside (V) was obtained in a 67% yield. Thus, the unsaturation was performed successfully in the uracil nucleoside series using the anhydronucleoside as a substrate. The structure of V could be easily confirmed by NMR. The vinylic protons at δ 6.50 and 5.70 with the characteristic coupling constant of $J_{2',3'}$= 10 Hz appeared in the spectrum.

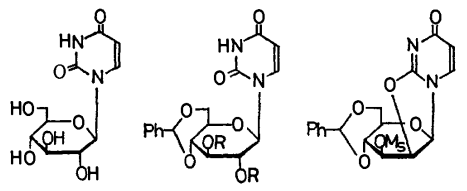

I

II R=H
III R=Ms

IV

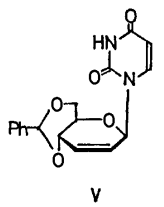

V

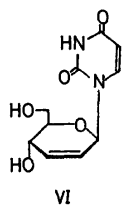

VI

After several screenings, DMF was found to be the most suitable solvent for the elimination reaction.

Compound (V) was treated with 80% aqueous acetic acid for 15 min under reflux to give a new crystalline product, VI, in a 50% yield. The overall yield of VI from I was 18%.

Experimental

All the melting points are uncorrected. The NMR data were recorded at 100 MHz with a JEOL PS-100 instrument.

1-(4′,6′-O-Benzylidene-β-D-glucopyranosyl)uracil (II). A suspension of 4 g of β-D-glucopyranosyluracil (I) and 13 g of freshly melted zinc chloride in 70 ml of benzaldehyde was shaken for 30 h. The resulting clear solution was stirred into ether (500 ml). The precipitate thus formed was filtered and then recrystallized from methanol to afford 3.6 g (68%) of the benzylidene nucleside (II) as colorless needles; mp 278—281 °C (dec);[5] $[\alpha]_D^{22}$ −8° (*c* 1.0 in DMF). Found: C, 55.91; H, 5.07; N, 7.56%. Calcd for $C_{17}H_{18}N_2O_7$: C, 56.35; H, 5.07; N, 7.73%.

1-(4′,6′-O-Benzylidene-2′,3′-di-O-methylsulfonyl-β-D-glucopyranosyl)uracil (III). Into a cooled (0 °C) suspension of the benzylidene nucleoside (II) (11 g) in pyridine (450 ml), we stirred drop by drop methanesulfonyl chloride (8.5 ml). The reaction mixture was kept for 15 h at room temperature. The subsequent addition of the reaction mixture, which had been concentrated to a small volume, into ice water (2 l) with vigorous stirring gave a colored precipitate. The subsequent crystallization of the precipitate from acetone–ethanol afforded 14 g (89%) of III; mp 189—192 °C (dec); $[\alpha]_D^{22}$ −12° (*c* 1.0 in DMF); UV (EtOH) λ_{max} 255 nm (log ε 3.74); NMR [$(CD_3)_2SO$] δ=7.80 (1H, d, $J_{5,6}$= 8.8 Hz, H-6), 7.38 (5H, C_6H_5), 6.20 (1H, broad d, $J_{1',2'}$= 7.5 Hz, H-1′), 5.68 (1H, d, $J_{5,6}$=8.8 Hz, H-5), 5.66 (1H, s, PhCH), 5.15—5.40 (2H, m, H-2′ and -3′), 3.30 (4H, m, H-4′, -5′, -6′, and -6″), 3.16 (3H, s, CH_3SO_2), and 3.10 (3H, s, CH_3SO_2). Found: C, 44.01; H, 4.25; N, 5.41%. Calcd for $C_{19}H_{22}N_2O_{11}S_2$: C, 44.26; H, 4.07; N, 5.33%.

2,2′-Anhydro-1-(4′,6′-O-benzylidene-3′-O-methylsulfonyl-β-D-mannopyranosyl)urasil (IV). A mixture of the methanesulfonylated nucleoside (III) (13.5 g, 26 mmol) and sodium benzoate (4.6 g, 32 mmol) in DMF (500 ml) was heated at 120—130 °C with stirring for 1.5 h. The reaction mixture was then vigorous stirred into ice water (4 l) to give a crystalline product. Recrystallization from acetone afforded 9.8 g (89%) of the anhydronucleoside (IV); mp 215—216 °C (dec); $[\alpha]_D^{22}$ −130° (*c* 0.5 in DMF); UV (EtOH) λ_{max} 225 and 245 nm (log ε 3.90 and 3.89); NMR [$(CD_3)_2SO$]

δ=7.95 (1H, d, $J_{5,6}$=8 Hz, H-6), 7.40 (5H, C_6H_5), 6.13 (1H, $J_{1',2'}$=3 Hz, H-1'), 5.90 (1H, d, $J_{5,6}$=8 Hz, H-5), 5.77 (1H, s, PhCH), 5.55 (1H, q, $J_{2',3'}$=5 Hz, $J_{3',4'}$=10 Hz, H-3'), 5.35 (1H, q, $J_{1',2'}$=3 Hz, $J_{2',3'}$=5 Hz, H-2'), 3.8—4.3 (4H, m, H-4', -5', -6', and -6"), 3.22 (3H, s, CH_3SO_2). Found; C, 50.87; H, 4.26; N, 6.60%. Calcd for $C_{18}H_{18}N_2O_8S$: C, 51.18; H, 4.27; N, 6.64%.

General Procedure for the Unsaturation of the Anhydronucleoside (IV). A mixture of IV (210 mg, 0.5 mmol) and sodium iodide (1.5 g, 10 mmol) in the appropriate solvent (DMF, hexamethylphosphotriamide, or 1,3-dimethyl-2-imidazolidinone,[6] 20 ml) was refluxed for an appropriate time with stirring. The addition of water (30 ml) to the reaction mixture while it was hot gave the crystalline starting material (IV), which was identified by IR. To the filtrate we then added ethyl acetate (50 ml), and the organic layer was washed with thiosulfate and water, dried over Na_2SO_4, and evaporated. The crystals thus obtained were recrystallized from acetone to afford *1-(4',6'-O-benzylidene-2',3'-dideoxy-β-*D-erythro-*hex-2'-enopyranosyl)uracil (V)*; mp 228—230 °C (dec); $[\alpha]_D^{22}$ +32° (*c* 0.75 in DMF); UV (EtOH) λ_{max} 257 nm (log ε 3.75); NMR [$(CD_3)_2SO$] δ=7.45 (1H, d, $J_{5,6}$=8 Hz, H-6), 7.40 (5H, C_6H_5), 6.52 (1H, d, $J_{1',2'}$=3 Hz, H-1'), 6.50 (1H, d, $J_{2',3'}$=10 Hz, H-3'), 5.70 (1H, d, $J_{2',3'}$=10 Hz, H-2'), 5.70 (1H, s, PhCH), 5.65 (1H, d, $J_{5,6}$=8 Hz, H-5), 3.7—4.5 (4H, m, H-4', -5', -6', and -6"). Found: C, 61.24; H, 4.84; N, 8.25%. Calcd for $C_{17}H_{16}N_2O_5 \cdot 1/4H_2O$: C, 61.29; H, 4.96; N, 8.41%.

*1-(2',3'-Dideoxy-β-*D-erythro-*hex-2'-enopyranosyl)uracil (VI).* A mixture of V (140 mg) in 80% aqueous acetic acid (10 ml) was refluxed for 15 min; then, after cooling, the clear solution was evaporated to a syrup. Preparative TLC (silica gel, 10 v/v% EtOH–benzene) of the syrup afforded a pure product (VI) (50 mg, 50%); mp 161—163°; $[\alpha]_D^{22}$ +84° (*c* 0.33 in EtOH); NMR [$(CD_3)_2SO$] δ=7.34 (1H, d, $J_{5,6}$=9 Hz, H-6), 6.28 (1H, q, $J_{1',2'}$=$J_{1',3'}$=2.0 Hz, H-1'), 6.15 (1H, dt, $J_{2',3'}$=10 Hz, $J_{1',3'}$=$J_{3',4'}$=2.0 Hz, H-3'), 5.64 (1H, dt, $J_{2',3'}$=10 Hz, $J_{1',2'}$=$J_{2',4'}$=2.0 Hz, H-2'), 5.62 (1H, d, $J_{5,6}$=9 Hz, H-5), 4.04 (1H, m, H-4'), and 3.2—3.8 (3H, m, H-5', -6', and -6"). Found: C, 50.35; H, 5.05; N, 11.79%. Calcd for $C_{10}H_{12}N_2O_5$: C, 50.0; H, 5.04; N, 11.66%.

The authors wish to thank Professor Sakurai, Tohoku University, for providing the 1,3-dimethyl-2-imidazolidinone.

References

1) T. Yamazaki, H. Sugiyama, N. Yamaoka, K. Matsuda, and S. Seto, *Carbohydr. Res.*, **50**, 278 (1976); *J. Chem. Soc., Perkin Trans. 1*, **1977**, 1981.

2) T. Yamazaki, H. Shiraishi, K. Matsuda, H. Sugiyama, S. Seto, and N. Yamaoka, *J. Chem. Soc., Chem. Commun.*, **1975**, 518. T. Yamazaki, K. Matsuda, H. Sugiyama, S. Seto, and N. Yamaoka, *J. Chem. Soc., Perkin Trans. 1*, **1977**, 1654.

3) R. J. Suhadolnik, "Nucleoside Antibiotics," Wiley Interscience, New York (1970), p. 170.

4) Compound (I) was prepared by the method used for nitromethane-mercury cyanide [N. Yamaoka, K. Aso, and K. Matsuda, *J. Org. Chem.*, **30**, 149 (1965)].

5) F. W. Lichtenthaler, T. Ueno, and P. Voss, *Bull. Chem. Soc. Jpn.*, **47**, 2304 (1974).

6) F. Kondo, D. Sc. Thesis, Tohoku University (1976).

BULLETIN OF THE CHEMICAL SOCIETY OF JAPAN, VOL. 50 (12), 3425—3426 (1977)

The Synthesis of the (Diacetylmethyl)tropylium Ion and Its Transformation to the 3-Acetyl-2-methylfurotropylium Ion

Koichi KOMATSU, Satoshi TANAKA, Seiki SAITO,* and Kunio OKAMOTO

Department of Hydrocarbon Chemistry, Faculty of Engineering, Kyoto University, Sakyo-ku, Kyoto 606

* *Department of Synthetic Chemistry, School of Engineering, Okayama University, Tsushima, Okayama 700*

(Received May 17, 1977)

Synopsis. The intramolecularly hydrogen-bonded cation, the (diacetylmethyl)tropylium ion (**3**), has been synthesized. The deprotonation of **3** does not afford 8,8-diacetylheptafulvene, but does give the intramolecularly cyclized cycloheptatriene derivative, which can be transformed to the peripheral ten-π-electron cation, **5**; **5** is characterized by means of ^{13}C NMR spectroscopy.

The deprotonation of substituted tropylium ions is known as the facile method to generate 8-substituted heptafulvenes.[1] Especially, the tropylium ion with an electron-withdrawing group at the α-carbon of the substituent can be regarded as a potential precursor for the stable 8-substituted heptafulvene. Here we wish to report on the synthesis of the (diacetylmethyl)tropylium ion (**3**), the "formal" precursor of 8,8-diacetylheptafulvene, and its transformation to the new ten-π-electron cation, the 3-acetyl-2-methylfurotropylium ion (**5**).

The whole reaction sequence is shown in Scheme 1. The reaction of the trityl cation with the 3-substituted cycloheptatriene, **2**, successfully afforded the **3** cation in a good yield, whereas the reaction with the 7-substituted cycloheptatriene, **1**, was found only to regenerate the unsubstituted tropylium ion in an 81.3% yield. The perchlorate of the **3** cation consists of brownish yellow crystals, stable in air. The IR and NMR spectral data indicated that the diacetylmethyl group of **1** is in the keto form, whereas those of **2** and **3** are in the intramolecularly hydrogen-bonded enol form. The spectrophotometric titration carried out in 23% EtOH indicated the pK_a value for the **3** cation to be 0.72.

As is suggested by the considerable acidity of **3**, a facile deprotonation occurred when **3** was treated with triethylamine in dichloromethane. However, contrary to what was expected, the product (a pale orange oil) was not 8,8-diacetylheptafulvene, but the cycloheptatriene derivative, **4**, that was possibly formed by the intramolecular nucleophilic attack of the enolate anion on the positively charged seven-membered ring.[2] The cyclization product, **4**, is somewhat unstable at room temperature and can be quantitatively reconverted to the **3** cation when treated with proton acids. On the other hand, the hydride abstraction of **4** with the trityl cation gave the perchlorate of the **5** cation as an air-stable, greenish-blue powder.

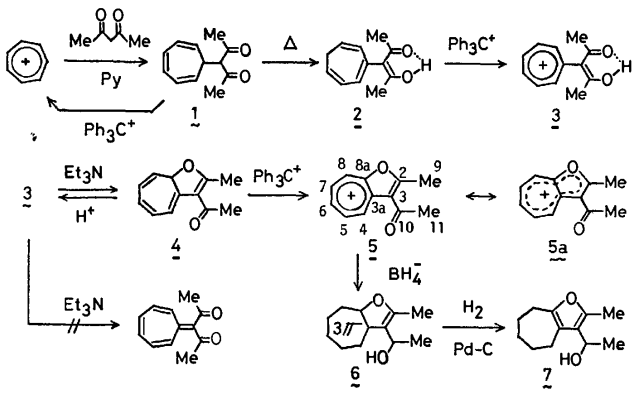

Scheme 1.

The structure of **5** was confirmed by the chemical transformations (**5**→**6**→**7**) shown in Scheme 1. The hydrogenated product, **7**, exhibited the UV spectrum characteristic of the substituted furans.[3] In the NMR spectrum of **5**, the one-proton multiplet resonating in the lowest field is assigned to H-4, taking into account the diamagnetic anisotropy effect of the acetyl-carbonyl group; therefore, the averaged conformation of the acetyl group appears to be almost coplanar to the molecular plane. The UV-visible spectrum of **5** exhibits the longest wavelength absorption at 634 nm (log ε, 2.46). A comparison of the UV-visible spectrum of **5** with that of 1-acetyl-2-methylazulene[4] suggests the resemblance of the electronic state of **5**, with its furan oxygen donating two unshared 2p electrons to the conjugated π-system, to that of the corresponding azulene derivative. Thus, there seems to be some contribution of the structure, **5a**, to the resonance hybrid of **5**.

Table 1. ^{13}C NMR data for **4** and **5** in CD_3CN

Carbon	δ (ppm from TMS)		Charge density
	4	**5**	**5**
2	178.7 s	176.9 s	+0.2982
3	116.3 s	122.6 s	−0.0834
3a	138.9 s	149.8 s	+0.1029
4	127.2 d	145.9 d	+0.1358
5	132.7 d	147.2 d	+0.1120
6	123.6 d	151.0 d	+0.1307
7	116.7 d	145.4 d	+0.1162
8	111.0 d	136.9 d	+0.1244
8a	84.7 d	165.2 s	+0.1357
9	17.2 q	17.6 q	—
10	194.0 s	194.3 s	+0.4431
11	31.1 q	31.9 q	—

The ^{13}C NMR spectral data for **5** are shown in Table 1, together with those for the neutral compound, **4**. The signal assignment for **5** was made on the basis of the peak multiplicity observed in the off-resonance spectrum and on that of the charge density obtained by the simple HMO calculation using the following parameters: $h_{\dot{O}}=2.0$, $k_{\dot{O}}=\sqrt{2}$; $h_{\ddot{O}}=2.0$, $k_{\ddot{O}}=0.6$. Each carbon in the seven-membered ring as well as the C-3 in the fused furan ring are shown to be definitely shifted to a lower

field upon transformation from **4** to **5**, corresponding to the introduction of the positive charge. Furthermore, it is indicated that the general trend in the π-electron distribution of **5** also resembles that of benzofuran,[5] by a comparison of the ^{13}C chemical shifts observed and reported for these compounds.

Experimental

(Diacetylmethyl)tropylium Perchlorate (3 ClO_4^-). The reaction of tropylium fluoroborate (7.12 g, 40.0 mmol) with acetylacetone (4.00 g, 40.0 mmol) in dry pyridine (80 ml) afforded 7-(diacetylmethyl)cycloheptatriene (**1**)† (7.30 g, 96.0%) as a white powder after a usual work-up; mp 122.1—123.1 °C (from benzene); IR (KBr) 1720 cm^{-1} (C=O); NMR ($CDCl_3$) δ=2.13 (s, 6, CH_3), 2.83 (dt, 1, H^7), 3.91 (d, 1, $CHAc_2$), 5.10 (dd, 2, $H^{1,6}$), 6.20 (m, 2, $H^{2,5}$), and 6.65 ppm (t, 2, $H^{3,4}$). The cycloheptatriene, **1** (2.18 g, 11.5 mmol), was sealed in an ampoule under a vacuum and heated at 155 °C for 2.5 h. Purification by preparative TLC (benzene–ether (97: 3)/SiO_2) and successive vacuum distillation gave 3-(diacetylmethyl)cycloheptatriene (**2**) (1.12 g, 51.4%) as white crystals; bp 89.5 °C/ 0.3 Torr; IR (KBr) 1600 cm^{-1} (C=O···HO); NMR (CCl_4) δ=2.00 (s, 6, CH_3), 2.33 (t, 2, CH_2), 5.38 (dt, 2, $H^{1,6}$), 5.97 (d, 1, H^2), 6.13 (dd, 1, H^5), 6.45 (d, 1, H^4), and 16.50 ppm (s, 1, OH). A mixture of trityl perchlorate (4.38 g, 12.8 mmol) and **2** (2.42 g, 12.7 mmol) in dry acetonitrile (10 ml) was stirred at room temp for 20 min and at 60 °C for 15 min. The addition of ethyl acetate (50 ml) and ether (20 ml) afforded **3** ClO_4^-† (3.14 g, 85.6%); mp 137.1—139.2 °C (dec); UV $\lambda_{max}^{MeCN-10\%HCl(1:1)}$ 222 nm (log ε, 4.42), 263 (3.86), 302 (3.68), and 425 (3.68); IR (KBr) 3200—2800 (O–H···O=C), 1598 (C=O···HO), and 1080 cm^{-1} (ClO_4^-); NMR (CF_3COOH) δ=2.23 (s, 6, CH_3) and 9.28 ppm (s, 6, $C_7H_6^+$). The pK_a value was determined by the spectrophotometric method described previously.[6]

3-Acetyl-2-methylfurotropylium Perchlorate (5 ClO_4^-). The reaction of triethylamine (0.399 g, 3.95 mmol) with **3** ClO_4^- (1.00 g, 3.47 mmol) in dichloromethane (80 ml) for 30 min at room temp and a subsequent work-up yielded **4** (0.705 g, 107%); UV λ_{max}^{MeCN} 229 nm (log ε, 4.22), 286 sh (3.76), and 320 (3.80); IR (neat) 1655 cm^{-1} (conj. C=O); 100 MHz NMR ($CDCl_3$; the numbering is the same as in **5**) δ=2.33 (s, 3, CH_3), 2.41 (s, 3, $COCH_3$), 4.85 (m, 1, >CH–), 5.15 (dd, 1, H^8), 6.00 (ddd, 1, H^7), 6.23 (ddt, 1, H^6), 6.39 (dm, 1, H^4), and 6.58 ppm (ddm, 1, H^5). The reaction of trityl perchlorate (1.43 g, 4.18 mmol) with **4** (0.720 g, 3.81 mmol) in dry acetonitrile (3 ml) for 35 min at room temp gave, after the addition of ethyl acetate and ether, **5** ClO_4^-† (0.907 g, 82.9%) as a greenish blue powder; mp 140.0—141.1 °C (dec); UV λ_{max}^{MeCN} 218 nm (log ε, 4.39), 260 (4.43), 363 (3.85), 590 sh (2.17), and 634 (2.46); IR (KBr) 1660 (conj. C=O) and 1090 cm^{-1} (ClO_4^-); NMR (CF_3COOH) δ=3.00 (s, 3, CH_3), 3.30 (s, 3, $COCH_3$), 9.15 (m, 4, H^{5-8}), and 10.20 ppm (m, 1, H^4).

Reduction of 5. A solution of **5** ClO_4^- (0.848 g, 2.96 mmol) in acetonitrile (50 ml) was added, dropwise, to a stirred suspension of sodium borohydride (0.179 g, 4.73 mmol) in acetonitrile (15 ml). After 1 h at room temp, the orange solution was worked up to give a crude product (0.668 g), from which **6** (0.274 g, 48.7%) was isolated by means of preparative TLC (benzene–ether (4: 1)/SiO_2); IR (neat) 3360 cm^{-1} (OH); NMR (CCl_4) δ=1.37 (br d, 3, CH_3), 2.00 (br s, 1, OH), 2.23 (sx3, 3, >C–CH_3), 3.05 (t, 2, CH_2), 4.73 (qx3, 1, >CH–), and 5.0—6.8 ppm (m, 4, =CH–). Then, **6** (0.151 g, 0.794 mmol) was hydrogenated over palladium–carbon in benzene–ether (3: 1), yielding **7** (0.0671 g, 43.6%) as a colorless oil after purification by preparative TLC (benzene/SiO_2); UV λ_{max}^{EtOH} 217 nm (log ε, 3.82); IR (neat) 3350 cm^{-1} (OH); NMR (CCl_4) δ=1.25 (d, 3, CH_3), 1.61 (br s, 6, $-(CH_2)_3-$), 2.07 (s, 4, >C–CH_3 +OH), 2.44 (br m, 4, >C–CH_2–), and 4.58 ppm (q, 1, >CH–); MS *m/e* 194 (M^+).

† Satisfactory analytical results were obtained.

References

1) a) K. Hafner, *Angew. Chem.*, **75**, 1041 (1963); b) H. J. Dauben, Jr., and R. B. Medz, Abstr., p. 7s, 145th Annual Meeting of the American Chemical Society, N. Y., 1963; c) D. J. Bertelli, C. Golino, and D. L. Dreyer, *J. Am. Chem. Soc.*, **86**, 3329 (1964); d) M. Oda and Y. Kitahara, *Chem. Commun.*, **1969**, 352; e) K. M. Rapp and J. Daub, *Tetrahedron Lett.*, **1976**, 2011; f) K. Komatsu, M. Fujimori, and K. Okamoto, *Tetrahedron*, in press.

2) A similar type of cyclization has been reported to take place at the deprotonation of the (1-benzoylethyl)tropylium ion; D. J. Bertelli, P. O. Crews, and S. Griffin, *Tetrahedron*, **24**, 1945 (1968).

3) See, for example, I. M. Heilbron, E. R. H. Jones, P. Smith, and B. C. L. Weedon, *J. Chem. Soc.*, **1946**, 54.

4) $\lambda_{max}^{cyclohexane}$ 240 nm (log ε 4.25), 297 (4.54), 383 (3.68), 548 (2.51), and 565 (2.50); E. Heilbronner and R. Gerdil, *Helv. Chim. Acta*, **39**, 1996 (1956).

5) The ^{13}C chemical shifts reported for benzofuran are δ (ppm from TMS in dioxane) 145.9 (C-2), 107.3 (C-3), 128.5 (C-3a), 123.6 (C-4), 125.1 (C-5), 122.0 (C-6), 112.1 (C-7), 155.9 (C-7a); R. J. Abraham, D. F. Wileman, G. R. Bedford, and D. Greatbanks, *J. Chem. Soc., Perkin Trans. 2*, **1972**, 1733.

6) K. Okamoto, K. Komatsu, O. Murai, O. Sakakguchi, and Y. Matsui, *Bull. Chem. Soc. Jpn.*, **46**, 1785 (1973).

BULLETIN OF THE CHEMICAL SOCIETY OF JAPAN, VOL. 50 (12), 3427—3428 (1977)

Reaction of Bis(*trans*-1-hexenyl)methylborane with Two Molar Equivalents of Methylcopper(I). Evidence for the Presence of *trans*-1-Hexenylcopper(I) as an Intermediate

Yoshinori YAMAMOTO, Hidetaka YATAGAI, Kazuhiro MARUYAMA, Akio SONODA,* and Shun-Ichi MURAHASHI*

Department of Chemistry, Faculty of Science, Kyoto University, Kyoto 606

** Faculty of Engineering Science, Osaka University, Osaka 560*

(Received May 18, 1977)

Synopsis. Bis(*trans*-1-hexenyl)methylborane, prepared by the reaction of bis(*trans*-1-hexenyl)chloroborane with methyllithium, was treated with 2 molar equivalents of methylcopper(I) at −78 °C to give (5*E*,7*E*)-5,7-dodecadiene quantitatively. The result indicates the presence of *trans*-1-hexenylcopper(I) intermediate.

It was reported that dialkenylchloroboranes (**1**) react with 3 molar equivalents of methylcopper(I) to give (*E*,*E*)-1,3-dienes (**2**) in a high yield.[1]

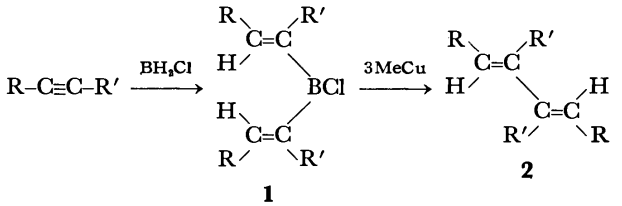

1 **2**

The transformation from **1** to **2** appears to involve the following sequence of reactions (Scheme 1), proceeding through an alkenylcopper(I) intermediate.[2] Actually, the reaction of (1-butyl-1-hexenyl)dimethylborane (**3**) with an equivalent amount of methylcopper(I) gave

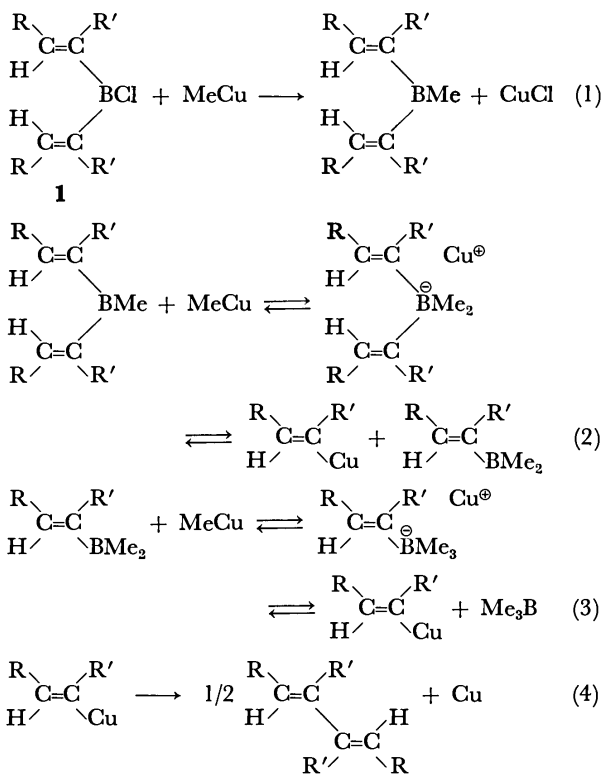

Scheme 1. Proposed mechanism.

(5*E*,7*E*)-6,7-dibutyl-5,7-dodecadiene (**4**) in *ca.* 100% yield.[2] The result strongly supports the process shown by Eq. 3. However, no verification of Eq. 2 was obtained.[2] We wish to report an experimental evidence, establishing the proposed mechanism in Scheme 1.

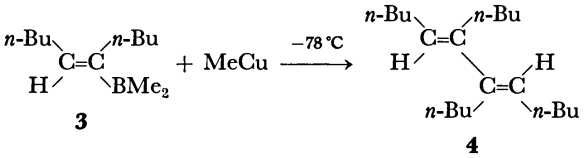

3 **4**

Results and Discussion

Bis(*trans*-1-hexenyl)methylborane (**5**) was prepared by the reaction of bis(*trans*-1-hexenyl)chloroborane with an equivalent amount of methyllithium at −78 °C. An ether solution of **5** was slowly added to an ether suspension of 2 molar equivalents of methylcopper(I) at −78 °C. The color immediately changed from yellow to black. GLPC analysis revealed the approximately quantitative formation of (5*E*,7*E*)-5,7-dodecadiene (**6**).

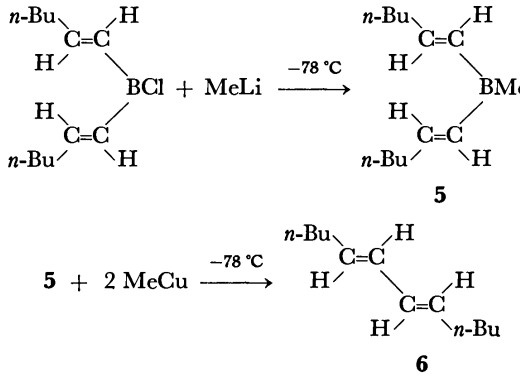

5 **6**

The result indicates that process (2) is involved in the transformation from **1** to **2**. Since an alkenylcopper(I) is far more unstable than methylcopper(I), it dimerizes even at low temperature (probably>−30 °C) (Eq. 4). Consequently, the equilibrium in Eqs. 2 and 3 lies to the right, two molar equivalents of methylcopper(I) being necessary for **5** to complete the reaction.

Process (1) was confirmed by GLPC examination of the borane product; the direct GLPC analysis (SE-30) of the reaction product from bis(*trans*-1-hexenyl)-chloroborane with an equivalent amount of methylcopper(I) at −78 °C revealed the quantitative formation of **5**.

As regards the copper(I) borates in Scheme 1, direct transmetalation from the alkenylboranes to the alkenyl-

copper(I) without passing through the copper(I) borates can be proposed as an alternative mechanism. So far we have no unambiguous evidence for such copper species. Copper(I) tetraarylborates were prepared by cation exchange reaction.[4] Recently copper(I) tetraalkylborates have been used for organic synthesis.[5] By analogy to these results, it is reasonable to assume the presence of copper(I) dialkenyldimethylborate and copper(I) alkenyltrimethylborate. The present results provide an evidence for the formation of alkenylcopper(I) species, confirming the mechanism in Scheme 1.

The lithium borates (**7**) prepared from bis(*trans*-1-hexenyl)chloroborane and 2 molar equivalents of methyllithium react with 2 molar equivalents of methylcopper(I) to give **6** in 82% yield.[1]

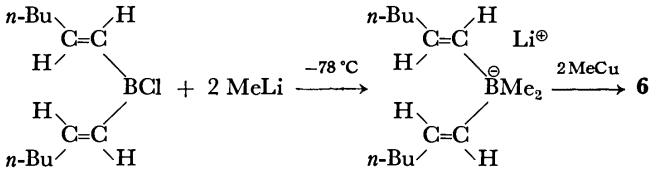

7

The result can be explained according to Scheme 1 by an equilibrium between the lithium borate (**7**) and the copper(I) borate (**8**).[6]

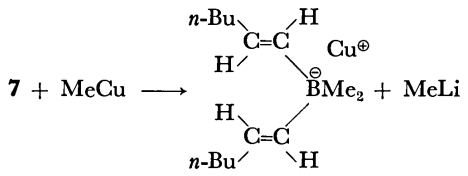

8

Experimental

All temperatures were uncorrected. The NMR spectra were obtained on a Jeol JNM-MH-60 spectrometer, TMS being chosen as an internal standard. GLPC analyses were carried out on a Yanagimoto GCG 550T using a 2 m column packed with SE-30 10 wt% on Celite 545 AW.

Materials. The reagent grade solvent and copper(I) iodide were purified by standard techniques. Commercial 1-hexene was used. $BH_2Cl:OEt_2$[7] and methyllithium[8] were prepared according to the known procedures. The titration of methyllithium was performed according to the method of Watson and Eastham.[9]

Preparation of **5**. To an ether solution of bis(*trans*-1-hexenyl) chloroborane, prepared from the reaction of 1-hexyne with $BH_2Cl:OEt_2$,[7] was added an equivalent amount of methyllithium ether solution at −78 °C. The temperature was regulated to reach room temperature in 1—2 h. Bis(*trans*-1-hexenyl)methylborane was then distilled under reduced pressure; 80—90% yield; bp 65—70 °C/0.5 mmHg NMR(δ in CCl_4, J=Hz) 6.73 (d—t, 2H, J_d=16, J_t=6), 6.16 (d, 2H, J_d=16) 2.44—1.80 (m, 4H), 1.80—1.20 (m, 8H), 0.90 (t, 6H, J_t=6), 0.70 (s, 3H).

Reaction of **5** *with Methyl Copper(I).* The reaction was carried out as described previously.[2] The reaction mixture was analyzed by GLPC with an appropriate internal standard (dodecane). The structure of **6** was assigned by comparison with an authentic sample.[1] Methanol should be produced according to Scheme 1. The peak corresponding to methanol was observed, but its precise yield could not be determined under the present analytical conditions.

*Reaction of the Lithium Borate (***7***).* To an ether solution of bis(*trans*-1-hexenyl) chloroborane was added 2 molar equivalents of methyllithium ether solution at −78 °C. The temperature was regulated to reach 0 °C in 1—2 h. In this case, lithium borate (**7**) was not isolated but directly reacted with methylcopper(I) as described above. The product was analyzed by GLPC with dodecane as an internal standard.

References

1) Y. Yamamoto, H. Yatagai, and I. Moritani, *J. Am. Chem. Soc.*, **97**, 5606 (1975).

2) Y. Yamamoto, H. Yatagai, K. Maruyama, A. Sonoda, and S-I. Murahashi, *J. Am. Chem. Soc.*, **99**, 5652 (1977).

3) G. M. Whitesides, C. P. Casey, and J. K. Krieger, *J. Am. Chem. Soc.*, **93**, 1379 (1971). For the stability of MeCu(I), see G. H. Posner, "Organic Reactions," Vol. 22, Wiley, New York (1975), p. 253.

4) A. N. Nesmeyanov, V. A. Sazonova, G. S. Liberman, and L. I. Yemelyanova, *Izv. Akad. Nauk SSSR, Otd. Khim. Nauk*, **1955**, 48.

5) N. Miyaura, M. Itoh, and A. Suzuki, *Tetrahedron Lett.*, **1976**, 255; *Synthesis*, **1976**, 618; N. Miyaura, N. Sasaki, M. Itoh, and A. Suzuki, *Terahedron Lett.*, **1977**, 173.

6) The complex (**7**) is stable and does not give the diene if it is not treated with methylcopper(I).

7) H. C. Brown, "Organic Syntheses *via* Boranes," Wiley, New York (1975).

8) "Organic Syntheses," Coll. Vol. V, Wiley, New York (1973), p. 859.

9) S. C. Watson and J. F. Eastham, *J. Organomet. Chem.*, **9**, 165 (1967).

BULLETIN OF THE CHEMICAL SOCIETY OF JAPAN, VOL. 50 (12), 3429—3430 (1977)

The Photochemical Synthesis of 2-Chloro-3-(2-furyl)-1,4-naphthoquinones

Kazuhiro MARUYAMA and Tetsuo OTSUKI

Department of Chemistry, Faculty of Sciences, Kyoto University, Kyoto 606

(Received May 31, 1977)

Synopsis. Upon the irradiation of a benzene solution of 2,3-dichloro-1,4-naphthoquinone, **1**, and furan derivatives, **2**, 2-chloro-3-(2-furyl)-1,4-naphthoquinones, **3**, were obtained, accompanyed by a liberation of hydrogen chloride. The formation of a CT-complex between **1** and **2** was essential for the progress of the reaction. The ^{1}H-CIDNP signals which were observed during irradiation suggest an intervention of a radical pair in the reaction.

Many workers have reported synthetic methods of a variety of quinones, applying the addition reaction of radicals to quinones,[1] the reaction of organometallic reagents with quinones,[1] and the photochemical reaction of quinones with aldehydes.[2] Here we wish to report on a new photochemical synthetic route to 2-furyl derivatives of 1,4-naphthoquinones.

Results and Discussion

As a typical example the photochemical reaction of 2,3-dichloro-1,4-naphthoquinone, **1**, with the **2a** furan will be illustrated. The irradiation of a benzene solution of **1** and **2a** by a high-pressure Hg arc lamp gave a photo-substitution product, **3a**, as red needles in a yield of 82%, accompanied by the liberation of hydrogen chloride. The hydrogen chloride liberated in the reaction was estimated by titration with a standardized aqueous sodium hydroxide solution; the amount of it reached 84% of that of **3a**. The structure of **3a** was compatible with its spectral data and was further confirmed by its chemical reactions (Scheme 1).[3-5]

When the photochemical reaction was examined by means of the ^{1}H-CIDNP technique, strongly polarized signals were observed during the course of the reaction (Fig. 1). The polarized signals, 1, 2, and 3, were all assignable to furyl-ring protons of **3a**. This suggests that the photo-substitution product, **3a**, is produced *via* a radical pair.

When **2a** was added to a benzene solution of **1** (λ_{max}: 439 nm), a new absorption band (λ_{max}: 465 nm) (shoulder) appeared which was ascribable to the CT-complex between **1** and **2a**.[6,7] When the CT-band was irradiated by the light of a selected wavelengthth (λ_{max}: 488 nm, $\Delta_{1/2}$=20 nm), the product, **3a**, was exclusively produced, the yield being improved to 92%. This result indicates an important contribution of the CT-complex in the initial stage of the reaction (Scheme 2).

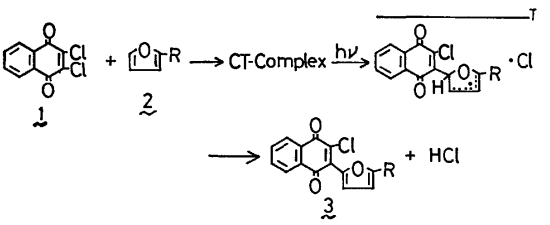

R=**a**: H, **b**: CH_3, **c**: CH_2OCH_3, **d**: $CH_2OC_2H_5$, **e**: $CH_2OC_3H_7$, **f**: CH_2O-phytyl **g**: CH_2O-tetra-*O*-acetyl-*β*-D-glycopyranosyl, **h**: CH_2OCOCH_3, **i**: CH_2OCO-CH_2N-phthaloyl.

Scheme 2.

Such furan derivatives as **2a**—**i**, which formed CT-complexes with **1**, behaved similarly in the photochemical reaction and gave photo-products, **3a**—**i**, in fairly good yields (*cf.* Experimental). Thus, the present reaction provides a good method of synthesizing 2-chloro-3-(2-furyl)-1,4-naphthoquinones. During the course of all the reactions, the ring- and α-protons of furyl ring due to the corresponding photo-substitution products, **3a**—**i**, showed polarized ^{1}H-CIDNP signals (Figs. 1—3). In contrast, such furan derivatives as **2j**—**n**, which gave no indication of CT-complex formation with **1**, did not undergo a similar photo-substitution reaction. The importance of the formation of the CT-complex was further supported by the results of the photochemical reactions of other 1,4-naphthoquinones with **2a**. That is, 2,3-dibromo-1,4-naphthoquinone gave a photo-substitution product, **10**, in the reaction with **2a**, but 2-chloro- and 2-bromo-1,4-naphthoquinone gave another types of products.[8]

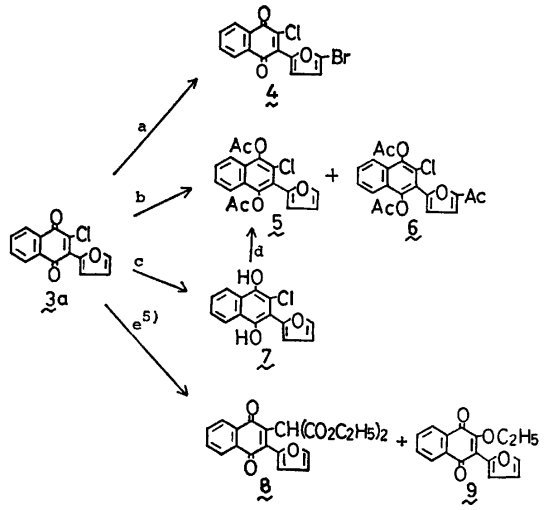

a) Br_2, $CHCl_3$, r.t., 1 h b) Zn–Ac_2O, reflux, 0.5 h c) H_2(Pd/C), ethanol, r.t., 0.5 h d) Ac_2O–Pyridine, r.t., 4 h e) NaCH $(CO_2C_2H_5)_2$, ethanol, r.t., 0.5 h.

Scheme 1.

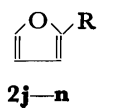

2j—**n**

R= **j**: CHO
k: $CH(SCH_2)_2$
l: CO_2H
m: CO_2CH_3
n: Benzofuran

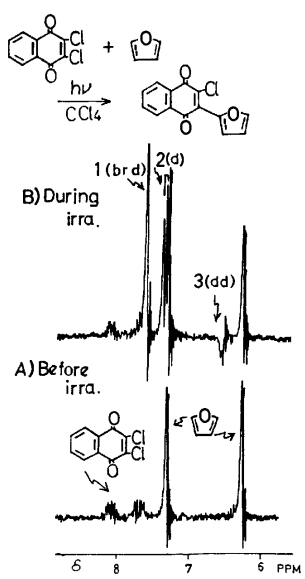

Fig. 1. ^{1}H-NMR spectra observed in the photochemical reaction of **1** with **2a** (Solvent: CCl_4). A) Before irradiation, B) during irradiation. Signal 1, 2, and 3 are polarized signals.

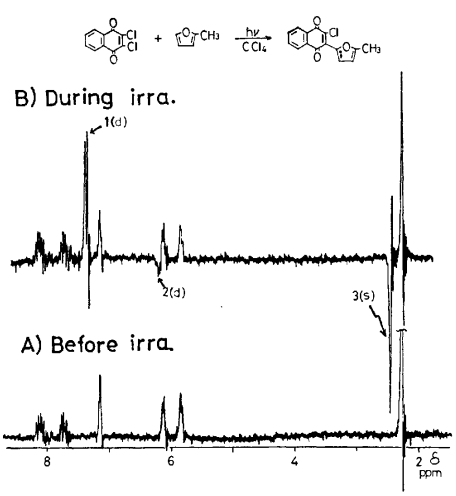

Fig. 2. ^{1}H-NMR spectra observed in the photochemical reaction of **1** with **2b** (Solvent: CCl_4). A) before irradiation, B) during irradiation. Signals 1, 2, and 3 are polarized signals.

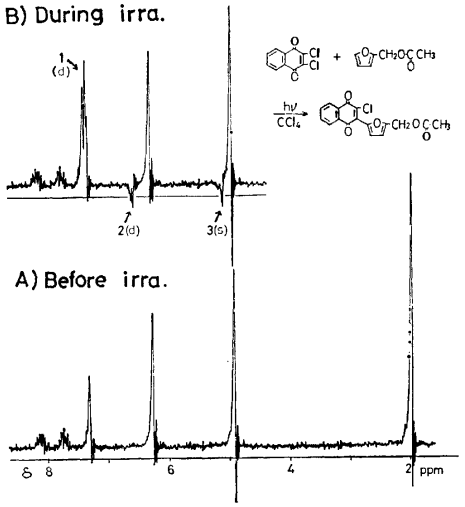

Fig. 3. ^{1}H-NMR spectra observed in the photochemical reaction of **1** with **2h** (Solvent: CCl_4). A) Before irradiation, B) during irradiation. Signals 1, 2, and 3 are polarized signals.

Experimental

General Procedure. A benzene solution of 2,3-dichloro-1,4-naphthoquinone, **1** (1.5×10^{-3} M), and an excess amount of a furan derivative, **2** (*ca.* 4.5×10^{-2} M), was irradiated by means of a high-pressure Hg arc lamp (300 W) at room temperature. After the complete consumption of **1**, the photosubstitution product, **3**, was isolated using chromatography on silica gel.

Identification of the Products. *2-Chloro-3-(2-furyl)-1,4-naphthoquinone (**3a**)*; red needles, mp 137—138 °C; yield, 82 %. Found: C, 64.95; H, 2.88; Cl, 13.69%. Calcd for $C_{14}H_7O_3Cl$: C, 65.00; H, 2.73; Cl, 13.71%. Mass *m/e*=260, 258 (M^+). IR(KBr) 1680, 1665 cm^{-1}. NMR($CDCl_3$) δ 6.60 (1H, d of d, J=4 and 2Hz), 7.40 (1H, d, J=4 Hz), 7.72 (1H, d, J=2 Hz), 7.6—7.8 (2H, m), 8.0—8.2 (2H, m). UV λ_{max} ($CHCl_3$): 443 nm (ε: 5.5×10^3), 321 (sh) (5.6×10^3), 272 (2.2×10^4). *2-Chloro-3-(5-methyl-2-furyl)-1,4-naphthoquinone (**3b**)*; red crystals, mp 123 °C; yield, 65%. Mass *m/e*=272 (M^+). *2-Chloro-3-(5-methoxymethyl-2-furyl)-1,4-naphthoquinone (**3c**)*; red crystals; mp 107—108 °C; yield, 49%. Mass *m/e*=304, 302 (M^+). *2-Chloro-3-(5-ethoxymethyl-2-furyl)-1,4-naphthoquinone (**3d**)*; red crystals; mp 68 °C; yield, 38%. Mass *m/e*=318, 316 (M^+). *2-Chloro-3-(5-propoxymethyl-2-furyl)-1,4-naphthoquinone (**3e**)*; red crystals; mp 51.5—53.0 °C; yield, 51%. Mass *m/e*=322,330 (M^+). *2-Chloro-3-(5-phytyloxymethyl-2-furyl)-1,4-naphthoquinone (**3f**)*; yellow oil; yield 7%. IR (KBr) 1680 cm^{-1}. NMR($CDCl_3$) δ 0.8—2.2 (36 H, m), 4.10 (2H, d, J=8 Hz), 4.54 (2H, s), 5.36 (1H, t, J=8 Hz), 6.56 (1H, d, J=4 Hz), 7.42 (1H, d, J=4 Hz), 7.7—7.9 (2H, m), 8.0—8.2 (2H, m). *2-Chloro-3-[5-(tetra-O-acetyl-β-D-glucopyranosyloxymethyl)-2-furyl]-1,4-naphthoquinone (**3g**)*; red crystals; mp 160 °C (dec); yield, 22%. IR(KBr) 1755, 1735, 1720, 1675 cm^{-1}. NMR($CDCl_3$) δ 2.00 (3H, s), 2.04 (6H, s), 2.12 (3H, s), 4.1—5.3 (9H, m), 6.64 (1H, d, J=4 Hz), 7.48 (1H, d, J=4 Hz), 7.7—7.9 (2H, m), 8.1—8.3 (2H, m). *2-Chloro-3-(5-acetoxymethyl-2-furyl)-1,4-naphthoquinone (**3h**)*; red crystals; mp 96—97 °C; yield, 47%. Mass *m/e*=322,330 (M^+). *2-Chloro-3-[5-(N-phthaloylglycyloxymethyl)-2-furyl]-1,4-naphthoqiunone (**3i**)*; red crystals; mp 140—142 °C; yield, 25%. IR(KBr) 1770, 1750, 1720, 1670 cm^{-1}. NMR($CDCl_3$) δ 4.48 (2H, s), 5.26 (2H, s), 6.66 (1H, d, J=4 Hz), 7.38 (1H, d, J=4 Hz), 7.6—8.0 (6H, m), 8.0—8.2 (2H, m). *2-Bromo-3-(2-furyl)-1,4-naphthoquinone (**10**)*; red crystals; mp 146—147 °C; yield, 40%. Mass *m/e*=304,302(M^+).

References

1) K. T. Finkley, in "The Chemistry of the Quinonoid Compounds," ed by S. Patai, John Wiley & Sons, London (1974), p. 877.

2) J. M. Bruce, in "The Chemistry of Quinonoid Compounds," ed by S. Patai, John Wiley & Sons, London (1974), p. 465; K. Maruyama and Y. Miyagi, *Bull. Chem. Soc. Jpn.*, **47**, 1303 (1974).

3) 2-Acetyl-3-(2-furyl)-1,4-naphthoquinone has been prepared by the thermal reaction of 2-acetyl-1,4-naphthoquinone with furan; *cf.* C. H. Eugster and P. Bosshard, *Helv. Chim. Acta*, **46**, 815 (1963); N. B. Bauman, S. Fumagalli, G. Weisgerber, and C. H. Eugster, *ibid.*, **49**, 1794 (1966).

4) In the present reaction neither cyclobutanes nor oxetanes were isolated, in contrast to the usual photochemical reaction of furan derivatives with 1,4-naphthoquinone; *cf.* C. H. Krauch and S. Farid., *Tetrahedron Lett.*, **1960**, 4783.

5) The substitution of the chlorine atom of 2,3-dichloro-1,4-naphthoquinone has been reported; *cf.* Fr. Michel, *Chem. Ber.*, **33**, 2402 (1900).

6) *K*, the equilibrium constant for complex formation, was estimated to be 2.8 l/mol by the aid of the Benesi-Hidebrand relation.

7) The new absorption band was comparable to that of the CT-complex between **1** and hexamethylbenzene; *cf.* S. Chatterjee, *J. Chem. Soc., B*, **1971**, 2194. Furan has been reported to form CT-complexes with some electron acceptors, such as chloranil; *cf.* Z. Yoshida and T. Kobayashi, *Tetrahedron*, **26**, 267 (1970).

8) Upon irradiation with 2-chloro- or 2-bromo-1,4-naphthoquinones, the **2a** furan yielded the usual [2+2] photoaddition products.

BULLETIN OF THE CHEMICAL SOCIETY OF JAPAN, VOL. 50 (12), 3431—3432 (1977)

Addition Reaction of Copper(I) Methyltrialkylborates with Ethyl Propiolate. Stereospecific Synthesis of (*E*)-α,β-Unsaturated Acid Esters

Kinji YAMADA, Norio MIYAURA, the late Mitsuomi ITOH, and Akira SUZUKI*

Faculty of Engineering, Hokkaido University, Sapporo 060

(Received June 27, 1977)

Synopsis. The reaction between ethyl propiolate and copper(I) methyltrialkylborates was found to give the corresponding addition products which are converted by hydrolysis into the α,β-unsaturated acid esters in relatively good yields. The α,β-unsaturated esters thus obtained are sclectively *E*-isomers.

Previously, we have reported that copper(I) methyltrialkylborates readily available by the reaction between lithium methyltrialkylborates and copper(I) halides undergo addition reactions to acrylonitrile, ethyl acrylate, and 1-acyl-2-vinylcyclopropanes.[1] These borates also react with alkyl halides such as benzylic,[2] allylic and propargylic halides,[3] and aroyl halides.[4] In the present paper, we wish to report the stereospecific synthesis of (*E*)-α,β-unsaturated carboxylic esters *via* the reaction of copper(I) methyltrialkylborates with ethyl propiolate.

No reaction occurs between ethyl propiolate and lithium methyltrialkylborates at room temperature. However, when copper(I) methyltrialkylborates prepared from lithium methyltrialkylborates and copper(I) halides are used, the reaction proceeds smoothly to give α,β-unsaturated esters together with ethyl 2-butenoate (Eqs. 1 and 2).

$$R_3B + MeLi \longrightarrow [R_3BMe]Li \xrightarrow{CuX} [R_3BMe]Cu \quad (1)$$

$$[R_3BMe]Cu + HC{\equiv}C\text{-}CO_2Et \longrightarrow RCH{=}CHCO_2Et + CH_3CH{=}CHCO_2Et \quad (2)$$

When copper(I) methyltripropylborate obtained from copper(I) bromide and lithium methyltripropylborate was treated with ethyl propiolate at 0 °C in tetrahydrofuran under nitrogen atmosphere, ethyl (*E*)-2-butenoate, ethyl (*E*)-2-hexenoate, and ethyl (*Z*)-2-hexenoate were formed in 32, 37, and 2% yields, respectively. Ethyl 2-butenoate, an undesirable by-product, is considered to be formed by the addition of methyl group of the methyltripropylborate as an alkylating group. It was found that yields and product ratios of the *E*-isomer depend markedly on the copper(I) halides and solvents employed. The reaction using copper(I) iodide as a halide and 1,2-dimethoxyethane (DME) as a solvent was effective for the prevention of formation of a by-product. Under such reaction conditions, the desired (*E*)-α,β-unsaturated acid esters were obtained in good yields from representative organoboranes. The results are summarized in Table 1. The new reaction is applicable to representative primary trialkylboranes such as propyl, butyl, isobutyl, and hexylboranes. Although the reaction mechanism is still unknown, the formation of (*E*)-α,β-unsaturated acid esters as main products seems to suggest that the reaction proceeds through the *cis*-addition process.[5]

Table 1. (*E*)-α,β-Unsaturated acid esters from copper(I) methyltrialkylborates and ethyl propiolate[a]

Organoborane R_3B, R=	CuX X=	Solvent	Reaction time (h)	Yield of products (%)[b] MeCH=CHCO$_2$Et	Yield of products (%)[b] RCH=CHCO$_2$Et (Ratio of *E*-isomer, %)
Propyl	Br	THF	0.5	32	39 (95)
	I	THF	0.5	36	36 (97)
	Br	DME	0.5	18	44 (98)
	Cl	DME	0.5	19	32 (94)
	I	DME	0.5	5	63 (>99)
Butyl	I	DME	0.5	—	61 (>99)
Isobutyl	I	DME	0.5	—	53 (99)
Hexyl	I	DME	1.0	—	42 (98)

a) All the reactions were carried out by using 20% excess borate complexes. b) Based on ethyl propiolate used. Analyzed by VPC.

The preparation of α,β-unsaturated esters from ethyl propiolate and dialkylboranes was reported by Negishi *et al.*[6] The present reaction, however, provides a more general synthetic method for (*E*)-α,β-unsaturated acid esters from organoboranes.

Experimental

Materials. Commercial copper(I) halides and ethyl propiolate were used. The solvents were purified by distillation before use. Trialkylboranes were prepared by the usual procedure.[7]

The IR and NMR spectra were taken on a Hitachi-Perkin-Elmer Model 125 spectrophotometer and a Hitachi R-22 spectrometer at 90 MHz using tetramethylsilane as an internal standard.

General Procedure. The following procedure for the preparation of ethyl (*E*)-2-hexenoate is representative. A dry 100 ml-flask equipped with a septum inlet and a magnetic stirring bar was flushed with dry nitrogen. The flask was charged with copper(I) iodide (4.68 g, 24 mmol) and dry DME (40 ml). Lithium methyltripropylborate[2] (24 mmol, prepared from equimolar amount of tripropylborane in THF and methyllithium in ether) was added to the solution at 0 °C with stirring. After 5 min, ethyl propiolate (1.9 ml, 20 mmol) was added and the reaction mixture was stirred at 0 °C for 30 min. The residual organoborane was then oxidized with 3 M-aqueous sodium hydroxide (8 ml) and 30% hydrogen peroxide (8 ml) at room temperature for 2 h. The products were extracted with ether and analyzed by VPC. Analysis indicated the presence of 12.6 mmol (63%) of ethyl (*E*)-2-hexenoate and 1.0 mmol (5%) of ethyl (*E*)-2-butenoate. Analytically pure materials were obtained by preparative

* Author to whom all correspondence should be addressed.

VPC. (15% SE-30 on Uniport B, 1.2 m) with Varian autoprep Model-2800.

Identification of the Products. *Ethyl (E)-2-Hexenoate*: n_D^{23} 1.4371. Found: C, 67.48; H, 9.78%. Calcd for $C_8H_{14}O_2$: C, 67.57; H, 9.93%. Mass: $m/e=142$ (M^+). IR (CCl_4); 1720, 1650, 985 cm^{-1}. NMR (CCl_4); τ, 9.02 (3H, t, $J=7.0$ Hz), 8.71 (3H, t, $J=7.0$ Hz), 8.47 (2H, m), 7.80 (2H, q), 5.84 (2H, q), 4.20 (1H, d, $J_{vinyl}=16.0$ Hz), 3.08 (1H, dt, $J=7.0$ and 7.0 Hz).

Ethyl (E)-2-Heptenoate: n_D^{23} 1.4393 (lit,[8] n_D^{25} 1.4355). Found: C, 69.36; H, 10.38%. Calcd for $C_9H_{16}O_2$: C, 69.19; H, 10.32%. Mass; $m/e=156$ (M^+). IR (CCl_4); 1720, 1650, 985 cm^{-1}. NMR (CCl_4); τ, 9.06 (3H, t, $J=7.0$ Hz), 8.75 (3H, t, $J=7.0$ Hz), 8.57 (4H, m), 7.78 (2H, q), 5.87 (2H, q), 4.23 (1H, d, $J_{vinyl}=16.0$ Hz), 3.10 (1H, dt, $J=7.0$ and 7.0 Hz).

Ethyl (E)-5-Methyl-2-hexenoate: n_D^{21} 1.4362. Found: C, 69.07; H, 10.29%. Calcd for $C_9H_{16}O_2$: C, 69.19; H, 10.32%. Mass; $m/e=156$ (M^+). IR (CCl_4); 1725, 1655, 990 cm^{-1}. NMR (CCl_4); τ, 9.03 (6H, d, $J=6.5$ Hz), 8.82 (3H, t, $J=7.0$ Hz), 8.21 (1H, m), 7.93 (2H, t, $J=7.0$ Hz), 5.86 (2H, q), 4.25 (1H, d, $J_{vinyl}=16.0$ Hz), 3.16 (1H, dt, $J=7.0$ and 7.0 Hz).

Ethyl (E)-2-Nonenoate: n_D^{22} 1.4417. Found: C, 71.50; H, 11.07%. Calcd for $C_{11}H_{20}O_2$: C, 71.69; H, 10.94%. Mass; $m/e=184$ (M^+). IR (CCl_4); 1725, 1655, 985 cm^{-1}. NMR (CCl_4); τ, 9.09 (3H, t, $J=6.0$ Hz), 8.72 (3H, t, $J=6.0$ Hz), 8.64 (8H, s), 7.79 (2H, q), 5.86 (2H, q), 4.43 (1H, d, $J_{vinyl}=16.0$ Hz), 3.10 (1H, dt, $J=6.5$ and 6.5 Hz).

References

1) N. Miyaura, M. Itoh, and A. Suzuki, *Tetrahedron Lett.*, **1976**, 255.

2) N. Miyaura, M. Itoh, and A. Suzuki, *Synthesis*, **1976**, 618.

3) N. Miyaura, M. Itoh, and A. Suzuki, *Bull. Chem. Soc. Jpn.*, **50**, 2199 (1977).

4) N. Miyaura, N. Sasaki, M. Itoh, and A. Suzuki, *Tetrahedron Lett.*, **1977**, 173.

5) E. J. Corey and J. A. Katzenellbogen, *J. Am. Chem. Soc.*, **91**, 1851 (1969).

6) E. Negishi, G. Lew, and T. Yoshida, *J. Org. Chem.*, **39**, 2321 (1974).

7) H. C. Brown, "Organic Synthesis *via* Boranes," John-Wiley & Sons, New York (1975).

8) C. J. Martin, A. I. Schepartz, and B. F. Daubert, *J. Am. Chem. Soc.*, **70**, 2601 (1948).